AWARD LECTURE / CONFÉRENCE D'HONNEUR

2003 Alfred Bader Award Lecture
Predicting the rates of chemical reactions

J. Peter Guthrie

Abstract: The dream of being able to predict the rate of a chemical reaction corresponding to a detailed mechanism is now almost within our grasp. No barrier theory (NBT), which makes the calculations relatively facile, is described, as are various applications of the approach to date. Illustrations are given of the use of NBT not just as a quantitative tool for predicting rates, but as a qualitative tool for thinking about which of a pair of reactions will have the higher intrinsic barrier, and thus be slower for similar thermodynamic driving force.

Key words: rate, equilibrium, thermodynamics, kinetics, no barrier theory, computational chemistry, chemical reactivity.

Résumé : Le rêve de pouvoir être capable de prédire la vitesse de réaction d'une réaction chimique correspondant à un mécanisme détaillé est à la portée de la main. On décrit la théorie sans barrière qui rend les calculs relativement faciles, comme c'est aussi le cas pour diverses applications de l'approche jusqu'à maintenant. On donne des exemples de l'utilisation de la théorie sans barrière non seulement comme un outil quantitatif permettant de prédire des vitesses, mais aussi comme outil qualitatif permettant de faire un choix entre deux réactions pour définir laquelle aura la barrière intrinsèque la plus élevée et, en conséquence, sera la plus lente pour des forces motrices thermodynamiques semblables.

Mots clés : vitesse, équilibre, thermodynamique, cinétique, théorie sans barrière, chimie quantique, réactivité chimique.

[Traduit par la Rédaction]

Introduction

The goal of my current research is to develop general methods for predicting the rates of chemical reactions. In reviewing the progress that has been made, and the research currently underway in my laboratory, I wish also to share with you the dream that motivates this research. "Dream" is a flexible word, with various meanings, of which I wish to focus on two:

"Dream: (n) 1.···2. A visionary creation of the imagination. 3.···4. A goal or purpose ardently desired" (1).

What then is this visionary creation, ardently desired? To have a general method, which any chemist could apply, to proceed from structures of starting material and products (written out in the detailed form of an organic reaction mechanism, as is illustrated in Fig. 1), to the free energy of activation for the corresponding reaction in the solvent of interest. This is an ambitious goal, and we will have to start with less ambitious targets, but this remains the ultimate dream.

Received 20 July 2004. Published on the NRC Research Press Web site at http://canjchem.nrc.ca on 3 February 2005.

J.P. Guthrie.[1] Department of Chemistry, University of Western Ontario, London, ON N6A 5B7, Canada.

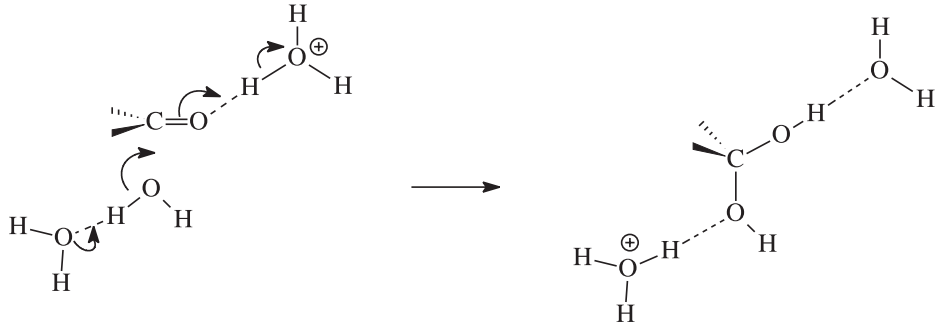
[1]Corresponding author (e-mail: peter.guthrie@uwo.ca).

Suppose for a moment that it were possible to achieve this dream. We would then have predictive power not just to say how fast a proposed reaction (perhaps never yet attempted in the laboratory) would be, but also to say how fast the likely alternative reactions were likely to be, and thus to predict whether the reaction would be clean or not. We would also have a mechanistic criterion, an unambiguous way to say how a reaction occurs, and which of the plausible mechanisms that could be written were viable contenders. The questions to ask would be: which mechanism leads to the fastest reaction, since this is the one that will be observed; and which predicted rate matches the experimental rate — they had better be the same or there is something badly wrong with the approach! Finally, we would have a new way of thinking about reactions, because the method that makes the dream possible imposes a new and different way of thinking about reactions, and why they have kinetic barriers.

To go from structure to rate is an ambitious goal; as a first stage one might think about going from equilibrium to rate. Would it be possible, given an equilibrium constant in solution, to calculate the corresponding rate constant by some manageably small computation? There is in fact a long history of using equilibrium constants as a guide to predicting rate constants. This began with linear free energy relations (LFER) such as the Bronsted relation (2). As Bronsted and Petersen recognized from the start (2), such a linear free energy relation is only an approximation, valid over a short

 doi: 10.1139/V04-172 © 2005 NRC Canada

Fig. 1. A typical organic reaction, with a detailed mechanism for the overall transformation, which is believed to occur in a single reactive collision, transforming one encounter complex into another.



range, to what must over the full range of possibility be a nonlinear relation. Nevertheless, LFERs have been very useful in organic chemistry, and can often be used for interpolative (or, with less confidence, extrapolative) estimation of rate constants. There was a considerable pause before this expected nonlinearity could be demonstrated, first by Bell (3) and Eigen (4). Marcus (5–11) developed a theory leading to quadratic relationships between rate and equilibrium constants; the theory was developed for electron transfer reactions (5–8), but has proven to be a very general description of the relation of rate to equilibrium (9–11), and Murdoch (12) has shown that a Marcus relationship is a logical consequence of the Hammond Postulate (13), Leffler's equation (14), and the assumption that interactions between substituents and reaction center are present in either starting material or products. Many of the extensions have been purely empirical (15–25).

If we accept that it will be necessary to start by calculating rate constants from equilibrium constants, what are the prospects for being able to calculate equilibrium constants from structure? In fact, this is now almost possible. For neutrals there are now fairly general and affordable procedures by which one can calculate $\Delta H_f^\circ(g)$ (26, 27) and $S^\circ(g)$ (28, 29). The solvation energy, or free energy of transfer from the gas phase to solution (ΔG_t) is still a bit trickier; sometimes the available methods work very well, but sometimes they fail badly. For ions it is much harder, both to match experimental precision in the gas phase, and to calculate solvation energies. Nonetheless it is almost possible, and a little more progress should bring this part of the dream within reach.

Results and discussion

No barrier theory (NBT)— The shape of the dream

The method that I have developed for calculating rates of reactions is called no barrier theory (NBT) to emphasize the key idea, namely that if only one thing were to happen in a chemical reaction there would be no kinetic barrier.[2] The reason that almost all real chemical reactions have an associated kinetic barrier is that most reactions require two or more things to happen in order for reaction to take place. This theory uses the same conceptual framework as Marcus Theory, namely that reaction proceeds from encounter complex of starting materials to encounter complex of products. Marcus Theory leads to the well-known eqs. [1] and [2]. The encounter complex of starting materials has them in position to begin the bond transformation, and the encounter complex of products has them in the position immediately resulting from bond transformation. The free energy cost of bringing reactants together, the work term, is called w_R, and the corresponding energy for the products is w_P. It should be possible to estimate the values of these work terms based on the entropic, electrostatic, desolvational, etc., contributions. Marcus Theory uses an intrinsic barrier ($\tilde{G}$), which operationally is the kinetic barrier when the thermodynamic barrier, within the encounter complex, is zero. Although the intrinsic barrier is often transferable within a family of similar reactions, it becomes a function of the equilibrium constant for large variation in equilibrium constant (24, 25, 30, 31). If the intrinsic barrier were constant for a family of reactions then it would be straightforward to calculate rate constants from equilibrium constants for further members of the family; if the intrinsic barrier is not constant this becomes impossible unless the intrinsic barrier is correlated with the equilibrium constant and even then is less satisfactory. The Marcus equation relating $\Delta G^\ddagger$, ΔG°, and, $\tilde{G}$ means that knowing any two allows one to calculate the third. Thus, if the free energy of activation can be calculated by some means from the standard free energy change, then in effect we have calculated the intrinsic barrier.

$$[1] \qquad \Delta G^\ddagger = w_r + \tilde{G}\left(1 + \frac{\Delta G^\circ - w_r + w_p}{4\tilde{G}}\right)^2$$

$$[2] \qquad \Delta G^\ddagger_{corr} = \tilde{G}\left(1 + \frac{\Delta G^\circ_{corr}}{4\tilde{G}}\right)$$

where

$$\Delta G^\ddagger_{corr} = \Delta G^\ddagger - w_r$$

$$\Delta G^\circ_{corr} = \Delta G^\circ - w_r + w_p$$

$\tilde{G}$ = the intrinsic barrier

w_r = work term for reactants

w_p = work term for products

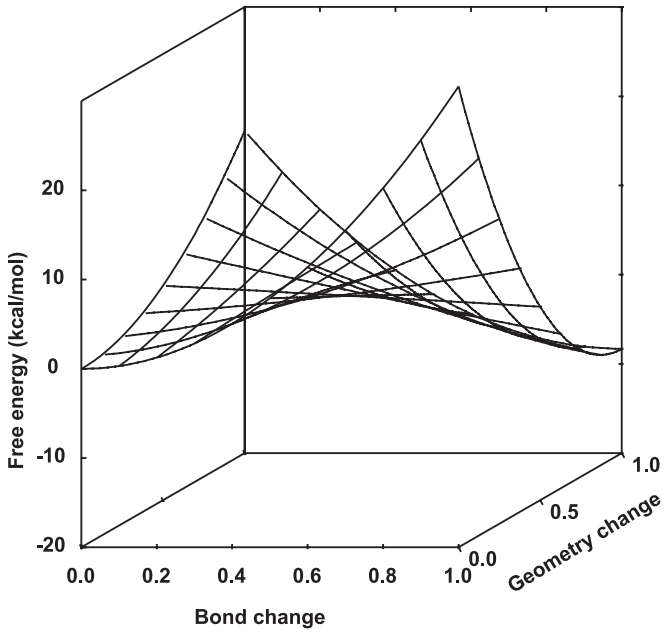
[2] "Kinetic barrier" is equivalent to free energy of activation and easily transformed into rate constant. This expression is used to emphasize that there is a barrier to overcome if reaction is to take place, even when the reaction is thermodynamically favorable.

© 2005 NRC Canada

The suggestion that "if only one thing happens then there is a quadratic relation between energy and the reaction coordinate" sounds like lunacy, because it is well-known that most reactions have a kinetic barrier, and that the energy as a function of reaction coordinate looks far more like a quartic (minima at starting material and product, maximum at transition state) than like a quadratic through initial and final energies. The saving thing is the clause "if only one thing happens" because the viewpoint of the theory is that for almost all real reactions more than one thing must happen. This is illustrated in Fig. 2; in this figure and in higher dimensional versions of it, such as Fig. 3, the origin (0,...,0) represents the initial state, while (1,...,1) represents the final state, and the other corners represent hypothetical states where one (or two or more in higher dimensional cases) of the simple reaction dimensions have gone to completion. The dimensions are chosen so that they run from 0 to 1 and so that the energy is a quadratic function of each dimension. Even when only two things happen, if the energy is a quadratic function of the reaction coordinate for any section, parallel to an axis, through the square reaction diagram, then there will be a barrier, and the simplest path from starting material to saddle point to product will look approximately quartic.

What kinds of simple, one thing at a time processes are we talking about? First, there is geometry change, from one hybridization to another. This is the same sort of change as a bending vibration, for which we expect Hooke's Law behavior; an appropriate coordinate would be some simple function of bond angles set up to run from 0 to 1, such as $(\theta - \theta_0)/(\theta_1 - \theta_0)$, where θ_0 is the initial angle, θ_1 is the final angle, and θ is any intermediate value. Then there are bond length changes, where again we expect Hooke's Law behavior, and an appropriate coordinate would be a simple function of bond length, scaled to run from 0 to 1, such as $(r - r_0)/(r_1 - r_0)$. Next there are bond making or breaking processes. For a pure bond making or breaking (with no accompanying geometry change) we would expect a Morse curve (32) (eq. [3]), which does not look much like a quadratic. However, if the bond length in the Morse curve is transformed into a bond order using the Pauling bond length – bond order relationship (33) (eq. [4]), then we obtain a quadratic in a coordinate related to bond order. Finally, proton transfer between two atoms (with no accompanying geometry change, as for oxygen to oxygen transfer) is at least an approximation to a simple process, because it is known that these reactions can be ultra-fast with rate constants greater than 10^{11} s^{-1} (34). However, it is also clear that this is only an approximation and that this is not truly a no barrier process. Reactions such as the water-mediated proton switch, which involve only proton transfers between electronegative atoms, and which are successfully described by Multidimensional Marcus Theory (with an intrinsic barrier for proton transfer between two atoms of 1 kcal/mol) are not satisfactorily treated by NBT with these proton transfers treated as simple processes. On the other hand, the approximation that proton transfer between two atoms can be treated as a simple process is quite satisfactory for reactions involving heavy atom bond making and geometry change coordinates, as for various carbonyl hydration reactions.

Fig. 2. The kind of energy surface implied by NBT. In this case, a two-dimensional reaction diagram was used, with one bond change and one geometry change dimension.



$$[3] \qquad E = D_e[1 - \exp(-\beta(r - r_0))]^2$$

$$[4] \qquad r_n = r_1 - \alpha \log(n)$$

The theory can be summarized in a few postulates:

(1) Reactants[3] are in equilibrium with starting material or product at each point along each reaction coordinate, with the minimum at the lower energy end of the coordinate.
(2) For any process where only one elementary reaction coordinate changes, the energy will be a quadratic function of the corresponding reaction coordinate with the minimum at the lower energy end of the coordinate.
(3) Heterolytic bond cleavage constitutes an elementary reaction coordinate.
(4) Proton transfer between two atoms constitutes an elementary reaction coordinate.

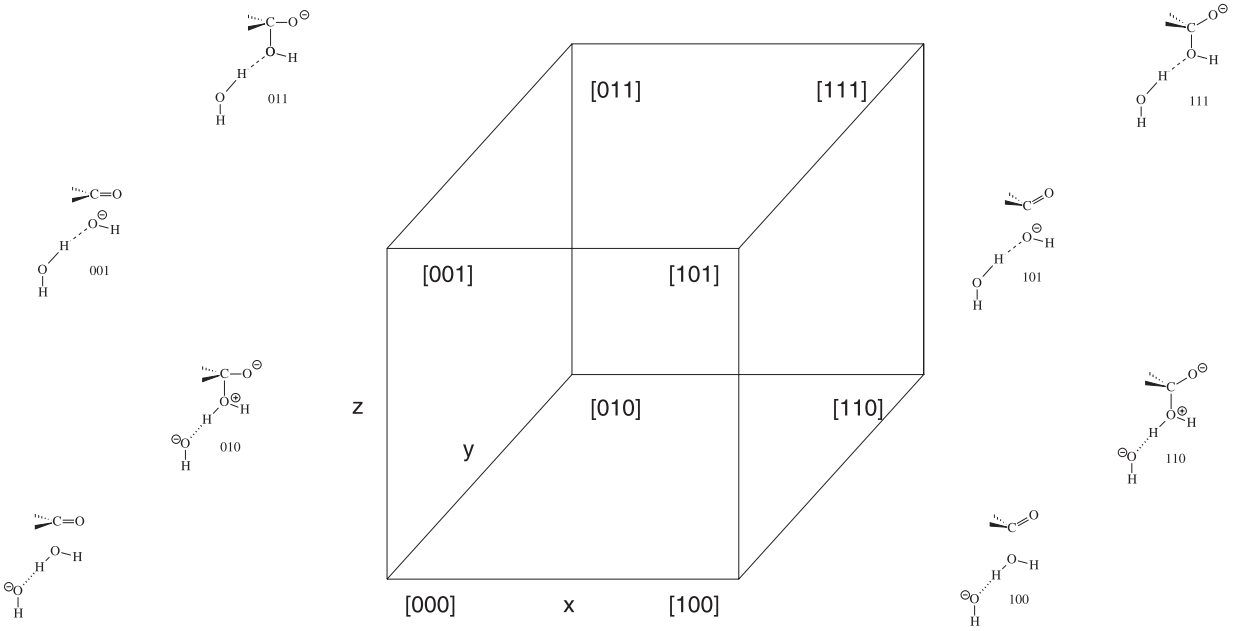
The first is the assumption underlying transition state theory. The second is the key assumption of the theory; if it is accepted then all else follows. The last two make explicit how reactions will be described. For convenience, all coordinates are defined to run from 0 to 1.

For an overall chemical reaction involving two or more simple reaction dimensions, we can construct a two, three, four,... dimensional reaction diagram (square, cube, hypercube,...). Once we have calculated the energy of each corner of the diagram, as will be illustrated in what follows, then, by postulate 2, we have defined the energy surface (or hypersurface) for the reaction. By finding the energy of the lowest saddle point on this surface between initial and final states we will determine the free energy of activation. This has been done for hundreds of reactions, and it works.

[3] Here we are using "reactants" to mean the molecular system involved in the chemical reaction at any point on the reaction hypersurface.

© 2005 NRC Canada

Fig. 3. The three-dimensional reaction diagram needed to describe addition of hydroxide to a reactive carbonyl compound. The structures corresponding to each corner are shown. Energy would be a fourth dimension, orthogonal to the three shown.



The assumptions stated above permit the calculation of rate constants for any reaction provided that the energies of all corners of the appropriate diagram can be calculated and that energy is a quadratic function of each coordinate: electron transfer or electronic state changes will not fit this pattern. The equilibrium constant in solution is a crucial input datum. Distortion energies are calculated relative to equilibrium species with the same bonding arrangement. This procedure leads to the rate constant for a particular step in a reaction. If the mechanism is complicated, and the rate-determining step is not known, then similar calculations for several different steps may be needed to determine the overall rate constant for the observable reaction.

To illustrate the process of calculating a free energy of activation, I will work through an example, the addition of hydroxide to acetaldehyde.



Three things happen in this transformation: there is a proton transfer between two oxygens; a carbon–oxygen bond forms; and there is a geometry change at the reaction center from sp^2 to sp^3. The first of these may seem superfluous — why not simply start with hydroxide in contact with the carbonyl carbon? The problem is that hydroxide is strongly solvated, by approximately three water molecules, and for hydroxide to be in contact with the carbonyl carbon, with one lone pair ready to begin bond formation, requires loss of one of these solvating water molecules. Comparison of the pK_a of water in water and in DMSO as solvent shows that losing hydrogen bonding solvation is very expensive. On the other hand, the carbonyl compound, dissolved in water, must have water molecules in contact with it, and thus the cost of putting a water molecule in contact is zero. The more elaborate process shown above avoids the cost of bringing hydroxide into contact with the carbonyl before reaction begins, but at the cost of a more elaborate transition state. The advantage of using a general model is that it allows the molecules to tell us what the lowest energy path is: if the cost of bringing hydroxide into contact with the carbonyl carbon is small with respect to the overall kinetic barrier, then it is found that progress along the proton transfer dimension is complete at the transition state. If this cost is high with respect to the kinetic barrier, then the more elaborate three-dimensional path is followed: this is the case for the more reactive carbonyl compounds. The three-dimensional reaction diagram, which is sufficient for all of the compounds discussed here, is shown in Fig. 3.

Now the energy of each corner of the diagram must be calculated. The starting material is the reference; from the overall equilibrium constant for the reaction, we know the free energy of the product corner. By using the experimental equilibrium constants we avoid the tough computational task of calculating solvation energies. Now the energy of each distorted form is calculated using the difference in MO energies between distorted and equilibrium structures. If the difference is calculated for structures differing only in geometry and not in bonding, then relatively low level molecular orbital calculations will suffice. To calculate the energy differences between structures differing in bonding would be much more difficult. If a proton transfer has taken place the free energy change is calculated from the pK_a values of the species involved (either measured or estimated using linear free energy relations). If hydrogen bonds are present, their free energies of formation from the separate species are calculated using the Stahl–Jencks equation (35). Electrostatic interactions, if present, are calculated using a simple model, scaled to the experimental ion-pairing energies in the solvent of interest. The statistical effects of encounter (if more than one nonsolvent species is present in

© 2005 NRC Canada

the corner species) are calculated using the simple model proposed by Hine (15).

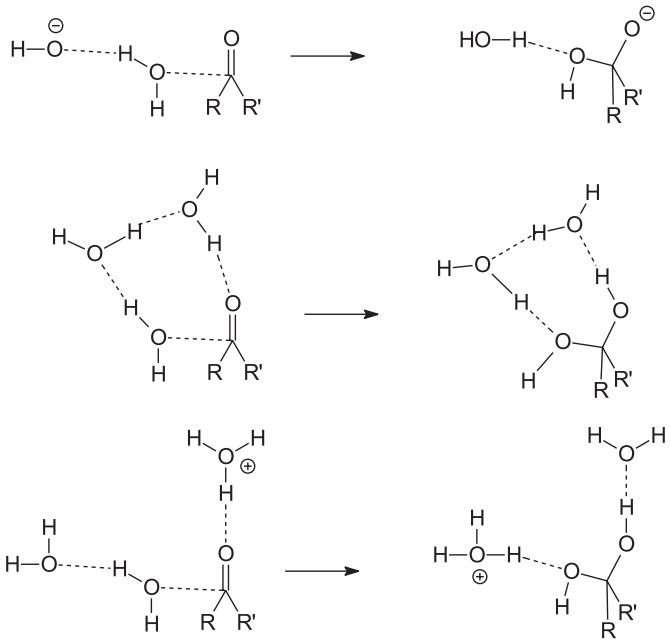
The corner energies, by postulate 2, define the free energy hypersurface for the reaction. Now we find the lowest saddle point between starting materials and products, by systematically searching the hyperspace. Computer programs have been written to do this. First, all candidate saddle points are found, which are points higher than a nearby point closer to the starting point and than a nearby point closer to the final point. These candidates are ranked in terms of energy level and tested starting with the lowest. The first one for which one can find both a path leading to starting point without going higher than the candidate, and a path leading to final point without going higher than the candidate is the lowest energy transition state on the energy surface.

At this stage, my dream may be sounding like your nightmare. There are lots of details to take care of, lots of fussy calculations, lots of corner structures to account for. (For a two-dimensional reaction diagram, there are four corners; for a 3-D diagram, eight corners; for a 4-D diagram, 16 corners; for a 5-D diagram, 32 corners;...). The solution is found in words of wisdom from Kernighan and Plauger: "Let the machine do the dirty work" (36). I am engaged in writing computer programs to make the calculations easier to perform. The initial implementation involved a sequence of four programs to carry out the four stages of the analysis. (1) To identify the reaction dimensions. (2) To generate structures of the corner intermediates, in the form of data files suitable for MO calculations: this allows calculation of the distortion energies. (3) To calculate energies for each corner species as described above. (4) To search for the transition state. The next revision, now underway, will combine the first two programs into one, which will set up the calculation of distortion energies. In addition, this revision will correct various deficiencies in the initial versions of the programs, which became quite apparent as we used them. Once the data files for the MO calculations of distortion energies are set up, there is a pause while these calculations are carried out, a pause that can take a while depending on the level of theory used and the size of the molecular species.

Dreams are all very well: does it work? A review of published examples

We have reported a thorough investigation of the application of NBT to carbonyl hydration reactions, examining the hydroxide-catalyzed, uncatalyzed, and acid-catalyzed paths, and covering the range of compounds for which rate and equilibrium constants are available (31). In all 121 rate constants were calculated, spanning a range of 16 powers of 10. For each path, a general mechanism was used, more complicated than necessary for some, but sufficient to cover all cases. The lowest energy transition state can easily involve fewer than the maximum number of reaction dimensions in the model. For hydroxide, the standard model involves a water molecule as actual nucleophile, with hydroxide acting as general base, although for unreactive carbonyl compounds the lowest energy path involves the simpler direct hydroxide attack path, which is a subset of the full mechanism. For uncatalyzed attack, the cyclic path shown is the most general, even though for many compounds a simpler two water

Fig. 4. The general mechanisms for hydroxide-catalyzed, uncatalyzed, and acid-catalyzed addition of water to carbonyl compounds. In particular cases, a simpler subset of these mechanisms may suffice to describe the transition state.



mechanism, leading to the hydronium ion complex of the anionic tetrahedral intermediate (with a water separating the charges) is preferred. For acid-catalyzed attack, the most general mechanism starts with a hydronium ion complexed with the carbonyl oxygen and involves two water molecules, one as nucleophile and one as general base. These three mechanisms are illustrated in Fig. 4. Again for many compounds a simper version, starting with the protonated carbonyl, may be the lowest energy transition state. In each case, the standard procedure allows the molecule to tell us if one of the possible dimensions should have a value of zero or one at the transition state, i.e., if the actual process should be of lower dimensionality than the general mechanism. For 121 reactions, the rms deviation was 1.1 in log k, or 1.4 kcal/mol in $\Delta G^{\ddagger}$. Although most of these reactions could also be described by Multidimensional Marcus Theory, with a constant intrinsic barrier for C—O bond formation, for the most reactive compounds the reactions with hydroxide required that the intrinsic barrier depend on the equilibrium constant (37).

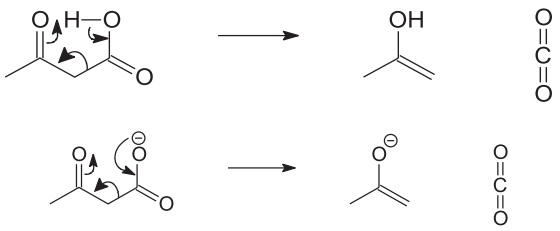
The first application of NBT was to the reaction of water or hydroxide as base removing the α hydrogen from carbonyl compounds to give enolates (38). Again, it was possible to cover the entire range of compounds for which both rate and equilibrium constants were available, and do so with an rms error of 1.08 in log k for monocarbonyl compounds and 0.65 in log k for dicarbonyl compounds.

Cyanohydrin formation, a simple carbon–carbon bond forming reaction, could also be treated by NBT, with an rms error of 1.3 in log k (39).

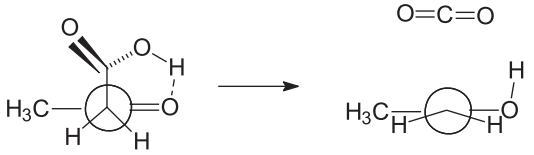
Thus far, the focus has been on demonstrating that the NBT method could calculate rate constants from equilibrium constants and distortion energies. In the case of decarboxylation

© 2005 NRC Canada

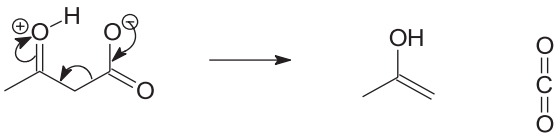
reactions, it could also be used as a mechanistic criterion to show that the textbook mechanism is incorrect (40). For the decarboxylation of acetoacetic acid, the commonly written mechanisms are:



For acetoacetate anion, the mechanism is unambiguous, and the observed rate constant is reproduced by NBT. For neutral acetoacetic acid, there is a problem with the mechanism shown if one considers it in stereoelectronic detail.



For direct proton transfer accompanying decarboxylation, not only is the carboxylic acid in the less stable conformation, with the H syn to the CH_2, but if the C—C bond, which breaks, is to be aligned parallel to the *p* orbitals of the ketone, then the proton must be transferred to the π bond and not to the lone pair. This is all energetically expensive, and if one follows through then the calculated free energy of activation is too high by 15 kcal/mol (40). In fact, the correct free energy of activation is obtained if one starts with the zwitterionic form of the starting material.



Current efforts

Currently, I am looking at the application of NBT to S_N1 reactions. As a part of that effort I have examined the feasibility of calculating the equilibrium constant for conversion of an alcohol of the type ArCRR′OH to the corresponding cation, the process measured by pK_R. pK_R values are now available for a number of such compounds (41–44). What we have found, in work which is nearing completion (45),[4] is that the absolute equilibrium constant can be calculated if the gas-phase thermodynamics are determined by calculations at the G3MP2B3 level (46), and solvation energies are calculated by the IPCM continuum model. These G3MP2B3 calculations are quite demanding of computer resources, and with the facilities available to me become impractical much beyond 100 valence shell electrons. For larger systems only lower level calculations are practical, and these do not lead to satisfactory absolute equilibrium constants. Instead, I found that calculated relative equilibrium constants, using cumyl alcohol and cation as the reference system, are linearly correlated with values derived from experiment. Presumably, there is massive cancellation of errors when one uses such a relative equilibrium constant. In any event, this made it possible to estimate pK_R values for a number of cases where no experimental values were available.

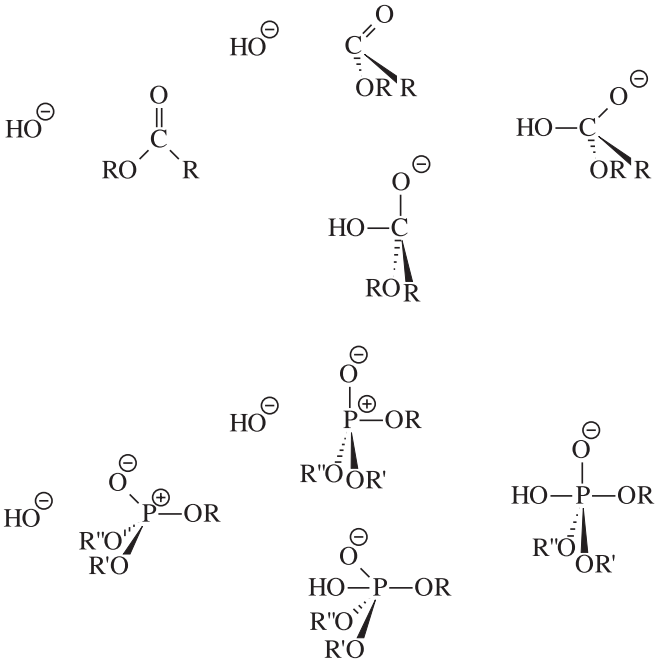
Given equilibrium constants, whether experimental or calculated, it is then possible to calculate the rate constants for trapping of the cation by water, for which numerous values are available from the work of Richard and co-workers (41–43, 47, 48), and McClelland and co-workers (49, 50). The model for these reactions involves three dimensions: (1) formation of the C—O bond; (2) change of the geometry at the reaction center from sp^2 to sp^3; (3) change of the bond lengths in the conjugated system from the alternating bonds of the cation to the aromatic ring arrangement of the alcohol. We considered adding a proton transfer step with a second water molecule acting as a general base, but when this four-dimensional model was tried the proton transfer was only advanced to a very small extent in the transition states and the free energy of activation was essentially the same as for the three-dimensional model. The first paper on this work has now been published (45).

Work on phosphate ester hydrolyses is incomplete, but I am encouraged to think that rates of phosphate ester reactions can also be treated by NBT. Phosphate esters also provide a nice example of the power of NBT as a qualitative way of thinking about how reactions happen. One of the striking things about phosphate esters is how unreactive they are relative to carboxylate esters. Phosphate diesters are anionic at physiological pH, which renders them even less reactive, and this unreactivity has been suggested as the reason why DNA is based on a phosphate sugar backbone. What is less widely recognized is that this unreactivity, even for neutral phosphate triesters, occurs despite the more favorable equilibrium constant for addition of hydroxide to trimethyl phosphate than for addition of hydroxide to methyl acetate. In Marcus language, the intrinsic barrier for addition to trimethyl phosphate must be considerably larger than for addition to methyl acetate to overcome the equilibrium constant effect, which would make phosphate more reactive if the intrinsic barriers were similar. Why then are phosphate esters inherently less reactive than carboxylate esters? This might be an embarrassment for an instructor teaching introductory organic chemistry, except that one can say: "This is easily explained by qualitative application of no barrier theory". Consider the two addition reactions in terms of NBT, as shown in Fig. 5. For the carboxylic ester, distortion of the starting material to the geometry of the product of addition involves the change of three angles from 120° to 109.5°, for a change of 10.5° each. For the corresponding distortion of trimethyl phosphate, three angles change from 109.5° to 120°, for a change of 10.5° each, and three angles change from 109.5° to 90°, for a change of 19.5° each. To the crude approximation that all bending force constants are the same (and in fact the force constants in molecular mechanics vary relatively little, which is why it is possible to use generalized values where no experimental data are available), it is clear that the distortion energy is larger for the phosphate es-

[4] Additional work is in progress.

© 2005 NRC Canada

Fig. 5. Comparison of the addition of hydroxide to a carboxylate and a phosphate ester in terms of NBT. Qualitatively, one can see that the total angular distortion is greater in the phosphate case, and thus that the intrinsic barrier for addition to phosphate will be greater.

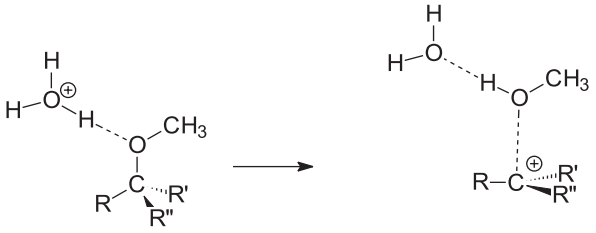


ter. The same conclusion follows from the analogous analysis of distortions of the adducts. If both distortions are larger for the phosphate ester, then for the same equilibrium constant it is clear that the free energy of activation will be larger for the phosphate ester, thereby explaining the phenomenon in qualitative terms. If the appropriate MO calculations are carried out, the distortions are indeed larger for phosphates, and lead to good values for the rate constants of the various methyl phosphate esters.

Leonardo Leandro[5] is examining the application of NBT to E2 elimination reactions. For simple alkyl halides, this requires a five-dimensional model: (1) C—Br bond breaking; (2) geometry at the carbon that makes or loses the bond to bromine; (3) C—C bond length; (4) proton transfer from C to O; (5) geometry at the carbon that makes or loses the bond to proton. With this model, the free energies of activation for ethyl bromide, isopropyl bromide, *tert*-butyl bromide, 1-phenethyl bromide, and 2-phenethyl bromide have been calculated with an rms deviation of 1.4. A manuscript describing this work is now in preparation.

Ian Greig[6] spent a month in my laboratory, and in this time was able to show that the rate constants for the hydrolysis of acetals and ortho esters could be calculated by NBT.

There were a few complications along the way. The pK_{BH^+} values for the acetals or orthoesters are not directly measurable, nor easily calculated (protonated acetals tend to fall apart in the gas phase), so values had to be estimated by linear free energy relations. Fortunately, the final results are quite insensitive to the pK_{BH^+} values used. To calculate distortion energies for protonated acetals or orthoesters, it was necessary to lock the C—O bond length at the value in the neutrals, again because otherwise this bond would simple stretch and break. With these provisos, it was possible to calculate the free energies of activation for acid-catalyzed hydrolysis for a set of compounds ranging from formaldehyde dimethyl acetal to tetramethyl orthocarbonate. A manuscript describing this work is now in preparation.



Conclusions and prospects

Although the dream is still far from achieved, the prospects are encouraging. No Barrier Theory (NBT) seems to be a general way to calculate rate constants. The programs I am developing, however imperfect and unfriendly they are at present, are already helping the research move forward. The prospects for being able to calculate equilibrium constants in solution from first principle are encouraging, even though this remains a challenging problem. There is abundant motivation to keep going, and the goal is still ardently desired.

Acknowledgments

We thank the Natural Sciences and Engineering Research Council of Canada (NSERC) for financial support of this work and the Canada Council for the Arts for a Killam Fellowship. We thank the Shared Hierarchical Academic Research Computing Network (SHARCNET) for use of computing resources.

References

1. P. Gove (*Editor*). Websters seventh new collegiate dictionary. Springfield, Mass., USA. 1965.
2. J.N. Bronsted and K. Pedersen. Z. Phys. Chem. Stoechiom. Verwandtschaftsl. **108**, 185 (1923).
3. R.P. Bell. The proton in chemistry. Cornell University Press, Ithaca, N.Y. 1973.
4. M. Eigen. Angew. Chem. Int. Ed. Engl. **3**, 1 (1964).
5. R.A. Marcus. J. Chem. Phys. **24**, 966 (1956).
6. R.A. Marcus. Discuss. Faraday Soc. **29**, 21 (1960).
7. R.A. Marcus. Annu. Rev. Phys. Chem. **15**, 155 (1964).
8. R.A. Marcus. J. Chem. Phys. **43**, 679 (1965).
9. A.O. Cohen and R.A. Marcus. J. Phys. Chem. **72**, 4249 (1968).
10. R.A. Marcus. J. Phys. Chem. **72**, 891 (1968).
11. R.A. Marcus. J. Am. Chem. Soc. **91**, 7224 (1969).
12. J. Murdoch. J. Am. Chem. Soc. **94**, 4410 (1972).
13. G.S. Hammond. J. Am. Chem. Soc. **77**, 334 (1955).
14. J.E. Leffler and E. Grunwald. Rates and equilibria of organic reactions. Wiley, New York. 1963. p. 157.
15. J. Hine. J. Am. Chem. Soc. **93**, 3701 (1971).

[5] J.P. Guthrie and L. Leandro. Manuscript in preparation.
[6] J.P. Guthrie and I.R. Greig. Manuscript in preparation.

© 2005 NRC Canada

16. W.J. Albery and M.M. Kreevoy. Adv. Phys. Org. Chem. **16**, 87 (1978).
17. G.W. Koeppl and A.J. Kresge. J. Chem. Soc. Chem. Commun. 371 (1973).
18. M.M. Kreevoy and D.E. Konasewich. Adv. Chem. Phys. **21**, 243 (1972).
19. M.M. Kreevoy and I.-S.H. Lee. J. Am. Chem. Soc. **106**, 2550 (1984).
20. D. Kim, I.H. Lee, and M.M. Kreevoy. J. Am. Chem. Soc. **112**, 1889 (1990).
21. J.P. Guthrie. J. Am. Chem. Soc. **100**, 5892 (1978).
22. J.P. Guthrie. J. Am. Chem. Soc. **113**, 7249 (1991).
23. J.P. Guthrie. J. Am. Chem. Soc. **118**, 12 878 (1996).
24. J.W. Bunting and D. Stefanidis. J. Am. Chem. Soc. **111**, 5834 (1989).
25. J.P. Richard, T.L. Amyes, and K.B. Williams. Pure Appl. Chem. **70**, 2007 (1998).
26. L.A. Curtiss and K. Raghavachari. Theor. Chem. Acc. **108**, 61 (2002).
27. J. Guthrie. J. Phys. Chem. A, **105**, 8495 (2001).
28. A.L.L. East and L. Radom. J. Chem. Phys. **106**, 6655 (1997).
29. J.P. Guthrie. J. Phys. Chem. A, **105**, 9196 (2001)
30. M.M. Kreevoy, D. Ostovic, I.-S.H. Lee, D.A. Binder, and G.W. King. J. Am. Chem. Soc. **110**, 524 (1988).
31. J.P. Guthrie and V. Pitchko. J. Am. Chem. Soc. **122**, 5520 (2000).
32. P.M. Morse. Phys. Rev. **34**, 57 (1929).
33. L. Pauling. The nature of the chemical bond. Cornell University Press, Ithaca, N.Y. 1960.
34. E. Grunwald. Prog. Phys. Org. Chem. **3**, 317 (1966).
35. N. Stahl and W.P. Jencks. J. Am. Chem. Soc. **108**, 4196 (1986).
36. B.W. Kernighan and P.J. Plauger. The elements of programming style. McGraw-Hill, New York. 1978.
37. J.P. Guthrie. J. Am. Chem. Soc. **122**, 5529 (2000).
38. J.P. Guthrie. J. Am. Chem. Soc. **119**, 1151 (1997).
39. J.P. Guthrie. J. Am. Chem. Soc. **120**, 1688 (1997).
40. J. Guthrie. Bioorg. Chem. **30**, 32 (2002).
41. J.P. Richard, M. Rothenberg, and W.P. Jencks. J. Am. Chem. Soc. **106**, 1361 (1984).
42. T.L. Amyes, J.P. Richard, and M. Novak. J. Am. Chem. Soc. **114**, 8032 (1992).
43. J.P. Richard, V. Jagannadham, T.L. Amyes, M. Mishima, and Y. Tsuno. J. Am. Chem. Soc. **116**, 6706 (1994).
44. J. Richard. Tetrahedron, **51**, 1535 (1995).
45. J.P. Guthrie and V. Pitchko. J. Phys. Org. Chem. **17**, 548 (2004).
46. A. Baboul, L. Curtiss, P. Redfern, and K. Raghavachari. J. Chem. Phys. **110**, 7650 (1999).
47. T.L. Amyes, I.W. Stevens, and J.P. Richard. J. Org. Chem. **58**, 6057 (1993).
48. J.P. Richard. J. Am. Chem. Soc. **111**, 1455 (1989).
49. F.L. Cozens, N. Mathivanan, R.A. McClelland, and S. Steenken. J. Chem. Soc. Perkin Trans. 2, 2083 (1992).
50. R.A. McClelland, F.L. Cozens, S. Steenken, T.L. Amyes, and J.P. Richard. J. Chem. Soc. Perkin Trans. 2, 1717 (1993).

© 2005 NRC Canada

Computational investigation of isomeric and conformeric structures of methyl iodoperoxide

Evangelos Drougas and Agnie M. Kosmas

Abstract: Quantum mechanical electronic structure methods are employed to investigate the isomeric and conformeric stuctures of methyl iodoperoxide. Optimized geometries and harmonic vibrational frequencies are calculated at the MP2 level of theory using two types of basis sets, the 6-311G(d,p) for all atoms and the 6-311G(d,p) combined with the LANL2DZ relativistic ECP procedure for iodine. Refinement of the energetics has been accomplished by performing single-point CCSD(T) calculations. Five isomers were determined in total among which iodomethyl hydroperoxide (ICH_2OOH) is found to be the lowest energy structure. Conformational barriers and transition states that connect the isomeric forms have been characterized.

Key words: methyl iodoperoxide, isomers, conformers.

Résumé : Méthodes quantomechaniques de structure electronique sont employées pour l' investigation des structures isomeriques and conformeriques de methyl iodoperoxide. Des géométries optimizées et des fréquances harmoniques vibrationales sont calculées à la méthode théorique MP2 avec l' usage de deux types de basis sets, 6-311G(d,p) et 6-311G(d,p) avec le procédé relativistique ECP de méthode LANL2DZ pour l' iodine. Des énergies totales et rélatives sont calculées avec CCSD(T). Cinq isomers sont determinés en total. Iodomethyl hydroperoxide (ICH_2OOH) est trouvé d' être la structure la plus stable. Des barrières conformeriques et des états de transition qui connectent les formes isomeriques sont characterizés.

Mots clés : methyl iodoperoxide, isomers, conformers.

Introduction

Iodine polyoxides (1) have been implicated in the atmospheric chemistry of iodine (2, 3) in the reactivity of iodine–ozone mixtures (4), in the reactions between iodine-containing compounds in the marine boundary layer (5, 6), and in the mechanism of oxygen–iodine lasers (7). Methyl iodoperoxide is an interesting relevant species suggested to be involved in the mechanism of the self-reaction of CH_3O_2 radicals formed in the photolysis of iodomethane (8) and the reactions of CH_3O radicals with iodine monoxide (9). It is the methyl analog of hydrogen iodoperoxide (HOOI) recently investigated theoretically (10) and similarly involved in the mechanism of HO + IO reaction (11). Other related systems include the isomeric forms of methyl hypoiodide (CH_3OI, CH_3IO, and ICH_2OH), extensively studied in the work of Misra et al. (12) where the novel species CH_2IOH has been computed at the MP2 level of theory that has no counterpart in the chemistry of lighter halomethanes.

In the current work we present the computational investigation of the isomeric structures of CH_3OOI species and the isomerization and conformational barriers. Five isomers, four interisomerization transition state configurations, and two conformational barriers were determined in total. Among the isomeric minimum energy structures, another novel species, the CH_2IOOH isomer, was found, which like the CH_2IOH species mentioned above, presents no analogs in the chemistry of lighter halo-methylperoxides (13, 14).

Received 19 May 2004. Published on the NRC Research Press Web site at http://canjchem.nrc.ca on 27 January 2005.

E. Drougas and A.M. Kosmas.[1] Department of Chemistry, University of Ionnina, Gr-451 10, Ionnina, Greece.

[1]Corresponding author (e-mail: amylona@cc.uoi.gr).

Methodology

The computations have been carried out using the Gaussian 98 A.9 series of programs (15). The main part of our work has been to select a suitable methodology and the appropriate basis sets to handle iodine-containing compounds. Two series of optimizations were performed at the MP2 level of theory. In the first series, the 6-311G(d,p) basis set, denoted hereafter as basis set A, was employed for all atoms involved in the system including iodine. In the second series of optimizations, all atoms except iodine were handled in the same way, i.e., with the 6-311G(d,p) basis set, but the iodine atom was treated differently using the relativistic effective-core-potential (ECP) LANL2DZ procedure of Wadt and Hay (16), which includes first-order relativistic effects. The LANL2DZ basis set was augmented with *d* and *f* polarization functions (exponents 0.292 and 0.441, respectively) and it is denoted hereafter as basis set B. The necessity of including extra polarization functions for the proper quantum description of I has been recognized on several occasions (10, 17–19). To refine the energetics, a final series of calculations were performed using coupled cluster techniques. Thus, the relative stability order among the various isomers was established by CCSD(T)/B computations carried out at the basis set B optimized geometries. All infor-

 doi: 10.1139/V04-156 © 2005 NRC Canada

Table 1. Structural parameters (Å, °) of isomeric and conformeric structures of CH_3OOI using the two optimization procedures described in the text.

Species	Coordinate	MP2/A	MP2/B
CH_3OOI	r(C-O)	1.419	1.418
	r(C-H)	1.096	1.096
	r(C-H)	1.092	1.092
	r(O-O)	1.416	1.438
	r(O-I)	2.103	2.005
	<) COO	107.2	106.4
	<) OOI	110.6	109.8
	<) HCO	104.4	104.2
	<) HCO	110.8	110.9
	<) HCH	110.3	110.9
	<)COOI	89.8	89.6
CH_3OOI (cis)	r(C-O)	1.409	1.408
	r(C-H)	1.095	1.095
	r(C-H)	1.093	1.093
	r(O-O)	1.475	1.480
	r(O-I)	2.076	1.990
	<) COO	116.2	115.9
	<) OOI	119.8	119.6
	<) HCO	102.3	104.2
	<) HCO	112.3	112.6
	<) HCH	110.7	110.9
	<)COOI	0.0	0.0
CH_3OOI (trans)	r(C-O)	1.413	1.408
	r(C-H)	1.094	1.095
	r(C-H)	1.092	1.093
	r(O-O)	1.477	1.480
	r(O-I)	2.047	1.990
	<) COO	102.0	101.9
	<) OOI	105.3	105.6
	<) HCO	104.0	104.2
	<) HCO	111.0	112.6
	<) HCH	110.4	110.9
	<)COOI	180.0	180.0
CH_3OIO	r(C-O)	1.432	1.437
	r(C-H)	1.096	1.096
	r(C-H)	1.091	1.090
	r(O-I)	2.038	1.948
	r(I-O)	1.831	1.777
	<) COI	112.7	106.4
	<) OIO	107.8	106.2
	<) HCO	105.6	105.7
	<) HCO	111.7	111.2
	<) HCH	110.3	110.9
	<)COOI	64.4	67.7
CH_3IO_2	r(C-I)	2.120	2.091
	r(C-H)	1.092	1.093
	r(C-H)	1.091	1.092
	r(I-O)	1.807	1.749
	<) CIO	97.6	98.5
	<) OIO	113.2	110.9
	<) HCI	109.2	109.1
	<) HCI	103.4	103.6
ICH_2OOH	r(C-O)	1.380	1.384
	r(C-I)	2.201	2.162
	r(C-H)	1.089	1.090
	r(O-O)	1.438	1.440
	r(O-H)	0.967	0.967
	<) ICO	113.3	113.4
	<) COO	107.4	107.3
	<) HCI	105.4	105.1
	<) HCI	106.3	106.1
	<) HCH	113.5	113.4
	<) OOH	100.0	100.0
	<) COOH	98.6	101.2
CH_2IOOH	r(C-I)	1.958	1.929
	r(C-H)	1.082	1.083
	r(I-O)	2.213	2.112
	r(O-O)	1.439	1.449
	r(O-H)	0.963	0.964
	<) HCI	118.1	118.2
	<) HCH	121.3	120.9
	<) CIO	115.6	116.2
	<) IOO	108.7	108.9
	<) OOH	99.7	99.4
	<) CIOO	76.1	78.3
	<) IOOH	–105.2	–109.9

mation about the basis sets was obtained from the Extensible computational chemistry environment basis set database, version 1.0 (20).

Full optimizations and harmonic vibrational frequency calculations were performed using both basis sets to identify the computed stationary points as energy minima or transition states. The transition states were characterized by one imaginary frequency and they were further confirmed as first-order saddle points by intrinsic reaction coordinate (IRC) calculations where they have shown to connect the appropriate isomeric species.

Geometry and frequency results

The structural results at both optimization levels are listed in Tables 1 and 2. Table 1 contains the optimized geometrical parameters of the minimum energy structures and the conformeric forms of CH_3OOI, while Table 2 lists the geometries of the isomerization barriers determined. Figure 1 displays the basis set B optimized structures for all species examined and Table 3 lists the harmonic frequency results from both optimization procedures. Table 4 lists the calculated electronic energies including the zero-point-energy (ZPE) corrections and the energy differences with respect to CH_3OOI, as well as the explicit ZPE values at the MP2/B level. Finally, Fig. 2 contains an energy profile of all species involved with respect to the most stable adduct, iodomethyl hydroperoxide (ICH_2OOH), based on the CCSD(T)/B single-point energy calculations.

The geometries obtained by both optimization procedures are, in general, fairly consistent with each other. However, the basis B results do exhibit significant overall tightening of the optimized structures wherever iodine bonding is involved, a tendency that reflects the considerable improve-

© 2005 NRC Canada

Table 2. Structural parameters (Å, °) of isomerization transition states of the CH_3IO_2 system using the two optimization procedures described in the text.

Species	Coordinate	MP2/A	MP2/B
TS1	r(C-O)	1.440	1.443
	r(C-H)	1.090	1.090
	r(O-O)	1.512	1.507
	r(CO-I)	2.124	2.095
	r(O-I)	2.448	2.370
	<) COI	118.9	106.4
	<) HCO	103.6	104.0
	<) HCO	109.9	109.5
	<) HCO	107.4	107.2
	<) HCH	110.4	110.2
	<) HCH	112.6	111.9
	<)HCOI	85.6	85.8
TS2	r(C-I)	2.362	2.314
	r(C-H)	1.084	1.086
	r(C-H)	1.080	1.082
	r(C-H)	1.094	1.096
	r(I-O)	1.828	1.772
	r(I-O)	1.913	1.861
	<) ICH	108.4	108.6
	<) ICH	113.2	115.9
	<) ICH	88.9	88.7
	<) HCH	115.0	114.7
	<) OIO	115.9	114.2
	<) OIC	86.9	86.6
	<) HCIO	157.6	160.7
TS3	r(C-I)	1.929	1.902
	r(C-H)	1.082	1.081
	r(I-O)	1.819	1.766
	r(I-O)	2.133	2.029
	r(O-H)	0.970	0.971
	<) HCI	118.6	119.1
	<) HCH	124.6	124.2
	<) CIO	104.1	103.5
	<) CIO	95.1	93.7
	<) OIO	119.5	121.9
	<) HOI	107.9	107.5
	<) HCIO	45.4	41.9
	<) CIOH	–159.6	–159.2
TS4	r(I-C)	2.102	2.074
	r(O-O)	1.285	1.281
	r(C-H)	1.087	1.087
	r(O-H)	0.986	0.986
	<) HCI	110.6	110.3
	<) HOO	106.5	106.7
	<) OCI	84.9	84.7
	<) OOC	93.8	93.5
	<) HCO	123.1	122.7

Table 3. Harmonic vibrational frequencies (cm^{-1}).[a]

CH_3OOI	115, 202, 272, 472, 524, 808, 1047, 1197, 1224, 1475, 1483, 1528, 306, 3157, 3198
	105, 215, 293, 461, 573, 1048, 1200, 1223, 1475, 1484, 1531, 3062, 3156, 3193
CH_3OIO	69, 160, 232, 296, 488, 897, 1038, 1187, 1191, 1486, 1499, 1525, 3050, 3134, 3180
	86, 151, 243, 307, 544, 920, 1037, 1189, 1193, 1486, 1502, 1527, 3060, 3148, 3191
CH_3IO_2	122, 198, 239, 279, 534, 868, 873, 900, 916, 1300, 1454, 1456, 3089, 3214, 3223
	135, 212, 257, 306, 558, 852, 855, 940, 961, 1287, 1454, 1457, 3079, 3206, 3213
CH_2IOOH	49, 158, 210, 327, 413, 568, 620, 781, 876, 908, 1352, 1427, 3190, 3330, 3837
	76, 171, 229, 308, 429, 594, 649, 809, 868, 894, 1345, 1423, 3181, 3319, 3839
ICH_2OOH	134, 228, 296, 461, 572, 859, 919, 1110, 1279, 1308, 1403, 1464, 3144, 3242, 3798
	134, 225, 299, 465, 589, 856, 916, 1101, 1276, 1303, 1398, 1466, 3135, 3230, 3804
CH_3OOH (cis)	249i, 222, 299, 386, 570, 762, 1060, 1176, 1222, 1464, 1475, 1532, 3056, 3149, 3174
	235i, 229, 303, 408, 585, 744, 1056, 1177, 1217, 1461, 1475, 1535, 3055, 3148, 3171
CH_3OOH (trans)	19i, 160, 232, 296, 488, 897, 1038, 1187, 1191, 1486, 1498, 1525, 3050, 3133, 3179
	40i, 218, 242, 330, 663, 808, 1073, 1199, 1226, 1470, 1474, 1541, 3073, 3164, 3194
TS1	535i, 216, 256, 382, 449, 858, 1037, 1192, 1203, 1457, 1487, 1501, 3098, 3219, 3225
	543i, 217, 251, 383, 459, 859, 1038, 1195, 1202, 1461, 1488, 1501, 3101, 3223, 3229
TS2	992i, 145, 210, 247, 442, 781, 854, 872, 879, 1252, 1421, 1503, 3078, 3251, 3322
	1003i, 149, 220, 252, 442, 791, 863, 885, 929, 1260, 1440, 1512, 3058, 3263, 3329
TS3	206i, 201, 247, 343, 405, 426, 471, 791, 799, 844, 905, 1366, 3195, 3350, 3765
	170i, 219, 267, 378, 398, 438, 487, 808, 822, 877, 928, 1356, 3197, 3354, 3759
TS4	223i, 82, 125, 187, 247, 475, 573, 820, 941, 1365, 1455, 1604, 3138, 3275, 3516
	217i, 84, 127, 197, 249, 477, 594, 819, 937, 1365, 1460, 1623, 3129, 3264, 3509

[a]The first series of results for each species corresponds to basis set A and the second series to basis set B.

ment achieved by the use of the LANL2DZ approach implicitly including first-order relativistic effects, and the employment of the extra *d* and *f* polarization functions.

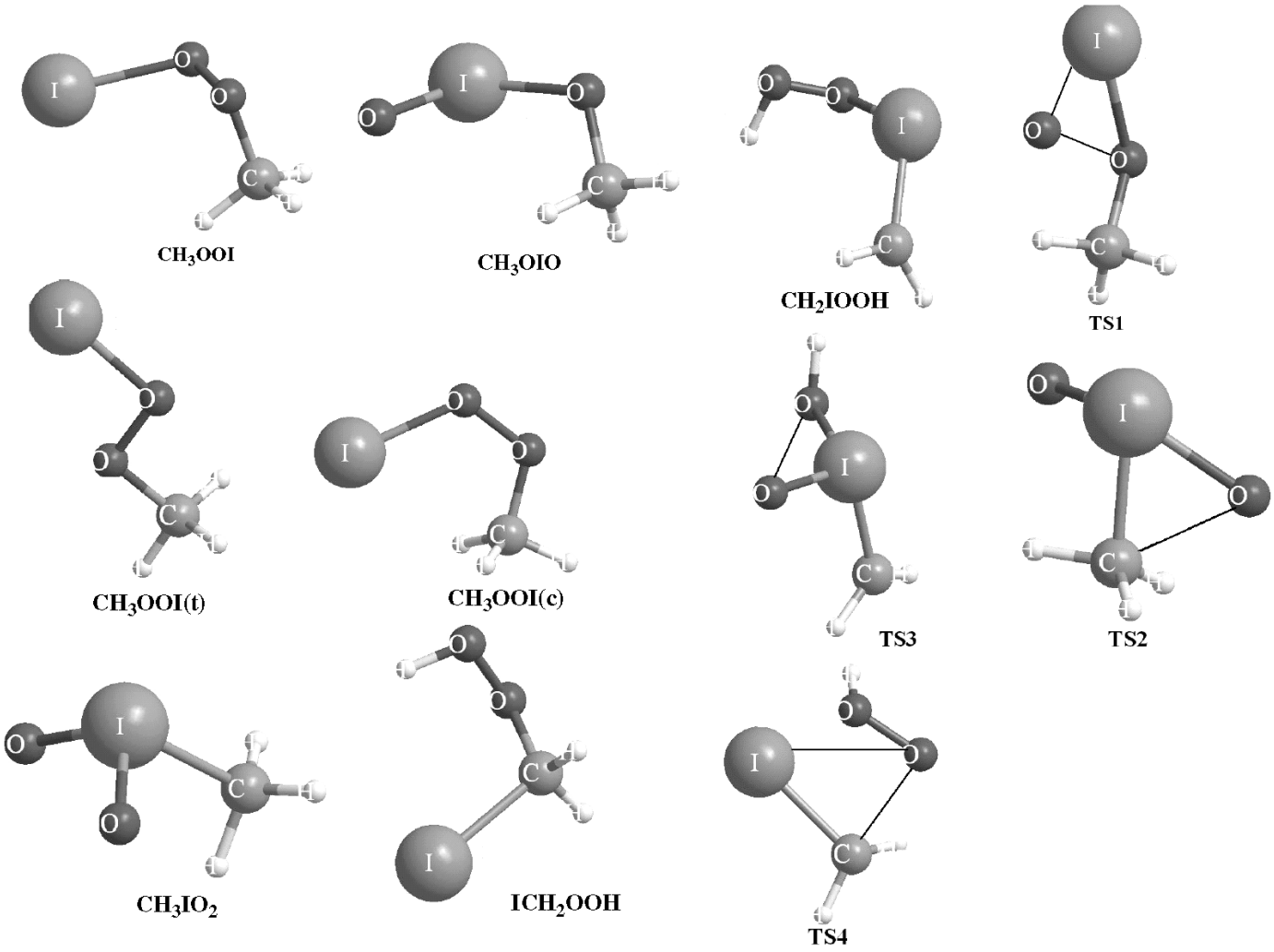
Energy minima

Five types of plausible connectivity for the isomeric forms of methyl iodoperoxide were examined: CH_3OOI, CH_3OIO, CH_3IO_2, ICH_2OOH, and CH_2IOOH.

The peroxide form (CH_3OOI) is one of the two nascent association minima that may be formed in the CH_3O + IO reaction. In the equilibrium state it possesses C_1 symmetry and shows a skew configuration with a COOI dihedral angle

© 2005 NRC Canada

Fig. 1. Optimized structures for CH_3OOI isomers and isomerization and conformational barriers at the MP2/B level of theory.



of 89.8° with basis set A and 89.6° with basis set B. The O-O-I bond angle is calculated to be 109.8° and the O—O and O—I bond distances are 1.438 and 2.005 Å, respectively, with the B basis set. The MP2/6-311G(d,p) calculations (basis A results) agree overall with the MP2/B results, e.g., 110.6° for the O-O-I bond angle and 1.416 and 2.103 Å for the O—O and O—I bond distances. The differences exhibit the tightening observed because of the LANL2DZ approach used for I, which shortens the O—I distance by 0.1 Å, and results in a slight enlargement of the O—O distance by 0.02 Å. The present results are consistent with the corresponding data for HOOI (10) where the LANL2DZ methodology augmented with extra polarization functions has also been used and where the O—O and O—I bond distances were found to be 1.428 and 2.058 Å, respectively.

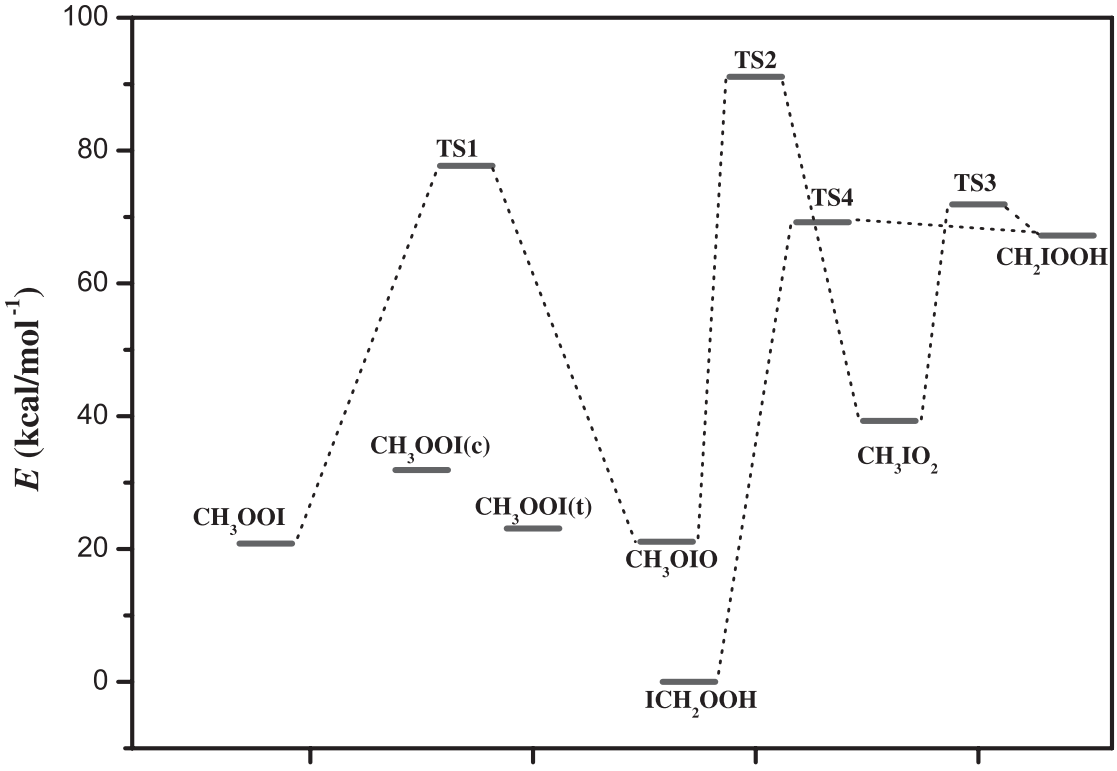
The other two isomeric forms that preserve the CH_3 group entity are CH_3OIO and CH_3IO_2, resulting from the hypervalent bonding of the I atom. CH_3OIO like CH_3OOI may also be formed as a nascent intermediate in the CH_3O + IO reaction and presents similar characteristics with the HOIO isomer. For example, the bond distances CO—I and OI—O at the MP2/B level were found to be 1.948 and 1.777 Å, respectively, in good agreement with the corresponding distances 1.989 and 1.812 Å in HOIO (10), but significantly shorter than the corresponding MP2/A values (2.038 and 1.831 Å). However, both basis sets' results show the interesting shrinkage that the iodine-terminal oxygen bond distance suffers compared to iodine-bridged oxygen bond length, as in all-bridged, halogen-terminal oxygen bonds, because of the partial double bond character that these bonds exhibit (21). The third isomer CH_3IO_2 with a C_s symmetry, presents the I-O multiple bond characteristics more enhanced because of the double pair of electrons that are shared with the terminal oxygen atoms. Thus, it presents the shortest I—O bond distance (1.807 Å with basis set A and 1.749 Å with basis set B) following the same trend as all X—O distances in the analogous YXO_2, X = Cl, Br structures (13, 14). The nature of the hypervalent halogen-terminal oxygen multiple bonding has been analyzed in great detail by Lee et al. (21) and it has found to present important consequences not only

© 2005 NRC Canada

Table 4. Electronic (Hartrees) and relative (kcal/mol) energies with respect to CH_3OOH including ZPE (kcal/mol) corrections for CH_3OOI isomers, conformers, and isomerization transition states.

Species	Basis set A	ΔE	Basis set B	ΔE	CCSD(T)	ΔE	ZPE
CH_3OOI	–7106.758 560	0.0	–201.046 102	0.0	–201.106 571	0.0	28.3
CH_3OIO	–7106.739 093	12.2	–201.054 082	–5.0	–201.106 201	0.2	28.0
CH_3IO_2	–7106.688 105	44.2	–201.028 626	10.9	–201.077 120	18.5	26.8
ICH_2OOH	–7106.799 527	–25.7	–201.082 553	–22.9	–201.139 765	–20.8	28.8
CH_2IOOH	–7106.680 959	48.7	–200.974 350	45.0	–201.030 719	47.6	25.9
CH_3OOI (cis)	–7106.740 571	11.3	–201.028 791	10.9	–201.087 712	11.8	27.9
CH_3OOI (trans)	–7106.754 657	2.4	–201.043 370	1.7	–201.102 981	2.2	28.1
TS1	–7106.660 685	61.4	–200.947 740	61.7	–201.015 908	56.9	28.0
TS2	–7106.600 078	99.4	–200.929 573	73.1	–200.9868 39	75.1	25.5
TS3	–7106.656 473	64.1	–200.979 870	41.6	–201.025 116	51.0	24.7
TS4	–7106.676 760	51.3	–200.960 027	54.0	–201.029 434	48.4	25.4

Fig. 2. Energy stability profile at the CCSD(T)/B level of theory with respect to CH_3OOI.



in the bond distances, but in the relative stability of the isomers as well, as we shall see in the next section.

The final isomeric structures examined are ICH_2OOH and CH_2IOOH, which contain the iodomethyl group and may be considered as possible intermediates in the reaction of the iodomethyl radical (ICH_2) with the hydroperoxy radical (HO_2). Iodomethyl hydroperoxide (ICH_2OOH) is found to be a very stable species, the most stable structure among all isomers of the CH_3OOI family. The compound presents interesting similarities with the $ClCH_2OOH$ species (22), found to be one of the products in the experimental investigation of the $ClCH_2O_2 + HO_2$ reaction (23). The equilibrium geometries using both basis sets are consistent and show the same structural and stability features observed in the $ClCH_2OOH$, CH_3OOCl system, namely the decrease in C—O bond distance and the lower energy of the halomethyl isomer, indicating a stronger interaction of the halogenated methylic group with the -OOH part, compared to the interaction of the plain methylic group with the -OOX fragment. Indeed, we have for example, C—O = 1.418 Å in CH_3OOI and C—O = 1.384 Å in ICH_2OOH (basis set B). The effect results in a very high stability for ICH_2OOH as we shall see in the next section.

The novel species CH_2IOOH presents the same type of C—I bonding as the CH_2IOH compound calculated by Misra et al. (12) at the MP2(full)/6-31G(d) level. In the present work, CH_2IOOH has been also optimized at the MP2 level using both types of basis sets. Both structures result from the hypervalent bonding of iodine with the carbon atom and present significantly shorter C—I bond distances compared

© 2005 NRC Canada

to the C—I single bonds in the iodomethyl C-O type derivatives. Thus, the C—I bond distances in CH_2IOOH and ICH_2OOH were found to be 1.958 and 1.929 Å, and 2.201, and 2.162 Å, with basis sets A and B, respectively. The results are consistent with the CH_2IOH and ICH_2OH cases (12) where the values 1.959 and 2.225 Å have been determined, respectively, at the MP2/6-31G(d) level. The partially double C—I bond is also demonstrated by the slight biradical character that the molecule appears to possess as reflected in the instability of the spin-restricted (RHF) wavefunction compared to the spin-unrestricted (UHF) one (12).

Isomerization and conformation barriers

Four transition state configurations have been determined for the following isomerization processes: CH_3OOI <–> CH_3OIO (TS1), CH_3OIO <–> CH_3IO_2 (TS2), CH_3IO_2 <–> CH_2IOOH (TS3), and ICH_2OOH <–> CH_2IOOH (TS4). The geometries calculated with basis set B are included in Fig. 1 and they are characterized by one imaginary frequency (Table 3) as first-order saddle-points. All transition state structures exhibit triangular geometries, and TS1 is characterized by the I atom migration to the carbon-bonded oxygen atom, while TS2, TS3, and TS4 result from the the I atom migration to the carbon atom and insertion between the oxygen atom and the carbon atom.

The cis and trans conformeric structures of CH_3OOI with respect to C, O, O, and I atoms are also depicted in Fig. 1. They are well-characterized as conformational barriers by the imaginary frequencies, 249i, 235i and 19i, 40i, respectively, with bases A and B and present the same variations in O—O bond distance and O-O-I bond angle with the torsional angle as the CH_3OOBr, CH_3OOCl conformational barriers (13, 14). Thus, the O—O bond varies from its largest value, 1.475 Å, 1.480 Å in the conformers to its shortest, 1.416 Å, 1.438 Å in the minimum, while the C-O-O bond angle decreases from a maximum value (116.2°, 115.9°) in the cis conformer to a minimum value (102.0°, 101.9°) in the trans, through an intermediate value in the minimum energy structure (107.2°, 106.4°) in the two basis sets, respectively. The same type of variation is followed by the I-O-O bond angle.

Electronic energy and relative stability results

Table 4 summarizes the electronic (including zero point energy corrections) and the relative energies at the MP2 level combined with both basis sets and also the CCSD(T)/B//MP2/B single point energy calculations, while Fig. 2 presents a relative energy profile based on the CCSD(T) procedure. All three series of energy calculations predict the iodomethyl hydroperoxide (ICH_2OOH) to be by far the most stable isomer. However, inspection of Table 2 also demonstrates significant discrepancies in the relative stability order among the various isomers, despite the general overall consistency in the structural results. The most striking difference is observed in the relative stability order between the CH_3OOI and the CH_3OIO forms. The MP2/A results locate CH_3OIO 12.2 kcal mol^{-1} higher than CH_3OOI, while the MP2/B calculations reverse this order and predict CH_3OIO to be more stable than CH_3OOI by 5 kcal mol^{-1}. This order is similar to that predicted for the HOOI, HOIO isomers where the latter is calculated to be lower by 13 kcal mol^{-1} using DFT techniques combined with the LANL2DZ procedure (10). The CCSD(T)/B results place both isomers at similar energy levels, locating CH_3OIO higher only by 0.2 kcal mol^{-1}. We attribute the considerable stability of the CH_3OIO structure to the stabilization acquired by the bonding between the highly positively charged I and the electronegative CH_3O partner. The comparison with the analogous Cl, Br species indicates indeed a progressive stabilization of the CH_3OXO form as the electronegativity of the halogen decreases. Thus, the energy difference (8.4 kcal mol^{-1}) of CH_3OClO decreases to 6.3 kcal mol^{-1} for Br and drops to 0.2 kcal mol^{-1} for I.

With the same reasoning, the CH_3IO_2 structure is clearly found to be the highest in energy at all levels of theory since, in this case, the bonding between the positively charged hypervalent iodine and the electropositive moiety CH_3 considerably increases the instability of the structure. Thus, CH_3IO_2 is higher located than CH_3OOI at the MP2 level by 44.2 kcal mol^{-1} with basis set A, 10.9 kcal mol^{-1} with basis set B, and 18.5 kcal mol^{-1} at the CCSD(T)/B level in agreement with the corresponding $XClO_2$, $XBrO_2$ species, whose stability has been found to depend strongly on the electronegativity of the X partner (13, 14, 21, 24–26). The results are consistent with the relative stability order of the HIO_2 isomer, which is also the most unstable in the HOOI family, calculated to be 26.5 kcal mol^{-1} higher compared to the peroxide isomer HOOI.

The two iodomethyl isomers, ICH_2OOH and CH_2IOOH, are found to be the most stable and unstable isomers, respectively. In particular, CH_2IOOH is found to be unstable compared to CH_3OOI by more than 40 kcal mol^{-1} in all three levels of energy calculations. Similar energy order is found also in the CH_3OI family where CH_2IOH is calculated to be 42 kcal mol^{-1} higher than CH_3OI.

The calculated isomerization barriers TS1–TS4 are very high located to allow any interconversion process in all series of energy calculations without notable differences in the results. No differences are observed for the cis and trans energy barriers, which range from 11.8 to 2.2 kcal mol^{-1}, respectively, at the CCSD(T)/B level.

Summary

Five isomeric forms have been optimized for methyl iodoperoxide at the MP2 level of theory using two basis sets, the 6-311G(d,p) for all atoms and the 6-311G(d,p) for all atoms combined with the LANL2DZ method for I augmented with additional *d* and *f* polarization functions. Consistent overall structural and harmonic frequency results are obtained by both methods, but the relativistic corrections and the additional polarization produces tighter O—I and C—I bond lengths.

The refinement of the energetics has been accomplished carrying out CCSD(T) calculations at the MP2/6-311G(d,p) + LANL2DZdf optimized geometries. The more stable isomer is found to be the iodomethyl hydroperoxide. Among the three CH_3- isomeric forms, competing stability is found for the CH_3OOI and CH_3OIO structures. The CH_3IO_2 adduct is the highest in energy among the three. The most unstable

© 2005 NRC Canada

structure is found to be the novel species CH_2IOOH containing hypervalent iodine–carbon bonding that presents no analog in the corresponding families of the lighter halogens.

The interisomerization transition states are very high located to present any probability for such processes to take place and they thus, reflect the stability of each isomeric form with respect to the others. Finally, the cis and trans torsional barriers are also calculated and they are found to be consistent in all three methods of energy calculations.

References

1. A. Misra and P. Marshall. J. Phys. Chem. A, **102**, 9056 (1998).
2. S. Solomon, R.R. Garcia, and A.R. Ravishankara. J. Geophys. Res. D: Atmos. **99**, 20 491 (1994).
3. S. Solomon, J.B. Burkholder, A.R. Ravishankara, and R.R. Garcia. J. Geophys. Res. D: Atmos. **99**, 20 929 (1994).
4. S.P. Sander. J. Phys. Chem. **90**, 2194 (1986).
5. C.D. Dowd, J.L. Jimenez, R. Bahreini, C.R. Flagan, H.J. Seinfeld, K. Hameri, L. Pirjola, M. Kulmala, S.G. Jennings, and T. Hoffmann. Nature (London), **417**, 632 (2002).
6. E.K. Charles. Nature (London), **417**, 597 (2002).
7. V.A. Zolotarev, D.V. Ishkov, Y.P. Podmarkov, M.P. Frolov, and N.N. Yuryshev. Sov. J. Quantum Electron. **21**, 826 (1991).
8. M.E. Jenkin and R.A. Cox. J. Phys. Chem. **95**, 3229 (1991).
9. D. Shah, C.E. Canosa-Mas, N.J. Hendy, M.J. Scott, A. Vipond, and R.P. Wayne. Phys. Chem. Chem. Phys. **3**, 4932 (2001).
10. N. Begovic, Z. Markovic, S. Anic, and L. Kolar-Anic. J. Phys. Chem. A, **108**, 651 (2004).
11. P. Campuzano-Jost and J.N. Crowley. J. Phys. Chem. A, **103**, 2712 (1999).
12. A. Misra, R.J. Berry, and P. Marshall. J. Phys. Chem. A, **101**, 7420 (1997).
13. D.K. Papayannis, V.S. Melissas, and A.M. Kosmas. Phys. Chem. Chem. Phys. **5**, 2976 (2003).
14. E. Drougas and A.M. Kosmas. Int. J. Quant. Chem. **98**, 335 (2004).
15. M.J. Frisch, G.W. Trucks, H.B. Schlegel, G.E. Scuseria, M.A. Robb, J.R. Cheeseman, V.G. Zakrzewski, J.A. Montgomery, Jr., R.E. Stratmann, J.C. Burant, S. Dapprich, J.M. Millam, A.D. Daniels, K.N. Kudin, M.C. Strain, O. Farkas, J. Tomasi, V. Barone, M. Cossi, R. Cammi, B. Mennucci, C. Pomelli, C. Adamo, S. Clifford, J. Ochterski, G.A. Petersson, P.Y. Ayala, Q. Cui, K. Morokuma, D.K. Malick, A.D. Rabuck, K. Raghavachari, J.B. Foresman, J. Cioslowski, J.V. Ortiz, B.B. Stefanov, G. Liu, A. Liashenko, P. Piskorz, I. Komaromi, R. Gomperts, R.L. Martin, D.J. Fox, T. Keith, M.A. Al-Laham, C.Y. Peng, A. Nanayakkara, C. Gonzalez, M. Challacombe, P.M.W. Gill, B. Johnson, W. Chen, M.W. Wong, J.L. Andres, M. Head-Gordon, E.S. Replogle, and J.A. Pople. GAUSSIAN 98 [computer program]. Gaussian, Inc., Pittsburgh, Penn. 1998.
16. W.R. Wadt and P.J. Hay. J. Chem. Phys. **82**, 284 (1985).
17. M.N. Glukhovtsev, A. Pross, M.P. McGrath, and L. Radom. J. Chem. Phys. **103**, 1878 (1995).
18. A.J. Sadlej. Theor. Chim. Acta, **81**, 339 (1992).
19. D.K. Papayannis, V.S. Melissas, and A.M. Kosmas. Chem. Phys. Lett. **349**, 299 (2001).
20. Molecular Science Computing Facility, Environmental and Molecular Sciences Laboratory. Extensible computational chemistry environment basis set database [online]. Version 1.0. Available from http:\\ecce.emsl.pnl.gov. Pacific Northwest Laboratory, Richland, Wash.
21. T.J. Lee, C.E. Dateo, and J.E. Rice. Mol. Phys. **96**, 633 (1999).
22. H. Sun, C.-J. Chen, and J.W. Bozzelli. J. Phys. Chem. A, **104**, 8270 (2000).
23. T.J. Wallington, M.D. Hurley, and W.F. Schneider. Chem. Phys. Lett. **251**, 164 (1996).
24. J.S. Francisco, S.P. Sander, T.J. Lee, and A.P. Rendell. J. Phys. Chem. **98**, 5644 (1994).
25. S. Guha and J.S. Francisco. J. Phys. Chem. A, **101**, 5347 (1997).
26. R.S. Zhu, Z.F. Xu, and M.C. Lin. J. Chem. Phys. **116**, 7452 (2002).

© 2005 NRC Canada

$InCl_3 \cdot 4H_2O$-promoted green preparation of xanthenedione derivatives in ionic liquids

Xuesen Fan, Xueyuan Hu, Xinying Zhang, and Jianji Wang

Abstract: A green procedure for the synthesis of xanthenedione derivatives (**3**) through $InCl_3 \cdot 4H_2O$-promoted condensation of aldehydes (**1**) and 5,5-dimethyl-1,3-cyclohexanedione (**2**) in ionic liquids is described in this paper. This novel method has such advantages as operational simplicity and environmental benignancy together with enhanced atom utilization. Moreover, the reaction media and the catalyst can be recovered conveniently and reused effectively for at least six times.

Key words: ionic liquid, xanthenedione derivatives, indium trichloride, green synthesis.

Résumé : Dans ce travail, on décrit une méthode verte de synthèse de dérivés **3** de la xanthènedione par le biais d'une condensation, catalysée par le $InCl_3 \cdot 4H_2O$, des aldéhydes (**1**) avec la 5,5-diméthylcyclohexane-1,3-dione (**2**), dans des liquides ioniques. Cette nouvelle méthode allie la simplicité d'opération et un caractère bénin pour l'environnement avec une utilisation accrue des atomes. De plus, le milieu réactionnel ainsi que le catalyseur peuvent être facilement récupérés et réutilisés d'une façon efficace jusqu'à six fois.

Mots clés : liquide ionique, dérivés de la xanthènedione, trichlorure d'indium, synthèse verte.

[Traduit par la Rédaction]

Introduction

Xanthene derivatives have attracted considerable interest in recent years because of their promising activity as positive allosteric modulators of metabotropic (mGlu) receptors (1) and potent nonpeptidic inhibitors of recombinant human calpain I (2). They have been used as rigid carbon skeletons for the construction of new chiral bidentate phosphine ligands with potential applications in catalytic processes (3). In particular, xanthenediones constitute a structural unit in a number of natural products (4) and have been used as versatile synthons because of the inherent reactivity of the inbuilt pyran ring (5). Up to now, several methods have been developed for the preparation of xanthenediones. Among them, the conventional procedures involve acid- or base-catalyzed condensation of appropriate active methylene carbonyl compounds with aldehydes (6). However, these methods are plagued by the limitation of prolonged reaction times, poor yields, and side reactions of aldehydes. Recently, Singh et al. (7*a*) reported a new method for the preparation of xanthenediones through carbon transfer reactions of 1,3-oxazinanes and oxazolidines with carbon nucleophiles. It has also been reported that xanthenedione derivatives could be obtained through condensation of aldehydes and 5,5-dimethyl-1,3-cyclohexanedione in glycol under microwave irradiation (7*b*). Most recently, Jin et al. (7*c*) reported a novel and interesting procedure in which the above condensation process was realized in water in the presence of a dodecylbenzenesulphonic acid catalyst. However, due to their great importance, there still needs to be development of novel methods for the preparation of xanthenediones.

The development of environmentally friendly catalysts and solvents for organic chemistry is an area of considerable importance. From both economical and environmental points of view, the use of nonvolatile solvents is very promising. In the last few years, room-temperature ionic liquids (RTILs), especially those based on 1,3-dialkylimidaxolium cations, have been recognized as a possible environmentally benign alternative to chemically volatile solvents. They are nonvolatile, recyclable, nonexplosive, easy to handle, and thermally robust. In many cases, the products are weakly soluble in the ionic liquid phase so that the products can be easily separated by simple filtration or extraction with ether. Because of the great potential of RTILs as novel reaction media for catalytic processes, much attention has currently been focused on their applications as novel media for various kinds of organic reactions (8). As a continuation of our interest in the area of clean synthesis using ionic liquids as a green recyclable alternative to classical molecular solvents (9), we report here a very simple and green procedure for the preparation of xanthenediones (**3**, Scheme 1) through a $InCl_3 \cdot 4H_2O$-promoted cascade reaction between aldehydes (**1**) and 5,5-

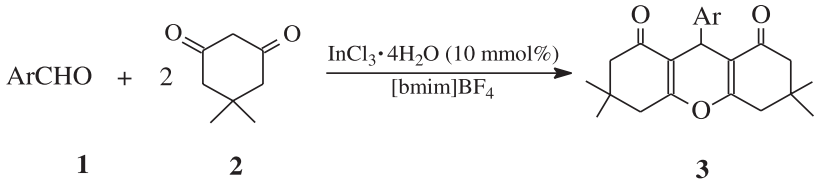
Received 17 May 2004. Published on the NRC Research Press Web site at http://canjchem.nrc.ca on 27 January 2005.

X. Fan,[1] **X. Zhang, and J. Wang.** School of Chemical and Environmental Sciences, Henan Key Laboratory for Environmental Pollution Control, Henan Normal University, Xinxiang, Henan 453007, P. R. China.
X. Hu. School of Chemical and Environmental Sciences, Henan Key Laboratory for Environmental Pollution Control, Henan Normal University, Xinxiang, Henan 453007, P. R. China and Chongqing University of Medical Sciences, Chongqing 400016, P.R. China.

[1]Corresponding author (e-mail: fanxs88@263.net).

 doi: 10.1139/V04-155 © 2005 NRC Canada

Scheme 1.



Scheme 2.

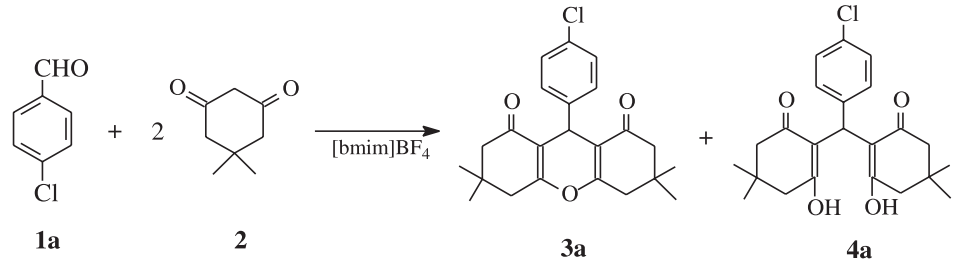


Table 1. Reaction condition screening for the condensation of **1a** and **2** in the ionic liquid.[a]

				Isolated yield (%)	
Entry	Amount of $InCl_3·4H_2O$ (mmol)	Reaction temp. (°C)	Reaction time (h)	**3a**	**4a**
1	0	r.t.	1.5	5	20
2	0	50	1.5	10	30
3	0	50	3	15	35
4	0	70	3	18	42
5	0	100	3	20	55
6	0	120	5	23	69
7	0.10	50	3	55	10
8	0.10	70	3	75	5
9	0.10	70	5	83	0
10	0.10	80	5	95	0

[a]Reaction conditions: 1 mL solvent, 0.5 mmol **1a**, and 1 mmol **2**.

dimethyl-1,3-cyclohexanedione (**2**) in ionic liquid 1-butyl-3-methylimidazolium tetra-fluoroborate ([bmim][BF_4]).

Results and discussion

The mixture of 5,5-dimethyl-1,3-cyclohexanedione (**2**) and 4-chlorobenzaldehyde (**1a**) in [bmim][BF_4] was prepared and stirred at room temperature. After 0.5 h, some solid was observed and TLC analysis gave a positive result for the formation of a new compound together with the remaining aldehyde **1a**. To have a complete conversion, stirring of the mixture was continued for 1 h. To our surprise, another compound was formed as indicated by the TLC analysis. At this stage, the reaction was quenched by the addition of 5 mL H_2O to the mixture. Then, the solid compound was collected and separated through column chromatography. Subsequent analysis in terms of physical and spectral data (IR, ^{1}H NMR, and MS) showed that these two compounds were 9-(4 chlorophenyl)-3,3,6,6-tetramethyl-3,4,5,6,7,9-exahydro-1*H*-xanthene-1,8(2*H*)-dione (**3a**) and bis(5,5-dimethyl-3-hydroxy-1-oxa-2-cyclohexen-2-yl)-4′-chlorophenylmethane (**4a**). Their yields were found to be 5% and 20%, respectively. In addition, it should be noted that the compound formed first in this process was **4a**. The reaction process is shown in Scheme 2.

To obtain **3a** alone, rather than the mixture of **3a** and **4a**, with more increased yield, the reaction mixture of **1a** and **2** was then stirred at different elevated reaction temperatures and (or) over a prolonged reaction time. The results obtained are shown in Table 1. It can be seen that with increased reaction temperature and (or) prolonged reaction time, although **3a** could be obtained in higher yields, the yields of **4a** were also increased to some extent. Thus, it seems impossible to get **3a** alone just by adjusting such factors as temperature and reaction time. Considering the fact that $InCl_3·4H_2O$, as an efficient Lewis acid catalyst, has been successfully used in promoting many kinds of organic reactions (10), especially in several condensation processes, we then added a catalytic amount of $InCl_3·4H_2O$ into the reaction mixture with the hope of obtaining an improved result in terms of both yield and selectivity of **3a**. To our delight, $InCl_3·4H_2O$ showed high efficiency for this process by affording **3a** not only in high yield, but also with excellent selectivity (entries 7–10, Table 1).

Based on the above results, this process was then extended to other structurally varied aldehydes to investigate its scope and generality. The results are listed in Table 2. It

© 2005 NRC Canada

Table 2. Preparation of xanthenediones promoted by $InCl_3 \cdot 4H_2O$ in [bmim][BF_4] at 80 °C.

Entry	Ar	Time (h)	Products	Yield (%)	mp (Lit. value) (ref.)
1	*p*-ClC_6H_4	5	**3a**	95	237–239 (230 to 231) (7*b*)
2	*p*-$CH_3C_6H_4$	4	**3b**	90	210–212 (218–220) (7*b*)
3	*p*-$NO_2C_6H_4$	5	**3c**	86	222–224 (222–224) (7*b*)
4	C_6H_5	4	**3d**	87	199–201 (198–200) (7*b*)
5	*o*-ClC_6H_4	10	**3e**	83	225–227 (228 to 229) (7*b*)
6	*p*-$CH_3OC_6H_4$	5	**3f**	87	241–243 (227–228) (10)
7	*p*-FC_6H_4	4	**3g**	90	224–226 (225–227) (10)
8	*o*-BrC_6H_4	10	**3h**	76	226–228
9	*p*-BrC_6H_4	4	**3i**	93	234–236
10	*m*-$NO_2C_6H_4$	4	**3j**	92	145–147

Table 3. Reusability of [bmim][BF_4] and the catalyst.[a]

Round	Ionic liquid recovered (%)	Isolated yield of **3a** (%)
1	98	95
2	99	98
3	98	93
4	99	91
5	98	88
6	97	87

[a]Reaction conditions: reaction temp. 80 °C, reaction time 5 h.

is shown that under the similar fashion, a wide range of aldehydes underwent smooth condensation with 5,5-dimethyl-1,3-cyclohexanedione (**2**) to give xanthenedione derivatives in high yields. One feature of the present procedure is that aldehydes both with electron-withdrawing groups and with electron-donating groups afforded the corresponding product in good yields, and para- and meta-substituted substrates reacted almost equally well. However, aldehydes bearing an ortho group turned out to be reluctant to undergo the condensation reaction probably because of steric hindrance. Thus, longer reaction time is required for these substrates to get the corresponding products in high yields (entries 5 and 8, Table 2).

Our attention was then directed toward the possibility of recycling the reaction media since the recovery and reuse of catalyst and solvent are highly preferable for a greener process. At completion, water was added into the reaction mixture, and the solid was collected by filtration to give the product. The filtrate containing [bmim][BF_4] and the dissolved In(III) was concentrated under reduced pressure to recover the ionic liquid and the catalyst. Then, their reusability was investigated by using **1a** and **2** again as the model substrates. It has been observed that even in the sixth round, the corresponding product could still be obtained with fairly good yield by using the ionic liquid and the catalyst recovered from the fifth (Table 3, entry 6).

For the sake of comparison with [bmim][BF_4], several conventional organic solvents including methanol, ethanol, toluene, and ethyl acetate, were also used in this catalytic process with **1c** (*p*-nitrobenzaldehyde) and **2** as model substrates. The results are summarized in Table 4.

Table 4. Reaction of **1c** and **2** in different solvents.[a]

				Isolated yield (%)	
Entry	Solvent	Reaction temp. (°C)	Reaction time (h)	**3c**	**4c**
1	Ethanol	Reflux	5	29	31
2	Methanol	Reflux	5	24	23
3	Toluene	80	5	25	27
4	Ethyl acetate	Reflux	5	59	Traces
5	[bmim][BF_4]	80	5	86	0

[a]Reaction conditions: 1 mL solvent, 0.5 mmol **1c**, and 1 mmol **2**.

It has been shown that of the five solvents used, [bmim][BF_4] gave the best result in terms of both yield and selectivity. In fact, only when [bmim][BF_4] was used as the reaction medium, can **3c** be obtained with a high yield (86%, Table 4, entry 5). On the other hand, when toluene, methanol, ethanol, or ethyl acetate was used, not only was the reaction incomplete after being stirred at reflux or at 80 °C for 5 h, but a mixture of **3c** and **4c** was also obtained with much lower yields (Table 4, entries 1–4). Actually, **3c** is in the solid state when the reaction is complete and therefore can be obtained through simple filtration because of its poor solubility in [bmim][BF_4]. On the contrary, when toluene, methanol, ethanol, or ethyl acetate was used, the product was dissolved in the solution. Therefore, with toluene or ethyl acetate as solvent, the product has to be obtained through tedious experimental operations, such as washing with water, drying over anhydrous sodium sulfate, concentrating under vacuum, and subsequent separation on column chromatography. When ethanol or methanol was used, the separation procedure turned out to be even more complicated. First, the solvent had to be removed and the residue was redissolved in another solvent immiscible with water. Then the solution was washed with water, dried, concentrated, and finally separated on column. Considering all of these differences, it may be safe to say that using [bmim][BF_4] in place of conventional organic solvents as the reaction medium actually results in a much enhanced reactivity, and avoids the disadvantages such as tedious operational procedure and potential experimental pollution in relation to the organic solvents.

It has been reported that another green solvent, water, has also been used as reaction medium for this procedure (11). However, due to the poor solubility of substrates in water, a

© 2005 NRC Canada

phase-transfer catalyst (quaternary ammonium salt) and a strong acid catalyst (such as TsOH) have to be used to facilitate the cyclodehydration reaction. Even so, xanthenedione derivatives **3** (Scheme 2) can only be obtained from para-substituted aromatic aldehydes through a much longer reaction period. In the case of ortho- and meta-substituted aromatic aldehydes, non-cyclodehydrated products **4** (Scheme 2) instead of **3** were obtained. In contrast, the substrates are well-dissolved in the [bmim][BF_4]/In^{3+} system, no phase-transfer catalyst is needed, and the reaction time is much shorter in our situation. Moreover, aromatic aldehydes with ortho- or meta-substituents can react smoothly with **2** to produce xanthenedione derivates **3** in good yields (Table 2, entries 5 and 10). In another case, microwave irradiation technique has also been successfully used in the condensation of aldehydes with 5,5-dimethyl-1,3-cyclohexanedione to give xanthenedione (7*b*). However, its potential use for larger scale preparation may be rather limited compared to the method presented in this paper.

In conclusion, we have found a novel procedure for the preparation of xanthenedione derivatives. The main advantages of this procedure include high yields, simple experimental procedure, and ease of recovering and reusing of the catalyst and the reaction media. Therefore, the present method is expected to serve as an alternative process for the preparation of xanthenedione derivatives.

Experimental

Melting points were measured by a Kofler micromelting point apparatus and the results were uncorrected. IR spectra were recorded on a Bruker Vector 22 spectrometer in KBr with absorption in cm^{-1}. ^1H NMR spectra were determined on a Bruker AC 400 spectrometer as $CDCl_3$ solutions. Chemical shifts (δ) are expressed in ppm downfield from the internal standard tetramethylsilane, and coupling constants (*J*) are given in Hz. Elemental analyses were performed on an EA-1110 instrument.

The ionic liquid [bmim][BF_4] was prepared and purified according to literature procedure (12). Other reagents were of reagent grade and were used without further purification.

General procedure for the preparation of xanthenedione derivatives

Aldehyde (**1**, 1 mmol), 5,5-dimethyl-1,3-cyclohexanedione (**2**, 2 mmol), and $InCl_3 \cdot 4H_2O$ (0.1 mmol) were added to a 10 mL round-bottomed flask containing 1 mL [bmim][BF_4]. Then the mixture was stirred at 80 °C for a certain period of time (shown in Table 2) to complete the reaction (monitored by TLC). At completion, water was added into the reaction mixture and the solid was collected by suction and rinsed with cold ethanol to give the product **3**. All the products were fully characterized by IR, ^1H NMR, and elemental analysis. The aqueous solution of ionic liquid together with the catalyst was concentrated under reduced pressure to recover the ionic liquid and catalyst for subsequent use.

*9-(4′-Flurophenyl)-3,3,6,6-tetramethyl-3,4,5,6,7,9-hexahydro-1***H***-xanthene-1,8-(2***H***)-dione (3g)*

Colorless needles, mp 224~226 (lit. value (10) mp 225~227). ν: IR (KBr, cm^{-1}) ν: 3030, 2950, 2878, 1685, 1660, 1627, 1467, 1357, 1203. ^1H NMR ($CDCl_3$) δ: 1.04 (s, 6H, 2 × CH_3), 1.11 (s, 6H, 2 × CH_3), 2.14~2.46 (m, 8H, 4 × CH_2), 4.77 (s, 1H, CH), 7.31(d, *J* = 8.4 Hz, 2H, ArH), 7.65 (d, *J* = 8.4 Hz, 2H, ArH). Anal. calcd. for $C_{23}H_{25}FO_3$: C 74.98, H 6.84; found: C 74.88, H 6.75.

*9-(2′-Bromophenyl)-3,3,6,6-tetramethyl-3,4,5,6,7,9-hexahydro-1***H***-xanthene-1,8-(2***H***)-dione (3h)*

Colorless needles, mp 226~228. IR (KBr, cm^{-1}) ν: 2959, 2871, 1679, 1666, 1627, 1469, 1357, 1203. ^1H NMR ($CDCl_3$) δ: 1.04 (s, 6H, 2 × CH_3), 1.11 (s, 6H, 2 CH_3), 2.14~2.46 (m, 8H, 4 CH_2), 5.04 (s, 1H, CH), 6.98 (t, *J* = 8.0 Hz, 1H, ArH), 7.21 (t, *J* = 4.0 Hz, 1H, ArH), 7.45 (m, 1H, ArH), 7.47 (d,d, *J* = 8.0, 0.9 Hz, 1H, ArH). Anal. calcd. for $C_{23}H_{25}BrO_3$: C 64.39, H 5.87; found: C 64.25, H 5.77.

*9-(4′-Bromophenyl)-3,3,6,6-tetramethyl-3,4,5,6,7,9-hexahydro-1***H***-xanthene-1,8-(2***H***)-dione (3i)*

Colorless needles, mp 234~236. IR (KBr, cm^{-1}) ν: 2953, 2878, 1679, 1662, 1625, 1487, 1470, 1362. ^1H NMR ($CDCl_3$) δ: 1.00 (s, 6H, 2 × CH_3), 1.12 (s, 6H, 2 × CH_3), 2.16~2.48 (m, 8H, 4 × CH_2), 4.72 (s, 1H, CH), 7.18 (d, *J* = 8.4 Hz, 2H, ArH), 7.35 (d, *J* = 8.4 Hz, 2H, ArH). Anal. calcd. for $C_{23}H_{25}BrO_3$: C 64.39, H 5.87; found: C 64.30, H 5.82.

*9-(3′-Nitrophenyl)-3,3,6,6-tetramethyl-3,4,5,6,7,9-hexahydro-1***H***-xanthene-1,8-(2***H***)-dione (3j)*

Colorless crystals, mp 145~147. IR (KBr, cm^{-1}) ν: 2958, 1677, 1655, 1622, 1525, 1475, 1363, 1202. ^1H NMR ($CDCl_3$) δ: 1.02 (s, 6H, 2 × CH_3), 1.14 (s, 6H, 2 × CH_3), 2.17~2.53 (m, 8H, 4 CH_2), 4.86 (s, 1H, CH), 7.43 (t, *J* = 8.0 Hz, 1H, ArH), 7.84 (d, *J* = 7.6 Hz, 1H, ArH), 7.99~8.04 (m, 2H, ArH). Anal. calcd. for $C_{23}H_{25}NO_5$: C 69.86, H 6.37, N 3.54; found: C 69.66, H 6.29, N 3.51.

Acknowledgements

This work was financially supported by the National Natural Science Foundation of China (No. 20273019) and the Science Foundation of Henan Normal University for Young Scholars (No. 0307032).

References

1. J. Wichmann, K. Bleicher, E. Vieira, T. Woltering, F. Knoflach, and V. Mutel. Farmaco, **57**, 989 (2002).
2. S. Chatterjee, M. Iqbal, J.C. Kauer, J.P. Mallamo, S. Senadhi, and S. Mallya. Bioorg. Med. Chem. Lett. **6**, 1619 (1996).
3. (*a*) Y. Hamada, F. Matsuura, M. Oku, K. Hatano, and T. Shioiri. Tetrahedron Lett. **38**, 8961 (1997); (*b*) S. Hillebrand, J. Bruckmann, C. Kruger, and M.W. Haenel. Tetrahedron Lett. **36**, 75 (1995); (*c*) G. Malaise, L. Barloy, and J.A. Osborn. Tetrahedron Lett. **42**, 7417 (2001).
4. (*a*) S. Hatakeyma, N. Ochi, H. Numata, and S. Takano. J. Chem. Soc. Chem. Commun. 1202 (1988), and refs. cited therein; (*b*) G.M. Cingolant and M. Pigini. J. Med. Chem. **12**, 531 (1988).
5. C.N. O'Callaghan and T.B.H. McMurry. J. Chem. Res. Synop. 214 (1995); J. Chem. Res. Miniprint, 1448 (1995), and refs. cited therein.
6. J. Kuthan, P. Sebek, and S. Bohm. *In* Advances in heterocyclic

© 2005 NRC Canada

chemistry. Vol. 62. Academic Press, Inc., New York. 1995. p. 19.
7. (*a*) K. Singh, J. Singh, and H. Singh. Tetrahedron, **52**, 14 273 (1996); (*b*) S.J. Tu, Y. Gao, X.H. Liu, S.F. Tang, and X.J. Qiu. Chin. J. Org. Chem. **21**, 1164 (2001); (*c*) T. Jin, J. Zhang, J. Xiao, A. Wang, and T. Li. Synlett, **5**, 866 (2004).
8. (*a*) J. Dupont, R.F. de Souza, and P.A.Z. Suarez. Chem. Rev. **102**, 3667 (2002); (*b*) D.B. Zhao, M. Wu, Y. Kou, and E.Z. Min. Catal. Today, **74**, 157 (2002); (*c*) H. Olivier-Bourbigou and L. Magna. J. Mol. Catal. A: Chem. **182–183**, 419 (2002); (*d*) T. Welton. Chem. Rev. **99**, 2071 (1999); (*e*) Z. Li and C.G. Xia. Tetrahedron Lett. **44**, 2069 (2003); (*f*) J.S. Yadav, B.V.B. Reddy, A.K. Basak, and A. Venkat Narsaiah. Tetrahedron Lett. **44**, 1047 (2003).
9. (*a*) X. Zhang, X. Fan, H. Niu, and J. Wang. Green Chem. **5**, 267 (2003); (*b*) X. Zhang, H. Niu, and J. Wang. J. Chem. Res. Synop. 33 (2003).
10. (*a*) T.P. Loh, L.C. Feng, and L.L. Wei. Tetrahedron, **57**, 4231 (2001); (*b*) Z.G. Li, J.H. Zhang, and C.J. Li. Tetrahedron Lett. **44**, 153 (2003); (*c*) D.S. Bose, A.P. Rudradas, and M.H. Babu. Tetrahedron Lett. **43**, 9195 (2002).
11. D.Q. Shi, Q.Y. Zhuang, J. Chen, S.X. Wang, S.J. Tu, and H.W. Hu. Chin. J. Org. Chem. **23**, 694 (2003).
12. J.D. Holbrey and K.R. Seddon. J. Chem. Soc. Dalton Trans. 2133 (1999).

© 2005 NRC Canada

Glycosides from the sea cucumber *Cucumaria frondosa*. III. Structure of frondosides A_2-1, A_2-2, A_2-3, and A_2-6, four new minor monosulfated triterpene glycosides

Alexandra S. Silchenko, Sergey A. Avilov, Alexandr S. Antonov, Anatoly I. Kalinovsky, Pavel S. Dmitrenok, Vladimir I. Kalinin, Valentin A. Stonik, Carl Woodward, and Peter D. Collin

Abstract: Frondosides A_2-1 (**1**), A_2-2 (**2**), A_2-3 (**3**), and A_2-6 (**4**) are new monosulfated holostane pentaosides isolated from the sea cucumber *Cucumaria frondosa*. Their structures have been elucidated on the basis of spectral data (2D NMR and MS). Frondoside A_2-2 (**2**) contains an α,β-unsaturated ketone fragment in the side chain of the aglycon, unique for triterpene glycosides of sea cucumbers.

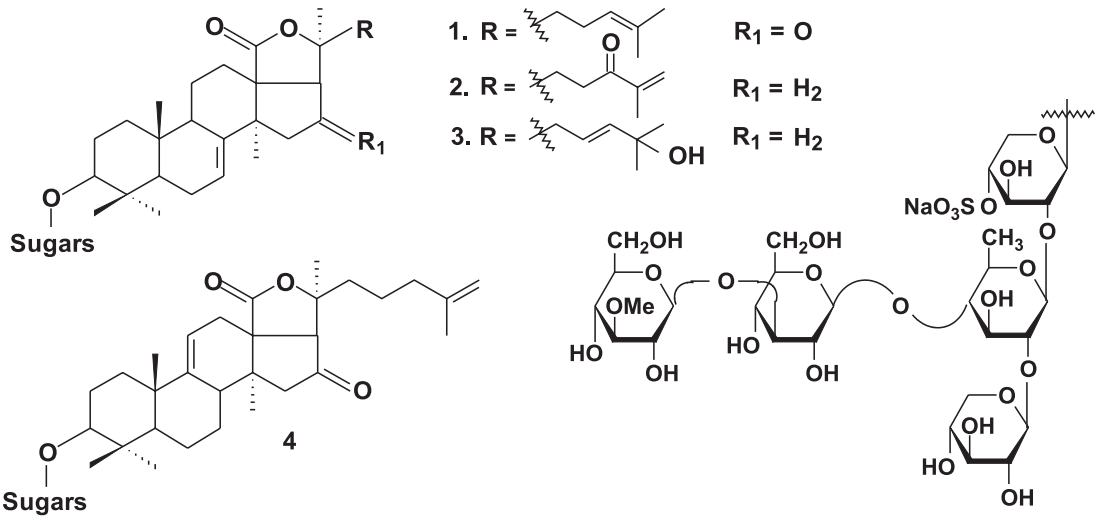
Key words: Cucumaria frondosa, sea cucumbers, frondosides, triterpene glycosides.

Résumé : Les frondosides A_2-1 (**1**), A_2-2 (**2**), A_2-3 (**3**) et A_2-6 (**4**) sont des pentaosides monosulfatés d'holostane isolés du concombre de mer *Cucumaria frondosa*. On a élucidé leurs structures sur la base de données spectrales (RMN 2D et SM). La chaîne latérale de l'aglycone du frondoside A_2-2 (**2**) comporte un fragment de cétone α,β-insaturée qui est unique pour les glycosides triterpéniques des concombres de mer.

Mots clés : Cucumaria frondosa, concombres de mer, frondosides, glycosides triterpéniques.

[Traduit par la Rédaction]

The sea cucumber *Cucumaria frondosa* Gunnerus (Cucumariidae, Dendrochirotida) is a widespread benthic animal common in the North Atlantic and Western Arctic seas that is harvested commercially. Although previous studies of this sea cucumber have yielded a series of new triterpene glycosides, *C. frondosa* remains poorly investigated because of the extreme complexity of its glycoside fraction (1–6). Previously, we isolated and reported a new minor monosulfated tetraoside frondoside A_1 along with the known frondoside A from the specimens of *C. frondosa* collected in the Barents



Received 5 July 2004. Published on the NRC Research Press Web site at http://canjchem.nrc.ca on 29 January 2005.

A.S. Silchenko, S.A. Avilov, A.S. Antonov, A.I. Kalinovsky, P.S. Dmitrenok, V.I. Kalinin,[1] and V.A. Stonik. Pacific Institute of Bioorganic Chemistry, Far East Division of the Russian Academy of Sciences, Vladivostok, 690022, Russia.
C. Woodward and P.D. Collin. Coastside Bio Resources Inc., P.O. Box 151, Stonington, ME 04681, USA.

[1]Corresponding author (e-mail: kalininv@piboc.dvo.ru).

 doi: 10.1139/V04-163 © 2005 NRC Canada

Table 1. ^{13}C and ^{1}H NMR chemical shifts, and selected HMBC and NOESY correlations of the carbohydrate moiety of frondosides **1–4**.

Position	δ_C[a,b,c]	δ_H mult. (*J* in Hz)[d]	HMBC	NOESY
Xyl1 (1→C-3)				
1	104.84	4.79 d (7.0)	C: 3	H-3,5-Xyl1, H-3, H-31
2	**81.33**	4.06 m	C: 1-Qui	H-1 Qui
3	75.93	4.47 t (9.3)		H-1,5 Xyl1
4	*75.60*	5.18 m		
5	64.46	4.81 dd (12.0; 5.3)		H-1,3 Xyl1
		3.89 m		H-1,3 Xyl1
Qui (1→2Xyl1)				
1	102.17	5.33 d (7.7)	C: 2-Xyl1	H-5 Qui, H-2 Xyl1
2	**82.15**	4.12 m		H-1 Xyl 2
3	75.72	4.12 m		
4	**86.70**	3.63 m		H-6 Qui, H-1 Glu
5	70.91	3.63 m		H-1 Qui
6	17.92	1.67 d (5.6)	C: 4,5-Qui	H-4 Qui, H-30
Glc (1→4Qui)				
1	104.65	4.93 d (7.8)	C: 4-Qui	H-4 Qui, H-3,5 Glu
2	73.64	4.03 m		
3	**87.87**	4.26 t (9.0)	C: 1-MeGlu	H-1 MeGlu, H-1,5 Glu
4	69.57	4.07 m		
5	77.75	4.01 m		H-1,3 Glu
6	61.87	4.48 brd (12.0)		
		4.18 dd (6.2; 12.0)		
MeGlc (1→3Glu)				
1	105.43	5.33 d (7.8)	C: 3-Glu	H-3 Glu, H-3,5 MeGlu
2	74.96	4.01 m		
3	87.71	3.73 t (8.9)	OMe	H-1,5 MeGlu
4	70.41	4.14 m		
5	78.22	3.99 m		H-1,3 MeGlu
6	62.06	4.50 dd (2.3;12.1)		
		4.26 dd (3.2; 12.3)		
OMe	60.69	3.89 s	C:3 -MeGlu	
Xyl 2 (1→2 Qui)				
1	105.43	5.41 d (6.7)	C: 2-Qui	H-3,5 Xyl 2, H-2 Qui
2	74.96	4.06 m		
3	76.41	4.14 m		H-1 Xyl2
4	70.50	4.12 m		
5	66.42	4.41 dd (3.9;11.0)		
		3.68 dd (9.0; 11.0)		H-1 Xyl2

[a]Recorded at 125 MHz in C_5D_5N.
[b]Bold = interglycosidic positions.
[c]Italic = sulfate position.
[d]Recorded at 500 MHz in C_5D_5N.

Sea (3). We also elucidated the structure of a novel and more polar trisulfated non-holostane (having no lactone cycle in the aglycon) pentaoside from this animal (4).

In continuation of our investigations on *C. frondosa* triterpene glycosides, we report herein results of the study on monosulfated pentaosides having a glucose residue as the third monosaccharide unit in the carbohydrate moiety in contrast to the major component of the glycoside fraction, frondoside A, having xylose as the corresponding residue.

Sea cucumbers were collected in the Gulf of Maine, Penobscot Bay, Maine, USA. Column chromatography on polychrom-1 (powdered Teflon) of the ethanolic extract of *C. frondosa* gave a mixture of glycosides that was separated by column chromatography on silica gel, affording a crude mixture of monosulfated pentaosides. Separation of the fraction by HPLC yielded four individual glycosides, frondosides A_2-1 (**1**), A_2-2 (**2**), A_2-3 (**3**), and A_2-6 (**4**) belonging to the cucumarioside A_2 group (7).

Signals of the carbohydrate chains in the NMR spectra of isolated glycosides (**1–4**) were coincident in all of them indicating the identity of the sugar parts of these compounds (Table 1). The presence of five characteristic doublets (J = 6.7–7.8 Hz) in the ^{1}H NMR spectra of **1–4** and corresponding signals of anomeric carbons in the ^{13}C NMR were indicative of a pentasaccharide chain and the β-configuration of glycosidic bonds (8). The characteristic proton resonances of methyl groups at δ 1.67 ppm (d, J = 5.6 Hz) and δ 3.89 ppm (s) suggested the presence of quinovose and 3-*O*-methyl glucose residues in the oligosaccharide chain. The comparison of carbon resonances belonging to the carbohydrate chains

© 2005 NRC Canada

Table 2. ^{13}C and ^{1}H NMR chemical shifts and selected HMBC and NOESY correlations of the frondoside A_2-1 (**1**) aglycon moiety.

Position	δ_C[a]	δ_H Mult. (*J* in Hz)[b]	HMBC	NOESY
1	35.71	1.46 m		H-19
2	26.74	1.89 m (a)		H-19, H-30
		2.06 m (e)		
3	88.83	3.29 dd (4.2, 11.3)		H-5, H-31, H-1 Xyl1
4	39.36			
5	48.24	1.03 m		H-3
6	23.14	2.04 m		
7	121.82	5.80 m		
8	143.92			
9	47.06	3.64		H-11, H-12, H-19
10	35.55			
11	22.34	1.93 m		H-1, H-12
12	29.60	1.26 m	C: 18	H-11, H-21
		2.36 m		H-32
13	56.80			
14	45.64			
15	51.92	2.45 br d (16.5)	C:16, 13, 17	
		2.78 br d (16.5)		
16	214.32			
17	63.44	3.04 s	C: 12, 13, 16, 18, 20, 21	H-12, H-21, H-32
18	179.32			
19	23.90	1.22 s	C: 3, 4, 9, 10	H-1, H-2, H-9
20	83.67			
21	26.03	1.62 s	C: 17, 20, 22	H-12
22	38.69	1.71 m		
		1.91 m		
23	23.02	2.14 m		
		2.43 m		H-21
24	123.92	5.14 m		H-27
25	132.01			
26	17.50	1.63 s	C: 24, 25, 27	
27	25.53	1.66 s	C: 24, 25, 26	
30	17.30	1.12 s	C: 3, 4, 5, 31	H-2, H-6 Qui
31	28.63	1.29 s	C: 3, 4, 5, 30	H-3, H-1 Xyl1
32	31.99	1.30 s	C: 8, 13, 14, 15	

[a]Recorded at 125.77 MHz in C_5D_5N.
[b]Recorded at 500 MHz in C_5D_5N.

of **1**–**4** (Table 1) showed complete coincidence with those in the spectrum of monosulfated pentaoside cucumarioside A_2-2 isolated from *Cucumaria japonica* (7). The structure of the carbohydrate chains of **1**–**4** was corroborated by HMBC and NOESY correlations (Table 1). Specifically, interglycosidic bonds were confirmed by NOESY cross peaks between H-1 of the first xylose residue and H-3 of the aglycon; between H-2 of quinovose and H-1 of the terminal xylose residue; between H-4 of quinovose and H-1 of the glucose residue; and between H-3 of the glucose residue and H-1 of the terminal 3-*O*-methyl-glucose residue.

The MALDI TOF MS of glycoside **1** exhibited pseudomolecular ion peaks at *m/z* 1341 $[M_{Na} + Na]^+$, 1342 $[M_{Na} + Na + H]^+$ along with the peak at *m/z* 1239 $[M_{Na} - SO_3Na + Na + H]^+$ in the positive ion mode, and pseudomolecular ion peaks at *m/z* 1295 $[M_{Na} - Na]^-$, 1296 $[M_{Na} - Na + H]^-$, and 1163 $[M_{Na} - Na - Xyl + H]^-$, and a peak at *m/z* 1119 $[M_{Na} - Na - 3\text{-O-Me-Glc} + H]^-$ (because of the loss of terminal monosaccharide residues) in the negative ion mode. The HR MALDI TOF MS (positive ion mode) showed the pseudomolecular ion $[M_{Na} + Na]^+$ at *m/z* 1341.5098, calculated for $C_{59}H_{91}O_{29}SNa_2$ as 1341.5160, which allowed us to determine the molecular formula of frondoside A_2-1 (**1**) as $C_{59}H_{91}O_{29}SNa$.

The aglycon moiety of glycoside **1** was found by extensive NMR spectroscopy (^1H and ^{13}C NMR, HMQC, HMBC, ^1H–^1H COSY, and NOESY) (Table 2) to be very similar with that of cucumarioside A_2-2 isolated from *C. japonica* (7). It is distinguished only by the presence of a 24(25)-double bond instead of a 25(26) one (7). The presence of a 7(8)-double bond was confirmed by signals at 121.82 (C-7) and 143.92 (C-8) ppm in the ^{13}C NMR spectrum and 5.80 ppm (m, H-7) in the ^1H NMR spectrum (7). The presence of a 24(25)-double bond was confirmed by the signals at 123.92 ppm (C-24) and 132.01 ppm (C-25) in the ^{13}C NMR spectrum and 5.14 ppm (m, H-24) in the ^1H NMR spectrum. Signals of the terminal methyl groups of the aglycon side chain at 17.50 ppm (C-26) and 25.53 ppm (C-27) in the ^{13}C NMR and 1.63 (s, H-26) and 1.66 (s, H-27) in the ^1H NMR spectra also indicated the position of a double

© 2005 NRC Canada

Table 3. ^{13}C and ^{1}H NMR chemical shifts and selected HMBC and NOESY correlations of the frondoside A_2-2 (**2**) aglycon moiety.

Position	δ_C[a]	δ_H Mult. (J in Hz)[b]	HMBC	NOESY
1	36.08	1.43 m, 1.49 m		
2	26.90	1.85 m, 2.05 m		H-19
3	89.09	3.25 dd (4.1, 11.5)	C: 1 Xyl1	H-5, H-31, H-1 Xyl1
4	39.51			
5	47.97	1.05	C: 4, 6, 10, 30	H-3, H-30
6	23.26	2.05 m, 2.07 m		
7	119.93	5.71 m		
8	146.53			
9	47.25	3.49 br d (13.3)		H-19
10	35.47			
11	22.79	1.55 m, 1.80 m		H-1, H-12
12	30.29	1.96 m, 2.05 m		H-21
13	58.70			
14	51.25			
15	34.18	1.64 m, 1.78 m		
16	24.21	1.90 m, 1.94 m		
17	53.29	2.24 m		H-21, H-32
18	179.85			
19	23.93	1.21 s	C: 1, 5, 9, 10	H-9
20	83.55			
21	25.86	1.42 m	C: 17, 20, 22	H-17
22	33.50	2.12 m, 2.22 m		
23	32.41	2.85 m	C: 24	
24	200.32			
25	144.50			
26	124.80	5.75 s, 6.06 s	C: 24, 27	
27	17.58	1.93 s	C: 24, 25, 26	
30	17.34	1.14 s	C: 3, 4, 5, 31	H-6 Qui
31	28.64	1.29 s	C: 3, 4, 5, 30	H-3
32	30.75	1.14 s	C: 8, 13, 14, 15	H-17

[a]Recorded at 125.77 MHz in C_5D_5N.
[b]Recorded at 500 MHz in C_5D_5N.

bond at C-24 (9). The signal at 214.32 ppm (C-16) in the ^{13}C NMR spectrum was characteristic for a C-16 keto group (7). The structure of the aglycon moiety was also confirmed by HMBC and NOESY data. In particular, the cross-peak between H-24 and H-27 corresponding to the 24(25)-double bond was observed in NOESY. Hence, frondoside A_2-1 (**1**) is 3-*O*-{3-*O*-methyl-β-D-glucopyranosyl-(1→3)-β-D-glucopyranosyl-(1→4)-[β-D-xylopyranosyl-(1→2)]-β-D-quinovopyranosyl-(1→2)-4-*O*-sodium sulfate-β-D-xylopyranosyl}-16-keto-3β-hydroxy-holosta-7,24-diene.

The MALDI TOF MS of glycoside **2** exhibited a pseudomolecular ion at *m/z* 1341 $[M_{Na} + Na]^+$ and 1239 $[M_{Na} - SO_3Na + Na + H]^+$ in the positive ion mode and a pseudomolecular ion at *m/z* 1295 $[M_{Na} - Na]^-$ and fragmentation peaks at *m/z* 1163 $[M_{Na} - Na - Xyl + H]^-$ and 1119 $[M_{Na} - Na - 3\text{-O-Me-Glc} + H]^-$ (because of the loss of terminal monosaccharide residues) in the negative ion mode. The HR MALDI TOF MS (positive ion mode) showed the pseudomolecular ion $[M_{Na} + Na]^+$ at *m/z* 1341.5148 ($C_{59}H_{91}O_{29}SNa_2$, calcd. 1341.5160), which allowed us to determine the molecular formula of frondoside A_2-2 (**2**) as $C_{59}H_{91}O_{29}SNa$.

The aglycon moiety of glycoside **2** was found by extensive NMR spectroscopy (^1H and ^{13}C NMR, HMBC, HMQC, ^1H–^1H COSY, and NOESY) (Table 3) to be very similar to that of cucumarioside A_7-3 isolated from *C. japonica*, having no oxygen functional group at C-16 and distinguished only by signals of the side chain (10). The signals of C-25 and C-26 at 144.50 and 124.80 ppm in the ^{13}C NMR spectrum and at 5.75 (s, H-26) and 6.06 (s, H-26′) ppm in the ^1H NMR spectrum indicated the presence of a terminal double bond. The signal at 200.32 ppm in the ^{13}C NMR spectrum showed the presence of a ketone group in the side chain. The position of a ketone group at C-24 was indicated by the cross-peaks between C-24 and protons H-26 and H-27 in the HMBC spectrum. The presence of an α,β-unsaturated ketone fragment in the side chain was also confirmed by the UV spectrum of glycoside **2** (λ_{max} = 249.6 nm, ε = 2127). Hence, frondoside A_2-2 (**2**) is 3-*O*-{3-*O*-methyl-β-D-glucopyranosyl-(1→3)-β-D-glucopyranosyl-(1→4)-[β-D-xylopyranosyl-(1→2)]-β-D-quinovopyranosyl-(1→2)-4-*O*-sodium sulfate-β-D-xylopyranosyl}-3β-hydroxy-holosta-7,25-diene-24-one.

The MALDI TOF MS of glycoside **3** exhibited a pseudomolecular ion at *m/z* 1343 $[M_{Na} + Na]^+$ and the ion peak at *m/z* 1241 $[M_{Na} - SO_3Na + Na + H]^+$ in the positive ion mode, and a pseudomolecular ion at *m/z* 1297 $[M_{Na} - Na]^-$ and fragmentation peaks at 1165 $[M_{Na} - Na - Xyl + H]^-$ and 1121 $[M_{Na} - Na - 3\text{-O-Me-Glc} + H]^-$ (because of the

© 2005 NRC Canada

Table 4. ^{13}C and ^{1}H NMR chemical shifts and selected HMBC and NOESY correlations of the frondoside A_2-3 (**3**) aglycon moiety.

Position	δ_C[a]	δ_H Mult. (*J* in Hz)[b]	HMBC	NOESY
1	36.07	1.41 m		
2	26.90	1.85 m		
		2.04 m		
3	89.10	3.25 dd (4.1; 11.1)		H-5, H-1, H-1 Xyl1
4	39.50			
5	47.97	1.04 m	C: 4, 10, 19, 30, 31	H-3
6	23.26	2.06 m		H-30, H-31
7	119.87	5.70 m		H-5, H-6, H-15
8	146.60			
9	47.27	3.48 m		H-19
10	35.46			
11	22.75	1.52 m, 1.78 m		
12	30.16	1.88 m, 1.99 m		
13	58.50			
14	51.20			
15	34.17	1.76 m, 1.65 m		
16	24.68	1.98 m		H-32, H-15
17	53.10	2.16 m		H-16, H-32
18	180.00			
19	23.91	1.21 s	C: 9, 10	H-2, H-9
20	83.68			
21	26.09	1.42 s	C: 17, 20, 22	
22	42.18	2.55 brd (7.0)	C: 20, 21, 23, 24	
23	119.74	5.87 dt (15.3; 7.2)	C: 25	
24	144.48	5.97 d (15.3)	C: 25	
25	69.60			
26	30.43	1.54 s	C: 24, 25, 27	
27	30.38	1.54 s	C: 24, 25, 26	
30	17.32	1.14 s	C: 3, 4, 5, 31	H-6 Qui
31	28.65	1.31 s	C: 3, 4, 5, 30	
32	30.78	1.07 s	C: 8, 13, 14, 15	

[a]Recorded at 125.77 MHz in C_5D_5N.
[b]Recorded at 500 MHz in C_5D_5N.

loss of terminal monosaccharide residues) in the negative ion mode. In the HR MALDI TOF MS (positive ion mode), the pseudomolecular ion $[M_{Na} + Na]^+$ at *m/z* 1343.5387 ($C_{59}H_{93}O_{29}SNa_2$, calcd. 1343.5317) was observed, allowing us to determine the molecular formula of frondoside A_2-3 (**3**) as $C_{59}H_{93}O_{29}SNa$.

The aglycon moiety of glycoside **3** was found by extensive NMR spectroscopy (^1H and ^{13}C NMR, HMBC, HMQC, ^1H–^1H COSY, and NOESY) (Table 4) also to be very similar with that of cucumarioside A_7-3 isolated from *C. japonica*, having no oxygen functional group at C-16 and distinguished only by signals of the side chain (10). However, signals of the side chain in the ^{13}C NMR spectrum were very similar with those of the known cucumarioside G_4 from *Eupentacta fraudatrix* (11) and eximisoside A from *Psolus eximius* (12) showing the presence of a 23(24)-double bond and a hydroxy group at C-25. Indeed, the position of the 23(24)-double bond was confirmed by cross-peaks between H-23 and C-25; H-24 and C-25; H_3-26 and H_3-27 of the terminal methyl groups, and C-24 in HMBC. The signal of C-25 was shifted downfield to 69.60 ppm in the ^{13}C NMR spectrum, indicating the presence of a hydroxy group in this position. Hence, frondoside A_2-3 (**3**) is 3-*O*-{3-*O*-methyl-β-D-glucopyranosyl-(1→3)-β-D-glucopyranosyl-(1→4)-[β-D-xylopyranosyl-(1→2)]-β-D-quinovopyranosyl-(1→2)-4-*O*-sodium sulfate-β-D-xylopyranosyl}-3β,25-dihydroxy-holosta-7,23-diene.

The MALDI TOF MS of glycoside **4** exhibited a pseudomolecular ion at *m/z* 1341 $[M_{Na} + Na]^+$ and a characteristic ion peak at *m/z* 1239 $[M_{Na} - SO_3Na + Na + H]^+$ in the positive ion mode, and a pseudomolecular ion at *m/z* 1295 $[M_{Na} - Na]^-$ along with fragmentation ion peaks at *m/z* 1163 $[M_{Na} - Na - Xyl + H]^-$ and 1119 $[M_{Na} - Na - 3\text{-}O\text{-}Me\text{-}Glc + H]^-$ (because of the loss of terminal monosaccharide residues) in the negative ion mode. In the HR MALDI TOF MS (positive ion mode), the pseudomolecular ion $[M_{Na} + Na]^+$ at *m/z* 1341.5160 was observed (calculated for $C_{59}H_{91}O_{29}SNa_2$ 1341.5145), which allowed us to determine the molecular formula of frondoside A_2-6 (**4**) as $C_{59}H_{91}O_{29}SNa$.

The aglycon moiety of glycoside **4** was found by extensive NMR spectroscopy (^1H and ^{13}C NMR, HMBC, HMQC, ^1H–^1H COSY, and NOESY) (Table 5) to be holotoxinogenin, already known from holotoxins A_1 and B_1 from *Stichopus* (= *Apostichopus*) *japonicus* (13) and widely distributed in sea cucumber glycosides (14), having 9(11)-, and 25(26)-double bonds and a 16-ketone group. Indeed, the signals at 151.17 (C-9) and 110.93 (C-11) ppm in the ^{13}C NMR spectrum and 5.33 (m, H-11) ppm in the ^1H NMR spectrum indi-

© 2005 NRC Canada

Table 5. ^{13}C and ^{1}H NMR chemical shifts and selected HMBC and NOESY correlations of the frondoside A_2-6 (**4**) aglycon moiety.

Position	δ_C[a]	δ_H Mult. (*J* in Hz)[b]	HMBC	NOESY
1	36.09	1.41 m		
		1.81 m		
2	26.78	1.92 m		
		2.14 m		
3	88.66	3.22 dd (3.5, 11.1)	C: 1 Xyl1, 30, 31	H-5, H-31, H-1 Xyl1
4	39.59			
5	52.74	0.93 m	C: 6	H-3
6	20.99	1.52 m		
		1.70 m		
7	28.38	1.60 m		
8	38.58	3.27 m		H-15β, H-19
9	151.17			
10	39.85			
11	110.93	5.33 m		
12	31.97	2.50 m	C: 11, 13	H-21
13	55.60			
14	41.95			
15	51.90	2.23 br d (12.6)	C; 14, 16, 32	H-8
		2.40 br d (12.6)	C; 13, 16, 17, 32	H- 32
16	213.12			
17	61.21	2.83 br s	C: 13, 16, 18, 20, 21	H-21, H-32
18	175.91			
19	21.94	1.38 s	C: 1, 5, 9, 10	H-2, H-8, H-30
20	82.98			
21	26.66	1.41 s	C: 17, 20, 22	H-12, H-17, H-22
22	38.36	1.66 m		
		1.80 m		H-21, H-23
23	22.27	1.53 m		
		1.82 m		H-21, H-22
24	37.88	2.00 m	C: 25, 26, 27	
25	145.46			
26	110.39	4.79 br s	C: 24, 27	
27	22.16	1.70 s	C: 24, 25, 26	H –23
30	16.66	1.11 s	C: 3, 4, 5, 31	H-2, H-6, H-19, H-6 Qui
31	27.97	1.28 s	C: 3, 4, 5, 30	H-3, H-1 Xyl1
32	20.55	0.91 s	C: 8, 13, 14, 15	H- 15 α, H-17

[a]Recorded at 125.77 MHz in C_5D_5N.
[b]Recorded at 500 MHz in C_5D_5N.

cated the presence of a 9(11)-double bond. The signals at 145.46 (C-25) and 110.39 (C-26) ppm in the ^{13}C NMR spectrum and at δ 4.79 (br s, H-26) ppm in the ^{1}H NMR spectrum showed the presence of a terminal 25(26)-double bond. The signal at 213.12 (C-16) ppm in the ^{13}C NMR spectrum was indicative of a keto-group at C-16. Hence, frondoside A_2-6 (**4**) is 3-*O*-{3-*O*-methyl-β-D-glucopyranosyl-(1→3)-β-D-glucopyranosyl-(1→4)-[β-D-xylopyranosyl-(1→2)]-β-D-quinovopyranosyl-(1→2)-4-*O*-sodium sulfate-β-D-xylopyranosyl}-3β-hydroxy-holosta-9,25-diene-16-one.

The glycosides **1**–**4** are new ones, the glycosides **1**–**3** have new aglycones, while **4** represents a new combination of a previously known carbohydrate chain and aglycone. The simultaneous presence of a 24-ketone group and the 25(26)-double bond as an α,β-unsaturated ketone fragment in the side chain of the aglycon of frondoside A_2-2 (**2**) is unique for sea cucumber glycosides.

Experimental section

General experimental procedures

All melting points were determined with a Kofler–Thermogenerate apparatus. Optical rotation was measured on a PerkinElmer 343 polarimeter. NMR spectra were recorded on a AMX Bruker 500 spectrometer at 500.12/125.67 MHz ($^{1}H/^{13}C$) and a Bruker DPX 300 spectrometer at 300/75 MHz ($^{1}H/^{13}C$) in C_5D_5N with TMS as an internal reference (δ = 0). The MALDI TOF MS (positive and negative ion modes) were recorded using a Bruker apparatus, model BIFLEX III, with impulse extraction of ions, on an α-cyano-4-hydroxycinnamic acid matrix. UV spectrum was recorded on a CECIL, CE 7250, 7000 series spectrophotometer in water solution. HPLC was performed using an Agilent 1100 chromatograph equipped with a differential refractometer on Diasphere-110 C_{18} and Chiradex 5 mμ columns.

© 2005 NRC Canada

Animal material

The sea cucumber *C. frondosa* (the family Cucumariidae; the order Dendrochirotida) was collected in Penobscot Bay (Gulf of Maine, Maine, USA) in September 2000 by commercial dragging. Taxonomic identification was carried out by Dr. E.N. Gudimova. A voucher specimen CF-09–2000 is on deposit in the collection of the Murmansk Marine Biological Institute of the Kolsky Scientific Center of the Russian Academy of Sciences, Murmansk, Russia.

Extraction and isolation of the fraction of glycosides belonging to the cucumarioside A_2 group

Body walls of 40 specimens of the sea cucumbers were separated, cut very small, and lyophylized to dryness and extracted twice with hot ethanol. The dry weight of the residue was 943 g. The combined extracts were concentrated to dryness and chromatographed on a polychrom-1 column (powdered Teflon, Biolar, Latvia) previously loaded in EtOH and washed with distilled water to give inorganic salts and polar impurities at elution with H_2O and the fraction containing glycosides at elution with 50% acetone. This fraction was twice chromatographed on silica gel columns eluting with $CHCl_3$–EtOH–H_2O (100:100:17 and 100:75:10) solvent systems to obtain a homogenous on TLC crude subfraction of glycosides belonging to the cucumarioside A_2 group (500 mg).

Isolation of glycosides 1–4

The subfraction was subsequently submitted for HPLC on a Diasphere-110 C_{18} (4 × 250) column (MeOH, water, $Na_2HPO_4 \cdot 12H_2O$ (540 mg in 100 mL of water) (72:27:3)) and a Chiradex 5 mμ (4 × 250) column (MeOH, water, $Na_2HPO_4 \cdot 12H_2O$ (540 mg in 100 mL of water) (60:37:3)) followed by desalting on a Teflon column as described above to give 2.4 mg of frondoside A_2-1 (**1**), $[\alpha]_D^{20}$ –70 (*c* 0.1, pyridine), mp 218–220 °C (see Tables 1 and 2 for ^{13}C and ^1H NMR data). MALDI TOF MS (positive ion mode) *m/z* (rel. intensity): 1341 ($C_{59}H_{91}O_{29}SNa_2$ $[M_{Na} + Na]^+$, 0.7), 1342 ($C_{59}H_{92}O_{29}SNa_2$ $[M_{Na} + Na + H]^+$, 1), 1239 ($[M_{Na} – SO_3Na + Na + H]^+$, 0.3). MALDI TOF MS (negative ion mode) *m/z* (rel. intensity): 1295 ($C_{59}H_{91}O_{29}S$ $[M_{Na} – Na]^–$, 1), 1296 ($C_{59}H_{92}O_{29}S$ $[M_{Na} – Na + H]^–$, 0.6), 1163 ($[M_{Na} – Na – Xyl + H]^–$, 0.03), 1119 ($[M_{Na} – Na – 3\text{-O-Me-Glc} + H]^–$, 0.03); 2.4 mg of frondoside A_2-2 (**2**), $[\alpha]_D^{20}$ –36 (*c* 0.1, pyridine), mp 198–200 °C (see Tables 1 and 3 for ^{13}C and ^1H NMR data). UV (λ_{max}, nm): 249.6, ε = 2127. MALDI TOF MS (positive ion mode) *m/z* (rel. intensity): 1341 ($C_{59}H_{91}O_{29}SNa_2$ $[M_{Na} + Na]^+$, 1) 1239 ($[M_{Na} – SO_3Na + Na + H]^+$, 0.3). MALDI TOF MS (negative ion mode) *m/z* (rel. intensity): 1295 ($C_{59}H_{91}O_{29}S$ $[M_{Na} – Na]^–$, 1), 1163 ($[M_{Na} – Na – Xyl + H]^–$, 0.04), 1119 ($[M_{Na} – Na – 3\text{-O-Me-Glc} + H]^–$, 0.04); 1.8 mg of frondoside A_2-3 (**3**), $[\alpha]_D^{20}$ –15 (*c* 0.1, pyridine), mp 213–215 °C (see Tables 1 and 4 for ^{13}C and ^1H NMR data). MALDI TOF MS (positive ion mode) *m/z* (rel. intensity): 1343 ($C_{59}H_{93}O_{29}SNa_2$ $[M_{Na} + Na]^+$, 1) 1241 ($[M_{Na} – SO_3Na + Na + H]^+$, 0.3), 1167 ($[M_{Na} – 3\text{-O-Me-Glc} + Na + H]^+$, 0.2). MALDI TOF MS (negative ion mode) *m/z* (rel. intensity): 1297 ($C_{59}H_{93}O_{29}S$ $[M_{Na} – Na]^–$, 1), 1165 ($[M_{Na} – Na – Xyl + H]^–$, 0.2), 1121 ($[M_{Na} – Na – 3\text{-O-Me-Glc} + H]^–$, 0.3); 3.1 mg of frondoside A_2-6 (**4**), $[\alpha]_D^{20}$ –51 (*c* 0.1, pyridine), mp 220–222 °C (see Tables 1 and 5 for ^{13}C and ^1H NMR data). MALDI TOF MS (positive ion mode) *m/z* (rel. intensity): 1341 ($C_{59}H_{91}O_{29}SNa_2$ $[M_{Na} + Na]^+$, 1) 1239 ($[M_{Na} – SO_3Na + Na + H]^+$, 0.3). MALDI TOF MS (negative ion mode) *m/z* (rel. intensity): 1295 ($C_{59}H_{91}O_{29}S$ $[M_{Na} – Na]^–$, 1), 1163 ($[M_{Na} – Na – Xyl + H]^–$, 0.05), 1119 ($[M_{Na} – Na – 3\text{-O-Me-Glc} + H]^–$, 0.05).

Acknowledgements

The authors acknowledge financial support from CRDF RB1-557-VL-02, a grant of the Presidium of the Russian Academy of Sciences "Molecular and Cell Biology", and of the President of the Russian Federation grant No. NSH-725.2003.4.

References

1. M. Girard, J. Belanger, J.W. ApSimon, F.-X. Garneau, C. Harvey, and J.-R. Brisson. Can. J. Chem. **68**, 11 (1990).
2. J. Findlay, N. Yayli, and L. Radics. J. Nat. Prod. **55**, 93 (1992).
3. S.A. Avilov, V.I. Kalinin, O.A. Drozdova, A.I. Kalinovsky, V.A. Stonik, and E.N. Gudimova. Khim. Prir. Soedin. 260 (1993).
4. S.A. Avilov, O.A. Drozdova, V.I. Kalinin, A.I. Kalinovsky, and V.A. Stonik. Can. J. Chem. **76**, 137 (1998).
5. N. Yayli and J. Findlay. Phytochemistry, **50**, 135 (1999).
6. N. Yayli. Indian J. Chem. **40B**, 399 (2001).
7. S.A. Avilov, V.A. Stonik, and A.I. Kalinovsky. Khim. Prir. Soedin. 787 (1990).
8. A.S. Shashkov and O.S. Chizhov. Bioorg. Khim. **2**, 437 (1976).
9. S.S. Afiyatullov, L.Y. Tishchenko, V.A. Stonik, A.I. Kalinovsky, and G.B. Elyakov. Khim. Prir. Soedin. 244 (1985).
10. O.A. Drozdova, S.A. Avilov, A.I. Kalinovsky, V.A. Stonik, Y.M. Milgrom, and J.W. Rashkes. Khim. Prir. Soedin. 242 (1993).
11. V.I. Kalinin, S.A. Avilov, A.I. Kalinovsky, V.A. Stonik, Y.M. Milgrom, and J.W. Rashkes. Khim. Prir. Soedin. 691 (1992).
12. V.I. Kalinin, S.A. Avilov, E.Y. Kalinina, O.G. Korolkova, A.I. Kalinovsky, V.A. Stonik, R. Riguera, and C. Jimenez. J. Nat. Prod. **60**, 817 (1997).
13. I.I. Maltsev, V.A. Stonik, A.I. Kalinovsky, and G.B. Elyakov. Comp. Biochem. Physiol. **78B**, 421 (1984).
14. V.A. Stonik, V.I. Kalinin, and S.A. Avilov. J. Nat. Toxins, **8**, 235 (1999).

© 2005 NRC Canada

Synthesis of novel optically pure β-lactams

Yan Yang, Fengyun Wang, Fernande D. Rochon, and Margaret M. Kayser

Abstract: Several new β-lactams were synthesized as racemates via a Staudinger reaction. The corresponding optically pure compounds were obtained in subsequent biotransformation steps either through baker's yeast reduction or lipase resolution. Their absolute configurations were established. The X-ray crystal structures of three new substituted β-lactams are reported here. These compounds represent key building blocks for a variety of medicinally important molecules, including inhibitors of aspartyl proteases and Taxol® analogues.

Key words: optically pure β-lactams, lipase resolutions, baker's yeast reductions, Staudinger reaction.

Résumé : Faisant appel à la réaction de Staudinger, on a réalisé la synthèse de plusieurs nouvelles β-lactames racémiques. On a obtenu les composés correspondants optiquement purs par le biais de biotransformations subséquentes impliquant une réduction par la levure de boulanger ou par résolution avec une lipase. On en a déterminé les configurations absolues. On a déterminé les structures cristallines de trois β-lactames substituées par diffraction des rayons X. Ces composés sont des unités pouvant servir à la synthèse de plusieurs molécules médicinalement importantes, y compris des inhibiteurs de protéases de l'aspartyle et des analogues du Taxol®.

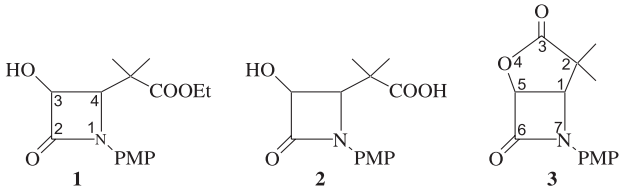
Mots clés : β-lactames optiquement pures, résolutions à la lipase, réductions avec de la levure de boulanger, réaction de Staudinger.

[Traduit par la Rédaction]

Introduction

The β-lactam skeleton represents a core structure of numerous natural and synthetic antibiotics (1). The 3-hydroxy-substituted β-lactams are convenient precursors of β-amino-α-hydroxy esters that constitute key fragments of many biologically important natural products such as aminosugars, α-hydroxy-β-amino acids, glycosphingolipids, peptidic enzyme inhibitors, and alkaloids (2). Furthermore, 3-hydroxy-β-lactams are used for the construction of analogues of the anticancer drug Taxol® (3). It is not surprising, therefore, that the development of enantioselective syntheses of such β-lactams has been pursued by numerous laboratories around the world.

The extensive structure–activity relationship (SAR) studies have shown that the phenylisoserine C-13 side chain of paclitaxel (Taxol®, Fig. 1), essential for anticancer activity, tolerates a variety of modifications (4), and even small changes significantly influence the bioactive properties of the drug (3, 5). The therapeutic potential of paclitaxel is limited by its high hydrophobicity and development of resistance. Search for analogues with better water solubility, easier to administer, fewer side effects, and active on multidrug-resistant (MDR) cells is an on-going process (6). We have been interested in developing the synthesis of optically pure C-13 side chains in which 3′-phenyl is replaced with bulky, polar groups. The preparation of side chains in the form of 3-hydroxy-β-lactams is particularly appealing since it is in this form that the prospective side chains are generally coupled with baccatin III. Here, we report the syntheses and characterizations of several isomers of 4-(1-ethoxycarbonyl-1-methylethyl)-3-hydroxy-β-lactam (**1**), the 4-(1-carboxy-1-methylethyl)-3-hydroxy-β-lactam (**2**), and the corresponding lactone (**3**).



A number of methods for the preparation of β-lactams, such as ketene–imine cycloaddition (1*a*, 7), metalloester enolate–imine condensation (8), isocyanate–alkene cycloaddition (9), and alkyne–nitrone cycloaddition (10), have been developed over the years. Among these, the most widely used is the Staudinger reaction, in which ketene–imine addition leads to a β-lactam ring system. Optically pure β-lactams prepared via asymmetric synthesis employed either a combination of chiral imine and achiral ketenes, achiral imines and chiral ketenes (1*a*, 11), or a direct cyclization of ketene–imine in the presence of a chiral catalyst (12). Only a few studies resorted to biocatalytic approaches such as lipase-catalyzed resolution (13) or baker's yeast reduction (14). Since our preliminary goal was to syn-

Received 22 March 2004. Published on the NRC Research Press Web site at http://canjchem.nrc.ca on 5 February 2005.

Dedicated to Professor Peter Stanetty on the occasion of his 60th birthday.

Y. Yang, F. Wang, and M.M. Kayser.[1] Department of Physical Sciences, University of New Brunswick, Saint John, NB E2L 4L5, Canada.
F.D. Rochon. Département de chimie, Université du Québec à Montréal, C. P. 8888, Succ. Centre-Ville Montréal, QC H3C 3P8, Canada.

[1]Corresponding author (e-mail: kayser@unbsj.ca).

 doi: 10.1139/V04-159 © 2005 NRC Canada

Scheme 1.

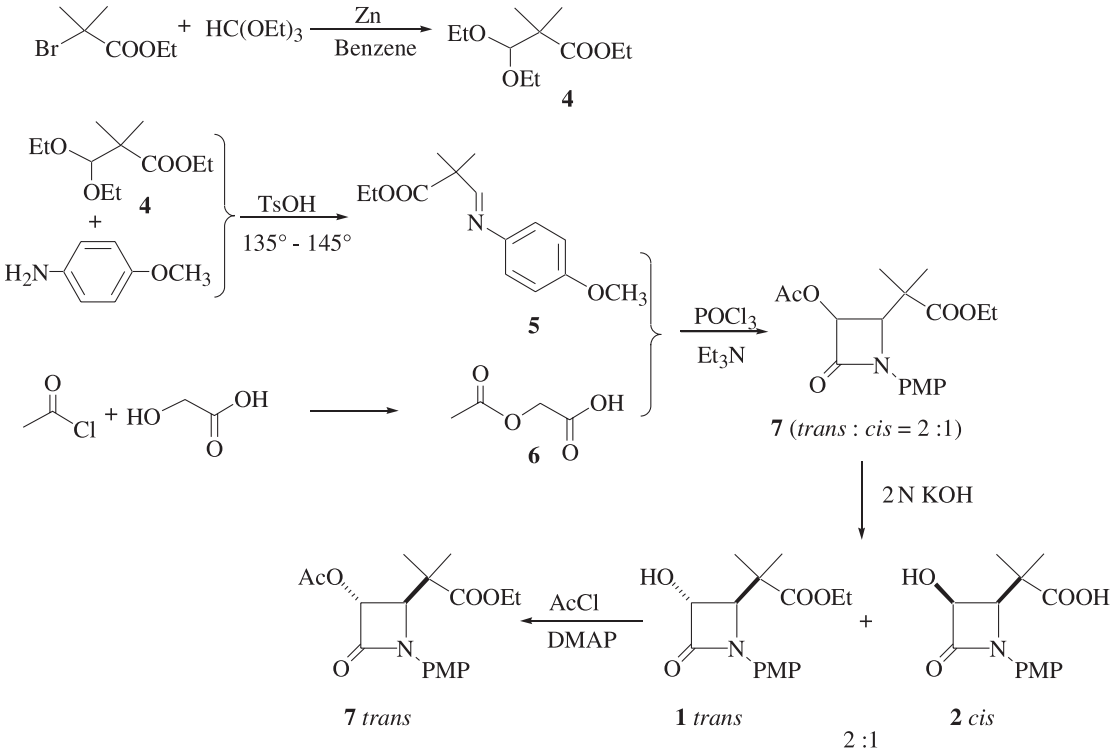
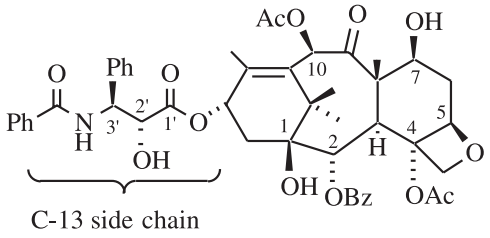


Fig. 1. Structure of paclitaxel (Taxol®).



thesize and characterize all the diastereomers and enantiomers, we decided to prepare the racemic β-lactams through Staudinger cyclization (Scheme 1) and to obtain enantiopure β-lactams in the subsequent biotransformation steps.

Results and discussion

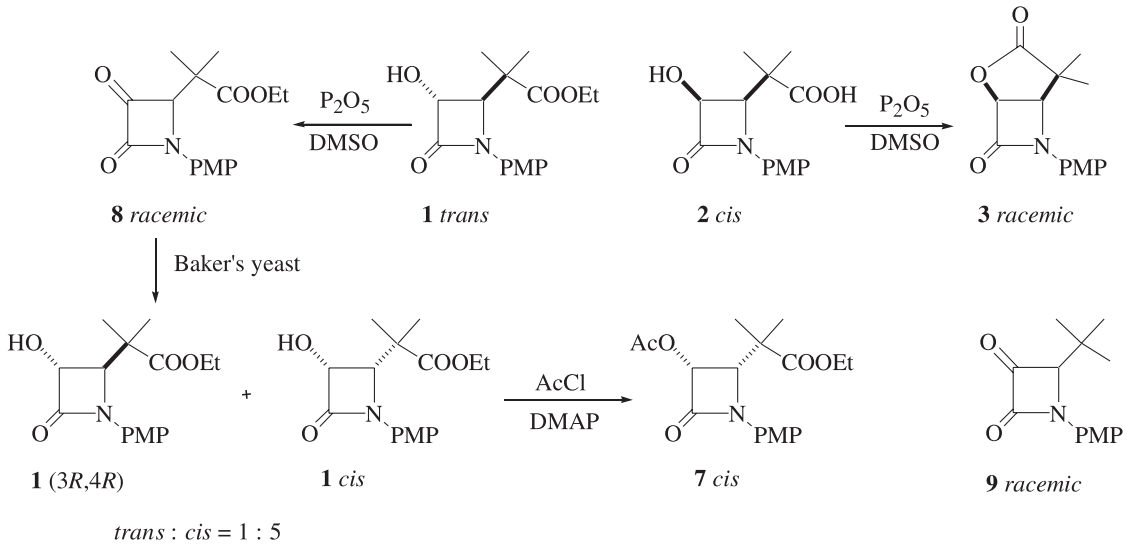
Condensation of 3,3-diethoxy-2,2-dimethylpropionic acid ethyl ester (**4**) (15) with *p*-anisidine gave 3-(4-methoxyphenylimino)-2,2-dimethylpropionic acid ethyl ester (**5**), which was used in the following step without purification. Cycloaddition of **5** with the in-situ-generated acetoxyacetyl chloride in the presence of anhydrous triethylamine gave acetyl β-lactam **7** (PMP = *p*-methoxyphenyl) in 53% yield after two steps. The β-lactam product **7** consisted of trans and cis diastereomers in the ratio of 2:1 based on the ^{1}H NMR spectrum of the product mixture. Hydrolysis of **7** (2 N KOH) gave two compounds as shown in Scheme 1. It was interesting to note that while the *trans*-acetyl β-lactam was selectively hydrolyzed to the corresponding *trans*-3-hydroxy β-lactam (**1**) as expected, its cis diastereomer was hydrolyzed at both acetyl and acetate groups, yielding *cis*-3-hydroxy β-lactam (**2**). Apparently in the cis isomer, the hindered ester function undergoes hydrolysis aided by the strategically located 3-OH group. The two compounds were easily separated during the extraction process (see Experimental). This turned out to be very useful in the characterization of **7**-*trans* and **7**-*cis*, since the original mixture from the Staudinger reaction was inseparable by chromatography. The pure sample of **7**-*trans* was prepared by acylation of **1**-*trans* (Scheme 1), while **7**-*cis* was obtained from baker's yeast reduction of the α-keto-β-lactam (**8**, Scheme 2). Their stereochemistry was assigned on the basis of coupling constants for the *cis*- and t*rans*-β-lactams (16). Oxidation of compound **1** with DMSO/phosphorus pentoxide provided the α-keto-β-lactam (**8**). Under the same conditions, **2**-*cis* was dehydrated to a racemic mixture of fused lactone–lactams **3** as shown in Scheme 2.

In an initial attempt to obtain optically pure 3-hydroxy-β-lactams (**1**), we performed baker's yeast reduction of the racemic 3-oxo-β-lactam (**8**). This strategy was successful for the *tert*-butyl analogue **9**, where it yielded easily separable 3-hydroxy diastereomers 3*R*,4*S*-*cis* and 3*R*,4*R*-*trans* (14). Unfortunately, in the case of ketone **8**, the reduction product consisted of an inseparable mixture of essentially racemic **1**-*cis* and an optically pure **1**-*trans* isomer, tentatively identified as 3*R*,4*R* (Scheme 2). The ratio of cis to trans (5:1) was measured from the ^{1}H NMR spectrum of the product mixture.

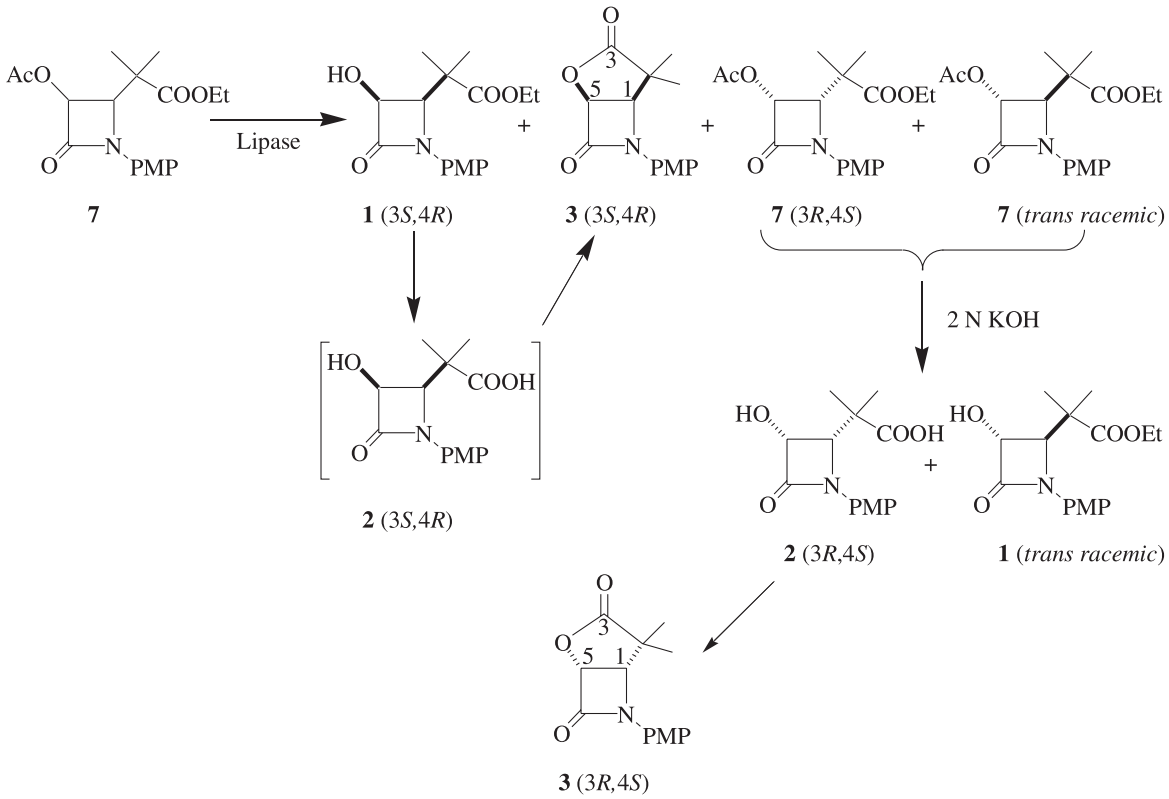
Since a racemic mixture of *cis*-3-acetoxy-4-phenyl-β-lactams was reported to be enantioselectively hydrolyzed by Amano lipase (13*a*), we decided to test the ability of this enzyme to resolve the mixture of lactams **7**. It turned out that the mixture of the isomers of **7** could be resolved efficiently, particularly since the **7**-*trans* is not a suitable substrate for the lipase PS "Amano" (Scheme 3).

© 2005 NRC Canada

Scheme 2.



Scheme 3.



Of the four products formed in the course of the lipase resolution, compounds **1** and **3** were easily separated by chromatography and the absolute configuration of **1** (3*S*,4*R*) was established with certainty by X-ray diffraction methods. The whole diffraction sphere was measured with Cu-Kα radiation. The absolute structure parameter (Flack) determined using the option TWIN/BASF 0.5 indicated the right configuration (Table 1).

The molecular structure of **1** (3*S*,4*R*) is shown in Fig. 2. The internal angles in the four-membered ring vary between 85.4(1)° and 95.1(2)°. The N—C and O—C bond distances close to the carbonyl groups are shorter than the others. For example, the distances N—C1 = 1.360(3) Å and O4—C5 = 1.335(3) Å, while N—C3 = 1.488(3) Å and O4—C6 = 1.461(3) Å.

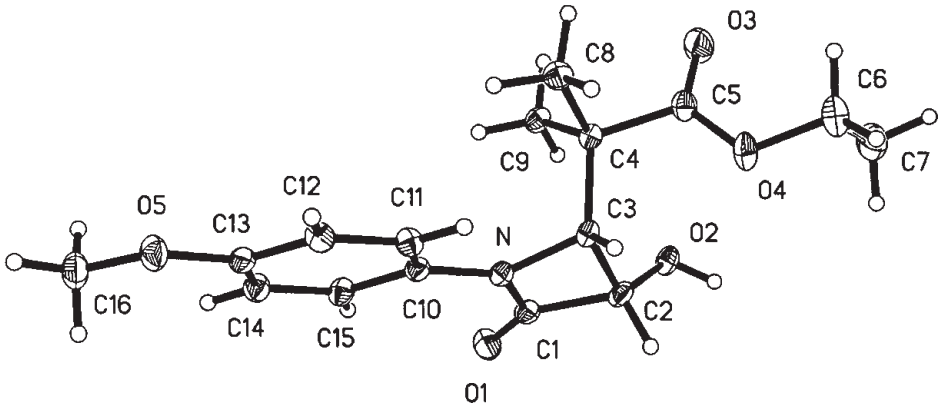
The lactone–lactam **3** (1*R*,5*S*), apparently resulting from hydrolysis of the ethoxy carbonyl group followed by cyclization, was isolated and its absolute configuration was initially established by chiral-phase HPLC analysis. This was possible because the four isomers of **7** are clearly re-

© 2005 NRC Canada

Table 1. Crystal data for compounds **1**, **3**, and **11**.

Compound	**1**	**3**	**11**
Empirical formula	$C_{16}H_{21}NO_5$	$C_{14}H_{15}NO_4$	$C_{23}H_{18}BrNO_4$
Formula weight	307.34	261.27	452.29
Temperature (K)	223(2)	223(2)	293
Wavelength (Å)	1.541 78	1.541 78	0.710 73
Crystal system	Monoclinic	Monoclinic	Orthorhombic
Space group	$P2_1$	$P2_1$	$P2_12_12_1$
a (Å)	11.383 2(2)	5.896 2(1)	8.901(3)
b (Å)	5.895 9(1)	18.571 0(2)	10.392(4)
c (Å)	12.270 9(2)	11.529 2(1)	21.842(8)
β (°)	110.431(1)	90.762(1)	90.
Volume (Å^3)	771.74(2)	1 262.32(3)	2020.4(13)
Z	2	4	4
D_{calcd} (Mg m^{-3})	1.323	1.375	1.487
Absorption coefficient (mm^{-1})	0.815	0.842	2.064
F(000)	328	552	920
θ range for data collection (°)	3.84–72.9	3.83–72.77	1.86–25.0
Reflections collected	9298	15 210	2052
Independent reflections (R_{int})	2711 (0.051 1)	4 802 (0.029 8)	2052
Observed reflections ($I > 2\sigma(I)$)	2656	4 570	899
Goodness-of-fit on F^2	1.041	1.045	1.048
Final R_1 [$I > 2\sigma(I)$]	0.051 5	0.035 0	0.063 6
wR_2 (all data)	0.139 6	0.073 0	0.108 2
Absolute structure parameter	0.1(2)	0.00(17)	0.00(3)

Fig. 2. Crystal structure of *cis*-3-hydroxy-β-lactam (**1**, 3*S*,4*R*).



solved on the chiral-phase HPLC. Furthermore, in the course of the HPLC-monitored lipase resolution we were able to observe that only *one* of the cis enantiomers was hydrolyzed; its antipode and the two trans diastereomers were unaffected. Additional evidence for the configuration of **3** (1*R*,5*S*) was obtained when a mixture of **1** (3*S*,4*R*) and **3** (1*R*,5*S*) under extended treatment with an excess of the lipase was transformed entirely into the lactone **3** (1*R*,5*S*). Finally, we were able to obtain a suitable crystal, and the proposed absolute configuration of **3** (1*R*,5*S*) was confirmed by X-ray diffraction. Again, the absolute structure parameter (Flack) confirmed the correct enantiomer (Table 1). The compound crystallized with two independent molecules in the unit cell. The two molecules are very similar as shown by identical equivalent bond distances and angles. The molecular structure of one of the two molecules is shown in Fig. 3.

The conformations of the two molecules are slightly different, especially in the region of the five-membered ring. For example, the torsion angles in the first molecule N1-C3-C4-C5 = –91.9(2)°, N1-C3-C4-C7 = 27.5(3)°, and N1-C3-C4-C6 = 153.8(2)°, while the corresponding angles in the second molecule are N2-C17-C19-C18 = –82.4(2)°, N2-C17-C19-C20 = 38.7(3)°, and N2-C17-C19-C27 = 165.3(2)°. Again, the N—C and O—C bond distances close to the carbonyl bonds are shorter than the others.

The remaining products from the lipase resolution, **7** (3*R*,4*S*) and **7**-*trans* (racemic), were hydrolyzed with 2 N

© 2005 NRC Canada

Fig. 3. Crystal structure of the fused lactone–lactam **3** (1*R*,5*S*).

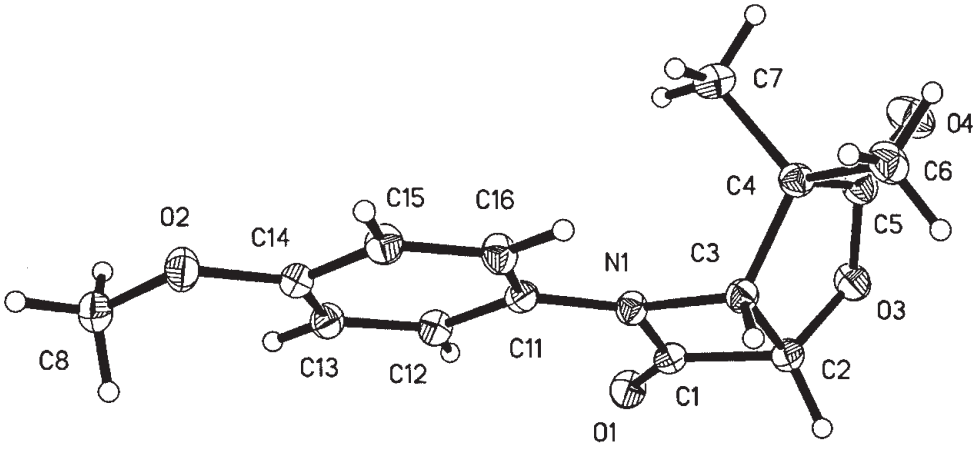
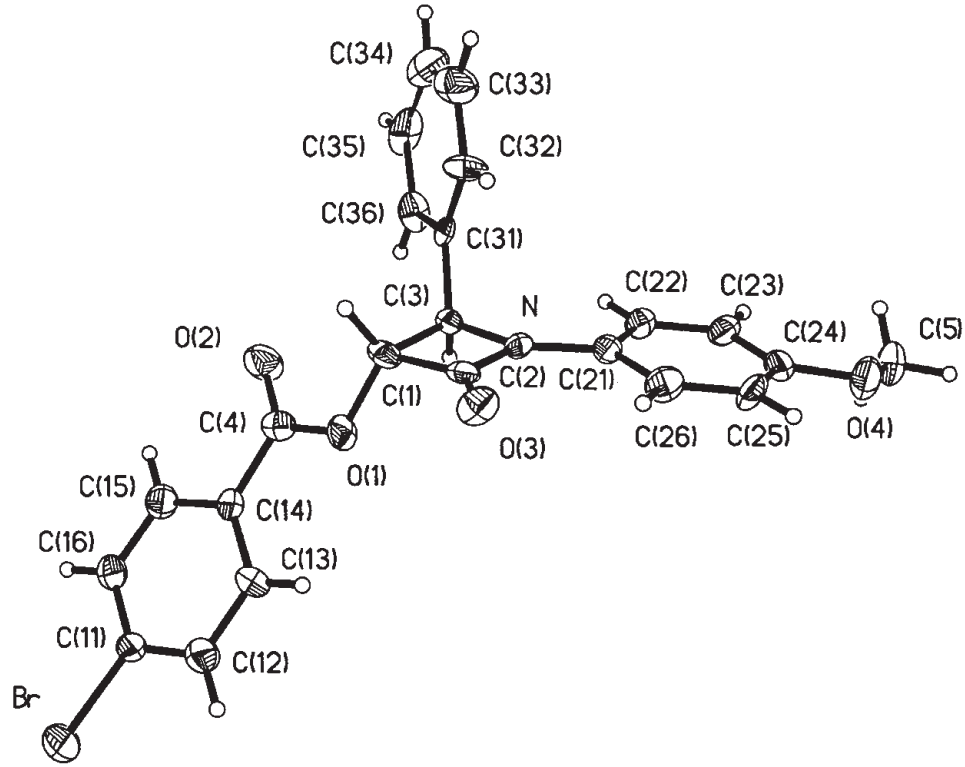


Fig. 4. Crystal structure of *trans*-β-lactam (**11**, 3*R*,4*R*).

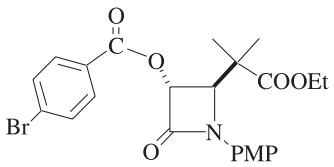


KOH to give **2** (3*R*,4*S*) and **1**-*trans* (racemic), which were separated during the work-up. The subsequent treatment of **2** (3*R*,4*S*) with DMSO/phosphorous pentoxide gave lactone **3** (1*S*,5*R*), which is clearly distinguishable from its antipode on the chiral-phase HPLC and has opposite specific rotation (Scheme 3).

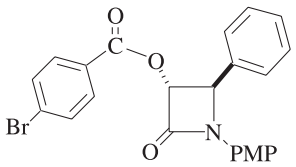
The attempts to resolve racemic **1**-*trans* using lipases PS "Amano", PS-C "Amano" II, AY "Amano", and AK "Amano" were not successful. To characterize fully and to establish unambiguously the absolute configurations of the trans products, we decided to separate and identify the **1**-*trans* enantiomer from the baker's yeast reduction (Scheme 2). We were unable to separate the overlapping cis and trans isomers, however, on treatment with 2 N KOH, only the racemic **1**-*cis* was hydrolysed to the corresponding acid and the enantiopure **1**-*trans* was separated during the work-up. Unfortunately, neither **1**-*trans* nor its *p*-bromobenzoyl derivative **10** could produce crystals suitable for X-ray crystallographic analysis. Thus, the (3*R*,4*R*) absolute configuration was tentatively assigned by analogy to other related *trans*-β-lactams obtained from yeast-catalyzed reductions: the phenyl-substituted **11** (3*R*,4*R*) (17) whose crystal structure was determined and is shown in Fig. 4 (Table 1), and *tert*-butyl-substituted lactam **12** (3*R*,4*R*) reported earlier (14).

In summary, we have synthesized and fully characterized several new β-lactams. The absolute configurations were deduced from chiral-phase HPLC and confirmed through X-ray crystal structure determination. We are currently developing and optimizing more efficient and better-yielding

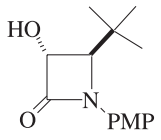
© 2005 NRC Canada



10 (3*R*,4*R*)



11 (3*R*,4*R*)



12 (3*R*,4*R*)

protocols for the preparations of these and several other related compounds.

Experimental

The X-ray crystallographic data for compounds **1** and **3** were collected using a Bruker Platform diffractometer, equipped with a Bruker SMART 2K charged-coupled device (CCD) area detector using the program SMART and normal focus sealed tube source graphite-monochromated Cu-Kα radiation. The crystal-to-detector distance was 4.908 cm, and the data collection was carried out in 512 pixel × 512 pixel mode, utilizing 4 pixel × 4 pixel binning. The initial unit cell parameters were determined by a least-squares fit of the angular setting of strong reflections, collected by a 9.0° scan in 30 frames over four different parts of the reciprocal space (120 frames total). One complete sphere of data was collected, to better than 0.8\Å resolution. Upon completion of the data collection, the first 101 frames were recollected to improve the decay correction analysis. The crystal structure of the bromo compound (**11**) was determined on a Siemens P4 instrument using graphite-monochromated Mo-Kα radiation and the XSCANS program (18). The intensity data were corrected for the effects of Lorentz and polarization. An absorption correction based on the equations of the crystal faces was applied for crystal **11**. The coordinates of the first set of atoms (Br for **11**) were determined by direct methods and the positions of all the other atoms were found by the standard Fourier methods. The structures were refined on F_0^2 using all reflections. The H atoms were fixed in idealized positions using a riding model with displacement parameters = $1.2U_{eq}$ (1.5 for methyl groups) of the parent atom. The SHELXTL system (19) was used for all calculations and drawings. The experimental details and crystal data are listed in Table 1. The absolute structure of the three compounds was established with certainty. For crystals **1** and **3**, the data were measured with Cu-Kα radiation on the entire sphere. Crystal **11** was measured with Mo-Kα, but it contains a heavy atom, which makes it very easy to determine the absolute configuration. The absolute Flack parameter was obtained using the option TWIN/BASF 0.5 in the refinement program. The crystal of compound **3** contains two independent molecules in the unit cell.

All chemicals were purchased from commercial suppliers and were used as received except where noted. Dry methylene chloride was freshly prepared by distillation from calcium hydride. Triethylamine was freshly distilled from sodium hydride. Commercially available DMSO was treated with molecular sieves (4 Å). Thin layer chromatography was performed on Sigma-Aldrich 0.2 mm aluminum-backed silica gel plates with UV indicator and was visualized under a UV lamp. Flash chromatography was performed on 230–400 mesh silica gel (Silicycle). Chiral-phase HPLC analyses were performed on a Chiracel OD-H column (4.6 mm × 150 mm) using hexane:iso-propanol (90:10) as the mobile phase. A UV detector set at 254 nm was used to monitor the reactions. Capillary gas chromatography was performed on a DB-1301 (15 m × 0.53 mm × 1.0 μm) column from J & W Scientific. Lipases were generous gifts from Amano Enzyme USA Co., Ltd. Commercial baker's yeast was obtained from a local grocery chain.

Melting points were determined on a Fisher–Johns melting point apparatus and are uncorrected. Specific rotation ($[\alpha]_D$) was measured on a PerkinElmer 241 polarimeter at room temperature with energy source Na 589 and is given in $10^{-1\circ}$ cm^2 g^{-1}. IR spectra were recorded as thin films on a Mattson Satellite FT IR spectrometer. ^{1}H NMR and ^{13}C NMR spectra were recorded in $CDCl_3$ solution, except where otherwise specified, at room temperature either on a Bruker AC-250 FT-NMR spectrometer or a Varian Unity 400 FT-NMR spectrometer; chemical shifts (δ) are reported in ppm using Me_4Si as the internal standard. *J* values are expressed in Hz. The high-resolution mass spectra were obtained on a Kratos MS50TC mass spectrometer.

(±)-3-Acetoxy-4-(1-ethoxycarbonyl-1-methylethyl)-1-(4-methoxyphenyl)-2-azetidinone (7)

A mixture containing *p*-anisidine (15.4 g, 0.125 mol), ethyl 3,3-diethoxy-2,2-dimethylpropanoate (**4**) (30.0 g, 0.137 mol), and *p*-toluenesulfonic acid monohydrate (0.100 g, 0.526 mmol) was heated at reflux for 5 h. The reaction mixture was cooled and evaporated under vacuum to remove the resulting ethanol. The imine **5** thus obtained was used in the next step without purification. Phosphorus oxychloride (28.0 g, 0.182 mol) in dry methylene chloride (100 mL) was added dropwise to a solution of imine **5**, acetoxyacetic acid **6** (23.4 g, 0.198 mol), and triethylamine (69.9 mL, 0.502 mol) in methylene chloride (500 mL) maintained at 5 °C. The stirred reaction was warmed to room temperature and monitored by TLC until complete disappearance of the imine (48 h). The reaction was quenched with 2 N HCl (400 mL) solution, and extracted with methylene chloride (3 × 400 mL). The combined organic layers were washed sequentially with a saturated solution of $NaHCO_3$ and brine, dried over magnesium sulfate, and concentrated under reduced pressure. The residue was purified by flash chromatography on silica gel to give compound **7** as a mixture of diastereomers (trans:cis = 2:1) with a yield of 23.0 g (53%) over two steps from *p*-anisidine. **7**-*trans*: IR ($CHCl_3$, cm^{-1}): 2981, 2940, 1765, 1731, 1513, 1372, 1221, 1149. ^{1}H NMR (400 MHz, $CDCl_3$) δ: 1.17 (3H, t, *J* = 7.2, CH_2CH_3), 1.21 (3H, s, CCH_3), 1.29 (3H, s, CCH_3), 2.17 (3H, s, $COCH_3$), 3.78 (3H, s, OCH_3), 4.03 (2H, q, *J* = 7.0, CH_2CH_3), 4.49 (1H, d, *J* = 1.8, NC*H*), 5.74 (1H, d, *J* = 1.8, OC*H*), 6.86 (2H, d, *J* = 9.1, Ar*H*), 7.21 (2H, d, *J* = 8.9, Ar*H*). ^{13}C NMR (100 MHz, $CDCl_3$) δ: 13.9 (CH_2CH_3), 20.0 (CCH_3), 20.7

© 2005 NRC Canada

(CCH_3), 22.9 ($COCH_3$), 43.5 (CCH_3), 55.5 (OCH_3), 61.3 (OCH_2), 66.7 (NCH), 75.4 (OCH), 114.4, 123.1, 128.7, 157.8, 162.5 (*C*O), 169.2 (*C*O), 175.3 (*C*O). **7**-*cis*: ^{1}H NMR (400 MHz; $CDCl_3$) δ: 1.26 (3H, t, *J* = 7.3, CH_2CH_3), 1.29 (3H, s, CCH_3), 1.32 (3H, s, CCH_3), 2.10 (3H, s, $COCH_3$), 3.80 (3H, s, OCH_3), 4.11 (2H, q, *J* = 7.0, CH_2CH_3), 4.76 (1H, d, *J* = 5.3, NCH), 5.74 (1H, d, *J* = 5.3, OCH), 6.89 (2H, d, *J* = 9.0, ArH), 7.33 (2H, d, *J* = 9.2, ArH). ^{13}C NMR (100 MHz, $CDCl_3$) δ: 13.9 (CH_2CH_3), 20.0 (CCH_3), 20.7 (CCH_3), 22.9 ($COCH_3$), 44.5 (CCH_3), 54.2 (OCH_3), 61.0 (OCH_2), 63.2 (NCH), 73.3 (OCH), 114.4, 121.5, 129.7, 157.3, 163.2 (*C*O), 168.8 (*C*O), 175.0 (*C*O). HR-MS calcd. for $C_{18}H_{23}NO_6$ (M^+): 349.1525; found: 349.1511.

3-Hydroxy-1-(4-methoxyphenyl)-2-azetidinone (1)

A solution of **7** (mixture) (5.0 g, 0.014 mol) in THF (100 mL) was slowly treated with 2 N KOH (50 mL) at 0 °C. The reaction was stirred at 0 °C until TLC indicated complete conversion (2 h). The solution was extracted with ethyl acetate (3 × 80 mL). The combined organic layers were washed with brine, dried over magnesium sulfate, filtered, and evaporated to dryness to afford racemic **1**-*trans* (2.8 g) as a colorless solid. The water layer was acidified with 2 N HCl to pH 2 ~ 3, and then extracted with ethyl acetate. The organic layers were combined and washed with brine, dried over magnesium sulfate, filtered, and evaporated to dryness to afford racemic **2**-*cis* (1.2 g) as a colorless solid. (±)-*trans*-4-(1-Ethoxycarbonyl-1-methylethyl)-3-hydroxy-1-(4-methoxyphenyl)-2-azetidinone (**1**): mp 78 to 79 °C. IR ($CHCl_3$, cm^{-1}): 3387, 2939, 1730, 1513, 1249, 1150. ^{1}H NMR (400 MHz, $CDCl_3$) δ: 1.16 (3H, s, CCH_3), 1.18 (3H, t, *J* = 7.2, CH_2CH_3), 1.27 (3H, s, CCH_3), 3.78 (3H, s, OCH_3), 4.05 (2H, q, *J* = 7.2, CH_2), 4.38 (1H, d, *J* = 1.7, NCH), 4.73 (1H, d, *J* = 1.7, HOCH), 6.84 (2H, d, *J* = 9.0, ArH), 7.16 (2H, d, *J* = 8.9, ArH). ^{13}C NMR (100 MHz, $CDCl_3$) δ: 14.0 (CH_2CH_3), 20.4 (CCH_3), 22.8 (CCH_3), 43.6 (CCH_3), 55.5 (OCH_3), 61.2 (OCH_2), 68.6 (NCH), 76.7 (OHCH), 114.4, 123.0, 129.0, 157.7, 167.2 (*C*O), 175.6 (*C*O). HR-MS calcd. for $C_{16}H_{21}NO_5$ (M^+): 307.1420; found: 307.1428. (±)-*cis*-4-(1-Carboxy-1-methylethyl)-3-hydroxy-1-(4-methoxyphenyl)-2-azetidinone (**2**): mp 168 to 169 °C. IR ($CHCl_3$, cm^{-1}): 3373, 2979, 2839, 1724, 1513, 1248, 1170. ^{1}H NMR (400 MHz, d_6-acetone) δ: 1.32 (3H, s, CCH_3), 1.35 (3H, s, CCH_3), 3.79 (3H, s, OCH_3), 4.74 (1H, d, *J* = 5.3, NCH), 5.16 (1H, d, *J* = 5.3, OHCH), 6.92 (2H, d, *J* = 9.0), 7.40 (2H, d, *J* = 9.0). ^{13}C NMR (100 MHz, d_6-acetone) δ: 22.1 (CCH_3), 26.8 (CCH_3), 45.6 (CCH_3), 56.5 (OCH_3), 65.7 (NCH), 77.7 (OCH), 115.7, 122.7, 132.8, 158.4, 168.8 (*C*O), 178.6 (*C*O). HR-MS calcd. for $C_{14}H_{17}NO_5$ (M^+): 279.1107; found: 279.1113.

(±)-4-(1-Ethoxycarbonyl-1-methylethyl)-1-(4-methoxyphenyl)-3-oxo-2-azetidinone (8)

Phosphorus pentoxide (6.0 g, 0.042 mol) was added to dry DMSO (90 mL) and stirred at room temperature for 30 min. Racemic **1**-*trans* (7.5 g, 0.025 mol) in DMSO (45 mL) was added over an 1 h period. The resulting mixture was stirred at room temperature until TLC showed complete conversion (48 h). The reaction was quenched with a cold saturated aqueous solution of sodium bicarbonate (100 mL) and extracted with ethyl acetate (3 × 100 mL). The combined organic phases were washed with water (5 × 150 mL), followed by brine and dried over sodium sulfate. The solvent was removed under vacuum. The residue was purified by flash chromatography on silica gel and crystallized from ethyl acetate – hexane to give 5.3 g (71%) of **8** as yellow crystals; mp 64 to 65 °C. IR ($CHCl_3$, cm^{-1}): 2981, 1815, 1764, 1513, 1253, 1149. ^{1}H NMR (400 MHz, $CDCl_3$) δ: 1.18 (3H, t, *J* = 7.0, CH_2CH_3), 1.27 (3H, s, CCH_3), 1.37 (3H, s, CCH_3), 3.82 (3H, s, OCH_3), 4.07 (2H, q, *J* = 7.2, CH_2), 4.95 (1H, s, NCH), 6.92 (2H, d, *J* = 9.0), 7.38 (2H, d, *J* = 9.2). ^{13}C NMR (100 MHz, $CDCl_3$) δ: 13.8 (CH_2CH_3), 21.0 (CCH_3), 23.6 (CCH_3), 44.9 (CCH_3), 55.5 (OCH_3), 61.7 (OCH_2), 76.7 (NCH), 114.6, 121.5, 128.9, 158.4, 161.0 (*C*O), 174.4 (*C*O), 193.3 (*C*O). HR-MS calcd. for $C_{16}H_{19}NO_5$ (M^+): 305.1263; found: 305.1274.

(±)-*cis*-7-(4-Methoxyphenyl)-2,2-dimethyl-4-oxa-7-aza-bicyclo[3.2.0]heptane-3,6-dione (3)

Phosphorus pentoxide 1.8 g (0.013 mmol) was added to dry DMSO (35 mL) and stirred at room temperature for 30 min. Racemic **2**-*cis* (2.4 g, 0.0090 mol) in DMSO (15 mL) was added over 30 min. The resulting mixture was stirred at room temperature until TLC indicated complete conversion (48 h). The reaction was quenched with a cold saturated aqueous solution of sodium bicarbonate (40 mL) and extracted with ethyl acetate (3 × 40 mL). The combined organic phases were washed with water (5 × 80 mL) and brine, dried over sodium sulfate, and concentrated under reduced pressure. Crystallization of the crude residue from ethyl acetate – hexane afforded 1.9 g (85%) of **3** as a colorless crystalline solid; mp 169–169.5 °C. IR ($CHCl_3$, cm^{-1}): 2976, 2936, 2838, 1781, 1513, 1385, 1247, 1149. ^{1}H NMR (250 MHz, $CDCl_3$) δ: 1.28 (3H, s, CCH_3), 1.39 (3H, s, CCH_3), 3.80 (3H, s, OCH_3), 4.49 (1H, d, *J* = 4.6, NCH), 5.44 (1H, d, *J* = 4.6, OCH), 6.90 (2H, d, *J* = 8.9), 7.31 (2H, d, *J* = 8.9). ^{13}C NMR (62.9 MHz, $CDCl_3$) δ: 20.4 (CCH_3), 25.1 (CCH_3), 42.8 (CCH_3), 55.5 (OCH_3), 61.2 (NCH), 79.8 (OCH), 114.6, 118.7, 130.3, 157.1, 160.7 (*C*O), 180.1 (*C*O). HR-MS calcd. for $C_{14}H_{15}NO_4$ (M^+): 261.1001; found: 261.1006.

Lipase-catalyzed hydrolysis of 7

The reaction was carried out in a 0.2 mol L^{-1} potassium phosphate buffer (pH 7.5, 50 mL) containing a mixture of cis and trans diastereomers of **7** (2.1 g, 0.006 mol) and lipase PS "Amano" (2.1 g). The reaction mixture was stirred at room temperature. The kinetic resolution of **7**-*cis* was monitored by chiral HPLC (the **7**-*trans* diastereomers were not hydrolysed by the lipase). After 26 h, 50% conversion of **7**-*cis* was observed. The mixture was extracted with ethyl acetate, and the combined ethyl acetate layers were washed with brine and dried over magnesium sulfate. Removal of the solvent afforded a mixture of unreacted **7** (3*R*,4*S*) and racemic **7**-*trans* as well as the compounds **1** (3S,4*R*) and **3** (1*R*,5*S*). Separation on a silica gel column gave unreacted material **7** (1.2 g), optically pure 3-hydroxy-β-lactam (**1**) (3S,4*R*) as a colorless crystal (0.080 g), and lactone **3** (1*R*,5*S*) as a colorless crystal (0.18 g). The recovered mixture **7** (7.5 g, 0.022 mol) was hydrolyzed with 2 N KOH, as described above, to yield optically pure **2** (3*R*,4*S*) as a white solid (1.1 g) and racemic **7**-*trans* as a colorless solid (5.0 g).

© 2005 NRC Canada

1 (3*S*,4*R*): mp 139–139.8 °C. $[\alpha]_D$ = –170 (*c* 1.00 in CH_2Cl_2). **3** (1*R*, 5*S*): mp 140 to 141 °C. $[\alpha]_D$ = –110 (*c* 1.00 in CH_2Cl_2). **3** (1*S*, 5*R*) prepared from **2** (3*R*,4*S*) in 91% yield: mp 139 to 140 °C. $[\alpha]_D$ = +108 (*c* 1.00 in CH_2Cl_2). **2** (3*R*, 4*S*): mp 158 to 159 °C. $[\alpha]_D$ = +13.4 (*c* 1.00 in CH_3COCH_3).

Procedure for baker's yeast reduction of 8

A suspension of baker's yeast (10 g) and dextrose (40 g) in sterilized water (500 mL) was stirred at 30 °C in a fermentor with aeration for 15 min. Compound **8** (1.00 g) was added and stirring continued for 26 h. The reaction was monitored by chiral HPLC. After complete conversion, the reaction mixture was saturated with salt and centrifuged at 3000× *g* for 10 min to remove yeast cells. The supernatant was extracted with ethyl acetate. The cell pellet was extracted three times with ethyl acetate. The combined organic layers were washed with brine, dried over magnesium sulfate, and filtered. Vacuum evaporation afforded the crude mixture (0.82 g) of optically pure **1**-*trans*, and mixtures of **1**-*cis* and **3**. The crude reaction product (0.29 g) was hydrolyzed with 2 N KOH as described before. Optically pure **1**-*trans* (3*R*,4*R*) was isolated as a colorless oil (0.029 g); **1**-*cis* and **3** were hydrolyzed to the racemic acid **2** and were isolated from the aqueous layer as a colorless solid (0.17 g). **1** (3*R*,4*R*): $[\alpha]_D$ = +84.9 (*c* 1.65 in CH_2Cl_2). ^{1}H NMR (250 MHz, $CDCl_3$) δ: 1.17 (3H, s, CCH_3), 1.18 (3H, t, *J* = 7.10, CH_2CH_3), 1.28 (3H, s, CCH_3), 3.78 (3H, s, OCH_3), 4.05 (2H, q, *J* = 7.05, CH_2CH_3), 4.35 (H, d, *J* = 1.70, NC*H*), 4.75 (1H, d, *J* = 1.6, OHC*H*), 6.82 (2H, d, *J* = 9.2, Ar*H*), 7.14 (2H, d, *J* = 9.2).[2]

Acknowledgements

Financial support by the Natural Sciences and Engineering Research Council of Canada (NSERC) (FDR and MMK) and Medical Research Fund of New Brunswick (MMK) are gratefully acknowledged. The NMR spectra were recorded at the Atlantic Regional Magnetic Resonance Centre at Dalhousie University, Halifax, Nova Scotia, Canada. The authors thank Dr. D.L. Hooper for the spectra with chiral solvating agents. The help of Stéphane M. Foulem, an undergraduate participant, is gratefully acknowledged.

References

1. For reviews on β-lactam antibiotics see: (*a*) G.I. Georg and V.T. Ravikumar. *In* The organic chemistry of β-lactams. *Edited by.* G.I. Georg. VCH, New York. 1993; (*b*) R. Southgate, C. Branch, S. Coulton, and E. Hunt. *In* Recent progress in the chemical synthesis of antibiotics and related microbial products. Vol. 2. *Edited by* G. Lukacs. Springer-Verlag, Berlin. 1993. p. 621; (*c*) F.H. Van der Steen and G. van Koten. Tetrahedron, **47**, 7503 (1991).
2. C. Palomo, J.M. Aizpurua, I. Ganboa, and M. Oiarbide. Synlett, 1813 (2001); C. Palomo, J.M. Aizpurua, and I. Ganboa. *In* Enantioselective synthesis of β-amino acids. *Edited by* E. Juaristi. Wiley-VCH, New York. 1997; C. Palomo, J.M. Aizpurua, I. Ganboa, and M. Oiarbide. Pure Appl. Chem. **72**, 1763 (2000); R. Herranz, J. Castro-Pichel, S. Vinuesa, and M.T. Garcia-Lopez. J. Org. Chem. **55**, 2232 (1990), and refs. cited therein; Y. Kobayashi, Y. Takemoto, Y. Ito, and S. Terashima. Tetrahedron Lett. **31**, 3031(1990); K. Iizuka, T. Kamijo, T. Kubota, K. Akahane, H. Umeyama, and Y. Kiso. J. Med. Chem. **31**, 701 (1988); T. Aoyagi, H. Tobe, F. Kojima, M. Hamada, T. Takeuchi, and H. Umezawa. J. Antibiot. **31**, 636 (1978).
3. R.A. Holton, R.J. Biedinger, and P.D. Boatman. Semisynthesis of Taxol® and Taxotere. *In* Taxol® science and applications. *Edited by* M. Suffness. Boca Raton, CRC Press, Florida. 1995.
4. S. Lin, X. Geng, C. Qu, R. Tynebor, D.J. Gallagher, E. Pollina, J. Rutter, and I. Ojima. Chirality, **12**, 431 (2000); I. Ojima, S. Lin, J.C. Slater, T. Wang, P. Pera, R.J. Bernacki, C. Ferlini, and G. Scambia. Bioorg. Med. Chem. **8**, 1619 (2000); T. Yamaguchi, N. Harada, K. Ozaki, H. Arakawa, K. Oda, N. Nakanishi, K. Tsujihara, and T. Hashiyama. Bioorg. Med. Chem. Lett. **9**, 1639 (1999); S.M. Ali, M.Z. Hoemann, J. Aube, G.I. Georg, and L.A. Mitscher. J. Med. Chem. **40**, 236 (1997); I. Ojima, J.C. Slater, E. Michaud, S.D. Kuduk, P.-Y. Bounaud, P. Vrignaud, M.-C. Bissery, J.M. Veith, P. Pera, and R.J. Bernacki. J. Med. Chem. **39**, 3889 (1996); G.I. Georg, T.C. Boge, Z.S. Cheruvallath, J.S. Clowers, G.C.B. Harriman, M. Hepperle, and H. Park. The medicinal chemistry of Taxol®. *In* Taxol® science and applications. *Edited by* M. Suffness. Boca Raton, CRC Press, Florida. 1995; S.M. Ali, M.Z. Hoemann, J. Aubé, L.A. Mitscher, and G.I. Georg. J. Med. Chem. **38**, 3821 (1995); G.I. Georg, G.C.B. Harriman, M. Hepperle, and R.H. Himes. Bioorg. Med. Chem. Lett. **4**, 1381 (1994).
5. For recent reviews see: X. Wang, H. Itokawa, and K.-H. Lee. *In* Taxus: The genus taxus. Medical and aromatic plants — Industrial profiles. Vol. 32. *Edited by* H. Itokawa and K.H. Lee. Taylor and Francis, London. 2003; D.G.I. Kingston. Chem. Commun. 867 (2001); D.G.I. Kingston. J. Nat. Prod. **63**, 726 (2000).
6. T. Konno, J. Watanabe, and K. Ishihara. J. Biomed. Mater. Res. **65A**, 210 (2003); A.L. Seligson, R.C. Terry, J.C. Bressi, J.G. Douglass III, and M. Sovak. Anti-Cancer Drugs, **12**, 305 (2001), and refs. cited therein; M.I. Nicoletti, T. Colombo, C. Rossi, C. Monardo, S. Stura, M. Zucchetti, A. Riva, P. Morazzoni, M.B. Donati, E. Bombardelli, M. D'Incalci, and R. Giavazzi. Cancer Res. **60**, 842 (2000); D. Sampath, C.M. Discafani, F. Loganzo, C. Beyer, H. Liu, X. Tan, S. Musto, T. Annable, P. Gallagher, C. Rios, and L.M. Greenberger. Mol. Cancer Ther. **2**, 873 (2003). For a review see: I. Ojima, S. Lin, and W. Tao. Curr. Med. Chem. **6**, 927 (1999).
7. For reviews see: C. Palomo, J.M. Aizpurua, I. Ganboa, and M. Oiarbide. Eur. J. Org. Chem. 3223 (1999). Some recent examples: M.D. Mihovilovic, A. Feicht, and M.M. Kayser. J. Prakt. Chem. (Weinheim, Ger.), **342**, 585 (2000); B.K. Banik and F.F. Becker. Tetrahedron Lett. **41**, 6551 (2000).
8. For reviews see: M. Benaglia, M. Cinquini, and F. Cozzi. Eur. J. Org. Chem. 563 (2000); D.J. Hart and D.-C. Ha. Chem. Rev. **89**, 1447 (1989). A recent example: S. Schunk and D. Enders. Org. Lett. **2**, 907 (2000).

[2] Supplementary data may be purchased from the Directory of Unpublished Data, Document Delivery, CISTI, National Research Council Canada, Ottawa, ON K1A 0S2, Canada (http://www.nrc.ca/cisti/irm/unpub_e.shtml for information on ordering electronically). CCDC 220029, 220030, and 225739 contain the crystallographic data for this manuscript. These data can be obtained, free of charge, via www.ccdc.cam.ac.uk/conts/retrieving.html (or from the Cambridge Crystallographic Data Centre, 12 Union Road, Cambridge CB2 1EZ, UK; fax +44 1223 336033; or deposit@ccdc.cam.ac.uk).

© 2005 NRC Canada

9. J.R. Malpass. *In* Comprehensive organic chemistry: The synthesis and reactions of organic compounds. Vol. 2. *Edited by* D. Barton and W.D. Ollis. Pergamon Press, Oxford. 1979. p. 22; M. Chmielewski, Z. Kaluza, and B. Furman. Chem. Commun. 2689 (1996).
10. A. Basak, S.C. Ghosh, T. Bhowmick, A.K. Das, and V. Bertolasi. Tetrahedron Lett. **43**, 5499 (2002); M.M.-C. Lo and G.C. Fu. J. Am. Chem. Soc. **124**, 4572 (2002); M. Miura, M. Enna, K. Okuro, and M. Nomura. J. Org. Chem. **60**, 4999 (1995); M. Kinugasa and S. Hashimoto. J. Chem. Soc. Chem. Commun. 466 (1972).
11. M. Arun, S.N. Joshi, V.G. Puranik, B.M. Bhawal, and A.R.A.S. Deshmukh. Tetrahedron, **59**, 2309 (2003); R. Fernández, A. Ferrete, J.M. Lassaletta, J.M. Llera, and E. Martin-Zamora. Angew. Chem. Int. Ed. **41**, 831(2002); S.N. Joshi, A.R.A.S. Deshmukh, and B.M. Bhawal. Tetrahedron: Asymmetry, **11**, 1477 (2000); S. Brown, A.M. Jordan, N.J. Lawrence, R.G. Pritchard, and A.T. McGown. Tetrahedron Lett. **39**, 3559 (1998); I. Ojima and F. Delaloge. Chem. Soc. Rev. **26**, 377 (1997); S. Matsui, Y. Hashimoto, and K. Saigo. Synthesis, 1161 (1998); Y. Hashimoto, A. Kai, and K. Saigo. Tetrahedron Lett. **36**, 8821 (1995); T. Fujisawa, A. Shibuya, D. Sato, and M. Shimizu. Synlett, 1067 (1995).
12. P.A. Magriotis. Angew. Chem. Int. Ed. **40**, 4377 (2001); B.L. Hodous and G.C. Fu. J. Am. Chem. Soc. **124**, 1578 (2002); A.E. Taggi, A.M. Hafez, H. Wack, B. Young, W.J. Drury III, and T. Lectka. J. Am. Chem. Soc. **122**, 7831 (2000); H. Wack, W.J. Drury III, A.E. Taggi, D. Ferraris, and T. Lectka. Org. Lett. **1**, 1985 (1999).
13. (*a*) R. Brieva, J.Z. Crich, and C.J. Sih. J. Org. Chem. **58**, 1068 (1993); (*b*) E. Forró and F. Fülöp. Tetrahedron: Asymmetry, **12**, 2351 (2001); (*c*) W. Adam, P. Groer, H.-U. Humpf, and C.R. Saha-Möller. J. Org. Chem. **65**, 4919 (2000); (*d*) A. Basak, T. Mahato, G. Bhattacharya, and B. Mukherjee. Tetrahedron Lett. **38**, 643 (1997); (*e*) J.A. Carr, T.F. Al-Azemi, T.E. Long, J.-Y. Shim, C.M. Coates, E. Turos, and K.S. Bisht. Tetrahedron, **59**, 9147 (2003).
14. M.M. Kayser, Y. Yang, M.D. Mihovilovic, A. Feicht, and F.D. Rochon. Can. J. Chem. **80**, 796 (2002).
15. N.C. Deno. J. Am. Chem. Soc. **69**, 2233 (1947).
16. It is generally recognized that *cis*- β-lactams have larger coupling constants than the corresponding trans diastereomers. C. Palomo, J.M. Aizpurua, F. Cabré, J.M. Garcia, and J.M. Odriozola. Tetrahedron Lett. **35**, 2721 (1994). Also see B.K. Banik and F.F. Becker, in ref. 7. In the case of compound **7**, the *J* coupling constant for cis isomers is 5.3 Hz, whereas that for the trans is 1.8 Hz.
17. M.M. Kayser, M.D. Mihovilovic, J. Kearns, A. Feicht, and J.D. Stewart. J. Org. Chem. **64**, 6603 (1999).
18. XSCANS. PC Version 5 [computer program]. Bruker AXS Inc., Madison, Wisconsin. 1995.
19. SHELXTL. Release 5.10 [computer program]. Bruker AXS Inc., Madison, Wisconsin. 1997.

© 2005 NRC Canada

A quantitative structure–activity relationship study for α-substituted acetamido-*N*-benzylacetamide derivatives — A novel anticonvulsant drug class

Albert Y. Jin, Harold Kohn, Cécile Béguin, Shridhar V. Andurkar, James P. Stables, and Donald F. Weaver

Abstract: A library of 35 benzylacetamide derivatives was evaluated for anticonvulsant activity as reflected in the ED_{50} (mg/kg) required to suppress seizure activity in the maximal electroshock seizure (MES) test. Using the method of partial least-squares regression in conjunction with cross-validation, the influence of 31 topological, electronic, physicochemical, and structural properties on anticonvulsant activity was investigated. A QSAR model of the $\log ED_{50}$ in the MES test was established ($R^2_{adj} = 0.77$) as a function of the following seven properties: the Wiener index on distance code (Wmean), the mean information index on atomic composition (rIac), the partial charge at the C-terminal carbonyl carbon (qCC), the sum of partial charges in the α substituent (qαtotal), the number of hydrogen bond donors and acceptors in the α substituent (Hdα and Haα), and the calculated value of the squared *n*-octanol/water partition coefficient. Based on this model, two new amido ketone compounds — (*R*,*S*)-2-acetamido-5-phenyl-3-pentanone and *cis*/*trans*-(*R*,*S*)-2-acetamido-5-phenyl-4-penten-3-one — were synthesized and shown to have significant anticonvulsant activity in the MES test.

Key words: QSAR, anticonvulsant, benzylacetamide, functionalized amino acid, amido ketones.

Résumé : On a évalué 35 dérivés du benzylacétamide pour leur activité anticonvulsivante telle que reflétée dans les ED_{50} (mg/kg) requises pour supprimer l'activité de crise dans le test de crise maximale d'électrochoc (MES). Faisant appel à la méthode de régression partielle des moindres carrés en conjonction avec contre validation, on a évalué l'influence de 31 propriétés topologiques, électroniques, physicochimiques et structurales sur l'activité anticonvulsivante. Dans le test MES, on a pu établir un modèle QSAR du $\log ED_{50}$ ($R^2_{adj} = 0{,}77$) en fonction des sept propriétés suivantes: l'indice de Wiener sur la distance code (Wmean), l'indice d'information moyenne sur la composition atomique (rIac), la charge partielle au niveau de l'atome de carbone du carbonyle C-terminal (qCC), la somme des charges partielles dans le substituant α (qαtotal), le nombre de donneurs et d'accepteurs de liaison hydrogène dans le substituant α (Hdα et Haα) et la valeur calculée du coefficient de partition *n*-octanol/eau mise au carré. Sur la base de ce modèle, on a synthétisé deux nouvelles amidocétones, les (*R*,*S*)-2-acétamido-5-phénylpentan-3-one et les *cis*/*trans*-(*R*,*S*)-2-acétamido-5-phénylpent-4-én-3-one, qui ont montré des activités anticonvulsivantes élevées dans le test de MES.

Mots clés : QSAR, anticonvulsivante, benzylacétamide, acide aminé fonctionnalisé, amidocétones.

[Traduit par la Rédaction]

Introduction

The search for safer and more potent anticonvulsant medications remains a drug design priority (1, 2). Quantitative structure–activity relationship (QSAR) studies have received widespread attention as a powerful drug design tool for the optimization of promising drug candidates (3–11). In this study, QSAR methodology was used to elucidate the structural correlates of anticonvulsant activity in a series of α-substituted acetamido-*N*-benzylacetamide compounds shown by Kohn et al. (12) to be a promising novel anticonvulsant class.

Received 20 July 2004. Published on the NRC Research Press Web site at http://canjchem.nrc.ca on 3 February 2005.

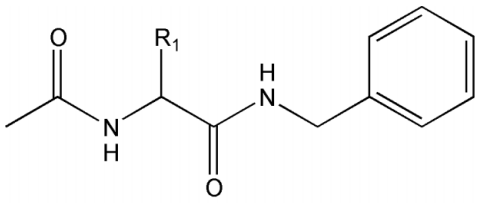
A.Y. Jin. Department of Medicine (Neurology), Queen's University, Kingston, ON K7L 3N6, Canada.
H. Kohn. Division of Medicinal Chemistry and Natural Products, School of Pharmacy, University of North Carolina, Chapel Hill, NC 27599-7360, USA.
C. Béguin. Department of Chemistry, University of Houston, Houston, TX 77204-5641, USA.
S.V. Andurkar. Department of Chemistry, University of Houston, Houston, TX 77204-5641, USA and School of Pharmacy, Midwestern University, 555 31st Street, Downers Grove, IL 60515, USA.
J.P. Stables. Epilepsy Branch, National Institute of Neurological Disorders and Stroke, National Institutes of Health, 6001 Executive Boulevard, Suite 2106, Rockville, MD 20852, USA.
D.F. Weaver.[1] Departments of Medicine (Neurology) and Chemistry, and School of Biomedical Engineering, Dalhousie University, Halifax, NS B3H 4J3, Canada.

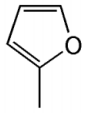
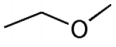
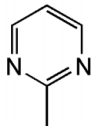
[1]Corresponding author (e-mail: donald.weaver@dal.ca).

 doi: 10.1139/V04-160 © 2005 NRC Canada

The putative benzylacetamide anticonvulsant pharmacophore or "bioactive face", shown in Fig. 1, consists of: a vicinal diamine linkage; an oxygen atom on the ethylene chain bridging two amino groups; and an aromatic ring one carbon removed from an amide group. Exploitation of this anticonvulsant design led to a diverse array of structural analogues with promising activity and low neurotoxicity (13–21), including *N*-acetyl-DL-alanine-*N*-benzylamide, and (*R*,*S*)-α-acetamido-*N*-benzyl-2-furancetamide. These and the discovery of several other highly active analogues suggest that the current anticonvulsant paradigm offers numerous avenues for improvement. However, the plethora of simultaneous synthetic changes embodied within the variety of active compounds can obscure potential directions for further structural modification. Multivariable regression through the method of partial least-squares regression (PLSR) provides an ideal approach to reveal physicochemical features that can be correlated with bioactivity. The substituted acetamido-*N*-benzylacetamide derivatives examined in this study were shown to influence anticonvulsant activity through seven physical and chemical properties. Through this QSAR study, promising directions for future drug design have lead to the synthesis of two new functionalized amido ketone compounds — (*R*,*S*)-2-acetamido-5-phenyl-3-pentanone and *trans*-(*R*,*S*)-2-acetamido-5-phenyl-4-penten-3-one — that show significant anticonvulsant activity.

Fig. 1. A novel anticonvulsant paradigm: α-substituted acetamido-*N*-benzylacetamides. Bioactivity expressed as ED_{50} (mg/kg) in the maximal electroshock seizure test.



R_1	Compound	ED_{50} (mg/kg)
	**11**	10.3
	**27**	8.3
	**30**	8.1

Methods

All compounds shown in Table 1 were synthesized and the racemates were pharmacologically evaluated as previously described (12–21). Anticonvulsant activity, measured as the ED_{50} (mg/kg) in the maximal electroshock seizure (MES) test, was evaluated through the Anticonvulsant Drug Development program at the National Institute of Neurologic Disorders and Stroke, Bethesda, Maryland, USA. All experiments with animals were performed with protocols that have received ethics approval for the humane treatment of experimental animals. These compounds displayed an $ED_{50} \leq 100$ mg/kg. By restricting the compound selection to those that displayed reasonable bioactivity, the confounding effect of including irrelevant and nonactive compounds was minimized.

Calculations were performed on an IBM RS/6000 RISC 550 workstation operating under AIX 3.2, and an IBM parallel 8-node SP2 computer operating under AIX4.1. Topological indices were calculated using the TOPOLOGY program provided by H.L. Gordon (22). Molecular volumes based on van der Waals' volume fragmental constants (23, 24) were calculated using the software package QUANTA, version 4.1 from Accelrys Inc. Molecular mechanics calculations were performed using the CHARMm force field (25, 26). Semiempirical molecular orbital calculations were done using the software package Gaussian94 (revision E3) from Gaussian, Inc. (27). Log *P* values were estimated using the fragment approach of Leo and Hansch (28) implemented in the MaclogP program (version 1.0.0) from Biobyte Corporation. Calculations for exploratory data analysis, modeling, and model analysis were done using the Splus (version 3.4) statistical analysis program from MathSoft Inc. The Splus function "pls1a" — an implementation of the algorithm presented by Marten and Naes (29) — was modified and used for partial least-squares regression during model development. Leave-one-out cross-validation was carried out using the modified Splus function "cv".

QSAR — Partial least-squares regression and leave-one-out cross-validation

Standard QSAR terminology is used (30, 31). "Property" refers to any characteristic of a molecule. "Response" refers to a property that is to be expressed in terms of other properties called "predictors" or "descriptors". A "model" expresses the response as a function of the set of predictors. In this study, bioactivity expressed as the $\log(ED_{50})$ in the MES test provided the response variable.

Partial least-squares regression (PLSR) in conjunction with cross-validation (CV) provides a robust means of revealing linear predictor–response relationships (32–37). In this study, PLSR and CV were used to develop and evaluate the QSAR model based on improvements in the adjusted R^2 (R^2_{adj}), the root mean square error of calibration (RMSEC), the predicted error sum of squares (PRESS), and the root mean square error of prediction (RMSEP):

$$[1] \qquad R^2_{adj} = 1 - (n - 1)/(n - p) \times (1 - R^2)$$

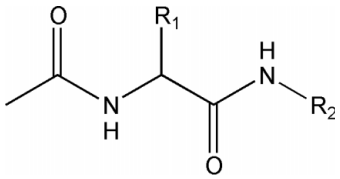
(where n = the number of observations, p = the number of PLSR components used in the model, and R^2 = the square of the correlation coefficient),

$$[2] \qquad \text{RMSEC} = \sum (y'_i - y_i)^2/n$$

(where the sum is over all compounds $i = 1$ to n, y'_i is the predicted bioactivity from the PLSR model, and y_i is the corresponding measured bioactivity),

© 2005 NRC Canada

Table 1. Anticonvulsant activity of substituted benzylacetamide derivatives.



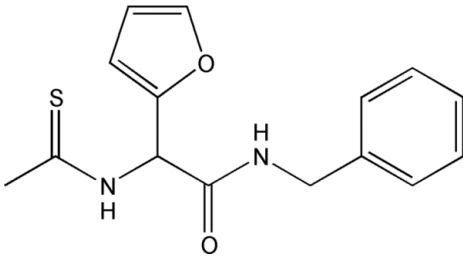
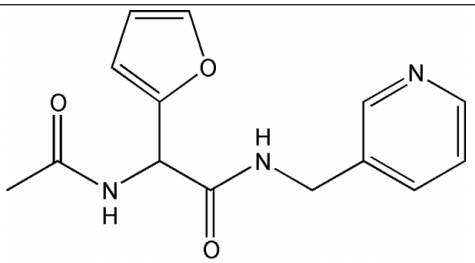
Compound	R_1 substituent	R_2 substituent	MES ED_{50}
1	CH_3	CH_2-Ph	76.54
2	CH_3	CH_2-Ph-*m*-F	77.38
3	2-Furanyl	CH_2-Ph-*o*-F	40
4	2-Furanyl	CH_2-Ph-*m*-F	13.3
5	2-Furanyl	CH_2-Ph-*p*-F	12.7
6	2-Furanyl	CH_2-2,5-$F_2C_6H_3$	23.8
7	2-Furanyl	CH_2-2,6-$F_2C_6H_3$	63
8	3-Allyl	CH_2-Ph	33.6
9	2-Tetrahydrofuranyl	CH_2-Ph	51.7
10	Ph	CH_2-Ph	20.31
11	2-Furanyl	CH_2-Ph	10.3
12	2-Furanyl-5-CH_3	CH_2-Ph	19.2
13	2-Pyrrolyl	CH_2-Ph	16.1
14	2-Pyrrolyl-5-CH_3	CH_2-Ph	36.5
15	2-Thienyl	CH_2-Ph	44.8
16	3-Thienyl	CH_2-Ph	87.8
17	1-Pyrrole	CH_2-Ph	80.2
18	1-Pyrazole	CH_2-Ph	16.5
19	2-Pyridyl	CH_2-Ph	10.8
20	$C(S)NH_2$	CH_2-Ph	86.5
21	$NHCH_2CH_3$	CH_2-Ph	42.4
22	$N(CH_3)_2$	CH_2-Ph	45.3
23	$N(CH_3)OH$	CH_2-Ph	~30
24	$NPhNH_2$	CH_2-Ph	42.79
25	OH	CH_2-Ph	79
26	OCH_2CH_3	CH_2-Ph	62
27	CH_2OCH_3	CH_2-Ph	8.3
28	$CH_2OCH_2CH_3$	CH_2-Ph	17
29	2-Pyrazinyl	CH_2-Ph	14.8
30	2-Pyrimidyl	CH_2-Ph	8.1
31	2-Oxazole	CH_2-Ph	10.5
32	2-Thiazole	CH_2-Ph	12.0
33	N(H)Ph(3-NH_2)	CH_2-Ph	98.6
34			18.4

Table 1 (*concluded*).

Compound	R_1 substituent	R_2 substituent	MES ED_{50}
35			~30

Note: All compounds were isolated as racemates. Compounds were orally administered to albino Sprague–Dawley rats and ED_{50} (mg/kg) was measured in the MES test, as conducted under the auspices of the National Institutes of Health's Anticonvulsant Screening Project.

$$[3] \quad \text{PRESS} = \sum (y'_{i(\text{cv})} - y_i)^2$$

$$[4] \quad \text{RMSEP} = (\text{PRESS}/n)^{1/2}$$

(where the sum is over all observations $i = 1$ to n, $y'_{i(\text{cv})}$ = the predicted $\log(ED_{50})$ obtained from leave-one-out CV, and y_i = the actual $\log(ED_{50})$).

In QSAR studies, the assumption of normality in the data distribution is tenuous as the large variety of data types are often not distributed evenly around a mean value. Also, the set of compounds in this study is not representative of the *entire* set of anticonvulsant compounds that contain the pharmacophore shown in Fig. 1. For example, the effect of a long alkyl R_1 substituent on anticonvulsant activity was not explored in this study. Also, the effect of benzyl substituents at the benzylacetamido moiety was examined only with respect to the arrangement of fluoro groups on the aromatic ring. Unlike random sampling done from a large population, the "sample" of compounds in this study was chosen based on the availability of accurate bioactivity data. Therefore, the application of "bootstrapping" methods to calculate population statistics, e.g., confidence intervals from limited samples cannot be justified. In this study, the uncertainty in the regression coefficients for the autoscaled data (see Data pretreatment section) was described using the range in the regression coefficients obtained during cross-validation.

Predictor selection

A set of 31 predictors was used to describe each compound. These predictors were chosen based on their ability to differentiate properties amongst a wide range of compounds. Four predictor categories were employed to describe topological, electronic, physicochemical, and ad hoc properties.

The topological predictors used in this study have been shown by Todeschini et al. (38) to differentiate a wide variety of molecules based on structural branching and elemental diversity. These included: the mean Randić connectivity index "r1mean"; the Kier–Hall flexibility index "phi"; the Wiener index on distance code "Wmean"; and the Balaban distance connectivity index "BJ". The following topological indices were based on the application of Shannon statistical information theory to both molecular graphs and atomic composition (39): the mean information content of the mag-

© 2005 NRC Canada

nitude of the distance degree "rIwdd"; the mean information on equality of the distance degree "rIedd"; the mean information index on atomic composition "rIac"; the multigraph information content index "rIc"; the bonding information content index "bIc"; and the complementary information content "cIc".

Electronic predictors were used to differentiate topologically similar compounds by elemental composition. These predictors were chosen to reflect changes in the local electronic environment near positions where substituents were frequently altered. Since there is a conformational dependence for properties based on the distribution of electron density, partial charges were used strictly as a means to differentiate molecules, and not as a reflection of the electron density distribution associated with an in vivo state. In the CHARMm force field, unfavorable steric contacts were removed through energy minimization starting from extended conformations (i.e., ϕ and ψ torsional angles at the α-carbon were initially set to 180°). For the subsequent semi-empirical molecular orbital calculations (27), each molecule was then further energy minimized using the PM3 Hamiltonian (40). Mulliken partial charges at selected atoms and molecular orbital energies were tabulated for each compound to generate the following predictors: partial charges at the α-carbon (qαC), the C-terminal carbonyl carbon (qCC), and the N-terminal amide nitrogen (qNN); the sum of the partial charges in the α-carbon substituent(s) (qαtotal); and the difference in energy ($\Delta E_{\text{LUMO–HOMO}}$) between the lowest unoccupied and highest occupied molecular orbitals (referred to as LUMO and HOMO, respectively).

Physicochemical predictors were based on estimated values of log *P*, where *P* is the *n*-octanol/water partition coefficient. Using the method originally proposed by Leo et al. (28) as implemented in the ClogP program, the predictors ClogP and ClogP^2 represented the estimated log *P* and (log *P*)^2, respectively. The log *P* has been strongly correlated to the extent of passive diffusion across the blood–brain barrier (41–45). Therefore, this predictor was included to delimit the hydrophobic constraints that must be considered in future syntheses.

Ad hoc predictors were devised to examine the influence of regiospecific substitutions. These included: molecular weight (MW); molecular volume calculated using van der Waals' volume fragmental constants (Vtotal); α-carbon substituent volume (Vαtotal); C-terminal substituent volume (VCterm) and N-terminal substituent volume (VNterm); the number of hydrogen bond donors and acceptors in the α-carbon substituent (Hdα and Haα, respectively), the C-terminal substituent (HdC and HaC) and the N-terminal substituent (HdN and HaN); the number of atoms between the α-carbon and the nearest heteroatom in the α-carbon substituent (*n*-α-het); and the number of nitrogen and oxygen atoms in the α-carbon substituent (Nα and Oα).

Data pretreatment

The predictor data was analyzed to minimize confounding effects. Predictors that showed little or no variance were discarded. These predictors contain information pertaining only to a few compounds and contribute greatly to data noise, thus obscuring trends in the data. Correlation among predictor variables with a correlation coefficient $|r| > 0.8$ were also identified. Predictor variables were then removed to reduce the number of highly correlated variables within the predictor data set. By removing these predictors, the likelihood of developing spurious predictor–response relationships can be greatly reduced. The remaining predictor data was then scaled and normalized through an "autoscaling" procedure, in which the data was scaled to the predictor's standard deviation and centered about the mean. This procedure allowed the predictors to carry approximately the same weight in model development, despite differences in their measurement scales.

Model development

The model was generated in a stepwise fashion using the following procedure:

1. The correlation between each predictor variable and the response variable was calculated.
2. A linear model was derived using the predictor with the highest correlation coefficient.
3. The R^2 was calculated for the model.
4. PLSR models were derived using all previously used predictor data plus one of the remaining predictors. For each model, the R^2_{adj} was calculated.
5. The added predictor was replaced with another one of the remaining predictors. R^2_{adj} was recalculated. This last step was repeated until all of the remaining predictors had been tested. Leave-one-out cross-validation was also performed on each model.
6. From all of the models generated, the one with the most improved R^2_{adj} and smallest PRESS was accepted. Steps 4 to 6 were then repeated until the improvement in R^2_{adj} was less than 0.02, yielding the final model. This limit was set to avoid overfitting.

Results

Of the 31 predictor variables initially evaluated in this study, six showed insignificant variance and were discarded. These variables were: VCterm, VNterm, HdC, HaC, HdN, and HaN. In addition, five variables were removed to eliminate excessive correlation within the predictor data set. The five discarded predictors were: BJ, rIwdd, cIc, MW, and Vtotal. The remaining 20 variables used in the study were: r1mean, Wmean, rIedd, rIac, rIc, bIc, phi, $\Delta E_{\text{LUMO–HOMO}}$, V$\alpha$total, q$\alpha$C, qCC, qNN, q$\alpha$total, Hd$\alpha$, Ha$\alpha$, *n*-$\alpha$-het, N$\alpha$, O α, ClogP, and ClogP^2. Of the 35 compounds used in the analysis, approximately 50% had $\log(ED_{50}) < 1.5$, with a $\log(ED_{50})$ range between 0.9 and 2.0. Exploratory analysis of the predictor data showed that most of the variables were not described by a normal distribution; similarly, the bioactivities were also not normally distributed (data not shown).

The majority of the compounds in Table 1 contain a benzylamide moiety at the C-terminal. Among these, the most active compounds incorporated a variety of different α-carbon groups, including: -CH_2OCH_3 (**27**, ED_{50} = 8.3 mg/kg), 2-pyrimidyl (**30**, ED_{50} = 8.1 mg/kg), and 2-furanyl (**11**, ED_{50} = 10.3 mg/kg). There was no consistent trend in the activity data on changing the α substituent from acyclic to cyclic or nonaromatic to aromatic structures. At the C-terminal, seven compounds with either fluoro-

© 2005 NRC Canada

Table 2. QSAR model statistics and regression coefficients.

Statistic	PLSR model (complete data set)	PLSR model (three outliers removed)
RMSEC	0.19	0.16
PRESS	2.29	1.31
RMSEP	0.25	0.20
R^2_{adj}	0.66	0.77
q^2	0.42	0.63
Regression coefficients for the autoscaled data (range of coefficients derived during cross-validation in brackets):		
Wmean	–0.27 (–0.38,–0.23)	–0.25 (–0.33, –0.22)
rIac	0.38 (0.27, 0.41)	0.26 (0.22, 0.29)
qCC	–0.37 (–0.44, –0.29)	–0.44 (–0.51, –0.37)
qαtotal	0.27 (0.16, 0.31)	0.21 (0.11, 0.24)
Hdα	0.58 (0.38, 0.62)	0.63 (0.46, 0.66)
Haα	–0.43 (–0.52, –0.37)	–0.52 (–0.56, –0.49)
$(ClogP)^2$	0.37 (0.29, 0.44)	0.29 (0.20, 0.34)

substituted phenyl rings or a pyridinyl ring also did not show any consistent trend in anticonvulsant activity when compared with the benzylamide-substituted compounds. There were also no consistent topological, electronic, or physicochemical trends in comparing acyclic and cyclic α substituents. The acyclic-containing structures generally showed a smaller α-substituent volume, as expected.

The initial PLSR model employed seven predictors and three PLSR components: Wmean, rIac, qCC, qαtotal, Hdα, $ClogP^2$, and Haα. The fit to the response data was good, with an R^2_{adj} value of 0.66. Predictions based on the first PLSR component alone accounted for 48% of the bioactivity displayed in Table 1. The contribution of each predictor to a PLSR component can be assessed by the predictor's "weighting" that arises from the PLSR algorithm. Weightings range from –1 to +1, with positive values indicating a positive correlation to the response variable. The predictor weightings for the first PLSR component showed the involvement of Hdα, Haα, qCC, rIac, qαtotal, and Wmean with corresponding weights of 0.567, –0.384, –0.553, 0.176, 0.309, and –0.312, respectively. The second PLSR component accounted for an additional 16% of the bioactivity in Table 1 and was weighted heavily towards $ClogP^2$, with a weight of 0.837. The third component accounted for about 2% of the bioactivity and was derived mainly from Hdα, Haα, rIac, and qαtotal, with minor contributions from the remaining predictors qCC, $ClogP^2$, and Wmean. Using three PLSR components, the RMSEC was 0.19 (see Table 2). The cross-validated q^2 value was 0.42 and the PRESS was 2.29, forewarning of poor predictive ability. Thus, from the RMSEP value of 0.25, one could expect that future predictions of $\log(ED_{50})$ will vary by ±0.25, a significant error for a logarithmic scale. One cause of this was the presence of three outliers identified as compounds **4**, **7**, and **13**. For compounds **4** and **13**, the $\log(ED_{50})$ was overestimated by 0.34 and 0.48, respectively. Compound **7** was estimated to have a $\log(ED_{50}) = 1.45$, compared to its actual value of 1.79. Removal of these outliers from the data set resulted in a second model with a slight change in the regression coefficients, as shown in Table 2. The cross-validated q^2 improved to 0.63, suggesting that the second model would be expected to account for approximately 60% of the variance in the anticonvulsant activity of newly synthesized compounds. Three components were also found to be ideal in the second model. The predictor weightings for the first and second components were similar to that seen in the initial model, whereas the third component was derived mainly from Hdα, Haα, and rIac, with minor contributions from qCC, qαtotal, and $ClogP^2$. The percentage of the bioactivity in Table 1 accounted for by the first and second components was 62% and 13%, respectively. The third component accounted for an additional 2%. From cross-validation, the range for each regression coefficient using the autoscaled data is shown in Table 2. Quantile–quantile plots of the regression coefficients derived during cross-validation showed significant deviations from a normal distribution suggesting that the use of standard error would be inappropriate (data not shown).

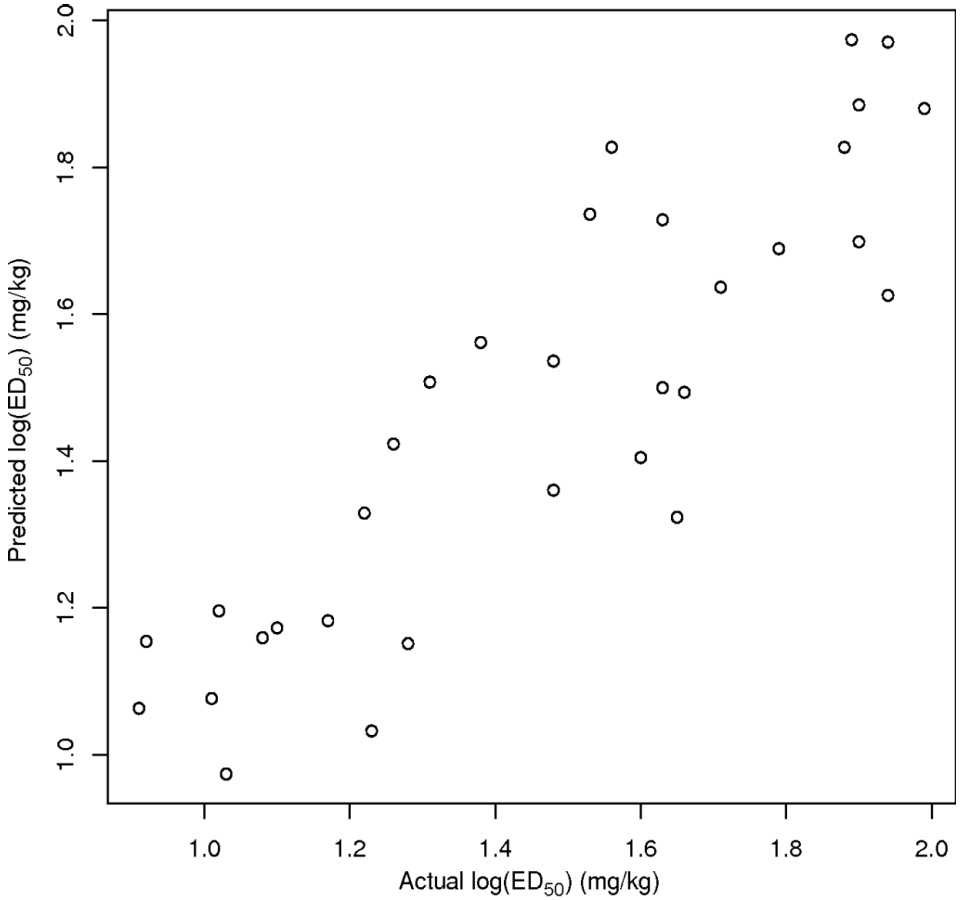
Using the approach outlined by Golbraikh and Tropsha (46), a measure of model robustness can be obtained by comparing the q^2 statistic of the PLSR model against q^2 values derived from models using randomly shuffled bioactivity data. For 10 sets of data with randomly shuffled $\log(ED_{50})$ values, models containing up to seven predictors and up to three removed outliers were generated using the same modeling strategy. The q^2 values for the random data sets varied from 0.26 to 0.59, with a mean value of 0.36 and a standard deviation of 0.13. The *Z*-score was calculated using $Z = (h - \mu)/\sigma$, where h is the q^2 for the PLSR model, μ is the mean q^2, and σ is the standard deviation in q^2 for the random data sets. For the PLSR model, $Z = 2.1$, indicating that the likelihood the model was derived by chance is 0.018, or 1 in 56. However, among the random data sets, the presence of two models with q^2 values of 0.58 and 0.59 indicated some instability in the model, perhaps reflecting the small size of the data set. This forewarns that predictions based on the model should be of a qualitative nature.

The chemical interpretation of the PLSR model can be facilitated by deriving the regression coefficients to generate the following prediction relation for the unscaled and uncentred data:

$$[5]\quad \log(ED_{50}) = (-0.434)\text{Wmean} + (0.738)\text{rIac} + (-7.36)\text{qCC} + (0.520)\text{q}\alpha\text{total} + (0.285)\text{Hd}\alpha + (0.163)\text{ClogP}^2 + (-0.272)\text{Ha}\alpha + 4.60$$

© 2005 NRC Canada

Fig. 2. Predicted log(ED_{50}) vs. actual log(ED_{50}) for 32 α-substituted acetamido-*N*-benzylacetamide derivatives. Predicted log(ED_{50}) = (–0.434)Wmean + (0.738)rIac + (–7.36)qCC + (0.520)qαtotal + (0.285)Hdα + (0.163)ClogP^2 + (–0.272)Haα + 4.60 (R^2_{adj} = 0.77; cross-validated q^2 = 0.63, three PLSR components).



(R^2_{adj} = 0.77; RMSEC = 0.16; cross-validated q^2 = 0.63; RMSEP = 0.20; three PLSR components).

A plot of the predicted log(ED_{50}) against the actual log(ED_{50}) is shown in Fig. 2. The statistical relevance in this QSAR equation can be summarized as follows: (*a*) from an original set of 31 predictors, seven predictors were found to be useful in describing anticonvulsant activity; (*b*) as suggested by R^2_{adj} = 0.77, this QSAR can account for 77% of the variance in the anticonvulsant activity displayed in Table 1; (*c*) for Table 1, this QSAR calculates the log(ED_{50}) within an error of ±0.16; (*d*) one can expect the QSAR equation to predict about 60% of the variance in the anticonvulsant activity of a new set of compounds (cross-validated q^2 = 0.63), with an error of ±0.20 in the predicted log(ED_{50}) (RMSEP = 0.20); (*e*) from the original 31 predictors examined (a potentially 31-dimensional data space), the "essential" data *that is relevant to anticonvulsant activity* can be described by a three-dimensional data space represented by the three PLSR components, which are mutually orthogonal.

Discussion

The potential of a QSAR analysis lays not only in the statistical characterization of favorable structure–activity trends, but also in the identification of irrelevance or redundancy among the many structural properties of initial interest. A well-constructed QSAR model should provide not only a range in which structural properties are correlated to some measure of bioactivity, but also a set of boundaries within which toxicity and bioavailability issues may be examined.

Chemical and structural interpretation of the model

The seven predictors employed by the PLSR model cover a range of topological, electronic, physicochemical, and ad hoc properties. Although the chemical meaning of predictors such as Hdα is self-evident, for others such as Wmean, the structural implications are less intuitive. Through examples drawn from Table 1, the significance of these predictors can be clearly illustrated.

The predictor Wmean spanned a range from 4.26 to 5.18. At the high end, compounds **5**, **24**, and **33** possess heteroatom-containing cyclic α substituents. Heteroatoms in the C-terminal benzylamide groups of **5** also increased Wmean. Thus, the presence of heteroatoms in either large branched α substituents or at the C-terminal benzylamide group was associated with a large Wmean value, which favoured anticonvulsant activity. Countering this, a large rIac value disfavours anticonvulsant activity. High values for rIac arose from the introduction of heteroatoms in small α-carbon and C-terminal substituents. Compounds such as **2**, **6**, and **20** possessed high rIac values of 1.40, 1.40, and 1.32, re-

© 2005 NRC Canada

spectively. Low values were seen in large compounds with little heteroatom diversity. For example, compounds **8**, **10**, and **19** displayed rIac values of 0.99, 0.89, and 1.02. As the size of a molecule increases, the probability of elemental diversity at a given nucleus diminishes, thus lowering rIac. This illustrates the interdependence of rIac and Wmean. This interpretation does not account for the possible influence of other possible R_1 moieties, such as alkyl chains of varying lengths. Thus, one cannot exclude that the current model is biased towards favouring large heteroatom-containing substituents.

The large difference in the regression coefficients for the electronic predictors qCC and qαtotal reflects the difference in the ranges for these variables. When this is taken into account, the contributions of the qCC and qαtotal terms are of comparable magnitude. Anticonvulsant activity was associated with increasing values of qCC. Large qCC values above 0.28 were attributed to the presence of electron-withdrawing centres adjacent to the α-carbon. For example, in compounds **5** (ED_{50} = 12.7 mg/kg, qCC = 0.282) and **11** (ED_{50} = 10.3 mg/kg, qCC = 0.281) the 2-furanyl α substituent places an aromatic center next to the α-carbon. In contrast, a low qCC value in compound **26** (ED_{50} = 62 mg/kg, qCC = 0.202) was due to the placement of an electron-rich -OCH_2CH_3 group next to the α-carbon. Differences in qαtotal were more difficult to interpret as most qαtotal values were close to zero. Both qαtotal and qCC were calculated using Mulliken population analysis and are therefore strongly dependent on conformation. For each molecule in the present study, in the absence of biologically relevant conformational data, the extended conformation was used to calculate the electron density distribution. This does not necessarily correspond to an in vivo state. Therefore, while qαtotal and qCC in this study were useful in distinguishing different compounds, it would be inappropriate to attribute any biological significance to these partial charges, e.g., with respect to receptor interactions. Clearly, for future analyses, it would be preferrable to substitute more relevant electronic predictors should the appropriate conformational data become available.

The physicochemical predictor $ClogP^2$ provided an indication of the hydrophobic requirements for activity. Most of the compounds in Table 1 showed a $ClogP^2$ value between 0 and 1. For compounds with $ClogP^2 < 1$, the small $ClogP^2$ coefficient of 0.163 indicates that the impact of the $ClogP^2$ term on $\log(ED_{50})$ is weak. This suggests that favourable activity is compatible with a wide range in hydrophobicity.

The chemical and physical interpretation of the current PLSR model complements the structure–activity relationship study of functionalized amino acids reported by Shen et al. (47). In that study, data sets using topological indices and atom pair descriptors were used to construct models employing up to 50 predictors using either the "k-nearest-neighbor" QSAR (kNN-QSAR) method or a "simulated annealing" partial least-squares (SA-PLS) approach. These techniques were capable of generating models with high q^2 values and good prediction capabilities. In addition, the use of atom pair descriptors was useful for revealing chemical substructures that were present in only the most active compounds. However, the relation between chemical *properties* and anticonvulsant activity can be obscured through the simultaneous use of many predictors, which have only an indirect correlation to physicochemical quantities. The current PLSR model complements the kNN-QSAR and SA-PLS models by revealing *chemical trends* that may be exploited by the synthetic chemist to design new compounds. Thus, for example, the PLSR model suggested that anticonvulsant activity may be enhanced by eliminating α-substituent hydrogen bond donors, incorporating α-substituent hydrogen bond acceptors, and increasing the partial positive charge at the C-terminal carbon. This information is difficult to obtain from the use of topological descriptors alone.

Outlier analysis

Compounds **4**, **7**, and **13** have been identified as outliers. The ED_{50} for compounds **4** and **13** are overestimated (i.e., the model predicts that they are less active than they actually are) while the ED_{50} for compound **7** is underestimated (i.e., the model predicts greater bioactivity than is actually seen). Compound **4** (R_2 = *meta*-fluorobenzyl) is comparable to compounds **3** (R_2 = *ortho*-fluorobenzyl) and **5** (R_2 = *para*-fluorobenzyl), with experimental ED_{50} values of 13.3, 40, and 12.7, respectively. The calculated ED_{50} values for **4**, **3**, and **5** are 28.7, 27.0, and 16.4. Thus, the model fails to recognise the favourable *meta*-fluorobenzyl group, and treats this as equivalent to the unfavourable ortho analogue.

Compound **7** contains a 2-furanyl group at R_1 and a -CH_2-2,6-$F_2C_6H_3$ group at R_2. It is comparable to compound **6**, which differs by having a -CH_2-2,5-$F_2C_6H_3$ group at R_2. The calculated and actual ED_{50} values for **7** are 27.9 and 63, respectively. The corresponding values for **6** are 41.4 and 23.8. The model fails to recognize the detrimental effect of two *ortho*-fluoro groups at the R_2 benzyl moiety. In fact, the model predicts the *opposite* trend for compounds **6** and **7**. As for compounds **3**, **4**, and **5**, the model fails to recognise the detrimental effect of the *ortho*-fluorobenzyl group.

Compound **13** contains a 2-pyrrolyl group at R_1 and a benzyl group at R_2, and is comparable to **14** (R_1 = 2-pyrrolyl-5-CH_3). Compounds **13** and **14** possess calculated ED_{50} values of 49.2 and 48.1, respectively. From the experimental ED_{50} values in Table 1, the presence of a 5-methyl group on the pyrrole ring in **14** is associated with lower activity. This suggests that the model doesn't account for the steric effect of the methyl group attached to the pyrrolyl ring in compound **14**.

This outlier analysis illustrates an inherent inability of this QSAR method to account for specific pharmacodynamic interactions. The substituent position in the R_2 benzyl moiety or in the R_1 2-pyrrolyl group was not specifically characterized in the original descriptor set. Specific descriptors focused on substituent effects would be appropriate in QSAR studies of future drug candidates containing an array of modifications at these sites. Additionally, this QSAR study did not utilize three-dimensional conformational data, which may be relevant to model specific drug–receptor interactions. The use of detailed conformational data is dependent on availability and the relevance of the structural information to the specific drug–receptor milieu. Conformational data is most useful in exploring trends within a series of closely related structural analogues. Consequently, this would not be appropriate in the present QSAR study, which examined a wide variety of α-substituted acetamido-*N*-benzylacetamide structures. It is certainly possible that for

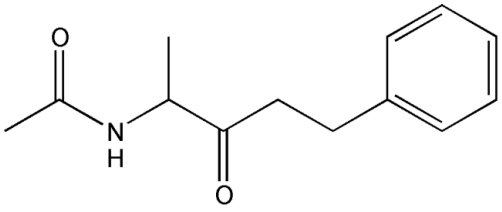
© 2005 NRC Canada

Table 3. Anticonvulsant activity of functionalized amido ketones.

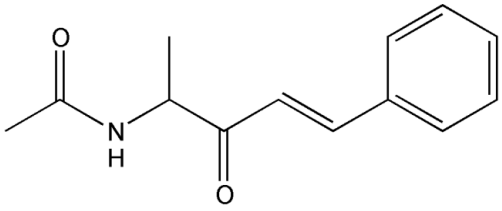
Compound	MES ED_{50} (mg/kg)
(*R*,*S*)-2-Acetamido-5-phenyl-3-pentanone	47
(*R*)-2-Acetamido-5-phenyl-3-pentanone	26
(*S*)-2-Acetamido-5-phenyl-3-pentanone	>30
trans-(*R*,*S*)-2-Acetamido-5-phenyl-4-penten-3-one	~30

Note: Compounds were administered to albino Sprague–Dawley rats (oral route, (po)) and ED_{50} was measured in the MES test, as conducted under the auspices of the National Institutes of Health's Anticonvulsant Screening Project.

Fig. 3. Functionalized amido ketones: (*R*,*S*)-2-acetamido-5-phenyl-3-pentanone and *trans*-(*R*,*S*)-2-acetamido-5-phenyl-4-penten-3-one.



(*R,S*)-2-Acetamido-5-phenyl-3-pentanone



trans-(*R,S*)-2-Acetamido-5-phenyl-4-penten-3-one

compounds **4**, **7**, and **13** specific steric and nonbonding interactions within the receptor microenvironment directly affected anticonvulsant activity. A future exploration of benzyl group substituent effects at the R_2 position or 2-pyrrolyl substituents at the R_1 position may be promising.

Functionalized amido ketones — a new anticonvulsant class

The PLSR model suggested that certain chemical modifications would be compatible with increased anticonvulsant activity. Increasing positive charge at the C-terminal carbonyl carbon and the removal of hydrogen bond donors in the α substituent could be obtained by modifications at either the α-carbon or at the C-terminal. Therefore, two functionalized amido ketones — (*R*,*S*)-2-acetamido-5-phenyl-3-pentanone, and *trans*-(*R*,*S*)-2-acetamido-5-phenyl-4-penten-3-one — were proposed to explore these possibilities (Fig. 3). The absence of a C-terminal benzylamide moiety not only increased the positive charge at the C-terminal carbonyl carbon, but also represented a substantial structural departure from the original pharmacophore shown in Fig. 1, removing a site for amide bond hydrolysis. These compounds satisfied the following structural guidelines derived from the model: (*a*) both had a large Wmean value of 4.258; (*b*) both had a low rIac value of 0.87; (*c*) both had qCC values greater than 0.28; (*d*) neither compound had a hydrogen bond donor in the α substituent. Using the PLSR model in conjunction with the previous experience with functionalized amino acid anticonvulsants, the synthesis, characterization, and pharmacologic testing of several substituted amido ketones was completed by Béguin et al. (48).

Significant anticonvulsant activity was seen in the MES test for (*R*,*S*)-2-acetamido-5-phenyl-3-pentanone, and *trans*-(*R*,*S*)-2-acetamido-5-phenyl-4-penten-3-one (see Table 3). Additionally, (*R*)-2-acetamido-5-phenyl-3-pentanone showed greater potency than the (*S*)-isomer. This finding mirrored the stereochemical influence exerted at the α-carbon in *N*-acetyl-DL-alanine-*N*-benzylamide, in which the D-isomer possessed 10 times the pharmacologic activity of the L-isomer (12). This suggested that anticonvulsant activity is mediated by a molecular scale interaction. The vinylic amido ketone *trans*-(*R*,*S*)-2-acetamido-5-phenyl-4-penten-3-one also demonstrated significant activity. The similar activities exhibited by functionalized amino acid, saturated amido ketone, and vinylic amido ketone anticonvulsants indicated the biological equivalence of the terminal substituents -N(H)CH_2Ph, -CH_2CH_2Ph, and *trans*-CH=CHPh. This raises the possibility that these groups attain a similar bioactive conformation.

Conclusions

The aim of the exploratory phase of rational drug design is to identify the most promising strategies for the future optimization of the lead compound. In the present study, a chemometric approach employing QSAR methodology was used to extract novel insight from a diverse collection of structural analogues. The resulting structure–activity model suggested possible directions for future synthetic design.

Modeling with the compounds shown in Table 1 yielded the following linear relationship after the removal of three outliers: log(ED_{50}) = (–0.434)Wmean + (0.738)rIac + (–7.36)qCC + (0.520)qαtotal + (0.285)Hdα + (0.163)ClogP^2 + (–0.272)Haα + 4.60 (R^2_{adj} = 0.77; cross-validated q^2 = 0.63; three PLSR components). This model explained 77% of the variance in the calibration set as a function of seven predictors. Through leave-one-out cross-validation, it was shown that the relevant structural and chemical information in Table 1 was described by three components, i.e., a three-dimensional predictor space. The cross-validated q^2 statistic of 0.63 indicated that the model should account for ~60% of the variance in future test set predictions.

The model provided statistical support for the validity of the proposed anticonvulsant pharmacophore for α-substituted acetamido-*N*-benzylacetamide compounds. From a structural perspective, favourable bioactivity was correlated with: highly branched, cyclic α substituents and a large *N*-benzylacetamido moiety (indicated by Wmean and rIac); the presence of α-substituent hydrogen-bond acceptors (from Ha

© 2005 NRC Canada

α); the absence of hydrogen-bond donors (Hdα); and, the presence of electron-withdrawing substituents at either the α-position or the benzyl moiety (from the qCC term). The ClogP[2] coefficient suggests that a wide range of hydrophobic compounds can be accomodated by the present pharmacophore. The synthesis of functionalized amido ketones represents a synthetic priority consistent with this QSAR study. These compounds possess appreciable activity in the maximal electroshock seizure test and represent a newly discovered class of anticonvulsant agents.

Acknowledgements

The authors thank Dr. Heather L. Gordon for the provision of her program TOPOLOGY.F" to calculate topological indices.

References

1. R. Diaz-Arrastia, M.A. Agostini, and P.C. Van Ness. JAMA, J. Am. Med. Assoc. **287**, 2917 (2002).
2. C.W. Bazil and T.A. Pedley. Annu. Rev. Med. **49**, 135 (1998).
3. J.S. Delaney, A. Mullaley, G.W. Mullier, G.J. Sexton, R. Taylor, and R.C. Viner. J. Chem. Inf. Comput. Sci. **33**, 174 (1993).
4. J.W. McFarland and D.J. Gans. Quant. Struct.–Act. Relat. **13**, 11 (1994).
5. Ajay. Chemom. Intell. Lab. Syst. **24**, 19 (1994).
6. J.S. Tokarski and A.J. Hopfinger. J. Med. Chem. **37**, 3639 (1994).
7. L. Belvisi, G. Bravi, C. Scolastico, A. Vulpetti, A. Salimbeni, and R. Todeschini. J. Comput. Aided Mol. Des. **8**, 211 (1994).
8. A.C. Good, T.J.A. Ewing, D.A. Gschwend, and I.D. Kuntz. J. Comput. Aided Mol. Des. **9**, 1 (1995).
9. K. Raghavan, J.K. Buolamwini, M.R. Fresen, Y. Pommier, K.W. Kohn, and J.N. Weinstein. J. Med. Chem. **38**, 890 (1995).
10. S. Sicsic, I. Serraz, J. Andrieux, B. Brémont, M. Mathé-Allainmat, A. Poncet, S. Shen, and M. Langlois. J. Med. Chem. **40**, 739 (1997).
11. J.W. McFarland and D.J. Gans. *In* Comprehensive medicinal chemistry. *Edited by* C. Hansch, P.G. Sammes, and J.B. Taylor. Pergamon Press, Oxford. 1990. pp. 667–689.
12. H. Kohn, J.D. Conley, and J.D. Leander. Brain Res. **457**, 371 (1988).
13. S. Cortes, Z.-K. Liao, D. Watson, and H. Kohn. J. Med. Chem. **28**, 601 (1985).
14. J.D. Conley and H. Kohn. J. Med. Chem. **30**, 567 (1987).
15. P. LeGall, K.N. Sawhney, J.D. Conley, and H. Kohn. Int. J. Pept. Protein Res. **32**, 279 (1988).
16. H. Kohn, K.N. Sawhney, P. LeGall, J.D. Conley, D.W. Robertson, and J.D. Leander. J. Med. Chem. **33**, 919 (1990).
17. H. Kohn, K.N. Sawhney, P. Legall, D.W. Robertson, and J.D. Leander. J. Med. Chem. **34**, 2443 (1991).
18. H. Kohn, K.N. Sawhney, P. Bardel, D.W. Robertson, and J.D. Leander. J. Med. Chem. **36**, 3350 (1993).
19. P. Bardel, A. Bolanos, and H. Kohn. J. Med. Chem. **37**, 4567 (1994).
20. H. Kohn, K.N. Sawhney, D.W. Robertson, and J.D. Leander. J. Pharm. Sci. **83**, 689 (1994).
21. D. Choi, J.P. Stables, and H. Kohn. J. Med. Chem. **39**, 1907 (1996).
22. H.L. Gordon and J.A. Bikker. TOPOLOGY [computer program]. 1995.
23. I. Motoc and G.R. Marshall. Chem. Phys. Lett. **116**, 415 (1985).
24. A. Bondi. J. Phys. Chem. **68**, 441 (1964).
25. B.R. Brooks, R.E. Bruccoleri, B.D. Olafson, D.J. States, S. Swaminathan, and M. Karplus. J. Comput. Chem. **4**, 187 (1983).
26. F.A. Momany and R. Rone. J. Comput. Chem. **13**, 888 (1992).
27. M.J. Frisch, G.W. Trucks, H.B. Schlegel, P.M.W. Gill, B.G. Johnson, M.A. Robb, J.R. Cheeseman, T. Keith, G.A. Petersson, J.A. Montgomery, K. Raghavachari, M.A. Al-Laham, V.G. Zakrzewski, J.V. Ortiz, J.B. Foresman, J. Cioslowski, B.B. Stefanov, A. Nanayakkara, M. Challacombe, C.Y. Peng, P.Y. Ayala, W. Chen, M.W. Wong, J.L. Andres, E.S. Replogle, R. Gomperts, R.L. Martin, D.J. Fox, J.S. Binkley, D.J. Defrees, J. Baker, J.P. Stewart, M. Head-Gordon, C. Gonzalez, and J.A. Pople. Gaussian 94. Revision E.3 [computer program]. Gaussian, Inc., Pittsburgh, Penn. 1995.
28. A. Leo, C. Hansch, and D. Elkins. Chem. Rev. **71**, 525 (1971).
29. H. Martens and T. Naes. Multivariate calibration. Wiley, Guildford, UK. 1989.
30. D. Livingstone. Data analysis for chemists: Applications to QSAR and chemical product design. Oxford University Press, Oxford. 1995.
31. C. Liang and D.A. Gallagher. Am. Lab. (Shelton, Conn.), 34 (1997).
32. Y.C. Martin, C.T. Lin, C. Hetti, and J. DeLazzer. J. Med. Chem. **38**, 3009 (1995).
33. S. de Jong. Chemom. Intell. Lab. Syst. **18**, 251 (1993).
34. E. Marengo and R. Todeschini. Chemom. Intell. Lab. Syst. **12**, 71 (1991).
35. S. Wold. Chemom. Intell. Lab. Syst. **14**, 71 (1992).
36. P. Geladi and B.R. Kowalski. Anal. Chim. Acta, **185**, 1 (1986).
37. K. Helland, H.E. Berntsen, O.S. Borgen, and H. Martens. Chemom. Intell. Lab. Syst. **14**, 129 (1992).
38. R. Todeschini, R. Cazar, and E. Collina. Chemom. Intell. Lab. Syst. **15**, 51 (1992).
39. D. Bonchev. Information theoretic indices for characterization of chemical structures. Research Studies Press, Letchworth, UK. 1983.
40. J.J.P. Stewart. J. Comput. Chem. **10**, 209 (1989).
41. M.H. Abraham, K. Takacs-Novak, and R.C. Mitchell. J. Pharm. Sci. **86**, 310 (1997).
42. M.H. Abraham, H.S. Chadha, and R.C. Mitchell. Drug Des. Discovery, **13**, 123 (1995).
43. A. Seelig, R. Gottschlich, and R.M. Devant. Proc. Natl. Acad. Sci. U.S.A. **91**, 68 (1994).
44. F. Lombardo, J.F. Blake, and W.J. Curatolo. J. Med. Chem. **39**, 4750 (1996).
45. T. Salminen, A. Pulli, and J. Taskinen. J. Pharm. Biomed. Anal. **15**, 469 (1997).
46. A. Golbraikh and A. Tropsha. J. Mol. Graphics Modell. **20**, 269 (2002).
47. M. Shen, A. LeTiran, Y. Xiao, A. Golbraikh, H. Kohn, and A. Tropsha. J. Med. Chem. **45**, 2811 (2002).
48. C. Béguin, S.V. Andurkar, A.Y. Jin, J.P. Stables, D.F. Weaver, and H. Kohn. Bioorg. Med. Chem. **11**, 4275 (2003).

© 2005 NRC Canada

Re-evaluation of the second thermodynamic dissociation constants of α-alanine, valine, and leucine using potentiometric data measured for aqueous potassium chloride solutions at 298.15 K

Jaakko I. Partanen, Pekka M. Juusola, and Virginie Verraes

Abstract: Equations were developed for the calculation of the second stoichiometric (molality scale) dissociation constants (K_{m2}) of α-alanine, valine, and leucine in aq. KCl solutions at 298.15 K from the revised thermodynamic dissociation constants (K_{a2}) of these acids and the ionic strength (I_m) of the solutions. The ionic strength of the solutions considered in this study is determined mostly by KCl alone, and the equations for K_{m2} were based on the single-ion activity coefficient equations of the Hückel type. The existing literature data obtained from Harned cell measurements and new potentiometric titration data were used to revise the K_{a2} values of the three amino acids. The values $(1.295 \pm 0.013) \times 10^{-10}$, $(1.894 \pm 0.009) \times 10^{-10}$, and $(1.685 \pm 0.011) \times 10^{-10}$ were obtained from the new potentiometric titration data for α-alanine, valine, and leucine, respectively. For alanine and valine, the new K_{a2} values are also supported by the Harned cell data used, but the value $(1.80 \pm 0.02) \times 10^{-10}$ obtained for leucine from these data is significantly different. The potentiometric values are recommended here. The activity coefficient equations for the calculation of K_{m2} values were also determined from the new potentiometric data. By means of the activity coefficient equations obtained for these three amino acids for KCl solutions, K_{m2} can be evaluated almost within experimental error up to an I_m of about 1.0 mol kg^{-1}. The K_{m2} values calculated by this method are also compared with the values suggested in the literature.

Key words: ionic strength dependence, stoichiometric dissociation constant, Debye–Hückel equation, potentiometry, α-alanine, valine, leucine.

Résumé : Des équations sont développées pour le calcul de K_{m2}, la deuxième constante de dissociation stœchiométrique (en molalité) de l'α-alanine, la valine et la leucine en solutions aqueuses de KCl à 298,15 K, à partir des constantes thermodynamiques révisées (K_{a2}) de ces acides et de la force ionique de la solution (I_m). La force ionique des solutions considérées dans la présente étude est imposée presque en totalité par KCl, et les équations des constantes K_{m2} sont déduites d'équations de type Hückel pour la détermination du coefficient d'activité d'un seul type d'ions en solution. Les données bibliographiques existantes, obtenues à partir de mesures faites sur des cellules de Harned, ainsi que de nouvelles données potentiométriques ont été utilizées pour réévaluer les valeurs des coefficients K_{a2} des ces trois acides aminés. Des valeurs de $(1{,}295 \pm 0{,}013) \times 10^{-10}$, $(1{,}894 \pm 0{,}009) \times 10^{-10}$ et $(1{,}685 \pm 0{,}011) \times 10^{-10}$ ont ainsi été obtenues pour l'α-alanine, la valine et la leucine, respectivement, à partir de nouvelles titrations potentiométriques. Pour l'alanine et la valine, les nouvelles valeurs de K_{a2} sont confirmées par les valeurs utilizées provenant de valeurs obtenues avec des cellules de Harned, mais la valeur de $(1{,}80 \pm 0{,}02) \times 10^{-10}$ obtenue pour la leucine diffère considérablement. Les valeurs potentiométriques sont recommandées dans la présente étude. Les équations pour les coefficients d'activités utilizées pour le calcul des constantes K_{a2} ont aussi été déterminées à partir de nouvelles données potentiométriques. Au moyen de la méthode de calcul obtenue pour ces trois acides aminés en solutions de KCl, leur constante K_{m2} peut être calculée dans la limites des erreurs expérimentales jusqu'à des valeurs de force ionique au moins de 1.0 mol kg^{-1}. Les valeurs de K_{m2} calculées par cette méthode sont aussi comparées aux valeurs suggérées dans la bibliographie.

Mots clés : dépendance à la force ionique, constante de dissociation stœchiométrique, équation de Debye–Hückel, potentiométrie, α-alanine, valine, leucine.

Received 14 January 2004. Published on the NRC Research Press Web site at http://canjchem.nrc.ca on 5 February 2005.

J.I. Partanen[1] and P.M. Juusola. Department of Chemical Technology, Lappeenranta University of Technology, P.O. Box 20, FIN-53851 Lappeenranta, Finland.
V. Verraes. Department of Chemical Technology, Lappeenranta University of Technology, P.O. Box 20, FIN-53851 Lappeenranta, Finland and KETEK Chemistry, Korpintie 8, FIN-67100, Kokkola, Finland.

[1]Corresponding author (e-mail: jpartane@lut.fi).

 doi: 10.1139/V04-164 © 2005 NRC Canada

Introduction

In this manuscript, we continue studies (ref. 1 and see refs. 1–17 therein) dealing with the thermodynamics of weak acid solutions. The purpose of these studies is to determine the stoichiometric dissociation constants (for example, the molality scale dissociation constants (K_m)) for salt solutions of different weak acids as reliably as possible from potentiometric titration data measured with glass electrodes. Additionally in these studies, calculation methods for experimental K_m values for weak acids are also developed for literature data measured with galvanic cells without a liquid junction. The used cells of this type (Harned cells) contain a hydrogen electrode and a silver–silver chloride electrode.

The other motivation for studies in this field is to develop equations for correlating experimental K_m values for different weak acids with the composition variables of salt solutions at 298.15 K and also at other temperatures (2, 3). In the present study, a Hückel equation is used for the analysis of potentiometric titration data for aq. KCl solutions of alanine, valine, and leucine, as well as Harned cell data for NaCl solutions of these three amino acids. Pitzer equations, which are nowadays most often used for interpretation of thermodynamic data, were not considered in this study because the necessary Pitzer parameters are missing for the component salts of sodium and potassium alaninate, valinate, and leucinate, and these parameters cannot be accurately determined solely from the existing data.

α-Alanine ($CH_3CH(NH_2)COOH$ = ala), valine ($(CH_3)_2CHCH(NH_2)COOH$ = val), and leucine ($(CH_3)_2CHCH_2CH(NH_2)COOH$ = leu) are simple aliphatic amino acids. Many studies have been published on the dissociation of these acids in aqueous solutions. A review of this research by IUPAC (4) shows, however, that only a few systematic studies on the influence of ionic strength I_m or other composition variables on K_{m1} and K_{m2} (i.e., on the first and second stoichiometric dissociation constant) of these three amino acids have been carried out. Systematic studies for other weak acids are also rare, and the existing studies in this field are usually concentrated on acids used as pH buffer substances. The existing systematic glass electrode studies have been considered in the reviews written by Daniele et al. (5) and Sastre de Vicente (6).

Stoichiometric dissociation constants of ala have been studied by Brandariz et al. (7) in aq. KNO_3 solutions (I_m = 0.3–1.6 mol kg^{-1}), by Fiol et al. (8) in NaCl solutions (I_m = 0.05–1.25 mol kg^{-1}), and by Fiol et al. (9) in artificial sea water (I_m = 0.087–0.62 mol kg^{-1}). K_{m1} and K_{m2} values for val have been investigated by Brandariz et al. (10) in KCl and KBr solutions (I_m = 0.1–1.7 mol kg^{-1}) and by Fiol et al. (11) in artificial sea water (I_m = 0.10–0.72 mol kg^{-1}). The existing systematic leu studies are the following: Rey et al. (12) in KNO_3 solutions (I_c = 0.025–0.5 mol dm^{-3}, I_c is the ionic strength on the molarity scale) and Fiol et al. (9) in artificial sea water (I_m = 0.087–0.62 mol kg^{-1}).

Harned cells have been used in the determination of the thermodynamic dissociation constants of amino acids. Though old, these studies are nowadays very important because the resulting K_a values at various temperatures are still the best values available for most of the amino acids. This is true also for ala, val, and leu. Nims and Smith (13) determined in this way the value 1.35×10^{-10} for the second thermodynamic dissociation constant (= K_{a2}) of ala at 298.15 K, and Smith et al. (14) determined the values of 1.36×10^{-10}, 1.91×10^{-10}, and 1.80×10^{-10} for K_{a2} of ala, val, and leu, respectively, at this temperature. In the present study, the calculation of these values is revised, and for the first time the K_{m2} values for the solutions of these three amino acids are calculated from the Harned cell data.

In the determination of the second dissociation constants of ala, val, and leu, the pH during titration was above 8, as in a recent glycine study (1). The solutions titrated had, therefore, to be protected against atmospheric carbon dioxide. This was achieved, as in the glycine study, by bubbling argon through the solution before titration. An argon blanket was thus formed over the solution and it protected the solution from absorption of CO_2. The glycine study (1) and the present study show that this experimental technique allows the determination of K_m values with a glass electrode for alkaline solutions almost with the same accuracy obtained by the best glass electrode techniques for acidic solutions.

Experimental

Potentiometric titrations of ala, val, and leu were carried out in aq. KCl solutions at 298.15 K. A series of KCl (pro analysi, Riedel–de Haën) solutions for each acid was prepared in RO-filtered water (Millipore). The concentrations in this series were as follows: 0.080, 0.160, 0.240, 0.320, 0.400, 0.500, 0.700, and 1.350 mol L^{-1}. Solutions at 0.0100 mol L^{-1} of L-ala (Aldrich), of L-val (Fluka), and of L-leu (Fluka) were prepared. A 0.1000 mol L^{-1} KOH (Titrisol, Merck) solution was also prepared in RO-filtered water (Millipore), and this solution was protected during titrations from atmospheric CO_2. The concentration of this solution was standardized using titrations of a potassium hydrogen phthalate solution, and the result of nine replicate determinations was (0.100 02 ± 0.000 03) mol L^{-1} where the standard deviation is given. The experimental data from the ala titrations are shown in Table 1, from the val titrations in Table 2, and from the leu titrations in Table 3.

The solutions for titration were prepared by mixing a volume of 100.0 cm^3 of a KCl solution, 25.00 cm^3 of water, and 10.00 cm^3 of the ala, val, or leu solution (for details, see ref. 15). The amino acid solutions were titrated with the KOH solution, and details of the titrations are given in ref. 1. The molalities were calculated from the experimental molarities (see below and ref. 15) using an equation reported by Harned and Owen (16) for this conversion in KCl solutions. To verify the stability of the measuring system, a titration of formic acid was carried out under similar conditions before the amino acid titration in each KCl solution. An argon gas blanket was also adjusted over the formic acid solutions before titration. From the results of these formic acid titrations, the K_m values were determined by the method suggested in ref. 17. This method is principally the same as the one used here for the three amino acids. The resulting K_m values are shown in Tables 1, 2, and 3 for ala, val, and leu cases, respectively. These K_m values from the formic acid titrations were very close to those calculated from the equations recommended in ref. 17 for K_m of this acid in KCl solutions (shown Table 1). The good agreement between the

© 2005 NRC Canada

Table 1. Data obtained from titrations of α-alanine in KCl solutions at different ionic strengths (I_m) with a base (KOH) solution at 298.15 K (series AKC).

Symbol	AKC1	AKC2	AKC3	AKC4	AKC5	AKC6	AKC7	AKC8
$I_m/(m^o)$[a]	0.0595	0.1193	0.1792	0.2393	0.2997	0.3755	0.5280	1.0331
V (cm^3)[b]				E (mV)[c]				
0.40	–148.2	–146.7	–146.0	–144.4	–145.6	–145.0	–143.2	–138.5
0.45	–152.5	–151.2	–150.6	–148.8	–149.9	–149.5	–147.4	–142.9
0.50	–156.7	–155.4	–154.6	–152.9	–154.0	–153.5	–151.5	–147.0
0.55	–160.7	–159.3	–158.6	–156.6	–158.0	–157.4	–155.2	–150.7
0.60	–164.4	–163.1	–162.2	–160.2	–161.5	–161.1	–158.8	–154.0
0.65	–167.8	–166.6	–165.6	–163.8	–165.1	–164.5	–162.2	–157.3
0.70	–171.1	–170.0	–169.0	–167.1	–168.3	–167.8	–165.6	–160.8
0.75	–174.4	–173.1	–172.1	–170.3	–171.5	–170.9	–168.6	–163.6
0.80	–177.6	–176.3	–175.2	–173.3	–174.5	–173.8	–171.5	–166.5
0.85	–180.5	–179.3	–178.2	–176.3	–177.6	–176.7	–174.4	–169.3
0.90	–183.5	–182.2	–181.1	–179.1	–180.4	–179.6	–177.1	–171.9
0.95	–186.3	–185.0	–183.9	–181.9	–183.2	–182.2	–179.9	–174.7
1.00	–189.0	–187.7	–186.4	–184.5	–185.8	–184.9	–182.4	–177.4
1.05	–191.6	–190.3	–189.1	–187.0	–188.3	–187.4	–184.9	–179.8
1.10	–194.0	–192.8	–191.5	–189.5	–190.7	–189.8	–187.2	–181.9
1.15	–196.4	–195.2	–193.9	–191.9	–193.0	–192.1	–189.5	–184.2
1.20	–198.8	–197.5	–196.2	–194.0	–195.3	–194.3	–191.6	–186.4
K(obsd)[d]	2.65	2.86	3.08	3.18	3.22	3.17	3.37	3.10
K(recd)[e]	2.73	3.00	3.16	3.25	3.32	3.36	3.36	3.05

[a] m^o = 1 mol kg^{-1}.
[b] Volume of titrant added.
[c] Measured cell potential difference.
[d] 10^4K_m for formic acid obtained from the titrations that were carried out before the amino acid titrations (see text).
[e] 10^4K_m for formic acid predicted by the equation recommended in ref. 17 for this acid in KCl solutions.

Table 2. Data obtained from titrations of valine in KCl solutions at different ionic strengths (I_m) with a base (KOH) solution at 298.15 K (series VKC).

Symbol	VKC1	VKC2	VKC3	VKC4	VKC5	VKC6	VKC7	VKC8
$I_m/(m^o)$[a]	0.0595	0.1193	0.1792	0.2393	0.2997	0.3755	0.5280	1.0331
V (cm^3)[b]				E (mV)[c]				
0.40	–139.3	–138.1	–137.5	–137.1	–137.2	–136.7	–136.9	–137.4
0.45	–143.9	–142.7	–142.1	–141.8	–141.9	–141.3	–141.5	–142.0
0.50	–148.3	–146.9	–146.4	–146.0	–146.2	–145.7	–145.8	–146.3
0.55	–152.3	–151.1	–150.5	–150.2	–150.2	–149.8	–149.9	–150.4
0.60	–156.2	–155.0	–154.4	–154.2	–154.2	–153.8	–153.9	–154.2
0.65	–160.1	–158.8	–158.2	–158.0	–158.0	–157.4	–157.7	–157.9
0.70	–163.7	–162.4	–161.9	–161.6	–161.6	–161.1	–161.3	–161.5
0.75	–167.3	–166.0	–165.4	–165.2	–165.1	–164.6	–164.7	–165.0
0.80	–170.7	–169.5	–168.8	–168.6	–168.6	–168.1	–168.1	–168.3
0.85	–174.1	–172.9	–172.2	–172.0	–172.0	–171.3	–171.4	–171.6
0.90	–177.6	–176.2	–175.4	–175.3	–175.1	–174.7	–174.8	–174.7
0.95	–180.8	–179.4	–178.7	–178.4	–178.3	–177.8	–177.9	–177.8
1.00	–183.9	–182.6	–181.8	–181.6	–181.5	–180.9	–180.9	–180.7
1.05	–186.9	–185.6	–184.8	–184.5	–184.4	–183.8	–183.8	–183.6
1.10	–189.8	–188.5	–187.6	–187.3	–187.2	–186.5	–186.5	–186.3
1.15	–192.5	–191.2	–190.3	–190.1	–190.0	–189.3	–189.2	–189.0
1.20	–195.2	–193.9	–192.9	–192.6	–192.6	–191.9	–191.8	–191.4
K(obsd)[d]	2.66	2.91	3.12	3.13	3.21	3.29	3.22	3.09

[a] m^o = 1 mol kg^{-1}.
[b] Volume of titrant added.
[c] Measured cell potential difference.
[d] 10^4K_m for formic acid obtained from the titrations that were carried out before the amino acid titrations (see text). The recommended K_m values for formic acid are given in Table 1.

© 2005 NRC Canada

Table 3. Data obtained from titrations of leucine in KCl solutions at different ionic strengths (I_m) with a base (KOH) solution at 298.15 K (series LKC).

Symbol	LKC1	LKC2	LKC3	LKC4	LKC5	LKC6	LKC7	LKC8
$I_m/(m^o)$[a]	0.0595	0.1193	0.1792	0.2393	0.2997	0.3755	0.5280	1.0331
V (cm^3)[b]				E (mV)[c]				
0.40	–142.4	–141.4	–141.1	–140.6	–140.4	–140.6	–139.9	–138.0
0.45	–147.0	–146.0	–145.7	–145.2	–145.1	–145.1	–144.4	–142.4
0.50	–151.3	–150.3	–150.0	–149.4	–149.3	–149.4	–148.7	–146.5
0.55	–155.3	–154.3	–154.0	–153.5	–153.3	–153.3	–152.6	–150.4
0.60	–159.2	–158.1	–157.9	–157.3	–157.1	–157.2	–156.5	–154.1
0.65	–163.0	–162.0	–161.5	–160.9	–160.7	–160.9	–160.0	–157.6
0.70	–166.5	–165.4	–165.0	–164.4	–164.3	–164.5	–163.5	–161.0
0.75	–170.0	–168.9	–168.5	–167.8	–167.7	–167.8	–166.9	–164.3
0.80	–173.4	–172.3	–171.9	–171.2	–171.0	–171.1	–170.3	–167.3
0.85	–176.5	–175.5	–175.1	–174.3	–174.2	–174.2	–173.3	–170.4
0.90	–179.8	–178.6	–178.3	–177.4	–177.2	–177.3	–176.4	–173.3
0.95	–182.9	–181.7	–181.2	–180.5	–180.3	–180.3	–179.3	–176.2
1.00	–185.9	–184.6	–184.2	–183.4	–183.2	–183.2	–182.2	–178.9
1.05	–188.7	–187.5	–187.0	–186.2	–186.0	–186.0	–184.9	–181.5
1.10	–191.4	–190.2	–189.7	–188.9	–188.7	–188.6	–187.4	–184.1
1.15	–194.0	–192.8	–192.3	–191.5	–191.3	–191.2	–190.1	–186.5
1.20	–196.5	–195.3	–194.8	–194.0	–193.7	–193.6	–192.5	–188.8
K(obsd)[d]	2.69	3.03	3.00	3.24	3.16	3.30	3.39	3.14

[a] m^o = 1 mol kg^{-1}.
[b] Volume of titrant added.
[c] Measured cell potential difference.
[d] $10^4 K_m$ for formic acid obtained from the titrations that were carried out before the amino acid titrations (see text). The recommended K_m values for formic acid are given in Table 1.

observed and recommended K_m values for this acid guarantees the quality of the new data for the amino acids considered.

Theory

In the Hückel method, the following equation is generally used for the calculation of the activity coefficient (γ) of a univalent ion i on the molality scale.

$$[1] \qquad \ln \gamma_i = -\frac{\alpha\sqrt{I_m}}{1 + B_i\sqrt{I_m}} + b_{i,MCl}\left(\frac{I_m}{m^o}\right)$$

where m^o = 1 mol kg^{-1}, I_m is the ionic strength on the molality scale, and α is the Debye–Hückel parameter at 298.15 K, equal to 1.174 44 (mol $kg^{-1})^{-1/2}$; see Archer and Wang (18). B_i and $b_{i,MCl}$ are the parameters that are dependent on ion i, and $b_{i,MCl}$ is also dependent on the salt MCl present in the system. Table 4 gives the parameter values determined previously for this equation and used here.

The thermodynamic value of the second dissociation constant (K_{a2}) of ala, val, or leu is given by

$$[2] \qquad K_{a2} = \frac{a_H a_A}{a_{HA}} = \left(\frac{\gamma_H \gamma_A}{\gamma_{HA}}\right) K_{m2}$$

where a is the activity, HA refers to amino acid molecules or zwitterions, and A to the anion resulted from the amino acid, i.e., to alaninate, valinate, or leucinate. It is assumed that the activity coefficient of the neutral species HA follows the Kirkwood equation (22, 23)

$$[3] \qquad \ln \gamma_{HA} = b_{HA}\left(\frac{I_m}{m^o}\right)$$

for zwitterions, where b_{HA} is a constant. The second stoichiometric dissociation constant of the amino acid, K_{m2} in eq. [2], is defined by $K_{m2} = m_H m_A/(m_{HA} m^o)$. The following equation can be derived from eqs. [1]–[3] for K_{m2} of these acids in aq. NaCl or KCl solutions:

$$[4] \qquad \ln K_{m2,MCl} = \ln K_{a2} + \alpha\sqrt{I_m}\left(\frac{1}{1 + B_H\sqrt{I_m}} + \frac{1}{1 + B_A\sqrt{I_m}}\right) - [b_{H,MCl} + (b_{A,MCl} - b_{HA,MCl})]\left(\frac{I_m}{m^o}\right)$$

where MCl refers to either NaCl or KCl. Here, the values of B_H = 1.25 (mol $kg^{-1})^{-1/2}$, B_A = 2.2 (mol $kg^{-1})^{-1/2}$, $b_{H,NaCl}$ = 0.238, and $b_{H,KCl}$ = 0.178 were used in this equation (see Table 4). The thermodynamic dissociation constants (K_{a2}) and the parameters $b_{A,KCl} - b_{HA,KCl}$ (= q_{KCl}) and $b_{A,NaCl} - b_{HA,NaCl}$ (= q_{NaCl}) were determined from the new potentiometric titration data and from the Harned cell data for the amino acids considered. The value of B_A = 2.2 (mol $kg^{-1})^{-1/2}$ was determined previously for glycine species (1), and it also applies to alaninate, valinate, and leucinate ions (see below).

© 2005 NRC Canada

Table 4. Ion parameters for the Hückel equation (eq. [1]) at 298.15 K and results of the regression analysis obtained by eq. [12] from the present glass electrode data and the hydrogen electrode data of Nims and Smith (13) and Smith et al. (14).

Parameter	H^+	Cl^-	Alaninate ion	Valinate ion	Leucinate ion
$10^{10}K_{a2}$[a]			1.29	1.89	1.68
pK_{a2}[b]			9.888	9.723	9.773
$10^{10}K_{a2}$(obsd)[c]			1.295±0.013	1.894±0.009	1.685±0.011
$p[K_{a2}(obsd)]$[c]			9.888±0.004	9.723±0.002	9.773±0.003
$10^{10}K_{a2}$(obsd)[d]			1.32		
$p[K_{a2}(obsd)]$[d]			9.880±0.002		
$10^{10}K_{a2}$(obsd)[e]			1.35	1.93	1.80
$p[K_{a2}(obsd)]$[e]			9.871±0.005	9.715±0.003	9.744±0.004
B(mol $kg^{-1})^{-1/2}$	1.25[f]	1.25[f]	2.2[g]	2.2[g]	2.2[g]
b_{LiCl}	0.298[h]	0.298[h]			
b_{NaCl}	0.238[f]	0.238[f]			
b_{KCl}	0.178[h]	0.178[h]			
q_{KCl}			0.46[i]	0.35[i]	0.45[i]
q_{KCl}(obsd)[j]			0.46±0.02	0.348±0.011	0.450±0.014
q_{NaCl}(obsd)[k]			0.79±0.07		
q_{NaCl}(obsd)[l]			1.3±0.2	0.15±0.15	0.5±0.2

[a]Recommended value of the second thermodynamic dissociation constant for the corresponding acid.
[b]$pK_{a2} = -\log K_{a2}$.
[c]Experimental value of K_{a2} of the corresponding amino acid (see also footnote *b*). It was estimated from the K_{m2} values obtained from glass electrode data (Tables 1–3) in this study, and the standard deviation is also given.
[d]Experimental value of K_{a2} of α-alanine (see also footnote *b*). It was estimated from the K_{m2} values obtained from hydrogen electrode data (Table 5) of Nims and Smith (13), and the standard deviation is also given.
[e]Experimental value of K_{a2} of of the corresponding amino acid (see also footnote *b*). It was estimated from the K_{m2} values obtained from hydrogen electrode data (Tables 6–8) of Smith et al. (14), and the standard deviation is also given.
[f]Determined from Harned cell data (19).
[g]Determined for glycine species from Harned cell data (20). The same value is used here for the anions considered.
[h]Determined from Harned cell data (21).
[i]Recommended in this study ($q = b_A - b_{HA}$).
[j]Estimated from the K_{m2} values obtained from glass electrode data (Tables 1–3) in this study, and the standard deviation is also given ($q = b_A - b_{HA}$).
[k]Estimated from the K_{m2} values obtained in this study from hydrogen electrode data (Table 5) of Nims and Smith (13), and the standard deviation is also given ($q = b_A - b_{HA}$).
[l]Estimated from the K_{m2} values obtained in this study from hydrogen electrode data (Tables 6–8) of Smith et al. (14), and the standard deviation is also given ($q = b_A - b_{HA}$).

The thermodynamic value of the ionic product of water ($K_{a,w}$) is defined by

$$[5] \qquad K_{a,w} = \frac{\gamma_H \gamma_{OH} m_H m_{OH}}{a_w (m^o)^2} = \frac{g_w m_H m_{OH}}{(m^o)^2}$$

where OH refers to hydroxide ions, w refers to water, and the quantity g_w is defined by $g_w = \gamma_H\gamma_{OH} / a_w$. Harned and Hamer (24) determined the value 1.008×10^{-14} for $K_{a,w}$ at 298.15 K. In a previous study (1), the following equation containing only one salt-dependent parameter (b_w) was used for $\ln g_w$ for KCl and NaCl solutions at 298.15 K:

$$[6] \qquad \ln g_w = \ln\left(\frac{\gamma_H\gamma_{OH}}{a_w}\right) = -\frac{2\alpha\sqrt{I_m}}{1 + B_H\sqrt{I_m}} + b_w\left(\frac{I_m}{m^o}\right)$$

For NaCl solutions, the value of parameter b_w is 0.412 (obtained in ref. 1 from the Harned cell data of Harned and Mannweiler (25)), and eq. [6] is valid up to an ionic strength of about 3 mol kg^{-1}. For KCl solutions, the value of this parameter is 0.482 (obtained from the data of Harned and Hamer (24)), and eq. [6] is valid in this case up to an I_m of about 2 mol kg^{-1}.

Results

Redetermination of the second thermodynamic dissociation constants of amino acids from Harned cell data

Nims and Smith (13) and Smith et al. (14) have measured cell potential differences (cpd = E) for ala, val, and leu solutions using cells of the type

$$[7] \qquad \text{Pt(s)} \mid H_2(g, f = 101.325\ \text{kPa}) \mid \text{HA(aq, } m_a\text{)}, \text{NaA(aq, } m_b\text{)}, \text{NaCl(aq, } m_s\text{)} \mid \text{AgCl(s)} \mid \text{Ag(s)}$$

where f is the fugacity. In the actual cell used (13, 14), the amino acid was partially neutralized by sodium hydroxide and the composition shown in cell [7] resulted from this neutralization. The ionic strength of the solutions varied from 0.010 to 0.151 mol kg^{-1}, and the molalities m_a, m_b, and m_s were approximately equal. Nims and Smith (13) measured 22 ala solutions, Smith et al. (14) seven ala, six val,

© 2005 NRC Canada

Table 5. Experimental K_{m2} values for α-alanine obtained from data measured by Nims and Smith (13) on cell [7] and those predicted by the present Hückel model.

I_m (mol kg^{-1})	$10^{10}K_m$(obsd)	$10^{10}K_m$(pred)	10^3e(pK_{m2})[a]
0.010 34	1.71	1.57	–36.1
0.011 79	1.67	1.59	–21.2
0.012 52	1.64	1.59	–11.5
0.015 24	1.67	1.62	–12.7
0.015 35	1.66	1.62	–9.9
0.019 61	1.68	1.66	–5.5
0.021 41	1.71	1.67	–9.3
0.030 12	1.73	1.73	+1.1
0.030 38	1.73	1.73	–0.4
0.032 16	1.75	1.74	–2.8
0.043 90	1.79	1.80	+1.4
0.045 63	1.81	1.81	–2.0
0.047 06	1.80	1.81	+3.5
0.061 58	1.84	1.86	+4.4
0.061 83	1.86	1.86	+1.1
0.063 66	1.86	1.87	+2.8
0.089 52	1.90	1.93	+8.2
0.094 40	1.94	1.94	+0.5
0.095 33	1.92	1.95	+5.1
0.114 78	1.95	1.98	+5.5
0.125 37	1.98	1.99	+2.7
0.151 21	1.98	2.02	+8.5

[a]Calculated by eq. [27].

and five leu solutions. The cell potential differences (E) of cell [7] are given by

$$[8] \qquad E = E^{o} - \frac{RT}{F}\ln\left(\frac{\gamma_H\gamma_{Cl}m_Hm_{Cl}}{(m^{o})^2}\right)$$

where Cl refers to chloride ions, and E^o is the standard cpd. A value of 0.222 50 V was used for E^o (see Harned and Ehlers (26)). In addition, these cpd data were updated by using the conversion factor 1 V = 1.000 34 int. V. The data in these sets were used to determine K_{a2} as follows.

The observed K_{m2} value was first calculated from each experimental point by using eq. [6] and the equations

$$[9] \qquad \ln\left(\frac{m_H}{m^{o}}\right) = \frac{(E^{o} - E)F}{RT} - \ln\left(\frac{\gamma_H\gamma_{Cl}m_{Cl}}{m^{o}}\right)$$

$$[10] \qquad m_{OH} = \frac{K_{a,w}(m^{o})^2}{g_w m_H}$$

$$[11] \qquad K_{m2} = \frac{m_H(m_b - m_{OH})}{(m_a + m_{OH})m^{o}}$$

For the activity coefficients of hydrogen and chloride ions in eq. [9], eq. [1] was used with the parameters given in Table 4. The experimental K_{m2} values calculated in this way from the data of Nims and Smith (13) and Smith et al. (14) are presented in Tables 5–8.

The values for K_{a2} of the three amino acids were determined from the K_{m2} values in Tables 5–8 using the equation:

Table 6. Experimental K_{m2} values for α-alanine obtained from data measured by Smith et al. (14) on cell [7] and those predicted by the present Hückel model.

I_m (mol kg^{-1})	$10^{10}K_{m2}$(obsd)	$10^{10}K_{m2}$(pred)	10^3e(pK_{m2})[a]
0.019 51	1.70	1.66	–9.4
0.020 26	1.74	1.66	–19.2
0.027 69	1.75	1.72	–8.6
0.030 84	1.76	1.73	–6.7
0.040 17	1.77	1.78	+3.2
0.060 15	1.83	1.86	+7.2
0.080 42	1.89	1.91	+5.5

[a]Calculated by eq. [27].

Table 7. Experimental K_{m2} values for valine obtained from data measured by Smith et al. (14) on cell [7] and those predicted by the present Hückel model.

I_m (mol kg^{-1})	$10^{10}K_m$(obsd)	$10^{10}K_{m2}$(pred)	10^3e(pK_{m2})[a]
0.018 46	2.47	2.42	–8.3
0.030 13	2.61	2.54	–11.5
0.039 98	2.70	2.62	–12.1
0.047 87	2.76	2.67	–14.4
0.059 82	2.87	2.74	–20.6
0.093 47	2.97	2.88	–13.8

[a]Calculated by eq. [27].

Table 8. Experimental K_{m2} values for leucine obtained from data measured by Smith et al. (14) on cell [7] and those predicted by the present Hückel model.

I_m (mol kg^{-1})	$10^{10}K_{m2}$(obsd)	$10^{10}K_{m2}$(pred)	10^3 e(pK_{m2})[a]
0.018 01	2.30	2.14	–30.4
0.020 40	2.35	2.17	–35.4
0.027 63	2.37	2.24	–25.2
0.036 20	2.46	2.30	–30.0
0.070 86	2.64	2.46	–29.6

[a]Calculated by eq. [27].

$$[12] \qquad \ln K_{m2,MCl} - \alpha\sqrt{I_m}\left(\frac{1}{1 + B_H\sqrt{I_m}} + \frac{1}{1 + B_A\sqrt{I_m}}\right) = y = \ln K_{a2} - (b_{H,MCl} + q_{MCl})\left(\frac{I_m}{m^{o}}\right)$$

where, in this case, MCl is NaCl. In preliminary calculations, it was observed that the value of B_A = 2.2 (mol kg^{-1})$^{-1/2}$ applies also to the three amino acids studied. This value has been determined for glycine species from the large Harned cell data sets of King (27) in ref. 20. Equation [12] represents an equation of the straight-line y vs. (I_m/m^o). K_{a2} can be obtained from the intercept of the line with the y-axis, and the slope of the straight line is $b_{H,NaCl} + q_{NaCl}$. The resulting K_{a2} values for the amino acids are shown in Table 4. As can also be seen in this table, each value obtained for q_{NaCl} of the amino acid species has a wide confidence interval, and thus is not very reliable. This is due to the fact that the Harned cell data are only for dilute solutions and the two

© 2005 NRC Canada

Debye–Hückel terms on the left hand side of eq. [12] are dominant in these solutions and the slope term on the right hand side is thus small. Therefore, the q_{NaCl} values obtained from Harned cell data were not used here.

Determination of the experimental values for the stoichiometric dissociation constants from potentiometric glass electrode data

In ref. 1, the following equation was derived for the molality of hydroxide ions (m_{OH}) at each point of the glycine titrations

$$[13] \quad m_{OH}^2 + \left(m_t - m_b + \frac{K_{a,w}m^o}{g_w K_{m2}}\right)m_{OH} - \frac{K_{a,w}m^o}{g_w K_{m2}}m_b = 0$$

The same equation can now be used for the ala, val, and leu titration data in Tables 1–3. In this equation, m_b is the molality of KOH, in the solution titrated and $m_b = c_b V / w_1$, where c_b is the concentration, V is the volume of the base solution added in the titration, and w_1 is the mass of water in the solution titrated. In eq. [13], m_t is the total molality of amino acid in the solution titrated, and $m_t = n_t/w_1$ where n_t is the total amount of this substance. Equation [13] is of the second degree in the molality of OH^- ions and can therefore be easily solved.

For the determination of K_{m2} of ala, val, and leu from the titration data, a glass electrode parameter (E_0) was estimated from each titration data set in addition to this dissociation constant. In the present titrations, the following equation is valid (see ref. 1) for the cell potential differences (E) measured with the glass electrode cell

$$[14] \quad E = E_0 + \frac{RT}{F}\ln\left(\frac{m_H}{m^o}\right)$$

where E_0 is constant during each titration at a constant ionic strength and must be estimated from the titration data.

K_{m2} and E_0 were calculated for each amino acid data set of N points presented in Tables 1–3 by the following set of equations:

$$[15] \quad \sum_{i=1}^{N}(E_i - E_{pred,i}) = 0$$

$$[16] \quad \ln\left(\frac{x_i}{m^o}\right) = \frac{(E_i - E_0)F}{RT}$$

$$[17] \quad o_i = \frac{K_{a,w}(m^o)^2}{g_w x_i}$$

$$[18] \quad K_{m2,i} = \frac{x_i(m_{b,i} - o_i)}{\left(\frac{n_t}{w_{1,i}} - m_{b,i} + o_i\right)m^o}$$

$$[19] \quad K_{m2} = \frac{\left(\sum_{i=1}^{N} K_{m2,i}\right)}{N}$$

$$[20] \quad y_i = \left(\frac{n_t}{w_{1,i}} - m_{b,i} + \frac{K_{a,w}m^o}{g_w K_{m2}}\right)^2 + 4m_{b,i}\left(\frac{K_{a,w}m^o}{g_w K_{m2}}\right)$$

$$[21] \quad m_{OH,i} = \frac{\left[\sqrt{y_i} - \left(\frac{n_t}{w_{1,i}} - m_{b,i} + \frac{K_{a,w}m^o}{g_w K_{m2}}\right)\right]}{2}$$

$$[22] \quad m_{H,i} = \frac{K_{a,w}(m^o)^2}{g_w m_{OH,i}}$$

$$[23] \quad E_{pred,i} = E_0 + \left(\frac{RT}{F}\right)\ln\left(\frac{m_{H,i}}{m^o}\right)$$

where x_i and o_i are the experimental molalities of hydrogen and hydroxide ions at point i, respectively. The results from the calculations of the titration data of Tables 1–3 are shown in Tables 9 (for ala), 10 (for val), and 11 (for leu).

Determination of the thermodynamic dissociation constants for amino acids and the activity parameters for the amino acid species from the experimental K_{m2} values obtained from titration data

The activity parameter q_{KCl} (= $b_{A,KCl} - b_{HA,KCl}$) and K_{a2} were determined from the new titration data. The experimental K_{m2} values shown in Tables 9–11 were used in these determinations with eq. [12] where, in this case, MCl is KCl. The results from these linear regressions are shown in Table 4.

The K_{a2} estimates from the titration data and from the Harned cell data (see Table 4) for ala and val agree quite well. On the other hand, the K_{a2} estimates for leu do not agree. The K_{a2} value 1.80×10^{-10} was obtained for leu from the data of Smith et al. (14), whereas the K_{a2} value 1.68×10^{-10} resulted from the new titration data. The new potentiometric K_{a2} values are recommended here because of the following arguments: (1) Good agreement was obtained between glass electrode and Harned cell values of K_{a2} for ala and val (see Table 4); (2) the glass electrode data for leu seem to be as reliable as those for ala and val; (3) the glass electrode K_{a2} value for leu was based on eight experimental potentiometric K_{m2} values (each of them was based on 17 titration points) instead of the five K_{m2} values from which the Harned cell value for K_{a2} was estimated (see Table 8). The recommended values are thus 1.29×10^{-10} (ala), 1.89×10^{-10} (val), and 1.68×10^{-10} (leu). The resulting values of q_{KCl} for the three amino acids and their standard deviations are also shown in Table 4.

Discussion

The Hückel parameters recommended above were tested with the titration data presented in Tables 1–3. The recommended K_{m2} values given in Tables 9–11 were used in these tests. Parameter E_0 for eq. [14] was calculated for each data set by using eqs. [20]–[22] and the following equations:

$$[24] \quad E_{0,i} = E_i - \left(\frac{RT}{F}\right)\ln\left(\frac{m_{H,i}}{m^o}\right)$$

© 2005 NRC Canada

Table 9. Results calculated from the titration data of α-alanine (see Table 1) (series AKC).

Symbol	AKC1	AKC2	AKC3	AKC4	AKC5	AKC6	AKC7	AKC8
I_m (mol kg^{-1})	0.0595	0.1193	0.1792	0.2393	0.2997	0.3755	0.5280	1.0331
$10^{10}K_{m2}$(obsd)[a]	1.86	2.06	2.07	2.08	2.13	2.06	1.96	1.67
$10^{10}K_{m2}$(recd)[b]	1.86	2.00	2.06	2.09	2.09	2.07	2.00	1.63
E_0 (mV)[c]	410.64	409.82	409.81	411.18	409.69	410.37	413.18	422.13

[a]Second stoichiometric dissociation constant of alanine determined from the titration data by means of the method described in the text.
[b]Second stoichiometric dissociation constant of alanine calculated by eq. [4] with $K_{a2} = 1.29 \times 10^{-10}$ and with the recommended activity parameters.
[c]Value of the glass electrode parameter E_0 used in the calculation of the errors for Fig. 1. It was determined by requiring that the sum of errors in the data set is zero (i.e., by eqs. [20]–[22], [24], and [25]).

Table 10. Results calculated from the titration data of valine (see Table 2) (series VKC).

Symbol	VKC1	VKC2	VKC3	VKC4	VKC5	VKC6	VKC7	VKC8
I_m (mol kg^{-1})	0.0595	0.1193	0.1792	0.2393	0.2997	0.3755	0.5280	1.0331
$10^{10}K_{m2}$(obsd)[a]	2.72	2.98	3.06	3.17	3.19	3.19	3.14	2.67
$10^{10}K_{m2}$(recd)[b]	2.75	2.97	3.08	3.14	3.16	3.17	3.11	2.68
E_0 (mV)[c]	411.44	410.55	410.12	409.76	409.45	409.85	410.04	413.21

[a]Second stoichiometric dissociation constant of valine determined from the titration data by means of the method described in the text.
[b]Second stoichiometric dissociation constant of valine calculated by eq. [4] with $K_{a2} = 1.89 \times 10^{-10}$ and with the recommended activity parameters.
[c]Value of the glass electrode parameter E_0 used in the calculation of the errors for Fig. 2. It was determined by requiring that the sum of errors in the data set is zero (i.e., by eqs. [20]–[22], [24], and [25]).

Table 11. Results calculated from the titration data of leucine (see Table 3) (series LKC).

Symbol	LKC1	LKC2	LKC3	LKC4	LKC5	LKC6	LKC7	LKC8
I_m (mol kg^{-1})	0.0595	0.1193	0.1792	0.2393	0.2997	0.3755	0.5280	1.0331
$10^{10}K_{m2}$(obsd)[a]	2.40	2.60	2.70	2.72	2.76	2.75	2.66	2.13
$10^{10}K_{m2}$(recd)[b]	2.43	2.61	2.69	2.72	2.73	2.71	2.62	2.15
E_0 (mV)[c]	410.88	409.90	409.25	409.40	409.33	409.24	410.63	417.43

[a]Second stoichiometric dissociation constant of leucine determined from the titration data by means of the method described in the text.
[b]Second stoichiometric dissociation constant of leucine calculated by eq. [4] with $K_{a2} = 1.68 \times 10^{-10}$ and with the recommended activity parameters.
[c]Value of the glass electrode parameter E_0 used in the calculation of the errors for Fig. 3. It was determined by requiring that the sum of errors in the data set is zero (i.e., by eqs. [20]–[22], [24], and [25]).

$$[25] \qquad E_0 = \frac{\left(\sum_{i=1}^{N} E_{0,i}\right)}{N}$$

The resulting E_0 values are included in Tables 9–11. The results of the tests are shown as error plots in Figs. 1*a* (ala), 2*a* (val), and 3*a* (leu) where the cpd error defined by

$$[26] \qquad e_E = E(\text{observed}) - E(\text{predicted})$$

is presented for each data set as a function of the added volume of the KOH solution. The error plots in these graphs are random and almost all of the errors are comparable to the resolution of the pH meter (i.e., to 0.1 mV). Therefore, the titration data presented in Tables 1–3 support quite well the calculation method.

From each point of the titrations presented in Tables 1–3, an experimental value of K_{m2} can also be calculated from eqs. [16]–[18] with the E_0 values shown in Tables 9–11. All of these values are compared with the recommended values in Figs. 1*b*, 2*b*, and 3*b*. In these graphs, the pK_m (= –log(K_m)) errors, defined by

$$[27] \qquad e(\text{p}K_{m2}) = \text{p}K_{m2}(\text{observed}) - \text{p}K_{m2}(\text{predicted})$$

are presented as a function of the added volume of the KOH solution. All pK_{m2} errors in Figs. 1*b*, 2*b*, and 3*b* are smaller than ±0.015 and they form a random pattern in almost every data set. The maximum error can also be compared to the conventional pK_m error of 0.06 suggested by Albert and Serjeant (28). These considerations also reveal how valuable the new activity coefficient models are.

The Harned cell data considered above were also compared with the results obtained using recommended models for ala, val, and leu. These data were measured in NaCl solutions, but the recommended values of q_{KCl} must be used for q_{NaCl} in these calculations because of the lack of better values (see Table 4). On the other hand, the solutions used to obtain these data were rather dilute and thus specific interactions between species in those were probably not very important. The predicted K_{m2} values and the pK_{m2} errors defined by eq. [27] are presented in Tables 5–8 as a function

© 2005 NRC Canada

Fig. 1. (*a*) The difference between the observed and predicted cpd values (e_E in eq. [26]), and (*b*) the difference between the observed and predicted pK_{m2} values (e(pK_{m2}) in eq. [27]) as a function of the titrant volume in the titrations of α-alanine with the KOH solution. The predicted cpd for (*a*) was calculated by eqs. [4]–[6], [13], and [14] using the thermodynamic value of 1.29×10^{-10} for the second dissociation constant, the recommended activity parameters, and the value of the glass electrode parameter E_0 shown in Table 9. The observed K_{m2} value for (*b*) was calculated from each titration point by eqs. [5], [6], [16]–[18] with the glass electrode parameter shown in Table 9, and the predicted K_{m2} value was calculated by eq. [4]. Symbols of the different sets are shown in the graphs.

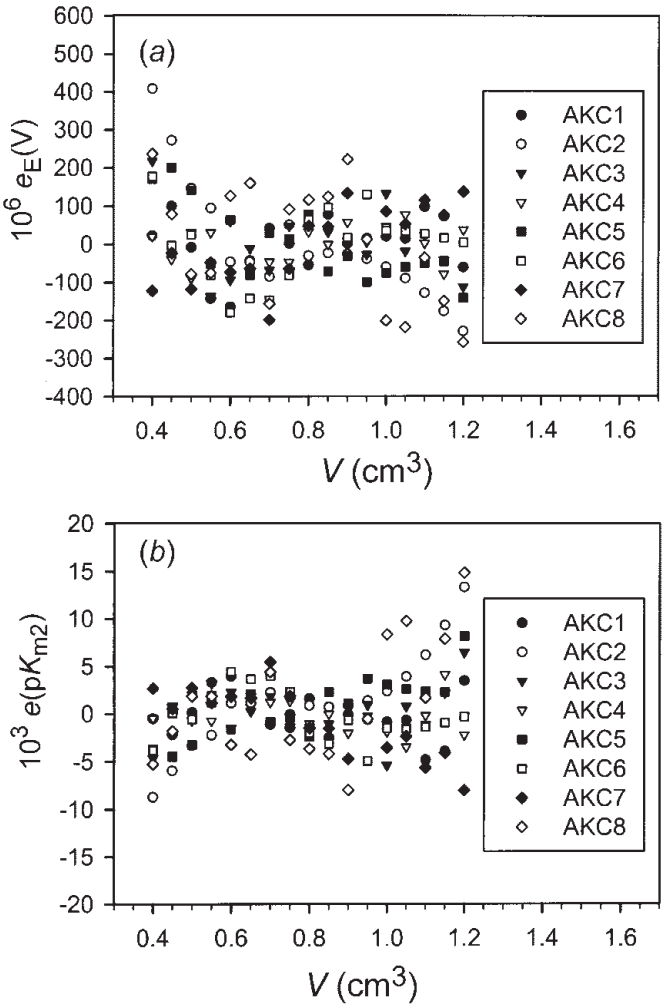
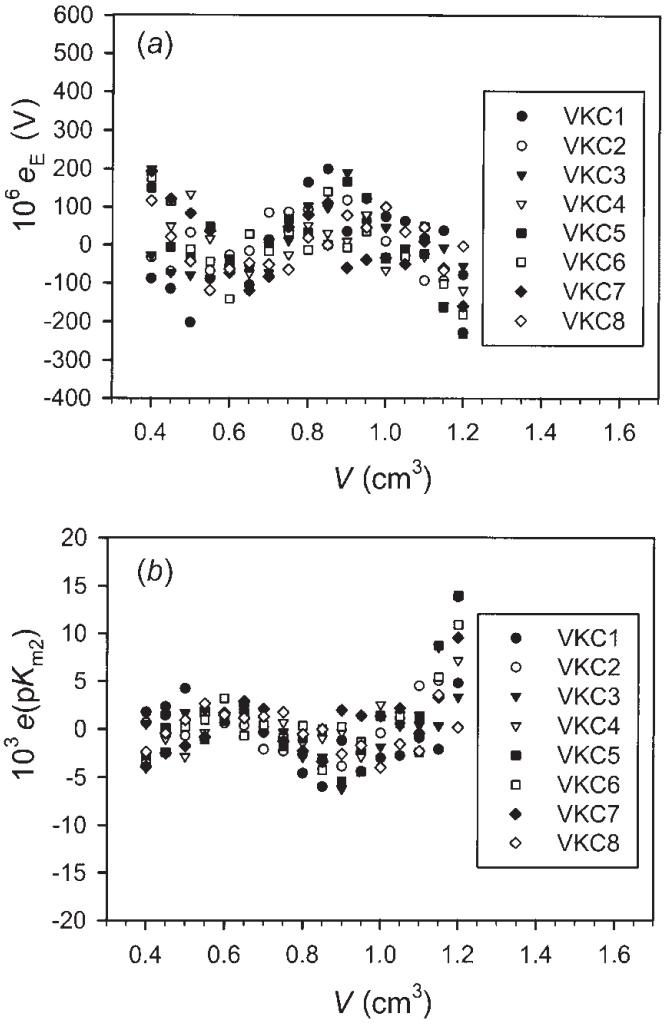


Fig. 2. (*a*) The difference between the observed and predicted cpd values (e_E in eq. [26]), and (*b*) the difference between the observed and predicted pK_{m2} values (e(pK_{m2}) in eq. [27]) as a function of the titrant volume in the titrations of valine with the KOH solution. The predicted cpd for (*a*) was calculated by eqs. [4]–[6], [13], and [14] using the thermodynamic value of 1.89×10^{-10} for the second dissociation constant, the recommended activity parameters, and the value of the glass electrode parameter E_0 shown in Table 10. The observed K_{m2} value for (*b*) was calculated from each titration point by eqs. [5], [6], [16]–[18] with the glass electrode parameter shown in Table 10, and the predicted K_{m2} value was calculated by eq. [4]. Symbols of the different sets are shown in the graphs.



of the ionic strength of the solution. The recommended K_{a2} values were used in these calculations. The errors in these tables also support quite well the new models for ala and val, but not for leu (see Table 8 and the discussion above).

Brandariz et al. (10) have determined K_{m1} and K_{m2} values for val in aq. KCl and KBr solutions at 298.15 K using potentiometric titrations. The experimental K_{m2} values in KCl solutions were tested with the present Hückel model. The results are shown as error plots in Fig. 4. In this figure, the pK_{m2} errors defined by eq. [27] are presented as a function of the ionic strength of the solution. The results in this figure show that the experimental data support only satisfactorily the new model. It can be seen by comparing Figs. 2*b* and 4 that the precision of the data of Brandariz et al. (10) is less than that of the present study. Therefore, it seems that more reliable K_{m2} values are obtained by using the new model.

Table 12 shows the recommended K_{m2} values for ala, val, and leu in aq. KCl solutions at 298.15 K at rounded ionic strengths. These values apply to the case where KCl alone determines the ionic strength of the solution. The K_{m2} values were calculated using eq. [4] with the recommended K_{a2} val-

© 2005 NRC Canada

Fig. 3. (*a*) The difference between the observed and predicted cpd values (e_E in eq. [26]), and (*b*) the difference between the observed and predicted pK_{m2} values (e(pK_{m2}) in eq. [27]) as a function of the titrant volume in the titrations of leucine with the KOH solution. The predicted cpd for (*a*) was calculated by eqs. [4]–[6], [13], and [14] using the thermodynamic value of 1.68×10^{-10} for the second dissociation constant, the recommended activity parameters, and the value of the glass electrode parameter E_0 shown in Table 11. The observed K_{m2} value for (*b*) was calculated from the titration points by eqs. [5], [6], [16]–[18] with the glass electrode parameter shown in Table 11, and the predicted K_{m2} value was calculated by eq. [4]. Symbols of the different sets are shown in the graphs.

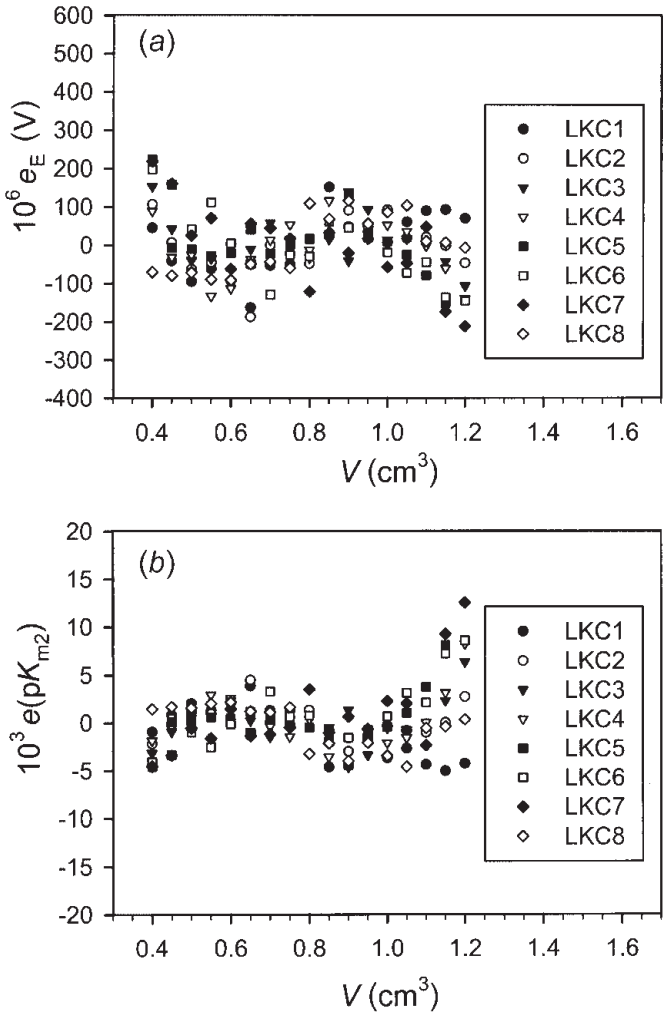
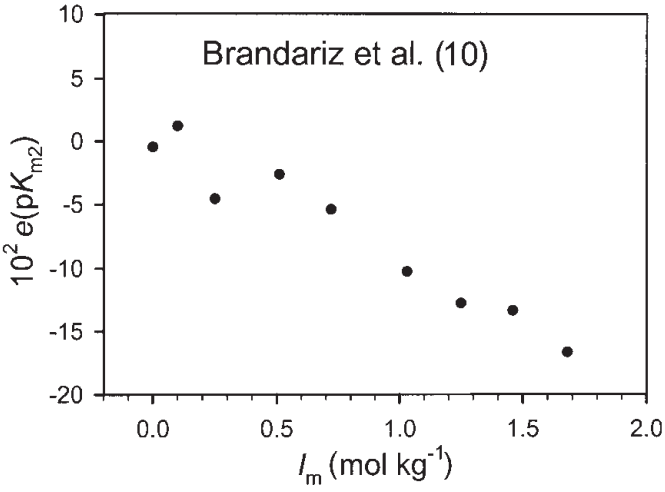


Table 12. The second stoichiometric dissociation constant (K_{m2}) at 298.15 K for α-alanine (ala), valine (val), and leucine (leu) as a function of the ionic strength (I_m) in aq. KCl solutions.

$I_m/(m^o)^a$	$10^{10}K_{m2}$(ala)	1010 K_{m2}(val)	$10^{10}K_{m2}$(leu)
0	1.29	1.89	1.68
0.01	1.57	2.30	2.04
0.02	1.66	2.44	2.17
0.03	1.73	2.55	2.26
0.04	1.79	2.63	2.33
0.05	1.83	2.70	2.38
0.06	1.87	2.75	2.43
0.07	1.90	2.80	2.47
0.08	1.92	2.84	2.51
0.09	1.95	2.88	2.54
0.10	1.97	2.91	2.56
0.15	2.04	3.03	2.66
0.20	2.07	3.10	2.70
0.30	2.09	3.16	2.73
0.40	2.06	3.16	2.70
0.50	2.02	3.12	2.64
0.70	1.89	2.98	2.47
1.00	1.66	2.71	2.18

[a] I_m is the same as m_{KCl} and m^o = 1 mol kg^{-1}.

Fig. 4. The difference (e(pK_{m2}) in eq. [27]) between the pK_{m2} values determined by Brandariz et al. (10) for valine in KCl solutions and those predicted by the recommended Hückel method (i.e., by eq. [4] with $K_{a2} = 1.89 \times 10^{-10}$ and with the recommended activity parameters) as a function of I_m.



ues and with the recommended parameter values shown in Table 4.

In Table 13, we have collected the parameters for the Hückel equations determined previously for the calculation of K_m values of various weak acids in aq. NaCl, KCl, and LiCl solutions at 298.15 K. The new parameter values for alaninate, valinate, and leucinate species in this table are close to the values obtained previously (1) for glycinate species. The present values for the difference of q_{KCl} (= $b_{A,KCl} - b_{HA,KCl}$) are also rather close to the b values of anions resulting from the light aliphatic carboxylic acids in KCl solutions. Therefore, the second stoichiometric dissociation constants of ala, val, and leu depend on the ionic strength in these solutions qualitatively, in the same way as the dissociation constants of aliphatic acids. In dilute solutions, the Debye–Hückel terms in the Hückel equations of ions (see eq. [1]) are dominant, and a strong dependence was observed (see Table 12). At molalities higher than about 0.05 mol kg^{-1}, the influence of these terms decreases and the terms taking into account the specific interactions between

© 2005 NRC Canada

Table 13. Parameter values for the calculation of K_m values of weak acids (H_2A^+ or HA) by the Hückel method (eq. [4]) in aq. KCl, NaCl, and LiCl solutions at 298.15 K (for activity coefficients of ionic species H_2A^+ and A^-, eq. [1] is used, and of neutral species HA, eq. [3] is used, see also Table 4).

Parameter	K_a[a]	B (mol kg^{-1})$^{-1/2}$	q_{KCl}	q_{NaCl}	q_{LiCl}	Ref.
$HCOO^-$	1.82×10^{-4}	1.4	0.308[b]	0.189[b]		17
CH_3COO^-	1.76×10^{-5}	1.6	0.308[b]	0.189[b]	–0.068[b]	21
$CH_3CH_2COO^-$	1.35×10^{-5}	1.7	0.308[b]	0.189[b]		29
$CH_3CH_2CH_2COO^-$	1.52×10^{-5}	2.0	0.26[b]	0.11[b]		30
CH_2OHCOO^-	1.47×10^{-4}	1.4	0.308[b]	0.04[b]	–0.068[b]	21, 31
$CH_3CH_2OHCOO^-$	1.38×10^{-4}	1.5	0.308[b]	0.189[b]	–0.24[b]	32
$C_6H_5COO^-$	6.33×10^{-5}	1.25	0.25[b]	0.09[b]		33
$^+NH_3CH_2COOH$	4.46×10^{-3}	2.2		–0.039[c]		20
$NH_2CH_2COO^-$	1.65×10^{-10}	2.2	0.39[d]	0.39[d]		1
Alaninate ion[e]	1.29×10^{-10}	2.2	0.46[d]			
Valinate ion[e]	1.89×10^{-10}	2.2	0.35[d]			
Leucinate ion[e]	1.68×10^{-10}	2.2	0.45[d]			

[a]The thermodynamic dissociation constant of the corresponding acid.
[b]$q_{MCl} = b_{A,MCl}$, where M = K^+, Na^+, or Li^+.
[c]$q_{NaCl} = b_{HA,NaCl} - b_{H2A,NaCl}$.
[d]$q_{MCl} = b_{A,MCl} - b_{HA,MCl}$, where M = K^+ or Na^+.
[e]Determined in the present study.

ions (the linear correction term in eq. [1]) become more important and will gradually overcome the effect of the Debye–Hückel terms.

Acknowledgements

J.P. and P.J. are indebted to the Research Foundation of Lappeenranta University of Technology (the Lahja and Lauri Hotinen's Fund) for financial support.

References

1. J.I. Partanen, P.M. Juusola, P.O. Minkkinen, and V. Verraes. Can. J. Chem. **81**, 1462 (2003).
2. J.I. Partanen and A.K. Covington. J. Chem. Eng. Data, **48**, 797 (2003).
3. J.I. Partanen and A.K. Covington. J. Chem. Eng. Data, **49**, 394 (2004).
4. I. Sóvágó, T. Kiss, and A. Gergely. Pure Appl. Chem. **65**, 1029 (1993).
5. P.G. Daniele, C. De Stefano, C. Foti, and S. Sammartano. Curr. Top. Solution Chem. **2**, 253 (1997).
6. M.E. Sastre de Vicente. Curr. Top. Solution Chem. **2**, 157 (1997).
7. I. Brandariz, S. Fiol, R. Herrero, T. Vilariño, and M. Sastre de Vicente. J. Chem. Eng. Data, **38**, 531 (1993).
8. S. Fiol, I. Brandariz, and M. Sastre de Vicente. Talanta, **42**, 797 (1995).
9. S. Fiol, I. Brandariz, R.F. Herrero, T. Vilariño, and M.E. Sastre de Vicente. J. Chem. Eng. Data, **40**, 117 (1995).
10. I. Brandariz, F. Arce, X.L. Armesto, F. Penedo, and M. Sastre de Vicente. Monatsh. Chem. **124**, 249 (1993).
11. S. Fiol, T. Vilariño, R. Herrero, M.E. Sastre de Vicente, and F. Arce. J. Chem. Eng. Data, **43**, 393 (1998).
12. F. Rey, A. Varela, J.M. Antelo, and F. Arce. J. Chem. Eng. Data, **34**, 35 (1989).
13. L.F. Nims and P.K. Smith. J. Biol. Chem. **101**, 401 (1933).
14. P.K. Smith, A.C. Taylor, and E.R.B. Smith. J. Biol. Chem. **122**, 109 (1937–1938).
15. J.I. Partanen, P.M. Juusola, and P.O. Minkkinen. Acta Chem. Scand. **49**, 163 (1995).
16. H.S. Harned and B.B. Owen. The physical chemistry of electrolytic solutions. 3rd ed. Reinhold Publishing Corp., New York. 1958. p. 725.
17. J. Partanen and P.M. Juusola. J. Chem. Eng. Data, **45**, 110 (2000)
18. D.G. Archer and P. Wang. J. Phys. Chem. Ref. Data, **19**, 371 (1990).
19. J. Partanen, P. Juusola, and P. Minkkinen. Acta Polytech. Scand. Chem. Technol. Ser. **231**, 1 (1995).
20. J.I. Partanen. Ber. Bunsenges. Phys. Chem. **102**, 855 (1998).
21. J.I. Partanen. Acta Chem. Scand. **52**, 985 (1998).
22. J.G. Kirkwood. J. Chem. Phys. **2**, 351 (1934).
23. J.G. Kirkwood. Chem. Rev. **24**, 233 (1939).
24. H.S. Harned and W.J. Hamer. J. Am. Chem. Soc. **55**, 2194 (1933).
25. H.S. Harned and G.E. Mannweiler. J. Am. Chem. Soc. **57**, 1873 (1935).
26. H.S. Harned and R.W. Ehlers. J. Am. Chem. Soc. **54**, 1350 (1932).
27. E.J. King. J. Am. Chem. Soc. **67**, 2178 (1945).
28. A. Albert and E.P. Serjeant. *In* The determination of ionization constants. A laboratory manual. 3rd ed. Chapman and Hall, London. 1984.
29. J.I. Partanen, P.M. Juusola, and P.O. Minkkinen. Acta Chem. Scand. **53**, 547 (1999).
30. J.I. Partanen, P.M. Juusola, and P.O. Minkkinen. Fluid Phase Equilib. **173**, 135 (2000).
31. J.I. Partanen, P.M. Juusola, and P.O. Minkkinen. Z. Phys. Chem. (Muenchen), **215**, 515 (2001).
32. J.I. Partanen, P.M. Juusola, and P.O. Minkkinen. Fluid Phase Equilib. **204**, 245 (2003).
33. J.I. Partanen, P.M. Juusola, and P.O. Minkkinen. J. Solution Chem. **30**, 443 (2001).

© 2005 NRC Canada

New cycloaddition of diarylazines with 1,2-dehydrobenzene, 1,1,2,2-tetracyanoethylene, and dibenzoylacetylene — Facile synthesis of acridinones, pyrazolidine, and pyridazine derivatives

Ashraf A. Aly and Mohsen A.-M. Gomaa

Abstract: Diarylazines were reacted with 1,2-dehydrobenzene (*o*-benzyne) to give 10-amino-3-substituted-9(10*H*)-acridinones. On the other hand, 1,1,2,2-tetracyanoethylene was reacted with diarylazines through Michael addition to yield 5-arylpyrazolidine-3,3,4,4-tetracarbonitriles. On reacting the same azines with dibenzoylacetylene, pyridazine derivatives were obtained via a Diels–Alder reaction.

Key words: diarylazines, 1,2-dehydrobenzene, tetracyanoethylene, dibenzoylacetylene.

Résumé : Les diarylazines réagissent avec le 1,2-dihydrobenzène (*o*-benzyne) pour conduire à la formation des 10-amino-9(10*H*)-acridones substituées en position 3. Par ailleurs, le 1,1,2,2-tétracyanoéthylène réagit avec les diarylazines par le biais d'une addition de Michael qui conduit à la formation de 5-arylpyrazolidine-3,3,4,4-tétracarbonitriles. Les mêmes azines, par réaction avec le dibenzoylacétylène, conduisent à la formation de dérivés de la pyridazine par le biais d'une réaction de Diels–Alder.

Mots clés : diarylazines, 1,2-dihydrobenzène, tétracyanoéthylène, dibenzoylacétylène.

[Traduit par la Rédaction]

Introduction

The reaction of diarylazines with various dienophiles has been valuable in the field of heterocyclic compounds (1–3). Azines derived from aromatic aldehydes undergo the so-called criss-cross addition with 2 equiv. of the dienophile to yield 1,5-diaza-bicyclo[3,3,0]octane of pyrazole derivatives (2, 3). On the basis that the reactions of azines with dienophiles are found to be susceptible to electronic and steric factors, various types of intramolecular rearrangements have been observed (4–6). Therefore, the chemistry of azines towards various dienophiles still needs more light shed on it because of the abnormality that sometimes accompanies their reactions. In this context, we aim to develop efficient, facile, and elegant syntheses of various heterocycles of biological interest, which basically depend upon cycloaddition reactions (7–11). As an extension of this strategy, we have now explored the chemistry of the aromatic azines towards some dienophiles such as 1,2-dehydrobenzene (*o*-benzyne), 1,1,2,2-tetracyanoethylene, and dibenzoylacetylene, which are known to undergo various types of cycloadditions (12–14).

Received 9 April 2004. Published on the NRC Research Press Web site at http://canjchem.nrc.ca on 5 February 2005.

A.A. Aly[1] and M.A.-M. Gomaa. Chemistry Department, Faculty of Science, El-Minia University, 61519, El-Minia, Egypt.

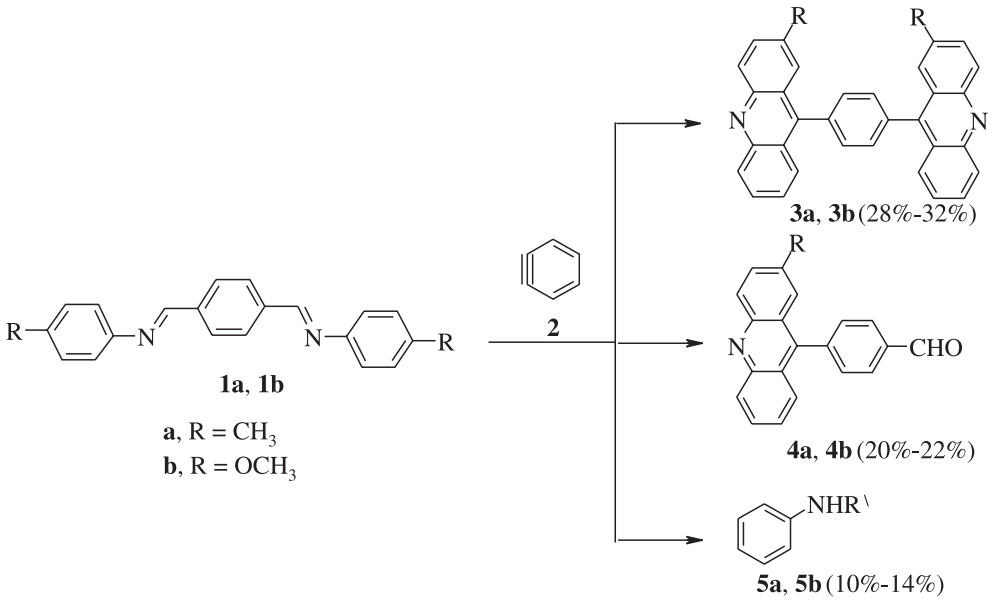
[1]Corresponding author (e-mail: ashraf160@yahoo.com).

Results and discussion

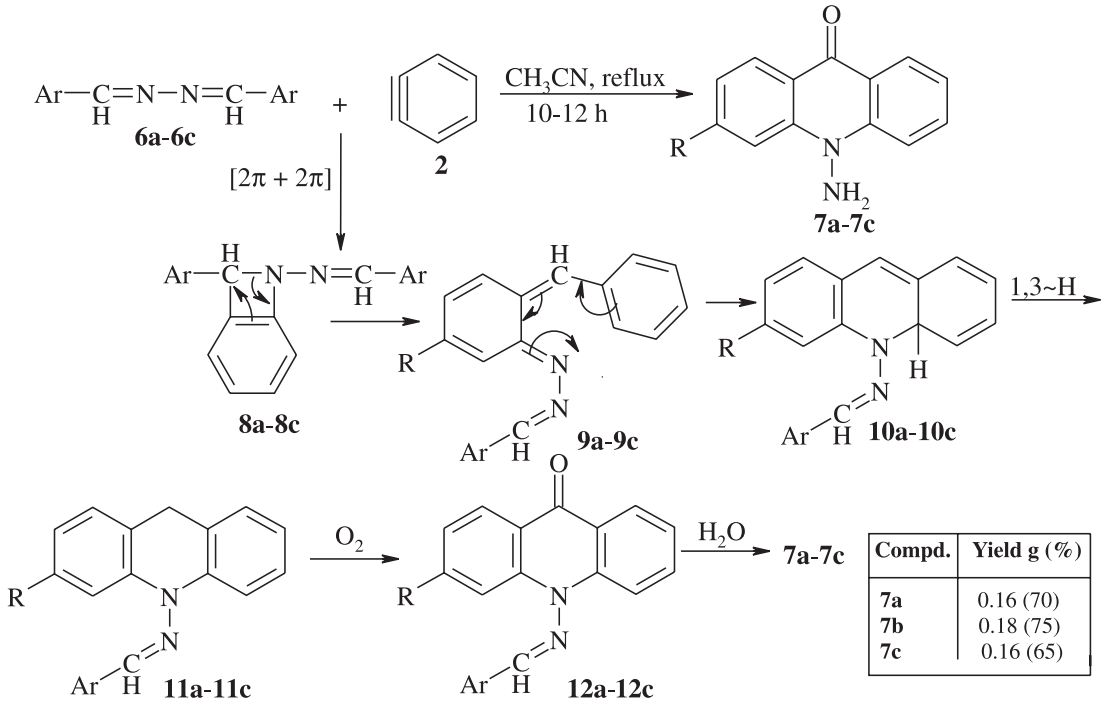
Some years ago, we examined the reaction of *N*,*N*′-bis-(aryl)-benzene-1,4-diyldimethylidene-diamines (**1a**, **1b**) with 1,2-dehydrobenzene (*o*-benzyne, **2**). The reaction gave 1,4-bis(2′-substituted-acridine-10-yl)benzenes (**3a**, **3b**), 10-(4′-formylphenyl)-2-substituted-acridines (**4a**, **4b**), and *N*-phenyl-arylamines (**5a**, **5b**) (Scheme 1). The reaction mechanism was described via [2π + 2π] cycloaddition between 2 mol of **2** and the azomethine groups in **1a** and **1b** (Scheme 1) (7). The formation of compounds **4a** and **4b** was explained as being due to the hydrolysis of one azomethine during the course of the reaction (Scheme 1) (7). 1,2-Dehydrobenzene (*o*-benzyne, **2**), which was generated by diazotization of 1,2-anthranilic acid, (7, 8, 11, 15) reacted with **6a**–**6c** (16) to afford **7a**–**7c** in yields of 65%–75% (Scheme 2). Mechanistically, the reaction of **2** with imines is undoubtedly based initially upon [2π + 2π] cycloaddition forming a benzazetidine ring (7, 8). Thus, we postulated that cycloaddition occurred between 1 mol of **2** and one azomethine group in **6a**–**6c** to form cycloadducts **8a**–**8c**. The benzazetidines **8a**–**8c** were converted by ring opening into their valence tautomers **9a**–**9c**. Subsequently, ring closure of **9a**–**9c** via electrocyclization, followed by a 1,3-hydrogen shift, would give the dehydroacridines **11a**–**11c**. One can expect that the acridinones **12a**–**12c** were obtained by aerial oxidation of **11a**–**11c**. Presumably, during chromatographic purification, the imine group is hydrolyzed to yield, ultimately, 10-amino-3-substituted-9(10*H*)-acridinones **7a**–**7c** (Scheme 2). It is worthwhile to mention that the reactions of

 doi: 10.1139/V04-170 © 2005 NRC Canada

Scheme 1.



Scheme 2. Synthesis of 10-amino-3-substituted-9(10*H*)-acridinones.

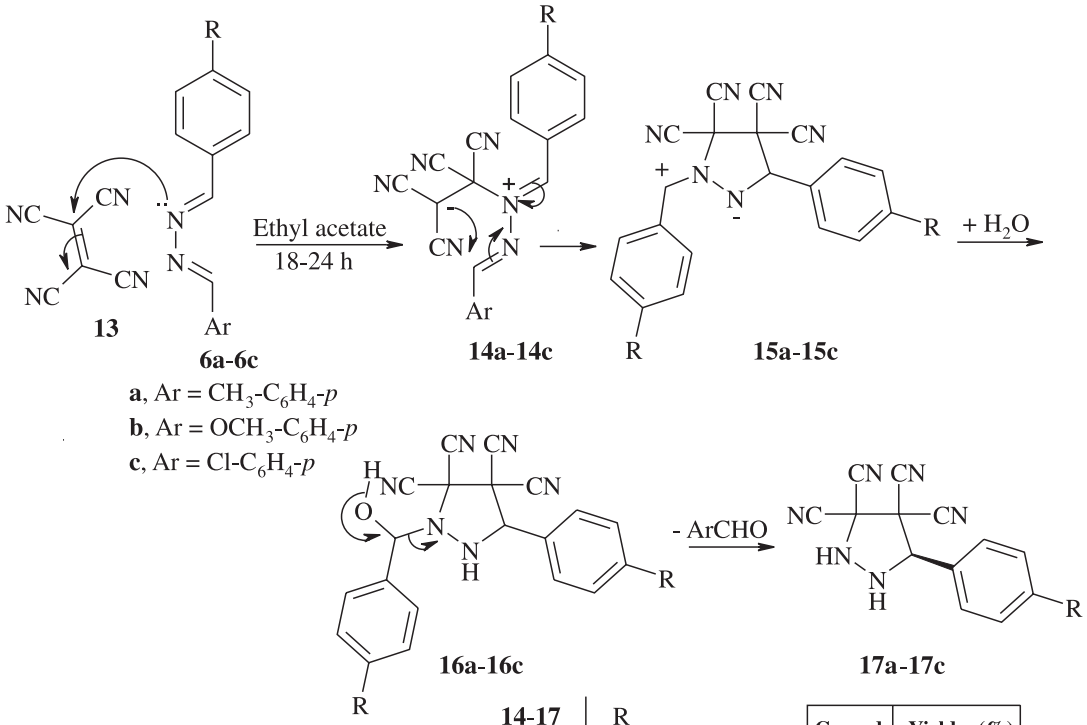


Compd.	Yield g (%)
7a	0.16 (70)
7b	0.18 (75)
7c	0.16 (65)

2 with diarylazines possessing electron-donating substitutents in the arylidene groups (such as **6a** and **6b**) yielded **7a** and **7b** in higher yields than **7c**. NMR spectra as well as COSY H-H and C-H spectral data of compounds **7a**–**7c** supported their structural proof. Additionally, NMR spectra of the isolated compounds **7a**–**7c** were compared with those of the known 3-substituted acridinones (17). Accordingly, some distinctive δ values of the protons and carbons of **7a**–**7c** were easily analyzed. For example, the ^{13}C NMR spectrum of **7a** showed 14 signals; seven signals were attributed to aromatic CH, one signal at higher field was identified as a methyl carbon atom, and six quaternary carbon atoms, one of them resonating downfield at δ = 178.80 was assigned as the carbonyl carbon atom C-9. In the IR spectrum of **7a**, absorptions at 3250 and 1695 cm^{-1} were assigned to the NH_2 and carbonyl groups, respectively. The importance of the

© 2005 NRC Canada

Scheme 3. Synthesis of 5-aryl-pyrazolidine-3,3,4,4-tetracarbonitrile derivatives.



14-17	R
a	CH_3
b	OCH_3
c	Cl

Compd.	Yield g (%)
17a	0.18 (68)
17b	0.21 (74)
17c	0.19 (66)

acridines' synthesis comes from their medical and industrial value (17, 18). Moreover, *N*-substituted acridinones have anticancer activity (19). Therefore, work is still directed towards utilization of facile methods such as microwave to synthesize acridine derivatives (20).

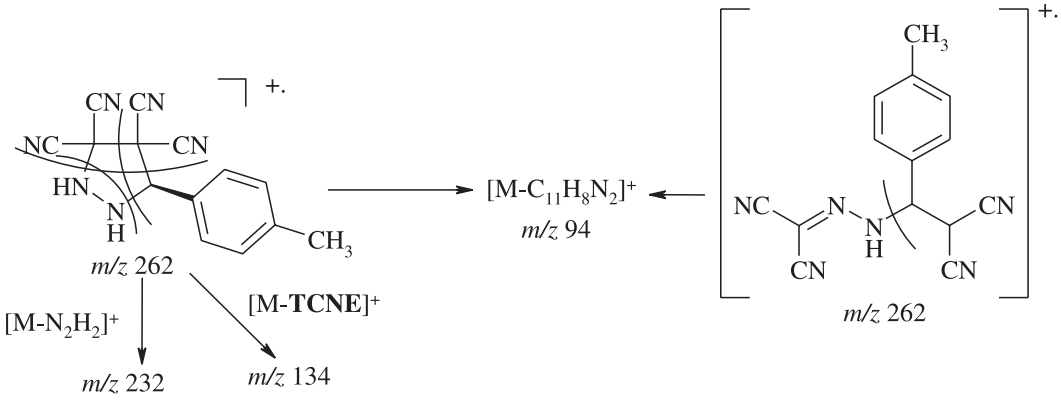
Recently, the synthesis of various pyrazolidines has been reported via 1,3-dipolar cycloaddition of azomethine-iminoylidene derivatives (21). However, on reacting **6a–6c** with 1,1,2,2-tetracyanoethylene (TCNE, **13**) in ethyl acetate, we obtained 5-aryl-pyrazolidine-3,3,4,4-tetracarbonitriles **17a–17c** (Scheme 3). Herein, the reaction can be described as being due to Michael addition followed by cyclization to form intermediate iminium ions **15a–15c**. Addition of moisture to **15a–15c** would, therefore, produce **16a–16c** (Scheme 3). Finally, elimination of arylaldehydes from **16a–16c** yielded **17a–17c** (Scheme 3). The structural assignment of **17a–17c** is unequivocally confirmed by mass, IR, ^{1}H NMR, and ^{13}C NMR, as well as elemental analysis. For example, mass spectra and elemental analysis of **17a** established its molecular formula as $C_{14}H_{10}N_6$. Particularly interesting is the ^{1}H NMR spectrum of **17a**, which showed a singlet at δ_H = 4.60 corresponding to H-5. The NH–NH proton signals were superimposed upon the aromatic ones at δ_H = 6.20–6.50. The ^{13}C NMR spectrum of **17a** showed four signals at δ_C = 20.90, 52.00, 54.60, and 60.40, which were assigned to the CH_3 group, C-4, C-3, and C-5, respectively. The ^{13}C DEPT 135/90 spectrum of **17a** showed a signal with a positive amplitude at δ_C = 60.40 confirming the existence of the methine carbon atom C-5. Conclusive evidence for the proposed structure of compounds **17a–17c** was obtained from COSY H-H and C-H experiments. The molecular modeling (MM2) (22) of **17a**, as an example, indicated the presence of its most stable geometric form in which the phenyl group in the same plane of the formed five-member ring as plotted in Scheme 3. Therefore, compounds **17a–17c** were identified as 5-aryl-pyrazolidine-3,3,4,4-tetracarbonitriles.

Earlier reports (23, 24) investigated the fragmentation patterns of 3,3,4,4,5-pentasubstituted pyrazolidines. Similar fragmentation processes were observed in the mass spectroscopy of compounds **17a–17c**. For example, the mass spectrum of **17a** showed a molecular ion at *m*/*z* 262 (Fig. 1). The fragmentation pattern of this compound also includes heterocycle cleavages with loss of $C_{11}H_8N_2^+$ (*m*/*z* = 94), which might indicate the existence of $M^{+\cdot}$ in its linear form. Figure 1 indicates the most expected fragmentation patterns of the mass spectrum in **17a**. For example, the ion peaks at *m*/*z* = 232 and 134 appeared in the mass spectrum of **17a** corresponding to the fragmentation patterns [$M^+ - N_2H_4$] and [M^+ – TCNE], respectively. Fragmentation through the N—N bond cleavage also appears, but less intensely (*m*/*z* 246, Fig. 1).

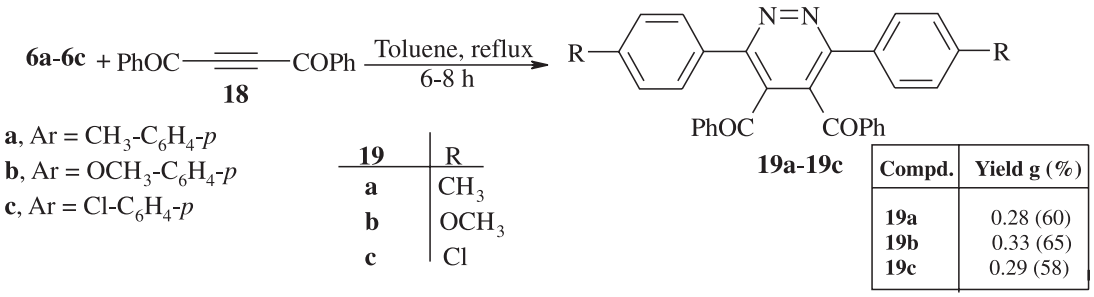
Surprisingly, reaction of **6a–6c** with dibenzoylacetylene (DBA, **18**) produced pyridazine derivatives **19a–19c** (Scheme 4). Apparently, the reaction between **6a–6c** and **18** occurred via [4π + 2π] cycloaddition followed by aromatization. The symmetrical structure of **19a–19c** was easily deduced from mass and NMR spectra (see Experimental). For example, mass spectroscopy of compound **19a**

© 2005 NRC Canada

Fig. 1. Specific fragmentation paths of compund **17a**.



Scheme 4. Synthesis of 3,6-diaryl-4,5-dibenzoyl-pyridazines.



Compd.	Yield g (%)
19a	0.28 (60)
19b	0.33 (65)
19c	0.29 (58)

showed a strong fragment ion at *m/z* 234 (60%) corresponding to half the molecular weight of this compound. The ^{13}C NMR spectrum of **19a** showed 16 signals, half the number of carbon atoms existing in the molecular formula. The carbonyl group, C-3, and C-4 appeared at δ_C = 190.20, 154.00, and 140.90, respectively (see Experimental). In the case of **19b**, the ^{13}C NMR spectrum revealed five characteristic carbon signals at δ_C = 188.00, 153.90, 148.20, 142.00, and 50.90 corresponding to the carbonyl group, C-3, Ar-C-OMe, C-4, and OCH_3, respectively. The obtained products **19a**–**19c** constitute a new class of pyridazine derivatives. Pyridazines have been reported to have antihypertensive activity (25), in addition to analgesic and anti-inflammatory activities (26).

Experimental

Melting points are uncorrected. NMR spectra were recorded in $CDCl_3$ or DMSO-d_6 on a Bruker AM 400 instrument (400.134 MHz for ^1H, 100.60 MHz for ^{13}C). The chemical shifts (δ) were measured relative to internal TMS. Coupling constants were expressed in Hz. Elemental analyses were performed by the Microanalysis Center of the Institut für Anorganische Chemie, Technische Universität Braunschweig. Mass spectra were obtained on a Finnigan MAT 8430 spectrometer at 70 eV. IR spectra were obtained on a Nicolet 320 FT-IR using KBr pellets. UV spectra were recorded on a Beckman UV 5230 spectrophotometer. For preparative layer chromatography (TLC), glass plates (20 cm × 48 cm) were covered by a slurry of silica gel PF254 (Merck) and air dried.

Reaction of 6a–6c with 2 — Synthesis of 10-amino-3-substituted-acridin-9(10*H*)-ones (7a–7c)

Benzenediazonium carboxylate was prepared by a published procedure (7, 8, 11, 14). Under a nitrogen atmosphere, 2 mmol of **2** precursor was slowly added to the stirred and refluxed solutions of **6a**–**6c** (2 mmol) in dry acetonitrile (250 mL) over 1 h. The reaction mixture was stirred at reflux until the consumption of the starting materials (monitored by TLC) in 10–12 h. The solvent was concentrated and the residue was filtered off. The precipitate was washed with dichloromethane (250 mL). The filtrate was concentrated in vacuum and the residue was separated by PLC using toluene as the eluant. The first migrating zones contained the arylaldehyde derivatives R_f 0.80 (CH_2Cl_2), which were identified by TLC comparison to authentic samples and were isolated in 3%–7% yields. This was followed by the zones containing compounds **7a**–**7c**. All zones were extracted with acetone and the recovered products were recrystallized from the stated solvents.

*10-Amino-3-methylacridin-9(10*H*)-one (7a)*

Pale green crystals (0.16 g, 70%), mp 200 °C (CH_3COCH_3). R_f 0.4 (CH_2Cl_2). IR ν (KBr, cm^{-1}): 3250 (NH_2), 3050–3018 (Ar-CH), 2980–2890 (ali.-CH), 1695 (CO). ^1H NMR ($CDCl_3$): 2.20 (3H, s, CH_3), 4.60 (2H, br s, NH_2), 5.92 (1H, dd, H-5, *J* = 8.4, 1.4 Hz), 6.00 (1H, d, H-4, *J* = 1.3 Hz), 7.30–7.50 (2H, m, H-6 and H-7), 7.60 (1H, dd, H-2, *J* = 8.2, 1.3 Hz), 7.84 (1H, dd, H-8, *J* = 8.4, 1.4 Hz), 8.15 (1H, d, *J* = 8.4 Hz, H-1). ^{13}C NMR ($CDCl_3$): 20.90 (CH_3), 118.40 (CH-5), 120.00 (CH-4), 126.60, 128.00, 129.40, 130.80 (Ar-CH), 132.40, 133.90 (Ar-C), 134.90 (Ar-CH), 136.00, 136.90, 138.20 (Ar-C), 178.80 (CO). MS *m/z* (%): 224 [M^+] (100), 208 (36), 192 (24), 180 (32), 102 (24),

© 2005 NRC Canada

76 (20). Anal. calcd. for $C_{14}H_{12}N_2O$ (224.258) %: C 74.98, H 5.39, N 12.49; found: C 74.80, H 5.30, N 12.40.

10-Amino-3-methoxyacridin-9(10H)-one (7b)

Green crystals (0.18 g, 75%), mp 180–182 °C (EtOH). R_f 0.6 (CH_2Cl_2). IR ν (KBr, cm^{-1}): 3260 (NH_2), 3056–3020 (Ar-CH), 2960–2870 (ali.-CH), 1700 (CO). ^1H NMR ($CDCl_3$): 3.70 (3H, s, OCH_3), 4.70 (2H, br s, NH_2), 6.10–6.30 (2H, m, H-4 and H-5), 7.36–7.54 (2H, m, H-6 and H-7), 7.80–8.00 (2H, m, H-2 and H-8), 8.24 (1H, d, J = 8.4 Hz, H-1). ^{13}C NMR ($CDCl_3$): 50.00 (OCH_3), 118.60 (CH-5), 121.00 (CH-4), 126.80, 128.40, 130.00, 131.20 (Ar-CH), 132.80, 134.40 (Ar-C), 135.20 (Ar-CH), 136.80, 137.20, 138.40 (Ar-C), 178.20 (CO). MS m/z (%): 240 [M^+] (100), 210 (30), 192 (28), 180 (30), 102 (20), 108 (18), 76 (20). Anal. calcd. for $C_{14}H_{12}N_2O_2$ (240.257) %: C 69.99, H 5.03, N 11.66; found: C 69.80, H 5.10, N 11.60.

10-Amino-3-chloroacridin-9(10H)-one (7c)

Yellowish-green crystals (0.16 g, 65%), mp 178–180 °C (acetone). R_f 0.3 (CH_2Cl_2). IR ν (KBr, cm^{-1}) 3230 (NH_2), 3040–3010 (Ar-CH), 1690 (CO). ^1H NMR ($CDCl_3$): 4.40 (2H, br s, NH_2), 5.80 (1H, dd, H-5, J = 8.4, 1.3 Hz), 5.92 (1H, d, H-4, J = 1.3 Hz), 7.20–7.40 (2H, m, H-6 and H-7), 7.56 (1H, dd, H-2, J = 8.4, 1.4 Hz), 7.74 (1H, dd, H-8, J = 8.4, 1.4 Hz), 8.10 (1H, d, J = 1.3 Hz, H-1). ^{13}C NMR ($CDCl_3$): 118.00 (CH-5), 119.20 (CH-4), 126.30, 127.60, 129.00, 130.00 (Ar-CH), 132.00, 133.20 (Ar-C), 134.30 (Ar-CH), 135.80, 136.60, 138.00 (Ar-C), 176.90 (CO). MS *m*/*z* (%): 246 [M + 2] (42), 244 [M^+] (100), 208 (32), 210 (34), 192 (20), 194 (26), 180 (28), 102 (24), 76 (24). Anal. calcd. for $C_{13}H_9ClN_2O$ (244.676) %: C 63.81, H 3.71, Cl 14.49, N 11.45; found: C 63.70, H 3.70, Cl 14.40, N 11.40.

Reaction of 6a–6c with 13 — Synthesis of 5-aryl-pyrazolidine-3,3,4,4-tetracarbonitriles (17a–17c)

To a stirred solution of **6a**–**6c** (1 mmol) in ethyl acetate (50 mL), a solution of **13** (0.13 g, 1 mmol) in ethyl acetate (20 mL) was added at room temperature over 30 min. The color of the reaction mixture changed from yellow to green during this period. The reaction mixture was stirred at ambient temperature for 18–24 h. The reaction was monitored by TLC until consumption of the starting materials (the color of the mixture became dark green). The reaction mixture was concentrated in vacuo and the residue was separated by PLC using toluene – ethyl acetate (10:1) as the eluent. The first migrating zones contained arylaldehydes. The second migrating zones contained compounds **17a**–**17c**, which were recrystallized from the solvents stated.

5-(4′-Methylphenyl)-pyrazolidine-3,3,4,4-tetracarbonitrile (17a)

Buff crystals (0.18 g, 68%), mp 220–222 °C (CH_3CN). R_f 0.2 (CH_2Cl_2). IR ν (KBr, cm^{-1}): 3240–3220 (NH), 3040–3010 (Ar-CH), 2990–2860 (ali.-CH), 2222–2210 (CN). ^1H NMR (DMSO-d_6): 2.38 (3H, s, CH_3), 4.60 (1H, s, H-5), 6.20–6.50 (4H, m, Ar-H and NH), 6.80–7.10 (2H, m, Ar-H). ^{13}C NMR (DMSO-d_6): 20.90 (CH_3), 52.00 (C-4), 54.60 (C-3), 60.40 (CH-5), 113.20 (2CN), 114.00 (2CN), 126.60 (2Ar-CH), 132.60 (2Ar-CH), 133.60 (Ar-C-CH_3), 135.40 (ArCH-3). MS *m*/*z* (%): 262 [M^+] (100), 246 (18), 232 (24), 220 (16), 192 (22), 134 (28), 94 (24). Anal. calcd. for $C_{14}H_{10}N_6$ (262.270) %: C 64.11, H 3.84, N, 32.04; found: C 64.38, H 3.90, N 32.10.

5(4′-Methoxyphenyl)-pyrazolidine-3,3,4,4-tetracarbonitrile (17b)

Pale brown crystals (0.21 g, 74%), mp 246–248 °C (EtOH). R_f 0.5 (CH_2Cl_2). IR ν (KBr, cm^{-1}): 3230–3216 (NH), 3050–3012 (Ar-CH), 2980–2850 (ali.-CH), 2210 (CN). ^1H NMR ($CDCl_3$): 3.90 (3H, s, OCH_3), 4.72 (1H, s, H-5), 6.10 (1H, br s, NH), 6.30–6.54 (3H, m, Ar-H and NH), 6.82–7.14 (2H, m, Ar-H). ^{13}C NMR ($CDCl_3$): 50.90 (OCH_3), 54.00 (C-4), 54.80 (C-3), 61.00 (CH-5), 113.90 (2CN), 114.60 (2CN), 127.40 (2Ar-CH), 134.00 (2Ar-CH), 136.90 (ArCH-3), 153.00 (Ar-C-OMe). MS *m*/*z* (%): 278 [M^+] (100), 246 (22), 232 (28), 220 (18), 192 (30), 134 (26), 94 (28). Anal. calcd. for $C_{14}H_{10}N_6O$ (278.269) %: C 60.43, H 3.62, N 30.20; found: C 60.30, H 3.70, N 30.10.

5(4′-Chlorophenyl)-pyrazolidine-3,3,4,4-tetracarbonitrile (17c)

Buff crystals (0.19 g, 66%), mp 200–202 °C (EtOH). R_f 0.4 (CH_2Cl_2). IR ν (KBr, cm^{-1}): 3220 (NH), 3020–3000 (Ar-CH), 2222 (CN). ^1H NMR (DMSO-d_6): 4.50 (1H, s, H-5), 6.00 (1H, br s, NH), 6.15–6.40 (3H, m, Ar-H and NH), 6.64–6.84 (2H, m, Ar-H). ^{13}C NMR (DMSO-d_6): 50.00 (C-4), 52.00 (C-3), 56.90 (CH-5), 113.60, (2CN), 114.20 (2CN), 124.00 (Ar-C-Cl), 125.60, (2Ar-CH), 128.00 (2Ar-CH), 134.00 (ArCH-3). MS *m*/*z* (%): 284 [M + 2] (38), 282 [M^+] (100), 246 (20), 244 (24), 232 (28), 224 (24), 222 (26), 192 (28), 134 (20), 94 (24). Anal. calcd. for $C_{13}H_7ClN_6$ (282.688) %: C 55.23, H 2.50, Cl 12.54, N 29.73; found: C 55.38, H 2.60, Cl 12.60, N 29.70.

Reaction of 6a–6c with 18 — Synthesis of 3,6-diaryl-4,5-dibenzoyl-pyridazines (19a–19c)

A mixture of **6a**–**6c** (1 mmol) and **18** (0.24 g, 1 mmol) in toluene (200 mL) was stirred at reflux for 6–8 h (the reaction was followed by TLC). The collected yellow precipitates of **19a**–**19c** were washed with hot toluene, and then recrystallized from the stated solvents.

4,5-Dibenzoyl-3,6-di-(4′-methylphenyl)-pyridazine (19a)

Pale yellow crystals (0.28 g, 60%), mp 260–262 °C (EtOH). IR ν (KBr, cm^{-1}): 3010–3000 (Ar-CH), 2890–2850 (ali.-CH), 1695 (CO), 1600 (C=N). ^1H NMR (DMSO-d_6): 2.40 (6H, s, $2CH_3$), 5.98 (4H, dd, J = 8.6, 1.4 Hz), 6.40–6.68 (4H, m), 6.80–7.10 (4H, m), 7.40–7.78 (4H, m), 7.90–8.10 (2H, m). ^{13}C NMR (DMSO-d_6): 30.90 (CH_3), 126.60, 127.00, 130.18, 130.60, 131.00 (Ar-CH), 132.16 (Ar-C), 132.80, 133.60 (Ar-CH), 133.90 (Ar-C), 134.80, 136.20 (Ar-CH), 138.60 (Ar-C), 140.90 (C-4), 154.00 (C-3), 190.20 (CO). MS *m*/*z* (%): 468 [M^+] (100), 452 (24), 426 (22), 364 (34), 348 (28), 270 (18), 234 (60), 220 (34), 178 (34), 92 (18), 76 (28). Anal. calcd. for $C_{32}H_{24}N_2O_2$ (468.545) %: C 82.03, H 5.16, N 5.98; found: C 82.15, H 5.05, N 5.90.

4,5-Dibenzoyl-3,6-di-(4′-methoxyphenyl)-pyridazine (19b)

Yellow crystals (0.33 g, 65%), mp 280–282 °C (EtOH). IR ν (KBr, cm^{-1}): 3024–3008 (Ar-CH), 2990–2890 (ali.-CH), 1695 (CO), 1590 (C=N). ^1H NMR (DMSO-d_6): 3.90

© 2005 NRC Canada

(6H, s, $2OCH_3$), 6.04 (4H, dd, J = 8.6, 1.4 Hz), 6.56–6.90 (4H, m), 7.10–7.38 (4H, m), 7.54–7.84 (4H, m), 8.00–8.18 (2H, m). ^{13}C NMR (DMSO-d_6): 50.90 (OCH_3), 126.64, 127.20, 130.22, 131.40, 131.90 (Ar-CH), 132.50 (Ar-C), 133.80, 134.20 (Ar-CH), 133.60 (Ar-C), 134.00, 136.90 (Ar-CH), 142.00 (C-4), 148.20 (Ar-C-OMe), 153.90 (C-3), 188.00 (CO). MS *m*/*z* (%): 500 [M^+] (100), 486 (20), 458 (20), 442 (20), 226 (60), 234 (30), 226 (48), 178 (26), 104 (18), 92 (22), 76 (34). Anal. calcd. for $C_{32}H_{24}N_2O_4$ (500.544) %: C 76.78, H 4.83, N 5.60; found: C 76.68, H 4.84, N 5.55.

4,5-Dibenzoyl-3,6-di-(4′-chlorophenyl)-pyridazine (19c)

Yellow crystals (0.29 g, 58%), mp 210–212 °C (CH_3CN). IR ν (KBr, cm^{-1}): 3020–3002 (Ar-CH), 1690 (CO), 1592 (C=N). ^1H NMR (DMSO-d_6): 5.84 (4H, dd, J = 8.3, 1.6 Hz), 6.30–6.60 (4H, m), 6.72–7.00 (4H, m), 7.30–7.60 (4H, m), 7.96–8.16 (2H, m). ^{13}C NMR (DMSO-d_6): 125.50, 126.60, 129.32, 130.18, 130.56 (Ar-CH), 130.30 (Ar-C), 132.20, 132.68 (Ar-CH), 133.00 (Ar-C), 133.80, 135.90 (Ar-CH), 137.40 (Ar-C), 140.00 (C-4), 152.80 (C-3), 186.90 (CO). MS *m*/*z* (%): 511 [M + 2] (48), 509 [M^+] (100), 507 (50), 474 (24), 472 (28), 406 (22), 404 (24), 300 (30), 298 (34), 256 (58), 224 (20), 222 (24), 176 (20), 104 (18), 92 (22), 76 (40). Anal. calcd. for $C_{30}H_{18}Cl_2N_2O_2$ (509.382) %: C 70.74, H 3.56, Cl 13.92, N 5.50; found: C 70.58, H 3.64, Cl 14.00, N 5.50.

Acknowledgement

The authors deeply thank Dr. Alan B. Brown, Department of Chemistry, F.I.T. Melbourne, FL 32901, USA for his review.

References

1. (*a*) T. Wagner-Jauregg. Synthesis, 349 (1976); (*b*) K. Burger, H. Schickaneder, and W. Thenn. Tetrahedron Lett. 1125 (1975); (*c*) A.E. Tipping and T.P. Forshaw. J. Chem. Soc. C, 2404 (1971); (*d*) K. Burger, H. Schickaneder, and M. Pinzel. Chem.-Ztg. **100**, 90 (1976); (*e*) S. Evans, R.C. Gearhart, L.J. Guggenberger, and E.E. Schweizer. J. Org. Chem. **42**, 452 (1977); (*f*) P.C. Jain, Y.N. Mukerjee, and N. Anand. J. Am. Chem. Soc. **96**, 2996 (1974). (*g*) S. Satsumabayashi, S. Motoki, and H. Nakano. J. Org. Chem. **41**, 156 (1976).
2. K. Burger, H. Schickaneder, W. Thenn, G. Ebner, and C. Zettl. Justus Liebigs Ann. Chem. 2156 (1976); (*b*) K. Burger, H. Schickaneder, and M. Pinzel. Justus Liebigs Ann. Chem. 30 (1976).
3. (*a*) K. Burger, W. Thenn, and H. Schickaneder. Chem. Ber. **108**, 1468 (1975); (*b*) K. Burger, W. Thenn, R. Rauh, H. Schickaneder, and A. Gieren. Chem. Ber. **108**, 1460 (1975), and refs. cited therein.
4. S.S. Mathur and H. Suschitzky. J. Chem. Soc. Perkin Trans. 1, 2479 (1975).
5. S.E. Armstrong and A.E. Tipping. J. Chem. Soc. Perkin Trans. 1, 1411 (1975).
6. N. Kise and N. Ueda. Tetrahedron Lett. **42**, 2365 (2001).
7. A.A. Aly, N.K. Mohamed, A.A. Hassan, and A.E. Mourad. Tetrahedron, **55**, 1111 (1999).
8. A.A. Aly. Tetrahedron, **59**, 1739 (2003).
9. M.A.-M. Gomaa. J. Chem. Soc. Perkin Trans. 1, 341 (2002).
10. M.A.-M. Gomaa and D. Döpp. Synthesis, 1545 (2003).
11. A.A. Aly, A.E. Mourad, K.M. El-Shaieb, and H. Hopf. Synth. Commun. **31**, 637 (2001).
12. M.R. Bryce and J.M. Vernon. Adv. Heterocycl. Chem. **28**, 183 (1981).
13. T.L. Gilchrist. *In* The chemistry of triple-bonded functional groups. *Edited by* S. Patai and Z. Rappoport. John Wiley and Sons, New York. 1983. Chap. 11.
14. J.A. Berson. Tetrahedron, **48**, 3 (1992).
15. A.A. Aly, H. Hopf, and L. Ernst. Eur. J. Org. Chem. 3021 (2000).
16. B.S. Furniss, A.J. Hannaford, P.W.G. Smith, and A.R. Tatchell. Vogel's textbook of practical organic chemistry. 5th ed. Longman, Harlow, Essex, UK. 1989. p. 1260.
17. E. Veverkova, M. Noskova, and S. Toma. Synth. Commun. **32**, 729 (2002).
18. P. Gambetti, R.B. Petersen, P. Parchi, S.G. Chen, S. Capellari, L. Goldfarb, R. Gabizon, P. Montagna, E. Lugaresi, P. Piccardo, and B. Ghetti. *In* Prion biology and diseases. *Edited by* S.B. Prusiner. Cold Spring Harbor Laboratory Press, Plainview, New York. 1999. pp. 509–583.
19. J.M.F. Gagan. *In* Acridines. *Edited by* R.M. Acheson. John Wiley and Sons, New York. 1973. pp. 141–377.
20. F. Charmantray, M. Demeunynck, D. Carrez, A. Croisy, A. Lansiaux, C. Bailly, and P. Colson. J. Med. Chem. **46**, 967 (2003).
21. A. Chauveau, T. Martens, M. Bonin, L. Micouin, and H.-P. Husson. Synthesis, 1885 (2002).
22. N.L. Allinger. MM2 (91) force field program [computer program]. Quantum Chemistry Program Exchange, Indiana University, Bloomington, Indiana; Molecular mechanics PM3 program (ACD/3D) [computer program]. Advanced Chemical Development Inc., Toronto, Ontario, Canada. 1988.
23. H. Wilde, R. Herzschuh, P. Lepom, and G. Mann. J. Prakt. Chem. (Leipzig), **323**, 14 (1981).
24. K.N. Zelenin, S.V. Oleinik, A.A. Potekhin, V.V. Ovcharenko, J. Sinkkonen, and K. Pihlaja. ARKIVOC, 94 (2003).
25. V. Curran and A. Ross. J. Med. Chem. **17**, 273 (1974).
26. G. Nannini, G. Biasoli, E. Perrone, A. Forgione, A. Buttinoni, and M. Ferrari. Eur. J. Med. Chem. **14**, 53 (1979).

© 2005 NRC Canada

N-Iodosuccinimide — An effective reagent for regioselective heterocyclization of *o*-cyclohex-2′-enylanilines for the synthesis of hexahydrocarbazoles

K.C. Majumdar, U.K. Kundu, U. Das, N.K. Jana, and B. Roy

Abstract: A number of carbazoles are synthesized in good yields by the *N*-iodosuccinimide mediated heterocyclization of *o*-cyclohex-2′-enylanilines in acetonitrile at –10 °C for 45 min followed by heating with palladium–charcoal (10%) in benzene (80 °C) for 18–20 h.

Key words: N-iodosuccinimide, hexahydrocarbazole, heterocyclization, carbazole, Claisen rearrangement.

Résumé : On a réalisé la synthèse de plusieurs carbazoles avec de bons rendements en faisant appel à une hétérocyclisation, catalysée par le *N*-iodosuccinimide, de *o*-cyclohex-2′-énylanilines, à –10 °C pendant 45 min, suivie par un chauffage avec du palladium sur charbon (10 %), dans le benzène, à 80 °C, pendant une période de 18 à 20 heures.

Mots clés : N-iodosuccinimide, hexahydrocarbazole, hétérocyclisation, carbazole, réarrangement de Claisen.

[Traduit par la Rédaction]

Introduction

There are several reports for the synthesis of carbazoles (1). Carbazole has been synthesized from diphenylamine either by photochemical cyclization (2) or by thermal cyclization (3), and also in the presence of iodine (4) at 350 °C. We have reported the synthesis of 1-alkoxy tetrahydrocarbazoles by the Hg(II)-mediated heterocyclization (5) of *o*-cyclohex-2′-enylanilines. This prompted the evaluation of the efficacy of *N*-iodosuccinimide for the heterocyclization of *o*-cyclohex-2′-enylanilines.

o-Cyclohex-2′-enylanilines **1a**–**1g** were prepared in 50%–90% yields by the acid-catalyzed aza-Claisen rearrangement of 3-*N*-alkyl, *N*-arylamino cyclohexene in refluxing ethanolic hydrochloric acid following the literature procedure (5).

Results and discussion

It was envisaged that heterocyclization of *o*-cyclohex-2′-enylanilines (**1a**–**1g**) would afford hexahydrocarbazoles. Previously, we have successfully utilized pyridinehydrotribromide (6) and hexaminehydrotribromide (7) for the heterocyclization of *o*-cyclohex-2′-enylphenols. However, our attempts at cyclization of *o*-cyclohex-2′-enylanilines with these reagents were of no avail (8). At this point our attention was drawn to *N*-iodosuccinimide, which is reported to effect the cyclization of unsaturated nitrogen-containing substrates. Electron-poor nitrogen species like amides and hydroxylic amines have so far been employed (9) for the preparation of *N*-*p*-toluenesulfonyl-3-hydroxy-4-pentenamides, *N*-protected 3-hydroxy-4-pentenyl-amines, 4-hydroxy-5-hexenylamines, and dialkylsubstituted pyrrolidines and piperidines from hydroxylic amines. Intramolecular cyclization of substrates by electron-poor nitrogen nucleophiles has been accomplished under various reaction conditions. However, there is no report so far on the iodoamination where arylamines have been used as electron-poor nucleophiles with *N*-iodosuccinimide. Therefore, substrate **1a** was stirred with 1 equiv. of *N*-iodosuccinimide in acetonitrile at –10 °C. The reaction was completed in ~45 min to give a viscous oil in 60% yield. This was characterized as 1,2,3,4,4a,9a-hexahydro-1-iodo-9-methylcarbazole (**2a**) from its elemental analysis and spectroscopic data. ^{13}C NMR spectral data and DEPT experiment corroborated the proposed structure for product **2a**. The degree of protonation of the 10 carbons were determined by DEPT experiment, which showed one -CH_3, three -CH_2-, and six >CH-. Substrates **1b**–**1g** were also similarly treated to give products **2b**–**2g** in 55%–70% yield (Scheme 1). It was found that the iodoamines (**2a**–**2g**) are not very stable and on standing decompose to intractable products. The products **2a**–**2e** were dehydrogenated with palladium-charcoal (10%) in refluxing benzene for 18–20 h to give corresponding carbazoles **3a**–**3e** in 60%–65% yield (10–13). These were characterized as substituted 9-methylcarbazoles (**3**) from their elemental analyses and spectroscopic data. The products **2f** and **2g** were similarly treated with 5% palladium–charcoal to give products **4f** and **4g** in 60% and 62% yield, respectively, contaminated with minor amounts of fully aromatized products. These minor products could not be isolated in pure form. The products (**4f** and **4g**) were characterized as 1,2,3,4-tetra-

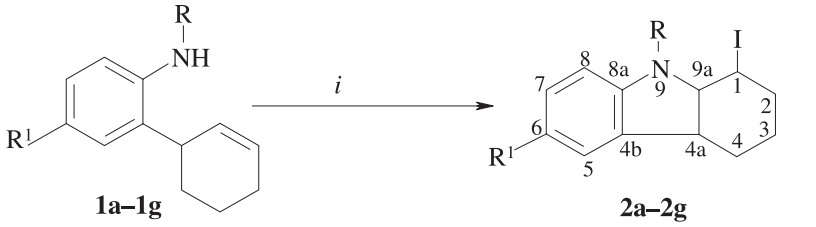
Received 24 June 2004. Published on the NRC Research Press Web site at http://canjchem.nrc.ca on 5 February 2005.

K.C. Majumdar,[1] U.K. Kundu, U. Das, N.K. Jana, and B. Roy. Department of Chemistry, University of Kalyani, Kalyani-741 235, W.B, India.

[1]Corresponding author (e-mail: kcm@klyuniv.ernet.in).

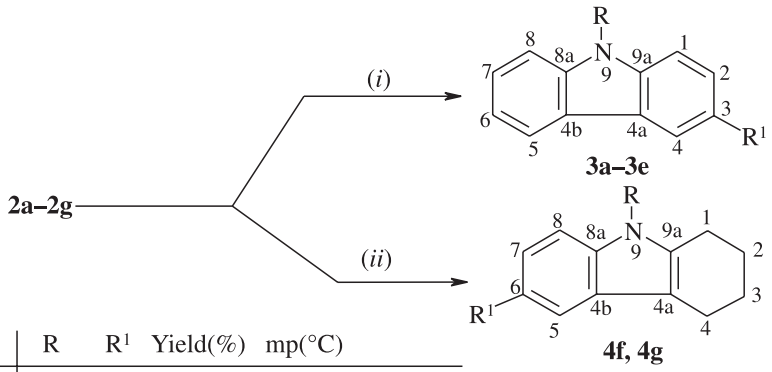
 doi: 10.1139/V04-162 © 2005 NRC Canada

Scheme 1. Reagents and conditions: (*i*) NIS, CH_3CN, –10 °C, 45 min.



(a) R = Me, R^1 = Br (e) R = Me, R^1 = H
(b) R = Me, R^1 = Et (f) R = Et, R^1 = H
(c) R = Me, R^1 = Me (g) R = Et, R^1 = Cl
(d) R = Me, R^1 = Cl

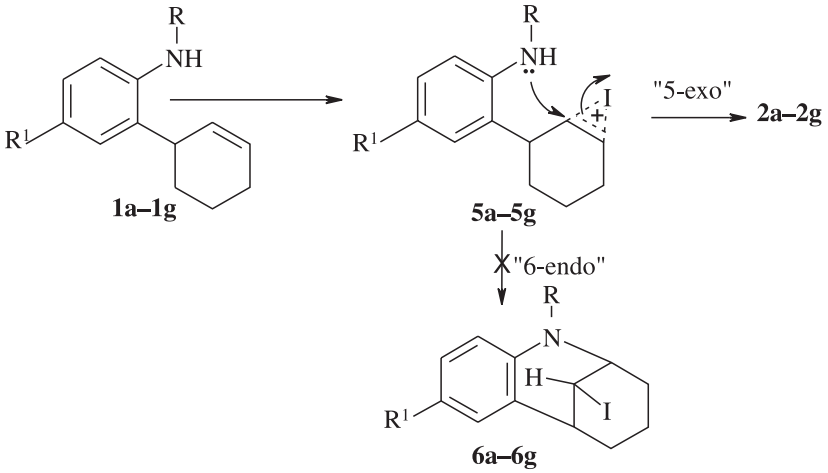
Scheme 2. Reagents and conditions: *(i)* Pd-C (10%), C_6H_6, ↓↑, 18–20 h; (*ii*) Pd-C (5%), ↓↑, 18–20 h.



	R	R^1	Yield(%)	mp(°C)
3a	Me	Br	63	76 (lit.(10) 78-79)
3b	Me	Et	60	——
3c	Me	Me	61	82 (lit.(11) 84)
3d	Me	Cl	55	38 (lit.(12) 38-40)
3e	Me	H	65	84 (lit.(13) 85)

	R	R^1	Yield(%)
4f	Et	H	60
4g	Et	Cl	62

Scheme 3.



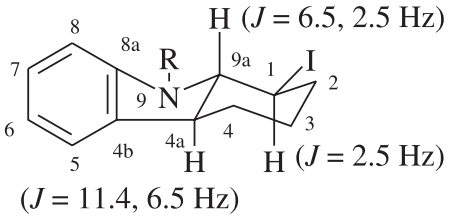
hydrocarbazoles from their elemental analyses and spectroscopic data (Scheme 2).

The regioselective formation of hexahydrocarbazoles **2a**–**2g** from substrates **1a**–**1g** may be easily explained by the initial formation of an intermediate iodonium ion (**5a**–**5g**), which may undergo a "5-*exo*" cyclization to give products **2a**–**2g**. An alternative "6-*endo*" cyclization to give bicyclic products is ruled out as no such product could be isolated from the reaction mixture (Scheme 3).

The relative stereochemistry of the product could not be determined from the observed coupling constants of protons (C4a-*H*, C9a-*H*, and C1-*H*) alone. However, we could assign

© 2005 NRC Canada

Fig. 1. Stereostructure of compound **2**.



the stereochemistry of the product by considering the mechanism of the reaction. As the product **2a** is formed via an iodonium intermediate, the N9—C9a and C1—I bonds in **2a** are antiperiplanar. Again, Pd-C-catalyzed dehydrogenation occurs via cis-elimination. Therefore, the C9a—*H* and C1—I bonds are expected to be cis. C4a-*H* is suggested to be axial because shifting of the double bond is facilitated by the axial hydrogen. Hence, C9a-*H* and C4a-*H* should be trans (J = 6.5 Hz because of the presence of nitrogen heteroatom). The iodine atom and N-R groups are bulky and likely to occupy equatorial positions (Fig. 1). The same heterocyclization was attempted with *N*-bromosuccinimide without any success, while pyridine hydrotribromide and hexamine hydrotribromide afforded the addition products along with ring-brominated products, and there also, no cyclization was observed (8). *N*-Iodosuccinimide is a mild reagent and reacts at low temperature bringing about regioselective heterocyclization of *o*-cyclohex-2′-enylanilines to give hexahydrocarbazoles. For the cases where pyridine hydrotribromide and hexamine hydrotribromide afforded bicyclic products, cyclizations occurred by a 6-*endo* mode. In contrast, *N*-iodosuccinimide gave linear hexahydrocarbazoles by a 5-*exo* cyclization. Recently, we reported the formation of bicylic heterocycles by *N*-iodosuccinimide-mediated reactions in cases of 2-cyclohex-2′-enyl phenols (14) and 3-cyclohex-2′-enyl-4-hydroxy coumarins (15). 2-(Cyclopent-2′-enyl)anilines have recently been cyclized using iodine (16) in the presence of $NaHCO_3$. Synthesis of tetrahydrocarbazoles by Ullmann cross coupling of *o*-halonitrobenzene and various related nitrobenzenes with a range of α-halo cyclohexenones followed by reaction with hydrogen in the presence of Pd on C has also been recently reported (17). The present work clearly demonstrates the viability of *N*-iodosuccinimide as an effective reagent for regioselective heterocyclization of *o*-allylanilines. In the cases of cyclization of electron-poor nitrogen species like amides and hydroxylic amines, different types of stereoisomers were obtained (9). However, in the present study only one type of regioselective product was obtained. Therefore, this is an effective reagent for the synthesis of hexahydrocarbazoles. We have, therefore, successfully demonstrated the use of aryl amines as electron-poor nucleophiles in the *N*-iodosuccinimide-mediated iodoaminations for the first time.

Experimental

Melting points were determined in an open capillary and are uncorrected. UV absorption spectra were recorded in EtOH on a Shimadzu UV-2401 PC spectrophotometer (λ_{max} in nm), and IR spectra were obtained on a PerkinElmer L 120-000A grating IR spectrophotometer and the frequency reported in cm^{-1}. ^1H NMR (300 MHz) and ^{13}C NMR (75.5 MHz) spectra were recorded in $CDCl_3$ (TMS was used as an internal standard) on a Bruker DPX-300 instrument at the Indian Institute of Chemical Biology, Kolkata, India (chemical shifts in δ ppm). Elemental analyses and recording of mass spectra were carried out by RSIC (CDRI) Lucknow on a JEOL D-300 (El) instrument. Silica gel (60–120 mesh, Spectrochem, India) was used for chromatographic separation. Petroleum ether refers to the fraction boiling between 40 and 60 °C. Palladium on activated charcoal (5% and 10%) was procured from S.D. Fine Chemicals Ltd. (India) and Loba Chemie, respectively.

General procedure for the synthesis of compounds 2a–2g

A solution of compound **1** (**1a**–**1g**) (1 mmol) in dry CH_3CN (50 mL) was stirred at –10 °C with *N*-iodosuccinimide (0.23 g, 1 mmol) for 45 min. The solvent was removed under reduced pressure at room temperature. The residual mass was dissolved in $CHCl_3$ (50 mL). The $CHCl_3$ was washed with a saturated solution of $NaHSO_3$ (2 × 25mL), water (2 × 25 mL), and dried (Na_2SO_4). A gummy residue was obtained after evaporation of the solvent. This was purified by column chromatography over silica gel. Elution of the column with petroleum ether (40–60 °C) gave compounds **2a**–**2g** as viscous oils.

Compound 2a

Viscous oil; yield 60%. UV (EtOH, nm) λ_{max}: 217, 265, 303. IR (neat, cm^{-1}) ν_{max}: 530, 1260, 1500, 1590, 2940, 3120. ^1H NMR ($CDCl_3$, 300 MHz) δ: 1.73–1.89 (m, 4H), 1.97–2.01 (m, 2H), 2.75 (s, 3H, N-*Me*), 3.29 (dt, J = 6.5, 11.4 Hz, 1H, ArC*H*), 3.57 (dd, J = 6.5, 2.5 Hz, 1H, -NC*H*), 4.86 (d, J = 2.5 Hz, 1H, -C*H*I), 6.40–6.43 (m, 1H, Ar*H*), 7.14–7.21 (m, 2H, Ar*H*). ^{13}C NMR ($CDCl_3$, 75.5 MHz) δ: at 21.24 (C3), 29.89 (C4), 30.83 (C1), 31.28 (C2), 35.19 (>N*C*H_3), 38.57 (C4a), 74.30 (C9a), 110.82 (C8), 126.37 (C5), 130.49 (C7), 137.03 (C6), 138.12 (C4b), and 148.03 (C8a). MS *m*/*z*: 391, 393 (M^+, M^+ + 2). Anal. calcd. for $C_{13}H_{15}BrIN$ (%): C 39.79, H 3.82, N 3.57; found: C 39.95, H 3.72, N 3.43.

Compound 2b

Viscous oil; yield 67%. UV (EtOH, nm) λ_{max}: 217, 264, 303. IR (neat, cm^{-1}) ν_{max}: 555, 1266, 1506, 1615, 2929, 3132. ^1H NMR ($CDCl_3$, 300 MHz) δ: 1.15 (t, J = 7.5 Hz, 3H), 1.28–1.89 (m, 4H), 2.28–2.33 (m, 2H), 2.46 (q, J = 7.5 Hz, 2H), 2.88 (s, 3H, N-*Me*), 3.29 (brs, 1H, -NC*H*), 3.83 (brs, 1H, ArC*H*), 4.84 (brs, 1H, -C*H*I), 6.43 (d, J = 8.7 Hz, 1H, Ar*H*), 6.67–7.22 (m, 2H, Ar*H*). MS *m*/*z*: 341 (M^+). Anal. calcd. for $C_{15}H_{20}IN$ (%): C 52.78, H 5.86, N 4.10; found: C 52.68, H 5.79, N 4.15.

Compound 2c

Viscous oil; yield 65%. UV (EtOH, nm) λ_{max}: 217, 264, 303. IR (neat, cm^{-1}) ν_{max}: 550, 1260, 1500, 1610, 2921, 3130. ^1H NMR ($CDCl_3$, 300 MHz) δ: 1.22–1.91 (m, 4H), 2.20 (s, 3H), 2.24–2.38 (m, 2H), 2.88 (s, 3H, N-*Me*), 3.05 (brs, 1H, -NC*H*), 3.48 (brs, 1H, ArC*H*), 4.83 (brs, 1H, -C*H*I), 6.42 (d, J = 8.7 Hz, 1H, Ar*H*) 6.65–6.93 (m, 2H,

© 2005 NRC Canada

Ar*H*). MS *m*/*z*: 327 (M^+). Anal. calcd. for $C_{14}H_{18}IN$ (%): C 51.37, H 5.50, N 4.28; found: C 51.29, H 5.48, N 4.32.

Compound 2d

Viscous oil; yield 58%. UV (EtOH, nm) λ_{max}: 218, 265, 304. IR (neat, cm^{-1}) ν_{max}: 590, 1261, 1470, 1600, 2924, 3132. ^1H NMR ($CDCl_3$, 300 MHz) δ: 1.28–2.00 (m, 4H), 2.20–2.50 (m, 2H), 2.88 (s, 3H, N-*Me*), 3.04 (brs, 1H, -NC*H*), 3.49 (brs, 1H, ArC*H*), 4.75 (brs, 1H, -C*H*I), 6.39 (d, *J* = 8.7 Hz, 1H, Ar*H*), 6.80–7.03 (m, 2H, Ar*H*). MS *m*/*z*: 347, 349 (M^+, $M^+ + 2$). Anal. calcd. for $C_{13}H_{15}ClIN$ (%): C 44.89, H 4.31, N 4.02; found: C 44.78, H 4.29, N 4.12.

Compound 2e

Viscous oil; yield 55%. UV (EtOH, nm) λ_{max}: 218, 264, 303. IR (neat, cm^{-1}) ν_{max}: 560, 1260, 1470, 1630, 2920, 3130. ^1H NMR ($CDCl_3$, 300 MHz) δ: 1.26–2.01 (m, 4H), 2.23–2.49 (m, 2H), 2.87 (s, 3H, N-*Me*), 3.08 (brs, 1H, -NC*H*), 3.42 (brs, 1H, ArC*H*), 4.76 (brs, 1H, -C*H*I), 6.53–7.49 (m, 4H, Ar*H*). MS *m*/*z*: 313 (M^+). Anal. calcd. for $C_{13}H_{16}IN$ (%): C 49.84, H 5.11, N 4.47; found: C 49.83, H 5.08, N 4.52.

Compound 2f

Viscous oil; yield 70%. UV (EtOH, nm) λ_{max}: 217, 264, 304. IR (neat, cm^{-1}) ν_{max}: 550, 1250, 1500, 1610, 2920, 3110. ^1H NMR ($CDCl_3$, 300 MHz) δ: 1.14–1.19 (m, 3H), 1.30–1.89 (m, 4H), 2.30–2.34 (m, 2H), 2.98 (brs, 1H, -NC*H*), 3.05–3.42 (m, 2H), 3.52 (brs, 1H, ArC*H*), 4.75 (brs, 1H, -C*H*I), 6.50–7.09 (m, 4H, Ar*H*). MS *m*/*z*: 327 (M^+). Anal. calcd. for $C_{14}H_{18}IN$ (%): C 51.37, H 5.50, N 4.28; found: C 51.28, H 5.43, N 4.32.

Compound 2g

Viscous oil; yield 63%. UV (EtOH, nm) λ_{max}: 217, 265, 303. IR (neat, cm^{-1}) ν_{max}: 560, 1260, 1490, 1590, 2930, 3100. ^1H NMR ($CDCl_3$, 300 MHz) δ: 1.13–1.17 (m, 3H), 1.28–1.80 (m, 4H), 2.26–2.40 (m, 2H), 2.99 (brs, 1H, -NC*H*), 3.14–3.36 (m, 2H), 3.51 (brs, 1H, ArC*H*), 4.65 (brs, 1H, -C*H*I), 6.30 (d, *J* = 8.7 Hz, 1H, Ar*H*), 7.09–7.31 (m, 2H, Ar*H*). MS *m*/*z*: 361, 363 (M^+, $M^+ + 2$). Anal. calcd. for $C_{14}H_{17}ClIN$ (%): C 46.47, H 4.70, N 3.87; found: C 46.52, H 4.68, N 3.79.

General procedure for the synthesis of compounds 3a–3e and 4f and 4g

Compound **2** (**2a**–**2e**, 0.2 g) was refluxed with 10% palladium on charcoal (0.02 g), and in the case of compounds **2f** and **2g**, 5% palladium on charcoal was used in benzene (20 mL) for 18–20 h. The mixture was filtered and benzene was distilled off. The residual mass was directly chromatographed over silica gel. Elution of the column with petroleum ether (40–60 °C) gave the compounds **3a**–**3e** and **4f** and **4g.** The solid compounds were recrystallized from ethanol.

Compound 3a

White crystalline solid, mp 76 to 77 °C (lit. value (10) mp 78 to 79 °C); yield 63%. UV (EtOH, nm) λ_{max}: 222, 265, 297. IR (KBr, cm^{-1}) ν_{max}: 1246, 1493, 1605, 2925, 3134. ^1H NMR ($CDCl_3$, 300 MHz) δ: 3.86 (s, 3H, N-*Me*), 7.71–7.48 (m, 4H, Ar*H*), 7.50–8.11 (m, 3H, Ar*H*). MS *m*/*z*: 259, 261 (M^+, $M^+ + 2$). Anal. calcd. for $C_{13}H_{10}BrN$ (%): C 60.00, H 3.84, N 5.38; found: C 60.11, H 3.76, N 5.32.

Compound 3b

Viscous oil; yield 60%. UV (EtOH, nm) λ_{max}: 222, 265, 297. IR (neat, cm^{-1}) ν_{max}: 1247, 1488, 1605, 2926, 3133. ^1H NMR ($CDCl_3$, 300 MHz) δ: 1.31 (t, *J* = 7.5 Hz, 3H), 2.79 (q, *J* = 7.5 Hz, 2H), 3.88 (s, 3H, N-*Me*), 7.17–7.47 (m, 5H, Ar*H*), 7.91–8.08 (m, 2H, Ar*H*). ^{13}C NMR (75.5 MHz, $CDCl_3$) δ: at 17.03 (C12), 29.37 (C11), 29.50 (>NCH_3), 108.60 (C1), 108.75 (C8), 118.95 (C6), 119.47 (C5), 120.61 (C2), 123.10 (C4a), 123.25 (C4b), 125.86 (C7), 126.37 (C4), 135.29 (C3), 139.91 (C9a), and 141.66 (C8a). MS *m*/*z*: 209 (M^+). Anal. calcd. for $C_{15}H_{15}N$ (%): C 86.12, H 7.17, N 6.69; found: C 86.22, H 7.11, N 6.60.

Compound 3c

Pale yellow crystalline solid, mp 81 to 82 °C (lit. value (11) mp 84 °C); yield 61%. UV (EtOH, nm) λ_{max}: 222, 265, 297. IR (KBr, cm^{-1}) ν_{max}: 1264, 1494, 1590, 2931, 3134. ^1H NMR ($CDCl_3$, 300 MHz) δ: 2.53 (s, 3H, ArCH_3), 3.83 (s, 3H, N-*Me*), 7.17–7.47 (m, 5H, Ar*H*), 7.89–8.07 (m, 2H, Ar*H*). MS *m*/*z*: 195 (M^+). Anal. calcd. for $C_{14}H_{13}N$ (%): C 86.15, H, 6.66, N 7.17; found: C 86.31, H 6.59, N 7.23.

Compound 3d

Pale yellow crystalline solid, mp 38–40 °C (lit. value (12) mp 38–40 °C); yield 55%. UV (EtOH, nm) λ_{max}: 221, 266, 297. IR (KBr, cm^{-1}) ν_{max}: 1246, 1474, 1596, 2939, 3130. ^1H NMR ($CDCl_3$, 300 MHz) δ: 3.84 (s, 3H, N-*Me*), 7.22–7.44 (m, 4H, Ar*H*), 7.47–8.05 (m, 3H, Ar*H*). MS *m*/*z*: 215, 217 (M^+, $M^+ + 2$). Anal. calcd. for $C_{13}H_{10}ClN$ (%): C 72.38, H 4.64, N 6.49; found: C 72.29, H 4.61, N 6.42.

Compound 3e

Pale yellow crystalline solid, mp 83 to 84 °C (lit. value (13) mp 85 °C); yield 65%. UV (EtOH, nm) λ_{max}: 222, 265, 297. IR (KBr, cm^{-1}) ν_{max}: 1245, 1468, 1600, 2926, 3133. ^1H NMR ($CDCl_3$, 300 MHz) δ: 3.86 (s, 3H, N-*Me*), 7.20–7.46 (m, 4H, Ar*H*), 7.48–8.11 (m, 4H, Ar*H*). MS *m*/*z*: 181 (M^+); Anal. calcd. for $C_{13}H_{11}N$ (%): C 86.18, H 6.07, N 7.73; found: C 86.12, H 6.11, N 7.68.

Compound 4f

Viscous oil; yield 60%. UV (EtOH, nm) λ_{max}: 229, 263, 293. IR (neat, cm^{-1}) ν_{max}: 1231, 1484, 1598, 2928, 3053. ^1H NMR ($CDCl_3$, 300 MHz) δ: 1.40–1.45 (m, 3H), 1.54–1.93 (m, 4H), 2.70–2.72 (m, 2H), 4.02–4.09 (m, 2H), 4.33–4.40 (m, 2H), 7.02–8.11 (m, 4H, Ar*H*). MS *m*/*z*: 199 (M^+). Anal. calcd. for $C_{14}H_{17}N$ (%): C 84.42, H 8.54, N 7.03; found: C 84.48, H 8.48, N 7.12.

Compound 4g

Viscous oil; yield 62%. UV (EtOH, nm) λ_{max}: 221, 265, 293. IR (neat, cm^{-1}) ν_{max}: 1231, 1485, 1599, 2928, 3052. ^1H NMR ($CDCl_3$, 300 MHz) δ: 1.41–1.45 (m, 3H), 1.60–2.02 (m, 4H), 2.71–2.74 (m, 2H), 4.03–4.13 (m, 2H, =CCH_2), 4.23–4.41 (m, 2H), 7.05–8.11 (m, 3H, Ar*H*). MS *m*/*z*: 233, 235 (M^+, $M^+ + 2$). Anal. calcd. for $C_{14}H_{16}ClN$ (%): C 71.94, H 6.85, N 5.99; found: C 71.83, H 6.87, N 5.23.

© 2005 NRC Canada

Acknowledgements

We thank the Council of Scientific and Industrial Research (CSIR, New Delhi) for financial assistance. Two of us (U.D. and N.K.J) are grateful to CSIR (New Delhi) for fellowships. We also thank Dr. S.K. Samanta for his assistance.

References

1. J.A. Joule. Advances in heterocyclic chemistry. Vol. 35. *Edited by* A.R. Katritzky. Academic Press, Inc., London. 1984. p. 83.
2. (*a*) E.J. Browen and J.H.D. Eland. Proc. Chem. Soc. London, 202 (1963); (*b*) W. Carruthers. Chem. Commun. 272 (1966); (*c*) K.H. Grelman, G.M. Sherman, and H. Linzchith. J. Am. Chem. Soc. **85**, 1881 (1963); (*d*) P. Bhattacharyya, S.S. Jash, and A.K De. J. Chem. Soc. Chem. Commun. 1668 (1984).
3. (*a*) S.H. Oakeshott and S.G. Plant. J. Chem. Soc. 1210 (1926); (*b*) E. Campaigne and R.D. Lake. J. Org. Chem. **24**, 478 (1959); (*c*) B. Akermark, E. Eberson, and E. Pettersson. J. Org. Chem. **40**, 1365 (1975); (*d*) D.P. Chakraborty, K.C. Das, and S.P. Basak. J. Indian Chem. Soc. **45**, 84 (1968); (*e*) K.H. Pausacker and R. Robinson. J. Chem. Soc. 1557 (1947).
4. A. Islam, P. Bhattacharyya, and D.P. Chakraborty. J. Chem. Soc. Chem. Commun. 537 (1972).
5. (*a*) K.C. Majumdar, R.N. De, and S. Saha. Tetrahedron Lett. **31**, 1207 (1990); (*b*) K.C. Majumdar and U. Das. Can. J. Chem. **74**, 1592 (1996).
6. (*a*) K.C. Majumdar and A.K. Kundu. Indian J. Chem. **32B**, 605 (1993); (*b*) K.C. Majumdar and A.K. Kundu. Can. J. Chem. **73**,1727 (1995).
7. K.C. Majumdar, A.K. Kundu, and P. Chatterjee. Synth. Commun. **26**, 893 (1996).
8. K.C. Majumdar, U. Das, and A.K. Kundu. Synth. Commun. **28**, 1593 (1998).
9. (*a*) Z. Yoshida, T. Tamura, S. Kawamura, and K. Tanaka. Tetrahedron Lett. **25**, 1063 (1984); (*b*) D.R. Williams, M.H. Osterhout, and J.M. McGill. Tetrahedron Lett. **30**, 1327 (1989); (*c*) Z. Yoshida, Y. Tamura, S. Kawamura, K. Tanaka, T. Bando, and M. Hojo. J. Org. Chem. **53**, 5491 (1988).
10. T. Stevans and S.H. Tucker. J. Chem. Soc. **123**, 2140 (1923).
11. P. Kubacek. Coll. Czech. Chem. Commun. **46**, 40 (1981).
12. M.D. Rosa, A.P. Quesada, and D.J. Dodsworth. J. Org. Chem. **52**, 173 (1987).
13. W.C. Sumpter and F.M. Miller. The chemistry of heterocyclic compounds. *Edited by* A. Weissberger. Interscience Publishers Ltd., London. 1954. p. 73.
14. K.C. Majumdar and P.K. Basu. Synth. Commun. **32**, 3719 (2002).
15. K.C. Majumdar and S. Sarkar. Tetrahedron, **58**, 8501 (2002).
16. R.R. Gataullin, F.F. Minnigulov, A.A. Fatykhov, L.V. Spirikhin, and I.B. Abdrakhmanov. Russ. J. Org. Chem. **37**, 1289 (2001).
17. M.G. Banwell, B.D. Kelly, O.J. Kokas, and D.W. Lupton. Org. Lett. **5**, 2497 (2003).

© 2005 NRC Canada

The 2-oxo-3,3,5,5-tetramethylcyclopentanecarboxylic acid keto–enol system in aqueous solution — Generation of the enol by flash photolytic Wolff rearrangement of 2-diazo-4,4,6,6-tetramethylcyclohexane-1,3-dione followed by hydration of the acylketene thus formed

Y. Chiang, A.J. Kresge, V.A. Nikolaev, I. Onyido, and X. Zeng

Abstract: Flash photolysis of 2-diazo-4,4,6,6-tetramethylcyclohexane-1,3-dione in aqueous solution produced 2-oxo-3,3,5,5-tetramethylcyclopentylideneketene, which underwent hydration to the enol of 2-oxo-3,3,5,5-tetramethylcyclopentanecarboxylic acid; the enol then isomerized to the keto form of the acid. Rates of hydration of the ketene and rates of ketonization of the enol were measured in perchloric acid, sodium hydroxide, and buffer solutions, and rate profiles were constructed. Rates of enolization of 2-oxo-3,3,5,5-tetramethylcyclopentanecarboyxlic acid were also measured, using bromine to scavenge the enol as it formed, and rates of enolization and ketonization were then combined to give the keto–enol equilibrium constant $pK_E = 1.65$. This and other results are discussed in comparison with the behavior of the unmethylated 2-oxocyclopentanecarboxylic acid system.

Key words: flash photolysis, photo-Wolff reaction, ketene hydration, enolization, ketonization, keto–enol equilibria, β-oxocarboxylic acids.

Résumé : La photolyse éclair de la 2-diazo-4,4,6,6-tétraméthylcyclohexane-1,3-dione en solution aqueuse conduit à la formation du 2-oxo-3,3,5,5-tétraméthylcyclopentylidènecétène qui subit ensuite une hydratation conduisant à l'énol de l'acide 2-oxo-3,3,5,5-tétraméthylcyclopentanecarboxylique qui se transforme éventuellement en forme cétonique de l'acide. On a mesuré les vitesses d'hydratation du cétène et les vitesses de cétonisation de l'énol dans des solutions d'acide perchlorique, d'hydroxyde de sodium et de tampons et on a construit des profils de vitesse. On a aussi mesuré les vitesses d'énolisation de l'acide 2-oxo-3,3,5,5-tétraméthylcyclopentanecarboxylique à l'aide de brome pour piéger l'énol qui se forme; ensuite on a combiné les vitesses d'énolisation et de cétonisation pour calculer la constante d'équilibre céto–énolique, $pK_E = 1{,}65$. On discute de ce résultat et d'autres en comparaison avec le comportement du système l'acide 2-oxocyclopentanecarboxylique non méthylé.

Mots clés : photolyse éclair, réaction de photo-Wolff, hydratation d'un cétène, énolisation, cétonisation, équilibre céto–énolique, acides β-oxocarboxyliques.

[Traduit par la Rédaction]

Introduction

Keto–enol tautomerizm of β-ketoesters has been investigated for more than a century and about which there is consequently an impressively large body of information.[2] In striking contrast to this, comparatively little is known about keto–enol tautomerizm of the parent keto acids themselves. In an effort to rectify this imbalanced situation, we have examined keto–enol tautomerizm of acetoacetic acid (**1**) (3), 2-oxocyclopentanecarboxylic acid (**2**) (4), trifluoroacetoacetic acid (**3**) (5), and 2-oxo-cyclohexanecarboxylic acid (**4**) (6). We now add to that a study of keto–enol tautomerizm of 2-oxo-3,3,5,5-teteramethylcyclopentane carboxylic acid (**5**).

We generated the enol of 2-oxo-3,3,5,5-tetramethylcyclopentanecarboxylic acid (**8**) by hydration of 2-oxo-3,3,5,5-tetramethylcyclopentylideneketene (**7**), itself produced by flash photolytic photo-Wolff reaction of 2-diazo-4,4,6,6-tetramethylcyclohexane-1,3-dione (**6**), as shown in eq. [1]. We were able to observe both the enol and the preceeding ketene as short-lived transient species, and we consequently

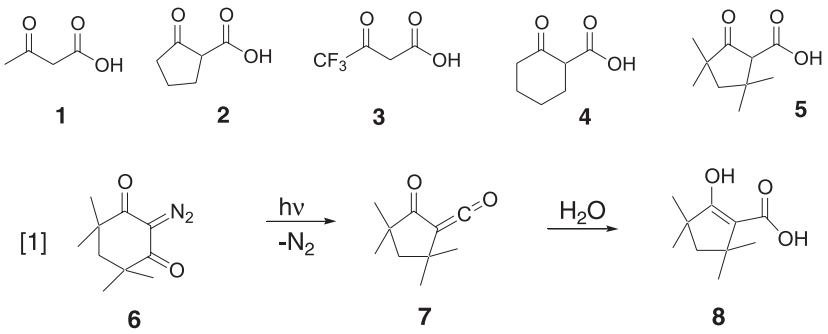
Received 18 June 2004. Published on the NRC Research Press Web site at http://canjchem.nrc.ca on 11 February 2005.

Y. Chiang, A.J. Kresge,[1] V.A. Nikolaev, I. Onyido, and X. Zeng. Department of Chemistry, University of Toronto, Toronto, ON M5S 3H6, Canada.

[1]Corresponding author (e-mail: akresge@chem.utoronto.ca).

[2]For reviews of the early work, see ref. 1, and for a summary of some more recent studies, see ref. 2.

 doi: 10.1139/V04-152 © 2005 NRC Canada



could study the chemistry of both. Our results provide some interesting comparisons with the behavior of the unmethylated 2-oxocyclopentanecarboxylic acid keto–enol system.

β-Ketocarboxylic acids such as that investigated here can, at least in principle, form two isomeric enols: a ketone enol and a carboxylic acid enol. High level ab initio calculations show, however, that the ketone enol is the more stable isomer by a considerable margin (7), and this is consistent with the much greater enol content of simple ketones than that of simple carboxylic acids, i.e., pK_E = 8.3 for acetone (8) vs. the reliable estimate pK_E = 20 for acetic acid (9). The enol studied here was consequently a ketone enol, as shown in eq. [1].

Experimental section

Materials

2-Diazo-4,4,6,6-tetramethylcyclohexane-1,3-dione (**6**) was prepared by diazo group transfer from *p*-toluenesulfonyl azide to 4,4,6,6-tetramethylcyclohexane-1,3-dione (10), and 2-oxo-3,3,5,5-tetramethylcyclopentanecarboxylic acid (**5**) was prepared by the photo-Wolff reaction of this diazo compound in the presence of water (11). All other materials were best available commercial grades.

Kinetics, ketone enolization

Rates of enolization of 2-oxo-3,3,5,5-tetramethylcyclopentanecarboxylic acid were measured under first-order conditions by bromine scavenging of the enol as it formed, with an excess of bromine over ketone substrate. Determinations were made in aqueous hydrobromic acid solutions and acetic acid buffers using sodium bromide to maintain a constant ionic strength (0.10 mol L^{-1}). At the concentrations employed, bromine existed largely as the tribromide ion, and reactions were followed by monitoring the absorbance of this ion at λ = 330 nm. Measurements were made using either a Cary 2200 spectrometer, with ketone substrate concentration = 5 × 10^{-5} mol L^{-1} or a Hi-Tech SF-51 stopped-flow system, with substrate concentration = 1 × 10^{-4} mol L^{-1}. In both cases, the temperature of the reacting solutions was controlled at 25.1 ± 0.05 °C. The data obtained using the stopped-flow system conformed to the first-order rate law well, and observed first-order rate constants were determined by least-squares fitting of a single exponential function. In the slower runs monitored with the Cary spectrometer, on the other hand, an exponential absorbance drop was followed by a considerably slower downward drift;[3] these data conformed well to a single exponential plus linear expression, and observed first-order rate constants were obtained by fitting of such a function.

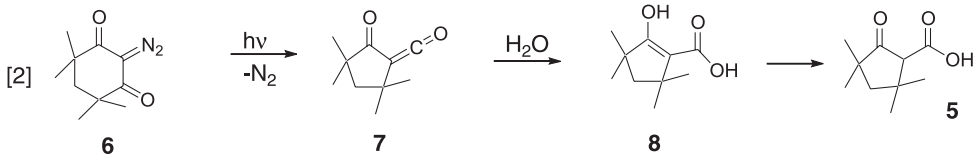
Kinetics, ketene hydration, and enol ketonization

Rates of hydration of 2-oxo-3,3,5,5-tetramethylcyclopentylideneketene were measured using a nanosecond laser flash photolysis system, operating at λ = 248 nm that has already been described (14), and rates of ketonization of 2-oxo-3,3,6,6-tetramethylcyclopentanecarboxylic acid enol were measured using a microsecond flash lamp system that has also already been described (15). Substrate concentrations were in the range (3–10) × 10^{-5} mol L^{-1}, and the temperature of all reacting solutions was maintained at 25.0 ± 0.1 °C. The data obtained conformed to the first-order rate law well, and observed first-order rate constants were determined by least-squares fitting of a single exponential function.

Results and discussion

Reaction identification

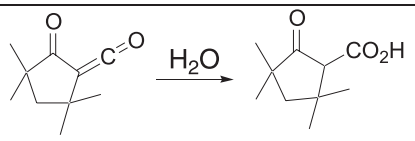
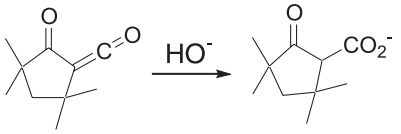
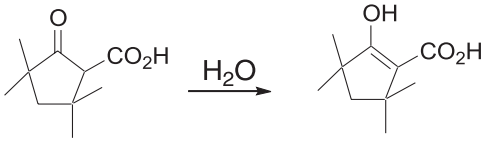
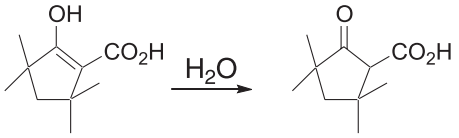
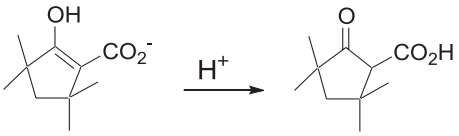
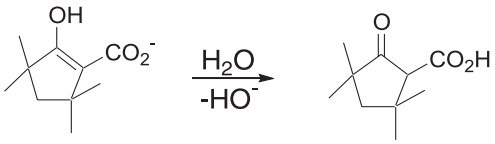
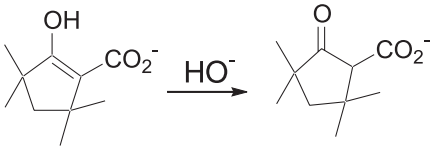
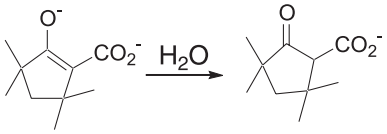
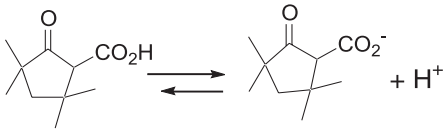
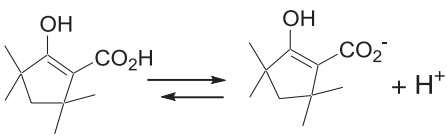
It was already known (11) that irradiation of 2-diazo-4,4,6–6-tetramethylcyclohexane-1,3-dione (**6**) with UV light gave a photo-Wolff rearrangement producing 2-oxo-3,3,5–5-tetramethylcyclopentylideneketene (**7**), which, in the presence of water, underwent rapid hydration to the enol of 2-oxo-3,3,5,5-tetramethylcyclopentanecarboxylic acid (**8**); ketonization of this enol then furnished 2-oxo-3,3,5,5-tetramethylcyclopentanecarboxylic acid itself (**5**) as the final



[3] Such consumption of additional amounts of halogen in enolization reaction studies has been observed before (4, 12) and has been attributed to subsequent hydrolysis and oxidation reactions of the initial halogenated products (12*a*); in the case of β-keto acids, such as the present substrate, decarboxylation followed by additional rapid halogenation is also known to occur (13).

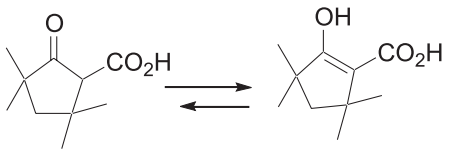
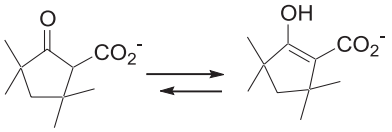
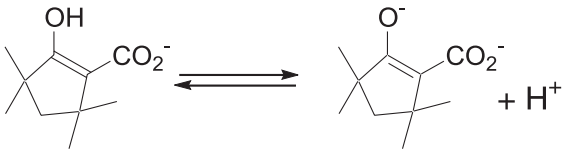
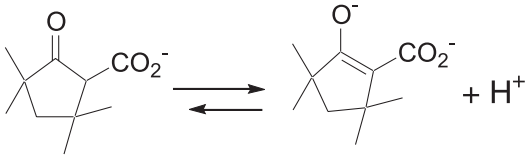
© 2005 NRC Canada

Table 1. Summary of rate and equilibrium constants for the 2-oxo-3,3,5,5-tetramethylcyclopentylideneketene and 2-oxo-3,3,5,5-tetramethylcyclopentanecarboxylic acid systems.[a]

Process	Constant
	$k_0 = 1.34 \times 10^6\ s^{-1}$
	$k_{HO} = 2.06 \times 10^6\ M^{-1}\ s^{-1}$
	$k_0^E = 1.73 \times 10^{-1}\ s^{-1}$
	$k_0^K = 7.66\ s^{-1}$
	$k'_{H^+} = 7.60 \times 10^4\ M^{-1}\ s^{-1}$
	$k'_0 = 1.74 \times 10^{-3}\ s^{-1}$
	$k'_{HO^-} = 8.49 \times 10^1\ M^{-1}\ s^{-1}$
	$k''_0 = 3.1 \times 10^2\ s^{-1}$
	$Q_{a,k} = 1.58 \times 10^{-4}$ mol L^{-1}[b] $pQ_{a,K} = 3.80$
	$Q_{a,E} = 1.03 \times 10^{-4}$ mol L^{-1}[b] $pQ_{a,E} = 3.99$

© 2005 NRC Canada

Table 1 (*concluded*).

Process	Constant
	$K_E = 2.26 \times 10^{-2}$ $pK_E = 1.65$
	$K'_E = 1.48 \times 10^{-2}$ $pK'_E = 1.83$
	$Q'^{E}_a = 4.4 \times 10^{-15}$ mol L^{-1}[b] $pQ'^{E}_a = 14.4$
	$Q'^{K}_a = 6.5 \times 10^{-17}$ mol L^{-1}[b] $pQ'^{K}_a = 16.2$

[a]Aqueous solution, 25 °C, ionic strength = 0.10 mol L^{-1}.
[b]Concentration quotient at 0.10 mol L^{-1} ionic strength.

reaction product (eq. [2]). We had observed analogous sequences of reactions before in previous flash photolytic studies of 2-diazo-1,3-diketones (3–6), where they appeared as a rapid microsecond absorbance rise in the region λ = 250–300 nm, attributable to ketene hydration, followed by a much slower millisecond decay of this absorbance, attributable to enol ketonization. Similar absorbance changes were observed in the present study. That and the chemistry provided by these absorbance changes, plus the known occurrence of the reactions of eq. [2], established the processes that we were monitoring as the hydration of 2-oxo-3,3,5–5-tetramethylcyclopentylideneketene (**7**), and the ketonization of 2-oxo-3,3,5,5-tetramethylcyclopentanecarboxylic acid enol (**8**).

Ketene hydration

Rates of hydration of 2-oxo-3,3,5,5-tetramethylcyclopentylideneketene were measured in aqueous perchloric acid and sodium hydroxide solutions and in acetic acid, biphosphate ion, and tris(hydroxymethyl)methylammonium ion buffers. The ionic strength of these solutions was maintained at 0.10 mol L^{-1}, except for four sodium hydroxide concentrations in the range 0.2–0.5 mol L^{-1} where ionic strength = [NaOH]: hydroxide ion catalysis of this reaction was weak, and measurements at hydroxide ion concentrations above 0.10 mol L^{-1} were required to obtain reliable values of the hydroxide ion catalytic coefficient. These data are summarized in Tables S1–S3.[4]

The measurements in buffers were made in a series of solutions of constant buffer ratio, and therefore constant hydronium ion concentration, but varying total buffer concentration. The data were analyzed by linear least-squares fitting of the buffer dilution expression shown as eq. [3]. Buffer catalysis proved to be either weak or

$$[3] \qquad k_{obs} = k_{int} + k_{buff}[\text{buffer}]$$

nonexistant, and buffer catalytic coefficients (k_{buff}) were not well-determined. This is typical of ketene reactions in the buffers employed, inasmuch as the buffer bases react as nucleophiles and the nucleophilic strength of the present buffer bases is weak (16). The zero-buffer-concentration intercepts (k_{int}), on the other hand, were accurately fixed. These, plus the rate constants determined in perchloric acid and sodium hydroxide solutions, are displayed as the upper rate profile of Fig. 1. Hydronium ion concentrations (written here as $[H^+]$) of the buffer solutions needed for this purpose were obtained by calculation using acidity constants of the buffer acids from the literature and activity coefficients recommended by Bates (17).

The present rate profile is typical of ketene hydrations, which generally show long uncatalyzed portions, weak hydroxide ion catalysis, and weak or nonexistant hydronium

[4]Tables of rate data (Tables S1–S10) may be purchased from the Depository of Unpublished data, Document Delivery, CISTI, National Research Council Canada, Ottawa, ON K1A OS2, Canada (http://www.nrc.ca/cisti/irm/unpub_e.shtml for information on ordering electronically).

© 2005 NRC Canada

ion catalysis (18). The rate law that applies in the present case is shown as eq. [4],

$$[4] \qquad k_{obs} = k_o + k_{HO}[HO^-]$$

and least-squares fitting of this expression gave $k_o = (1.34 \pm 0.01) \times 10^6$ s^{-1} and $k_{HO} = (2.06 \pm 0.113) \times 10^6$ M^{-1} s^{-1} (Table 1).

Enol ketonization

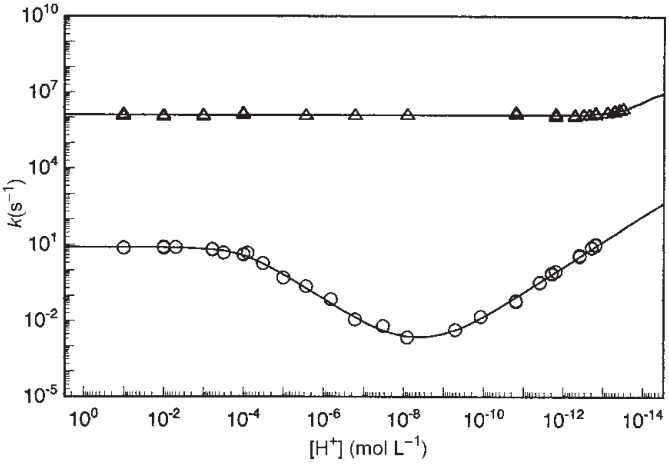
Rates of ketonization of 2-oxo-3,3,5,5-tetramethylcyclopentanecarboxylic acid enol were measured in aqueous perchloric acid and sodium hydroxide solutions and also in formic acid, acetic acid, biphosphate ion, tris(hydroxymethyl)methylammonium ion, ammonium ion, and bicarbonate ion buffers. The ionic strength of these solutions was maintained at 0.10 mol L^{-1}. The data are summarized in Tables S4–S6.[4]

The measurements in buffers were once again done in a series of solutions of constant buffer ratio, and therefore constant hydronium ion concentration, but varying total buffer concentration, and the data were analyzed by least-squares fitting of the buffer dilution expression of eq. [3]. Buffer catalysis was now strong, which is typical of enol ketonization reactions where buffers serve as proton transfer reagents. The zero-buffer-concentration intercepts together with the rate constants measured in perchloric acid and sodium hydroxide solutions are displayed as the lower rate profile shown in Fig. 1.

This rate profile is characteristic of enol ketonizations and may be understood in terms of the accepted mechanism for this reaction, which involves rate-determining β-carbon protonation of enol or enolate ion by any available acid (19). Because this profile refers to solvent-related species, the protonating acid will be either the hydronium ion or a water molecule. Since ketonization is an electrophilic addition reaction, successively ionized forms of the enol will be more reactive than their precursors, and ketonization will take place through them even when they are relatively minor substrate species.

Over the acidity range represented by the present rate profiles, the enol will react through either its monoanionic or dianionic form, as shown in eq. [5]. This produces a horizontal uncatalyzed rate profile segment at the high acidity end, where ketonization is through carbon protonation of the enol carboxylate ion by H$^+$ while un-ionized enol is still the major substrate species. Such a reaction produces H$^+$ in the rapidly established pre-equilibrium step and then uses it up in the rate-determining step, giving an overall process independent of H$^+$ concentration.

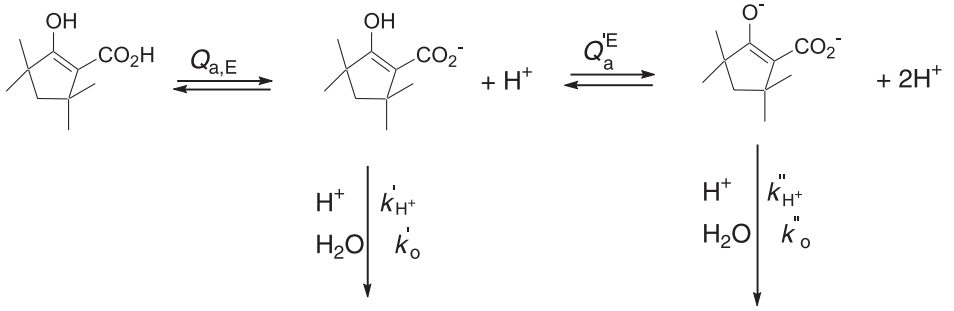
Fig. 1. Rate profiles for the hydration of 2-oxo-3,3,5,5-tetramethylcyclopentylideneketene (Δ) and the ketonization of 2-oxo-3,3,5,5-tetramethylcyclo-pentanecarboxylic acid enol (O) in aqueous solution at 25 °C.



As the acidity drops this uncatalyzed ketonization gives way to a reaction where H$^+$ is still the protonating agent, but now the enol exits mainly in its carboxylate ion form. This produces a downward bend in the profile, corresponding to the carboxylic acid group ionization constant $Q_{a,E}$, and leading to a diagonal acid-catalyzed segment of slope = –1. At sufficiently low acidity, this acid catalysis gives way to a narrow second horizontal plateau, whose origin is sometimes uncertain, as discussed below. Beyond this plateau, ketonization takes place through the dianionic form of the enol while its monoanion is still the dominant substrate form, with water as the carbon-protonating agent. This gives a pre-equilibrium that produces H$^+$, but the latter is now not used up in the rate-determining step; this produces a process whose rate is inversely proportional to H$^+$ concentration and has the appearance of hydroxide ion catalysis.

In the rate profiles for ketonization of some of the previous β-oxocarboxylic acid enols that we investigated, this apparent hydroxide ion catalysis became saturated and gave way to a third horizontal plateau as the fully ionized enol became the dominant substrate species (3–5). This did not happen in the present case because the acidity constant of this enol ($pQ'^{E}_{a} = 14.4$, vide infra) is well beyond the rate profile limit (p[H$^+$] = 12.8) imposed by the requirement that ionic strength be kept constant at 0.10 mol L^{-1}.

[5]



© 2005 NRC Canada

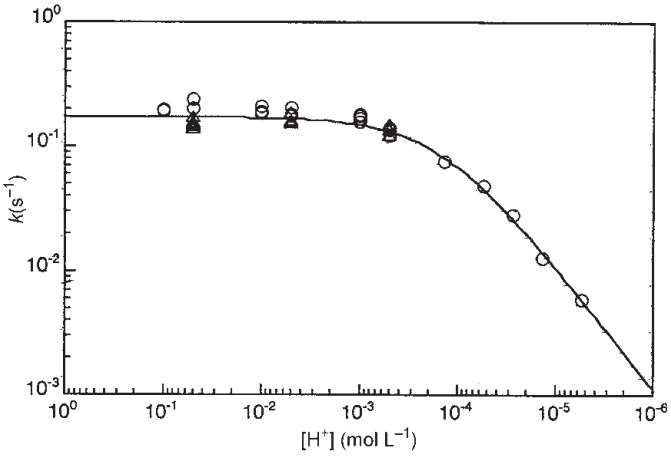
The rate law that corresponds to this reaction scheme is given in eq. [6],

$$[6] \qquad k_{obs} = \frac{k'_{H^+}Q_{a,E}[H^+]}{Q_{a,E} + [H^+]} + k'_{uc} + k'_{HO^-}[HO^-]$$

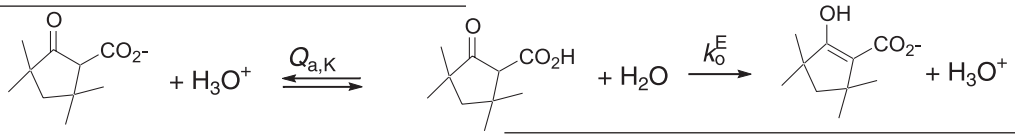
with (k'_{uc}) as the rate constant for the process of uncertain origin responsible for the horizontal plateau at the center of the rate profile, and k'_{HO^-} as the rate constant for the apparent hydroxide ion catalysis; the other constants are defined by eq. [5]. Least-squares fitting of this expression gave $k'_{H^+} = (7.60 \pm 0.63) \times 10^4$ M^{-1} s^{-1}, $Q_{a,E} = (1.03 \pm 0.11) \times 10^{-4}$ mol L^{-1}, $pQ_{a,E} = 3.99 \pm 0.05$,[5] $k'_{uc} = (1.74 \pm 0.37) \times 10^{-3}$ s^{-1}, and $k'_{HO^-} = (8.49 \pm 0.34) \times 10^1$ M^{-1} s^{-1}.

It was pointed out above that the origin of the rate profile plateau with rate constant k'_{uc} is sometimes uncertain. This is because it could be due either to ketonization of the monoanionic form of the enol through carbon protonation by a water molecule or to equilibrium ionization of the monoanion to the dianion followed by carbon protonation of that by H^+. In the latter case, k'_{uc} would be equal to $k''_{H^+}Q'^{E}_{a}$, and use of the estimate $pQ'^{E}_{a} = 14.4$ (vide infra) then provides $k''_{H^+} = (4.0 \pm 2.1) \times 10^{11}$ M^{-1} s^{-1}. This is a very large rate constant whose value exceeds the encounter-controlled limit ($k \cong 10^{10}$ M^{-1} s^{-1}) for two particles in aqueous solution at 25 °C (20). This suggests that k'_{uc} does not represent reaction of the dianionic form of the enol with H^+, but is rather due to carbon protonation of the monoanionc form by a water molecule.

Fig. 2. Rate profile for the enolization of 2-oxo-3,3,5,5-tetramethylcyclopentanecarboxylic acid in aqueous solution at 25 °C based on rate constants measured with conventional (O) and stopped-flow (Δ) spectrometers.



that involved rate-determining carbon protonation of the carboxylate ion form of the enol by hydronium ion, providing un-ionized 2-oxo-3,3,5,5-tetramethylcyclopentanecarboxylic acid and a water molecule as reaction products (vide supra). Enolization will therefore occur by the rate-determining reaction of the un-ionized carboxylic acid with a water molecule, giving the horizontal uncatalyzed region seen at the high acidity end of the rate profile of Fig. 2. The un-ionized acid, however, will also be in equilibrium with its less reactive carboxylate ion, as shown in eq. [7], and the

[7] 

need to convert this ion to the more reactive un-ionized acid before enolization can take place will give the acid-catalyzed region seen at the lower acidity end of the rate profile of Fig. 2. The bend in the profile connecting these two regions, of course, corresponds to the ionization constant of the substrate acid.

The rate law that fits this reaction scheme is shown as eq. [8] whose rate and

$$[8] \qquad k_{obs} = k_o^E[H^+]/([H^+] + Q_{a,K})$$

equilibrium constants are defined in eq. [7]. Least-squares analysis of the data using this expression gave $k_o^E = (1.73 \pm 0.04) \times 10^{-1}$ s^{-1} and $Q_{a,K} = (1.55 \pm 0.11) \times 10^{-4}$ mol^{-1}, $pQ_{a,K} = 3.81 \pm 0.03$.[5]

The acidity constant $Q_{a,K}$ of the carboxylic acid group of 2-oxo-3,3,5,5-tetramethylcyclopentanecarboxylic acid was also determined spectrophotometrically by monitoring the reversible absorbance change at λ = 225 nm that occurred as this acid ionized. Absorbance measurements (A) were made in aqueous perchloric acid solutions and acetic acid and biphosphate ion buffers, using a fixed stoichiometric concentration (7.15×10^{-4} mol L^{-1}) of the cyclopentanecarboxylic

Ketone enolization

Rates of enolization of 2-oxo-3,3,5,5-tetramethylcyclopentanecarboxylic acid were measured in aqueous hydrobromic acid solutions over the concentration range [HBr] = 0.1–0.0005 mol L^{-1} and in acetic acid buffers that extended this acidity range down to 5×10^{-6} mol L^{-1}. The data so obtained are summarized in Tables S7 and S8.[4]

The measurements in buffers were once again made in a series of solutions of constant buffer ratio, and therefore constant hydronium ion concentration, but varying total buffer concentration. Buffer catalysis was strong, and the data were analyzed by least-squares fitting of the buffer dilution expression given in eq. [3]. The k_{int} obtained in this way, together with the rate constants measured in hydrobromic acid solution, are displayed as the rate profile shown in Fig. 2. It may be seen that rate constants measured using conventional and stopped-flow spectrometers agree very well with one another.

This enolization reaction is the microscopic reverse of the ketonization of 2-oxo-3,3,5–5-tetramethylcyclopentanecarboxylic acid enol, which was assigned a reaction mechanism in the acidity region of these enolization rate measurements

[5] This is a concentration acidity constant applicable at ionic strength = 0.10 mol L^{-1}.

© 2005 NRC Canada

acid substrate. The ionic strength of these solutions was maintained at 0.10 mol L^{-1}. The data so obtained are summarized in Table S9.[5]

These results were analysed by least-squares fitting of the titration curve expression shown as eq. [9], in which A_{HA} is the absorbance of un-ionized acid and A_A is

$$[9] \qquad A = (A_{HA}[H^+] + A_A Q_{a,K})/(Q_{a,K} + [H^+])$$

the absorbance of its carboxylate ion. This gave $Q_{a,K}$ = (1.59 ± 0.08) ×10^{-4} mol L^{-1}, in very good agreement with the result obtained from the enolization rate measurements ($Q_{a,K}$ = (1.55 ± 0.11) × 10^{-4} mol L^{-1}). The weighted average of the two values is (1.58 ± 0.06) × 10^{-4} mol L^{-1}, $pQ_{a,K}$ = 3.80 ± 0.02.[5]

Keto–enol equilibria

The enolization and ketonization rate constants determined here can be combined to provide keto–enol equilibrium constants for the 2-oxo-3,3,5,5-tetramethylcyclopentanecarboxylic acid system. Two such equilibrium constants may be defined: one (K_E), relating keto and enol isomers with the carboxylic acid group in its un-ionized form and another (K'_E), with this group in its ionizied carboxylate form.

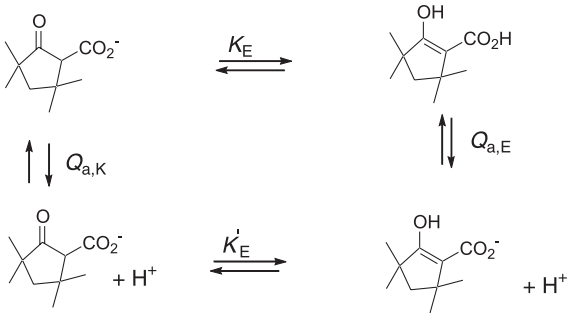
The first of these equilibrium constants can be formulated as the ratio of enolization to ketonization rate constants, as shown in eq. [10], using rate constants that

$$[10] \qquad K_E = k_o^E/k_o^K$$

refer to enolization in the uncatalyzed reaction of the rate profile shown in Fig. 2 and ketonization in the corresponding region of the rate profile of Fig. 1. The rate profile of Fig. 1, however, was constructed using rates of decay of enol, which, because ketonization is slightly reversible (K_E = 0.02, vide infra) are actually rates of approach to equilibrium and contain a small (2%) enolization component. The quantity $k'^K_{H^+}Q_{a,E}$ that represents the acid-region plateau of the profile in Fig. 1 must therefore be corrected by subtracting off k_o^E to convert it into a pure ketonization rate constant: $k_o^K = k'^K_{H^+}Q_{a,E} - k_o^E$ = (7.66 ± 0.44) s^{-1}. Rates of enolization, of course, require no correction because they were determined by bromine scavenging under nonreversible conditions. The rate and equilibrium constants determined here when applied in this way then lead to K_E = (2.26 ± 0.14) × 10^{-2}, pK_E = 1.65 ± 0.03.

The second keto–enol equilibrium constant (K'_E) involving carboxylate ion species, can be evaluated from K_E using the thermodynamic cycle shown in eq. [11]. The relationship $K'_E = K_E Q_{a,E}/Q_{a,K}$ using values of $Q_{a,E}$ and $Q_{a,K}$ determined here then leads to K'_E = (1.48 ± 0.20) × 10^{-2}, pK'_E = 1.83 ± 0.06.

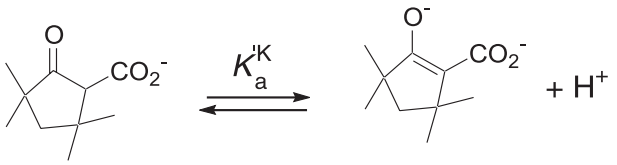
[11]



Carbon acid strength

The acidity constant of 2-oxo-3,3,5,5-tetramethylcyclopentanecarboxylate ion ionizing further as a carbon acid (eq. [12]) was determined spectrophotometrically by monitoring the reversible absorbance change at λ = 280 nm that accompanies this reaction. Absorbance measurements were made in aqueous potassium hydroxide solutions over the concentration range [KOH] = 0.2–14 mol L^{-1} using a constant stoichiometric concentration (7.2 × 10^{-5} mol L^{-1}) of substrate. The data so obtained are summarized in Table S10.[4]

[12]



Because these measurements were made in concentrated potassium hydroxide solutions, the results should be analyzed using a basicity function to express solvent basic strength. Three basicity functions were tried: an H_- scale based on neutral indole indicators (21), an $H_=$ scale based on indoles bearing carboxylate groups (21), and an $H_=$ scale based on aromatic amines bearing carboxylate and sulfonate groups (22). The absorbance data were first transformed into values of I (= [basic form]/[acidic form]) and the fit of log I to each of these basicity scales was determined. Each basicity scale gave an adequately linear plot of log I vs. the basicity function. The slope of the plot using H_-, however, was significantly different from unity (1.26 ± 0.02), and this function was consequently deemed unsuitable for analyzing the present results. The slopes of the two plots using $H_=$ scales, on the other hand, were both indistinguishable from unity and were in fact the same: 1.02 ± 0.02. The data were therefore analyzed using each of these functions: least-squares fitting using eq. [9] with $10^{-H_=}$ in place of $[H^+]$ gave K_a = (3.65 ± 0.09) × 10^{-17} mol L^{-1} with the Yagil $H_=$ scale and K_a = (1.34 ± 0.03) × 10^{-17} mol L^{-1} with the Halle $H_=$ scale.

It is not clear which of these results is to be preferred. We therefore took the simple average, which gave K_a = (2.50 ± 1.16) × 10^{-17} mol L^{-1}, pK_a = 16.60 ± 0.20. It is unfortunate that this gives a result with a rather large uncertainty (ca. 50%), but this value is still sufficiently precise to allow some interesting conclusions to be drawn (vide infra).

Basicity functions such as the $H_=$ scales used here are anchored to an infinitely dilute standard state, and the acidity constant K_a determined here is therefore a thermodynamic value applicable at zero ionic strength. It may be converted to a concentration dissociation constant (Q'^K_a) appropriate to the ionic strength (0.10 mol L^{-1}) used for the other measurements made here, by applying appropriate activity coefficients. Use of f = 0.83 for the hydronium ion (17), plus the

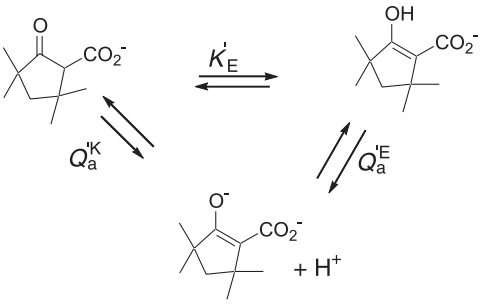
© 2005 NRC Canada

acetate ($f = 0.775$) (17) and hydrogen citrate ($f = 0.36$) (17) values as surrogates for the mono- and dianions of eq. [12], then gives $Q_a'^K = (6.48 \pm 3.00) \times 10^{-17}$ mol L^{-1}, $pQ_a'^K = 16.19 \pm 0.20$.[5]

pK_E' and k_0'' determination

The thermodynamic cycle given in eq. [13] shows that $Q_a'^K = K_E' Q_a'^E$. This relationship then allows the enol acidity constant $Q_a'^E$ to be determined from the now known values of

[13]

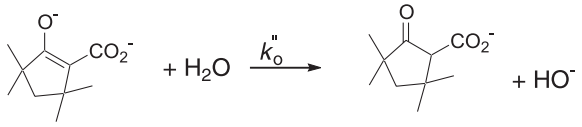


K_E' and $Q_a'^K$: $Q_a'^E = Q_a'^K/K_E' = (4.38 \pm 2.11) \times 10^{-15}$ mol L^{-1}, $pQ_a'^E = 14.36 \pm 0.21$.[5]

It was pointed out above that values of this acidity constant for some other β-oxocarboxylic acid systems were obtained from bends at the low acidity ends of their rate profiles. The very low value of this acidity constant estimated here for the present system shows why such a rate-profile-derived determination could not be made in this case: the relevant bend would have come well beyond the lowest acidity available ([H$^+$] = 10^{-13} mol L^{-1}), consistent with maintaining an ionic strength of 0.10 mol L^{-1}.

This presently determined estimate of $Q_a'^E$ can in turn be used to obtain a value of the rate constant k_0'' for ketonization by the uncatalyzed route beyond the unobserved rate profile bend, i.e., through carbon protonation of the enol dianion by a water molecule, as shown in eq. [14]. This

[14]

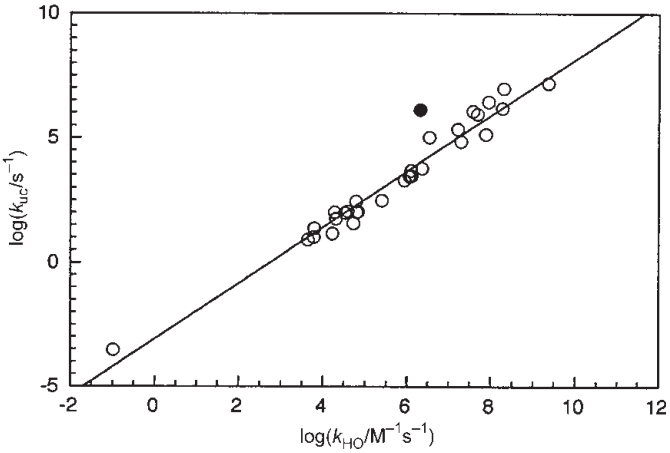


rate constant is related to the hydroxide ion rate constant of eq. [6], $k'^K_{HO^-}$: $k'^K_{HO^-} = k_0'' Q_a'^E / Q_w$, and use of the known values of $Q_a'^E$ and the autoprotolysis constant of water (Q_w) gives $k_0'' = (3.07 \pm 1.48) \times 10^2$ s^{-1}. This result is considerably above the largest rate constant measured at the low acidity end of the rate profile of Fig. 1, which again points to the incompatibility of making measurements in this profile region while maintaining an ionic strength of 0.10 mol L^{-1}.

Comparison with the unmethylated cyclopentyl system

The rate of uncatalyzed hydration of 2-oxo-3,3,5,5-tetramethylcyclopentylideneketene determined here is virtually the same as that for the unmethylated 2-oxocyclopentylideneketene (4): the two rate constants differ by less than 5%. The rates of the hydroxide-ion-catalyzed hydrations of the ketenes, on the other hand, differ by a factor of 37, with the present ketene being the more slowly reacting substrate.

Fig. 3. Correlation of rate constants for the hydroxide-ion-catalyzed and uncatalyzed hydration reactions of ketenes. The filled circle represents hydration of the presently examined substrate.



The reason for this striking difference in behavior of the uncatalyzed and hydroxide-ion-catalyzed reactions is not at all clear. The methylated ketene would, of course, be expected to be the more slowly reacting substrate, inasmuch as both water and hydroxide ion serve as nucleophiles in these reactions, adding to the ketene carbonyl carbon atom through approach in the ketene molecular plane (23); such approach is hindered by the methyl groups in the methylated cyclopentyl system. Some difference in the hindrance encountered by water and hydroxide ion is also to be expected, for hydroxide is strongly solvated in aqueous solution and is consequently a considerably larger nucleophile than is a water molecule. A change from identical rate constants to a factor of 37 difference in going from water to hydroxide ion is, however, surprising.

At any rate, this retardation of the hydroxide-ion-catalyzed ketene hydration, but not of the water reaction, produces a striking deviation from a correlation of rate constants for the hydroxide ion and water reactions of some 30 other ketenes (24). This deviation is shown in Fig. 3.

There are also interesting differences between the methylated and unmethylated systems in their keto–enol interconversions. The rate of water-catalyzed enolization, for example, in the methylated system is 3.3 times faster than in the unmethylated system. The rate of enol ketonization, on the other hand, is 2.2 times slower in the methylated than in the unmethylated system. These differences propagate into a difference in keto–enol equilibrium constants through the relationship that expresses the equilibrium constant as a ratio of enolization to ketonization rate constants: $K_E = k_E/k_K : K_E$ for the methylated system is 7.3 times that for the unmethylated system, which is nicely consistent with the product $3.3 \times 2.2 = 7.3$.

This difference can be understood in terms of strain produced by eclipsing interactions in the keto isomer between the carboxylic acid group and hydrogen atom at position 1 and the substituents at position 5. This strain is relieved as the keto form isomerizes to the enol form and the state of

© 2005 NRC Canada

hybridization of carbon number 1 changes from sp^3 to sp^2. This eclipsing strain is, of course, greater in the methylated system with its methyl groups at position 5 than in the unmethylated system with only hydrogen atoms at this location. The methylated system consequently has more to gain from this relief of strain, thus making its keto–enol equilibrium constants greater than that for the unmethylated system.

Acknowledgement

We are grateful to the Natural Sciences and Engineering Research Council of Canada (NSERC) for financial support of this work.

References

1. C.K. Ingold. *In* Structure and mechanism in organic chemistry. 2nd ed. Cornell University Press, Ithaca, N.Y. 1969. pp. 794–837; G.W. Wheland. *In* Advanced organic chemistry. 3rd ed. Wiley, New York. 1960. pp. 663–703.
2. J. Toullec. *In* The chemistry of enols. *Edited by* Z. Rappoport. Wiley, New York. 1990. pp. 353–378.
3. Y. Chiang, H.-X. Guo, A.J. Kresge, and O.S. Tee. J. Am. Chem. Soc. **118**, 3386 (1996).
4. Y. Chiang, A.J. Kresge, V.A. Nikolaev, and V.V. Popik. J. Am. Chem. Soc. **119**, 11 183 (1997).
5. Y. Chiang, A.J. Kresge, Q. Meng, Y. Morita, and Y. Yamamoto. J. Am. Chem. Soc. **121**, 8345 (1999).
6. J.A. Chang, A.J. Kresge, V.A. Nikolaev, and V.V. Popik. J. Am. Chem. Soc. **125**, 6478 (2003).
7. S. Hoz and A.J. Kresge. J. Phys. Org. Chem. **10**, 182 (1997).
8. Y. Chiang, A.J. Kresge, and N.P. Schepp. J. Am. Chem. Soc. **111**, 3977 (1989).
9. J.P. Guthrie. Can. J. Chem. **71**, 2123 (1993); J.P. Guthrie and Z. Liu. Can. J. Chem. **73**, 1395 (1995).
10. K. Korobitsyna and V.A. Nikolaev. J. Org. Chem. USSR (Engl. Transl.), **12**, 1245 (1976).
11. K. Korobitsyna and V.A. Nikolaev. J. Org. Chem. USSR (Engl. Transl.), **12**, 1252 (1976).
12. (*a*) J.P. Guthrie and J. Cossar. Can. J. Chem. **68**, 397 (1990); J.P. Guthrie, J. Cossar, and J. Lu. Can. J. Chem. **69**, 1904; (*b*) R.P. Bell and M.I. Page. J. Chem. Soc. Perkin Trans. 2, 1681 (1973).
13. E.J. Corey. J. Am. Chem. Soc. **75**, 3297 (1953).
14. J. Andraos, Y. Chiang, C.G. Huang, A.J. Kresge, and J.C. Scaiano. J. Am. Chem. Soc. **115**, 10 605 (1993).
15. Y. Chiang, M. Hojatti, J.R. Keeffe, A.J. Kresge, N.P. Schepp, and J. Wirz. J. Am Chem. Soc. **109**, 4000 (1993).
16. J. Andraos and A.J. Kresge J. Am. Chem. Soc. **114**, 5643 (1992).
17. R.G. Bates. *In* Determination of pH theory and practice. Wiley, New York. 1973. p. 49.
18. Y. Chiang, A.J. Kresge, and V.V. Popik. J. Am. Chem. Soc. **117**, 9165 (1995).
19. J.R. Keeffe and A.J. Kresge. *In* The chemistry of enols. *Edited by* Z. Rappoport. Wiley, New York. 1990. Chap. 7.
20. E.F. Caldin. *In* The mechanism of fast reactions in solution. IOS Press, Washington, D.C. 2001. pp. 33–36.
21. G. Yagil. J. Phys. Chem. **71**, 1034 (1967).
22. J.-C. Halle, F. Terrier, and R. Schall. Bull. Soc. Chim. Fr. 4569 (1969).
23. T.T. Tidwell. *In* Ketenes. Wiley-Interscience, New York. 1995. pp. 571–587.
24. J. Andraos and A.J. Kresge. Can. J. Chem. **78**, 508 (2000).

© 2005 NRC Canada

AWARD LECTURE / CONFÉRENCE D'HONNEUR

2004 Alcan Award Lecture
From dinuclear to triakontahexanuclear complexes — Adventures in supramolecular coordination chemistry[1]

Laurence K. Thompson

Abstract: Polynuclear coordination complexes result from the interplay between the arrangement of the binding sites of a ligand, and their donor content, and the coordination preferences of the metal ion involved. Rational control of the ligand properties, such as denticity, geometry, and size, can lead to large, and sometimes predictable, polynuclear assemblies. This Alcan Award Lecture highlights our "adventures" with polynucleating ligands over the last 25 years, with examples ranging from simple dinucleating to more exotic high-denticity ligands. Complexes with nuclearities ranging from 2 to 36 have been produced, many of which have novel magnetic, electrochemical, and spectroscopic properties. Self-assembly strategies using relatively simple "polytopic" ligands have been very successful in producing high-nuclearity clusters in high yield. For example, linear "tritopic" ligands produce M_9 (M = Mn(II), Fe(II), Fe(III), Co(II), Ni(II), Cu(II), Zn(II)) [3 × 3], flat grid-like molecules, which have quantum dot-like arrays of nine closely spaced metal centers in electronic communication. Some of these grids are discussed in terms of their novel magnetic and electrochemical properties, and also as multistable nanometer-scale platforms for potential molecular device behaviour. Bigger ligands with extended arrays of coordination pockets, and the capacity to self-assemble into much larger grids, are highlighted to illustrate our current and longer term goals of generating polymetallic molecular two-dimensional layers on surfaces.

Key words: Alcan Award Lecture, transition metal, polynuclear, structure, magnetism, electrochemistry, surface studies, molecular device.

Résumé : Les complexes de coordination polynucléaires résultent de l'interaction entre l'arrangement des sites de fixation d'un ligand et leur contenu en donneur et les préférences de coordination de l'ion métallique impliqué. Un contrôle rationnel des propriétés du ligand, par exemple, la denticité, la géométrie et la taille, peuvent conduire à d'importants assemblages polynucléaires qui quelquefois peuvent être prédites. Cette conférence du prix Alcan met en relief notre aventure de plus de ving-cinq ans avec les ligands de polynucléation et comporte des exemples allant de simples dinucléations à des ligands plus exotiques de denticité plus élevée. On a produit des complexes comportant des nucléarités allant de deux à trente-six dont plusieurs présentent de nouvelles propriétés magnétiques, électrochimiques et spectroscopiques. Les stratégies d'autoassemblage faisant appel à des ligands polytopes relativement simples ont connu de grands succès dans la production d'agrégats de nucléarité élevée avec d'excellents rendements. Par exemple, les ligands tritopiques conduisent à la formation de M_9 [M = Mn(II), Fe(II), Fe(III), Co(II), Ni(II), Cu(II), Zn(II)] [3 × 3], des molécules planes et en forme de réseaux qui possèdent des arrangements pointillés quantiques de neuf centres métalliques en proche proximité et en communication électronique. Certains de ces réseaux peuvent être discutés en termes de leurs nouvelles propriétés magnétiques et électrochimiques ainsi que leur rôle potentiel de plates-formes multistables d'échelle nanométrique pour le comportement de dispositifs moléculaires. Afin d'illustrer nos objectifs tant courant que ceux à long terme relatif à la génération de molécules polynucléaires à couches bidimensionnelles sur des surfaces, on présentera des ligands plus gros comportant des arrangements plus étendus de poches de coordination ayant la capacité de s'autoassembler en réseaux plus grands.

Mots clés : conférence du prix Alcan, métal de transition, polynucléaire, structure, magnétisme, électrochimie, études de surface, dispositif moléculaire.

[Traduit par la Rédaction]

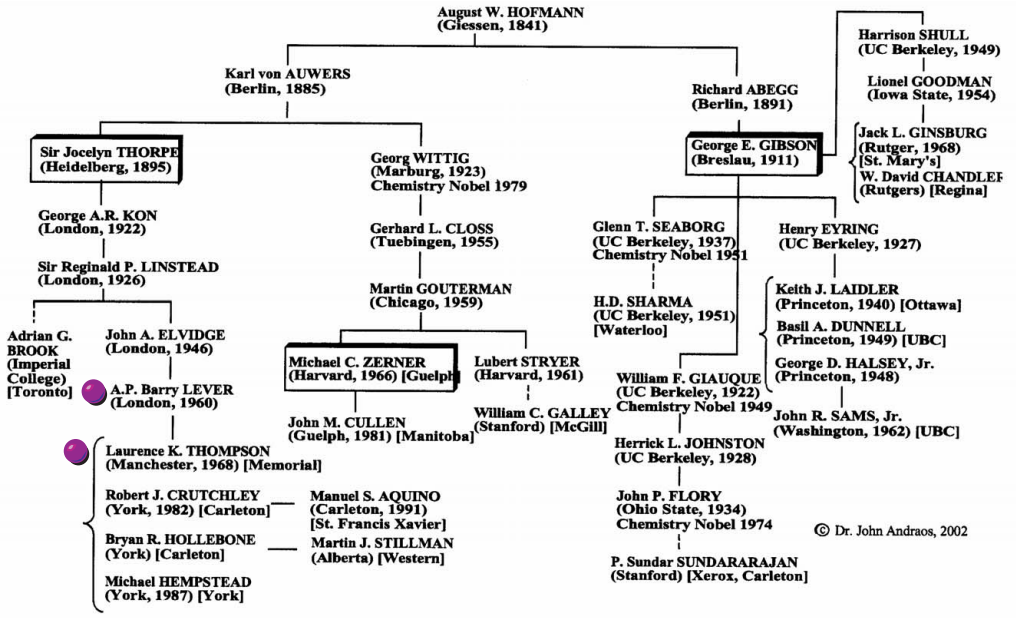
Received 9 September 2004. Published on the NRC Research Press Web site at http://canjchem.nrc.ca on 25 February 2005.

L.K. Thompson. Department of Chemistry, Memorial University, St. John's, NL A1B 3X7, Canada. (e-mail: lthomp@mun.ca).

[1]Presented at the 87th Canadian Chemistry Conference and Exhibition, London, Ontario, May 29–June 1, 2004.

 doi: 10.1139/V04-173 © 2005 NRC Canada

Fig. 1. Academic family tree and portrait of August Hofmann.





August Wilhelm Hofmann (1818-1892)

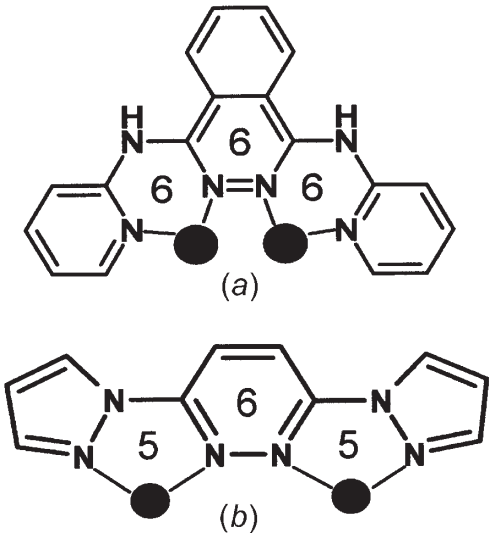
Introduction

A major influence in one's approach to research inevitably stems from the research interests of one's Ph.D. advisor, and also on one's academic lineage. My academic family tree (Fig. 1) shows that organic chemistry is a strong influence in this background, with connections through Sir Reginald P. Linstead and Sir Jocelyn Thorpe to August W. Hofmann. In this context, it is interesting to note that Hofmann attended the University of Giessen in the 1830s with the intention of studying law and philosophy but, after attending Liebig's lectures, became most interested in chemistry. In the mid 1800s, he was instrumental in establishing the Royal College of Chemistry in London.

As an undergraduate at UMIST (University of Manchester Institute of Science and Technology) in the mid 1960s,

© 2005 NRC Canada

Fig. 2. (*a*) Model 6–6–6 dinuclear phthalazine complex. (*b*) Model 5–6–5 dinuclear pyridazine complex.



blending core science and "technology" was a natural focus. It is perhaps ironic that in the current chemical "arena" this is suddenly seen as an important direction, with e.g., "Materials Applications" being a major platform in departmental and university strategic plans. Barry Lever (Ph.D. advisor) had broad interests in coordination chemistry and spectroscopy and provided a rich opportunity for a raw graduate student to get a quick start in an interesting and productive research area. I chose a project on phthalazine coordination chemistry (Fig. 2*a*), which started my journey into the realm of polynuclear complexes, with the interesting properties provided by the presence of more than one metal ion in a molecule, e.g., electronic and magnetic communication.

Research summary

Complexes derived directly from polyfunctional ligands

The successful developments and advances in X-ray crystallography in the 1950s, coupled with improvements in computing power, expanded the scope of biological chemistry, and in particular metallo-protein chemistry, with the successful solution of the structures of a number of metal-containing proteins and enzymes. These were restricted to fairly small systems, and yet interest in probing and understanding active-site protein structure and function led to the emergence of a new field combining biological and inorganic chemistry — bioinorganic chemistry. "Model" compounds were synthesized in their thousands by coordination chemists trying to "mimic" metallo-protein active-site structures on the basis of, e.g., spectroscopic and magnetic properties.

Polydentate aromatic diazine ligands, e.g., phthalazines (Fig. 2*a*; 1,4-di(2′-pyridyl)aminophthalazine (pap); defined as a 6–6–6 system based on the sequence of chelate ring and diazine ring sizes) provided a unique platform for the systematic examination of magnetic properties as a function of structure in a series of dinuclear copper(II) complexes. These were studied as active-site models for the dinuclear centers in, e.g., hemocyanin, laccase, and ascorbate oxidase. The parent compound in this class, $[Cu_2(pap)(\mu_2\text{-}OH)(\mu_2\text{-}Cl)Cl_2]\cdot 1.5H_2O$ (**1**) (Fig. 3), is formed by simply reacting pap with $CuCl_2\cdot 2H_2O$ in water. A crystal structure revealed a dinuclear center, with two square-pyramidal copper(II) ions spaced at 2.99 Å (avg.), with μ_2-OH (Cu-O-Cu bridge angle 100.9° (avg.)) and phthalazine N_2 groups bridging the metals (1). The copper(II) ions are antiferromagnetically exchange-coupled through the diazine and hydroxide bridges with a singlet–triplet splitting ($-2J$) of 200 cm^{-1} (2). It was observed that changing the anion in a series of related complexes led to a variation in exchange coupling. The anionic replacement occurred at the apical bridging position and caused a dramatic change in the dinuclear center dimensions, with increasing Cu–Cu distances (3.14–3.22 Å) and Cu-OH-Cu bridge angles (111–116°) as single-atom bridges (e.g., Cl) were replaced by triatomic bridges (e.g., SO_4^{2-}, ClO_4^-, IO_3^-, NO_3^-) (see Fig. 4 for the IO_3^--bridged complex $[Cu_2(pap)(\mu_2\text{-}OH)(\mu\text{-}IO_3)(IO_3)_2]\cdot 4H_2O$ (**2**); Cu-OH-Cu 113.8(2)°). The $-2J$ values increased accordingly (280–600 cm^{-1}) (3–6), and in all cases the hydroxide bridge remained intact.

To increase the dinuclear dimensions further, a ligand modification strategy was employed, which involved changing the size of the chelate rings formed on coordination. Reducing the ring size from six in the phthalazine ligands to five in ligands like 3,6-bis(1-pyrazolyl)pyridazine (ppd) (Fig. 2*b*; 5–6–5 system) results in a dramatic expansion of the dinuclear center with a much larger increase in dinuclear center dimensions (Cu–Cu 3.29–3.46 Å; Cu-OH-Cu 117–127°), and a resulting increase in exchange coupling ($-2J$ =

Fig. 3. Structural representation of $[Cu_2(pap)(\mu_2\text{-}OH)(\mu_2\text{-}Cl)Cl_2]\cdot 1.5H_2O$ (**1**).

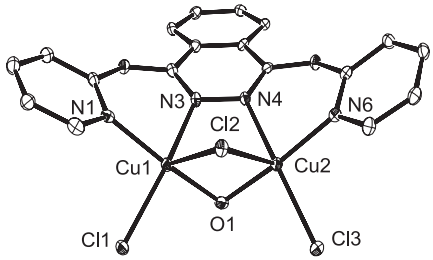
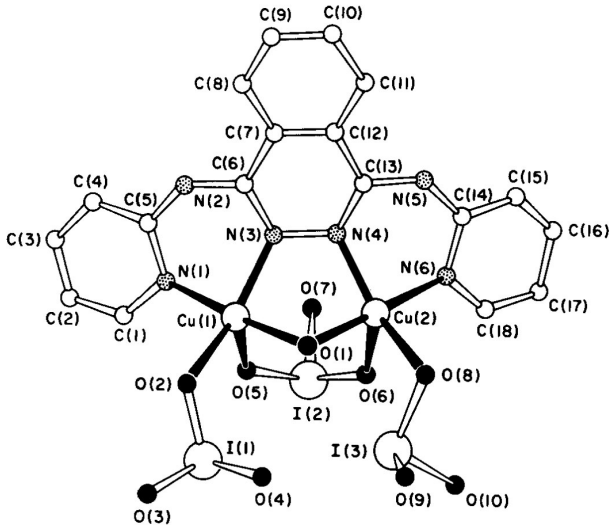
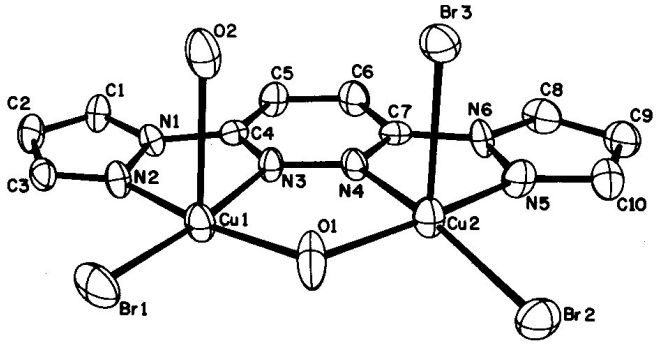


Fig. 4. Structural representation of $[Cu_2(pap)(\mu_2\text{-}OH)(\mu\text{-}IO_3)(IO_3)_2]\cdot 4H_2O$ (**2**).



© 2005 NRC Canada

Fig. 5. Structural representation of $[Cu_2(ppd)(\mu_2\text{-}OH)Br_3(H_2O)]$ (**3**).



770–1305 cm^{-1}) (5, 6). A typical example, $[Cu_2(ppd)(\mu_2\text{-}OH)Br_3(H_2O)]$ (**3**), is shown in Fig. 5. In all cases, the copper ions are bridged by the diazine (N_2) and hydroxide groups.

The magnetic exchange interactions in the diazine complexes result from alignment and overlap of the copper magnetic orbitals with appropriate symmetry orbitals (e.g., *p* orbitals) on the bridging groups. In most cases, the copper ions have square-pyramidal geometries resulting in $d_{x^2-y^2}$ magnetic ground states, which places the unpaired *d* electron in an ideal molecular orbital environment for exchange coupling via both equatorial bridges in the copper basal planes (e.g., as in Fig. 5). In cases where an axial bridge exists, e.g., in **1**, this results in an orthogonal magnetic connection and does not contribute to antiferromagnetic exchange. The exchange integrals for a large number of complexes in this class were analyzed as a function of hydroxide bridge angle, and a reasonable straight line plot gave the relationship $-2J = 23.06\alpha - 2143$ cm^{-1} (where α is the Cu-OH-Cu bridge angle, and the diazine bridge is assumed to make a small, and roughly constant, contribution to overall exchange) (6).

Studies on laccase (*Rhus vernicifera*) ($-2J \geq 1000$ cm^{-1}) and oxy-hemocyanin (*Megathura crenulata*) ($-2J \geq 1250$ cm^{-1}) extracts in the late 1970s using superconducting quantum interference device (SQUID) measurements revealed very strong antiferromagnetic exchange between the two copper(II) ions at the dinuclear active-site centers (7, 8). The limited structural information available at that time suggested oxygen bridge(s) between the copper(II) centers, and given estimates of copper–copper separations of ~3.5 Å, a projected Cu-O-Cu bridge angle of ~140° results. Substituting this angle into the correlation equation above gives $-2J \approx 1100$ cm^{-1}, consistent with the experimentally observed protein values, strongly supporting an oxygen-based bridge between the copper centers. Definitive model studies (9), and ultimately an X-ray structure on oxy-hemocyanin (*Limulus polyphemus*) (10), revealed that this structural motif is correct, although two oxygen atoms are found between the copper ions, in the form of bridging η_2–η_2 peroxide.

In the early 1980s, the chemistry of azide-bridged dicopper complexes attracted much attention because of the unusual ferromagnetic properties of a few μ_2-1,1-azide bridged dicopper(II) systems (Fig. 6) reported by Kahn and co-workers (11–14) and the suggestion by those authors that, owing to a "spin-polarization" mechanism, ferromagnetic exchange would persist at all Cu-N_3-Cu angles (12). This was based on the interaction of *d* electron spin in the copper

Fig. 6. Spin polarization models for μ_2-1,1 and μ_2-1,3 bridging azides.

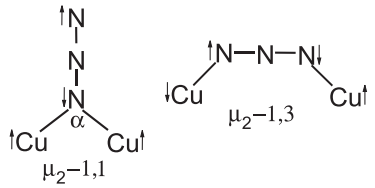
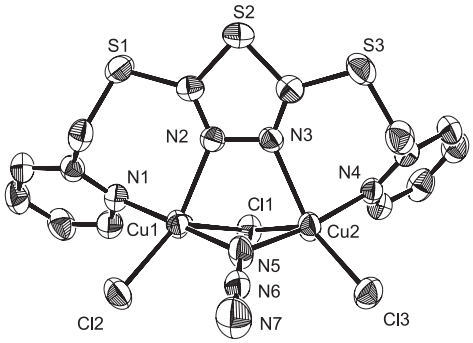


Fig. 7. Structural representation of $[Cu_2(dmptd)(\mu_2\text{-}1,1\text{-}N_3)(\mu_2\text{-}Cl)Cl_2]\cdot CH_3CN$ (**4**).



ion with a π_g symmetry MO on azide, which has a preponderance of α and β spin localized at the end nitrogen atoms. The antiferromagnetic behaviour of "all known" μ_2-1,3-azide bridged dicopper(II) complexes was explained conveniently using the same model (Fig. 6).

Our interest in azide-bridged systems rested with our ability to adjust dinuclear center dimensions successfully in hydroxide-bridged dinuclear copper(II) complexes and the knowledge that azide would replace hydroxide as a μ_2-1,1 bridge. We were therefore able to produce a large series of μ_2-1,1-azide bridged diazine complexes and were able to vary the Cu-N_3-Cu angle in a very broad range (98°–125°), in complexes where the $d_{x^2-y^2}$ copper electrons overlapped directly with the azide bridge orbitals. The 2,5-bis((pyridylmethyl)thio)thiadiazole (dmptd) ligand in the complex $[Cu_2(dmptd)(\mu_2\text{-}1,1\text{-}N_3)(\mu_2\text{-}Cl)Cl_2]\cdot CH_3CN$ (**4**) (Fig. 7; Cu-N_3-Cu 105.9(1)°) is a 7–5–7 ring system, which forces the copper ions to be quite close together (Cu–Cu 3.1215(7) Å), leading to a small azide bridge angle (15, 16). This complex exhibits strong intramolecular ferromagnetic exchange ($2J = 118(3)$ cm^{-1}), consistent with the observations of Kahn and co-workers. The complex $[Cu_2(pap)(\mu_2\text{-}1,1\text{-}N_3)(\mu\text{-}Br)Br_2]\cdot CHCl_3$ (**5**) (Fig. 8; Cu-N_3-Cu 108.7°) and others with the 6–6–6 ring configuration have somewhat larger Cu-N_3-Cu bridge angles than their hydroxide counterparts (108–112°) and exhibit intramolecular antiferromagnetic exchange ($-2J > 100$ cm^{-1}) (16). The 5–6–5 complex $[Cu_2(ppd)(\mu_2\text{-}1,1\text{-}N_3)(ClO_4)(N_3)_2(H_2O)]$ (**6**) (Fig. 9; Cu-N_3-Cu 123.2(2)°, Cu–Cu 3.409(2) Å) has a much larger dinuclear center owing to the presence of five-membered chelate rings, typical of similar systems in this group, which exhibit very strong antiferromagnetic exchange ($-2J = 770$–1100 cm^{-1}) (16).

A magnetostructural analysis of the exchange data for the 1,1-azide-bridged complexes shows a good straight line relationship between exchange integral ($2J$) and Cu-N_3-Cu

© 2005 NRC Canada

Fig. 8. Structural representation of $[Cu_2(pap)(\mu_2\text{-}1,1\text{-}N_3)(\mu\text{-}Br)Br_2]\cdot CHCl_3$ (**5**).

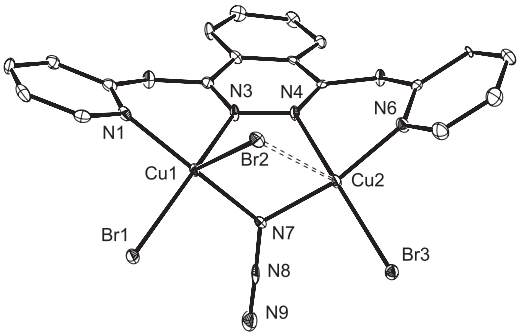
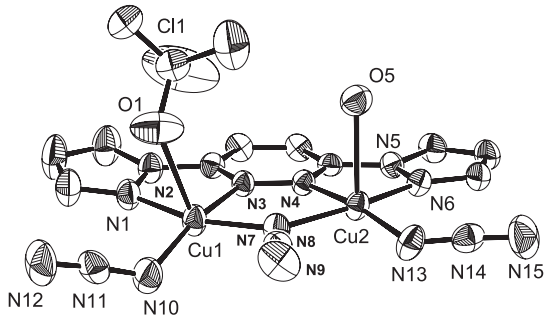


Fig. 9. Structural representation of $[Cu_2(ppd)(\mu_2\text{-}1,1\text{-}N_3)(ClO_4)(N_3)_2(H_2O)]$ (**6**).



bridge angle, with $2J = -41.94\alpha + 4440$ cm^{-1} (17). The changeover from antiferromagnetic to ferromagnetic behavior occurs at ~106° ($2J = 0$ cm^{-1}). Since in all cases the exchange is mediated by two bridging groups (azide and diazine), a correction for the diazine contribution must be included. This is estimated to be of the order $2J \approx -100$ cm^{-1} in all cases from baseline studies of dinuclear complexes with just diazine bridges. This therefore means that the actual angle at which the azide bridge causes a change in sign of the magnetic exchange behavior is ~108°, consistent with the angle of accidental orthogonality of 103° calculated using extended Hückel theory (11, 18). These results indicate that an orbital overlap model involving metal *d* orbital and bridge atom *p* orbital participation is the controlling influence in the exchange process for μ_2-1,1-azide bridged dicopper(II) systems and that it is not necessary to invoke spin polarization theory. It is of interest to note that a polarized neutron diffraction study on the complex $[Cu_2(t\text{-bupy})_4(\mu_2\text{-}1,1\text{-}N_3)_2](ClO_4)_2$ (**7**; *t*-bupy = *p-tert*-butylpyridine) (12) shows positive spin density on the copper ions and the azide bridging nitrogen atoms, thus contradicting spin polarization theory (19).

Increasing the nuclearity in a complex can be achieved by increasing the number of donor pockets in the ligand. This becomes more difficult to achieve and control with increasing nuclearity, but ligands like pap (Fig. 2*a*) can effectively be doubled by starting with tetracyanobenzene, rather than dicyanobenzene, to produce a tetrapyridyl-benzodipyridazine ligand (Fig. 10). Reaction of this and related ligands with copper(II) salts produces novel tetranuclear complexes with two dinuclear halves connected by the planar, fused aromatic network. Figure 11 illustrates the structure of the complex

Fig. 10. Synthetic scheme for tetranuclear benzodipyridazine complexes.

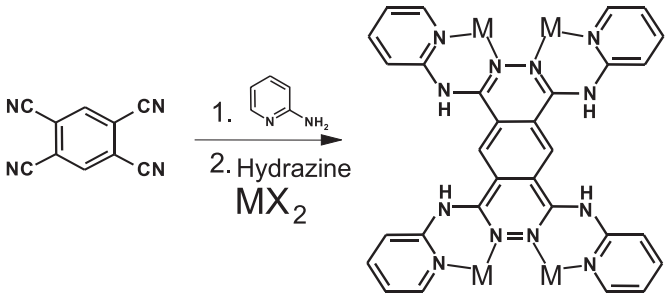


Fig. 11. Structural representation of $[Cu_4(tnl4)(\mu_2\text{-}OH)_2(H_2O)_8](CF_3SO_3)_6\cdot 6H_2O$ (**8**).

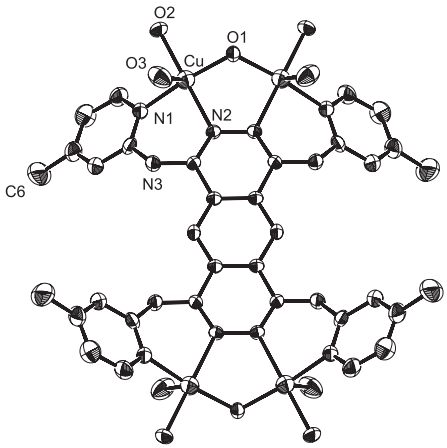
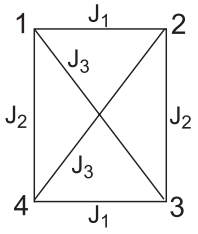


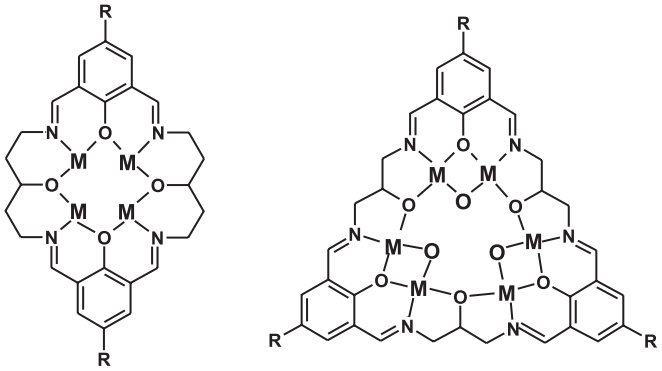
Fig. 12. Magnetic exchange model for a rectangular tetranuclear complex.



$[Cu_4(tnl4)(\mu_2\text{-}OH)_2(H_2O)_8](CF_3SO_3)_6\cdot 6H_2O$ (**8**) (where tnl4 is a tetrapyridyl-benzodipyridazine ligand with a 4-methyl substituent on each pyridine ring) (20, 21). Fairly large Cu-OH-Cu bridge angles lead to intramolecular antiferromagnetic exchange; however, the magnetic data for this class of compound cannot be fitted successfully to a simple dinuclear exchange expression ($H_{ex} = -2JS_1\cdot S_2$) but can instead be fitted successfully to a rectangular exchange scheme (Fig. 12), in which $J_2 = J_3$ ($H_{ex} = -2J_1(S_1\cdot S_2 + S_3\cdot S_4) - 2J_2(S_2\cdot S_3 + S_1\cdot S_4)$). Fairly large $-J_1$ values (167–338 cm^{-1}) and substantial $-J_2$ values (36–210 cm^{-1}) indicate that exchange coupling is split between the direct diazine/hydroxide interaction and the cross-ligand interaction. While μ-OH/μ-diazine interactions are well documented (4–6), the long coupling pathway across the fused aromatic network is most unusual.

© 2005 NRC Canada

Fig. 13. Template cyclized [2:2] and [3:3] formyl-phenol based macrocyclic structures.



(*a*) (*b*)

Fig. 14. Structural representation of $[Cu_6(L)(\mu_2\text{-}OH)_3]_2(NO_3)_6\cdot 10H_2O$ (**9**) illustrating one hexacopper ring.

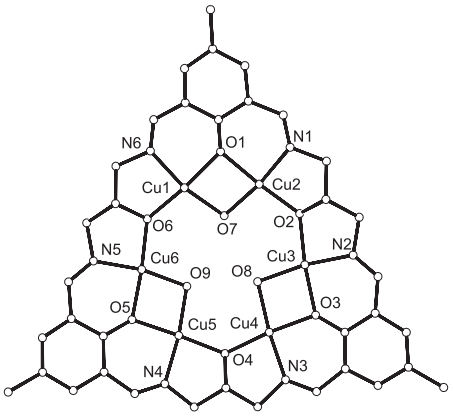
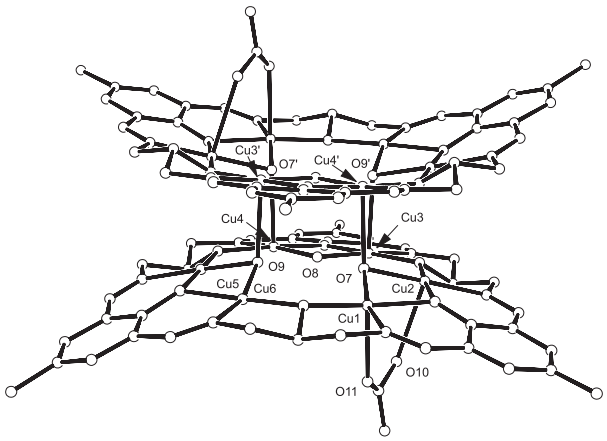


Fig. 15. Structural representation of the dimeric form of $[Cu_6(L)(\mu_2\text{-}OH)_3]_2(NO_3)_6\cdot 10H_2O$ (**9**).



Template cyclization as a method to achieve higher nuclearity

Increasing the nuclearity of a complex beyond four metals with a single ligand approach presents special synthetic challenges, and so other routes, e.g., metal ion templating and self-assembly, are more desirable. With appropriately chosen precursor subunits, this can lead to novel, and in some cases "predictable", outcomes. Macrocyclic ligands based on the diformyl-phenol building block are well known, and reaction with 1,5-diamino-3-pentanol in the presence of metal ions like copper(II) readily templates the formation of 2:2 tetranuclear complexes (22–24) (Fig. 13*a*; e.g., R = CH_3). The alkoxide and phenoxide bridges lead to intramolecular antiferromagnetic exchange between the copper(II) ions. The chelate rings are all six-membered.

The use of a smaller diamino-alcohol linker, e.g., 1,3-diaminopropan-2-ol, would generate five-membered chelate rings and prevent the formation of a 2:2 macrocycle, and one would expect that if a macrocycle formed on reaction with a diformyl phenol, the ring size would be larger. In reality, template condensation of 2,6-diformyl-4-methylphenol with 1,3-diaminopropan-2-ol in the presence of $Cu(NO_3)_2$ leads to a 3:3 condensation and the formation of a hexanuclear complex $[Cu_6(L)(\mu_2\text{-}OH)_3]_2(NO_3)_6\cdot 10H_2O$ (**9**) in high yield (Fig. 13*b*) (25, 26). The X-ray structure (Fig. 14) shows the square-planar copper(II) centers connected by an alternation of phenoxide and alkoxide bridges around the hexagonal copper ring. The structure also reveals that adventitious hydroxide bridges (O(7), O(8), O(9)) between Cu(1) and Cu(2), Cu(3) and Cu(4), and Cu(5) and Cu(6) actually lead to an alternation of single and double oxygen bridges. The overall structure is, in fact, a dodecanuclear dimer (Fig. 15), with two saucer-shaped hexagonal macrocyclic rings joined at their bases by axial Cu–O interactions (e.g., Cu(4)′-O(7) 2.43 Å, Cu(3)′-O(9) 2.45 Å). Oxygen bridge angles (alkoxide 131°–136°, phenoxide 96°–98°, hydroxide 96°–99°) are in ranges that would suggest that intramolecular spin exchange would be dominated by antiferromagnetic coupling, and this is borne out by experiment. Variable-temperature magnetic data were fitted to an alternating exchange Hamiltonian (eq. [1]),

$$[1] \qquad H_{ex} = -2J_1\{S_i\cdot S_{i-1}\} - 2J_2\{S_i\cdot S_{i+1}\}$$

and best fit results were obtained for $-2J_1 = -2J_2 = 318$ cm^{-1} (g = 2.05). An alternate fitting procedure suggested weak antiferromagnetic exchange between the rings in the dimer structure (26). The results suggest that electron delocalization occurs throughout the whole Cu_6 ring structure via the oxygen bridges, which connect the copper magnetic orbitals directly, and the ring can be considered as a metallacyclic analogue of the benzene structure.

Self-assembly as a strategy to higher nuclearity

Large polynuclear systems can be approached by the method of self-assembly, in which coordination information is encoded into a ligand by the creation of suitable coordination pockets in an appropriate spatial arrangement. On reaction with a metal ion, the metal decodes this information according to its own coordination preferences.

This is illustrated in the simplest example by considering the hydrazone ligands poap, pzoap, and poapz (Fig. 16), which contain two coordination pockets (ditopic) and form five-membered chelate rings on coordination, as shown in Fig. 16 for pzoap. The proximity of these rings and the presence of a bridging oxygen atom allow the high-yield self-assembly of [2 × 2] square-based grid complexes with a variety of transition-metal ions (Fig. 16). The complex $[Cu_4(pzoap\text{-}H)_4](NO_3)_4\cdot 3H_2O$ (**10**) (Fig. 17) shows a [2 × 2]

© 2005 NRC Canada

Fig. 16. Ditopic hydrazone ligands, bonding mode, and self-assembly model.

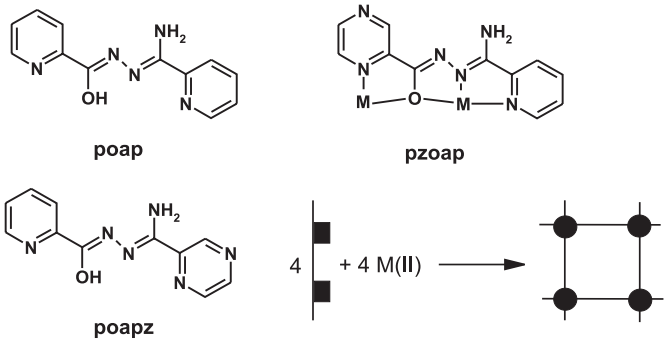
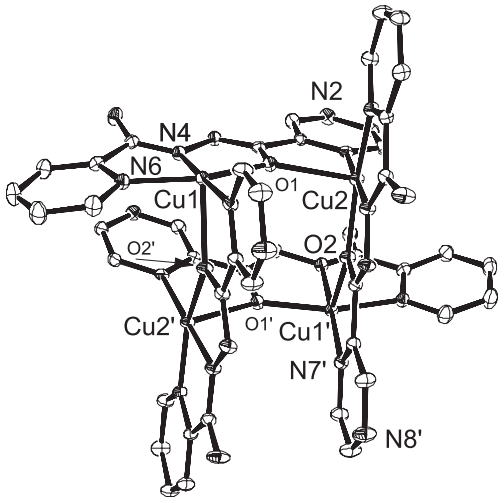


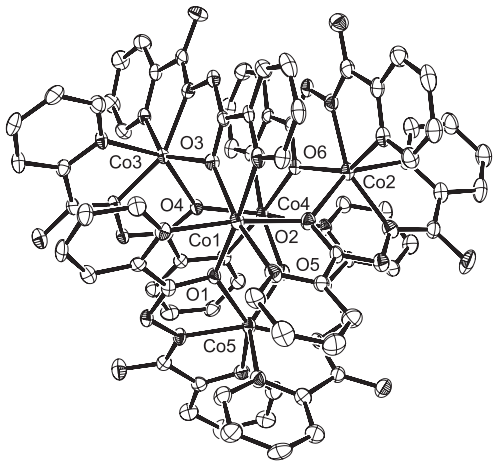
Fig. 17. Structural representation of $[Cu_4(pzoap\text{-}H)_4](NO_3)_4{\cdot}3H_2O$ (**10**).



square grid arrangement of four ligands and four five-coordinate square-pyramidal copper(II) ions, with the four copper ions bridged by four μ_2-O (deprotonated hydrazone) oxygen atoms (27). The tetradentate ligands are arranged in parallel pairs above and below the metal plane. Cu–Cu distances are ~4.05 Å, with Cu-O-Cu angles in the range 140°–141°.

A close examination of the Cu—O bond lengths in the square core reveals that they alternate short–long (Cu(1)—O(1) 2.015(1) Å; Cu(2)—O(1) 2.294(2) Å; Cu(2)—O(2) 2.036(2) Å; Cu(1)—O(2) 2.261(1) Å), with the copper-ion basal planes twisted by 90° from neighbouring copper centers. Since in a square-pyramidal ($d_{x^2-y^2}$ ground state) copper ion the unpaired electron resides in the $d_{x^2-y^2}$ orbital, it follows that there can be no magnetic overlap of the copper ion spin through the oxygen bridge connections, and so there can be no significant intramolecular antiferromagnetic exchange. Given the large Cu-O-Cu angles, this would not be expected. Variable-temperature magnetic data are in accord with this prediction, with a magnetic moment (per mole) increasing from a value of 4.0 μ_B at 300 K to 5.0 μ_B at 5 K. Fitting of the data to the exchange Hamiltonian shown in eq. [2] (which assumes all exchange couplings are the same) for a sequence of four S = 1/2 spin centers arranged in a square gave g = 2.221(5), J = 8.2(4) cm^{-1}, TIP (temperature-independent paramagnetism) = 242 × 10^{-6} cm^3 mol^{-1}, and θ (Weiss-like correction) = –0.4 K. The presence of intramolecular ferromagnetic coupling is clear proof of the internal orthogonal connectivity between the copper(II) ions. Other similar examples have also been studied (27).

Fig. 18. Structural representation of $[Co_5(poap\text{-}H)_6](ClO_4)_4{\cdot}3H_2O$ (**14**).



[2] $$H_{ex} = -J\{S_1{\cdot}S_2 + S_2{\cdot}S_3 + S_3{\cdot}S_4 + S_1{\cdot}S_4\}$$

Nickel(II) and manganese(II) square grid complexes, e.g., $[Ni_4(poap\text{-}H)_4(H_2O)_4](NO_3)_4{\cdot}8H_2O$ (**11**) and $[Mn_4(poapz\text{-}H)_4(H_2O)_4](NO_3)_4{\cdot}H_2O$ (**12**), have also been obtained, with similar [2 × 2] $M_4(\mu_2\text{-}O)_4$ structures and dimensions (27, 28). Orthogonality issues do not arise with these metal ions, and the large M-O-M bridge angles (Ni complex: 132°–140°; Mn complex: 127–130°) lead to intramolecular antiferromagnetic exchange (–J = 10–16 cm^{-1} (Ni); –J = 2.9 cm^{-1} (Mn)). Six-coordinate metal-ion geometries occur in these systems, and since each ligand only fills five donor positions, heteroleptic structures result with co-ligands (e.g., water or an anion) occupying the four vacant coordination sites. Self-assembly leaves the structural outcome to the whims of nature in large measure, and while square [2 × 2] grids are one outcome, there are theoretically others. The lowest ligand/metal combination that would satisfy the bonding requirements for a homoleptic assembly would be 6/5 (i.e., 30 coordination sites for each). It has been found that in some cases, where weakly coordinating anions are involved (e.g., perchlorate), homoleptic pentanuclear clusters are formed in preference to the [2 × 2] square grids (29, 30). Typical examples are $[Mn_5(poap\text{-}H)_6](ClO_4)_4$ (**13**) and $[Co_5(poap\text{-}H)_6](ClO_4)_4{\cdot}3H_2O$ (**14**). The structure of **14** is shown in Fig. 18. The pentanuclear cation has a trigonal bipyramidal arrangement of cobalt(II) ions bonded to six tetradentate ligands, with the core comprising a $Co_5(\mu_2\text{-}O)_6$ subunit. The core structure is shown in Fig. 19. M-O-M bridge angles fall in the range 125–136°, suggesting significant intramolecular antiferromagnetic exchange. Magnetic moments fall from 13.4 μ_B at 300 K to 5.8 μ_B at 5 K (**13**) and from 10.6 μ_B at 300 K to 2.7 μ_B at 2 K (**14**), confirming the expected behavior. Analysis of the magnetic data for the manganese complex, using a full isotropic model (eq. [3]; atom numbering as in Fig. 19), gave g = 2.02 and J = –1.8 cm^{-1}.

© 2005 NRC Canada

Fig. 19. Core structure of $[Co_5(poap\text{-}H)_6](ClO_4)_4 \cdot 3H_2O$ (**14**).

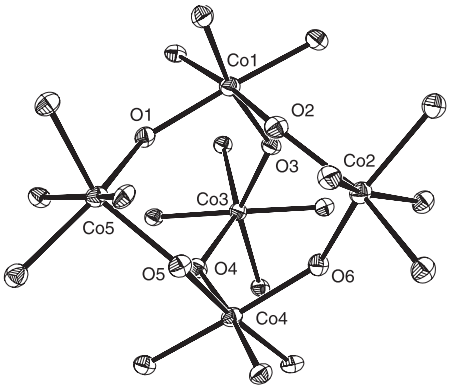
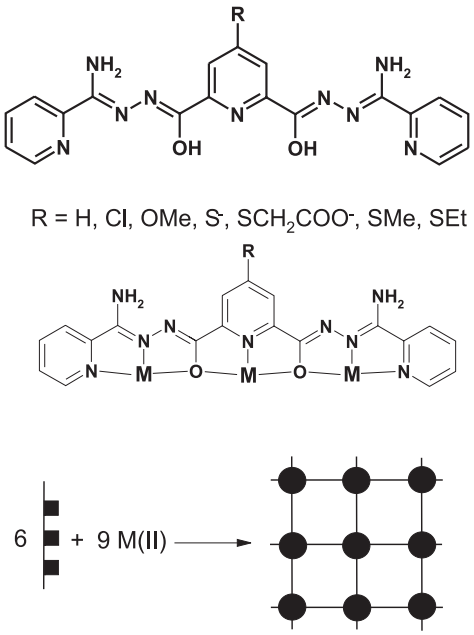


Fig. 20. Tritopic pyridine-dihydrazone ligands, bonding mode, and self-assembly model.



[3] $$H_{ex} = -J\{S_1 \cdot S_2 + S_1 \cdot S_3 + S_1 \cdot S_5 + S_4 \cdot S_5 + S_4 \cdot S_3 + S_4 \cdot S_2\}$$

The creation of larger grid molecules requires the incorporation of extra coordination sites in the ligand. This can be achieved by extending the ligand backbone in Fig. 16 using substituted 2,6-picolinic dihydrazones as the building blocks. Extension with capping pyridine ends can be achieved simply by reaction of the dihydrazone with methyl-2-pyridyl imidate to produce the tritopic ligands shown in Fig. 20 (R = H). Variants of this ligand type can readily be made by changing R, and also incorporating other end groups, e.g., pyrazine. The formation of five-membered chelate rings on coordination ensures that the metal ions are arranged in a roughly linear fashion. Self-assembly in the presence of, e.g., Mn(II), Fe(II), Fe(III), Ni(II), Co(II), Cu(II), and Zn(II) occurs in high yield to produce [3 × 3] nonanuclear grid complexes (31–42). A typical grid structure of the complex $[Mn_9(Cl2poap\text{-}2H)_6](ClO_4)_6 \cdot 10H_2O$ (**15**)

Fig. 21. Structural representation of $[Mn_9(Cl2poap\text{-}2H)_6](ClO_4)_6 \cdot 10H_2O$ (**15**). Colour code: Mn, magenta; C, black; O, red; N, blue; Cl, green.

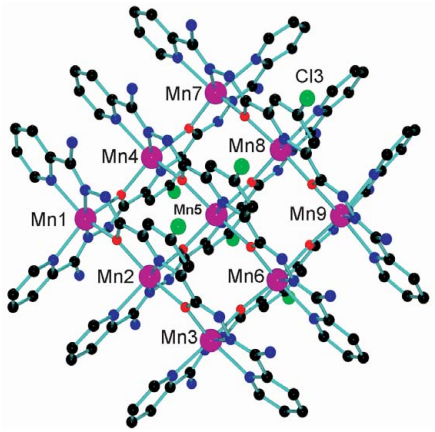
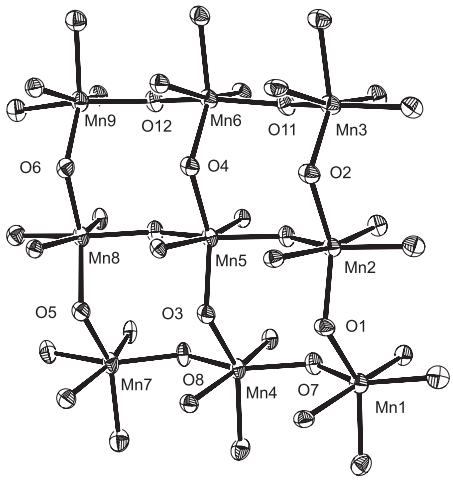


Fig. 22. Core structure of $[Mn_9(Cl2poap\text{-}2H)_6](ClO_4)_6 \cdot 10H_2O$ (**15**).



is shown in Fig. 21. The $[Mn_9(\mu_2\text{-}O)_{12}]$ core structure is shown in Fig. 22 (35). The grid consists of a pseudo-square core with nine six-coordinate Mn(II) centers bridged by 12 deprotonated hydrazone oxygen atoms, with Mn–Mn separations in the range 3.88–4.06 Å and Mn-O-Mn angles in the range 126.4°–130.7°. Six ligands are arranged in two parallel groups above and below the metal plane, with separations between the rings in the range 3.5–4.0 Å, indicating the likely contribution of π interactions to the overall stability of the grid.

The magnetic properties of the $Mn(II)_9$ grids are typified by **15,** which shows a drop in magnetic moment from 17 μ_B at 300 K to close to 6 μ_B at 2 K (Fig. 23), indicating dominant intramolecular antiferromagnetic exchange. The ground state is confirmed by M/H (magnetization at variable field) measurements (2 K) for this and all other $Mn(II)_9$ grids to be $S = 5/2$. The full isotropic magnetic exchange model (Fig. 24; eq. [4]) involves two J values but cannot be conveniently solved because of the enormous dimensions of the matrices involved.

© 2005 NRC Canada

Fig. 23. Magnetic moment as a function of temperature for $[Mn_9(Cl2poap\text{-}2H)_6](ClO_4)_6 \cdot 10H_2O$ (**15**). The solid line represents the best fit of the magnetic data to a chain model. See text for fitted parameters.

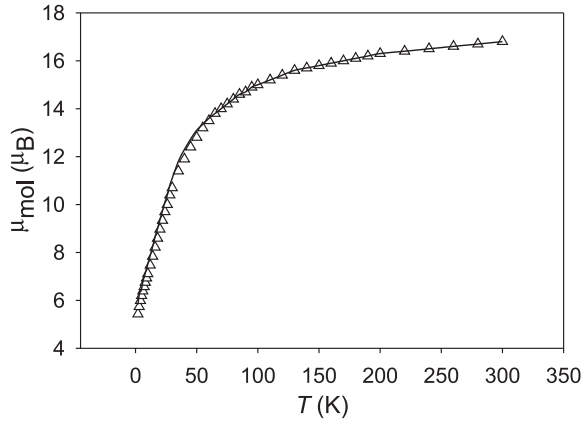
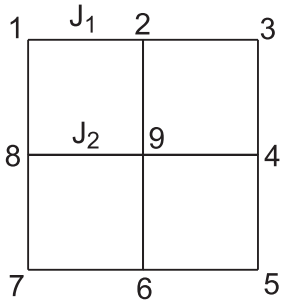


Fig. 24. Magnetic model for [3 × 3] nonanuclear grid.



$$[4] \quad H_{ex} = -J_1\{S_1 \cdot S_2 + S_2 \cdot S_3 + S_3 \cdot S_4 + S_4 \cdot S_5 + S_5 \cdot S_6 + S_6 \cdot S_7 + S_7 \cdot S_8 + S_1 \cdot S_8\} - J_2\{S_2 \cdot S_9 + S_4 \cdot S_9 + S_6 \cdot S_9 + S_8 \cdot S_9\}$$

Even when D_4 rotational symmetry is employed, the computer memory (RAM) requirement is ~4 GB. In the low-temperature antiferromagnetic limit, the ground state for the outer ring of eight Mn(II) centers is $S = 0$, and so a reasonable simplification of the model involves the assumption that J_2 can be ignored in comparison with J_1. A further simplification includes the representation of the ring as a chain using an $S = 5/2$ chain model (38). Typically, $-J_1$ values are found in the range 4–5 cm^{-1} ($g = 2.0$, $J_1 = -4.6$ cm^{-1} for **15**) for $Mn(II)_9$ grids in this class. The solid line in Fig. 23 represents the best fit of the data using this model for **15**.

Three different metal-ion chromophores are found in the M_9 grids: *trans*-N_2O_4 at the center, *cis*-N_4O_2 at the corners, and *mer*-N_3O_3 on the sides (Figs. 21 and 22). This should lead to different electronic properties at these sites, and this is reflected quite clearly in the electrochemical properties. Figure 25 illustrates the cyclic voltammetry for the complex $[Mn_9(MeS2poap\text{-}2H)_6](CF_3SO_3)_6$ (**16**) (Fig. 20; R = SMe) in acetonitrile solution (Pt electrode). The large, fairly broad quasi-reversible single wave at $E_{1/2} = 0.62$ V corresponds to a four-electron process associated with oxidation of the four isolated, but similar, corner Mn(II) centers to Mn(III). The

Fig. 25. Cyclic voltammetry in acetontirile for $[Mn_9(MeS2poap\text{-}2H)_6](CF_3SO_3)_6$ (**16**) (Pt electrode).

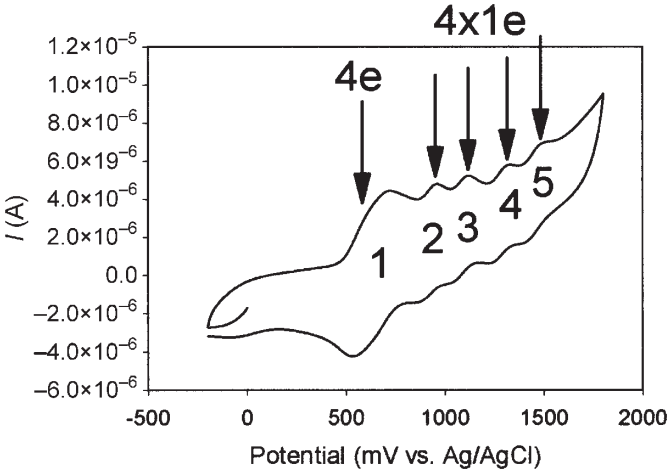
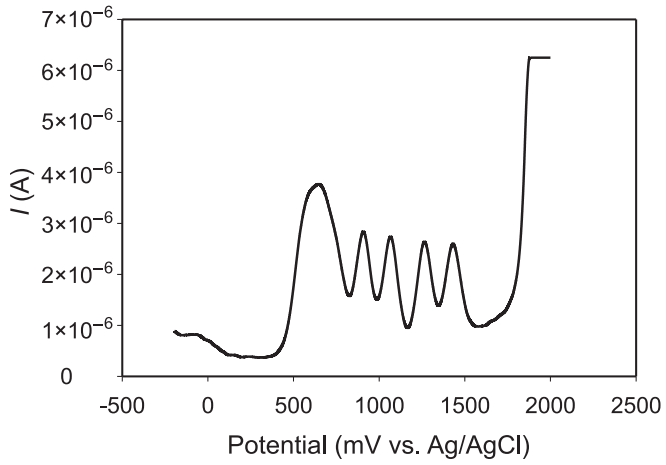


Fig. 26. Differential pulse voltammetry in acetonitrile for $[Mn_9(MeS2poap\text{-}2H)_6](CF_3SO_3)_6$ (**16**).



four higher potential waves are reversible in nature and correspond to one-electron oxidations of four Mn(II) centers, which are clearly in communication, in that as one Mn(II) center oxidizes, it influences the potential at which a neighbour is oxidized. These waves are assigned to the side Mn centers, which can communicate electronically through the central metal ion and also by electrostatic coulombic interactions. Differential pulse voltammetry (Fig. 26) shows these redox events much more clearly. All other $Mn(II)_9$ grid complexes have similar voltammetric responses, with $E_{1/2}$ values varying with the 4-pyridine ring substituent (Fig. 20).[2]

Oxidation of the $Mn(II)_9$ grids proceeds smoothly using bulk electrolysis, to produce examples with $[Mn(III)_3Mn(II)_6]$ and $[Mn(III)_4Mn(II)_5]$ cores. Chemical oxidants, e.g., Cl_2(aq.) and Br_2(aq.), can also be used. The complex $[Mn(III)_3Mn(II)_6(Cl2poap\text{-}2H)_6](ClO_4)_9 \cdot 7H_2O$ (**17**), isolated from the reaction of the complex $[Mn(II)_9(Cl2poap\text{-}2H)_6](ClO_4)_6 \cdot 10H_2O$ (**15**) with Cl_2(aq.), has three corner metal-ion centers oxidized to Mn(III), with considerably shortened Mn—L distances (M—$L_{avg.}$ 2.055–2.066 Å), but

[2] References 31 and 38; V.A. Milway, D.J. Pond, and L.K. Thompson. Unpublished results.

© 2005 NRC Canada

the Mn—L distance for the fourth corner metal ion is much longer (M—$L_{avg.}$ 2.174 Å) and closer to expected values for Mn(II) (38). Complete corner metal-ion oxidation can be achieved using bulk electrolysis (applied potential of +20 V in CH_3CN) of the complex $[Mn_9(2poap\text{-}2H)_6](ClO_4)_6\cdot 10H_2O$ (**18**) (31). An X-ray structure shows the space group symmetry $I\bar{4}$ with four equivalent corner centers oxidized to Mn(III) (M—$L_{avg.}$ 2.062(4) Å) in the complex $[Mn(III)_4Mn(II)_5(2poap\text{-}2H)_6](ClO_4)_{10}\cdot 18H_2O$ (**19**) (43). The grid structures remain intact on oxidation with almost no change in the overall grid dimensions, leading to slightly higher Mn-O-Mn angles in all oxidized cases. Oxidation of the side Mn(II) centers has not yet been clearly documented, although with persulfate oxidation preliminary evidence indicates removal of more than four electrons.

As each metal ion is oxidized to Mn(III), the electron complement of the grid diminishes, with $S = 4/2$ spin centers replacing $S = 5/2$ spin centers at the corners. This leads not only to lowered room temperature magnetic moments but also to changes in the ground-state spin. For compound **17** with three $S = 4/2$ centers at the corners (Fig. 24; $S = 4/2$ at sites 1, 3, and 5) in the low-temperature antiferromagnetic limit ($J_1 < 0$ cm^{-1}), the ground-state spin of the outer eight-membered metallic ring is $S = 3/2$. Coupling of the ring to the central Mn(II) for $J_2 < 0$ cm^{-1} results in an overall ground state spin of 5/2 – 3/2 = 2/2. Magnetization studies at 2 K as a function of field confirm the $S = 2/2$ ground state (38). Variable-temperature and variable-field magnetic data for **18**, which has all four corner sites oxidized (Fig. 24; $S = 4/2$ at sites 1, 3, 5, and 7), reveals that the ground state has $S = 1/2$, as a result of antiferromagnetic exchange between the $S = 4/2$ ring and the central $S = 5/2$ site. Magnetic data are thus definitive in assessing the state of oxidation of the grids.

Reaction of copper(II) salts with ligands in this class provides some surprises, in that examples of trinuclear, octanuclear, and nonanuclear complexes can be obtained depending on the anion used and the synthetic conditions. Copper acetate forms a linear trinuclear complex, $[Cu_3(2poap\text{-}2H)(CH_3COO)_4]\cdot 3H_2O$ (**19**), on reaction with 2poap, in which the ligand adopts a different coordination conformation, with a copper ion bound to a N_3 central ligand pocket and bridged to its neighbours by N_2 diazine groups (Fig. 27). The hydrazone oxygen atoms are bound terminally to the peripheral copper ions. This and related complexes exhibit magnetic properties typical of linear trinuclear systems with intramolecular antiferromagnetic exchange. Fitting of the variable-temperature magnetic data for **19** to the exchange expression derived from the Hamiltonian (eq. [5]) gave $g = 2.19(1)$ and $J = -75.5(2)$ cm^{-1} (44).

$$[5] \qquad H_{ex} = -2J\{S_1\cdot S_2 + S_2\cdot S_3\}$$

Reaction of other copper salts, e.g., $Cu(NO_3)_2\cdot 3H_2O$ and $Cu(ClO_4)_2\cdot 6H_2O$, under mild (room temperature) conditions in CH_3CN/MeOH and MeOH/H_2O mixtures leads to octanuclear complexes as the major products. $[Cu_8(Cl2poap\text{-}2H)_4(NO_3)_8]\cdot 20H_2O$ (**20**) (Fig. 28) is a typical example. Four heptadentate Cl2poap ligands (Fig. 20; R = Cl) intersect via their end pockets to produce a $Cu_4(\mu_2\text{-}O)_4$ inner core involving six-coordinate Cu(II) ions, with the ends of the ligands radiating outwards in a "pinwheel" shape to bind four extra

Fig. 27. Structural representation of $[Cu_3(2poap\text{-}2H)(CH_3COO)_4]\cdot 3H_2O$ (**19**).

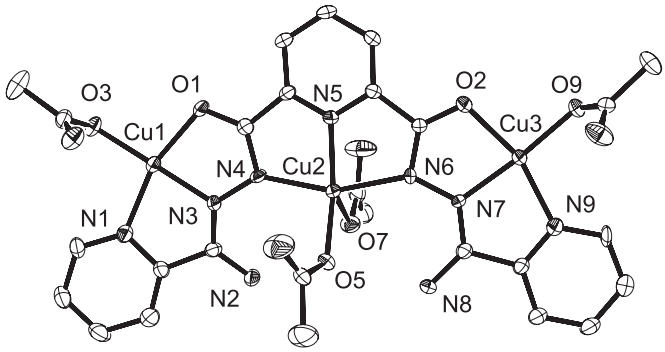
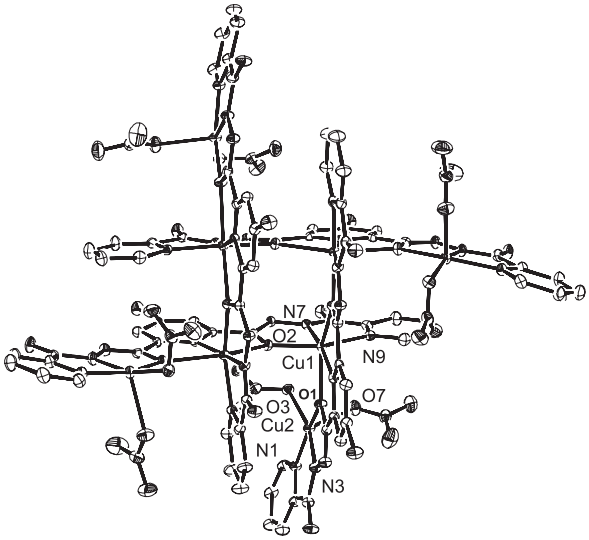


Fig. 28. Structural representation of $[Cu_8(Cl2poap\text{-}2H)_4(NO_3)_8]\cdot 20H_2O$ (**20**).



square-pyramidal Cu(II) ions. The terminal ligand pockets provide three donors (N_2O), and two monodentate nitrates fill the two remaining coordination sites. The terminal copper ions are bridged to the core with μ_2-O connections. The core structure is shown more clearly in Fig. 29. Cu–Cu distances vary from 4.01 to 4.06 Å, with Cu-O-Cu angles in the range 138.6–140.0°. Cu—O bond distances throughout the cluster alternate between long (axial) and short (equatorial) from one copper center to the next. This leads to strict magnetic orbital orthogonality between adjacent pairs of $d_{x^2-y^2}$ ground-state metal ions (45).

More forcing conditions lead to the formation of Cu_9 grids, and in the case of M2poap (Fig. 20; R = OMe), reaction with $Cu(NO_3)_2\cdot 3H_2O$ in MeOH/H_2O with heating to reflux forms the complex $[Cu_9(M2poap\text{-}H)_2(M2poap\text{-}2H)_4](NO_3)_8\cdot 17H_2O$ (**21**) (45). The structure (Fig. 30) shows the familiar [3 × 3] square grid arrangement, with nine six-coordinate Cu(II) centers bridged by μ_2-O hydrazone oxygen atoms. The core structure is shown in Fig. 31. The grid dimensions are similar to those of the Mn(II) systems, with Cu–Cu separations in the range 3.97–4.21 Å and Cu-O-Cu angles in the range 135.4°–142.4°. An examination of the bond distances at the eight metal ions in the outer ring re-

© 2005 NRC Canada

Fig. 29. Core structural representation of $[Cu_8(Cl2poap\text{-}2H)_4(NO_3)_8]\cdot 20H_2O$ (**20**).

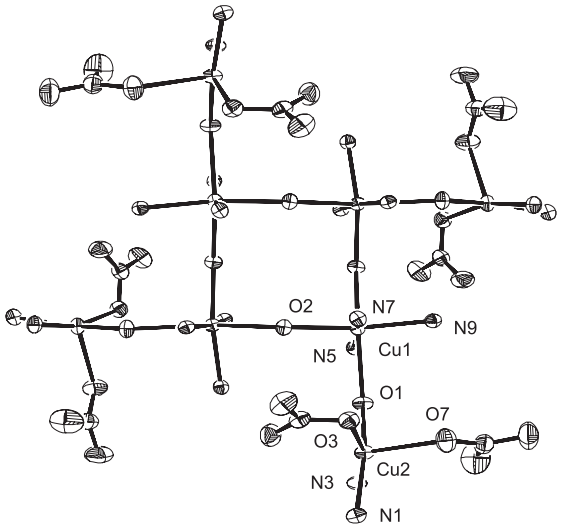
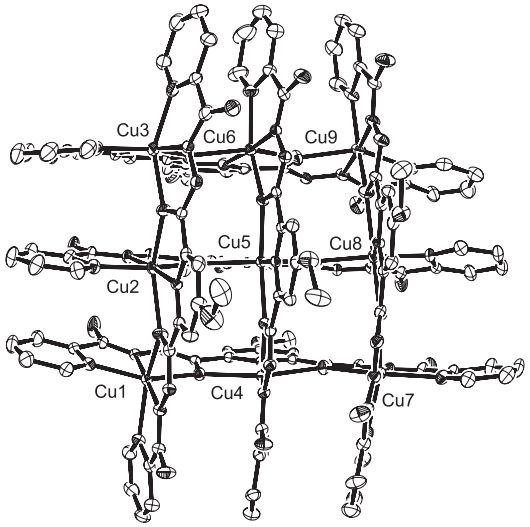


Fig. 30. Structural representation of $[Cu_9(M2poap\text{-}H)_2(M2poap\text{-}2H)_4](NO_3)_8\cdot 17H_2O$ (**21**).



veals axially elongated geometries indicating $d_{x^2-y^2}$ ground states, with the central atom having a compressed tetragonal geometry, suggestive of a d_{z^2} ground state. The magnetic orbital arrangement in the ring is most unusual but parallels that in the "pinwheel" complexes, with all copper magnetic planes arranged with strict magnetic orbital orthogonality. This leads to ferromagnetic exchange within the ring (vide infra). All other Cu_9 grid molecules in this class have similar magnetic orbital topologies. The central d_{z^2} copper ion is also expected to be orthogonally connected, but magnetic studies indicate that this is not the case (32, 39, 45).

The magnetic exchange models for the copper "grid" and "pinwheel" complexes (see eqs. [4] and [6] for the exchange

Fig. 31. Core structural representation of $[Cu_9(M2poap\text{-}H)_2(M2poap\text{-}2H)_4](NO_3)_8\cdot 17H_2O$ (**21**).

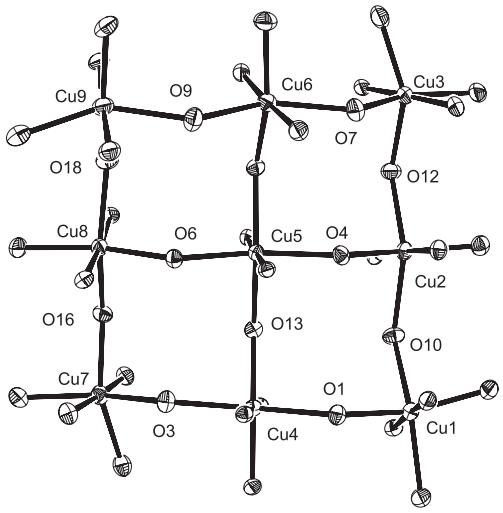
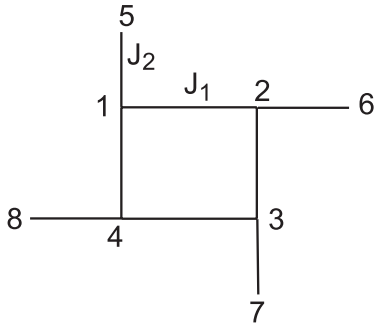


Fig. 32. Magnetic exchange model for Cu_8 pinwheel cluster.



Hamiltonian expressions and Figs. 24 and 32) are quite different.

$$[6]\qquad H_{ex} = -J_1\{S_1\cdot S_2 + S_2\cdot S_3 + S_3\cdot S_4 + S_1\cdot S_4\} - J_2\{S_1\cdot S_5 + S_2\cdot S_6 + S_3\cdot S_7 + S_4\cdot S_8\}$$

A reasonable simplification for the Cu_8 systems is to assume that $J_1 \approx J_2$, since the Cu–Cu separations and Cu-O-Cu angles are similar throughout the cluster. The large number of spin centers in these and other high-nuclearity clusters prompted us to create a software package that would deal with the complex calculations of the total spin quantum number situations and their energies using a typical Kambe vector summation approach (46) and then substitute these internally into the van Vleck equation (eq. [7]) to generate a theoretical magnetic susceptibility (χ_m)/temperature profile.

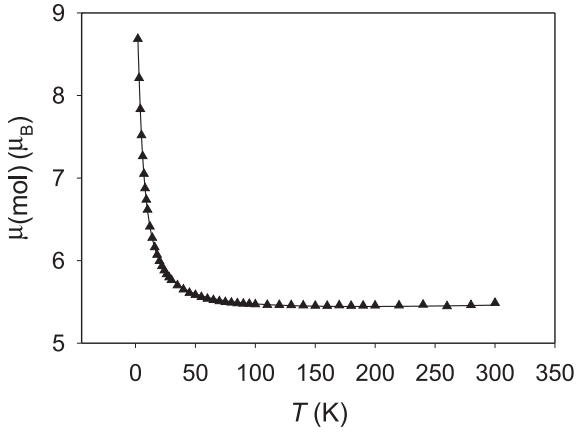
$$[7]\qquad \chi_m = \frac{N\beta^2 g^2[\Sigma S'(S'+1)(2S'+1)\,e^{-E(S')/kT}}{3k(T-\theta)[\Sigma(2S'+1)e^{-E(S')/kT}} + \text{TIP}$$

The software package that we created, MAGMUN4.0,[3] runs on a Windows™ platform, deals with a variety of spin-

[3] MAGMUN4.0 is available free of charge from http://www.ucs.mun.ca/ ~lthomp/index.html. It has been developed by Dr. Zhiqiang Xu (Memorial University), in conjunction with Dr. O. Waldmann (oliver.waldmann@iac.unibe.ch). We do not distribute the source codes. The programs may be used only for scientific purposes, and economic utilization is not allowed. If the routine is used to obtain scientific results that are published, the origin of the programs should be quoted.

© 2005 NRC Canada

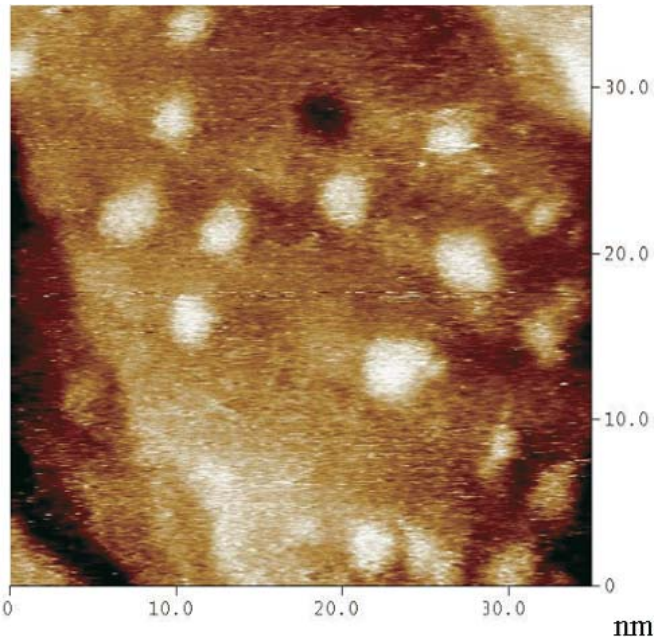
Fig. 33. Magnetic moment variation as a function of temperature for **20** (solid line calculated using fitted parameters quoted in the text).



coupled situations irrespective of geometry, and can provide a full fitting of both simple and quite complex exchange situations using nonlinear regression fitting procedures. Such calculations are, however limited by the computer RAM available (vide supra), because of the size of the matrices involved in the spin coupling schemes. As an illustration, for a fully isotropic calculation based on eq. [4] ($J_1 = J_2$), the RAM requirements for $S = 3/2$ (largest dimension 5300), 4/2 (largest dimension 25 200), and 5/2 (largest dimension 88 900) [3 × 3] grids are 215 MB, 4.8 GB, and 60.3 GB, respectively. Imposing D_4 rotational symmetry can reduce the requirements significantly, and for the $S = 5/2$ case (largest dimension 22 210), only 3.8 GB are required. This still places such calculations beyond the capability of most PCs.

The magnetic exchange for the Cu_8 clusters and Cu_9 grids can be solved successfully using MAGMUN4.0. For compound **20**, the magnetic moment rises from 5.5 μ_B at 300 K to 8.7 μ_B at 2 K, which is indicative of intramolecular ferromagnetic exchange (Fig. 33). Fitting of the data to eqs. [6] and [7] gave $g = 2.15(1)$, $J = 7.8(5)$ cm^{-1}, and TIP = 540 × 10^{-6} cm^3 mol^{-1} for a system with an $S = 8/2$ ground state (M/H data at 2K) (the solid line in Fig. 33 corresponds to this data fitting). This is entirely consistent with strict *d* orbital orthogonality within the cluster. The magnetic moment of compound **21** exhibits a different response as a function of temperature, with a room temperature moment of 5.84 μ_B, dropping steadily to 5.16 μ_B at 26 K, followed by a sharp rise to 6.39 μ_B at 2 K. Such a profile, which is typical of all the $Cu(II)_9$ grids studied, implies the presence of both antiferromagnetic and ferromagnetic exchange within the grids. Analysis of the variable-temperature magnetic data for **21** according to eqs. [4] and [7] gave $g = 2.17(1)$, $J_1 = 0.5(1)$ cm^{-1}, $J_2 = -23(1)$ cm^{-1}, and TIP = 790 × 10^{-6} cm^3 mol^{-1}, confirming the presence of ferromagnetic coupling in the Cu_8 ring. The negative J_2, which is typical of all Cu_9 grids, indicates that despite an expected ferromagnetic J_2 term based on magnetic orbital orthogonality arguments, the central copper ion plays an unusual role in the overall coupling scheme and must undergo some sort of dynamic Jahn–Teller distortion, which allows it to interact in an antiferromagnetic sense with its four neighbours. The net reduction in total spin is therefore 2/2, which means that the overall spin ground state for the grid is 9/2 – 2/2 = 7/2. This is confirmed by magnetization data as a function of field at 2 K.

Fig. 34. STM imagery for complex **15** attached to a Au(111) surface. The bright spots represent grid molecular ions attached in a flat conformation to the surface.

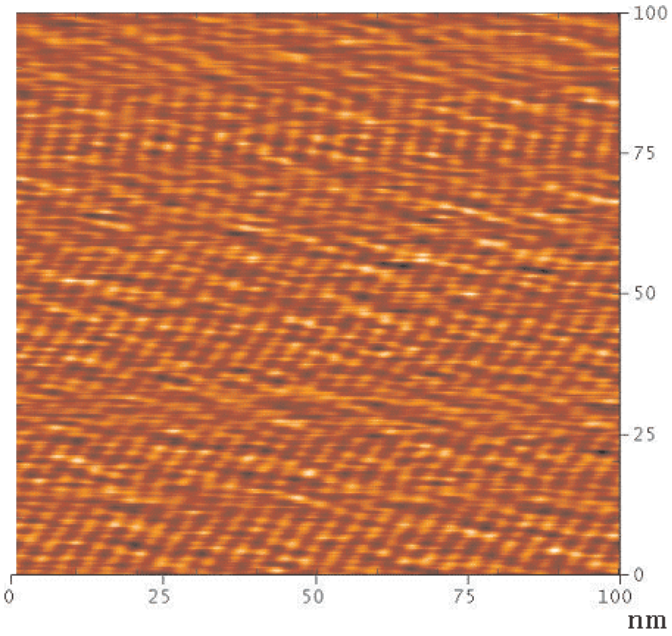


The [3 × 3] grid molecules have generated great interest in the physics community, as simple quantum dot models, and in the case of Mn(II) quantum oscillation effects have been demonstrated in the field dependence of the magnetic torque at low temperature (41). The novel, and close to reversible, electrochemical properties observed in bulk solution, and the demonstrated ability of these systems to exist in mixed oxidation state structures, suggests that an individual molecule may exhibit similar properties if it can be appropriately addressed in the solid state. The flat nature of the grids implies that they may adhere well to certain surfaces. As a simple test, electrochemistry was carried out on compound **15**, which has chlorine atoms exposed prominently on both faces of the grid (Fig. 21), using a gold electrode in place of platinum. Similar redox responses were observed to those obtained with platinum. The gold electrode was then thoroughly cleaned and immersed in a solution of **15** in acetonitrile for an extended period. The electrode was then rinsed thoroughly, and cyclic voltammetry performed on the electrode in the absence of dissolved grid. Redox responses in the 0–1.2 V range clearly indicated gold-bound grid molecules.

Surface studies were then carried out on Au(111) films formed on mica substrates, and imaging performed using scanning tunneling microscopy (STM) techniques. Compound **15** was deposited from a dilute solution in acetonitrile. STM imagery shows that individual molecules are attached to the gold surface (Fig. 34). The grid dimensions are consistent with the "footprint" of the grid observed from the X-ray structural determination and indicate that the mol-

© 2005 NRC Canada

Fig. 35. STM imagery for complex $[Mn_9(S2poap)_6](ClO_4)_{10}\cdot 12H_2O$ (**22**) bound as a self-assembled monolayer (SAM) to Au(111).



ecules are bound in a flat conformation, with the chlorine atoms as the likely points of surface attachment (47). Surface binding on gold would be much stronger with sulphur-based groups attached at the 4-position of the central ligand pyridine ring. This has been achieved with a $Mn(II)_9$ grid complex of the ligand S2poap (Fig. 20; R = S^-), $[Mn_9(S2poap)_6](ClO_4)_{10}\cdot 12H_2O$ (**22**). The Au(111) surface imagery in this case is quite remarkable (Fig. 35) and indicates that a self-assembled monolayer (SAM) has formed from a dilute acetonitrile solution of the complex. The bright spots have dimensions on the order of 2.6 nm across, completely consistent with the molecular structural dimensions obtained for grids in this class by X-ray crystallographic techniques (48). Spaces between the grids (dark spots) are comparable in size to the grids themselves.

The [2 × 2] and [3 × 3] grids are novel systems with molecular-based properties that rely on the close juxtaposition of the metal ions themselves and the simple oxygen atom bridges that connect them. This leads to considerable electron delocalization within the grids, and electronic properties that are manifested in terms of rich electrochemistry in the case of the Mn_9 systems and magnetic properties that reflect electron communication throughout the grids. Future and ongoing studies are aimed at addressing individual molecules on surfaces, as already demonstrated by STM imagery, by probing the electronic properties at the molecular level, and even detecting individual molecules based on the presence of unpaired spins. This has recently been demonstrated using a combination of STM and ESR on organic radicals bound to a highly oriented pyrolytic graphite (HOPG) surface (49). The Mn_9 grids are considered to have significant potential for device behaviour at the molecular level, in, e.g., a switching or data storage capacity.

Fig. 36. The extended ligand dpocco and bonding motif with copper(II).

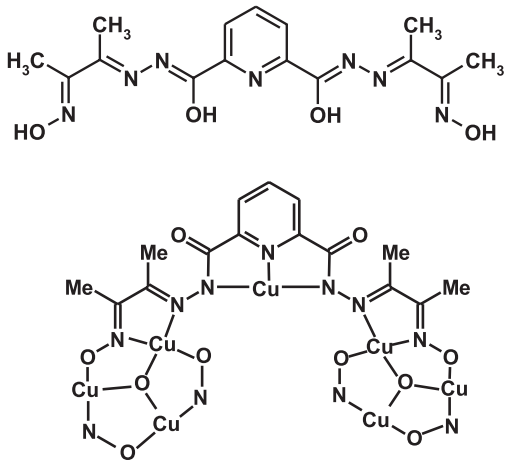
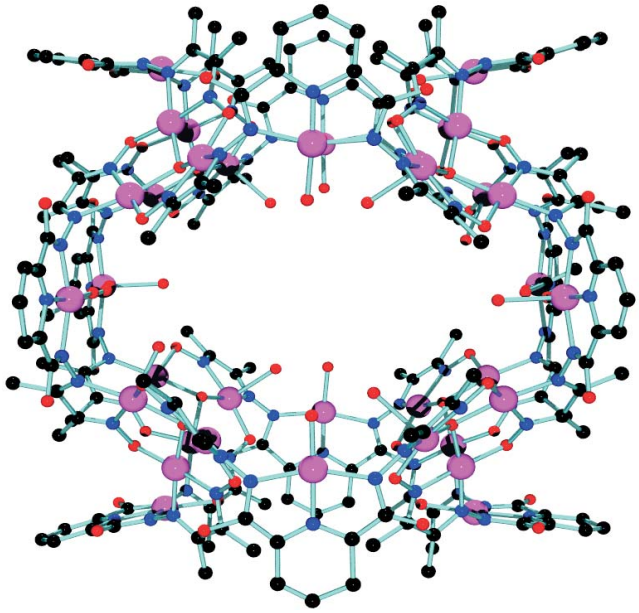


Fig. 37. Structural representation of $[Cu_{36}(dpocco\text{-}4H)_{12}(\mu_3\text{-}OH)_8](CH_3COO)_{16}\cdot xH_2O$ (**23**). Colour code: Cu, magenta; C, black; O, red; N, blue.



Larger grids and clusters are a logical extension of the work achieved so far, and they can be approached in a more or less systematic way using extended ligands. Extension of the 2,6-picolinic-dihydrazone core by reaction with butanedione monoxime leads to the ligand dpocco (Fig. 36), which has the tritopic core found in, e.g., 2poap, but with peripheral ligating groups capable of additional coordination. Reaction of dpocco with $[Cu(OAc)_2(H_2O)]_2$ led to dark crystals whose structure revealed a most unusual Cu_{36} cluster $[Cu_{36}(dpocco\text{-}4H)_{12}(\mu_3\text{-}OH)_8](CH_3COO)_{16}\cdot xH_2O$ (**23**) (50). The ligand adopts a different conformation from that observed in the [3 × 3] grids, with a copper bound in a central N_3 pocket, but bridged via μ_2-N–N groups to two peripheral copper ions (Fig. 37). The oxime function at the end of each ligand takes part in additional bonding to two more similar

© 2005 NRC Canada

Fig. 38. Core structural representation for **23**.

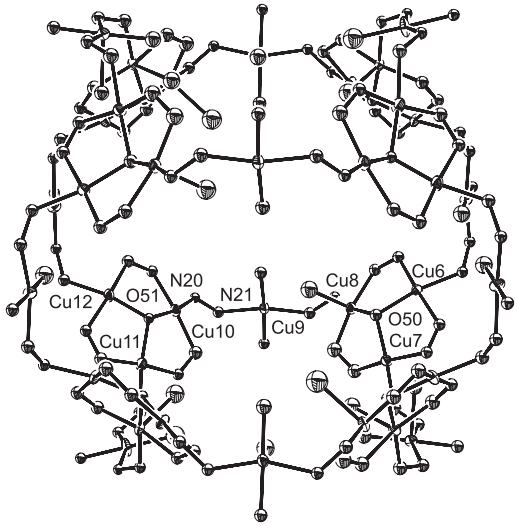


Fig. 39. Extended grid models.

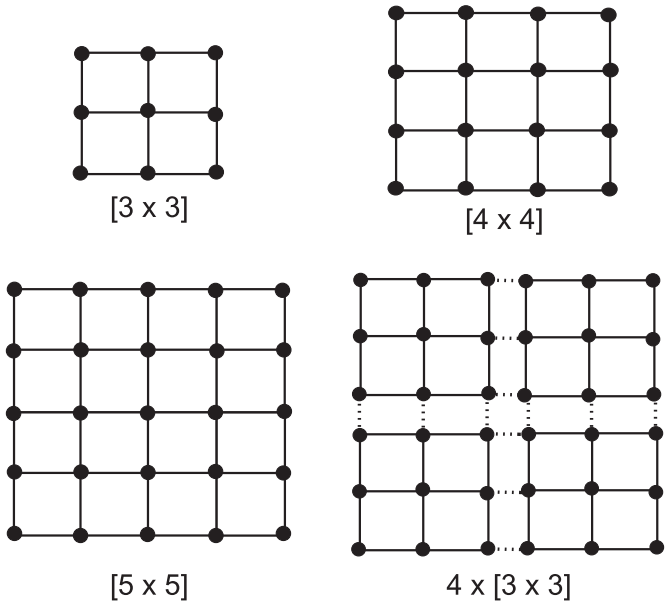
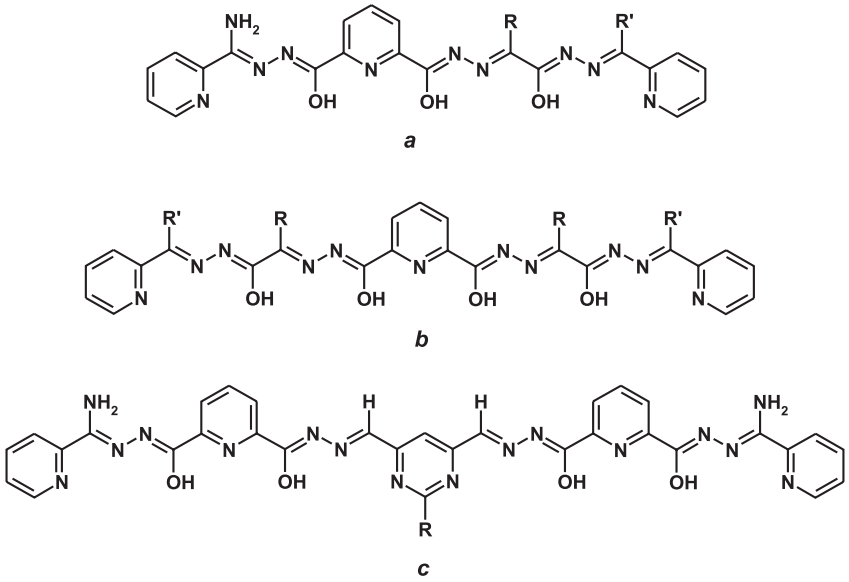


Fig. 40. Extended "polytopic" picolinic hydrazone ligands.



copper subunits, forming a μ_3-OH bridged trinuclear, triangular fragment. This arrangement extends throughout the collection of 12 such subunits forming the Cu_{36} cluster (Fig. 37). A simplified core representation is shown in Fig. 38. The magnetic properties of this unique cluster indicate intramolecular antiferromagnetic exchange, with a moment at room temperature of 10.1 μ_B dropping to 4.5 μ_B at 2 K. The large spin state associated with this cluster has thus far prevented solution of the exchange problem.

Conclusion

The formation of polynuclear coordination complexes can be achieved up to a certain size by combining metal ions with single ligands, providing they have a large number of coordination pockets. Synthetic difficulties with large ligands, and adverse entropy situations, seriously impede the formation of systems with high nuclearities, and in our case four was the largest number. Metal-ion template cyclizations can produce larger systems by the controlled organization of appropriate subunits into, e.g., large macrocycles, and nuclearities up to six have been achieved in this way. The pursuit of higher nuclearity clusters and grids has been a challenge, but the design and synthesis of polyfunctional ligands with appropriately arranged coordination pockets can lead to nuclearities up to 36 by taking advantage of, for instance, self-assembly processes. Generally, this approach produces stable clusters and grids in high yield and provides a thermodynamic driving force to counterbalance the negative entropy effects involved in organizing large numbers of particles into the same unit. This method is again based on ligand synthesis, but in principle it is a simpler way to

© 2005 NRC Canada

achieve novel high-nuclearity systems. The M_9 grids, particularly those with manganese, have proven to be unique systems in terms of their magnetic and electronic properties.

The synthesis of larger [$n \times n$] grids (e.g., $n = 4$, 5) and compartmental grids (e.g., $4 \times [3 \times 3]$) based on 2,6-picolinic-dihydrazone subunits (Fig. 39) depends on the extension of this type of ligand with suitable additional coordination pockets. This would involve maintaining the linear sequence of five-membered chelate rings, and also the repeating arrangement of "enolic" oxygen donors. Figure 40 illustrates examples of tetratopic, pentatopic, and hexatopic ligands (*a*, *b*, and *c*, respectively), which could be synthesized by extension of the picolinic hydrazone framework. Examples of ligands in all three classes have been synthesized, and preliminary results indicate that extended [4 × 4] grids can be produced.

Acknowledgements

The work described in this paper has been the result of many contributions from undergraduate students, high school students, graduate students, postdoctoral fellows, research associates, and sabbatical associates with whom I have had the privilege of working over the years. Also I must thank and acknowledge numerous collaborators both within and outside Canada, whose expertise and interest have fostered, advanced and encouraged our work. These numerous researchers should all share in the Alcan Lecture Award.

Pursuing research in a smaller university always presents special challenges, but Memorial University has always been supportive financially, logistically and in terms of teaching loads. Generous financial support from the Natural Sciences and Enginerring Research Council of Canada (NSERC) over the years has been a major component in financing our research programme, but international support via collaborative research projects from NATO, the Engineering and Physical Sciences Research Council (UK) Monbusho, and the Norwegian Research Council has also played a significant role.

Finally, it is indeed an honour to have been chosen to receive the Alcan Lecture Award. Thanks are extended to the Aluminum Company of Canada for providing the award and to the Canadian Society for Chemistry for sponsoring it.

References

1. L.K. Thompson, V.T. Chacko, J.A. Elvidge, A.B.P. Lever, and R.V. Parish. Can. J. Chem. **47**, 4141 (1969).
2. G. Bullock, F.W. Hartstock, and L.K. Thompson. Can. J. Chem. **61**, 57 (1983).
3. L.K. Thompson. Can. J. Chem. **61**, 579 (1983).
4. L.K. Thompson, A.W. Hanson, and B.S. Ramaswamy. Inorg. Chem. **23**, 2459 (1984).
5. L.K. Thompson, T.C. Woon, D.B. Murphy, E.J. Gabe, F.L. Lee, and Y. LePage. Inorg. Chem. **24**, 4719 (1985).
6. L.K. Thompson, F.L. Lee, and E.J. Gabe. Inorg. Chem. **27**, 39 (1988).
7. D.M. Dooley, R.A. Scott, J. Ellinghaus, E.I. Solomon, and H.B. Gray. Proc. Natl. Acad. Sci. U.S.A. **75**, 3019 (1978).
8. E.I. Solomon, D.M. Dooley, R.H. Wang, H.B. Gray, M. Cerdonio, F. Mogno, and G.L. Romani. J. Am. Chem. Soc. **98**, 1029 (1976).
9. N. Kitajima, K. Fujisawa, Y. Moro-oka, and K. Toriumi. J. Am. Chem. Soc. **111**, 8975 (1989).
10. K.A. Magnus, B. Hazes, H. Ton-That, C. Bonaventura, J. Bonaventura, and W.G.J. Hol. Proteins Struct. Funct. Genet. **19**, 302 (1994).
11. O. Kahn. Inorg. Chim. Acta, **62**, 3 (1982).
12. S. Sikorav, I. Bkouche-Waksman, and O. Kahn. Inorg. Chem. **23**, 490 (1984).
13. J. Cormarmond, P. Plumeré, J.-M. Lehn, Y. Agnus, R. Loius, R. Weiss, O. Kahn, and I. Morgenstern-Badarau. J. Am. Chem. Soc. **104**, 6330 (1982).
14. O. Kahn, S. Sikorav, J. Gouteron, S. Jeannin, and Y. Jeannin. Inorg. Chem. **22**, 2877 (1983).
15. S.S. Tandon, L.K. Thompson, and J.N. Bridson. J. Chem. Soc. Chem. Commun. 804 (1993).
16. S.S. Tandon, L.K. Thompson, M.E. Manuel, and J.N. Bridson. Inorg. Chem. **33**, 5555 (1994).
17. L.K. Thompson, S.S. Tandon, and M.E. Manuel. Inorg. Chem. **34**, 2356 (1995).
18. O. Kahn. Comments Inorg. Chem. **3**, 105 (1984).
19. M.A. Aebersold, B. Gillon, O. Plantevin, L. Pardi, O. Kahn, P. Bergeret, I. von Seggren, F. Tuczek, L. Öhrström, A. Grand, and E. Lelièvre-Berna. J. Am. Chem. Soc. **120**, 5238 (1998).
20. S.S. Tandon, S.K. Mandal, L.K. Thompson, and R.C. Hynes. J. Chem. Soc. Chem. Commun. 1572 (1991).
21. S.S. Tandon, S.K. Mandal, L.K. Thompson, and R.C. Hynes. Inorg. Chem. **31**, 2215 (1992).
22. V. McKee and S.S. Tandon. J. Chem. Soc. Chem. Commun. 385 (1988).
23. V. McKee and S.S. Tandon. Inorg. Chem. **28**, 2901 (1989).
24. V. McKee and S.S. Tandon. J. Chem. Soc. Dalton Trans. 221 (1991).
25. S.S. Tandon, L.K. Thompson, and J.N. Bridson. J. Chem. Soc. Chem. Commun. 911 (1992).
26. S.S. Tandon, L.K. Thompson, J.N. Bridson, and C. Benelli. Inorg. Chem. **34**, 5507 (1995).
27. C.J. Matthews, K. Avery, Z. Xu, L.K. Thompson, L. Zhao, D.O. Miller, K. Biradha, K. Poirier, M.J. Zaworotko, C. Wilson, A.E. Goeta, and J.A.K. Howard. Inorg. Chem. **38**, 5266 (1999).
28. L.K. Thompson, C.J. Matthews, L. Zhao, D.O. Miller, C. Wilson, M.A. Leech, J.A.K. Howard, S.L. Heath, A.G. Whittaker, and R.E.P. Winpenny. J. Solid State Chem. **159**, 308 (2001).
29. C.J. Matthews, Z. Xu, S.K. Mandal, L.K. Thompson, K. Biradha, K. Poirier, and M.J. Zaworotko. J. Chem. Soc. Chem. Commun. 347 (1999).
30. C.J. Matthews, L.K. Thompson, S.R. Parsons, Z. Xu, D.O. Miller, and S.L. Heath. Inorg. Chem. **40**, 4448 (2001).
31. L. Zhao, C.J. Matthews, L.K. Thompson, and S.L. Heath. J. Chem. Soc. Chem. Commun. 265 (2000).
32. L. Zhao, Z. Xu, L.K. Thompson, S.L. Heath, D.O. Miller, and M. Ohba. Angew. Chem. Int. Ed. **39**, 3114 (2000).
33. L. Zhao, Z. Xu, L.K. Thompson, and D.O. Miller. Polyhedron, **20**, 1159 (2001).
34. Z. Xu, L.K. Thompson, and D.O. Miller. Polyhedron, **21**, 1715 (2002).
35. L.K. Thompson, L. Zhao, Z. Xu, D.O. Miller, and W.M. Reiff. Inorg. Chem. **42**, 128 (2003).
36. L. Weeks, L.K. Thompson, J.G. Shapter, K.J. Pope, and Z. Xu. J. Microsc. (Oxford), **212**, 102 (2003).

© 2005 NRC Canada

37. V.A. Milway, V. Niel, T.S.M. Abedin, Z. Xu, L.K. Thompson, H. Grove, D.O. Miller, and S.R. Parsons. Inorg. Chem. **43**, 1874 (2004).
38. L. Zhao, Z. Xu, H. Grove, V.A. Milway, L.N. Dawe, T.S.M. Abedin, L.K. Thompson, T.L. Kelly, R.G. Harvey, D.O. Miller, L. Weeks, J.G. Shapter, and K.J. Pope. Inorg. Chem. **43**, 3812 (2004).
39. O. Waldmann, R. Koch, S. Schromm, P. Müller, L. Zhao, and L.K. Thompson. Chem. Phys. Lett. **332**, 73 (2000).
40. O. Waldmann, L. Zhao, and L.K. Thompson. Phys. Rev. Lett. **88**, 066 401 (2002).
41. O. Waldmann, S. Carretta, P. Santini, R. Koch, A.G.M. Jansen, G. Amoretti, R. Caciuffo, L. Zhao, and L.K. Thompson. Phys. Rev. Lett. **92**, 096 403 (2004).
42. T. Guidi, S. Carretta, P. Santini, E.W. Liviotti, N. Magnani, C. Mondelli, O. Waldmann, L.K. Thompson, L. Zhao, C.D. Frost, G. Amoretti, and R. Caciuffo. Phys. Rev. B: Condens. Matter, **69**, 104 432 (2004).
43. L.K. Thompson, T.L. Kelly, L.N. Dawe, H. Grove, M.T. Lemaire, J.A.K. Howard, E.C. Spencer, C.J. Matthews, S.T. Onions, S.J. Coles, P.N. Horton, M.B. Hursthouse, and M.E. Light. Inorg. Chem. **43**, 7605 (2004).
44. L. Zhao, L.K. Thompson, Z. Xu, D.O. Miller, and D.R. Stirling. J. Chem. Soc. Dalton Trans. 1706 (2001).
45. V.A. Milway, V. Niel, T.S.M. Abedin, Z. Xu, L.K. Thompson, H. Grove, D.O. Miller, and S.R. Parsons. Inorg. Chem. **43**, 1874 (2004).
46. K. Kambe. J. Phys. Soc. Jpn. **5**, 58 (1950).
47. J.G. Shapter, L. Weeks, L.K. Thompson, K.J. Pope, Z. Xu, and M. Johnston. Proc. SPIE Int. Soc. Opt. Eng. **5275**, 59 (2004).
48. L. Weeks, L.K. Thompson, J.G. Shapter, K.J. Pope, and Z. Xu. J. Microsc. (Oxford), **212**, 102 (2003).
49. C. Durkan and M.E. Welland. Appl. Phys. Lett. **80**, 458 (2002).
50. T.S.M. Abedin, L.K. Thompson, D.O. Miller, and E. Krupicka. J. Chem. Soc. Chem. Commun. 708 (2003).

© 2005 NRC Canada

Stereoselective synthesis of multiply substituted [1,2]oxazinan-3-ones via ring-closing metathesis

Gennady V. Shustov, Melanie K. Chandler, and Saul Wolfe

Abstract: The title compounds are α-amino acids whose nitrogen atoms are enclosed within 4,5-disubstituted, six-membered cyclic hydroxamates and they are of interest as potential β-lactam surrogates. The compounds have been synthesized in the present work by functionalization of the double bonds of *N*-substituted 6*H*-[1,2]oxazin-3-ones, which are obtained upon successive reaction of the triflates of *S*-α-hydroxy esters with *O*-allylhydroxylamine and acryloyl chloride, followed by cyclization of the resulting *R*-α-*N*-acryloyl-*N*-allyloxyamino esters in the presence of the ring-closing metathesis (RCM) catalyst bis(tricyclohexylphosphine)benzylideneruthenium dichloride. The olefins are also accessible, but less efficiently so, by a Wittig sequence that employs bromoacetyl bromide in place of acryloyl chloride, followed successively by triphenylphosphine, silver triflate, ozonolysis, and cyclization. Asymmetric dihydroxylation of these chiral olefins affords a single diastereomer in high yield having either the α*R*,4*S*,5*S*- or the α*R*,4*R*,5*R* configuration, depending on the auxiliary. The configuration of the α*R*,4*R*,5*R* isomer has been confirmed by its conversion to (α*R*,4*S*,5*R*)-2-(α-carboxyethyl)-4-phenylacetylamino-5-hydroxy-1,2-oxazinan-3-one, whose α*R*,4*R*,5*S* diastereomer was previously prepared from L-ascorbic acid. With *N*-bromosuccinimide in aqueous dimethylformamide, a 6*H*-[1,2]oxazin-3-one afforded a separable 1:1 mixture of bromohydrins, which could be cyclized to epoxides or hydrogenolyzed to 5-hydroxy-1,2-oxazinan-3-ones.

Key words: penicillin surrogates, asymmetric dihydroxylation, bis(tricyclohexylphosphine)benzylideneruthenium dichloride, cyclic sulfite, epoxides, azidohydrin, bromohydrin.

Résumé : Les composés mentionnés dans le titre sont des acides α-aminés dont l'atome d'azote fait partie d'hydroxamates cycliques à six chaînons substitués dans les positions 4 et 5 qui présentent de l'intérêt comme substituts de β-lactames. Dans ce travail, les composés ont été synthétisés par le biais d'une fonctionnalisation de doubles liaisons de 6*H*-[1,2]oxazin-3-ones *N*-substituées qui sont obtenues par la réaction successive des triflates des esters *S*-α-hydroxylés avec de la *O*-allylhydroxylamine et du chlorure d'acryloyle, suivie d'une cyclisation des esters *R*-α-*N*-acryloyl-*N*-allyloxyamino en présence du catalyseur RCM, dichlorure du bis(tricyclohexylphosphine)benzylidène ruthénium. Les oléfines sont aussi accessibles, mais d'une façon moins efficace, par le biais d'une séquence de Wittig faisant appel au bromure de bromoacétyle, à la place du chlorure d'acryloyle, suivie successivement d'une réaction avec le triphénylphosphine, le triflate d'argent, d'une ozonolyse et d'une cyclisation. La dihydroxylation asymétrique de ces oléfines chirales conduit à un seul diastéréoisomère, avec un rendement élevé, de configuration α*R*,4*S*,5*S*- ou α*R*,4*R*,5*R*- suivant la nature de l'auxiliaire. La configuration de l'isomère α*R*,4*R*,5*R* a été confirmée par sa conversion en (α*R*,4*S*,5*R*)-2-(α-carboxyéthyl)-4-phénylacétylamino-5-hydroxy-1,2-oxaziran-3-one, dont le diastéréoisomère a antérieurement été préparé à partir de l'acide L-ascorbique. La réaction du *N*-bromosuccinimide, dans le diméthylformamide aqueux, avec une 6*H*-[1,2]oxazin-3-one conduit à la formation d'un mélange 1 : 1 de bromohydrines qui peut facilement être séparé alors que les deux isomères peuvent être cyclisés en époxydes ou hydrogénolysés en 5-hydroxy-1,2-oxazinan-3-ones.

Mots clés : substituts de pénicilline, dihydroxylation asymétrique, dichlorure de bis(tricyclohexylphosphine)benzylidèneruthénium, sulfite cyclique, époxydes, azidohydrine, bromohydrine.

[Traduit par la Rédaction]

The final stage of bacterial cell wall peptidoglycan biosynthesis proceeds in two steps (1). The first is displacement of the terminal D-alanine from an RCO-D-ala-D-ala chain by the hydroxyl group of a serine peptidase (**1** → **2**). The second is a cross-linking reaction in which the enzyme is displaced from the depsipeptide by an amino group of another chain (**2** → **3**). These serine peptidases, also known as penicillin-binding proteins (PBPs) (2), are the targets of β-lactam antibiotics (**4** → **5**).

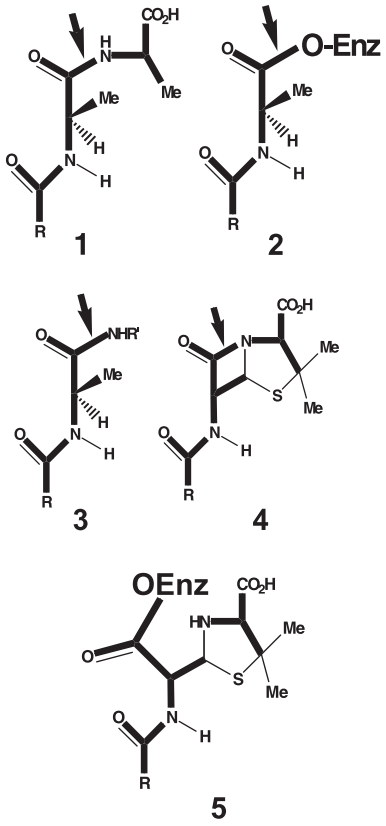
It has been recognized for many years that **1** and **4** are structural analogs (3), i.e., that β-lactam antibiotics are *N*-acyl-D-ala-D-ala surrogates. Since lactivicin (**6**), an antibiotic

Received 9 August 2004. Published on the NRC Research Press Web site at http://canjchem.nrc.ca on 25 February 2005.

G.V. Shustov, M.K. Chandler, and S. Wolfe.[1] Department of Chemistry, Simon Fraser University, 8888 University Drive, Burnaby, BC V5A 1S6, Canada.

[1]Corresponding author (e-mail: swolfe@sfu.ca).

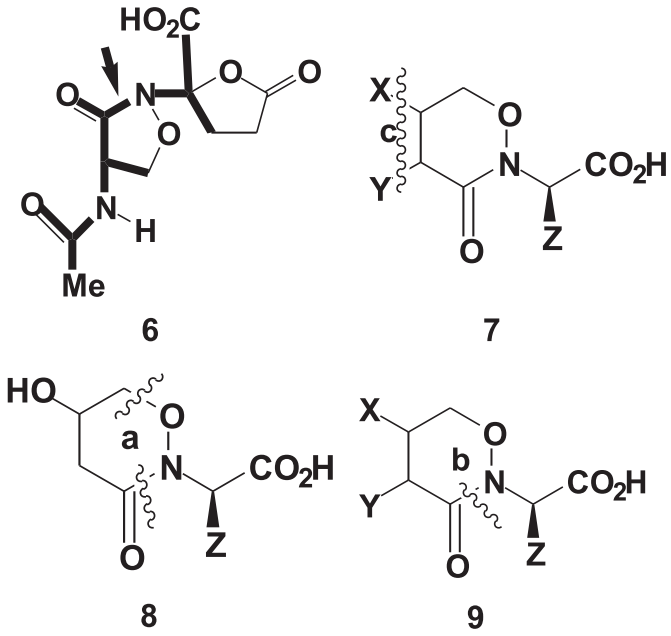
 doi: 10.1139/V04-174 © 2005 NRC Canada



isolated from culture filtrates of *Empedobacter lactagenus* YK-258 and *Lysobacter albus* YK-422, also functions by acylation of the serine hydroxyl groups of PBPs and other penicillin-recognizing enzymes (4), it seems likely that lactivicin is a penicillin and *N*-acyl-D-ala-D-ala analog, and that an isoxazolidin-3-one ring, a five-membered cyclic hydroxamate, is a β-lactam surrogate.

We have recently reported that *six*-membered cyclic hydroxamates of general structure **7** may also serve as β-lactam and D-ala-D-ala surrogates. In a first synthetic approach to such compounds (**8**, Z = H, Me) (5), based on disconnection **a**, protected *N*-hydroxyglycine and *N*-hydroxyalanine were coupled to racemic protected β-hydroxy-γ-bromobutyric acid, and the cyclic hydroxamate was generated by O1-C5 ring closure. In a second approach (6), based on disconnection **b** (**9**), the cyclic hydroxamate was prepared by trimethylaluminium-promoted cyclization of an ε-aminooxyester. These initial syntheses suggested that a stereocontrolled approach to **7**, with extensive variation of X, Y, and Z via **a** would be difficult, because of significant competing *O*-acylation when Z ≠ H, and that syntheses via **b** would also be unsatisfactory because of the large number of steps (11 steps from L-ascorbic acid to **7**, Z = Me, X = α-hydroxy, Y = β-phenylacetamido) and low overall yield (0.9%).

This paper reports a stereocontrolled route to **7**, based on **c**, the functionalization of olefins **13**, which are accessible in three steps from the benzyl, benzhydryl or *tert*-butyl L-α-hydroxyesters **10** by a ring-closing metathesis (RCM) strategy (7).



Scheme 1 summarizes the results obtained starting with the α-hydroxy acids available from the nitrous acid deaminations of L-alanine, L-valine and L-phenylglycine. In situ reaction of allyloxyamine (8) with the triflates of **10** proceeded with inversion of configuration (6, 9) to yield the *R*-α-allyloxyamino esters **11**, which were converted to the RCM precursors **12** with acryloyl chloride. With the exception of the phenyl compound (R_2 = Ph), cyclization to **13** was achieved in 80%–90% yield in refluxing methylene chloride in the presence of the first generation Grubbs catalyst bis(tricyclohexylphosphine)benzylideneruthenium dichloride (4 to 5 mol%).

The synthetic improvement provided by the RCM approach can be seen upon comparison of the cyclizations of **12a** and of the Wittig precursor **16**. Thus (Scheme 2), successive reaction of **11a** with bromoacetyl bromide, triphenylphosphine, and silver triflate, followed by ozonolysis and treatment with potassium carbonate led to cyclization to **13a** in 27% yield.

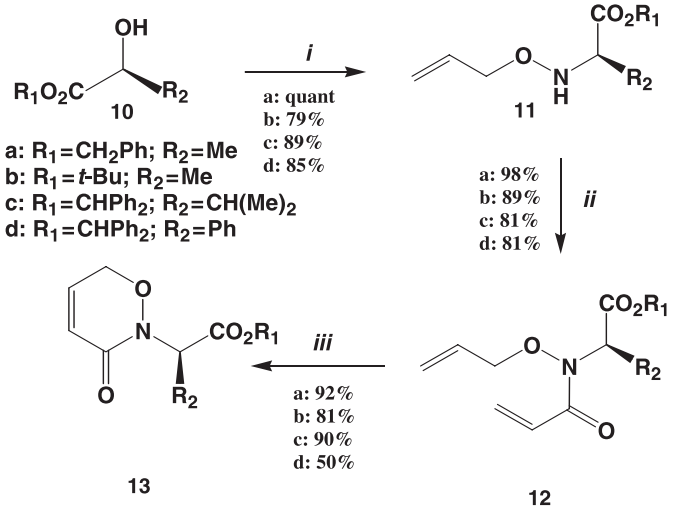
Schemes 3 and 4 exemplify reaction sequences that have been applied to the olefins **13**. In Scheme 3, Sharpless asymmetric dihydroxylation (10) leads, depending on the auxiliary, either to a β-diol **17** or an α-diol **19** as a single diastereomer in each case, and these diols can be deprotected to carboxylic acids **18** or **20**, respectively. The cyclic sulfi*te* (11) of **19** afforded the *trans*-azidohydrin **22** (12),[2] which was converted in 81% overall yield, into **25**, the (α*R*,4*S*,5*R*)-isomer of 2-(α-carboxyethyl)-4-phenylacetylamino-5-hydroxy-1,2-oxazinan-3-one (**25**), which was different from the (α*R*,4*R*,5*S*)-isomer (**7**) synthesized previously from L-ascorbic acid.

As summarized in Scheme 4, **26**, the 6*H*-[1,2]oxazin-3-one prepared from benzhydryl *S*-lactate, reacted with *N*-bromosuccinimide in aqueous dimethylformamide to give, in addition to the dibromides **27**, a separable mixture of bromo-

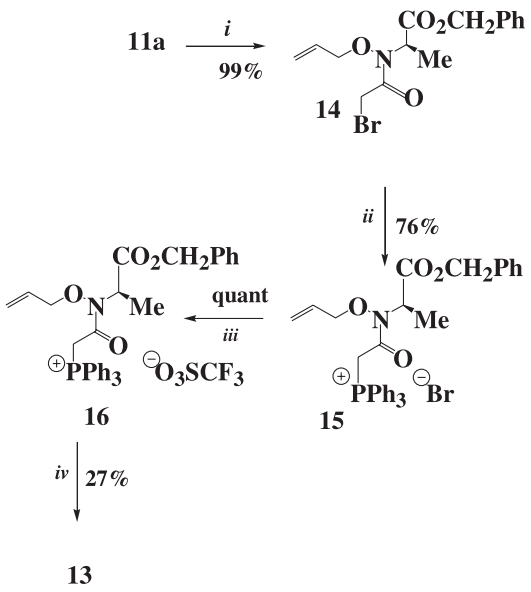
[2] No attempt was made to improve the (nonoptimized) 18% yield of this reaction (11). Cyclic sulfates (13) are, in general, more effective substrates for this reaction than cyclic sulfites, but this route was also not pursued (14).

© 2005 NRC Canada

Scheme 1. (*i*) $(CF_3SO_2)_2O$, 2,6-lutidine, *O*-allylhydroxylamine, CH_2Cl_2; (*ii*) CH_2=CHCOCl, Et_3N or 2,6-lutidine, CH_2Cl_2; (*iii*) PhCH=$RuCl_2[P(Cychex)_3]_2$ (Grubbs'catalyst), CH_2Cl_2 or toluene.



Scheme 2. (*i*) $BrCH_2COBr$, Et_3N, CH_2Cl_2; (*ii*) PPh_3, toluene; (*iii*) CF_3SO_3Ag, MeCN; (*iv*) O_3, CH_2Cl_2, then Me_2S, then K_2CO_3, H_2O.

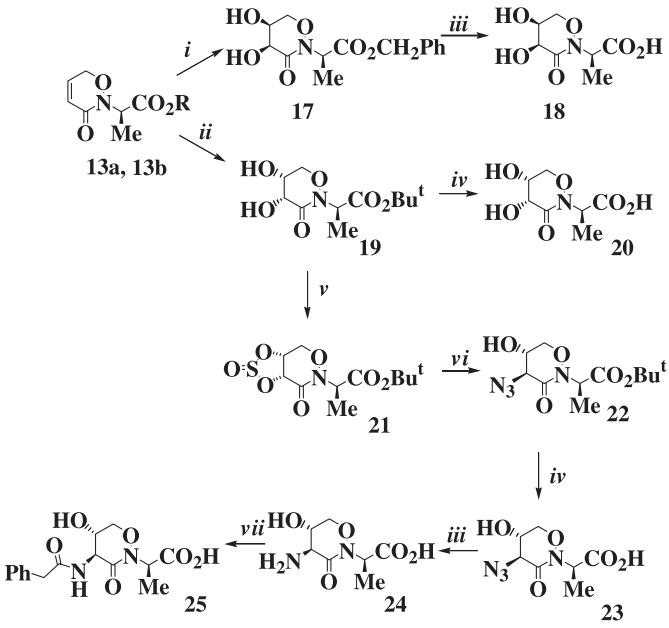


hydrins **28**, in 26% (less polar isomer) and 20% (more polar isomer) yields. Both bromohydrins could be cyclized to epoxides **29**, and the less polar bromohydrin could be hydrogenolyzed in the presence of triethylamine to a single stereoisomer of **30**.

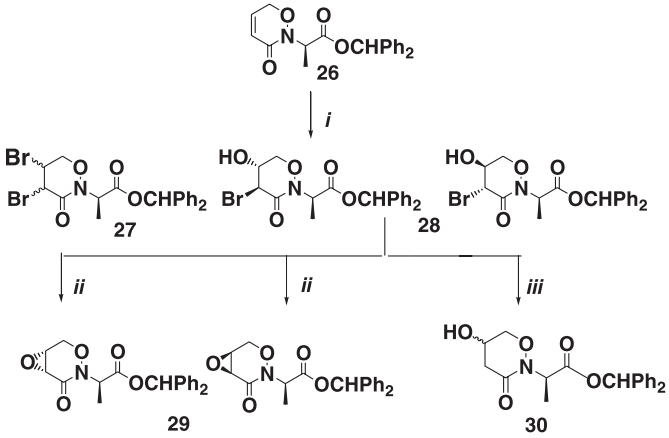
Experimental

Solvents were dried and distilled before use according to standard literature procedures (15). Except where indicated, chemicals were of the highest available purity from Aldrich. All reactions were performed under dry nitrogen using oven-

Scheme 3. (*i*) AD-mix-β, $(DHQD)_2PHAL$, $K_2OsO_4(OH)_4$, $MeSO_2NH_2$, *t*-BuOH, H_2O; (*ii*) AD-mix-α, $(DHQ)_2PHAL$, $K_2OsO_4(OH)_4$, $MeSO_2NH_2$, *t*-BuOH, H_2O; (*iii*) H_2, Pd/C, EtOAc; (*iv*) CF_3CO_2H, CH_2Cl_2; (*v*) $SOCl_2$, Et_3N, CH_2Cl_2; (*vi*) NaN_3, DMF; (*vii*) $PhCH_2COCl$, $NaHCO_3$, MeCN, H_2O.



Scheme 4. (*i*) NBS, DMF, H_2O; (*ii*) K_2CO_3, acetone; (*iii*) H_2, Pd/C, Et_3N, MeOH.



dried (140 °C, 24 h) glassware. The glassware was allowed to cool in a desiccator under vacuum and assembled cold, capped with rubber septa, and evacuated with dry nitrogen gas. Both ^1H and ^{13}C nuclear magnetic resonance (NMR) spectra were recorded on a Bruker model AMX 400 spectrometer operating at 400.1 and 100.6 MHz, respectively. Chemical shifts (δ) are reported in parts per million (ppm) relative to tetramethylsilane (TMS) in an appropriate deuterated solvent. ^{1}HMR data are reported in the following manner: chemical shift, integration, peak multiplicity, coupling constants, and identification. The peak multiplicities are abbreviated as s (singlet), d (doublet), t (triplet), q (quartet), dd (doublet of doublets), ddd (doublet of doublets of doublets), m (multiplet), etc. ^{13}CMR data are reported as δ values in ppm downfield from tetramethylsilane. Infrared (IR)

© 2005 NRC Canada

spectra were recorded on a Bomen-Hartmann-Braun spectrometer (1% KBr or 1% solution). Mass spectra refer to direct inlet EI measurements or CI measurements, using isobutane, or fast-atom bombardment (FAB) employing xenon gas, on a Kratos MS50 spectrometer operated at 70 eV by G. Owens at Simon Fraser University. Melting points (mp) were determined on a Fisher-Johns apparatus, and are uncorrected. Analytical thin layer chromatography (TLC) was carried out on precoated Merck silica gel 60 F-254 plates with aluminium backing. Spots were observed under short-wavelength UV light, or were visualized with iodine vapour, ninhydrin, or ceric sulfate. Flash column chromatography (16*a*) and dry-column flash chromatography (16*b*) were carried out on Merck silica gel 60 (230–400 mesh), using only distilled solvents under dry nitrogen gas. Elemental analyses were performed by M.K. Yang on a Carlo Erba model 1106 elemental analyzer at Simon Fraser University.

Allyloxyamine

DBU (46.36 mL, 0.31 mol) was added in one portion, with stirring, to a cooled solution (5–10 °C) of *N*-hydroxyphthalimide (53.80 g, 0.33 mol) in DMF (120 mL). After 10 min, allyl bromide (25.96 mL, 0.30 mol) was added dropwise. When the addition was complete, the cooling bath was removed and the reaction mixture was stirred at room temperature for 1 h, until the color turned from dark burgundy to yellow. Ethyl acetate (300 mL) and water (150 mL) were added, the aqueous phase was separated, and the organic phase was washed with water (4 × 50 mL). The combined aqueous extracts were back-extracted with EtOAc (3 × 50 mL) and the combined organic layers were washed with satd. $NaHCO_3$ (10 × 50 mL) until the aqueous phase was pale yellow, then with brine (2 × 75 mL), dried over anhydr. $MgSO_4$ and concentrated to give *N*-allyloxyphthalimide 58.83 g (96%), mp 59 to 60 °C (lit. value (3) mp 59 to 60 °C) as a white solid. A solution of the *N*-allyloxyphthalimide (58.70 g, 0.289 mol) in dry ethanol (295 mL) was treated dropwise, with stirring, with a solution of hydrazine hydrate (14.01 mL, 0.289 mol) in EtOH (44 mL). The reaction mixture immediately turned yellow and a white precipitate formed. The mixture was refluxed for 2 h, stirred at room temperature for 17 h, cooled (10–15 °C), concentrated, and concd. HCl (30.24 mL, 0.37 mol) was added dropwise. The white precipitate was removed by filtration and washed with water (160 mL). The filtrate was concentrated under reduced pressure and the residue was maintained at 1 torr (1 torr = 133.322 4 Pa) for 3 h. Water (100 mL) was added, the solution was filtered, and the filtrate was concentrated to 50 mL and added portionwise to KOH pellets in a distillation apparatus. The product was collected at 80–100 °C. A second distillation over KOH pellets afforded 18.96 g (89%) of allyloxyamine as a colorless liquid, bp 94–97 °C (lit. value (17) bp 98 to 99 °C).

(*R*)-*N*-Allyloxyalanine benzyl ester (11a)

A solution of triflic anhydride (10.86 g, 38.5 mmol) in dry CH_2Cl_2 (20 mL) was added dropwise to a solution of benzyl (*S*)-lactate (**10a**) (6.31 g, 35 mmol) in dry CH_2Cl_2 (100 mL) with cooling (–68 to –72 °C) and stirring. After 5–7 min, a solution of 2,6-lutidine (4.31 g, 40.3 mmol) in dry CH_2Cl_2 (15 mL) was added dropwise at the same temperature and the reaction mixture was stirred for 30 min at –68 to –72 °C. A solution of allyloxyamine (4.55 g, 77 mmol) in dry CH_2Cl_2 (15 mL) was then added dropwise, with cooling (–68 to –72 °C) and stirring. The reaction mixture was stirred for 15 min at ca. –72 °C and then was allowed to warm to room temperature. Stirring was continued for 15 h and the reaction mixture was then shaken with satd. $NaHCO_3$ (200 mL) and dried over $MgSO_4$. After removal of the solvent, the residue was purified by dry flash chromatography (silica gel 60H for TLC, 10% EtOAc – hexanes) to afford 8.20 g (quant) of the product as a pale yellowish oil. IR (film, cm^{-1}): 3264, 1740, 1456, 1208, 1170. ^{1}H NMR (100 MHz, $CDCl_3$ + 1 drop of D_2O) δ: 1.28 (3H, d, ^3J = 7.1 Hz, *Me*CH), 3.82 (1H, q, ^3J = 7.1 Hz, MeC*H*), 4.22 (2H, dt, ^3J = 5.7 Hz, ^4J = 1.2 Hz, OCH_2CH=CH$_2$), 5.16–5.37 (2H, m, CH=CH_2), 5.23 (2H, CH_2Ph), 5.76–6.15 (1H, m, ^3J = 5.7 Hz, $^3J^{cis}$ = 9.9 Hz, $^3J^{trans}$ = 17.1 Hz, C*H*=CH$_2$), 7.38 (5H, *Ph*).^{13}C NMR (100 MHz, $CDCl_3$) δ: 14.81, 59.09, 66.63, 75.22, 117.53, 128.06, 128.24, 128.56, 134.37, 135.84, 174.01. Anal. calcd. for $C_{13}H_{17}NO_3$ (%): C 66.4, H 7.3, N 5.95; found: C 66.3, H 7.4, N 6.15.

(*R*)-*N*-Acryloyl-*N*-allyloxyalanine benzyl ester (12a)

A solution of acryloyl chloride (3.26 g, 36 mmol) in dry CH_2Cl_2 (20 mL) was added dropwise with cooling (–5 to –10 °C) and stirring to a solution of (*R*)-*N*-allyloxyalanine benzyl ester (**11a**) (7.06 g, 30 mmol) and Et_3N (4.55 g, 45 mmol) in dry CH_2Cl_2 (80 mL). The reaction mixture was stirred for 1 h at 0–5 °C and then for 4.5 h at room temperature. After dilution with CH_2Cl_2 (ca. 150 mL), the mixture was washed successively with water (3 × 50 mL), 1 N HCl (50 mL), brine (100 mL), and dried over $MgSO_4$. Removal of the solvent gave 9.16 g of a yellow oil, which was purified by dry flash chromatography (silica gel 60H for TLC, 3% EtOAc – hexanes to 15% EtOAc – hexanes) to afford 8.52 g (98%) of the product as a colorless oil. IR (film, cm^{-1}): 1746, 1667, 1621, 1411. ^{1}H NMR (100 MHz, $CDCl_3$) δ: 1.61 (3H, d, ^3J = 7.3 Hz, *Me*CH), 4.45 (2H, dq, ^3J = 6.0 Hz, ^4J = 1.1 Hz, OCH_2CH=CH$_2$), 5.09 (1H, q, ^3J = 7.3 Hz, MeC*H*,), 5.21 (2H, CH_2Ph), 5.25–5.47 (2H, m, CH=CH_2, allyl), 5.76–6.15 (1H, m, ^3J = 6.0 Hz, $^3J^{cis}$ = 10.0 Hz, $^3J^{trans}$ = 17.3 Hz, C*H*=CH$_2$, allyl), 5.83 (1H, dd, ^2J = 2.7 Hz, $^3J^{cis}$ = 7.6 Hz, CH=CH_AH$_B$, acryloyl), 6.48 (1H, dd, ^2J = 2.7 Hz, $^3J^{trans}$ = 17.2 Hz, CH=CH$_A$$H_B$, acryloyl), 6.80 (1H, dd, $^3J^{cis}$ = 7.6 Hz, $^3J^{trans}$ = 17.2 Hz, C*H*=CH$_2$, acryloyl) 7.39 (5H, *Ph*). ^{13}C NMR (100 MHz, $CDCl_3$) δ: 14.06, 56.45, 67.10, 78.27, 120.28, 126.21, 128.07, 128.21, 128.48, 130.04, 130.91, 135.47, 168.22, 170.35. MS (CI, isobutane), *m/z*: 290 (M^+ + 1). Anal. calcd. for $C_{16}H_{19}NO_4$ (%): C 66.4, H 6.6, N 4.8; found: C 66.4, H 6.7, N 5.1.

(*R*)-2-(3-Oxo-3,6-dihydro[1,2]oxazin-2-yl)-propionic acid benzyl ester (13a)

A solution of (*R*)-*N*-acryloyl-*N*-allyloxyalanine benzyl ester (**12a**) (7.32 g, 25.3 mmol) and bis(tricyclohexylphosphine)benzylideneruthenium dichloride (1.04 g, 1.26 mmol, 5 mol%) in dry CH_2Cl_2 (250 mL) was refluxed for 6 h under nitrogen, with stirring. Stirring was continued for 20 h at room temperature and the dark brown reaction mixture was then filtered through a short pad of silica gel 60H (for TLC), which was washed with CH_2Cl_2 (50 mL). After concentra-

© 2005 NRC Canada

tion of the filrate, the dark oily residue was purified by dry flash chromatography (silica gel 60H for TLC, 5% EtOAc – hexanes to 15% EtOAc – hexanes) to afford 6.05 g (92%) of the product. IR (film, cm^{-1}): 1745, 1675, 1214, 1189. ^1H NMR (400 MHz, $CDCl_3$) δ: 1.53 (3H, d, ^3J = 7.3 Hz, *Me*CH), 4.46 (1H, dq, ^2J = –15.9 Hz, ^3J = 3.4 Hz, ^4J = 1.8 Hz, OCH_ACH=CH), 4.56 (1H, dq, ^2J = 15.9 Hz, ^3J = 3.4 Hz, ^4J = 1.8 Hz, OCH_BCH=CH), 5.15 (1H, d, ^2J = 12.4 Hz, CH_APh), 5.19 (1H, q, MeC*H*, ^3J = 7.3 Hz), 5.22 (1H, d, ^2J = 12.4 Hz, CH_BPh), 6.04 (1H, dt, $^3J^{cis}$ = 10.0 Hz, ^4J = 1.8 Hz, CH=C*H*CO), 6.72 (1H, dt, $^3J^{cis}$ = 10.0 Hz, ^3J = 3.4 Hz, CH_2C*H*=CHCO), 7.27–7.40 (5H, m, *Ph*). ^{13}C NMR (100 MHz, $CDCl_3$) δ: 13.71, 53.57, 67.08, 67.57, 122.32, 128.02, 128.26, 128.52, 135.49, 139.67, 164.64, 170.09. MS (CI, isobutane), *m*/*z*: 262 (M^+ + 1). Anal. calcd. for $C_{14}H_{15}NO_4$ (%): C 64.4, H 5.8, N 5.4; found: C 64.3, H 5.85, N 5.6.

(*R*)-*N*-(Bromoacetyl)-*N*-allyloxyalanine benzyl ester (14)

A solution of bromoacetyl bromide (2.22 g, 11 mmol) in dry CH_2Cl_2 (20 mL) was added dropwise with cooling (–25 to –30 °C) and stirring to a solution of (*R*)-*N*-allyloxyalanine benzyl ester (**11a**) (2.59 g, 11 mmol) and Et_3N (1.11 g, 11 mmol) in dry CH_2Cl_2 (30 mL). The reaction mixture was stirred for 1 h at 0–5 °C and then allowed to warm to room temperature. After dilution with CH_2Cl_2 (ca. 30 mL), the mixture was washed successively with water (2 × 30 mL), 1 N HCl (30 mL), satd. $NaHCO_3$ (30 mL), dried over $MgSO_4$, and evaporated to yield **14** as a yellowish oil. IR (film, cm^{-1}): 1746, 1678, 1455, 1214. ^1H NMR (100 MHz, $CDCl_3$) δ: 1.60 (3H, d, ^3J = 7.3 Hz, *Me*CH), 4.08 (2H, CH_2Br), 4.49 (2H, dt, ^3J = 6.1 Hz, ^4J = 0.9 Hz, OCH_2CH=CH_2), 4.98 (1H, q, MeC*H*, ^3J = 7.3 Hz), 5.16–5.48 (2H, m, CH=CH_2), 5.20 (2H, CH_2Ph), 5.76–6.15 (1H, m, ^3J = 6.1 Hz, $^3J^{cis}$ = 10.0 Hz, $^3J^{trans}$ = 17.3 Hz, C*H*=CH_2), 7.29–7.41 (5H, m, *Ph*). MS (CI, isobutane), *m*/*z*: 358, 356 (M^+ + 1).

Conversion of 14 to 15

A solution of **14** (3.90 g, 11 mmol) in dry toluene (10 mL) was added dropwise to a solution of triphenylphosphine (2.88 g, 11 mmol) in dry toluene (20 mL), and the reaction mixture was stirred for 24 h at room temperature. The precipitated yellow oil was separated, washed with toluene, and dried in vacuo to give a solid yellowish hygroscopic foam, which was reprecipitated from a mixture of dry CH_2Cl_2 (10 mL) and absolute ether (ca. 100 mL) to afford 5.16 g (76%) of **15** as a white hygroscopic foam.

Conversion of the bromide salt 15 to the triflate salt 16

A solution of silver trifluoromethanesulfonate (2.56 g, 10 mmol) in dry MeCN (20 mL) was added dropwise with stirring to a solution of **15** (6.18 g, 10 mmol) in dry MeCN (25 mL). The yellow precipitate was collected on a sintered glass funnel using a short pad of Celite® 545, and washed with MeCN (ca. 50 mL). The filtrate was concentrated under reduced pressure and the residual yellow foam was dissolved in CH_2Cl_2 (100 mL) and a small amount of $MgSO_4$ was added to coagulate small particles of AgBr. The solution was filtered again and the filtrate was concentrated to provide 6.52 g (quant) of **16** as a yellow highly hygroscopic foam. ^1H NMR (400 MHz, $CDCl_3$, major isomer) δ: 1.50 (3H, d, ^3J = 7.4 Hz, *Me*CH), 4.84 (1H, dd, ^2J = 11.5 Hz, ^3J = 6.1 Hz, OCH_ACH=CH_2), 4.80 (1H, q, MeC*H*, ^3J = 7.4 Hz), 4.84 (1H, dd, ^2J = 11.5 Hz, ^3J = 6.1 Hz, OCH_BCH=CH_2), 4.89 (1H, dd, $^2J_{HH}$ = 17.8 Hz, $^2J_{HP}$ = 12.7 Hz, CH_AP), 5.06 (1H, d, ^2J = 12.4 Hz, CH_APh), 5.10 (1H, d, ^2J = 12.4 Hz, CH_BPh), 5.31 (1H, br.d, $^3J^{cis}$ = 10.4 Hz, CH=CH_D), 5.35 (1H, dd, $^2J_{HH}$ = 17.8 Hz, $^2J_{HP}$ = 13.8 Hz, CH_BP), 5.49 (1H, dd, $^3J^{trans}$ = 17.2 Hz, ^2J = 1.2 Hz, CH=CH_E), 5.92–6.02 (1H, m, ^3J = 6.1 Hz, $^3J^{cis}$ = 10.4 Hz, $^3J^{trans}$ = 17.2 Hz, C*H*=CH_2), 7.4–7.8 (5H, m, *Ph*CH_2), 7.6–7.7 (15H, m, *Ph*$_3$P).

Ozonolysis and cyclization of 16

A solution of **16** (6.52 g, 9.95 mmol) in CH_2Cl_2 (180 mL) was cooled to –76 to –78 °C, stirred, and saturated with ozone (moderate bubbling until a persistent blue color remained). Excess ozone was removed by bubbling nitrogen through the reaction mixture at –76 to –78 °C, and Me_2S (3.1 g, 50 mmol) was added dropwise with stirring. The reaction mixture was allowed to warm to room temperature and a solution of K_2CO_3 (6.91 g, 50 mmol) in water (20 mL) was added with vigorous stirring. Water (100 mL) was added and the organic layer was separated, washed with water (2 × 30 mL), dried over $MgSO_4$, and concentrated to a yellow semisolid, which was purified by flash chromatography (silica gel 60H, 20% EtOAc – hexanes) to afford 0.70 g (27%) of **13** as a colorless oil, identical with the material prepared previously.

(*R*)-*N*-Acryloyl-*N*-allyloxyalanine *tert*-butyl ester (12b)

A solution of triflic anhydride (15.52 g, 55 mmol) in dry CH_2Cl_2 (25 mL) was added dropwise to a solution of *tert*-butyl (*S*)-lactate (**10b**) (6.71 g, 46 mmol) in dry CH_2Cl_2 (130 mL) with cooling (–68 to –72 °C) and stirring. After 5–7 min, a solution of 2,6-lutidine (6.16 g, 57.5 mmol) in dry CH_2Cl_2 (20 mL) was added dropwise and stirring was continued for 1.5 h at –68 to –72 °C. A solution of allyloxyamine (6.57 g, 90 mmol) in dry CH_2Cl_2 (20 mL) was then added dropwise, with continued cooling and stirring. After an additional 15 min stirring at –72 °C, the reaction mixture was allowed to warm to room temperature, and stirring was continued for 15 h. The reaction mixture was then shaken with satd. $NaHCO_3$ and the organic layer was dried over magnesium sulfate and evaporated to give 14.31 g (79% yield) of a 1.0:0.97 mixture of (*R*)-*N*-allyloxyalanine *tert*-butyl ester (**11b**) and 2,6-lutidine. Additional 2,6-lutidine (2.66 g, 24.8 mmol) was added to a solution of this mixture in dry CH_2Cl_2 (100 mL), the solution was cooled to –15 to –20 °C, and a solution of acryloyl chloride (5.09 g, 56.3 mmol) in dry CH_2Cl_2 (20 mL) was added dropwise, with stirring. Stirring was continued for 1 h at 0–5 °C and then 20 h at room temperature. After dilution with CH_2Cl_2 (ca. 150 mL), the mixture was washed successively with water (4 × 50 mL), 1 mol L^{-1} citric acid (2 × 50 mL), satd. $NaHCO_3$ (2 × 50 mL), dried over $MgSO_4$, and concentrated to give 12.73 g of a red oil, which was purified by dry flash chromatography (silica gel 60H for TLC, 1% EtOAc – hexanes to 7% EtOAc – hexanes) to afford 8.91 g (70% over the two steps) of **12b** as a colorless oil. IR (film, cm^{-1}): 2981, 1738, 1667, 1622, 1411. ^1H NMR (100 MHz, $CDCl_3$) δ: 1.47 (9H, *Me*$_3$C), 1.53 (3H, d, ^3J = 7.3 Hz, *Me*CH), 4.48 (2H, dq,

© 2005 NRC Canada

^3J = 5.9 Hz, ^4J = 1.2 Hz, OCH_2CH=CH_2), 4.93 (1H, q, ^3J = 7.3 Hz, MeC*H*,), 5.26–5.50 (2H, m, CH=CH_2, allyl), 5.76–6.18 (1H, m, ^3J = 5.9 Hz, $^3J^{cis}$ = 10.1 Hz, $^3J^{trans}$ = 15.6 Hz, C*H*=CH_2, allyl), 5.81 (1H, dd, ^2J = 2.6 Hz, $^3J^{cis}$ = 9.5 Hz, CH=CH_AH$_B$, acryloyl), 6.46 (1H, dd, ^2J = 2.6 Hz, $^3J^{trans}$ = 17.0 Hz, CH=CH$_A$$H_B$, acryloyl), 6.80 (1H, dd, $^3J^{cis}$ = 9.5 Hz, $^3J^{trans}$ = 17.0 Hz, C*H*=CH_2, acryloyl). ^{13}C NMR (100 MHz, $CDCl_3$) δ: 14.12, 27.91, 57.28, 78.22, 81.83, 120.02, 126.42, 129.75, 131.09, 132.41, 168.34, 169.55. MS (CI, isobutane), *m*/*z*: 256 (M^+ + 1).

Cyclization of 12b to 13b

A solution of (*R*)-*N*-acryloyl-*N*-allyloxyalanine *tert*-butyl ester (**12b**) (3.39 g, 13.27 mmol) and bis(tricyclohexylphosphine)benzylideneruthenium dichloride (Grubbs' catalyst) (0.48 g, 0.58 mmol, 4.4 mol%) in dry benzene (120 mL) was refluxed with stirring under nitrogen for 6 h. Additional amounts (0.23 g, 0.28 mmol and 0.21 g, 0.25 mmol) of the catalyst were added and the reaction mixture was refluxed for 8 h after each of these additions. The dark brown reaction mixture was then filtered through a short pad of silica gel 60H (for TLC), which was washed with CH_2Cl_2 (100 mL). The filtrate was concentrated and the dark oily residue was purified by dry flash chromatography (silica gel 60H for TLC, 5% EtOAc – hexanes to 20% EtOAc – hexanes) to afford 2.45 g (81%) of **13b** as an oil. IR (film, cm^{-1}): 2979, 1737, 1677, 1368, 1162. ^{1}H NMR (400 MHz, $CDCl_3$) δ: 1.46 (9H, *Me*$_3$C), 1.53 (3H, d, ^3J = 7.3 Hz, *Me*CH), 4.49 (1H, dq, ^2J = 15.8 Hz, ^3J = 3.4 Hz, ^4J = 1.8 Hz, OCH_ACH=CH), 4.64 (1H, dq, ^2J = –15.8 Hz, ^3J = 3.4 Hz, ^4J = 1.8 Hz, OCH_BCH=CH), 5.03 (1H, q, MeC*H*, ^3J = 7.3 Hz), 6.05 (1H, dt, $^3J^{cis}$ = 10.0 Hz, ^4J = 1.8 Hz, CH=C*H*CO), 6.74 (1H, dt, $^3J^{cis}$ = 10.0 Hz, ^3J = 3.4 Hz, CH_2C*H*=CHCO). ^{13}C NMR (100 MHz, $CDCl_3$) δ: 13.77, 27.95, 54.16, 67.53, 81.82, 122.46, 139.47, 164.67, 169.28. MS (CI, isobutane), *m*/*z*: 228 (M^+ + 1). Anal. calcd. for $C_{11}H_{17}NO_4$ (%): C 58.1, H 7.5, N 6.2; found: C 58.4, H 7.7, N 6.3.

(*R*)-3-Methyl-2-(3-oxo-3,6-dihydro[1,2]oxazin-2-yl)-butyric acid (13, R_1 = H, R_2 = CH(Me)$_2$)

A solution of **13c** (2.00 g, 5.47 mmol) in 98% formic acid (120 mL) was stirred vigorously at room temperature for 6 h. The solvent was then removed in vacuo, and the residue, in dry CH_2Cl_2 (100 mL), was dried over anhydr. $MgSO_4$. Removal of the solvent gave 2.22 g of a yellow oil, which was purified via dry flash chromatography (silica gel 60H for TLC, 30% EtOAc – hexanes → 100% EtOAc) to afford 0.82 g (75%) of the product as a yellow solid. ^{1}H NMR (100 MHz, $CDCl_3$) δ: 1.10 (d, 3H, -CH_3), 1.15 (d, 3H, -CH_3), 2.20–2.80 (m, 1H, C*H*Me$_2$), 4.40–4.75 (m, 2H, NOCH_2), 4.90 (d, 1H, NC*H*), 6.15 (dt, 1H, NOCH$_2$CH=C*H*), 6.81 (dt, 1H, NOCH$_2$C*H*), 8.33 (br. s, 1H, CO_2H). MS (CI, isobutane), *m*/*z*: 200 (M^+ + 1).

(*S*)-2-Hydroxy-3-methylbutyric acid benzhydryl ester (10c)

A solution of diphenyldiazomethane (0.70 g, 3.60 mmol) in EtOAc (5 mL) was added portionwise with cooling (ice bath) and stirring to a solution of (*S*)-2-hydroxy-3-methylbutyric acid (0.51 g, 4.36 mmol) in EtOAc (5 mL). The resulting purple solution was stirred at room temperature for 6 h until the color faded to pale yellow, and then was washed successively with satd. $NaHCO_3$ (3 × 5 mL) and brine (2 × 5 mL), dried over anhydr. $MgSO_4$, and concentrated to give 0.99 g of a yellow solid. Recrystallization from hexanes yielded 0.82 g (80%) of **10c** as white crystals, mp 71 to 72 °C. ^{1}H NMR (400 MHz, $CDCl_3$) δ: 0.76 (d, 3H, -CH_3), 1.02 (d, 3H, -CH_3), 2.12–2.23 (m, 1H, C*H*Me$_2$), 2.68 (br. s, 1H, OH), 4.16 (d, 1H, C*H*OH), 6.96 (s, 1H, C*H*Ph$_2$), 7.20–7.45 (m, 10H, Ar*H*). MS (CI, isobutane), *m*/*z*: 285 (M^+ + 1). Anal. calcd. for $C_{18}H_{20}O_3$ (%): C 76.03, H 7.09; found: C 76.13, H 7.12.

(*R*)-2-Allyloxyamino-3-methylbutryic acid benzhydryl ester (11c)

A solution of triflic anhydride (4.42 mL, 26.29 mmol) in dry CH_2Cl_2 (12 mL) was added dropwise via syringe to a solution of **10c** (6.50 g, 22.86 mmol) in dry CH_2Cl_2 (70 mL), with cooling (–68 to –70 °C) and stirring. After 5 min, a solution of 2,6-lutidine (3.19 mL, 27.43 mmol) in dry CH_2Cl_2 (10 mL) was added dropwise. The pale yellow reaction mixture was stirred at –68 °C for 1 h, warmed to room temperature, and stirred for an additional 17 h. The solvent was removed under reduced pressure and the residue (in EtOAc) was washed with 1 N citric acid (5 × 100 mL), dried over anhydr. $MgSO_4$, and evaporated to give 9 g of a red semisolid. This was purified via dry flash chromatography (silica gel 60H for TLC, 5% EtOAc – hexanes) to afford 8.04 g of the triflate as a pale yellow solid. ^{1}H NMR (400 MHz, $CDCl_3$) δ: 0.89 (d, 3H, -CH_3), 1.05 (d, 3H, -CH_3), 2.38–2.46 (m, 1H, C*H*Me$_2$), 5.04 (d, 1H, C*H*OSO$_2$CF$_3$), 7.00 (s, 1H, C*H*Ph$_2$), 7.20–7.42 (m, 10H, Ar*H*). MS (CI, isobutane), *m*/*z*: 417 (M^+ + 1). Anal. calcd. for $C_{19}H_{19}O_5SF_3$ (%): C 54.80, H 4.60; found: C 54.55, H 4.63.

A solution of allyloxylamine (5.41 g, 0.074 mol) in dry CH_3CN (35 mL) was added, with stirring, to a solution of the above triflate (7.71 g, 0.018 mol) in dry CH_3CN (80 mL). The reaction mixture was refluxed for 3 h, cooled to room temperature, and evaporated under reduced pressure. The residue, in EtOAc (100 mL), was washed successively with satd. $NaHCO_3$ (3 × 100 mL) and brine (2 × 100 mL), dried over anhydr. $MgSO_4$, and concentrated to give 6.67 g of a pale yellow oil. Purification by dry flash chromatography (silica gel 60H for TLC, 10% EtOAc – hexanes) afforded 5.62 g (89%) of **11c** as a colorless oil. ^{1}H NMR (400 MHz, $CDCl_3$) δ: 0.86 (d, 3H, -CH_3), 0.92 (d, 3H, -CH_3), 1.85–1.94 (m, 1H, C*H*Me$_2$), 3.57 (d, 1H, NC*H*), 4.17–4.19 (m, 2H, OCH_2), 5.14–5.18 (m, 1H, OCH$_2$CH=C*H*H), 5.22 (dd, 1H, OCH$_2$CH=CH*H*), 5.83–5.93 (m, 1H, OCH$_2$C*H*), 6.98 (s, 1H, C*H*Ph$_2$), 7.23–7.40 (m, 10H, Ar*H*). MS (CI, isobutane), *m*/*z*: 340 (M^+ + 1). Anal. calcd. for $C_{21}H_{25}NO_3$ (%): C 74.31, H 7.42, N 4.13; found: C 74.49, H 7.46, N 4.40.

(*R*)-2-(*N*-Acryloyl, *N*-allyloxyamino)-3-methylbutyric acid benzhydryl ester (12c)

A solution of **11c** (5.08 g, 14.98 mmol) in dry CH_2Cl_2 (50 mL) was treated in one portion with triethylamine (3.13 mL, 22.47 mmol). The solution was stirred at room temperature for 5 min, cooled to 0 °C, and 97% acryloyl chloride (1.50 mL, 17.98 mmol) was added dropwise via syringe. This mixture was stirred at 0 °C for 45 min, then allowed to warm to room temperature, and stirring was continued for 2.5 h. The light orange reaction mixture was

© 2005 NRC Canada

then diluted with CH_2Cl_2 (150 mL) and washed successively with water (3 × 50 mL), 1 N HCl (50 mL), and brine (100 mL), dried over anhydr. $MgSO_4$, and evaporated to 5.67g of an orange oil. Purification by dry flash chromatography (silica gel 60H for TLC, 3% EtOAc – hexanes → 5% EtOAc – hexanes) gave 4.79 g (81%) of **12c** as a yellow oil. ^{1}H NMR (400 MHz, $CDCl_3$) δ: 0.95 (d, 3H, -CH_3), 0.96 (d, 3H, -CH_3), 2.44–2.54 (m, 1H, C*H*Me_2), 4.15 (dd, 1H, OC*H*H), 4.32 (dd, 1H, OCH*H*), 4.87 (d, 1H, NC*H*), 5.17–5.22 (m, 2H, OCH_2CH=CH_2), 5.73–5.82 (m, 2H, OCH_2CH + NC=OC*H*), 6.48 (dd, 1H, NC=OCH=C*H*H), 6.71 (dd, 1H, NC=OCH=CH*H*), 6.91 (s, 1H, C*H*Ph_2), 7.20–7.40 (m, 10H, Ar*H*). MS (CI, isobutane), *m*/*z*: 394 (M^+ + 1).

(*R*)-3-Methyl-2-(3-oxo-3,6-dihydro[1,2]oxazin-2-yl)-butyric acid benzhydryl ester (13c)

Bis(tricyclohexylphosphine)benzylideneruthenium dichloride (0.34 g, 0.42 mmol) was weighed directly into a 250 mL flask, placed under a nitrogen atmosphere, and dry CH_2Cl_2 (25 mL) was added, followed by a solution of **12c** (3.28 g, 8.33 mmol) in dry CH_2Cl_2 (60 mL). The dark purple reaction mixture was refluxed for 4 h, cooled to room temperature, filtered through a short, densely packed pad of silica gel 60H for TLC (ϕ ~ 3.8 cm, *l* ~ 2 cm), which was washed with CH_2Cl_2 (5 × 20 mL). Removal of the solvent gave 3.18 g of a brown oil, which was purified via dry flash chromatography (silica gel 60H for TLC, 5% EtOAc – hexanes → 20% EtOAc – hexanes) to afford 3.57 g (90%) of the product as a brown oil. ^{1}H NMR (400 MHz, $CDCl_3$) δ: 0.99 (d, 3H, -CH_3), 1.01 (d, 3H, -CH_3), 2.44–2.53 (m, 1H, C*H*Me_2), 4.38 (ddd, 2H, NOCH_2), 4.97 (d, 1H, NC*H*), 6.05 (dt, 1H, $NOCH_2CH$=C*H*), 6.68 (dt, 1H, $NOCH_2$C*H*), 6.92 (s, 1H, C*H*Ph_2), 7.20–7.40 (m, 10H, Ar*H*). MS (CI, isobutane), *m*/*z*: 366 (M^+ + 1).

(*S*)-α-Hydroxyphenylacetic acid benzhydryl ester (10d)

A solution of diphenyldiazomethane (0.53 g, 2.72 mmol) in EtOAc (5 mL) was added portionwise with cooling (ice bath) and stirring to a solution of (*S*)-mandelic acid (0.50 g, 3.29 mmol) in EtOAc (5 mL). The purple reaction mixture was stirred at room temperature for 1 h and was then washed successively with satd. $NaHCO_3$ (3 × 5 mL) and brine (2 × 5 mL), dried over anhydr. $MgSO_4$, and concentrated to 0.99 g of a yellow solid, which was recrystallized from hexanes to give 0.67 g (80%) of the ester, mp 87 to 88 °C (lit. value (18) mp 87 to 88 °C). ^{1}H NMR (400 MHz, $CDCl_3$) δ: 3.45 (d, 1H, O*H*), 5.28 (d, 1H, C*H*OH), 6.75 (s, 1H, C*H*Ph_2), 7.20–7.45 (m, 15H, Ar*H*).

(*R*)-α-Allyloxyaminophenylacetic acid benzhydryl ester (11d)

A solution of triflic anyhydride (10.80 mL, 64.47 mmol) in dry CH_2Cl_2 (25 mL) was added dropwise via syringe to a solution of **10d** (17.85 g, 56.1 mmol) in dry CH_2Cl_2 (175 mL), with cooling (–68 to –70 °C) and stirring. After 5 min, a solution of 2,6-lutidine (7.80 mL, 67.28 mmol) in dry CH_2Cl_2 (25 mL) was added dropwise. The pale yellow reaction mixture was stirred at –68 °C for 1 h, and a solution of allyloxyamine (7.29 g, 99.8 mmol) in dry CH_2Cl_2 (25 mL) was added dropwise with continued cooling and stirring. The yellow reaction mixture was stirred for 30 min and the cooling bath was then removed and the mixture allowed to warm to room temperature. Stirring was continued at room temperature for 17 h and the dark yellow solution was mixed in a separatory funnel with 250 mL of satd. $NaHCO_3$. The two layers were gently mixed by bubbling nitrogen for 20 min, and then shaken manually. The organic phase was separated, washed successively with satd. $NaHCO_3$ (2 × 250 mL) and brine (250 mL), dried over $MgSO_4$, and evaporated to 24.05 g of a mixture of **11d** and 2,6-lutidine (1:0.37, mol:mol), which was used in the next step without further purification. ^{1}H NMR (100 MHz, $CDCl_3$) δ: 4.28 (dt, 2H, NOCH_2), 4.95 (br. d, 1H, NC*H*), 5.10–5.45 (m, 2H, $NOCH_2CH$=CH_2), 5.72–6.15 (m, 1H, $NOCH_2$C*H*), 6.22 (br. d, 1H, N*H*), 6.98 (s, 1H, C*H*Ph_2), 7.02–7.50 (m, 10H, Ar*H*).

(*R*)-(*N*-Acryloyl, *N*-α-allyloxyamino)phenylacetic acid benzhydryl ester (12d)

2,6-Lutidine (4.24 mL, 36.4 mmol) was added dropwise, with stirring, to a solution of **11d** (9.06 g, 24.26 mmol) in dry CH_2Cl_2 (75 mL). After 5 min at room temperature, the reaction mixture was cooled to 0 °C and a solution of 97% acryloyl chloride (2.44 mL, 29.12 mmol) in dry CH_2Cl_2 (25 mL) was added dropwise with stirring. This mixture was stirred at 0 °C for 45 min, then allowed to warm to room temperature and stirred for 17 h. The reaction mixture was diluted with CH_2Cl_2 (50 mL) and washed successively with water (50 mL), 1 N citric acid (2 × 100 mL), satd. $NaHCO_3$ (2 × 75 mL), and brine (100 mL), dried over anhydr. $MgSO_4$, and evaporated to a dark orange oil, which was purified via dry flash chromatography (silica gel 60H for TLC, 3% EtOAc – hexanes → 20% EtOAc – hexanes) to afford 8.36 g (81%) of **12d** as a yellow oil. ^{1}H NMR (400 MHz, $CDCl_3$) δ: 3.60 (dd, 1H, NOC*H*H), 4.07 (dd, 1H, NOCH*H*), 5.04 (dd, 1H, $NOCH_2CH$=C*H*H), 5.10 (dd, 1H, $NOCH_2CH$=CH*H*), 5.53–5.63 (m, 1H, $NOCH_2$C*H*), 5.84 (dd, 1H, C=OC*H*), 6.28 (s, 1H, NC*H*), 6.49 (dd, C=OCHC*H*H), 6.77 (dd, 1H, C=OCHCH*H*), 6.94 (s, 1H, C*H*Ph_2), 7.02–7.46 (m, 15H, Ar*H*). MS (CI, isobutane), *m*/*z*: 428 (M^+ + 1).

(*R*)-(3-Oxo-3,6-dihydro[1,2]oxazin-2-yl)-phenylacetic acid benzhydryl ester (13d)

Bis(tricyclohexylphosphine)benzylideneruthenium dichloride (0.11 g, 0.13 mmol) was weighed directly into a 50 mL flask, placed under a nitrogen atmosphere, and dry CH_2Cl_2 (10 mL) was added, followed by a solution of **12d** (1.10 g, 2.58 mmol) in dry CH_2Cl_2 (15 mL). The purple reaction mixture was refluxed for 3 h, an additional 0.11 g of the catalyst was added, and refluxing was continued for another 2 h. The mixture was then allowed to cool to room temperature and filtered through a short, densely packed pad of silica gel 60H for TLC (ϕ ~ 3.8 cm, *l* ~ 2 cm), which was washed with CH_2Cl_2 (5 × 20 mL). Evaporation gave a brown oil, which was purified via column chromatography (5% EtOAc – hexanes → 30% EtOAc – hexanes) to afford 0.50 g (50%) of **13d** as a brown oil. ^{1}H NMR (400 MHz, $CDCl_3$) δ: 4.34 (ddd, 1H, NOC*H*H), 4.61 (ddd, 1H, NOCH*H*), 6.04 (dt, 1H, $NOCH_2CH$=C*H*), 6.37 (s, 1H, NC*H*), 6.70 (dt, 1H, $NOCH_2$C*H*), 6.96 (s, 1H, C*H*Ph_2), 7.10–7.40 (m, 15H, Ar*H*). MS (CI, isobutane), *m*/*z*: 410 (M^+ + 1).

© 2005 NRC Canada

(α*R*,4*S*,5*S*)-2-(α-Benzoxycarbonylethyl)-4,5-dihydroxy-1,2-oxazinan-3-one (17)

A mixture of $K_2OsO_2(OH)_4$ (0.0063 g, 0.017 mmol), $(DHQD)_2PHAL$ (0.032 g, 0.041 mmol), and AD-mix-β (1.41 g) was dissolved in a mixture of *tert*-butanol (5 mL) and water (5 mL). After dissolution of the salts, methanesulfonamide (0.099 g, 1.04 mmol) was added and the mixture was cooled to –2 °C. The benzyl ester **13a** (0.26 g, 1.01 mmol) was added in one portion and the heterogeneous slurry was stirred vigorously for 14 h at –2 to +2 °C. Sodium sulfite (1.5 g) was added to quench the reaction and stirring was continued for 1 h at room temperature. Methylene chloride (10 mL) was added and the organic layer was separated. The aqueous phase was extracted with CH_2Cl_2 (5 × 5 mL) and the combined organic extracts were dried over $MgSO_4$. After removal of the solvent, the yellowish semisolid residue was purified by dry flash chromatography (silica gel 60H for TLC, 15% EtOAc – hexanes to EtOAc) to afford 0.158 g (81%) of the product as a white solid. ^{1}H NMR (400 MHz, $CDCl_3$ + 2 drops of CD_3OD) δ: 1.53 (3H, d, ^3J = 7.3 Hz, α-*Me*CH), 3.96 (1H, dd, ^2J = –11.8 Hz, ^3J = 2.5 Hz, 6-H_A), 4.41 (1H, d, ^3J = 4.1 Hz, 4-*H*), 4.44 (1H, dd, ^2J = –11.8 Hz, ^3J = 6.8 Hz, 6-H_B), 4.55–4.51 (1H, m, 5-H), 5.11 (1H, q, ^3J = 7.3 Hz, -C*H*), 5.13 (1H, s, CH_2Ph), 7.34–7.24 (5H, m, *Ph*).

(α*R*,4*S*,5*S*)-2-(α-Carboxyethyl)-4,5-dihydroxy-1,2-oxazinan-3-one (18)

A suspension of 5% Pd-C (0.137 g) in EtOAc (10 mL) was stirred for 1 h in a hydrogen atmosphere and a solution of the benzyl ester **17** (0.137 g, 0.464 mmol) in EtOAc (15 mL) was added dropwise. The reaction mixture was stirred for 8 h under hydrogen and filtered through a short pad of silica gel 60H (for TLC) followed by washing with MeOH (7 × 5 mL). After evaporation of the filtrate under reduced pressure, the residue was triturated with dry ether and dried in vacuo to provide 0.093 g (98%) of the product as a white solid. ^{1}H NMR (400 MHz, CD_3CN) δ: 1.44 (3H, d, ^3J = 7.3 Hz, α-*Me*CH), 3.00 (2H, br. s, O*H*, O*H*), 3.90 (1H, m, 6-H_A), 4.37 (1H, d, ^3J = 4.4 Hz, 4-*H*), 4.49–4.43 (2H, m, 6-H_B, 5-H), 5.01 (1H, q, ^3J = 7.3 Hz, -C*H*), 5.31 (1H, br. s, COO*H*). ^{13}C NMR (100 MHz, CD_3CN) δ: 13.55, 54.34, 70.15, 70.64, 78.41, 171.22, 172.85.

(α*R*,4*R*,5*R*)-2-(α-*tert*-Butoxycarbonylethyl)-4,5-dihydroxy-1,2-oxazinan-3-one (19)

This compound was obtained in 83% yield from **13b** as a white solid (mp 93 to 94 °C) as described above, but with $(DHQ)_2PHAL$ as the auxiliary. ^{1}H NMR (400 MHz, $CDCl_3$ + 2 drops of CD_3OD) δ: 1.44 (3H, d, ^3J = 7.3 Hz, α-*Me*CH), 1.45 (9H, *Me*$_3$C), 2.25 (2H, br. s, O*H*, O*H*), 4.30 (1H, dd, ^2J = –11.9 Hz, ^3J = 2.8 Hz, 6-H_A), 4.37 (1H, d, ^3J = 4.5 Hz, 4-*H*), 4.38 (1H, dd, ^2J = –11.9 Hz, ^3J = 7.3 Hz, 6-H_B), 4.56–4.52 (1H, br. m, 5-H), 4.96 (1H, q, ^3J = 7.3 Hz, α-C*H*). ^{13}C NMR (100 MHz, $CDCl_3$) δ: 13.96, 27.92, 54.89, 68.89, 69.98, 76.55, 83.01, 169.46, 169.94. IR (KBr), cm^{-1}: 3423, 2985, 1739, 1662, 1415, 1152. MS (CI, isobutane), *m/z*: 262 (M^+ + 1). Anal. calcd. for $C_{11}H_{19}NO_6$ (%): C 50.6, H 7.3, N 5.4; found: C 50.5, H 7.4, N 5.4.

(α*R*,4*R*,5*R*)-2-(α-Carboxyethyl)-4,5-dihydroxy-1,2-oxazinan-3-one (20)

Trifluoroacetic acid (0.9 mL) was added in one portion to a cooled (ca. 0 °C) stirred solution of the *tert*-butyl ester **19** (0.0467 g, 0.179 mmol) in CH_2Cl_2 (0.9 mL). The reaction mixture was maintained at room temperature for 1 h and was concentrated under reduced pressure. The semisolid residue was triturated with dry ether and dried in vacuo to afford 0.0295 g (80%) of the product as a white solid. ^{1}H NMR (400 MHz, CD_3CN) δ: 1.41 (3H, d, ^3J = 7.3 Hz, α-*Me*CH), 3.60 (2H, br. s, O*H*, O*H*, COO*H*), 4.14 (1H, dd, ^2J = –11.6 Hz, ^3J = 2.3 Hz, 6-H_A), 4.34 (1H, d, ^3J = 4.1 Hz, 4-*H*), 4.40 (1H, dd, ^2J = –11.6 Hz, ^3J = 7.4 Hz, 6-H_B), 4.49–4.45 (2H, m, 5-H), 5.01 (1H, q, ^3J = 7.3 Hz, α-C*H*), 5.31 (1H, br. s, COO*H*). ^{13}C NMR (100 MHz, CD_3CN) δ: 14.45, 54.48, 70.05, 70.99, 77.77, 167.30, 171.82.

(α*R*,1*R*,6*R*)-2-(α-*tert*-Butoxycarbonylethyl)-8-thia-3,7,9-trioxa-4-azabicyclo[4.3.0]nona-5,8-dione (21)

A solution of thionyl chloride (1.64 g, 13.75 mmol) in dry CH_2Cl_2 (15 mL) was added dropwise with cooling (–15 to –20 °C) and stirring to a solution of the diol **19** (2.40 g, 9.17 mmol) and Et_3N (3.71 g, 36.67 mmol) in dry CH_2Cl_2 (45 mL). After stirring for 1 h at –2 to 2 °C, the reaction mixture was diluted with CH_2Cl_2 (60 mL) and washed successively with water (20 mL), 1 mol L^{-1} citric acid (20 mL), satd. $NaHCO_3$ (20 mL), dried over $MgSO_4$, and evaporated to give the cyclic sulfite **21** (2.52 g, 90%) as a 1:1 mixture of diastereomers. ^{1}H NMR (400 MHz, $CDCl_3$) δ: 1.45 (9H, *Me*$_3$C), 1.46 (9H, *Me*$_3$′C), 1.47 (3H, d, ^3J = 7.3 Hz, α-*Me*CH), 1.49 (3H, d, ^3J = 7.3 Hz, α-*Me*′CH), 4.43 (1H, dd, ^2J = –12.4 Hz, ^3J = 5.5 Hz, 2-H_A), 4.48 (1H, dd, ^2J = –11.5 Hz, ^3J = 5.0 Hz, 2-H_A′), 4.51 (1H, dd, ^2J = –11.5 Hz, ^3J = 5.0 Hz, 2-H_B), 4.60 (1H, dd, ^2J = –12.4 Hz, ^3J = 6.5 Hz, 2-H_B′), 5.01 (1H, q, ^3J = 7.3 Hz, α-C*H*), 5.05 (1H, q, α-C*H*, ^3J = 7.3 Hz), 5.18 (1H, d, ^3J = 8.2 Hz, 6-*H*), 5.22 (1H, m, ^3J = 8.2, 6.5, 5.5 Hz, 1-*H*), 5.37 (1H, d, ^3J = 7.3 Hz, 6-*H*′), 5.50 (1H, m, ^3J = 7.3, 5.0 Hz, 1-*H*′). The compound was used in the next reaction without further purification.

(α*R*,4*S*,5*R*)-2-(α-*tert*-Butoxycarbonylethyl)-4-azido-5-hydroxy-1,2-oxazinan-3-one (22)

Sodium azide (1.60 g, 24.6 mmol) was added in one portion to a stirred solution of the cyclic sulfite (2.52 g, 8.21 mmol) in HMPA (15 mL), and the solution was stirred for 24 h at room temperature. Then EtOAc (50 mL) was added and the resultant mixture was washed successively with water (2 × 15 mL) and 1 mol L^{-1} citric acid (15 mL). The combined aqueous layers were extracted with EtOAc (3 × 15 mL). The combined organic extracts were washed successively with satd. $NaHCO_3$ (50 mL), brine (2 × 50 mL), dried over $MgSO_4$, and concentrated. The dark oily residue was purified by flash chromatography (silica gel 60H, 1% MeCN – CH_2Cl_2 to 10% MeCN – CH_2Cl_2) to afford 0.37 g (16%) of the product as a yellowish oil. IR (film, cm^{-1}): 3436, 2981, 2116, 1739, 1685, 1256, 1158. ^{1}H NMR (400 MHz, $CDCl_3$) δ: 1.46 (9H, *Me*$_3$C), 1.48 (3H, d, ^3J = 7.3 Hz, α-*Me*CH), 2.65 (1H, d, ^3J = 4.5 Hz, O*H*), 4.08–4.02 (1H, m, 5-H), 4.08 (1H, dd, ^2J = –11.6 Hz, ^3J = 3.5 Hz, 6-H_A), 4.27 (1H, dd, ^2J = –11.6 Hz, ^3J = 6.1 Hz, 6-H_B), 4.37

© 2005 NRC Canada

(1H, d, ^3J = 7.6 Hz, 4-*H*), 4.93 (1H, q, ^3J = 7.3 Hz, α-C*H*). ^{13}C NMR (100 MHz, $CDCl_3$) δ: 13.32, 27.98, 55.25, 64.62, 70.52, 75.25, 82.79, 167.33, 168.37. MS (CI, isobutane), *m*/*z*: 287 (M^+ + 1). Anal. calcd. for $C_{11}H_{18}N_4O_5$ (%): C 46.2, H 6.3, N 19.6; found: C 46.4, H 6.3, N 19.4.

(α*R*,4*S*,5*R*)-2-(α-Carboxyethyl)-4-azido-5-hydroxy-1,2-oxazinan-3-one (23)

Precooled (ca. 0 °C) trifluoroacetic acid (6.5 mL) was added dropwise to a cooled (0 to –5 °C) stirred solution of the *tert*-butyl ester **21** (0.469 g, 1.64 mmol) in CH_2Cl_2 (8 mL). The reaction mixture was maintained at room temperature for 1.5 h and was then concentrated under reduced pressure. Traces of trifluoroacetic acid were removed by repeated addition and evaporation of dry ether (3 × 15 mL). After drying in vacuo, 0.373 g (99%) of the product was obtained as a yellowish semisolid. IR (film, cm^{-1}): 3456, 2959, 2125, 1746, 1654, 1284. ^{1}H NMR (400 MHz, $CDCl_3$) δ: 1.58 (3H, d, ^3J = 7.4 Hz, α-*Me*CH), 4.10–4.06 (1H, m, 5-H), 4.13 (1H, dd, ^2J = –11.7 Hz, ^3J = 4.1 Hz, 6-H_A), 4.31 (1H, dd, ^2J = –11.7 Hz, ^3J = 5.9 Hz, 6-H_B), 4.43 (1H, d, ^3J = 7.4 Hz, 4-*H*), 5.12 (1H, q, ^3J = 7.4 Hz, α-C*H*), 6.51 (2H, br. s, O*H*, COO*H*). ^{13}C NMR (100 MHz, CD_3CN) δ: 13.51, 54.74, 65.75, 71.38, 78.21, 167.55, 170.91. MS (CI, isobutane), *m*/*z*: 231 (M^+ + 1). The compound was used in the next reaction without further purification.

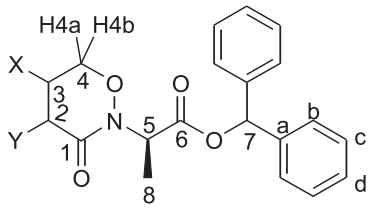
(α*R*,4*S*,5*R*)-2-(α-Carboxyethyl)-4-amino-5-hydroxy-1,2-oxazinan-3-one (24)

A suspension of 5% Pd-C (0.175 g) in EtOAc (10 mL) was stirred for 1.5 h under a hydrogen atmosphere and a solution of the azido alcohol **23** (0.37 g, 1.62 mmol) in EtOAc (15 mL) was added dropwise. The reaction mixture was stirred under hydrogen for 17 h and then evaporated to dryness. The residue was washed with dry ether (3 × 15 mL) and the product was extracted from the dried residue with hot (ca. 70 °C) water (30 mL). The aqueous solution was filtered through a paper filter and the black solid was washed with hot water (3 × 10 mL). Evaporation of the filtrate provided 0.296 g (90%) of the product **24** as a white solid, mp 200–202 °C (dec.). IR (KBr, cm^{-1}): 3158, 1684, 1599, 1568, 1400. ^{1}H NMR (400 MHz, CD_3OD + 1 drop of CF_3CO_2H) δ: 1.52 (3H, d, ^3J = 7.4 Hz, α-*Me*CH), 4.08 (1H, dd, ^2J = –11.7 Hz, ^3J = 2.5 Hz, 6-H_A), 4.18–4.16 (2H, m, 4-H, 5-H), 4.46–4.41 (1H, dd, ^2J = –11.7 Hz, ^3J = 6.4 Hz, 6-H_B), 4.98 (1H, q, ^3J = 7.4 Hz, α-C*H*). ^{13}C NMR (100 MHz, D_2O) δ: 17.62, 59.62, 61.42, 73.69, 82.48, 169.06, 180.86. MS (CI, isobutane), *m*/*z*: 205 (M^+ + 1). Anal. calcd. for $C_7H_{12}N_2O_5 \cdot 0.5H_2O$ (%): C 39.4, H 6.1, N 13.1; found: C 39.3, H 6.2, N 13.2.

(α*R*,4*S*,5*R*)-2-(α-Carboxyethyl)-4-phenylacetylamino-5-hydroxy-1,2-oxazinan-3-one (25)

A solution of phenylacetyl chloride (0.191 g, 1.24 mmol) in dry MeCN (3 mL) was added dropwise with cooling (–5 to –6 °C) and stirring to a solution of the amino acid **24** (0.290 g, 1.36 mmol) and $NaHCO_3$ (0.343 g, 4.08 mmol) in water (7 mL). The reaction mixture was stirred for 2 h at 0 to –2 °C and for 1 h at room temperature and was then concentrated under reduced pressure to a volume of ca. 5 mL, cooled to ca. 5 °C and the pH was adjusted to 2 to 3 with 1 mol L^{-1} HCl (2.8 mL). The white precipitate was collected, washed with water, and dried in vacuo to afford 0.364 g (91%) of **25** as a white solid, mp 194 to 195 °C (dec.) (from isopropanol). IR (KBr, cm^{-1}): 3361, 2913, 1729, 1666, 1630, 1542, 1440, 1233. ^{1}H NMR (400 MHz, CD_3OD) δ: 1.47 (3H, d, ^3J = 7.3 Hz, α-*Me*CH), 3.62 (1H, d, ^2J = –14.8 Hz, CH_APh), 3.67 (1H, d, ^2J = –14.8 Hz, CH_BPh), 4.06 (1H, dd, ^2J = –11.4 Hz, ^3J = 3.7 Hz, 6-H_A), 4.12–4.06 (1H, m, 5-H), 4.33 (1H, dd, ^2J = –11.4 Hz, ^3J = 5.6 Hz, 6-H_B), 4.66 (1H, d, ^3J = 8.0 Hz, 4-H), 4.96 (1H, q, ^3J = 7.3 Hz, α-C*H*), 7.38–7.17 (5H, m, *Ph*). ^{13}C NMR (100 MHz, CD_3OD) δ: 13.71, 43.63, 55.70, 57.54, 71.84, 79.10, 127.85, 129.51, 130.37, 136.63, 169.61, 172.71, 174.89. MS (CI, isobutane), *m*/*z*: 323 (M^+ + 1). Anal. calcd. for $C_{15}H_{18}N_2O_6$ (%): C 55.9, H 5.6, N 8.7; found: C 55.7, H 5.7, N 8.6.

Functionalization of a 6*H*[1,2]oxazin-3-one with aq. *N*-bromosuccinimide — Bromohydrins, epoxides, and alcohols



The olefin **26** was prepared from the triflate of benzhydryl *S*-lactate by sequential reactions with allyloxyamine, acryloyl chloride, and bis(tricyclohexylphosphine)benzylideneruthenium dichloride. ^{1}H NMR (100 MHz, $CDCl_3$) δ: 1.60 (3H), 4.40 (2H), 4.57 (1H), 6.05 (1H), 6.68 (1H), 6.91 (1H) 7.35 (10H). *N*-Bromosuccinimide (1.06 g, 2 equiv., 5.92 mmol) was added with rapid stirring to a solution of **26** (1.00 g, 2.96 mmol) in DMF (2.3 mL, 10 equiv., 29.6 mmol) and H_2O (110 μL, 2 equiv., 5.92 mmol). The resulting mixture was stirred for 24 h at room temperature. Water (20 mL) was then added and the mixture was extracted with Et_2O (3 × 30 mL). The combined organic extracts were dried over $MgSO_4$, and concentrated under reduced pressure to an oil. Flash column chromatography (5%–30% EtOAc – hexanes, gradient) provided, in order of elution, a mixture of dibromides (**27**) (199 mg), unreacted starting material (212 mg), and two diastereomeric bromohydrins **28** (268 and 206 mg, 26% and 20%, respectively). There was no reaction after 48 h when the experiment was performed in aq. THF.

Dibromides 27

^{1}H NMR (400 MHz, $CDCl_3$) δ: 7.33–7.34 (m, Ar-H), 6.92 (s, H-7), 6.91 (s, H-7′), 5.30 (q, *J* = 7.3 Hz, H-5), 5.27 (q, *J* = 7.3 Hz, H-5′), 4.73 (d, *J* = 4.0 Hz, H-2), 4.68 (d, *J* = 4.1 Hz, H-2′), 4.54–4.65 (m, containing 4.63 (dd, *J* = 4.3, 12.6 Hz, H-4a), 4.51 (dd, *J* = 5.7, 12.3 Hz, H-4a′)), 4.31 (dd, *J* = 12.3, 5.8 Hz, H-4b′), 4.15 (dd, *J* = 12.7, 4.1 Hz, H-4b), 1.58 (d, *J* = 7.3 Hz, H-8), 1.56 (d, *J* = 7.3 Hz, H-8′).^{13}C NMR (75 MHz, $CDCl_3$) δ: 168.4 and 138.3 (C-6, C-6′), 163.5 and 162.5 (C-1, C-1′), 139.5 and 139.3 (Ar-a, Ar-a′), 128.6, 128.5, 128.3, 128.2, 128.1, 127.4, 127.3, 127.2,

© 2005 NRC Canada

126.9, 126.8, 126.5, 78.5 and 78.4 (C-7, C-7′), 73.5 and 72.4 (C-4, C-4′), 54.5 and 54.3 (C-5, C-5′), 46.5 and 45.6 (C-2, C-2′), 43.5 and 43.3 (C-3, C-3′), 13.3 (C-8, C-8′).

28 (Less polar isomer)

^{1}H NMR (400 MHz, $CDCl_3$) δ (ppm): 7.29–7.34 (m, Ar-H), 6.89 (s, H-7), 5.27 (q, *J* = 7.3 Hz, H-5), 4.44 (dd, *J* = 5.0, 11.7 Hz, H-4a), 4.42 (dd, *J* = 0.7, 4.6 Hz, H-2), 4.34–4.36 (br m, H-3), 4.06 (dd, *J* = 11.7, 2.5 Hz, H-4b), 3.25 (br s, -OH), 1.59 (d, *J* = 7.3 Hz, H-8). ^{13}C NMR (75 MHz, $CDCl_3$) δ (ppm): 169.3 (C-6), 167.0 (C-1), 139.2, 139.1 (Ar-a), 128.6 (Ar-c), 128.3, 128.1 (Ar-d), 127.2, 126.8 (Ar-b), 78.8 (C-7), 73.0 (C-3), 71.6 (C-4), 54.6 (C-5), 44.7 (C-1), 13.2 (C-8). MS (CI, isobutane), *m/z*: 435, 433 (M^+ + 1).

28 (More polar isomer)

^{1}H NMR (400 MHz, $CDCl_3$) δ (ppm): 7.29–7.35 (m, Ar-H), 6.89 (s, H-7), 5.23 (q, *J* = 7.3 Hz, H-5), 4.56 (d, *J* = 6.1 Hz, H-2), 4.46 (dd, *J* = 11.7, 5.8 Hz, H-4a), 4.28–4.35 (br m, H-3), 3.90 (dd, *J* = 11.7, 3.5 Hz, H-4b), 2.86 (br s, -OH), 1.56 (d, *J* = 7.3 Hz, H-8). ^{13}C NMR (75 MHz, $CDCl_3$) δ (ppm): 168.7 (C-6), 164.0 (C-1), 139.3 (Ar-a), 128.6 (Ar-c), 128.3, 128.1 (Ar-d), 127.3, 126.8 (Ar-b), 78.5 (C-7), 74.4 (C-3), 73.0 (C-4), 54.6 (C-5), 49.0 (C-1), 13.7 (C-8). MS (CI, isobutane), *m/z*: 435, 433 (M^+ + 1).

Epoxides 29

Potassium carbonate (62 mg, 1.1 equiv.) was added to a solution of **28** (171 mg, 0.41 mmol) in acetone (2 mL). The resulting mixture was stirred at room temperature for 24 h, concentrated under reduced pressure, and the residue shaken with a mixture of 10% NH_4Cl (50 mL) and Et_2O (50 mL). The aqueous phase was extracted with Et_2O (3 × 20 mL) and the combined ether layers were dried over $MgSO_4$ and evaporated. Flash column chromatography of the residue (20%–25% EtOAc – hexanes) afforded the appropriate epoxide (39.6 mg, 29%).

***29** Isomer I (from the less polar **28**)*

^{1}H NMR (400 MHz, $CDCl_3$) δ (ppm): 7.31–7.37 (m, Ar-H), 6.83 (s, H-7), 5.16 (q, *J* = 7.3 Hz, H-5), 4.40 (d, *J* = 12.5 Hz, H-4a), 4.02 (d, *J* = 12.5 Hz, H-4b), 3.65–3.67 (m, H-2 and H-3), 1.50 (d, *J* = 7.3 Hz, H-8). ^{13}C NMR (75 MHz, $CDCl_3$) δ (ppm): 168.1 (C-6), 165.2 (C-1), 139.8, 139.7 (Ar-a), 128.5, 128.4 (Ar-c), 127.9, 127.8 (Ar-d), 127.0, 126.9 (Ar-b), 78.3 (C-7), 67.3 (C-4), 53.9 (C-2), 52.6 (C-5), 48.7 (C-3), 13.1 (C-8).

***29** Isomer II (from the more polar **28**)*

^{1}H NMR (400 MHz, $CDCl_3$) δ (ppm): 7.30–7.37 (m, Ar-H), 6.89 (s, H-7), 5.31 (q, *J* = 7.3 Hz, H-5), 4.18 (d of multiplets, *J* = 12.7 Hz, H-4a), 4.06 (d, *J* = 12.7 Hz, H-4b), 3.63 (d, *J* = 4.1 Hz, H-2), 3.60 (dd, *J* = 4.1, 1.3 Hz, H-3), 1.55 (d, *J* = 7.3 Hz, H-8). ^{13}C NMR (75 MHz, $CDCl_3$) δ (ppm): 169.0 (C-6), 163.7 (C-1), 139.4, 139.3 (Ar-a), 128.5, 128.5 (Ar-c), 128.3, 128.1 (Ar-d), 127.3, 126.7 (Ar-b), 78.3 (C-7), 66.9 (C-4), 53.8 (C-2), 53.3 (C-5), 48.9 (C-3), 13.8 (C-8).

Debromination of 28

A solution of the less polar isomer of **28** (200 mg, 0.196 mmol) in MeOH (1.5 mL) containing Et_3N (36 μL) and 10% Pd-C (10 mg) was stirred under hydrogen for 18 h and then filtered through a pad of Celite®. The pad was washed with ethanol and the combined filtrates were concentrated. The residue was partitioned between H_2O (10 mL) and Et_2O (10 mL). The ether layer was dried ($MgSO_4$) and evaporated to a viscous yellow oil. Flash column chromatography (10%–80% EtOAc – hexanes) provided the debromination product **30** (27 mg). ^{1}H NMR (400 MHz, $CDCl_3$) δ (ppm): 7.31–7.37 (m, Ar-H), 6.90 (s, H7-), 5.32 (q, *J* = 7.3 Hz, H-5), 4.35–4.42 (m, H-3), 4.13 (dd, *J* = 11.8, 5.4 Hz, H-2a), 4.01 (ddd, *J* = 11.8, 3.2, 1.0 Hz, H-2b), 2.77 (dd, *J* = 15.7, 5.0 Hz, H-4a), 2.64 (ddd, *J* = 15.7, 3.8, 1.0 Hz, H-4b), 1.56 (d, *J* = 7.3 Hz, H-8). ^{13}C NMR (75 MHz, $CDCl_3$) δ (ppm): 169.9 (C-6), 169.2 (C-1), 139.4, 139.3 (Ar-a), 128.6, 128.6 (Ar-c), 128.2, 128.1 (Ar-d), 127.2, 126.8 (Ar-b), 78.5 (C-7), 76.2 (C-4), 66.2 (C-3), 53.5 (C-5), 38.6 (C-2), 13.6 (C-8).

Acknowledgements

The authors thank Sarah Chinapoo for technical assistance, and the Natural Sciences and Engineering Research Council of Canada (NSERC), the Western Technology Seed Investment Fund, and the BC Science Council for financial support.

References

1. J.-M. Frère and N. Joris. Crit. Rev. Microbiol. **16**, 299 (1985); T.D.H. Bugg and C.T. Walsh. Nat. Prod. Rep. **9**, 199 (1992).
2. J.M. Frère, M. Nguyen-Distèche, J. Coyette, and B. Joris. *In* The chemistry of beta-lactams. *Edited by* M. Page. Chapman and Hall, Glasgow. 1992. p 148.
3. D.J. Tipper and J.L. Strominger. Proc. Natl. Acad. Sci. U.S.A. **54**, 1133 (1965).
4. S. Harada, S. Tsubotani, T. Hida, H. Ono, and H. Okazaki. Tetrahedron Lett. **27**, 6229 (1986); Y. Nozaki, N. Katayama, H. Ono, S. Tsubotani, T. Harada, H. Okazaki, and Y. Nakao. Nature (London), **325**, 179 (1987).
5. S. Wolfe, C.I. Akuche, S. Ro, M.-C. Wilson, C.-K. Kim, and Z. Shi. Can. J. Chem. **81**, 915 (2003).
6. S. Wolfe, M.-C. Wilson, M.-H. Cheng, G.V. Shustov, and C.I. Akuche. Can. J. Chem. **81**, 937 (2003).
7. R.H. Grubbs, S.J. Miller, and G.C. Fu. Acc. Chem. Res. **28**, 446 (1995); T.M. Trnka and R.H. Grubbs. Acc. Chem. Res. **34**, 18 (2001); R.H. Grubbs (*Editor*). Handbook of metathesis. Vols. 1 and 2. Wiley-VCH, Chichester. 2003; A. Deiters and S.F. Martin. Chem. Rev. **104**, 2199 (2004).
8. R.F. Kleinschmidt and A.C. Cope. J. Am. Chem. Soc. **66**, 1929 (1944).
9. T.P. Kogan and T.E. Rawson. Tetrahedron Lett. **33**, 7089 (1992).
10. K.B.Sharpless. Tetrahedron, **50**, 4235 (1994); H.C. Kolb, M.S. VanNieuwenhze, and K.B. Sharpless. Chem. Rev. **94**, 2483 (1994).
11. H.S. Byun, L. He, and R. Bittman. Tetrahedron, **56**, 7051 (2000).
12. G.V. Shustov, A.V. Kachanov, V.A. Korneev, R.G. Kostyanovsky, and A. Rauk. J. Am. Chem. Soc. **115**, 10 267 (1993).
13. Y. Gao and K.B. Sharpless. J. Am. Chem. Soc. **110**, 7538 (1988).
14. B.M. Kim and K.B. Sharpless. Tetrahedron Lett. **31**, 4317 (1990).

© 2005 NRC Canada

15. D.D. Perrin and W.L.F. Armarego. *In* Purification of laboratory chemicals. 3rd ed. Pergamon Press, New York. 1988.
16. (*a*) W.C. Still, M. Kahn, and A. Mitra. J. Org. Chem. **43**, 2923 (1978); (*b*) J. Grochowski. Synthesis, 682 (1976); L.M. Harwood. Aldrichimica Acta, **18**, 25 (1985); A.J. Shusterman, P.G. McDougal, and A. Glasfeld. J. Chem. Ed. **74**, 1222 (1997).
17. R.F. Kleinschmidt and A.C. Cope J. Am. Chem. Soc. **66**, 1929 (1944).
18. M. Ohtani, T. Matsuura, F. Watanabe, and M. Narisada. J. Org. Chem. **56**, 4120 (1991).

© 2005 NRC Canada

Synthesis, characterization, and biological activity of a new palladium(II) complex with deoxyalliin

Pedro P. Corbi, Antonio C. Massabni, Andréia G. Moreira, Francisco J. Medrano, Miriam G. Jasiulionis, and Claudio M. Costa-Neto

Abstract: Synthesis, characterization, and biological activity of a new water-soluble Pd(II)–deoxyalliin (*S*-allyl-L-cysteine) complex are described in this article. Elemental and thermal analysis for the complex are consistent with the formula $[Pd(C_6H_{10}NO_2S)_2]$. ^{13}C NMR, ^1H NMR, and IR spectroscopy show coordination of the ligand to Pd(II) through S and N atoms in a square planar geometry. Final residue of the thermal treatment was identified as a mixture of PdO and metallic Pd. Antiproliferative assays using aqueous solutions of the complex against HeLa and TM5 tumor cells showed a pronounced activity of the complex even at low concentrations. After incubation for 24 h, the complex induced cytotoxic effect over HeLa cells when used at concentrations higher than 0.40 mmol/L. At lower concentrations, the complex was nontoxic, indicating its action is probably due to cell cycle arrest, rather than cell death. In agreement with these results, the flow cytometric analysis indicated that after incubation for 24 h at low concentrations of the complex cells are arrested in G0/G1.

Key words: palladium(II), deoxyalliin, *S*-allyl-L-cysteine, tumor cells, cancer.

Résumé : On décrit la synthèse, la caractérisation et l'activité biologique d'un nouveau complexe, soluble dans l'eau, de Pd(II)–désoxyalliine (*S*-allyl-L-cystéine). Les analyses élémentaire et thermique du complexe sont en accord avec la formule $[Pd(C_6H_{10}NO_2S)_2]$. Les spectres de RMN du ^{13}C et du ^1H ainsi que la spectroscopie infrarouge permettent de montrer que la coordination du ligand au Pd(II) se fait par les atomes de soufre et d'azote dans une géométrie plan carré. Le résidu final du traitement thermique a été identifié comme un mélange de PdO et de Pd métallique. Des essais antiprolifération à l'aide de solutions aqueuses du complexe ont permis de démontrer l'activité prononcée du complexe contre les cellules cancéreuses HeLa et TM5, même à faibles concentrations. Après une incubation de 24 h, le complexe utilisé à des concentrations supérieures à 0,40 mmol/L induit un effet cytotoxique vis-à-vis des cellules HeLa. À des concentrations plus faibles, le complexe n'est pas toxique, ce qui indique que son action est probablement due à un arrêt du cycle cellulaire plutôt qu'à une mort de la cellule. En accord avec ces résultats, l'analyse de l'écoulement cytométrique indique que, après une incubation de 24 h à de faibles concentrations de complexe, les cellules de G0/G1 s'arrêtent.

Mots clés : palladium(II), désoxyalliine, *S*-allyl-L-cystéine, cellules cancéreuses, cancer.

[Traduit par la Rédaction]

Introduction

The most largely used metal-based drug is cisplatin (*cis*-diammindichloroplatinum(II)), which has been used for the treatment of several human cancers, particularly testicular, ovarian, bladder, head, and neck (1, 2). For a review see ref. 3. The anticancer properties of cisplatin were first observed by Barnet Rosenberg at the Michigan State University in 1965 (4), but only in 1978 was this compound approved worldwide for cancer treatment (5). Toxic side effects of cisplatin, mainly nephrotoxicity, neurotoxicity (2), and ototoxicity (6), have limited its use and led to the development of second generation drugs. Interest in developing new complexes with lower side effects than cisplatin, but at the same time with high activity against tumors, has stimulated syntheses of many new complexes of platinum(II) and

Received 12 July 2004. Published on the NRC Research Press Web site at http://canjchem.nrc.ca on 12 February 2005.

P.P. Corbi[1] and A.C. Massabni. Departamento de Química Geral e Inorgânica, Instituto de Química – UNESP, CP 355, CEP 14801–970, Araraquara, SP, Brazil.
A.G. Moreira. Departamento de Química Geral e Inorgânica, Instituto de Química – UNESP, CP 355, CEP 14801-970, Araraquara, SP, Brazil and Departamento de Bioquímica e Imunologia, Faculdade de Medicina de Ribeirão Preto – USP, 14049-900, Ribeirão Preto, SP, Brazil.
F.J. Medrano. Laboratório Nacional de Luz Síncrotron – LNLS, CP 6192, CEP 13084-971, Campinas, SP, Brazil.
M.G. Jasiulionis. Departamento de Micro-Imuno-Parasitologia, Escola Paulista de Medicina – UNIFESP, 04023-062, São Paulo, Brazil.
C.M. Costa-Neto. Departamento de Bioquímica e Imunologia, Faculdade de Medicina de Ribeirão Preto – USP, 14049-900, Ribeirão Preto, SP, Brazil.

[1]Corresponding author (e-mail: pedrocorbi@yahoo.com).

 doi: 10.1139/V05-003 © 2005 NRC Canada

also of palladium(II) (7, 8). Pd(II) complexes containing S and N donor ligands have been prepared and biological assays showed their activities against several tumor lines (HL-60, HeLa, 3T3, JURKAT, Pam212, and Pam-ras) (7).

Deoxyalliin (*S*-allyl-L-cysteine, $C_6H_{11}NO_2S$), a sulfur-containing amino acid derived from cysteine, is a product of vegetal origin present in onion and garlic bulbs (9, 10). More recent studies have shown that deoxyalliin may be considered a biological antagonist of nitrosomorpholine, the substance responsible for the development of hepatic cancer in humans (11). It also exhibits the capacity to inhibit proliferation of malignant cells from the human nervous system and thorax (12, 13).

Complexes containing Pt(II) or Pd(II) with mixed ligands such as amino acids and 1,10-phenanthroline displayed cytotoxic activities in vitro against Molt-4, a human leukaemia cell line (1). A study of *S*-alkyl and *S*-alkylaryl cysteine complexes with platinum(II) characterized by ^{13}C NMR, ^{1}H NMR, and IR absorption spectroscopy has also been reported (14). Biological tests were not performed for the latter complexes. The present article describes the synthesis and characterization of a new palladium(II) complex with deoxyalliin and its biological action against proliferation of tumor cells.[2]

Experimental

Materials

L-Deoxyalliin of analytical purity was purchased from LKT Laboratories. Palladium(II) chloride and lithium chloride of analytical purity were purchased respectively from Acros and Mallinckrodt Laboratories. Elemental analyses for carbon, hydrogen, nitrogen, and sulfur were performed with a CHNS-O EA1110 analyzer (CE Instruments); cystine was used as a reference substance. IR spectra were recorded on a FT-IR spectrophotometer spectrum 2000 (PerkinElmer) with samples prepared as KBr or CsI pellets. ^{13}C NMR and ^{1}H NMR were recorded on a Varian 500 MHz spectrometer; samples were analyzed in deuterium oxide solutions. Thermal analyses were performed on a Thermoanalyzer TG/DTA simultaneous SDT 2960 (TA Instruments) in the following conditions: synthetic air, 100 cm^3/min and heating rate of 10 °C/min, from 40 to 1100 °C. Palladium content was determinated by analyzing the residue of the thermal treatment at 900 °C. Powder X-ray analysis was performed on a D 5000 Siemens diffractometer using $CuK_{\alpha 1}$ radiation (λ = 1.5406 Å) with a graphite diffracted beam monochromator. The sample was scanned over the 2θ range from 4° to 70° in 0.05° steps. The counting time was 1.0 s/step. Cisplatin was purchased from Acros and MTT from Sigma. Media (DMEM and RPMI) and antibiotics for cell culture were purchased from Life Technologies, Inc. (Gaithersburg, Maryland) and FCS from Cultilab (Campinas, Brazil). Flasks and 24-well plates for cell culture were purchased from Costar (Corning Inc., Corning, N.Y.).

Preparation of the Pd(II) complex

The potassium salt solution of deoxyalliin was prepared by adding 1.12×10^{-3} mol of potassium hydroxide to a methanolic solution containing 1.12×10^{-3} mol of deoxyalliin (molar proportion of 1:1). This reaction was carried out at room temperature with stirring for 1 h.

The Pd(II) complex was synthesized by adding 5.6×10^{-4} mol of a freshly prepared methanolic solution of Li_2PdCl_4 to the solution of the potassium salt of deoxyalliin previously prepared, containing 1.12×10^{-3} mol of the ligand (molar proportion Pd(II):deoxyalliin of 1:2). This reaction was carried out at room temperature with stirring. A pale yellowish solid of the complex was precipitated slowly. After 2 h of constant stirring, the complex was filtered, washed with cooled methanol, and dried in a desiccator under P_4O_{10}. Final yield of the synthesis was about 70%. Anal. calcd. for $[Pd(C_6H_{10}NO_2S)_2]$ (%): C 33.8, H 4.72, N 6.56, S 15.0, Pd 24.9; found: C 33.4, H 4.60, N 6.40, S 14.7, Pd 23.7. No single crystals of the complex were obtained for X-ray structure determination. The lithium tetrachloropalladate solution was prepared by the reaction of $PdCl_2$ and LiCl in methanol under stirring and reflux for 30 min.

Cell culture

HeLa (human cervix cancer, ATCC CCL-2) and TM5 (murine melanoma, (15)) cell lines were cultured at 37 °C in a humidified atmosphere containing 5% CO_2, using, respectively, DMEM supplemented with 10% of Fetal Calf Serum (FCS) and RPMI at pH 6.9 with 5% FCS. Penicillin (100 U/mL) and streptomycin (100 µg/mL) were used as antibiotics.

Determination of the cell number and cell viability

A stock sample solution was prepared by dissolving the Pd(II) complex in a phosphate-buffered saline solution (PBS). PBS was used as the vehicle for the Pd(II) complex in all biological experimental procedures. Final different concentrations of the complex were achieved by dilution of the stock solution directly into the cell's medium. Cells were plated (25×10^4 cells/60 mm dish) 24 h prior to the beginning of the experiment. 48 h after addition of the complex or the vehicle, cells were detached and counted in individual samples using an impedance-based automated counter (CELM, Barueri, Brazil). To evaluate the immediate cytotoxic action of the Pd(II) complex, the MTT method (16) was applied to the cells after incubation for 24 h. Briefly, 24 h after plating 2.5×10^4 cells/well in a 24-well plate, the complex or the vehicle was added and the cells incubated for 24 h in culture conditions. After that, 100 µL of a MTT solution (5 mg/mL in PBS) were added and the cells were incubated for another period of 3 h. After washing with PBS, 200 µL of isopropanol were added, and cell viability was determined by absorbance measurements at 570 nm.

Cell cycle analysis by flow cytometry

Flow cytometric analysis of the Pd(II)-complex-treated TM5 cells was performed using a FACScan (Becton Dickinson). For synchronization, the cells were submitted to

[2] Abbreviations: phosphate-buffered saline (PBS), Dulbecco's modified Eagle's medium (DMEM), Roswell Park Memorial Institute medium (RPMI), fetal calf serum (FCS), American type cell collection (ATCC).

© 2005 NRC Canada

a serum depletion for 24 h to induce M block, followed by addition of fresh serum to stimulate growth in the presence (0.20 mmol/L) or absence of the Pd(II) complex. After 24 h, cells were washed, fixed with ice-cold ethanol (70% final concentration), resuspended in 0.5 mL of a solution of propidium iodide (20 µg/mL) and 200 µg/mL of Dnase-free Rnase in PBS, and incubated for 30 min at 37 °C. For flow cytometric analysis, at least 10 000 cells were evaluated using a FACSCalibur™. Cell cycle distribution and pre-G1 fraction were determined and quantified using the CellQUEST™ program.

Effect of the complex on melanoma growth in C57BL/6 mice

Groups of six C57BL/6 mice weighing between 25 and 30 g were selected. For tumor induction, melanoma TM5 cells (2×10^5) were injected subcutaneously into the dorsal-side of each mouse. In the subsequent 5 days, the complex (24 mg/kg and 72 mg/kg) or the vehicle (PBS) was administrated subcutaneously into the dorsal-side of each animal at a distance (1 cm) from the site of the cells injection. Detection of tumors were followed for 30 days, after which animals were sacrificed. C57BL/6 mice were kept at Centro de Desenvolvimento de Modelos Experimentais para Medicina e Biologia (CEDEME, UNIFESP, SP, Brasil) under the International Guiding Principles for Biomedical Research Involving Animals (CIOMS), Genebra (1985), and the Guide to the Care and Use of Experimental Animals, Canadian Council on Animal Care (www.ccac.ca).

Results and discussion

IR spectroscopy

The IR spectra of deoxyalliin, potassium *S*-allyl-L-cysteinate, and $[Pd(C_6H_{10}NO_2S)_2]$ complex are shown in Fig. 1.

Two very well resolved bands in the range 3400–3000 cm^{-1} are an indication of coordination of the amino group to Pd(II) (17). The IR spectrum of potassium *S*-allyl-L-cysteinate shows a broad band at 3350–2575 cm^{-1}, which corresponds to the NH_2 vibrational frequencies, while in the spectrum of deoxyalliin, the frequencies related to the amino group are observed in the range 3160–2675 cm^{-1} (broad band). Enlargement and shifting of the band show that the two hydrogen atoms of the amino group are involved in the formation of hydrogen bonds, which occur with cysteine and its derivatives, as deoxyalliin (17). The amino group involvement in the ligand coordination is attested by the presence of two very well resolved bands at 3220 and 3079 cm^{-1} for the Pd(II) complex (17). Moreover, the absence of the band at 2050–2150 cm^{-1} in the complex spectrum, in comparison to the free ligand and its potassium salt, confirms coordination through the amino group. The band at 2050–2150 cm^{-1} is assigned to a noncoordinated NH_2 group, as it occurs for the free ligand (18).

The IR spectrum of $[Pd(C_6H_{10}NO_2S)_2]$ also shows a strong absorption band at 1617 cm^{-1}, which can be assigned to a free ionized carboxylate group. In the case of Pt(II) complexes with *S*-alkyl cysteine derivatives, in which the carboxylate group was not coordinated to the metal ion, the band attributed to the free ionized carboxylate group appears at 1620 cm^{-1} (14).

Fig. 1. IR absorption spectra for: (*a*) deoxyalliin, (*b*) potassium *S*-allyl-L-cysteinate, and (*c*) the Pd(II) complex.

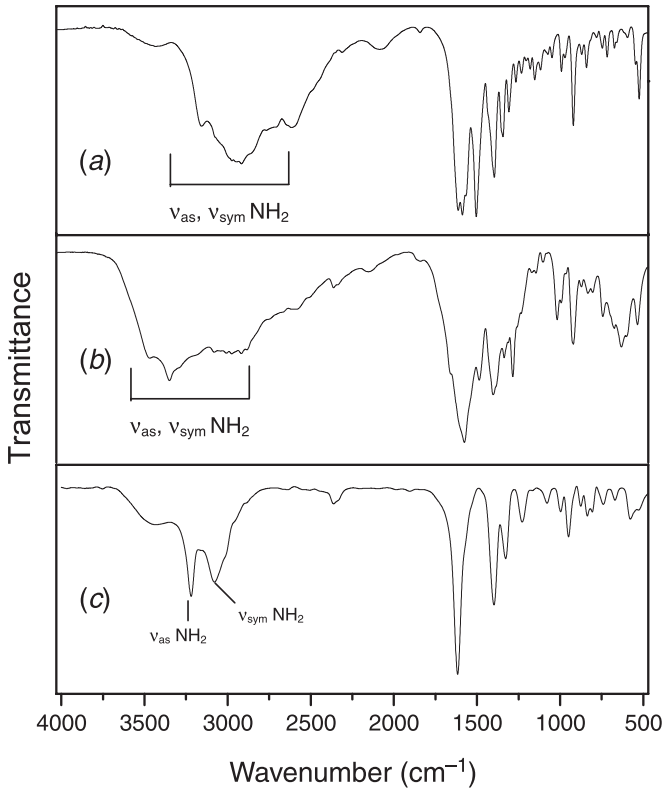
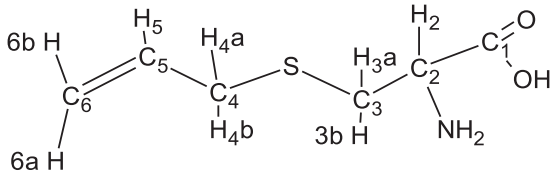


Fig. 2. The schematic structure of deoxyalliin.



The IR spectra of the complexes were also measured in the region 700–150 cm^{-1} to identify frequencies related to M—S and M—N bonds. The IR spectrum shows frequencies at 342 cm^{-1} and at 554 cm^{-1}, which could be assigned to ν(M-S) and ν(M-N), respectively. These attributions are in agreement with the literature values, being similar to those found for an ethyl cysteinate complex of palladium(II) (19) and for other metal complexes with amino acids (14). Considering the presence of two well-defined bands for ν(M-N) and ν(M-S), a trans configuration could be proposed for the Pd(II) complex, as it occurs for complexes of the type $[Pt(L\text{-}H^+)_2]$, where L is an *S*-alkyl-L-cysteine derivative (14).

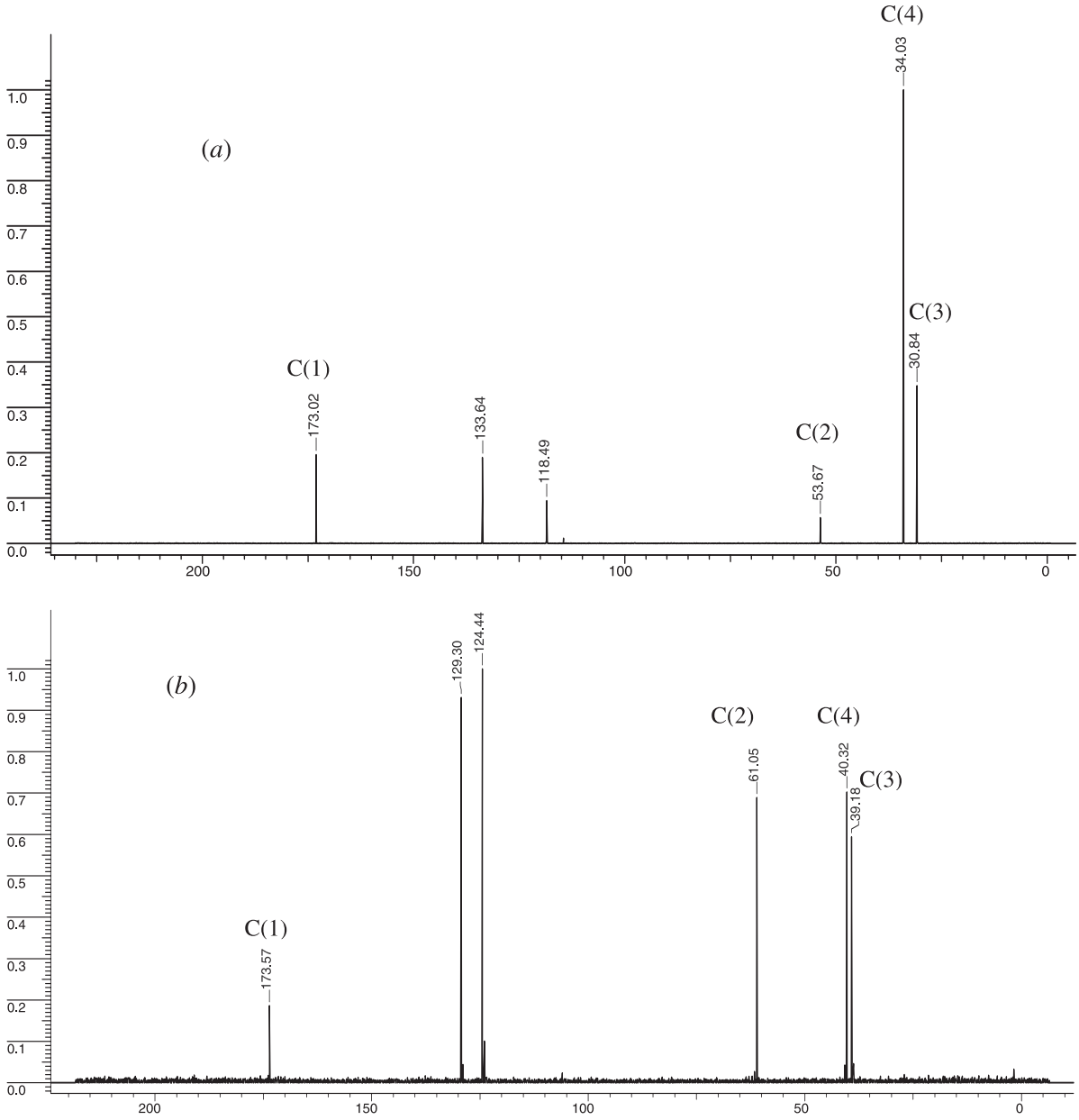
^1H and ^{13}C NMR spectrometry

^1H NMR and ^{13}C NMR spectra of the Pd(II) complex are useful for assigning ligand to metal bonding sites. The NMR spectra of the complex were analyzed in comparison to the spectra of the free ligand. The ligand structure is shown in Fig. 2.

The ^1H NMR spectrum of the Pd(II) complex with deoxyalliin is consistent with coordination of the ligand to

© 2005 NRC Canada

Fig. 3. ^{13}C NMR for: (*a*) deoxyalliin and (*b*) the Pd(II) complex.



the metal through the S and N atoms. Protons near the coordination sites are shifted downfield by 0.2–0.7 ppm. It was also observed that the chemical shifts for H(4a, 4b) (see Fig. 2) varies from 2.9 ppm for the ligand spectrum to 3.6 ppm for the complex. It was also observed that H(2a) varies from 3.8 ppm for the ligand to 4.0 ppm for the complex. These results are in agreement with the literature for Pd(II) and Pt(II) complexes involving amino acid derivatives showing *S*,*N*-coordination sites to the metal ions (14).

^{13}C NMR data are in agreement with S and N coordination proposed by analyzing the ^{1}H NMR and IR spectra. ^{13}C NMR chemical shifts for deoxyalliin and the Pd(II) complex are shown in Fig. 3.

According to the ^{13}C NMR data, the chemical shift at 173 ppm in the spectrum of the ligand is assigned to the carbon atom of the COOH group (C1 in Figs. 2, 3*a*, and 3*b*). In the spectrum of the complex, no changes are observed for the chemical shift of the COOH group. Pronounced changes are observed for the chemical shifts of C2, C3, and C4 in the spectrum of the Pd(II) complex when compared to the free ligand (see Figs. 2, 3*a*, and 3*b*). These changes are other indications for coordination of deoxyalliin to Pd(II) through the N and S atoms of the amino acid structure.

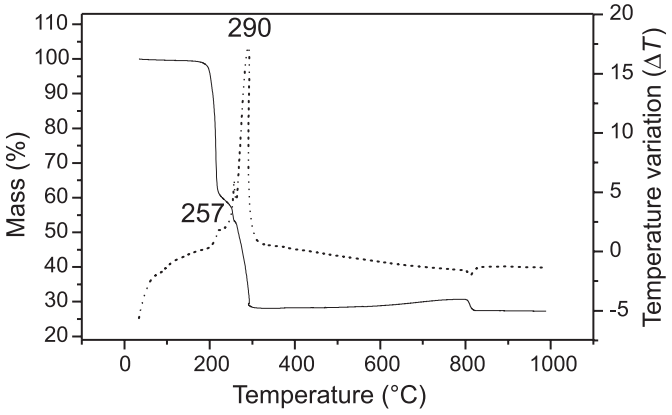
Thermal analysis

TG and DTA curves for the Pd(II) complex are shown in Fig. 4. According to the thermogravimetric data, the composition of the complex formulated as $[Pd(C_6H_{10}NO_2S)_2]$ is confirmed. Oxidation of the coordinated ligand starts at temperatures near 200 °C. The residue formed after the thermal treatment of the Pd(II) complex at 900 °C was identified by powder X-ray diffractometry as a mixture of PdO (20) and metallic Pd (21).

DTA of the Pd(II) complex shows a strong exothermic

© 2005 NRC Canada

Fig. 4. TG (solid) and DTA (dot) curves for $[Pd(C_6H_{10}NO_2S)_2]$.



peak with a maximum at 290 °C and a weak peak at 257 °C (see Fig. 4). These effects are assigned to ligand oxidation of the complex in two steps.

Powder X-ray diffractometry

Powder X-ray diffraction data for $[Pd(C_6H_{10}NO_2S)_2]$ have been successfully indexed in supposition of an orthorhombic system with the following lattice cell parameters: a = 10.740 Å, b = 19.999 Å, and c = 5.2470 Å. A complete discussion of the powder X-ray indexation of this new complex has already been described (22).

Antiproliferative and cell viability analyses

The profile of the cell proliferation assays using HeLa and TM5 cells (Fig. 5) shows a blockage action of the Pd(II) complex starting at low concentrations such as 0.050 mmol/L, especially for HeLa cells. At 0.40 mmol/L, HeLa proliferation was totally eliminated and TM5 cell proliferation was only about 25% when compared to the control. Similar results were obtained when cisplatin was used: ~70% inhibition at 0.40 mmol/L (data not shown here).

The Pd(II) complex was also analyzed for HeLa cells after a longer exposure period of time (Fig. 6). The results showed that after 7 days of exposure to the Pd(II) complex (concentrations of 0.10 and 0.20 mmol/L), cell proliferation was about 75% inhibited. When the concentration was increased to 0.40 or 0.80 mmol/L, cell proliferation was completely inhibited.

The evaluation of the immediate cytotoxic action of the Pd(II) complex was analyzed after an incubation time of 24 h. After this period of incubation, a relevant effect was found only at high concentrations of the complex (0.40 and 0.80 mmol/L) suggesting that the antiproliferative action of the Pd(II) complex observed at lower concentrations is probably due to cell cycle arrest rather than cell death. In the case of cell death, cell viability would appear reduced at lower concentrations of the complex when compared to the control.

Flow cytometry analysis

As can be observed in Fig. 7, TM5 melanoma cells treated during 24 h with the Pd(II) complex at the concentration of 0.20 mmol/L did not present an apoptosis pattern, as seen by the low level of hypodiploid cells, which are detected when DNA fragmentation and (or) loss of DNA is occurring. On the other hand, cells were mainly arrested in G0/G1, when compared to the vehicle treated group. These results corroborate the data discussed here for the cytotoxic action of the compound after an incubation time of 24 h.

Fig. 5. Proliferation profiles for HeLa and TM5 cells after treatment with the Pd(II) complex in different concentrations for 48 h. The data represent an average of three to six independent experiments done in duplicate.

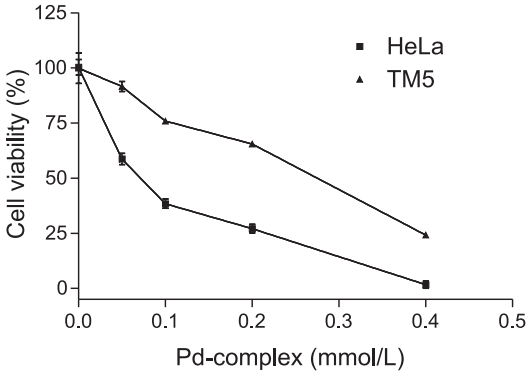
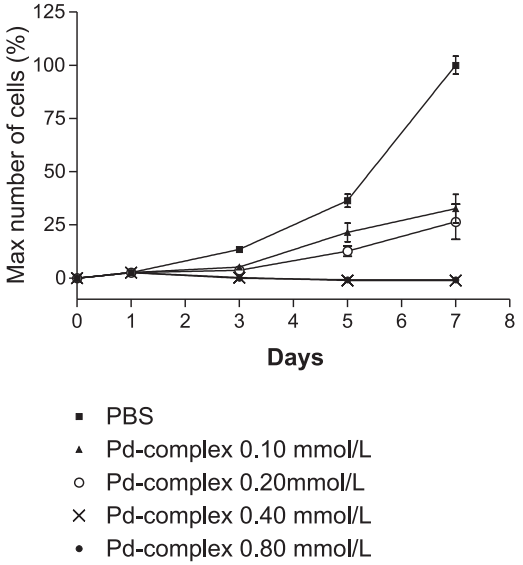


Fig. 6. Profiles for HeLa proliferation after treatment with the Pd(II) complex in different concentrations. The data represent an average of three independent experiments done in duplicate.



In vivo assays

The results obtained for the melanoma growth assay using C57/BL6 mice were considered nonsignificant due to the short delay (~48 h) observed for the appearance of tumors in the group treated with the complex (72 mg/kg body weight) when compared to the control group. No side effects, e.g., weight loss, were detected. This modest result warrants further in vivo investigation and optimization of dosage of the complex.

Final conclusions

Based on the chemical and spectroscopic results, a schematic structure for the Pd(II) complex with deoxyalliin is proposed in Fig. 8.

© 2005 NRC Canada

Fig. 7. Flow cytometric analysis of TM5 cells subjected to 0.20 mmol/L of Pd(II) complex or the vehicle (PBS) for 24 h. Hypodiploid cells correspond to cells that are undergoing apoptosis. The data represent an average of two independent experiments.

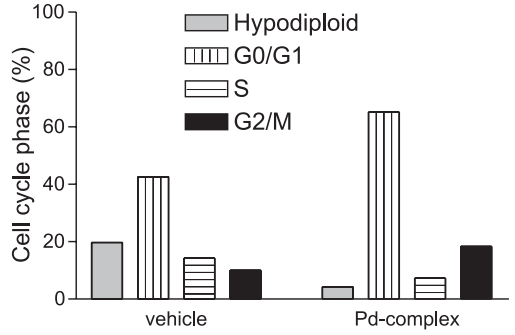
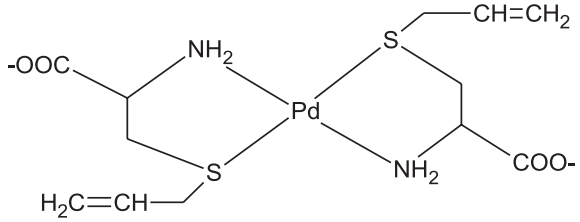


Fig. 8. The schematic structural formula proposed for $[Pd(C_6H_{10}NO_2S)_2]$.



Antiproliferative activity of the Pd(II) complex with deoxyalliin over HeLa and TM5 cells started at the concentration 0.050 mmol/L leading to a proliferation inhibition of about 40% for HeLa and 10% for TM5 cells. At the concentration 0.40 mmol/L, proliferation of HeLa cells was totally eliminated while inhibition of the proliferation of TM5 cells was about 75%. The MTT assay, used to evaluate the immediate cytotoxic effect of the complex, after an incubation of 24 h, indicated that at low concentrations, the Pd(II) complex action is probably due to cell cycle arrest rather than cell death, which was observed only under concentrations equal or higher than 0.40 mmol/L. In agreement with this conclusion, the flow cytometry analysis indicated that TM5 cells are mainly arrested at G0/G1 after a period of 24 h of incubation for the concentration 0.20 mmol/L of the complex. It is well-established that cisplatin treatment arrests cells in G2 with subsequent induction of apoptosis (3). In the present work, it was also possible to observe that, using the concentration 0.20 mmol/L of the Pd(II) complex, an apoptosis pattern was not triggered, as evidenced by a low percentage of hypodiploid cells (see Fig. 7). To our knowledge up to this date, a pattern of cell arresting by palladium complexes has not been described in the literature. We have also tested this Pd(II) complex against the development of melanoma tumors in mice in a preliminary trial. A slight delay (~48 h compared to untreated controls) in tumor appearance for the 72 mg/kg Pd(II)-complex-treated group was observed.

This work describes a new palladium(II) complex with in vitro biological activity in the μmol/L concentration. Its action is similar to other palladium complexes and also to cisplatin when tested against HeLa cells (8, 23–25).

Acknowledgments

This study was supported by grants from FAPESP (São Paulo State Research Foundation, Proc. 03/02616-7) and CNPq (Brazilian National Research Council). The authors are grateful to Dr. Nivaldo Boralle for the NMR spectra and also to Dra. Marisa S. Crespi for thermal analyses.

References

1. V.X. Jin and J.D. Ranford. Inorg. Chim. Acta, **304**, 38 (2000).
2. Y.S. Sohn, H. Baek, Y.H. Cho, Y. Lee, O. Jung, C.O. Lee, and Y.S. Kim. Int. J. of Pharm. **153**, 79 (1997).
3. M. Kartalou and J.M. Essigman. Mutat. Res. **478**, 1 (2001).
4. B. Rosenberg, L. Van Camp, and T. Krigas. Nature (London), **205**, 698 (1965).
5. D. Lebwohl and R. Canetta. Eur. J. Cancer, **34**, 1522 (1998).
6. J.L. Butour, S. Wimmer, and P. Castan. Chem. Biol. Interact. **104**, 165 (1997).
7. A.G. Quiroga and C.N. Ranninger. Coord. Chem. Rev. **248**, 119 (2004).
8. G.B. Onoa, V. Moreno, E. Freisinger, and B. Lippert. J. Inorg. Biochem. **89**, 237 (2002).
9. H.E. Renis and R.E. Henze. Food Res. **23**, 345 (1958).
10. T. Suzuki, M. Sugii, T. Kakimoto, and N. Tsuboi. Chem. Pharm. Bull. **9**, 251 (1961).
11. M.E. Dion, M. Agler, and A. John. Nutr. Cancer, **28**, 1 (1997).
12. C. Welch, L. Wuarin, and N. Sidell. Cancer Lett. **63**, 211 (1992).
13. G. Li, C.H. Quiao, R.I. Lin, J. Pinto, M.P. Osborne, and R.K. Tiwari. Oncol. Rep. **2**, 787 (1995).
14. V. Theodorou and N. Hadjiliadis. Polyhedron, **4**, 1283 (1985).
15. M. Correa, J. Machado, Jr., C.R.W. Carneiro, J.B. Pesquero, M. Bader, L.R. Travassos, R. Chammas, and M.G. Jasiulionis. Int. J. Cancer. In press.
16. T. Mosmann. J. Immun. Methods, **65**, 55 (1983).
17. K. Nakamoto. Infrared and raman spectra of inorganic and coordination compounds. Part B. 5th ed. John Wiley and Sons, New York. 1997. p. 385.
18. R.M. Silverstein and F.X. Webster. Spectrometric identification of organic compounds. 6th ed. John Wiley and Sons, New York. 1998. p. 482.
19. M. Chandrasekharan, M.R. Udupa, and G. Avaramudan. J. Inorg. Nucl. Chem. **36**, 1417 (1974).
20. The International Centre for Diffraction Data. Powder diffraction database. [CD-ROM]. File 30-1556 (JCPDS-ICDD). 1996.
21. The International Centre for Diffraction Data. Powder diffraction database. [CD-ROM]. File 5-0681 (JCPDS-ICDD). 1994.
22. P.P. Corbi, A.C. Massabni, and C.M. Costa-Neto. Powder Diffr. **19**, 270 (2004).
23. A.G. Quiroga, J.M. Perez, E.I. Montero, J.R. Masaguer, C. Alonso, and C. Navarro-Ranninger. J. Inorg. Biochem. **70**, 117 (1998).
24. A. Basu, B.A. Teicher, and J.S. Lazo. J. Biol. Chem. **265**, 8451 (1990).
25. G. Faraglia, D. Fregona, S. Sitran, L. Giovagnini, C. Marzano, F. Baccichetti, U. Casellato, and R. Graziani. J. Inorg. Biochem. **83**, 31 (2001).

© 2005 NRC Canada

Mild, efficient, and chemoselective dehydrogenation of 2-imidazolines, bis-imidazolines, and *N*-substituted-2-imidazolines with potassium permanganate supported on montmorillonite K-10

Iraj Mohammadpoor-Baltork and Mohammad Abdollahi-Alibeik

Abstract: Different types of 2-imidazolines, bis-imidazolines, and *N*-substituted-2-imidazolines are efficiently oxidized to their corresponding imidazoles with potassium permanganate ($KMnO_4$) supported on montmorillonite K-10 under very mild conditions. The procedure is very simple and no strict conditions were required. Selective dehydrogenation of 2-alkyl-2-imidazolines in the presence of 2-aryl-2-imidazolines is a noteworthy advantage of this method and can be considered as a useful practical achievement in these reactions.

Key words: 2-imidazolines, imidazoles, dehydrogenation, potassium permanganate, montmorillonite K-10.

Résumé : Utilizant des conditions réactionnelles très douces impliquant du permanganate de potassium ($KMnO_4$) déposé sur de la montmorillonite K-10, il est possible d'oxyder divers types de 2-imidazolines, de bis-imidazolines et de 2-imidazolines substituées en imidazoles correspondants. La méthode est simple et ne demande pas de conditions strictes. La déshydrogénation sélective des 2-alkyl-2-imidazolines en présence de 2-aryl-2-imidazolines est un avantage important de cette méthode et elle peut être considérée comme la plus grande réalisation de ces réactions.

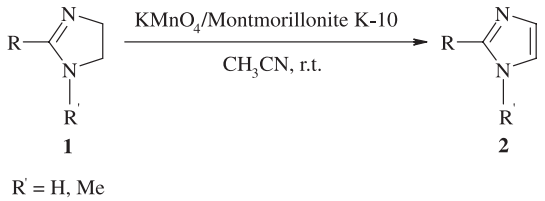
Mots clés : 2-imidazolines, imidazoles, déshydrogénation, permanganate de potassium, montmorillonite K-10.

[Traduit par la Rédaction]

Introduction

Compounds with an imidazole ring system have many pharmaceutical and biological activities including antihypertensive, antiinflammatory, antibacterial, and antidiabetic (1). Several methodologies for the direct synthesis of substituted imidazoles have been published (2–4). 2-Substituted imidazoles are also prepared by the oxidation of the corresponding 2-imidazolines. However, the oxidation of 2-imidazolines to the resonance-stabilized imidazoles is surprisingly difficult. Several methods and reagents such as Zn-Al_2O_3 (5), Ni (6), Se (7), Pd/C (8), MnO_2 (9), $BaMnO_4$ (10), and DMSO (11) have been developed for this purpose in the literature. The reported reagents suffer from one or more of the following disadvantages such as low yields of the products, very long reaction times, toxicity, harsh reaction conditions, and the use of large excess of the reagents. Also, some of these methods are not effective for the oxidation of 2-alkyl-2-imidazolines. Potassium permanganate has also been used for the oxidation of 2-imidazolines (12). However, this method suffers from drawbacks such as long reaction times (12–16 h), low yields of the products (40%–72%), and strict reaction conditions (reflux in dioxane). Thus, the development of a new improved protocol for a high yielding oxidation of 2-imidazolines and bis-imidazolines to their corresponding imidazoles using inexpensive reagents such as $KMnO_4$ under very mild reaction conditions is still in demand.

Scheme 1.



Results and discussion

It was recently shown that adsorption onto solid supports can change the reactivity and selectivity of $KMnO_4$ in oxidation reactions (13). Along this line, herein, we wish to disclose that $KMnO_4$ adsorbed on the very inexpensive and readily available support, montmorillonite K-10, oxidizes 2-imidazolines, bis-imidazolines, and *N*-substituted-2-imidazolines to their corresponding imidazoles efficiently under very mild reaction conditions (Scheme 1).

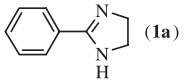
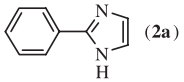
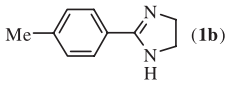
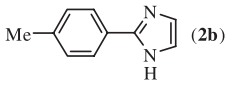
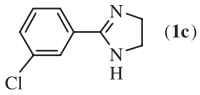
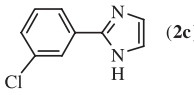
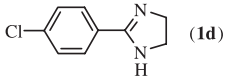
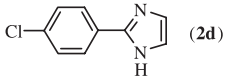
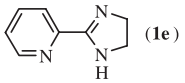
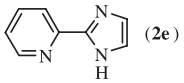
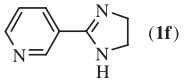
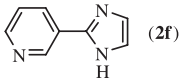
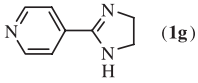
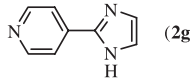
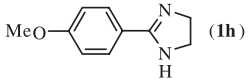
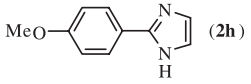
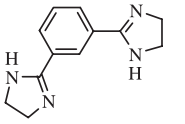
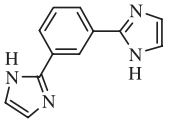
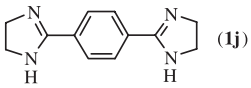
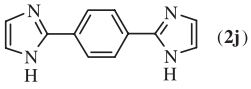
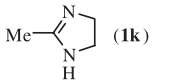
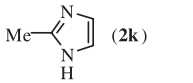
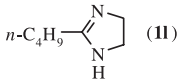
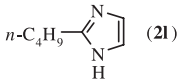
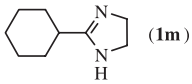
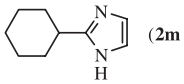
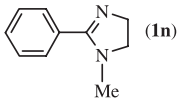
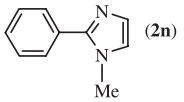
Received 9 August 2004. Published on the NRC Research Press Web site at http://canjchem.nrc.ca on 12 February 2005.

I. Mohammadpoor-Baltork[1] and M. Abdollahi-Alibeik. Department of Chemistry, Isfahan University, Isfahan 81746–73441, Iran.

[1]Corresponding author (e-mail: imbaltork@sci.ui.ac.ir).

 doi: 10.1139/V04-171 © 2005 NRC Canada

Table 1. Oxidation of 2-imidazolines and bis-imidazolines with $KMnO_4$ – montmorillonite K-10 in CH_3CN at room remperature.

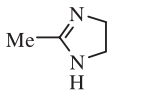
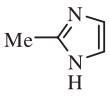
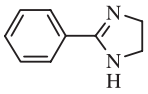
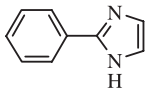
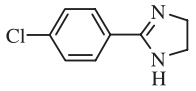
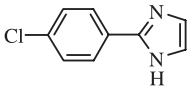
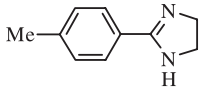
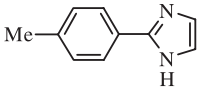
Substrate (**1**)	Product[a] (**2**)	Time (min)	Yield (%)[b]	$KMnO_4$/Imidazoline[c]
 (**1a**)	 (**2a**)	60	95	2
 (**1b**)	 (**2b**)	45	95	2.2
 (**1c**)	 (**2c**)	105	86	2
 (**1d**)	 (**2d**)	115	89	2.2
 (**1e**)	 (**2e**)	50	89	2
 (**1f**)	 (**2f**)	75	97	2
 (**1g**)	 (**2g**)	55	90	2
 (**1h**)	 (**2h**)	50	70	2
 (**1i**)	 (**2i**)	70[d]	75	4
 (**1j**)	 (**2j**)	75[d]	70	4
 (**1k**)	 (**2k**)	10	88	1
 (**1l**)	 (**2l**)	20	88	1
 (**1m**)	 (**2m**)	45	93	1.5
 (**1n**)	 (**2n**)	50	85	2

[a]All products were identified by comparison of their physical and spectral data with those of authentic samples (10–12, 16–21).
[b]Yields refer to isolated products.
[c]Molar ratio.
[d]Reaction was performed in mixture of CH_3CN–DMF (1:2) at room temperature.

Our goals in undertaking this work were: (*i*) to achieve rapid reaction rates, higher yields, and milder reaction conditions; (*ii*) to overcome the drawbacks of the reported methods; (*iii*) to develop a high-yielding synthesis of imidazoles using a cheap commercially available reagent. We first examined the oxidation of 2-phenyl-2-imidazoline (**1a**) using $KMnO_4$ (2 equiv.) alone in CH_3CN at room temperature. Only 20% of the 2-phenylimidazole was isolated from the

© 2005 NRC Canada

Table 2. Comparison of some of the results obtained from $KMnO_4$ – montmorillonite K-10 (I) and some of those reported with DMSO (II) (11), 10%Pd/C (III) (11), and $KMnO_4$ – refluxing dioxane (IV) (12).

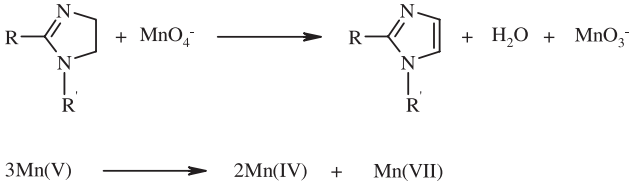
Substrate	Product	Yield (%) (Time, h)			
		I	II	III	IV
		88 (0.16)	0 (48)	0 (48)	72 (12)
		95 (1)	51 (48)	77 (48)	40 (16)
		89 (1.9)	51(48)	30 (48)	—
		95 (0.75)	71 (48)	57 (48)	—

reaction mixture after 2 h. Once again, we attempted a similar reaction with $KMnO_4$ (2 equiv.) in the presence of different amounts of montmorillonite K-10 and observed that to achieve a quantitative yield of the corresponding imidazole, the weight ratio 1:2 of $KMnO_4$:montmorillonite K-10 is required (entry 1, Table 1). It is worth mentioning that in the oxidation of 2-phenyl-2-imidazoline with $KMnO_4$ (3 equiv.) in refluxing dioxane, only 40% of the related imidazole was obtained after 16 h (12).

Similarly, different types of 2-aryl-2-imidazolines (**1b**–**1h**) were reacted with $KMnO_4$ in the presence of montmorillonite K-10 and their corresponding imidazoles **2b**–**2h** were obtained in good to excellent yields. Under these conditions, the 2-aryl-2-imidazolines do not exhibit significantly different reactivities. The influence of the substituents on the yields of the products is also not significant. Bis-imidazolines (**1i**–**1j**) were also oxidized with this reagent system, affording the corresponding bis-imidazoles (**2i**–**2j**) in high yields. The oxidation of 2-alkyl-2-imidazolines (**1k**–**1m**) was also investigated. It was found that in comparison with 2-aryl-2-imidazolines, the oxidation of 2-alkyl-2-imidazolines can proceed effectively with lower amounts of $KMnO_4$ (1–1.5 equiv.) in the presence of montmorillonite K-10 in CH_3CN at room temperature. Under these conditions, 2-alkylimidazoles (**2k**–**2m**) were obtained in excellent yields (Table 1). *N*-Substituted-2-imidazolines such as *N*-methyl-2-phenylimidazoline (**1n**) underwent oxidation with $KMnO_4$ – montmorillonite K-10 to afford the corresponding imidazole **2n** in 85% yield. Therefore, in addition to oxidation of 2-imidazolines and bis-imidazolines, it seems that this method can be applied successfully for the oxidation of *N*-substituted 2-imidazolines.

To show the efficiency of montmorillonite K-10 in these reactions, the dehydrogenation of 2-phenylimidazoline (**1a**) and 2-(4-chlorophenyl)imidazoline (**1d**) was investigated with potassium permanganate in the presence of untreated montmorillonite clay. Under these conditions, the corresponding imidazoles **2a** and **2d** were obtained in 50% and 35% yields, respectively. This difference seems to indicate the importance of the acidity of montmorillonite K-10 in the dehydrogenation of 2-imidazolines.

Scheme 2.



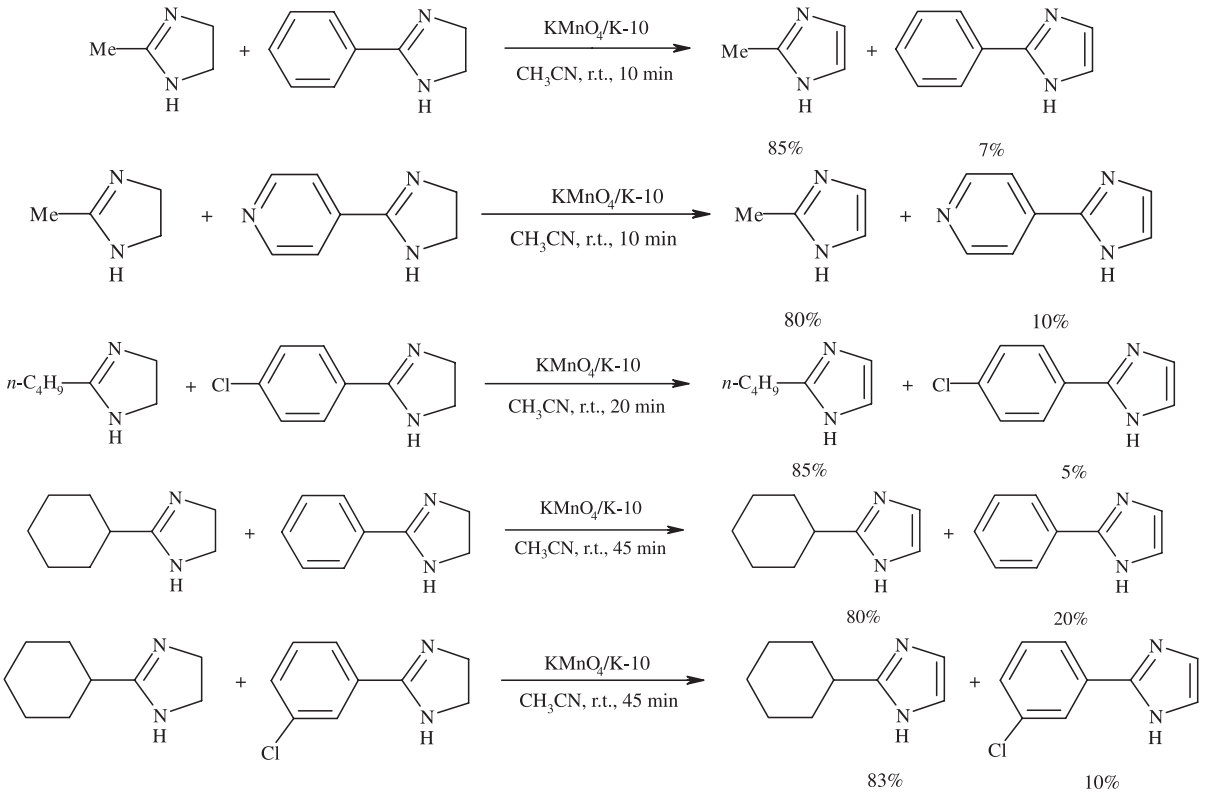
After completion of the reaction, the waste brown MnO_2 precipitate is formed, which is removed by filtration. The exact mechanism of these reactions is unclear at present. However, on the basis of the above observation, a plausible explanation is that 2-imidazolines are oxidized to their corresponding imidazoles and permanganate ion is reduced from Mn(VII) to Mn(V). The Mn(V) ion formed disproportionates to Mn(VII) and Mn(IV) (Scheme 2). Thus, the end product of manganese in these dehydrogenation reactions is MnO_2 (14).

In Table 2, some of the results of our experiments are compared with those reported by other methods. As can be seen, this method is superior to the previously reported methods in terms of yields, reaction times, the amount of the reagent used for successful oxidation, and reaction conditions. Also, this is the first report in which the reactions have been carried out at room temperature and under very mild conditions.

To extend the scope of this reagent system further, the competitive oxidation of 2-alkyl-2-imidazolines and 2-aryl-2-imidazolines was also examined. The results are shown in Scheme 3 and the product ratios were determined by NMR spectroscopy. It was found that 2-alkyl-2-imidazolines are oxidized in the presence of 2-aryl-2-imidazolines with high selectivity. It is worth mentioning that such a selectivity has not been reported previously and can be considered as a useful practical achievement in oxidation of 2-imidazolines.

© 2005 NRC Canada

Scheme 3.



In conclusion, we have demonstrated a remarkably mild, efficient, and simple method for the oxidation of 2-imidazolines, bis-imidazolines, and *N*-substituted-2-imidazolines using $KMnO_4$ – montmorillonite K-10 at room temperature. In addition, short reaction times, low cost of the reagents, the ease of use, high yields of the products, and chemoselectivity are noteworthy advantages of this method and offer significant improvements over the existing procedures for the oxidation of 2-imidazolines.

Experimental

Melting points were determined using a Stuart Scientific apparatus and are uncorrected. IR spectra were run on a Shimadzu IR-435 spectrophotometer. ^{1}H NMR spectra were recorded in DMSO-d_6 solvent on a Brucker 500 MHz spectrometer. Yields refer to isolated products. 2-Imidazolines, bis-imidazolines, and *N*-methyl-2-phenylimidazoline were prepared according to the described procedure (15).

Dehydrogenation of 2-imidazolines, bis-imidazolines, and *N*-substituted-2-imidazolines — General procedure

Potassium permanganate (1.58 g, 10 mmol) and montmorillonite K-10 (3.16 g) were ground together in a mortar until a fine homogeneous powder was obtained.

To a solution of substrate (1 mmol) in CH_3CN (25 mL), $KMnO_4$ – montmorillonite K-10 (0.474–1.90 g, 1–4 mmol) was added portionwise and the mixture was stirred at room temperature for 10–115 min. The progress of the reaction was monitored by TLC (eluent: EtOAc–MeOH, 4:1). Ethanol (1 mL) was added to reduce excess oxidant and after stirring for an additional 20 min, the mixture was filtered through a short pad of Celite or silica gel and the solid material was washed with CH_3CN (20 mL). The filtrate was evaporated and the resulting crude material was purified by chromatography on SiO_2 or Al_2O_3 with an appropriate eluent. The pure products were obtained in 70%–97% yields (Table 1). Selected physical and spectroscopy data: Compound **2b**: mp 218–220 °C (lit. value (11) mp 223 °C). IR ν_{max} (KBr, cm^{-1}): 3435, 3150, 2985, 1658, 1610, 1575, 1514, 1435, 1100, 815, 725. ^{1}H NMR (500 MHz, DMSO-d_6) δ_H: 12.39 (s, 1H, NH), 7.81 (d, J = 8 Hz, 2H, Ar), 7.23 (d, J = 7.5 Hz, 2H, Ar), 7.18 (br s, 1H, =CH), 6.99 (br s, 1H, =CH), 2.31 (s, 3H, CH_3). Compound **2i**: mp 290–292 °C (lit. value (18) mp 287 to 288 °C). IR ν_{max} (KBr, cm^{-1}): 3400, 3105, 3010, 1610, 1592, 1517, 1496, 1478, 1370, 1108, 968, 938, 745, 704. ^{1}H NMR (500 MHz, DMSO-d_6) δ_H: 12.63 (s, 2H, 2NH), 8.57 (d, J = 1.1 Hz, 1H, Ar), 7.86 (d, J = 7.7 Hz, 2H, Ar), 7.49 (t, J = 7.7 Hz, 1H, Ar), 7.23 (br s, 2H, 2 × =CH), 7.07 (br s, 2H, 2 × =CH). Compound **2k**: mp 139–141 °C (lit. value (12) mp 140–142 °C). IR ν_{max} (KBr, cm^{-1}): 3115, 3012, 1670, 1595, 1440, 1298, 1110, 990, 935, 750, 738. ^{1}H NMR (500 MHz, DMSO-d_6) δ_H: 9.00 (s, 1H, NH), 6.82 (s, 2H, 2 × =CH), 2.24 (s, 3H, CH_3).

Acknowledgment

We are thankful to the Isfahan University Research Council for partial support of this work.

References

1. (*a*) M.R. Grimmett. Comprehensive heterocyclic chemistry. Vol. 4. *Edited by* K.T. Potts. Pergamon Press, Oxford. 1984.

© 2005 NRC Canada

p. 345; (*b*) J.G. Lambardino and E.H. Wiseman. J. Med. Chem. **17**, 1182 (1974); (*c*) H.G. Kim, J.K. Lee, J.T. Lee, and C.S. Lee. Bull. Korean Chem. Soc. **21**, 345 (2000).
2. A.Y. Usyatinsky and Y.L. Khmelnitsky. Tetrahedron Lett. **41**, 5031 (2000).
3. S. Balalaie, M.M. Hashemi, and M. Akhbari. Tetrahedron Lett. **44**, 1709 (2003), and refs. cited therein.
4. C.M. Coleman, J.M.D. MacElroy, J.F. Gallagher, and D.F. O'Shea. J. Comb. Chem. **4**, 87 (2002).
5. T. Dockner and A. Frank. Ger. Offen. 2 729 017 (1979).
6. L.P. Kyrudes, F.B. Zienty, G.W. Steahly, and H.L. Morrill. J. Org. Chem. 577 (1947).
7. R.E. Klem, H.F. Skinner, H. Walba, and R.W. Isensee. J. Heterocycl. Chem. 403 (1970).
8. Y. Amemiya, D.D. Miller, and F.L. Hsu. Synth. Commun. **20**, 2483 (1990).
9. P.K. Martin, H.R. Matthews, H. Rapoport, and G. Thyagarajan. J. Org. Chem. 3758 (1968).
10. J.L. Hughey IV, S. Knapp, and H. Schugar. Synthesis, 489 (1980).
11. M. Anastassiadou, G. Baziard-Mouysset, and M. Payard. Synthesis, 1814 (2000).
12. M.E. Campos, R. Jimenez, F. Martinez, and H. Salgado. Heterocycles, **40**, 841 (1995).
13. (*a*) D.G. Lee. Encyclopedia of reagents for organic synthesis. *Edited by* L.A. Paquette. Wiley, New York. 1995. p. 4274; (*b*) A. Shaabani, A. Bazgir, F. Teimouri, and D.G. Lee. Tetrahedron Lett. **43**, 5165 (2002); (*c*) I. Mohammadpoor-Baltork, M.M. Khodaei, A.R. Hajipour, and E. Aslani. Monatsh. Chem. **134**, 539 (2003).
14. H.O. House. Modern synthetic reactions. 2nd ed. W.A. Benjamin, Inc., Menlo Park, Calif. 1972. p. 274.
15. I. Mohammadpoor-Baltork and M. Abdollahi-Alibeik. Bull. Korean Chem. Soc. **24**, 1354 (2003).
16. J.J. Baldwin, P.K. Lumma, F.C. Novello, G.S. Ponticello, and J.M. Sprague. J. Med. Chem. **20**, 1189 (1977).
17. R.D. Miller, V.Y. Lee, and C.R. Moylan. Chem. Mater. **6**, 1023 (1994).
18. N. Sawa. Nippon Kagaku Zasshi, **89**, 868 (1968).
19. W.E. Erner. US Patent 2 847 417 (1958); Chem. Abstr. **53**, 4305 (1959).
20. H. Schubert and S. Hofmann. J. Prakt. Chem. (Leipzig), **7**, 119 (1958).
21. Y. Kikugawa. Synthesis, 124 (1981).

© 2005 NRC Canada

3-Carboxypyridinium chlorochromate – aluminium chloride — An efficient and inexpensive reagent system for the selective oxidation of sulfides to sulfoxides and sulfones in solution and under microwave irradiation

Iraj Mohammadpoor-Baltork, Hamid R. Memarian, and Kiumars Bahrami

Abstract: 3-Carboxypyridinium chlorochromate (CPCC) in the presence of aluminium chloride is a very efficient reagent for the selective oxidation of sulfides to sulfoxide and sulfones in solution and under microwave irradiation. It is noteworthy that different functional groups including carbon–carbon double bonds, ketones, oximes, aldehydes, ethers, and acetals were tolerated under these reaction conditions.

Key words: sulfoxides, sulfones, oxidation, chlorochromate, Lewis acid.

Résumé : Le chlorochromate de 3-carboxypyridinium (CCCP) en présence de chlorure d'aluminium est un réactif très efficace pour l'oxydation des sulfures en sulfoxydes et en sulfones effectuée en solution et sous irradiation de micro-ondes. Il est notable que divers groupes fonctionnels, y compris les doubles liaisons carbone–carbone, les cétones, les oximes, les aldéhydes, les éthers et les acétals, sont tolérés dans les conditions de la réaction.

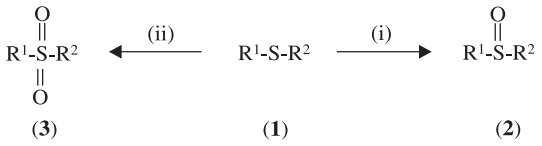
Mots clés : sulfoxydes, sulfones, oxydation, chlorochromate, acide de Lewis.

[Traduit par la Rédaction]

Introduction

Sulfoxides and sulfones are useful synthetic intermediates for the construction of various chemically and biologically significant molecules (1). The most popular and straightforward method for preparing sulfoxides or sulfones involves the oxidation of sulfides. Various methods are available for the oxidation of sulfides to sulfoxides and (or) sulfones (2–29). However, some of these methods suffer from drawbacks such as long reaction times, low yields of the products, the use of expensive reagents, and undesired reactions of other functional groups. On the other hand, selective oxidation of sulfides to sulfoxides and sulfides to sulfones with the same reagent system under the adjusted reaction conditions is an important process in synthetic organic chemistry, and only a few reports are available in the literature for this purpose (30). Consequently, introduction of a new method and inexpensive reagent for the oxidation of sulfides to sulfoxides and sulfones is still in demand. The chemoselective oxidation of sulfides without affecting the other functional groups is also another point of interest. Along this line, we wish to report that sulfides are efficiently oxidized to their corresponding sulfoxides and sulfones with 3-carboxypyridinium chlorochromate in solution and under microwave irradiation.

Scheme 1. (*i*) CPCC (0.8–1 equiv.), $AlCl_3$ (1 equiv.), CH_3CN, reflux or MW; (*ii*) CPCC (1–2.5 equiv.), $AlCl_3$ (1 equiv.), CH_3CN, reflux or MW.



Results and discussion

3-Carboxypyridinium chlorochromate (CPCC) is an inexpensive reagent and is easily prepared from the commercially available starting materials. We have recently reported CPCC as a convenient reagent for the oxidative cleavage of carbon–nitrogen double bonds, oxidative deprotection of trimethylsilyl and tetrahydropyranyl ethers, oxidation of 1,4-dihydropyridines, and deprotection of thiocarbonyl compounds (31). In the course of further exploration on the application in synthetic organic chemistry, we found that CPCC in the presence of aluminium chloride can be used as an efficient reagent for the oxidation of sulfides to sulfoxides and sulfones (Scheme 1).

Initially, benzyl 4-methylphenyl sulfide (entry **1g**, Table 1) was used as a model compound for sulfoxidation by CPCC alone in refluxing acetonitrile. It was found that the reaction did not proceed at all after 2 h.

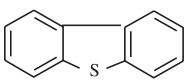
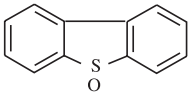
Received 20 July 2004. Published on the NRC Research Press Web site at http://canjchem.nrc.ca on 19 February 2005.

I. Mohammadpoor-Baltork,[1] H.R. Memarian, and K. Bahrami. Department of Chemistry, Isfahan University, Isfahan 81746-73441, Iran.

[1]Corresponding author (e-mail: imbaltork@sci.ui.ac.ir).

 doi: 10.1139/V05-008 © 2005 NRC Canada

Table 1. Oxidation of sulfides to sulfoxides using CPCC–$AlCl_3$.

Sulfide (**1**)	Sulfoxide (**2**)[a]	Time (min)		Yield (%)[d]		
		Solution[b]	MW[c]	Solution	MW	Ref.
$(C_6H_5)_2S$ (**1a**)	$(C_6H_5)_2SO$ (**2a**)	120	3	83	82	2
$C_6H_5CH_2SC_6H_5$ (**1b**)	$C_6H_5CH_2SOC_6H_5$ (**2b**)	75	1.5	93	92	2
$(C_6H_5CH_2)_2S$ (**1c**)	$(C_6H_5CH_2)_2SO$ (**2c**)	20	0.33	87	90	2
4-$MeC_6H_4CH_2SC_6H_5$ (**1d**)	4-$MeC_6H_4CH_2SOC_6H_5$(**2d**)	60	1	95	95	35*a*
4-$BrC_6H_4CH_2SC_6H_5$ (**1e**)	4-$BrC_6H_4CH_2SOC_6H_5$ (**2e**)	45	0.75	93	95	35*b*
4-$O_2NC_6H_4CH_2SC_6H_5$ (**1f**)	4-$O_2NC_6H_4CH_2SOC_6H_5$ (**2f**)	30	0.5	94	94	—
4-$MeC_6H_4SCH_2C_6H_5$ (**1g**)	4-$MeC_6H_4SOCH_2C_6H_5$ (**2g**)	40	0.75	94	95	30*b*
4-$BrC_6H_4SCH_2C_6H_5$ (**1h**)	4-$BrC_6H_4SOCH_2C_6H_5$ (**2h**)	90	2	91	93	35*b*
4-$ClC_6H_4SCH_2C_6H_5$ (**1i**)	4-$ClC_6H_4SOCH_2C_6H_5$ (**2i**)[e]	100	2	87	85	30*b*
4-$BrC_6H_4CH_2SCH_2C_6H_5$ (**1j**)	4-$BrC_6H_4CH_2SOCH_2C_6H_5$ (**2j**)	20	0.33	93	95	—
4-$BrC_6H_4CH_2SC_6H_4$4-Me (**1k**)	4-$BrC_6H_4CH_2SOC_6H_4$4-Me (**2k**)	30	0.5	94	94	35*c*
4-$BrC_6H_4CH_2SC_6H_4$4-Br (**11**)	4-$BrC_6H_4CH_2SOC_6H_4$4-Br (**2l**)	80	1.5	93	92	35*b*
4-$BrC_6H_4CH_2SC_6H_4$4-Cl (**1m**)	4-$BrC_6H_4CH_2SOC_6H_4$4-Cl (**2m**)[e]	80	1.5	90	90	35*b*
4-$O_2NC_6H_4CH_2SC_6H_4$4-Cl (**1n**)	4-$O_2NC_6H_4CH_2SOC_6H_4$4-Cl (**2n**)[e]	70	1.25	82	83	35*c*
2-$ClC_6H_4CH_2SC_6H_4$4-Cl (**1o**)	2-$ClC_6H_4CH_2SOC_6H_4$4-Cl (**2o**)	100	2	93	94	35*b*
$(n\text{-}C_3H_7)_2S$ (**1p**)	$(n\text{-}C_3H_7)_2SO$ (**2p**)[e]	20	0.33	75	79	34
$(n\text{-}C_4H_9)_2S$ (**1q**)	$(n\text{-}C_4H_9)_2SO$ (**2q**)[e]	30	0.5	75	77	35*i*
$n\text{-}C_8H_{17}SCH_2CH_2CHMe_2$ (**1r**)	$n\text{-}C_8H_{17}SOCH_2CH_2CHMe_2$ (**2r**)	135	3.25	95	98	—
 (**1s**)	 (**1s**)[e]	180	4	73	75	2

Note: MW refers to microwave irradiation.
[a]All products were identified by comparison of their physical and spectral data with those of authentic samples.
[b]Sulfide:CPCC:$AlCl_3$ = 1:1:1.
[c]Sulfide:CPCC:$AlCl_3$ = 1:0.8:1.
[d]Isolated yields.
[e]Sulfone (3%–16%) was obtained from the reaction mixture.

Table 2. Oxidation of benzyl 4-methylpheny sulfide to benzyl 4-methylpheny sulfoxide with CPCC in the presence of different Lewis acids in refluxing CH_3CN.

Entry	Lewis acid[a]	Time (min)	Yield (%)[b]
1	$AlCl_3$	40	94
2	$BiCl_3$	40	73
3	$SnCl_2{\cdot}2H_2O$	40	72
4	$NiCl_2{\cdot}6H_2O$	40	63
5	$FeCl_3{\cdot}6H_2O$	40	68
6	$CoCl_2{\cdot}6H_2O$	40	65

[a]Sulfide:CPCC:Lewis acid = 1:1:1.
[b]Isolated yields.

Table 3. Oxidation of benzyl 4-methylpheny sulfide to benzyl 4-methylpheny sulfoxide with CPCC in the presence of $AlCl_3$ in different solvents under reflux conditions.

Entry	Solvent[a]	Time (min)	Yield (%)[b]
1	CH_3CN	40	94
2	CH_3COCH_3	40	75
3	$CHCl_3$	40	65
4	CH_2Cl_2	40	60
5	*n*-Hexane	40	12

[a]Sulfide:CPCC:$AlCl_3$ = 1:1:1.
[b]Isolated yields.

Recently, Lewis-acid-promoted oxidation of organic compounds has been reported in the literature (32). Therefore, the oxidation of benzyl 4-methylphenyl sulfide to the corresponding sulfoxide with CPCC in the presence of different Lewis acids such as $AlCl_3$, $BiCl_3$, $FeCl_3{\cdot}6H_2O$, $SnCl_2{\cdot}2H_2O$, $NiCl_2{\cdot}6H_2O$, and $CoCl_2{\cdot}6H_2O$ in refluxing acetonitrile was investigated. The best result was achieved using $AlCl_3$ (Table 2).

We have also examined this reaction in different solvents such as CH_2Cl_2, $CHCl_3$, CH_3CN, CH_3COCH_3, and *n*-hexane, and it was observed that CH_3CN is the only solvent of choice for this purpose (Table 3).

The applicability of the CPCC–$AlCl_3$ system was then examined for sulfoxidation of diaryl, dibenzyl, aryl benzyl, dialkyl, and cyclic sulfides in refluxing acetonitrile. The optimum molar ratio of sulfide to CPCC to $AlCl_3$ was found to be 1:1:1. Under these conditions, the corresponding sulfoxides were obtained in high yields (Table 1).

Recently, there has been a growing interest in the application of microwave irradiation in chemical reactions (33). The salient features of the microwave approach are the much im-

© 2005 NRC Canada

proved reaction rates, formation of cleaner products, and operational simplicity. Therefore, the sulfoxidation of the above-mentioned sulfides with CPCC–$AlCl_3$ was performed under microwave irradiation with a dramatic reduction of reaction time. Under these conditions, the optimum molar ratio of sulfide to CPCC to $AlCl_3$ was found to be 1:0.8:1. When the sulfides, dissolved in 2 mL of CH_3CN, were treated with CPCC–$AlCl_3$ and irradiated for 0.33–4 min, the corresponding sulfoxides were obtained in high yields (Table 1).

However, in the oxidation of alkyl aryl sulfides such as 4-chlorophenyl methyl sulfide and methyl phenyl sulfide, a mixture of sulfoxide (~55%) and sulfone (~40%) were isolated from the reaction mixture.

To show the efficiency and applicability of the CPCC–$AlCl_3$ system further, the oxidation of sulfides to their corresponding sulfones was also carried out in solution and under microwave irradiation. The reaction conditions specified in Table 4 were optimized for use in both solution (sulfide to CPCC to $AlCl_3$ = 1:1.5–2.5:1) and under microwave irradiation (sulfide to CPCC to $AlCl_3$ = 1:1–2:1). It was found that a wide variety of diaryl, dialkyl, dibenzyl, aryl benzyl, alkyl aryl, and cyclic sulfides were oxidized to their sulfones in excellent yields in refluxing acetonitriles. It should be noted that some of these oxidation reactions were also performed in dry acetonitrile and no improvement was observed under these conditions. The oxidation of these sulfides with the CPCC–$AlCl_3$ system under microwave irradiation afforded the corresponding sulfones in excellent yields in very short reaction times (0.25–4.5 min) without any special precautions. The results are presented in Table 4. Under microwave irradiation, acetonitrile was used for the homogenization of the reaction mixture. The polar character of this solvent also seems to increase the reaction temperature, so the reaction is completed in a short time (33*c*). Inspection of the data in Tables 1 and 4 show that the yields of the reactions in solution and under microwave irradiation are comparable, but under microwave irradiation, the reaction times are considerably shorter. Also, the molar ratio of CPCC to sulfide is lower under microwave irradiation.

We investigated some of these reactions with 3-carboxypyridine–$AlCl_3$ and it was found that the reactions did not proceed at all. Also, during the reaction with CPCC, the colour of the mixture turned from yellow-orange to green. Further, the reaction times and yields were comparable when the reactions were carried out in air and under an inert atmosphere. These are good indications that the oxygens transferred to sulfides are those bound to chromium in the CPCC reagent.

As mentioned in our previous publications (32), some of the reagents under investigation were effective oxidizing agents only in the presence of aluminium chloride. This trend has been also observed in the oxidation of sulfides with CPCC. Unfortunately, we have not been able to assign a reasonable mechanism for these reactions at present.

It is worth mentioning that the CPCC–$AlCl_3$ system is chemoselective, tolerating various functional groups such as carbon–carbon double bonds, ketones (Table 4, entries **1t**, **1c′**, and **1d′**), oximes, aldehydes, ethers, and acetals (Scheme 2). These observations clearly suggest that this method can be applied for the chemoselective oxidation of sulfides in the presence of the above-mentioned functional groups in multifunctional molecules.

To show the advantage of 3-carboxypyridinium chlorochromate (CPCC) over pyridinium chlorochromate (PCC), we compared the results obtained for some of the reactions using these two reagents. It was found that the yields of the reactions are higher with CPCC (Table 5).

In conclusion, we have demonstrated that the CPCC–$AlCl_3$ system is an inexpensive and excellent reagent for the oxidation of a variety of structurally diverse sulfides to their corresponding sulfoxides and sulfones. It is noteworthy that the reaction can tolerate oxidatively sensitive functional groups and that the sulfur atom is selectively oxidized.

Experimental

The sulfides **1a**, **1p**, **1q**, **1s**, **1t**, and **1d′** were purchased from the Merck chemical company. The other sulfides were prepared according to the described procedure (34). Microwave irradiation was carried out using a commercial microwave oven (Samsung M9G45) operating at 2450 MHz (900 W). The yields refer to isolated pure products. Melting points were determined using a Mettler FP5 apparatus and are uncorrected. IR spectra were run on a Philips PU9716 spectrophotometer. ^1H NMR spectra were recorded on a Bruker 80 or 200 and (or) 500 MHz spectrometer with $CDCl_3$ as the solvent and TMS as the internal standard. The elemental analysis was performed by the Research Institute of Petroleum Industry, Tehran, Iran. CPCC was prepared according to the reported procedure (31*a*).

General procedure for the oxidation of sulfides to sulfoxides in solution

In a round-bottomed flask (50 mL) equipped with a condenser and a magnetic stirrer, a solution of sulfide (1 mmol) in CH_3CN (10 mL) was prepared. CPCC (1 mmol) and $AlCl_3$ (1 mmol) were added and the mixture was stirred under reflux conditions for the time indicated in Table 1. The progress of the reaction was monitored by TLC (eluent: *n*-hexane – ethyl acetate, 7:2). The mixture was filtered and the solid material was washed with CH_3CN (10 mL). The filtrate was evaporated and the crude product was purified by recrystallization or chromatography on silica gel to afford the pure sulfoxide (Table 1).

General procedure for the oxidation of sulfides to sulfoxides under microwave irradiation

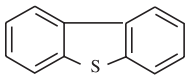
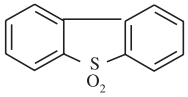
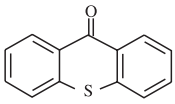
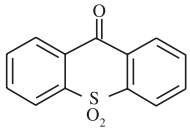
A mixture of sulfide (1 mmol), CPCC (0.8 mmol), and $AlCl_3$ (1 mmol) and CH_3CN (2 mL) was exposed to microwave irradiation (900 W) for 0.33–4 min (at 20 s intervals). The progress of the reaction was followed by TLC. After completion of the reaction, the mixture was extracted with ethyl acetate (2 × 20 mL). Evaporation of the solvent followed by recrystallization or chromatography on silica gel afforded the pure sulfoxide (Table 1).

General procedure for the oxidation of sulfides to sulfones in solution

To a solution of sulfide (1 mmol) in CH_3CN (10 mL) in a round-bottomed flask (50 mL) equipped with a condenser and a magnetic stirrer, CPCC (1.5–2.5 mmol) and $AlCl_3$

© 2005 NRC Canada

Table 4. Oxidation of sulfides to sulfones using CPCC–$AlCl_3$.

Sulfide (**1**)	Sulfone (**3**)[a]	Time (min)		Yield (%)[d]		
		Solution[b]	MW[c]	Solution	MW	Ref.
$(C_6H_5)_2S$ (**1a**)	$(C_6H_5)_2SO_2$ (**3a**)	120	3	95	95	35*i*
$C_6H_5CH_2SC_6H_5$ (**1b**)	$C_6H_5CH_2SO_2C_6H_5$ (**3b**)	65	1	97	99	30*a*
$(C_6H_5CH_2)_2S$ (**1c**)	$(C_6H_5CH_2)_2SO_2$ (**3c**)	30	0.5	96	97	34
4-$MeC_6H_4CH_2SC_6H_5$ (**1d**)	4-$MeC_6H_4CH_2SO_2C_6H_5$ (**3d**)	60	1	96	95	35*d*
4-$BrC_6H_4CH_2SC_6H_5$ (**1e**)	4-$BrC_6H_4CH_2SO_2C_6H_5$ (**3e**)	60	1	95	98	35*d*
4-$O_2NC_6H_4CH_2SC_6H_5$ (**1f**)	4-$O_2NC_6H_4CH_2SO_2C_6H_5$ (**3f**)	40	0.75	98	98	—
4-$MeC_6H_4SCH_2C_6H_5$ (**1g**)	4-$MeC_6H_4SO_2CH_2C_6H_5$ (**3g**)	60	1	95	95	30*b*
4-$BrC_6H_4SCH_2C_6H_5$ (**1h**)	4-$BrC_6H_4SO_2CH_2C_6H_5$ (**3h**)	100	2.5	96	97	35*b*
4-$ClC_6H_4SCH_2C_6H_5$ (**1i**)	4-$ClC_6H_4SO_2CH_2C_6H_5$ (**3i**)	100	2.5	94	94	30*b*
4-$BrC_6H_4CH_2SCH_2C_6H_5$ (**1j**)	4-$BrC_6H_4CH_2SO_2CH_2C_6H_5$ (**3j**)	30	2.5	95	99	—
4-$BrC_6H_4CH_2SC_6H_4$4-Me (**1k**)	4-$BrC_6H_4CH_2SO_2C_6H_4$4-Me (**3k**)	45	0.75	95	97	35*c*
4-$BrC_6H_4CH_2SC_6H_4$4-Br (**1l**)	4-$BrC_6H_4CH_2SO_2C_6H_4$4-Br (**3l**)	100	2.5	95	95	35*b*
4-$BrC_6H_4CH_2SC_6H_4$4-Cl (**1m**)	4-$BrC_6H_4CH_2SO_2C_6H_4$4-Cl (**3m**)	110	2.5	94	95	35*b*
4-$O_2NC_6H_4CH_2SC_6H_4$4-Cl (**1n**)	4-$O_2NC_6H_4CH_2SO_2C_6H_4$4-Cl (**3n**)	60	1	95	95	35*c*
2-$ClC_6H_4CH_2SC_6H_4$4-Cl (**1o**)	2-$ClC_6H_4CH_2SO_2C_6H_4$4-Cl (**3o**)	120	2.5	93	94	35*b*
$(n\text{-}C_3H_7)_2S$ (**1p**)	$(n\text{-}C_3H_7)_2SO_2$ (**3p**)	50	1	92	95	34
$(n\text{-}C_4H_9)_2S$ (**1q**)	$(n\text{-}C_4H_9)_2SO_2$ (**3q**)	90	2	95	95	35*i*
$n\text{-}C_8H_{17}SCH_2CH_2CHMe_2$ (**1r**)	$n\text{-}C_8H_{17}SO_2CH_2CH_2CHMe_2$ (**3r**)	120	3	94	96	—
 (**1s**)	 (**3s**)	180	4	92	95	35*i*
 (**1t**)	 (**3t**)	200	4.5	91	93	35*g*
$n\text{-}C_8H_{17}SMe$ (**1u**)	$n\text{-}C_8H_{17}SO_2Me$ (**3u**)	60	1	95	94	—
$n\text{-}C_8H_{17}SCH_2CH_3$ (**1v**)	$n\text{-}C_8H_{17}SO_2CH_2CH_3$ (**3v**)	60	1	94	94	—
C_6H_5SMe (**1w**)	$C_6H_5SO_2Me$ (**3w**)	30	0.5	94	96	30*b*
4-MeC_6H_4SMe (**1x**)	4-$MeC_6H_4SO_2Me$ (**3x**)	20	0.33	91	92	35*h*
4-ClC_6H_4SMe (**1y**)	4-$ClC_6H_4SO_2Me$ (**3y**)	100	2.5	94	94	—
$C_6H_5S(n\text{-}C_3H_7)$ (**1z**)	$C_6H_4SO_2(n\text{-}C_3H_7)$ (**3z**)	45	0.75	92	95	35*e*
$C_6H_5S(n\text{-}C_4H_9)$ (**1a′**)	$C_6H_5SO_2(n\text{-}C_4H_9)$ (**3a′**)	60	1	96	95	35*e*
$C_6H_5SCHMe_2$ (**1b′**)	$C_6H_5SO_2CHMe_2$ (**3b′**)	65	1	92	92	35*e*
$C_6H_5SCH_2CH{=}CH_2$ (**1c′**)	$C_6H_5SO_2CH_2CH{=}CH_2$ (**3c′**)	30	0.5	91	94	30*b*
$(CH_2{=}CHCH_2)_2S$ (**1d′**)	$(CH_2{=}CHCH_2)_2SO_2$ (**3d′**)	5	0.25	94	97	35*f*

Note: MW refers to microwave irradiation.
[a]All products were identified by comparison of their physical and spectral data with those of authentic samples.
[b]Sulfide:CPCC:$AlCl_3$ = 1:2.5:1 and 1:1.5:1 for entries **1a**–**1v** and **1w**–**1d′**, respectively.
[c]Sulfide:CPCC:$AlCl_3$ = 1:2:1 and 1:1:1 for entries **1a**–**1v** and **1w**–**1d′**, respectively.
[d]Isolated yields.

(1 mmol) were added and the mixture was stirred under reflux conditions for the appropriate time according to Table 4. The progress of the reaction was monitored by TLC (eluent: *n*-hexane – ethyl acetate, 7:1). The reaction mixture was filtered and the solid material was washed with CH_3CN (10 mL). Evaporation of the solvent, followed by recrystallization or chromatography on silica gel afforded the pure sulfone (Table 4).

General procedure for the oxidation of sulfides to sulfones under microwave irradiation

A mixture of sulfide (1 mmol), CPCC (1 to 2 mmol), $AlCl_3$ (1 mmol), and CH_3CN (2 mL) was prepared. The mixture was irradiated (900 W) for 0.25–4.5 min (at 20 s intervals) and the completion of the reaction was monitored by TLC examination. After completion of the reaction, the mixture was extracted with ethyl acetate (2 × 20 mL). The

© 2005 NRC Canada

Scheme 2. A = CPCC:substrates:$AlCl_3$ = 1:1:1:1, CH_3CN, reflux; B = CPCC:substrates:$AlCl_3$ = 0.8:1:1:1, CH_3CN, MW; C = CPCC:substrates:$AlCl_3$ = 2.5:1:1:1, CH_3CN, reflux; D = CPCC:substrates:$AlCl_3$ 2:1:1:1, CH_3CN, MW.

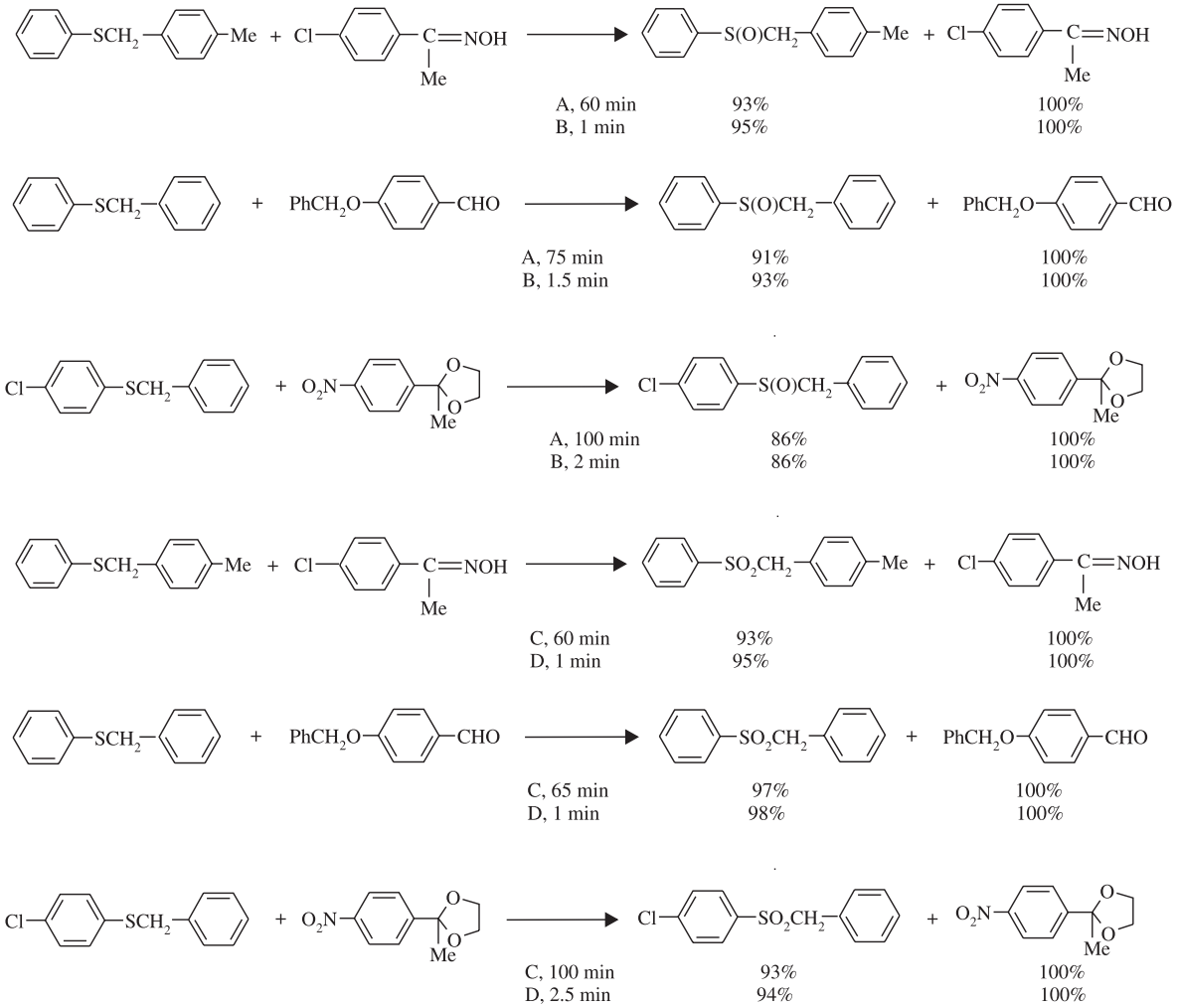


Table 5. Comparison of some of the results obtained with CPCC and PCC.

		CPCC: Yield%[a] (time, min)		PCC: Yield%[a] (time, min)	
Substrate	Product	Solution	MW	Solution	MW
1c	**2c**	87 (20)	90 (0.33)	65 (20)	70 (0.33)
1e	**2e**	93 (45)	95 (0.75)	70 (45)	74 (0.75)
1c	**3c**	96 (30)	97 (0.5)	75 (30)	78 (0.5)
1e	**3e**	95 (60)	98 (1)	73 (60)	74 (1)

Note: MW refers to microwave irradiation.
[a]Isolated yields.

solvent was evaporated and purification was achieved by recrystallization or chromatography on silica gel to afford the pure sulfone (Table 4).

Spectroscopic data

Compound **2f**: mp 161–163 °C. IR ν_{max} (KBr, cm^{-1}): 1515, 1345, 1026. ^1H NMR (200 MHz, $CDCl_3$) δ_H: 8.12 (d, J = 6.5 Hz, 2H, Ph-H), 7.51–7.40 (m, 5H, Ph-H), 7.13 (d, J = 6.5 Hz, 2H, Ph-H), 4.24 (d, J = 12.0 Hz, 1H, CH_2), 4.04 (d, J = 12.0 Hz, 1H, CH_2). Anal. calcd. for $C_{13}H_{11}NSO_3$: C 59.76, H 4.24, N 5.36, S 12.27; found: C 59.63, H 4.40, N 5.25, S 12.41.

Compound **2j**: mp 139 to 140 °C. IR ν_{max} (KBr, cm^{-1}): 1028. ^1H NMR (500 MHz, $CDCl_3$) δ_H: 7.54 (d, J = 8.27 Hz, 2H, Ph-H), 7.44–7.40 (m, 3H, Ph-H), 7.33–7.32 (m, 2H, Ph-H), 7.2 (d, J = 8.27 Hz, 2H, Ph-H), 3.95 (s, 2H, CH_2), 3.89 (d, J = 13.09 Hz, 1H, CH_2), 3.78 (d, J = 13.09 Hz, 1H, CH_2). Anal. calcd. for $C_{14}H_{13}SOBr$: C 54.38, H 4.24, S 10.37; found: C 54.30, H 4.22, S 10.50.

Compound **2r**: mp 42 to 43 °C. IR ν_{max} (KBr, cm^{-1}): 1018. ^1H NMR (200 MHz, $CDCl_3$) δ_H: 2.80–2.55 (m, 4H, -CH_2-SO-CH_2-), 1.90–1.60 (m, 5H, 2CH_2, CH), 1.50–1.15 (m, 10H, 5CH_2), 0.94–0.88 (m, 9H, 3CH_3). Anal. calcd. for $C_{13}H_{28}SO$: C 67.18, H 12.14, S 13.80; found: C 66.98, H 12.08, S 14.10.

Compound **3f**: mp 204 to 205 °C. IR ν_{max} (KBr, cm^{-1}): 1515, 1345, 1300, 1142. ^1H NMR (200 MHz, $CDCl_3$) δ_H: 8.18 (d, J = 6.5 Hz, 2H, Ph-H), 7.70–7.40 (m, 5H, Ph-H), 7.10 (d, J = 6.5 Hz, 2H, Ph-H), 4.44 (s, 2H, CH_2). Anal. calcd. for $C_{13}H_{11}NSO_4$: C 56.31, H 3.99, N 5.05, S 11.56; found: C 56.17, H 4.10, N 4.96, S 11.75.

Compound **3j**: mp 176–178 °C. IR ν_{max} (KBr, cm^{-1}): 1299, 1116. ^1H NMR (80 MHz, $CDCl_3$) δ_H: 7.60–7.17 (m,

© 2005 NRC Canada

9H, Ph-H), 4.14 (s, 2H, CH_2), 4.02 (s, 2H, CH_2). Anal. calcd. for $C_{14}H_{13}BrSO_2$: C 51.70, H 4.03, S 9.86; found: C 51.60, H 4.10, S 9.97.

Compound **3r**: mp 39–41 °C. IR ν_{max} (KBr, cm^{-1}): 1266, 1110. ^1H NMR (80 MHz, $CDCl_3$) δ_H: 2.90–2.65 (m, 4H, $-CH_2-SO_2-CH_2-$), 1.90–0.80 (m, 24H, alkyl). Anal. calcd. for $C_{13}H_{28}SO_2$: C 62.85, H 11.36, S 12.91; found: C 62.70, H 11.45, S 13.10.

Compound **3u**: mp 63 to 64 °C. IR ν_{max} (KBr, cm^{-1}): 1275, 1122. ^1H NMR (80 MHz, $CDCl_3$) δ_H: 3.0–2.70 (m, 5H, $-CH_2-SO_2-CH_3$), 1.85–0.80 (m, 15H, alkyl). Anal. calcd. for $C_9H_{20}SO_2$: C 56.21, H 10.48, S 16.67; found: C 56.15, H 10.40, S 16.85.

Compound **3v**: mp 66 to 67 °C. IR ν_{max} (KBr, cm^{-1}): 1272, 1114. ^1H NMR (80 MHz, $CDCl_3$) δ_H: 3.0–2.65 (m, 4H, $-CH_2-SO_2-CH_2-$), 1.85–0.80 (m, 18H, CH_3, alkyl). Anal. calcd. for $C_{10}H_{22}SO_2$: C 58.21, H 10.74, S 15.54; found: C 58.20, H 10.70, S 15.65.

Compound **3y**: mp 95–97 °C. IR ν_{max} (KBr, cm^{-1}): 1304, 1142. ^1H NMR (500 MHz, $CDCl_3$) δ_H: 7.90 (d, J = 8.5 Hz, 2H, Ph-H), 7.60 (d, J = 8.5 Hz, 2H, Ph-H), 3.10 (s, 3H, CH_3). Anal. calcd. for $C_7H_7ClSO_2$: C 44.10, H 3.70, S 16.82; found: C 43.90 H 3.80, S 17.10.

Acknowledgments

We are thankful to the Isfahan University Research Council for partial support of this work.

References

1. (*a*) E. Block. Reactions of organosulfur compounds. Academic Press, New York. 1978; (*b*) P. Page. Organosulfur chemistry: Synthetic aspects. Academic Press, New York. 1995.
2. Y. Watanabe, T. Numata, and S. Oae. Synthesis, 204 (1981).
3. (*a*) M. Hirano, J.-I. Tomaru, and T. Morimoto. Chem. Lett. 523 (1991); (*b*) M. Hirano, S. Yakabe, J.H. Clark, H. Kudo, and T. Morimoto. Synth. Commun. **26**, 1875 (1996).
4. F. Bonadies, F.D. Angelis, L. Locati, and A. Scettri. Tetrahedron Lett. **37**, 7129 (1996).
5. K.-T. Liu and Y.-C. Tong. J. Org. Chem. **43**, 2717 (1978).
6. S.H. Mashraqui, C.D. Mudaliar, and M.A. Karnik. Synth. Commun. **28**, 939 (1998).
7. Y.H. Kim and D.C. Yoon. Tetrahedron Lett. **29**, 6453 (1988).
8. M.H. Ali, D.R. Leach, and C.E. Schmitz. Synth. Commun. **28**, 2969 (1998).
9. K.S. Ravikumar, J.-P. Begue, and D. Bonnet-Delpon. Tetrahedron Lett. **39**, 3141 (1998).
10. G. Song, F. Wang, H. Zhang, X. Lu, and C. Wang. Synth. Commun. **28**, 2783 (1998).
11. Y.-J. Chen and Y.-P. Huang. Tetrahedron Lett. **41**, 5233 (2000).
12. A. Shaabani, M.B. Teimouri, and H.R. Safaei. Synth. Commun. **30**, 265 (2000).
13. A. Bravo, B. Dordi, F. Fontana, and F. Minisci. J. Org. Chem. **66**, 3232 (2001).
14. D.J. Procter. J. Chem. Soc. Perkin Trans. 1, 335 (2001).
15. F. Batigalhia, M. Zaldini-Hernandes, A.G. Ferreira, I. Malvestiti, and Q.B. Cass. Tetrahedron, **57**, 9669 (2001).
16. S.E. Martin and L.I. Rossi. Tetrahedron Lett. **42**, 7147 (2001).
17. Z.-X. Xiong, N.-P. Huang, and P. Zhong. Synth. Commun. **31**, 245 (2001).
18. (*a*) A.R. Hajipour, S.E. Mallakpour, and H. Adibi. J. Org. Chem. **67**, 8666 (2002); (*b*) A.R. Hajipour, H.R. Bagheri, and A.E. Ruoho. Phosphorus Sulfur Silicon Relat. Elem. **178**, 2441 (2003).
19. B. Pelotier, M.S. Anson, I.B. Campbell, S.J.F. Macdonald, G. Priem, and R.F.W. Jackson. Synlett, 1055 (2002).
20. S.S. Kim, K. Nehru, S.S. Kim, D.W. Kim, and H.C. Jung. Synthesis, 2484 (2002).
21. (*a*) H. Firouzabadi and M. Seddighi. Synth. Commun. **21**, 211 (1991); (*b*) H. Firouzabadi and I. Mohammadpoor-Baltork. Bull. Chem. Soc. Jpn. **65**, 1131 (1992); (*c*) N. Iranpoor, H. Firouzabadi, and A.-R. Pourali. Tetrahedron, **58**, 5179 (2002); (*d*) N. Iranpoor, H. Firouzabadi, and A.-R. Pourali. Synlett, 347 (2004).
22. G. Kar, A.K. Saikia, U. Bora, S.K. Dehury, and M.K. Chaudhuri. Tetrahedron Lett. **44**, 4503 (2003).
23. W.L. Xu, Y.Z. Li, Q.S. Zhang, and H.S. Zhu. Synthesis, 227 (2004).
24. B.M. Trost and D.P. Curran. Tetrahedron Lett. **22**, 1287 (1981).
25. K.R. Guertin and A.S. Kende. Tetrahedron Lett. **34**, 5369 (1993).
26. V. Khanna, G.C. Maikap, and J. Iqbal. Tetrahedron Lett. **37**, 3367 (1996).
27. M.H. Ali and G.J. Bohnert. Synth. Commun. **28**, 2983 (1998).
28. D.H.R. Barton, W. Li, and J.A. Smith. Tetrahedron Lett. **39**, 7055 (1998).
29. D.A. Alonso, C. Najera, and M. Varea. Tetrahedron Lett. **43**, 3459 (2002).
30. (*a*) C.G. Venier, T.G. Squires, Y.-Y. Chen, G.P. Hussmann, J.C. Shei, and B.F. Smith. J. Org. Chem. **47**, 3773 (1982); (*b*) B.M. Choudary, B. Bharathi, C.V. Reddy, and M.L. Kantam. J. Chem. Soc. Perkin Trans. 1, 2069 (2002); (*c*) A. McKillop and J.A. Tarbin. Tetrahedron Lett. **24**, 1505 (1983); (*d*) R.P. Greenhalgh. Synlett, 235 (1992); (*e*) S. Yamazaki. Bull. Chem. Soc. Jpn. **69**, 2955 (1996); (*f*) R.S. Varma, R.K. Saini, and H.M. Meshram. Tetrahedron Lett. **38**, 6525 (1997).
31. (*a*) I. Mohammadpoor-Baltork and Sh. Pouranshirvani. Synth. Commun. **26**, 1 (1996); (*b*) I. Mohammadpoor-Baltork and Sh. Pouranshirvani. Synthesis, 756 (1997); (*c*) I. Mohammadpoor-Baltork, M.M. Sadeghi, H.R. Memarian, and R. Pairow J. Chem. Res. (S), 40 (2000); (*d*) I. Mohammadpoor-Baltork, H.R. Memarian, and K. Bahrami. Monatsh. Chem. **135**, 411 (2004).
32. (*a*) H. Firouzabadi and I. Mohammadpoor-Baltork. Synth. Commun. **24**, 1065 (1994); (*b*) H. Firouzabadi and I. Mohammadpoor-Baltork. Bull. Chem. Soc. Jpn. **68**, 2319 (1995); (*c*) H. Firouzabadi, A.R. Sardarian, and H. Badparva. Bull. Chem. Soc. Jpn. **69**, 685 (1996); (*d*) I. Mohammadpoor-Baltork and A.R. Nourozi. Synthesis, 487 (1999); (*e*) I. Mohammadpoor-Baltork, M.M. Sadeghi, and A.-H. Adibi. Molecules, 900 (2001); (*f*) M. Gholizadeh, I. Mohammadpoor-Baltork, and B. Kharamesh. Bull. Korean Chem. Soc. **25**, 566 (2004).
33. (*a*) S. Caddick. Tetrahedron, **51**, 10 403 (1995); (*b*) S. Deshayes, M. Liagre, A. Loupy, J.-L. Luchi, and A. Petit. Tetrahedron, **55**, 10 851 (1999); (*c*) L. Perreux and A. Loupy. Tetrahedron, **57**, 9199 (2001).
34. A.I. Vogel, A.R. Tatchell, B.S. Furnis, A.J. Hannaford, and P.W.G. Smith. Vogel's textbook of practical organic chemistry. 5th ed. Prentice-Hall, New Jersey. 1989. p. 789.
35. (*a*) Y. Guo and W. S. Jenks. J. Org. Chem. **60**, 5480 (1995); (*b*) N.G. Clark, J.E. Cranham, D. Greenwood, J.R. Marshall, and H.A. Stevenson. J. Sci. Food Agric. 566 (1957); (*c*) R.F. Brookes, N.G. Clark, J.E. Cranham, D. Greenwood, J.R. Marshall, and H.A. Stevenson. J. Sci. Food Agric. 111 (1958); (*d*) D.L. Dalrymple, J.D. Reinheimer, D. Barnes, and R. Baker. J. Org. Chem. **29**, 2647 (1964); (*e*) W.A. Baldwin and R. Rob-

© 2005 NRC Canada

inson. J. Chem. Soc. 1445 (1932); (*f*) A.C. Serra, C.M.M. Da Silva Correa, M.A.M.S.A. Vieira, and M.A. Gomes. Tetrahedron, **46**, 3061 (1990); (*g*) B. Taljaard, A. Goosen, and C.W. McCleland. J. Chem. Soc. Perkin Trans. 1, 931 (1989); (*h*) D.N. Harpp, J.G. Gleason, and D.K. Ash. J. Org. Chem. **36**, 322 (1971); (*i*) Aldrich handbook of fine chemicals and laboratory equipment. 1999–2000.

© 2005 NRC Canada

Conformational study of internally retrograde and quasi-retrograde molecules — An ab initio and DFT study

Miguel A. Zamora, Luis N. Santágata, Marcelo F. Masman, José A. Bombasaro, Mónica L. Freile, and Ricardo D. Enriz

Abstract: A conformational study of the symmetrical and nonsymmetrical homologue series was carried out. In this study, ab initio (RHF/3-21G and RHF/6-31G(d)) and density functional theory (B3LYP/6-31G(d)) calculations were performed. The presence of two symmetrical aromatic systems (identical or not) reduces notably the conformational possibilities of these compounds. Our results indicate that RHF/3-21G calculations are sufficient to use in a preliminary form. However, from our results it is prudent to use this technique only for a preliminary or exploratory conformational analysis. Thus, at least, the HF level of theory in conjunction with more extended basis sets and the inclusion of electron correlation appear to be necessary to confirm critical points at the potential energy hyper surfaces (PEHSs) and to assign the conformational preferences of these compounds. In the present paper, we report a complete and comprehensive picture of the conformational intricacies of the compounds with a small flexible connecting chain (n = 1–5). In addition, an "educated guess" for the conformational behaviour of large-size homologues (n = 6–10) is also reported.

Key words: ab initio and DFT calculations, conformational study, homologue series.

Résumé : On a effectué une étude conformationnelle de séries homologues symétrique et non-symétrique en procédant à des calculs ab initio (RHF/3-21G et RHF/6-31G(d)) et à des calculs de densité fonctionnelle (B3LYP/6-31G(d)). La présence de deux systèmes aromatiques symétriques (identiques ou pas) réduit considérablement les possibilités conformationnelles de ces composés. Nos résultats indiquent que les calculs RHF/3-21G sont suffisants pour être utilisés dans une forme préliminaire. Toutefois, sur la base de nos résultats, il serait prudent de n'utiliser cette technique que pour une analyse conformationnelle préliminaire ou exploratoire. Il semble en effet nécessaire d'utiliser au moins le niveau HF de la théorie en combinaison avec des ensembles de bases plus étendus et d'inclure une corrélation d'électron pour confirmer les points critiques des hypersurfaces d'énergie potentielle (HSEP) et pour attribuer les préférences conformationnelles de ces composés. Dans ce travail, on rapporte une image complète de la complexité de ces composés comportant de petites chaînes de liaison flexibles (n = 1–5). On rapporte de plus une évaluation probable du comportement conformationnel des homologues plus grands (n = 6–10).

Mots clés : calculs ab initio et de la théorie de la densité fonctionnelle, étude conformationelle, séries homologues.

[Traduit par la Rédaction]

Introduction

Life disfavours symmetry, just look at a familiar face as it is reflected by the mirror and you immediately recognize that the apparent symmetry of the human body is nothing but a disguise. Life's dislike of symmetry is even more evident at the molecular level. Our body uses D-glucose, L-amino acids, and many more molecules chosen discriminatively from the two mirror-image forms of chiral molecules. In contrast, for computational calculation purposes, symmetry is a very advantageous situation because it reduces notably the conformational possibilities of symmetrical compounds.

On the other hand, nature is efficient in producing compounds with a high degree of symmetry. It is now claimed that symmetry involving forces, including electromagnetic forces, are important in biology, particularly for the assembly of macromolecules. In addition, the ordering of water in organized systems and the symmetry of interactions may play important roles in biological processes (1, 2). Symmetrical natural compounds present generally a C_2 or C_{2v} symmetry axis; examples are the alkaloids lobelanine and sparteine, the anticoagulant dicumarol, and the antispermatogenic gossypol (Fig. 1).

Besides drugs of natural origin, twin drugs combining two structural components in a single molecule have been de-

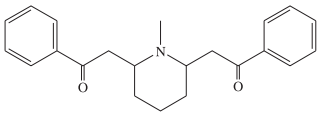
Received 31 August 2004. Published on the NRC Research Press Web site at http://canjchem.nrc.ca on 25 February 2005.

M.A. Zamora, L.N. Santágata, M.F. Masman, J.A. Bombasaro, and R.D. Enriz.[1] Departamento de Química, Facultad de Química, Bioquímica y Farmacia, Universidad Nacional de San Luis, Chacabuco 917, 5700 San Luis, Argentina.
M.L. Freile. Departamento de Química, Facultad de Ciencias Naturales U.N.P.S.J.B. km 4. 9000, Comodoro Rivadavia, Chubut, Argentina.

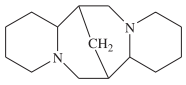
[1]Corresponding author (e-mail: denriz@unsl.edu.ar).

 doi: 10.1139/V05-002 © 2005 NRC Canada

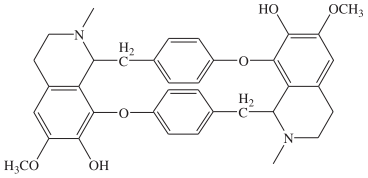
Fig. 1. Symmetrical natural compounds.



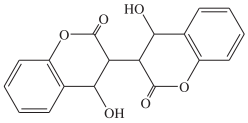
Lobelanine



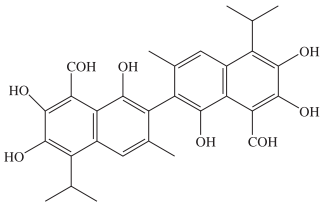
Sparteine



Isochondrodendrine



Dicumarol



Gossypol

scribed in numerous domains of medicinal chemistry. Identical twin drugs acting on receptors have been efficient in several cases. The development of polyamine disulphides such as APC or benextramine (Fig. 2) allowed the hypothesis of symmetrical properties of α-adrenergic receptors (3). Melthoctramine (Fig. 2) is a useful probe for characterizing acetylcholine muscarinic receptor subtypes where it appears as a selective M_2 antagonist (4). In addition, many twin drugs have been reported acting as enzyme inhibitors (HIV-enzyme (5), protein kinase (6, 7)), DNA ligands (8, 9), as well as surface-active antibacterial agents (9).

It should be noted that, in general, the twin drugs of interest in medicinal chemistry are large; implying that relatively large compounds possess a great number of different spatial orderings. Thus, a complete conformational analysis for these compounds appears to be, at least in principle, a very difficult task. However, it is well-known that symmetry reduces notably the conformational possibilities of a symmetrical homologue series. The question that arises is: is the number of identical or enantiomeric conformations by symmetrical reasons enough to keep the number of different conformations "manageable" using high levels of theory calculations?

To better understand how the presence of symmetrical aromatic systems reduces the conformational possibilities in a homologue series, we performed a comparative conformational study for four series of compounds possessing different degrees of symmetry (Fig. 3).

Method of calculation

Molecular geometry optimizations were performed at three levels of theory, RHF/3-21G, RHF/6-31G(d), and B3LYP/6-31G(d), for the compounds **Ia**, **IIa**, **IIIa**, **IVa**, **IIb**, **IIc**, and **IId** (Fig. 3). The rest of the compounds reported here were evaluated only from RHF/3-21G calculations. Partially relaxed potential energy surface (PES) scan calculations for compounds **Ia**, **IIa**, **IIIa**, **IVa**, **IIb**, **IIc**, and **IId** (Fig. 3) were calculated at the RHF/3-21G level of theory. In the partially relaxed PES scan calculations, the variables were rotated with 30° increments to produce plots consisting of 13 × 13 = 169 points, keeping the bond lengths and internal angles fixed. The partially relaxed PES scan calculations (opt = z-matrix), were all critical points possessing gradients less than 4.5×10^{-4} a.u.

All the calculations reported here were carried out with the GAUSSIAN 03 program (10).

Results and discussion

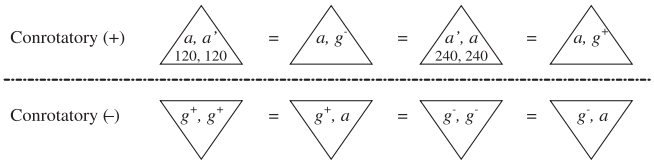
Compounds Ia, IIa, IIIa, and IVa (n = 1)

These compounds look like a simple conformational problem with two torsional angles (θ and ϕ). When a planar moiety of twofold symmetry is connected to a tetrahedral carbon of threefold symmetry, the torsional conformational potential about that single bond does not necessarily have three minima; in principle it may have six minima, as in the case of methylbenzene. In ethylbenzene (11), however, the six degenerate minima are reduced to two unique structures.

Compounds **Ia** (12, 13) and **IIa** (14) have been studied previously from ab initio and DFT calculations. In these compounds, the rotation along θ and ϕ are expected to show some symmetry since the two sides of the aromatic rings are identical. By the same rationale, such symmetry is not expected to be present when rotations are carried out along θ in compound **IIIa** and along θ and ϕ in compound **IVa**.

Figure 4 shows the PES obtained for compound **Ia**. This surface possesses eight clearly defined potential wells; however, the eight minima energy values obtained are degenerate, implying that we can have only identity and enantiomeric relationships, but not diastereoisomerism.

Observing Fig. 4, we can note that the pair of minima, located in one of the quadrants, is repeated four times in the full cycle of rotation. The pairs of minima are lying along the conrotatory mode of motion. Thus, we can classify the eight minima to two sets of four structures. In each set, the four structures are identical and the two sets imply an enantiomeric relationship.

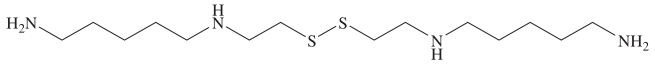


The -·-·-·-·- line symbolizes a mirror, which is called upon to indicate the enantiomeric relationship. The results obtained for compound **Ia** are identical to those reported earlier (12, 13).

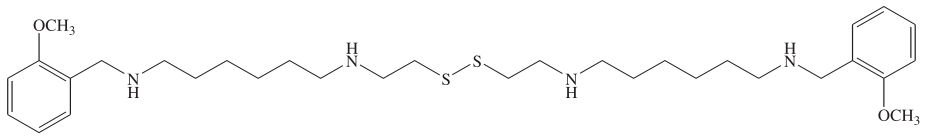
The conformational PES of **IIa** looks quite different from that of compound **Ia** (Fig. 4). Each of the four pairs of minima, together with their corresponding TS, collapsed to a single minimum. The result of such annihilation of critical points is that instead of eight only four minima are located on the conformational PES. The θ and ϕ values for these four

© 2005 NRC Canada

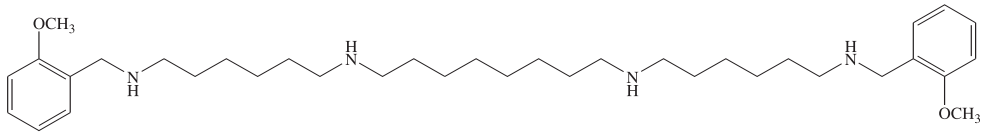
Fig. 2. Symmetrical ligands with a connecting flexible chain.



APC

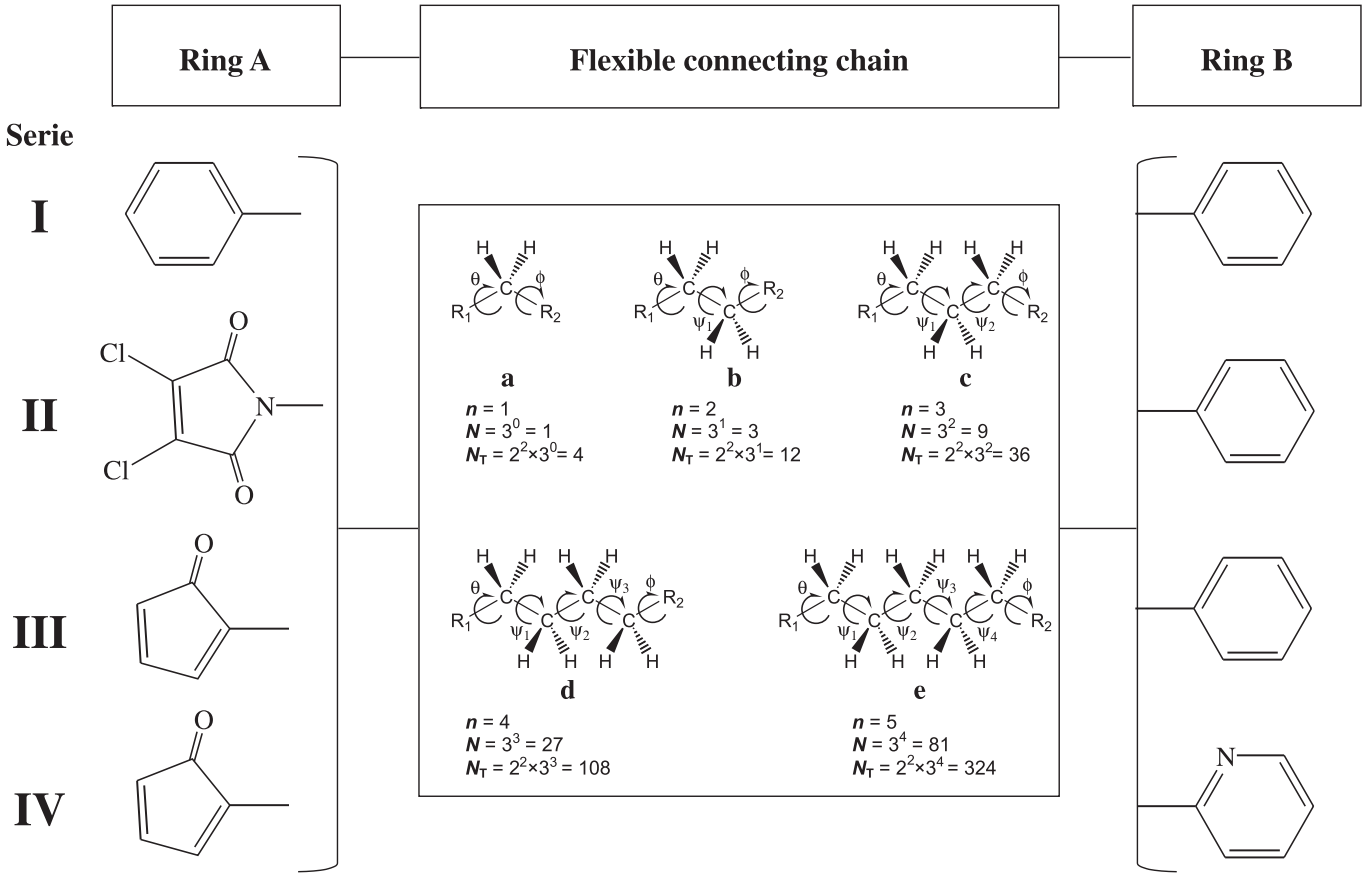


Benextramine



Melthoctramine

Fig. 3. General structural features of the four homologue series reported here. The torsional angles θ, ψ_1, ψ_2, ψ_3, ψ_4, ψ_5, and ϕ are also shown. n = number of methylenes; $N = 3^{(n-1)}$: number of backbone conformers without rotation about the θ and ϕ angles; $N_T = 2^2 \times 3^{(n-1)}$: total number of conformers.

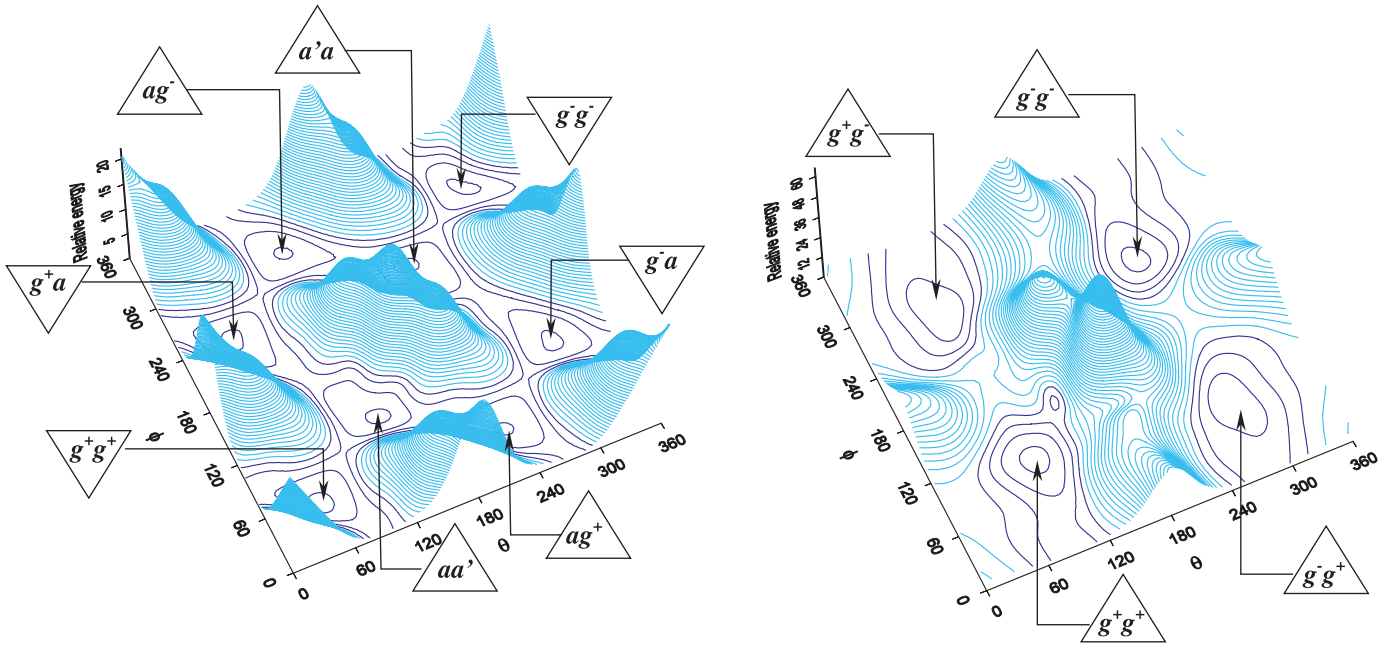


minima are close to the location of the annihilated TS, namely ±90°. Interestingly enough, the four minima are identical.

The PES obtained for compound **IIIa** (Fig. 5) displays six potential wells. It is interesting to note that the total energetic degeneracy observed in the above compounds is now removed. This implies that we now have a diastereoisomeric relationship as the result of axis chirality. The form g^+, g^+ is identical to g^+, g^-, whereas g^-, g^- is identical to g^-, g^+; in turn, a, g^+ is identical to a, g^-, which is 0.4 kcal/mol above

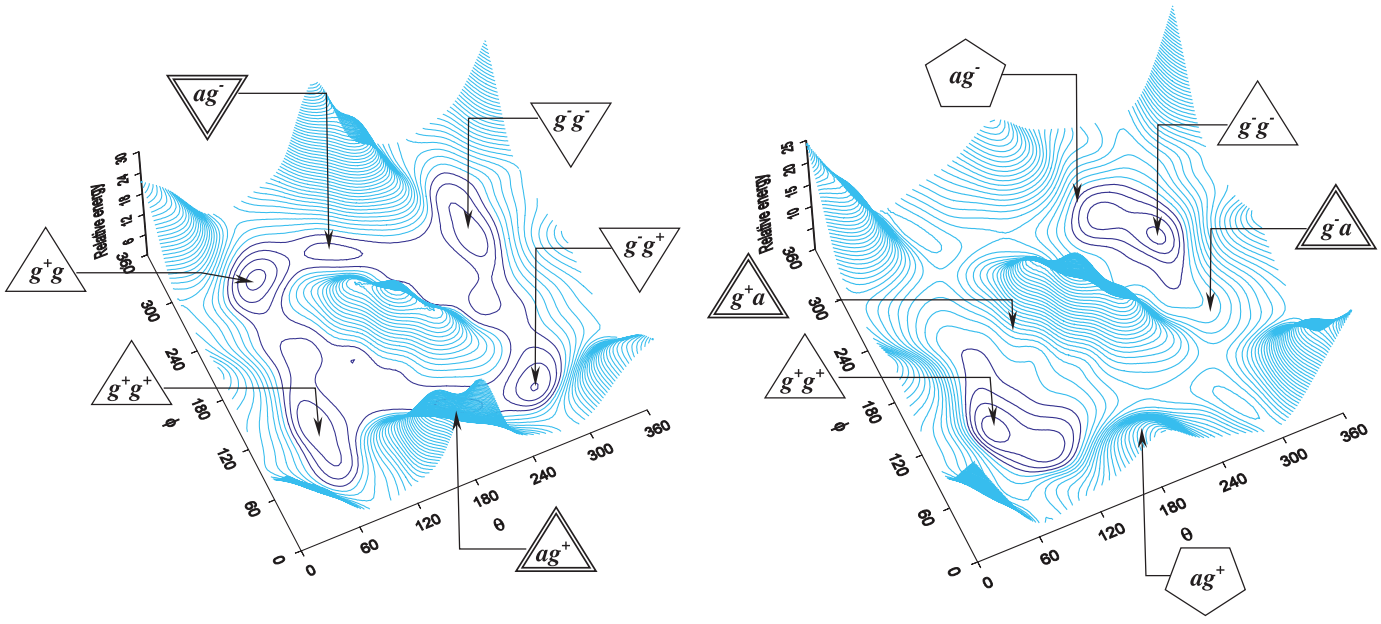
© 2005 NRC Canada

Fig. 4. Conformational PES obtained for compounds **Ia** and **IIa** from RHF/3-21G calculations. Full cycle of rotation (from 0° to 360°) for variables θ and ϕ.



Compound Ia **Compound IIa**

Fig. 5. Conformational PES obtained for compounds **IIIa** and **IVa** from RHF/3-21G calculations. Full cycle of rotation (from 0° to 360°) for variables θ and ϕ.



Compound IIIa **Compound IVa**

the global minima at the RHF/3-21G level. However, the global minimum varies as a function of the basis set or level of theory; g^+, g^+ at the RHF/3-21G and *a*, g^+ at the RHF/6-31G(d) and DFT levels (Table 1). From Fig. 5 and Table 1, it is easy to note that g^+, g^+ is the enantiomeric form of g^-, g^- and g^+, g^- is the enantiomeric form of g^-, g^+.

The PES obtained for compound **IVa** is shown in Fig. 5. This PES looks quite different from those obtained for compound **Ia**, showing six critical points that were confirmed at higher levels of theory. The global minimum at the three levels of theory reported here is the conformer g^+, g^+, which has a mirror image in the form g^-, g^-. Conformation *a*, g^+

© 2005 NRC Canada

Table 1. Torsional angles and relative energies obtained for the conformations of compounds **Ia**, **IIa**, **IIIa**, and **IVa** using RHF/3-21G, RHF/6-31G(d), and B3LYP/6-31G(d) calculations.

Compound	Basis set	Conformation	θ (°)	ϕ (°)	Energy gap (kcal/mol)
Ia	RHF/3-21G	g^+ g^+	57.65[a]	57.53[a]	
	RHF/6-31G(d)	g^+ g^+	58.30[a]	58.30[a]	
	B3LYP/6-31G(d)	g^+ g^+	58.31	61.26	
IIa	RHF/3-21G	g^+ g^+	86.64	89.08	
	RHF/6-31G(d)	g^+ g^+	87.64	89.95	
	B3LYP/6-31G(d)	g^+ g^+	87.87	89.38	
IIIa	RHF/3-21G	g^+ g^+	81.23	101.81	0.00
		a g^+	179.94	89.35	0.44
	RHF/6-31G(d)	g^+ g^+	80.59	93.72	0.62
		a g^+	–179.97	89.65	0.00
	B3LYP/6-31G(d)	g^+ g^+	82.85	100.94	0.13
		a g^+	179.99	89.35	0.00
IVa	RHF/3-21G	g^+ g^+	82.03	104.63	0.00
		a g^+	127.69	64.48	1.02
		g^+ a	71.04	–147.77	2.62
	RHF/6-31G(d)	g^+ g^+	83.55	91.80	0.00
		a g^+	Not found		
		g^+ a	70.51	–151.45	1.76
	B3LYP/6-31G(d)	g^+ g^+	83.15	97.95	0.00
		a g^+	120.16	69.77	0.42
		g^+ a	70.83	–149.41	1.65

Note: Energy gap (ZPE-corrected electronic energy difference).
[a]Data obtained from ref. 12.

possesses a mirror image in the form a, g^-, and is 1.02 and 0.42 kcal/mol above the global minimum at RHF/3-21G and DFT levels, respectively. This form is not a minimum at the RHF/6-31G(d) level of calculation. Conformation g^+, a was found at the three levels of theory and possesses a mirror image in the form g^-, a.

To avoid misleading terminology, from now on the term "different conformations" will be used only for different spatial orderings with different energies (the so-called diastereoisomers) without consideration of the mirror images. Thus, the enantiomeric forms will be considered "equivalent conformations". In summary, compounds **Ia** and **IIa** have only one conformation, whereas compounds **IIIa** and **IVa** display two and three different conformations, respectively.

Compounds Ib, IIb, IIIb, and IVb (n = 2)

In these compounds, the orientations of the ring systems are described by the dihedral angles θ and ϕ; whereas the orientations of the alkyl chain are described by the dihedral angle ψ_1. The multidimensional conformational analysis (MDCA) (15–17) predicts the existence of 2 × 3 × 2 = 12 legitimate minima for triple rotors with these multiplicities.

The three torsional angles (θ, ψ_1, ϕ) span a three-dimensional (i.e., 3D) conformational hyper surface. The PEHS is therefore labelled as a 3D-PEHS even though such a PEHS is, in fact, a four-dimensional where the dependent variable, the energy, is the fourth dimension. We, of course, may generate 2D cross-sections of this 3D-PEHS by singling out one torsional angle (for example, ψ_1).

The overall expression for the 3D-PEHS in which energy is the function of the three independent variables, can thus be partitioned into three 2D-PES of the type:

$$[1] \qquad E^{\psi_1 = g^+} = E(\theta, \phi)$$

$$[2] \qquad E^{\psi_1 = a} = E(\theta, \phi)$$

$$[3] \qquad E^{\psi_1 = g^-} = E(\theta, \phi)$$

where g^+ (gauche plus) ≅ 60°, a (anti) ≅ 180°, and g^- (gauche minus) ≅ 300°.

Each of the above equations represents a 2D-PES for compounds **Ib** and **IIb**. These surfaces are shown topologically in Fig. 6.

Using RHF/3-21G calculations, 12 forms were found. However, observing the results shown in Fig. 6, it is clear from the topology of the hyper surface $E = E(\theta, \psi_1, \phi)$ that the four minima obtained in each 2D-PES (eqs. [1]–[3]) are identical. Figure 7 illustrates this situation very well for eq. [2]. It is interesting to note that the four forms with ψ_1 in g^+ (eq. [1]) are equivalents (enantiomeric forms) to those with ψ_1 in g^- (eq. [3]). Thus, compounds **Ib** and **IIb** possess only two different spatial orderings: a folded conformation ("gauche") and an extended one ("anti"), which are shown in Fig. 8. These conformations were also obtained using RHF/6-31G(d) and DFT calculations (Table 2).

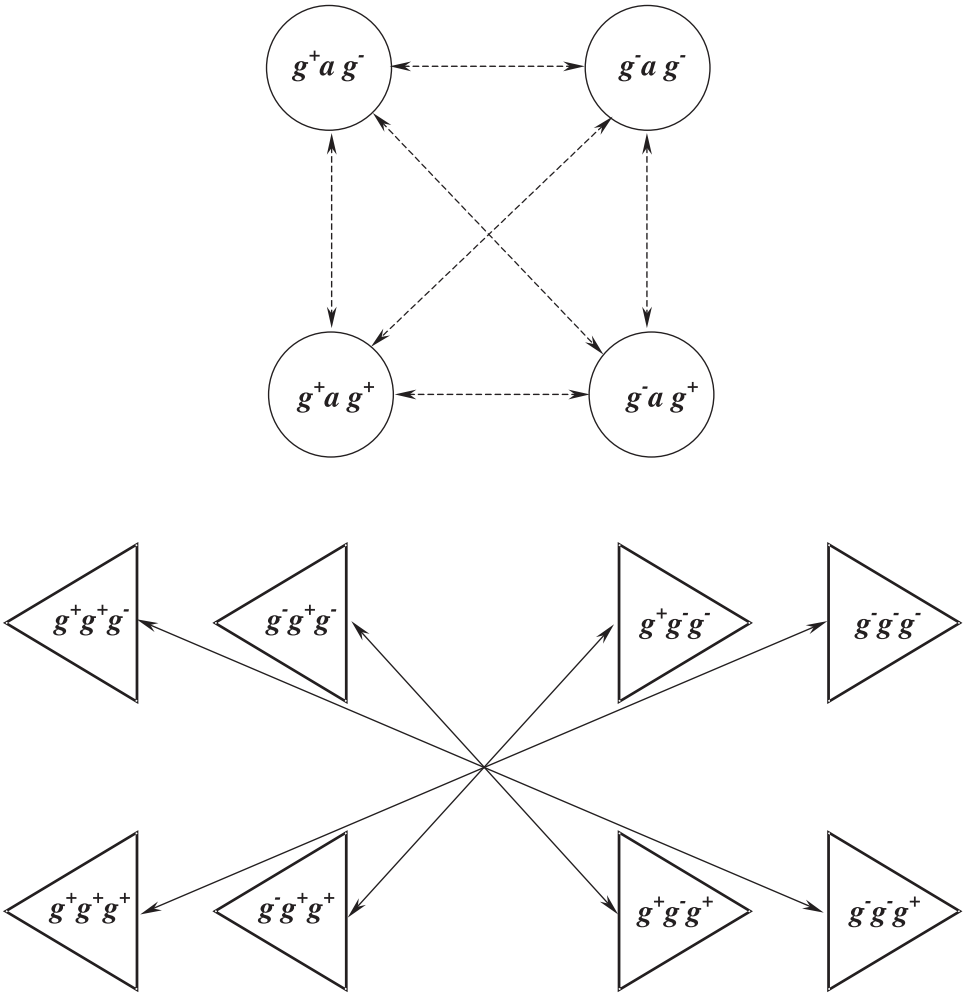
Compound **IIIb** possesses six different conformations as a function of the planar (pln), perpendicular (perp), or antiperpendicular (antp) position of the benzene ring (Table 2). Compound **IVb**, in turn, possesses 11 different conformations owing to the lack of symmetry between A and B rings (Table 2).

Compounds Ic, IIc, IIIc, and IVc (n = 3)

These compounds are, in principle, a quadruple rotor and therefore its conformational change is governed by four cir-

© 2005 NRC Canada

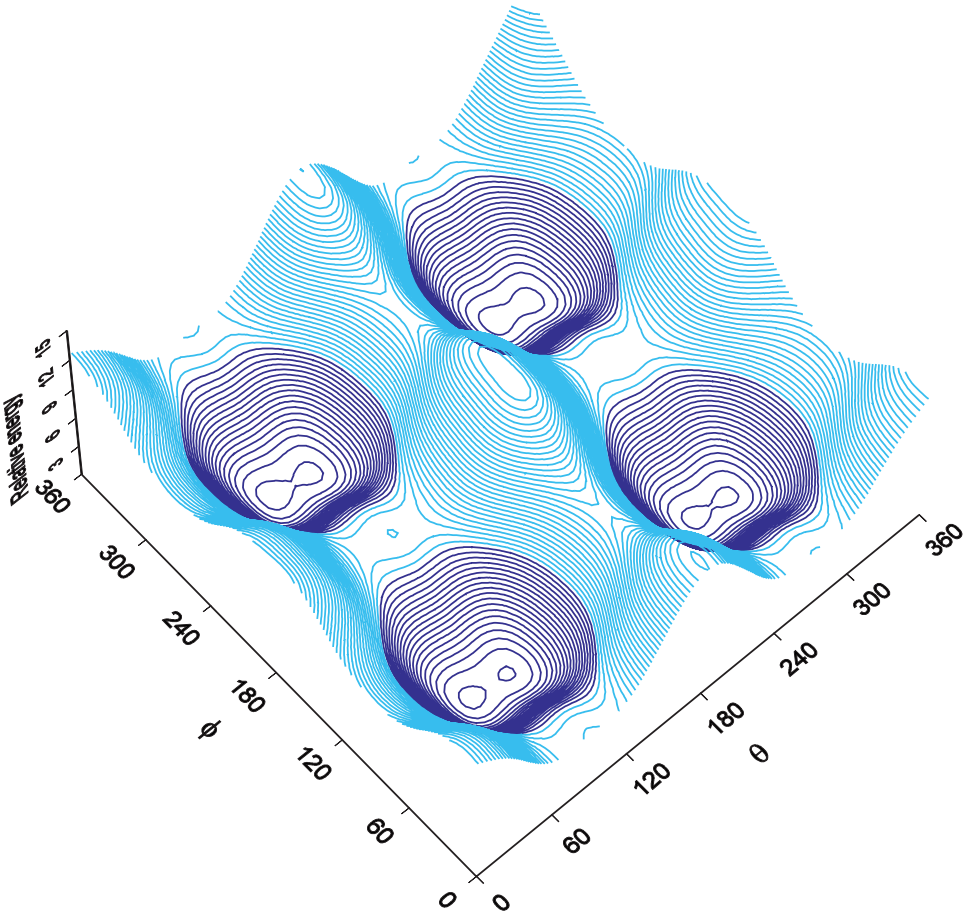
Fig. 6. Topological view for the three 2D-PESs represented in eqs. [1]–[3]. The enantiomeric conformers are shown with the same geometrical figure.



cular motions involving θ, ψ_1, ψ_2, and ϕ torsional angles. MDCA predicts the existence of 2 × 3 × 3 × 2 = 36 legitimate minima for a quadruple rotor with these multiplicities. Observing the results obtained for compounds **Ic**, **IIc**, and **IIIc** in Table 3, it is clear that the conformational intricacies of these compounds are mainly determined by two torsional angles (ψ_1 and ψ_2) instead of four dihedrals. In contrast to the idealized topology, instead of 36, only three different conformations were found for compound **Ic**. In principle, it appears to be nine conformations, however, fully relaxed computations indicate only three different conformations for this molecule. The topological features of the ψ_1 vs. ψ_2 surface is given in Fig. 9; these nine stable conformations, however, encompass only three unique conformers. The degenerate conformations (enantiomeric and identical forms) are denoted by circles and squares, in this figure. To categorize the different structures obtained for this compound, we introduced, intuitively rather than by a precise definition, three forms: fully folded (FF), partially folded (PF), and fully extended (FE). By the FF form,we mean a closed structure with relatively short distances between the aromatic rings. By the FE form, we mean a form with a linearized connecting chain. By PF, we denote a form intermediate between folded and extended (Fig. 8). The PES scanning ψ_1 vs. ψ_2 for compound **IIc** is shown in Fig. 10. In principle, it appears to be nine conformations, however, fully relaxed computations indicate only five different conformations for this molecule. The topological features of this surface is given in Fig. 9. It is interesting to note that RHF/3-21G calculations found six different conformations the last one being a conformation with the torsional angle ϕ in a planar form (g^+ *a* g^+ *a*) (Table 3). However, this conformation was not found at high levels of theory. Considering that the g^+ *a* g^+ *a* conformation only exists on the RHF/3-21G less accurate PES, it is reasonable to assume that this form is a very flat minimum on the hypersurface and at higher levels of calculation this minimum just disappears. Again, the global minimum varies as a function of the basis set or level of theory: FF (g^+ g^+ g^+ g^+) at RHF/3-21G and FE (g^+ *a* *a* g^+) at RHF/6-31G(d) and B3LYP/6-31G(d). It should be noted that the torsional angles obtained for the different conformations using different levels of theory are closely related suggesting that RHF/3-21G calculations are sufficient to use in a preliminary and exploratory form. However, RHF/6-31G(d) or DFT calculations appear to be necessary to confirm critical points and to assign conformational preferences. This is par-

© 2005 NRC Canada

Fig. 7. 2D-PES obtained for eq. [2] of compound **IIb**. Calculations were performed using RHF/3-21G computations.



Compound IIb *anti*

ticularly apparent considering that the number of conformations and the global minimum varies as a function of the basis set or level of theory.

RHF/3-21G calculations predict 13 and 20 different conformations for compounds **IIIc** and **IVc**, respectively. It is instructive to note that for these compounds several planar conformations for both aromatic rings are allowed (Table 3). This is a striking difference with respect to the above results suggesting that from now on the planar forms for the aromatic rings would be taken into account in the conformational analysis.

Compounds Id, IId, IIId, and IVd (n = 4)

These compounds are a quintuple rotor and therefore its conformational change is governed by five circular motions involving θ, ψ_1, ψ_2, ψ_3, and φ torsional angles. MDCA predicts the existence of 2 × 3 × 3 × 3 × 2 = 108 legitimate minima for a quintuple rotor with the above multiplicities. In the particular case of compounds **Id** and **IId**, the overall expression for the 5D-PEHS in which energy is the function of the five independent variables (θ, ψ_1, ψ_2, ψ_3, and φ), can be partitioned into three 2D-PES keeping θ and φ ≅90°. In contrast, this is not the case of compounds **IIId** and **IVd**, where the torsional angles θ and φ can adopt planar forms. Instead of 108, only seven different conformations were found for compound **Id**, one of them possessing the torsional angle θ at about 180° (Table 4).

Figure 8 gives the spatial view for the seven different conformations obtained for compound **Id**. The following types of structures were found:

(1) Fully extended (FE) structures with three torsional angles (ψ_1–ψ_3) in anti (≅ ± 180°).
(2) Open extended (OE) structures with one torsional angle in gauche (≅ ± 60°) and two in anti.
(3) Open folded (OF) structures with two torsional angles in gauche and one in anti.
(4) Fully folded (FF) structures with the three torsional angles in gauche.

Figure 11 gives the topological features obtained for the respective PESs (eqs. [4]–[6]) of compound **IId**.

[4] $E^{\psi_2 = g^+} = E(\psi_1, \psi_3)$

[5] $E^{\psi_2 = a} = E(\psi_1, \psi_3)$

[6] $E^{\psi_2 = g^-} = E(\psi_1, \psi_3)$

The 25 stable conformations encompass only 13 unique conformers. The energetically degenerated conformations (identical and enantiomeric forms) are denoted by double arrows and with the same notation. Figure 12 shows the PES ob-

© 2005 NRC Canada

Fig. 8. Spatial view of the different conformations obtained for compounds **Ib**, **Ic**, and **Id** (geometries were obtained from RHF/3-21G calculations).

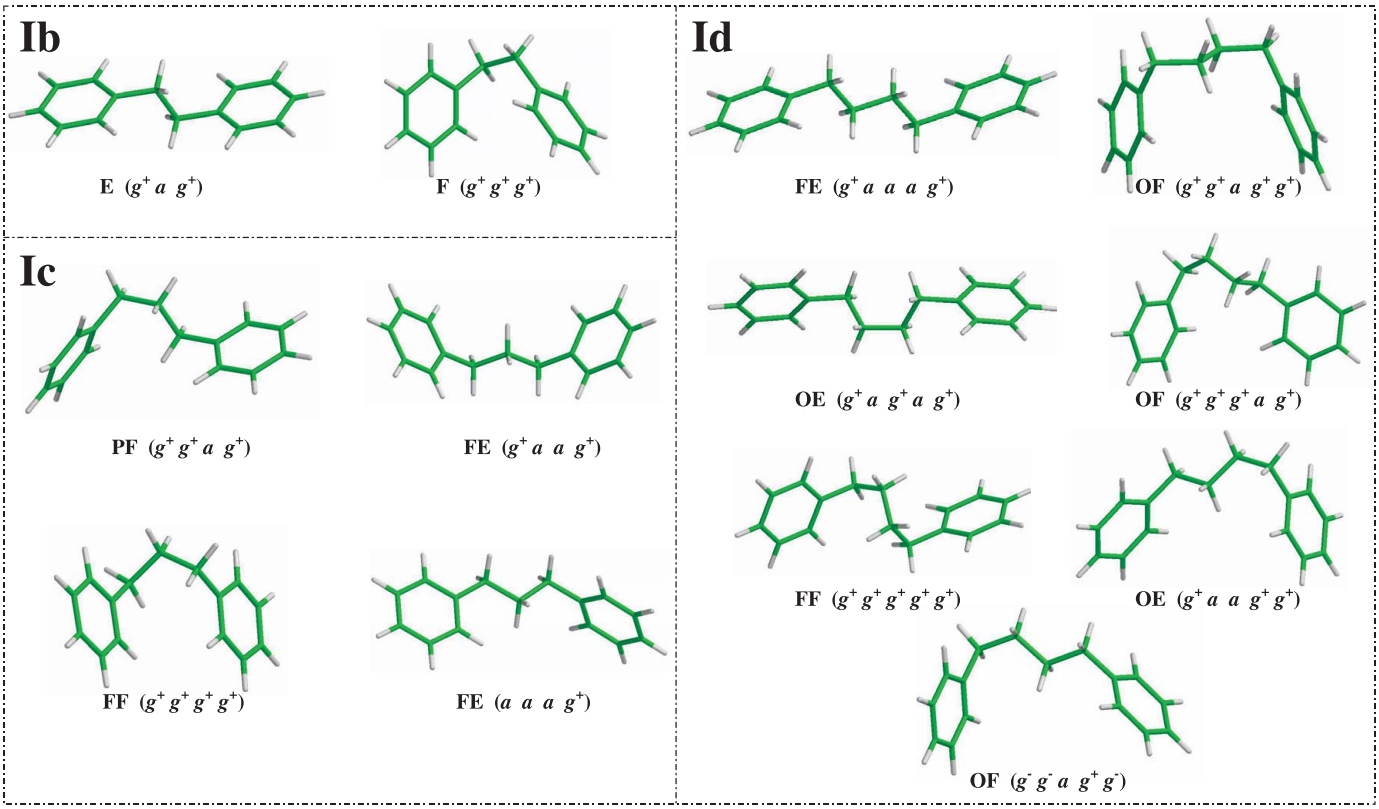


Table 2. Torsional angles and relative energies obtained for the conformations of compounds **Ib**, **IIb**, **IIIb**, and **IVb** using RHF/3-21G calculations.

Compound	Basis set	Conformation	θ (°)	ψ_1 (°)	ϕ (°)	Energy gap (kcal/mol)
Ib	RHF/3-21G	g^+ *a* g^+	89.17	179.97	88.83	0.00
		g^+ g^+ g^+	83.20	69.97	83.15	0.63
IIb	RHF/3-21G	g^+ *a* g^+	80.64	180.36	89.40	0.00
		g^+ g^+ g^+	57.87	53.61	75.11	0.26
	RHF/6-31G(d)	g^+ *a* g^+	88.88	180.02	89.20	0.00
		g^+ g^+ g^+	67.90	55.60	72.90	0.91
	B3LYP/6-31G(d)	g^+ *a* g^+	88.56	180.05	89.08	0.00
		g^+ g^+ g^+	66.27	56.88	74.15	0.73
IIIb	RHF/3-21G	g^+ *a* g^+	65.90	–178.76	88.03	0.00
		g^+ g^+ g^+	65.96	66.83	79.94	0.43
		g^- g^+ g^+	–105.20	62.23	79.49	2.41
		g^- g^+ g^+	–116.15	60.83	27.18	2.89
		a a g^+	0.00	180.00	89.07	3.47
		a a a	–0.02	179.89	0.01	6.03
IVb	RHF/3-21G	g^+ g^+ g^+	65.55	66.42	52.59	0.00
		g^+ *a* g^-	64.41	177.83	–59.51	0.22
		a g^+ g^-	174.59	72.18	–105.73	1.04
		g^+ g^+ g^-	60.56	62.56	–91.49	1.86
		a a g+	–173.32	–177.52	62.85	2.07
		a g^+ g^+	161.52	73.33	43.67	2.22
		g^- g^+ g^+	–98.96	67.23	71.45	2.65
		g^- g^+ *a*	–117.56	63.48	–161.44	2.72
		g^- g^+ g^-	–94.20	65.18	–91.90	3.24
		a g^+ *a*	–126.83	64.67	5.01	3.31
		a a a	–179.90	179.74	–178.94	4.10

Note: For compound **IIb**, RHF/6-31G(d) and B3LYP/6-31G(d) computations are also included.

© 2005 NRC Canada

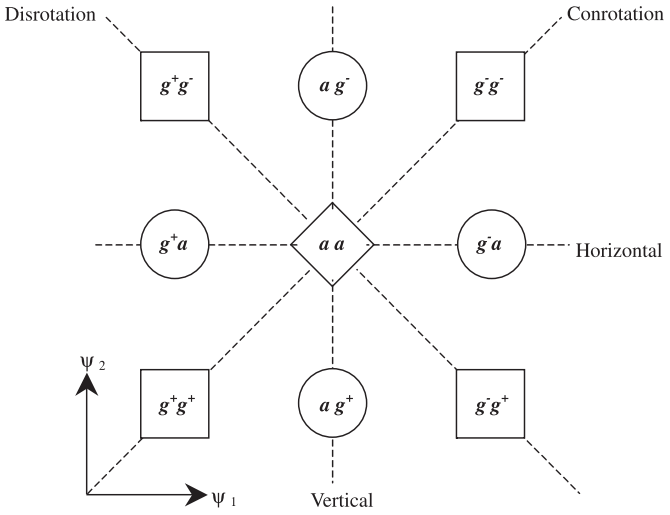
Table 3. Torsional angles and relative energies obtained for the conformations of compounds **Ic**, **IIc**, **IIIc**, and **IVc** using RHF/3-21G calculations.

Compound	Basis set	Conformation	θ (°)	ψ_1 (°)	ψ_2 (°)	ϕ (°)	Energy gap (kcal/mol)
Ic	RHF/3-21G	$g^+ g^+ a g^+$	74.90	65.81	–179.51	88.92	0.00
		$g^+ a a g^+$	89.08	180.00	180.00	89.01	0.13
		$g^+ g^+ g^+ g^+$	66.37	65.87	65.85	66.35	0.32
		$a a a g^+$	175.40	–178.64	–179.70	89.11	2.10
IIc	RHF/3-21G	$g^+ g^+ g^+ g^+$	73.99	71.79	74.34	83.25	0.00
		$g^+ g^+ g^- g^+$	64.68	65.96	–73.81	121.83	1.58
		$g^+ a a g^+$	93.97	179.81	179.98	88.27	1.76
		$g^+ a g^+ g^+$	104.26	177.27	62.86	72.53	1.78
		$g^+ g^+ a g^+$	69.42	60.29	176.24	85.22	1.81
		$g^+ a g^+ a$	71.56	–170.57	64.99	–162.10	2.22
	RHF/6-31G(d)	$g^+ g^+ g^+ g^+$	78.77	74.43	74.22	77.54	0.94
		$g^+ g^+ g^- g^+$	69.70	74.64	–74.91	123.62	1.22
		$g^+ a a g^+$	88.65	–179.98	–179.99	89.18	0.00
		$g^+ a g^+ g^+$	90.41	175.78	62.69	70.94	0.61
		$g^+ g^+ a g^+$	79.65	63.32	176.73	85.72	0.67
		$g^+ a g^+ a$	Not found				
	B3LYP/6-31G(d)	$g^+ g^+ g^+ g^+$	77.40	73.76	73.66	81.28	0.22
		$g^+ g^+ g^- g^+$	70.08	65.11	–74.4	122.10	1.05
		$g^+ a a g^+$	88.76	–179.99	–179.99	88.92	0.00
		$g^+ a g^+ g^+$	91.28	176.97	62.88	71.20	0.43
		$g^+ g^+ a g^+$	79.59	63.17	176.73	85.87	0.42
		$g^+ a g^+ a$	Not found				
IIIc	RHF/3-21G	$g^- g^+ g^+ g^+$	–88.00	78.78	71.68	80.26	0.00
		$g^+ g^+ g^+ g^+$	71.74	66.41	65.01	70.44	0.87
		$g^- a g^+ g^+$	–67.31	179.09	64.97	74.43	0.89
		$g^+ g^+ a g^+$	65.13	65.38	179.21	85.09	1.05
		$g^+ a a g^-$	68.52	–178.27	–179.78	–85.08	1.13
		$g^+ a g^+ g^+$	66.32	–169.24	65.00	20.49	1.31
		$g^+ a g^+ g^+$	63.65	177.49	62.43	70.16	1.44
		$g^+ g^- a g^+$	93.53	–59.82	–174.53	90.25	1.79
		$a a a g^+$	–179.79	–179.94	–179.96	88.88	2.06
		$a a g^+ g^+$	–174.79	179.17	66.40	76.35	2.36
		$g^+ g^+ g^- g^-$	56.91	75.15	–70.22	–58.00	4.09
		$g^+ g^- g^+ g^+$	94.54	–62.84	95.03	58.58	4.22
		$a a a a$	179.91	179.97	179.90	–179.63	4.40
IVc	RHF/3-21G	$g^+ g^+ g^+ g^-$	85.19	65.07	64.14	–92.02	0.00
		$g^- g^+ g^+ g^+$	–87.48	77.23	71.88	73.53	0.03
		$g^+ g^+ g^+ g^+$	64.98	63.14	63.68	49.27	1.25
		$a g^+ a g^+$	–178.10	71.57	–152.08	64.67	1.46
		$g^+ a g^+ a$	67.30	–168.49	67.94	–166.26	1.51
		$g^+ a g^- g^+$	65.34	178.09	–71.76	85.64	1.63
		$g^+ g^+ a g^-$	65.45	65.03	175.61	–69.23	1.71
		$g^+ a a g^+$	69.32	–178.39	–176.43	71.01	1.83
		$g^+ a g^+ g^-$	64.56	178.75	66.31	–93.28	1.91
		$g^+ g^+ a g^+$	69.05	67.78	–177.50	67.83	2.26
		$g^- g^+ a g^+$	–93.66	57.98	175.86	61.48	2.45
		$g^- g^+ a g^-$	–91.97	62.67	172.41	–57.58	2.52
		$g^- a a g^+$	–69.81	–179.97	–178.18	66.16	2.52
		$g^+ a g^+ g^+$	69.14	177.73	68.08	63.15	2.53
		$a a g^+ g^+$	–172.07	–179.84	68.29	58.01	2.58
		$a a a g^+$	174.66	179.73	–177.31	61.08	2.80
		$a a g^- g^+$	178.45	178.00	–71.25	86.92	3.33
		$a g^+ g^+ g^-$	–134.17	58.03	58.34	–87.59	3.91
		$a g^+ g^+ g^-$	–166.58	73.70	73.44	–85.69	3.92
		$a a a a$	179.97	180.00	179.95	–179.81	5.17

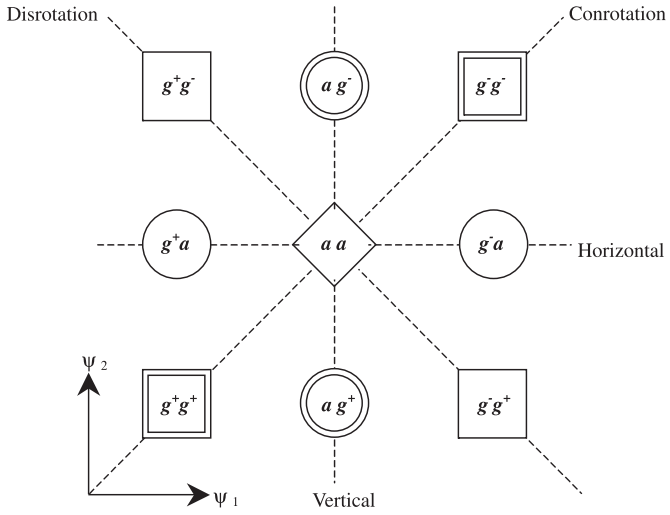
Note: For compound **IIc**, RHF/6-31G(d) and B3LYP/6-31G(d) computations are also included.

© 2005 NRC Canada

Fig. 9. Topological view of the 2D-PESs (ψ_1 vs. ψ_2) for compounds **Ic** and **IIc** keeping θ and ϕ in ±90°. Enantiomeric and identical forms are denoted with the same geometrical figure.



Compound Ic



Compound IIc

tained for eq. [5] using RHF/3-21G calculations; the symmetry of this surface might be appreciated in this figure.

In addition to the 13 conformations with torsional angles θ and ϕ in perpendicular or antiperpendicular form, another conformation with ϕ = 164.6° (quasi-planar) was found (Table 4).

The 14 different conformations attained for compound **IId** from RHF/3-21G computations were also obtained using RHF/6-31G(d) and DFT calculations. Whereas for RHF/3-21G calculations, the global minimum is the $g^+\ g^+\ g^+\ a\ g^-$ conformation, for RHF/6-31G(d) and DFT calculations, the preferred form is the $g^+\ a\ a\ a\ g^+$ (Table 4).

Compound **IIId** possess 32 different conformations from RHF/3-21G calculations. Obviously, the conformational behaviour of compound **IVd** is even more complex considering the lack of symmetry of ring B. Thus, 59 different conformations were obtained for this compound from RHF/3-21G calculations.

Compounds Ie and IIe (n = 5)

These compounds are a sextuple rotor and therefore its conformational change is governed by six circular motions involving θ, ψ_1, ψ_2, ψ_3, ψ_4, and ϕ torsional angles. MDCA predicts the existence of $2 \times 3 \times 3 \times 3 \times 3 \times 2 = 324$ minima for a sextuple rotor with these multiplicities. RHF/3-21G calculations found 14 and 37 different conformations for compounds **Ie** and **IIe**, respectively (Table 5).

Since the PEHS of large and flexible homologues is highly multidimensional, it is not an easy task to explore all possibilities from ab initio calculations. Thus, we cannot be absolutely sure that the conformations reported here are the only possible structures for these compounds. This is particularly apparent considering that the criterion chosen to obtain the starting geometries was that postulated by MDCA. It is instructive to note that MDCA is not a fool-proof strategy (18). However, to ameliorate such situations we have performed additional calculations considering, for example, different planar forms for the aromatic ring systems. Thus, we have carried out sufficient calculations to feel confident that the results reported here possess an adequate degree of accuracy.

At this stage of our work, some observations can be made with respect to the conformational intricacies of compounds reported here. Table 5 shows the conformations predicted by MDCA and also those obtained from RHF/3-21G calculations (denoted in italics). Figure 13 gives a graphic representation of the values shown in Table 5. This figure shows the increasing complexity of conformational space as a function of the lengthening of the saturated carbon connecting chain for the different series reported here.

What about the large-size homologues?

Our results indicate that conformationally restricted retrograde or quasi-retrograde molecules (n = 1) have only one structure; small-size compounds have an enumerable number of conformers. However, nobody can make even an "educated guess" how many conformers might be associated with a medium- or large-size flexible twin drug ($n = 5 - n$) taking into account redundancy owing to symmetry. We have not performed ab initio calculations for large-size homologues, therefore it is not yet possible to do more than speculate.

Let us first consider the case of MDCA. This approach predicts the possible total number of different conformations (f) using a general equation that might be expressed as:

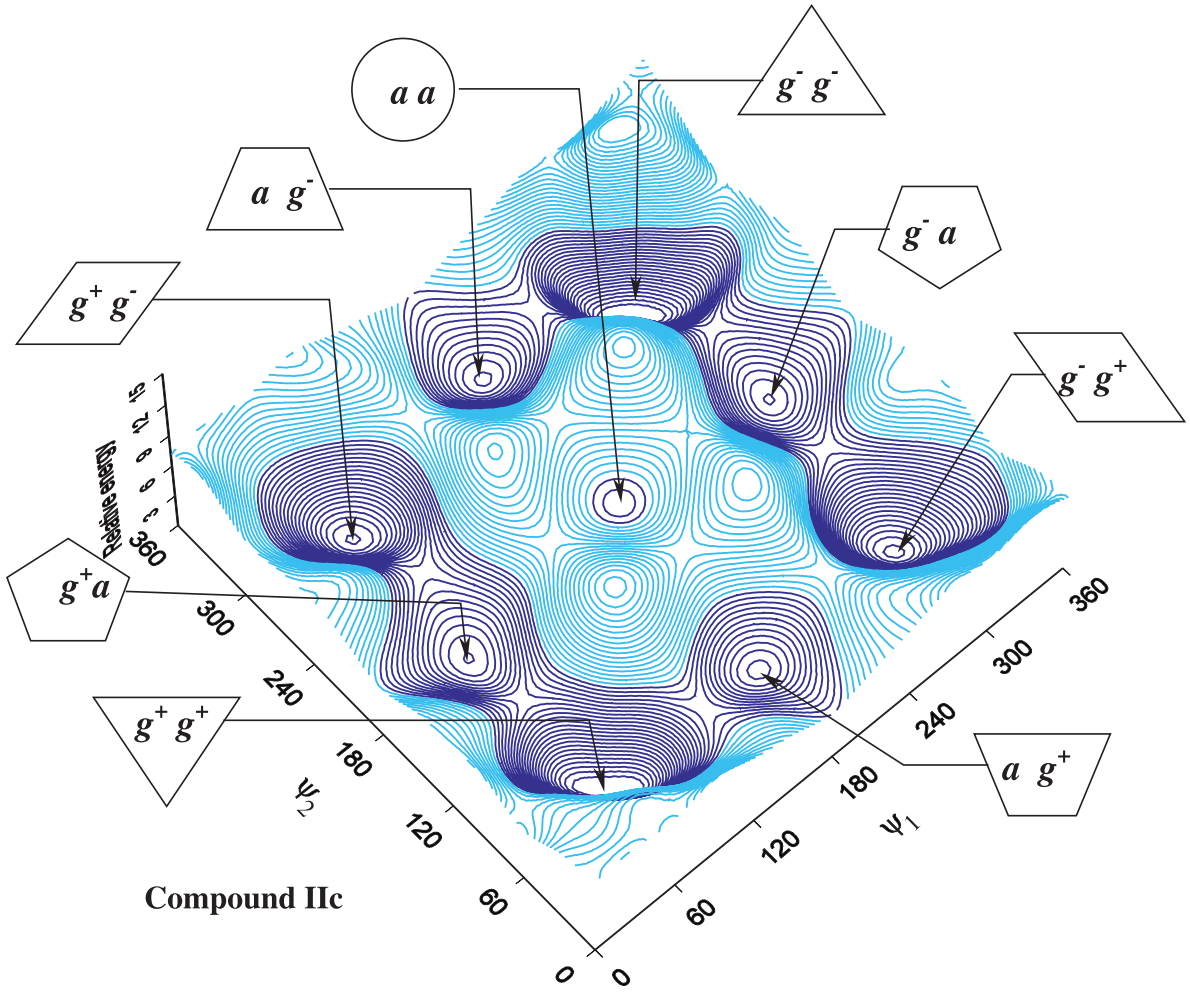
$$[7] \qquad N_T = 2^2 \times 3^{(n-1)}$$

where $N_T = f$ (total number of different conformations) and numbers 2 and 3 are due to the sp^2 and sp^3 torsional modes, respectively (see Fig. 3).

In the case of series **I–IV**, we may assume that the total number of different conformers ($f(n)$) of these compounds

© 2005 NRC Canada

Fig. 10. PES obtained for compound **IIc** varying ψ_1 vs. ψ_2. Computations were performed using RHF/3-21G calculations. Enantiomeric forms are denoted with the same geometrical figure.



follows a similar behaviour to that given in eq. [7]. Thus, we can obtain a general equation as follows:

$$[8] \qquad f_{\mathrm{MDCA}} = \alpha 3^{\beta(n-1)}$$

However, in this case, both constants α and β loose the significance given by MDCA and therefore, they only play a mathematical role, adjusting in a convenient way the corresponding function with the calculated $f(n)$ values in each series. Thus, it would be possible to compare the respective equations of each series with eq. [8].

The potential number of different conformations $f(n)$ for the different series may be adjusted using a linear-regression equation such that:

$$[9] \qquad \log_{10} f(n) = (\log_{10} \alpha - \beta \log_{10} 3) + (\beta \log_{10} 3)n$$

Equation [9] may be summarized in the following form:

$$[10] \qquad \log_{10} f(n) = A + B \times n$$

It is necessary to adjust A and B to obtain the corresponding α and β constants. These results are shown in Table 6 where in the last column the correlation coefficients (r) are also given.

The small value obtained for β in the series **I** is a direct consequence of the slight increase of $f(n)$ in **I** with respect to the other series reported here.

On the basis of results shown in Table 6, it is possible now to predict the possible total number of different conformations ($f(n)$) for any homologue of each series. Thus, Table 5 gives the number of $f(n)$ obtained from RHF/3-21G calculations (grey zone), and the predicted number of $f(n)$ (white zone) for the four series.

Figure 13 gives a graphic representation of the values shown in Table 5. The increasing complexity of the conformational space as a function of the lengthening of the saturated carbon connecting chain from $n = 1$ to $n = 10$ might be appreciated in this figure. It is clear, however, that the symmetry reduces notably the conformational possibilities in series **I** and **II**; this is particularly apparent in the case of identical twin compounds (series **I**).

Table 7 gives the percentage relative differences obtained for the calculated values of $f(n)$. These values were obtained from eq. [11]

$$[11] \qquad \Delta\% = [|f_{\mathrm{eq.[8]}}(n) - f(n)| \,/\, f(n)]100$$

where $f_{\mathrm{eq.[8]}}(n)$ is obtained from eq. [8] and $f(n)$ is obtained from the RHF/3-21G calculations.

© 2005 NRC Canada

Table 4. Torsional angles and relative energies obtained for the conformations of compounds **Id** and **IId** using RHF/3-21G calculations.

Compound	Basis set	Conformation	θ (°)	ψ_1 (°)	ψ_2 (°)	ψ_3 (°)	ϕ (°)	Energy gap (kcal/mol)
Id	RHF/3-21G	$g^+ a a a g^+$	89.01	180.00	–179.96	–179.99	88.69	0.00
		$g^+ a a g^+ g^+$	91.68	–179.32	–179.45	67.09	76.59	0.26
		$g^- g^- a g^+ g^-$	–75.12	–65.89	–179.98	65.90	–104.36	0.42
		$g^+ g^+ a g^+ g^+$	72.79	64.75	178.07	64.65	72.69	0.63
		$g^+ a g^+ a g^+$	89.93	177.57	68.74	177.57	89.45	0.72
		$g^+ g^+ g^+ a g^+$	71.14	60.82	66.86	177.88	80.79	1.01
		$g^+ g^+ g^+ g^+ g^+$	74.32	64.07	69.38	63.89	74.44	1.20
IId	RHF/3-21G	$g^+ g^+ g^+ a g^-$	77.18	59.20	65.63	–176.63	–89.12	0.00
		$g^+ a g^+ g^+ g^-$	89.78	–170.39	72.14	65.90	–95.04	0.72
		$g^+ g^+ g^+ g^+ g^-$	72.26	58.32	61.33	56.52	–114.64	1.04
		$g^+ g^+ a g^- g^+$	69.73	61.11	176.45	–65.68	105.12	1.52
		$g^+ a a a g^+$	89.71	180.00	–179.97	179.98	88.77	1.53
		$g^+ a a g^+ g^+$	74.14	179.71	178.78	64.90	74.97	1.73
		$g^+ g^+ a a g^+$	67.63	60.36	176.47	178.65	87.57	1.74
		$g^+ g^+ a g^+ g^+$	73.75	63.76	178.02	66.78	76.37	1.92
		$g^+ a g^+ a g^-$	102.04	178.36	69.28	177.40	–88.62	2.36
		$g^+ g^- g^+ a g^-$	98.10	–64.86	90.48	–175.42	–102.58	2.42
		$g^+ a g^+ g^- g^-$	75.05	–173.81	85.17	–73.86	–81.00	2.57
		$g^+ g^- g^- g^+ g^-$	101.34	–69.91	–98.89	56.18	–117.65	3.06
		$g^+ a a a a$	79.08	179.02	179.75	–179.85	164.63	3.86
		$g^+ g^- g^+ g^+ g^-$	109.87	–89.53	74.14	63.00	–108.81	4.82
	RHF/6-31G(d)	$g^+ g^+ g^+ a g^-$	80.23	63.53	68.26	179.26	–89.18	0.83
		$g^+ a g^+ g^+ g^-$	93.23	–177.13	71.51	65.90	–99.14	1.29
		$g^+ g^+ g^+ g^+ g^-$	78.23	63.03	65.66	60.27	–112.03	1.70
		$g^+ g^+ a g^- g^+$	79.38	63.57	178.06	–65.65	106.52	1.05
		$g^+ a a a g^+$	88.91	180.00	179.99	180.00	89.40	0.00
		$g^+ a a g^+ g^+$	84.92	179.95	177.32	64.54	73.83	0.68
		$g^+ g^+ a a g^+$	77.73	62.60	176.77	178.87	87.29	0.82
		$g^+ g^+ a g^+ g^+$	81.71	66.23	177.41	66.75	74.99	1.30
		$g^+ a g^+ a g^-$	90.37	176.65	67.21	175.85	–89.18	1.19
		$g^+ g^- g^+ a g^-$	103.81	–67.52	87.68	179.90	–96.53	2.88
		$g^+ a g^+ g^- g^-$	87.68	175.61	79.12	–71.51	–68.20	2.45
		$g^+ g^- g^- g^+ g^-$	105.56	–71.55	–97.91	59.57	–109.22	3.56
		$g^+ a a a a$	88.96	179.99	–179.90	–179.54	–1.76	1.89
		$g^+ g^- g^+ g^+ g^-$	107.36	–59.90	95.40	68.53	–102.61	3.82
	B3LYP/6-31G(d)	$g^+ g^+ g^+ a g^-$	80.63	62.26	66.28	–179.00	–90.00	0.16
		$g^+ a g^+ g^+ g^-$	93.57	–173.61	71.27	65.70	–95.11	0.63
		$g^+ g^+ g^+ g^+ g^-$	78.85	61.94	64.33	60.24	–111.74	0.93
		$g^+ g^+ a g^- g^+$	80.96	62.48	176.46	–65.76	104.98	0.66
		$g^+ a a a g^+$	88.63	180.00	180.00	180.00	89.07	0.00
		$g^+ a a g^+ g^+$	85.23	–179.71	179.56	65.07	73.34	0.49
		$g^+ g^+ a a g^+$	77.12	61.90	177.50	178.69	87.01	0.58
		$g^+ g^+ a g^+ g^+$	83.67	66.29	178.15	65.99	75.67	0.90
		$g^+ a g^+ a g^-$	91.12	176.85	66.07	176.11	–90.44	0.97
		$g^+ g^- g^+ a g^-$	101.24	–68.08	86.43	–178.15	–96.15	2.15
		$g^+ a g^+ g^- g^-$	86.91	177.38	75.73	–72.54	–67.71	1.80
		$g^+ g^- g^- g^+ g^-$	103.06	–71.97	–95.01	58.85	–109.98	2.71
		$g^+ a a a a$	88.48	–179.96	–179.91	–179.50	–1.82	1.53
		$g^+ g^- g^+ g^+ g^-$	105.98	–59.05	93.20	67.41	–99.35	2.82

Note: For compound **IId**, RHF/6-31G(d) and B3LYP/6-31G(d) computations are also included.

It is interesting to note that $f(n)$ functions displayed bigger differences for $n = 1$ and 2 with respect to $n = 3$–5. It appears that there is more difficult to simulate the conformational intricacies of torsional angles θ and ϕ than those of the connecting flexible chain. On the other hand, it is clear that more ab initio calculations performed on medium- and large-size homologues will help us to obtain more accurate predictive equations.

There exists the possibility that eq. [8] itself is perhaps inappropriate for obtaining the total number of different conformations in the series reported here. If, however, this equation is correct in postulating the above conformations,

© 2005 NRC Canada

Fig. 11. Topological view of the three 2D-PES (eqs. [4]–[6]) of compound **IId**. The enantiomeric forms are denoted with the same geometrical figure.

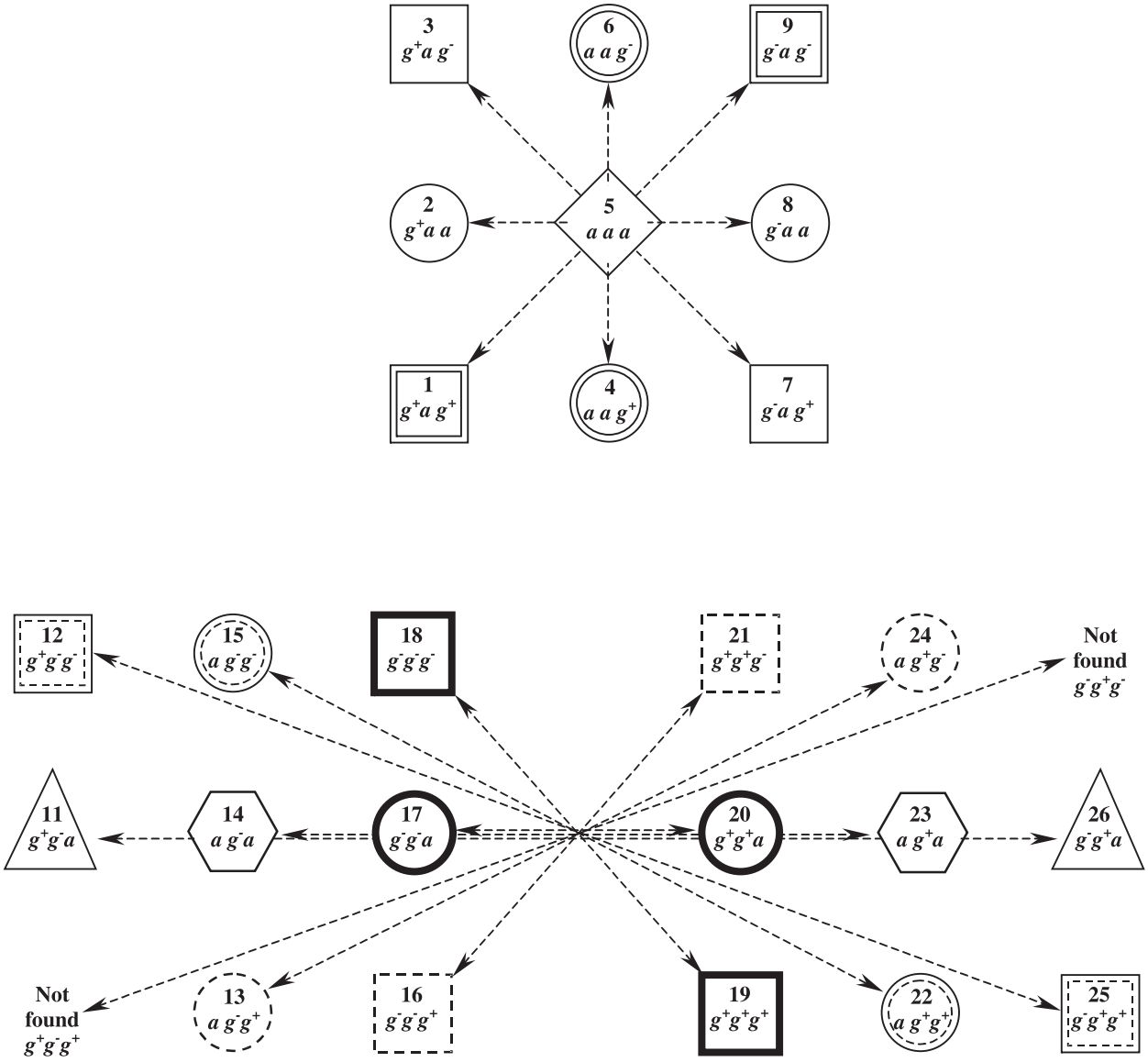


Table 5. Predicted number of $f(n)$ for the four series from n = 1–10.

n	1	2	3	4	5	6	7	8	9	10	20	50
$f_{MDCA}(n)$	**4**	**12**	**36**	**108**	**324**	**972**	**2916**	**8748**	**26 244**	**78 732**	**4.65×10^{9}**	**9.57×10^{23}**
$f_{I}(n)$	*1*	*2*	*3*	*7*	*11*	21	38	70	129	235	99 698	7.60×10^{12}
$f_{II}(n)$	*1*	*2*	*6*	*14*	*37*	90	225	562	1 405	3 514	3.37×10^{7}	2.96×10^{19}
$f_{III}(n)$	*2*	*6*	*13*	*32*	81	201	497	1230	3 047	7 549	6.56×10^{7}	4.32×10^{19}
$f_{IV}(n)$	*3*	*11*	*20*	*59*	152	395	1026	2661	6 904	17 914	2.47×10^{8}	6.55×10^{20}

Note: RHF/3-21G calculations were performed in the zone denoted in italics; the rest of the values were obtained from eq. [8]. MDCA values are shown in bold.

we can obtain the possible number of different conformations of any large homologue in each series. For example, eq. [8] predicts about 99 698 different conformations for $\mathbf{I}_{n=20}$ and the amazing number of 7.60×10^{12} different conformations for homologue $\mathbf{I}_{n=50}$.

It is clear that eq. [8] is highly speculative, therefore further calculations to confirm its validity are necessary. However, accepting the validity of this equation, we may form at least a superficial idea about the conformational possibilities of large-size homologues possessing symmetrical or non-symmetrical aromatic rings.

Conclusions

The presence of two symmetrical rings (identical or not) reduces notably the conformational possibilities of flexible

© 2005 NRC Canada

Fig. 12. 2D-PES obtained for eq. [5] of compound **IId** from RHF/3-21G calculations. Enantiomeric forms are denoted with the same geometrical figure.

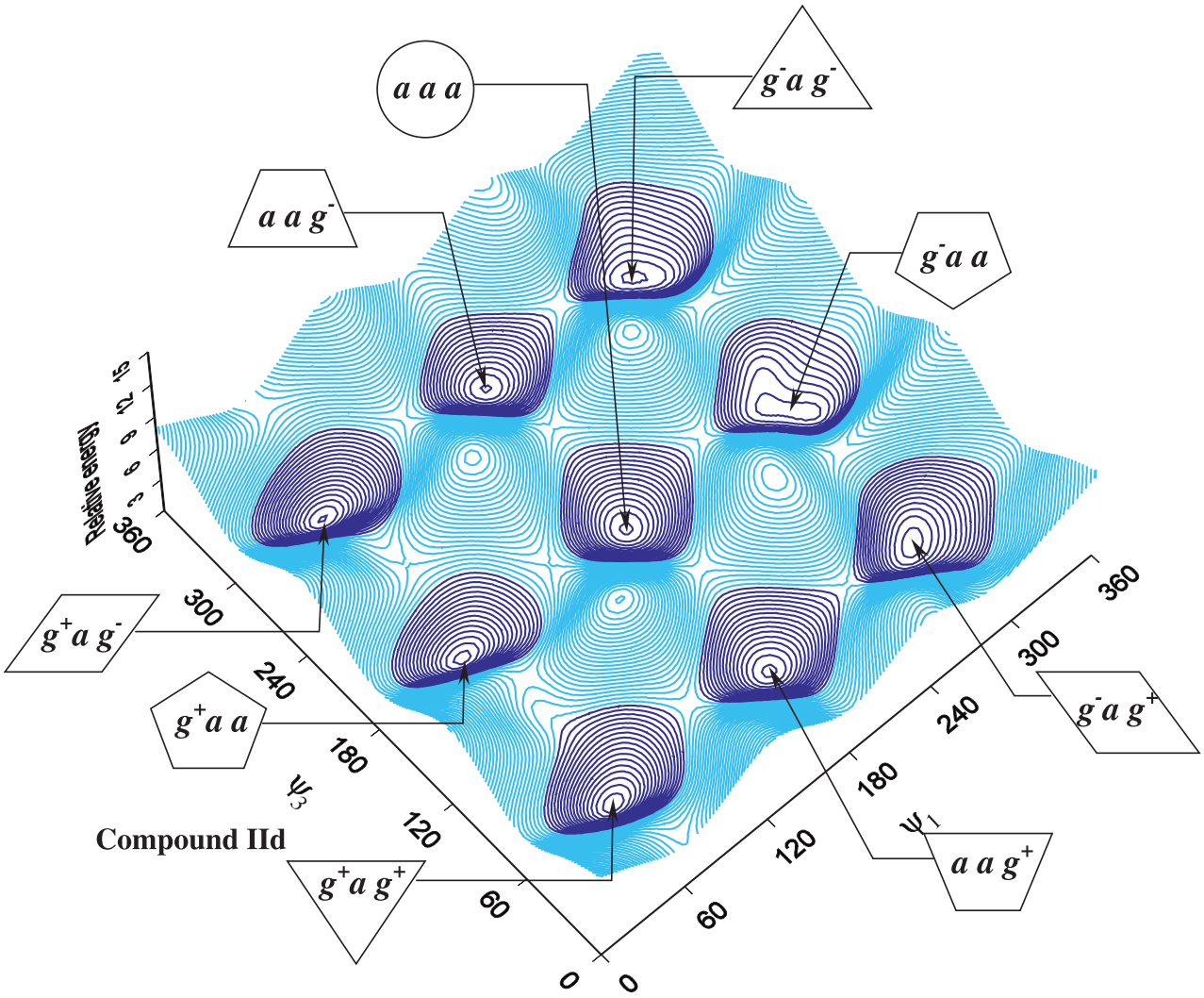


Table 6. Different values obtained for constants *A*, *B*, α and β for the different series.

Series	*A*	*B*	α	β	*r*
I	–0.255 13	0.262 69	1.017 599	0.550 573	0.995 07
II	–0.435 75	0.398 15	0.917 065	0.834 484	0.998 23
III	–0.062 47	0.394 82	2.149 562	0.825 677	0.997 58
IV	0.112 39	0.414 08	3.361 012	0.867 872	0.991 09

Note: The last column shows the respective correlation coeficient (*r*).

homologues. Thus, the conformational behaviour of compounds, which in principle appears to be a very complex problem, could be evaluated using relatively high levels of theory.

The three levels of theory reported here (RHF/3-21G, RHF/6-31G(d)), and B3LYP/6-31G(d)) displayed closely related results indicating that RHF/3-21G calculations are sufficient to use in a preliminary form. However, caution is needed when using RHF level of theory with a modest basis set for a final and complete conformational analysis involving flexible homologues. From our results, it is prudent to use this technique only for a preliminary or exploratory conformational analysis. At least, the HF level of theory in conjunction with more extended basis sets and the inclusion of electron correlation appear to be necessary to confirm critical points at the PEHSs and to assign the conformational preferences of these compounds.

Chemists working in the field of twin drugs, in particular with flexible homologue series, must have been frequently exposed to the problem of multiconformation the most. How many conformers are expected for flexible homologues considering the redundancy owing to symmetry?

For compounds with a small-size connecting chain (*n* = 1–5), our results give a complete and comprehensive picture

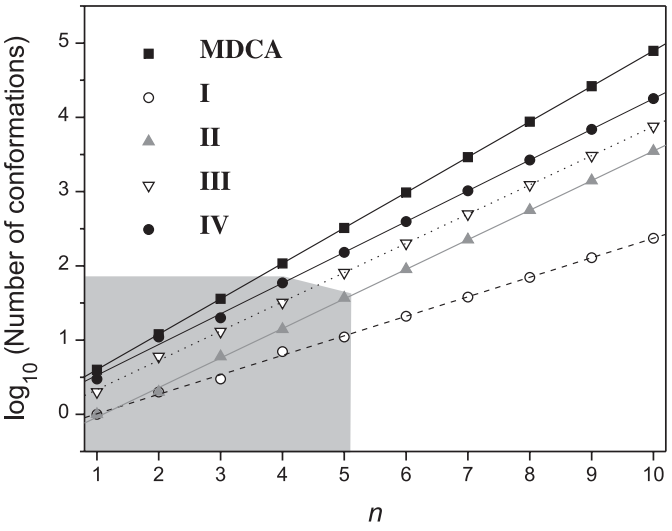
© 2005 NRC Canada

Table 7. Possible number of different conformations obtained from: RHF/3-21G calculations (calcd.) and eq. [8] ($f(n)$).

n	1	2	3	4	5
calcd.	1	2	3	7	11
f_{I}(n)	1.017 599	1.863 231	3.411 589	6.246 646	11.437 66
Δ%	1.76	6.84	13.72	10.76	3.98
calcd.	1	2	6	14	37
$f_{II}(n)$	0.917 065	2.293 771	5.737 203	14.349 946	35.892 22
Δ%	8.29	14.69	0.73	2.5	2.99
calcd.	2	6	13	32	
$f_{III}(n)$	2.149 562	5.324 735	13.190 039	32.673 384	
Δ%	7.48	11.25	1.46	2.1	
calcd.	3	11	20	59	
$f_{IV}(n)$	3.361 012	8.720 678	22.627 18	58.709 799	
Δ%	12.03	20.72	13.14	0.49	

Note: The percentage relative difference (Δ%) for the homologues in the four series is also shown.

Fig. 13. Effect of chain length (homologues n = 1–10) on the increasing complexity of conformational space. RHF calculations were performed in the grey zone; the rest of the values were obtained from eq. [8].



of their respective conformational behaviours. In the case of large-size homologues (n = 6–10), accepting the validity of our educated guess (eq. [8]), we may form at least a superficial idea about the conformational intricacies of these homologues possessing symmetrical and nonsymmetrical rings.

Acknowledgments

This work was supported by a grant from the Universidad Nacional de San Luis (UNSL). Some calculations were carried out on "Clementina" of the Centro de Supercomputación, Buenos Aires, Argentina. RDE is member of the scientific staff of the Consejo Nacional de Investigaciones Científicas y Tecnológicas (CONICET, Argentina).

References

1. J.P. Changeux. *In* Symmetry and function of biological systems at the macromolecular level. *Edited by* A. Engström and B. Strandberg. Almquist and Wiksell, Stockholm. 1969. pp. 235–256.
2. T. Blundell, T. Sewell, and B. Turnbell. *In* Structural studies on molecules of biological interest: A volume in honour of Professor Dorothy Hodgkin. *Edited by* G. Dodson, J.P. Glusker, and D. Sayre. Oxford University Press, London. 1981. pp. 390–403.
3. C. Melchiorre. Tr. Pharmacol. Sci. **2**, 209 (1981).
4. C. Melchiorre, M.L. Bolognesi, A. Chiarini, A. Minarini, and S. Spampinato. J. Med. Chem. **36**, 3734 (1993).
5. G.T. Tan, A. Wickramasinghe, S. Verma, R. Singh, S.H. Hugher, J.M. Pezzuto, M. Baba, and P. Nohan. J. Med. Chem. **35**, 4846 (1992).
6. I. Takahashi, S. Makanishi, E. Kobayashi, H. Nakano, K. Suzuki, and T. Yamaoki, Biochem. Biophys. Res. Commun. **165**, 1207 (1987).
7. B. Stefanska, M. Dziederszycka, J. Martelli, J. Tarasiuk, M. Bontemps-Gracz, and E. Borowski. J. Med. Chem. **36**, 38 (1993).
8. T.P. Wunz, R.T. Dorr, D.S. Alberts, C.L. Tunget, J. Einspanr, S. Milton, and W. Remers. J. Med. Chem. **30**, 1313 (1987).
9. I. Brandt, J. Lund, A. Bergman, E. Klasson-Wheler, L. Poellinger, and J.A. Gustafsson. Drug Metab. Dispos. **13**, 490 (1985).
10. M.J. Frisch, G.W. Trucks, H.B. Schlegel, G.E. Scuseria, M.A. Robb, J.R. Cheeseman, J.A. Montgomery, Jr., T. Vreven, K.N. Kudin, J.C. Burant, J.M. Millam, S.S. Iyengar, J. Tomasi, V. Barone, B. Mennucci, M. Cossi, G. Scalmani, N. Rega, G.A. Petersson, H. Nakatsuji, M. Hada, M. Ehara, K. Toyota, R. Fukuda, J. Hasegawa, M. Ishida, T. Nakajima, Y. Honda, O. Kitao, H. Nakai, M. Klene, X. Li, J.E. Knox, H.P. Hratchian, J.B. Cross, C. Adamo, J. Jaramillo, R. Gomperts, R.E. Stratmann, O. Yazyev, A.J. Austin, R. Cammi, C. Pomelli, J.W. Ochterski, P.Y. Ayala, K. Morokuma, G.A. Voth, P. Salvador, J.J. Dannenberg, V.G. Zakrzewski, S. Dapprich, A.D. Daniels, M.C. Strain, O. Farkas, D.K. Malick, A.D. Rabuck, K. Raghavachari, J.B. Foresman, J.V. Ortiz, Q. Cui, A.G. Baboul, S. Clifford, J. Cioslowski, B.B. Stefanov, G. Liu, A. Liashenko, P. Piskorz, I. Komaromi, R.L. Martin, D.J. Fox, T. Keith, M.A. Al-Laham, C.Y. Peng, A. Nanayakkara, M. Challacombe, P.M.W. Gill, B. Johnson, W. Chen, M.W. Wong, C. Gonzalez, and J.A. Pople. GAUSSIAN 03. Revision B.05 [computer program]. Gaussian, Inc., Pittsburgh, Penn. 2003.
11. Ö. Farkas, S.J. Salpietro, and I.G. Csizmadia. J. Mol. Struct: THEOCHEM, **367**, 25 (1996).
12. S.E. Villagra, M.B. Santillan, A.M. Rodriguez, G.A. Chasse, M.L. Freile, S.A. Zacchino, P. Matyus, and R.D. Enriz. J. Mol. Struct: THEOCHEM, **549**, 217 (2001).

© 2005 NRC Canada

13. M. Feigel. J. Mol. Struct: THEOCHEM, **366**, 83 (1966).
14. M.A. Zamora, M.F. Masman, J.A. Bombasaro, M.L. Freile, V. Cechinel Filho, S.M. Lopez, S.A. Zacchino, and R.D. Enriz. Int. J. Quant. Chem. **93**, 32 (2003).
15. I.G. Csizmadia. The chemistry of the thiol group. John Wiley and Sons, New York. 1974. Chap. 1.
16. M.P. Peterson and I.G. Csizmadia. J. Am. Chem. Soc. **100**, 6911 (1978).
17. M.R. Peterson and I.G. Csizmadia. Progress of theoretical organic chemistry. Vol. 3. Elsevier, Amsterdam. 1982. pp. 190–266.
18. M. Ramek, C.-H. Yu, and L. Schäfer. Can. J. Chem. **76**, 566 (1998).

© 2005 NRC Canada

Échelles pK_{HB} et enthalpique du pouvoir accepteur de liaison hydrogène de thioéthers, thiols et disulfures

Christian Laurence, Michel Berthelot, Karine Evain et Bertrand Illien

Résumé : Le pouvoir accepteur de liaison hydrogène (liaison H) de 31 bases soufrées tétraédriques (thioéthers, thiols, disulfures) a été mesuré par spectrométrie infrarouge à partir (*i*) de leurs constantes de complexation 1 : 1 avec le 4-fluorophénol dans CCl_4 à 25 °C (échelle pK_{HB}), (*ii*) de l'enthalpie de liaison H, et (*iii*) du déplacement de fréquence $\Delta\nu$(OH) du 4-fluorophénol par liaison H. La comparaison des échelles pK_{HB}, $\Delta H°$ et $\Delta\nu$(OH) met en évidence certaines particularités de chaque échelle. Le pouvoir accepteur de liaison H dépend (*i*) de la nature de l'atome accepteur (O > S, en accord avec le principe des acides et des bases durs et mous), (*ii*) de sa fonctionnalité (pour les bases soufrées : sulfure de phosphine > thioamide > thiocétone > thioéther > thiol > isothiocyanate ~ disulfure) et (*iii*) des effets de substituant sur la fonction. Les principaux effets de substituant sont (*i*) l'effet de polarisabilité des substituants alkyles, (*ii*) l'effet inductif, (*iii*) l'effet de résonance, et (*iv*) l'effet de cyclisation, qui fait varier le pourcentage de caractère *s* des paires libres du soufre. Les spectres infrarouges montrent que le 4-fluorophénol, outre sa fixation sur le soufre, établit également une liaison H avec l'atome de chlore de $MeSCH_2Cl$ et $MeSCH_2CH_2Cl$ et avec le nuage π de PhSMe, Ph_2S, $PhCH_2SMe$ et $EtSCH{=}CH_2$.

Mots clés : liaison hydrogène, thioéthers, thiols, disulfures, échelle pK_{HB}.

Abstract: The hydrogen bond acceptor (HBA) strength of 31 tetrahedral sulfur bases (thioethers, thiols, disulfides) has been measured by IR spectrometry from: (*i*) their 1:1 complexation constants with 4-fluorophenol in CCl_4 at 25 °C (the pK_{HB} scale); (*ii*) their HB enthalpies; and (*iii*) the frequency shifts, $\Delta\nu$(OH), of the ν(OH) band of 4-fluorophenol hydrogen bonded to sulfur. The comparison of the pK_{HB}, $\Delta H°$, and $\Delta\nu$(OH) scales points to their distinctive features. The HBA strength depends on: (*i*) the nature of the atomic site: oxygen bases are always stronger than sulfur bases, in agreement with the hard and soft acids and bases principle; (*ii*) the functionality of this atom (for sulfur bases: phosphine sulfur > thioamide > thioketone > thioether > thiol > isothiocyanate ~ disulfide); and (*iii*) the substituent effects on the function. The main substituent effects are: (*i*) the polarizability effect of alkyl groups; (*ii*) the field-inductive effect; (*iii*) the resonance effect; and (*iv*) the cyclization effect, which changes the percentage of the *s* character of sulfur lone pairs. In addition to the attachment to the sulfur atom, IR spectra show the attachment of 4-fluorophenol to the chlorine of $MeSCH_2Cl$ and $MeSCH_2CH_2Cl$, and the interaction to the π cloud of PhSMe, Ph_2S, $PhCH_2SMe$, and $EtSCH{=}CH_2$.

Key words: hydrogen bond, thioethers, thiols, disulfides, pK_{HB} scale.

Introduction

Nous construisons actuellement (1) une échelle thermodynamique du pouvoir accepteur de liaison hydrogène (liaison H) des molécules organiques. Reprenant l'idée initiale de Gurka et Taft (2), cette échelle, notée pK_{HB}, repose sur la constante de formation de liaison H entre des bases organiques B et un donneur de liaison H de référence, le 4-fluorophénol, dans des conditions standard de solvant (CCl_4), de température (298 K) et de stœchiométrie (1 : 1) (équations [1]–[3]). Le choix de ces conditions permet de mesurer la constante d'équilibre K_c

$$[1] \qquad B + 4\text{-}FC_6H_4OH \rightleftarrows 4\text{-}FC_6H_4OH\cdots B$$

$$[2] \qquad K_c = \frac{[4\text{-}FC_6H_4OH\cdots B]}{[B][4\text{-}FC_6H_4OH]} \text{ en } M^{-1}$$

$$[3] \qquad pK_{HB} = \log_{10} K_c$$

avec précision dans une large gamme s'étendant d'environ pK_{HB} = –1 pour les bases très faibles à pK_{HB} = +4 pour les bases fortes. Il suffit de déterminer la concentration de 4-fluorophénol non lié à l'équilibre, par exemple par spectrométrie infrarouge (IR) à l'aide de la bande ν(OH) à 3614 cm^{-1} (3). L'échelle pK_{HB} permet une comparaison

Reçu le 8 juillet 2004. Publié sur le site Web des Presses scientifiques du CNRC à http://revcanchim.cnrc.ca, le 24 février 2005.

C. Laurence,[1] M. Berthelot, K. Evain et B. Illien. Université de Nantes, Laboratoire de spectrochimie et modélisation EA 1149, FR Centre national de la recherche scientifique (CNRS) 2465, Faculté des sciences et des techniques, 2, rue de la Houssinière, B.P. 92208, 44322, Nantes CEDEX 3, France.

[1]Auteur correspondant (courriel : Christian.Laurence@chimie.univ-nantes.fr).

 doi: 10.1139/V05-007 © 2005 CNRC Canada

quantitative des énergies de Gibbs (ΔG° = –5,7 pK_{HB}, ΔG° en kJ mol^{-1}) de formation de liaison H, interaction moléculaire omniprésente en chimie (4) et en biologie (5).

Nous avons déjà mesuré pK_{HB} pour un grand nombre de bases carbonées, halogénées, oxygénées, azotées et soufrées (1). Dans cette dernière famille, nous avons étudié une série de molécules à soufre trigonal : thioamides et thiourées (6), isothiocyanate de méthyle (7) et thiocamphre (7). Le présent travail concerne la mesure par spectrométrie infrarouge à transformée de Fourier (IRTF) de l'échelle pK_{HB} de bases soufrées tétraédriques : 27 thioéthers, deux disulfures et deux thiols.

De manière à déterminer les principaux effets structuraux modifiant le pouvoir accepteur de liaison H des bases soufrées tétraédriques, nous avons sélectionné 11 thioéthers avec des groupes alkyles de longueur et de ramification différentes, huit thioéthers cycliques, cinq thioéthers substitués par différents groupes inductifs électroattracteurs et trois thioéthers où les paires libres du soufre peuvent se conjuguer avec un système π. Nous obtenons ainsi une échelle qui s'étend sur 1,3 unité de pK_{HB}, soit environ 7,6 kJ mol^{-1}, du sulfure de diphényle (pK_{HB} = –0,93) au sulfure de di-*tert*-butyle (pK_{HB} = +0,40).

La mesure de la constante d'équilibre à différentes températures permet de déterminer l'enthalpie et l'entropie de complexation du 4-fluorophénol par ces bases soufrées, en vue d'étudier l'existence de la relation de compensation enthalpie–entropie (8).

La spectrométrie IRTF permet la mesure des déplacements par liaison H, Δν(OH), de la fréquence d'élongation OH du 4-fluorophénol. Ces déplacements constituent une échelle spectroscopique du pouvoir accepteur de liaison H. Ils permettent de tester l'existence de la relation controversée de Badger–Bauer (9, 10) entre enthalpies de complexation et déplacements de fréquence OH. De plus la spectrométrie IRTF est une méthode de choix pour révéler d'autres sites accepteurs de liaison H que l'atome de soufre. Par exemple, elle met en évidence deux complexes pour la molécule $MeSCH_2Cl$, l'un sur l'atome de soufre, l'autre sur l'atome de chlore, et permet de séparer les contributions respectives de ces deux sites à la constante de complexation globale.

Partie expérimentale

Produits

Toutes les bases soufrées, le solvant CCl_4, et le donneur de liaison H 4-fluorophénol sont des composés commerciaux soigneusement purifiés et desséchés. Ils sont manipulés en boîte sèche pour préparer les solutions et remplir la cellule IR.

Spectres IR

Ils sont enregistrés sur un spectromètre Bruker Vector 22 avec une résolution de 1 cm^{-1}. La cellule en quartz possède un trajet optique de 1 cm pour permettre l'étude de solutions très diluées de 4-fluorophénol (4 mmol L^{-1}) et donc éviter l'autoassociation de ce dernier. À cette concentration il n'y a effectivement aucune bande ν(OH···O) à 3480 cm^{-1} correspondant au dimère du 4-fluorophénol (11). La cellule est thermorégulée à 25,0 ± 0,2 °C, pour la mesure de pK_{HB} et Δν(OH). Sa température est variée de –5 à +60 °C, pour les déterminations d'enthalpie, à l'aide d'un système thermoélectrique.

Constantes K_c, enthalpies ΔH°, entropies ΔS° et déplacements $\Delta\nu$(OH)

Les méthodes de détermination ont déjà été publiées (12, 13). Un choix rigoureux des concentrations initiales en 4-fluorophénol et base soufrée, dans CCl_4, permet de former essentiellement des complexes de liaison H de stœchiométrie 1 : 1 (c.-à-d. l'équilibre [1] prédomine très largement). Par exemple, un excès de base soufrée permet de rendre minimale la présence de complexes 1 : 2 (1 base : 2 phénols) pour les composés à plusieurs sites accepteurs de liaison H.

Résultats

Nous rapportons les valeurs pK_{HB}, $\Delta G^\circ_{x,298}$, ΔH°_{298}, $\Delta S^\circ_{x,298}$ et Δν(OH) pour la liaison H du 4-fluorophénol avec 31 bases soufrées dans le tableau 1. Les constantes K_c relatives aux concentrations molaires sont transformées en K_x relatives aux fractions molaires (14), et les grandeurs thermodynamiques sont calculées par les équations [4]–[6]. Le déplacement Δν(OH) en passant du 4-fluorophénol libre au 4-fluorophénol lié au soufre est donné par l'équation [7].

$$[4] \qquad \Delta G^0_x = -RT \ln K_x$$

$$[5] \qquad \Delta H^0 = RT^2 \, [d(\ln K_x)/dT]$$

$$[6] \qquad \Delta S^0_x = (\Delta H^0 - \Delta G^0_x)/T$$

$$[7] \qquad \Delta\nu(OH) = \nu(OH \text{ libre}) - \nu(OH\cdots S) = 3614 - \nu(OH\cdots S)$$

Pour six thioéthers possédant un site potentiel accepteur de liaison H supplémentaire (site π ou Cl), nous observons sur le spectre IR, entre la bande fine ν(OH) du 4-fluorophénol libre à 3614 cm^{-1} (fig. 1, bande 1) et la bande large ν(OH···S) (fig. 1, bande 3) correspondant au complexe sur le soufre, une bande supplémentaire (fig. 1, bande 2). Nous attribuons cette bande supplémentaire à un deuxième complexe de liaison H se formant soit sur un atome de chlore (composés **19** et **20**), soit sur un nuage π aromatique (**17**, **21** et **22**) ou éthylénique (**23**). En effet ces bandes supplémentaires sont bien aux positions attendues pour une liaison H sur un atome de chlore (15) ou sur un site π aromatique (16) ou éthylénique (16).

Puisque nous avons contrarié la formation de complexes 2:1 par un excès de base soufrée, nous avons essentiellement en solution deux complexes 1 : 1, un complexe OH···S sur l'atome de soufre et un complexe OH···X (π ou Cl) sur le site supplémentaire. Dans ce cas la constante de complexation mesurée à partir de l'absorbance de la bande ν(OH) du 4-fluorophénol libre correspond à la formation de ces deux complexes, et il est facile de montrer (18) qu'elle est la somme de deux constantes, K_c(S) et K_c(X), ou 2K_c(X) pour Ph_2S. La constante propre à l'atome de soufre peut donc être calculée à partir de l'équation [8], s'il

$$[8] \qquad K_c(\text{totale}) = K_c(S) + xK_c(X) \; (x = 1 \text{ ou } 2)$$

© 2005 CNRC Canada

Tableau 1. Valeurs pK_{HB}, $\Delta G^{\circ}_{x,298}$ (kJ mol^{-1}), ΔH°_{298} (kJ mol^{-1}), $\Delta S^{\circ}_{x,298}$ (J K^{-1} mol^{-1}) et $\Delta\nu$(OH) (cm^{-1}) pour la liaison H du 4-fluorophénol avec 31 bases soufrées dans CCl_4.

N°	Base	Formule	pK_{HB}	$-\Delta G^{\circ}_{x,298}$	$-\Delta H^{\circ}_{298}$	$-\Delta S^{\circ}_{x,298}$	$\Delta\nu$(OH)
1	Disulfure de méthyle	Me_2S_2	–0,19(–0,49)[a]	4,77(3,06)[a]	8,8	13,4(19,2)[a]	147
2	Disulfure d'éthyle	Et_2S_2	–0,10(–0,40)[a]	5,19(3,48)[a]			157
3	Ethanethiol	EtSH	–0,16	4,94	10,4	18,2	176
4	Isopropanethiol	*i*-PrSH	–0,10	5,18	11,0	19,6	182
5	Sulfure de diméthyle	Me_2S	0,12	6,51	12,8	21,2	253
6	Sulfure d'éthyle et de méthyle	EtSMe	0,18	6,85	13,4	21,8	258
7	Sulfure de *n*-propyle et de méthyle	*n*-PrSMe	0,16	6,71	13,5	22,6	260
8	Sulfure de *n*-butyle et de méthyle	*n*-BuSMe	0,17	6,76	13,5	22,7	262
9	Sulfure de *n*-octyle et de méthyle	*n*-OctSMe	0,17	6,84	13,6	22,6	263
10	Sulfure de *c*-hexyle et de méthyle	*c*-HexSMe	0,24	7,27	14,6	24,7	274
11	Sulfure de *tert*-butyle et de méthyle	*t*-BuSMe	0,25	7,27	14,8	25,4	271
12	Sulfure de diéthyle	Et_2S	0,25	7,06	14,7	25,7	266
13	Sulfure de di *n*-butyle	*n*-Bu_2S	0,23	6,88	15,5	28,8	270
14	Sulfure de di *n*-propyle	*i*-Pr_2S	0,30	7,49	16,0	28,4	276
15	Sulfure de di *tert*-butyle	*t*-Bu_2S	0,40	8,03	18,1	33,9	300
16	Sulfure d'allyle et de méthyle	CH_2=$CHCH_2SMe$	0,08	6,29	~12,0[b]		244
17	Sulfure de benzyle et de méthyle	$PhCH_2SMe$	–0,02[c]	5,67	~11,5[b]		238
18	Bisméthyle thiométhane	$MeSCH_2SMe$	–0,22[a]	6,28(4,56)[a]	~10,0	12,5 (18,3)[a]	216
19	Sulfure de méthyle et de 2-chloroéthyle	$MeSCH_2CH_2Cl$	–0,12[d]	5,01			200
20	Sulfure de méthyle et de chlorométhyle	$MeSCH_2Cl$	–0,37[d]	4,87			140
21	Thioanisole	PhSMe	–0,32[c]				185
22	Sulfure de diphényle	PhSPh	–0,93[c]				163
23	Sulfure de vinyle et d'éthyle	$EtSCH=CH_2$	–0,13[c]		~10,2[b]		181
24	Sulfure d'éthylène	$\underline{CH_2CH_2}S$	0,03	5,97	11,6	18,9	231
25	Sulfure de propylène	$CH_3\underline{CHCH_2}S$	0,10	6,47	13,0	21,9	253[e]
26	Sulfure de triméthylène	$\underline{CH_2CH_2CH_2}S$	0,13	6,59	12,7	20,5	253
27	Tétrahydrothiophène	$\underline{CH_2CH_2CH_2CH_2}S$	0,32	7,45	14,3	22,9	279
28	1,3-Dithiolane	$S\underline{CH_2CH_2S}CH_2$	–0,07(–0,38)[a]	5,35(3,64)[a]	~12,4	23,7(29,5)[a]	207
29	1,4-Dithiane	$S\underline{CH_2CH_2SCH_2}CH_2$	0,16(–0,14)[a]	6,72(5,00)[a]	11,0	14,3(20,0)[a]	210
30	1,3-Dithiane	$S\underline{CH_2SCH_2CH_2}CH_2$	0,24(–0,06)[a]	7,16(5,44)[a]	~11,5	14,5(20,3)[a]	201
31	Sulfure de pentaméthylène	$\underline{CH_2CH_2CH_2CH_2CH_2}S$	0,23	7,12	14,2	23,8	266

[a]Valeur par atome de soufre (supposés équivalents) après correction statistique de log 2 (pK_{HB}), RT ln 2(ΔG) et $-R$ ln 2(ΔS).
[b]Valeur indicative à cause du deuxième site.
[c]Après soustraction de la contribution du site π (voir tableau 2).
[d]Après soustraction de la contribution du chlore (voir tableau 2).
[e]Un épaulement, observé à $\Delta\nu$ = 186 cm^{-1}, pourrait être attribué à une stéréochimie de complexation (voir réf. 17 pour les éthers).

est possible d'évaluer K_c(X). Nous l'avons fait à partir des déplacements de fréquence IR $\Delta\nu$(OH), en utilisant les corrélations entre pK_{HB} et $\Delta\nu$(OH) établies dans des travaux précédents pour les familles des chloroalcanes (15) et des bases π aromatiques (16) et éthyléniques (16). Le détail des calculs est donné dans le tableau 2.

Nous n'avons trouvé dans la littérature que des travaux partiels et hétérogènes (se rapportant à des donneurs de liaison H et des solvants différents) sur les paramètres thermodynamiques de liaison H des bases soufrées tétraédriques (19–26). Ils ne permettent pas de construire une échelle homogène du pouvoir accepteur de liaison H des bases soufrées.

Avec le 4-fluorophénol dans CCl_4, nous n'avons trouvé que la valeur pK_{HB} = 0,11 pour Et_2S (2) qui diffère sensiblement de notre valeur 0,25. Nous pensons que la valeur 0,11 déterminée par RMN du ^{19}F est moins précise que notre valeur IR, car la méthode RMN se rapporte à deux inconnues (K_c et résonance ^{19}F du complexe) au lieu d'une en IR (K_c).

Par contre Arnett et al. (27) ont déterminé par calorimétrie les enthalpies de complexation du 4-fluorophénol avec six thioéthers (tableau 3), par la méthode (approchée) de la base pure. Pour trois thioéthers, les écarts relatifs entre les valeurs calorimétriques et les valeurs IR (van't Hoff) ne dépassent pas 8 %. Trois autres thioéthers ont un autre site accepteur de liaison H, et la calorimétrie montre ici ses limites, puisqu'elle ne peut mettre en évidence l'existence de deux complexes 1 : 1 (S et π ou S et Cl) à la différence de l'IR.

Nous considérons donc que ce travail constitue quasiment la première étude thermodynamique cohérente sur le pouvoir accepteur de liaison H des thioéthers, thiols et disulfures. Les données sont nombreuses et structuralement diversifiées. De plus, elles nous semblent fiables dans la mesure où la précision photométrique de l'IRTF et la méthode de détermination des enthalpies et des entropies (13) doivent garantir des résultats reproductibles et probablement précis. La reproductibilité est de l'ordre de ±0,03 sur pK_{HB}, de ±0,5 kJ mol^{-1} sur ΔH°, et de ±1,5 J K^{-1} mol^{-1} sur ΔS°.

© 2005 CNRC Canada

Tableau 2. Évaluation de la constante de complexation (M^{-1}) sur le soufre, K_c(S), dans le cas des thioéthers possédant un autre site X accepteur de liaison H.

N°	Base	X	K_c (totale)[a]	Δν(OH)[b]	K_c(X)[c]	K_c(S)[d]	pK_{HB}(S)
17	$MeSCH_2Ph$	π	1,33	55	0,38	0,95	–0,02
19	$MeSCH_2CH_2Cl$	Cl	1,07	52	0,30	0,77	–0,12
20	$MeSCH_2Cl$	Cl	0,69	46	0,26	0,43	–0,37
21	PhSMe	π	0,81	50	0,33	0,48	–0,32
22	PhSPh	2π	0,74	47	0,62	0,12	–0,93
23	$EtSCH=CH_2$	π	0,88	61	0,15	0,73	–0,13

[a]Valeur mesurée.
[b]Déplacement (cm^{-1}) de fréquence de la bande OH du 4-fluorophénol lié sur le site X.
[c]Calculée à partir des relations pK_{HB} = 1,04 [Δν(OH)/100] – 1,06 pour les bases chlorées, pK_{HB} = 1,09 [Δν(OH)/100] – 1,02 pour les bases π aromatiques et pK_{HB} = 1,26 [Δν(OH)/100] – 1,60 pour les bases π éthyléniques.
[d]$K_c(S) = K_c(\text{totale}) - xK_c(X)$.

Discussion

Position des bases soufrées sur les échelles pK_{HB} et enthalpique du pouvoir accepteur de liaison H

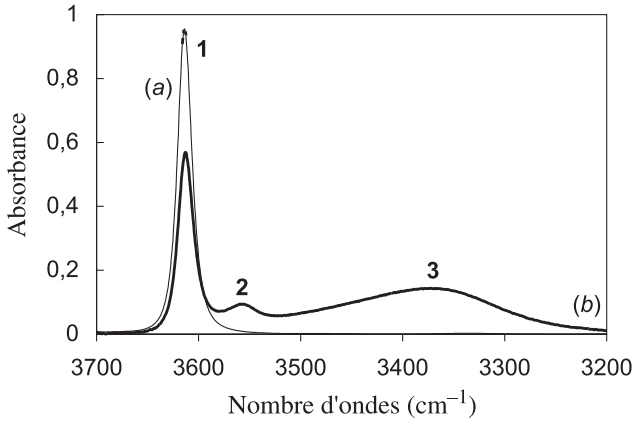
Pour les bases soufrées tétraédriques nous observons :

Fonction	Disulfure	<	Thiol	<	Thioéther
Composé	Me_2S_2		EtSH		Me_2S
$-\Delta H°$ (kJ mol^{-1})	8,8		10,4		12,8

Ces valeurs sont intéressantes pour comparer les enthalpies de liaison H de donneurs OH aux résidus cystine, cystéine, et méthionine dans la reconnaissance moléculaire de ligands par des récepteurs biologiques. Elles sont par ailleurs en accord avec un travail (28) soulignant que, dans l'organisation des cristaux organiques, les contacts intermoléculaires par liaison H à un soufre tétraédrique, quoique peu fréquents, ne peuvent être négligés.

Pour l'ensemble des bases soufrées, à part la fonction isothiocyanate le soufre tétraédrique est moins accepteur que le soufre trigonal :

Fig. 1. Spectres IR dans la région ν(OH) (*a*, traits fins) d'une solution 4 mmol L^{-1} de 4-fluorophénol dans CCl_4 (*b*, traits gras) de la même solution après ajout de 0,49 mol L^{-1} de $PhCH_2SMe$, montrant (1) la bande ν(OH) du 4-fluorophénol libre à 3614 cm^{-1}, (2) la bande ν(OH···π) d'un premier complexe 1 : 1 à 3559 cm^{-1}, et (3) la bande ν(OH···S) très large d'un deuxième complexe 1 : 1 à 3376 cm^{-1}.



Fonction	Isothiocyanate	<	Thioéther	<	Thiocétone	<	Thioamide	<	Sulfure de phosphine
Composé	MeN=C=S		Me_2S		Thiocamphre		$HCSNMe_2$[2]		$(n\text{-Oct})_3PS$[2]
$-\Delta H°$ (kJ mol^{-1})	9,0		12,8		14,7		19,1		20,7

Ces résultats sont en accord avec les calculs MP2/6-311++G(d,p) de Platts et al. (29) sur le pouvoir accepteur de liaison hydrogène de H_2S et $H_2C=S$.

Comme le montre le tableau 4, quelle que soit la fonctionalité du chalcogène, les bases soufrées sont toujours de moins bons accepteurs de liaison H que les bases oxygénées correspondantes. Ceci vérifie banalement le principe HSAB des acides et des bases durs et mous (30), puisque les donneurs de liaison H sont des acides durs dans la classification de Pearson (30) et que l'oxygène est plus dur (η(H_2O) = 7,0 eV) que le soufre (η(H_2S) = 5,3 eV) (31). D'une manière plus intéressante, les données du tableau 4 permettent de quantifier le principe HSAB : pour les complexes de liaison H considérés, la perte d'énergie de Gibbs en passant d'une base dure oxygénée à une base molle soufrée varie de 2,0 kJ mol^{-1} (0,35 pK_{HB}) pour le couple *t*-Bu_2S–*t*-Bu_2O à 12,5 kJ mol^{-1} (2,2 pK_{HB}) pour le couple Et_3PS–Et_3PO.

Relation de Badger–Bauer entre Δ*H* et Δν(OH)

Badger et Bauer (9, 10) ont proposé que le déplacement Δν(OH) pouvait permettre d'estimer l'enthalpie de la liaison H. Cette proposition a été très controversée (3, 27, 34–40). Nous observons sur la figure 2 une bonne relation pour beaucoup de bases soufrées tétraédriques; le 1,3-dithiane **30** et le 1,3-dithiolane **28** dévient de cette relation, probablement à cause de la non-équivalence de leurs deux atomes de soufre, et donc de l'inadaptation de l'équation de van't Hoff pour décrire la variation avec la température d'une constante d'équilibre qui est la somme de deux constantes différentes (vide supra). De même les thiols **3** et **4** et le disulfure **1**

[2]Résultats non publiés du Laboratoire.

© 2005 CNRC Canada

Tableau 3. Comparaison des enthalpies de complexation (kJ mol^{-1}) du 4-fluorophénol par des thioéthers déterminées par calorimétrie (cal.) ou par variation de la constante de complexation avec la température (vH).

Thioéther	$-\Delta H°$ (cal.)	Thioéther	$-\Delta H°$ (cal.)	$-\Delta H°$ (vH)	Écart (%)
Ph_2S[a]	5,90	*n*-Bu_2S	14,39	15,5	–7
PhSMe[a]	6,99	Et_2S	15,19	14,7	+3
$ClCH_2SMe$[b]	7,91	$CH_2CH_2CH_2CH_2S$	15,52	14,3	+8

[a]Base à la fois π et S.
[b]Base à la fois Cl et S.

Tableau 4. Comparaison des valeurs pK_{HB} pour trois familles de bases oxygénées (*E* = oxygène) et soufrées (*E* = soufre) : oxydes (sulfures) de phosphine, (thio)amides et (thio)éthers.

	pK_{HB}			
Bases	Oxygène	Réf.	Soufre	Réf.
$(MeO)_3PE$	2,50	33	0,58	2
$(EtO)_3PE$	2,68	33	0,76	2
Ph_3PE	3,16	33	1,00	2
Et_3PE	3,66	33	1,46	2
Oct_3PE	3,59	33	1,54	a
$ClCENMe_2$	1,00	32	0,50	6
$PhCENMe_2$	2,23	32	1,02	6
$HCENMe_2$	2,10	32	1,05	6
$MeCENMe_2$	2,44	32	1,22	6
$Me_2NCENMe_2$	2,44	32	1,35	6
$(Me)NCH_2CH_2N(Me)C{=}E$	2,46	32	1,32	6
t-Bu*E*Me	1,19	17	0,25	a
Et_2E	1,01	17	0,25	a
n-Bu_2E	0,88	17	0,23	a
i-Pr_2E	1,11	17	0,30	a
t-Bu_2E	0,75	17	0,40	a
$EtECH{=}CH_2$	0,10	17	–0,13	a
$MeCHCH_2E$	0,97	17	0,10	a
$CH_2CH_2CH_2E$	1,36	17	0,13	a
$CH_2CH_2CH_2CH_2E$	1,28	17	0,32	a
$CH_2CH_2ECH_2E$	0,45	17	–0,38	a
$CH_2CH_2ECH_2CH_2E$	0,73	17	–0,14	a
$CH_2CH_2CH_2ECH_2E$	0,63	17	–0,06	a
$CH_2CH_2CH_2CH_2CH_2E$	1,23	17	0,23	a

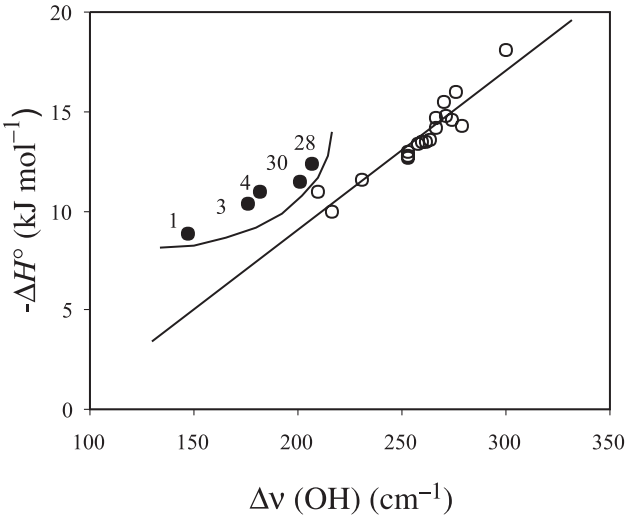
[a]Ce travail.

n'obéissent pas à la relation des thioéthers. En excluant ces cinq composés, nous observons l'équation [9] de coefficient de correlation r = 0,941 et d'écart type s = 0,65 kJ mol^{-1} pour

[9] $-\Delta H° = 8{,}04\ (\Delta\nu(OH)/100) - 7{,}08$

n = 18 thioéthers. La relation de Badger–Bauer peut donc rendre des services, puisque l'écart type de l'estimation est de l'ordre de grandeur des erreurs expérimentales. Cependant il faut prendre garde à son caractère très dépendant de la famille (thiols, thioéthers et disulfures forment ici des familles différentes).

Fig. 2. Relation entre l'enthalpie de liaison H, $-\Delta H°$, et le déplacement Δν(OH) pour les complexes du 4-fluorophénol avec des bases soufrées. Le disulfure **1** et les thiols **3** et **4** n'appartiennent pas à la famille des thioéthers. Dans celle-ci, le 1,3-dithiane **30** et le 1,3-dithiolane **28** dévient (voir texte).



Relation de compensation entre l'enthalpie et l'entropie

Il existe un dilemme dans la construction des échelles de basicité. Doit-on les définir à partir d'énergies de Gibbs, comme l'échelle pK_{BH}^{+}, ou d'enthalpies, comme l'échelle du nombre donneur de Gutmann (41) ? Cette question ne se pose pas s'il existe une relation extrathermodynamique, appelée relation de compensation, entre l'enthalpie et l'entropie (équation [10] dans laquelle δ est un opérateur de variation de structure) dans la série de réactions considérées, car alors ΔH et ΔG sont reliés par l'équation [11]. Cette dernière

[10] $\delta\Delta H = \beta\delta\Delta S$

[11] $\delta\Delta G = [1 - (T/\beta)]\delta\Delta H$

équation est appelée relation d'isoéquilibre, car lorsque T = β, $\delta\Delta G$ = 0.

Le système de coordonnées ΔH, ΔS est à éviter pour étudier l'existence de la relation de compensation, car une relation entre ces deux grandeurs peut ne traduire que leurs erreurs liées quand elles ont été déterminées par la loi de van't Hoff. Exner a montré (8) que le système de coordonnées ln K, T^{-1}, c'est-à-dire l'équation [12], était mathématiquement équivalent au système ΔH, ΔS, c'est-à-dire à l'équation [10], mais qu'il était cette fois

© 2005 CNRC Canada

[12] $\ln K_{ij} = (\Delta H_i^\circ / R)(\beta^{-1} - T_{ij}^{-1}) + y_0$

statistiquement correct, puisque ln K et T^{-1} sont des coordonnées a priori indépendantes. L'équation [12], dans laquelle i et j se rapportent respectivement au thioéther et à la température, correspond à celle d'un faisceau de droites de van't Hoff se coupant en un point commun de coordonnées β^{-1} et y_0. Le problème se réduit donc à la démonstration de l'existence d'un point commun à plusieurs droites de régression (ici droites de van't Hoff). Ouvrard et al. (42) ont développé un programme permettant de répondre à cette question.

Nous avons appliqué ce programme aux thiols, thioéthers et disulfures de notre étude (sauf aux thioéthers possédant un site π ou Cl secondaire ou deux atomes de soufre suspectés d'être non équivalents). Avec cet échantillonnage le test F de Fischer au niveau 95 % rejette l'existence d'un point d'intersection unique. Nous avons essayé d'autres échantillonnages et trouvons qu'il faut enlever les quatre thioéthers Et_2S, n-Bu_2S, i-Pr_2S et t-Bu_2S pour que l'existence de la relation d'isoéquilibre [11] soit statistiquement démontrée. La température d'isoéquilibre β est alors égale à 778 K, et son intervalle d'erreur est 685 à 931 K.

Les statistiques indiquent donc que dans la famille des bases soufrées tétraédriques, la relation d'isoéquilibre est obéie par (*i*) les thiols, (*ii*) les thioéthers cycliques et (*iii*) les thioéthers aliphatiques, dont un des substituants alkyles est moins volumineux que le groupe éthyle (ce qui inclut MeSEt et même *t*-BuMeS, mais exclut EtSEt). Une explication moléculaire, qui pourrait être basée sur l'effet stérique, reste à trouver pour ces observations statistiques sur l'entropie de liaison H.

Effet des substituants alkyles sur le pouvoir accepteur de liaison H

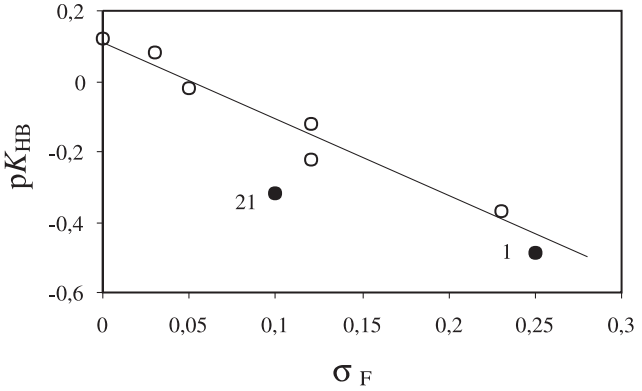
Les substituants alkyles peuvent *augmenter* le pouvoir accepteur de liaison H du soufre par leur effet de polarisabilité ou le *diminuer* par leur effet stérique. Ces deux effets sont corrélés significativement pour les substituants alkyles, car l'augmentation du nombre d'atomes (de carbone et d'hydrogène) augmente à la fois le nombre d'électrons (la polarisabilité) et la taille (l'effet stérique). Pour l'échantillon de substituants alkyles considéré (Me, Et, *n*-Pr, *n*-Bu, *n*-Oct, *c*-Hex, *i*-Pr, *t*-Bu) et l'hydrogène, c.-à-d. pour neuf points, il existe un coefficient de corrélation significatif (0,935) entre la constante σ_α de polarisabilité (43, 44) et la constante υ d'effet stérique (45). Un seul paramètre peut donc être utilisé pour décrire l'effet des groupes alkyles; nous avons choisi la constante σ_α de polarisabilité (43, 44). C'est le signe du coefficient de la régression de ΔH° en σ_α qui déterminera si les groupes alkyles agissent majoritairement par effet stérique (coefficient négatif, diminution de $-\Delta H^\circ$) ou par effet de polarisabilité (coefficient positif, augmentation de $-\Delta H^\circ$). L'équation [13] montre que pour 11 thioéthers RSR′ **5**–**15** et deux thiols RSH **3**, **4**, le pouvoir accepteur de liaison H

[13] $-\Delta H^\circ = 6{,}92\ (-\Sigma\sigma_\alpha) + 7{,}4$

$n = 13$, $r = 0{,}983$, $s = 0{,}38$

augmente quand le nombre, la longueur et la ramification des substituants alkyles R et R′ (c.-à-d. $-\Sigma\sigma_\alpha$) du soufre augmentent. Ceci indique que l'effet de polarisabilité l'emporte sur l'effet stérique pour l'enthalpie de liaison H. Grâce à cette relation on estime à environ 7,4 kJ mol^{-1} l'enthalpie de complexation avec H_2S (pour lequel $\Sigma\sigma_\alpha = 0$) dont l'état gazeux rend l'étude expérimentale difficile.

Fig. 3. Relation entre pK_{HB} et la constante inductive σ_F du substituant XCH_2 dans la série XCH_2SMe : pK_{HB} = –2,189 σ_F + 0,11; n = 6; r = 0,977. Le disulfure MeSSMe **1** obéit à cette corrélation, tandis que le thioanisole PhSMe **21** dévie vers le bas (voir texte).



Effet inductif

Nous avons étudié l'effet inductif de substituants électroattracteurs dans la série XCH_2SMe (**5**, **16**, **17**, **18**, **19** et **20**). La figure 3 montre que la diminution de pK_{HB} par cet effet électroattracteur est bien reliée à la constante inductive σ_F du groupe XCH_2 (44). Le thioanisole PhSMe **21** dévie vers le bas, car à l'effet inductif du substituant Ph s'ajoute son effet de résonance électroattracteur. Au contraire le disulfure MeSSMe **1** se place sur la droite de régression. Ceci indique que la diminution du pouvoir accepteur de liaison H en passant d'un thioéther à un disulfure est principalement due à l'effet inductif du substituant SR. Ainsi la constante σ_F = +0,25 du substituant SMe en fait le substituant inductif le plus électroattracteur de notre échantillon; en conséquence le disulfure MeSSMe a la valeur pK_{HB} la plus faible (–0,49) de la série. Il a également l'enthalpie de liaison H la plus petite de toutes les bases soufrées, dont l'enthalpie a été mesurée dans ce travail.

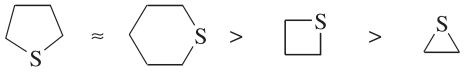
Effet de résonance

L'effet de résonance électroattracteur des groupes Ph et $CH{=}CH_2$ s'ajoute à leur effet inductif électroattracteur pour diminuer la densité électronique des paires libres du soufre dans les thioéthers aromatiques et éthyléniques PhSMe, Ph_2S et $EtSCH{=}CH_2$. Ces derniers sont donc significativement moins accepteurs de liaison H que leurs analogues aliphatiques. Ainsi l'écart entre PhSMe et *c*-HexSMe est de 0,56 unité de pK (3,2 kJ mol^{-1}) et celui entre $EtSCH{=}CH_2$ et EtSEt de 0,38 unité de pK (2,2 kJ mol^{-1}).

Effet de cyclisation

La cyclisation modifie le pouvoir accepteur de liaison H des thioéthers cycliques. L'ordre observé sur l'échelle enthalpique est le suivant :

© 2005 CNRC Canada



$-\Delta H°$ (kJ mol^{-1})	14,3	≈	14,2	>	12,7	>	11,6
% *s* moyen des paires libres du S	35,6	≈	35,2	<	37,5	<	41,4

Une explication simple pourrait provenir d'une modification de l'hybridation des paires libres du soufre par variation de l'angle CSC. Quand celui-ci se ferme en allant vers les plus petits cycles, leur pourcentage de caractère *s* augmente. En conséquence le pouvoir accepteur de liaison H diminue, puisque la basicité de liaison H d'une paire libre diminue généralement avec l'augmentation de son caractère *s* (par exemple, pour l'azote la basicité diminue dans l'ordre Me_3N > pyridine > acétonitrile). Nous avons analysé les paires libres du soufre par la méthode NBO (« natural bond orbital ») (46, 47) au niveau B3LYP/6-31+G** (48). Nous trouvons un accord satisfaisant (r = 0,967, n = 4) entre le pourcentage moyen de caractère *s* des paires libres calculé par cette méthode et l'enthalpie de complexation.

Remerciements

Les auteurs remercient le Centre de calcul intensif des Pays de la Loire (CCIPL), l'Institut du développement et des ressources en informatique scientifique (IDRIS) et le Centre informatique national de l'enseignement supérieur (CINES) pour leurs allocations de ressource informatique.

Bibliographie

1. C. Laurence et M. Berthelot. Perspect. Drug Discovery Des. **18**, 39 (2000).
2. R.W. Taft, D. Gurka, L. Joris, P.v.R. Schleyer et J.W. Rakshys. J. Am. Chem. Soc. **91**, 4801 (1969).
3. E.M. Arnett, L. Joris, E. Mitchell, T.S.S.R. Murty, T.M. Gorrie et P.v.R. Schleyer. J. Am. Chem. Soc. **92**, 2365 (1970).
4. G.C. Pimentel et A.L. McClellan. The hydrogen bond. Freeman, San Francisco. 1960.
5. G.A. Jeffrey et W. Saenger. Hydrogen bonding in biological structures. Springer-Verlag, Berlin. 1991.
6. C. Laurence, M. Berthelot, J.-Y. Le Questel et M.J. El Ghomari. J. Chem. Soc. Perkin Trans. 2, 2075 (1995).
7. B. Illien, K. Evain, M. Berthelot et C. Laurence. J. Phys. Org. Chem. **16**, 608 (2003).
8. O. Exner. Prog. Phys. Org. Chem. **10**, 411 (1973).
9. R.M. Badger et S.H. Bauer. J. Chem. Phys. **5**, 839 (1937).
10. R.M. Badger. J. Chem. Phys. **8**, 288 (1940).
11. C. Laurence, M. Berthelot et J. Graton. *Dans* The chemistry of phenols. Vol. part 1. *Sous la direction de* Z. Rappoport. Wiley, New York. 2003.
12. J. Graton, F. Besseau, M. Berthelot, E.D. Raczynska et C. Laurence. Can. J. Chem. **80**, 1375 (2002).
13. C. Ouvrard, M. Berthelot et C. Laurence. J. Phys. Org. Chem. **14**, 804 (2001).
14. R. Foster. Organic charge-transfer complexes. Academic Press, Londres. 1969.
15. C. Ouvrard, M. Berthelot et C. Laurence. J. Chem. Soc. Perkin Trans. 2, 1357 (1999).
16. F. Besseau, C. Laurence et M. Berthelot. Bull. Soc. Chim. Fr. **133**, 381 (1996).
17. M. Berthelot, F. Besseau et C. Laurence. Eur. J. Org. Chem. 925 (1998).
18. C. Ouvrard, M. Lucon, J. Graton, M. Berthelot et C. Laurence. J. Phys. Org. Chem. **17**, 56 (2004).
19. R. West, D.L. Powell, L.S. Whatley, M.K.T. Lee et P.v.R. Schleyer. J. Am. Chem. Soc. **84**, 3221 (1962).
20. R. West, D.L. Powell, M.K.T. Lee et L.S. Whatley. J. Am. Chem. Soc. **86**, 3227 (1964).
21. R. West, L.S. Wilson et D.L. Powell. J. Organomet. Chem. **178**, 5 (1979).
22. J. Chojnowski et W.W. Brandt. J. Am. Chem. Soc. **90**, 1384 (1968).
23. V. Sara, J. Moravec, V. Horak et M. Horak. Collect. Czech. Chem. Commun. **34**, 2390 (1969).
24. G.C. Vogel et R.S. Drago. J. Am. Chem. Soc. **92**, 5347 (1970).
25. A.D. Sherry et K.F. Purcell. J. Am. Chem. Soc. **94**, 1848 (1972).
26. J.L.M. Abboud, C. Roussel, E. Gentric, K. Sraidi, J. Lauransan, G. Guiheneuf, M.J. Kamlet et R.W. Taft. J. Org. Chem. **53**, 1545 (1988).
27. E.M. Arnett, E.J. Mitchell et T.S.S.R. Murty. J. Am. Chem. Soc. **96**, 3875 (1974).
28. F.H. Allen, C.M. Bird, R.S. Rowland et P.R. Raithby. Acta Crystallogr. B, **B53**, 680 (1997).
29. J.A. Platts, S.T. Howard et B.R.F. Bracke. J. Am. Chem. Soc. **118**, 2726 (1996).
30. R.G. Pearson. J. Am. Chem. Soc. **85**, 3533 (1963).
31. R.G. Parr et R.G. Pearson. J. Am. Chem. Soc. **105**, 7512 (1983).
32. J.Y. Le Questel, C. Laurence, A. Lachkar, M. Helbert et M. Berthelot. J. Chem. Soc. Perkin Trans. 2, 2091 (1992).
33. A. Chardin. Thèse de doctorat, Université de Nantes, Nantes, France. 1997.
34. E.D. Becker. Spectrochim. Acta, **17**, 436 (1961).
35. D.L. Powell et R. West. Spectrochim. Acta, **20**, 983 (1964).
36. S. Singh, A.S.N. Murthy et C.N.R. Rao. Trans. Faraday Soc. **62**, 1056 (1966).
37. T. Gramstad et J. Sandstrom. Spectrochim. Acta, Part A, **25**, 31 (1969).
38. P. Goralski. J. Chem. Soc. Faraday Trans. **89**, 2433 (1993).
39. J. Rossarie, J.P. Gallas, C. Binet et R. Romanet. J. Chim. Phys. Phys.–Chim. Biol. **75**, 63 (1978).
40. M.H. Abraham, D.V. Prior, R.A. Schulz, J.J. Morris et P.J. Taylor. J. Chem. Soc. Faraday Trans. **94**, 879 (1998).
41. V. Gutmann. Electrochim. Acta, **21**, 661 (1976).
42. C. Ouvrard, M. Berthelot, T. Lamer et O. Exner. J. Chem. Inf. Comput. Sci. **41**, 1141 (2001).
43. W.J. Hehre, C.F. Pau, A.D. Headley, R.W. Taft et R.D. Topsom. J. Am. Chem. Soc. **108**, 1711 (1986).
44. C. Hansch, A. Leo et R.W. Taft. Chem. Rev. **91**, 165 (1991).
45. M. Charton. Top. Curr. Chem. **114**, 57 (1983).
46. A.E. Reed, R.B. Weinstock et F. Weinhold. J. Chem. Phys. **83**, 735 (1985).
47. E.D. Glendening, A.E. Reed, J.E. Carpenter et F. Weinhold. Natural Bond Orbital (NBO). Version, 3,1.
48. M.J. Frisch, G.W. Trucks, H.B. Schlegel, G.E. Scuseria, M.A. Robb, J.R. Cheeseman, J.A. Montgomery, J.T. Vreven, K.N. Kudin, J.C. Burant, J.M. Millam, S.S. Iyengar, J. Tomasi, V. Barone, B. Mennucci, M. Cossi, G. Scalmani, N. Rega, G.A. Petersson, H. Nakatsuji, M. Hada, M. Ehara, K. Toyota, R. Fukuda, J. Hasegawa, M. Ishida, T. Nakajima, Y. Honda, O. Kitao, H. Nakai, M. Klene, X. Li, J.E. Knox, H.P. Hratchian, J.B. Cross, C. Adamo, J. Jaramillo, R. Gomperts, R.E. Stratmann, O. Yazyev, A.J. Austin, R. Cammi, C. Pomelli,

© 2005 CNRC Canada

J.W. Ochterski, P.Y. Ayala, K. Morokuma, G.A. Voth, P. Salvador, J.J. Dannenberg, V.G. Zakrzewski, S. Dapprich, A.D. Daniels, M.C. Strain, O. Farkas, D.K. Malick, A.D. Rabuck, K. Raghavachari, J.B. Foresman, J.V. Ortiz, Q. Cui, A.G. Baboul, S. Clifford, J. Cioslowski, B.B. Stefanov, G. Liu, A. Liashenko, P. Piskorz, I. Komaromi, R.L. Martin, D.J. Fox, T. Keith, M.A. Al-Laham, C.Y. Peng, A. Nanayakkara, M. Challacombe, P.M.W. Gill, B. Johnson, W. Chen, M.W. Wong, C. Gonzalez et J.A. Pople. GAUSSIAN 03. Rev C,01 [programme d'ordinateur]. Wallingford, USA. 2004.

© 2005 CNRC Canada

An intriguing effect of lithium perchlorate dispersed on silica gel in the bromination of aromatic compounds by *N*-bromosuccinimide

Mojtaba Bagheri, Najmedin Azizi, and Mohammad R. Saidi

Abstract: A convenient and efficient procedure for electrophilic aromatic bromination has been developed by mixing of *N*-bromosuccinimide and an aromatic compound at room temperature on the surface of silica gel mixed with solid anhydrous $LiClO_4$. All of the substrates examined underwent clean electrophilic aromatic bromination in reaction times of a few minutes to afford the corresponding bromoarenes under neutral conditions in excellent yield. In the case of thiophenol, no substitution reaction occurred, and the corresponding disulfide was obtained in excellent yield.

Key words: LP-SiO_2, NBS, arenes, electrophilic bromination, regioselectivity.

Résumé : On a mis au point une méthode pratique et efficace d'effectuer une bromation aromatique électrophile donnant d'excellents rendements et qui implique la mise en contact, à la température ambiante et pendant quelques minutes, de *N*-bromosuccinimide et d'un composé aromatique à la surface d'un gel de silice mélangé avec du $LiClO_4$ anhydre solide. Tous les substrats ont donné lieu à des bromations aromatiques électrophiles propres conduisant, dans des conditions neutres, aux bromoarènes correspondants. Dans le cas du thiophénol, il ne se produit pas de réaction de substitution et le disulfure correspondant est obtenu avec un excellent rendement.

Mots clés : LP-SiO_2, NBS, arènes, bromation électrophile, régiosélectivité.

[Traduit par la Rédaction]

Introduction

Brominated arenes are versatile intermediates in the synthesis of a wide variety of biologically active compounds. They are also widely used for the preparation of products of commercial importance such as pharmaceuticals, agrochemicals, synthetic colorants, and performance chemicals (1). A popular method for the bromination of aromatic compounds is the reaction of molecular bromine with an arene, in a halogenated hydrocarbon (2) or acetic acid (3). However, in many cases, mixtures of mono-, di-, and polybrominated products are obtained. Another popular and mild, less hazardous, and inexpensive reagent that has been used for electrophilic aromatic bromination is *N*-bromosuccinimide (NBS) in CCl_4 (4). The major advantage of the use of NBS as a brominating agent is that the by-product succinimide can be easily recovered, converted to NBS, and reused. A variety of methods for such a reaction with NBS have been reported in the literature, including NBS-PTZ (5), NBS-PTSA (5), NBS-Amberlyst (6), NBS-NaOH (7), NBS-HZSM (8), and NBS-HBF_4/Et_2O (9). In addition, electrophilic bromination of activated aromatic compounds has been reported to be favored in polar solvents such as propylene carbonate (10), DMF (11), CH_3CN (12), and ionic liquids (13). Despite the apparent utility of these reagents, they have not been widely used for electrophilic aromatic bromination, which may be due to the variable results reported in terms of both products and yields. More recently, green protocols such as solid-state bromination (14) and Oxone®/sodium bromide (15) have been reported in the literature.

Results and discussion

In recent years, the use of lithium perchlorate in diethyl ether (LPDE) as a polar medium has attracted attention owing to the enhanced rate and selectivity observed for various organic transformations in this medium (16). The LPDE medium provides a convenient means to carry out reactions under neutral and easy workup conditions.

In continuation of our interest on the application of lithium perchlorate for various organic transformations (17), we herein describe a simple, efficient, and general method for the electrophilic bromination of aromatic rings by using NBS in CH_2Cl_2 catalyzed by solid lithium perchlorate dispersed on silica gel ($LiClO_4$–SiO_2). The general applicability of this reagent for a large number of aromatic compounds was investigated, and the results are summarized in Tables 1 and 2. The brominated compounds were identified on the basis of their ^{1}H NMR and mass spectral data, and by comparison of these data with those reported in the literature. The

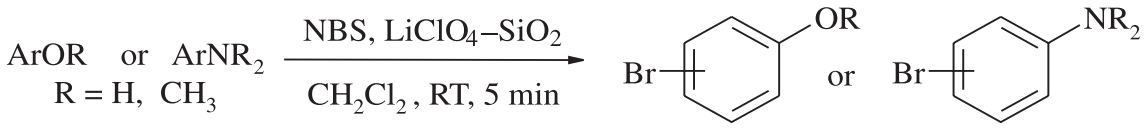
Received 26 July 2004. Published on the NRC Research Press Web site at http://canjchem.nrc.ca on 24 February 2005.

M. Bagheri, N. Azizi, and M.R. Saidi.[1] Department of Chemistry, Sharif University of Technology, P.O. Box 11365–9516, Tehran, Iran.

[1]Corresponding author (e-mail: saidi@sharif.edu).

 doi: 10.1139/V05-001 © 2005 NRC Canada

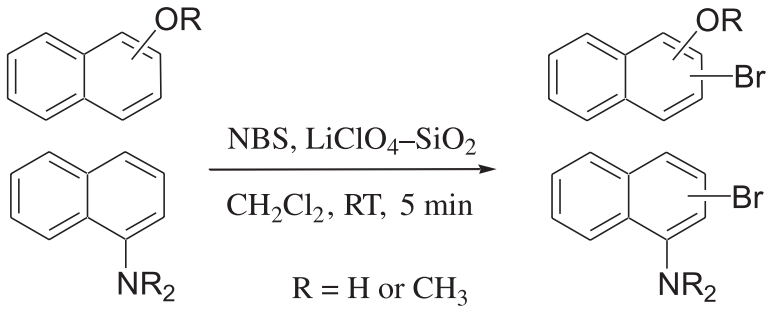
Table 1. Bromination of activated benzene derivatives by NBS in the presence of $LiClO_4$–SiO_2.



Entry	Substrate	NBS (equiv.)	Product(s)	Yield (%)
1	Phenol	2	2,4-Dibromophenol	85
			4-Bromophenol	15
2	Aniline	2	2,4-Bromoaniline	98
3	*p*-Cresol	1	2-Bromo-4-methylphenol	95
4	*p*-Toluidine	1	2-Bromo-4-methyltoluidine	98
5	4-Hydroxyacetophenone	2	3,5-Dibromo-4-hydroxyacetophenone	80
			3-Bromo-4-hydroxyacetophenone	20
6	4-Aminoacetophenone	2	3,5-Dibromo-4-aminoacetophenone	90
7	4-Nitrophenol	2	2,6-Dibromo-4-nitrophenol	80
			2-Bromo-4-nitrophenol	20
8	4-Nitroaniline	2	2,6-Dibromo-4-nitroaniline	98
9[a]	Anisole	1	4-Bromoanisole	98
10	*N,N*-Dimethylaniline	1	4-Bromo-*N,N*-dimethylaniline	98
11	4-(*N,N*-Dimethylamino)benzaldehyde	1	3-Bromo-4-(*N,N*-dimethylamino)benzaldehyde	90
12	2-Aminobenzonitrile	1	2-Amino-4-bromo-benzonitrile	95
13	3-Anisidine	2.5	2,4,6-Tribromo-3-anisidine	10
			2,4-Dibromo-3-anisidine	90
14	4-Bromoaniline	1	2,4-Dibromoaniline	98
15	4-Chloroaniline	1	2-Bromo-4-chloroaniline	98

[a]Reaction time was 2 h, and 1.0 g of $LiClO_4$–SiO_2 was used.

Table 2. Bromination of naphthalene derivatives by NBS in the presence of $LiClO_4$–SiO_2.



Entry	Substrate	NBS (equiv.)	Product(s)	Yield (%)
1	2-Naphthol	1	1-Bromo-2-naphthol	98
2	1-Naphthol	2	2,4-Dibromo-1-naphthol	98
3	1-Naphthylamine	2	2,4-Dibromo-1-naphthylamine	98
4	2,7-Dihydroxynaphthalene	1	1-Bromo-2,7-dihydroxynaphthalene	98
5[a]	2-Methoxynaphthalene	2	1,4-Dibromo-2-methoxynaphthalene	98
6	Anthracene	2	9,10-Dibromoanthracene	100

[a]1.0 g of $LiClO_4$–SiO_2 was used.

starting materials used in this study were commercially available. The bromination reaction was studied at different temperatures and in solvents of different polarities (CH_3CN, CH_2Cl_2, CCl_4, MeOH, and 5 mol/L LPDE), using different molar ratios of NBS/arene. The optimized reaction conditions were found to be the simple stirring of a solution of arene (1 equiv.), NBS (1 equiv.), and 0.4 g $LiClO_4$–SiO_2 (1:4) in CH_2Cl_2 at room temperature, which afforded the product in good yield (Table 1). Without using solid $LiClO_4$ or SiO_2, the reaction is less selective and the reaction time is longer.

The data in Table 1 clearly show the general applicability of this method for a variety of aromatic compounds. In most cases, one product (either the monobromo- or the

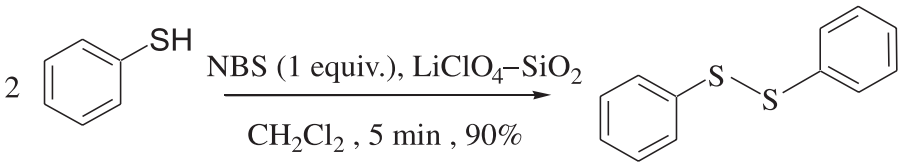
© 2005 NRC Canada

Table 3. Bromination of activated pyridine and quinoline derivatives by NBS in the presence of $LiClO_4$–SiO_2.

Entry	Substrate	NBS (equiv.)	Product(s)	Yield (%)
1	2-Aminopyridine	2	5-Bromo-2-aminopyridine	90
			3,5-Dibromo-2-aminopyridine	10
2	8-Aminoquinoline	2	5,7-Dibromo-8-aminoquinoline	98

Note: Reaction time: 5 min.

Scheme 1.



dibromoarene) was formed in a short reaction time and in good yield. In all cases, the crude products were monitored by GC and checked for the presence of any by-products. Some general trends are apparent from the data in Table 1. First, the reactivity of the substrate seems to be related to the electron density on the aromatic ring. Thus, the nucleus must be sufficiently activated before significant reactions occurred. This reagent is not effective for benzene, toluene, or naphthalene, and amino derivatives give slightly easier and cleaner reaction than hydroxyl derivatives. The presence of electron-donating or electron-withdrawing groups on the aniline or phenol did not affect the rates or the yields of the reactions. For example, *p*-methylaniline, *p*-nitroaniline, *N,N*-dimethylaniline, and *p*-(*N,N*-dimethylamino)benzaldehyde gave the monobromo product in short reaction times and in high yields (Table 1, entries 4, 8, 10, and 11). *p*-*S*ubstituted anilines were brominated at the ortho position. In the case of aniline (Table 1, entry 2), 1-naphthylamine (Table 2, entry 3), and 4-aminoacetophenone (Table 1, entry 6), as well as 8-aminoquinoline (see Table 3, entry 2), in the presence of 2 equiv. of NBS dibromination occurred at the 2 and 4 positions in high yields. It is noteworthy that the direct bromination of aniline with bromine in solution often results in polybromination and requires the protection of amino groups. The results with the derivatives of phenol are somewhat different. For example, under the above reaction conditions, phenol gave dibromophenol (Table 1, entry 1), while 2-naphthol (Table 2, entry 1), 2,7-dihydroxynaphthalene (Table 2, entry 4), and *p*-substituted phenols gave only monobrominated products in short reaction times and with high yields (except in the case of 4-nitrophenol). 1-Naphthol (Table 2, entry 2) and 3-anisidine (Table 1, entry 13) produced the corresponding dibromo derivatives. The bromination of methoxybenzene required a long reaction time with 1 g of $LiClO_4$–SiO_2 (Table 1, entry 9), but 2-methoxynaphthalene gave the dibromo product in excellent yield with 1 g of $LiClO_4$–SiO_2 (Table 1, entry 13). Comparison of our results with those reported in the literature clearly shows that higher reactivity and higher selectivity are obtained with $LiClO_4$–SiO_2 than with SiO_2 (18).

We next investigated bromination of 2-aminopyridine and 8-aminoquinoline. The most direct approach to the bromination of pyridine derivatives is the direct electrophilic halogenation of the activated pyridines in polar protic solvents, such as water and ethanol. In the reported procedures, with the use of common organic solvents such as CH_3CN, CS_2, CH_2Cl_2, and CCl_4, mixtures of monobromo and dibromo products were formed, with long reaction times (19, 20). We have found that NBS/$LiClO_4$–SiO_2 is suitable for the regioselective monobromination of aminopyridine and dibromination of 8-aminoquioline with excellent yields and a reaction time of a few minutes (Table 3).

To extend the scope of this reagent, we have also investigated bromination of anthracene and thiophenol. NBS in CCl_4 is a common brominating agent for anthracene and affords a mixture of mono- and dibromoanthracene in good yields (21). We found that bromination of anthracene with 2 equiv. of NBS using the NBS/$LiClO_4$–SiO_2 reagent yieled 9,10-dibromoanthracene as the sole product. On the other hand, bromination of thiophenol was not successful, and coupling of thiol groups to form the disulfide in excellent yields was observed (Scheme 1).

In conclusion, we have developed a simple, general, and efficient method for electrophilic bromination of activated arenes under mild conditions, mediated by $LiClO_4$ dispersed on SiO_2 in CH_2Cl_2. The absence of side-chain bromination products in this procedure clearly indicates that an electrophilic aromatic substitution mechanism operates in this reaction medium; the remarkable enhancement in reaction rates and regioselectivity could be explained by increased polarization of the N—Br bond of NBS in this ionic process. This procedure also can be applied to polycyclic aromatic compounds. Furthermore, the $LiClO_4$–SiO_2 reagent is cheap, stable, easy to handle, and nontoxic. The present method would be useful in organic synthesis. We are currently extending this methodology to the use of NXS (X = Cl, I).

Experimental

General procedure for the bromination of aromatic compounds with NBS

NBS (1–2 eqiuv.) was added slowly to a stirred solution of an aromatic compound (2 mmol) and 0.4 g of $LiClO_4$–SiO_2 (1:4) in CH_2Cl_2 (20 mL). When the addition was complete, the reaction mixture was stirred at room temperature and the progress of the reaction monitored by TLC and GC. Complete conversion was achieved for most of the substrates. The reaction mixture was filtered, and the catalyst

© 2005 NRC Canada

was recovered and washed with CH_2Cl_2 (2 × 10 mL). The combined organic layer was washed with water and dried over anhydrous sodium sulfate and concentrated under reduced pressure using a rotary evaporator. Almost pure crude product was obtained in most cases. Further purification was carried out by short column chromatography on silica gel (ethyl acetate: petroleum ether). All compounds are known and were characterized on the basis of their spectroscopic data (GC, MS, NMR) and by comparison of these data with those reported in the literature.

Acknowledgements

We are grateful to the Research Council of Sharif University of Technology for financial support. We also thank Volkswagen-Stiftung (Federal Republic of Germany) for financial support towards the purchase of chemicals.

References

1. (*a*) C. Chrisophersen. Acta Chem. Scand. **39B**, 517 (1985); (*b*) B. Iddon and B.J. Wakefield. *In* Bromine compounds. *Edited by* D. Price, B. Iddon, and B.J. Wakefield. Elsevier, Amsterdam. 1988. pp. 181–251; (*c*) A. Brancale, C. McGuigan, A. Graciela, R. Snoeck, E. De Clercq, and J. Balzarini. Bioorg. Med. Chem. Lett. **10**, 1215 (2000); (*d*) P.D. Leeson, R. Baker, R.W. Carling, N.R. Curtis, K.W. Moore, B.J. Williams, A.C. Foster, A.E. Donald, J.A. Kemp, and G.R. Marshall. J. Med. Chem. **34**, 1243 (1991).
2. (*a*) S.M. Kelly and H. Schadt. Helv. Chim. Acta, **68**, 813 (1985); (*b*) K.H. Dotz and M. Popall. Chem. Ber. **121**, 665 (1988). (*c*) S. Torii, H. Tanaka, T. Siroi, and M. Akada. J. Org. Chem. **49**, 2061 (1984).
3. C.E. Coburn, D.K. Anderson, and J.S. Swenton. J. Org. Chem. **48**, 1455 (1983).
4. J.C. Roberts and P. Roffey. J. Chem. Soc. C, 160 (1966).
5. (*a*) P. Bovonsombat and E. McNelis. Synthesis, 237 (1993); (*b*) R.J. Lahoti and K.V. Srinivasan. J. Mol. Catal. **210**, 165 (2004).
6. Y. Goldberg and H. Alper. J. Mol. Catal. **88**, 377 (1994).
7. J. Auerbach, S.A. Weissmann, T.J. Blacklock, M.R. Angles, and K. Hoogsteen. Tetrahedron Lett. **34**, 931 (1993).
8. P. Vincent, A. Sudalai, D. Thomas, and K.V. Srinivasan. Tetrahedron Lett. **35**, 7055 (1994).
9. T. Oberhauser. J. Org. Chem. **62**, 4504 (1997).
10. S.D. Ross, M. Finkelstein, and R.C. Petersen. J. Am. Chem. Soc. **80**, 4327 (1958).
11. (*a*) J.M. Gnaim, P.M. Keehn, and B.S. Green. Tetrahedron Lett. **33**, 2883 (1992); (*b*) R.H. Mitchell, Y.H. Lai, and R.V. Williams. J. Org. Chem. **44**, 4733 (1979).
12. M.C. Carreno, J.L. Garcia Ruano, G. Sanz, M.A. Toledo, and A. Urbano. J. Org. Chem. **60**, 5328 (1995).
13. (*a*) R. Rajagopal, D.V. Jarikote, R.J. Lahoti, T. Daniel, and K.V. Srinivasan. Tetrahedron Lett. **44**, 1815 (2003); (*b*) J.S. Yadav, B.V.S. Reddy, P.S.R. Reddy, A.K. Basak, and A.V. Narsaiah. Adv. Synth. Catal. **77**, 346 (2004).
14. F. Toda and J. Schmeyers. Green Chem. **5**, 701 (2003).
15. K.-J. Lee, H.-K. Cho, and C.-E. Song. Bull. Korean Chem. Soc. **23**, 773 (2002).
16. S. Sankara Raman and J.E. Nesakumar. Eur. J. Org. Chem. 2003 (2000).
17. (*a*) M.R. Saidi and N. Azizi. Tetrahedron: Asymmetry, **13**, 2523 (2002); (*b*) M.R. Saidi and N. Azizi. Tetrahedron: Asymmetry, **14**, 389 (2003); (*c*) N. Azizi and M.R. Saidi. Tetrahedron Lett. **43**, 4305 (2002); (*d*) M.R. Saidi and N. Azizi. Synlett, 1347 (2002); (*e*) N. Azizi and M.R. Saidi. Tetrahedron, **59**, 5329 (2003).
18. H. Konishi, K. Aritomi, T. Okano, and T. Kiji. Bull. Chem. Soc. Jpn. **62**, 304 (1989).
19. (*a*) F.S. Yates. *In* Comprehensive heterocycle chemistry. Vol. 2. *Edited by* A.R. Katritzky and C.W. Rees. Pergamon Press, Oxford. 1984. pp. 198–205; (*b*) R.H. Mitchell, Y.-H. Lai, and R.V. Williams. J. Org. Chem. **44**, 4733 (1979); (*c*) P.J. Brignell, P.E. Jones, and A.R. Katrizky. J. Chem. Soc. B, 117 (1970).
20. V. Canibano, J.F. Rodriguez, M. Santos, M.A. Sanz-Tejedor, M.C. Carrefio, G. Gonzalez, and J.-L. Gareia-Ruano. Synthesis, 2175 (2001).
21. S. Duan, F. Turk, J. Speigle, J. Corbin, J. Masnovi, and R.-J. Baker. J. Org. Chem. **65**, 3005 (2000).

© 2005 NRC Canada

Synthesis, characterization, and coordination chemistry of phosphines with ethylenedioxythiophene substituents

M'hamed Chahma, Daniel J.T. Myles, and Robin G. Hicks

Abstract: The preparation of several new phosphines bearing one or more 3,4-ethylenedioxythiophene (EDOT) units as substituents linked at the 2-thienyl position is described. The phosphines were prepared by reaction of lithiated EDOT intermediates with appropriate chlorophosphines to afford (3,4-ethylenedioxy-2-thienyl)diphenylphosphine (**1**), (bis(3,4-ethylenedioxy-2-thienyl)phenylphosphine (**2**), tris(3,4-ethylenedioxy-2-thienyl)phosphine (**3**), 2,5-bis(diphenylphosphino)-3,4-ethylenedioxythiophene (**4**), and 2-diphenylphosphino-5-mesitylthio-3,4-ethylenedioxythiophene (**5**). Molybdenum carbonyl complexes of compounds **1**–**3** were prepared by reaction of the phosphine ligands with *cis*-$Mo(CO)_4(pip)_2$. In all cases, spectroscopic evidence is fully consistent with the phosphines acting as monodentate, P-bound ligands. Electrochemical studies on the phosphines as well as their metal complexes indicate that the normal electrochemical redox robustness of the EDOT group is dramatically decreased by the presence of phosphine substituents: all compounds exhibited irreversible oxidation processes and no evidence of electropolymerization was observed for the phosphines bearing two or three EDOT groups.

Key words: phosphines, thiophene, 3,4-ethylenedioxythiophene, EDOT, electrochemistry, coordination complexes.

Résumé : On décrit la préparation de plusieurs nouvelles phosphines portant un ou plusieurs unités de 3,4-éthylènedioxythiophène (EDOT) comme substituants liés à la position 2-thiényle. On a préparé les phosphines par la réaction d'intermédiaires EDOT lithiés avec les chlorophosphines appropriées qui ont conduit à la formation des (3,4-éthylènedioxy-2-thiényl)diphénylphosphine (**1**), bis(3,4-éthylènedioxy-2-thiényl)phénylphosphine (**2**), tris(3,4-éthylènedioxy-2-thiényl)phosphine (**3**), 2,5-bis(diphénylphosphino)-3,4-éthylènedioxythiophène (**4**) et 2-diphénylphosphino-5-mésitylthio-3,4-éthylènedioxythiophène (**5**). La réaction des ligands phosphines avec les *cis*-$Mo(CO)_4(pip)_2$ a permis de préparer les complexes du molybdène carbonyle des composés **1**–**3**. Dans tous les cas, les données spectroscopiques sont en total accord avec le fait que les phosphines agissent comme des ligands monodentates liés par le phosphore. Des études électrochimiques sur les phosphines ainsi que sur leurs complexes métalliques indiquent que la solidité redox électrochimique normale du groupe EDOT est dramatiquement abaissée par la présence des substituants phosphines : tous les composés donnent lieu à des processus d'oxydation irréversibles et aucune électropolymérisation n'a été observée avec les phosphines portant deux ou trois groupes EDOT.

Mots clés : phosphines, thiophène, 3,4-éthylènedioxythiophène, EDOT, électrochimie, complexes de coordination.

[Traduit par la Rédaction]

Introduction

The importance of phosphine ligands in (organo)transition metal chemistry cannot be overstated. The ability to modulate steric and electronic properties of phosphines (1) and their resulting metal complexes has facilitated the development of metal phosphine-based catalysis in a wide range of forums, particularly in late metal-catalyzed cross-coupling reactions (Suzuki, Stille, Kumada–Corriu, etc.) (2). As one of the prototypical members of this ligand class, triphenylphosphine is a true benchmark ligand. In recent years, other arylphosphine derivatives have been explored in which some or all of the phenyl groups have been replaced by heteroaromatic rings such as pyridine (3) and furan (4). Phosphines containing thiophene subtitutents have also received attention. Although they typically behave as simple P-monodentate ligands (5), thienylphosphines can also act as bridging ligands via the thiophene sulfur atom (6), or as chelating ligands involving cyclometallation of one of the thiophene rings (7).

Thienylphosphine complexes have also attracted interest because of the possibility of making phosphine-substituted conjugated polythiophenes in which the electronic properties of the polymer can be tuned via metal coordination at the phosphine (8). Metal–organic polymers have received a great deal of interest stemming from the potential properties that may arise from polymers containing both organic and inorganic elements (9). There has been a particularly strong emphasis on polymers containing metals as part of, or attached to, conjugated frameworks (10). The main motivation behind

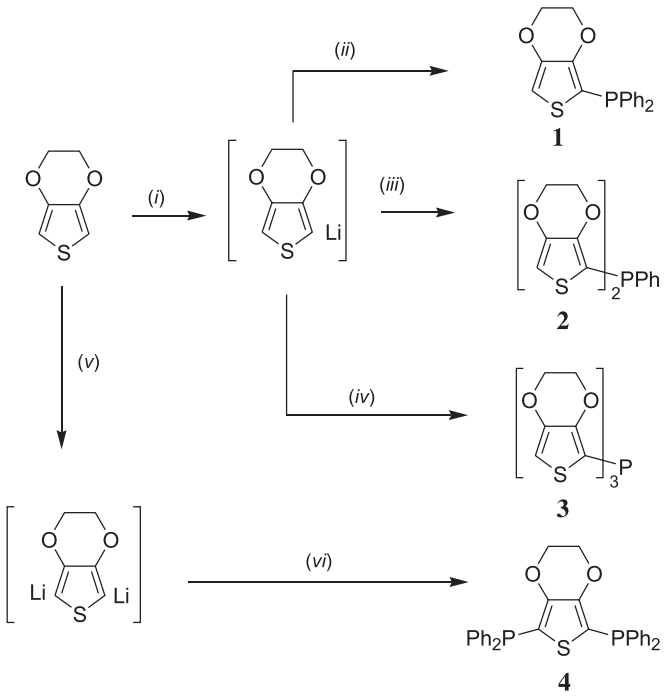
Received 5 August 2004. Published on the NRC Research Press Web site at http://canjchem.nrc.ca on 24 February 2005.

M. Chahma, D.J.T. Myles, and R.G. Hicks.[1] Department of Chemistry, University of Victoria, PO Box 3065 STN CSC, Victoria, BC V8W 3V6, Canada.

[1]Corresponding author (e-mail: rhicks@uvic.ca).

 doi: 10.1139/V05-004 © 2005 NRC Canada

Scheme 1.



these studies is to explore the possibilities of making new materials, which combine inherent functional properties of purely organic conjugated polymers (11) such as conductivity, electrochromism, and light emission with the electronically interesting features of metal complexes (magnetic, optical, etc.).

Among the many thiophenes that have been incorporated into conjugated organic polymers, 3,4-ethylendioxythiophene (EDOT) stands out as an electron-rich derivative. The strongly electron-donating oxygen atoms render EDOT relatively easily oxidized and impart exceptional stability to the resulting homopolymer. The outstanding properties of poly(EDOT) have led to the synthesis and study of a wide range of hybrid materials of EDOT with other organic and inorganic moieties (12). However, no EDOT-substituted phosphines have been reported. It occurred to us that such species should be useful ligands and may lead to interesting materials from hybrid EDOT–phosphine–metal complexes and polymers. To this end, herein we describe the synthesis, characterization, and preliminary coordination chemistry of triarylphosphine derivatives bearing 3,4-ethylenedioxy-2-thienyl groups as substituents.

Synthesis and characterization of EDOT phosphines

The EDOT–phosphine derivatives were prepared by reactions of in-situ-generated, lithiated EDOT compounds with the appropriate chlorophosphine (Scheme 1). Thus, Li^+EDOT^- reacts with chlorodiphenylphosphine, dichlorophenylphosphine, and trichlorophosphine to give $Ph_2P(EDOT)$ (**1**), $PhP(EDOT)_2$ (**2**), and $P(EDOT)_3$ (**3**), respectively. In addition, 2,5-bis(diphenylphosphino)-3,4-ethylenedioxythiophene (Ph_2P-EDOT-PPh_2) (**4**) was prepared by reaction of chlorodiphenylphosphine with doubly lithiated EDOT.

Scheme 2.

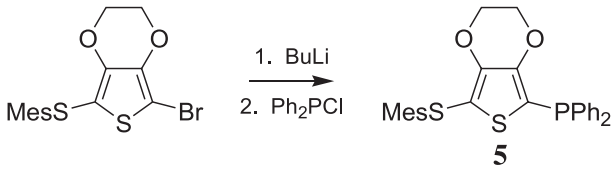


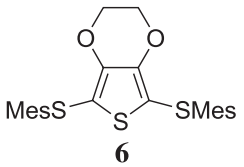
Table 1. Characterization data for EDOT–phosphines **1**–**5** and related compounds.

Compound	λ_{max} (nm)	^{31}P NMR δ (ppm)	E_p (V vs. Fc/Fc^+)
EDOT	260	—	+0.93
$EDOT–PPh_2$ (**1**)	274	–28.1	+0.79
$(EDOT)_2PPh$ (**2**)	274	–50.5	+0.68
$(EDOT)_3P$ (**3**)	277	–68.5	+0.60
Ph_2P-EDOT-PPh_2 (**4**)	292	–26.5	+0.52
MesS-EDOT-PPh_2 (**5**)	288, 305	–27.6	+0.57
MesS-EDOT-SMes (**6**)	305	—	+0.40[a]

[a]Reversible.

In addition to compounds **1**–**4**, an EDOT derivative with one diphenylphosphine (Ph_2P) and one mesitylthio (MesS) substituent was prepared for comparison of electrochemical properties. Compound **5** was synthesized from 5-bromo-2-(mesitylthio)-3,4-ethylenedioxythiophene) (13) via lithium–halogen exchange followed by treatment with Ph_2PCl using analogous protocols employed in the synthesis of **1**–**4**. (Scheme 2).

Although some EDOT derivatives with unsubstituted thiophene α-carbon atoms are unstable to air and moisture, all of the EDOT phosphines are air-stable compounds. Table 1 summarizes pertinent physicochemical data for the new EDOT-substituted phosphines as well as EDOT itself and 2,5-bis(mesitylthio)3,4-ethylenedioxythiophene (**6**), a disubstituted EDOT derivative previously made in our lab.(13) The UV–vis spectra all have lowest energy absorption maxima in the neighborhood of 277–290 nm. These are all slightly red-shifted relative to EDOT itself (λmax = 260 nm) indicative of a weak electronic perturbation of the EDOT chromophore by the phosphine moieties. The ^{31}P NMR chemical shifts of the series $(EDOT)_nPPh_{3-n}$ progress smoothly to more negative values as phenyl groups are successively replaced by more electron-rich EDOT moieties. Analogous behaviour is observed in the related series of unsubstituted 2-thienyl–phenylphosphines $(2\text{-Th})_nPPh_{3-n}$ (Fig. 1) (6*a*). Similar trends can also be found in triarylphosphines bearing para substituents, for which the more electron-donating groups give rise to more negative δ ^{31}P NMR values (14).



The redox properties of compounds **1**–**5** were examined by cyclic voltammetry. All new compounds **1**–**5** exhibited irreversible oxidation waves at the potentials given in Table 1.

© 2005 NRC Canada

Table 2. Characterization data for Mo complexes of EDOT phosphines and related compounds.

Compound	^{31}P NMR δ (ppm)	ν(CO) (cm^{-1})	E_p (V vs. Fc/Fc$^+$)
cis-Mo(CO)$_4$(EPPh$_2$)$_2$ (**7**)	+24.3	2023m, 1924s, 1908s, 1878m	+0.32
Mo(CO)$_5$(E$_2$PPh) (**8**)	+7.6	1992w, 1946sh	+0.67
Mo(CO)$_5$(E$_3$P) (**9**)	–8.5	1990w, 1947sh	+0.69
cis-Mo(CO)$_4$(ThPPh$_2$)$_2$[6c]	+26.7	2010, 1900, 1880	—
Mo(CO)$_5$(Th$_2$PPh)[6c]	+15.0	2020, 1945, 1905, 1885	—
Mo(CO)$_5$(Th$_3$P)[6c]	+6.6	2020, 1945, 1910, 1890	—

Fig. 1. ^{31}P NMR chemical shifts for (2-thienyl)phenylphosphines (data from ref. 14) and (3,4-ethylenedioxy-2-thienyl)phenylphosphines.

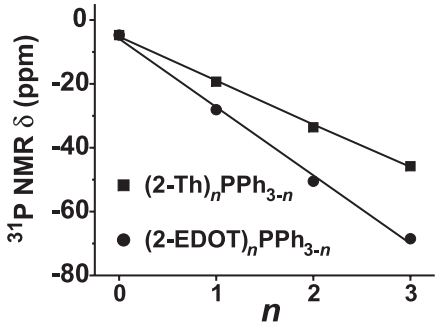
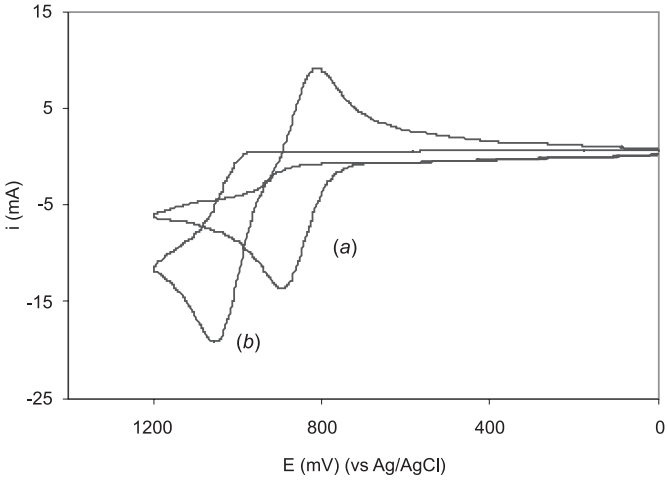


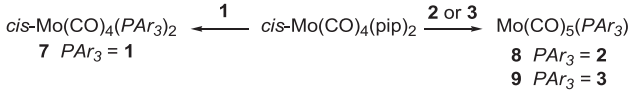
Fig. 2. CV of 2 × 10^{-4} mol/L of **6** (*a*) alone and (*b*) with 1 equiv. of Ph$_3$P added.



For compounds **1**–**3**, the irreversible nature of the oxidation was not unexpected because the EDOT groups in these compounds contain unsubstituted positions on the thiophene ring. These unsubstituted positions are known to be highly reactive sites in oxidized thiophenes. However, the bis(phosphine)-substituted EDOT **4** and 5-mesitylthio-2-diphenylphosphine-3,4-ethylenedioxythiohene (**5**) also exhibited irreversible behaviour upon oxidation. Thiophenes containing substituents at all the 2 (or 5) positions generally can be electrochemically oxidized to give radical cations that are stable at least on electrochemical timescales, For example, bis(mesitylthio)EDOT **6** undergoes a fully reversible oxidation to its radical cation at +0.40 mV. Evidently, the presence of a phosphine group on one of the a carbon atoms of EDOT render the oxidation of the latter moiety irreversible. In general, the oxidation of thiophene derivatives bearing two or more unsubstituted α-carbon atoms are irreversibly oxidized because the resulting radical cations couple at these carbons — this is the first step in the electropolymerization of thiophene and its derivatives. The source of instability in compounds **1**–**5** appears to arise from reactions specific to phosphine-containing thiophenes: although, in principle, compounds **2** and **3** could lead to poly(thiophene–phosphine) materials upon oxidation, repeated electrochemical cycling lead to passivation of the electrode and no formation of polymer was observed. Similar behavior was observed in related phosphinoterthiophenes (8*e*). As a final piece of supporting evidence, the reversibility of the electrochemical oxidation of **6** is dramatically decreased upon addition of triphenylphosphine (Fig. 2).

Coordination complexes

Preliminary investigations into the coordination chemistry of the phosphines involved reactions with molybdenum carbonyl species; related complexes of other 2-thienylphosphines have been reported (6*b*, 6*c*, 6*f*). Reactions of **1** with the reagent *cis*-Mo(CO)$_4$(piperidine)$_2$ (15) led to the expected cis-disubstituted product *cis*-Mo(CO)$_4$(EPPh$_2$)$_2$ (**7**). However, reactions of **2** or **3** with *cis*-Mo(CO)$_4$(piperidine)$_2$ in a 2:1 ratio did gave mixtures of products, which appeared to contain the *mono*substituted products Mo(CO)$_5$(PAr$_3$) in addition to the anticipated disubstituted products. Changing the stoichiometric ratio of phosphines to Mo to 1:1 produced the monosubstituted products **8** and **9** in high yields. These unexpected products must result from intermolecular CO transfer and may be a consequence of the larger steric bulk of the phosphines bearing multiple EDOT substituents. The qualitative similarity of an EDOT group to a naphthyl group would lead to approximately similar steric features between (EDOT)$_3$P (**3**) and tris(1-naphthyl)phosphine, the latter of which has a cone angle of ~200° (1*c*).



The product identities were confirmed through a combination of IR, NMR, and mass spectroscopies. The ^{31}P NMR chemical shifts (see Table 2) of the complexes are 52–60 ppm upfield relative to the chemical shifts of the free ligand, indicative of P-coordinated phosphines. The proton and carbon NMR suggest simple P-monodentate coordination modes for all three phosphines; no evidence of either cyclometallation of S-donating binding is detected. The ^{13}C

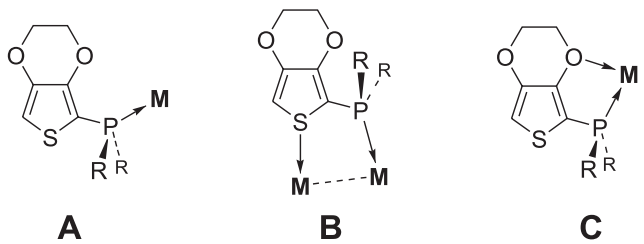
© 2005 NRC Canada

NMR spectra were particularly informative as the magnitude of the carbon–phosphorus coupling constants to the carbonyl groups provided strong support for the cis-disubstituted geometry of **7** as well as the monosubstituted nature of **8** and **9**. Parent molecular anions were observed in the mass spectra of all three complexes. However, these are all relatively weak compared with the base peaks, which in each case correspond to the loss of two carbonyls. This process may well be facilitated by chelation of an ethylenedioxy oxygen atom of the EDOT–phosphines (see the following). The ν(CO) frequencies are quite similar to those observed in related molybdenum carbonyl complexes of 2-thienylphosphines, a feature that suggests that the π-electron-rich nature of the EDOT moiety is not strongly felt by the metal center in these complexes.

Cyclic voltammetry studies on complexes **7**–**9** revealed irreversible oxidations for all three compounds. Interestingly, the oxidation peak potential for complexes **8** and **9** are very similar to the peak potentials for the corresponding free ligand, whereas the peak potential for **7** is some 0.4 V lower than its free phosphine ligand. This may be related to the fact that **7** has two EDOT phosphine ligands whereas **8** and **9** have one each, although the irreversibility of the oxidations renders direct comparisons difficult owing to the scan rate dependence of these processes. Attempts to electropolymerize **7**–**9** by repeated electrochemical cycling failed, instead leading to electrode passivation.

Conclusions

We have described the synthesis and characterization of a new series of phosphines bearing ethylenedioxythiophene substituents. Characterization of the phosphines as well as metal complexes thereof suggest there is little electronic perturbation of the EDOT group by the phosphine and vice versa. In sharp contrast to other lone-pair-containing substituents (e.g., -OR, -SR) that can enhance the redox stability of thiophenes, phosphine groups do not offer much in the way of electrochemical stability at all and in fact can destabilize the otherwise inherently robust redox characteristics of the EDOT moiety. In a similar vein, it appears that the electron richness of the EDOT ring is not manifested in a more "electron-rich" metal center in coordination complexes — at least for the ones presented herein. Nonetheless, these compounds should be useful additions to the stable of arylphosphine ligands because of their ease of synthesis, variable steric bulk, and in particular because of the potential modes of coordination they offer: As simple monodentate mode **A**, bidentate (P/S) bridging ligands in polynuclear systems **B**, or chelating (P/O) chelating **C** — the latter two having the potential to be hemilabile coordination modes (16). Studies aimed at exploring the potential coordinative versatility of these ligands are in progress.



Experimental

General considerations

All reagents were purchased from Aldrich and used as received; $Mo(CO)_4(piperdine)_2$ was prepared according to literature procedures (15). All reactions were performed under an atmosphere of dry argon using standard Schlenk or glove box techniques. Solvents were dried and distilled under argon prior to use (CH_2Cl_2, CaH_2; THF, Na–benzophenone). Mass spectra were recorded on a Kratos Concept IH mass spectrometer system. IR spectra were recorded as Nujol mulls or KBr presses on a PerkinElmer Spectrum One spectrometer. NMR spectra were recorded on a Bruker AMX360 spectrometer. Cyclic voltammetry experiments were performed using a CV-50W voltammetric analyzer (BAS) at room temperature (22 ± 2 °C). Voltammetric measurements were performed in CH_2Cl_2 containing 1 mol/L of *n*-Bu_4NBF_4. The platinum electrode (BAS, diameter 1.6 mm) was used as the working electrode. Platinum and silver wires were used as auxiliary and reference electrodes, respectively. The reference electrode was calibrated vs. ferrocene/ferrocenium redox ($E°$ = 0.440 vs. Ag/AgCl) internal reference. The working electrode was polished on alumina before use. *iR* compensations were applied for all experiments.

General synthesis of (3,4-ethylenedioxy-2-thienyl) phosphine derivatives

The synthesis of EDOT-substituted phosphines **1**–**4** is exemplified by the synthesis of **1**. EDOT (1.313 g, 9.25 mmol) was dissolved in THF (50 mL) and treated with *n*-BuLi (1.6 mol/L, 3 mL, 9.36 mmol) at room temperature. After 2 h of stirring, the mixture was cooled to –78 °C and chlorodiphenylphosphine (3 mL, 3.1 mmol) was added dropwise to the reaction mixture. The mixture was stirred at –78 °C for 2 h and gradually brought to room temperature. The mixture was then poured into water (100 mL) and extracted using CH_2Cl_2 (2 × 100 mL). The organic layers were combined and dried over anhydr. $MgSO_4$. Removal of the solvent gave a crude product, which was purified by chromatography using silica gel and chloroform as the eluent. The product was then recrystallized in CH_2Cl_2–methanol.

(3,4-Ethylenedioxy-2-thienyl)diphenylphosphine (EDOT-PPh_2, 1)

Yield: 74%; mp 84 °C. UV–vis (CH_2Cl_2): λ_{max} (ε) 274 nm (16 450 M^{-1} cm^{-1}). ^1H NMR (CD_2Cl_2, 300 MHz) δ: 4.20 (m, 4H), 6.60 (s, 1H), 7.40 (m, 10H). ^{13}C NMR (CD_2Cl_2, 125 MHz) δ: 64.94 (CH_2), 65.41 (CH_2), 106.22 (CH), 109.95 (C, d, J = 28.6 Hz), 128.75 (4CH, d, J = 6.8 Hz), 129.23 (2CH), 133.54 (4CH, d, J = 20.2 Hz), 137.24 (2C, d, J = 8.6 Hz), 142.72 (C, d, J = 3.7 Hz), 147.01 (2C, d, J = 18.9 Hz). ^{31}P NMR (CD_2Cl_2, 145 MHz) δ: –28.12. HR-MS calcd. for $C_{18}H_{15}O_2PS$: 326.0530; found: 326.0535. Anal. calcd. for $C_{18}H_{15}O_2P$ (%): C 66.25, H 4.63, O 9.80; found: C 66.21, H 4.17, O 9.95.

© 2005 NRC Canada

Bis(3,4-ethylenedioxy-2-thienyl)phenylphosphine ((EDOT)$_2$PPh, 2)

Yield: 74%; mp 137 °C. UV–vis (CH_2Cl_2): λ_{max} (ε) 274 nm (21 500 M^{-1} cm^{-1}). ^{1}H NMR (CD_2Cl_2, 300 MHz) δ: 4.20 (m, 8H), 6.60 (s, 2H), 7.40 (m, 5H). ^{13}C NMR (CD_2Cl_2, 125 MHz) δ: 64.91 ($2CH_2$), 65.42 ($2CH_2$), 106.31 (2CH), 109.22 (C, d, *J* = 25.5 Hz), 128.62 (2CH, d, *J* = 6.8 Hz), 129.12 (CH), 132.48 (2CH, d, *J* = 19.8 Hz), 136.95 (2C, d, *J* = 6.3 Hz) 142.53 (2C, d, *J* = 4 Hz), 146.90 (2 C, d, *J* = 20.5 Hz). ^{31}P NMR (CD_2Cl_2, 145 MHz) δ: –50.5. HR-MS calcd. for $C_{18}H_{15}O_4PS_2$: 390.0149; found: 390.0144. Anal. calcd. for $C_{18}H_{15}O_4PS_2$ (%): C 55.38, H 3.87, O 16.39; found: C 54.60, H 3.89, O 16.39.

Tris(3,4-ethylenedioxy-2-thienyl)phosphine ((EDOT)$_3$P, 3)

Yield: 77%; mp 181 °C. UV–vis (CH_2Cl_2): λ_{max} (ε) 277 nm (25 450 M^{-1} cm^{-1}). ^{1}H NMR (CD_2Cl_2, 300 MHz) δ: 4.20 (m, 12H), 6.60 (s, 3H). ^{13}C NMR (CD_2Cl_2, 125 MHz) δ: 64.90 (CH_2), 65.43 (CH_2), 106.15 (CH), 108.75 (C, d, *J* = 22.6 Hz), 142.47 (C, d, *J* = 4.5 Hz), 146.14 (C, d, *J* = 21.5 Hz). ^{31}P NMR (CD_2Cl_2, 145 MHz) δ: –50.54. HR-MS calcd. for $C_{18}H_{15}O_6PS_3$: 453.9768; found: 453.9757. Anal. calcd. for $C_{18}H_{15}O_6PS_3$ (%): C 47.57, H 3.33, O 21.12; found: C 47.07, H 3.17, O 21.97.

2,5-Bis(diphenylphosphinyl)-3,4-ethylenedioxythiophene (Ph$_2$P-EDOT-PPh$_2$, 4)

Yield: 63%; mp 101 °C. UV–vis (CH_2Cl_2): λ_{max} (ε) 292 nm (25 230 M^{-1} cm^{-1}). ^{1}H NMR (CD_2Cl_2, 300 MHz) δ: 4.20 (s, 4H), 7.40 (m, 20H). ^{13}C NMR (CD_2Cl_2, 125 MHz) δ: 65.14 (CH_2), 116.35 (C, d, *J* = 31.3 Hz), 128.74 (CH, d, *J* = 7.5 Hz), 129.29 (CH), 133.57 (CH, d, *J* = 20.4 Hz), 136.79 (C, d, *J* = 8.8 Hz), 146.91 (C, dd, *J* = 2.9 Hz, *J* = 17.9 Hz). ^{31}P NMR (CD_2Cl_2, 145 MHz) δ: –26.5. HR-MS calcd. for $C_{30}H_{24}O_2P_2S$: 510.0972; found: 510.0963. Anal. calcd. for $C_{30}H_{24}O_2P_2S$ (%): C 70.58, H 4.74, O 6.27, P 12.13; found: C 67.97, H 4.48, O 6.67, P 11.67.

2-Diphenylphosphinyl-5-mesitylthio-3,4-ethylenedioxythiophene (MesS-EDOT-PPh$_2$, 5)

Yield: 70%; mp 102 °C. ^{1}H NMR (CD_2Cl_2, 300 MHz) δ: 2.30 (s, 3H), 2.50 (s, 6H), 4.2 (m, 4H), 6.90 (s, 2H), 7.30 (m, 10H). ^{13}C NMR (CD_2Cl_2, 125 MHz) δ: 21.33 (CH_3), 22.34 ($2CH_3$), 65.35 (CH_2), 65.37 (CH_2), 110.97 (2C, d, *J* = 31.6 Hz), 116.00 (2C), 128.97 (4CH, d, *J* = 6.8 Hz), 129.48 (2CH), 129.79 (2CH) 133.68 (4CH, d, *J* = 19.2 Hz), 137.12 (C, d, *J* = 7.9), 139.65 (C), 142.65 (C, d, *J* = 3.4 Hz), 143.21 (C), 146.71 (2C, d, *J* = 19.2 Hz). ^{31}P NMR (CD_2Cl_2, 145 MHz) δ: –27.6. HR-MS calcd. for $C_{27}H_{25}O_6PS_2$: 476.1034; found: 476.1033. Anal. calcd. for $C_{27}H_{25}O_6PS_2$ (%): C 68.04, H 5.29, O 6.71, P 7.93; found: C 67.58, H 4.96, O 7.12, P 6.08.

***Syntheses of* cis-*Mo(CO)$_4$*(PAr$_3$)$_2$ (7, PAr$_3$ = 1)**

A solution of **1** (0.652 g, 2 mmol) in CH_2Cl_2 (2 mL) was added dropwise to a stirred slurry of *cis*-$Mo(CO)_4$(piperidine)$_2$ (0.380 g, 1 mmol) in CH_2Cl_2 (10 mL) at room temperature. The mixture was stirred overnight and filtered through a pad of silica gel. After filtration, the solution was concentrated and the product was precipitated by the addition of pentane. The complex was isolated as a white solid (yield 43%); mp 115 °C. IR ν(CO) cm^{-1}: 2023, 1924, 1908, 1878. ^{1}H NMR (CD_2Cl_2, 300 MHz) δ: 4.10 (m, 8H), 6.60 (d, *J* = 2.10 Hz, 2H), 7.20 (m, 8H), 7.40 (m, 12). ^{13}C NMR (CD_2Cl_2, 125 MHz) δ: 64.60 (CH_2), 64.80 (CH_2), 105.50 (CH), 109.80 (C, dd, *J* = 12.5 Hz), 128.30 (C, t, *J* = 4.6 Hz), 130.00 (CH) 133.40 (C, t, *J* = 6.8 Hz), 135.90 (C, dt, *J* = 15.5 Hz), 143.20 (C, t, *J* = 3 Hz), 145.70 (C, t, *J* = 3.7 Hz), 210.20 (C, t, *J* = 9.4 Hz), 215.6 (C, t, *J* = 9.3 Hz). ^{31}P NMR (CD_2Cl_2, 145 MHz) δ: 24.3. HR-MS calcd. for $C_{40}H_{30}MoO_8P_2S_2$: 861.9912; found: 861.9911. Anal. calcd. for $C_{40}H_{30}MoO_8P_2S_2$ (%): C 55.82, H 3.51, O 14.87, P 7.20; found: C 54.70, H 3.67, O 15.36, P 7.07.

***Syntheses of Mo(CO)$_5$*(PAr$_3$) (8, PAr$_3$ = 2)**

Complex **8** was prepared in an analogous fashion to **9**. Yield: 70%; mp 172 °C. Irν(CO) cm^{-1}: 1946. ^{1}H NMR (CD_2Cl_2, 300 MHz) δ: 4.20 (s, 8H) 6.70 (d, *J* = 2.2 Hz, 2H), 7.40 (m, 3H), 7.60 (m, 3H). ^{13}C NMR (CD_2Cl_2, 125 MHz) δ: 64.90 (CH_2), 65.30 (CH_2),106.70 (CH, d, *J* = 2.4 Hz), 128.8 (CH, d, *J* = 9.8 Hz), 130.8 (CH), 132.20 (CH, d, *J* = 13.1 Hz), 135.30 (C, d, *J* = 39.9 Hz), 143.20 (C, d, *J* = 6.4 Hz), 146.4 (C, d, *J* = 8.1 Hz), 206.40 (C, d, *J* = 9.5 Hz), 211.60 (C, d, *J* = 24.7 Hz). ^{31}P NMR (CD_2Cl_2, 145 MHz) δ: 7.6. HR-MS calcd. for $C_{23}H_{15}MoO_9PS_2$: 627.8950; found: 627.8985.

***Syntheses of Mo(CO)$_5$*(PAr$_3$) (9, PAr$_3$ = 3)**

cis-$Mo(CO)_4$(piperidine)$_2$ (1.154 g, 3 mmol) was added to a solution of **3** (0.422 g, 0.9 mmol) in CH_2Cl_2 (10 mL) at room temperature. The mixture was stirred overnight and filtered through a pad of silica gel. The product was isolated by precipitation from pentane. Yield: 60%; mp 202 °C. IR ν(CO) cm^{-1}: 1947. ^{1}H NMR (CD_2Cl_2, 300 MHz) δ: 4.10 (m, 8H), 6.60 (d, *J* = 2.9 Hz, 2H). ^{13}C NMR (CD_2Cl_2, 125 MHz) δ: 64.70 (CH_2), 65.00 (CH_2), 106.30 (CH), 107.10 (C, d, *J* = 36.7 Hz), 142.70 (C, d, *J* = 7.3 Hz), 145.8 (C, d, *J* = 10.6 Hz), 206.0 (C, d, *J* = 9.5 Hz), 211.60 (C, d, *J* = 24.6 Hz). ^{31}P NMR (CD_2Cl_2, 145 MHz) δ: –8.5. HR-MS calcd. for $C_{23}H_{15}MoO_{11}PS_3$: 691.8569; found: 691.8618. Anal. calcd. for $C_{23}H_{15}MoO_{11}PS_3$ (%): C 40.01, H 2.19, O 25.49, S 13.93, P 4.49; found: C 39.99, H 2.22, O 25.65, S 14.34, P 4.44.

Acknowledgements

We thank the University of Victoria, the Natural Sciences and Engineering Research Council of Canada (NSERC), and Defence R&D Canada-Atlantic for support.

References

1. (*a*) C.A. Tolman. Chem. Rev. **77**, 313 (1977); (*b*) M.M. Rahman, H.Y. Liu, K. Eriks, A. Prock, and W.P. Giering. Organometallics, **8**, 1 (1989); (*c*) P.B. Dias, M.E. Minas de Piedade, and J.A. Martinho Simões. Coord. Chem. Rev. **135**–**136**, 737 (1994).
2. (*a*) K. Tamao, T. Hiyama, and E.I. Negishi. J. Organomet. Chem. **653**, 1 (2002), and subsequent papers; (*b*) J.K. Stille. Angew. Chem. Int. Ed. Engl. **25**, 508 (1986); (*c*) I. Miyaura and A. Suzuki. Chem. Rev. **95**, 2457 (1995); (*d*) P.W.N.M. van Leeuwen, P.C.J. Kamer, J.N.H. Reek, and P. Dierkes. Chem. Rev. **100**, 2741 (2000).

© 2005 NRC Canada

3. G.R. Newkome. Chem. Rev. **93**, 2067 (1993).
4. N.G. Andersen and B.A. Keay. Chem. Rev. **101**, 997 (2001).
5. (*a*) D.W. Dick and D.W. Stephan. Can. J. Chem. **64**, 1970 (1985); (*b*) A.R. Sanger. Can. J. Chem. **62**, 2168 (1984); (*c*) J.D. King, M. Monari, and E.J. Nordlander. J. Organometal. Chem. **573**, 272 (1999); (*d*) U. Bodenseick, H. Vahrenkamp, G. Rehinwald, and H. Stoeckli-Evans. J. Organometal. Chem. **488**, 85 (1995); (*e*) T.M. Räsäsen, S. Jääskeläinen, and T.A. Pakkanen. J. Organometal. Chem. **553**, 453 (1998); (*f*) J. Chantson, H. Gorls, and S. Lotz. Inorg. Chim. Acta, **305**, 32 (2000).
6. (*a*) D.W. Allen and B.F. Taylor. J. Chem. Soc. Dalton Trans. 51 (1982); (*b*) A. Varshney and G.M. Gray. Inorg. Chim. Acta, **148**, 215 (1988); (*c*) V.K. Jain, V.S. Sagoria, and M.S. Gill. Indian J. Chem. **28A**, 164 (1989); (*d*) A.J. Deeming, M.K. Shinhmar, A.J. Arce, and Y.J. De Sanctis. J. Chem. Soc. Dalton Trans. 1153 (1999); (*e*) O. Clot, M.O. Wolf, G.P.A. Yap, and B.O. Patrick. J. Chem. Soc. Dalton Trans. 2729 (2000); (*f*) S.P. Tunik, I.O. Koshevoy, A.J. Poë, D.H. Farrar, E. Nordlander, M. Haukka, and T.A.J. Pakkanen. J. Chem. Soc. Dalton Trans. 2457 (2003).
7. (*a*) A.J. Deeming, S.N. Jayasuria, A.J. Arce, and Y. De Sanctis. Organometallics, **15**, 786 (1996); (*b*) D. Cauzzi, C. Graiff, C. Massera, G. Predieri, and A. Tiripicchio. Inorg. Chim. Acta, **300–302**, 471 (2000); (*c*) C. Moorlag, O. Clot, M.O. Wolf, and B.O. Patrick. Chem. Commun. 3028 (2002).
8. (*a*) D.A. Weinberger, T.B. Higgins, C.A. Mirkin, L.M. Liable-Sands, and A.L. Rheingold. Angew. Chem. Int. Ed. **38**, 2565 (1999); (*b*) D.A. Weinberger, T.B. Higgins, C.A. Mirkin, C.L. Stern, L.M. Liable-Sands, and A.L. Rheingold. J. Am. Chem. Soc. **123**, 2503 (2001); (*c*) C. Hay, C. Fischmeister, M. Hissler, L. Toupet, and R. Reau. Angew. Chem. Int. Ed. **39**, 1812 (2000); (*d*) O. Clot, M.O. Wolf, and B.O. Patrick. J. Am. Chem. Soc. **122**, 10 456 (2000); (*e*) O. Clot, M.O. Wolf, and B.O. Patrick. J. Am. Chem. Soc. **123**, 9963 (2001); (*e*) O. Clot, Y. Akahori, C. Moorlag, D.B. Leznoff, M.O. Wolf, R.J. Batchelor, B.O. Patrick, and M. Ishii. Inorg. Chem. **42**, 2704 (2003).
9. (*a*) I. Manners. Angew. Chem. Int. Ed. Engl. **35**, 1603 (1996); (*b*) P. Nguyen, P. Gomez-Elipe, and I. Manners. Chem. Rev. **99**, 1515 (1999); (*c*) A. Abd-El-Aziz and E.K. Todd. Coord. Chem. Rev. **246**, 3 (2003); (*d*) D.R. Tyler. Coord. Chem. Rev. **246**, 291 (2003).
10. (*a*) R.P. Kinsborough and T.M. Swager. Prog, Inorg. Chem. **48**, 123 (1999); (*b*) P.G. Pickup. J. Mater. Chem. **9**, 1641 (1999); (*c*) M.O. Wolf. Adv. Mater. **13**, 545 (2001); (*d*) T. Hirao. Coord. Chem. Rev. **226**, 81 (2002); (*e*) T.L. Stott and M.O. Wolf. Coord. Chem. Rev. **246**, 89 (2003); (*f*) N.J. Long and C.K. Williams. Angew. Chem. Int. Ed. **42**, 2586 (2003).
11. T.J. Skotheim, R.L. Elsenbaumer, and J.R. Reynolds (*Editors*). Handbook of conducting polymers. 2nd ed. Marcel Dekker, New York. 1998.
12. (*a*) B.L. Groenendaal, F. Jonas, D. Freitag, H. Pielartzik, and J.R. Reynolds. Adv. Mater. **12**, 481 (2000); (*b*) B.L. Groenendaal, G. Zotti, P.H. Aubert, S.M. Waybright, and J.R. Reynolds. Adv. Mater. **15**, 855 (2003).
13. R.G. Hicks and M.B. Nodwell. J. Am. Chem. Soc. **122**, 6746 (2000).
14. S.O. Grim, A.W. Yankowsky, S.A. Bruno, W.J. Bailey, E.F. Davidoff, and T.J. Marks. J. Chem. Eng. Data, **15**, 497 (1970).
15. D.J. Darensbourg and R.L. Kump. Inorg. Chem. **17**, 2680 (1978).
16. C.S. Slone, D.A. Weinberger, and C.A. Mirkin. Prog. Inorg. Chem. **48**, 233 (1999).

© 2005 NRC Canada

^{1}H NMR studies on the solution conformation of the [L-Ser^{10}] and [D-Ser^{10}] analogues of contulakin-G

Lill Kindahl, Lennart Kenne, and Corine Sandström

Abstract: The synthesis of the *O*-glycosylated serine-10 analogue of contulakin-G yielded both the [L-] and the [D-Ser^{10}] analogues. The ^{1}H NMR study indicated that the sugars of the two Ser^{10}-glycosylated peptides lacked the hydrogen bond to the peptide backbone that exists in contulakin-G. NOEs showed that the glycan part of the [D-Ser^{10}] analogue had a different orientation to the peptide backbone than that of the [L-Ser^{10}] analogue. The peptide backbones in the two compounds were found to exist mainly in random coil conformations, with transient turns at the site of glycosylation. A transient turn was also found at the C-terminus of the [D-Ser^{10}] glycopeptide. The NMR data indicated that the average conformation of the [D-Ser^{10}] analogue resembles the conformation of contulakin-G more than the [L-Ser] does. Since biological data showed that the [D-Ser^{10}] glycopeptide was as active as contulakin-G, while the [L-Ser^{10}] glycopeptide was only slightly active at more than 100 times the dose, it is possible that it is the orientation of the glycan relative to the peptide chain that is actually recognized by the proteolytic enzyme.

Key words: conformation, contulakin-G analogues, NMR, *O*-linked glycopeptide.

Résumé : La synthèse de l'analogue sérine-10 *O*-glycosylée de la contulakine-G conduit à la formation des deux analogues [L-] et [D-Ser^{10}]. Une étude de RMN du ^{1}H indique que dans les sucres des deux peptides Ser^{10}-glucosylés on ne retrouve pas la liaison hydrogène avec le squelette du peptique qui existe dans la contulakine-G. Des études d'effet Overhauser nucléaire montrent que l'orientation de la partie glycane de l'analogue [D-Ser^{10}] par rapport au squelette du peptide est différente de celle de l'analogue avec [L-Ser^{10}]. On a trouvé que les squelettes peptidiques des deux composés existent principalement sous la forme de pelote aléatoire avec des revirements transitoires au site de la glycosylation. On a aussi observé un revirement transitoire au C-terminal de l'analogue [D-Ser^{10}] du glycopeptide. Les données de la RMN indiquent la conformation moyenne de l'analogue [D-Ser^{10}] ressemble plus à la conformation de la contulakine-G que celle de l'analogue [L-Ser]. Comme les données biologiques montrent que l'analogue [D-Ser^{10}] du glycopeptide est aussi actif que la contulakine-G alors que l'analogue [L-Ser^{10}] du glycopeptide n'est que faiblement actif à plus de cent fois la dose, il est possible que ce soit l'orientation du glycane par rapport à la chaîne peptidique qui soit reconnue par l'enzyme protéolytique.

Mots clés : conformation, analogues de la contulakine-G, RMN, glycopeptide à liaison par l'oxygène.

[Traduit par la Rédaction]

Introduction

Contulakin-G (**1**, Scheme 1) is an invertebrate neurotensin analogue, which has recently entered phase II clinical trials for short-term management of postoperative pain (1–3). Contulakin-G is a 16 amino acid *O*-glycosylated glycopeptide, which was isolated from the venom of the Cone snail *Conus geographus*. In a previous study, the conformations of contulakin-G (**1**) and three analogues (**2**–**4**, Scheme 1) were investigated by ^{1}H NMR spectroscopy, and an attempt was made to correlate the NMR data to the biological activity of these compounds (4). The analogues were the nonglycosylated peptide (**2**), one analogue with the monosaccharide α-D-Gal*p*NAc at Thr^{10} (**3**), and one analogue with the disaccharide β-D-Gal*p*-(1→3)-α-D-Gal*p*NAc at Ser^7 (**4**).

The potency of compounds **1**–**4** was assessed by testing their ability to induce latency of tail flick in mice in an assay of acute pain.[2] Contulakin-G (**1**) was found to be significantly more potent than the analogue with the monosaccharide α-D-Gal*p*NAc at Thr^{10} (**3**). The latter was in turn more potent than the nonglycosylated peptide **2**, which was found to have an activity comparable to that of the analogue *O*-glycosylated at Ser^7 (**4**). These results suggested that the presence of the glycan, its size and position are important factors for the activity of contulakin-G. The NMR study showed that contulakin-G and the three analogues mainly existed in random coil conformations (4). Some transient populations of folded conformations were also present in the glycopeptides, and turns, probably induced by the sugars, were found in the peptide chain around the site of

Received 24 June 2004. Published on the NRC Research Press Web site at http://canjchem.nrc.ca on 25 February 2005.

L. Kindahl, L. Kenne, and C. Sandström.[1] Department of Chemistry, Swedish University of Agricultural Sciences, P.O. Box 7015, SE-750 07 Uppsala, Sweden.

[1]Corresponding author (e-mail: corine.sandstrom@kemi.slu.se).

[2]A.G. Craig, T. Norberg, J. Kang, J. Wagstaff, R. Layer, J. Imperial, and B.M. Olivera. Manuscript in preparation.

 doi: 10.1139/V04-176 © 2005 NRC Canada

Scheme 1. Structure of contulakin-G (**1**), and the analogues (**2**–**6**).

pGlu[1]-Ser-Glu-Glu-Gly[5]-Gly-Ser-Asn-Ala-Thr[10]-Lys-Lys-Pro-Tyr-Ile[15]-Leu-OH (**1**)

↑

β-D-Gal*p*-(1→3)-α-D-Gal*p*NAc-(1

pGlu[1]-Ser-Glu-Glu-Gly[5]-Gly-Ser-Asn-Ala-Thr[10]-Lys-Lys-Pro-Tyr-Ile[15]-Leu-OH (**2**)

pGlu[1]-Ser-Glu-Glu-Gly[5]-Gly-Ser-Asn-Ala-Thr[10]-Lys-Lys-Pro-Tyr-Ile[15]-Leu-OH (**3**)

↑

α-D-Gal*p*NAc-(1

pGlu[1]-Ser-Glu-Glu-Gly[5]-Gly-Ser[7]-Asn-Ala-Thr[10]-Lys-Lys-Pro-Tyr-Ile[15]-Leu-OH (**4**)

↑

β-D-Gal*p*-(1→3)-α-D-Gal*p*NAc-(1

pGlu[1]-Ser-Glu-Glu-Gly[5]-Gly-Ser-Asn-Ala-DSer[10]-Lys-Lys-Pro-Tyr-Ile[15]-Leu-OH (**5**)

↑

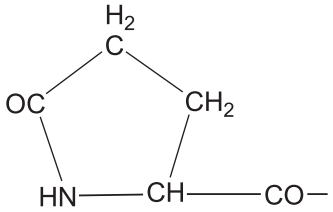
β-D-Gal*p*-(1→3)-α-D-Gal*p*NAc-(1

pGlu[1]-Ser-Glu-Glu-Gly[5]-Gly-Ser-Asn-Ala-LSer[10]-Lys-Lys-Pro-Tyr-Ile[15]-Leu-OH (**6**)

↑

β-D-Gal*p*-(1→3)-α-D-Gal*p*NAc-(1

pGlu = pyroglutamic acid:



glycosylation. In the two peptides *O*-glycosylated at Thr[10] (**1** and **3**), the presence of a transient hydrogen bond between the α-D-Gal*p*NAc residue and the peptide was found. An intramolecular hydrogen bond between the carbohydrate and the peptide chain did not exist in the peptide *O*-glycosylated at the Ser[7] residue (**4**). In contulakin-G (**1**), an additional transient turn was formed at the C-terminal end of the peptide chain. When the stability towards enzymatic degradation with proline specific endopeptidase was investigated,[2] the nonglycosylated peptide (**2**) and the peptide *O*-glycosylated at the Ser[7] residue (**4**) showed significantly more susceptibility to enzymatic hydrolysis than contulakin-G (**1**) and the analogue with the monosaccharide α-D-Gal*p*NAc at Thr[10] (**3**). It was concluded that the glycan was able to exert significant protection against enzymatic degradation, and this protection appeared to be completely abolished in the Ser[7]-glycosylated analogue (**4**). The analogue **3**, which is glycosylated with the monosaccharide α-D-Gal*p*, was also more readily degraded than contulakin-G (**1**), which is glycosylated with the disaccharide β-D-Gal*p*-(1→3)-α-D-Gal*p*NAc. This indicated that the glycan might sterically inhibit the enzyme from inactivating the peptide by hydrolysis of the linkage between Pro[13] and Tyr[14]. The stabilization against enzymatic degradation correlated with the increased

© 2005 NRC Canada

antinociceptive activity of the compounds,[2] and it is possible that the reduced proteolysis of contulakin-G, as compared to that of the nonglycosylated peptide, may be responsible for the increased activity of this peptide. Since the data obtained in the proteolysis study indicated that the main role of the glycan is a steric inhibition of enzymatic degradation, it was of interest to study the Ser^{10}-glycosylated analogue of contulakin-G (Scheme 1). Previous NMR studies have reported differences in glycan mobility and orientation relative to the peptide backbone depending on if the glycosylated residue was a threonine or a serine (5, 6). In this work, we have studied the solution conformations of [Ser^{10}]-contulakin-G by ^{1}H NMR spectroscopy.

Results and discussion

The synthesis of [Ser^{10}]-contulakin-G was performed in a similar way as previously described (1). As the synthetic product was purified with reverse phase HPLC, two components with different retention times were found; one fraction with shorter retention time containing compound **5**, and one fraction with longer retention time containing compound **6**. The mass spectrum showed that both compounds had the correct mass, and that both were glycopeptides. In the antinociceptive assay of acute pain (7) of the two samples, it was found that glycopeptide **5** was active at about the same potency as contulakin-G (**1**), whereas glycopeptide **6** only was slightly active at more than 100 times the dose.[3] The structures of the two compounds were determined by ^{1}H NMR spectroscopy using a combination of standard two-dimensional COSY, DQF-COSY, TOCSY, and NOESY experiments. The chemical shifts of the signals from the protons of the peptide chains are given in Table 1, and those of the sugars in Table 2.

Structure determination

The disaccharide

Figure 1 shows the one-dimensional proton NMR spectra of compounds **5** and **6** in D_2O recorded at 25 °C. In both spectra, the downfield signal at δ 4.90 ppm in **5** and 4.89 ppm in **6** ($^3J_{1,2}$ = 3.8 Hz) was assigned to the anomeric proton of α-D-Gal*p*NAc. The signal from the anomeric proton of the β-D-Gal*p* residue was found at δ 4.48 ppm in **5** and 4.46 ppm in **6** ($^3J_{1,2}$ = 7.8 Hz). In the 2D NOESY spectra, the strong NOE between H-1 of β-D-Gal*p* and H-3 of α-D-Gal*p*NAc confirmed that the two sugars are connected through a 1,3-linkage (β-D-Gal*p*-(1→3)-α-D-Gal*p*NAc).

The primary structure of the peptide chain

The amino acid sequence of the peptide was confirmed by sequential assignment using the $d_{\alpha N}(i,i+1)$ NOE connectivities. The primary structure at the Lys^{12}–Pro^{13} junction was confirmed by the observation of an NOE between the α-H of Lys^{12} and the δ-CH_2 protons of Pro^{13}.

The site of glycosylation

The site of glycosylation at Ser^{10} of compounds **5** and **6** was confirmed by the existence of an NOE between the H-1 of α-D-Gal*p*NAc and the β-H of Ser^{10}. The two β protons of Ser^{10} in compounds **5** and **6** had signals that were slightly more separated than those of Ser^2 and Ser^7. This separation was also observed for the methine protons of the Ser^7 residue in compound **4**, and is due to the effect of glycosylation.

Differences in NMR spectra

The 2D COSY, TOCSY, and NOESY spectra of compounds **5** and **6** were very similar and Table 1 shows that most of the chemical shift differences between the signals from the amino acid protons in **5** and **6** were <0.04 ppm. An exception was found for the α-H signal of Ser^{10}, which showed a difference of 0.06 ppm between compounds **5** and **6**. Also, the NH signals of Lys^{11} and α-D-Gal*p*NAc showed differences between compounds **5** and **6** of 0.16 and 0.17 ppm, respectively. A major difference was found in the fine structure of the α-H–β-H and α-H–β′-H cross-peaks of Ser^{10} in the phase-sensitive DQF–COSY spectra. In the spectrum of compound **5**, the downfield proton had a $^3J_{H\alpha,H\beta}$ = 6 Hz, whereas the upfield proton had a $^3J_{H\alpha,H\beta}$ = 4 Hz (no stereospecific assignments of the geminal β-H protons of Ser^{10} were made). In the spectrum of compound **6**, the peak pattern of these two cross-peaks was reversed; the downfield proton had a *J* value of 4 Hz, while the upfield proton had a *J* value of 6 Hz. These data indicated that the structure of the two compounds differed by the configuration of α-C of the Ser^{10} amino acid, which means that the serine residue substituted by the glycan would have been racemized during peptide synthesis.

Determination of configuration at [Ser^{10}]

The absolute configuration of the serine residues in the peptide chains of **5** and **6** was determined using the GC–MS method of Ström et al. (8) (see Experimental). The analysis showed that **5** contained L-Ser and D-Ser in the ratio 2:1, while **6** only contained L-Ser. Since two L-serine are present at the 2 and 7 positions in the peptide chain of compounds **5** and **6**, this indicates that **5** has a D-Ser at the site of glycosylation, whereas **6** has a L-Ser.

Conformational analysis of the peptide chain

Chemical shifts

The ^{1}H NMR chemical shifts measured for most of the amino acid residues in compounds **5** and **6** (Table 1) had values similar to those in random coils (9, 10). An exception was found for the α-protons of the residues at and around the glycosylation sites, α-H of Lys^{12} and α-H of Leu^{16} (Table 1, Fig. 2). The α-H signal of Ser^{10} in **5** and **6** showed downfield shifts of 0.17 and 0.11 ppm, respectively, as compared to the random coil values. In the Ser^{10}-glycosylated peptides **5** and **6**, the α-H signal of the preceding residue, Ala^9, had a chemical shift value close to that of random coil, whereas in the Thr^{10}-glycosylated peptides **1** and **3**, the α-H

[3] The mice were administrated intrathecally with a constant volume (5 μL) and then gently wrapped in a towel with the tail exposed. At various time points following the intrathecal injection, the tail was dipped in a water bath maintained at 54 °C and the time taken for the mouse to withdraw its tail recorded. If there was no withdrawal by 8 s, the tail was withdrawn to avoid tissue damage (A.G. Craig, unpublished results).

© 2005 NRC Canada

Table 1. ^{1}H NMR chemical shifts (ppm) of **1**,[a] **5**, and **6** at 25 °C in 95% H_2O – 5% D_2O (pH 5.6).

Residue	Cpd	NH	α-H	β-H	Others
pGlu[1]	**1**	7.90	4.41	1.99	γ-CH_2 2.41, 2.56
	5		4.41	2.11	γ-CH_2 2.44, 2.55
	6		4.41	2.11	γ-CH_2 2.45, 2.56
Ser[2]	**1**	8.46	4.48	3.89	
	5	8.46	4.50	3.89	
	6	8.46	4.51	3.89	
Glu[3]	**1**	8.58	4.43	1.99	γ-CH_2 2.47, 2.15
	5	8.69	4.36	1.96	γ-CH_2 2.33, 2.10
	6	8.72	4.34	1.96	γ-CH_2 2.28, 2.09
Glu[4]	**1**	8.44	4.38	1.99	γ-CH_2 2.47, 2.15
	5	8.49	4.32	1.96	γ-CH_2 2.33, 2.10
	6	8.52	4.29	1.95	γ-CH_2 2.28, 2.08
Gly[5]	**1**	8.47	3.99		
	5	8.48	3.98		
	6	8.49	3.98		
Gly[6]	**1**	8.29	4.02		
	5	8.29	4.01		
	6	8.29	4.01		
Ser[7]	**1**	8.33	4.46	3.89	
	5	8.34	4.46	3.92, 3.86	
	6	8.34	4.43	3.90, 3.87	
Asn[8]	**1**	8.48	4.75	2.85, 2.77	γ-NH_2 6.91, 7.57
	5	8.52	4.73	2.87, 2.78	γ-NH_2 6.94, 7.59
	6	8.49	4.72	2.86, 2.78	γ-NH_2 6.93, 7.61
Ala[9]	**1**	8.10	4.49	1.41	
	5	8.11	4.36	1.40	
	6	8.07	4.35	1.40	
Thr[10]	**1**	8.55	4.52	4.33	γ-CH_3 1.30
L-Ser[10]	**5**	8.50	4.64	3.98, 3.81	
D-Ser[10]	**6**	8.49	4.58	4.02, 3,83	
Lys[11]	**1**	8.45	4.38	1.81	γ-CH_2 1.47, δ-CH_2 1.47, ε-CH_2 2.99
	5	8.20	4.33	1.80	γ-CH_2 1.36, δ-CH_2 1.66, ε-CH_2 3.00
	6	8.36	4.33	1.81	γ-CH_2 1.43, δ-CH_2 1.68, ε-CH_2 3.00
Lys[12]	**1**	8.35	4.45	1.78	γ-CH_2 1.48, δ-CH_2 1.74, ε-CH_2 3.03
	5	8.36	4.57	1.76	γ-CH_2 1.47, δ-CH_2 1.70, ε-CH_2 3.02
	6	8.32	4.52	1.75	γ-CH_2 1.46, δ-CH_2 1.70, ε-CH_2 3.01
Pro[13]	**1**		4.39	1.84, 2.25	γ-CH_2 2.01, δ-CH_2 3.84, 3.62
	5		4.38	1.81, 2.23	γ-CH_2 1.99, δ-CH_2 3.79, 3.62
	6		4.38	1.81, 2.23	γ-CH_2 2.00, δ-CH_2 3.79, 3.62
Tyr[14]	**1**	8.17	4.57	3.00	^{2,6}H 7.13, 6.84
	5	8.08	4.59	3.01	^{2,6}H 7.12, 6.84
	6	8.10	4.58	3.01	^{2,6}H 7.13, 6.84
Ile[15]	**1**	7.93	4.14	1.78	γ-CH_2 1.40, 1.11, γ-CH_3 0.88, δ-CH_3 0.83
	5	7.92	4.14	1.80	γ-CH_2 1.40, 1.10, γ-CH_3 0.88, δ-CH_3 0.83
	6	7.92	4.14	1.81	γ-CH_2 1.40, 1.11, γ-CH_3 0.88, δ-CH_3 0.83
Leu[16]	**1**	8.13	4.26	1.62	γ-CH_3 1.63, δ-CH_3 0.94, 0.89
	5	7.80	4.17	1.57	γ-CH_3 1.58, δ-CH_3 0.92, 0.88
	6	7.76	4.15	1.56	γ-CH_3 1.57, δ-CH_3 0.92, 0.88

[a]Taken from ref. 4.

signal showed a large downfield shift of 0.17 and 0.13 ppm, respectively (4). The α-H signal of the second residue from the site of glycosylation (α-H Lys[12]) in **5** and **6** showed a large downfield shift of 0.20 and 0.25 ppm, respectively, as compared to the random coil value. This signal of Lys[12] was also shifted downfield with 0.25 ppm for the nonglycosylated peptide **2**, 0.24 ppm for the Ser[7] analogue **4**, and 0.14 and 0.15 ppm for the Thr[10] analogues **3** and **4**, respectively (4). This suggests that the downfield shift is mainly due to the neighbouring Pro[13], which is known to be "turn-inducing". In **5** and **6**, the α-H signal of Leu[16] is shifted upfield 0.17 and 0.19 ppm, respectively, as compared to the random coil values.

$^3\mathbf{J}_{NH,\alpha H}$ values

The $^3J_{NH,\alpha H}$ values were in the range 5.7–9.0 Hz in **5** and

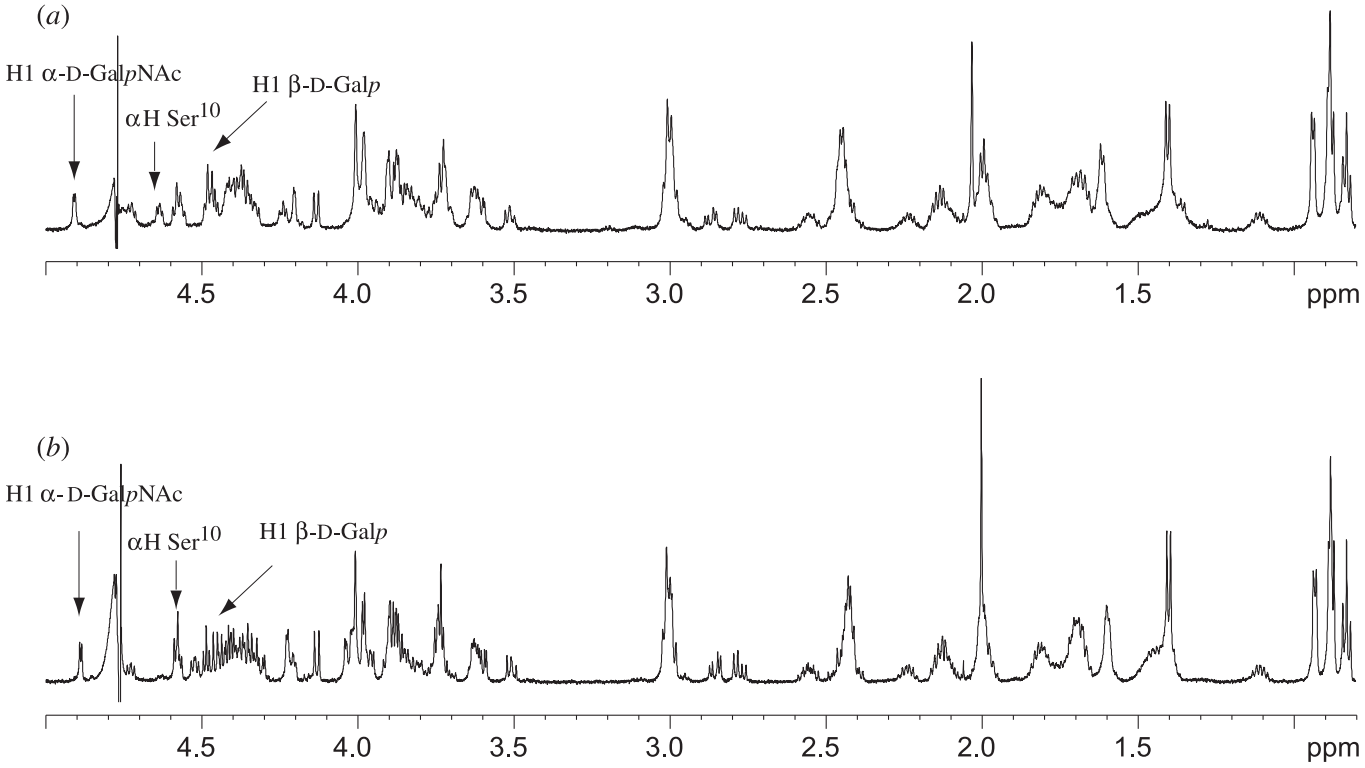
© 2005 NRC Canada

Table 2. ^{1}H NMR chemical shifts (ppm) for the sugar signals in **1**,[a] **5**, and **6** at 25 °C in 95% H_2O – 5% D_2O (95:5, pH 5.6).

	Cpd	H-1	H-2	H-3	H-4	H-5	H-6	NH	NAc
β-D-Gal*p*	**1**	4.45	3.54	3.60	3.91	3.61	3.73, 3.70		
	5	4.48	3.51	3.61	3.91	n.d.	n.d.		
	6	4.46	3.51	3.61	3.91	n.d.	n.d.		
α-D-Gal*p*NAc	**1**	4.88	4.23	4.03	4.21	4.05	~3.6, ~3.7	7.66	2.02
	5	4.90	4.36	3.95	4.21	3.95	3.83	8.14	2.04
	6	4.89	4.31	4.03	4.23	n.d.	n.d.	7.97	2.00

Note: n.d. (not determined because of spectral overlap).
[a]Taken from ref. 4.

Fig. 1. One-dimensional ^{1}H NMR spectra of (*a*) **5** and (*b*) **6** recorded at 25 °C in D_2O. The arrows show the anomeric H-1 of α-D-Gal*p*NAc and β-D-Gal*p*, and the α-H of Ser^{10}.



6 (Table 3) and were very similar to the values measured in the (glyco-)peptide analogues **1**–**4** (4). These values suggested random coil or extended conformations. The $^3J_{NH,\alpha H}$ values of 8.6 and 9.0 Hz measured for Thr^{10} in contulakin-G (**1**) and in the analogue with α-D-Gal*p*NAc at Thr^{10}(**3**) were slightly larger than the corresponding value of 7.5 Hz measured in the nonglycosylated peptide (**2**) (4). This increase in the *J* value of **1** and **3** as compared to **2** was attributed to the presence of some ordered secondary structures in **1** and **3**. A larger $^3J_{NH,\alpha H}$ value was also measured for [D-Ser^{10}] in **5** (8.5 Hz) as compared to [L-Ser^{10}] in **6** (6.6 Hz) (Table 3). It should be noted that in analogue **4**, a value of 6.4 Hz was measured for the glycosylated Ser^7 (4). Furthermore all the nonglycosylated Ser residues in **1**–**6** had *J* values from 6.0 to 6.8 Hz.

Temperature coefficients for the NH protons

The temperature coefficients ($\Delta\delta/\Delta T$) for the NH proton signals from **5** and **6** were obtained in 95% H_2O – 5% D_2O solutions from a series of one-dimensional spectra recorded at sample temperatures between 5 and 45 °C (Table 3). The large $\Delta\delta/\Delta T$ values indicated that no hydrogen bonds or amide protons protected from solvent were present in the peptide chains.

NOEs in the peptide chain

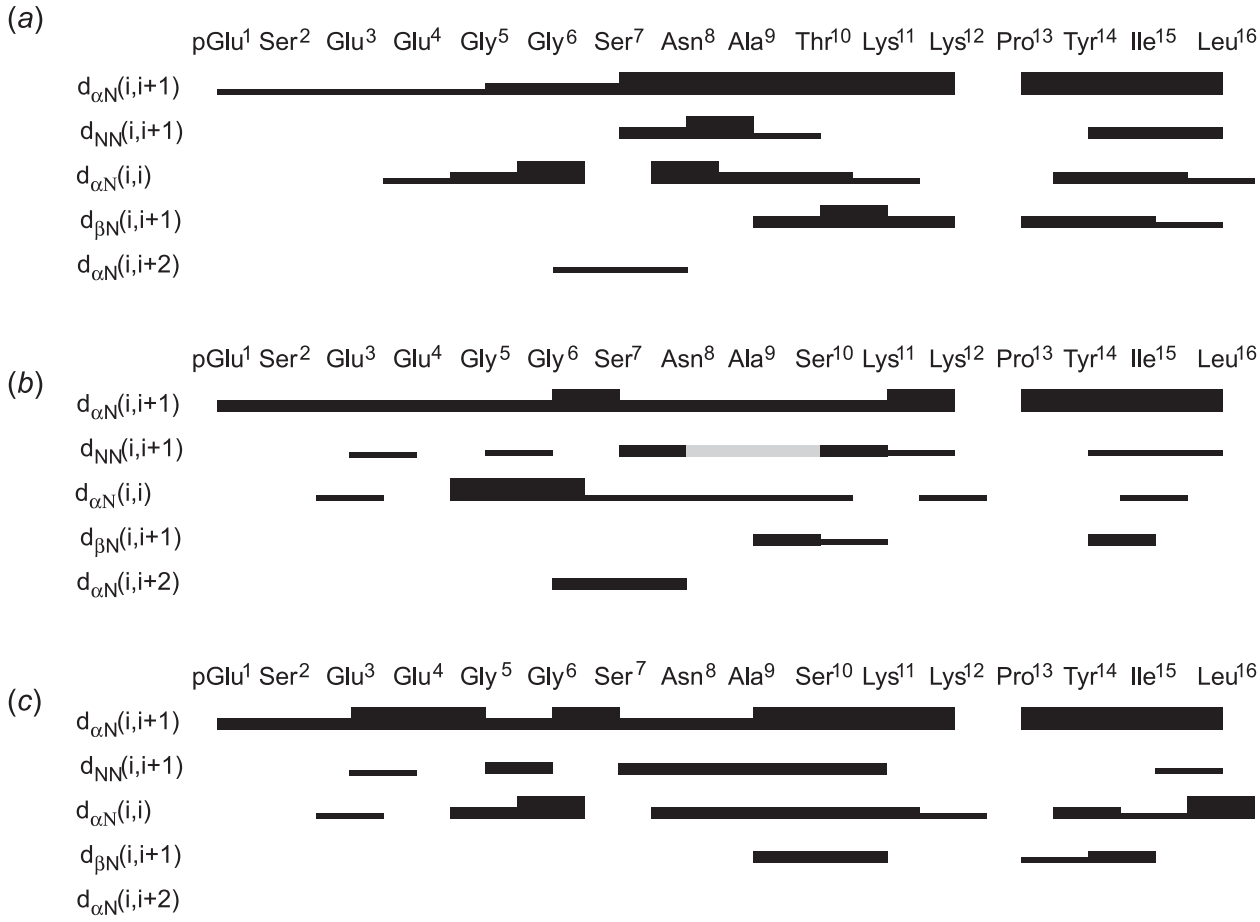
In **5** and **6**, the sequential $d_{\alpha N}(i,i+1)$ NOE pattern characteristic of extended conformations was observed along the whole peptide chain (Fig. 2). Sequential $d_{NN}(i,i+1)$ NOEs were observed for residues 7–12 and 14–16 in **5**, and 7–11 in **6** (Fig. 3). However, none of the $d_{NN}(i,i+1)$ NOEs found in **5** and **6** were strong, suggesting a high degree of flexibility in glycopeptides **5** and **6**. The [D-Ser^{10}] glycopeptide **5** had a Gly^6-Asn^8 $d_{NN}(i,i+2)$ NOE indicative of a turn, also found in contulakin-G (**1**), but not in the [L-Ser^{10}] analogue **6**.

Carbohydrate–peptide interaction

In contulakin-G (**1**) and the α-D-Gal*p*NAc analogue **3**, a $\Delta\delta/\Delta T$ of –5.8 ppb/°C was measured for the NH of α-D-

© 2005 NRC Canada

Fig. 2. Intra- and inter-residue NOE signals involving the backbone NH protons in (*a*) contulakin-G (**1**) (taken from ref. 4), (*b*) **5**, and (*c*) **6**. The thickness of the lines represents the relative intensities of the NOE signals. Greyish lines represent overlapping NOEs. The NOESY were recorded at 5 °C with a mixing time of 300 ms.



Gal*p*NAc in water solution. This together with the NOEs between the glycan and the peptide chain and with the small $^3J_{H\alpha,H\beta}$(Thr^{10}) value (1.5 Hz in **1** and 2 Hz in **3**) indicated a torsional rigidity between the sugar and the peptide, enforced by a hydrogen bond interaction between the NH of α-D-Gal*p*NAc and Thr^{10}. In **5** and **6**, *O*-glycosylated at a serine residue, the large $\Delta\delta/\Delta T$ value obtained for the NH of α-D-Gal*p*NAc (–11.3 ppb/°C in **5** and –8.3 ppb/°C in **6**) showed that these protons are not protected from exchange with the solvent through hydrogen bond formation. Also, in **5** and **6**, the two $^3J_{H\alpha,H\beta}$ of Ser^7 had values in the range 4–6 Hz and the relative intensities of the two α-H–βH NOEs were similar. This indicated that the C_α—C_β bond is subject to conformational averaging, and that there is motion around the sugar–peptide linkage. The $^3J_{H\alpha,H\beta}$ value characteristic for conformational averaging ($^3J_{H\alpha,H\beta}$ ~ 6–8 Hz) is, however, not easy to distinguish from the corresponding value for the gauche rotamer ($^3J_{H\alpha,H\beta}$ ~ 4 Hz) only from the fine structure of the DQF-COSY cross-peaks, since there is a limitation in digital resolution and line widths. A few NOEs were found between the peptide and the carbohydrate moiety in **5** and **6** (Fig. 4). These were the NH(Ser^{10})–H-1(α-D-Gal*p*NAc), β-H(Ser^{10})–H-1(α-D-Gal*p*NAc), β′-H(Ser^{10})–H-1(α-D-Gal*p*NAc), β-H(Ser^{10})–H2(α-D-Gal*p*NAc), β′-H(Ser^{10})–H-2(α-D-Gal*p*NAc), and NH(Lys^{11})–H-1(α-D-Gal*p*NAc) NOEs. Two additional NOEs, NH(Ser^{10})–NH(α-D-Gal*p*NAc) and NH(Ser^{10})–CH_3CO(α-D-Gal*p*NAc), were found for compound **5**. These additional NOEs together with a larger $^3J_{NH,\alpha H}$(Ser^{10}) value of 8.5 Hz indicated that the average orientations of the glycan in the [D-Ser^{10}] analogue **5** and in the [L-Ser^{10}] analogue **6** were different. The $^3J_{NH,H2}$ of 9.7 Hz measured for Gal*p*NAc of **5** and **6** demonstrated a trans orientation of NH relative to C(2)H.

Our previous NMR study (4) on contulakin-G and analogues **1**–**4** together with the present work on **5** and **6** suggest that there is more local rigidity around the threonine segment, as in **1** and **3**, than around the serine segment, as in **4**–**6**. These conformational differences have previously been shown from NMR and molecular modelling studies for other *O*-linked glycopeptides (5, 6). In these studies, the galactosamine units at the Thr residue were in close contact with several peptide atoms, whereas the galactosamine units attached to Ser residues assumed more apical positions with the surrounding peptide backbones distanced from the sugar, allowing more rotational freedom around the glycosidic bond. On the other hand, another study showed that a Thr-linked glycan was positioned perpendicular to the peptide backbone, and had no hydrogen bond to the peptide (11). A recent NMR study on MUC1 glycopeptides also showed that glycosylation produced only localized effects on the confor-

© 2005 NRC Canada

Table 3. $^3J_{NH,\alpha H}$ vicinal coupling constants (Hz) and NH temperature coefficients ($\Delta\delta/\Delta T$, ppb/°C) for the NH protons in **1**,[a] **5**, and **6** in 95% H_2O – 5% D_2O (95:5, pH 5.6).

	$^3J_{NH,\alpha H}$			$\Delta\delta/\Delta T$		
Residue	**1**	**5**	**6**	**1**	**5**	**6**
pGlu[1]	<1	—	—	13.4	—	—
Ser[2]	6.2	6.8	6.0	[b]	9.6	7.1
Glu[3]	7.0	6.4	6.4	15.2	8.7	8.7
Glu[4]	7.0	6.5	6.6	9.1	8.9	8.3
Gly[5]	11.5[c]	11.8[c]	11.5	7.2	9.2	9.9
Gly[6]	11.7[c]	11.8[c]	11.8	6.9	7.2	7.0
Ser[7]	6.8	6.1	9.5[d]	7.8	8.8	9.2
Asn[8]	7.5	7.7	7.0	7.9	8.4	7.3
Ala[9]	5.9	5.7	5.7	6.7	6.4	6.0
Thr[10]–Ser[10]	8.6	8.5	6.6	8.4	8.6	11.0
Lys[11]	7.2	6.8	7.0[d]	10.8	6.9	11.9
Lys[12]	6.2	6.6	7.2	9.9	10.6	10.4
Pro[13]	—	—	—	—	—	—
Tyr[14]	7.3	7.2	7.2	13	13.0	14.1
Ile[15]	8.8	8.6	9.0	8.3	9.7	9.6
Leu[16]	7.1	7.4	7.5	8.8	8.9	8.7
NHGal*p*NAc	10.1	9.7	9.7	5.8	11.3	8.3

[a]Taken from ref. 4.
[b]Not calculated because of spectral overlap.
[c]$^3J_{NH,\alpha H} + {}^3J_{NH,\alpha' H}$.
[d]Measured from DQF-COSY because of spectral overlap in the one-dimensional NMR spectrum.

mation and the backbone dynamics of residues at or close to the site of glycosylation (12). The NMR data for **5** and **6** together with models obtained by MM2 suggested that, while there was no hydrogen bond interaction in the L- and D-serine analogues, the contacts between the peptide chain and the glycan were closer with a D-serine that with an L-serine. Because of the difference in chirality of the Ser[10] residue of **5** as compared to **6**, the backbone from Ser[10] to the amino acid 16 extended in opposite directions relative to the glycan in these two compounds. The disaccharide was bent away from the peptide chain in the [L-Ser[7]] enantiomer (**6**) whereas in the [D-Ser[7]] enantiomer (**5**), the glycan was positioned over the Lys[10]–Leu[16] chain.

Conclusions

Because of racemization, the synthesis of [Ser[10]]-contulakin-G yielded two diatereoisomers that have been characterized by ^{1}H NMR spectroscopy and GC–MS as the [D-Ser[10]]- and [L-Ser[10]]-contulakin-G. The absence of strong $d_{NN}(i,i+1)$ NOEs together with the temperature coefficients and $^3J_{NH,\alpha H}$ values indicated that the peptide chain in glycopeptides **5** and **6** predominantly existed in random coil or extended conformations. The NMR data also showed that there was no hydrogen bond between the peptide chain and the glycan. Thus, the hydrogen bond previously found in contulakin-G (4) does not seem to be of crucial importance for the biological activity. In contulakin-G (**1**) and in the [D-Ser[10]] analogue **5**, the NH(Ser[10])–NH(Gal*p*NAc), αH(Glu[6])–NH(Asn[8]), and consecutive NH(Tyr[14])–NH(Ile[15]) and NH(Ile[15])–NH(Leu[16]) NOEs were found, but these NOEs were not found in the [L-Ser[10]] analogue **6**. These differences in NOEs, together with the larger $^3J_{NH,\alpha H}$-value of 8.6 Hz for Thr[10] in contulakin-G (**1**) and of 8.5 Hz for D-Ser[10] in **5**, suggest that the ensemble average conformation of the [D-Ser[10]] analogue **5** resembles the conformation of contulakin-G (**1**) more than the [L-Ser[10]] analogue **6** does. The transient turn between residues 14 to 16 found in contulakin-G (**1**) and in [D-ser[10]]-contulakin-G (**5**), both with high biological activity, is probably not of importance for the biological activity. Previously, Craig et al. (1) concluded that *O*-glycosylation was a strategy of contulakin-G to enhance the binding affinity to neurotensin receptors. If the biological activity was due to binding of the glycopeptides to neurotensin receptors, and this transient C-terminal turn would be beneficial in the binding to these receptors, the turn would probably also have been found in conformational studies of this neurotensin. This is, however, not the case (13, 14). Previous proteolytic degradation studies showed that the glycan sterically inhibited the enzyme from hydrolysing the Pro[13]—Tyr[14] bond, and that this was a likely explanation to the high biological activity of contulakin-G.[2] The difference in the biological activity of [D-Ser[10]]-contulakin-G and [L-Ser[10]]-contulakin-G indicates that the orientation of the sugar relative to the peptide chain is important to protect against proteolytic degradation.

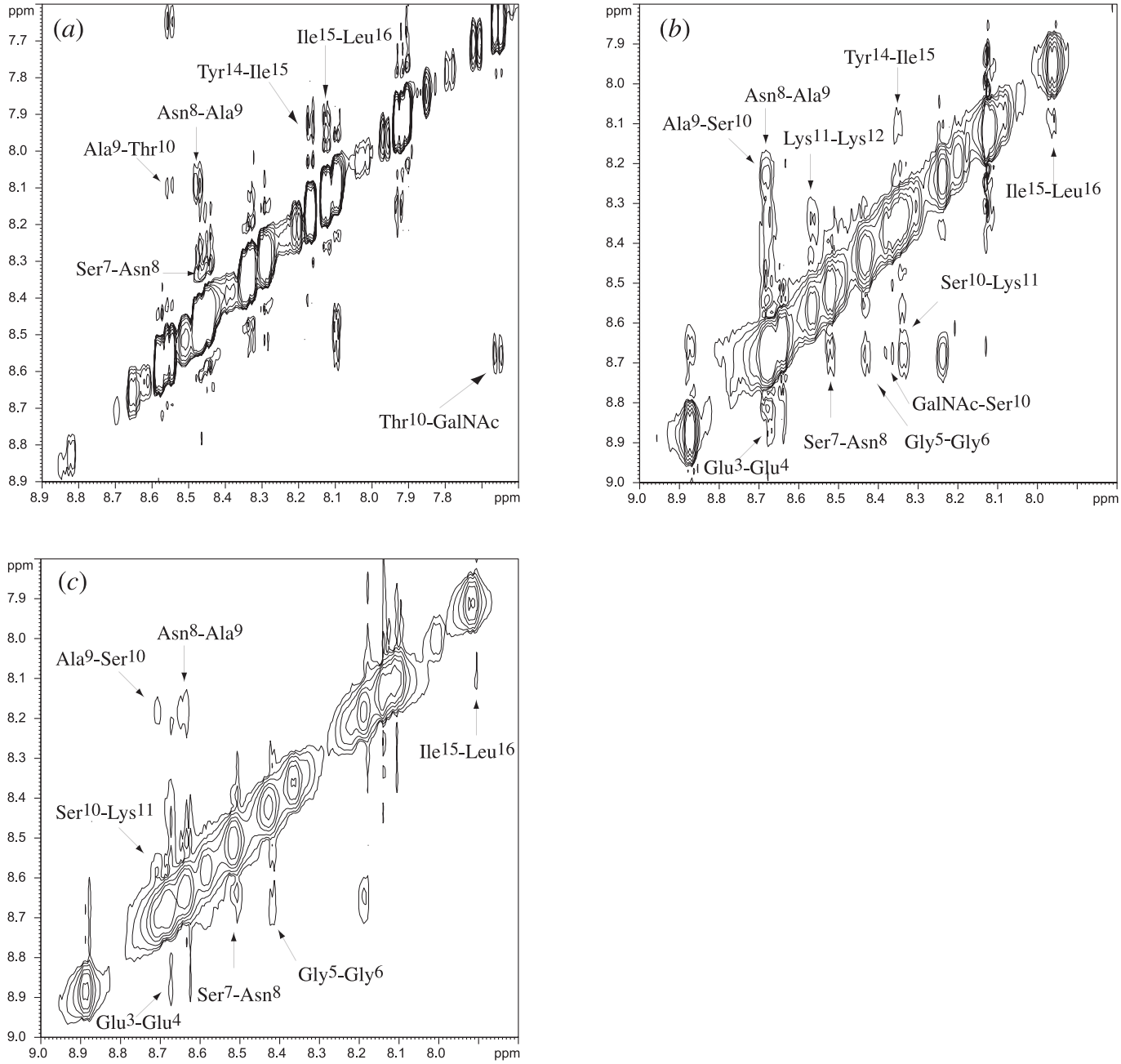
Experimental

Synthesis

Glycopeptides **5** and **6** were manually synthesized using a solid phase approach and Fmoc protection strategy, in a similar fashion as previously described (1). After cleavage of the peptide from the resin (100 °C, 2 h), the precipitate from the diethylether was dried. The product was then dissolved in 0.1% trifluoroacetic acid (TFA) and separated by HPLC

© 2005 NRC Canada

Fig. 3. The NH–NH region of the 2D NOESY spectra (mixing time 300 ms) of the glycopeptides **1**, **5**, and **6** in 95% H_2O – 5% D_2O. (*a*) Contulakin-G (**1**) (25 °C) (from ref. 4), (*b*) [D-Ser^{10}] analogue **5** (5 °C), and (*c*) [L-Ser^{10}] analogue **6** (5 °C).



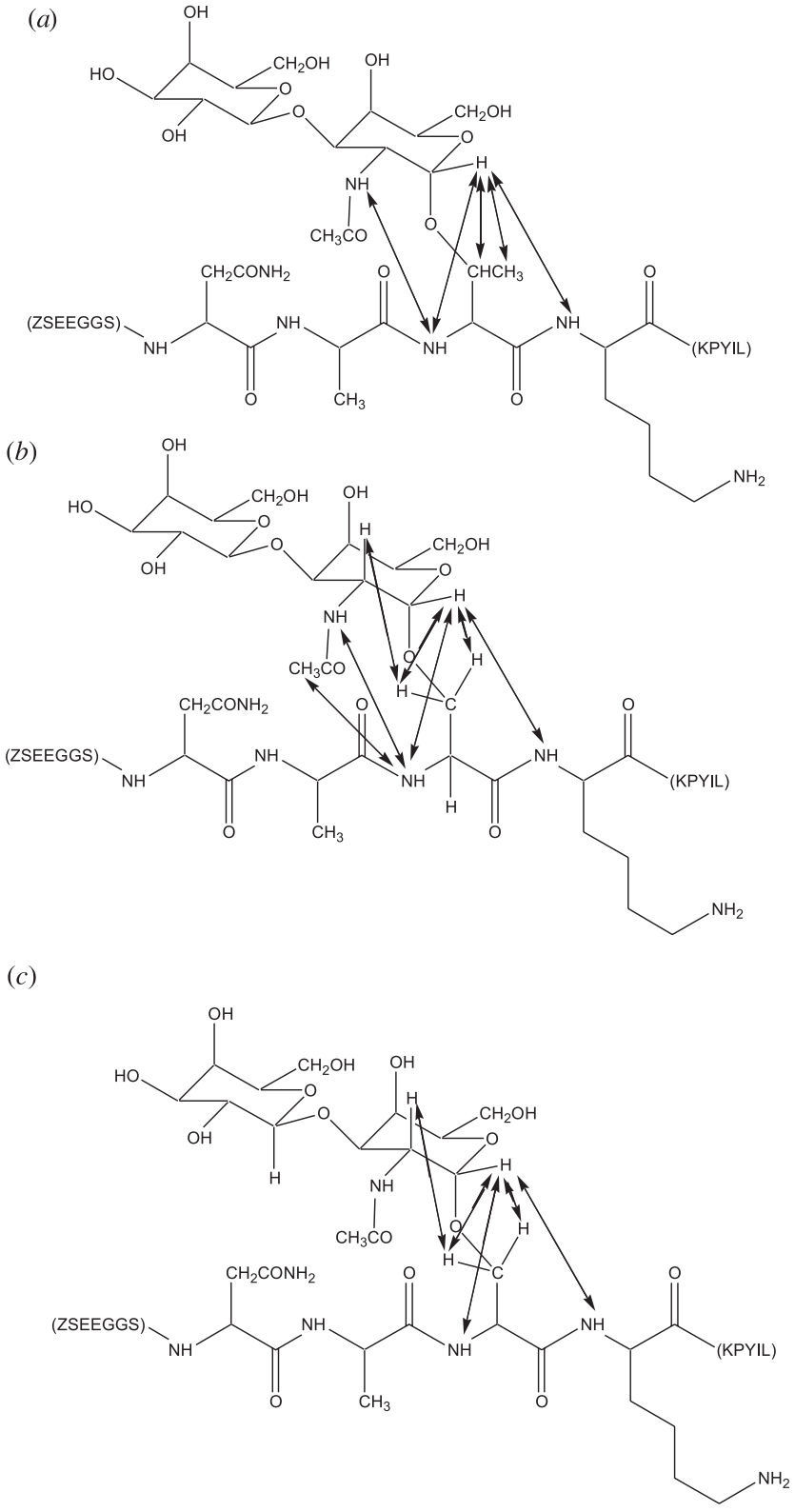
using a C18 column, a buffer A = 0.1% TFA and a buffer B = 60% acetonitrile in 1% TFA; 1 min gradient from 20% B to 60% B. Two separate HPLC fractions eluted, the first at approximately the same time as contulakin-G and the second about 2 min later. The samples were lyophilised separately, and the glycan deprotected in a similar way as previously described (1). The samples were again purified by HPLC under the same conditions as described above. The purity of the final samples was >95% based on RP-HPLC with triethylamine (pH 6) as the ion pairing agent, and capillary zone electrophoresis. Analysis of the protected glyco amino acid on TLC indicated a pure starting material. The mass spectrum yielded the information that both compounds had the correct mass, and that both were glycopeptides. The samples were characterized with electrospray-MS on an ion trap instrument and MALDI-TOF MS, and both samples were found to have identical monoisotopic masses and superimposable isotope distributions.

Determination of absolute configuration by GC–MS

The absolute configuration of the serine residues in the peptide chains of **5** and **6** was determined by using the GC–MS method of Ström et al. (8). A small amount (<0.1 mg) of each peptide was hydrolysed by 6 mol L^{-1} hydrochloric acid.

© 2005 NRC Canada

Fig. 4. Schematic representation of inter-residual NOEs observed at the junction between the peptide and the glycan in (*a*) **1**, (from ref. 4), (*b*) **5**, and (*c*) **6**.



Prior to injection on the column, the acid function was esterified with (*S*)-(+)-butanol, and perfluoropropanoic acid was allowed to react with the amine and alcohol functions to make the amino acids more volatile. Reference samples were prepared by derivatisation of commercially available D- and L-serine as outlined above.

© 2005 NRC Canada

NMR spectroscopy

The samples were prepared by dissolving ~1 mg of glycopeptide in 50 µL 99.98% D_2O, H_2O–D_2O (95:5), or in a pH 5.6 buffer containing H_2O–D_2O (95:5, v:v), 100 mmol L^{-1} sodium chloride and 13.5 mmol L^{-1} sodium acetate. The solutions were then transferred into 1.7 mm NMR capillaries. All NMR experiments were performed on a Bruker DRX-600 spectrometer equipped with a 2.5 mm microprobe. The NMR spectra, unless specified, were recorded at 5, 15, or 25 °C. The temperature coefficients were calculated for the amide protons in H_2O–D_2O solutions using ^{1}H NMR chemical shift data measured by variation of the temperature from 5 to 45 °C in steps of 5 °C. The two-dimensional NMR spectra were recorded in the phase-sensitive mode using the TPPI method (15). For experiments on samples in D_2O, the residual HDO peak was suppressed by preirradiation at low decoupler power. For experiments in 95% H_2O – 5% D_2O, the WATERGATE pulse sequence was used for water suppression (16). The DQF–COSY and TOCSY spectra were typically acquired with 4K data points in t_2 and 512 points in t_1, and a repetition delay of 1.5 s. TOCSY were recorded with a mixing time of 100 ms. NOESY and ROESY spectra were recorded with mixing times (t_m) from 100 to 600 ms for NOESY and 150 ms for ROESY. 256 Spectra of 4K data points were acquired, and a repetition delay of 2.5 s was used. The ^{1}H NMR chemical shifts were measured relative to the resonance of the methyl signal of acetone (δ 2.225 ppm) added as an internal reference.

MM2 representations

Chem3D (R) version 4.0 for Windows 95 and NT was used. Minimization was performed with the "MM2" force field. The default convergence criterion was used (rms (root mean square) force 0.1 kcal mol^{-1} $Å^{-1}$).

Acknowledgements

This work was supported by grants from the Swedish Research Council. Professor Thomas Norberg is acknowledged for providing the sugars used in the synthesis of the glycopeptides. Many thanks to Dr. A.G. Craig for providing the two glycosylated contulakin-G analogues and the biological data.

References

1. A.G. Craig, T. Norberg, D. Griffin, C. Hoeger, M. Akhtar, K. Schmidt, W. Low, J. Dykert, E. Richelson, V. Navarro, J. Mazella, M. Watkins, D. Hillyard, J. Imperial, L.J. Cruz, and B.M. Olivera. J. Biol. Chem. **274**, 13752 (1999)
2. J.D. Wagstaff, R.T. Layer, A.G. Craig, B.-M. Olivera, and R.T. McCabe. Proc. 29th Annu. Meet. Soc. Neurosci. **25**, 1944 (1999).
3. R.M. Jones and G. Bulaj. Curr. Opin. Drug Discovery Dev. **3**, 141 (2000).
4. L. Kindahl, C. Sandström, A.G. Craig, T. Norberg, and L. Kenne. Can. J. Chem. **80**, 1022 (2002).
5. X.L. Huang, J.J. Barchi, E.D.T. Lung, P.P. Roller, P.L. Nara, J. Muschik, and R.R. Garrity. Biochemistry, **36**, 10 846 (1997).
6. G.A. Naganagowda, T.L. Gururaja, J. Satyanarayana, and M.J. Levine. J. Pept. Res. **54**, 290 (1999).
7. J.L. Nieto, M. Rico, J. Santoro, J. Herranz, and F.J. Bermejo. Int. J. Pept. Protein Res. **28**, 315 (1986).
8. K.S. Ström, J. Sjögren, A. Broberg, and J. Schnürer. J. Appl. Environ. Microbiol. **68**, 4322 (2002).
9. D.S. Wishart, B.D. Sykes, and F.M. Richards. Biochemistry, **31**, 1647 (1992).
10. D.S. Wishart, C.G. Bigam, A. Holm, R.S. Hodges, and B.D. Sykes. J. Biomol. NMR, **5**, 67 (1995).
11. L. Kirnarsky, O. Prakash, S.M. Vogen, M. Nomoto, M.A. Hollingsworth, and S. Sherman. Biochemistry, **39**, 12076 (2000).
12. J.S. Grinstead, R.R. Koganty, M.J. Krantz, B.M. Longenecker, A.P. Campbell. Biochemistry, **41**, 9946 (2002).
13. G.Y. Xu and C.M. Deber. Int. J. Pept. Protein Res. **37**, 528 (1991).
14. J.L. Hylden and G.L. Wilcox. Eur. J. Pharmacol. **67**, 313 (1980).
15. D. Marion and K. Wüthrich. Biochem. Biophys. Res. Commun. **113**, 967 (1983).
16. M. Piotto, V. Saudek, and V. Sklenar. J. Biomol. NMR, **2**, 661 (1992).

© 2005 NRC Canada

Theoretical studies on the absorption and luminescent properties of a series of derivatives of 1,3-diphenyl-5-pyrene-2-yl-4,5-dihydro-1*H*-pyrazole

Xiao-Juan Liu, Ji-Kang Feng, Ai-Min Ren, Xin Zhou, and Hong Cheng

Abstract: The absorption and emission spectra for a series of substituted 1,3-diphenyl-5-pyrene-2-yl-4,5-dihydro-1*H*-pyrazole (DPPyP) molecules are computed by TDDFT methods. The solvent effect is modeled using the self-consistent reaction field (SCRF) method with Tomasi's polarized continuum model (PCM). The ground-state geometries were optimized by the Hartree–Fock method with the 6-31G basis set (and also with 3-21G* for molecule A) (HF/6-31G), and the lowest singlet excited-state geometries were optimized at the ab initio CIS level with the 6-31G basis set (CIS/6-31G). The calculated results indicate that the TDDFT method can reproduce the experimental values. We consider the effects of different basis sets on the optimization of the ground-state geometries. Specially, some insights on the differences observed for these compounds in changing the substituted donors (H, CH_3, and NH_2) and acceptor group (CN) are given; the results indicate that introduction of the donor groups will lead emission to be red-shifted, while introduction of the acceptor will induce the emission to be blue-shifted, which provides useful information for modulating light-emitting material colors.

Key words: absorption and emission, TDDFT, CIS, SCRF–PCM.

Résumé : Les spectres d'absorption et d'émission d'une série de 1,3-diphényl-5-pyrène-2-yl-4,5-dihydro-1*H*-pyrazole (DPPyP) ont été calculés par des méthodes « TDDFT ». On a modélisé l'effet du solvant faisant appel à la méthode de champ réactionnel autocohérent (« SCRF ») avec le modèle du continuum polarisé de Tomasi (« PCM »). On a optimizé les géométries de l'état fondamental par la méthode de Hartree–Fock, avec l'ensemble de base 6-31G (ainsi q'avec l'ensemble 3-21G* pour la molécule A) (HF/6-31G), et les géométries de l'état excité singulet d'énergie la plus faible ont été optimizées au niveau ab initio CIS avec un ensemble de base 6-31G (CIS/6-31G). Les résultats calculés indiquent que la méthode TDDFT permet de reproduire les valeurs expérimentales. Les effets des différents ensembles de base sur l'optimization des géométries de l'état fondamental ont été considérés. En particulier, on discute quelques explications possibles des différences observées pour ces composés lorsqu'on remplace des substituants donneurs (H, CH_3 ou NH_2) par un groupe accepteur (CN); les résultats indiquent que l'introduction de groupes donneurs conduit à une émission déplacée vers le rouge alors que l'introduction d'un groupe accepteur induit un déplacement de l'émission vers le bleu et que ces différences fournissent une méthode de moduler les couleurs émises par les matériaux qui émettent de la lumière.

Mots clés : adsorption, émission, TDDFT, CIS, SCRF–PCM.

[Traduit par la Rédaction]

Introduction

Considerable research efforts in recent years have been dedicated to the development of electroluminescent polymers and organic materials for use in light-emitting diodes (LEDs). The efforts were stimulated by the potential applications of these devices in the electronics industry. The main advantages of such LEDs over inorganic ones are that they are lightweight and have a large active area and flexibility. These factors favor their use in display technology. For ex-

Received 12 April 2004. Published on the NRC Research Press Web site at http://canjchem.nrc.ca on 25 February 2005.

X.-J. Liu, A.-M. Ren, and X. Zhou. State Key Laboratory of Theoretical and Computational Chemistry, Institute of Theoretical Chemistry, Jilin University, Changchun 130023, P.R. China.
H. Cheng. The college of Chemistry, Jilin University, Changchun 130023, P. R. China.
J.-K. Feng.[1] State Key Laboratory of Theoretical and Computational Chemistry, Institute of Theoretical Chemistry, Jilin University, Changchun 130023, P.R. China and The College of Chemistry, Jilin University, Changchun 130023, P.R. China.

[1]Corresponding author (e-mail: Jikangf@yahoo.com).

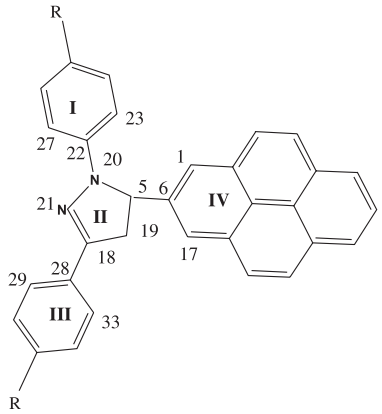
 doi: 10.1139/V04-168 © 2005 NRC Canada

ample in 1987, Tang and Van Slyke (1) reported on the interesting electroluminescent properties of multilayer devices using an organic material (Alq_3) as an emitter.

The basic structure of these stacked light-emitting devices typically has up to four organic semiconductor layers. Starting from the anode, the construction of a hole-injection layer (HIL) with a low ionization potential lowers the barrier controlling the injection of holes. It is covered by a hole-transport layer (HTL), which conducts the positive carriers to the confinement zone. In a symmetrical fashion, an electron-transport layer (ETL) and an electron-injection layer (EIL) just below the cathode perform the same functions but for negative carriers. The emitting layer is generally one of the transport layers. It can be intrinsically luminescent or doped with fluorescent molecules. The discovery of several important classes of organic materials with excellent transport, injection, and luminescent properties has enabled fabrication of high-performance multilayer device structures (2, 3). Recently, many hole-transport materials (HTM) with high glass transition temperatures (T_g), including starburst amines (4), spiro-linked amines (5), and those with rigid groups (6), have been investigated, such as *N*,*N*′-di-1-naphthenyl-*N*,*N*′-diphenyl-1,1′-bephenyl-4,4′-damine (α-NPD) (7) and 1,3,5-triaryl-2-pyrazoline compounds. But most of these compounds have low melting points and show poor thermal stability. Sano et al. (8) have demonstrated that pyrazoline dimers have higher melting points than pyrazoline monomers, and that stable amorphous films can be obtained by using these dimers. Some other works found that the introduction of condensed rings into the pyrazoline ring could also increase the melting point of the compounds (9–11). In these experiments, phenanthryl and pyrene groups were introduced into the 5-position of the pyrazoline ring. X-ray diffraction analysis shows that these molecules have nonplanar structure (10), and that there is strong π-stacking interaction in the solid state. This particular structure endues these molecules with good film forming ability and a high T_g of 96 °C. One popular approach to modulating the emissive color of organic materials is to introduce electron-withdrawing and (or) electron-releasing groups into the molecules. For example, tris (4-methyl-8-hydroxyquinoline) aluminum(III) (4-$Almq_3$) has received attention, because it has significantly higher photoluminescence and electroluminescence quantum yields.

However, few theoretical investigations of the luminescent properties for the pyrazoline derivatives mentioned above have appeared in the literature owing to the fact that the calculation of excited-state properties typically requires significantly more computational effort than is needed for the ground states. In present work, the geometries, absorption and emission properties of 1,3-diphenyl-5-pyrene-2-yl-4,5-dihydro-1*H*-pyrazole (DPPyP) derivatives, with the pyrene group introduced into the 5-position of the pyrazoline, were theoretically studied with the quantum chemical calculations. The transition energies were calculated at the ground-state and excited-state geometries using time-dependent density functional theory (TDDFT), and the results are compared with the available experimental data. The excited-state geometries were optimized at the ab initio CIS level of theory. Since the introduction of electron-withdrawing and (or) electron-releasing groups can modulate the emissive color, we connected donors (amino and methyl) and acceptor (cyanic) to the two phenyls to investigate their effects on the absorption and emission properties.

Fig. 1. The investigated molecules and the numbers for the pyrazoline ring.



Calculation details

The ground-state structures of the molecules were optimized at the Hartree–Fock level with the 6-31G basis set (HF/6-31G). The ab initio CIS (12) method was adopted to obtain the first singlet excited-state structures of the molecules. Vertical transition energies were evaluated with TDDFT (B3LYP/6-31G) as implemented in GAUSSIAN 98 at the optimized geometries obtained with 6-31G basis sets. The solvent effect is modeled using the self-consistent reaction field (SCRF) method with the Tomasi's polarized continuum model (PCM). The PCM model defines the solvent cavity as the union of a series of interlocking atomic spheres. The effect of the polarization of the solvent continuum is represented numerically: it is computed by numerical integration rather than by an approximation to the analytical form used in the Onsager model. Ionization potentials are obtained by calculating energy differences in the neutral ground-state and the cation ground-state geometries (the cation ground-state geometries are calculated using the restricted open shell Hartree–Fock–ROHF/6-31G method). These calculations were all carried out with the program package GAUSSIAN 98 (13).

Results and discussion

Molecular ground-state structures

The investigated molecules are shown in Fig. 1, their ground-state geometries are predicted at HF levels with 6-31G basis sets. Taking molecule A as an example, its equilibrium geometry is optimized using the HF method with both 3-21G* and 6-31G basis sets to investigate the basis set effect on the geometrical and electronic structures. Some selected interatomic bond lengths and bond angles of molecule A (DPPyP) are listed in Table 1, along with those of 1,3-diphenyl-5-(9-phenanthryl)-4,5-dihydro-1*H*-pyrazole (DPPhP), which is an analog of our investigated molecules given in the literature (14), while the dihedral angles among the planes of DPPyP are listed in Table 2. It can be seen that the calculated geometrical parameters are in good agreement

© 2005 NRC Canada

Table 1. Selected bond lengths (Å) and angles (°) of molecule A (DPPyP) with different basis sets and its analog (DPPhP).

	DPPyP		
	3-21G*	6-31G	DPPhP[a]
Bond lengths (Å)			
N(20)—N(21)	1.411	1.381	1.365
N(20)—C(5)	1.480	1.472	1.466
C(5)—C(19)	1.560	1.554	1.539
C(19)—C(18)	1.519	1.512	1.502
N(21)—C(18)	1.266	1.272	1.292
N(20)—C(22)	1.395	1.395	1.388
C(18)—C(28)	1.469	1.469	1.454
C(6)—C(5)	1.522	1.523	1.520
Bond angles (°)			
N(21)-N(20)-C(22)	118.29	119.13	121.16
N(21)-N(20)-C(5)	111.26	111.76	112.82
C(22)-N(20)-C(5)	126.02	126.57	125.70
C(5)-C(19)-C(18)	102.29	102.54	101.63
C(19)-C(18)-N(21)	113.54	112.48	102.00
C(19)-C(18)-C(28)	123.81	124.84	112.97
N(21)-C(18)-C(28)	122.65	122.68	125.31
C(18)-N(21)-C(20)	110.24	111.06	121.70
C(6)-C(5)-C(19)	112.78	113.59	109.16
C(6)-C(5)-H(43)	108.04	107.05	110.4

[a]From ref. 10, which are 1,3-diphenyl-5-(9-phenanthryl)-4,5-dihydro-1*H*-pyrazole molecules and it is different in that the condensed ring is pyrene in our paper and phenanthryl in ref. 10.

Table 2. The dihedral angles (°) between planes.

	Plane I	Plane II	Plane III
Plane II	9.6°(14.3°)		
Plane III	9.0°(10.9°)	1.9°(4.7°)	
Plane IV	87.6°(86.1°)	81.0°(79.8°)	89.7°(84.0°)

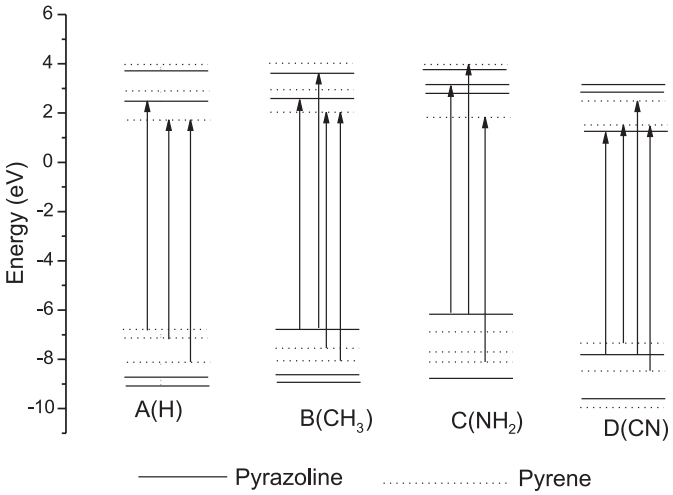
Note: The numbers in parentheses are from the single-crystal X-ray diffraction analysis of 1,3-diphenyl-5-(9-phenanthryl)-4,5-dihydro-1*H*-pyrazole molecules. From ref. 10.

Table 3. The HF calculated orbital energies and ionization potentials (in eV).

Orbital	A	B	C	D
Virtual orbitals				
LUMO + 4	3.85	3.94	3.98	3.04
LUMO + 3	3.77	3.62	3.88	2.95
LUMO + 2	2.85	2.85	3.17	2.48
LUMO + 1	2.47	2.64	2.90	1.43
LUMO	1.71	2.01	1.85	1.29
Occupied orbitals				
HOMO	–6.99	–6.89	–6.13	–7.42
HOMO – 1	–7.10	–7.66	–6.86	–7.91
HOMO – 2	–8.20	–8.02	–7.65	–8.54
HOMO – 3	–8.85	–8.67	–8.08	–9.67
HOMO – 4	–9.02	–8.82	–8.78	–9.76
IP	6.45(5.61)[a]	6.41	4.93	6.80

[a]Reference 11.

Fig. 2. Molecular orbital diagram summarizing the HF predicted energies and the main excitations.



with the X-ray diffraction experimental values. The bond length differences between molecule DPPyP and its analog DPPhP are 0.01~0.02 Å and the angles have a discrepancy within 1.5° except for the angles C(1)-C(6)-C(5), C(6)-C(7)-H(43), and C(6)-C(5)-C(19). Considering the different sterical effect between phenanthryl and pyrene, the discrepancy is reasonable. Table 2 shows that the two phenyl groups are conjugated with the pyrazoline ring and form a large conjugated π system, just like DPP. The dihedral angles formed by planes IV and I, II, III (see Fig. 1) in the investigated molecules are all a little larger than those in the analog DPPhP. These discrepancies between the two molecules are due to the sterically hindered group difference between phenanthryl and pyrene.

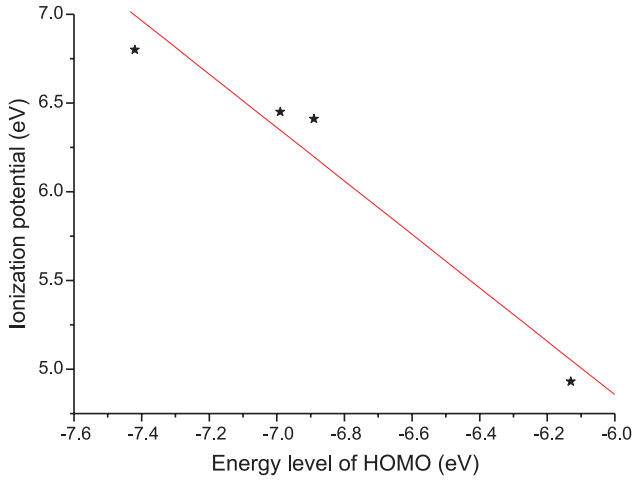
The bond angle of C(6)-C(7)-H(43) of 107.11° and the dihedral angle between planes II and IV of 81.0° suggest that the pyrene group extends outside the pyrazoline ring. Therefore, the introduction of the large polycyclic pyrene group decreases the symmetry of the compound and the resultant compounds A and other investigated molecules have nonplanar molecular structures, which is in agreement with the experimental results (10). Experimental results indicated that the nonplanar structure can prevent regular packing of molecules, and hence allows the formation of stable, amorphous films (10).

Molecular electronic structure

Electronic structures are fundamental to the interpretation and understanding of the absorption spectra. It has been found that the relative ordering of the occupied and virtual orbitals provides a reasonable qualitative indication of the excitation energies. The five highest occupied and five lowest virtual orbital energies for all the studied molecules calculated by HF/6-31G are given in Table 3. For a simple comparison, the schematic representation of the energy level of the orbitals and the main related electronic energy transitions are shown in Fig. 2. In Fig. 2, the solid lines represent that the molecular orbital is mainly made up of the atomic orbitals on pyrazoline; the dotted lines represent that the molecular orbital is mainly made up of the atomic orbitals on the pyrene. It can be found from Fig. 2 that introduction of donor groups (molecules B-CH_3 and C-NH_2) raises the

© 2005 NRC Canada

Fig. 3. The relationship between the energy of the HOMOs and ionization potentials.



HOMO a little, while introduction of an acceptor (molecule D-CN) lowers the frontier orbitals, when compared to molecule A, which has no substituted group.

Ionization energy (IP) is defined as the minimum energy necessary to bring an electron from the material into vacuum. According to Koopmans theorem, this energy value can be compared to the computed highest occupied molecular orbital energy level (HOMO). In this paper, the IPs are obtained by differences in the total self-consistent energies of the cation and the neutral states at the cation and neutral ground-state optimized geometries, respectively. The calculated values are also listed in Table 3. The calculated ionization potential energies are 6.45, 6.41, and 4.93 eV for molecules A, B, and C, respectively, and the 6.45 eV for molecule A corresponds to its experimental value of –5.61 eV. As for molecule D, its ionization potential is 6.80 eV. Comparing the values of IP with the energy values of HOMO, we found that they are indeed approximately equivalent with each other. To indicate their relationship, we plot the lines of IP vs. the energy of HOMO in Fig. 3. Fig. 3 shows that these points are almost in line, which verifies the Koopmans theory. In photoluminescent materials, the ionization potential of HTL is higher than that of HIL, so holes would enter from the HIL to the HTL layer freely after being injected from ITO (indium tin oxide). From this point of view, molecule C is a better candidate for use in a device than molecules B and D.

Electronic absorption spectra

Since the accuracy of the computed spectra are dependent upon the structural parameters used in the calculations, it is important to establish the quality of the computed structures by comparing the calculated spectra to available experimental data. Taking molecule A as an example, we calculated the absorptions on the optimized ground-state (S_0) geometries obtained with the HF/6-31G and HF/3-21G* methods, respectively. The calculated results are listed in Table 4, along with the experimental values. The TDDFT results indicate that there is a comparatively large discrepancy between the absorptions for the two geometries. This phenomenon indicates that the TDDFT method is sensitive to the molecular geometries, and comparing both the calculated absolute geometrical parameters and absorption with the experimental values, it was found that the 6-31G basis set based on the HF method is suitable for our investigated molecules, and the TDDFT (B3LYP/6-31G) model is good enough to predict the investigated molecular absorption spectra.

Table 4. The TDDFT calculated absorption properties in the gas phase, based on the HF-optimized geometries with 6-31G and 3-21G* basis sets.

3-21G*			6-31G			
Energy (eV)	λ (nm)	*f*	Energy (eV)	λ (nm)	*f*	In CH_3CN solution[a] (nm)
3.69	336	0.45	3.65	340		345
						330
4.08	314	0.32	3.94	314		315
						275
5.04	246	0.17	4.87	255		265
5.06	245	0.17	5.26	236		240
5.40	230	0.40	5.31	233		
			5.56	223		

[a]Reference 11.

It is well-known, both experimentally (15–20) and theoretically (21–26), that the presence of solvent strongly influences the optical response for many polar and nonpolar molecules compared to the gas phase. For our investigated molecules, based on the HF/6-31G optimized geometries, using the SCRF–PCM model, we calculated the absorptions both in the gas phase and in the acetonitrile (CH_3CN) solvent. The results are tabulated in Table 5. Firstly, we found that the solvent has a much stronger effect on molecule C than the other molecules. This result indicates that the introduction of a strong donor group (-NH_2) makes the molecule more polarized. Secondly, it was found that only when the solvent effect is considered in the calculation, the calculated results are in agreement with the change tendency with the substituent group. And the tendency is that with the substituent group strength increasing, the absorption is red-shifted (the absorption is 336, 338, and 360 nm for molecules A, B, and C, respectively). So it is necessary for our investigated molecules that the solvent effect should be considered in the spectra calculation. For all the studied molecules, the calculated excited energies (in nm), dominant orbital excitations, and oscillator strengths (*f*) from TDDFT calculations in the CH_3CN solvent are listed in Table 6. In the table we have reported only the active bands that are important for a complete characterization for the compounds. We begin with the spectrum of molecule A, and then discuss the donors (amine and methyl) and acceptor (cyanyl) substitution effects.

The strongest absorption of molecule A is located at 336 nm with 0.51 oscillator strength, which is in accordance with the experimental value of 345 nm, and this excited state mainly involves the transition from HOMO to LUMO + 1; the other two absorptions of 314 and 254 nm are mainly from the transitions of HOMO – 1 to LUMO and HOMO – 2 to LUMO, respectively (this also is shown in Fig. 2). In Fig. 4*a*, these molecular orbitals are plotted to provide a qualitative indication of the excitations. From Fig. 4, it can be easily found that the absorption at 336 nm comes from

© 2005 NRC Canada

Table 5. The absorptions in gas and in the acetonitrile solvent for the HF/6-31G optimized geometries.

A(H)		$B(CH_3)$		$C(NH_2)$		D(CN)	
Gas	Solution	Gas	Solution	Gas	Solution	Gas	Solution
340(0.48)	336(0.51)	349(0.52)	338(0.45)		360(0.47)	375(0.58)	368(0.75)
315(0.34)	314(0.28)	322(0.35)	326(0.17)	313(0.29)	306(0.22)	315(0.36)	319(0.36)
				312(0.18)			
			308(0.35)	305(0.33)		263(0.42)	271(0.29)
255(0.26)	254(0.29)	258(0.28)		262(0.47)	269(0.28)	255(0.35)	256(0.17)
236(0.13)		243(0.35)	248(0.33)		268(0.27)		253(0.13)
233(0.25)		226(0.14)	239(0.33)				
223(0.12)		223(0.17)		247(0.35)	247(0.32)		235(0.18)
217(0.17)							

the electron transition within the pyrazoline, while the other two absorptions of 314 and 254 nm can be seen as coming from the electron transitions within the pyrene. This result indicates that the absorption of molecule A is the combination of the absorption of the two chromophores (the pyrene and pyrazoline groups). This opinion is consistent with the experiment (10, 11). In the experiment (10), it was found that the absorption and emission are not affected by the introduction of the bulky phenanthryl substitution both in acetonitrile solution and in the solid film when comparing molecules DPPhP and DPP.

Similarly, the absorption characters of other molecules are analyzed in the same way as molecule A. Such as in molecule C (shown in Fig. 4*b*), the 360 nm absorption comes from the electron transition within the pyrazoline; the 268 and 247 nm absorptions come from the electron transitions within the pyrene, while the 306 nm absorption comes from the electron transition from pyrazoline to pyrene. In all, the introduction of the substituent of the amino group induces more electrons to distribute on the pyrazoline group. For molecule B from Fig. 2, we found that its absorptions are all within its constituent chromophores. Molecule D's absorption occurs mainly as an electron transition within constituent chromophores, with an absorption coming from pyrazoline to pyrene. In all, for our investigated molecules, their absorptions mainly come from the electron transitions within individual chromophores; and if a strong substituent group is introduced on pyrazoline, there exists some electron transition between the two chromophores, such as in molecules C and D.

Excited-state geometry calculations

Excited-state optimized geometries are important for the investigation of emission properties because structural relaxation after photoexcitation cannot be reproduced by ground-state optimization. The excited-state geometries were optimized at the ab initio CIS levels with the 6-31G basis set. We found that the geometry changes mainly happen on the pyrazoline group, especially on plane II (see Fig. 1), such as the R bond (18, 21) length is decreased by 0.037 Å from ground to excited state, and the angles related to plane II are all changed about 0.5°. We investigated the geometry relaxations upon excitation by consideration of the nodal patterns of the HOMO and LUMO orbitals (15). It is considered that if there are no nodes across the bond on HOMO, while there are nodes across the same bond on LUMO, then this bond will be elongated when the molecule changes from the ground state to the excited state; in contrast, if there is no nodal across the bond on LUMO, while there is a nodal across the same bond on HOMO, then this bond will be contracted. According to this rule, we investigated the bond length changes in molecule A. The nodal patterns are plotted in Fig. 5*b*, only plane II being shown. The HOMO has nodes across C(5)-C(19), C(5)-C(20), and C(18)-C(19) on plane II (for labelling see Fig. 5*a*), while LUMO has no nodes across these bonds; one would expect contraction of these bonds. Fig. 5*a* shows that these bonds are in fact considerably shorter in the excited state. The HOMO has no node across C(18)-C(28), while on LUMO this bond shows a node across it, and the data in Fig. 5*a* confirms the anticipated elongation of these bonds.

Emission properties

Based on the excited-state geometry optimization by CIS/6-31G, we carried out the emission calculation using TDDFT/6-31G in the CH_3CN solvent (using the same model as absorption). The calculated results are shown in Table 7; the experimental data are included for comparison. The TDDFT calculated value of molecule A is located at 423 nm, which is in agreement with the experimental value of 440 nm in CH_3CN solvent. When the substituent groups are amine and methyl for molecules B and C, their emissions are red-shifted, positioned at 431 and 501 nm, respectively, while the cyanyl substituent makes the emission blue-shift (418 nm).

The calculated Stokes shift values, the differences between the absorption and emission λ_{max} values, are compared with the experimental values. TDDFT calculated results (B3LYP/6-31G model) based on the excited-state optimized geometries by CIS/6-31G reproduced experimental emission well. The TDDFT-calculated Stokes shift (87 nm) for molecule A is in good agreement with the experimental data (95 nm). Furthermore, molecule C has the largest Stokes shift in these molecules, indicating that during the excitation the nuclei position has a comparatively large change in molecule C than incompared with the other molecules.

Conclusions

We have calculated the ground- and excited-state geometries using the HF/6-31G and CIS/6-31G methods, respectively. The calculated geometrical parameters are in good agreement with available X-ray diffraction data. Comparison of the CIS/6-31G optimized excited-state structures and the

© 2005 NRC Canada

Table 6. Calculated excited energies (λ_{max} in nm), dominant orbital excitations, and oscillator strengths (f) in CH_3CN solvent from TDDFT calculations on the HF/6-31G optimized geometries for all the investigated molecules.

A			B			C			D		
λ (nm)	Dominant orbital excitation	f	λ (nm)	Dominant orbital excitation	f	λ (nm)	Dominant orbital excitation	f	λ (nm)	Dominant orbital excitation	f
336	HOMO → LUMO + 1	0.51	338	HOMO → LUMO + 1	0.45	360	HOMO → LUMO + 2	0.47	368	HOMO – 1 → LUMO	0.75
						306	HOMO → LUMO + 4	0.22	319	HOMO → LUMO + 1	0.36
314	HOMO – 1 → LUMO	0.28	326	HOMO → LUMO + 2	0.17						
			308	HOMO – 1 → LUMO	0.35	268	HOMO – 5 → LUMO	0.27	271	HOMO – 1 → LUMO + 2	0.29
254	HOMO – 2 → LUMO	0.29	248	HOMO – 2 → LUMO	0.33	247	HOMO – 3 → LUMO	0.32	256	HOMO – 3 → LUMO + 1	0.17
			239	HOMO – 3 → LUMO + 1	0.33				235	HOMO – 4 → LUMO	0.18

Fig. 4. Absorption property diagrams shown by the frontier orbital electron transition plot.

© 2005 NRC Canada

Fig. 5. (*a*) The selected bond lengths (Å) of molecule A in the ground and the first excited state (in parentheses). (*b*) The nodal picture of HOMO and LUMO.

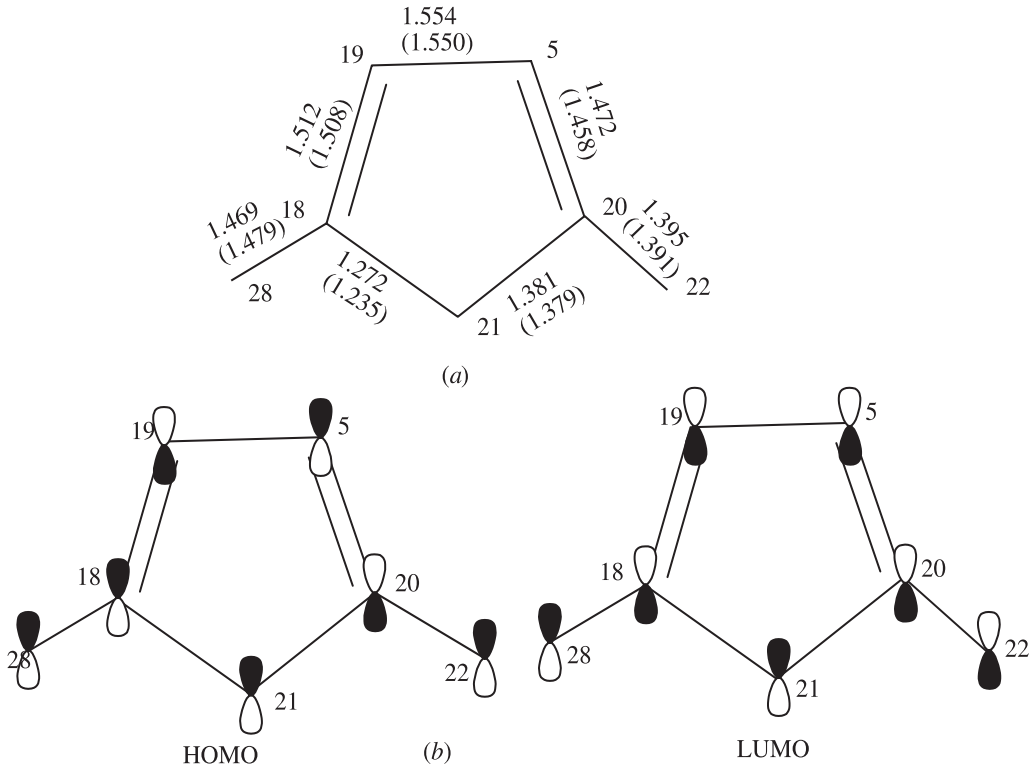


Table 7. Emission wavelengths (λ_{max} in nm) computed with the TDDFT[a] method using the CIS/6-31G optimized geometry.

Molecules	TDDFT (nm)	Stokes shift[b]	In 1×10^{-6} mol L^{-1} acetonitrile solution[c] (nm)
A	423	95(87)[d]	440
B	431	93	
C	501	141	
D	418	50	

Note: Oscillator strengths are in parentheses.
[a]The B3LYP/6-31G model was used.
[b]The TDDFT calculated results.
[c]Reference 11.
[d]Reference 10.

HF/6-31G ground-state structures indicates that the geometric shift is mainly confined to the pyrazoline part (plane II). Basis sets effects on the absorption properties are discussed taking molecule A as an example. The absorptions on these two geometries (optimized here using HF/6-31G and HF/3-21G*) were calculated by TDDFT methods, the results indicating that the TDDFT method is sensitive to the geometries and can give reliable results for the absorption values. Using the CIS-optimized structure of the excited state, TDDFT calculations predict an emission wavelength of 423 nm, which is comparable to 440 nm, which is observed experimentally in the acetonitrile solvent. The Stokes shift calculated by TDDFT is 87 nm, in agreement with the observed value of 95 nm. The TDDFT provides a good method to calculate the Stokes shift for these molecules.

The calculated results indicate that the introduction of donor groups will lead the molecular emissions to be red-shifted, and introduction of an acceptor will lead the luminescence to be blue-shifted, which is useful for modulating the emission color in practical light-emitting materials and the holes transition.

Acknowledgments

This work is supported by the Major State Basis Research Development Program (No. 2002CB 613406) and the National Nature Science Foundation of China (No. 90101026 20173021), and the Key Laboratory for Supramolecular Structure and Material of Jillin University.

References

1. C.W. Tang and S.A. Van Slyke. Appl. Phys. Lett. **51**, 913 (1987).
2. C.W. Tang. SID 96 Digest. 181 (1996).
3. S. Roth, M. Burghard, and G. Leising. Curr. Opin. Solid State Mater. Sci. **23**, 209 (1998).
4. M. Thelakkat and H. W. Schmidt. Adv. Mater. (Weinheim, Ger.), **10**, 219 (1998).
5. J. Salbeck and F. Weissortel. Macromol. Symp. **125**, 121 (1997).
6. B.E. Koene, D.E. Loy, and M.E. Thompson. Chem. Mater. **10**, 2235 (1998).
7. C.H. Chen, J. Shi, and C.W. Tang. Macromol. Symp. **125**, 1(1997).
8. T. Sano, T. Fujii, Y. Nishio, F. Famada, K. Shibata, and K. Kuroki. Jpn. J. Appl. Phys. **34**, 3124 (1995).

© 2005 NRC Canada

9. C.W. Ma, L.Q. Zhang, X.H. Li, X.S. Wang, B.W. Zhang, Y. Cao, D.M. Wang, X.Y. Jiang, Z.L. Zhang, D.Q. Zhang, and Y. Qiu. Acta Chim. Sin. **60**, 847 (2002).
10. C.Q. Ma, L.Q. Zhang, J.H. Zhou, X.S. Wang, B.W. Zhang, Y. Cao, P. Bugnon, M. Schaer, F. Nüsech, D.Q. Zhang, and Y. Qiu. J. Mater. Chem. **12**, 3481 (2002).
11. X.C. Gao, H. Cao, L.Q. Zhang, B.W. Zhang, Y. Cao, and C.H. Huang. J. Mater. Chem. **9**, 1077 (1999).
12. J.B. Foresman, M. Head-Gordon, J.A. Pople, and M.J. Frisch. J. Phys. Chem. **96**, 135 (1992).
13. M.J. Frish, G.W. Trucks, H.B. Schlegel, G.E. Scuseria, M.A. Robb, J.R. Cheeseman, V.G. Zakrzewski, J.A. Montgomery, R.E. Stratmann, J.C. Burant, S. Dapprich, J.M. Millam, A.D. Daniels, K.N. Kudin, M.C. Stain, O. Farkas, J. Tomasi, V. Barone, M. Cossi, A.D. Daniels, K.N. Kudin, M.C. Strain, O. Farkas, J. Tomasi, V. Barone, M. Cossi, R. Cammi, B. Mennucci, C. Pomelli, C. Adamo, S. Clifford, J. Ochterski, G.A. Petersson, P.Y. Ayala, Q. Cui, K. Morokuma, D.K. Malick, A.D. Rabuck, K. Raghavachari, J.B. Foresman, J. Cioslowski, J.V. Oritz, B.B. Stefanov, G. Liu, A. Liashenko, P. Piskorz, I. Komaromi, R. Gomperts, R.L. Martin, D.J. Fox, T. Keith, M.A. AI-Laham, C.Y. Peng, A. Nanayakkara, C. Gonzalez, M. Challacombe, P.M.W. Gill, B.G. Johnson, W. Chen, M.W. Wong, J.L. Andres, M. Head-Gordon, E.S. Replogle, and J.A. Pople. GAUSSIAN 98 [computer program]. Gaussian, Inc., Pittsburgh, Penn. 1998.
14. B. Buffin. Acta Crystallogr. **B24**, 1256 (1968).
15. B.F. Levine and C.G. Bethea. J. Chem. Phys. **65**, 2429 (1976).
16. L.J. Cheng, W. Tam, S.R. Marder, A.E. Stiegman, G. Rikken, and C.W. Spangler. J. Phys. Chem. **95**, 10643 (1991).
17. S.R. Marder, D.N. Bretan, and L.T. Cheng. Science (Washington, D.C.), **252**, 103 (1991).
18. K. Calys, E. Hendrickx, M. Triest, T. Verbiest, A. Persoons, C. Dehu, J.L. Brédas. Science (Washington, D.C.), **262**, 632 (1993).
19. G. Bourhill, J.L. Brédas, L.T. Cheng, S.R. Marder, F. Meyers, J.W. Perry, and B.G. Tiemann. J. Am. Chem. Soc. **116**, 2619 (1994).
20. F.L. Huyskens, P.L. Huskens, and A.P. Persoons. J. Chem. Phys. **108**, 8161 (1998).
21. C.C. Teng and A.F. Garito. Phys. Rev. Lett. **50**, 350 (1983).
22. C.C. Teng and A.F. Garito. Phys. Rev. B: Condens. Matter, **28**, 6766 (1983).
23. Y. Luo, A. Cesar, and H. Ågren. Chem. Phys. Lett. **252**, 389 (1995).
24. R. Cammi, B. Mennucci, and J. Tomasi. J. Phys. Chem. A, **104**, 4690 (2000).
25. W. Bartkowiak and J. Lipiński. J. Comput. Chem. **22**, 31 (1998).
26. W. Bartkowiak and T. Misiaszek. Chem. Phys. **261**, 353 (2000).

© 2005 NRC Canada

A synthetic, structural, and ^{113}Cd NMR study of cadmium complexes of 1,3-thiazolidine-2-thionate, including the structures of $Cd(C_3H_4NS_2)_2$, $(Cd(C_3H_4NS_2)_2(C_5H_5N)_3 \cdot C_5H_5N$, and $(Ph_4P)_2[I_2Cd(\mu\text{-}C_3H_4NS_2)_2CdI_2]$

Donald C. Craig, Ian G. Dance, Philip A.W. Dean, James M. Hook, Hilary A. Jenkins, Christopher W. Kirby, Marcia L. Scudder, and Umarani Rajalingam

Abstract: The crystallization of cadmium bis(1,3-thiazolidine-2-thionate), $Cd(C_3H_4NS_2)_2$ (**1**), is reported. Freshly prepared **1** reacts with $Ph_4P^+X^-$ in a 1:2 ratio to give $(Ph_4P)_2[Cd_2(C_3H_4NS_2)_2X_4]$ (X = I (**4**) or Br (**5**)). Crystallization of **1** from pyridine produces a solvate **7**, which loses pyridine readily. X-ray analyses show that **1** has a polymeric sheet structure in which the $C_3H_4NS_2^-$ ligands act as bidentate bridges through N and the exocyclic S and the Cd has a CdN_2S_2 kernel; **5** is isomorphous with **4**, which contains a dimeric anion again with bridging through the N and exocyclic S of the heterocyclic ligands; and **7** is $Cd(C_3H_4NS_2)_2(C_5H_5N)_3 \cdot C_5H_5N$, containing trigonal bipyramidal $Cd(C_3H_4NS_2)_2(C_5H_5N)_3$ molecules, in which the $C_3H_4NS_2^-$ ligands, both of which are monodentate and in equatorial positions, occur as a unique combination of S- and N-bound. Cadmium-113 NMR data for **1** in pyridine solution and solid-state CP-MAS ^{113}Cd data for **1**, **7**, bis(pyridinium-4-thiolate)cadmium, and tetrakis(pyridinium-2-thiolate)cadmium nitrate are reported and discussed. The compound **1** has chemical and NMR spectroscopic properties that make it a useful standard for solid-state CP-MAS ^{113}Cd NMR spectroscopy.

Key words: cadmium, 1,3-thiazolidine-2-thionate, X-ray analysis, solid-state ^{113}Cd NMR, ^{113}Cd NMR standard compound.

Résumé : On a effectué la cristallisation du bis(1,3-thiazolidine-2-thionate) de cadmium, $Cd(C_3H_4NS_2)_2$ (**1**). Le composé **1** fraîchement préparé réagit avec le $Ph_4P^+X^-$ dans un rapport 1 : 2 pour conduire à la formation de $(Ph_4P)_2[Cd_2(C_3H_4NS_2)_2X_4]$ (X = I (**4**) et Br (**5**)). La cristallisation du composé **1** dans la pyridine conduit à la formation du produit solvaté **7** qui perd facilement de la pyridine. Les données de la diffraction des rayons X montrent que le composé **1** existe dans une structure en feuillets polymériques dans laquelle les ligands $C_3H_4NS_2^-$ agissent comme ponts bidentates entre l'azote et le soufre exocyclique et que le cadmium se trouve dans un noyau CdN_2S_2; que le composé **5** est isomorphe de **4** qui contient un anion dimère qui se lie lui aussi par des ponts à l'azote et au soufre exocyclique des ligands hétérocycliques; que **7**, $Cd(C_3H_4NS_2)_2(C_5H_5N)_3 \cdot C_5H_5N$, comporte des molécules bipyramidales trigonales $Cd(C_3H_4NS_2)_2(C_5H_5N)_3$ dans lesquelles les ligands $C_3H_4NS_2^-$, qui sont tous les deux monodentates et dans des positions équatoriales, se retrouvent comme une combinaison unique avec des liaisons au soufre et à l'azote. On a obtenu et on discute des données de RMN du ^{113}Cd pour le composé **1**, en solution dans la pyridine, et des données de « CP-MAS » à l'état solide du ^{113}Cd pour les composés **1** et **7**, le bis(pyridinium-4-thiolate)cadmium et le nitrate de tétrakis(pyridinium-2-thiolate)cadmium. Le composé **1** a des propriétés chimiques et spectroscopiques qui pourraient le rendre utile comme standard pour la spectroscopie RMN ^{113}Cd « CP-MAS » à l'état solide.

Mots clés : cadmium, 1,3-thiazolidine-2-thionate, diffraction des rayons X, RMN du ^{113}Cd à l'état solide, composé standard pour la RMN du ^{113}Cd.

[Traduit par la Rédaction]

Received 29 August 2004. Published on the NRC Research Press Web site at http://canjchem.nrc.ca on 25 February 2005.

D.C. Craig, I.G. Dance, and M.L. Scudder. School of Chemistry, University of New South Wales, Sydney 2052, Australia.
P.A.W. Dean,[1] H.A. Jenkins,[2] C.W. Kirby, and U. Rajalingam.[3] Department of Chemistry, University of Western Ontario, London, ON N6A 5B7, Canada.
J.M. Hook. NMR Facility, University of New South Wales, Sydney 2052, Australia.

[1]Corresponding author (e-mail: pawdean@uwo.ca).
[2]Present address: Department of Chemistry, Saint Mary's University, Halifax, NS B3H 3C3, Canada.
[3]Present address: Vice President, Urecoats Technologies Inc., 4100 North PowerlineBusiness Park, Pompano Beach, FL 33073, USA.

 doi: 10.1139/V04-177 © 2005 NRC Canada

Introduction

An interest (1) in cadmium complexes of heterocyclic thione donor ligands, including 1,3-thiazolidine-2-thione (tztH), has led us into an investigation of complexes containing cadmium and the 1,3-thiazolidine-2-thionate anion (tzt^-). The compound $Cd(tzt)_2$ was first reported in this journal in 1976 (2*a*). It was suggested that the structure was polymeric and based on tetrahedrally coordinated metal ions. However, the compound has never been characterized structurally, and to our knowledge there are no other structurally characterized examples of complexes of Cd with the tzt^- ligand either.

Heterocyclic thionates, including tzt^-, are known to be versatile ligands (3, 4). A search of the Cambridge Structural Database[4] (CSD) (5) revealed that the following bonding modes occur for the tzt^- ligand in structurally characterized examples: monodentate bonding through sulfur (found in only two examples, MeHg(tzt) (6) and $(Ph_3P)Au(tzt)$ (7)); a single example of monodentate bonding through N, reported since the completion of our work (8); N,S-chelation; and bridging, which usually involves both N and the exocyclic S, although a single example of bridging solely through the exocyclic S is known (9). Of these, the N,S-bridging mode predominates.

In this paper, we describe the structure of $Cd(tzt)_2$, as well as the synthesis and characterization of two other cadmium complexes of tzt^-.

Experimental

Materials

Tetraphenylphosphonium bromide and iodide, pyridine-2- and pyridine-4-thiols (py2SH and py4SH), $Cd(NO_3)_2{\cdot}4H_2O$, and $Cd(OAc)_2{\cdot}2H_2O$ were commercial products and used as received. Thiazolidine-2-thione (Aldrich) was recrystallized from water before use. Spectroscopic-grade pyridine was dried over NaOH before use. All other solvents were spectroscopic grade and were stored over 3 Å molecular sieves.

Synthesis of $Cd(tzt)_2$ (1) and $Cd(py2S)_2$ (2)

Compounds **1** and **2** were synthesized (and, for **2**, recrystallized) by the literature methods (2, 10). The salt $[Cd(py2SH)_4](NO_3)_2$ was prepared as reported previously (1*a*, 11).

Synthesis of $Cd(py4S)_2$ (3)

Compound **3** was prepared in the same way as **2**. Anal. calcd. for $C_{10}H_8CdN_2S_2$: C 36.08, H 2.42, N 8.42; found: C 35.85, H 2.38, N 8.48.

Synthesis of $(Ph_4P)_2[I_2Cd(\mu\text{-}C_3H_4NS_2)_2CdI_2]$ (4)

A solution of tztH (0.066 g, 0.55 mmol) and Et_3N (0.075 mL, 0.53 mmol) in CH_2Cl_2 (3 mL) was added with stirring to a mixture of $Cd(NO_3)_2{\cdot}4H_2O$ (0.076 g, 0.27 mmol) in 10 mL of MeCN, causing formation of a white precipitate. To the mixture was added solid Ph_4PI (0.233 g, 0.500 mmol), causing the precipitate to dissolve. Diethyl ether was added until turbidity was apparent, at which point the container and contents were placed in a freezer for several days. The colourless crystals that formed were washed with diethyl ether and dried in vacuo. Yield: 0.029 g, 14%. Anal. calcd. for $C_{54}H_{48}Cd_2I_4N_2P_2S_4$: C 39.36, H 2.94, N 1.70; found: C 40.29, H 2.87, N 2.11. The formulation of the compound was confirmed by a single-crystal X-ray analysis (see below).

Synthesis of $(Ph_4P)_2[Br_2Cd(\mu\text{-}C_3H_4NS_2)_2CdBr_2]$ (5)

A solution of $Cd(NO_3)_2{\cdot}4H_2O$ (0.076 g, 0.25 mmol) in 3 mL of MeCN was added with stirring to a mixture of tztH (0.058 g, 0.49 mol) and Et_3N (0.069 mL, 0.49 mmol) in 3 mL of MeCN. To the white precipitate was added solid Ph_4PBr (0.206 g, 0.491 mmol), causing dissolution of the precipitate. Thereafter, diethyl ether was added, and colourless crystals were obtained and isolated as for **4**. Yield: 0.074 g, 41%. Anal. calcd. for $C_{54}H_{48}Br_4Cd_2N_2P_2S_4$: C 44.43, H 3.31, N 1.92; found: C 44.77, 44.89, H 3.04, 2.82, N 2.07, 2.07. Unit cell parameters for **5** at 294 K: monoclinic, a = 9.650(2) Å; b = 16.156(3) Å; c = 18.361 Å; β = 102.78(1)°.

Other attempted syntheses of $(Ph_4P)_2$ $[Cd_2(tzt)_2X_4]$

Attempts to prepare **4** and **5** rationally, by the stoichiometric reaction of $Cd(tzt)_2$, Ph_4PX, and CdX_2 (X = Br or I) in MeCN, were not successful; dissolution of the reactants was incomplete, and the colourless crystals isolated from the supernatant liquor were found by X-ray analysis to be $(Ph_4P)_2[Cd_2X_6]$.

Crystallization of 1

Colourless crystals of **1** were obtained by liquid diffusion at room temperature: in a vial of approximate dimensions 2.5 cm o.d. × 8 cm, a solution of tztH (0.120 g, 1.01 mmol) in a mixture of EtOH (8.5 mL) and DMSO (1.5 mL) was allowed to diffuse into a solution of $Cd(OAc)_2{\cdot}2H_2O$ (0.135 g, 0.51 mmol) in 10 mL of water, through an intervening 10 mL layer of EtOH and H_2O (1:1 (*v*/*v*)).

Attempted crystallization of 3

An attempt was made to crystallize **3**, by the method used to crystallize **1** (see preceding section). The yellow crystals that were produced were found, by complete X-ray analysis, to be $Cd(py4S)_2(py4SH)_2$ (**6**), which had been characterized independently (12).

Crystallization of 7, the pyridine solvate of 1

Following ref. 10, an attempt was made to crystallize **1** from pyridine. The colourless crystals that were produced were shown by X-ray analysis to be $Cd(tzt)_2(py)_3{\cdot}py$ (**7**) (see below). This adduct loses pyridine on standing at room temperature, although the loss is not complete even after pumping the adduct under preparative vacuum for 24 h. Anal. calcd. for $3Cd(tzt)_2{\cdot}py$, $C_{23}H_{29}Cd_3N_7S_{12}$ of the pumped product: C 24.54, H 2.60, N 8.71; found: C 24.54, 24.27, H 2.62, 2.28, N 9.12, 8.72.

NMR spectra

Solutions of $Cd(tzt)_2$ in pyridine were prepared in 10 mm o.d. NMR tubes under an atmosphere of argon. Their ^{113}Cd NMR spectra were measured using a Varian INOVA 400

[4] Version 5.25, including three updates.

© 2005 NRC Canada

spectrometer system, at 88.663 MHz, without a field-frequency lock; negligible field drift occurred. Decoupling was inverse-gated since ^{113}Cd has a negative Overhauser effect. The pulse width used was 9.5 μs (68°), the acquisition time was 1 s, and the re-cycle time was 4 s. After each temperature change, 30 min was allowed to reach a steady state before the spectrum was measured. External referencing was carried out by sample interchange using an aqueous solution of $Cd(ClO_4)_2$ (0.1 mol/L), at 299 K. Temperatures were calibrated using the ^{1}H NMR spectrum of MeOH (13) when no decoupling was used, and the heating effect of decoupling was measured using a 1:1 (*v*/*v*) CCl_4–Me_2CO mixture (14).

CP-MAS solid-state ^{113}Cd NMR spectra were measured at either the University of New South Wales (UNSW), using a Varian Inova-300 spectrometer system operating at 66.5 MHz, or the University of Western Ontario (UWO), using a Varian Infinity Plus 400WB spectrometer system operating at 88.6 MHz, at 303 and 293 K, respectively, with a range of spinning speeds. The samples, dry powders, except for microcrystalline **7**, which was damp with pyridine, were contained in 4 mm (UNSW) or 7.5 mm (UWO) pencil-design spinners made of partially stabilized ZrO_2. Optimal conditions were found by experimentation. Typical conditions (MAS rates, ^{1}H pulsewidth (μs and degrees), contact time, re-cycle time, acquisition time, spectral window) used at UNSW were: 2–8 kHz, 3.3 μs (90°), 20 ms, 60 s, 10 ms, and 100 kHz. Those at UWO were 3–6 kHz, 6 μs (90°), 15 ms, 60 s, 3.0 ms, and 166.67 kHz. Referencing was by sample interchange with solid $CdSO_4{\cdot}8H_2O$ (δ_{Cd} = –64.6/–77.4 relative to 0.1 mol/L $Cd(ClO_4)_2$ (aq) (15)) and with solid $Cd(tzt)_2$ at UNSW and UWO, respectively. Isotropic signal positions were found by comparing spectra measured at two or more spinning rates.

All simulations of the MAS spectra were carried out by first converting to Bruker format and then using the Bruker WINFIT program to obtain the following parameters: the principal components δ_{11}, δ_{22}, and δ_{33} with $\delta_{11} > \delta_{22} > \delta_{33}$; δ_{iso} (= $1/3(\delta_{11} + \delta_{22} + \delta_{33})$); and asymmetry factor η (= $(\delta_{11} - \delta_{22})/(\delta_{iso} - \delta_{33})$). The span Ω and the skew κ were calculated as $\Omega = \delta_{33} - \delta_{11}$, and $\kappa = 3(\delta_{iso} - \delta_{22})/\Omega$. (16). The values of δ have an estimated error of ±1 ppm.

X-ray structure determinations

Crystals of **1**, **6**, and **7** were obtained as described above. Crystals of **4** were obtained from a saturated solution in CH_2Cl_2, while crystals of **5** were obtained during the synthesis. The data crystals were mounted on silica (UNSW), glass (UWO), or mohair (University of Sydney) fibres.

Data for **1** and **6** were collected at ambient temperature (294 K) at UNSW using a Nonius CAD4 diffractometer, equipped with CAD4 software.[5] Data reduction used the CAD4 software and a local program. Structure solution and refinement on *F* were accomplished using SIR92 (17) and RAELS (18), respectively. All non-hydrogen atoms were refined with anisotropic thermal parameters. Hydrogen atoms were included in calculated positions and were assigned the isotropic equivalent thermal parameter of the atom to which they are bonded.

Data for **4** and unit cell data for **5** were obtained at 294(2) K at UWO with a Siemens P4 diffractometer, using XSCANS software. The data for **4** were processed, and full-matrix least-squares refinement on F^2 was performed, using direct methods and the SHELXTL 5.03 program package (19). All non-hydrogen atoms of both the cations and the anion were refined with anisotropic thermal parameters. Hydrogen atoms were included in positions calculated on geometric grounds and were included as riding atoms in the structure factor calculations.

Data for **7** were collected at Sydney University using a Bruker SMART 1000 CCD diffractometer. The temperature used was 250(2) K, with the crystal being cooled by a cold nitrogen gas stream from an Oxford Cryosystems Cryostream. (Crystals of **7** lose pyridine at room temperature, as noted above, and were also observed, during setting up of the X-ray diffractometer for data collection at reduced temperature, to undergo a destructive phase transition at approximately 212 K). Data processing, structure solution, and refinement for **7** were as for **1** and **6**, except that TLX group thermal parameters were used for the four independent pyridine rings (where T is the translation tensor, L is the libration tensor, and X is the origin of libration).

Details of data collection and refinement for **1**, **4**, and **7** are given in Table 1. Selected interatomic distances and angles for the three structures appear in Tables 2, 3, and 4, respectively. Full crystallographic data for **1**, **4**, **6**, and **7** have been deposited as Supplementary data.[6] All figures resulting from the X-ray analyses were created using CrystalMaker (20).

Elemental microanalyses

C, H, and N microanalyses were carried out by Campbell Microanalytical Laboratory (University of Otago, New Zealand) (for **3**) and Guelph Analytical Laboratories Ltd. (Guelph, Ont.) (for **4** and **5**, and for **7** after pumping).

Results and discussion

Bulk **1** is easily prepared but, once isolated, is intractable, and a polymeric structure has been suggested (2); that suggestion is confirmed in the present work. Our attempts to solubilize pre-prepared **1**, by addition of $Ph_4P^+X^-$ (X = Br or I) in a $Cd(tzt)_2$:$Ph_4P^+X^-$ ratio of 1:2 to break up the polymeric structure as $Cd(tzt)_2X_2^-$, were unsuccessful. However, mixtures in which Cd^{2+}:tzt^-:$Ph_4P^+X^-$ = 1:2:2, with the $Cd(tzt)_2$ freshly prepared in situ, gave $(Ph_4P)_2[X_2Cd(tzt)_2CdX_2]$ (X = I (**4**) or Br (**5**)) in low yield as the unexpected products. The compound **4** has been characterized structurally in this work, and **5** has been found to be isomorphous, and presumably

[5] Version 5.0. 1989.

[6] Supplementary data may be purchased from the Directory of Unpublished Data, Document Delivery, CISTI, National Research Council Canada, Ottawa, ON K1A 0S2, Canada (http://www.nrc.ca/cisti/irm/unpub_e.shtml for information on ordering electronically). CCDC 247585–247588 contain the crystallographic data for this manuscript. These data can be obtained, free of charge, via www.ccdc.cam.ac.uk/conts/retrieving.html (or from the Cambridge Crystallographic Data Centre, 12 Union Road, Cambridge CB2 1EZ, U.K.; fax +44 1223 336033; or deposit@ccdc.cam.ac.uk).

© 2005 NRC Canada

Table 1. Crystallographic data for **1**, **4**, and **7**.

	1	**4**	**7**
	$Cd(tzt)_2$	$(Ph_4P)_2[Cd_2I_4(tzt)_2]$	$Cd(tzt)_2(py)_3$·py
Empirical formula	$C_6H_8CdN_2S_4$	$C_{54}H_{48}Cd_2I_4N_2P_2S_4$	$C_{26}H_{28}CdN_6S_4$
Formula mass	348.8	1647.6	665.2
Colour, habit	Colourless, prism	Colourless, block	Colourless, irregular
Crystal dimensions (mm)	0.10 × 0.12 × 0.26	0.30 × 0.40 × 0.40	0.21 × 0.26 × 0.43
Crystal system	Orthorhombic	Monoclinic	Monoclinic
Space group	*Pbcn*	$P2_1/c$	$C2/c$
Z	8	2	8
a (Å)	15.076(4)	9.865(1)	31.178(5)
b (Å)	9.436(2)	16.247(2)	11.920(2)
c (Å)	15.828(6)	18.523(2)	16.738(3)
β (°)	90	102.292(9)	112.245(5)
Collection ranges	$0 \le h \le 17$; $0 \le k \le 11$; $0 \le l \le 18$	$-1 \le h \le 11$; $-19 \le k \le 1$; $-22 \le l \le 21$	$-39 \le h \le 39$; $-15 \le k \le 15$; $-22 \le l \le 22$
Temperature (K)	294(2)	294(2)	250(2)
V (Å^3)	2252(1)	2900.7(6)	5758(2)
D_{calcd} (Mg m^{-3})	2.06	1.89	1.53
Radiation	MoKα (λ = 0.71073 Å)	MoKα (λ = 0.71073 Å)	MoKα (λ = 0.71073 Å)
μ (mm^{-1})	2.604	3.097	1.06
Absorption correction	Analytical	Empirical	Gaussian
F(000)	1360	1576	2704
θ range for data collection (°)	1.5–25.0	2.11–25.00	2.72–28.05
Number of reflections measured	1978	5113	6789
Independent observed reflections	1606	4628 (R_{int} = 0.029)	5991 (R_{int} = 0.034)
Data/restraints/parameters	1606/0/119	4628/0/308	5991/0/238
Maximum shift/error	0.017	0.013	0.025
Goodness-of-fit	1.19	1.10	1.62
Final R indices ($I > 2\sigma(I)$)	R_1 = 0.024,[a] wR_2 = 0.035[b]	R_1 = 0.043,[a] wR_2 = 0.089[c]	R_1 = 0.028,[a] wR_2 = 0.043[b]
Absolute structure parameter	NA	NA	NA
Extinction coefficient	NA	NA	NA
Largest diff. peak and hole (e Å^{-3})	0.45 and –0.71	0.87 and –0.84	0.75 and –0.73

[a] $R_1 = \Sigma(||F_o| - |F_c||)/\Sigma|F_o|)$ for $F_o^2 > 2\sigma(F_o^2)$ ($I > 2\sigma(I)$).
[b] $wR_2 = \{[\Sigma w(F_o - F_c)^2]/[\Sigma w(F_o^2)^2]\}^{1/2}$ for $F_o^2 > 2\sigma(F_o^2)$.
[c] $wR_2 = \{[\Sigma w(F_o^2 - F_c^2)^2]/[\Sigma w(F_o^2)]\}^{1/2}$ for $F_o^2 > 2\sigma(F_o^2)$.

Table 2. Selected bond distances and angles for $Cd(tzt)_2$ (**1**).

Bond distances (Å)							
Cd—S1A	2.498(1)	Cd—N1A[a]	2.259(3)	Cd—S1B	2.557(1)	Cd—N1B[b]	2.201(3)
S1A—C1A	1.729(4)	S2A—C1A	1.755(4)	N1A—Cd	2.259(3)	N1A—C1A	1.291(5)
N1A—C2A	1.463(5)	S1B—C1B	1.711(4)	S2B—C1B	1.770(4)		
N1B—Cd	2.201(3)	N1B—C1B	1.281(5)	N1B—C2B	1.481(4)		
Bond angles (°)							
S1A-Cd-N1A[a]	103.61(8)	S1A-Cd-S1B	106.69(4)	S1A-Cd-N1B[b]	123.37(9)	N1A-Cd-S1B	100.86(9)
N1A[a]-Cd-N1B[b]	104.0(1)	S1B-Cd-N1B[b]	115.16(8)	Cd-S1A-C1A	97.3(1)	C1A-S2A-C3A	91.7(2)
Cd[a]-N1A-C1A	121.4(3)	Cd[a]-N1A-C2A	124.2(3)	C1A-N1A-C2A	113.5(3)	S1A-C1A-S2A	119.6(2)
S1A-C1A-N1A	124.9(3)	S2A-C1A-N1A	115.6(3)	Cd-S1B-C1B	103.7(1)	C1B-S2B-C3B	90.5(2)
Cd[c]-N1B-C1B	124.5(3)	Cd[c]-N1B-C2B	122.4(2)	C1B-N1B-C2B	113.1(3)	S1B-C1B-S2B	121.2(2)
S1B-C1B-N1B	124.4(3)	S2B-C1B-N1B	114.4(3)				

[a] Symmetry operator: $1 - x, y, 1/2 - z$.
[b] Symmetry operator: $1/2 - x, 1/2 + y, z$.
[c] Symmetry operator: $1/2 - x, -1/2 + y, z$.

isostructural, with **4**. Isolated **1** does dissolve readily in pyridine. A similar solubility of polymeric $Cd(py2S)_2$ (**2**) in pyridine has been reported (10). Unlike **2**, **1** is obtained from pyridine as a solvate, $Cd(tzt)_2(py)_3$·py (**7**), the remarkable structure of which is described below. Pyridine is readily lost from **7**; a material analyzing, approximately, as

© 2005 NRC Canada

Table 3. Selected bond distances and bond angles for $(Ph_4P)_2[I_2Cd(tzt)_2CdI_2]$ (**4**).

Bond distances (Å)							
Cd—N1[a]	2.245(5)	Cd—S1	2.531(2)	Cd—I2	2.7222(7)	Cd—I1	2.8057(7)
S1—C1	1.714(7)	C1—N1	1.293(8)	C1—S2	1.757(6)	N1—C2	1.460(8)
C2—C3	1.53 (1)	C3—S2	1.795(8)				
Bond angles (°)							
N1[a]-Cd-S1	107.88(15)	N1[a]-Cd-I2	116.21(14)	S1-Cd-I2	117.86(5)		
N1[a]-Cd-I1	98.39(13)	S1-Cd-I1	96.19(5)	I2-Cd-I1	117.01(2)		
C1-S1-Cd	105.8(2)	N1-C1-S1	126.3(5)	N1-C1-S2	115.6(5)		
S1-C1-S2	118.0(4)	C1-N1-C2	113.3(5)	C1-N1-Cd[a]	122.2(4)		
C2-N1-Cd[a]	124.2(4)	N1-C2-C3	109.4(6)	C2-C3-S2	105.1(5)		
C1-S2-C3	91.1(3)						

[a]Symmetry operator: $-x + 1, -y + 1, -z$.

Table 4. Selected bond distances and angles for $Cd(tzt)_2(py)_3{\cdot}py$ (**7**).

Bond distances (Å)							
Cd—S1A	2.551(1)	Cd—N1B	2.227(2)	Cd—$N1_{Py1}$	2.471(2)	Cd—$N1_{Py2}$	2.365(2)
Cd—$N1_{Py3}$	2.455(2)	S1A—C1A	1.727(2)	S2B—C1A	1.772(2)	N1A—C1A	1.270(3)
N1A—C2A	1.465(4)	S1B—C1B	1.701(2)	S2B—C1B	1.774(2)		
N1B—C1B	1.294(3)	N1B—C2B	1.458(3)				
Bond angles (°)							
S1A-Cd-N1B	133.35(4)	S1A-Cd-$N1_{Py1}$	96.49(5)	S1A-Cd-$N1_{Py2}$	90.49(4)		
S1A-Cd-$N1_{Py3}$	93.01(5)	N1B-Cd-$N1_{Py1}$	84.32(6)	N1B-Cd-$N1_{Py2}$	135.79(6)		
N1B-Cd-$N1_{Py3}$	92.59(6)	$N1_{Py1}$-Cd-$N1_{Py2}$	85.23(6)	$N1_{Py1}$-Cd-$N1_{Py3}$	169.39(7)		
$N1_{Py2}$-Cd-$N1_{Py3}$	89.99(6)	Cd-S1A-C1A	99.82(7)	C1A-S21-C3A	90.4(2)		
C1A-N1A-C2A	111.5(2)	S1A-C1A-S2B	115.5(1)	S1A-C1A-N1A	127.7(2)		
S2B-C1A-N1A	116.8(2)	C1B-S2B-C3B	91.1(1)	Cd-N1B-C1B	114.6(1)		
Cd-N1B-C2B	128.1(1)	C1B-N1B-C2B	114.5(2)	S1B-C1B-S2B	119.5(1)		
S1B-C1B-N1B	125.9(2)	S2B-C1B-N1B	114.6(2)				

$3Cd(tzt)_2{\cdot}py$ remains after **7** has been pumped for 24 h. The pumped material gave no solid-state ^{113}Cd NMR spectrum in our hands; thus, it is not simply a mixture of **1** and **7**.

Crystal structure of $Cd(tzt)_2$ (1)

The structure of **1** is polymeric, as predicted (2), with puckered sheets lying perpendicular to the *c* axis (Figs. 1 and 2). Within a sheet (Fig 1*a*), each tzt^- ligand acts in an N,S-bridging manner, through N and the exocyclic S, as is commonly found for this ligand (see Introduction). Accordingly, each cadmium atom is four-coordinate, the coordination kernel being CdN_2S_2. The organic moieties are on the surface of the layers and "insulate" each layer from the next (Fig 1*b*), as is frequently observed in metal–organic layer structures. Selected bond distances and angles are given in Table 2.

Within the CdN_2S_2 kernels of **1**, the Cd—S1A and Cd—S1B distances are 2.498(1) and 2.557(1) Å, respectively, which can be compared with the known ranges of 2.41–2.68 Å for Cd bound to a terminal thiolate S atom and 2.45–2.65 Å for Cd bound to a terminal thione S atom, as reported in the CSD, and with Cd—S bond distances of 2.531(2) Å in **4** and 2.551(1) Å in **7** (see below). The Cd—N1A and Cd—N1B distances, 2.259(3)and 2.201(3) Å, can be compared with the Cd—N distance of 2.245(5) Å found for the bridging ligands in **4** and that of 2.227(2) Å found for the monodentate N-bound tzt^- in **7** (see below). The bond angles at Cd range from 100.86(9)° to 123.37(9)°, so that the geometry is distorted tetrahedral, a common situation for Cd.

In the structure, there are eight-membered Cd-S-C-N-Cd-S-C-N rings in the boat conformation, with twofold symmetry. The two heterocyclic rings (A) that are joined to the eight-membered ring are in *syn* positions. Each A ring together with its exocyclic S is essentially planar (the maximum deviation from the least-squares plane is 0.04 Å). The N1A–Cd vector makes an angle of 77.9(1)° with the perpendicular to the plane. The C1A-S1A-Cd bond angle is 97.3(1)°.

Within the tzt^- ligands B, which are not involved in the eight-membered Cd-S-C-N-Cd-S-C-N rings, the twisted conformation is found, with C2B and C3B on opposite sides of the N1B,C1B,(S1B),S2B plane (for which the maximum deviation is 0.01 Å) and 0.24 and 0.32 Å out of the plane. The N1B–Cd vector makes an angle of 81.8(1)° with the perpendicular to the N1B,C1B,(S1B),S2B plane. The C1B-S1B-Cd bond angle is 103.7(1)°.

Crystal structure of $(Ph_4P)_2[I_2Cd(tzt)_2CdI_2]$ (4)

The crystal structure of **4** contains segregated columns of Ph_4P^+ cations and $[I_2Cd(tzt)_2CdI_2]^{2-}$ anions, along the *a* direction (Fig. 3). The cation chains are made up of pairs of Ph_4P^+ ions linked through sixfold phenyl embraces (21), with a P···P distance of 5.96 Å; adjacent pairs are linked through offset face-to-face interactions (21) with a longer

© 2005 NRC Canada

Fig. 1. Views of the structure of $Cd(tzt)_2$ (**1**): (*a*) along *c* showing a sheet and the two different types of tzt^- ligands; (*b*) along *b*, showing the corrugated sheets. Colour code: Cd, black; S, yellow; N, blue; C, green; H, cyan.

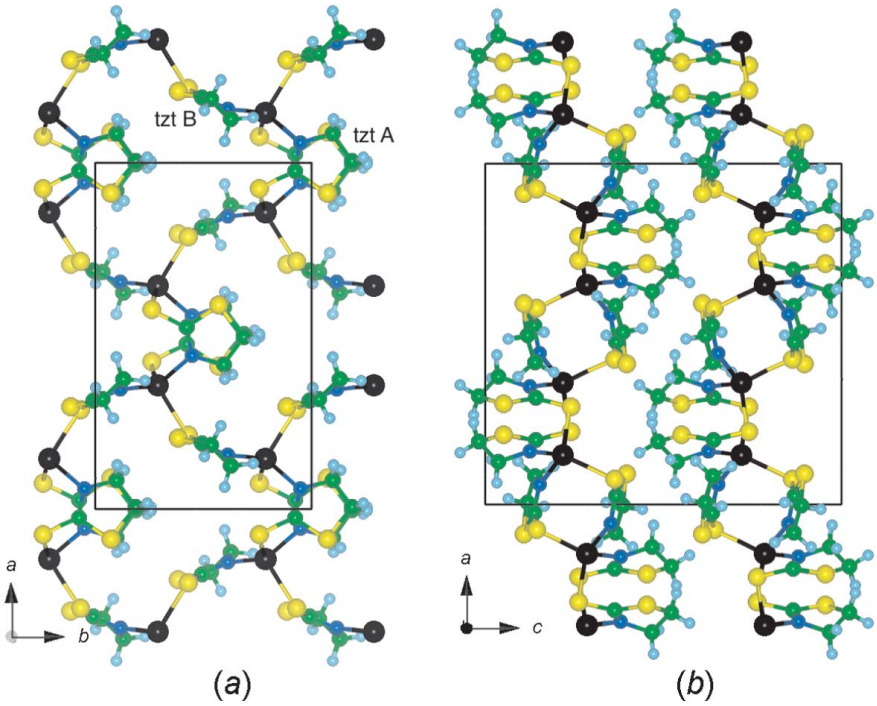
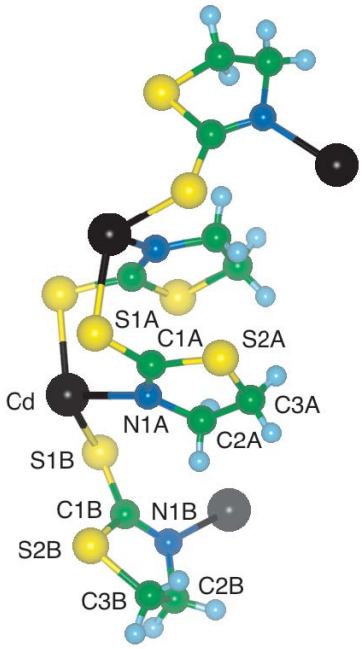


Fig. 2. A fragment of the structure of $Cd(tzt)_2$, giving the numbering scheme and showing the eight-membered Cd-S-C-N-Cd-S-C-N ring in the boat conformation.



P···P distance of 8.14 Å. The cations are otherwise unremarkable. Within the chains of anions, the repeat distance is *a* (9.87 Å). Figure 4 shows an anion, with the numbering scheme used. Selected bond distances and angles for the anion in **4** are presented in Table 3.

The centrosymmetric anion contains an eight-membered Cd-S-C-N-Cd-S-C-N ring in the chair conformation, with the tzt rings bonded through N and exocyclic S and occupying *anti* positions at the head and the foot of the chair. We note that eight-membered rings are found in the structure of **1** also; however, the conformation of the eight-membered rings in the (discrete) anions of **4** differs from that found for the eight-membered rings found in (polymeric) **1**. Within the anion, the tzt rings have an envelope conformation (the flap, C3, is 0.39 Å out of the least-squares plane of C2,N1,C1,(S1),S2; the N1–Cd vector lies essentially *in* this plane, the mean deviation of the atoms in the C2,N1,Cd,C1,(S1),S2 plane being 0.014 Å. The coordination kernel of Cd is $CdNSI_2$. The Cd—S distance is 2.531(2) Å, which falls between the two Cd—S distances of **1**. The Cd—N distance, 2.245(5) Å, is not statistically different from the longer Cd—N distance of **1** (2.259(3) Å) but is longer than the Cd—N distance of 2.227(2) Å found for the N-bonded tzt^- in **7** (see below). The Cd—I1 and Cd—I2 distances, 2.8057(7) and 2.7222(7) Å, fall within the range reported in the CSD for the terminal bonds of $[I_2CdI_2CdI_2]^{2-}$ and $[I_2Cd(\mu\text{-}SEt)(\mu\text{-}I)CdI_2]^{2-}$ (2.68–2.81 Å). The bond angles at Cd range from 96.19(5)° to 117.86(5)°, and the coordination geometry about Cd is again distorted tetrahedral. The C1-S1-Cd bond angle is 105.8(2)°, while the C1-N1-Cd angle is 122.2(4)°.

Crystal structure of $Cd(tzt)_2(py)_3{\cdot}py$ (7)

The structure of **7** consists of discrete $Cd(tzt)_2(py)_3$ molecules and lattice py molecules. As can be seen in Fig. 5 (in which the C atoms of bound and lattice py molecules are coloured orange and magenta, respectively), the crystal structure reveals regions that are rich in free and bound py and regions within which tzt^- ligands of adjacent $Cd(tzt)_2(py)_3$ molecules interdigitate. Each Cd-containing molecule is associated with four lattice py molecules. The

© 2005 NRC Canada

Fig. 3. A view along *a* of the structure of $(Ph_4P)_2[I_2Cd(\mu\text{-}tzt)_2CdI_2]$ (**4**), showing segregated columns of cations and anions. Colour code: Cd, black; I, magenta; P, red; S, yellow; N, blue; C, green; H, cyan.

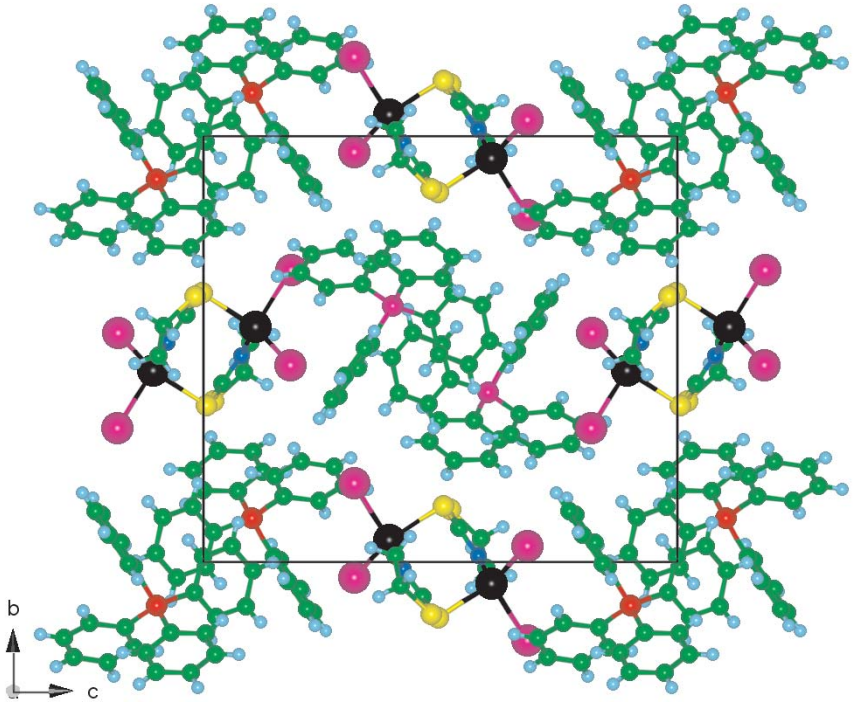
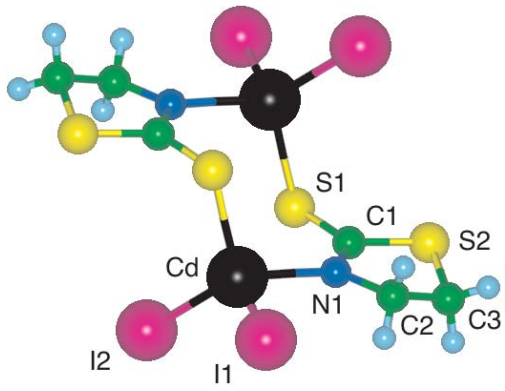


Fig. 4. The anion in $(Ph_4P)_2[I_2Cd(\mu\text{-}tzt)_2CdI_2]$ (**4**), giving the numbering scheme and showing the eight-membered Cd-S-C-N-Cd-S-C-N ring in the chair conformation.



geometry of the lattice py molecules is normal. Figure 6 shows a $Cd(tzt)_2(py)_3$ molecule and gives a partial numbering scheme. Table 4 gives selected bond distances and angles for this molecule.

As can be seen in Fig. 6, the Cd atom in $Cd(tzt)_2(py)_3$ exhibits distorted trigonal bipyramidal geometry, neither the coordination number nor the coordination geometry being unusual for Cd, according to a search of the CSD. We regard the Cd···S1B distance of 3.3 Å as indicating a nonbonding interaction — the sum of the Cd and S van der Waals radii is 3.38 Å (22) — but if the additional S were included in the first coordination sphere of Cd (within the angle $N1_{Py2}$-Cd-N1B), the coordination geometry of the Cd would be distorted octahedral, with S1B approximately *trans* to S1A. A unique feature of the $Cd(tzt)_2(py)_3$ molecule is that it contains examples of *both* rare S-bonded monodentate tzt^- (tzt(A)) *and* rare N-bonded monodentate tzt^- (tzt(B)).

Within $Cd(tzt)_2(py)_3$, pyridine molecules 1 and 3 occupy the axial positions, the $N1_{Py1}$-Cd-$N1_{Py3}$ bond angle being 169.39(7)°. The Cd is close to being coplanar with the atoms $N1_{Py2}$, S1A, and N1B, which occupy the equatorial sites of $Cd(tzt)_2(py)_3$ (the maximum deviation of the four atoms from the least-squares plane is 0.06 Å). The angles between the perpendicular to the mean Cd,$N1_{Py2}$,S1A,N1B plane and the $N1_{Py1}$–Cd and $N1_{Py3}$–Cd vectors are 8.7° and 2.3°, respectively.

The Cd—$N1_{Py1}$ and Cd—$N1_{Py3}$ distances are 2.471(2) and 2.455(2) Å, respectively, which fall in the known range for Cd–py bonds in the CSD (2.276–2.554 Å). In the equatorial plane, the Cd—$N1_{Py2}$, Cd—S1A, and Cd—N1B distances are 2.365(2), 2.551(1) and 2.227(2), respectively. Thus, the bond between Cd and the equatorial pyridine molecule, Py2, is significantly shorter than those to the axial pyridine molecules; such a relationship between equatorial and axial bond lengths is not unusual (23). The Cd—S1A bond length does not differ significantly from the longer Cd—S distance in **1**, while the Cd—N1B distance falls between the two Cd—N distances observed in **1**. Within the equatorial plane, the S1A-Cd-$N1_{Py2}$ angle is 90.49(4)°, while the N1B-Cd-$N1_{Py2}$ and S1A-Cd-$N1_{Py2}$ angles are considerably larger (135.79(6)° and 133.35(4)°, respectively). The origin of this difference is probably steric: the S1A-Cd-$N1_{Py2}$ angle can close up because the Py2 and tzt(A) rings are relatively far apart, as a result of the bend-back at S1A, the exocyclic sulfur atom of tzt(A). In addition, the presence of the nonbonded S1B (see above) may cause the $N1_{Py2}$-Cd-N1B angle to open up.

© 2005 NRC Canada

Fig. 5. A view along *b* of the structure of $Cd(tzt)_2(py)_3$·py (**7**), revealing pyridine-rich regions and tzt-rich regions. Colour code: Cd, black; S, yellow; N, blue; bound-pyridine C, orange; lattice-pyridine C, magenta; non-pyridine C, green; H, cyan.

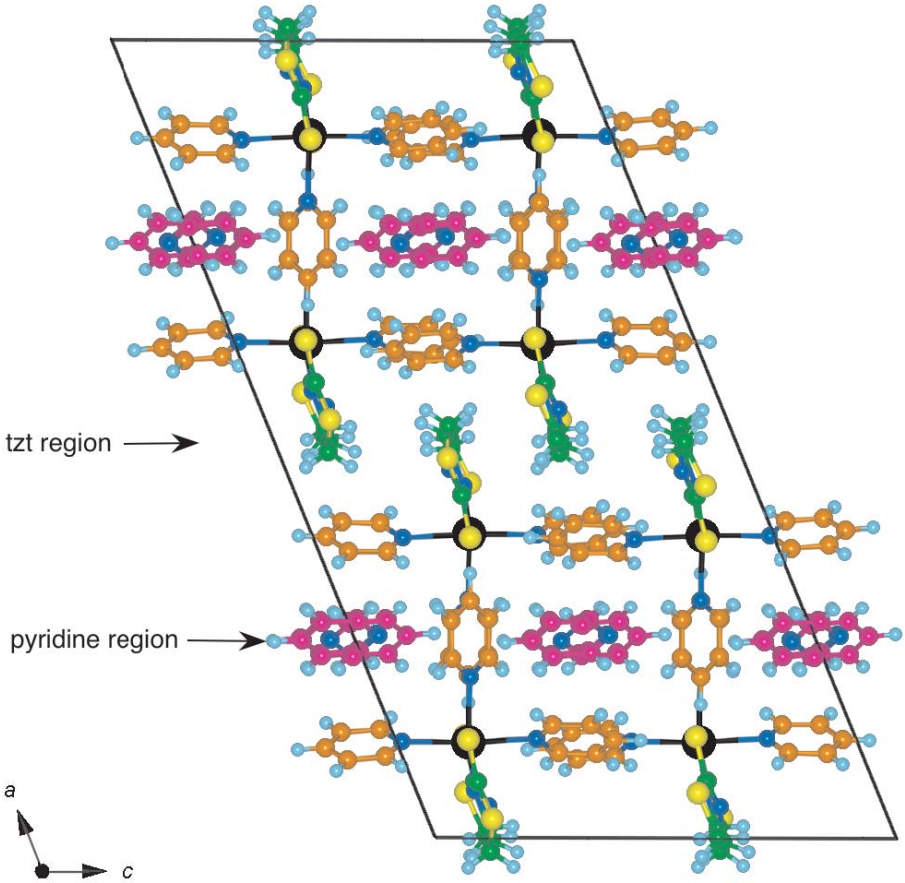
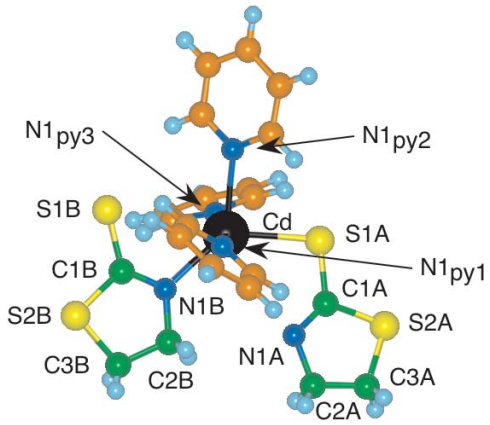


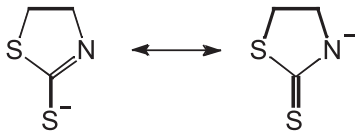
Fig. 6. The trigonal bipyramidal $Cd(tzt)_2(py)_3$ molecule found in $Cd(tzt)_2(py)_3$·py (**7**), viewed in the axial direction, giving a partial numbering scheme and showing the S- and N-bound tzt^- ligands in the equatorial plane.



Both tzt rings have the envelope conformation (the flaps C3A and C3B are 0.21 and 0.24 Å out of their respective C2,N1,C1,(S1),S2 planes). The Cd–N1B vector makes an angle of 78.4° with the C2B,N1B,C1B,(S1B),S2B mean plane.

The structure of **7** provides a unique opportunity to compare the geometries of S- and N-bound tzt^- ligands within the same complex. In both ligands, the expected planar geometry occurs at C1. The changes in the thioamide region are quite small but are in the direction expected from a consideration of the resonance structures of tzt^-, **IA** and **IB** (Scheme 1): more C–N multiple bonding and less C–(exocyclic)S multiple bonding in the S-bound ligand (labelled A), which promotes resonance structure **IA**, than in the N-bound ligand (labelled B), which promotes resonance structure **IB**. Thus, the C1—N1 distance in the A ring is 1.270(3) Å, while that in the B ring is 1.294(3) Å, and the C1—S1 distance is 1.727(2) Å in the A ring and 1.701(2) Å in the B ring. In addition, the N1-C1-S2 and S1-C1-N1 angles are larger in the S-bound (A) ligand (116.8(2)° and 127.2(2)°, respectively) than in the N-bound (B) ligand (114.6(2)° and 125.9(2)°, respectively), while C1-N1-C2 and S1-C1-S2 angles are larger in the N-bound ligand (115.5(2)° and 119.5(1)°, respectively) than in the S-bound ligand (111.5(2)° and 115.5(1)°, respectively).

Scheme 1. Resonance structures of tzt^-.



I A **I B**

Comparison of the geometry of the monodentate ligands with those of the bidentate ligands in **1** and **4** is complicated

© 2005 NRC Canada

Table 5. ^{113}Cd NMR spectral parameters of **1**, **7**, and related compounds.

Substrate	Kernel	δ_{iso}	δ_{11}	δ_{22}	δ_{33}	Ω	κ	Ref.
1	CdN_2S_2	411[a]	559	375	301	258	0.4	—[b]
7	CdN_4S	361	477	477	129	348	–1.0	—[b]
$Cd(py2S)_2$[c]	$CdN_2S_2S'_2$	326	411	362	205	206	–0.5	—[b,d]
	$CdN_2S_2S'_2$	311	398	382	152	246	–0.9	—[b,d]
$Cd(py2S)_2$[e]	$CdN_2S_2S'_2$	321	429	367	167	262	–0.5	—[b,d]
$Cd(py4S)_2$	CdS_4[f]	516	734	599	216	518	–0.5	—[b]
$Cd(btzS)_2$[c,g]	$CdN_2S_2S'_2$(?)	340	—[h]	—[h]	—[h]	—[h]	—[h]	10
	$CdN_2S_2S'_2$(?)	329	—[h]	—[h]	—[h]	—[h]	—[h]	10
$Cd(btzS)_2$[e]	$CdN_2S_2S'_2$	327	—[h]	—[h]	—[h]	—[h]	—[h]	10
$[Cd(py2SH)_4](NO_3)_2$	CdS_4	635[i]						—[b]
$[Cd(tztH)_4](CF_3SO_3)_2$	CdS_4	586	622	582	558	61	0.2	1*b*
$[Cd(tztH)_4][Cd(O_2NO)_4]$	CdS_4[j]	557[i]						1*b*

[a]At 88.66 MHz, a saturated solution of **1** in pyridine had δCd($\Delta\nu_{1/2}$, approx.) = 207(450), 198(250), 191(40 Hz) at 298, 253, 244 K.
[b]This work.
[c]Before recrystallization from pyridine.
[d]This signal could not be observed by Hursthouse et al. (10).
[e]After recrystallization from pyridine.
[f]Tentative assignment; see text.
[g]btzSH = mercaptobenzothiazole.
[h]Not reported in ref 10.
[i]Isotropic down to a spinning speed of 1500 Hz at 66.549 MHz.
[j]Cation only; for the anion, δiso = –131 ppm (1*b*).

by the fact that the structures were measured at different temperatures. In addition, the supporting ligands at Cd differ in these complexes, and this must have an effect. However, we note that planarity at C1 is maintained, as expected, and also that the C1-N1-C2 angle in the bridging ligands is remarkably constant at 113.1(3)°–113.5(3)°, a value intermediate between those found in tzt(A) and tzt(B) in **7**.

Cadmium-113 NMR spectra of 1, 7, and related compounds

Solid-state (SS) ^{113}Cd NMR spectra of **1** and **7** have been measured, together with the variable-temperature solution ^{113}Cd NMR spectrum of **1** in pyridine and several other solid-state ^{113}Cd NMR spectra, for comparison. The NMR results are detailed in Table 5, and Fig. 7 shows representative solid-state NMR spectra.

Compound **1** gives a CP-MAS ^{113}Cd NMR spectrum with a single isotropic chemical shift, consistent with the finding of a single Cd atom in the single-crystal X-ray analysis. The chemical shift, 411 ppm, can be compared with the values of 557–586 ppm found for $[Cd(tztH)_4]^{2+}$ in solid compounds containing the S-bound neutral thione, and hence a CdS_4 kernel (1*b*). In **1**, the kernel is CdS_2N_2, and replacement of an S-donor by an N-donor is expected to lead to increased shielding, as is observed. (Few ^{113}Cd NMR data are available for established CdN_4 kernels, but a tetrahedral CdN_4 kernel in statically disordered $Cd(CN)_2$ has a ^{113}Cd NMR chemical shift of ca. 360 ppm (24), while, perhaps coincidentally, the *square-planar* CdN_4 kernel in (*meso*-tetraphenylporphyrinato)cadmium has an isotropic ^{113}Cd NMR chemical shift of 399 ppm (25)). Compound **1** has many of the properties that are desirable in a ^{113}Cd NMR reference material useful for solid-state ^{113}Cd NMR, including: ease of preparation, stability (we have kept **1** for months in a refrigerator with no obvious change in its CP-MAS ^{113}Cd NMR spectrum), and a single Cd environment giving a relatively sharp signal (e.g., ca. 750 Hz, S/N ≈ 18 after 8 transients, at UWO).

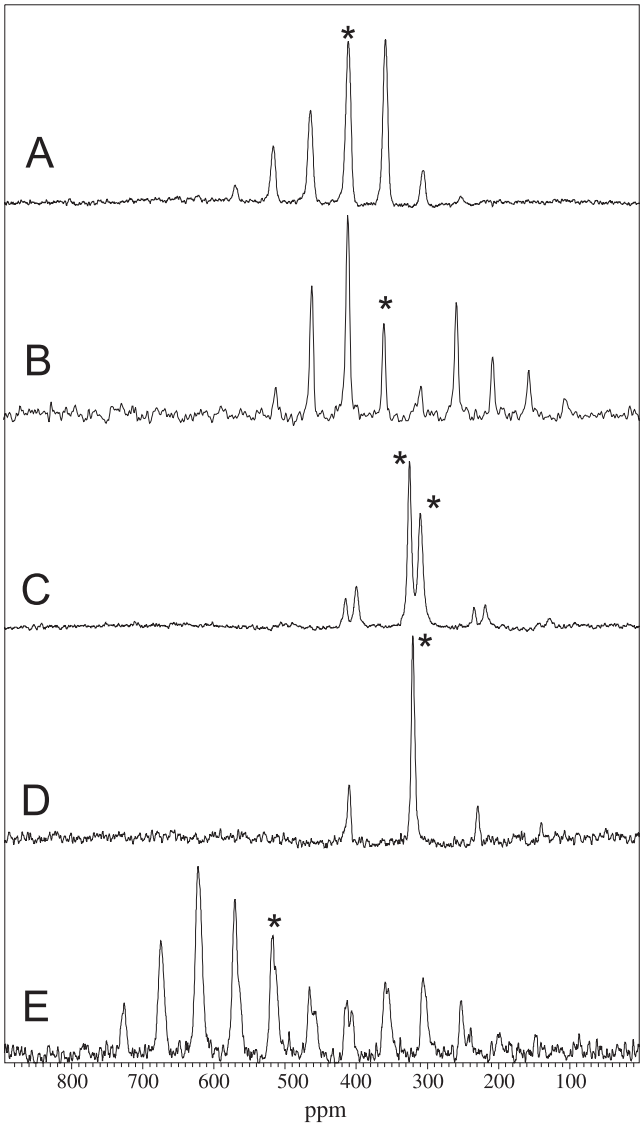
When **1** is converted into its pyridine adduct, which contains $Cd(py)_3$(tzt-*N*)(tzt-*S*) molecules (see above), the ^{113}Cd NMR chemical shift in the solid state changes to 361 ppm. Though the observed shielding is relatively slight, both increasing coordination number and increasing nitrogen/sulfur ratio in the coordination kernel are expected to lead to shielding. We were unable to find a ^{113}Cd NMR signal for the compound "3Cd(tzt)$_2$·(py)" that is obtained by pumping on **7**; certainly, it is not simply a mixture of **1** and **7**.

The change in chemical shift when **1** is dissolved in pyridine is surprisingly large: the ^{113}Cd NMR signal is found at 191 ppm at 244 K, at which temperature the linewidth is relatively narrow (ca. 40 Hz). This chemical shift is more shielded than δ_{iso} of $Cd(py)_3$(tzt-*N*)(tzt-*S*), by an amount that exceeds expectation for an effect of the medium only. Tentatively, we suggest that either the tzt$^-$ ligands are both N-bound in solution or the number of bound pyridines exceeds three in the solution in pyridine, or both.

The ^{113}Cd NMR chemical shift of solid **1** is larger than that of solid $Cd(btzS)_2$ (btzS$^-$ = mercaptobenzothiazolate), in which a $CdN_2S_2S'_2$ kernel occurs (10). Thus, it seems that of the two competing effects — larger coordination number, producing shielding, versus larger sulfur/nitrogen ratio in the coordination sphere. producing deshielding — the former is dominant for $Cd(btzS)_2$, although the effect on the chemical shift of N,S-chelation, which occurs in the solid, is an unknown and complicating factor in this comparison. As expected from its similar structure, again with a $CdN_2S_2S'_2$ kernel (10), solid $Cd(py2S)_2$ has an isotropic chemical shift similar to that of $Cd(btzS)_2$; the similarity between the two compounds extends even to the simplification of their solid-state ^{113}Cd NMR spectra from two signals to a single isotropic signal that occurs when the samples are recrystallized from pyridine. The CP-MAS ^{113}Cd NMR spectrum of

© 2005 NRC Canada

Fig. 7. CP-MAS ^{113}Cd NMR spectra of: (A) compound **1**, $Cd(ttz)_2$, 3.5 kHz, 66.5 MHz, 303 K; (B) compound **7**, $Cd(tzt)_2py$, 4.5 kHz, 88.6 MHz, 293 K; (C) compound **2**, $Cd(py2S)_2$, before recrystallization, 6 kHz, 66.5 MHz, 303 K; (D) compound **2**, $Cd(py2S)_2$, after recrystallization from pyridine, 6 kHz, 66.5 MHz, 303 K; and (E) compound **3**, $Cd(py4S)_2$, 3.5 kHz, 66.5 MHz, 303 K. An asterisk indicates the isotropic signal.



$Cd(py2S)_2$ could not be observed by the previous workers (10), but insufficient experimental detail is available in ref. 10 to explain the discrepancy between the previous work and our current work. The $[Cd(py2SH)_4]^{2+}$ cation in its solid nitrate salt has a CdS_4 kernel (1*a*); its isotropic ^{113}Cd NMR signal is considerably deshielded, by ≈300 ppm relative to that of either $Cd(py2S)_2$ or $Cd(btzS)_2$, consistent with both the smaller coordination number and the larger sulfur/nitrogen ratio found in the coordination sphere of $[Cd(py2SH)_4]^{2+}$.

Finally, the isotropic ^{113}Cd NMR chemical shift of $Cd(py4S)_2$ is significantly deshielded, by ≈200 ppm, compared with those of $Cd(py2S)_2$ and $Cd(btzS)_2$, and the 4-thiolate must therefore have a different structure from the other two thiolates. Although the structure of $Cd(py4S)_2$ remains unknown — as noted above, attempts to crystallize this compound by the method used for $Cd(tzt)_2$ yielded $Cd(py4SH)_2(py4S)_2$ — the chemical shift approaches the region where resonances from CdS_4 kernels are found (see, e.g., Table 5 and refs. 26 and 27), although it is smaller than those found (12) for $[Cd(py4S)_{4-n}(py4SH)_n]^{(2-n)+}$ (n = 0, 2, 4) in a DMF–MeOH solvent mixture (616–617 ppm at 213 K).

Acknowledgements

We thank Dr. Peter Turner, Professional Officer, Crystallography, School of Chemistry, University of Sydney, Australia, for collecting single-crystal X-ray data on compound **7**, and Dr. Michael Jennings, Manager, Crystallography Facility, Department of Chemistry, UWO, for assistance in preparing the manuscript. Much progress with this work was made possible by a sabbatical leave from UWO, and by Visiting Professorships at UNSW in 2001–2002 and 2004, for which PAWD is grateful. IGD acknowledges the support of the Australian Research Council.

References

1. (*a*) U. Rajalingam, P.A.W. Dean, and H.A. Jenkins. Can. J. Chem. **78**, 590 (2000); (*b*) U. Rajalingam, P.A.W. Dean, H.A. Jenkins, M. Jennings, and J.M. Hook. Can. J. Chem. **79**, 1330 (2001).
2. (*a*) C. Preti and G. Tosi. Can. J. Chem. **54**, 1558 (1976); (*b*) N.A. Bell, W. Clegg, S.J. Coles, C.P. Constable, R.W. Harrington, M.B. Hursthouse, M.E. Light, E.S. Raper, C. Sammon, and M.R. Walker. Inorg. Chim. Acta, **357**, 2091 (2004).
3. E.S. Raper. Coord. Chem. Rev. **153**, 199 (1996); **165**, 475 (1997).
4. P.D. Akrivos. Coord. Chem. Rev. **213**, 181 (2001).
5. F.H. Allen, J.E. Davies, J.J. Galloy, O. Johnson, O. Kennard, C.F. Macrae, E.M. Mitchell, G.F. Mitchell, J.M. Smith, and D.G. Watson. J. Chem. Inf. Comput. Sci. **31**, 187 (1991).
6. A.R. Norris, A. Palmer, and A.L. Beauchamp. J. Crystallogr. Spectrosc. Res. **20**, 23 (1990).
7. T.A. Grant, J.M. Forward, and J.P. Fackler, Jr. Z. Kristallogr. **211**, 483 (1996)
8. L.F. Soares, D.C. Menezes, R.M. Silva, A.C. Doriguetto, J. Ellena, Y.P. Mascarenhas, and E.E. Castellano. Polyhedron, **23**, 204 (2004).
9. A.M. Brodie, H.D. Holden, J. Lewis, and M.J. Taylor. J. Chem. Soc. Dalton Trans. 633 (1986)
10. M.B. Hursthouse, O.F.Z. Khan, M. Mazid, M. Motevalli, and P. O'Brien. Polyhedron, **9**, 541 (1990).
11. B.P. Kennedy and A.B.P. Lever. Can. J. Chem. **50**, 3488 (1972).
12. K.S. Anjali, J.J. Vittal, and P.A.W. Dean. Inorg. Chim. Acta, **351**, 79 (2003).
13. C. Amman, P. Meier, and A.E. Merbach. J. Magn. Reson. **46**, 319 (1982).
14. J. Led and S.B. Petersen. J. Magn. Reson. **32**, 1 (1978).
15. G.S.H. Lee, K.J. Fisher, A.M. Vassallo, J.V. Hanna, and I.G. Dance. Inorg. Chem. **32**, 66 (1993).
16. R.K. Harris. Solid State Nucl. Magn. Reson. **10**, 177 (1998).
17. A. Altomare, M.C. Burla, M. Camalli, G. Cascarano, C. Giacovazzo, A. Guagliardi, and G. Polidori. J. Appl. Crystallogr. **27**, 435 (1994).

© 2005 NRC Canada

18. A.D. Rae. RAELS [computer program]. Australian National University, Canberra. 2000.
19. SHELXTL Reference Manual, Version 5.03, Siemens Energy and Automation, Inc., Analytical Instrumentation, Madison, Wis. 1996.
20. D. Palmer. CrystalMaker, Version 6.3 [computer program]. CrystalMaker Software, Yarnton, UK. 2004.
21. I.G. Dance and M.L. Scudder. Chem. Eur. J. **2**, 481 (1996); J. Chem. Soc. Dalton Trans. 3755 (1996).
22. A. Bondi. J. Phys. Chem. **68**, 441 (1964).
23. D.L. Kepert. *In* Inorganic stereochemistry, inorganic chemistry concepts. Vol. 6. *Edited by* C.K. Jørgensen, M.F. Lappert, S.J. Lippard, J.L. Margarve, K. Niedenzu, H. Nöth, R.W. Parry, and H. Yamatera. Springer-Verlag, Berlin. 1982. Chap. 4. pp. 36–41
24. S. Nishikiori, C.I. Ratcliffe, and J.A. Ripmeester. Can. J. Chem. **68**, 2270 (1990).
25. P.D. Ellis, R.R. Inners, and H.J. Jakobsen. J. Phys. Chem. **86**, 1506 (1982).
26. M.F. Summers. Coord. Chem. Rev. **86**, 43 (1988).
27. R.J. Goodfellow. *In* Multinuclear NMR. *Edited by* J. Mason. Plenum, New York. 1987. Chap. 21.

© 2005 NRC Canada

AWARD LECTURE / CONFÉRENCE D'HONNEUR

2002 W.A.E. McBryde Award Lecture — Affinity recognition, capillary electrophoresis, and laser-induced fluorescence polarization for ultrasensitive bioanalysis

X. Chris Le, Victor Pavski, and Hailin Wang

Abstract: The combination of affinity recognition, capillary electrophoresis (CE), laser-induced fluorescence (LIF), and fluorescence polarization for the ultrasensitive determination of compounds of biological interest is described. Competitive immunoassays using CE–LIF eliminate the need for fluorescently labeling trace analytes of interest and are particularly useful for determination of small molecules, such as cyclosporine, gentamicin, vancomycin, and digoxin. Fluorescence polarization allows for differentiation of the antibody-bound from the unbound small molecules. Noncompetitive affinity CE–LIF assays are shown to be highly effective in the determination of biomarkers for DNA damage and HIV-1 infection. An antibody (or aptamer) is used as a fluorescent probe to bind with a target DNA adduct (or the reverse transcriptase of the HIV-1 virus), with the fluorescent reaction products being separated by CE and detected by LIF. Aptamers are attractive affinity probes for protein analysis because of high affinity, high specificity, and the potential for a wide range of target proteins. Fluorescence polarization provides unique information for studying molecular interactions. Innovative integrations of these technologies will have broad applications ranging from cancer research, to biomedical diagnosis, to pharmaceutical and environmental analyses.

Key words: capillary electrophoresis, laser-induced fluorescence, fluorescence polarization, immunoassay, affinity probes, antibodies, aptamers, DNA damage, toxins, therapeutic drugs.

Résumé : On décrit une méthode de détermination ultrasensible de l'intérêt biologique de composés qui est basée sur une combinaison de la reconnaissance d'affinité, l'électrophorèse capillaire (EC), de la fluorescence induite au laser (FIL) et de la polarisation de fluorescence. Les essais immunologiques compétitifs faisant appel à la combinaison EC–FIL éliminent la nécessité de marquages fluorescents de traces de l'analyte examiné. Aussi, ils sont particulièrement utiles pour la détermination de petites molécules, telle la cyclosporine, la gentamicine, la vancomycine et le digoxine. La polarisation de fluorescence permet de différencier de l'anticorps lié des petites molécules non liées. On a montré que les essais EC–FIL d'affinité non compétitive sont très efficaces dans la détermination de biomarqueurs pour le dommage à l'ADN et les infections du HIV-1. On a utilisé un anticorps (ou aptamère) comme sonde fluorescente qui se lie à un adduit d'ADN cible (ou la transcriptase inverse du virus HIV-1), alors que les produits fluorescents de la réaction sont séparés par EC et détectées par FIL. Les aptamères sont des sondes d'affinité qui présentent de l'attrait pour l'analyse des protéines en raison de leur grande affinité, de leur spécificité élevée et du potentiel pour un large éventail de protéines cibles. La polarisation de fluorescence permet de recueillir de l'information unique pour l'étude des interactions moléculaires. Des intégrations innovatrices de ces technologies donneront lieu à un vaste éventail d'applications allant de la cancérologie aux diagnostics biomédicaux et aux analyses pharmaceutiques et environnementales.

Mots clés : électrophorèse capillaire, fluorescence induite au laser, polarisation de fluorescence, essai immunologique, sondes d'affinité, anticorps, aptamères, dommage à l'ADN, toxines, médicaments.

[Traduit par la Rédaction]

Received 9 September 2004. Published on the NRC Research Press Web site at http://canjchem.nrc.ca on 18 March 2005.

X.C. Le.[1] Environmental Health Sciences, Department of Public Health Sciences, University of Alberta, Edmonton, AB T6G 2G3, Canada and Department of Chemistry, University of Alberta, Edmonton, AB T6G 2G2, Canada.
V. Pavski and H. Wang. Environmental Health Sciences, Department of Public Health Sciences, University of Alberta, Edmonton, AB T6G 2G3, Canada.

[1]Corresponding author (e-mail: xc.le@ualberta.ca).

 doi: 10.1139/V04-175 © 2005 NRC Canada

Introduction

Affinity recognition is widely used as a means of achieving specificity for a range of bioanalytical applications. As an example, immunoassays that make use of the preferential binding affinity of antibody to specific antigen (or hapten) are widely used for the ultrasensitive and selective detection of a large variety of biological substances, including, but not limited to, whole microorganisms, viruses, proteins and peptides, therapeutic drugs, chemical warfare agents, natural and man-made toxins, and environmental contaminants (1–3). In an immunoassay, antibodies are used as analytical reagents to bind with a target analyte. The distribution of the analyte between bound and free forms is related to the total analyte concentration.

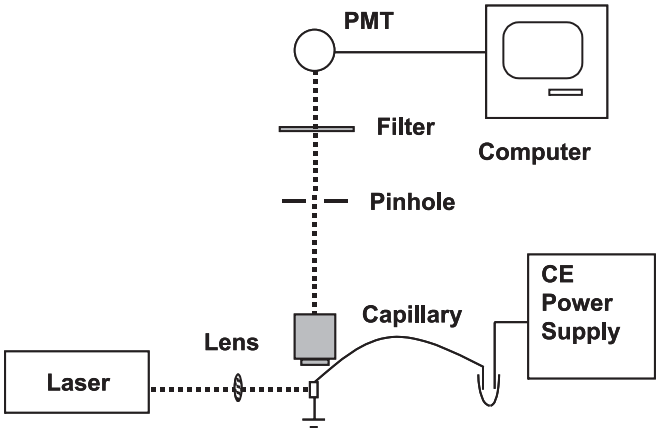
Immunological recognition is based on the spatial complementarity of the epitope of the antigen with the paratope in the antibody. Because antibodies target epitopes, not the whole antigen, antibodies can fail to discriminate structurally similar species by cross-reacting. One way to improve the specificity of the technique is to combine the immunoassay with chromatography–electrophoresis separation. Capillary electrophoresis (CE) is a high efficiency analytical separation technique (4, 5). Fast and efficient separation and a small sample volume requirement make CE a powerful technique for bioanalysis (6–8). Laser-induced fluorescence (LIF) offers extremely sensitive detection for CE, leading to a single molecule detection limit (9–13). However, fluorescent labeling of trace levels of analyte in the presence of a sample matrix can be problematic because of nonquantitative derivatization at trace levels and matrix interference on the labeling reactions.

By developing innovative combinations of affinity recognition with CE–LIF, these problems can be circumvented. Ourselves and others have demonstrated the potential of competitive immunoassay using CE with LIF or laser-induced fluorescence polarization (LIFP) detection, and affinity capillary electrophoresis (14–20). Affinity CE–LIF has been demonstrated for biological and environmental applications, including studies of antibody–antigen interactions, determination of therapeutic drugs and natural toxins, and assays for DNA damage (see refs. 17–20 for reviews). This paper describes recent work in this area, part of which has been presented in the W.A.E. McBryde Medal address at the 85th Canadian Society for Chemistry Conference held in Vancouver. Here, we summarize CE–LIF, competitive immunoassays, noncompetitive immunoassays, aptamers as affinity probes, and fluorescence polarization.

Capillary electrophoresis with laser-induced fluorescence detection (CE–LIF)

Electrophoresis is defined as the movement of ions in an applied electric field, typically through an anticonvective medium. Fused silica capillaries, essentially the polyimide-coated fused silica tubing produced for gas chromatography, are attractive as anticonvective media, and are relatively inexpensive. Although the earliest prototypes of capillary electrophoresis (CE) systems were developed between 1958 and 1965 (21), it was not until the early 1980s that potential detection systems became sufficiently affordable to permit the development of CE on a practical basis (4, 5). In a typical free zone CE experiment, the capillary ends are inserted into electrophoretic buffer reservoirs, into which electrodes are also inserted. Samples are introduced either hydrodynamically (pressure injection) or electrophoretically using a short (5–10 s) application of voltage from a high voltage (5–30 kV) power supply. When voltage is once more applied, during the electrophoresis of the sample, electroosmotic flow (EOF) develops as the result of the negatively charged silanol groups on the fused silica walls. Driven by the EOF, analyte species migrate to the detection window according to their respective electrophoretic mobilities, effectively their charge to mass ratios. The plug flow character of the EOF permits separation efficiencies of a million theoretical plates (5).

Fig. 1. A schematic diagram showing a CE–LIF system used in this laboratory (adapted from ref. 48).



Owing to their small inner diameter (typically 10–100 μm), fused silica capillaries have very small internal volumes. Samples injected into the capillary have volumes of around 1–10 nL. To provide high sensitivity detection, the detection system must be compatible with the small sample volume. Because absorbance is dependent on the path length (Beer's law, $A \propto L$), it is not a very sensitive detection mode for CE, owing to the very small path length (i.e., internal diameter) of the capillary.

Fluorescence, however, is independent of sample path length. Because of this, laser-induced fluorescence (LIF) excitation of the CE sample volume, provided the analyte is natively fluorescent or fluorescently labeled, has provided the best detection limits in CE applications. A schematic diagram of a CE–LIF system used in our laboratory is given in Fig. 1. The set-up consists of a CE unit and an LIF detection system. The LIF detection system consists of a laser for excitation (e.g., argon ion laser, primary laser line 488 nm or green helium–neon laser at 543.5 nm), laser beam focusing and fluorescence collection optics (lens, filter, aperture, microscope objective), and a detector (e.g., a photomultiplier tube (PMT)). Output from the PMT is passed through an analogue-to-digital (A/D) converter into a data acquisition board in a personal computer. Fluorescence intensity is usually obtained from the peak area of the species of interest, and calibration plots of fluorescence intensity vs. the concentration of standard solutions of the species of interest are used to quantify the analyte.

© 2005 NRC Canada

We have demonstrated the sensitivity of CE–LIF in studies of oligosaccharides (22, 23). Because of the very low UV absorption of oligosaccharides, their direct spectrophotometric detection is problematic. Improvements in sensitivity have been obtained mainly through derivatization with chromophores or fluorophores, with fluorophore labeling and LIF detection providing the best limits of detection (24–26). We chose tetramethylrhodamine (TMR) as the fluorescent label because of its high molar absorptivity and quantum yield. The oligosaccharides were aminated and then reacted with the *N*-hydroxysuccinimide ester of tetramethylrhodamine to produce TMR-labeled compounds. Using an inexpensive green helium–neon laser with an excitation wavelength of 543.5 nm, we were able to generate intense orange fluorescence, which was collected through a 580 nm bandpass filter and detected by a PMT. The limit of detection was 8×10^{-23} mol (80 yoctomol) or 50 molecules of TMR-labeled saccharides (22).

Figure 2 shows an example of the detection of βGal(1→3)βGlcNAc and βGal(1→4)βGlcNAc (LacNAc) series oligosaccharide standards and enzyme products from human colon adenocarcinoma HT-29 cells by CE–LIF. A TMR-labeled oligosaccharide (βGal(1→4)βGlcNAc (LacNAc)) was used as a substrate and incubated with the cells for 20 h. The cells were then centrifuged and lysed, with the purified lysate being isolated for analysis. Unreacted substrate (βGal(1→4)βGlcNAc-O-TMR) is the major component of the cell sample, with minor components being the linker arm ($HO(CH_2)_8CONHCH_2CH_2NHCO$-TMR), βGlcNAc-O-TMR, αFuc(1→2)βGal(1→4)βGlcNAc-O-TMR, βGal(1→4)[αFuc(1→3)]βGlcNAc-O-TMR, and αFuc(1→2)βGal(1→4)[αFuc(1→3)]βGlcNAc-O-TMR.

Because CE requires only minute amounts of sample and LIF provides excellent detections, we have further developed the CE–LIF technique for the analysis of single cells. Analysis of single cells is important because it may permit the study of cell heterogeneity from the same cell line as a function of age and culturing conditions. We studied enzymatic hydrolysis of TMR-labeled trisaccharides in Baker's yeast cells (23). Cells (*Saccharomyces cerevisiae*, baker's yeast) were incubated with the TMR-labeled trisaccharide, α-D-Glc(1→2)α-D-Glc(1→3)α-D-Glc-O-$(CH_2)_8$CO-$NHCH_2CH_2$-NHCO-TMR, with shaking at 25 °C for 24 h. At various intervals during the incubation, microlitres of the cell suspension were removed and washed thoroughly with phosphate-buffered saline (PBS), prior to analysis by confocal laser scanning microscopy to ascertain the degree of uptake in the cells of the TMR-labeled trisaccharide. Fluorescence from the cells increased with time, and short-term incubations of cells with the TMR-labeled substrate exhibited no detectable fluorescence, indicating the increased fluorescence over time is related to actual incorporation of the substrate, rather than simple adsorption of the fluorescent dye at the cell surface. To facilitate the insertion of single cells into the CE, the bare capillary end was etched with hydrofluoric acid. A 2–5 μL volume of spheroplast suspension was placed on a glass slide under an inverted fluorescence microscope. An appropriate spheroplast was located, the capillary was moved proximate to it with the micromanipulators, and an airtight syringe or syringe pump was used to provide gentle suction from the detection end of the capillary. After a single spheroplast was introduced into the capillary, suction was stopped, the capillary was placed in running buffer, and a high (20–25 kV) voltage was applied for 10 s to drive the electrophoresis buffer into the capillary. The nonphysiological pH running buffer (containing SDS) lyses the cell. The CE separates the trisaccharide substrate and its enzymatic products that are originated from the single spheroplast.

Fig. 2. Electropherogram of oligosaccharide standards (top trace), the enzyme products from the HT-29 cells (middle trace), and the fluorescent substrate (bottom trace). The major component of the cell sample is unreacted substrate, βGal(1→4)βGlcNAc-O-TMR (peak 3), with minor components being the linker arm ($HO(CH_2)_8CONHCH_2CH_2NHCO$-TMR (peak 1)), βGlcNAc-O-TMR (peak 2), αFuc(1→2)βGal(1→4)βGlcNAc-O-TMR (peak 4), βGal(1→4)[αFuc(1→3)]βGlcNAc-O-TMR (peak 5), and αFuc(1→2)βGal(1→4)[αFuc(1→3)]βGlcNAc-O-TMR (peak 6) (adapted from ref. 22).

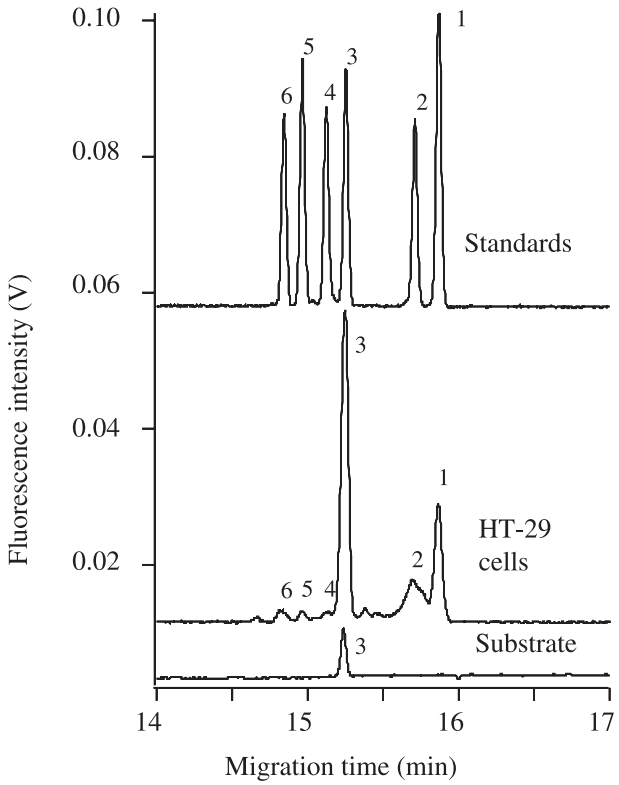
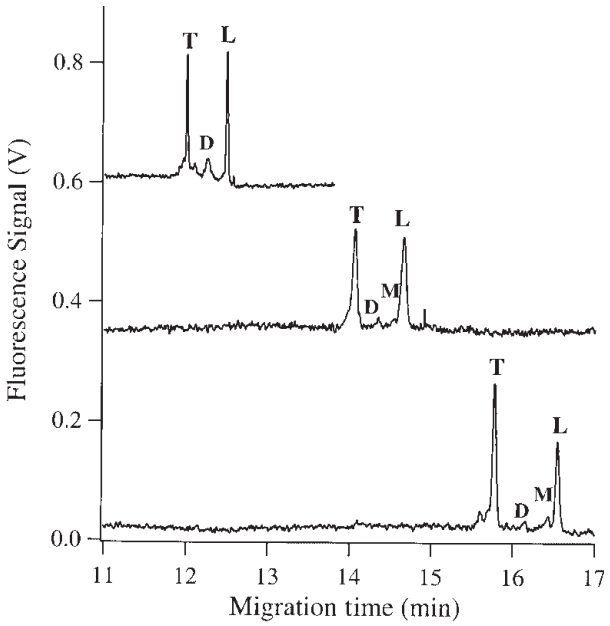


Figure 3 shows the electropherograms obtained from different individual spheroplasts. The major fluorescent compounds, the TMR-labeled trisaccharide and free linker arm, were detected at a concentration of approximately 500–1000 molecules. TMR-labeled disaccharide and monosaccharide were also detected at concentrations of less than 100 molecules. The variations among the electropherograms presumably reflect the heterogeneity of the cell population and their different stages of maturity. This methodology can be expanded to any class of enzymes for which a fluorescent substrate may be synthesized, ultimately permitting enzyme activity to be assayed on a cell-by-cell basis. Determining the distribution of enzyme activity in a cell population may prove useful in the diagnostic and prognostic determination of cancer and other diseases, as well as in in vivo studies on

© 2005 NRC Canada

Fig. 3. Electrophoresis of the contents of three different single yeast spheroplasts introduced into the capillary. The major fluorescent compounds, the TMR-labeled trisaccharide (T) and free linker arm (L), are present at a concentration of approximately 500–1000 molecules. TMR-labeled disaccharide (D) and monosaccharide (M) are also detected, at concentrations of less than 100 molecules (adapted from ref. 23).



the development of enzyme inhibitors in the pharmaceutical industry.

Other groups have also developed highly sensitive CE–LIF techniques for single cell analysis (27–33). These included analyses of amino acids in a single giant neuron from a snail (27), glutathione in single human erythrocytes (28), amines in individual rat pheochromocytoma cells (29), carbohydrate metabolites in single cancer cells (30), kinase activities (31), RNA synthesis (32), and protein fingerprint (33) in single cells.

Competitive CE–LIF immunoassays

Although CE–LIF permits the study of single molecules and single cells, it usually requires the analyte of interest to be fluorescently labeled. While some biological analytes exhibit native fluorescence (34), the fluorescent wavelengths required tend to be in the UV, where commercial lasers are few, expensive, and have limited excitation wavelengths. While it is possible to fluorescently label the target analyte, in practice fluorescent labeling of trace or ultratrace levels of analyte in the presence of the sample matrix is challenging owing to nonquantitative labeling and poor specificity. One way to overcome this limitation and be able to detect (directly or indirectly) nonfluorescent analytes is to form complexes between them and a fluorescently labeled partner. Immunoassays are an elegant way of accomplishing this.

Two immunoassay formats combined with CE–LIF are discussed in the following two sections. In a competitive immunoassay, a fluorescently labeled antigen (analyte; Ag*) is used, and the unlabeled target analyte (Ag) competes with labeled Ag* for binding to a limiting amount of unlabeled antibody (Ab), as illustrated by eq. [1].

$$[1] \qquad Ag^* + Ag + 2Ab \leftrightarrows Ab\text{–}Ag + Ab\text{–}Ag^*$$

Provided they possess sufficiently different electrophoretic mobilities, two peaks corresponding to the free Ag* and bound Ab–Ag* complex should be observed. As the concentration of unlabeled analyte (Ag) increases, more Ag* is displaced from the Ab–Ag* complex, and the fluorescence intensity of the complex peak decreases with increasing analyte concentration, while the free Ag* peak increases. Both peaks may be used for quantitation.

The first CE–LIF immunoassay was reported by Schultz and Kennedy (14). They used a fluorescein isothiocyanate (FITC) labeled insulin as a probe and Fab fragments of anti-insulin mouse monoclonal antibody IgG_{2a} served as the analyte. A calibration curve constructed from both the free FITC-insulin and the bound FTIC-insulin-Fab complex exhibited linear dynamic ranges of two orders of magnitude. The concentration detection limit for Fab was 2 nmol/L, and the mass detection limit was 2.8×10^{-19} mol (280 zeptomol). These authors also performed a competitive assay in which unlabeled insulin competed with FITC-insulin for a limiting amount of anti-insulin antibody, attaining linear dynamic ranges and limits of detection similar to those found with their initial immunoassay for antibody IgG_{2a}.

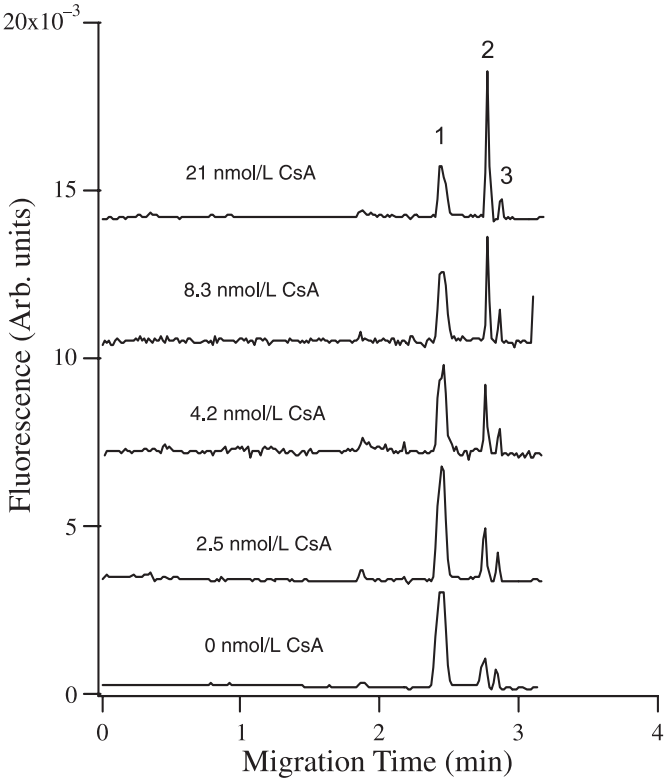
Using a competitive immunoassay and CE–LIF detection, we were able to detect the immunosuppressive drug, cylcosporine A (CsA), in the whole blood of organ transplant patients (16). Cyclosporine is believed to suppress T-cell activation (35), and must be maintained within a narrow therapeutic concentration range in blood (150–450 ng/mL) (36), or adverse effects such as nephrotoxicity, hepatoxicity, and neurotoxicity may result. Using the fluorescently labeled tracer (CsA*) and antibody (Ab) from a commercially available cyclosporine test kit, we were able to quantify CsA in whole blood samples with a limit of detection of 0.9 nmol/L and a mass detection limit of 9×10^{-19} mol. Figure 4 displays electropherograms that illustrate the effect of increasing nonfluorescent CsA (analyte) concentration at fixed concentrations of Ab and CsA*. In the presence of a limiting amount of Ab, CsA and fluorescently labeled CsA* react as shown in eq. [2].

$$[2] \qquad 2Ab + CsA^* + CsA \leftrightarrows Ab\text{–}CsA^* + Ab\text{–}CsA$$

As the CsA concentration increases, more fluorescently labeled CsA* is displaced from the immunocomplex, and the peak corresponding to the Ab–CsA* complex decreases, while the free CsA* peak increases. CsA was quantified from a calibration curve using the free CsA* peak in the electropherogram. Methanol, used in preparation of the blood samples, was found to weaken the stability of the Ab–CsA* complex somewhat, but otherwise did not interfere with the analysis. Similarly, binding of the antibody (Ab) with two CsA metabolites, AM9 and AM19, which were reported to have the highest cross reactivity (37), was assessed and the antibody was found to exhibit a cross reactivity of only 13.3 ± 0.1% with AM9 and 2.0 ± 0.1% with AM19 (16). Excellent agreement for the quantification of CsA in

© 2005 NRC Canada

Fig. 4. Electropherograms showing the competition of the analyte (CsA) with the fluorescent tracer (CsA*) for the antibody (Ab) with increasing concentration of CsA (adapted from ref. 16).



whole blood was found for our assay and for CsA obtained by a standard fluorescence polarization immunoassay.

We have also applied the competitive CE–LIF assay to the analysis of digoxin (38), gentamicin (38), and vancomycin (39). A minimum detectable concentration of vancomycin in clinical samples (heparinized plasma) was found to be 0.98 ng/mL (1.1 fg of vancomycin), which is approximately 10 times better than conventional assays. Like cyclosporine A, digoxin and gentamicin are drugs whose therapeutic serum concentrations fall into narrow ranges. Digoxin, prescribed for congestive heart failure and supraventricular arrhythmias, must be monitored not to exceed the range of 0.8–2.0 ng/mL, whereas gentamicin, prescribed to treat infections caused by Gram-negative bacteria, must be maintained in the range of 5–10 μg/mL. Fluorescently labeled tracers (digoxin* and gentamicin*) and corresponding antibodies for digoxin and gentamicin were obtained from commercially available test kits. At pH below 11.1, the Ab–digoxin* complex was poorly resolved and subsequent experiments were performed at a running buffer pH of 12. Calibration curves were readily constructed from both free digoxin* and bound Ab–digoxin* complex peaks, with a concentration limit of detection of 0.02 ng/mL (26 pmol/L) and a mass detection limit of 2.6×10^{-20} mol (26 zeptomol) being attained for digoxin. Cross-calibration with another commercially available digoxin immunoassay showed good agreement with our assay for the determination of digoxin in whole blood. Calibration curves could be constructed as with digoxin and a concentration limit of detection of 25 ng/mL (52 nmol/L) and a mass detection limit of 5.2×10^{-19} mol was obtained for gentamicin. Because of the incomplete resolution of the gentamicin* and bound Ab–gentamicin* complex, as well as the tendency of the immunocomplex to dissociate at high pH, it was not possible to determine gentamicin levels in whole blood samples.

While the above examples deal with the analysis of relatively small molecules, we have also applied competitive immunoassay and CE–LIF to the detection of larger molecules, such as toxins. Staphylococcal enterotoxins (SE) are a family of serologically distinct proteins capable of causing food poisoning when ingested at levels as low as 1 μg (40). In particular, we investigated the detection of staphylococcal enterotoxins A and B (SEA and SEB) (41, 42). Fluorescently labeled SEA (SEA*) was obtained by incubating SEA at room temperature with FITC for 30 min. The Ab–SEA* complex forms at 3 min in the electropherogram, roughly 1 min before the free SEA* peak. Using the Ab–SEA* complex peak for quantitation, a calibration curve linear from 0.3–6.5 nmol/L SEA was obtained. As little as 3×10^{-18} mol of SEA could be detected, for a concentration detection limit of 0.3 nmol/L. No cross-reactivity of the SEA antibody with SEB was observed. For detection of SEB, tetramethylrhodamine isothiocyanate (TRITC) was used to label SEB. It was found that TRITC-labeled SEB (SEB*) exhibited the highest binding affinity with the SEB antibody at pH 7.0. The addition of 5 mmol/L phytic acid to the running buffer increased the resolution between the bound Ab–SEB* and free SEB* peaks sufficiently that both peaks could be used for quantitation. It is possible that the ion-pairing properties of phytic acid reduce the adsorption of proteins to the capillary wall, thus improving both peak shape and resolution. Calibration plots exhibited linear dynamic ranges of nearly two orders of magnitude, and recovery of SEB spiked into a skim milk sample matrix was essentially quantitative.

Our group has also employed competitive CE–LIF immunoassay in our extensive studies of DNA damage and repair. DNA damage by environmental and endogenous agents is considered to be a critical step leading to mutation and subsequent neoplastic transformation and cancer induction. Damage to DNA is also critical in the cytotoxicity induced by anti-cancer treatments such as ionizing radiation and chemotherapeutic agents. In reaction to the insult to their DNA caused by genotoxic agents, cells have adapted a number of DNA repair pathways, each of which deals with a different type of lesion (43). Because DNA damage and repair plays a critical role in cancer development and treatment, it is important to be able to detect and quantify the damage. Assays for DNA damage are important not only for general studies in biochemistry and genetics of mutagenesis and DNA repair, but also because they present the potential to use DNA damage as an endpoint in monitoring environmental and occupational exposure to carcinogens, as well as cellular exposure to anti-cancer agents in clinical dosimetry.

Tan et al. (44) developed a competitive CE–LIF immunoassay for DNA adducts of benzo[*a*]pyrene diol epoxide in a human lung carcinoma cell line (A549). Benzo[*a*]pyrene-7,8-diol 9,10-epoxide (BPDE) is a reactive carcinogenic species produced in vivo when benzo[*a*]pyrene is metabolized by cytochrome P450 and epoxide hydrolase. The reactive epoxide moiety of BPDE binds to DNA, primarily at the N^2

© 2005 NRC Canada

position of deoxyguanosine, forming the bulky adduct BPDE-N^2-dG, which can affect DNA replication and transcription. To detect this DNA damage, a fluorescently labeled single-stranded DNA oligonucleotide (90-mer*) containing a BDPE-N^2 deoxyguanosine (dG) adduct in the middle of the strand was synthesized and used as a detection probe (45). Such an oligonucleotide, which contains a known amount of specific damage type, functions effectively as a fluorescent probe that can be used for sensitive, selective, and specific detection of DNA damage by CE–LIF. The assay itself involves binding of the fluorescently labeled 90-mer DNA probe (90-mer*) with an unlabeled anti-BPDE antibody, typically mouse monoclonal 8E11. BPDE–DNA adducts in a sample compete with the fluorescently labeled probe for the limiting amount of antibody. Electropherograms of the unbound DNA probe (90-mer*) and DNA–antibody complex (Ab–90-mer*) obtained from DNA from A549 cells incubated with 9.4–300 μmol/L BPDE, appear in Fig. 5. The Ab–90-mer* complex is observed to migrate before the unbound DNA. This is because both antibody-bound and unbound DNA are negatively charged and the direction of their electrophoretic mobilities is opposite to that of the electroosmotic flow (EOF). The decrease in total charge-to-mass ratio after antibody binding decreases the mobility of the bound DNA adduct moving toward the injection end of the capillary (positive polarity). Because the magnitude of EOF is larger than that of the electrophoretic mobility, the net result is faster migration directed towards the detector end of the capillary (direction of EOF). As DNA from cells subjected to incubation with increasing levels of BPDE are used, more fluorescently labeled DNA probe (90-mer*) is displaced from the DNA–antibody complex (Ab–90-mer*), and the complex peak decreases while the free 90-mer* peak increases. In this instance, the affinity complex is composed of two distinct peaks (peaks 1 and 2 in Fig. 5). Since antibodies are bidentate, they are capable of binding with up to two antigen molecules. Peak 1 corresponds to the complex formed between the antibody and one DNA adduct (1:1 complex), whereas peak 2 corresponds to the complex formed between the antibody and two DNA adducts (1:2 complex). Therefore, antibody binding stoichiometry can be studied using rationally designed fluorescent oligonucleotide probes (46).

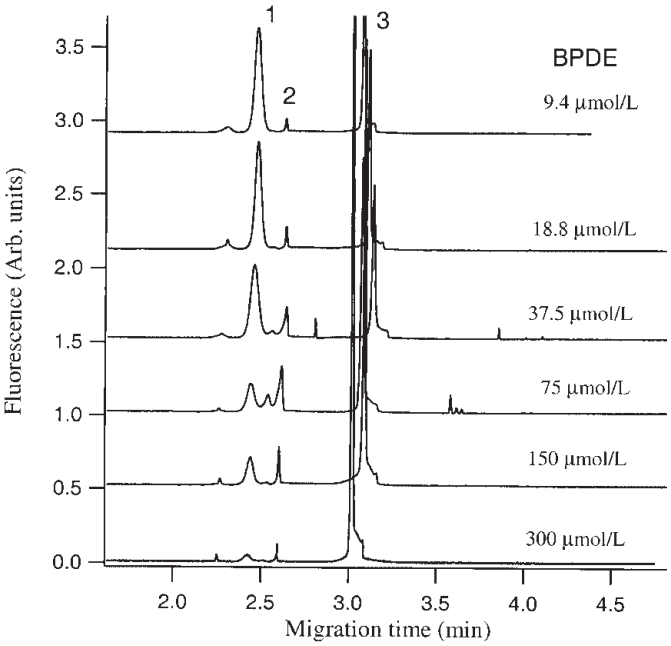
Noncompetitive CE–LIF immunoassays

In a noncompetitive immunoassay, a probe (usually an antibody) is fluorescently labeled (Ab*) and is used to bind with the analyte (Ag), forming a fluorescent Ab*–Ag complex. The chemical reaction illustrating this behavior is given in eq. [3].

$$[3] \qquad Ab^* + Ag \leftrightarrows Ab^*\text{–}Ag$$

The Ab*–Ag complex and uncomplexed free Ab* are separated by CE and detectable by LIF. As the analyte (Ag) concentration increases, more free Ab* (which is held at a constant or limiting concentration) is consumed in binding to form the Ab*–Ag complex, the fluorescence of which increases. Ultimately, all the free Ab* should be consumed into the bound Ab*–Ag complex. On electrophoresis, the Ab* and Ab*–Ag species appear as separate peaks and the

Fig. 5. Electropherograms showing the competitive assays for DNA adducts of BPDE in A549 cells. The cells had been incubated with 9.4–300 μmol/L BPDE for 2 h prior to extraction of the DNA for adduct analysis. Peaks 1 and 2 correspond to the 1:1 and 1:2 stoichiometric complexes formed by the 8E11 antibody and the BPDE–90mer* oligonucleotide. Peak 3 represents the free BPDE–90mer* probe (adapted from ref. 44).

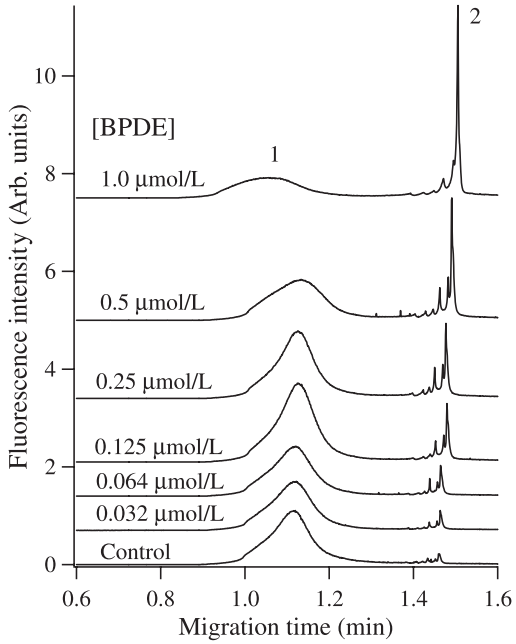


analyte concentration in an unknown sample may be obtained by a calibration curve against known standards. Either the increase in the fluorescence intensity of the Ab*–Ag peak, or the decrease in fluorescence intensity of the Ab* peak with increasing analyte concentration, may be used for quantitation.

Our group has also developed a noncompetitive CE–LIF immunoassay for BDPE–DNA adducts (47, 48). Instead of using the synthetic 90-mer DNA as a probe, a fluorescently labeled antibody (secondary antibody, $F(ab')_2$ fragment of goat anti-mouse IgG, Ab''_{IgG}*) is used to bind to the anti-BDPE antibody (primary antibody, mouse monoclonal 8E11, Ab'_{8E11}), rendering the Ab'_{8E11}–BPDE adduct complex fluorescent. Electropherograms for the fluorescent secondary antibody, the secondary antibody bound to the primary antibody, and the immunocomplex of the two antibodies with the DNA damage are shown in Fig. 6. To maximize formation of the fluorescent complex so that DNA damage may be quantified, excess amounts of secondary antibody (Ab''_{IgG}*) were used to saturate the primary antibody (Ab'_{8E11}), which in turn was added in excess to saturate the DNA damage. Peak 1 corresponds to the primary–secondary antibody species, and peak 2 corresponds to the Ab''_{IgG}*–Ab'_{8E11}–BPDE adduct affinity complex. The BPDE–DNA adducts from A549 human lung carcinoma cells were formed by incubating the cells with BPDE (0.032–1.0 μmol/L) for 2 h (48). With increasing concentration of BPDE, the fluorescence signal from the DNA adducts (peak 2) increases, indicating a clear dose–response relationship. Using the results from the complex that had been incubated with 0.032 μmol/L BPDE,

© 2005 NRC Canada

Fig. 6. Electropherograms showing the noncompetitive assays for BPDE–DNA adducts in A549 cells. The cells had been incubated with 0.032–1.0 µmol/L BPDE for 2 h prior to extraction of the DNA for adduct analysis. Peak 1 corresponds to the complex formed between the primary 8E11 antibody (Ab'_{8E11}) and the fluorescently labeled secondary antibody, the $F(ab')_2$ fragment of goat anti-mouse IgG (Ab''_{IgG}*). Peak 2 corresponds to the affinity complex of BPDE–DNA adducts with the two antibodies (Ab''_{IgG}*–Ab'_{8E11}–BPDE adducts) (adapted from ref. 48).



a detection limit of approximately three BPDE adducts per 10^9 nucleotides was obtained. This is comparable with the most sensitive method available for detecting DNA damage, the ^{32}P post-labeling assay (49).

Use of aptamers as affinity probes

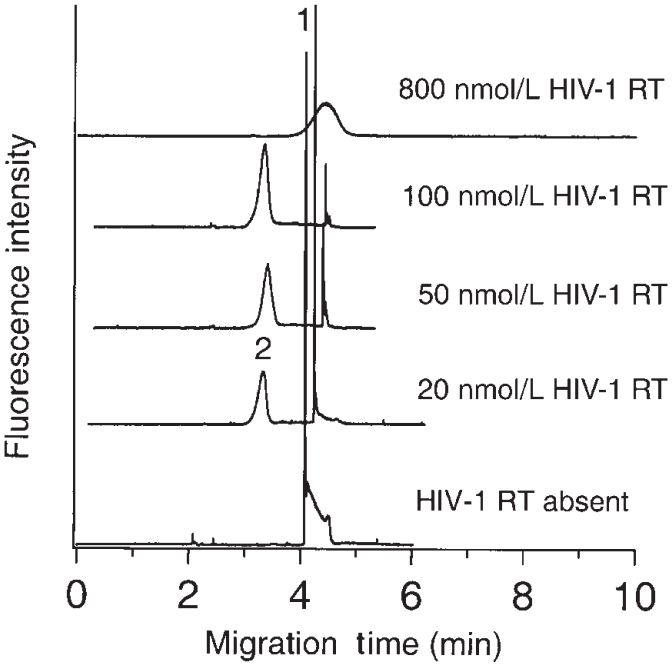
Most immunoassays or affinity assays use antibodies as probes. Although antibodies are highly selective and sensitive probes for immunoassays, they have shortcomings. For example, fluorescent labeling of proteins is not always facile, and a fluorescent label can interfere with binding if it is too close to the binding site. Because they need to be generated within an organism, the binding characteristics and analytical performance of antibodies can vary from lot to lot. Finally, antibodies must be carefully handled as they denature at much lower temperatures than oligonucleotides. Recently, there has been much interest in generating, as alternatives to antibodies, synthetic oligonucleotides, which have binding properties similar to antibodies. Termed aptamers from the Latin *aptus* meaning "fitting", these are synthetic RNA or DNA molecules generated in vitro from a combinatorial chemistry process termed SELEX or systematic evolution of ligands by exponential enrichment (50, 51). A large pool of oligonucleotides of the same length with randomized sequences is tested for binding, typically by filter assays, to a specific target ligand. The oligonucleotides that bind most tightly to the target ligand are then separated and amplified by the polymerase chain reaction (PCR), and the process is repeated until the pool evolves to a subset of sequences with the highest binding affinity to the target ligand. At the end of the process, the aptamers produced have binding constants typically many orders of magnitude greater than the original oligonucleotide mixture (typically nmol/L to pmol/L) (50), making the aptamers highly selective for their target ligands. Aptamers may be produced in a matter of weeks to months with the traditional SELEX process, or in a matter of days with the automated SELEX process (52) and the modified capillary electrophoresis process (53). Once the sequence of the aptamer is known, it can be easily synthesized and readily and specifically labeled. Because of this specificity in synthesis, aptamers should not be subject to the lot-to-lot variability that can sometimes be problematic with antibody production. Although both RNA and DNA aptamers are produced, successful analytical applications have overwhelmingly employed DNA aptamers, likely because RNA aptamers are particularly vulnerable to degradation by ribonucleases because of the presence of the 2′-hydroxyl group on the ribose sugar.

German et al. (54) first used a fluorescently labeled DNA aptamer and CE–LIF for the determination of nanomolar levels of IgE in reconstituted human serum, and thrombin in standard solution, yielding calibration curves having linearity of five orders of magnitude. Although used in a number of applications including being immobilized on stationary phases in capillary electrochromatography (55–57), affinity chromatography (58), and affinity mass spectrometry (59), aptamers have been sparingly used in affinity CE–LIF (60, 61). Schneider et al. (62) described the synthesis of single-stranded DNA aptamers for the reverse transcriptase (RT) of the type 1 human immunodeficiency virus (HIV-1). Two oligonucleotides, an 81-mer termed RT 26 and an 84-mer termed RT 12, were developed. They have binding constants with HIV-1 RT of 1 nmol/L and 2 nmol/L, respectively. This represents a 1000-fold increase over binding to wild-type DNA. These aptamers represent excellent potential probes for binding to HIV-1 RT, which is significant in that HIV-1 RT is a biomarker for the HIV-1 virus, and HIV-1 RT activity is used to determine HIV-1 viral load.

Figure 7 illustrates the formation of the RT26-HIV-1 RT affinity complex as HIV-1 RT concentration is increased at a constant concentration of aptamer (61). As expected, the affinity complex increases with HIV-1 RT concentration, whereas the free aptamer peak decreases, ultimately completely being incorporated into the affinity complex at 800 nmol/L HIV-1 RT. Calibration curves were linear to 6 µg/mL HIV-1 RT. The aptamer-based assay provides the first sensitive, selective, and rapid assay for HIV-1 RT, although the extremely low levels of HIV-1 RT present in the sera of HIV-positive individuals (9×10^{-4} to 1 pg/mL) (63), would restrict its application to cell culture. Other current HIV-1 RT assays are laborious and time-consuming, typically involving PCR and gel electrophoresis of the PCR products. None detect HIV-1 RT directly. They also suffer interference from the human T-cell leukemia virus type 1 (HTLV-1), the avian myeloblastosis virus (AMV), and the Moloney murine leukemia virus (MMLV), among others. In contrast, the CE–LIF assay using aptamer showed no cross reaction to AMV-RT, or MMLV-RT, or heat-denatured HIV-1 RT.

© 2005 NRC Canada

Fig. 7. Electropherograms demonstrating the effect of increasing HIV-1 RT concentration (0–800 nmol/L) at a fixed concentration (17 nmol/L) of fluorescently labeled RT 26 aptamer. The bottom electropherogram contains data representing only the RT 26 aptamer. Peak 1 corresponds to the unbound aptamer and Peak 2 corresponds to the affinity complex formed between the aptamer and the HIV-1 RT protein (adapted from ref. 60).



Fluorescence polarization

An additional property that can be used to enhance detection and studies of molecular binding is fluorescence polarization. Fluorescence polarization is governed by the orientation of a molecule in the excited state relative to the electric vector of excitation (64–67). A molecule that loses its orientation as the result of rotational diffusion is said to be depolarized. A fluorescent molecule, when excited by polarized light, emits fluorescence with its polarization (P) controlled by rotational correlation time (ϕ), and fluorescence lifetime (τ) as shown below (65).

$$[4] \qquad \frac{1}{P} - \frac{1}{3} = \left(\frac{1}{P_o} - \frac{1}{3}\right)\left(1 + \frac{\tau}{\phi}\right)$$

where P_o is the intrinsic polarization in the absence of rotational diffusion. The fluorescence is depolarized when the rotational correlation time is small relative to the fluorescence lifetime. When the fluorescence lifetime is constant for a given fluorophore, an increase in fluorescence polarization may be observed with increasing rotational correlation time. The Debye–Stokes–Einstein equation (68) permits an estimation of rotational correlation time.

$$[5] \qquad \phi = \frac{M\eta(v + h)}{RT}$$

where M is the mass of the molecule, η is the viscosity of the solution, v is the specific volume of the molecule, h is the degree of hydration, T is the absolute temperature, and R is the ideal gas constant.

When vertically polarized light is used for excitation, I_v is the intensity of the vertically polarized fluorescence and I_h is the intensity of the horizontally polarized fluorescence.

The degree of polarization (P) is defined as follows:

$$[6] \qquad P = \frac{I_v - I_h}{I_v + I_h}$$

Similarly, fluorescence anisotropy (A) can be obtained from I_v and I_h as follows:

$$[7] \qquad A = \frac{I_v - I_h}{I_v + 2I_h}$$

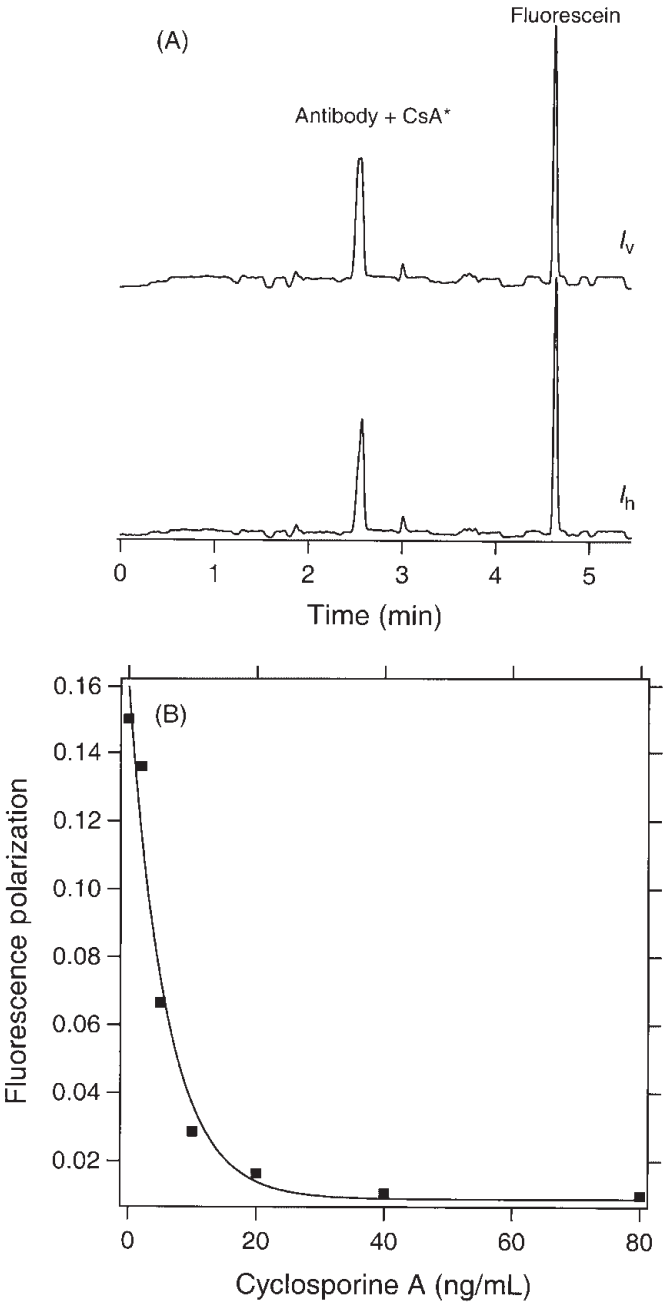
Measurement of fluorescence polarization provides additional analytical information because polarization is affected by changes in molecular size. When a molecule is excited by polarized light, it fluoresces with a degree of polarization that is primarily determined by the rotational motion of the molecule, which is inversely proportional to molecular size. Small molecules rotate rapidly in solution, causing the molecule's fluorescence to be depolarized (low fluorescence polarization). In contrast, when a small fluorescent molecule binds to a much larger molecule (e.g., antibody, ~150 000 Da), the rotational motion slows down and the fluorescence polarization of the large bound complex is higher. Changes in fluorescence polarization can therefore be used to monitor binding or dissociation of molecules, making polarization very useful in affinity binding studies.

We utilized fluorescence polarization in a competitive immunoassay to quantify CsA in electrophoretic conditions under which free fluorescently labeled tracer (CsA*) and bound tracer–antibody complex (Ab–CsA*) co-eluted (i.e., homogeneous immunoassay) (69). As antibody concentration is increased, fluorescence polarization increases, consistent with the small fluorescent tracer (CsA*) binding to the much larger antibody (Ab). The resulting increase in molecular size, coupled with restricted molecular motion, is responsible for the fluorescence polarization. When the concentration of unlabeled analyte (CsA) is increased, CsA displaces CsA* from the Ab–CsA* complex, and the fluorescence polarization decreases as a result. An electropherogram of the co-eluted antibody–tracer complex, along with the calibration curve appears in Fig. 8.

We also examined the fluorescence polarization in fluorescently labeled vancomycin binding to its antibody (70). The binding of vancomycin to its antibody results in an increase in molecular volume and a slower rotation of the molecule; consequently, the vancomycin–antibody immunocomplex exhibits significant polarization. A mean fluorescence polarization was found to be 0.28 ± 0.02. This value represents the intrinsic polarization of the complex, which is dependent on the rotational diffusion of the molecule, but is independent of the concentration of vancomycin and antibody added. We also investigated the polarization of fluorescently labeled Staphylococcal enterotoxin A (SEA). Free labeled SEA exhibited appreciable polarization (0.14), making it identifiable in the presence of residual dyes. This finding suggests that CE–LIFP may be used to monitor the

© 2005 NRC Canada

Fig. 8. (A) Electropherograms of a mixture containing fluorescently labeled cyclosporine A (CsA*) and its antibody in a 1:1 volume ratio. The upper and lower traces correspond to vertically (I_v) and horizontally (I_h) polarized fluorescence, respectively. The unbound CsA* and the Ab–CsA* complex were made to co-elute. (B) Fluorescence polarization as a function of unlabeled cyclosporine A. This represents a homogeneous competitive immunoassay (adapted from ref. 69).



progress of labeling reactions to verify the purity of reaction products.

LIFP is capable of providing information on the formation of affinity complexes prior to or during CE separation. An example of on-line monitoring of affinity complex formation was demonstrated in a study of protein–DNA interaction (71). Because of lower binding affinity, dynamic formation of the affinity complexes was achieved and was monitored using LIFP. Both the fluorescence polarization and mobility shift information enabled studies of the DNA–protein binding. Unlike the mobility shift method that required the use of an internal marker to correct for unwanted changes of mobility, the LIFP method does not have this limitation. Prior to our studies, most fluorescence measurements for CE detection have been based on the fluorescence intensity. The CE–LIFP technique maintains the advantage of excellent sensitivity as in the case of laser-induced fluorescence detection. It provides the additional capability of identifying complex formation, suitable for studies of molecular interactions. Applications of the CE–LIFP technique to such binding systems as vancomycin and its antibody, staphylococcal enterotoxin and its antibody, and *trp* operator and *trp* repressor represent peptide–protein, protein–protein, and DNA–protein interactions (70, 72). The affinity complexes were readily distinguished from the unbound molecules on the basis of their fluorescence polarization. Studies of these common binding systems demonstrate potential wide applications of CE–LIFP.

Conclusions

CE–LIF provides an excellent means for the rapid and ultrasensitive (tens to hundreds of molecules) determination of bioanalytical compounds of interest from a wide variety of samples. The application of immunoassay by CE–LIF permits the determination of unlabeled analyte in a sensitive and selective manner, in the presence of many potential interfering components in the sample matrix. The range of immunoassays or affinity CE–LIF assays is limited only by the ability to generate a suitable antibody or aptamer to a target of interest. We have successfully used CE–LIF for the analysis of components of single cells, for the determination of therapeutic drugs in human sera, for the determination of natural toxins, and for the detection of biomarkers for DNA damage and HIV-1 infection. The use of LIFP provides additional benefits in studying molecular interactions and improving affinity assays. The use of aptamers as affinity probes presents new opportunities for a wide range of analytical applications.

Acknowledgements

The authors thank the group members and collaborators for their contribution to the research described in this manuscript. The Natural Sciences and Engineering Research Council of Canada (NSERC), the Canadian Water Networks NCE, the Canada Research Chairs Program, and the National Institutes of Health are acknowledged for financial support of our research.

References

1. R.M. Nakamuro, Y. Kasahara, and G.A. Rechnitz. Immunochemical assays and biosensor technologies for the 90s. American Society for Microbiology, Washington, D.C. 1992.
2. J.P. Gosling and L.V. Basso (*Editors*). Immunoassay: laboratory analysis and clinical applications. Butterworth-Heinemann, Boston. 1994.

© 2005 NRC Canada

3. D. Wild (*Editor*). The immunoassay handbook. 2nd ed. Nature Publishing Group, London. 2001.
4. J.W. Jorgenson and K.D. Luckas. Anal. Chem. **53**, 1298 (1981).
5. J.W. Jorgenson and K.D. Luckas. Science (Washington, D.C.), **222**, 266 (1983).
6. P. Camilleri (*Editor*). Capillary electrophoresis theory and practice. 2nd ed. CRC Press, Boca Raton, Florida. 1998.
7. J.P. Landers (*Editor*). Handbook of capillary electrophoresis. 2nd ed. CRC Press, Boca Raton, Florida. 1997.
8. P.G. Righetti (*Editor*). Capillary electrophoresis in analytical biotechnology. CRC series in analytical biotechnology. CRC Press, Boca Raton, Florida. 1996.
9. A. Castro and E.B. Shera. Anal. Chem. **67**, 3181 (1995).
10. D.Y. Chen and N.J. Dovichi. Anal. Chem. **68**, 690 (1996).
11. J.C. Fister III, S.C. Jacobson, L.M. Davis, and J.M. Ramsey. Anal. Chem. **70**, 431 (1998).
12. M.R. Shortreed, H. Li, W.-H. Huang, and E.S. Yeung. Anal. Chem. **72**, 2879 (2000).
13. R.A. Keller, W.P. Ambrose, A.A. Arias, H. Cai, S.R. Emory, P.M. Goodwin, and J.H. Jett. Anal. Chem. **74**, 316A (2002).
14. N.M. Schultz and R.T. Kennedy. Anal. Chem. **65**, 3161 (1993).
15. K. Shimura and B.L. Karger. Anal. Chem. **66**, 9 (1994).
16. L. Ye, X.C. Le, J.Z. Xing, M. Ma, and R. Yatscoff. J. Chromatogr. B, **714**, 59 (1998).
17. X.C. Le, Q.-H. Wan, and M.T. Lam. Electrophoresis, **23**, 903 (2002).
18. N.H.H. Heegaard, S. Nilsson, and N.A. Guzman. J. Chromatogr. B, **715**, 29 (1998).
19. R.M. Guijt-van Duijn, G.W.K. van Dedem, and E. Baltussen. Electrophoresis, **21**, 3905 (2000).
20. D. Schmalzing, S. Buonocore, and C. Piggee. Electrophoresis, **21**, 3919 (2000).
21. S. Hjertén. Chromotogr. Rev. **9**, 122 (1967).
22. X.C. Le, Y. Zhang, N.J. Dovichi, C.A. Compston, M.M. Palcic, R.J. Beever, and O. Hindsgaul. J. Chromatogr. A, **781**, 515 (1997).
23. X.C. Le, W. Tan, C.H. Scaman, A. Szpacenko, E. Arriaga, Y. Zhang, D.N.J.O. Hindsgaul, and M.M. Palcic. Glycobiology, **9**, 219 (1999).
24. J. Liu, O. Shirota, and M. Novotny. Anal. Chem. **64**, 973 (1992).
25. M. Stefansson and M. Novotny. Anal. Chem. **66**, 1134 (1994).
26. J.Y. Zhao, P. Diedrich, Y. Zhang, O. Hindsgaul, and N.J. Dovichi. J. Chromatogr. B, **657**, 307 (1994).
27. R.T. Kennedy, M.D. Oates, B.R. Cooper, B. Nickerson, and J.W. Jorgenson. Science (Washington, D.C.), **246**, 57 (1989).
28. B.L. Hogan and E.S. Yeung. Anal. Chem. **64**, 2841 (1992).
29. S.D. Gilman and A.G. Ewing. Anal. Chem. **67**, 58 (1995).
30. S.N. Krylov, Z. Zhang, N.W.C. Chan, E. Arriaga, M.M. Palcic, and N.J. Dovichi. Cytometry, **37**, 15 (1999).
31. G.D. Meredith, C.E. Sims, J.S. Soughayer, and N.L. Allbritton. Nat. Biotechnol. **18**, 309 (2000).
32. F.T. Han and S.J. Lillard. Anal. Biochem. **302**, 136 (2002).
33. S. Hu, L. Zhang, S.N. Krylov, and N.J. Dovichi. Anal. Chem. **75**, 3495 (2003).
34. E.S. Yeung. Anal. Chem. **71**, 522A (1999).
35. B.D. Kahan. N. Engl. J. Med. **321**, 1725 (1989).
36. D. Soy, M. Campistol, M. Brunet, M. Roca, E. Carreras, H. Andreu, C. Codina, and J. Ribas. Transplant. Proc. **27**, 2415 (1995).
37. R.W. Yatscoff, T.G. Rosano, and L.D. Bowers. Clin. Biochem. **24**, 23 (1991).
38. Q.-H. Wan and X.C Le. J. Chromatogr. B, **734**, 31 (1999).
39. M.T. Lam, Q.-H. Wan, C.A. Boulet, and X.C. Le. J. Chromatogr. A, **853**, 545 (1999).
40. L. Spero, A. Johnson-Winegar, and J.J. Schmidt. *In* Handbook of natural toxins. Vol. 4. *Edited by* M.C. Hardegree and A.T. Tu. Marcel Dekker, New York. 1988. Chap. 4.
41. M.T. Lam, Q.-H. Wan, C.A. Boulet, and X.C. Le. J. Chromatogr. A, **853**, 545 (1999).
42. M.T. Lam, C.A. Boulet, and X.C. Le. Anal. Chim. Acta, **457**, 21 (2002).
43. E.C. Friedberg, G.C. Walker, and W. Siede. DNA repair and mutagenesis. ASM Press, Washington, D.C. 1995.
44. W.G. Tan, T.J. Carnelley, P. Murphy, H. Wang, J. Lee, S. Barker, M. Weinfeld, and X.C. Le. J. Chromatogr. A, **924**, 377 (2001).
45. T.J. Carnelley, S. Barker, H. Wang, W.G. Tan, M. Weinfeld, and X.C. Le. Chem. Res. Toxicol. **14**, 1513 (2001).
46. H. Wang, J. Xing, W. Tan, M. Lam, T. Carnelley, M. Weinfeld, and X.C. Le. Anal. Chem. **74**, 3714 (2002).
47. J.Z. Xing, T. Carnelley, J. Lee, W.P. Watson, E. Booth, M. Weinfeld, and X.C. Le. *In* Methods in molecular biology. Vol. 162. Capillary electrophoresis of nucleic acids. Vol. 1. *Edited by* K.R. Mitchelson and J. Cheng. 2001. Chap. 30.
48. H. Wang, M. Lu, N. Mei, J. Lee, M. Weinfeld, and X.C. Le. Anal. Chim. Acta, **500**, 13 (2003).
49. A.C. Beach and R.C. Gupta. Carcinogenesis, **13**, 1053 (1992).
50. K.W. Uphoff, S.D. Bell, and A.D. Ellington. Curr. Opin. Struct. Biol. **6**, 281 (1996).
51. C. Turek and L. Gold. Science (Washington, D.C.), **249**, 505 (1990).
52. L.J. Sooter, T. Riedel, E.A. Davidson, M. Levy, J.C. Cox, and A.D. Ellington. Biol. Chem. **382**, 1327 (2001).
53. S.D. Mendonsa and M.T. Bowser. J. Am. Chem. Soc. **126**, 20 (2004).
54. I. German, D.D. Buchanan, and R.T. Kennedy. Anal. Chem. **70**, 4540 (1998).
55. R.B. Kotia, L. Li, and L.B. McGown. Anal. Chem. **72**, 827 (2000).
56. M.A. Rehder and L.B. McGown. Electrophoresis, **22**, 3759 (2001).
57. J.A.M. Charles and L.B. McGown. Electrophoresis, **23**, 1599 (2002).
58. Q. Deng, I. German, D. Buchanan, and R.T. Kennedy. Anal. Chem. **73**, 5415 (2001).
59. L.W. Dick, Jr. and L.B. McGown. Anal. Chem. **76**, 3037 (2004).
60. V. Pavski and X.C. Le. Anal. Chem. **73**, 6070 (2001).
61. M. Berezovski, R. Nutiu, Y. Li, and S.N. Krylov. Anal. Chem. **75**, 1382 (2003).
62. D.J. Schneider, J. Feignon, Z. Hostomsky, and L. Gold. Biochemistry, **34**, 9599 (1995).
63. J.G. García-Lerma, R.F. Schinazi, A.S. Juodawlkis, V. Soriano, Y. Lin, K. Tatti, D. Rimland, T.M. Folks, and W. Heneine. Antimicrob. Agents Chemother. **43**, 264 (1999).
64. J.R. Lakowicz. Principles of fluorescence spectroscopy. Kluwer Academic/Plenum Press, New York. 1999.
65. F. Perrin. J. Phys. Radium, **7**, 390 (1926).
66. G. Weber. Adv. Protein Chem. **8**, 415 (1953).
67. W.B. Dandliker and V.A. de Saussure. Immunochemistry, **7**, 799 (1970).
68. D.S. Gottfried, A. Kagan, B.M. Hoffman, and J.M. Friedman. J. Phys. Chem. B, **103**, 2803 (1999).
69. Q.-H. Wan and X.C. Le. J. Chromatogr. A, **853**, 555 (1999).
70. Q.-H. Wan and X.C. Le. Anal. Chem. **71**, 4183 (1999).
71. Q.-H. Wan and X.C. Le. Anal. Chem. **72**, 5583 (2000).
72. V. Pavski and X.C. Le. Curr. Opin. Biotechnol. **14**, 65 (2003).

© 2005 NRC Canada

Kinetic and spectroscopic studies on α- and β-cyclodextrin rotaxanes with (μ-*N*,*N*′-bis(4-pyridinylmethylene)-α,ω-alkanediimine)bis[pentacyanoferrate(II)] threads

Victor X. Jin, Donal H. Macartney, and Erwin Buncel

Abstract: [2]Pseudorotaxanes have been prepared by threading *N*,*N*′-bis(4-pyridinylmethylene)-1,2-ethanediimine (**L2**), -1,4-butanediimine (**L4**), and -1,6-hexanediimine (**L6**) ligands through α-cyclodextrin (α-CD) and β-cyclodextrin (β-CD), and have subsequently been converted to the corresponding [2]rotaxane species by coordinating bulky $[Fe(CN)_5]^{3-}$ end groups. The stability constants for the [2]pseudorotaxanes were determined by ^{1}H NMR chemical shift titrations and increase with the polymethylene chain length *n*. The rate constants for both the formation of the $[Fe(CN)_5(\mathbf{Ln})]^{3-}$ complexes from the $[Fe(CN)_5OH_2]^{3-}$ ion and **Ln**, and the rate constants for the dissociation of **Ln** from the metal complexes, exhibit significant diminutions in the presence of α- and β-CD, owing to inclusions of the free and coordinated ligands, respectively. The lability of the iron(II)–pyridine bonds also permits the spontaneous self-assembly of the [2]rotaxane upon the addition of cyclodextrin to the iron dimer complexes. The mechanism for this process involves the rate-determining dissociation of a $[Fe(CN)_5]^{3-}$ unit from $[(NC)_5Fe(\mathbf{Ln})Fe(CN)_5]^{6-}$, followed by CD inclusion of the **Ln** ligand to form a semirotaxane, and subsequent recomplexation by the $[Fe(CN)_5OH_2]^{3-}$ ion.

Key words: cyclodextrins, rotaxanes, pentacyanoferrate(II), ligand substitution, kinetics.

Résumé : En enfilant les ligands *N*,*N*′-bis(4-pyrimidylméthylène)-éthane-1,2-diimine (**L2**), -butane-1,4-diimine (**L4**) et -hexane-1,6-diimine (**L6**) à travers la α-cyclodextrine (α-CD) et la β-cyclodextrine (β-CD), il y a formation de [2]pseudorotaxanes qui ont été subséquemment transformés en espèces [2]rotaxanes par coordination avec les groupes terminaux volumineux, $[Fe(CN)_5]^{3-}$. On a déterminé les constantes de stabilité des [2]pseudorotaxanes titrages des déplacements chimiques en RMN du ^{1}H et par augmentation avec la longueur de la chaîne polyméthylène, *n*. Les constantes de formation des complexes de $[Fe(CN)_5(\mathbf{Ln})]^{3-}$ à partir de l'ion $[Fe(CN)_5OH_2]^{3-}$ et de **Ln** ainsi que de dissociation de **Ln** à partir des complexes métalliques présentent toutes des diminutions significatives en présence de α-CD et de β-CD en raison des inclusions respectivement de ligands libres et coordinés. La labilité des liaisons fer(II)–pyridine permet aussi l'auto-assemblage du [2]rotaxane lors de l'addition de cyclodextrine aux complexes dimère du fer. Le mécanisme de ce processus implique une dissociation qui détermine la vitesse d'une unité de $[Fe(CN)_5]^{3-}$ de $[(NC)_5Fe(\mathbf{Ln})Fe(CN)_5]^{6-}$, suivie d'une inclusion de CD du ligand **Ln** pour former une semirotaxane et une recomplexation subséquente par l'ion $[Fe(CN)_5OH_2]^{3-}$.

Mots clés : cyclodextrines, rotaxanes, pentacyanoferrate(II), substitution de ligand, cinétique.

[Traduit par la Rédaction]

Introduction

Rotaxanes (1, 2) are supramolecular species (3) in which a cyclic molecular bead is threaded by a linear chain and stoppered by bulky end units, thus preventing the complex from dissociating into its cyclic and linear molecular components. The syntheses of a number of [2]rotaxanes ([*n*] indicates the number of components in the rotaxane) containing a variety of cyclic beads, with alkyl or polyether chains as the threads and bulky organic groups or metal complexes as the end groups, have been reported (4–10). The cyclodextrins (CD) (11, 12), a class of cyclic oligosaccharides normally comprising six (α-CD), seven (β-CD), or eight (γ-CD) α-(1→4)-linked D(+)-glucopyranose units with a toroidal hydrophobic cavity capable of including a wide variety of guest substances (13), have also been employed as the cyclic component in the syntheses of rotaxanes in recent years (14). [2]Rotaxanes, stoppered by transition metal complexes (15–20), have generally been prepared by reacting a semirotaxane (bearing one bulky end unit) with a second metal complex or organic end unit.

In our laboratory, we have investigated the kinetics and mechanisms of the formation of a series of stable α-cyclodextrin rotaxanes of the type $[(NC)_5Fe\{R(CH_2)_nR'\text{-}CD\}Fe(CN)_5]^{4-}$, with symmetric and asymmetric threads where R and R′ = 3- and 4-cyanopyridine or 4,4′-bipyridine and (or) pyrazine, with *n* = 8–12 (20–23). These [2]rotaxanes will

Received October 24, 2004. Published on the NRC Research Press Web site at http://canjchem.nrc.ca on 1 March 2005.

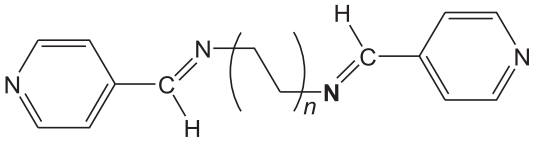
V.X. Jin, D.H. Macartney,[1] and E. Buncel. Department of Chemistry, Queen's University, Kingston, ON K7L 3N6, Canada.

[1]Corresponding author (e-mail: donal@chem.queensu.ca).

 doi: 10.1139/V05-019 © 2005 NRC Canada

self-assemble irrespective of the order of the addition of the α-CD, the $[R(CH_2)_nR']^{2+}$ ligand, and the $[Fe(CN)_5]^{3-}$ stopper components. The slower route involves initial formation of an iron dimer complex, $[(NC)_5Fe(R(CH_2)_nR')Fe(CN)_5]^{4-}$, which will not permit direct threading through α-CD because of the bulky pentacyanoferrate(II) stoppers. Slow dissociation of a $[Fe(CN)_5]^{3-}$ unit, however, followed by the α-CD inclusion of the coordinated bridging ligand yields a semirotaxane, which may be rapidly recomplexed by $[Fe(CN)_5OH_2]^{3-}$. The rate constants for this self-assembly process are dependant on the lability of the iron–nitrogen bond. We have recently reported the results of kinetic and spectroscopic investigations on similar α- and β-CD [2]rotaxanes containing shorter, conjugated neutral bis(4′-pyridyl) bridging ligands (24).

In this paper we report the results of kinetic and spectroscopic studies on the formation of α- and β-cyclodextrin [2]rotaxanes of the type $[(NC)_5Fe\{\mathbf{Ln}\cdot CD\}Fe(CN)_5]^{6-}$ in basic solution, where the neutral **Ln** bridging ligands are *N*,*N*′-bis(4-pyridinylmethylene)-1,2-ethanediimine (**L2**), -1,4-butanediimine (**L4**), and –1,6-hexanediimine (**L6**).



n = 1 **L2**
n = 2 **L4**
n = 3 **L6**

The **L2** ligand has recently been employed as a bridging ligand in the construction of a number of one-, two-, and three-dimensional coordination polymers of transition metals (25–28) and as a component in photochromic co-crystals with 1,2-diaryl-1,2-ethanediols (29). The structure of **L2** has been determined by X-ray crystallography (26).

The end group precursor, $[Fe(CN)_5OH_2]^{3-}$, is generated in basic solution by the aquation of the $[Fe(CN)_5(SO_3)]^{5-}$ ion, instead of the $[Fe(CN)_5NH_3]^{3-}$ ion, which is normally employed in acidic or neutral solutions. The stability constants for the [2]pseudorotaxanes, {**Ln**·CD}, have been determined by means of ^{1}H NMR spectroscopic titrations. We report the results of kinetic and spectroscopic studies on the ligand substitution reactions involving α- and β-cyclodextrin inclusion complexes of the neutral diimine ligands **Ln** in basic solution. In addition, the kinetics and mechanism of the self-assembly of $[(NC)_5Fe\{\mathbf{Ln}\cdot CD\}Fe(CN)_5]^{6-}$ rotaxanes from the corresponding iron dimer complex have been studied using ^{1}H NMR spectroscopic techniques.

Experimental

Materials

The α- and β-cyclodextrins (Aldrich) were dried at 80 °C under reduced pressure for at least 12 h prior to use. The 4-pyridinecarboxaldehyde, 1,2-diaminoethane, 1,4-diaminobutane, and 1,6-diaminohexane (Aldrich) were used as received. Sodium pentacyano(sulphito)ferrate(II) hydrate ($Na_5[Fe(CN)_5SO_3]\cdot 3H_2O$) was prepared by a literature method (30). The $[Fe(CN)_5OH_2]^{3-}$ ion was generated in basic solution by the rapid aquation of the sulphite salt ($t_{1/2} \approx$ 1 min, I = 0.05 mol/L (31)). The sulphite salt is relatively stable at concentrations up to 10^{-3} mol/L without dimerization and oxidation (32).

Syntheses of *N*,*N*′-bis(4′-pyridinylmethylene)-α,ω-alkanediimines (L2, L4, and L6)

4-Pyridinecarboxaldehyde (1 mL, 1.136 g, 10.32 mmol) and 5.2 mmol of the appropriate α,ω-diaminoalkane were dissolved in 1 and 2 mL of methanol, respectively. The two methanolic solutions were mixed rapidly and stirred at room temperature for approximately 30 min. The methanol was then removed under vacuum to yield a pale yellow semi-solid. The reaction product was then recrystallized from ether:methanol (2:1) to give white crystals.

L2

Yield: 80% (0.98 g); mp 134 to 135 °C (lit. value (26) mp 125–128 °C, lit. value (29, 33) mp 130 °C, lit. value (34) mp 136–138 °C). ^{1}H NMR (DMSO-d_6, ppm) δ: 8.63 (d, 4H, H_2, $J_{2,3}$ = 11 Hz), 8.38 (s, 2H, -C*H*=N), 7.62 (d, 4H, H_3), 3.94 (s, 4H, H-α) (lit. ($CDCl_3$) 8.63 (d), 8.22 (s), 7.49 (d), 3.99 (s) ppm (29)). ^{13}C NMR (DMSO-d_6, ppm) δ: 161.9 (C-1), 150.5 (C-2), 142.7 (C-3), 121.9 (C-4), 60.7 (C-α) (lit. ($CDCl_3$) 160.84, 150.42, 142.63, 121.83, 61.27 ppm (29)). Anal. calcd. for $C_{14}H_{14}N_4$: C 70.56, H 5.92, N 23.51; found: C 70.21, H 5.91, N 23.65.

L4

Yield: 85% (1.16 g); mp 73 to 74 °C (lit. value (33) mp 75 °C). ^{1}H NMR (DMSO-d_6, ppm) δ: 8.64 (d, 4H, H_2, $J_{2,3}$ = 11 Hz), 8.38 (s, 2H, -C*H*=N), 7.64 (d, 4H, H-3), 3.65 (s, 4H, H-α), 1.68 (m, 4H, H-β). ^{13}C NMR (DMSO-d_6, ppm) δ: 160.0 (C-2), 150.8 (C-3), 143.1 (C-4), 121.9 (-*C*H=N), 60.4 (C-α), 28.0 (C-β). Anal. calcd. for $C_{16}H_{18}N_4$: C 72.08, H 6.80, N 21.02; found: C 71.90, H 6.73, N 21.01.

L6

Yield: 82% (1.24 g); mp 101 to 102 °C. ^{1}H NMR (DMSO-d_6, ppm) δ: 8.64 (d, 4H, H-2, $J_{2,3}$ = 11 Hz), 8.35 (s, 2H, -C*H*=N), 7.64 (d, 4H, H-2), 3.60 (m, 4H, H-α), 1.61 (t, 4H, H-β), 1.34 (m, 4H, H-γ). ^{13}C NMR (DMSO-d_6, ppm) δ: 160.0 (C-2), 150.9 (C-3), 143.4 (C-4), 122.4 (-*C*H=N), 61.3 (C-α), 30.9 (C-β), 27.3 (C-γ). Anal. calcd. for $C_{18}H_{22}N_4$: C 73.33, H 7.53, N 19.02; found: C 73.32, H 7.51, N 18.97.

Physical measurement

The kinetics of the ligand substitution reactions of the substituted pentacyanoferrate(II) complexes ($[Fe(CN)_5L]^{3-}$) were determined spectrophotometrically by stopped-flow (Applied Photophysics SX-17MV) or conventional (Hewlett-Packard 8452A) mixing techniques. The formation reactions were carried out under pseudo-first-order conditions of excess entering ligand concentrations over the concentrations of freshly prepared $[Fe(CN)_5OH_2]^{3-}$ ion solutions (λ_{max} = 440 nm, ε = 660 M^{-1} cm^{-1} (35)). The dissociations of the substituted $[Fe(CN)_5\mathbf{Ln}]^{3-}$ complexes involved the use of 0.10 mol/L DMSO to scavenge the dissociated metal center. Plots of $\ln(A_t - A_\infty)$ or $\ln(A_\infty - A_t)$ against time were linear for at least three half-lives, with six to eight replicate experiments performed for the stopped-flow measurements and

© 2005 NRC Canada

Table 1. Limiting ^{1}H NMR chemical shift changes ($\Delta\delta_{lim}$) and inclusion stability constants for the **L2**, **L4**, and **L6** ligands with α- and β-cyclodextrins.[a]

	$\Delta\delta_{lim}$ (ppm)					
	L2		**L4**		**L6**	
Proton[b]	α-CD	β-CD	α-CD	β-CD	α-CD	β-CD
H-2	0.105	0.089	0.094	0.052	0.233	0.108
H-3	0.121	0.093	0.080	0.040	0.258	0.112
-C*H*=N	0.082	0.067	0.106	0.066	0.175	0.065
H-β			0.104	0.069	0.103	0.088
H-γ					0.102	0.073
K_L (M^{-1})	129±11 (α)		370±20 (α)		730±38 (α)	
	354±78 (β)		898±90 (β)		1011±150 (β)	

[a]In 8 mmol/L NaOD at 25 °C, I = 0.05 mol/L (NaCl).
[b]The H-α proton was obscured by the solvent peak in the presence of cyclodextrin.

one experiment for the ligand dissociation reactions (the first-order rate constants are available in the Supplementary material).[2] The reaction temperature was maintained to within 0.1 °C over the range 20.0–32.5 °C by means of external circulating water baths. The ionic strength was kept at 0.05 mol/L by using sodium chloride.

The ^{1}H NMR spectra were recorded on Bruker AC-200 and AM-400 instruments in D_2O or DMSO-d_6, utilizing the residual solvent proton signal as the reference. The cyclodextrin inclusion stability constants for the ligands in this study were determined by ^{1}H NMR titrations of the ligands with α- or β-cyclodextrins, as described previously (36, 37). The mass spectrometry measurements were obtained on a VG Quattro quadrupole mass spectrometer, with an atmospheric pressure electrospray source. Samples, as solutions in 1:1 mixture of methanol and distilled water with 0.010 mol/L α-cyclodextrin, were introduced into the source at a flow rate of 5 mL min^{-1}. Elemental analyses were performed by Canadian Microanalytical Services, Delta, British Columbia.

The stability constants for the α- and β-cyclodextrin pseudorotaxanes of the **L2**, **L4**, and **L6** ligands were calculated from ligand substitution kinetic data and ^{1}H NMR chemical shift titrations by the application of nonlinear least-squares and Simplex optimization programs to the equations for a 1:1 guest–host model as described previously (36, 37).

Results and discussion

[2]Pseudorotaxane complexes

While the neutral *N,N′*-bis(4′-pyridylmethylene)-α,ω-alkanediimine ligands, **L2**, **L4**, and **L6** prepared in this study are easily hydrolysed in the acid and neutral aqueous solution, they are relatively stable in basic solution (pH > 12). The stabilities of α- and β-cyclodextrin in the basic solution permit an investigation of their inclusion interactions with the ligands in this medium. The additions of α- or β-CD to aqueous solutions of the neutral ligands result in the formation of [2]pseudorotaxane complexes (eq. [1]).

$$[1] \qquad \mathbf{Ln} + \mathrm{CD} \underset{}{\overset{K_L}{\rightleftharpoons}} \{\mathbf{Ln}\cdot\mathrm{CD}\}$$

The formations of the [2]pseudorotaxane complexes {**Ln**·CD} result in downfield chemical shifts for the threaded ligand proton resonances with respect to their positions for the free ligand. The observed chemical shift changes ($\Delta\delta_{obs}$) are proportional to the fraction of the ligand that is included in the CD cavity (eq. [2]).

$$[2] \qquad \Delta\delta_{obs} = \frac{\Delta\delta_{lim}[\mathbf{Ln}\cdot\mathrm{CD}]}{[\mathbf{Ln}]_T}$$

Using a global fit of the changes in the chemical shifts ($\Delta\delta_{obs}$) of the aromatic and aliphatic protons, the stability constants (K_L) for **L2**, **L4**, and **L6** with α- and β-CD, were determined at 25 °C at I = 0.05 mol/L (NaCl), and are presented in Table 1, along with the values of $\Delta\delta_{lim}$. The values of $\Delta\delta_{lim}$ for the included ligands are greater with α-CD than with β-CD as a result of the tighter fit of the ligand in the smaller α-CD cavity.

The stability constants K_L for the formation of cyclodextrin inclusion complexes of diimine neutral ligands increase with an increase in the methylene chain length n. This trend has already been observed previously in our laboratory (20–23) for other ligands with *N*-heterocyclic end groups ($R(CH_2)_nR^{2+}$, n = 8–12). With a shorter polymethylene chain linking the end group, the hydrophilic 4-pyridyl group is inserted further into the hydrophobic cyclodextrin interior, resulting in a destabilization of the pseudorotaxane. The cyclodextrin stability constant determined for {**L6**·α-CD} (730 ± 38 M^{-1}) is similar to the values measured previously for related ligands ($R(CH_2)_{10}R^{2+}$) with similar chain lengths; 1400 ± 130 M^{-1} for $\{pyz(CH_2)_{10}pyz\cdot\alpha\text{-CD}\}^{2+}$ (22), 1500 ± 100 M^{-1} for $\{bpy(CH_2)_{10}bpy\cdot\alpha\text{-CD}\}^{2+}$ (21), 1300 M^{-1} for $\{pyr(CH_2)_{10}pyr\cdot\alpha\text{-CD}\}^{2+}$ (38), 610 ± 130 M^{-1} for $\{3CNpyr(CH_2)_{10}3CNpyr\cdot\alpha\text{-CD}\}^{2+}$, and 900 ± 230 M^{-1} for $\{4CNpyr(CH_2)_{10}4CNpyr\cdot\alpha\text{-CD}\}^{2+}$ (23). From the present and previous studies (39), it has been concluded that the stability constants are dependent more on the length of polymethylene chain than on the size and charge of the end groups. Due to the poorer aqueous solubility of the present neutral ligands with more than six methylene groups in the chain, data are limited in this study to two-, four-, and six-methylene chain ligands.

[2]Supplementary data may be purchased from the Directory of Unpublished Data, Document Delivery, CISTI, National Research Council Canada, Ottawa, ON K1A 0S2, Canada (http://cisti-icist.nrc-cnrc.gc.ca/irm/unpub_e.shtml for information on ordering electronically).

© 2005 NRC Canada

Table 2. Spectroscopic and kinetic parameters associated with the ligand substitution reactions of pentacyanoferrate(II) complexes with the **L2**, **L4**, and **L6** ligands in the presence of α- and β-cyclodextrins.[a]

	Ligand		
Parameter	**L2**	**L4**	**L6**
λ_{max} (nm)	456	456	464
ε (M^{-1} cm^{-1})	714	927	1162
λ_{max}^{CD} (nm)	464 (α)	464 (α)	476 (α)
	466 (β)	466 (β)	478 (β)
k_f^0 (M^{-1} s^{-1})	771±7	757±11	721±29
$\Delta H^{\ddagger}_f{}^0$ (kJ mol^{-1})	74±4	78±6	76±4
$\Delta S^{\ddagger}_f{}^0$ (J K^{-1} mol^{-1})	58±10	53±3	59±3
k_f^{CD} (M^{-1} s^{-1})	652±3(α)	641±3 (α)	588±14 (α)
	634±3 (β)	604±5 (β)	504±14 (β)
$\Delta H^{\ddagger}_f{}^{CD}$ (kJ mol^{-1})	65±6 (α)	62±4 (α)	63±4 (α)
	66±4 (β)	64±2 (β)	66±3 (β)
$\Delta S^{\ddagger}_f{}^{CD}$ (J K^{-1} mol^{-1})	29±5 (α)	28±4 (α)	29±3 (α)
	31±7 (β)	30±7 (β)	31±2 (β)
K_L (M^{-1}) (kinetics)	154±20 (α)	168±26 (α)	233±30 (α)
	410±52 (β)	464±56 (β)	794±104 (β)
$10^3 k_d^0$ (s^{-1})	2.33±0.13	1.84±0.09	1.34±0.05
$\Delta H^{\ddagger}_d{}^0$ (kJ mol^{-1})	97±2	100±3	96±3
$\Delta S^{\ddagger}_d{}^0$ (J K^{-1} mol^{-1})	30±9	38±9	22±10
$10^3 k_d^{CD}$ (s^{-1})	0.98±0.10 (α)	0.88±0.11 (α)	0.82±0.08 (α)
	0.89±0.09 (β)	0.80±0.09 (β)	0.79±0.07 (β)
$\Delta H^{\ddagger}_d{}^{CD}$ (kJ mol^{-1})	103±7 (α)	93±8 (α)	98±7 (α)
	100±8 (β)	102±11 (β)	99±5 (β)
$\Delta S^{\ddagger}_d{}^{CD}$ (J $K^{-1}mol^{-1}$)	45±15 (α)	19±3 (α)	25±10 (α)
	43±13 (β)	39±10 (β)	29±13 (β)
K_{ML} (M^{-1}) (kinetics)	913±180 (α)	1155±155 (α)	1246±123 (α)
	1134±189 (β)	1316±139 (β)	1889±154 (β)

[a]Kinetic measurements at 25.0 °C, I = 0.05 mol/L (NaCl). The α and β symbols refer to limiting parameters measured for α-CD and β-CD, respectively.

The presence of the [2]pseudorotaxanes of the **Ln** ligands with α-CD ({**Ln**·α-CD}$^{2+}$) was also detected by electrospray mass spectroscopy (ES-MS). In the ES-MS spectra, signals were observed at m/z = 1266.9 for {**L6**·α-CD+H}$^+$ (expected at m/z = 1267.2) and 1288.9 for {**L6**·α-CD+Na}$^+$. A signal observed at m/z = 1088.9 was assigned to the {$NH_2(CH_2)_6NH_2$·α-CD} fragment. Similar molecular ions and fragments were observed in the ES-MS spectra of the [2]pseudorotaxanes with the other **Ln** ligands.

Cyclodextrin semirotaxane and rotaxane complexes

The ligand substitution reactions between the $[Fe(CN)_5OH_2]^{3-}$ ion and the neutral ligands (**Ln**) result in the rapid formation of $[Fe(CN)_5(\mathbf{Ln})]^{3-}$ complexes, which exhibit metal-to-ligand charge transfer (MLCT) bands in the 460–480 nm range. The addition of 1 equiv. of $[Fe(CN)_5OH_2]^{3-}$ ion to a solution containing the cyclodextrin-included ligands produces a semirotaxane species (eq. [3]). The visible spectra of the semirotaxanes exhibit a bathochromic shift in the MLCT bands (Table 2), as observed previously for pentacyanoferrate(II) complexes containing several neutral 4-substituted pyridine ligands (24, 37). The addition of one or more further equivalents of the $[Fe(CN)_5OH_2]^{3-}$ ion yields the corresponding rotaxane complex, $[(NC)_5Fe\{\mathbf{Ln}\cdot CD\}Fe(CN)_5]^{6-}$ (eq. [4]).

$$[3]\quad [Fe(CN)_5OH_2]^{3-} + \{\mathbf{Ln}\cdot CD\} \underset{k_d^{CD}}{\overset{k_f^{CD}}{\rightleftharpoons}} [Fe(CN)_5\{\mathbf{Ln}\cdot CD\}]^{3-} + H_2O$$

$$[4]\quad [Fe(CN)_5\{\mathbf{Ln}\cdot CD\}]^{3-} + [Fe(CN)_5OH_2]^{3-} \rightleftharpoons [(NC)_5Fe\{\mathbf{Ln}\cdot CD\}Fe(CN)_5]^{6-}$$

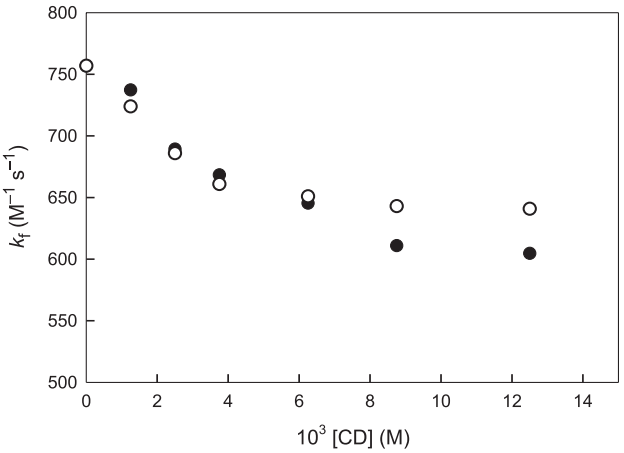
Ligand substitution kinetics

In this study, the labile $[Fe(CN)_5OH_2]^{3-}$ ion was generated in basic solution by the aquation of the $[Fe(CN)_5SO_3]^{5-}$ ion (31, 40) rather than the $[Fe(CN)_5NH_3]^{3-}$ ion more commonly employed in neutral solutions. The ligand substitution reactions of the $[Fe(CN)_5OH_2]^{3-}$ ion with the neutral ligands in basic solution (eq. [5]) may be monitored by following the appearance of the MLCT bands of the $[Fe(CN)_5(\mathbf{Ln})]^{3-}$ products (Table 2) and measured by using stopped-flow

$$[5]\quad [Fe(CN)_5OH_2]^{3-} + \mathbf{Ln} \underset{k_d^0}{\overset{k_f^0}{\rightleftharpoons}} [Fe(CN)_5\mathbf{Ln}]^{3-} + H_2O$$

© 2005 NRC Canada

Fig. 1. Dependences of k_f on[α-CD] (●) and [β-CD] (o) for the reaction of the $[Fe(CN)_5OH_2]^{3-}$ ion with the **L4** ligand at 25.0 °C, I = 0.05 mol/L (NaCl).



techniques. The reactions were carried out under pseudo-first-order conditions of excess entering ligand concentration. The observed pseudo-first-order rate constants display a first-order dependence on [**Ln**], and the second-order rate constants (k_f^0) determined at 25.0 °C and an ionic strength of 0.05 mol/L (NaCl), are presented in Table 2. The formation rate constants (771 ± 7 M^{-1} s^{-1} for **L2**, 757 ± 11 M^{-1} s^{-1} for **L4**, and 721 ± 29 M^{-1} s^{-1} for **L6**) are of similar magnitude as the literature (24, 37, 40) values for other neutral bis(4-pyridyl) ligands and significantly less than those of the singly and doubly positive charged bis(4-pyridyl) ligands (21–23, 36, 40–42), as discussed in the following. The rate constants for the formation of $[Fe(CN)_5(\mathbf{Ln})]^{3-}$ also decrease with an increase in the methylene chain length. Upon inclusion of the ligand by α- or β-CD (Scheme 1), the rate constant for the substitution reaction is observed to decrease (Fig. 1), reaching a limiting value of k_f^{CD} at high α- or β-CD concentrations.

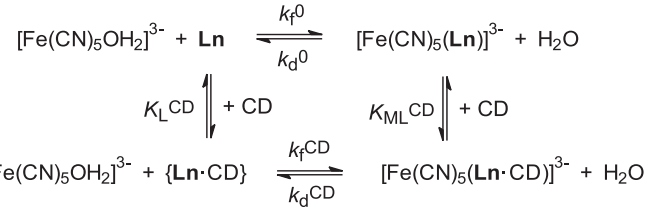
The second-order rate constants (k_f^{CD}) for the reactions of the included ligands and the inclusion stability constants (K_L) were obtained from nonlinear least-squares fits of the experimental rate constants (k_f^{obs}) to eq. [6].

$$[6] \qquad k_f^{obs} = \frac{k_f^0 + k_f^{CD} K_L^{CD} [CD]}{1 + K_L^{CD} [CD]}$$

The values of k_f^0, k_f^{CD}, and K_L at 25 °C and the corresponding activation parameters are presented in Table 2.

The ligand substitution reactions of the $[Fe(CN)_5OH_2]^{3-}$ are commonly accepted to proceed by an ion pair dissociative (D_{IP}) mechanism (40) in which the rate-determining step involves the dissociation of the aqua ligand from the metal center within a $[Fe(CN)_5OH_2//L]^{(3-n)-}$ ion-pair complex. The observed rate constants (k_f) are therefore dependent on the magnitude of the ion-pair stability, which increases with the charge on the entering ligand. The decrease in the formation rate constants results from an increase in the methylene chain length from two to six carbons, as the donor nitrogens are placed further apart and the efficiency of the precusor ion pair $[Fe(CN)_5OH_2//L]^{3-}$ leading to substitution decreases. In the presence of excess cyclodextrin, the rate constants for the formation of semirotaxanes were reduced to approximately 75% of the corresponding value of free ligand. The decrease also results from a decrease in the proportion of "effective" ion pairs that lead to substitution by placing the donor atom of the ligand in close proximity to the site of the leaving aqua ligand. Upon inclusion of the ligand within the cyclodextrin cavity, the neutral ligand is less accessible to form an ion pair with the $[Fe(CN)_5OH_2]^{3-}$ ions. In addition, the included ligand is much larger than the free ligand, such that its donor nitrogen atom is accessible on a smaller portion of the surface of the cyclodextrin-ligand host–guest complex. The larger β-CD host allows for deeper insertion and therefore the limiting rate constants in the presence of high [β-CD] are generally somewhat lower relative to those measured at high [α-CD]. These diminutions are small compared with the decreases reported previously for the $[bpy(CH_2)_{10}bpy]^{2+}$ (21) and $[4CNpyr(CH_2)_{10}4CNpyr]^{2+}$ (23) ligands in the presence of α-CD, for example. With positively charged ligands the charges are "separated" by the cyclodextrin cavity, resulting in a reduction of the effective charge. The enthalpies of activation associated with k_f^0 and k_f^{CD} are the same within the experimental errors, which are attributed to the same rate-determining step by loss of the aqua ligand. There is reasonable agreement between the stability constants for cyclodextrin guest–host complexes {**Ln**·CD} determined from NMR chemical shift titrations (Table 1) and from the ligand substitution kinetic data (Table 2). Similar differences, resulting from the use of these different techniques, have been observed previously for other substituted pentacyanoferrate(II) complexes with cyclodextrins (36, 37).

Scheme 1.



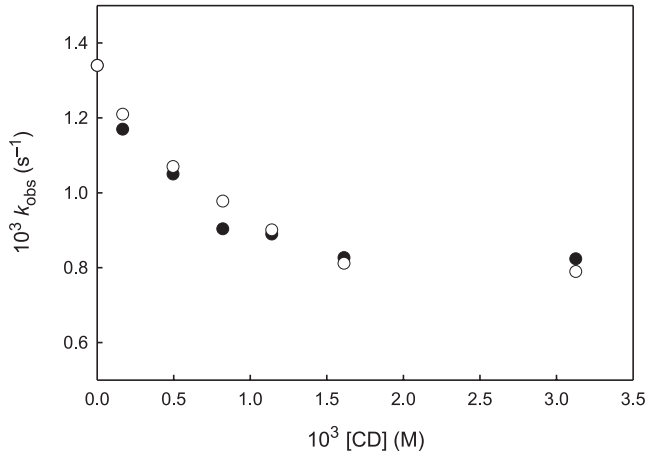
The kinetics of the dissociation of the ligands **Ln** from the $[Fe(CN)_5(\mathbf{Ln})]^{3-}$ complexes have been investigated. The reaction may be followed by the addition of an excess of dimethyl sulfoxide (0.10 mol/L) to trap the $[Fe(CN)_5]^{3-}$ intermediate and form a very inert (k_{-DMSO} = 7.5 × 10^{-5} s^{-1} at 25.0 °C (I = 1.0 mol/L ($LiClO_4$) (43)), colorless (λ_{max} = 352 nm) $[Fe(CN)_5DMSO]^{3-}$ product Limiting first-order rate constants (k_d^0) are observed at 0.10 mol/L DMSO. The addition of either α- or β-CD, which forms a semirotaxane complex ($[Fe(CN)_5(\mathbf{Ln}\cdot CD)]^{3-}$), resulted in a decrease in the rate constant for dissociation of included coordinated **Ln** ligand (Fig. 2). The observed first-order dissociation rate constants (k_d^{obs}) may be expressed in terms of the specific rate constants k_d^0 and k_d^{CD} and the cyclodextrin inclusion stability constants (eq. [7]).

$$[7] \qquad k_d^{obs} = \frac{k_d^0 + k_d^{CD} K_{ML}^{CD} [CD]}{1 + K_{ML}^{CD} [CD]}$$

The limiting rate constants for the included complexes k_d^{CD} and the inclusion stability constants were determined by the nonlinear least-squares fit of the experimental rate constants

© 2005 NRC Canada

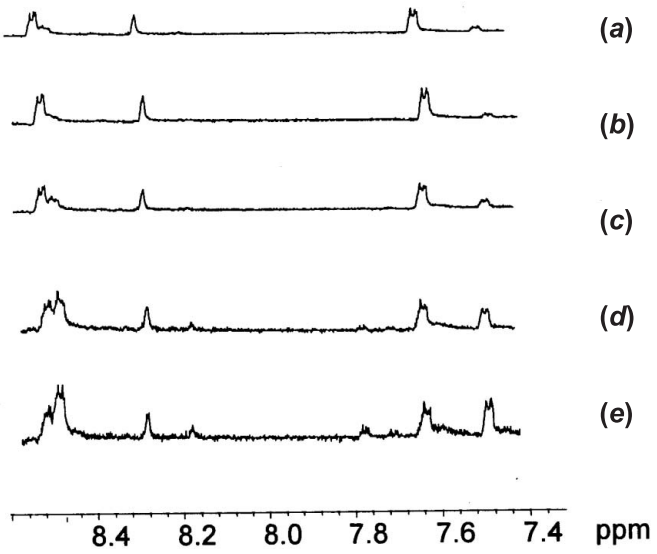
Fig. 2. Dependences of k_d on [α-CD] (●) and [β-CD] (o) for the reaction of the $[Fe(CN)_5\mathbf{L6}]^{3-}$ ion with DMSO (0.10 mol/L) at 25.0 °C, I = 0.05 mol/L (NaCl).



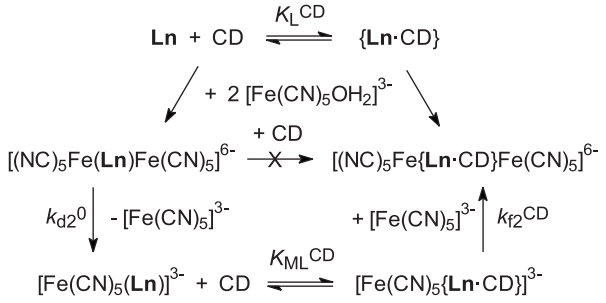
k_d^{obs} to eq. [7]. The dissociation rate constants and activation parameters for the $[Fe(CN)_5(\mathbf{Ln})]^{3-}$ complexes and the corresponding semirotaxanes $[Fe(CN)_5\{\mathbf{Ln}\cdot CD\}]^{3-}$ species are presented in Table 2.

The ligand dissociation reactions of substituted pentacyanoferrate(II) complexes procede by a dissociative (D) mechanism (40), with the rate constant for loss of the L^{n+} from $[Fe(CN)_5L]^{(3-n)-}$ being independent of the nature of the entering ligand, and reaching a limiting value at high entering ligand (such as DMSO) concentrations. The diminution of rate constant decreases with the length of the polymethylene chain, with decreases of 58% (ethane), 51% (butane), and 39% (hexane) from the nonincluded ligand rate constants (Table 2). The magnitudes of the decreases in the ligand dissociation rate constants are comparable to the trends observed for other neutral (24, 36) and cationic (21–23, 36) ligands and are attributed, in part, to a stabilization of the ground state through greater π-back-bonding from the metal to the CD-included, 4′-substituted pyridine ring.

Fig. 3. ^{1}H NMR spectra of the aromatic pyridine protons as a function of time for the self-assembly of the $[(NC)_5Fe\{\mathbf{L2}\cdot\alpha\text{-}CD\}Fe(CN)_5]^{6-}$ rotaxane upon addition of α-CD (5×10^{-2} mol/L) to the $[(NC)_5Fe\{\mathbf{L2}\cdot\alpha\text{-}CD\}Fe(CN)_5]^{6-}$ dimer (5×10^{-3} mol/L) in 8 mmol/L NaOD (I = 0.05 mol/L (NaCl)) at: (*a*) 1 min, (*b*) 5 min, (*c*) 9 min, (*d*) 30 min, and (*e*) 45 min.



Scheme 2.



Rotaxane self-assembly

The addition of an excess of α-cyclodextrin to solutions of the dimer complexes resulted in a slow formation of the corresponding [2]rotaxane. The kinetics of this process may be monitored by ^{1}H NMR spectroscopy. The symmetry-related proton resonances of the bridging ligand of the dimer are separated into pairs of peaks as rotaxane is formed, as indicated in Fig. 3 for the complex containing the **L2** ligand. The direct inclusion of the dimer by threading through the α-CD cavity (5.5 Å diameter) is prevented by the bulky $[Fe(CN)_5]^{3-}$ units (9.0 Å diameter). The self-assembly of [2]rotaxanes has been shown to proceed by two possible routes (20–24), depending on the order of addition of the three components (Scheme 2).

The first route, resulting from the addition of the labile aquapentacyanoferrate(II) ion to the corresponding preassembled [2]pseudorotaxane species (eqs. [1], [3], and [4]), is very rapid. A second, slower route involves the addition of cyclodextrin to the dimeric $[(NC)_5Fe(\mathbf{Ln})Fe(CN)_5]^{6-}$ species. This pathway involves the rate-determining dissociation of a pentacyanoferrate(II) ion from the bridging ligand, followed by the threading of the cyclodextrin by the free end of the coordinated ligand, and the rapid recomplexation by an aquapentacyanoferrate(II) ion (Scheme 2). The extent of the rotaxane formation is determined by the stability constant of the semirotaxane species (K_{ML}) and the kinetics of approach to equilibrium is given by $\ln[([L]_0\text{-}[L\cdot CD]_e)/([L\cdot CD]_t\text{-}[L\cdot CD]_e)] = kt$, where $[L]_0$ is the initial dimer concentration, and $[LCD]_t$ and $[LCD]_e$ are the concentrations of the rotaxane at time t and at equilibrium, respectively. The first-order rate constants determined for the self-assembly process at 25 °C, using [α-CD] = 5×10^{-2} mol/L, are $(1.82 \pm 0.28) \times 10^{-3}$ s^{-1}, $(1.77 \pm 0.21) \times 10^{-3}$ s^{-1}, and $(1.45 \pm 0.16) \times 10^{-3}$ s^{-1} for **L2**, **L4**, and **L6**, respectively. The rate constants for this process are very similar in magnitude to values (k_d^0) determined for the ligand dissociation reactions of iron complexes (Table 2). The self-assembly by the latter route may be related to the lability of the iron–nitrogen bond. More rapid self-assembly processes were observed for the pentacyanoferrate(II) complexes with greater lability of the iron–nitrogen bond in the complexes containing the 4-cyanopyridine head groups ($k = (3.8 \pm 0.1) \times 10^{-2}$ s^{-1} (23)),

© 2005 NRC Canada

while with the more inert bond to the pyrazinium (pyz) nitrogen, in a threading ligand such as $pyz(CH_2)_{10}pyz^{2+}$ (k = $(2.6 \pm 0.1) \times 10^{-4}$ s^{-1} (22)), results in much slower self-assembly of the rotaxane.

Acknowledgements

The authors thank the Natural Sciences and Engineering Research Council of Canada (NSERC) for financial support in the form of research and equipment grants (D.H.M. and E.B.). Scholarship support (V.X.J.) from Queen's University and the Ontario Ministry of Training, Colleges and Universities is gratefully acknowledged.

References

1. G. Schill. Catenanes, rotaxanes, and knots. Academic Press, New York. 1971.
2. J.-P. Sauvage and C. Dietrich-Buchecker (*Editors*). Molecular catenanes, rotaxanes, and knots. Wiley-VCH, Weinheim. 1999.
3. J.-M. Lehn. Supramolecular chemistry: Concepts and perspectives. VCH, Weinheim. 1995.
4. J.-C. Chambron. *In* Transition metals in supramolecular chemistry. *Edited by* J.-P. Sauvage. Wiley, New York. 1999. Chap. 6.
5. H.W. Gibson, M.C. Bheda, and P.T. Engen. Prog. Polym. Sci. **19**, 843 (1994).
6. D.B. Amabilino and J.F. Stoddart. Chem. Rev. **95**, 2725 (1995).
7. A. Harada. Coord. Chem. Rev. **148**, 111 (1996).
8. R. Jäger and F. Vögtle. Angew. Chem. Int. Ed. Engl. **36**, 930 (1997).
9. J.-P. Sauvage. Acc. Chem. Res. **31**, 611 (1998).
10. F. Raymo and J.F. Stoddart. Chem. Rev. **99**, 1643 (1999).
11. J. Szejtli and T. Osa. *In* Comprehensive supramolecular chemistry. Vol. 3. *Edited by* J.L. Atwood, J.E.D. Davies, D.D. MacNicol, and F. Vögtle. Permagon, Oxford. 1996.
12. J. Szejtli. Chem. Rev. **98**, 1743 (1998).
13. K.A. Connors. Chem. Rev. **97**, 1325 (1997).
14. S.A. Nepogodiev and J.F. Stoddart. Chem. Rev. **98**, 1959 (1998).
15. H. Ogino. New J. Chem. **17**, 683 (1993), and refs. therein.
16. T.V.S. Rao and D.S. Lawrence. J. Am. Chem. Soc. **112**, 3614 (1990).
17. R. Isnin and A.E. Kaifer. J. Am. Chem. Soc. **113**, 8188 (1991).
18. R.B. Hannak, G. Farber, G. Konrat, and B. Krauter. J. Am. Chem. Soc. **119**, 2313 (1997).
19. A.D. Shukla, H.C. Bajaj, and A. Das. Angew. Chem. Int. Ed. **40**, 446 (2001).
20. R.S. Wylie and D.H. Macartney. J. Am. Chem. Soc. **114**, 3136 (1992).
21. R.S. Wylie and D.H. Macartney. Supramol. Chem. **3**, 29 (1993).
22. D.H. Macartney and C.A. Waddling. Inorg. Chem. **33**, 5912 (1994).
23. A.P. Lyon and D.H. Macartney. Inorg. Chem**. 36**, 729 (1997).
24. A.J. Baer and D.H. Macartney. Inorg. Chem. **39**, 1410 (2000).
25. Y. Kiskin-Posner, G.K. Patra, and I. Goldberg. Cryst. Eng. Comm. **4**, 296 (2002).
26. G.K. Patra and I. Goldberg. J. Chem. Soc. Dalton Trans. 1051 (2002).
27. W.-Y. Sun, B.-L. Fei, T.-A. Okamura, W.-X. Tang, and N. Ueyama. Eur. J. Inorg. Chem. 1855 (2001)
28. X.-M. Ouyang, B.-L. Fei, T.-A. Okamura, H.-W. Bu, W.-Y. Sun, W.-X. Tang, and N. Ueyama. Eur. J. Inorg. Chem. 618 (2003).
29. M. Felderhoff, T. Smolka, R. Sustmann, I. Steller, H.-C. Weiss, and R. Boese. J. Prakt. Chem. **341**, 639 (1999).
30. E.J. Baran and A. Muller. Z. Anorg. Chem. **368**, 144 (1969).
31. E.B. Borghi, M.A. Blesa, P.J. Aymonino, and J.A. Olabe. J. Inorg. Nucl. Chem. **43**, 1849 (1981).
32. Z. Bradic, M. Pribanic, and S. Asperger. J. Chem. Soc. Dalton Trans. 353 (1975).
33. H.A. Staab and F. Voegtle. Chem. Ber. **98**, 2681 (1965).
34. K. Lohs. Z. Chem. **5**, 147 (1965).
35. H.E. Toma, A.A. Batista, and H.B. Gray. J. Am. Chem. Soc. **104**, 7509 (1982).
36. M.E. Shortreed, R.S. Wylie, and D.H. Macartney. Inorg. Chem. **32**, 1824 (1993).
37. R.S. Wylie and D.H. Macartney. Inorg. Chem. **32**, 1830 (1993).
38. H. Saito, H. Yonemura, H. Nakamura, and T. Matsuo. Chem. Lett. 535 (1990).
39. M.V. Rekharsky and Y. Inoue. Chem. Rev. **98**, 1875 (1998).
40. D.R. Eaton and J.M. Watkins. Inorg. Chem. **24**, 1424 (1985).
41. D.H. Macartney. Rev. Inorg. Chem. **9**, 101 (1988), and refs. therein.
42. D.H. Macartney and L.J. Warrack. Can. J. Chem. **67**, 1774 (1989).
43. D.A. Foucher, D.H. Macartney, L.J. Warrack, and J.P. Wilson. Inorg. Chem. **32**, 3425 (1993).
44. H.E. Toma, J.M. Malin, and E. Giesbrecht. Inorg. Chem. **12**, 2084 (1973).

© 2005 NRC Canada

Stereoselective synthesis and stereochemistry of *r*-2-alkoxycarbonyl-*c*-3-*o*-substituted phenyl-1,4-thiazane 1,1-dioxides

N. Bhavani, S. Perumal, and R. Banureka

Abstract: *r*-2-Alkoxycarbonyl-*c*-3-aryl-1,4-thiazane 1,1-dioxides were obtained as the stereoselective product, when the aldehyde used was *o*-substituted benzaldehyde while the *p*-substituted benzaldehydes gave a trans product. The relative configuration of the adjacent alkoxycarbonyl and aryl groups was assigned from the vicinal coupling constant, ^3J = 10.6 Hz in the trans isomer and 3.2 Hz in the cis isomer, and from the multiplicity pattern, i.e., a doublet for the H-2 proton of the trans isomer and a triplet for the H-2 proton of the cis isomer. The unusual, large long-range coupling (^4J = 2.8 Hz) because of the "W" arrangement between H-2e and H-6e across the ring type was very useful for confirming the cis configuration and chair conformation of the isomer. The various ^{1}H and ^{13}C NMR assignments were made with the help of ^{1}H–^{1}H COSY, ^{1}H–^{13}C COSY, HMBC, and NOESY spectral analyses.

Key words: ^{1}H and ^{13}C NMR, ^{1}H–^{1}H COSY, ^{1}H–^{13}C COSY, HMBC, NOESY, stereoselectivity, 1,4-thiazane.

Résumé : Les 1,1-dioxydes de *r*-2-alkoxycarbonyl-*c*-3-aryl-1,4-thiazane sont obtenus comme produit stéréosélectif lorsque l'aldéhyde utilisé est un benzaldéhyde ortho substitué alors que les benzaldéhydes substitués en para conduisent au produit trans. Les configurations relatives des groupes alkoxycarbonyle et aryle adjacents ont été attribuées sur la base de la constante de couplage vicinale, ^3J = 10,6 Hz dans l'isomère trans et 3,2 Hz dans l'isomère cis, et du patron de multiplicité, c'est-à-dire la présence d'un doublet pour le proton H-2 de l'isomère trans et d'un triplet pour le proton H-2 de l'isomère cis. La constante de couplage à longue distance relativement importante (^4J = 2,8 Hz) causée par l'arrangement en « W » des protons H-2e et H-6e à travers ce type de cycle a été très utile pour confirmer la configuration cis et la conformation chaise de l'isomère. Les diverses attributions des spectres RMN du ^{1}H et du ^{13}C ont été faites sur la base d'analyses spectrales ^{1}H–^{1}H COSY, ^{1}H–^{13}C COSY, HMBC et NEOSY.

Mots clés : ^{1}H et ^{13}C RMN, ^{1}H–^{1}H COSY, ^{1}H–^{13}C COSY, HMBC, NEOSY, stéréosélectivité, 1,4-thiazane.

[Traduit par la Rédaction]

Introduction

Stereochemistry is an intrinsic universal feature of organic compounds and influences virtually all pharmacodynamic, pharmacokinetic, and biotransformation processes (1). Drug molecules having the proper absolute configuration only react with the receptor sites in the human body (2). Hence, the stereoselectivity (3) gains importance in organic synthesis. Thiazanes are widely used in new drug development (4, 5). Thiazane derivatives stimulate calcium uptake (6) used as antitumour, antiviral (7), bactericidal, parasiticidal (8), antituberculotic (9), and cardiovascular (10) agents, and they are also used as local anesthetics (11).

So far 3,5-disubstituted (12), 2,3,5-trisubstituted (13, 14), and 2,3,5,6-tetrasubstituted (15, 16) 1,4-thiazanes have been reported. Eliel and co-workers (17) reported the synthesis of *cis*-2,3-diphenyl-1,4-thiazane 1,1-dioxide from optically active starting material, and there too after several (more than 10 steps) tedious procedures. There has been no report on the synthesis of 2,3-disubstituted-1,4-thiazane 1,1-dioxides where the two substituents are different and in less stable cis configuration. Here, we report an one-pot synthesis of *cis*-2-alkoxycarbonyl-3-aryl-1,4-thiazane 1,1-dioxides, where the position of a substituent in the aryl ring controls the stereochemistry of the product.

For a 2,3-disubstituted 1,4-thiazane (in the rigid chair form), two configurational isomers, cis and trans, are possible. Generally, the thermal reaction will lead to the thermodynamically more stable trans isomer with the preferred diequatorial orientation of the substituents. The cis isomer with one axial substituent and one equatorial substitutent will be the less stable, kinetic-controlled product. In the present work, the trans isomer was obtained with benzaldehyde and *p*-substituted benzaldehydes, but the cis isomer was the product with *o*-substituted benzaldehydes.

Received 5 July 2004. Published on the NRC Research Press Web site at http://canjchem.nrc.ca on 9 March 2005.

N. Bhavani and R. Banureka.[1] Department of Chemistry, Annamalai University, Annamalainagar – 608 002, India.
S. Perumal. School of Chemistry, Madurai Kamaraj Universit, Madurai, India.

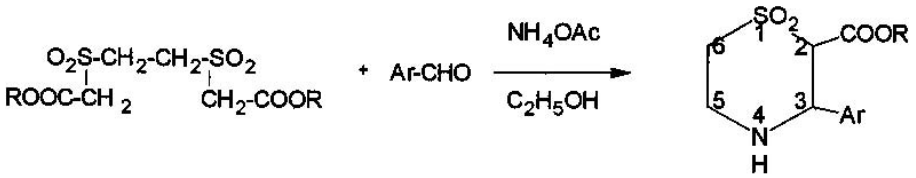
[1]Corresponding author (banurekar@yahoo.co.in).

Results and discussion

Synthesis of 2-alkoxycarbonyl-3-aryl-1,4-thiazane 1,1-dioxides (Scheme 1) has been carried out by the condensation of dialkyl ethane – 1,2-disulphonylacetate (18) with 1 mol of araldehyde and ammonium acetate. Formation of a six-

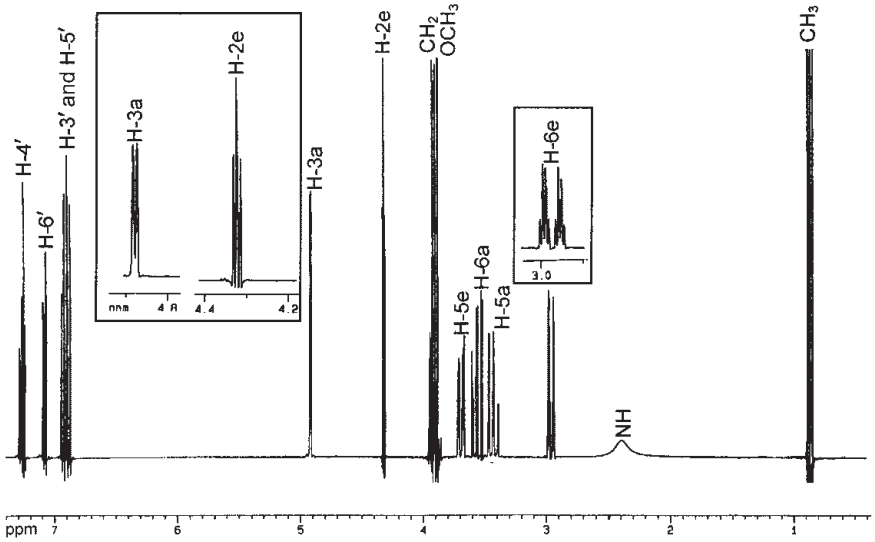
 doi: 10.1139/V05-020 © 2005 NRC Canada

Scheme 1.



	R	Ar
1	C_2H_5	C_6H_5
2	C_2H_5	*p*-$CH_3C_6H_4$
3	CH_3	C_6H_5
4	C_2H_5	*p*-$OCH_3C_6H_4$
5	C_2H_5	*p*-ClC_6H_4
6	C_2H_5	*o*-$OCH_3C_6H_4$
7	C_2H_5	*o*-ClC_6H_4

Spectrum 1. ^{1}H NMR spectrum of **6**.



membered 1,4-thiazane ring was confirmed by microanalysis, IR, and mass spectra. Their stereochemistry was studied through NMR spectra.

The ^{1}H NMR chemical shift values with multiplicity patterns and coupling constants, along with their assignments are given in Table 1.

The diaxial coupling constant (10.6 Hz) between the H-2 and H-3 protons for the compounds (**1**–**3**) gives evidence for the trans (17) configuration with the preferred diequatorial orientation of the two substituents for the *p*-substituted phenyl compounds.

Stereochemistry of *o*-substituted phenyl compounds (6 and 7)

The H-2 and H-3 protons do not appear as two simple doublets with diaxial coupling constants. From the small coupling (17) constant (Table 1) between H-2 and H-3 protons, it is inferred that there is a change in configuration from *e*, *e* to *a*, *e*. For the cis configuration of the substituents with an *a*, *e* conformation, there are two possibilities, i.e., aryl group equatorial and ethoxycarbonyl group axial or aryl group axial and ethoxycarbonyl group equatorial. The benzylic proton signal appears as a doublet ($^3J_{a,e}$ = 3.2 Hz) so it has only one coupling partner. But the triplet (Spectrum 1) for the H-2 proton indicates that it has one more coupling partner, and that should be necessarily a long-range coupling partner (19). Long-range coupling is possible only with a "W" arrangement (20), and hence, the H-2 proton must be equatorial and ester group axial; consequently, the aryl group should be equatorial. In the ^{1}H–^{1}H COSY (21) spectrum (Spectrum 2), there is a cross peak (A) between the H-2e triplet and the doublet of the quartet signal at 2.96 ppm (i.e., H-6e), and this is an added evidence for the long-range coupling. The large cross peak (B) is due to the coupling be-

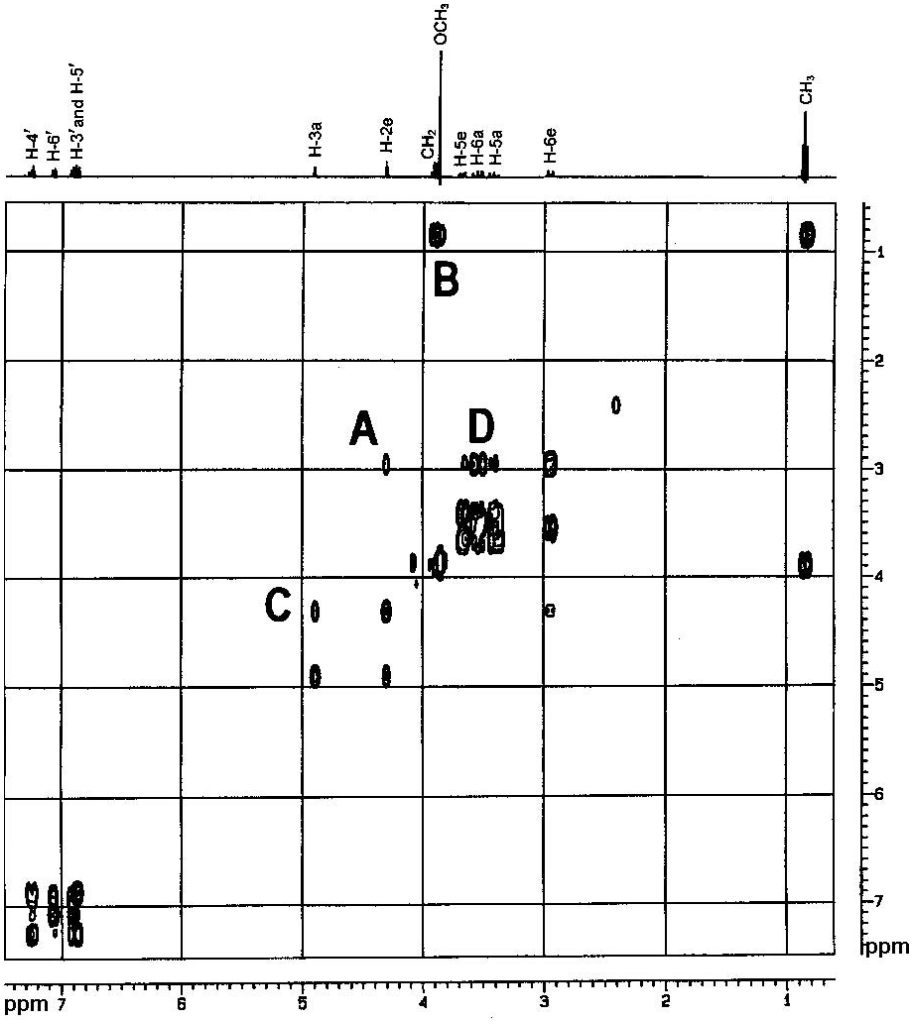
© 2005 NRC Canada

Table 1. ^{1}H NMR spectral data of 2-alkoxycarbonyl-3-aryl-1,4–thiazane 1,1-dioxides (**1**–**3**, **6**, **7**).[a]

Compound	NH	H-6a	H-6e	H-5a	H-5e	H-2[b]	H-3[c]
1	1.88 (s)	3.22 (m, 13.7, 10.3, 3.8)	3.15 (m, 13.7, 3.0)	3.47[d] (m)	3.47[d] (m)	4.06 (d, 10.6)	4.46 (d, 10.6)
2	2.05 (s)	3.12 (m)	3.12 (m)	3.40[d] (m)	3.40[d] (m)	4.04 (d, 10.6)	4.38 (d, 10.6)
3	2.05 (s)	3.22 (m)	3.22 (m)	3.48[d] (m)	3.48[d] (m)	4.09 (d, 10.6)	4.48 (d, 10.6)
6	2.39 (s)	3.56 (td, 13.4 12.5, 2.2)	2.96 (dq, 13.4, 2.4)	3.42 (td, 14.1 12.5, 2.2)	3.68 (m, 14.1, 2.2)	4.32 (t, 3.0)[e]	4.38 (d, 3.2)
7	2.32 (s)	3.58 (ddd,13.3, 12.1, 3.8)	2.99 (dq, 13.3 2.4)	3.44 (ddd, 14.1, 12.1, 2.4)	3.68 (m, 14.1, 3.8)	4.26 (t, 3.0)	4.98 (d, 3.2)

[a]NMR could not be recorded for compounds **4** and **5** because of their low solubility in $CDCl_3$ and DMSO-d_6.
[b]H-2 is axial for **1**–**3** and equatorial for **6** and **7**.
[c]H-3 is axial for **1**–**3**, **6**, and **7**.
[d]Overlapped signals correspond to 2H.
[e]$^4J_{e,e}$ for H-2 is calculated as the total width (6 Hz) – $^3J_{a,e}$ for H-3a (3.2 Hz) = 2.8 Hz.

Spectrum 2. ^{1}H–^{1}H COSY spectrum of **6**.



tween ester methylene and methyl protons. The cross peak (C) (between H-2e and H-3a) and a group of cross peaks (D) (between H-6e and H-5a, H-6a, H-5e) are obvious since they are coupling partners.

If the aryl group were to be axial, there would be steric interaction (from the Drieding model) between the *o*-substituent in the aryl group and the axial S=O bond of the sulphonyl group (Fig. 1).

^{13}C NMR assignments are given in Table 2. The carbon signals, especially for the aromatic and ipso carbons, are assigned only with the help of the HMBC (21) spectrum (Spectrum 3). For example, between the two high frequency

© 2005 NRC Canada

Spectrum 3. HMBC spectrum of **6**.

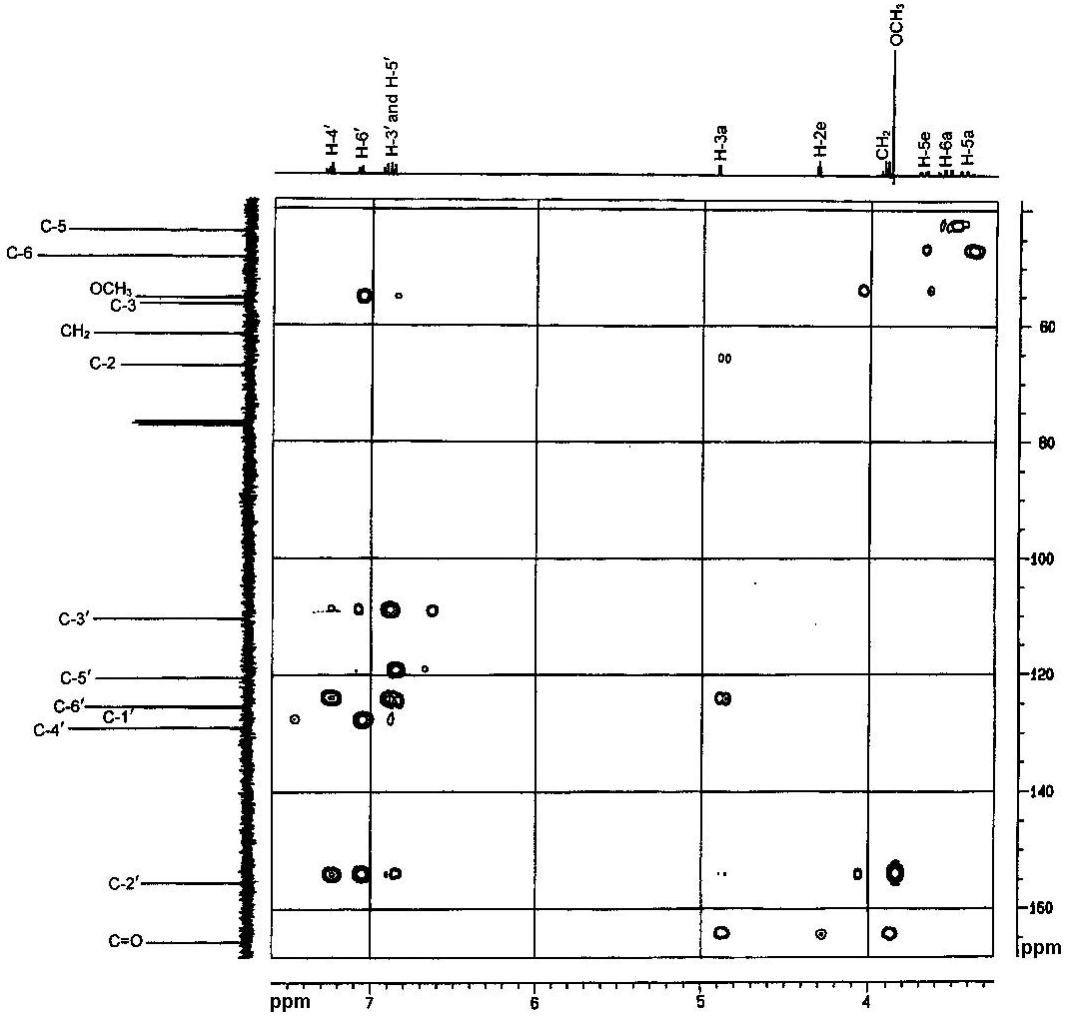


Fig. 1. Steric interaction between the *o*-OCH_3 group and the axial S=O group.

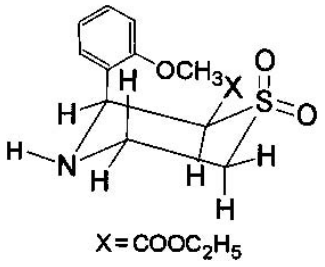


Table 2. ^{13}C NMR chemical shift values (ppm) of the ring carbons of 2-alkoxycarbonyl-3-aryl-1,4-thiazane 1,1-dioxides (**1**–**3**, **6**, **7**).[a]

Compound	C-2	C-3	C-5	C-6
1	72.65	62.78	43.71	52.89
2	72.58	62.42	43.62	52.77
3	72.44	62.67	43.58	52.73
6	67.04	56.39	43.90	48.32
7	66.72	58.56	43.92	48.35

[a]NMR could not be recorded for compounds **4** and **5** because of their low solubility in $CDCl_3$ and DMSO-d_6.

signals, 155.41 and 165.67 ppm, the former is assigned to the methoxy group bearing the ipso carbon (C-2′) since it gives multiple bond correlations with aromatic protons and methoxy methyl protons, and the latter is assigned to the carbonyl carbon since it gives multiple bond correlations with H-3a, H-2e, and ester methylene protons.

The orientation of the NH proton, whether axial or equatorial, is derived only from the NOE (21) spectrum (Spectrum 4). The NH proton gives a NOE with the H-6′ proton (A) and a strong NOE with the H-5a proton (B); the latter excludes the axial orientation of the NH proton and there is no NOE cross peak between the NH proton and the methoxy methyl protons. The various NOE cross peaks confirm the equatorial orientation of the NH proton and the perpendicular orientation of the *o*-methoxyphenyl ring to the plane of the thiazane ring (Fig. 2). The absence of NOE between the NH and ethoxycarbonyl methyl and methylene protons (which are relatively in the 1,3-diaxial position, if N-H is axial) excludes the possibility of an equilibrium between axial NH and equatorial NH.

Thus, the axial orientation of the ester group at the C-2 position, the equatorial and perpendicular orientation of the

© 2005 NRC Canada

Spectrum 4. NOESY spectrum of **6**.

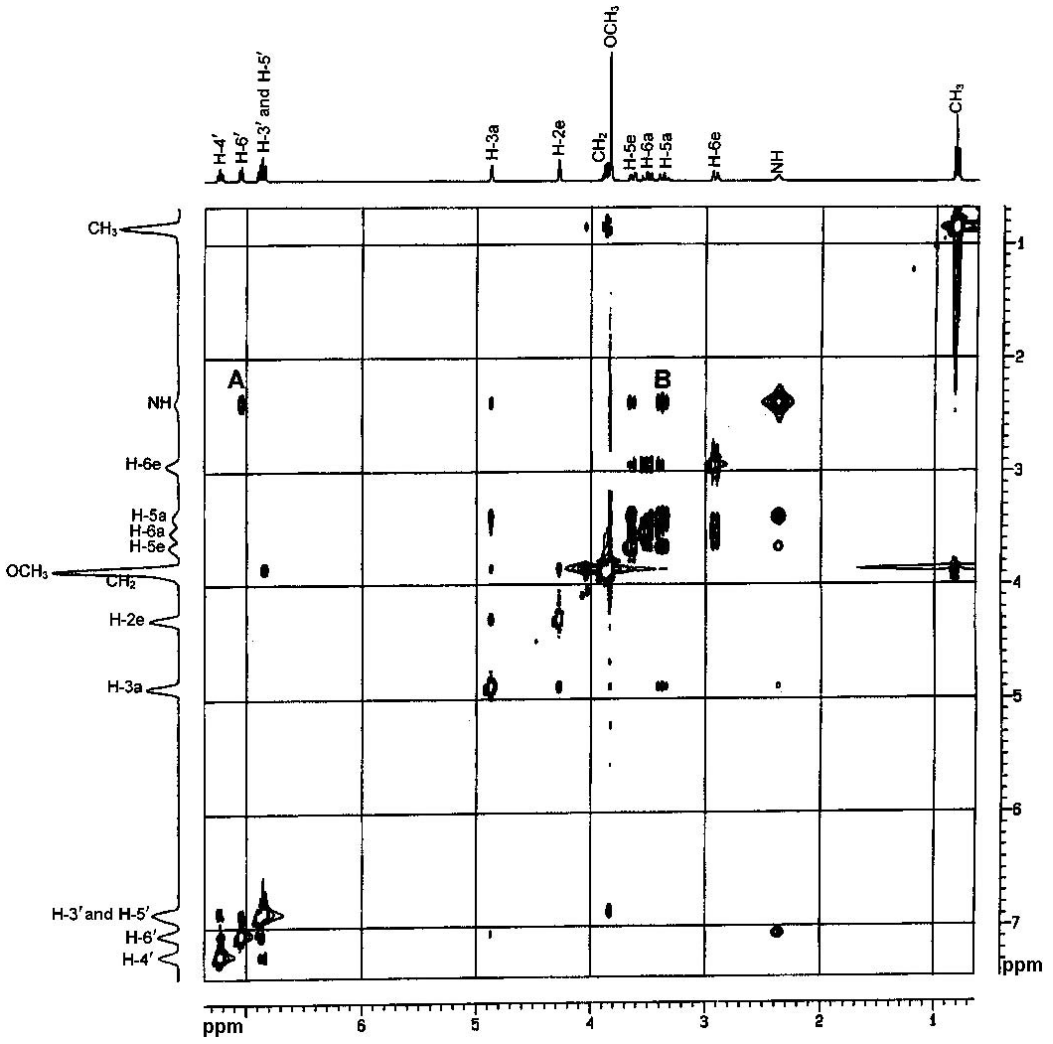


Fig. 2. Relative configuration and conformation of compound **6**.

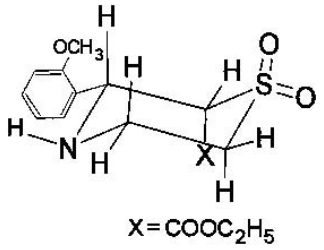
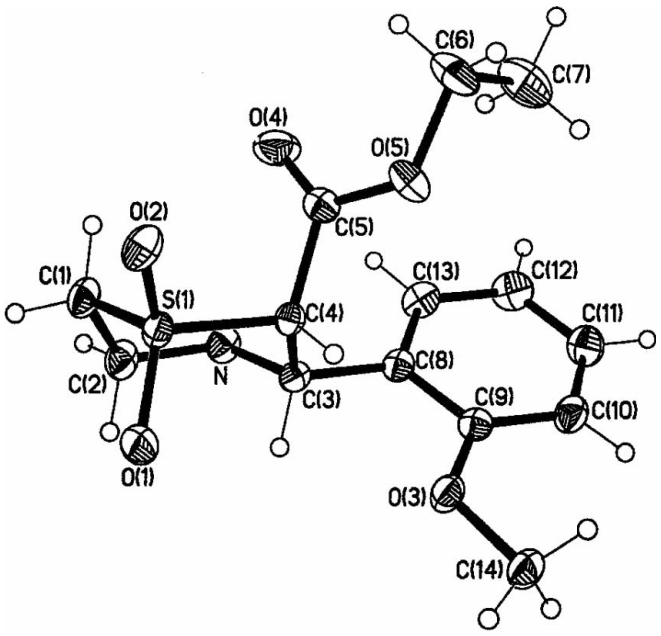


Fig. 3. ORTEP diagram of **6**.



o-substituted phenyl group at the C-3 position, and the chair conformation of the thiazane ring are derived from NMR spectra and confirmed by single crystal X-ray diffraction study. The ORTEP diagram is given in Fig. 3.

Conclusion

o-Substituted benzaldehydes give *r*-2a-alkoxycarbonyl-*c*-3-*o*-substituted phenyl-1,4-thiazane 1,1-dioxides when treated with dialkyl ethane – 1,2–disulphonylacetate and ammonium acetate as the stereoselective cis product. On the other hand, benzaldehyde and *p*-substituted benzaldehydes

© 2005 NRC Canada

give stereoselectively the trans product. The cis configuration with the axial ethoxycarbonyl group and equatorial aryl group is a consequence of the steric hindrance between the *o*-substituent in the phenyl ring and the ethoxycarbonyl group if it were in an equatorial orientation.

Experimental

Melting points are uncorrected. Microanalytical data were obtained from IISc, Bangalore-12, India. IR spectra were recorded on a JASCO-IR-700 IR spectrophotometer as potassium bromide discs of the sample. Mass spectra were obtained from RSIC, IIT, Chennai, India.

NMR spectra were recorded at 27 °C on a Bruker AMX 400 instrument operating at 400 MHz at a concentration of 20 mg/mL in $CDCl_3$ for ^1H NMR and 100 MHz at a concentration of 40 mg/mL in $CDCl_3$ for ^{13}C NMR, and chemical shifts were referenced internally to TMS in all cases.

The experimental parameters for the ^1H–^1H COSY spectra were: number of scans 16, number of data points 1 K, relaxation delay 1 s, acquisition time 0.1348 s, and spectral width 3817 Hz. The ^1H–^{13}C COSY spectra were obtained using the following parameters: number of scans 64, number of data points 2 K, acquisition time 0.666 s, relaxation delay 1 s, and spectral width 9981 Hz in F_1 and 15 576 Hz in F_2.

Crystallogrpahic data (22)

Compound **6** forms monoclinic crystals, a = 25.706 Å (5), b = 9.7180 Å (19), c = 12.245 Å (2), β = 93.44(3)°, Z = 8, space group $C2/c$. The structure was solved from 3132 observed reflections (Mo Kα radiation), and refined to R = 0.093 and R_w = 0.100.

Compounds

r-2e-Ethoxycarbonyl-*t*-3-phenyl-1,4-thiazane 1,1-dioxide (1)

A mixture of diethyl ethane – 1,2-disulphonylacetate (0.05 mol) (18), benzaldehyde (0.05 mol), and ammonium acetate (0.06 mol) in ethanol (100 mL) was heated under reflux for 6 h. The excess of solvent was removed by distillation and the mixture was kept overnight. The separated solid was filtered, washed with water, dried and recrystallized from ethanol. Yield: 55%; mp 164 to 165 °C. IR (cm^{-1}): 3400 (NH), 1722 (C=O), 1292 (asy. SO_2), 1126 (sym. SO_2). ^1H NMR (ppm): 1.00 (3H, t, CH_3), 1.88 (1H, br.s, NH), 3.19 (2H, m, H-6a, H-6e), 3.47 (2H, m, H-5a, H-5e), 4.01 (2H, q, CH_2), 4.06 (1H, d, $^3J_{a,a}$ = 10.6 Hz, H-2a), 4.46 (1H, d, $^3J_{a,a}$ = 10.6 Hz, H-3a), 7.32–7.38 (5H, m, aromatic). ^{13}C NMR (ppm): 13.69 (CH_3), 43.71 (C-5), 52.89 (C-6), 62.20 (CH_2), 62.78 (C-3), 72.65 (C-2), 127.71–128.92 (aromatic carbon), and 138.05 (ipso carbon). MS (*m*/*z*): 283, 238, 211, 196, 191, 172, 146, 133, 131, 130, 119, 118, 105, 104. Anal. calcd. for $C_{13}H_{17}NO_4S$: C 55.12, H 6.01, N 4.94; found: C 55.45, H 6.10, N 4.81.

r-2e-Ethoxycarbonyl-*t*-3-*p*-tolyl-l,4-thiazane 1,1-dioxide (2)

r-2e-Ethoxycarbonyl-*t*-3-*p*-tolyl-l,4-thiazane 1,1-dioxide (**2**) was obtained following the procedure of compound **1**. Yield: 50%; mp 145 to 146 °C. IR (cm^{-1}): 3420 (NH), 1724 (C=0), 1290 (asy. SO_2), 1125 (sym. SO_2). ^1H NMR (ppm): 0.99 (3H, t, CH_3), 2.05 (1H, br.s, NH), 2.29 (3H, s, tolyl), 3.12 (2H, m, H-6a, H-6e), 3.40 (2H, m, H-5a, H-5e), 3.99 (2H, q, CH_2), 4.04 (1H, d, $^3J_{a,a}$ = 10.6 Hz, H-2a), 4.38 (1H, d, $^3J_{a,a}$ = 10.6 Hz, H-3a), 7.10 (2H, d, aromatic), 7.23 (2H, d, aromatic). ^{13}C NMR (ppm): 13.66 (CH_3), 21.03 (tolyl), 43.62 (C-5), 52.77 (C-6), 62.08 (CH_2), 62.42 (C-3), 72.58 (C-2), 125.49–138.62 (aromatic), 161.71 (C=O). Anal. calcd. for $C_{14}H_{19}NO_4S$: C 56.56, H 6.40, N 4.71; found: C 56.43, H 6.46, N 4.63.

r-2e-Methoxycarbonyl-*t*-3-phenyl-1,4-thiazane 1,1-dioxide (3)

r-2e-Methoxycarbonyl-*t*-3-phenyl-1,4-thiazane 1,1-dioxide (**3**) was obtained following the procedure of compound **1**. Yield: 45%; mp 144–146 °C. IR (cm^{-1}), 3425 (NH), 1715 (C=0), 1295 (asy. SO_2), 1130 (sym. SO_2). ^1H NMR (ppm): 2.05 (1H, s, NH), 3.22 (2H, m, H-6a, H-6e), 3.48 (2H, m, H-5a, H-5e), 3.59 (3H, s, CH_3), 4.09 (1H, d, $^3J_{a,a}$ = 10.6 Hz, H-2a), 4.48 (1H, d, $^3J_{a,a}$ = 10.6 Hz, H-3a), 7.31 (5H, m, aromatic). ^{13}C NMR (ppm): 43.58 (C-5), 52.73 (C-6), 52.92 (CH_3), 62.67 (C-3), 72.44 (C-2), 127.48–128.83 (aromatic), 138.07 (ipso), 162.28 (C=O). Anal. calcd. for $C_{12}H_{15}NO_4S$: C 53.53, H 5.58, N 5.20; found: C 53.38, H 5.62, N 5.14.

r-2e-Ethoxycarbonyl-*t*-3-(*p*-methoxyphenyl)-1,4–thiazane 1,1-dioxide (4)

Diethylethane-1,2-disulphonyl acetate (0.05 mol), *p*-methoxybenzaldehyde (0.05 mol), and ammonium acetate (0.06 mol) in ethanol (100 mL) was refluxed for 15 h. The excess solvent was removed by distillation and the residue was poured into water. It solidified after 15 days. The solid was filtered, washed with water, then with ether, dried, and recrystallized from an ethanol–acetone mixture. Yield: 25%; mp 165–167 °C. IR (cm^{-1}): 3450 (NH), 1735 (C=O), 1290 (asy. SO_2), 1115 (sym. SO_2). Anal. calcd. for $C_{14}H_{19}NO_5S$: C 53.67, H 6.07, N 4.47; found: C 53.60, H 6.03, N 4.38. Very low solubility in $CDCl_3$.

r-2e-Ethoxycarbonyl-*t*-3-(*p*-chlorophenyl)-1,4-thiazane 1,1-dioxide (5)

r-2e-Ethoxycarbonyl-*t*-3-(*p*-chlorophenyl)-1,4-thiazane 1,1-dioxide (**5**) was obtained following the procedure of compound **4**. Yield: 30%; mp 178–180 °C. IR (cm^{-1}): 3420 (NH), 1687 (C=O), 1290 (asy. SO_2), 1120 (sym. SO_2). Anal. calcd. for $C_{13}H_{16}NO_4SCl$: C 49.21, H 5.05, N 4.42; found: C 49.24, H 5.02, N 4.38. Very low solubility in $CDCl_3$.

r-2a-Ethoxycarbonyl-*c*-3-(*o*-methoxyphenyl)-1,4-thiazane 1,1-dioxide (6)

r-2a-Ethoxycarbonyl-*c*-3-(*o*-methoxyphenyl)-1,4-thiazane 1,1-dioxide (**6**) was obtained following the procedure of compound **4**; reaction time 20 h. Yield: 20%; mp 143–145 °C. IR (cm^{-1}): 3475 (NH), 1740 (C=O), 1295 (asy. SO_2), 1114 (sym. SO_2). ^1H NMR (ppm): 0.86 (3H, s, CH_3), 2.39 (1H, br.s, NH), 2.96 (1H, dt, J = 13.4, 2.2 Hz, H-6e), 3.42 (1H, td, J = 14.1, 12.5, 2.2 Hz, H-5a), 3.56 (1H, td, J = 13.4, 12.5, 2.2 Hz, H-6a), 3.68 (1H, m, J = 14.1, 2.2 Hz, H-5e), 3.87 (3H, s, methoxy), 3.90 (2H, Dq, CH_2), 4.32 (1H, t, J = 3.2, 2.8 Hz, H-2e), 4.91 (1H, d, J = 3.2 Hz, H-3a), 7.07 (4H, m, aromatic). ^{13}C NMR (ppm): 13.44 (CH_3), 43.90 (C-

© 2005 NRC Canada

5), 48.32 (C-6), 55.31 (methoxy), 56.39 (C-3), 61.57 (CH_2), 67.04 (C-2), 110.28 (C-3′), 120.51 (C-5′), 125.37 (C-6′), 125.57 (C-1′), 129.03 (C-4′), 155.41 (C-2′), 165.67 (C=O). Anal. calcd. for $C_{14}H_{19}NO_5S$: C 53.67, H 6.07, N 4.47; found: C 53.58, H 5.59, N 4.38.

r-2a-Ethoxycarbonyl-*c*-3-(*o*-chlorophenyl)-1,4-thiazane 1,1-dioxide (7)

r-2a-Ethoxycarbonyl-*c*-3-(*o*-chlorophenyl)-1,4-thiazane 1,1-dioxide (**7**) was obtained following the procedure of compound **4**; reaction time 20 h. Yield: 20%; mp 134–136 °C. IR (cm^{-1}): 3410 (NH) 1682 (C=0), 1303 (asy. SO_2), 1115 (sym. SO_2). Anal. calcd. for $C_{13}H_{16}NO_4SCl$: C 49.21, H 5.05, N 4.42; found: C 49.13, H 5.09, N 4.36.

References

1. M.S. Chorghade, M.K. Gurjar, and A. Talukdar. Chem. Today, 20 (2002)
2. M.S. Chorghade, M.K. Gurjar, and C.V. Ramana. Chem. Today, 13 (2003)
3. P.A. Bartlett. Tetrahedron, **36**, 2 (1980).
4. E. Pitzus. J. Int. Med. Res. **6**, 414 (1978).
5. L. Aguirre-Cruz, O. Velasco, and J. Sotelo. J. Parasitol. **84**, 1032 (1998).
6. S.M. Liebowitz, J.B. Lombardine, and C.I. Allen. Eur. J. Pharmacol. **120**, 111 (1986).
7. I.A. Shehata, H.I. Elsubbagh, A.M. Abdelal, M.A. Elsherbeny, and A.A. Alobaide. Med. Chem. Res. **6**, 148 (1996).
8. A.J. Boulton and A. Mckillop. Comprehensive hetrocyclic chemistry. 1st ed. Vol. 3. Pergmon, Oxford. 1984. p. 1038.
9. L. Bukowski. Pharmazie, **56**, 23 (2001).
10. T. Yamamoto, M. Hori, I. Watanabe, K. Harada, S. Ikeda, and H. Ohtaka. Chem. Pharm. Bull. **48**, 843 (2000).
11. V. Paul, D. Rene, and R. Paul. Bull. Soc. Chim. Fr. 1252 (1962).
12. V. Baliah and T. Rangarajan. J. Chem. Soc. 3069 (1954).
13. D. Bhaskar Reddy, S. Reddy, N. Subba Reddy, and M.V. Ramana Reddy. Indian J. Chem. **30B**, 529 (1991).
14. D. Bhaskar Reddy, S. Reddy, N. Subba Reddy, and M.V. Ramana Reddy. Indian J. Chem. **34B**, 816 (1995).
15. S. Selvaraj, A. Dhanabalan, A. Mercypushpalatha, and N. Arumugam. Phosphorus Sulphur Silicon, **63**, 295 (1991).
16. S. Selvaraj, A. Dhanabalan, and N. Arumugam. Indian J. Chem. **33B**, 67 (1994).
17. J.L. Garcia Ruano, M.C. Martinez, J.H. Rodriguez, E.M. Olefirowicz, and E.L. Eliel. J. Org. Chem. **57**, 4215 (1992).
18. V. Baliah and G. Prema. Indian J. Chem. **9**, 1310 (1971).
19. Atta-ur-Rahman. Nuclear magnetic resonance. Basic principles. Springer, New York. 1986. p. 86.
20. J.C. Jochima, G. Taigel, A. Seeliger, P. Lutz, and H.E. Driesen. Tetrahedron Lett. 4363 (1967).
21. R.M. Silverstein and F.X. Webster. Spectrometric identification of organic compounds. 6th ed. Wiley and Sons, New York. 1997.
22. M. Subha Nandhini, R. Banurekha, R.V. Krishnakumar, A. Mostad, N. Bhavani, S. Perumal, and S. Natarajan. Acta Crystallogr. **E59**, o1400 (2003).

© 2005 NRC Canada

A novel enamination of β-dicarbonyl compounds catalyzed by $Bi(TFA)_3$ immobilized on molten TBAB

Mohammad M. Khodaei, Ahmad R. Khosropour, and Mehdi Kookhazadeh

Abstract: Enamination of a wide variety of primary amines was successfully carried out in the presence of catalytic amounts of bismuth(III) trifluoroacetate immobilized on molten tetrabutylammonium bromide as "green" media under mild conditions. This new system of the catalyst is recyclable and reusable. Generally, the results of the reaction in tetrabutylammonium bromide is better than the previously obtained results in water because of their yields and reaction times.

Key words: amine, bismuth compounds, β-dicarbonyl compounds, enamination, ionic liquid.

Résumé : On a procédé avec succès à une évaluation d'une grande variété d'amines primaires, en présence de quantités catalytiques de trifluoroacétate de bismuth(III) immobilisé sur de bromure de tétrabutylammonium fondu comme milieu « vert », dans des conditions douces. Ce nouveau système de catalyseur est recyclable et réutilisable. En général, les résultats de la réaction dans le bromure de tétrabutylammonium sont meilleurs que ceux obtenus antérieurement dans l'eau en raison de leurs rendements et de leurs temps de réaction.

Mots clés : amine, composés du bismuth, composés β-dicarbonylés, énamination, liquide ionique.

[Traduit par la Rédaction]

Introduction

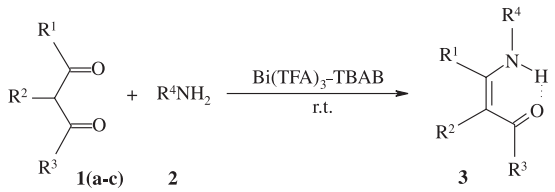
The increasing attention during the last decades for environmental protection has influenced both modern academic and industrial groups to develop chemical processes with maximum yield under minimum amounts of harmful reagents. Therefore, much attention has been devoted to the use of alternative reaction media (1, 2). Besides the use of water or supercritical fluids, organic reaction in ionic liquids (ILs) as new reaction media, are aimed toward green chemistry (3). The use of these liquids in place of conventional organic solvents can lead to significant improvements in the rates and yields of reactions. In addition, they possess a number of interesting properties, especially their lack of vapor pressure, a widely accessible temperature range with lack of flammability, and ease of recycling that facilitates product recovery and may reduce environmental emissions (4–8). Also, ILs often contain poorly coordinating anions and thus form a new class of polar, noncoordinating solvents (9). Consequently, ionic liquids have been used in several catalytic reactions involving many different catalysts. Several catalysts have been immobilized in ionic liquids and successfully recycled as a result of the involatile nature of these media. Some reactions that have been investigated in these catalytic media are the use of palladium catalysts for Suzuki (10), Stille (11), and Heck coupling reactions (12, 13), a chromium catalyst for asymmetric epoxide openings (14), a ruthenium catalyst for asymmetric alkenes hydrogenations (15), and etc. (16–19). Recently, molten tetrabutylammonium bromide (TBAB) as an ionic liquid for immobilization of some catalysts has been used successfully (20–25).

Received 12 July 2004. Published on the NRC Research Press Web site at http://canjchem.nrc.ca on 16 March 2005.

M.M. Khodaei,[1] A.R. Khosropour,[2] and M. Kookhazadeh. Department of Chemistry, Faculty of Science, Razi University, Kermanshah 67149, Iran.

[1]Corresponding author (e-mail: mmkhoda@razi.ac.ir).
[2]Corresponding author (e-mail: arkhosropour@razi.ac.ir).

Scheme 1.



1a: $R^1 = CH_3$, $R^2 = H$, $R^3 = CH_3$
1b: $R^1 = CH_3$, $R^2 = H$, $R^3 = Ph$
1c: $R^1 = CH_3$, $R^2 = H$, $R^3 = OC_2H_5$
1d: $R^1 = CH_3$, $R^2 = CH_2CH_2R^3$, $R^3 = O$

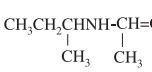
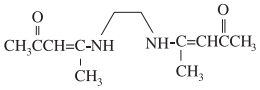
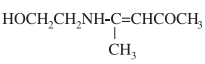
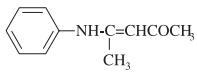
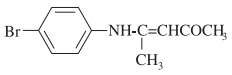
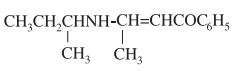
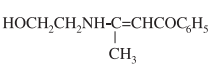
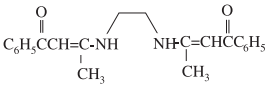
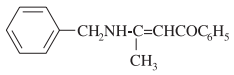
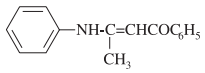
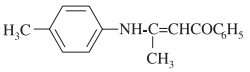
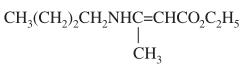
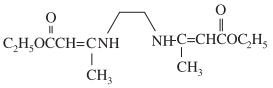
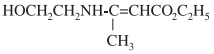
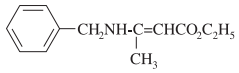
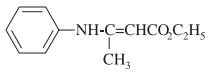
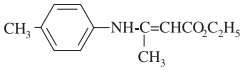
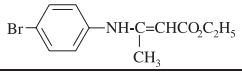
Results and discussion

As part of our program aimed at developing new selective and environmentally friendly methodologies for the preparation of fine chemicals (26–27), we were interested in investigating another method (28–31) for the enamination reaction.

Very recently, we have reported that $Bi(TFA)_3$, as an efficient and water-tolerant Lewis acid, catalyzes the enamination of β-dicarbonyl compounds in aqueous media (32). Herein, we would like to report another modified procedure on the enamination reaction of various primary amines with β-dicarbonyl compounds in the presence of catalytic amounts of $Bi(TFA)_3$ immobilized on molten TBAB as inexpensive ionic liquid at room temperature (Scheme 1).

 doi: 10.1139/V05-021 © 2005 NRC Canada

Table 1. Enamination reaction catalyzed with $Bi(TFA)_3$ immoblized on TBAB.

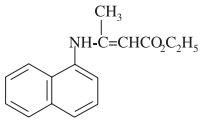
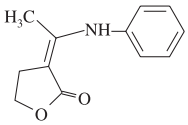
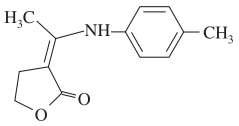
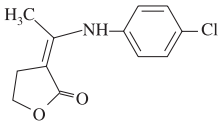
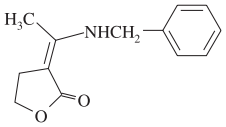
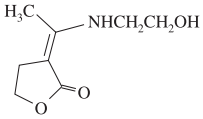
Entry		R^4	Product[a]	Time (min)	Yield (%)[b]
1	**1a**	$CH_3CH_2CHCH_2$		5	93
2	**1a**	$H_2NCH_2CH_2$		15	90
3	**1a**	$HOCH_2CH_2$		10	87
4	**1a**	C_6H_5		Immediately	99
5	**1a**	4-BrC_6H_4		20	85
6	**1b**	$CH_3CH_2CHCH_2$		15	78
7	**1b**	$HOCH_2CH_2$		30	74
8	**1b**	$H_2NCH_2CH_2$		10	86
9	**1b**	$C_6H_5CH_2$		5	91
10	**1b**	C_6H_5		10	83
11	**1b**	4-$CH_3C_6H_4$		10	85
12	**1c**	$CH_3(CH_2)_2CH_2$		Immediately	99
13	**1c**	$H_2NCH_2CH_2$		Immediately	97
14	**1c**	$HOCH_2CH_2$		Immediately	98
15	**1c**	$C_6H_5CH_2$		Immediately	98
16	**1c**	C_6H_5		10	84
17	**1c**	4-$CH_3C_6H_4$		5	92
18	**1c**	4-BrC_6H_4		15	60

This condensation reaction with a wide range of aromatic and aliphatic primary amines and β-dicarbonyl compounds proceeded effectively in these conditions. The results are summarized in Table 1. The reaction is performed at ambient temperature with very short reaction times and does not require the use of an inert atmosphere (16).

In all cases, in comparison to the reaction under aqueous media, the reactions were very rapid and in excellent yields.

© 2005 NRC Canada

Table 1 (*concluded*).

Entry		R^4	Product [a]	Time (min)	Yield (%)[b]
19	**1c**	α-naphthyl		25	74
20	**1d**	C_6H_5		60	83
21	**1d**	4-$CH_3C_6H_4$		60	80
22	**1d**	4-ClC_6H_4		5	93
23	**1d**	$C_6H_5CH_2$		15	93
24	**1d**	$HOCH_2CH_2$		10	96

[a]All products were identified by comparison of their physical and spectral data with those of authentic samples (17).
[b]Isolated yields.

For example, the yield from the enamination of 1-butyl amine with acetyl acetone in the presence of $Bi(TFA)_3$ under aqueous media was only 63% for 3 h while, the reaction yield and rate were improved significantly using 50 mol % of molten TBAB instead of water (entry 1, Table 1). It was also observed that these reactions could not be performed in the absence of the Lewis acid.

This method was successfully applied to enamination of diketones (entries 1–11, Table 1), linear (entries 12–19, Table 1), and cyclic β-ketoesters (entries 20–24, Table 1). The regiochemistry observed from these β-dicarbonyls is similar to that in aqueous media, which was limited to preferential amines' attack at the acetyl position and no by-product was observed.

Interestingly, when $Bi(TFA)_3$ was added to the molten TBAB, the mixture did not result in solidification after cooling to room temperature and remained a liquid paste in such a way that the magnetic bar stirred well.

Another advantage of this method for the transformation is recyclability of this catalyst. Since $Bi(TFA)_3$–TBAB was weakly soluble in Et_2O, it was separated by washing with Et_2O and dried at 60 °C under reduced pressure and reused in five runs without any loss of activity.

In conclusion, $Bi(TFA)_3$–TBAB is a new, highly efficient, and reusable catalyst for the enamination of 1,3-dicarbonyl compounds. Mild reaction conditions, short reaction times, excellent yields, and high chemoselectivity are noteworthy advantages of this procedure. Moreover, stability and low toxicity of the Lewis acid and the ionic liquid are the other merits of this method.

Experimental

General experimental procedure

To a solution of the amine (1 mmol) and β-dicarbonyl compound (1 mmol) in molten TBAB (0.5 mmol), $Bi(TFA)_3$ (0.05 mmol) was added and the reaction mixture stirred at room temperature for the appropriate time according to Table 1. After completion of the reaction as indicated by GLC or TLC, the mixture was washed with Et_2O (3 × 10 mL). Crude products were purified by preparative chromatography on silica gel using *n*-heptane–AcOEt (10:1) as the eluent. The β-enaminones were thus prepared in 60%–99% yields.

Spectroscopic data

Compound **5**: mp 49 to 50 °C. IR (KBr, cm^{-1}) ν_{max}: 3290, 3162, 2906 1604, 1573, 1475, 1360, 903, 839. ^1H NMR (200 MHz, $CDCl_3$) δ_H: 12.4 (br, 1H, NH), 7.55–6.9 (m, 4H,

© 2005 NRC Canada

Ar), 5.22 (s, 1H, =CH), 2.18 (s, 3H, CH_3), 1.98 (s, 3H, CH_3). ^{13}C NMR (50 MHz, $CDCl_3$) δ_c: 196.7, 159.7, 138.3, 132.2, 126.2, 118.8, 117.1, 100.8, 98.7, 29.6, 20.2. Anal. calcd. for $C_{11}H_{12}BrNO$: C 51.99, H 4.76, N 5.51; found: C 52.0, H 4.9, N 5.8.

Compound **10**: mp 99–102 °C. IR (KBr, cm^{-1}) ν_{max}: 3150, 3003, 2900, 1610, 1602, 1587, 1534, 1427, 1317, 1188, 1060, 803. ^1H NMR (200 MHz, $CDCl_3$) δ_H: 13.2 (br, 1H, NH), 8.3–8.0 (m, 5H. Ph), 7.5–7.2 (m, 5H, Ph), 6.2 (s, 1H, C=CH), 2.2 (s, 3H, CH_3). ^{13}C NMR (50 MHz, $CDCl_3$) δ_c: 189.1, 162.7, 140.4, 139.1, 131.4, 129.6, 129.1, 128.7, 127.5, 126.2, 125.2, 94.7, 20.9. Anal. calcd. for $C_{16}H_{15}NO$: C 80.98, H 6.37, N 5.90; found: C 80.6, H 6.3, N 6.1.

Compound **21**: mp 92–94 °C. IR (KBr, cm^{-1}) ν_{max}: 3182, 3072, 2900, 1666, 1637, 1245, 1019, 955. ^1H NMR (200 MHz, $CDCl_3$) δ_H: 9.9 (br, 1H, NH), 7.25–7 (m, 4H, Ar), 4.42 (t, J = 8 Hz, 2H, OCH_2), 3.03 (t, J= 8.1 Hz, 2H, =C-CH_2-), 2.45 (s, 3H, CH_3), 2.08 (s, 3H, CH_3). ^{13}C NMR (50 MHz, $CDCl_3$) δ_c: 174.4, 154.5, 147.8, 136.8, 135.2, 130.1, 124.9, 88.9, 65.8, 26.9, 21.3. Anal. calcd. for $C_{13}H_{15}NO_2$: C 71.86, H 6.95, N 6.45; found: C 71.6, H 7.0, N 6.7.

Acknowledgments

We are thankful to the Razi University Research Council for partial support of this work.

References

1. J.M. DeSimone. Science, **297**, 799 (2002).
2. P. Tunda and P.T. Anastas. Green chemistry: Theory and practice. Oxford University Press, Oxford. 1998.
3. J. Dupont, R.F. de Souza, and P.A.Z. Suarez. Chem. Rev. **102**, 3667 (2002).
4. R. Rajagopal, D.V. Jarikote, and K.V. Srinivasan. Chem. Commun. 616 (2002).
5. K. Jin, X. Huang, L. Pang, J. Li, A. Appel, and S. Wherland. Chem. Commun. 2872 (2002).
6. D. Zhao, M. Wu, Y. Kou, and E. Min. Catal. Today, **74**, 157 (2002).
7. S. Harrisson, S.R. Mackenzie, and D.M. Haddleton. Chem. Commun. 2850 (2002).
8. J.H. Clark. Green Chem. 1 (1999).
9. R. Sheldon. Chem. Commun. 2399 (2001).
10. C.J. Matthews, P.J. Smith, and T. Welton. Chem. Commun. 1249 (2000).
11. S.T. Handy and X. Zhang. Org. Lett. **3**, 233 (2001).
12. H. Hagiwara, Y. Shimizu, T. Hoshi, M. Ando, K. Ohkubo, and C. Yokoyama. Tetrahedron Lett. **41**, 4349 (2001)
13. A.J. Carmichael, M.J. Earle, J.D. Holbrey, P.B. McCormac, and K.R. Seddon. Org. Lett. **1**, 997 (1999).
14. C.E. Song, C.R. Oh, E.J. Roh, and D.J. Choo. Chem. Commun. 1743 (2000).
15. R.A. Brown, P. Pollet, E. McKoon, C.A. Eckert, C.L. Liotta, and P.G. Jessop. J. Am. Chem. Soc. **123**, 1254 (2001).
16. S.L. Chen, S.J. Ji, and T.P. Loh. Tetrahedron Lett. **44**, 2405 (2003).
17. J.M. Fraile, J.I. Garcia, C.I. Herrerias, J.A. Mayoral, D. Carrie, and M. Vaultier. Tetrahedron: Asymmetry, **12**, 1891 (2001)
18. J.N. Rosa, C.A.M. Afonso, and A.G. Santos. Tetrahedron, **57**, 4189 (2001).
19. C.E. Song, W.H. Shim, E.J. Roh, S. Lee, and J.H. Choi. Chem. Commun. 1695 (2001).
20. J. Dupont, M. Pfeffer, and J. Spencer. Eur. J. Inorg. Chem. 1917 (2001).
21. M.T. Reetz and E. Westermann. Angew. Chem. Int. Ed. **39**, 165 (2000).
22. J. Silberg, T. Schareina, R. Kempe, K. Wurst, and M.R. Buchmeiser. J. Organomet. Chem. **622**, 6 (2001).
23. V. Calo, A. Nacci, A. Monopoli, L. Lopez, and A. di Cosmo. Tetrahedron, **57**, 6071 (2001).
24. V. Calo and A.Z. Nacci. Z. Naturforsch. A: Phys. Sci. **56a**, 702 (2001).
25. M.M. Khodaei, A.R. Khosropour, and K. Ghozati. Tetrahedron Lett. **45**, 3525 (2004).
26. M.M. Khodaei, A.R. Khosropour, and S.J. Hoseini Jomor. J. Chem. Res. (S), **10**, 638 (2003).
27. A.R. Khosropour, M.M. Khodaei, and K. Ghozati. Chem. Lett. **33**, 304 (2004).
28. B. Rechsteiner, F. Texier-Boullet, and J. Hamelin. Tetrahedron Lett. **34**, 5071 (1993).
29. C.J. Valduga, A. Squizani, H.S. Braibante, and M.E.F. Braibante. Synthesis, 1019 (1998).
30. A. Arcadi, G. Bianchi, S. Di Giuseppe, and F. Marinelli. Green Chem. 64 (2003).
31. H.A. Stefani, I.M. Costa, and D.O. Silva. Synthesis, 1526 (2000).
32. A.R. Khosropour, M.M. Khodaei, and M. Khookhazadeh. Tetrahedron Lett. **45**, 1725 (2004).

© 2005 NRC Canada

Efficient one-pot transformation of aminoarenes to haloarenes using halodimethylisulfonium halides generated in situ

Woonphil Baik, Wanqiang Luan, Hyun Joo Lee, Cheol Hun Yoon, Sangho Koo, and Byeong Hyo Kim

Abstract: Halodimethylsulfonium halide **1**, which is readily formed in situ from hydrohaloic acid and DMSO, is a good nucleophilic halide. This activated nucleophilic halide rapidly converts aryldiazonium salt prepared in situ by the same hydrohaloic acid and nitrite ion to aryl chlorides, bromides, or iodides in good yield. The combined action of nitrite ion and hydrohaloic acid in DMSO is required for the direct transformation of aromatic amines, which results in the production of aryl halides within 1 h. Substituted compounds with electron-donating or -withdrawing groups or sterically hindered aromatic amines are also smoothly transformed to the corresponding aromatic halides. The only observed by-product is the deaminated arene (usually <7%). The isolated aryldiazonium salts can also be converted to the corresponding aryl halides using **1**. The present method offers a facile, one-step procedure for transforming aminoarenes to haloarenes and lacks the environmental pollutants that usually accompany the Sandmeyer reaction using copper halides.

Key words: aminoarenes, haloarenes, halodimethylsulfonium halide, halogenation, amination.

Résumé : Les halogénures d'halogénodiméthylsulfonium (**1**) qui se forment facilement à partir des acides hydrohaloïques et du DMSO sont de bons halogénures nucléophiles. Sous l'action de ce type d'halogénure nucléophile, les sels d'aryldiazonium préparés in situ à l'aide du même acide hydrohaloïque et de l'ion nitrite peuvent facilement être transformés en chlorures, bromures ou iodures d'aryles, avec de bons rendements. L'action combinée de l'ion nitrite et d'un acide hydrohaloïque dans le DMSO est requise pour la transformation directe des amines aromatiques qui conduit à la formation d'halogénures d'aryles en moins d'une heure. Les composés substitués par des groupes électrodonneurs ou électroattracteurs ainsi que les amines stériquement empêchées sont aussi transformées facilement en halogénures d'aryles correspondants. Le seul produit secondaire observé est l'arène désaminé (généralement moins de 7 %). Sous l'action des produits **1**, les sels d'aryldiazonium isolés peuvent aussi être transformés en halogénures d'aryles correspondants. Cette méthode est présentée comme une procédure facile, en une étape, qui permet de transformer des aminoarènes en halogénoarènes et qui n'est pas entachée des polluants environnementaux qui accompagnent généralement la réaction de Sandmeyer qui utilise des halogénures de cuivre.

Mots clés : aminoarènes, halogénoarènes, halogénure d'halogénodiméthylsulfonium, halogénation, amination.

[Traduit par la Rédaction]

Introduction

Aromatic halides are versatile reagents that can be converted to a wide variety of materials. Representative processes for preparing aromatic halides include: (*i*) direct aromatic halogenation (1), wherein the hydrogen atom is replaced by a halogen atom, and (*ii*) the Sandmeyer reaction (2, 3), which involves the substitution of an amino group by a halogen atom via a diazonium salt. Since aromatic amines are generally more economical to produce, most methods for preparing highly substituted aromatic halides have centered around improving the Sandmeyer reaction. The Sandmeyer reaction is a two-step process: diazotization followed by halogenation (3). The typical Sandmeyer reaction is generally carried out in the presence of more than one equimolar amount of cuprous halide (3*b*–3*d*), and the discharge of excess copper salt can cause environmental pollution. In addition, since the stability and formation of the diazonium salt are the important factors in the Sandmeyer reaction, special conditions such as a low reaction temperature and filtration are necessary (2, 3). Considering the wide range of potential applications for aromatic halides, the development of a simple method that requires a low manufacturing cost while minimizing environmental pollution is required. Some modi-

Received 10 August 2004. Published on the NRC Research Press Web site at http://canjchem.nrc.ca on 9 March 2005.

W. Baik,[1] W. Luan, H.J. Lee, C.H. Yoon, and S. Koo. Department of Chemistry, Myong Ji University, Yong In City, Kyung Ki Do, 449–728, Korea.
B.H. Kim. Department of Chemistry, Kwangwoon University, Seoul, Korea.

[1]Corresponding author (e-mail: wpbaik@mju.ac.kr).

 doi: 10.1139/V05-026 © 2005 NRC Canada

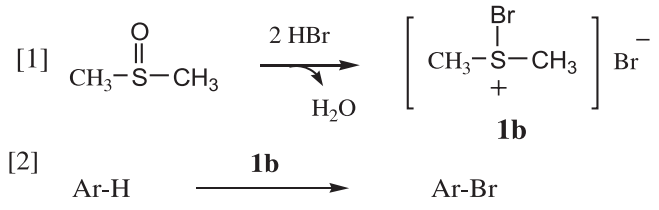
Table 1. Transformation of *p*-nitroaniline to *p*-bromoaniline under various conditions.[a]

Entry	HBr (equiv.)	KNO_2 (equiv.)	Solvent	Conditions	Yield (%)[b] 3	4	2
1	1.5	1.5	DMSO	12 h, 80 °C	35 (6)[c]	tr	40
2	4.0	4.0	DMSO	10 min, 35 °C	86 (7)[c]	0	tr
3	4.0	4.0	H_2O	24 h, 35 °C	0	~10	(Salt)[d]
4	4.0	4.0	DMF[e]	12 h, 35 °C	0	~5	Sluggish
5	3.0	0	DMSO	24 h, rt	0	26	tr
6	0	4.0	DMSO	24 h, 35 °C	0	0	98

[a]Reactions were performed by adding 10.0 mmol of *p*-nitroaniline and the indicated amount of HBr to KNO_2 in 50 mL of solvent.
[b]Yields were determined by GLC analysis by comparison to dodecane as an internal standard.
[c]The deaminated product, nitrobenzene.
[d]The aryldiazonium salt was formed.
[e]Other solvents (THF, HMPA, hexane, and benzene) were also examined, but none gave the desired product.

fied Sandmeyer reactions (4) that involve a diazonium salt have been developed for the purpose of simplicity. Unlike the sodium nitrite and acidic conditions needed for the preparation of diazonium salt, alkyl nitrite is a useful in situ diazotizing agent for the one-step preparation of aromatic halides (4*a*–4*d*). This method also uses anhyd. $CuCl_2$ (4*a*–4*b*) or $CuBr_2$ (4*a*–4*b*) and I_2 with CH_2I_2 for iodination (4*d*). Iodination suffers in this case in that it is difficult to separate the product from excess diiodomethane. A similar direct replacement of the aromatic amino group by iodine or bromine through reactions with gaseous nitrogen dioxide, but without an added metal activator, has been reported (4*h*, 4*k*). Although there are specific advantages to each of these methods, none of the modified variations has received wide application. To simplify the reaction and minimize the environmental problems and manufacturing cost, several factors should be considered: (*i*) the development of in situ diazotization for a single-step reaction, and (*ii*) the development of an activated halogen nucleophile that can replace CuX_2, I_2, CH_2I_2, etc.

Bromodimethylsulfonium bromide **1b** has been used as a bromide nucleophile in the substitution of hydrogen atom(s) of aromatic compounds (5–7). As shown in eqs. [1] and [2], when HBr is added with DMSO as the solvent, bromodimethylsulfonium bromide **1b** is formed instantly, and replacement of a hydrogen atom of the benzene ring by bromide occurs simultaneously (5).

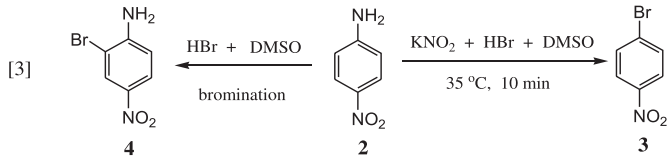


Despite the synthetic utility of **1b** in the bromination of arenes, it has not been investigated as an activated halogen nucleophile in the replacement of a diazonium group. An aromatic amine would be converted to a diazonium salt by the addition of nitrite salt and hydrohaloic acid, while at the same time an activated halide nucleophile **1** (X = Cl (**1a**), X = Br (**1b**), X = I (**1c**)) would be prepared readily in situ from the same hydrohaloic acid and DMSO. Thus, the transformation of an amine group to a halogen group in aromatic compounds may occur in a single-step process via concurrent diazotization–displacement using the combination of NO_2^-–HX–DMSO. Therefore, we sought to use **1** in the halogenation of the diazonium salt that is prepared in situ using the same halohydric acid and nitrite ion.

Results and discussion

Bromination and (or) chlorination

Preliminary studies on the bromination of *p*-nitroaniline were carried out using KNO_2 and 48% aq. HBr[2] in DMSO. *p*-Nitroaniline **2** with KNO_2 (4 equiv.) and HBr (4 equiv.) in DMSO at 35 °C afforded *p*-bromonitrobenzene **3** in 86% yield within 10 min along with a 7% yield of nitrobenzene (Table 1 and eq. [3]). None of the brominated product, 2-bromo-4-nitroaniline **4**, was observed. However, when *p*-nitroaniline was reacted with a mixture of HBr and DMSO in the absence of KNO_2, 2-bromo-4-nitroaniline **4** was observed in 26% yield, as reported by Chauhan and co-workers (6). The transformation to *p*-bromonitrobenzene was not observed without the nitrite ion. With stoichiometric amounts of HBr and KNO_2 in DMSO, 35% of *p*-bromonitrobenzene and 40% of the starting material were observed, but even after 24 h the brominated product was only formed in a trace amount (~2%). Presumably, the diazonium salt that is instantly formed by the action of KNO_2 and HBr prevents the bromination of *p*-nitroaniline.



The molar ratio of HBr to aromatic amine for this reaction should be from about 3:1 to about 5:1; preferably, about 4:1. A higher molar ratio of HBr will lead to the formation of brominated product as a by-product. For example, with 7 equiv. of HBr and 4 equiv. of KNO_2 in DMSO, *p*-bromoaniline was transformed to 76% *p*-dibromobenzene and 15%

[2]Due to safety and handling considerations, aqueous hydrohaloic acid or hydrohaloic acid in glacial acetic acid solution is preferred. It is generally available commercially and contains about 48%–57% by weight H_2O solution or acetic acid.

© 2005 NRC Canada

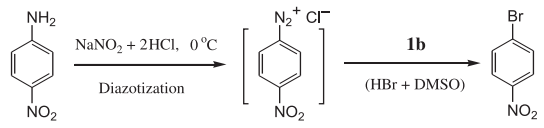
Table 2. Transformation of Ar-NH_2 by KNO_2 and HX in DMSO.[a]

Entry	Substrate	Time (min)	Product	Yield (%)[b]
1	*o*-$O_2NC_6H_4NH_2$	15	*o*-$O_2NC_6H_4Br$	82 (78)
2	*o*-$O_2NC_6H_4NH_2$	30	*o*-$O_2NC_6H_4Cl$	79 (73)
3	*p*-CH_3CO $C_6H_4NH_2$	10	*p*-CH_3CO C_6H_4Br	88
4	*p*-CH_3CO $C_6H_4NH_2$	60	*p*-CH_3CO C_6H_4Cl	69
5	5-Cl-2-$O_2NC_6H_4NH_2$	10	5-Cl-2-$O_2NC_6H_4Br$	77
6	3,5-$(O_2N)_2C_6H_4NH_2$	10	3,5-$(O_2N)_2C_6H_4Br$	83 (80)
7	3,5-$(O_2N)_2C_6H_4NH_2$	60	3,5-$(O_2N)_2C_6H_4Cl$	69
8	2-MeO-5-$O_2NC_6H_4NH_2$	20	2-MeO-5-$O_2NC_6H_4Br$	81
9	*p*-HOOC $C_6H_4NH_2$	20	*p*-HOOC C_6H_4Br	78
10	*p*-HOOC $C_6H_4NH_2$	120	*p*-HOOC C_6H_4Cl	67
11	4-CH_3-2-$O_2NC_6H_4NH_2$	10	4-CH_3-2-$O_2NC_6H_4Br$	81
12	2,6-$(CH_3)_2C_6H_4NH_2$	30	2,6-$(CH_3)_2C_6H_4Br$	79
13	2,6-$(CH_3)_2C_6H_4NH_2$	120	2,6-$(CH_3)_2C_6H_4Cl$	69
14	2,6-$F_2C_6H_4NH_2$	20	2,6-$F_2C_6H_4Br$	85
15	*p*-$CH_3OC_6H_4NH_2$	10	*p*-$CH_3OC_6H_4Br$	85
16	4-Aminobenzophenone	10	4-Bromobenzophenone	89 (85)
17	4-Aminobenzophenone	60	4-Chlorobenzophenone	77
18	4-Aminoacetophenone	15	4-Bromoacetophenone	91
19	4-Aminobiphenyl	20	4-Bromobiphenyl	85 (78)
20	1-Aminonaphthalene	20	1-Bromonaphthalene	61
21	2-Aminoanthraquinone	20	2-Bromoanthraquinone	80
22	2-Amino-3-nitropyridine	30	2-Bromo-3-nitrophridine	54
23	5-Aminoisoquinoline	30	5-Bromoisoquinoline	61 (54)
24	1-Aminoisoquinoline	120	1-Chloroisoquinoline	51
25	3-Aminoquinoline	30	3-Bromoquinoline	59

[a]Reactions were performed by adding 10.0 mmol of the aniline and 40.0 mmol of 48% aq. HBr (or 37% aq. HCl) in 25 mL of DMSO to 40.0 mmol of KNO_2 in 25 mL of DMSO. The reaction temperature was 35 °C.

[b]Yields were generally determined by GLC analysis by comparison to an internal standard. Isolated yields after column chromatography or recrystallization are given in parentheses.

tribromobenzene. Thus, the use of excess HBr results in dibromobenzene, which is further brominated to give the tribromobenzene. The molar ratio of nitrite to aromatic amine should be about 3:1 to 5:1. The use of low molar ratios may cause a drop in product yields. To investigate the role of DMSO in the transformation of *p*-nitroaniline to *p*-bromonitrobenzene, other solvents were studied. However, none of the other solvents (H_2O, DMF, THF, HMPA, hexane, benzene, etc.) gave the desired product under the same conditions. The formation of the diazonium salt was observed in H_2O, and the reaction was very sluggish in DMF. No further reaction was seen in the absence of DMSO. Thus, DMSO has two roles; first, it reacts with HBr to form bromodimethylsulfonium bromide **1b**, and second, it readily dissolves nitrite ion. In fact, the reaction is too fast to observe the formation of the diazonium salt. To prove that the reaction proceeds via aryldiazonium salt under our conditions, isolated diazonium salt that was prepared by the general method (8) using sodium nitrite and HCl was treated with a premixed solution of HBr and DMSO as shown in eq. [4]. As expected, *p*-bromonitrobenzene was produced in 52% yield. According to this two-step protocol (diazotization–replacement), the activated bromodimethylsulfonium bromide **1b** directly converted the diazonium salt to provide the aryl bromide compound.

[4] 

The present method is characterized by the simultaneous in-situ formation of the activated bromide **1b** and aryldiazonium salt of the same HBr at room temperature and the smooth one-pot transformation of aminoarenes to monohaloarenes without further halogenated by-products.

The reaction is carried out by dissolving KNO_2 in DMSO and then adding *p*-nitroaniline and HBr to the resulting mixture at ambient temperature. The order in which the nitrite ion, hydrobromic acid, and an aromatic amine are added is not critical to the reaction.

The general applicability of this procedure for several other aminoarenes was then investigated, and the results are presented in Table 2. As can be seen, clean transformation occurs in good to excellent yields. The products were checked for purity by GLC and ^1H NMR. All of the products were also checked by GC–MSD to ensure the absence of any brominated by-products.

Reactions of sterically hindered aminobenzenes took place in reasonable yields within 1 h. Furthermore, anilines, even those with electron-withdrawing substituents, such as an aldehyde, ketone, nitro group, or carboxylic group, also showed good reactivity. For example, with 2,4-dinitroaniline

© 2005 NRC Canada

Table 3. Effect of CuX in the transformation of Ar-NH_2 by KNO_2 and HX in DMSO.[a]

Entry	Substrate	Time (min)	Product	Yield (%)[b]
1	*p*-$CH_3COC_6H_4NH_2$	10	*p*-$CH_3COC_6H_4Br$	94
2	*p*-$CH_3COC_6H_4NH_2$	20	*p*-$CH_3COC_6H_4Cl$	82
3	3,5-$(O_2N)_2C_6H_4NH_2$	10	3,5-$(O_2N)_2C_6H_4Br$	91
4	3,5-$(O_2N)_2C_6H_4NH_2$	20	3,5-$(O_2N)_2C_6H_4Cl$	88
5	*p*-HOOC $C_6H_4NH_2$	10	*p*-HOOC C_6H_4Br	83
6	*p*-HOOC $C_6H_4NH_2$	30	*p*-HOOC C_6H_4Cl	77
7	2,6-$F_2C_6H_4NH_2$	10	2,6-$F_2C_6H_4Br$	97
8	1-Aminonaphthalene	20	1-Bromonaphthalene	76
9	2-Amino-3-nitropyridine	30	2-Bromo-3-nitrophridine	74
10	5-Aminoisoquinoline	30	5-Bromoisoquinoline	81
11	1-Aminoisoquinoline	30	1-Chloroisoquinoline	79

[a]Reactions were performed by adding 2.0 mmol of CuX (0.2 equiv.) under the same conditions as in Table 2.
[b]Yields were generally determined by GLC analysis by comparison to an internal standard.

or 2,6-dimethylaniline, transformation took place to predominantly produce 1-bromo-2,4-dinitrobenzene or 1-bromo-2,6-dimethylbenzene, respectively. Furthermore, bromination or side-chain bromination was not observed, which suggests a highly effective transformation that is fully controlled by electronic and steric factors. However, in most cases, deaminated product was observed in trace (~7%) yields, and this was not affected by the amount of either HX or KNO_2. Conventional diazotization of electron-deficient anilines such as dinitroanilines is usually carried out using concentrated sulfuric acid as the reaction medium (4*c*, 8). Thus, the present method is especially attractive for anilines bearing electron-withdrawing groups. In addition, the present method was effective for preparing highly halogen-substituted benzenes. For example, 2,4-difluoroaniline reacts with KNO_2–HBr–DMSO to give 1-bromo-2,4-difluorobenzene in 87% yield within 30 min. For electron-rich anilines, the yields were also modest to high. However, conversion of aromatic diamines to the corresponding dibromo or monobromo products was unsatisfactory.

Having demonstrated the superiority of the aminoarenes, we then turned our attention to the evaluation of heterocyclic amine compounds. Reactions with aminopyridines also showed good transformations to their corresponding bromopyridines without any noticeable side reactions (Table 2, entries 22~25). Typically, during the reactions with aminopyridines, such as 5-aminoisoquinoline, 1-aminoisoquinoline, 2-amino-3-nitropyridine, or aminoquinoline, complete conversion was observed even though the pyridinium salt was formed by the action of HBr. We believe that the positively charged nitrogens of the pyridinium salt and the diazonium salt exert some electronic and inductive effects to enhance the electrophilicity of the carbon atom of the ring.

We successfully performed this transformation on a semi-preparatory scale (1000 g)[3] and a microscale (<0.1 g). In any case, this one-pot procedure is superior to the classical or modified Sandmeyer reactions in terms of yield, convenience, cost, and reaction time. In addition, the ease with which the product can be purified due to the use of the water-miscible solvent DMSO and aq. HX allows a large-scale preparation in an efficient one-pot reaction.

The versatility of halodimethylsulfonium halide, especially chlorodimethylsulfonium chloride **1a**, is also demonstrated in Table 2. Upon treatment of 37% aq. HCl with KNO_2 in DMSO, the amino group is transformed to give a chlorinated arene. The yields were relatively low compared to the bromination, indicating that the pK_a values of HX may affect the stabilities of both the halodimethylsulfonium halide and the diazonium salt.

In an attempt to increase the product yield for some aminoarenes and aminopyridines, we examined the effect of a copper halide. The typical conversion of arenediazonium ions to aryl halides requires a quantitative amount of Cu(II) halide (Sandmeyer reaction). We observed that the addition of 0.2 equiv. of CuBr (or CuCl) to the reaction mixture under our conditions increased the yield and reduced the reaction time (Table 3).

Iodination

Since some reactions, such as the Ullmann (9, 10), Suzuki (11), and Heck reactions (12), are facile for iodoarenes, a simple and reliable preparation method is still under investigation. Attractive methods have been proposed by several groups (4*d*–4*j*), such as using "isoamyl nitrite" as the diazotizing agent and "diiodomethane" as both a solvent and halogen source (4*d*). However, it can be difficult to separate the product from excess diiodomethane and the use of sterically hindered anilines is problematic. To evaluate the sequence using iododimethylsulfonium iodide **1c**[4] prepared in situ by HI and DMSO, the conversion of anilines to iodobenzenes was also investigated. Most of the conversions to iodobenzenes were successful under these conditions. Furthermore, the yields were excellent with a very short reaction time and in most cases by-products were not observed. We were surprised by the high transformation efficiency of sterically hindered and electron-withdrawing group substi-

[3]A high-speed mechanical stirrer with a multiblade paddle was adequate for dissolving KNO_2 for the preparatory-scale reaction.
[4]It is likely that the mechanism of the formation of halodimethylsulfonium halides (**1c**) iododimethylsullfonium iodide, involves reversible formation of a sulfur dichloride (R_2SCl_2) intermediate. See ref. 5*b*. Bromodimethylsulfonium iodide prepared from HBr, DMSO, and I^- via the formation of bromodimethylsulfonium bromide was treated followed by the replacement of bromide with a more nucleophilic iodide, as shown in eq. [6].

© 2005 NRC Canada

Table 4. Transformation of Ar-NH_2 to Ar-I using halodimethylsulfonium iodide.[a]

Entry	Substrate	Halide	Time (min)	Product	Yield (%)[b]
1	*o*-$O_2NC_6H_4NH_2$	**1c**	15	*o*-$O_2NC_6H_4I$	89
2	2-CH_3O-5-O_2N-$C_6H_4NH_2$	**1c**	10	2-CH_3O-5-O_2N-C_6H_4I	93 (88)
3	5-Cl-2-$O_2NC_6H_4NH_2$	**1c**	10	5-Cl-2-$O_2NC_6H_4I$	95 (91)
4	3,5-$(O_2N)_2C_6H_4NH_2$	**1c**	10	3,5-$(O_2N)_2C_6H_4I$	89
5	4-CH_3-2-$O_2NC_6H_4NH_2$	**1c**	10	4-CH_3-2-$O_2NC_6H_4I$	81
6	2,6-$(CH_3)_2C_6H_4NH_2$	**1c**	10	2,6-$(CH_3)_2C_6H_4I$	87
7	2,6-$F_2C_6H_4NH_2$	**1c**	20	2,6-$F_2C_6H_4I$	84
8	*p*-$CH_3OC_6H_4NH_2$	**1c**	10	*p*-$CH_3OC_6H_4I$	85
9	2-CH_3O-5-O_2N-$C_6H_4NH_2$	**1c′**	30	2-CH_3O-5-O_2N-C_6H_4I	81 (73)
10	2,6-$F_2C_6H_4NH_2$	**1c′**	30	2,6-$F_2C_6H_4I$	74
11	4-Aminobenzophenone	**1c′**	30	4-Iodobenzophenone	90
12	2-Aminoanthraquinone	**1c**	20	2-Iodoanthraquinone	90
13	1-Aminonaphthalene	**1c**	30	1-Iodonaphthalene	59
14	1-Aminonaphthalene	**1c′**	30	1-Iodonaphthalene	65
15	1-Aminonaphthalene	**1c** (CuI)[c]	30	1-Iodonaphthalene	93 (88)
16	2-Amino-3-nitropyridine	**1c**	60	2-Iodo-3-nitrophridine	59
17	2-Amino-3-nitropyridine	**1c** (CuI)[c]	60	2-Iodo-3-nitrophridine	89 (81)

[a]**1c**: Reactions were performed by adding 10.0 mmol of the aniline and 40.0 mmol of 57% aq. HI in 25 mL of DMSO to 40.0 mmol of KNO_2 in 25 mL of DMSO. **1c′**: 48% aq. HBr and KI were used instead of HI. The reaction temperature was 35 °C.
[b]Yields were generally determined by GLC analysis by comparison to an internal standard. Isolated yields after column chromatography or recrystallization are given in parentheses.
[c]CuI (0.1 equiv.) was added.

tuted anilines in Table 4 (entries 3–6), where 1-iodo-2,6-dinitrobenzene and 1-iodo-2,6-dimethylbenzene were formed in respective yields of 89% and 87% with a very short reaction time. The reported yield of 1-iodo-2,6-dinitrobenzene for the route with isoamyl nitrite in diiodomethane is only 36% at 105 °C (6). The present method is highly attractive for the preparation of aryl iodides because of the simple one-pot conversion and high yields.

Similar to the formation of bromodimethylsulfonium bromide **1b** from HBr and DMSO, iododimethylsulfonium iodide **1c** is prepared by HI and DMSO (eq. [5]). To confirm the halogen source of halodimethylsulfonium halide, bromodimethylsulfonium iodide **1c′**, prepared from HBr, DMSO, and KI via the formation of bromodimethylsulfonium bromide **1b**, was examined (eq. [6]). As shown in Table 4 (entries 9–11), similar results were obtained using HBr–KI–KNO_2–DMSO, which indicates that bromodimethylsulfonium iodide **1c′** also acts as an excellent halogen source for the replacement of aryldiazonium salt.

[5] $CH_3SOCH_3 \xrightarrow[H_2O]{2HI} [CH_3SCH_3]^+ I^-$ **1c**

[6] $CH_3SOCH_3 \xrightarrow[H_2O]{2\,HBr} [CH_3SCH_3]^+ Br^- \xrightarrow{I^-} [CH_3SCH_3]^+ I^-$ **1c′**

Fluorination

In addition to our study of the direct transformation of aryldiazonium salt to fluoroarenes, some halodimethylsulfonium fluorides were also investigated. Similar reaction protocols were used with various fluoride sources, however, the conversion of aminoarenes to fluoroarenes was not successful even in the presence of CuF. Presumably, the weak nucleophilicity and low acidity of HF may not lead to the formation of halodimethylsulfonium fluoride.

Conclusions

We have described an efficient protocol for the transformation of aminoarenes to iodo-, bromo-, or chloroarenes using in-situ-generated halodimethylsulfonium halides. The present method offers several advantages: (*i*) the amino group in an aromatic compound can be transformed to a halide in reasonable to high yields regardless of a substituent effect; (*ii*) the process is simple and consists of a single step; (*iii*) the reaction time is very short (generally 10~60 min), and the reaction temperature is mild (e.g., at 35 °C); (*iv*) the cost of the hardware is very low; and (*v*) the reaction can minimize environmental pollution.

Experimental section

General

All reagents were used without further purification. Mass spectra were obtained at a 70 eV via GC–MSD coupling. ^1H NMR spectra were recorded on a 300 MHz spectrometer in $CDCl_3$ solution. GLC analyses were performed using a capillary column (25 m × 0.2 mm i.d.). Melting points were determined on a Mel-Temp II apparatus and were uncorrected. All known products were identical in all respects (mp, IR, MS, and NMR) to those previously reported.

© 2005 NRC Canada

General procedure for microscale production — Use of bromodimethylsulfonium bromide prepared by HBr and DMSO

A solution of 48% aq. HBr (2.49 mL, 20.0 mmol) dissolved in DMSO (25 mL) was added dropwise to a solution of aminoarene (5 mmol) in a mixture of 25 mL of DMSO and KNO_2 (1.70 g, 20.0 mmol) at 35 °C with stirring. The added mixture was stirred at 35 °C for the time given in Table 2 and then transferred to a solution of K_2CO_3 (5 g) in 100 mL of ice water. The reaction mixture was then taken up in ether, and the ethereal extracts were washed with water and dried over anhydrous magnesium sulfate. Removal of the solvent under reduced pressure gave the crude product. The crude product was further purified by column chromatography (or recrystallization) to give the product, the mp, and spectral data (^{1}H NMR and GC–MS) all of which were in full agreement with those of an authentic sample.

General procedure for preparative-scale production

A mixture of 2.5 L of DMSO and KNO_2 (85.1 g, 1.0 mol) was vigorously stirred at 60 °C to rapidly dissolve KNO_2, and aminoarene (0.25 mol) was then added.[3] The resulting solution was then cooled to room temperature. Aqueous HBr solution (48%, 124.5 mL, 1.0 mol) diluted with 2.0 L of DMSO was added dropwise at a rate of 20 mL/min, and the mixture was then warmed to 35 °C. The DMSO solution of HBr added to the reaction mixture can be carried off through a long condenser tube. After the usual workup, the crude product was purified by recrystallization.

Preparation of 4-bromoanisole

A mixture of 4-methoxyaniline (0.25 mol, 30.75 g), KNO_2 (85.1 g, 1.0 mol), HBr solution (48%, 124.5 mL, 1.0 mol), and 4.5 L of DMSO was stirred at 60 °C for 2 h. The product was recovered by the standard procedure, yielding 37.87 g of pure 4-bromoanisole (81%).

General procedure for microscale production — Use of iododimethylsulfonium iodide prepared by HI and DMSO

Aminoarene (5.0 mmol) was added to a solution of KNO_2 (1.70 g, 20.0 mmol) in DMSO (25 mL) at 35 °C. Aqueous HI (57%, 2.64 mL, 20 mmol) in DMSO (25 mL) was added, and the reaction mixture was stirred for the time given in Table 4. After the reaction was completed, the cooled reaction mixture was neutralized with 10% aq. Na_2CO_3 and extracted with methylene chloride (3 × 10 mL). The combined methylene chloride extracts were washed with brine and dried over magnesium sulfate. The solvent was removed in vacuo and the residue was chromatographed to give the product, the mp, and spectral data (^{1}H NMR and GC–MS) all of which were in full agreement with those of an authentic sample.

General procedure for microscale production — Use of bromodimethylsulfonium iodide prepared by HBr, KI, and DMSO

To a solution of aminoarene (5.0 mmol) in a mixture of 25 mL of DMSO and KNO_2 (1.70 g, 20 mmol) was added dropwise a solution of 47% HBr (2.49 mL, 20 mmol) and KI (4.15 g, 25 mmol) dissolved in DMSO (25 mL) at 35 °C. When the addition was complete, the mixture was further stirred at 35 °C for an additional 10 min and then transferred to a solution containing K_2CO_3 (5 g) in 100 mL ice water. The reaction mixture was then taken up in ether, and the ethereal extracts were washed with water and dried over anhydrous magnesium sulfate. Removal of the solvent under reduced pressure gave the crude product.

Acknowledgments

This work was supported by the Regional Research Center program of the Ministry of Science and Technology (MOST) and KOSEF-Kyungkido.

References

1. (*a*) E.B. Merkushev. Synthesis, 923 (1988); (*b*) R.C. Larock. Comprehensive organic transformations. 2nd ed. Wiley, New York. 1999. pp. 619–626.
2. (*a*) D.S. Wulfman. The chemistry of diazonium and diazo groups. *Edited by* S. Patai. Wiley, New York. 1978. Chap. 8; (*b*) R.C. Larock. Comprehensive organic transformations. 2nd ed. Wiley, New York. 1999. pp. 678–679; (*c*) J.K. Kochi. J. Am. Chem. Soc. **79**, 2942 (1957); (*d*) S.C. Dickerman, D.J. Desouza, and N. Jacobson. J. Org. Chem. **34**, 710 (1969); (*e*) C.J. Galli. J. Chem. Soc. Chem. Perkin Trans. 2, 897 (1984).
3. (*a*) H.H. Hodgen. Chem. Rev. **40**, 251 (1947); (*b*) L.A. Bigelow. *In* Organic syntheses, collective volumes. Vol. 1. Wiley, New York. 1941. p. 135; (*c*) W.W. Hartman and M.R Brethen. *In* Organic syntheses, collective volumes. Vol. 1. Wiley, New York. 1941. p. 162; (*d*) J.L Hartwell. *In* Organic syntheses, collective volumes. Vol. 3. Wiley, New York. 1955. p. 185.
4. (*a*) M.P. Dolye, B. Siegried, and J.F. Dellaria. J. Org. Chem. **42**, 2426 (1977); (*b*) M.P. Dolye, M.A. Van Lente, R. Mowat, and W.F. Fobare. J. Org. Chem. **45**, 2570 (1980); (*c*) M.P. Dolye and W.J. Bryker. J. Org. Chem. **44**, 1572 (1979); (*d*) W.B. Smith and O.C. Ho. J. Org. Chem. **55**, 2543 (1990); (*e*) V. Nair and S.G. Richardson. J. Org. Chem. **45**, 3969 (1980); (*f*) L. Friedman and J.F. Chlebowski. J. Org. Chem. **33**, 1636 (1967); (*g*) J.G. Lee and H.T. Cha. Tetrahedron Lett. **33**, 3167 (1992); (*h*) H. Suzuki and N. Nonoyama. Tetrahedron Lett. **39**, 4533 (1998); (*i*) C. Giordano, L. Coppi, and M. Paiocchi. US Patent 5 142 093, 1992; (*j*) M.J. Evers, L.E. Christiaens, M.R. Guillaume, and M.J. Renson. J. Org. Chem. **50**, 1779 (1985); (*k*) M.S. Newman and W. Fones. J. Am. Chem. Soc. **69**, 1221 (1947).
5. (*a*) G. Majetich, R. Hicks, and S. Reister. J. Org. Chem. **62**, 4321 (1997); (*b*) K. Mislow, T. Simmons, J. Melillo, and A. Ternary. J. Am. Chem. Soc. **86**, 1452 (1964); (*c*) D. Landini and F. Montari. J. Chem. Soc. Chem. Commun. 86 (1968).
6. S.K. Srivastava, P.M.S. Chauhan, and A.P. Bhaduri. J. Chem. Soc. Chem. Commun. 2679 (1996).
7. (*a*) G. Megyeri and T. Keve. Synth. Commun. **19**, 3415 (1989); (*b*) T. Fletcher and H. Pan. J. Am. Chem. Soc. **78**, 4812 (1956).
8. W.W. Hartman and M.R. Brethen. Organic syntheses, collective volumes. Vol. 1. Wiley, New York. 1941. pp. 162.
9. For reviews, see: (*a*) P.E. Fanta. Synthesis, 9 (1974); (*b*) M. Goshaev, O.S. Otroshchenko, and A.S. Sadykov. Russ. Chem. Rev. **41**, 1046 (1972); (*c*) G. Bringmann, R. Walker, and R. Weirich. Angew. Chem. Int. Ed. Engl. **29**, 977 (1990).
10. (*a*) T.D. Nelson and A.I. Meyers. J. Org. Chem. **59**, 2655 (1994); (*b*) J.C. Salfeld and E. Baume. Tetrahedron Lett. **7**,

© 2005 NRC Canada

3365 (1966); (*c*) A.G. Mack, H. Suschitzy, and B.J. Wakefield. J. Chem. Soc. Perkin Trans. 1, 1682 (1980).
11. (*a*) For reviews, see: N. Miyaura and A. Suzuki. Chem. Rev. **95**, 2457 (1995); (*b*) V. Fiandanese, L. Mazzone, and F. Naso. J. Chem. Soc. Chem. Commun. 2523 (1995).
12. (*a*) J.J. Bozell and C.E. Vogt. J. Am. Chem. Soc. **110**, 2655 (1988); (*b*) R.C. Larock and P.L. Johnson. J. Chem. Soc. Chem. Commun. 1368 (1989); (*c*) R.C. Larock and B.E. Baker. Tetrahedron Lett. **30**, 2603 (1989).

© 2005 NRC Canada

Dew points of quaternary ethane + carbon dioxide + water + methanol mixtures — Measurement and modelling

C. Jarne, S.T. Blanco, S. Avila, C. Berro, S. Otín, and I. Velasco

Abstract: Dew points have been measured for eight ethane + carbon dioxide + water + methanol mixtures at pressures from 0.11 to 2.17 MPa and temperatures from 249.0 to 288.7 K. The results are analysed in terms of a predictive excess-function equation of state (EF-EOS) method based on the zeroth approximation of Guggenheim's reticular model. This method can be used to adequately predict the dew points of the mixtures in the temperature and pressure ranges used in the present study. In fact, the model reproduces the experimental dew point temperature data with ≤3.1 K average absolute deviation.

Key words: dew point, equation of state, excess function.

Résumé : On a mesuré les points de rosée de huit mélanges d'éthane + dioxyde de carbone + eau + méthanol, à des pressions allant de 0,11 à 2,17 MPa et à des températures allant de 249,0 à 288,7 K. On a analysé les résultats en termes d'une méthode basée sur une équation d'état de fonction d'excès permettant de faire des prédictions basées sur l'approximation zéro du modèle réticulaire de Guggenheim. On peut utilizer cette méthode pour prédire adéquatement les points de rosée de mélanges dans les plages de température et de pression utilizées dans la présente étude. En fait, le modèle permet de reproduire les données expérimentales de points de rosée avec une déviation absolue moyenne de moins de 3,1 K.

Mots clés : point de rosée, équation d'état, fonction d'excès.

[Traduit par la Rédaction]

Introduction

To investigate the influence of carbon dioxide, water, methanol and heavy hydrocarbons on the vapour–liquid equilbrium (VLE) of natural gas within the usual pressure and temperature conditions of natural gas transported by pipeline, we have previously studied the following systems: carbon dioxide + water and carbon dioxide + water + methanol (1), methane + carbon dioxide + water (2), ethane + carbon dioxide + water (2) and methane + carbon dioxide + water + methanol (3). Dew point data for the quaternary ethane + carbon dioxide + water + methanol system, which are not available in the literature, are reported in the present work. In addition, we have developed a theoretical model for dew point prediction.

A water + methanol dew point generation device was built and tested in previous studies (4, 5). The results for eight ethane + carbon dioxide + water + methanol mixtures at pressures from 0.11 to 2.17 MPa and temperatures from 249.0 to 288.7 K are presented here. The experimental results obtained for the quaternary mixtures are analysed in terms of a predictive excess-function equation of state (EF-EOS) method based on the zero-order approximation of Guggenheim's reticular model, which reproduces the experimental dew point temperature data with an average absolute deviation (AAD) less than or equal to 3.1 K.

Experimental procedure

The experimental method used in this work is based on the generation of gases saturated with water and methanol by condensation of these components in a temperature-controlled condenser with continuous gas flow at specified pressures.

A schematic diagram of the experimental apparatus is shown in Fig. 1. The gas supply bottles that contain ethane + carbon dioxide mixtures (Table 1) were prepared by weight by Abello-Linde (6). After controlled expansion (RV1), the gas from the ethane + carbon dioxide bottle was saturated with water and methanol vapour by flowing the gas through a saturator containing a liquid mixture of water and methanol at laboratory temperature (TI1). The temperature of con-

Received 9 February 2004. Published on the NRC Research Press Web site at http://canjchem.nrc.ca on 22 March 2005.

C. Jarne, S.T. Blanco, S. Otín, and I. Velasco.[1] Departamento de Química Orgánica y Química Física. Facultad de Ciencias. Universidad de Zaragoza, 50.009 – Zaragoza, Spain.
S. Avila. Technology, Environment and Construction Direction, ENAGAS, S. A., Spain.
C. Berro. Laboratoire de Chimie Physique de Marseille. Faculté des Sciences de Luminy. Université de la Méditerranée, 13.288 – Marseille CEDEX 9, France.

[1]Corresponding author (e-mail: curra@posta.unizar.es).

 doi: 10.1139/V05-040 © 2005 NRC Canada

Fig. 1. Schematic diagram of the experimental apparatus used in this work. Control valve (RV), ball valve (V), three-way valve (HV), temperature measurement (TI), pressure measurement (PI), water content analyser (QI), volume measurement (XI).

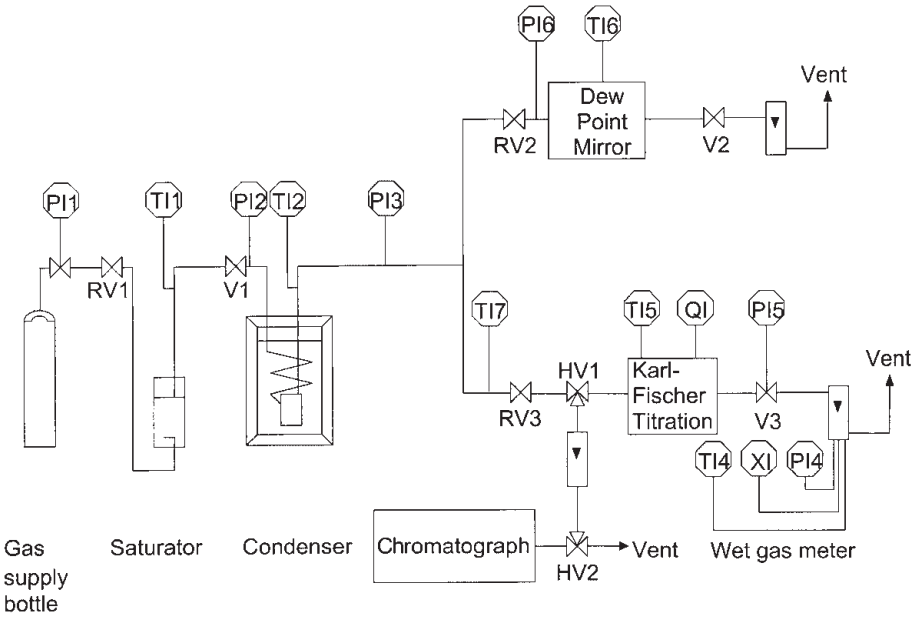


Table 1. Composition of ethane + carbon dioxide mixtures and relative accuracy specified by the supplier.

Component	Gas 1 (%)	Gas 2 (%)
Ethane	55±1	5±1
Carbon dioxide	45±1	95±1

densation of water and methanol was then achieved in a stainless-steel condenser, which was located in a thermostatic bath set at the desired temperature of condensation (TI2). This temperature (TI2) is lower than the temperature in the saturator (TI1). The values for the water and methanol contents in the gas phase of the generated VLE are obtained at the outlet of the condenser using the Karl Fischer titration (7) for water content and by gas chromatographic analysis for methanol content.

The dew point values for the ethane + carbon dioxide + water + methanol mixtures were measured by means of a chilled mirror instrument. The input pressure (PI6) of the gas in the chilled-mirror instrument was set using a regulator valve (RV2). When the apparatus reached a stable dew point temperature (TI6), both the pressure and temperature were recorded.

The following instrumentation is used in the experimental apparatus: a Mitsubishi CA 06 Karl Fischer titrator, coupled with an Elster wet gasmeter Type Gr. 00, E51 to measure the water content (0.2% accuracy); a HP 5890 gas chromatograph fitted with a Haysep Q column and a thermal conductivity detector to measure the methanol content; a MBW dew point instrument (model DP3-D-HP-K2) to measure the dew point temperatures. The cooling of the mirror as achieved by a cascaded-element Peltier cooling unit and the dew-point mirror temperature was opto-electronically controlled; a pressure transmitter to measure the dew point pressures (max error of 0.1%).

Prior to the study of ethane + carbon dioxide + water + methanol mixtures, the precision of the dew point measurements was determined as described previously (4, 5).

Results

We calculated the dew-point curves for gas 1 and gas 2 (Table 1) using the Peng–Robinson equation of state (8). The experimental dew points for the quaternary systems range from 0.11 to 2.17 MPa at temperatures from 249.0 to 288.7 K to avoid the presence of liquid ethane and carbon dioxide in the apparatus.

The water and methanol mol fractions and the dew point temperatures and pressures for the quaternary systems are collected in Table 2.

As shown in Table 2 for ethane + carbon dioxide + water + methanol mixtures with the same ethane and carbon dioxide contents and similar water mol fractions (such as gas 1 + 0.00048 water mol fraction + 0.0033 methanol mol fraction and gas 1 + 0.00040 water mol fraction + 0.0086 methanol mol fraction), increasing the methanol mol fraction in the mixture leads to an increase of the dew point temperature at a given pressure.

For the quaternary mixtures with the same ethane and carbon dioxide contents and similar methanol mol fractions (such as gas 1 + 0.00029 water mol fraction + 0.0049 methanol mol fraction and gas 1 + 0.00083 water mol fraction + 0.0053 methanol mol fraction), increasing the water content also increases the dew point temperature at a given pressure.

On the other hand, the dew point curve of gas 2 is on the right hand side of that of gas 1 in the pressure–temperature diagram. However, if we consider the mixtures gas 1 + 0.00040 water mol fraction + 0.0086 methanol mol fraction and gas 2 + 0.00044 water mol fraction + 0.0083 methanol mol fraction, we observe that, for a given pressure, the values of the dew temperatures are practically the same for the

© 2005 NRC Canada

Table 2. Experimental contents of water and methanol and dew point temperatures and pressures for ethane + carbon dioxide + water ($\bar{x}_{water}$) + methanol ($\bar{x}_{methanol}$) systems.

T (K)	P (10^5 Pa)	T (K)	P (10^5 Pa)
Gas 1: $\bar{x}_{water}$ *= 0.00029 and* $\bar{x}_{methanol}$ *= 0.0049*			
249.0	1.1	278.6	9.7
251.3	1.3	281.8	12.3
255.6	1.9	284.1	14.6
261.0	2.8	284.7	15.2
266.1	4.0	286.4	17.2
270.3	5.5	287.3	18.3
273.9	7.1	287.9	19.1
276.4	8.4	288.6	20.0
Gas 1: $\bar{x}_{water}$ *= 0.00040 and* $\bar{x}_{methanol}$ *= 0.0086*			
255.3	1.1	277.1	4.8
256.2	1.2	281.3	6.3
262.6	1.8	284.1	7.6
265.9	2.3	287.3	9.3
271.1	3.2	288.6	10.1
275.0	4.2		
Gas 1: $\bar{x}_{water}$ *= 0.00048 and* $\bar{x}_{methanol}$ *= 0.0033*			
249.3	1.1	278.9	10.7
252.0	1.4	280.1	11.9
259.5	2.5	281.4	13.1
260.5	2.7	282.5	14.0
265.2	3.9	283.7	15.7
269.4	5.3	284.8	16.9
271.7	6.3	285.5	17.9
273.9	7.4	286.6	19.4
276.1	8.8	287.3	20.5
277.3	9.6	288.1	21.7
Gas 1: $\bar{x}_{water}$ *= 0.00083 and* $\bar{x}_{methanol}$ *= 0.0053*			
255.1	1.1	280.8	7.0
261.7	1.8	283.2	8.3
266.7	2.6	284.2	9.0
271.6	3.7	285.9	10.1
273.9	4.4	287.6	11.1
276.9	5.4	288.2	11.6
279.4	6.4		
Gas 2: $\bar{x}_{water}$ *= 0.00035 and* $\bar{x}_{methanol}$ *= 0.0047*			
249.6	1.1	278.9	9.9
257.3	2.0	282.1	12.5
263.3	3.2	282.9	13.3
267.1	4.2	284.7	15.3
269.7	5.1	286.1	17.0
272.0	6.0	287.2	18.7
274.4	7.1	288.5	21.0
Gas 2: $\bar{x}_{water}$ *= 0.00044 and* $\bar{x}_{methanol}$ *= 0.0083*			
255.9	1.1	280.9	6.1
259.3	1.4	282.9	7.0
263.9	1.9	285.5	8.2
268.0	2.6	287.2	9.2
272.2	3.4	288.7	10.1
277.2	4.8		
Gas 2: $\bar{x}_{water}$ *= 0.00057 and* $\bar{x}_{methanol}$ *= 0.0034*			
250.4	1.1	279.9	10.6
250.9	1.1	281.5	12.0
256.8	1.8	284.1	14.7
260.8	2.4	285.1	16.1
266.8	3.9	286.0	17.1
270.6	5.2	286.9	18.2
274.2	6.9	287.8	20.0
276.3	8.0	288.3	20.9
Gas 2: $\bar{x}_{water}$ *= 0.00086 and* $\bar{x}_{methanol}$ *= 0.0056*			
255.4	1.2	281.5	7.3
262.7	1.8	283.0	8.1
267.1	2.6	284.8	9.3
268.9	3.0	286.0	10.1
273.2	4.1	287.3	11.0
276.0	5.0	288.2	11.7
279.0	6.1		

two quaternary mixtures. Therefore, it seems that the values of dew temperature and pressure for the quaternary mixtures are more sensitive to the water and methanol content than to the ethane and carbon dioxide content. Similar results were found for methane + carbon dioxide + water + methanol mixtures in an earlier work (3).

In a previous study (2), the dew points of ethane + carbon dioxide + water mixtures were studied. When comparing the results from the present work for ethane + carbon dioxide + water + methanol with the results of the previous study (2) for mixtures with the same ethane, carbon dioxide, and water content, we found that the presence of methanol in the mixtures leads to a displacement of the dew point curves to higher values of dew point temperature and pressure. This is observed for gas 1 + 0.00083 water mol fraction + 0.0053 methanol mol fraction (Table 2), gas 1 + 0.00082 water mol fraction (2), gas 2 + 0.00086 water mol fraction + 0.0056 methanol mol fraction (Table 2) and gas 2 + 0.00091 water mol fraction (2). At a given pressure, the difference between the dew temperature values of the mixture with methanol and without methanol are up to 7 K.

Discussion

As mentioned earlier, this work is part of a program of research investigating the influence of carbon dioxide, water, methanol, and heavy compounds of natural gases on the VLE of natural gas. Therefore, the ranges of dew temperature and pressure are studied within the typical ranges for natural gas transmission through pipelines, which means temperatures from 249 to 288 K and pressures up to 10 MPa. Although classical models such as UNIQUAC (9), DISQUAC (10), or modified UNIFAC (11) allow the prediction of vapour–liquid equilibria at low pressures for systems that contain polar compounds, they are not suitable for the present work. Instead, we use in this work the EF-EOS model, which is based on the zeroth-order approximation of Guggenheim's quasi-reticular model. In the EF-EOS model, which is an extension of the development originally presented by Vidal (12), the connection between excess functions and equations of state is established by equating excess

© 2005 NRC Canada

functions derived from Guggenheim's quasi-lattice theory to expressions derived from equations of state (13).

A comparison between experimental and calculated dew point temperatures was carried out. The values of dew temperature for the system investigated were calculated by means of the EF-EOS method (13) using the experimental values of pressure and composition obtained in the present work.

The EF-EOS model has been chosen because it can be used to adequately predict the dew points of all the mixtures of present interest in the temperature and pressure ranges. The model satisfies two important conditions: (1) the Helmholtz energies of the pure components are calculated by an equation of state; (2) the excess functions are defined at a constant packing fraction described by v^0/v, where v^0 is the molar close-packed volume and v the molar volume. It is assumed that it is possible to define a "co-volume" b proportional to v^0, which allows the evaluation of the packing fraction η by the ratio $\eta = b/v$. The packing fraction for the pure components and for the mixture is assumed to be the same, which means that the lattice on which the pure components are placed undergoes no distortion during the mixing process.

Regarding the EOS used in the EF-EOS model, given that the thermodynamic properties of carbon dioxide, such as saturation density, are often represented by cubic equations of state with poor accuracy, we have used for this component the more accurate IUPAC equation of state (14).

For ethane, water, and methanol, the translated Peng–Robinson cubic equation of state is used (13, 15). The name for this equation is due to the use of a translated molar volume $\bar{v}$ called the pseudo-molar volume (16) instead of the molar volume as for the Peng–Robinson cubic equation of state.

$$[1] \qquad P = \frac{RT}{\bar{v} - \bar{b}} - \frac{a(T)}{\bar{v}(\bar{v} + \gamma\bar{b})}$$

where P and T are the system pressure and temperature, R is the gas constant, $\bar{b}$ is the pseudo-co-volume, and γ is a constant. For ethane, the equations proposed by Rauzy (15) are used to calculate a, and for $\bar{b}$, the equations proposed by Péneloux et al. (13) and Rauzy (15) are used.

For water and methanol, the attractive parameter a is calculated using the equations taken from Carrier et al. (16) and Carrier (17). For the pseudo co-volume $\bar{b}$, the equations used are those of Péneloux et al. (13) and Rauzy (15).

The excess function of the EF-EOS model is the residual excess Helmholtz energy ($A^{\mathrm{E}}_{\mathrm{res}}$), which contributes to the molar Helmholtz energy (A) of the mixtures as follows

$$[2] \qquad A = A^{\mathrm{id}} - RT\ln(1-\eta) - \sum_{i=1}^{p} \frac{x_i}{b_i}\psi_i(\eta) + A^{\mathrm{E}}_{\mathrm{res}}$$

where A^{id} is the ideal mixture molar Helmholtz energy, b_i is the molar co-volume for the component i, $\psi_i(\eta)$ is a function of the packing fraction, and x_i is the molar fraction for component i in the mixture. The residual excess Helmholtz energy ($A^{\mathrm{E}}_{\mathrm{res}}$) is a function in which composition x and packing fraction η are separated variables

Table 3. Values for E^0_{ij} and r used in this work (eq. [6]).

Binary	E^0_{ij} (J cm^{-3})	r
CO_2 + CH_3OH	673.15	–1.319
H_2O + CH_3OH	253.20	–3.068

$$[3] \qquad A^{\mathrm{E}}_{\mathrm{res}}(T, x, \eta) = E(T, x)\int_0^{\eta} (Q'(\eta)/\eta)\mathrm{d}\eta$$

where $Q'(\eta)$ is a function of the packing fraction.

For the first factor on the right-hand side of eq. [3], different equations are used depending on the binary interaction that is present in the mixture. For binary interactions between carbon dioxide and water, carbon dioxide and methanol, carbon dioxide and ethane, and water and methanol (18), we used

$$[4] \qquad E(T, x) = \frac{1}{2}\sum_{i=1}^{p}\sum_{j=1}^{p} \frac{q_i q_j x_i x_j}{q_{\mathrm{m}}} E_{ij}(T)$$

where the subscripts i and j refer to the components i and j of the mixture with p components, q_i is the molecular surface of the component i, q_{m} is the mean molecular surface, and E_{ij} is the interaction energy between components i and j. E_{ij} is calculated using the following equation for binary interactions between carbon dioxide and water (18)

$$[5] \qquad E_{ij} = \alpha - \beta T\ln(T) + \lambda T$$

where α = 5018.172 J cm^{-3}, β = 13.645 J cm^{-3} K^{-1}, and λ = 102.580 J cm^{-3} K^{-1} are adjusted parameters taken from Rauzy and Péneloux (1986) (18).

E_{ij} is calculated for binary interactions between carbon dioxide and methanol, and between water and methanol (18) using

$$[6] \qquad E_{ij} = E^0_{ij}\left[\frac{T^0}{T}\right]^r$$

E^0_{ij} is the interaction energy at the reference temperature T^0 and r is an adjusted parameter taken from Rauzy and Péneloux (18) and listed in Table 3.

E_{ij} is calculated for binary interactions between carbon dioxide and ethane by means of a group contribution method as follows (19)

$$[7] \qquad E_{ij} = -\frac{1}{2}\sum_{k=1}^{N}\sum_{l=1}^{N} (\alpha_{ik} - \alpha_{jk})(\alpha_{il} - \alpha_{jl})A_{kl}(T)$$

where the subscripts k and l refer to the groups k and l of the components of the mixture with N groups, α_{ik} is the surface area fraction of group k in molecule i, and A_{kl} is the group interaction parameter between groups k and l taken from ref. 19.

The binary interactions between ethane and water and between ethane and methanol (20) were calculated using

© 2005 NRC Canada

Table 4. Values of the group interaction parameters ${}_1A_{kl}^0$, ${}_1B_{kl}^0$, ${}_2A_{kl}^0$, and ${}_2B_{kl}^0$ used in this work (eqs. [13] and [15]).

Binary	${}_1A_{kl}^0$	${}_1B_{kl}^0$	${}_2A_{kl}^0$	${}_2B_{kl}^0$
$C_2H_6 + H_2O$	1288.287 (20)	–1.56 (20)	5946.637 (21)	0.39 (21)
$C_2H_6 + CH_3OH$	264.046[a]	0.783[a]	1272.672[a]	–0.931[a]

[a]This work.

$$[8] \quad E(T,x) = \frac{1}{2q_m}\left[\sum_{i=1}^{p} q_i x_i \left(\sum_{j=1}^{p} q_j x_j K_{ij}\right) + \sum_{i=1}^{p} q_i x_i \left(\sum_{j=1}^{p} q_j^{1/3} x_j L_{ji}^{1/3}\right)\right]$$

where K_{ij}, L_{ij} are binary interaction parameters calculated using the following equations

$$[9] \quad K_{ij} = \frac{E_{ij}^1 + E_{ij}^2}{2}$$

$$[10] \quad L_{ij} = E_{ij}^2 - E_{ij}^1$$

$$[11] \quad L_{ij} = -L_{ji}$$

E_{ij}^1 the interchange energy between components i and j in a binary mixture where the mol fraction of j tends to zero, while E_{ij}^2 is the interchange energy in a binary mixture of i and j where the mol fraction of i tends to zero. E_{ij}^1 and E_{ij}^2 are calculated using a group contribution method as follows (20)

$$[12] \quad E_{ij}^1 = -\frac{1}{2}\sum_{k=1}^{N}\sum_{l=1}^{N}(\alpha_{ik} - \alpha_{jk})(\alpha_{il} - \alpha_{jl})A_{kl}^1(T)$$

with

$$[13] \quad A_{kl}^1 = {}_1A_{kl}^0\left(\frac{T^0}{T}\right)^{{}_1B_{kl}^0}$$

$$[14] \quad E_{ij}^2 = -\frac{1}{2}\sum_{k=1}^{N}\sum_{l=1}^{N}(\alpha_{ik} - \alpha_{jk})(\alpha_{il} - \alpha_{jl})A_{kl}^2(T)$$

$$[15] \quad A_{kl}^2 = {}_2A_{kl}^0\left(\frac{T^0}{T}\right)^{{}_2B_{kl}^0}$$

Superscripts 1 and 2 for A_{kl}^1 and A_{kl}^2 have the same meaning as previously explained for E_{ij}^1 and E_{ij}^2 and ${}_1A_{kl}^0$, ${}_1B_{kl}^0$ and ${}_2A_{kl}^0$, ${}_2B_{kl}^0$ are group interaction parameters at the reference temperature T^0. The values for these parameters are presented in Table 4. The parameters for interchange energies between ethane + water were taken from previous studies (20, 21). In the present work, these parameters for the interchange energy between ethane and methanol are calculated using previously reported vapour–liquid equilibrium data for ethane + methanol mixtures (22–24).

Conclusions

The measured dew point curves and calculated values using the EF-EOS method are presented in Figs. 2–5. Values of AAD are calculated using eq. [16] and listed for each dew point curve in Table 5.

$$[16] \quad \text{AAD} = \frac{1}{N}\sum_{n=1}^{N}\left|T_n^{exp} - T_n^{calc}\right|$$

where N is the number of measured dew points that constitute an experimental dew point curve and T is the dew temperature.

Fig. 2. Comparison of measured dew points (symbols) and calculated values using the EF-EOS method (curves) for {Gas 1 + $\bar{x}_{water}$ + $\bar{x}_{methanol}$} systems: $\bar{x}_{water}$ = 0.000 29, $\bar{x}_{methanol}$ = 0.0049 (●); $\bar{x}_{water}$ = 0.000 40, $\bar{x}_{methanol}$ = 0.0086 (○).

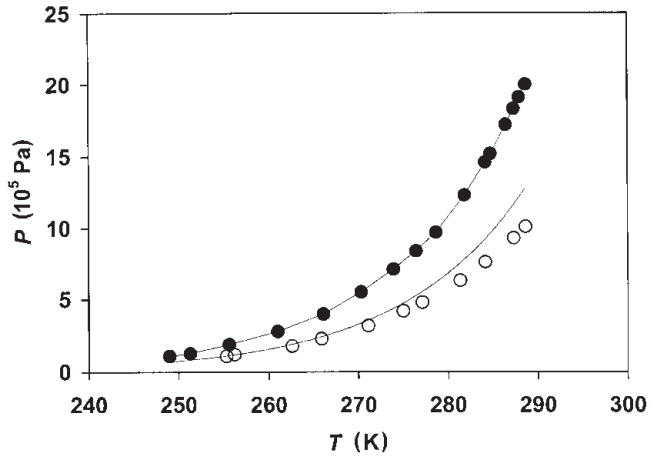
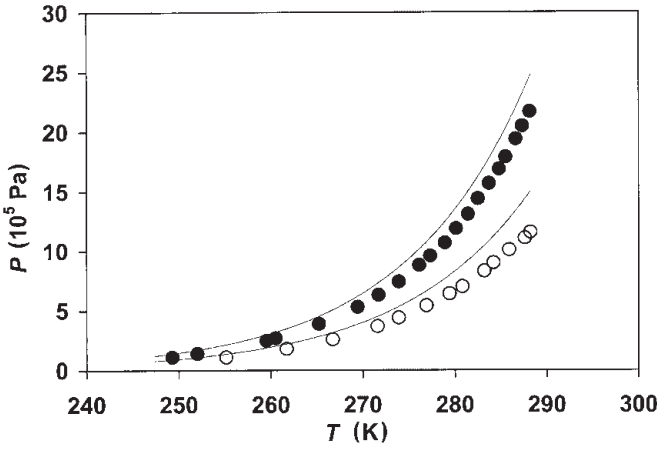


Fig. 3. Comparison of measured dew points (symbols) and calculated values using the EF-EOS method (curves) for {Gas 1 + $\bar{x}_{water}$ + $\bar{x}_{methanol}$} systems: $\bar{x}_{water}$ = 0.000 48, $\bar{x}_{methanol}$ = 0.0033 (●); $\bar{x}_{water}$ = 0.000 83, $\bar{x}_{methanol}$ = 0.0053 (○).



© 2005 NRC Canada

Table 5. Water and methanol contents for ethane + carbon dioxide + water ($\bar{x}_{water}$) + methanol ($\bar{x}_{methanol}$) systems, experimental ranges of dew temperatures and pressures and values of AAD for the dew point curves.

Ethane + carbon dioxide mixture	$\bar{x}_{water}$	$\bar{x}_{methanol}$	T range (K)	P range (10^5 Pa)	AAD (K)
Gas 1	0.000 29	0.0049	249.0–288.6	1.1–20.0	0.0
Gas 1	0.000 40	0.0086	255.3–288.6	1.1–10.1	1.7
Gas 1	0.000 48	0.0033	249.3–288.1	1.1–21.7	2.0
Gas 1	0.000 83	0.0053	255.1–288.2	1.1–11.6	3.0
Gas 2	0.000 35	0.0047	249.6–288.5	1.1–21.0	0.7
Gas 2	0.000 44	0.0083	255.9–288.7	1.1–10.1	1.2
Gas 2	0.000 57	0.0034	250.4–288.3	1.1–20.9	1.9
Gas 2	0.000 86	0.0056	255.4–288.2	1.2–11.7	3.1

Fig. 4. Comparison of measured dew points (symbols) and calculated values using the EF-EOS method (curves) for {Gas 2 + $\bar{x}_{water}$ + $\bar{x}_{methanol}$} systems: $\bar{x}_{water}$ = 0.000 35, $\bar{x}_{methanol}$ = 0.0047 (●); $\bar{x}_{water}$ = 0.000 44, $\bar{x}_{methanol}$ = 0.0083 (○).

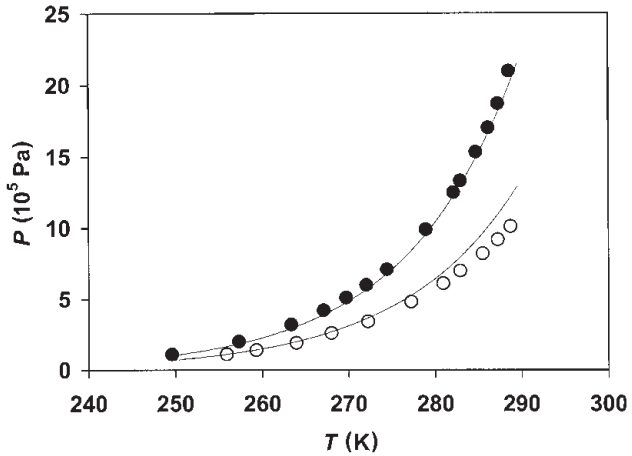
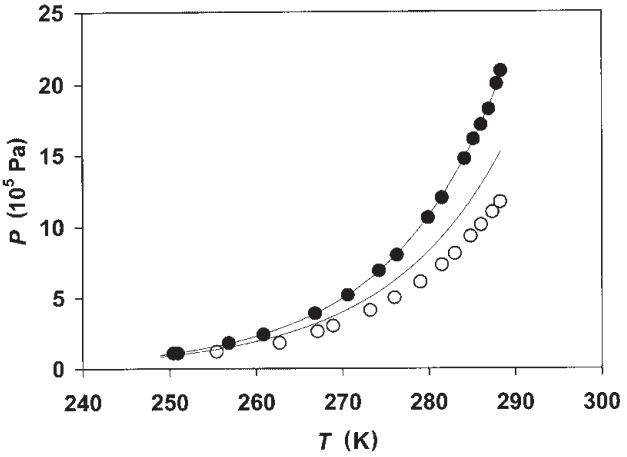


Fig. 5. Comparison of measured dew points (symbols) and calculated values using the EF-EOS method (curves) for {Gas 2 + $\bar{x}_{water}$ + $\bar{x}_{methanol}$} systems: $\bar{x}_{water}$ = 0.000 57, $\bar{x}_{methanol}$ = 0.0034 (●); $\bar{x}_{water}$ = 0.000 86, $\bar{x}_{methanol}$ = 0.0056 (○).



The AAD values for the studied quaternary systems are ≤3.1 K. No influence of temperature and pressure is found for the values of the deviations. The good agreement with the predictions obtained in this paper using the EF-EOS method validates this model for the prediction of dew points of the investigated ethane + carbon dioxide + water + methanol mixtures in our work.

Because the EF-EOS model uses a group contribution model, the availability of binary experimental data corresponding to every binary interaction in the mixture is not necessary. In view of this feature and the good results obtained with this model in this work and previous studies (1–3, 25), the EF-EOS model could be used to predict reliable dew points for hydrocarbons, water and water + methanol in real natural gases, even though binary experimental data for all components of the so-called C_6 + fraction are not available.

Acknowledgments

This work is part of research project 2FD97-2078 financially supported by the Science and Technology Ministry of Spain and FEDER funds. The authors also acknowledge the technical support of ENAGAS, S. A.

References

1. C. Jarne, S.T. Blanco, M. Artal, E. Rauzy, S. Otín, and I. Velasco. Fluid Phase Equilib. **216**, 85 (2004).
2. C. Jarne, S.T. Blanco, M.A. Gallardo, E. Rauzy, S. Otín, and I. Velasco. Energy Fuels, **18**, 396 (2004).
3. C. Jarne, S.T. Blanco, J. Fernández, E. Rauzy, S. Otín, and I. Velasco. Ind. Eng. Chem. Res. **43**, 662 (2004).
4. S.T. Blanco, I. Velasco, E. Rauzy, and S. Otín. Fluid Phase Equilib. **161**, 107 (1999).
5. S.T. Blanco, I. Velasco, E. Rauzy, and S. Otín. Can. J. Chem. **78**, 1587 (2000).
6. ISO 6142:2001.
7. ISO 10101:1993.
8. D.Y. Peng and D.B. Robinson. Ind. Eng. Chem. Fundam. **15**, 59 (1976).
9. D.S. Abrams and J.M. Prausnitz. AIChE J. **2**, 116 (1975).
10. H.V. Kehiaian. Fluid Phase Equilib. **13**, 243 (1983).
11. B.L. Larsen, P. Rasmussen, and A. Fredenslund. Ind. Eng. Chem. Res. **26**, 2274 (1987).
12. J. Vidal. Chem. Eng. Sci. **33**, 787 (1978).
13. A. Péneloux, W. Abdoul, and E. Rauzy. Fluid Phase Equilib. **47**, 115 (1989).
14. S. Angus, B. Armstrong, and K.M. de Reuck. IUPAC international thermodynamic tables of the fluid state. Vol. 3. Carbon dioxide. Peramon Press, Oxford. 1976. pp. 44–79.

© 2005 NRC Canada

15. E. Rauzy. Thèse d'Etat–Sciences, Université Aix-Marseille II, France. 1982.
16. B. Carrier, M. Rogalski, and A. Péneloux. Ind. Eng. Chem. Res. **27**, 1714 (1988).
17. B. Carrier. Thèse de Docteur en Sciences, Université Aix-Marseille III, France. 1989.
18. E. Rauzy and A. Péneloux. Int. J. Thermophys. **7**, 635 (1986).
19. C. Berro, L. Barna, and E. Rauzy. Fluid Phase Equilib. **114**, 63 (1996).
20. H. Hocq. Thèse en Sciences, Université de Droit, d'Economie et des Sciences d'Aix-Marseille III, France. 1994.
21. S. Blanco, S. Ávila, I. Velasco, E. Rauzy, and S. Otín. Fluid Phase Equilib. **171**, 233 (2000).
22. C.B. Kretschmer and R. Wiebe. J. Am. Chem. Soc. **74**, 1276 (1952).
23. X. Nanping, D. Junhaug, W. Yanru, and S. Jun. Fluid Phase Equilib. **81**, 175 (1992).
24. W. Weber, S. Zeck, and H. Knapp. Fluid Phase Equilib. **18**, 253 (1984).
25. C. Jarne, S. Avila, S.T. Blanco, E. Rauzy, S. Otín, and I. Velasco. Ind. Eng. Chem. Res. **43**, 209 (2004).

List of symbols

- a equation of state attractive energy parameter (Pa m^6 mol^{-2})
- A molar Helmholtz energy (J mol^{-1})
- A_{kl} group interaction parameter between groups k and l (J m^{-3})
- AAD absolute average deviation (K)
- b co-volume; equation of state size parameter (m^3 mol^{-1})
- $\bar{b}$ pseudo co-volume (m^3 mol^{-1})
- E_{ij} interchange energy (J m^{-3})
- E_{ij}^0 interaction energy at the reference temperature T^0 for binary interactions between carbon dioxide and methanol, and between water and methanol (J m^{-3})
- E_{ij}^1, E_{ij}^2 interchange energy between ethane and water or methanol (J m^{-3})
- K_{ij}, L_{ij} binary interaction parameters for ethane–water and ethane–methanol (J m^{-3})
- N number of groups in a solution
- N for calculating AAD, number of dew points that constitute a dew point curve
- p number of components in the mixture
- P pressure (Pa)
- q molecular surface (m^2); $q_i = \delta_i b_i$ with d_i an adjustable parameter and b_i the co-volume for component i
- Q' a packing fraction function
- r adjusted parameter in the EF-EOS model
- R gas constant (8.314 J mol^{-1} K^{-1})
- T temperature (K)
- T^0 reference temperature (298.15 K)
- v molar volume (m^3 mol^{-1})
- v^0 molar close packed volume (m^3 mol^{-1})
- $\bar{v}$ molar pseudo volume (m^3 mol^{-1})
- x mol fraction
- $\bar{x}_{water}$ experimental mean value of the water mol fraction
- $\bar{x}_{methanol}$ experimental mean value of the methanol mol fraction
- α adjusted parameter in the EF-EOS model (J cm^{-3})
- α_{ik} surface area fraction of group k in molecule i
- β adjusted parameter in the EF-EOS model (J cm^{-3} K^{-1})
- γ constant in the translated PR-EOS
- η packing fraction
- λ adjusted parameter in the EF-EOS model (J cm^{-3} K^{-1})
- Ψ function of the packing fraction

Superscripts and subscripts

- calc calculated
- exp experimental
- E excess property
- id ideal solution property
- i, j referring to components i, j
- k, l referring to groups k, l
- m referring to a mean molecular value
- n referring to a point of a dew point curve in the calculation of AAD
- res residual

© 2005 NRC Canada

Substituent effects of the cycloaddition reaction of 7-substituted 5*H*-benzocycloheptenes with singlet oxygen and the chemistry of the benzocycloheptene endoperoxides

Murat Güney, Zeynep Çelik Ceylan, Arif Daştan, and Metin Balci

Abstract: The cycloaddition reaction of 7-substituted 5*H*-benzocycloheptenes with singlet oxygen and the chemistry of the obtained endoperoxides were investigated. Reaction of carboethoxy-substituted endoperoxide with NEt_3 gave a mixture of products; hydroxyketone, diketone, and carboethoxy-substituted keto–enol tautomers, whereas the reaction of methyl-substituted endoperoxide only formed a diketone under the same reaction conditions. Thermolysis, thiourea, and CoTPP reactions of the endoperoxides were also studied. The reaction mechanism and electronic effect of substituents were discussed.

Key words: benzocycloheptene, photooxygenation, endoperoxides, rearrangement, CoTPP.

Résumé : On a étudié la réaction de cycloaddition de 5*H*-benzocycloheptènes substitués en position 7 avec de l'oxygène singulet et la chimie des endoperoxydes obtenus. Alors que la réaction du NEt_3 avec de l'endoperoxyde substitué par un groupe méthyle conduit uniquement à la formation d'une dicétone, la réaction dans les mêmes conditions de l'endoperoxyde substitué par un groupe carboéthoxy fournit des mélanges de produits, tels des hydroxycétone, dicétone et tautomères céto–énoliques substitués par un groupe carboéthoxy. On a aussi étudié la thermolyse des endoperoxydes et leurs réactions avec la thiourée et le CoTPP. On discute du mécanisme réactionnel et de l'effet électronique des substituants.

Mots clés : benzocycloheptène, photooxygénation, endoperoxydes, réarrangement, CoTPP.

[Traduit par la Rédaction]

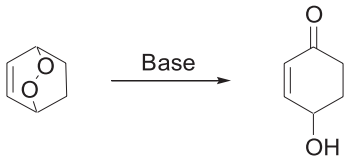
Introduction

Bicyclic endoperoxides serve as key substances in a variety of chemical and biological transformations (1). They can be readily synthesized by the photooxygenation of the appropriate dienes (1). The peroxide linkage is highly susceptible to reductive cleavage as well as to acid- and base-catalyzed rearrangements. The base-catalyzed decomposition of unsaturated bicyclic endoperoxides is a general type of elimination reaction (1, 2). The application of this reaction to bicyclic endoperoxides results in the formation of hydroxyenones (Scheme 1) (3).

The reaction of unsaturated bicyclic endoperoxides derived from cycloheptatriene and its derivatives with bases should open up an entry to the synthesis of tropone and tropolone derivatives. For example, cycloheptatriene endoperoxide gives tropone upon treatment with a base such as triethylamine (4). In earlier research, we applied the triethylamine-catalyzed reaction of the endoperoxide **3** derived from benzocycloheptene, to the synthesis of benzotropone and benzotropolone derivatives. Instead of the expected hydroxy-ketone **4**, the saturated 1,4-diketone **5** was isolated as the sole product in an almost quantitative yield (5). This rearrangement, the transformation of **3** into **5**, is an unusual reaction observed in the chemistry of bicyclic endoperoxides (Scheme 2).

To shed some light onto the generality of this reaction and to study the applicability (6) of the bicyclic endoperoxides derived from benzocycloheptene to the synthesis of benzotropone derivatives, we have synthesized two derivatives **10** and **13** containing electron-withdrawing and electron-donating substituents. In this paper, we report on the synthesis of these compounds and their photooxygenation reactions and transformations.

Scheme 1.



1 **2**

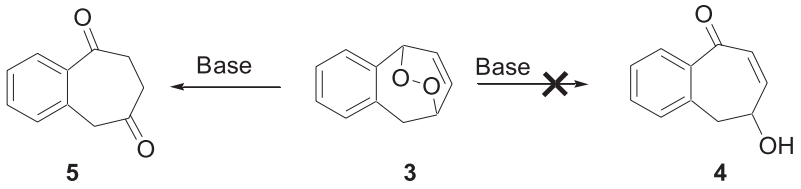
Received 27 August 2004. Published on the NRC Research Press Web site at http://canjchem.nrc.ca on 23 March 2005.

M. Güney and A. Daştan.[1] Department of Chemistry, Atatürk University, 25240, Erzurum, Turkey.
Z.Ç. Ceylan. Department of Environmental Engineering, Atatürk University, 25240, Erzurum, Turkey.
M. Balci.[2] Department of Chemistry, Middle East Technical University, 06531, Ankara, Turkey.

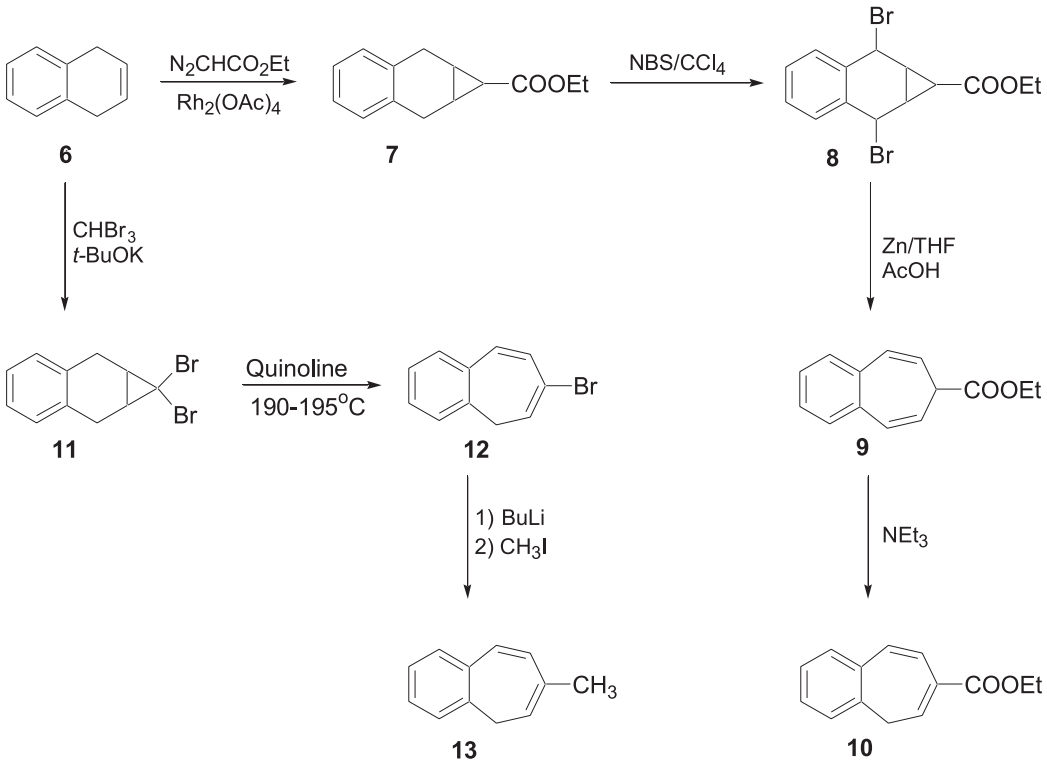
[1]Corresponding author (e-mail: adastan@atauni.edu.tr).
[2]Corresponding author (e-mail: mbalci@metu.edu.tr).

 doi: 10.1139/V05-046 © 2005 NRC Canada

Scheme 2.



Scheme 3.



Results and discussion

The starting materials **10** and **13** were synthesized starting from dihydronaphthalene **6**. The addition of carbenes to an aromatic compound is an important method for the construction of seven-membered rings (7). However, the yields are usually not good and the reactions are without selectivity. Therefore, the Rh(II)-catalyzed cyclopropanation of the dihydronaphthalene **6** was performed with ethyl diazoacetate to give **7** (8). Bromination of **7** with NBS followed by Zn elimination produced the benzocycloheptatriene derivative **9** (9). The base-catalyzed isomerization of **9** with triethylamine afforded the conjugated isomer **10** in a 94% yield. For the synthesis of methyl derivative **13**, dibromocarbene was added to **6** to afford **11**. The ring expansion with quinoline followed by HBr elimination of **11** produced the vinyl bromide **12** (9) in a high yield. The halogen-metal exchange of the bromine atoms in **12** with *n*-BuLi followed by quenching with CH_3I furnished the target compound, methylbenzocycloheptene **13** (10) (Scheme 3).

The photooxygenation of benzocycloheptene derivatives **10** and **13** was carried out by the bubbling of oxygen in carbon tetrachloride while irradiating with a 500 W lamp in the presence of tetraphenylporphine as a sensitizer. ^{1}H NMR monitoring indicated complete consumption of **13** after 24 h, but ester **10** only after 9 days (Scheme 4).

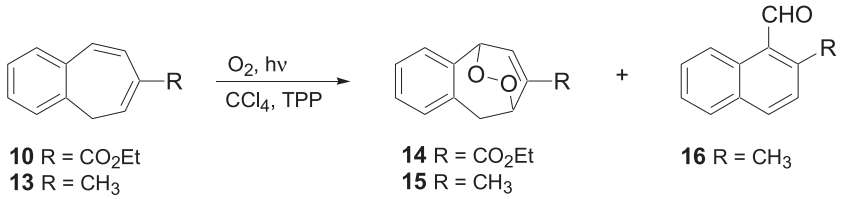
In contrast to the parent hydrocarbon,[3] the ester derivative **10** formed the endoperoxide **14** as the sole compound in 94% yield. On the other hand, the photooxygenation of **13** formed a mixture consisting of the expected bicyclic endoperoxide **15** and naphthalene derivative **16**. Formation of naphthaldehyde **16** from **13** may be explained by the [2 + 2]-cycloaddition of singlet oxygen to the electron-rich double bond. The formed dioxetane can easily undergo a ring cleavage reaction to give the dicarbonyl compound **18**, which in turn can undergo intramolecular Aldol-type condensation reactions (11) to form naphthaldehyde **16** (Scheme 5).

In the case of ester **10**, a [2 + 2]-cycloaddition product was not observed, which was probably due to the electron-withdrawing effect of the ester group, which decreases the electron density at the double bond. The deactivation effect

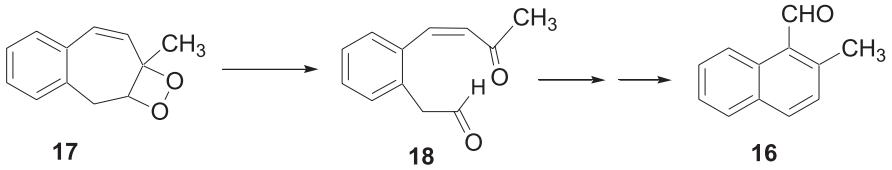
[3] See ref. 5. The parent compound forms four products: a [2 + 4]-cycloaddition product, a dialdehyde formed by the cleavage of the initially formed dioxetane, naphthalene, and naphthaldehyde.

© 2005 NRC Canada

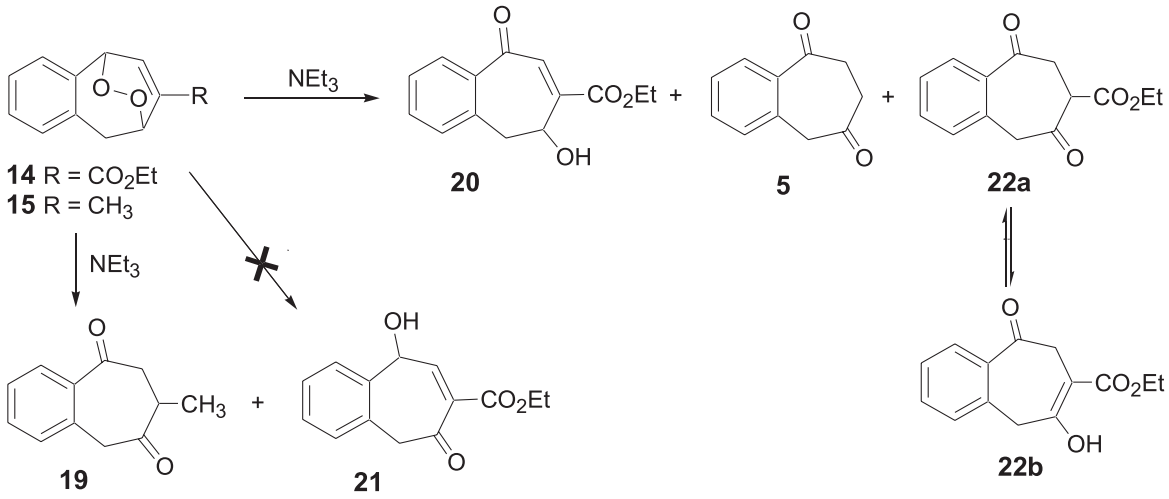
Scheme 4.



Scheme 5.



Scheme 6.



of the ester group was also reflected in the reaction time of **10**, which was converted in 9 days to endoperoxide **14**.

NEt_3-catalyzed reaction of the endoperoxides 14 and 15

The NEt_3-catalyzed reaction of endoperoxide **15** gave only diketone **19** in 90% yield, whereas the reaction of **14** under the same reaction conditions resulted in the formation of three products: hydroxy ketone **20** (37%), diketone **5** (18%), and **22a/22b** (45%) (Scheme 6).

The formation of diketones during the NEt_3-catalyzed reaction of the bicyclic endoperoxide was observed before (5). Contrary to diketone **19**, diketoester **22a** was in equilibrium with its enol form **22b** because of the conjugation of the enol double bond with the ester carbonyl group. Both isomers were observed by NMR spectroscopy in a ratio of 64:36. The signal at δ 12.49 ppm showed the hydroxyl proton of the enol form, which was exchanged upon treatment with D_2O. The singlets at 3.91 and 3.73 ppm were assigned to the methylene protons of the enol form. In the keto form, these methylenic protons appear as AB systems. It is noteworthy that the compound prefers to crystallize in enol form, which allowed us to observe the enol structure **22b** spectroscopically. When the crystalline enol **22b** was dissolved in $CDCl_3$ and the NMR spectrum measured immediately only the enol was observed, and on standing the equilibrium mixture was formed after 2 h. The product **20** was an expected, rearranged product. Methyl derivative **15** did not form any trace of the corresponding hydroxyenone. According to the mechanism of base-catalyzed endoperoxide rearrangement (12), the first step of the reaction includes an abstraction of the α-proton to give a carbanion intermediate. In the second step, the electron pair of the carbanion causes heterolytic cleavage of the peroxide linkage. Finally, in the last step, the formed alkoxide anion captures a proton to form the expected rearranged product **20** (Scheme 7).

The isolated hydroxyketone **20** was treated under the same reaction conditions with NEt_3, to see whether **20** will be converted into **22a/22b** or not. It was shown that ketone **20** was stable. Therefore, it may be assumed that hydroxyketone **20** was not an intermediate. To observe the nature of the intermediate, the reaction of endoperoxide **15** (5*c*) with NEt_3 was monitored by ^1H NMR spectroscopy. After 25 h, we observed a new AB system at 3.92 and 3.68 ppm with a coupling constant of J_{AB} = 14.0 Hz. This coupling constant indicated the formation of a ring-contracted product **28** as we have observed previously (5). We assume that the primarily formed alkoxide **26** attacks the carbonyl group and forms a cyclic ether **28**, which can then rearrange rapidly

© 2005 NRC Canada

Scheme 7.

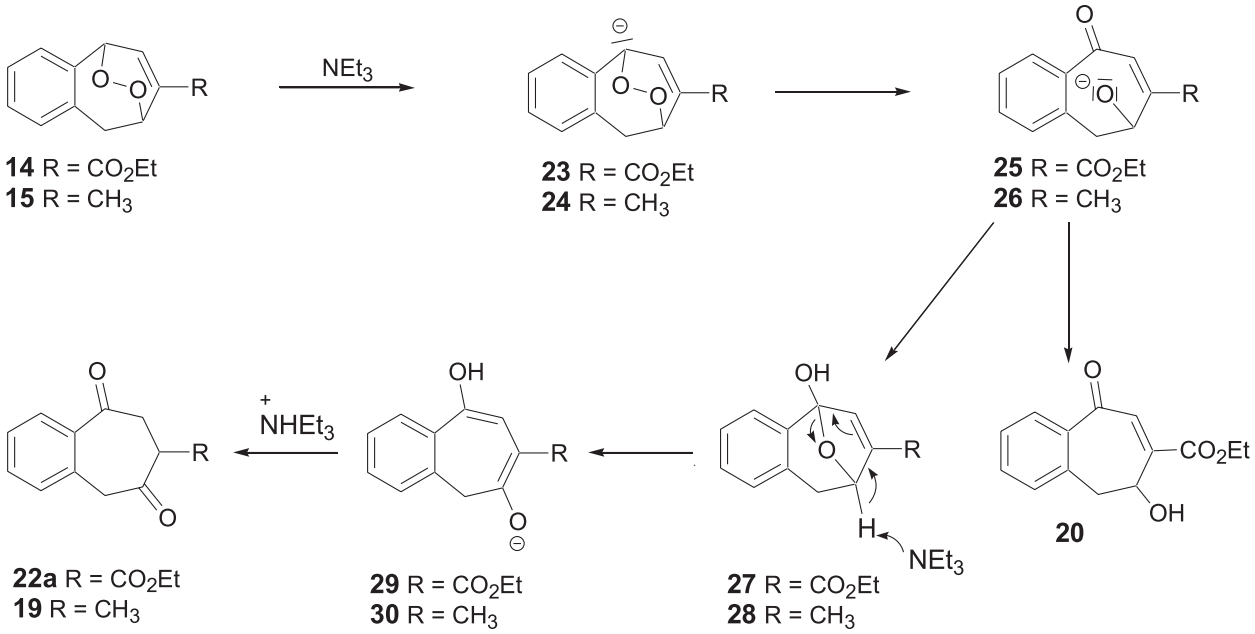
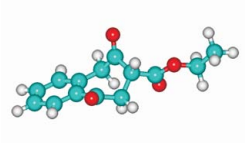
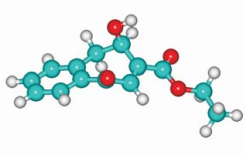
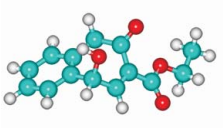
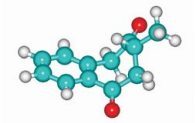
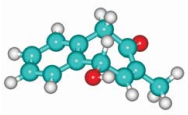
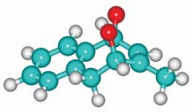


Fig. 1. AM1 optimized geometries, relative energies of the diketones, and the corresponding hydroxyketones.

Compounds	 **22a**	 **20**	 **21**
Relative energies in kcal/mol	0.0	12.22	14.15
Compounds	 **19**	 **37**	 **38**
Relative energies in kcal/mol	0.0	8.23	9.56

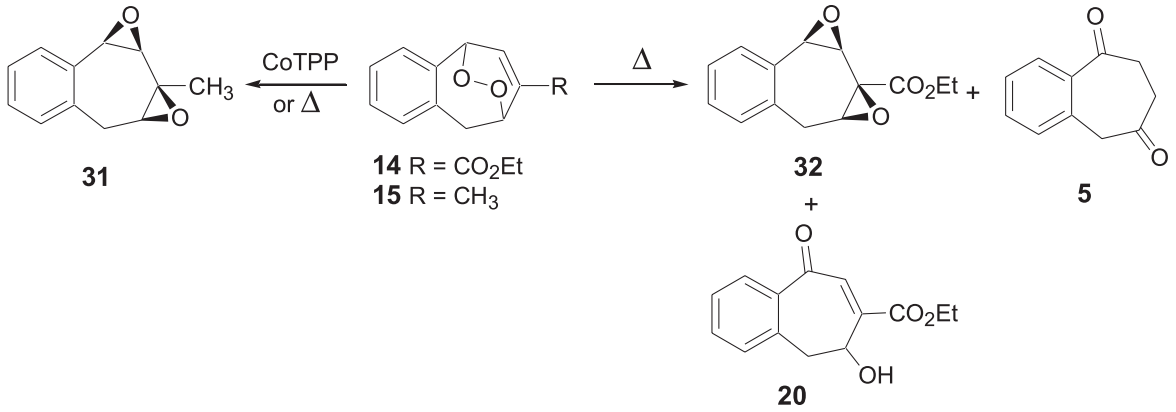
into the dienol **30** by removal of the bridgehead proton. Tautomerization of **30** forms diketone **19**. A hydroxyenone having the structure of **20** was not formed in the case of the methyl derivative **15**. This difference in the reactivity of these bicyclic endoperoxides **14** and **15** upon treatment with NEt_3 may tentatively be attributed to electronic interaction between the alkoxide and neighboring ethyl carboxylate group, which probably partially hinders the formation of cyclic ether **27**. The interesting feature of this reaction was the formation of diketone **5** from **14** where the ester group was removed from the molecule. The formation mechanism of the product **5** is not clear. However, we assume that the neighbouring hydroxyl groups support the decarboxylation reaction. Heating of **22a** up to 109 °C also resulted in the formation of **5**. Therefore, we assume that diketone **5** is a secondary product.

Since both endoperoxides **14** and **15** formed different products by way of a NEt_3 reaction, we evaluated the relative stability of the possible isomers. To do this we carried out AM1 calculations. Our computational investigation of these isomers indicated that the formed diketones **19** and **22a** are thermodynamically more stable isomers, by from 8 to 14 kcal/mol, compared with the isomeric hydroxyketones **20**, **21**, **37**, and **38** (Fig. 1).

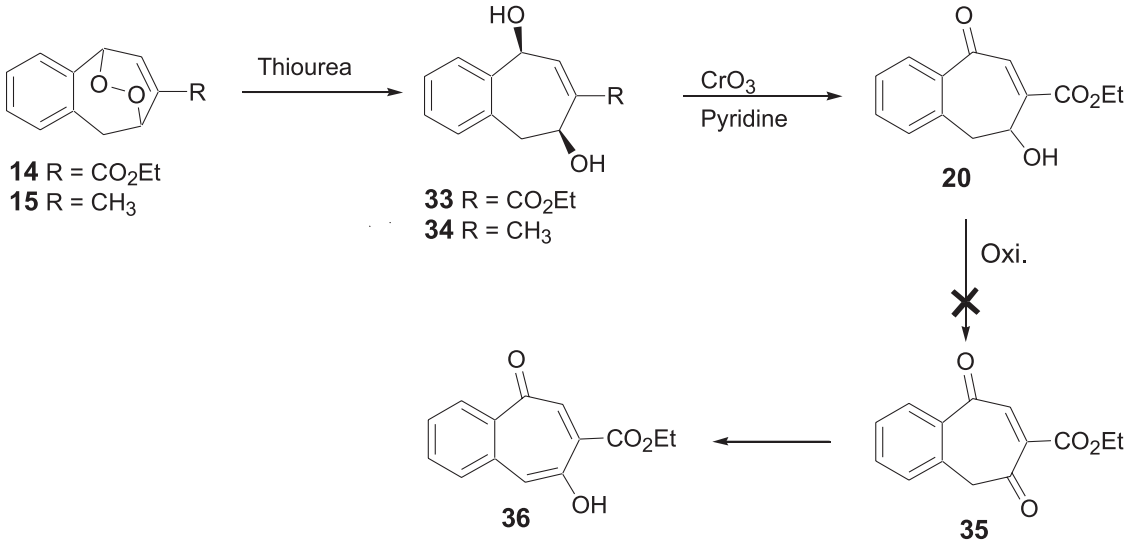
Since bicyclic endoperoxides have a large synthetic potential from the point of view of the mechanistic and synthetic

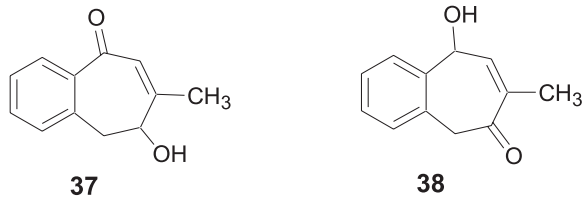
© 2005 NRC Canada

Scheme 8.



Scheme 9.





aspect (5, 6), we were interested in the further transformation of these bicyclic endoperoxides. For the conversion of the endoperoxides into synthetically useful intermediates we studied their thermolysis and tetraphenylporphine (Co-TPP)-catalyzed (13) reactions. It is well-established that unsaturated bicyclic endoperoxides undergo thermal homolytic cleavage of the weak oxygen–oxygen bond followed by the addition of the formed oxygen radicals to the adjacent double bond to give bis(epoxides) with a syn configuration.

Thermolysis or the CoTPP-catalyzed reaction of endoperoxide **15** gave bis(epoxide) **31** (in 45% yield) as expected, whereas the reaction of the endoperoxide **14** with CoTPP produced a complex mixture. On the other hand, the thermal decomposition of endoperoxide **14** resulted in the formation of bis(epoxide) **32** (51%), hydroxy ketone **20** (7%), and diketone **5** (5%), respectively (Scheme 8).

Thiourea reduction of bicyclic endoperoxides provides convenient and efficient access to 2-ene-1,4-diols with a syn configuration. In previous studies, we showed that the reaction of endoperoxides derived from cycloheptatriene derivatives with thiourea formed tropone and tropolone derivatives (6). We, therefore, turned our attention to the thiourea reaction of the endoperoxides **14** and **15**. When the reduction of endoperoxides **14** and **15** with thiourea in methanol was carried out, the diols **33/34** were formed as the sole products. The oxidation of diol **33** gave the hydroxyenone **20**. All of the efforts to oxidize the second hydroxyl group in **33** failed. No other benzotroponoid compounds such as **35** and **36** were observed. This resistance against the oxidation reagent can be attributed to the strong electrostatic interaction between the hydroxyl group and the ester carbonyl group (Scheme 9).

In summary, the results of the present work demonstrate that the photooxygenation of benzocycloheptene derivatives **10** and **13** mainly provided [2 + 4]-cycloaddition products. In the case of **13**, 2-methyl-naphthalene-1-carbaldehyde **16** was isolated as the side product. The fact that the isomer **10** did not form any trace of a naphthalene derivative can be attributed to the effect of the ester group, which decreases the electron density in the seven-membered ring. The base-

© 2005 NRC Canada

catalyzed reaction of the endoperoxide **15** resulted in the formation of the rearranged diketone **19**. This transformation is unusual in the chemistry of the bicyclic endoperoxides. On the other hand, the endoperoxide **14** also gave a diketone **22a** in only a 45% yield besides the normally expected hydroxy ketone **20** and unusual diketone **5**. These results show that an electron-withdrawing substituent attached to the double bond decreases the ratio of the diketone **22a** compared to the methyl-substituted endoperoxide **15**. Furthermore, the formation of the diketone **5** where the ester group is removed from the molecule is also unusual in peroxide chemistry and is observed here for the first time. Thiourea reduction of **14** and **15** provided the ene-2,4-diol derivatives **33** and **34**, which could not be converted into benzotropone derivatives.

Experimental

General

The melting points are uncorrected. IR spectra were obtained from a solution in 0.1 mm cells or KBr pellets on a regular instrument. The ^{1}H and ^{13}C NMR spectra were recorded on 400 (100) and 200 (50) MHz spectrometers. Apparent splitting is given in all of the cases. Column chromatography was performed on silica gel (60-mesh, Merck). TLC was carried out on Merck 0.2 mm silica gel 60 F_{254} analytical aluminum plates. All substances reported in this paper were in racemic form.

Synthesis of ethyl 7*H*-benzo[*a*]cycloheptene-7-carboxylate (9)

Synthesis of 8 (14)

Dibromide **8** was synthesized according to the procedure (8) for methyl ester analogies in a 30% overall yield starting from dihydronaphthalene **6**.

A solution of **8** (2.0 g, 5.35 mmol) in THF (10 mL) and 0.1 mL glacial AcOH was stirred with powdered Zn (0.86 g, 13.17 mmol) for 20 min at rt and 2 h at 45 ± 5 °C. The solution was filtered, the solvent was removed under vacuum, and the oily residue was dissolved in ether (60 mL). The ether solution was washed with satd. NH_4Cl (2 × 60 mL) and dried over $MgSO_4$. Removal of the solvent under vacuum gave crude **9** (0.95 g, 83%), which was recrystallized from *n*-hexane to give **9** (7), but it melted at below room temperature. ^{1}H NMR (200 MHz, $CDCl_3$) δ: 7.41–7.29 (AA′BB′ system, 4H, H_{aryl}), 6.70 (dd, A part of AB system, $J_{5,6} = J_{8,9} = 10.0$ Hz, $J_{5,7} = J_{7,9} = 1.7$ Hz, 2H, H_5 and H_9), 6.05 (dd, B part of AB system, $J_{5,6} = J_{8,9} = 10.0$ Hz, $J_{6,7} = J_{7,8} = 5.2$ Hz, 2H, H_6 and H_8), 4.26 (q, $J = 7.2$ Hz, 2H, OCH_2), 3.19 (tt, $J_{6,7} = J_{7,8} = 5.2$ Hz, $J_{5,7} = J_{7,9} = 1.7$ Hz, 1H, H_7), 1.30 (t, $J = 7.2$ Hz, 3H, CH_3). ^{13}C NMR (50 MHz, $CDCl_3$) δ: 174.8, 138.4, 132.3, 131.6, 129.1, 128.5, 63.2, 45.1, 16.2. Anal. calcd. for $C_{14}H_{14}O_2$: C 78.48, H 6.59; found: C 78.71, H 6.53.

Ethyl 5*H*-benzo[*a*]cycloheptene-7-carboxylate (10)

A solution of **9** (1.1 g, 5.1 mmol) and triethylamine (74 mg, 0.73 mmol) in 5 mL of CCl_4 was refluxed for 16 h. After removing the solvent and triethyl amine, the residue was filtered on a short silica gel column (10 g) eluting with *n*-hexane to give 1.01 g (93%) of **10** as a colorless wax. ^{1}H NMR (200 MHz $CDCl_3$) δ: 7.37–7.19 (m, 5H, H_{aryl} and H_9), 6.99 (d, B part of AB system, $J_{8,9} = 11.7$ Hz, 1H, H_8), 6.97 (t, $J_{5,6} = 7.4$ Hz, 1H, H_6), 4.22 (q, $J = 7.2$ Hz, 2H, OCH_2), 3.16 (d, $J_{5,6} = 7.4$ Hz, 2H, H_5), 1.30 (t, $J = 7.2$ Hz, 3H, CH_3). ^{13}C NMR (50 MHz, $CDCl_3$) δ: 168.3, 138.2, 137.8, 137.2, 136.3, 131.9, 131.1, 130.0, 129.7, 128.2, 127.9, 62.8, 36.2, 16.3. Anal. calcd. for $C_{14}H_{14}O_2$: C 78.48, H 6.59; found: C 78.67, H 6.48.

Synthesis of 7-methyl-5*H*-benzo[*a*]cycloheptene (13)

To a magnetically stirred solution of monobromide **12** (10) (3.0 g, 13.6 mmol) in tetrahydrofuran (150 mL) was added dropwise 6.8 mL of BuLi (2 mol/L, hexane, 13.6 mmol) under N_2 at –78 °C by a syringe. The reaction mixture was stirred for 3 h at the given temperature, then CH_3I (1.1 mL, 2.32 g, 13.6 mmol) was added. The reaction mixture was stirred for an additional 1 h at –78 °C, and then the temperature was increased to 0 °C. Tetrahydrofuran was removed at a reduced pressure and water (50 mL) was added to the residue. The resulting mixture was extracted with *n*-hexane (3 × 100 mL). The combined extracts were washed with water and dried ($MgSO_4$). Removal of the solvent and chromatography of the residue on a silica gel (100 g) column, with *n*-hexane as eluant, gave **13** (9) as a colorless liquid (1.5 g, 70%). ^{1}H NMR (200 MHz $CDCl_3$) δ: 7.40–7.15 (m, 4H, H_{aryl}), 7.05 (d, A part of AB system, $J_{8,9} = 11.6$ Hz, 1H, H_9), 6.45 (d, B part of AB system, $J_{8,9} = 11.6$ Hz, 1H, H_8), 5.62 (t, 1H, H_6), 3.02 (d, 2H, H_5), 1.90 (bs, 3H, CH_3).

Photooxygenation of ethyl 5*H*-benzo[*a*]cycloheptene-7-carboxylate (10)

The ester **10** (0.34 g, 1.59 mmol) and tetraphenylporphrine (10 mg) were dissolved in 20 mL of CCl_4. The solution was put in a 100 mL round-bottomed (Pyrex glass) flask equipped with a cooling jacket and was then irradiated with a projection lamp (500 W) while a slow stream of dry oxygen was passed through the solution at room temperature. To keep the reaction temperature constant, water was circulated through the cooling jacket. After 9 days, the solvent was evaporated at low temperature (20 °C). Chromatography of the residue on a silica gel (50 g) column, with *n*-hexane – ethyl acetate (97:3) as the eluant, gave **14**. After recrystallization of the residue from CH_2Cl_2–*n*-hexane (1/2) the endoperoxide **14** was obtained as colorless crystals (367 mg, 94%, mp 82 °C).

Ethyl 10,11-dioxatricyclo[7.2.2.0^{2,7}]trideca-2,4,6,12-tetraene-13-carboxylate (14)

IR (KBr, cm^{-1}): 3069, 2976, 2907, 1723, 1484, 1453, 1392, 1353, 1269, 1215, 1107, 1069, 1023, 961. ^{1}H NMR (200 MHz, $CDCl_3$) δ: 7.64 (dd, $J_{1,12} = 7.4$ Hz, $J_{9,12} = 1.5$ Hz, 1H, H_{12}), 7.33–7.13 (m, 4H, H_{aryl}), 5.53 (m, 1H, H_9), 5.42 (dd, $J_{1,12} = 7.4$ Hz, $J_{1,9} = 1.5$ Hz, 1H, H_1), 4.25 (q, $J = 7.1$ Hz, 2H, OCH_2), 3.71 (dd, A part of AB system, $J_{8,8'} = 18.3$ Hz, $J_{8,9} = 3.9$ Hz, 1H, H_8), 3.19 (dd, B part of AB system, $J_{8',8} = 18.3$ Hz, $J_{8',9} = 3.0$ Hz, 1H, $H_{8'}$), 1.30 (t, $J = 7.1$ Hz, 3H, CH_3). ^{13}C NMR (50 MHz, $CDCl_3$) δ: 165.4, 141.7, 139.8, 137.7, 133.1, 132.6, 130.8, 129.1, 128.0, 81.0, 77.0, 63.1, 39.3, 16.1. EI-MS (70 eV) *m/z* (%): 246 (M^+, 1), 228 (4), 201 (28), 172/171 (60), 116/115 (100), 103 (26), 91

© 2005 NRC Canada

(60), 89 (32), 65 (33). Anal. calcd. for $C_{14}H_{14}O_4$: C 68.28, H 5.73; found: C 67.93, H 5.66.

Photooxygenation of 7-methyl-*5H*-benzocycloheptene (13)

The reaction was carried out according to the above mentioned procedure by using 3.0 g (19.2 mmol) of **13** and TPP (10 mg) in 400 mL of carbon tetrachloride. After 24 h, the solvent was evaporated and the residue was chromatographed on silica gel (80 g) eluting with hexane. The first fraction was TPP and the second fraction was identified as 2-methyl-naphthalene-1-carbaldehyde (6%) (15). The third fraction was identified as 13-methyl-10,11-dioxatricyclo[7.2.2.$0^{2,7}$]trideca-2,4,6,12-tetraene (**15**) as a pale yellow wax (1.2 g, 36%). IR (KBr, cm^{-1}) 2910, 1490, 1450, 1410, 1330, 1230, 1190, 1000, 920, 840, 760. ^{1}H NMR (200 MHz, $CDCl_3$) δ: 7.30–7.05 (m, 4H, H_{aryl}), 6.43 (bd, $J_{1,12}$ = 7.4 Hz, 1H, H_{12}), 5.21 (dd, $J_{1,12}$ = 7.4 Hz, $J_{1,9}$ = 1.5 Hz, H_1), 4.77 (m, 1H, H_9), 3.61 (dd, A part of AB system, $J_{8,8'}$ = 18.2 Hz, $J_{8,9}$ = 4.3 Hz, 1H, H_8), 3.18 (dd, B part of AB system, $J_{8',8}$ = 18.2 Hz, $J_{8',9}$ = 2.7 Hz, 1H, $H_{8'}$), 1.92 (d, $J_{12,methyl}$ = 1.7 Hz, 3H, methyl). ^{13}C NMR (50 MHz, $CDCl_3$) δ: 140.5, 136.3, 136.1, 131.4, 128.5, 127.2, 126.6, 126.3, 80.7, 80.4, 37.1, 20.3. Anal. calcd. for $C_{12}H_{12}O_2$: C 76.27, H 6.43; found: C 75.91, H 6.61.

Reaction of the endoperoxide 14 with NEt_3

Freshly distilled triethylamine (1 mL) in 3 mL of CH_2Cl_2 was added dropwise to a solution of the endoperoxide **14** (1.0 g, 4.10 mmol) in 50 mL of CH_2Cl_2 at 0 °C during 15 min. The mixture was then stirred at 0 °C for 2 h and at room temperature for 20 h and the solvent evaporated. The residue was submitted to column chromatography (silica gel, 50 g) eluting with *n*-hexane – ethyl acetate (9:1). The first fraction (450 mg, 45%) was identified as keto–enol equilibrium tautomers **22a/22b**. It was recrystallized from CH_2Cl_2–*n*-hexane (4:1) (mp 76 to 77 °C). The rapidly measured NMR spectrum of the crystals showed only the enol form **22b**; however, at standing at room temperature for 2 h, equilibrium between the tautomers **22a/22b** was established consisting of 64% enol **22b** and 36% ketone **22a**.

Ethyl 8-hydroxy-5-oxo-6,9-dihydro-5H-benzo[a]cycloheptene-7-carboxylate (22b)

^{1}H NMR (400 MHz, $CDCl_3$) δ: 12.49 (bs, 1H, OH), 8.14 (dd, $J_{3,4}$ = 7.7 Hz, $J_{2,4}$ = 1.5 Hz, 1H, H_{4aryl}), 7.49–7.28 (m, 3H, H_{aryl}), 4.23 (q, *J* = 7.1 Hz, 2H, OCH_2), 3.92 (s, 2H, H_6), 3.74 (s, 2H, H_9), 1.33 (t, *J* = 7.1 Hz, 3H, CH_3).

Ethyl 5,8-Dioxo-6,7,8,9-tetrahydro-5H-benzocycloheptene-7-carboxylate (22a)

IR (KBr, cm^{-1}): 2976, 1684, 1661, 1461, 1415, 1361, 1338, 1269, 1192, 1100, 1061. ^{1}H NMR (400 MHz, $CDCl_3$) δ: 7.94 (dd, $J_{3,4}$ = 7.7 Hz, J_{24} = 1.5 Hz, 1H, H_{4aryl}), 7.54–7.24 (m, 3H, H_{aryl}), 4.15 (d, A part of ABX system, $J_{9,9'}$ = 15.2 Hz, 1H, H_9), 4.06 (m, 2H, OCH_2), 3.97 (d, B part of ABX system, $J_{9,9'}$ = 15.2 Hz, 1H, $H_{9'}$), 3.70 (dd, J_{67} = 9.5 Hz, $J_{6'7}$ = 2.9 Hz, 1H, H_7), 3.45 (dd, A part of AB system, $J_{6,6'}$ = 18.0 Hz, $J_{6,7}$ = 9.5 Hz, 1H, H_6), 3.19 (dd, B part of AB system, $J_{66'}$ = 18.0 Hz, $J_{6',7}$ = 2.9 Hz, $H_{6'}$), 1.12 (t, *J* = 7.2 Hz, 1H, CH_3).^{13}C NMR for the mixture **22a/22b** (50 MHz, $CDCl_3$) δ: 202.6, 200.2, 195.5, 178.6, 173.4, 169.9, 140.1, 138.4, 137.1, 135.6, 134.8, 134.7, 134.6, 132.7, 132.5, 132.1, 131.9, 130.2, 129.7, 63.8, 63.0, 54.4, 51.1, 43.8, 43.2, 42.3, 16.1, 15.8. Anal. calcd. for $C_{14}H_{14}O_4$: C 68.28, H 5.73; found: C 67.88, H 5.67.

The second fraction was 6,7-dihydro-9*H*-benzocycloheptene-5,8-dione (**5**) (4) as a colorless wax (127 mg, 18%). IR (NaCl, film, cm^{-1}): 3072, 2972, 2914, 1722, 1684, 1603, 1483, 1452, 1418, 1379, 1325, 1287, 1240, 1094. ^{1}H NMR (200 MHz, $CDCl_3$) δ: 8.01 (dd, $J_{3,4}$ = 7.6 Hz, $J_{2,4}$ = 1.4, 1H, H_{4aryl}), 7.98–7.20 (m, 3H, H_{aryl}), 4.01 (s, 2H, H_9), 3.08 (AA′ part of AA′BB′ system, 2H, H_6), 2.68 (BB′ part of AA′BB′ system, 2H, H_7). ^{13}C NMR (50 MHz, $CDCl_3$) δ: 208.1, 201.9, 138.05, 135.8, 135.5, 132.6, 132.0, 130.0, 52.2, 41.0, 37.4.

The last fraction was identified as ethyl 6-hydroxy-9-oxo-6,9-dihydro-5*H*-benzocycloheptene-7-carboxylate (**20**) as a colorless wax (370 mg, 37%). IR (KBr, cm^{-1}): 3446, 2984, 2900, 1715, 1623, 1584, 1446, 1423, 1400, 1369, 1246, 1123, 1076, 1023, 930. ^{1}H NMR (200 MHz, $CDCl_3$) δ: 7.66 (bd, $J_{1,2}$ = 7.6 Hz, 1H, H_{1aryl}), 7.51–7.28 (m, 3H, H_{aryl}), 7.12 (s, 1H, H_8), 4.92 (t, $J_{5,6}$ = $J_{5',6}$ = 5.2 Hz, 1H, H_6), 4.32 (q, *J* = 7.2 Hz, 2H, OCH_2), 3.33 (d, $J_{5,6}$ = $J_{5',6}$ = 5.2 Hz, 2H, H_5, $H_{5'}$), 1.35 (t, *J* = 7.2 Hz, 3H, CH_3). ^{13}C NMR (APT, 50 MHz, $CDCl_3$) δ: 195.2, 169.6, 146.0, 141.1, 138.5(–), 136.9, 134.7(–), 132.9(–), 131.2(–), 129.4(–), 68.1(–), 64.1, 42.4, 16.0(–). EI-MS (70 eV) *m/z* (%): 246 (M^+, 1), 217 (7), 201 (100), 172/171 (47), 144 (43), 132 (53), 116/115 (83), 90/89 (40), 65 (18). Anal. calcd. for $C_{14}H_{14}O_4$: C 68.28, H 5.73; found: C 68.78, H 5.67.

Reaction of the endoperoxide 15 with NEt_3

The reaction was carried out according to the above procedure by using 100 mg (532 mmol) of **15** and NEt_3 (2 to 3 drops) in 50 mL of chloroform. After 5 days, the solvent was removed and the residue was chromatographed on silica gel (50 g) eluting with *n*-hexane–$CHCl_3$ (1:1). 7-Methyl-6,7-dihydro-9*H*-benzocycloheptene-5,8-dione (**19**) was obtained as the sole product. Colorless crystals from *n*-hexane–$CHCl_3$ (1:1) mp 216–218 °C (90 mg, 90%). IR (KBr, cm^{-1}): 2970, 2910, 1730, 1690, 1590, 1440, 1370, 1270, 1160, 1050, 1030, 950, 920. ^{1}H NMR (200 MHz, $CDCl_3$) δ: 7.99 (dd, $J_{3,4}$ = 7.6 Hz, $J_{2,4}$ = 1.6 Hz, 1H, H_{4aryl}), 7.54–7.20 (m, 3H, H_{aryl}), 4.15 (d, A part of AB system, $J_{9,9'}$ = 14.6 Hz, 1H, H_9), 3.90 (d, B part of AB system, $J_{9,9'}$ = 14.6 Hz, 1H, $H_{9'}$), 3.13–3.03 (m, 2H, H_6 and $H_{6'}$), 2.78 (m, 1H, H_7), 1.18 (d, $J_{7,methyl}$ = 7.0 Hz, 3H, CH_3). ^{13}C NMR (50 MHz, $CDCl_3$) δ: 209.1, 200.5, 136.2, 134.5, 134.2, 131.4, 130.6, 129.6, 51.4, 47.4, 40.3, 16.7. Anal. calcd. for $C_{12}H_{12}O_2$: C 76.57, H 6.43; found: C 76.71, H 6.57.

Thermolysis of 22a/22b

In a sealed tube, the keto–enol tautomers **22a/22b** (100 mg, 0.41 mmol) in toluene (3 mL) were heated to 109 °C for 3 days. After removing the solvent, the ^{1}H NMR spectrum of the residue showed the formation of the diketone **5** in 55% yield.

Thermolysis of endoperoxide 14

Endoperoxide **14** (990 mg, 4.02 mmol) was dissolved in toluene (10 mL) and heated to 173 °C for 24 h in a sealed

© 2005 NRC Canada

tube. After evaporation of the solvent, the residue was crystallized from CH_2Cl_2–*n*-hexane to give bis(epoxide) **32** (500 mg, 51%). The NMR spectrum of the filtrate showed that diketone **5** (5%) and hydroxy ketone **20** (7%) were also formed.

Ethyl 5R(S),6R(S),7S(R),8S(R)-diepoxy-6,7,8,9-tetrahydro-5H-benzocycloheptene-7-carboxylate (32)

IR (KBr, cm^{-1}): 3000, 2938, 1753, 1461, 1438, 1376, 1292, 1184, 1123, 1076, 1038, 992, 930, 915. ^{1}H NMR (200 MHz, $CDCl_3$) δ: 7.47–7.11 (m, 4H, H_{aryl}), 4.17 (d, A part of AB system, $J_{5,6}$ = 4.1 Hz, 1H, H_5), 4.15 (m, 2H, OCH_2), 4.08 (d, B part of AB system, $J_{5,6}$ = 4.1 Hz, 1H, H_6), 3.72 (dd, A part of ABX system, $J_{9,9'}$ = 13.6 Hz, $J_{8,9}$ = 7.3 Hz, 1H, H_9), 3.46 (dd, $J_{8,9}$ = 7.3 Hz, $J_{8,9'}$ = 6.6 Hz, 1H, H_8), 3.01 (dd, B part of ABX system, $J_{9',9}$ = 13.6 Hz, $J_{8,9'}$ = 6.6 Hz, 1H, $H_{9'}$), 1.25 (t, J = 7.1 Hz, 3H, CH_3). ^{13}C NMR (50 MHz, $CDCl_3$) δ: 170.8, 136.7, 134.1, 133.1, 132.6, 130.1, 129.2, 63.9, 61.6, 58.0, 57.0, 54.1, 34.6, 15.9. EI-MS (70 eV) *m/z* (%): 246 (M^+, 1), 228 (4), 201 (30), 172/171 (37), 144/145 (34), 115 (100), 103 (26), 91 (36), 77 (32), 65 (33). Anal. calcd. for $C_{14}H_{14}O_4$: C 68.28, H 5.73; found: C 68.54, H 5.69.

CoTPP-catalyzed reaction of 15

Cobalt-*meso*-tetraphenylporphyrin (CoTPP, 5 mg) was added in portions to a magnetically stirred solution of endoperoxide **15** (100 mg, 532 mmol) in 5 mL of $CHCl_3$ at –10 °C. The mixture was then stirred for 2 h and the solvent evaporated. ^{1}H NMR spectral analysis of the reaction mixture indicated the formation of compounds **31** and the residue was submitted to column chromatography (silica gel, 50 g) eluting with $CHCl_3$–*n*-hexane (3:2) and gave 5*R*(*S*),6*R*(*S*),7*S*(*R*),8*S*(*R*)-diepoxy-7-methyl-6,7,8,9-tetrahydro-5*H*-benzocycloheptene (**31**) as colorless crystals (45 mg, 45%) from CH_2Cl_2–*n*-hexane (1:3), mp 85 to 86 °C. IR (KBr, cm^{-1}): 2940, 1490, 1430, 1370, 1210, 1190, 1090, 1030, 990, 910, 880, 840, 790, 750. ^{1}H NMR (200 MHz, $CDCl_3$) δ: 7.41–7.11 (m, 4H, H_{aryl}), 4.08 (d, A part of AB system, $J_{5,6}$ = 4.0 Hz, 1H, H_5), 3.65 (dd, $J_{9,9'}$ = 12.8 Hz, $J_{8,9}$ = 6.2 Hz, 1H, H_9), 3.55 (d, B part of AB system, $J_{5,6}$ = 4.0 Hz, 1H, H_6), 3.06–2.87 (m, 2H, $H_{9'}$ and H_8), 1.37 (s, 3H, CH_3). ^{13}C NMR (50 MHz, $CDCl_3$) δ: 136.7, 132.7, 131.4, 131.0, 129.1, 127.4, 60.3, 58.3, 56.2, 56.1, 33.4, 21.4. Anal. calcd. for $C_{12}H_{12}O_2$: C 76.57, H 6.43; found: C 76.64, H 6.54.

Thermolysis of endoperoxide 15

The reaction was carried out according to the above procedure by using 50 mg (266 mmol) of **23** in 5 mL of toluene at 190–210 °C. After 1 h, the solvent was removed and the residue was chromatographed on silica gel (50 g) eluting with *n*-hexane–$CHCl_3$ (1:1). The bis(epoxide) **31** was obtained as the sole product (13 mg, 27%).

The reaction of endoperoxide 14 with thiourea

The endoperoxide **14** (350 mg, 1.42 mmol) was dissolved in 12 mL of CH_3OH. A solution of thiourea (114 mg, 1.5 mmol) in 5 mL of methanol was then added dropwise in 10 min. After stirring of the solution at room temperature for 3.5 h, the residue was filtered through silica gel (5 g) eluting with ethyl acetate – *n*-hexane (1:1) to give ethyl 6*S*(*R*),9*S*(*R*)-6,9-dihydroxy-6,9-dihydro-5*H*-benzo[*a*]cycloheptene-7-carboxylate (**33**) (335 mg, 95%), mp 63 to 64 °C from $CHCl_3$. IR (KBr, cm^{-1}): 3502, 3378, 3131, 2993, 2900, 2800, 1697, 1465, 1380, 1265, 1041, 879. ^{1}H NMR (200 MHz, CD_3OD) δ: 7.53 (d, $J_{1,2}$ = 6.9 Hz, 1H, H_{1aryl}), 7.30–7.21 (m, 3H, H_{aryl}), 7.10 (m, 1H, H_8), 5.69 (m, 1H, H_9), 4.84 (m, 1H, H_6), 4.19 (q, J = 7.1 Hz, 2H, OCH_2), 3.27 (bd, A part of AB system, $J_{5,5'}$ = 14.3 Hz, 1H, H_5), 3.01 (dd, B part of AB system, $J_{5',5}$ = 14.3 Hz, $J_{5',6}$ = 4.4 Hz, 1H, $H_{5'}$), 1.28 (t, J = 7.1 Hz, 3H, CH_3). ^{13}C NMR (50 MHz, $CDCl_3$) δ: 170.8, 149.8, 146.7, 136.2, 135.4, 134.1, 129.6, 129.4, 125.5, 70.9, 67.0, 63.9, 41.5, 16.4. Anal. calcd. for $C_{14}H_{16}O_4$: C 67.73, H 6.50; found: C 68.09, H 6.44.

The reaction of endoperoxide 15 with thiourea

The reaction was carried out according to the above procedure by using 140 mg (745 mmol) of **15** in 10 mL of CH_3OH at –10 °C. After 24 h, the solvent was removed and the residue was chromatographed on silica gel (5 g) eluting with *n*-hexane–$CHCl_3$ (1:1). (5*S(R)*,8*S*(*R*))-7-methyl-8,9-dihydro-5*H*-benzo[*a*]cycloheptene-5,8-diol (**34**) was obtained as a pale yellow wax (90 mg, 64%). IR (KBr, cm^{-1}): 3580, 2900, 2840, 1640, 1590, 1370, 1120, 1060, 1000, 900, 870. ^{1}H NMR (200 MHz, $CDCl_3$) δ: 7.56–715 (m, 4H, H_{aryl}), 5.68 (m, 1H, H_6), 5.58 (m, 1H, H_5), 4.14 (m, 1H, H_8), 3.25 (bd, A part of AB system, $J_{9,9'}$ = 14.6 Hz, 1H, H_9), 3.05 (dd, A part of AB system, $J_{9,9'}$ = 14.6 Hz, $J_{8,9'}$ = 4.5 Hz, 1H, $H_{9'}$), 1.80 (bs, 3H, CH_3). Anal. calcd. for $C_{12}H_{14}O_2$: C 75.76, H 7.42; found: C 76.21, H 7.37.

Oxidation of 33 with CrO_3

To a magnetically stirred solution of CrO_3 (360 mg, 3.6 mmol) in 16 mL of CH_2Cl_2 and pyridine (284 mg, 3.6 mmol) cooled to 0 ± 5 °C was added dropwise a solution of diol **33** (297 mg, 1.20 mmol) in 4 mL methylene chloride during 5 min. This solution was stirred for 2 h at 0 ± 5 °C and for an additional 22 h at room temperature. The solvent was removed by rotoevaporation. Methylene chloride (100 mL) was added to the residue, and then filtered to remove the precipitated material. The organic layer was washed with 1 mol/L (20 mL) HCl solution, water, and then dried over $MgSO_4$. After removal of the solvent, the residue was filtered through a short silica gel column eluting with *n*-hexane–EtOAc (85:15) to give hydroxy ketone **20** (206 mg, 70%).

Acknowledgments

The authors are indebted to Atatürk University and the Middle East Technical University for technical support. This work also has been supported by the Turkish Academy of Sciences in the framework of the Young Scientist Award Program (AD/TUBA-GEBIP / 2001-1-3). The authors are also indebted to Dr. Fabrizio Fabris (Ca Foscari University) for mass spectral measurements.

References

1. (*a*) M. Balci. Pure Appl. Chem. **69**, 97 (1997); (*b*) E.L. Clennan and C.S. Foote. *In* Organic peroxides. *Edited by* W.

© 2005 NRC Canada

Ando. Wiley, Chichester. 1992; (*c*) A.J. Bloodwoth and H.J. Eggelte. *In* Singlet oxygen O_2. Vol. II. Reaction modes and products part 1. *Edited by* A.A. Frimer. CRC Press, Boca Raton, Florida. 1985; (*d*) H.H. Wasserman and R.W. Murray. Singlet oxygen. Academic Press, New York. 1979; (*e*) M. Balci. Chem. Rev. **81**, 91 (1981).

2. N. Kornblum and H.E. Delamare. J. Am. Chem. Soc. **73**, 880 (1951).
3. (*a*) K.H. Schulte-Elte, B. Willhalm, and G. Ohloff. Angew. Chem. Int. Ed. Engl. **8**, 985 (1969); (*b*) W. Skorianetz, K.H. Schulte-Elte, and G. Ohloff. Helv. Chim. Acta, **54**, 1913 (1971); (*c*) T. Asao, M. Yagihara, and Y. Kitahara. Heterocycles, **15**, 985 (1981); (*d*) W. Adam and M. Balci. Angew. Chem. **90**, 1014 (1978); (*e*) W. Adam, M. Balci, B. Pietrzak, and H. Rebollo. Synthesis, 820 (1980); (*f*) Y. Kayama, M. Oda, and Y. Kitahara. Chem. Lett. 345 (1974); (*g*) W. Adam, O. Cueto, O. de Lucchi, K. Peters, E.-M. Peters, and H.G. von Schnering. J. Am. Chem. Soc. **103**, 5822 (1981); (*h*) A.D. Meijere, D. Kaufmann, and I. Erden. Tetrahedron, **42**, 6487 (1986); (*i*) B.M. Kwon, C.S. Foote, and S.I. Khan. J. Org. Chem. **54**, 3378 (1989); (*j*) A.G. Griesbeck, T. Deufel, K. Peters, E.-M. Peters, and H.G. von Schnering. J. Org. Chem. **60**, 1952 (1995); (*k*) W. Adam and I. Erden. Angew. Chem. Int. Ed. Engl. **17**, 210 (1978).
4. (*a*) T. Asao, M. Yagihara, and Y. Kitahara. Bull. Chem. Soc. Jpn. **51**, 2131 (1978); (*b*) A.S. Kende and J.J.-C. Chu. Tetrahedron Lett. 4837 (1970); (*c*) W. Adam and M. Balci. J. Am. Chem. Soc. **101**, 7537 (1979); (*d*) W. Adam and M. Balci. J. Am. Chem. Soc. **101**, 7542 (1979).
5. (*a*) B. Atasoy and M. Balci. Tetrahedron, **42**, 1461 (1986); (*b*) M. Balci and B. Atasoy. Tetrahedron Lett. **25**, 4033 (1984); (*c*) M.E. Sengül, Z. Ceylan, and M. Balci, Tetrahedron, **53**, 10401 (1997).
6. A. Dastan, N. Saraçoglu, and M. Balci. Eur. J. Org. Chem. 3519 (2001).
7. (*a*) M. Matsumoto, T. Shiono, H. Mutoh, M. Amano, and S. Arimitsu. J. Chem. Soc. Chem. Commun. 101 (1995); (*b*) A.J. Anciaux, A. Demonceau, A.F. Noels, A.J. Hubert, R. Warin, and P. Teyssie. J. Org. Chem. **46**, 873 (1981); (*c*) F. Pietra. Chem. Rev. **73**, 294 (1973).
8. For the methyl ester derivative of **10** see: (*a*) D.M. Madigan and J.S. Swenton. J. Am. Chem. Soc. **92**, 7513 (1970); (*b*) J.S. Swenton and D.M. Madigan. Tetrahedron, **28**, 2703 (1972); (*c*) J.S Swenton, A. Kenneth, D.M. Madigan, and P.D. Rosso. J. Org. Chem. **40**, 1280 (1975).
9. Benzocycloheptatriene carboxylate **9** was obtained as a by-product by Rh(II)-catalyzed cyclopropanation of naphthalene with ethyl diazoacetate. The physical properties of **9** were not reported. See: P. Müller, J.-L. Toujas, and G. Bernardinelli. Helv. Chim. Acta, **83**, 1525 (2000).
10. C. Mayor and W.M. Jones. Tetrahedron Lett. **44**, 3855 (1977).
11. For the formation of aromatic aldehydes from cycloheptatriene derivatives see: (*a*) W. Adam and M. Balci. J. Am. Chem. Soc. **101**, 7542 (1979); (*b*) W. Adam and H. Rebollo. Tetrahedron Lett. **22**, 3049 (1981).
12. (*a*) M.G. Zagorski and R.G. Salomon. J. Am. Chem. Soc. **102**, 2501 (1980); (*b*) M.G. Zagorski and R.G. Salomon. J. Am. Chem. Soc. **104**, 3498 (1982); (*c*) R.G. Salomon, D.B. Miller, M.G. Zagorski, and J. Coughlin. J. Am. Chem. Soc. **106**, 6049 (1984); (*d*) M. Yoshida, M. Miura, M. Nojima, and S. Kusabayashi. J. Am. Chem. Soc. **105**, 6279 (1983); (*f*) E. Mete, R. Altundaş, H. Secen, and M. Balci. Turk. J. Chem. **27**, 145 (2003).
13. (*a*) J.D. Boyd, C.S. Foote, and D.K. Imagawa. J. Am. Chem. Soc. **102**, 3641 (1980); (*b*) Y. Sütbeyaz, H. Secen, and M. Balci. J. Org. Chem. **53**, 2312 (1988).
14. I.A. D'yakonov, T.V. Mandel'shtam, and E.M. Kharicheva. Zh. Org. Khim. **6**, 2252 (1970).
15. T.C. Walsgrove and F. Sondheimer. Tetrahedron Lett. **30**, 2719 (1978).

© 2005 NRC Canada

Investigation of the density dependence of the shear relaxation time of dense fluids

Mehrdad Bamdad, Saman Alavi, Bijan Najafi, and Ezat Keshavarzi

Abstract: The shear relaxation time, a key quantity in the theory of viscosity, is calculated for the Lennard–Jones fluid and fluid krypton. The shear relaxation time is initially calculated by the Zwanzig–Mountain method, which defines this quantity as the ratio of the shear viscosity coefficient to the infinite shear modulus. The shear modulus is calculated from highly accurate radial distribution functions obtained from molecular dynamics simulations of the Lennard–Jones potential and a realistic potential for krypton. This calculation shows that the density dependence of the shear relaxation time isotherms of the Lennard–Jones fluid and Kr pass through a minimum. The minimum in the shear relaxation times is also obtained from calculations using the different approach originally proposed by van der Gulik. In this approach, the relaxation time is determined as the ratio of shear viscosity coefficient to the thermal pressure. The density of the minimum of the shear relaxation time is about twice the critical density and is equal to the common density, which was previously reported for supercritical gases where the viscosity of the gas becomes independent of temperature. It is shown that this common point occurs in both gas and liquid phases. At densities lower than this common density, even in the liquid state, the viscosity increases with increasing temperature.

Key words: dense fluids, radial distribution function, shear modulus, shear relaxation time, shear viscosity.

Résumé : Le temps de relaxation de cisaillement, une quantité clé dans la théorie de la viscosité, a été calculé pour le fluide de Lennard–Jones et pour le krypton solide. Le temps de relaxation de cisaillement a été initialement calculé par la méthode de Zwanzig–Mountain qui définit cette quantité comme le rapport du coefficient de viscosité de cisaillement au module de cisaillement infini. Le module de cisaillement est calculé à partir de fonctions de distribution radiale très précises obtenues à partir de simulations dynamiques moléculaires du potentiel de Lennard–Jones et d'un potentiel réaliste pour le krypton. Ce calcul permet de montrer que la dépendance entre la densité et les isothermes du temps de relaxation de cisaillement du fluide de Lennard–Jones et du krypton passe par un minimum. On a aussi calculé le minimum du temps de relaxation de cisaillement en utilisant les différentes approches proposées originalement par van der Gulik. Dans cette approche, le temps de relaxation est déterminé comme le rapport du coefficient de viscosité de cisaillement et de la pression thermique. La densité du minimum du temps de relaxation de cisaillement est égale à environ deux fois la densité critique et elle est égale à la densité commune qui a été rapportée antérieurement pour les gaz supercritiques où la viscosité du gaz devient indépendante de la température. Il est démontré que ce point commun se retrouve dans les phases tant gazeuses que liquides. À des densités inférieures à cette densité commune, même à l'état liquide, la viscosité augmente avec une augmentation de la température.

Mots clés : fluides denses, fonction de distribution radiale, module de cisaillement, temps de relaxation associé au cisaillement, viscosité de cisaillement.

[Traduit par la Rédaction]

1. Introduction

The flow of linear momentum, thermal energy, or mass in a fluid can result from local fluctuations inside an equilibrium system or from external driving forces in nonequilibrium systems. In nonequilibrium states of a fluid, the velocity distribution differs from the Maxwell distribution. Internal collisions reestablish a new Maxwell distribution in the system, and the timescale for reestablishing a new equilibrium state is determined by the relaxation time (τ) of the system (1).

The notion that viscosity and elasticity are two different aspects of the same phenomenon and that ordinary liquids behave elasticity at short enough times was first suggested by Maxwell and put on a firm molecular footing in 1965 by Zwanzig and Mountain (2). By starting with the Green–Kubo time-correlation expression for the frequency-dependent shear viscosity they derived that

$$[1] \qquad \eta_0 = \tau G_\infty$$

where η_0 is the zero-frequency shear viscosity and G_∞ the infinite-frequency shear modulus.

Zwanzig and Mountain (2) derived the formula relating the infinite-frequency shear modulus to the radial distribu-

Received 6 October 2004. Published on the NRC Research Press Web site at http://canjchem.nrc.ca on 29 March 2005.

M. Bamdad, B. Najafi, and E. Keshavarzi. Department of Chemistry, Isfahan University of Technology, Isfahan 84154, Iran.
S. Alavi.[1] Steacie Institute for Molecular Sciences, National Research Council of Canada, 100 Sussex Dr., Ottawa, ON K1A 0R6, Canada.

[1]Corresponding author (e-mail: saman.alavi@nrc.ca).

 doi: 10.1139/V05-047 © 2005 NRC Canada

tion function (RDF) for fluids interacting with a spherically symmetric potential

$$[2] \qquad G_\infty = \rho kT + \frac{2\pi}{15}\rho^2 \int_0^\infty g(r)\frac{\mathrm{d}}{\mathrm{d}r}\left[r^4 \frac{\mathrm{d}\phi(r)}{\mathrm{d}r}\right]\mathrm{d}r$$

where $g(r)$, $\phi(r)$, k, T, and ρ are the radial distribution function, intermolecular pair potential, Boltzmann constant, absolute temperature, and density, respectively. Zwanzig and Mountain (2, 3) calculated relaxation times for monatomic fluids using the Lennard–Jones potential. For more general classes of fluids, this approach requires a proper selection of intermolecular potential and mathematical form for the radial distribution function.

Van der Gulik (4–6) showed that the viscosity coefficient of a dense fluid is directly proportional to the thermal pressure, i.e., the sum of the external and internal pressure. By using the classical ideas of Maxwell regarding the equivalence of elasticity and viscosity and the modern basis given by Zwanzig and Mountain, van der Gulik interpreted the Maxwell relaxation time as the slope of the linear viscosity–pressure curve. In this approach, the relaxation time is the time in which a perturbation to the Maxwellian distribution decreases to $1/e$ of its original magnitude, and is related to the average collision interval. This approach can yield precise relaxation times since the method is based on the accurate viscosity and thermal pressure values and does not depend on the form of the intermolecular potential.

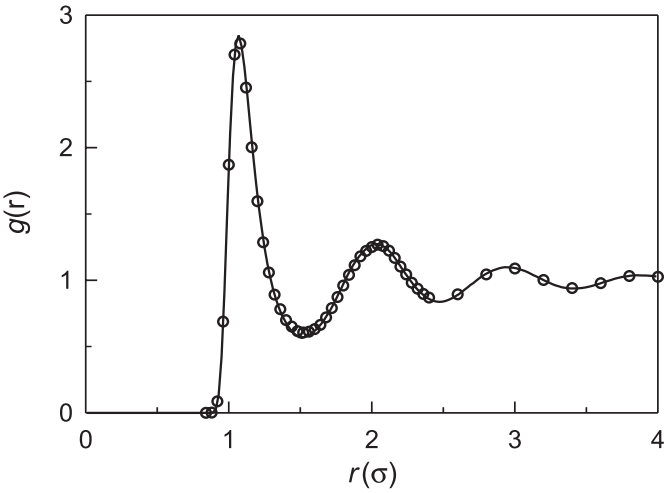
This paper is organized as follows. In section 2, molecular dynamics simulations of highly accurate radial distribution functions (RDF) for the Lennard–Jones fluid and krypton using a realistic potential are described. These functions are used to study the density dependence of the shear relaxation time in the Zwanzig–Mountain approach (section 3). The density dependence of the shear relaxation time will also be studied using the van der Gulik scheme for Lennard–Jones fluids and some real fluids (section 4). Both approaches show that the shear relaxation times for Lennard–Jones (LJ) fluids and real fluids pass through a minimum at a specific reduced density and this minimum is related to the intersection point observed in viscosity–density isotherms (7) at which the temperature variation of viscosity is reversed (section 5).

2. The radial distribution function of LJ fluids and krypton

To obtain the shear modulus for the LJ potential, the integral in eq. [2] is evaluated numerically using the RDF of LJ fluids. Although a number of analytical functions are available for the calculation of the RDF for the LJ fluids (8), they are based on fitting the simulated values of Verlet (9) over a limited density and temperature range. In this work, the RDF at each density and temperature is obtained by a standard molecular dynamics simulation.

The RDF is calculated (10, 11) from the spatial distributions of atoms in a system with 864 particles enclosed in a cube of side L with periodic boundary conditions interacting through a two-body LJ potential

Fig. 1. The agreement between the Verlet (9) RDF (open circles) for the LJ fluid with those calculated in the present work (solid line) at $T^* = kT/\varepsilon = 1.095$ and $\rho^* = \rho\sigma^3 = 0.88$.



$$[3] \qquad \phi(r) = 4\varepsilon\left(\left(\frac{\sigma}{r}\right)^{12} - \left(\frac{\sigma}{r}\right)^{6}\right)$$

A cutoff of at $r_v = 2.5\sigma$ is used for the potential. The simulation was run for a total of 50 000 time steps and the step size for the velocity – Verlet integrator was set to $\Delta t^* = 0.001$. The RDF calculated for the LJ fluids is compared to the accurate Verlet RDF (9) in Fig. 1 for a sample temperature and density, and the agreement between the points indicates the accuracy of the simulations. The RDFs required at each density and temperature are determined in a similar manner without introducing uncertainties involved in the construction of a correlation function.

Similar calculations were performed for krypton using the highly accurate krypton HFD-B2 potential (12). This potential (E_{int}) is based on partitioning the interaction energy of Kr into uncorrelated (ΔE_{SCF}, Hartree–Fock) and correlated (ΔE_{corr}) parts. The parameters in the HFD-B2 potential are adjusted by fitting to precise spectroscopic and transport properties of krypton. The form of this potential is

$$[4] \qquad E_{int} = A\exp(-\alpha R + \beta R^2) - [C_6F^{-6} + C_8R^{-8} + C_{10}R^{-10}]F(R)$$

with

$$[5] \qquad F(R) = \exp[-(DR_mR^{-1} - 1)^2] \qquad R < DR_m$$

$$= 1 \qquad R \geq DR_m$$

where A, α, β, C_6, C_8, C_{10}, and D are adjustable parameters and R_m is the interatomic separation at the minimum of the potential. The molecular dynamics simulations for this potential were run for a total of 50 000 time steps with a step size of $\Delta t^* = 0.001$. The RDFs calculated for Kr with this potential show good agreement with available RDF data for this gas.

© 2005 NRC Canada

3. The relaxation time from the Zwanzig–Mountain approach

There are several semiemperical and analytical expressions for the viscosity of LJ fluids (13), but there is little data and no unique formula for predicting the shear relaxation time. In this section, the RDF for the LJ and accurate krypton potentials are used to calculate G_∞, which along with the viscosity, is used to determine the density dependence of the shear relaxation time of the fluids.

In the first approach, the Mountain–Zwanzig (3) relation (eq. [1]) is used along with the analytical expression for reduced shear viscosity of (supercritical) LJ fluids given by Rowley and Painter (13) to determine the shear relaxation time. The reduced viscosity is defined as $\eta^* = \eta\sigma^2/\sqrt{m\varepsilon}$, where m is molecular weight. The reduced shear modulus ($G_\infty^* = G_\infty\sigma^3/\varepsilon$) for the LJ fluid is obtained from the numerical solution of eq. [2] and is tabulated for several reduced temperatures and densities in Table 1. In Fig. 2, the reduced shear relaxation time ($\tau^* = \eta^*/G_\infty^*$) of a LJ fluid is plotted as a function of the reduced density for three isotherms. The relaxation time goes through a minimum at $\rho^* = 0.69$ for the $T^* = 1.3$ isotherm ($\rho^* = \rho\sigma^3$ and $T^* = kT/\varepsilon$). This minimum shifts to $\rho^* = 0.78$ for $T^* = 2.1$. The reduced relaxation times and densities at different temperatures are given in Table 2. The presence of the minima is discussed in section 5.

Argon, krypton, nitrogen, and carbon dioxide can be considered as examples of LJ fluids and the viscosities of these fluids from the NIST Standard Reference Database (14) along with eq. [2] can be used to predict their infinite-limit shear modulus and then shear relaxation time. The best values of ε and σ for these fluids (7, 12) are given in Table 3. As shown in Fig. 3, the use of experimental viscosities for LJ fluids gives shear relaxation time isotherms, which also show a minima at certain densities (Table 2).

To obtain the relaxation time for a fluid described with a realistic potential, the RDF of krypton is determined from a molecular dynamics simulation using a highly accurate HFD-B2 potential (12). The integral in eq. [2] is evaluated numerically using this RDF. Viscosities from the NIST Standard Reference Database (14) are used to determine the shear relaxation time for krypton. The values of the reduced infinite shear modulus for this potential are given in Table 1. The shear relaxation time of Kr calculated at $T^* = 1.6$ is plotted vs. density and compared to the similar curve for the LJ potential in Fig. 4. The location of the minimum of the krypton potential is at $\rho^* = 0.65$ compared to $\rho^* = 0.70$ for the LJ potential. The value of the relaxation time for the krypton potential at the minimum is also ~10% lower than the LJ potential.

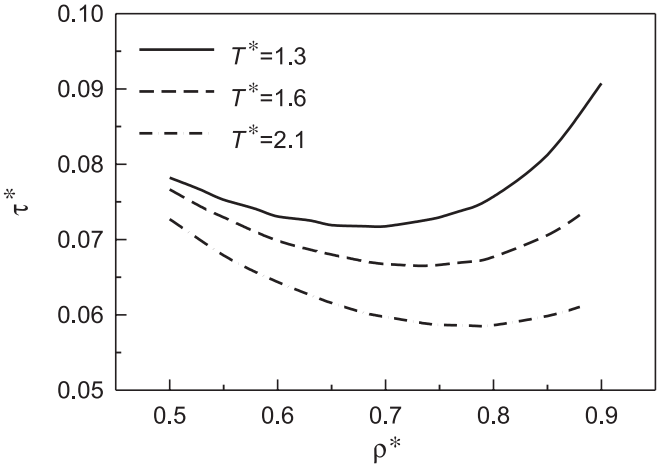
4. Relaxation time from the thermal pressure approach

In the second approach, the relaxation time is calculated from an expression recently proposed by van der Gulik (6) who derived the relaxation time as the ratio of the shear viscosity to thermal pressure

Table 1. The reduced shear modulus ($G_\infty^* = G_\infty\sigma^3/\varepsilon$) from the numerical solution of eq. [2] for LJ and krypton potentials.

	LJ			Krypton		
ρ^*	T^*			T^*		
	1.3	1.6	2.1	1.3	1.6	2.1
0.50	7.24	7.92	9.02	8.64	9.10	9.92
0.55	9.07	9.94	11.36	10.62	11.25	12.23
0.60	11.29	12.41	14.13	12.93	13.74	15.05
0.65	13.93	15.28	17.47	15.65	16.67	18.28
0.70	17.10	18.80	21.43	18.80	20.06	22.02
0.75	20.90	22.96	26.16	22.53	24.05	26.38

Fig. 2. The reduced relaxation time of the LJ fluid vs. reduced density for three reduced isotherms using the Zwanzig–Mountain method with the viscosity values of Rowley and Painter (13).



$$[6] \qquad \tau = \frac{\eta}{p_{th}}$$

where $p_{th} = T(\partial p/\partial T)_\rho$ is the thermal pressure. The thermal pressure can be calculated directly from eq. [7], which covers the entire fluid range

$$[7] \qquad \left(\frac{\partial p}{\partial T}\right)_\rho = R\rho\left[1 + \sum_{i=1}^{6}\left(a_i + \frac{b_i}{T_r} + \frac{c_i}{T_r^2}\right)\rho_r^i\right]$$

where a_i, b_i, and c_i are the adjustable parameters, and $T_r = T/T_C$ and $\rho_r = \rho/\rho_C$ are the reduced temperature and density, respectively, T_C and ρ_C are the critical temperature and density, and R is the gas constant.[2]

In the zero-density limit, the thermal pressure equals the external pressure (p) and the result of eq. [6] is in agreement with the Maxwell relation for ideal gases ($\eta = p\tau$). This implies that viscosity exists because the velocity distribution in a nonequilibrium system cannot adjust instantaneously to an equilibrium distribution. The importance of this formula lies in the fact that it can be generalized to all fluids in the form $\eta = G\tau$, where G is the shear modulus, which for ideal gases equals the pressure p. At low densities, the external pressure is related to the average number of collisions between gas

[2] M. Bamdad, S. Alavi, and B. Najafi. Submitted.

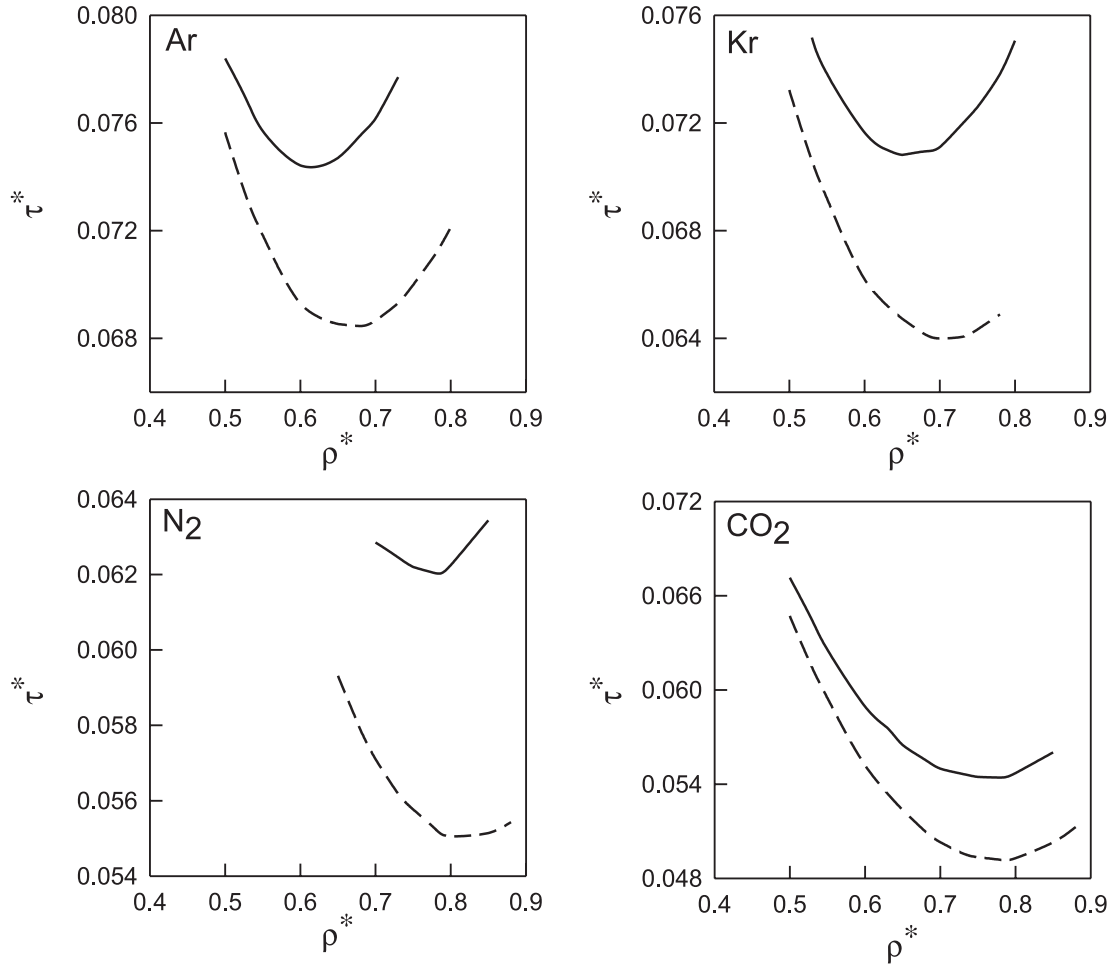
© 2005 NRC Canada

Table 2. Location of the minima of relaxation time for different isotherms from the Zwanzig–Mountain approach and the thermal pressure approach, and common density (ρ^*_{com}) of the intersection of viscosity–density isotherms (7, 18).

		Zwanzig–Mountain approach		Thermal pressure approach		
		Location of the minima		Location of the minima		Density at the common point
Fluid	T^*	ρ^*	τ^*	ρ^*	τ^*	(ρ^*_{com})
LJ	1.3	0.69	0.072	0.66	0.300	~0.78[a]
	1.6	0.73	0.067	0.66	0.265	
	2.1	0.78	0.059	0.68	0.223	
Ar	1.3	0.60	0.074	0.60	0.306	~0.73[b]
	1.6	0.67	0.069	0.60	0.266	
Kr	1.3	0.65 (0.60)[c]	0.071 (0.063)[c]	0.65	0.291	~0.71[b]
	1.6	0.70 (0.65)[c]	0.063 (0.059)[c]	0.68	0.247	
N_2	1.3	0.78	0.062	0.78	0.293	~0.73[b]
	1.6	0.80	0.055	0.75	0.243	
CO_2	1.3	0.78	0.054	0.75	0.235	~0.70[b]
	1.6	0.78	0.049	0.73	0.197	

[a]From Meier et al. (18).
[b]From Najafi et al. (7).
[c]Values from the krypton potential (12) are given in parentheses.

Fig. 3. The reduced relaxation time of Ar, Kr, N_2, and CO_2 vs. reduced density for T^* = 1.3 (solid line) and T^* = 1.6 (dashed line) using the Zwanzig–Mountain method, and experimental viscosity values for each fluid from the NIST database (14).



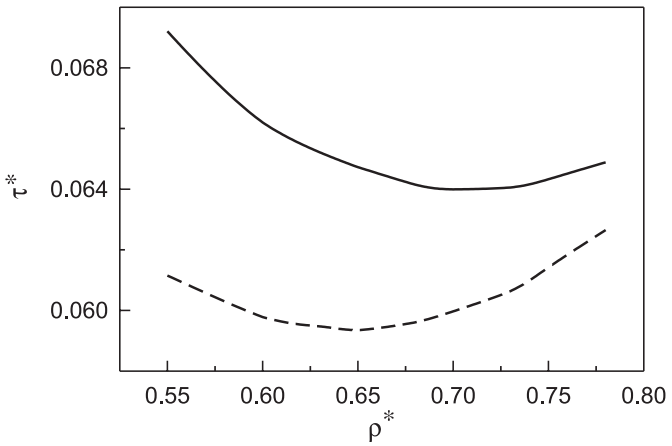
© 2005 NRC Canada

Table 3. Intermolecular parameters used in the Zwanzig–Mountain approach.

Fluid	σ (nm)	ε/*k* (K)
Ar	0.3350	143.23
Kr	0.3571	201.30
N_2	0.3728	85.229
CO_2	0.3800	233.03

Note: Parameters for Kr are from ref. 12 and the other parameters from ref. 7.

Fig. 4. The reduced relaxation time of krypton as a function of the reduced density for $T^* = 1.6$ isotherm for the LJ potential (solid line) and the krypton HFD-2B potential (dashed line).

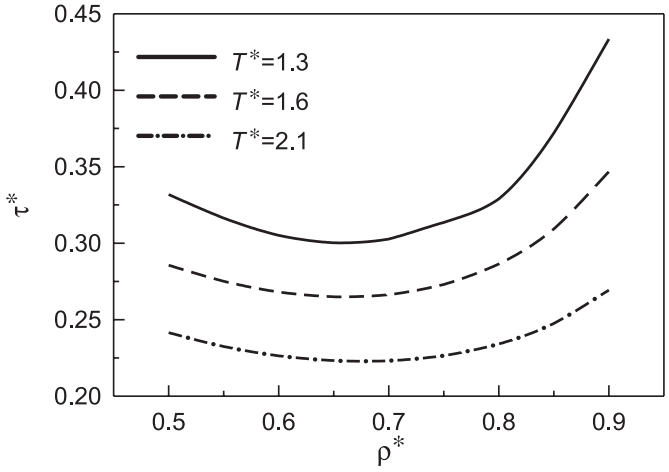


particles and the container wall. At high densities, the intermolecular forces change the number and intensity of molecule–wall collisions, and as a result, the effective pressure that the particles exert is not equal to the external pressure, but rather to the thermal (or kinetic) pressure (15). This result is plausible since the shear viscosity of dense fluids is related to the exchange of momentum between molecular layers via collisions. The viscosity coefficient is thus determined by the number of collisions per unit volume per unit time and by the efficiency of the exchange of momentum during collisions (5).

To obtain the shear relaxation time of LJ potentials, we use the analytical expression for reduced shear viscosity of LJ (supercritical) fluids given by Rowley and Painter (13), and the thermal pressure of the LJ fluids is calculated using an equation of state for LJ fluids (16). The reduced relaxation time ($\tau^* = \eta^*/p^*_{th}$, where $p^*_{th} = p_{th}\sigma^3/\varepsilon$) is plotted vs. reduced density for three isotherms in Fig. 5. The reduced relaxation times and densities for the different isotherms are given in Table 2. The density of the minimum increases from about $\rho^* = 0.66$ to $\rho^* = 0.68$ as we go from $T^* = 1.3$ to $T^* = 2.1$.

The density dependence of the reduced shear relaxation times of argon, krypton, nitrogen, and carbon dioxide using eq. [6] for $T^* = 1.3$ and $T^* = 1.6$ are shown in Fig. 6, and the locations of the minima are given in Table 2. The viscosities from the NIST Standard Reference Database (14) are used. These results show that the shear relaxation times for different isotherms of real fluids pass through a minimum at a reduced density, which is about twice the critical density.

Fig. 5. The reduced relaxation time of LJ fluid vs. reduced density for three reduced isotherms using the thermal pressure approach with the viscosity values of Rowley and Painter (13).



The relaxation time at the minima occur at densities that are very close to those calculated in section 3 and shown in Fig. 3.

5. Conclusion

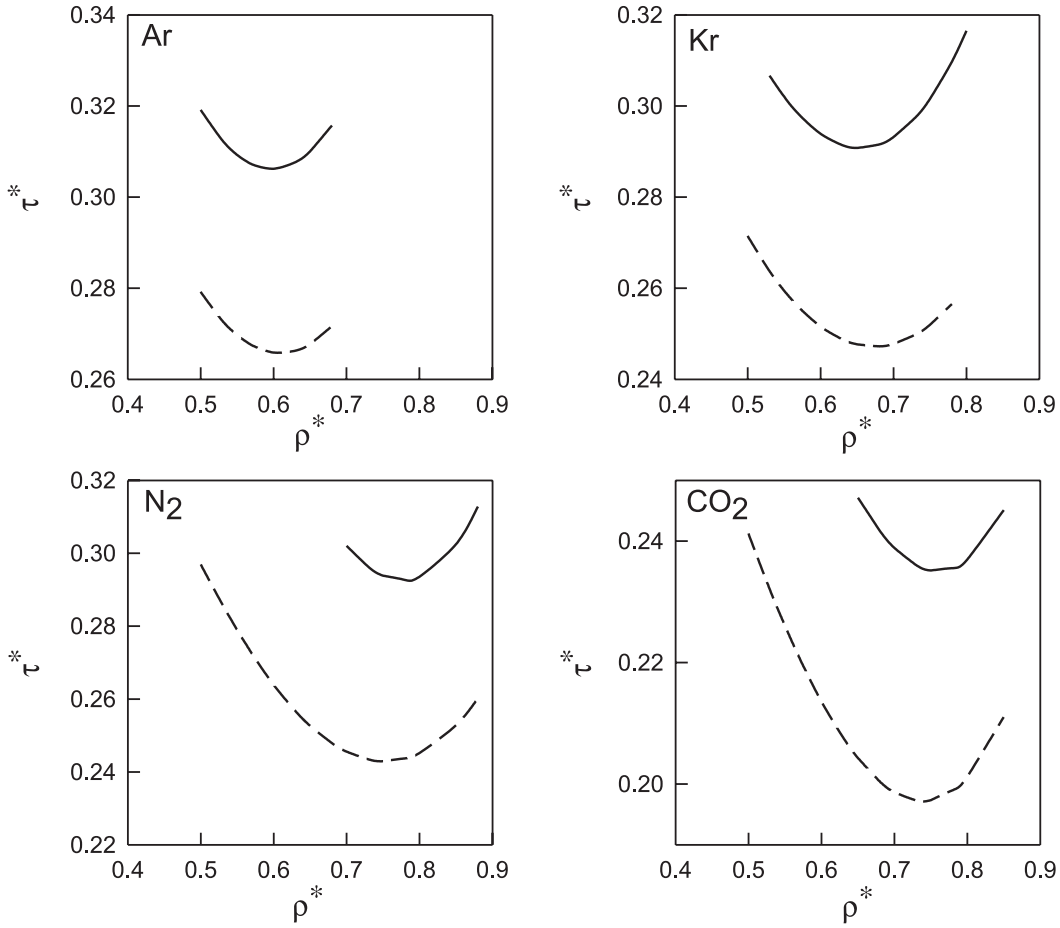
Although relaxation time is a key parameter for transport phenomena, data for this quantity in the literature are very rare. In this study, the shear relaxation time for LJ and real fluids are calculated using the Zwanzig and Mountain (2, 3) and van der Gulik (4–6) approaches. Although these methods use very different data to calculate the shear relaxation time, they predict similar trends for the density and temperature dependence of the relaxation times.

As Figs. 2 (based on the Zwanzig–Mountain method) and 5 (based on the van der Gulik method) show, the shear relaxation time – density isotherms of LJ fluids have minima at densities located at $\rho^* \approx 0.7$. This minimum density is about twice the critical density of LJ fluids and real fluids such as argon, krypton, nitrogen, and carbon dioxide. The minimum density is very close to the common density point (ρ_{com}), which was previously reported for the viscosity of supercritical gases (7). This common density point was determined by Najafi et al. (7) and Michels et al. (17) based on the experimental viscosity data of argon. They showed for supercritical isotherms at densities lower than ρ_{com}, $(\partial\eta/\partial T)_\rho > 0$ as is the normal case for gases and at densities higher than ρ_{com}, $(\partial\eta/\partial T)_\rho < 0$ as is normal for liquids. This is shown in Fig. 7 for the LJ fluid and argon. The change in the temperature dependence of viscosity is observed in the supercritical region and is therefore not due to the gas–liquid phase transition. The density minima of the relaxation time and the common-viscosity density point are in the same general region of the phase diagram. The values of the density at the common point for the different fluids studied in this work are given in Table 2.

Recently, Meier et al. (18) performed extensive molecular dynamic simulations for the viscosity of LJ fluids and some of their observations overlap with those discussed in this work. Based on the time-correlation function approach, they

© 2005 NRC Canada

Fig. 6. The density dependence of the reduced relaxation time of Ar, Kr, N_2, and CO_2 for $T^* = 1.3$ (solid line) and $T^* = 1.6$ (dashed line) using the thermal pressure method, and experimental viscosities from the NIST database (14).



calculated the temperature and density dependence of the three different contributions to the viscosity

$$[8] \qquad \eta(\rho,T) = \eta_{KK}(\rho,T) + \eta_{KP}(\rho,T) + \eta_{PP}(\rho,T)$$

where η_{KK}, η_{KP}, and η_{PP} represent kinetic–kinetic, kinetic–potential, and potential–potential contributions, respectively. In the zero-density limit, the sole contributor is the kinetic–kinetic term, which is the Chapman–Enskog viscosity. They showed that the density isotherms of η_{KK} and η_{PP} vary monotonically for densities greater than the critical density. However, the density isotherms of η_{KP} have a maximum in the range of $0.6 < \rho^* < 0.75$, which is approximately 2–2.5 times the critical density of the LJ fluid ($\rho_c^* \approx 0.3$). The maximum of the η_{KP} isotherms shifts to higher densities as the temperature increases in a manner similar to the increase in the minimum of the shear relaxation time. This behaviour of η_{KP} causes the viscosity–density isotherms to intersect in the $0.75 < \rho^* < 0.80$ density range.

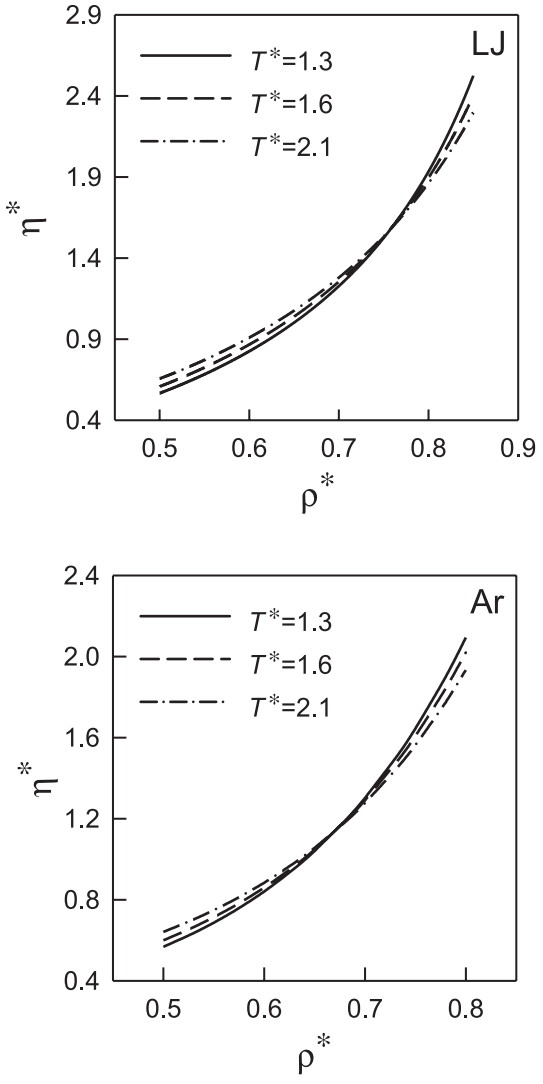
The existence of the minimum in the shear relaxation time can be further clarified by studying the density dependence of $(\partial G_\infty/\partial\rho)_T$ or $(\partial p_{th}/\partial\rho)_T$ and $(\partial\eta/\partial\rho)_T$ for a typical a LJ isotherm in Fig. 8. Although both $(\partial G_\infty/\partial\rho)_T$ and $(\partial p_{th}/\partial\rho)_T$ increase monotonically with density, $(\partial\eta/\partial\rho)_T$ decreases slowly at first, but then increases very rapidly after $\rho^* \approx 0.6$. This contrast in the behavior of viscosity at densities higher than the common point density can be attributed to the collisional transfer mechanism, which becomes dominant and yields higher viscosities than the kinetic transfer mechanism, which is dominant at low densities. By noting that the shear relaxation time is the ratio of the viscosity to the shear modulus or thermal pressure, the origin of the minimum in the relaxation time at the common point density will be evident.

The origin of the relaxation time minimum can be investigated from the molecular view point. For supercritical isotherms at lower densities, as the density is increased, the relaxation time decreases. This behaviour is expected since at low densities the viscosity is density-independent. At the same time, with increasing density, the number of molecular momentum carriers increases and so the relaxation time must decrease. The viscosity arises from the transport of momentum between the fluid layers during laminar flow. By increasing the correlation between layers, the relaxation time required for a system to eliminate any velocity gradients decreases. Momentum transfer in a fluid can occur by mass carriers (represented by the η_{KK} contributions) and by the effect of intermolecular forces (represented by the η_{PP} and η_{KP} contributions). The former mechanism predominates at low, and the latter at high densities (15).

In the intermediate density range ($\rho^* < 0.70$), the role of attractive forces becomes more important than in dilute fluids, as is evident from the molecular dynamics calculations.

© 2005 NRC Canada

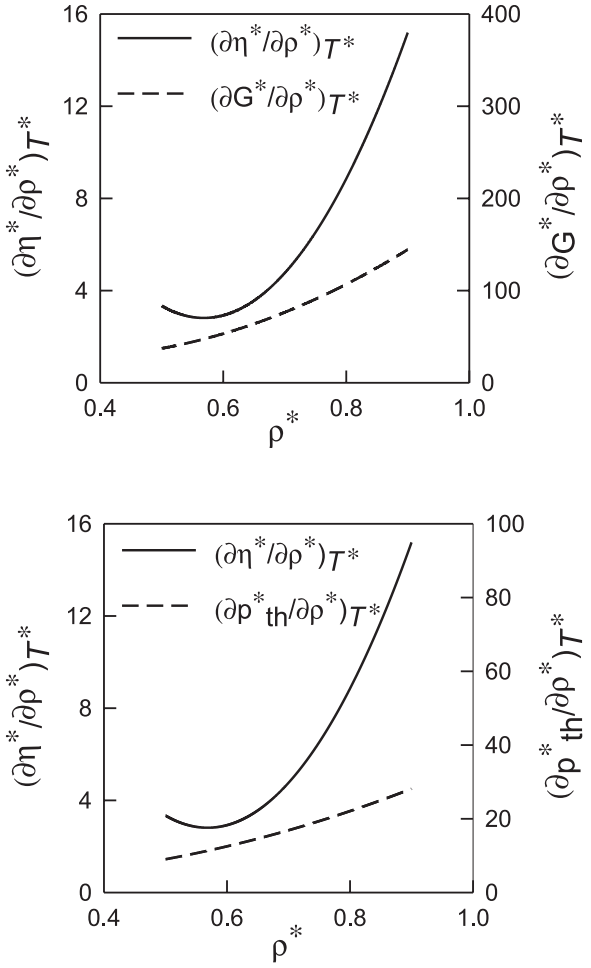
Fig. 7. Intersection of the reduced viscosity–density isotherms of the LJ fluid (top) and argon (bottom).



Molecular dynamics calculations show the viscosity of a square-well fluid increases with a greater slope as a function of density as the attractive well depth becomes larger (19). Although in molecular dynamics simulations temperature and well depth are not separable, for small changes of ε/kT it is possible to assume the well depth has been varied for an isotherm. An intersection point at about twice the critical density for isotherms of viscosity vs. density is found in molecular dynamics simulations of square-well fluids (20). In this intermediate density range, attraction between adjacent fluid layers becomes the dominant contributor to viscosity and causes a decrease in the relaxation time. For $\rho^* > 0.70$, the fluid becomes more compressed and the repulsive contribution of the intermolecular potential becomes dominant and cancels the effects of attractive forces. Consequently, the relaxation time increases for $\rho^* > 0.70$. Weeks et al. (21) pointed out that for LJ liquids, repulsive forces are dominant for densities higher than $\rho^* = 0.65$, which is twice the critical density in real fluids.

In addition to the gas phase, the density of the minima in the shear relaxation time isotherms are observable in the liquid phase, as shown for subcritical isotherms of *liquid* argon in Fig. 9. The density at which the viscosity isotherms for liquid argon intersect is also given in Fig. 9. This figure shows that for $\rho/\rho_c < 2.23$, the viscosity of liquid argon increases with increasing temperature, which is a behaviour usually associated with the gas phase. Although the increase of the viscosity with temperature is small, it is nonetheless measurable. This increase in viscosity with increasing temperature is observed in the experimental viscosity of liquid carbon dioxide (5) and liquid methane (22). Molecular dynamics simulations of Meier et al. (18) for the LJ fluid show that at densities lower than $\rho^* \approx 0.75$, the viscosity increases with temperature, while for densities higher than $\rho^* \approx 0.75$ in the liquid region in the range, the viscosity decreases with temperature.

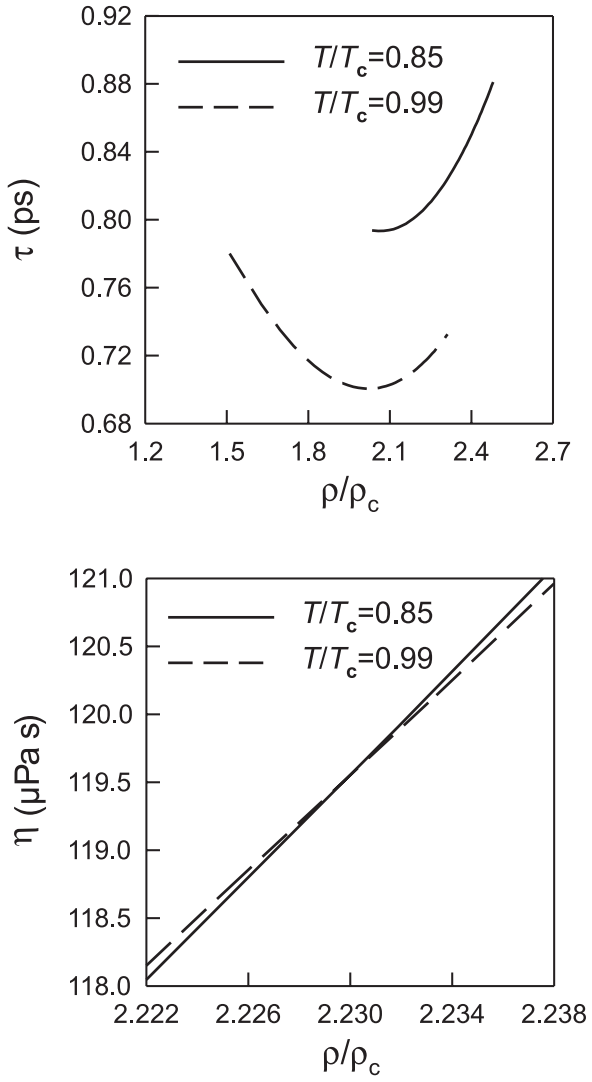
Fig. 8. Slope of reduced viscosity (left vertical axes) and G^*_∞ or p^*_{th} (right vertical axes) with respect to density vs. reduced density for the LJ fluid at $T^* = 1.6$.



The reason why most texts (23, 24) state that the viscosity of liquids decreases with increasing temperature is that viscosity data for liquids are normally measured at liquid densities greater than twice that of the critical density ($\rho/\rho_c > 2.23$ for the case of argon). Our results emphasize that the trend of increasing viscosity with increasing temperature depends only on the density of the fluid, regardless of its gas or liquid state. A similar behavior is observed for the metal-to-nonmetal transition where metallic or nonmetallic behavior

© 2005 NRC Canada

Fig. 9. Relaxation time (top) and viscosity (bottom) vs. reduced density, where ρ_C and T_C are the critical density and temperature, respectively, for liquid argon. Experimental data for Ar are obtained from the NIST database (14).



depends only on the density and not on the physical state of the fluid metal (25).

As a final note, it is necessary to emphasize that eq. [2] is derived for two-body potentials (2). At high densities, three and further many-body terms yield contributions to the macroscopic properties that can cause the difference between the relaxation times obtained by the Zwanzig–Mountain and thermal pressure approaches. These many body terms are not taken into account in the present simulations and might yield some contribution to the magnitude of the shear modulus. However, since the density minima obtained from the two approaches are close, the effect of many body forces on the density of the minimum of the relaxation time will not be large.

Acknowledgement

We wish to acknowledge the research council of the Isfahan University of Technology for financial support (Grant No. 1CHA811).

References

1. R.S. Berry, S.A. Rice, and J. Ross. Physical chemistry. John Wiley and Sons, Inc., New York. 1980.
2. R. Zwanzig and R.D. Mountain. J. Chem. Phys. **43**, 4464 (1965).
3. R.D. Mountain and R. Zwanzig. J. Chem. Phys. **44**, 2777 (1966).
4. P.S. van der Gulik, R. Mostert, and H.R. van den Berg. Physica, **151A**, 153 (1988).
5. P.S. van der Gulik. Physica, **238A**, 81 (1997).
6. P.S. van der Gulik. Physica, **256A**, 39 (1998).
7. B. Najafi, Y. Ghayeb, and G.A. Parsafar. Int. J. Thermophys. **21**, 1011 (2000).
8. E. Matteoli and G.A. Mansoori. J. Chem. Phys. **103**, 4672 (1995).
9. L. Verlet. Phys. Rev. **165**, 201 (1968).
10. J.M. Haile. Molecular dynamics simulation: elementary methods. John Wiley and Sons, Inc., New York. 1992.
11. M.P. Allen and D.J. Tildesley. Computer simulation of liquids. Clarendon Press, New York. 1987.
12. A.K. Dham, A.R. Allnatt, W.J. Meath, and R.J. Aziz. Mol. Phys. **67**, 1291 (1989).
13. R.L. Rowley and M.M. Painter. Int. J. Thermophys. **18**, 1109 (1997).
14. E.W. Lemmon, M.O. McLinden, and D.G. Friend. Thermophysical properties of fluid systems. NIST Chemistry WebBook, NIST Standard Reference Database Number 69 [online]. *Edited by* P.J. Linstrom and W.G. Mallard. National Institute of Standards and Technology, Gaithersburg Maryland. Available from http://webbook.nist.gov. March 2003.
15. H.C. Longuet-Higgins and J.A. Pople. J. Chem. Phys. **25**, 884 (1956).
16. M. Mecke, A. Muller, J. Winkelmann, J. Vrabec, J. Fischer, R. Span, and W. Wagner. Int. J. Thermophys. **17**, 391 (1996); Erratum, **19**, 1493 (1998).
17. A. Michels, A. Botzen, and W. Schuurman. Physica, **20**, 1141 (1954).
18. K. Meier, A. Laesecke, and S. Kabelac. J. Chem. Phys. **121**, 3671 (2004).
19. J.P.J. Michels and N.J. Trappeniers. Physica, **104A**, 243 (1980).
20. J.P.J. Michels and N.J. Trappeniers. Physica, **101A**, 156 (1980).
21. J.D. Weeks, D. Chandler, and H.C. Andersen. J. Chem. Phys. **54**, 5237 (1971).
22. B.A. Younglove and J.F. Ely. J. Phys. Chem. Ref. Data, **16**, 577 (1987).
23. I.N. Levine. Physical chemistry. 4th ed. McGraw-Hill Inc., New York. 1995.
24. P.W. Atkins. Physical chemistry. 6th ed. Oxford University Press, New York. 1998.
25. E. Keshavarzi and G. Parsafar. J. Phys. Chem. **103B**, 6584 (1999).

© 2005 NRC Canada

Oxidation of 1-(4′-substituted phenyl)-2-(4-methylphenyl)diazene — Benzylic substitution vs. C–azo bond breaking

Alexandru C. Razus, Carmen Nitu, Claudia Pavel, Crinu-Anghel Ciuculescu, Valentin Cimpeanu, Corneliu Stanciu, and Philip P. Power

Abstract: The low oxidation potential of 1-phenyl-2-(4-methylphenyl)diazene 4′-substituted with a dimethylamino or methoxy group (**10** and **11**) allows the easy single electron transfer with radical cation generation in the presence of $FeCl_3$. At the same time, the stabilizing effect of the positive charge exerted by 4-dimethylaminophenyl > 4-methoxy groups on the intermediate carbocation favors the hydrogen atom elimination in comparison with proton loss. Whereas benzylic substitution towards di- and triarylmethane derivatives takes place starting from diazene **11**, the oxidation of diazene **10** leads mainly to products of C–azo breaking. This difference is well-supported by the idea that the electron, in the first step of oxidation, is extracted from the azo and (or) from the amino nitrogen atom.

Key words: diazenes, oxidation, single electron transfer, benzylic substitution, C–azo bond breaking.

Résumé : Le faible potentiel d'oxydation des 1-phényl-2-(4-méthylphényl)diazènes substitués en position 4′ par des groupes diméthylamino (**10**) ou méthoxy (**11**) permet, en présence de $FeCl_3$ le transfert facile d'un seul électron avec la formation d'un cation radical. En même temps, l'effet stabilisant de la charge positive des groupes 4-diméthylamino-phényle > 4-méthoxy sur le carbocation intermédiaire favorise l'élimination de l'atome d'hydrogène par rapport à une perte de proton. Alors que la substitution benzylique vers les dérivés di- et triarylméthanes se fait à partir du diazène **11**, l'oxydation du diazène **10** conduit principalement à des produits résultant d'une rupture de la liaison C–azo. Cette différence est bien expliquée par l'idée que l'électron, dans la première étape de l'oxydation, est extrait de l'atome d'azote de l'azo et (ou) amino.

Mots clés : diazènes, oxydation, transfert d'un seul électron, substitution benzylique, rupture d'une liaison C–azo.

[Traduit par la Rédaction]

Introduction

In a previous paper (1), we investigated the oxidation of *para*-methyl substituted (*E*)-1-azulen-1-yl-2-phenyldiazene (**1**), with iron(III) chloride (Scheme 1). The reaction was performed in benzene, with good conversion of the starting diazene (between 60% and 80%) to afford products that are mono- and diphenyl-substituted at the methyl group. As shown in the scheme, the di- and triphenylmethane derivatives, the corresponding carbinols, and compounds resulting from hydroxyl oxidation or intramolecular water elimination were also generated. When chlorinated diazene **1**(Cl) was oxidized, 3,3′-dichloro-1,1′-biazulene was also separated from the reaction mixture.

The proposed oxidation mechanism shown in Scheme 2 (1) is based on an initial single electron transfer (SET), **1** → $\mathbf{1}^{+\cdot}$, and on the efficient stabilization of the positive charge on a tropylium ion moiety both in the radical cation $\mathbf{1}^{+\cdot}$ (the most favoured resonance structure is represented) and in the subsequent cation **8**.

We now extend these results on the azulenic diazenes to compounds having the azulenic moiety replaced by other groups, which lower the oxidation potential and stabilize the positive charge, such as 4-dimethylamino- and 4-methoxyphenyl groups (compounds **10** (2) and **11** (3), respectively).

Oxidation of diazenes 10 and 11

The previously used reaction conditions (1) were maintained: the ratio of diazene : ferric chloride = 1:4 in benzene (1 mmol diazene in 25 mL benzene), without atmospheric protection. Because of the lower reactivity of the starting compounds and the rather high number of formed products, a longer reaction time was necessary. The reaction was monitored by TLC and when no changes in the compound ratio were detected, the reaction mixture was worked-up, and the products were separated by liquid chromatography on alumina. Not all of the compounds could be separated and individually characterized. Some products were identified by the careful analysis of GC–MS and NMR spectra of the eluted chromatographic fractions. Along with the main products, the reaction mixtures also contained other unidentified deriv-

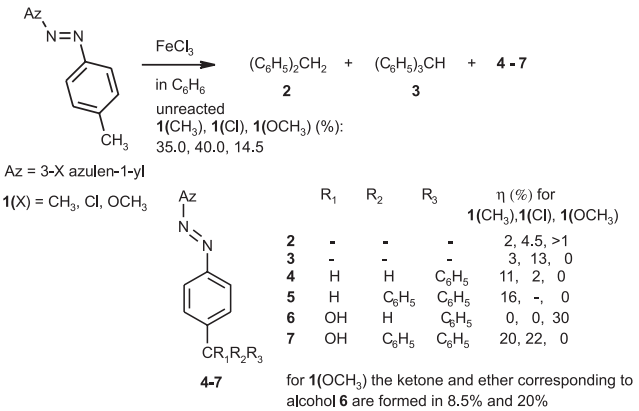
Received 15 July 2004. Published on the NRC Research Press Web site at http://canjchem.nrc.ca on 29 March 2005.

A.C. Razus,[1] C. Nitu, C. Pavel, C.-A. Ciuculescu, and V. Cimpeanu. C.D. Nenitzescu Institute of Organic Chemistry, Romanian Academy, Spl. Independentei 202B, sector 6, P.O. Box 15-254, 060023-Bucharest, Romania.
C. Stanciu and P.P. Power. Department of Chemistry, One Shields Avenue, University of California, Davis, CA 95616, USA.

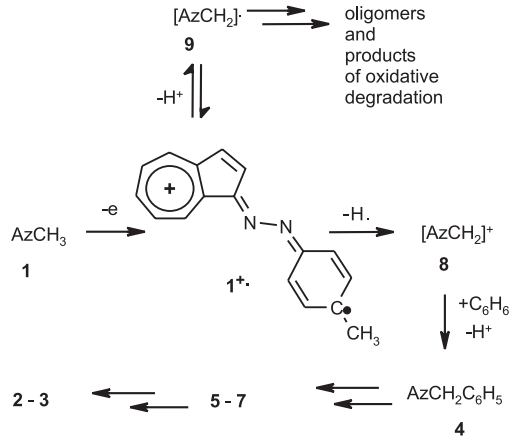
[1]Corresponding author (e-mail: acrazus@cco.ro).

 doi: 10.1139/V05-044 © 2005 NRC Canada

Scheme 1.



Scheme 2.



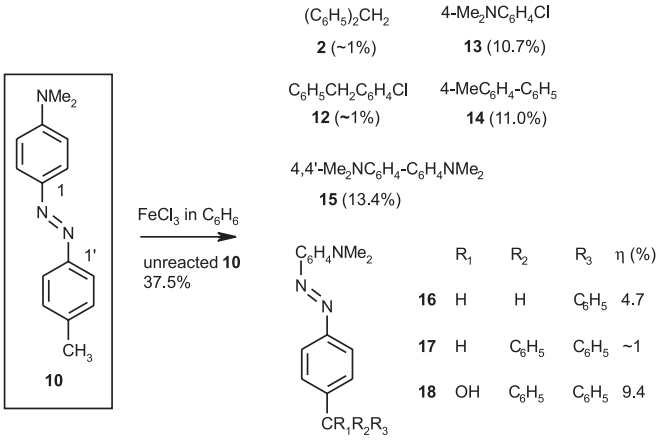
atives in very small amounts (under 1%) as well as a small quantity of a complex tar mixture.[2]

The reaction of diazene 10

The reaction mixture was stirred for 1 week and after work-up, six fractions were chromatographically separated. The main products obtained and their yields are given in Scheme 3. In this case, a significant amount of tar product was not eluted, but remained on the column.

The GC–MS of fraction 1 indicated the presence of three compounds in the molar ratio of 10:1:1.[3] The first two components had the same M^+ (molecular ion) (*m/z*): 168 ($C_{13}H_{12}^{+\cdot}$). For the last compound, the fragments 202/204 in abundances of 40%/12% indicated the presence of one chlorine atom in the molecule ($C_{13}H_{11}Cl^{+\cdot}$). The first compound with an M^+ of 168 had the same mass spectral features as 4-methyl-substituted biphenyl **14** (4), whereas the mass spectrum of the second compound resembled that of diphenylmethane **2**. In the ^{1}H NMR spectrum of fraction 1, the singlet at δ 3.92 ppm, near the methylene protons of **2** (δ 3.96 ppm) (5), supported the presence of the second compound that also possessed a methylene group. On the basis of chemical shifts and integrations in the ^{1}H NMR spectrum, the diphenylmethane type of structure was attributed to the

Scheme 3.



halogenated compound **12**. Unfortunately, the chlorine position in the molecule could not be accurately assigned, however, the para position seems to be a plausible assumption. The MS of the single compound contained in fraction 2 displayed the characteristic peak of a monochlorinated derivative, M^+ 155/157 (76%/25%). The structure of this compound (**13**) (6) was ascertained on the basis of the AB group signal at δ 7.16 and 6.63 ppm (J = 9.1 Hz) for 1,4-disubstituted benzene as well as on the singlet peak corresponding to six methyl protons at 2.86 ppm. Fraction 3 consisted of the unreacted diazene **10**. The GC–MS of fraction 4 showed the presence of two compounds (**16** and **17**) with M^+ at 315 and 391, in a molar ratio of 6:1 (5), with very similar retention times on the chromatographic column. In the ^{1}H NMR spectrum of this fraction, the singlets at δ 4.03 and 5.60 ppm proved the presence of diaryl- and triarylmethane protons, respectively (other signals characteristic to the proposed structures (**16** and **17**) were also present). The dimeric compound **15** (4, 5, 7) was isolated from fraction 5, whereas fraction 6 contained the carbinol **18** (8).

The reaction of diazene 11

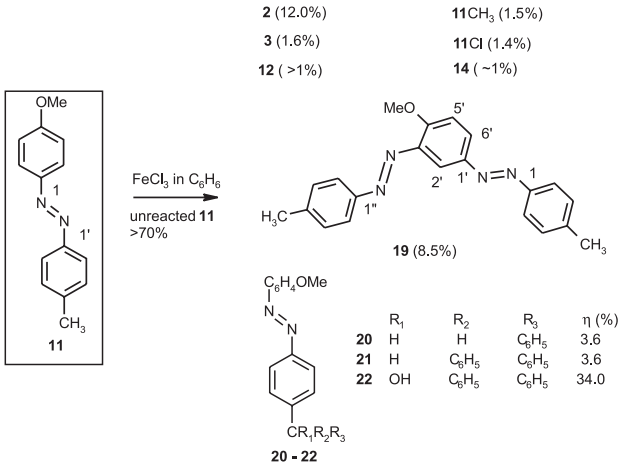
The reaction mixture was maintained at reflux for 48 h and after work-up, seven fractions were separated chromatographically. The results are described in Scheme 4.

Lower yields of the products were obtained in this case because of the very low reactivity of **11**, even under severe reaction conditions. For this reason, the separation and identification of the products from this diazene were more difficult in comparison to those of **10**. The GC–MS of fraction 1 was consistent with the presence of compounds **2**, **12** (in traces), and **14**, products also obtained from the oxidation of **10**, together with triphenylmethane (**3**) (4), in a molar ratio **2**:**3**:**14** of 12:1.6:1. The GC–MS of fraction 2 showed the presence of two compounds in a molar ratio of 1.1:1 with M^+ at (*m/z*) 241 and 260/262 (36%/84%) corresponding to the methylated and monochlorinated starting diazenes (**11**(CH_3) and **11**(Cl)), respectively. Unfortunately, the position of substitution could not be established. Fraction 3 was the starting material (**11**). The diaryl- and triarylmethanic compounds (**21** and **22**) (8) were present in an equimolar ra-

[2] The search for eventually formed products soluble in aqueous solution at work-up (as, for instance, phenols) was unsuccessful.
[3] The ratio between the integral of singlets in the ^{1}H NMR spectrum is in accord with the ratio from the GC–MS.

© 2005 NRC Canada

Scheme 4.



tio in fraction 4 as can be concluded from both MS (M^+ 302 and 378) and ^{1}H NMR spectra (δ 4.06 and 5.62 ppm for methylene and methyne protons). The value of M^+ = 344 for compound **19**, eluted in fraction 5, corresponded to the structure of starting diazene **11** substituted by the 4-methylphenylazo group. In the ^{1}H NMR spectrum of **19**, two phenyl moieties were present, both with para positions substituted by N=N and CH_3 (the AB group signal at δ 7.28–7.34 ppm corresponding to 4H, and at δ 7.81 and 7.87 ppm each accounting for 2H). The two singlets very closely placed (at δ 2.43 and 2.44 ppm each making for 3H) and the singlet at δ 4.11 ppm accounting for 3H corresponded to two benzylic and one methoxy methyl groups, respectively. The chemical shifts and the coupling values for other signals of **19** are consistent with methoxybenzene 2,4-di-substituted by 4-methylphenylazo groups. Unfortunately, the elemental analysis of compound **19** failed because of the presence of a very small amount of an unidentified compound, present in fraction 5, which could not be eliminated by chromatography. Fraction 6 contained some unidentified compounds in traces (as shown by GC–MS), and in fraction 7, the carbinol **22** (8) was separated and characterized.

Discussion

The experimental and spectroscopic data described previously support the following conclusions.

The increase in the amount of unreacted diazenes along the series **1**(CH_3) = **1**(Cl) > **10** > **11** (Schemes 1, 3, and 4) reflects the decrease in their reactivity. This trend follows their oxidation potentials (9).[4] The high oxidation potential of the diazenes that have no activating groups, for example 1-(4-methylphenyl)-2-phenyldiazene, prevents the reaction (90% of starting material remains unreacted after 2 weeks and an amount of tar is formed).

The most unexpected difference among the reactivities of the diazenes is the nature and ratio of the oxidation products. The products obtained can be classified by: (*a*) compounds formed by C–azo bond breaking, and (*b*) benzylic substituted compounds (in some cases the substitution was followed by C–azo bond breaking as for **2**, **3**, and **12**).

For the oxidation of the diazene **10**, the major products **13** and **15** belong to group (*a*) and preserve 4-dimethylaminophenyl moiety. A moderate amount of compound **14** with a 4-tolyl moiety is also formed. When diazene **11** was reacted, such products were not generated except for a small amount of compound **14**, which formed in only 1% yield.

The products of benzylic substitution, i.e., **3**, **12**, and **20**–**22**, were obtained by the oxidation of diazene **11** in about 46% yield. In contrast, for the diazene **10,** the compounds of the type (*b*), **2**, **12**, and **16**–**20**, result only in 17% yield.

In the reaction mixture of diazene **11**, the interesting bisdiazene **19** and a very small amount of compounds **11**(CH_3) and **11**(Cl) were also present. However, the assignment of the structures of the last two products as methyl- or chlorine-substituted starting diazene **11** was based only on their mass spectra.

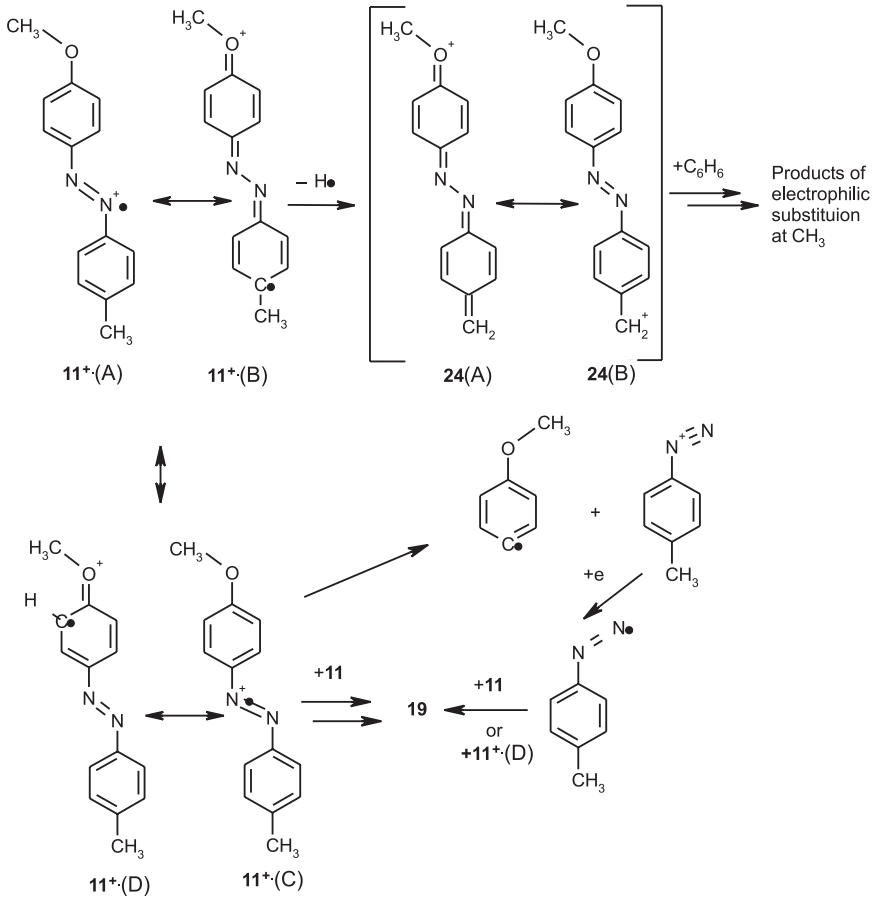
Accordingly, the benzylic substitution without C–azo bond breaking represents the major oxidation route for the diazenes **1** and **11** (Schemes 1 and 4). The main compounds formed in the reaction mixture of **10** were, however, generated by C–azo breaking followed by subsequent stabilization of the fragments **13**–**15** (Scheme 3). Another feature of the reactivity of diazene **10** is the higher amount of the product conserving the 4-dimethylaminophenyl moiety in comparison with those with a 4-tolyl group. This illustrates the difference between the two types of C–azo bond breaking in **10**, which involves the =N-dimethylaminophenyl and =N-tolyl moieties.

As for all oxidations with $FeCl_3$ that we studied, the first reaction step consists of a SET with radical cation generation. Based on the results of EPR and theoretical investigations of the diphenyldiazene radical cation, Rhodes and coworkers (10) suggested the structure [–:N=$N^{+\bullet}$– ↔ –$^{+\bullet}$N=N:–] for the azo group, with the possibility of spin delocalization on the phenyl ring. A good electron donor group, such as the methoxy at one of the phenyl moieties, as in compound **11** or azulene, as in the diazene **1**, enhances the spin delocalization. Some resonance structures for the radical cation **11**$^{+\bullet}$ are presented in Scheme 5.[5] If the structure **11**$^{+\bullet}$ (B) is the most favoured (11), the intermediates formed during the most important oxidation route, namely benzylic substitution, would resemble those for the azulenic diazene **1** (Scheme 2). The presence of a significant amount of bisdiazene **19** in the oxidation mixture of **11** can be considered a surprising result. Thus, the electrophilic substitution of diazene **11** by the diazonium cation, formed in a homolytic breaking of the C–azo bond (12),[6] is prevented by the presence of the deactivating azo double bond (in spite of the existence of the electron donor methoxy substituent).[7]

[4] The overall yield of all products is almost the same for each of the oxidized diazenes.
[5] Other structures could also be written as, for instance, a structure with one electron transferred from the oxygen atom; however, the obtained products seem to infringe on this possibility.
[6] The similar C–azo breaking in structure **11**$^{+\bullet}$ (A), if it takes place, leads to the formation of a low reactive diazonium salt. Possibly, at the work-up of the reaction mixture, the small amount of stabilization products formed from diazonium salts was lost.
[7] The coupling at the anisole succeeds only with very reactive diazonium salts.

© 2005 NRC Canada

Scheme 5.

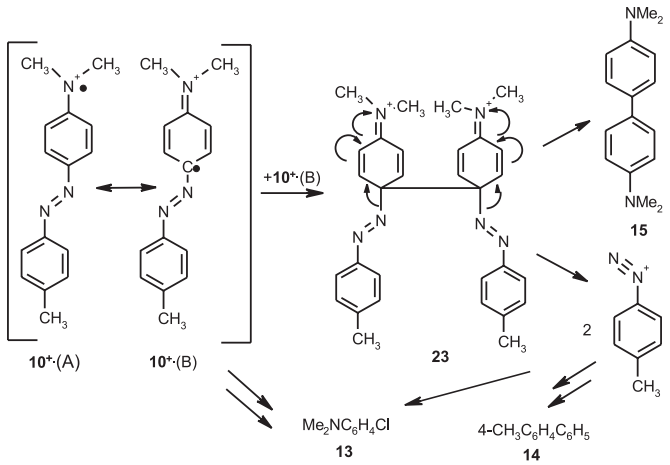


The radicalic route for generation of **19** seems to be more realistic. Thus, the attack of the nitrogen spin of the radical cation $\mathbf{11}^{+\cdot}$ (C) on the *ortho*-CH_3O position in **11** gives a new radical cation. The subsequent proton elimination and anisyl radical cleavage results in the formation of compound **19**. An alternative route that can be also considered starts from the above-mentioned diazonium salt. The diazonium radical obtained by reduction of this salt with $FeCl_2$, present in the medium, substitutes the radical cation $\mathbf{11}^{+\cdot}$ (D) or, more probably, the compound **11**. Incertitude remains, however, in connection with the aryl diazonium radical lifetime. Some results obtained in the thermic decomposition of such intermediates (13) indicate a rate constant for loss of nitrogen between 10^7 and 10^9 s^{-1}; therefore, it is difficult to imagine another faster reaction even if the reaction is diffusion controlled (14).

At the oxidation of diazene **10**, the di- and triarylmethane derivatives originate in a radical cation similar to $\mathbf{11}^{+\cdot}$. However, it is difficult to say whether this intermediate is formed, namely, by single electron transfer from the azo nitrogen (Scheme 5) or from the amino nitrogen (Scheme 6) or by both ways.

One further question remains to be answered: what is the reaction route by which diazene **10** can generate significant amounts of the products **13** and **15**, which have the 4-dimethylaminophenyl moiety, but no azo bond? The best fit to the experimental data involves, as the first reaction step, the SET from the amino nitrogen atom. This interpretation is

Scheme 6.



supported by the reported structure of the radical cation that was obtained by the anodic oxidation of dimethylaniline (15). This intermediate possesses both the charge and the spin at the nitrogen atom with the possibility of spin delocalization to the para position followed by spin coupling. In contrast with our chemical oxidation, the electrochemical oxidation of **10** did not allow the separation of products and only formation of a thin film was reported (16). The key intermediate for the generation of the product **15** seems to be the radical cation $\mathbf{10}^{+\cdot}$ with a charge distribution depicted by

© 2005 NRC Canada

structure (B) (Scheme 6). The dimerization of $\mathbf{10}^{+\cdot}$ (B) by spin-spin coupling to **23** and the diazonium salt elimination gives the biphenyl **15** (the same reaction route explains the presence of the azulene dimer coupled at the 1,1′ positions during the oxidation of **1**(Cl)). The generation of **15** from the free 4-dimethylaminophenyl radical can be excluded because no products of cross coupling were found in the reaction mixture. The chlorine (atom or anion) attack on $\mathbf{10}^{+\cdot}$ (B) provides the compound **13**. It seems possible that the 4-methylbiphenyl **14** is a result of the radical arylation of benzene (17). The 4-tolyl radical is formed by the reduction of the diazonium salt obtained at the decomposition of **23** and the subsequent nitrogen elimination.

Conclusion

In conclusion, the low oxidation potentials of the diazenes **10** and **11**, as well as of **1**, result in an easy single electron transfer with radical cation generation. At the same time, the stabilizing effects exerted by the azulene > 4-dimethylaminophenyl > 4-methoxyphenyl groups on the carbocations favour hydrogen atom elimination over proton loss (1). Therefore, the superacidic behaviour of the radical cation intermediates proposed earlier (18) must be carefully considered. Factors such as the type of substituent or the polarity of reaction medium can favour either the homolytic or the heterolytic breaking of the C—H bond. The differences in the nature and the product ratios for diazenes oxidation are complex. Whereas di- and triarylmethane derivatives are the major products starting from **1** and **11**, diazene **10** leads mainly to products of C–azo breaking. This difference can be satisfactorily explained by the different position from which the electron is lost in the first step of the oxidation process to generate the radical cation intermediate.

Experimental

^{1}H and ^{13}CNMR: Bruker Avance DRX4 (^{1}H: 400 MHz, ^{13}C: 100.62 MHz) and Varian Gemini 300BB (^{1}H: 300 MHz, ^{13}C: 75.47 MHz) spectrometers; chemical shifts (δ) are expressed in ppm, and *J* values are given in Hz; TMS was used as internal standard in $CDCl_3$ as solvent; in a few cases the signals were assigned on the basis of COSY and HETCOR experiments. IR: Beckmann IR 5A. Mass spectra were recorded on a JEOL JMS-DX303 spectrometer coupled to a Shimadzu GC-14B gas chromatograph with a DB-1 capillary column and a C-R6A integrator. Column chromatography: basic alumina (activity BII-III (Merck)). Dichloromethane (DCM) was distilled over CaH_2 and ethyl acetate was distilled over Na_2CO_3. The numbering of the positions in the compounds is reported in Schemes 3 and 4.

Starting diazenes

N,*N*-Dimethyl-*N*-{4-[(*E*)-(4′-methylphenyl)diazenyl]phenyl}amine (**10**) was obtained as described in literature (2).

(*E*)-1-(4-Methoxyphenyl)-2-(4-methylphenyl)diazene (**11**) was obtained by coupling of the 4-tolyldiazonium salt with phenol (18) and reacting the diazene with diazomethane. Compound **11** shows the ^{1}H NMR spectrum as described (18): δ_H ($CDCl_3$): 2.42 (3H, s, CH_3), 3.89 (3H, s, OCH_3), 7.00 (2H, d, J = 9.2 Hz, 3-, 5-H), 7.29 (2H, d, J = 8.1 Hz, 3′-, 5′-H), 7.79 (2H, d, J = 8.3 Hz, 2′-, 6′-H), 7.90 (2H, d, J = 9.2 Hz, 2-, 6-H). ^{13}C NMR ($CDCl_3$) δ_C: 21.44 (CH_3), 55.54 (OCH_3), 114.15 (C-3, -5), 122.52 (C-2′, -6′), 124.55 (C-2, -6), 129.67 (C-3′, -5′), 140.79 (C-4′), 147.03 (C-1), 150.81 (C-1′), 161.80 (C-4).

Oxidation with ferric chloride — General procedure

In a round-bottomed flask to a magnetically stirred solution of diazene **10** or **11** in benzene (1 mmol diazene for 25 cm^3), anhydrous ferric chloride was added at room temperature (the oxidation of diazene **11** occurred at reflux of the solvent) without air protection (ratio between $FeCl_3$ and diazene is 4:1). From time to time the separated viscous oily product was mechanically removed from the flask wall for a better contact between the reactants. The reaction was monitored by TLC (homogenous samples were collected, washed with a saturated sodium bicarbonate solution, and dried), and it was stopped when the spot of the starting compound vanished or maintained a stationary intensity (the reaction time will be indicated for each diazene). The reaction mixture was quenched with a saturated sodium bicarbonate solution and the major amount of the benzene was evaporated in vacuum. The suspension was extracted three times with 200 cm^3 DCM, the organic extracts were washed once with water, dried (Na_2SO_4), and the solvent was evaporated in vacuum. The residue was fractionated by column chromatography under conditions described in the following. To establish the ratio between the compounds in the eluted fractions, GC–MS and ^{1}H NMR signal integrals were considered and the product yields were calculated towards the reacted diazene. For some of the obtained compounds, mass spectra and (or) ^{1}H NMR spectra, available in the spectra libraries, were used for identification.

Reaction of 10

After 7 days at room temperature, the reaction mixture was worked-up and from 1.5 mmol of **10**, an amount of 367 mg of the rough product was separated on an alumina column (d = 3 cm; l = 13 cm) in six fractions, the first five with *n*-pentane:DCM (4:1), the last one with ethyl acetate. Fraction 1: (the ratio between the compounds was calculated on the basis of GC–MS and ^{1}H NMR spectra of the fraction) 4-methyl-1,1′-biphenyl (**14**, 17 mg, 0.102 mmol, 11%), benzylbenzene (**2**, ~2 mg, 0.010 mmol, ~1%), 1-benzyl-chlorobenzene (**12**, ~2 mg, 0.010 mmol, ~1%). Fraction 2: *N*-(4-chlorophenyl)-*N*,*N*-dimethylamine (**13**, 16 mg, 0.100 mmol, 10.7%). Fraction 3: unreacted **10** (135 mg, 0.564 mmol, conversion 62.4%). Fraction 4: 17 mg, *N*,*N*-dimethyl-*N*-{4-[(*E*)-(4-(phenylmethyl)phenyl)diazenyl]phenyl}amine (**16**) and *N*,*N*-dimethyl-*N*-{4-[(*E*)-(4-(diphenylmethyl)phenyl)diazenyl]phenyl}amine (**17**) with a molar ratio (determined by GC–MS and ^{1}H NMR) of 5.8:1 (4.7% and ~1%, respectively). Fraction 5: *N*,*N*,*N*′,*N*′-tetrametyl-1,1′-biphenyl-4,4′-diamine (**15**, 15 mg, 0.063 mmol, 13.4%). Fraction 6: *N*,*N*-dimethyl-*N*-{4-[(*E*)-(4-(diphenylhydroximethyl)phenyl)diazenyl]phenyl}amine (**18**, 36 mg, 0.088 mmol, 9.4%).

Spectra of resultant fractions or compounds

Mixture of **16** and **17** in fraction 4: yellow powder. ^{1}H NMR ($CDCl_3$) δ_H: 3.07 (40.8H, s, $N(CH_3)_2$), 4.03 (11.6H, s,

© 2005 NRC Canada

CH_2), 5.60 (1H, s, C*H*), 6.75 (13.6H, d, *J* = 9.3 Hz, 3-, 5-H), 7.12–7.31 (52.6H, m, 3′-, 5′-H, and phenyl protons), 7.77 (13.6H, d, *J* = 9.2 Hz, 2-, 6-H), 7.86 (13.6H, d, *J* = 9.2 Hz, 2-, 6-H). GC–MS, *m*/*z* (70 eV): 317 (M(**16**)$^+$ + 2, 2%), 316 (M^+ + 1, 13), 315 (M^+, 71), 165 (13), 157 (15), 152 (18), 148 (10), 121 (6), 120 (100), 118 (8), 105 (15), 104 (20), 91 (23), 77 (22); 392 (M(**17**)$^+$ + 1, 16%), 391 (M^+, 68), 167 (17), 165 (55), 120 (100), 105 (18), 104 (20), 91 (19), 77 (26).

Because only the melting point, elemental analysis, and ^{1}H NMR spectrum for compound **18** were reported in the literature (8) without the proton assignments, we now report the complete characterization of this compound: yellow crystals with mp 210 °C (lit. value (8) mp 209 °C). ν_{max} (CH_2Cl_2) cm^{-1}: 3580 weak (OH). ^{1}H NMR ($CDCl_3$) δ_H: 3.07 (6H, s, N(CH_3)$_2$), 6.74 (2H, d, *J* = 9.3 Hz, 3-, 5-H), 7.30–7.32 (10H, m, phenyl protons), 7.39 (2H, d, *J* = 8.7 Hz, 3′-, 5′-H), 7.76 (2H, d, *J* = 8.7 Hz, 2-, 6-H), 7.86 (2H, d, *J* = 9.2 Hz, 2′-, 6′-H). ^{13}C NMR ($CDCl_3$) δ_C: 40.23 (N(CH_3)$_2$), 81.91 (*C*-OH), 111.43 (t), 121.59 (t), 124.94 (t), 127.29 (t), 127.89 (t), 127.94 (t), 128.55 (t), 143.67 (q), 146.66 (q), 147.86 (q), 152.21 (q), 152.38 (q). GC–MS *m*/*z* (70 eV): 409 (M^+ + 2, 1%), 408 (M^+ + 1, 5), 407 (M^+, 15), 121 (13), 120 (69), 105 (34), 95 (15), 93 (17), 91 (11), 81 (46), 77 (23), 69 (100), 67 (11).

Reaction of 11

After 2 days at reflux, the reaction mixture was worked-up and from 3.54 mmol of **11**, an amount of 826 mg of the rough product was separated on an alumina column (*d* = 4 cm, *l* = 15 cm) in seven fractions, the first two with *n*-pentane:DCM (4:1), the next fractions with increasing ratios of ethyl acetate : *n*-pentane from 1:10 to pure ester for the last fraction. Fraction 1: (the molar ratio between the compounds resulted from the GC–MS and ^{1}H NMR spectra of the fraction) compound **2** (4 mg, 0.022 mmol, 2%), compound **14** (~2 mg, 0.012 mmol, ~1%), benzhydrylbenzene (**3**, 4 mg, 0.018 mmol, 1.6%), and in traces, chlorinated compound **12**. Fraction 2: (the ratio between the compounds resulted from the GC–MS of the fraction): **11**(CH_3) (4 mg, 0.017 mmol, 1.5%) and **11**(Cl) (4 mg, 0.016 mmol, 1.4%). Fraction 3: unreacted **11** (558 mg, 2.46 mmol, conversion 30%). Fraction 4: (the molar ratio was determined by GC–MS and ^{1}H NMR): (*E*)-1-(4-methoxyphenyl)-2-(4-(phenylmethyl)phenyl)diazene (**20**, 12 mg, 0.038 mmol, 3.6%), (*E*)-1-(4-methoxyphenyl)-2-(4-(diphenylmethyl)phenyl)diazene (**21**, 14 mg, 0.038 mmol, 3.6%). Fraction 5: (*E*)-1-{2-methoxy-5-[(*E*)-(4-methylphenyl)diazenyl]phenyl}-2-(4-methylphenyl)diazene (**19**, 16 mg, 0.046 mmol, 8.5%), and traces from an unknown product. Fraction 6: a mixture of unidentified products (28 mg). Fraction 7: (*E*)-1-(4-methoxyphenyl)-2-(4-(hydroxydiphenylmethyl)phenyl)diazene (**22**, 144 mg, 0.36 mmol, 34%).

Spectra of resultant fractions or compounds

Compound **11**(Cl) *m*/*z* (70 eV): 262/260 (M^+, 36%/84%), 261 (83), 153 (17), 135 (96), 125 (93), 107 (91), 92 (90), 77 (100), 63 (91).

Compound **11**(CH_3) *m*/*z* (70 eV): 241 (M^+ + 1, 14%), 240 (M^+, 80), 149 (47%), 122 (20), 121 (99), 119 (17), 92 (30), 91 (100), 77 (57), 65 (97).

Compound **19**: ^{1}H NMR ($CDCl_3$) δ_H: 2.43 and 2.44 (two singlets, 3H + 3H, two CH_3), 4.11 (3H, s, OCH_3), 7.21 (1H, d, *J* = 8.9 Hz, 5′-H), 7.28–7.34 (4H, m, 2-, 2″-H), 7.81 (2H, d, *J* = 8.2 Hz, 3- or 3″-H), 7.87 (2H, d, *J* = 8.2 Hz, 3″- or 3-H), 8.05 (1H, dd, *J* = 8.8 and 2.4 Hz, 6′-H), 8.22 (1H, d, *J* = 2.4 Hz, 2′-H). GC–MS *m*/*z* (70 eV): 344 (M^+, 1.5%), 255 (2), 119 (45), 91 (100), 76 (16), 65 (65).

Mixture of **20** and **21** (8) in fraction 4: yellow powder. ^{1}H NMR ($CDCl_3$) δ_H: 3.87 (6H, s, OCH_3), 4.06 (2H, s, CH_2), 5.61 (1H, s, C*H*), 7.00 (4H, d, *J* = 8.9 Hz, 3-, 5-H), 7.05–7.40 (19H, m, 3′-, 5′-H, and phenyl protons), 7.80 (4H, d, *J* = 8.3 Hz, 2′-, 6′-H), 7.85 (4H, d, *J* = 9.2 Hz, 2-, 6-H). GC–MS *m*/*z* (70 eV): 302 (M(**20**)$^+$, 71%), 239 (1), 228 (3), 215 (6), 180 (6), 168 (9), 165 (100), 163 (19), 152 (66), 139 (25), 135 (44), 115 (37), 107 (77), 91 (92), 89 (45), 77 (99), 63 (99); 378 (M(**21**)$^+$, 15%), 334 (2), 310 (1), 189 (3), 162 (5), 134 (20), 106 (12), 104 (20), 91 (100), 90 (22), 77 (10), 65 (60).

Because only the melting point, elemental analysis, and ^{1}H NMR spectrum were reported for compound **22** (8), without the proton position assignments, the compound was now completely characterized by us: yellow crystals with mp 181 to 182 °C (lit. value (8) mp 182 °C). ν_{max} (CH_2Cl_2) cm^{-1}: 3590 weak (OH). ^{1}H NMR ($CDCl_3$) δ_H: 3.87 (3H, s, OCH_3), 6.99 (2H, d, *J* = 8.9 Hz, 3-, 5-H), 7.29–7.31 (10H, m, phenyl protons), 7.43 (2H, d, *J* = 8.6 Hz, 3′-, 5′-H), 7.80 (2H, d, *J* = 8.3 Hz, 2′-, 6′-H), 7.90 (2H, d, *J* = 9.2 Hz, 2-, 6-H). GC–MS *m*/*z* (70 eV): 396 (M^+ + 2, 2%), 395 (M^+ + 1, 11), 394 (M^+, 42), 318 (2), 317 (10), 289 (10), 259 (5), 242 (4), 241 (22), 239 (13), 183 (8), 135 (47), 107 (100), 105 (55), 92 (22), 77 (52).

Acknowledgments

Authors A.C.R. and C.E.N. thank the Alexander von Humboldt Foundation for fellowships and Professor Klaus Hafner from the Technical University of Darmstadt, Institute of Organic and Bioorganic Chemistry, for hosting during their fellowships and for his full support, both material and scientific.

References

1. A.C. Razus and Carmen Nitu. J. Chem. Soc. Perkin Trans. 1, 989 (2000), and refs. therein.
2. S. Yamamoto, N. Nishimura, and S. Hasegawa. Bull. Chem. Soc. Jpn. **55**, 2018 (1982).
3. M. Okubo, T. Takahashi, and K. Koga. Bull. Chem. Soc. Jpn. **56**, 199 (1983).
4. MS Library: for **2**: Rev. 808, NIST 14808; for **3**: Rev. 757, NIST 32822; for **14**: Rev. 972, NIST 14810; for **15**: Rev. 928, NIST 32051.
5. C.J. Pouchert and J. Behnke. The Aldrich library of ^{1}H and ^{13}C FT NMR spectra. For compound **2**: **7C**; for compound **3**: **8C**; for compound **14**: **32C**; for compound **15**: **486C**.
6. T. Heidelberg. Chem. Ber. **20**, 149 (1887); J.R.L. Smith, L.C. McKeer, and J.M. Taylor. J. Chem. Soc. Perkin Trans 2, 385 (1988).
7. A.G. Giumanini and G. Lercker. J. Org. Chem. **35**, 3756 (1970).
8. D. Hellwinkel and H. Fritsch. Chem. Ber. **123**, 2207 (1990).
9. The increase in oxidation potential was approximated from the increasing values of half-wave potentials for azulene,

© 2005 NRC Canada

dimethylaniline, and anisole. N.L. Weinberg (*Editor*). *In* Techniques of Chemistry. Vol. V, part. II. John Wiley and Sons, New York. 1974. Appendix.
10. C.J. Rhodes. J. Chem. Soc. Chem. Commun. 799 (1990); C.J. Rhodes, H. Agirbas, M. Lindgren, and O.N. Antzutkin. J. Chem. Soc. Perkin Trans. 2, 2135 (1993).
11. The effective dimerization of (*E*)-1-azulen-1-yl-2-phenyldiazene in the para position at the oxidation with $FeCl_3$ attests to the important contribution of structures such as $\mathbf{11}^{+\cdot}$ for the spin density in the radical cation. A.C. Razus. J. Chem. Soc. Perkin Trans. 1, 981 (2000).
12. The generation of the phenyl cation by transfer of both bond electrons toward the azo group requires high energy. L. Friedman. *In* Carbonium ions. Vol. II. *Edited by* G.A. Olah and P. von R. Schleyer. Wiley-Interscience, New York. 1970. p. 701.
13. N.A. Porter, L.J. Marnett, C.H. Lochmuller, G.L. Closs, and M. Shobataki. J. Am. Chem. Soc. **94**, 3664 (1972).
14. The same order of the diffusion-controlled rate constant (10^{-10} L/mol s at 20 °C) was estimated for a radicalic reaction in benzene. J.G. Calvert and J.N. Pitts. Photochemistry. John Wiley and Sons, New York. 1966. p. 627.
15. T. Mizogouchi and R.N. Adams. J. Am. Chem. Soc. **84**, 2058 (1962).
16. T.A. Gough and M.E. Peover. Polarography. 1964 ed. McMillan, London. 1965. p. 1017; N.L. Weinberg (*Editor*). *In* Techniques of chemistry. Vol. V, part I. John Wiley and Sons, New York. 1974. Table 5.29. p. 763.
17. X. Zhang and F.G. Bordwell. J. Org. Chem. **57**, 4163 (1992); V.D. Parker, Y.T. Chao, and G. Zheng. J. Am. Chem. Soc. **119**, 11 390 (1997); E. Baciocchi, M. Bietti, and O. Lanzalunga. Acc. Chem. Res. **33**, 243 (2000), and refs. therein.
18. S.-J. Yeh and H.H. Jaffe. J. Am. Chem. Soc. **81**, 3274 (1959).

© 2005 NRC Canada

Synthesis of some heterocyclic systems of anticipated biological activities via 6-aryl-4-pyrazol-1-yl-pyridazin-3-one

A.S.A. Youssef, M.I. Marzouk, H.M.F. Madkour, A.M.A. El-Soll, and M.A. El-Hashash

Abstract: 6-Aryl-4-pyrazol-1-yl-pyridazin-3-one (**1**) reacted with a PCl_5–$POCl_3$ mixture to give the 3-chloropyridazine derivative **3**. Reaction of **3** with 2-hydroxybenzoylhydrazide and semicarbazide hydrochloride afforded **4** and **5**. Reaction of **1** with ethyl chloroacetate gave **8**. Reaction of **8** with hydrazine hydrate yielded the hydrazide **9**. The hydrazide **9** condensed with the acetylenic ketones and esters **10a**–**10d** and acetylacetone to give the adducts **11a**, **11b**, **12**, **13**, and **14**. Reacting **1** with formaldehyde and piperidine, morpholine, or piperazine, 3-bromopropanoic acid, acetic anhydride, *p*-toluenesulphonyl chloride, succinyl chloride, oxalyl chloride, ethanolamine, or ethyl chloroacetate gave the adducts **15**–**22**. The structures of all newly synthesized compounds were evidenced from their spectral and microanalytical data.

Key words: 6-aryl-4-pyrazol-1-yl-pyridazinone derivative, 6-aryl-3-chloropyridazine derivative, 3,6-diaryl-1,2,4-triazino[4,3-*b*]pyridazine derivative, 6-aryl-3-ethoxycarbonylmethoxypyridazine derivative, 6-aryl-3-(ω-benzoylacetophenone)hydrazinocarbonylmethoxypyridazine.

Résumé : La 6-aryl-4-pyrazol-1-yl-pyridazin-3-one (**1**) réagit avec un mélange de PCl_5–$POCl_3$ pour conduire à la formation du dérivé 3-chloropyridazine **3**. La réaction de **3** avec le 2-hydroxybenzoylhydrazide et le chlorhydrate de semicarbazide conduit aux dérivés **4** et **5**. La réaction de **1** avec le chloroacétate d'éthyle conduit à **8**. La réaction de **8** avec l'hydrate d'hydrazine permet d'obtenir l'hydrazide **9**. L'hydrazide **9** se condense avec les cétones acétyléniques, les esters **10a**–**10d** et l'acétylacétone pour fournir les produits **11a**, **11b**, **12**, **13** et **14**. La réaction de **1** avec le formaldéhyde et la pipéridine, la morpholine ou la pipérazine, l'acide 3-bromopropanoïque, l'anhydride acétique, le chlorure de *p*-toluènesulfonyle, le chlorure de succinyle, le chlorure d'oxalyle, éthanolamine ou le chloroacétate d'éthyle conduit aux adduits **15**–**22**. Les structures de tous les composés nouvellement synthétisés ont été caractérisés par leurs données microanalytiques et spectroscopiques.

Mots clés : dérivé de la 6-aryl-4-pyrazol-1-yl-pyridazinone, dérivé de la 6-aryl-3-chloropyridazine, dérivé de la 3,6-diaryl-1,2,4-triazino[4,3-*b*]pyridazine, dérivé de la 6-aryl-3-éthoxycarbonylméthoxypyridazine, 6-aryl-3-(ω-benzoylacétophénone)hydrazinocarbonylméthoxypyridazine.

[Traduit par la Rédaction]

Introduction

In a recent previous publication (1) we reported the reaction of β-aroylacrylic acid with some nitrogen nucleophiles and active methylene reagents and the utility of some of the reaction products in heterocyclic synthesis. A large number of pyridazin-3-ones were reported to exhibit insecticidal (2–6), allergenic (7), antihypertensive (8–12), analgesic (13, 14), anti-inflammatory, and bactericidal (15, 16) activities. This prompted us to study the behaviour of 6-(4-chloro-3-methyl) phenyl-4-(3,5-dimethyl-pyrazol-1-yl)-4,5-dihydropyridazin-3-one toward various reagents, hoping to get new compounds of anticipated biological activities.

Results and discussion

It has been reported (17, 18) that the reaction of 6-(4-chloro-3-methyl)phenyl-4-(3,5-dimethylpyrazol-1-yl)-**1a** or 6-(4-chloro-3-methyl) phenyl-4-(5-isopropyl-2-methyl)phenyl-**1b**-2,3,4,5-tetrahydropyridazin-3-one with a phosphorous pentachloride – phosphorous oxychloride mixture yielded 4,6-diaryl-3-chloro-4,5-dihydropyridazine derivatives **2a** and **2b**, respectively. In the present investigation, similar treatment of **1a** with the same reagent afforded 6-aryl-3-chloropyridazine derivative **3**. The previous reports suggested structure **2** for the products where there was a lack of spectroscopic data.

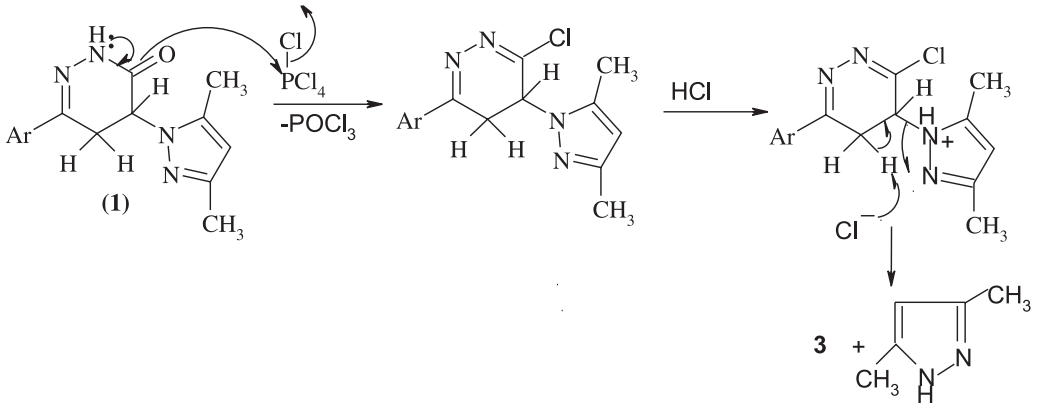
Received 8 April 2004. Published on the NRC Research Press Web site at http://canjchem.nrc.ca on 30 March 2005.

A.S.A. Youssef,[1] M.I. Marzouk, H.M.F. Madkour, and M.A. El-Hashash. Chemistry Department, Faculty of Science, Ain Shams University, Abbassia, Cairo, Egypt.
A.M.A. El-Soll. Chemistry Department, Faculty of Science, El-Tahdi University, Libya.

[1]Corresponding author (e-mail: ahmedy93@hotmail.com).

 doi: 10.1139/V05-045 © 2005 NRC Canada

Scheme 1.



(1)

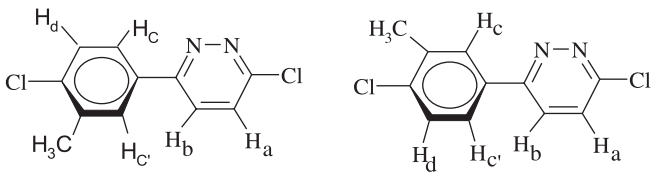
a, Ar = 3,5-dimethylpyrazolyl
b, Ar = 5-*i*-Pr-2-$CH_3C_6H_3$
c, Ar = 2,5-$(CH_3)_2C_6H_3$

(2)

a, Ar = 3,5-dimethylpyrazolyl
b, Ar = 5-*i*-Pr-2-$CH_3C_6H_3$

(3)

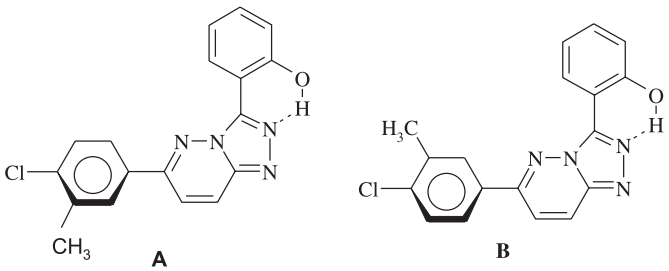
The ^{1}H NMR spectrum of compound **3** shows the aromatic proton resonances and doesn't exhibit the signals of the ABX pattern of the CH_2-CH- group as well as the signals of the methyl protons of the dimethylpyrazole ring. This infers the absence of these moieties. It discloses AB quartet signals owing to the two protons H_a and H_b of the pyridazine ring. The appearance of extra signals correlated with methyl and the aromatic protons is good evidence for the existence of **3** in the two conformations **A** and **B**, as a result of the limited rotation of the aryl group around the pyridazine ring as shown. The same phenomenon was observed for strucrures **4**, **5**, **8**, **9**, **14**, and **22**. The structure of **3** gets further support from mass spectroscopy. Thus, its EI-MS exhibits a molecular ion peak.



A (3) B

The formation of **3** has been rationalized in terms of the route mentioned in Scheme 1.

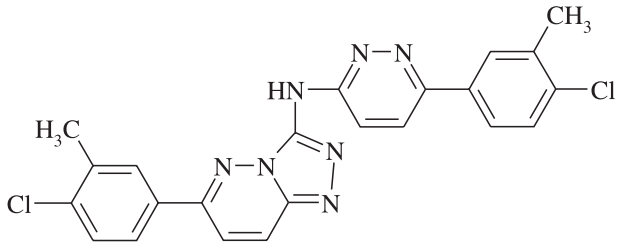
Treating an equimolar amount of 6-aryl-3-chloropyridazine derivative **3** with 2-hydroxybenzoylhydrazide in pyridine gave 3-(2-hydroxy) phenyl-6-aryl-1,2,4-triazolo[4,3-*b*]pyridazine derivative **4**. The structure of compound **4** is substantiated from its microanalytical and spectral data. The ^{1}H NMR spectrum of **4** is in accord with the proposed structure. The higher δ value of the OH proton is in accord with the existence of **4** as its chelated form as shown. Further support for the assigned structure of **4** was gained from EI-MS that revealed the molecular ion peak.



A B

(4)

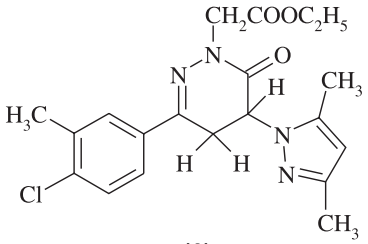
Reacting **3** with semicarbazide hydrochloride in the presence of triethylamine as a base afforded 3-[6-(4-chloro-3-methyl)phenylpyridazin-3-yl]amino-6-(4-chloro-3-methyl)-phenyl-1,2,4-triazolo[4,3-*b*]pyridazine (**5**).



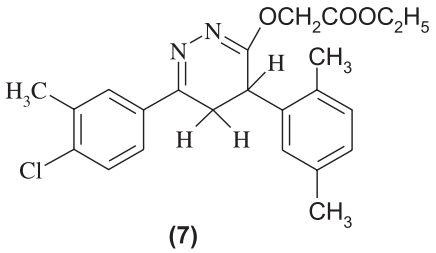
(5)

The structure of compound **5** is evidenced from its microanalytical and spectral data. The ^{1}H NMR spectrum exhibits exchangeable NH as well as two well-separated singlets consistent with protons of two methyl groups. The

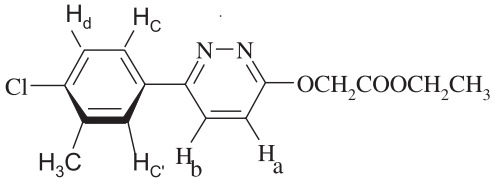
© 2005 NRC Canada



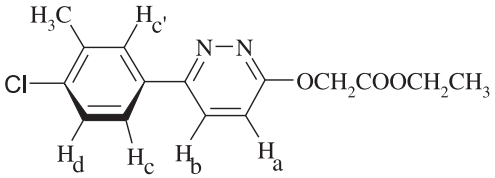
(6)



(7)



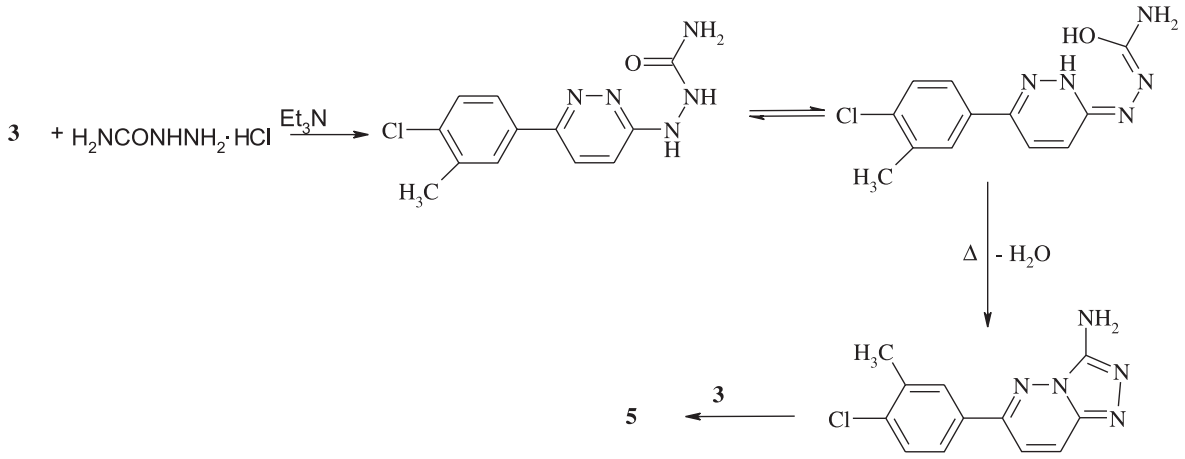
(A)



(B)

(8)

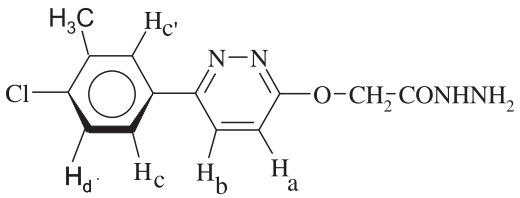
Scheme 2.



complexity of signals in the aromatic region suggests the existence of more than two diastereomers. The EI-MS spectrum of **5** doesn't show the molecular ion peak, but instead shows the ($M^{+\cdot}$ – Cl) peak. The formation of **5** is outlined in Scheme 2.

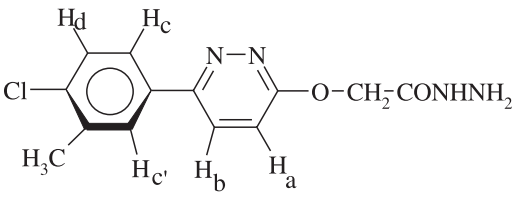
It has been reported (17, 19) that 4,6-diaryl pyridazinone derivatives **1a** and **1c** reacted with ethyl chloroacetate in the presence of potassium carbonate in dry acetone to give the adducts **6** (17) and **7** (19), respectively. In the present work, treatment of **1a** with ethyl chloroacetate in dioxane instead of dry acetone yielded the adduct **8** as a mixture of two conformers **8A** and **8B**. Although compounds **6–8** have the same melting point, the conflict in structure is probably due to the lack in the spectroscopic evidence used by previous authors (17, 19) in the assignment of structures.

The structure of compound **8** is evidenced from its microanalytical and spectral data. Thus, its IR spectrum shows absorptions correlated with the $\nu_{C=O}$ (ester). The ^{1}H NMR spectrum shows absorption signals correlated with the OCH_2 and $COOCH_2CH_3$ protons. Moreover, the structure of **8** gets further support from its EI-MS as it shows the molecular ion peak and some of the abundant peaks. On the other hand, the treatment of **8** with hydrazine hydrate afforded the hydrazides **9**.



A

(9)



B

© 2005 NRC Canada

The structure of compound **9** is established from its microanalytical and spectral data. Thus, its IR spectrum shows absorptions characteristic for ν_{NH} and $\nu_{C=O}$ (amide). The ^{1}H NMR spectrum supports the proposed structure as it is devoid of any signals corresponding to the protons of the ethyl group, but instead to signals correlated with the hydrazino group. The suggested structure gets further support from the EI-MS as it shows the correct molecular ion peak beside some of the abundant peaks.

The reaction of hydrazide **9** with acetylenic ketones and ester **10a**–**10d** in refluxing dioxane afforded the adducts **11a**, **11b**, **12**, and **13**, respectively. The structures of compounds **11a**, **11b**, **12**, and **13** are deduced from their microanalytical and spectral data. Thus, their IR spectra reveal characteristic bands for ν_{NH} and $\nu_{C=O}$. The lower absorption values for the C=O and NH groups in **11** and **13** are in good agreement with the existence of compounds **11** and **13** in their chelated forms as shown. Further support for the suggested structure of compounds **11a** and **11b** was gained from their ^{1}H NMR spectra, which revealed two ABqs representing AB systems, one owing to the methylene protons of the CH_2COR group and the other owing to the OCH_2CO protons (20–22). The fact that these methylene protons behave as AB systems can be attributed either to the large anisotropic effect of the C=N or C=O groups and the nitrogen lone pair or to the restriction of rotation at the aroyl group by the weak hydrogen bonding between the NH and carbonyl group. The ^{1}H NMR spectra of **12** and **13** are in good agreement with the proposed structures.

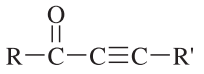
Furthermore, the electron impact mass spectra of compounds **11a** and **11b** don't show the molecular ion peaks, instead they show the ($M^{+\cdot}$ – $ArCOCH_2C(Ar')$=N·NH) peak beside some of the abundant peaks. On the other hand, the EI-MS spectra of compounds **12** and **13** show molecular ion peaks beside some of the abundant peaks.

The formation of **11** and **13** seems to proceed by Michael addition of the hydrazide **9** at the β-carbon of the acetylenic compounds **10**. Similarly, compound **12** is formed, followed by ring closure.

On the other hand, the reaction of the hydrazide **9** with acetylacetone in boiling methanol yielded the adduct **14**. The structure of **14** is evidenced by microanalytical, ^{1}H NMR, and mass spectral data. Thus, its IR spectrum shows bands characteristic for $\nu_{C=O}$, $\nu_{C=N}$, and (or) $\nu_{C=C}$. Moreover, the assigned structure of compound **14** gets further support from the ^{1}H NMR spectrum.

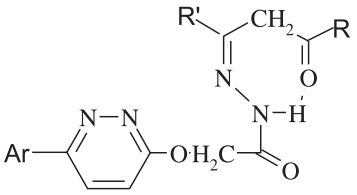
Inspection of the ^{1}H NMR spectrum revealed the existence of two closely spaced singlets for the methyl protons attached at position 5 in the pyrazole ring, probably because the rate of rotation of the pyrazole ring around the hindered "partial double bond" is slow (23). This allows the existence of this methyl group in two different conformations (**A** and **B**) under different magnetic environments as shown in the following. Furthermore, the mass spectrum of **14** shows the molecular ion peak in addition to some abundant peaks. Compound **14** is formed through condensation of the hydrazide **9** with one of the two carbonyl groups of acetylacetone followed by ring closure.

Treatment of pyridazinone derivative **1a** with piperidine or morpholine and an excess of 40% formaldehyde solution in refluxing dioxane afforded 6-aryl-2-piperidin-1-yl-methyl-



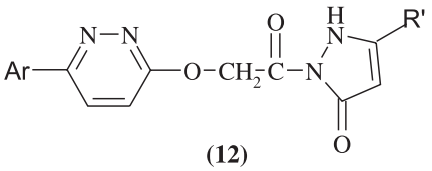
(10)

a, R = 4-Cl-C_6H_4, R' = C_6H_5
b, R = R' = C_6H_5
c, R = OC_2H_5, R' = 4-ClC_6H_4
d, R = OC_2H_5 , R' = $CO_2C_2H_5$



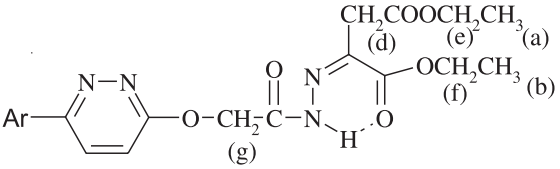
(11)

a, Ar = 4-Cl-3-$CH_3C_6H_3$, R = 4-ClC_6H_4 , R' = C_6H_5
b, Ar = 4-Cl-3-$CH_3C_6H_3$, R = R' = C_6H_5



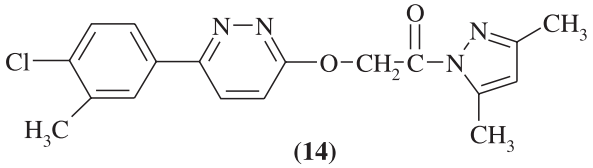
(12)

Ar = 4-Cl-3-$CH_3C_6H_3$, R' = 4-Cl-C_6H_4-

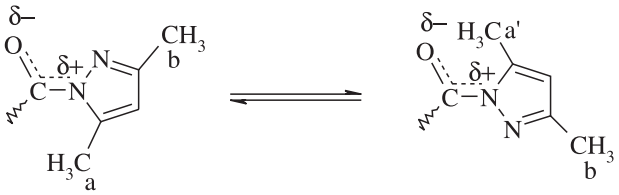


(13)

Ar = 4-Cl-3-$CH_3C_6H_3$

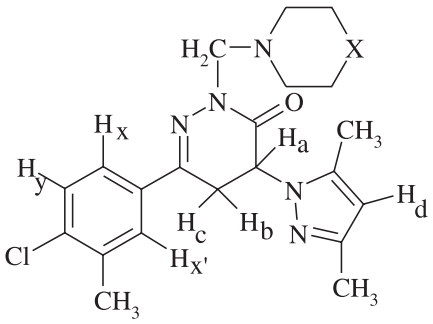


(14)



A **(14)** **B**

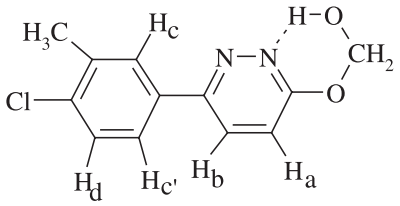
© 2005 NRC Canada



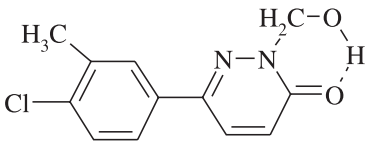
(15)

a, X = CH_2

b, X = O



(16)

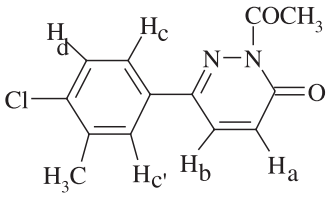


(17)

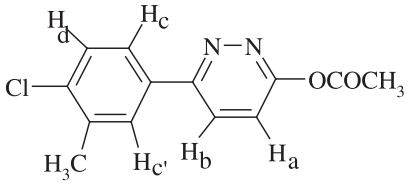
15a or 6-aryl-2-morpholin-4-yl-methyl-**15b**-4-(3,5-dimethyl pyrazol-1-yl)-2,3,4,5-tetrahydropyridazin-3-one. However, similar treatment of **1a** with piperazine yielded a mixture of the two isomeric compounds (**3**-hydroxymethoxy-6-arylpyridazine derivative **16** and 2-hydroxymethyl-6-aryl-2,3-dihydropyridazin-3-one derivative **17**, respectively).

The structures of compounds **15**–**17** are evidenced from their microanalytical and spectral data. Thus, their IR spectra show absorptions characteristic for $\nu_{C=O}$, $\nu_{C=N}$, and (or) $\nu_{C=C}$ in addition to ν_{OH} for structures **16** and **17**. The lower absorption values for the OH and C=O groups for compounds **16** and **17** are in good agreement with their existence in the chelated forms shown. The ^{1}H NMR spectra of compounds **15a** and **15b** disclosed ABX patterns consistent with -CH_X-CH_AH_B-CO moieties in which each of these coupled protons appears as a doublet of doublet with a geminal coupling constant $J \approx 16.8$ Hz and a vicinal coupling constant of ≈13 or 7 Hz. In addition, they show two central peaks of ABq corresponding to the -CH_2-N group. Analysis of the observed ^{1}H NMR spectrum of the mixture containing **16** and **17** inferred that they exist in deuterated dimethylsulphoxide in a ratio of 2:1, respectively. Moreover, the structures of compounds **15a** and **15b** and the mixture containing **16** and **17** get further support from the EI-MS spectra, where the spectra of compounds **15b** and the mixture of **16** and **17** show molecular ion peaks, whereas that of compound **15a** doesn't show the molecular ion peak, but does show a peak corresponding to [$M^{+\cdot}$ – dimethylpyrazole].

The reaction of equimolar amounts of **1a** and 3-bromopropanoic acid in refluxing dioxane and in the presence of potassium carbonate as a base gave a mixture of the two isomeric products 6-aryl-2-(2-carboxy) ethylpyridazinone derivative **18** and 6-aryl-3-(2-carboxyl)ethoxy pyridazine derivative **19**.



(20)



(21)

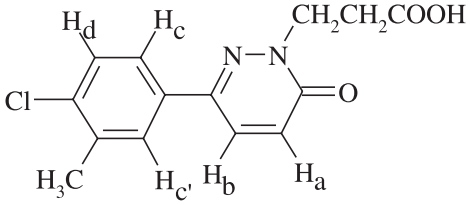
The structures of compounds **18** and **19** are substantiated from microanalytical and spectral data. Thus, the IR spectrum shows absorptions characteristic for $\nu_{OH(br.)}$, $\nu_{C=O}$ (acid), and $\nu_{C=O}$ (amide). Analysis of the ^{1}H NMR spectrum inferred that compounds **18** and **19** exist in deuterated dimethylsulphoxide as a mixture in a ratio of 1:1.2. Existence of compounds **18** and **19** as a mixture has been evidenced from the location of two triplet signals consistent with the protons of the NCH_2 and OCH_2 groups for structures **18** and **19**, respectively. The EI-MS spectrum of compounds **18** and **19** doesn't show the molecular ion peak, but does show a peak at *m*/*e* 220, which corresponds to the [$M^{+\cdot}$ – CH_2=CHCOOH] peak beside some of the abundant peaks.

Treatment of **1a** with acetic anhydride yielded a mixture of equimolar amounts of 2-acetyl-6-aryl-2,3-dihydropyridazin-3-one derivative **20** and 3-acetoxy-6-arylpyridazine derivative **21**.

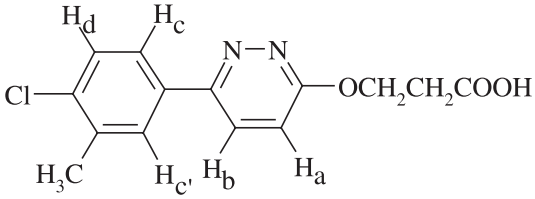
The structures of compounds **20** and **21** are deduced from microanalytical and spectral data. The IR spectrum shows absorptions characteristic for $\nu_{C=O}$, $\nu_{C=N}$, and (or) $\nu_{C=C}$. Moreover, the ^{1}H NMR spectrum supports the structures of **20** and **21** as it shows two closely spaced singlets at δ 2.75 and 2.78 correlated with the methyl protons of the $NCOCH_3$ and $OCOCH_3$ groups, respectively. The EI-MS spectrum of the mixture doesn't show the molecular ion peak, but instead the [$M^{+\cdot}$ – CH_2=C=O] peak as a base peak.

It has been reported (17) that 6-aryl-4-pyrazolylpyridazinone derivative **1a** reacted with benzenesulphonyl chloride in refluxing acetone and in the presence of potassium carbonate as a base to give the *N*-benzenesulphonyl derivative **23**. However, in the present work, treatment of equimolar amounts of **1** with *p*-toluenesulphonyl chloride, succinyl

© 2005 NRC Canada

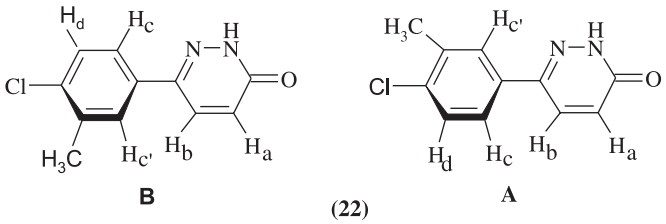


(18)

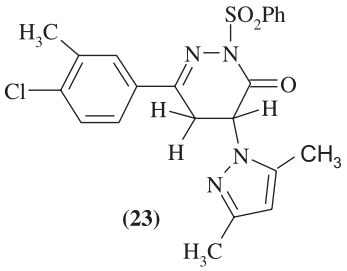


(19)

chloride, oxalyl chloride, or ethanolamine in refluxing pyridine or with ethyl chloroacetate in boiling dimethylformamide afforded 6-aryl-2,3-dihydro pyridazin-3-one (**22**) as a mixture of two conformations **22A** and **22B**. Compounds **22** and **23** have identical melting points although they have different structures, as there is a lack in the spectroscopic evidence used by previous authors (17) in their assignment of structure **23**.



(22)



(23)

The structure of compound **22** is deduced spectroscopically and chemically. Its IR spectrum shows ν_{NH} and $\nu_{C=O}$. The ^{1}H NMR spectrum is in good agreement with the proposed structure considering the existence of the conformations **22A** and **22B**. Further support for the proposed structure was gained from the EI-MS spectrum as it shows the molecular ion peak beside some of the abundant peaks. A chemical proof for the structure of compound **22** was given by comparison (mp, mixed mp, and TLC) with an authentic sample prepared by treating **1a** with hydrazine hydrate in boiling ethanol. Also, by refluxing compound **1a** with pyridine to give compound **22**. This supports the role of pyridine as a base in the removal of the dimethylpyrazolyl group.

The formation of compounds **16** and **17** (mixture), **18** and **19** (mixture), **20** and **21** (mixture), and **22** upon treating **1** with piperazine–HCHO, 3-bromopropanoic acid – K_2CO_3, acetic anhydride, *p*-toluenesulponyl chloride – pyridine, succinyl chloride – pyridine, oxalyl chloride – pyridine, ethanolamine – pyridine, or ethyl chloroacetate – DMF can be explained on the basis of an acid- or base-catalysed removal of the dimethylpyrazolyl moiety, as in case of **22**, followed by nucleophilic attacks of the lactam–lactim tautomer to the reagents used in the other cases.

Experimental

All melting points are uncorrected. The IR spectra were recorded on FT IR Mattson (infinity series) spectrometers as KBr discs. The ^{1}H NMR spectra were measured on a Varian Gemini 200 MHz instrument with chemical shifts (δ) expressed in ppm downfield from TMS. Mass spectra were recorded on a Shimadzu GC-MS-QP 1000 Ex instrument operating at 70 eV. TLC was run using TLC aluminum sheets silica gel F_{254} (Merck). Note: All attempts to separate all of the isomeric mixtures mentioned, including column chromatography, failed possibly because of isomerization taking place during separation.

Reaction of 1a with the PCl_5–$POCl_3$ mixture — Formation of 3

A mixture of **1a** (5 mmol), PCl_5 (5 mmol), and $POCl_3$ (10 mL) was gently heated for 3 h, cooled, poured into crushed ice, and the precipitated solid was filtered and recrystallized from benzene to give **3**.

6-(4-Chloro-3-methyl) phenyl-3-chloropyridazine (3)

Yield: 60%; white crystals, mp 175 to 176 °C, lit. value (17, 18) mp 176 °C. IR (cm^{-1}): 3078 (CH_{aryl}), 2924, 2854 (CH_{alkyl}), 1672, 1600 (C=N and (or) C=C), 821 (C-Cl). ^{1}H NMR (200 MHz, $CDCl_3$) δ: 2.439, 2.461 (two singlets, $2CH_3$), 7.37, 7.481 (two doublets, H_d, J_o = 8.2 Hz), 7.559 (d, H_a, J_{ab} = 9.2 Hz), 7.764 (dd, $H_{c'}$, J_o = 8.2 Hz, J_m = 2.2 Hz), 7.806 (d, H_b, J_{ab} = 9.0 Hz), 7.95, 8.041 (two doublets, Hc, J_m = 2.2 Hz). EI-MS *m*/*z*: 238 ($M^{+\cdot}$, 56), 210 ($M^{+\cdot} - N_2$, 23), 150 (4-Cl-3$CH_3C_6H_3C{\equiv}CH$, base), 115 (89), 90 (6), 89 (29), 64 (10), 63 (44). Anal. calcd. for $C_{11}H_8N_2Cl_2$ (%): C 55.26, H 3.37, N 11.72; found: C 55.44, H 3.51, N 11.82.

Reaction of 3 with 2-hydroxybenzoylhdyrazide — Formation of 4

A mixture of **3** (5 mmol) and 2-hydroxybenzoylhydrazide (5 mmol) in pyridine (10 mL) was refluxed for 6 h. The reaction mixture was left to cool then poured into ice-cold water. The precipitated solid was filtered off, washed, dried, and then recrystallized from methanol to give **4**.

*3-(2-Hydroxyphenyl)-6-(4-chloro-3-methyl) phenyl1,2,4-triazolo[4,3-*b*]pyridazine (4)*

Yield: 33%; dark brown crystals, mp 249 to 250 °C. IR (cm^{-1}): 3427 (OH), 3062 (CH_{aryl}), 2924, 2858 (CH_{alkyl}), 1623, 1585 (C=N and (or) C=C). ^{1}H NMR (200 MHz, $CDCl_3$) δ: 2.506, 2.528 (two singlets, 2 CH_3), 7.049–8.932 (m, 9, ArH), 11.92 (br.s, 1, OH exchangeable). EI-MS *m*/*z* (%): 338 ($M^{+\cdot}$ + 2, 22), 337 ($M^{+\cdot}$ + 1, base), 336 ($M^{+\cdot}$, 60), 184 (49), 183 (58), 157 (16), 156 (16), 127 (34), 126 (15),

© 2005 NRC Canada

125 (20), 102 (14), 101 (15), 89 (50), 77 (35), 76 (18), 65 (18), 64 (34), 63 (52), 52 (22), 51 (59), 50 (28). Anal. calcd. for $C_{18}H_{13}N_4OCl$ (%): C 64.19, H 3.89, N 16.64, Cl 10.53; found: C 64.26, H 3.92, N 16.76, Cl 10.65.

Reaction of 3 with semicarbazide hydrochloride — Formation of 5

A solution of **3** (3 mmol) and semicarbazide hydrochloride (3.5 mmol) in dry dioxane (20 mL) was refluxed for 12 h in the presence of potassium carbonate (1.0 g). The reaction mixture was concentrated, cooled, and then poured into ice-cold water. The solid formed was filtered off, washed, dried, and then recrystallized from methanol to give **5**.

3-[6-(4-Chloro-3-methyl)phenylpyridazin-3-yl]amino-6-(4-chloro-3-methyl)phenyl-1,2,4-triazolo[4,3-b]pyridazine (5)

Yield: 54%; violet crystals, mp 194–196 °C. IR (cm^{-1}): 3447 (NH), 3057 (CH_{aryl}), 2983, 2900, 2859 (CH_{alkyl}), 1687, 1603, 1573 (C=N and (or) C=C). ^1H NMR (200 MHz, $CDCl_3$) δ: 2.423, 2.491 (two singlets, $2CH_3$), 7.146–8.184 (m, 11, ArH + NH). EI-MS *m/z*: 426 ($M^{+\cdot}$ – Cl, 11), 390 (40), 360 (14), 297 (14), 244 (24), 216 (25), 164 (77), 151 (37), 150 (15), 125 (25), 115 (40), 89 (82), 63 (80). Anal. calcd. for $C_{23}H_{17}N_7Cl_2$ (%): C 59.75, H 3.71, N 21.21, Cl 15.34; found: C 60.01, H 3.79, N 21.36, Cl 15.41.

Reaction of 1a with ethyl chloroacetate — Formation of 8

A solution of **1a** (5 mmol) in dry dioxane (20 mL) was heated with ethyl chloroacetate (5 mmol) for 24 h in the presence of potassium carbonate (3 g). The reaction mixture was concentrated, cooled then poured into ice-cold water. The precipitated solid was filtered off, dried, and then recrystallized from petroleum ether 80–100 °C.

6-(4-Chloro-3-methyl)phenyl-3-ethoxycarbonylmethoxypyridazine (8)

Yield: 70%; pale yellow crystals, mp 100 °C, lit. value (17, 19) mp 96 °C, 89 °C. IR (cm^{-1}): 3071 (CH_{aryl}), 2987, 2911 (CH_{alkyl}), 1749 (C=O), 1672, 1596 (C=N and (or) C=C). ^1H NMR (200 MHz, $CDCl_3$) δ: 1.292 (t, 3, CH_3CH_2O, J = 7.2 Hz), 2.403, 2.421 (two singlets, $2CH_3$), 4.255 (q, 2, CH_3CH_2O, J = 7.2 Hz), 4.956 (s, 2, OCH_2CO), 7.041, 7.646 (two doublets, H_a, J_{ab} = 9.8 Hz), 7.292, 7.399 (two doublets, H_d, J_o = 8.4 Hz), 7.551, 7.501 (two doublet doublets, H_c, J_o = 8.6 Hz, J_m = 1.8 Hz), 7.557, 7.771 (two doublets, $H_{c'}$, J_m = 1.8 Hz), 7.676, 7.682 (two doublets, H_b, J_{ba} = 9.6 Hz). EI-MS *m/z*: 308 ($M^{+\cdot}$ + 2, 20), 306 ($M^{+\cdot}$, 55), 263 ($M^{+\cdot}$ + 2-OC_2H_5, 9), 261 ($M^{+\cdot}$ – OC_2H_5, 4), 233 ($M^{+\cdot}$ + 2-$COOC_2H_5$, base), 231 ($M^{+\cdot}$ – $COOC_2H_5$, 41), 205 (19), 198 (13), 170 (17), 163 (51), 128 (23), 115 (15), 89 (17), 63 (73). Anal. calcd. for $C_{15}H_{15}N_2O_3Cl$ (%): C 58.73, H 4.93, N 9.13, Cl 11.56; found: C 58.81, H 5.00, N 9.22, Cl 11.63.

Reaction of 8 with hydrazine hydrate

A solution of **8** (3 mmol) in ethanol (20 mL) was refluxed with hydrazine hydrate (5 mmol) for 4 h. The reaction mixture was cooled. The precipitated solid was filtered off and recrystallized from methanol.

6-(4-Chloro-3-methyl) phenyl-3-hydrazinocarbonylmethoxypyridazine (9)

Yield: 82%; white crystals, mp 210–212 °C. IR (cm^{-1}): 3409, 3306, 3205 (NH), 3055 (CH_{aryl}), 2953, 2921, 2853 (CH_{alkyl}), 1667 (C=O), 1589, 1533 (C=N and (or) C=C). ^1H NMR (200 MHz, DMSO-d_6) δ: 2.393, 2.413 (two singlets, $2CH_3$), 4.306 (br.s, 2, NH_2 exchangeable), 4.742 (s, 2, OCH_2), 7.078, 7.090 (two doublets, H_a, J_{ab} = 9.78 Hz), 7.491, 7.541 (two doublets, H_d, J_o = 8.4 Hz), 7.732, 7.774 (two doublet doublets, H_c, J_o = 8.52 Hz, J_m = 1.86 Hz), 7.885, 7.929 (two doublets, $H_{c'}$, J_m = 1.82 Hz), 8.086, 8.110 (two doublets, H_b, J_{ba} = 9.8 Hz), 9.316 (br.s, 1, NH exchangeable). EI-MS *m/z*: 292 ($M^{+\cdot}$, 5), 263 ($M^{+\cdot}$ + 2-$NHNH_2$, 59), 261 ($M^{+\cdot}$ – $NHNH_2$, 17), 235 ($M^{+\cdot}$ + 2-$CONHNH_2$, 29), 231 ($M^{+\cdot}$ – $CONHNH_2$, base), 205 (12), 198 (13), 170 (15), 163 (21), 151 (10), 89 (15), 63 (20). Anal. calcd. for $C_{13}H_{13}N_4O_2Cl$ (%): C 53.34, H 4.48, N 19.14, Cl 12.11; found: C 53.46, H 4.52, N 19.24, Cl 12.35.

Reactions of 9 with acetylenic ketones, esters 10a–10d, and with acetylacetone

General procedure

A mixture of **9** (3 mmol) and **10a**–**10d** (3 mmol) in dioxane (15 mL) or acetylacetone (3 mmol) in methanol (20 mL) was refluxed for 10 h. The reaction mixture was concentrated, left to stand at room temperature. The solid formed was recrystallized from a suitable solvent to give **11a**, **11b**, **12**, **13**, and **14**.

6-(4-Chloro-3-methyl)phenyl-3-[ω-(4-chlorobenzoyl)acetophenone]hydrazonocarbonylmethoxypyridazine (11a)

Yield: 62%; white crystals, mp 198–200 °C (from methanol). IR (cm^{-1}): 3391 (NH), 3039 (CH_{aryl}), 2954, 2906, 2843 (CH_{alkyl}), 1662 (C=O). ^1H NMR (200 MHz, $CDCl_3$) δ: 2.421 (s, 3, CH_3), 3.371, 3.752 (ABq, 2, CH_2CO, J = 18.5 Hz), 4.848 (br.s, 1, NH), 5.355, 5.688 (ABq, 2, OCH_2CO, J = 16.4 Hz), 7.005–7.756 (m, 14, Ar-H). EI-MS *m/z*: 533 ($M^{+\cdot}$, missed), 272 (3.5), 263 (8.4), 261 (24.5), 256 (38.5), 254 (base), 235 (5.3), 233 (15), 170 (56.4), 153 (10.1), 151 (27), 115 (12.9), 113 (6.1), 111 (9.1), 103 (3.8), 89 (27.7), 82 (4.2), 63 (24.1). Anal. calcd. for $C_{28}H_{22}N_4O_3Cl_2$ (%): C 63.30, H 4.16, N 10.50; found: C 63.54, H 4.23, N 10.67.

6-(4-Chloro-3-methyl)phenyl-3-(ω-benzoylacetophenone)hydrazonocarbonylmethoxypyridazine (11b)

Yield: 21%; pale yellow crystals, mp 118–120 °C (from benzene). IR (cm^{-1}): 3435 (NH), 3063, 3032 (CH_{aryl}), 2960, 2920, 2859 (CH_{alkyl}), 1668 (C=O). ^1H NMR (200 MHz, $CDCl_3$) δ: 2.418 (s, 3, CH_3), 3.409, 3.756 (ABq, 2, CH_2CO, J = 18.3 Hz), 4.905 (br.s, 1, NH exchangeable), 5.410, 5.590 (ABq, 2, OCH_2CO, J = 16.6 Hz), 6.988–7.755 (m, 15, Ar-H). EI-MS *m/z*: 498 ($M^{+\cdot}$, missed), 240 (8.2), 238 (24.2), 263 (41.2), 261 (base), 235 (23.5), 233 (79.1), 220 (40.9), 170 (27.8), 153 (5.1), 151 (14.5), 118 (2), 115 (12.4), 77 (61.2), 103 (9.3), 89 (17.9), 87 (3.1), 63 (22.3). Anal. calcd. for $C_{28}H_{23}N_4O_3Cl$ (%): C 67.40, H 4.65, N 11.23; found: C 67.65, H 4.81, N 11.44.

6-[4-Chloro-3-methyl)phenyl-3-[3-(4-chlorophenyl-5-oxo-2,5-dihydro-pyrazol-1-yl)carbonylmethoxypyridazine (12)

Yield: 19%; white crystals, mp > 300 °C (from methanol).

© 2005 NRC Canada

IR (cm^{-1}): 3154 (NH), 3032 (CH_{aryl}), 2958, 2920, 2850 (CH_{alkyl}), 1673 (C=O), 1628, 1586 (C=N and (or) C=C). ^1H NMR (200 MHz, DMSO-d_6) δ: 2.478 (s, 3, CH_3), 4.855 (s, 2, OCH_2), 7.090–8.135 (m, 10, ArH + CH=), 10.469 (br.s, 1, NH exchangeable). EI-MS *m*/*z*: 454 ($M^{+\cdot}$, 6), 234 (18), 208 (10), 163 (base), 64 (10). Anal. calcd. for $C_{22}H_{16}N_4O_3Cl_2$ (%): C 58.04, H 3.54, N 12.31, Cl 15.57; found: C 58.22, H 3.62, N 12.44, Cl 15.68.

6-(4-Chloro-3-methyl) phenyl-3-(1,2-diethoxycarbonyl acetaldehyde hydrazonocarbonyl)methoxypyridazine (13)

Yield: 36%; white crystals, mp 179 to 180 °C (from methanol). IR (cm^{-1}): 3233, 3150 (NH), 3090 (CH_{aryl}), 2920, 2851 (CH_{alkyl}), 1736, 1711 (C=O ester), 1661 (C=O amide), 1626, 1592 (C=N and (or) C=C). ^1H NMR (200 MHz, DCl_3) δ: 1.287 (t, 3, $CH_{3(a)}$, J = 7.02 Hz), 1.346 (t, 3, $CH_{3(b)}$, J = 7.05 Hz), 2.409, 2.426 (two singlets, CH_3(Ar)), 3.662 (s, 2, $CH_{2(d)}$), 4.129 (q, 2, $CH_{2(e)}$, J = 7.08 Hz), 4.311 (q, 2, $CH_{2(f)}$, J = 7.08 Hz), 5.468 (s, 2, $CH_{2(g)}$), 7.051–7.731 (m, 5, ArH), 10.099 (br.s, 1, NH exchangeable). EI-MS *m*/*z*: 462 ($M^{+\cdot}$, 3), 391 ($M^{+\cdot}$ + 2-$CO_2C_2H_5$, 12), 289 ($M^{+\cdot}$ – $CO_2C_2H_5$, 36), 261 (64), 233 (84), 205 (10), 170 (57), 115 (13), 89 (20), 63 (23), 54 (base). Anal. calcd. for $C_{21}H_{23}N_4O_6Cl$ (%): C 54.49, H 5.01, N 12.01; found: C 54.61, H 5.28, N 12.31.

6-(4-Chloro-3-methyl)phenyl-3-[(3,5-dimethylpyrazole-1-yl)carbonylmethoxypyridazine (14)

Yield: 38%; white crystals, mp 164–166 °C (from petroleum ether 60–80 °C – benzene). IR (cm^{-1}): 3047, 3011 (CH_{aryl}), 2968, 2925, 2854 (CH_{alkyl}), 1739 (C=O), 1668, 1591 (C=N and (or) C=C). ^1H NMR (200 MHz, $CDCl_3$) δ: 2.257, 2.274 (two singlets, $CH_{3a'}$, CH_{3a}), 2.407, 2.421 (two singlets, CH_3 (aryl)), 2.529 (s, 3, CH_{3b}), 5.765 (s, 2, OCH_2), 6.001 (s, 1, CH=), 7.057–7.734 (m, 5, ArH). EI-MS *m*/*z*: 356 ($M^{+\cdot}$, 2), 260 (base), 261 (26), 233 (40), 170 (79), 151 (20), 116 (24), 89 (13), 63 (14). Anal. calcd. for $C_{18}H_{17}N_4O_2Cl$ (%): C 60.59, H 4.80, N 15.70, Cl 9.94; found: C 60.67, H 4.91, N 15.89, Cl 10.02.

Reactions of 1a with piperidine, morpholine, or piperazine and 40% formaldehyde

A mixture of **1a** (5 mmol), formaldehyde (15 mL) and piperidine (5 mmol), morpholine (5 mmol), or piperazine (5 mmol) in dioxane (20 mL) was refluxed for 20 h. The reaction mixture was concentrated, cooled, and poured into ice-cold water. The precipitated solid was filtered off, then recrystallized from a suitable solvent to give **15a**, **15b** and **16**, **17** as a mixture.

6-(4-Chloro-3-methyl)phenyl-2-piperidin-1-yl-methyl-4-(3,5-dimethyl-pyrazol-1-yl)-2,3,4,5-tetrahydropyridazin-3-one (15a)

Yield: 42%; white crystals, mp 188–190 °C (from petroleum ether 80–100 °C). IR (cm^{-1}): 1672 (C=O), 1596, 1557 (C=N and (or) C=C). ^1H NMR (200 MHz, $CDCl_3$) δ: 1.391 (m, 2, $CH_2CH_2CH_2$), 1.523 (m, 4, $CH_2CH_2CH_2$), 2.229, 2.257 (two singlets, $2CH_3$ of pyrazol ring), 2.413 (s, 3, CH_3), 2.570 (m, 4, $N(CH_2)_2$), 3.444 (dd, H_b, J_{bc} = 16.9 Hz, J_{ba} = 7 Hz), 3.881 (dd, H_c, J_{cb} = 16.8 Hz, J_{ca} = 13.8 Hz), 4.682, 4.925 (ABq, -CH_2-N, J = 13 Hz), 4.842 (q, H_a, J_{HaHb} = 6.4 Hz, J_{HaHc} = 13.8 Hz), 5.897 (s, 1, H_d), 7.385 (d, H_y, J_o = 8.4 Hz), 7.599 (dd, H_x, J_o = 8.4 Hz, J_m = 2 Hz), 7.64 (d, $H_{x'}$, J_m = 2 Hz). EI-MS *m*/*z*: 317 ($M^{+\cdot}$ – dimethylpyrazole, 1), 221 (3), 220 (2), 163 (2), 109 (3), 99 (7), 98 (base), 97 (12). Anal. calcd. for $C_{22}H_{28}N_5OCl$ (%): C 63.83, H 6.82, N 16.92; found: C 63.94, H 6.97, N 17.02.

6-(4-Chloro-3-methyl)phenyl-2-morpholin-4-yl)methyl-4-(3,5-dimethyl-pyrazol-1-yl)-2,3,4,5-tetrahydropyridazin-3-one (15b)

Yield: 44%; white crystals, mp 186 to 187 °C (from petroleum ether 80–100 °C). IR (cm^{-1}): 1672 (C=O), 1597, 1557 (C=N and (or) C=C). ^1H NMR (200 MHz, $CDCl_3$) δ: 2.219, 2.555 (two sinlgets, $2CH_3$ of pyrazol ring), 2.409 (s, 3, CH_3), 2.715 (m, 4, N $(CH_2)_2$), 3.442 (dd, H_b, J_{bc} = 16.7 Hz, J_{ba} = 7.0 Hz), 3.675 (m, 4, $O(CH_2)_2$), 3.892 (dd, H_c, J_{cb} = 15.3 Hz, J_{ca} = 14.4 Hz), 4.691, 4.869 (ABq, CH_2-N, J = 13.1 Hz), 4.858 (m, 1, H_a), 5.895 (s, 1, H_d), 7.383 (d, H_y, J_o = 8.2 Hz), 7.554 (dd, H_x, J_o = 8.4 Hz, J_m = 2 Hz), 7.628 (d, $H_{x'}$, J_m = 1.8 Hz). EI-MS *m*/*z*: 415 ($M^{+\cdot}$, 1), 397 ($M^{+\cdot}$ – H_2O, 1), 319 ($M^{+\cdot}$ – dimethylpyrazole, 1), 221 (4), 220 (4), 100 (base), 99 (4), 97 (15), 96 (4), 56 (19), 54 (4). Anal. calcd. for $C_{21}H_{26}N_5O_2Cl$ (%): C 60.64, H 6.30, N 16.84, Cl 8.52; found: C 60.75, H 6.44, N 16.96, Cl 8.68.

3-Hydroxymethoxy-6-(4-chloro-3-methyl)phenylpyridazine (16) and 2-hydroxymethyl-6-(4-chloro-3-methyl)phenyl-2,3-dihydropyridazin-3-one (17)

Yield: 30%; white crystals, mp 152 to 153 °C (from aqueous ethanol). IR (cm^{-1}): 3335 ($OH_{br.}$), 3072 (CH_{aryl}), 2958, 2918, 2852 (CH_{alkyl}), 1652 (C=O), 1601, 1515 (C=N and (or) C=C). For **16**: ^1H NMR (200 MHz, DMSO-d_6) δ: 2.421 (s, 3, CH_3), 5.418 (d, 2, OCH_2), 6.802 (t, 1, OH, exchangeable), 7.061 (d, 1, H_a, J_{ab} = 10.1 Hz), 7.529 (d, 1, H_d, J_o = 8.48 Hz), 7.742 (dd, 1, $H_{c'}$, J_o = 8.4 Hz, J_m = 2.8 Hz), 7.862 (d, 1, H_c, J_m = 2.9 Hz), 8.042 (d, 1, H_b, J_{ba} = 9.7 Hz). For **17**: ^1H NMR (200 MHz, DMSO-d_6) δ: 2.400 (s, 3, CH_3), 4.464 (d, 2, NCH_2), 6.802 (t, 1, OH, exchangeable), 7.061 (d, 1, H_a, J_{ab} = 10.1 Hz), 7.529 (d, 1, H_d, J_o = 8.48 Hz), 7.742 (dd, 1, $H_{c'}$, J_o = 8.4 Hz, J_m = 2.8 Hz), 7.862 (d, 1, H_c, J_m = 2.9 Hz), 8.042 (d, 1, H_b, J_{ba} = 9.7 Hz). EI-MS *m*/*z*: 252 ($M^{+\cdot}$ + 2, 4), 250 ($M^{+\cdot}$, 12), 185 ($M^{+\cdot}$ – CH_2O-Cl, 19), 163 (61), 128 (37), 89 (12), 63 (39). Anal. calcd. for $C_{12}H_{11}N_2O_2Cl$ (%): C 57.49, H 4.42, N 11.17, Cl 14.14; found: C 57.58, H 4.57, N 11.01, Cl 14.20.

Reaction of 1a with 3-bromopropanoic acid

A mixture of **1a** (5 mmol) and 3-bromopropanoic acid (5 mmol) in dry dioxane (20 mL), in the presence of potassium carbonate (3 g), was refluxed for 10 h. The reaction mixture was concentrated, cooled, and poured into ice-cold water. The precipitated solid was filtered off, washed, dried, and recrystallized from methanol to give a mixture of **18** and **19**.

6-(4-Chloro-3-methyl)phenyl-2-(2-carboxy)ethyl-2,3-dihydropyridazin-3-one (18) and 6-(4-chloro-3-methyl) phenyl-3-(2-carboxy)ethoxypyridazine (19)

Yield: 68%; yellowish white crystals, mp > 300 °C. IR (cm^{-1}): 3197 ($OH_{br.}$), 1710, 1668 (C=O). ^1H NMR (200 MHz, DMSO-d_6) δ: 2.095 (t, 2, CH_2COOH, J = 6.8 Hz), 2.408 (two singlets, $2CH_3$), 3.496 (t, 2, NCH_2CH_2, J = 6.8 Hz),

© 2005 NRC Canada

7.017 (d, H_a, J_{ab} = 9.6 Hz), 7.528 (d, H_d, J_o = 8.6), 7.761 (dd, H_c, J_o = 8.6 Hz, J_m = 1.8 Hz), 7.904 (d, H_c', J_m = 1.9 Hz), 8.043 (d, H_b, J_{ba} = 9.6 Hz), 11.5 (br.s, 1, OH exchangeable). EI-MS *m/z*: 222 ($M^{+\cdot}$ + 2-CH_2=CHCOOH, 38), 220 ($M^{+\cdot}$ – CH_2=CH-COOH, base), 192 ($M^{+\cdot}$ – CH_2=CHCOOH-CO, 19), 185 ($M^{+\cdot}$ – CH_2=CHCOOH-Cl, 20), 165 (34), 163 (76), 157 (14), 128 (36), 102 (16), 89 (18), 72 (50), 63 (46), 55 (61). Anal. calcd. for $C_{14}H_{13}N_2O_3Cl$ (%): C 57.44, H 4.48, N 9.57; found: C 57.62, H 4.53, N 9.74.

Acetylation of 1a with acetic anhydride

A solution of **1a** (5 mmol) in acetic anhydride (15 mL) was heated for 3 h. The reaction mixture was cooled and then poured into ice-cold water. The precipitated solid was filtered off, washed, dried, and then recrytallized from benzene to give a mixture of **20** and **21**.

2-Acetyl-6-(4-chloro-3-methyl)phenyl-2,3-dihydropyridazin-3-one (20) and 3-acetoxy-6-(4-chloro-3-methyl)phenylpyridazine (21)

Yield: 72%; white crystals, mp 167 to 168 °C. IR (cm^{-1}): 1764, 1674 (C=O), 1616, 1595 (C=N and (or) C=C). ^{1}H NMR (200 MHz, $CDCl_3$) δ: 2.424, 2.442 (two singlets, $2CH_3$), 2.75 (s, 3, $NCOCH_3$), 7.044 (d, H_a, J_{ab} = 9.8 Hz), 7.437 (d, H_d, J_o = 8.4 Hz), 7.547–7.601 (m, 2, H_c, H_c'), 7.65 (d, H_b, J_{ba} = 9.8 Hz). EI-MS *m/z*: 222 ($M^{+\cdot}$ + 2-CH_2=C=O, 36), 220 ($M^{+\cdot}$ – CH_2=C=O, base), 185 ($M^{+\cdot}$ – CH_2=C=O-Cl, 17), 163 (88), 157 (14), 128 (49), 89 (14), 63 (75). Anal. calcd. for $C_{13}H_{11}N_2O_2Cl$ (%): C 59.44, H 4.22, N 10.66; found: C 59.61, H 4.35, N 10.81.

Reaction of 1a with *p*-toluenesulphonyl chloride, succinyl chloride, oxalyl chloride, ethanolamine, or ethyl chloroacetate

A mixture of **1a** (5 mmol) and ethyl chloroacetate (5 mmol) in DMF (10 mL) or *p*-toluene sulphonyl chloride (5 mmol), succinyl chloride (5 mmol), oxaylchloride (5 mmol), or ethanolamine (5 mmol) in pyridine (10 mL) was heated for 12 h. The reaction mixture was cooled then poured into ice-cold water in the former case or ice-cold HCl in the latter cases. The precipitated solid was filtered, washed, dried, and then recrystallized from ethanol to give **22**.

6-(4-Chloro-3-methyl)phenyl-2,3-dihydropyridazin-3-one (22)

Yield: 50%; white crystals, mp 232 to 233 °C, lit. value (17) mp 238 °C. IR (cm^{-1}): 3189, 3146 (NH), 3041 (CH_{aryl}), 2929, 2836 (CH_{alkyl}), 1679 (C=O), 1592, 1548 (C=N and (or) C=C). ^{1}H NMR (200 MHz, DMSO-d_6) δ: 2.358, 2.380 (two singlets, $2CH_3$), 6.998, 7.009 (two doublets, H_a, J_{ab} = 9.8 Hz), 7.446, 7.496 (two doublets, H_d, J_o = 8.4 Hz), 7.696, 7.736 (two doublet doublets, H_c, J_o = 8.2 Hz, J_m = 2.0 Hz), 7.847, 7.879 (two doublets, H_c', J_m = 1.8 Hz), 8.034, 8.059 (two doublets, H_b, J_{ba} = 9.8), 13.271 (br.s, 1, NH exchangeable). EI-MS *m/z*: 222 ($M^{+\cdot}$ + 2, 28), 221 ($M^{+\cdot}$ + 1, base), 220 ($M^{+\cdot}$, 88), 206 (15), 192 ($M^{+\cdot}$ – CO, 10), 185 (17), 166 (20), 165 (19), 163 (55), 157 (12), 129 (44), 128 (30), 127 (23), 78 (18), 77 (27), 75 (15), 64 (23), 63 (45), 50 (20). Anal. calcd. for $C_{11}H_9N_2OCl$ (%): C 59.87, H 4.09, N 12.69, Cl 16.07; found: C 59.96, H 4.27, N 12.76, Cl 16.25.

References

1. A.S.A. Youssef, H.M.F. Madkour, M.I. Marzouk, A.M.A. El-Soll, and M.A. El-Hashash. Afinidad, **61**, 304, (2003).
2. S. Aurelia, G. Stanislov, J. Julia, and H. Anna. Agrochemia (Bratislava), **9**, 129 (1969).
3. V. Konečný. Pestic. Sci. **4**, 775 (1973).
4. N. Meki, H. Tomioka, K. Fujimot, T. Imahase, and K. Mikya. Jpn. Kokai Tokyo Koho, JP 02 45 471 [9045, 471] (Cl C07 D 237/18), 15 February 1990; Chem. Abstr. **113**, 54 361 (1990).
5. F. Bettarini, L. Capuzzi, S. Massimini, P. Castoro, and V. Caprioli. Eur. Pat. Appl. EP 391 390 (Cl C07 D237/16), 10 October 1990; Chem. Abstr. **114**, 12 239 (1991).
6. M. Taniguchi, M. Baba, Y. Ochiai, M. Hirose, and K. Hirsta. Can. Patent 1 270 830 (Cl C07 D237/18) 26 June 1990; Chem. Abstr. **114**, 228 933 (1991).
7. S. Barlogova and J. Grunt. Cesk. Hyg. **20**, 5 (1975).
8. W.V. Curran and A. Ross. J. Med. Chem. **17**, 237 (1974).
9. F.J. McEvoy and C.R. Allen. J. Med. Chem. **17**, 284 (1974).
10. R. Bergmann and R. Gericke. J. Med. Chem. **33**, 492 (1990).
11. W. Schoen. Eur. Pat. Appl. EP 347 987 (Cl C07 K5/02) 27 December 1989; Chem. Abstr. **114**, 229 391 (1991).
12. H. Blaschke, H. Stroissnig, H. Fellier, and R. Enzenhofer. Eur. Pat. Appl. EP. 372 305 (Cl C07 D 403/12) 13 June 1990; Chem. Abstr. **113**, 231 393 (1990).
13. R. Jaunin. Chim. Ther. **2**, 317 (1967).
14. C. Rubat, P. Coudert, P. Tronche, J. Bastide, and A.M. Privat. Chem. Pharm. Bull. **37**, 2832 (1989).
15. S. Kamiya, A. Nakamira, T. Itai, K. Koshinuma, and G. Okusa. Yakugaku Zasshi, **86**, 1099 (1966).
16. G.H. Sayed, A.A. Ismail, S. El-Nagdy, and S.M. Mohamed. Egypt. J. Chem. **29**, 433 (1986).
17. G.H. Sayed, A.A. Ismail, M. El-Mobayed, and S.M. Mohamed. Commun. Fac. Sci. Univ. Ankara Ser. B: Chem. Chem. Eng. **36**, 53 (1990); Chem. Abstr. **123**, 256 625v (1995).
18. M.A. El-Hashash, M.M. Mohamed, A.A. Sayed, and O.A. Abo-Baker. Pak. J. Sci. Ind. Res. **28**, 229 (1985).
19. M.A. El-Hashash and S.I. El-Nagdy. J. Chem. Eng. Data, **29**, 361 (1983).
20. Y.A. Al-Farkh, F.H. Al-Hajjar, N.R. El-Rayyes, and H.S. Hamoud. J. Heterocycl. Chem. **15**, 759 (1978).
21. F.G. Baddar, F.H. Al-Hajjar, and N.R. El-Rayyes. J. Heterocycl. Chem. **15**, 385 (1978).
22. F.G. Baddar, F.H. Al-Hajjar, and N.R. El-Rayyes. J. Heterocycl. Chem. **13**, 257 (1976).
23. R.M. Silverestin. Spectrometric identification of organic compounds. 6th ed. John Wiley and Sons, Inc., New York. 1997. Chap. 4. p. 173.

© 2005 NRC Canada

Efficient, microwave-assisted intramolecular 1,3-dipolar cycloadditions of oximes and *N*-methylnitrones derived from *o*-alkenylmethoxy-acetophenones

Surinderjit Singh, M.P.S. Ishar, Gajendra Singh, and Rajinder Singh

Abstract: Contrary to literature reports, the *o*-allyloxy- and crotyloxy-acetophenone-oximes (**2a**, **2b**) are transformed to nitrones, which undergo regio- and stereoselective intramolecular 1,3-dipolar cycloadditions, both on microwave heating under solvent free conditions and refluxing in toluene, to afford novel cycloadducts (**5a**, **5b**); the oxazepine-*N*-oxide (**3a**) reported to be formed in 98% yield was obtained only as a minor product (~10%). However, *o*-cinnamyloxy-acetophenone-oxime (**2c**) under similar conditions undergoes intramolecular *N*-alkylation to afford nitrone (**3c**). The reactions carried out under microwave irradiation are cleaner, require shorter reaction times, and have higher yields. Corresponding intramolecular 1,3-dipolar cycloadditions of *N*-methylnitrones (**B**), generated in situ from *o*-alkenylmethoxy-acetophenones (**1a**–**1c**) and *N*-methylhydroxylamine under solvent-free microwave irradiation conditions, are completely regio- and stereoselective, require much shorter reaction times, and afford adducts (**4a**–**4c**) in higher yields, as compared with their thermal counterparts.

Key words: cycloadditions, nitrones, oximes, *o*-alkenylmethoxy-acetophenones, microwave, isoxazolidines.

Résumé : Contrairement à ce qui a déjà été rapporté dans la littérature, les oximes des *o*-allyloxy- et crotyloxy-acétophénones (**2a**, **2b**) se transforment en nitrones qui subissent des cycloadditions 1,3-dipolaires intramoléculaires régio- et stéréosélectives aussi bien par chauffage micro-onde dans des conditions n'impliquant pas de solvant que par reflux dans du toluène pour conduit à la formation de nouveaux cycloadduits (**5a**, **5b**); il avait été rapporté que cette réaction conduisant à la formation du *N*-oxyde de l'oxazépine (**3a**) se formait avec un rendement de 98 %; toutefois au cours de la présente étude, il ne forme qu'un produit mineur obtenu qu'avec environ 10 % de rendement. Toutefois, dans les mêmes conditions, l'oxime de la *o*-cinnamyloxy-acétophénone (**2c**) subit une *N*-alkylation intramoléculaire qui conduit à la formation de la nitrone **3c**. Les réactions effectuées dans des conditions d'irradiation micro-onde sont plus propres, demandent moins de temps et conduisent à de meilleurs rendements. Dans des conditions d'irradiation micro-onde sans solvant, les cycloadditions 1,3-dipolaires intramoléculaires correspondantes des *N*-méthylnitrones (**B**) générées in situ conduisent à des formations complètement régio- et stéréosélectives de *o*-alcénylméthoxy-acétophénones (**1a**–**1c**) et de *N*-méthylhydroxylamine; ces réactions nécessitent des temps de réaction plus courts et conduisent à la formation des produits **4a**–**4c** avec des rendements plus élevés que ceux obtenus dans les réactions thermiques équivalentes.

Mots clés : cycloadditions, nitrones, oximes, *o*-alcénylméthoxy-acétophénones, micro-onde, isoxazolidines.

[Traduit par la Rédaction]

Introduction

Considerable interest is centered on nitrone cycloadditions (1), including the nitrones derived from 1,2-*H* shifts in oximes (2), for generating biologically active molecules or precursors and scaffolds for the same (1–3). However, there are only few examples wherein oxime–nitrone transformation and intramolecular cycloadditions of keto-oximes have been investigated (4). Recently, it has been reported that oximation of *o*-allyloxy-acetophenone and -benzophenone (**1**) affords *E*-oximes (**2**), which are quantitatively converted to dipoles (**3**, Scheme 1) on refluxing in xylene for 14 h (5).

On the other hand, reaction of **1a** (R = CH_3, R^1 = H) with *N*-methylhydroxylamine hydrochloride in the presence of NaOH in aqueous ethanol, under reflux for 36 h, has been reported to furnish cycloadduct **4** (78% yield) derived from intramolecular 1,3-dipolar cycloaddition of an in-situ-generated nitrone (6) (Scheme 1). The same adduct has also been obtained in 49% yield by reaction of *o*-allyloxyphenylacetylene with *N*-methylhydroxylamine in a sealed tube at 110 °C for 46 h (6). Recently, microwave-assisted organic transformations, particularly under solvent free conditions, have emerged as an important component of the modern nonconventional green organic synthetic methodologies,

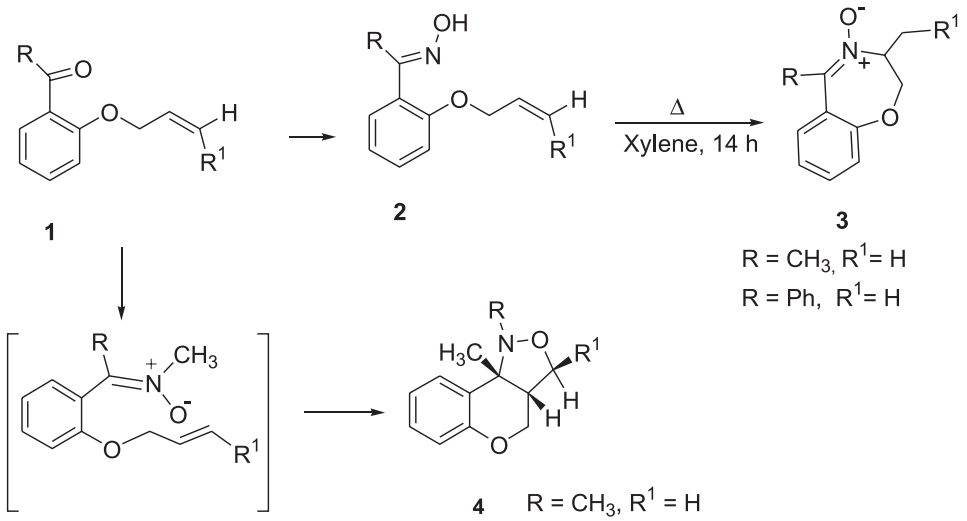
Received 20 October 2004. Published on the NRC Research Press Web site at http://canjchem.nrc.ca on 29 March 2005.

S. Singh, M.P.S. Ishar,[1] G. Singh, and R. Singh.
Department of Pharmaceutical Sciences, Guru Nanak Dev University, Amritsar-143005, Punjab, India.

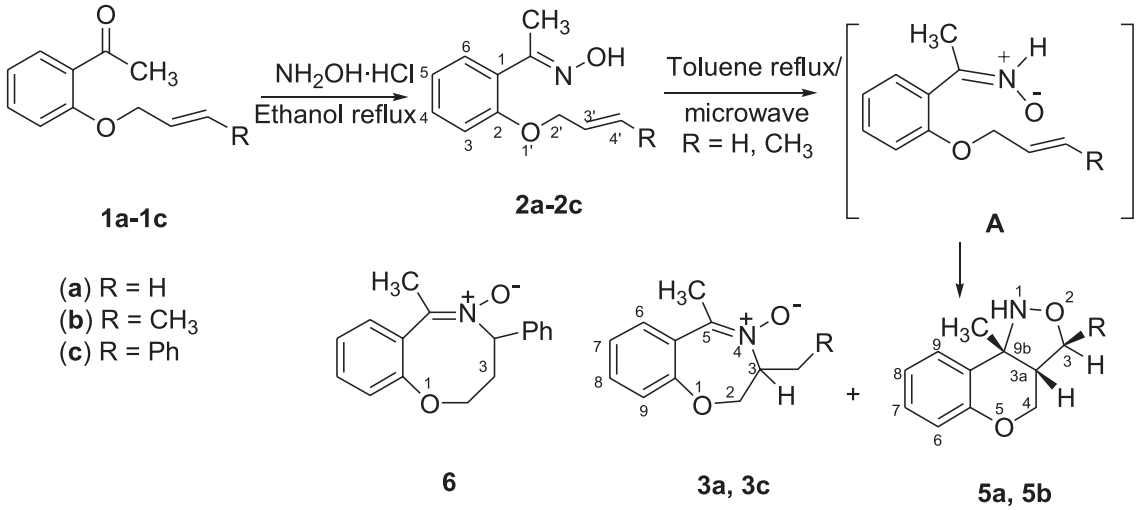
[1]Corresponding author (e-mail: mpsishar@yahoo.com).

 doi: 10.1139/V05-049 © 2005 NRC Canada

Scheme 1.



Scheme 2.



whose effectiveness has also been demonstrated for intramolecular cycloadditions (7). As a part of our ongoing investigations on 1,3-dipolar cycloadditions (8), and with the aim of developing scaffolds for some peptidomimetics, we have investigated the intramolecular 1,3-dipolar cycloaddition of *N*-methylnitrones and nitrones generated from oximes, derived from *o*-allyloxy-, -crotyloxy-, -cinnamyloxy-acetophenones (**1a**–**1c**). The reactions have been carried out under microwave-assisted, solvent-free conditions and the results compared with those of the reactions carried out under conventional (toluene–ethanol reflux) conditions.

Results and discussion

Oximes (**2a**–**2c**) were obtained in high yields (93%–95%) by refluxing corresponding ketones **1a**–**1c** (9) and hydroxylamine hydrochloride in dry ethanol as crystalline solids and characterized spectroscopically. Although oxime **2a** has been reported previously (5) and assigned a geometry –*E*, its melting point has not been reported; the spectroscopic data determined for **2a** is comparable with the data reported in the literature (5). Oximes **2a**–**2c** were adsorbed on silica gel and exposed to microwave heating (500 W, 75 °C) and products **5a**–**5b** and **3a** and **3c** (Scheme 2) were separated by column chromatography over silica gel.

The products were characterized by rigorous spectroscopic (IR, ^{1}H and ^{13}C NMR including COSY, hetero-COSY, and NOESY 2D NMR measurements, and mass spectra) and microanalytical data, and comparison of the data with the data reported for related systems (2, 3, 5). The assigned mode and regiochemistry of the addition in the case of **5a** and **5b** is based on the chemical shift of the C9b-methyl group, which indicated that it is no longer attached to an unsaturated carbon in the product and chemical shift of C3-H(s), which indicated the proximity of C3 to the oxygen; C3-H(s) resonances were easily identified from their multiplicity. The stereochemical disposition between the C9b-methyl group and C3a-H, i.e., the cis arrangement is based on spatial proximity established by the NOESY spectrum. Compound **3a** has been identified from its NMR spectral data (5). The assigned structure of compound **3c** is based, inter alia, on the observation of a 3H singlet (methyl)

© 2005 NRC Canada

Table 1. Reaction conditions, reaction times, and % yields of the products.

Serial No.	Compound	Toluene reflux Temp (°C)	Time (min)	Yield (%)	Microwave irradiation Temp (°C)[a]	Time (min)	Yield (%)
1	**5a**	110	4320	33	75	15	58
2	**5b**	110	4320	35	75	15	61
3	**3c**	110	4320	34	75	15	59

[a]The final temperature was measured at the end of microwave irradiation by introducing a glass thermometer into the reaction mixture.

Scheme 3.

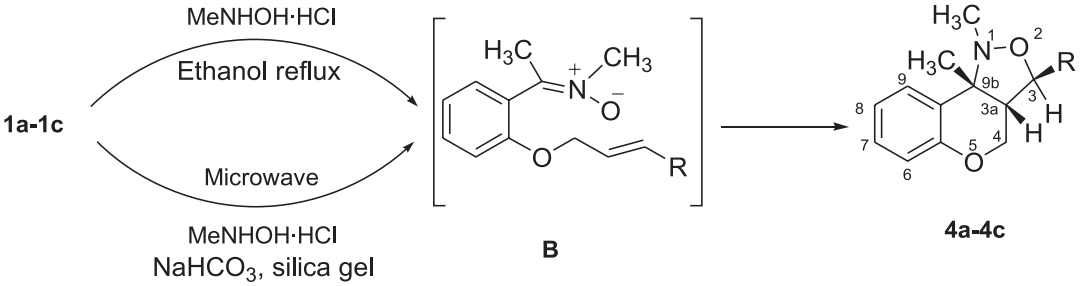


Table 2. Reaction conditions, reaction times, and % yields of the products.

Serial No.	Compound	Ethanol reflux Temp (°C)	Time (min)	Yield (%)	Microwave irradiation Temp (°C)[a]	Time (min)	Yield (%)
1	**4a**	78 to 79	720	82	75	15	96
2	**4b**	78 to 79	720	84	75	15	97
3	**4c**	78 to 79	720	80	75	15	95

[a]The final temperature was measured at the end of microwave irradiation by introducing a glass thermometer into the reaction mixture.

at δ 2.54 indicating that the methyl group is attached to an unsaturated carbon and the presence of an intense band in its IR spectrum at 1218 cm^{-1}, which is characteristic of the nitrone functionality (10). The alternative structure **6** for this compound was ruled out by ^1H multiplicities and connectivities as well as ^{13}C NMR assignments established by rigorous 2D NMR measurements. For instance, two 1H double doublets at δ 3.50 (^2J = 13.8 Hz and ^3J = 4.9 Hz) and δ 2.87 (^2J = 13.8 Hz and ^3J = 8.2 Hz) have been attributed to benzylic-Hs in **3c**, and such a pattern is not anticipated for C3-Hs in **6**; the hetero-COSY – 2D NMR spectrum revealed the corresponding benzylic-C resonance at δ 32.90.

As the formation of **5a** and **b** was contrary to the reported production (5) of only oxazepine-*N*-oxides (**3**) (5), in the thermal transformations of related oximes, thermal reactions of **2a**–**2c** were reinvestigated by refluxing dry toluene solutions and the products were similarly isolated by column chromatographic separation of the reaction concentrates. The results of thermal and corresponding microwave-assisted transformations are summarized in Table 1 and clearly indicate that similar results are obtained under both sets of conditions as far as the nature of the major products is concerned. However, the reactions carried out under microwave irradiation are attended with higher yields of the cycloadducts (**5a** and **5b**) as well as nitrones (**3c**) with much shortened reaction times.

For reactions of *N*-methylnitrones derived from ketones **1a**–**1c** under microwave heating, the ketones **1a**–**1c** were mixed with *N*-methylhydroxylamine hydrochloride and sodium bicarbonate, adsorbed on silica gel, and exposed to microwave radiation; products were isolated and purified by column chromatography. For corresponding thermal reactions, equimolar solutions of **1a**–**1c** and *N*-methylhydroxylamine hydrochloride in anhydrous ethanol were refluxed and products **4a**–**4c**) were similarly isolated by column chromatography. The results are summarized in Scheme 3 and Table 2.

Compound **4a** could be easily identified from the comparison of its spectroscopic data with the data reported in the literature (6); the assigned structures and stereochemistry in the case of **4b** and **4c** are again based on rigorous spectroscopic analysis, particularly, the NMR spectral data, and comparison of the same with that of the related systems (2, 3*k*, 6).

Thus, contrary to the reported (5) thermal transformation of oxime **2a** and corresponding *o*-allyloxybenzophenone oxime, leading, quantitatively, to bicyclic nitrones such as **3a**, and the recorded observation (5) that the formation of these bicyclic nitrones is related to the preferred *E* geometry of these oximes, the present investigations reveal that intramolecular 1,3-dipolar cycloaddition is the preferred mode of transformation of oximes **2a** and **2b**, both under thermal and

© 2005 NRC Canada

microwave irradiation conditions. Though, the precise reasons for the differential behavior of the oximes under comparable conditions, leading to **3a** and **3c** in the present investigations, are not very clear, in general, the exo-trig processes leading to seven-membered rings are favored (11). Mechanistically, as far as the regiochemistry of addition is concerned, i.e., the preferential formation of annelated products **5a**, **5b**, and **4a**–**4c**) vis-à-vis the bridged products, molecular modeling (MOPAC) studies on both *E* and *Z* forms of the involved nitrones revealed that the obtained regiochemistry as well as stereochemistry of addition are a consequence of the only feasible, less-cumbersome approach for intramolecular cycloadditions of these nitrones.

Conclusions

The present report thus describes regio- and stereoselective microwave-assisted intramolecular 1,3-dipolar cycloadditions of nitrones derived from *o*-allyloxy- and -crotyloxy-acetophenone oximes and *N*-methylnitrones derived from *o*-allyloxy-, -crotyloxy-, and -cinnamyloxy-acetophenones. A comparison with their thermal counterparts reveals that the reactions carried out under microwave irradiation conditions are cleaner, attended with higher yields, along with a drastic reduction in the reaction times. The obtained cycloadducts will be utilized, after opening of the isoxazolidine moiety, for synthesis of some peptidomimetics.

Experimental

Instrumentation and general procedures

Bruker AC-200FT (200 MHz) and JEOL AL-300FT (300 MHz) spectrometers were used to record ^{1}H and ^{13}C NMR spectra. IR spectra were recorded on a Shimadzu DR-2001 FT-IR spectrophotometer in $CHCl_3$ solution or as KBr pellets. Mass spectra, EI and ESI methods were recorded on Shimadzu GC–MS QP-2000A and Bruker Daltonics Esquire 300 mass spectrometers, respectively. Elemental analyses were carried out on a PerkinElmer 240C elemental analyzer and are reported in % atomic abundance. All melting points are uncorrected and were measured in open glass capillaries. Thin layer chromatography (TLC) was carried out on silica gel G-coated (Loba Chemie, containing 13% $CaSO_4$ as a binder) (1 mm thick layer) glass plates.

General procedure for preparation of oximes

Solutions of ketones **1a**–**1c** (200 mg, (9)) and hydroxylamine hydrochloride (1.0 molar equiv.) in dry ethanol were refluxed for 15–18 h. After the completion of the reaction (TLC, $CHCl_3$ solvent), the solvent was removed under reduced pressure. The residue was taken up in chloroform (20 mL) and washed successively with aqueous bicarbonate and water. After drying over anhydr. Na_2SO_4, the solutions were concentrated to one-fifth of their volume and triturated with hexane when colorless solids separated out.

o-*Allyloxyacetophenone oxime (2a)*

Yield: 95%; colorless solid, mp 48–50 °C (hexane:chloroform, 2:1). IR (KBr, cm^{-1}): 3260, 1610, 1595, 1480, 1440, 1380, 1355, 1280. ^{1}H NMR ($CDCl_3$, 200 MHz) δ: 8.75 (br, 1H, -OH), 7.34–7.28 (m, 2H, arom.-Hs), 6.99–6.88 (m, 2H, arom.-Hs), 6.03 (ddt, 1H, *J* = 5.0, 10.5, and 17.3 Hz, C3′-H), 5.39 (dd, 1H, *J* = 1.3 and 17.3 Hz, C4′-H), 5.27 (dd, 1H, *J* = 1.1 and 10.5 Hz, C4′-H), 4.57 (d, 2H, *J* = 5.0 Hz, C2′-Hs), 2.26 (s, 3H, CH_3). ^{13}C NMR ($CDCl_3$, 75 MHz) δ: 158.20 (quat.), 156.42 (quat.), 133.01 (CH), 130.08 (CH), 129.48 (CH), 127.19 (C1), 120.82 (CH), 117.41 (=*C*H$_2$), 112.39 (CH), 69.09 (O*C*H$_2$), 15.38 (*C*H$_3$). MS (EI) *m*/*z*: 192 (M$^+$ + 1), 191 (M$^+$).

o-*Crotyloxyacetophenone oxime (2b)*

Yield: 93%; colorless solid, mp 43–45 °C (hexane:chloroform, 2:1). IR (KBr, cm^{-1}): 3280, 1605, 1490, 1440, 1368, 1275. ^{1}H NMR ($CDCl_3$, 200 MHz) δ: 8.63 (br, 1H, -OH), 7.33–7.26 (m, 2H, arom.-Hs), 6.97–6.87 (m, 2H, arom.-Hs), 5.81–5.63 (m, 2H, C3′-H and C4′-H), 4.49 (d, 2H, *J* = 5.5 Hz, C2′-Hs), 2.25 (s, 3H, CH_3), 1.76 (dd, 3H, *J* = 1.0 and 5.9 Hz, C4′-CH_3). ^{13}C NMR ($CDCl_3$, 75 MHz) δ: 157.12 (quat.), 156.60 (quat.), 130.03 (CH), 129.93 (CH), 128.30 (CH), 127.20 (C1), 125.91 (CH), 120.60 (CH), 112.47 (CH), 69.03 (OCH_2), 17.80 (CH_3), 15.34 (CH_3). MS (ESI) *m*/*z*: 228 (M + Na)$^+$.

o-*Cinnamyloxyacetophenone oxime (2c)*

Yield: 95%; colorless solid, mp 106–108 °C (hexane:chloroform, 2:1). IR (KBr, cm^{-1}): 3285, 1605, 1495, 1430, 1368, 1225. ^{1}H NMR ($CDCl_3$, 200 MHz) δ: 9.10 (br, 1H, -OH), 7.45–7.28 (m, 7H, arom-Hs), 6.99 (td, 2H, arom.-Hs, *J* = 1.0 and 8.8 Hz), 6.74 (d, 1H, *J* = 15.9 Hz, C4′-H), 6.41 (dt, 1H, *J* = 5.6 and 15.9 Hz, C3′-H), 4.76 (dd, 2H, *J* = 1.1 and 5.6 Hz, C2′-Hs), 2.31 (s, 3H, CH_3). ^{13}C NMR ($CDCl_3$, 75 MHz) δ: 156.96 (quat.), 156.46 (quat.), 136.38 (quat.), 132.79 (CH), 130.12 (CH), 129.52 (CH), 128.57 (CH), 127.86 (CH), 127.27 (C1), 126.55 (CH), 124.27 (CH), 120.89 (CH), 112.58 (CH), 69.05 (OCH_2), 15.43 (CH_3). MS (ESI) *m*/*z*: 290 (M + Na)$^+$.

General procedure for the transformations of oximes under microwave irradiation

Oximes **2a**–**2c** (200 mg) were dissolved in chloroform (10 mL) and to the solution was added silica gel (G, 3.0 g) and the solvent was removed under vacuum. The obtained powder was exposed to microwave irradiation (500 W) for 15 min (five cycles, 3 min each); the exposure time optimization is based on TLC ($CHCl_3$ solvent) monitoring. The adsorbed material was then extracted with ethyl acetate (25 mL) and dried over anhydr. Na_2SO_4. The solvent was then distilled off under reduced pressure. The products were isolated by column chromatographic separation over silica gel (60–120 mesh, 30 g). The column was packed in hexane and hexane – ethyl acetate gradients were used for elution.

(3aS,9bR)-9b-Methyl-1,3a,4,9b-tetrahydro-3H-chromeno[4,3-c]isoxazole (5a)

Elution of the column initially with hexane – ethyl acetate (9:1) afforded **1a** (14 mg, 7%) and unreacted oxime **2a** (30 mg, 15%) with hexane – ethyl acetate (7:1). Further elution with hexane – ethyl acetate (3:1) afforded cycloadduct **5a** (116 mg, 58%) as a yellow oil. R_f 0.37 ($CHCl_3$). IR ($CHCl_3$, cm^{-1}): 3260, 1585, 1510, 1482, 1430, 1290. ^{1}H

© 2005 NRC Canada

NMR ($CDCl_3$, 200 MHz) δ: 7.48 (dd, 1H, J = 1.7 and 7.7 Hz, arom.-H), 7.21 (ddd, 1H, arom.-H, J = 8.8, 7.3, and 1.7 Hz), 7.24–6.89 (m, 2H, arom.-Hs), 4.34 (unresolved dd, 1H, $^2J \cong {}^3J \sim 8.3$ Hz, C3-H), 4.21 (dd, 1H, ^2J = 11.6 and J = 4.6 Hz, C4-H), 3.78 (dd, 1H, ^2J = 11.6 and J = 8.1 Hz, C4-H), 3.73 (dd, 1H, ^2J = 8.1 and 5.1 Hz, C3-H), 2.78–2.69 (m, 1H, C3a-H), 1.56 (s, 3H, C9b-CH_3). ^{13}C NMR ($CDCl_3$, 75 MHz) δ: 154.69 (C5a), 128.92 (CH), 128.69 (CH), 124.67 (C9a), 121.89 (CH), 117.15 (CH), 72.50 (C3), 65.41 (C9b), 61.13 (C4), 47.66 (C3a), 26.29 (CH_3). MS (EI) m/z: 192 (M^+ + 1), 191 (M^+). Anal. calcd. for $C_{11}H_{13}NO_2$: C 69.09, H 6.85, N 7.32; found: C 68.97, H 6.99, N 7.20. Further elution with hexane – ethyl acetate (1:1) afforded **3a** as a reddish oil (20 mg, 10%) (5). R_f 0.16 ($CHCl_3$).

*(3S,3aS,9bR)-9b-Dimethyl-1,3a,4,9b-tetrahydro-3*H*-chromeno[4,3-*c*]isoxazole (5b)*

Elution of the column initially with hexane – ethyl acetate (9:1) afforded **1b** (20 mg, 10%) and unreacted oxime **2b** (30 mg, 15%) with hexane – ethyl acetate (7:1). Further elution with hexane – ethyl acetate (3:1) afforded cycloadduct **5b** (122 mg, 61%) as a yellow oil. R_f 0.37 ($CHCl_3$). IR ($CHCl_3$, cm^{-1}): 3270, 1615, 1585, 1490, 1450, 1380, 1298, 1235, 1125. ^{1}H NMR ($CDCl_3$, 300 MHz) δ: 7.43 (dd, 1H, J = 1.2 and 7.9 Hz, arom.-H), 7.22–7.16 (m, 1H, arom.-H), 7.00–6.83 (m, 2H, arom.-Hs), 4.17 (dd, 1H, ^2J = 11.7 and J = 4.3 Hz, C4-H), 3.95 (dd, 1H, J = 4.2 and 6.0 Hz, C3-H), 3.88 (dd, 1H, J = 6.1 and 11.7 Hz, C4-H), 2.19–2.14 (m, 1H, C3a-H), 1.60 (s, 3H, C9b-CH_3), 1.45 (d, 3H, J = 6.0 Hz, C3-CH_3). ^{13}C NMR ($CDCl_3$, 75 MHz) δ: 154.37 (C5a), 128.86 (CH), 128.13 (CH), 125.86 (C9a), 122.08 (CH), 117.29 (CH), 81.37 (C3), 65.52 (C9b), 61.96 (C4), 56.12 (C3a), 27.98 (C9b-*C*H_3), 18.84 (C3-*C*H_3). MS (ESI) m/z: 228 (M + Na)$^+$. Anal. calcd. for $C_{12}H_{15}NO_2$: C 70.22, H 7.37, N 6.82; found: C 70.15, H 7.49, N 6.73.

3-Benzyl-5-methyl-2,3-dihydro-benzo[f][1,4]oxazepine-4-oxide (3c)

Elution of the column initially with hexane – ethyl acetate (9:1) afforded **1c** (20 mg, 10%) and unreacted oxime **2c** (40 mg, 20%) with hexane – ethyl acetate (7:1). Further elution with hexane – ethyl acetate (1:1) afforded cycloadduct **3c** (118 mg, 59%) as a yellow oil. R_f 0.16 ($CHCl_3$). IR ($CHCl_3$, cm^{-1}): 1600, 1573, 1490, 1447, 1288, 1218. ^{1}H NMR ($CDCl_3$, 200 MHz) δ: 7.41–6.91 (m, 9H, arom-Hs), 4.65–4.55 (m, 2H, C2-Hs), 4.49–4.41 (m, 1H, C3-H), 3.50 (dd, 1H, ^2J = 13.8 and ^3J = 4.9 Hz, benzylic-H), 2.87 (dd, 1H, ^2J = 13.8 and ^3J = 8.2 Hz, benzylic-H), 2.54 (s, 3H, CH_3). ^{13}C NMR ($CDCl_3$, 75 MHz) δ: 154.48 (C9a), 142.97 (quat.), 136.93 (CH), 130.75 (CH), 129.26 (CH), 128.74 (CH), 126.94 (C5a), 124.12 (CH), 123.11 (CH), 121.39 (CH), 75.64 (C3), 71.85 (C2), 32.90 (benzylic-*C*), 18.89 (CH_3). MS (ESI) m/z: 290 (M + Na)$^+$. Anal. calcd. for $C_{17}H_{17}NO_2$: C 76.48, H 7.29, N 6.94; found: C 76.38, H 6.41, N 5.24.

General procedure for thermal transformations of oximes

Oximes **2a**–**2c** (200 mg) were refluxed in dry toluene (50 mL) for 72 h. After the completion of the reaction (TLC, $CHCl_3$ solvent), the solvent was removed under reduced pressure and the products were isolated by similar column chromatographic separations of the concentrate. From the reaction of **2a** were obtained **1a** (84 mg, 42%), **2a** (30 mg, 15%), and **5a** (66 mg, 33%), eluted with hexane – ethyl acetate 9:1, 7:1, and 3:1, respectively.

From the reaction of **2b** were obtained **1b** (80 mg, 40%), **2b** (32 mg, 16%), and **5b** (70 mg, 35%), eluted, respectively, with hexane – ethyl acetate 9:1, 7:1, and 3:1.

From the reaction of **3c** were isolated **1c** (86 mg, 43%), **2c** (28 mg, 14%) and **3c** (68 mg, 34%), eluted with hexane – ethyl acetate 9:1, 7:1, and 1:1, respectively.

General procedure for the reactions of ketones 1a–1c with *N*-methylhydroxylamine hydrochloride under microwave irradiation

Ketones **1a**–**1c** (200 mg) were mixed with *N*-methylhydroxylamine hydrochloride (equimolar) and sodium bicarbonate (1.0 g), and adsorbed on silica gel (G, 3.0 g) as described earlier. The reaction mixture was exposed to microwave radiation (500 W) for 15 min (five cycles, 3 min each); exposure time optimization is based on TLC ($CHCl_3$ solvent) monitoring. The adsorbed material was then extracted with ethyl acetate (25 mL), and dried over anhydr. Na_2SO_4. The solvent was then distilled off under reduced pressure. The products were isolated by column chromatographic separation over silica gel (60–120 mesh, 30 g). The column was packed in hexane and hexane – ethyl acetate gradients were used for elution.

*(3S,3aS,9bR)-1,3,9b-Trimethyl-1,3a,4,9b-tetrahydro-3*H*-chromeno[4,3-*c*]isoxazole (4b)*

Elution with hexane – ethyl acetate (3:1) afforded cycloadduct **4b** (223 mg, 97%) as a colorless oil. R_f 0.35 ($CHCl_3$). IR ($CHCl_3$, cm^{-1}): 1610, 1575, 1490, 1430, 1290, 1245, 1235. ^{1}H NMR ($CDCl_3$, 300 MHz) δ: 7.35 (d, 1H, J = 7.5 Hz, arom.-H), 7.16 (unresolved dd, 1H, $J \sim 7.5$ Hz, arom.-H), 6.96 (unresolved dd, 1H, $J \sim 7.5$ Hz, arom.-H), 6.82 (d, 1H, J = 8.1 Hz, arom.-H), 4.27–4.09 (m, 3H, C3-H and C4-Hs), 2.89 (s, 3H, *N*-CH_3), 2.27–2.19 (m, 1H, C3a-H), 1.51 (s, 3H, C9b-CH_3), 1.42 (d, 3H, J = 6.3 Hz, C3-CH_3). ^{13}C NMR ($CDCl_3$, 75 MHz) δ: 154.59 (C5a), 128.29 (CH), 128.09 (CH), 126.1 (quat.), 121.16 (CH), 117.03 (CH), 74.89 (C3), 65.0 (C4), 63.64 (C9b), 39.29 (*N*-CH_3), 54.04 (C3a), 20.33 (C3-CH_3 and C9b-CH_3, hetero-COSY). MS (EI) m/z: 220 (M^+ + 1, 6), 219 (M^+, 40). Anal. calcd. for $C_{13}H_{17}NO_2$: C 71.21, H 7.81, N 6.39; found: C 71.34, H 7.70, N 6.21.

*(3R,3aS,9bR)-1,9b-Dimethyl-3-phenyl-1,3a,4,9b-tetrahydro-3*H*-chromeno[4,3-*c*]isoxazole (4c)*

Elution with hexane – ethyl acetate (3:1) afforded cycloadduct **4b** (211 mg, 95%) as a colorless solid, mp 43–45 °C (hexane:chloroform, 2:1). R_f 0.35 ($CHCl_3$). IR (KBr, cm^{-1}): 1610, 1575, 1495, 1430, 1290, 1245, 1235. ^{1}H NMR ($CDCl_3$, 200 MHz) δ: 7.48–7.16 (m, 7H, arom.-Hs), 7.03–6.90 (m, 2H, arom.-Hs), 5.05 (d, 1H, J = 7.5 Hz, C3-H), 4.26–4.18 (m, 2H, C4-Hs), 2.78 (s, 3H, *N*-CH_3), 2.67–2.60 (m, 1H, C3a-H), 1.59 (s, 3H, CH_3). ^{13}C NMR ($CDCl_3$, 75 MHz) δ: 54.77 (C5a), 140.92 (quat.), 128.56 (CH), 128.14 (CH), 127.71 (CH), 126.29 (quat.), 125.98 (CH), 121.39 (CH), 117.20 (CH), 80.58 (C3), 64.76 (C9b), 64.07

© 2005 NRC Canada

(C4), 56.15 (C3a), 39.98 (N-CH_3), 23.43 (CH_3). MS (ESI) *m/z*: 304 $(M + Na)^+$. Anal. calcd. for $C_{18}H_{19}NO_2$: C 76.84, H 6.81, N 4.98; found: C 76.69, H 6.97, N 4.82.

General procedure for the reactions of ketones 1a–1c with *N*-methylhydroxylamine hydrochloride under thermal conditions

Solutions of ketones **1a**–**1c** (200 mg) and *N*-methylhydroxylamine hydrochloride (equimolar) in anhydrous ethanol (50 mL) were refluxed in the presence of sodium bicarbonate (1.0 g, excess) for 12 h. After the completion of the reaction (TLC, $CHCl_3$ solvent), the solvent was removed under reduced pressure. The residue was taken up in chloroform (20 mL) and washed with water. After drying over anhydr. Na_2SO_4, the products were isolated by similar column chromatographic separations of the concentrate over a silica gel column employing hexane – ethyl acetate (3:1) as the eluent. The cycloadducts **4a**–**4c** were obtained in 191 mg (82%), 193 mg (84%), and 178 mg (80%) yields, respectively.

References

1. (*a*) J.J. Tufariello. *In* Nitrones in 1,3-dipolar cycloaddition chemistry. Vol. 2. *Edited by* A. Padwa. Wiley Interscience, New York. 1984; (*b*) A. Padwa and A.M. Schoffstall. *In* Advances in cycloaddition. *Edited by* D. Curran. JAI Press, Greenwich. 1990. p. 2; (*c*) S.E. Denmark and A. Thorarensen. Chem. Rev. **96**, 1371 (1996); (*d*) W. Carruthers. *In* Cycloaddition reactions in organic synthesis — Tetrahedron organic chemistry series. Vol. 8. *Edited by* J.E. Baldwin and P.D. Magnus. Pergamon Press, Oxford. 1990. Chap. 6. p. 269; (*e*) A. Hassner, R. Maurya, O. Friedman, H.E. Gottlieb, A. Padwa, and D. Austin. J. Org. Chem. **58**, 4539 (1993); (*f*) L.A. Paquette. *In* Comprehensive organic synthesis. Vol. 5. *Edited by* B.M. Trost and I. Fleming. Pergamon Press, Oxford. 1991. Chap. 3; (*g*) K.V. Gothelf and K.A. Jorgensen. Chem. Rev. **98**, 863 (1998); (*h*) K.V. Gothelf and K.A. Jorgensen. *In* Synthetic applications of 1,3-dipolar cycloaddition chemistry towards heterocycles and natural products. Vol. 59. *Edited by* A. Padwa and W. Pearson. Wiley-VCH, Weinheim. 2002. p. 864.
2. (*a*) Q. Cheng, W. Zhang, Y. Tagami, and T. Oritani. J. Chem. Soc. Perkin Trans. 1, 452 (2001); (*b*) O. Tamura, T. Mitsuya, and H. Ishibashi. J. Chem. Soc. Chem. Commun. 1128 (2002); (*c*) M. Noguchi, H. Okoda, S. Nishimura, Y. Yamagata, S. Takamura, M. Tanaka, A. Kakehi, and H. Yamamoto. J. Chem. Soc. Perkin Trans. 1, 185 (1999).
3. (*a*) M. Frederickson. Tetrahedron, **53**, 403 (1997); (*b*) H.G. Aurich, M. Geiger, C. Genetes, K. Harms, and H. Koster. Tetrahedron, **54**, 3181 (1998); (*c*) G. Broggini, C. La Rosa, T. Pilati, A. Terraneo, and G. Zecchi. Tetrahedron, **57**, 8323 (2001); (*d*) F.M. Cordero, M. Gensini, A. Goti, and A. Brandi. Org. Lett. **2**, 2475 (2000); (*e*) W. Carruthers, P. Coggins, and J.B. Weston. J. Chem. Soc. Perkin Trans. 1, 2323 (1990); (*f*) A. Long and S.W. Baldwin. Tetrahedron Lett. **42**, 5343 (2001); (*g*) P. Merino, S. Anoro, S. Franco, F.L. Merchan, T. Tejero, and V. Tunon. J. Org. Chem. **65**, 1590 (2000); (*h*) S.W. Baldwin, B.G. Young, and A.T. McPhail. Tetrahedron Lett. **39**, 6819 (1998); (*i*) S. Hanessian and M. Bayrakdarian. Tetrahedron Lett. **43**, 967 (2002).
4. E. Abele and E. Lukevics. Heterocycles, **53**, 2285 (2000), and refs. cited therein.
5. F. Heaney and C. O'Mahony. J. Chem. Soc. Perkin Trans. 1, 341 (1998).
6. A. Padwa and G.S.K. Wong. J. Org. Chem. **51**, 3125 (1986).
7. (*a*) A. Loupy, F. Maurel, and A. Sabatie-Gogova. Tetrahedron, **60**, 1683 (2004); (*b*) A. Loupy (*Editor*). Microwave in organic synthesis. Wiley-VCH, Weinheim. 2002; (*c*) L. Perreux and A. Loupy. Tetrahedron, **57**, 9199 (2001); (*d*) P. Lidstrom, J. Ticrney, B. Waltey, and J. Wesfman. Tetrahedron, **57**, 9225 (2001); (*e*) L. Ohberg and J. Westman. Synlett, 1296 (2001); (*f*) P. Wipf, J. Janjic, and C.R.J. Stephenson. Org. Biol. Chem. **2**, 443 (2004).
8. (*a*) M.P.S. Ishar, K. Kumar, and R. Singh. Tetrahedron Lett. **39**, 6547 (1998); (*b*) M.P.S. Ishar and K. Kumar. Tetrahedron Lett. **40**, 175 (1999); (*c*) N.K. Girdhar and M.P.S. Ishar. Tetrahedron Lett. **39**, 7551 (2000); (*d*) M.P.S. Ishar, G. Singh, K. Kumar, and R. Singh. Tetrahedron, **56**, 7817 (2000).
9. R. Singh and M.P.S. Ishar. Tetrahedron, **58**, 7595 (2002).
10. P.A.S. Smith and J.E. Robertson. J. Am. Chem. Soc. **84**, 1197 (1962).
11. (*a*) J.E. Baldwin. J. Chem. Soc. Chem. Commun. 734 (1976); (*b*) J.E. Baldwin, J. Cutting, W. Dupont, L. Kruse, L. Silberman, and R.C. Thomas. J. Chem. Soc. Chem. Commun. 736 (1976).

© 2005 NRC Canada

MINIREVIEW / MINISYNTHÈSE

Review on green chemistry — Suzuki cross coupling in aqueous media

Robert Franzén and Youjun Xu

Abstract: The Suzuki cross-coupling reaction is a very efficient, reliable, and environmentally friendly method for the introduction of novel carbon–carbon bonds into molecules. This review summarizes recent advances in the use of the reaction in aqueous media with a focus on different types of ligands and the ligandless protocols currently in use. Several synthetic targets for the reaction have been mentioned. The work summarizes recent results from studies on asymmetric Suzuki reactions performed in organic – aqueous mixed solvents.

Key words: Suzuki reaction, green chemistry, metal-catalyzed cross-coupling reactions, aqueous synthesis media.

Résumé : La réaction de couplage croisé de Suzuki est une méthode très efficace, fiable et environnementalement correcte pour l'introduction de nouvelles liaisons carbone–carbone dans des molécules. Cette revue résume les progrès récents réalisés dans l'utilisation de la réaction en milieu aqueux, en se concentrant sur les divers types de ligands et les protocoles sans ligands actuellement en usage. Plusieurs cibles de synthèse pour cette réaction sont mentionnées. Le travail résume les résultats récents obtenus à partir d'études sur les réactions de Suzuki asymétriques effectuées dans des solvants mixtes organique – aqueux.

Mots clés : réaction de Suzuki, chimie verte, réactions de couplage croisé catalysées par les métaux, milieu de synthèse aqueux.

[Traduit par la Rédaction]

Introduction

The chemical industry is a major contributor to environmental pollution, largely because of the use of hazardous solvents. These solvents released or disposed by the chemical industry include methanol, toluene, xylene, methyl ethyl ketone, and methylene chloride (1). With sharpened regulatory pressure focusing on organic solvents, the search for alternatives is of increasing importance. In this respect, organic transformations in aqueous media (2), have received much attention because water is easily available, economical, and harmless to the environment. The cross-coupling reaction of alkenyl and aryl halides with organoborane derivatives in the presence of a palladium catalyst and a base, known as the Suzuki reaction, has often been carried out in an organic–aqueous mixed solvent. Although Davidson and Triggs (3) discovered in 1968 that arylboronic acids reacted with palladium(II) acetate to give corresponding biaryls, and Garves (4) in 1970 that arylsulfinic acids could be coupled to biaryls using Pd(II) in aqueous solvents, it was not until 1979 when biaryls could efficiently be prepared by a palladium-catalyzed reaction. Miyaura and Suzuki (5) reported that cross-coupling reactions between alkenylboranes and organic halides were efficiently catalyzed by a catalytic amount of tetrakis(triphenylphoshine) palladium ($Pd(PPh_3)_4$) in the presence of a suitable base. Starting from these observations, the reaction has developed to become one of the most utilized methods for the introduction of novel carbon–carbon bonds in solution (6) and on solid phase (7). This current paper summarizes recent developments in Suzuki-type, palladium-catalyzed coupling reactions in water. This short review summarizes the advantages of using the Suzuki protocol instead of other similar cross-coupling reactions in aqueous media, several structurally different ligands that promote the reaction in water, recent results from ligandless Suzuki protocols, and target molecules mainly produced by the method. The paper ends with a few examples for the utilization of the reaction in an asymmetric manner.

Received 28 September 2004. Published on the NRC Research Press Web site at http://canjchem.nrc.ca on 29 March 2005.

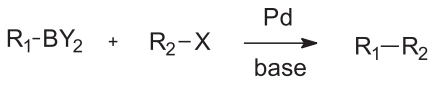
R. Franzén.[1] Tampere University of Technology, Institute of Materials Chemistry, Korkeakoulunkatu 8, FIN-33720 Tampere, Finland.
Y. Xu. Shenyang Pharmaceutical University, School of Pharmaceutical Engineering, Wenhua Road 103, Shenyang 110016, Peoples Republic of China.

[1]Corresponding author (e-mail: robert.franzen@tut.fi).

 doi: 10.1139/V05-048 © 2005 NRC Canada

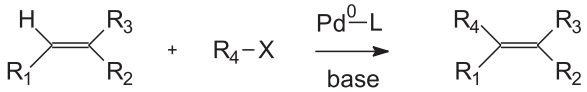
Fig. 1. Selected palladium-catalyzed cross-coupling reactions.

Suzuki coupling: Pd-catalyzed cross coupling of organic halides or perfluorinated sulfonates with organoboron derivatives.



X = I, Br, Cl, OSO_2
BY_2 = $B(OR_2)$, 9-BBN, $B(alkyl)_2$
R_1 or R_2 = various aromatic or alifatic hydrocarbons

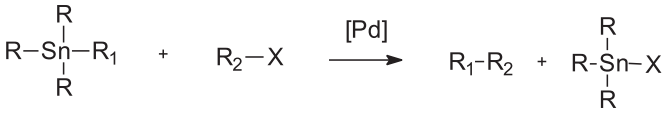
Heck reaction: Pd-catalyzed coupling of an alkyl, aryl, or vinyl entity to an alkene



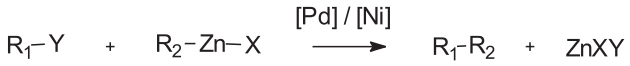
Kumada coupling: Ni- or Pd-catalyzed substitution of aryl halides with Grignard reagents



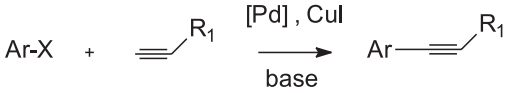
Stille coupling: Pd-catalyzed reaction of organostannanes with halides, acetates, or perfluorinated sulfonates lacking a sp^3-hybridized β-hydrogen



Negishi coupling : Ni- or Pd-catalyzed coupling of a alkenyl, aryl, allylic, or benzylic halide with alkyl- or arylzinc reagents



Sonogashira coupling: Cu(I) mediated and Pd-driven alkyne coupling to aromatic halides in the presence of a base



Suzuki cross coupling vs. other palladium-catalyzed reactions

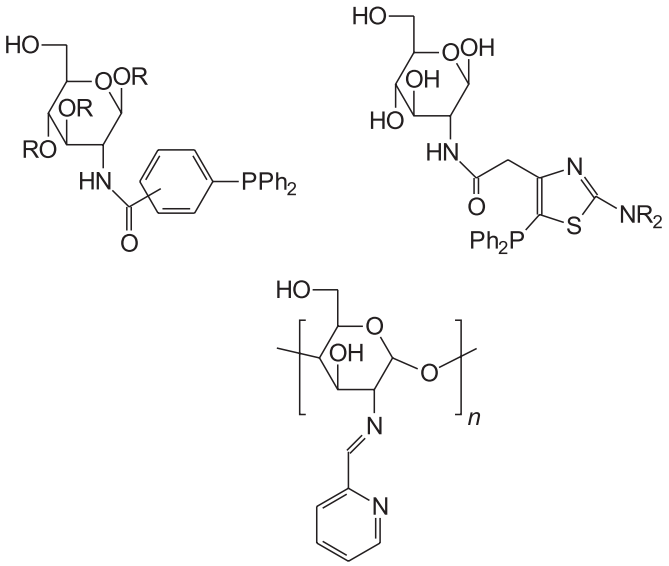
In the Suzuki reaction (5, 6), the Heck reaction (8), the Kumada reaction (9), the Stille reaction (10), the Negishi reaction (11), and the Sonogashira reaction (12), palladium is known to be particularly effective in activating sp^2-carbon–halogen bonds even in aqueous media (13) (Fig. 1). All reaction types have drawbacks that limit the use in synthesis. Suzuki cross coupling has, on the other hand, less limitations than the other reactions mentioned. In the Heck reaction, for example, where an aryl or vinyl halide and an alkene are converted to a more highly substituted alkene under Pd catalysis, the intermolecular reaction often proceeds well when the alkene is electrophilic. With nucleophilic substituents, the reaction gives less satisfactory results. The Kumada coupling is very sensitive to air and the presence of radical inhibitors, and this has limited the use of the reaction in aqueous media. In the Stille reaction, stannates are used as substrates, and many of these are environmentally hazardous. There is no toxicity issue involved in organoborane reagents. For a large-scale setting, a Suzuki coupling is an attractive choice. The organoborane reagents are usually more easy to prepare in the laboratory, and the workup procedures are more simple than using other cross-coupling methods (14–17).

Ligands

The vast majority of ligands applied in modern synthesis possess low water solubility. Many strategies have been used to enhance the solubility of metal–ligand complexes in water of which three are mostly utilized (18). The catalytic reaction is performed in the presence of micelle-forming surfactants, solubilizing functionalities are added to the ligand, i.e., ionic groups to poorly soluble ligands and easily accessible, water-soluble sources from nature are utilized as ligands. These include, for example, carbohydrates and the

© 2005 NRC Canada

Fig. 2. Ligand alternatives from nature suitable for Suzuki cross coupling.



biopolymer chitosan suitable for the Suzuki reaction (19) (Fig. 2). Ligands based on monosaccharides usually have only moderate solubility in water and often require incorporation of extra hydrophilic groups to improve the ligand property. Also, a co-solvent or a surfactant is sometimes needed for optimum efficiency. Dissaccharide ligands have the advantage of higher aqueous solubility, but the synthesis of these is usually tedious. Chitosan, on the other hand (20–23), has proven to be a very promising material for organic synthesis and catalysis. For example, Suzuki and Heck reactions have successfully been completed using metal–chitosan complexes as catalysts in aqueous solutions (24). The complexes have offered both economically and environmentally more favourable conditions for many reactions. Catalysts for the Suzuki reaction heterogenized through covalent attachment to organic or inorganic supports have also been synthesized (25). The supports have included organic polymers (7, 26), silica (27), and layered clays (28).

Ligandless Suzuki cross coupling

From an environmental point of view, development of a new catalytic system without the use of stabilizing phosphine ligands in aqueous media under mild conditions has attracted much attention. The reaction with ligandless catalysts such as Pd/C in water has, for example, very recently been investigated (16, 29) (Fig.3). Compared to air-sensitive and expensive homogenous palladium catalysts, palladium charcoal can safely be handled and removed from the reaction mixture by simple filtration. The recovered palladium charcoal can be purified and reused as palladium metal. These features are also of great advantage in industrial processes. Other palladium catalysts useful for the ligandless Suzuki reaction in water include $Pd(OAc)_2$ and $PdCl_2$ (30, 31).

Targets for the Suzuki cross coupling

The synthesis of biaryl compounds, reviewed by Stanforth (32), is of importance for numerous agrochemical and pharmaceutical applications (Fig. 4). The classic Ullmann methology (33) is well-known in this context. Owing, on the other hand, to the versatile chemistry of palladium compounds in carbon–carbon bond-forming reactions, several palladium-catalyzed prosesses have been proposed as eco-friendly replacement for this stoichiometric protocol. Essentially based on the Pd(II)–Pd(0) redox cycle, these processes require in situ regeneration of the active palladium catalyst, which can be achieved, for example, during the Suzuki reaction by various reagents, e.g., 2-propanol, hydrogen gas, or aqueous alkali salts. In the synthesis of heterocyclic compounds, the aqueous Suzuki reaction has found many applications (34). A few examples include the structural modifications and preparations of pyrroles (35), indoles (36), pyridines (37), quinoxalines (38), benzofurans (39),

Fig. 3. Pd/C-catalyzed ligandless Suzuki coupling.

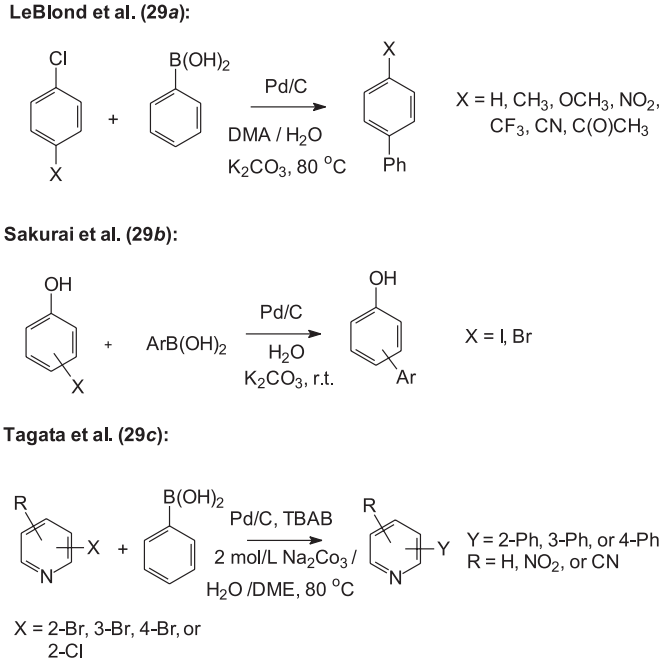
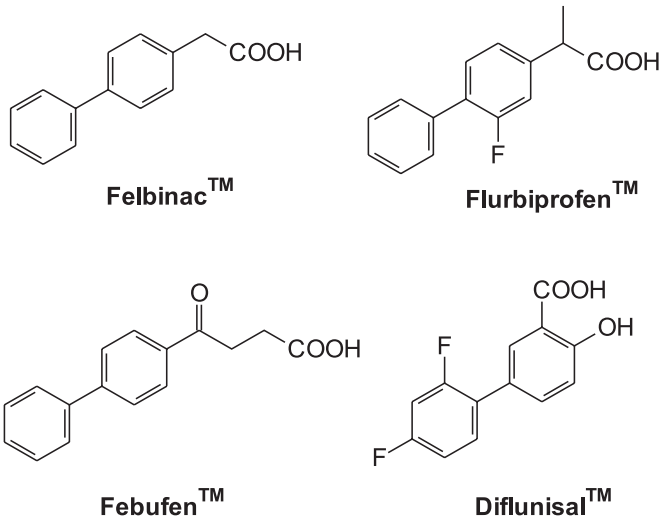
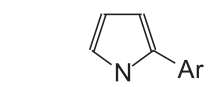


Fig. 4. Examples of non-steroidal anti-inflammatory drugs bearing biaryl fragments.

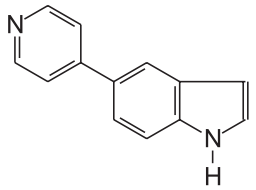


© 2005 NRC Canada

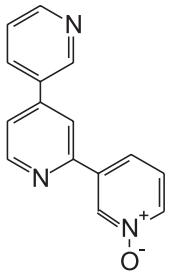
Fig. 5. Examples of heterocycles prepared by an aqueous Suzuki reaction.



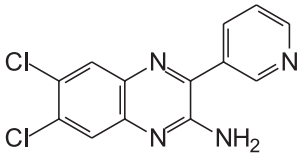
Ar = Ph, 4-MePh, 4-ClPh, 1-naphtyl, 2-thienyl, 3-pyridyl
(Johnson et al. (35))



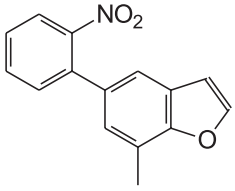
(Yang and Martin (36*b*))



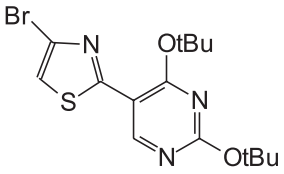
(Zoltewicz and Cruskie (37))



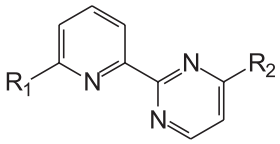
(Li and Yue (38))



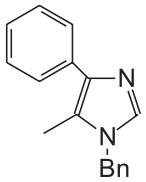
(Soos et al. (39))



(Wellmar et al. (40*a*))



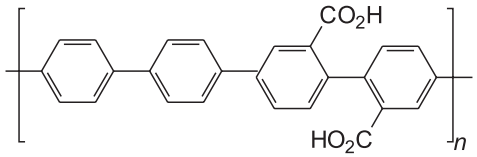
R_1 = Ph, 1-pyridyl, benzyl
R_2 = H or CH_3
(Hargreaves et al. (40*b*))



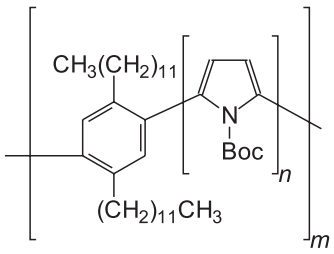
(Wang and Haseltine (41))

pyrimidyl thiazoles (40*a*), pyridyl pyrimidines (40*b*), and imidazoles (41) (Fig. 5). The Suzuki reaction of boronic acids in water and a variety of heteroaryl halides has been conducted to prepare 5-substitued heteroaryl pyrimidines, which can be hydrolyzed to 5-substituted uracils as potential antiviral agents (42*a*). Using a palladium(0) complex having a monosulfated phosphine as a ligand, Casalnuovo and Calabrese (42*b*) performed an alkylation of biomolecules in an aqueous medium. The reaction could tolerate a broad range of functional groups, including those present in unprotected nucleotides and amino acids. In the preparation of purines on solid phase, Pd catalyses have also successfully been utilized (43). In the synthesis of polymeric materials (Fig. 6), the Suzuki reaction has found applications in water. A hydrocarbon nonmetallic conducting polymer with a rigid rod of benzene rings was synthesized recently in water (44). Another example is the synthesis of phenyl–pyrrole mixed

Fig. 6. Two recent examples of the utilization of the Suzuki reaction in the preparation of polymers.

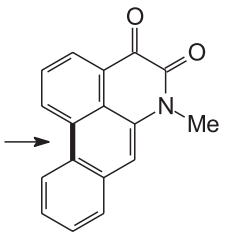


(Wallow and Novak (44))

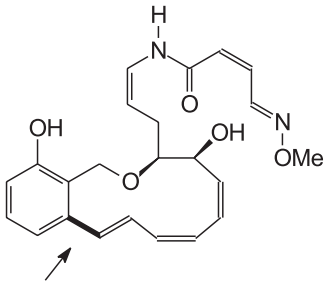


(Martina and Schluter (45))

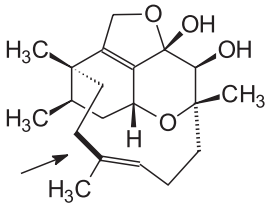
Fig. 7. Complex organic molecules prepared using a Suzuki reaction as the key step.



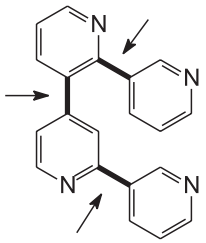
4,5-Dioxoaporphines
(Suau et al. (47))



Oximidine II
(Molander and Dehmel (48))

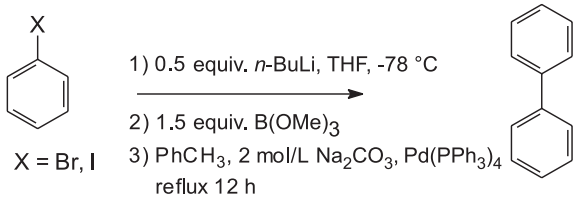


Phomactin A
(Mohr and Halcomb (49))



Nemertelline
(Bouillon et al (51))

Fig. 8. Initial attempts to prepare C_2-symmetric biaryls.



© 2005 NRC Canada

Fig. 9. Preparation of axially chiral biaryls.

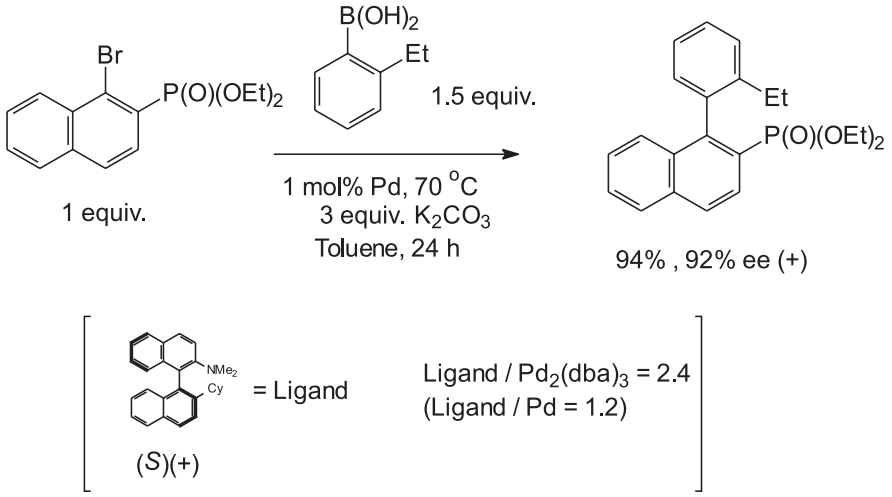
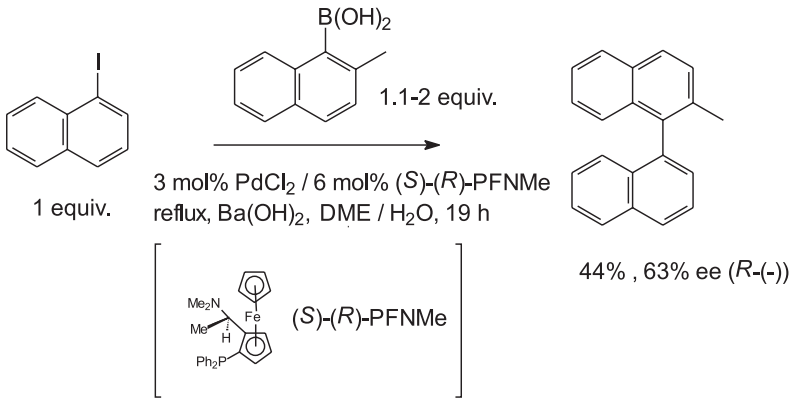


Fig. 10. Asymmetric Suzuki cross coupling performed in organic–aqueous mixed solvents for the preparation of binaphtalene derivatives.



polymers (45) using a method where originally β-octasubstituted tetramethylporphyrins were crafted by various arylboronic acids (46). In the total synthesis of complex molecules, such as aporphinoids (47), oximidine II (48), (+)-phomactin (49), gymnocin-A (50), quaterpyridine nemertelline (51), and ristocetin aglycon (52), an organic solvent – aqueous mixed Suzuki reaction has successfully been used as a key step (Fig. 7). These mentioned molecules are only a few very recent examples. The Suzuki cross coupling has, since its discovery, been used for a large group of different natural products (53).

Catalytic asymmetric Suzuki cross coupling

The asymmetric Suzuki cross-coupling reaction has successfully been accomplished in both organic solvents and inorganic–aqueous mixed solvents. For the preparation of C_2-symmetric biaryls, a modified Suzuki cross-coupling method of haloarenes was designed in 1996 by Keay and co-workers (54) (Fig. 8). The catalytic asymmetric version of the reaction for the synthesis of axially chiral biaryl compounds was later developed by the Buchwald group (55) (Fig. 9). The first, asymmetric Suzuki cross coupling performed in an organic–aqueous mixed solvent resulting in binaphthalene derivatives in up to 63% ee, was described by Cammidge and Crepy (56) (Fig. 10). In DME, the reaction gave up to 85% ee. Following these discoveries, other reports on the asymmetric synthesis for chiral binaphhyls or biaryls have been reported, for example, by Castanet et al. (57) in the study on chirality reverseal depending on the palladium – chiral phosphine ratio in the reaction of sterically hindered arylboronic acids. The reaction was performed in DME–water or toluene–EtOH–water. An atropo-enantioselective Suzuki cross coupling towards an axially chiral antimitotic biaryl has very recently been prepared by Herrbach et al. (58) in dioxane–water. Chiral atropisomeric binaphthalenes have also been synthesized in water–DME and a mixture of water–EtOH–toluene.

Concluding remarks

Suzuki cross coupling as a method for carbon–carbon bond formation has been a highly useful and versatile method needed for the development of modern drug discovery and in the synthesis of many natural products and polymers. Although the method has found many applications in synthesizing hitherto different molecules, there is still much work on the development towards an efficient catalyst applicable for structurally different substrates. The work on developing a catalyst working entirely in water has resulted in

© 2005 NRC Canada

a few remarkable discoveries. However, during the next few years, it is anticipated that new and more efficient catalysts will be discovered, giving even more excellent results in aqueous media.

Acknowledgements

This collaborative work has financially been supported by the Magnus Ehrnrooths Foundation.

References

1. P.T. Anastas, L.G. Heine, and T.C. Williamson. Green chemical syntheses and processes. American Chemical Society, Washington, D.C. 2000.
2. C.-J. Li and T.-H. Chan. Organic reactions in aqueous media. John Wiley and Sons Inc., New York. 1997.
3. J.M. Davidson and C.J. Triggs. J. Chem. Soc. A, **6**, 1324 (1968).
4. K. Garves. J. Org. Chem. **43**, 2870 (1978).
5. N. Miyaura and A. Suzuki. J. Chem. Soc. Chem. Commun. 866 (1979).
6. N. Miyaura and A. Suzuki. Chem. Rev. **95**, 2457 (1995).
7. R. Franzén. Can. J. Chem. **78**, 957 (2000).
8. R.F. Heck. Org. React. **27**, 345 (1982).
9. T. Hayashi and M. Kumada. Acc. Chem. Res. **15**, 395 (1982).
10. J.W. Labadie, D. Tueting, and S.K. Stille. J. Org. Chem. **48**, 4634 (1983).
11. E.-I. Negishi. Acc. Chem. Res. **15**, 340 (1982).
12. K. Sonogashira. J. Organomet. Chem. **653**, 46 (2002).
13. J. Tsuji. Transition metal reagents and catalysts: Innovations in organic synthesis. John Wiley and Sons, New York. 2002.
14. F. Lipton, M.A. Mauragis, M.T. Maloney, M.F. Veley, D.W. VanderBor, J.J. Newby, R.B. Appell, and E.D. Daugs. Org. Process Res. Dev. **7**, 385 (2003).
15. M. Beller and A. Zapf. *In* Handbook of organopalladium chemistry for organic synthesis. *Edited by* E. Negishi. Wiley, Hoboken, New Jersey. Vol. 1. 2002. p. 1209.
16. D.S. Ennis, J. McManus, W. Wood-Kaczmar, J. Richardson, G.E. Smith, and A. Carstairs. Org. Process Res. Dev. **3**, 248 (1999).
17. Y. Mori, M. Nakamura, T. Wakabayashi, K. Mori, and S. Kobayashi. Synlett, **4**, 601 (2002).
18. A. Herrmann and C.W. Kohlpaintner. Angew. Chem. Int. Ed. Engl. **32**, 1524 (1993).
19. (*a*) U.M. Lindström. Chem. Rev. **102**, 2751 (2002); (*b*) R. Kolodziuk, A. Penciu, M. Tollabi, E. Framery, C. Goux-Henry, A. Iourtchenko, and D. Sinou. J. Organomet. Chem. **687**, 384 (2003); (*c*) S. Parisot, R. Kolodziuk, C. Goux-Henry, A. Iourtchenko, and D. Sinou. Tetrahedron Lett. **43**, 7397 (2002); M. Bellar, J.G.E. Krauter, and A. Zapf. Angew. Chem. Int. Ed. Engl. **36**, 772 (1997).
20. J. Zhang and C.-G. Xia. J. Mol. Catalysis A, **206**, 59 (2003).
21. T. Vincent and E. Guibal. Ind. Eng. Chem. Res. **41**, 5158 (2002).
22. F. Quignard, A. Choplin, and A. Domard. Langmuir, **16**, 9106 (2000).
23. M.-A. Yin, G.-L. Yuan, Y.-Q. Wu, M.-Y. Huang, and Y.-Y. Jiang. J. Mol. Catalysis, **147**, 93 (1999).
24. J.J.E. Hardy, S. Hubert, D.C. Macquarrie, and A.J. Wilson. Green Chem. **6**, 53 (2004).
25. D.E. De Vos, I.F.J. Vankelecom, and P.A. Jacobs. Chiral catalyst immobilization and recycling. Wiley-VCH, Weinheim. 2000.
26. W. Gu, W.-J. Zhou, and D.L. Gin. Chem. Mater. **13**, 1949 (2001).
27. J. Jamis, J.R. Anderson, R.S. Dickson, E.M. Campi, and W.R. Jackson. J. Organomet. Chem. **603**, 80 (2000).
28. G. Sartori, F. Bigi, R. Maggi, A. Mazzacani, and G. Oppici. Eur. J. Org. Chem. 2513 (2001).
29. (*a*) C.R. LeBlond, A.T. Andrews, Y. Sun, and J.R. Sowa, Jr. Org. Lett. **3**, 1555 (2001); (*b*) H. Sakurai, T. Tsukuda, and T. Hirao. J. Org. Chem. **67**, 2721 (2002); (*c*) T. Tagata and M. Nishida. J. Org. Chem. **68**, 9412 (2003); (*d*) D.A. Conlon, B. Pipik, S. Ferdinand, C.R. LeBlond, J.R. Sowa, B. Izzo, P. Collins, G.J. Ho, J.M. Williams, Y.J. Shi, and Y. Sun. Adv. Synth. Catal. **345**, 931 (2003).
30. M.T. Reetz and E. Westermann. Angew. Chem. **112**, 170 (2000).
31. G.W. Kabalka, V. Namboodiri, and L. Wang. J. Chem. Soc. Chem. Commun. 775 (2001).
32. S.P. Stanforth. Tetrahedron, **54**, 263 (1998).
33. F. Ullmann. Ber. **36**, 2389 (1903).
34. J.J. Li and G.W. Gribble. Palladium in heterocyclic chemistry. Pergamon, New York. 2000.
35. C.N. Johnson, G. Stemp, N. Anand, S.C. Stephen, and T. Gallagher. Synlett, 1025 (1998).
36. (*a*) R.J. Sundberg. Indoles. Academic Press, London. 1996; (*b*) Y. Yang and A.R. Martin. Heterocycles, **34**, 1395 (1992).
37. A. Zoltewicz and M.P. Cruskie, Jr. Tetrahedron, **51**, 11 393 (1995).
38. J. Li and W.S. Yue. Tetrahedron Lett. **40**, 4507 (1999).
39. T. Soos, G. Timari, and G. Hajos. Tetrahedron Lett. **40**, 8607 (1999).
40. (*a*) U. Wellmar, A.-B. Hörnfeldt, and S. Gronowitz. J. Heterocycl. Chem. **32**, 1159 (1995); (*b*) S.L. Hargreaves, B.L. Pilkington, S.E. Russell, and P.A. Worthington. Tetrahedron Lett. **41**, 1653 (2000).
41. D. Wang and J. Haseltine. J. Heterocycl. Chem. **31**, 1637 (1994).
42. (*a*) D. Peters, A.-B. Hörnfeldt, and T. Musil. J. Heterocycl. Chem. **27**, 2165 (1990); (*b*) A.L. Casalnuovo and J.C. Calabrese. J. Am. Chem. Soc. **112**, 4324 (1990).
43. R. Franzén and J. Tois. Comb. Chem. High Throughput Scr. **6**, 433 (2003).
44. T.I. Wallow and B.M. Novak. J. Am. Chem. Soc. **113**, 7411 (1991).
45. S. Martina and A.-D. Schluter. Macromolecules, **25**, 3607 (1992).
46. X. Zhou, Z. Zhou, T.C.W. Mak, and K.S. Chan. J. Chem. Soc. Perkin Trans. 1, 2519 (1994).
47. R. Suau, R. Rico, F. Najera, F.J. Ortiz-Lopez, J.M. Lopez-Romero, M. Moreno-Manas, and A. Roglans. Tetrahedron, **60**, 5725 (2004)
48. G.A. Molander and F. Dehmel. J. Am. Chem. Soc. **126**, 10 313 (2004).
49. P.J. Mohr and R.L. Halcomb. J. Am. Chem. Soc. **125**, 1712 (2003).
50. C. Tsukano and M. Sasaki. J. Am. Chem. Soc. **125**, 14 294 (2003).
51. A. Bouillon, A.S. Voisin, A. Robic, J.-C. Lancelot, V. Collot, and S. Rault. J. Org. Chem. **68**, 10 178 (2003).
52. B.M. Crowley, Y. Mori, C.C. McComas, D. Tang, and D.L. Boger. **126**, 4310 (2004)
53. K.C. Nicolaou and E.J. Sorensen. Classics in total synthesis. VCH Verlagsgesellschaft mbH, Weinheim. 1996.
54. N.G. Andersen, S.P. Maddaford, and B.A. Keay. J. Org. Chem. **61**, 9556 (1996).

© 2005 NRC Canada

55. J. Yin and S.L. Buchwald. J. Am. Chem. Soc. **122**, 12 051 (2000).
56. A.N. Cammidge and K.V.L. Crepy. Chem. Commun. 1723 (2000).
57. A.-S. Castanet, F. Colobert, P.-E. Broutin, and M. Obringer. Tetrahedron: Asymmetry, **13**, 659 (2002).
58. A. Herrbach, A. Marinetti, O. Baudoin, D. Guenard, and F. Gueritte. J. Org. Chem. **68**, 4897 (2003).

© 2005 NRC Canada

RAPID COMMUNICATION / COMMUNICATION RAPIDE

Aromatization of 1,4-dihydropyridines with selenium dioxide

Xiao-hua Cai, Hai-jun Yang, and Guo-lin Zhang

Abstract: 1,4-Dihydropyridines were aromatized to corresponding pyridines using stoichiometric selenium dioxide at ambient temperature in a yield of 87%~98%.

Key words: 1,4-dihydropyridines, aromatization, oxidation, pyridine derivatives, selenium dioxide.

Résumé : Les 1,4-dihydropyridines sont aromatisés en pyridines correspondantes avec des rendements allant de 87 %~98 % par traitement avec une quantité stoechiométrique de dioxyde de sélénium, à la température ambiante.

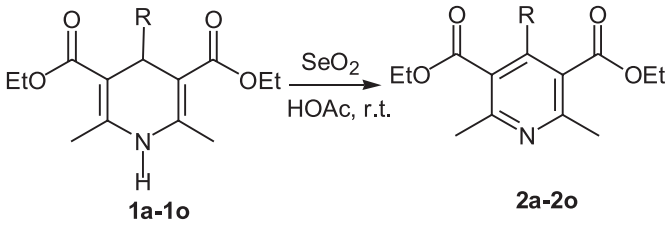
Mots clés : 1,4-dihydropyridines, aromatisation, oxydation, dérivés de la pyridine, dioxyde de sélénium.

[Traduit par la Rédaction]

Introduction

1,4-Dihydropyridines are calcium antagonists (1), antitubercular agents (2), and neuropeptide Y Y1 receptor antagonists (3). They possess neuroprotective (4), platet anti-aggregration (5), and antidiabetic (6) activities. Aromatization of 1,4-dihydropyridines has received considerable attention owing to the fact that 1,4-dihydropyridine-based calcium channel blockers are oxidatively converted to pyridine derivatives by the action of cytochrome P-450 in the liver (7). In addition, the corresponding pyridine derivatives show antihypoxic and antiischemic activites (8). 1,4-Dihydropyridines can easily be synthesized by Hantzsch condensation of aldehydes, β-keto esters, and ammonia or ammonium acetate (7*b*, 9). 1,4-Dihydropyridines have been aromatized to pyridines by various reagents such as $KMnO_4$ (10), HNO_3 (11), DDQ (12), $NaNO_2$ (13), $Zr(NO_3)_4$ (14), $Cu(NO_3)$ (15), $Bi(NO_3)\cdot 5H_2O$ (16), $Mn(OAc)_3$ (17), $(NH_4)_4Ce(NO_3)_6$ (18), urea nitrate and $K_2S_2O_8$–Co^{2+} (19), Pd/C (20), Pt(II) complex – *h*ν (21), GSNO (22), and O_2 – activated carbon (23). Despite these intensive efforts, most of the reported oxidation procedures require long reaction time, utilize strong oxidants in large excess, and afford products with only modest yields. In particular, the aromatization reaction with these reagents leads to dealkylation of the 4-position or formation of side products (11, 24). Therefore, the development of more effective methods for aromatization of 1,4-dihydropyridines is still necessary.

Scheme 1.



Selenium dioxide was widely used for the oxidation of a methylene group activated allyically or benzylically, or by an adjacent carbonyl group (25). Here, we wish to describe a simple and efficient precodure for the aromatization of 1,4-dihydropyridines with selenium dioxide at room temperature (Scheme 1).

Our initial attempts to aromatize 1,4-dihydropyridines (**1a**) as a test case in EtOH, CH_3CN, or THF at ambient or thermal conditions led to corresponding pyridine **2a** in very low yield (<40%). But the aromatization of **1a** in acetic acid occurred smoothly to give the expected pyridine at room temperature in 96% yield. The success of this reaction prompted us to examine the aromatization of some 4-alkyl, aryl, and alkenyl 1,4-dihydropyridines under the same conditions. All reactions proceeded efficiently within 20~60 min to provide the corresponding pyridines in good yields (87%~98%, Table 1). With respect to the yields of the products, a 1:1 mol ratio of 1,4-dihydropyridines and selenium dioxide in HOAc was optimal. The salient features for this procedure are milder reaction conditions, shorter reaction

Received 30 September 2004. Published on the NRC Research Press Web site at http://canjchem.nrc.ca on 29 March 2005.

X.-h. Cai. Chengdu Institute of Biology, the Chinese Academy of Sciences, Chengdu 610041, P.R. China and Chengdu Institute of Organic Chemistry, the Chinese Academy of Sciences, Chengdu 610041, P.R. China.
H.-j. Yang, and G.-l. Zhang.[1] Chengdu Institute of Biology, the Chinese Academy of Sciences, Chengdu 610041, China.

[1]Corresponding author (e-mail: zhanggl@cib.ac.cn).

Can. J. Chem. Downloaded from www.nrcresearchpress.com by China University of Science and Technology on 09/11/12
For personal use only.

 doi: 10.1139/V05-058 © 2005 NRC Canada

Can. J. Chem. Downloaded from www.nrcresearchpress.com by China University of Science and Technology on 09/11/12
For personal use only.

Table 1. Aromatization of 1,4-dihydropyridines to pyridines by SeO_2 at room temperature.

Product[a]	R	Time (min)	Yield (%)[b]	mp (°C)
2a	C_6H_5	30	96	63–65 (62 to 63 (14))
2b	H	20	97	71–72 (68 to 69 (14))
2c	Me	20	97	Yellow oil (liq (17))
2d	*n*-Propyl	40	92	Yellow oil (yellow oil (19))
2e	C_6H_5-CH_2	40	90	Yellow oil (liq (26))
2f	C_6H_5-CH=CH	50	96	162–164 (162 to 163 (17))
2g	4-F-C_6H_5	40	94	88–90
2h	4-Cl-C_6H_5	50	98	63–65 (65 to 66 (14))
2i	4-MeO-C_6H_5	20	95	55–57 (56–58 (19))
2j	4-HO-C_6H_5	40	94	172 to 173 (171–173 (17))
2k	2-NO_2-C_6H_5	60	89	72 to 73 (74–76 (27))
2l	2-Furyl	60	87	Yellow oil (liq (17))
2m	4-HO-3-MeO-C_6H_5	50	92	159 to 160
2n	4-MeO-3-OH-C_6H_5	30	95	140–142
2o	3,4-2Cl-C_6H_5	40	94	63–65 (66–68 (28))

[a]All known compounds were characterized by comparing their spectral data with those reported.
[b]Isolated yields.

time, higher yield, avoidance of dealkylation or debenzylation at C-4, and stoichiometric oxidants used. Moreover, this is a simple procedure for the separation of the products.

Conclusion

An efficient and simple procedure for the aromatization of 1,4-dihydropyridines to correponding pyridine derivatives with stoichiometric selenium dioxide was developed.

Experimental

In a typical procedure, a mixture of **1a** (165 mg, 0.5 mmol), selenium dioxide (66 mg, 0.5 mmol), and HOAc (4 mL) was stirred at room temperature for 30 min. After completion monitored by TLC, the reaction mixture was quenched with a satd. aqueous $NaHCO_3$ solution and the red solid selenium was filtered off. The filtrate was extracted with Et_2O. The organic layer was washed with water, dried over anhydr. $MgSO_4$, and concentrated to give the pure product **2a** (156 mg, 96%), mp 63–65 °C (lit. value (14) mp 62 to 63 °C). Under similar conditions, various substituted 1,4-dihydropyridines were converted to corresponding pyridines (Table 1).

Diethyl 2,6-dimethyl-4-(*p*-fluorinephenyl)pyridine-3,5-dicarboxylate (2g)

Yellow solid. IR (KBr, cm^{-1}) ν_{max}: 2989, 2928, 2905, 2856, 1736, 1716, 1607, 1559, 1513, 1446, 1385, 1294, 1235, 1163, 1106, 1047, 867, 851, 796. ^1H NMR ($CDCl_3$, 400 MHz) δ_H: 1.02 (t, 6H, J = 7.2 Hz), 2.62 (s, 6H), 4.06 (q, 4H, J = 7.2 Hz), 7.06~7.10 (m, 2H), 7.23~7.26 (m, 2H). *m/z* (ESI): 346 (100%, $[M + 1]^+$), 330 (21%, $[M - CH_3]^+$).

Diethyl 2,6-dimethyl-4-(4-hydroxy-3-methoxyphenyl)pyridine-3,5-dicarboxylate (2m)

Yellow solid. IR (KBr, cm^{-1}) ν_{max}: 3424, 3064, 2997, 2934, 1740, 1721, 1613, 1569, 1514, 1441, 1384, 1281, 1215, 1130, 1043, 1008, 866, 836, 757, 691. ^1H NMR ($CDCl_3$, 400 MHz) δ_H: 1.01 (t, 6H, J = 7.2 Hz), 2.59 (s, 6H), 3.86 (s, 3H, OCH_3), 4.06 (q, 4H, J = 7.2 Hz), 5.68 (br s, 1H, OH), 6.74 (dd, 1H, J = 8.8 Hz, J = 2.4 Hz), 6.77~6.79 (m, 2H). *m/z* (ESI): 396 (100%, $[M + Na^+]$), 374 (100%, $[M + 1]^+$).

Diethyl 2,6-dimethyl-4-(3-hydroxy-4-methoxyphenyl)pyridine-3,5-dicarboxylate (2n)

Yellow solid. IR (KBr, cm^{-1}) ν_{max}: 3432, 3045, 2984, 2934, 1738, 1724, 1613, 1559, 1507, 1441, 1382, 1267, 1213, 1130, 1045, 1008, 862, 841, 815, 755, 672. ^1H NMR ($CDCl_3$, 400 MHz) δ_H: 1.02 (t, 6H, J = 7.2 Hz), 2.58 (s, 6H), 3.91 (s, 3H, OCH_3), 4.06 (q, 4H, J = 7.2 Hz), 5.62 (br s, 1H, OH), 6.74 (dd, 1H, J = 8.4 Hz, J = 2.4 Hz), 6.83~6.87 (m, 2H). *m/z* (ESI): 374 (100%, $[M + 1]^+$).

References

1. (*a*) G.W. Zamponi, S.C. Stotz, R.J. Staples, T.M. Andro, J.K. Nelson, V. Hulubei, A. Blumenfeld, and N.R. Natale. J. Med. Chem. **46**, 87 (2003); (*b*) S. Visentin, B. Rolando, A. Di Stilo, R. Frutterro, M. Novara, E. Carbone, C. Roussel, N. Vanthuyne, and A. Gasco. J. Med. Chem. **47**, 2688 (2004); (*c*) A. Zarghi, H. Sadeghi, A. Fassihi, M. Faizi, and A. Shafiee. Farmaco, **58**, 1077 (2003); (*d*) R. Peri, S. Padmanabhan, A. Rutledge, S. Singh, and D.J. Triggle. J. Med. Chem. **43**, 2906 (2000).
2. P.S. Kharkar, B. Desai, H. Gaveria, B. Varu, R. Loriya, Y. Naliapara, A. Shah, and V.M. Kulkarn. J. Med. Chem. **45**, 4858 (2002).
3. (*a*) G.S. Poindexter, M.A. Bruce, J.G. Breitenbucher, M.A. Higgins, S.-Y. Sit, J.L. Romine, S.W. Martin, S.A. Ward, R.T. McGovern, W. Clarke, J. Russell, and I. Antal-Zimanyi. Bioorg. Med. Chem. **12**, 507 (2004); (*b*) G.S. Poinder, M.A. Bruce, K.L. LeBoulluec, I. Monkovic, S.W. Martin, E.M. Parker, L.G. Iben, R.T. McGovem, A.A. Ortiz, J.A. Stanley, G.K. Mattson, M. Kozlowski, M. Arcuri, and I.A. Zimanyi. Bioorg. Med. Chem. Lett. **12**, 379 (2002).
4. V. Klusa. Drugs Fut. **20**, 135 (1995).
5. R.G. Bretzel, C.C. Bollen, E. Maeser, and K.F. Federlin. Drugs Fut. **17**, 465 (1992).

© 2005 NRC Canada

Can. J. Chem. Downloaded from www.nrcresearchpress.com by China University of Science and Technology on 09/11/12
For personal use only.

6. (*a*) J.G. McCormack, N. Westergaard, M. Kristiansen, C.L. Brand, and J. Lau. Curr. Pharm. Des. **7**, 1457 (2001); (*b*) A.K. Ogawa, C.A. Willoughby, B. Raynald, K.P. Ellsworth, W.M. Geissler, R.W. Myer, J. Yao, H. Georgianna, and K.T. Chapman. Bioorg. Med. Chem. Lett. **13**, 3405 (2003).
7. (*a*) R. Boer and V. Gekeler. Drugs Fut. **20**, 499 (1995); (*b*) G. Sabitha, G.S. Kiran Kumar Reddy, Ch. Srinivas Reddy, and J.S. Yadav. Tetrahedron Lett. **44**, 4129 (2003).
8. B. Khadikar and S. Borkat. Synth. Commun. **28**, 207 (1998), and refs. cited therein.
9. (*a*) L. Öhberg and J. Westman. Synlett, 1296 (2001); (*b*) M.A. Zolfigol and M. Safaiee. Synlett, 827 (2004).
10. J.-J. Vanden Eynde, A. Mayence, and A. Maquestiau. Tetrahedron, **48**, 463 (1992).
11. R.H. Böker and F.P. Guengerich. J. Med. Chem. **29**, 1596 (1986).
12. A.I. Meyers and N.R. Narale. Heterocycles, **29**, 1596 (1982).
13. B. Loev and K.M. Snader. J. Org. Chem. **30**, 1914 (1964).
14. G. Sabitha, G.S.K. Kumar Reddy, Ch.S. Reddy, N. Fatima, and J.S. Yadav. Synthesis, 1267 (2003).
15. A. Maquestiau and J.-J. Vanden Eynde. Tetrahedron Lett. **32**, 3839 (1991).
16. S.H. Mashraqui and M.A. Karnik. Synthesis, 713 (1998).
17. R.S. Varma and D. Kumar. Tetrahedron Lett. **40**, 21(1999).
18. J.R. Pfister. Synthesis, 689 (1990).
19. A. Marimuthu, D. Muralidharan, and T.P. Paramasivan. Tetrahedron, **58**, 5069 (2002).
20. N. Nakamichi, Y. Kawashita, and M. Hayashi. Org. Lett. **4**, 3955 (2002).
21. D. Zhang, L.-Z. Wu, L. Zhou, X. Han, Q.-Z. Yang, L.-P. Zhang, and C.-J. Tung. J. Am. Chem. Soc. **126**, 3440 (2004).
22. (*a*) Y.-Z. Mao, M.-Z. Jin, Z.-L. Liu, and L.-M. Wu. Org. Lett. **2**, 741 (2000); (*b*) $RuCl_3$–O_2: S.H. Mashraqui and M.A. Karnik. Tetrahedron Lett. **39**, 4895 (1998); (*c*) $h\nu$ – high pressure: Z.-L. Liu and M.-Z. Jin. Chem. Commun. 2451 (1998); (*d*) CrO_2: K.-Y. Koi and J.-Y. Kim. Tetrahedron Lett. **40**, 3207 (1999); (*e*) NO: J.-P. Cheng and X.-O. Zhu. J. Org. Chem. **65**, 8158 (2000); (*f*) conaphthenate–O_2: S.P. Chavan, R.K. Kharul, U.R. Kalkote, and I. Shivakumar. Synth. Commun. **33**, 1333 (2003).
23. N. Nakamichi, Y. Kawashita, and M. Hayashi. Synthesis, 1015 (2004).
24. (*a*) F. Delgado, C. Alvarez, O. Garcia, G. Penieres, and C. Marquez. Synth. Commun. **21**, 2137 (1991); (*b*) Y.L. Hu, J.H. Yu, S.Y. Yang, J.X. Wang, and Y.Q. Yin. Synth. Commun. **28**, 2793 (1998).
25. (*a*) S. Takami, A. Oshida, Y. Tawada, S. Kashino, K. Satake, and M. Kimura. J. Org. Chem. **65**, 6093 (2000); (*b*) T.J. Sommer. Synthesis, 161 (2004); (*c*) R.K. Boeckman, Jr. and L.M. Reeder. Synlett, 1399 (2004); (*d*) J.G. Lee and K.C. Kim. Tetrahedron Lett. **33**, 6363 (1992).
26. J.S. Yadav, B.V. Subba Reddy, G. Sabitha, and G.S. Kiran Kumar Reddy. Synthesis, 1532 (2000).
27. B.X. Wang, Y.F. Hu, and H.W. Hu. Synth. Commun. **29**, 4193 (1999).
28. J. Liu, Y.J. Bai, Z.J. Wang, B.Q. Yang, and W.H. Li. Synth. Commun. **31**, 2625 (2001).

© 2005 NRC Canada

Bert Allen and the first complex of dinitrogen[1]

G.J. Leigh

Abstract: A personal account is given of the effect that the report of the first dinitrogen complex by Allen and Senoff in 1965 had on people who were working in this area of nitrogen fixation.

Key words: history, ruthenium, dinitrogen, ammonia, complex, serendipity.

Résumé : Un témoignage personnel est offert sur les effets de la caractérisation du premier complexe diazote par Allen et Senoff en 1965 sur les intervenants du domaine de la fixation de l'azote.

Mots clés : historique, ruthénium, diazote, ammoniac, complexe, sérendipité.

[Traduit par la Rédaction]

The 1960s saw the birth of an enormous effort to uncover the mystery of biological nitrogen fixation. The hopes that this might enable mankind to develop radically new ways of maintaining soil fertility have, alas, yet to be fulfilled (1). In biological terms, the isolation of cell-free extracts of nitrogenase in 1960 (2) for the first time enabled us to study the structure and function of the enzyme. Parallel developments in chemistry were rather later, but it had long been known (3) that molybdenum (or, in its absence, vanadium, though this metal was long overlooked) seemed to be necessary to sustain biological nitrogen fixation, and the obvious inference was that dinitrogen complexes were somehow involved. Although dinitrogen complexes had long been expected, simply on the basis that dinitrogen and carbon monoxide are isoelectronic, and that a multitude of metal carbonyls were known, none had been found. Indeed, Orgel (4) had suggested a side-on structure for them, analogous to the binding of acetylenes to metals.

The discovery of the first dinitrogen complex by Allen and Senoff (5) was apparently accidental. Bert was trying to repeat a literature preparation of $[Ru(NH_3)_6]^{2+}$ from $RuCl_3 \cdot 3H_2O$ and $N_2H_4 \cdot H_2O$. The vigorous reaction of these two materials generates lots of N_2 and NH_3, as well as causing the reduction of the ruthenium(III) to ruthenium(II) (6). If ammonium chloride is added to the reaction mixture, then $[Ru(NH_3)_6]Cl_2$ can indeed be isolated, but in its absence $[Ru(NH_3)_5(N_2)]^{2+}$ is formed (5). Bert was undertaking an IR study of ruthenium(II) poly(ammine) complexes, and the use of IR spectroscopy gave him information that was not really available to the original investigators of this reaction, who had to rely on analysis and magnetic properties alone to characterize their materials. In fact, the dinitrogen complex may even have been prepared by those who originally prepared $[Ru(NH_3)_6]^{2+}$, but they could not have recognised it. Bert must have seen immediately the strong band at ca. 2130 cm^{-1}, which he assigned correctly to $\nu(N{\equiv}N)$. He formulated the compound $[Ru(NH_3)_5(N_2)]^{2+}$ though he did not then note that the strong IR band meant that the dinitrogen must have been bound end-on to the ruthenium. As dinitrogen complexes go, this ruthenium complex is actually not a very interesting compound, but its discovery and announcement (once the reluctant referees of *Chemical Communications* had been convinced that Bert's claim was a reasonable one) had tremendous implications. Some of these are outlined in the following.

First, it established that metal complexes of dinitrogen could indeed be isolable materials. I myself repeated the preparation described in *Chemical Communications* within a couple of hours of receiving the paper. Other claims for further dinitrogen complexes soon followed. It confirmed that we were probably on the right track in trying to model the function of the enzyme using metal complexes, even though the dinitrogen in this particular ruthenium complex turned out not to be reducible to ammonia.

Secondly, it became evident that $[Ru(NH_3)_5(N_2)]^{2+}$could be formed not just from hydrazine, but also from dinitrogen gas in aqueous media, such as from the reduction under N_2 of $[Ru(NH_3)_5Cl]^{2+}$ by zinc in dilute sulphuric or from the reduction of a solution of ruthenium trichloride by zinc amalgam in aqueous tetrahydrofuran (7). In fact, dinitrogen can displace the ligand water from $[Ru(NH_3)_5(H_2O)]^{2+}$. At the time (8, 9), this observation was a considerable surprise.

$$[Ru(NH_3)_5(H_2O)]^{2+} + N_2 \rightarrow [Ru(NH_3)_5(N_2)]^{2+} + H_2O$$

Almost at the same time, experiments with cobalt complexes (10) showed that, in favourable circumstances, dinitrogen could also displace the ligand ammonia. Thus, Bert's compound gave us the first indication of the ligand properties of dinitrogen. This was not the end of the story, because it was soon discovered by Taube and co-workers (8) and others (11) that the bound dinitrogen could also act as a donor to further metal ions, and this was the first suggestion that the bound dinitrogen was polarized in the sense Ru-

Received 10 February 2005. Published on the NRC Research Press Web site at http://canjchem.nrc.ca on 22 March 2005.

G.J. Leigh. Department of Chemistry, School of Life Sciences, University of Sussex, Brighton BN1 9QJ, UK. (e-mail: G.J.Leigh@sussex.ac.uk).

[1]This article is part of a Special Issue dedicated to Dinitrogen Chemistry.

 doi: 10.1139/V05-056 © 2005 NRC Canada

$N^+\equiv N^-$. This direction of polarization was confirmed by an ESCA study of rhenium–dinitrogen complexes (12).

$$[Ru(NH_3)_5(H_2O)]^{2+} + [Ru(NH_3)_5(N_2)]^{2+} \rightarrow [Ru(NH_3)_5(\mu\text{-}N_2)Ru(NH_3)_5]^{4+} + H_2O$$

There are now numerous examples of dinitrogen bridging between metal ions. Later workers (13) showed that this polarization of dinitrogen in complexes such as those of molybdenum and tungsten could lead to the protonation of coordinated N_2.

Thirdly, initial reports (5, 14) claimed that by addition of sodium borohydride the dinitrogen in $[Ru(NH_3)_5(N_2)]^{2+}$ was convertible to ammonia. Bearing in mind that the compound itself contains a lot of ammonia, and also that it was formed from hydrazine, well-known to be reducible to ammonia, this claim needed to be treated with some caution. Subsequently, my colleagues in the Unit of Nitrogen Fixation prepared samples of $[Ru(NH_3)_5(^{15}N_2)]^{2+}$, as well as dinitrogen compounds of iridium and cobalt. In all three cases, the dinitrogen ligands were unequivocally obtained from $^{15}N_2$ (15) rather than from hydrazine or ammonia. Treatment of these labelled dinitrogen complexes with acid or with reducing agents caused general decomposition in all three cases, but in no case was $^{15}NH_3$ obtained. This brought to the attention of the community that extreme care needs to be taken in assessing claims both of dinitrogen fixation and of dinitrogen reduction, and that positive results from isotopic labelling were a requirement for definitive proof. Considering that some dinitrogen complexes are formed with very slow dinitrogen uptake (over hours or even days), and that scavenging of impurities such as nitrogen oxides from the dinitrogen gas stream was always possible, the same consideration must apply to the formation of dinitrogen complexes as well as to dinitrogen reduction.

In summary, the compound first identified by Bert Allen and his student Caesar Senoff was the first dinitrogen complex, and although its chemistry is not very exciting in terms of the dinitrogen reactivity it facilitates, its formation and the circumstances of its formation demonstrated that dinitrogen complexes are indeed feasible models for the interaction of metal centres in nitrogenases with N_2. It shed the first light on the remarkable ligating properties of dinitrogen. It stimulated the discovery of the large number of dinitrogen complexes known today, and it allowed the uncovering of the completely new range of dinitrogen activity that is still being developed 40 years later.

References

1. G.J. Leigh. The world's greatest fix — A history of nitrogen and agriculture. Oxford University Press, New York. 2004.
2. J.E. Carnahan, L.E. Mortenson, H.F. Mower, and J.E. Castle. Biochim. Biophys. Acta, **44**, 520 (1960).
3. H. Bortels. Arkiv. Mikrobiol. **1**, 333 (1930); **7**, 13 (1936).
4. L.E. Orgel. An introduction to transition metal chemistry, ligand field theory. 2nd ed. Methuen, London. 1966. p. 142.
5. A.D. Allen and C.V. Senoff. Chem. Commun. 621 (1965).
6. A.D. Allen and C.V. Senoff. Can. J. Chem. **45**, 1337 (1967).
7. D.E. Harrison and H. Taube. J. Am. Chem. Soc. **89**, 5706 (1967); A.E. Shilov, A.K. Shilova, and Yu. G. Borodko. Kinet. Katal. **7**, 768 (1966).
8. D.E. Harrison, E. Weissberger, and H. Taube. Science (Washington, D.C.), **159**, 320 (1968).
9. A.D. Allen and F. Bottomley. Can. J. Chem. **46**, 469 (1968).
10. L.S. Pu, A. Yamamoto, and S. Ikeda. J. Am. Chem. Soc. **90**, 7170 (1968).
11. J. Chatt, J.R. Dilworth, G.J. Leigh, and R.L. Richards. Chem. Commun. 955 (1970).
12. G.J. Leigh, J.R. Murrell, W. Bremser, and W.G. Proctor. Chem. Commun. 1661 (1970).
13. J. Chatt, G.A. Heath, and R.L. Richards. J. Chem. Soc. Chem. Commun. 1014 (1972).
14. A.D. Allen, F. Bottomley, R.O. Harris, V.P. Reinsalu, and C.V. Senoff. J. Am. Chem. Soc. **89**, 5595 (1967).
15. J. Chatt, R.L. Richards, J.R Sanders, and J.E. Fergusson. Nature (London), **221**, 551 (1969).

© 2005 NRC Canada

Ligand-assisted reduction of Co(II) to Co(I) and subsequent coordination of dinitrogen[1]

Jennifer Scott, Sandro Gambarotta, and Ilia Korobkov

Abstract: Reaction of the bis-aminopyridine dianion {[2,6-[2,6-(*i*-Pr)$_2$PhN-C=(CH$_2$)]$_2$(C$_5$H$_3$N)]Li(THF)}{Li(THF)$_4$} with $CoCl_2(THF)_{1.5}$ under Ar afforded the dinuclear complex {[2,6-(*i*-Pr)$_2$PhN-C=(CH$_2$)](C$_5$H$_3$N)[2,6-(*i*-Pr)$_2$PhN=C(CH$_2$)]}$_2$[Co(μ-Cl)Li(THF)$_3$]$_2$·4(THF) (**1**) in which the ligand is coupled to a second identical unit at a terminal methylene carbon. In turn, the C—C bond formation caused reduction of the Co(II) center to the monovalent state. The same reaction performed under a nitrogen atmosphere afforded the double dinitrogen complex {[2,6-(*i*-Pr)$_2$PhN-C=(CH$_2$)](C$_5$H$_3$N)[2,6-(*i*-Pr)$_2$PhN=C(CH$_2$)]}$_2$[Co(N$_2$)]$_2$·2(toluene) (**2**).

Key words: low-valent Co, diiminopyridinato, dinitrogen fixation.

Résumé : La réaction du dianion bis-aminopyridine {[2,6-[2,6-(*i*-Pr)$_2$PhN-C=(CH$_2$)]$_2$(C$_5$H$_3$N)]Li(THF)}{Li(THF)$_4$} avec le $CoCl_2(THF)_{1,5}$, sous atmosphère d'argon, conduit à la formation du complexe dinucléaire {[2,6-(*i*-Pr)$_2$PhN-C=(CH$_2$)](C$_5$H$_3$N)[2,6-(*i*-Pr)$_2$PhN=C(CH$_2$)]}$_2$[Co(μ-Cl)Li(THF)$_3$]$_2$·4(THF) (**1**) dans lequel le ligand est couplé à une deuxième unité identique au niveau d'un carbone méthylénique terminal. Par ailleurs, la formation d'une liaison C—C provoque une réduction du Co(II) vers l'état monovalent. La même réaction réalisée sous atmosphère d'azote conduit au complexe double de diazote {[2,6-(*i*-Pr)$_2$PhN-C=(CH$_2$)](C$_5$H$_3$N)[2,6-(*i*-Pr)$_2$PhN=C(CH$_2$)]}$_2$[Co(N$_2$)]$_2$·2(toluène) (**2**).

Mots clés : cobalt de basse valence, diiminopyridinato, fixation de diazote.

[Traduit par la Rédaction]

Introduction

The catalytic transformation of dinitrogen into ammonia is the driving force behind the flourish of interest towards coordination of dinitrogen by transition metal complexes. However, despite the amount of research dedicated to this topic in the last 40 years, this coveted catalytic transformation has been documented in only a handful of cases and has remained limited to the occurrence of a few turnovers (1). A significant step in this direction was recently achieved by Yandulov and Schrock (2) with the cobaltocene-promoted reduction of the molybdenum-coordinated dinitrogen complex [HIPTN$_3$N]MoN$_2$, {[HIPTN$_3$N]$^{3-}$ = [{3,5-(2,4,6-*i*-Pr$_3$C$_6$H$_2$)$_2$C$_6$H$_3$NCH$_2$CH$_2$}$_3$N]$^{3-}$}. Chirik and co-workers (3) have also reported an exciting development in the dinitrogen chemistry of zirconium by observing the formation of ammonia after the addition of H_2 to a zirconocene dinitrogen dimer. On the same line, albeit not catalytic, is the formation of a metal-bound NH_2 unit from N_2 cleavage, as obtained during the reduction of a tetra-aryloxide actinide system (4).

The possibility of performing cleavage of coordinated dinitrogen into the corresponding nitride moieties has fueled research towards the use of strongly reducing, low-valent, early metal systems (2–5). However, a metal whose redox potential is sufficiently reducing to transfer several electrons to a coordinated dinitrogen molecule might not necessarily have the chance to perform efficient catalytic transformations. Accordingly, the versatile nitrogenase enzyme initially forms a dinitrogen complex, possibly *weakly* bound, which receives electrons from the pyruvate electron pool via multiple association–dissociation rounds between the Fe-protein and the Fe-Mo protein (6, 7). This is possibly suggesting the puzzling idea that a system capable of performing *weak* reduction of dinitrogen (e.g., labile coordination instead of multi-electron reduction) might actually be the starting point for the search for catalytic transformations. The premise of employing a labile dinitrogen complex as a prelude to a multi-metallic cooperative interaction is somewhat substantiated by recent observations in Sm-dipyrrolide chemistry (8).

Dinitrogen chemistry involving late transition metals is substantially less developed when compared with low-valent early metals and *f*-block elements. The large volume and variety of transformations involving early metal dinitrogen systems, including partial reduction followed by elemental modifications or incorporation into the ligand system, has made early metal complexes the most popular targets for these studies and several recent reviews have detailed the latest developments in this area (9). On the other hand, late metal complexes have a definite inclination towards labile coordination of dinitrogen and, interestingly, Fe is the protagonist of the unique performances of the nitrogenase enzyme. Recent encouraging observations in this direction

Received 15 September 2004. Published on the NRC Research Press Web site at http://canjchem.nrc.ca on 3 March 2005.

J. Scott, S. Gambarotta,[2] and I. Korobkov. Department of Chemistry, University of Ottawa, Ottawa, ON K1N 6N5, Canada.

[1]This article is part of a Special Issue dedictated to Dinitrogen Chemistry.
[2]Corresponding author (e-mail: sgambaro@science.uottawa.ca).

 doi: 10.1139/V05-010 © 2005 NRC Canada

have been made by Holland and co-workers (10) with the reduction of dinitrogen coordinated to an Fe(*nacnac*) system. The reduction formed a new complex in which the dinitrogen unit undergoes only a relatively minor elongation of the N—N bond, thus suggesting that, similar to the case of a tetranuclear Sm dinitrogen complex (8*a*), electron density is mainly stored on the metal rather than in the N_2 unit. We believe that this may be particularly significant because if the strengthening of the Fe—N bond as a result of the reduction is minute, an increased reactivity of the coordinated N_2 unit could be found.

Dinitrogen complexes of cobalt are scarce (11–24). In addition, the few reported complexes all appear to be rather similar, the main differences arising from the skeleton of the supporting phosphine ligand and the oxidation state of the Co center, which varies from –1 to +1. In some cases, the coordination of dinitrogen is assisted by another metal center (13–18, 21, 22). An alternative to the main phosphine theme is provided by a cobalt complex of the bis-iminopyridine ligand system (24). A Co(II) derivative was specifically prepared for ethylene polymerization purposes. However, activation of the catalyst caused the reduction of the metal to the monovalent state, which, while cationized by a Lewis acid, performed dinitrogen coordination. Furthermore, the behavior of the bis-iminopyridine ligand is truly unique. Not only has it shown much promise as a supporting ligand for catalytic olefin polymerization (25, 26), but it has also displayed a desirable ability to store electrons in the large, delocalized π system (27). In addition, it may engage in a number of metal-promoted transformations (28–31). The fact that this ligand system can stabilize a NdI_2 moiety via internal redox (31) raises questions about the possibility of its use for electron storage towards promoting catalytic dinitrogen activation.

Recent work in our lab has demonstrated that the bis-imino pyridinato ligand can be further transformed into the corresponding dianion via deprotonation of the two methyl groups attached to the imine function (31). The electron-accepting ability is still very strong in the dianionic version of this ligand. Therefore, as part of an ongoing program, we have now probed the reactivity of the dianionic {[2,6-[2,6-(*i*-Pr)$_2$PhN-C=(CH$_2$)]$_2$(C$_5$H$_3$N)]Li(THF)}{Li(THF)$_4$} with divalent cobalt with the hope of preparing a new family of labile, yet reactive, dinitrogen complexes. In this paper, we describe the preparation of a double dinitrogen complex supported by a ligand system capable of holding a substantial amount of negative charge.

Experimental section

All operations were performed either under an argon atmosphere using standard Schlenk techniques or in a dry box filled with purified nitrogen. The THF complex of $CoCl_2$ was prepared according to the standard procedure and 2,6-[2,6-(*i*-Pr)$_2$PhN-C(CH$_3$)]$_2$(C$_5$H$_3$N) (32), LiCH$_2$Si(CH$_3$)$_3$ (33), and {[2,6-[2,6-(*i*-Pr)$_2$PhN-C=(CH$_2$)]$_2$(C$_5$H$_3$N)]Li(THF)}{Li(THF)$_4$} (31) were prepared following published procedures. IR spectra were recorded on a Mattson 9000 and Nicolet 750-Magna FT-IR instrument from Nujol mulls prepared in a dry box. Samples for magnetic susceptibility measurements were weighed inside a dry box equipped with an analytical balance and sealed into calibrated tubes, and the measurements were carried out at room temperature with a Gouy balance (Johnson Matthey). Elemental analyses were performed on a PerkinElmer 2400 CHN analyzer. Data for X-ray crystal structure determinations were obtained with a Bruker diffractometer equipped with a Smart CCD area detector. NMR spectra were recorded on a Bruker AMX-500 spectrometer.

Preparation of {[2,6-(*i*-Pr)$_2$PhN-C=(CH$_2$)](C$_5$H$_3$N)[2,6-(*i*-Pr)$_2$PhN=C(CH$_2$)]}$_2$[Co(μ-Cl)Li(THF)$_3$]$_2$·(THF)$_4$ (1)

A solution of {[2,6-[2,6-(*i*-Pr)$_2$PhN-C=(CH$_2$)]$_2$(C$_5$H$_3$N)]Li(THF)}{Li(THF)$_4$} (1.25 g, 1.5 mmol) in THF was added to a stirred suspension of $CoCl_2(THF)_{1.5}$ (0.35 g, 1.5 mmol) in THF. The solution instantly became dark burgundy. The reaction was allowed to stir for 5 min and centrifuged to remove small amounts of insoluble material. The solvent was evaporated in vacuo until a small volume, and the resulting solution was allowed to stand at room temperature for 24 h upon which large, dark-burgundy crystals of **1** were isolated (0.92 g, 0.48 mmol, 65%). IR (Nujol mull, cm^{-1}) ν: 3058 (w), 2895 (s), 1640 (m), 1565 (vs), 1517 (m), 1466 (vs), 1399 (m), 1378 (m), 1323 (w), 1304 (m), 1260 (s), 1200 (w), 1174 (s), 1160 (w), 1099 (vs), 1048 (vs), 1026 (vs), 1003 (vs), 936 (m), 913 (s), 892 (m), 801 (vs), 778 (m), 764 (m), 748 (m), 726 (s), 694 (m). Anal. calcd. for $C_{106}H_{164}N_6Cl_2Li_2O_{10}Co_2$: C 67.54, H 8.77, N 4.46; found: C 67.78, H 9.01, N 4.55.

Preparation of {[2,6-(*i*-Pr)$_2$PhN-C=(CH$_2$)](C$_5$H$_3$N)[2,6-(*i*-Pr)$_2$PhN=C(CH$_2$)]}$_2$[Co(N$_2$)]$_2$·2(toluene) (2)

A solution of {[2,6-[2,6-(*i*-Pr)$_2$PhN-C=(CH$_2$)]$_2$(C$_5$H$_3$N)]Li(THF)}{Li(THF)$_4$} (1.25 g, 1.5 mmol) in toluene was added to a stirred suspension of $CoCl_2(THF)_{1.5}$ (0.35 g, 1.5 mmol) in toluene under an argon atmosphere. The solution instantly became dark-burgundy red. The mixture was stirred overnight and centrifuged to remove small amounts of insoluble residue. The solution was then exposed to nitrogen gas causing an extreme deepening of the colour with standing overnight. The black-coloured solution was evaporated in vacuo down to a small volume. Small dark brown crystals of **2** were obtained after allowing the solution to stand at room temperature for 48 h (0.59 g, 0.45 mmol, 60%). IR (Nujol mull, cm^{-1}) ν: 3057 (w), 2895 (s), 2153 (vs), 1598 (w), 1583 (m), 1548 (m), 1533 (m), 1494 (m), 1464 (vs), 1418 (w), 1372 (vs), 1323 (s), 1250 (s), 1203 (w), 1176 (s), 1142 (w), 1098 (m), 1073 (m), 1057 (m), 1038 (m), 1006 (s), 935 (m), 915 (m), 894 (w), 869 (w), 800 (s), 780 (vs), 762 (m), 747 (s), 729 (vs), 694 (m). ^{1}H NMR (500 MHz, C$_6$D$_6$, 25 °C) δ: 0.917 (d, 12H, (C*H*$_3$)$_2$CH), 1.21 (m, 24H, (C*H*$_3$)$_2$CH), 1.42 (d, 12H, (C*H*$_3$)$_2$CH), 2.47 (quint, 4H, (CH$_3$)$_2$C*H*), 3.16 (quint, 4H, (CH$_3$)$_2$C*H*), 3.53 (br s, 4H, N=C-C*H*$_2$-C*H*$_2$-C=N), 4.01 (s, 2H, NC=C*H*$_2$), 4.67 (s, 2H, NC=C*H*$_2$), 6.74 (d, 4H, *m*-C$_6$*H*$_3$-*i*-Pr$_2$), 6.88 (d, 4H, *m*-C$_6$*H*$_3$-*i*-Pr$_2$), 7.01 (t, 2H, *p*-C$_6$*H*$_3$-*i*-Pr$_2$), 7.10 (t, 2H, *p*-C$_6$*H*$_3$-*i*-Pr$_2$), 7.30 (t, 2H, *p*-C$_5$*H*$_3$N), 7.41 (d, 2H, *m*-C$_5$*H*$_3$N), 8.26 (d, 2H, *m*-C$_5$*H*$_3$N). Anal. calcd for $C_{80}H_{98}Co_2N_{10}$: C 72.93, H 7.50, N 10.63; found: C 72.71, H 7.83, N 10.88.

X-ray crystallography

Compounds **1** and **2** consistently yielded crystals that dif-

© 2005 NRC Canada

fracted weakly and the results presented are the best of several trials. The crystals were mounted on thin glass fibers using paraffin oil and cooled to the data collection temperature. Data were collected on a Bruker AXS SMART 1K CCD diffractometer. To obtain acceptable redundancy data, compounds **1** and **2** were collected with the sequence of 0.3° ω scans at 0°, 120°, and 240° in φ. Initial unit cell parameters were determined from 50 data frames collected at the different sections of the Ewald sphere. Semi-empirical absorption corrections based on equivalent reflections were applied. Systematic absences in the diffraction data set and unit-cell parameters were consistent with monoclinic, $P2_1/n$ for **1** and triclinic, $P\bar{1}$ for **2**. Solutions in the centrosymmetric space groups yielded chemically reasonable and computationally stable results of refinement. The structures were solved by direct methods, completed with difference Fourier syntheses and refined with full-matrix least-squares procedures based on F^2. The compound molecule was located in the inversion center in the structure of **1**. Two molecules of THF with full occupancy not located on any symmetry operators were found in the lattice of **1**. Two molecules of toluene with a full occupancy not located on any symmetry operators were found in the asymmetric unit of **2**. All non-hydrogen atoms, except those of the THF solvent molecules in **1**, were refined with anisotropic displacement coefficients. THF solvent molecules in the structure of **1** were refined isotropically. All hydrogen atoms were treated as idealized contributions. All scattering factors are contained in several versions of the SHELXTL program library with the latest version used being v.6.12 (34). Crystallographic data and relevant bond distances and angles are reported in Tables 1 and 2.[3]

Table 1. Crystal data and structure analysis results.

	1	**2**
Formula	$C_{106}H_{164}Cl_2Co_2Li_2N_6O_{10}$	$C_{80}H_{98}Co_2N_{10}$
fw	1885.07	1317.54
Space group	Monoclinic, $P2(1)/n$	Triclinic, $P\bar{1}$
a (Å)	12.193(4)	10.6951(18)
b (Å)	17.861(5)	15.299(3)
c (Å)	24.904(7)	24.071(4)
α (°)		74.320(3)
β (°)	99.632(6)	89.344(3)
γ (°)		69.659(3)
V (Å^3)	5347(3)	3540.5(10)
Z	2	2
Radiation (Kα, Å)	0.710 73	0.710 73
T (K)	203(2)	125(2)
D_{calcd} (g cm^{-3})	1.171	1.236
μ_{calcd} (mm^{-1})	0.417	0.520
F_{000}	2032	1404
R, R_w[2a]	0.0804, 0.2319	0.0772, 0.1845
GoF	1.107	1.022

[a] $R = S||F_0| - |F_c||/\Sigma|F|$, $R_w = [\Sigma(|F_0| - |F_c|)^2/\Sigma wF_0^2]^{1/2}$.

Table 2. Selected bond distances (Å) and angles (°).

1		**2**	
Bond lengths (Å)			
Co—N(1)	1.902(5)	Co(1)—N(1)	1.850(4)
Co—N(2)	1.816(5)	Co(1)—N(2)	1.821(4)
Co—N(3)	1.882(5)	Co(1)—N(3)	1.856(4)
Co—Cl	2.2677(19)	Co(1)—N(4)	1.808(5)
Cl—Li	2.397(14)	N(4)—N(5)	1.095(6)
N(1)—C(2)	1.388(8)	N(1)—C(2)	1.372(6)
C(1)—C(2)	1.359(9)	C(1)—C(2)	1.341(7)
N(3)—C(8)	1.359(8)	N(3)—C(8)	1.353(6)
C(8)—C(9)	1.498(9)	C(8)—C(9)	1.492(6)
C(9)—C(9′)	1.554(13)	C(9)—C(42)	1.536(7)
Bond angles (°)			
N(2)-Co-N(3)	82.1(2)	N(4)-Co(1)-N(2)	177.6(2)
N(2)-Co-N(1)	83.0(2)	N(4)-Co(1)-N(1)	96.88(18)
N(3)-Co-N(1)	165.1(2)	N(2)-Co(1)-N(1)	82.95(17)
N(2)-Co-Cl	177.29(17)	N(4)-Co(1)-N(3)	98.14(18)
N(3)-Co-Cl	98.05(17)	N(2)-Co(1)-N(3)	82.00(18)
N(1)-Co-Cl	96.76(16)	N(1)-Co(1)-N(3)	164.95(18)
Co-Cl-Li	155.2(4)	N(5)-N(4)-Co(1)	178.9(5)

Results and discussion

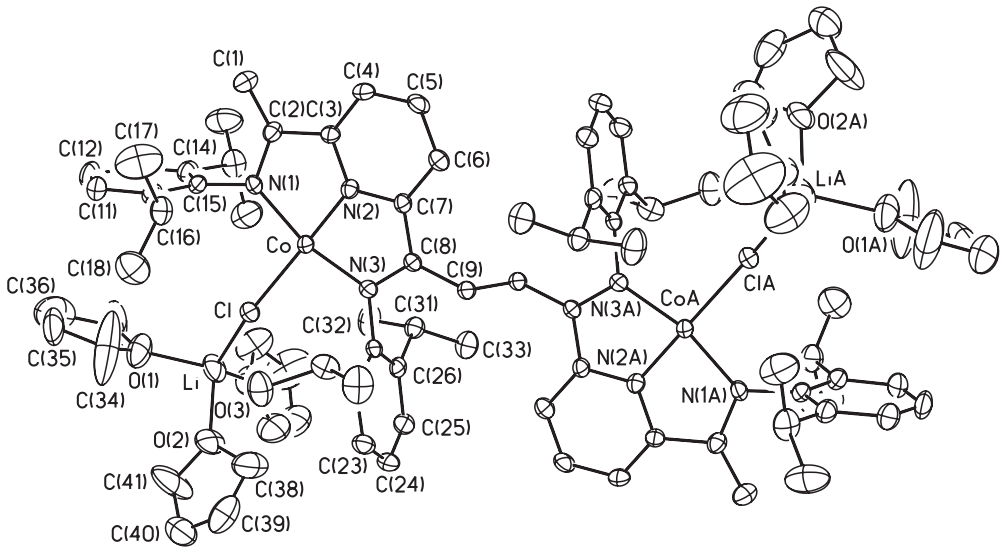
The reaction of $CoCl_2(THF)_{1.5}$ with the dilithium salt of the bis-aminopyridine dianion {[2,6-[2,6-(*i*-Pr)$_2$PhN-C=(CH$_2$)]$_2$(C$_5$H$_3$N)]Li(THF)}{Li(THF)$_4$} was carried out under an Ar atmosphere affording a dark-burgundy solution from which very dark red crystals of the dimeric {[2,6-(*i*-Pr)$_2$PhN-C=(CH$_2$)](C$_5$H$_3$N)[2,6-(*i*-Pr)$_2$PhN=C(CH$_2$)]}$_2$[Co(μ-Cl)Li-(THF)$_3$]$_2$·4(THF) (**1**) were isolated in 65% yield.

The formula and connectivity of **1** were elucidated by an X-ray crystal structure. The molecule consists of a symmetry-generated dimer (Fig. 1) where the metal is surrounded by the ligand system (Co-N(1) = 1.902(5) Å, Co-N(2) = 1.816(5) Å, Co-N(3) = 1.882(5) Å) and one chlorine atom (Co-Cl = 2.2677(19) Å) in a lightly folded square-planar arrangement (N(1)-Co-N(2) = 83.0(2)°, N(2)-Co-N(3) = 82.1(2)°, N(1)-Co-N(3) = 165.1(2)°, N(1)-Co-Cl = 96.76(16)°, N(3)-Co-Cl = 98.05(17)°, N(2)-Co-Cl = 177.29(17)°). The chlorine atom bridges one Li cation solvated by three molecules of THF (Cl-Li = 2.397(14) Å). Of the two -ene functions originally present in the dilithium salt, only one remained intact after the reaction, exhibiting a short C—C bond distance (C(1)-C(2) = 1.359(9) Å) as expected for a C—C double bond. The other -ene function was reduced to a single bond (C(8)-C(9) = 1.498(9) Å). The terminal C atom of this function now forms a C—C single bond with an identical C atom of a second unit (C(9)-C(9A) = 1.554(13) Å), thereby assembling the dinuclear structure. Consequently, the adjacent C-N distance was shortened to a length exhibiting substantial double bond character (N(3)-C(8) = 1.359(8) Å). The

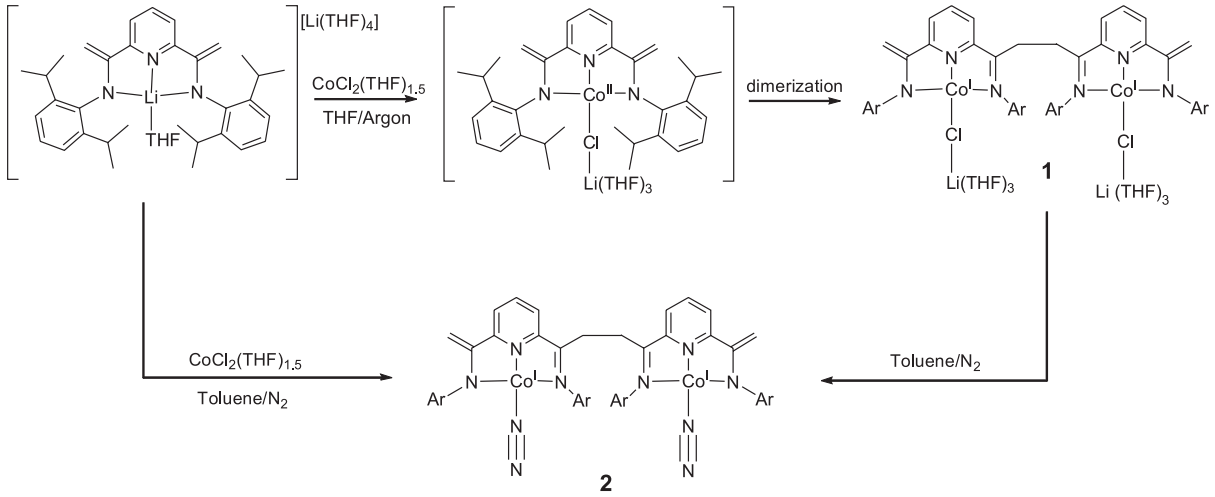
[3] Supplementary data may be purchased from the Directory of Unpublished Data, Document Delivery, CISTI, National Research Council Canada, Ottawa, ON K1A 0S2, Canada (http://cisti-icist.nrc-cnrc.gc.ca/irm/unpub_e.shtml for information on ordering electronically). CCDC 261291 and 261292 contain the crystallographic data for this manuscript. These data can be obtained, free of charge, via ww.ccdc.cam.ac.uk/conts/retrieving.html (or from the Cambridge Crystallographic Data Centre, 12 Union Road, Cambridge CB2 1EZ, UK; fax +44 1223 336033; or deposit@ccdc.cam.ac.uk).

© 2005 NRC Canada

Fig. 1. Thermal ellipsoid plot of **1**. Thermal ellipsoids are drawn at the 30% probability level.



Scheme 1.



slightly large values of the final convergence parameters are due to the disorder encountered in the THF molecules, which could not be properly modeled.

The chemical connectivity, as summarized in Scheme 1, doubtlessly assigns the monovalent state to the two Co atoms. Accordingly, complex **1**, which is extremely air-sensitive and turns brown immediately upon exposure to air, is diamagnetic in the solid state as expected for a d^8 species in a square-planar field. Unfortunately, the very low solubility of **1** in most common deuterated solvents prevented the recording of informative NMR spectra. The coupling of the ligand at the expense of a C=C double bond as observed during the formation of **1** has two precedents in the chemistry of Mn(II) (28) and Ln(III) (Ln = Nd, La) (31). However, in both cases, the coupling required the presence of a strong reducing agent. By contrast, the coupling affording complex **1** occurred via *spontaneous reduction* to Co(I). In other words, the electron necessary for the reduction is supplied by the C=C double bond undergoing a radical type of coupling. This is particularly striking considering that Co(I) has a very strong reducing power and is usually regarded as far more reactive than the divalent congener.

We have observed that the preparation of **1** in toluene and under a dinitrogen atmosphere afforded a much deeper colour and precipitation of a dark-coloured microcrystalline solid. Its solid state IR showed the presence of a sharp and intense band at 2153 cm^{-1}, possibly diagnosing the presence of weakly bound dinitrogen. The recrystallization of this new compound was unsuccessful, and thus, crystals of sufficient quality could only be obtained from the reaction mixture. The X-ray crystal structure revealed this new species to be a double dinitrogen complex formulated as $\{[2,6\text{-}(i\text{-}Pr)_2PhN\text{-}C{=}(CH_2)](C_5H_3N)[2,6\text{-}(i\text{-}Pr)_2PhN{=}C(CH_2)]\}_2\text{-}[Co(N_2)]_2\cdot 2(\text{toluene})$ (**2**).

The basic structure of complex **2** (Fig. 2) is very similar to that of **1** where each cobalt center is connected to one moiety of the binucleating ligand (Co-N(1) = 1.850(4) Å, Co-N(2) = 1.821(4) Å, Co-N(3) = 1.856(4) Å). The dinuclear structure is realized through the coupling of one methylene unit with that of a second identical entity. The bond dis-

© 2005 NRC Canada

Fig. 2. Thermal ellipsoid plot of **2**. Thermal ellipsoids are drawn at the 30% probability level.

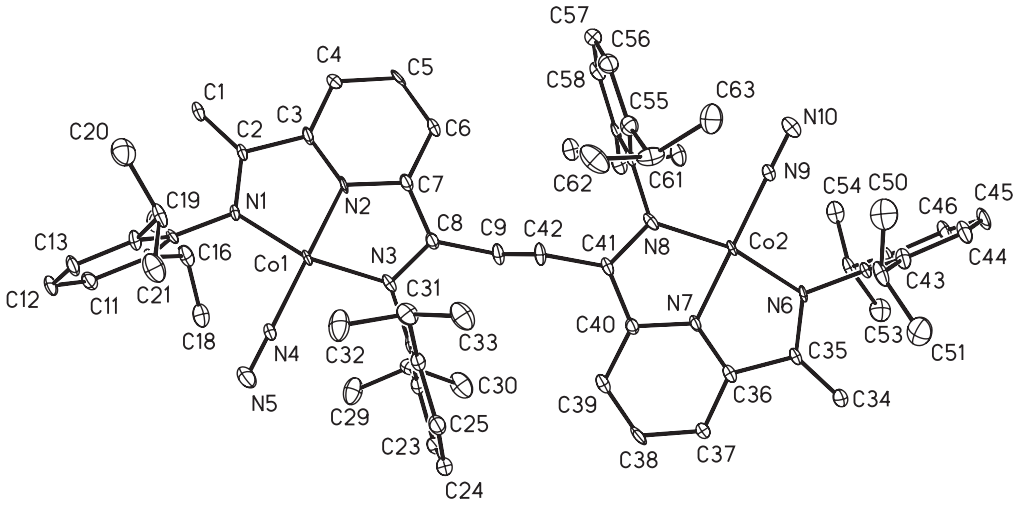


Table 3. Co–N_2 complexes.

Complex	ν_{NN} (cm^{-1})	d_{NN} (Å)	Ref.
$CoH(PPh_3)_3N_2$	2088	1.112(11)	11
$[Co(PPh_3)_3N_2]Mg(THF)_2$	1840	NS[a]	12
$[Co(PPh_3)_3N_2]_2Mg(THF)_4$	1840	NS[a]	13
$[Co(PPh_3)_3N_2]Li(Et_2O)_3$	1900	1.167(16)	13
$[Co(PPh_3)_3N_2]Li(THF)_3$	1890	1.19(4)	13
$[Co(PPh_3)_3N_2]Na(THF)_3$	1910	NS[a]	13, 14
$[Co(PPh_3)_3]_2N_2$	sym	NS[a]	14
$\{[Co(PMe_3)_3N_2]K\}_6$	2056	1.16	15
$[Co(PMe_3)_3N_2]_2Mg(THF)_4$	1830	1.18	16
$[Co(PMe_3)_3N_2MgC(CH_3)_3(Et_2O)]_2$	1660	1.211(4)	17
$[Co(PMe_3)_3N_2Al(CH_3)_2]_2$	Not given	1.252(6)	18
$[CoP(CH_2CH_2PPh_2)_3N_2]PF_6$–$BPh_4$	2125	1.084	19
$[Co(PMe_3)(N_2)(m\text{-}t\text{-}Bu_2P)]_2$	1910	1.092(5)	20
$[Co\{(PPh_2CH_2)_3CCH_3\}]_2N_2$	sym	1.18(2)	21
$\{Co[(P\text{-}i\text{-}Pr_2CH_2)_3BPh]N_2\}_2Mg(THF)_4$	1863	1.155(3)	22
$[\{Co[(P\text{-}i\text{-}Pr_2CH_2)_3BPh]\}_2N_2]Na(THF)_6$	Not given	1.147(4)	22
$CoTp'N_2$	2046	NS[a]	23
$[CoLN_2][MeB(C_6F_5)_3]$	Not given	1.112(6)	24

Note: Tp′ = hydridotris(3-*tert*-butyl-5-methylpyrazolyl)borate and L = 2,6-[CMe=N(2,6-C_6H_3-*i*-Pr_2)]$_2C_5H_3N$.
[a]No structure reported to date.

tances and angles are comparable to those found for complex **1**. The geometry around the cobalt is once again distorted square-planar (N(1)-Co-N(2) = 82.95(17)°, N(2)-Co-N(3) = 82.00(18)°, N(1)-Co-N(3) = 164.95(18)°, N(1)-Co-N(4) = 96.88(18)°, N(3)-Co-N(4) = 98.14(18)°, N(2)-Co-N(4) = 177.6(2)°), the only difference being that the pendant Cl-Li(THF)$_3$ unit has been replaced by a terminally bound N_2 unit (Co-N(4) = 1.808(5) Å).

The ^{1}H NMR spectrum of **1** showed the terminal =CH_2 groups as two rather broad singlets at 4.67 and 4.01 ppm coupled to the same resonance at 72.53 ppm of the ^{13}C NMR spectrum. Two sets of *i*-Pr groups are present, while the CH_2CH_2 bridge between the two units gives a broad resonance at 3.53 ppm.

The N-N distance of the coordinated N_2 unit of **2** (N(4)-N(5) = 1.095(6) Å) suggests very little if no activation of the N—N triple bond. This is in good agreement with the stretching frequency of the coordinated dinitrogen, which displays an unusually high value (ν = 2153 cm^{-1}). The result of a search on existing cobalt dinitrogen complexes is summarized in Table 3. Of the 18 complexes listed, nine contain cobalt in the formal monovalent state. All of these species display stretching frequencies substantially lower than that of **2**, thus indicating the lowest level of activation among all

© 2005 NRC Canada

the Co–N_2 complexes reported to date. As mentioned above, the majority of these species are phosphine derivatives, and the only closely related compound is the cationic bis-iminopyridinato complex (24). However, the ligand is formally neutral in this complex, and it is the Lewis acidity of a Co(I) cationic complex that is regarded as the driving force for the labile coordination of dinitrogen. Unfortunately, no IR data were reported for this complex. Its N-N distance (N-N = 1.112(6) Å) is slightly longer than that observed for **2**. From these observations, it is conceivable to expect that the coordination of N_2 in **2** might be especially labile. In sharp contrast with these expectations, the dinitrogen moiety could *not* be expelled from the complex even in boiling toluene or THF. Nevertheless, ethylene polymerization was observed upon activation with MAO, which demonstrates that the dinitrogen unit must be labile to free at least one coordination site necessary for the ensuing polymerization.

In summary, in this preliminary study aimed at assessing the reactivity of labile N_2 complexes, we have prepared a Co(I) dimer from the reaction of Co(II) with a dianionic tridentate bis-aminopyridine ligand system via coupling of the ligand and subsequent reduction of the metal center. In the absence of THF, the Co(I) species coordinates dinitrogen and shows the weakest perturbation of a N—N multiple bond among the existing Co–N_2 complexes. Nevertheless, the coordination of the N_2 unit appears to be robust.

Acknowledgments

This work was supported by the Natural Sciences and Engineering Research Council of Canada (NSERC). We are grateful to Dr. G.P.A. Yap for solving the crystal structure of **1**.

References

1. (*a*) T.A. Bazhenova and A.E. Shilov. Coord. Chem. Rev. **144**, 69 (1995); (*b*) M.E. Vol'pin, M.A. Ilatovskaya, L.V. Kosyakova, and V.B. Shur. Chem. Commun. 1074 (1968); (*c*) G.N. Schrauzer, G. Schlesinger, and P.A. Doemeny. J. Am. Chem. Soc. **93**, 1803 (1971); (*d*) G.N. Schrauzer, P.R. Robinson, E.L. Moorehead, and T.M. Vickrey. J. Am. Chem. Soc. **98**, 2815 (1976); (*e*) P. Sobota and B. Jezowska-Trzebiatowska. J. Organomet. Chem. **131**, 341 (1977); (*f*) C.R. Dickson and A.J. Nozik. J. Am. Chem. Soc. **100**, 8007 (1978); (*g*) K. Tanaka, Y. Hozumi, and T. Tanaka. Chem. Lett. 1203 (1982); (*h*) A.E. Shilov. J. Mol. Catal. **41**, 221 (1987); (*i*) K. Komori, H. Oshita, Y. Mizobe, and M. Hidai. J. Am. Chem. Soc. **111**, 1939 (1989); (*j*) J.O. Dziegielewski and R. Grzybek. Polyhedron, **9**, 645 (1990).
2. D.V. Yandulov and R.R. Schrock. Science, **301**, 76 (2003).
3. J.A. Pool, E. Lobkovsky, and P.J. Chirik. Nature (London), **427**, 527 (2004).
4. I. Korobkov, S. Gambarotta, and G.P.A. Yap. Angew. Chem. Int. Ed. **42**, 4958 (2003).
5. (*a*) P. Berno and S. Gambarotta. Angew. Chem. Int. Ed. Engl. **34**, 822 (1995); (*b*) C.E. Laplaza and C.C. Cummins. Science (Washington, D.C.), **268**, 861 (1995); (*c*) Q. Cui, D.G. Musaev, M. Svensson, S. Sieber, and K. Morokuma. J. Am. Chem. Soc. **117**, 12 366 (1995); (*d*) C.E. Laplaza, M.J.A. Johnson, J.C. Peters, A.L. Odom, E. Kim, C.C. Cummins, G.N. George, and I.J. Pickering. J. Am. Chem. Soc. **118**, 8623 (1996); (*e*) A. Zanotti-Gerosa, E. Solari, L. Giannini, C. Floriani, A. Cheisi-Villa, and C. Rizzoli. J. Am. Chem. Soc. **120**, 437 (1998); (*f*) H. Ishino, S. Tokunaga, H. Seino, Y. Ishii, and M. Hidai. Inorg. Chem. **38**, 2489 (1999); (*g*) J.C. Peters, J.P.F. Cherry, J.C. Thomas, L. Baraldo, D.J. Mindiola, W.M. Davis, and C.C. Cummins. J. Am. Chem. Soc. **121**, 10 053 (1999); (*h*) Y.C. Tsai, M.J.A. Johnson, D.J. Mindiola, C.C. Cummins, W.T. Klooster, and J.F. Koetzle. J. Am. Chem. Soc. **121**, 10 426 (1999); (*i*) G.K.B. Clentsmith, V.M.E. Bates, P.B. Hitchcock, and F.G.N. Cloke. J. Am. Chem. Soc. **121**, 10 444 (1999); (*j*) A. Caselli, E. Solari, R. Scopelliti, C. Floriani, N. Re, C. Rizzoli, and A. Chiesi-Villa. J. Am. Chem. Soc. **122**, 3652 (2000); (*k*) D.J. Mindiola, K. Meyer, J.P.F. Cherry, T.A. Baker, and C.C. Cummins. Organometallics, **19**, 1622 (2000); (*l*) E. Solari, C.D. Silva, B. Iacono, J. Hesschenbrouck, C. Rizzoli, R. Scopelliti, and C. Floriani. Angew. Chem. Int. Ed. **40**, 3907 (2001); (*m*) V. Yandulov and R.R. Schrock. J. Am. Chem. Soc. **124**, 6252 (2002); (*n*) M.D. Fryzuk, C.M. Kozak, M.R. Bowdridge, B.O. Patrick, and S.J. Rettig. J. Am. Chem. Soc. **124**, 8389 (2002); (*o*) H. Kawaguchi and T. Matsuo. Angew. Chem. Int. Ed. **41**, 2792 (2002); (*p*) M.D. Fryzuk, B.A. MacKay, S.A. Johnson, and B.O. Patrick. Angew. Chem. Int. Ed. **41**, 3709 (2002); (*q*) Y.-C. Tsai and C.C. Cummins. Inorg. Chim. Acta, **345**, 63 (2003); (*r*) M.D. Fryzuk, B.A. MacKay, and B.O. Patrick. J. Am. Chem. Soc. **125**, 3234 (2003); (*s*) M.D. Fryzuk and S.A. Johnson. Coord. Chem. Rev. **200–202**, 379 (2000); (*t*) M.P. Shaver and M.D. Fryzuk. Adv. Synth. Catal. **345**, 1061 (2003).
6. L.C. Seefeldt, I.G. Dance, and D.R. Dean. Biochemistry, **43**, 1401 (2004).
7. L.C. Seefeldt and D.R. Dean. Acc. Chem. Res. **30**, 260 (1997).
8. (*a*) M. Ganesan, M.P. Lalonde, S. Gambarotta, and G.P.A. Yap. Organometallics, **20**, 2443 (2001); (*b*) S. Gambarotta and J. Scott. Angew. Chem. Int. Ed. **43**, 5298 (2004).
9. (*a*) C.M. Kozak and P. Mountford. Angew. Chem. Int. Ed. **43**, 1186 (2004); (*b*) B.A. MacKay and M.D. Fryzuk. Chem. Rev. **104**, 385 (2004); (*c*) M.D. Fryzuk, J.B. Love, S.J. Rettig, and V.G. Young. Science (Washington, D.C.), **275**, 1445 (1997); (*d*) H. Basch, D.G. Musaev, K. Morokuma, M.D. Fryzuk, J.B. Love, W.W. Seidel, A. Albinati, T.F. Koetzle, W.T. Klooster, S.A. Mason, and J. Eckert. J. Am. Chem. Soc. **121**, 523 (1999); (*e*) M.D. Fryzuk, S.A. Johnson, and S.J. Rettig. J. Am. Chem. Soc. **120**, 11 024 (1998); (*f*) M.D. Fryzuk, S.A. Johnson, B.O. Patrick, A. Albinati, S.A. Mason, and T.F. Koetzle. J. Am. Chem. Soc. **123**, 3960 (2001).
10. J.M. Smith, R.J. Lachicotte, K.A. Pittard, T.R. Cundari, G. Lukat-Rodgers, K.R. Rodgers, and P.L. Holland. J. Am. Chem. Soc. **123**, 9222 (2001).
11. (*a*) J.H. Enemark, B.R. Davis, J.A. McGinnety, and J.A. Ibers. Chem. Commun. 96 (1968); (*b*) B.R. Davis, N.C. Payne, and J.A. Ibers. Inorg. Chem. **8**, 2719 (1969).
12. Y. Miura and A. Yamamoto. Chem. Lett. 937 (1978).
13. A. Yamamoto, Y. Miura, T. Ito, H.-L. Chen, K. Iri, F. Ozawa, K. Miki, T. Sei, N. Tanaka, and N. Kasai. Organometallics, **2**, 1429 (1983).
14. M. Aresta, C.F. Nobile, M. Rossi, and A. Sacco. Chem. Commun. 781 (1971).
15. H.-F. Klein, R. Hammer, J. Wenninger, P. Friedrich, and G. Huttner. Z. Naturforsch. **33b**, 1267 (1978).
16. R. Hammer, H.-F. Klein, U. Schubert, A. Frank, and G. Huttner. Angew. Chem. Int. Ed. Engl. **15**, 612 (1976).
17. H.-F. Klein, H. Koenig, S. Koppert, K. Ellrich, and J. Riede. Organometallics, **6**, 1341 (1987).

© 2005 NRC Canada

18. H.-F. Klein, K. Ellrich, and K. Ackermann. J. Chem. Soc. Chem. Commun. 888 (1983).
19. (*a*) C. Bianchini, M. Peruzzini, and F. Zanobini. Organometallics, **10**, 3415 (1991); (*b*) C. Bianchini, C. Mealli, A. Meli, M. Peruzzini, and F. Zanobini. J. Am. Chem. Soc. **110**, 8725 (1988).
20. R.A. Jones, A.L. Stuart, J.L. Atwood, and W.E. Hunter. Organometallics, **2**, 1437 (1983).
21. F. Cecconi, C.A. Ghilardi, S. Midollini, S. Moneti, A. Orlandini, and M. Bacci. J. Chem. Soc. Chem. Commun. 731 (1985).
22. T.A. Betley and J.C. Peters. J. Am. Chem. Soc. **125**, 10 782 (2003).
23. J.W. Egan, Jr., B.S. Haggerty, A.L. Rheingold, S.C. Sendlinger, and K.H. Theopold. J. Am. Chem. Soc. **112**, 2445 (1990).
24. V.C. Gibson, M.J. Humphries, K.P. Tellmann, D.F. Wass, A.J.P White, and D.J. Williams. Chem. Commun. 2252 (2001).
25. B.L. Small, M. Brookhart, and A.M.A. Bennett. J. Am. Chem. Soc. **120**, 4049 (1998).
26. G.J.P. Britovsek, V.C. Gibson, B.S. Kimberley, P.J. Maddox, S.J. McTavish, G.A. Solan, A.J.P. White, and D.J. Williams. Chem. Commun. 849 (1998).
27. D. Enright, S. Gambarotta, G.P.A. Yap, and P.H.M. Budzelaar. Angew. Chem. Int. Ed. **41**, 3873 (2002).
28. H. Sugiyama, G. Aharonian, S. Gambarotta, G.P.A. Yap, and P.H.M. Budzelaar. J. Am. Chem. Soc. **124**, 12 268 (2002).
29. D. Reardon, F. Conan, S. Gambarotta, G.P.A. Yap, and Q. Wang. J. Am. Chem. Soc. **121**, 9318 (1999).
30. I. Korobkov, S. Gambarotta, and G.P.A. Yap. Organometallics, **21**, 3088 (2002).
31. H. Sugiyama, I. Korobkov, S. Gambarotta, A. Mueller, and P.H.M. Budzelaar. Inorg. Chem. **43**, 5771 (2004).
32. L.K. Johnson, C.M. Killian, and M.S. Brookhart. J. Am. Chem. Soc. **117**, 6414 (1995).
33. C. Tessier-Youngs and O.T. Beachley, Jr. Inorg. Synth. **24**, 95 (1986).
34. G.M. Sheldrick. SHELXTL. Version 6.12 [computer program]. Brucker AXS, Madison, Wisconsin. 2001.

© 2005 NRC Canada

The importance of cyclopentadienyl substituent effects in group 4 metallocene dinitrogen chemistry[1]

Jaime A. Pool and Paul J. Chirik

Abstract: This article highlights some of our recent efforts and presents new data on the importance of cyclopentadienyl substituent effects on group 4 metallocene dinitrogen chemistry. Reactions such as the coordination of N_2 to an isolated titanium sandwich complex, alkali-metal reductions of zirconocene dihalide complexes, alkane reductive elimination reactions, and the hydrogenation of zirconium dinitrogen complexes are all extremely sensitive to the groups present on the cyclopentadienyl rings. These results are promising for the future of N_2 fixation, as the reactivity of a specific metallocene can be dramatically altered by subtle manipulations in ligand substituents.

Key words: cyclopentadienyl, zirconium, dinitrogen, ammonia, sandwich.

Résumé : Ce travail met en relief des travaux récents de notre équipe et présente de nouvelles données sur l'importance des effets des substituants du cyclopentadiényle sur la chimie du diazote des métallocènes du groupe 4. Les réactions, telle la coordination du N_2 sur un complexe sandwich isolé, les réductions par les métaux alcalins des complexes dihalogénés du zirconocène, les réactions d'éliminations réductrices d'alcane et l'hydrogénation des complexes de diazote du zirconium sont toutes extrêmement sensibles aux groupes présents sur les cycles cyclopentadiényles. Ces résultats sont remplis de promesses pour la fixation future du N_2 puisque la réactivité spécifique d'un métallocène spécifique peut être dramatiquement altérée par des manipulations subtiles des ligands substituants.

Mots clés : cyclopentadiényle, zirconium, diazote, ammoniac, sandwich.

[Traduit par la Rédaction]

Introduction

The isolation and characterization of the first homogeneous transition metal dinitrogen complex, $[(H_3N)_5Ru(N_2)]^{2+}$, by Allen and Senoff (1) spawned a new era in nitrogen fixation. As demonstrated by Shepherd and Taube (2), synthetic chemists were presented with the unprecedented opportunity to rationally assemble and investigate the metal–N_2 linkage (3, 4), and, more significantly, determine its proclivity to participate in functionalization reactions. One pervasive theme common to all subsequent work on well-defined transition metal dinitrogen compounds is the ability to tune metal–ligand combinations and explore structure–reactivity relationships. This prospect paved the way for Chatt et al.'s pioneering work (5), highlighted by the fixation of N_2 to ammonia by successive proton and electron transfers with zerovalent group 6 dinitrogen compounds. Recently, this cycle has been extended to include iron complexes (6), systems where ruthenium dihydrogen complexes serve as the H-atom source (7), and molybdenum compounds that are catalytically competent (8, 9).

In addition to studies with group 6 and 8 compounds, there has been a long-standing interest in early transition metal complexes for nitrogen fixation. Not long after Allen and Senoff's report (1), Vol'pin and Shur (10) described ammonia production from N_2 by protonation of a $(\eta^5\text{-}C_5H_5)_2TiCl_2$–alkyllithium mixture. Subsequently, van Tamelen (11) and Brintzinger (12) independently explored the mechanism of this reaction, leading to the pioneering synthesis by the latter's research group of the first well-defined titanium dinitrogen compound, $[(\eta^5\text{-}C_5Me_5)_2Ti]_2(\mu_2, \eta^1, \eta^1\text{-}N_2)$ (13). This molecule, as well as its zirconium congener, $[(\eta^5\text{-}C_5Me_5)_2Zr(\eta^1\text{-}N_2)]_2(\mu_2, \eta^1, \eta^1\text{-}N_2)$, can be protonated with mineral acids to yield hydrazine (14). Since these seminal discoveries, group 4 transition metal dinitrogen chemistry has experienced remarkable growth and numerous successes (15). A few recent highlights include the synthesis by Mori and co-workers (16) of *N*-heterocycles and natural products from N_2 using modified Vol'pin chemistry and Fryzuk and co-workers' (17, 18) side-on bound dinitrogen complex that undergoes partial hydrogenation and reacts with both silanes and terminal alkynes.

Inspired by these advances, we initiated a program in July 2001 aimed at incorporating atmospheric N_2 into value-added nitrogen-containing products using well-defined group 4 transition metal dinitrogen compounds. Specifically, we hoped to gain an understanding of how dinitrogen is acti-

Received 9 September 2004. Published on the NRC Research Press Web site at http://canjchem.nrc.ca on 3 March 2005.

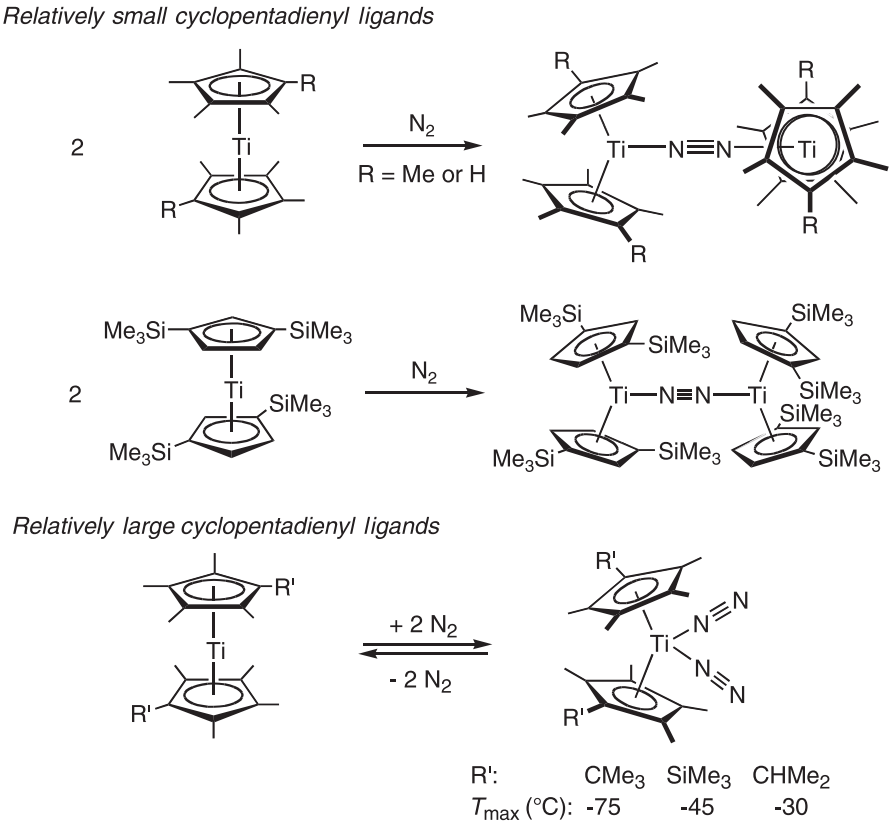
J.A. Pool[2] and P. Chirik.[3] Department of Chemistry and Chemical Biology, Baker Laboratory, Cornell University, Ithaca, NY 14853, USA.

[1]This article is part of a Special Issue dedicated to Dinitrogen Chemistry.

[2]Present address: Chemistry Division, Los Alamos National Laboratory, Los Alamos, NM 87545, USA.
[3]Corresponding author (e-mail: pc92@cornell.edu).

 doi: 10.1139/V05-009 © 2005 NRC Canada

Fig. 1. Effect of cyclopentadienyl ligand substitution on N_2 coordination to titanium sandwich complexes. T_{max} refers to the maximum temperature at which N_2 coordination is observed. Temperature values are ±2 °C.



vated by low-valent metal centers, elucidate the factors that govern its hapticity (e.g., "side-on" vs. "end-on"), and translate these findings onto reactions that transform and liberate a functionalized nitrogen fragment from the metal center. Here, we recount some of our previous results as well as present new data that underscore the importance of cyclopentadienyl substituent effects in group 4 metallocene dinitrogen chemistry. Particularly striking is how seemingly modest changes in substitution, such as the replacement of a methyl group with a hydrogen atom or a *tert*-butyl with an isopropyl group, can completely alter the course of N_2 activation and functionalization.

Results and discussion

Activation of N_2 by low-valent group 4 metallocenes

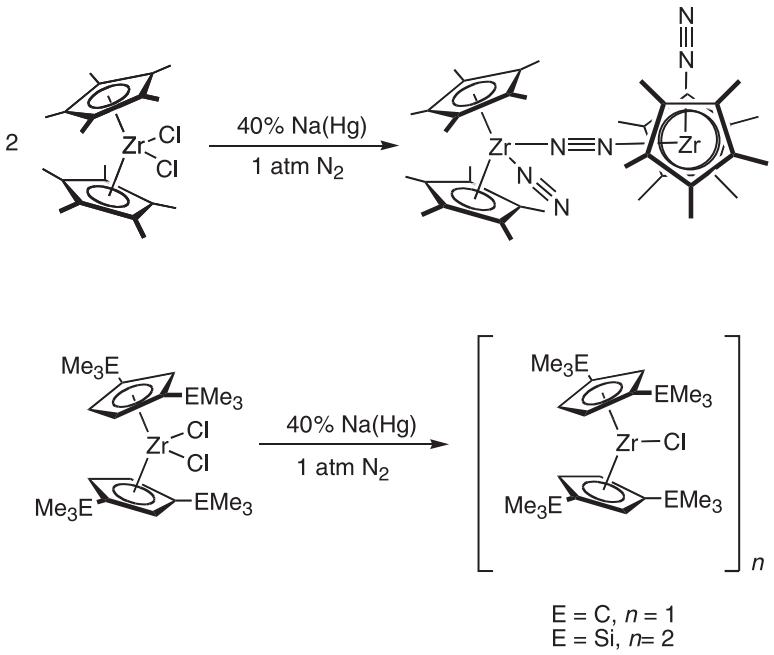
Our illustration of the importance of cyclopentadienyl substituent effects on N_2 activation begins with one of the simplest reactions imaginable for dinitrogen reduction — the coordination of N_2 to a preformed, low-valent titanium(II) sandwich compound (Fig. 1). Previous reports from the literature hinted at subtle, yet interesting substituent effects. The transiently generated titanium(II) sandwiches, $(\eta^5\text{-}C_5Me_5)_2Ti$ (13), $(\eta^5\text{-}C_5H_3\text{-}1,3\text{-}(SiMe_3)_2)_2Ti$ (19), and presumably $(\eta^5\text{-}C_5Me_4H)_2Ti$ (20), react rapidly with N_2 to afford end-on bound, bridged, dimeric dinitrogen complexes. In contrast, Lawless and co-workers (21) have isolated and crystallographically characterized $(\eta^5\text{-}C_5Me_4SiMe_2\text{-}t\text{-}Bu)_2Ti$, which is unreactive toward N_2 at ambient temperature and pressure. Mach and co-workers (22) have since independently prepared a family of silyl-substituted titanocenes that are reported to resist N_2 coordination up to pressures of 50 atm (1 atm = 101.325 kPa).

Intrigued by these reactivity differences, we sought to understand the steric and electronic properties of cyclopentadienyl ligands that govern N_2 activation by the titanium sandwiches. In an attempt to separate steric and electronic contributions, two new titanium(II) complexes, $(\eta^5\text{-}C_5Me_4R)_2Ti$ (R = $CHMe_2$, CMe_3), were prepared. The presence of 10 alkyl substituents on the ligand framework served to simulate the electronic environment of N_2-reactive $(\eta^5\text{-}C_5Me_5)_2Ti$ while large isopropyl or *tert*-butyl groups mimicked the steric disposition of reportedly N_2-inert $(\eta^5\text{-}C_5Me_4SiMe_3)_2Ti$ (22). The magnetic and NMR spectroscopic data collected at 23 °C, in addition to elemental analyses, were consistent with isolation of the sandwich complexes, $(\eta^5\text{-}C_5Me_4CHMe_2)_2Ti$ and $(\eta^5\text{-}C_5Me_4CMe_3)_2Ti$ (23).

Attempts to grow X-ray quality crystals of $(\eta^5\text{-}C_5Me_4CHMe_2)_2Ti$ by cooling a concentrated pentane solution to –35 °C in an N_2 atmosphere produced a spectacular color change from red to intense blue. Warming the solutions back to room temperature resulted in vigorous evolution of gas and regeneration of the diagnostic red color of the sandwich compound. A combination of in situ React-IR spectroscopy, Toepler pump analysis, and X-ray diffraction were used to identify the blue compound as the monomeric titanocene bis-dinitrogen complex, $(\eta^5\text{-}C_5Me_4CHMe_2)_2Ti(N_2)_2$ (23). Further investigation of other titanium sandwiches such

© 2005 NRC Canada

Fig. 2. Cyclopentadienyl substituent effects on the outcome of alkali-metal reduction of zirconocene dichloride complexes (1 atm = 101.325 kPa).

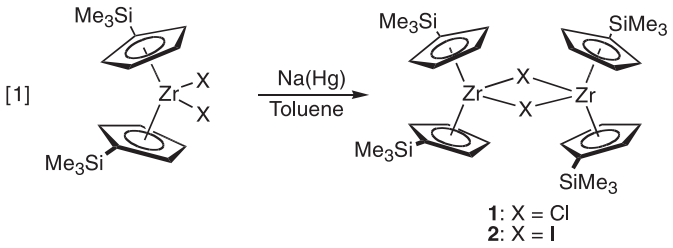


as $(\eta^5\text{-}C_5Me_4CMe_3)_2Ti$ and $(\eta^5\text{-}C_5Me_4SiMe_3)_2Ti$ by in situ React-IR studies established reversible dinitrogen coordination for these molecules as well, although N_2 loss is observed at much lower temperatures (Fig. 1). While N_2 and CO are isoelectronic, these molecules are the first examples of bent metallocene dinitrogen complexes with a bonding motif frequently encountered with more familiar titanocene dicarbonyl complexes.

Importantly, these studies have demonstrated the effect that cyclopentadienyl substitution can have on the coordination of dinitrogen to a low-valent transition metal center. Changing two methyl groups on the ligand array to isopropyl, *tert*-butyl, or silyl substituents blocks formation of dimeric dinitrogen compounds and thus allows reversible dinitrogen coordination.

For zirconium, the situation is more complicated. Isolation of a bona fide bis-cyclopentadienyl zirconium sandwich complex, $[(CpR_n)_2Zr]$, has not been achieved, most likely owing to the increased thermodynamic potential for the second-row metal to attain its highest oxidation state. Typically, access to zirconium dinitrogen compounds proceeds by reduction of the appropriate Zr(IV) dihalide complex with an alkali metal or its equivalent (e.g., KC_8). Again, significant cyclopentadienyl substituent effects are operative in these reactions. Whereas $(\eta^5\text{-}C_5Me_5)_2ZrCl_2$ undergoes smooth reduction with 40% sodium amalgam in the presence of N_2 to yield $[(\eta^5\text{-}C_5Me_5)_2Zr(\eta^1\text{-}N_2)]_2(\mu_2, \eta^1, \eta^1\text{-}N_2)$ (14), related zirconocenes such as $(\eta^5\text{-}C_5H_3\text{-}1,3\text{-}(EMe_3)_2)_2ZrCl_2$ (E = C (24), Si (25)) only undergo a one-electron reduction to produce the corresponding Zr(III) monochloride under similar conditions (Fig. 2).

These results prompted further investigation into the reduction of various substituted zirconocene dihalide complexes. Reduction of $(\eta^5\text{-}C_5H_4SiMe_3)_2ZrCl_2$ with 0.5% sodium amalgam in toluene under 1 atm of N_2 (1 atm = 101.325 kPa) afforded deep-purple, diamagnetic crystals identified as the zirconium(III) monochloride dimer, $[(\eta^5\text{-}C_5H_4SiMe_3)_2Zr(\mu_2\text{-}Cl)]_2$ (**1**) (eq. [1]). Stronger reducing agents such as KC_8, CsC_8, and sodium potassium alloy also yielded **1**. The ^1H NMR spectrum of **1** in benzene-d_6 is consistent with a C_{2v} symmetric compound. The cyclopentadienyl resonances, observed at 5.31 and 5.44 ppm, are relatively upfield-shifted as compared to the analogous resonances of the starting dichloride complex, which appear at 6.09 and 6.69 ppm.



Cooling a concentrated pentane solution of **1** afforded purple blocks suitable for X-ray diffraction. The solid-state structure, presented in Fig. 3, establishes a dimeric molecule possessing a planar Zr_2Cl_2 core where the $[SiMe_3]$ substituents are oriented away from the metallocene wedge in a *cisoid* arrangement. The Zr–Zr distance of 3.512(12) Å is shorter than the values of 3.86 and 3.94 Å reported for the two molecules in the unit cell of paramagnetic $[(\eta^5\text{-}C_5H_3\text{-}1,3\text{-}(SiMe_3)_2)_2Zr(\mu_2\text{-}Cl)]_2$ (25), but is significantly longer than the value of 2.96 Å for the sum of the covalent radii for zirconium. The presence of only one $[SiMe_3]$ on the cyclopentadienyl ring affords a more open metallocene compared to $[(\eta^5\text{-}C_5H_3\text{-}1,3\text{-}(SiMe_3)_2)_2Zr(\mu_2\text{-}Cl)]_2$ and, as a result, a much shorter Zr–Zr distance is observed.

Reduction of the corresponding zirconocene diiodide complex, $(\eta^5\text{-}C_5H_4SiMe_3)_2ZrI_2$, with the range of reductants described above again resulted in one-electron reduction to

© 2005 NRC Canada

Fig. 3. Molecular structure of **1** at 30% probability ellipsoids. Hydrogen atoms are omitted for clarity.

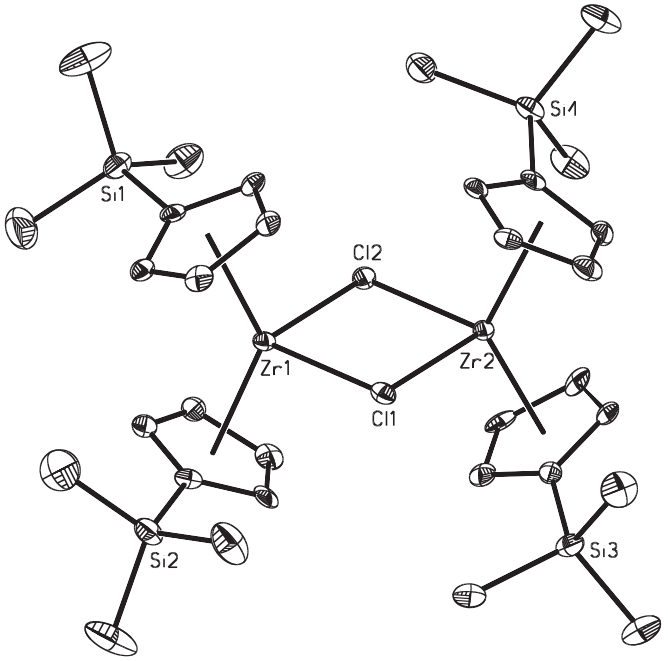
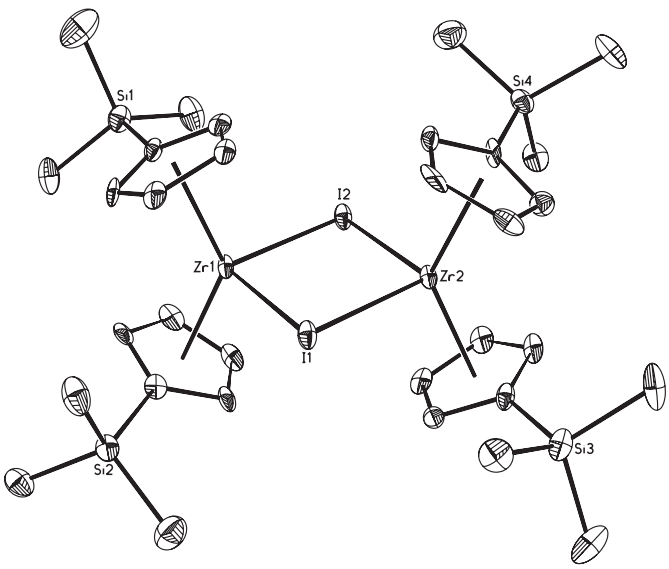


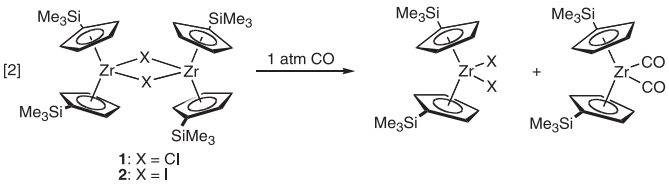
Fig. 4. Molecular structure of **2** at 30% probability ellipsoids. Hydrogen atoms are omitted for clarity.



the zirconium(III) monoiodide complex, $[(\eta^5\text{-}C_5H_4SiMe_3)_2Zr(\mu_2\text{-}I)]_2$ (**2**) (eq. [1]). As with **1**, **2** is diamagnetic and has been characterized by NMR spectroscopy, elemental analysis, and X-ray diffraction (Fig. 4). As expected with the larger iodide ligands, the Zr–Zr distance has expanded to 3.6855(8) Å and the I(1)-Zr(1)-I(2) angle has opened to 101.870(19)° as compared to 93.24(8)° for **1**. Similar chemistry is also observed for the reduction of $(\eta^5\text{-}C_5H_4SiMe_2\text{-}t\text{-}Bu)_2ZrCl_2$ (26), where only one-electron reduction to the diamagnetic Zr(III) monohalide dimer results (27).

Dimeric, diamagnetic Zr(III) monohalide complexes have been prepared previously by Gambarotta and co-workers (28, 29). Independent computational studies by DeKock et al. (30) and Bénard and Rohmer (31) have established that a partial Zr–Zr bonding interaction accounts for the observed spin pairing. However, the metal–metal interaction can be attenuated, and therefore the spin state of the molecule altered, by both the bridging ligand and cyclopentadienyl substituents. Relatively unhindered cyclopentadienyl ligands such as those found in **1** and **2** allow close contact (3.512–3.685 Å) of the two zirconium centers, allowing a metal–metal interaction and spin pairing. Interestingly, in the case of the larger iodide ligands present in **2**, the I-Zr-I angle opens to allow electronic communication between the two zirconium centers. Introduction of an additional [$SiMe_3$] substituent as in the case of $[(\eta^5\text{-}C_5H_3\text{-}1,3\text{-}(SiMe_3)_2)_2Zr(\mu_2\text{-}Cl)]_2$ limits the contact of the metal centers, and the compound is paramagnetic (25).

The inability to reduce the silylated zirconocenes to zirconium(II) dinitrogen compounds with potent reducing agents such as CsC_8 and NaK suggested that a kinetic rather than a thermodynamic barrier inhibited the desired two-electron reduction. Considering that an array of formally zirconium(II) dicarbonyl complexes can be prepared by straightforward reduction of the dihalide complexes with activated Mg and CO (32), the affinity of the zirconium for the incoming ligand appears to influence the outcome of the reduction. Addition of 1 atm of CO (1 atm = 101.325 kPa) to both **1** and **2** induced disproportionation into the known zirconocene dicarbonyl, $(\eta^5\text{-}C_5H_4SiMe_3)_2Zr(CO)_2$ (33), and the dihalide complex, $(\eta^5\text{-}C_5H_4SiMe_3)_2ZrX_2$ (eq. [2]). Similar reactivity has also been observed by Gambarotta and co-workers with the unsubstituted zirconium cyclopentadienyl compounds (29).

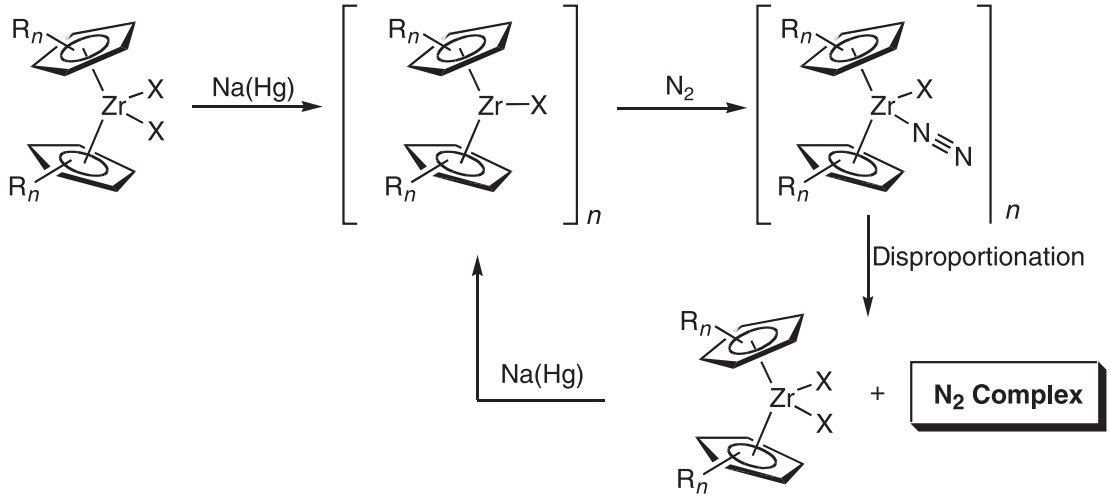


A mechanism that accounts for these observations is presented in Fig. 5. Following the initial reduction to Zr(III), an exogenous ligand coordinates (N_2 is shown in this case) and forms the intermediate dinitrogen complex, $(CpR_n)_2ZrX(N_2)$, which then disproportionates into the Zr(IV) dihalide and the Zr(II) dinitrogen complex. The resulting zirconocene dihalide is then recycled back to Zr(III) by the reducing agent and the process continues. Lappert and co-workers (34) have obtained EPR evidence for a monomeric, side-on bound Zr(III) dinitrogen compound, $Cp_2Zr(CH_2SiMe_3)(\eta^2\text{-}N_2)$, providing experimental support for such an intermediate. Thus, the ability of the Zr(III) compound to bind dinitrogen, not the strength of the reducing agent, appears to dictate whether a two-electron reduction occurs.

This model, in conjunction with the known steric and electronic properties of zirconocene complexes (32), accounts

© 2005 NRC Canada

Fig. 5. Proposed mechanism for the synthesis of zirconocene dinitrogen complexes by alkali-metal reduction.



for the observed reduction chemistry. Zirconocenes with sterically demanding, electron-donating ligands such as (η^5-C_5Me_5) or (η^5-C_5Me_4H) inhibit dimerization of the Zr(III) intermediate and stabilize the Zr–N_2 interaction through π-backbonding. In contrast, zirconocenes with single silyl substituents are prone to form robust halide-bridged dimers and have less electron density for back donation. These effects should be considered when exploring zirconocene complexes for dinitrogen activation.

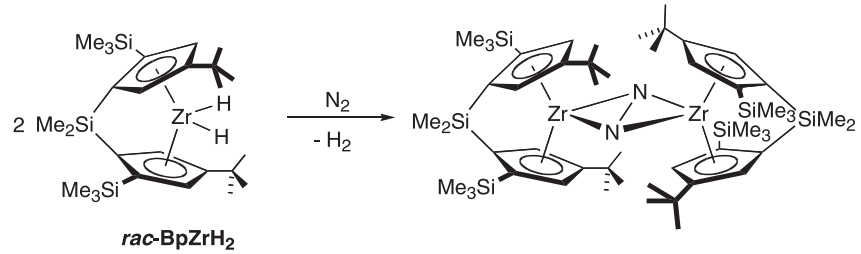
The limitations of the alkali-metal reduction reactions, in particular with cyclopentadienyl ligands containing electron-withdrawing substituents, demonstrated the need for alternative methods for the synthesis of zirconocene dinitrogen complexes. Alkane or dihydrogen reductive elimination from the appropriate Zr(IV) precursor could also achieve the desired two-electron reduction. Importantly, ground-state considerations (vide infra) also suggest that reductive elimination will be favored for electron-poor zirconocenes and would therefore complement reduction by alkali metals in terms of the class of metallocenes that could be targeted.

Inspiration for this aspect of the chemistry derived from several sources. Teuben and co-workers (20) had reported the synthesis of an end-on bound titanocene dinitrogen complex upon loss of dihydrogen from the corresponding titanium(III) monohydride. Fryzuk et al. (35) also had described a similar reaction with a dinuclear tantalum tetrahydride to yield an unusual dinitrogen complex with a N_2 ligand that can be classified as being both side-on and end-on. This molecule has since exhibited rich reaction chemistry (36).

Another major inspiration stems from a serendipitous discovery made by one of us (PJC) while working with John Bercaw at Caltech. We were studying rates of olefin insertion and β-hydrogen elimination with zirconocene dihydrides and alkyl hydrides to gain an understanding of molecular weight control in metallocene-catalyzed olefin polymerization. Having worked with a number of model complexes, we became interested in extending our studies to isospecific *ansa*-zirconocenes. A stock solution of *rac*-$BpZrH_2$ (Bp = $Me_2Si(C_5H_2$-2-$SiMe_3$-4-$CMe_3)_2$) in toluene was prepared for kinetic studies and placed in the drybox freezer and essentially forgotten. About a year later during one of John's famous group cleanups, the vial (clearly labeled of course!) was found, and we discovered that beautiful pleochroic crystals had formed. X-ray diffraction established a side-on bound, modestly activated N_2 ligand (37). Subsequent NMR experiments demonstrated that loss of H_2 and coordination of dinitrogen took place over the course of hours at ambient temperature (eq. [3]).

In July 2001 at Cornell, we began a systematic investigation of the rate of alkane reductive elimination as a function of cyclopentadienyl ligand. Zirconocene isobutyl hydrides were chosen because these molecules could be conveniently prepared by addition of 2 equiv. of *tert*-butyllithium to the corresponding dichloride complex (38). Using this methodology, a series of "mixed-ring" zirconocene isobutyl hydrides, (η^5-C_5Me_5)(CpR_n)$Zr(CH_2CHMe_2)H$, were prepared. Their relative rates of reductive elimination were measured and the products formed from alkane loss identified. In each case, loss of isobutane afforded a single diastereomer of a cyclometalated zirconium hydride rather than the desired dinitrogen complex. Importantly, however, it was established that the rate of alkane reductive elimination increased with incorporation of [$SiMe_3$] substituents, an effect ascribed to both steric and electronic destabilization of the Zr(IV) alkyl

[3]



***rac*-$BpZrH_2$**

© 2005 NRC Canada

hydride ground state (39). Subsequent experiments with the $(\eta^5\text{-}C_5Me_5)(\eta^5\text{-}C_5H_3\text{-}1,3\text{-}(SiMe_3)_2)Zr(R)H$ (R = alkyl) family of complexes demonstrated increased rates of elimination with increasing size of the alkyl group, a phenomenon also attributed to ground-state destabilization (40).

These results led to the design and synthesis of the purely silyl-substituted zirconocene neopentyl hydride, $(\eta^5\text{-}C_5H_3\text{-}1,3\text{-}(SiMe_3)_2)_2Zr(CH_2CMe_3)H$, which undergoes facile loss of neopentane at ambient temperature to afford the corresponding cyclometalated zirconocene hydride. Exposure of this molecule to a blanket of N_2 at –35 °C afforded crystals of the dinitrogen complex $[(\eta^5\text{-}C_5H_3\text{-}1,3\text{-}(SiMe_3)_2)_2Zr]_2(\mu_2, \eta^2, \eta^2\text{-}N_2)$ (eq. [4]). X-ray diffraction revealed a side-on bound N_2 ligand with an elongated N—N bond of 1.47 Å. Thus, alkane reductive elimination provides a unique synthetic pathway to a dinitrogen complex that cannot be accessed by alkali-metal reduction. Unfortunately, the yield of the dinitrogen complex is low owing to the propensity of the cyclometalated zirconocene hydride to participate in numerous side reactions. However, preliminary reactivity studies with $[(\eta^5\text{-}C_5H_3\text{-}1,3\text{-}(SiMe_3)_2)_2Zr]_2(\mu_2, \eta^2, \eta^2\text{-}N_2)$ are encouraging as reaction with ethyl chloroformate yields diethylazodicarboxylate, a useful precursor for the synthesis of amino acids and other organic molecules.

Low-valent bis-indenyl zirconium chemistry

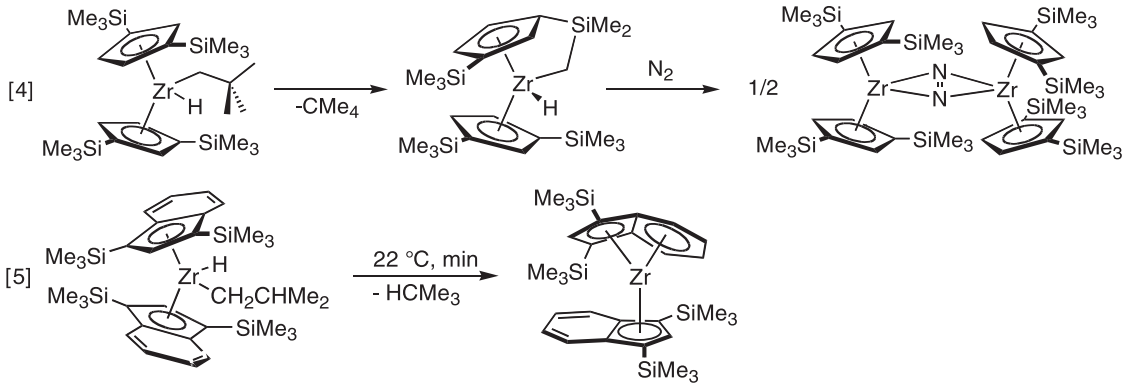
Because incorporation of $[SiMe_3]$ groups into the cyclopentadienyl ligand array afforded N_2-reactive cyclometalated hydride complexes, we have also explored similar reactions with the corresponding silylated indenyl complexes. The indenyl anion, the benzo-substituted version of the cyclopentadienyl ligand, has enjoyed considerable success as a supporting ligand in metallocene-catalyzed olefin polymerization (41), although investigations into the chemistry of low-valent species have been limited. Moreover, replacement of the cyclopentadienyl anion with an indenyl ligand often results in enhanced or even unique reactivity. This behavior, when applied to associative substitution reactions, has been termed the "indenyl effect" (42).

Treatment of the silylated bis-indenyl zirconocene dichloride, $(\eta^5\text{-}C_9H_5\text{-}1,3\text{-}(SiMe_3)_2)_2ZrCl_2$, with 2 equiv. of isobutyllithium allows observation of the transient bis-indenyl zirconocene isobutyl hydride, which undergoes rapid reductive elimination of isobutane to yield a unique bis-indenyl zirconium sandwich (43). Recent crystallographic studies have established an unprecedented η^9 bonding interaction of one of the indenyl rings, where the planarity of the carbocycle is compromised to engage in bonding with the zirconium (eq. [5]) (44). These molecules have proven to be isolable sources of Zr(II), participating in numerous coupling and ligand addition reactions, although N_2 activation has not been observed. Thus, the chemistry of low-valent zirconium cyclopentadienyl and indenyl-substituted complexes is distinctly different, again highlighting the sensitivity to "ancillary" ligand environment.

End-on vs. side-on coordination and the hydrogenation of N_2

The elongated N—N bond in $[(\eta^5\text{-}C_5H_3\text{-}1,3\text{-}(SiMe_3)_2)_2Zr]_2(\mu_2, \eta^2, \eta^2\text{-}N_2)$ and the reaction of this complex with electrophiles prompted further investigation into the origins of side-on coordination of the dinitrogen ligand. Particularly, we were interested in elucidating the effect of cyclopentadienyl substituents on N_2 hapticity and exploring reactivity differences between the side-on and end-on coordination modes. Based on the observed end-on coordination in $[(\eta^5\text{-}C_5Me_5)_2Zr(\eta^1\text{-}N_2)]_2(\mu_2, \eta^1, \eta^1\text{-}N_2)$, we hypothesized that side-on coordination was in fact electronically favored and should be observed in the absence of overriding steric effects. To test this assertion, we decided to systematically investigate the hapticity of the N_2 ligand as methyl groups were removed from the pentamethylcyclopentadienyl ligand. Ideally, the methyl substitution would maintain sufficient electron density and steric protection to promote complete reduction to the zirconium(II) dinitrogen complex yet allow close contact of the metal centers for η^2-coordination of the bridging N_2 ligand (Fig. 6).

The bis-tetramethyl zirconocene dichloride, $(\eta^5\text{-}C_5Me_4H)_2ZrCl_2$ (45), was first explored owing to the commercial availability of the ligand and the relative ease of synthesis of homoleptic zirconocene dichloride compounds. Reduction of the Zr(IV) dihalide with 0.5% sodium amalgam under N_2 afforded a green solid. Diagnostic reactions with CO and I_2 afforded the zirconocene dicarbonyl and diiodide complexes, respectively, suggesting that the product was indeed a dinitrogen complex. Not long after the initial synthesis, beautiful single crystals were obtained for a diffraction experiment. The solid-state structure confirmed our formulation of the molecule's identity, but revealed that the N_2 had changed hapticity to side-on as compared to end-on in the case of permethylzirconocene (eq. [6]) (46). Another important feature of the solid-state structure was the peculiar arrangement of the cyclopentadienyl ligands in the dimer. The two metallocene wedges are canted with respect to each



© 2005 NRC Canada

Fig. 6. Exploration of cyclopentadienyl substituent effects on N_2 hapticity.

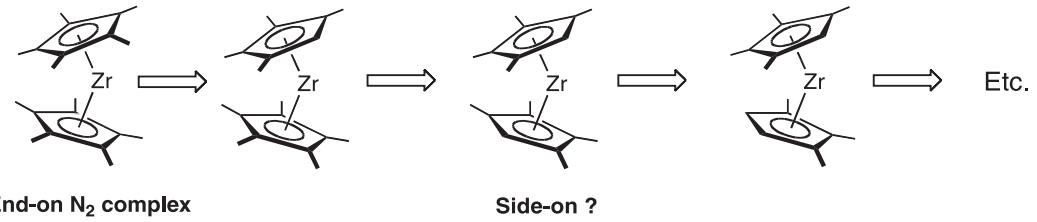
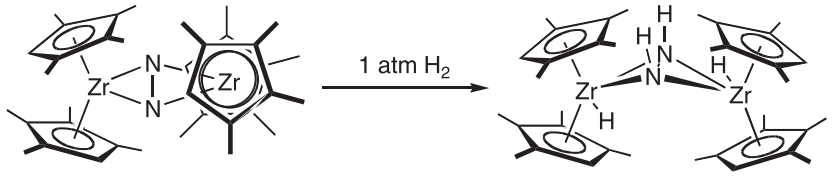
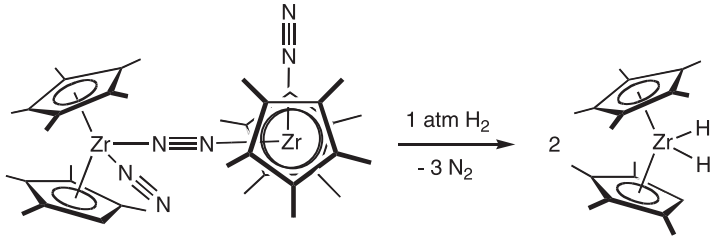


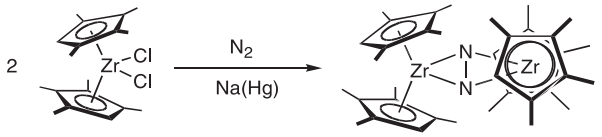
Fig. 7. Side-on vs. end-on coordination of dinitrogen and comparison of hydrogenation reactivity (1 atm = 101.325 kPa).

Eight methyl groups - side-on coordination and N_2 hydrogenation



Nine methyl groups - end-on coordination and N_2 loss

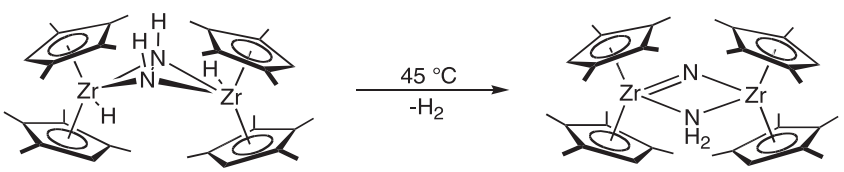


[6] 

other, forming a dihedral angle of 65.3°. This angle is significantly distorted from the electronically preferred coplanar arrangement observed in less-substituted dinitrogen complexes (39).

Having isolated and crystallographically characterized a new, side-on bound N_2 complex, we were anxious to explore its reactivity. Given the long-standing interest in the synthesis of ammonia from its elements, we first studied hydrogenation. Based on literature precedent, we anticipated that this nitrogen complex would behave like most others — addition of H_2 would induce loss of free N_2 with concomitant formation of the zirconocene dihydride. Addition of 1 atm of H_2 (1 atm = 101.325 kPa) to $[(\eta^5\text{-}C_5Me_4H)_2Zr]_2(\mu_2, \eta^2, \eta^2\text{-}N_2)$ in benzene-d_6 immediately bleached the intense purple solution and resulted in a sparingly soluble white solid. Much to our surprise (and delight!), we isolated not the expected dihydride complex but rather the zirconocene hydrazido compound, $[(\eta^5\text{-}C_5Me_4H)_2ZrH]_2(\mu_2, \eta^2, \eta^2\text{-}N_2H_2)$, arising from hydrogenation of the N_2 ligand (Fig. 7). IR and NMR experiments in conjunction with isotopic labeling studies quickly established the molecule's identity, but a crystal structure was essential. The zirconocene hydrazido complex was sparingly soluble in both aromatic and aliphatic hydrocarbons, making crystallization difficult. Fortunately, slow diffusion of hydrogen into a concentrated benzene-d_6 solution of the dinitrogen complex afforded a very large single crystal that yielded high-quality diffraction data.

Having hydrogenated atmospheric nitrogen to a hydrazido ligand, we next explored the possibility of fixation to ammonia. Mild thermolysis of $[(\eta^5\text{-}C_5Me_4H)_2ZrH]_2(\mu_2, \eta^2, \eta^2\text{-}N_2H_2)$ resulted in loss of H_2 along with N_2 scission, forming the zirconocene amido, nitrido complex, $[(\eta^5\text{-}C_5Me_4H)_2Zr]_2\text{-}(\mu_2\text{-}N)(\mu_2\text{-}NH_2)$ (eq. [7]). Protonolysis of this molecule with mineral acids does indeed yield free ammonia. Although this was an interesting result, N_2 fixation where H_2 was the sole hydrogen source was desired. Warming heptane solutions of

[7] 

© 2005 NRC Canada

$[(\eta^5\text{-}C_5Me_4H)_2ZrH]_2(\mu_2, \eta^2, \eta^2\text{-}N_2H_2)$ to 85 °C under 1 atm of H_2 (1 atm = 101.325 kPa) yielded small quantities of free ammonia, the zirconocene dihydride, and several Zr(IV) products arising from the reaction of the two.

The remarkable hydrogenation activity observed with $[(\eta^5\text{-}C_5Me_4H)_2Zr]_2(\mu_2, \eta^2, \eta^2\text{-}N_2)$ prompted us to investigate the reduction of $(\eta^5\text{-}C_5Me_5)(\eta^5\text{-}C_5Me_4H)ZrCl_2$. Reaction of the zirconocene dichloride or diiodide with KC_8 afforded a purple solution from which the end-on dinitrogen complex, $[(\eta^5\text{-}C_5Me_5)(\eta^5\text{-}C_5Me_4H)Zr(\eta^1\text{-}N_2)_2](\mu_2,\eta^1,\eta^1\text{-}N_2)$, was isolated. Exposure to 1 atm of H_2 (1 atm = 101.325 kPa) resulted in loss of N_2 and formation of the zirconocene dihydride (47). The reactions of zirconocene dinitrogen complexes again emphasize the sensitivity of the observed chemistry to cyclopentadienyl substituent effects. Replacing a single methyl group by a hydrogen atom completely alters the course of N_2 fixation. In the more substituted cases, trivial N_2 loss is observed whereas in the less-hindered example, ammonia synthesis can be achieved under mild conditions in solution.

Recent work in our laboratory has focused on the origin of the unprecedented reactivity of $[(\eta^5\text{-}C_5Me_4H)_2Zr]_2(\mu_2, \eta^2, \eta^2\text{-}N_2)$. Both computational and isotopic labeling studies (47) are consistent with the "twist" of the dimer as the origin of N_2 hydrogenation. Canting of the zirconium centers permits increased π back donation to the π^* molecular orbital of the side-on bound N_2 ligand, imparting significant Zr=N character and allowing facile 1,2-addition of H_2 across the zirconium–nitrogen bond (48, 49). Thus, both side-on coordination of N_2 and twisting of the zirconium dimer appear to be essential ingredients for nitrogen fixation.

Conclusions and future outlook

Over the past 3 years, our laboratory has observed the profound consequences that cyclopentadienyl ligand manipulations have on the activation, hapticity, and reactivity of dinitrogen with group 4 metallocenes. For titanium sandwich complexes, introduction of large substituents into $[C_5Me_4R]^-$ ligands allowed observation of monomeric, bis-dinitrogen complexes that are isoelectronic and isostructural to titanocene di-carbonyl complexes. In zirconium chemistry, access to the desired Zr(II) dinitrogen complex can be controlled by manipulation of the electronic properties of the cyclopentadienyl substituents. For electron-deficient metallocenes, reductive elimination is facile, whereas for electron-rich compounds, alkali-metal reduction is the preferred synthetic route. Significantly, either alkali-metal reduction or reductive elimination with the corresponding bis-indenyl zirconocene complexes affords unusual zirconium sandwich compounds in which one of the ligands is engaged in η^9 bonding.

Investigation into the substituent effects on the hapticity of dinitrogen allowed observation of the first hydrogenation of N_2 to ammonia in solution under relatively mild conditions. The $[C_5Me_4H]^-$ ligand supports a side-on bound zirconocene dinitrogen complex in which two metallocene wedges are twisted with respect to one another. This distortion from the electronically preferred planar geometry imparts zirconium-imido character to the N_2 ligand, resulting in facile 1,2-addition of H_2 at ambient temperature. Because such subtle changes in ligand structure produce such significant consequences, the prospects for stoichiometric and possibly even catalytic nitrogen functionalization reactions are promising.

Experimental

General considerations

All air- and moisture-sensitive manipulations were carried out using standard vacuum line, Schlenk, or cannula techniques or in an M. Braun inert-atmosphere drybox containing an atmosphere of purified nitrogen. The M. Braun drybox was equipped with a cold well designed for freezing samples in liquid nitrogen. All glassware was predried in an oven at 150 °C. Solvents for air- and moisture-sensitive manipulations were initially dried and deoxygenated using literature procedures (50). Deuterated solvents for NMR spectroscopy were distilled from sodium metal under an atmosphere of argon and stored over 4 Å molecular sieves. Argon and hydrogen gas were purchased from Airgas Incorporated and passed through a column containing manganese oxide on vermiculite and 4 Å molecular sieves before admission to the high-vacuum line.

^1H and ^{13}C NMR spectra were recorded on a Varian Inova 400 spectrometer operating at 399.860 MHz (^1H) and 100.511 MHz (^{13}C). All chemical shifts are reported relative to $SiMe_4$ using ^1H (residual) or ^{13}C NMR chemical shifts of the solvent as a secondary standard. Elemental analyses were performed by Robertson Microlit Laboratories, Inc. (Madison, N.J.).

Single crystals suitable for X-ray diffraction were coated with polyisobutylene oil in a drybox and were quickly transferred to the goniometer head of a Siemens SMART CCD area detector system equipped with a molybdenum X-ray tube (λ = 0.710 73 Å). Preliminary data revealed the crystal system. A hemisphere routine was used for data collection and determination of lattice constants. The space group was identified and the data were processed using the Bruker SAINT program and corrected for absorption using SADABS. The structures were solved using direct methods (SHELXS) completed by subsequent Fourier synthesis and refined by full-matrix least-squares procedures. The crystallographic data for complexes **1** and **2** are provided in the supplementary data.[4]

Preparation of $[(\eta^5\text{-}C_5H_4SiMe_3)_2Zr(\mu_2\text{-}Cl)]_2$

A 250 mL round-bottomed flask was charged with 0.901 g (2.06 mmol) of $(\eta^5\text{-}C_5H_4SiMe_3)_2ZrCl_2$ (51) and approximately 100 mL of toluene. In a separate flask, 5 equiv.

[4] Supplementary data may be purchased from the Directory of Unpublished Data, Document Delivery, CISTI, National Research Council Canada, Ottawa, ON K1A 0S2, Canada (http://cisti-icist.nrc-cnrc.gc.ca/irm/unpub_e.shtml for information on ordering electronically). CCDC 261388 and 261389 contain the crystallographic data for this manuscript. These data can be obtained, free of charge, via www.ccdc.cam.ac.uk/conts/retrieving.html (or from the Cambridge Crystallographic Data Centre, 12 Union Road, Cambridge CB2 1EZ, UK; fax +44 1223 336033; or deposit@ccdc.cam.ac.uk).

© 2005 NRC Canada

of 0.5% (by weight) Na(Hg) was prepared. The solution of the zirconocene dichloride was added to the amalgam and the reaction mixture was stirred for 4 days. The resulting purple solution was separated from the amalgam by pipette and filtered through Celite. The solvent was removed in vacuo, and the purple oil was triturated with pentane to yield a purple solid. Recrystallization from pentane at –35 °C afforded 0.553 g (67% yield) of $[(\eta^5\text{-}C_5H_4SiMe_3)_2ZrCl]_2$. ^{1}H NMR (benzene-$d_6$) δ: 0.40 (s, 36H, Si$Me_3$), 5.31 (s, 8H, Cp), 5.44 (s, 8H, Cp). ^{13}C NMR (benzene-d_6) δ: 1.29 (SiMe_3), 104.10, 107.31, 113.12 (Cp). Anal. calcd. for $C_{32}H_{52}Si_4Zr_2Cl_2$: C 47.89, H 6.53; found: C 48.20, H 6.31.

Preparation of $(\eta^5\text{-}C_5H_4SiMe_3)_2ZrI_2$

A 100 mL round-bottomed flask was charged with 1.445 g (3.32 mmol) of $(\eta^5\text{-}C_5H_4SiMe_3)_2ZrCl_2$ and approximately 50 mL of CH_2Cl_2. A CH_2Cl_2 solution containing 1.552 g (3.959 mmol) of BI_3 was prepared and added to the metallocene solution with stirring. The reaction mixture was stirred for 2 days, after which time the solvent was removed in vacuo. The resulting yellow solid was extracted into pentane and the yellow solution filtered through Celite. The pentane was removed in vacuo, leaving 0.586 g (29%) of a yellow solid identified as $(\eta^5\text{-}C_5H_4SiMe_3)_2ZrI_2$. ^{1}H NMR (benzene-$d_6$) δ: 0.29 (s, 18H, Si$Me_3$), 6.07 (d, 4H, Cp), 6.68 (d, 4H, Cp). ^{13}C NMR (benzene-d_6) δ: 0.57 (SiMe_3), 115.95, 123.74, 125.40 (Cp).

Preparation of $[(\eta^5\text{-}C_5H_4SiMe_3)_2Zr(\mu_2\text{-}I)]_2$

This molecule was prepared in a similar manner to $[(\eta^5\text{-}C_5H_4SiMe_3)_2ZrCl]_2$ with 0.143 g (0.234 mmol) of $(\eta^5\text{-}C_5H_4SiMe_3)_2ZrI_2$ yielding 0.087 g (77% yield) of deep-purple crystals identified as $[(\eta^5\text{-}C_5H_4SiMe_3)_2ZrI]_2$. ^{1}H NMR (benzene-$d_6$) δ: 0.41 (s, 36H, Si$Me_3$), 5.21 (d, 8H, Cp), 5.36 (d, 8H, Cp). ^{13}C NMR (benzene-d_6) δ: 1.14 (SiMe_3), 102.04, 103.44, 113.64 (Cp). Anal. calcd. for $C_{32}H_{52}Si_4Zr_2I_2$: C 39.00, H 5.32; found: C 38.90, H 4.93.

Acknowledgements

We would like to thank the US National Science Foundation, the US National Institutes of Health, the Petroleum Research Fund administered by the American Chemical Society, and the Research Corporation (Cottrell Scholar award to PJC) for financial support for N_2 chemistry. PJC would also like to thank the team of dedicated graduate students and postdocs who have made the chemistry happen.

References

1. A.D. Allen and C.V. Senoff. J. Chem. Soc. Chem. Commun. 621 (1965).
2. R.E. Shepherd and H. Taube. Inorg. Chem. **12**, 1392 (1973).
3. J.N. Armor and H. Taube. J. Am. Chem. Soc. **92**, 2560 (1970).
4. F. Bottomley and S.C. Nyburg. J. Chem. Soc. Chem. Commun. 897 (1966).
5. J. Chatt, J.R. Dilworth, and R.L. Richards. Chem. Rev. **78**, 589 (1978).
6. T.A. Betley and J.C. Peters. J. Am. Chem. Soc. **125**, 10 782 (2003).
7. Y. Nishibayashi, S. Iwai, and M. Hidai. Science (Washington, D.C.), **279**, 540 (1998).
8. D.V. Yandulov and R.R. Schrock. Science, **301**, 76 (2003).
9. V. Ritleng, D.V. Yandulov, W.W. Weare, R.R. Schrock, A.S. Hock, and W.M. Davis. J. Am. Chem. Soc. **126**, 6150 (2004).
10. M.E. Vol'pin and V.B. Shur. Nature (London), **209**, 1236 (1966).
11. E.E. van Tamelen. Acc. Chem. Res. **3**, 361 (1970).
12. H.H. Brintzinger. J. Am. Chem. Soc. **88**, 4305 (1966).
13. J.E. Bercaw and H.H. Brintzinger. J. Am. Chem. Soc. **93**, 2045 (1971).
14. J.M. Manriquez and J.E. Bercaw. J. Am. Chem. Soc. **96**, 6229 (1974).
15. M.D. Fryzuk and S.A. Johnson. Coord. Chem. Rev. **200**, 379 (2000).
16. (*a*) M. Mori, K. Hori, M. Akashi, M. Hori, Y. Sato, and M. Nishida. Angew. Chem. Int. Ed. **37**, 636. (1998); (*b*) M. Akashi, M. Nishida, and M. Mori. Chem. Lett. 465 (1999); (*c*) K. Hori and M. Mori. J. Am. Chem. Soc. **120**, 7651 (1998); (*d*) M. Akashi, Y. Sato, and M. Mori. J. Org. Chem. **66**, 7873 (2001).
17. M.D. Fryzuk, J.B. Love, and S.J. Rettig. Science (Washington, D.C.), **275**, 1445 (1997).
18. L. Morello, J.B. Love, B.O. Patrick, and M.D. Fryzuk. J. Am. Chem. Soc. **126**, 9480 (2004).
19. T.E. Hanna, I. Keresztes, E. Lobkovsky, W.H. Bernskoetter, and P.J. Chirik. Organometallics, **23**, 3448 (2004).
20. J.M. De Wolf, R. Blaauw, A. Meetsma, J.H. Teuben, R. Gyepes, V. Varga, K. Mach, N. Veldman, and A.L. Spek. Organometallics, **15**, 4977 (1996).
21. P.B. Hitchcock, F. Kerton, and G.A. Lawless. J. Am. Chem. Soc. **120**, 10 264 (1998).
22. (*a*) L. Lukesová, M. Horácek, P. Stepnicka, K. Fejfarová, R. Gyepes, I. Cisorová, J. Kubista, and K. Mach. J. Organomet. Chem. **663**, 134 (2002); (*b*) M. Horácek, V. Kupfer, U. Thewalt, P. Stepnicka, M. Polasek, and K. Mach. Organometallics, **18**, 3572 (1999).
23. T.E. Hanna, E. Lobkovsky, and P.J. Chirik. J. Am. Chem. Soc. **126**, 14 688 (2004).
24. I.F. Urazowski, V.I. Ponomaryev, I.E. Nifantev, and D.A. Lemenovskii. J. Organomet. Chem. **368**, 287 (1989).
25. P.B. Hitchcock, M.F. Lappert, G.A. Lawless, H. Oliver, and E.J. Ryan. J. Chem. Soc. Chem. Commun. 474 (1992).
26. P.A. Deck, X. Cheng, E.J. Stoebenau, C. Slebonick, D.R. Billodeaux, and F.R. Fronczek. Organometallics, **19**, 5404 (2000).
27. J.A. Pool. Ph.D. thesis, Cornell University, Ithaca, N.Y. 2004.
28. Y. Wielstra, S. Gambarotta, A. Meetsma, and J.L. de Boer. Organometallics, **8**, 250 (1989).
29. Y. Wielstra, S. Gambarotta, A. Meetsma, and A.L. Spek. Organometallics, **8**, 2948 (1989).
30. R.L. DeKock, M.A. Peterson, L.E.L. Reynolds, L.-H. Chen, E.J. Baerends, and P. Vernooijs. Organometallics, **12**, 2794 (1993).
31. M. Bénard and M.-M. Rohmer. J. Am. Chem. Soc. **114**, 4785 (1992).
32. C.E. Zachmanoglou, A. Docrat, B.M. Bridgewater, G.E. Parkin, C.G. Brandow, J.E. Bercaw, C.N. Jardine, M. Lyall, J.C. Green, and J.B. Kiester. J. Am. Chem. Soc. **124**, 9525 (2002).
33. A. Antifiolo, M.F. Lappert, A. Singh, D.J.W. Winterborn, L.M. Engelhardt, C.L. Raston, A.H. White, A.J. Carty, and N.J. Taylor. J. Chem. Soc. Dalton Trans. 1463 (1987).
34. J. Jeffrey, M.F. Lappert, and P.I. Riley. J. Organomet. Chem. **181**, 25 (1979).
35. M.D. Fryzuk, S.A. Johnson, and S.J. Rettig. J. Am. Chem. Soc. **120**, 11 024 (1998).
36. M.D. Fryzuk, B.A. MacKay, and B.O. Patrick. J. Am. Chem. Soc. **125**, 3234 (2003).

© 2005 NRC Canada

37. P.J. Chirik, L.M. Henling, and J.E. Bercaw. Organometallics, **20**, 534 (2001).
38. J.A. Pool, C.A. Bradley, and P.J. Chirik. Organometallics, **21**, 1271 (2002).
39. J.A. Pool, E. Lobkovsky, and P.J. Chirik. J. Am. Chem. Soc. **125**, 2241 (2003).
40. J.A. Pool, E. Lobkovsky, and P.J. Chirik. Organometallics, **22**, 2797 (2003).
41. G.W. Coates. Chem. Rev. **100**, 1223 (2000).
42. M.E. Rerek and F. Basolo. J. Am. Chem. Soc. **106**, 5908 (1984).
43. C.A. Bradley, E. Lobkovsky, and P.J. Chirik. J. Am. Chem. Soc. **125**, 8110 (2003).
44. C.A. Bradley, I. Keresztes, E. Lobkovsky, V.G. Young, and P.J. Chirik. J. Am. Chem. Soc. **126**, 16 937 (2004).
45. C. Janiak, U. Versteeg, K.C.H. Lange, R. Weiman, and E. Hahn. J. Organomet. Chem. **501**, 219 (1995).
46. J.A. Pool, E. Lobkovsky, and P.J. Chirik. Nature (London), **427**, 529 (2004).
47. J.A. Pool, W.H. Bernskoetter, and P.J. Chirik. J. Am. Chem. Soc. **126**, 14 326 (2004).
48. C.C. Cummins, S.M. Baxter, and P.T. Wolczanski. J. Am. Chem. Soc. **110**, 8731 (1988).
49. A.P. Duncan and R.G. Bergman. Chem. Rec. **2**, 431 (2002).
50. A.B. Pangborn, M.A. Giardello, R.H. Grubbs, R.K. Rosen, and F.J. Timmers. Organometallics, **15**, 1518 (1996).

© 2005 NRC Canada

Low-coordinate iron complexes as synthetic models of nitrogenase[1]

Patrick L. Holland

Abstract: Three-coordinate iron sites are potentially important intermediates in the reduction of dinitrogen by the enzyme nitrogenase, but synthetic work to outline the behavior of three-coordinate iron complexes is in its infancy. Recent work shows that bulky diketiminate ligands give a general route to three-coordinate iron complexes with a variety of third ligands. The low coordination number leads to exciting new reactions in which N—N bonds are weakened or broken. Such complexes show great promise for evaluating the ability of low-coordinate iron to perform bond cleavage reactions akin to the individual steps of the nitrogenase system.

Key words: nitrogenase, three-coordinate iron, diketiminate, N–N cleavage.

Résumé : Les sites de fer tricoordiné sont potentiellement d'importants intermédiaires dans la réduction du diazote par l'enzyme nitrogénase, mais le travail de synthèse pour ébaucher le comportement des complexes de fer tricoordiné n'en est qu'à ses débuts. Des travaux récents montrent que des ligands dicétiminates volumineux permettent de tracer une route générale conduisant à des complexes de fer tricoordiné avec une variété de troisièmes ligands. Le faible nombre de coordination conduit à d'excitantes nouvelles réactions dans lesquelles les liaisons N—N sont affaiblies ou rompues. De tels complexes offrent de grandes possibilités pour évaluer l'habilité du fer à faible coordination à provoquer des réactions de bris de liaisons ressemblant aux étapes individuelles du système de la nitrogénase.

Mots clés : nitrogénase, fer tricoordiné, dicétiminate, clivage N–N.

[Traduit par la Rédaction]

Introduction — Nitrogenase and synthetic models

The discovery of facile reactions through which N_2 may be transformed into more useful nitrogen-containing molecules is a chemical challenge that has occupied chemists for more than a century. The greatest success in this quest happened roughly a century ago, when Haber and Bosch developed the high-temperature iron-based hydrogenation of N_2 that is performed on a staggering scale today (1). When Haber was awarded the Nobel Prize, he recognized in his address an attractive route for learning how to reduce N_2 more easily: "Nitrogen bacteria teach us that Nature, with her sophisticated forms of the chemistry of living matter, still understands and utilizes methods which we do not as yet know how to imitate" (2). Inorganic chemists still believe that mimicking the biological fixation of nitrogen is an important goal, but have not yet been able to elucidate the "methods" of which Haber spoke.

One guide in this effort is the study of the *nitrogenase* enzymes, which have been reviewed (3, 4). Particular attention has fallen on iron–molybdenum nitrogenase, because it is the most active nitrogenase and because it has been crystallographically characterized to high resolution (5). The site at which N_2 is bound and reduced to ammonia (the limiting stoichiometry is shown in eq. [1]) is the *iron–molybdenum cofactor* or *FeMoco*.

$$[1] \qquad N_2 + 8H^+ + 8e^- + 16\text{MgATP} \rightarrow 2NH_3 + H_2 + 16\text{MgADP} + 16\text{phosphate}$$

Figure 1 shows the isolated form of the cluster (5). X represents a hypervalent light atom, most likely nitrogen (6–10), which is coordinated to the six central iron atoms of the cluster. These six iron atoms have a geometry that is intermediate ($\tau = 0.46$) between trigonal pyramidal ($\tau = 1$) and tetrahedral ($\tau = 0$) (11). The oxidation states of the metals are thought to be $Fe_4^{2+}Fe_3^{3+}Mo^{4+}$ in this isolated form (10), but unfortunately this picture is not strictly relevant to the reaction with N_2 because the cluster must be reduced by several electrons before substrates bind. The reduced, activated form is unstable, reducing protons to hydrogen in the absence of substrate. Therefore, the active form of the cofactor is frustratingly obscured from crystallographic view, and chemists can only speculate as to its topology, geometry, and modes of reactivity.

The *synthetic modeling approach* has been a valuable strategy for many outstanding issues in bioinorganic chemistry (12). Synthetic inorganic compounds that have structural, spectroscopic, and (or) functional similarity to the enzyme active site are studied in detail and profitably compared with data for the enzymatic system. In the case of nitrogenase, this quest has involved synthesis and characterization of iron–sulfur and iron–molybdenum–sulfur clusters, and the

Received 10 August 2004. Published on the NRC Research Press Web site at http://canjchem.nrc.ca on 9 March 2005.

P.L. Holland. Department of Chemistry, University of Rochester, Rochester, NY 14627, USA. (e-mail: holland@chem.rochester.edu).

[1]This article is part of a Special Issue dedicated to Dinitrogen Chemistry.

 doi: 10.1139/V05-005 © 2005 NRC Canada

Scheme 1.

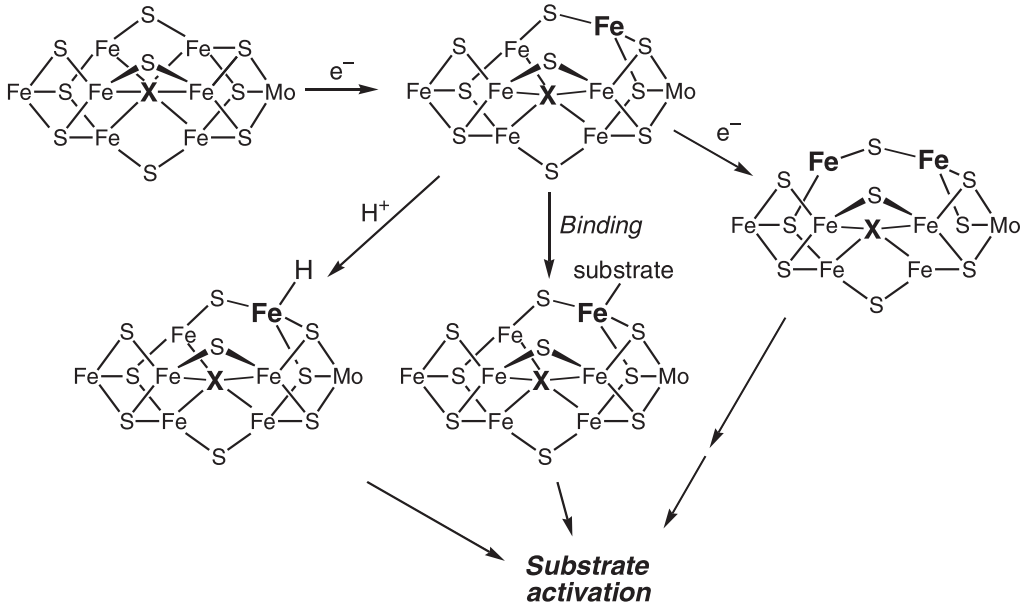
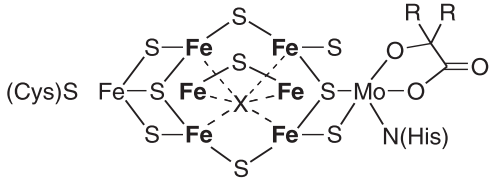


Fig. 1. The isolated form of the iron–molybdenum cofactor of nitrogenase. X represents a light atom that is thought to be C, N, or O.



binding and reduction of N_2 by metals. An important step along this road came with the synthesis of metal–N_2 complexes, as first reported by Allen and Senoff (13). As the known chemistry of N_2 has grown, increasing effort has been devoted to the study of molybdenum and iron compounds as synthetic models that teach us about the geometric and chemical capabilities of these metals.

In the synthetic literature, most modeling efforts have focused on molybdenum, with especially important contributions from the research groups of Chatt (14), Cummins (15), and Schrock (16), who have each completely broken the N—N bond of N_2. Despite the feasibility of molybdenum for N_2 reduction, recent work shows several pieces of evidence that N_2 binding may occur instead at iron in the enzyme! (*a*) There are nitrogenases that contain no molybdenum and have only somewhat lower activity (17). (*b*) The selectivity of the iron–molybdenum enzyme changes drastically with mutations near the *iron* sites of the FeMoco (18). (*c*) The six iron atoms at the center of the cluster have unusual, low-coordinate geometries. In view of these findings, there is an urgent need to explore the nitrogenase-relevant chemistry of iron complexes to gain the level of insight that has been accomplished for molybdenum.

The relevance of three-coordinate iron

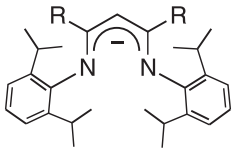
Scheme 1 shows the framework for a nitrogenase mechanism that guides our experiments on low-coordinate iron compounds. Reduction of metal–sulfur clusters is known to place electrons into orbitals that have metal–ligand antibonding character (19). Therefore, one expects weakening and (or) breaking of cluster bonds upon FeMoco reduction. Bonds to the hypervalent X atom are presumably weak, and breaking an Fe—X bond generates a three-coordinate, unsaturated, and highly reactive iron center. This iron atom may directly bind N_2, or be protonated to form a low-coordinate iron hydride (with electrons coming from the cluster). This process may be repeated without reducing the coordination number of X to an unstable level. The binding of substrates would then occur at the belt of the FeMoco, as implicated by ingenious studies on nitrogenase mutants (18, 20).

Despite the fact that three-coordinate iron is unprecedented in biological compounds, this deduction is persuasive for a number of reasons. First, a highly coordinatively unsaturated, low-valent iron atom could conceivably coordinate the weak donor N_2. Second, the role of X would be explained as a hemilabile ligand (21) that coordinates and saturates iron in the inactive form but releases it for activity in the reduced form. This role of X is consistent with several lines of evidence that indicate that X is *not* from turnover N_2 (namely, ENDOR/ESEEM studies do not show a signal after turnover with $^{15}N_2$ (22, 23), and nitrogenase mutants that are incapable of turning over N_2 are spectroscopically identical to the wild-type enzyme (18)). Finally, the research of Wolczanski and of Cummins has shown that three-coordinate transition-metal complexes have extensive bond-breaking ability (24), suggesting that exploration of analogous iron complexes could yield important clues about N—N bond breaking by the FeMoco.

A number of computational studies (using density functional theory (DFT)) have given a picture of potential N_2 binding modes and intermediates. However, only one reported study has taken the essential step of determining the energetic cost of the barriers between the intermediates (25). The mechanism with catalytically relevant activation barriers

© 2005 NRC Canada

Fig. 2. The bulky diketiminate ligands used to stabilize three-coordinate iron(II) complexes. R = methyl or *tert*-butyl.



has N_2 bound between two iron atoms that have lost some bonds to X and to the bridging sulfide. Although the synthetic compounds described below do not have perfect topological congruence with the theoretical models, it is heartening that calculations are consistent with Scheme 1 in that bond breaking within the cofactor is important in the process of binding nitrogen.

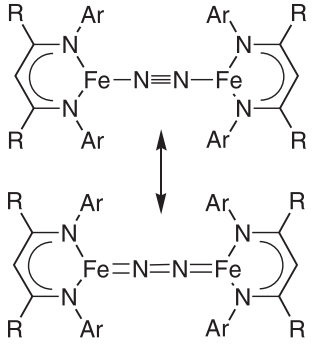
Synthesis and spectroscopy of three-coordinate iron(II) complexes

To test the ideas outlined in Scheme 1, it is necessary to study low-coordinate iron compounds, and there are few in the literature. The following research builds on the discovery that bulky β-diketiminate ligands (Fig. 2) are useful bidentate ligands that stabilize three-coordinate compounds, even with copper(II) where three-coordination previously had been unprecedented (26). In initial work, we demonstrated that coordination of β-diketiminate ligands to iron(II), cobalt(II), and nickel(II) gives three-coordinate halide complexes, which are sometimes in equilibrium with four-coordinate dimers or lithium halide adducts (27, 28). Substitution of the halide ligand leads to complexes in which the third ligand coordinates through C, N, O, S, Cl, and H, giving great variety in electronic and steric properties of the three-coordinate iron(II) complexes (29).

In collaborative work with Eckard Münck and his research group, the electronic structure of these compounds was elaborated (30). The three-coordinate iron(II) compounds are invariably high-spin (S = 2), with four half-filled d orbitals and one filled d orbital. This filled orbital is the d_{z^2} orbital, using an axis system where z is perpendicular to the coordination plane of iron. Interestingly, there is substantial unquenched orbital angular momentum, arising from mixing between the d_{z^2} orbital and another low-lying d orbital (mediated by spin-orbit coupling). This unusual electronic structure leads to large negative zero-field splitting, which was quantified using Mössbauer and EPR spectroscopies. Interestingly, DFT calculations separated the Mössbauer quadrupole splitting into components attributable to specific ligands, which helped to understand the Mössbauer parameters for the FeMoco. More recently, the Münck group has used these parameters to show that the bonding between iron and X in the FeMoco is ionic and relatively weak (10). That is, X does not greatly perturb the electronic structure of the iron atoms to which it is attached.

The possession of well-characterized three-coordinate iron(II) complexes with one differentiated site allowed us to experimentally ask certain questions about the potential roles of low-coordinate iron in the FeMoco. The remainder of this review will consist of three specific questions, along with the results of initial studies that have started to answer these questions.

Fig. 3. Diiron complex with weakened N_2 ligands (N–N distances are 1.18–1.19 Å). The lower resonance structure suggests the weakening of N_2 through backbonding from the iron d orbitals into the π* orbital of N_2. Ar = 2,6-diisopropylphenyl. R = *tert*-butyl.



Does low coordination number enable iron to interact strongly with N_2 and to weaken the N—N triple bond?

Prior to the year 2001, all known complexes in which N_2 was coordinated only by iron had the metal in a coordination number of five or greater. In these iron(0) and iron(II) compounds, the N—N bond lengths were 1.13 Å or less, and N–N stretching frequencies were greater than 1900 cm^{-1}, corresponding to a nearly unperturbed N—N triple bond. Hence, iron–nitrogen complexes were categorized as "unactivated", based on the numerous precedents from iron in five- or six-coordinate geometries (31).

The bulky diketiminate ligands lead to iron–N_2 complexes that have a coordination number of only three (Fig. 3). These were synthesized by reduction of the iron chloride complexes under an atmosphere of N_2 (32). The crystal structures of the formally iron(I) and iron(0) complexes show that the N—N bonds are stretched to lengths of 1.18–1.24 Å, distances that are characteristic of N—N double bonds. Confirming the weakening of the bonds, resonance Raman spectra show N–N stretching bands below 1800 cm^{-1}. DFT calculations indicate that the molecules have high-lying filled orbitals with substantial Fe–N π-bonding character; these same orbitals have antibonding π interactions between the two nitrogen atoms. Therefore, there is backbonding of iron d orbitals into the π* orbital of the bridging N_2 ligand, weakening the N—N bond by shifting charge from Fe to N_2.

To confirm that the weakening of the bonds is attributable to the low coordination number, we performed comparative calculations on the five-coordinate and three-coordinate diiron–dinitrogen models illustrated in Fig. 4. The former model closely resembles literature N_2 complexes of iron(0) (33), and the latter is a modification in which the coordination number forcibly has been changed from five to three. Interestingly, despite retention of the π-withdrawing CO ligands in the three-coordinate model, the optimized N–N distance is quite long (1.173 Å), and similar to that in the diketiminate compound. The stretching of N_2 upon reducing the coordination number of iron from five to three supports a

© 2005 NRC Canada

Scheme 2.

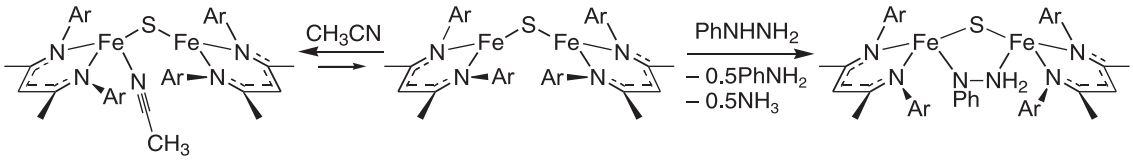


Fig. 4. A theoretical test of the effect of coordination number on iron–N_2 bonding. According to DFT calculations, removal of the two axial ligands shortens the Fe—N bonds and stretches the N—N bond, demonstrating the link between coordination number and N_2 weakening.

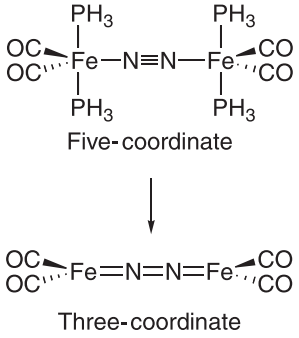
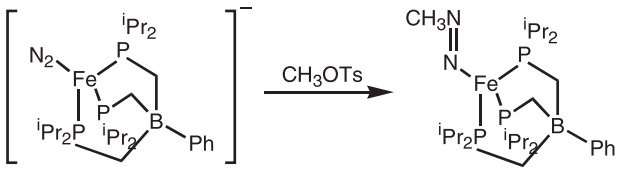


Fig. 5. A four-coordinate iron-dinitrogen complex that has a weakened N—N bond and reacts with electrophiles at the N_2 ligand.



fundamental connection between coordination number and the ability to weaken the N—N bond of coordinated N_2.

Does this anomalous ability to weaken N_2 extend to four-coordinate iron? An affirmative answer to this question comes from recent work from Betley and Peters (34) in which tris(phosphino)borate ligands stabilize tetrahedral iron complexes. Notably, the four-coordinate iron–dinitrogen complexes have weakened and stretched N—N bonds. In the example shown in Fig. 5, the weakening from iron(0) was demonstrated with the N-N stretching frequency of 1884 cm^{-1}. Therefore, the principle that low coordination number engenders anomalous N_2-weakening ability appears to be general to three- and four-coordination, and the strength of the N—N bond is perhaps more sensitive to the coordination number than to the oxidation state. Further studies will use this weakening to enable reactions at the N_2 unit; for example, the Fe–N_2 complex in Fig. 5 reacts with methyl tosylate to give a methyldiazenido complex.

Do sulfide-bridged diiron complexes react with nitrogenase-relevant compounds?

One potential reduced form of the FeMoco has a pair of iron atoms that have been "freed" from the central X ligand (Scheme 1). The juxtaposition of two coordinatively unsaturated sites in one complex is a good recipe for activating N_2 toward reactivity, based on the work of Fryzuk et al. (35). Because diketiminates differentiate one coordination site, it was possible to access a complex in which two three-coordinate iron atoms are bridged by sulfide. When one of the N_2 complexes was treated with elemental sulfur, we isolated a bridging sulfidodiiron(II) complex in high yield. Scheme 2 shows this compound and some of its reactivity (11). Variable-field Mössbauer spectroscopy experiments demonstrate that in the compound, the two iron(II) ions are high-spin but magnetically coupled.

The X-ray crystal structure of the sulfido complex shows that the Fe_2S core is bent at sulfur (Fe-S-Fe = 102°), but the angle at sulfur is not as acute as its analogue in the FeMoco (Fe-S-Fe ~ 71°). This difference may be due to the absence of the X bridge in the model compound, or to steric interactions between the large diketiminate ligands. However, the steric clash is not sufficient to keep the iron centers from coordinating additional weak ligands like acetonitrile, ammonia, and alkylhydrazines. For example, the 1:1 adduct with acetonitrile is shown at the left of Scheme 2.

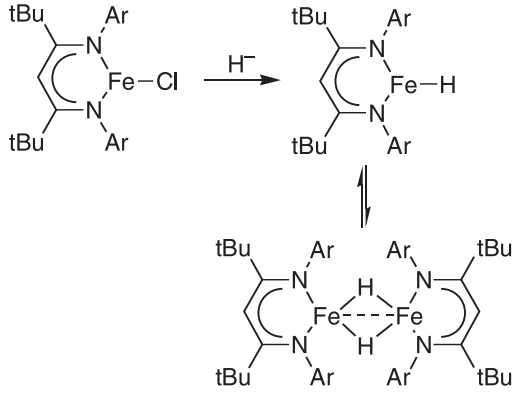
The sulfido compound undergoes a very interesting reaction with phenylhydrazine, giving the mixed-valence iron(II)–iron(III) complex at the right side of Scheme 2. In this product, the hydrazine is converted into a hydrazido ligand concurrent with oxidation of iron. The oxidizing agent in the reaction is phenylhydrazine itself, which is reduced to aniline and ammonia! Titration experiments showed that 1.5 equiv. of the hydrazine react, and the ammonia was distilled out of the reaction to verify the reaction stoichiometry shown in Scheme 2. We liken the cleavage of N—N bonds by this diiron compound to the rupture of N—N single bonds that must take place during the catalytic cycle of nitrogenase. More generally, the reaction indicates that the Fe_2S core is a substantial reducing agent and a reactive functionality.

Are iron hydrides reactive enough to be considered as potential FeMoco intermediates?

Thorough studies on the time course of H_2 production upon rapid acidification of the FeMoco during nitrogenase turnover strongly implied that several protonations of the enzyme occur prior to N_2 binding (36). There are many potential sites on the FeMoco that could be protonated, including the metal centers: protonation of a metal formally oxidizes the metal by two units and reduces H^+ to H^-. The possibility of hydride species as nitrogenase intermediates is persuasive to organometallic chemists, because nitrogenase reduces organic substrates in a manner that is reminiscent of the reac-

© 2005 NRC Canada

Fig. 6. Synthesis of a low-coordinate iron(II) hydride complex. Ar = 2,6-diisopropylphenyl. The iron–iron distance in the dimer is only 2.62 Å.



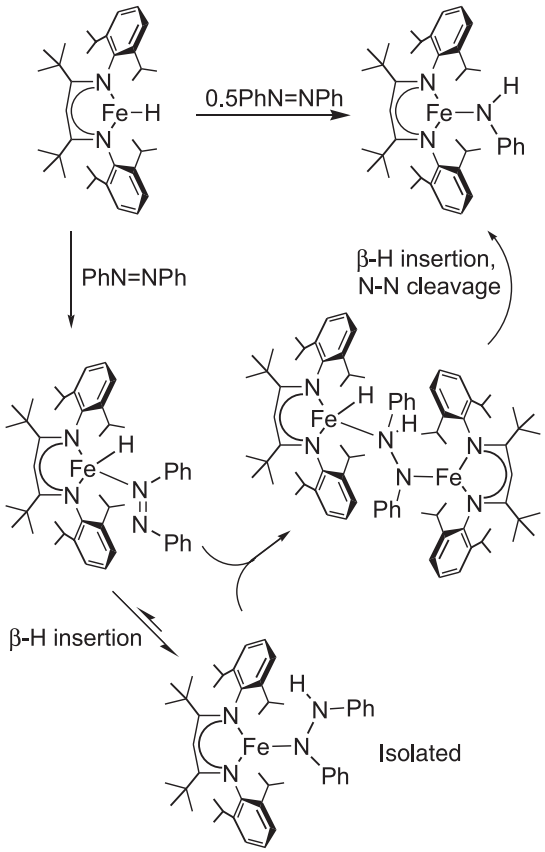
tions of metal-hydride species (37). However, *all* iron-hydride complexes in the literature had a coordination number of five or higher, and a low-spin electronic configuration (38). The surprising stability of high-spin, three-coordinate alkyliron(II) complexes (39, 40) suggested that it would be possible to make the first low-coordinate, high-spin iron hydride. This compound would allow evaluation of a high-spin iron-hydride functionality toward nitrogenase-relevant substrates.

The transformation shown in Fig. 6 leads to the isolation of a stable hydride complex, as long as the BEt_3 by-product is promptly removed (41). This synthetic strategy can be used to generate gram quantities of the hydride complex shown. Surprisingly, hydride (the smallest possible ligand!) bridges the two metals. The short bridge holds the two iron atoms very close together, and the Fe–Fe distance is nearly identical to the 2.63 Å Fe–Fe distance between pairs of iron atoms in the FeMoco.

In solution, the hydride dimer is in equilibrium with a three-coordinate monomer. The monomeric hydridoiron(II) complex was characterized by its high-temperature UV–vis and ^{1}H NMR spectra and magnetism, which are very similar to three-coordinate alkyl analogues (40). Because the position of ^{1}H NMR resonances in paramagnetic compounds is very sensitive to the electronic structure at the metal, the similarity of the NMR spectra is good evidence that the monomeric hydride has the same trigonal-planar geometry seen in the crystal structures of the alkyl complexes (40). Another interesting feature is the ^{1}H NMR spectrum of the dimer, which consists of a multitude of peaks for analytically pure material. We believe that the complicated ^{1}H NMR spectrum results from hindered C—C bond rotations in the ligand. Consistent with decreased flexibility, the dimeric hydride is much less soluble in alkanes than the other diketiminate–iron complexes.

In an amazing transformation, reaction of the hydride complex with 0.5 molar equiv. of diphenyldiazene ("azobenzene") quantitatively gives a phenylamido complex. This reaction, shown in Scheme 3, represents the first example of complete N—N double bond cleavage by an iron-hydride complex. Other examples of N—N double bond cleavage by synthetic compounds occur with four-electron oxidation of the metal and formation of two imido ligands. In contrast,

Scheme 3.



the reaction in Scheme 3 results in no overall change in oxidation state at the metal: the reducing equivalents formally come from oxidation of the hydride ligands. In our view, the possibility of hydride as a reducing agent for biological bond cleavage is persuasive because drastic changes in oxidation state at the metal would not be required to accomplish the necessary reduction chemistry.

We have isolated and crystallographically characterized the hydrazido intermediate shown in Scheme 3. Isolated samples of this compound independently convert to a mixture of the amido complex and 0.5 equiv. of diazene, with a reaction rate that is first-order in iron concentration. Ongoing mechanistic experiments suggest the mechanism shown in Scheme 3, but confirmation of this mechanism requires further study.

Summary and implications

The biological reduction of N_2 is a stunning transformation for which the mechanism is quite unclear. By conceptually breaking down the cofactor into monoiron and diiron units, and by hypothesizing that low coordination is the key feature that engenders high reactivity by the FeMoco, we have been able to identify specific questions that can be answered by small, well-characterized iron complexes. In contrast to the established chemistry of five- and six-coordinate iron complexes that show "normal" organometallic reductions and little N_2 weakening, three- and four-coordinate iron complexes are more active. It is not yet clear whether the major determinant of this higher reactivity is the high-

© 2005 NRC Canada

spin electronic configuration or the low coordination number. Thus, the conventional wisdom that iron is not reactive enough to be responsible for nitrogenase activity needs to be reconsidered in light of these studies.

Acknowledgments

I thank the Rochester Department of Chemistry, the National Science Foundation, the National Institutes of Health, and the Alfred P. Sloan Foundation for financial support of the work described. Thanks are due to the faculty and staff at Rochester for assistance, to Dennis Dean for thoughtful comments, and to Jonas Peters and his group for insightful discussions. Most of all, I thank the students, collaborators, and co-workers who are responsible for these research accomplishments: Jeremy Smith, Nathan Eckert, and Javier Vela at the University of Rochester, Hanspeter Andres, Sebastian Stoian, Emile Bominaar, and Eckard Münck at Carnegie Mellon University, Kenton Rodgers and Gudrun Lukat-Rodgers at North Dakota State University, and Karl Pittard and Thomas Cundari at the University of North Texas.

References

1. V. Smil. Sci. Am. **277**, 76 (1997).
2. Nobel Foundation. Nobel lectures in chemistry 1901–1921. Elsevier, Amsterdam. 1966.
3. B.K. Burgess and D.J. Lowe. Chem. Rev. **96**, 2983 (1996).
4. P.L. Holland. *In* Comprehensive coordination chemistry 2. Vol. 8. *Edited by* J. McCleverty and T.J. Meyer. Elsevier, Oxford. 2003. pp. 569–599.
5. O. Einsle, F.A. Tezcan, S.L.A. Andrade, B. Schmid, M. Toshida, J.B. Howard, and D.C. Rees. Science, **297**, 1696 (2002).
6. I. Dance. Chem. Commun. 324 (2003).
7. T. Lovell, T. Liu, D.A. Case, and L. Noodleman. J. Am. Chem. Soc. **125**, 8377 (2003).
8. B. Hinnemann and J.K. Norskøv. J. Am. Chem. Soc. **125**, 1466 (2003).
9. U. Huniar, R. Ahlrichs, and D. Coucouvanis. J. Am. Chem. Soc. **126**, 2588 (2004).
10. V. Vrajmasu, E. Münck, and E.L. Bominaar. Inorg. Chem. **42**, 5974 (2003).
11. J. Vela, S. Stoian, C.J. Flaschenriem, E. Münck, and P.L. Holland. J. Am. Chem. Soc. **126**, 4522 (2004).
12. R.H. Holm and E.I. Solomon. Chem. Rev. **104**, 347 (2004).
13. D. Allen and C.W. Senoff. Chem. Commun. 621 (1965).
14. J. Chatt, J.R. Dilworth, and R.L. Richards. Chem. Rev. **78**, 589 (1978).
15. J.C. Peters, J.-P.F. Cherry, J.C. Thomas, L. Baraldo, D.J. Mindiola, W.M. Davis, and C.C. Cummins. J. Am. Chem. Soc. **121**, 10 053 (1999).
16. D.V. Yandulov and R.R. Schrock. Science, **301**, 76 (2003).
17. E. Krahn, B.J.R. Weiss, M. Kröckel, J. Groppe, G. Henkel, S.P. Cramer, A.X. Trautwein, K. Schneider, and A. Müller. J. Biol. Inorg. Chem. **7**, 37 (2002).
18. J. Christiansen, D.R. Dean, and L.C. Seefeldt. Annu. Rev. Plant Physiol. Plant Mol. Biol. **52**, 269 (2001).
19. H. Beinert, R.H. Holm, and E. Münck. Science (Washington, D.C.), **277**, 653 (1997).
20. H.-I. Lee, R.Y. Igarashi, M. Laryukhin, P.E. Doan, P.C. Dos Santos, D.R. Dean, L.C. Seefeldt, and B.M. Hoffman. J. Am. Chem. Soc. **126**, 9563 (2004).
21. C.S. Slone, D.A. Weinberger, and C.A. Mirkin. Prog. Inorg. Chem. **48**, 233 (1999).
22. H. Thomann, T.V. Morgan, H. Jin, S.J.N. Burgmayer, R.E. Bare, and E.I. Stiefel. J. Am. Chem. Soc. **109**, 7913 (1987).
23. H.-I. Lee, P.M.C. Benton, M. Laryukhin, R.Y. Igarashi, D.R. Dean, L.C. Seefeldt, and B.M. Hoffman. J. Am. Chem. Soc. **125**, 5604 (2003).
24. C.C. Cummins. Prog. Inorg. Chem. **47**, 685 (1998).
25. J. Schimpl, H.M. Petrilli, and P.E. Blöchl. J. Am. Chem. Soc. **125**, 15 772 (2003).
26. P.L. Holland and W.B. Tolman. J. Am. Chem. Soc. **121**, 7270 (1999).
27. J.M. Smith, R.J. Lachicotte, and P.L. Holland. Chem. Commun. 1542 (2001).
28. N.A. Eckert, E.M. Bones, R.J. Lachicotte, and P.L. Holland. Inorg. Chem. **42**, 1720 (2003).
29. N.A. Eckert, J.M. Smith, R.J. Lachicotte, and P.L. Holland. Inorg. Chem. **43**, 3306 (2004).
30. H. Andres, E. Bominaar, J.M. Smith, N.A. Eckert, P.L. Holland, and E. Münck. J. Am. Chem. Soc. **124**, 3012 (2002).
31. F. Tuczek and N. Lehnert. Angew. Chem. Int. Ed. **37**, 2636 (1998).
32. J.M. Smith, R.J. Lachicotte, K.A. Pittard, T.R. Cundari, G. Lukat-Rodgers, K.R. Rodgers, and P.L. Holland. J. Am. Chem. Soc. **123**, 9222 (2001).
33. H. Berke, W. Bankhardt, G. Huttner, J. Von Seyerl, and L. Zsolnai. Chem. Ber. **114**, 2754 (1981).
34. T.A. Betley and J.C. Peters. J. Am. Chem. Soc. **125**, 10 782 (2003).
35. M.D. Fryzuk, S.A. Johnson, B.O. Patrick, A. Albinati, S.A. Mason, and T.F. Koetzle. J. Am. Chem. Soc. **123**, 3960 (2001); M.D. Fryzuk, B.A. MacKay, S.A. Johnson, and B.O. Patrick. Angew. Chem. Int. Ed. **41**, 3709 (2002); M.D. Fryzuk, C.M. Kozak, M.R. Bowdridge, B.O. Patrick, and S.J. Rettig. J. Am. Chem. Soc. **124**, 8389 (2002).
36. D.J. Lowe and R.N.F. Thorneley. Biochem. J. **224**, 877 (1984); R.N.F. Thorneley and D.J. Lowe. Biochem. J. **224**, 887 (1984); D.J. Lowe and R.N.F. Thorneley. Biochem. J. **224**, 895 (1984); R.N.F. Thorneley and D.J. Lowe. Biochem. J. **224**, 903 (1984).
37. G.J. Leigh and C.N. McMahon. J. Organomet. Chem. **500**, 219 (1995).
38. M. Peruzzini and R. Poli. Recent advances in hydride chemistry. Elsevier, New York. 2001.
39. P.L. Holland, T.R. Cundari, L.L. Perez, N.A. Eckert, and R.J. Lachicotte. J. Am. Chem. Soc. **124**, 14 416 (2002).
40. J.M. Smith, R.J. Lachicotte, and P.L. Holland. Organometallics, **21**, 4808 (2002).
41. J.M. Smith, R.J. Lachicotte, and P.L. Holland. J. Am. Chem. Soc. **125**, 15 752 (2003).

© 2005 NRC Canada

Portability of the RNNMo(3+) core — Application to the synthesis of dinitrogen-derived trialkoxymolybdenum organodiazenido complexes[1]

John-Paul F. Cherry, Paula L. Diaconescu, and Christopher C. Cummins

Abstract: An alcoholysis strategy has been employed in the synthesis of new oligo- or polymeric trialkoxymolybdenum diazenido complexes $[R^1NNMo(O\text{-}1\text{-}Ad)_3]_x$ (R^1 = Me or C(O)OMe) as well as their mononuclear THF solvates $R^1NNMo(O\text{-}1\text{-}Ad)_3(THF)$. Dinitrogen-derived diazenido precursor complexes $R^1NNMo(N[R]Ar)_3$ (R = *i*-Pr, Ar = 3,5-$C_6H_3Me_2$) react smoothly with 3 equiv. 1-adamantanol to liberate 3 equiv. HN(R)Ar without disruption of the diazenidomolybdenum(3+) core. X-ray structural investigations were carried out for diazenido complex $MeNNMo(O\text{-}1\text{-}Ad)_3(THF)$ and for the corresponding cationic dimethyldiazenido complex $[Me_2NNMo(O\text{-}1\text{-}Ad)_3(THF)]^+$, obtained as its triflate salt. The latter cation was found upon cobaltocene reduction to undergo N—N bond cleavage, producing nitride $NMo(O\text{-}1\text{-}Ad)_3$ (synthesized independently) and dimethylamine.

Key words: molybdenum, dinitrogen, bond cleavage, hydrazido, diazenido.

Résumé : On a utilisé une stratégie d'alcoolyse dans la synthèse de nouveaux complexes oligo- et polymériques du diazénido trialkoxymolybdène $[R^1NNMo(O\text{-}1\text{-}Ad)_3]_x$ (R^1 = Me ou C(O)OMe) et celle de leurs complexes monomoléculaires monosolvatés par le THF $R^1NNMo(O\text{-}1\text{-}Ad)_3(THF)$. Les complexes précurseurs diazénido dérivés du diazote $R^1NNMo(N[R]Ar)_3$ (R = *i*-Pr, Ar = 3,5-$C_6H_3Me_2$) réagissent sans problème avec trois équivalents d'adamant-1-ol pour libérer trois équivalents de HN(R)Ar sans disruption du noyau diazénidomolybdène(3+). On a examiné les structures du complexe diazénido $MeNNMo(O\text{-}1\text{-}Ad)_3(THF)$ et du complexe diméthyldiazénido cationique correspondant $[Me_2NNMo(O\text{-}1\text{-}Ad)_3(THF)]^+$ isolé sous la forme de triflate. On a trouvé que la réduction de ce dernier cation par le cobaltocène conduit à un clivage de la liaison N—N qui conduit à la formation du nitrure $NMo(O\text{-}1\text{-}Ad)_3$ (qui a été synthétisé par une voie indépendante) et de la diméthylamine.

Mots clés : molybdène, diazote, clivage d'une liaison, hydrazido, diazénido.

[Traduit par la Rédaction]

Introduction

Amide (NR_2^{1-}) ligands (1) and tripodal variants incorporating them have become established supporting ligands for the dinitrogen chemistry of metals from groups 4, 5, and 6 (2–16). In contrast, while early metal alkoxides and (or) aryloxides are abundant and their chemistry is well-established (17), the combination of alkoxide supporting ligands and dinitrogen activation–functionalization remains rare. A prime example of dinitrogen binding, activation, and cleavage to nitride by an early metal aryloxy system is provided by the niobium-calix[4]arene system reported by Floriani and co-workers (18). Furthermore, N_2 splitting in combination with intermetal N-atom transfer has been reported in a system that produces $^{15}NMo(O\text{-}t\text{-}Bu)_3$ from $^{15}N_2$ (19).

Since a common mode of reactivity for coordinated dinitrogen is that involving treatment with simple electrophiles (e.g., H^+, Me^+ synthons) and conversion to diazenido (NNH^{1-} or $NNMe^{1-}$) units (20–24), and since such conversions are essentially absent from the known chemistry of early-metal alkoxides, we sought an alternative synthetic entry to trialkoxymolybdenum(IV) diazenido systems. Dinitrogen-derived diazenido, hydrazido, and related ligands have interested theoreticians for at least a quarter century (25).

We have shown recently that certain Mo-ligand multiply bonded functional groups are "portable" in the sense that they can be retained while exchanging all the supporting ligands. Accordingly, the monomeric terminal phosphide (P^{3-}) complex $PMo(O\text{-}1\text{-}MeCy)_3$ was synthesized by treatment of $PMo(N[i\text{-}Pr]Ar)_3$ with 3 equiv. of 1-methyl cyclohexanol (26). In addition, a variety of Schrock-type alkyne metathesis catalysts $R^1CMo(OR^2)_3$ could be synthesized by an analogous alcoholysis protocol, involving treatment of precursor $R^1CMo(N[i\text{-}Pr]Ar)_3$ with 3 equiv. of the desired alcohol or phenol, R^2OH (27, 28). The latter two examples reveal the "portability" of the MoP and MoC triple bond functional groups, attributable to their compatibility with the required protic reaction conditions in concert with the protolytic sen-

Received 12 September 2004. Published on the NRC Research Press Web site at http://canjchem.nrc.ca on 9 March 2005.

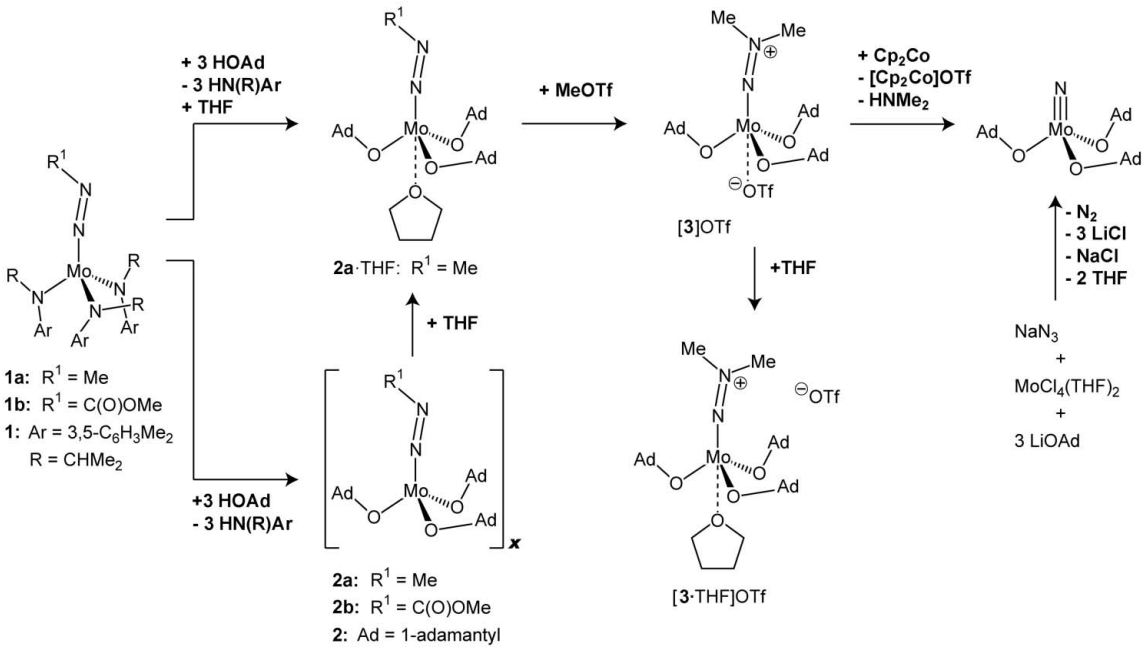
J.-P.F. Cherry, P.L. Diaconescu, and C.C. Cummins.[2] Department of Chemistry, Room 2-227, Massachusetts Institute of Technology, 77 Massachusetts Avenue, Cambridge, MA 02139-4307, USA.

[1]This article is part of a Special Issue dedicated to Dinitrogen Chemistry.

[2]Corresponding author (e-mail: ccummins@mit.edu).

 doi: 10.1139/V05-025 © 2005 NRC Canada

Scheme 1.



sitivity of the molybdenum–amide bonds. In the present work, we show that the same approach lends itself to the synthesis of a diazenido trialkoxymolybdenum(IV) system.

Results and discussion

Prepared by treatment of the corresponding anionic dinitrogen complex (29) (sodium salt) with, respectively, methyl tosylate (MeOTs) and methyl chloroformate are the diazenido complexes $R^1NNMo(N[i\text{-}Pr]Ar)_3$ **1a** ($R^1 = CH_3$, synthesis and structure reported previously) (29) and **1b** (R^1 = C(O)OMe). Gram quantities of **1a** could be obtained as red blocks in 58% isolated yield, as crystallized from ether (23). In contrast, **1b** was recovered in 94% yield as an analytically pure dark oil that dissolves in benzene to give a yellow solution.

The choice of MeOTs as the CH_3^+ source in the synthesis of **1a** was not random (29). A mild and non-oxidizing methylating agent is required to avoid both over-methylation and 1e oxidation of the anionic dinitrogen complex to its labile neutral counterpart (7). Furthermore, we had shown previously that sodium amalgam reduction of three-coordinate $Mo(N[t\text{-}Bu]Ar)_3$ in the presence of MeOTs under N_2 constituted a one-pot synthesis of $MeNNMo(N[t\text{-}Bu]Ar)_3$ (7). Structural precedent for molecules containing the [N=N C(O)OMe](1–) ligand, as found in **1b**, is extant (30).

Adamantanolysis of **1a** (Scheme 1) was accomplished by treating with 3 equiv. of 1-AdOH in THF at –25 °C, followed by warming to 25 °C and stirring for 4 h (Scheme 1). Solvent removal in vacuo, followed by suspension in pentane of the resulting orange solid, and subsequent collection by filtration, gave $MeNNMo(OAd)_3(THF)$ (**2a**·THF) in 81% isolated yield. The filtrate was shown to contain, essentially exclusively, pure HN(*i*-Pr)Ar. A band at 1544 cm^{-1} in the IR spectrum of **2a**·THF is assigned to ν_{NN}, and this diamagnetic derivative exhibits ^1H and ^{13}C NMR spectra consistent with a single 1-adamantyl environment.

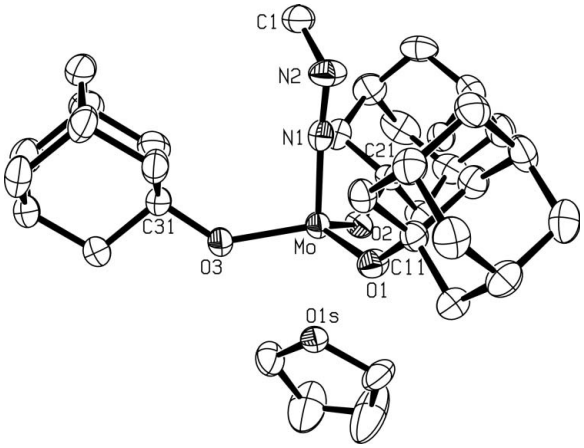
The specific choice of adamantanol in this work derives from a combined consideration of steric bulk and solubility properties. The steric protection afforded by adamantoxide in complexes such as **2a**·THF is often sufficient to favor a mononuclear formulation, but in addition, such complexes have sufficiently low solubility in saturated hydrocarbon media for efficient separation from the nonvolatile HN(*i*-Pr)Ar aniline liberated in the alcoholysis reaction. In the latter respect, adamantoxy is superior to, for example, *tert*-butoxy.

Adamantanolysis of **1a** was also possible in the absence of THF, under more forcing conditions (toluene, 92 °C, 39 h). In this case, the orange product precipitated from the brown reaction mixture while still hot. The product obtained in this manner (**2a**, 30% yield) was only sparingly soluble in benzene, toluene, or chloroform, but dissolved quantitatively in THF to provide solvate **2a**·THF. The properties of solvent-free **2a** are reminiscent of those reported for nitrosyl $ONW(O\text{-}t\text{-}Bu)_3$ (31), and both compounds are presumably polymeric in the solid state, though the nature of the bridging interactions is not known in either case. For **2a**, it may be surmised that the nucleophilic β-N atom of the diazenido ligand serves to provide the bridging contact, leading to infinite polymer formation. If so, then by analogy, the nitrosyl oxygen in $ONW(O\text{-}t\text{-}Bu)_3$ may behave similarly. Such structural features (i.e., topologically linear bridging N=NR or NO) are of interest given the paucity of data concerning such interactions (32), and their potential relevance to oxygen-atom or nitrene-group transfer reactions (33).

The molecular structure of **2a**·THF (Fig. 1) was determined via single-crystal X-ray diffraction. The overall molecular conformation is quite reminiscent of that observed for nitrosyl $ONW(O\text{-}t\text{-}Bu)_3(py)$ (31), with local threefold axial symmetry in the trialkoxymetal core, an apical metal–ligand multiple bond, and a solvent adduct trans thereto. The

© 2005 NRC Canada

Fig. 1. Thermal ellipsoid representation at 50% probability of **2a**·THF. Selected interatomic distances (Å) and angles (°): Mo-N1, 1.773(3); N1-N2, 1.250(4); Mo-O2, 1.902(2); Mo-O1s, 2.300(2); Mo-N1-N2, 171.8(3); N1-N2-C1, 118.7(3).

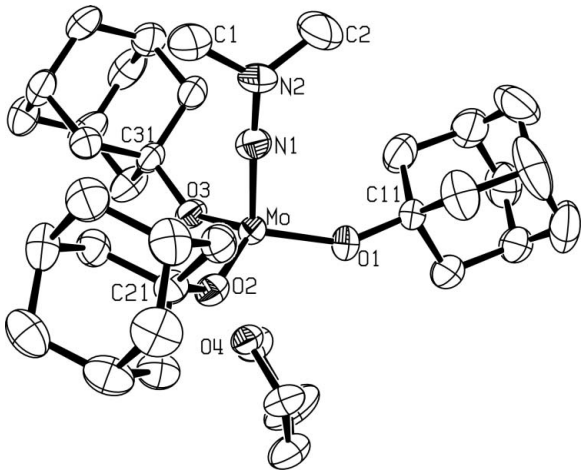


key structural parameters for the diazenidomolybdenum core in **2a**·THF (see caption to Fig. 1) are essentially unperturbed relative to those reported previously for **1a** (26), indicating that the exchange of alkoxide for anilide ligation, along with the inclusion of a trans solvent molecule, alters little the apical metal–ligand multiple bonding. The bond angles in the diazenido core reveal *sp* and sp^2 hybridization at, respectively, N1 and N2, as is typical of this functional group. The Mo-N1 distance is elongated by only ca. 0.1 Å relative to values typical of terminal MoN triple bonds (6), such that the resonance structure used to represent **2a**·THF in Scheme 1 is not by itself a complete description of the Mo—N bonding.

While **1b** was obtained only as a dark oil, its conversion to a solid derivative was accomplished via room-temperature adamantanolysis. Product **2b** was obtained accordingly as a yellow powder in 62% yield. The low solubility of **2b** in toluene suggests that like **2a**, the complex is polymeric in the solid phase. While in **2a** the β-N atom is likely to provide a bridging contact, in the case of **2b**, the carbonyl oxygen atom in the carboxylmethyl residue may alternatively serve this function. Carboethoxydiazenido molybdenum 3+ systems have been obtained from $O_2Mo(dtc)_2$ (dtc = *N*,*N*-dimethyldithiocarbamate) by treatment with the corresponding hydrazine, or by ethylchloroformate derivitization of dinitrogen complexes $(N_2)_2Mo(dppe)_2$ (dppe = 1,2-diphenylphosphinoethane) (34).

Nucleophilicity of the β-N in **2a**·THF was demonstrated by reaction of the complex with methyl triflate. The triflate salt [**3**]OTf was thereby produced as an orange powder in 82% isolated yield. Dimethylhydrazido complexes related to [**3**]OTf include the triaryloxy system $Me_2NNV(dipp)_3$ (dipp = 2,6-diisopropylphenoxy) studied with reference to vanadium-containing nitrogenase (35). The latter system displayed a short metal–nitrogen interatomic distance: V-N = 1.653(3) Å, an elongated N—N bond: N-N = 1.311(4) Å, and near linearity at the α-N atom: V-N-N = 175.8(3)° (35). While the structure of unsolvated [**3**]OTf is unknown, solvate [**3**·THF]OTf was obtained straightforwardly and its structure determined crystallographically (Fig. 2). Structural parameters for the dimethylhydrazido ligand in [**3**·THF]OTf are very similar to those seen for the aforementioned triaryloxy vanadium system. Accordingly, the methylation event leading to [**3**]OTf may be viewed as a redox event, the metal undergoing a formal oxidation state change from 4+ to 6+ concomitantly. The bonding between metal and α-N is then accurately described as for a metal imido complex (25). On the other hand, donation of the dimethylamino lone pair of electrons into the metal-α-N π* system leads to its observed planarity and suggests the alternative formulation, as drawn in Scheme 1 for the line drawings of [**3**]OTf and [**3**·THF]OTf. A related, structurally characterized molybdenum dimethylhydrazido complex cation was obtained by methyl triflate treatment of a trimethylsilyldiazenido complex (36).[3]

Fig. 2. Thermal ellipsoid representation at 50% probability of [**3a**·THF][OTf] (disordered triflate anion omitted for clarity). Selected interatomic distances (Å) and angles (°): Mo-N1, 1.745(3); N1-N2, 1.296(5); Mo-O2, 1.860(3); Mo-O4, 2.297(3); Mo-N1-N2, 177.2(3); N1-N2-C2, 119.5(4); N1-N2-C2, 120.0(4); C2-N2-C1, 118.2(4).



There has long been interest in the conversion of dinitrogen-derived hydrazido systems to amines, and it has been shown that treatment of cationic hydrazido complexes with $LiAlH_4$ can effect the conversion (37). Although not a clean transformation, it has been shown that [{ArN_3N}$MoNNMe_2$]OTf upon reduction with Na–Hg in THF undergoes N—N bond cleavage producing nitride [ArN_3N]MoN together with dimethylamine and other products (38), implying that neutral dimethylhydrazido complex [ArN_3N]$MoNNMe_2$ lacks sufficient stability for isolation. Presumably, fragmentation of the latter neutral system leads to nitride along with the [NMe_2] radical, the latter being

[3] Supplementary data may be purchased from the Directory of Unpublished Data, Document Delivery, CISTI, National Research Council Canada, Ottawa, ON K1A 0S2, Canada (http://cisti-icist.nrc-cnrc.gc.ca/irm/unpub_e.shtml for information on ordering electronically). CCDC 262546 and 262547 contain the crystallographic data for this manuscript. These data can be obtained, free of charge, via ww.ccdc.cam.ac.uk/conts/retrieving.html (or from the Cambridge Crystallographic Data Centre, 12 Union Road, Cambridge CB2 1EZ, UK; fax +44 1223 336033; or deposit@ccdc.cam.ac.uk).

© 2005 NRC Canada

capable of hydrogen atom abstraction from THF solvent to produce dimethylamine. Sodium amalgam reduction of dimethylhydrazido $[Me_2NNMo(N[t\text{-}Bu]Ar)_3][OTf]$ likewise gave rise to dimethylamine and the corresponding nitrido complex, $NMo(N[t\text{-}Bu]Ar)_3$ (7). Similarly, in the present work we find (Scheme 1) that cobaltocene reduction of [**3**]OTf produced cobaltocenium triflate, nitride $NMo(O\text{-}1\text{-}Ad)_3$, and dimethylamine, as determined spectroscopically. Nitride $NMo(O\text{-}1\text{-}Ad)_3$ was prepared independently using the method described by Chisholm and co-workers (39) for the synthesis of $NMo(O\text{-}t\text{-}Bu)_3$, for determination of the NMR spectroscopic characteristics of the former. The existence of neutral molybdenum(V) dimethylhydrazido complexes has been probed for electrochemically (38), and such systems remain interesting as putative reactive intermediates in this manifold of amine-producing N—N bond cleavage reactions.

Concluding remarks

Diazenido complexes synthesized from N_2 in the context of a simple supporting platform, namely the $Mo(N[R]Ar)_3$ (R = *i*-Pr, Ar = 3,5-$C_6H_3Me_2$) fragment, have been shown to be amenable to replacement of the full complement of ancillary ligands. Accordingly, trialkoxymolybdenum-supported diazenido systems have become available for study, expanding the scope of systems combining the chemistry of N_2 or N_2-derived ligands with an O-donor supporting framework. This approach, harnessing the portability of the diazenidomolybdenum(3+) core, provides an opportunity to study this functional group's behavior in a variety of contexts.

Experimental

General considerations

All operations were performed in a drybox under an atmosphere of purified nitrogen. Anhydrous ether, toluene, benzene, pentane, and hexane were purified according to the procedure of Grubbs and co-workers (40). Deuterated solvents were degassed and dried over molecular sieves (4 Å) and transferred under vacuum into a storage vessel. Molecular sieves (4 Å) and Celite® were activated in vacuo overnight at a temperature above 180 °C. Other chemicals were purified and dried by standard procedures or were used as received. IR spectra were recorded on a Bio-Rad 135 Series FT IR spectrometer. ^{1}H and ^{13}C NMR spectra were recorded on a Varian VXR-500, Varian Mercury-300, Varian XL-300, or Varian Unity-300 spectrometer. ^{1}H and ^{13}C NMR chemical shifts are reported with reference to solvent resonances. Dinitrogen complex $[Na(THF)][N_2Mo(N[i\text{-}Pr]Ar)_3]$ and compound **1a** were prepared as previously reported (29, 41).

Synthesis of $(Ar[i\text{-}Pr]N)_3MoN_2C(O)OMe$ (1b) (41)

To a solution of $[Na(THF)][N_2Mo(N[i\text{-}Pr]Ar)_3]$ (151 mg, 0.214 mmol) in ether (8 mL) was added a solution of methyl chloroformate (18 µL, 0.235 mmol) at –25 °C. The mixture was allowed to warm to room temperature and was stirred for a total of 3 h. The resultant mixture was filtered through a pad of Celite® on a sintered glass frit. The solvent was removed from the filtrate in vacuo to give **1b** as a dark brown oil (135 mg, 94% yield). FT IR (C_6D_6, KBr, cm^{-1}): ν_{NN} 1654, ν_{CO} 1212. ^{1}H NMR (C_6D_6, 25 °C) δ: 6.46 (3H, para), 6.32 (6H, ortho), 4.81 (3H, methine), 3.62 (3H, $N_2C(O)OCH_3$), 1.93 (18H, Ar-CH_3). ^{13}C NMR (C_6D_6, 25 °C) δ: 165.1 ($N_2C(O)OCH_3$), 148.0 (ipso), 138.8 (meta), 127.5 (ortho), 125.2 (para), 64.4 ($CH(CH_3)_2$), 52.6 ($N_2C(O)OCH_3$), 25.4 ($CH(CH_3)_2$), 21.7 (aryl-CH_3). Anal. calcd. for $C_{35}H_{51}N_5O_2Mo$: C 62.77, H 7.68, N 10.46; found: C 62.55, H 7.79, N 10.41.

Synthesis of $(AdO)_3Mo(N_2Me)(THF)$ (2a·THF) (41)

A solution of 1-adamantanol (667 mg, 4.38 mmol) in THF (4 mL) was added to a solution of **1a** (884 mg, 1.41 mmol) in THF (8 mL) at –25 °C. The mixture was then stirred for 4.5 h at room temperature after which the solvent was removed in vacuo. The resultant orange powder was suspended in pentane and stirred for 20 min. This gave a suspension that was chilled to –25 °C, and from which orange powder was collected by filtration and washed with cold pentane. The filtrate was subjected twice to the same concentration–suspension–cooling–washing procedure to maximize the yield. The combined orange precipitate was dried in vacuo to yield **2a** (759 mg, 81% yield). FT IR (THF, KBr, cm^{-1}): ν_{NN} 1544. ^{1}H NMR (THF-d_8, 25 °C) δ: 3.75 (3H, N_2CH_3), 3.60 (4H, THF), 2.13 (9H, C*H*), 1.92 (18H, CH_2), 1.76 (4H, THF), 1.66 (18H, CH_2). ^{13}C NMR (THF-d_8, 25 °C) δ: 78.8 ($OC(CH_2\text{-})_3$), 68.4 (THF), 47.6 ($CH\text{-}CH_2$), 43.8 (N_2CH_3), 37.5 ($C(CH_2\text{-})_3$), 32.7 ($CH\text{-}CH_2$), 26.5 (THF). Anal. calcd. for $C_{35}H_{56}N_2O_4Mo$: C 63.24, H 8.49, N 4.22; found: C 63.16, H 8.4, N 4.16.

Synthesis of $(AdO)_3Mo(N_2Me)$ (2a) (41)

$(Ar[i\text{-}Pr]N)_3MoN_2Me$ (**1a**, 328 mg, 0.524 mmol), 1-adamantanol (239 mg, 1.57 mmol), and toluene (12 mL) were installed in a flask equipped with a Teflon stopcock. The reaction mixture was stirred for 39 h at 92 °C. Then, the mixture was cooled to –25 °C, and the resulting orange precipitate was filtered off and washed with cooled toluene to give **2a** as an orange powder (92 mg, 30% yield). ^{1}H NMR ($CDCl_3$, 25 °C) δ: 3.77 (3H, $NNCH_3$), 2.10 (9H, C*H*), 1.88 (18H, CH_2), 1.56 (18H, CH_2). Anal. calcd. for $C_{31}H_{48}N_2O_3Mo$: C 62.82, H 8.16, N 4.73; found: C 62.58, H 8.25, N 4.67.

Synthesis of $(AdO)_3MoNNC(O)OMe$ (2b) (41)

A toluene (4 mL) solution of $(Ar[i\text{-}Pr]N)_3MoN_2C(O)OMe$ (**1b**, 190 mg, 0.284 mmol) was added to 1-adamantanol (134 mg, 0.879 mmol). The mixture was stirred for 12 h, producing a yellow solution with a yellow precipitate. The yellow precipitate was filtered off, washed with cold toluene, and dried in vacuo to give **2b** as a yellow powder (113 mg, 62% yield). FT IR (C_6D_6, KBr, cm^{-1}) ν: 2915, 2852, 1113, 1086, 1061. ^{1}H NMR ($CDCl_3$, 25 °C) δ: 3.70 (3H, $N_2C(O)OCH_3$), 2.32 (9H, C*H*), 2.10 (18H, CH_2), 1.65/1.62 (18H, CH_2). ^{13}C NMR ($CDCl_3$, 25 °C) δ: 163.9 ($N_2C(O)OCH_3$), 86.8 ($C(CH_2\text{-})_3$), 52.9 ($CH\text{-}CH_2$), 45.4 ($N_2C(O)OCH_3$), 36.2 ($C(CH_2\text{-})_3$), 31.9 ($CH\text{-}CH_2$). Anal. calcd. for $C_{32}H_{48}N_2O_5Mo$: C 60.37, H 7.60, N 4.40; found: C 60.84, H 7.71, N 4.48.

Synthesis of $[(AdO)_3Mo(NNMe_2)][OTf]$ ([3][Otf]) (41)

Methyl triflate (258 µL, 2.28 mmol) was added to a toluene (8 mL) suspension of $(AdO)_3MoN_2Me(THF)$ (**2a**·THF, 759 mg, 1.14 mmol) at –25 °C. The mixture was stirred for

© 2005 NRC Canada

3 h at room temperature. The resultant purple-red mixture was filtered through Celite® and the solvent was removed from the filtrate in vacuo. The crude red solid thereby obtained was suspended in ether–pentane 1:1 and cooled to –25 °C. An orange precipitate of [**3**][OTf] was collected by filtration and dried in vacuo (709 mg, 82%). FT IR (C_6D_6, KBr, cm^{-1}) ν: 2915, 2852, 1113, 1086, 1061. ^1H NMR (C_6D_6, 25 °C) δ: 3.34 (6H, NN(CH_3)$_2$), 2.11 (9H, C*H*), 2.06 (18H, CH_2), 1.52/1.49 (18H, CH_2). ^{13}C NMR (C_6D_6, 25 °C) δ: 86.6 (*C*(CH$_2$-)$_3$), 45.8 (*C*H-CH$_2$), 45.3 (NN(*C*H$_3$)$_2$), 36.6 (C(*C*H$_2$-)$_3$), 32.0 (*C*H-CH$_2$). Anal. calcd. for $C_{33}H_{51}N_2O_6F_3SMo$: C 52.37, H 6.79, N 3.70; found: C 52.48, H 6.74, N 3.78.

Synthesis of [(AdO)$_3$Mo(NNMe$_2$)(THF)][OTf] ([3·THF][OTf]) (41)

The complex [(AdO)$_3$Mo(NNMe$_2$)(THF)][OTf] ([**3**·THF][OTf]) was obtained simply by dissolving [**3**]OTf in THF. Unlike **2a**·THF, the THF ligand in [**3**·THF][OTf] can be removed by simply dissolving the complex in toluene and removing the solvent. A single crystal suitable for X-ray structure analysis was obtained by recrystallization from toluene–THF. ^1H NMR (C_6D_6, 25 °C) δ: 3.76 (4H, THF), 3.46 (6H, NN(CH_3)$_2$), 2.12 (9H, C*H*), 2.00 (18H, CH_2), 1.57/1.54 (18H, CH_2), 1.48 (4H, THF).

Independent synthesis of (AdO)$_3$MoN (41)

Sodium azide (801 mg, 12.3 mmol) was added to a THF (50 mL) suspension of $MoCl_4(THF)_2$ (3.92 g, 10.3 mmol) at room temperature, and the mixture was stirred for 1 h. Then, Li(OAd) (4.74 g, 30.0 mmol) was added, and the mixture was stirred for 4 h at room temperature. The resulting mixture was filtered through Celite®, and the solvent was removed from the filtrate to give a dark, red-brown solid. The solid was stirred in boiling toluene (125 mL) and filtered through a pad of Celite® on a sintered glass frit, and the solid collected on the frit was washed with toluene. The filtrate was condensed and allowed to stand at room temperature for 36 h. The white precipitate was collected by filtration, washed with pentane, and dried in vacuo. The resulting powder was further suspended in cold toluene (25 mL), collected by filtration, and dried in vacuo to give (AdO)$_3$MoN as a white powder (0.98 g, 17% yield). FT IR (pyridine-d_5, KBr, cm^{-1}) ν: 2938, 2893, 2851, 1453, 1104, 1077, 940, 745. ^1H NMR (pyridine-d_5, 25 °C) δ: 2.24 (18H, CH_2), 2.17 (9H, C*H*), 1.63/1.61 (18H, CH_2). ^{13}C NMR (pyridine-d_5, 25 °C) δ: 78.1 (*C*(CH$_2$-)$_3$), 46.1 (*C*H-CH$_2$), 36.9 (C(*C*H$_2$-)$_3$), 32.0 (CH-*C*H$_2$). Anal. calcd. for $C_{30}H_{45}NO_3Mo$: C 63.93, H 8.05, N 2.49; found: C 64.06, H 8.12, N 2.58.

Acknowledgments

The authors wish to thank Joshua S. Figueroa and Tetsuro Murahashi for technical assistance. We are also grateful to the United States National Science Foundation for funding this work (grant CHE-0316823).

References

1. R. Kempe. Angew. Chem. Int. Ed. **39**, 468 (2000).
2. D.V. Yandulov and R.R. Schrock. Science, **301**, 76 (2003).
3. R.R. Schrock. Chem. Commun. 2389 (2003).
4. V. Ritleng, D.V. Yandulov, W.W. Weare, R.R. Schrock, A.S. Hock, and W.M. Davis. J. Am. Chem. Soc. **126**, 6150 (2004).
5. C.E. Laplaza and C.C. Cummins. Science (Washington, D.C.), **268**, 861 (1995).
6. C.E. Laplaza, M.J.A. Johnson, J.C. Peters. A.L. Odom, E. Kim, C.C. Cummins, G.N. George, and I.J. Pickering. J. Am. Chem. Soc. **118**, 8623 (1996).
7. J.C. Peters, J.-P.F. Cherry, J.C. Thomas, L. Baraldo, D.J. Mindiola, W.M. Davis, and C.C. Cummins. J. Am. Chem. Soc. **121**, 10 053 (1999).
8. Y.-C. Tsai and C.C. Cummins. Inorg. Chim. Acta, **345**, 63 (2003).
9. P. Berno and S. Cambarotta. Organometallics, **14**, 2159 (1995).
10. J.-I. Song, P. Berno, and S. Gambarotta. J. Am. Chem. Soc. **116**, 6927 (1994).
11. N. Desmangles, H. Jenkins, K.B. Ruppa, B. Kamalesh, and S. Gambarotta. Inorg. Chim. Acta, **250**, 1 (1996).
12. L. Morello, J.B. Love, B.O. Patrick, and M.D. Fryzuk. J. Am. Chem. Soc. **126**, 9480 (2004).
13. M.P. Shaver, R.K. Thomson, B.O. Patrick, and M.D. Fryzuk. Can. J. Chem. **81**, 1431 (2003).
14. M.D. Fryzuk, B.A. MacKay, S.A. Johnson, and B.O. Patrick. Angew. Chem. Int. Ed. **41**, 3709 (2002).
15. M.D. Fryzuk, C.M. Kozak, M.R. Bowdridge, B.O. Patrick, and S.J. Rettig. J. Am. Chem. Soc. **124**, 8389 (2002).
16. M.D. Fryzuk. *In* Modern coordination chemistry — The legacy of Joseph Chatt. *Edited by* G.J. Leigh and N. Winterton. Royal Society of Chemistry, Cambridge. 2002. pp. 187–207.
17. D.C. Bradley, R.C. Mehrotra, I.P. Rothwell, and A. Singh. Alkoxo and aryloxo derivatives of metals. Academic Press, San Diego, Calif. 2001.
18. A. Caselli, E. Solari, R. Scopelliti, C. Floriani, N. Re, C. Rizzoli, and A. Chiesi-Villa. J. Am. Chem. Soc. **122**, 3652 (2000).
19. C.E. Laplaza, A.R. Johnson, and C.C. Cummins. J. Am. Chem. Soc. **118**, 709 (1996).
20. J. Chatt, J.R. Dilworth, and R.L. Richards. Chem. Rev. **78**, 589 (1978).
21. M. Hidai and Y. Mizobe. Met. Ions Biol. Syst. **39**, 121 (2002).
22. M. Hidai and Y. Mizobe. React. Coord. Ligands, **2**, 53 (1989).
23. G.J. Leigh and N. Winterton (*Editors*). Modern coordination chemistry — The legacy of Joseph Chatt. Royal Society of Chemistry, Cambridge. 2002.
24. B.A. MacKay and M.D. Fryzuk. Chem. Rev. **104**, 385 (2004).
25. D.L. DuBois and R. Hoffmann. Nouv. J. Chim. **1**, 479 (1977).
26. F.H. Stephens, J.S. Figueroa, P.L. Diaconescu, and C.C. Cummins. J. Am. Chem. Soc. **125**, 9264 (2003).
27. Y.-C. Tsai, P.L. Diaconescu, and C.C. Cummins. Organometallics, **19**, 5260 (2000).
28. J.M. Blackwell, J.S. Figueroa, F.H. Stephens, and C.C. Cummins. Organometallics, **22**, 3351 (2003).
29. J.-P.F. Cherry, F.H. Stephens, M.J.A. Johnson, P.L. Diaconescu, and C.C. Cummins. Inorg. Chem. **40**, 6860 (2001).
30. T. Nicholson and J. Zubieta. Inorg. Chem. **26**, 2094 (1987).
31. M.H. Chisholm, F.A. Cotton, M.W. Extine, and R.L. Kelly. Inorg. Chem. **18**, 116 (1979).
32. No examples of either turned up in a search of the Cambridge Structural Database. On the other hand, some transition-metal nitrosyl complexes are known to interact with Lewis acids (e.g., BF_3) at their nitrosyl oxygen atom. For a structurally characterized example see: W.B. Sharp, P. Legzdins, and B.O. Patrick. J. Am. Chem. Soc. **123**, 8143 (2001).
33. A.L. Odom, C.C. Cummins, and J.D. Protasiewicz. J. Am. Chem. Soc. **117**, 6613 (1995).

© 2005 NRC Canada

34. G. Butler, J. Chatt, W. Hussain, G.J. Leigh, and D.L. Hughes. Inorg. Chim. Acta, **30**, L287 (1978).
35. R.A. Henderson, Z. Janas, L.B. Jerzykiewicz, R.L. Richards, and P. Sobota. Inorg. Chim. Acta, **285**, 178 (1999).
36. M.B. O'Donoghue, W.M. Davis, and R.R. Schrock. Inorg. Chem. **37**, 5149 (1998).
37. P.C. Bevan, J. Chatt, G.J. Leigh, and E.G. Leelamani. J. Organomet. Chem. **139**, C59 (1977).
38. G.E. Greco and R.R. Schrock. Inorg. Chem. **40**, 3861 (2001).
39. D.M.T. Chan, M.H. Chisholm, K. Folting, J.C. Huffman, and N.S. Marchant. Inorg. Chem. **25**, 4170 (1986).
40. A.B. Pangborn, M.A. Giardello, R.H. Grubbs, R.K. Rosen, and F.J. Timmers. Organometallics, **15**, 1518 (1996).
41. J.-P.F. Cherry. Ph.D. thesis, Massachusetts Institute of Technology (M.I.T.), Cambridge, Mass. 2001.

© 2005 NRC Canada

Mesoporous tantalum oxide photocatalysts for Schrauzer-type conversion of dinitrogen to ammonia[1]

Chaoyang Yue, Michel L. Trudeau, and David Antonelli

Abstract: Mesoporous tantalum oxide, Fe^{3+}-doped mesoporous tantalum oxide, and bis(toluene) titanium reduced mesoporous tantalum oxide were used for the first time as Schrauzer-type photocatalysts for the conversion of dinitrogen to ammonia. The materials were characterized by XRD, TEM, XPS, and nitrogen absorption before and after catalytic runs. The results showed low to moderate activities depending on the composition. In contrast to previously studied Ti catalysts, Fe doping and heat pretreatment were not prerequisites for photocatalytic activity, but did improve the turnover rates by up to a factor of two. The optimal Fe loading for the tantalum oxides was found to be 1 wt% and the optimal heating condition at 300 °C for 3 h. Increased surface area and heat treatment were also found to improve activities. Contrary to our expectations, reduction of the mesostructure with bis(toluene) titanium had little effect on the catalytic activity. In spite of the dramatically higher surface areas of the mesoporous tantalum oxides as compared with bulk titanias used previously in this process, the overall catalytic activities were still less than those obtained in the Schrauzer system. This suggests that the increase in diffusion and surface area offered by the mesoporous structure is offset by the smaller crystalline domain sizes in the walls of the structure, leading to poor electron-hole separation and a reduction in catalytic efficiency.

Key words: mesoporous, Schrauzer, ammonia, photocatalysis, tantalum oxide.

Résumé : On a utilisé pour la première fois de l'oxyde de tantale mésoporeux, de l'oxyde de tantale mésoporeux dopé au Fe^{3+} et de l'oxyde de tantale mésoporeux réduit par du bis(toluène)titane comme photocatalyseurs de type Schrauzer pour la conversion du diazote en ammoniac. Les matériaux ont été caractérisés par XRD, TEM, XPS et adsorption d'azote avant et après les réactions catalytiques. Les résultats démontrent la présence d'activités allant de faibles à modérées suivant la composition. Par opposition aux catalyseurs de titane étudiés antérieurement, le dopage au Fe et le prétraitement à la chaleur ne sont pas des prérequis pour l'activité catalytique, mais ils améliorent les vitesses d'échange par des facteurs pouvant atteindre deux. On a trouvé que les additions optimales de Fe aux oxydes de tantale sont de 1 % en poids et que les conditions de chauffage sont de 300 °C pendant 3 h. On a aussi observé qu'une augmentation de l'aire de la surface et le traitement par la chaleur améliorent les activités. Contrairement à ce qui avait été prévu, la réduction de la mésostructure à l'aide de bis(toluène)titane n'a que peu d'effet sur l'activité catalytique. Malgré une augmentation dramatique des aires de la surface des oxydes de tantale mésoporeux en comparaison aux titanes en masse utilisés antérieurement dans ce procédé, les activités catalytiques globales étaient inférieures à celles obtenues dans le système Schrauzer. Cette observation suggère que l'augmentation de la diffusion et de l'aire de la surface offerte par la structure mésoporeuse sont contrebalancées par des tailles plus faibles du domaine cristallin dans les parois de la structure qui conduisent à une séparation plus mauvaise des trous électroniques et à une réduction de l'efficacité catalytique.

Mots clés : mésoporeux, Schrauzer, ammoniac, photocatalyse, oxyde de tantale.

[Traduit par la Rédaction]

Introduction

In the past decade, a variety of photocatalytic systems using semiconducting transition metal oxides have been developed for oxidative degeneration of organic chemicals (1, 2), fixation of carbon dioxide (3, 4), evolution of H_2 from water (5, 6), and reduction of metal ions (7). Coupling the controlled pore size and high surface areas of mesoporous materials with the photocatalytic properties of many oxides would represent an important advance in terms of reaction

Received 11 August 2004. Published on the NRC Research Press Web site at http://canjchem.nrc.ca on 9 March 2005.

C. Yue and D. Antonelli.[2] Department of Chemistry and Biochemistry, The University of Windsor, 401 Sunset Avenue, Windsor, ON N9B 3P4, Canada.
M.L. Trudeau. Emerging Technologies, Hydro-Québec Research Institute, 1800 Boul. Lionel-Boulet, Varennes, QC J3X 1S1, Canada.

[1]This article is part of a Special Issue dedicated to Dinitrogen Chemistry.
[2]Corresponding author (e-mail: danton@uwindsor.ca).

 doi: 10.1139/V05-018 © 2005 NRC Canada

rates and overall efficiency because of better diffusion rates and a greater number of reactive surface sites per mol of catalyst. One of the more unusual photocatalytic processes is the conversion of dinitrogen and water over a metal-doped titanium oxide catalyst (8–10). This process uses water as the reductant with high-energy UV light as the driving force and contrasts to other methods of dinitrogen activation, which are the subject of much current interest (11–16). Initial work by Schrauzer demonstrated that electron-hole separation on Fe-doped titania led to highly reactive sites on the surface, which could trap and reduce dinitrogen. Oxidation of water by the hole provided a source of protons and electrons to complete the cycle and make the process catalytic. The doping of the metal oxide was found to be a necessary step for high activity for reasons that are still not clear, but may be related to the creation of a permanent space-charge region in the material. Further work by Hoshino demonstrated that activities of n-doped titania could be increased by incorporation of a conducting polymer on the surface, creating a p–n junction, which aided in the electron-hole separation, and thus increased the efficiency (10). The rates quoted for these reactions are on the order of mmol/h/g of catalyst. While modest, these rates could be improved by increasing the surface area and a judicious choice of dopant. Recent work in our group demonstrated that mesoporous Ti and Nb oxides when treated with bis(toluene) niobium or bis(toluene) titanium gave materials that readily cleaved dinitrogen under ambient conditions, leading to the formation of surface ammonia in 1% to 2% levels in the presence of low levels of moisture (17, 18). Since these materials are based on oxides that normally display photocatalytic activity in the bulk phase, it appears that the development of a related mesoporous transition-metal-oxide-based photocatalytic process for nitrogen fixation may indeed be feasible. However, to date there have been numerous difficulties in exploiting the surface area of mesoporous titanium in photocatalytic processes. In 1998, Stone and Davis (19) studied the photocatalytic activity of phosphated titania based mesoporous molecular sieves. The well-known oxidative dehydrogenation of 2-propanol to acetone was used as a probe to measure the photocatalytic activity of the materials. The lower photocatalytic activity of mesoporous titania compared to the anatase phase was attributed to the amorphous nature of the walls of these materials and the presence of phosphorous in the case of the titania materials: the low degree of crystalline wall and the high surface concentration of defects lead to surface electron-hole recombination, and (or) the poisoning of catalytic surface sites by the phosphorus remaining from the templates. Since high surface area phosphate-free mesoporous titania are now readily available, the presence of phosphorous in these materials should no longer hinder applications (20), however it appears that the low crystallinity of the walls of the structure may be the tallest hurdle to overcome before the development of functional mesoporous titanium oxide photocatalysts can be realized (21).

Although mesoporous Ti oxide has been disappointing as a photocatalyst, Takahara, Domen, and co-workers (22) reported more promising activity for mesoporous Ta oxide in the photocatalytic decomposition of water. When as-synthesized tantalum oxide, prepared by the method of Antonelli and Ying (23), was used as a photocatalyst, H_2 evolved in a rate of 50 μmol/h. In contrast, a sample calcined at 600 K after template removal by acid treatment and solvent extraction showed higher photocatalytic activity and released both H_2 and O_2 in a stoichiometric ratio, even though a brief induction period was observed. The initial H_2 evolution was attributed to the decomposition reaction of the remaining surfactants and the stoichiometric evolution of H_2 and O_2 started after complete consumption of the surfactant template. A NiO-loaded sample showed higher photocatalytic activity and shorter induction time than those samples without NiO since NiO can act as co-catalyst in the water decomposition reaction. The optimal NiO loading level for the overall water decomposition was found to be 4.0 wt%. The NiO loaded samples showed an important trend in increasing photocatalytic activity. Thus, mesoporous Ta_2O_5 showed better photocatalytic activity than the bulk amorphous and crystallized samples because of its higher surface area. These high activities as compared to those reported above for titania and niobia were explained by the different band gaps of the respective materials. The authors suggest that mesoporous Ta oxide functions as an efficient photocatalyst in this case (22) because the very thin walls of the structure ensure that virtually all electron-hole pairs generated are close enough to the surface to allow rapid migration and reaction with water.

Recent work in our group has shown that mesoporous Ta oxide, when treated with bis(toluene) titanium, converts dinitrogen to ammonia on the surface (24). This is important because it demonstrates that the Ti-reduced surface of the Ta oxide mesostructure can split dinitrogen, the first part of the Schrauzer process, and this reduced species can react with ambient moisture to form ammonia. Further, the activity of mesoporous Ta oxide as a photocatalyst in water splitting, suggests it may also be useful in the Schrauzer process. The use of a Ta oxide surface is also of special interest owing to recent work by Fryzuk and co-workers (25) demonstrating that organometallic Ta hydrides are capable of coordinating and partially reducing dinitrogen. In this paper, we focus on the photocatalytic behavior of pure mesoporous tantalum oxide, Fe^{3+}-doped tantalum oxide, and semiconducting bis(toluene) titanium reduced mesoporous tantalum oxide. Fe was used in this system because both Schrauzer and Guth (8) and Palmisano et al. (9) showed that Fe was the best dopant for the photocatalysis in the case of titanium oxide and also because Fe species are important as active centers in the commercial Haber process. Furthermore, X-ray studies on biological nitrogen fixation have suggested that a seven-Fe cluster in Fe–Mo nitrogenase is the site of N_2 reduction.

Experimental section

Chemicals and catalysts preparation

All chemicals, except tantalum ethoxides from Alfa Aesar, were obtained from Aldrich. Mesoporous tantalum oxides were synthesized following the ligand-assisted templating method introduced by Antonelli and Ying (23). Fe^{3+}-doped catalysts were prepared by aqueous impregnation of iron nitrate nonahydrates with mesoporous tantalum oxide for 4 h with stirring and dried in oven at 110 °C overnight, then cal-

© 2005 NRC Canada

cined in a furnace at 300 °C for 3 to 4 h. Bis(toluene) titanium reduced catalysts were prepared by stirring 0.5 g of the mesoporous solid with 0.5 g of bis(toluene) titanium in 50 mL of toluene. The mesoporous solid immediately turns from a light faun color to a deep blue-black. After 1 day of additional stirring to ensure complete absorption of the organometallic, the reduced material was collected by suction filtration under nitrogen and washed several times with toluene. The resulting black material was dried in vacuo at 10^{-3} torr (1 torr = 133.322 4 Pa) on a Schlenk line until all condensable volatile had been removed.

Apparatus and procedure for photocatalysis

All experiments were conducted in a U-shaped Pyrex reactor with a sintered glass frit as the fixed bed. A 450 W UV photochemical lamp was set up parallel to the reactor at a distance of about 8 cm. The photocatalytic reactions were initialized by feeding N_2 (ultrahigh purity), bubbled through deionized water at a constant flow rate of 60 cm^3/min, into the reaction tube. NH_3 produced from the reaction was absorbed by a 60 mL 0.01 N HCl aqueous solution, which was replaced every hour and kept for subsequent quantitative determination by the indophenol blue method (9). This method detects both NH_4^+ and NH_3 forms of N and the detection limit was reported to be about 10 μg NH_3-N/L, and Beer's law was obeyed up to about 1200 μg NH_3-N/L. After a 3 h run, samples were flushed again by pure helium to measure the adsorbed NH_3 on the powder surface. However, complete release of trapped NH_3 may require heating at 573 K or higher for several hours. Comparison experiments were also conducted under the same operation conditions, but using inert helium instead of the mixture of N_2 + H_2O as the feeding gas. These experiments are important for the $Fe(NO_3)_3$-doped catalysts to eliminate trace amounts of ammonia formed by heat treatment of the surface nitrate.

Characterization

Nitrogen adsorption and desorption data were collected on a Micromeritics ASAP 2010. X-ray diffraction (XRD) patterns (Cu Kα) were recorded on a Siemens D500δ-2δ diffractometer. All X-ray photoelectron spectroscopy (XPS) peaks were referenced to the carbon C–(C, H) peak at 284.8 eV, and the data were obtained using a Physical Electronics PHI-5500 using charge neutralization. Transmission electron microscopy (TEM) pictures were obtained by using a H9000 HR-TEM operated at 300 kV. The powder was deposited on a SiO_2-coated Cu grid.

Results and discussion

Pure mesoporous tantalum oxide

The X-ray diffraction patterns for a sample of mesoporous tantalum oxide, and that of the material treated in an oven at 300 °C for 3 h are shown in Fig. 1. The intense (100) reflection at d = 2.7 nm without resolved (110) and (200) reflections, is consistent with a wormhole structure rather than a highly ordered hexagonal structure. Apart from a slight broadening and diminishing in intensity, the XRD pattern of the calcined material shows little difference from that of the starting material, demonstrating that the initial mesostructure is largely retained after heat treatment. Figure 2 shows the

Fig. 1. X-ray powder diffraction patterns for (*a*) mesoporous Ta oxide (S1); (*b*) mesoporous Ta oxide after calcination at 300 °C for 3 h (S7); and (*c*) 1% Fe^{3+}-doped mesoporous Ta oxide after calcination at 300 °C for 3 h (S8).

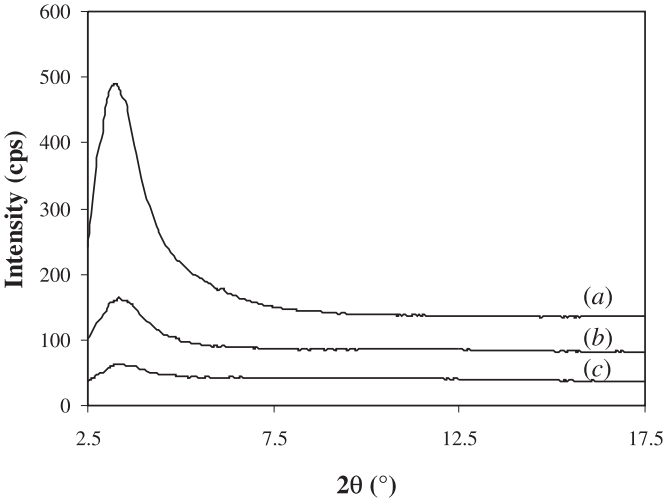
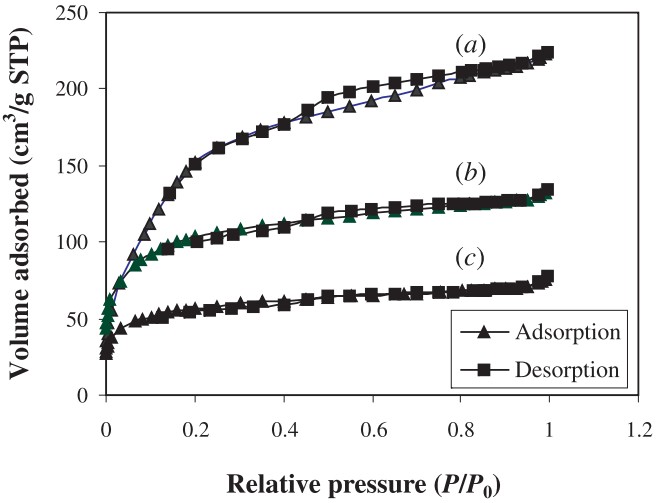


Fig. 2. Nitrogen adsorption–desorption isotherms for (*a*) mesoporous Ta oxide (S1); (*b*) mesoporous Ta oxide after calcination at 300 °C for 3 h (S7); and (*c*) 1% Fe^{3+}-doped mesoporous Ta oxide after calcination at 300 °C for 3 h (S8).



nitrogen adsorption and desorption isotherms of these materials. Heat treatment results in a decrease in specific BET surface area from 624 m^2/g to 366 m^2/g, and a corresponding decrease in the cumulative Horvan–Kawazoe (HK) pore volume from 0.304 cm^3/g to 0.103 cm^3/g, with the pore size remaining at 23 Å. Unlike MCM-41, which has a sharp pore-size distribution and a typical type IV isotherm, these materials possess a broader pore-size distribution and an isotherm somewhere between that of type I and IV because of the pore size, which is on the cusp between the microporous and mesoporous regimes. TEM was used to directly image mesoscopic order, particle morphology, as well as pore size and wall thickness of this material. Figure 3 clearly shows spherical particles with a wormhole pore structure consistent with XRD pattern; the measured pore size is about 25 Å, in good agreement with the results from nitrogen adsorption;

© 2005 NRC Canada

Table 1. Effects of thermal pretreatment and Fe^{3+} doping on photocatalytic activity.

Sample	Catalyst composition and pretreatment conditions	BET surface area (m^2/g)	Average activity (over 3 h) (μmol/g/h)
S1	Pure Ta oxide without any treatment	624	0.263
S2	Pure Ta oxide fired at 300 °C for 4 h	319	0.47
S3	0.3% Fe^{3+}-doped Ta oxide, 300 °C for 4 h	225	0.312
S4	0.5% Fe^{3+}-doped Ta oxide, 300 °C for 4 h	199	0.739
S5	1% Fe^{3+}-doped Ta oxide, 300 °C for 4 h	196	0.79
S6	2% Fe^{3+}-doped Ta oxide, 300 °C for 4 h	196	0.35
S7	Pure Ta oxide fired at 300 °C for 3 h	366	0.683
S8	1% Fe^{3+}-doped Ta oxide, 300 °C for 3 h	199	0.794
S9	Pure Ta oxide fired at 300 °C for 3 h, then reduced with bis(toluene) titanium	293	0.702

Fig. 3. TEM of pure mesoporous Ta oxide (S1).

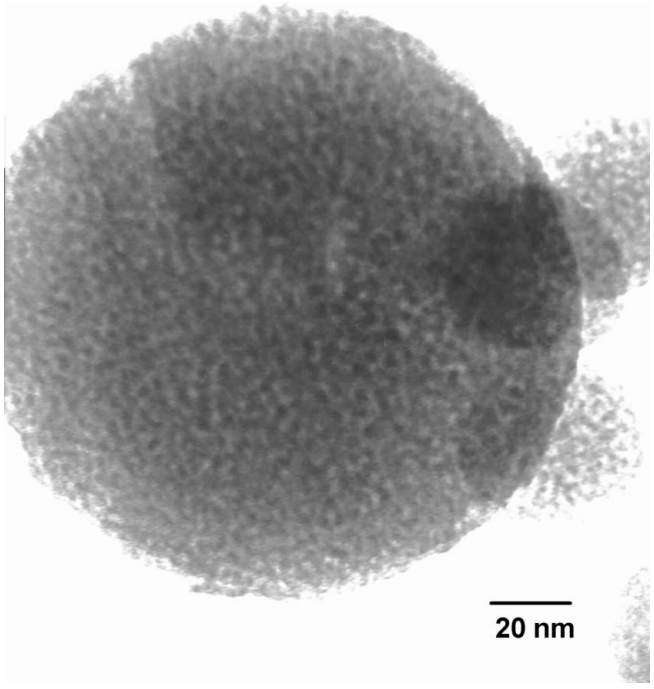


Fig. 4. XPS spectra of the Ta 4*f* region for S7 (*a*) before photocatalytic reaction and (*b*) after a 3 h photocatalytic reaction.

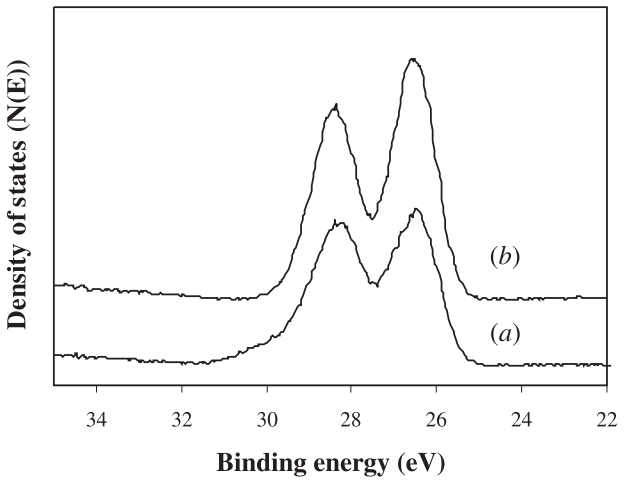
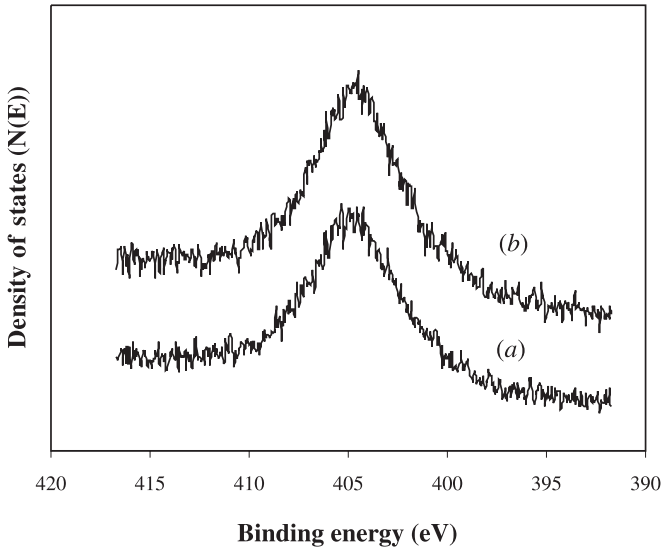


Fig. 5. XPS spectra of the N 1*s* region for S7 (*a*) before photocatalytic reaction and (*b*) after a 3 h photocatalytic reaction.



the wall is roughly 15 Å, differing slightly from the calculated value of 8 Å on the basis of *d* spacing and HK pore size assuming a perfectly hexagonal unit cell.

Photocatalytic activities of pure Ta oxide (S1) and Ta oxide after heat treatment (S2, S7) are listed in Table 1. Pure tantalum oxide without any treatment only shows low activity of 0.263 μmol/g/h and thermal treatment at 300 °C for 3 h (S7) improves the activity to 0.683 μmol/g/h. Prolonged heating time decreases the activity again to 0.47 μmol/g/h (S2). To examine the oxidation states of surface Ta and possible N species in these materials, XPS measurements were carried out. Figure 4 shows the Ta $4f_{5/2,\ 7/2}$ region for pure mesoporous Ta oxide before and after the photocatalytic reaction. The emissions at 26.6 eV and 28.5 eV are characteristic of Ta (V) and demonstrate that there has been little or no change in the oxidation state of the Ta over the course of the reaction. The N 1*s* region of this spectrum before and after the photocatalytic run are also similar (Fig. 5), showing a single peak at 405 eV for the Ta $4p_{3/2}$ emission. The expected N 1*s* emission for ammonia or other nitrogen species (396–403 eV) are not seen either because the Ta emission is too large and obscures the N emission, or because the quantities of N on the surface after the reaction are too small to be detected by XPS.

© 2005 NRC Canada

The improved activity on heat treatment is not unexpected because it increases local crystallization of materials, which often leads to more efficient migration of electrons and holes through the lattice to the surface. In Schrauzer and Guth's work (8), conversion from the anatase phase to the rutile modification by heat treatment at 1000 °C was a prerequisite for the high activity. In contrast, mesoporous tantalum oxide is considerably photoactive without heat treatment, as Domen and co-workers reported (22), most probably because of the small wall thickness, which enables the excited electron to migrate to the surface. While heat treatment in the case of the mesoporous Ta oxides initially improves the activity, prolonged calcination causes a diminution of the active surface in addition to an increasing loss of surface metal hydroxide groups, both contributing to a decrease of photocatalytic activity. In the case of very high surface mesoporous materials, this problem becomes even more prominent because of the apparent incompatibility of the presence of the mesostructure and the crystallinity of the walls. All mesoporous materials reported so far have either amorphous wall structures or disconnected nanocrystalline grains embedded in the walls. Crystallization of the walls to bulk oxides occurs upon exhaustive thermal treatment, resulting in a collapse of the mesostructure. Thus, high surface area and porosity is normally offset by crystallinity. In light of these observations, the difference of activity between S2 and S7 likely results from their different surface areas.

Fe^{3+}-doped mesoporous tantalum oxides

To get higher activities, we prepared a series of Fe^{3+}-doped Ta oxides with different loading levels. The XRD pattern and the N_2 adsorption and desorption isotherm of the 1 wt% Fe^{3+}-doped sample are also shown in Figs. 1 and 2, respectively. Surprisingly, the BET surface area of this sample decreased by more than two-thirds, i.e., from the original 624 m^2/g to 199 m^2/g, although the HK pore size remains unchanged. After carefully examining each step of preparation, we found the loss in surface area originates mainly from the aqueous impregnation of $Fe(NO_3)_3$. This phenomena is not uncommon as (26, 27) the Davis group reported that Ru/MCM-41, when impregnated with $CsNO_3$ in aqueous solution, experiences a loss of surface area to 623 m^2/g from 1058 m^2/g and a loss of total pore volume to 0.417 cm^3/g from 1.015 cm^3/g. This effect is likely related to the surface tension of water confined in the nanopores. Liquid water has a much higher surface tension (72.75×10^{-3} N m^{-1} at 20 °C) than organic solvents (23.7 0^{-3} N m^{-1} for acetone, at 20 °C).

XPS spectra of Fe^{3+}-doped tantalum oxides for Ta 4*f* and N 1*s* regions are quite similar to those of pure mesoporous tantalum oxides, except that the two peaks of Ta $4f_{5/2,\ 7/2}$ show slight broadening and are relatively weaker in intensity, which can be attributed to a broader distribution of Ta sites in the walls of the material. The Fe 2*p* region in all materials could not be resolved due to the very low content of this element.

The activities of all Fe^{3+}-doped catalysts from the experiments are listed in Table 1. Clearly, the highest activities appear on the 1 wt% Fe^{3+}-doped samples, S5 and S8. Although the underlying reason for this Fe-induced enhancement of activity is not completely clear, it may be related to a modification of the band-gap region and (or) formation of a permanent space charge region in the walls. Fe has always been one of the best choices for the photocatalytic conversion of dinitrogen to ammonia (9). For example, Palmisano et al. (9) demonstrated that the pure TiO_2, with band-gap energy in the near-UV, is not active under visible light, but doping with Fe extends the light absorbed by TiO_2 to the visible region. An optimal doping is achieved when a space charge region exists with an electric force more than 0.2 eV, whose thickness is more or less equal to the light penetration depth, which ensures all the generated electron-hole pairs are efficiently separated. Tantalum oxides possess a band-gap energy of 4.0 eV and absorb in the near-UV without doping, so that the modification of the bang-gap region should not be necessary. In fact, pure tantalum oxide (S7) demonstrates moderate photocatalytic activity, while the activity of the 0.3% Fe^{3+}-doped sample (S3) is actually lower than that of pure tantalum oxide (S2, S7). However, this surprising observation can be rationalized when considering the additional and offsetting effect of the loss of surface area resulting from aqueous impregnation.

The nearly identical activities of S5 and S8 are also of some interest. From the standpoint of surface area alone, S8 should have higher activity than S5. After careful examination of the experimental data presented in Figs. 6 and 7, it becomes evident that S5 has more preadsorbed NH_3 than S8 although they have theoretically the same wt% of $Fe(NO_3)_3$-doping content. This suggests that more catalytically active Fe is present in S5 than in S8, possibly because of the longer calcination time. Since we cannot identify the exact phase(s) of Fe(III) from XRD and XPS because of the low level of Fe, it is not possible at this stage to establish any structure–property relationships that might elucidate the nature of the active Fe centers. The higher content of more active Fe in S5 counteracts the disadvantage of lower surface area, bringing the two samples to the same level of activity.

Mesoporous Ta oxide reduced with bis (toluene) titanium

To improve the activities of these catalysts by improving electron-hole separation on the surface of the Ta oxide mesostructure, we pursued methods of improving surface conductivity in these otherwise insulating structures. The development of a stoichiometric process for fixing dinitrogen on the surface of a mesoporous oxide reduced with a bis(toluene) metal species (17, 18) was an extension of previous work in which organometallic sandwich compounds were used as reducing agents to make low-dimensional molecular conductors in the pores of the mesostructure (28–32). The introduction of the organometallic into the pores was similar to a classical redox intercalation reaction in which an electron donor reduces the walls of the inorganic host to create a material with periodic charge regions consisting of a anionic metal oxide phase and a cationic dopant intercalate phase. In the case of bis(toluene) titanium and mesoporous Ta oxide, the organometallic acts as a reductant, but does not retain its structural integrity on loss of electrons, instead losing the toluene ligands to essentially deposit Ti atoms on the surface of the mesostructure while also reducing the mesostructure. XPS studies show that there are several Ta and Ti environments in this material, including a low-valent Ti species that

© 2005 NRC Canada

Fig. 6. Comparison experiments on S8 under an UV lamp: (*a*) helium is the only feeding gas and (*b*) a mixture of N_2 + H_2O is the feeding gas.

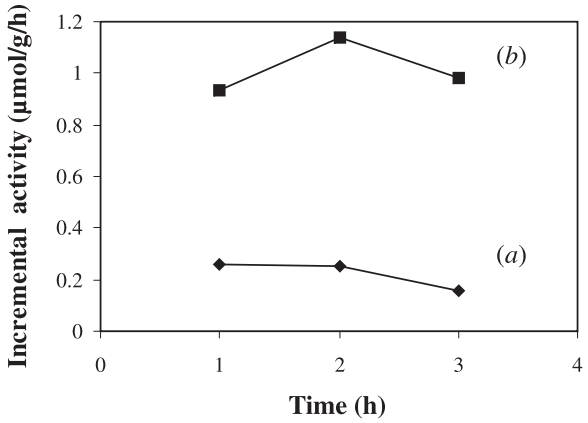
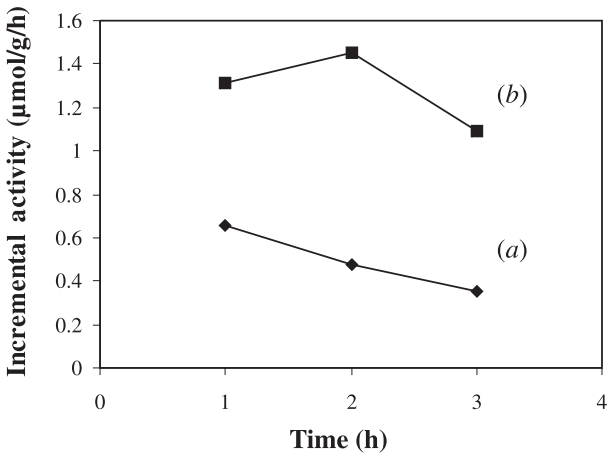


Fig. 7. Comparison experiments on S5 under an UV lamp: (*a*) helium is the only feeding gas and (*b*) a mixture of N_2 + H_2O is the feeding gas.



reacts almost spontaneously with dinitrogen to create surface nitride (24). Charge balancing of this highly reduced mesoporous system requires that the electron-depleted, low-valent coat have a cationic charge and the partially reduced higher valent coat have a negative charge. This morphology should create a depletion zone between the two layers similar to that between a p–n junction, which may be useful in promoting electron-hole separation in a photocatalytic process involving dinitrogen, since coating of n-doped titania with a p-doped conducting polymer creates a p–n junction with a depletion region that improves the thermodynamics of nitrogen reduction by water (10). By analogy, the bis(toluene)-Ti-reduced mesoporous Ta oxide may thus show very high activity towards dinitrogen in photocatalysis. These reduced materials are metallic or semiconductors depending on the degree of reduction, while other reduced mesoporous oxides are insulators. The highly conducting nature has been attributed to the low-valent coat on the surface, and implies that the surface states are continuous in nature. This may provide a further advantage in photocatalysis, as surface defects and localized electron traps have been indicated as reasons why amorphous oxides usually have poor electron-hole separation properties (19). Thus, the modification of mesoporous Ta oxide with bis(toluene) titanium to create a metallic oxide coat on the surface of the material may represent a strategy of overcoming electron localization leading to electron-hole pair recombination, since electrons tend to drift towards metallic regions on the surfaces of photocatalysts, and these reduced mesoporous oxides must have a more continuous band structure with fewer surface defects to display such high conductivities.

Surprisingly, our catalytic runs with the bis(toluene)-Ti-reduced mesoporous Ta oxide catalyst did not give better results than pure tantalum oxide (see Table 1, S7 vs. S9). The most likely explanation for this is that although bis (toluene) titanium increases the surface conductivity and creates sites capable of splitting dinitrogen, this surface coat is very air sensitive and possibly degrades as O_2 is formed over the course of the reaction. For this reason, it may be more effective to coat the inner surface of the material with a more robust semiconducting polymer to create an internal p–n junction capable of effecting superior electron-hole separation without degrading during the catalytic process. Since uniformly coating the inside mesoporous materials without clogging the pores is not trivial, requiring careful selection of catalyst dopants on the inner surface and control of polymer substrate concentrations, this strategy represents the body of an independent study.

Conclusion

For the first time, we have studied the photocatalytic conversion of dinitrogen to ammonia over a mesoporous Ta-oxide-based catalyst. All catalysts studied showed low to moderate activity and the 1 wt% Fe-doped catalysts show comparable molar activities to Schrauzer's initial results. Higher surface area, heat treatment, and Fe content were found to increase the activities, however, the latter two factors have an adverse effect on the first, i.e., surface area, such that optimization is hindered. Treatment of the material with bis(toluene) Ti had little effect on the photocatalytic activity, most likely because of the oxygen sensitivity of this material.

References

1. R.J. Davis, J. Gainer, G. O'Neal, and I.-W. Wu. Water Environ. Res. **66**, 50 (1994).
2. G. Al-sayyed, J.C. D'Oliveira, and P. Pichat. J. Photochem. Photobiol. A, **58**, 99 (1991).
3. F. Saladin, L. Forss, and I. Kamber. J. Chem. Soc. Chem. Commun. 533 (1995).
4. S. Yamagata, M. Nishijo, N. Murao, S. Ohta, and I. Mizoguchi. Zeolites, **15**, 490 (1995).
5. A.J. Bard and M.A. Fox. Acc. Chem. Res. **28**, 141 (1995).
6. K. Sayama, A. Tanaka, K. Domen, K. Maruya, and T. Onishi. J. Catal. **124**, 541 (1990).
7. K. Tanaka, K. Harada, and S. Murata. Sol. Energy, **36**, 159 (1986).
8. G.N. Schrauzer and T.D. Guth. J. Am. Chem. Soc. **99**, 7189 (1977).
9. L. Palmisano, V. Augugliaro, A. Sclafani, and M. Schiavello. J. Phys. Chem. **92**, 6710 (1988).

© 2005 NRC Canada

10. K. Hoshino. Chem. Eur. J. **7**, 2727 (2001).
11. M.D. Fryzuk and S.A. Johnson. Coord. Chem. Rev. **200**, 379 (2000).
12. M. Hidai and Y. Mizobe. Chem. Rev. **95**, 1115 (1995).
13. T.A. Bazhenova and A.E. Shilov. Coord. Chem. Rev. **144**, 69 (1995).
14. C.E. Laplaza and C.C. Cummins. Science (Washington, D.C.), **268**, 861 (1995).
15. M.D. Fryzuk, J.B. Love, S.J. Rettig, and V.G. Young. Science (Washington, D.C.), **275**, 1445 (1997).
16. D.V. Yandulov and R.R. Schrock. Science, **301**, 76 (2003).
17. M. Vettraino, X. He, M. Trudeau, R. Schurko, and D.M. Antonelli. J. Am. Chem. Soc. **124**, 9567 (2002).
18. M. Vettraino, X. He, M. Trudeau, J.E. Drake, and D.M. Antonelli. Adv. Funct. Mater. **3**, 174 (2002).
19. V.F. Stone, Jr. and R.J. Davis. Chem. Mater. **10**, 1468 (1998).
20. Y. Wang, X. Tang, L. Lin, W. Huang, Y.R. Hacohen, and A. Gedanken. Adv. Mater. **12**, 1183 (2000).
21. M. Mamak, N. Coombs, and G. Ozin. Adv. Mater. **12**, 198 (2000).
22. Y. Takahara, J.N. Kondo, T. Takata, D. Lu, and K. Domen. Chem Mater. **13**, 1194 (2001).
23. D.M. Antonelli and J.Y. Ying. Angew. Chem. Int. Ed. Engl. **35**, 426 (1996).
24. A. Lezau, B. Skadtchenko, M. Trudeau, and D.M. Antonelli. J. Chem. Soc. Dalton Trans. 4115 (2003).
25. S.A. Johnson, S.J. Rettig, and M.D. Fryzuk. J. Am. Chem. Soc. **123**, 3960 (2001).
26. C.T. Fishel, R.J. Davis, and J.M. Garces. J. Catal. **163**, 148 (1996).
27. F. Rosowski, A. Hornung, O. Hinrichson, D. Herein, M. Muhler, and G. Ertl. Appl. Catal. A, **151**, 443 (1997).
28. B. Ye, M. Trudeau, and D.M. Antonelli. Adv. Mater. **13**, 561 (2001).
29. B. Ye, M. Trudeau, and D.M. Antonelli. Chem. Mater. **14**, 2774 (2002).
30. X. He, M. Trudeau, and D.M. Antonelli. Adv. Mater. **12**, 1036 (2000).
31. X. He and D.M. Antonelli. Angew. Chem. Int. Ed. **41**, 214 (2002).
32. S. Murray, M. Trudeau, and D.M. Antonelli. Adv. Mater. **12**, 1339 (2000).

© 2005 NRC Canada

Functionalization and cleavage of coordinated dinitrogen via hydroboration using primary and secondary boranes[1]

Bruce A. MacKay, Samuel A. Johnson, Brian O. Patrick, and Michael D. Fryzuk

Abstract: The reaction of the side-on, end-on ditantalum dinitrogen complex $([NPN]Ta)_2(\mu\text{-}\eta^1\text{:}\eta^2\text{-}N_2)(\mu\text{-}H)_2$ (where NPN = $PhP(CH_2SiMe_2NPh)_2$) with a variety of secondary and primary boranes is reported. With 9-BBN, hydroboration of the Ta_2N_2 unit occurs via B-H addition, which in turn triggers a cascade of reactions that result in N—N bond cleavage, ancillary ligand rearrangement involving silicon group migration, and finally elimination of benzene from the N-Ph group and a B-H moiety to generate the imide–nitride derivative. In the presence of excess 9-BBN, the Lewis acid – base adduct of the imide–nitride ($[NP\mu\text{–}N]Ta(=NBC_8H_{14})(\mu\text{-}NB(H)C_8H_{14})Ta[NPN]$) is formed. A similar set of reactions is observed for dicyclohexylborane (Cy_2BH), which hydroborates the dinitrogen complex to generate $[NPN]Ta(H)(\mu\text{-}\eta^1\text{:}\eta^2\text{-}NNBCy_2)(\mu\text{-}H)_2Ta[NPN]$, followed by loss of H_2 and silicon group migration to yield the imide–nitride $[NP\mu\text{–}N]Ta(=NBCy_2)(\mu\text{-}N)(Ta[NPN]$. With thexyl borane ($H_2BCMe_2CHMe_2$), a similar sequence of reactions is suggested starting with hydroboration to generate $[NPN]Ta(H)(\mu\text{-}\eta^1\text{:}\eta^2\text{-}NNB(H)C_6H_{13})(\mu\text{-}H)_2Ta[NPN]$, followed by loss of H_2 and ancillary ligand rearrangement. When bis(pentafluorophenyl)borane ($HB(C_6F_5)_2$) is used, no hydroboration of coordinated N_2 is observed, rather simple adduct formation to give $([NPN]Ta)_2(\mu\text{-}\eta^1\text{:}\eta^2\text{-}NN\text{-}B(H)(C_6F_5)_2)(\mu\text{-}H)_2$ occurs.

Key words: dinitrogen, tantalum, hydroboration, N—N bond cleavage.

Résumé : On rapporte les résultats de la réaction du complexe de diazote ditantale $([NPN]Ta)_2(\mu\text{-}\eta^1\text{:}\eta^2\text{-}N_2)(\mu\text{-}H)_2$ (dans lequel NPN = $PhP(CH_2SiMe_2NPh)_2$) avec une variété de boranes secondaires et primaires. Avec le 9-BBN, l'hydroboration de l'unité Ta_2N_2 se produit par une addition B-H, qui provoque à son tour une cascade de réactions conduisant à une rupture de la liaison N—N, un réarrangement du ligand impliquant une migration du groupe du silicium et finalement l'élimination du benzène du groupe N-Ph et une portion B-H pour générer la formation du dérivé imide–nitrure ($[NP\mu\text{–}N]Ta(=NBC_8H_{14})(\mu\text{-}NB(H)C_8H_{14})Ta[NPN]$). On observe un ensemble de réactions semblables avec le dicyclohexylborane (Cy_2BH) qui provoque une hydroboration du complexe de diazote pour générer le $[NPN]Ta(H)(\mu\text{-}\eta^1\text{:}\eta^2\text{-}NNBCy_2)(\mu\text{-}H)_2Ta[NPN]$, suivie d'une perte de H_2 et de la migration du groupe du silicium pour conduire à la formation de l'imide nitrure $[NP\mu\text{–}N]Ta(=NBCy_2)(\mu\text{-}N)Ta[NPN]$. Avec le thésylborane ($H_2BCMe_2CHMe_2$), la réaction suivrait un cours semblable qui débuterait avec une hydroboration pour générer le $[NPN]Ta(H)(\mu\text{-}\eta^1\text{:}\eta^2\text{-}NNB(H)C_6H_{13})\text{-}(\mu\text{-}H)_2Ta[NPN]$, suivie d'une perte de H_2 et d'un réarrangement de ligand. Avec le bis(pentafluorophényl)borane ($HB(C_6F_5)_2$), on n'observe pas l'hydroboration du N_2 coordiné, uniquement la formation d'un adduit simple qui génère le $([NPN]Ta)_2(\mu\text{-}\eta^1\text{:}\eta^2\text{-}NN\text{-}B(H)(C_6F_5)_2)(\mu\text{-}H)_2$.

Mots clés : diazote, tantale, hydroboration, scission de la liaison N—N.

[Traduit par la Rédaction]

Introduction

The activation of small molecules by metal complexes is a mature area of inorganic chemistry. Nevertheless, molecular nitrogen, one of the most abundant small molecules in the biosphere, continues to frustrate inorganic chemists because of its intrinsic lack of reactivity (1–5). Under extreme conditions, N_2 will react with H_2 over an activated iron surface to generate ammonia; this energy-intensive catalytic transformation, known as the Haber–Bosch process, supplies the global need for NH_3-derived fertilizers (6). While discovery of a homogeneous version of the Haber–Bosch process is the goal of a number of groups around the world (7, 8), another worthwhile goal is to develop a process that converts molecular nitrogen to high-value organonitrogen materials, such as amines, substituted hydrazines, and *N*-heterocycles (9–15).

A key challenge in devising any homogeneous catalytic cycle involving molecular nitrogen is coordination of N_2 to the metal centre. Because dinitrogen is intrinsically unreactive, formation of N_2 complexes is not straightforward.

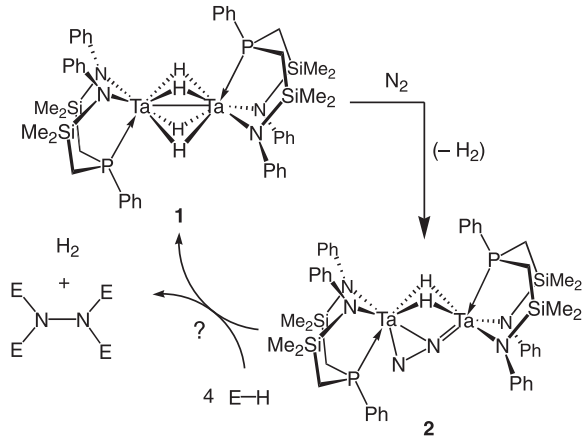
Received 15 September 2004. Published on the NRC Research Press Web site at http://canjchem.nrc.ca on 16 March 2005.

B.A. MacKay, S.A. Johnson, B.O. Patrick, and M.D. Fryzuk.[2] Department of Chemistry, University of British Columbia, 2036 Main Mall, Vancouver, BC V6T 1Z1, Canada.

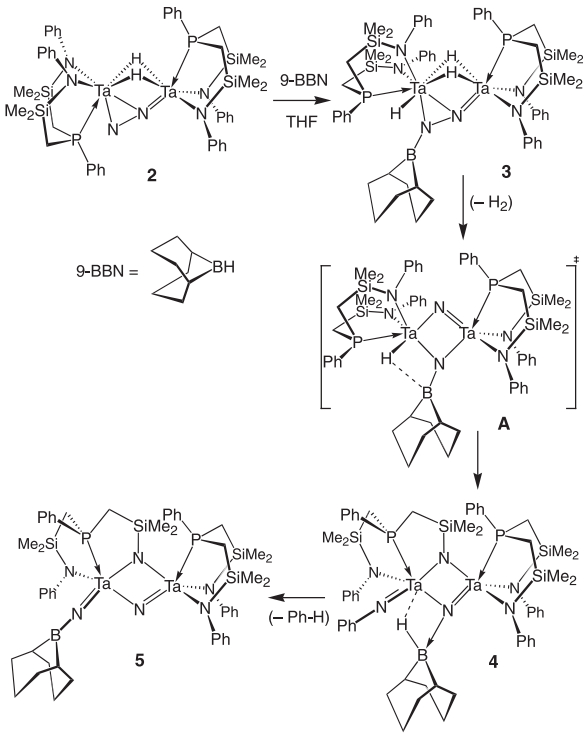
[1]This article is part of a Special Issue dedicated to Dinitrogen Chemistry.
[2]Corresponding author (e-mail: fryzuk@chem.ubc.ca).

 doi: 10.1139/V04-161 © 2005 NRC Canada

Scheme 1.



Scheme 2.



Since the first report of a dinitrogen complex in 1965 (16), many N_2 derivatives have been synthesized (17–20). The most common method of synthesis generally requires strongly reducing conditions, which unfortunately is incompatible with many functionalization protocols. Recently, we reported (21) a facile method for the formation of a ditantalum dinitrogen complex that involves reaction of N_2 with the ditantalum tetrahydride **1** (Scheme 1). This reaction proceeds smoothly to generate the side-on, end-on dinitrogen complex **2** without the necessity of added reducing agents. It occurred to us that multiple additions of some simple hydride reagent (E-H) across the Ta_2N_2 core of **2** could regenerate the starting tetrahydride **1** and produce a functionalized hydrazine moiety (N_2E_4). Since addition of N_2 to **1** reforms the dinitrogen complex **2**, this could result in a catalytic sequence.

To test this hypothesis, we have examined the reaction of **2** with a number of simple hydride reagents, and preliminary communications have already been published (22, 23). In the case where E-H is 9-borabicyclo[3.3.1]nonane (9-BBN), one E-H addition occurs cleanly; however, a catalytic cycle was precluded because of an ancillary ligand dominated rearrangement. Nevertheless, this work did allow the discovery of a new type of N—N bond cleavage process that results from functionalization of coordinated N_2. In this paper, we report the full details of the reaction of the dinitrogen complex **2** with some primary and secondary boranes.

Results and discussion

As summarized in Scheme 2, our initial attempt at E-H addition to **2** using 9-BBN resulted in the first example of a hydroborated dinitrogen complex (**3**). It was found that addition product **3** is thermally unstable and undergoes H_2 elimination and N—N bond cleavage, presumably via the unobserved intermediate **A**, followed by silicon migration from the ancillary ligand to the bridging nitride to generate **4**. We presume that the final step is elimination of benzene via the B—H bond and the phenyl of the Ta=N-Ph unit to generate the final imide-nitride **5**. Postulation of this proposed scheme was facilitated by the X-ray crystal structures of intermediates **3** and **4**, and final product **5**, along with detailed labeling experiments (22).

Attempted second hydroboration — Synthesis and characterization of [NPN]Ta(H)(μ-N_2-B(C_6H_{11})$_2$)(μ-H)$_2$Ta[NPN] (6)

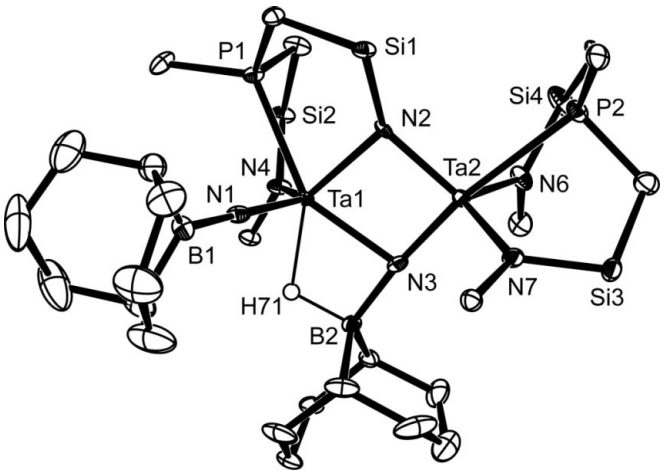
Having established that hydroboration of **2** with 9-BBN leads to N—N bond cleavage and the formation of reactive nitrides, we examined multiple additions of 9-BBN to further test the catalytic plan shown in Scheme 1. Addition of 2 or more equiv. of 9-BBN to **2** resulted in a complicated mixture of products as observed by ^{31}P NMR spectroscopy. Although none of the products were immediately identifiable, there did seem to be a major product present; unfortunately, it could not be separated from the other materials present. Fortuitously, addition of 1 equiv. of 9-BBN to imide–nitride **5** resulted in the clean formation of this same major product unencumbered by impurities. This new complex **6** has two resonances (1:1 integration) in its ^{31}P NMR spectrum that are distinct from those of **5**, and the ^{1}H NMR spectrum does not feature resonances indicative of tantalum hydrides. To determine its identity, crystals of **6** were obtained from a cooled THF solution and subjected to X-ray diffraction analysis.

The solid-state molecular structure of **6** (Fig. 1) shows that a simple Lewis acid – base reaction between the bridging nitride in **5** and the B atom of 9-BBN has taken place. This second equiv. of 9-BBN occupies a position roughly equal to that of the single 9-BBN fragment in intermediate **4** (Scheme 2). The N3—B2 bond length of 1.516(5) Å suggests a N—B single bond (24). The borylimido group is deflected towards the phosphine donor Pl by the presence of the second equiv. of 9-BBN. Other than this, complex **6** is very similar in structure to **5**.

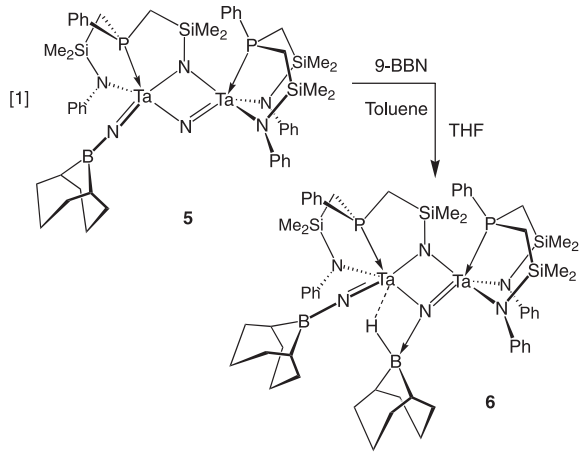
In solution, the presence of the boron hydride is implied by a broad ^{1}H NMR resonance integrating to one proton at δ 4.32 ppm. In the solid state, hydrogen atom H71 was re-

© 2005 NRC Canada

Fig. 1. ORTEP drawing of the solid-state molecular structure of **6** as determined by X-ray crystallography (ellipsoids at 50% probability). Silyl methyls and phenyl ring carbons other than ipso are omitted for clarity. H71 was refined isotropically. Selected bond lengths (Å), bond angles (°), and torsion angles (°): Ta1—N1 1.824(3), N1—B1 1.404(5), Ta1—N2 2.175(3), N2—Ta2 1.947(3), Ta2—N3 1.854(3), N3—Ta1 2.156(3), N3—B2 1.516(5), N2—Si1 1.738(3), Ta1—N4 2.126(3), Ta1—P1 2.5825(10), Ta2—N5 2.091(3), Ta2—N6 2.048(3), Ta2—P2 2.7737(10); Ta1-N2-Ta2 93.87(11), N2-Ta2-N3 91.05(12), Ta2-N3-Ta1 97.23(13), N3-Ta1-N2 77.58(11), Ta1-N1-B1 179.3(3), Ta1-N3-B2 88.6(3), N1-Ta1-P1 86.99(10), N1-Ta1-N4 123.12(13), Ta1-N2-Si1 139.05(16), N3-Ta2-N5 101.25(13), N3-Ta2-N6 103.04(12), N3-Ta2-P2 171.01(9), Ta1-N2-Ta2-N3 3.87(11), Ta1-Ta2-N2-Si1 6.9(6), N1-Ta1-N2-Ta2 –117.54(13), P1-Ta1-Ta2-P2 13.46(4), Ta2-N2-Ta1-N4 98.92(14).



fined isotropically, and thus its position as shown in Fig. 1 is likely based on the structures obtained for **4** as well as the position and coordination geometry of B2. This reaction is shown in eq. [1]. Significantly, the intramolecular reaction to give **5** from **3** proceeds whether additional hydroboration

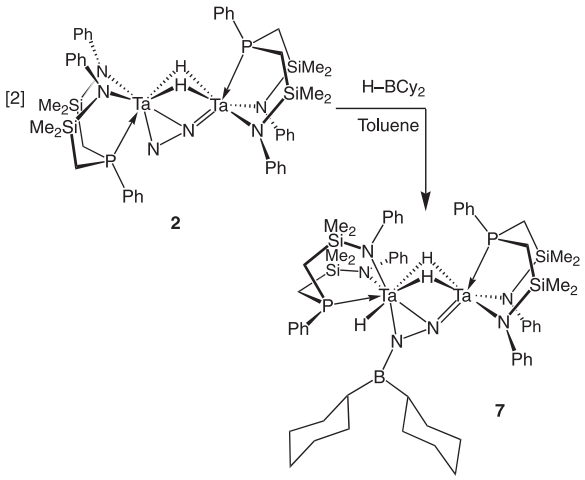


reagent is present or not; as mentioned above, the 2:1 reaction between 9-BBN and **2** also gives mostly **6** when this reaction is monitored by ^{31}P NMR spectroscopy, indicating that 9-BBN is not competent to intercept the nascent nitrido intermediate postulated in the transformation of **4** to **5**, either by hydroboration or simple Lewis acid adduct formation. This precludes hydroboration as the appropriate E-H addition to completely satisfy the proposal of Scheme 1.

A homologous series of complexes prepared with dicyclohexylborane (Cy_2BH) and thexyl borane ($H_2BCMe_2CHMe_2$)

We wondered about the generality of the cascade of reactions shown in Scheme 2. The ability to cleave coordinated N_2 and to generate a new N—B bond was incentive to examine whether or not other borane reagents would engage in similar outcomes or in fact open up new reaction pathways. Given the ready availability of different organoborane reagents, this seemed worthwhile.

The reaction of 1 equiv. of dicyclohexylborane (Cy_2BH) with **2** in toluene gives [NPN]Ta(H)(μ-η^1:η^2-NNBCy_2)(μ-H)$_2$Ta[NPN] (**7**) in 93% yield after stirring for 12 h (eq. [2]).



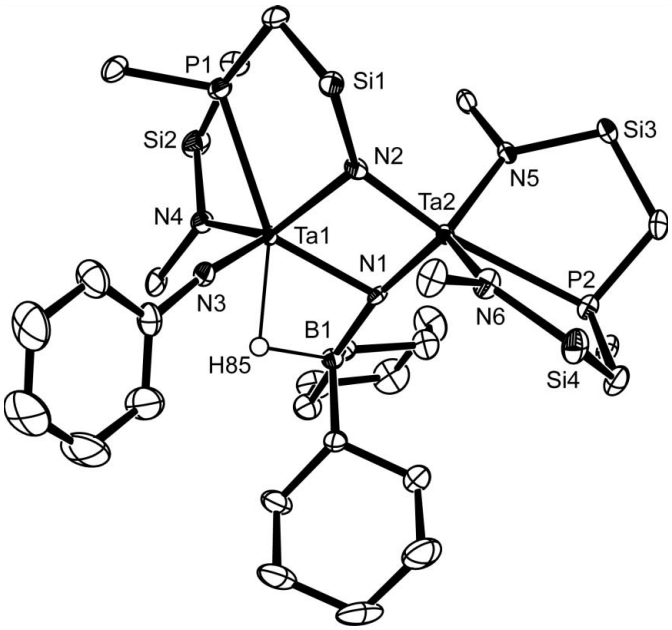
Identification of **7** was facilitated by the similarity of its ^{1}H and ^{31}P NMR spectra to those of the initial 9-BBN adduct (**3**). Thus, the ^{1}H NMR spectrum of **7** indicates C_1 solution symmetry (eight silyl methyl resonances and two separate one-proton resonances associated with bridging hydrides are present), and a new resonance at δ 16.04 ppm implies the existence of a new terminal hydride, as was found for **3**. The solid-state molecular structure of **7** was not established.

Does **7** decompose in the same manner as **3** (Scheme 2)? Toluene or THF solutions of **7** show conversion to [NPμ-N]Ta(=NPh)(μ-NB(H)Cy_2)Ta[NPN] (**8**) in similar yield and on a time scale comparable to the decomposition of **3** into **4**. Therefore, hydroboration and N—N bond cleavage are both possible using Cy_2BH interchangeably with 9-BBN. The solid-state molecular structure of **8** has been determined and it is shown in Fig. 2. The relative orientations of the phenylimido ligand and H85 are similar to **4**. The fact that N—N bond scission and silyl group migration from an [NPN] ligand amide to the new dinitrogen-derived nitrido ligand have occurred in an exactly analogous fashion is evident. Bond lengths and angles are comparable to those of **4**, except that the [NPN] ancillary ligand bound to Ta2 of complex **8** is rotated by 70° about the Ta-Ta axis as compared to its position in **4**.

Like its 9-BBN analogue **4**, **8** is observed via NMR spectroscopy to eliminate benzene in d^8-THF solution, and at the

© 2005 NRC Canada

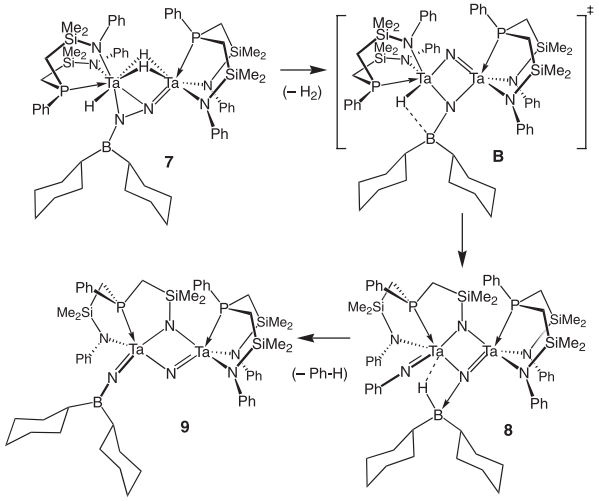
Fig. 2. ORTEP drawing (spheroids at 50% probability) of **8** ([NPμ-N]Ta(=NPh)(μ-NB(H)Cy_2)Ta[NPN]). Silyl methyl and phenyl ring carbons other than ipso omitted for clarity. H85 was located in the electron difference map and refined isotropically. Selected bond lengths (Å), bond angles (°), and torsion angles (°): Ta1—N1 2.142(3), Ta1—N2 2.191(3), Ta1—N3 1.788(3), Ta1—N4 2.146(3), Ta1—P1 2.6370(11), N1—B1 1.532(7), B1—H1 1.59(6), Ta1—H1 1.90(8), N2—Si1 1.738(3), N1—N2 2.675(3), Ta2—N5 2.070(3), Ta2—N6 2.066(3), Ta2—P2 2.7897(10); N1-Ta1-N2 76.31(12), Ta1-N2-Ta2 94.88(12), N2-Ta2-N1 90.40(13), Ta2-N1-Ta1 98.41(13), Ta1-N1-B1 89.8(2), N1-B1-H1 90.2(6), N1-Ta1-N3 117.17(13), N1-Ta1-N4 114.08(11), N1-Ta1-P1 136.84(8), N1-Ta2-N5 114.35(12), N1-Ta2-N6 117.00(13), N1-Ta2-P2 99.46(9), Ta1-N2-Ta2-N1 0.25(11), P1-Ta1-Ta2-P2 –143.96(4), N1-Ta1-N2-Si1 –176.8(2), N2-Ta1-N1-B1 –169.8(2).

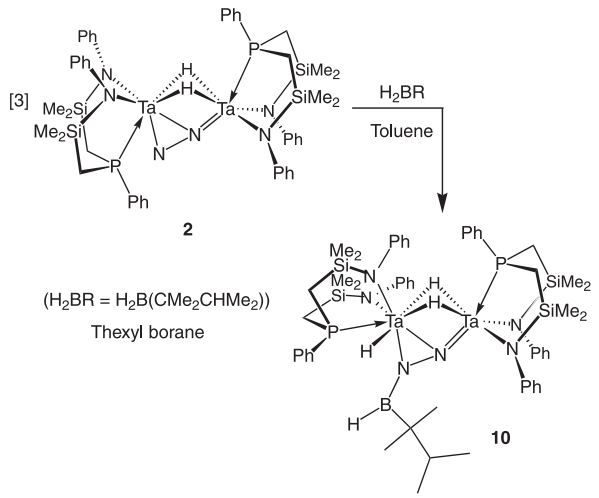


same time, ^{31}P NMR resonances of a new species (**9**) arise. Identification of this complex as ([NPμ–N]Ta(=NBCy_2)(μ-N)Ta[NPN] was made by ^{1}H and ^{31}P NMR spectroscopy in analogy to that already shown in Scheme 2. This new imide–nitride **9** forms cleanly from **8** in an overall yield of 83% as measured by ^{31}P NMR spectroscopy against an internal reference. This is an improvement over the conversion of **4** to **5**, in which many other ^{31}P NMR-active side-products were detected. Although the change from 9-BBN to dicyclohexylborane does not significantly attenuate hydroboration of **1** or N—N bond cleavage, it did increase the yield of **9** vs. the yield of **5**. In Scheme 3, this chemistry is summarized starting with hydroboration adduct **7**; loss of H_2 triggers N—N bond cleavage, presumably through an unobserved intermediate such as **B**, which then undergoes silicon migration from the ancillary [NPN] ligand to generate **8** and finally **9** via loss of benzene. Presumably, addition of another equivalent of dicyclohexylborane to **9** would produce an adduct similar to **6** in eq. [1]; however, this was not pursued.

Since hydroboration of **2** and N—N bond cleavage occurred for the secondary boranes 9-BBN and Cy_2BH, it was of interest to examine the course of the reactions with a primary borane. The presence of another boron hydride for intramolecular reactions after an initial hydroboration suggested the possibility of different post-hydroboration reaction paths including another potential opportunity to form N—H bonds. The 1:1 reaction between **2** and thexyl borane ($H_2BCMe_2CHMe_2$) proceeds to completion over 12 h as shown in eq. [3] to give [NPN]Ta(H)(μ-η^1:η^2-NNB(H)C_6H_{13})(μ-H)$_2$Ta[NPN] (**10**) in 92% yield.

Scheme 3.

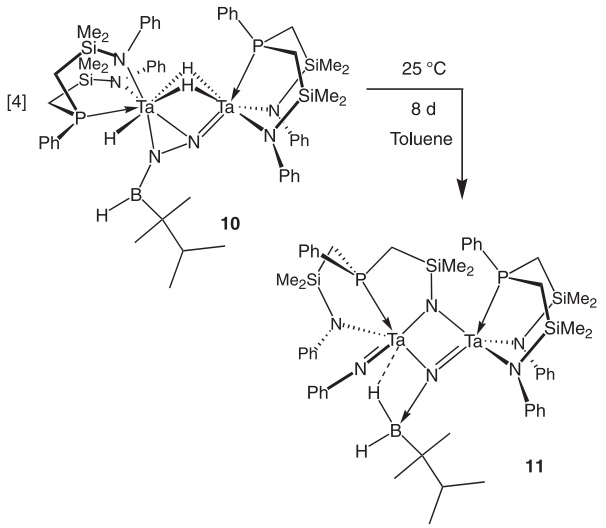




Although crystals suitable for X-ray diffraction were not isolated, the ^{1}H NMR spectrum of **10** shows the expected C_1 symmetry and the new resonance characteristic of a terminal hydride at δ 15.52 ppm, analogous to that already observed for **3** and **7**. The remaining boron hydride is evident as a broad singlet at δ 4.42 ppm that integrates to one proton.

As for complexes **3** and **7**, solutions of **10** are thermally unstable. The rearranged product (**11**) has no resonances suggestive of bridging or terminal hydride ligands in its ^{1}H NMR spectrum, and the ^{31}P NMR resonances of **11** do not unequivocally make it a sister complex to **4** or **8**. The ^{1}H NMR spectrum is indicative of C_1 symmetry, and the resonances can be assigned as [NPμ-N]Ta(=NPh)(μ-N$B(H)_2C_6H_{13}$)Ta[NPN], as shown in eq. [4].

© 2005 NRC Canada

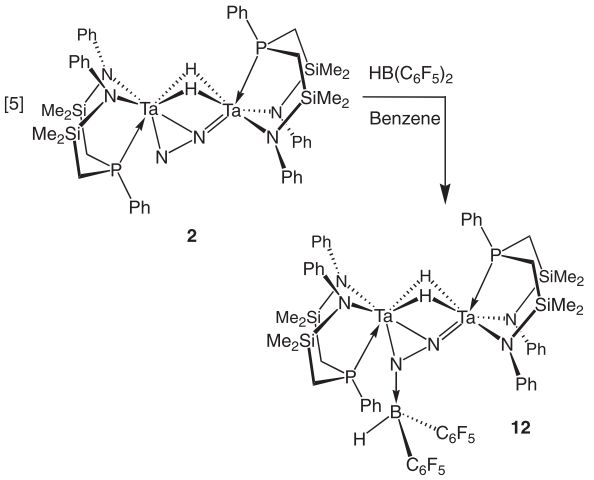


Satisfactory elemental analysis was obtained for this formulation, but the solid-state molecular structure of **11** has not been established. The only indication that **11** might be other than that suggested is that it does not degrade via elimination of benzene to a congener of **5** or **9**. Instead it can be observed by ^{31}P NMR spectroscopy to convert into a number of different products over a week. None of these were spectrally related to **5** or **9**. Hydroboration of **2** with thexyl borane may lead to new rearrangements for **8** that were not observed with secondary boranes, but characterization of the resulting complexes has not been possible. It is likely that the additional B-H functionality coupled with the already documented propensity for ancillary ligand rearrangements in this system renders this combination too reactive. With group 6 dinitrogen complexes, the reaction with thexyl borane results in a totally different and distinct outcome than described herein (25) (Table 1).

Synthesis of ([NPN]Ta)$_2$(μ-η^1:η^2-NN-B(H)(C$_6$F$_5$)$_2$)(μ-H)$_2$ (12)

Although the dinitrogen unit of **2** can be derivatized by hydroboration, it is not clear how to remove the functionalized dinitrogen moiety or the dinitrogen-derived atoms in the descendant complexes from the bimetallic core, because the Ta–N interactions remain quite strong. It was postulated that a more Lewis acidic borane might react in a similar manner to 9-BBN, but would remove additional electron density from the dinitrogen moiety, and thus greatly weaken the Ta—N bonds. A straightforward synthesis of the strongly Lewis acidic secondary borane HB(C$_6$F$_5$)$_2$ has recently been reported (26, 27), and so the reactivity of this borane with **2** was investigated.

The reaction of HB(C$_6$F$_5$)$_2$ with complex **2** occurs immediately; however, the colour of the solution changes from the red-brown of **2** to a dark yellow-brown colour, rather than to an orange colour as observed for the B-H addition adducts **3**, **7**, and **10**. Two new resonances are observed in the ^{31}P NMR spectrum at δ 10.0 and δ 22.8 with a J_{PP} value of 25.1 Hz. A broad peak at δ 4.7 in the ^{1}H NMR spectrum integrates to a single proton. The location and broadness of this resonance identifies it as a hydrogen atom bound to boron. A similar peak is observed in the ^{1}H NMR spectrum of the starting borane HB(C$_6$F$_5$)$_2$. The ^{15}N NMR spectrum of the ^{15}N$_2$-enriched complex ***^{15}N$_2$*-12**, which was prepared by the reaction of ***^{15}N$_2$*-2** with HB(C$_6$F$_5$)$_2$, contains two resonances, at δ –46.9 and δ 24.0. The resonance at δ –46.9 is a doublet of doublets, with a $^2J_{NP}$ value of 25.9 Hz and a $^1J_{NN}$ value of 15.3 Hz. As for ***^{15}N$_2$*-2**, the chemical shift of this resonance and the large coupling to ^{31}P indicates that this is the end-on nitrogen. The chemical shift of the second ^{15}N resonance (δ = 24.0) is much closer to that observed in the B(C$_6$F$_5$)$_3$ adduct of ***^{15}N$_2$*-2** (δ 2.4) than to ***^{15}N$_2$*-3** (δ –114.8), where a tantalum hydride bond is formed. This reaction product is, therefore, not related to complexes **3**, **7**, and **10**, which are the products of B-H addition. Rather, this spectral information indicates that **12** is more closely related to the Lewis acid – base adducts of **2** with B(C$_6$F$_5$)$_3$, GaMe$_3$, and AlMe$_3$, (28) and can be assigned as [NPN]Ta(μ-η^1:η^2-NN-B(H)(C$_6$F$_5$)$_2$)(μ-H)$_2$Ta[NPN]. As for these complexes and parent complex **2**, the solution symmetry of **12** is C_s as evidenced by the four unique silyl methyl resonances in its ^{1}H NMR spectrum. The formation of complex **12** is illustrated in eq. [5].



This assignment was confirmed by X-ray crystallography. An ORTEP drawing of the solid-state molecular structure of **12** is shown in Fig. 3. Hydrides were not located in the diffraction experiment, but the Ta$_2$N$_2$ core bonding and the relative disposition of the ancillary [NPN] ligands is reminiscent of parent complex **2** and of its Lewis acid adducts.

Upon hydroboration, the N—N bond was elongated from 1.319(4) Å in **2** to 1.411(15) Å in **3**. The same bond in **12** is only marginally elongated as compared to the starting dinitrogen complex and the other metric parameters of the Ta$_2$N$_2$ core are similar. Therefore, derivatizaton of the coordinated N$_2$ unit of **2** with strongly Lewis acidic boranes does not affect core bonding. Like **2** and its Lewis adducts, **12** is a stable molecule as compared to **3**, **7**, and **10**, and it shows no propensity to undergo the reductive elimination and N—N bond scission common to these complexes. It seems that addition of the H—B bond across the exposed Ta=N bond of **2** is a precondition for these processes. The theoretically predicted reversal of the polarity of this bond in HB(C$_6$F$_5$)$_2$ vs. dialkylboranes may preclude this reaction, implying that E—H bond polarity is a important consideration in selecting

© 2005 NRC Canada

Table 1. X-ray crystallographic information for complexes **6**, **8**, and **11**.[3]

	[NPμ-N]Ta(=N-BC_8H_{14})(μ-N-B(H)C_8H_{14})Ta[NPN] (**6**)	[NPμ-N]Ta(=NPh)(μ-N-B(H)(C_6H_{11})$_2$)Ta[NPN] (**8**)	([NPN]Ta)$_2$(μ-NN-B(H)(C_6H_5)$_2$)(μ-H)$_2$ (**11**)
CCDC registry	250128	250129	250130
Formula	$C_{58}H_{86}N_6P_2Ta_2$ $Si_4B_2[C_6H_6]$	$C_{67}H_{93}N_6Ta_2P_2Si_4B$	$C_{60}H_{65}BF_{10}N_6P_2Si_4Ta_2(C_6H_6)_{2.5}$
FW	1581.39	1518.70	1802.46
Colour, habit	Yellow, chip	Yellow, chip	Dark, block
Crystal dimensions (mm)	0.20 × 0.15 × 0.15	0.35 × 0.20 × 0.10	0.32 × 0.24 × 0.16
Crystal system	Monoclinic	Triclinic	Monoclinic
Space group	$P2_1/n$ (No. 14)	$P\bar{1}$(No. 2)	$P2_1/n$ (No. 14)
a (Å)	11.7634(4)	12.0875(4)	17.2272(3)
b (Å)	25.6823(8)	13.7220(4)	24.5044(2)
c (Å)	24.0178(9)	20.9574(8)	18.4711(3)
α (°)	90	91.266(3)	90
β (°)	96.180(2)	90.784(3)	95.071(1)
γ (°)	90	84.952(3)	90
V (Å^3)	7213.9(4)	3461.5(2)	7766.9(2)
Z	4	2	4
ρ_{calcd} (g/cm^3)	1.46	1.46	1.54
F(000)	3208.00	1538.00	3596.00
μ(MoKα) (mm^{-1})	3.181	3.312	2.988
Transmission factors	0.6368–1.0000	0.7278–1.0000	0.8192–1.0000
$2\theta_{max}$ (°)	55.8	55.7	56.0
Total no. of reflns.	62 376	31 854	46 043
No. of unique reflns.	16 351	14 230	15 345
R_{merge}	0.053	0.062	0.043
No. reflns with $I \geq n\sigma(I)$	12 735 (n = 2)	11 678 (n = 2)	15 345 (n = 2)
No. of variables	775	720	881
R (F^2, all data)	0.043	0.039	0.036
R_w (F^2, all data)	0.068	0.074	0.076
R (F, $I > n\sigma(I)$)	0.029	0.029	0.046
R_w (F, I > $n\sigma(I)$)	0.062	0.071	0.081
GOF	0.94	0.098	1.088

Note: Rigaku/ADSC CCD diffractometer, $R = \Sigma ||F_o^2| - |F_c^2||/\Sigma|F_o^2|$; $R_w = (\Sigma w(|F_o^2| - |F_c^2|)^2/\Sigma w|F_o^2|^2)^{1/2}$.

reagents for any scheme bent on using **2** for catalytic functionalization of N_2.

Summary

The initial study of the hydroboration of a dinuclear tantalum dinitrogen complex with 9-BBN has been extended to other monoalkyl- and dialkylboranes. In all cases, the N_2 complexes, derivatized by H—B bond addition across the exposed Ta=N bond, spontaneously undergo reductive elimination of two bridging hydrides as H_2 coupled to N—N bond cleavage without loss of the new B—N bond. This cascade of reactions is only somewhat attenuated by different substituents on the hydroboration reagent. Subsequent addition reactions across new Ta=N moieties do not occur, but the additional equivalents of hydroboration reagent can be incorporated into the complex as alkylborohydride adducts. Bis(pentafluorophenyl)borane $HB(C_6F_5)_2$ fails to react with the starting dinitrogen complex **2** in the same manner as the alkylboranes; instead, a stable adduct is formed, likely a result of the enhanced Lewis acidity of the boron centre owing to the presence of the perfluorophenyl substituents. This is summarized in Scheme 4.

Experimental section

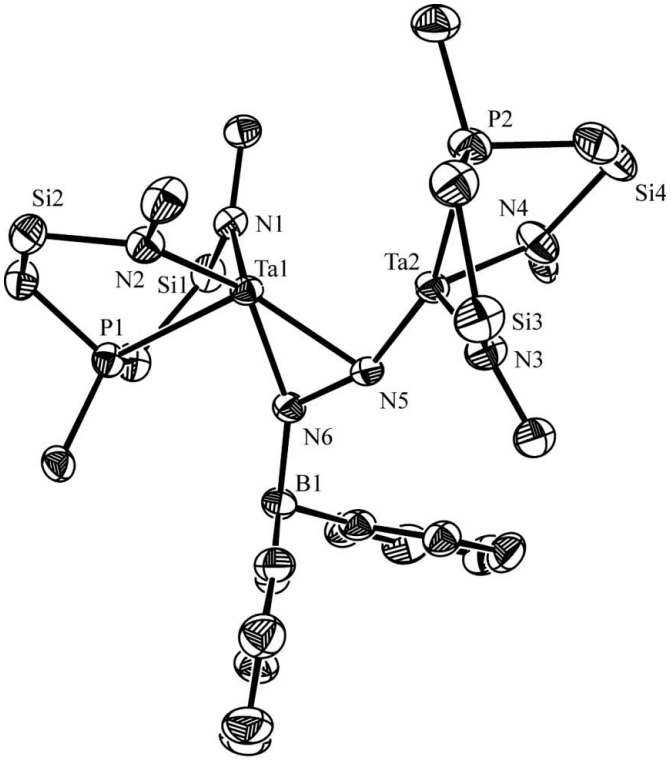
General considerations

Unless otherwise stated, all manipulations were performed under an atmosphere of dry oxygen-free dinitrogen by means of standard Schlenk or glovebox techniques (Vacuum Atmospheres HE-553-2 glovebox equipped with a MO-40-2H purification system and a –60 °C freezer). Anhydrous hexanes and toluene were purchased from Aldrich, sparged with dinitrogen, and passed through columns containing activated alumina and Ridox catalyst before use. Anhydrous diethylether was stored over sieves and distilled from so-

[3] Supplementary data may be purchased from the Directory of Unpublished Data, Document Delivery, CISTI, National Research Council Canada, Ottawa, ON K1A 0S2, Canada (http://cisti-icist.nrc-cnrc.gc.ca/irm/unpub_e.shtml for information on ordering electronically). CCDC 250128–250130 contain the crystallographic data for this manuscript. These data can be obtained, free of charge, via ww.ccdc.cam.ac.uk/conts/retrieving.html (or from the Cambridge Crystallographic Data Centre, 12 Union Road, Cambridge CB2 1EZ, UK; fax +44 1223 336033; or deposit@ccdc.cam.ac.uk).

© 2005 NRC Canada

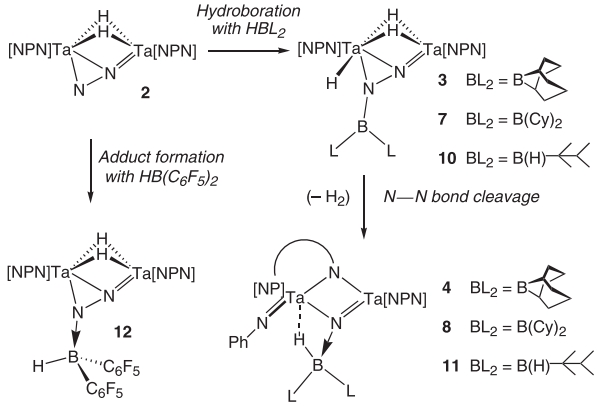
Fig. 3. ORTEP depiction of the solid-state molecular structure of $([NPN]Ta)_2(\mu\text{-}\eta^1\text{:}\eta^2\text{-NN-B(H)}(C_6F_5)_2)(\mu\text{-H})_2$ (**12**) as determined by X-ray crystallography. The bridging hydrides and the hydrogen bound to boron were not located. The silyl methyl groups and fluorine atoms are omitted for clarity, and only the ipso carbons of the PPh and NPh groups are shown. Selected bond lengths (Å) and bond angles (°): N5—N6 1.368(4), Ta1—Ta2 2.8903(2), Ta1—N5 2.186(3), Ta1—N6 1.964(3), Ta2—N5 1.878(3), N6—B1 1.557(5), Ta1—P1 2.6089(10), Ta2—P2 2.6265(10); Ta1-N5-Ta2 90.36(12), Ta1-N6-N5 79.8(2), Ta1-N6-B1 155.6(3).



dium benzophenone ketyl under argon. Pentane was stored over sieves and distilled from sodium benzophenone ketyl solublized by tetraglyme under dry dinitrogen prior to storage over a potassium mirror. Tetrahydrofuran was heated at reflux over CaH_2 prior to distillation from sodium benzophenone ketyl under argon. Nitrogen gas was dried and deoxygenated by passage through a column containing activated molecular sieves and MnO.

Deuterated benzene was dried by heating at reflux with sodium–potassium alloy in a sealed vessel under partial pressure, then trap-to-trap distilled, and freeze–pump–thaw degassed three times. Deuterated tetrahydrofuran and toluene were dried by refluxing with molten potassium metal in a sealed vessel under vacuum, then trap-to-trap-distilled, and freeze–pump–thaw degassed three times. Unless otherwise stated, ^{1}H, ^{31}P, ^{1}H{^{31}P}, ^{13}C, ^{11}B, ^{15}N, ^{29}Si-DEPT, and two-dimensional NMR spectra were recorded on either a Bruker AMX-500 instrument (5 mm BBI probe) operating at 500.1 MHz for ^{1}H or a Bruker AVA-400 instrument (5 mm BBI probe) operating at 400.1 MHz for ^{1}H. ^{1}H NMR spectra were referenced to residual proton in deuterated solvent as follows: C_4D_7HO (δ 3.58 ppm), C_6D_5H (δ 7.15 ppm), and

Scheme 4.



C_7D_7H (δ 2.09 ppm). ^{31}P NMR spectra were referenced to external $P(OMe)_3$ (δ 141.0 ppm with respect to 85% H_3PO_4 at δ 0.0 ppm) or internal $P(OMe)_3$ flame-sealed inside a 1 mm × 25 mm glass capillary tube if required, ^{13}C NMR spectra to $^{13}CC_5D_6$ (δ 128.4 ppm) and $^{13}CD_2Cl_2$ (δ 54.0 ppm), ^{11}B spectra to neat $BF_3{\cdot}Et_2O$ (δ 0.0 ppm), ^{15}N spectra to external nitromethane at 0.0 ppm, and ^{29}Si to Me_4Si 50% in $CDCl_3$ (δ 0.0 ppm). Elemental analyses were performed by Mr. P. Borda and Mr. M. Lakha, of The University of British Columbia Department of Chemistry.

The syntheses of complexes **1**, **2** (21), **3**, **4**, and **5** (22), dicyclohexylborane (29), thexyl borane (30), and $HB(C_6F_5)_2$ (27) were performed as described in the literature.

[NPμ-N]Ta(=N-BC$_8$H$_{14}$)(μ-NB(H)C$_8$H$_{14}$)Ta[NPN] (6)

To a stirred 15 mL toluene solution of **5** (298 mg, 0.229 mmol) was added dropwise 0.25 mL (1.1 equiv.) of 1.0 mol/L 9-BBN solution in THF. The resulting mixture was stirred overnight and the ^{31}P NMR spectrum of a small portion indicated that the reaction had proceeded to consume all of complex **5**, giving exclusively resonances of **6**. After evaporation of solvent and precipitation from pentane, 241 mg (0.169 mmol, 74% yield) of **6** was recovered on a frit. ^{1}H NMR (C_6D_6, 300 K, 400 MHz) δ: –0.69, –0.21, 0.05, 0.13, 0.25, 0.34, 0.43, (s, 3H each) SiCH_3; 0.84, 0.97 (d, 1H each) PCH_2, complicated overlapping multipets from 0.70 to 2.26 (total 39H), B-C_8H_{14} and PCH_2 (solvent was contaminated with a small amount of hexanes) 4.32 (b, 1H), B-*H*; 6.73, 6.79, 6.81, 6.85, 6.93, 7.07, 7.09, 7.20 (s, d, t, some peaks obscured by solvent) C_6H_5-N and C_6H_5-P; (7.51 (d, 2H, J_{HH} = 6.95 Hz), 7.94 (d, 2H, J_{HH} = 7.05 Hz), *o*-C_6H_5-P. ^{31}P NMR (C_6D_6, 300 K, 161.9 MHz) δ: –12.52 (b), 27.26 (s). Anal. calcd. for $C_{58}H_{86}B_2N_6P_2Si_4Ta_2$: C 48.88, H 6.08, N 5.90; found: C 49.12, H 6.23, N 5.81.

[NPN]Ta(H)(μ-η^1:η^2-NNBCy$_2$)(μ-H)$_2$Ta[NPN](7)

Toluene (25 mL) was added to an intimate mixture of dry **2** (0.412 g, 0.327 mmol) and white solid dicyclohexylborane (58.2 mg, 1 equiv.) in a glove box. The resulting mixture was stirred vigorously overnight, the solvent was evaporated, and the residues were triturated under hexanes, giving 0.438 mg (0.305 mmol, 93.2% yield) of **7**. ^{1}H NMR (500.1 MHz, C_6D_6, 300 K) δ: –0.37, –0.22, –0.17, –0.05, –0.10, –0.01, 0.09, 0.14 (s, 24H total), SiCH_3; 0.28, 0.40, 0.64, 0.73, 0.77, 0.86, 1.09, 1.15 to 1.34 (broad), 1.47, 1.59,

© 2005 NRC Canada

and 1.77 (broad overlapping resonances), cyclohexyl and PCH_2; 6.61, 6.66, 6.73, 6.82, 6.88, 6.96, 7.13 to 7.26 (overlapping), 7.29, 7.38, and 7.70 (overlapping doublets, triplets, 20H total, some resonances obscured by solvent) P-C$_6H_5$ and N-C$_6H_5$; 8.14 (d, J_{PH} = 6.38 Hz), 8.24 (d, J_{PH} = 6.82 Hz), *o*-P-C$_6H_5$; 10.70 and 11.51 (d, 1H each, J_{HH} = 10.0 Hz) μ-H; 16.04 (d, J_{PH} = 14.6 Hz), Ta-*H*. ^{13}C NMR was not recorded. ^{31}P NMR (202.5 MHz, C$_6$D$_6$, 300 K) δ: 7.98 (d, J_{PP} = 10.2 Hz), 20.0 (d, J_{PP} = 10.2 Hz). Anal. calcd. for $C_{60}H_{87}BN_6P_2Si_4Ta_2$: C 50.07, H 6.09, N 5.84; found: C 50.35, H 6.34, N 5.48.

Decomposition of 7 to [NPμ-N]Ta(=NPh)(μ-NB(H)Cy$_2$)Ta[NPN] (8)

A capped THF solution of 396 mg (0.275 mmol) **7** was left in a glove box at ambient temperature for 3 weeks and then cooled in a –60 °C freezer, giving crystals of **8**. Yield 0.186 g, 0.129 mmol, 47%. ^{1}H NMR (400.1 MHz, C$_7$D$_8$, 300 K) δ: –1.13, –0.90, –0.09, –0.15, –0.36, 0.18, 0.34 (s, 24H total), SiCH_3; 0.50, 1.16 (d, 1H each) PCH_2; –0.01, 0.68, 0.87, 1.06, 1.33, 1.45, 1.48 (broad overlapping multiplets, total 26H) B-C$_6H_{11}$ and PCH_2; 4.09 (b, FWHM 32 Hz, 1H) B*H*; 6.28, 6.30, 6.34, 6.40, 6.50, 6.74, 6.83, 6.94, 7.00, 7.11, 7.18 (overlapping doublets, triplets, 20H total, some resonances obscured by solvent) P-C$_6H_5$ and N-C$_6H_5$; 7.84 (d, J_{PH} = 6.59 Hz), 7.49 (d, J_{PH} = 7.06 Hz), (10H total) *o*-P-C$_6H_5$. ^{13}C NMR (100.6 MHz, C$_7$D$_8$, 300 K) δ: –1.77, –0.80, –0.64, 0.30, 2.67, 2.75, 3.30, 5.39, Si*C*H$_3$; 32.85 (b), B-C_{ipso} of cyclohexyl; 11.14, 15.45, 18.19, 25.93, 26.05, *C*H$_2$ of cyclohexyl; 20.99, 25.32, 26.05, 26.41, 27.16, 29.99, 30.49, 31.58, P-*C*H$_2$; 118.27, 119.03, 120.98, 122.79, 123.16, 123.29, 125.70, 126.98, 127.15, 127.51, 127.74, 128.56, 133.56, 135.84 (some resonances obscured by solvent), P-*C*$_6$H$_5$ and N-*C*$_6$H$_5$; 127.62, 131.96, *o*-P-*C*$_6$H$_5$; 151.24, 158.19, ipso-P-*C*$_6$H$_5$. ^{31}P NMR (161.9 MHz, C$_7$D$_8$, 300 K) δ: –2.30 (d, J_{PP} = 3.1 Hz), 28.30 (d, J_{PP} = 3.1 Hz). Anal. calcd. for $C_{60}H_{85}BN_6P_2Si_4Ta_2$: C 50.14, H 5.96, N 5.85; found: C 50.28, H 6.13, N 5.46.

Decomposition of 8 to [NPμ-N]Ta(=NBCy$_2$)(μ-N)Ta[NPN] (9)

A d^8-THF solution of **8** suitable for NMR spectroscopy in a Wilmad NMR tube capped with a plastic stopper and sealed with ParaFilm laboratory film and bearing a sealed capillary containing internal standard was left in a glove box for 3 weeks. Spectra were acquired intermittently. After this time, the ^{31}P and ^{1}H NMR spectra were exclusively that of **8**, and the integration with respect to internal standard allowed evaluation of 83% yield. The total integration of other ^{31}P NMR active resonances was 6%. ^{1}H NMR (400.1 MHz, C$_7$D$_8$, 300 K) δ: –1.10, –0.88, –0.34, –0.13, –0.02, 0.18, 0.20, 0.33 (s, 3H each), SiCH_3; 0.49, 0.75, 0.89, 1.17, 1.21, 1.31, 1.55 (d, 1H each), P-CH_2; 0.6–1.6 (complicated overlapping multiplets, 22H total), B-(C$_6H_{11}$)$_2$; 3.81 (b, FWHM 28 Hz, 1H) B-*H*; 6.27, 6.34, 6.51, 6.57, 6.63, 6.67, 6.77, 6.83, 6.86, 6.95, 6.99, 7.03, 7.11, 7.16, 7.42, 7.57 (d, t, overlapping, 26H total) P-*C*$_6$H$_5$ and N-*C*$_6$H$_5$; 7.47, 7.83 (d, 2H each), *o*-P-*C*$_6$H$_5$. ^{31}P NMR (161.9 MHz, C$_7$D$_8$, 300 K) δ: 0.76 (d, J_{PP} = 5.94 Hz), 17.41 (d, J_{PP} = 5.94 Hz). Elemental analysis was not obtained.

[NPN]Ta(H)(μ-η^1:η^2-NNB(H)C$_6$H$_{13}$)(μ-H)$_2$Ta[NPN] (10)

To a stirred toluene solution of **1** (0.336 g, 0.266 mmol) was added 0.54 mL (0.27 mmol, 1.02 equiv.) of freshly prepared thexyl borane (0.5 mol/L in THF). After stirring overnight the solvents were evaporated, leaving an orange residue that was triturated under hexanes and recovered on a frit, giving 0.332 g (0.244 mmol, 91.8% yield) of solid pale orange **10**. ^{1}H NMR (400 MHz, C$_6$D$_6$, 300 K) δ: –0.32, –0.14, –0.05, 0.11, 0.17, 0.19, 0.25, 0.34 (s, 3H each), SiCH_3; 1.21, 1.41, 1.45, 1.59, 1.61, 1.67, 1.78, 1.81 (d, 1H each) PCH_2; 0.82, 0.89 (d, 3H each) 1.11, 1.23 (s, 3H each), B-C(CH_3)$_2$CH(CH_3)$_2$; 1.64 (m, ^{1}H) B-C(CH$_3$)$_2$C*H*(CH$_3$)$_2$; 4.42 (b, ^{1}H) B-*H*; 5.96, 6.07, 6.22, 6.28, 6.35, 6.66, 6.91, 6.94, 7.01, 7.12, 7.20, 7.22, 7.25 (d, t, total 26H), P-C$_6H_5$ and N-C$_6H_5$; 7.71, 7.92 (d, 2H each) *o*-P-C$_6H_5$; 10.2, 11.6 (d, ^{1}H each) Taμ*H*; 15.52 (s, ^{1}H) Ta*H*. ^{31}P NMR (161.9 MHz, C$_6$H$_6$, 300 K) δ: 8.73 (d, J_{PP} = 15.3 Hz), 24.16 (d, J_{PP} = 15.3 Hz). Anal. calcd. for $C_{54}H_{79}BN_6P_2Si_4Ta_2$: C 47.72, H 5.86, N 6.18; found: C 47.32, H 6.26, N 6.12.

[NPμ-N]Ta(=NPh)(μ-NB(H)$_2$C$_6$H$_{13}$)Ta[NPN] (11)

A 15 mL toluene solution of 0.328 g (0.241 mmol) **11** was allowed to stand in a glove box at ambient temperature for 8 days. The ^{31}P NMR spectrum of a portion of this solution showed no remaining **10**, and solvent was evaporated. Solid **11** (134 mg, 41% yield) was recovered on a frit after trituration under hexanes. ^{1}H NMR (400 MHz, C$_4$D$_8$O, 300 K) δ: –0.48, –0.43, –0.08, –0.02, 0.08, 0.11, 0.27, 0.34 (s, 3 H each, 24H total), SiCH_3; 0.55, 0.78, 1.20, 1.30, 1.57, 1.81, 2.22, 2.36 (d, 1H each), PCH_2; 0.73, 0.81, 1.40, 1.57 (s, 3H each), B-C(CH_3)$_2$CH(CH_3)$_2$; 3.58, 4.32 (b, 1H each), B-*H*; 6.76, 6.80, 6.96, 7.02, 7.05, 7.06, 7.09, 7.12, 7.14, 7.16, 7.19, 7.30, 7.33 (d, t, 1 and 2H each, 26H total) P-C$_6H_5$ and N-C$_6H_5$; 7.61, 8.02 (d, 2H each) P-C$_6H_5$. ^{31}P NMR (161.9 MHz, C$_4$D$_8$O, 300 K) δ: –6.68 (b), 18.55 (s). Anal. calcd. for $C_{54}H_{77}BN_6P_2Si_4Ta_2$: C 47.79, H 5.72, N 6.19; found: C 47.42, H 6.10, N 6.38.

([NPN]Ta)$_2$(μ-η^1:η^2-NNB(H)(C$_6$F$_5$)$_2$)(μ-H)$_2$ (12)

To a solution of **2** (0.7589 g, 0.6017 mmol) in 10 mL of C$_6$H$_6$ was added solid HB(C$_6$F$_5$)$_2$ (0.2081 g, 0.6017 mmol, 1.0 equiv.). The solution was allowed to stir for 3 h, and the product was then allowed to crystallize by slow evaporation. The solid was collected and dried, to yield ([(NPN]$_2$TaH)$_2$N$_2$(HB(C$_6$F$_5$)$_2$) as a brown solid (0.943 g, 97%). ^{1}H NMR (500 MHz, C$_7$D$_8$, 350 K) δ: –0.28, –0.07, –0.03, 0.03 (s, 24H total, SiCH_3), 0.61, 1.45, 1.68, 2.03 (AMX, 8H total, CH_2 ring), 4.7 (br, $W_{1/2}$ = 250 Hz, 1H, B*H*), 6.77, 6.87, 6.94, 6.98, 7.06, and 7.20 (overlapping m, 26 H, NPh and PPh), 7.02 and 7.57 (m, 4H total, PPh *o*-*H*), 11.56 (dd, $^2J_{HP}$ = 20.9 Hz, $^2J_{HP}$ = 17.3 Hz, 2H, Ta*H*). ^{1}H NMR (500 MHz, C$_7$D$_8$, 245 K) δ: –0.26, –0.26, –0.24, –0.17, 0.00, 0.09, 0.11, 0.41 (s, 24H total, SiCH_3), 0.63, 1.05, 1.20, 1.28, 1.36, 1.39, 1.67, 2.73 (AMX, 8H total, CH_2 ring), 4.7 (br, 1H, B*H*), 5.80, 6.16, 6.51, 6.75, 6.85 (m, 1H each, NPh or PPh) 6.91–7.37 (overlapping m, 18 H, NPh and PPh), 7.49 (m, 2H, PPh-*o*-*H*), 7.53 (m, 2H, PPh or NPh), 7.88 (m, 2H, PPh-*o*-*H*), 11.00 (br m, $^2J_{HH}$ = 14.2 Hz, 1H, Ta*H*), 11.67 (ddd, $^2J_{HH}$ = 14.2 Hz, $^2J_{HP}$ = 14.7 Hz, $^2J_{HP}$ = 31.9 Hz, 1H, Ta*H*). ^{31}P NMR (C$_7$D$_8$, 299 K) δ: 10.0 (d, $^2J_{PP}$ = 25.1, [NPN] ligand), 22.8 (d, $^2J_{PP}$ = 25.1, [NPN]

© 2005 NRC Canada

ligand). Anal. calcd. for $C_{60}H_{65}BF_{10}N_6P_2Si_4Ta_2$: C 44.84, H 4.08, N 5.23; found: C 44.77, H 4.13, N 5.10.

([NPN]Ta)$_2$(μ-η^1:η^2-^{15}N^{15}NB(H)(C$_6$F$_5$)$_2$)(μ-H)$_2$ (*$^{15}N_2$*-12)

The ^{15}N-labeled analogue was prepared in a manner identical to that used for **12**, except for using the ^{15}N-labeled precursor ***$^{15}N_2$*-2**. ^{31}P NMR (C_7D_8, 299 K) δ: 10.0 (dd, J_{PP} = 25.1 Hz, $^2J_{PN}$ = 17.2 Hz, [NPN] ligand), 22.8 (d, J_{PP} = 25.1 Hz, [NPN] ligand). ^{15}N NMR (C_7D_8, 299 K) δ: −48.1 (dd, $^1J_{NN}$ = 16.2 Hz, $^2J_{NP}$ = 25.1 Hz), 11.5 (d, $^1J_{NN}$ = 16.2 Hz).

Acknowledgements

The authors thank the Natural Sciences and Engineering Research Council of Canada (NSERC) for funding (PGS-A, PGS-B, and PDF awards to B.A.M. and S.A.J., Discovery Grant to M.D.F.).

References

1. M.D. Fryzuk and S.A. Johnson. Coord. Chem. Rev. **200–202**, 379 (2000).
2. S. Gambarotta. J. Org. Chem. **500**, 117 (1995).
3. M. Hidai and Y. Mizobe. Chem. Rev. **95**, 1115 (1995).
4. B.A. MacKay and M.D. Fryzuk. Chem. Rev. **104**, 381 (2004).
5. C.M. Kozak and P. Mountford. Angew. Chem. Int. Ed. **43**, 1186 (2004).
6. R. Schlögl. Angew. Chem. Int. Ed. **42**, 2004 (2003).
7. D.V. Yandulov and R.R. Schrock. Science, **301**, 76 (2003).
8. J.A. Pool, E. Lobkovsky, and P.J. Chirik. Nature (London), **427**, 527 (2004).
9. M. Hidai. Coord. Chem. Rev. **185–186**, 99 (1999).
10. K. Hori and M. Mori. J. Am. Chem. Soc. **120**, 7651 (1998).
11. M. Hori and M. Mori. J. Org. Chem. **60**, 1480 (1995).
12. M. Akashi, Y. Sato, and M. Mori. J. Org. Chem. **66**, 7873 (2001).
13. K. Komori, H. Oshita, Y. Mizobe, and M. Hidai. J. Am. Chem. Soc. **111**, 1939 (1989).
14. M. Mori, K. Hori, M. Akashi, M. Hori, Y. Sato, and M. Nishida. Angew. Chem. Int. Ed. **37**, 636 (1998).
15. K. Ueda, Y. Sato, and M. Mori. J. Am. Chem. Soc. **122**, 10 722 (2000).
16. A.D. Allen and C.V. Senoff. Chem. Commun. 621 (1965).
17. M.P. Shaver and M.D. Fryzuk. Adv. Synth. Catal. **345**, 1061 (2003).
18. M. Hidai and Y. Mizobe. Metal Ions Biol. Syst. **39**, 121 (2002).
19. S. Gambarotta. *In* Inorganic chemistry highlights. *Edited by* G. Meyer, D. Naumann, and L. Weseman. John Wiley and Sons, New York. 2002. p. 285.
20. J. Chatt, J.R. Dilworth, and R.L. Richards. Chem. Rev. **78**, 589 (1978).
21. M.D. Fryzuk, S.A. Johnson, B.O. Patrick, A. Albinati, S.A. Mason, and T.F. Koetzle. J. Am. Chem. Soc. **123**, 3960 (2001).
22. M.D. Fryzuk, B.A. MacKay, S.A. Johnson, and B.O. Patrick. Angew. Chem. Int. Ed. **41**, 3709 (2002).
23. M.D. Fryzuk, B.A. MacKay, and B.O. Patrick. J. Am. Chem. Soc. **125**, 3234 (2003).
24. M. Yalpani, R. Koester, and R. Boese. Chem. Ber. **126**, 285 (1993).
25. H. Ishino, Y. Ishii, and M. Hidai. Chem. Lett. 677 (1998).
26. D.J. Parks, R.E.v.H. Spence, and W.E. Piers. Angew. Chem. Int. Ed. Engl. **34**, 809 (1995).
27. D.J. Parks, W.E. Piers, M. Parvez, R. Atencio, and M.J. Zaworotko. Organometallics, **17**, 1369 (1998).
28. F. Studt, B.A. MacKay, S.A. Johnson, B.O. Patrick, M.D. Fryzuk, and F. Tuczek. Chem. Eur. J. **11**, 604 (2005).
29. H.C. Brown, M.C. Desai, and P.K. Jadhav. J. Org. Chem. **47**, 5065 (1982).
30. G. Zweifel and H.C. Brown. J. Am. Chem. Soc. **85**, 2066 (1963).

© 2005 NRC Canada

Synthesis and structure of a (NacNac)rhodium terminal dinitrogen complex[1]

Jason D. Masuda and Douglas W. Stephan

Abstract: Reaction of the ligand salt $CH[C(Me)(N\text{-}i\text{-}Pr_2C_6H_3)]_2Li(Et_2O)$ with $[Rh(COE)(\mu\text{-}Cl)]_2$ proceeds to give the brown crystalline product $CH[C(Me)(N\text{-}i\text{-}Pr_2C_6H_3)]_2Rh(N_2)(COE)$ (**1**) in 38% yield. X-ray crystallographic study of **1** confirmed the formulation and revealed that the terminally bound dinitrogen molecule exhibits a Rh—N distance of 1.943(4) Å and an N—N distance of 1.091(6) Å. Comparison to other Rh–N_2 complexes shows that the N—N distances reflect a complex admixture of the trans influence and the net electron density at the metal center.

Key words: rhodium, dinitrogen, diimine, structure.

Résumé : La réaction du sel ligand $CH[C(Me)(N\text{-}i\text{-}Pr_2C_6H_3)]_2Li(Et_2O)$ avec le $[Rh(COE)(\mu\text{-}Cl)]_2$ conduit à la formation d'un produit cristallin de couleur brune, le $CH[C(Me)(N\text{-}i\text{-}Pr_2C_6H_3)]_2Rh(N_2)(CEO)$ (**1**), avec un rendement de 38 %. Une étude du composé **1** par diffraction des rayons X a permis de confirmer sa formule et a révélé que, pour la molécule de diazote liée en position terminale, la distance Rh—N est égale à 1,943(4) Å et la distance N—N est égale à 1,091(6) Å. Une comparaison avec d'autres complexes Rh–N_2 montre que les distances N—N sont un reflet d'un mélange complexe de l'influence trans et d'une densité électronique nette au niveau du centre métallique.

Mots clés : rhodium, diazote, diimine, structure.

[Traduit par la Rédaction]

Introduction

The 40th anniversary of the discovery of dinitrogen complexes is being commemorated with this issue of the *Canadian Journal of Chemistry*. During the time since the initial discovery of a Ru–N_2 complex by Allen and Senoff (1), a variety of other metals have been shown to interact with N_2 in either a terminal or bridging fashion. Moreover, the reactivity of such species, have led to significant breakthroughs in the understanding of N_2 chemistry. This work has been reviewed (2–6). In continuing studies towards N_2 reduction, metals capable of both N_2 and H_2 activation have been targeted. While Rh complexes have a well-known ability to react with hydrogen, few Rh–N_2 complexes are known. Several examples of bridging bimetallic species have been described including $[Me_2C_6H(CH_2P\text{-}i\text{-}Pr_2)_2Rh]_2(\mu\text{-}N_2)$ (7), $[Me_2C_6H(CH_2P\text{-}t\text{-}Bu_2)(CH_2NEt_2)Rh]_2(\mu\text{-}N_2)$ (8), $[MeC_6H_2(CH_2P\text{-}t\text{-}Bu_2)_2ORh]_2(\mu\text{-}N_2)$ (9), $[(i\text{-}Pr_3P)_2RhH]_2(\mu\text{-}N_2)$ (10), and $[CH_2(P\text{-}t\text{-}Bu_2)_2RhCH_2\text{-}t\text{-}Bu]_2(\mu\text{-}N_2)$ (11) (Scheme 1). In addition, terminally bound N_2 complexes that have been characterized include $(Ph\text{-}t\text{-}Bu_2P)_2RhH(N_2)$ (12), $(i\text{-}Pr_3P)_2RhCl(N_2)$ (13), and $MeCH(CH_2CH_2P\text{-}t\text{-}Bu_2)_2Rh(N_2)$ (14). In these complexes, the presence of strong σ-donor ligands (phosphine, alkyl, aryl) is thought to strengthen the Rh to N_2 interaction via π backbonding (Scheme 2).

In this manuscript, we report the synthesis and X-ray structural study of the terminal N_2–Rh complex, $CH[C(Me)(N\text{-}i\text{-}Pr_2C_6H_3)]_2Rh(N_2)(COE)$ (COE = cyclooctene), containing a bulky diimine ligand (NacNac). In a very recent communication, Chirik and co-workers (15) reported the analogous Ir complex.

Received 12 October 2004. Published on the NRC Research Press Web site at http://canjchem.nrc.ca on 17 March 2005.

J.D. Masuda and D.W. Stephan.[2] Department of Chemistry and Biochemistry, University of Windsor, Windsor, ON N9B3P4 Canada.

[1]This article is part of a Special Issue dedicated to Dinitrogen Chemistry.

[2]Corresponding author (e-mail: stephan@uwindsor.ca).

Experimental

General data

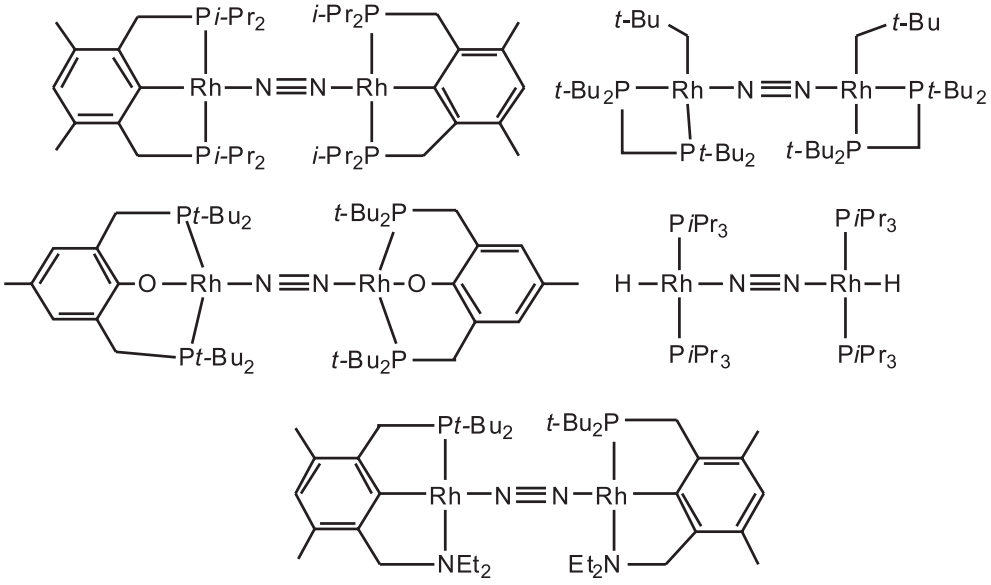
All preparations were done under an atmosphere of dry, O_2-free N_2 in a Vacuum Atmospheres inert atmosphere glovebox. Solvents were purified employing a Grubbs' type solvent purification system manufactured by Innovative Technology. Deuterated solvents were purified using the appropriate techniques. All organic reagents were purified by conventional methods. ^1H and ^{13}C NMR spectra were recorded on Bruker Avance-300 and -500 spectrometers. Trace amounts of protonated solvents were used as references and chemical shifts are reported relative to $SiMe_4$. Combustion analyses were done in house employing a PerkinElmer CHN analyzer. $CH[C(Me)(N\text{-}i\text{-}Pr_2C_6H_3)]_2Li(Et_2O)$ was prepared following the literature procedure (16). $[Rh(COE)_2(\mu\text{-}Cl)]_2$ was purchased from the Strem Chemical Co.

Synthesis of $CH[C(Me)(N\text{-}i\text{-}Pr_2C_6H_3)]_2Rh(N_2)(COE)$ (1)

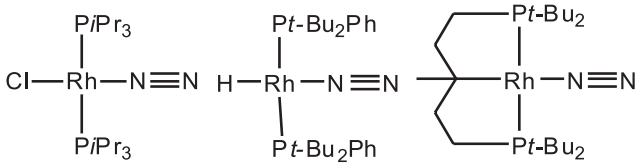
To a solution of $CH[C(Me)(N\text{-}i\text{-}Pr_2C_6H_3)]_2Li(Et_2O)$ (0.500 g, 1.00 mmol) in 10 mL Et_2O was added $[Rh(COE)_2(\mu\text{-}Cl)]_2$ (0.249 g, 0.50 mmol). The mixture was allowed to stir overnight whereupon the solution became dark brown-black. The mixture was filtered through Celite® and solvent was removed to give a dark semisolid. This material was dissolved

 doi: 10.1139/V05-012 © 2005 NRC Canada

Scheme 1. Bridged Rh–N_2 complexes.



Scheme 2. Terminal Rh–N_2 complexes.



in pentane (5 mL) and again filtered through Celite®. Cooling the pentane solution to –35 °C gave 263 mg of a dark brown crystalline solid after work-up. Yield: 38%. IR (KBr pellet, cm^{-1}): 2175 (ν_{NN}), 1535 (ν_{NC}). ^1H NMR (0 °C): 6.98–7.13 (m, 6H, *m*, *p*-Ar, C_7D_7H), 5.12 (s, 1H, CH), 3.73 (br sept, 2H, CH, $J_{H\text{-}H}$ = 7 Hz), 3.46 (br sept, 2H, CH, $J_{H\text{-}H}$ = 7 Hz), 3.27 (br d, 2H, HC=CH, $J_{H\text{-}H}$ = 10 Hz), 1.59 (6H, Me), 1.58 (d, 6H, *i*-Pr, $J_{H\text{-}H}$ = 7 Hz), 1.47 (d, 6H, *i*-Pr, $J_{H\text{-}H}$ = 7 Hz), 1.41 (br m, 4H, CH_2), 1.20 (d, 6H, *i*-Pr, $J_{H\text{-}H}$ = 7 Hz), 1.14–1.29 (m, 8H, CH_2), 1.02 (d, 6H, *i*-Pr, $J_{H\text{-}H}$ = 7 Hz). ^{13}C NMR (25 °C, partial): 157.8, 152.0, 143.1, 142.7, 141.6, 130.3, 127.8–129.0 (m, obscured by toluene-d_8) 126.2, 125.4, 123.9, 123.7, 123.3, 97.3 (C-H, 74.9, (broad s, H-C=C-H), 30.7, 29.5, 28.9, 28.1, 26.5, 25.8, 25.0, 24.7, 24.4, 23.6. Anal. calcd. for $C_{37}H_{55}N_4Rh$: C 67.46, H 8.42, N 8.50; found: C 67.46, H 8.49, N 8.30.

X-ray data collection and reduction

Crystals were manipulated and mounted in capillaries in a glovebox, thus maintaining a dry, O_2-free environment for each crystal. Diffraction experiments were performed on a Siemens SMART System CCD diffractometer. The data were collected in a hemisphere of data in 1448 frames with 10 s exposure times. The observed extinctions were consistent with the space groups in each case. The data sets were collected (4.5° < 2θ < 45–50.0°). The intensities of reflections within these frames showed no statistically significant change over the duration of the data collections. The data were processed using the SAINT and XPREP processing packages. An empirical absorption correction based on redundant data was applied to each data set. Subsequent solution and refinement was performed using the SHELXTL solution package.

Structure solution and refinement

Non-hydrogen atomic scattering factors were taken from the literature tabulations (17, 18). The heavy atom positions were determined using direct-methods employing the SHELXTL direct-methods routine. The remaining non-hydrogen atoms were located from successive difference Fourier map calculations. The refinements were carried out by using full-matrix least-squares techniques on *F*, minimizing the function $\omega (F_o - F_c)^2$ where the weight ω is defined as $4F_o^2/2\sigma(F_o^2)$, and F_o and F_c are the observed and calculated structure factor amplitudes. In the final cycles of each refinement, all non-hydrogen atoms were assigned anisotropic temperature factors in the absence of disorder or insufficient data. In the latter cases, atoms were treated isotropically. C-H atom positions were calculated and allowed to ride on the carbon to which they are bonded assuming a C—H bond length of 0.95 Å. H atom temperature factors were fixed at 1.10 times the isotropic temperature factor of the C atom to which they are bonded. The H-atom contributions were calculated, but not refined. The locations of the largest peaks in the final difference Fourier map calculation as well as the magnitude of the residual electron densities in each case were of no chemical significance. Additional details are provided in the supplementary data.[3]

[3] Supplementary data may be purchased from the Directory of Unpublished Data, Document Delivery, CISTI, National Research Council Canada, Ottawa, ON K1A 0S2, Canada (http://cisti-icist.nrc-cnrc.gc.ca/irm/unpub_e.shtml for information on ordering electronically). CCDC 252431 contains the crystallographic data for this manuscript. These data can be obtained, free of charge, via ww.ccdc.cam.ac.uk/conts/retrieving.html (or from the Cambridge Crystallographic Data Centre, 12 Union Road, Cambridge CB2 1EZ, UK; fax +44 1223 336033; or deposit@ccdc.cam.ac.uk).

© 2005 NRC Canada

Scheme 3. $CH[C(Me)(N\text{-}i\text{-}Pr_2C_6H_3)]_2Rh(N_2)(COE)$.

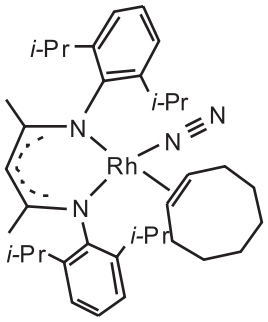


Table 1. Crystallographic data.

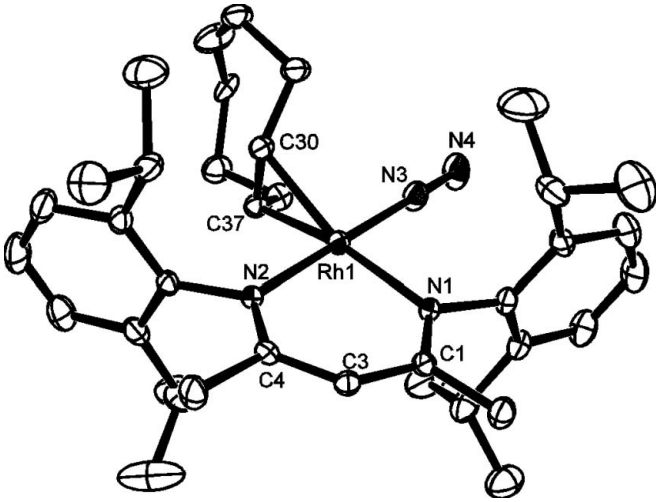
	1
Formula	$C_{37}H_{55}N_4Rh$
Molecular weight	630.72
Crystal system	Monoclinic
Space group	$P2_1/c$
a (Å)	8.9010(6)
b (Å)	17.2004(12)
c (Å)	23.4064(16)
β (°)	92.926(2)
V (Å^3)	3578.9(4)
Z	4
D(calcd.) (gcm^{-1})	1.167
Abs. coeff. (μ, mm^{-1})	0.502
Data collected	17 436
Data $F_o^2 > 3\sigma(F_o^2)$	5 150
Variables	384
R	0.0450
Rw	0.1138
GOF	1.035

Results and discussion

Reaction of the ligand salt $CH[C(Me)(N\text{-}i\text{-}Pr_2C_6H_3)]_2Li(Et_2O)$ with $[Rh(COE)(\mu\text{-}Cl)]_2$ proceeds with stirring overnight to give a dark brown-black solution. Work-up of this reaction afforded the dark brown crystalline product **1** in 38% yield. The NMR data were consistent with a disymmetric environment about Rh as two sets of resonances attributable to the isopropyl groups on the aryl rings of the ligand. NMR data were also consistent with the presence of a COE ring bound to Rh. The nature of the fourth ligand on Rh was unclear although IR spectrometry revealed an absorption at 2175 cm^{-1}. This compares with the absorption at 2126 cm^{-1} observed for the Ir analog of **1** suggesting the possibility of coordinated N_2. The higher N–N stretching frequency further suggests a shorter N—N bond distance in **1**. All of these data are consistent with the formulation of **1** as $CH[C(Me)(N\text{-}i\text{-}Pr_2C_6H_3)]_2Rh(N_2)(COE)$ (Scheme 3).

X-ray crystallographic study of **1** confirmed the formulation and revealed the pseudo-square-planar coordination geometry about Rh (Table 1). The coordination sphere is comprised of the two nitrogen atoms of the diimine ligand, a side-bound olefinic fragment of COE, and a terminally bound dinitrogen molecule. The metal-bound nitrogen of the N_2 fragment forms angles of 179.04(16)° and 88.93(15)° with the N atoms of the diimine ligand consistent with the pseudo-square-planar coordination geometry (Fig. 1).

Fig. 1. ORTEP drawing of **1**; 30% thermal ellipsoids are shown. Hydrogen atoms are omitted for clarity. Distances (Å) and angles (°): Rh(1)—N(1) 2.076(3), Rh(1)—N(2) 2.074(3), Rh(1)—N(3) 1.943(4), Rh(1)—C(30) 2.167(5), Rh(1)—C(37) 2.179(5), N(1)—C(1) 1.320(6), N(2)—C(4) 1.332(6), N(3)—N(4) 1.091(6), C(37)—C(30) 1.382(6), N(3)-Rh(1)-N(2) 179.04(16), N(3)-Rh(1)-N(1) 88.93(15), N(2)-Rh(1)-N(1) 90.11(13), N(3)-Rh(1)-C(30) 87.94(17), N(2)-Rh(1)-C(30) 92.99(15), N(1)-Rh(1)-C(30) 161.49(16), N(3)-Rh(1)-C(37) 86.29(17), N(2)-Rh(1)-C(37) 94.59(15), N(1)-Rh(1)-C(37) 160.58(16), C(30)-Rh(1)-C(37) 37.08(17), N(4)-N(3)-Rh(1) 179.6(6).



The diimine ligand is N-bound to Rh with Rh—N distances of 2.076(3) and 2.074(3) Å. The "bite-angle" (N-Rh-N) for the diimine ligand is 90.11(13)°. These compare with the Rh—N distance and bite angle of 1.955(2) Å and 91.3(1)° observed in the three coordinate Rh–olefin complex $CH[C(Me)(NMe_2C_6H_3)]_2Rh(COE)$ (19). The imine C—N bond distances are typical at 1.320(6) and 1.332(6) Å, respectively.

The olefinic fragment of a COE ligand is π bound to Rh with Rh—C distances of 2.167(5) and 2.179(5) Å, and a corresponding C—C distance of 1.382(6) Å. In comparison, the coordinated olefinic C—C bond distance of $CH[C(Me)(N\text{-}Me_2C_6H_3)]_2Rh(COE)$ (19) gives rise to Rh—C distances of 2.072(5) and 2.066(6) Å, with a C—C distance of 1.398(7) Å. The longer Rh—C distances in **1** are consistent with the lesser Lewis acidity of the Rh center as a result of its four-coordinate nature.

The terminally bound dinitrogen molecule exhibits a Rh—N distance of 1.943(4) Å. This is shorter than the Rh—N bond distance in $(Ph\text{-}t\text{-}Bu_2P)_2RhH(N_2)$ (1.970(4) Å) (12) and yet much longer than that in $(i\text{-}Pr_3P)_2RhCl(N_2)$ (1.885(4) Å) (13) (Table 2). The Rh-N-N angle is essentially linear with an angle of 179.6(6)° and the N—N distance is 1.091(6) Å. In general, the N—N distance in **1** is shorter than those observed for the bridging $Rh_2(\mu\text{-}N_2)$ complexes, consistent with interaction with only one metal center. The N—N distance in **1** is also longer than the N—N distances seen in $(i\text{-}Pr_3P)_2RhCl(N_2)$, $MeCH(CH_2CH_2P\text{-}t\text{-}Bu_2)_2Rh(N_2)$, and the Ir

© 2005 NRC Canada

Table 2. Metric parameters for selected Rh/Ir–N_2 complexes.

Compound	M–N	N–N	ν (cm^{-1})	Ref.
$[Me_2C_6H(CH_2P\text{-}i\text{-}Pr_2)_2Rh]_2(\mu\text{-}N_2)$	1.9687(17)	1.108(3)	2165	7
$[Me_2C_6H(CH_2P\text{-}t\text{-}Bu_2)(CH_2NEt_2)Rh]_2(\mu\text{-}N_2)$	2.021	1.130	n/a	8
$[MeC_6H_2(CH_2P\text{-}t\text{-}Bu_2)_2ORh]_2(\mu\text{-}N_2)$	1.912(2)	1.129(4)	2095	9
$[(i\text{-}Pr_3)_2RhH]_2(\mu\text{-}N_2)$	1.981(5) 1.973(5)	1.134(5)	2140	10
$[CH_2(P\text{-}t\text{-}Bu_2)_2RhCH_2\text{-}t\text{-}Bu]_2(\mu\text{-}N_2)$	1.973(3)	1.106(6)	n/a	11
$(Ph\text{-}t\text{-}Bu_2P)_2RhH(N_2)$	1.970(4)	1.074(7)	2155	12
$(i\text{-}Pr_3P)_2RhCl(N_2)$	1.885(4)	0.958(5)	2100	13
$MeCH(CH_2CH_2P\text{-}t\text{-}Bu_2)_2Rh(N_2)$	2.032(1)	0.963(14	2110	14
$CH[C(Me)(N\text{-}i\text{-}Pr_2C_6H_3)]_2Ir(N_2)(COE)$	1.903(3)	1.107(4)	2126	15
$CH[C(Me)(N\text{-}i\text{-}Pr_2C_6H_3)]_2Rh(N_2)(COE)$	1.943(4)	1.091(6)	2175	Herein
$CH[C(Me)(NMe_2C_6H_3)]_2Rh(N_2)(COE)$	n/a	n/a	2172	19

Note: n/a = not available.

analog of **1**. While the Rh—N distance in the terminal-N_2 complexes correlates the expected trend based on the trans influence of the ligand opposite dinitrogen, there is no direct correlation between the Rh—N and the N—N distances in the compiled list of Rh–N_2 complexes (Table 2). The N—N distance appears to reflect a complex mixture of the trans influence and the net electron density at the metal center. It is these features together that impact on the π donation to N_2, and thus the resulting N—N bond length.

Acknowledgments

Financial support from the Natural Sciences and Engineering Research Council of Canada (NSERC) is gratefully acknowledged. JDM is grateful for the award of an Ontario Graduate Scholarship and a Bayer Inc. Award from the Macromolecular Science and Engineering Division of the Canadian Institute for Chemistry.

References

1. A.D. Allen and C.W. Senoff. Chem. Commun. 621 (1965).
2. B.A. MacKay and M.D. Fryzuk. Chem. Rev. **104**, 385 (2004).
3. M. Hidai and Y. Mizobe. Pure Appl. Chem. **73**, 261 (2001).
4. M.D. Fryzuk and S.A. Johnson. Coord Chem. Rev. **200**–**202**, 379 (2000).
5. R.R. Schrock. Pure Appl. Chem. **69**, 2197 (1997).
6. M. Hidai and Y. Mizobe. Chem. Rev. **95**, 1115 (1995).
7. R. Cohen, B. Rybtchinski, M. Gandelman, H. Rozenberg, J.M.L. Martin, and D. Milstein. J. Am. Chem. Soc. **125**, 6532 (2003).
8. R. Cohen, B. Rybtchinski, M. Gandelman, L.J.W. Shimon, J.M.L. Martin, and D. Milstein. Angew. Chem. Int. Ed. **42**, 1949 (2003).
9. M.E. van der Boom, S.-Y. Liou, Y. Ben-David, L.J.W. Shimon, and D. Milstein. J. Am. Chem. Soc. **120**, 6531 (1998).
10. T. Yoshida, T. Okano, D.L. Thorn, T.H. Tulip, S. Otsuka, and J.A. Ibers. J. Organomet. Chem. **181**, 183 (1979).
11. H. Urtel, C. Meier, F. Eisentraeger, F. Rominger, J.P. Joschek, and P. Hofmann. Angew. Chem. Int. Ed. **40**, 781 (2001).
12. P.R. Hoffmann, T. Yoshida, T. Okano, S. Otsuka, and J.A. Ibers. Inorg. Chem. **15**, 2462 (1976).
13. D.L. Thorn, T.H. Tulip, and J.A. Ibers. J. Chem. Soc. Dalton Trans. 2022 (1979).
14. A. Vigalok, H.-B. Kraatz, L. Konstantinovsky, and D. Milstein. Chem. Eur. J. **3**, 253 (1997).
15. W.H. Bernskoetter, E. Lobkovsky, and P.J. Chirik. Chem. Commun. 764 (2004).
16. Y. Ding, H.W. Roesky, M. Noltemeyer, H.-G. Schmidt, and P.P. Power. Organometallics, **20**, 1190 (2001).
17. D.T. Cromer and J.B. Mann. Acta Crystallogr. A, **A24**, 321 (1968).
18. D.T. Cromer and J.T. Waber. Int. Tables X-Ray Crystallogr. **4**, 71 (1974).
19. P.H.M. Budzelaar, R. De Gelder, and A.W. Gal. Organometallics, **17**, 4121 (1998).

© 2005 NRC Canada

Synthesis and structure of a terminal dinitrogen complex of nickel[1]

Rory Waterman and Gregory L. Hillhouse

Abstract: Reaction of petroleum ether solutions of $[(dtbpe)Ni]_2(\eta^2,\mu\text{-}C_6H_6)$ (**1**, dtbpe = 1,2-bis(di-*tert*-butylphosphino)ethane) with triphenylphosphine under a dinitrogen atmosphere gives the Ni(0) dinitrogen adduct $(dtbpe)Ni(N_2)(PPh_3)$ (**2**), which can be isolated as dark red crystals in 87% yield. The X-ray crystal structure of **2** reveals pseudotetrahedral geometry about Ni and a terminal dinitrogen ligand with Ni—N(1) = 1.830(2) Å, N(1)—N(2) = 1.112(2) Å, and Ni-N(1)-N(2) = 177.5(2)°.

Key words: dinitrogen, nickel, X-ray.

Résumé : La réaction du $[(dtbpe)Ni]_2(\eta^2,\mu\text{-}C_6H_6)$ (**1**, dtbpe = 1,2-bis(di-*tert*-butylphosphino)éthane) en solution dans l'éther de pétrole avec de la triphénylphosphine, sous une atmosphère de diazote, conduit à la formation de l'adduit Ni(0) diazote $(dtbpe)Ni(N_2)(PPh_3)$ (**2**) que l'on peut isoler sous la forme de cristaux rouges avec un rendement de 87 %. Une étude du composé **2** par diffraction des rayons X révèle une géométrie pseudotétraédrique autour du Ni et la présence d'un ligand diazote terminal avec des distances Ni—N(1) = 1,830(2) Å, N(1)—N(2) = 1,112(2) Å et un angle Ni-N(1)-N(2) = 177,5(2)°.

Mots clés : diazote, nickel, rayons X.

[Traduit par la Rédaction]

Introduction

The 1965 report from University of Toronto chemistry professor Bert Allen and his graduate student Caesar Senoff of the isolation of stable dinitrogen complex salts of the formulation $[(NH_3)_5Ru(N_2)^{2+}][X^-]_2$ from the reaction of ruthenium trichloride with hydrazine hydrate in aqueous solution rocked the scientific community (1, 2). The crystallographic determination of the solid-state structure of the Allen and Senoff complex definitively corroborated the proposed binding mode of the N_2 ligand as end-on bound to Ru in an approximately linear fashion (3). In the intervening 40 years since that landmark discovery, nearly every transition metal has been reported to utilize dinitrogen as a ligand, and many binding modes, including bridging and side-bound, have been observed for N_2 ligands (4). Because the dinitrogen ligand is often quite labile, N_2 complexes can serve as useful starting materials for a variety of synthetic purposes. Over the years much research effort has focused on designing systems containing ligated N_2 in which coordination to a metal sufficiently activates the N—N triple bond that it can be subsequently functionalized (or "fixed"), such as in processes that cleave the N—N triple bond (5) or model enzymatic systems that perform catalytic N_2 reduction (6).

Only a few examples of isolated nickel complexes possessing a dinitrogen ligand have appeared in the literature. Most Ni–N_2 species have been dimeric or polynuclear (7–9). The dinitrogen-bridged complex $[(PCy_3)_2Ni]_2(\mu\text{-}N_2)$ has been reported and structurally characterized (9), and an unusual side-bound N_2 complex, $[(C_6H_5Li)_6Ni_2(N_2)(Et_2O)_2]_2$, has been reported (7). Surprisingly, no structural data exist for simple end-on N_2 complexes of nickel, even though this is by far its most common coordination mode. Herein we report the preparation and structural characterization of the first example of an isolable nickel complex containing a terminal, end-on bound N_2 ligand.

Experimental

General considerations

Unless otherwise stated, all operations were performed in a M. Braun Lab Master dry box under an atmosphere of purified nitrogen. Petroleum ether was dried by passage through activated alumina and Q-5 columns. C_6D_6 was purchased form Cambridge Isotope Laboratory (CIL), degassed, and dried over CaH_2 or activated 4 Å molecular sieves. Celite®, alumina, and 4 Å molecular sieves were activated under vacuum overnight at a temperature above 180 °C. Anhydrous solvents such as benzene and diethylether were purchased from Acros or Fischer, stirred over sodium metal, and filtered through activated alumina. $[(dtbpe)Ni]_2(\eta^2,\mu\text{-}C_6H_6)$ (**1**, dtbpe = 1,2-bis(di-*tert*-butylphosphino)ethane) was

Received 9 September 2004. Published on the NRC Research Press Web site at http://canjchem.nrc.ca on 22 March 2005.

R. Waterman[2] and G.L. Hillhouse.[3] Department of Chemistry, The University of Chicago, 5735 S. Ellis Avenue, Chicago, IL 60637, USA.

[1]This article is part of a Special Issue dedicated to Dinitrogen Chemistry.
[2]Present address: Department of Chemistry, University of California at Berkeley, Berkeley, CA 94720, USA.
[3]Corresponding author (e-mail: g-hillhouse@uchicago.edu).

 doi: 10.1139/V05-011 © 2005 NRC Canada

prepared according to the literature procedure (10). All other chemicals were used as received. IR data (Fluorolube S-20 mulls, CaF_2 plates) were measured with a Nicolet 670 FT-IR instrument. Elemental analyses were performed by Desert Analytics (Tucson, Arizona). ^1H, ^{13}C, and ^{31}P NMR spectra were recorded on Bruker 500 and 400 MHz NMR spectrometers. ^1H and ^{13}C NMR data are reported with reference to solvent resonances (residual C_6D_5H in C_6D_6, 7.16 ppm; C_6D_6, 128.0 ppm). ^{31}P NMR spectra are reported with respect to external 85% H_3PO_4 (0 ppm).

Preparation of (dtbpe)Ni(N_2)(PPh_3) (2)

In a nitrogen-filled, inert-atmosphere glovebox, a 25 mL round-bottomed flask was charged with 72 mg (0.087 mmol) of [(dtbpe)Ni]$_2$(η^2,μ-C_6H_6) (**1**) and 45 mg (0.174 mmol) of PPh_3 followed by 14 mL of petroleum ether. The solution immediately became blood red in color and was filtered after stirring for 90 min. The volume of the solution was reduced to ca. 5 mL, and upon cooling to –35 °C, dark red crystals were deposited, which were collected by filtration and dried to give **2** (100 mg, 0.149 mmol, 87% yield). IR (Fluorolube mull, CaF_2, cm^{-1}): 3050–2850 (vs br), 2072 (ν_{NN}, vs), 1585 (m), 1479 (s), 1434 (s), 1392 (m), 1360 (m). ^1H NMR (22 °C, 500 MHz, C_6D_6) δ: 7.94 (t, C_6H_5, 6H), 7.15 (d, C_6H_5, 6H), 7.07 (t, C_6H_5, 3H), 1.55 (m, CH_2, 4H), 1.17 (mult, CH_3, 36H). ^{13}C NMR (22 °C, 125.8 MHz, C_6D_6) δ: 133.8 (d, J_{PC} = 14.5 Hz, C_6H_5), 129.8 (s, C_6H_5), 127.9 (s, C_6H_5), 127.7 (s, C_6H_5), 34.6 (m, J_{PC} = 4.4 Hz, $C(CH_3)_3$), 30.7 (br t, J_{PC} = 3.6 Hz, CH_3), 23.4 (m, CH_2). ^{31}P NMR (22 °C, 202.4 MHz, C_6D_6) δ: 73.5 (d, J_{PP} = 95.7 Hz, PtBu$_2$), 28.7 (t, J_{PP} = 95.7 Hz, PPh$_3$). Anal. calcd for $C_{36}H_{55}N_2NiP_3$: C 64.78, H 8.31, N 4.20; found: C 65.11, H 8.28, N 3.31.

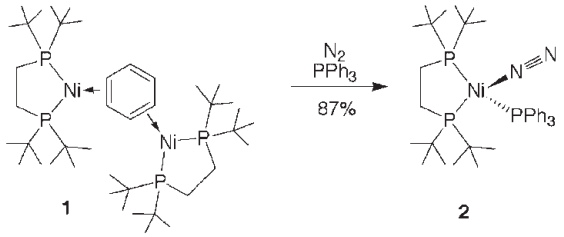
Crystallographic data collection, structure solution, and refinement

A dark red block of **2** was selected under a stereomicroscope while immersed in mineral oil to avoid possible reaction with air. The crystal was removed from the oil using a tapered fiber that also served to hold the crystal for data collection, and mounted and centered on a Bruker SMART APEX system in a nitrogen cold stream. Rotation and still images showed diffractions to be sharp, while frames separated in reciprocal space were obtained and provided an orientation matrix and initial cell parameters. Final cell parameters were obtained from the full data set. A "hemisphere" data set was obtained, which samples approximately 1.2 hemispheres of reciprocal space to a resolution of 0.84 Å using 0.3° steps in ω using 10 s integration times for each frame. The space group was determined as *P*-1 based on systematic absences and intensity statistics. Direct methods were used to locate non-hydrogen atoms from the electron difference map. All heavy atoms were converted to and refined anisotropically. Hydrogen atoms were refined isotropically and fixed at calculated positions. A semiempirical absorption correction was applied from ψ-scans. All software and sources of scattering factors are contained in the SHELXTL (version 5.1) program library (G. Sheldrick, Bruker Analytical X-ray Systems, Madison, Wisconsin). Details of the data set and the refinement are given in Table 1. Table 2 lists selected metrical parameters of the structure of **2**.[4]

Results and discussion

Reaction of petroleum ether solutions of the benzene complex [(dtbpe)Ni]$_2$(η^2,μ-C_6H_6) (**1**) with PPh_3 under a nitrogen atmosphere gives a dark red solution from which the dinitrogen complex (dtbpe)Ni(N_2)(PPh_3) (**2**) can be isolated as analytically pure dark red crystals in 87% yield (eq. [1]).

[1]



Even in the presence of excess PPh_3, only **2** is formed and no tetrakisphosphine species is observed. Characterization of **2** followed from its NMR (^1H, ^{13}C, and ^{31}P) and IR spectra, and a single crystal X-ray diffraction study. The ^{31}P NMR spectrum of **2** exhibits a single resonance for the dtbpe ligand (δ 73.5, doublet) and a single resonance for the PPh_3 ligand (δ 28.7, triplet) with $^2J_{PP}$ = 95.7 Hz for both, indicating pseudotetrahedral geometry about nickel. The solid-state IR spectrum of **2** shows a strong ν_{NN} at 2072 cm^{-1}.

Single crystals of **2** were grown by slowly cooling concentrated hexane solutions of the complex. A perspective view of the molecular structure of **2** is shown in Fig. 1 with select metrical parameters given in Table 2. The complex features a pseudotetrahedral nickel center with a terminal N_2 ligand with a short N—N bond of 1.112(2) Å. The nitrogen ligand is approximately linear with Ni-N(1)-N(2) = 177.5(2)° and Ni—N(1) = 1.830(2) Å. These values can be compared with those found in the structure of the bridged dinitrogen complex [(PCy_3)$_2$Ni]$_2$(μ-N_2) (9) which exhibits Ni—N bond lengths of 1.77 and 1.79 Å, and N—N = 1.12 Å (standard errors were not given in the report).

Complex **2** is, to the best of our knowledge, the only example of an *isolated* nickel complex with a terminal N_2 ligand. It is noteworthy that a family of nickel(II) complexes of the formula L_2NiX_2 (X = Cl or Br; L = PEt_3, PEt_2Ph, or P-*n*-Bu_3) can be reduced in the presence of phosphine to generate $L_3Ni(N_2)$ species that have not been isolated, but lose N_2 to give tetrakisphosphine nickel(0) complexes L_4Ni upon precipitation (11). Solution IR, ^{31}P NMR, and electronic spectra for these $L_3Ni(N_2)$ complexes led to their formulation as pseudotetrahedral at Ni with terminal N_2 ligands

[4] Supplementary data may be purchased from the Directory of Unpublished Data, Document Delivery, CISTI, National Research Council Canada, Ottawa, ON K1A 0S2, Canada (http://cisti-icist.nrc-cnrc.gc.ca/irm/unpub_e.shtml for information on ordering electronically). CCDC 261287 contains the crystallographic data for this manuscript. These data can be obtained, free of charge, via ww.ccdc.cam.ac.uk/conts/retrieving.html (or from the Cambridge Crystallographic Data Centre, 12 Union Road, Cambridge CB2 1EZ, UK; fax +44 1223 336033; or deposit@ccdc.cam.ac.uk).

© 2005 NRC Canada

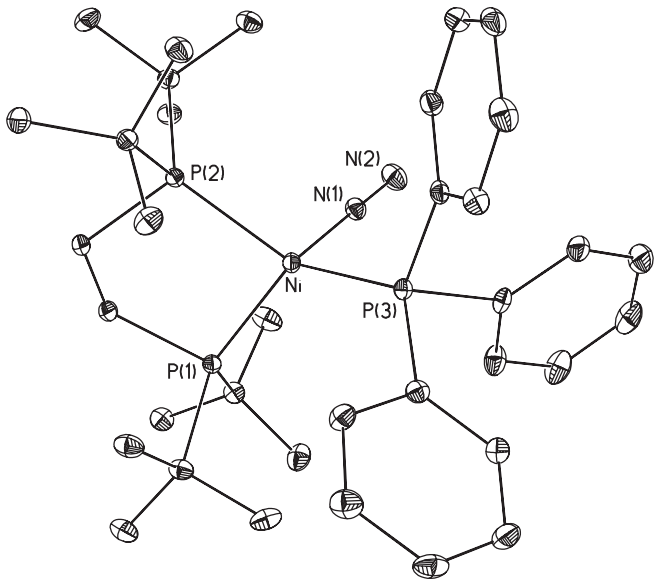
Table 1. Crystal and structure refinement for (dtbpe)Ni(N_2)(PPh_3) (**2**).

Empirical formula	$C_{36}H_{55}N_2NiP_3$
Formula weight	667.44
Temperature (K)	100
Wavelength (Å)	0.710 73
Crystal system	Triclinic
Space group	*P*-1
Unit cell dimensions	
a (Å)	9.7911(7)
b (Å)	13.7423(10)
c (Å)	13.8687(10)
α (°)	81.6860(10)
β (°)	76.5680(10)
γ (°)	80.1250(10)
Volume (Å^3)	1777.4(2)
Z	2
Density (calculated) (Mg/m^3)	1.247
Absorption coefficient (mm^{-1})	0.707
F(000)	716
Crystal size, description	210 μm × 200 μm × 200 μm, dark red cube
θ Range for data collection	2.02–28.30
Index ranges	$-12 \le h \le 12$, $-18 \le k \le 18$, $-18 \le l \le 18$
Reflections collected	19 902
Independent reflections	8 305 (R_{int} = 0.0336)
Completeness to θ = 28.30	94.0%
Absorption correction	Semiempirical from ψ scans
Max and min transmission	0.8714 and 0.8656
Refinement method	Full-matrix least-squares on F^2
Data/restraints/parameters	8 305/0/379
Goodness-of-fit on F^2	1.058
Final *R* indices ($I > 2\sigma(I)$)	R_1 = 0.0403, wR_2 = 0.0968
R indices (all data)	R_1 = 0.0461, wR_2 = 0.0999
Largest diff. peak and hole (e Å^{-3})	1.188 and –0.365

Table 2. Selected bond lengths and angles for (dtbpe)Ni(N_2)(PPh_3) (**2**).

Bond lengths (Å)	
Ni—N(1)	1.830(2)
Ni—P(3)	2.2048(6)
Ni—P(1)	2.2302(6)
Ni—P(2)	2.2328(5)
N(1)—N(2)	1.112(2)
Bond angles (°)	
N(2)-N(1)-Ni	177.5(2)
N(1)-Ni-P(3)	96.12(5)
N(1)-Ni-P(1)	112.07(5)
P(3)-Ni-P(1)	123.66(2)
N(1)-Ni-P(2)	109.03(5)
P(3)-Ni-P(2)	122.60(2)
P(1)-Ni-P(2)	93.62(2)

Fig. 1. A perspective view of the structure of (dtbpe)Ni(N_2)(PPh_3) (**2**). Hydrogen atoms have been omitted for clarity.



(11*a*). These transient complexes have N–N stretching frequencies in the range of 2050–2100 cm^{-1}, which can be compared to the corresponding stretch at 2072 cm^{-1} in **2** and 2028 cm^{-1} in [(PCy_3)$_2$Ni]$_2$(μ-N_2), although the latter value, recorded in solution, has been suggested to be for mono-

© 2005 NRC Canada

meric $(PCy_3)_2Ni(N_2)$ that results from dissociation of the dimer in toluene (9). In the light of these previous reports, the stability of **2** is undoubtedly the result of the steric bulk of the dtbpe ligand, which prevents expulsion of N_2 and coordination of a second PPh_3 ligand to give the hypothetical $(dtbpe)Ni(PPh_3)_2$. Finally, an unusual "Ni(I)" complex, $(PEt_3)_2Ni(H)(N_2)$, has been formulated on the basis of UV–vis and IR data (12), but the absence of magnetic susceptibility or ^1H NMR information and the similarity of the IR and UV–vis spectra to $(PEt_3)_3Ni(N_2)$ (vide supra) casts doubts on the identity of this compound (11*a*).

Acknowledgments

We are grateful to the National Science Foundation for financial support of this research through Grant CHE-0244239 to G.L.H., and to the Department of Education for a GAANN Fellowship to R.W.

References

1. A.D. Allen and C.V. Senoff. Chem. Commun. 621 (1965).
2. A.D. Allen and F. Bottomley. Acc. Chem. Res. **1**, 360 (1968).
3. F. Bottomley and S.C. Nyberg. Acta Crystallogr. **B24**, 1289 (1968).
4. (*a*) J. Chatt, J.R. Dilworth, and R.L. Richards. Chem. Rev. **78**, 589 (1978); (*b*) M.D. Fryzuk and S.A. Johnson. Coord. Chem. Rev. **200**, 379 (2000); (*c*) F. Barriere. Coord. Chem. Rev. **236**, 71 (2003); (*d*) B.A. MacKay and M.D. Fryzuk. Chem. Rev. **104**, 385 (2004).
5. C.E. Laplaza and C.C. Cummins. Science (Washington, D.C.), **268**, 861 (1995).
6. (*a*) D.V. Yandulov and R.R. Schrock. Science, **301**, 76 (2003); (*b*) R.R. Schrock. Chem. Commun. 2389 (2003).
7. C. Krüger and T.-Y. Tsay. Angew. Chem. Int. Ed. Engl. **12**, 998 (1973).
8. K. Jonas, D.J. Brauer, C. Krüger, P.J. Roberts, and Y.-H. Tsay. J. Am. Chem. Soc. **98**, 74 (1976).
9. P.W. Jolly, K. Jonas, C. Krüger, and Y.-H. Tsay. J. Organomet. Chem. **33**, 109 (1971).
10. I. Bach, R. Goddard, C. Kopiske, K. Seevogel, and K.R. Pörschke. Organometallics, **18**, 10 (1999).
11. (*a*) G.A. Tolman, D.H. Gerlach, J.P. Jesson, and R.A. Schunn. J. Organomet. Chem. **65**, C23 (1974); (*b*) M. Aresta, G.F. Nobile, and A. Sacco. Inorg. Chim. Acta, **12**, 167 (1975).
12. S.C. Srivastava and M. Bigorgne. J. Organomet. Chem. **18**, 30 (1969).

© 2005 NRC Canada

Synthesis and characterization of cationic iron complexes supported by the neutral ligands $NP^{i\text{-}Pr}_3$, $NArP^{i\text{-}Pr}_3$, and $NS^{t\text{-}Bu}_3$[1]

Cora E. MacBeth, Seth B. Harkins, and Jonas C. Peters

Abstract: This paper compares the local geometries, spin states, and redox properties of a series of iron complexes supported by neutral, tetradentate NP_3 (tris(phosphine)amine) and NS_3 (tris(thioether)amine) ligands. Our consideration of an Fe-mediated N_2 fixation scheme similar to that proposed by Chatt for molybdenum motivates our interest in systems of these types. This report specifically describes the synthesis and characterization of cationic Fe(II) chloride complexes supported by the neutral ligands $NP^{i\text{-}Pr}_3$ ($NP^{i\text{-}Pr}_3$ = $[N(CH_2CH_2P\text{-}i\text{-}Pr_2)_3]$), $NArP^{i\text{-}Pr}_3$ ($NArP^{i\text{-}Pr}_3$ = [N(2-diisopropylphosphine-4-methylphenyl)$_3$]), and $NS^{t\text{-}Bu}_3$ ($NS^{t\text{-}Bu}_3$ = $[N(CH_2CH_2S\text{-}t\text{-}Bu)_3]$). The solid-state structures, electrochemistry, and magnetic properties of these complexes are reported. Whereas the $NP^{i\text{-}Pr}_3$ and $NArP^{i\text{-}Pr}_3$ ligands provide pseudotetrahedral $S = 2$ ferrous cations $[Fe(NP^{i\text{-}Pr}_3)Cl]PF_6$ (**1**[PF_6]) and $[Fe(NArP^{i\text{-}Pr}_3)Cl]BPh_4$ (**2**[BPh_4]) featuring a long Fe—N bond distance, the $NS^{t\text{-}Bu}_3$ ligand gives rise to a trigonal bipyramidal structure with a $S = 1$ ground state and a much shorter Fe–N interaction. The complexes **1**[BPh_4] and **2**[BPh_4] can be reduced under CO to give rise to the five-coordinate Fe(I) monocarbonyls $[Fe(NP^{i\text{-}Pr}_3)CO]BPh_4$ (**4**[BPh_4]) and $[Fe(NArP^{i\text{-}Pr}_3)CO]BPh_4$ (**5**[BPh_4]). The solid-state structures and electrochemistry of **4**[BPh_4] and **5**[BPh_4] are described, as is the EPR spectrum of **4**[BPh_4]. The synthesis and characterization of the hydride–dinitrogen complex $[Fe(NP^{i\text{-}Pr}_3)(N_2)(H)]PF_6$ (**6**[PF_6]) has also been accomplished and its properties are also reported.

Key words: nitrogenase, iron, polydentate phosphines, thioether ligands, N_2 chemistry, nitrogen, Fe(I).

Résumé : Dans ce travail, on compare les géométries locales, états de spin et propriétés redox d'une série de complexes de fer supportés par les ligands neutres et tridentates NP_3 (tris(phosphine)amine) et NS_3 (tris(thioéther)amine). Notre considération d'un schéma de fixation du N_2 catalysé par le Fe semblable à celui proposé par Chatt pour le molybdène motive notre intérêt dans les systèmes de ce type. Dans ce travail, on décrit spécifiquement la synthèse et la caractérisation de complexes cationiques du chlorure de Fe(II) supportés par les ligands neutres $NP^{i\text{-}Pr}_3$ ($NP^{i\text{-}Pr}_3$ = $[N(CH_2CH_2P\text{-}i\text{-}Pr_2)_3]$), $NArP^{i\text{-}Pr}_3$ ($NArP^{i\text{-}Pr}_3$ = [N(2-diisopropylphosphine-4-méthylphényl)$_3$]) et $NS^{t\text{-}Bu}_3$ ($NS^{t\text{-}Bu}_3$ = $[N(CH_2CH_2S\text{-}t\text{-}Bu)_3]$), y compris les structures à l'état solide, l'électrochimie et les propriétés magnétiques de ces complexes. Alors que les ligands $NP^{i\text{-}Pr}_3$ et $NArP^{i\text{-}Pr}_3$ conduisent à des cations ferreux pseudotétraédriques $S = 2$ $[Fe(NP^{i\text{-}Pr}_3)Cl]PF_6$ (**1**[PF_6]) et $[Fe(NArP^{i\text{-}Pr}_3)Cl]BPh_4$ (**2**[BPh_4]) comportant une longue liaison Fe—N, le ligand $NS^{t\text{-}Bu}_3$ conduit à la formation d'un complexe de structure bipyramidale trigonale avec un état fondamental $S = 1$ et une interaction Fe–N beaucoup plus courte. Les complexes **1**[BPh_4] et **2**[BPh_4] peuvent être réduits sous l'influence du CO pour conduire à des complexes monocarbonylés et pentacoordinés du Fe(I), $[Fe(NP^{i\text{-}Pr}_3)CO]BPh_4$ (**4**[BPh_4]) et $[Fe(NArP^{i\text{-}Pr}_3)CO]BPh_4$ **5**[BPh_4]. On décrit aussi les structures solides et l'électrochimie des complexes **4**[BPh_4] et **5**[BPh_4] ainsi que le spectre RPE du composé **4**[BPh_4]. On a aussi réalisé la synthèse et la caractérisation du complexe hydrure–diazote $[Fe(NP^{i\text{-}Pr}_3)(N_2)(H)]PF_6$ (**6**[PF_6]) et on rapporte ses propriétés.

Mots clés : nitrogénase, fer, phosphines polydentates, ligands thioéther, chimie du N_2, azote, Fe(I).

[Traduit par la Rédaction]

Introduction

The site(s) of substrate binding and reactivity (e.g., N_2, HC≡CH, H^+, CO) at the inorganic cofactors of nitrogenase enzymes is a fascinating and complicated issue (1). Because crystallographic data is presently available only for the FeMo-nitrogenase (FeMo-N_2ase) enzyme (2), the biochemical (3), theoretical (4), and synthetic (1, 5), model communities have focused the bulk of their attention on understanding its mode of mechanistic action. The presence of a single molybdenum center in the FeMo-cofactor (2, 3*a*), in addition to a wealth of structurally diverse functional

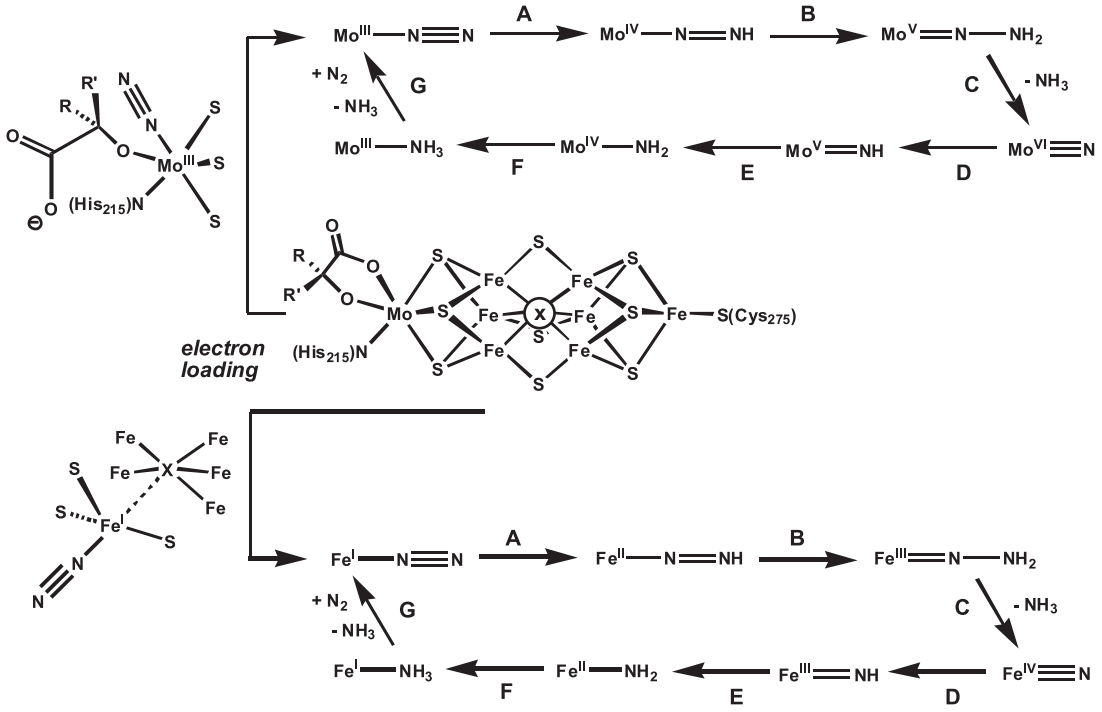
Received 9 September 2004. Published on the NRC Research Press Web site at http://canjchem.nrc.ca on 23 March 2005.

C.E. MacBeth, S.B. Harkins, and J.C. Peters.[2] California Institute of Technology, Division of Chemistry and Chemical Engineering, Mail Code 127-72, 1200 E. California Blvd., Pasadena, CA 91125, USA.

[1]This article is part of a Special Issue dedicated to Dinitrogen Chemistry.
[2]Corresponding author (e-mail: jpeters@caltech.edu).

 doi: 10.1139/V05-017 © 2005 NRC Canada

Scheme 1.



model systems (6), has reinforced the suggestion that a single molybdenum site may be responsible for mediating N_2 uptake and reduction in FeMo-N_2ase. Particularly attractive is a scheme akin to that originally put forward by Chatt et al. (7) and later modified by Pickett (8) in which a vacant Mo^{III} site, perhaps generated via homocitrate dechelation under electron loading conditions, binds N_2 to mediate its successive reduction to NH_3 by the successive transfer of protons and electrons. Such a scenario is schematically outlined in the top portion of Scheme 1. Significant in this regard is the recent work of Yandulov and Schrock (9), who have demonstrated that such a cycle can be accomplished in a small molecule synthetic system. They have shown that certain triamidoamine-supported molybdenum complexes are capable of catalytically shuttling among various oxidation states ($Mo^{III}/Mo^{IV}/Mo^{V}/Mo^{VI}$) as nitrogen is taken up and reduced to ammonia.

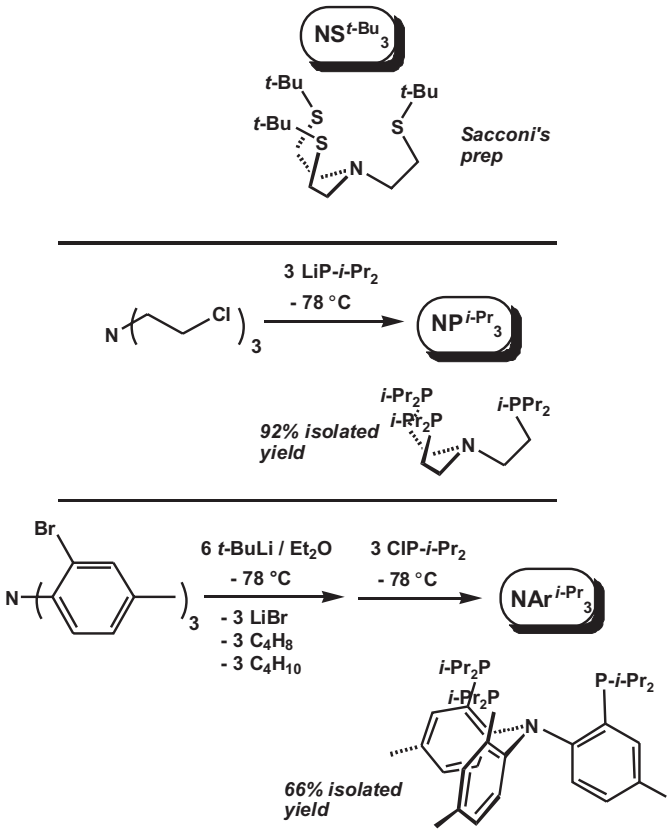
These successes not withstanding, it needs to be emphasized that iron is the only metal *known* to be ubiquitous to all nitrogenase enzymes (10) (also true of hydrogenase enzymes), and biochemical and spectroscopic data (11) are available to suggest that the iron sites of the FeMo-cofactor play a critical, albeit ill-defined, role in facilitating N_2 reduction, and myriad proposals have been put forth stressing an Fe-mediated N_2 fixation scheme. Problematic is that the inorganic dinitrogen chemistry of iron is far less well-developed than that for molybdenum, and therefore evaluating the chemical feasibility of such schemes is at present difficult. Most of the Fe-mediated scenarios being considered in the literature invoke multiple iron centers during N_2 uptake–reduction (5). This is due to the presence of multiple iron centers in the cofactor, and perhaps more importantly, to the implicit assumption that a single iron site cannot support the various N_x intermediates, oxidation states, and multi-electron transformations that would need to be invoked *en route* to NH_3 production from N_2 (bottom of Scheme 1, steps A–G), in sharp contrast to the case of redox-rich molybdenum.

Inorganic coordination chemistry can play a key role with respect to expanding our understanding of the N_2 chemistry available to iron, and in testing the validity of the assumptions mentioned above. The recent structural assignment of a central light atom in the MoFe-cofactor core (2) suggests that, if one or more iron atoms in the central section of the cofactor provides an initial site for N_2 uptake (3*a*), then coordinatively unsaturated iron centers provide plausible starting points for inorganic iron model chemistry (12). At the bottom of Scheme 1 we sketch a N_2 reduction scenario that mirrors that of the molybdenum postulate, but in this case invokes a hemi-labile role for the central light atom that exposes a low-valent iron site for N_2 uptake under electron loading conditions. Such a scenario would set the stage for the further reduction of N_2 to ammonia, perhaps via a Chatt-type cycle based upon iron (steps A–G). Fe–N_x model complexes will help to evaluate the chemical feasibility of this mechanistic scheme. Depending on the degree to which the Fe–X linkage is broken during the cycle, four- and (or) five-coordinate complexes may be considered as the most appropriate starting points.

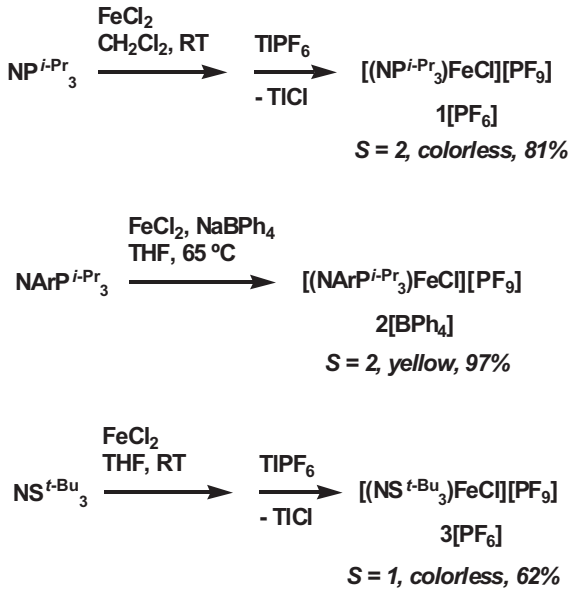
In this context, our own group has recently developed four-coordinate iron, phosphine-supported systems of the generic type $L_3Fe–N_x$ (13). These pseudotetrahedral platforms exhibit: (*i*) an unprecedented degree of redox flexibility for mononuclear iron systems; (*ii*) a fascinating propensity to populate low-spin, ground-state configurations for pseudotetrahedral Fe^{2+}, Fe^{3+}, and Fe^{4+} species; and (*iii*) a capacity to accommodate strongly π-basic (e.g., N^{3-}, NR^{2-}), π-acidic (e.g., N_2), and intermediate type (e.g., N_2R^-, NR_2^-) ligands

© 2005 NRC Canada

Scheme 2.



Scheme 3.



at a single coordination site. An obvious question that emerges is whether five-coordinate iron scaffolds will display similar properties.

In the present paper, we compare the local geometries, spin states, and redox properties of a series of iron complexes supported by neutral, tetradentate NP_3 (tris(phosphine)amine) and NS_3 (tris(thioether)amine) ligands (14). Two new NP_3-type ligands are introduced, $NP^{i\text{-Pr}}_3$ ($NP^{i\text{-Pr}}_3$ = $N(CH_2CH_2P\text{-}i\text{-}Pr_2)_3$) and $NArP^{i\text{-Pr}}_3$ ($NArP^{i\text{-Pr}}_3$ = N(2-diisopropylphosphine-4-methylphenyl)$_3$) are described, and we establish the nature of their ferrous "$(NP_3)Fe^{II}$–X" ions. For comparison, we also describe a structurally related "$(NS^{t\text{-Bu}}_3)Fe^{II}$–X" system ($NS^{t\text{-Bu}}_3$ = (e.g., $N(CH_2CH_2S\text{-}t\text{-}Bu)_3$)) (14). It is established that the $NP^{i\text{-Pr}}_3$ and $NArP^{i\text{-Pr}}_3$ scaffolds support unusual monovalent, trigonal bipyramidal monocarbonyl derivatives. Additionally, it is demonstrated that the $NP^{i\text{-Pr}}_3$ ligand supports N_2 coordination to iron.

Results and discussion

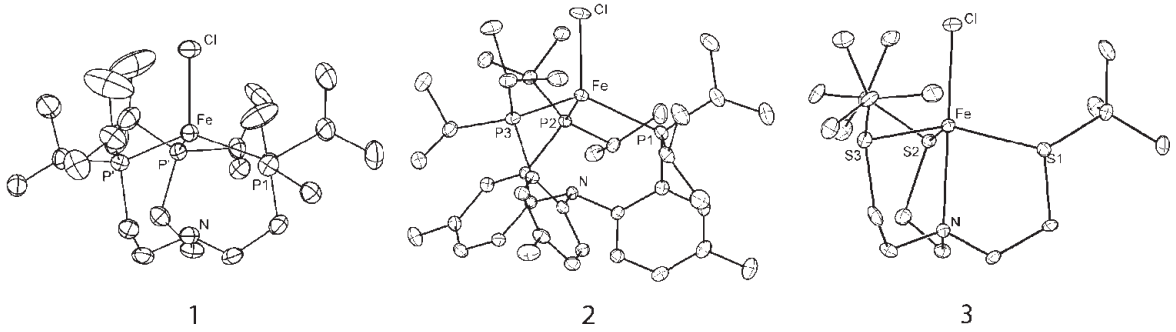
Five-coordinate iron complexes supported by neutral, tetradentate NP_3 (15, 16) and PP_3 (17) ligands are well-known, dating back to the early pioneering efforts of Sacconi and co-workers (14, 15). Despite the general utility of these types of polydentate phosphines, little attention has been paid to derivatives with sterically encumbering phosphine substituents. To begin to explore such systems we have targeted the preparation of the isopropyl-substituted systems $NP^{i\text{-Pr}}_3$ and $NArP^{i\text{-Pr}}_3$ (Scheme 2). Isopropyl-substituted $NP^{i\text{-Pr}}_3$ can be prepared by a straightforward modification of the literature procedure for NP^{Ph}_3 (NP^{Ph}_3 = $N(CH_2CH_2PPh_2)_3$) (14). Accordingly, the addition of 3 equiv. of lithium diisopropylphosphide to an ethereal solution of tris(2-chloroethyl)amine at low temperature affords $NArP^{i\text{-Pr}}_3$ in excellent isolated yield (92%) following work-up. Preparation of $NArP^{i\text{-Pr}}_3$ requires a combination of a suitable carbanion nucleophile and chlorophosphine electrophile. We find that the addition of chlorodiisopropylphosphine to an ethereal solution of $[2\text{-Li-4-Me-}C_6H_3]_3N$, generated in situ by the addition of *tert*-butyllithium to tris(*o*-bromo-*p*-tolyl)amine, affords crystalline $NArP^{i\text{-Pr}}_3$ in good yield (66%) after work-up.

As shown in Scheme 3, cationic Fe(II)–chloride complexes of these NP_3-type ligands can be prepared by reacting the neutral phosphine ligands with $FeCl_2$ in the presence of a halide abstraction reagent ($TlPF_6$ or $NaBPh_4$) in either CH_2Cl_2 or THF, providing colorless $[Fe(NP^{i\text{-Pr}}_3)Cl]PF_6$ (**1**[PF_6]) and yellow $[Fe(NArP^{i\text{-Pr}}_3)Cl]BPh_4$ (**2**[BPh_4]). For structural and magnetic comparison, we also prepared the colorless complex $[Fe(NS^{t\text{-Bu}}_3)Cl]PF_6$ (**3**[PF_6]) by the addition of $FeCl_2$ to a THF solution of $NS^{t\text{-Bu}}_3$ followed by chloride abstraction with $TlPF_6$. The isolated yield of **3**[PF_6] is fairly good (62%), although not in comparison to the high yields obtained for **1**[PF_6] and **2**[BPh_4]. Somewhat surprising is that the iron chemistry of Sacconi's $NS^{t\text{-Bu}}_3$ ligand has not been previously described, though its coordination to the first row transition metals Co (18), Ni (19), and Cu (20) has been known for some time. Given the sulfur-rich environment of the central iron sites of the MoFe-cofactor, and the possible presence of an interstitial N atom, $NS^{t\text{-Bu}}_3$ and related ligands provide an interesting structural starting point for functional iron model studies.

X-ray diffraction analyses of single crystals of **1**[PF_6], **2**[BPh_4], and **3**[PF_6] (Fig. 1) establishes that each complex is monomeric. NP_3-supported **1**[PF_6] and **2**[BPh_4] are best described as tetrahedral complexes and are structurally quite similar to the ferrous cation of NP^{Ph}_3 (15*b*). Accordingly, **1**[PF_6] features an elongated Fe-N distance of 2.801(3) Å

© 2005 NRC Canada

Fig. 1. Displacement ellipsoid (50%) representation of **1**[PF_6], **2**[BPh_4], and **3**[PF_6]. Hydrogen atoms and counteranions have been removed for clarity. Selected bond lengths (Å) and angles (°) for **1**[PF_6]: Fe—Cl 2.262(2), Fe—P1 2.455(1), Fe—N 2.801(3), N-Fe-Cl 180.00(11), P1-Fe-P′ 112.10(2), P1-Fe-Cl 106.70(2). For **2**[BPh_4]: Fe—Cl 2.253(2), Fe—P1 2.467(2), Fe—P2 2.485(2), Fe—P3 2.481(2), Fe—N 2.701(2), P1-Fe-C1 103.83(6), P2-Fe-Cl 115.89(5), P3-Fe-Cl 105.64(4), Fe-N 2.701(2). For **3**[PF_6]: Fe—Cl 2.298(1), Fe—S1 2.447(1), Fe—S2 2.453(1), Fe—S3 2.407(1), Fe—N 2.378(3), N-Fe-Cl 178.32(8), S1-Fe-Cl 101.38(4), S2-Fe-Cl 97.54(4), S3-Fe-Cl 100.11(4).



1 2 3

(2.701(2) Å for **2**[BPh_4]) (21). The iron centers in **1**[PF_6] and **2**[BPh_4] lie above the P_3 plane, projected into the hemisphere opposite the apical N atom. Both systems are high spin (S = 2), expected for conventional pseudotetrahedral iron(II) systems.

It is interesting that the local geometry of sulfur-supported **3**[PF_6] is better described as trigonal bipyramidal. It displays a much shorter Fe–N interaction (2.378(3) Å), which in turn places the Fe center closer to the plane created by its three sulfur donor atoms. The trigonal bipyramidal geometry of **3**[PF_6] gives rise to an average S-Fe-Cl bond angle of 99.7°. For comparison, the average P-Fe-Cl angles of **1**[PF_6] and **2**[BPh_4] are 106.7° and 108.5°, respectively, closer to that expected for an idealized tetrahedral geometry (109.5°). The fact that complex **3**[PF_6] adopts a higher coordination number is perhaps reflective of the decreased electron-releasing character of sulfur relative to phosphorus, resulting in a more electron-deficient iron center that draws the additional N-atom donor inward. The spin state of **3**[PF_6] (S = 1) also reflects the change in coordination number. Two unpaired electrons are expected for an σ-only *d*-orbital splitting scheme under a trigonal bipyramidal ligand field.

Electrochemical characterization of **1**[PF_6] and **2**[BPh_4] shows that each system supports a reversible $Fe^{II/I}$ redox process (–1.65 V for **1**[PF_6] and –1.51 V for **2**[BPh_4]; internally referenced to Cp_2Fe in THF). Only **1**[PF_6] affords a reversible $Fe^{III/II}$ couple (0.54 V). Cationic **2**[BPh_4] is irreversibly oxidized at above ca. 0.5 V. For comparison, we note that NS_3-supported **3**[PF_6] does not feature any well-defined redox processes in the potential window scanned, although problematic adsorption of the complex to the glassy carbon electrode cannot be discounted. Electrochemical data for **1**[PF_6] and **2**[BPh_4] suggests that Fe(I) species should be accessible, at least for the phosphine-supported complexes. While the neutral iron(I) chloride complexes of $NP^{i\text{-}Pr}{}_3$ and $NArP^{i\text{-}Pr}{}_3$ have proven synthetically elusive, formal replacement of the chloride by CO leads to well-defined cationic iron(I) species. Thus, tetraphenylborate salts of $\mathbf{1}^+$ and $\mathbf{2}^+$ can be reduced by Na/Hg amalgam in THF under a blanket of CO to provide deep red, crystalline material. Thorough analysis establishes the products to be the cationic, monocarbonyl derivatives [$Fe(NP^{i\text{-}Pr}{}_3)CO$]$BPh_4$ (**4**[BPh_4]) and [$Fe(NArP^{i\text{-}Pr}{}_3)CO$]$BPh_4$ (**5**[BPh_4]), each of which is isolated in high yield (>85%). Attempts to prepare the related iron(I) $NS^{t\text{-}Bu}{}_3Fe(CO)^+$ species by similar strategies have not been successful.

Structurally characterized, Fe(I) monocarbonyl complexes are rare. To our knowledge, Parkin and co-workers (22) have reported the only crystallographically characterized example of such a species, which is pseudotetrahedral, using an anionic substituted tris(pyrazolyl)borate ligand auxiliary. Recently, we have reported the structural characterization of an iron(I) dicarbonyl complex, which is approximately square pyramidal, supported by an anionic tris(phosphino)borate ligand (13*a*). The solid-state structures of **4**[BPh_4] and **5**[BPh_4] were obtained for comparison and are shown in Fig. 2. Each cationic complex is rigorously trigonal bipyramidal. The Fe—N bond distances observed for **4**[BPh_4] (2.150(2) Å) and **5**[BPh_4] (2.164(2) Å) are dramatically contracted (>0.6 Å) compared with their Fe(II)–chloride precursors. Each carbonyl derivative also displays an unusually short Fe—C bond length (1.680(4) Å for **4**[BPh_4], 1.709(2) Å for **5**[BPh_4]) because of the presence of very strong π backbonding from the iron(I) centers into the π* orbitals of the coordinated CO ligand. The strength of this interaction is also reflected by the observation of very low ν(CO) stretching frequencies (1881 cm^{-1} for **4**[BPh_4], 1880 cm^{-1} for **5**[BPh_4]; THF/KBr). For comparison, Parkin's four-coordinate iron(I) monocarbonyl [$PhTp^{t\text{-}Bu}$]Fe(CO) exhibits a longer Fe—C bond length of 1.789(3) Å, and a ν(CO) value of 1907 cm^{-1} (22). Despite their cationic nature, the π-backbonding ability of **4**[BPh_4] and **5**[BPh_4] is appreciably stronger than in Parkin's tetrahedral derivative, presumably resulting from the presence of a fifth donor group.

The cyclic voltammetry of complexes **4**[BPh_4] and **5**[BPh_4] was also studied. As shown in Fig. 3, both species exhibit two fully reversible redox processes that we assign as $Fe^{I/0}$ (–1.6 V for **4**[BPh_4] and **5**[BPh_4]) and $Fe^{II/I}$ (–0.3 V for **4**[BPh_4], –0.2 V for **5**[BPh_4]) redox events. Bianchini et al. (23) have explored the cyclic voltammetry of a related iron system, [$(PP_3)Fe(C{\equiv}CPh)$]BPh_4, which shows a reversible $Fe^{II/I}$ process but an irreversible $Fe^{I/0}$ event. The neutral π-acidic CO ligand of $\mathbf{4}^+$ and $\mathbf{5}^+$ is better able to stabilize the zero-valent state of iron than the anionic phenylacetylide ligand of [$(PP_3)Fe(C{\equiv}CPh)$]BPh_4.

Because complexes **4**[BPh_4] and **5**[BPh_4] represent rather

© 2005 NRC Canada

Fig. 2. Displacement ellipsoids (50%) of **4**[BPh_4], **5**[BPh_4], and **6**[PF_6]. Hydrogen atoms and counteranions have been removed for clarity. Selected bond lengths (Å) and angles(°) for **4**[BPh_4]: Fe—C 1.680(4), Fe—N 2.150(2), Fe—P1 2.2939(8), Fe—P2 2.2379(8), Fe—P3 2.2851(8), C-Fe-N 177.43(11). For **5**[BPh_4]: Fe—C 1.709(3), Fe—N 2.164(2), Fe—P1 2.3091(7), Fe—P2 2.2936(7), Fe—P3 2.2722(7), C-Fe-N 177.6(1). For **6**[PF_6]: Fe—N2 1.804(3), Fe—N1 2.142(3), Fe—H 1.53(4), Fe—P1 2.245(1), Fe—P2 2.250(1), Fe—P3 2.286(1), N1-Fe-N2 176.4(1).

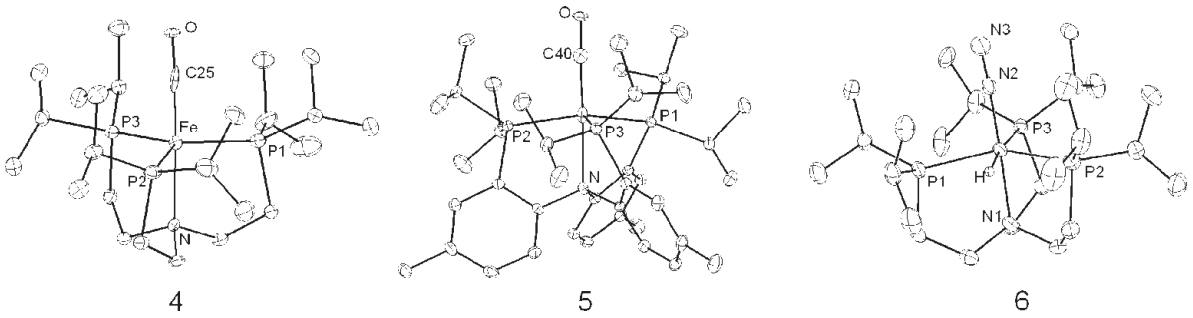


Fig. 3. Cyclic voltammograms of **5**[BPh_4] and **4**[BPh_4] recorded at 100 mV/s in THF vs. $Ag/AgNO_3$.

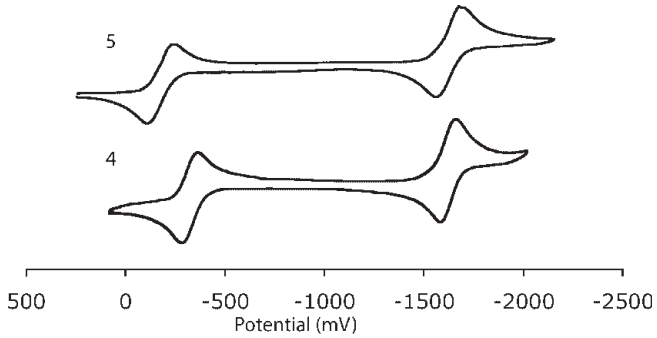
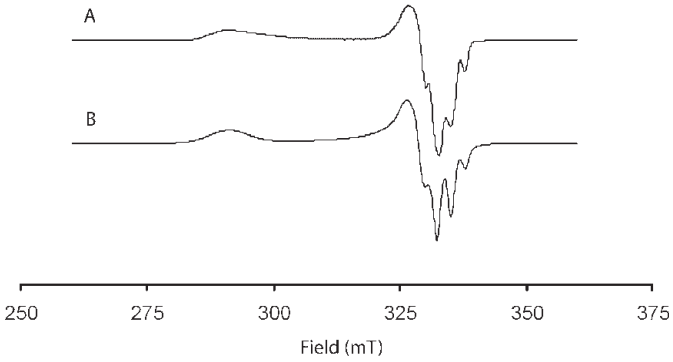


Fig. 4. EPR spectrum of **4**[BPh_4] (5.4 K, ν = 9.475 GHz) recorded in a frozen glass of 1-methyltetrahydrofuran. (A) Experimental spectrum, (B) simulated spectrum: g_1 = 2.302, $a_{1(P)}$ = 30 G; g_2 = 2.0365, $a_{2(P)}$ = 15 G; g_3 = 2.0075, $a_{3(P)}$ = 28 G.



unusual examples of mononuclear iron(I) carbonyls it was prudent to undertake their magnetic characterization. Solution moments for **4**[BPh_4] and **5**[BPh_4] (24, d_8-THF) were measured to be 2.05 μ_B and 1.96 μ_B, respectively, implying a doublet ground state for each species. We also collected a glassy 1-methyltetrahydrofuran EPR spectrum of **4**[BPh_4] at 5.4 K (Fig. 4A). The observed signal, which is rhombic with three components at g_1 = 2.3020, g_2 = 2.0365, and g_3 = 2.0075, shows well-resolved superhyperfine coupling to the phosphorus nuclei of the ligand (3 × P, I_p = 1/2). The spectrum can be satisfactorily simulated as an S = 1/2 spin system by inclusion of the superhyperfine interactions (Fig. 4B). The three-component, rhombic signal observed is qualitatively comparable to that reported by Bianchini et al. (23) for the iron(I) derivative (PP_3)Fe(C≡CPh). However, Bianchini notes the absence of superhyperfine interactions between the unpaired electron and the phosphorous nuclei of PP_3 as a result of a spin-spin exchange narrowing processes occurring at sufficiently fast rates. The presence of resolvable superhyperfine interactions in the spectrum of **4**[BPh_4] likely benefits from the acquisition of the spectrum in the glassy phase.

The reduction of the cationic complexes **1**, **2**, and **3** under dinitrogen is a topic of ongoing study. For the present contribution, we note that N_2 uptake can be achieved by the ($NP^{i\text{-}Pr}_3$)Fe system by slight modification of the route used for the original preparation of [(NP^{Ph}_3)Fe(H)(N_2)][BPh_4] (NP^{Ph}_3 = $N(CH_2CH_2PPh_2)_3$) (15*a*, 16). Addition of a THF solution of Li[BEt_3H] to **1**[PF_6] under N_2 generates yellow, diamagnetic [Fe($NP^{i\text{-}Pr}_3$)(N_2)(H)]PF_6 (**6**[PF_6]) in good yield. Complex **6**[PF_6] has been thoroughly characterized and its X-ray crystal structure is shown in Fig. 2. The spectroscopic and structural data for **6**[PF_6] compare favorably with those reported for [(NP^{Ph}_3)Fe(H)(N_2)][BPh_4] (16). The ν(N_2) vibration is observed at only slightly lower energy for **6**[PF_6] (2087 vs. 2090 cm^{-1} in THF/KBr), and the Fe—N_{N2} bond distances are indistinguishable (1.81(1) Å). The ν(Fe-H) vibration for **6**[PF_6], which has been confirmed by preparation of a deuterated sample, is shifted to a much lower frequency than for [(NP^{Ph}_3)Fe(H)(N_2)][BPh_4] (1865 vs. 1913 cm^{-1}), likely reflecting the presence of an isopropyl-substituted rather than a phenyl-substituted phosphine donor trans to the hydride.

In conclusion, we have attempted to motivate renewed interest in the small molecule coordination chemistry of five-coordinate iron systems supported by ligands that allow access to low-valent states. Understanding potential reactivity patterns for local iron sites of the cofactor of nitrogenase provides one such impetus. In this regard, we have expanded the versatile NP_3 ligand set popularized by Sacconi and co-workers (15) to include the bulkier, more electron-releasing $NArP^{i\text{-}Pr}_3$ and $NP^{i\text{-}Pr}_3$ derivatives that feature isopropyl-substituted phosphine donors. The iron coordination chemistry of these new generation polyphosphine ligands is well-defined, and iron(I) carbonyl and iron(II)

© 2005 NRC Canada

dinitrogen adducts have been described. A key feature of these tetradentate ligands concerns the flexibility of the ligand. The apical Fe–N donor interaction reacts to the nature of the ligand in the fifth binding site: it contracts for π-acidic CO (Fe(I) relative to chloride (Fe(II)). The related but less electron-releasing $NS^{t\text{-}Bu}_3$ ligand supports a well-defined, cationic $(NS_3)Fe^{II}$–Cl species whose local geometry and donor ligands are interesting given the local geometry of the central iron sites of the MoFe-cofactor of nitrogenase. A difference in spin state is observed when comparing the $(NS^{t\text{-}Bu}_3)Fe^{II}$–Cl complex **3**[$PF_6$] ($S = 1$) and its $(NP_3)Fe^{II}$–Cl analogues ($S = 2$). This difference results from a severe contraction of the apical Fe–N linkage to lend a trigonal bipyramidal rather than a tetrahedral geometry for the divalent iron center in **3**[PF_6]. Future work will examine the installation of nitrogenous donor ligands in the fifth binding site of these scaffolds.[3]

Experimental section

All manipulations were carried out using standard Schlenk or glovebox techniques under a nitrogen atmosphere. All solvents were deoxygenated and dried by sparging with N_2 gas and passage through an activated alumina column. Non-halogenated solvents were tested with a standard purple solution of sodium benzophenone ketyl in tetrahydrofuran to ensure dioxygen and water removal. Deuterated solvents were purchased from Cambridge Isotopes Laboratories, Inc. and were degassed and stored over activated 3 Å molecular sieves prior to use. All other reagents and solvents were purchased from commercial vendors and used without further purification unless otherwise noted. $NS^{t\text{-}Bu}_3$ (14), LiP-*i*-Pr_2 (25), and $N(CH_2CH_2Cl)_3$ (26) were prepared according to literature procedures. *CAUTION: $N(CH_2CH_2Cl)_3$ (a mustard agent) and thallium reagents are toxic and should be handled with extreme care.*

Elemental analyses were performed by Desert Analytics, Tucson, Arizona. A Varian Mercury-300 spectrometer was used to record ^1H and ^{31}P NMR spectra at room temperature. ^1H and ^{13}C NMR chemical shifts were referenced to residual solvent. ^{31}P NMR are reported relative to an external standard of 85% H_3PO_4 (0 ppm). Abbreviations for reported signal multiplicites are as follows: singlet (s), doublet (d), triplet (t), quartet (q), multiplet (m), broad (br). IR spectra were recorded on a Bio-Rad Excalibur FTS 3000 spectrometer controlled by Win-IR Pro software using a KBr solution cell. MS data were obtained by injection of a hydrocarbon solution onto a Hewlett-Packard 1100MSD mass spectrometer (ES^+) or an Agilent 5973 mass selective detector (EI). UV–vis measurements were recorded on a Varian Cary 50 Bio spectrophotometer controlled by Cary WinUV Software. All measurements were recorded using a quartz cell fitted with a Teflon® cap.

Room temperature solution magnetic susceptibilities were determined using the method of Evans (24). Electrochemical measurements were recorded in a glovebox under a dinitrogen atmosphere using a BAS CV 100 W (Bioanalytical Systems Inc., West Lafayette, Indiana). A glassy carbon working electrode, a platinum wire auxiliary electrode, and a $Ag/AgNO_3$ nonaqueous reference electrode were used in all studies. All measurements were carried out in THF solutions of electrolyte (0.32 mol/L tetra-*n*-butylammonium hexafluorophosphate) and analyte. All electrochemical measurements are referenced to Fc/Fc^+ as an internal standard.

X-band EPR measurements were recorded using a Bruker EMX spectrometer (controlled by Bruker Win EPR software version 3.0) equipped with a rectangular cavity working in the TE_{102} mode. Low-temperature measurements were conducted with an Oxford continuous-flow helium cryostat. Accurate frequency values were recorded from a frequency counter on the microwave bridge. Solution spectra were acquired in 1-methyltetrahydrofuran. Samples were prepared in a glovebox under dinitrogen in a quartz EPR tube equipped with a ground glass joint.

Crystallographic data for complexes **1**–**6** appear in Tables 1 and 2. X-ray diffraction studies were carried out at the Beckman Institute Crystallographic Facility on a Bruker Smart 1000 CCD diffractometer. Crystals were mounted on a glass fiber with Paratone-N oil. Crystallographic data were collected on a Bruker P4 diffractometer (0.710 73 Å MoKα) with a CCD area detector. Data were collected using the Bruker SMART program, collecting scans at five settings. Data reduction was performed using Bruker SAINT v6.2. Structure solution and structure refinement were performed using SHELXS-97 (Sheldrick, 1990) and SHELXL-97 (Sheldrick, 1997).

Refinement of F^2 against all reflections

The weighted *R* factor (*wR*) and goodness of fit (S) are based on F^2, conventional *R* factors (*R*) are based on *F*, with *F* set to zero for negative F^2. The threshold expression of $F^2 > 2\sigma(F^2)$ is used only for calculating *R* factors(gt), etc., and is not relevant to the choice of reflections for refinement. *R* factors based on F^2 are statistically about twice as large as those based on *F*, and *R* factors based on *all* data will be even larger.

All esds (except the esd in the dihedral angle between two l.s. planes) are estimated using the full covariance matrix. The cell esds are taken into account individually in the estimation of esds in distances, angles, and torsion angles; correlations between esds in cell parameters are only used when they are defined by crystal symmetry. An approximate (isotropic) treatment of cell esds is used for estimating esds involving l.

Synthesis of $NP^{i\text{-}Pr}_3$

In a 100 mL flask, tris(2-chloroethyl)amine (1.72 g, 8.41 mmol) was dissolved in THF (100 mL) and cooled to –78 °C, while stirring, for 30 min. Diisopropyllithiophosphine (3.34 g, 26.9 mmol) was dissolved in THF (50 mL)

[3] Supplementary data may be purchased from the Directory of Unpublished Data, Document Delivery, CISTI, National Research Council Canada, Ottawa, ON K1A 0S2, Canada (http://cisti-icist.nrc-cnrc.gc.ca/irm/unpub_e.shtml for information on ordering electronically). CCDC 261768–261770 and 240830–240832 contain the crystallographic data for this manuscript. These data can be obtained, free of charge, via ww.ccdc.cam.ac.uk/conts/retrieving.html (or from the Cambridge Crystallographic Data Centre, 12 Union Road, Cambridge CB2 1EZ, UK; fax +44 1223 336033; or deposit@ccdc.cam.ac.uk).

© 2005 NRC Canada

Table 1. Crystallographic data and detail of refinement for **1**[PF_6], **2**[BPh_4], and **3**[PF_6].

Crystal	[Fe(NP$^{i\text{-Pr}}_3$)Cl]PF_6	[Fe(NArP$^{i\text{-Pr}}_3$)Cl]BPh_4	[Fe(NS$^{t\text{-Bu}}_3$)Cl]PF_6
Empirical formula	$C_{24}H_{54}NP_4ClF_6Fe$	$C_{63}H_{80}BClFeNP_3$	$C_{18}H_{39}NPS_3ClF_6Fe$
Formula weight	685.86	1046.30	601.95
Crystal system	Cubic	Triclinic	Monoclinic
Space group	$P2_13$	P-1 (No. 2)	$P2_1/n$
a (Å)	14.8923(8)	10.992(9)	16.7388(15)
b (Å)		14.940(12)	12.0505(11)
c (Å)		17.893(15)	27.017(3)
α (°)		83.95(3)	
β (°)		79.03(3)	101.593(2)
γ (°)		89.11(3)	
V (Å^3)	3 302.8(3)	2 869(4)	5 338.4(8)
Z	4	2	8
D_{calcd} (Mg/m^3)	1.379	1.211	1.498
Radiation (MoKα)	λ = 0.710 73 Å	λ = 0.710 73 Å	λ = 0.710 73 Å
T (K)	100(2)	100(2)	100(2)
θ Range (°)	2.36–29.47	1.37–34.70	1.86–31.49
Total reflections	43 333	70 110	52 733
Unique reflections	3 511	21 858	15 469
Parameters	116	646	605
R_1, w$R2$ ($I > 2\sigma(I)$)[a]	0.045, 0.072	0.0452, 0.0836	0.0595, 0.0977
Goodness-of-fit on F^2	2.594	1.236	1.460

[a] $R_1 = \Sigma||F_o| - |F_c|| / \Sigma|F_o|$; $wR2 = \{\Sigma[w(F_o^2 - F_c^2)^2] / \Sigma[w(F_o^2)^2]\}^{1/2}$.

Table 2. Crystallographic data and detail of refinement for **4**[BPh_4], **5**[BPh_4], and **6**[PF_6].

Crystal	[Fe(NP$^{i\text{-Pr}}_3$)CO]BPh_4	[Fe(NArP$^{i\text{-Pr}}_3$)CO]BPh_4·THF	[Fe(NP$^{i\text{-Pr}}_3$)N_2(H)]PF_6
Empirical formula	$C_{48}H_{74}BNOP_3Fe$	$C_{64}H_{80}BFeNOP_3$·C_4H_8O	$C_{24}H_{55}F_6FeN_3P_4$
Formula weight	852.66	1110.96	679.44
Crystal system	Monoclinic	Monoclinic	Triclinic
Space group	$P2_1/c$	P 1 21/c 1 (No. 14)	P-1
a (Å)	17.4370(9)	11.1069(6)	9.9335(9)
b (Å)	11.3322(6)	22.6213(13)	11.2697(10)
c (Å)	24.3169(13)	23.9289(14)	14.8239(14)
α (°)			99.275(2)
β (°)	104.5680(10)°	91.349(2)	97.251(2)
γ (°)			95.764(2)
V (Å^3)	4 650.5(4)	6 010.5(6)	1 612.3(3)
Z	4	4	2
D_{calcd} (Mg/m^3)	1.218	1.228	1.400
Radiation (MoKα, Å)	λ = 0.710 73	λ = 0.710 73	λ = 0.710 73
T (K)	100(2)	100(2)	100(2)
θ Range (°)	1.73–28.43	1.70–33.81	1.9–32.7
Total reflections	61 863	102 345	52 733
Unique reflections	11 004	21 841	8 000
Parameters	517	700	378
R_1, w$R2$ ($I > 2\sigma(I)$)[a]	0.0626, 0.0988	0.0678, 0.1397	0.0604, 0.1519
Goodness-of-fit on F^2	2.206	1.006	1.09

[a] $R_1 = \Sigma||F_o| - |F_c|| / \Sigma|F_o|$; $wR2 = \{\Sigma[w(F_o^2 - F_c^2)^2] / \Sigma[w(F_o^2)^2]\}^{1/2}$.

and added dropwise to the stirring, cold solution of tris(2-chloroethyl)amine over the course of 30 min. After addition of the diisopropyllithiophosphine was complete, the reaction was slowly warmed to room temperature and stirred for 3 h. All volatiles were removed in vacuo to yield a pale yellow oil and white precipitate. The reaction mixture was then stirred in diethylether (30 mL) for 20 min. The resulting mixture was then filtered through a 60 mL, medium porosity, scintered glass frit that was layered with 1 inch (1 inch = 25.4 mm) of Celite® and 1 inch (1 inch = 25.4 mm) of silica gel. The white solids collected on the frit where then washed with two 20 mL portions of petroleum ether. All volatiles

© 2005 NRC Canada

were removed from the filtrate to yield $NP^{i\text{-}Pr}_3$ as a very viscous, pale yellow oil (3.48 g, 92%). ^{1}H NMR (300 MHz, C_6D_6): 2.87 (dt, 5.4 Hz, 6H), 1.5–1.75 (m, 12H) 1.05 (m, 36H). ^{13}C NMR (75 MHz, C_6D_6): 53.2 (d, 29.5 Hz), 24.1 (d, 14.3 Hz), 20.6 (t, 16.6 Hz), 19.4 (d, 9.7 Hz). ^{31}P NMR (121.4 MHz, C_6D_6): 0.78 (br s). FAB-MS (*m*/*z*): 450.3526 ($NP^{i\text{-}Pr}_3$ + H^+).

Synthesis of $NArP^{i\text{-}Pr}_3$

In a 100 mL flask, tris(2-bromo-*p*-tolyl)amine (3.0 g, 5.73 mmol) was dissolved in ether (50 mL) and cooled to –78 °C. Solid *t*-BuLi (2.2 g, 34.4 mmol) was added portionwise over 15 min. The reaction was warmed to room temperature after 30 min. Following 3 h of stirring, the reaction mixture was yellow in color with LiBr precipitate. The reaction vessel was cooled to –78 °C and chlorodiisopropylphosphine (2.8 g, 18.0 mmol) was added over 5 min. The mixture was stirred at ambient temperature for 18 h at which time it was filtered through a plug of silica gel and the solvent removed in vacuo. The resulting tacky solid was dissolved in CH_2Cl_2 (50 mL), filtered through Celite®, and dried to a solid. Trituration of the filtrate in methanol (150 mL) afforded an analytically pure fine white solid, which was collected on a fritted glass funnel and dried thoroughly under reduced pressure (2.4 g, 66%). ^{1}H NMR (300 MHz, $CDCl_3$): 7.25 (s), 7.16 (br s), 6.95 (s), 6.93 (s), 6.87 (dd, 2.0 Hz, 8.0H), 6.48 (dd, 4.0 Hz, 8.0H), 2.54 (m), 2.30 (s), 2.28 (s), 1.51 (d sept, 2.0 Hz, 7.0H), 1.21 (q, 7.5 Hz, 14.5H), 1.13 (dd, 7.0 Hz, 10.0H), 1.00 (br s), 0.91 (dd, 7.5 Hz, 10.0H), 0.825 (br s), 0.41 (7.5 Hz, 14H). ^{13}C NMR (126 MHz, $CDCl_3$): 155.1 (m), 154.5 (m), 135.0 (m), 134.7 (s), 133.9 (br s), 131.9 (s), 129.9 (br s), 129.3 (s), 127.7 (s), 23.9 (m), 23.4 (m), 21.9 (m), 21.1 (s), 21.0 (s), 19.2 (m). ^{31}P NMR (121 MHz, $CDCl_3$): –2.87 (br m), –11.28 (s). Anal. calcd. for $C_{39}H_{60}NP_3$: C 73.67, H 9.51, N 2.20; found: C 73.57, H 9.25, N 2.05.

Synthesis of $[Fe(NP^{i\text{-}Pr}_3)Cl]PF_6$ (1[PF_6])

Solid $FeCl_2$ (0.335 g, 2.65 mmol) was added to a stirring solution of $NP^{i\text{-}Pr}_3$ (1.19 g, 2.56 mmol) dissolved in CH_2Cl_2 (2.0 mL). The slurry was stirred for 10 min and $TlPF_6$ was added dropwise as a THF (4.0 mL) solution over 15 min. A white precipitate began to form immediately. The reaction was stirred for 4 h and then filtered through Celite®. The pad of Celite® was washed with two portions of CH_2Cl_2 (5.0 mL). All volatiles were then removed in vacuo to yield a white solid. The white solid was extracted into CH_2Cl_2 (5.0 mL) and again filtered through a pad of Celite®. The colorless solution was then layered with Et_2O and stored at –35 °C for 2 days to afford colorless crystals of the desired product (1.48 g, 81.3%). μ_{eff} (CD_2Cl_2, 298 K): 5.04 μ_B. ^{1}H NMR (300 MHz, CD_2Cl_2): 27.5 (b), 3.2 (b), –8.5 (b). ^{31}P NMR (121.4 MHz, CD_2Cl_2): –141.5 (septet, 711 Hz, PF_6). Anal calcd. for $C_{24}H_{54}ClF_6FeNP_4$: C 42.03, H 7.94, N 2.04; found: C 42.13, H 8.00, N 2.05.

Synthesis of $[Fe(NP^{i\text{-}Pr}_3)Cl]BPh_4$ (1[BPh_4])

The tetraphenylborate salt was synthesized in a similar maner as **1**, with the following exceptions: sodium tetraphenylborate was used in place of $TlPF_6$, and methanol was used in place of THF.

Synthesis of $[Fe(NArP^{i\text{-}Pr}_3)Cl]BPh_4$ (2[BPh_4])

A 50 mL reaction vessel was charged with $NArP^{i\text{-}Pr}_3$ (1.0 g, 1.57 mmol), $FeCl_2$ (0.20 g, 1.57 mmol), sodium tetraphenylborate (0.540 g, 1.57 mmol), and THF (25 mL) and sealed with a Teflon® stopper. The reaction was heated at 65 °C for 12 h, cooled, and the solvent was removed in vacuo. The resultant yellow solids were washed with petroleum ether (2 × 20 mL) and dried under reduced pressure. The product was extracted into CH_2Cl_2, filtered through a plug of Celite® and layered petroleum ether, which afforded analytically pure yellow crystals upon standing (1.60 g, 97%). Crystals suitable for X-ray diffraction were obtained by layering an CH_2Cl_2 solution with diethylether. μ_{eff} (acetone-d_6, 298 K): 5.3 μ_B. ^{1}H NMR (300 MHz, CD_2Cl_2): 140.9 (br s), 30.2 (br s), 19.4 (br s), 15.3 (s), 15.0 (s), 9.76 (s), 7.32 (s), 7.03 (t, 7.8 Hz), 6.87 (m), 5.03 (s), –3.05 (br s), –16.1 (br s), –20.7 (br s). Anal. calcd. for $C_{63}H_{80}BClFeNP_3$: C 72.32, H 7.71, N 1.34; found: C 72.08, H 7.53, N 1.46.

Synthesis of $[Fe(NS^{t\text{-}Bu}_3)Cl]PF_6$ (3[PF_6])

$NS^{t\text{-}Bu}_3$ (0.133 g, 0.364 mmol) was stirred in 5.0 mL of THF and solid $FeCl_2$ (0.0457 g, 0.364 mmol) was added. A THF solution (4.0 mL) of $TlPF_6$ (0.127 g, 0.364 mmol) was added to the reaction dropwise over 20 min. A white precipitate began to form immediately. The reaction mixture was stirred for 3 h, concentrated to dryness, dissolved in CH_2Cl_2 (3.0 mL), and filtered through a pad of Celite®. Layering the resulting colorless filtrate with Et_2O produced colorless crystals (0.136 g, 62%) of the desired product. ^{1}H NMR (300 MHz, d_8 -THF): 20.5 (b), 10.9 (b), 2.6 (b). ^{31}P NMR (121.4 MHz, THF-d_8): –143.5 (septet, 711 Hz, PF_6). Anal. calcd. for $C_{18}H_{39}ClF_6FeNP$: C 35.91, H 6.16, N 2.33; found: C 35.23, H 6.16, N 2.46.

Synthesis of $[Fe(NP^{i\text{-}Pr}_3)(CO)]BPh_4$ (4[BPh_4])

A 0.23 weight% amalgam was prepared in a 25.0 mL Shlenk flask by dissolving solid Na (5.1 mg, 0.22 mmol) in mercury (2.21 g). The flask was then charged with $[Fe(NP^{i\text{-}Pr}_3)Cl]BPh_4$ (0.190 g, 0.221 mmol) dissolved in THF (5.0 mL) and a stir bar. The headspace of the flask was quickly evacuated and refilled three times with 1 atm of CO(g) (1 atm = 101.325 kPa). After the third cycle, the flask was sealed under 1 atm of CO(g) (1 atm = 101.325 kPa) and stirring commenced. The reaction mixture changed immediately from colorless to bright yellow. The reaction mixture was stirred for 12 h over which the color changed again from golden yellow to dark red. All volatiles were removed in vacuo and the resulting red-brown solid was extracted into THF (3.0 mL) and filtered through a pad of Celite® to remove insoluble material. The resulting red solution was layered with Et_2O and stored at –35 °C overnight. The next day, large red crystals of the product were isolated on a medium porosity frit and dried. IR (THF, KBr, cm^{-1}) ν(CO): 1881. μ_{eff} (THF-d_8, 298 K): 2.15 μ_B. ^{1}H NMR (THF-d_8): 19.1 (b), 7.65 (b), 7.2 (b), 7.0 (b), 3.6 (b), –0.47 (b). Anal. calcd. for $C_{49}H_{75}BFeNOP_4$: C 68.94, H 8.86, N 1.64; found: C 68.96, H 8.62, N 1.66.

Synthesis of $[Fe(NArP^{i\text{-}Pr}_3)(CO)]BPh_4$ (5[BPh_4])

In a 50 mL Schlenk flask, $[(NArP^{i\text{-}Pr}_3)FeCl][BPh_4]$ (60 mg, 0.057 mmol) was dissolved in THF (50 mL) and so-

© 2005 NRC Canada

dium metal (1.3 mg, 0.057 mmol) amalgamated in mercury (1.84 g, 9.17 mmol) was added. The solution was sparged with CO(g) for 10 min and then stirred vigorously for 18 h during which time the solution became green in color. The solvent was removed under reduced pressure, and the resultant green solids were extracted with THF (5 mL) and then filtered. The green filtrate was layered with petroleum ether (15 mL) and the desired product precipitated as analytically pure red crystals (49 mg, 83%). μ_{eff} (THF-d_8, 298 K): 2.1 μ_B. IR (THF, KBr, cm^{-1}) ν(CO): 1880. Anal. calcd. for $C_{63}H_{80}BFeNOP_3$: C 73.99, H 7.76, N 1.35; found: C 73.76, H 7.70, N 1.47.

Synthesis of $[Fe(NP^{i\text{-}Pr}{}_3)(N_2)(H)]PF_6$ (6[PF_6])

Solid **1**[PF_6] (0.222 g, 0.324 mmol) was dissolved in THF (10 mL) and cooled to –78 °C. To this solution a solution of $Li(HBEt_3)$ (1.0 mol/L in ether) (356 μL, 0.356 mmol) was added dropwise via syringe. The reaction mixture changed slowly from colorless to pale yellow over 1 h. The reaction mixture was warmed to room temperature and filtered through a pad of Celite®. The yellow filtrate was dried in vacuo to yield a yellow-brown solid. The solid was extracted into THF (4.0 mL) and filtered through a pad of Celite®. The filtrate was layered with Et_2O (4.0 mL) and stored at –35 °C for 3 days to afford light yellow crystals of the desired product (0.142 g, 66%). IR (THF, KBr, cm^{-1}): ν(N_2) 2090, ν(FeH) 1865. ^{1}H NMR (300 MHz, THF-d_8): –8.77 (dt, J_{PH} = 74.1 Hz (cis), J_{PH} = 38.1 Hz (trans)), 1.4–1.6 (m, 36H), 1.8 (t, 2H), 1.94 (m, 4H), 1.98 (m, 2H), 2.15–2.25 (m, 4H), 2.32 (m, 2H), 2.48 (m, 2H) 2.70 (m, 2H). ^{31}P NMR (121.4 MHz, THF-d_8): 67.6 (d, 2P J_{pp}= 41.4 Hz), 62.2 (t, 1P), –141.5 (septet, 1P, J_{FP} = 711 Hz, PF_6). Anal. calcd. for $C_{24}H_{55}F_6FeN_3P_4$: C 42.43, H 8.16, N 6.18; found: C 42.82, H 8.16, N 5.72.

Synthesis of $[Fe(NP^{i\text{-}Pr}{}_3)(N_2)(D)]PF_6$

$Fe(NP^{i\text{-}Pr}{}_3)(N_2)(D)]PF_6$ was prepared by following the synthetic protocol outlined for **6**[PF_6] and using $Li(DBEt_3)$ in place of $Li(HBEt_3)$. The IR (THF, KBr) for this complex exhibits a ν(FeD) = 1341 cm^{-1}.

Acknowledgement

We acknowledge the DOE (Department of Energy) (PECASE), the NSF (National Science Foundation) (CHE-0132216), and the Beckman Institute Senior Research Fellows Program (CEM) for financial support. Larry Henling and Dr. Michael Day provided crystallographic assistance.

References

1. (*a*) S.C. Lee and R.H. Holm. Proc. Natl. Acad. Sci. U.S.A. **100**, 3595 (2003); (*b*) P.L. Holland. *In* Comprehensive coordination chemistry 2. Vol. 8. *Edited by* J.A. McLeverty and T.J. Meyer. Elsevier, New York. 2003. pp. 569–599.
2. O. Einsle, F.A. Tezcan, S.L.A. Andrade, B. Schmid, M. Yoshida, J.B. Howard, and D.C. Rees. Science, **297**, 1696 (2002).
3. (*a*) L.S. Seefeldt, I.G. Dance, and D.R. Dean. Biochemistry, **43**, 1401 (2004); (*b*) B.K. Burgess and K.J. Lowe. Chem. Rev. **96**, 2983 (1996).
4. (*a*) V. Vrajmasu, E. Münch, and E.L. Bominaar. Inorg. Chem. **42**, 5974 (2003); (*b*) H. Uwe, R. Ahlrichs, and D. Coucouvanis. J. Am. Chem. Soc. **126**, 2588 (2004).
5. (*a*) D. Coucouvanis, J. Han, and N. Moon. J. Am. Chem. Soc. **124**, 216 (2002); (*b*) J. Vela, S. Stoian, C.J. Flashenriem, E. Münck, and P.L. Holland. J. Am. Chem. Soc. **126**, 4522 (2004).
6. (*a*) J. Chatt, J.R. Dilworth, and R.L. Richards. **78**, 589 (1978); (*b*) F. Barriere. Coord. Chem. Rev. **236**, 71 (2003).
7. J. Chatt, J.R. Dilworth, and R.L. Richards. Chem. Rev. **78**, 589 (1978).
8. C.J. Pickett. J. Biol. Inorg. Chem. **1**, 601 (1996).
9. D.V. Yandulov and R.R. Schrock. Science, **301**, 76 (2003).
10. J.B. Howard and D.C. Rees. Chem. Rev. **96**, 2965 (1996).
11. H. Lee, R.Y. Igarashi, M. Laryukhin, P.E. Doan, P.C. Dos Santos, D.R. Dean, L.C. Seefeldt, and B.M. Hoffman. J. Am. Chem. Soc. **126**, 9563 (2004).
12. J.M. Smith, R.J. Lachicotte, K.A. Pittard, T.R. Cundari, G. Lukat-Rodgers, K.R. Rodgers, and P.L. Holland. J. Am. Chem. Soc. **123**, 9222 (2001).
13. (*a*) S.D. Brown, T.A. Betley, and J.C. Peters. J. Am. Chem. Soc. **125**, 322 (2003); (*b*) T.A. Betley and J.C. Peters. J. Am. Chem. Soc. **125**, 10 782 (2003); (*c*) T.A. Betley and J.C. Peters. J. Am. Chem. Soc. **126**, 6252 (2004).
14. R. Morassi and L. Sacconi. Inorg. Synth. **16**, 174 (1976).
15. (*a*) P. Stoppioni, F. Mani, and L. Sacconi. Inorg. Chim. Acta, **11**, 227 (1974); (*b*) L. Sacconi and M.D. Vaira. Inorg. Chem. **17**, 810 (1978); (*c*) M. Di Vaira, C.A. Ghilardi, and L. Sacconi. Inorg. Chem. **15**, 1555 (1976); (*d*) M. Di Vaira, S. Minollini, and L. Sacconi. Inorg. Chem. **16**, 1518 (1977).
16. T.A. George, D.J. Rose, and Y. Chang, Q. Chen, J. Zubieta. Inorg. Chem. **34**, 1295 (1995).
17. For examples see: (*a*) C. Bianchini, A. Meli, M. Peruzzini, C. Bohanna, M.A. Esteruelas, and L.A. Oro. Organometallics, **11**, 138 (1992); (*b*) L.D. Field, B.A. Messerle, and R.J. Smernik. Inorg. Chem. **36**, 5984 (1997); (*c*) L.D. Field, B.A. Messerle, R.J. Smernik, T.W. Hambley, and P. Turner. Inorg. Chem. **36**, 2884 (1997).
18. G. Fallani, R. Morassi, and F. Zanobini. Inorg. Chim. Acta, **12**, 147 (1975).
19. (*a*) P. Stavropoulos, M. Carrie, M.C. Muetterties, and R.H. Holm. J. Am. Chem. Soc. **112**, 5385 (1990); (*b*) P. Stavropoulos, M.C. Muetterties, M. Carrie, and R.H. Holm. J. Am. Chem. Soc. **113**, 8485 (1991).
20. (*a*) J.M. Baumeister, R. Alberto, K. Ortner, and O.B. Spingler. J. Chem. Soc. Dalton Trans. 4143 (2002); (*b*) E.A. Ambundo, A.J. Grall, N. Aguera-Vega, L.T. Dressel, T.H. Cooper, M.J. Heeg, L.A. Ochrymowyc, and D.B. Rorabacher. Inorg. Chem. **38**, 4233 (1999).
21. Long M-N distances are often observed for $[(NP_3)M(II)–X]^+$ complexes. See for example: (*a*) C.A. Ghilardi, C. Mealli, S. Midollini, and A. Orlandini. Inorg. Chem. **24**, 164 (1985); (*b*) M. Di Vaira and A.B. Orlandini. Inorg. Chem. **12**, 1292 (1973).
22. J.L. Kisko, T. Hascall, and G. Parkin. J. Am. Chem. Soc. **120**, 10 561 (1998).
23. C. Bianchini, F. Laschi, D. Masi, F.M. Ottavini, A. Pastor, M. Peruzzini, P. Zanello, and F. Zanobini. J. Am. Chem. Soc. **115**, 2723 (1993).
24. (*a*) S.K. Sur. J. Magn. Reson. **82**, 169 (1989); (*b*) D.F. Evans. J. Chem. Soc. 2003 (1959).
25. (*a*) A.H. Cowely, R.H. Jones, M.A. Mardones, and C.M. Nunn. Organometallics, **10**, 1635 (1991); (*b*) K. Issleib and F. Krech. J. Organomet. Chem. **13**, 283 (1968).
26. J.P. Mason and D.J. Gasch. J. Am. Chem. Soc. **60**, 2816 (1938).

© 2005 NRC Canada

Synthesis of tungsten complexes that contain hexaisopropylterphenyl-substituted triamidoamine ligands, and reactions relevant to the reduction of dinitrogen to ammonia

Dmitry V. Yandulov and Richard R. Schrock

Abstract: [$HIPTN_3N$]WCl (**W**Cl) can be synthesized readily by adding H_3[$HIPTN_3N$] to WCl_4(DME) followed by $LiN(SiMe_3)_2$ ([$HIPTN_3N$]$^{3-}$ = [(HIPTNCH$_2$CH$_2$)$_3$N]$^{3-}$ where HIPT = 3,5-(2,4,6-*i*-Pr$_3$C$_6$H$_2$)$_2$C$_6$H$_3$ = HexaIsoPropylTerphenyl). Reduction of **W**Cl with KC_8 in benzene under N_2 yields **W**N=NK. **W**N=NK is readily oxidized in THF by $ZnCl_2$ to yield zinc metal and **W**N_2. Reduction of **W**N_2 to [**W**N_2]$^-$ is reversible at –2.27 V vs. $FeCp_2^{+/0}$ in 0.1 mol/L [Bu_4N][BAr$'_4$]/PhF electrolyte (Ar′ = 3,5-(CF$_3$)$_2$C$_6$H$_3$), while oxidation of **W**N_2 to [**W**N_2]$^+$ is also reversible at –0.66 V. Protonation of **W**N=NK by [Et_3NH][OTf] in benzene yields **W**N=NH essentially quantitatively. Protonation of **W**N=NH at N_β with [H(OEt)$_2$][BAr$'_4$] in ether affords [**W**=NNH_2][BAr$'_4$] quantitatively. Electrochemical reduction of [**W**=NNH_2][BAr$'_4$] in 0.1 mol/L [Bu_4N][BAr$'_4$]/PhF is irreversible at scan rates of up to 1 V/s. Addition of NaBAr$'_4$ and NH_3 to **W**Cl in PhF yields [**W**(NH_3)][BAr$'_4$]. Electrochemical reduction of [**W**(NH_3)][BAr$'_4$] in 0.1 mol/L [Bu_4N]-[BAr$'_4$]/PhF is irreversible at –2.06 V vs. $FeCp_2^{+/0}$ at a scan rate of 0.5 V/s. Treatment of [**W**(NH_3)][BAr$'_4$] with triethylamine and [$FeCp_2$][PF_6] in C_6D_6, followed by $LiN(SiMe_3)_2$, yielded **W**≡N. Treatment of [**W**(NH_3)][BAr$'_4$] with $LiBHEt_3$ (1 mol/L in THF) results in formation of **W**H, which is converted to **W**H_3 upon exposure to an atmosphere of H_2. Attempts to prepare **W**N=NH by treating **W**N_2 with [2,6-LutH][BAr$'_4$] and $CoCp_2$ yielded only [**W**=NNH_2][BAr$'_4$]. [**W**=NNH_2][BAr$'_4$] is reduced to **W**=NNH_2 by $CoCp_2^*$, but this species disproportionates to yield **W**N=NH, **W**≡N, and ammonia. Reduction of [**W**(NH_3)][BAr$'_4$] with $CoCp_2^*$ does not yield any observable **W**(NH_3). Attempted catalytic reduction of dinitrogen using **W**N_2 as the catalyst under conditions identical or similar to those employed for catalytic reduction of dinitrogen by **Mo**N_2 and related Mo complexes failed. Single crystal X-ray studies were carried out on **W**-N=NK, **W**N_2, **W**-N=NH, [**W**=NNH_2][BAr$'_4$], and [**W**(NH_3)][BAr$'_4$].

Key words: dinitrogen, reduction, tungsten, ammonia.

Résumé : Le complexe [$HIPTN_3N$]WCl (**W**Cl) peut facilement être synthétisé par l'addition de H_3[$HIPTN_3N$] à du WCl_4(DME), suivie d'une additon de $LiN(SiMe_3)_2$ ([$HIPTN_3N$]$^{3-}$ = [(HIPTNCH$_2$CH$_2$)$_3$N]$^{3-}$ dans lequel HIPT = 3,5-(2,4,6-*i*-Pr$_3$C$_6$H$_2$)$_2$C$_6$H$_3$ = HexaIsoPropylTerphényle). La réduction de **W**Cl par du KC_8, dans du benzène, sous atmosphère d'azote, conduit à la formation de **W**N=NK. Sous l'action du $ZnCl_2$ dans du THF, le **W**N=NK s'oxyde facilement pour conduire à la formation de zinc métallique et de **W**N_2. Dans un électrolyte à 0,1 mol/L de [Bu_4N][BAr$'_4$]/PhF (Ar′ = 3,5-(CF$_3$)$_2$C$_6$H$_3$), la réduction du **W**N_2 en [**W**N_2]$^-$ est réversible à –2,27 V vs. $FeCp_2^{+/0}$ alors que l'oxydation du [**W**N_2] en [**W**N_2]$^+$ est aussi réversible à –0,66 V. La protonation du **W**N=NK par le [Et_3NH][OTf], dans le benzène, conduit à la formation de **W**N=NH, avec un rendement pratiquement quantitatif. La protonation du **W**N=NH au niveau du N_β avec du [H(OEt)$_2$][BAr$'_4$], dans l'éther, conduit à la formation de [**W**=NNH_2][BAr$'_4$] avec un rendement quantitatif. La réduction électrochimique du [**W**=NNH_2][BAr$'_4$] dans du [Bu_4N][BAr$'_4$]/PhF à 0,1 mol/L est irréversible à des vitesses de balayage allant jusqu'à 1 V/s. L'addition de NaBAr$'_4$ et de NH_3 au **W**Cl dans du PhF conduit à la formation de [**W**(NH_3)][BAr$'_4$]. La réduction électrochimique du [**W**(NH_3)][BAr$'_4$] dans du [Bu_4N][BAr$'_4$]/PhF à 0,1 mol/L est irréversible à –2,06 V vs. $FeCp_2^{+/0}$, à une vitesse de balayage de 0,5 V/s. Le traitement du [**W**(NH_3)][BAr$'_4$] par de la triéthylamine et du [$FeCp_2$][PF_6] dans du C_6D_6, suivi de $LiN(SiMe_3)_2$ conduit à la formation de **W**≡N. Le traitement de [**W**(NH_3)][BAr$'_4$] par du $LiBHEt_3$ (1 mol/L dans du THF) conduit à la formation de **W**H qui peut être transformé en **W**H_3 par exposition à un atmosphère de H_2. Des essais en vue de préparer le **W**N=NH par traitement du **W**N_2 avec du [2,6-LutH][BAr$'_4$] et du $CoCp_2$ ne fournissent que du [**W**=NNH_2][BAr$'_4$]. Sous l'influence du $CoCp_2^*$, le [**W**=NNH_2]-[BAr$'_4$] est réduit en **W**=NNH_2, mais cette espèce subit une réaction de dismutation conduisant à la formation de **W**N=NH, de **W**≡N et d'ammoniac. La réduction du [**W**(NH_3)][BAr$'_4$] par le $CoCp_2^*$ ne fournit aucune trace de **W**(NH_3). Des essais en vue d'effectuer la réduction du diazote en utilisant du **W**N_2 comme catalyseur, dans des

Received 11 August 2004. Published on the NRC Research Press Web site at http://canjchem.nrc.ca on 30 March 2005.

D.V. Yandulov[1] and R.R. Schrock.[2] Department of Chemistry, Massachusetts Institute of Technology, Cambridge, MA 02139, USA.

[1]Present address: Department of Chemistry, Stanford University, Stanford, CA 94305-5080, USA.
[2]Corresponding author (e-mail: rrs@mit.edu).

 doi: 10.1139/V05-013 © 2005 NRC Canada

conditions identiques ou semblables à celles utilisées pour la réduction catalytique du diazote par le **Mo**N_2 et les complexes apparentés du molybdène n'ont pas donné les résultats escomptés. Des études de diffraction des rayons X sur un cristal unique ont été effectuées sur le **W**-N=NK, le **W**N_2, le **W**-N=NH, le [**W**=NNH_2][BAr'_4] et le [**W**(NH_3)][BAr'_4].

Mots clés : diazote, réduction, tungstène, ammoniac.

[Traduit par la Rédaction]

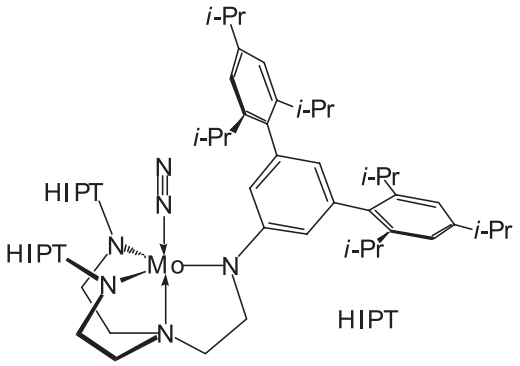
Introduction

Discovery of the first dinitrogen complex of a transition metal, $[Ru(NH_3)_5(N_2)]^{2+}$, in 1965 (1) provided support for the proposal that dinitrogen might be reduced to ammonia at a molybdenum center in nitrogenase (only the FeMo nitrogenase was known at the time (2–4)). As more and more types of transition-metal-catalyzed reactions were discovered in the following decades, scientists became optimistic that catalysts would be discovered for the reduction of dinitrogen to ammonia, or for the combination of dinitrogen with elements other than hydrogen (5–16). Unfortunately, although hundreds of man years have been directed toward this goal in the last 40 years, and although hundreds of dinitrogen complexes of all transition metals in groups 4 through 10 (if we include those detected at low temperature in matrices) are now known, progress has been relatively slow.

Chatt, a pioneer, along with Hidai, in dinitrogen chemistry involving W(0) and Mo(0) phosphine complexes (5–7, 12, 14) believed that dinitrogen could be reduced to ammonia at a single metal center through end-on binding of dinitrogen, and was the first to show that up to 2 equiv. of ammonia per metal could be formed from M(0) dinitrogen complexes (M = Mo or W) upon addition of protons, the six electrons being provided by the metal (5). If dinitrogen could be reduced to ammonia catalytically through the addition of six external protons and six external electrons, and if a distinct intermediate were formed upon addition of each proton and electron, then 12 intermediates could be imagined, or a total of 14 if one includes a dinitrogen complex and a complex that contains no nitrogen or nitrogen-derived ligand. Although examples of almost all of the proposed intermediates for reduction of dinitrogen at a single Mo or W center in a "Chatt cycle" have been isolated, the ligand environment (L_x) of the metal has varied from compound to compound, and no catalytic reaction to give ammonia was ever achieved (see, however, the synthesis of silylamines catalytically (17)). Significant progress has been made toward utilizing atmospheric dinitrogen to make organic molecules (6, 7, 18–26). One catalytic reduction is known in which dinitrogen is reduced to a mixture of hydrazine (largely) and ammonia (9, 27, 28). This system requires molybdenum, is catalytic with respect to molybdenum, produces >90% hydrazine, and takes place in methanol in the presence of $Mg(OH)_2$ and a strong reducing agent (e.g., Na amalgam). Unfortunately, few details concerning the mechanism of this intriguing reaction have been established. In this context, it should be noted that ammonia can be formed from hydrazine via disproportionation (to dinitrogen and ammonia) in the presence of transition metals. In fact, $[Ru(NH_3)_5(N_2)]^{2+}$ was first prepared by treating Ru salts with hydrazine (1).

We have been interested in dinitrogen chemistry of early metals in relatively high oxidation states for more than two decades (29). Approximately 4 years ago, we began to explore the chemistry of Mo complexes that contain a triamidoamine ($[(ArNCH_2CH_2)_3N]^{3-}$ = $[ArN_3N]^{3-}$, Ar = aryl) ligand (30, 31). To prevent formation of what we believe to be relatively stable and unreactive bimetallic [ArN_3N]Mo-N=N-Mo[ArN_3N] complexes, maximize steric protection of a metal coordination site in a monometallic species, and provide increased solubility in nonpolar solvents, we synthesized species that contain a $[HIPTN_3N]^{3-}$ ligand, where HIPT = 3,5-(2,4,6-*i*-$Pr_3C_6H_2)_2C_6H_3$ (HexaIsoPropylTerphenyl, see Fig. 1) (32, 33). Starting with **Mo**Cl (**Mo** = [$HIPTN_3N$]Mo), we showed that we could isolate and characterize many intermediates in a hypothetical Chatt-like reduction of dinitrogen, all of which contain the same $[HIPTN_3N]^{3-}$ supporting ligand (Fig. 2). These intermediates include paramagnetic **Mo**(N_2) (**1**), diamagnetic [**Mo**(N_2)]$^-$ (**2**), diamagnetic **Mo**-N=N-H (**3**), diamagnetic {**Mo**=N-NH_2}{BAr'_4} (**4**; Ar′ = 3,5-$(CF_3)_2C_6H_3$), diamagnetic Mo≡N (**7**), diamagnetic {**Mo**=NH}{BAr'_4} (**8**), paramagnetic {**Mo**(NH_3)}{BAr'_4} (**12**), and paramagnetic **Mo**(NH_3) (**13**). Extensive ^{15}N labeling studies, NMR studies, and X-ray studies (of **1**, **2** (as two different Mg derivatives), **7**, and **12** (33), and **3**, **4**, **8**, and **13** (34)) all reveal a trigonal pocket in which N_2 or its reduced products are protected to a dramatic degree by three 3,5-(2,4,6-*i*-$Pr_3C_6H_2)_2C_6H_3$ (HIPT) rings clustered around it. Compounds **5**, **6**, **10**, and **14** (Fig. 2) have not yet been observed. The oxidation state of the metal varies between Mo(III) and Mo(VI) in the species as they are drawn in Fig. 2. No other unambiguous example of one of these complexes (**3**) is known, presumably either because in other systems bimolecular processes that involve H radical or proton transfer result in facile decomposition, or the synthetic methods are incompatible with the ligands that are present. Steric protection of the nitrogen entities within the pocket provided by the bulky HIPT groups are believed to be an important reason why several of the most unusual species can be prepared.

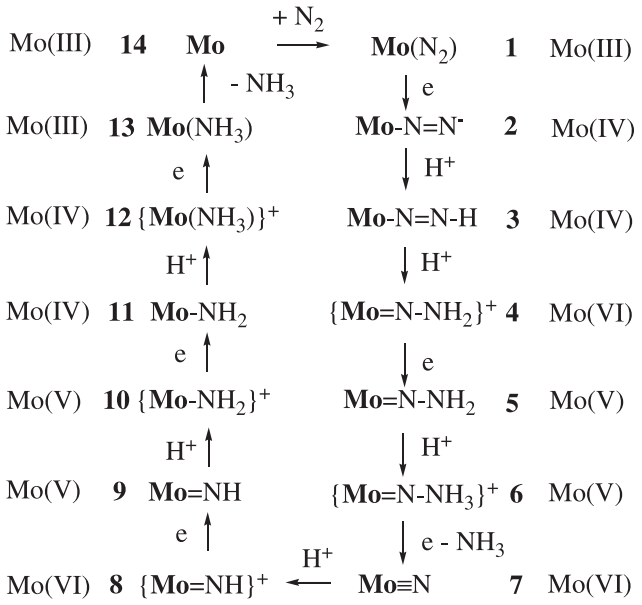
Fig. 1. A drawing of [$HIPTN_3N$]Mo(N_2) = **Mo**N_2.



1

© 2005 NRC Canada

Fig. 2. Proposed intermediates in the reduction of dinitrogen at a [HIPTN$_3$N]Mo (**Mo**) center through the step-wise addition of protons and electrons.



We then showed that it is possible in fact to reduce dinitrogen catalytically in heptane using {2,6-lutidinium}{BAr$'_4$} as the proton source and decamethylchromocene as the electron source (35). The results of 16 runs using four different Mo derivatives (**1**, **3**, **7**, or **12**) revealed that ~8 equiv. of ammonia are formed with an efficiency of 63%–66% based on reducing equivalents available. A run employing **Mo**(^{15}N^{15}NH) under ^{15}N$_2$ yielded entirely ^{15}N-labeled ammonia. We assume at this stage that any equivalents of reducing agent that are not consumed in making ammonia are consumed to form hydrogen, and we now know that no hydrazine is formed.[3] The fact that compounds that contain hexamethylterphenyl or hexa-*tert*-butylterphenyl variations of the [HIPTN$_3$N]$^{3-}$ ligand are relatively inefficient catalysts for catalytic reduction of dinitrogen to ammonia (37) suggests that the catalytic reaction is extremely finely balanced and that perhaps most or all of the intermediates shown in Fig. 2 are actually involved. All are likely to be equilibria with exception of the actual N—N bond cleavage reaction (**Mo**=N-NH$_3^+$ + e → **Mo**≡N + NH$_3$).

It has been known for some time that certain bacteria grown in the presence of tungsten will produce a "FeW nitrogenase", but that enzyme will not reduce dinitrogen to ammonia (2, 3, 38). Therefore, we became interested in preparing some tungsten analogs of the [HIPTN$_3$N]Mo species shown in Fig. 2, exploring conversion of one to another, and testing at least one of them for catalytic dinitrogen reduction activity. We report this work here.

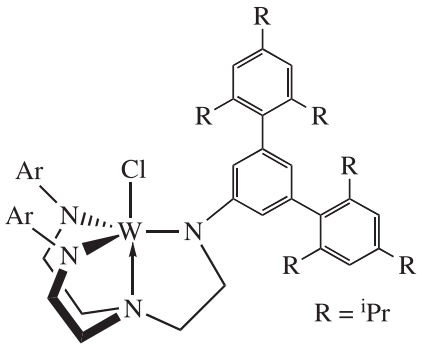
Results

Synthesis of WCl and diazenido species

The starting material for this chemistry ([HIPTN$_3$N]WCl (**W**Cl)) can be readily synthesized by a two-step method analogous to that used to prepare [HIPTN$_3$N]MoCl (33) as shown in eq. [1]. The ^{1}H NMR spectrum of high-spin **W**Cl (d^2) contains sharper resonances than does the spectrum of **Mo**Cl; this difference, and the pattern of relative shifts of the corresponding resonances between Mo and W complexes is very similar to that observed previously for a series of related [ArN$_3$N]MCl (M = Mo, W) (30, 39, 40) and [Me$_3$SiN$_3$N]MCl (41–43) complexes. Like **Mo**Cl, **W**Cl is exceedingly air- and moisture sensitive, so the utmost care is required to ensure that solvents are pure, dry, and free of oxygen.

Reduction of **Mo**Cl with magnesium in THF under an atmosphere of dinitrogen led to salts that contain the [**Mo**(N$_2$)]$^-$ anion (33). However, attempts to prepare [**W**(N$_2$)]$^-$ salts in this manner were not successful; **W**Cl was slowly converted into a complex mixture of unidentified products. Reduction of **W**Cl is markedly accelerated when potassium graphite (KC$_8$) is employed as the reductant in THF or DME, but a complex mixture of products is still formed. However, when **W**Cl is treated with KC$_8$ in benzene under dinitrogen, clean and nearly quantitative conversion of **W**Cl to diamagnetic **W**-N=NK takes place over a period of 1 to 2 days at room temperature (eq. [2]). No intermediates could be detected by ^{1}H NMR when this reaction was performed in C$_6$D$_6$. Deep red **W**-N=NK was isolated in good yield and was fully characterized. Since **W**-N=NK can be dissolved in THF without decomposition (vide infra), failure of the reductions in THF and DME must be attributed to a some side reaction or reactions prior to binding of dinitrogen to the metal, presumably at the W(III) stage. **W**N=NK is readily soluble in aliphatic

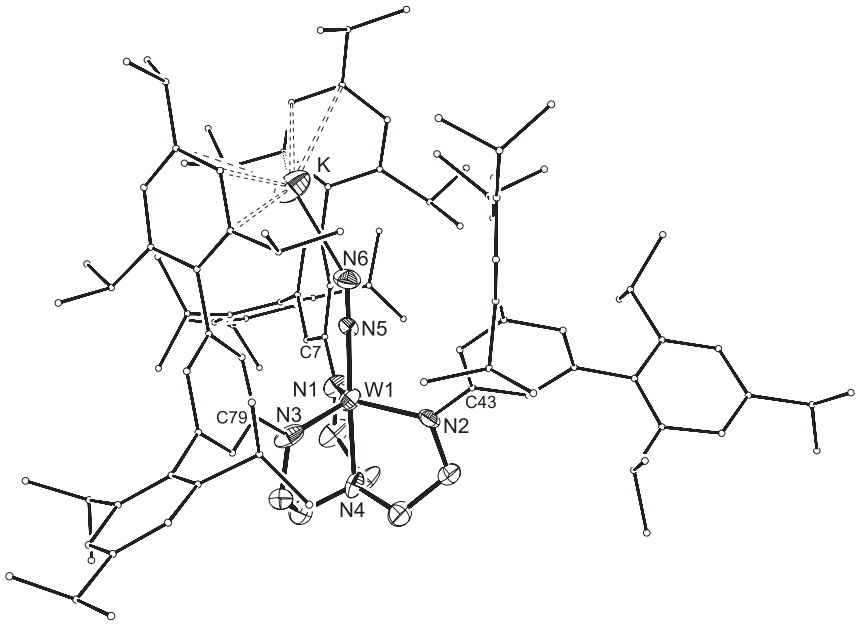
[1] WCl$_4$(DME) —(1. H$_3$[HIPTN$_3$N], C$_6$H$_6$, 2 h; 2. 3.1 LiN(SiMe$_3$)$_2$, 2 h)→ **W**Cl

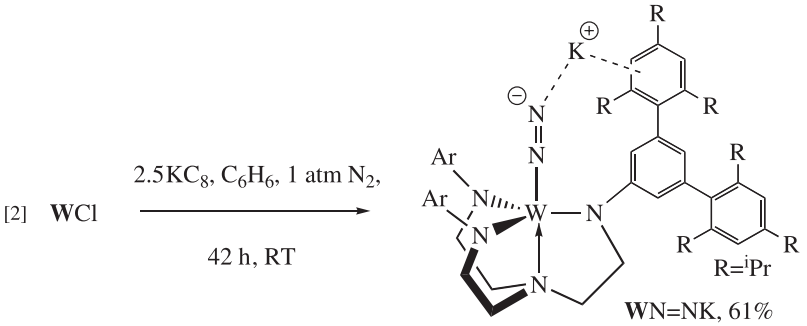


[3] W. Weare. Unpublished results.

© 2005 NRC Canada

Fig. 3. Thermal ellipsoid drawing of **W**N=NK (50% probability level, hydrogen atoms omitted).





solvents and can be recrystallized without change from pentane.

The structure of **W**-N=NK, as determined through a single crystal X-ray study, is shown in Fig. 3 (see also Table 1 for crystal data and Table 2 for selected M—N and N—N bond distances and angles in W and Mo analogs, along with selected IR and NMR data. A full set of X-ray data is available as supporting information.[4] The potassium ion is 2.536(7) Å from N6, the β nitrogen in the unsubstituted diazenido ligand, and is supported through six interactions with aryl carbon atoms in two Trip (2,4,6-*i*-$Pr_3C_6H_2$) aromatic rings of two HIPT substituents. The potassium ion resides 3.229 and 3.301 Å from the ring centroids, and all K···H contacts are >2.92 Å. Interaction between the potassium and the aromatic rings is not symmetric, with K···C distances spanning a range of 0.52 Å for each ring. The presence of the potassium ion has no noticeable effect on the C—C bond distances in the two aryl rings with which it interacts. Understandably, the orientations of the three HIPT groups are significantly different, with one HIPT group in contact with K being rotated by only 10° out of the plane of the amide nitrogen (N1), while the other two HIPT groups are rotated by an average of 28.3° outside of the plane of the amide nitrogen to which they are attached. "Encapsulation" of the K ion between two aryl rings accounts for the high solubility of **W**-N=NK in aliphatic solvents (binding of sodium or potassium ions to aryl rings in high oxidation state amido complexes has considerable precedent in the literature (44–47)). The N—N (1.220(8) Å) and W—N (1.849(7) Å) bond distances are consistent with a considerably greater degree of reduction of the N_2 unit in **W**-N=NK relative to that in **Mo**-N=NMgBr$(THF)_3$ (1.156(8) and 1.863(7) Å, respectively) (33). Greater backbonding from the tungsten center in **W**-N=NK (vs. the molybdenum center in **Mo**-N=NMgCl$(THF)_3$ (33)) is also evident from the relative values for ν_{NN} in the two species (1745 cm^{-1} (W) and 1812 cm^{-1} (Mo), respectively, in benzene). The W-N_α-N_β angle is essentially linear (177.3(6)°), as expected.

[4] Supplementary data may be purchased from the Directory of Unpublished Data, Document Delivery, CISTI, National Research Council Canada, Ottawa, ON K1A 0S2, Canada (http://cisti-icist.nrc-cnrc.gc.ca/irm/unpub_e.shtml for information on ordering electronically). CCDC 261864–261868 contain the crystallographic data for this manuscript. These data can be obtained, free of charge, via ww.ccdc.cam.ac.uk/conts/retrieving.html (or from the Cambridge Crystallographic Data Centre, 12 Union Road, Cambridge CB2 1EZ, U.K.; fax +44 1223 336033; or deposit@ccdc.cam.ac.uk).

© 2005 NRC Canada

Table 1. Crystal data and structure refinement for [HIPTN$_3$N]W-N=NK, [HIPTN$_3$N]WN$_2$, [HIPTN$_3$N]W-N=NH, {[HIPTN$_3$N]W=N-NH$_2$}[BAr$'_4$], and {[HIPTN$_3$N]W(NH$_3$)}[BAr$'_4$].[a]

	W-N=NK	**W**N$_2$	**W**-N=NH	{**W**-N=NH$_2$}[BAr$'_4$]	{**W**(NH$_3$)}[BAr$'_4$]
Empirical formula	$C_{114}H_{159}KN_6W$	$C_{114}H_{159}N_6W$	$C_{114}H_{160}N_6W$	$C_{146}H_{173}BF_{24}N_6W$	$C_{146}H_{174}BF_{24}N_5W$
Formula weight	1 836.42	1 797.32	1 798.33	2 662.56	2649.56
Crystal system	Monoclinic	Monoclinic	Triclinic	Triclinic	Triclinic
Space group	*P*2(1)/*n*	*Cc*	$P\bar{1}$	$P\bar{1}$	$P\bar{1}$
a (Å)	18.297(4)	16.0231(9)	18.2377(14)	15.7795(10)	15.8411(9)
b (Å)	40.166(9)	40.125(2)	20.1004(15)	20.6647(14)	20.5894(11)
c (Å)	19.528(4)	17.9933(10)	37.763(3)	26.2549(17)	26.3012(14)
α (°)	90	90	86.923(2)	85.2740(10)	84.9740(10)
β (°)	117.600(5)	93.8110(10)	85.346(2)	83.6730(10)	83.8560(10)
γ (°)	90	90	75.098(2)	81.9220(10)	81.8820(10)
Volume (Å^3)	12 718(5)	11 542.7(11)	13 326.0(17)	8405.1(10)	8420.7(8)
Z	4	4	4	2	2
Density (calcd., Mg/m^3)	0.959	1.034	0.896	1.052	1.045
Absorption coeff. (mm^{-1})	0.981	1.044	0.904	0.755	0.754
F(000)	3912	3836	3840	2772	2760
Crystal size (mm^3)	0.20 × 0.18 × 0.07	0.27 × 0.15 × 0.14	0.20 × 0.10 × 0.03	0.21 × 0.14 × 0.12	0.18 × 0.16 × 0.13
θ range (°)	1.01–25.00	1.37–27.00	1.05–25.00	0.78–27.00	0.78–27.00
Index ranges	$-14 \le h \le 21$	$-20 \le h \le 20$	$-21 \le h \le 18$	$-18 \le h \le 20$	$-20 \le h \le 20$
	$-47 \le k \le 47$	$-50 \le k \le 51$	$-23 \le k \le 15$	$-26 \le k \le 25$	$-15 \le k \le 26$
	$-21 \le l \le 23$	$-10 \le l \le 22$	$-44 \le l \le 44$	$-33 \le l \le 33$	$-33 \le l \le 33$
Reflections collected	62 953	35 587	69 284	57 366	57 597
Indep. reflections (*R*(int))	22 389 (0.1916)	16 642 (0.0509)	46 258 (0.1000)	36 498 (0.0387)	36 583 (0.0817)
Compl. to θ max (%)	99.9	99.9	98.6	99.4	99.5
Absorption correction	None	None	Empirical[b]	Empirical[b]	None
Data/restraints/param.	22 389/0/1 135	16 642/2/1 126	46 258/21/2 251	36 498/0/1 639	36 583/0/1 631
Goodness-of-fit on F^2	0.938	0.965	0.928	0.961	0.776
Final *R* indices (I > 2σ(*I*))	*R*1 = 0.0733	*R*1 = 0.0434	*R*1 = 0.1026	*R*1 = 0.0611	*R*1 = 0.0612
	*wR*2 = 0.1517	*wR*2 = 0.0984	*wR*2 = 0.2264	*wR*2 = 0.1489	*wR*2 = 0.1147
R indices (all data)	*R*1 = 0.1362	*R*1 = 0.0504	*R*1 = 0.2094	*R*1 = 0.0805	*R*1 = 0.1048
	*wR*2 = 0.1732	*wR*2 = 0.1004	*wR*2 = 0.2632	*wR*2 = 0.1577	*wR*2 = 0.1235
Peak and hole (e Å^{-3})	2.872 and –1.777	1.765 and –1.530	1.295 and –1.619	2.172 and –1.566	1.244 and –1.090

[a]In all cases the temperature = 193(2) K, the wavelength = 0.710 73 Å, and the refinement method full-matrix least-squares on F^2.
[b]Empirical absorption correction was applied using the SADABS v2.10 program (36).

Table 2. A comparison of structural and spectroscopic properties of selected [HIPTN$_3$N]W and [HIPTN$_3$N]Mo complexes.[a]

Compound property	**Mo**N$_2$	**W**N$_2$	**W**N=NK	**Mo**N=NH	**W**N=NH	**Mo**=NNH$_2^{+b}$	**W**=NNH$_2^{+b}$
M-N$_\alpha$ (Å)	1.963(5)	1.945(6)	1.849(7)	1.810(7)	1.732(9)	1.737(3)	1.745(3)
N$_\alpha$-N$_\beta$ (Å)	1.061(7)	1.132(8)	1.220(8)	1.25(1)	1.29(1)	1.310(5)	1.315(5)
ν(^{14}N$_\alpha$^{14}N$_\beta$) (cm^{-1})	1990	1888	1745	1587	1542	—	—
ν(^{15}N$_\alpha$^{15}N$_\beta$) (cm^{-1})	1924	1826	1688	1523	1499	—	—
δ(^{15}N$_\alpha$^{15}N$_\beta$) (ppm)	—	—	357, 350	409, 233	394, 229	358, 140	344, 131
^1J(^{15}N$_\beta$^{15}N$_\alpha$, H) (Hz)	—	—	11.2	15.9, 53.6	15.4, 53.1	11.2, 90.5	10.1, 83.6

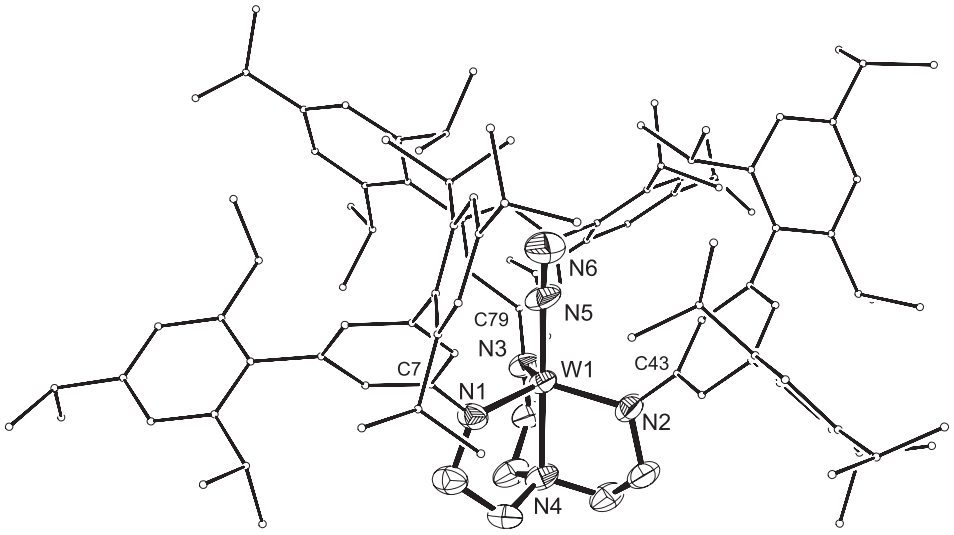
[a]IR and ^{15}N NMR data in C_6D_6 at 22 °C, unless stated otherwise. The Mo compounds can be found in refs. 33 and 34.
[b]Anion = BAr$'_4^-$.

Doubly labeled **W**-^{15}N=^{15}NK reveals sharp doublet resonances for ^{15}N$_\alpha$ (at 357 ppm) and ^{15}N$_\beta$ (at 350 ppm) in the ^{15}N NMR spectrum in C_6D_6 at room temperature. The ^{15}N$_\alpha$ and ^{15}N$_\beta$ resonances in **W**-^{15}N=^{15}NK are relatively close together, yet fall well within the range typical for compounds of this general type (48, 49). The ^{1}H NMR spectrum of **W**-N=NK in C_6D_6 at room temperature features slightly broadened resonances, yet is otherwise consistent with a C_{3v}-symmetric structure. Apparently the interactions between the potassium ion and the aryl rings are weak enough so that intramolecular ligand fluxionality in **W**-N=NK, including rotation of the HIPT rings around the N—C$_{ipso}$ bonds, is not hindered significantly at room temperature.

Treatment of a C_6D_6 solution of **W**-N=NK with Bu$_4$NCl results in a rapid color change from maroon-red to dark green. Both IR and ^{1}H NMR spectra of the green solution show complete conversion of **W**-N=NK to a single diamagnetic product with a ν_{NN} frequency shifted to higher energy

© 2005 NRC Canada

Fig. 4. Thermal ellipsoid drawing of $\mathbf{W}N_2$ (50% probability level, hydrogen atoms omitted).



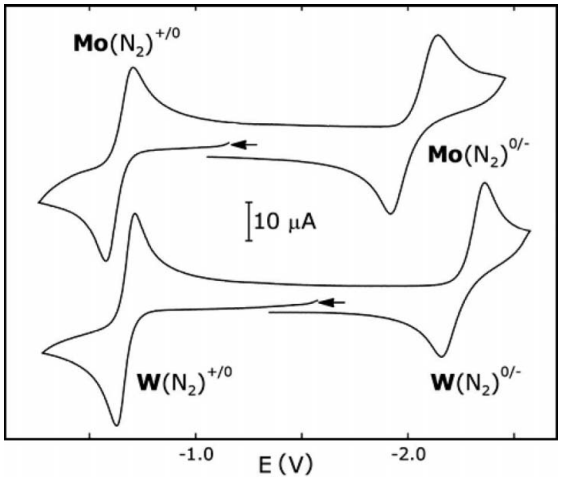
by 56 cm^{-1} from what it is in **W**-N=NK. These observations are analogous to those made for related **Mo** diazenides (33) and indicate formation of a species in which there is essentially no interaction between the cation and the β nitrogen, i.e., formation of $[\mathbf{W}\text{-}N{=}N]^-$. However, all attempts to crystallize [**W**-N=N][Bu_4N] (e.g., by precipitation with pentane) have failed. This compound appears to decompose to yield two major pentane-soluble diamagnetic tungsten complexes and Bu_3N. We speculate that part of the decomposition consists of a reaction between $[\mathbf{W}N_2]^-$ and Bu_4N^+ to yield **W**-N=NBu and Bu_3N. In contrast, [**Mo**-N=N][Bu_4N] can be isolated and is stable at room temperature (33). A greater nucleophilicity of $[\mathbf{W}N_2]^-$ compared to $[\mathbf{Mo}N_2]^-$ at N_β would be consistent with the observed greater degree of backbonding from tungsten to the N_2 unit and would not be surprising.

Synthesis of a terminal dinitrogen complex of W(III)

Like various $\{\mathbf{Mo}\text{-}N{=}N\}^-$ salts (33), **W**N=NK is readily oxidized in THF by $ZnCl_2$ to yield zinc metal and the neutral dinitrogen complex, $\mathbf{W}N_2$, essentially quantitatively. The $\mathbf{W}N_2$ complex was isolated as an orange solid in 53% yield starting from **W**Cl and has been fully characterized. The ^1H NMR spectrum of $\mathbf{W}N_2$ in C_6D_6 resembles that of the low-spin d^3 $\mathbf{Mo}N_2$ analog (33), although the ligand backbone resonances of the **W** complex are broader and shifted with respect to those for $\mathbf{Mo}N_2$ (at 35, –11, and –23 ppm for $\mathbf{W}N_2$ and at 23 (NCH_2), –5 (4,6-*H*), and –34 (NCH_2) ppm in $\mathbf{Mo}N_2$). $\mathbf{W}N_2$ is the only known terminal dinitrogen complex of tungsten in which a triamido/amine ligand is present and the only one of W(III) to our knowledge.

A single crystal X-ray study of $\mathbf{W}N_2$ (Fig. 4) shows it to have a structure analogous to that of $\mathbf{Mo}N_2$ (33) with an N—N bond distance of 1.132(8) Å (cf. 1.098 Å in free N_2 and 1.061(7) Å in $\mathbf{Mo}N_2$). The observed "shorter" N—N bond length in $\mathbf{Mo}N_2$ than in free dinitrogen is believed to be a consequence of a slight "libration" of the bound dinitrogen about the center of the N—N bond, which would make the N—N bond appear slightly shorter than it actually is (34). The actual N—N bond distance in $\mathbf{W}N_2$ therefore actually also could be somewhat longer than what is observed, although one might expect the degree of this type of libration of a bound dinitrogen to decrease as backbonding to dinitrogen increases. There is clearly a greater degree of backbonding to N_2 in $\mathbf{W}N_2$ than in $\mathbf{Mo}N_2$ also according to ν(N-N) frequencies, i.e., the value for ν(N-N) is nearly 100 cm^{-1} lower in $\mathbf{W}N_2$ (1888 cm^{-1}) than in $\mathbf{Mo}N_2$ (1990 cm^{-1}). All other structural details are normal for $[HIPTN_3N]^{3-}$ complexes (see supporting information).[4]

Fig. 5. Electrochemical behavior of $\mathbf{M}N_2$ (**M** = **Mo** or **W**) in 0.1 mol/L [Bu_4N][BAr'_4]/PhF, recorded at a glassy carbon electrode (3 mm diam.) at a scan rate of 500 mV/s. The potential scale is referenced to $FeCp_2^{+/0}$.



Electrochemical reduction of $\mathbf{W}N_2$ to $[\mathbf{W}N_2]^-$ is reversible and takes place at –2.27 V vs. $FeCp_2^{+/0}$ in 0.1 mol/L [Bu_4N][BAr'_4]/PhF electrolyte (Fig. 5) (the advantages of $[Bu_4N]^+$ salts of relatively unreactive and weakly coordinating anions as electrolytes in polar, but relatively unreactive solvents such as fluorobenzene, were demonstrated more than 10 years ago (50), and have been explored more systematically by Geiger and co-workers in the last several years (51–55)). The $\mathbf{W}N_2^{0/-}$ potential is 260 mV more negative than the corresponding $E^{\circ\prime}(\mathbf{Mo}N_2^{0/-})$ value (34), consistent with tungsten being more difficult to reduce than

© 2005 NRC Canada

molybdenum, as expected. The tungsten dinitrogen complex also undergoes a reversible electrochemical oxidation, but at the *same* potential as the molybdenum dinitrogen complex (–0.66 V, Fig. 5). The similarity in the $\mathbf{M}N_2^{+/0}$ potentials for Mo and W can be ascribed to an effective "leveling" of the HOMO energies in the two $\mathbf{M}N_2$ complexes as a consequence of increased π donation from the metal to N_2 in $\mathbf{W}N_2$ ($\Delta\nu$(N-N) = 102 cm^{-1}, vide supra). However, the HOMO energies in $[\mathbf{Mo}N_2]^-$ and $[\mathbf{W}N_2]^-$ are not approximately the same, and $[\mathbf{W}N_2]^-$ therefore remains a stronger one-electron reductant than $[\mathbf{Mo}N_2]^-$ by 260 mV under the conditions described.

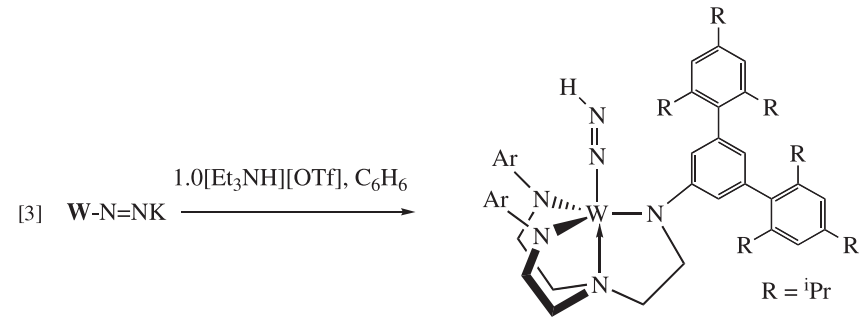
Synthesis of WN=NH and $[W{=}NNH_2][BAr'_4]$

Protonation of **W**N=NK by [Et_3NH][OTf] in benzene is virtually instantaneous and yields **W**N=NH essentially quantitatively (eq. [3]). Diamagnetic **W**N=NH was isolated in 55% yield starting from **W**Cl and has been fully characterized. The N=N*H* resonance appears at 8.43 ppm in the ^{1}H NMR spectrum in C_6D_6, flanked by ^{183}W satellites with $^3J(^{183}W\text{-}H)$ = 17.4 Hz. The IR spectrum in C_6D_6 exhibits a ν(N-N) absorption at 1542 cm^{-1}, a frequency 45 cm^{-1} lower than the corresponding value in **Mo**N=NH (34). The ^{1}H NMR spectrum of doubly labeled **W**-^{15}N=^{15}NH features a doublet of doublets for the ^{15}N=^{15}N*H* resonance ($^1J(^{15}N_\beta\text{-}H)$ = 53.1 Hz, $^2J(^{15}N_\alpha\text{-}H)$ = 6.7 Hz) and two doublets of doublets at 394 ($^{15}N_\alpha$) and 229 ($^{15}N_\beta$) ppm ($^1J(^{15}N\text{-}^{15}N)$ = 15.4 Hz) in the ^{15}N NMR spectrum. These NMR data are similar to those observed for **Mo**N=NH (Table 2). Unlike **Mo**N=NH, however, **W**N=NH is quite stable thermally, suffering only minor decomposition after a solution in C_6D_6 had been heated to 65 °C for 11 days. In contrast, **Mo**N=NH decays in C_6D_6 with a half-life of ~7 h at 61 °C, forming predominantly **Mo**H, when prepared via a method analogous to that shown in eq. [3]. This decomposition was shown to be promoted by traces of acid (33) that are believed to remain after the Mo reaction analogous to that shown in eq. [3].

The X-ray crystal structure of **W**N=NH is shown in Fig. 6. Owing to the presence of two independent molecules in the unit cell and the difficulty of obtaining adequately sized crystals of this compound, the quality of this structure is mediocre (*R*1 = 10%). However, it was possible to refine all non-hydrogen atoms anisotropically. The critical geometrical parameters of the two crystallographically independent molecules are statistically indistinguishable (within 3σ). The average W—N_α (1.732(9) Å) and N_α—N_β (1.286(11) Å) distances are shorter and longer, respectively, than those in **Mo**N=NH (1.810(7) and 1.25(1) Å, Table 2), consistent with a greater degree of backbonding from tungsten into the N=NH group. A greater degree of backbonding from W is also evident from a lower value for ν(N-N) in **W**N=NH (1542 cm^{-1}) than in **Mo**N=NH (1587 cm^{-1}). Each molecule of **W**N=NH is noticeably asymmetric within the $[HIPTN_3N]^{3-}$ ligand. One W—N(amide) distance is slightly shorter than the other two in each molecule, and the HIPT group attached to that amido nitrogen is rotated out of its plane by an average of 68° in the direction *opposite* to the average turn of 28° found for the other two HIPT groups in each molecule. As a result, the three HIPT groups in each molecule do not form a pseudo three-fold symmetric propeller arrangement around the apical pocket similar to what is found in 13 other [HIPTN_3N]Mo and [HIPTN_3N]W derivatives. The hydrazide ligand is bent at both W (N5-W-N4 = 173.1(4)°) and N5 (W-N5-N6 = 173.6(9)°) in the same direction, primarily toward the unique N(amide) (N3A in the molecule shown in Fig. 6). The diazenide hydrogen was not located, but was added and refined in the position shown. It should be noted that N_α-N_β-R angles in diazenido compounds vary, e.g., from 132° in [$(Me_3SiNCH_2CH_2)_2NCH_2CH_2NMe_2$)]-Mo($CH_3$)($N_2$TMS) to 170° in {[$(Me_3SiNCH_2CH_2)_2$N-$CH_2CH_2NMe_2$]Mo-N=N$SiMe_3$}OTf (56). Therefore, we cannot say with any degree of certainty exactly where H_β is located. To our knowledge, **Mo**N=NH (33, 34) and **W**N=NH are the only structurally characterized examples of parent diazenide complexes of any metal.

Protonation of **W**N=NH at N_β with [H$(OEt)_2$][BAr'_4] in ether affords the hydrazido(2–) species $[\mathbf{W}{=}NNH_2][BAr'_4]$ essentially quantitatively (eq. [4]). This W(VI) species can be isolated in good yield as a pale-yellow solid and has been fully characterized. The NNH_2^+ resonance appears at 5.96 ppm in the ^{1}H NMR spectrum in C_6D_6, flanked by barely resolved ^{183}W satellites ($^1J(^{183}W\text{-}H)$ = 6 Hz). Labeled $[\mathbf{W}{=}{}^{15}N^{15}NH_2][BAr'_4]$ features a doublet of doublets for the $^{15}N^{15}NH_2^+$ resonance in the ^{1}H NMR spectrum ($^1J(^{15}N_\beta\text{-}H)$ = 83.6 Hz, $^2J(^{15}N_\alpha\text{-}H)$ = 1.8 Hz) and a doublet at 344 ($^{15}N_\alpha\text{-}^{15}N_\beta H_2^+$) and a triplet of doublets at 131 ppm ($^{15}N_\alpha\text{-}^{15}N_\beta H_2^+$, $J(^{15}N\text{-}^{15}N)$ = 10.1 Hz) in the ^{15}N NMR spectrum. While the spectra of $[\mathbf{W}{=}NNH_2][BAr'_4]$ are generally similar to those of $[\mathbf{Mo}{=}NNH_2][BAr'_4]$, ^{15}N NMR data for $[\mathbf{W}{=}NNH_2][BAr'_4]$ reveal a reduction of $^1J(^{15}N_\beta\text{-}H)$ to 83.6 Hz in $[\mathbf{W}{=}NNH_2][BAr'_4]$ from 90.5 Hz in $[\mathbf{Mo}{=}NNH_2]$-$[BAr'_4]$ (34), consistent with an increased *p* character in the bonding at N_β as a consequence of a greater degree of backbonding to the NNH_2 unit in $[\mathbf{W}{=}NNH_2][BAr'_4]$.

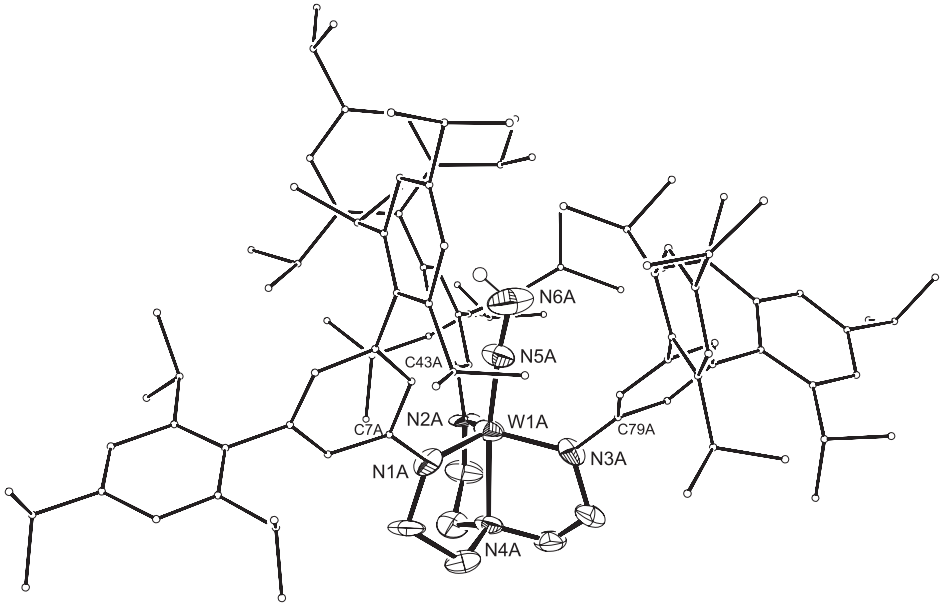
The structure of $[\mathbf{W}{=}NNH_2][BAr'_4]$ (Fig. 7) is similar to other {[HIPTN_3N]M}[BAr'_4] (M = Mo, W) derivatives that have been characterized in an X-ray study. The N_α—N_β distance (1.315(5) Å) is essentially identical to that in



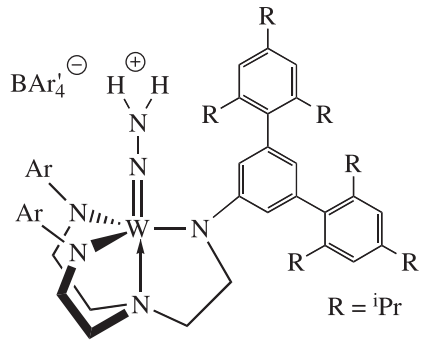
W-N=NH, 55%

© 2005 NRC Canada

Fig. 6. Thermal ellipsoid drawing of **W**-N=NH (50% probability level, selected hydrogen atoms omitted).



[4] **W**-N=NH —1.05[H(OEt$_2$)$_2$][BAr$'_4$], Et$_2$O, -35 °C to RT, 1 h→ [**W**=NNH$_2$][BAr$'_4$], 72%



[**Mo**=NNH$_2$][BAr$'_4$] (1.310(5) Å). Since the N$_\alpha$—N$_\beta$ distance in [**W**=NNH$_2$][BAr$'_4$] is similar to that in **W**N=NH (1.29(1) Å), the amount of N$_\alpha$—N$_\beta$ double bond character must be significant, as one would expect in a M-N-N π system of this type. The NNH$_2^+$ hydrogens were not located, but were refined in calculated positions. Regardless of the particular orientation chosen for their representation, their presence in the model had a slight, but constant, effect on the refined N—N distance.

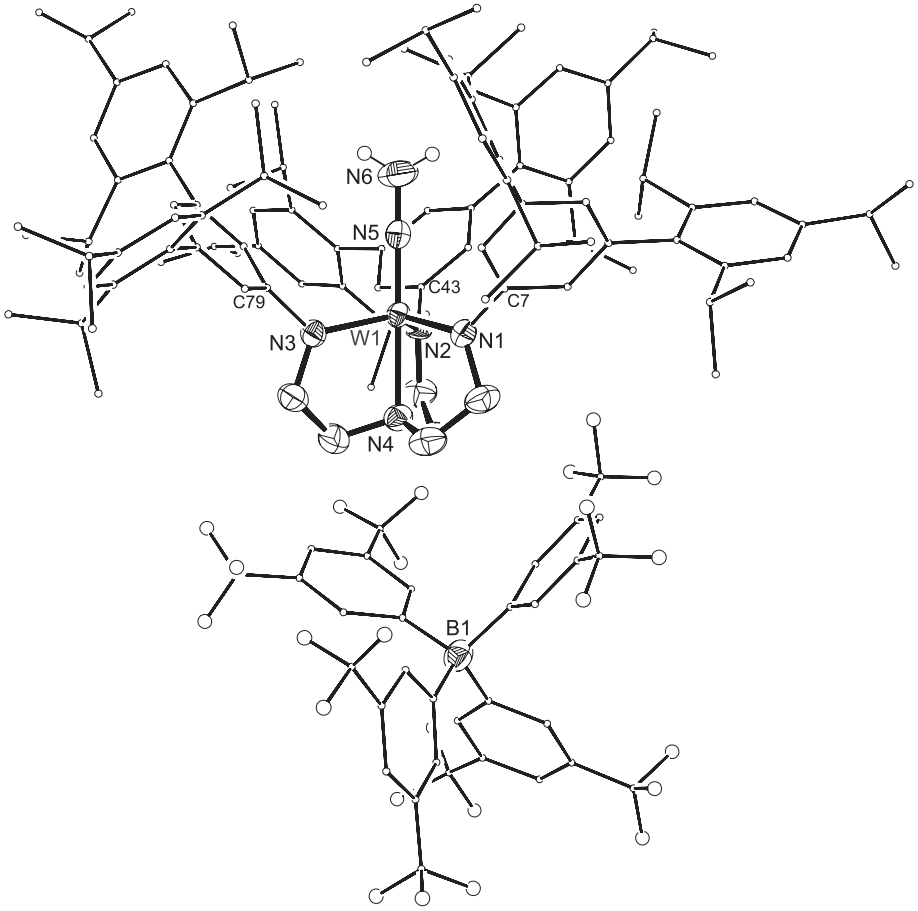
Electrochemical reduction of [**W**=NNH$_2$][BAr$'_4$] in 0.1 mol/L [Bu$_4$N][BAr$'_4$]/PhF at a glassy carbon electrode is irreversible at scan rates of up to 1 V/s and takes place at I_{pc} = –2.2 V vs. FeCp$_2^{+/0}$ (100 mV/s scan rate). The **Mo** analog, [**Mo**=NNH$_2$][BAr$'_4$], undergoes a quasi-reversible reduction at –1.56 V under the same conditions (34), which allows us to estimate the difference between the **Mo**=NNH$_2^{+/0}$ and **W**=NNH$_2^{+/0}$ couples as being 400–500 mV. The magnitude of this difference is considerably greater than that found for [**M**N$_2$]$^{0/-}$ (260 mV) and [**M**N$_2$]$^{+/0}$ (0 mV) potentials (M = Mo or W, vide supra). Apparently π donation of electron density from M into the [NNH$_2$]$^{2-}$ system does not differ substantially for Mo and W, and the **M**=NNH$_2^{+/0}$ potential difference therefore better reflects the difference in the HOMO energy that results from substitution of W for Mo alone. Consistent with this hypothesis, a large difference between Mo and W is also found for the **M**(NH$_3$)$^{+/0}$ potentials (vide infra).

Synthesis of [W(NH$_3$)][BAr$'_4$], its structure, and reactivity

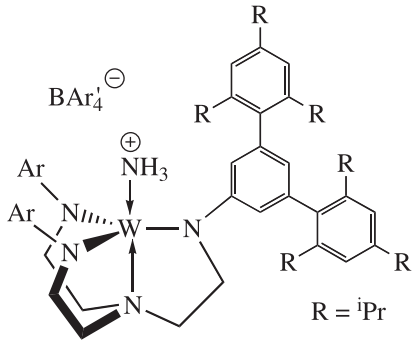
When **W**Cl is treated with NaBAr$'_4$ and NH$_3$ in PhF [**W**(NH$_3$)][BAr$'_4$] is formed nearly quantitatively (eq. [5]). This reactivity mirrors that established for **Mo**Cl (33), except that fluorobenzene had to be used as a solvent because **W**Cl was found to be incompatible with dichloromethane. The ammonia adduct was isolated in good yield and fully characterized. Its ^{1}H NMR spectrum in C$_6$D$_6$ features a pattern of paramagnetically shifted and broadened resonances characteristic of a high-spin d^2 **W** environment in complexes of this general type. The resonances in **W**(NH$_3$)$^+$ are paramagnetically shifted to a greater extent than those of **W**Cl, a phenomenon that was also observed for **Mo**(NH$_3$)$^+$ vs. **Mo**Cl.

© 2005 NRC Canada

Fig. 7. Thermal ellipsoid drawing of [**W**=NNH_2][BAr'_4] (50% probability level, selected hydrogen atoms omitted).



[5] **W**Cl —(2.2$NaBAr'_4$, 4NH_3; PhF, 2 h)→ [**W**(NH_3)][BAr'_4], 87%



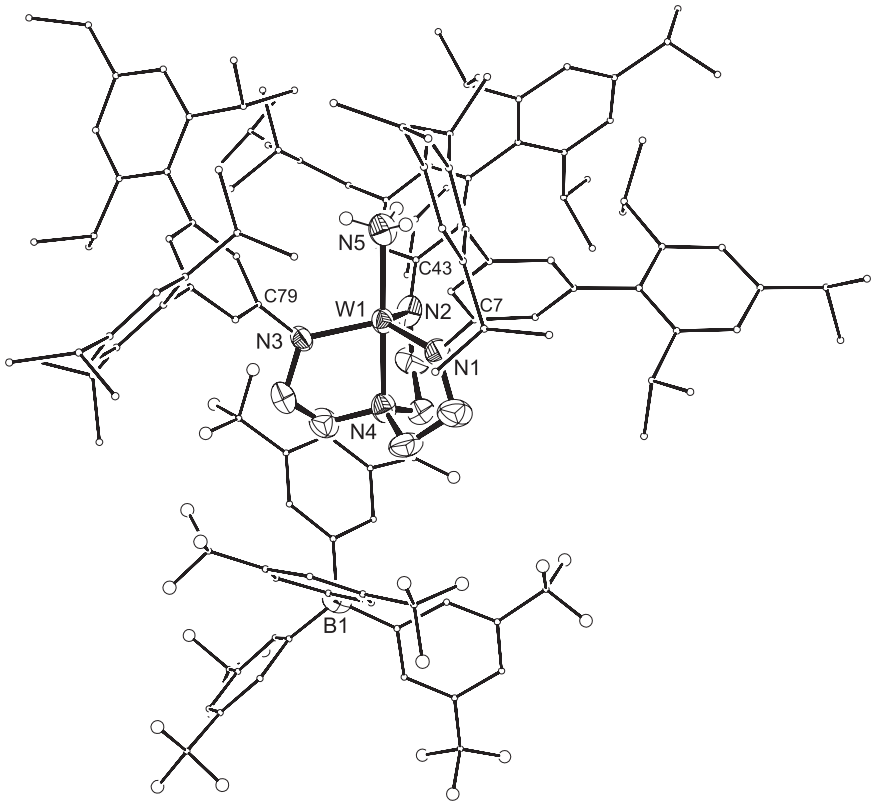
The X-ray crystal structure of [**W**(NH_3)][BAr'_4] (Fig. 8) is essentially identical to that of [**Mo**(NH_3)][BAr'_4] (33). The M—N(ammonia) distances are 2.210(4) Å in [**W**(NH_3)][BAr'_4] vs. 2.24(1) Å in [**Mo**(NH_3)][BAr'_4] (Table 2). The ammonia protons were not located, but are shown in calculated positions.

Electrochemical reduction of [**W**(NH_3)][BAr'_4] in 0.1 mol/L [Bu_4N][BAr'_4]/PhF at a glassy carbon electrode reveals an irreversible wave at a scan rate of 0.5 V/s (Fig. 9). The couple appears to become more reversible at faster scan rates (1 and 2 V/s) at –2.06 V vs. $FeCp_2^{+/0}$, although it cannot be called reversible even at 2 V/s. In contrast, one-electron reduction of [**Mo**(NH_3)][BAr'_4] is fully reversible both in PhF (0.1 mol/L [Bu_4N][BAr'_4]) at a glassy carbon electrode and THF (0.4 mol/L [Bu_4N][PF_6]) at a platinum disk at all scan rates and takes place at $E^{o\prime}$(**Mo**(NH_3)$^{+/0}$) = –1.63 V vs. $FeCp_2^{+/0}$ in PhF (0.1 mol/L [Bu_4N][BAr'_4]). The difference in **M**(NH_3)$^{+/0}$ potentials (M = Mo or W) is thus ~430 mV, similar to the difference between the **Mo**=$NNH_2^{+/0}$ and **W**=$NNH_2^{+/0}$ potentials (vide supra). Chemical reductions of both [**W**=NNH_2][BAr'_4] and [**W**(NH_3)][BAr'_4] are described below.

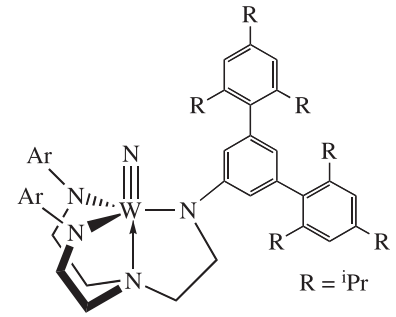
Deprotonation of [**W**(NH_3)]$^+$ with $LiN(SiMe_3)_2$/4TMEDA in C_6D_6 yields a single paramagnetic product, which we pre-

© 2005 NRC Canada

Fig. 8. Thermal ellipsoid drawing of [**W**(NH$_3$)][BAr$'_4$] (50% probability level, selected hydrogen atoms omitted).



[6] [**W**(NH$_3$)][BAr$'_4$] → (1) 2.2[Cp$_2$Fe][PF$_6$], 4Et$_3$N; (2) 3LiN(SiMe$_3$)$_2$, C$_6$D$_6$ → **W**≡N



sume to be (at least initially) **W**(NH$_2$). However, attempts to isolate the product in analytically pure crystalline form so far have failed. Treatment of [**W**(NH$_3$)][BAr$'_4$] with triethylamine and [FeCp$_2$][PF$_6$] in C$_6$D$_6$, followed by LiN(SiMe$_3$)$_2$ yielded **W**≡N essentially quantitatively (eq. [6]). The nitride can be prepared more conveniently via salt metathesis of **W**Cl with 3 equiv. of NaN$_3$ in a mixture of C$_6$H$_6$ and MeCN over a period of 16 h at room temperature (eq. [7]), the method utilized originally in the synthesis of [Me$_3$SiN$_3$N]W≡N (42). The IR spectra of **W**≡N and **Mo**≡N in C$_6$D$_6$ are virtually identical in the 1200–900 cm^{-1} region, with the exception of an absorption at 1012 cm^{-1} in the **Mo**≡N spectrum (ν(Mo-N)) and at 1024 cm^{-1} in the **W**≡N spectrum. Therefore, we assign the 1024 cm^{-1} absorption to the ν(W-N) stretch. As in [Me$_3$SiN$_3$N]M≡N complexes, ν(M-N) is slightly higher for **W**≡N than it is in **Mo**≡N. The ^{15}N NMR spectrum of **W**≡^{15}N shows a resonance for the nitride at 827 ppm (vs. 898 ppm in **Mo**≡^{15}N).

[7] **W**Cl → (3NaN$_3$, C$_6$H$_6$: MeCN, 16 h, RT, 58%) → **W**≡N

Treatment of a C$_6$D$_6$ solution of [**W**(NH$_3$)][BAr$'_4$] with LiBHEt$_3$ (1 mol/L in THF) results in a color change to brown and formation of a largely one paramagnetic species, which is tentatively assigned as the monohydride complex, **W**H, on the basis of reactivity similar to that exhibited by **Mo**H (33). However, a small amount of a diamagnetic product is present initially, which becomes the sole observable species when the reaction mixture is exposed to an atmosphere of H$_2$ for ~10 min (eq. [8]); this diamagnetic species (**W**H$_3$) can be isolated in 42% yield. This compound was identified on the basis of the similarity of its NMR and IR spectra with those of the crystallographically characterized

© 2005 NRC Canada

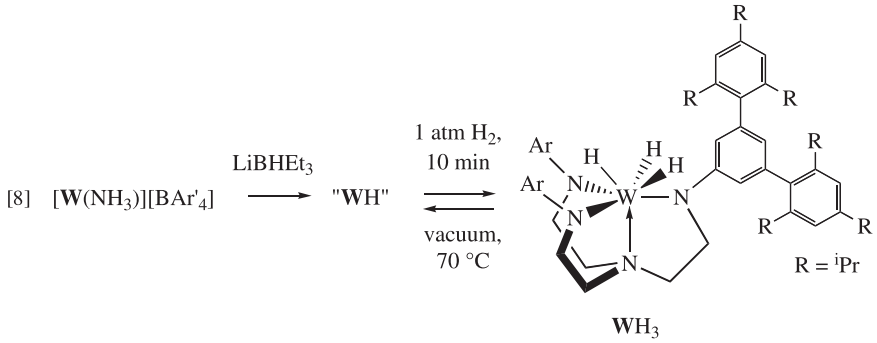
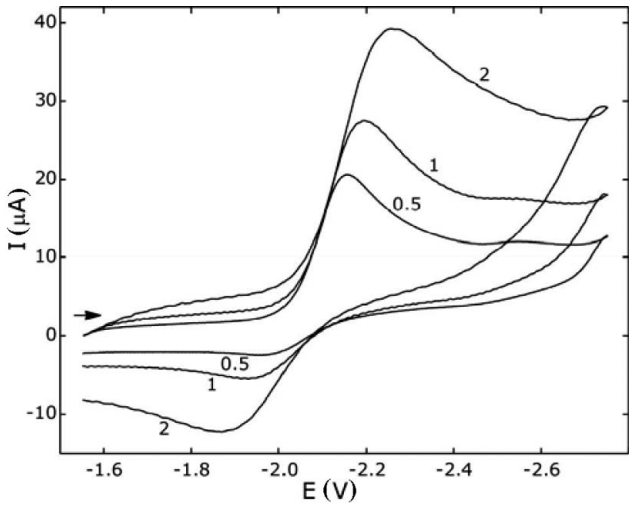


Fig. 9. Electrochemical behavior of $[\mathbf{W}(NH_3)][BAr'_4]$ in 0.1 mol/L $[Bu_4N][BAr'_4]$/PhF, recorded at a glassy carbon electrode (3 mm diam.) at the scan rates shown in V/s. The potential scale is referenced to $FeCp_2^{+/0}$.

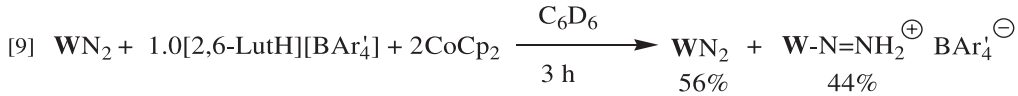


complex, $[Me_3SiN_3N]WH_3$ (57). Like $[Me_3SiN_3N]WH_3$, $\mathbf{W}H_3$ features a low-field resonance of intensity three in its ^1H NMR spectrum in C_6D_6 at 11.99 ppm with $^1J(^{183}W\text{-}H)$ = 24 Hz (cf. 10.01 ppm and 23 Hz in $[Me_3SiN_3N]WH_3$), in addition to characteristic ligand resonances. The IR spectrum of $\mathbf{W}H_3$ in C_6D_6 shows two broad absorptions at 1958 and 1966 cm^{-1} consistent with ν(W-H) stretching modes (cf. 1903 and 1887 cm^{-1} in $[Me_3SiN_3N]WH_3$ in Nujol). However, unlike $[Me_3SiN_3N]WH_3$, $\mathbf{W}H_3$ can be induced to lose H_2, by exposure to a high vacuum at 70 °C to yield a mixture that contains a considerable amount of **W**H after a few hours. This difference in behavior can be attributed to less electron donation by the $[HIPTN_3N]^{3-}$ ligand compared to the $[Me_3SiN_3N]^{3-}$ ligand. It should be noted that what is proposed to be $[HIPTN_3N]MoH_3$ cannot be isolated since it readily loses dihydrogen to form $[HIPTN_3N]MoH$ at room temperature (34).

Reduction of dinitrogen on W with protons and electrons

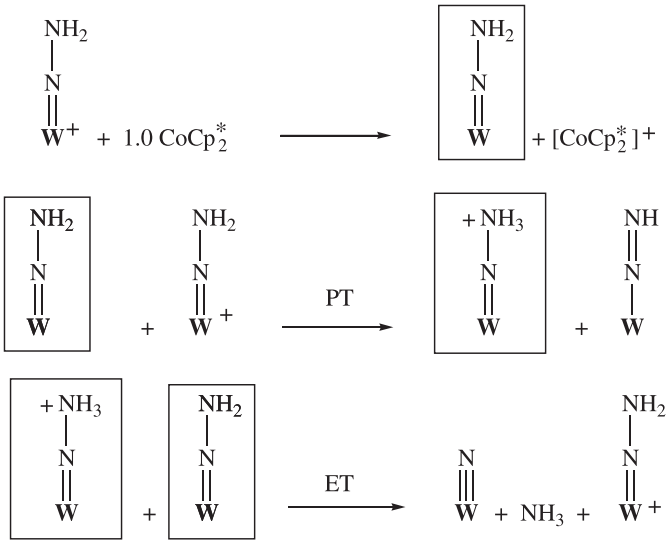
Treatment of $\mathbf{W}N_2$ with 1 equiv. of $[2,6\text{-LutH}][BAr'_4]$ (2,6-Lut = 2,6-lutidine) and 2 equiv. of $CoCp_2$ in C_6D_6 results in a subtle color change, formation of a yellow precipitate of $[CoCp_2][BAr'_4]$, complete consumption of the acid, and conversion of approximately half of the starting $\mathbf{W}N_2$ to $[\mathbf{W}{=}NNH_2][BAr'_4]$ in 3 h at 22 °C (eq. [9]). This mixture remains unchanged over a period of 24 h. **W**N=NH is converted quantitatively into $[\mathbf{W}{=}NNH_2][BAr'_4]$ upon reaction with 1 equiv. of $[2,6\text{-LutH}][BAr'_4]$ in C_6D_6. Therefore, we propose that **W**N=NH is formed in the reduction of $\mathbf{W}N_2$ in the presence of $[2,6\text{-LutH}][BAr'_4]$ and that **W**N=NH then consumes a proton relatively irreversibly to give $[\mathbf{W}{=}NNH_2][BAr'_4]$, thereby limiting consumption of $\mathbf{W}N_2$ when 1 equiv. of acid is present to ~50%. In contrast, the analogous reaction between $\mathbf{Mo}N_2$ and $[2,6\text{-LutH}][BAr'_4]$ and $CoCp_2$ rapidly yields **Mo**N=NH quantitatively (34). $[\mathbf{Mo}{=}NNH_2][BAr'_4]$ is considerably more acidic than $[\mathbf{W}{=}NNH_2][BAr'_4]$, as judged from the fact that treatment of **Mo**N=NH with 1 equiv. of $[2,6\text{-LutH}][BAr'_4]$ in C_6D_6 gives an equilibrium mixture of **Mo**N=NH and $[\mathbf{Mo}{=}NNH_2][BAr'_4]$ (44:56); therefore, conversion of $\mathbf{Mo}N_2$ to **Mo**N=NH can be complete when $\mathbf{Mo}N_2$ is treated with only 1 equiv. of $[2,6\text{-LutH}][BAr'_4]$ and $CoCp_2$. The most important point is that a one-electron reduction–protonation of $\mathbf{W}N_2$ to yield **W**N=NH is feasible, although this process appears to be slower than conversion of $\mathbf{Mo}N_2$ to **Mo**N=NH under analogous conditions.

Isolated $[\mathbf{W}{=}NNH_2][BAr'_4]$ reacts rapidly with 2 equiv. of $CoCp_2^*$ ($E^{\circ\prime}$ = –2.01 V vs. $FeCp_2^{+/0}$ in PhF) in C_6D_6, as indicated by the formation of a yellow precipitate of $[CoCp_2^*][BAr'_4]$. However, instead of the expected one-electron reduced (W(V)) product ($\mathbf{W}{=}NNH_2$), a proton NMR spectrum of the reaction mixture recorded 20 min after mixing $[\mathbf{W}{=}NNH_2][BAr'_4]$ and $CoCp_2^*$ revealed that only **W**N=NH and **W**≡N were present in a 52:48 ratio. After 17 h, the ratio of **W**N=NH to **W**≡N had not changed, but a well-resolved triplet for free ammonia could be observed. This ammonia was collected by vacuum transfer and shown (using the indophenol analytical method) to amount to 0.43 equiv. of the original $[\mathbf{W}{=}NNH_2][BAr'_4]$. Therefore, one-electron reduction of $[\mathbf{W}{=}NNH_2][BAr'_4]$ predominantly results in the net reaction shown in eq. [10]. In fact, this reaction was used to prepare $\mathbf{W}{\equiv}{}^{15}N$ from $[\mathbf{W}{=}{}^{15}N^{15}NH_2][BAr'_4]$. This stoichiometry is consistent with the disproportionation of the initial reduction product, $\mathbf{W}{=}NNH_2$, a W(V) species, into a W(IV) and a W(VI) species, **W**N=NH and **W**≡N, respectively. A plausible sequence of elementary electron- and



© 2005 NRC Canada

Scheme 1. A proposed sequence of reactions that yields the net process shown in eq. [10]. Unobservable intermediates are shown in boxes. The counterion ($BAr'_4{}^-$) is excluded for clarity. PT = proton transfer, ET = electron transfer.



proton-transfer steps that comprises the overall process is proposed in Scheme 1.

[10] $[\mathbf{W}{=}N\text{-}NH_2]BAr'_4 + 1.0CoCp^*_2 \xrightarrow{C_6D_6} 0.5\mathbf{W}\text{-}N{=}NH + 0.5\mathbf{W}{\equiv}N + 0.5\,NH_3 + [CoCp^*_2]BAr'_4$

Initial one-electron reduction of $\mathbf{W}{=}NNH_2^+$ yields as yet unobserved $\mathbf{W}{=}NNH_2$, possibly in a rapid equilibrium. A small amount of $\mathbf{W}{=}NNH_2^+$ then protonates $\mathbf{W}{=}NNH_2$ to yield the proposed hydrazidium(2–) species ($\mathbf{W}{=}NNH_3^+$), while $\mathbf{W}{=}NNH_2^+$ is transformed into **W**N=NH. The hydrazidium(2–) species ($\mathbf{W}{=}NNH_3^+$) then oxidizes $\mathbf{W}{=}NNH_2$ to regenerate $\mathbf{W}{=}NNH_2^+$, and in the process is reduced to form $\mathbf{W}{\equiv}N$ and ammonia. Essentially, the disproportionation of $\mathbf{W}{=}NNH_2$ is catalyzed by $\mathbf{W}{=}NNH_2^+$.

It is possible that the disproportionation shown in Scheme 1 requires some time to proceed to completion and that the initial "**W**(V) = NNH_2" exists in a fast electron-transfer equilibrium with $\mathbf{W}{=}NNH_2^+$ and (or) $CoCp^{*+}_2$, which causes extensive broadening and (or) complete disappearance of the resonances for $\mathbf{W}{=}NNH_2^+$ and $CoCp^{*+}_2$ in the ^{1}H NMR spectrum. A similar situation was encountered in the reversible reduction of{[$HTBTN_3N$]Mo(NH_3)}[BAr'_4] with $CrCp^*_2$ in C_6D_6 (37). However, irreversibility of the electrochemical reduction of $[\mathbf{W}{=}NNH_2][BAr'_4]$ suggests that the sequence of reactions following the initial electron transfer takes place rapidly at 22 °C. We are puzzled by the apparently fast rate of net proton transfer in the absence of conspicuous proton-transfer mediators. However, we note that small amounts of the free ligand, H_3[$HIPTN_3N$], are typically formed in a decomposition reaction, and could easily mediate the proton-transfer step. The actual mechanism of the proton-transfer step remains to be clarified.

Reduction of $[\mathbf{Mo}{=}NNH_2][BAr'_4]$ at room temperature proceeds in a manner closely analogous to that shown in eq. [10] and (it is proposed) Scheme 1 (34). One of the reasons to investigate the chemistry of $[\mathbf{W}{=}NNH_2][BAr'_4]$ was the possibility that $\mathbf{W}{=}NNH_2$ would be more stable than $\mathbf{Mo}{=}NNH_2$ and that $\mathbf{W}{=}NNH_2$, therefore, could at least be observed. Instead, however, we find that $\mathbf{W}{=}NNH_2$ is even less stable than $\mathbf{Mo}{=}NNH_2$. In each case, the high propensity of $\mathbf{M}{=}NNH_2$ to disproportionate can be attributed to a combination of a high Brønsted basicity of N_β in combination with strong reducing properties. We attribute the strong reducing properties to the presence of one of the five electrons in the M-N_α-N_β π system in a π orbital that has a node at N_α; four electrons are in the two perpendicular lowest energy bonding molecular orbitals. This combination of properties makes $\mathbf{M}{=}NNH_2$ susceptible to *both* protonation by its own oxidized form *and* oxidation by its own protonated form, at least in a thermodynamic sense. If both steps are kinetically feasible, then disproportionation proceeds readily, perhaps in part because of the fact that the step in which ammonia is formed (N—N bond cleavage) is almost certainly irreversible. It is important to note that disproportionation of $\mathbf{M}{=}NNH_2$ intermediates has no adverse consequences for overall reduction of dinitrogen to ammonia, since it merely leads to species that are themselves susceptible to further reactions that lead to the formation of ammonia. Disproportionations of d^1 species and related intermolecular proton or electron transfer reactions are likely to complicate the mechanism of ammonia formation depicted in Fig. 2, when all species are in solution.

Attempted conversion of $W(NH_3)^+$ to WN_2, and catalytic reduction of N_2

The results discussed in the previous section show that it is possible to reduce $\mathbf{W}N_2$ to yield ammonia and $\mathbf{W}{\equiv}N$ in the presence of acid and reductant. Since reduction of $\mathbf{Mo}{\equiv}N$ to $\mathbf{Mo}(NH_3)^+$ is a relatively easy transformation in the **Mo** dinitrogen reduction cycle (35), while reduction of $\mathbf{Mo}(NH_3)^+$ to $\mathbf{Mo}(NH_3)$ and transformation of $\mathbf{Mo}(NH_3)$ into $\mathbf{Mo}N_2$ can be observed (34), we examined the feasibility of converting $\mathbf{W}(NH_3)^+$ into $\mathbf{W}N_2$.

Reduction of $[\mathbf{W}(NH_3)][BAr'_4]$ with 2 equiv. of $CoCp^*_2$ in C_6D_6 proceeds to some extent, as judged by the rapid formation of a yellow precipitate of $[CoCp^*_2][BAr'_4]$. However, the ^{1}H NMR spectrum of the resulting solution is unusually featureless, i.e., few resonances beyond isopropyl methyl resonances and some aryl resonances can be observed. Since the ^{1}H NMR spectrum of $\mathbf{Mo}(NH_3)$ is similar to that of other d^3 Mo complexes in this general family, we expected $\mathbf{W}(NH_3)$ to be observable and to have a very similar spectrum to that of $\mathbf{Mo}(NH_3)$.

The mixture of $[\mathbf{W}(NH_3)][BAr'_4]$ and $\mathbf{W}(NH_3)$ remained unchanged for days and also did not change after being exposed to 800 psi (1 psi = 6.894 757 kPa) of N_2 for 48 h. Thermolysis at 60 °C for a day resulted only in minor decomposition and formation of $\mathbf{W}{\equiv}N$ and $\mathbf{W}H_3$. Treatment of $\mathbf{W}N_2$ with ~4 equiv. of NH_3 in C_6D_6 under argon also resulted in no change after 15 days, again in sharp contrast to the behavior in the analogous molybdenum system where an equilibrium between $\mathbf{Mo}(NH_3)$ into $\mathbf{Mo}N_2$ is readily established in a closed system over a period of several hours. Although it has not been possible to transform $\mathbf{W}(NH_3)$ into $\mathbf{W}N_2$, $\mathbf{W}(NH_3)$ appears to be relatively stable, at least as

© 2005 NRC Canada

Table 3. Results of the attempted catalytic reduction of dinitrogen with $\mathbf{W}N_2$.[a]

Reductant	$E^{o\prime}$(THF)[b]	$E^{o\prime}$(PhF)[c]	Acid	pK_a (H_2O)	Equiv. of NH_3[d]
$CrCp^*_2$	–1.47	–1.63	[2,6-LutH][BAr'_4]	6.68	1.31
$CoCp^*_2$	–1.84	–2.01	[2,6-LutH][BAr'_4]	6.68	1.51
$CoCp^*_2$	–1.84	–2.01	[Et_3NH][BAr'_4]	10.67	0.62

[a]Single runs of all experiments were carried out with 5.84 μmol of $\mathbf{W}N_2$, 36 equiv. of the reductant, and 48 equiv. of the acid, under conditions otherwise identical to those previously described (35, 37).
[b]V vs. $FeCp_2^{+/0}$ in 0.4 mol/L [Bu_4N][PF_6].
[c]V vs. $FeCp_2^{+/0}$ in 0.1 mol/L [Bu_4N][BAr'_4].
[d]The maximum possible is 12 equiv. of ammonia (36 electrons available).

generated by reduction of [$\mathbf{W}(NH_3)$][BAr'_4] with $CoCp^*_2$. However, this conclusion is difficult to reconcile with a limited degree of reversibility of the electrochemical reduction of [$\mathbf{W}(NH_3)$][BAr'_4] ([Bu_4N][BAr'_4]/PhF) (Fig. 9). Therefore, the exact nature of the putative "$\mathbf{W}(NH_3)$" remains obscure, and we cannot exclude the possibility that some reaction involving oxidation of W(III) (e.g., intramolecular NH addition) is facile. In any case, it seems likely that $\mathbf{W}(NH_3)$ is not strictly analogous to well-behaved $\mathbf{Mo}(NH_3)$ (34).

Treatment of the mixture containing partly reduced $\mathbf{W}(NH_3)^+$ in C_6D_6 with [Et_3NH][BAr'_4] produced a new paramagnetic species that gave rise to considerable quantities of both $\mathbf{W}(NH_3)^+$ and $\mathbf{W}H_3$ after several days, but no $\mathbf{W}N_2$ or products of its reduction. The net reaction of $\mathbf{W}(NH_3)^+$ with a reductant and an acid thus results primarily in reduction of protons (presumably) and formation (ultimately) of $\mathbf{W}H_3$ (eq. [11]), but dinitrogen is not bound or reduced.

$$[11]\quad [\mathbf{W}(NH_3)][BAr'_4] + 4CoCp^*_2 + 3[Et_3NH][BAr'_4] \longrightarrow \mathbf{W}H_3 + NH_3 + 4[CoCp^*_2][BAr'_4] + 3Et_3N$$

In view of the previous observations, it is perhaps not surprising that attempted catalytic reduction of dinitrogen using $\mathbf{W}N_2$ as the catalyst under conditions identical or similar to those employed for catalytic reduction of dinitrogen by Mo complexes (35) failed (Table 3). This can be attributed chiefly to the inability to convert $\mathbf{W}(NH_3)^+$ into $\mathbf{W}N_2$ to any significant extent on the timescale of a typical catalytic experiment (6 h), as was independently established in the experiments previously described. Ammonia is formed, but less than 2 equiv., i.e., at most 1.51 equiv. with $CoCp^*_2$ as the reductant and [2,6-LutH][BAr'_4] as the acid. Therefore, while it is possible to cleave the N—N bond and form the first equivalent of ammonia, and to form some $\mathbf{W}NH_x^{y+}$ species that yield additional ammonia upon workup, dinitrogen is not bound and reduced further under the conditions employed.

Conclusions

We have been able to synthesize a number of [$HIPTN_3N$]W complexes analogous to the [$HIPTN_3N$]Mo species that are proposed intermediates in the catalytic reduction of dinitrogen to ammonia (35), among them the first terminal dinitrogen complex of W(III) ($\mathbf{W}N_2$), the second structurally characterized example of a parent diazenide of any metal ($\mathbf{W}$N=NH), and three other tungsten derivatives containing dinitrogen at various stages of reduction ($\mathbf{W}N{=}NH_2^+$, $\mathbf{W}{\equiv}N$, and $\mathbf{W}(NH_3)^+$). As expected, tungsten variants of known molybdenum complexes are characterized by greater nucleophilicities (at N_β) and lower reduction potentials. Interestingly, however, the differences between Mo and W potentials are considerably less pronounced for complexes that contain a dinitrogen ligand, e.g., 260 mV for $\mathbf{M}N_2^{0/-}$ and 0 mV for $\mathbf{M}N_2^{+/0}$. Structural and spectroscopic data (Table 2) signify the more electron-rich nature of all other tungsten derivatives without exception. We had hoped to observe and possibly isolate W variants of several proposed Mo species that are either exceedingly difficult to isolate, and in some cases even observe in situ. However, many of the W complexes, e.g., [$\mathbf{W}N_2$][Bu_4N] and $\mathbf{W}(NH_3)$, were in fact less stable than the analogous Mo complexes. Also $\mathbf{W}{=}NNH_2$ disproportionates into a mixture of $\mathbf{W}$N=NH, $\mathbf{W}{\equiv}$N, and ammonia much faster than does $\mathbf{Mo}{=}NNH_2$. Although dinitrogen in $\mathbf{W}N_2$ could be reduced to ammonia with acid and reductant combinations similar to those used in the catalytic reduction of dinitrogen with [$HIPTN_3N$]Mo species, catalytic turnover could not be achieved as a consequence of (inter alia) major difficulties in converting $\mathbf{W}(NH_3)^+$ into $\mathbf{W}N_2$. Complications of this magnitude in a system where Mo analogs are intermediates in the catalytic reduction of dinitrogen to ammonia would appear to doom tungsten as a plausible site for dinitrogen reduction. *If* MoFe and WFe nitrogenases are structurally analogous, and *if* dinitrogen is reduced at Mo in the MoFe nitrogenase, then one can imagine why reduction of dinitrogen by the WFe nitrogenase might fail.

Experimental section

General

All air- and moisture-sensitive compounds were manipulated using standard Schlenk and glovebox techniques under an atmosphere of nitrogen in flame- and oven-dried glassware (including NMR tubes). Ether, pentane, and toluene were purged with nitrogen, passed through activated alumina columns (58), and freeze–pump–thaw degassed three times. THF, DME, 1,4-dioxane, and benzene were distilled from dark purple Na–benzophenone ketyl solutions. Dichloromethane and acetonitrile were distilled from CaH_2, while fluorobenzene was distilled from P_2O_5 under N_2. All dried and deoxygenated solvents were stored over molecular sieves in a nitrogen-filled glovebox. Small quantities of hydrocarbon and ether solvents, as well as all such deuterated NMR solvents, were purified a second time by vacuum transfer from dark-purple solutions and (or) suspensions of Na–benzophenone ketyl (or CaH_2 for CH_2Cl_2, PhF, and

© 2005 NRC Canada

CD_2Cl_2), degassed, and stored in gas-tight solvent bulbs inside a glovebox. Molecular sieves (3 Å) and Celite® were activated in vacuo at 230 °C for several days. Cobaltocene (sublimed), $CrCp^*_2$ (sublimed), $[CoCp^*_2][PF_6]$ (Strem), $(Me_3Si)_2NLi$ (sublimed), anhydr. $ZnCl_2$, $LiBHEt_3$ (1 mol/L THF), and NaN_3 (Aldrich) were used as received, unless indicated otherwise. WCl_4(DME) (59), $H_3[HIPTN_3N]$ (33), $NaBAr'_4$ (60), $[H(OEt_2)_2][BAr'_4]$ (60), and [2,6-LutH][BAr'_4] (35) were prepared according to the published procedures or slight modifications thereof. Potassium graphite (KC_8) was prepared by stirring potassium metal, freshly cut in a nitrogen-filled glovebox, and graphite in 1:8 stoichiometry with a glass-coated stirbar under 700 torr (1 torr = 133.322 Pa) of Ar at 140 °C for an hour. $CoCp^*_2$ was prepared from $[CoCp^*_2][PF_6]$ and a slight excess of KC_8 in THF over 4 h and sublimed. $[Et_3NH][BAr'_4]$ was prepared from Et_3NHCl and 1.05 equiv. of $NaBAr'_4$ in CH_2Cl_2. All metal complexes were stored in the dark, under N_2 at –35 °C. ^1H, ^{19}F, and ^{15}N NMR spectra were recorded on a Varian Mercury 300 (^1H 300 MHz, ^{19}F 282 MHz), Varian Unity 300 (^1H 300 MHz) or a Varian Inova 500 (^1H 500 MHz, ^{15}N 50.7 MHz) spectrometers and referenced to the residual protio solvent peaks (^1H) or external neat PhF (^{19}F, –113.15 ppm relative to $CFCl_3$) and neat MeCN (^{15}N, +245.5 ppm relative to neat NH_3 at 303 K (61)). Attempted catalytic dinitrogen reduction runs and analyses of ammonia by the indophenol method (62–65) utilized procedures, equipment, and reagents described previously (35, 37). IR spectra were recorded on a Nicolet Avatar 360 FT-IR spectrometer in 0.2 mm KBr solution cells; frequencies are given in cm^{-1}. Elemental analyses were performed by H. Kolbe Mikroanalytisches Laboratorium, Mülheim an der Ruhr, Germany.

Electrochemistry

Electrochemical measurements were carried out using a BAS CV-50W potentiostat, 0.1 mol/L $[Bu_4N][BAr'_4]$ in PhF electrolyte, and a standard three-electrode cell assembly with glassy carbon (3.0 mm diam.) disk working electrode, platinum wire auxiliary electrode, and a AgCl-coated silver wire reference electrode. All measurements were referenced internally with $FeCp_2$, $CoCp_2$, or **Mo**N_2 (35), as appropriate. Compensation of internal solution resistance was used to lower the peak separation of reversible couples to 100–200 mV using the standard routines available with the BAS CV-50W potentiostat and accompanying software. An explanation of the technique can be found on the web at http://www.epsilon-web.net/Ec/manual/Setup/ir_comp.html.

[$HIPTN_3N$]WCl

A mixture of WCl_4(DME) (3.897 g, 9.37 mmol) and $H_3[HIPTN_3N]$ (14.93 g, 9.40 mmol) was stirred vigorously in benzene (100 mL) for 2 h to give a dark red-brown homogeneous solution. Solid $(Me_3Si)_2NLi$ (4.868 g, 29.1 mmol) was added in portions over a period of 10 min. The solution was stirred for an additional 2 h and taken to dryness in vacuo. The residue was dried at 70 °C overnight and extracted with benzene. The extracts were filtered through Celite®, and the filtrates were concentrated and centrifuged in portions to remove residual LiCl. The resulting homogeneous solution was then taken to dryness in vacuo and the residue was heated at 85 °C for several hours. Trituration of the residue with pentane (60 mL) afforded a dark orange microcrystalline solid, which was collected by filtration on a glass frit after standing the mixture at –35 °C overnight, washed with cold pentane, and dried in vacuo at 85 °C for several hours. Yield: 11.28 g (6.25 mmol, 67%). ^1H NMR (C_6D_6, 20 °C) δ: 18.81 (s, 6H, 4′,6′-*H*), 7.49 (s, 12H, 3,5,3″,5″-*H*), 3.47 (br s, 12H, 2,6,2″,6″-C*H*Me_2), 3.18 (sept, J_{HH} = 6.6 Hz, 6H, 4,4″-C*H*Me_2), 2.98 (s, 3H, 2′-*H*), 1.58 (d, J_{HH} = 6.6 Hz, 36H, 4,4″-CH(CH_3)$_2$), 1.34 (s, 36H, 2,6,2″,6″-CH(CH_3)$_2$), 0.83 (br s, 36H, 2,6,2″,6″-CH(CH_3)$_2$), –27.06 (s, 6H, NCH_2), –50.1 (br s, 6H, NCH_2). Anal. calcd. for $C_{114}H_{159}ClN_4W$ (%): C 75.87, H 8.88, N 3.10, Cl 1.96; found: C 75.97, H 8.78, N 2.97, Cl 2.10.

[$HIPTN_3N$]WN=NK

A mixture of **W**Cl (500 mg, 0.277 mmol) and KC_8 (93.6 mg, 0.692 mmol) was stirred in benzene (6 mL) under 1 atm of N_2 (1 atm = 101.325 kPa) with a glass-coated magnetic stirbar for 42 h. The resulting dark maroon-red mixture was taken to dryness in vacuo and the solid residue was extracted with pentane. The pentane extracts were filtered through Celite® and concentrated to 5 mL; a black-red crystalline solid formed within in minutes. The mixture was kept at –35 °C for several days and the product was then collected on a frit, washed with cold pentane, and dried in vacuo at 35 °C for 2 h. Yield: 310 mg (0.169 mmol, 61%). IR (C_6D_6): 1745 ($\nu_{N\text{-}N}$). IR (pentane): 1747 ($\nu_{N\text{-}N}$). ^1H NMR (C_6D_6, 20 °C) δ: 7.54 (br s, 6H, 4′,6′-*H*), 7.16 (s, 12H, 3,5,3″,5″-*H*), 6.61 (s, 3H, 2′-*H*), 3.75 (br s, 6H, NCH_2), 3.42 (sept, J_{HH} = 6.8 Hz, 12H, 2,6,2″,6″-C*H*Me_2), 2.84 (br sept, J_{HH} = 6 Hz, 6H, 4,4″-C*H*Me_2), 1.93 (br s, 6H, NCH_2), 1.26 (d, J_{HH} = 6.5 Hz, 36H, 4,4″-CH(CH_3)$_2$), 1.24 (d, J_{HH} = 6.0 Hz, 36H, 2,6,2″,6″-CH(CH_3)$_2$), 1.2 (br sh, 36H, 2,6,2″,6″-CH(CH_3)$_2$). Anal. calcd. for $C_{114}H_{159}KN_6W$ (%): C 74.56, H 8.73, N 4.58; found: C 74.43, H 8.59, N 4.45.

X-ray quality crystals were obtained from a supersaturated heptane solution at room temperature.

[$HIPTN_3N$]W^{15}N=^{15}NK

A mixture of **W**Cl (500 mg, 0.277 mmol) and KC_8 (93.6 mg, 0.692 mmol) in benzene (6 mL), prepared under regular N_2 in a 25 mL flask fitted with a Teflon® valve, was freeze–pump–thaw degassed five times, pressurized to 1 atm (1 atm = 101.325 kPa) with $^{15}N_2$ purified with solid Na–Ph_2CO and stirred with a glass-coated magnetic stirbar for 50 h. A work-up procedure analogous to that used in the preparation of the unlabeled complex yielded 285 mg (0.155 mmol, 56%) of a black-red solid, identified by spectroscopic data as the labeled compound enriched with ^{15}N at the N_α and N_β diazenido sites to the extent of only 92% as a consequence of some initial reaction under $^{14}N_2$ to yield [$HIPTN_3N$]W^{14}N=^{14}NK. IR (C_6D_6): 1745 ($\nu_{14N\text{–}14N}$), 1688 ($\nu_{15N\text{–}15N}$). ^{15}N NMR (C_6D_6, 20 °C) δ: 356.6 (d, $J(^{15}N_\alpha\text{-}^{15}N_\beta)$ = 11.2 Hz, $^{15}N_\alpha$), 349.5 (d, $J(^{15}N_\alpha\text{-}^{15}N_\beta)$ = 11.2 Hz, $^{15}N_\beta$).

[$HIPTN_3N$]WN_2

A mixture of **W**Cl (500 mg, 0.277 mmol) and KC_8 (93.6 mg, 0.692 mmol) was stirred in benzene (6 mL) under 1 atm of N_2 (1 atm = 101.325 kPa) with a glass-coated mag-

© 2005 NRC Canada

netic stirbar for 42 h. The resulting mixture was filtered through Celite® and brought to dryness in vacuo. Solid $ZnCl_2$ (30.2 mg, 0.222 mmol) and THF (6 mL) were added to the residue. After stirring the solution for a few minutes, a dark orange-red solution and a precipitate of Zn metal formed. The mixture was taken to dryness in vacuo and heated to 75 °C for 2 h. The solid residue was extracted with pentane and the pentane extracts were filtered through Celite®. The extracts were taken to dryness in vacuo. Addition of Me_4Si (7 mL) to the solid residue led to the formation of a microcrystalline orange solid after 1 h. The mixture was kept at –35 °C for several days and the solid product was collected on a frit, washed with cold Me_4Si, and dried in vacuo at 75 °C for 2 h. Yield: 265 mg (0.147 mmol, 53%). IR (C_6D_6): 1888 ($\nu_{N\text{-}N}$). ^{1}H NMR (C_6D_6, 20 °C) δ: 35.2 (br s, 6H, NCH_2), 6.79 (s, 12H, 3,5,3″,5″-*H*), 2.83 (s, 6H, 4,4″-C*H*Me_2), 2.58 (br s, 36H, 2,6,2″,6″-CH(CH_3)$_2$), 1.29 (s, 36H, 4,4″-CH(CH_3)$_2$), 0.66 (s, 36H, 2,6,2″,6″-CH(CH_3)$_2$), –0.25 (s, 2H, 2′-*H*), –0.95 (s, 12H, 2,6,2″,6″-C*H*Me_2), –11.1 (br s, 6H, 4′,6′-*H*), –22.5 (br s, 6H, NCH_2). Anal. calcd. for $C_{114}H_{159}N_6W$ (%): C 76.18, H 8.92, N 4.68; found: C 75.93, H 9.08, N 4.57.

X-ray quality crystals were obtained from a supersaturated heptane solution at room temperature.

[HIPTN$_3$N]W(^{15}N$_2$)

A mixture of **W**^{15}N=^{15}NK (10 mg) and $ZnCl_2$ (0.6 mg, 0.8 equiv.) in THF (0.6 mL) was stirred for 10 min. The mixture was filtered through Celite® and the filtrate was taken to dryness in vacuo. The solid residue was dissolved in C_6D_6 for spectroscopic analysis. IR (C_6D_6): 1888 ($\nu_{14N\text{–}14N}$), 1826 ($\nu_{15N\text{–}15N}$).

[HIPTN$_3$N]WN=NH

A mixture of **W**Cl (500 mg, 0.277 mmol) and KC_8 (93.6 mg, 0.692 mmol) was stirred in benzene (6 mL) with a glass-coated magnetic stirbar for 42 h under 1 atm of N_2 (1 atm = 101.325 kPa). The resulting dark maroon-red mixture was treated with solid [Et_3NH][OTf] (69.6 mg, 0.277 mmol), stirred for 30 min, and taken to dryness in vacuo. The solid residue was extracted with pentane and the pentane extracts were filtered through Celite®. Upon concentration of this solution to ~5 mL, the product precipitated as a cotton-like solid. Repeated warming and cooling of the mixture to –35 °C induced crystallization of the product in the form of a microcrystalline solid sufficiently dense to allow isolation by filtration. The resulting beige solid was washed with cold pentane and dried in vacuo at 60 °C. Yield: 273 mg (0.152 mmol, 55%). IR (C_6D_6): 1542 ($\nu_{N\text{-}NH}$). ^{1}H NMR (C_6D_6, 20 °C) δ: 8.43 (s, 1H, J(^{183}W-H) = 17.4 Hz, N=N*H*), 7.30 (br d, 6H, 4′,6′-*H*), 7.20 (s, 12H, 3,5,3″,5″-*H*), 6.64 (br t, 3H, 2′-*H*), 3.68 (br t, 6H, NCH_2), 3.14 (sept, J_{HH} = 6.6 Hz, 12H, 2,6,2″,6″-C*H*Me_2), 2.93 (sept, J_{HH} = 6.9 Hz, 6H, 4,4″-C*H*Me_2), 1.88 (br t, 6H, NCH_2), 1.37 (d, J_{HH} = 6.6 Hz, 36H, 4,4″-CH(CH_3)$_2$), 1.24 (d, J_{HH} = 6.6 Hz, 36H, 2,6,2″,6″-CH(CH_3)$_2$), 1.14 (d, J_{HH} = 6.6 Hz, 36H, 2,6,2″,6″-CH(CH_3)$_2$). Anal. calcd. for $C_{114}H_{160}N_6W$ (%): C 76.14, H 8.97, N 4.67; found: C 76.00, H 8.96, N 4.55.

X-ray quality crystals were obtained from a supersaturated heptane solution at room temperature.

[HIPTN$_3$N]W^{15}N=^{15}NH

W^{15}N=^{15}NK (40 mg) was treated with [Et_3NH][OTf] (1.05 equiv.) in C_6D_6 in an NMR tube to yield the title compound, 92% ^{15}N-enriched, essentially quantitatively. The solution was taken to dryness in vacuo and the residue was dissolved in C_6D_6 for spectroscopic analysis. IR (C_6D_6): 1499 ($\nu_{^{15}N-^{15}NH}$). ^{1}H NMR (C_6D_6, 20 °C) δ: 8.42 (s, 0.08H, ^{14}N$_\alpha$=^{14}N$_\beta$*H*), 8.41 (dd, ^1J(^{15}N$_\beta$-H) = 53.1 Hz, ^2J(^{15}N$_\alpha$-H) = 6.7 Hz, J(^{183}W-H) = 17.1 Hz, 0.92H, ^{15}N$_\alpha$=^{15}N$_\beta$*H*) (other resonances are identical to those measured for the unlabeled sample). ^{15}N NMR (C_6D_6, 20 °C) δ: 393.5 (dd, J(^{15}N$_\alpha$-^{15}N$_\beta$) = 15.8 Hz, ^2J(^{15}N$_\alpha$-H) = 6.5 Hz, $^{15}N_\alpha$=^{15}N$_\beta$H), 229.3 (dd, ^1J(^{15}N$_\beta$-H) = 53.9 Hz, J(^{15}N$_\alpha$-^{15}N$_\beta$) = 14.9 Hz, ^{15}N$_\alpha$=$^{15}N_\beta$H).

{[HIPTN$_3$N]W=NNH$_2$}[BAr′$_4$]

An ether (4 mL) solution of **W**N=NH (100 mg, 55.6 μmol) was stirred and treated with solid [H(OEt$_2$)$_2$][BAr′$_4$] (59.1 mg, 58.4 μmol) at –35 °C. The solution was stirred for 1 h while being allowed to warm up to room temperature, and then taken to dryness in vacuo. The resulting solid was extracted with pentane and the pentane extracts were filtered through Celite® and concentrated to ~3 mL. Seeding this solution with a minute amount of {[HIPTN$_3$N]Mo=NNH$_2$}[BAr′$_4$] (33) led to a gradual formation of pale yellow microcrystals over a period of ~1 h. The mixture stood at –35 °C for several days and the product was isolated by filtration, washed with cold pentane, and dried in vacuo at 60 °C. Yield: 106 mg (39.8 μmol, 72%). ^{1}H NMR (C_6D_6, 20 °C) δ: 8.36 (br s, 8H, C_6H_3-3,5-(CF_3)$_2$-2,6-*H*), 7.66 (br s, 4H, C_6H_3-3,5-(CF_3)$_2$-4-*H*), 7.13 (s, 12H, 3,5,3″,5″-*H*), 6.79 (br d, 6H, 4′,6′-*H*), 6.62 (br t, 3H, 2′-*H*), 5.96 (s, 2H, J(^{183}W-H) ~ 6 Hz, N-NH_2), 3.78 (br t, 6H, NCH_2), 2.88 (sept, J_{HH} = 6.9 Hz, 6H, 4,4″-C*H*Me_2), 2.67 (sept, J_{HH} = 6.8 Hz, 12H, 2,6,2″,6″-C*H*Me_2), 2.32 (br t, 6H, NCH_2), 1.33 (d, J_{HH} = 6.6 Hz, 36H, 4,4″-CH(CH_3)$_2$), 1.11 (d, J_{HH} = 6.8 Hz, 36H, 2,6,2″,6″-CH(CH_3)$_2$), 0.98 (d, J_{HH} = 6.8 Hz, 36H, 2,6,2″,6″-CH(CH_3)$_2$). ^{19}F NMR (C_6D_6, 20 °C) δ: –62.4 (s, CF_3). Anal. calcd. for $C_{146}H_{173}BF_{24}N_6W$ (%): C 65.86, H 6.55, N 3.16; found: C 65.74, H 6.46, N 3.08.

X-ray quality crystals were obtained from a supersaturated heptane solution at room temperature.

{[HIPTN$_3$N]W=^{15}N^{15}NH$_2$}[BAr′$_4$]

W^{15}N=^{15}NH, generated in situ as described above, was treated with 1 equiv. of [H(OEt$_2$)$_2$][BAr′$_4$] in C_6D_6 in an NMR tube to yield the title compound, 92% ^{15}N-enriched, essentially quantitatively. ^{1}H NMR (C_6D_6, 20 °C) δ: 5.99 (s, 0.08 H, ^{14}N$_\alpha$-^{14}N$_\beta H_2$), 5.99 (dd, ^1J(^{15}N$_\beta$-H) = 83.6 Hz, ^2J(^{15}N$_\alpha$-H) = 1.8 Hz, 0.92 H, ^{15}N$_\alpha$-^{15}N$_\beta H_2$) (other resonances are identical to those measured for the unlabeled sample). ^{15}N NMR (C_6D_6, 20 °C) δ: 343.8 (d, J(^{15}N$_\alpha$-^{15}N$_\beta$) = 10.2 Hz, 1N, $^{15}N_\alpha$-^{15}N$_\beta H_2$), 131.1 (td, ^1J(^{15}N$_\beta$-H) = 83.8 Hz, J(^{15}N$_\alpha$-^{15}N$_\beta$) = 9.9 Hz, 1N, ^{15}N$_\alpha$-$^{15}N_\beta H_2$).

[HIPTN$_3$N]W≡N

A mixture of **W**Cl (500 mg, 0.277 mmol) and NaN_3 (54.0 mg, 0.831 mmol) in a mixture of benzene and acetonitrile (4:6 mL) was stirred vigorously for 16 h. The mixture became lighter in color and was taken to dryness in vacuo. The solid residue was dried at 80 °C in vacuo and ex-

© 2005 NRC Canada

tracted with benzene. The benzene extracts were filtered through Celite® and the filtrates were taken to dryness in vacuo. Addition of pentane (3 mL) led to the precipitation of a pale beige solid after 1 h at room temperature. The mixture was allowed to stand at –35 °C for several days, and the product was then isolated by filtration, washed with cold pentane, and dried at 70 °C in vacuo. Yield: 286 mg (0.160 mmol, 58%). IR (C_6D_6): 1024 ($\nu_{Mo\text{-}N}$). ^{1}H NMR (C_6D_6, 20 °C) δ: 8.01 (br s, 6H, 4′,6′-*H*), 7.21 (s, 12H, 3,5,3″,5″-*H*), 6.59 (s, 3H, 2′-*H*), 3.66 (br t, 6H, NCH_2), 3.10 (sept, J_{HH} = 6.6 Hz, 12H, 2,6,2″,6″-C*H*Me$_2$), 2.93 (sept, J_{HH} = 6.8 Hz, 6H, 4,4″-C*H*Me$_2$), 1.66 (br t, 6H, NCH_2), 1.37 (d, J_{HH} = 6.9 Hz, 36H, 4,4″-CH(CH_3)$_2$), 1.24 (d, J_{HH} = 6.6 Hz, 36H, 2,6,2″,6″-CH(CH_3)$_2$), 1.10 (br d, J_{HH} = 6.3 Hz, 36H, 2,6,2″,6″-CH(CH_3)$_2$). Anal. calcd. for $C_{114}H_{159}N_5W$ (%): C 76.78, H 8.99, N 3.93; found: C 76.57, H 9.01, N 3.94.

[HIPTN$_3$N]W≡^{15}N

[**W**=^{15}N^{15}NH$_2$][BAr′$_4$], generated in situ as described above, was treated with 2 equiv. of $CoCp_2^*$ in C_6D_6 in an NMR tube to yield a mixture consisting predominantly of **W**^{15}N=^{15}NH and the title compound. ^{15}N NMR (C_6D_6, 20 °C) δ: 827.0 (s, W≡^{15}*N*), 393.5 (dd, W$^{15}N_\alpha$=^{15}N$_\beta$H), 229.3 (dd, W^{15}N$_\alpha$=$^{15}N_\beta$H).

{[HIPTN$_3$N]W(NH$_3$)}[BAr′$_4$]

Ammonia (57 mL, 360 torr (1 torr = 133.322 Pa), ~1.11 mmol) was vacuum transferred from a bronze-colored Na solution to a frozen mixture of **W**Cl (500 mg, 0.277 mmol) and NaBAr′$_4$ (540.2 mg, 0.610 mmol) in fluorobenzene (10 mL). The mixture was thawed and stirred at room temperature for 2 h, at which time ^{1}H NMR analysis of an aliquot taken from the reaction mixture showed complete consumption of **W**Cl. The mixture was taken to dryness in vacuo, and the solid residue was dried at 60 °C and extracted with pentane. The pentane extracts were filtered through Celite® and the filtrate was concentrated to 3 mL. This solution was seeded with a minute quantity of crystalline {[HIPTN$_3$N]Mo(NH$_3$)}[BAr′$_4$], which led to rapid formation of a bright yellow microcrystalline solid. The mixture was left standing at –35 °C for several days and the product was then isolated by filtration, washed with cold pentane, and dried in vacuo at 60 °C, turning light orange. Yield: 642 mg (242 mmol, 87%). ^{1}H NMR (C_6D_6, 20 °C) δ: 18.66 (s, 6H, 8.27, 4′,6′-*H*), 7.41 (s, 12H, 3,5,3″,5″-*H*), 7.34 (s, 8H, C$_6H_3$-3,5-(CF$_3$)$_2$-2,6-*H*), 7.21 (s, 4H, C$_6H_3$-3,5-(CF$_3$)$_2$-4-*H*), 3.15 (sept, J_{HH} = 6.9 Hz, 6H, 4,4″-C*H*Me$_2$), 2.7 (v br s, 12H, 2,6,2″,6″-C*H*Me$_2$), 1.54 (d, J_{HH} = 6.6 Hz, 36H, 4,4″-CH(CH_3)$_2$), 1.01 (br s, 36H, 2,6,2″,6″-CH(CH_3)$_2$), 0.6 (v br s, 36H, 2,6,2″,6″-CH(CH_3)$_2$), –0.20 (s, 3H, 2′-*H*), –28.79 (s, 6H, NCH_2), –63.7 (br s, 6H, NCH_2). Anal. calcd. $C_{146}H_{174}BF_{24}N_5W$ (%): C 66.16, H 6.62, N 2.64; found: C 65.97, H 6.68, N 2.52.

X-ray quality crystals were obtained from a supersaturated heptane solution at room temperature.

[HIPTN$_3$N]WH$_3$

A benzene (5 mL) solution of [**W**(NH$_3$)][BAr′$_4$] (700 mg, 0.264 mmol) was treated with LiBHEt$_3$ (1 mol/L THF, 264 μL, 0.264 mmol) at room temperature. The resulting brown-red mixture was stirred for 30 min, freeze–pump–thaw degassed, and exposed to 1 atm of H_2 (1 atm = 101.325 kPa), which caused some lightening in color. The mixture was stirred for 1 h and brought to dryness in vacuo. The resulting solid was dried at 80 °C and extracted with benzene. The benzene extracts were filtered through Celite® and the filtrate was taken to dryness. Addition of pentane (4 mL) to the residue led to a gradual formation of a light brown solid. The mixture was left standing at –35 °C for several days and the product was then isolated by filtration, washed with cold pentane, and dried in vacuo at 70 °C. As was explained in the text, **W**H$_3$ loses hydrogen in the solid state at elevated temperatures under vacuum, forming an observable quantity of a paramagnetic compound tentatively assigned as the monohydride **W**H. Thus, solid **W**H$_3$ isolated as described previously was stored under an atmosphere of H_2 overnight, which nearly eliminated the **W**H impurity. Yield: 208 mg (0.117 mmol, 44%). IR (C_6D_6): 1966, 1958 (both broad, $\nu_{W\text{-}H}$). ^{1}H NMR (C_6D_6, 20 °C) δ: 11.99 (s, 3H, J(^{183}W-H) = 24 Hz, W(*H*)$_3$), 7.66 (s, 6H, 4′,6′-*H*), 7.21 (s, 12H, 3,5,3″,5″-*H*), 6.54 (s, 3H, 2′-*H*), 3.65 (s, 6H, NCH_2), 3.10 (sept, J_{HH} = 6.8 Hz, 12H, 2,6,2″,6″-C*H*Me$_2$), 2.93 (sept, J_{HH} = 6.9 Hz, 6H, 4,4″-C*H*Me$_2$), 2.01 (s, 6H, NCH_2), 1.37 (d, J_{HH} = 6.9 Hz, 36H, 4,4″-CH(CH_3)$_2$), 1.24 (d, J_{HH} = 6.9 Hz, 36H, 2,6,2″,6″-CH(CH_3)$_2$), 1.12 (d, J_{HH} = 6.6 Hz, 36H, 2,6,2″,6″-CH(CH_3)$_2$). Anal. calcd. for $C_{114}H_{162}N_4W$ (%): C 77.25, H 9.21, N 3.16; found: C 77.08, H 9.28, N 3.06.

Acknowledgements

R.R.S. is grateful to the National Institutes of Health (GM 31978) for research support and both R.R.S. and D.V.Y. are grateful to William E. Geiger for advice on electrochemistry in weakly polar media.

References

1. A.D. Allen and C.V. Senoff. J. Chem. Soc. Chem. Commun. 621 (1965).
2. B.K. Burgess and D.J. Lowe. Chem. Rev. **96**, 2983 (1996).
3. B.K. Burgess. ACS Symp. Ser. **535**, 144 (1993).
4. B.K. Burgess. Chem. Rev. **90**, 1377 (1990).
5. J. Chatt, J.R. Dilworth, and R.L. Richards. Chem. Rev. **78**, 589 (1978).
6. M. Hidai and Y. Mizobe. Chem. Rev. **95**, 1115 (1995).
7. M. Hidai. Coord. Chem. Rev. **185–186**, 99 (1999).
8. M.D. Fryzuk and S.A. Johnson. Coord. Chem. Rev. **200–202**, 379 (2000).
9. T.A. Bazhenova and A.E. Shilov. Coord. Chem. Rev. **144**, 69 (1995).
10. C.J. Pickett. J. Biol. Inorg. Chem. **1**, 601 (1996).
11. F. Barriere. Coord. Chem. Rev. **236**, 71 (2003).
12. R.L. Richards. Coord. Chem. Rev. **154**, 83 (1996).
13. R.A. Henderson, G.J. Leigh, and C.J. Pickett. Adv. Inorg. Chem. Radiochem. **27**, 197 (1983).
14. J. Chatt and G.J. Leigh. Chem. Soc. Rev. **1**, 121 (1972).
15. A.D. Allen, R.O. Harris, B.R. Loescher, J.R. Stevens, and R.N. Whiteley. Chem. Rev. **73**, 11 (1973).
16. B.A. MacKay and M.D. Fryzuk. Chem. Rev. **104**, 385 (2004).
17. K. Komori, H. Oshita, Y. Mizobe, and M. Hidai. J. Am. Chem. Soc. **111**, 1939 (1989).

© 2005 NRC Canada

18. M. Mori, K. Hori, M. Akashi, M. Hori, Y. Sato, and M. Nishida. Angew. Chem. Int. Ed. **37**, 636 (1998).
19. K. Hori and M. Mori. J. Am. Chem. Soc. **120**, 7651 (1998).
20. M. Mori, M. Hori, and Y. Sato. J. Org. Chem. **63**, 4832 (1998).
21. M. Akashi and M. Mori. Heterocycles, **59**, 661 (2003).
22. K. Ueda and M. Mori. Tetrahedron Lett. **45**, 2907 (2004).
23. M. Mori. J. Heterocycl. Chem. **37**, 623 (2000).
24. M. Akashi, Y. Sato, and M. Mori. J. Org. Chem. **66**, 7873 (2001).
25. M. Akashi, M. Nishida, and M. Mori. Chem. Lett. 465 (1999).
26. M. Mori. J. Organometal. Chem. **689**, 4210 (2004).
27. A.E. Shilov. J. Mol. Catal. **41**, 221 (1987).
28. A.E. Shilov. Russ. Chem. Bull. Int. Ed. **52**, 2555 (2003).
29. R.R. Schrock. Pure Appl. Chem. **69**, 2197 (1997).
30. G.E. Greco and R.R. Schrock. Inorg. Chem. **40**, 3850 (2001).
31. G.E. Greco and R.R. Schrock. Inorg. Chem. **40**, 3860 (2001).
32. D.V. Yandulov and R.R. Schrock. J. Am. Chem. Soc. **124**, 6252 (2002).
33. D.V. Yandulov, R.R. Schrock, A.L. Rheingold, C. Ceccarelli, and W.M. Davis. Inorg. Chem. **42**, 796 (2003).
34. D. Yandulov and R.R. Schrock. Inorg. Chem. **44**, 1103 (2005).
35. D.V. Yandulov and R.R. Schrock. Science, **301**, 76 (2003).
36. G.M. Sheldrick. SADABS: A program for absorption correction of crystallographic data. Version 2.10 [computer program]. University of Goettingen, Goettingen, Germany. 1996.
37. V. Ritleng, D.V. Yandulov, W.W. Weare, R.R. Schrock, A.R. Hock, and W.M. Davis. J. Am. Chem. Soc. **126**, 6150 (2004).
38. S. Siemann, K. Schneider, M. Oley, and A. Mueller. Biochemistry, **42**, 3846 (2003).
39. G.E. Greco, A.I. Popa, and R.R. Schrock. Organometallics, **17**, 5591 (1998).
40. S.W. Seidel, R.R. Schrock, and W.M. Davis. Organometallics, **17**, 1058 (1998).
41. R.R. Schrock, S.W. Seidel, N.C. Mösch-Zanetti, K.-Y. Shih, M.B. O'Donoghue, W.M. Davis, and W.M. Reiff. J. Am. Chem. Soc. **119**, 11 876 (1997).
42. N.C. Mösch-Zanetti, R.R. Schrock, W.M. Davis, K. Wanninger, S.W. Seidel, and M.B. O'Donoghue. J. Am. Chem. Soc. **119**, 11 037 (1997).
43. R.R. Schrock, K.-Y. Shih, D. Dobbs, and W.M. Davis. J. Am. Chem. Soc. **117**, 6609 (1995).
44. M.G. Fickes, A.L. Odom, and C.C. Cummins. Chem. Commun. 1993 (1997).
45. J.C. Peters, A.L. Odom, and C.C. Cummins. Chem. Commun. 1995 (1997).
46. J.B. Greco, J.C. Peters, T.A. Baker, W.M. Davis, C.C. Cummins, and G. Wu. J. Am. Chem. Soc. **123**, 5003 (2001).
47. J.S. Figueroa and C.C. Cummins. Angew. Chem. Int. Ed. **43**, 984 (2004).
48. J. Mason. Chem. Rev. **81**, 205 (1981).
49. J. Mason. *In* Multinuclear NMR. *Edited by* J. Mason. Plenum Press, New York. 1987.
50. M.G. Hill, W.M. Lamanna, and K.R. Mann. Inorg. Chem. **30**, 4687 (1991).
51. N.G. Connelly and W.E. Geiger. Chem. Rev. **96**, 877 (1996).
52. R.J. LeSuer and W.E. Geiger. Angew. Chem. Int. Ed. **39**, 248 (2000).
53. N. Camire, U.T. Mueller-Westerhoff, and W.E. Geiger. J. Organomet. Chem. **637–639**, 823 (2001).
54. N. Camire, A. Nafady, and W.E. Geiger. J. Am. Chem. Soc. **124**, 7260 (2002).
55. S. Trupia, A. Nafady, and W.E. Geiger. Inorg. Chem. **42**, 5480 (2003).
56. M.B. O'Donoghue, W.M. Davis, and R.R. Schrock. Inorg. Chem. **37**, 5149 (1998).
57. D.A. Dobbs, R.R. Schrock, and W.M. Davis. Inorg. Chim. Acta, **263**, 171 (1997).
58. A.B. Pangborn, M.A. Giardello, R.H. Grubbs, R.K. Rosen, and F.J. Timmers. Organometallics, **15**, 1518 (1996).
59. C. Persson and C. Andersson. Inorg. Chim. Acta, **203**, 235 (1993).
60. M. Brookhart, B. Grant, and A.F. Volpe, Jr. Organometallics, **11**, 3920 (1992).
61. M. Witanowski, L. Stefaniak, S. Szymanski, and H. Januszewski. J. Magn. Reson. **28**, 217 (1977).
62. A.L. Chaney and E.P. Marbach. Clinical Chem. **8**, 130 (1962).
63. M.W. Weatherburn. Anal. Chem. **39**, 971 (1967).
64. T.T. Ngo, A.P.H. Phan, C.F. Yam, and H.M. Lenhoff. Anal. Chem. **54** (1982).
65. M.J. Dilworth and K. Fisher. Anal. Biochem. **256**, 242 (1998).

© 2005 NRC Canada

Research inspired by the chemistry of nitrogenase — Novel metal complexes and their reactivity toward dinitrogen, nitriles, and alkynes[1]

Masanobu Hidai and Yasushi Mizobe

Abstract: Summarized here are our continuous studies of the last three decades concerning syntheses of new types of complexes learned from nitrogenase and their reactivites toward dinitrogen, nitriles, and alkynes. For Mo and W dinitrogen complexes with tertiary phosphine coligands, a variety of their intriguing reactivities have been demonstrated, and novel transformations of the N_2 ligands into numerous nitrogen-containing ligands and compounds have been developed. The C≡N bond cleavage of certain nitriles also proceeds on the Mo site surrounded by tertiary phosphines. Stimulated by the sophisticated structure of the active site of nitrogenase, multinuclear metal–sulfur complexes have been synthesized in rational ways. New types of stoichiometric and catalytic reactions of alkynes have been found by using the thiolato-bridged diruthenium complexes and some cubane-type sulfido clusters containing a noble metal.

Key words: nitrogen fixation, molybdenum and tungsten dinitrogen complexes, ruthenium thiolato complexes, metal sulfido clusters, nitriles, alkynes.

Résumé : Dans ce travail, on présente un résumé des études qui se poursuivent dans notre laboratoire et qui ont été réalisées depuis au moins trente ans sur des synthèses de nouveaux types de complexes basées sur la façon de faire de la nitrogénase et sur leurs réactivités vis-à-vis du diazote, des nitriles et des alcynes. Pour les complexes du diazote avec le molybdène et le tungstène comportant des coligands de nature phosphine tertiaire, on a mis en évidence une variété de réactivités intrigantes et on a développé de nouvelles transformations de ligands N_2 en de nombreux ligands et composés contenant de l'azote. Le clivage de la liaison C≡N de certains nitriles procède au niveau d'atomes de molybdène entourés de phosphines tertiaires. Stimulés par la structure sophistiquée du site actif de la nitrogénase, on a synthétisé de façons rationnelles des complexes sulfurés de métaux polynucléaires. On a aussi découvert de nouveaux types de réactions stoechiométriques et catalytiques des alcynes en faisant appel à des complexes de diruthénium comportant des ponts thiolato et quelques agrégats sulfido de type cubane contenant des métaux nobles.

Mots clés : fixation de l'azote, complexes de diazote avec le molybdène et le tungstène, complexes thiolato du ruthénium, agrégats sulfido métalliques, nitriles, alcynes.

[Traduit par la Rédaction]

Introduction

Dinitrogen and carbon monoxide are isoelectronic and both molecules have a triple bond. However, their reactivities are quite different. The Haber–Bosch process developed in the early 20th century requires drastic reaction conditions to form ammonia from dinitrogen and dihydrogen. Thus, about 40 years ago, dinitrogen was recognized to be chemically inert. In contrast, a variety of metal carbonyl complexes were known at that time and carbon monoxide was widely used as a carbon source for organic synthesis under relatively mild conditions, as typically found in hydroformylation. Nobody believed that a dinitrogen complex, in which dinitrogen is bound to a transition meal, is readily isolated as a stable compound. Therefore, the discovery of the first dinitrogen complex $[Ru(NH_3)_5(N_2)]X_2$ (X = Br, I, BF_4, PF_6) by Allen and Senoff in 1965 (1) was a great surprise to chemists. This finding, together with the observation by Vol'pin in 1964 that ammonia was formed after hydrolysis of the mixture of a Ti complex and a reducing agent under dinitrogen (2), had spurred chemists to have a dream that dinitrogen is converted into ammonia under mild conditions as observed in biological nitrogen fixation. In 1967, Yamamoto et al. (3) succeeded in synthesis of the cobalt dinitrogen complex $[CoH(N_2)(PPh_3)_3]$ from dinitrogen itself. However, those dinitrogen complexes did not show the favorable reactivity of the coordinated N_2: i.e., treatment of the complexes with acids resulted in release of N_2 gas. At that time, molybde-

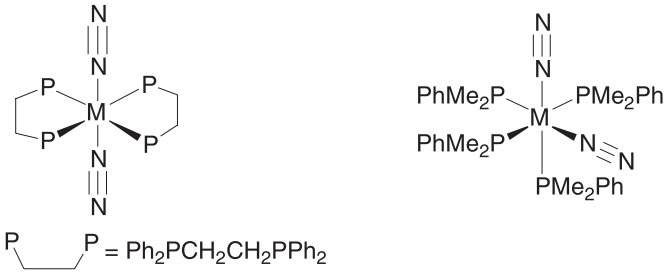
Received 9 September 2004. Published on the NRC Research Press Web site at http://canjchem.nrc.ca on 14 April 2005.

M. Hidai.[2] Department of Materials Science and Technology, Faculty of Industrial Science and Technology, Tokyo University of Science, Noda, Chiba 278-8510, Japan.
Y. Mizobe. Institute of Industrial Science, The University of Tokyo, Komaba, Meguro-ku, Tokyo 153-8505, Japan.

[1]This article is part of a Special Issue dedicated to Dinitrogen Chemistry.
[2]Corresponding author (e-mail: hidai@rs.noda.tus.ac.jp).

 doi: 10.1139/V05-016 © 2005 NRC Canada

Fig. 1. Typical Mo and W dinitrogen complexes.



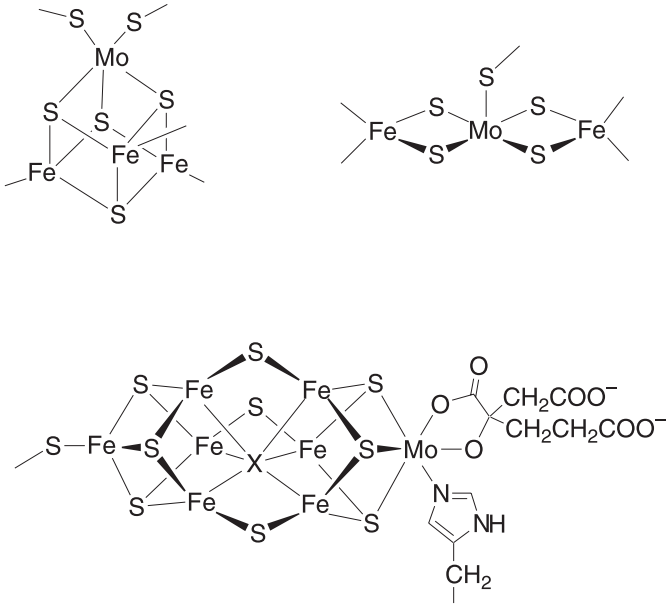
1a: M = Mo, **1b**: M = W

2a: M = Mo, **2b**: M = W

num was believed to be a key metal in biological nitrogen fixation. Fortunately, we succeeded in the preparation of the first molybdenum dinitrogen complex *trans*-$[Mo(N_2)_2(dppe)_2]$ (**1a**, dppe = $Ph_2PCH_2CH_2PPh_2$) in 1969 (4). Later, Chatt et al. (5) prepared a series of molybdenum and tungsten dinitrogen complexes of the type $[M(N_2)_2(L)_4]$ (M = Mo, W, L = tertiary phosphine). Typical dinitrogen complexes are shown in Fig. 1. Noteworthy is that these molybdenum and tungsten dinitrogen complexes are outstanding in the reactivity of the coordinated N_2, as compared with other dinitrogen complexes containing almost all transition metals prepared later. The N—H and N—C bond formation of the coordinated N_2 is readily achieved to form ammonia, hydrazine, and organo-nitrogen compounds. The first part of this review focuses on our long-standing studies on the chemistry of molybdenum and tungsten dinitrogen complexes. Readers should refer to comprehensive reviews to fully understand the chemistry of dinitrogen complexes (6).

In the middle 1980s, we embarked on our second approach toward activation of dinitrogen as well as nitriles and alkynes by learning more precisely from biological nitrogen fixation. Biological nitrogen fixation proceeds under mild conditions with the aid of nitrogenase (7). In 1978, the active site of nitrogenase was believed to be a molybdenum–iron–sulfur cluster, the structure of which was proposed mainly on the basis of EXAFS studies of nitrogenase as shown in Fig. 2 (8). The single-crystal X-ray analysis of nitrogenase has very recently revealed the $MoFe_7S_9$ cluster structure with an interstitial light atom, probably nitrogen, in the FeMo cofactor of the MoFe protein (9), which is directly involved in reduction of dinitrogen. It is to be noted that the molybdenum and iron atoms are coordinated by sulfur atoms, which is in sharp contrast to the above molybdenum and tungsten dinitrogen complexes with phosphine ligands. Extensive studies by Holm, Coucouvanis, and other groups (10) have been directed toward synthesis of iron–molybdenum–sulfur clusters with a similar structure to the active site of nitrogenase. However, our studies have intentionally been directed to synthesis of noble metal–sulfur clusters and development of their unique reactivities towards small molecules including not only dinitrogen, but also nitriles and alkynes. We are aware that the natural enzyme "nitrogenase" does not use noble metals to build the active site, but we are able to employ noble metals to prepare analogous metal–sulfur clusters, which might exhibit unique catalysis for transformation of dinitrogen as well as other small molecules. The second part of this review summarizes our studies of the chemistry of noble metal–sulfur clusters (11).

Fig. 2. Structures of the FeMo-cofactor. Upper: Structures proposed in 1978 based on Mo EXAFS analysis of the MoFe protein (8). Lower: Structure revealed very recently by the single-crystal X-ray analysis (9).



Chemistry of molybdenum and tungsten dinitrogen complexes with phosphine ligands

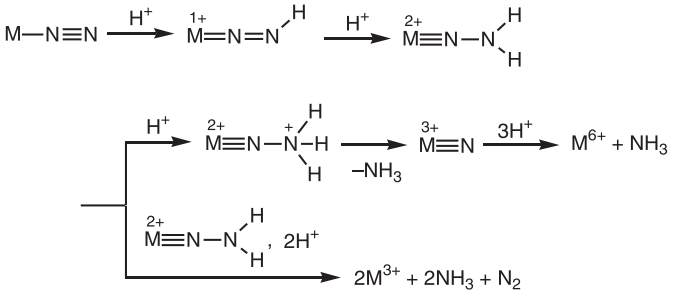
N—H bond formation

Although the first molybdenum dinitrogen complex *trans*-$[Mo(N_2)_2(dppe)_2]$(**1a**) was prepared by our group, well-defined protonation of the coordinated N_2 in dinitrogen complexes of the type $[M(N_2)_2(L)_4]$ (M = Mo, W, L = tertiary phosphine) was discovered by Chatt et al. (13) for the reactions of *trans*-$[M(N_2)_2(dppe)_2]$ with HX (M = Mo (**1a**): X = Br; M = W (**1b**): X = Cl, Br), affording the hydrazido(2–) complexes *trans*-$[MX(NNH_2)(dppe)_2]X$ (12), just after their novel finding of the N—C bond formation by treatment of **1b** with RCOCl or RCOCl–HCl to give *trans*-$[WCl(NNCOR)(dppe)_2]$ or *trans*-$[WCl(NNHCOR)(dppe)_2]Cl$, respectively (vide infra). Single-crystal X-ray analysis of hydrazido(2–) complexes has been undertaken for *trans*-$[WCl(NNH_2)(dppe)_2][BPh_4]$ (14), and also for *trans*-$[MoF(NNH_2)(dppe)_2][BF_4]$ obtained by our group from the reaction of **1a** with aq. HBF_4 in THF (15). These crystallographic studies disclosed the linear M–N–N linkage, the trigonal planar geometry around the terminal N atom, and the N—N bond order greater than unity, as the common structural features of the hydrazido(2–) ligand derived from the coordinated N_2.

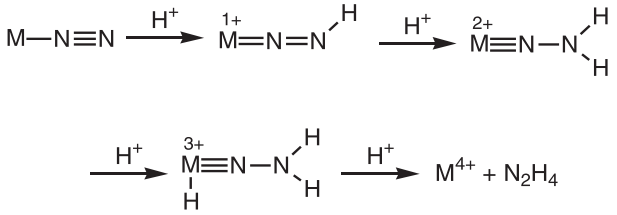
Although the reactions of **1** with protic acids stop at the hydrazido(2–) stage except for those under quite drastic conditions, subsequent extensive studies mainly done by Chatt and co-workers (16) on the reactions of complexes of the type $[M(N_2)_2(L)_4]$ have clarified the pathway to convert one N_2 ligand in *cis*-$[W(N_2)_2(PMe_2Ph)_4]$ (**2b**) almost quantitatively into ammonia under ambient conditions. Thus, **2b** re-

© 2005 NRC Canada

Scheme 1.



Scheme 2.

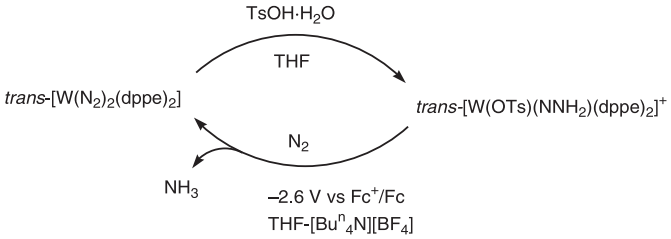


acts with sulfuric acid in MeOH at room temperature to give ammonia (ca. 1.9 mol/W atom) together with uncharacterized W(VI) species. Sequence of the N_2 reduction is shown in Scheme 1, which involves the dianenido (WNNH), hydrazido(2–) ($WNNH_2$), hydrazidium ($WNNH_3^+$), and nitrido (WN) intermediates formed by the stepwise protonation of the N_2 ligand coupled with the electron transfer from the central metal to the nitrogenous ligands. Ammonia formation from the Mo analogue *cis*-$[Mo(N_2)_2(PMe_2Ph)_4]$ (**2a**) proceeds less effectively (ca. 0.65 mol/Mo atom), since the disproportionation of the hydrazido(2–) intermediates predominates over the formation of the hydrazidium intermediate owing to the weaker electron-donating ability of Mo than W (Scheme 1). Not only the central metal, but also the nature of the acid and solvent remarkably affects the yields of the nitrogen hydrides from **2**. For example, we observed the preferential formation of hydrazine from both **2a** and **2b** upon treatment with HCl gas in ethereal solvents like $MeOCH_2CH_2OMe$ (17). The mechanism operating in this system involves the hydrido-hydrazido(2–) species as the other isolable intermediate after the hydrazido(2–) stage (Scheme 2).

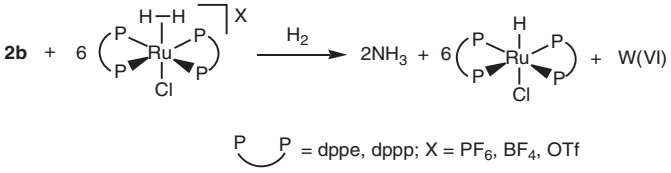
Important advances in the reduction of the coordinated N_2 in **1** and **2** have then been achieved by employment of electroreductive conditions or by application of bimetallic systems. Thus, Pickett and co-workers (18) found that the controlled-potential electrolysis of the hydrazido(2–) complex *trans*-$[W(OTs)(NNH_2)(dppe)_2]^+$ (TsO = *p*-$MeC_6H_4SO_3$) in THF produced ammonia (0.21 mol/W atom) with concomitant regeneration of the parent N_2 complex **1b** in high yield. By repeating the cycle of protonation and electro-reduction shown in Scheme 3 three times, the yield of ammonia reached 0.73 mol/W atom.

We and other groups (19) have independently found that treatment of **2b** with a series of metal hydrides in MeOH gives ammonia in low to moderate yields after base distillation of the reaction mixtures. The metal hydrides employed include the "acidic" metal hydrides such as $H_2Fe(CO)_4$, $HCo(CO)_4$, and $HFeCo_3(CO)_{12}$, as well as the "hydridic"

Scheme 3.



Scheme 4.

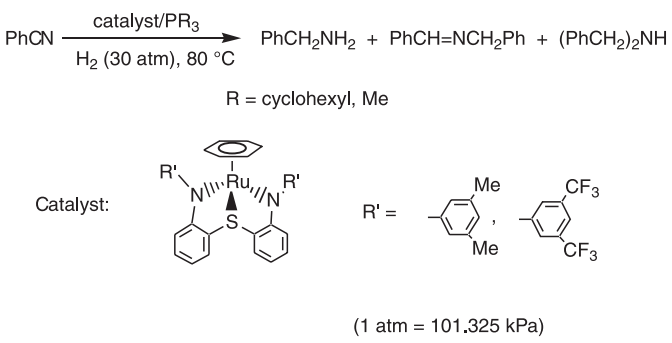


metal hydride $[Cp_2ZrHCl]$ (Cp = η^5-C_5H_5). Reactions of **1** with the acidic hydridometal carbonyls in ROH afforded the hydrazido(2–) complexes *trans*-$[M(OR)(NNH_2)(dppe)_2]X$ (X = $Co(CO)_4$, $FeCo_3(CO)_{12}$) (19*b*), suggesting that this reaction course forming ammonia also involves the hydrazido(2–) complexes as the intermediate. As for the protonation of the N_2 ligand in **1** and **2** by using bimetallic systems, several intriguing reactions have more recently been developed by our group (20).

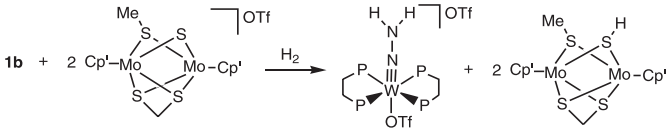
The η^2-H_2 complexes are now variously known, and in certain complexes the η^2-H_2 ligand is quite acidic to undergo the heterolytic cleavage by a base. Morris and co-workers (21) reported the reaction of **1b** with 2 equiv. of $[CpRu(dtpfe)H_2][BF_4]$ (dtpfe = $(p\text{-}CF_3C_6H_4)_2PCH_2CH_2P(C_6H_4CF_3\text{-}p)_2$), which exists as a slowly interconverting mixture of the dihydrogen and dihydrido species in solution, to form *trans*-$[WF(NNH_2)(dppe)_2][BF_4]$ and [CpRu(dtpfe)H], although $[CpRu(dtpfe)H_2][BF_4]$ is not available directly from gaseous H_2. Recently, we have found that when **2b** is treated with 10 equiv. of dihydrogen complexes *trans*-$[RuCl(\eta^2\text{-}H_2)(\mathbf{P_2})_2]X$ ($\mathbf{P_2}$ = dppe, dppp; dppp = $Ph_2PCH_2CH_2CH_2PPh_2$; X = PF_6, BF_4, TfO; TfO = CF_3SO_3), which are derived from $[RuCl(\mathbf{P_2})_2]X$ and H_2 gas, ammonia is obtained in the yields of 0.45–0.79 mol/W atom after the reactions at 55 °C under H_2 (Scheme 4) (22). Analogous treatment of **1b** with *trans*-$[RuCl(\eta^2\text{-}H_2)(dppp)_2]X$ (X = PF_6, BF_4) afforded the hydrazido(2–) complexes *trans*-$[WF(NNH_2)(dppe)_2]X$ as expected. Isolation of *trans*-$[M(OTf)(NNH_2)(PMe_2Ph)_4][OTf]$ from the reaction of **2b** with *trans*-$[RuCl(\eta^2\text{-}H_2)(dppe)_2][OTf]$ at room temperature more straightforwardly confirmed the presence of the hydrazido(2–) complexes as the intermediates for the formation of ammonia shown in Scheme 4. In these reactions, the N—H bond formation presumably occurs via the direct attack of the basic terminal N atom in **2b** and **1b** on the η^2-H_2 ligand, leading to the heterolytic cleavage of the H—H bond to give the N–H protons and the Ru–H hydrides. Since the N_2 ligand in Mo complexes **1a** and **1b** behaves as a weaker base, the N—H bond forming reactions did not take place upon treatment with these Ru η^2-H_2 complexes. This result is reminiscent of the reactions of **2** with MeOH, EtOH, and water at 50 °C, in which ammonia is obtained only from the W complex **2b** and not from the Mo

© 2005 NRC Canada

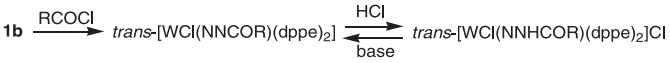
Scheme 5.



Scheme 6.



Scheme 7.



complex **2a** (23). Replacement of the above Ru η^2-H_2 complexes by less acidic *trans*-[RuH(η^2-H_2)(**P_2**)$_2$]X (X = BF_4, TfO) resulted in a dramatic decrease in the yields of ammonia.

Although the above reaction of the coordinated N_2 and the coordinated H_2 forming ammonia is of great interest, electrons for the reduction of the coordinated N_2 are supplied from the metal, and hence the reaction is no more than stoichiometric. Our extensive study has led to the finding that Ru bis(diarylamido)-thioether complexes are effective in the presence of an alkylphosphine for catalytic hydrogenation of benzonitrile to give benzylamine and benzylidenebenzylamine at 80 °C. The reaction was presumed to proceed through the heterolytic cleavage of H_2 on the Ru—N bond. Dinitrogen was also bound to the metal center, however, no ammonia was observed from the reaction of N_2 and H_2 (Scheme 5) (24).

It is to be noted that catalytic conversion of N_2 into ammonia by using a well-defined N_2 complex has very recently been achieved for the first time by Schrock and co-workers (25): a Mo dinitrogen complex having a triamidoamine ligand is treated with 2,6-lutidinium salt as the proton source and decamethylchromocene as the reductant to produce ammonia (ca. 4 mol/Mo atom).

When **2b** is treated under H_2 with 10 equiv. of sulfur-bridged dimolybdenum complex [(CpMo)$_2$(μ-S_2CH_2)(μ-S)(μ-SH)][OTf], which is known to mediate the reductive cleavage of the C≡N bond in nitriles by H_2 gas (26), ammonia is obtained in the yield of 0.38 mol/W atom (27). The reaction of **1b** with 2 equiv. of the related dimolybdenum complex [(Cp′Mo)$_2$(μ-S_2CH_2)(μ-S)(μ-SMe)][OTf] (Cp′ = η^5-C_5H_4Me) under H_2, which has been reported to split H_2 heterolytically in the presence of base such as pyridine (28), results in the formation of the hydrazido(2–) complex *trans*-[W(OTf)(NNH_2)(dppe)$_2$][OTf] together with [(Cp′Mo)$_2$(μ-S_2CH_2)(μ-SH)(μ-SMe)] (Scheme 6) (27). Although the detailed mechanism is yet unknown, the NH protons are apparently supplied through the heterolytic cleavage of H_2.

Protonation of the coordinated N_2 has also been attempted by using hydrosulfido complexes as the proton source. This has led to the finding that the μ-hydrosulfido complexes [(Cp*Ir)$_3$(μ-SH)$_3$]Cl (Cp* = η^5-C_5Me_5) and [{Fe[PhP(CH_2CH_2PPh_2)$_2$]}$_2$(μ-SH)$_3$][BF_4] react with **2b** to yield 0.78 and 0.38 mol ammonia per W atom, respectively (29). Dance (30) has proposed that the mechanism for the N_2 reduction in the FeMo-cofactor of nitrogenase involves the μ-SH intermediate generated by the protonation of the μ-sulfides of the $MoFe_7S_9$ core, whose protons are then transferred to the adjacent N_2 molecule bonded to the Fe_4 face. The reactivities of the μ-SH complexes toward **2b** observed here are therefore quite interesting because of their relevance to the biological N_2-reducing system. It is to be noted that the reactions of both H_2S and PhSH with **2b** result in the loss of all N_2 ligands as N_2 gas.

N—C bond formation

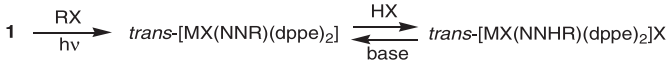
Extensive studies on the protonation of the N_2 ligand in **1** and **2** have demonstrated many reaction systems that transform molecular nitrogen into ammonia, and less commonly hydrazine, under mild conditions. In some cases, the mechanisms have been clarified in a well-defined manner. These results, which are of great importance in their own right, provide much information for gaining insight into biological nitrogen fixation. However, as far as the ammonia synthesis is concerned, it is highly improbable that the homogeneous system surpassing the modern Haber-Bosch process will be realized practically in the near future. On the other hand, direct conversion of molecular N_2 into nitrogen-containing organic compounds might be of more industrial significance than the ammonia synthesis. Development of the N—C bond forming reactions on the N_2 ligand is therefore quite interesting.

As already described, acyl- and aroyldiazenido complexes *trans*-[WCl(NNCOR)(dppe)$_2$] and their hydrazido(2–) derivatives *trans*-[WCl(NNHCOR)(dppe)$_2$]Cl have first been obtained through the C—N bond formation of the coordinated N_2 (13) (Scheme 7). The structure of the diazenido complex was clarified in detail for *trans*-[MoCl(NNCOPh)(dppe)$_2$] derived from the reaction of *trans*-[Mo(N_2)(NCR)(dppe)$_2$] with PhCOCl (31).

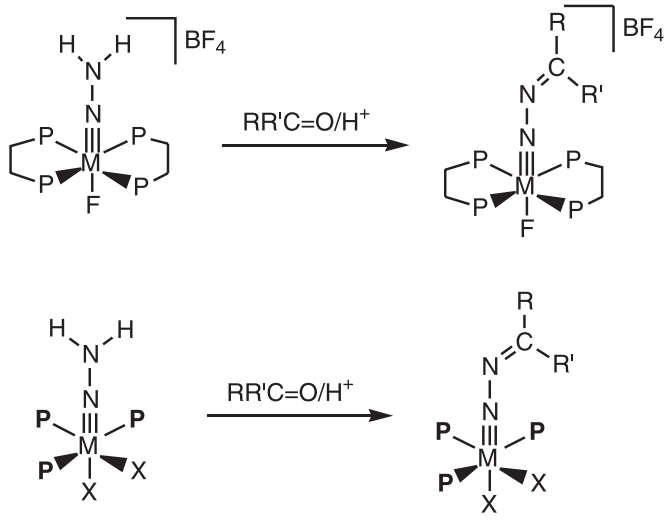
These reactions of **1** with acyl and aroyl chlorides involving the nucleophilic attack of the coordinated N_2 on the carbonyl C atoms as the principal step have further been extended by Chatt, George, and co-workers (32) to those with alkyl halides RX, yielding the corresponding alkyldiazenido complexes *trans*-[MX(NNR)(dppe)$_2$], although the latter reactions proceed via the reaction of the terminal N atom of the N_2 ligand with the alkyl radical generated through the homolysis of RX in the coordination sphere of Mo or W under irradiation with a W lamp. Interconversion between these diazenido complexes and their alkylhydrazido(2–) derivatives *trans*-[MX(NNHR) (dppe)$_2$]X readily proceeds through protonation and deprotonation (Scheme 8). Dialkylhydrazido(2–) complexes *trans*-[MBr(NNMe_2)(dppe)$_2$]Br and

© 2005 NRC Canada

Scheme 8.



Scheme 9.

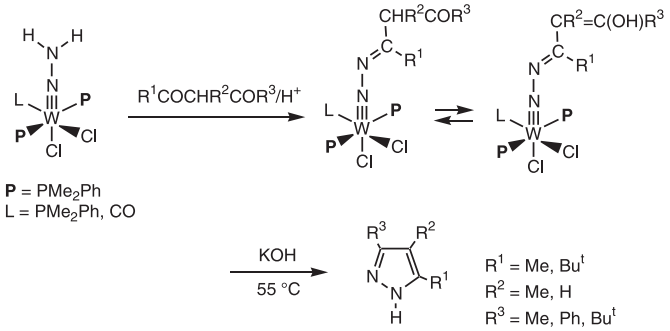


trans-[MBr(NN(CH$_2$)$_{n-1}$CH$_2$)(dppe)2]Br can be obtained directly, when complexes **1** were treated with MeBr or Br(CH$_2$)$_n$Br (n = 3–5) (33). For *trans*-[MoBr(NN(CH$_2$)$_4$CH$_2$)(dppe)$_2$]Br, the cyclic system producing H$_2$NN(CH$_2$)$_4$CH$_2$ from N_2 has been attained by coupling with the electrolysis of the dialkylhydrazido(2–) complex under N_2 to regenerate **1a** (34). Unfortunately, the N—C bond formation using alkyl halides is not applicable to the monophosphine complexes **2** under these conditions because of the loss of all N_2 ligands as N_2 gas.

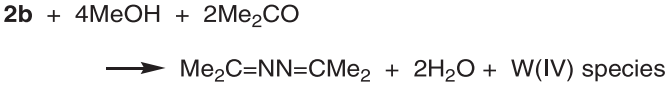
As for the more convenient and general methods to form the N—C bonds from the N_2 ligand in complexes **1** and **2**, we have demonstrated the condensation reactions of hydrazido(2–) complexes with aldehydes and ketones to give a variety of diazoalkane complexes. Thus, hydrazido(2–) complexes *trans*-[MF(NNH$_2$)(dppe)$_2$][BF$_4$] and *cis*,*mer*-[MX$_2$(NNH$_2$)(PMe$_2$Ph)$_3$] (X = Br, Cl) both react with various aldehydes and ketones RR′C=O to afford *trans*-[MF(NN=CRR′)(dppe)$_2$][BF$_4$] (35) and *cis*,*mer*-[MX$_2$(NN=CRR′)(PMe$_2$Ph)$_3$] (36) (Scheme 9). Addition of a catalytic amount of acid enhances these condensation reactions remarkably, especially for those with ketones. Treatment of *cis*,*mer*-[WBr$_2$(NN=CMe$_2$)(PMe$_2$Ph)$_3$] with HBr gives a mixture of N_2H_4 and acetone azine (Me$_2$C=NN=CMe$_2$), while that with LiAlH$_4$ yields a mixture of *i*-Pr-NH$_2$ and NH$_3$ (36*a*).

From the reactions of these hydrazido(2–) complexes and *cis*,*trans*-[WCl$_2$(NNH$_2$)(PMe$_2$Ph)$_2$(CO)] (37) with 1,3-diketones R^{1}COCHR^{2}COR^3, diazoalkane complexes *trans*-[MF{NN=CMe(CH$_2$COMe)}](dppe)$_2$]BF$_4$ (35) and *cis*,*mer*- or *cis*,*trans*-[MX$_2$\{NN=CR^1(CHR^{2}COR^3)\}(PMe$_2$Ph)$_2$(L)] (M = Mo: L = PMe$_2$Ph; M = W: L = PMe$_2$Ph, CO) were prepared analogously. From the latter complexes *cis*,*mer*- or *cis*,*trans*-[WCl$_2$\{NN=CR^1(CHR^{2}COR^3)\}(PMe$_2$Ph)$_2$(L)], pyrazoles were obtained by reaction with KOH in EtOH (38) (Scheme 10).

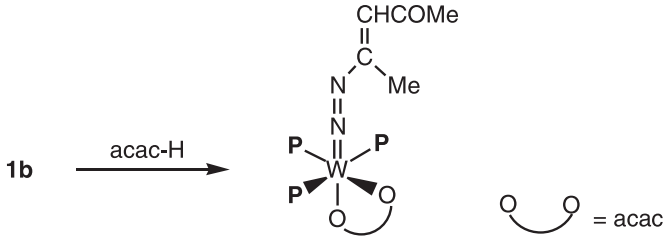
Scheme 10.



Scheme 11.



Scheme 12.



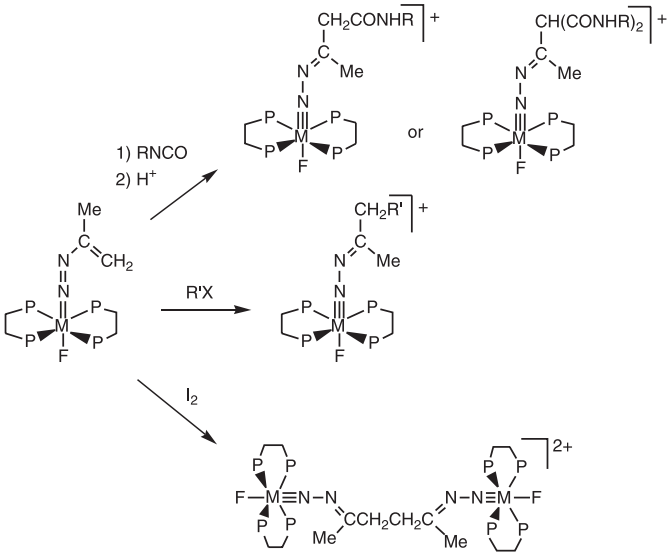
Treatment of *cis*,*mer*- or *cis*,*trans*-[WCl$_2$(NNH$_2$)(PMe$_2$Ph)$_2$(L)] with 1,3,5-triketones resulted in the formation of either the mononuclear complexes with diazoalkane (e.g., NN=CMeCH=C(OH)CH=C(OH)Ph) ligand or the dinuclear complexes with bridging bis(diazo)alkane (e.g., NN=CPh-CH$_2$COCH$_2$CPh=NN) ligand (39).

It is noteworthy that the reaction of the N_2 complex **2b** with a mixture of MeOH–acetone at 50 °C gives acetone azine directly (Scheme 11), which presumably proceeds through the formation of the hydrazido(2–) intermediate and the subsequent condensation with acetone forming a diazoalkane species (23). The yield of the azine increases significantly by addition of KOH to the reaction mixture. On the other hand, an alkenyldiazenido complex *mer*-[W(acac)\{NN-CMe(=CHCOMe)\}(PMe$_2$Ph)$_3$] (acac = acetylacetonante) was isolated from the reaction of **2b** with acetylacetone in MeOH (Scheme 12). The related diazenido complexes *trans*-[MF\{NNCMe(=CHCOMe)\}(dppe)$_2$] were derived by deprotonation from the diazoalkane complexes *trans*-[MF\{NN=CMe-(CH$_2$COMe)\}](dppe)$_2$][BF$_4$] by the use of NaOMe (40).

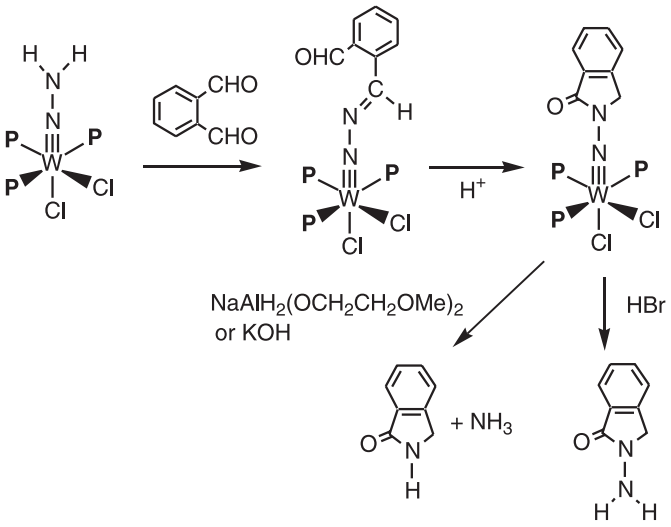
Diazenido complexes *trans*-[MF\{NNCMe(=CH$_2$)\}](dppe)$_2$] have been prepared similarly from *trans*-[MF(NN=CMe$_2$-(dppe)$_2$][BF$_4$] and LDA or NaN(SiMe$_3$)$_2$, which are converted to a series of new mononuclear diazoalkane complexes with NN=CMe(CH$_2$CONHR) and NN=CMe(CH$_2$R) ligands as well as dinuclear complexes with μ-bis(diazo)alkane ligand NN=CMeCH$_2$CH$_2$CMe=NN by treatment with RNCO/H$^+$, RX, and I$_2$, respectively (41) (Scheme 13). From the cationic diazoalkane complex *mer*-[WCl(NN=CMe$_2$)(PMe$_2$Ph)$_3$(CO)]$^+$, the μ-alkyldiazenido complex [{*trans*,*trans*-WCl(PMe$_2$Ph)$_2$(CO)$_2$}$_2$(μ-NNCMe$_2$CMe$_2$NN)] was isolated by reduction with Mg under CO (42).

© 2005 NRC Canada

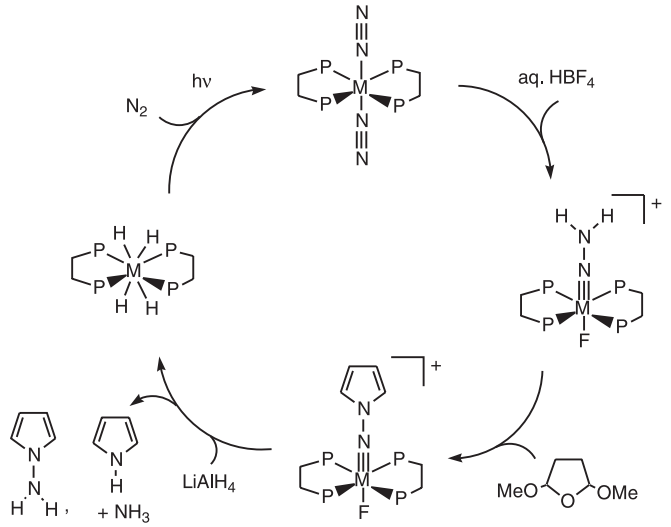
Scheme 13.



Scheme 14.



Scheme 15.



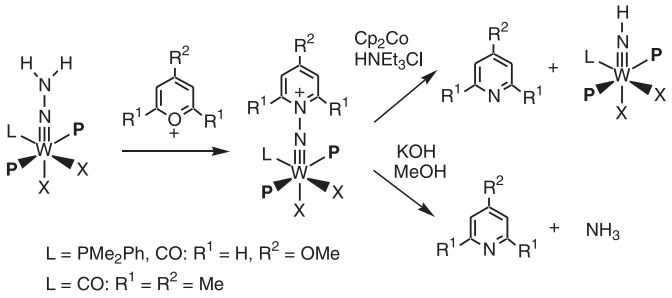
Condensation reactions of the hydrazido(2–) complexes as the versatile methods for the N—C bond formation have further been studied, aiming at the syntheses of *N*-heterocyclic ligands and compounds. Treatment of *cis*,*mer*-[$WCl_2(NNH_2)(PMe_2Ph)_3$] with phthalaldehyde at room temperature in the presence of a catalytic amount of aq. HCl gives (phthalimidin-2-yl)imido complex *cis*,*mer*-[$WCl_2(NNCH_2C_6H_4CO)(PMe_2Ph)_3$] via the condensation of the hydrazido(2–) ligand with one formyl group of the aldehyde to give a diazoalkane complex, followed by the cyclization forming the phthalimidine ring (43). In the absence of the acid, the reaction stops at the intermediate diazoalkane stage, which is converted into the (phthalimidin-2-yl)imido complex by addition of the acid. In the case of *trans*-[$WF(NNH_2)(dppe)_2]^+$, the reaction catalyzed by the acid gives the diazoalkane complex at room temperature, which can be transformed into the corresponding (phthalimidin-2-yl)imido complex by heating the reaction mixture in the presence of $AlCl_3$. Reaction of *cis*,*mer*-[$WCl_2(NNCH_2C_6H_4CO)(PMe_2Ph)_3$] with HBr gives 2-aminophthalimidine, while that with $NaAlH_2(OCH_2CH_2OMe)_2$ or KOH affords a mixture of phthalimidine and NH_3 (Scheme 14).

A cyclic acetal of succinaldehyde, i.e., 2,5-dimethoxytetrahydrofuran, also reacts with the hydrazido(2–) complexes *trans*-[$MX(NNH_2)(dppe)_2]^+$ (X = F, Cl) and *cis*,*mer*-[$WX_2(NNH_2)(PMe_2Ph)_3$] (X = Cl, Br) to give the condensation products *trans*-[$MX(NNCH{=}CHCH{=}CH)(dppe)_2]^+$ and *cis*,*mer*-[$WX_2(NNCH{=}CHCHC{=}CH)(PMe_2Ph)_3$], respectively (44). Interestingly, electrophilic substitution reactions at the pyrrole ring in the former dppe complexes occur selectively at the β position because of the steric effect of the dppe ligands giving *trans*-[$MX(NNCH{=}C(E)CH{=}CH)(dppe)_2]^+$ (E = Br, CN, COR). Complexes *trans*-[$MX(NNCH{=}CHCH{=}CH)(dppe)_2]^+$ are reduced by $LiAlH_4$, yielding pyrrole and *N*-aminopyrrole together with [$MH_4(dppe)_2$]. These hydrido complexes are known to be converted to the parent N_2 complexes **1** under certain conditions, so that the cycle forming pyrrole and *N*-aminopyrrole from N_2 has been accomplished (Scheme 15). In the degradation of the PMe_2Ph complex *cis*,*trans*-[$WX_2(NNCH{=}CHCHC{=}CH)(PMe_2Ph)_2(L)$], it has turned out that the reaction conditions and the nature of L (L = PMe_2Ph, CN-*t*-Bu, CO, PhC≡CH, PhCHO, Br) significantly affect the yield of the products: either pyrrole and ammonia or aminopyrrole (45). For example, treatment of *cis*,*trans*-[$WBr_2(NNCH{=}CHCHC{=}CH)(PMe_2Ph)_2$(CN-*t*-Bu)] with $LiAlH_4$ followed by methanolysis gives pyrrole and ammonia quantitatively, whereas the reactions of the CO, PhC≡CH, and PhCHO complexes with KOH in alcohol produce aminopyrrole selectively.

Reactions of hydrazido(2–) complexes *cis*,*mer*- or *cis*,*trans*-[$WX_2(NNH_2)(PMe_2Ph)_2(L)$] (L = PMe_2Ph, CO, C_2H_4) with pyrylium cations result in the formation of (1-pyridinio)imido complexes such as [$WX_2(NNC_5H_4OMe)(PMe_2Ph)_2(L)]^+$ and [$WX_2(NNC_5H_2Me_3)(PMe_2Ph)_2(L)]^+$, which

© 2005 NRC Canada

Scheme 16.

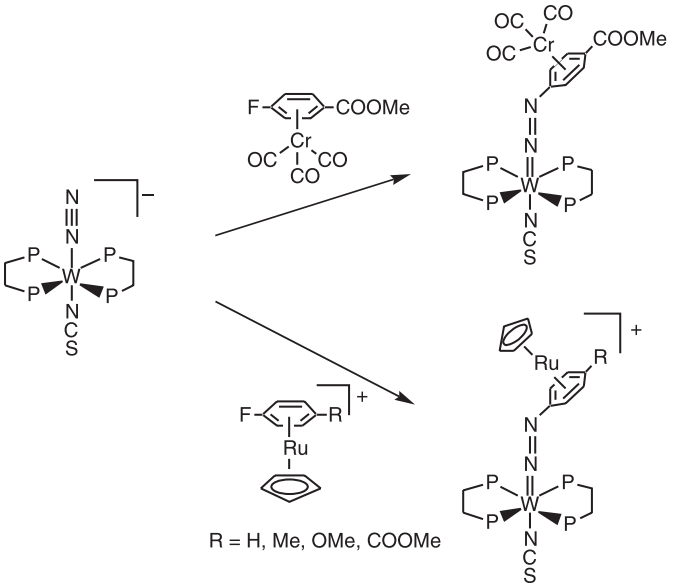


liberate pyridines by treatment with $CoCp_2$/$HNEt_3Cl$ in THF or KOH in MeOH (46) (Scheme 16).

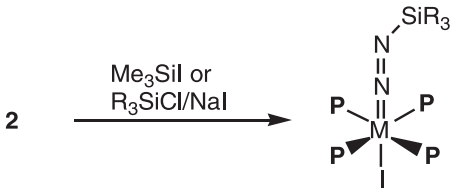
As summarized above, the Mo and W hydrazido(2–) complexes are quite potential compounds that readily condense with numerous carbonyl compounds and related oxygen-containing organic compounds. The hydrazido(2–) ligands also react as the nucleophiles with organic acid halides and heteroallenes to give the substitution products and addition products. These include, for example, a diacylated complex *trans*-[WF(NNCOCH$_2$CH$_2$CO)(dppe)$_2$][BF4] from *trans*-[WF(NNH$_2$)(dppe)$_2$][BF$_4$] and succinyl chloride (47), and *cis*,*mer*-[WCl$_2$(NNHCOCHPh$_2$)(PMe$_2$Ph)$_3$] from *cis*,*mer*-[WCl$_2$(NNH$_2$)(PMe$_2$Ph)$_3$] and diphenylketene (48), respectively.

Finally, arylation of the coordinated N_2 is shown. Alkylation of the N_2 ligand in **1** is the well-demonstrated reaction applicable to a series of alkyl halides and dihalides (vide supra). However, arylation of the coordinated N_2 by aryl halides is hardly accessible except for the pathway via the reaction of the highly activated aryl fluoride 2,4-$(O_2N)_2C_6H_3F$ with the diazenido complexes [WX(NNH)(dppe)$_2$] (X = F, Br, CF_3COO) generated in situ from the corresponding hydrazido(2–) complexes with bases (49). We have found that the anionic N_2 complex [W(NCS)(N$_2$)(dppe)$_2$]$^-$ reacts with π-fluoroarene complexes such as [(*p*-FC$_6$H$_4$CO-OMe)Cr(CO)$_3$] and [(*p*-FC$_6$H$_4$R)RuCp]$^+$ (R = H, Me, OMe, COOMe) to give the bimetallic complexes with bridging aryldiazenido ligands (50) (Scheme 17), where by activating both the N_2 ligand and the fluoroarenes, arylation of the coordinated N_2 has been attained.

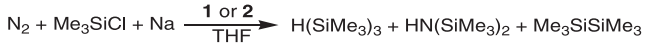
Scheme 17.



Scheme 18.



Scheme 19.



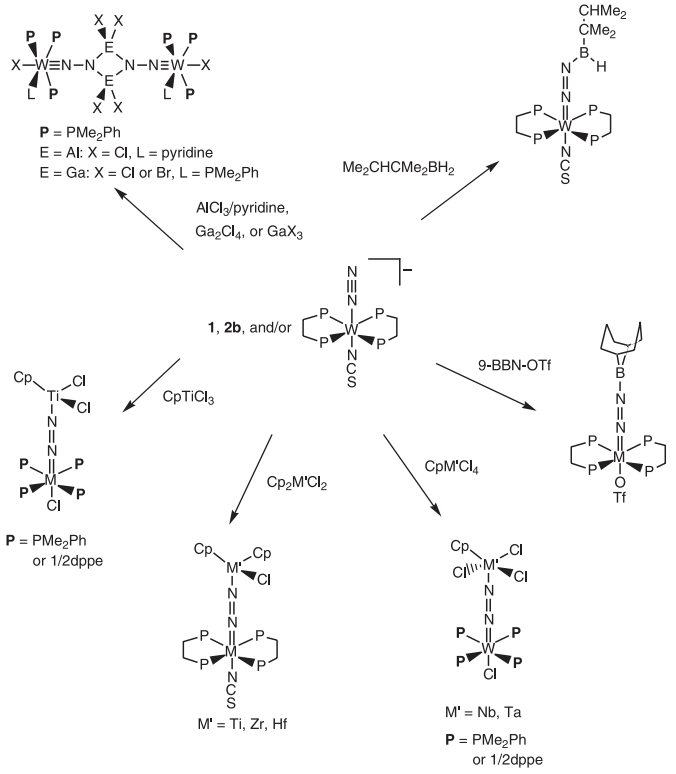
Formation of the N—heteroatom bond

The terminal N atom having the nucleophilic character of the N_2 ligand in **1** and **2** reacts with electrophilic heteroatom centers in addition to protons and electron-deficient C atoms. Thus, by treatment with Me_3SiI in benzene at 50 °C under dry conditions, **1** and **2** give the silyldiazenido complexes [MI(NNSiMe$_3$)(dppe)$_2$] and *trans*-[MI(NNSiMe$_3$)(PMe$_2$Ph)$_4$]. In the presence of adventitious moisture, silylhydrazido(2–) complexes [MI(NNHSiMe$_3$)(dppe)$_2$]I and *cis*,*mer*-[MI$_2$(NNHSiMe$_3$)(PMe$_2$Ph)$_3$] are obtained in addition to the diazenido complexes (51). Although Me_3SiCl does not react with **1** and **2** under these conditions, it has turned out that treatment of **2b** with a mixture of Me_3SiCl–NaI gives *trans*-[MI(NNSiMe$_3$)(PMe$_2$Ph)$_4$]. Following this procedure, synthesis of a variety of silyldiazenido complexes becomes available by the use of numerous silyl chlorides obtained commercially (52) (Scheme 18). From the reaction of **2b** with ClSiMe$_2$CH$_2$CH$_2$SiMe$_2$Cl–NaI followed by treatment with certain π-acceptor molecules L, disilylated complexes *cis*,*trans*-[WI(NNSiMe$_2$CH$_2$CH$_2$SiMe$_2$)(PMe$_2$Ph)$_2$(L)] (L = CO, alkene, isonitrile, nitrile) were isolated (53). Germylation also proceeds similarly at the N_2 ligand in **2b** upon reacting with R_3GeCl–NaI (52). Bimetallic silylation systems were also explored, which resulted in the finding that the silylcobalt complex [Ph$_2$MeSiCo(CO)$_4$] prepared from Ph$_2$MeSiH and [Co$_2$(CO)$_8$] reacts with **1** and **2** to give silyldiazenido complexes *trans*-[{MI(NNSiPh$_2$Me)(**P**)$_4$}(μ-OC)Co(CO)$_3$] (**P** = PMe$_2$Ph, 1/2dppe) (54).

Reduction of *trans*-[MI(NNSiMe$_3$)(PMe$_2$Ph)$_4$] with Na under N_2 in THF has been revealed to give N_1 products including NH_3, HN(SiMe$_3$)$_2$, $NaNH_2$, $NaNHSiMe_3$, and NaN(SiMe$_3$)$_2$, accompanied by the regeneration of the parent N_2 complexes **2** (55). Detailed study on this and related reactions has led to the development of the novel catalytic system converting molecular N_2 into silylamines. Thus, when Me_3SiCl is treated with an equimolar amount of Na dispersion in THF under N_2 at 30 °C in the presence of **2a**, N(SiMe$_3$)$_3$ was obtained in the yield of 24 mol/Mo atom to-

© 2005 NRC Canada

Scheme 20.

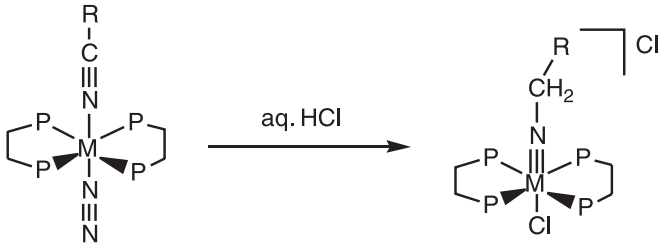


gether with a small amount of $HN(SiMe_3)_2$ after 15 h (Scheme 19) (55*a*). A major by-product is $Me_3SiSiMe_3$. For the N_2 complexes **1** and **2**, the catalytic activities decrease in the order **2a** > **1a** > **2b**, **1b**. The reactions in which molecular N_2 is converted catalytically into nitrogenous compounds under mild conditions are quite rare and those using well-defined N_2 complexes as a catalyst or catalyst precursor are still limited to only two systems: one is the present system and the other is the reaction of a Mo dinitrogen complex having a triamidoamine ligand (vide supra) (25).

With respect to the Group 13 elements, reactions of **1** and **2** with AlR_3 (R = Me, Et) forming Lewis acid – base adducts containing the $MNNAlR_3$ moieties were known for some time (56). In contrast, treatment of **2b** with $AlCl_3$–pyridine and $GaCl_3$ gives the ditungsten complexes having the $ClWNN(ECl_2)_2NNWCl$ array (E = Al (57), Ga (58)) (Scheme 20). As for boron compounds, by treating the anionic W complex $[W(NCS)(N_2)(dppe)_2]^-$ with 1,1,2-trimethylpropylborane and 9-borabicyclo[3.3.1]nonane, or by reacting **1** with 9-borabicyclo[3.3.1]nonyl triflate, novel borylation of coordinated N_2 was successful (59) (Scheme 20). The boryldiazenido complexes obtained were fully characterized, which demonstrated the bent N–N–B linkages for the complexes with the NCS anion, and the essentially linear N–N–B linkages for the triflate complexes.

Lewis acidic compounds containing Group 4 and Group 5 metals such as $CpTiCl_3$, Cp_2MCl_2 (M = Ti, Zr, Hf), and $CpMCl_4$ (M = Nb, Ta) also react with the coordinated N_2 in **1**, **2b**, and (or) $[W(NCS)(N_2)(dppe)_2]^-$ to form dinuclear complexes containing an essentially linear XWNNM array (60) (Scheme 20). Interestingly, heterobimetallic dinitrogen complexes $[Cp'TiCl_2(\mu\text{-}N_2)WCl(L)_4]$ (Cp′ = Cp, Cp*, etc.; L = 1/2dppe, 1/2depe, PMe_2Ph) obtained from similar reactions exhibit high catalytic activity for olefin polymerization when combined with modified methylaluminoxane, in which the W dinitrogen fragment acts as a novel metallodinitrogen ligand to the catalytically active Ti center (61).

Scheme 21.



Reactions of coordinated nitriles — C≡N bond cleavage

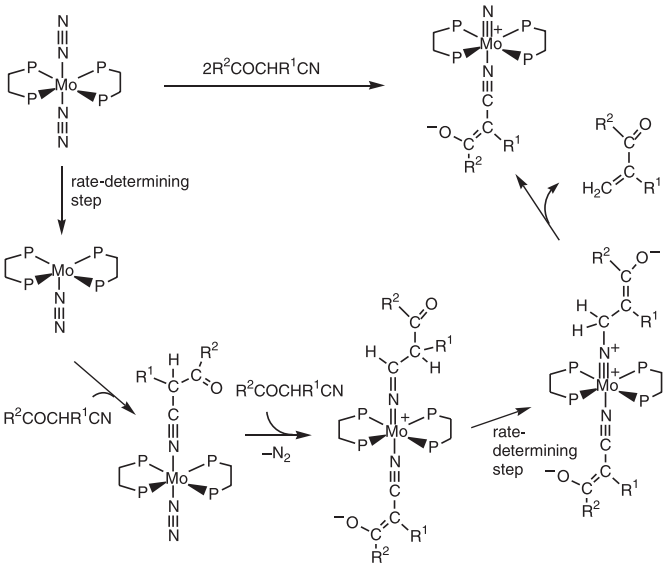
When nitrile–dinitrogen complexes *trans*-$[M(N_2)(NCR)(dppe)_2]$ (M = Mo (62), W (63)), which are readily derived from **1** and RCN, are treated with aq. HCl in THF, imido complexes *trans*-$[MCl(NCH_2R)(dppe)_2]Cl$ (R = Me, aryl) are obtained (Scheme 21). Reactions with aq. HBF_4 proceed in a similar manner to give *trans*-$[MF(NCH_2R)(dppe)_2]BF_4$ (64). The nitriles bound to the $M(dppe)_2$ site are susceptible to the attack by protons because of the strong π back donation from the electron-rich M centers. It is to be noted, however, that the protonation of *trans*-$[M(N_2)(NC\text{-}n\text{-}Pr)(dppe)_2]$ with HCl or H_2SO_4 has been reported to occur at the N_2 ligand to give the hydrazido(2–) complexes *trans*-$[M(NNH_2)(NC\text{-}n\text{-}Pr)(dppe)_2]^{2+}$ (63), and the reactions of *trans*-$[Mo(N_2)(NCR)(dppe)_2]$ with PhCOCl afford *trans*-$[MoCl(NNCOPh)(dppe)_2]$ (vide supra) (31, 62).

It is quite interesting that in the reactions of **1a** with 2 equiv. of β-ketonitriles R^2COCHR^1CN, unique C≡N bond cleavage takes place under mild conditions, yielding the complexes with nitrido- and nitrile-enolato ligands *trans*-$[Mo(N)(NCCR^1COR^2)(dppe)_2]$ (65). This reaction is initiated by the dissociation of one N_2 ligand as the first rate-determining step. The vacant site is occupied by one β-ketonitrile, which undergoes rapid protonation at the cyano C atom by the second β-ketonitrile, yielding the alkylideneamido (or azavinylidene) complex with the nitrile-enolato ligand *trans*-$[Mo(N{=}CHCHR^1COR^2)(NCCR^1COR^2)(dppe)_2]$. Migration of the β-proton in the alkylideneamido ligand to the α-C atom leading to the imido ligand constitutes the second rate-determining step in this reaction, which is followed by the rapid elimination of vinylketone $CH_2{=}CR^1COR^2$ to give the final product (Scheme 22). The mechanism of the present C≡N bond cleavage is quite rare, which is in sharp contrast with the precedented metathesis-type mechanism demonstrated for the reactions promoted by, e.g., $[W(C\text{-}t\text{-}Bu)(OC_6H_3\text{-}i\text{-}Pr_2\text{-}2,6)_3]$ and $[W_2(OR)_6]$ (R = *t*-Bu, CMe_2CF_3) (66).

As observed in the reactions of **1a** with β-ketonitriles, the N_2 complexes **1** can serve as good precursors to generate in situ the highly reactive, coordinatively unsaturated species "Mo(dppe)(N_2)" and "Mo(dppe)$_2$", which can activate not only nitriles but also a number of other small molecules including dihydrogen, isocyanide, alkynes, alkenes, etc. Such

© 2005 NRC Canada

Scheme 22.



remarkable reactivities characteristic of **1** have recently been reviewed by the authors elsewhere (67).

Chemistry of noble metal–sulfur cluster complexes

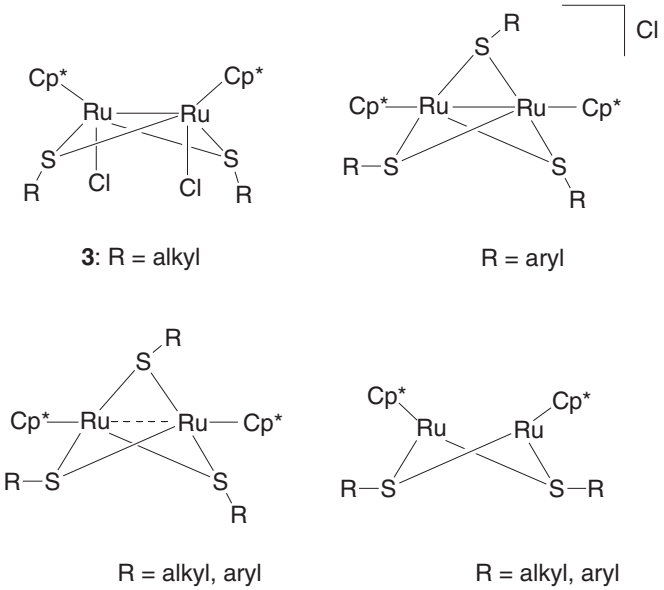
As summarized above, the zero-valent Mo and W dinitrogen complexes with phosphine co-ligands **1** and **2** display numerous outstanding reactivities, which include those relating intimately to the function of nitrogenase. However, this natural enzyme consists of the multimetallic site with a sulfur environment to activate dinitrogen and so-called "alternative substrates" such as N_2H_4, acetylene, nitrile, etc. Recent studies have further revealed that a modified MoFe protein reduces, under turnover conditions, alkynes larger than acetylene, including propargyl alcohol (68). Hence, our studies have been done to synthesize the multimetallic complexes with sulfur ligands and to clarify their reactivities toward these small molecules. It is to be noted that fully characterized N_2 complexes with sulfur ligands are quite limited, which include the thioether (69), thiolato (70), and dithiocarbamato (71) complexes, and either the N_2 complexes with the sulfide ligands or those with sulfur-bridged multimetallic cores are yet unknown.

Diruthenium complexes with bridging thiolato ligands

Our studies on the polynuclear metal–sulfur compounds started about 20 years ago from synthesis of a new series of thiolato-bridged diruthenium complexes. Although the chemistry of transition metal – thiolato complexes was already the subject of much interest, this was almost limited to the compounds containing the biologically important metals. With respect to the Group 8 metals, extensive studies had been carried out on the Fe thiolato complexes, however, studies on the corresponding Ru complexes were developed only poorly at that time.

By treating the Ru(III) complex $[(Cp^*RuCl)_2(\mu\text{-}Cl)_2]$ (72) with certain thiolato sources, we isolated four types of diruthenium complexes with bridging thiolato ligands; i.e.,

Fig. 3. Structures of thiolato-bridged diruthenium complexes.

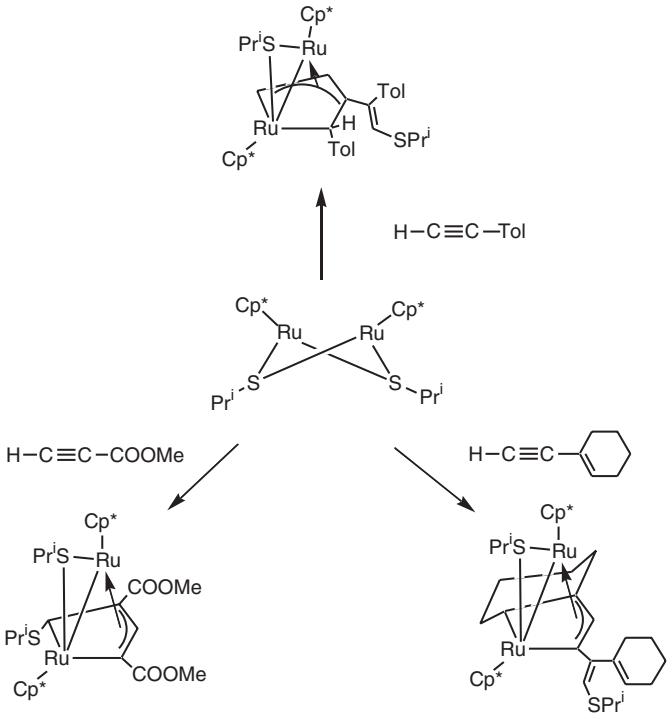


Ru(III)–Ru(III) complexes $[(Cp^*RuCl)_2(\mu\text{-}SR)_2]$ (**3**) and $[(Cp^*Ru)_2(\mu\text{-}SR)_3]Cl$ (73), paramagnetic Ru(III)–Ru(II) complexes $[(Cp^*Ru)_2(\mu\text{-}SR)_3]$, and Ru(II)–Ru(II) complexes $[(Cp^*Ru)_2(\mu\text{-}SR)_2]$ (74) (Fig. 3). The latter Ru(II)–Ru(II) complexes were prepared more readily (75) via the Ru(II) complexes $[(Cp^*Ru)_2(\mu\text{-}OMe)_2]$ (76) or $[(Cp^*Ru)_4(\mu_3\text{-}Cl)_4]$ (77) derived from $[(Cp^*RuCl)_2(\mu\text{-}Cl)_2]$. Studies on the reactivities toward small molecules were first done intensively for Ru(II)–Ru(II) and Ru(II)–Ru(III) complexes $[(Cp^*Ru)_2(\mu\text{-}S\text{-}i\text{-}Pr)_n]$ (n = 2, 3), which disclosed that these are quite versatile complexes that display various novel reactivities as already summarized elsewhere (11*e*). It is noteworthy that the reactions at the diruthenium site including coordination of neutral π-acceptor molecules such as CO and *t*-BuNC, dinuclear oxidative addition of H_2 and alkyl halides, and incorporation of two or three terminal alkyne molecules proceed with retention of the dinuclear core owing to the strong bridging ability of the thiolato ligand. Among these interesting reactions, those of alkynes with $[(Cp^*Ru)_2(\mu\text{-}S\text{-}i\text{-}Pr)_n]$ (n = 2, 3) are especially unique, which may be exemplified by the preparation of various dinuclear ruthenacyclopentenyl complexes from $[(Cp^*Ru)_2(\mu\text{-}S\text{-}i\text{-}Pr)_2]$ with a series of terminal alkynes (78) (Scheme 23) as well as the formations of bis(alkynyl) complexes (79) and diruthenacyclopentanone or diruthenacyclopentenone complexes (80) from $[(Cp^*Ru)_2(\mu\text{-}S\text{-}i\text{-}Pr)_3]$ with monoarylacetylenes and propargyl alcohols (Scheme 24), respectively. Extension of these studies on the reactions of Ru(II)–Ru(II) and Ru(II)–Ru(III) complexes with alkynes to those of Ru(III)–Ru(III) complexes **3** and the cationic complexes $[(Cp^*RuCl)(\mu\text{-}SR)_2\{Cp^*Ru(H_2O)\}][OTf]$ (**4**) derived from **3** through the anion metathesis has led more recently to the finding of new catalytic reactions promoted at their thiolato-bridged diruthenium sites.

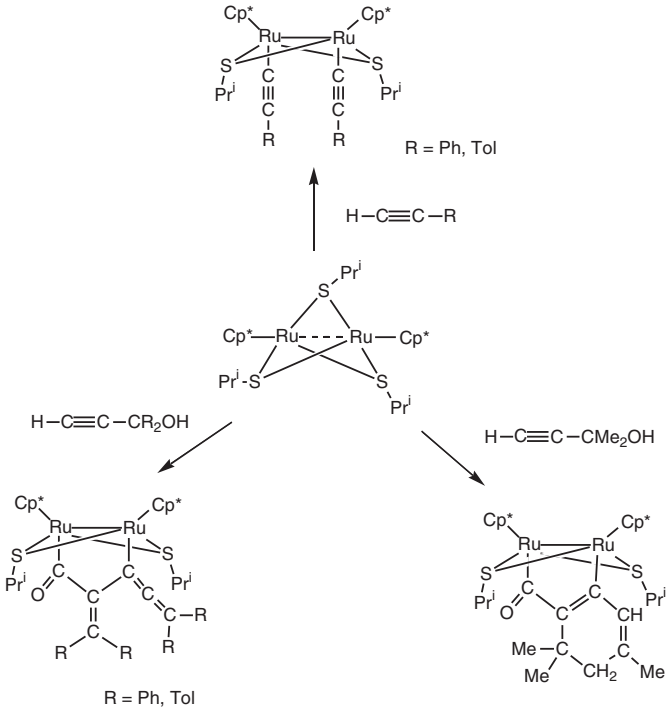
In the presence of NH_4BF_4 at 60 °C, complexes **3** (R = Me, Et, *n*-Pr) catalyze the head-to-head dimerization of various terminal alkynes into (*Z*)-en-ynes (81). It is noteworthy that aliphatic alkynes having chloro, hydroxy, and ester groups at the ω-positions are also converted to the corre-

© 2005 NRC Canada

Scheme 23.

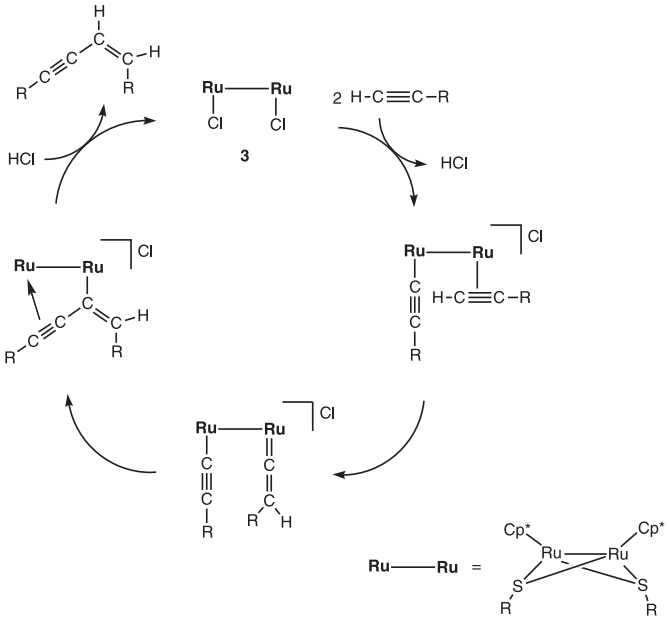


Scheme 24.

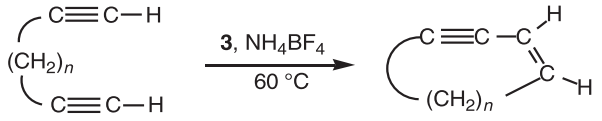


sponding (*Z*)-en-ynes in moderate to high yields. The mechanism involving the alkynyl-alkyne, alkynyl-vinylidene, and butenynyl intermediates was proposed (Scheme 25) on the basis of the isolation of vinylidene complexes [(Cp*Ru-Cl)(μ-S-*i*-Pr)$_2${Cp*Ru(=C=CHR)}][OTf] (R = H, COOMe, COMe) from the reaction of **4** (R = *i*-Pr) with HC≡CR (82)

Scheme 25.



Scheme 26.

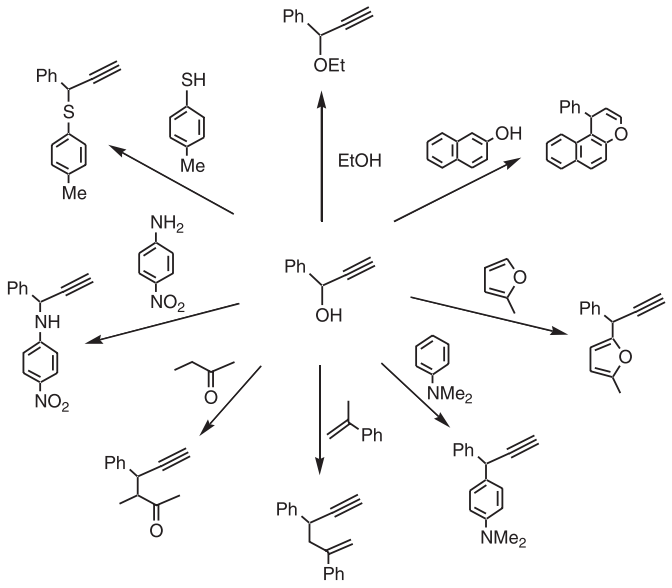


and the butenynyl complex [{Cp*Ru(C(=CHFc)C≡CFc)}(μ-S-*i*-Pr)$_2$(Cp*Ru)][OTf] (Fc = ferrocenyl) from **4** (R = *i*-Pr) and HC≡CFc (83). The latter butenynyl complex has turned out to catalyze the regio- and stereoselective dimerization of FcC≡CH to *Z*-FcCH=CHC≡CFc. This catalysis was later applied to the intramolecular reactions of α,ω-diynes HC≡C(CH$_2$)$_n$C≡CH (*n* = 6, 8, 10, 12), leading to a new method for synthesizing *endo*-macrocyclic (*Z*)-1-en-3-ynes (84) (Scheme 26).

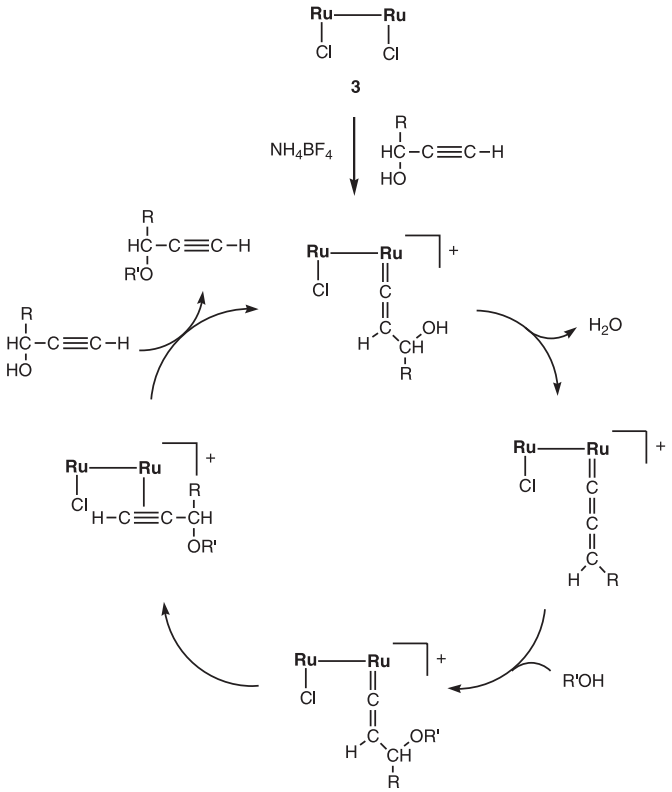
Noteworthy is that complexes **3** display the catalytic activity for the propargylic substitution reactions of propargylic alcohols HC≡CCHROH with a number of nucleophiles, which include not only heteroatom-centered nucleophiles such as alcohols, amines, and thiols (85), but also carbon-centered nucleophiles such as simple ketones (86), alkenes (87), phenols (88), and aromatic compounds (89) (Scheme 27). The above reactions proceed catalytically with complete regioselectivities, which are in sharp contrast to the Nicholas reaction effective for the propargylic substitution, but requiring a stoichiometric amount of Co_2CO_8 (90). It is also to be emphasized that conventional mononuclear ruthenium complexes are not effective for these propargylation reactions and the diruthenium core is essential for this catalysis. In Scheme 28, the mechanism proposed for the catalytic reaction of a propargylic alcohol with alcohol R′OH is shown as a typical example. Thus, the reaction is initiated by the formation of a vinylidene complex from **3** and the propargylic alcohol, which is then transformed into an allenylidene complex via dehydration. Nucleophilic attack of the alcohol on the γ-carbon atom in the allenylidene ligand gives another vinylidene complex,

© 2005 NRC Canada

Scheme 27.

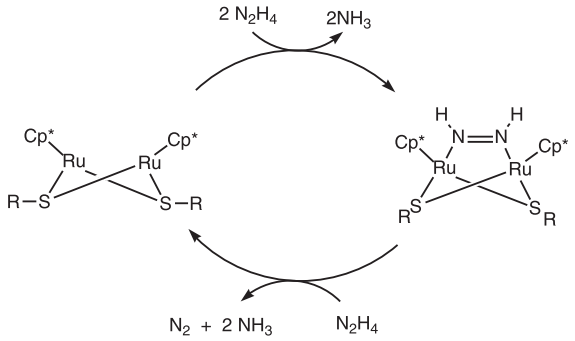


Scheme 28.



which subsequently isomerizes to a π-propargylic ether complex. The ether is liberated from the metal by reaction with excess of the propargylic alcohol to regenerate the initial vinylidene species. Formation of an allenylidene complex from the reaction of **3** with a propargylic alcohol was demonstrated by reacting **3** (R = Me) with $HC{\equiv}CC(Tol)_2OH$ in the presence of NH_4BF_4 at room temperature, whereby the isolated allenylidene complex $[\{Cp^*Ru(=C=C=CTol_2)\}(\mu\text{-}SMe)_2(Cp^*RuCl)][BF_4]$ liberated the ether $HC{\equiv}CC(Tol)_2OEt$ by treatment with EtOH at 60 °C.

Scheme 29.



The propargylation of ketones with propargylic alcohols has further been extended to convenient direct synthesis of tri- and tetra-substituted furans and pyrroles by employing a combination of two catalysts **3** and $PtCl_2$ (91). Quite interestingly, when the cationic diruthenium complex **4** (R = Me) was employed as catalyst, propargylation of aromatic compounds proceeds by using propargylic alcohols bearing not only a terminal acetylene group, but also an internal acetylene group (92), although elucidation of the reaction mechanism requires further investigation. Complex **4** also works effectively as a catalyst for the propargylic substitution reactions of various propargylic alcohols with thiols (93).

As the reaction that is relevant more closely to nitrogen fixation, disproportionation of hydrazine has been demonstrated to proceed at the thiolato-bridged diruthenium site. Thus, the Ru(II)–Ru(II) complex $[(Cp^*Ru)_2(\mu\text{-}S\text{-}i\text{-}Pr)_2]$ catalyzes the transformation of hydrazine into ammonia and dinitrogen, a balance equation of which is shown as $3N_2H_4 \rightarrow 4NH_3 + N_2$. Spectroscopic data of the reaction mixture suggested the presence of the μ-diazene complex as the intermediate (Scheme 29) (94).

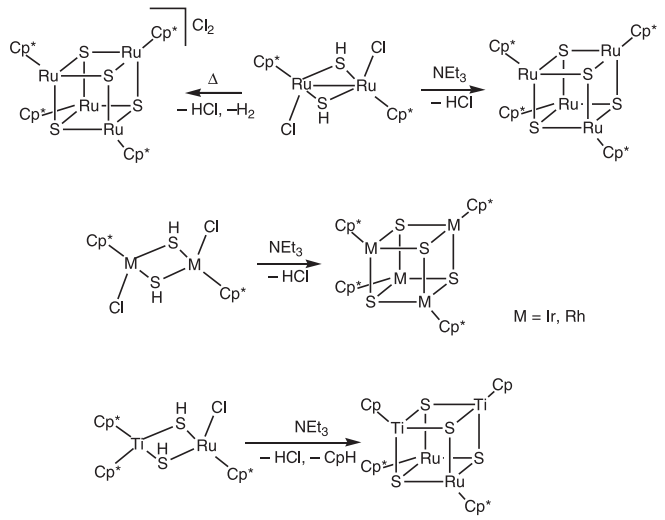
Chemistry of metal–sulfur cubane-type complexes

Metal–sulfur cubane-type M_4S_4 clusters have long been attracting much attention since the Fe_4S_4 core was demonstrated as the active site of bacterial ferredoxin in the early 1970s. Several years later, the mixed-metal, cubane-type $MoFe_3S_4$ core was proposed as a model of the metal–sulfur active site of the FeMo-cofactor (vide supra). In this context, cubane-type $MoFe_3S_4$ clusters had been prepared intensively as the model compounds of the nitrogenase active site (10). To be noted is that the cores of these clusters were prepared by the self-assembly methods in solution. Although subsequent studies on their reactivities have made some success in the cluster-catalyzed nitrogenase model reactions, e.g., reduction of N_2 into ammonia in a protic media under electrolytic conditions (95) and catalytic conversion of hydrazine into ammonia in the presence of certain proton and electron sources (96), development of intriguing reactivities of these clusters toward small molecules has been only poorly realized.

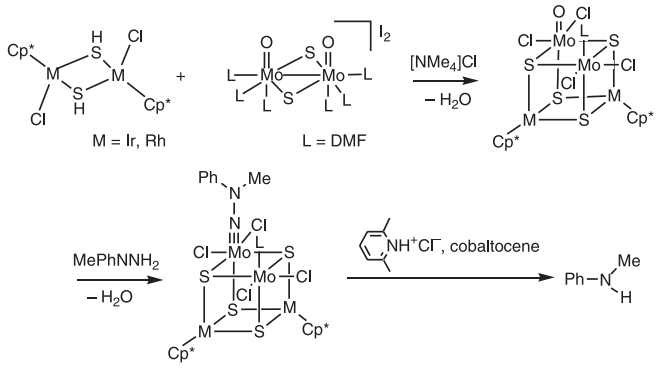
We have long been interested in synthesis and reactivities of noble metal-containing sulfur clusters and much effort has

© 2005 NRC Canada

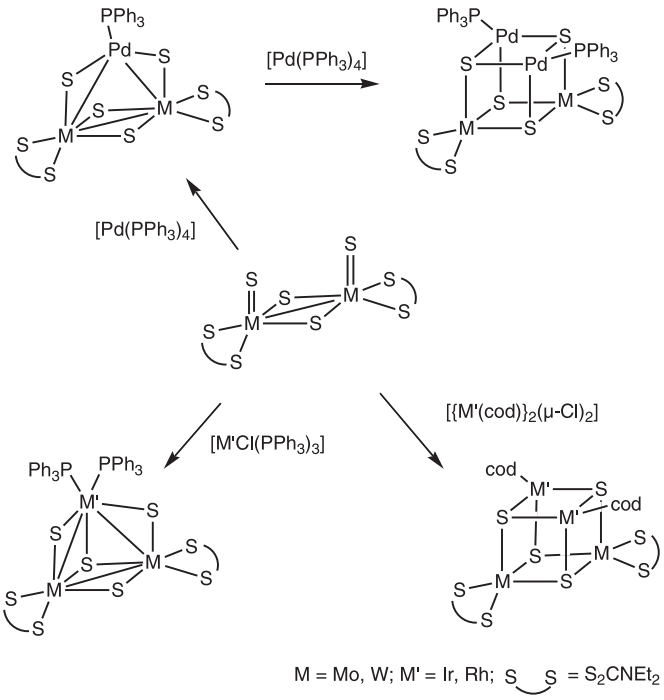
Scheme 30.



Scheme 31.



Scheme 32.



been devoted to the exploration of the *reliable* synthetic routes to prepare the sulfido clusters of this type with the desired atom composition in high yields (11*b*). These studies in this laboratory have resulted in the finding of several versatile methods to construct the cubane-type, metal–sulfido cores as summarized below.

A series of hydrosulfido-bridged dinuclear complexes with homometallic $M(\mu\text{-}SH)_2M$ (M = Ru (97), Ir, Rh (98)) and heterometallic $Ti(\mu\text{-}SH)_2Ru$ cores (99) have proved to be excellent precursors to prepare the homo- and heterometallic cubane-type clusters (Scheme 30). Thermal reaction of $[(Cp^*RuCl)_2(\mu\text{-}SH)_2]$ gives the cationic cluster $[(Cp^*Ru)_4(\mu_3\text{-}S)_4]Cl_2$ via the dimerization accompanied by dehydrogenation and dehydrochlorination (97), while treatment of $[(Cp^*MCl)_2(\mu\text{-}SH)_2]$ or $[(Cp_2Ti)(Cp^*RuCl)(\mu_2\text{-}SH)_2]$ with NEt_3 affords the neutral clusters $[(Cp^*M)_4(\mu_3\text{-}S)_4]$ (M = Ru, Ir, Rh) (100) or $[(CpTi)_2(Cp^*Ru)_2(\mu_3\text{-}S)_4]$ (99) through the dimerization with concomitant loss of HCl or HCl–CpH, respectively. By mixing $[(Cp^*RuCl)_2(\mu\text{-}SH)_2]$ and $[(Cp_2Ti)(Cp^*RuCl)(\mu_2\text{-}SH)_2]$ in the presence of NEt_3, the crossed condensation product $[(CpTi)(Cp^*Ru)_3(\mu_3\text{-}S)_4]$ is formed selectively (101).

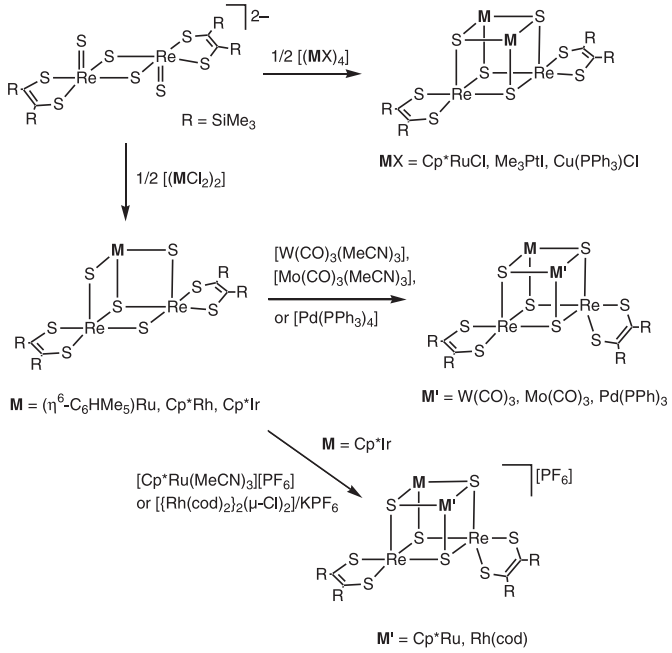
Condensation of the hydrosulfido-bridged complexes $[(Cp^*MCl)_2(\mu\text{-}SH)_2]$ (M = Ir, Rh) with the sulfido-bridged dimolybdenum oxo complex $[\{MoO(DMF)_3\}_2(\mu\text{-}S)_2]I_2$ in the presence of excess $[NMe_4]Cl$ gives the mixed-metal, cubane-type clusters with an oxo group on one Mo atom $[(MoOCl_2)\{MoCl_2(DMF)\}(Cp^*M)_2(\mu_3\text{-}S)_4]$ via dehydration. Further reaction of this Mo_2Ir_2 cluster with $MePhNNH_2$ affords the hydrazido(2–) cluster $[\{Mo(NNMePh)Cl_2\}\{MoCl_2(DMF)\}(Cp^*Ir)_2(\mu_3\text{-}S)_4]$, for which reductive cleavage of the N—N bond proceeds to form *N*-methylaniline by treatment with a lutidinium chloride – cobaltocene mixture (Scheme 31). Catalytic formation of *N*-methylaniline occurs when $MePhNNH_2$ is reacted with lutidinium chloride – cobaltocene in the presence of the oxo clusters $[(MoOCl_2)\{MoCl_2(DMF)\}(Cp^*M)_2(\mu_3\text{-}S)_4]$ (102). This reaction provides a rare example of catalytic reactions promoted by metal–sulfido clusters (103).

Sulfido-bridged dinuclear complexes $[\{MS(dtc)\}_2(\mu\text{-}S)_2]$ (M = Mo, W; dtc = diethyldithiocarbamate) also serve as good precursors to afford mixed-metal, cubane-type clusters by incorporating two metal fragments into their $MS(\mu\text{-}S)_2MS$ cores. Cubane-type clusters derived from this method are $[\{Pd(PPh_3)\}_2\{MS(dtc)\}_2(\mu_3\text{-}S)_4]$ (104) and $[\{M'(cod)\}_2\{MS(dtc)\}_2(\mu_3\text{-}S)_4]$ (M′ = Rh, Ir) (105). The trinuclear clusters $[\{Pd(PPh_3)\}\{MS(dtc)\}_2(\mu_3\text{-}S)(\mu_2\text{-}S)_3]$ as an intermediate are isolable from the reaction of $[\{MS(dtc)\}_2(\mu\text{-}S)_2]$ with an equimolar amount of $[Pd(PPh_3)_4]$. Although the formation of trinuclear clusters was not observed for the reaction of $[\{MS(dtc)\}_2(\mu\text{-}S)_2]$ with $[\{M'(cod)\}_2(\mu\text{-}Cl)_2]$ to give $[\{M'(cod)\}_2\{MS(dtc)\}_2(\mu_3\text{-}S)_4]$ (M′ = Rh, Ir), the incomplete cubane-type clusters $[\{M'(PPh_3)_2\}\{MS(dtc)\}_2(\mu_3\text{-}S)(\mu_2\text{-}S)_3(\mu_2\text{-}Cl)]$ (M′ = Rh, Ir) were obtained as the sole products from the reactions of $[\{MS(dtc)\}_2(\mu\text{-}S)_2]$ with $[M'Cl(PPh_3)_3]$ (Scheme 32).

Employment of the Re dithiolene complex $[PPh_4]_2[\{ReS(L)\}_2(\mu\text{-}S)_2]$ (L = $S_2C_2(SiMe_3)_2$) (106) as the alternative $MS(\mu\text{-}S)_2MS$ source gives rise to a new series of bimetallic cubane-type and incomplete cubane-type clusters.

© 2005 NRC Canada

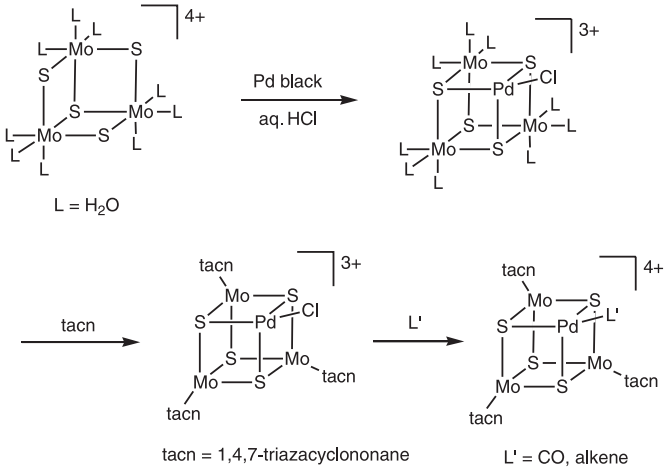
Scheme 33.



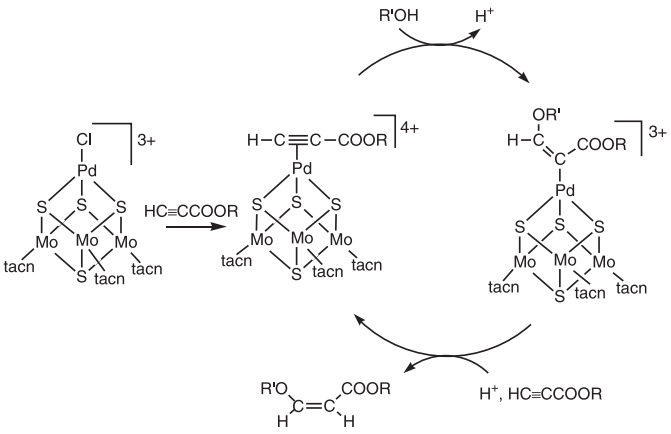
It is noteworthy that from the incomplete cubane-type clusters $[(Cp^*M)\{Re(L)_2\}(\mu_3\text{-}S)(\mu_2\text{-}S)_3]$ (M = Ir, Rh) and $[\{(\eta^6\text{-}C_6HMe_5)Ru\}\{Re(L)_2\}(\mu_3\text{-}S)(\mu_2\text{-}S)_3]$ obtained here, novel trimetallic cubane-type clusters containing $MM'Re_2(\mu_3\text{-}S)_4$ cores (M = Ir, Rh: M′ = W, Mo, Ru, Rh, Pd; M = Ru: M′ = W, Pd) could be prepared (Scheme 33). This contrasts sharply with the previous observation that such trimetallic cubane-type clusters were not available from the trinuclear PdM_2, RhM_2, and IrM_2 clusters derived from $[\{MS(dtc)\}_2(\mu\text{-}S)_2]$ (M = Mo, W) shown above.

Incorporation of a metal fragment into the void of the incomplete cubane-type $M_3(\mu_3\text{-}S)(\mu_2\text{-}S)_3$ core had earlier proved to be a versatile method to prepare bimetallic cubane-type $M_3M'(\mu_3\text{-}S)_4$ cores. Thus, Shibahara (107) reported the syntheses of a series of $Mo_3M'(\mu_3\text{-}S)_4$ clusters by the reaction of zero-valent M′ with an incomplete cubane-type Mo aqua cluster $[Mo_3(\mu_3\text{-}S)(\mu_2\text{-}S)_3(H_2O)_9]^{4+}$ in acidic solutions. We attempted for the first time the reactions of this aqua cluster $[\{Mo(H_2O)_3\}_3(\mu_3\text{-}S)(\mu_2\text{-}S)_3]^{4+}$ with noble metals and succeeded in the isolation of $Mo_3Pd(\mu_3\text{-}S)_4$ clusters $[\{Mo(H_2O)_3\}_3(PdCl)(\mu_3\text{-}S)_4]^{3+}$ and $[\{Mo(H_2O)_3\}_6(\mu_3\text{-}S)_6Pd_2(\mu_4\text{-}S)_2]^{8+}$ (108). A $Mo_3Pt(\mu_3\text{-}S)_4$ cluster was also available, which was isolated as the crystallographically characterizable cluster $[\{Mo(dppe)Cl\}_3(PtCl)(\mu_3\text{-}S)_4]$ (109). Related aqua clusters containing $Mo_3M'(\mu_3\text{-}S)_4$ and $W_3M'(\mu_3\text{-}S)_4$ cores with various M′ including noble metals were also synthesized later by Sykes and co-workers (110). The Mo_3Pd clusters have an unique tetrahedral Pd site and coordination of alkenes and CO occurs on the Pd site in $[\{Mo(tacn)\}_3(PdCl)(\mu_3\text{-}S)_4]^{3+}$ (tacn = 1,4,7-triazacyclononane) (Scheme 34). More interestingly, it has turned out that this cluster catalyzes the stereoselective addtion of alcohols and carboxylic acids to electron-deficient alkynes such as methyl propiolate (108, 111). A plausible mechanism for the addition of an alcohol to alkyl propiolate is shown in Scheme 35, where the coordinated tacn ligands on thee Mo atoms are omitted for clarity. The reaction is initiated by coordination

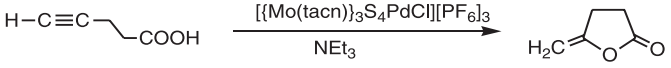
Scheme 34.



Scheme 35.



Scheme 36.

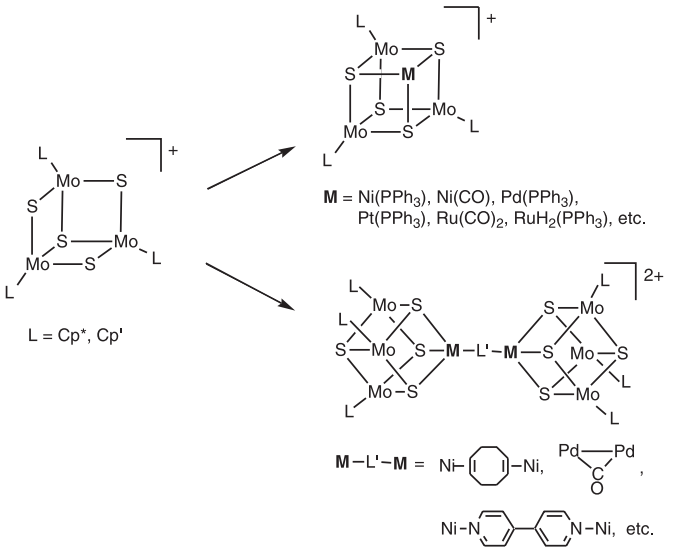


of the alkyne to the unique Pd atom, which is followed by nucleophilic attack of the alcohol to the activated alkyne to form a vinylpalladium intermediate. Liberation of the trans addition product from the metal occurs by protonolysis, and the cubane-type core is retained during the catalysis. This type of reaction was further extended to the intramolecular cyclization of alkynoic acids to afford enol lactones. The lactonization of 4-pentynoic acid catalyzed by this cluster proceeds very efficiently and the turnover reaches 100 000 after 19 h (112) (Scheme 36). Such catalytic activities were not observed for conventional mononuclear Pd complexes. These reactions are noteworthy since reactions efficiently catalyzed by well-defined metal–sulfido clusters are still rare.

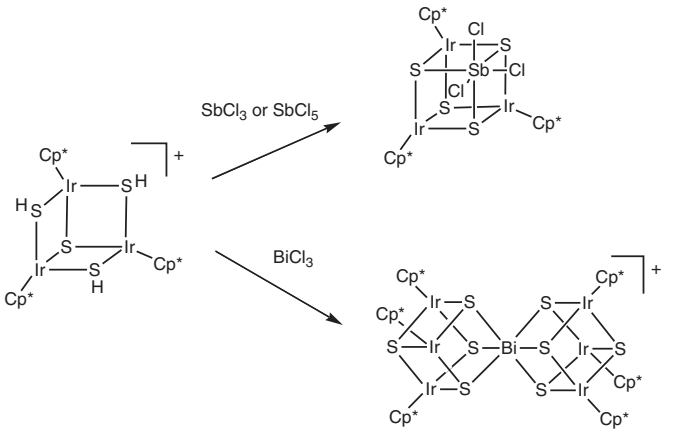
Incomplete cubane-type Mo clusters with cyclopentadienyl ligands $[(Cp^*Mo)_3(\mu_3\text{-}S)(\mu_2\text{-}S)_3]^+$ (113) and $[(Cp'Mo)_3(\mu_3\text{-}S)(\mu_2\text{-}S)_3]^+$ (Cp′ = $\eta^5\text{-}C_5MeH_4$) (114) have also been prepared recently, which incorporate various transition metal fragments to form cubane-type organometallic clusters (113, 115) (Scheme 37). Coordination of the alkyne

© 2005 NRC Canada

Scheme 37.



Scheme 38.



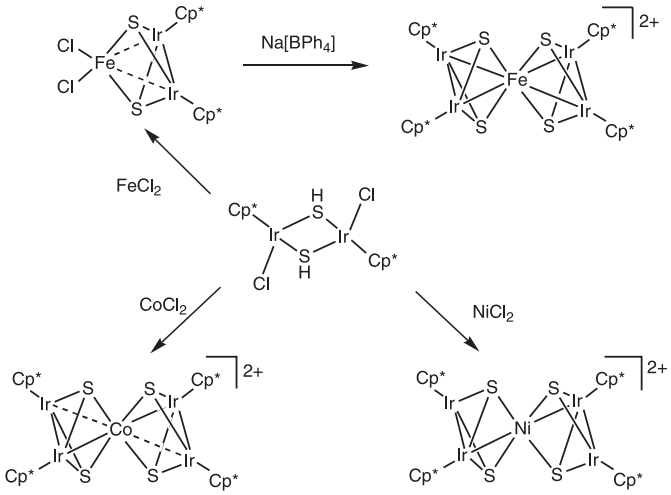
MeOCOC≡CCOOMe (DMAD) to the nickel site embedded in the Mo_3S_4 aggregate has been demonstrated by isolation of $[(Cp^*Mo)_3\{Ni(\eta^2\text{-DMAD})\}(\mu_3\text{-}S)_4][PF_6]$, whereas treatment of 4-pentynoic acid with a small amount of $(Cp^*Mo)_3Ni(\mu_3\text{-}S)_4$ clusters gives rise to the catalytic formation of an enol lactone as shown in Scheme 36 (115*a*).

Another new versatile precursor having an incomplete cubane-type core is the Ir sulfido – hydrosulfido cluster $[(Cp^*Ir)_3(\mu_3\text{-}S)(\mu_2\text{-}SH)_3]Cl$ (116). It is noteworthy that in contrast to the $Mo_3S_4^{4+}$ core containing relatively electron-deficient d^2 Mo(IV) centers described above, this Ir cluster has more electron-rich d^6 Ir(III) centers. This difference is reflected in the reactivities of these clusters: incorporation of the formal M(0) species including Sb(0) and Bi(0) occurs in the case of the $Mo_3S_4^{4+}$ clusters, whereas $[(Cp^*Ir)_3(\mu_3\text{-}S)(\mu_2\text{-}SH)_3]Cl$ does react with $SbCl_5$ and MCl_3 (M = Sb, Bi) to give a single cubane-type cluster $[(Cp^*Ir)_3(SbCl_3)(\mu_3\text{-}S)_4]$ and a corner-shared double cubane-type cluster $[\{(Cp^*Ir)_3(\mu_3\text{-}S)_4\}_2Bi]Cl$ containing high valent Sb(V) and Bi(V) centers (Scheme 38) (117).

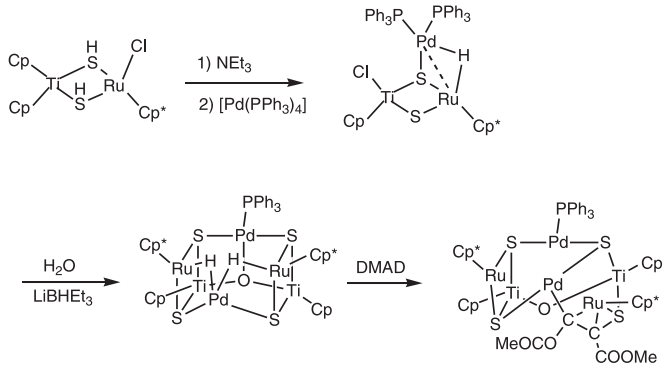
Penta- and hexanuclear sulfido complexes

Pentanuclear bow-tie clusters $[\{(Cp^*Ir)_2(\mu_3\text{-}S)_2\}_2M]^{2+}$ are

Scheme 39.



Scheme 40.



derived from the reaction of the hydrosulfido-bridged diiridium complex $[(Cp^*IrCl)_2(\mu\text{-}SH)_2]$ with MCl_2 (M = Fe, Co, Ni). In the reaction with $FeCl_2$, a trinuclear cluster $[(Cp^*Ir)_2(\mu_3\text{-}S)_2(FeCl_2)]$ is produced initially, which is then transformed into the pentanuclear cluster by treatment with $NaBPh_4$ (Scheme 39) (118).

As a metal–sulfido cluster with higher nuclearity, a novel hexanuclear trimetallic cluster $[(CpTi)_2(Cp^*Ru)_2Pd_2(PPh_3)\text{-}(\mu_3\text{-}S)_4(\mu_3\text{-}O)(\mu_2\text{-}H)_2]$ is formed from the reaction of the trinuclear cluster $[(CpTiCl)(Cp^*Ru)\{Pd(PPh_3)_2\}(\mu_3\text{-}S)(\mu_2\text{-}S)(\mu_2\text{-}H)]$ with water and $LiBHEt_3$. The latter trinuclear cluster is derived from the hydrosulfido-bridged complex $[(Cp_2Ti)(Cp^*RuCl)(\mu_2\text{-}SH)_2]$ and $[Pd(PPh_3)_4]$ in the presence of NEt_3 (Scheme 40) (119). Incorporation of the alkyne DMAD into the hexanuclear cluster core takes place to afford a new cluster depicted in Scheme 40 through the insertion of the alkyne into a Pd—S bond with concurrent loss of two hydrides.

Conclusion

We have summarized here our two approaches toward activation of dinitrogen, nitriles, and alkynes by using novel complexes learned from nitrogenase. During the last three decades, various types of reactions of those small molecules by employment of molybdenum and tungsten complexes have been developed, revealing that dinitrogen is not a chemically

© 2005 NRC Canada

inert molecule if it is bound to a transition metal surrounded by appropriate ligands. On the other hand, stimulated by the active site of nitrogenase, a variety of metal–sulfur clusters containing noble metals ranging from dinuclear to hexanuclear cores have been prepared in rational ways, and their structures and reactivities toward small molecules have been extensively investigated. This has led to the finding of the unique catalysis of dinuclear and tetranuclear cubane-type metal–sulfur complexes. Further studies from both approaches may lead to the development of new types of catalytic reactions of small molecules, which are not attainable by conventional mononuclear complexes, and hopefully to the development of a new generation of chemical nitrogen fixation that efficiently transforms dinitrogen into nitrogen hydrides and organo-nitrogen compounds under mild conditions.

Acknowledgements

We are deeply indebted to the enthusiastic and unwavering efforts of many students and collaborators whose names are listed in the papers in the references.

References

1. A.D. Allen and C.V. Senoff. Chem. Commun. 621 (1965).
2. (*a*) M.E. Vol'pin and V.B. Shur. Dokl. Akad. Nauk. SSSR, **156**, 1102 (1964); (*b*) M.E. Vol'pin. Pure Appl. Chem. **30**, 607 (1972).
3. A. Yamamoto, S. Kitazume, and S. Ikeda. Chem. Commun. 79 (1967).
4. (*a*) M. Hidai, K. Tominari, Y. Uchida, and A. Misono. Chem. Commun. 1392 (1969); (*b*) M. Hidai, K. Tominari, and Y. Uchida. J. Am. Chem. Soc. **94**, 110 (1972).
5. J. Chatt, J.R. Dilworth, and R.L. Richards. Chem. Rev. **78**, 589 (1978).
6. (*a*) M. Hidai and Y. Mizobe. *In* Molybdenum and tungsten. Their roles in biological processes. *Edited by* A. Sigel and H. Sigel. Marcel Dekker, Inc., New York. 2002. pp. 121–161; (*b*) M. Hidai and Y. Mizobe. *In* Activation of unreactive bonds and organic synthesis. *Edited by* S. Murai. Springer-Verlag, Berlin. 1999. pp. 227–241; (*c*) M. Hidai. Coord. Chem. Rev. **185–186**, 99 (1999); (*d*) M. Hidai and Y. Ishii. Bull. Chem. Soc. Jpn. **69**, 819 (1996); (*e*) M. Hidai and Y. Mizobe. Chem. Rev. **95**, 1115 (1995); (*f*) B.A. MacKay and M.D. Fryzuk. Chem. Rev. **104**, 385 (2004); (*g*) M.D. Fryzuk. Chem. Rec. **3**, 2 (2003); (*h*) M.P. Shaver and M.D. Fryzuk. Adv. Synth. Catal. **345**, 1061 (2003); (*i*) M.D. Fryzuk and S.A. Johnson. Coord. Chem. Rev. **200–202**, 379 (2000); (*j*) G.J. Leigh. *In* Nitrogen fixation at the millennium. *Edited by* G.J. Leigh. Elsevier, Amsterdam. 2002. pp. 299–332; (*k*) S. Gambarotta. J. Organomet. Chem. **500**, 117 (1995); (*l*) R.L. Richards. Coord. Chem. Rev. **154**, 83 (1996); (*m*) R.L. Richards. *In* Modern coordination chemistry. The legacy of Joseph Chatt. *Edited by* G.J. Leigh and N. Winterton. Royal Society of Chemistry, Cambridge. 2002. pp. 171–186.
7. (*a*) P.M.C. Benton, S. Sen, and J.W. Peters. *In* Nitrogen fixation at the millennium. *Edited by* G.J. Leigh. Elsevier, Amsterdam. 2002. pp. 35–71; (*b*) D.C. Rees and J.B. Howard. Curr. Opin. Chem. Biol. **4**, 559 (2000); (*c*) B.E. Smith. Adv. Inorg. Chem. **47**, 159 (1999); (*d*) B.K. Burgess and D.J. Lowe. Chem. Rev. **96**, 2983 (1996).
8. S.P. Cramer, K.O. Hodgson, W.O. Gillum, and L.E. Mortenson. J. Am. Chem. Soc. **100**, 3398 (1978).
9. O. Einsle, F.A. Tezcan, S.L.A. Andrade, B. Schmid, M. Yoshida, J.B. Howard, and D.C. Rees. Science, **297**, 1696 (2002).
10. (*a*) S.C. Lee and R.H. Holm. Chem. Rev. **104**, 1135 (2004); (*b*) S.C. Lee and R.H. Holm. Proc. Natl. Acad. Sci. U.S.A. **100**, 3595 (2003); (*c*) D. Coucouvanis. Acc. Chem. Res. **24**, 1 (1991); (*d*) H. Kawaguchi, K. Yamada, S. Ohnishi, and T. Tatsumi. J. Am. Chem. Soc. **119**, 10 871 (1997); (*e*) G. Christou and C.D. Garner. J. Chem. Soc. Dalton Trans. 2354 (1980).
11. (*a*) M. Hidai. *In* Perspectives in organometallic chemistry. *Edited by* C.G. Screttas and B.R. Steele. Royal Society of Chemistry, Cambridge. 2003. pp. 62–73; (*b*) M. Hidai, S. Kuwata, and Y. Mizobe. Acc. Chem. Rec. **33**, 46 (2000); (*c*) M. Hidai and Y. Mizobe. *In* Transition metal sulfur chemistry: Biological and industrial significance. *Edited by* E.I. Stiefel and K. Matsumoto. American Chemical Society, Washington, D.C. 1996. pp. 310–323; (*d*) M. Hidai, Y. Ishii, and S. Kuwata. *In* Modern coordination chemistry. The legacy of Joseph Chatt. *Edited by* G.J. Leigh and N. Winterton. Royal Society of Chemistry, Cambridge. 2002. pp. 208–216; (*e*) M. Hidai, Y. Mizobe, and H. Matsuzaka. J. Organomet. Chem. **473**, 1 (1994).
12. (*a*) J. Chatt, G.A. Heath, and R.L. Richards. J. Chem. Soc. Chem. Commun. 1010 (1972); (*b*) J. Chatt, G.A. Heath, and R.L. Richards. J. Chem. Soc. Dalton Trans. 2074 (1974).
13. J. Chatt, G.A. Heath, and G.J. Leigh. J. Chem. Soc. Chem. Commun. 444 (1972).
14. G.A. Heath, R. Mason, and K.M. Thomas. J. Am. Chem. Soc. **96**, 259 (1974).
15. M. Hidai, T. Kodama, M. Sato, M. Harakawa, and Y. Uchida. Inorg. Chem. **15**, 2694 (1976).
16. (*a*) J. Chatt, A.J. Pearman, and R.L. Richards. Nature (London), **253**, 39 (1975); (*b*) J. Chatt, A.J. Pearman, and R.L. Richards. J. Chem. Soc. Dalton Trans. 1852 (1977).
17. T. Takahashi, Y. Mizobe, M. Sato, Y. Uchida, and M. Hidai. J. Am. Chem. Soc. **102**, 7461 (1980).
18. (*a*) C.J. Pickett and J. Talarmin. Nature (London), **317**, 652 (1985); (*b*) C.J. Pickett, K.S. Ryder, and J. Talarmin. J. Chem. Soc. Dalton Trans. 1453 (1986).
19. (*a*) M. Hidai, T. Takahashi, I. Yokotake, and Y. Uchida. Chem. Lett. 645 (1980); (*b*) H. Nishihara, T. Mori, Y. Tsurita, K. Nakano, T. Saito, and Y. Sasaki. J. Am. Chem. Soc. **104**, 4367 (1982).
20. M. Hidai and Y. Nishibayashi. *In* Recent advances in hydride chemistry. *Edited by* M. Peruzzini and R. Poli. Elsevier, Amsterdam. 2001. pp. 117–138.
21. G. Jia, R.H. Morris, and C.T. Schweitzer. Inorg. Chem. **30**, 593 (1991).
22. (*a*) Y. Nishibayashi, S. Iwai, and M. Hidai. Science (Washington, D.C.), **279**, 540 (1998); (*b*) Y. Nishibayashi, S. Takemoto, S. Iwai, and M. Hidai. Inorg. Chem. **39**, 5946 (2000).
23. A. Watakabe, T. Takahashi, D.-M. Jin, I. Yokotake, Y. Uchida, and M. Hidai. J. Organomet. Chem. **254**, 75 (1983).
24. T. Takemoto, H. Kawamura, Y. Yamada, T. Okada, A. Ono, E. Yoshikawa, Y. Mizobe, and M. Hidai. Organometallics, **21**, 3897 (2002).
25. (*a*) D.V. Yandulov and R.R. Schrock. Science, **301**, 76 (2003); (*b*) V. Ritleng, D.V. Yandulov, W.W. Weare, R.R. Schrock, A.S. Hock, and W.M. Davis. J. Am. Chem. Soc. **126**, 6150 (2004).
26. P. Bernatis, J.C.V. Laurie, and M. Rakowski DuBois. Organometallics, **9**, 1607 (1990).

© 2005 NRC Canada

27. Y. Nishibayashi, I. Wakiji, K. Hirata, M. Rakowski DuBois, and M. Hidai. Inorg. Chem. **40**, 578 (2001).
28. J.C.V. Laurie, L.D. Duncan, R.C. Haltiwanger, R.T. Weberg, and M. Rakowski DuBois. J. Am. Chem. Soc. **108**, 6234 (1986).
29. Y. Nishibayashi, S. Iwai, and M. Hidai. J. Am. Chem. Soc. **120**, 10 559 (1998).
30. I. Dance. Chem. Commun. 523 (1998).
31. M. Sato, T. Kodama, M. Hidai, and Y. Uchida. J. Organomet. Chem. **152**, 239 (1978).
32. (*a*) J. Chatt, A.A. Diamantis, G.A. Heath, N.E. Hooper, and G.J. Leigh. J. Chem. Soc. Dalton Trans. 688 (1977); (*b*) G.E. Bossard, D.C. Busby, M. Chang, T.A. George, and S.D.A. Iske, Jr. J. Am. Chem. Soc. **102**, 1001 (1980); (*c*) W. Hussain, G.J. Leigh, H. Mohd-Ali, and C.J. Pickett. J. Chem. Soc. Dalton Trans. 1473 (1986).
33. M. Abu Bakar, D.L. Hughes, and G.J. Leigh. J. Chem. Soc. Dalton Trans. 2525 (1988).
34. C.J. Pickett and G.J. Leigh. J. Chem. Soc. Chem. Commun. 1033 (1981).
35. (*a*) M. Hidai, Y. Mizobe, M. Sato, T. Kodama, and Y. Uchida. J. Am. Chem. Soc. **100**, 5740 (1978); (*b*) Y. Mizobe, R. Ono, Y. Uchida, M. Hidai, M. Tezuka, S. Moue, and A. Tsuchiya. J. Organomet. Chem. **204**, 377 (1981).
36. (*a*) P.C. Bevan, J. Chatt, M. Hidai, and G.J. Leigh. J. Organomet. Chem. **160**, 165 (1978); (*b*) Y. Mizobe, M. Hidai, and Y. Uchida. Bull. Chem. Soc. Jpn. **53**, 1781 (1980).
37. T. Aoshima, T. Tamura, Y. Mizobe, and M. Hidai. J. Organomet. Chem. **435**, 85 (1992).
38. Y. Harada, Y. Mizobe, and M. Hidai. Bull. Chem. Soc. Jpn. **71**, 2701 (1988).
39. Y. Harada, Y. Mizobe, and M. Hidai. J. Organomet. Chem. **574**, 24 (1999).
40. M. Hidai, S. Aramaki, K. Yoshida, T. Kodama, T. Takahashi, Y. Uchida, and Y. Mizobe. J. Am. Chem. Soc. **108**, 1562 (1986).
41. Y. Ishii, H. Miyagi, S. Jitsukuni, H. Seino, B.S. Harkness, and M. Hidai. J. Am. Chem. Soc. **114**, 9890 (1992).
42. T. Aoshima, T. Tanase, Y. Mizobe, Y. Yamamoto, and M. Hidai. J. Chem. Soc. Chem. Commun. 586 (1992).
43. H. Seino, Y. Ishii, and M. Hidai. Inorg. Chem. **36**, 161 (1997).
44. H. Seino, Y. Ishii, T. Sasagawa, and M. Hidai. J. Am. Chem. Soc. **117**, 12 181 (1995).
45. T. Sasagawa, H. Seino, Y. Ishii, Y. Mizobe, and M. Hidai. Bull. Chem. Soc. Jpn. **72**, 425 (1999).
46. H. Ishino, S. Tokunaga, H. Seino, Y. Ishii, and M. Hidai. Inorg. Chem. **38**, 2489 (1999).
47. K. Iwanami, Y. Mizobe, T. Takahashi, T. Kodama, Y. Uchida, and M. Hidai. Bull. Chem. Soc. Jpn. **54**, 1773 (1981).
48. T. Aoshima, Y. Mizobe, M. Hidai, and J. Tsuchiya. J. Organomet. Chem. **423**, 39 (1992).
49. H.M. Colquhoun. J. Chem. Res. Synop. 325 (1979).
50. Y. Ishii, M. Kawaguchi, Y. Ishino, T. Aoki, and M. Hidai. Organometallics, **13**, 5062 (1994).
51. M. Hidai, K. Komori, T. Kodama, D.-M. Jin, T. Takahashi, S. Sugiura, Y. Uchida, and Y. Mizobe. J. Organomet. Chem. **272**, 155 (1984).
52. H. Oshita, Y. Mizobe, and M. Hidai. J. Organomet. Chem. **456**, 213 (1993).
53. H. Oshita, Y. Mizobe, and M. Hidai. Organometallics, **11**, 4116 (1992).
54. A.C. Street, Y. Mizobe, F. Gotoh, I. Mega, H. Oshita, and M. Hidai. Chem. Lett. 383 (1991).
55. (*a*) K. Komori, H. Oshita, Y. Mizobe, and M. Hidai. J. Am. Chem. Soc. **111**, 1939 (1989); (*b*) K. Komori, S. Sugiura, Y. Mizobe, M. Yamada, and M. Hidai. Bull. Chem. Soc. Jpn. **62**, 2953 (1989).
56. (*a*) M. Aresta. Gazz. Chim. Ital. **102**, 781 (1972); (*b*) J. Chatt, R.H. Crabtree, E.A. Jeffery, and R.L. Richards. J. Chem. Soc. Dalton Trans. 1167 (1973).
57. T. Takahashi, T. Kodama, A. Watakabe, Y. Uchida, and M. Hidai. J. Am. Chem. Soc. **105**, 1680 (1983).
58. K. Takagahara, H. Ishino, Y. Ishii, and M. Hidai. Chem. Lett. 897 (1998).
59. H. Ishino, Y. Ishii, and M. Hidai. Chem. Lett. 677 (1998).
60. H. Ishino, T. Nagano, S. Kuwata, Y. Yokobayashi, Y. Ishii, M. Hidai, and Y. Mizobe. Organometallics, **20**, 188 (2001).
61. H. Ishino, S. Takemoto, K. Hirata, Y. Kanaizuka, M. Hidai, M. Nabika, Y. Seki, T. Miyatake, and N. Suzuki. Organometallics, **23**, 4544 (2004).
62. T. Tatsumi, M. Hidai, and Y. Uchida. Inorg. Chem. **14**, 2530 (1975).
63. J. Chatt, G.J. Leigh, H. Neukomm, C.J. Pickett, and D.R. Stanley. J. Chem. Soc. Dalton Trans. 121 (1980).
64. H. Seino, Y. Tanabe, Y. Ishii, and M. Hidai. Inorg. Chim. Acta, **280**, 163 (1998).
65. Y. Tanabe, H. Seino, Y. Ishii, and M. Hidai. J. Am. Chem. Soc. **122**, 1690 (2000).
66. (*a*) R.R. Schrock, M.L. Listemann, and L.G. Sturgeoff. J. Am. Chem. Soc. **104**, 4291 (1982); (*b*) J.H. Freudenberger and R.R. Schrock. Organometallics, **5**, 398, (1986); (*c*) M.H. Chisholm, K. Folting, M.L. Lynn, D.B. Tiedrke, F. Lemoigno, and O. Eisenstein. Chem. Eur. J. **5**, 2318 (1999).
67. H. Seino, Y. Mizobe, and M. Hidai. Chem. Rec. **1**, 349 (2001).
68. (*a*) H.I. Lee, R.Y. Igarashi, M. Laryukhin, P.E. Dean, P.C. Dos Santos, D.R. Dean, L.C. Seefeldt, and B.M. Hoffman. J. Am. Chem. Soc. **126**, 9563 (2004); (*b*) I. Dance. J. Am. Chem. Soc. **126**, 11 852 (2004).
69. (*a*) T. Yoshida, T. Adachi, M. Kaminaka, T. Ueda, and T. Higuchi. J. Am. Chem. Soc. **110**, 4872 (1988); (*b*) T. Yoshida, T. Adachi, T. Ueda, M. Kaminaka, N. Sasaki, T. Higuchi, T. Aoshima, I. Mega, Y. Mizobe, and M. Hidai. Angew. Chem. Int. Ed. Engl. **28**, 1040 (1989).
70. For example: (*a*) D. Sellmann, A. Hille, A. Rösler, F.W. Heinemann, M. Moll, G. Brehm, S. Schneider, M. Reiher, B.A. Hess, and W. Bauer. Chem. Eur. J. **10**, 819 (2004); (*b*) D. Sellmann, B. Hautsch, A. Rösler, and F.W. Heinemann. Angew. Chem. Int. Ed. **40**, 1505 (2001); (*c*) R.R. Schrock, M. Wesolek, A.H. Liu, K.C. Wallace, and J.C. Dewan. Inorg. Chem. **27**, 2050 (1988); (*d*) D. Cruz-Garritz, S. Gelover, H. Torrens, J. Leal, and R.L. Richards. J. Chem. Soc. Dalton Trans. 2393 (1988).
71. J.R. Dilworth, R.A. Henderson, A. Hills, D.L. Hughes, C. McDonald, A.N. Stephens, and D.R. Walton. J. Chem. Soc. Dalton Trans. 1077 (1990).
72. N. Oshima, H. Suzuki, and Y. Moro-oka. Chem. Lett. 1161 (1984).
73. S. Dev, K. Imagawa, Y. Mizobe, G. Cheng, Y. Wakatsuki, H. Yamazaki, and M. Hidai. Organometallics, **8**, 1232 (1989).
74. S. Dev, Y. Mizobe, and M. Hidai. Inorg. Chem. **29**, 4797 (1990).
75. (*a*) A. Takahashi, Y. Mizobe, H. Matsuzaka, S. Dev, and M. Hidai. J. Organomet. Chem. **456**, 243 (1993); (*b*) U. Kölle, Chr. Rietmann, and U. Englert. J. Organomet. Chem. **423**, C20 (1992).
76. S.D. Loren, B.K. Campion, R.H. Heyn, T.D. Tilly, B.E. Bursten, and K.W. Ruth. J. Am. Chem. Soc. **111**, 4712 (1989).

© 2005 NRC Canada

77. (*a*) U. Kölle and J. Kossakowski. J. Organomet. Chem. **362**, 383 (1989); (*b*) P.J. Fagan, M.D. Ward, and J.C. Calabrese. J. Am. Chem. Soc. **111**, 1698 (1989).
78. (*a*) M. Nishio, H. Matsuzaka, Y. Mizobe, T. Tanase, and M. Hidai. Organometallics, **13**, 4214 (1994); (*b*) M. Nishio, H. Matsuzaka, Y. Mizobe, and M. Hidai. Organometallics, **15**, 965 (1996).
79. H. Matsuzaka, Y. Hirayama, M. Nishio, Y. Mizobe, and M. Hidai. Organometallics, **12**, 36 (1993).
80. H. Matsuzaka, H. Koizumi, Y. Takagi, M. Nishio, and M. Hidai. J. Am. Chem. Soc. **115**, 10 396 (1993).
81. J.-P. Qü, D. Masui, Y. Ishii, and M. Hidai. Chem. Lett. 1003 (1998).
82. Y. Takagi, H. Matsuzaka, Y. Ishii, and M. Hidai. Organometallics, **16**, 4445 (1997).
83. H. Matsuzaka, Y. Takagi, Y. Ishii, M. Nishio, and M. Hidai. Organometallics, **14**, 2153 (1995).
84. Y. Nishibayashi, M. Yamanashi, I. Wakiji, and M. Hidai. Angew. Chem. Int. Ed. **39**, 2909 (2000).
85. Y. Nishibayashi, I. Wakiji, and M. Hidai. J. Am. Chem. Soc. **122**, 11 019 (2000).
86. Y. Nishibayashi, I. Wakiji, Y. Ishii, S. Uemura, and M. Hidai. J. Am. Chem. Soc. **123**, 3393 (2001).
87. Y. Nishibayashi, Y. Inada, M. Hidai, and S. Uemura. J. Am. Chem. Soc. **125**, 6060 (2003).
88. Y. Nishibayashi, Y. Inada, M. Hidai, and S. Uemura. J. Am. Chem. Soc. **124**, 7900 (2002).
89. Y. Nishibayashi, M. Yoshikawa, Y. Inada, M. Hidai, and S. Uemura. J. Am. Chem. Soc. **124**, 11 846 (2002).
90. K.M. Nicholas. Acc. Chem. Res. **20**, 207 (1987).
91. Y. Nishibayashi, M. Yoshikawa, Y. Inada, M.D. Milton, M. Hidai, and S. Uemura. Angew. Chem. Int. Ed. **42**, 2681 (2003).
92. Y. Nishibayashi, Y. Inada, M. Yoshikawa, M. Hidai, and S. Uemura. Angew. Chem. Int. Ed. **42**, 1495 (2003).
93. Y. Inada, Y. Nishibayashi, M. Hidai, and S. Uemura. J. Am. Chem. Soc. **124**, 15 172 (2002).
94. S. Kuwata, Y. Mizobe, and M. Hidai. Inorg. Chem. **33**, 3619 (1994).
95. K. Tanaka, Y. Hozumi, and T. Tanaka. Chem. Lett. 1203 (1982).
96. (*a*) D. Coucouvanis, K.D. Demadis, S.M. Malinak, P.E. Mosier, M.A. Tyson, and L.J. Laughlin. *In* Transition metal sulfur chemistry: Biological and industrial significance. *Edited by* E.I. Stiefel and K. Matsumoto. American Chemical Society, Washington, D.C. 1996. pp. 117–134; (*b*) D. Coucouvanis, K.D. Demadis, S.M. Malinak, P.E. Mosier, M.A. Tyson, and L.J. Laughlin. J. Mol. Cat. A: Chem. **107**, 123 (1996); (*c*) K.D. Demadis, S.M. Malinak, and D. Coucouvanis. Inorg. Chem. **35**, 4038 (1996).
97. K. Hashizume, Y. Mizobe, and M. Hidai. Organometallics, **15**, 3303 (1996).
98. Z. Tang, Y. Nomura, Y. Ishii, Y. Mizobe, and M. Hidai. Inorg. Chim. Acta, **267**, 73 (1998).
99. S. Kabashima, S. Kuwata, and M. Hidai. J. Am. Chem. Soc. **121**, 7837 (1999).
100. Z. Tang, Y. Nomura, Y. Ishii, Y. Mizobe, and M. Hidai. Organometallics, **16**, 151 (1997).
101. S. Kabashima, S. Kuwata, K. Ueno, M. Shiro, and M. Hidai. Angew. Chem. Int. Ed. **39**, 1128 (2000).
102. H. Seino, T. Masumori, M. Hidai, and Y. Mizobe. Organometallics, **22**, 3424 (2003).
103. (*a*) M. Rakowski DuBois. Chem. Rev. **89**, 1 (1989); (*b*) J.C. Bayon, C. Claver, and A.M. Masdeu-Bulto. Coord. Chem. Rev. **193–195**, 73 (1999).
104. T. Ikada, S. Kuwata, Y. Mizobe, and M. Hidai. Inorg. Chem. **37**, 5793 (1998).
105. T. Ikada, S. Kuwata, Y. Mizobe, and M. Hidai. **38**, 64 (1999).
106. H. Seino, T. Kaneko, S. Fujii, M. Hidai, and Y. Mizobe. Inorg. Chem. **42**, 4585 (2003).
107. (*a*) T. Shibahara. Adv. Inorg. Chem. **37**, 143 (1991); (*b*) T. Shibahara. Coord. Chem. Rev. **123**, 73 (1993).
108. T. Murata, Y. Mizobe, H. Gao, Y. Ishii, T. Wakabayashi, F. Nakano, T. Tanase, S. Yano, M. Hidai, I. Echizen, H. Nanikawa, and S. Motomura. J. Am. Chem. Soc. **116**, 3389 (1994).
109. D. Masui, Y. Ishii, and M. Hidai. Bull. Chem. Soc. Jpn. **73**, 931 (2000).
110. R. Hernandez-Molina, M.N. Sokolov, and A.G. Sykes. Acc. Chem. Res. **34**, 223 (2001).
111. T. Wakabayashi, Y. Ishii, T. Murata, Y. Mizobe, and M. Hidai. Tetrahedron Lett. **36**, 5585 (1995).
112. T. Wakabayashi, Y. Ishii, K. Ishikawa, and M. Hidai. Angew. Chem. Int. Ed. Engl. **35**, 2123 (1996).
113. I. Takei, K. Suzuki, Y. Enta, K. Dohki, T. Suzuki, Y. Mizobe, and M. Hidai. Organometallics, **22**, 1790 (2003).
114. B. Rink, M. Brorson, and I.J. Scowen. Organometallics, **18**, 2309 (1999).
115. (*a*) I. Takei, Y. Wakebe, K. Suzuki, Y. Enta, T. Suzuki, Y. Mizobe, and M. Hidai. Organometallics, **22**, 4639 (2003); (*b*) K. Herbst, M. Monari, and M. Brorson. Inorg. Chem. **40**, 2979 (2001); (*c*) K. Herbst, B. Rink, L. Dahlenburg, and M. Brorson. Organometallics, **20**, 3655 (2001); (*d*) K. Herbst, P. Zanello, M. Corsini, N. D'Amelio, L. Dahlenburg, and M. Brorson. Inorg. Chem. **42**, 974 (2003).
116. F. Takagi, H. Seino, Y. Mizobe, and M. Hidai. Organometallics, **21**, 694 (2002).
117. A. Shinozaki, H. Seino, M. Hidai, and Y. Mizobe. Organometallics, **22**, 4636 (2003).
118. Z. Tang, Y. Nomura, S. Kuwata, Y. Ishii, Y. Mizobe, and M. Hidai. Inorg. Chem. **37**, 4909 (1998).
119. S. Kuwata, S. Kabashima, Y. Ishii, and M. Hidai. J. Am. Chem. Soc. **123**, 3826 (2001).

© 2005 NRC Canada

Early developments in lanthanide-based dinitrogen reduction chemistry[1]

William J. Evans and David S. Lee

Abstract: Although the first crystallographically characterized lanthanide dinitrogen complex was reported in 1988 with samarium, it is only in recent years that this field has expanded to include fully characterized examples for the entire series of lanthanides. The development of lanthanide dinitrogen chemistry has been aided by a series of unexpected results that present some good lessons in the development of science. This review presents a chronological account of the lanthanide dinitrogen chemistry discovered in our laboratory through the summer of 2004.

Key words: lanthanides, dinitrogen, reduction, alkali metal, nitrogen fixation, diazenido.

Résumé : Même si un premier complexe de diazote et d'un lanthanide a été caractérisé en 1988 avec le samarium, ce n'est que dans les années récentes que ce domaine a connu une expansion au cours de laquelle des exemples de complexes de chacun des membres de la série des lanthanides ont finalement été complètement caractérisés. Le développement de la chimie des complexes du diazote et des lanthanides a été aidé par une série de résultats inattendus qui présentent de bonnes leçons dans le développement de la science. Cette revue présente un exposé chronologique de la chimie des complexes de diazote et de lanthanides telle que développée dans notre laboratoire jusqu'au milieu de l'été 2004.

Mots clés : lanthanides, diazote, réduction, métal alcalin, fixation du diazote, diazénido.

[Traduit par la Rédaction]

Initial discovery

Just as Allen and Senoff's discovery of the first transition metal complex of dinitrogen (1) resulted from trying to rationalize data that did not quite match that expected, lanthanide dinitrogen chemistry in our laboratory was initiated by pursuing an experimental irregularity. While investigating the chemistry of the bent metallocene, $(C_5Me_5)_2Sm$ (**1**) (2), graduate student Tamara Ulibarri noticed that the C_6D_6 ^1H NMR spectra of samples of this compound occasionally contained an extra resonance at –0.6 ppm. This was observed in addition to the usual broad resonance of pure $(C_5Me_5)_2Sm$ in the 1 to 2 ppm region, a peak that varied depending on the concentration of this paramagnetic compound (3). Although the highly reactive $(C_5Me_5)_2Sm$ was freshly prepared each time by the same procedure, this small "impurity" peak was only occasionally present in the spectrum.

This intermittent extra resonance could easily have been ignored as an artifact. However, Tamara noticed that it was present only in samples prepared in the nitrogen-containing glovebox and not in samples prepared on the high vacuum line. Once she made this correlation, a sample prepared under nitrogen was cooled and the –0.6 resonance was observed to grow at the expense of the $(C_5Me_5)_2Sm$ signal. Subsequent crystallization of the sample gave a mixture of green and red crystals. Separation of the red crystals by hand from the green $(C_5Me_5)_2Sm$ and subsequent X-ray analysis revealed the structure of the first crystallographically characterized *f* element dinitrogen complex, $[(C_5Me_5)_2Sm]_2(\mu\text{-}\eta^2\text{:}\eta^2\text{-}N_2)$ (**2**) shown in Fig. 1 (4).

Received 13 September 2004. Published on the NRC Research Press Web site at http://canjchem.nrc.ca on 15 April 2005.

W.J. Evans[2] and D.S. Lee. Department of Chemistry, University of California, Irvine, CA 92697-2025, USA.

[1]This article is part of a Special Issue dedicated to Dinitrogen Chemistry.

[2]Corresponding author (e-mail: wevans@uci.edu).

The unusual $Sm_2(\mu\text{-}\eta^2\text{:}\eta^2\text{-}N_2)$ structure

Isolation of a dinitrogen complex of a lanthanide was most unexpected considering the traditional view of lanthanide bonding (5). The limited radial extension of the 4*f* orbitals gave these metal ions primarily ionic chemistry in which hard donor atom anions were the preferred ligands. In fact, for many years it was even believed that only oxygen donor ligands were hard enough for the lanthanides: nitrogen donor ligands were thought to be incapable of forming stable complexes with lanthanides (6, 7). This misconception was formed because much of the early chemistry was done in aqueous solution in which water was the predominant ligand. It was subsequently found that a variety of harder nitrogen ligands like $(NR_2)^-$, pyridine, nitriles, etc., would bind the trivalent ions (8). However, reactions with a neutral, soft ligand like dinitrogen seemed unlikely for these hard metal ions.

$[(C_5Me_5)_2Sm]_2(\mu\text{-}\eta^2\text{:}\eta^2\text{-}N_2)$ was unusual not only because it was the first dinitrogen complex of an *f* element, but also because it was the first dinitrogen complex *of any metal* in which the metals and N_2 were coplanar (structure **I** in Fig. 2). A variety of bimetallic dinitrogen complexes had been identified in 1988 when **2** was discovered (9), but they

 doi: 10.1139/V05-014 © 2005 NRC Canada

Fig. 1. Thermal ellipsoid plot of $[(C_5Me_5)_2Sm]_2(\mu\text{-}\eta^2\text{:}\eta^2\text{-}N_2)$ (**2**).

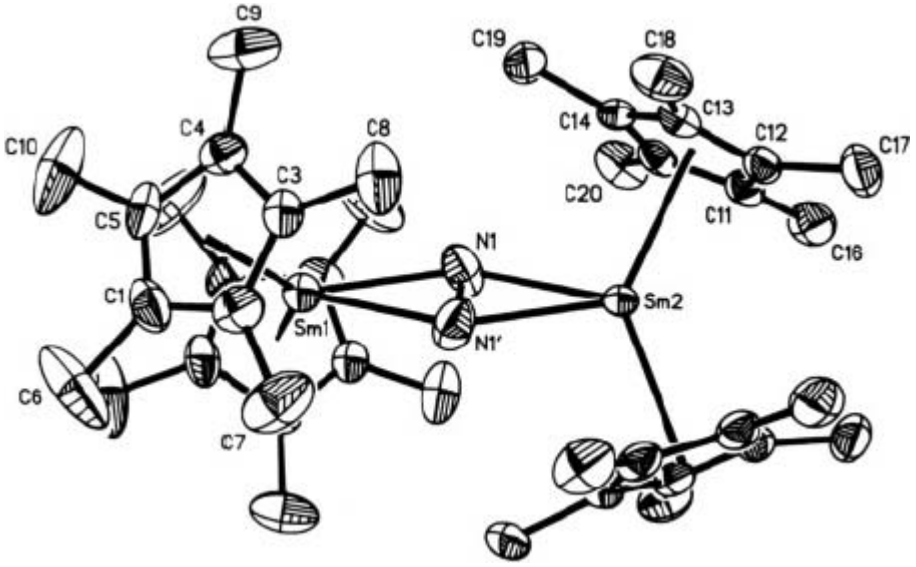
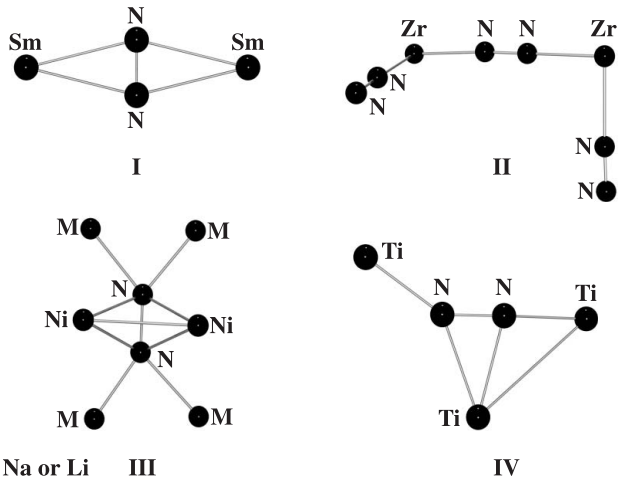


Fig. 2. Metal dinitrogen core structures: (**I**) found in $[(C_5Me_5)_2Sm]_2(\mu\text{-}\eta^2\text{:}\eta^2\text{-}N_2)$ (**2**) (4); (**II–IV**) other M_XN_2 arrangements known at that time (9–14).



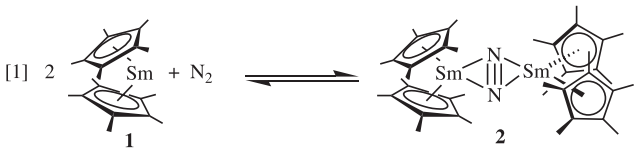
typically displayed end-on coordination of N_2, as in $[(C_5Me_5)_2Zr(\eta^1\text{-}N_2)]_2(\mu\text{-}\eta^1\text{:}\eta^1\text{-}N_2)$ (10), whose core structure is shown as **II** in Fig. 2. The closest dinitrogen examples to the coplanar $M_2(\mu\text{-}\eta^2\text{:}\eta^2\text{-}N_2)$ binding in **2** at that time in the literature were the tetrahedral M_2N_2 components of $[(PhLi)_6Ni_6N_2(OEt_2)_2]_2$ (11, 12) and $[Ph_5Ni_2N_2Na_3Li_6(OEt)_4(OEt_2)_3]_2$ (13) (structure **III**), and the triply bridging M_3N_2 unit in $(C_{10}H_8)(C_5H_5)_5(C_5H_4)Ti_4(\mu_3\text{-}\eta^2\text{:}\eta^2\text{-}N_2)$ (14) (structure **IV**, Fig. 2).

As is often the case with discoveries, the unusual structure found in **2** was also being observed at about the same time in another system in another laboratory. The Fryzuk group, investigating the $[(i\text{-}Pr_2PCH_2SiMe_2)_2N]^{1-}$ ligand system, independently found a structure of this type in the complex $\{[(i\text{-}Pr_2PCH_2SiMe_2)_2N]ClZr\}_2(\mu\text{-}\eta^2\text{:}\eta^2\text{-}N_2)$. This was published (15) shortly after $[(C_5Me_5)_2Sm]_2(\mu\text{-}\eta^2\text{:}\eta^2\text{-}N_2)$ was revealed.

The isolation of $[(C_5Me_5)_2Sm]_2(\mu\text{-}\eta^2\text{:}\eta^2\text{-}N_2)$ is all the more remarkable because of its unusual structural features and chemical behavior. $[(C_5Me_5)_2Sm]_2(\mu\text{-}\eta^2\text{:}\eta^2\text{-}N_2)$ is clearly a trivalent complex on the basis of its metrical parameters in the solid state and its ^{13}C NMR characteristics in solution. Hence, the Sm-C(C_5Me_5) distances are clearly in the trivalent range, which is distinct from that of divalent complexes (16). Likewise, the ^{13}C NMR shift pattern is characteristic of Sm^{3+} (ring carbons at 112 ppm, methyl carbons at 27 ppm) and is distinct from that of the more paramagnetic Sm^{2+} complexes, which have ring carbons around –100 ppm and methyl carbons around +100 ppm (4, 17).

Since the Sm^{3+} centers in $[(C_5Me_5)_2Sm]_2(\mu\text{-}\eta^2\text{:}\eta^2\text{-}N_2)$ indicate that dinitrogen was reduced to $(N_2)^{2-}$, an N—N bond distance of around 1.25 Å would be expected. However, the N—N distance in **2** (1.088(12) Å) was equivalent to that in free dinitrogen (1.0975 Å). In contrast, the N—N distance in the Fryzuk analog, $\{[(i\text{-}Pr_2PCH_2SiMe_2)_2N]ClZr\}_2(\mu\text{-}\eta^2\text{:}\eta^2\text{-}N_2)$ (1.548(7) Å), was among the longest of those observed for activated dinitrogen.

The short distance in $[(C_5Me_5)_2Sm]_2(\mu\text{-}\eta^2\text{:}\eta^2\text{-}N_2)$ could be connected with the fact that the structure of **2** was determined at room temperature, but it could also be associated with the unusual equilibrium shown in eq. [1]. Complex **2** exists in equilibrium with $(C_5Me_5)_2Sm$ (eq. [1]). This is a



strange situation since it involves a reversible Sm^{3+} to Sm^{2+} interconversion. Since Sm^{2+} is a strong reducing agent (18–20) (Table 1), once Sm^{3+} complexes are formed, they generally do not revert to Sm^{2+} (21, 22).

Hiatus

For the next 12 years, no dinitrogen complexes were dis-

© 2005 NRC Canada

Table 1. Calculated values of the Ln^{3+} + $e^- \rightarrow Ln^{2+}$ half reaction vs. NHE (18).

Ln	$Ln^{3+} + e^- \rightarrow Ln^{2+}$ ($E_{1/2}$ vs. NHE, V)
Eu	–0.35
Yb	–1.15
Sm	–1.5
Tm	–2.3
Dy	–2.5
Nd	–2.6
Pr	–2.7
Ho	–2.9
Er	–3.1
La	–3.1
Ce	–3.2
Tb	–3.7
Gd	–3.9
Lu	[a]
Y	[a]

[a]No values calculated.

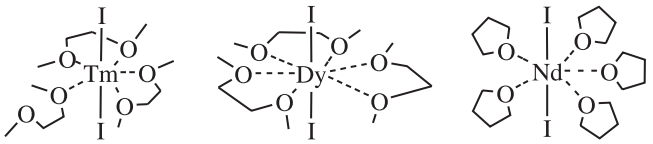
covered in our laboratory. This appeared to be a testament to the special properties of $(C_5Me_5)_2Sm$ (19, 20). Apparently, the analogous Eu and Yb metallocenes (23, 24) were not reducing enough to make the analogous isolable complexes (25), and Eu, Yb, and Sm were the only lanthanides that had molecular divalent complexes at that time. None of the other molecular Sm^{2+} complexes known at the time, such as $SmI_2(THF)_5$ (26, 27), $Sm[N(SiMe_3)_2]_2(THF)_2$ (28), $[C_5H_3(SiMe_3)_2]_2Sm(THF)$ (29), and $[(C_5Me_5)SmI(THF)]_2$ (30) appeared to be strong enough reductants to reduce N_2.

However, samarium dinitrogen chemistry did continue to advance. In 1994, Gambarrotta and co-workers began investigating the chemistry of Sm^{2+} in the coordination environments of tetrapyrrole tetraanion and dipyrrole dianion ligands. Tetrametallic $(N_2)^{4-}$ complexes were obtained from dinitrogen (31–36) as well as one $Sm_2(\mu\text{-}\eta^2\text{:}\eta^2\text{-}N_2)$ complex with an apparently short 1.08(3) Å N—N distance like that found in **2**. In some cases, these complexes were made from Sm^{2+} precursors and in others they were obtained from Sm^{3+} precursors and Li or Na in reactions that presumably made Sm^{2+} intermediates. In 1998, Floriani and co-workers (37) published a report on tetrapyrrole tetraanion Nd and Pr dinitrogen complexes prepared in the presence of Na. Interestingly, all of these polypyrrole lanthanide dinitrogen complexes also displayed the $Ln_2(\mu\text{-}\eta^2\text{:}\eta^2\text{-}N_2)$ coplanar arrangement found in $[(C_5Me_5)_2Sm]_2(\mu\text{-}\eta^2\text{:}\eta^2\text{-}N_2)$.

A new approach to lanthanide dinitrogen chemistry based on Tm^{2+}, Dy^{2+}, and Nd^{2+}

Significant expansion of dinitrogen chemistry in our laboratory resulted from the crystallographic identification of three new divalent molecular lanthanide diiodides, $TmI_2(DME)_3$ (38), $DyI_2(DME)_3$ (39), and $NdI_2(THF)_5$ (40). For many years it was expected that the only lanthanide ions that would form isolable, soluble, divalent, molecular species were Eu^{2+}, Yb^{2+}, and Sm^{2+}. As shown in Table 1, these three ions are the least reducing of the entire series (18). The next most reducing ions (Tm^{2+}, Dy^{2+}, and Nd^{2+}) were known in solid-

Fig. 3. Structures of the first molecular complexes of Tm^{2+}, Dy^{2+}, and Nd^{2+}, $TmI_2(DME)_3$ (38), $DyI_2(DME)_3$ (39), and $NdI_2(THF)_5$ (40).

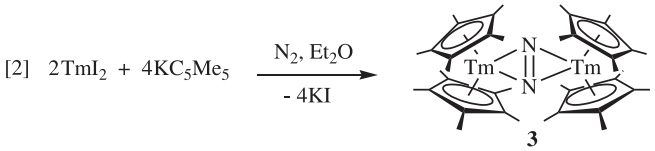


state materials obtained from Ln and I_2 in sealed tantalum vessels at high temperature (41), but attempts to isolate fully characterizable molecular species from these ions were unsuccessful. Transient, intensely colored solutions were reported to contain these ions, but their lifetimes were typically short (42–44). It was generally believed that these ions were too reactive to isolate and utilize in solution.

This belief was overturned in 1997, when the first crystallographic data on a stable, soluble, molecular Tm^{2+} complex were obtained (Fig. 3) (38). The existence of $TmI_2(DME)_3$ clearly showed that molecular divalent lanthanide chemistry was not limited only to Eu, Yb, and Sm.

On the basis of the rich chemistry previously observed for Sm^{2+} (19, 20), much was anticipated from the new divalent ion (Tm^{2+}). However, initial attempts to obtain chemistry from Tm^{2+} were not particularly productive (45–48). It readily formed Tm^{3+} products, but without generating any significantly new inorganic or organometallic reduction products. Attempts to utilize Tm^{2+} in situ in organic reaction chemistry as a replacement for SmI_2–HMPA suggested that in situ chemistry might be the best way to pursue this highly reactive divalent chemistry (49).

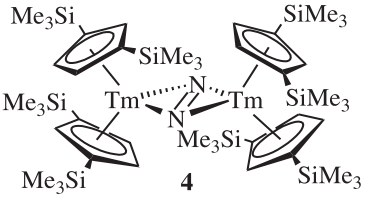
The reappearance of lanthanide dinitrogen chemistry in our laboratory came during the exploration of this in situ Tm^{2+} chemistry. In a reaction designed to mimic in situ the organometallic reduction chemistry of $(C_5Me_5)_2Sm$ (19, 20), TmI_2 was combined with 2 equiv. of KC_5Me_5. However, before a substrate could be added to this mixture, a reaction occurred. The product that was isolated from this reaction was $[(C_5Me_5)_2Tm]_2(\mu\text{-}\eta^2\text{:}\eta^2\text{-}N_2)$ (**3**), a complex analogous to the first lanthanide dinitrogen complex, $[(C_5Me_5)_2Sm]_2(\mu\text{-}\eta^2\text{:}\eta^2\text{-}N_2)$ (**2**). This result (eq. [2]) (50) showed that the supposedly inert atmosphere of dinitrogen provided the substrate for this in situ Tm^{2+} reaction!



This discovery advanced both divalent lanthanide chemistry and lanthanide dinitrogen chemistry. It revealed a new route to lanthanide-based reduction of dinitrogen and it showed one reason why the previous attempts to isolate molecular Ln^{2+} complexes might have failed.

Further studies of in situ TmI_2–cyclopentadienide chemistry showed that eq. [2] was not limited to $(C_5Me_5)^{1-}$ ligands. Dinitrogen complexes of $[C_5H_3(SiMe_3)_2]^{1-}$ (51) and even the mono-substituted $[C_5H_4(SiMe_3)]^{1-}$ ligand (52) could be isolated: $\{[C_5H_3(SiMe_3)_2]_2Tm\}_2(\mu\text{-}\eta^2\text{:}\eta^2\text{-}N_2)$ (**4**) (eq. [3]), and

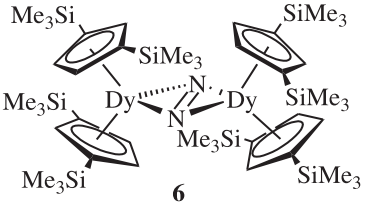
© 2005 NRC Canada

[3] $2TmI_2 + 4KC_5H_3(SiMe_3)_2 \xrightarrow[-4KI]{N_2,\ Et_2O}$ 

4

[4] $2TmI_2 + 4KC_5H_4(SiMe_3) \xrightarrow[-4KI]{N_2,\ THF}$ 

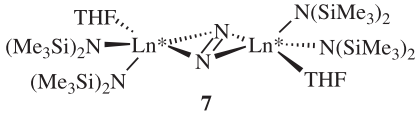
5

[5] $2DyI_2 + 4KC_5H_3(SiMe_3)_2 \xrightarrow[-4KI]{N_2,\ Et_2O}$ 

6

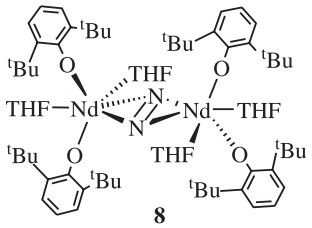
[6] $2Ln^*I_2 + 4KN(SiMe_3)_2 \xrightarrow[-4KI]{THF}$ "$2Ln^*[N(SiMe_3)_2]_2$" $\xrightarrow{N_2}$

Ln^* = Tm, Dy, Nd



7

[7] $2NdI_2 + 4KOC_6H_3{}^tBu_2\text{-}2,6 \xrightarrow[-4KI]{THF}$ "$2Nd(OC_6H_3{}^tBu_2\text{-}2,6)_2$" $\xrightarrow{N_2}$



8

$\{[C_5H_4(SiMe_3)]_2Tm\}_2(\mu\text{-}\eta^2\text{:}\eta^2\text{-}N_2)$ (**5**) (eq. [4]) (50). With the smaller, monosubstituted, cyclopentadienyl ligand in complex **5**, the thulium ions were solvated with THF, but the internal structure of the complex still maintained the formerly unusual $M_2(\mu\text{-}\eta^2\text{:}\eta^2\text{-}N_2)$ arrangement.

While the Tm^{2+} chemistry was being developed, new syntheses of divalent Dy^{2+} and Nd^{2+} compounds were reported (53), and crystallographic confirmation of the existence of these molecular divalent complexes of Dy^{2+} (39) and Nd^{2+} (40) was also obtained (Fig. 3). These advances allowed the dinitrogen reduction chemistry of these two elements to be studied. On the basis of the Tm^{2+} chemistry above, it was no surprise that DyI_2–$KC_5H_3(SiMe_3)_2$ would extend lanthanide dinitrogen chemistry to Dy (54). Again, a $M_2(\mu\text{-}\eta^2\text{:}\eta^2\text{-}N_2)$ structure was observed in the product, $\{[C_5H_3(SiMe_3)_2]_2Dy\}_2(\mu\text{-}\eta^2\text{:}\eta^2\text{-}N_2)$ (**6**) (eq. [5]).

Attempts to make analogous cyclopentadienyl neodymium dinitrogen complexes were unsuccessful. This seemed reasonable considering the high reactivity of Nd^{2+} (Table 1). For example, the TmI_2–$2KC_5Me_5$ combination had been found to be reactive enough to decompose Et_2O (in the absence of N_2) (50). However, more reactive NdI_2 would decompose THF at room temperature without any added ligand (55). It appeared that the combination of this more reducing Nd^{2+} ion and the electron-donating cyclopentadienyl ligand might be "too reactive" for dinitrogen reduction. This suggested that other ligands should be tried with Nd^{2+}.

To determine if the divalent ions of Tm^{2+}, Dy^{2+}, and Nd^{2+} could reduce dinitrogen without the aid of cyclopentadienyl ligands, in situ reactions of other "Ln^*Z_2" combinations were examined (Ln^* = Tm, Dy, Nd; $(Z)^{1-}$ = monoanion). The first two $(Z)^{1-}$ ligands studied were the amide and aryloxide ligands most commonly used in lanthanide chemistry, $[N(SiMe_3)_2]^{1-}$ (56) and $[OC_6H_3\text{-}t\text{-}Bu_2\text{-}2,6]^{1-}$ (57, 58). As shown in eqs. [6] and [7], in situ reactions of Ln^*I_2 with $KN(SiMe_3)_2$ and $KOC_6H_3\text{-}t\text{-}Bu_2\text{-}2,6$ generated two new series of lanthanide dinitrogen complexes, the amides, $\{[(Me_3Si)_2N]_2(THF)Ln^*\}_2(\mu\text{-}\eta^2\text{:}\eta^2\text{-}N_2)$ (**7**), and the aryloxides exemplified by $[(2,6\text{-}t\text{-}Bu_2C_6H_3O)_2(THF)_2Nd]_2(\mu\text{-}\eta^2\text{:}\eta^2\text{-}N_2)$ (**8**) (59). The $[N(SiMe_3)_2]^{1-}$ lanthanide dinitrogen complexes (**7**) were

© 2005 NRC Canada

analogous to the $[C_5H_4(SiMe_3)]^{1-}$ thulium complex (**5**) above, and contained one THF of solvation per metal. With NdI_2 and $[OC_6H_3$-*t*-Bu_2-2,6$]^{1-}$, the isolated product (**8**) contained *two* THF molecules of solvation per metal center.

Preponderance of the $Ln_2(\mu$-η^2:η^2-$N_2)$ structure

As shown in eqs. [6] and [7], despite the variation in metals, ligands, and degree of THF solvation, the new amide and aryloxide lanthanide dinitrogen complexes retained the formerly rare $M_2(\mu$-η^2:η^2-$N_2)$ structure first reported for $[(C_5Me_5)_2Sm]_2(\mu$-η^2:η^2-$N_2)$. Hence, the coplanar arrangement of two metals and dinitrogen that originally was unusual, subsequently became the structure found in all of the lanthanide cyclopentadienyl, amide, aryloxide, and polypyrrole polyanion dinitrogen complexes isolated. Although this structure originally could have been attributed to some constraints in the coordination environment enforced by the ancillary ligands, e.g., the four $(C_5Me_5)^{1-}$ ligands in $[(C_5Me_5)_2Sm]_2(\mu$-η^2:η^2-$N_2)$ (60) or the cyclic tetrapyrrole tetraanions (31–37), this was not possible with the new THF-solvated dinitrogen complexes with these simple monodentate amides and aryloxides. The fact that this $M_2(\mu$-η^2:η^2-$N_2)$ structure formed with both mono- and polydentate ligands and in unsolvated, mono-solvated, and di-solvated complexes, suggested that this was in fact the preferred structure for a Ln_2N_2 unit regardless of the ancillary ligands.

Although the $M_2(\mu$-η^2:η^2-$N_2)$ structure may have appeared to be unusual on the basis of transition metal chemistry, which initially had many more η^1 end-on bound dinitrogen complexes, it is actually a quite reasonable structure for the more ionic lanthanides. Bradley et al. (61, 62) discovered bimetallic lanthanide complexes of the $(O_2)^{2-}$ ligand in 1974 that had a $Ln_2(\mu$-η^2:η^2-$O_2)$ structure analogous to the $Ln_2(\mu$-η^2:η^2-$N_2)$ arrangement and similar structures have subsequently been identified (63). Calculations on the electrostatic stabilization of that $Ln_2(\mu$-η^2:η^2-$O_2)$ peroxide vs. a $Ln_2(\mu$-η^1:η^1-$O_2)$ arrangement, i.e., Ln-O-O-Ln, indicated that the μ-η^2:η^2-option was quite favored (62). The same argument could apply to $(N_2)^{2-}$ complexes of the lanthanides if the bonding is largely electrostatic.

In contrast to the predominance of the $M_2(\mu$-η^2:η^2-$N_2)$ structure in lanthanide dinitrogen chemistry, this arrangement still tends to be rare in transition metal chemistry. The structures of $\{[(Me_3Si)_2N]Cl(TMEDA)Ti\}_2(\mu$-$\eta^1$:$\eta^1$-$N_2)$ vs. $\{[(Me_3Si)_2N]_2Ti\}_2(\mu$-$\eta^2$:$\eta^2$-$N_2)_2$ were early examples of how changes in the ligand set can affect the preference for $M_2(\mu$-η^2:η^2-$N_2)$ bonding in transition metal complexes (64). The recent example of the $M_2(\mu$-η^2:η^2-$N_2)$ structure in $[(C_5Me_4H)_2Zr]_2(\mu$-η^2:η^2-$N_2)$ (65), in contrast to the end-on bonding in $[(C_5Me_5)_2Zr(\eta^1$-$N_2)]_2(\mu$-η^1:η^1-$N_2)$ (10), indicates that only small changes in the ancillary ligands can affect the stability of the $M_2(\mu$-η^2:η^2-$N_2)$ structure in transition metal chemistry. Examples of the $M_2(\mu$-η^2:η^2-$N_2)$ geometry have also been found with actinide metals, which often display chemistry intermediate between the lanthanides and transition metals. These include $[\{N(CH_2CH_2NSi$-*t*-$BuMe_2)_3\}U]_2(\mu$-η^2:η^2-$N_2)$ (66) and $[(C_5Me_5)(C_8H_4\{Si$-*i*-Pr_3-1,4$\}_2)U]_2(\mu$-η^2:η^2-$N_2)$ (67).

Paramagnetism in lanthanide dinitrogen complexes

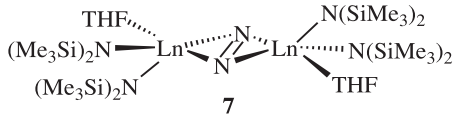
Although the advent of molecular complexes of the divalent ions of Tm^{2+}, Dy^{2+}, and Nd^{2+} expanded lanthanide dinitrogen chemistry to a wider range of metals, further studies of the reactivity of these reduced dinitrogen complexes remained challenging because of their paramagnetism. In the $(N_2)^{2-}$ complexes (**3**–**7**), the Tm^{3+} and Dy^{3+} ions have magnetic moments of 6.9 and 9.9 μ_B, respectively, and the compounds do not give observable NMR spectra. The Nd^{3+} complex (**8**) with a magnetic moment of 3.5 μ_B, gave observable spectra, but the broad resonances were still not very definitive. No ^{15}N NMR data were obtained on any of these species.

A new approach based on LnZ_3–K reactivity — The $Ln[N(SiMe_3)_2]_3$–K reduction system

If the presumed divalent "$Ln[N(SiMe_3)_2]_2$" intermediates thought to be responsible for the formation of the dinitrogen complexes in the syntheses from LnI_2 and $KN(SiMe_3)_2$ (eq. [6]) could be generated in situ from the readily accessible $Ln[N(SiMe_3)_2]_3$ complexes (56) and potassium (68), the synthesis of **7** would be improved since it did not depend on the highly reactive Ln^{*2+} ions. Accordingly, $Tm[N(SiMe_3)_2]_3$ was prepared (56) and treated with K under nitrogen. As shown in eq. [8], this "LnZ_3/K" approach (where Z is a monoanionic ligand that allows this chemistry) to dinitrogen reduction was successful and generated $\{[(Me_3Si)_2N]_2$-$(THF)Tm\}_2(\mu$-η^2:η^2-$N_2)$ (**7-Tm**).

This was a significant synthetic breakthrough, since it meant that **7-Tm** could be obtained from $Tm[N(SiMe_3)_2]_3$ rather than TmI_2. $Tm[N(SiMe_3)_2]_3$ is readily available from $LnCl_3$ and $KN(SiMe_3)_2$ by literature methods dating back to 1973 (56). Since $Tm[N(SiMe_3)_2]_3$ is much less reactive than TmI_2, this made the experimental procedure to make the **7-Tm** complex less demanding. Since Tm has a –2.3 V (vs. NHE) calculated Ln^{3+}/Ln^{2+} reduction potential (Table 1, (18)), and K has a –2.9 V reduction potential, eq. [8] was reasonable on the basis of redox potentials.

Although eq. [8] was successful with thulium, no evidence of a highly colored, divalent intermediate consistent with "$Tm[N(SiMe_3)_2]_2$" was observed. Similar results were obtained with the $Dy[N(SiMe_3)_2]_3$–K reaction (eq. [8], Ln = Dy). $\{[(Me_3Si)_2N]_2(THF)Dy\}_2(\mu$-$\eta^2$:$\eta^2$-$N_2)$ (**7-Dy**) could be synthesized by this method, but the intense color expected from "$Dy[N(SiMe_3)_2]_2$" generated via a –2.5 V Dy^{3+}/Dy^{2+} reduction by K was not visible. Although it was possible that the divalent intermediates reacted so fast that they were not seen, we decided to examine eq. [8] with a lanthanide for which no molecular divalent complex had been crystallographically characterized. Using Ho, which has a –2.9 V

[8] $2Ln[N(SiMe_3)_2]_3 + 2K \xrightarrow[-\,2KN(SiMe_3)_2]{N_2,\ THF}$ 

7

© 2005 NRC Canada

Ln^{3+}/Ln^{2+} reduction potential, eq. [8] was similarly successful and the first holmium dinitrogen complex was isolated ($\{[(Me_3Si)_2N]_2(THF)Ho\}_2(\mu\text{-}\eta^2\text{:}\eta^2\text{-}N_2)$, **7-Ho**).

Encouraged by these results, eq. [8] was examined with Y and Lu, for which no molecular divalent chemistry has previously been reported. These were important elements, because their trivalent complexes are diamagnetic. If eq. [8] was successful with these metals, this would produce the first diamagnetic $\{[(Me_3Si)_2N]_2(THF)Ln\}_2(\mu\text{-}\eta^2\text{:}\eta^2\text{-}N_2)$ complexes (68). Much to our delight, the $Ln[N(SiMe_3)_2]_3$–K reactions were also successful with yttrium and lutetium and produced **7-Y** and **7-Lu**. Subsequent studies showed that $\{[(Me_3Si)_2N]_2(THF)Ln\}_2(\mu\text{-}\eta^2\text{:}\eta^2\text{-}N_2)$ compounds could also be obtained in this way with Gd, Tb, and, Er, metals with Ln^{3+}/Ln^{2+} reduction potentials of –3.9, –3.7, and –3.1 V (vs. NHE), respectively. These reactions were all the more remarkable in that they could be accomplished with Na (–2.7 V) as well as K (69).

The success of eq. [8] not only with Tm and Dy, but also with Nd, Gd, Tb, Ho, Y, Er, and Lu suggested several mechanistic possibilities that are still under investigation at this time. If eq. [8] proceeds through divalent $Ln[N(SiMe_3)_2]_2$ intermediates, these reactions represent the first examples of molecular Gd^{2+}, Tb^{2+}, Er^{2+}, Ho^{2+}, Y^{2+}, and Lu^{2+} chemistry. Alternatively, if the trivalent $Ln[N(SiMe_3)_2]_3$ complexes were activating dinitrogen for reduction by potassium in THF, e.g., by formation of a "$(N_2)Ln[N(SiMe_3)_2]_3$" complex, which would allow alkali metal reduction to occur, this would be the first evidence of dinitrogen complexation to a trivalent lanthanide. Although this type of dinitrogen activation is common with transition metals (70, 71), and is known for actinides (72), formation of a dinitrogen complex of a trivalent lanthanide in the presence of a much larger concentration of a more polar, harder Lewis base, namely THF, is not precedented in lanthanide chemistry. An additional possibility involves activation of dinitrogen by the alkali metal reductant with subsequent electron transfer in the presence of $Ln[N(SiMe_3)_2]_3$. If this option is operating, it must occur with Na as well as K and potassium graphite.

Regardless of the mechanism, the LnZ_3 – alkali metal reduction system when applied to dinitrogen as a substrate using $[N(SiMe_3)_2]^{1-}$ as the $(Z)^{1-}$ ligand generates a series of isomorphous $\{[(Me_3Si)_2N]_2(THF)Ln\}_2(\mu\text{-}\eta^2\text{:}\eta^2\text{-}N_2)$ complexes (**7**) for Nd, Gd–Tm, Y, and Lu without the need for divalent reagents. Interestingly, this reaction did not give isolable crystalline complexes for the larger metals in the series, La, Ce, and Pr. Since these metals have Ln^{3+}/Ln^{2+} reduction potentials of –3.1, –3.2, and –2.7 V (vs. NHE), respectively, and since reactions with Gd (–3.9 V) and Tb (–3.7 V) were successful, it seems that reduction potential was not the determining factor here.

^{15}N NMR spectroscopy — The first diamagnetic data

The ability to extend reductive lanthanide dinitrogen chemistry to Y and Lu using the LnZ_3–K approach provided the opportunity for the first time to use NMR spectroscopy to study diamagnetic lanthanide dinitrogen complexes. Obtaining ^{15}N NMR data on $\{[(Me_3Si)_2N]_2(THF)Ln\}_2(\mu\text{-}\eta^2\text{:}\eta^2\text{-}N_2)$ (Ln = Y, Lu) was not easy, however (68). To insure the validity of the measurement only crystalline samples were examined and the yields of X-ray quality crystals whose identity could be verified by unit cell determination were small. Ultimately, the ^{15}N NMR shifts were obtained and found to be 513 and 557 ppm (vs. $MeNO_2$) for the **7-Y** and **7-Lu** analogs, respectively. These are compared with other complexes in Table 2.

Table 2. ^{15}N NMR shifts for some selected dinitrogen complexes.

Compound	^{15}N NMR shift referenced to $MeNO_2$
$[(C_5Me_5)_2(THF)La]_2(\mu\text{-}\eta^2\text{:}\eta^2\text{-}N_2)$	569
$\{[(Me_3Si)_2N]_2(THF)Lu\}_2(\mu\text{-}\eta^2\text{:}\eta^2\text{-}N_2)$	557
$\{[(Me_3Si)_2N]_2(THF)La\}_2(\mu\text{-}\eta^2\text{:}\eta^2\text{-}N_2)$	516
$\{[(Me_3Si)_2N]_2(THF)Y\}_2(\mu\text{-}\eta^2\text{:}\eta^2\text{-}N_2)$	513
$[(C_5Me_4H)_2(THF)La]_2(\mu\text{-}\eta^2\text{:}\eta^2\text{-}N_2)$	495
$[(C_5Me_4H)_2Zr]_2(\mu\text{-}\eta^2\text{:}\eta^2\text{-}N_2)$ (65)	240
$[(C_5Me_5)_2Zr(\eta^1\text{-}N_2)]_2(\mu\text{-}\eta^1\text{:}\eta^1\text{-}N_2)$ (10)	183 (Bridging)
	85 (Terminal)
$\{[(i\text{-}Pr_2PCH_2SiMe_2)_2N]ZrCl\}_2(\mu\text{-}\eta^2\text{:}\eta^2\text{-}N_2)$ (15)	82

Detection of a $La_2(\mu\text{-}\eta^2\text{:}\eta^2\text{-}N_2)$ complex

Once an estimate of the ^{15}N NMR shifts of diamagnetic Ln_2N_2 complexes was in hand, it was possible to look for the success of eq. [8] with Ln = La via ^{15}N NMR spectroscopy. Although the $La[N(SiMe_3)_2]_3$–K reaction did not give a crystalline **7-La** product, it was possible that the reaction occurred, but **7-La** just did not crystallize well under these conditions (69). When the $La[N(SiMe_3)_2]_3$–K reaction was conducted under $^{15}N_2$, a signal at 516 ppm was observed, which suggested that this LnZ_3–K reaction also succeeded with the largest metal in the lanthanide series (Table 2). This suggested that the LnZ_3–K–N_2 reaction was indeed general for the lanthanides, but that for the larger metals, the products did not readily crystallize. Since the radial size of the lanthanides changes by 0.18 Å from La to Lu (73), it is rare that the size of a given ligand set is ideal for crystallizing isomorphous examples for all the metals.

The $Ln(C_5Me_4H)_3$–K system

If the only factor that prevented identification of N_2 reduction via $Ln[N(SiMe_3)_2]_3$–K with the larger metals, La–Pr, involved the crystallizability of the $\{[(Me_3Si)_2N]_2(THF)Ln\}_2(\mu\text{-}\eta^2\text{:}\eta^2\text{-}N_2)$ products, then a change in the ligand environment could lead to success with these other metals. Accordingly, a new $(Z)^{1-}$ was sought for the LnZ_3–K–N_2 reaction (eq. [9]). It was further desirable to examine the LnZ_3–K reaction with other $(Z)^{1-}$ ligands to determine if the success of this approach to dinitrogen reduction in eq. [8] was involved with the fact that $(Z)^{1-}$ was specifically $[N(SiMe_3)_2]^{1-}$.

$$[9]\quad 2LnZ_3 + 2K \xrightarrow[THF]{N_2} [Z_2(THF)_XLn]_2(\mu\text{-}\eta^2\text{:}\eta^2\text{-}N_2) + 2KZ$$

© 2005 NRC Canada

A key factor in choosing $(Z)^{1-}$ was that LnZ_3 could be easily synthesized for all the lanthanides from readily available precursors, preferably the chloride, $LnCl_3$ (74), or from the elemental metal (75, 76). A $(Z)^{1-}$ ligand that met this requirement was $(C_5Me_4H)^{1-}$ (eq. [10]) (77, 78).

[10] $LnCl_3 + 3KC_5Me_4H \xrightarrow[-3KCl]{THF} (C_5Me_4H)_3Ln$

Hence, the $Ln(C_5Me_4H)_3$–K dinitrogen reduction reaction was examined. The Ln = La case was of particular interest since crystallographic evidence had not yet been obtained on this diamagnetic system. As shown in eq. [11], $(C_5Me_4H)_3La$ and $(C_5Me_4H)_3Nd$ in the presence of K and dinitrogen generate the new lanthanide dinitrogen complexes $[(C_5Me_4H)_2(THF)Ln]_2(\mu\text{-}\eta^2\text{:}\eta^2\text{-}N_2)$ (**9**) (79). Each has the $Ln_2(\mu\text{-}\eta^2\text{:}\eta^2\text{-}N_2)$ internal structure previously observed with other lanthanide complexes. The overall structure was similar to that of the $\{[(Me_3Si)_2N]_2(THF)Ln\}_2(\mu\text{-}\eta^2\text{:}\eta^2\text{-}N_2)$ complexes (**7**), except that C_5Me_4H groups had replaced the $[N(SiMe_3)_2]^{1-}$ ligands. This result demonstrated that with the proper ligand set, La_2N_2 complexes analogous to those of the other metals could be isolated in crystalline form. The ^{15}N NMR shift of this lanthanum complex was in the same region as the other diamagnetic lanthanides (495 ppm, Table 2).

The extension of the LnZ_3–K reaction to the organometallic $(C_5Me_4H)_3Ln$ starting materials showed that this reaction was not limited to $(Z)^{1-} = [N(SiMe_3)_2]^{1-}$. It provided another advance in that the yield of the reduced dinitrogen products was high. In contrast, the $Ln[N(SiMe_3)_2]_3$–K–N_2 reactions did not give yields that exceeded 50%, a factor that hindered subsequent reactivity studies of the $(N_2)^{2-}$ moiety. In addition, purification of the $\{[(Me_3Si)_2N]_2(THF)Ln\}_2(\mu\text{-}\eta^2\text{:}\eta^2\text{-}N_2)$ products was achieved only through crystallization as this was the primary means of separating the product (**7**) from the soluble $KN(SiMe_3)_2$ by-product of eq. [8]. The organometallic LnZ_3–K–N_2 system was superior in that the unwanted KZ by-product, in this case, KC_5Me_4H would precipitate from solution. Formation of an insoluble KZ by-product may prove to be useful in obtaining high yields in eq. [9] and may be an important point to consider in future applications of the LnZ_3–K reduction system.

LnZ_3–K reduction with heteroleptic precursors (LnZ_2Z'–K)

Since $(C_5Me_5)^{1-}$ is such a heavily investigated ligand with the lanthanides and since the first lanthanide dinitrogen complex (**2**) was obtained with $(C_5Me_5)^{1-}$ ligands (4), it was desirable to investigate the LnZ_3–K–N_2 reaction with Z = $(C_5Me_5)^{1-}$. However, the $(C_5Me_5)_3Ln$ complexes are not viable starting materials for a LnZ_3–K reaction. They are not known for all the lanthanides and in addition, they are not stable to the THF solvent typically used for eq. [9] (80). Specifically, $(C_5Me_5)_3Ln$ complexes ring-open THF to make $(C_5Me_5)_2Ln[O(CH_2)_4C_5Me_5]$ (80).

Since the LnZ_3–K reaction (eq. [9]) sacrifices one $(Z)^{1-}$ ligand per lanthanide in the reduction process, it is not necessary to have a homoleptic precursor composed of three identical $(Z)^{1-}$ ligands. In fact, a LnZ_2Z' precursor in which KZ′ is insoluble could be superior to LnZ_3 as a starting material. Accordingly, we examined the precursors to the $(C_5Me_5)_3Ln$ complexes, the $[(C_5Me_5)_2Ln][(\mu\text{-}Ph)_2BPh_2]$ salts, as starting materials for the LnZ_3–K reduction with the expectation that elimination of $KBPh_4$ would be favorable. These lanthanide tetraphenylborate salts are readily prepared from $LnCl_3$ for all of the lanthanides (81, 82).

As shown in eq. [12], $[(C_5Me_5)_2La][(\mu\text{-}Ph)_2BPh_2]$ can function as a precursor for a LnZ_3–K reduction of N_2 (79). $[(C_5Me_5)_2(THF)La]_2(\mu\text{-}\eta^2\text{:}\eta^2\text{-}N_2)$ (**10**) was isolated from this reaction and characterized by X-ray crystallography and ^{15}N NMR spectroscopy (Table 2). Hence, eq. [12] was the first example of the successful use of a heteroleptic LnZ_2Z' precursor in the LnZ_3–K reduction system. It also provided the first good crystallographic data on a $(C_5Me_5)^{1-}$ lanthanide dinitrogen complex since the isolation of $[(C_5Me_5)_2Sm]_2(\mu\text{-}\eta^2\text{:}\eta^2\text{-}N_2)$. Interestingly, the lanthanum complex is isolated as a THF solvate, whereas the samarium complex is not.

LnZ_3–K overview

The preliminary results obtained to date on the LnZ_3–K reduction reaction (eq. [9]) suggest it is a general method to make reduced dinitrogen complexes of all the lanthanides. The range of Z ligands that is possible in these reactions has barely been explored, and it has been shown to be possible to use LnZ_2Z' precursors as well. This LnZ_3–K reduction system allows, for the first time, high-yield syntheses of diamagnetic Ln_2N_2 complexes. This should be very helpful in

[11] $2\ (C_5Me_4H)_2Ln + 2KC_8 \xrightarrow[-2KC_5Me_4H,\ -graphite]{THF,\ N_2} [(C_5Me_4H)_2(THF)Ln]_2(\mu\text{-}\eta^2\text{:}\eta^2\text{-}N_2)$ **9**

Ln = La and Nd

[12] $2\ (C_5Me_5)_2La[(\mu\text{-}Ph)_2BPh_2] + 2KC_8 \xrightarrow[-2KBPh_4,\ -graphite]{THF,\ N_2} [(C_5Me_5)_2(THF)La]_2(\mu\text{-}\eta^2\text{:}\eta^2\text{-}N_2)$ **10**

© 2005 NRC Canada

allowing the dinitrogen chemistry of the lanthanides to be fully explored. Certainly, the low yield and paramagnetism and the need to work only with crystallized samples inhibited earlier development.

More generally, the LnZ_3–K reduction system brings reductive, divalent-like chemistry to all the lanthanides. This should allow size optimization of this reductive chemistry (80) and selective choice of the metals with the most favorable spectroscopic and magnetic properties. The LnZ_3–K reduction system also should be applicable to substrates other than dinitrogen.

Retrospective

With the helpful advantage of hindsight, it is interesting to consider alternative routes by which lanthanide dinitrogen chemistry could have been developed. For example, if it had been suspected that the divalent lanthanide ions Tm^{2+}, Dy^{2+}, and Nd^{2+} would reduce dinitrogen, the preliminary investigations of these ions might have been done differently. It is likely that the short lifetimes observed for at least Tm^{2+} and Dy^{2+} in the early spectroscopic studies reviewed in 1984 (44) could have been prolonged by using Ar instead of N_2 as an inert atmosphere. Lanthanide dinitrogen complexes could have been discovered at that time and by using Ar, the molecular divalent chemistry of these ions could have been developed starting in the 1980s instead of in 1997 (38). Since the more reactive Nd^{2+} even attacks THF at room temperature, more than an Ar atmosphere might have been needed to identify dinitrogen complexes with that divalent ion.

Likewise, if, in the 1970s, potassium had been used in any reaction in the presence of the $Ln[N(SiMe_3)_2]_3$ complexes (56) under N_2, the series of $\{[(Me_3Si)_2N]_2(THF)Ln\}_2(\mu\text{-}\eta^2\text{:}\eta^2\text{-}N_2)$ compounds might have been discovered. The $(O_2)^{2-}$ complex of similar structure, $\{[(Me_3Si)_2N]_2(PPh_3\text{-}O)La\}_2(\mu\text{-}\eta^2\text{:}\eta^2\text{-}O_2)$, was identified in 1974 (61).

The recent results also raise questions about the intermediacy of divalent states of the polypyrrole polyanion chemistry reported for Sm, Pr, and Nd (33, 37). These dinitrogen reduction reactions, which used Li and Na, were assumed to involve divalent intermediates, but they could also have been forerunners of the LnZ_3–K chemistry that we now know is available for the entire lanthanide series. Related to these possibilities, we recently became aware of Russian papers from the 1980s in which Vol'pin, Bochkarev, and co-workers reported that ammonia was generated from hydrolysis of combinations of lanthanide complexes and excess sodium naphthalenide under dinitrogen (83, 84). Interestingly, of all the metals examined in those studies, the use of divalent Yb^{2+} starting materials gave the most ammonia, about 0.25 NH_3/Yb. This is one of the lanthanides for which no dinitrogen complex is known, nor expected to be very stable on the basis of spectroscopic data and calculations (25). It is possible that with slightly different starting materials, these sodium naphthalenide reactions could also have led to crystallographically characterizable lanthanide dinitrogen complexes via a LnZ_3–K reaction before the 1988 discovery of **2**.

Hence, hints of $(N_2)^{2-}$ complexes of the lanthanides, which have now been fully defined in many examples by X-ray crystallography and ^{15}N NMR spectroscopy, were in the literature many years earlier. This is probably the case for many discoveries. The challenge is to identify and follow up on these early clues. In the case of the chemistry described here, it was the strange extra peak in the ^1H NMR spectrum of $(C_5Me_5)_2Sm$, the decision to do in situ chemistry with the reactive new Ln^{*2+} ions, and the absence of the appropriate color in the $Ln[N(SiMe_3)_2]_3$–K–N_2 reaction that provided us with key suggestions.

Conclusion

Lanthanide dinitrogen chemistry has grown enormously since the discovery of $[(C_5Me_5)_2Sm]_2(\mu\text{-}\eta^2\text{:}\eta^2\text{-}N_2)$ in 1988. Although the first example depended on the special reductive chemistry of Sm^{2+} and many of the subsequent examples resulted from the reactive divalent Tm^{2+} and Dy^{2+} ions, the discovery of the LnZ_3–K reduction system opened this chemistry to all the metals in the lanthanide series. Trivalent lanthanide complexes of the reduced dinitrogen $(N_2)^{2-}$ moiety have now been crystallographically characterized for all of the lanthanides in the series except the one radioactive member, Pm, the two most easily reduced elements, Eu and Yb, and Ce, which has not yet yielded to crystallization. These $(N_2)^{2-}$ compounds are available with a variety of simple ligands common in lanthanide chemistry, including cyclopentadienyls, amides, and aryloxides. Further diversity is likely to be possible via the LnZ_3–K and LnZ_2Z'–K reduction routes. More importantly, with the advent of high-yield routes to diamagnetic complexes, the stage is set for the first time for development of the chemical reactivity of these $(N_2)^{2-}$ ligands.

Acknowledgement

We thank the National Science Foundation for support of this research.

References

1. A.D. Allen and C.V. Senoff. J. Chem. Soc. Chem. Commun. **621** (1965).
2. W.J. Evans, L.A. Hughes, and T.P. Hanusa. J. Am. Chem. Soc. **106**, 4270 (1984).
3. W.J. Evans, L.A. Hughes, and T.P. Hanusa. Organometallics, **5**, 1285 (1986).
4. W.J. Evans, T.A. Ulibarri, and J.W. Ziller. J. Am. Chem. Soc. **110**, 6877 (1988).
5. A.J. Freeman and R.E. Watson. Phys. Rev. **127**, 2058 (1962).
6. F.A. Hart and F.P. Laming. Proc. Chem. Soc. London, 107 (1963).
7. J.H. Forsberg. Coord. Chem. Rev. **10**, 195 (1973).
8. F.A. Hart. *In* Comprehensive coordination chemistry. Vol. 3. *Edited by* G. Wilkinson, R.D. Gillard, and J.A. McCleverty. Pergamon Press, Oxford, UK. 1987. Chap. 39.
9. P. Pelikan and R. Boca. Coord. Chem. Rev. **55**, 55 (1984).
10. R.D. Sanner, J.M. Manriquez, R.E. Marsh, and J.E. Bercaw. J. Am. Chem. Soc. **98**, 8351 (1976).
11. K. Jonas. Angew. Chem. Int. Ed. Engl. **12**, 997 (1973).
12. C. Kruger and Y.H. Tsay. Angew. Chem. Int. Ed. Engl. **12**, 998 (1973).
13. K. Jonas, D.J. Brauer, C. Kruger, P.J. Roberts, and Y.H. Tsay. J. Am. Chem. Soc. **98**, 74 (1976).

© 2005 NRC Canada

14. G.P. Pez, P. Apgar, and R.K. Crissey. J. Am. Chem. Soc. **104**, 482 (1982).
15. M.D. Fryzuk, T.S. Haddad, and S.J. Rettig. J. Am. Chem. Soc. **112**, 8185 (1990).
16. W.J. Evans and S.E. Foster. J. Organomet. Chem. **433**, 79 (1992).
17. W.J. Evans and T.A. Ulibarri. J. Am. Chem. Soc. **109**, 4292 (1987).
18. L.R. Morss. Chem. Rev. **76**, 827 (1976).
19. W.J. Evans. Polyhedron, **6**, 803 (1987).
20. W.J. Evans. J. Organomet. Chem. **652**, 61 (2002).
21. W.J. Evans, T.A. Ulibarri, and J.W. Ziller. J. Am. Chem. Soc. **112**, 219 (1990).
22. W.J. Evans, S.L. Gonzales, and J.W. Ziller. J. Am. Chem. Soc. **116**, 2600 (1994).
23. W.J. Evans, L.A. Hughes, and T.P. Hanusa. Organometallics, **5**, 1285 (1986).
24. M. Schultz, C.J. Burns, D.J. Schwartz, and R.A. Andersen. Organometallics, **19**, 781 (2000).
25. L. Perrin, L. Maron, O. Eisenstein, D.J. Schwartz, C.J. Burns, and R.A. Andersen. Organometallics, **22**, 5447 (2003).
26. J.L. Namy, P. Girard, and H.B. Kagan. Nouv. J. Chim. **1**, 5 (1977).
27. W.J. Evans, T.S. Gummersheimer, and J.W. Ziller. J. Am. Chem. Soc. **117**, 8999 (1995).
28. W.J. Evans, D.K. Drummond, H. Zhang, and J.L. Atwood. Inorg. Chem. **27**, 575 (1988).
29. W.J. Evans, R.A. Keyer, and J.W. Ziller. J. Organomet. Chem. **394**, 87 (1990).
30. W.J. Evans, J.W. Grate, H.W. Choi, I. Bloom, W.E. Hunter, and J.L. Atwood. J. Am. Chem. Soc. **107**, 941 (1985).
31. J. Jubb and S. Gambarotta. J. Am. Chem. Soc. **116**, 4477 (1994).
32. T. Dube, S. Conoci, S. Gambarotta, G.P.A. Yap, and G. Vasapollo. Angew. Chem. Int. Ed. **38**, 3657 (1999).
33. J. Guan, T. Dube, S. Gambarotta, and G.P.A. Yap. Organometallics, **19**, 4820 (2000).
34. T. Dube, M. Ganesan, S. Conoci, S. Gambarotta, and G.P.A. Yap. Organometallics, **19**, 3716 (2000).
35. C.D. Berube, M. Yazdanbakhsh, S. Gambarotta, and G.P.A. Yap. Organometallics, **22**, 3742 (2003).
36. M. Ganesan, M.P. Lalonde, S. Gambarotta, and G.P.A. Yap. Organometallics, **20**, 2443 (2001).
37. E. Campazzi, E. Solari, C. Floriani, and R. Scopelliti. Chem. Commun. 2603 (1998).
38. M.N. Bochkarev, I.L. Fedushkin, A.A. Fagin, T.V. Petrovskaya, J.W. Ziller, R.N.R. Broomhall-Dillard, and W.J. Evans. Angew. Chem. Int. Ed. Engl. **36**, 133 (1997).
39. W.J. Evans, N.T. Allen, and J.W. Ziller. J. Am. Chem. Soc. **122**, 11 749 (2000).
40. M.N. Bochkarev, I.L. Fedushkin, S. Dechert, A.A. Fagin, and H. Schumann. Angew. Chem. Int. Ed. **40**, 3176 (2001).
41. G. Meyer and L.R. Morss (*Editors*). Synthesis of lanthanide and actinide compounds. 1991. p. 159.
42. A.N. Kamenskaya, K. Bukietynska, N.B. Mikheev, V.I. Spitsyn, and B.J. Trzebiatowska. Zh. Neorg. Khim. **24**, 1139 (1979).
43. A.N. Kamenskaya, N.B. Mikheev, and N.P. Kholmogorova. Zh. Neorg. Khim. **28**, 2499 (1983).
44. A.N. Kamenskaya. Zh. Neorg. Khim. **29**, 439 (1984).
45. W.J. Evans, R.N.R. Broomhall-Dillard, S.E. Foster, and J.W. Ziller. J. Coord. Chem. **46**, 565 (1999).
46. W.J. Evans, R.N.R. Broomhall-Dillard, and J.W. Ziller. Polyhedron, **17**, 3361 (1998).
47. M.N. Bochkarev, A.A. Fagin, I.L. Fedushkin, T.V. Petrovskaya, W.J. Evans, M.A. Greci, and J.W. Ziller. Russ. Chem. Bull. **9**, 1804 (1999).
48. M.N. Bochkarev, I.L. Fedushkin, A.A. Fagin, H. Schumann, and J. Demtschuk. Chem. Commun. 1783 (1997).
49. W.J. Evans and N.T. Allen. J. Am. Chem. Soc. **122**, 2118 (2000).
50. W.J. Evans, N.T. Allen, and J.W. Ziller. J. Am. Chem. Soc. **123**, 7927 (2001).
51. M.F. Lappert, A. Singh, J.L. Atwood, and W.E. Hunter. J. Chem. Soc. Chem. Commun. 1190 (1981).
52. M.F. Lappert, P.I.W. Yarrow, J.L. Atwood, and R. Shakir. J. Chem. Soc. Chem. Commun. 987 (1980).
53. M.N. Bochkarev and A.A. Fagin. Chem. Eur. J. **5**, 2990 (1999).
54. W.J. Evans, N.T. Allen, and J.W. Ziller. Angew. Chem. Int. Ed. **41**, 359 (2002).
55. W.J. Evans, P.S. Workman, and N.T. Allen. Org. Lett. **5**, 2041 (2003).
56. D.C. Bradley, J.S. Ghotra, and F.A. Hart. J. Chem. Soc. Dalton Trans. 1021 (1973).
57. P.B. Hitchcock, M.F. Lappert, and R.G. Smith. Inorg. Chim. Acta, **139**, 183 (1987).
58. H.A. Stecher, A. Sen, and A.L. Rheingold. Inorg. Chem. **27**, 1130 (1988).
59. W.J. Evans, G. Zucchi, and J.W. Ziller. J. Am. Chem. Soc. **125**, 10 (2003).
60. W.J. Evans. J. Alloys Comp. **192**, 205 (1993).
61. D.C. Bradley, J.S. Ghotra, F.A. Hart, M.B. Hursthouse, and P.R. Raithby. J. Chem. Soc. Chem. Commun. 40 (1974).
62. D.C. Bradley, J.S. Ghotra, F.A. Hart, M.B. Hursthouse, and P.R. Raithby. J. Chem. Soc. Dalton Trans. 1166 (1977).
63. M. Niemeyer. Z. Anorg. Allg. Chem. **628**, 647 (2002).
64. R. Duchateau, S. Gambarotta, N. Beydoun, and C. Bensimon. J. Am. Chem. Soc. **113**, 8986 (1991).
65. J.A. Pool, E. Lobkovsky, and P.J. Chirik. Nature (London), **427**, 527 (2004).
66. P. Scott and P. Roussel. J. Am. Chem. Soc. **120**, 1070 (1998).
67. F.G.N. Cloke and P.B. Hitchcock. J. Am. Chem. Soc. **124**, 9352 (2002).
68. W.J. Evans, D.S. Lee, and J.W. Ziller. J. Am. Chem. Soc. **126**, 454 (2004).
69. W.J. Evans, D.S. Lee, D.B. Rego, J.M. Perotti, S.A. Kozimor, E.K. Moore, and J.W. Ziller. J. Am. Chem. Soc. **126**, 14 574 (2004).
70. J.C. Peters, J.P.F. Cherry, J.C. Thomas, L. Baraldo, D.J. Mindiola, W.M. Davis, and C.C. Cummins. J. Am. Chem. Soc. **121**, 10 053 (1999).
71. M.B. O'Donoghue, W.M. Davis, R.R. Schrock, and W.M. Reiff. Inorg. Chem. **38**, 243 (1999).
72. W.J. Evans, S.A. Kozimor, and J.W. Ziller. J. Am. Chem. Soc. **125**, 14 264 (2003).
73. R.D. Shannon. Acta Crystallogr. **A32**, 751 (1976).
74. F.T. Edelmann. Synth. Methods Organomet. Inorg. Chem. **6**, 32 (1997).
75. G.B. Deacon and A.J. Koplick. Inorg. Nucl. Chem. Lett. **15**, 263 (1979).
76. G.B. Deacon, T.D. Tuong, and D.L. Wilkinson. Inorg. Synth. **27**, 136 (1990).
77. H. Schumann, M. Glanz, H. Hemling, and F.E. Hahn. Z. Anorg. Allg. Chem. **621**, 341 (1995).
78. M.A. Johnston. Ph.D. thesis, University of California, Irvine, California, USA. 2000.
79. W.J. Evans, D.S. Lee, C. Lie, and J.W. Ziller. Angew. Chem. Int. Ed. **43**, 5517 (2004).

© 2005 NRC Canada

80. W.J. Evans and B.L. Davis. Chem. Rev. **102**, 2119 (2002).
81. W.J. Evans, T.A. Ulibarri, L.R. Chamberlain, J.W. Ziller, and D. Alvarez, Jr. Organometallics, **9**, 2124 (1990).
82. W.J. Evans, C.A. Seibel, and J.W. Ziller. J. Am. Chem. Soc. **120**, 6745 (1998).
83. M.N. Bochkarev, A.A. Trifonov, G.A. Razuvaev, M.A. Ilatovskaya, and V.B. Shur. Izv. Akad. Nauk. SSSR Ser. Khim. **8**, 1898 (1986).
84. M.N. Bochkarev, A.A. Trifonov, G.A. Razuvaev, M.A. Ilatovskaya, V.B. Shur, M.E. Vol'pin. Dokl. Akad. Nauk. SSSR, **295**, 1381 (1987).

© 2005 NRC Canada

Bonding, activation, and protonation of dinitrogen on a molybdenum pentaphosphine complex — Comparison to *trans*-bis(dinitrogen) and -nitrile – dinitrogen complexes with tetraphosphine coordination[1]

Gerald C. Stephan, Gerhard Peters, Nicolai Lehnert, Carsten M. Habeck, Christian Näther, and F. Tuczek

Abstract: The molybdenum-N_2 pentaphosphine complex [$Mo(N_2)$(dpepp)(dppm)] (**1**) containing a bi- and a tridentate phosphine ligand (dpepp = $PhP(CH_2CH_2PPh_2)_2$, dppm = $Ph_2PCH_2PPh_2$) has been prepared and characterized. By protonation of **1** with triflic acid the NNH_2 complex [$Mo(NNH_2)$(dpepp)(dppm)]$(CF_3SO_3)_2$ (**2**) is formed without loss of the pentaphosphine coordination. The electronic properties of **1** and **2** and their ^{15}N and (or) ^2H counterparts are investigated by NMR, IR, and Raman spectroscopy coupled to DFT frequency and NMR shift calculations. Force constants are evaluated from experimental frequencies and isotope shifts by the quantum chemistry based normal coordinate analysis procedure (QCB-NCA). The results for the N_2 complex **1** are compared with those obtained earlier for bis(dinitrogen) and *trans*-nitrile dinitrogen systems. Importantly, the N_2 in the pentaphosphine complex is more strongly activated compared to corresponding bis(dinitrogen) compounds and more weakly activated compared to *trans*-nitrile N_2 systems. The activation of the NNH_2 ligand in complex **2** is similar to *trans*-nitrile systems and weaker compared to corresponding NNH_2 complexes with coordinated anions like [$MoF(NNH_2)(dppe)_2$](BF_4). These results are discussed based on the relative donor–acceptor properties of the respective trans ligands, demonstrating the influence of σ donation and π acceptance on the activation of N_2 in transition metal complexes.

Key words: nitrogen fixation, phosphine complexes, NMR shifts, DFT calculations, normal coordinate analysis.

Résumé : On a préparé et caractérisé le complexe pentaphosphine de molybdène-N_2 [$Mo(N_2)$(dpepp)(dppm)] (**1**) qui contient un ligand phosphine bidentate et un tridentate (dpepp = $PhP(CH_2CH_2PPh_2)_2$; dppm = $Ph_2PCH_2PPh_2$). Par protonation du complexe **1** avec l'acide triflique, le complexe NNH_2 [$Mo(NNH_2)$(dpepp)(dppm)]$(CF_3SO_3)_2$ (**2**) se forme sans perte de la coordination pentaphosphine. Les propriétés électroniques des composés **1** et **2** et de leurs contreparties ^{15}N et (ou) ^2H ont été étudiées par spectroscopie RMN, infrarouge et Raman couplées à des calculs de fréquences et de déplacements en RMN par la théorie de la densité fonctionnelle. Les constantes de force ont été évaluées à partir des fréquences expérimentales et les déplacements isotopiques par la chimie quantique en se basant sur une méthode d'analyse de coordonnées normales (QBC-NCA). Les résultats pour le complexe de N_2 (**1**) ont été comparés à ceux obtenus antérieurement avec les systèmes bis(diazote) et diazote nitrile *trans*. Le plus important est que, par comparaison avec les composés bis(diazote) correspondants, l'activation du complexe N_2 avec la pentaphosphine est plus forte alors que celle des systèmes nitriles *trans*. L'activation du ligand NNH_2 dans le complexe **2** est semblable à celle des systèmes nitriles *trans* et plus faible par comparaison aux complexes correspondants avec des anions coordinés comme le [$MoF(NNH_2)(dppe)_2$](BF_4). Une discussion de ces résultats sur la base des propriétés donneur–accepteur relatives des ligands trans respectifs permet de démontrer l'influence des caractères σ donneur et π accepteur sur l'activation du N_2 dans les complexes de métaux de transition.

Mots clés : fixation de l'azote, complexes de phosphines, déplacements chimiques en RMN, calculs de la théorie de la densité fonctionnelle, analyse de coordonnées normales.

[Traduit par la Rédaction]

Received 12 September 2004. Published on the NRC Research Press Web site at http://canjchem.nrc.ca on 13 April 2005.

G.C. Stephan, G. Peters, N. Lehnert, C.M. Habeck, C. Näther, and F. Tuczek.[2] Institut für Anorganische Chemie, Christian Albrechts Universität zu Kiel, Ohlshausenstr. 40, 24098 Kiel, Germany.

[1]This article is part of a Special Issue dedicated to Dinitrogen Chemistry.

[2]Corresponding author (e-mail: ftuczek@ac.uni-kiel.de).

 doi: 10.1139/V05-015 © 2005 NRC Canada

Introduction

Since the discovery of the first dinitrogen complex, synthetic nitrogen fixation in analogy to the biological process has presented a continuing challenge (1). Today, two systems exist that mediate the full conversion of N_2 to ammonia in a step-wise and well-defined manner. The first one of these is based on molybdenum or tungsten dinitrogen complexes with mono- or diphosphine coligands that can be protonated to give the corresponding NNH, NNH_2, and NNH_3 complexes (2). We have studied these systems with the help of spectroscopy coupled to DFT calculations (3). If monophosphine ligands are employed, protonation of the bis(dinitrogen) complex leads to formation of ammonia and a Mo(VI)/W(VI) species. Protonation of the corresponding Mo(0)/W(0) N_2 complexes with diphosphine ligands (dppe = $Et_2PCH_2CH_2PEt_2$ or depe = $Ph_2PCH_2CH_2PPh_2$) stops at the NNH_2 or NNH_3 stage (2). The N—N bond can be cleaved after two-electron reduction of the NNH_2 complex, generating the first molecule of NH_3 and a nitrido or imido complex (4). Protonation and reduction of these species produces a second molecule of ammonia and regenerates the Mo(0)/W(0) complex, which is able to bind N_2 (5). Importantly, a catalytic conversion of N_2 to ammonia has been reported for this system, achieving three cycles (6). More recently, a second system, able to fix dinitrogen, has been developed, which is based on a sterically shielded Mo(III) triamidoamine complex. For the conversion of complex-bound N_2 to NH_3, analogous intermediates have been evidenced and characterized, respectively, as for the classic Mo/W diphos compounds. Catalytic production of NH_3 from N_2 has been evidenced for this system as well, achieving six cycles with an efficiency of 65%. This represents a considerable improvement over the Mo/W diphos systems and a major breaktrough in the field of synthetic nitrogen fixation (7).

As compared to the novel Mo(triamidoamine) system that provides a sterically shielded site for the reduction and protonation of N_2, the Mo/W diphos complexes suffer from three disadvantages: (*i*) two molecules of N_2 are bound at the zero valent stage, one of which is replaced upon conversion to the NNH_2 stage by the conjugate base of the acid employed for protonation or the solvent. This already limits the maximum efficiency of the overall process to 50% with respect to the substrate, N_2; (*ii*) the different intermediates of the Mo/W diphos system along the pathway from N_2 to NH_3 react with each other. This in particular relates to Mo/W(IV) NNH_2 complexes, which are fairly acidic and protonate their two-electron reduced counterparts according to the simplified equation (co-ligands omitted).

$$[1] \quad Mo(IV)(NNH_2)^{2+} + Mo(II)(NNH_2) \rightarrow Mo(0)(N_2) + Mo(IV)(NH)^{2+} + NH_3$$

Analogous reactions are possible between Mo(IV) imido complexes and their two-electron reduced derivatives, and accordingly, between Mo(IV) and Mo(II) NNH_2 and NH species, respectively (5). It is obvious that these cross reactions further decrease the overall efficiency of the transition-metal-mediated conversion of N_2 to ammonia based on Mo/W diphos complexes. Efforts have been presented to overcome these problems by attachment of Mo/W dinitrogen complexes with phosphine co-ligands to polymers or electrodes (8).

The third and perhaps most serious disadvantage of the Mo/W mono- and diphosphine systems appears to be the fact that the phosphine ligation becomes labile at the Mo/W(IV) stage (3*c*). This leads to irreversible replacement of these ligands by Lewis-basic species present in solution, i.e., the conjugate bases of the acids employed for protonation or solvent molecules. Regeneration of zero valent tetraphosphine species capable of binding N_2 then is not possible any more, and the catalytic circle is interrupted. In an effort to increase the thermodynamic and kinetic stability of the phosphine ligation in Mo or W dinitrogen complexes, we have recently synthesized the tetraphosphine ligand prP_4 ($Ph_2P(CH_2)_2PPh(CH_2)_3PPh(CH_2)_2PPh_2$) and investigated the stereochemistry and coordination properties of this ligand based on $Fe(NCS)_2$ complexes (9). The synthesis and characterization of a corresponding Mo/W(0) complex is currently under investigation.

One step further along this line would correspond to binding of N_2 on a Mo(0)/W(0) complex with a pentaphosphine ligand. This would also solve the first one of the above-mentioned problems as only formation of mono-dinitrogen complexes is possible. While a linear pentaphosphine ligand is known (10), we have chosen to first investigate the properties of a ligand sphere with five phosphine donors based on a complex containing a combination of a bidentate and a tridentate ligand. Such a compound, $Mo(N_2)$(dpepp)(dppm) (**1**), has been synthesized and investigated by George et al. (11) (dpepp = $PhP(CH_2CH_2PPh_2)_2$, dppm = $Ph_2PCH_2PPh_2$). In the present paper, the electronic structure and the spectroscopic properties of this complex are determined. Moreover, the complex is protonated to generate the NNH_2 complex $[Mo(NNH_2)(dpepp)(dppm)](CF_3SO_3)_2$ (**2**). ^{15}N and ^{31}P NMR spectroscopic data of **1** and **2** are presented. IR and Raman data of **1** and **2** are evaluated with the QCB-NCA procedure, which has been developed to analyze the vibrational structure of large molecules (12). DFT calculations are performed for the model systems $[Mo(N_2)(PH_3)_5]$ (**Ia**), $[Mo(N_2)(P3)(dpm)]$ (**Ib**), $[Mo(NNH_2)(PH_3)_5]^{2+}$ (**IIa**), and $[Mo(NNH_2)(P3)(dpm)]^{2+}$ (**IIb**) of compounds **1** and **2**, respectively, (dpm = $H_2PCH_2CH_2PH_2$, P3 = $HP(CH_2CH_2PH_2)_2$). Based on spectroscopic and quantum chemical data, the activation of N_2 in complex **1** is compared to that present in the bis(dinitrogen) complex $[Mo(N_2)_2(dppe)_2]$ (**3**) and the dinitrogen complex with a *trans*-nitrile ligand $[Mo(N_2)(NCCH_3)(dppe)_2]$ (**4**) (dppe = $Ph_2PCH_2CH_2PPh_2$) (3*c*, 13). The general implications of these results are discussed.

Experimental

Synthesis, isotopic substitution, and sample preparation

All reactions were performed under an inert gas atmosphere using Schlenk techniques. The solvents were dried and freshly destilled under argon. All other reagents were used without further purification. The phosphine ligands were obtained from Strem Chemicals, CF_3SO_3D from Sigma-Aldrich, and $^{15}N_2$ from Deutero GmbH. All sample manipulations for vibrational and NMR spectroscopy were performed in a glovebox.

© 2005 NRC Canada

The dinitrogen complex [Mo(N_2)(dpepp)(dppm)] was prepared following the literature procedure with slight variations (see the following) (11). The ^{15}N isotopomer [Mo($^{15}N_2$)(dpepp)(dppm)] was synthesized using $^{15}N_2$ (98%). The NNH_2 complex [Mo(NNH_2)(dpepp)(dppm)](CF_3SO_3)$_2$ was obtained by protonation of the dinitrogen complex with triflic acid. The preparation of the protonated, ^{15}N-labeled complex [Mo($^{15}N^{15}NH_2$)(dpepp)(dppm)](CF_3SO_3)$_2$ was carried out from the ^{15}N-substituted dinitrogen complex. The deuterated complex [Mo(NND_2)(dpepp)(dppm)](CF_3SO_3)$_2$ was prepared using CF_3SO_3D. [$MoCl_3$(dpepp)] was prepared following a published method (14).

*[Mo(N_2)(dpepp)(dppm)] (**1**^{14})*

In a 100 mL Schlenk flask, a suspension of 820 mg (1.07 mmol) [$MoCl_3$(dpepp)] and 455 mg (1.2 mmol) dppm in 30 mL THF was added to sodium amalgam (250 mg Na, 30 g Hg). The mixture was stirred for 3 h at 0 °C and 18 h at ambient temperature under N_2. The red solution was decanted, filtered, and reduced to 8 mL in vacuum. Upon adding 10 mL of methanol, an orange precipitate formed. The product was filtered off, washed (3 × 4 mL) with methanol, and dried in vacuo for 6 h. Yield: 583 mg (0.56 mmol, 51%). Anal. calcd. for $C_{59}H_{55}MoN_2P_5$: C 67.9, H 5.3, N 2.7; found: C 67.3, H 5.4, N 2.5.

*[Mo($^{15}N_2$)(dpepp)(dppm)] (**1**^{15})*

The synthesis was performed analogous to **1**^{14} with 433 mg (1.2 mmol) dppm and 753 mg (1.02 mmol) [$MoCl_3$(dpepp)]. Instead of using a continuous N_2 flow, the flask was filled with $^{15}N_2$. Yield: 551 mg (0.53 mmol, 52%). Anal. calcd. for $C_{59}H_{55}Mo^{15}N_2P_5$: C 67.8, H 5.3, N 2.9; found: C 67.3, H 5.7, N 2.3.

*[Mo(NNH_2)(dpepp)(dppm)](CF_3SO_3)$_2$ (**2**^{14})*

In a 25 mL Schlenk flask, 0.05 mL (0.57 mmol) triflic acid was added to a solution of 300 mg (0.29 mmol) [Mo(N_2)(dpepp)(dppm)] in 8 mL THF at –78 °C. While the solution was stirred for 10 min, the colour changed from orange to green. Leaving the solution for 2 h at –78 °C led to the formation of a dark green solid. The product was filtered and dried in vacuo. The solution was cooled overnight to produce more of the product. Overall yield was 264 mg (0.2 mmol, 70%).

*[Mo($^{15}N^{15}NH_2$)(dpepp)(dppm)](CF_3SO_3)$_2$ (**2**^{15})*

The synthesis was performed analogous to **2**^{14} with 240 mg (0.23 mmol) [Mo(N_2)(dpepp)(dppm)] and 0.04 mL (0.46 mmol) triflic acid. Yield: 180 mg (0.13 mmol, 58%).

*[Mo(NND_2)(dpepp)(dppm)](CF_3SO_3)$_2$ (**2**^{D})*

The synthesis was performed analogous to **2**^{14} with 270 mg (0.27 mmol) [Mo(N_2)(dpepp)(dppm)] and 0.05 mL (0.57 mmol) deuterated triflic acid CF_3SO_3D. Yield: 110 mg (0.08 mmol, 30%).

Spectroscopy

IR spectroscopy

Mid-IR and far-IR spectra were obtained from KBr or PE pellets using a Bruker IFS v66/S FT-IR spectrometer.

Raman spectroscopy

Raman spectra were obtained on a Bruker IFS 66/CS NIR FT-Raman spectrometer at 294 K. The setup involves a 350 mW Nd-YAG laser with an excitation wavelength of 1064 nm. The samples were pressed into the groove of a holder that can be sealed with a glass plate to ensure inert gas conditions.

NMR spectroscopy

NMR spectra were recorded on a Bruker Avance 400 pulse Fourier transform spectrometer operating at a ^1H frequency of 400.13 MHz (^{31}P NMR 161.98 MHz, ^{15}N NMR 40.55 MHz, ^{19}F NMR 376.50 MHz) using a 5 mm inverse triple-resonance probe head. References as substitutive standards: H_3PO_4 85% pure, $\delta(^{31}P)$ 0 ppm; CH_3NO_2 neat, $\delta(^{15}N)$ 0 ppm; $CFCl_3/CDCl_3$, $\delta(^{19}F)$ 0 ppm. Samples of **1**^{14} and **1**^{15} were measured in THF-d^8 at 300 K. Samples of **2**^{14}, **2**^{15}, and **2**^{D} were measured in CD_2Cl_2 at 243 K. Because of the instability of the NNH_2 compound, sample preparation was performed at 263 K. Spin simulations were performed using the WinDNMR Calculation V.7.1.6 software package by Hans J. Reich.

DFT calculations

Spin-restricted DFT calculations were performed for the model systems [Mo(N_2)(PH_3)$_5$] (**Ia**), [Mo(N_2)(P3)(dpm)] (**Ib**), [Mo(NNH_2)(PH_3)$_5$]$^{2+}$ (**IIa**), and [Mo(NNH_2)(P3)(dpm)]$^{2+}$ (**IIb**) of compounds **1** and **2**, respectively, using Becke's three parameter hybrid functional with the correlation functional of Lee, Young, and Parr (B3LYP) (15). The LANL2DZ basis set was used for the calculations. It applies Dunning–Huzinaga full-double ξ basis functions (16) on the first row and Los Alamos effective core potentials plus DZ functions on all other atoms (17). Charges were analysed using the natural bond orbital (NBO) formalism (natural population analysis, NPA) (18). For the calculation of magnetic shielding tensors, the gauge invariant shielding atomic orbitals (GIAO) method was used. The calculations are based on the models **Ia**, **IIa**, [Mo(N_2)$_2$(PH_3)$_4$] (**III**), [Mo(N_2)($NCCH_3$)(PH_3)$_4$] (**IV**), and [MoF(NNH_2)(PH_3)$_4$]$^+$ (**V**), respectively (3, 13). All computational procedures were used as implemented in the GAUSSIAN 03 package (19). Wave functions were plotted with GaussView03 (20).

Normal coordinate analysis

Normal coordinate calculations were performed using the QCPE computer program by Peterson and McIntosh (21). It involves solutions of the secular equation **GFL** = Λ**L** by the diagonalisation procedure of Miyazawa. The calculations were based on a general valence force field, and the force constants were refined using the nonlinear optimization of the simplex algorithm according to Nelder and Mead (22). Normal coordinate analysis was based on the QCB-NCA procedure, which involves generation of an initial force field by DFT methods (3). For this purpose, models **Ib** and **IIb** of compounds **1** and **2**, respectively, were used. In the QCB-NCA procedure, the frequencies of the optimized models **Ib** and **IIb** were determined. No negative frequencies were found. The *f* matrix that derived from these calculations had its force constants in cartesian coordinates. These cartesian coordinates were transformed to internal coordinates using

© 2005 NRC Canada

Table 1. Crystallographic data for [Mo(N_2)(dpepp)(dppm) (**1**).

Crystal	[Mo(N_2)(dpepp)(dppm)]
Empirical formula	$C_{59}H_{55}MoN_2P_5$
Formula mass	1042.84
Colour, habit	Red, block
Crystal dimensions (mm^3)	0.4 × 0.4 × 0.3
Crystal system	Triclinic
Space group	*P*-1
Z	6
a (Å)	13.449(1)
b (Å)	20.827(2)
c (Å)	28.821(2)
α (°)	80.60(1)
β (°)	78.83(1)
γ (°)	85.29(1)
Volume ($Å^3$)	7802.5(8)
Scan range (°)	3–45
HKL range	$-14 \le h \le 13$, $-22 \le k \le 22$, $-30 \le l \le 30$
Temperature (K)	220(2)
D_{calcd} (Mg m^{-3})	1.332
Radiation	Mo Kα (λ = 0.710 73 Å)
Absorption coeff. (μ, mm^{-1})	0.446
Absorption correction	Numerical
F(000)	3240
θ range for data collection (°)	1.55–22.31
Observed reflections	36 899
Independent reflections	18 778 (R_{int} = 0.0381)
Reflections with $I > 2\sigma(I)$	14 567
Data/parameters	18 778/1 896
Maximum shift and error	≤0.001
Goodness-of-fit on F^2	1.062
Final *R* indices ($I > 2\sigma(I)$)	*R*1 = 0.072 5, *wR*2 = 0.188 3
R indices (all data)	*R*1 = 0.092 6, *wR*2 = 0.213 4
Extinction coefficient	0.007 4(4)
Largest diff. peak and hole (e $Å^{-3}$)	1.785 and –2.803

the program REDONG (23). The resulting *f* matrix in internal coordinates was put into FFIT, a fit program for force constants. In the last step, only the force constants of interest were fitted to the experimental frequencies. In contrast to QCA-NCA where only the large force constants were retained in the fitting procedure (3), no force constants were deleted in the QCB-NCA.

X-ray structure analysis

Intensity data were collected using a STOE image plate diffraction system with Mo Kα radiation. The structure was solved using direct methods using SHELXS-97 (24). Refinement was done against F^2 using SHELXS-97. Three of the phenyl rings of the ligands were disordered and were refined using a split model. All non-hydrogen atoms were refined with anisotropic displacement parameters except the carbon atoms of one disordered phenyl ring. The hydrogen atoms were placed in ideal positions and were refined isotropically using the riding model. Selected crystallographic data are presented in Table 1. Bond lengths and angles of the Mo-NN unit are presented in Table 2.[3]

Table 2. Selected bond lengths and angles for **1**.

[Mo(N_2)(dpepp)(dppm)]	
Bond lengths (Å)	
N_α—N_β	1.119(8)
Mo—N_α	2.025(6)
Mo—$P_{a,b,c,d,e}$	2.418(2)–2.497(2)
Bond angles (°)	
N_α-N_β-Mo	179.2(6)
N_β-Mo-P_e	167.0(2)
P_a-Mo-P_b	68.3(1)
P_c-Mo-P_d	97.9(1)

[3] Supplementary data may be purchased from the Directory of Unpublished Data, Document Delivery, CISTI, National Research Council Canada, Ottawa, ON K1A 0S2, Canada (http://cisti-icist.nrc-cnrc.gc.ca/irm/unpub_e.shtml for information on ordering electronically). CCDC 261394 contains the crystallographic data for this manuscript. These data can be obtained, free of charge, via ww.ccdc.cam.ac.uk/conts/retrieving.html (or from the Cambridge Crystallographic Data Centre, 12 Union Road, Cambridge CB2 1EZ, UK; fax +44 1223 336033; or deposit@ccdc.cam.ac.uk).

© 2005 NRC Canada

Results and analysis

Crystal structure determination of [Mo(N$_2$)(dpepp)(dppm)] (1)

The crystal structure of [Mo(N$_2$)(dpepp)(dppm)] (Fig. 1) represents the first structural characterization of a molybdenum(0) dinitrogen complex having a P_5 ligand set. The compound crystallizes in the triclinic space group *P*-1 with $Z = 6$ and three crystallographically independent complexes in the asymmetric unit. Bond lengths and angles in all three independent complexes are comparable. In each of the complexes, the molybdenum atoms are coordinated by five phosphorus atoms of one dpepp and one dppm ligand and one nitrogen atom of the dinitrogen molecule within distorted octahedra. The two phosphorus atoms of the dppm ligand and the two terminal phosphorus atoms of the dpepp ligand form the basal plane of the octahedra, whereas the nitrogen atom and the central phosphourus atom of the dpepp ligand are located in the axial positions. The dinitrogen molecule is located nearly above the center of the basal plane and is oriented almost perpendicular to this plane. The Mo—P bond lengths to the dppm ligand are significantly longer than those to the dpepp ligand. The Mo—P bond lengths to the central phosphorus atom of the dpepp ligand, which is located in the axial position trans to the dinitrogen molecule, are shorter than those to the terminal phosphorus atoms.

NMR spectroscopy

NMR spectroscopy of [Mo(N$_2$)(dpepp)(dppm)] (1^{14}, 1^{15})

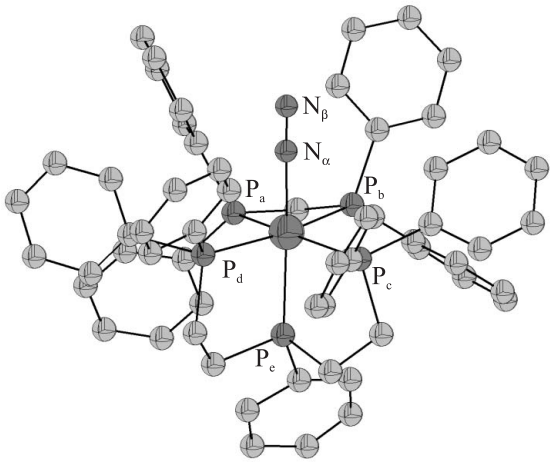
^{31}P NMR spectra and spin simulation

Complex **1^{14}** has an AMM′XX′-type ^{31}P NMR spectrum. Chemical shifts and signal multiplicities agree with the data reported by George et al. (11). For a better understanding of the coupling scheme, a spin simulation with the program WinDNMR was performed. In the simulation of this five-spin system, the chemical shifts of the signals and all known coupling constants were fixed. The unknown constants were varied until optimal agreement between the simulated and measured spectrum was achieved (Fig. 2).

The central phosphorus atom of the dpepp ligand P_e is in the trans position to the dinitrogen ligand (Fig. 3), which can be inferred from the absence of a large $^2J_{PP,trans}$ coupling. The signal of P_e (1, δ 89.5 ppm) has a triplet structure by coupling with P_a and P_b deriving from the dppm ligand ($^2J_{PP,cis}$ = –13.9 Hz). The coupling constant to the other phosphine donors P_c and P_d is below 1 Hz and therefore not resolved. The small value is due to the combination of a negative $^2J_{pp}$ cis coupling constant transmitted by the metal center and a positive $^3J_{PP}$ coupling constant mediated by the alkyl bridge with $^2J_{PP} \approx -^3J_{PP}$ (25). The signals of P_c and P_d (2, δ 66.4 ppm) show a large trans coupling ($^2J_{PP,trans}$ = 106.0 Hz) and a smaller cis coupling ($^2J_{PP,cis}$ = –23.1 Hz) with P_a and P_b. The simulation reveals an additional coupling constant, $^2J_{Pc,Pd}$ = –15 Hz. Another group of signals (2, δ 9.8 ppm) is assigned to the phosphorus atoms of dppm, P_a, and P_b. All coupling constants are listed in Table 3.

The ^{31}P NMR spectrum of the ^{15}N-containing complex **1^{15}** exhibits no changes in the signals of P_a, P_b, P_c, and P_d because the $^2J_{PN,cis}$ coupling constant is smaller than the line width. The signal of P_e in **1^{15}** is a quartet. This structure is caused by the $^2J_{NP,trans}$ coupling, which accidentally has the same value as the $^2J_{PP,cis}$ coupling to P_a, P_b (14 Hz) and by the fact that $^2J_{PP,cis}$ to P_c, $P_d \approx 0$.

Fig. 1. Crystal structure of [Mo(N$_2$)(dpepp)(dppm)] (**1**). Split phenyl rings and hydrogen atoms are not shown for clarity.



^{15}N NMR spectra and GIAO calculations

The ^{15}N NMR spectrum of complex **1^{15}** shows a doublet (δ –15.7 ppm) for the terminal nitrogen atom N_β ($^1J_{NN}$ = 5.7 Hz) whereas the coordinated nitrogen N_α (δ –30.5 ppm) exhibits a broad multiplet caused by $^2J_{cis/trans}$ couplings to the phosphorus atoms. Especially, N_β exhibits a remarkable low-field shift compared to bis(dinitrogen) complexes like [Mo(N$_2$)$_2$(dppe)$_2$] (**3**, δ(N_α) –43.1 ppm, δ(N_β) –42.8 ppm) (26) and even compared to *trans*-nitrile dinitrogen complexes like [Mo(N$_2$)(NCMe)(dppe)$_2$] (**4**, δ(N_α) –31.2 ppm, δ(N_β) –34.0 ppm) (27). These experimental results are supported by DFT GIAO calculations of the ^{15}N NMR shifts. The calculations were performed for models **Ia**, **III**, and **IV** of compounds **1**, **3**, and **4**, respectively, (cf. the Electronic structure section); the results are collected in Table 4.

The calculated chemical shifts of **Ia** referenced to nitromethane (–136 ppm) are δ 9.6 ppm for N_α and δ 3.9 ppm for N_β (expt. values –15.7 and –30.5 ppm, respectively; Table 4). ^{15}N shifts calculated for **III** and **IV** show a comparable discrepancy to the experimental data, but the *relative* magnetic shieldings Δδ of the different models exhibit good agreement to the experimentally observed trend (Table 5). Specifically, N_α of **Ia** is 12.5 ppm (expt. 12.6 ppm) low-field shifted compared to the bis(dinitrogen) complex **III** and 2.1 ppm (expt. 0.8 ppm) low-field shifted compared to the *trans*-nitrile dinitrogen complex **IV**. The terminal nitrogen atom N_β of **Ia** shows a calculated low-field shift of 24.0 ppm (expt. 27.2 ppm) compared to **III** and a calculated low-field shift of 11.3 ppm (expt. 18.3 ppm) compared to **IV**.

Magnetic shieldings consist of a paramagnetic and a diamagnetic term (25), and the calculations show that the differences among the magnetic shieldings of **Ia**, **III**, and **IV** are entirely caused by the paramagnetic term, which depends on $\sigma \rightarrow \pi$ and $\pi \rightarrow \sigma$ calculations (27, 28). For complex bound ligands like N_2, the $d_{xz/yz}(\pi) \rightarrow d_{z2}(\sigma)$ ligand field transitions of the central atom are important in this respect. The $d_{xz/yz}$ and d_{z2} orbitals are admixed with N_α/N_β π and σ atomic orbitals, respectively. The value of the paramagnetic term on

© 2005 NRC Canada

Fig. 2. Simulated (top) and experimental (bottom) ^{31}P NMR spectra of $[Mo(N_2)(dpepp)(dppm)]$ **1**[14].

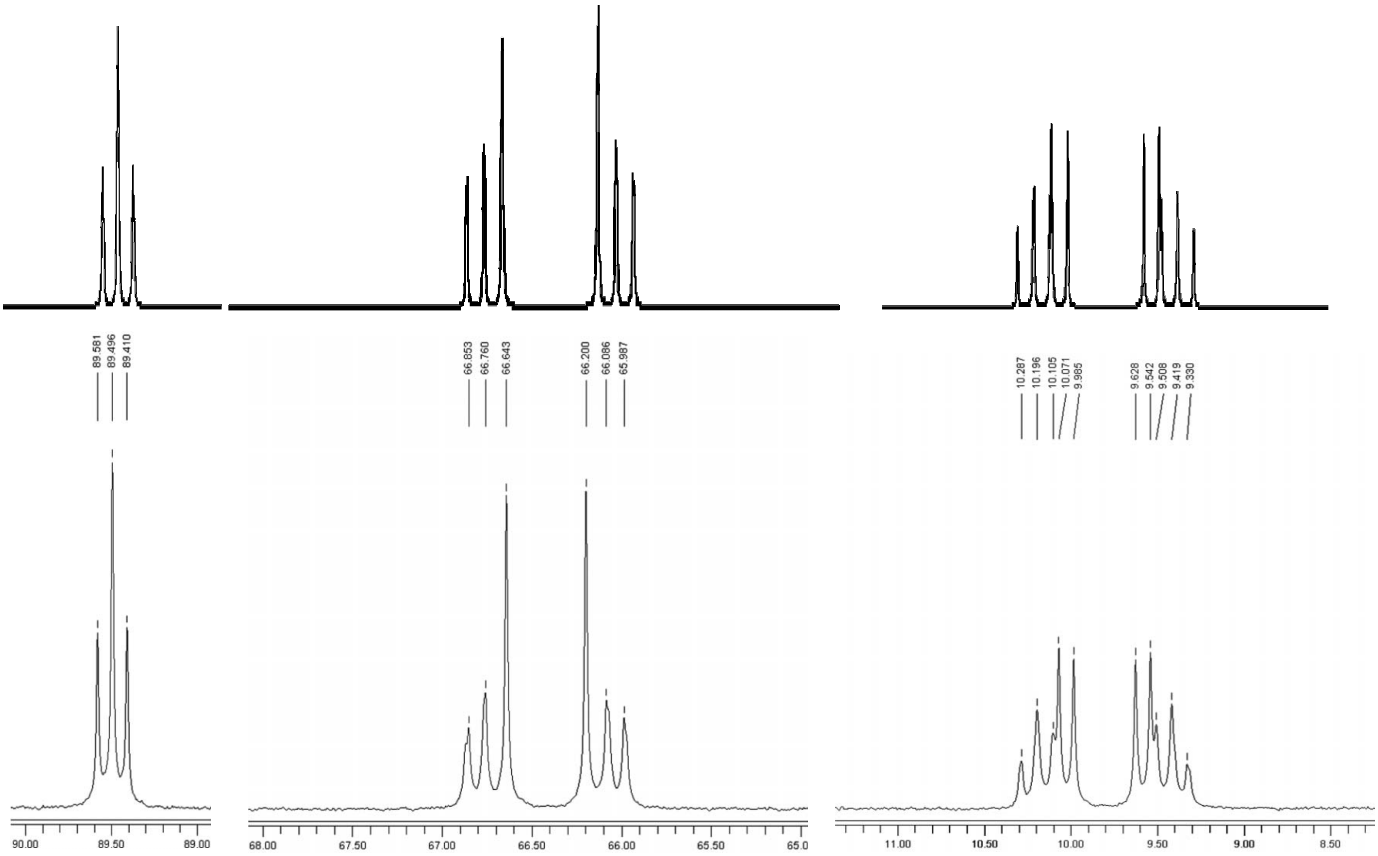
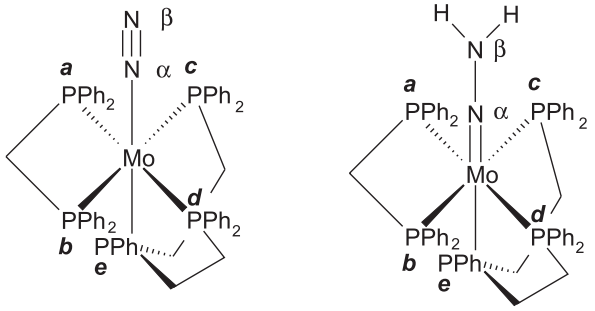


Fig. 3. $[Mo(N_2)(dpepp)(dppm)]$ (**1**) and $[Mo(NNH_2)(dpepp)(dppm)](Cf_3SO_3)_2$ (**2**).



a particular nitrogen atom is then determined by the energy of the ligand field transition and by the contribution of the nitrogen atomic orbitals to the $d_{xz/yz}$ and d_{z2} molecular orbitals involved in this transition, i.e., the lower the energy of the LF transition and the higher the contribution of N_α or N_β to the respective σ/π molecular orbitals, the higher the paramagnetic shift. The unusual low-field shift of the ^{15}N NMR resonances of **1** is explained in the framework of this concept in the Discussion.

*NMR spectroscopy of $[Mo(NNH_2)(dpepp)(dppm)](CF_3SO_3)_2$ (**2**[14], **2**[15], **2**[D])*

^{31}P NMR spectra

The ^{31}P NMR spectra of **2**[14], **2**[15], and **2**[D] are identical. They exhibit three broad signals (P_c, P_d, δ 54.5 ppm; P_e, δ 48.6 ppm; P_a, P_b δ –2.9 ppm). The signals of P_c, P_d and P_a, P_b are split by the strong $^2J_{PP,trans}$ coupling; the weaker $^2J_{PP,cis}$ and $^2J_{PN,trans}$ couplings are not resolved.

Table 3. Simulated coupling constants (J_{PP}) of **1**[14].

Coupling constant	Value (Hz)
J_{P_a,P_b}	0
J_{P_a,P_c}	–23.1
J_{P_a,P_d}	106.0
J_{P_a,P_e}	–13.9
J_{P_b,P_c}	106.0
J_{P_b,P_d}	–23.1
J_{P_b,P_e}	–13.9
J_{P_c,P_d}	–15
J_{P_c,P_e}	0.8
J_{P_d,P_e}	0.8

^{19}F NMR spectra

^{19}F NMR spectroscopy exhibits one sharp singlet at –79.5 ppm caused by the $CF_3SO_3^-$ counterion. There are no indications for a coordination of the counterion at the complex.

^{15}N NMR spectra and GIAO calculations

The protonated nitrogen N_β in complex **2**[15] shows a sharp signal at –216.1 ppm; in an INEPT experiment, this signal exhibits a triplet structure ($^1J_{NH}$ = 93.8 Hz). The coordinated nitrogen N_α gives a weak signal at –22.4 ppm and no signal

© 2005 NRC Canada

Table 4. Calculated magnetic shieldings for N_2 (**Ia**, **III**, **IV**) and NNH_2 model systems (**IIa**, **V**).

Model		Diamagnetic shielding (ppm)	Paramagnetic shielding (ppm)	Magnetic shielding (ppm)	Magnetic shielding ref. to $MeNO_2$ (ppm)	Expt. value (ppm)
$[Mo(N_2)(PH_3)_5]$ (**Ia**)	N_α	320.9	–460.8	–139.9	+3.9	–15.7
	N_β	335.9	–480.8	–145.6	+9.6	–30.5
$[Mo(N_2)_2(PH_3)_4]$ (**III**)	N_α	321.8	–452.6	–130.8	–5.2	–43.1
	N_β	334.9	–456.6	–121.6	–14.4	–42.8
$[Mo(N_2)(NCMe)(PH_3)_4]$ (**IV**)	N_α	321.2	–458.5	–137.8	+1.8	–31.2
	N_β	335.2	–469.5	–134.3	–1.7	–34.0
$[Mo(NNH_2)(PH_3)_5]^{2+}$ (**IIa**)	N_α	332.8	–414.0	–81.2	–54.8	–22.4
	N_β	323.9	–246.9	77.0	–213.0	–216.1
$[MoF(NNH_2)_2(PH_3)_4]^+$ (**V**)	N_α	329.0	–348.1	–19.1	–116.9	–79.9
	N_β	322.3	–220.5	101.8	–237.8	–240.5

Table 5. Calculated and measured chemical shieldings of **III** (**3**) and **IV** (**4**) relative to **I** (**1**).

Chemical shielding	**III** → **I** (ppm)	**IV** → **I** (ppm)
$\Delta\delta(N_\alpha)$ calcd.	+12.5	+2.1
$\Delta\delta(N_\alpha)$ expt.	+12.6	+0.8
$\Delta\delta(N_\beta)$ calcd.	+24.0	+11.3
$\Delta\delta(N_\beta)$ expt.	+27.2	+18.3

in the INEPT spectrum. The signals of $\mathbf{2^{15}}$ are low-field shifted compared to the corresponding *trans*-fluoro NNH_2 complex $[MoF(NNH_2)(dppe)_2](BF_4)$ (**5**, $\delta(N_\alpha)$ –79.9 ppm, $\delta(N_\beta)$ –240.5 ppm) (29). These results can again be reproduced by GIAO calculations based on models **IIa** and **V** of compounds **2** and **5**, respectively (Table 4). Again, the absolute values of the calculated magnetic shielding are too low compared to the experimental data, but the *relative* shifts show good agreement to the observed trend. Specifically, the magnetic shielding of N_α in $\mathbf{2^{15}}$ is calculated to be 62.1 ppm lower than in **V** (expt. 57.5 ppm). The N_β of $\mathbf{2^{15}}$ shows a calculated low-field shift of 24.7 ppm with respect to **5**, which exactly reproduces the measured value. As for the dinitrogen complexes, the variations in magnetic shielding are dominated by the paramagnetic term.

^1H NMR spectra

The hydrazido protons of complex $\mathbf{2^{14}}$ give rise to a singlet at 9.9 ppm. In the ^{15}N compound $\mathbf{2^{15}}$, the signal appears as a doublet (10.1 ppm, $^1J_{HN}$ = 93.9 Hz) because of coupling with ^{15}N. In the deuterated complex $\mathbf{2^D}$, only a very weak signal at 9.9 ppm can be observed, which is caused by $[Mo(NNHD)(dpepp)(dppm)](CF_3SO_3)_2$).

Vibrational spectra and normal coordinate analysis

Vibrational spectra of [Mo(N$_2$)(dpepp)(dppm)] (1^{14}, 1^{15})

The FT-Raman spectra of $\mathbf{1^{14}}$ (Fig. 4) exhibits two peaks at 2003/1984 and 454 cm^{-1}, which shift in the spectra of the ^{15}N compound $\mathbf{1^{15}}$. The split peak at 2003/1984 shifts about 66 cm^{-1} to 1935/1918 cm^{-1} and is assigned to the N-N stretch ν(NN). The peak at 454 cm^{-1} is assigned to the Mo-N stretching vibration ν(MoN) and shifts by about 5 cm^{-1} to 449 cm^{-1} in the spectrum of $\mathbf{1^{15}}$. Other intense signals in the Raman spectra at 526, 1000, 1028, 1096, and 1585 cm^{-1} remain unshifted in the ^{15}N compound. These vibrations are due to the phenyl residues of the dpepp and dppm ligands: the peak at 1585 cm^{-1} belongs to the C=C stretch; the peaks at 1093 and 1028 cm^{-1}correspond to plane bending vibrations δ(CC) and δ(CH) and the signal at 526 cm^{-1} is either an out-of-plane bend γ(CC) or a P-phenyl stretch (30).

IR spectra of the complexes $\mathbf{1^{14}}$ and $\mathbf{1^{15}}$ are given in Fig. 5. The N-N stretching vibration exhibits an intense band at 1979 cm^{-1} that shifts by 65 cm^{-1} to 1914 cm^{-1} in the ^{15}N compound. In the far-IR region, two other isotope-sensitive signals are found. The two bands at 505 and 497 cm^{-1}, which are part of a broad feature, show a slight shift to 503 and 493 cm^{-1}, respectively, and are assigned to the linear bending vibrations δ(MoNN). The Mo-N stretching vibration gives a weak signal in the far-IRspectra of $\mathbf{1^{14}}$ and $\mathbf{1^{15}}$ (453 and 448 cm^{-1}, respectively). The intense bands at 1584, 1571, 1480, and 1432 cm^{-1} are assigned to four C=C stretching modes of the phenyl residues (30, 3).

DFT frequency calculation of [Mo(N$_2$)(dpepp)(dppm)] (1^{14}, 1^{15})

Besides isotopic substitution, spectral analysis was assisted by a DFT frequency calculation based on the optimized model complex of **1**, $[Mo(N_2)(P3)(dpm)]$ (**Ib**). For the N-N stretching ν(NN), a frequency of 1973 cm^{-1} was obtained. The corresponding model containing ^{15}N $\mathbf{Ib^{15}}$ gives a frequency of 1908 cm^{-1}. The Mo-N stretching frequencies are calculated to 433 cm^{-1} ($\mathbf{Ib^{14}}$) and 428 cm^{-1} ($\mathbf{Ib^{15}}$). The calculated linear bending vibrations δ(MoNN) ($\mathbf{Ib^{14}}$ 521/502 cm^{-1}, $\mathbf{Ib^{15}}$ 489/474 cm^{-1}) show a stronger splitting as well as a stronger isotope shift than the experiment. For the ν(NN) vibration, **Ib** seems to be a good model, but for the ν(MoN) and δ(MoNN) vibrations, interactions with the hydrogen-substituted ligands are possibly influencing the predicted frequencies.

Quantum chemistry based normal coordinate analysis (QCB-NCA) of [Mo(N$_2$)(dpepp)(dppm)] (1a, 1b)

To analyze the vibrational properties of the dinitrogen complex **1**, a QCB-NCA has been applied that uses the full *f* matrix generated from the GAUSSIAN frequency calculation. This procedure is useful for the treatment of large molecules with low symmetry like **Ib**. Besides the force constants of the Mo-N-N unit (f_{NN}, f_{MoN}, f_{MoNN}), some off-

© 2005 NRC Canada

Fig. 4. FT-Raman spectra of [Mo(N_2)(dpepp)(dppm)] (**1**^{14}, **1**^{15}).

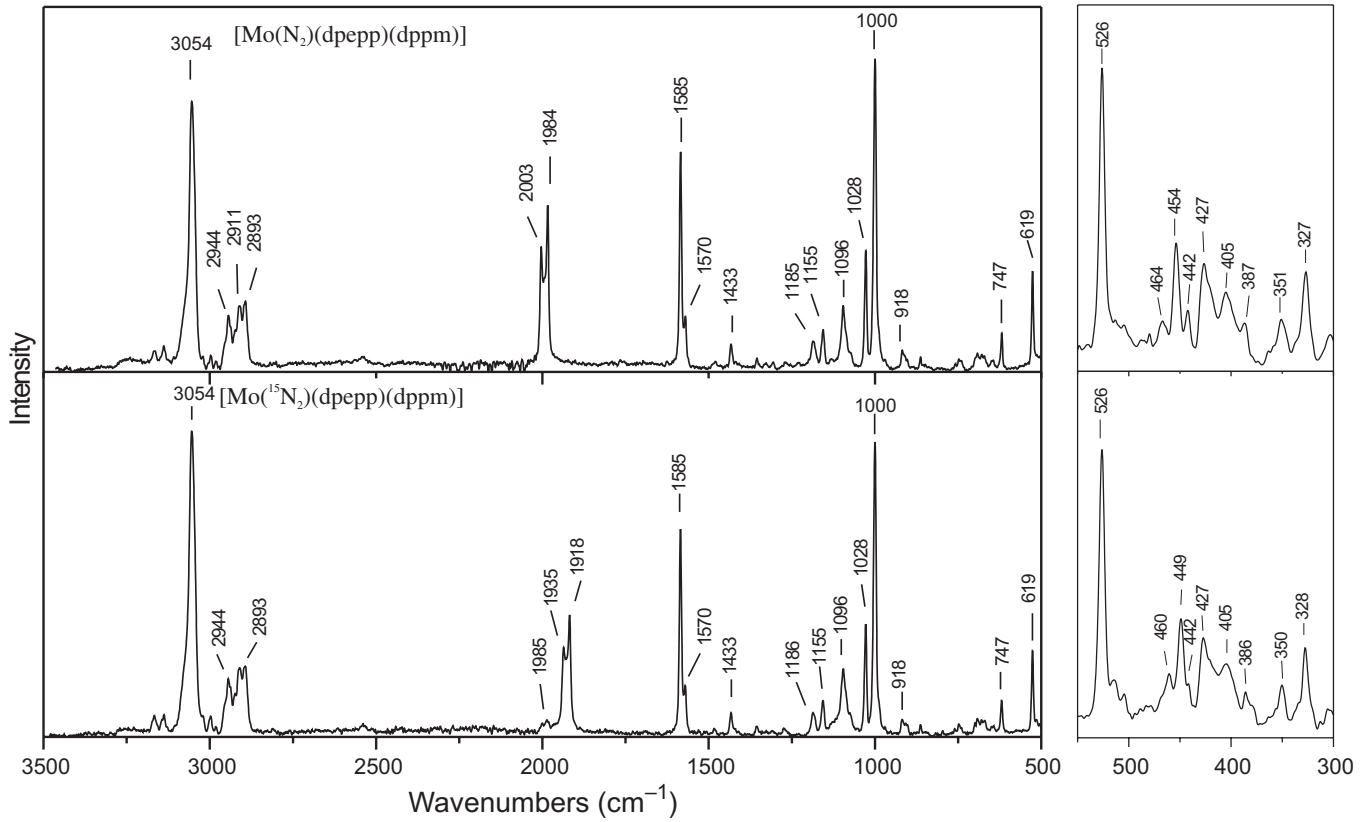
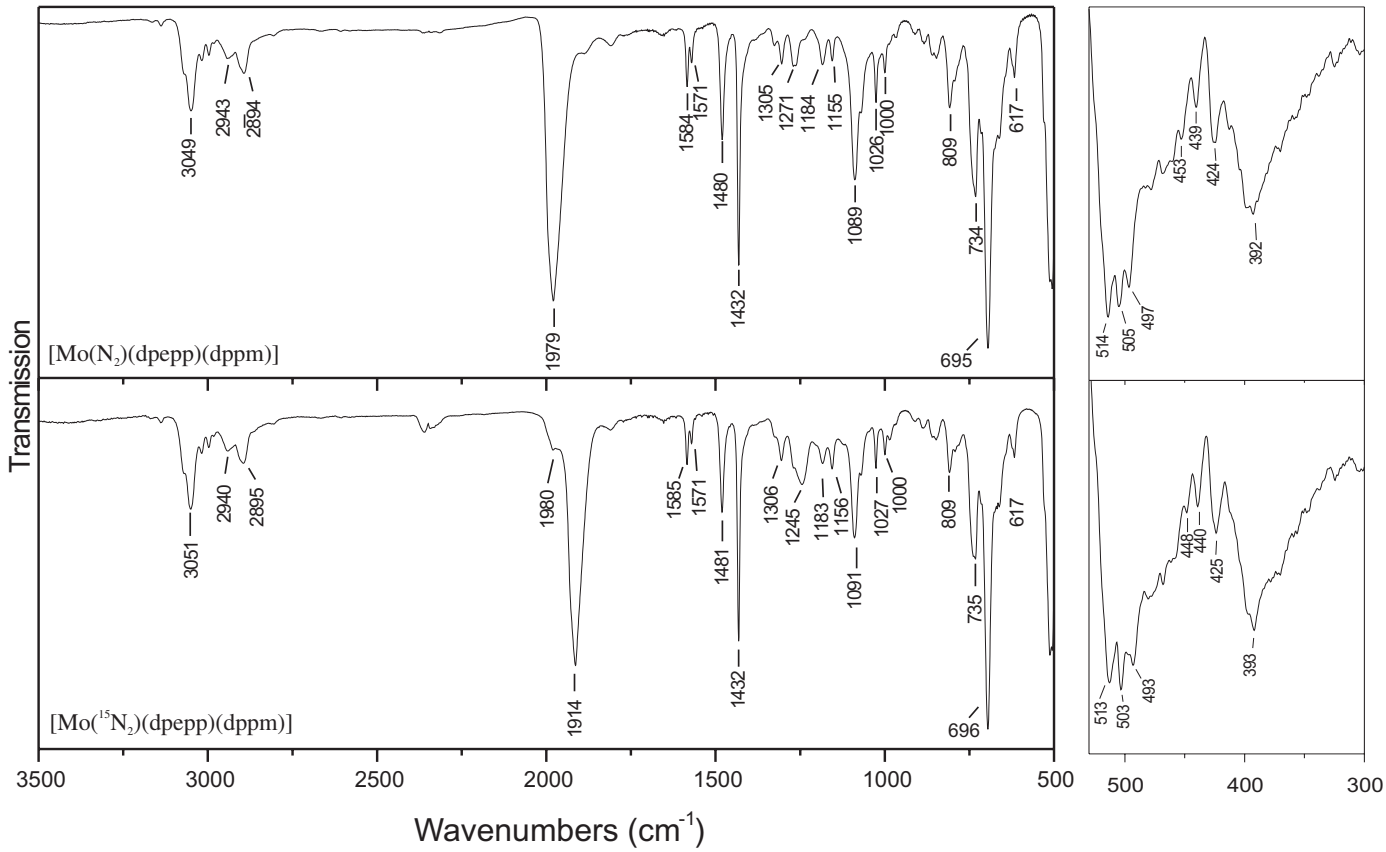


Fig. 5. IR spectra of [Mo(N_2)(dpepp)(dppm)] (**1**^{14}, **1**^{15}).

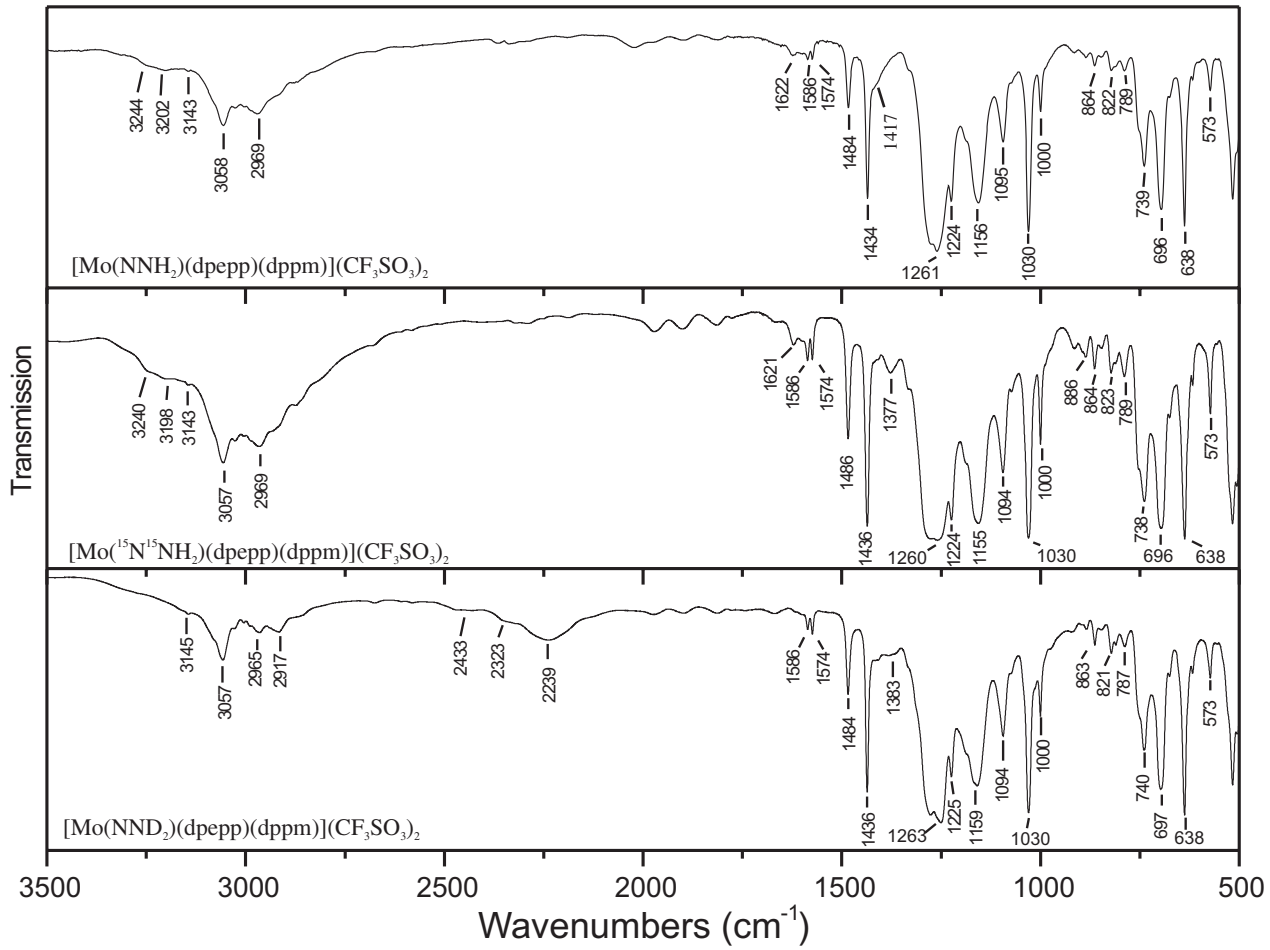


© 2005 NRC Canada

Table 6. Comparison of the observed and calculated frequencies of [Mo(N_2)(dpepp)(dppm)] (**1**).

	Experimental		QCB-NCA		B3LYP	
Vibration	^{14}N (cm^{-1})	^{15}N (cm^{-1})	^{14}N (cm^{-1})	^{15}N (cm^{-1})	^{14}N (cm^{-1})	^{15}N (cm^{-1})
ν(NN)	1979 (IR)	1914 (IR)	1980	1915	1973	1908
	1984/2003 (R)	1918/1935 (R)				
δ(MoNN)	505/497 (IR)	503/493 (IR)	509/493	502/492	521/502	489/474
ν(MoN)	453 (IR)	448 (IR)	454	451	433	428
	454 (R)	449 (R)				

Fig. 6. IR spectra of [Mo(NNH_2)(dpepp)(dppm)](CF_3SO_3)$_2$ (**2^{14}**, **2^{15}**, **2^{D}**).



diagonal elements were also included in the fit. The resulting *f* matrix is shown in the supplemental material (Table D5).[3] The resulting frequencies are collected in Table 6. Comparison between the experimental frequencies and the results from QCB-NCA shows overall good agreement. The calculated force constants for the Mo-N-N unit of **1** are f_{NN} = 16.3 mdyn/Å for the N—N bond, f_{MoN} = 2.8 mdyn/Å for the Mo—N bond, and f_{MoNN} = 0.44/0.43 mdynÅ for the bending coordinates. Compared to the corresponding bis(dinitrogen) complex [Mo(N_2)$_2$(dppe)$_2$] (**3**, f_{NN} = 17.22 mdyn/Å, f_{MoN} = 2.04 mdyn/Å) (3), the N—N bond is weaker and the Mo—N bond is stronger.

Vibrational spectra of [Mo(NNH_2)(dpepp)(dppm)](CF_3SO_3)$_2$ (2^{14}, 2^{15}, 2^{D})

The mid-IR spectrum of **2^{14}** (Fig. 6) shows a band at 3244 cm^{-1}, which can be attributed to the N-H stretching vibration. Because the signal is very broad and overlaps with C-H bands, the small shift to lower energy in **2^{15}** cannot be resolved. However, this feature shows a strong shift in the corresponding deuterium compound **2^{D}**. In this case, the broad band has a maximum at 2239 cm^{-1} and a shoulder at 2323 cm^{-1}, possibly indicating the presence of two N-D vibrations (symmetric and antisymmetric). In the mid-IR region below 1500 cm^{-1}, another isotope sensitive signal can be found. Specifically, the peak at 1377 cm^{-1} in the spectra of the ^{15}N compound **2^{15}** is missing in the spectra of **2^{14}** and **2^{D}**. Instead, the deuterium compound **2^{D}** shows a weak, broad band around 1383 cm^{-1}. In the IR spectra of **2^{14}**, the peak is partly masked by the ligand signal, causing a shoulder at 1417 cm^{-1}. All of these features are assigned to the N-N stretch. In addition to ligand signals at 1486, 1436,

© 2005 NRC Canada

Fig. 7. FT-Raman spectra of $[Mo(NNH_2)(dpepp)(dppm)](CF_3SO_3)_2$ (**2^{14}**, **2^{15}**, **2^{D}**).

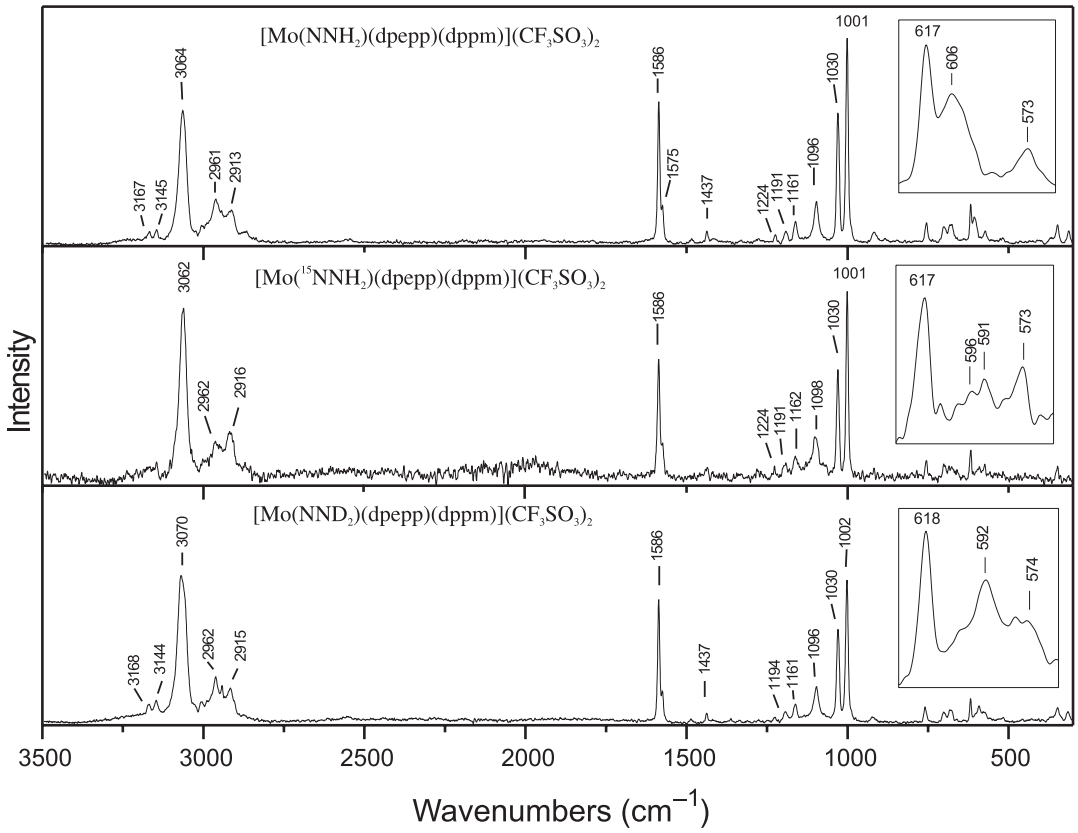


Table 7. Comparison of the observed and calculated frequencies of $[Mo(NNH_2)(dpepp)(dppm)](CF_3SO_3)_2$ (**2**).

	Experimental			QCB-NCA			B3LYP		
Vibration	$^{14}N^{14}NH_2$ (cm^{-1})	$^{15}N^{15}NH_2$ (cm^{-1})	NND_2 (cm^{-1})	$^{14}N^{14}NH_2$ (cm^{-1})	$^{15}N^{15}NH_2$ (cm^{-1})	NND_2 (cm^{-1})	$^{14}N^{14}NH_2$ (cm^{-1})	$^{15}N^{15}NH_2$ (cm^{-1})	NND_2 (cm^{-1})
$\nu(NH)_{as}$	3244	3240	2323	3245	3233	2411	3672	3660	2724
$\nu(NH)_{s}$	—	—	2239	3105	3101	2240	3522	3518	2538
$\nu(NN)$	(1417)	1377	(1383)	1422	1375	1398	1483	1433	1474
$\nu(MoN)$	606	596	592	607	596	591	622	607	599

1030, and 1001 cm^{-1}, very intense bands appear at 1250 and 1094 cm^{-1}; these can be assigned to the symmetric and antisymmetric S=O modes of the $CF_3SO_3^-$ counterions. The signals of the linear bending vibrations δ(MoNN) are not observed in the far-IR spectra because of a very intense band around 500 cm^{-1}. The far-IR spectrum of **2** does not contain any isotope-sensitive bands, and therefore is not shown.

Raman spectra of the NNH_2 complexes **2^{14}**, **2^{15}**, and **2^{D}** (Fig. 7) show one isotope-sensitive peak, which shifts from 606 cm^{-1} in the ^{14}N compound to 596 cm^{-1} in the ^{15}N and 592 cm^{-1} in the deuterium compound, respectively. These signals can be identified as Mo-N stretching vibrations. In the IR spectra, no signals are observed at the corresponding frequencies.

DFT frequency calculations of $[Mo(NNH_2)(dpepp)(dppm)](CF_3SO_3)_2$ (2^{14}, 2^{15}, 2^{D})

The DFT calculations indicate a splitting of the N-H vibration into an antisymmetric component at higher energy and a symmetric component at lower energy (Table 7). The same applies to the deuterated model. In all cases, the absolute values of the ν_{as} and ν_s vibrations are calculated too high. This is attributed to the absence of anharmonic terms in the calculation. The calculated frequency of the N-N stretching vibration is 1483 cm^{-1}, considerably higher than observed experimentally (~1417 cm^{-1}). Better agreement with the measured values is achieved for the Mo-N stretching vibrations (**IIb^{14}** 622 cm^{-1}, **IIb^{15}** 607 cm^{-1}, **IIb^{D}** 599 cm^{-1}). The relative magnitude of isotopic shifts ($\Delta\nu(^{15}N) < \Delta\nu(D)$) is in agreement with the experimental (Table 7).

QCB-NCA of $[Mo(NNH_2)(dpepp)(dppm)](CF_3SO_3)_2$ (2^{14}, 2^{15}, 2^{D})

The QCB-NCA of the NNH_2 complex **2** was performed in analogy to the QCB-NCA of the dinitrogen complex **1**. Based on the DFT treatment of model **IIb**, an *f* matrix in internal coordinates was generated using the program REDONG. The force constants of the Mo-NNH_2 unit were fitted to the experimental vibrational frequencies. Moreover, some off-diagonal force constants that correspond to interac-

© 2005 NRC Canada

tions between NN, MoN, and NH vibrations were included in the fitting process. The corresponding *f* matrix is shown in the supplemental material (Table D7).[3] The obtained frequencies are collected and compared to the experimental data in Table 7. Taking into account the limited spectroscopic information, especially for the NH and NN vibrations, good agreement between the QCB-NCA and the measured spectra was achieved. The calculated force constants are 7.65 mdyn/Å for the N—N bond and 5.94 mdyn/Å for the Mo—N bond. The NH force constants both have a value of 5.60 mdyn/Å.

Electronic structure

Model systems for [Mo(N$_2$)(dpepp)(dppm)]

DFT calculations of [Mo(N$_2$)(dpepp)(dppm)] (**1**) have been performed based on two different models. For the determination of the molecular orbital scheme and the NMR shift calculations, model [Mo(N$_2$)(PH$_3$)$_5$] (**Ia**) (Fig. 8) has been used. For the frequency calculations (vide supra) a more sophisticated model, [Mo(N$_2$)(P3)(dpm)] (**Ib**), (Fig. 8) has been employed. In this model, the phenyl residues are substituted by hydrogen atoms, but all alkyl bridges of the dppm and dpepp ligands, respectively, are included.

Optimized geometry of Ia and Ib

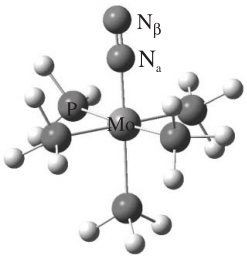
The optimized structures of **Ia** and **Ib** are shown in Fig. 8. The parameters of the MoNN unit are similar in both models: $\Delta_{\mathbf{Ia}}$(NN) = 1.17 Å, $\Delta_{\mathbf{Ib}}$(NN) = 1.17 Å, $\Delta_{\mathbf{Ia}}$(MoN) = 1.99 Å, $\Delta_{\mathbf{Ib}}$(NN) = 2.00 Å. In **Ib**, the dppm ligand has a P-Mo-P bite angle of 70.2°. Moreover, owing to the presence of the dpepp ligand, the N-Mo-P$_{trans}$ unit is bent; the corresponding angle is 168.3°. Cartesian coordinates of the optimzed structures of **Ia** and **Ib** are given in the supplemental material.[3]

Electronic structure of Ia

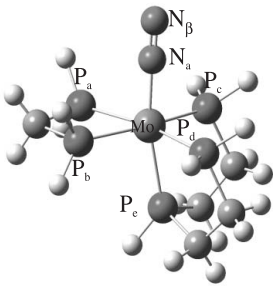
The molecular orbital scheme of **Ia** is shown in Fig. 9. For comparison, the MO schemes of the bis(dinitrogen) model complex [Mo(N$_2$)$_2$(PH$_3$)$_4$] (**III**) and the *trans*-nitrile dinitrogen model complex [Mo(N$_2$)(NCCH$_3$)(PH$_3$)$_4$] (**IV**) are given. Models **III** and **IV** have been studied earlier (3, 30). Countour plots of some relevant orbitals are displayed in Fig. 10.

The MO scheme of **Ia** is very similar to that of **III** and **IV**. The three highest occupied orbitals <32>, <33>, <34> are bonding combinations of d_{xz}, d_{yz}, and d_{xy} with the π_x* and π_y* orbitals of N$_2$. In contrast to **III** and **IV**, the d_{xy} orbital is mixed with the d_{yz} orbital in **Ia**, and thus becomes part of metal-N backdonation. This is caused by a reduction of the symmetry (**III** has C_{2v} symmetry, whereas **Ia** has C_s symmetry). Moreover, the contribution of N$_\beta$ to the backbonding orbitals is noticeably larger in **Ia** (Table 8) than in **III** (Table 9). Even compared to the strongest activated model complex **IV** (Table 9), the N$_\beta$ of **Ia** seems to have a slightly larger component in the backbonding orbitals. This is of relevance with respect to the magnitude of the ^{15}N NMR shift (vide infra). The Mo-N$_2$ σ-bonding interaction is represented by orbital <27>, a combination of σ(NN) with the d_{z2} orbital and a strong contribution of the four in-plane phosphine donors. <29> is the bonding combination of p_σ(P$_{trans}$) and d_{z2}, which is antibonding to p_σ(NN).

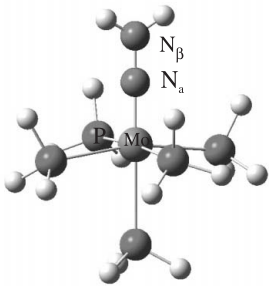
Fig. 8. Optimized structures of models **Ia**, **Ib**, **IIa**, and **IIb**.



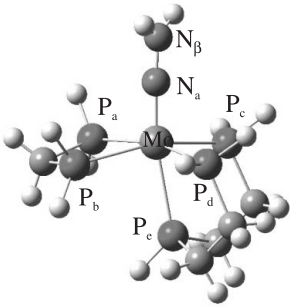
[Mo(N$_2$)(PH$_3$)$_5$] **Ia**



[Mo(N$_2$)(P3)(dpm)] **Ib**



[Mo(NNH$_2$)(PH$_3$)$_5$]$^{2+}$ **IIa**



[Mo(NNH$_2$)(P3)(dpm)]$^{2+}$ **IIb**

NPA charges of the three model complexes **Ia**, **III**, and **IV** are collected in Table 10. Importantly, the *trans*-nitrile model **IV** exhibits the highest charge (–0.21) on the N$_2$ unit, followed by **Ia** with a total charge of –0.17. The bis(dinitrogen) system **III** has the lowest total charge of –0.13. Based on these values, the activation of N$_2$ increases in the sequence **III** < **I** < **IV**. More detailed insight into the electronic-structural origin of this trend is provided by the partition of the atomic charges into atomic orbitals ($2s$, $3s$, $2p_x$, $2p_y$, $2p_z$, $3p_x$, $3p_y$, $3p_z$), which is given in

© 2005 NRC Canada

Fig. 9. Molecular orbital schemes of **Ia**, **III**, and **IV** (**III** and **IV** are from refs. 3*b*, 13).

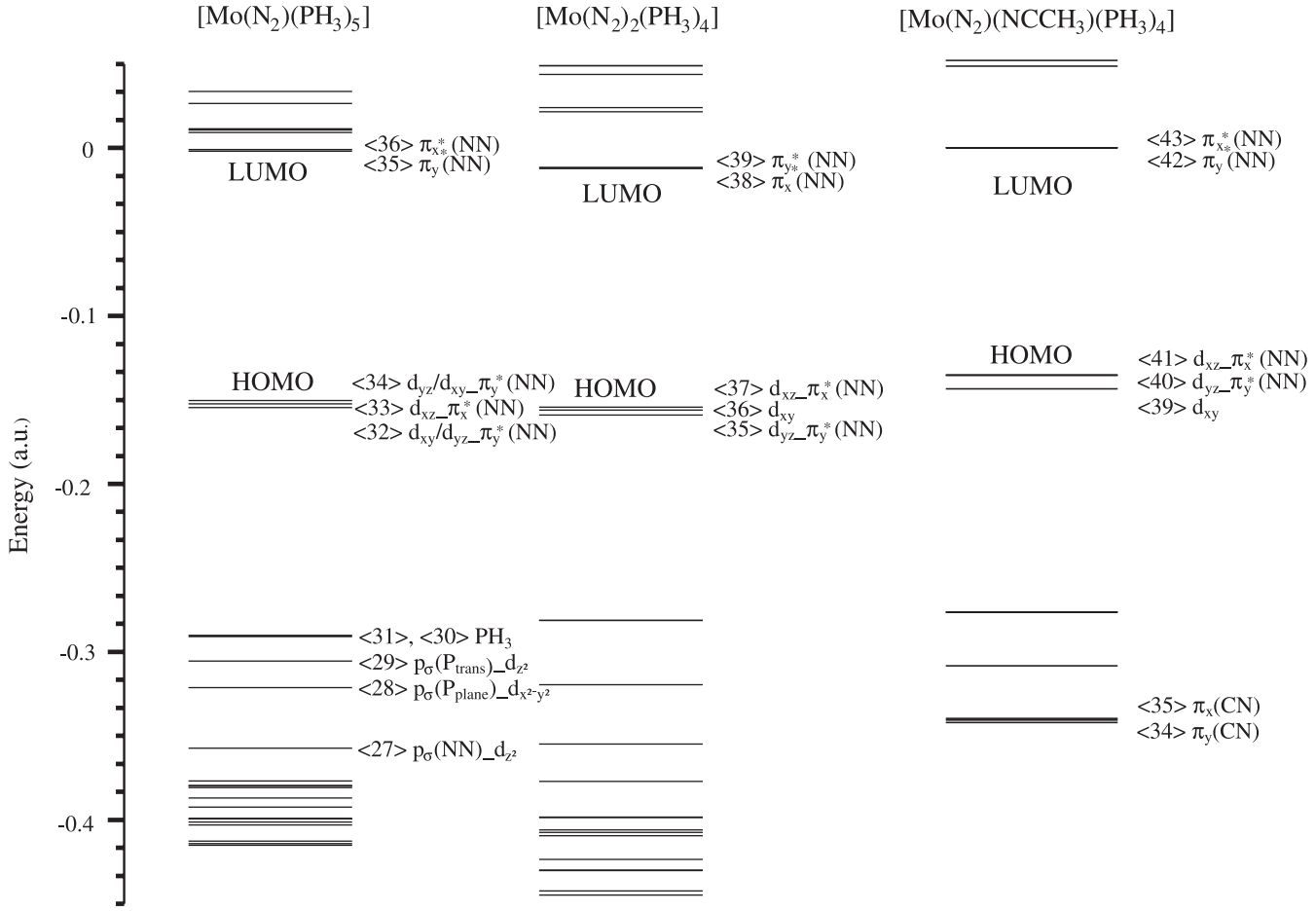
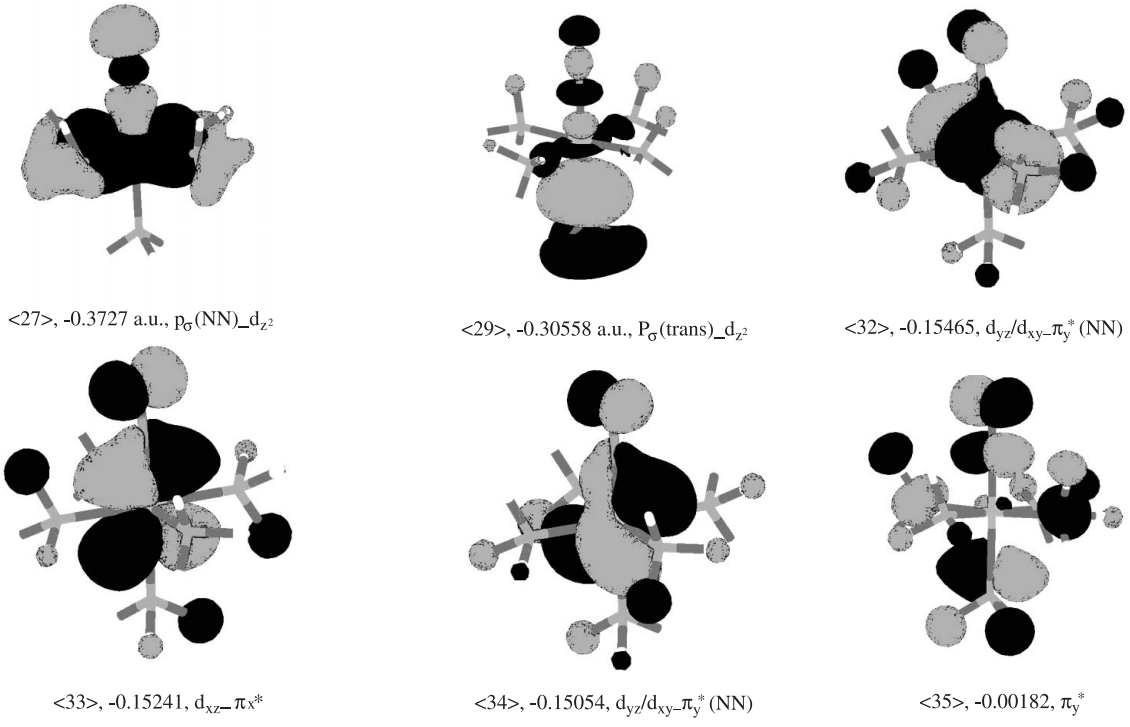


Fig. 10. Contour plots of some relevant orbitals of [Mo(N$_2$)(PH$_3$)$_5$] **Ia**.



© 2005 NRC Canada

Table 8. Charge contributions of $[Mo(N_2)(PH_3)_5]$ (**Ia**).

			Charge contribution (%)				
Orbital	Label	Energy (Hartree)	Mo	N_α	N_β	P(trans)	P(plane)
d_{yz}/d_{xy}–π_y*(NN)	34	–0.150 54	67	1	14	1	2
d_{xz}–π_x*(NN)	33	–0.152 41	63	1	14	1	2
d_{xy}/d_{yz}–π_y*(NN)	32	–0.154 65	65	0	5	1	2
PH_3	31	–0.290 22	0	1	2	0	79
PH_3	30	–0.290 96	0	1	2	0	79
$p_\sigma(P_{trans})$–d_{z2}	29	–0.305 58	5	5	4	63	5
$p_\sigma(P_{plane})$–d_{x2-y2}	28	–0.321 31	22	0	0	0	68
p_σ(NN)–d_{z2}	27	–0.372 7	9	13	22	1	43
p_σ(NN)	26	–0.376 64	1	42	32	5	10
π_x	25	–0.379 48	0	16	12	2	27
π_y	24	–0.379 79	0	23	17	5	19

Table 9. Charge contributions of backbonding orbitals of $[Mo(N_2)_2(PH_3)_4]$ (**III**) and $[Mo(N_2)(NCCH_3)(PH_3)_4]$ (**V**).

			Charge contribution (%)			
Orbital	Label	Energy (Hartree)	Mo	N_α (2x)	N_β (2x)	P
*$[Mo(N_2)_2(PH_3)_4]$ (**III**)*						
d_{xz}–π_x*(NN)	37	–0.1544	65	3	24	0
d_{xy}	36	–0.1561	67	0	0	3
d_{yz}–π_y*(NN)	35	–0.1591	60	2	23	2
*$[Mo(N_2)(NCCH_3)(PH_3)_4]$ (**V**)*						
d_{xz}–π_x*(NN)	41	–0.1372	61	1	15	2
d_{yz}–π_y*(NN)	40	–0.1373	60	1	14	2
d_{xy}	39	–0.1456	68	0	0	3

Table 10. NPA charges of **I**, **III**, and **IV**.

	Atom				
Model	Mo	N_α	N_β	PH_3(trans)	PH_3(plane)
$[Mo(N_2)(PH_3)_5]$ (**I**)	–1.18	–0.07	–0.10	0.23	0.29
$[Mo(N)_2(PH_3)_4]$ (**III**)	–1.01	–0.07	–0.06	—	0.31
$[Mo(N_2)(NCCH_3)(PH_3)_4]$ (**IV**)	–0.89	–0.10	–0.12	—	0.29

Table 11. $\Sigma\sigma$ corresponds to the summed contribution of σ-type atomic orbitals $2s$, $3s$, $2p_z$, $3p_z$ to the total NPA charge, and $\Sigma\pi$ corresponds to the summed contributions of the π-type atomic orbitals $2p_x$, $2p_y$, $3p_x$, $3p_y$. σ Donation from N_2 to the metal can be inferred from the value of $\Delta\sigma = 3 - \Sigma\sigma$ and π acceptance of N_2 from the metal is evident from $\Delta\pi = 2 - \Sigma\pi$. Strictly speaking, $\Delta\pi$ has two contributions: in the N_2 π-bonding orbitals π_x and π_y, a polarization of the dinitrogen unit occurs such that N_α gets negatively and N_β positively charged (Table 8). π backbonding almost exclusively transfers electron density to N_β, such that this atom gets negatively charged as well.

As evidenced from Table 11, both σ donation and π acceptance are largest in the *trans*-nitrile system **IV**, effectively leading to the highest activated N_2 ligand (vide supra). This can be explained by the fact that a high degree of σ donation leads to an elongation of the N—N bond, which acts to enhance the degree of π backbonding, overcompensating the effect of σ donation. The N_2 ligand of the pentaphosphine complex **Ia**, on the other hand, exhibits a significantly smaller degree of σ donation because of the presence of a strong donor in the trans position; therefore, π acceptance is not as large as in **IV**, and a lower activation of N_2 as compared to the *trans*-nitrile complex **IV** results. The activation of N_2 in **Ia**, on the other hand, is larger than in the bis(dinitrogen) complex **III**, as one backbonding ligand (N_2) has been exchanged by a σ-donor ligand (phosphine). In agreement with this description, $\Delta\pi$ values of N_α and N_β are more negative in **Ia** than in **III**. Based on the higher backbonding, N_2 is also slightly more σ donating in **Ia** as compared to **III**, but in sum the N_2 ligand in **Ia** is more strongly activated than in the bis(dinitrogen) complex **III**.

Model systems for $[Mo(NNH_2)(dpepp)(dppm)](CF_3SO_3)_2$

In analogy to the N_2 complex, two different models have been used for the NNH_2 complex. The molecular orbital scheme and the magnetic shielding calculation are based on $[Mo(NNH_2)(PH_3)_5]^{2+}$ (**IIa**) (Fig. 8). For the calculation of

© 2005 NRC Canada

Table 11. NPA charges of **Ia**, **III**, and **IV**.

	$[Mo(N_2)(PH_3)_5]$ (**Ia**)		$[Mo(N_2)_2(PH_3)_4]$ (**III**)		$[Mo(N_2)(NCCH_3)(PH_3)_4]$ (**IV**)	
	N_α	N_β	N_α	N_β	N_α	N_β
2*s*	1.427 09	1.625 42	1.422 38	1.594 72	1.436 95	1.627 48
3*s*	0.013 66	0.009 66	0.020 92	0.013 57	0.014 86	0.010 92
$2p_x$	1.174 45	1.104 92	1.153 22	1.065 72	1.279 84	1.275 10
$2p_y$	1.169 14	1.094 67	1.148 99	1.057 51	1.170 09	1.093 27
$2p_z$	1.258 42	1.253 85	1.294 53	1.317 99	1.169 25	1.099 53
$3p_x$	0.005 83	0.004 25	0.003 66	0.004 92	0.018 94	0.003 34
$3p_y$	0.005 37	0.004 42	0.003 10	0.004 15	0.003 23	0.004 86
$3p_z$	0.017 00	0.003 56	0.019 62	0.003 66	0.002 74	0.004 50
$\Sigma\sigma$	2.716 17	2.892 49	2.757 45	2.929 94	2.623 8	2.736 17
$\Sigma\pi$	2.354 79	2.208 26	2.308 97	2.132 30	2.474 84	2.376 57
σ *Donation*						
$\Delta\sigma = 3 - \Sigma\sigma$	0.283 83	0.107 51	0.242 55	0.070 06	0.376 2	0.263 83
π *Acceptance*						
$\Delta\pi = 2 - \Sigma\pi$	–0.354 79	–0.208 26	–0.308 97	–0.132 30	–0.474 84	–0.376 57
Total charge	–0.070 96	–0.100 75	–0.066 42	–0.062 24	–0.098 6	–0.112 74

the vibrational properties, the more realistic model $[Mo(NNH_2)(P3)(dpm)]^{2+}$ (**IIb**) (Fig. 8) was used, which included the alkyl bridges.

Optimized geometry of IIa and IIb

The bond distances of the NNH_2 unit are very similar in both models. Compared to the N_2 complex in **IIa**, the N—N bond is lengthened to 1.31 Å (**IIb**, 1.32 Å) by protonation. Simultaneously, the Mo—N bond is shortened to 1.77 Å (**IIa**) (**IIb**, 1.78 Å). In both models, the N—H bond distance is calculated to 1.02 Å. The geometric structure of the ligand framework in **IIb** is similar to that found for **Ib**. Cartesian coordinates of the optimized structures of **IIa** and **IIb** are collected in the supplemental material.[3]

Electronic structure of IIa

Figure 11 shows the molecular orbital scheme of **IIa**. For comparison, the MO schemes of the *trans*-fluoro NNH_2 model complex $[MoF(NNH_2)(PH_3)_4]^+$ (**V**) (3) and the *trans*-nitrile NNH_2 model complex $[Mo(NNH_2)(NCCH_3)(PH_3)_4]^{2+}$(**VI**) are given (9).

The MO scheme of **IIa** basically corresponds to those of **V** and **VI.** In all model systems, the nonbonding d_{xy} orbital is the HOMO. Below the HOMO are the bonding combinations of d_{xz} with π_v* (π* orbital perpendicular to the NNH_2 plane) <33> and d_{yz} with π_h* (π* orbital in the NNH_2 plane) <29>, respectively. The protonation of the dinitrogen model complex **Ia** causes a shortening of the Mo—N bond, which is accompanied by an enlargement of the N—N distance. This causes a decrease of the π_v* in energy, thus increasing the contribution of π_v* to the bonding combination d_{xz}–π_v* to 52% (Table 12). As a consequence, the backbonding interaction to d_{xz} orbital is strengthened. The bonding combination of π_h* with d_{yz} has 62% N_2 and 22% Mo character, and therefore a preponderance of π_h*. This represents an inverted bonding situation compared to the N_2 system, which is accounted for by the π_h*–d_{yz} labeling. The π_h* orbitals of the NNH_2 ligand in model systems **IIa**, **V**, and **VI** have the properties of a *p* donor at N_α (Table 13, Fig. 12). Therefore, the NNH_2 ligand receives electrons via π_v* and donates electron density via π_h*. In summary, the charge of the NNH_2 unit is not "2–", but slightly positive (**IIa**, +0.20) or negative (**V**, –0.03 from NPA, Table 14), respectively (3*b*). In contrast to the d_{xz}–π_v* and π_h*–d_{yz} orbitals of **V**, which have considerable contributions of the fluoride and phosphine ligands, the d_{xz}–π_v* and π_h*–d_{yz} orbitals of $[Mo(NNH_2)(PH_3)_5]^{2+}$ have almost no contributions besides the metal and the dinitrogen. LUMO <35> and <36> are the antibonding combinations of the NNH_2 π orbitals with the d_{xz} and d_{yz} orbitals, respectively.

Discussion

In the preceding sections, the structural, spectroscopic, and electronic properties of a molybdenum dinitrogen complex with a pentaphosphine coordination and its NNH_2 derivative were studied. The pentaphosphine coordination was achieved by combination of a tridentate (dpepp) and a bidentate (dppm) ligand. In this constitution, the complex exists in only one isomeric form and the pentaphosphine coordination sphere is stable towards protonation with triflic acid. Besides the investigated protonated compound **2**, only one more NNH_2 complex with five-coordinated phosphines is known; i.e., the complex with dimethylphosphinomethane (dmpm) instead of dppm (6). On this complex George et al. (11) demonstrated that only triflic acid forms the corresponding NNH_2 system, whereas protonation with other acids like HCl or HBr leads to different hydrido complexes under a loss of dinitrogen.

In the vibrational data of **1**[14] and **1**[15], all vibrations of the MoNN unit were identified, i.e., the NN stretch (1979 cm^{-1}), the MoN stretch (453 cm^{-1}), and the two bending vibrations (505/497 cm^{-1}). Especially for the NN stretch, good agreement between calculated frequencies and observed values was achieved (**IIb**, 1973 cm^{-1}). Based on the vibrational data and the DFT calculations of model **IIb**, a QCB-NCA was performed. The force constants of the N—N and Mo—N bonds, which are correlated with the activation of N_2 (1), were calculated as f_{NN} = 16.3 mdyn/Å and f_{MoN} = 2.8 mdyn/Å, respectively (free N_2 = 22.42 mdyn/Å). Therefore, the vibra-

© 2005 NRC Canada

Fig. 11. Molecular orbital schemes of **IIa**, **V**, and **VI** (**V** and **VI** are from refs. 3*b*, 13).

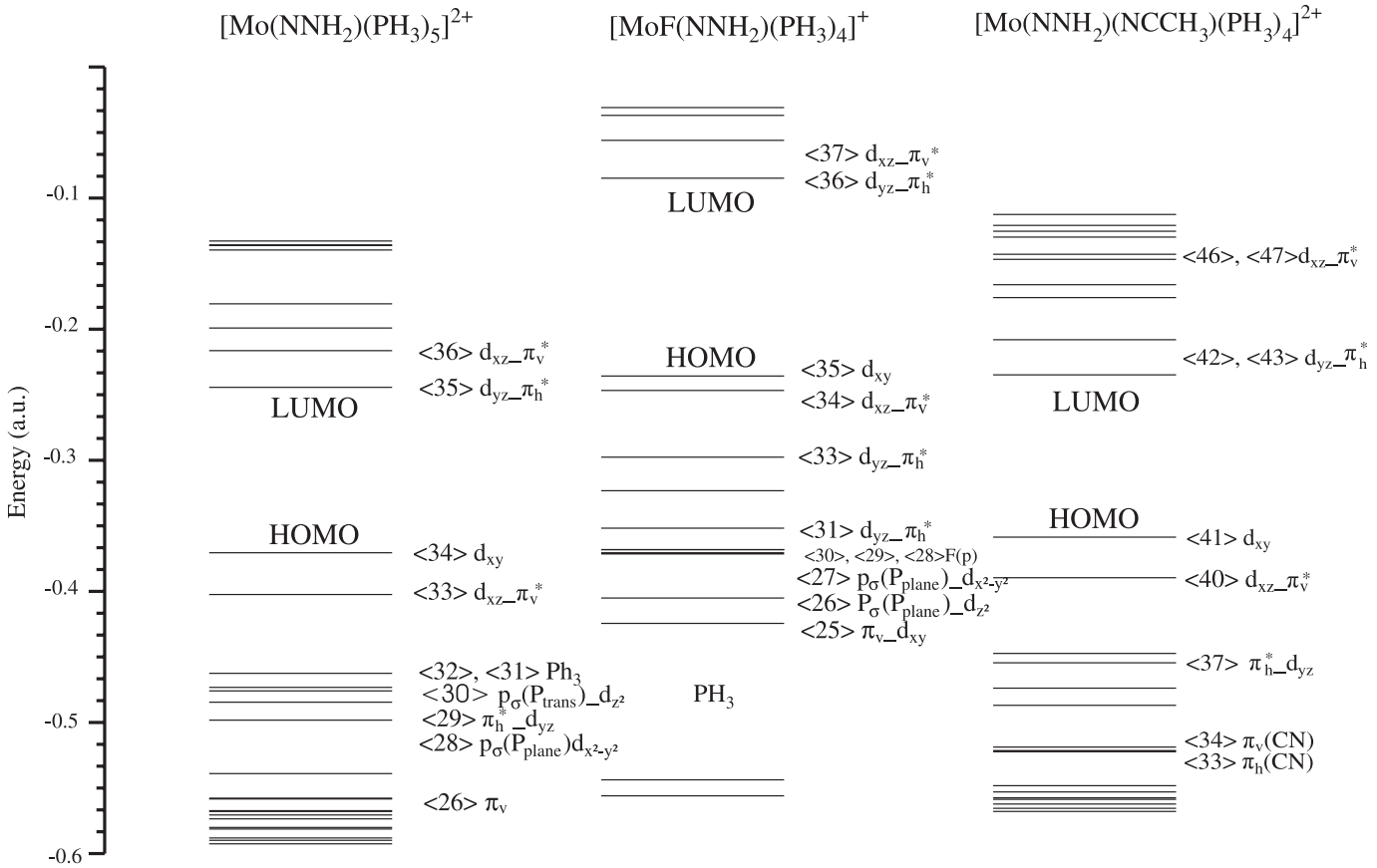


Table 12. Charge contributions of $[Mo(NNH_2)(PH_3)_5]^{2+}$ (**IIa**).

			Charge contribution (%)					
Orbital	Label	Energy (Hartree)	Mo	N_α	N_β	$H(NNH_2)$	P(trans)	P(plane)
d_{xz}_π_v*	36	–0.316 26	25	33	14	0	2	11
d_{yz}_π_h*	35	–0.344 37	46	24	0	6	1	11
d_{xy}	34	–0.470 53	87	0	0	0	0	0
d_{xz}_π_v*	33	–0.502 46	44	10	42	0	0	0
PH_3	32	–0.562 46	1	0	1	0	1	73
PH_3	31	–0.573 28	7	1	0	0	5	69
$p_\sigma(P_{trans})$_d_{z2}	30	–0.575 86	9	8	2	0	57	5
π_h*_d_{yz}	29	–0.584 38	22	58	4	7	0	3
$p_\sigma(P_{plane})$_d_{x2-y2}	28	–0.598 18	35	0	0	0	0	55
PH_3	27	–0.639 01	8	1	0	0	6	56
π_v	26	–0.657 88	1	13	17	0	2	30

tional spectra show a *stronger* activation of N_2 in the molybdenum pentaphosphine complex than in (bis)dinitrogen complexes like $[Mo(N_2)_2(dppe)_2]$ (f_{NN} = 17.2 dyn/Å and f_{MoN} = 2.0 mdyn/Å). Force constants for *trans*-nitrile dinitrogen systems are only known for W complexes that are more strongly activated by the metal center, and therefore, not directly comparable to **1** ($[W(N_2)(NCEt)(dppe)_2]$: f_{NN} = 14.95 mdyn/Å and f_{WN} = 3.15 mdyn/Å) (13). However, $[Mo(N_2)(NCCH_3)(dppe)_2]$ has an N-N stretching frequency of 1906 cm^{-1} (13); therefore, in *trans*-nitrile molybdenum dinitrogen systems the NN force constant should be smaller as compared with pentaphosphine complexes, corresponding to a higher activation of N_2. This is in agreement with the calculation (see the following). Interestingly, $[Mo(N_2)(dpepp)(dmpm)]$ exhibits an N-N stretching frequency of 1966 cm^{-1} (11), reflecting a stronger activation of N_2 by alkylphosphine as compared with the phenylphosphine ligands. This has been already known for bis(dinitrogen) complexes with diphosphine co-ligands (3).

The results of the DFT calculations on $[Mo(N_2)(PH_3)_5]$ (**Ia**) were compared with the parallel treatments of the bis(dinitrogen) and *trans*-nitrile dinitrogen model systems

© 2005 NRC Canada

Table 13. Charge contributions of selected MOs of $[MoF(NNH_2)(PH_3)_4]^+$ (**V**).

			Charge contribution (%)					
Orbital	Label	Energy (Hartree)	Mo	N_α	N_β	$H(NNH_2)$	F	P
d_{yz}–π_h*	36	–0.1848	53	20	2	13	5	2
d_{xy}	35	–0.3356	84	0	0	0	0	0
d_{xz}–π_v*	34	–0.3467	30	14	35	0	11	8
d_{yz}–π_h*(1)	33	–0.3977	7	26	1	3	19	39
d_{yz}–π_h*(2)	31	–0.4519	19	28	2	5	3	34

Fig. 12. Contour plots of some relevant orbitals of $[Mo(NNH_2)(PH_3)_5]^{2+}$ **IIa**.

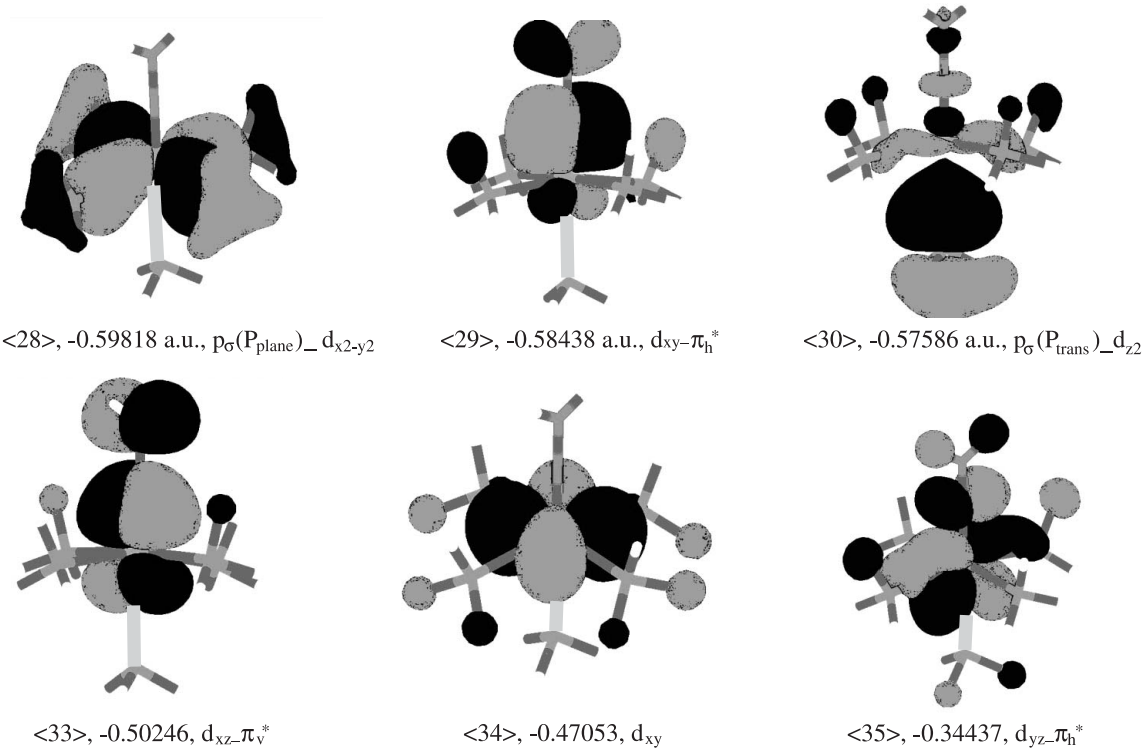


Table 14. NPA charges of **IIa**, **V**, and **IV**.

	Atom						
Model	Mo	N_α	N_β	H	PH_3(trans)	PH_3(plane)	F
$[Mo(NNH_2)(PH_3)_5]^{2+}$ (**IIa**)	–0.13	–0.10	–0.57	0.44	0.30	0.35	—
$[MoF(NNH_2)(PH_3)_4]^+$ (**V**)	0.04	–0.21	–0.68	0.43	—	0.24	–0.55
$[Mo(NNH_2)(NCCH_3)(PH_3)_4]^{2+}$ (**IV**)	–0.02	–0.10	–0.58	0.44	—	0.30	—

III and **IV**, respectively. Based on the calculated charges, the activation of N_2 follows the sequence **III** < **I** < **IV**. Specifically, the mono-dinitrogen complexes **Ia** and **IV** exhibit a stronger activation of the N_2 unit compared to **III** because of the absence of a second strong π acceptor (NPA charges of the N_2 unit: **Ia** (–0.17), **IV** (–0.21), **III** (–0.13)). The *trans*-nitrile system **IV** has the highest activated N_2 because of the fact that the nitrile is a weak σ donor and π acceptor (13). Therefore, σ donation of the coordinated N_2 to the metal is high, as evidenced from the large Δσ value in the NPA charge analysis. As a consequence, the energy of the π* orbitals is lowered and π backbonding is enforced. Strong backbonding overcompensates the stronger σ donation, and thus causes the high activation of the N_2 in the *trans*-nitrile system **IV**. This synergetic effect is missing in the pentaphosphine complex $[Mo(N_2)(PH_3)_5]$ (**Ia**) where because of the strongly σ-donating phosphine group in the *trans*-position, N_2 is a weaker σ donor than in **IV**. Therefore, the energy of the π* orbitals is not lowered as much as in **IV**, and no increase of backbonding occurs.

Another remarkable result is the low-field shift of the terminal nitrogen atom N_β in **1**. In fact, with a chemical shift of –16.7 ppm, N_β exhibits one of the largest low-field shifts recorded for end-on coordinated dinitrogen (23). Based on

© 2005 NRC Canada

DFT GIAO calculations, it can be shown that the origin of this unusual shift is the paramagnetic term. In analogy to observations on ^{31}P NMR shifts in ruthenium carbonyl phosphine complexes (31), the paramagnetic term to the ^{15}N NMR shift in mono-dinitrogen complexes appears to increase with the nitrogen contribution in the backbonding orbitals, going parallel to the activation of N_2. Besides the relatively high activation of N_2, there is an additional effect that increases the paramagnetic shift on N_β in **1**: The d_{xy} orbital <32>, which is nonbonding in the bis(dinitrogen) and *trans* nitrile complexes **III** and **IV**, respectively, is also involved in a backbonding interaction with N_2 and gets a N_β contribution. As a consequence, *all* $t_{2g} \rightarrow d_{z2}$ ligand-field transitions contribute to the paramagnetic shift of N_β in **I**, in contrast to **III** and **IV**.

The results of the vibrational and NMR spectroscopy confirm the structure of the NNH_2 complex with pentaphosphine coordination. Based on vibrational spectroscopy and DFT calculations, a QCB-NCA could be accomplished. The resulting force constants (f_{NN} = 7.65 mdyn/Å, f_{MoN} = 5.94 mdyn/Å) reflect the decrease of the N—N bond strength and the increase of the Mo—N bond strength caused by the protonation. They are similar to other molybdenum NNH_2 complexes like $[MoCl(NNH_2)(depe)_2]Cl$ (f_{NN} = 7.16 mdyn/Å, f_{MoN} = 5.52 mdyn/Å) (3). Unfortunately, no vibrational data for molybdenum-dppe NNH_2 complexes with coordinated counterions (Cl^-, F^-) or *trans*-nitrile ligands exist, which precludes a spectroscopic comparison of **2** to related NNH_2 systems in analogy to that performed for the N_2 complexes **1**, **3**, and **4**. However, DFT calculations of the model complex $[Mo(NNH_2)(PH_3)_5]^{2+}$ (**IIa**) show a NPA charge of +0.20 on the NNH_2 group while the corresponding *trans*-fluoro model **V** has a corresponding charge of –0.03. This reflects a lower activation of the NNH_2 ligand in **IIa** towards further protonation, which is due to weaker charge donation of a neutral phosphine group as compared to the anionic fluoride ligand in the *trans* position to the NNH_2 group of **V**.

The measured ^{15}N NMR data of $\mathbf{2^{15}}$ exhibit a considerable low-field shift compared with the *trans*-fluoro systems, i.e., the signal of the protonated nitrogen N_β in $\mathbf{2^{15}}$ is shifted by 24.7 ppm and the signal of the coordinated nitrogen N_α by 57.5 ppm. By employing GIAO shielding tensor calculations, it could be shown that these shifts are caused by the paramagnetic term. This result is explained by the fact that the Mo-NNH_2 metal–ligand π-bonding orbitals have considerable F and P parts in model $[MoF(NNH_2)(PH_3)_4]^+$ (**V**) of the fluoro system. In contrast, the corresponding orbitals of $\mathbf{2^{15}}$ are not admixed by the co-ligands and almost exclusively consist of Mo and N contributions. Therefore, they cause a greater paramagnetic shift of the nitrogen atoms than the corresponding orbitals of the *trans*-fluoro complex.

Remarkably, the pentaphosphine ligation of **1** is stable against exchange reactions induced by treatment with acid, in analogy to the $[Mo(N_2)(dpepp)(dmpm)]$ complex prepared by George et al. (11). An even higher stability could be achieved by using just one ligand with five phosphine donors. King and Cloyd (10) have synthesized linear and branched pentaphosphines with ethylene bridges. However, these ligands may be too small to accommodate Mo(0) or W(0) centers owing to a P-Mo-P angle of about 80° for ethyl-bridged phosphines. Possibly, the introduction of propylene bridges would offer a better ligand system for this purpose.

In summary, an octahedral mono-dinitrogen complex containing five phosphine groups and its NNH_2 counterpart was described and characterized. Based on the results of NMR, IR, and Raman spectroscopy coupled to DFT calculations, the dinitrogen complex was shown to exhibit a stronger activation compared to bis(dinitrogen) and a weaker activation compared to *trans*-nitrile N_2 complexes. The spectroscopic and theoretical investigations of the analogous hydrazido system with pentaphosphine ligation suggest a relatively low activation of the NNH_2 ligand towards further protonation, comparable to that present in *trans*-nitrile NNH_2 systems.

Acknowledgments

FT thanks DFG Tu58/13-1, Fonds der chemischen Industrie (FCI), and Christian Albrechts Universität Kiel for funding of this research.

References

1. (*a*) A.D. Allen and C.V. Senoff. Chem Commun. 621, (1965); (*b*) M.D. Fryzuk and B.A. MacKay. Chem. Rev. **104**, 385 (2004).
2. (*a*) R.A. Henderson, G.J. Leigh, and C. Pickett. Adv. Inorg. Chem. Radiochem. **27**, 197 (1983); (*b*) G.J. Leigh. Acc. Chem. Res. **25**, 177 (1992); (*c*) M. Hidai and Y. Mizobe. Chem. Rev. **95**, 1115 (1995); (*d*) M. Hidai. Coord. Chem. Rev. **99**, 185 (1999).
3. (*a*) N. Lehnert and F. Tuczek. Inorg. Chem. **38**, 1659 (1999); (*b*) N. Lehnert and F. Tuczek. Inorg. Chem. **38**, 1671 (1999); (*c*) K.H. Horn, N. Lehnert, and F. Tuczek. Inorg. Chem. **42**, 1076 (2003); (*d*) F. Tuczek, K.H. Horn, and N. Lehnert. Coord. Chem. Rev. **107**, 245 (2003); (*e*) F. Tuczek. Adv. Inorg. Chem. **55**, 27 (2004).
4. C.J. Pickett and G.J. Leigh. J. Chem. Soc. Dalton Trans. 1033 (1981).
5. Y. Aliah, S.K. Ibrahim, M.A. Queiros, A. Fonseca, J. Talarmin, F. Volant, and C.J. Pickett. J. Chem. Soc. Dalton Trans. 4807 (1997).
6. C.J. Pickett and J. Talarmin. Nature (London), **317**, 652 (1985).
7. (*a*) D.V. Yandulov and R.R. Schrock. Science, **301**, 76 (2003); (*b*) D.V. Yandulov and R.R. Schrock. J. Am. Chem. Soc. **124**, 6252 (2002); (*c*) D.V. Yandulov, R.R. Schrock, A.L. Rheingold, C. Ceccarelli, and W.M. Davis. Inorg. Chem. **42**, 796 (2003); (*d*) V. Ritleng, D.V. Yandulov, W.W. Weare, R.R. Schrock, A.S. Hock, and W.S. Davis. J. Am. Chem. Soc. **104**, 6150 (2004).
8. (*a*) T.A. George and B.B. Kaul. Inorg. Chem. **29**, 4969 (1990); (*b*) G.J. Leigh and C.J. Pickett. J. Chem. Soc Dalton Trans. 1797 (1977); (*c*) D.L. DuBois. Inorg. Chem. **23**, 2047 (1984).
9. C.M. Habeck, C. Hoberg, G. Peters, C. Näther, and F. Tuczek. Organometallics, **23**, 3252 (2004).
10. (*a*) R.B. King and J.C. Cloyd. Z. Naturforsch. **27b**, 1432 (1972); (*b*) R.B. King and J.C. Cloyd. Phosphorus, **3**, 213 (1973).
11. (*a*) T.A. George and R.C. Tisdale. Inorg. Chem. **27**, 2909, (1988); (*b*) T.A. George and R.C. Tisdale. J. Am. Chem. Soc. **107**, 5157 (1985); (*c*) T.A. George, L. Ma, S.N. Shailh, R.C. Tisdale, and J. Zubieta. Inorg. Chem. **29**, 4789 (1990).

© 2005 NRC Canada

12. F. Studt, B.A. MacKay, M.D. Fryzuk, and F. Tuczek. J. Am. Chem. Soc. **126**, 280 (2004).
13. C.M. Habeck, N. Lehnert, C. Näther, and F. Tuczek. Inorg. Chim. Acta, **337**, 11 (2002).
14. T.A. George and R.A. Kovar. Inorg. Chem. **20**, 285 (1981).
15. (*a*) A.D. Becke. Phys. Rev. A, **38**, 3098 (1988); (*b*) A.D. Becke. J. Chem. Phys. **98**, 1372 (1993); (*c*) A.D. Becke. J. Chem. Phys. **98**, 5648 (1993).
16. T.H. Dunning and P.J. Hay. *In* Modern theoretical chemistry. Plenum Press, New York. *Edited by* H.F. Schaefer III. 1976.
17. (*a*) P.J. Hay and W.R. Wadt. J. Chem. Phys. **82**, 270 (1985); **82**, 299 (1985); (*b*) W.R. Wadt and P.J. Hay. J. Chem. Phys. **82**, 284 (1985).
18. (*a*) J.P. Foster and F.J. Weinhold. J. Am. Chem. Soc. **102**, 7211 (1980); (*b*) A.B. Rives and F. Weinhold. Int. J. Quantum Chem. Symp. **14**, 201 (1980); (*c*) A.E. Reed, R.B. Weinstock, and F. Weinhold. J. Chem. Phys. **83**, 735 (1985); (*d*) A.E. Reed, L.A. Curtiss, and F. Weinhold. Chem. Rev. **88**, 899 (1988).
19. M.J. Frisch, G.W. Trucks, H.B. Schlegel, G.E. Scuseria, M.A. Robb, J.R. Cheeseman, J.A. Montgomery, Jr., T. Vreven, K.N. Kudin, J.C. Burant, J.M. Millam, S.S. Iyengar, J. Tomasi, V. Barone, B. Mennucci, M. Cossi, G. Scalmani, N. Rega, G.A. Petersson, H. Nakatsuji, M. Hada, M. Ehara, K. Toyota, R. Fukuda, J. Hasegawa, M. Ishida, T. Nakajima, Y. Honda, O. Kitao, H. Nakai, M. Klene, X. Li, J.E. Knox, H.P. Hratchian, J.B. Cross, C. Adamo, J. Jaramillo, R. Gomperts, R.E. Stratmann, O. Yazyev, A.J. Austin, R. Cammi, C. Pomelli, J.W. Ochterski, P.Y. Ayala, K. Morokuma, G.A. Voth, P. Salvador, J.J. Dannenberg, V.G. Zakrzewski, S. Dapprich, A.D. Daniels, M.C. Strain, O. Farkas, D.K. Malick, A.D. Rabuck, K. Raghavachari, J.B. Foresman, J.V. Ortiz, Q. Cui, A.G. Baboul, S. Clifford, J. Cioslowski, B.B. Stefanov, G. Liu, A. Liashenko, P. Piskorz, I. Komaromi, R.L. Martin, D.J. Fox, T. Keith, M.A. Al-Laham, C.Y. Peng, A. Nanayakkara, M. Challacombe, P.M.W. Gill, B. Johnson, W. Chen, M.W. Wong, C. Gonzalez, and J.A. Pople. GAUSSIAN 03. Revision B.03 [computer program]. Gaussian, Inc., Pittsburgh, Penn. 2003.
20. GaussView 3.07. Gaussian, Inc., Pittsburgh, Penn. 2003.
21. M.R. Peterson and D.F. McIntosh. QCPE program 576. Quantum chemistry program exchange [computer program]. Department of Chemistry, Indiana University, Bloomington, Indiana. 1988.
22. J.A. Nelder and R. Mead. Comput. J. **7**, 308 (1965).
23. A. Allouche and J. Pourcin. Spectrochim. Acta, **49A**, 571 (1993).
24. G.M. Sheldrick. SHELXS-97 and SHELXL-97 [computer programs]. University of Göttingen, Göttingen, Germany. 1997.
25. P.S. Pregosin and R.W. Kunz. ^{31}P and ^{13}C NMR of transition metal phosphine complexes. Springer-Verlag, Berlin. 1979.
26. S. Donovan-Mtunzi, R.L. Richards, and J. Mason. J. Chem. Soc. Dalton. Trans. 469 (1984).
27. S. Donovan-Mtunzi, R.L. Richards, and J. Mason. J. Chem. Soc. Dalton. Trans. 2729 (1984).
28. J.W. Gleeson and W.R. Vaughan. J. Chem. Phys. **78**, 5385 (1983).
29. S. Donovan-Mtunzi, R.L. Richards, and J. Mason. J. Chem. Soc. Dalton. Trans. 1329 (1984).
30. N.B. Colthup, L.H. Daly, and S.E. Wiberley. Introduction to infrared and Raman spectroscopy. 3rd ed. Academic Press, Orlando, Florida. 1990.
31. K. Eichele, R.E. Wasylishen, J.F. Corrigan, N.J. Taylor, A.J. Carty, K.W. Feindel, and G.M. Bernard. J. Am. Chem. Soc. **124**, 1541 (2001).

© 2005 NRC Canada

FOREWORD / AVANT-PROPOS

This issue of the *Canadian Journal of Chemistry* commemorates the 40th anniversary of a landmark Canadian discovery by A.D. Allen and C.V. Senoff at the University of Toronto in the mid-60s. In 1965, a paper appeared in *Chemical Communications*, entitled "Nitrogenopentaammineruthenium(II) Complexes" that detailed the serendipitous formation of the $[Ru(NH_3)_5N_2]^{2+}$ complex cation, *the first dinitrogen complex*, from the reaction of $RuCl_3$ with hydrazine hydrate. Instead of ending up as a curiosity and relegated to secondary literature reviews of esoteric inorganic complexes, this report sparked an intense effort in the coordination chemistry and reactivity of molecular nitrogen that continues to this day.

Research into nitrogen fixation is a topic with great historical perspective and continues even today on three fronts. The first front stems from the early work by Haber on ammonia synthesis, and is concerned with efforts to further improve the efficiency of the heterogeneous reaction of N_2 and H_2 over activated metal surfaces to produce NH_3. Another active front involves understanding the biological fixation of nitrogen by certain enzymes. The third front involves homogeneous activation and functionalization of molecular nitrogen by metal complexes, an area that overlaps with the previous two fronts from a modeling point of view, but also is concerned with expanding the known reactivity patterns of the simple N_2 molecule.

In this issue, an international slate of authors who are active in the area of dinitrogen chemical research were contacted to submit an article, either original or a minireview of their work. Authors from Japan, Germany, the United States, and Canada have submitted 13 articles that provide retrospective and updates of current research in this important area. It is interesting that four of the principal authors were not even born in 1965, a testament to the importance of this long-standing problem in chemistry. A number of the other authors clearly indicate how important this complex was to this area of research.

In the following pages, the original article from 1965 is reproduced (by permission of The Royal Society of Chemistry). In addition, a brief historical perspective is given by G.J. Leigh on A.D. (Bert) Allen and this discovery. The goal of this commemorative issue is to provide a forum for recent work in dinitrogen coordination chemistry and celebrate an important Canadian milestone. I want to personally thank all of the contributors for their enthusiasm and support of this project.

Michael D. Fryzuk
Vancouver, 2005

Ce numéro de la *Revue canadienne de chimie* souligne le 40^{e} anniversaire d'une découverte historique canadienne au milieu des années 60 par A.D. Allen et C.V. Senoff de l'Université de Toronto. En effet, en 1965, on note la parution d'un article dans *Chemical Communications* intitulé « Nitrogenopentaammineruthenium(II) Complexes » dans lequel les auteurs exposent en détail la formation fortuite du cation du complexe $[Ru(NH_3)_5N_2]^{2+}$, *le premier complexe diazoté*, à partir de la réaction du $RuCl_3$ avec de l'hydrate d'hydrazine. Plutôt que d'être considéré comme une simple trouvaille inusitée et d'être relégué aux rapports de synthèses secondaires sur les complexes inorganiques ésotériques, ce rapport a profondément dynamisé la chimie de coordination et la réactivité de l'azote moléculaire et cet intérêt est toujours aussi manifeste aujourd'hui.

L'étude de la fixation de l'azote est un domaine de grande perspective historique qui repose, encore de nos jours, sur trois composantes. La première est le fruit des travaux initiaux de Haber sur la synthèse de l'ammoniac visant à améliorer l'efficacité de la réaction hétérogène de l'azote (N_2) et de l'hydrogène (H_2) sur des surfaces métalliques activées menant à la production de l'ammoniac (NH_3). La deuxième composante consiste à approfondir les connaissances sur les mécanismes de la fixation biologique de l'azote par certains enzymes. La troisième composante porte sur la fonctionnalisation et l'activation homogène de l'azote moléculaire par des complexes métalliques, un domaine de recherche qui chevauche les deux premières composantes sur le plan de la modélisation, mais qui vise également le développement des modes réactionnels de l'azote comme simple molécule.

Pour réaliser ce numéro commémoratif, un éventail international d'auteurs oeuvrant dans le domaine de la chimie du diazote ont été invités à soumettre un article original ou une minisynthèse sur leurs travaux. Des auteurs du Japon, de l'Allemagne, des États-Unis et du Canada ont soumis 13 articles qui présentent un historique des travaux réalisés dans le domaine en plus de faire le point sur la recherche actuelle. Par ailleurs, il est intéressant de noter que quatre des principaux auteurs qui ont contribué à ce numéro n'étaient même pas nés en 1965, ce qui témoigne de l'importance de ce problème de longue date en chimie. De plus, plusieurs autres auteurs ont clairement indiqué à quel point ce complexe est important pour ce domaine de recherche.

On y retrouve notamment l'article original de 1965 (reproduit avec l'autorisation de la Royal Society of Chemistry). De plus, G.J. Leigh présente un bref historique sur A.D. (Bert) Allen et cette découverte. Ce numéro commémoratif a pour but d'offrir un forum pour les travaux récents menés dans le domaine de la chimie de la coordination du diazote et de souligner cet important jalon canadien. Je tiens à remercier personnellement toutes les personnes qui ont contribué leur enthousiasme et leur appui à ce projet.

Michael D. Fryzuk
Vancouver, 2005

© 2005 NRC Canada

The following is a reproduction of the original article by Allen and Senoff published by The Royal Society of Chemistry in *Chemical Communications* in 1965.

Voici une reproduction de l'article original de Allen et Senoff publié dans *Chemical Communications* en 1965 par la Royal Society of Chemistry.

Number 24, 1965 621

Nitrogenopentammineruthenium(II) Complexes

By A. D. Allen and C. V. Senoff

(*Lash Miller Chemical Laboratories, University of Toronto, Toronto 5, Canada*)

Vol'pin and Shur have recently explored the possibility of fixing molecular nitrogen under mild conditions.[1–3] We now report that from aqueous solutions of ruthenium trichloride (free from nitric oxide) and hydrazine hydrate at 25° it is possible to isolate complexes which appear to be of the type $[Ru(NH_3)_5N_2]X_2$ where X = Br^-, I^-, BF_4^-, and PF_6^-. These salts are the first reported compounds in which N_2 is co-ordinated to a transition metal. The iodide salt is diamagnetic and has the following analysis: N, 20·52; H, 3·96; NH_3, 17·84; I, 54·05%. (Calc. for $H_{15}N_7I_2Ru$: N, 20·94; H, 3·21; NH_3, 18·16; I^-, 54·27%). The complexes are only moderately stable towards air

[1] M. E. Vol'pin and V. B. Shur, *Doklady Akad. Nauk S.S.S.R.*, 1964, **156**, 1102.
[2] M. E. Vol'pin and V. B. Shur, *Vestnik Akad. Nauk S.S.S.R.*, 1965, 51.
[3] M. E. Vol'pin, V. B. Shur, and L. P. Bichin, *Izvest. Akad. Nauk S.S.S.R., Ser. Khim.*, 1965, 720.

and decompose fairly rapidly in water. The conductance of solutions of the di-iodide salt in dimethyl sulphoxide is exactly the same as solutions of the reference compound $[Ru^{III}(NH_3)_5I]I_2$ over the concentration range measured (1—10 × 10^{-5} M).

The infrared spectra of these compounds contain a strong, sharp, band between 2170—2115 $cm.^{-1}$ (see Table) which is assigned to the N_2 stretch. Upon co-ordination to the metal the N_2 stretching mode has undergone a shift to lower frequency of about 200 $cm.^{-1}$ from that observed for molecular nitrogen (2331 $cm.^{-1}$).[4] It is not possible at present to ascertain whether co-ordination occurs through the lone pair of electrons on one of the nitrogen atoms or through the π-electron system of the molecule, but the crystal structure of these compounds is being investigated.

If the iodide salt is treated with 20% aqueous $NaBH_4$ solution and 40% NaOH solution the amount of ammonia evolved corresponds to 24%, compared with 18% found on normal treatment with alkali, indicating that nearly all of the co-ordinated nitrogen is converted into ammonia by the action of the borohydride ion.[1–3]

When the fluoborate salt is treated with 95% sulphuric acid under high vacuum the non-condensable gas (77° K) that is liberated was shown to be nitrogen by mass spectrometry. A maximum of about 40% of the theoretical amount of nitrogen has been obtained in this way, and it is thought that the remaining nitrogen may have been converted into ammonia or oxidized by the acid. The complexes, $[Ru(NH_3)_6](BF_4)_2$, $[Ru(NH_3)_6]Cl_3$, and $FeCl_2,2N_2H_4$ were treated with sulphuric acid in a similar manner. No nitrogen was evolved, indicating that the source of the nitrogen is not hydrazine or ammonia.

We have considered the possibility that the complex contains a co-ordinated di-imide molecule, *i.e.*, $[Ru^{II}(NH_3)_5.NH{=}NH]^{2+}$. Evidence against this is (a) that the $\nu_{N=N}$ frequency should be at about 1400 $cm.^{-1}$,[5] (b) that the n.m.r. spectrum in dimethyl sulphoxide contains no bands other than those attributed to the ammonia hydrogens, and (c) that the gas liberated on treatment with sulphuric acid contains no hydrogen.

Because of the lability of the N_2 ligand these complexes are ideal starting materials for the preparation of a number of ruthenium(II) and ruthenium(III) complexes. Mild treatment with the hydrohalic acids leads to the formation of the corresponding halogenopentammineruthenium(III) salts. The following ruthenium(II) complexes have also been prepared by the reaction of the nitrogenopentammine complexes with the appropriate ligand: $[Ru(NH_3)_6]X_2$, $[Ru(NH_3)_4py_2]X_2$, $[Ru(NH_3)_2py_4]X_2$, $[Ru(NH_3)_5DMSO]X_2$ where X = I^-, BF_4^-, PF_6^-, and DMSO = dimethyl sulphoxide.

Table

X =	Br^-	I^-	BF_4^-	PF_6^-
ν_{N_2}	2118s	2129s	2154s	2167s

(*Received, September 20th*, 1965; *Com.* 598.)

[4] K. Nakamoto, "Infrared Spectra of Inorganic and Co-ordination Compounds," Wiley, New York, 1963, p. 72.
[5] E. J. Blau, B. F. Hochheimer, and H. J. Unger, *J. Chem. Phys.*, 1961, **34**, 1060.

© The Royal Society of Chemistry 1965

© 2005 NRC Canada

AWARD LECTURE / CONFÉRENCE D'HONNEUR

2004 Fred Beamish Award Lecture — Analytical – materials chemistry on old CDs — Beyond self-assembly

Cassie Ho, Dinah M. Soolaman, and Hua-Zhong Yu

Abstract: This review describes a variety of new chemistry that has been established in our research laboratory and by other scientists worldwide related to optical compact disc (CD) technology. In particular, we have discovered that gold substrates from CD-Rs can be used to prepare high-quality, self-assembled monolayers (SAMs) after removing the protective polymer films with concentrated nitric acid. It was proven that these substrates are feasible for electrochemical, spectroscopic, and surface wetting studies. We have also demonstrated that CD-R gold films are ideal micropatterned conductive substrates for the "customized" fabrication of material microstructures. In addition, we have been working on the micropatterning of DNA probes on CD-R substrates, and exploring the possibility of using the CD-R writing/reading system for biochip fabrication and gene analysis.

Key words: compact disc-recordable (CD-R), self-assembled monolayers (SAMs), electrochemical analysis, material micro- and (or) nanostructures, biomedical diagnosis.

Résumé : Cette revue décrit plusieurs aspects d'une nouvelle chimie développée dans notre laboratoire ainsi que par d'autres chimistes à travers le monde en relation avec la technologie du disque compact optique (CD). En particulier, on a découvert que des substrats d'or obtenus à partir de CD-R peuvent être utilisés pour préparer des monocouches autoassemblées de haute qualité après avoir enlevé les films de polymères protecteurs à l'aide d'acide nitrique concentré. Il a été prouvé que ces substrats peuvent être réalisés pour des études électrochimiques, spectroscopiques et de mouillage de surface. On a aussi démontré que les films d'or de CD-R sont les substrats conducteurs à micromotifs idéaux pour la fabrication de matériaux à microstructures « personnalisées ». De plus, des travaux ont aussi été effectués sur le micromodelage de sondes d'ADN sur des substrats CD-R et dans le domaine de l'exploration des possibilités d'utiliser un système d'écriture/lecture d'un CD-R dans la fabrication d'une biopuce et de l'analyse des gènes.

Mots clés : disque compact enregistrable (CD-R), monocouches autoassemblées, analyse électrochimique, matériaux à micro- et (ou) nanostructures, diagnostic biomédical.

[Traduit par la Rédaction]

Introduction

Compact discs are the most commonly used optical information storage media because of their versatility and ease of use (1). The structures of the compact disc read-only memory (CD-ROM) and the compact disc-recordable (CD-R) differ significantly; while the CD-ROM contains pits and plateaus that represent binary data, the CD-R uses organic dyes that decompose when it is "burnt" and the alternating "burnt – not burnt" pattern is then used to represent data.

Received 2 September 2004. Published on the NRC Research Press Web site at http://canjchem.nrc.ca on 22 April 2005.

C. Ho, D.M. Soolaman, and H.-Z. Yu.[1] Department of Chemistry, Simon Fraser University, Burnaby, BC V5A 1S6, Canada.

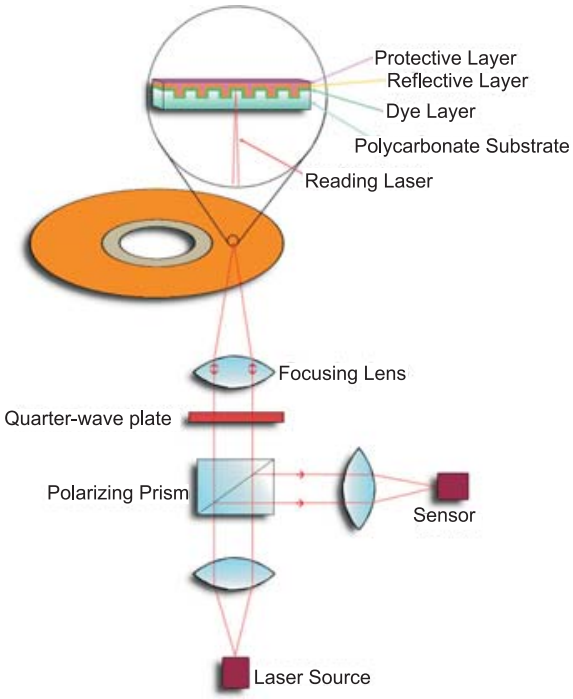
[1]Corresponding author (e-mail: hzyu@sfu.ca).

The structure of a CD-ROM consists of three layers: (1) a polycarbonate (PC) layer that forms the support for the entire structure, (2) a reflective layer that is usually made from sputtered aluminium, silver or gold, and (3) a protective layer of lacquer that protects the reflective layer from everyday wear. The properties of the polycarbonate often differ slightly among manufacturers (1*a*). The PC substrate is normally created via injection moulding from a master pattern and good flow properties are essential for easy moulding (2). A pattern of pits and plateaus that represents the binary data is stamped onto the PC. Then, a thin reflective layer that is used to reflect the CD reading laser back into the reading head is sputtered over top. Finally, a protective lacquer layer is spin-coated on top of it all.

The CD reader uses polarized light to read the data (Fig. 1). The laser beam is circularly polarized in the polarizing prism; it then goes through the quarter-wave plate to be polarized in one direction. After it is reflected from the CD,

 doi: 10.1139/V05-006 © 2005 NRC Canada

Fig. 1. Schematic illustration of the construction of a compact disc-recordable (CD-R) and the optical reading/writing system. Reprinted from ref. 1*b*. Reproduced by permission of The Royal Society of Chemistry.



the light will go back through the quarter-wave plate and be polarized in the other direction. The prism will direct the light to the sensors (3). When the incident light hits the PC, it will be refracted (n = 1.55) and the laser spot will be focused even further into a smaller spot (2). The wavelength of the light in the PC will be 1.55 times shorter than in the air (λ = 780 nm in air, $\lambda \approx$ 500 nm in the PC). The depth of the pits in the PC layer is designed to be $\lambda/4$, so that when the light is reflected back it will have travelled $\lambda/2$. This causes destructive interference and no light travels back into the reading head. In this manner, the pattern on the CD represents binary data.

CD-Rs contain four layers that are sandwiched together on top of a polycarbonate substrate (Fig. 1). Unlike CD-ROMs, the PC substrate does not contain any pits or plateaus, but rather contains many racks that spiral around the entire PC; these tracks are used to position the reading and writing laser. They impart a "mountain-and-valley" topography to all the other layers in the disc (3). The distance between each valley is approximately 1.3 μm.

The most commonly used dyes in CD-R medias are derivatives of cyanine and phthalocyanine, although azo-based dyes are also used (1*a*). During the recording process, the CD writer focuses an IR laser beam on the dye layer. The dye layer absorbs the laser light and darkens, blocking the reflective layer from the visible laser light used by regular CD drives and (or) players. The actual darkening process has not been very well understood; some dye formulations seem to change colour chemically and become opaque, while others absorb enough IR laser light and they deform from the heat, literally "burning" a dark spot into the dye layer.

Over top of the dye layer is a reflective layer made of silver, gold, or aluminium that is more common today. This layer is very thin (ca. 50–100 nm) and serves to reflect the reading laser back through the polarizing prism into the CD reading head (1*b*). A protective lacquer film goes on top of the reflective layer to protect it from being scratched or damaged during everyday use. Depending on the brand, there might also be another layer over top that allows the CD-R to be labelled.

Aside from being a popular information storage media, CD-Rs have proven to be very versatile in modern chemical research. Extended from our short report published in *Chemical Communications* as a Focus Article (1*b*), this review provides a comprehensive summary of the recent developments in the use of compact disc technology in a (bio-)chemical laboratory setting. Herein, we will focus on the work carried out in our laboratory during the past few years, while brief descriptions of related research work from other laboratories worldwide will be included in corresponding sections.

Surface chemistry on CD-Rs — Self-assembly and beyond

The surface chemistry of materials plays an important role in determining their behaviour in different chemical and biological environments. The surface property of the reflective gold layer in a CD-R was characterized with wetting measurements, electrochemistry, and a scanning tunnelling microscope (STM). It was found to be a suitable substrate for the formation of self-assembled monolayers (SAMs) (4).

Self-assembly is one of the most remarkable and ubiquitous events in chemical and biological processes. It has been employed by chemists to prepare highly organized monolayers on solid substrates. For the past two decades, the use of SAMs to modify the surface characteristics of solid materials has been very popular. An extensive review of SAMs was written by Ulman (5) more than 10 years ago and many more applications of SAMs have been proposed since that time. For example, alkanethiolate SAMs on gold electrodes have been used as model systems to study the kinetics of long-range electron transfer (6, 7). In the field of nanofabrication, SAMs can be used to protect nanoparticles to avoid coalescence; more details can be found in Murray's recent review on monolayer-protected nanocrystals (8). As well, SAMs of thiol-terminated oligonucleotides have potential applications in gene analysis; several recent reviews on advances in electrochemical DNA sensors are available (9–11).

One of the key issues in preparing high quality SAMs is the choice and pretreatment of substrates. In 2001, we reported the formation of high quality SAMs on gold substrates from CD-Rs (4). These SAMs were compared with those formed on commercially available gold slides purchased from Evaporated Metal Films (EMF), Inc. (Ithaca, New York) using FT IR, contact angle measurements, electrochemical measurements, and STM.

The preparation of the CD-R gold substrates is very simple: gold CD-Rs (Kodak CD-R Gold Ultima) are cut into pieces using a pair of regular scissors and stripped of their protective layer via immersion in concd. HNO_3 for 3–5 min. After the protective layer is peeled off, the CD pieces can be

© 2005 NRC Canada

used to prepare SAMs by submersing them in a dilute solution of organothiols in absolute ethanol for 18–24 h (Fig. 2).

The SAMs formed on two different gold substrates were initially characterized by contact angle measurements. As expected, gold substrates modified with 1-octadecanethiolate SAMs were found to be more hydrophobic than the bare ones in both cases. The comparisons between the bare gold substrates were more complicated because of their time-dependent nature. However, the equilibrated contact angles of both substrates agree within experimental uncertainties. The contact angles of the bare CD-R gold substrate was found to be 60 ± 2° and the EMF gold substrate was found to be 62 ± 2°; the SAM-modified CD-R gold substrate, on the other hand, was found to be 100 ± 3° and the EMF gold substrate was found to be 100 ± 2°. From these wetting studies, we can conclude that the CD-R gold substrates are comparable to the commercial EMF samples and that the SAMs formed on these two substrates show similar quality. This certainly confirms that CD-R gold substrates can be used in place of commercial gold substrates in wetting property studies.

The results from the wetting studies are rather macroscopic because the resolution of the contact angle is limited by the size of the water drops that were around 2–4 mm in diameter, depending on the hydrophobicity of the surface. Electrochemical measurements were carried out using cyclic voltammetry (CV) because this technique has been shown to be sensitive to the quality and thickness of monolayers on gold (12). The CV scans of both the bare gold substrates and the SAM-modified substrates were done with a 1.0 mmol/L solution of $Fe(CN)_6^{3-}$ acting as the electroactive species in a 1.0 mol/L KCl electrolyte (Fig. 3). The scans of the bare gold surfaces were of the same shape and so were the scans of the modified surfaces. The current in the scans of the modified surfaces is lower and mostly capacitive; it is also independent of scan rate, indicating that the reduction of $Fe(CN)_6^{3-}$ is kinetically limited, which is the result of the decreased interfacial electron transfer rate as electrons have to tunnel through the monolayer to reach the electrode. Both decreases in current from the monolayer on CD-R and EMF substrates are in the same order of magnitude, indicating that the packing and coverage of both monolayers are approximately the same.

As a further confirmation of the integrity of SAMs on CD-R gold substrates, infrared spectroscopy (IR) was carried out. All the assigned peaks in their IR spectra agreed with each other within experimental uncertainties, while their intensities differed only slightly (Fig. 4). The band at 2964 cm^{-1} is assigned to the CH_3 asymmetric in-plane CH stretching mode (ν_a), while the bands at 2937 and 2877 cm^{-1} are assigned to the CH_3 symmetric CH stretching mode (ν_s), which is split due to Fermi resonance interactions with the lower frequency asymmetric CH_3 deformation. The bands at 2917 and 2850 cm^{-1} are assigned to the $\nu_a(CH_2)$ and $\nu_s(CH_2)$ modes, respectively. These two modes were generally chosen for structural interpretation because of the minimal overlap of their bands with those of other modes. For example, the absorbance band of $\nu_a(CH_2)$ at 2917 cm^{-1} indicates a crystalline structure in the alkyl chains of the SAMs on both substrates. We can conclude from the IR data that the packing and orientation of the alkyl chains in the monolayers were comparable on the CD-R and the commercial substrate.

Fig. 2. Self-assembly of 1-octadecanethiol on gold substrates prepared from CD-Rs: (*a*) polycarbonate base, (*b*) dye-photosensitive layer, (*c*) gold reflective layer, (*d*) protective polymer films, and (*e*) self-assembled monolayers. Reprinted in part with permission from ref. 4. Copyright 2001 American Chemical Society.

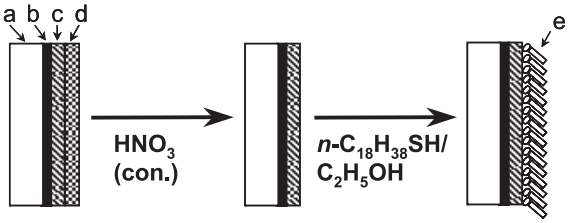
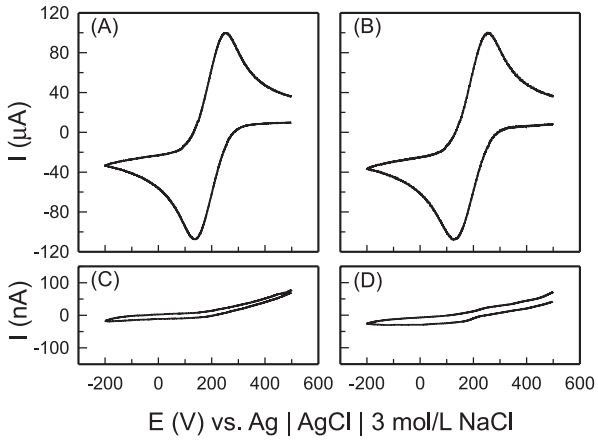


Fig. 3. Cyclic voltammgrams for (A) bare gold from CD-Rs, (B) bare gold from EMF, (C) $CH_3(CH_2)_{17}S$-Au(CD-Rs), and (D) $CH_3(CH_2)_{17}S$-Au(EMF) in 1.0 mmol/L $K_3Fe(CN)_6$ and 0.1 mol/L KCl. The scanning rate is 50 mV/s. Reprinted in part with permission from ref. 4. Copyright 2001 American Chemical Society.



STM images provided a close look at the surface morphology of the substrates. Both CD-R and EMF gold substrates showed a polycrystalline structure, i.e., a "rolling hills" topography in their respective STM images (Fig. 5). However, the CD-R substrates show a more uniform grain size with diameters of 20–40 nm and a more even peak-to-valley height of around 3 to 4 nm. The EMF substrates were not as uniform and the peak-to-valley height was significantly higher. Neither one of the bare gold substrates is atomically flat; this means they are suitable only for microscale studies.

Based on the above studies, it can be clearly seen that gold substrates prepared from CD-Rs are suitable for self-assembly. The resulting monolayers are comparable to those formed from commercial gold substrates and give very reproducible results. The best advantage of using a CD-R substrate is that it does not require the use of highly corrosive and dangerous "piranha" (H_2O_2:H_2SO_4, 1:3) solution, which will explode when in contact with organic materials. CD-R substrates are also considerably less expensive when compared with commercial gold substrates, because each CD will produce many smaller pieces that can be used in individual studies.

We have extended the application of gold CD-R substrates to other surface chemistry studies. In our study of the evapo-

© 2005 NRC Canada

Fig. 4. IR external reflection spectra for self-assembled monolayers of $CH_3(CH_2)_{17}SH$ on (A) gold substrates prepared from CD-Rs and (B) gold plates purchased from EMF. The *p*-polarized light was incident at 80°. Reprinted in part with permission from ref. 4. Copyright 2001 American Chemical Society.

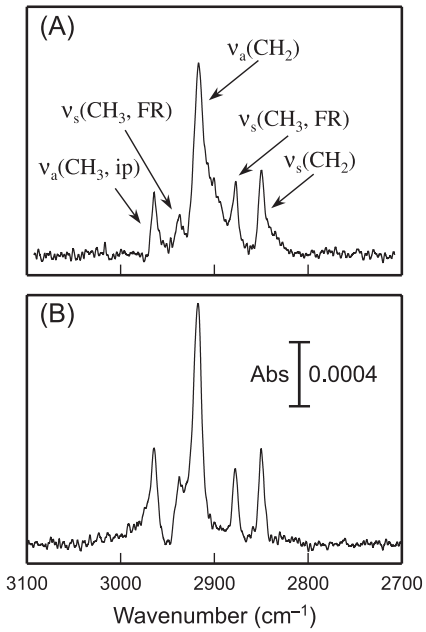
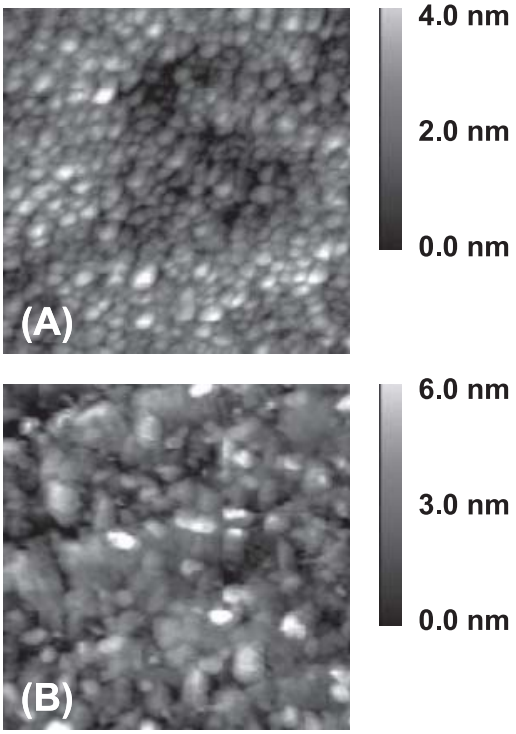


Fig. 5. STM images with grayscale encoding of gold substrates in 500 nm × 500 nm ranges obtained in air: (A) prepared from CD-Rs and (B) purchased from EMF. Imaging conditions: Pt/Ir tip, 0.2 V (sample positive), 0.2 nA. Reprinted with permission from ref. 4. Copyright 2001 American Chemical Society.



ration of water microdroplets (13), mixed SAMs of *n*-decanethiol and 11-mercaptoundecanol on both CD-R and EMF gold substrates were used as the model surfaces. The property of the SAMs, and in turn, the property of the surface, could be tuned with the relative concentrations of each component in the SAM. The evaporation of liquid droplets from a solid surface is a commonplace phenomenon and has been the subject of continuous investigation for quite some time. Picknett and Bexon (14) proposed that there are two modes of evaporation of liquid droplets on solid surfaces and they are: (1) the constant contact angle mode, where the area changes while the contact angle remains constant, and (2) the constant area mode, where the contact angle changes while the area remains constant. However, up to 30 years of experimental observations have yet to validate the theory.

Despite the difference in their initial contact angle, it was found in our study that for all the SAMs, regardless of their composition, the evaporation begins in the constant area mode and reaches an equilibrium contact angle that was approximately 10° less than the initial contact angle. At the point where this equilibrium contact angle is reached, the evaporation mode switches to the constant contact angle mode, whereby the area begins to shrink. It is believed that the change in the contact mode is due to the equilibration of the different interfacial forces acting on the droplet and not because of surface orientation reorganization. Although the SAMs have a different ratio of *n*-decanethiol to 11-mercaptoundecanol, nevertheless, they all exhibited the identical behaviour. In addition, no significant differences were found between the CD-R and commercial gold substrates.

CD-R gold substrates were also utilized in the study of surface reaction kinetics. For example, we studied the formation process of titanium(IV) dioxide on functionalized gold surfaces (15). Titanium dioxide (TiO_2) is a widely used photocatalyst and semiconducting material that has many potential applications. Due to their higher surface areas and enhanced activity, research into nanocrystalline TiO_2 particles and TiO_2 thin films has been very active during the past decade. It has been shown that hydrolysis and condensation of titanium(IV) alkoxides can yield thermally stable, nanocrystalline thin films (16). In our studies, the gold surface was first modified with dithiolreitol (DTT) and then it was immersed into a solution of titanium(IV) alkoxide to immobilize the titanium complex. The surface was then examined with contact angle measurements and it was found that as time passes, the water contact angle decreases. This change is believed to be caused by the hydrolysis of the titanium(IV) alkoxides on the surface to form more hydrophilic titanium dioxide. These experiments were completed on both CD-R and EMF gold substrates with equal success; this again demonstrates the versatility of the CD-R gold substrates.

Electrochemical analysis using CDtrodes

Once the protective layer is removed from the gold CD-Rs, the revealed reflective layer is suitable for use as an electrode for electrochemical analysis. Such electrodes were named CDtrodes and can be produced via a similar procedure as depicted in Fig. 2. This field of research has been pioneered by Angnes and his colleagues during the past 5 years (17–20). They have shown that the performance of

© 2005 NRC Canada

these CDtrodes are very reproducible and are comparable to commercial gold electrodes (Fig. 6). Thin-layer flow cells using CDtrodes were designed to analyse both organic (e.g., dipyrone (18)) and inorganic analytes (e.g., copper (19) and mercury (20)). Independently, De Strycker and co-workers (21) used CDtrode flow cells to analyze the cerium content during polymerization reactions. The detection limit of the CDtrode flow cells was shown to be similar to that of atomic absorption spectroscopy (19). With little to no loss in performance, the advantage of using CDtrodes over commercial electrodes is obvious as the low-cost electrodes allows for "single-use" cells that are convenient and, unlike commercial electrodes, do not require stringent cleaning before use.

A spectroelectrochemical cell that allows simultaneous detection using UV–vis spectroscopy and flow injection analysis was constructed by Daniel and Gutz (22) using two gold CDtrodes inside a cuvette (Fig. 7). The CDtrodes were glued with epoxy onto two acrylic plates for stability and served as both the working and auxiliary electrode in the cell. A 200 μm silicon rubber spacer was placed between the two electrodes to provide space for the light to pass through the cell (22). Using these cells, the electrochemical and UV–vis spectroscopic analyses can be conducted simultaneously.

Tailored electrode arrays have also been constructed from the reflective layer of a gold CD-R using heat transferred masks and wet etching techniques (23). This innovative method uses a laser printout as a positive mask for the electrode. After the desired electrode pattern is printed out onto wax paper, it is then transferred onto the gold surface via thermal pressing. The toner, but not the wax paper, sticks to the gold and prevents the aqueous etching solution from taking away the gold underneath. The minimum size of the electrodes was determined mainly by the resolution of the printer and the size of the toner particles. These custom-designed electrodes were then used to create microfluidic cells that showed very good reproducibility during amperometric analysis.

Aside from gold CD-Rs, similar CDtrodes have also been made using silver CD-Rs (24). These silver electrodes were used for quantification of chloride and cyanide in flow injection analysis and for lead analysis in voltammetry. The reproducibility of these silver CDtrodes was found to be quite good, and the detection limit was fairly low (i.e., 0.2, 50, and 200 μg/L for Pb^{2+}, Cl^-, and CN^-, respectively). This further demonstrates that the use of reflective layers from CD-Rs as an inexpensive source for noble metal electrodes is very attractive owing to its ideal performance in the electrochemical analysis.

Micro-fabrication with CD-Rs

Micro- and nano-fabrication has many potential applications in advanced technologies, such as miniaturized electronic and biomedical devices. The use of the unique CD-R substrates with their prepatterned grooves to create inorganic material microstructures is described in the following.

To explore the applications of CD-R substrates in microfabrication, we used controlled electrochemical deposition to create zirconia thin films on top of the mountain-and-valley structure of these substrates as shown in Fig. 8*a* (25). This research stems from the fact that zirconia thin films have potential applications as photocatalysts and oxygen sensors, and that electrochemical deposition is a common method of preparing oxide thin films (26, 27). We investigated the zir-

Fig. 6. Comparative cyclic voltammograms with (A) a commercial gold electrode (area, 3.15 mm^2) and (B) a CDtrode (area, 2.83 mm^2) in 0.2 mol/L H_2SO_4 (scan rate, 20 mV s^{-1}). Reprinted in part with permission from ref. 17. Copyright 2000 American Chemical Society.

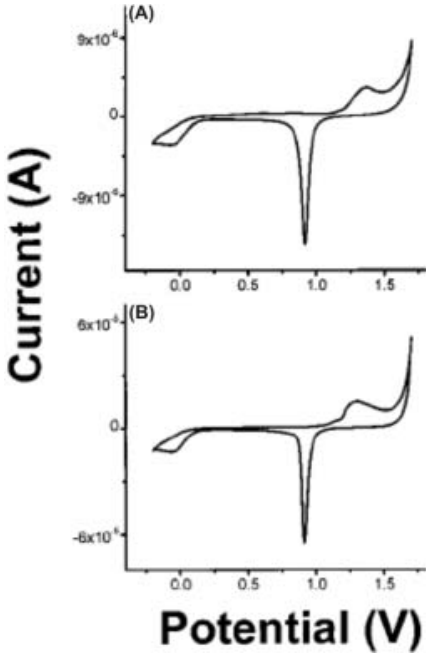
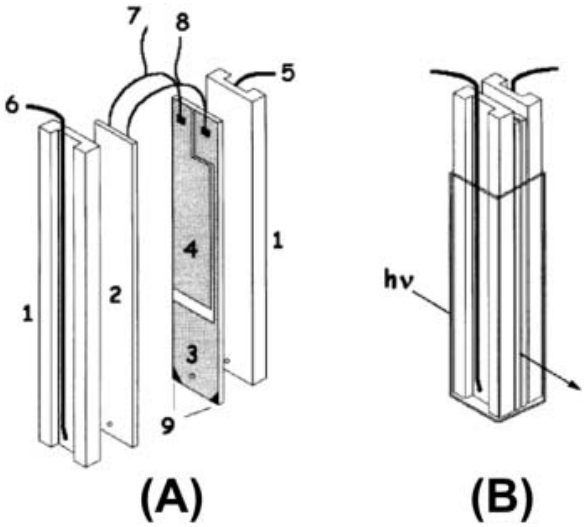
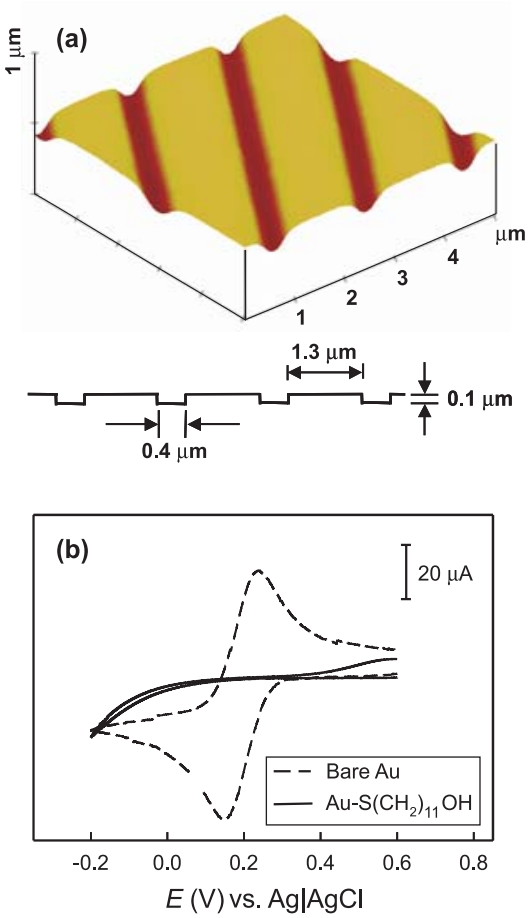


Fig. 7. Schematic illustration of the spectroelectrochemical cell in (A) exploded view and (B) assembled into the cuvette. Components: (1) acrylic plate; (2) Au-CDtrode polycarbonate back plane; (3) Au-CDtrode working electrode area; (4) auxiliary electrode area; (5) solution inlet; (6) salt bridge to (not shown) reference electrode (Ag/AgCl); (7) electric interconnection of the twin auxiliary electrodes; (8) electric interconnection of the twin working electrodes; (9) silicone rubber spacer, 200 mm thick. Adapted from ref. 22, copyright 2001 by John Wiley and Sons, Inc., used with permission.



© 2005 NRC Canada

Fig. 8. Microscopic morphology and electrochemical response of gold substrates prepared from CD-Rs. (*a*) AFM image of the pregrooved features of CD-R gold substrates and the schematic cross-sectional profile. (*b*) Cyclic voltammgrams for bare gold substrates from CD-Rs (dashed line) and Au-$S(CH_2)_{11}OH$ (solid line) in 1.0 mmol/L $K_3[Fe(CN)_6]$ and 0.1 mol/L aqueous KCl solution at a scan rate of 20 mV/s. Reprinted in part with permission from ref. 25. Copyright 2002 American Chemical Society.

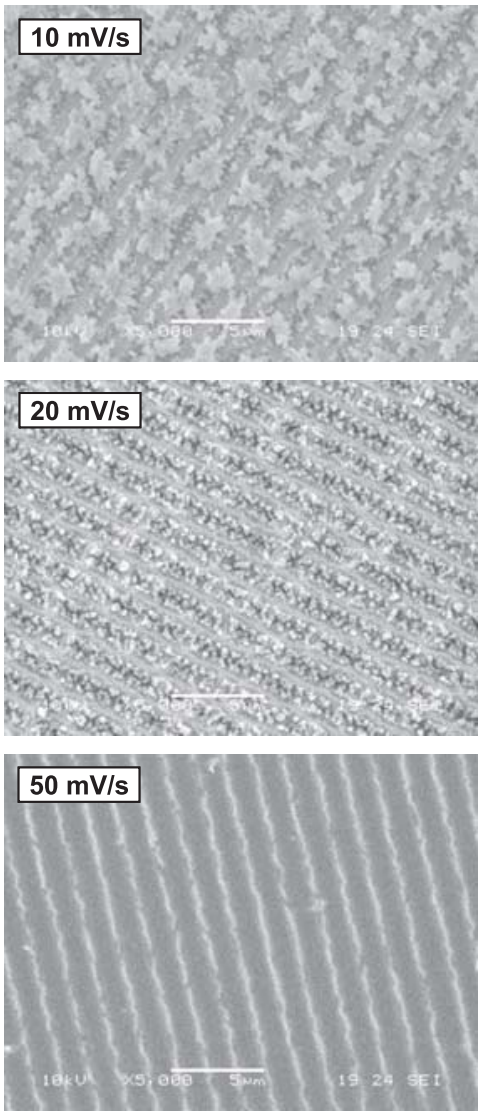


conia electrodeposition on bare gold CD-R surfaces and those modified with ω-terminated SAMs.

Cyclic voltammetry was used to deposit the zirconia thin film onto the gold substrate in an aqueous electrolyte of 5.0 mmol/L $ZrOCl_2 \cdot 8H_2O$ and 0.1 mol/L KCl. A zirconium thin film was formed on all of the surfaces after 10 cycles between –1.1 and +0.7 V (vs. Ag/AgCl). After each cycle, the cathodic current at the electrode would drop because of the buildup of zirconia on the surface, giving a greater resistance. It is believed that the $ZrOCl_2$ in the electrolyte coordinates to the surface and is hydrolyzed by the cathodically generated hydroxyl ions.

The SEM images show that the growth of zirconia thin films is dependent on the electrochemical conditions. Higher scan rates gave even more uniform surfaces that had pronounced growth on the mountains compared with the valleys (Fig. 9). For example, at a scan rate of 50 mV/s, the zirconia film was uniform on the mountains while the formation in the valleys was significantly less. The sample cycled at 20 mV/s, on the other hand, had zirconia particle formation

Fig. 9. SEM images of zirconium thin film formed on Au-$S(CH_2)_{11}OH$. Samples were prepared by cyclic voltammetry at different scan rates in 5.0 mmol/L $ZrOCl_2$ and 0.1 mol/L aqueous KCl solution. The accelerating voltage of the electron beam used was 10 kV and the magnification setting used for imaging was ×5000. Reprinted in part with permission from ref. 25. Copyright 2002 American Chemical Society.



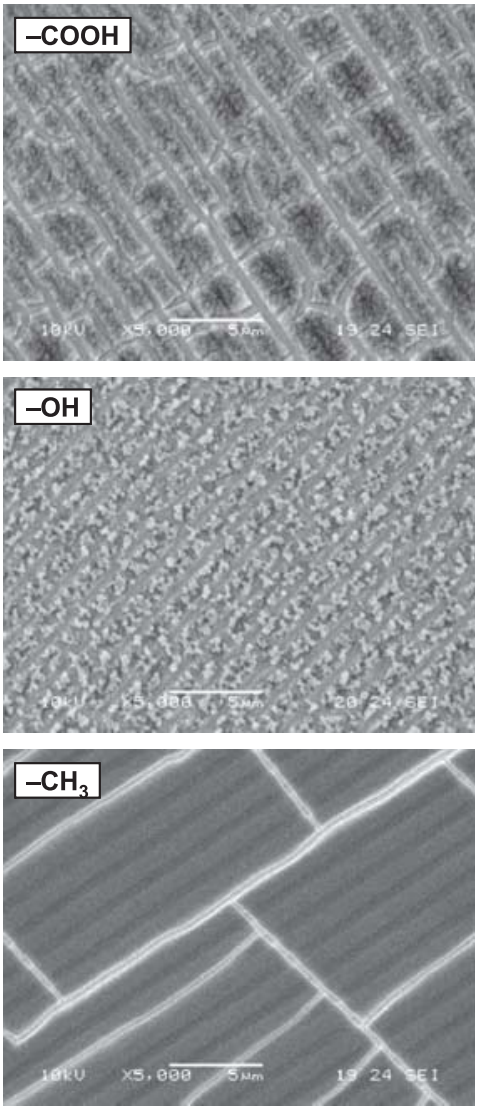
very much confined to the mountains In addition, the particles were only a few hundred nanometres in size and oriented along the mountains to give microscale strips of zirconia particles. At a lower scan rate (e.g., 10 mV/s), the film showed a larger, more amorphous growth with nucleation appearing on top of or starting from smaller particles without any confinement to the mountains It is believed that the two main factors contributing to these unique structures are: (1) the charge builds up on the corners and edges of the ridged substrate, and (2) the impeded diffusion of the electrolyte to the valleys; both of these factors favour the growth of zirconia on the mountains over the valleys. On flat gold substrates, however, the zirconia thin films had a characteristic racked-mud appearance that signifies an amorphous film (28).

© 2005 NRC Canada

The zirconia thin films formed on the CD-R substrate modified with differently functionalized SAMs (i.e., with different terminal groups, such as -COOH, -OH, and -CH_3) showed different types of growth (Fig. 10). The thin film formed on top of the Au-S$(CH_2)_{10}$COOH SAM showed some preferential growth along the mountains, but not as distinctive as the Au-S$(CH_2)_{11}$OH sample. The Au-S$(CH_2)_{11}CH_3$ sample, on the other hand, showed almost no preferences, but formed an almost uniform thin film that cracked along the valleys of the CD-R substrate as a result of the dehydration of the films. Because the interactions between the terminating groups and the $ZrOCl_2$ in solution are important to the formation of the films, we believe that the different SAMs contributed differently to the film formation. For the CH_3-terminated SAMs, the uniformly hydrophobic surface did not favour the selective nucleation and growth of the zirconia. In the case of the carboxyl-terminated SAM, the surface charge, which is sensitive to the local pH, will help the formation of the films. The preliminary X-ray diffraction studies showed all these zirconium thin films to be amorphous, despite the different substrates and scan rates. While the simple patterns on the CD-R substrate do not allow for fabrication of more complex structures, it is suitable for studies in selective crystal growth and template-directed deposition of inorganic thin films.

Aside from the metal reflective layer, the polycarbonate base of the CD-R has also been found useful in micro- and (or) nanostructural fabrications. For example, the microscale "track-and-trail" structure of the polycarbonate base was used as the pattern and mould to form microstructures on glass and plastic substrates (29). A soft-lithographic method for synthesis and transfer of materials to and from polymers (STOMP) was developed by Batteas and co-workers (30) to create nanostructures in gold film on mica by using "naked" PC substrates as stamps. The reflective layer and the dye layer were first removed via vigorous rinsing with ultrapure water and sonication with a 1:4 methanol–water mixture. The polycarbonate base was then pressed onto the gold and, while still pressed together, both the stamp and the gold were submerged into an etching solution. The resulting fine gold wires (ca. 200–500 nm wide) will be embedded in the stamp. If two PC stamps with embedded gold wires are compressed together, 3-D crosshatched structures can be created.

Fig. 10. SEM images of zirconium thin film formed on differently functionalized CD-R gold substrates (i.e., Au-S$(CH_2)_{11}CH_3$, Au-S$(CH_2)_{10}$COOH, and Au-S$(CH_2)_{11}$OH). All samples were prepared and imaged under experimental conditions otherwise identical to those in Fig. 9. Reprinted in part with permission from ref. 25. Copyright 2002 American Chemical Society.



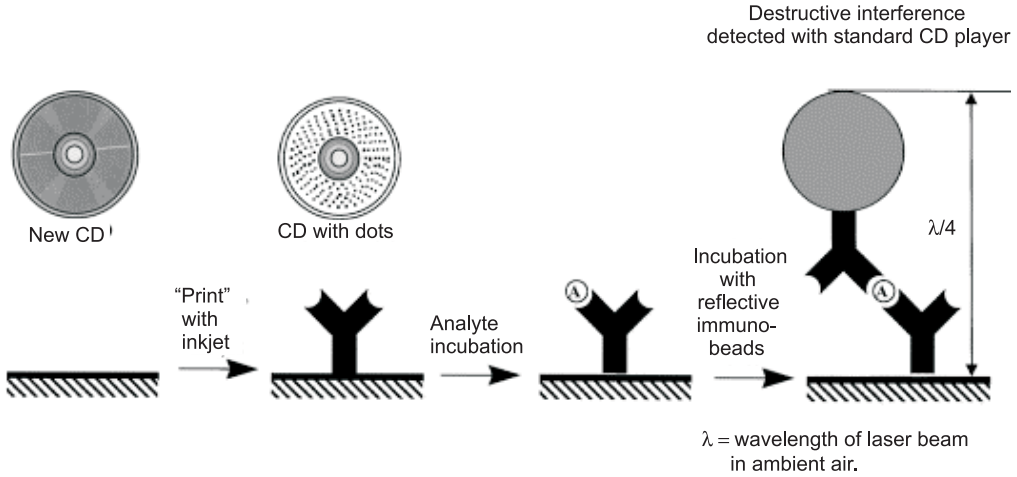
Biomedical diagnosis with CDs

Plastic disks having the same shape as conventional CDs have been found to be useful in the design of microfluidic platforms. Microfluidic devices based on these circular plastic disks have been pioneered and reviewed by Madou et al. (31). In one of their designs, multiple sets of interconnected fluid reservoirs on a polycarbonate disk were created by a computer numerically controlled (CNC) machine and were used to perform an enzyme-linked immunosorbent assay (ELISA) for rat IgG from a hybridoma cell culture (32). Each step of the assay was controlled by the rotation speed of the disk; the centrifugal and capillary forces were used to control the flow sequence of the solutions through the microchannels. Detection was carried out using a fluorescence microscope at the end of the sequence. The results of the microfluidic disks are similar to that of a microtiter plate within the same detection range; however, it only consumed one-tenth of the same reagents as a microtiter plate. This would lower the cost of each assay by reducing the amount of expensive antigens and antibodies needed. Although these developments are significant, it should be noted that these devices are not based on conventional CDs and are thus not covered in detail in this review.

The detection of a DNA hybridization event is done mostly through the use of fluorescence labels that are either directly incorporated into the target and (or) probe DNA strand or via a second labelling step in most assays; however, fluorescence detection on DNA microarrays created on regular CDs may not be ideal because of the autofluorescense of the polycarbonate substrate. The search for alter-

© 2005 NRC Canada

Fig. 11. Concept of reflective immunobead-based sandwich assay on CD. Light reflected from the reflective surface of the disc would be detected. However, light reflected from the reflective beads would cause destructive interference and would not be detected. The difference in height between the top of the bead and the reflective disc layer would be equal to one-quarter of the wavelength of the laser beam used (λ/4). This system would allow the use of standard CD ROM drives for analysis of the disc without any modifications. Reprinted from Anal. Chim. Acta, Vol. 411. H. Kido, A. Maquieira, and B.D. Hammock. Disc-based immunoassay microarrays pp. 1–11. Copyright (2000), with permission from Elsevier.

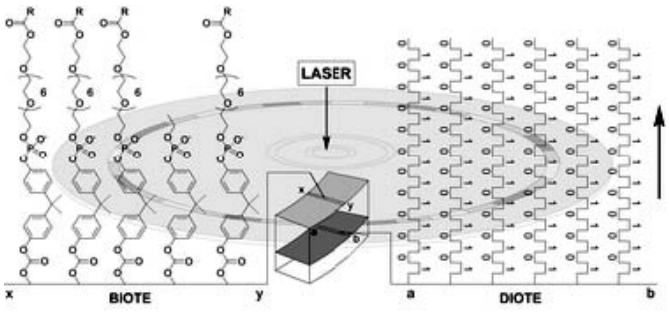


native methods of detection on CD-based microarrays has produced several other options as described in the following.

An innovative concept of detecting biological molecules on CDs by disrupting the laser beam in a conventional CD reader was proposed by Hammock and co-workers (33). As shown in Fig. 11, arrays of protein or DNA probes can be deposited onto the polycarbonate of the CD by hand, using a pipette, or it can be "printed" onto the CD using an inkjet printer using modified ink. The target proteins would be modified with a reflective substance, such as a gold or silver particles and when the two bind, the reflective particle would be immobilized to the surface. Ideally, the distance between the top of the reflective particle and the CD reflective surface would be λ/4, where λ is the wavelength of the reading laser. This would cause the same destructive interference that occurs when the reading laser hits a pit in the CD-ROM. This method of detection would allow the use of conventional CD readers to conduct the analysis of the microarrays. However, up to date, no experimental work based on this idea followed from that laboratory.

In the work of La Clair and Burkart (34), a similar method of CD-reading laser disruption is employed in the detection of large protein molecules. Numerical data were first written onto specific regions on a CD-R (DIOTE); these regions were then later modified with phosphodiesterated ligands (BIOTE) (Fig. 12). These biological ligands were chosen for their activity with streptavidin and concanavalin A, and were deposited onto the polycarbonate layer via inkjet printing Once the BIOTE–DIOTE construct was complete, the CD-R was read on a standard CD reader on a computer and the digital information was obtained and analyzed. This data should contain a certain amount of errors caused by the introduction of the ligands in the path of the optical laser and these errors will form the baseline for subsequent error analysis. After this, the regions containing the ligands, including nonbinding ligands to serve as blanks, were incubated with solutions of streptavidin in PBS buffer or concanavalin A in

Fig. 12. Pictorial representation of the BIOTE layer containing biological ligands and the DIOTE layers containing digital binary data on the sectors of a CD-R; details explained in the text. Reprinted from ref. 34. Reproduced by permission of The Royal Society of Chemistry.

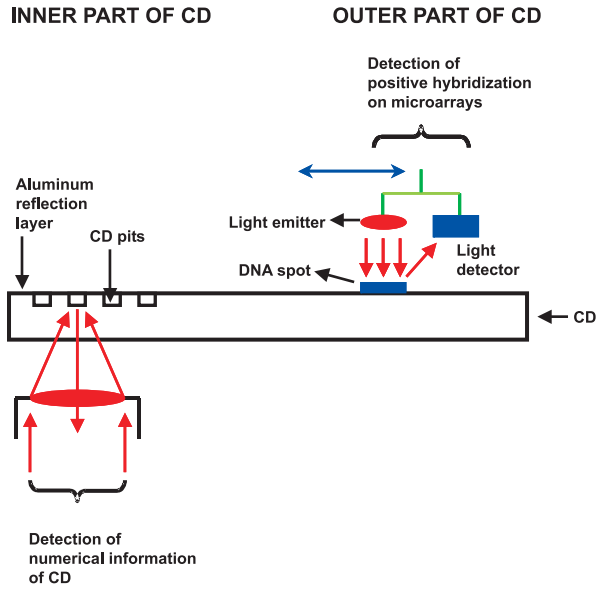


acetate buffer and then washed in deionized water. The data from the CD-R was read again to obtain the higher error rate that is generated by the even larger molecules (streptavidin and concanavalin A) now bound to the surface. By comparing the second set of error rates to the blank, it was possible to determine the binding efficiency of the protein molecules to the respective ligands. It was also possible to determine the concentration of streptavidin by the level of errors that were generated.

Besides the method of disrupting the CD-reading laser, there are also other protocols of detecting DNA hybridization and protein interactions. Remacle and co-workers (35) designed a colorimetric detection protocol to recognize the hybridization of DNA. Their DNA microarray platform contains both numerical and genomic information on a single CD (Bio-CD) (35). As shown in Fig. 13, there are two sections in these specially manufactured Bio-CDs: (1) the inner section of the disk is similar to a conventional CD and contains numerical data used to identify the DNA probes and to control the Bio-CD reader, and (2) the outer section is a

© 2005 NRC Canada

Fig. 13. Schematic representation of a reading system for colorimetric CD detection composed of two laser-based devices. The first one is a classic laser CD reader reading the numeric information registered in the inner phase of the CD, and the second one is a photodiode head detecting the laser light diffraction in the presence of positive hybridization onto the microarray of the CD. Adapted from ref. 35, copyright 2002 by Eaton Publishing Co., used with permission.

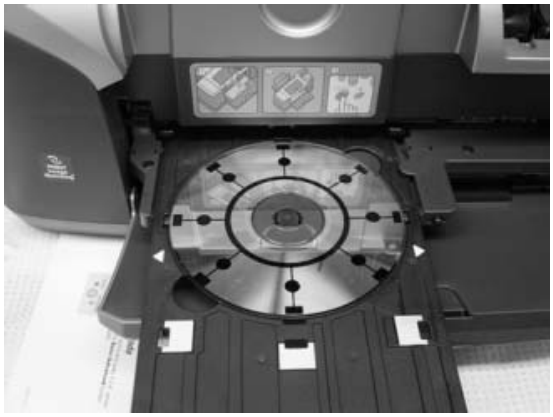


polycarbonate substrate that contains the genomic information in several sets of DNA probes. It is similar to the Hammock concept (33) in that a reflective entity is attached to the target to allow for laser detection, but dissimilar in that a separate diode is used to collect the information on the microarray. The target DNA (the *fem A* gene of various *Staphylococci*) was first modified with biotin so that after hybridization with the DNA probe on the polycarbonate substrate the biotin will stand up from the polycarbonate surface (36). The microarray is then incubated with a solution of streptavidin – colloidal gold conjugate. After washing with a Silver Blue solution that contained silver nitrate and hydroquinone (37), a silver layer will be plated on the surface of the gold particles. When the Bio-CD is read with the doubled-sided Bio-CD reader, the silver-coated gold particles reflect the laser into a photodiode detector and show up as bright spots. A computer program will then analyze and quantify the data collected by the photodiode. It should be noted that a specially designed CD reader/writer is required to utilize their Bio-CDs.

We find the idea of directly using conventional CD/CD-R technology for biosensing applications most appealing, and thus it is our current research goal. We have been attempting to immobilize DNA directly onto the CD polycarbonate surface via either chemical or photochemical routes. Inspired by the Hammock concept (33), we have been working on the data error comparison method to monitor DNA hybridization on CDs.

We are also working on electrochemical methods of detecting DNA hybridization for a potentially more sensitive and cost effective gene analysis (38, 39). We have created electrode microarrays on a gold CD-R using soft lithography

Fig. 14. Demonstration of printing electrode-patterns on a gold CD-R with an Epson PhotoStylus R300 printer.



and inkjet technology. Soft lithographic techniques, such as microcontact printing, do not require expensive laser equipment such as those of conventional photolithography. It uses self-assembly and replica moulding to fabricate micro- and nanostructures; a comprehensive review has been written on this subject by Xia and Whitesides (40). In place of the microcontact printing used by Kumar and Whitesides (41) to stamp patterns onto their gold substrates, we use inkjet printing technology to print masks of hydrophobic ink with our electrode patterns onto the gold CD-R substrates (Fig. 14). After forming the electrode array on the polycarbonate substrate by etching away the gold, we can modify the surface of each electrode with different DNA probes. In principle, by employing a large array of electrodes, simultaneous detection and quantification of many different strands of DNA is feasible.

Conclusions

Rather than being discarded or used as coasters for hot drinks, old CD-Rs are very useful in modern research. CD-R gold substrates can be used to prepare high-quality, self-assembled monolayers (SAMs) after removing the protective polymer films with concentrated nitric acid. These substrates are comparable to other commercial gold substrates in terms of the quality of the monolayers formed, and are well suited for surface wetting, electrochemical, and spectroscopic studies. CD-R polycarbonate bases are also ideal micropatterned substrates for the fabrication of material microstructures and miniaturized devices. The potential applications of micropatterned DNA probes on CDs used in combination with conventional CD technology for biomedical and gene analysis are very appealing.

Acknowledgements

H.Z.Y. wishes to thank Eli Lilly Canada, Inc. and the CSC Division of Analytical Chemistry for sponsoring the Fred Beamish Award; in particular, it was created to recognize early career achievement in the field of analytical chemistry. Over the past 4 years, at both Acadia and Simon Fraser, H.Z.Y. has had the privilege of working with a number of extremely talented undergraduate and graduate students, and post-doctoral fellows. Besides the coauthors of this review

© 2005 NRC Canada

paper, the contributions of Aaron W. Rowe, Tina T.T. Yu, Damien M. Waugh, Dr. Zhen Wang, Ming Zhou, and Dr. Jeffrey T. Banks (The University of New Brunswick) to this project deserve special recognition. We are grateful to the Natural Sciences and Engineering Research Council of Canada (NSERC), Simon Fraser University, and the World Gold Council (UK) for financial support of the research described in this review.

References

1. (*a*) D. Birkett. J. Chem. Ed. **79**, 1081 (2002); (*b*) H.-Z. Yu. Chem. Commun. 2633 (2004).
2. K.J. Kuhn. Audio compact disk — An introduction [online]. Available from http://www.ee.washington.edu/conselec/CE/kuhn/cdaudio/95x6.htm [accessed on 24 August 2004]. 2003.
3. K.C. Pohlman. The compact disc handbook. 2nd ed. A-R Editions, London. 1992.
4. H.-Z. Yu. Anal. Chem. **73**, 4743 (2001).
5. A. Ulman. An introduction to ultrathin organic films: From Langmuir-Blodgett to self-assembly. Academic Press, Boston. 1991.
6. H.O. Finklea and D.D. Hanshew. J. Am. Chem. Soc. **112**, 3173 (1992).
7. D.E. Khoshtariya, J. Wei, H. Liu, H. Yue, and D.H. Waldeck. J. Am. Chem. Soc. **125**, 7704 (2003).
8. C. Templeton, W.P. Wuelfing, and R.W. Murray. Acc. Chem. Res. **33**, 27 (2000).
9. T.G. Drummond, M.G. Hill, and J.K. Barton. Nat. Biotechnol. **21**, 1192 (2003).
10. W. Vercoutere and M. Akeson. Curr. Opin. Chem. Biol. **6**, 816, (2002).
11. M. Fojta. Electroanalysis, **14**, 1149 (2002).
12. H.-Z. Yu, Y.Q. Wang, J.Z. Cheng, J.W. Zhao, S.M. Cai, H. Inokuchi, A. Fujishima, and Z.F. Liu. Langmuir, **12**, 2843 (1996).
13. H.-Z. Yu, D.M. Soolaman, A.W. Rowe, and J.T. Banks. Chem. Phys. Chem. **5**, 1035 (2004).
14. R.G. Picknett and R. Bexon. J. Colloid Interface Sci. **61**, 336 (1977).
15. J.T. Banks, T.T. Yu, and H.-Z. Yu. J. Phys. Chem. B, **106**, 3538 (2002).
16. H. Sakai, H. Kawahara, M. Shimazaki, and M. Abe. Langmuir, **14**, 2008 (1998).
17. L. Angnes, E.M. Richter, M.A. Augelli, and G.H. Kume. Anal. Chem. **72**, 5503 (2000).
18. R.A.A. Muñoz, R.C. Matos, and L. Angnes. J. Pharm. Sci. **90**, 1972 (2001).
19. E.M. Richter, M.A. Augelli, S. Magarotto, and L. Angnes. Electroanalysis, **13**, 760 (2001).
20. E.M. Richter, M.A. Augelli, G.H. Kume, R.N. Mioshi, and L. Angnes. Fresenius' J. Anal. Chem. **366**, 444 (2000).
21. P. Westbroek, J. De Strycker, P. Dubruel, E. Temmerman, and E.H. Schacht. Anal. Chem. **74**, 915 (2002).
22. D. Daniel and I.G.R. Gutz. Electroanalysis, **13**, 681 (2001).
23. D. Daniel and I.G.R. Gutz. Electrochem. Commun. **5**, 782 (2003).
24. E.M. Richter, D.P. de Jesus, C.A. Neves, C.L. do Lago, and L. Angnes. Quim. Nova, **26**, 839 (2003).
25. H.-Z. Yu, A.W. Rowe, and D.M. Waugh. Anal. Chem. **74**, 5742 (2002).
26. R. Shacham, D. Mandler, and D. Avnir. Chem. Eur. J. **10**, 1936 (2004).
27. G.H.A. Therese and P.V. Kamath. Chem. Mater. **12**, 1195 (2000).
28. R. Chaim, I. Silberman, and L. Gal-Or. J. Electrochem. Soc. **138**, 1942 (1991).
29. P. Hazarika, D. Chowdhury, and A. Chattopadhyay. Lab-on-a-Chip **3**, 128 (2003).
30. J.M. Helt, C.M. Drain, and J.D. Batteas. J. Am. Chem. Soc. **126**, 628 (2004).
31. M.J. Madou, L.J. Lee, S. Daunert, S. Lai, and C.H. Shih. Biomed. Microdevices, **3**, 245 (2001).
32. S. Lai, S. Wang, J. Luo, L.J. Lee, S.T. Yang, and M.J. Madou. Anal. Chem. **76**, 1832 (2004).
33. H. Kido, A. Maquieira, and B.D. Hammock. Anal. Chim. Acta, **411**, 1 (2000).
34. J.J. La Clair and M.D. Burkart. Org. Biomol. Chem. **1**, 3244 (2003).
35. I. Alexandre, Y. Houbion, J. Collet, S. Hamels, J. Demarteau, J.L. Gala, and J. Remacle. BioTechniques, **33**, 435 (2002).
36. S. Hamels, J.L. Gala, S. Dufour, P. Vannuffle, N. Zammatteo, and J. Remacle. BioTechniques, **31**, 1364 (2001).
37. I. Alexandre, S. Hamels, S. Dufour, J. Collet, N. Zammatteo, F. De Longueville, J.L. Gala, and J. Remacle. Anal. Biochem. **295**, 1 (2001).
38. H.-Z. Yu, C.Y. Luo, C.G. Sankar, and D. Sen. Anal. Chem. **75**, 3902 (2003).
39. L. Su, C.G. Sankar, D. Sen, and H.-Z. Yu. Anal. Chem. **76**, 5953 (2004).
40. Y. Xia and G.M. Whitesides. Annu. Rev. Mater. Sci. **28**, 153 (1998).
41. N.A. Kumar and G. Whitesides. Appl. Phys. Lett. **63**, 2002 (1993).

© 2005 NRC Canada

Synthesis and evaluation of 7-hydroxyindan-1-one-derived chiral auxiliaries

Arun A. Narine and Peter D. Wilson

Abstract: A series of novel chiral acetals were prepared from 7-hydroxyindan-1-one and a variety of substituted chiral nonracemic C_2-symmetric 1,2-ethanediols (R = Me, Ph, CH_2OMe, CH_2OBn, CH_2O(1-Np), and *i*-Pr). These acetals were evaluated as chiral auxiliaries for use in asymmetric synthesis. A high degree of stereochemical induction was observed in the diethylaluminum chloride-promoted Diels–Alder reaction of an acrylate derivative (R = *i*-Pr) with cyclopentadiene (91:9 dr). This demonstrated that these acetals could serve as effective chiral directors in asymmetric substrate-directed reactions.

Key words: 7-hydroxyindan-1-one, chiral nonracemic C_2-symmetric 1,2-diols, acetals, chiral auxiliaries, Diels–Alder reaction.

Résumé : On a préparé une série de nouveaux acétals chiraux à partir de la 7-hydroxyindan-1-one et une variété d'éthane-1,2-diols substitués, de symétrie C_2, non racémiques et chiraux (R = Me, Ph, CH_2OMe, CH_2OBn, CH_2O(1-Np) et *i*-Pr). On a évalué ces acétals comme auxiliaires chiraux dans des synthèses asymétriques. On a observé un degré élevé d'induction stéréochimique dans la réaction de Diels–Alder, catalysée par le chlorure de diéthylaluminium, d'un acrylate (R = *i*-Pr) avec le cyclopentadiène (91 : 9 dr). Ce résultat démontre que ces acétals peuvent servir de directeurs chiraux efficaces dans des réactions asymétriques dirigées par le substrat.

Mots clés : 7-hydroxyindan-1-one, 1,2-diols de symétrie C_2 non racémiques et chiraux, acétals, auxiliaires chiraux, réaction de Diels–Alder.

[Traduit par la Rédaction]

Introduction

The development and evaluation of new chiral auxiliaries, ligands, and catalysts for use in asymmetric synthesis is a central focus of modern synthetic organic chemistry. To date, a variety of chiral acetals have been designed and employed as chiral directors in a broad range of asymmetric reactions (1, 2). We have designed a series of novel cyclic acetals (**1**) as a general class of conformationally constrained chiral auxiliaries, ligands, and catalysts for use in asymmetric synthesis (Fig. 1). These acetals should be readily accessible from the parent ketones (**2**) (such as functionalized indan-1-one (n = 1) and tetral-1-one (n = 2) derivatives as well as their heterocyclic analogues) and a series of chiral nonracemic C_2-symmetric 1,2-diols (**3**) via experimentally simple acid-catalyzed condensation reactions.

The atom or substituent X is the attachment or binding site of the chiral auxiliary, ligand, or catalyst. The substituent Y can be varied to alter the electronic properties of this system and could also serve as an attachment site to a polymeric support. Thus, the structure of these chiral directors could be optimized using automated synthesis or used to prepare polymer-supported reagents. Similarly, the substituents of the cyclic acetal moiety could be varied to alter the electronic and steric environment of the chiral auxiliary, ligand, or catalyst. The use of chiral nonracemic C_2-symmetric 1,2-diols **3** to prepare these acetals ensures that only a single diastereoisomer is produced in these condensation reactions (3). Of note, the two planes of the acetal moiety are positioned in an approximately orthogonal manner that results in one of the diastereotopic faces of these molecules being effectively blocked by one of the substituents of the cyclic acetal.

In this paper, the synthesis of a series of 7-hydroxyindan-1-one-derived chiral auxiliaries (**4**) is described (Fig. 2) (4). These structurally rigid chiral auxiliaries were synthesized in a modular and convergent manner from readily available 7-hydroxyindan-1-one (**5**) and a series of chiral nonracemic C_2-symmetric 1,2-diols (**3**). In addition, these chiral auxiliaries were evaluated by undertaking a study of the Lewis acid-promoted Diels–Alder reactions of the corresponding acrylate derivatives **6** (5).

Results and discussion

7-Hydroxyindan-1-one (**5**) was prepared on a multi-gram scale by a known three-step, two-pot, procedure (Scheme 1) (6, 7). This involved conversion of 3-chloropropanoic acid to

Received 12 November 2004. Published on the NRC Research Press Web site at http://canjchem.nrc.ca on 27 April 2005.

A.A. Narine and P.D. Wilson.[1] Department of Chemistry, Simon Fraser University, 8888 University Drive, Burnaby, BC V5A 1S6, Canada.

[1]Corresponding author (e-mail: pwilson@sfu.ca).

 doi: 10.1139/V05-052 © 2005 NRC Canada

Scheme 1. Synthesis of 7-hydroxyindan-1-one-derived chiral auxiliaries **4a** (R = Me) and **4b** (R = Ph). Reagents and conditions: (*a*) 3-chloropropanoic acid, PCl_3, ~115 °C, 3 h; then phenol, toluene, reflux, 3 h; $AlCl_3$, 90–180 °C, ~6 h (ref. 6); (*b*) AcCl, pyridine, CH_2Cl_2, 0 °C to room temperature, 19 h, 89%; (*c*) 1,2-diols **3a** (R = Me) and **3b** (R = Ph), *p*-TsOH, benzene, reflux, 16–40 h, 90% **8a** (R = Me), 83% **8b** (R = Ph); (*d*) LiOH, THF–H_2O (3:1), room temperature, 16–40 h, 84% **4a** (R = Me), 90% **4b** (R = Ph). The compound used in this study was the enantiomer of that indicated in the reaction scheme (*).

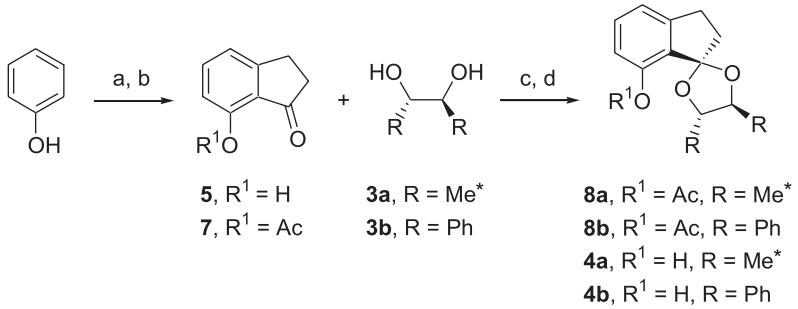


Fig. 1. Novel chiral acetals **1** as auxiliaries, ligands, and catalysts for asymmetric synthesis.

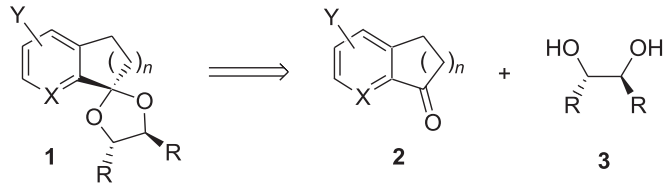
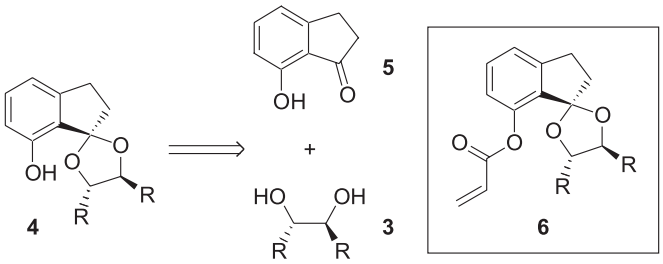


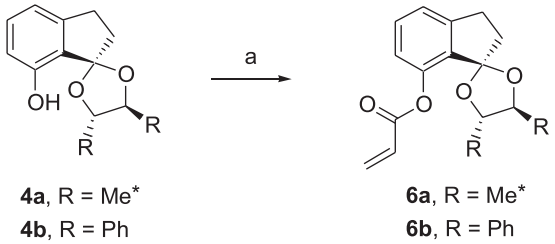
Fig. 2. 7-Hydroxyindan-1-one-derived chiral auxiliaries **4**.



the corresponding acid chloride, on heating with phosphorous trichloride, which in turn was reacted with phenol to afford phenyl 3-chloropropanoate. This ester was purified by distillation and then reacted with aluminum trichloride. Following the addition of aqueous hydrochloric acid, 7-hydroxyindan-1-one (**5**) was isolated directly from the reaction mixture by steam distillation and purified by recrystallization.

It was found that 7-hydroxyindan-1-one (**5**) could not be condensed directly with a series of chiral nonracemic 1,2-diols **3** or with 1,2-ethanediol (8). Various reaction conditions and acid catalysts were screened, without success, to effect this key acetal formation reaction. We consider that this finding is due to the acid-catalyzed enolization of the ketone moiety. This results in a decrease in the reactivity of the carbonyl centre of 7-hydroxyindan-1-one (**5**) towards nucleophilic attack by the diol. To solve this problem, the phenol moiety of 7-hydroxyindan-1-one (**5**) was protected as an acetate using acetyl chloride and pyridine as reagents (8). Condensation of the acetate **7** with commercially available (2*R*,3*R*)-2,3-butanediol **3a** (R = Me) and (1*S*,2*S*)-1,2-diphenyl-1,2-ethanediol **3b** (stilbenediol, R = Ph), using *para*-toluenesulfonic acid (*p*-TsOH) as a catalyst, afforded the acetals **8a** (R = Me) and **8b** (R = Ph) in good yield (9). These acetals were then converted efficiently to the target chiral auxiliaries **4a** (R = Me) and **4b** (R = Ph) on hydrolysis of the acetate moieties with lithium hydroxide.[2]

Scheme 2. Synthesis of Diels–Alder reaction substrates, acrylates **6a** (R = Me) and **6b** (R = Ph). Reagents and conditions: (*a*) acryloyl chloride, Et_3N, benzene, 0 °C to room temperature, 2–2.5 h, 88% **6a** (R = Me), 86% **6b** (R = Ph). The compound used in this study was the enantiomer of that indicated in the reaction scheme (*).



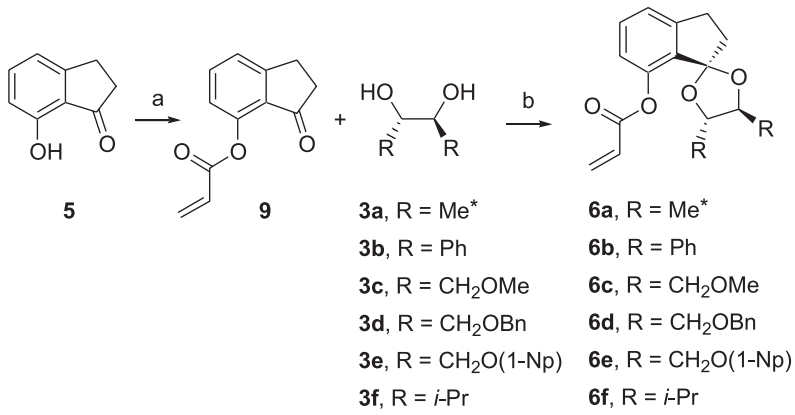
The 7-hydroxyindan-1-one-derived chiral auxiliaries **4a** (R = Me) and **4b** (R = Ph) were then reacted with acryloyl chloride and triethylamine (Scheme 2). This afforded the required Diels–Alder reaction substrates **6a** (R = Me) and **6b** (R = Ph) in 88% and 86% yields, respectively.

To prepare a more extensive series of Diels–Alder reaction substrates and to determine the effect of the chiral acetal substituents in subsequent substrate-directed reactions, a more direct route was developed (Scheme 3). In this instance, 7-hydroxyindan-1-one (**5**) was converted to the ketoester **9** on reaction with acryloyl chloride and triethylamine in good yield. Condensation of the ketoester **9** with (2*R*,3*R*)-

[2] The chiral auxiliaries **4a** (R = Me) and **4b** (R = Ph) are stable compounds and can be stored in a capped vial at 4 °C for several months without any sign of decomposition.

© 2005 NRC Canada

Scheme 3. Direct synthesis of Diels–Alder reaction substrates, acrylates **6a**–**6f** (R = Me, Ph, CH_2OMe, CH_2OBn, CH_2O(1-Np), and *i*-Pr). Reagents and conditions: (*a*) acryloyl chloride, Et_3N, CH_2Cl_2, 0 °C to room temperature, 12 h, 93%; (*b*) 1,2-diols **3a**–**3f** (R = Me, Ph, CH_2OMe, CH_2OBn, CH_2O(1-Np), and *i*-Pr), *p*-TsOH or PPTS, benzene, reflux, 4 h–4 days, 93% **6a** (R = Me), 93% **6b** (R = Ph), 82% **6c** (R = CH_2OMe), 80% **6d** (R = CH_2OBn), 56% **6e** (R = CH_2O(1-Np)), 80% **6f** (R = *i*-Pr). The compound used in this study was the enantiomer of that indicated in the reaction scheme (*).



2,3-butanediol **3a** (R = Me) and (1*S*,2*S*)-1,2-diphenyl-1,2-ethanediol **3b** (R = Ph) afforded the acrylates **6a** (R = Me) and **6b** (R = Ph), which were prepared earlier by the less direct route, again in good yield.[3,4] In addition, the ketoester **9** was condensed with (2*S*,3*S*)-1,4-dimethoxy-2,3-butanediol **3c** (R = CH_2OMe) (10), (2*S*,3*S*)-1,4-dibenzyloxy-2,3-butanediol **3d** (R = CH_2OBn) (11), (2*S*,3*S*)-1,4-bis(1-naphthoxymethyl)-2,3-butanediol **3e** (R = CH_2O(1-Np)) (12), and (1*S*,2*S*)-1,2-diisopropyl-1,2-ethanediol **3f** (R = *i*-Pr) (13). These chiral nonracemic 1,2-diols were all prepared from (2*R*,3*R*)-(+)-diethyltartrate based on literature procedures. The condensation reactions afforded the acrylates **6c**–**6f** (R = CH_2OMe, CH_2OBn, CH_2O(1-Np), and *i*-Pr) in 56%–93% yield.

The Diels–Alder reactions of all of the acrylates **6** with cyclopentadiene were performed in the presence of either diethylaluminum chloride or titanium tetrachloride in dichloromethane or toluene (Table 1). For the (2*R*,3*R*)-acrylate **6a** (R = Me), the diethylaluminum chloride-promoted cycloaddition reaction afforded the desired products **10a** and **11a** (R = Me) in good yield and was moderately diastereoselective (63:37 dr in dichloromethane and 64:36 dr in toluene). Thus, the outcome of this reaction was found to be independent of the reaction solvent employed (Table 1, entries 1 and 2). Repeating these reactions using titanium tetrachloride as the Lewis acid resulted in cleavage of the acetal moiety. The Diels–Alder reaction of the (1*S*,2*S*)-acrylate **6b** (R = Ph) with cyclopentadiene, using diethylaluminum chloride as the Lewis acid in dichloromethane, afforded the desired products **10b** and **11b** (R = Ph) in good yield and again was moderately diastereoselective (74:26 dr, Table 1, entry 3). However, a significant improvement in the diastereoselectivity of the reaction was observed when this reaction was performed in toluene (83:17 dr, Table 1, entry 4). When titanium tetrachloride (0.75 equiv.) was used to effect this cycloaddition reaction in dichloromethane, the adducts **10b** and **11b** (R = Ph) were isolated in this instance (26:74 dr, Table 1, entry 5).[5] Of note, it is of interest that the stereochemical outcome of the reaction was reversed with this dibasic Lewis acid. However, no reaction was observed when the reaction was repeated in toluene (14).[6] For the (2*S*,3*S*)-acrylate **6e** (R = CH_2O(1-Np)), the diethylaluminum chloride-promoted cycloaddition reaction afforded the desired products **10e** and **11e** (R = CH_2O(1-Np)) in good yield, but was only moderately diastereoselective (68:32 dr, Table 1, entry 6).[7] However, the diethylaluminum chloride-promoted Diels–Alder reaction of the (1*S*,2*S*)-acrylate **6f** (R = *i*-Pr) in toluene finally proved to be highly stereoselective (91:9 dr, Table 1, entry 7).

The absolute stereochemistry of the major diastereoisomers of the reaction products from all of the Diels–Alder reactions was determined unequivocally. This was achieved

[3] In the case of the formation of acrylate **6b** (R = Ph) from ketoester **9** and diol **3b** (R = Ph), a mixture of *p*-TsOH and PPTS was employed as the catalyst for this condensation reaction.

[4] Of note, the acrylates **6a** (R = Me) and **6b** (R = Ph) are highly crystalline compounds, as compared to the acetates **8a** (R = Me) and **8b** (R = Ph), which facilitates their purification. They can also be hydrolyzed with lithium hydroxide at room temperature to prepare the 7-hydroxyindan-1-one-derived chiral auxiliaries **4a** (R = Me) and **4b** (R = Ph) in 97% and 73% yield (18 and 40 h, respectively). The acrylate **6b** (R = Ph) can be converted more efficiently to the auxiliary **4b** (R = Ph) using lithium aluminum hydride in 82% yield.

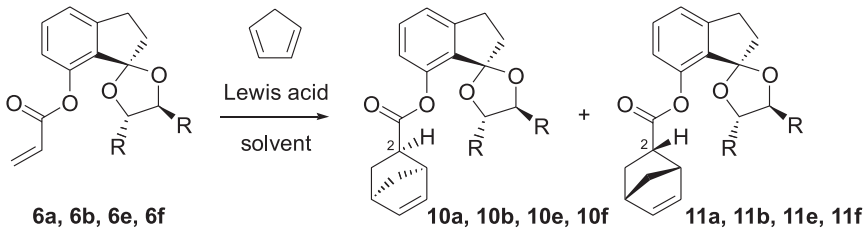
[5] The use of titanium tetrachloride (1.5 equiv.) in this reaction resulted in the decomposition of the starting material.

[6] A variety of other Lewis acids were screened to effect the Diels–Alder reaction of acrylate **6b** (R = Ph) and cyclopentadiene. Zinc chloride, tin tetrachloride, bis(cyclopentadienyl)titanium dichloride ($(C_5H_5)_2TiCl_2$), boron trifluoride diethyl etherate, and titanium tetraisopropoxide afforded the Diels–Alder adducts **10b** and **11b** (R = Ph) in ~20%, 50%, 65%, 80%, and 90% combined yields, respectively. However, these reactions afforded ~1:1 mixtures of adducts **10b** and **11b** (R = Ph). The use of boron trichloride (1.5 equiv.) resulted in the decomposition of the starting material.

[7] The Lewis acid-promoted Diels–Alder reactions of acrylates **6c** (R = CH_2OMe) and **6d** (R = CH_2OBn) were not diastereoselective (54:46 and 55:45 dr, respectively).

© 2005 NRC Canada

Table 1. Illustrative Lewis acid-promoted Diels–Alder reactions of chiral acrylates **6a**, **6b**, **6e**, and **6f** (R = Me, Ph, CH_2O(1-Np), and *i*-Pr) with cyclopentadiene.



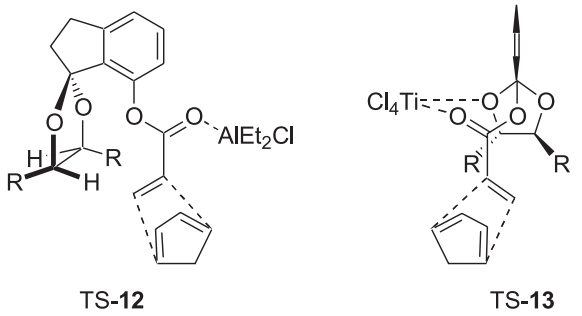
Entry	Acrylate	R	Acetal conf.	Lewis acid[a]	Solvent	Yield[b]	dr[c] (**10**:**11**)	Conf.[d]
1	**6a**	Me	*R*,*R*	Et_2AlCl	CH_2Cl_2	72	63:37[e]	*S*
2	**6a**	Me	*R*,*R*	Et_2AlCl	Toluene	72	64:36[e]	*S*
3	**6b**	Ph	*S*,*S*	Et_2AlCl	CH_2Cl_2	83	74:26	*R*
4	**6b**	Ph	*S*,*S*	Et_2AlCl	Toluene	89	83:17	*R*
5	**6b**	Ph	*S*,*S*	$TiCl_4$[f]	CH_2Cl_2	76	26:74	*S*
6	**6e**	CH_2O(1-Np)	*S*,*S*	Et_2AlCl	Toluene	76	68:32	*R*
7	**6f**	*i*-Pr	*S*,*S*	Et_2AlCl	Toluene	71	91:9	*R*

[a]The reactions were performed at –78 °C with excess cyclopentadiene and 1.5 equiv. of the Lewis acid for 10–60 min unless stated otherwise.
[b]Combined yields of the Diels–Alder adducts (**10** and **11**) after purification by flash chromatography.
[c]Determined by ^{1}H NMR spectroscopy (400 or 600 MHz) of the crude reaction mixtures. In all cases, the endo:exo stereoselectivity was greater than 98:2.
[d]Refers to the stereochemical configuration at C-2 of the major norbornene Diels–Alder adduct.
[e]The compound used in this study was the enantiomer of that indicated in the reaction scheme.
[f]0.75 equiv. of the Lewis acid was employed and the reaction mixture was allowed to warm to room temperature overnight.

by the facile and efficient removal of the chiral auxiliary and comparison of the specific rotation of the resultant norbornene Diels–Alder adducts to literature values (see Supplementary material)[8] (15). These reactions were either performed by hydrolysis with lithium hydroxide, transesterification with sodium methoxide, or reduction with lithium aluminum hydride. Of note, the chiral auxiliaries **4a**, **4b**, **4e**, and **4f** were recovered in good yield (78%, 87%, 60%, and 79%, respectively, on hydrolysis with lithium hydroxide) for use in subsequent asymmetric transformations.

The stereochemical outcome of the diethylaluminum chloride-promoted Diels–Alder reaction of the acrylate derivates **6** can be rationalized in terms of the transition state shown below (Fig. 3, TS-**12**) (16). Here, cyclopentadiene attacks from the top face of the complex. This is due to the steric influence of one of the substituents of the chiral acetal moiety that projects directly over the bottom face of the complex. In the case of the titanium tetrachloride-promoted Diels–Alder reaction, we suggest that the acrylate moiety is rotated and coordinated to the more accessible acetal oxygen (TS-**13**). Attack of cyclopentadiene, again from the top face of the complex, would result in the observed reversal in the stereochemical outcome of the reaction.

Fig. 3. Transition states for the Lewis acid-promoted Diels–Alder reactions (TS-**12** and TS-**13**).



Conclusions

A series of acrylate derivatives **6a**–**6f** (R = Me, Ph, CH_2OMe, CH_2OBn, CH_2O(1-Np), and *i*-Pr) of the 7-hydroxyindan-1-one-derived chiral auxiliaries **4** were prepared. A high degree of stereochemical induction was observed in a diethylaluminum chloride-promoted Diels–Alder reaction of the acrylate derivative **6f** (R = *i*-Pr) with cyclopentadiene (91:9 dr). This demonstrated that these designed chiral acetals could serve as effective chiral directors in asymmetric processes. Current studies involve the synthesis of additional derivatives of these chiral auxiliaries for use in other asymmetric substrate-directed reactions. Studies are also focused on the elaboration of the 7-hydroxyindan-1-one-derived acetals **4**, by regioselective functionalization at C-6, to prepare a variety of chiral ligands for use in catalytic asymmetric synthesis. In addition, the preparation and evaluation of related chiral pyridine, *N*,*N*-dialkylaminopyridine,

[8]Detailed experimental procedures and complete product characterization data for all of the additional compounds synthesized as well as ^{1}H and ^{13}C NMR spectra for compounds **4a**, **4b**, **6b**, and **6f**. In addition, the experimental procedures for the stereochemical proof of the major Diels–Alder adducts **10b** and **10f** are provided. Supplementary data for this article are available on the Web site or may be purchased from the Depository of Unpublished Data, Document Delivery, CISTI, National Research Council Canada, Ottawa, ON K1A 0S2, Canada. DUD 3652. For more information on obtaining material refer to http://cisti-icist.nrc-cnrc.gc.ca/irm/unpub_e.shtml.

© 2005 NRC Canada

and bipyridine catalysts and ligands is being actively pursued. Moreover, we have recently completed an efficient and modular synthesis of a series of chiral nonracemic *P*,*N*-ligands based on the design concept described in this paper (17). These ligands were evaluated in palladium(II)-catalyzed asymmetric allylic substitution reactions. A *P*,*N*-ligand derived from (1*S*,2*S*)-1,2-diphenyl-1,2-ethanediol **3b** (R = Ph) was found to be highly stereoselective (up to 90% ee).

Experimental section

For general experimental details refer to the Supplementary material.[8]

7-Acetoxyindan-1-one (7) (18)

To a stirred solution of 7-hydroxyindan-1-one (**5**) (101 mg, 0.682 mmol) in dichloromethane (3 mL) at 0 °C were added pyridine (164 μL, 2.03 mmol) and acetyl chloride (96 μL, 1.4 mmol). The reaction mixture was stirred at 0 °C for 1 h and then at room temperature for 18 h. The resultant mixture was poured into a saturated aqueous solution of ammonium chloride (25 mL) and was extracted with dichloromethane (3 × 10 mL). The combined organic extracts were then dried over anhydrous magnesium sulfate, filtered and concentrated to afford a yellow oil. Purification by flash chromatography using hexanes–ether (2:1) as the eluant afforded the title compound **7** (115 mg, 89%) as a white crystalline solid; mp 75–77 °C (hexanes–ether), lit. value (18) mp 78 to 79 °C (ether). IR (ef) cm^{-1}: 1770, 1710, 1610, 1472, 1368, 1245, 1187, 1013. ^1H NMR (400 MHz, $CDCl_3$) δ: 2.40 (3H, s, C*H*$_3$), 2.67 (2H, m, ArC*H*$_2$), 3.14 (2H, m, C*H*$_2$CO), 6.97 (1H, ddd, *J* = 7.9, 1.5, 0.9 Hz, Ar*H*), 7.34 (1H, ddd, *J* = 7.6, 1.5, 0.9 Hz, Ar*H*), 7.58 (1H, m, Ar*H*). ^{13}C NMR (101 MHz, $CDCl_3$) δ: 20.9, 25.6, 36.7, 120.6, 124.5, 128.7, 135.9, 147.7, 157.0, 169.3, 203.8. MS (C.I.) *m*/*z*: 191 (M + H), 149. Anal. calcd. for $C_{11}H_{10}O_3$: C 69.46, H 5.30; found: C 69.30, H 5.35.

7-Acetoxyindan-1-one (*S*,*S*)-stilbenediol acetal (8b) — Representative procedure for the preparation of acetal 8a

A stirred solution of the acetate **7** (196 mg, 1.03 mmol), diol **3b** (258 mg, 1.20 mmol), and *para*-toluenesulfonic acid monohydrate (20 mg, 0.10 mmol) in benzene (2 mL) was heated at reflux for 40 h with azeotropic removal of water. After allowing the reaction mixture to cool to room temperature, potassium carbonate (0.1 g) was added and the mixture was stirred for 10 min. Direct purification of the reaction mixture by flash chromatography using hexanes–ether (4:1) as the eluant afforded the title compound **8b** (332 mg, 83%) as a colourless gum. $[\alpha]_D^{20}$ –158 (*c* 1.70, chloroform). IR (ef) cm^{-1}: 1746, 1616, 1590, 1473, 1403, 1307, 1225, 1153, 1114, 1084. ^1H NMR (400 MHz, C_6D_6) δ: 1.82 (3H, s, C*H*$_3$), 2.28–2.44 (2H, m, ArCH$_2$C*H*$_2$), 2.63 (1H, ddd, *J* = 15.9, 8.5, 2.1 Hz, ArC*H*H), 2.72–2.83 (1H, m, ArCH*H*), 4.80 (1H, d, *J* = 8.5 Hz, PhC*H*), 5.17 (1H, d, *J* = 8.5 Hz, PhC*H*), 6.82 (1H, dd, *J* = 5.5, 2.7 Hz, Ar*H*), 7.09–7.12 (3H, m, Ar*H*), 7.13–7.19 (5H, m, Ar*H*), 7.34 (2H, m, Ar*H*), 7.40 (2H, m, Ar*H*). ^{13}C NMR (101 MHz, C_6D_6) δ: 20.9, 28.6, 39.2, 85.9, 87.0, 118.4, 121.9, 122.8, 127.0, 127.2, 128.6, 128.7, 128.8, 130.9, 133.3, 136.8, 137.9, 147.0, 148.1, 168.1. MS (MALDI-TOF) *m*/*z*: 409 (M + Na). Anal. calcd. for $C_{25}H_{22}O_4$: C 70.06, H 6.61; found: C 70.30, H 6.52.

7-Hydroxyindan-1-one (*S*,*S*)-stilbenediol acetal (4b) — Representative procedure for the preparation of chiral auxiliary 4a

To a solution of the acetate **8b** (91 mg, 0.24 mmol) in tetrahydrofuran (6 mL) and water (2 mL) was added lithium hydroxide monohydrate (50 mg, 1.2 mmol). The resultant opaque solution was stirred at room temperature for 40 h and then diluted with a saturated aqueous solution of ammonium chloride (25 mL) and extracted with dichloromethane (3 × 10 mL). The combined organic extracts were dried over anhydrous magnesium sulfate, filtered and concentrated to afford a pale orange oil. Purification by flash chromatography using hexanes–ether (4:1) as the eluant afforded the title compound **4b** (74 mg, 90%) as a white solid; mp 50–52 °C (hexanes–ether). $[\alpha]_D^{20}$ –100 (*c* 3.16, chloroform). ^1H NMR (400 MHz, C_6D_6) δ: 2.25 (1H, ddd, *J* = 12.8, 7.6, 3.7 Hz, ArCH$_2$C*H*H), 2.30–2.39 (1H, m, ArCH$_2$CH*H*), 2.67 (1H, ddd, *J* = 15.9, 8.2, 4.0 Hz, ArC*H*H), 2.71–2.80 (1H, m, ArCH*H*), 4.85 (1H, d, *J* = 8.2 Hz, C*H*Ph), 5.02 (1H, d, *J* = 8.5 Hz, CHPh), 6.58 (1H, s, O*H*), 6.68 (1H, d, *J* = 7.6 Hz, Ar*H*), 6.82 (1H, d, *J* = 8.2 Hz, Ar*H*), 7.01–7.19 (9H, m, Ar*H*), 7.26–7.30 (2H, m, Ar*H*). ^{13}C NMR (101 MHz, C_6D_6) δ: 28.9, 38.9, 85.9, 86.1, 114.7, 117.3, 119.6, 125.9, 126.7, 127.2, 128.3, 128.7, 128.8, 128.9, 132.1, 136.5, 138.3, 146.0, 154.7. IR (ef) cm^{-1}: 3446, 1619, 1598, 1469, 1317, 1166, 1123, 1047, 936, 745. MS (CI) *m*/*z*: 345 (M + H), 238. Anal. calcd. for $C_{23}H_{20}O_3$: C 80.21, H 5.85; found: C 80.02, H 5.97.

7-Acryloyloxyindan-1-one (*S*,*S*)-stilbenediol acetal (6b) from the chiral auxiliary 4b — Representative procedure for the preparation of Diels–Alder substrate 6a from the chiral auxiliary 4a

To a stirred solution of the chiral auxiliary phenol **4b** (80 mg, 0.23 mmol), in benzene (3 mL) at 0 °C was added triethylamine (39 μL, 0.28 mmol) and acryloyl chloride (23 μL, 0.28 mmol). After 2 h, the reaction mixture was allowed to warm to room temperature over 30 min. The resultant mixture was diluted with a saturated aqueous solution of ammonium chloride (25 mL) and extracted with dichloromethane (2 × 15 mL). The combined organic extracts were washed with brine (10 mL), dried over anhydrous magnesium sulfate, filtered and concentrated to afford a colourless gum. Purification by flash chromatography using hexanes–ether (5:1) as the eluant afforded the title compound **6b** (79 mg, 86%) as a white solid. An analytical sample of the product, as large colourless crystals, was prepared by recrystallization from hexanes–ether by slow evaporation; mp 82 to 83 °C (hexanes–ether). $[\alpha]_D^{20}$ –197 (*c* 1.98, chloroform). IR (ef) cm^{-1}: 1746, 1473, 1403, 1316, 1224, 1146, 1048, 751. ^1H NMR (400 MHz, C_6D_6) δ: 2.29–2.45 (2H, m, ArCH$_2$C*H*$_2$), 2.57 (1H, ddd, *J* = 15.6, 8.2, 1.8 Hz, ArC*H*H), 2.78 (1H, m, ArCH*H*), 4.80 (1H, d, *J* = 8.5 Hz, C*H*Ph), 5.14 (1H, d, *J* = 8.5 Hz, C*H*Ph), 5.18 (1H, dd, *J* = 10.4, 0.9 Hz, CH=C*H*H), 6.11 (1H, dd, *J* = 17.4, 10.4 Hz, C*H*=CH$_2$), 6.34 (1H, dd, *J* = 17.4, 1.1 Hz, CH=CH*H*), 6.82 (1H, d, *J* = 7.0 Hz, Ar*H*), 7.01–7.20 (10H, m, Ar*H*), 7.28 (2H, d, *J* =

© 2005 NRC Canada

6.4 Hz, Ar*H*), 7.35 (2H, d, *J* = 6.4 Hz, Ar*H*). ^{13}C NMR (101 MHz, C_6D_6) δ: 28.6, 39.2, 86.0, 86.8, 118.3, 121.9, 123.0, 127.1, 127.2, 128.5, 128.6, 128.7, 132.2, 133.7, 136.7, 137.9, 147.1, 147.9, 163.9. MS (CI) *m*/*z*: 399 (M + H), 292, 203. Anal. calcd. for $C_{26}H_{22}O_4$: C 78.37, H 5.57; found: C 78.51, H 5.55.

7-Acryloyloxyindan-1-one (9)

To a stirred solution of 7-hydroxyindan-1-one (**5**) (1.00 g, 6.75 mmol) and triethylamine (1.0 mL, 7.2 mmol) in dichloromethane (15 mL) at 0 °C was added acryloyl chloride (0.60 mL, 7.4 mmol) over 5 min. The reaction mixture was then allowed to warm slowly to room temperature over 12 h. The resultant mixture was diluted with ether (50 mL) and washed with saturated aqueous solutions of ammonium chloride (2 × 10 mL) and sodium bicarbonate (2 × 10 mL), brine (10 mL), and water (10 mL). The organic layer was then dried over anhydrous magnesium sulfate, filtered and concentrated to afford a white solid. Purification by flash chromatography using hexanes–ether (3:2) as the eluant afforded the title compound **9** (1.27 g, 93%) as a white crystalline solid. An analytical sample of the product, as large colourless crystals, was prepared by recrystallization from hexanes–ether by slow evaporation; mp 83 to 84 °C (hexanes–ether). IR (ef) cm^{-1}: 1737, 1699, 1607, 1150. ^{1}H NMR (400 MHz, $CDCl_3$) δ: 2.67 (2H, m, ArCH_2), 3.14 (2H, m, CH_2C=O), 6.06 (1H, dd, *J* = 10.4, 1.2 Hz, CH=C*H*H), 6.40 (1H, dd, *J* = 17.4, 10.4 Hz, C*H*=CH$_2$), 6.65 (1H, dd, *J* = 17.1, 1.2 Hz, CH=CH*H*), 7.03 (1H, d, *J* = 7.9 Hz, Ar*H*), 7.35 (1H, d, *J* = 7.6, Ar*H*), 7.59 (1H, m, Ar*H*). ^{13}C NMR (101 MHz, $CDCl_3$) δ: 25.7, 36.8, 120.7, 124.5, 127.6, 128.8, 133.1, 135.9, 147.6, 157.0, 164.2, 203.6. MS (CI) *m*/*z*: 203 (M + H), 149. Anal. calcd. for $C_{12}H_{10}O_3$: C 71.28, H 4.98; found: C 71.26, H 4.95.

7-Acryloyloxyindan-1-one (3*S*,4*S*)-2,5-dimethyl-3,4-hexanediol acetal (6f) from the ketoester 9 — Representative procedure for the preparation of the Diels–Alder substrates 6a–6e from the ketoester 9

A stirred solution of the ketoester **9** (132 mg, 0.653 mmol), diol **3f** (16) (109 mg, 0.745 mmol), and *para*-toluenesulfonic acid monohydrate (7 mg, 0.04 mmol) in benzene (6 mL) was heated at reflux for 20 h with azeotropic removal of water. The reaction mixture was then allowed to cool to room temperature and potassium carbonate (0.2 g) was added. After 30 min, the resultant mixture was filtered and concentrated to afford a light brown oil (231 mg). Purification by flash chromatography using hexanes–ether (8:1) as the eluant afforded the title compound **6f** (173 mg, 80%) as a white crystalline solid; mp 83 to 84 °C (hexanes–ether). $[\alpha]_D^{20}$ –76 (*c* 0.78, tetrahydrofuran). IR (ef) cm^{-1}: 1750, 1617, 1591, 1471, 1403, 1316, 1254, 1232, 1225, 1153, 1048, 985, 799, 755. ^{1}H NMR (400 MHz, C_6D_6) δ: 0.94 (3H, d, *J* = 7.0 Hz, CH_3CH), 0.95 (3H, d, *J* = 6.7 Hz, CH_3CH), 1.01 (3H, d, *J* = 6.7 Hz, CH_3CH), 1.04 (3H, d, *J* = 6.7 Hz, CH_3CH), 1.60–1.69 (1H, m, C*H*CH$_3$), 1.76–1.86 (1H, m, C*H*CH$_3$), 2.08 (2H, dd, *J* = 5.5, 5.2 Hz, ArCH$_2$CH_2), 2.47 (1H, dt, *J* = 15.9, 5.5 Hz, ArC*H*H), 2.66–2.76 (1H, m, ArCH*H*), 3.56 (1H, dd, *J* = 8.2, 4.9 Hz, C*H*O), 3.79 (1H, dd, *J* = 8.2, 4.6 Hz, C*H*O), 5.36 (1H, dd, *J* = 10.4, 1.5 Hz, CH=C*H*H), 6.21 (1H, dd, *J* = 17.4, 10.1 Hz, C*H*=CHH), 6.46 (1H, dd, *J* = 17.4, 1.5 Hz, CH=CH*H*), 6.74 (1H, d, *J* = 7.6 Hz, Ar*H*), 6.91 (1H, d, *J* = 8.2 Hz, Ar*H*), 6.97–7.02 (1H, m, Ar*H*). ^{13}C NMR (101 MHz, C_6D_6) δ: 17.4, 17.7, 20.1, 20.4, 28.6, 30.5, 31.0, 39.3, 83.5, 84.4, 116.7, 121.8, 122.8, 128.8, 130.6, 131.5, 134.1, 146.8, 148.0, 163.8. MS (CI) *m*/*z:* 331 (M + H), 203, 183. Anal. calcd. for $C_{20}H_{26}O_4$: C 72.70, H 7.93; found: C 72.41, H 7.99.

7-((1*R*,2*R*,4*R*)-Bicyclo[2.2.1]hept-5-ene-2-carboxyl)indan-1-one (3*S*,4*S*)-2,5-dimethyl-3,4,-hexanediol acetal (10f) using diethylaluminum chloride as the Lewis acid and toluene as the solvent — Representative procedure for the Lewis acid-promoted Diels–Alder reactions

To a stirred solution of the acrylate **6f** (85 mg, 0.26 mmol) in toluene (7 mL) at –78 °C was added diethylaluminum chloride (1.0 mol/L in hexanes, 0.39 mL, 0.39 mmol) over 1 min. Cyclopentadiene (1.0 mL, 12 mmol) was added to the resultant solution. After 1 h, the reaction mixture was poured into a saturated aqueous solution of sodium bicarbonate (25 mL). The resultant mixture was extracted with dichloromethane (2 × 25 mL) and the combined organic extracts were washed with brine (10 mL), dried over anhydrous magnesium sulfate, filtered and concentrated to afford a pale yellow gum (112 mg). Purification by flash chromatography using hexanes–ether (10:1) as the eluant afforded an inseparable mixture of the title compound **10f** and a trace amount of the diastereoisomer **11f** (73 mg, 71%) as a colourless oil, which solidified on standing. As determined by analysis of the ^{1}H NMR (600 MHz) spectrum of the crude reaction product, the diastereoisomeric ratio of the products was 91:9 (**10f**:**11f**) and the endo:exo ratio of the major product **10f** was >98:2; mp 81 to 82 °C (hexanes–ether). $[\alpha]_D^{20}$ –39 (*c* 0.86, tetrahydrofuran). IR (ef) cm^{-1}: 1763, 1616, 1591, 1472, 1316, 1234, 1176, 1164, 1147, 1130, 1106, 1041, 755, 711. ^{1}H NMR (600 MHz, C_6D_6) (major diastereoisomer **10f**) δ: 0.97 (3H, d, *J* = 7.0 Hz, CH_3CH), 1.00 (3H, d, *J* = 7.0 Hz, CH_3CH), 1.03 (3H, d, *J* = 6.7 Hz, CH_3CH), 1.08 (1H, m, C*H*H-bridge), 1.12 (3H, d, *J* = 6.7 Hz, CH_3CH), 1.40 (1H, dq, *J* = 8.2, 1.8 Hz, CH*H*-bridge), 1.62–1.72 (1H, m, C*H*CH$_3$), 1.73–1.83 (2H, m, CH$_2$C*H*C=O), 1.83–1.95 (1H, m, C*H*CH$_3$), 1.99–2.12 (2H, m, ArCH$_2$CH_2), 2.46 (1H, ddd, *J* = 15.9, 7.9, 2.4 Hz, ArC*H*H), 2.67 (1H, broad s, C*H*-bridgehead), 2.69–2.79 (1H, m, ArCH*H*), 3.23–3.29 (1H, m, C*H*C=O), 3.41 (1H, broad s, C*H*-bridgehead), 3.60 (1H, dd, *J* = 7.9, 4.6 Hz, C*H*O), 3.90 (1H, dd, *J* = 7.9, 5.2 Hz, C*H*O), 6.13 (1H, dd, *J* = 5.6, 2.9 Hz, C*H*=CH), 6.17 (1H, dd, *J* = 5.7, 2.7 Hz, C*H*=CH), 6.75 (1H, dd, *J* = 7.5, 0.7 Hz, Ar*H*), 6.88 (1H, d, *J* = 7.9 Hz, Ar*H*), 7.02 (1H, m, Ar*H*). ^{13}C NMR (101 MHz, C_6D_6) (major diastereoisomer **10f**) δ: 17.5, 17.7, 20.2, 20.4, 28.6, 29.6, 30.7, 31.3, 39.3, 43.2, 43.9, 46.5, 50.1, 83.4, 84.6, 116.9, 122.0, 122.5, 130.4, 132.3, 133.8, 138.2, 146.7, 148.4, 172.1. MS (CI) *m*/*z*: 397 (M + H), 269, 249, 183, 121. Anal. calcd. for $C_{26}H_{22}O_4$: C 75.73, H 8.13; found: C 75.42, H 8.23.

Acknowledgments

We are grateful to the Natural Sciences and Engineering Research Council of Canada (NSERC) and Simon Fraser University (SFU) for financial support. We also wish to ac-

© 2005 NRC Canada

knowledge the Canadian Foundation for Innovation (CFI) and the British Columbia Knowledge Development Fund (BCKDF) for support of our research program. A.A.N. thanks SFU for graduate research fellowships. Mr. J.M. Belli is thanked for preliminary investigations. Mr. M.P.A. Lyle is thanked for preparing the chiral nonracemic diol **3f** (R = *i*-Pr) and for discussion.

References

1. For the use of chiral acetals as auxiliaries in substrate-directed reactions see, for example: (*a*) R. Alibés, F. Busquè, P. de March, M. Figueredo, J. Font, M.E. Gambino, and B.A. Keay. Tetrahedron: Asymmetry, **12**, 1747 (2001); (*b*) J. Cossy and S. BouzBouz. Tetrahedron Lett. **37**, 5091 (1996); (*c*) A. Alexakis and P. Mangeney. Tetrahedron: Asymmetry, **1**, 477 (1990).
2. For reviews on the applications of two prominent classes of chiral acetals (Seebach's TADDOLs and Ley's 1,2-diacetals) in asymmetric synthesis, see: (*a*) D. Seebach, A.K. Beck, and A. Heckel. Angew. Chem. Int. Ed. **40**, 92 (2001); (*b*) S.V. Ley, D.K. Baeschlin, D.J. Dixon, A.C. Foster, S.J. Ince, H.W.M. Priepke, and D.J. Reynolds Chem. Rev. **101**, 53 (2001).
3. For a review on C_2-symmetry concepts in synthesis, see: J.K. Whitesell. Chem. Rev. **89**, 1581 (1989).
4. For reviews on chiral auxiliaries see, for example: (*a*) K. Rück-Braun and H. Kunz. Chiral auxiliaries in cycloadditions. Wiley-VCH, Weinheim. 1999; (*b*) J. Seyden-Penne. Chiral auxiliaries and ligands in asymmetric synthesis. John Wiley and Sons, New York. 1995.
5. For reviews on the Diels–Alder reaction, see: (*a*) E.J. Corey. Angew. Chem. Int. Ed. **41**, 1650 (2002), and refs. therein; (*b*) F. Fringuelli and A. Taticchi. The Diels–Alder reaction: Selected practical methods. John Wiley and Sons, Chichester, UK. 2002.
6. (*a*) F. Mayer and L. van Zutphen. Chem. Ber. **57**, 200 (1924); (*b*) S. Wagatsuma, S. Higuchi, H. Ito, T. Nakano, Y. Naoi, K. Sakai, T. Matsui, Y. Takahashi, A. Nishi, and S. Sano. Org. Prep. Proc. Int. **5**, 65 (1973).
7. For a recent synthesis of 7-haloindan-1-ones, see: P. Nguyen, E. Corpuz, T.M. Heidelbaugh, K. Chow, and M.E. Garst. J. Org. Chem. **68**, 10 195 (2003).
8. Wipf and co-workers have also reported that a derivative of an 8-hydroxytetral-1-one could not be condensed with 1,2-ethanediol. However, on protection of the phenol moiety as an acetate the desired reaction proceeded smoothly on using pyridinium *para*-toluenesulfonate (PPTS) as an acid catalyst, see: P. Wipf, J.K. Jung, S. Rodríguez, and J.S. Lazo. Tetrahedron, **57**, 283 (2001). The lack of reactivity of the carbonyl functional group of 7-hydroxyindan-1-one (**5**) could also be explained if it behaves as a vinylogous acid. Of note, the carbonyl stretch for 7-hydroxyindan-1-one (**5**) is at 1676 cm^{-1} and the carbonyl stretch for the acetate **7** is at 1710 cm^{-1}. This indicates that there is intramolecular hydrogen bonding in 7-hydroxyindan-1-one (**5**), but no significant enolization. Similarly, the hydroxyl stretch for 7-hydroxyindan-1-one (**5**), at 3364 cm^{-1}, is sharp.
9. (1*S*,2*S*)-1,2-Diphenyl-1,2-ethanediol **3b** (R = Ph) was also prepared from (*E*)-stilbene on a multi-gram scale according to a literature procedure, see: K.B. Sharpless, W. Amberg, Y. Bennani, G. Crispino, J. Hartung, K. Jeong, H. Kwong, K. Morikawa, Z. Wang, D. Xu, and X. Zhang. J. Org. Chem. **57**, 2768 (1992).
10. D. Seebach, H.O. Kalinowski, B. Bastani, G. Crass, H. Daum, H. Dörr, N.P. DuPreez, V. Ehrig, W. Langer, C. Nüssler, H.-A. Oei, and M. Schmidt. Helv. Chim. Acta, **60**, 301 (1977).
11. E.A. Mash, K.A. Nelson, S. van Deusen, and S.B. Hemperly. Org. Synth. Coll. Vol. **VIII**, 155 (1993).
12. J. Yamashita, M. Minagawa, A. Sonobe, S. Ohashi, M. Kawamura, K. Shimizu, and H. Hashimoto. Chem. Lett. 1409 (1982).
13. The noncommercially available chiral nonracemic diol **3f** was prepared by Mr. M.P.A. Lyle from L-diethyl tartrate according to literature procedures, see: (*a*) X. Wang, S.D. Erickson, T. Iimori, and W.C. Still. J. Am. Chem. Soc. **114**, 4128 (1992); (*b*) D.S. Matteson, E.C. Beedle, and A.A. Kandil. J. Org. Chem. **52**, 5034 (1987).
14. In preliminary studies using the acrylate **6b** (R = Ph) and diethylaluminum chloride as the Lewis acid (~1 mol/L, hexanes, Aldrich) in which a small amount of white precipitate had been deposited in the reagent bottle, diastereoselectivities of 92:8 and combined yields of 85%–90% were consistently achieved when these reactions were performed in toluene. In the case of the acrylate **6e** (R = CH_2O(1-Np)), the diastereoselectivity of the reaction was 87:13 (74% yield). In efforts to duplicate these initial findings, experiments were performed using freshly prepared diethylaluminum chloride solutions (1.5 equiv.) in which aliquots of water (0.25–1.5 equiv.) were added. However, in these instances only slight increases in the diastereoselectivities of the reactions were observed (up to 86:14) for acrylate **6b** (R = Ph). Also, there was no significant change in the reaction yields. Methylalumoxane afforded adducts **10b** and **11b** (R = Ph) as a 68:32 mixture of diastereoisomers in 90% yield, see: M. Akakura and H. Yamamoto. Synlett, 277 (1997). The use of trimethylaluminum as a less active Lewis acid with acrylate **6b** (R = Ph) afforded the expected product in only ~25% yield (58:42 dr, endo:exo = 82:18). A more active Lewis acid, methylaluminum dichloride, also afforded the expected products (82:18 dr). In this case, it was not possible to determine the yield of the reaction because of co-eluting decomposition products. No reaction of this acrylate with cyclopentadiene was observed when aluminum trichloride was employed as the Lewis acid.
15. (*a*) W. Oppolzer, M.J. Kelly, and G. Bernardinelli. Tetrahedron Lett. **25**, 5889 (1984); (*b*) J.A. Berson, J.S. Walia, A. Remanick, S. Suzuki, P. Reynolds-Warnhoff, and D. Willner. J. Am. Chem. Soc. **83**, 3986 (1961); (*c*) J.A. Berson and D.A. Ben-Efraim. J. Am. Chem. Soc. **81**, 4083 (1959).
16. It would be expected that the acrylate moiety reacts in a s-trans conformation with cyclopentadiene on complexation with the Lewis acid, see: R.J. Loncharich, T.R. Schwartz, and K.N. Houk. J. Am. Chem. Soc **109**, 14 (1987). For additional discussion see: ref. 5*b*.
17. M.P.A. Lyle, A.A. Narine, and P.D. Wilson. J. Org. Chem. **69**, 5060 (2004).
18. R. Criegee and K. Klonk. Liebigs Ann. Chem. **564**, 1 (1949).

© 2005 NRC Canada

Thermodynamic properties of water in the water-poor region of binary water + alcohol mixtures

Karin Liltorp, Peter Westh, and Yoshikata Koga

Abstract: In our previous thermodynamic studies, we suggested that alcohol molecules in water-poor water + alcohol mixtures exist as alcohol clusters in a form similar to the pure alcohols. Here, we use calorimetry and densitometry to investigate how H_2O interacts with alcohol clusters in water-poor binary aqueous mixtures of 12 different alcohols. The composition dependence of the measured excess partial molar enthalpy and volume of water (H_W^E and V_W^E), along with entropy data calculated from H_W^E and literature data for excess chemical potentials, showed that in water-poor solutions of small alcohols such as methanol, ethanol, and 1-propanol, mutual water–water interactions are endothermic, but entropically favorable. Conversely, in long-chain solvents such as 1-octanol and 1-decanol, the interaction is exothermic and entropically unfavorable. We suggest that these observations reflect water–alcohol hydrogen bonding in short-chain solvents and water clustering with more hydrogen bonding than in pure water or "dewetting" in mixtures of the longer alcohols, respectively. The composition dependence of H_W^E was also used to locate anomalies that specify the boundary between the mixing schemes characterizing the intermediate and the water-poor regions of alcohol + water mixtures.

Key words: aqueous alkane-mono-ols, excess partial molar enthalpy, entropy and volume, mixing schemes.

Résumé : Dans des études thermodynamiques antérieures réalisées dans ces laboratoires, il a été suggéré que les molécules d'alcool dans des mélanges eau + alcool pauvres en eau existent sous la forme d'agrégats d'alcool semblable à celle qu'on retrouve dans les alcools purs. Dans ce travail, on fait appel à la calorimétrie et à la densitométrie pour étudier la façon dont H_2O interagit avec les agrégats d'alcool dans des mélanges aqueux binaires pauvres en alcool de douze alcools différents. La relation qui existe entre la composition et l'enthalpie molaire partielle en excès et le volume d'eau (H_W^E et V_W^E) ainsi que les données d'entropie calculées à partir des valeurs de H_W^E obtenues à partir de la littérature et les données de la littérature relatives aux potentiels chimiques en excès ont montré que dans des solutions pauvres en eau de petites molécules d'alcool, telles le méthanol, l'éthanol et le propan-1-ol, les interactions sont endothermiques, mais favorables d'un point de vue entropique. Par ailleurs, dans des solvants à longue chaîne, tels l'octan-1-ol et le décan-1-ol, l'interaction est exothermique mais défavorisée d'un point de vue entropique. Il est suggéré que ces observations sont un reflet respectivement des liaisons hydrogènes eau–alcool dans les solvants à courte chaîne et de l'agrégation de l'eau avec plus de liaison hydrogène que dans l'eau pure ou d'une « déshydratation » dans les mélanges impliquant des alcools à plus longues chaînes. On a aussi utilisé la relation de dépendance entre la composition et le H_W^E pour localiser les anomalies qui déterminent la frontière entre les schémas de mélange et qui caractérisent les régions intermédiaires et les pauvres en eau des mélanges eau + alcool.

Mots clés : alcane-monoalcools aqueux, enthalpie molaire partielle en excès, entropie et volume, schémas de mélange.

[Traduit par la Rédaction]

Introduction

Aqueous mixtures of small alcohols have been extensively studied, and they continue to be one of the most important model systems for the fundamental elucidation of the hydrophobic effect, and thus for the understanding of biomolecular self-assembly. The vast majority of these studies address dilute (water-rich) alcohol solutions in which the drive towards expelling hydrophobic solutes is large, and hence the characteristics of hydrophobicity are readily studied. However, an increasing amount of biochemical information suggests that water-poor model systems might also be important. Thus, the living cell is "crowded" with macromolecules and solutes (1, 2) to the extent where most water is surface associated, and thus has properties that are likely to be different from those of bulk water or dilute solutions. Another interesting aspect comes from recent research that has questioned the conventional wisdom of the so-called "bound" water. It has been shown that water at biopolymer interfaces may be characterized by high mobility and (or) high entropy (3–7), in obvious conflict with the properties expected for a bound molecule. To account for these and similar observations it has been speculated that water is a "plasticizer" (8, 9) or "lubricant" (10), which promotes fast

Received 5 July 2004. Published on the NRC Research Press Web site at http://canjchem.nrc.ca on 6 May 2005.

K. Liltorp and P. Westh. Department of Life Sciences and Chemistry, Roskilde University, PO Box 260, DK-4000 Roskilde, Denmark.
Y. Koga.[1] Department of Chemistry, The University of British Columbia, 2036 Main Mall, Vancouver, BC V6T 1Z1, Canada.

[1]Corresponding author (e-mail: koga@chem.ubc.ca).

 doi: 10.1139/V05-050 © 2005 NRC Canada

dynamics, and hence the function of biopolymers and biomolecular aggregates. Such effects are to be understood in terms of direct (or "contact") interactions of water and the biomolecules, and they are not readily elucidated by water-rich model systems, in which strong solute-induced changes in mutual water interactions, sometimes denoted "iceberg formation" (11), dominate solution properties. Such cooperative changes in water–water hydrogen bonding will vanish at low water concentration, and the thermodynamic properties in this composition range might consequently more clearly provide information on direct interactions of water and organic nonelectrolytes.

We have previously used aqueous solutions of alkane-mono-ols (AL) as model systems in an attempt to elucidate molecular interactions in aqueous mixtures. As summarized in review articles (12–14), we have found that there are three distinctive composition regions in each of which the mixing scheme is qualitatively different from the other regions. Starting from the water-rich side, we named them Mixing scheme I, II, and III, respectively. Details of each mixing scheme were discussed earlier (11–17). In the water-poor region in particular, AL molecules form clusters with structures and properties similar to the pure alcohol. Water molecules, on the other hand, interact with the AL clusters in a manner depending on the identity of the alcohol. These conclusions were deduced from the excess partial molar quantities of the alcohols, H^E_{AL}, S^E_{AL}, and V^E_{AL}, and the composition derivatives of these quantities

$$[1] \qquad F^E_{AL-AL} \equiv N\left(\frac{\partial F^E_{AL}}{\partial n_{AL}}\right) = (1 - x_{AL})\left(\frac{\partial F^E_{AL}}{\partial x_{AL}}\right) \qquad (F = H, S, \text{ or } V)$$

The H^E_{AL-AL} function, for example, reflects the effect of incoming AL on the enthalpic situation of an existing AL in solution. Hence, H^E_{AL-AL} signifies the enthalpy change generated by mutual AL interactions. A positive sign for H^E_{AL-AL}, which has been generally found for dilute aqueous solutions, shows that AL–AL interactions act to increase H^E_{AL}, i.e., that mutual AL interactions are endothermic in the sense that they are energetically less favorable than the mixed AL–water interaction. Analysis of H^E_{AL-AL} data was the key information that led to the details of the mixing scheme in the water-rich region. In particular, some anomalous behaviors of H^E_{AL-AL} and of the analogous functions for excess entropy and volume were instrumental in locating the boundary between Mixing schemes I and II. In the water-poor region, however, the absolute values of H^E_{AL} and other excess partial molar functions of AL and their composition derivatives were found to be almost zero, which indicated that AL molecules exist as clusters purely consisting of AL molecules as in their pure state (11–18). Because the values of the excess partial molar quantities of AL are nearly zero and constant, the resulting values of H^E_{AL-AL} and its entropy and volume analogues in the water-poor region are therefore almost zero, and possible anomalies are rather difficult to identify. In contrast, the excess partial molar enthalpy of water (H^E_W) together with other partial molar quantities of water are expected to be sizable in this range, which of course contains thermodynamic information as to how water molecules interact with AL clusters. It follows that measurements of H^E_W and subsequent analysis with respect to the function,

$$[2] \qquad H^E_{W-W} \equiv N\left(\frac{\partial H^E_W}{\partial n_W}\right) = (1 - x_W)\left(\frac{\partial H^E_W}{\partial x_W}\right)$$

which is analogous to the AL–AL interaction function in eq. [1], could identify anomalies more conspicuously, and consequently shed some light on the mixing schemes in the water-poor composition range.

In the light of this, we have conducted a series of this type of measurements in the water-poor region and a number of parallel investigations on the volumetric behavior of the same systems. Here, we report these results and discuss the mode of interactions of water molecules with AL clusters, and the mixing scheme boundaries in the water-poor composition region.

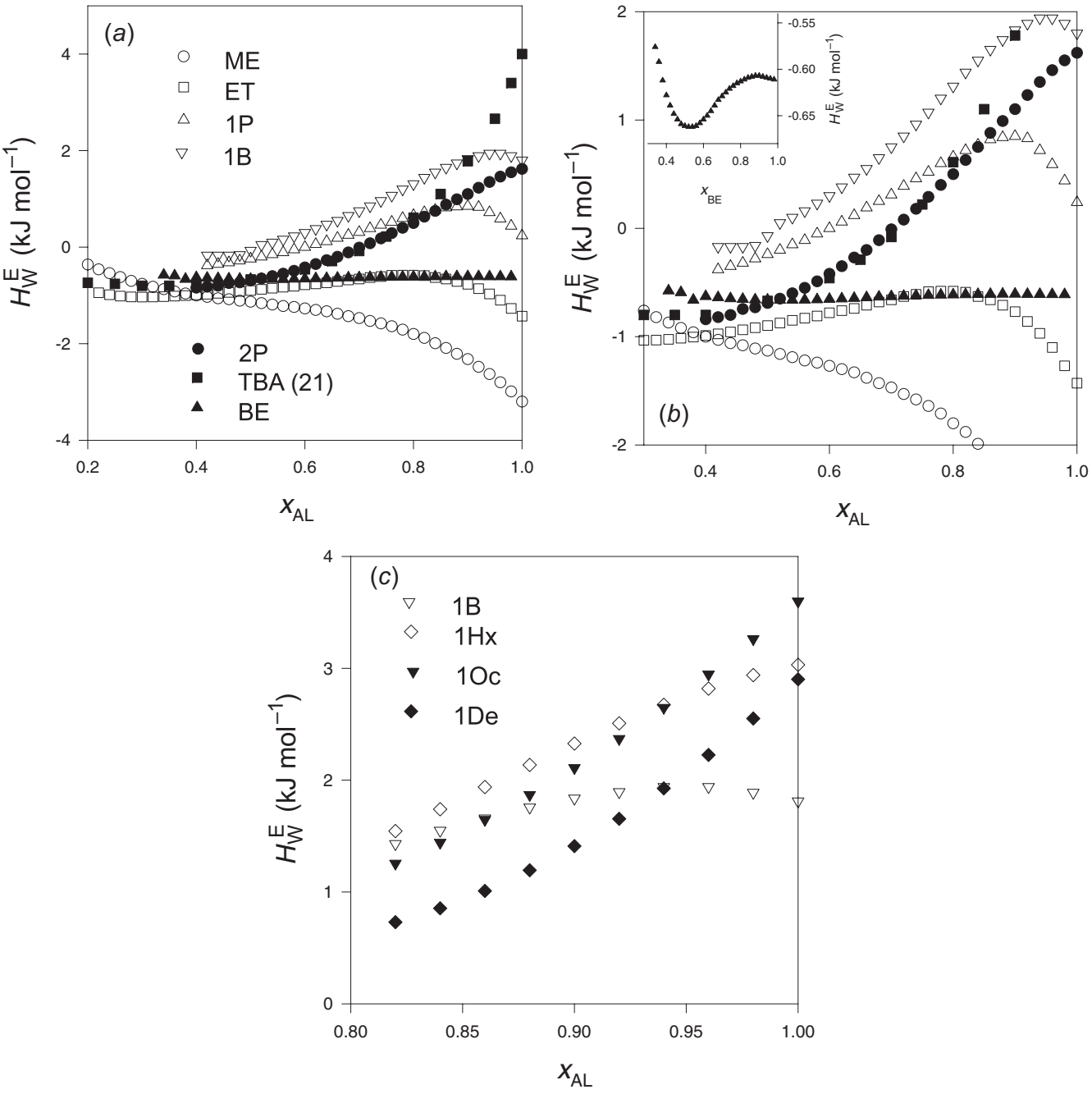
Experimental

The alcohols used as solvents were methanol (ME, 99.9%, Fluka), ethanol (ET, 99.8%, Fluka), 1-propanol (1P, 99.8%, Fluka), 2-propanol (2P, 99.5%, Sigma, St. Louis, Missouri), 1-butanol (1B, 99.9%, Merck, Darmstadt, Germany), 1-pentanol (1Pe, 8.5%, Merck), 1-hexanol (1Hx, 99%, Fluka), 1-octanol (1Oc, 99.5%, Fluka), 1-decanol (1De, 99.5%, Fluka), 2-butoxyethanol (i.e., ethylene glycol monobutyl ether) (BE, 99.5%, Sigma), and glycerol (Gly, 99.5%, Merck). A spot check by an analytical gas chromatograph equipped with mass spectroscopy, indicated the purity quoted by the supplier were correct. Due care was exercised in handling all the alcohol samples so as not to contaminate them with moisture. Water was freshly prepared using MilliQ equipment (Millipore, Bedford, Mass.). For ethanol–water, the calorimetric data were retrieved on a home-made instrument similar to the LKB Bromma 8700 (18). The uncertainty of this data is ±30 J mol^{-1}. All other calorimetric measurements were conducted on a TAM 2277 isothermal calorimeter (Thermometric, Järfälla, Sweden), equipped with a nW amplifier module. Type 2250 titration modules (Thermometric) with a 1 mL stainless steel cell and a gold stirrer were used. The cell initially contained pure alcohol quantified by weight, which was subsequently titrated with 1 µL aliquots of water. The experimental scatter upon repeated injections of water ranged from ±5 J mol^{-1} for the smaller water miscible alcohols to about ±50 J mol^{-1} for the most hydrophobic solvents. All calorimetric measurements were made at 25.0 °C. For the large alcohols (1Pe, 1Hx, 1Oc, and 1De), the measurements were limited to the composition region, $x_{AL} > 0.8$, since near the phase separation, the rate of dissolution becomes too slow for the determination of H^E_W within the stated uncertainty.

The densities of the alcohol–water mixtures were determined in a DMA 602 vibrating tube measuring cell (Anton Parr, Graz, Austria). The measuring cell was built into a set-up allowing automated cycles of "titrate–mix–measure" (19). In the present work, samples of pure alcohol (about 7 mL) were weighed in the instrument mixing cell and titrated with a number of 10 µL aliquots of pure water. For the most hydrophobic alcohols, this method showed increased scatter, probably because of incomplete mixing. Thus, for

© 2005 NRC Canada

Fig. 1. (*a*) Measured (this work) excess partial molar enthalpy of water in water + alcohol mixtures at 25 °C. (*b*) Expanded version of panel (*a*). (*c*) The same for longer alcohols. The inset in (*b*) is further expanded for BE.



these systems, parallel trials were made in which samples were prepared manually by weight and stirred for 24–48 h prior to density measurements. As discussed in the following, this method of mixing seems satisfactory. The experimental temperature was 25.000 ± 0.005 °C. The equipment was calibrated against air and pure water, and the experimental repeatability was $\pm 5 \times 10^{-6}$ g cm^{-3}.

Results

Calorimetry

Measured values of H_W^E dissolved in ME, ET, 1P, 2P, 1B, 1Hx, 1Oc, 1De, BE, and Gly are listed in Table A1.[2] Based on these data and the literature values of the excess chemical potential of water (μ_W^E) (16, 20), the excess partial molar en-

[2] Supplementary data for this article (Tables A1–A3) are available on the Web site or may be purchased from the Depository of Unpublished Data, Document Delivery, CISTI, National Research Council Canada, Ottawa, ON K1A 0S2, Canada. DUD 3651. For more information, on obtaining material refer to http://cisti-icist.nrc-cnrc.gc.ca/irm/unpub_e.shtml.

© 2005 NRC Canada

tropy of water × temperature (TS^E_W) can be calculated using $TS^E_W = H^E_W - \mu^E_W$. We used values of H^E_W and μ^E_W read off smooth curves at a mol fraction interval of 0.02. The resulting TS^E_W data are listed in Table A2[2], together with the smooth values of H^E_W and μ^E_W. Data from the calorimetric measurements are plotted in Fig. 1 together with those for *tert*-butanol (TBA) determined earlier (21). The derived TS^E_W values are plotted as a function of x_{AL} in Fig. 2. It is clear from Figs. 1 and 2 that the values of H^E_W and TS^E_W have some modest dependence on x_{AL} in this water-rich region, though certainly not as much as H^E_{AL} and TS^E_{AL} in the water-rich end.

For some of the systems, where data for both H^E_W and H^E_{AL} are available in an extended concentration range, the consistency of the measurements can be tested against the Gibbs–Duhem relation

$$[3] \qquad x_{AL}\delta H^E_{AL} + x_W H^E_W = 0$$

From the previous H^E_{AL} data (17, 22), the Gibbs–Duhem sums (left hand side of eq. [3]) were calculated at increments of $\delta x_{AL} = 0.02$ for ME, ET, 1P, 2P, and BE. The resulting sums are within ±0.003 kJ mol^{-1} with a few sporadic exceptions of ±0.01 kJ mol^{-1}. Considering the experimental uncertainties, we conclude that the Gibbs–Duhem consistency is satisfactory.

The quality of the present measurements was further tested by calculating the excess (integral) molar enthalpy (H^E_m)

$$[4] \qquad H^E_m = x_{AL}H^E_{AL} + x_W H^E_W$$

from H^E_W measured here and previously published values of H^E_{AL} for ME, ET, 1P, 2P, and BE (17, 22). The calculated H^E_m values were compared with previously published data (17, 22–31) and it was found that the current results fell within the scatter of the literature values. We point out that this analysis only serves to check the reliability of the current methodology. The H^E_W needed for the present discussion cannot be derived with sufficient precision from the literature data on H^E_m (32). The values of H^E_W and TS^E_W at infinite dilution ($x_{AL} \to 1$) are listed in Table 1 for comparison together with the available literature data for H^E_{AL} and TS^E_{AL} for $x_{AL} \to 0$.

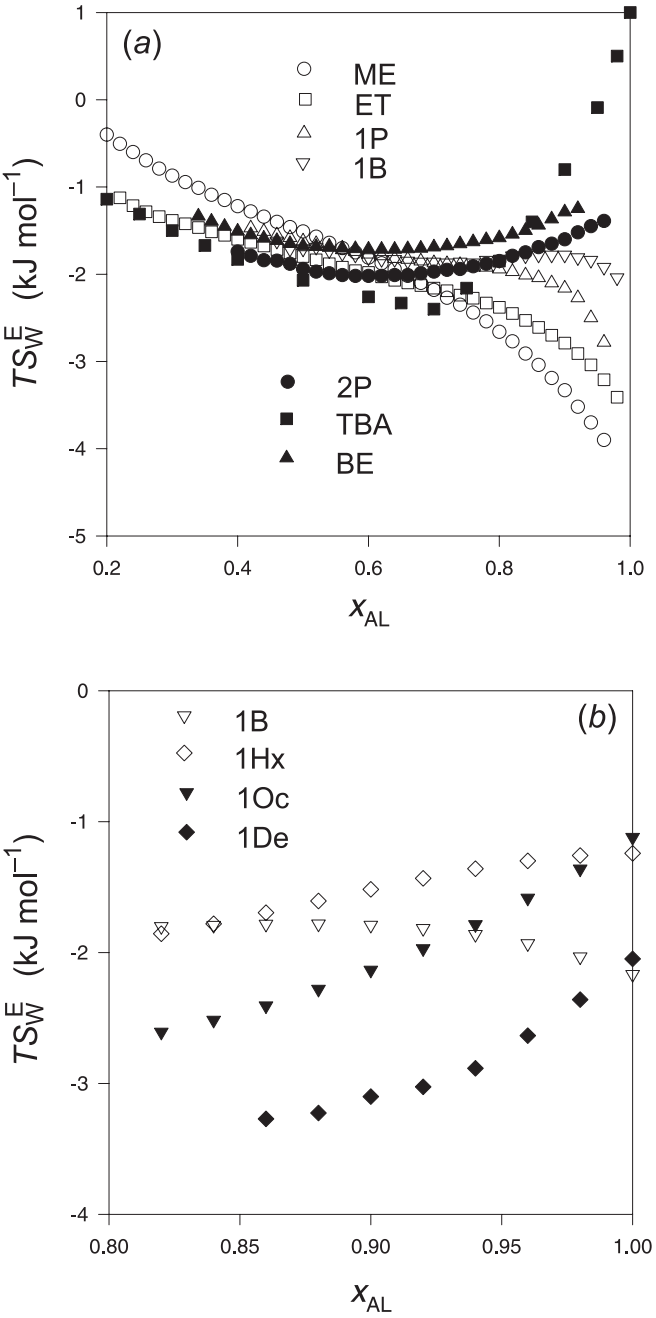
Density measurements

The measured density data for the water-poor solutions of ME, ET, 1P, 1B, 1Pe, 1Hx, 1Oc, 1De, and BE are listed in Table A3.[2] Figure 3 shows the representative data illustrated as the excess molar volumes of the mixtures (V^E_m) plotted against the mol fraction of the alcohol (x_{AL}). The excess volumes are calculated as:

$$[5] \qquad V^E_m = V_m - x_{AL}V^*_{AL} - x_W V^*_W$$

where V_m is the measured molar volume and the asterisk signifies pure liquid (water or alcohol). For small alcohols, the match with the literature data (33–38) is acceptable within the respective uncertainties. In the subsequent analysis, we use the literature data since the latter cover wider composition ranges. For 1Hx, 1Oc, and 1De, however, the existing data (39) for V^E_m are scattered by about 10-fold of our data shown in Fig. 3. For these alcohols, therefore, we used our data for further analysis.

Fig. 2. Excess partial molar entropy of water × the temperature (TS^E_W) at 25 °C calculated from the literature μ^E_W values and the H^E_W values measured in this work. (*a*) For shorter alcohols; (*b*) For longer alcohols.



The excess molar volume reflects changes in "free volume" (or molecular packing) when a mixture is made from its constituents in their standard (pure) state. The results in Fig. 3 confirm earlier observations (40) that the dissolution of water in small alcohols is accompanied with increased packing ($V^E_m < 0$), and that this negative volume change tapers off as the chain length of the solvent increases. For ME, ET, 1P, and 1B, V^E_m is a weakly concave function. However,

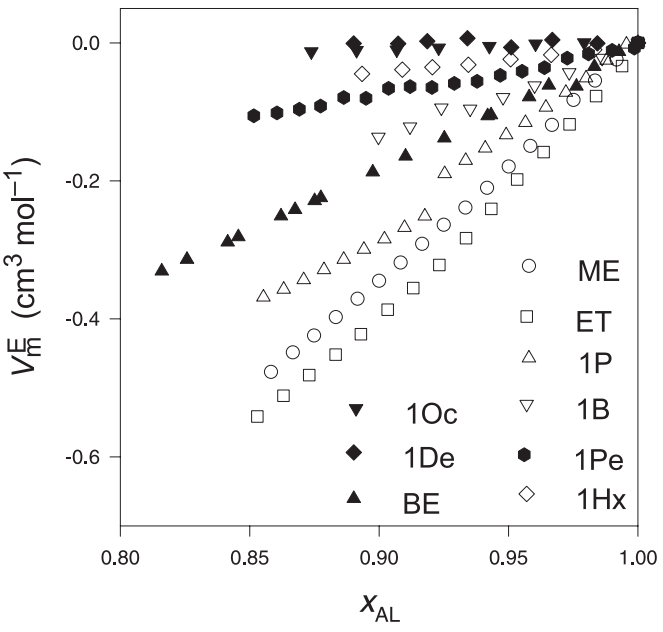
© 2005 NRC Canada

Table 1. Excess partial molar quantities at infinite dilution.

	Excess partial molar property of alcohol at $x_{AL} = 0$			Excess partial molar property of water at $x_W = 0$		
Alcohol	H^E_{AL} (kJ mol^{-1})	TS^E_{AL} (kJ mol^{-1})	V^E_{AL} (cm^3 mol^{-1})	H^E_W (kJ mol^{-1})	TS^E_W (kJ mol^{-1})	V^E_W (cm^3 mol^{-1})
ME	–7.4[a]	–8.7[b]	–2.2[c]	–3.2[d]	–4.3[d,e]	–3.6[d,f]
ET	–10.2[a]	–13.5[b]	–3.5[c]	–1.4[d]	–3.6[d,e]	–4.1[d,f]
1P	–10.4[a]	–17.0[b]	–4.4[g]	0.2[d]	–3.2[d,e]	–3.0,[d] –2.6[f]
2P	–13.1[a]	–18.1[b]	–4.1[h]	1.6[d]	–1.2[d,e]	–3.6,[i] –3.1[f]
1B	–9.3[j]	–19.3[j]	–5.4[g]	1.8[d]	–2.2[d,j]	–1.6,[d] –1.9[f]
TBA	–17.0[k]	–23.6[l]	–6.3[m]	4.0[k]	1.0[k,l]	–1.1,[n] –1.5[f]
1Pe	–7.8[o]	–21.3[o]	–6.1[g]			–0.7[d]
1He			–6.7[g]	3.0[d]	–1.0[d,e]	–0.6,[d] 0.0,[p] –0.7[q]
1Oc			–8.0[g]	3.5[d]	–1.1[d,r]	–0.1,[d] 0.3,[p] –0.2[q]
1De				2.9[d]	–1.6[d,r]	0.1,[d] 0.4[p]
BE	–17.0[s]	–26.2[t]	–8.2[u]	–0.6[d]	–1.0[d,t]	–1.8[d]
Gly	–5.6[v]	–3.5[v]	–2.3[v]	–1.6[d]	0.3[d,v]	

[a]Reference 17.
[b]Reference 15.
[c]Reference 33.
[d]This work.
[e]Reference 16.
[f]Reference 40.
[g]Reference 46.
[h]Reference 47.
[i]Reference 34.
[j]Reference 48.
[k]Reference 18.
[l]Reference 42.
[m]Reference 49.
[n]Reference 35.
[o]Reference 50.
[p]Reference 39.
[q]Reference 51.
[r]Reference 20.
[s]Reference 22.
[t]Reference 52.
[u]Reference 53.
[v]Reference 54.

Fig. 3. Measured (this work) excess molar volume of aqueous alcohols (V^E_m) at 25 °C.



for alcohols larger than BE, V^E_m becomes small and is practically linear in the mol fraction. To further analyze this volumetric behavior, we calculated the excess partial molar volume of AL ($V^E_{AL} = V^E_m + (1 - x_{AL})(dV^E_m/dx_{AL})$), and that of water ($V^E_W = V^E_m - x_{AL}(dV^E_m/dx_{AL})$). The slope ($dV^E_m/dx_{AL}$) was determined from the smooth curves.

The results are shown in Fig. 4 for V^E_{AL} and in Fig. 5 for V^E_W. It is clear that V^E_{AL} is generally very small in this region. Earlier, we suggested from the H^E_{AL} and S^E_{AL} data (11–18) that alcohols form clusters in a form similar to pure AL in the water-poor region. The fact that the V^E_{AL} values are close to zero (Fig. 4*b*) is consistent with this cluster formation, particularly so for large alcohols (Fig. 4*b*). Figure 5*a* provides a general overview of V^E_W based primarily on literature data (34–38), while Fig. 5*b* shows a close-up of the most water-poor range in solutions of 1B, 1Hx, 1Oc, or 1De. Table 1 lists the respective V^E_{AL} and V^E_W data at their respective infinite dilutions. It appears that the limiting value of V^E_W for small alcohols (ME, ET, 1P, and 2P) is about –3 to –4 cm^3 mol^{-1}. In other words, water is about 20% more densely packed in small alcoholic solvents than in pure water (V^*_W = 18.07 cm^3 mol^{-1}). If H_2O was considered to be a van der Waals liquid, its molar volume would be about 12 cm^3 mol^{-1}, assuming that a water molecule is a sphere of radius 1.5 Å

© 2005 NRC Canada

Fig. 4. Excess partial molar volumes of alcohols (V^{E}_{AL}) at 25 °C calculated using: (*a*) literature data; (*b*) data reported in the present work.

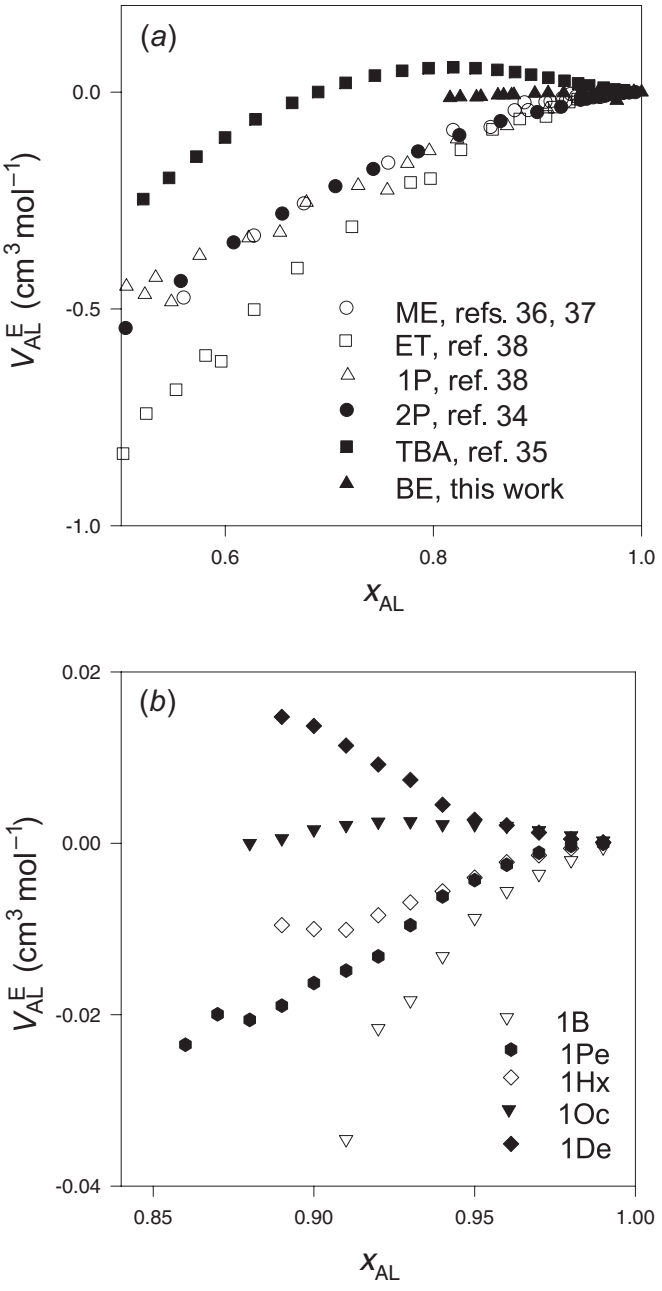
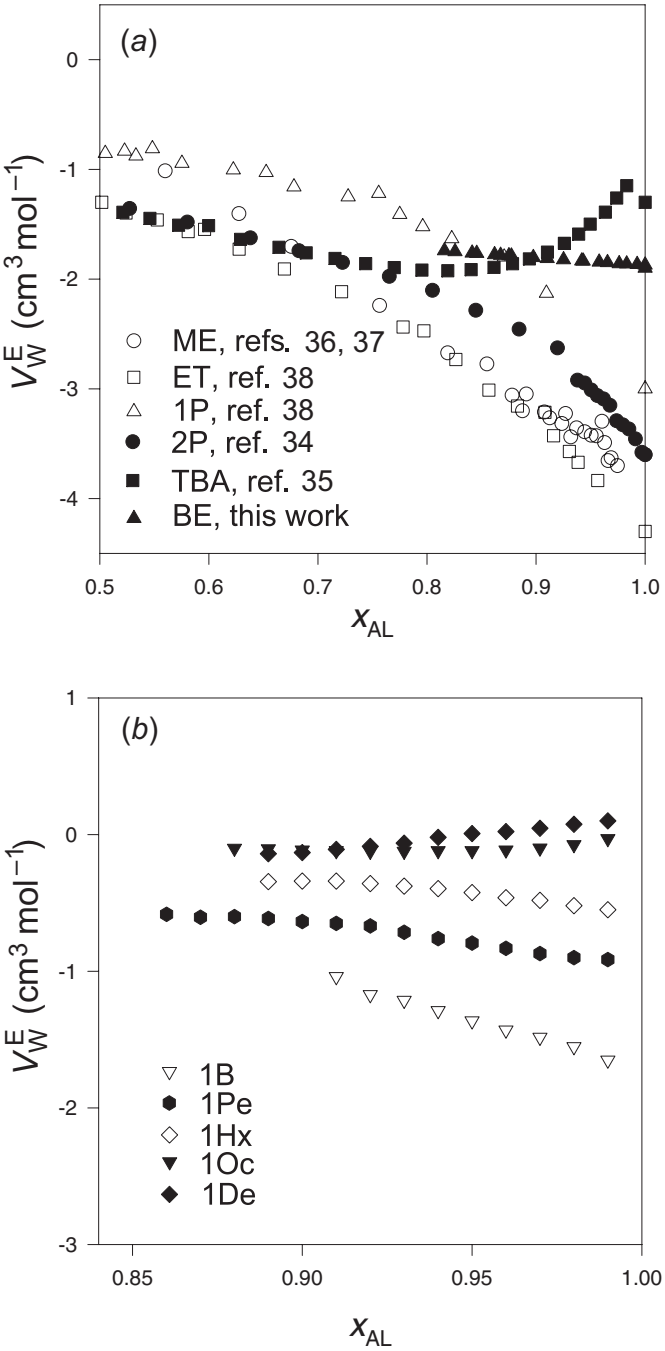


Fig. 5. Excess partial molar volume of water (V^{E}_{W}) at 25 °C calculated using: (*a*) literature data, (the infinite dilution data are from ref. 33); (*b*) data reported in this work.



using the van der Waals radii of H and O atoms (41), and assuming close packing. For water dissolved in longer alcohols, on the other hand, V^{E}_{W} gradually becomes less negative, and for the most hydrophobic solvents it is practically zero. This suggests that the packing density of water in hydrophobic alcohols deviates only a percent or so from the pure state.

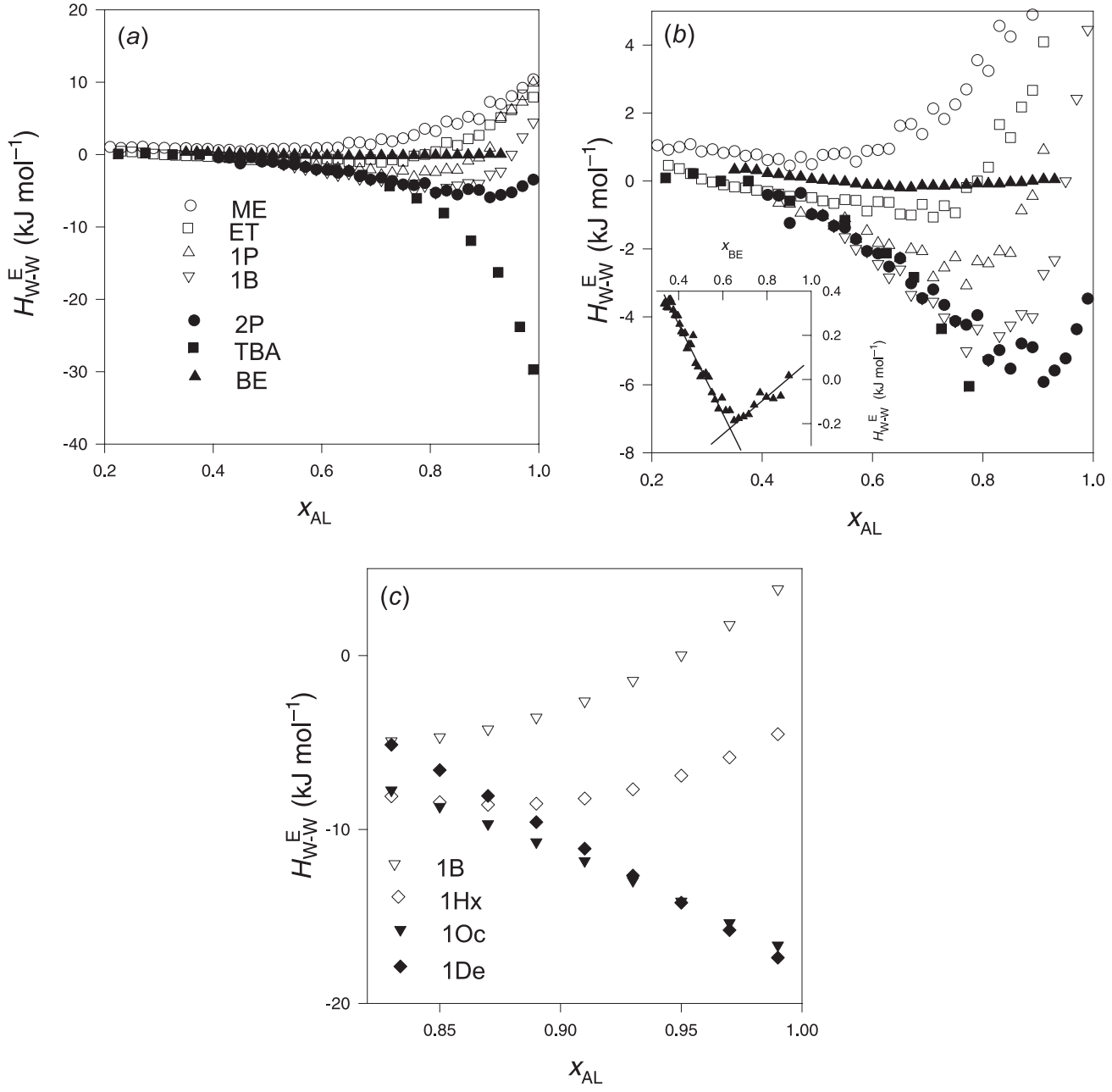
Discussion

Mixing scheme boundaries

As pointed out elsewhere (12–14) and in references quoted therein, comparative analysis of the higher order derivatives of the excess Gibbs energy is a powerful technique for detecting subtleties of molecular interactions in solutions. In particular, we have found that classification of the observed thermodynamic behavior according to the specific mixing schemes, reflecting characteristic modes of interactions, or "solution structures" is most helpful in singling out important general effects in aqueous solutions. In most aqueous alcohol solutions, changes in mixing schemes have been identified from the composition dependence of the AL–AL interaction (H^{E}_{AL-AL}), eq. [1], and its entropy and volume analogues. The same is true for aqueous nonelectrolytes in

© 2005 NRC Canada

Fig. 6. (*a*) H_2O–H_2O interaction in terms of enthalpy (H^E_{W-W}) at 25 °C. (*b*) Expanded version of panel (*a*). (*c*) The same for larger alcohols. The inset in (*b*) is further expanded for BE.

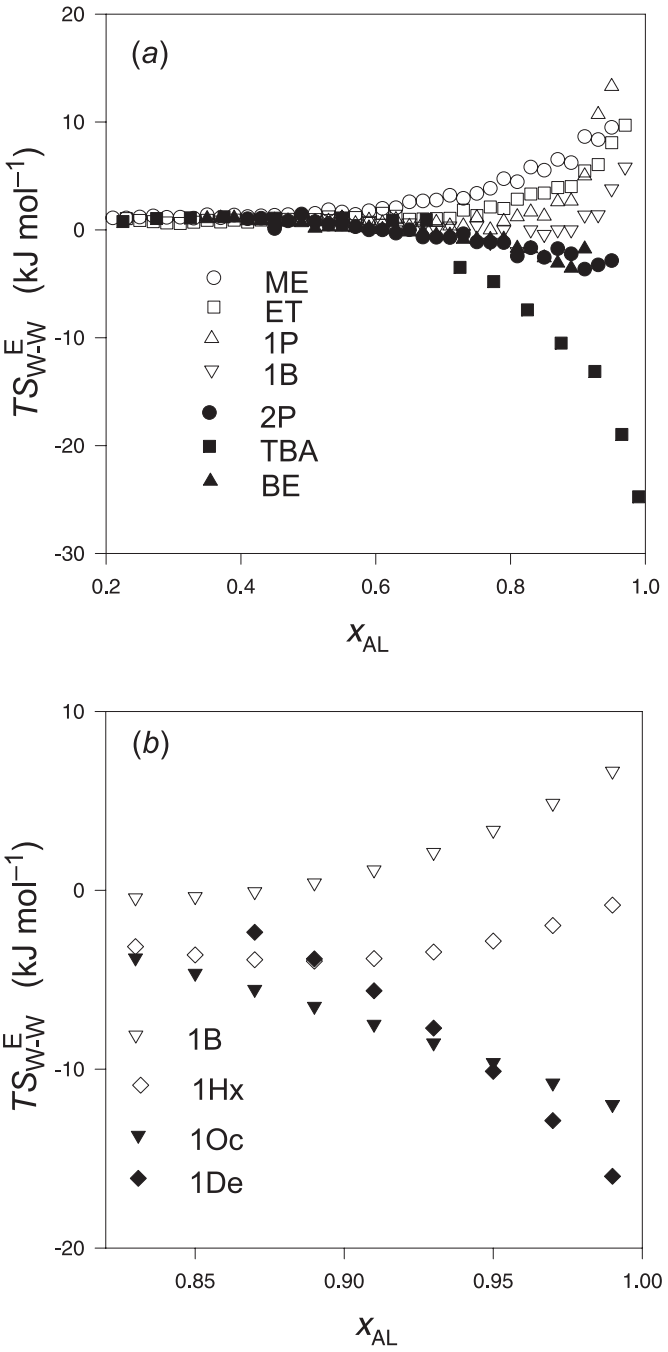


general (12–14). However, the data of H^E_{AL} and H^E_{AL-AL} are also inevitably small in their absolute values in the water-poor composition range, and it follows that H^E_W (measured in this work) and other partial molar quantities of water are potentially more sensitive parameters to identify changes in mixing schemes. Hence, the data in Figs. 1 and 2 have been used to reappraise previous discussions of mixing scheme boundaries in aqueous alcohols.

For this purpose, we calculated H^E_{W-W} using a smooth curve in Fig. 1 and the approximation ($\partial H^E_W/\partial x_W \approx \delta H^E_W/\delta x_W$) with $\delta x_W = 0.02$. The results are plotted in Fig. 6 and the data for the analogous entropy interaction function is given in Fig. 7. For ME, ET, 1P, 1B, and BE, H^E_{W-W} starts with a positive value, but decreases on increasing x_W, and reaches a minimum and starts to increase (Fig. 6). This minimum is the inflection point of the H^E_W vs. x_{AL} curve in Fig. 1, which corresponds to the boundary between Mixing schemes II and III. Best estimates for the location of this boundary are listed in Table 2. In general, the minimum in H^E_{AL-AL} is rather broad and it is difficult to pinpoint its location. However, the current method is much more reliable than identifying an anomaly from the H^E_{AL-AL} function, since the absolute values of the latter are close to zero (17). For 2P, although the value of H^E_{W-W} starts negative at $x_{AL} = 1$ ($x_W = 0$), it decreases as x_W increases to the minimum, and then increases just as for the other *n*-alkanols. For TBA, H^E_{W-W} in Fig. 6 in-

© 2005 NRC Canada

Fig. 7. H_2O–H_2O interaction in terms of entropy × temperature (TS^E_{W-W}) at 25 °C. (*a*) For shorter alcohols; (*b*) For longer alcohols.



creases smoothly to the maximum at about x_{TBA} = 0.05, which is the boundary between Mixing schemes I and II. Thus, there seems to be no sign of Mixing scheme III in terms of H^E_{W-W} for TBA. In Fig. 7, however, TS^E_{W-W} shows a sharp bend at about x_{TBA} = 0.62, which was argued to be the transition point between Mixing schemes II and III (42). This sharp bend in TS^E_{W-W} comes from a sharp bend at about x_{TBA} = 0.6 in μ^E_W obtained from the vapor pressure data (42). At x_{TBA} = 0.6, the TBA–H_2O system has an azeotrope, at which the data analysis used in the original paper (42) becomes difficult. A method of circumventing difficulties associated with azeotropy was subsequently developed (16), and its application to TBA–H_2O is warranted. Until such reexamination, we postpone any conclusion in this regard.

Table 2. Loci of the boundary in x_{AL} between Mixing schemes II and III for aqueous alcohols at 25 °C.

AL	From H^E_{W-W} (this work)	From H^E_{AL-AL} (ref. 15)
ME	0.47	0.54
ET	0.68	0.38
1P	0.74	0.30
2P	0.88	0.19
1B	0.80	
TBA	?	0.62[a]
BE	0.63	0.43

[a]The value of 0.38 quoted in ref. 15 is the value of x_W, not that of x_{AL}.

Interactions of water in the water-poor region

As discussed in the Introduction, there is some interest in the interrelationships of solvent hydrophobicity and the properties of water at high dilution (i.e., for $x_{AL} \rightarrow 1$). One straightforward approach to this is a comparison of the data for excess partial molar enthalpy, entropy, and volume of water at infinite dilution compiled in Table 1. Several interesting features can be identified from these data. Comparing, for example, the series of 1-alkanols, reveals that the H^E_W increases gradually with the alkyl chain length of the solvent, from –3 kJ mol^{-1} for ME to about +3 kJ mol^{-1} for 1Hx, 1Oc, and 1De. This course may seem intuitive for highly polar water molecules, which must (*a*) break away from mutual interactions, and (*b*) disperse into increasingly nonpolar environments, with limited capacity for establishing favorable interactions. While of some relevance, this picture turns out to be an oversimplification as discussed in more detail in the following. The competing thermodynamic effect of each of the two processes (*a*) and (*b*) must be an order of magnitude larger than the net result of a few kJ mol^{-1}. For example, the enthalpy of vaporization for alcohols is known to be about 50 kJ mol^{-1}. Hence, subtle differences for each alcohol in the energetics of each step (*a*) and (*b*) may result in a sizable difference in the net result. Thus, comparison among alcohols at the H^E_W or TS^E_W level must be exercised with caution. The relative changes in these quantities within the same alcohol, on the other hand, may be safer parameters to discuss the detailed molecular interactions. In the following, we use the relative changes in these quantities on changing the mol fraction, i.e., H^E_{W-W}, eq. [2], and TS^E_{W-W} extensively.

Another interesting trend to note in Table 1 is that V^E_W increases from large negative values in small solvents (ME, ET, 1P, and 2P) and levels off at a value near zero for more hydrophobic solvents such as 1Hx, 1Oc, and 1De.

To assess the characteristic properties of water more specifically in a predominantly nonpolar environment, we now focus on four of the more hydrophobic solvents, 1B, 1Hx, 1Oc, and 1De. Volumetric properties of dilute solutions of water in these solvents are presented in Figs. 4*b* and 5*b*. The calorimetric data for these systems is illustrated in Fig. 1*c*. Figure 2*b* shows TS^E_W calculated from the literature data for the excess chemical potential (16, 20). Based on the data in

© 2005 NRC Canada

Figs. 1*c* and 2*b*, the enthalpy and entropy interaction functions (H^E_{W-W} and TS^E_{W-W}) were calculated (eq. [2]) and are plotted in Figs. 6*c* and 7*b*. The results show that in 1B, H^E_{W-W} is positive at the highest x_{AL} values, but changes sign around x_{AL} = 0.95. This behavior resembles that of water dissolved in smaller alcohols (see Figs. 6*a* and 7*a*), and suggests that at very low water concentrations, mutual water interactions are less favorable in terms of enthalpy than water–alcohol interactions. Upon addition of more water, this picture changes H^E_{W-W} (becomes more negative) and water–water interactions become more enthalpically favorable. For water in 1Hx, H^E_{W-W} is slightly negative even at x_{AL} = 1, and for still longer alcohols, H^E_{W-W} attains sizable negative values in the most water-poor samples. This signifies that the first water molecules, on entering the alcohol, exhibit mutual interactions that are strongly enthalpically favored over water–alcohol contacts. The composition dependence of TS^E_{W-W} shown in Fig. 7 follows a very similar pattern, taking into account the opposite sign for the stability criterion. Thus, for water–1B, TS^E_{W-W} is positive in very water-poor samples, but changes sign around x_{AL} = 0.88. In other words, mutual water interactions are entropically favored over water–alcohol contacts for $x_{AL} > 0.88$. For the higher alcohols shown in Fig. 7*b*, TS^E_{W-W} remains negative over the investigated composition range, suggesting that water–water interactions bring about a decrease in entropy, i.e., that they are entropically unfavorable.

These observations may be rationalized in terms of a balance or a competition between strong alcohol–water interactions predominantly in mixtures of small alcohols and, on the one hand, the formation of water clusters more organized than in pure water predominantly in large alcohols. Thus, we suggest that the formation of water clusters around the alcohol -OH groups even in very water-poor mixtures becomes increasingly important as the solvent alkyl chain becomes longer (and the average distance between -OH groups increases). In 1Oc and 1De, this sequestering of water is associated with strong negative TS^E_{W-W} and H^E_{W-W} values (Figs. 6 and 7), which reflect ordering of water into more organized clusters with favorable enthalpic, but entropically unfavorable water–water interactions. In smaller alcohol solvents with a higher density of -OH groups, positive TS^E_{W-W} and H^E_{W-W} values probably reflect polar interactions of the alcohol hydroxyl group and a single molecule of water. This conclusion is supported by the volume data. In general, the volume behaviour of AL + water in the water-poor range is governed by a balance between a volume increase of organized clusters and a decrease by the direct interaction of a single molecule of water with AL clusters. For the larger alcohols (1Hx, 1Oc, 1-De), the remarkable composition independence of V^E_W (Figs. 4 and 5) suggests that the former effect is much larger. We point out that this organized clustering may be closely related to the so-called "dewetting" near large hydrophobic surfaces (43).

The suggestion that putative organized water clusters form primarily around the large alcohol -OH group is supported by data on the solubility of water in nonpolar solvents. Water is rather soluble in long-chain 1-alkanols and interestingly, the solubility becomes independent of the size of the alkyl group for solvents larger than 1-heptanol. Hence, the mol fraction of water at saturation remains at about 0.25 (x_{AL} = 0.75) for C8, C9, C10, C11, and C12 1-alkanols (44). For comparison, the solubility of water in normal alkanes, such as hexane, is almost three orders of magnitude smaller (45). The solubility data stress the importance of the -OH group and to reconcile this with the present observations, we suggest that the properties of water-poor aqueous solutions of long-chain 1-alkane-mono-ols are governed by the formation of (short-lived) organized clusters around the alcohol hydroxyl group. A similar conclusion was recently reached by Segatin and Klofutar (39).

Conclusions

We suggest that in the water-poor region of water + alcohol mixtures, alcohol molecules form clusters, presumably with -OH groups pointing outwards. Water molecules, on the other hand, interact with the -OH groups of alcohol clusters predominantly as single molecules for small alcohols. The H_2O–H_2O interaction is enthalpically repulsive and entropically favorable for small alcohols. As the alkyl group becomes larger, this interaction weakens to almost zero for BE. For even larger alcohols such as 1De, water molecules tend to cluster together in a more organized manner than in pure H_2O around the -OH groups of AL clusters.

In the Introduction we argued that information on the direct interaction of water and nonpolar molecules may be relevant for a number of biochemically important processes. Examples include the permeation of water through bilayer membranes and the roles of water bound to amphiphilic surfaces of biomolecules. We suggest here that some fundamental information on this may be derived from studies of water-poor aqueous alcohols. The present work concludes that even in 1-decanol, whose accessible surface area is dominated by the nonpolar alkyl chain, the properties of water around the hydroxyl group may be governed by the formation of clusters with more hydrogen bonds than in pure water. This behavior of water at low concentrations may be highly relevant for the understanding of some of its roles in biochemistry and indeed for the general elucidation of ubiquitous "hydrophobic interactions" among biomolecules. However, since clustering will reduce water – alkyl chain contacts, it may very well disqualify long-chain alkanols as model compounds for studies of "contact interactions" between water and hydrophobic interfaces, if the concept of contact interactions is important at all.

Acknowledgements

This research was supported by the Carlsberg Foundation, the Danish Technical Research Council, and the Natural Sciences and Engineering Research Council of Canada (NSERC).

References

1. A.P. Minton. J. Biol. Chem. **276**, 10 577 (2001).
2. P.R. Davis-Searles, A.J. Saubders, D.A. Erie, D.J. Winzor, and G.J. Pielal. Annu. Rev. Biophys. Biomol. Struct. **30**, 271 (2001).
3. H. Binder, B. Kohlstrunk, and H.H. Heerklotz. Chem. Phys. Lett. **304**, 329 (1999).
4. N. Markova, E. Sparr, L. Wadso, and H. Wennerstrom. J. Phys. Chem. B, **104**, 8053 (2000).
5. R. Ishima and D.A. Torchia. Nat. Struct. Biol. **7**, 740 (2000).

© 2005 NRC Canada

6. S.R. Kabir, K. Yokoyama, K. Mihashi, T. Kodama, and M. Suzuki. Biophys. J. **85**, 3154 (2003).
7. S.K. Pal, J. Peon, and A.H. Zewail. Proc. Natl. Acad. U.S.A. **99**, 15 297 (2002).
8. H.G. Nagendra, N. Sukumar, and M. Vijayan. Proteins: Struct. Funct. Bioinf. **32**, 229 (1998).
9. W.Q. Sun. Plant Physiol. **124**, 1203 (2000).
10. L.D. Barron, L. Hecht, and G. Wilson. Biochemistry, **36**, 13 143 (1997).
11. Y. Koga, K. Nishikawa, and P. Westh. J. Phys. Chem. A, **108**, 3873 (2004).
12. Y. Koga. J. Crystallogr. Soc. Jpn. **37**, 172 (1995)
13. Y. Koga. J. Phys. Chem. **100**, 5172 (1996).
14. Y. Koga. Netsu Sokutei, **30**, 54 (2003). Available in pdf form upon request to the corresponding author.
15. Y. Koga, P. Westh, and K. Nishikawa. Can. J. Chem. **81**, 150 (2003).
16. J. Hu, C.A. Haynes, A.H.Y. Wu, C.M.W. Cheung, M.M. Chen, E.G.M. Yee, T. Ichioka, K. Nishikawa, P. Westh, and Y. Koga. Can. J. Chem. **81**, 141 (2003).
17. S.H. Tanaka, H.I. Yoshihara, A.W.-C. Ho, F.W. Lau, P. Westh, and Y. Koga. Can. J. Chem. **74**, 713 (1996).
18. Y. Koga. Can. J. Chem. **66**, 1187 (1988).
19. P. Westh and C. Trandum. J. Phys. Chem. B, **104**, 11 334 (2000).
20. N. Segatin and C. Kloufutar. Monatsh. Chem. **135**, 241 (2004).
21. Y. Koga. Can. J. Chem. **66**, 3171 (1988).
22. W. Siu and Y. Koga. Can. J. Chem. **67**, 671 (1989).
23. L. Benjamin and G.C. Benson. J. Phys. Chem. **67**, 858 (1963).
24. M.J. Costigen, L.J. Hodges, K.N. Marsh, R.H. Stokes, and C.W. Tuxford. Aust. J. Chem. **33**, 2103 (1980).
25. J.A. Larkin. J. Chem. Thermodyn. **7**, 137 (1975).
26. M.I. Davis and E.S. Ham. Thermochim. Acta, **190**, 251 (1991).
27. M.I. Davis, J.B. Rubio, and J.B. Douheret. Thermochim. Acta, **259**, 177 (1995).
28. J.A. Boyne and A.G. Williams. J. Chem. Eng. Data, **12**, 318 (1967).
29. B. Marongiu, I. Ferino, R. Monaci, V. Solinas, and S. Torrazza. J. Mol. Liq. **28**, 229 (1984).
30. J.R. Battler and R.L. Rowlet. J. Chem. Thermodyn. **17**, 719 (1985).
31. A. Lietzmann, B. Lowen, and S. Schulz. J. Chem. Eng. Data, **39**, 785 (1994).
32. Y. Koga. *In* Comprehensive handbook of calorimetry and thermal analysis. *Edited by* M. Sorai. J. Wiley, New York. 2004. pp. 195–199.
33. C. Dethlefsen. Ph.D. thesis, University of Copenhagen, Copenhagen, Denmark. 1985.
34. M. Sakurai. J. Solution Chem. **17**, 267 (1988).
35. M. Sakurai. Bull. Chem. Soc. Jpn. **60**, 1 (1987).
36. M. Sakurai and T. Nakagawa. Bull. Chem. Soc. Jpn. **55**, 1641 (1982).
37. M. Sakurai and T. Nakagawa. J. Chem. Thermodyn. **14**, 269 (1982).
38. G.C. Benson and O. Kiyohara. J. Solution Chem. **9**, 791 (1980).
39. N. Segatin and C. Klofutar. Monatsh. Chem. **135**, 161 (2004).
40. M. Sakurai, K. Nakamura, and N. Takenaka. Bull. Chem. Soc. Jpn. **67**, 352 (1994).
41. K. Suzuki. Water and aqueous solutions. Kyouritsu Shuppan, Tokyo. 1980. p. 28.
42. Y. Koga, W.W.Y. Siu, and T.Y.H. Wong. J. Phys. Chem. **90**, 7700 (1990).
43. P. Ball. Nature (London), **423**, 25 (2003).
44. A.F.M. Barton. IUPAC solubility data series: Alcohols in water. Vol. 15. Pergamon, Oxford. 1984.
45. J.W. Roddy and C.F. Coleman. Talanta, **15**, 1281 (1968).
46. E. Vikingstad. J. Colloid Interface Sci. **72**, 75 (1979).
47. H.A. Akers and D.G. Gabler. Naturwissenschaften, **78**, 417 (1991).
48. K. Tamura, J. Hu, C. Trandum, P. Westh, C.A. Haynes, and Y. Koga. Phys. Chem. Chem. Phys. **2**, 355 (2000).
49. A. Hvidt, R. Moss, and G. Nielsen. Acta Chem. Scand. Ser. B, **32**, 274 (1978).
50. C. Tanford. The hydrophobic effect: formation of micelles and biological membranes. J. Wiley, New York. 1979.
51. M. Sakurai and T. Nakagawa. J. Chem. Thermodyn. **16**, 171 (1984).
52. Y. Koga. J. Phys. Chem. **95**, 4119 (1991).
53. Y. Koga, J. Kristiansen, and A. Hvidt. J. Chem. Thermodyn. **25**, 51 (1993).
54. E.C.H. To, J.V. Davies, M. Tucker, P. Westh, C. Trandum, K.S.H. Suh, and Y. Koga. J. Solution Chem. **28**, 1137 (1999).

© 2005 NRC Canada

Homoleptic magnesium bis-phosphinimide derivatives

Emily Hollink, Pingrong Wei, and Douglas W. Stephan

Abstract: The homoleptic Mg-phosphinimide complexes $Mg_2(\mu\text{-NP-}t\text{-Bu}_3)_2(\text{NP-}t\text{-Bu}_3)_2$ (**1**) and $Mg_3(\mu\text{-NP-}i\text{-Pr}_3)_4(\text{NP-}i\text{-Pr}_3)_2$ (**2**) were obtained from the reaction of 2 equiv. of the phosphinimines $HNPR_3$ (R = *t*-Bu, *i*-Pr) with $MgBu_2$. Spectroscopic and crystallographic studies confirmed the dimeric and trimeric structures of compounds **1** and **2**, respectively.

Key words: magnesium, phosphinimides, homoleptic, crystal stuctures.

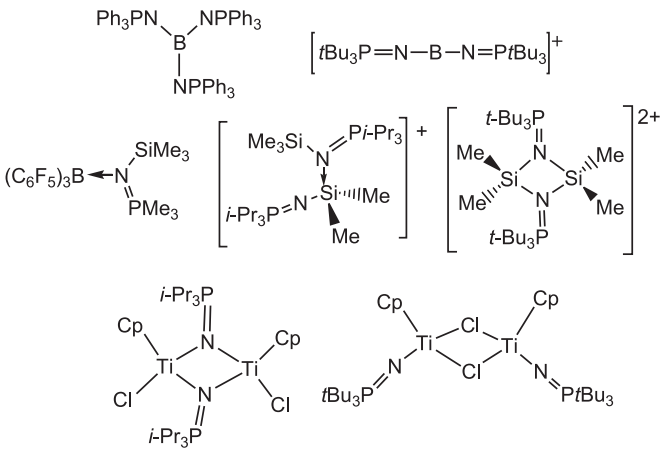
Résumé : On a obtenu les complexes homoleptiques Mg-phosphinimides $Mg_2(\mu\text{-NP-}t\text{-Bu}_3)_2(\text{NP-}t\text{-Bu}_3)_2$ (**1**) et $Mg_3(\mu\text{-NP-}i\text{-Pr}_3)_4(\text{NP-}i\text{-Pr}_3)_2$ (**2**) par réaction de 2 équiv. des phosphinimides $HNPR_3$ (R = *t*-Bu, *i*-Pr) avec du $MgBu_2$. Les études spectroscopiques et cristallographiques ont permis de confirmer la nature dimère et trimère des structures des composés **1** et **2**, respectivement.

Mots clés : magnésium, phosphinimides, homoleptique, structures cristallines.

[Traduit par la Rédaction]

Introduction

Main group derivatives of phosphinimine and phosphinimide ligands have been investigated and a large number of species have been structurally characterized. Much of the early work was reviewed by Dehnicke and Weller (1). In more recent studies of such species, we have prepared cationic silicon, germanium, tin, aluminum, and boron derivatives (2–4). Marked structural changes for phosphinimide derivatives as a result of steric effects have been previously seen for both main group and transition metal derivatives. For example, in the reactions of the phosphinimines with $B(C_6F_5)_3$, simple adducts, mono and dicationic species such as $Me_3PN(SiMe_3)\cdot B(C_6F_5)_3$, $[R_3PNSiMe_2(N(PR_3)SiMe_3)][MeB(C_6F_5)_3]$ (R = *i*-Pr, Ph), and $[((\mu\text{-}t\text{-}Bu_3PN)SiMe_2)_2][MeB(C_6F_5)_3]_2$ were characterized (2). In a similar sense, steric effects played a role in the formation of the linear cationic B species $[(t\text{-}Bu_3PN)_2B]^+X^-$, regardless of the ligand to boron stoichiometry used in the reaction (3). This stands in contrast to the species $B(NPPh_3)_3$, where the sterically less demanding phosphinimide accommodates a trigonal planar geometry at boron (5). One example of such steric effects in transition metal – phosphinimide complexes is represented by the contrasting structures of the Ti(III) species $[CpTi(\text{NP-}t\text{-}Bu_3)(\mu\text{-Cl})]_2$ and $[CpTiCl(\mu\text{-NP-}i\text{-}Pr_3)]_2$ (6). In this note, we probe the related steric effects for Mg-phosphinimide species. Herein, we report the first homoleptic Mg-phosphinimide complexes, $Mg_2(\mu\text{-NP-}t\text{-}Bu_3)_2(\text{NP-}t\text{-}Bu_3)_2$ and $Mg_3(\mu\text{-NP-}i\text{-}Pr_3)_4(\text{NP-}i\text{-}Pr_3)_2$ to be characterized. Preliminary examinations of the reactivity of these species are also reported.



Experimental section

All syntheses were performed employing an atmosphere of dry, oxygen-free nitrogen in a Vacuum Atmospheres inert atmosphere glovebox using oven-dried (140 °C) glassware unless otherwise stated. ^{1}H NMR data were acquired on a Bruker Avance 500 MHz spectrometer, while ^{13}C and ^{31}P NMR data were obtained from a Bruker Avance 300 MHz spectrometer. ^{1}H and ^{13}C NMR chemical shifts are listed relative to $SiMe_4$ in ppm, and were referenced to the residual solvent peak. ^{31}P NMR data were referenced using 85% H_3PO_4 as an external standard. All NMR spectra were recorded in C_6D_6. The University of Windsor Analytical Services (PerkinElmer 2400 series II Instrument) performed the combustion analyses.

Received 19 November 2004. Published on the NRC Research Press Web site at http://canjchem.nrc.ca on 22 April 2005.

E. Hollink, P. Wei, and D.W. Stephan.[1] Department of Chemistry and Biochemistry, University of Windsor, Windsor, ON N9B 3P4, Canada.

[1]Corresponding author (e-mail: Stephan@uwindsor.ca).

 doi: 10.1139/V05-059 © 2005 NRC Canada

Synthesis of $Mg_2(\mu\text{-NP-}t\text{-Bu}_3)_2(\text{NP-}t\text{-Bu}_3)_2$ (1) and $Mg_3(\mu\text{-NP-}i\text{-Pr}_3)_4(\text{NP-}i\text{-Pr}_3)_2$ (2)

These compounds were prepared employing similar procedures and thus only one is detailed. To a solution of Mg-*n*-Bu_2 (2.40 mL, 2.4 mmol; 1.0 mol/L in hexanes) in toluene (40 mL) was added a clear, colorless solution of HNP-*t*-Bu_3 (1.04 g, 4.8 mmol) in toluene (40 mL). After stirring at 25 °C for 10 h, all volatiles were removed in vacuo, affording a white solid (980 mg, 89%). Colorless crystals suitable for X-ray diffraction were grown from pentanes at –35 °C. **1**: ^{1}H NMR: 1.49 (d, 54H, $^3J_{P\text{-}H}$ = 11 Hz, *t*-Bu), 1.42 (d, 54H, $^3J_{P\text{-}H}$ = 12 Hz, *t*-Bu). ^{13}C NMR: 40.8 (d, $^1J_{P\text{-}C}$ = 46 Hz), 40.1 (d, $^1J_{P\text{-}C}$ = 52 Hz), 31.1, 30.9. ^{31}P NMR: 43.2 (s, 2P, μ-NP), 25.2 (s, 2P, σ-NP). Anal. calcd. for $C_{48}H_{108}Mg_2N_4P_4$: C 63.08, H 11.91, N 6.13; found: C 63.12, H 12.28, N 6.16. **2**: White solid (1.23 g, 87%). ^{1}H NMR: 2.25 (m, 12H, CH), 1.85 (m, 6H, CH), 1.32 (dd, 72H, $^3J_{P\text{-}H}$ = 12 Hz, $^3J_{H\text{-}H}$ = 7 Hz, Me), 1.27 (dd, 36H, $^3J_{P\text{-}H}$ = 12 Hz, $^3J_{H\text{-}H}$ = 7 Hz, Me). ^{13}C NMR: 28.8 (d, $^1J_{P\text{-}C}$ = 57 Hz), 26.1 (d, $^1J_{P\text{-}C}$ = 64 Hz), 18.8, 18.2. ^{31}P NMR: 27.6 (s, 4P, μ-NP), 7.9 (s, 2P, σ-NP). Anal. calcd. for $C_{54}H_{126}Mg_3N_6P_6$: C 57.99, H 11.36, N 7.51; found: C 57.85, H 11.67, N 7.26.

X-ray data collection and reduction

Crystals were manipulated and mounted in capillaries in a glovebox, thus maintaining a dry, O_2-free environment for each crystal. Diffraction experiments were performed on a Siemens SMART System CCD diffractometer. The data were collected in a hemisphere of data in 1448 frames with 10 s exposure times. The observed extinctions were consistent with the space groups in each case. The data sets were collected ($4.5° < 2\theta < 45°$–$50.0°$). The intensities of reflections within these frames showed no statistically significant change over the duration of the data collections. The data were processed using the SAINT and XPREP processing packages. An empirical absorption correction based on redundant data was applied to each data set. Subsequent solution and refinement was performed using the SHELXTL solution package.

Structure solution and refinement

Non-hydrogen atomic scattering factors were taken from the literature tabulations (7). The heavy atom positions were determined using direct methods employing the SHELXTL direct-methods routine. The remaining non-hydrogen atoms were located from successive difference Fourier map calculations. The refinements were carried out by using full-matrix least-squares techniques on *F*. In the final cycles of each refinement, all non-hydrogen atoms were assigned anisotropic temperature factors in the absence of disorder or insufficient data. In the latter cases, atoms were treated isotropically. C-H atom positions were calculated and allowed to ride on the carbon to which they are bonded assuming a C—H bond length of 0.95 Å. H-atom temperature factors were fixed at 1.10 times the isotropic temperature factor of the C atom to which they are bonded. The H-atom contributions were calculated, but not refined. The locations of the largest peaks in the final difference Fourier map calculation as well as the magnitude of the residual electron densities in each case were of no chemical significance. Additional details are provided in the supplementary data[2] and in Table 1.

Table 1. Crystallographic data.[a]

	1	2
Formula	$C_{48}H_{108}Mg_2N_4P_4$	$C_{54}H_{120}Mg_3N_6P_6$
Formula weight	913.88	1 112.31
a (Å)	13.479(9)	21.191(12)
b (Å)	19.999(14)	12.574(7)
c (Å)	22.441(15)	28.135(15)
α (°)	101.729(12)	90
β (°)	93.182(13)	106.867(10)
γ (°)	94.803(13)	90
Crystal system	Triclinic	Monoclinic
V (Å^3)	5 886(7)	7 174(7)
Space group	*P*-1	*P*2(1)/*c*
D(calcd.) (g cm^{-1})	1.031	1.030
Z	4	4
Abs. coeff. (μ, mm^{-1})	0.181	0.210
Data collected	24 379	29 801
Data $F_o^2 > 3\sigma(F_o^2)$	16 700	10 152
Variables	1045	622
R	0.0913	0.0609
Rw	0.1551	0.1133
GOF	0.885	1.030

[a]All data were collected at 25 °C and using Mo radiation (λ = 0.710 73 Å).

Results and discussion

The reaction of 2 equiv. of the phosphinimine HNP-*t*-Bu_3 with $MgBu_2$ resulted in the formation of the product **1** in 87% yield (Scheme 1). This species is extremely soluble in pentanes (ca. 1 g in 2 mL), but can be isolated from a saturated solution as colorless crystals at –35 °C. NMR characterization of **1** revealed two sets of resonances attributable to *tert*-butyl groups in the ^{1}H and ^{13}C NMR spectra, as well as two equal-intense signals in the ^{31}P NMR spectrum at 43.2 and 25.2 ppm. This is suggestive of a dimeric structure, in which two Mg centers are coordinated to both terminal and bridging phosphinimide units. The formulation of **1** as $Mg_2(\mu\text{-NP-}t\text{-Bu}_3)_2(\text{NP-}t\text{-Bu}_3)_2$ was confirmed by a crystallographic study (Fig. 1). As indicated by the spectroscopic data, two phosphinimide ligands bridge the two Mg centers with Mg—N distances in the range from 2.043(5) to 2.101(6) Å, giving rise to a Mg–Mg separation of 2.773(3) Å. Terminal phosphinimide ligands complete the coordination sphere of both Mg atoms. The terminal Mg—N distances of 1.922(6) and 1.902(6) Å are much shorter than the bridging Mg—N distances, as expected. The geometries about the Mg atoms

[2] Supplementary data for this article are available on the Web site or may be purchased from the Depository of Unpublished Data, Document Delivery, CISTI, National Research Council Canada, Ottawa, ON K1A 0S2, Canada. DUD 3654. For more information on obtaining material refer to http://cisti-icist.nrc-cnrc.gc.ca/irm/unpub_e.shtml. CCDC 256377 and 256378 contain the crystallographic data for this manuscript. These data can be obtained, free of charge, via www.ccdc.cam.ac.uk/conts/retrieving.html (or from the Cambridge Crystallographic Data Centre, 12 Union Road, Cambridge CB2 1EZ, UK; fax +44 1223 336033; or deposit@ccdc.cam.ac.uk).

© 2005 NRC Canada

Scheme 1. Synthesis of Mg bis-phosphinimides.

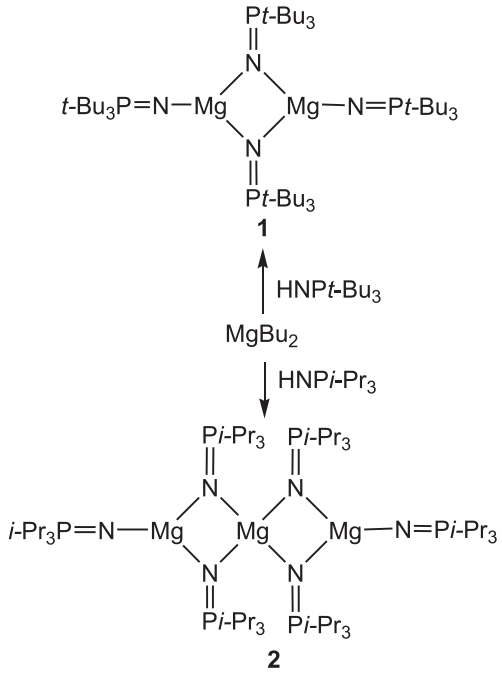
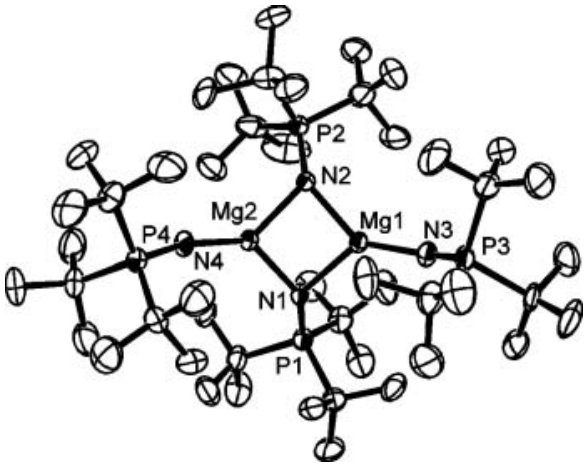
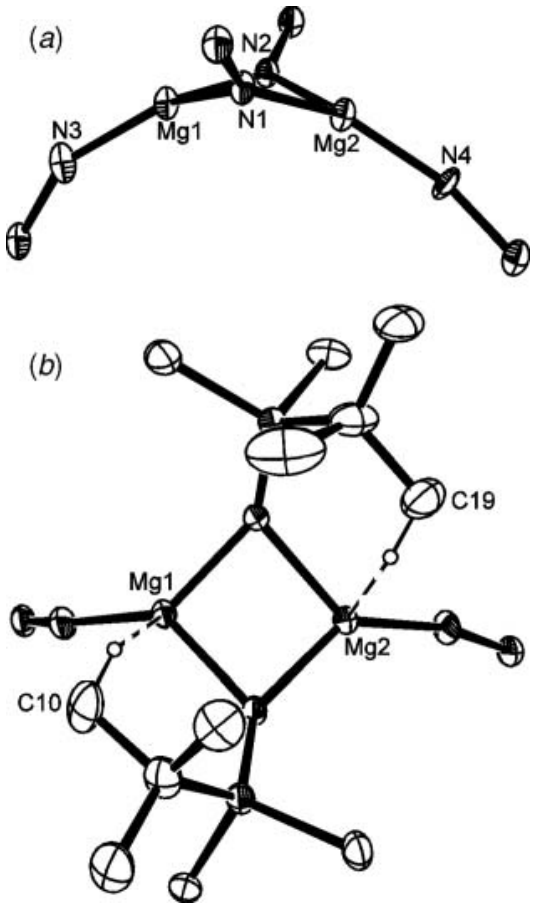


Fig. 1. ORTEP drawing of one of the two molecules of **1** in the asymmetric unit, hydrogen atoms omitted. Distances (Å): Mg(1)—N(3) 1.922(6), Mg(1)—N(2) 2.043(5), Mg(1)—N(1) 2.101(6), Mg(1)—Mg(2) 2.773(3), Mg(2)—N(4) 1.902(6), Mg(2)—N(1) 2.050(5), Mg(2)—N(2) 2.089(6), N(1)—P(1) 1.541(5), N(2)—P(2) 1.545(5), N(3)—P(3) 1.541(6), N(4)—P(4) 1.543(5). Angles (°): N(3)-Mg(1)-N(2) 134.2(3), N(3)-Mg(1)-N(1) 131.6(3), N(2)-Mg(1)-N(1) 90.4(2), N(4)-Mg(2)-N(1) 134.9(3), N(4)-Mg(2)-N(2) 132.0(3), N(1)-Mg(2)-N(2) 90.5(2), Mg(2)-N(1)-Mg(1) 83.8(2), Mg(1)-N(2)-Mg(2) 84.3(2), P(1)-N(1)-Mg(2) 144.0(3), P(1)-N(1)-Mg(1) 130.1(3), P(2)-N(2)-Mg(1) 143.4(3), P(2)-N(2)-Mg(2) 128.6(3), P(3)-N(3)-Mg(1) 150.3(4), P(4)-N(4)-Mg(2) 164.5(4).



are planar and three coordinate. The N-Mg-N angles in the Mg_2N_2 core are 90.4(2)°, while the N-Mg-N angles between the bridging and terminal phosphinimides are much larger, varying from 131.6(3)° to 134.9(3)°. The angles at N within these cores are 83.8(2)° and 84.3(2)°. Of the four P-N-Mg

Fig. 2. ORTEP drawings of: (*a*) the heavy atom core of **1**; (*b*) agostic C-H-Mg interactions in **1**.

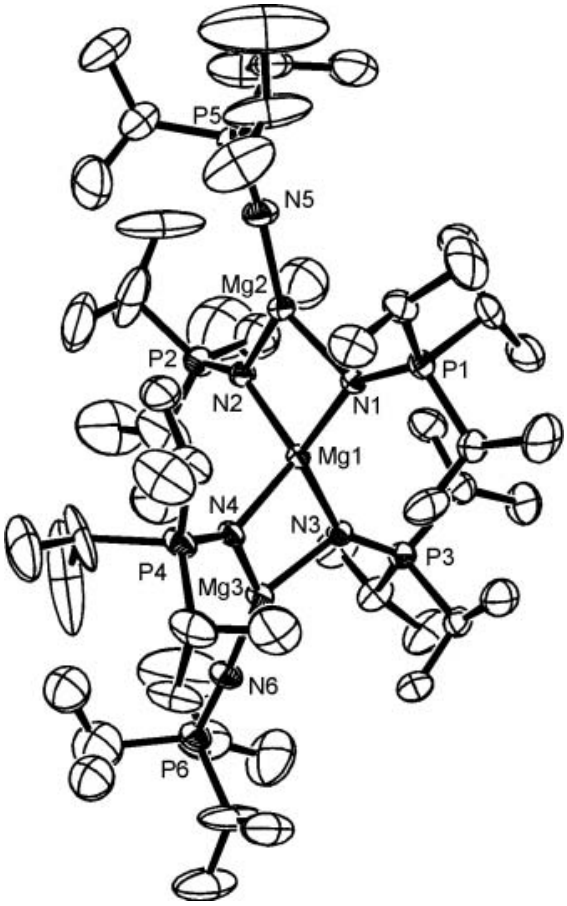


angles with this core, two are similar at 144.0(3)° and 143.4(3)°, while the others are 130.1(3)° and 128.6(3)°. This structural formulation of **1** is similar to the related three-coordinate Mg species $Mg_2(\mu\text{-}NBn_2)_2(NBn_2)_2$ (8), although the Mg_2N_4 core geometries are markedly different. In the amido derivative, the Mg_2N_4 core is planar, while in contrast, the core in **1** exhibits a significant distortion. The average angle between the N-Mg-N planes of the Mg_2N_2 core is 36.2°, while the angle between the terminal N(3)-P(3) and N(4)-P(4) vectors is 77.5° (Fig. 2*a*). These distortions are a consequence of the sterically demanding phosphinimide ligands. Interestingly, the Lewis acidic, three-coordinate Mg centers also give rise to close interactions in the solid state with H atoms of a *tert*-butyl group at distances from 2.298 to 2.487 Å (Fig. 2*b*). Similar intramolecular agostic interactions have been described for $Mg_2(\mu\text{-}t\text{-}Bu)_2(t\text{-}Bu)_2$ (9), while related intermolecular agostic interactions were observed for $Mg(CH(SiMe_3)_2)_2$ (10). The phosphinimide ligands exhibit consistent P—N bond lengths, averaging 1.543(5) Å. The terminal P-N-Mg angles vary significantly as demonstrated by a P(3)-N(3)-Mg(1) angle of 150.3(4)° and a P(4)-N(4)-Mg(2) angle of 164.5(4)°. This variation is a further reflection of the steric crowding in this molecule.

The analogous reaction of the less bulky phosphinimine HNP-*i*-Pr_3 with $MgBu_2$ proceeded in a similar manner to afford the highly soluble species **2** in 89% yield (Scheme 1). The ^1H and ^{13}C NMR data revealed two sets of resonances

© 2005 NRC Canada

Fig. 3. ORTEP drawing of **2**, hydrogen atoms omitted. Distances (Å): Mg(1)—N(3) 2.082(4), Mg(1)—N(4) 2.098(5), Mg(1)—N(1) 2.099(4), Mg(1)—N(2) 2.110(5), Mg(1)—Mg(3) 2.868(3), Mg(1)—Mg(2) 2.880(3), Mg(2)—N(5) 1.917(5), Mg(2)—N(2) 2.010(5), Mg(2)—N(1) 2.048(5), Mg(3)—N(6) 1.915(5), Mg(3)—N(4) 2.006(5), Mg(3)—N(3) 2.030(5), P(1)—N(1) 1.551(4), P(2)—N(2) 1.559(5), P(3)—N(3) 1.560(4), P(4)—N(4) 1.560(4), P(5)—N(5) 1.514(5), P(6)—N(6) 1.511(5). Angles (°): N(3)-Mg(1)-N(4) 87.94(17), N(3)-Mg(1)-N(1) 127.69(18), N(4)-Mg(1)-N(1) 122.57(19), N(3)-Mg(1)-N(2) 120.46(19), N(4)-Mg(1)-N(2) 112.07(18), N(1)-Mg(1)-N(2) 88.59(17), N(5)-Mg(2)-N(2) 136.6(2), N(5)-Mg(2)-N(1) 130.4(2), N(2)-Mg(2)-N(1) 92.80(18), N(6)-Mg(3)-N(4) 137.4(2), N(6)-Mg(3)-N(3) 130.4(2), N(4)-Mg(3)-N(3) 91.97(18), Mg(2)-N(1)-Mg(1) 87.96(17), Mg(2)-N(2)-Mg(1) 88.65(18), Mg(3)-N(3)-Mg(1) 88.42(17), Mg(3)-N(4)-Mg(1) 88.63(18), P(1)-N(1)-Mg(2) 124.5(2), P(1)-N(1)-Mg(1) 147.3(2), P(2)-N(2)-Mg(2) 131.9(3), P(2)-N(2)-Mg(1) 139.1(3), P(3)-N(3)-Mg(3) 124.8(2), P(3)-N(3)-Mg(1) 145.9(3), P(4)-N(4)-Mg(3) 134.6(3), P(4)-N(4)-Mg(1) 136.7(3), P(5)-N(5)-Mg(2) 174.9(4), P(6)-N(6)-Mg(3) 175.0(4).



for isopropyl groups, as well as two distinct resonances in the ^{31}P NMR spectrum at 27.6 and 7.9 ppm. However, in contrast to **1**, the ratio of these resonances was 2:1, with the downfield resonances being the more abundant. This suggested a 2:1 ratio of bridging to terminal phosphinimide ligands. Based on this information, **2** was formulated to be $Mg_3(\mu\text{-NP-}i\text{-Pr}_3)_4(\text{NP-}i\text{-Pr}_3)_2$. Despite some degree of disorder in the peripheral isopropyl groups, a crystallographic study of **2** confirmed the trimetallic nature of **2**, in which two pairs of phosphinimide ligands link two Mg centers to a central four-coordinate pseudo-tetrahedral Mg (Fig. 3). Terminal phosphinimide ligands complete the coordination sphere of terminal, tri-coordinate Mg centers. Similar to **1**, the average terminal Mg—N distances in **2** of 1.916(5) Å are significantly shorter than the bridging Mg—N distances that range from 2.082(4) to 2.110(5) Å. The resulting Mg–Mg separations of 2.868(3) and 2.880(3) Å in **2** are slightly longer than that seen in **1**. The angles about the central Mg atom are significantly distorted from pseudo-tetrahedral with the chelate N-Mg-N angles within the Mg_2N_2 units being 87.94(17)° and 88.59(17)°. The corresponding N-Mg-N angles at the three-coordinate Mg centers are 92.80(18)° and 91.97(18)°, while the N(bridging)-Mg-N(terminal) angles range from 130.4(2)° to 137.4(2)°. The Mg-N-Mg angles for the bridging phosphinimides are slightly larger than those in **1**, ranging from 87.96(17)° to 88.65(18)°. This is attributed to steric interactions among the four bridging phosphinimide ligands. The remaining N-Mg-N angles range from 112.07(18)° to 127.69(18)°. The P—N distances in **2** fall in the range of those in **1**, however, the terminal P-N-Mg angles are closer to linearity at 174.9(4)° and 175.0(4)°. The trimeric nature of **2** in comparison to the dimeric nature of **1** is attributed to the diminished steric demands of *i*-Pr vs. *t*-Bu substitutents on the phosphinimide ligand. Agostic Mg···H interactions analogous to those seen in **1** were not seen for **2**.

Preliminary examination of the reactivity of **1** revealed that reaction of $Ti(N\text{-}t\text{-Bu})Cl_2(t\text{-BuPy})_3$ (11) with **1** gave a mixture of products. In contrast, reaction of $CpZr(N\text{-}t\text{-Bu}_3)Cl_2$ with **1** proceeded cleanly to transfer a phosphinimide ligand from the Mg reagent to Zr, yielding the known species $CpZr(N\text{-}t\text{-Bu}_3)_2Cl$ in 85% yield (12). These results suggest that Mg-bis-phosphinimide derivatives may be highly soluble, effective ligand transfer reagents in our continuing studies of the chemistry of phosphinimide compounds.

Acknowledgements

Financial support from the Natural Sciences and Engineering Research Council of Canada (NSERC) and NOVA Chemicals Corporation is gratefully acknowledged.

References

1. K. Dehnicke and F. Weller. Coord. Chem. Rev. **158**, 103 (1997).
2. S. Courtenay, C.M. Ong, and D.W. Stephan. Organometallics, **22**, 818 (2003).
3. S. Courtenay, J.Y. Mutus, R.W. Schurko, and D.W. Stephan. Angew. Chem. Int. Ed. **41**, 498 (2002).
4. C.M. Ong, P. McKarns, and D.W. Stephan. Organometallics, **18**, 4197 (1999).
5. M. Moehlen, B. Neumueller, and K. Dehnicke. Z. Anorg. Allg. Chem. 177 (1998).
6. T.W. Graham, J. Kickham, S. Courtenay, P. Wei, and D.W. Stephan. Organometallics, **23**, 3309 (2004).
7. D.T. Cromer and J.T. Waber. Int. Tables X-Ray Crystallogr. **4**, 71 (1974).
8. W. Clegg, F.J. Craig, K.W. Henderson, A.R. Kennedy, R.E. Mulvey, P.A. O'Neil, and D. Reed. Inorg. Chem. **36**, 6238 (1997).

© 2005 NRC Canada

9. K.B. Starowieyski, J. Lewinski, R. Wozniak, J. Lipkowski, and A. Chrost. Organometallics, **22**, 2458 (2003).
10. P.B. Hitchcock, J.A.K. Howard, M.F. Lappert, W.-P. Leung, and S.A. Mason. Chem. Commun. 847 (1990).
11. P. Mountford. Chem. Commun. 2127 (1997).
12. E. Hollink, P. Wei, and D.W. Stephan. Organometallics, **23**, 1562 (2004).

© 2005 NRC Canada

Construction and application of a single-molecule fluorescence microscope

Sangram Bagh and Matthew F. Paige

Abstract: In this paper, we describe the construction, optimization, and testing of an epifluorescence microscope that has single-molecule (SM) resolution and sensitivity. The microscope makes use of a novel new type of wide-area charge-coupled device (CCD) photodetector with on-chip multiplier gain. Sensitivity and spatial resolution of the instrument are demonstrated by imaging individual Rhodamine 6G (R6G) molecules and characterizing their basic photophysical behaviour under a variety of imaging conditions. A simple, general method for calibrating the photodetector (correlating CCD counts with incident photons) using a highly attenuated laser beam is presented, and the performance of the photodetector is compared with that of other detectors commonly used in SM fluorescence imaging applications. We also demonstrate the versatility of the microscope system by characterizing the SM photophysical behaviour of several other fluorescent molecules, including bodipy-FL and the enhanced green fluorescent protein (EGFP).

Key words: single molecule, fluorescence, microscopy, CCD camera, calibration, photobleaching.

Résumé : Dans ce travail, on a construit, optimisé et vérifié d'un microscope à épifluorescence à résolution et sensibilité d'une seule molécule (SM). Le microscope fait appel à nouveau type de photodétecteur avec un dispositif à couplage de charge (« CCD ») à grand angle et un multiplicateur du gain sur la puce. On a démontré la sensibilité et la résolution spatiale de l'instrument en faisant l'image des molécules individuelles de Rhodamine 6G (R6G) et en caractérisant leur comportement photophysique dans diverses conditions. On présente une méthode générale et simple de calibrer le photodétecteur (qui relie le comptage du CCD avec les photons incidents) qui fait appel à un faisceau laser fortement atténué et on a comparé la performance du photodétecteur avec celle d'autres détecteurs régulièrement utilisés dans des applications d'imagerie de fluorescence SM. On démontre aussi la versatilité de ce système de microscope en caractérisant le comportement photophysique SM de plusieurs autres molécules fluorescentes, y compris le bodipy-FL et la protéine de fluorescent à vert exalté (« EGFP »).

Mots clés : molécule unique, fluorescence, microscopie, caméra à CCD, calibration, photolessivage.

[Traduit par la Rédaction]

Introduction

Single-molecule (SM) fluorescence spectroscopy is a rapidly growing field of research in which the fluorescence emission of individual, isolated molecules is directly measured. The principal motivation for carrying out SM experiments is that one can directly observe the behaviour of molecules in the absence of ensemble averaging. In standard, "bulk" chemical assays, the behaviour of individual molecules is blurred out through averaging; it has been shown on numerous occasions, however, that many chemical systems are heterogeneous when probed at the SM level, and that these hidden heterogeneities can play an important role in dictating the overall properties of the system (1–3). Studies of individual molecules have been extended beyond simple proof-of-principle experiments, and are now being used in a wide range of disciplines, including investigations of biological systems, polymers, and inorganic materials, to name a few (2, 4–7).

Fluorescence microscopy has become one of the primary tools used by researchers in the field of SM fluorescence spectroscopy, as the technique can provide both high sensitivity and good (diffraction-limited) spatial resolution. A number of different experimental methods for carrying out SM fluorescence microscopy have been demonstrated, including epifluorescence, wide-field total-internal reflection (TIR), confocal, and near-field scanning optical microscopies (3, 8, 9). There are a number of common criteria that these microscopy methods must meet to achieve SM detection; these include optimization of fluorescence collection efficiency, reduction of unwanted background signal, and the use of extremely sensitive, low-noise photodetectors. Optimal collection efficiency is achieved through careful alignment of the microscope, selection of suitable emission filters to attenuate residual excitation and scattered light, and by use of colour-corrected, oil-immersion microscope objectives with high numerical apertures (typically NA = 1.4) to maximize the number of collected photons. Background signals are typically minimized through a combination of careful sample preparation that makes use of only the highest purity solvents and buffers, and again through careful selec-

Received 2 November 2004. Published on the NRC Research Press Web site at http://canjchem.nrc.ca on 29 April 2005.

S. Bagh and M.F. Paige.[1] Department of Chemistry, University of Saskatchewan, 110 Science Place, Saskatoon, SK S7N 5C9, Canada.
[1]Corresponding author (e-mail: matthew.paige@sask.usask.ca).

 doi: 10.1139/V05-053 © 2005 NRC Canada

tion of emission filters to maximize rejection of excitation and scattered light.

Perhaps the most important component of a fluorescence microscope system with SM imaging capabilities is the photodetector. The primary requirements for photodetectors in SM experiments are both high-sensitivity, preferably over the visible region of the spectrum where fluorophores commonly used for biological fluorescent labeling purposes emit, and a high data acquisition rate. The latter is important for detecting rapid photophysical events and processes, and also because most fluorophores undergo rapid, irreversible photobleaching and the photodetector should ideally acquire many data points before photobleaching takes place. There are a number of photodetectors currently available that meet these requirements. Photomultiplier tubes (PMTs), for example, were used in some of the earliest SM fluorescence detection measurements (for a recent review, see ref. 8). However, PMTs typically suffer from low quantum efficiencies (photoelectrons generated per incident photon) in the visible region of the spectrum and require the use of sophisticated electronics to operate in single-photon counting mode, which is often desirable for SM experiments. Researchers in SM fluorescence microscopy more often make use of silicon-based photon-counting modules (avalanche photodiodes (APDs)) for scanned techniques such as confocal and near-field, and high-sensitivity charge-coupled device (CCD) cameras for wide-field illumination approaches such as epifluorescence or wide-field TIR. Both types of devices have high quantum efficiencies over the visible to near-IR regions of the spectrum. Also, both types of devices often have substantial gain, which is vital for overcoming the detector read-noise that can be a limiting factor in low-light level experiments.

CCD cameras have proven to be particularly useful for SM fluorescence microscopy experiments. They are parallel devices; that is, the entire sample illumination area can be imaged onto the CCD chip, allowing many individual molecules to be imaged simultaneously. This allows large data sets to be accumulated in just a few experiments. Modern CCD detectors also have a sufficiently rapid data acquisition rate (fastest acquisition time per single whole chip frame is typically ~30 ms) for SM measurements. The most sensitive of commercial CCD cameras often make use of image intensification, typically through the application of a known voltage to a multichannel plate (MCP) between the detector's photocathode and phosphor screen, to enhance signal levels. While offering superb sensitivity and good data acquisition rates, intensified CCD cameras are both expensive and prone to light-induced damage; a sudden jump in light levels while operating the image intensifier can cause severe damage to the detector chip.

Recently, a new type of CCD camera capable of ultrasensitive imaging without the use of an image intensifier has become commercially available. This new class of cameras, now available from several different manufacturers, makes use of a process termed on-chip multiplication gain to overcome detector read-noise at low light levels. In the on-chip multiplication process, a serial register of pixels is placed between the detector chip and the camera preamplifier. When electrons are transferred from the detector chip through the serial register, they are accelerated by an applied potential. This leads to the generation of secondary electrons through an impact-ionization process. The degree of amplification (gain) can be controlled by adjusting the magnitude of the potential applied to the serial register. With the use of multiplier gain and thermoelectric cooling of electronic elements, photodetector read-noise and dark current can be overcome and ultra-low light levels can be detected (10). Cameras with on-chip multiplier gain are significantly less expensive than conventional intensified CCD cameras, and since amplification takes place after the signal has reached the photodetector chip, the camera is relatively insensitive to damage caused by sudden increases in signal intensity. This new class of camera has tremendous potential in SM imaging applications, and their full capabilities in this regard should be explored.

In this paper, we describe our recent efforts at constructing and testing an epifluorescence microscope with SM sensitivity, which makes use of a CCD camera with on-chip multiplication gain for a photodetector. We demonstrate that our system has sufficient sensitivity and spatial resolution for imaging individual molecules of several different fluorophores, including Rhodamine 6G (R6G), enhanced green fluorescent protein (EGFP), and bodipy-FL, a fluorophore that has never before been characterized at the SM level. Basic photophysical measurements, including characterizing signal-to-noise ratios, generation of histograms of photobleaching rates, and characterization of photobleaching dynamics ("blinking") have been carried out for all of these fluorophores and are compared with data available from the literature. In addition, we present a simple, approximate procedure for calibrating the CCD photodetector such that the detector counts can be directly converted into numbers of photons, and discuss the overall potential of this class of camera for SM fluorescence imaging applications.

Materials and methods

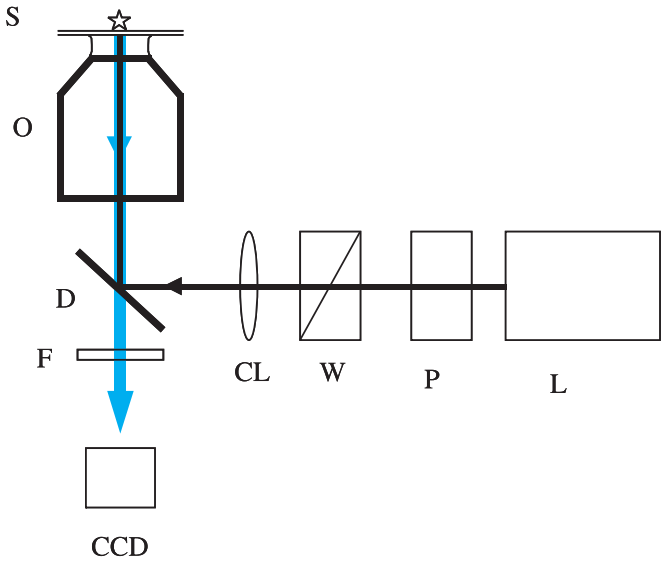
Microscope setup

The epifluorescence microscope used in these experiments is based on a commercial Nikon TE2000 inverted optical microscope (Nikon, Canada). A schematic diagram of the instrument is shown in Fig. 1. Briefly, a collimated, linearly polarized output beam from a tunable argon-ion laser (Melles Griot, Carlsbad, California, USA) was passed through neutral density filters to adjust laser power and a quarter waveplate to generate circularly polarized light. The beam was then focused onto the back focal plane of a 60×, 1.4NA oil-immersion objective lens (PlanApo, Nikon, Canada) by means of a 500 mm focal length lens. Excitation light was reflected onto the sample by a dichroic beamsplitter (for 488 nm excitation, a DRLP 500 nm, Omega Optical, Brattleboro, Vermont, USA; for 514 nm, a DRLP 540 nm).

After excitation, fluorescence emission from the sample was filtered through two long-pass emission filters (500AELP, Omega Optical, Brattleboro, Vermont, USA) to remove residual excitation light and directed onto a wide-area, front-illuminated CCD photodetector (Cascade 512F, Photometrics, Tucson, Arizona, USA). Unless stated otherwise, the CCD was operated at a fixed multiplication gain of 2907 arbitrary units for imaging. Operation of the CCD photodetector and data analysis was carried out through the soft-

© 2005 NRC Canada

Fig. 1. Schematic diagram of the single-molecule epifluorescence microscope used in these experiments. L (tunable Ar^+ laser), P (Glan–Thomson polarizing prism), W (quarter waveplate), CL (focusing lens (f = 500 mm)), D (dichroic beamsplitter), O (microscope objective (NA = 1.4, 60×)), S (sample and coverglass), F (longpass emission filter(s)), CCD (CCD photodetector). The lens focuses the excitation light onto the back focal plane of the microscope objective, resulting in an approximately 10 μm diameter excitation spot. The resulting fluorescence is collected back through the objective, passed through the dichroic and emission filters, and finally directed onto the CCD photodetector.



ware package MetaMorph (Universal Imaging, Downington, Pennsylvania, USA), which allows both static and time-resolved (time-lapse) imaging.

Sample preparation

Samples were prepared from very dilute dye solutions (~10^{-10} mol/L) in water, phosphate buffer, or methanol. Dyes used in these experiments included R6G (Sigma-Aldrich, Canada), bodipy-FL (Molecular Probes, Eugene, Oregon, USA), and EGFP (a kind gift from Professor H. Iwai, University of Saskatchewan). Aliquots of dye solution were deposited directly onto microscope coverglass (No. 1 thickness, borosilicate float glass, VWR, Canada) and the solvent allowed to evaporate, or were deposited by spin-casting. Coverglass was precleaned by first thoroughly rinsing with methanol and then repeatedly passing through the flame of a propane torch. Control samples of coverglass cleaned in this way showed no fluorescent impurities when imaged under conditions typically used for single-molecule measurements. For some samples, the dye-treated coverglass was also coated with a thin film of polymethylmethacrylate (PMMA; Polysciences, Warrington, Pennsylvania, USA), deposited by spin-casting a 5% *w*/*v* ethyl acetate solution of the polymer onto the coverglass. Samples of EGFP were prepared by diluting stock EGFP in phosphate buffer (pH 7.0), and mixing the sample in a 2% *w*/*v* agarose gel, prepared from the same buffer, at approximately 37 °C. A 5 μL aliquot of molten agarose was sandwiched between two clean pieces of coverglass and allowed to cool before imaging in the microscope.

Results and discussion

Initial characterization and testing of the microscope

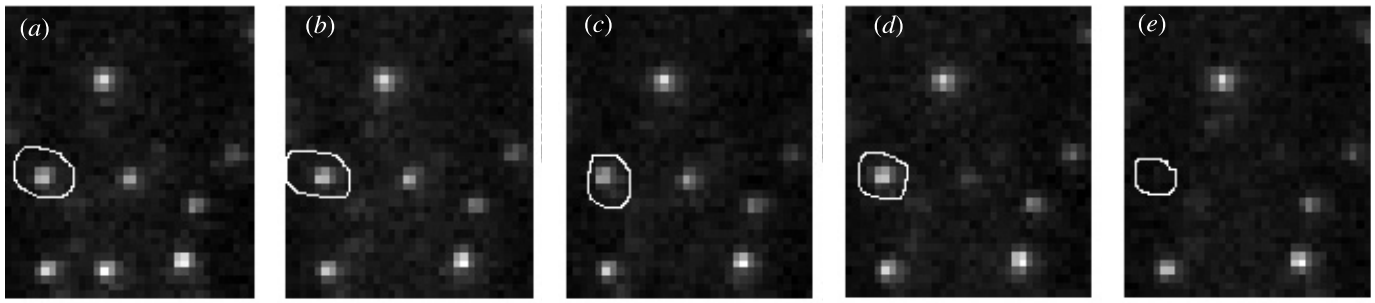
The SM fluorescence microscope was constructed as described in the Materials and methods section. Overall efficiency of the optical system in terms of light transmission in the microscope was determined by measuring the initial laser power entering the epi-illumination port and comparing this value to the laser power at different points in the optical train. Relative to this initial value, ~60% of the incident light is reflected off of the dichroic beamsplitter into the microscope objective and ~50% of the incident light is projected through the objective onto the sample plane. Losses are likely caused by reflection, scattering, and partial blocking of the excitation beam by optical elements that are not readily accessible in a commercial microscope. Based on experimentally measured light losses, the known values for numerical aperture of the objective lens and the transmission efficiency of the emission filters, we estimate the overall fluorescence collection efficiency of our microscope to be ~3% to 4%. This compares well with collection efficiency values reported by other researchers in this discipline (e.g., ref. 11).

After basic construction of the microscope system was complete, we tested its ability to detect individual molecules of R6G that had been immobilized in a PMMA matrix. When these samples (preparation described previously) were placed in the microscope and illuminated with an intensity of ~0.5–6.0 kW/cm^2, we observed images consisting of multiple (~5–10, depending on preparation conditions), well-dispersed spots on a dark background. In these experiments, illumination intensity is reported as the total laser power at the microscope objective, divided by the illumination area at the sample plane. A typical image of a sample prepared and imaged in this manner is shown in Fig. 2*a*. The fluorescent spots had diameters of approximately 300 nm, as determined by calibrating the CCD pixel size against a standard United States Air Force (USAF) test target. The sizes of the fluorescent spots are in reasonable agreement with the diffraction-limited size (~λ/2) that is anticipated when measuring individual molecules. When imaged under constant illumination conditions, the bright spots showed abrupt (single-step) photobleaching behaviour. That is, the emission intensity of a spot dropped down to the background level of the experiment during the time course of a single 100 ms integration period. This is shown in Figs. 2*a*–2*d*, in which a series of consecutive images is displayed. One particular spot has been circled to highlight the single-step photobleaching event. Single-step photobleaching, when observed in conjunction with low concentration levels and diffraction-limited size, is a well-known signature of single-molecule fluorescence experiments (1, 12), indicating that the fluorescent spots we observe are individual R6G molecules.

A simple and useful approach to data analysis in SM fluorescence experiments is to generate plots of fluorescence emission intensity of an individual molecule as a function of illumination time. These plots can provide basic "analytical" information about a fluorophore and detection system (i.e., signal-to-noise ratio, background signal intensity) that is

© 2005 NRC Canada

Fig. 2. Consecutive CCD images (*a*–*e*) of individual R6G molecules immobilized in a PMMA matrix. One molecule is circled for reference. The single step photobleaching of a bright spot in frame (*e*) is a characteristic signature of a single molecule (image size is approximately 5.0 μm × 5.7 μm, integration time = 100 ms per frame, excitation intensity = 0.6 kW/cm^2, excitation wavelength = 514 nm).

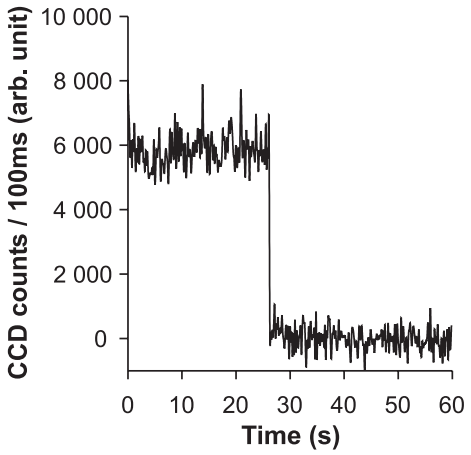


useful for optimizing the apparatus and sample preparation, and can also provide fundamental insight into the basic photophysical behaviour of the fluorophore. A typical plot showing fluorescence emission intensity vs. time for an individual molecule of R6G in PMMA is shown in Fig. 3. We operationally define the signal-to-noise (SNR) ratio as the mean signal (corrected for background and detector offset) measured with a 100 ms integration period for the entire duration of the molecule's on-time, divided by the standard deviation of the same signal. For R6G, we measured SNRs of around 11. This compares well with other SNRs for typical, good laser dyes found in the literature (e.g., ref. 9). It is worth noting that not every molecule in a SM measurement will have the same SNR. One primary reason for this is a distribution of effective absorption cross-sections for molecules resulting from the different orientation of molecules along the *z* axis when excitation light is circularly polarized in the *x*–*y* plane (see for example, ref. 13).

In general, we found that for R6G in PMMA, photobleaching takes place in a single-step after which the vast majority (>95%) of molecules remain in a permanently nonemissive state. Occasionally, we observed a molecule that displays blinking — that is, the fluorophore undergoes multiple transitions between an emissive and nonemissive state, but this was rare. Samples that were not coated with PMMA show a considerably larger fraction of molecules that undergo blinking, and the molecules photobleach much more rapidly than those coated with polymer (data not shown). This observation is in good agreement with numerous other studies, which suggest that blinking is connected to environmental factors such as interactions with glass surface sites and photochemical reactions with atmospheric oxygen (8, 14–16).

Another useful approach to analyzing single-molecule properties in chemical systems is to generate frequency histograms of fluorescence "on-times", the time required for a molecule to undergo irreversible photobleaching. This can provide insight into the presence of inhomogeneities in the chemical system, as well as more complex photophysical phenomena. For example, simple, homogeneous systems in which all molecules are subjected to identical local environmental conditions have fluorescence on-times that follow simple Poisson-type statistics, a consequence of selecting a small, random number of sample molecules from a large overall population. That is, the frequency of fluorescence

Fig. 3. A plot showing fluorescence emission intensity as a function of integration time for a single R6G molecule immobilized in a PMMA matrix (excitation intensity = 0.6 kW/cm^2, excitation wavelength = 514 nm). The intensity is shown in CCD counts/100 ms (arb. unit) after subtracting the mean background signal.



on-times can be expected to show a simple, single-exponential decrease (17). However, if there are several different sub-populations of molecules in the system, for instance a small subset of molecules bound to defects on a surface or molecules located in a region of the sample that has a different chemical composition, then one would observe significantly more complicated (typically multi-exponential) histograms. We show a histogram of fluorescence on-times for our test system of R6G in PMMA in Fig. 4, along with a simple, single-exponential fit. As seen in Fig. 4, the system shows an excellent fit to a single-exponential function, which is the expected result for the measurement of fluorescence on-time for a simple fluorophore like R6G in a uniform polymer matrix. These measurements are in reasonable agreement with those collected by a number of researchers (for example, refs. 15 and 18). We take these results, in combination with those described in the preceding paragraphs, as evidence that our microscope system (and most notably the photodetector) is sufficiently sensitive to detect individual molecules and can produce SM data that is consistent with the literature.

© 2005 NRC Canada

Fig. 4. The histogram and single exponential fit of on-time distribution for R6G in PMMA coating. The fitting function is $N = A_0 \exp(-t/\tau_{ON})$ where N = number of molecules at time t, τ_{ON} = photobleaching time constant, and A_0 = amplitude. The corresponding photobleaching time constant is $\tau_{ON} = 2.00$ s. The excitation intensity used was 0.6 kW/cm^2.

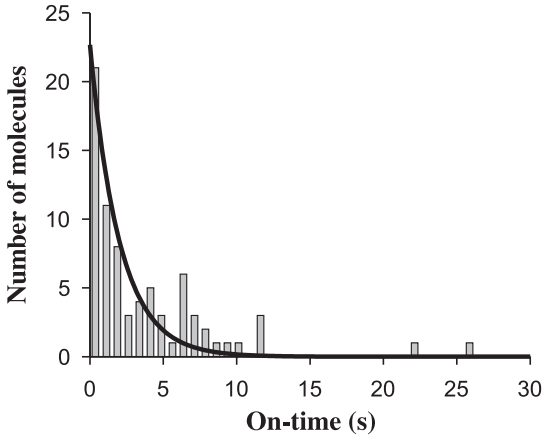
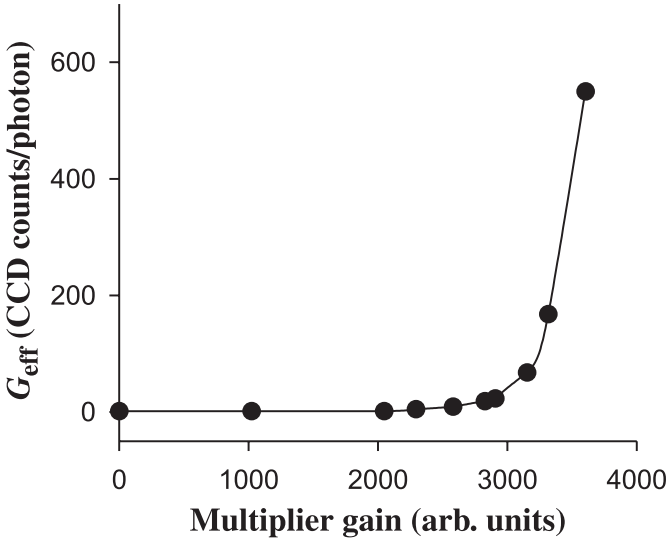


Fig. 5. A plot showing experimentally measured effective gain (see eq. [1] for the definition) as a function of applied multiplier gain. The experiment was carried out at an excitation power of 190 μW and wavelength of 514 nm.



Characterization and calibration of the CCD photodetector

While CCD photodetectors offer excellent sensitivity, the ability to monitor many molecules at a time, and good data acquisition rates, they suffer from a disadvantage to photon-counting modules in that they do not directly yield the number of photons emitted by a fluorophore. Since the ability to directly count numbers of emitted photons is often of great value in single-molecule fluorescence experiments, this limitation is somewhat problematic. The main challenge with correlating CCD counts to emitted photons is that the true gain factor for the detector is generally not well-known. In the Cascade 512F camera, for example, the gain factor is altered by changing the magnitude of the voltage between different pixels in the serial transfer register, which in turn affects the number of secondary electrons generated as charge is moved through the register. While the gain factor is, of course, correlated to the serial register voltages, the quantitative relationship between the two is not well-defined. A further complication is that CCD devices do not necessarily show fixed multiplicative gain; since the electron impact ionization process is, itself, a stochastic process, the gain factor itself can show statistical variations (so-called excess noise).

In an effort to quantify some of these effects for our photodetector, we have developed a simple procedure for calibrating our CCD detector against a well-defined source of photons such that CCD counts can be approximately converted into the number of incident photons. For the sake of simplicity, we will give an overall, working definition of effective gain as follows:

$$[1] \qquad \text{CCD counts} = N_{\text{photons}} \times G_{\text{eff}}$$

where CCD counts is the average number of analog-to-digital unit counts read from the CCD after subtracting dark counts, N_{photons} is the average number of photons hitting the detector chip in a known integration period, and G_{eff} is the overall effective gain of the system. We will include several operational factors in G_{eff}, including the quantum efficiency of the photodetector chip, the conversion gain that relates CCD electrons and CCD counts, and finally the on-chip multiplication gain. Our procedure for measuring G_{eff} is to align a heavily attenuated laser beam of known wavelength and power (the latter measured using a calibrated power meter) onto the chip, and record the average number of CCD counts over a known integration period. The value N_{photons} is then simply calculated from eq. [2]:

$$[2] \qquad N_{\text{photons}} = \frac{\lambda P_0 \Delta t}{hc}$$

where λ, P, Δt, h, and c are the laser wavelength, power, integration period, Planck's constant, and the speed of light, respectively. It should be noted that while using an attenuated laser beam for camera calibration can be very effective, great care must be taken to avoid causing photo damage to the chip; this procedure must be applied with particular care if applied to an intensified CCD camera, as it could easily lead to instrument damage.

Figure 5 shows a plot of G_{eff} as a function of the applied multiplier gain (λ = 514 nm, P_0 = 190 μW). At low values of applied multiplier gain, G_{eff} increases very slowly, but shows an exponential increase at higher values (2000–3000 arb. units). An exponential increase in gain with applied voltage is common in devices that make use of a series of elements to generate electron cascades (19). We found that at multiplier gains greater than 3500, dark counts begin to play a significant role in the overall signal, so the measurement range was restricted to below this value. For the single-molecule experiments described in the previous section, multiplication gains around 1000–2000 arb. units were sufficient to allow detection of only the brightest individual molecules; however, many molecules could be readily discerned in the range of 2000–3000 arb. units. We carried out the majority of our measurements at a setting of 2907 arb. units, which corresponds to a G_{eff} of 22.3 ± 0.2 CCD counts per

© 2005 NRC Canada

photon. At these settings, typical R6G molecules yield a photon count rate of around 250–400 counts per 100 ms time interval, which is in reasonable agreement with results collected using photon-counting modules (see for example, ref. 15).

We note that there are several sources of experimental error in this calibration procedure that limit its accuracy. For the Cascade 512F, the quantum efficiency of the photodetector chip increases by approximately 25% over the spectral range of 500–650 nm (20). Because of this and the finite width of emission peaks of fluorescent molecules, order one corrections in G_{eff} are needed. One can estimate the amount of error this causes by weighting the emission intensities from a bulk spectrum by the quantum efficiency of the detector at that wavelength. For R6G, this effect leads to an underestimate in G_{eff} of ~10%. While significant, this problem with the calibration procedure can be corrected for in a reasonable way. It is also worth noting that the latest generation of on-chip multiplier gain CCD cameras from Photometrics have a moderately invariant quantum efficiency over the spectral range of 500–700 nm, and for these cameras, the inaccuracy in the calibration procedure caused by this effect will become negligible.

Another potential source of error in this calibration procedure is the excess noise that is intrinsic to devices that do not have fixed, multiplicative gain. The excess noise factor (F) can be defined as (19):

$$[3] \qquad F = 1 + \frac{\sigma_G^{\,2}}{\langle G \rangle^2}$$

where σ_G^2 and $\langle G \rangle$ are the variance and mean of the gain, respectively. For a detector with deterministic gain, F should be equal to unity (zero variance in gain); for devices that have random gain, the excess noise factor can be considerably larger. Intensified CCD cameras typically have F values in the range of 1.5–3.5, though under some conditions this can go as high as 60, making calibration problematic (19, 21). For the Cascade camera, the manufacturer reports experimentally measured F values of around 1.4 at the highest gain of the instrument. To measure an upper limit on the excess noise that is relevant for the gain levels used in our typical SM measurements, we estimated F using our experimentally measured mean effective gain and variance in effective gain. While not the most accurate method for measuring the excess noise factor (for a more rigorous method see ref. 21), this approach will provide a reasonable "order of magnitude" measure of F. From our measurements, the F value works out to be ~1.005, indicating that, at the settings we use in SM experiments, excess noise effects are minimal. Variations in quantum efficiency with wavelength for the detector will be the dominant factor in terms of limiting the overall accuracy of the calibration procedure. It is worth noting that the selection of a multiplier gain level for use in SM experiments must take into account several factors; one must carefully balance the enhancement in signal levels that can be attained with high gains against the overall increase in system noise caused by excess noise. Overall, the SNR of the measurement will be lowered by the excess noise factor, so it is important in SM experiments not to use a multiplier gain that is higher than absolutely necessary.

Comparison of different fluorophores (R6G, bodipy-FL, and EGFP)

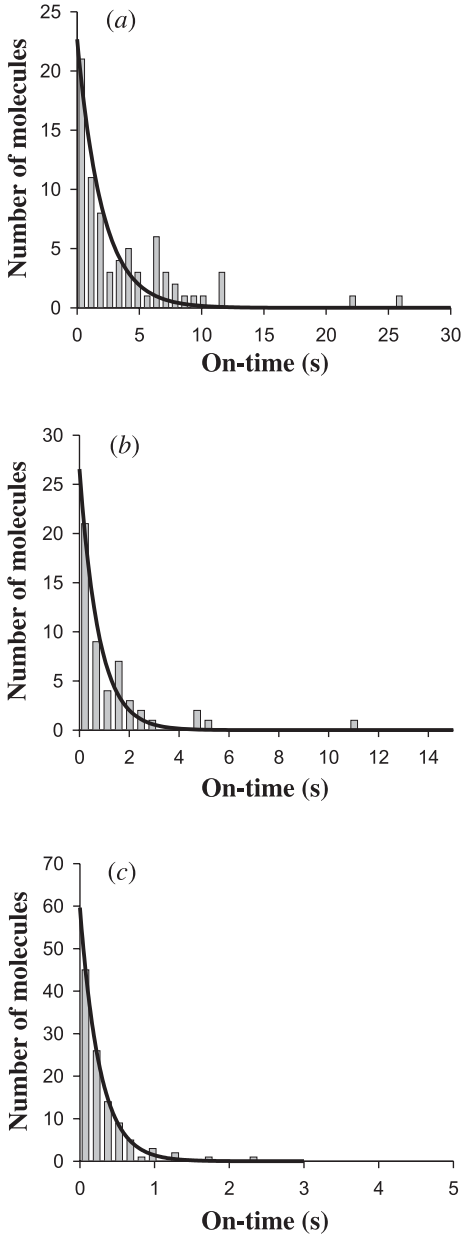
To further explore the capabilities of our microscope system, we have carried out a comparative study of the photophysical properties of several different fluorophores that have significant utility in biological applications. In particular, we have focused on two fluorophores, EGFP and bodipy-FL, which have both found extensive use as fluorescent labels of biological molecules (22, 23). As SM fluorescence techniques are increasingly applied to studies of biological systems, characterizing the basic optical properties of fluorophores that are used in these applications is of increasing importance.

As noted in the first section, a particularly useful approach for characterizing fluorophores in SM systems is to generate frequency histograms of on-times for individual molecules. In Figs. 6*a*–6*c*, we compare on-time histograms for R6G, EGFP, and bodipy-FL, all taken under the same illumination intensity and with molecules immobilized in a matrix (PMMA for R6G and bodipy-FL, a water-filled agarose gel for EGFP). For each of these fluorophores, the on-time histograms follow simple, single-exponential decay curves (fitting constants shown in the figure captions). The decay constant for the exponential fits provides a direct measure of the photobleaching stability of the different fluorophores, with the general photostability of the molecules measured here following the order: R6G > bodipy-FL > EGFP. It is important to note that the photobleaching time of a fluorophore represents a fundamental limit on a SM measurement, because once a molecule photobleaches, the experiment is over. This is a particular problem for studies that involve imaging the movement of labeled molecules during the time course of a biological process (e.g., refs. 24–27).

Of particular importance in this regard is the on-time histogram for EGFP, shown in Fig. 6*c*. EGFP has revolutionized many aspects of in vivo molecular biology experiments, as it allows proteins to be fluorescently labeled exclusively through the use of a cell's genetic machinery (for a recent review, see ref. 23). However, as is clear from the on-time frequency histogram measurements shown here, EGFP has very poor photostability (τ_{ON} = 0.27 s, in excellent agreement with ref. 28), and if one were to use EGFP for SM imaging applications, the amount of information that could be gathered before photobleaching ends the experiment is minimal. R6G is significantly more photostable than EGFP (τ_{ON} = 2.00 s), though ideally, one would prefer mean photobleaching times that are on the order of many minutes to hours. This has been one of the major driving forces behind the development of semiconductor "quantum dots" for fluorescence imaging applications (29, 30). Quantum dots have many properties that are similar to individual fluorescent molecules, but in general have much greater photostability than organic dyes. An additional complication arising from the use of EGFP as a fluorescent label is that the molecule shows unusual blinking behaviour; that is, EGFP has been reported to undergo multiple transitions between an emissive and nonemissive state over several different timescales (28, 31). In our measurements, we have noted that a small, but significant population of EGFP molecules undergoes repeated on–off blinking, even after illumination for many tens of minutes (data not shown). Despite a great deal of in-depth

© 2005 NRC Canada

Fig. 6. The histograms and single exponential fits of on-time distribution of: (*a*) R6G; (*b*) BODIPY in PMMA coating; and (*c*) EGFP in agarose gel (pH 7.0). The corresponding photobleaching time constants are: (*a*) τ_{ON} = 2.00 s; (*b*) τ_{ON} = 0.78 s; and (*c*) τ_{ON} = 0.27 s. The excitation intensity in each case was 0.6 kW/cm^2.



study, the underlying cause of this photophysical behaviour is still poorly understood. What is clear, however, is that the poor photostability and complex photophysics of EGFP make it a far from ideal label for use in SM biological imaging experiments.

As a possible alternative to EGFP for SM imaging experiments, we have also characterized bodipy-FL, a member of the boron-based "bodipy" (4,4-difluoro-4-bora-3a,4a-diaza-*s*-indacene) class of dyes marketed by Molecular Probes. While bodipy-FL would have to be directly coupled to a biomolecule to be used in imaging applications, it has a number of properties that make it a strong potential candidate for use as a SM fluorophore in biological imaging. It has a high quantum yield and extinction coefficient (quantum yield ~ 0.8, extinction coefficient ~ 90 000 M^{-1} cm^{-1} in methanol (32) and confirmed independently in our lab), and can be readily coupled to proteins or nucleic acids through a reactive amine group. As shown in the histogram of fluorescent on-times for bodipy-FL (Fig. 6*b*), the fluorophore has a characteristic on-time decay constant that is approximately three times greater than that of EGFP. Bodipy-FL also shows no evidence of blinking even after many minutes of observation under constant illumination conditions. A further possible benefit of using bodipy-FL dyes for SM experiments is that, under appropriate conditions, the molecule can form several different types of aggregates, including a quenched H dimer (33, 34). This has a huge number of possible SM applications, including the high-resolution measurement of distances between labeled protein residues by means of fluorescence quenching. One can envision monitoring single-molecule enzyme kinetics by observing substrate molecules that have been heavily labeled with bodipy-FL; the sudden onset of fluorescence when one member of the quenched H dimer has been removed could be used as an indicator that an enzymatic event has occurred. A similar approach, based upon quenching of dimeric cyanine dyes (the BOBO, TOTO, and YOYO classes of dyes, for example), has found useful applications for both bulk and single-molecule labeling studies of DNA (22, 35, 36). In general, intermolecular dimerization has the potential to be of great impact in this important discipline.

Summary

In this work, we have described the design, construction, and characterization of a fluorescence microscope with single-molecule sensitivity and resolution. Our microscope makes use of a new type of CCD camera with on-chip multiplier gain. A test system, consisting of molecules of the laser dye R6G immobilized in a polymer matrix, was studied in terms of SNR, photobleaching statistics, and photophysical behaviour, to allow comparison of our apparatus' performance and capabilities with other SM microscope systems reported in the literature. The microscope system attained comparable sensitivity, collection efficiency, and resolution to that reported by others in the field, indicating that the apparatus and in particular the CCD photodetector, was well-suited for SM measurements. We characterized the CCD detector performance in greater detail through the development of a simple calibration procedure to extract photon counts from CCD detector counts. Finally, we have compared and contrasted the photophysical properties of several fluorescent molecules that are commonly used as labels in fluorescence imaging, and, for the fluorophore bodipy-FL, have suggested some research directions that will be pursued in future experiments.

Acknowledgements

Funding for this work was provided by the Natural Sciences and Engineering Research Council of Canada (NSERC) and by the University of Saskatchewan.

© 2005 NRC Canada

References

1. T. Basche, W.E. Moerner, M. Orrit, and U.P. Wild. Single molecule optical detection, imaging and spectroscopy. Verlag-Chemie, Munich. 1997.
2. W.E. Moerner. J. Phys. Chem. B, **106**, 910 (2002).
3. W.E. Moerner and D.P. Fromm. Rev. Sci. Instrum. **74**, 3597 (2003).
4. S.M. Nie and R.N. Zare. Annu. Rev. Biophys. Biomol. Struct. **26**, 567 (1997).
5. X.S. Xie and J.K. Trautman. Annu. Rev. Phys. Chem. **49**, 441 (1998).
6. D.A. Vanden Bout, W.-T. Yip, D. Hu, D.-K. Fu, T.M. Swager, and P.F. Barbara. Science (Washington, D.C.), **277**, 1074 (1997).
7. S. Weiss. Science, **283**, 1676 (1999).
8. W.P. Ambrose, P.M. Goodwin, J.H. Jett, A. Van Orden, J.H. Werner, and R.A. Keller. Chem. Rev. **99**, 2929 (1999).
9. M.F. Paige, E.J. Bjerneld, and W.E. Moerner. Single Mol. **2**, 191 (2001).
10. Roper Scientific, Inc. Technical note No. 14: On-chip multiplication gain. 2003.
11. T. Schmidt, G.J. Schutz, W. Baumgartner, H.J. Gruber, and H. Schindler. Proc. Natl. Acad. Sci. U.S.A. **93**, 2926 (1996).
12. W.E. Moerner and M. Orrit. Science, **283**, 1670 (1999).
13. R.M. Dickson, D.J. Norris, and W.E. Moerner. Phys. Rev. Lett. **81**, 5322 (1998).
14. W.-T. Yip, D. Hu, J. Yu, D.A. Vanden Bout, and P.F. Barbara. J. Phys. Chem. A, **102**, 7564 (1998).
15. R. Zondervan, F. Kulzer, S.B. Orlinskii, and M. Orrit. J. Phys. Chem. A, **107**, 6770 (2003).
16. F. Vargas, O. Hollricher, O. Marti, G. de Schaetzen, and G. Tarrach. J. Chem. Phys. **117**, 866 (2002).
17. T. Basche, W.P. Ambrose, and W.E. Moerner. J. Opt. Soc. Am. B, **9**, 829 (1992).
18. E.W. Mei, S. Vinogradov, and R.M. Hochstrasser. J. Am. Chem. Soc. **125**, 13 198 (2003).
19. B.E.A. Saleh and M.C. Teich. Fundamentals of photonics. John Wiley and Sons, New York. 1991.
20. Roper Scientific, Inc. Cascade camera data sheet [online]. Available from http://www.photomet.com/qe_cascade.html [accessed 2005].
21. M.S. Robbins and B.J. Hadwen. IEEE Trans. Electron Devices, **50**, 1227 (2003).
22. R.P. Haugland. Handbook of fluorescent probes and research products. Molecular Probes, Inc., Eugene, Oregon. 2002.
23. R.Y. Tsien. Annu. Rev. Biochem. **67**, 509 (1998).
24. K. Adachi, H. Noji, and K. Kinosita. *In* Methods in enzymology. Biophotonics Part B. Vol. 361. *Edited by* G. Marriott and I. Parker. Elsevier B.V., Amsterdam, The Netherlands. p. 211. 2003.
25. K. Adachi, R. Yasuda, H. Noji, H. Itoh, Y. Harada, M. Yoshida, and K. Kinosita. Proc. Natl. Acad. Sci. U.S.A. **97**, 7243 (2000).
26. E.J.G. Peterman, H. Sosa, L.S.B. Goldstein, and W.E. Moerner. Biophys. J. **81**, 2851 (2001).
27. R.D. Vale, T. Funatsu, D.W. Pierce, L. Romberg, Y. Harada, and T. Yanagida. Nature (London), **380**, 451 (1996).
28. E.J.G. Peterman, S. Brasselet, and W.E. Moerner. J. Phys. Chem. A, **103**, 10 553 (1999).
29. P. Alivisatos. Nat. Biotechnol. **22**, 47 (2004).
30. S. Empedocles and M. Bawendi. Acc. Chem. Res. **32**, 389 (1999).
31. M.F. Garcia-Parajo, G.M.J. Segers-Nolten, J.A. Veerman, J. Greve, and N.F. van Hulst. Proc. Natl. Acad. Sci. U.S.A. **97**, 7237 (2000).
32. J. Karolin, L.B.A. Johansson, L. Strandberg, and T. Ny. J. Am. Chem. Soc. **116**, 7801 (1994).
33. D. Tleugabulova, Z. Zhang, and J.D. Brennan. J. Phys. Chem. B, **106**, 13 133 (2002).
34. I. Mikhalyov, N. Gretskaya, F. Bergstrom, and L.B.A. Johansson. Phys. Chem. Chem. Phys. **4**, 5663 (2002).
35. B.P. Bowen, J. Enderlein, and N.W. Woodbury. Photochem. Photobiol. **78**, 576 (2003).
36. B.P. Bowen and N.W. Woodbury. Photochem. Photobiol. **78**, 582 (2003).

© 2005 NRC Canada

Synthesis and spectra of aldehyde- and ketone-*O*-(2,5-dihydro-2-methoxy-5,5-dimethyl-1,3,4-oxadiazol-2-yl)oximes — Thermal sources of some methoxy(oximino)carbenes

Arkadiusz Klys, Malgorzata Dawid, and John Warkentin

Abstract: Ten new oxadiazoline sources of methoxy(oximino)carbenes were synthesized by exchanging the acetoxy group of 2-acetoxy-2-methoxy-Δ^3-1,3,4-oxadiazoline with an oximino group. The new compounds were characterized by means of spectroscopy and the formation of carbenes upon thermolysis of a few was demonstrated by means of interception with *tert*-butyl alcohol. The carbenes fragmented to form methoxycarbonyl and iminyl radicals.

Key words: 2,2-dioxyoxadiazoline, methoxy(oximino)carbene, oxadiazole, radical pair, rearrangement.

Résumé : On a effectué la synthèse de 10 nouvelles oxadiazolines sources de méthoxy(oximino)carbènes en procédant à l'échange du groupe acétoxy de la 2-acétoxy-2-méthoxy-Δ^3-1,3,4-oxadiazoline avec un groupe oximino. On a caractérisé les nouveaux composés par spectroscopie et la formation de carbènes par thermolyse de quelques-unes de ces sources a été mise en évidence par leur interception par l'alcool *tert*-butylique. Les carbènes se fragmentent avec formation des radicaux méthoxycarbonyle et iminyle.

Mots clés : 2,2-dioxyoxadiazoline, méthoxy(oximino)carbène, oxadiazole, paire de radicaux, réarrangement.

[Traduit par la Rédaction]

Introduction

Some 2,5-dihydro-5,5-dimethyl-2,2-dioxy-1,3,4-oxadiazoles (**1a**–**1d**) (also known as 5,5-dimethyl-2,2-dioxy-Δ^3-1,3,4-oxadiazolines) have been shown to be versatile reagents for the generation of carbenes including alkoxymethoxy-, acetoxymethoxy-, alkoxyaryloxy-, and diaryloxycarbenes. (1) Having shown that an alkyne functional group in the carbene from **1e** (2) and a carbonyl group in the carbene from **1f** (3) can intercept a dialkoxycarbene in an intramolecular reaction, leading to interesting products, and that thiocarbonyl groups are effective interceptors in intermolecular reactions (4), we decided to try the oxadiazoline approach to generate carbenes containing other functional groups (Scheme 1).

We now report the preparation of some aldehyde and ketone-*O*-(2,5-dihydro-2-methoxy-5,5-dimethyl-1,3,4-oxadiazol-2-yl)oximes (**2**) (also known as corresponding oxadiazolinyl oximes) that are precursors of carbenes of type **3** (Scheme 2), and show that carbenes **3d** and **3e** are indeed generated by thermolysis of **2d** and **2e**. Some potential intramolecular reactions of a generalized carbene **3** are shown in Scheme 3.

Received 11 November 2004. Published on the NRC Research Press Web site at http://canjchem.nrc.ca on 6 May 2005.

A. Klys,[1] M. Dawid,[2] and J. Warkentin.[3] Department of Chemistry, McMaster University, Hamilton, ON L8S 4M1, Canada.

[1]Present address: Department of Organic Chemistry, The University of Łódź, Łódź, Poland.
[2]Present address: Torcan Chemicals, Aurora, ON L4G 3H4, Canada.
[3]Corresponding author (e-mail: warkent@mcmaster.ca).

Methods, results, and discussion

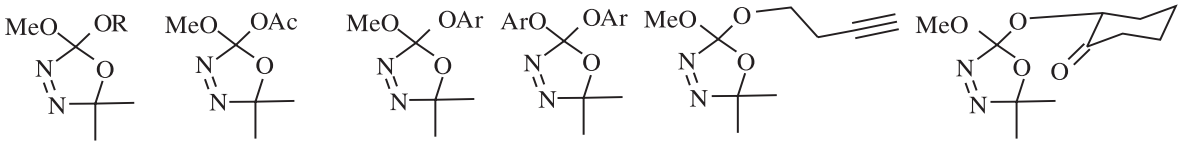
Compounds **2** were prepared by the exchange method (5), from 2-acetoxy-2-methoxy-2,5-dihydro-5,5-dimethyl-1,3,4-oxadiazole (also known as 2-acetoxy-2-methoxy-5,5-dimethyl-Δ^3-1,3,4-oxadiazoline) (**4**) and the appropriate oxime (**5**) in the presence of catalytic *p*-toluenesulfonic or trifluoroacetic acid (Scheme 4). All of the oximes used in this work are known compounds and compounds **2**, with the exception of **2b**, were the (*E*)-isomers. In the case of **2b**, a mixture of (*E*)- and (*Z*)-isomers was obtained. They were not separated and the ^{13}C NMR spectrum of the major isomer was assigned on the basis of signal intensities.

The oximes **5** were prepared by standard methods, including the (*Z*)-oxime of benzaldehyde (6). Exchange with the latter gave the same product (**2c**) as that obtained with the (*E*)-oxime of benzaldehyde, indicating that the oxime isomerizes under the acidic exchange conditions or that the product isomerizes after exchange has occurred (or both). To date we have been unable to prepare analogues of **2** with a (*Z*)-aldoxime unit.

Structural assignments are based on ^{1}H and ^{13}C NMR spectra, as well as high-resolution mass spectra of more complex samples. In some cases, the connectivity was supported with gradient HSQC spectra, to correlate ^{1}H and ^{13}C NMR chemical shifts. The ^{13}C NMR spectra of 2,2-

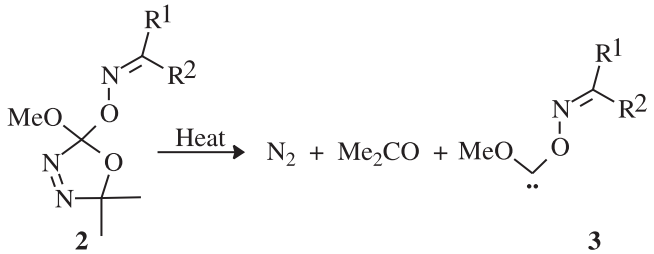
 doi: 10.1139/V05-061 © 2005 NRC Canada

Scheme 1.



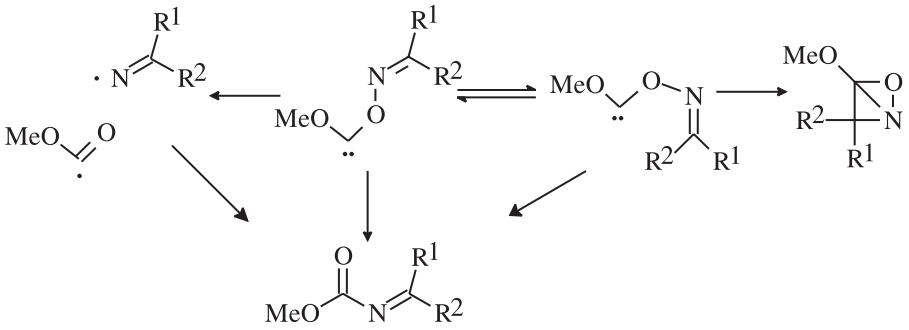
1a **1b** **1c** **1d** **1e** **1f**

Scheme 2. For **2a** and **3a**: $R^1 = R^2 = Me$; **2b** and **3b**: $R^1 = Et$, $R^2 = Me$ (major), $R^1 = Me$, $R^2 = Et$ (minor); **2c** and **3c**: $R^1 = Ph$, $R^2 = H$; **2d** and **3d**: $R^1 = Ph$, $R^2 = Me$; **2e** and **3e**: $R^1 = R^2 = Ph$; **2f** and **3f**: CR_1R_2 = 9-fluorenylidene; **2g** and **3g**: $R_1R_2 = (PhCH)_4$; **2h** and **3h**: $R^1R^2 = (CH_2)_4$; **2i** and **3i**: $R_1R_2 = (CH_2)_5$; **2j** and **3j**: $R^1 = MeCO$, $R^2 = Me$.

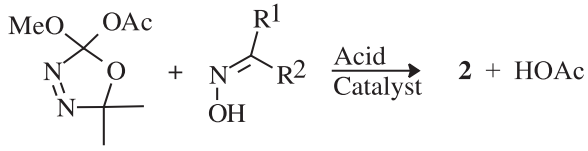


2 **3**

Scheme 3.



Scheme 4.



4 **5**

dialkoxy-5,5-dimethyl-Δ^3-1,3,4-oxadiazolines have the C-2 and C-5 signals near 137 and 119 δ, respectively (7). Values of the ^{13}C NMR chemical shift of iminyl carbons in 25 ketoximes fall between δ = 157.7 and 170.1 (8).

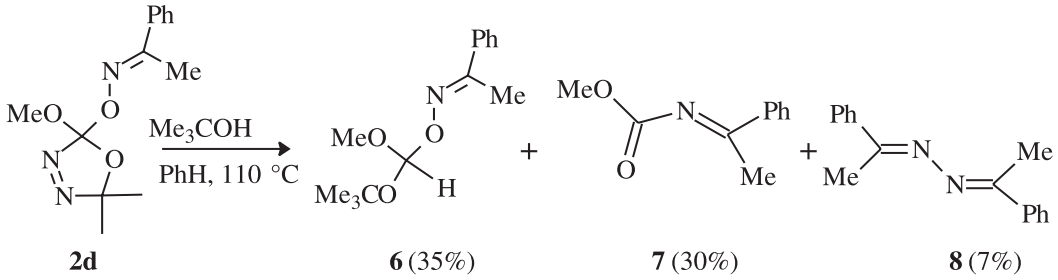
IR spectra were generally not informative enough to provide strong evidence of structure, with a weak band attributed to C=N stretching (9) near 1650 cm^{-1}. The carbonyl frequency of **2j**, as well as strong fingerprint bands for a few of the compounds **2** are included.

To test for the intermediacy of a carbene **3**, the potential precursor **2** was thermolysed in dry benzene, and in benzene containing *tert*-butyl alcohol (1.05 mol/L). Compounds chosen for initial study, namely **2d** and **2e**, are members of the family **2** with unsaturation in the group(s) attached to the iminyl carbon.

Thermolysis of **2d** in benzene containing *tert*-butyl alcohol (1.05 mol/L) gave **6** (35%) and **7** (30%) as major products. Acetophenone azine was also isolated. Capture of a carbene intermediate by the alcohol would afford **6**, while intramolecular rearrangment, by 1,2-migration of the iminyl function, or fragmentation to radicals and radical pair coupling, would lead to **7** (Scheme 5). There is precedent for the capture of carbenes by alcohols (10), and for rearrangement of acyloxycarbenes (1*f*, 11), which are models for **3**. Concerted rearrangement of carbene **3d** to **7** need not necessarily involve a large rate constant, even though rearrangement competed with bimolecular capture by *tert*-butyl alcohol. Capture of dimethoxycarbene by alcohols, in acetonitrile at room temperature, occurs with pseudo-first-order rate constants lying between about 10^4 s^{-1} (ethanol) and 10^5 s^{-1} (methanol) (10*a*). Capture occurs by protonation to form an ion pair, and would be slowed in benzene, accelerated by the higher temperature used in this work, and probably slowed for *tert*-butyl alcohol, given that ethanol reacts more slowly than methanol.

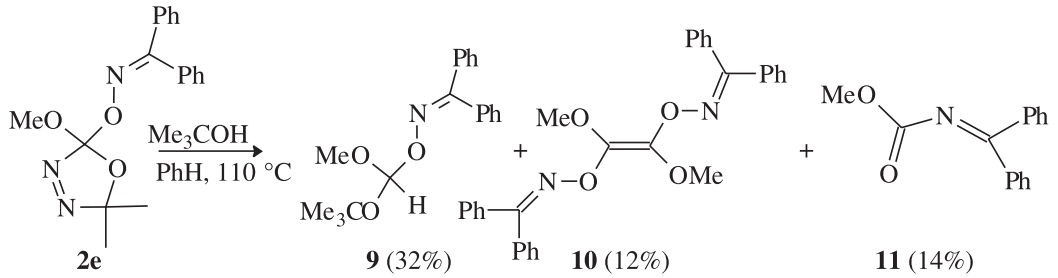
© 2005 NRC Canada

Scheme 5.

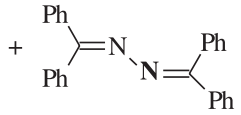


2d **6** (35%) **7** (30%) **8** (7%)

Scheme 6.



2e **9** (32%) **10** (12%) **11** (14%)



12 (5%)

Alternatively, **7** could arise by coupling of the methoxycarbonyl- and methylphenyliminyl radical pair. Some dialkoxycarbenes have been shown to fragment to radical pairs at 110 °C (10*d*, 12). The fact that acetophenone azine was isolated means that the radical-pair mechanism plays some role because the azine is almost certainly derived from coupling of the appropriate iminyl radicals. The fraction of **7** that arises by that route, as opposed to intramolecular rearrangement of **3d**, is not known at this time.

Compound **2e** afforded four products (**9**–**12**) when thermolysed in benzene containing *tert*-butyl alcohol (1.05 mol/L). Orthoformate **9** (32%) is the product of capture of carbene **3e** with *tert*-butyl alcohol while compound **10** (12%) is the carbene dimer and **11** (14%) appears to be the product of a 1,2-migration of the diphenyliminyl group to the carbene site of **3e**, either in a concerted intramolecular rearrangement or by means of coupling of methoxycarbonyl radicals and diphenyliminyl radicals (Scheme 6).

Analogous rearrangements, which are known for some acyloxycarbenes (1*f*, 11), appear to be concerted, in general. In the present case, the formation of diphenyliminyl radicals is strongly implied by the finding of compound **12**, which is most likely the product of coupling of the latter radicals. This conclusion was reinforced when thermolysis of **2e** in the presence of dimethyl acetylenedicarboxylate (DMAD) gave a mixture of products from which **13** was isolated. Presumably, **13** arose from intramolecular, radical aromatic substitution following addition of the diphenyliminyl radical to DMAD. Thus, the rearrangement of **3e** occurred, at least in part, by the carbene homolysis – radical combination mechanism.

There isn't any evidence for or against intramolecular addition of carbenes **3** to the iminyl functional group to generate the bicyclic intermediate of Scheme 3. Survival of such materials at 110 °C is unlikely, and alternative methods for generating carbenes **3** at lower temperatures will need to be investigated.

Summary

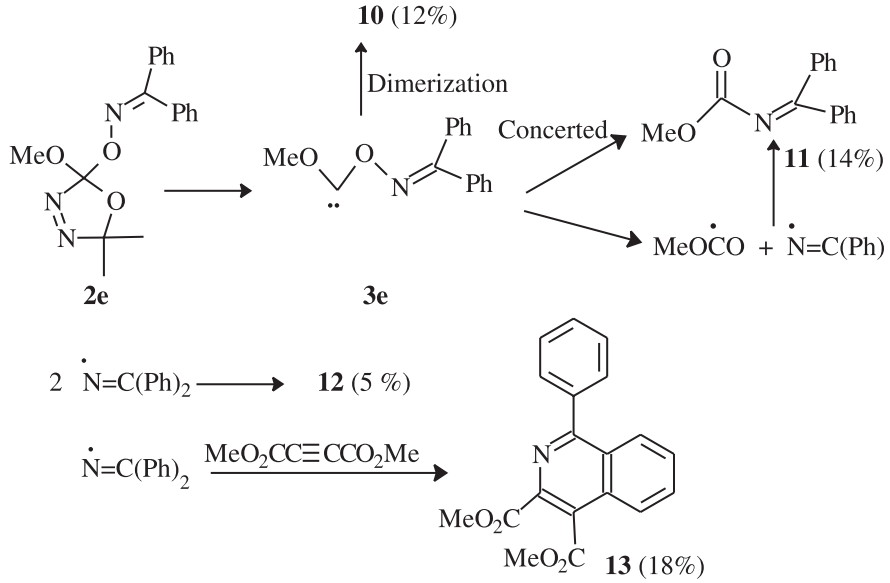
Ten new oxadiazolines, with a methoxy and an oximino substituent at C-2, were prepared and characterized. All of them can be expected to afford methoxy(oximino)carbenes upon thermolysis in benzene, as demonstrated for two of them by means of trapping with *tert*-butyl alcohol. In the absence of the alcohol a carbene dimer, as well as products from carbene fragmentation to a radical pair, were isolated (Scheme 7).

Experimental

IR spectra were taken with a Bruker Tensor 27 FT-IR instrument equipped with a Harrick ATR accessory and a ZnSe crystal. Neat samples in the solid or liquid state were used. NMR spectra were obtained with Bruker AV 200 or AV 600 instruments and, in one case, with a Varian Geminii 200BB machine. ^{1}H NMR chemical shifts in $CDCl_3$ and in C_6D_6 were referenced to the signal from $CHCl_3$ at δ =

© 2005 NRC Canada

Scheme 7.



7.26 ppm and the C_6HD_5 signal at 7.16 ppm, respectively. ^{13}C NMR shifts for solutions in $CDCl_3$ were referenced to the center line of the $CDCl_3$ triplet at δ = 77.16 ppm. Mass spectra were taken with a Micromass (Waters) GCT, TOF mass spectrometer, with ammonia for CI spectra. Most of the oxadiazolines gave $(M + H)^+$ masses, as well as the base peak corresponding to the 2-methoxy-5,5-dimethyl-Δ^3-1,3,4-oxadiazolinyl species ($C_5H_9N_2O_2$). A few did not afford $(M + H)^+$ masses, but gave the base peak instead. The mass corresponding to loss of N_2 was not generally observed.

Synthesis

The standard procedure involved 20 mmol of the acetoxymethoxyoxadiazoline (**4**) in methylene chloride containing a catalytic amount of toluenesulfonic acid and 20 mmol of the relevant oxime, except in the case of the preparation of **2g**, where the oxime was used in fourfold excess. The solution was kept at room temperature for 2 days before aq. KOH (5 mL H_2O plus ca. 0.4 g of KOH) was added and the resulting two-phase mixture was left for 1 day, except in the case of **2d**, which is rapidly destroyed by strong base. In that case, the catalytic acid and acetic acid were removed by means of a quick extraction with aq. $NaHCO_3$. After separation of the phases, washing with water, and drying with Na_2SO_4, the solvent was evaporated and the residue was column chromatographed on SiO_2 with 10% EtOAc in hexane for elution. The first fraction to be eluted was always the oxadiazoline. Yields (unoptimized) were about 40% in all cases except for **2g**, which was obtained in 15%–25% yield.

Acetone-O-(2,5-dihydro-2-methoxy-5,5-dimethyl-1,3,4-oxadiazol-2-yl)oxime (2a)

Colourless oil. ^1H NMR (200.1 MHz, $CDCl_3$) δ: 1.56 (s, 3H), 1.61 (s, 3H), 1.87 (s, 3H), 1.95 (s, 3H), 3.60 (s, 3H). ^{13}C NMR (50.3 MHz, $CDCl_3$) δ: 15.58, 21.40, 22.55, 24.13, 52.26, 119.91, 137.69, 158.65. MS (CI, NH_3) *m/z*: calcd. for $C_8H_{16}N_3O_3$ $(M + H)^+$: 202.23; found: 202.2.

2-Butanone-O-(1,5-dihydro-2-methoxy-5,5-dimethyl-1,3,4-oxadiazol-2-yl)oximes (2b) (E/Z mixture, not separated except for ^{13}C NMR of the major isomer)

Colourless oil. IR (most intense peaks, cm^{-1}): 1165, 1112, 898. ^1H NMR (600 MHz, $CDCl_3$) (major : minor isomer ratio ca. 2.5:1, integrations separate for each isomer) δ: (major isomer) 1.028 (t, *J* = 7.6 Hz, 3H), 1.556 (s, 3H), 1.625 (s, 3H), 1.933 (s, 3H), 2.191 (q, *J* = 7.6 Hz, 2H), 3.629 (s, 3H); (minor isomer) 1.087 (t, 3H), 1.558 (s, 3H), 1.611 (s, 3H), 1.845 (s, 3H), 2.418 (m, 2H), 3.608 (s, 3H). ^{13}C NMR (200 MHz, $CDCl_3$) (major isomer) δ: 10.62, 14.67, 19.52, 23.21, 24.22, 29.46, 52.95, 120.50, 163.10. HR-MS (CI, NH_3) *m/z*: calcd. for $C_9H_{18}N_3O_3$ $(M + H)^+$: 216.1348; found: 216.1345.

Benzaldehyde-O-(1,5-dihydro-2-methoxy-5,5-dimethyl-1,3,4-oxadiazol-2-yl)(E)-oxime (2c)

White solid, mp 65 °C. ^1H NMR (200.1 MHz, $CDCl_3$) δ: 1.60 (s, 3H), 1.69 (s, 3H), 3.69 (s, 3H), 7.33-7.55 (m, 5H), 8.23 (s, 1H). ^{13}C NMR (50.3 MHz, $CDCl_3$) δ: 23.22, 24.87, 53.12, 121.22, 127.71, 128.88, 130.89, 131.09, 138.31, 152.51. HR-MS (CI, NH_3) *m/z* calcd. for $C_{12}H_{16}N_3O_3$ $(M + H)^+$: 250.1192; found: 250.1171.

Acetophenone-O-(1,5-dihydro-2-methoxy-5,5-dimethyl-1,3,4-oxadiazol-2-yl)oxime (2d)

Colourless oil. IR (most-intense peaks, cm^{-1}): 1166.0, 1109.3, 904.8, 762.3, 693.5. ^1H NMR (200.1 MHz, $CDCl_3$) δ: 1.59 (s, 3H), 1.65 (s, 3H), 2.36 (s, 3H), 3.71 (s, 3H), 7.33–7.36 (m, 3H), 7.53–7.58 (m, 2H). ^{13}C NMR (50.3 MHz, $CDCl_3$) δ: 13.53, 23.12, 24.89, 53.13, 120.97, 126.52, 128.50, 129.90, 135.62, 138.51, 158.68. In the *E*-oxime itself, the chemical shift of the iminyl carbon ($CDCl_3$) is 155.9 δ (8). HR-MS (CI, NH_3) *m/z* calcd. for $C_{13}H_{18}N_3O_3$ $(M + H)^+$: 264.1348; found: 264.1361.

Benzophenone-O-(1,5-dihydro-2-methoxy-5,5-dimethyl-1,3,4-oxadiazol-2-yl)oxime (2e)

Colourless solid, mp 63 to 64 °C. IR (strongest sig-

© 2005 NRC Canada

nals, cm^{-1}: 1028.26, 923.09, 700.03. ^1H NMR (200.1 MHz, $CDCl_3$) δ: 1.58 (s, 3H), 1.68 (s, 3H), 3.54 (s, 3H), 7.29–7.44 (m, 10H). ^{13}C NMR (50.3 MHz, $CDCl_3$) δ: 23.21, 24.96, 53.16, 121.02, 128.17, 128.34, 128.47, 129.26, 130.16, 132.60, 135.59, 160.73. HR-MS (CI, NH_3) *m/z* calcd. for $C_{18}H_{21}N_3O_3$ $(M + H)^+$: 326.1505; found: 326.1482.

Fluorenone*-O-*(1,5-dihydro-2-methoxy-5,5-dimethyl-1,3,4-oxadiazol-2-yl)oxime (2f)

Pale yellow solid, mp 105 to 106 °C. IR (most intense peaks, cm^{-1}): 1166.18, 1098.28, 899.09. ^1H NMR (600 MHz, $CDCl_3$) δ: 1.65 (s, 3H), 1.78 (s, 3H), 3.81 (s, 3H), 7.23 (t, *J* = 7.2 Hz, 1H), 7.36, 7.33 (t, *J* = 7.2 Hz, 1H), 7.38 (t, *J* = 7.2 Hz, 1H), 7.45 (t, *J* = 7.2 Hz, 1H), 7.58 (d, *J* = 7.2 Hz, 1H), 7.60 (d, *J* = 7.2 Hz, 1H), 7.63 (d, *J* = 7.2 Hz, 1H), 8.33 (d, *J* = 7.2 Hz, 1H). ^{13}C NMR (150 MHz, $CDCl_3$) δ: 23.27, 24.94, 53.47, 120.13, 120.17, 121.80, 122.41, 128.17, 128.59, 129.99, 130.35, 130.91, 132.01, 135.00, 138.80, 140.88, 142.13, 155.33. HR-MS (CI, NH_3) *m/z* calcd. for $C_{18}H_{18}N_3O_3$ $(M + H)^+$: 324.1348; found: 324.1331.

2,3,4,5-Tetraphenylcyclopentadienone*-O-*(1,5-dihydro-2-methoxy-5,5-dimethyl-1,3,4-oxadiazol-2-yl)oxime (2g)

Reddish foam. ^1H NMR (200 MHz, $CDCl_3$) δ: 1.05 (s, 3H), 1.38 (s, 3H), 3.03 (s, 3H), 6.73–6.85 (m, 4H), 6.99–7.27 (m, 16H). ^{13}C NMR (50.3 MHz, $CDCl_3$) δ: 21.99, 25.10, 53.30, 121.60, 124.69, 126.75, 126.98, 127.21, 127.47, 127.61, 127.76, 130.01, 130.08, 130.66, 131.32, 132.66, 132.51, 132.66, 133.60, 134.05, 136.30, 138.16, 145.61, 151.57, 160.88. HR-MS (CI, NH_3) *m/z* calcd. for $C_{34}H_{29}N_3O_3$: 527.2209; found: 527.2213.

Cyclopentanone*-O-*(1,5-dihydro-2-methoxy-5,5-dimethyl-1,3,4-oxadiazol-2-yl)oxime (2h)

Colourless oil. ^1H NMR (200 MHz, $CDCl_3$) δ: 1.57 and 1.62 (2s, superimposed on m, total 10H), 2.18 (m, 2H), 2.53 (m, 2H), 3.60 (s, 3H). ^{13}C NMR (150 MHz, $CDCl_3$) δ: 23.19, 24.77, 25.48, 25.70, 25.99, 26.82, 32.18, 52.86, 120.34, 138.46, 164.34. MS (CI, NH_3) *m/z* calcd. for $C_5H_9N_2O_2$ $(M - C_5H_8NO)^+$: 129.14; found: 129.1 (100%).

Cyclohexanone*-O-*(1,5-dihydro-2-methoxy-5,5-dimethyl-1,3,4-oxadiazol-2-yl)oxime (2i)

Colourless oil. IR (C=N and four most intense peaks, cm^{-1}): 1763.2, 1164.3, 1101.8, 897.8, 862.3. ^1H NMR (600 MHz, $CDCl_3$) δ: 1.57 (s, 3H), 1.61 (s, 3H), 1.70–1.80 (m, 6H), 2.36 (distorted t, 2H), 2.52 (distorted t, 2H), 3.59 (s, 3H). ^{13}C NMR (150 MHz, $CDCl_3$) δ: 23.33, 24.70, 25.23, 28.43, 31.31, 52.87, 120.49, 125.67, 138.29, 171.14. MS (CI, NH_3) *m/z* calcd. for $C_5H_9N_2O_2$ $(M - C_6H_{10}NO)^+$: 129.14; found: 129.1 (100%).

Biacetyl*-O-*(1,5-dihydro-2-methoxy-5,5-dimethyl-1,3,4-oxadiazol-2-yl)]monoxime (2j)

Colourless oil. IR (neat, cm^{-1}): 1702.4 (C=O), 913.3 (most intense fingerprint peak). ^1H NMR (200.2 MHz, $CDCl_3$) δ: 1.59 (s, 3H), 1.67 (s, 3H), 2.05 (s, 3H), 2.28 (s, 3H), 3.70 (s, 3H). ^1H NMR (200.2 MHz, C_6D_6) δ: 1.27 (s, 3H), 1.40 (s, 3H), 1.76 (s, 3H), 1.90 (s, 3H), 3.44 (s, 3H). ^{13}C NMR (50.3 MHz, $CDCl_3$) δ: 9.54, 23.30, 24.81, 25.59, 53.35, 99.78, 147.40, 188.23, 220.02. MS (CI, NH_3) *m/z* calcd. for $C_9H_{16}N_3O_4$ $(M + H)^+$: 230.24; found: 230.1.

Thermolysis procedure

The oxadiazoline (1.5 mmol) in 5 mL of benzene, added to 5.25 mmol of *tert*-butyl alcohol, was heated in a sealed vessel at 110 °C for 24 h. The tube was then opened, and the solvent and volatile products were evaporated with a rotary evaporator. The residue was column chromatographed on silica gel with petroleum ether – ethyl acetate as the eluent. Some fractions had to be rechromatographed on a 2 mm silica plate in a Chromatotron apparatus, with the same solvents for elution. Thermolysis of **2d** afforded products **6**–**8**. The carbene dimer was not found.

Acetophenone*-O-(tert-*butoxy)(methoxymethylene)oxime (6)

Colourless oil, yield 35%. ^1H NMR (600 MHz, $CDCl_3$) δ: 1.35 (s, 9H), 2.29 (s, 3H), 3.42 (s, 3H), 6.00 (s, 1H), 7.35–7.36 (m, 3H), 7.65–7.67 (m, 2H). ^{13}C NMR (150 MHz, $CDCl_3$) δ: 13.48, 14.27, 28.97, 31.74, 51.31, 113.90, 126.42, 128.51, 129.43, 156.07.

Methyl (phenylethylidene)carbamate (7)

Colourless oil, in 30% yield. ^1H NMR (600 MHz, $CDCl_3$) δ: 2.39 (s, 3H), 3.92 (s, 3H), 7.39–7.45 (m, 3H), 7.72–7.73 (m, 2H). ^{13}C NMR (150 MHz, $CDCl_3$) δ: 13.88, 54.81, 126.53, 128.12, 130.15, 134.09, 153.99 (C=N), 162.22 (C=O).

Acetophenone azine (8) (13)

Yield: 7%. ^1H NMR (200.2 MHz, $CDCl_3$) δ: 2.33 (s, 6H), 7.42–7.45 (m, 6H), 7.91–7.93 (m, 4H). ^{13}C NMR (150 MHz, $CDCl_3$) δ: 15.25, 126.82, 128.51, 129.83, 138.51, 158.15. HR-MS (CI, NH_3) *m/z* calcd. for $C_{16}H_{16}N_2$: 236.1313; found: 236.1313 and 237.1387 $(M + H)^+$.

Thermolysis of **2e** afforded benzophenone-*O*-(*tert*-butoxy)(methoxymethylene)oxime (**9**), the carbene dimer (**10**), methyl (diphenylmethylene)carbamate ($MeOCON{=}CPh_2$, **11**) (14), and benzophenone azine (**12**, 5%) (15).

Benzophenone*-O-(tert-*butoxy)(methoxymethylene)oxime (9)

Compound **9** was very susceptible to hydrolysis and was not obtained in a pure state. Yield: ca. 32%. ^1H NMR (200.2 MHz, $CDCl_3$) δ: 1.29 (s, 9H), 3.40 (s, 3H), 5.99 (s, 1H), 7.31–7.52 (m, 10H). ^{13}C NMR (50.3 MHz, $CDCl_3$) δ: 28.92, 51.38, 114.01, 128.02–129.58 (eight signals visible in this range, but not resolved). A meaningful mass spectrum could not be obtained.

1,2-Dimethoxy-1,2-(diphenyliminoxy)ethene (10)

Colourless oil, yield 12%. ^1H NMR (200.2 MHz, $CDCl_3$) δ: 3.66 (s, 6H), 7.33–7.27 (m, 10H). ^{13}C NMR (50.3 MHz, $CDCl_3$) δ: 55.40, 128.45, 128.55, 129.03, 129.17, 129.94, 131.08, 132.20, 134.70, 154.67, 164.63. A correlation between the ^1H and ^{13}C NMR signals was established by means of gradient HSQC spectra. The trans isomer was assumed.

© 2005 NRC Canada

Methyl (diphenylmethylene)carbamate (11) (14)

Pale yellow oil, yield 14%. ^{1}H NMR (200.2 MHz, $CDCl_3$) δ: 3.86 (s, 3H), 7.33–7.59 (m, 10H). ^{13}C NMR (50.3 MHz, $CDCl_3$) δ: 53.26, 128.46, 129.10, 131.30, 136.48, 163.31 (C=O), 171.55 (C=N). The signals at 128.46 and 129.10 are much more intense than the other ArH signals, and probably correspond to several coincident chemical shifts.

Dimethyl 1-phenylisoquinoline-3,4-dicarboxylate (13)

Oxadiazoline **2e** (488 mg, 1.5 mmol) in benzene, heated with DMAD (745 mg, 5.25 mmol) and worked up as described previously, gave 85 mg (2.7 mmol, 18%) of **13**.[4]

White solid, mp 126 to 127 °C. ^{1}H NMR (600 MHz, $CDCl_3$) δ: 4.03 (s, 3H), 4.12 (s, 3H), 7.52–7.56 (m, 3H), 7.68–7.71 (m, 3H), 7.83 (t, J = 7.5 Hz, 1H), 8.01 (d, J = 8.4 Hz, 1H), 8.17 (d, J = 8.4 Hz, 1H). ^{13}C NMR (150 MHz, $CDCl_3$) δ: 53.3, 53.4, 125.7, 127.6, 127.8, 128.3, 128.7, 129.5, 129.8, 130.3, 131.8, 132.2, 133.8, 138.5, 162.3, 166.1, 168.2. The structure of **13** was determined by means of X-ray crystallography.

Acknowledgements

The authors are grateful to the Natural Sciences and Engineering Research Council of Canada (NSERC) for generous financial support and to Dr. Patton Giles, Chemical Abstracts, Columbus Ohio, for assistance with some of the nomenclature. The work of Professor J. Britten, who determined the structure of **13** by means of X-ray crystallography, is greatly appreciated. Preliminary work on the synthesis of a few of the oxadiazolines by Dr. Paramashivappa Rangappa is also acknowledged.

References

1. (*a*) J. Warkentin. J. Chem. Soc. Perkin Trans. 1, 2161 (2000); (*b*) X. Lu, D.L. Reid, and J. Warkentin. Can. J. Chem. **79**, 319 (2001); (*c*) X. Lu and J. Warkentin. Can. J. Chem. **79**, 364 (2001); (*d*) X. Lu and J. Warkentin. Can. J. Chem. **80**, 228 (2002); (*e*) N. Merkley and J. Warkentin. Can. J. Chem. **80**, 1187 (2002); (*f*) W. Czardybon, A. Klys, J. Warkentin, and N.H. Werstiuk. Can. J. Chem. **81**, 1438 (2003).
2. (*a*) K. Kassam and J. Warkentin. J. Org. Chem. **59**, 5071 (1994); (*b*) K. Kassam and J. Warkentin. Can. J. Chem. **75**, 120 (1997); (*c*) K. Kassam, P.C. Venneri, and J. Warkentin. Can. J. Chem. **75**, 1256 (1997).
3. M. Dawid and J. Warkentin. Can. J. Chem. **81**, 598 (2003).
4. (*a*) M. Dawid, G. Mloston, and J. Warkentin. Org. Lett. **3**, 2455 (2001); (*b*) M. Dawid, G. Mloston, and J. Warkentin. Chem. Eur. J. **8**, 2184 (2002); (*c*) M. Dawid, D.L. Reid, G. Mloston, and J. Warkentin. Can. J. Chem. **81**, 1025 (2003).
5. K. Kassam, D.L. Pole, M. El-Saidi, and J. Warkentin. J. Am. Chem. Soc. **116**, 1161 (1994).
6. M. Blackwell, P.J. Dunn, A.B. Graham, R. Grigg, P. Higginson, I.S. Saba, and M. Thornton-Pett. Tetrahedron, **58**, 7715 (2002).
7. M. El-Saidi, K. Kassam, D.L. Pole, T. Tadey, and J. Warkentin. J. Am. Chem. Soc. **114**, 8751 (1992).
8. (*a*) G.W. Buchanan and B.A. Dawson. Can. J. Chem. **55**, 1437 (1977); (*b*) P. Geneste, R. Durand, J.-M. Kamenka, H. Beierbeck, R. Martino, and J.K. Saunders. Can. J. Chem. **56**, 1940 (1978).
9. J.F. Brown. J. Am. Chem. Soc. **77**, 6341 (1955).
10. (*a*) X.-M. Du, H. Fan, J.L. Goodman, M.A. Kesselmayer, K. Krogh-Jespersen, J.A. LaVilla, R.A. Moss, S. Shen, and R.S. Sheridan. J. Am. Chem. Soc. **112**, 1920 (1990); (*b*) G. Hömberger, W. Kirmse, and R. Lelgemann. Chem. Ber. **124**, 1867 (1991); (*c*) W. Kirmse. *In* Advances in carbene chemistry. Vol 1. *Edited by* U.H. Brinker. JAI Press, Greenwich, Connecticut. 1994. p. 1; (*d*) N. Merkley and J. Warkentin. Can. J. Chem. **78**, 942 (2000); (*e*) W. Kirmse. *In* Advances in carbene chemistry. Vol 3. *Edited by* U.H. Brinker. JAI Press, Greenwich, Connecticut. 2001. p. 1.
11. (*a*) R.F.C. Brown, F.W. Eastwood, and G.L. McMullen. Chem. Commun. 328 (1975); (*b*) M. Békhazi and J. Warkentin. J. Org. Chem. **47**, 4870 (1982); (*c*) R.F.C. Brown, N.R. Browne, and F.W. Eastwood. Aust. J. Chem. **36**, 2355 (1983); (*d*) R.A. Moss, S. Xue, and W. Liu. J. Am. Chem. Soc. **116**, 1583 (1994); (*e*) R.A. Moss, S. Xue, W. Liu, and K. Krogh-Jespersen. J. Am. Chem. Soc. **118,** 12 588 (1996); (*f*) R.A. Moss, S. Xue, W. Ma, and H. Ma. Tetrahedron Lett. **38**, 4379 (1997); (*g*) R.A. Moss and D.C. Merrer. Tetrahedron Lett. **39**, 8067 (1998).
12. (*a*) N. Merkley, M. El-Saidi, and J. Warkentin. Can. J. Chem. **78**, 256 (2000); (*b*) D.L. Reid and J. Warkentin. J. Chem. Soc. Perkin Trans. 2, 1980 (2000); (*c*) D.L. Reid, J. Hernandez-Trujillo, and J. Warkentin. J. Phys. Chem. A, **104**, 3398 (2000); (*d*) P.C. Venneri and J. Warkentin. J. Am. Chem. Soc. **120**, 11 182 (1998).
13. D.H. Kenny. J. Chem. Ed. **57**, 462 (1980).
14. (*a*) E.-U. Wuerthwein, R. Kupfer, S. Meier, M. Krestel, and R. Allmann. Chem. Ber. **121**, 591 (1988); (*b*) R. Kupfer, S. Meier, and E.-U. Wuerthwein. Synthesis, 688 (1984).
15. R. Ahmed and J.P. Anselme. Tetrahedron, **28**, 4939 (1972).

[4] Supplementary data for this article are available on the Web site or may be purchased from the Depository of Unpublished Data, Document Delivery, CISTI, National Research Council Canada, Ottawa, ON K1A 0S2, Canada. DUD 3655. For more information on obtaining material refer to http://cisti-icist.nrc-cnrc.gc.ca/irm/unpub_e.shtml. CCDC 264346 contains the crystallographic data for this manuscript. These data can be obtained, free of charge, via www.ccdc.cam.ac.uk/conts/retrieving.html (or from the Cambridge Crystallographic Data Centre, 12 Union Road, Cambridge CB2 1EZ, UK; fax +44 1223 336033; or deposit@ccdc.cam.ac.uk).

© 2005 NRC Canada

Lanthanide complexes of an oxazoline-phenoxide hybrid chelate

David J. Berg, Chuanjian Zhou, Tosha Barclay, Xuening Fei, Shengyu Feng, Kevin A. Ogilvie, Robert A. Gossage, Brendan Twamley, and Mark Wood

Abstract: The synthesis of 2-(2′-hydroxy-3′-allylphenyl)-4,4-dimethyl-2-oxazoline, H-Allox (**3**), and lanthanide tris chelate complexes, *mer*-Ln(Allox)$_3$ (Ln = La (**4**), Ce (**5**), Sm (**6**), Er (**7**), and Y (**8**)), derived from it are reported. A six-coordinate mer geometry without alkene coordination was confirmed in the solid state by X-ray crystallography for **5** and **7**. Variable-temperature NMR experiments suggested that this is the most stable isomer in solution as well, although the inequivalent ligand environments undergo rapid averaging at room temperature for all five complexes. A mechanistic investigation indicated that this fluxional process is an intramolecular six-coordinate rearrangement, but it was not possible to distinguish between a Bailar (trigonal) or Rây–Dutt (rhombic) twist. Kinetic parameters for the fluxional process were determined by line shape analysis for **8** yielding $\Delta H^{\ddagger}$ = 24 ± 2 kJ mol^{-1} and $\Delta S^{\ddagger}$ = –99 ± 10 J mol^{-1} K^{-1}. The structural and dynamic features of **4**–**8** were compared with the related In, Ga, and Al tris(2-oxazolylphenoxides).

Key words: oxazoline, phenoxide, lanthanide, Group 3, Rây–Dutt twist, Bailar twist, Eyring plot, X-ray crystallography, mer isomer, variable-temperature NMR, line shape analysis, dynamic NMR, paramagnetic NMR, bidentate ligands.

Résumé : On rapporte la synthèse de la 2-(2′-hydroxy-3′-allylphényl)-4,4-diméthyl-2-oxazoline, H-Allox (**3**) et de complexes de lanthanide trischélates, *mer*-Ln(Allox)$_3$ (Ln = La (**4**), Ce (**5**), Sm (**6**), Er (**7**) et Y (**8**)) qui en dérivent. Pour les complexes **5** et **7**, les données cristallographiques ont permis de confirmer que, à l'état solide, ces complexes adoptent une géométrie mer six coordinnées sans coordination d'alcène. Les données d'expériences de RMN à température variable suggèrent que, en solution, cet isomère est aussi le plus stable même si les environnements inéquivalents des ligands de chacun de ces cinq complexes sous soumis à une moyenne rapide. Une investigation mécanistique indique que ce processus fluxionnel correspond à un réarrangement intramoléculaire à six coordonnées, mais il n'a pas été possible de faire une distinction entre une torsion de Bailar (trigonale) ou de Rây–Dutt (rhombique). On a déterminé les paramètres cinétiques du processus fluxionnel par une analyse de la forme des bandes du composé **8** et on en a déduit des valeurs de $\Delta H^{\ddagger}$ = 24 ± 2 kJ mol^{-1} et $\Delta S^{\ddagger}$ = –99 ± 10 J mol^{-1} K^{-1}. Les caractéristiques structurales et dynamiques des composés **4**–**8** avec celles des composés apparentés des tris(2-oxazolylphénolates) d'indium, de gallium et d'aluminium.

Mots clés : oxazoline, phénolate, lanthanide, Groupe 3, torsion de Rây–Dutt, torsion de Bailar, courbe de Eyring, cristallographie par diffraction des rayons X, isomère mer, RMN à température variable, analyse de la forme des bandes, RMN dynamique, RMN paramagnétique, ligands bidentates.

[Traduit par la Rédaction]

Introduction

The transition metal and Group 13 chemistry of chelating 2-(2′-hydroxyphenyl)-2-oxazoline ligands (H-**I**) has been extensively studied for two principal reasons. First, this chelate type is found in nature as part of microbial metal transport agents, especially the Fe(III) transporting siderophores (1, 2). Second, asymmetric ligands of this kind are easily prepared from readily available chiral β-aminoalcohols and the resulting chiral metal complexes have proven useful as

Received 14 January 2005. Published on the NRC Research Press Web site at http://canjchem.nrc.ca on 10 May 2005.

D.J. Berg[1] and M. Wood. Department of Chemistry, University of Victoria, P.O. Box 3065, Victoria, BC V8W 3V6, Canada.
C. Zhou. School of Materials Science and Engineering, Shandong University, 73 Jing Shi Lu Ji'nan City, Shandong Province, P.R. China 250061.
T. Barclay. Chemistry Department, North Harris College, 2700 W.W. Thorne Blvd. Houston, TX 77073-3499, USA.
X. Fei. Tianjin Institute of Urban Construction, 26 Jinjing Road, Xiqing District, Tianjin, P.R. China 300384.
S. Feng. Department of Chemistry and Chemical Engineering, Shandong University, 27 Shandu Nanlu, Ji'nan City, Shandong Province, P.R. China 250100.
K.A. Ogilvie and R.A. Gossage. The Chester Woodleigh Small Laboratory of Organic Chemistry, Department of Chemistry, Acadia University, Wolfville, NS B4P 2R6, Canada.
B. Twamley. University Research Office, 109 Morrill Hall, University of Idaho, Moscow, ID 83844-3010, USA.

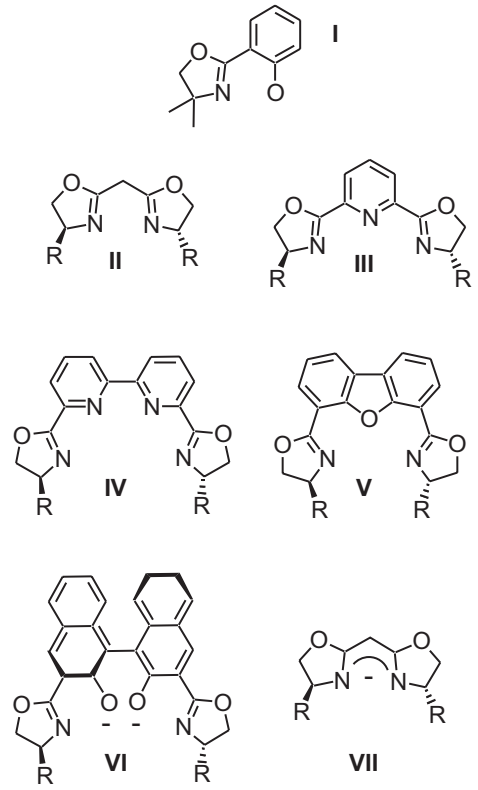
[1]Corresponding author (e-mail: djberg@uvic.ca).

 doi: 10.1139/V05-069 © 2005 NRC Canada

asymmetric oxidation catalysts (2). Despite the interest in 2-(2′-hydroxyphenyl)-2-oxazolines, and oxazolines in general, as ligands in transition metal chemistry, the Group 3 and lanthanide chemistry of such complexes has not been very well explored. To date, the limited oxazoline coordination chemistry that has been disclosed with these elements has been almost exclusively restricted to the neutral methylene-bis(oxazolines) (**II**, box) (3) or their close relatives containing additional donors: pyridine-bis(oxazolines) (**III**, *pybox*) (3, 4), 2,2′-bipyridine-bis(oxazolines) (**IV**) (3), and dibenzofuran-bis(oxazolines) (**V**) (3). This is remarkable considering the success of these ligands in catalytically active complexes of the *d*-block metals (2). Indeed, even though little work has been done so far, enantiomerically pure **II**–**V** have proven successful in Group 3 and lanthanide chemistry for asymmetric hetero-Diels–Alder (3), glyoxylate-ene (4*a*), Mukayama–Michael (4*b*), and annulation and addition reactions of allenylsilanes with aldehydes (4*c*).

Recently, examples of lanthanide complexes with anionic oxazoline-containing ligands (**I**, **VI**, and **VII**) have been reported (5–7). The tetrakis complex of 2-(2′-hydroxyphenyl)-4,4-dimethyl-2-oxazoline (**I**) with Ce^{4+} was prepared as a possible precursor to CeO_2 films by thermal decomposition. Lanthanide complexes of **VI** proved effective as asymmetric catalysts for the 1,3-dipolar cycloaddition of nitrones to alkenes, although the structure of the actual catalyst was not established (being formed in situ from $Yb(OTf)_3$ and **VI**) (6). The deprotonated box ligand **VII** has been used to prepare Ln[**VII**][NR_2]$_2$ (Ln = Y and R = $SiHMe_2$; Ln = La, Nd, Sm, Lu, and R = $SiMe_3$) and Ln[**VII**][$CH(SiMe_3)_2$]$_2$ (7) complexes that serve as hydroamination catalysts.

In this paper, we report the synthesis, solid-state structure, and solution behaviour of lanthanide complexes containing deprotonated 2-(2′-hydroxy-3′-allylphenyl)-4,4-dimethyl-2-oxazoline (Allox). The goal of this work is to understand the structural chemistry of tris(oxazoline-phenoxide) complexes of the lanthanides in solid state and solution. Although the present complexes are achiral, their solution behaviour should provide useful information about the suitability of enantiomerically pure variants as asymmetric Lewis acid catalysts. Besides providing some additional steric bulk, the allyl substituent was deliberately incorporated to assess whether coordination of the tethered alkene can occur. We have previously observed rare examples of alkene coordination with lanthanide centres for a phenoxide ligand bearing a tethered allyl group so it was of interest to see if this also occurred with Allox.[2]



Experimental

General procedures

All manipulations were carried out under an argon or nitrogen atmosphere, with the rigorous exclusion of oxygen and water, using standard glovebox (Braun MB150-GII) or Schlenk techniques. Tetrahydrofuran (THF), hexane, and toluene were dried by distillation from sodium benzophenone ketyl under argon immediately prior to use. The appropriate lanthanide tris(silylamides), Ln[$N(SiMe_3)_2$]$_3$, were prepared according to literature procedures (8). All NMR spectra (^{1}H, ^{13}C) including variable-temperature experiments were recorded on a Bruker AMX-360 MHz spectrometer and referenced to residual solvent resonances. All deuterated solvents were dried over activated 4 Å molecular sieves and spectra were recorded using 5 mm tubes fitted with a Teflon® valve (Brunfeldt). Variable-temperature NMR spectra and plots of δ vs. $1/T$ for paramagnetic complexes **5**–**7** are included in the Supplementary material,[3] while a representative high-temperature spectrum is included in the experimental data for each complex given below. Melting points were recorded using a Büchi melting point apparatus and are not corrected. Elemental analyses were performed by Canadian Microanalytical, Delta, British Columbia. Mass spectra were recorded on a Kratos Concept H spectrometer using electron impact (70 eV) ionization. The molecular ion simulation for complex **6** is shown in Fig. 1; simulations for **4**–**7** are included in the Supplementary material.[3]

2-(2′-Hydroxyphenyl)-4,4-dimethyl-2-oxazoline (1)

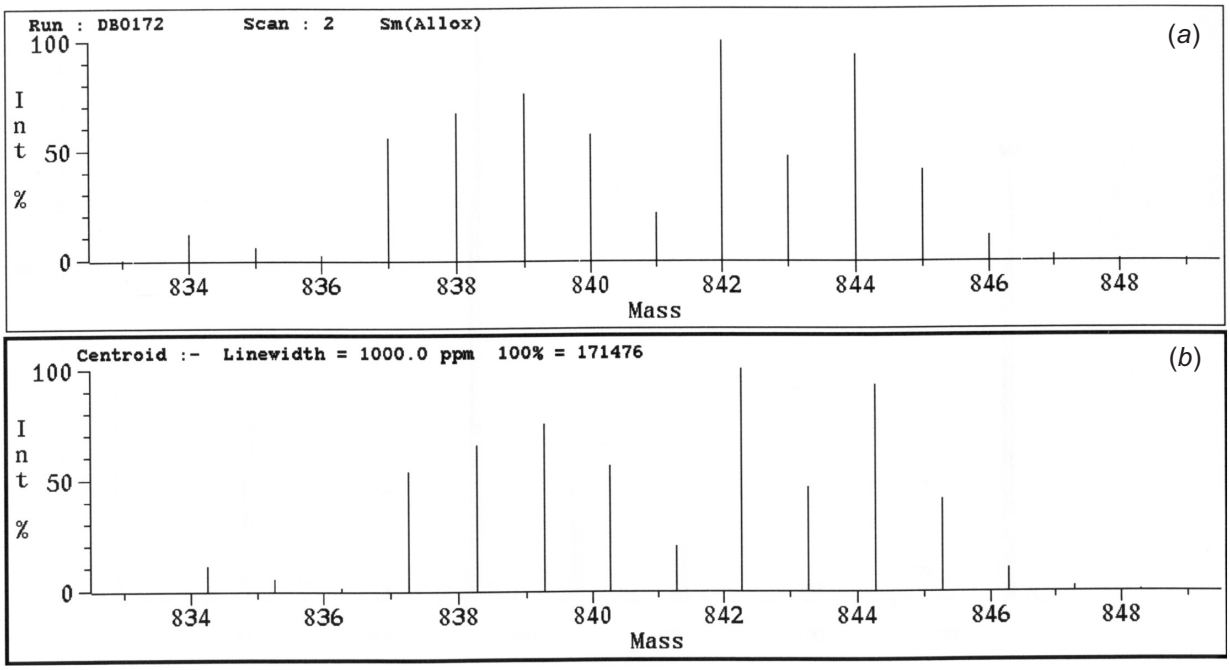
2-Cyanophenol (10.0 g, 0.0840 mol), $Yb(CF_3SO_3)_3$ (0.52 g, 1.0 mol%), and 2-amino-2-methylpropanol (11.22 g,

[2] D.J. Berg, T. Barclay, and X. Fei. Manuscript in preparation. Presented in part as contribution #764 at the 85th Canadian Society for Chemistry Conference, Vancouver, British Columbia, 1–6 June 2002.

[3] Supplementary data for this article are available on the Web site or may be purchased from the Depository of Unpublished Data, Document Delivery, CISTI, National Research Council Canada, Ottawa, ON K1A 0S2, Canada. DUD 3656. For more information on obtaining material refer to http://cisti-icist.nrc-cnrc.gc.ca/irm/unpub_e.shtml. CCDC 260761 and 260762 contain the crystallographic data for this manuscript. These data can be obtained, free of charge, via www.ccdc.cam.ac.uk/conts/retrieving.html (or from the Cambridge Crystallographic Data Centre, 12 Union Road, Cambridge CB2 1EZ, UK; fax +44 1223 336033; or deposit@ccdc.cam.ac.uk).

© 2005 NRC Canada

Fig. 1. (*a*) Experimental and (*b*) calculated isotopic patterns for the molecular ion of $Sm(Allox)_3$ (**6**).



0.126 mol) were suspended in dry 1,2-dichlorochlorobenzene (150 mL) in a Kontes flask under argon. The flask was sealed and the reaction mixture was heated to 170 °C for 24 h; all solids dissolved upon heating. After cooling, the flask was opened and the contents were poured onto ice (200 g). Dichloromethane (200 mL) was added and the two-phase mixture was separated. The organic layer was washed repeatedly with water, dried over anhydr. $MgSO_4$, filtered, and the solvent removed from the filtrate under vacuum to afford 2-(2′-hydroxyphenyl)-4,4-dimethyl-2-oxazoline (9) as white crystals. Yield: 12.5 g (78%); mp 58–60 °C. ^{1}H NMR (*d*-chloroform) δ: 12.17 (br s, 1H, O*H*), 7.65 (d, 1H, 6′-aryl*H*, J = 7.5 Hz), 7.34 (t, 1H, 4′-aryl*H*, J = 7.5 Hz), 6.98 (d, 1H, 3′-aryl*H*, J = 8.0 Hz), 6.83 (t, 1H, 5′-aryl*H*, J = 7.8 Hz), 4.07 (s, 2H, CH_2), 1.37 (s, 6H, CH_3). ^{13}C NMR (*d*-chloroform) δ: 164.2 (*C*=N), 159.9 (2′-aryl*C*), 133.2, 127.9, 118.6, 116.7 (aryl*C*H), 112.4 (1′-aryl*C*), 78.4 (CMe_2CH_2O), 67.1 (CMe_2), 28.5 (CH_3).

2-(2′-Allyloxyphenyl)-4,4-dimethyl-2-oxazoline (2)

The crude 2-(2′-hydroxyphenyl)-4,4-dimethyloxazoline (4.0 g, 0.021 mol) was placed in a round bottomed flask and dissolved in 100 mL of acetone. Excess allylbromide (3.19 g, 0.0264 mol), K_2CO_3 (12.1 g, 0.0872 mol), and *n*-$Bu_4N^+Br^-$ (0.34 g, 0.0017 mol), as a phase-transfer catalyst, were added. The suspension was stirred vigorously at room temperature for 6 days. The salts were removed by filtration and the solvent was stripped under vacuum. The residue was redissolved in diethyl ether (100 mL), filtered to remove further solids, and again taken to dryness under vacuum. The residue was columned on silica gel (hexane) and the pure allyl ether was isolated as a yellow oil. Yield: 4.11 g (85%). ^{1}H NMR (*d*-chloroform) δ: 7.61 (d, 1H, 6′-aryl*H*, J = 7.8 Hz), 7.24 (t, 1H, 4′-aryl*H*, J = 7.6 Hz), 6.87 (d, 1H, 3′-aryl*H*, J = 7.9 Hz), 6.81 (t, 1H, 5′-aryl*H*, J = 7.8 Hz), 5.95 (m, 1H, C*H*=CH_2), 5.46 (d, 1H, CH=CH_{trans}, J = 16.9 Hz), 5.17 (d, 1H, CH=CH_{cis}, J = 11.1 Hz), 4.46 (d, 2H, OCH_2CH=CH_2, J = 6.6 Hz), 3.98 (s, 2H, CH_2), 1.32 (s, 6H, CH_3). HR-MS (EI) calcd.: M^+ 231.1259; found: 231.1271.

2-(2′-Hydroxy-3′-allylphenyl)-4,4-dimethyl-2-oxazoline (H-Allox, 3)

Neat allyl ether **2** (3.3 g, 0.014 mol) was placed in a Kontes flask and heated with rapid stirring at 160 °C for 36 h. The resulting brown oil was chromatographed on silica gel (hexane – diethyl ether, 30:1) to afford **3** as a straw-colored oil. Carrying out the Claissen rearrangement at higher temperatures decreases the time required, but results in considerable production of the 4′-allyl isomer that is difficult to remove chromatographically. Yield: 2.9 g (88%). ^{1}H NMR (*d*-chloroform) δ: 12.42 (br s, 1H, O*H*), 7.43 (d, 1H, 6′-aryl*H*, J = 7.7 Hz), 7.18 (d, 1H, 4′-aryl*H*, J = 7.8 Hz), 6.72 (t, 1H, 5′-aryl*H*, J = 7.7 Hz), 5.95 (m, 1H, C*H*=CH_2), 5.05 (d, 1H, CH=CH_{trans}, J = 16.5 Hz), 5.02 (d, 1H, CH=CH_{cis}, J = 10.1 Hz), 4.01 (s, 2H, CH_2), 3.39 (d, 2H, CH_2CH=CH_2, J = 6.7 Hz), 1.30 (s, 6H, CH_3). ^{13}C NMR (*d*-chloroform) δ: 164.1 (*C*=N), 158.0 (2′-aryl*C*), 136.9 (*C*H=CH_2), 133.6 (aryl*C*H), 127.8 (3′-aryl*C*), 126.2, 118.4 (aryl*C*H), 115.8 (CH=*C*H_2), 112.4 (1′-aryl*C*), 78.6 (CMe_2CH_2O), 67.3 (CMe_2), 34.3 ($CH_2CH=CH_2$), 28.8 (CH_3). HR-MS (EI) calcd.: M^+ 231.1259; found: 231.1265.

La(Allox)$_3$ (4)

A solution of **3** (0.069 g, 0.30 mmol) in 4 mL of toluene was added to a solution of $La[N(SiMe_3)_2]_3$ (0.062 g, 0.10 mmol) in 4 mL of toluene in the glovebox. The solution immediately turned pale yellow and all solids dissolved. The solution was stirred overnight at room temperature and the solvent was removed under reduced pressure to yield a granular white solid. The solid was redissolved in a minimum of hot hexane–toluene (80:20), filtered though a Celite® pad, and the filtrate was then allowed to slowly cool to room tem-

© 2005 NRC Canada

perature. The clear, colorless blocks of **4** that deposited from solution were collected by vacuum filtration and dried under vacuum. Yield: 0.061 g (73%); mp 180–182 °C. ^{1}H NMR (d_8-toluene) δ: 7.90 (dd, 1H, 6′-aryl*H*, *J* = 7.7, 1.8 Hz), 7.20 (dd, 1H, 4′-aryl*H*, *J* = 7.2, 1.8 Hz), 6.59 (t, 1H, 5′-aryl*H*, *J* = 7.5 Hz), 5.98 (m, 1H, C*H*=CH$_2$), 5.00 (d, 1H, CH=CH_{trans}, *J* = 17.1 Hz), 4.90 (d, 1H, CH=CH_{cis}, *J* = 10.3 Hz), 3.47 (s, 2H, OCH_2), 3.45 (d, 2H, CH_2CH=CH$_2$, *J* = 6.7 Hz), 1.27 (s, 6H, CMe_2). ^{13}C NMR (d_8-toluene) δ: 168.0 (*C*=N), 157.8 (2′-aryl*C*), 137.6 (*C*H=CH$_2$), 135.1 (aryl*C*H), 130.9 (aryl*C*), 115.3 (aryl*C*H), 115.0 (CH=*C*H$_2$), 112.0 (1′-aryl*C*), 78.0 (CMe$_2$*C*H$_2$O), 67.4 (*C*Me$_2$), 35.5 (*C*H$_2$CH=CH$_2$), 28.5 (*C*H$_3$). The remaining aryl C resonance was not discernible. MS (EI) *m*/*z* (amu): 829 (M$^+$ ^{139}La, 44%), 599 (M$^+$ – L, 10%), 527 (M$^+$ – L – (C$_4$H$_8$O), 7%), 455 (M$^+$ – L – 2(C$_4$H$_8$O), 100%). Anal. calcd. for C$_{42}$H$_{48}$N$_3$O$_6$La (%): C 60.80, H 5.83, N 5.06; found: C 61.22, H 5.52, N 5.00.

Ce(Allox)$_3$ (5)

Complex **5** was prepared using a procedure analogous to **4** from Ce[N(SiMe$_3$)$_2$]$_3$ (0.062 g, 0.10 mmol) and 3 equiv. of **3**. Small, bright yellow blocks of **5** were isolated by allowing a warm (60 °C) hexane–toluene solution to cool to room temperature. Yield: 0.072 g (87%); mp 196–199 °C. ^{1}H NMR (d_8-toluene, 323 K) δ: 11.86 (d, 3H, 6′-aryl*H*, *J* = 7.4 Hz), 10.63 (d, 3H, 4′-aryl*H*, *J* = 6.8 Hz), 9.37 (t, 3H, 5′-aryl*H*, *J* = 6.3 Hz), 8.06 (m, 3H, C*H*=CH$_2$), 5.65 (d, 3H, CH=CH_{trans}, *J* = 14 Hz), 5.39 (d, 3H, CH=CH_{cis}, *J* = 8 Hz), 4.27 (br s, $\upsilon_{1/2}$ = 18 Hz, 6H, CH_2CH=CH$_2$), 1.00 (s, $\upsilon_{1/2}$ = 8 Hz, 6H, CH_2), –9.48 (br s, $\upsilon_{1/2}$ = 34 Hz, 18H, CH_3). MS (EI) *m*/*z* (amu): 830 (M$^+$ ^{140}Ce, 43%), 516 (100%). Anal. calcd. for C$_{42}$H$_{48}$N$_3$O$_6$Ce (%): C 60.71, H 5.82, N 5.06; found: C 61.05, H 5.71, N 4.92.

Sm(Allox)$_3$ (6)

Complex **6** was isolated as colorless crystals in the same manner as **4** and **5** previously starting from Sm[N(SiMe$_3$)$_2$]$_3$ (0.063 g, 0.10 mmol) and 3 equiv. of **3**. Yield: 0.052 g (62%); mp 173–176 °C. IR (Nujol, NaCl, cm^{-1}): 1652 (vw), 1635 (sh w), 1597 (s), 1558 (w), 1345 (w), 1260 (s), 1226 (vw), 1190 (w), 1160 (w), 1132 (m), 1096 (m), 1065 (w), 1055 (w), 862 (w), 822 (w), 768 (m), 750 (w), 720 (w), 667 (m). The IR spectra of complexes **4**, **5**, **7**, and **8** were superimposable with that of **6**. ^{1}H NMR (d_8-toluene, 373 K) δ: 9.23 (d, 3H, 6′-aryl*H*, *J* = 8.7 Hz), 7.87 (d, 3H, 4′-aryl*H*, *J* = 6.5 Hz), 7.68 (t, 3H, 5′-aryl*H*, *J* = 8.5 Hz), 6.10 (m, 3H, C*H*=CH$_2$), 4.97 (d, 3H, CH=CH_{trans}, *J* = 16 Hz), 4.85 (d, 3H, CH=CH_{cis}, *J* = 11 Hz), 2.83 (d, 6H, CH_2CH=CH$_2$, *J* = 6.4 Hz), 2.73 (s, 6H, CH_2), –2.94 (br s, $\upsilon_{1/2}$ = 4 Hz, 18H, CH_3). MS (EI) *m*/*z* (amu): 842 (M$^+$ ^{152}Sm, 68%), 612 (M$^+$ – L, 10%), 540 (M$^+$ – L – (C$_4$H$_8$O), 16%), 468 (M$^+$ – L – 2(C$_4$H$_8$O), 100%). Anal. calcd. for C$_{42}$H$_{48}$N$_3$O$_6$Sm (%): C 59.97, H 5.75, N 5.00; found: C 60.30, H 5.58, N 5.01.

Er(Allox)$_3$ (7)

Complex **7** was obtained as well-formed, bright pink prisms using the procedure outlined for **4** previously starting from Er[N(SiMe$_3$)$_2$]$_3$ (0.065 g, 0.10 mmol) and 3 equiv. of **3**. Yield: 0.077 g (90%); mp 168–170 °C. ^{1}H NMR (d_8-toluene, 373 K, all resonances are broad singlets) δ: 80.1 ($\upsilon_{1/2}$ = 4400 Hz, 18H, CH_3), 37.8 ($\upsilon_{1/2}$ = 480 Hz, 6H, CH_2), –1.51 ($\upsilon_{1/2}$ = 68 Hz, 3H, alkene*H*), –7.0 ($\upsilon_{1/2}$ = 180 Hz, 3H, alkene*H*), –12.1 ($\upsilon_{1/2}$ = 50 Hz, 3H, aryl*H*), –15.3 ($\upsilon_{1/2}$ = 35 Hz, 3H, aryl*H*), –20.8 ($\upsilon_{1/2}$ = 80 Hz, 3H, aryl*H*). One CH$_2$ (6H) resonance was not observable. MS (EI) *m*/*z* (amu): 858 (M$^+$ ^{168}Er, 100%), 628 (M$^+$ – L, 7%), 554 (M$^+$ – L – (C$_4$H$_8$O), 12%), 482 (M$^+$ – L – 2(C$_4$H$_8$O), 43%). Anal. calcd. for C$_{42}$H$_{48}$N$_3$O$_6$Er (%): C 58.79, H 5.64, N 4.90; found: C 60.71, H 5.92, N 4.62.

Y(Allox)$_3$ (8)

Complex **8** was isolated as colorless crystals using the procedure described for **4** starting from Y[N(SiMe$_3$)$_2$]$_3$ (0.057 g, 0.10 mmol) and 3 equiv. of **3**. Yield: 0.036 g (63%); mp 185 to 186 °C. ^{1}H NMR (d_8-toluene) δ: 7.90 (dd, 3H, 6′-aryl*H*, *J* = 8.0, 1.9 Hz), 7.16 (dd, 3H, 4′-aryl*H*, *J* = 7.3, 1.9 Hz), 6.57 (t, 3H, 5′-aryl*H*, *J* = 7.7 Hz), 5.89 (m, 3H, C*H*=CH$_2$), 4.95 (d, 3H, CH=CH_{trans}, *J* = 17.0 Hz), 4.86 (d, 3H, CH=CH_{cis}, *J* = 10.0 Hz), 3.51 (s, 6H, CH_2), 3.40 (d, 6H, CH_2CH=CH$_2$, *J* = 6.7 Hz), 1.25 (s, 18H, CMe_2). ^{13}C NMR (d_8-toluene) δ: 138.1 (*C*H=CH$_2$), 134.8 (aryl*C*H), 132.2 (aryl*C*), 115.1 (aryl*C*H), 114.7 (CH=*C*H$_2$), 112.5 (1′-aryl*C*), 78.1 (CMe$_2$*C*H$_2$O), 67.8 (*C*Me$_2$), 35.4 (*C*H$_2$CH=CH$_2$), 28.4 (*C*H$_3$). The remaining aryl C resonances and the oxazoline C=N resonance were not discernible. MS (EI) *m*/*z* (amu): 779 (M$^+$ ^{89}Y, 100%), 405 (M$^+$ – L – 2(C$_4$H$_8$O), 26%). Anal. calcd. for C$_{42}$H$_{48}$N$_3$O$_6$Y (%): C 64.69, H 6.20, N 5.39; found: C 65.01, H 6.44, N 5.15.

X-ray crystallographic studies

Crystals of **5** and **7** suitable for X-ray crystallography were grown by allowing a hot, concentrated, toluene–hexane solution to slowly cool to room temperature. Typical crystallographic procedures are illustrated for compound **5** in the following section. Crystals of **5** suitable for X-ray diffraction were removed from the flask, covered with a layer of hydrocarbon oil, attached to a glass fiber, and placed in the low-temperature nitrogen stream (10). Data was collected at 83(2) K using a Bruker/Siemens SMART APEX instrument (Mo Kα radiation, λ = 0.710 73 Å) equipped with a Cryocool NeverIce low-temperature device. Data were measured using ω scans of 0.3° per frame for 30 s, and a full sphere of data was collected. A total of 2132 frames were collected with a final resolution of 0.77 Å. The first 50 frames were recollected at the end of data collection to monitor for decay. Cell parameters were retrieved using SMART (11) software and refined using SAINTPlus (12) on all observed reflections. Data reduction and correction for Lorentzian polarization and decay were performed using the SAINTPlus (12) software. Absorption corrections were applied using SADABS (13). The structure was solved by direct methods and refined by the least-squares method on F^2 using the SHELXTL program package (14). The structure was solved in the space group $P2_1/n$ (No. 14) by analysis of systematic absences. All atoms were refined anisotropically. One of the terminal vinyl groups was disordered. This was modeled with an occupancy of 66% for the major fraction. Soft restraints were applied to maintain the correct geometry. No decomposition was observed during data collection. Details of the data collection and refinement are given in Ta-

© 2005 NRC Canada

Table 1. Crystallographic data for $Ln(Allox)_3$ (**5** (Ce), **7** (Er)).

Empirical formula	$C_{42}H_{48}CeN_3O_6$	$C_{42}H_{48}ErN_3O_6$
Formula weight	831.0	858.1
Temperature (K)	83	223
Wavelength (Å)	0.710 73	0.710 73
Crystal system	Monoclinic	Monoclinic
Space group	$P2_1/n$ (No. 14)	$P2_1/n$ (No. 14)
a (Å)	14.641 1(10)	14.426(3)
b (Å)	15.057 6(10)	15.186(3)
c (Å)	17.102 3(11)	17.065(4)
β (°)	94.976(1)	93.849(4)
Volume (Å^3)	3756.2(4)	3781.5(13)
Z	4	4
Density (calcd., g/cm^3)	1.47	1.51
Absorption coeff. (μ, mm^{-1})	1.264	2.27
F(000)	1708	1748
Crystal size (mm)	0.13 × 0.08 × 0.07	0.16 × 0.17 × 0.37
Crystal color and habit	Yellow needle	Pink needle
Diffractometer	Bruker Smart APEX	Bruker Smart 1000
θ range (°)	1.80–27.50	2.0–25.0
Reflections collect., independent	48 791, 8 624	19 548, 6 679
Max and min transmission	0.92 and 0.85	1.00 and 0.85
Data / restraints / parameters	8 624 / 7 / 482	6 679 / 2 / 488
Goodness-of-fit on F^2	1.01	0.92
Final R indices ($I > 2\sigma(I)$)	$R1$ = 0.045, $wR2$ = 0.093	$R1$ = 0.024, $wR2$ = 0.046
R (all data)	$R1$ = 0.092	$R1$ = 0.057
Largest diff. peak and hole (e/Å^3)	2.351 and –0.745	0.50 and –0.29

ble 1. Further details are provided in the Supplementary material.[3]

Results and discussion

Synthesis and characterization

The chelating neutral ligand 2-(2′-hydroxy-3′-allylphenyl)-4,4-dimethyl-2-oxazoline (HAllox, **3**) was prepared in three steps from 2-cyanophenol as illustrated in Scheme 1. The oxazoline ring was first introduced by the Lewis-acid-catalyzed cyclization of 2-cyanophenol and 2-amino-2-methylpropanol using ytterbium triflate as the catalyst. Although this reaction proceeds slowly at 170 °C in 1,2-dichlorobenzene, we prefer this route to the $ZnCl_2$-catalyzed cyclization (9) because the product is cleaner and yields are comparable. Introduction of the 3′-allyl group was achieved in two steps by the Claissen rearrangement of the allyl phenyl ether **2**.

Lanthanide complexes **4**–**8** of the new oxazoline-phenoxide ligand were most readily prepared by an acid–base reaction between the neutral ligand **3** and $Ln[N(SiMe_3)_2]_3$ in toluene (Scheme 1: Ln = La **4**, Ce **5**, Sm **6**, Er **7**, Y **8**). Metathesis reactions between the lithium salt LiAllox and YCl_3 or $LaCl_3$ in THF produced **4** or **8**, respectively, but the yields were much lower by this route (20%–30%). The complexes displayed the characteristic colour of each ion (Ce yellow, Er pink, La, Sm, Y colourless). Complexes **4**–**8** display similar melting points and their IR spectra as Nujol mulls are superimposable suggesting that these complexes are isostructural in the solid state. This observation was confirmed for **5** and **7** by X-ray crystallography (vide infra). All complexes gave an acceptable elemental analysis, but the carbon percentage was slightly high in all cases, possibly indicating retention of toluene solvent (from recrystallization).

All of the $Ln(Allox)_3$ complexes prepared gave well-behaved mass spectra with molecular ions as the base peaks for complexes of the smaller metals (Er **7** and Y **8**). Simulation of the molecular ion pattern provided unequivocal evidence for the formation of the tris chelate complexes, especially for **4**–**7**, since these metals have distinctive isotopic patterns. An example of the match between the experimental and calculated molecular ion pattern is shown in Fig. 1 for $Sm(Allox)_3$ (**6**). The dominant fragments in the mass spectra of **4**–**8** represent the loss of one or two ligands and the loss of C_4H_8O, presumably from cleavage of the oxazoline ring. The latter has been observed previously during the thermal decomposition of $Ce(Me_2\text{-phenox})_4$ (Me_2-phenox, ligand **I**) (5).

Solid-state structures

Crystallographic data for **5** and **7** are summarized in Table 1. Selected distances and angles are given in Table 2, and ORTEP3 (15) plots of the structures are shown in Figs. 2 (**5**, Ce) and 3 (**7**, Er). The structures of **5** and **7** are very similar to one another, showing a distorted octahedral coordination environment and a mer arrangement of the three chelating Allox ligands. The allyl groups clearly are not within bonding distance of the metal as the closest contacts between the internal or terminal alkene carbons and the metals are more than 4 Å.

More than 40 structures have been reported of metal complexes containing derivatives of the 2-oxazolylphenoxide chelate unit. These structures span all groups of the *d*-block and the Group 13 metals, but there are no examples contain-

© 2005 NRC Canada

Scheme 1.

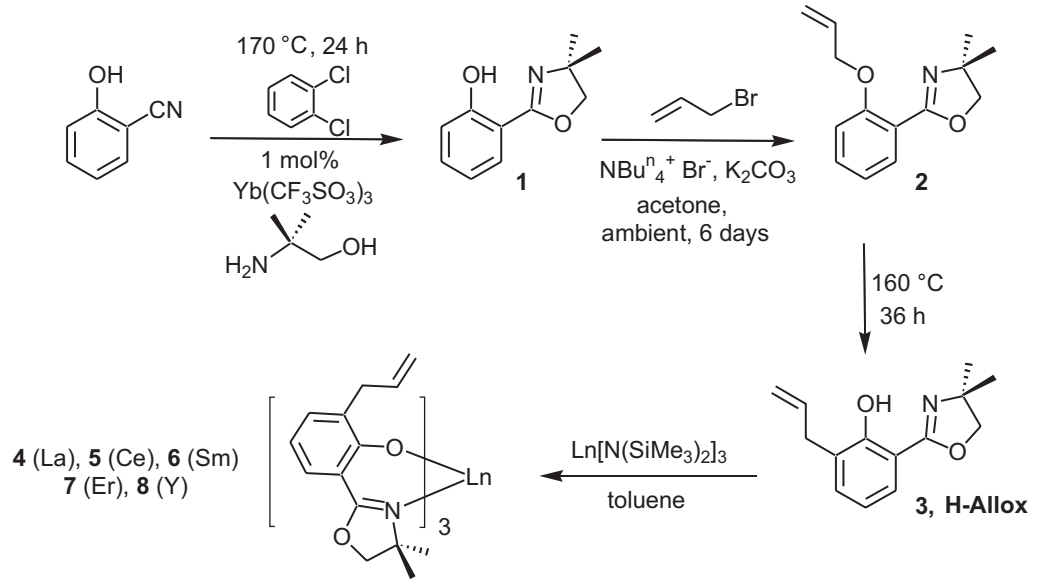


Table 2. Selected distances and angles for $Ln(Allox)_3$ (**5** (Ce), **7** (Er)).[a]

5		**7**	
Bond distances (Å)			
Ce(1)—N(1A)	2.697(3)	Er(1)—N(1)	2.420(3)
Ce(1)—N(1B)	2.584(4)	Er(1)—N(2)	2.433(3)
Ce(1)—N(1C)	2.577(4)	Er(1)—N(3)	2.541(3)
Ce(1)—O(1A)	2.260(3)	Er(1)—O(1)	2.148(2)
Ce(1)—O(1B)	2.251(3)	Er(1)—O(3)	2.124(3)
Ce(1)—O(1C)	2.275(3)	Er(1)—O(5)	2.140(2)
Bond angles (°)			
Ce(1)-O(1A)-C(1A)	148.9(3)	Er(1)-O(1)-C(1)	142.7(2)
Ce(1)-O(1B)-C(1B)	147.3(3)	Er(1)-O(3)-C(15)	143.9(2)
Ce(1)-O(1C)-C(1C)	146.2(3)	Er(1)-O(5)-C(29)	146.4(2)
N(1A)-Ce(1)-N(1B)	107.79(11)	N(1)-Er(1)-N(2)	160.7(9)
N(1A)-Ce(1)-N(1C)	92.92(11)	N(1)-Er(1)-N(3)	91.02(10)
N(1A)-Ce(1)-O(1A)	68.62(11)	N(1)-Er(1)-O(1)	75.41(9)
N(1A)-Ce(1)-O(1B)	161.41(11)	N(1)-Er(1)-O(3)	90.72(9)
N(1A)-Ce(1)-O(1C)	92.23(11)	N(1)-Er(1)-O(5)	100.61(9)
N(1B)-Ce(1)-N(1C)	156.48(12)	N(2)-Er(1)-N(3)	105.77(10)
N(1B)-Ce(1)-O(1A)	95.78(11)	N(2)-Er(1)-O(1)	94.46(9)
N(1B)-Ce(1)-O(1B)	69.94(11)	N(2)-Er(1)-O(3)	75.14(10)
N(1B)-Ce(1)-O(1C)	97.49(10)	N(2)-Er(1)-O(5)	93.50(9)
N(1C)-Ce(1)-O(1A)	102.22(11)	N(3)-Er(1)-O(1)	90.87(9)
N(1C)-Ce(1)-O(1B)	93.90(11)	N(3)-Er(1)-O(3)	166.86(9)
N(1C)-Ce(1)-O(1C)	70.02(11)	N(3)-Er(1)-O(5)	73.24(9)
O(1A)-Ce(1)-O(1B)	93.01(11)	O(1)-Er(1)-O(3)	102.16(9)
O(1A)-Ce(1)-O(1C)	159.36(11)	O(1)-Er(1)-O(5)	163.67(9)
O(1B)-Ce(1)-O(1C)	106.36(11)	O(3)-Er(1)-O(5)	93.65(9)

[a]Estimated standard deviations are in parentheses.

ing Group 3, lanthanide, (or actinide) ions.[4] Of the published structures, the best comparisons to **5** and **7** are the six-coordinate, tris chelate complexes of Al, Ga, and In, all of which also adopt a mer geometry (16). In fact, the other known tris chelates of this ligand type, three for Mn (2*d*, 2*h*) and one for Fe (17), crystallize exclusively in the mer geometry. There appears to be a pronounced trans influence operative in **5** and **7** as the M—N distance trans to oxygen is ca. 0.12 Å longer than that trans to nitrogen in both cases. A similar, but much smaller, effect is observed in the tris che-

[4]A complete listing of these structures and a table summarizing important metrical parameters is given in the Supplementary material.[3]

© 2005 NRC Canada

Fig. 2. ORTEP3 (16) plot (30% probability) of Ce(Allox)$_3$ (**5**).

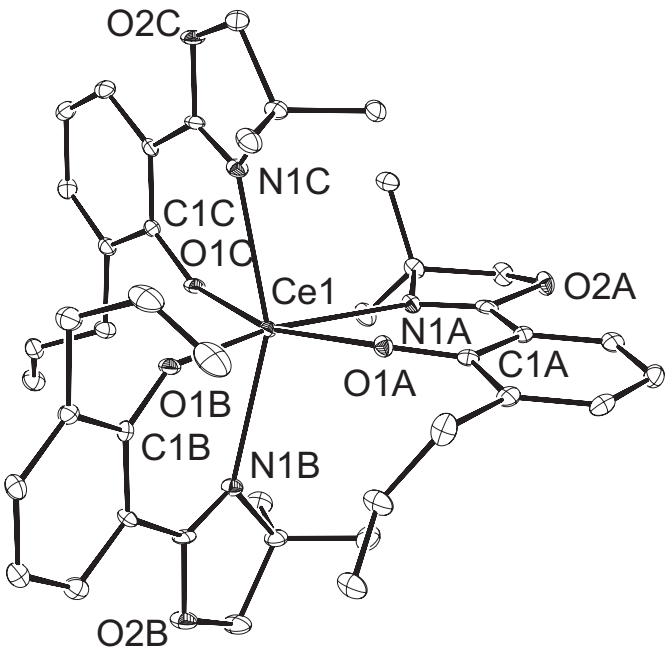
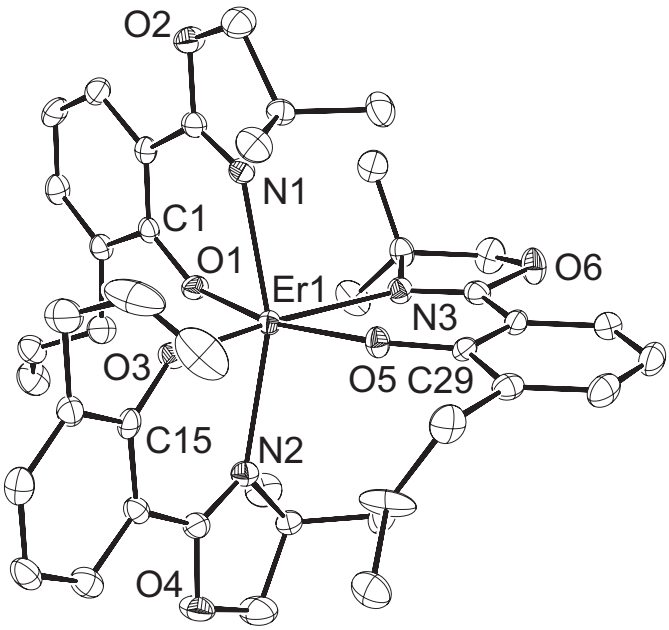


Fig. 3. ORTEP3 (16) plot (30% probability) of Er(Allox)$_3$ (**7**).



late complexes of Group 13 where the average difference is only ca. 0.03 Å (16). The Ln—O bond lengths in **5** and **7** are 0.07 Å *shorter* than predicted from In(Phox)$_3$ (PhoxH = 2-(2′-hydroxyphenyl)-2-oxazoline) (16*a*) after adjustment for differences in ionic radii[5] (18). In contrast, the Ln—N distances are 0.20 (**5**, Ce) and 0.17 (**7**, Er) Å *longer* than expected using this same comparison. All of these observations are consistent with a greater affinity for oxygen vs. nitrogen for the lanthanides.

There are only two structures reported of any type that contain a neutral oxazoline ring bonded to a Group 3 or lanthanide ion and both complexes contain the oxazoline ring as part of a chiral, tridentate "pybox" ligand (Sc(Ph-pybox)(OTf)$_3$(H$_2$O) (4*c*) and [La(Ph$_2$-pybox)(OTf)$_2$(H$_2$O)$_4$]$^+$-[OTf]$^-$ (4*b*)). The Sc—N(ox) distances in the seven-coordinate Sc complex predict Ce—N and Er—N distances of 2.56 and 2.44 Å, respectively, almost exactly matching those observed in **5** and **7** for the trans pair of oxazoline Ln—N bonds.[5] The La—N(ox) distances in the nine-coordinate La complex predict Ce—N and Er—N distances of 2.47 and 2.35 Å, respectively, far shorter than those actually observed. However, the La comparison is based on the nine-coordinate radius of La^{3+} and since the La centre is bound by four small water molecules, this radius is likely an overestimation of the size of the metal ion.

Subtle differences are detectable between the structures of **5** and **7**. In particular, although the difference in Ln—O bond lengths in the two structures (0.125 Å) matches the difference in ionic radii for the two metals (18), the difference in Ln—N bond distance (0.155 Å) is slightly larger than expected. Thus, the Er—N(oxazoline) distance in **7** is relatively short compared to that in **5**. Since Er is the smaller of the two metals, this runs counter to steric arguments; stronger oxazoline binding owing to the higher charge to size ratio of Er may explain this effect. In any case, it seems quite clear from the foregoing discussion that these complexes are not significantly crowded, as we might expect for a six-coordinate lanthanide center and relatively small ligand substituents.

The Ln-O-C angles of the phenoxide group are considerably less bent in **5** (146.2(3)°–148.9(3)°) and **7** (142.7(2)°–146.4(2)°) than those in the Group 13 tris chelates (122°–135°) (16), and only complexes of the Group 4 metals show M-O-C angles of more than 140° (19). Terminal Ln-O-C(aryl) angles are usually greater than 160° (20) so the observed angles are in fact more bent than usual because of the constraints of the chelate geometry.[6] The chelate bite itself (O-Ln-N (**5** (68.62(11)°–70.02(11)°), **7** (73.24(9)°–75.41(9)°)) is the smallest of any reported 2-oxazolylphenoxide structure (range (76°–96°), median (87°)),[4] but this is primarily a reflection of the fact that Ce and Er are the largest metals to which this ligand has been complexed.

Solution behaviour

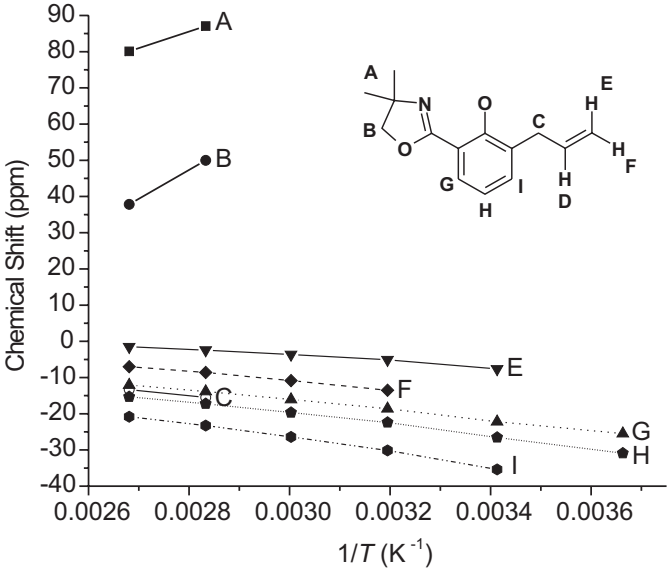
The NMR spectra of **4**–**8** in d_8-toluene each show a single set of nine resonances for the Allox ligand consistent with average C_{3v} molecular symmetry. Since this symmetry is unlikely in a static structure, we investigated the variable-temperature ^{1}H NMR spectra of all complexes at both high and low temperature. In all cases, lowering the temperature resulted in decoalescence into at least 17, and usually more, resonances (vide infra). The resonances for paramagnetic complexes **5**–**7** showed good linear behaviour in δ vs. 1/*T*

[5] Ionic radii from ref. 18: coordination number (CN) = 6 for In^{3+} 0.800 Å, Ce^{3+} 1.01 Å, Y^{3+} 0.90 Å, Er^{3+} 0.89 Å; CN = 7, Sc^{3+} 0.81 Å; CN = 9, La^{3+} 1.22 Å.

[6] The mean Ln-O-C angle in terminal phenoxides bearing only H or Me groups in the ortho positions is 167° with a standard deviation of 8° and an overall range of 144°–180°. Some typical examples are given in ref. 20.

© 2005 NRC Canada

Fig. 4. ^{1}H NMR chemical shift (δ) vs. the inverse temperature ($1/T$) plot for Er(Allox)$_3$ (**7**) above coalescence (d_8-toluene, 360 MHz).



plots above and below coalescence, consistent with a single species in each temperature regime. A sample plot for **7** above coalescence is shown in Fig. 4; remaining plots are included in the Supplementary material.[3] The line widths below coalescence were quite broad for Er, but the wider chemical shift window made it possible to distinguish 30 peaks in the low-temperature spectra. This is consistent with the low symmetry environment found in the solid-state structure since 36 resonances are expected if the molecule possesses C_1 symmetry.

In the case of Ce and Sm, resonances clearly overlap with one another, but the observation of six methyl signals in the low-temperature spectra of **6** indicates that the low-temperature limiting structure of this complex also possesses C_1 symmetry (Fig. 5). Addition of d_8-THF to a d_8-toluene solution of **6** had a minor effect on the chemical shifts observed, but did not alter the coalescence behaviour. Changing the concentration of **6** over a fivefold range also caused no changes in dynamic behaviour. Taken together, the observation of linear δ vs. $1/T$ behaviour above or below coalescence and the lack of concentration or coordinating solvent effects strongly imply that an intramolecular fluxional process is operative.

The diamagnetic complexes **4** and **8** show similar behaviour to their paramagnetic counterparts except that the smaller spectral dispersion leads to a much lower coalescence temperature and more overlap in the low-temperature spectra. The full VT NMR spectra of **8** are shown in Fig. 6 and an expansion of the most downfield aryl resonance is shown in Fig. 7. Most of the resonances that have decoalesced in the 193 K spectrum (Fig. 6) appear to be in 2:1 intensity ratio (resonances near 6.0 and 8.2 ppm, for example). However, closer inspection reveals that this is most likely due to accidental overlap of resonances. This is clear in the expansion of the downfield aryl resonance (6′-aryl H) because this proton cannot give rise to a true triplet given the coupling constants involved for this aryl position. The observation of an

Fig. 5. A portion of the low temperature ^{1}H NMR spectrum of Sm(Allox)$_3$ (**6**, d_8-toluene, 500 MHz, diamagnetic peaks between 0 and 1 ppm suppressed).

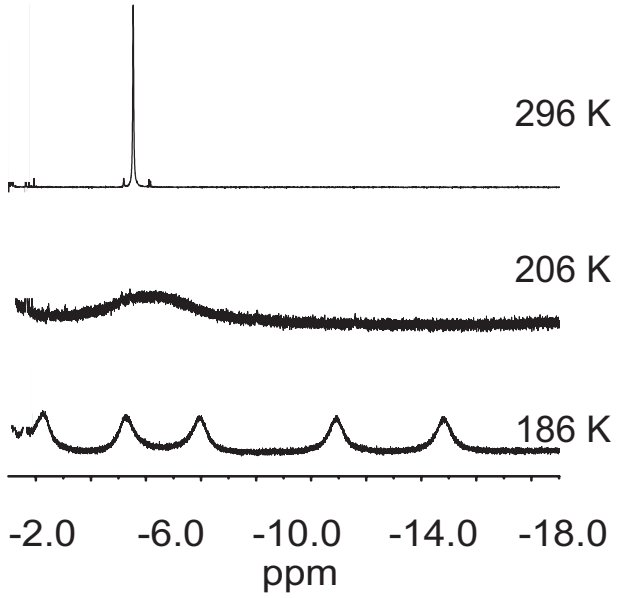
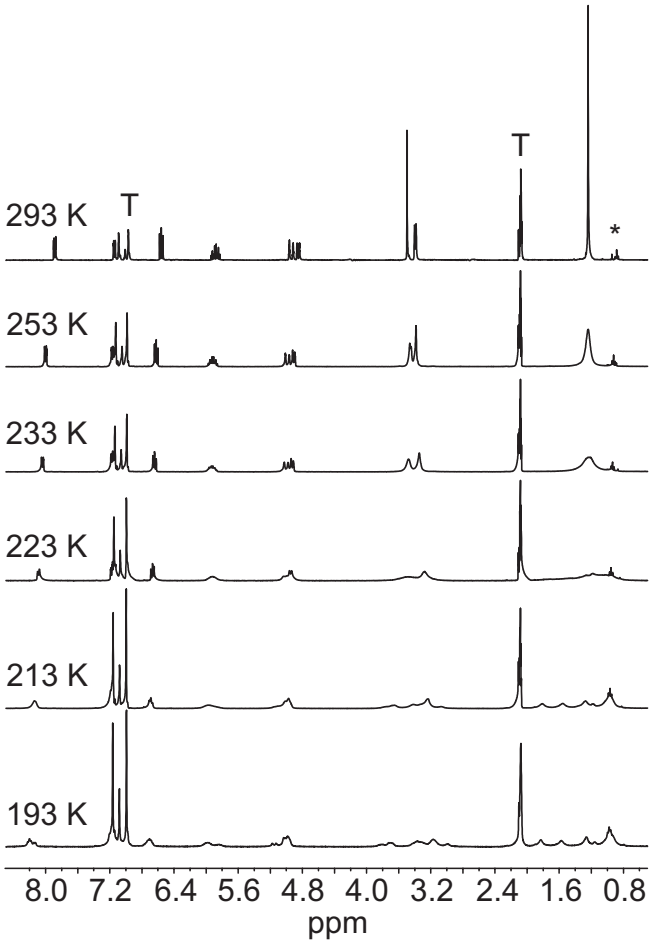


Fig. 6. Variable-temperature ^{1}H NMR spectra of Y(Allox)$_3$ (**8**) (d_8-toluene, 360 MHz, T = toluene, * = impurity).



© 2005 NRC Canada

Fig. 7. Expansion of the downfield aryl region of Fig. 6.

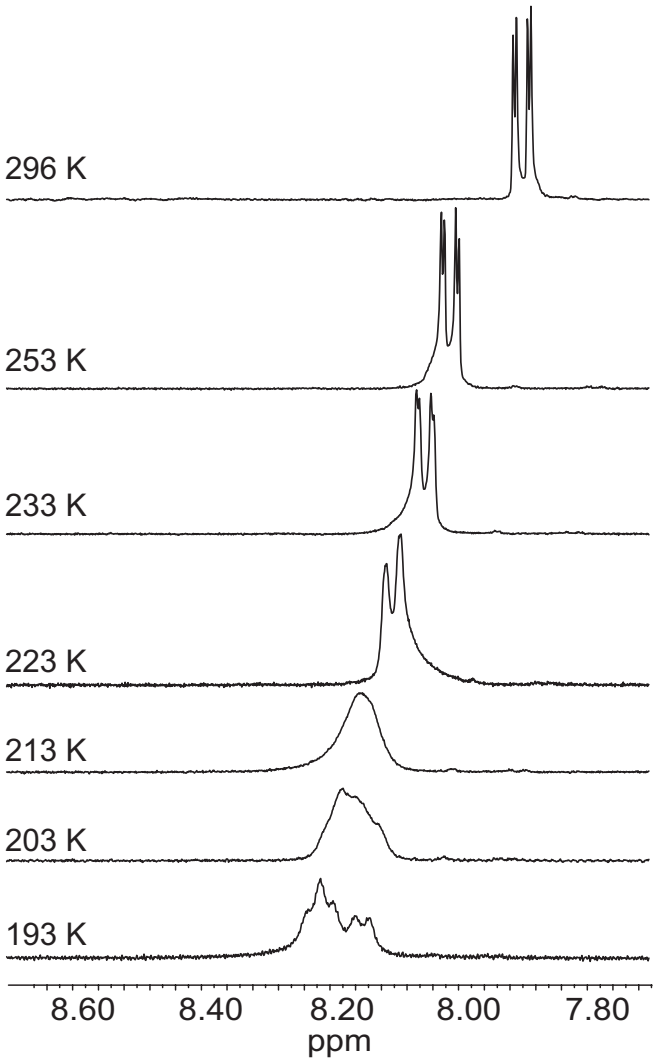


Fig. 8. Experimental and simulated (DNMR3) lineshapes for the 6′-aryl resonance of $Y(Allox)_3$ (**8**) at selected temperatures.

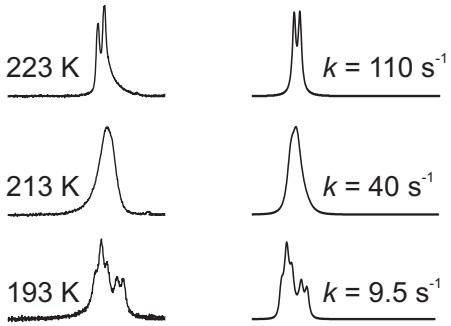
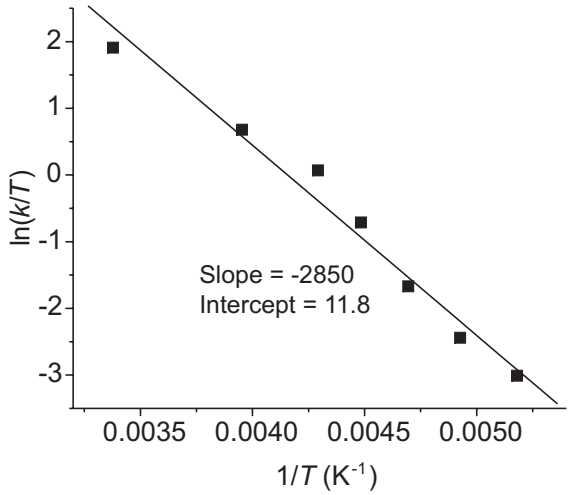


Fig. 9. Eyring plot for the exchange process of $Y(Allox)_3$ (**8**).



apparent triplet can only be explained by the overlap of two doublets (a doublet of doublets pattern is expected, but the smaller coupling is not resolvable given the line widths in this spectrum). The four methyl resonances between 1.0–1.8 ppm in the 193 K spectrum integrate as 3:3:3:9, which also can only be explained by accidental overlap of three (of the six) inequivalent methyl groups at 1.0 ppm.

The VT behaviour of the downfield aryl resonance was simulated by DNMR3 assuming that a single process exchanges all three inequivalent resonances; a subset of the simulated and observed spectra is shown in Fig. 8. The Eyring plot for this process (Fig. 9) gave $\Delta H^{\ddagger} = 24 \pm 2$ kJ mol^{-1} and $\Delta S^{\ddagger} = -99 \pm 15$ J mol^{-1} K^{-1}. While the errors in these parameters are admittedly quite large, the large negative entropy of activation is inconsistent with a dissociative mechanism (21). An associative process to produce a seven-coordinate complex is also highly unlikely given the lack of solvent and concentration dependence. A process involving a "hinged" five-coordinate intermediate cannot be entirely excluded, but most examples of rearrangements proceeding by partial dissociation of a chelate ligand show positive activation entropies (22). Conversely, a six-coordinate rearrangement of the anion in $K_3[Ga(catecholate)_3]$ has been established that shows a negative activation entropy of –20 to –47 J mol^{-1} K^{-1} depending on the solvent and conditions (23).

The foregoing discussion suggests that **4**–**8** undergo a six-coordinate fluxional process in solution. The options include the familiar Bailar (trigonal) or Rây–Dutt (rhombic) twists (Figs. 10 and 11) (24). Negative entropies of activation are often associated with both of these processes (23, 25).

The Bailar twist cannot interconvert mer and fac isomers, but it can scramble ligands between sites within the mer geometry and cause racemization (*mer*-Δ with *mer*-Λ). The Rây–Dutt twist can interconvert all four isomers (*mer*-Δ, *mer*-Λ, *fac*-Δ, *fac*-Λ) (26). We cannot distinguish between these two possibilities because we would need to observe fac and mer exchange to confirm a Rây–Dutt twist (26) and the fac isomer is not observed in the low-temperature NMR spectra of **4**–**8**.

Theoretically, it is also possible to distinguish between these two mechanisms kinetically since the Bailar twist exchanges ligand environments at different rates [$\mathbf{A} \rightarrow \mathbf{C}$, $\mathbf{B} \rightarrow \mathbf{B}$, $\mathbf{C} \rightarrow \mathbf{A}$] while a Rây–Dutt twist permutes ligand environments at an equal rate [$\mathbf{A} \rightarrow \mathbf{C}$, $\mathbf{B} \rightarrow \mathbf{A}$, $\mathbf{C} \rightarrow \mathbf{B}$] (Figs. 10*a*–10*c*) (26, 27). Unfortunately, the spectral dispersion in the VT NMR of diamagnetic complexes **4** and **8** is not sufficient to model exchange by anything more than a single process.

© 2005 NRC Canada

Fig. 10. Interconversion of geometric and optical isomers by the Rây–Dutt (rhombic) twist mechanism.

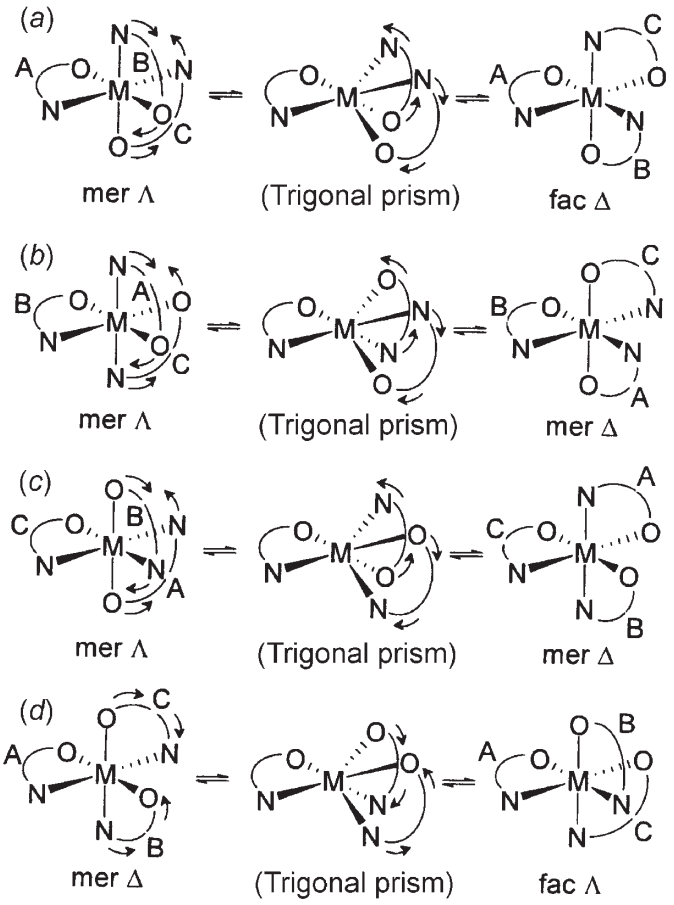
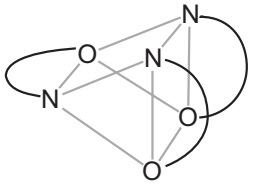


Fig. 11. The trigonal prismatic Rây–Dutt intermediate.



If the fac isomer is present and exchanging with the mer isomer, it must be in low concentration at all temperatures or we would not observe linear behaviour in plots of δ vs. $1/T$ for **5**–**7**.[7]

The relative energetics of the Rây–Dutt and Bailar twist mechanisms have been assessed theoretically by Rodger and Johnson (28). They suggest that the Bailar twist will generally be favoured if the ratio of chelate bite angle (b) to hard sphere contact distance (l) between adjacent ligand atoms (not part of the same chelate) is small ($b/l \approx 0.5$), and the Rây–Dutt twist will be favoured if this ratio is large ($b/l \approx 1.5$). According to these calculations, there is no energetic difference between the two mechanisms at $b/l = 0.914$. This ratio is 0.76 (Ce) and 0.82 (Er) in complexes **5** and **7**. It should also be pointed out that a recent experimental study on *mer*-Ga(fox)$_3$ (Hfox = 5-fluoro-8-hydroxyquinoline) using 2D EXSY NMR was able to kinetically distinguish between the two twist mechanisms and found that *both* contributed to the fluxional behaviour of this compound (27). Interestingly, the b/l ratio for *mer*-Ga(ox)$_3$ (Hox = 8-hydroxyquinoline) is 0.90 (29), almost exactly the value predicted by Rodger and Johnson to give equal energetics for either twist mechanism. Thus, while theoretical treatments suggest that **4**–**8** should undergo a Bailar rather than a Rây–Dutt twist, the mechanisms may be close enough in energy that both are operative.[8]

The fluxional Group 13 tris chelates (M(3′-MePhox)$_3$, M = Al, Ga, In) were previously investigated by VT NMR spectroscopy (16*a*). These complexes also undergo intramolecular rearrangement of inequivalent ligands within the mer geometry on the NMR timescale at, or just above, room temperature. In the case of In, there was some evidence for formation of the fac isomer as a distinct (nonexchanging) species at high temperature. The authors did not determine $\Delta S^{\ddagger}$ and were unable to rule out a bond rupture (five-coordinate Berry pseudorotation) mechanism. However, $\Delta G^{\ddagger}$ values were calculated at the coalescence temperatures and as might be expected, they decrease in the order Al (72 kJ mol^{-1}) > Ga (64 kJ mol^{-1}) > In (<42 kJ mol^{-1}). The value reported for In was based on the lowest temperature attained of 213 K; using the activation parameters for **8**, we calculate a value of $\Delta G^{\ddagger}$ = 45 kJ mol^{-1} at this temperature. While it might seem surprising that the much larger[4] Y complex has a larger $\Delta G^{\ddagger}$ value, the oxazoline rings in the In structure are unsubstituted while those in **8** bear two methyl groups in the 4 position. These methyl groups are relatively close to the metal centre (avg. 3.89 Å in **7**) and may well increase the barrier to a six-coordinate rearrangement.

Concluding remarks

Lanthanide complexes of the hybrid oxazoline-phenoxide chelating ligand Allox are readily accessible and adopt a six-coordinate mer geometry in the solid state without coordination of the pendant allyl substituents. NMR evidence suggests that this structure is maintained in solution over a wide temperature range, but exchange of inequivalent ligands within the mer geometry occurs rapidly on the NMR timescale at room temperature for all complexes studied. A more detailed study of the exchange process for Y complex **8** supports an intramolecular six-coordinate rearrangement, although it is not possible to distinguish between a Bailar (trigonal) or Rây–Dutt (rhombic) twist mechanism.

Acknowledgment

The support of the Natural Sciences and Engineering Research Council of Canada (NSERC) is gratefully acknowledged.

References

1. (*a*) A. Chimiak and J.B. Nielands. Struct. Bonding (Berlin), **58**, 90 (1984); (*b*) R.J. Bergeron. Chem. Rev. **84**, 587 (1984);

[7] Assuming that the ratio of fac and mer isomers varies significantly with temperature.
[8] For a discussion of electronic factors in six-coordinate rearrangements see ref. 30.

© 2005 NRC Canada

(*c*) P.J. Maurer and M.J. Miller. J. Am. Chem. Soc. **105**, 240 (1983); (*d*) Y. Nagao, T. Miyasaka, T. Hagiwara, and E. Fujita. J. Chem. Soc. Perkin Trans. 1, 183 (1984).
2. (*a*) C. Bolm, G. Schlingloff, and K. Wieghardt. Angew. Chem. Int. Ed. Engl. **33**, 1848 (1994); (*b*) C. Bolm and G. Schlingloff. J. Chem. Soc. Chem. Comm. 1247 (1995); (*c*) M. Gómez-Simón, S. Jansat, G. Muller, D. Panyella, M. Font-Bardia, and X.-J. Solans. J. Chem. Soc. Dalton Trans. 3755 (1997); (*d*) M. Hoogenraad, K. Ramkisoening, H. Kooijman, A.L. Spek, E. Bouwman, J.G. Haasnoot, and J. Reedjik. Inorg. Chim. Acta, **279**, 217 (1998); (*e*) M. Hoogenraad, K. Ramkisoening, H. Kooijman, A.L. Spek, E. Bouwman, J.G. Haasnoot, and J. Reedjik. Inorg. Chim. Acta, **320**, 117 (2001); (*f*) G. Mugesh, H.B. Singh, and R.J. Butcher. Eur. J. Inorg. Chem. 669 (2001); (*g*) M. Gómez, S. Jansat, G. Muller, G. Noguera, H. Teruel, V. Molines, E. Cerrada, and M. Hursthouse. Eur. J. Inorg. Chem. 1071 (2001); (*h*) M. Hoogenraad, K. Ramkisoening, S. Gorter, W.L. Driessen, E. Bouwman, J.G. Haasnoot, J. Reedjik, T. Mahabiersing, and F. Hartl. Eur. J. Inorg. Chem. 377 (2002); (*i*) W. Zhao, Y. Qian, J. Huang, and J. Duan. J. Organomet. Chem. **689**, 2614 (2004); (*j*) J. Arias, C.R. Newlands, and M.M. Abu-Omar. Inorg. Chem. **40**, 2185 (2001); (*k*) M. Gómez, G. Muller, and M. Rocamora. Coord. Chem. Rev. **193–195**, 769 (1999); (*l*) H.A. McManus and P.J Guiry. Chem. Rev. **104**, 4151 (2004).
3. C. Qian and L. Wang. Tetrahedron Lett. **41**, 2203 (2000).
4. (*a*) C. Qian and L. Wang. Tetrahedron: Asymmetry, **11**, 2347 (2000); (*b*) G. Desmoni, G. Faita, S. Filippone, M. Mella, M.G. Zampori, and M. Zema. Tetrahedron, **57**, 10 203 (2001); (*c*) D.A. Evans, Z.K. Sweeney, T. Rovis, and J.S. Tedrow. J. Am. Chem. Soc. **123**, 12 095 (2001); (*d*) G. Desimoni, G. Faita, and P. Quadrelli. Chem. Rev. **103**, 3119 (2003); (*e*) G. Desimoni, G. Faita, M. Guala, and C. Pratelli. J. Org. Chem. **68**, 7862 (2003).
5. H. Guillon, S. Daniele, L.G. Hubert-Pfalzgraf, and J.M. Letoffe. Polyhedron, **23**, 1467 (2004).
6. H. Kodama, J. Ito, K. Hori, T. Ohta, and I. Furakawa. J. Organomet. Chem. **603**, 6 (2000).
7. S. Hong, S. Tian, M.V. Metz, and T.J. Marks. J. Am. Chem. Soc. **125**, 14 768 (2003).
8. D.C. Bradley, J.S. Ghotra, and F.A. Hart. J. Chem. Soc. Dalton Trans. 1021 (1973).
9. (*a*) K.M. Button, R.A. Gossage, and R.K.R. Phillips. Synth. Commun. **32**, 363 (2002); (*b*) J.T. Banks, K.M. Button, R.A. Gossage, T.D. Hamilton, and K.E. Kershaw. Heterocycles, **55**, 2251 (2001); (*c*) K.M. Button and R.A. Gossage. J. Heterocyclic Chem. **40**, 513 (2003); (*d*) H. Witte and W. Seeliger. Angew. Chem. Int. Ed. Engl. **11**, 287 (1972); (*e*) H. Witte and W. Seeliger. Justus Liebigs Ann. 996 (1974); (*f*) C. Bolm, K. Weickhardt, M. Zehnder, and T. Ranff. Chem. Ber. **124**, 1173 (1991); (*g*) C. Bolm, K. Weickhardt, M. Zehnder, and D. Glasmacher. Helv. Chim. Acta, **74**, 717 (1991).
10. H. Hope. Prog. Inorg. Chem. **41**, 1 (1995).
11. SMART. Version 5.626 [computer program]. Bruker AXS, Madison, Wisconsin. 2002.
12. SAINTPlus. Version 6.22 [computer program]. Bruker AXS, Madison, Wisconsin. 2001.
13. G.M. Sheldrick. SADABS. Version 2.01 [computer program]. Bruker AXS, Madison, Wisconsin. 2001.
14. G.M. Sheldrick. SHELXTL. Version 6.10 [computer program]. Bruker AXS, Madison, Wisconsin. 2001.
15. L.J. Farrugia. J. Appl. Crystallogr. **30**, 565 (1997).
16. (*a*) H.R. Hoveyda, V. Karunaratne, S.J. Rettig, and C. Orvig. Inorg. Chem. **31**, 5408 (1992); (*b*) H.R. Hoveyda, C. Orvig, and S.J. Rettig. Acta Crystallogr. Sect. C, **C50**, 1906 (1994).
17. H. Kooijman, A.L. Spek, M. Hoogenraad, E. Bouwman, J.G. Haasnoot, and J. Reedjik. Acta Crystallogr. Sect. C, **C58**, 390 (2002).
18. R.D. Shannon. Acta Crystallogr. Sect. A, **A32**, 751 (1976).
19. (*a*) P.G. Cozzi, C. Floriani, A. Chiesi-Villa, and C. Rizzoli. Inorg. Chem. **34**, 2921 (1995); (*b*) P.G. Cozzi, E. Gallo, C. Floriani, A. Chiesi-Villa, and C. Rizzoli. Organometallics, **14**, 4994 (1995).
20. (*a*) W.J. Evans, T.P. Hanusa, and K.R. Levan. Inorg. Chim. Acta, **110**, 191 (1985); (*b*) W.J. Evans, M.A. Ansari, J.W. Ziller, and S.I. Khan. J. Organomet. Chem. **553**, 141 (1998); (*c*) W.J. Evans, J.M. Olafson, and J.W. Ziller. Inorg. Chem. **28**, 4308 (1989); (*d*) W.J. Evans, M.A. Greci, and J.W. Ziller. J. Chem. Soc. Chem. Comm. 2367 (1998); (*e*) G.R. Giesbrecht, J.C. Gordon, D.L. Clark, B.L. Scott, J.G. Watkin, and K.J. Young. Inorg. Chem. **41**, 6372 (2002); (*f*) S. Daniele, L. Hubert-Pfalzgraf, and J. Vaissermann. Polyhedron, **22**, 127 (2003); (*g*) W.J. Evans, M.A. Ansari, and J.W. Ziller. Inorg. Chem. **34**, 3079 (1995); (*h*) H.C. Aspinall and M. Williams. Inorg. Chem. **35**, 255 (1996); (*i*) M.E.G. Skinner, B.R. Tyrrell, B.D. Ward, and P. Mountford. J. Organomet. Chem. **647**, 145 (2002); (*j*) A.C. Hiller, S.-Y. Liu, A. Sella, and M.R.J. Elsegood. Inorg. Chem. **39**, 2635 (2000); (*k*) G.B. Deacon, C.M. Forsyth, and N.M. Scott. Eur. J. Inorg. Chem. 2501 (2000).
21. R.B. Jordan. Reaction mechanisms of inorganic and organometallic systems. 2nd ed. Oxford University Press, New York. 1998. pp. 102–133.
22. (*a*) C.P. Casey, J.F. Klein, and M.A. Fagan. J. Am. Chem. Soc. **122**, 4320 (2000); (*b*) T.K. Hollis, Y.J. Ahn, and F.S. Tham. J. Chem. Soc. Chem. Comm. 2996 (2002); (*c*) H. Mutsuzaki, H. Kawaguchi, P. Voth, K. Noda, S. Itoh, H.D. Takagi, K. Kashiwabara, and K. Tatsumi. Inorg. Chem. **42**, 5320 (2003).
23. B. Kersting, J.R. Telford, M. Meyer, and K.N. Raymond. J. Am. Chem. Soc. **118**, 5712 (1996).
24. (*a*) J.C. Bailar, Jr. J. Inorg. Nucl. Chem. **8**, 165 (1958); (*b*) P.C. Rây and N.K. Dutt. J. Indian Chem. Soc. **20**, 81 (1943); (*c*) M.L. Tobe and J. Burgess. Inorganic reaction mechanisms. Adison Wesley Longman, Ltd., New York. 1999. pp. 224–239.
25. (*a*) L. Kakaliou, W.J. Scanlan, B. Qian, S.W. Baek, and M.R. Smith III. Inorg. Chem. **38**, 5964 (1999); (*b*) M. Rahim, N.J. Taylor, S. Xin, and S. Collins. Organometallics, **17**, 1315 (1998); (*c*) D.J. Darensbourg and R.L. Gray. Inorg. Chem. **23**, 2993 (1984).
26. R.C. Fay and T.S. Piper. Inorg. Chem. **3**, 348 (1964).
27. M. Gromova, O. Jarjayes, S. Hamman, R. Nardin, C. Béguin, and R. Willem. Eur. J. Inorg. Chem. 545 (2000).
28. A. Rodger and B.F.G. Johnson. Inorg. Chem. **27**, 3602 (1988).
29. Calculated from the reported crystal structure data: (*a*) Y. Wang, W. Zhang, Y. Li, L. Ye, and G. Yang. Chem. Mater. **11**, 530 (1999); (*b*) H. Schmidbaur, J. Lettenbauer, D.L. Wilkinson, G. Muller, and O. Kumberger. Z. Naturforsch. B: Chem. Sci. **46**, 901 (1991); (*c*) L. Peck, Y. Bankovsky, V. Bel'sky, E. Silina, J. Ashaks, and A. Sturis. Latv. J. Chem. **3**, 3 (2000). CCDC code: YINRIW01.
30. C.D. Montgomery and C.J. Shorrock. Inorg. Chim. Acta, **328**, 259 (2002).

© 2005 NRC Canada

Oxo-rhenium(V) complexes with 8-hydroxyquinoline derivatives

Olivier Sigouin and André L. Beauchamp

Abstract: Compounds of the types $ReOCl_2(L)(PPh_3)$ and $ReOCl(L)_2$ were prepared by reacting $ReOCl_3(PPh_3)_2$ with 8-hydroxyquinoline (HL) and its 2-methyl, 2-chloro, 5-chloro, 5-nitro, 5,7-dichloro, 5,7-dibromo, and 5,7-diiodo derivatives. With the bulky 2-phenyl-8-hydroxyquinoline, only $ReOCl_2(L)(PPh_3)$ could be isolated, whereas the still bulkier 2-*tert*-butyl derivative did not react. For $ReOCl_2(L)(PPh_3)$, the coordination of the quinoline oxygen trans to the Re=O bond and the cis-dichloro arrangement in the equatorial plane were established from crystallographic studies on the 2-chloro and the 5,7-dibromo complexes. From the combined data for these various derivatives, the ^{1}H NMR signals could be fully assigned. With both series of compounds, a complex *d–d* absorption pattern is observed in the visible spectra, corresponding to the excitation of a *d* electron from the interaxial *d* orbital in the equatorial plane to the empty d_{xz} and d_{yz} orbitals, which are inequivalent in these low-symmetry systems. Deconvolution revealed the presence of two very weak low-energy components (~10 000 and ~12 000 cm^{-1}), which are assigned to the two expected singlet–triplet transitions, whereas two stronger bands at higher energy (~14 000 and ~17 000 cm^{-1}) originate from the two singlet–singlet transitions. These bands are not substantially displaced by substitution on the 8-hydroxyquinoline rings.

Key words: rhenium, quinoline, crystal structure, *d–d* electron transitions.

Résumé : Des composés de types $ReOCl_2(L)(PPh_3)$ et $ReOCl(L)_2$ ont été préparés par réaction de $ReOCl_3(PPh_3)_2$ avec la 8-hydroxyquinoline (HL) et ses dérivés 2-méthyl, 2-chloro, 5-chloro, 5-nitro, 5,7-dichloro, 5,7-dibromo et 5,7-diiodo. Avec le ligand encombré 2-phényl-8-hydroxyquinoline, seul $ReOCl_2(L)(PPh_3)$ a pu être isolé, alors que le dérivé 2-*tert*-butyl encore plus encombré n'a pas réagi. Pour $ReOCl_2(L)(PPh_3)$, la coordination de l'oxygène de la quinoline en trans de la liaison Re=O et l'arrangement cis-dichloro dans le plan équatorial ont été déterminés au moyen d'études cristallographiques sur les complexes des ligands 2-chloro et 5,7-dibromo. L'ensemble des données pour ces différents dérivés a permis de faire une attribution complète des signaux RMN ^{1}H. Pour les deux séries de composés, un motif d'absorption *d–d* compliqué est observé dans le spectre visible, qui correspond à l'excitation d'un électron *d* depuis l'orbitale *d* interaxiale dans le plan équatorial vers les orbitales vacantes d_{xz} et d_{yz}, qui ne sont pas équivalentes dans ces systèmes de basse symétrie. La déconvolution révèle la présence de deux composantes très faibles à basse énergie (~10 000 et ~12 000 cm^{-1}), qui sont attribuées aux deux transitions singulet–triplet attendues, tandis que les bandes plus fortes à énergie supérieure (~14 000 et ~17 000 cm^{-1}) proviennent de deux transitions singulet–singulet. Ces bandes ne sont pas déplacées appréciablement par substitution sur le cycle de la 8-hydroxyquinoline.

Mots clés : rhénium, quinoline, structure cristalline, transitions électroniques *d–d*.

Introduction

Systems giving rise to electronic transitions between low-spin and high-spin states at low energy cost present considerable interest, since they may provide a basis for developing molecular switches and devices for efficient information storage. The d^2 oxo-rhenium(V) core is a stable unit in which the ground state is low-spin and diamagnetic, since the strong π bonds formed via the oxygen p_x and p_y orbitals raise the d_{xz} and d_{yz} orbitals (LUMO) above the other interaxial *d* orbital (HOMO) in which the two *d* electrons are coupled. However, if the HOMO–LUMO gap could be reduced and become comparable with the pairing energy, the molecule could adopt a high-spin triplet ground state or possess a readily accessible high-spin excited state that could be involved in spin crossover processes.

In a previous study (1), the HOMO–LUMO gap was found to be relatively small in $ReOCl(P{\sim}O)_2$ compounds containing bidentate mixed $P{\sim}O^-$ ligands. To better understand the factors affecting the HOMO–LUMO gap, we recently examined various $ReOX_3$(dppe) and $ReO(OR)X_2$-(dppe) complexes, where the coordination sphere remained close to that of the $ReOCl(P{\sim}O)_2$ species and the equatorial *cis-P,P* arrangement was provided by bis(diphenylphosphino)-ethane(dppe) (2). The presence of a strong π-donor RO^- group trans to the Re=O bond in $ReO(OR)X_2$(dppe) was found to produce an energy gap greater than those of the $ReOX_3$(dppe) compounds, where the trans position is occu-

Received 6 October 2004. Published on the NRC Research Press Web site at http://canjchem.nrc.ca on 12 May 2005.

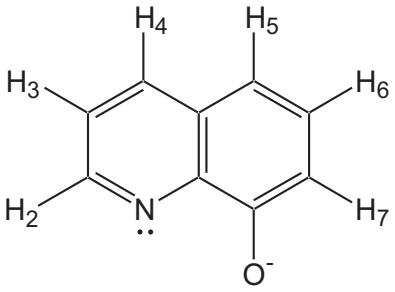
O. Sigouin and A.L. Beauchamp.[1] Département de chimie, Université de Montréal, C.P. 6128, Succursale Centre-ville, Montréal, QC H3C 3J7, Canada.

[1]Corresponding author (e-mail: andre.beauchamp@umontreal.ca).

 doi: 10.1139/V05-063 © 2005 NRC Canada

pied by a halogen. The present study was intended to determine to what extent the energy gap is sensitive to π interactions with donor atoms in the equatorial plane. To this end, we selected the 8-hydroxyquinoline ligand. Although little is known about the influence of this ligand on *d–d* transitions, it was hoped that the Re(V) complexes could provide information about the interaction of its aromatic π system with the interaxial *d* orbitals: when coordinated in the equatorial plane, the π system should interact with the d_{xz} and d_{yz} orbitals, whereas coordination parallel to the Re=O direction would generate interactions with the third interaxial orbital.

We are reporting here the preparation and characterization of $ReOCl_2(L)(PPh_3)$ and $ReOCl(L)_2$ compounds with a series of variously substituted deprotonated 8-hydroxyquinolines (L^-) (**I**). The low-energy UV–vis spectra were found to be rather insensitive to ring substitution, but in contrast with the dppe compounds studied earlier, all four expected low-energy *d–d* bands could be unraveled from the complicated spectral pattern observed.



I

Experimental section

Reactants and methods

8-Hydroxyquinoline (Hqn),[2] most of its derivatives (2-methyl, 5-monosubstituted and 5,7-disubstituted), $KReO_4$, and all other reactants were obtained from Aldrich and used without further purification. 2-Phenyl- and 2-*tert*-butyl-8-hydroxyquinoline were prepared as described by Delapierre et al. (3). The preparation of 2-chloro-8-hydroxyquinoline is described in the following. $ReOCl_3(PPh_3)_2$ (4) was prepared by the literature method.

IR spectra were recorded on PerkinElmer Spectrum One (4000–400 cm^{-1}, KBr pellets) or Bio-Rad Excalibur series FTS 3000FX (4000–200 cm^{-1}, CsI pellets). The NMR spectra were measured with Bruker AV-300, AMX-300, AV-400, or ARX-400 spectrometers. For the ^1H spectra, the residual solvent signal (DMSO-d_6 (2.50 ppm), acetone-d_6 (2.17 ppm), $CDCl_3$ (7.26 ppm), CD_3OD (3.31 ppm)) was used as internal reference. H_3PO_4 was used as an external reference (δ = 0) for the ^{31}P spectra. Electronic spectra were recorded as DMSO, chloroform, or dichloromethane solutions in quartz cells with a UV–vis–near-IR Cary 5E spectrometer. Elemental analyses were run at the Laboratoire d'Analyse Élémentaire de l'Université de Montréal.

Preparation of 2-chloro-8-hydroxyquinoline

This ligand was prepared by reacting $POCl_3$ with 2,8-dihydroxyquinoline obtained from Hqn via the *N*-oxide (5–7).

In glacial acetic acid (25 mL) and 30% H_2O_2 (10 mL) were dissolved 4.00 g (27.6 mmol) of Hqn. The mixture was heated at 70 °C for 16 h and after cooling to room temperature (RT), pH was adjusted to 12 with NH_4OH. The brown solid was collected by filtration and extracted with a hexane–acetone (10:1) mixture. Solvent evaporation yielded yellow crystals of Hqn-*N*-oxide (1.47 g, yield 33%); mp 138 °C (lit. value (5) mp 138–140 °C).

The Hqn-*N*-oxide (3.85 g, 23.9 mmol) was dissolved in acetic anhydride and heated at 140 °C for 5 h. The solvent was removed under reduced pressure and the dark-gray solid was washed with ethanol to give light-yellow 8-acetoxy-2-hydroxyquinoline (1.90 g, yield 39%). ^1H NMR ($CDCl_3$, ppm) δ: 10.17 (br s, 1H, OH), 7.80 (d, J = 9.5 Hz, H4), 7.44 (dd, J_1 = 7.9 Hz, J_2 = 1.2 Hz, H5), 7.37 (dd, J_1 = 7.9 Hz, J_2 = 1.2 Hz, H7), 7.21 (t, J = 7.9 Hz, H6), 6.68 (d, J = 9.6 Hz, H3), 2.51 (s, CH_3COO). Anal. calcd. for $C_{11}H_9NO_3$ (%): C 65.02, H 4.46, N 6.89; found: C 64.89, H 4.56, N 6.83.

The 8-acetoxy-2-hydroxy derivative was dissolved in methanol with 1 equiv. of K_2CO_3 and the reaction mixture was stirred at RT for 1 h. The solvent was evaporated, the brown product was dissolved in water, and a 10% HCl solution was slowly added. Colorless 2,8-dihydroxyquinoline was collected by filtration (1.40 g, yield 93%). ^1H NMR (CD_3OD, ppm) δ: 7.99 (d, J = 9.5 Hz, H4), 7.18 (dd, J_1 = 7.9 Hz, J_2 = 1.2 Hz, H5), 7.12 (t, J = 7.8 Hz, H6), 7.02 (dd, J_1 = 7.7 Hz, J_2 = 1.2 Hz, H7), 6.66 (d, J = 9.5 Hz, H3). Anal. calcd. for $C_9H_7NO_2$ (%): C 67.07, H 4.38, N 8.69; found: C 66.31, H 4.22, N 8.40.

The dihydroxy compound was dissolved in excess $POCl_3$ (10 mL) and heated on a steam bath for 1 h. The mixture was slowly transferred into a mixture of ice (75 g) and NH_4OH (37 mL). The white solid was filtered and dissolution in concd. HCl (75 mL) gave a clear yellow solution, which was heated on a steam bath for 1 h. A Na_2CO_3 solution (1.8 mol/L, 200 mL) was then added to precipitate the light-brown solid, which was collected by filtration and purified by chromatography on silica gel with hexane – ethyl acetate (80:20) as eluent. After solvent evaporation, the solid was dissolved in methanol, water was added to cloudiness, and the mixture was placed in the freezer for a few hours. The white crystalline solid (0.68 g, yield 41%) was filtered and dried in vacuo. ^1H NMR ($CDCl_3$): see Table 1. Anal. calcd. for C_9H_6ClNO (%): C 60.19, H 3.37, N 7.80; found: C 59.81, H 3.17, N 7.80.

Preparation of the $ReOCl_2(L)(PPh_3)$ compounds

These compounds were prepared following the method of Mazzi et al. (8), but benzene was replaced by THF as the solvent and reaction time was adjusted for each system.

In a typical run, $ReOCl_3(PPh_3)_2$ (0.12 mmol) was stirred in a refluxing solution of the ligand (0.12 mmol) in THF (10 mL). The colorless or yellow solution turned green first

[2] The neutral ligand is represented by Hqn and the coordinated deprotonated form by qn^-. The various derivatives are identified by an appropriate prefix showing the positions of the substituents: for instance, 2-Cl-qn^- for the 2-chloro-8-hydroxyquinoline anion.

© 2005 NRC Canada

Table 1. ^{1}H NMR chemical shifts (ppm) and coupling constants (Hz) for the free hydroxyquinolines (Hqn).[a]

	H-2	H-3	H-4	H-5	H-6	H-7	H-10
qn	8.84 (dd, 4.0, 1.6)	7.54 (dd, 8.4, 4.2)	8.32 (dd, 8.3, 1.6)	7.38 (dd, 8.3, 1.7)	7.44 (t, 7.7)	7.07 (dd, 7.1, 1.6)	9.83 (s, br)
2-Me-qn	2.66 (s, CH_3)	7.41 (d, 8.4)	8.18 (d, 8.4)	7.32 (d, 6.5)	7.35 (t, 8.0)	7.04 (d, 6.6)	9.41 (s, br)
2-Cl-qn[b]		7.40 (d, 8.6)	8.10 (d, 8.6)	7.33 (dd, 8.2, 1.1)	7.47 (t, 7.9)	7.22 (dd, 7.7, 1.1)	7.68 (s, br)
2-Ph-qn[b,c]		7.68 (d, 8.4)	8.28 (d, 8.3)	7.37 (d, 6.6)	7.47 (dd, 7.0, 2.4)	7.26 (d)[d]	8.68 (s, br)
2-*t*-Bu-qn[b]	1.47 (s, *t*-Bu)	7.55 (d, 8.7)	8.08 (d, 8.7)	7.28 (d, 8.1)	7.39 (t, 7.9)	7.15 (d, 7.4)	8.37 (s, br)
5-Cl-qn	8.95 (dd, 4.0, 1.0)	7.85 (dd, 8.4, 5.2)	8.49 (dd, 8.5, 1.5)		7.60 (d, 8.4)	7.08 (d, 8.4)	10.14 (s, br)
5-NO_2-qn	9.01 (d, 3.8)	7.88 (dd, 8.8, 4.1)	8.54 (d, 8.8)		9.15 (d, 8.9)	7.19 (d, 8.8)	*e*
5,7-Cl_2-qn	9.00 (dd, 4.0, 1.1)	7.77 (dd, 8.5, 4.3)	8.52 (dd, 8.5, 1.1)		7.84 (s)		*e*
5,7-Br_2-qn	8.96 (dd, 4.0, 0.9)	7.90 (dd, 8.5, 4.1)	8.45 (dd, 8.5, 1.0)		8.07 (s)		*e*
5,7-I_2-qn	8.87 (dd, 4.1, 1.0)	7.73 (dd, 8.5, 4.1)	8.29 (dd, 8.6, 1.0)		8.34 (s)		*e*

[a]In DMSO-d_6, except when otherwise stated.
[b]In $CDCl_3$.
[c]Phenyl resonances: 7.49–7.62 ppm (m, 3H), 8.17 (dd, 2H, ^3J = 5.8 Hz, ^4J = 1.6 Hz).
[d]Interference with the $CDCl_3$ peak.
[e]Not observed.

and then became very dark. When the reaction was stopped, the solvent was evaporated to dryness, the solid was redissolved in dichloromethane (acetone for the 2-Cl-qn compound), precipitated with diethyl ether, filtered, washed with acetone and diethylether, and dried in vacuo. For the less soluble Hqn complex, a precipitate was present at the end of the reaction and solvent evaporation was unnecessary.

Details for each compound are provided in the following. In all cases, the ^{1}H NMR spectra showed multiplets between 7.2 and 7.5 ppm for coordinated PPh_3. The remaining signals are listed in Table 1.

$ReOCl_2$(qn)(PPh_3)

The brown precipitate was filtered from the reaction mixture after 19 h. Yield: 87%. IR (CsI, cm^{-1}): 976 (s) ν(Re=O), 347 (w), 293 (w) ν(Re-Cl). ^{31}P NMR (DMSO-d_6) (ppm) δ: –12.5 (s). Anal. calcd. for $C_{27}H_{21}Cl_2NO_2PRe$ (%): C 47.72, H 3.11, N 2.06; found: C 47.57, H 3.02, N 2.13.

$ReOCl_2$(2-Me-qn)(PPh_3)

Reaction time: 24 h. Green-brown solid. Yield: 77%. IR (CsI, cm^{-1}): 972 (s) ν(Re=O), 314 (w), 284 (w) ν(Re-Cl). ^{31}P NMR (DMSO-d_6, ppm) δ: –17.4 (s). Anal. calcd. for $C_{28}H_{23}Cl_2NO_2PRe$ (%): C 48.49, H 3.34, N 2.02; found: C 48.37, H 3.42, N 2.01.

$ReOCl_2$(2-Cl-qn)(PPh_3)

Reaction time: 2 h. Recrystallization in acetone gave a green solid containing one lattice acetone molecule per formula. Yield: 63%. IR (CsI, cm^{-1}): 977 (s) ν(Re=O), 324 (w), 281 (w) ν(Re-Cl). ^{31}P NMR (DMSO-d_6, ppm) δ: –18.0 (s). Anal. calcd. for $C_{30}H_{26}Cl_3NO_3PRe$ (%): C 46.67, H 3.39, N 1.81; found: C 46.71, H 3.28, N 1.75.

$ReOCl_2$(2-Ph-qn)(PPh_3)

Reaction time: 23 h. Green-brown solid. Yield: 42%. IR (CsI, cm^{-1}): 974 (s) ν(Re=O), 328 (w), 279 (w) ν(Re-Cl). ^{31}P NMR (DMSO-d_6, ppm) δ: –16.7 (s). Anal. calcd. for $C_{33}H_{25}Cl_2NO_2PRe$ (%): C 50.03, H 3.27, N 1.74; found: C 49.82, H 3.31, N 1.79.

$ReOCl_2$(5-Cl-qn)(PPh_3)

Reaction time: 24 h. Brown solid. Yield: 91%. IR (CsI, cm^{-1}): 980 (s) ν(Re=O), 345 (w), 296 (w) ν(Re-Cl). ^{31}P NMR (DMSO-d_6, ppm) δ: –12.1 (s). Anal. calcd. for $C_{27}H_{20}Cl_3NO_2PRe$ (%): C 45.42, H 2.82, N 1.97; found: C 45.21, H 2.75, N 2.02.

$ReOCl_2$(5,7-Cl_2-qn)(PPh_3)

Reaction time: 21 h. Brown solid. Yield: 85%. IR (CsI, cm^{-1}): 980 (s) ν(Re=O), 311 (w), 282 (w) ν(Re-Cl). ^{31}P NMR (DMSO-d_6, ppm) δ: –12.4 (s). Anal. calcd. for $C_{27}H_{19}Cl_4NO_2PRe$ (%): C 43.33, H 2.56, N 1.87; found: C 43.03, H 2.57, N 1.78.

$ReOCl_2$(5,7-Br_2-qn)(PPh_3)

Reaction time: 21 h. Brown solid. Yield: 83%. IR (CsI, cm^{-1}): 984 (s) ν(Re=O), 324 (w), 279 (w) ν(Re-Cl). ^{31}P NMR (DMSO-d_6, ppm) δ: –10.8 (s). Anal. calcd. for $C_{27}H_{19}Br_2Cl_2NO_2PRe$ (%): C 38.73, H 2.29, N 1.67; found: C 37.43, H 2.07, N 1.66.

© 2005 NRC Canada

$ReOCl_2(5,7\text{-}I_2\text{-}qn)(PPh_3)$

Reaction time: 21 h. Brown solid. Yield: 93%. IR (CsI, cm^{-1}): 984 (s) ν(Re=O), 324 (w), 290 (w) ν(Re-Cl). ^{31}P NMR (DMSO-d_6, ppm) δ: –10.9 (s). Anal. calcd. for $C_{27}H_{19}Cl_2I_2NO_2PRe$ (%): C 34.82, H 2.06, N 1.50; found: C 34.87, H 1.75, N 1.49.

$ReOCl_2(5\text{-}NO_2\text{-}qn)(PPh_3)$

Prepared according to Chen et al. (9). Deep-green solid. Yield: 81%. IR (CsI, cm^{-1}): 977 (s) ν(Re=O), 324 (w), 285 (w) ν(Re-Cl). ^{31}P NMR (DMSO-d_6, ppm) δ: –9.3 (s). Anal. calcd. for $C_{27}H_{20}Cl_2N_2O_4PRe$ (%): C 44.76, H 2.78, N 3.87; found: C 44.71, H 2.78, N 3.87.

Preparation of the $ReOCl(L)_2$ compounds

These compounds were obtained according to Mazzi et al. (8), but the solvent used was THF instead of benzene. In a typical run, $ReOCl_3(PPh_3)_2$ (500 mg, 0.60 mmol) was added to a refluxing solution of the ligand (1.3 mmol) and Et_3N (0.2 mL, 1.44 mmol) in THF (50 mL). The mixture was stirred and the dark-brown or greenish-brown solid was filtered, washed with diethylether, rinsed with water to remove $(Et_3NH)Cl$, and finally dried in vacuo. Individual details are provided in the following and the ^1H NMR data are given in Table 1.

$ReOCl(qn)_2$

Reaction time: 20 h. Brown solid. Yield: 82%. IR (CsI, cm^{-1}): 968 (s) ν(Re=O), 312 (w) ν(Re-Cl). Anal. calcd. for $C_{18}H_{12}ClN_2O_3Re$ (%): C 41.11, H 2.30, N 5.33; found: C 40.49, H 2.20, N 5.26.

$ReOCl(2\text{-}Me\text{-}qn)_2$

Reaction time: 20 h. Brownish-green solid. Yield: 56%. IR (CsI, cm^{-1}): 970 (s) ν(Re=O), 320 (w), ν(Re-Cl). Anal. calcd. for $C_{20}H_{16}ClN_2O_3Re$ (%): C 43.36, H 2.91, N 5.06; found: C 42.72, H 2.88, N 4.97.

$ReOCl(2\text{-}Cl\text{-}qn)_2$

Reaction time: 3 h. Green solid. The compound recrystallized from CH_2Cl_2 contained 0.8 lattice solvent molecules per formula. Yield: 57%. IR (CsI, cm^{-1}): 968 (s) ν(Re=O), 324 (w), ν(Re-Cl). Anal. calcd. for $C_{18.8}H_{11.6}Cl_{4.6}N_2O_3Re$ (%): C 34.07, H 1.76, N 4.23; found: C 34.19, H 1.91, N 4.17.

$ReOCl(5\text{-}Cl\text{-}qn)_2$

Reaction time: 21 h. Dark-brown solid. Yield: 31%. IR (CsI, cm^{-1}): 976 (s) ν(Re=O), 324 (w) ν(Re-Cl). Anal. calcd. for $C_{18}H_{10}Cl_3N_2O_3Re$ (%): C 36.34, H 1.69, N 4.71; found: C 36.29, H 1.74, N 4.34.

$ReOCl(5\text{-}NO_2\text{-}qn)_2$ and $ReOCl(5,7\text{-}X_2\text{-}qn)_2$ for X = Cl, Br, I

The dark-brown raw solids contained a small amount of $ReOCl_2(L)(PPh_3)$ that could not be totally removed by chromatography on silica gel. The ^1H NMR data for these 2:1 species are included in Table 1.

Crystallographic measurements and structure determination

Dark-green crystals of $ReOCl_2(2\text{-Cl-qn})(PPh_3)$ were obtained by slow evaporation of an acetone solution. A crystal was mounted on a Bruker SMART CCD 2K diffractometer operating with graphite-monochromatized CuKα radiation and controlled by the SMART software (10). Sets of 30 oscillation frames of 0.3° over a range of 9° were recorded in four regions of the reciprocal space, from which the reduced cell was determined by least-squares refinement. For data collection, frames were recorded for different orientations of the crystal and detector so as to cover at least 95% of the reciprocal sphere. At the end, the first 101 frames were remeasured and the intensities of the 907 reflections did not show any decomposition of the crystal. The frames were analyzed with the SAINT software (11), which determined the intensity and the position of each spot. Accurate cell parameters were obtained by least-squares refinement over the positions of the whole data set. Irregular crystal shapes precluded the calculation of an analytical correction for absorption, but an empirical correction was applied using SADABS (12).

The SHELXTL system (13) was used for all calculations and drawings. The coordinates of the Re atoms were determined by direct methods and the positions of all other non-hydrogen atoms were found by the standard Fourier method. The structures were refined on F_o^2 using all reflections. The H atoms were fixed using a riding model with $U_{iso} = 1.2 \times U_{eq}$ of the atom to which they are bonded. Crystal data are listed in Table 2.[3]

Brown crystals of $ReOCl_2(5,7\text{-}Br_2\text{-qn})(PPh_3)$ were obtained by recrystallization in CH_2Cl_2–pentane. The crystallographic study was carried out with an Enraf-Nonius CAD-4 diffractometer operating with CuKα radiation under the control of the CAD-4 software (14). The reduced cell was initially determined from 20–25 spots located on a preliminary rotation photograph and centered in the detector aperture. Accurate cell parameters were then determined from the positions of 25 high-angle reflections centered with the SETANG and DETTH procedures. The intensities were recorded by ω/2θ scan. Possible crystal decomposition was monitored by measuring five standard reflections every hour. All data in the whole sphere were collected at room temperature. An absorption correction based on the crystal geometry was applied. The data were finally corrected for the effects of Lorentz and polarization, and averaged to provide the basic two-octant set.

The non-hydrogen atoms of the complex molecule were located and refined as stated previously. In the subsequent ΔF map, two regions centered on the inversion centers at (0, 0, 1/2) and (0, 0, 0), respectively, contained a number of small peaks owing to severely disordered solvent. No consis-

[3] Supplementary data for this article are available on the Web site or may be purchased from the Depository of Unpublished Data, Document Delivery, CISTI, National Research Council Canada, Ottawa, ON K1A 0S2, Canada. DUD 3653. For more information on obtaining material refer to http://cisti-icist.nrc-cnrc.gc.ca/irm/unpub_e.shtml. CCDC 251781 and 251782 contain the crystallographic data for this manuscript. These data can be obtained, free of charge, via www.ccdc.cam.ac.uk/conts/retrieving.html (or from the Cambridge Crystallographic Data Centre, 12 Union Road, Cambridge CB2 1EZ, U.K.; fax +44 1223 336033; or deposit@ccdc.cam.ac.uk).

© 2005 NRC Canada

Table 2. Crystal data.

	$ReOCl_2$(2-Cl-qn)(PPh_3)	$ReOCl_2$(5,7-Br_2-qn)(PPh_3)
Formula	$C_{27}H_{20}Cl_3NO_2PRe$	$C_{27}H_{19}Br_2Cl_2NO_2PRe$–$(CH_2Cl_2)_{0.75}(C_5H_{12})_{0.40}$
Formula weight	713.96	929.91
Crystal shape	Dark-green blocks	Brown platelets
T (K)	220(2)	220(2)
Diffractometer	Smart CCD	CAD-4
Crystal system	Monoclinic	Monoclinic
Space group	Cc (No. 9)	$P2_1/c$ (No. 14)
a (Å)	9.8861(2)	16.967(8)
b (Å)	15.0186(3)	10.168(3)
c (Å)	17.4254(3)	18.366(6)
α (°)	90	90
β (°)	96.144(1)	96.88(3)
γ (°)	90	90
Volume (Å^3)	2572.4(1)	3146(2)
Z	4	4
d_{calcd} (g/cm^3)	1.844	1.963
Crystal dimensions (mm)	0.40 × 0.27 × 0.14	0.46 × 0.29 × 0.04
Radiation (λ, Å)	CuKα, 1.541 78	CuKα, 1.541 78
μ (cm^{-1})	129.1	138.5
Rfls. measured	10 492	22 767
Rfls. independent	4060 (R_{int} = 0.052)	5972 (R_{int} = 0.102)
Rfls. obs. ($I > 2\sigma$)	3982	4579
R^a ($I > 2\sigma$)	0.0477	0.0455
$wR2^a$ ($I > 2\sigma$)	0.1203	0.1080
S^a ($I > 2\sigma$)	1.056	0.965

$^aR = \Sigma||F_o| - |F_c||/\Sigma|F_o|$; $wR2 = \{\Sigma[w(F_o^2 - F_c^2)^2]/\Sigma w(F_o^2)^2\}^{1/2}$; $S = \{\Sigma[w(F_o^2 - F_c^2)^2]/(N_{obs} - N_{param})\}^{1/2}$.

tent models for CH_2Cl_2 or pentane molecules could be assembled from these peaks. Therefore, this part of the structure was modeled by using the SQUEEZE procedure of the PLATON software (15), which indicated the presence of two cavities of 310 Å^3, each occupied by 95 electrons. Considering that CH_2Cl_2 and pentane both contain 42 electrons and that their volumes are 106 and 191 Å^3, respectively, each cavity should contain, on average, 0.8 pentane and 1.5 CH_2Cl_2 molecules. The contribution of the disordered solvent was calculated with the BYPASS procedure of van der Sluis and Spek (16) and a new hkl/F_o^2 list bypassing the solvent contribution was generated. The final model consisting of the ordered part only, without the disordered solvent contribution, was refined against this new data list, which is the one corresponding with the CIF file. Refinement converged normally to R = 0.0455. The solvent molecules were taken into account in the calculation of the derived quantities given in Table 2.

Results and discussion

The chemistry used by Mazzi et al. (8) to prepare $ReOCl_2$(qn)(PPh_3) and $ReOCl$(qn)$_2$ is applied here to obtain a series of complexes with various substituted 8-hydroxyquinolines. Refluxing equivalent amounts of the ligand and $ReOCl_3(PPh_3)_2$ leads to $ReOCl_2$(L)(PPh_3) compounds, in which one phosphine and the chlorine atom trans to the Re=O bond are displaced. By reacting 2 equiv. of ligand in the presence of 2 equiv. of Et_3N, the $ReOCl$(L)$_2$ products were obtained. No complexes could be prepared when a bulky *tert*-butyl substituent was present α to the N atom, whereas only the 1:1 complex was isolated with the phenyl-substituted ligand.

IR and NMR spectroscopies

Beside the large number of vibrations because of the quinolinate and PPh_3 ligands, all compounds show strong IR bands in the 968–984 cm^{-1} range for the Re=O stretching mode. Weaker features at ~325 and ~285 cm^{-1} are likely due to Re-Cl stretching, bands in this region being commonly found for similar systems (17).

The ^{1}H NMR signals of the free ligands are listed in Table 1 and identified following the numbering scheme **I**. Except for the 2-substituted compounds, a typical doublet of doublets is observed for H-3 at 7.4–7.9 ppm with couplings of 4 to 5 and 8 to 9 Hz, respectively. From the coupling constants and the COSY spectrum of Hqn, the adjacent protons are identified at 8.1–8.6 ppm (J = 8 to 9 Hz) and 8.8–9.0 ppm (J = 4 to 5 Hz). The latter signal must originate from H-2, since it disappears for the 2-substituted derivatives, whereas the remaining doublets for H-3 and H-4 show the larger coupling. Systematically, the H-2 and H-4 protons appear downfield from H-3, as expected from the mesomeric effect in the six-membered nitrogen heterocycle.

For the 5,7-disubstituted compounds, the remaining C-H signal is a singlet obviously due to H-6. When the phenol ring is not substituted, H-6 usually appears as a pseudo-triplet at ~7.4 ppm, resulting from roughly equal couplings (7–9 Hz) to two adjacent protons at ~7.1 and ~7.35 ppm, respectively. The latter signal is assigned to H-5, since it

© 2005 NRC Canada

Table 3. ^{1}H NMR chemical shifts (ppm) and coupling constants (Hz) for the quinolinate signals in the complexes.[a]

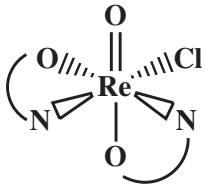
	H-2	H-3	H-4	H-5	H-6	H-7
$ReOCl_2(L)(PPh_3)$						
qn	8.37 (d, 5.0)	7.70 (dd, 8.3, 5.2)	8.21 (d, 8.3)	[b]	[b]	6.79 (d, 7.7)
2-Me-qn[c]	2.87 (s, CH_3)	7.70 (d, 8.0)	8.11 (d, 8.1)	[b]	[b]	6.62 (d, 7.1)
2-Cl-qn		7.89 (d, 8.6)	8.26 (d, 8.6)	[b]	[b]	6.81 (d, 7.1)
2-Ph-qn	7.04–7.10 (m, Ph)	7.68 (d, 8.4)	8.28 (d, 8.3)	[b]	[b]	6.70 (7.1)
5-Cl-qn	8.51 (d, 5.0)	7.85 (dd, 8.4, 5.2)	8.23 (d, 8.3)		7.57 (d, 8.3)	6.82 (d, 8.3)
5,7-Cl_2-qn	8.61 (d, 4.9)	7.89 (dd, 8.4, 5.3)	8.26 (d, 8.4)		7.79 (s)	
5,7-Br_2-qn	8.59 (d, 5.0)	7.90 (dd, 8.4, 5.2)	8.16 (d, 8.4)		7.99 (s)	
5,7-I_2-qn	8.52 (d, 5.1)	7.84 (dd, 8.5, 5.2)	7.99 (d, 8.2)		8.21 (s)	
5-NO_2-qn	8.63 (d, 5.0)	8.00 (dd, 8.7, 5.2)	8.49 (d, 8.8)		8.88 (d, 8.8)	6.90 (d, 8.8)
$ReOCl(L)_2$[d]						
qn	8.88 (d, 4.7)	8.00 (dd, 8.2, 5.2)	8.27 (m, H-2′/H-4)	7.42 (d, 8.1)	7.51 (t, 7.9)	6.61 (d, 7.6)
	8.27 (m, H-2′/H-4)	7.71 (dd, 8.2, 5.2)	8.83 (d, 8.2)	7.64 (d, 8.0)	7.86 (t, 8.0)	7.62 (d, 7.4)
2-Me-qn	3.56 (s, CH_3)	7.96 (d, 8.5)	8.18 (d, 8.4)	7.31 (m)	7.31 (m)	6.40 (dd, 6.5, 2.2)
	2.34 (s, CH_3)	7.55 (d, 8.4)	8.48 (d, 8.4)	7.47 (d, 8.3)	7.74 (t, 8.0)	7.49 (d, 7.9)
2-Cl-qn		8.14 (d, 8.6)	8.41 (d, 8.6)	7.45 (m)	7.45 (m)	6.67 (dd, 6.7, 2.1)
		7.81 (d, 8.6)	8.77 (d, 8.8)	7.64 (d, 8.7)	7.85 (t, 8.0)	7.66 (d, 8.4)
5-Cl-qn	8.99 (d, 4.8)	8.15 (dd, 8.6, 5.1)	8.34 (d, 8.3)		7.62 (d, 8.6)	6.62 (d, 8.4)
	8.48 (d, 4.9)	7.83 (dd, 8.5, 5.1)	8.90 (d, 8.6)		8.06 (d, 8.4)	7.66 (d, 8.6)
5,7-Cl_2-qn	9.02 (d, 4.3)	8.19 (dd, 8.5, 5.2)	8.41 (d, 8.5)		7.94 (s)	
	8.62 (d, 5.1)	7.88 (dd, 8.5, 5.2)	8.96 (d, 7.4)		8.34 (s)	
5,7-Br_2-qn	9.01 (d, 4.7)	8.19 (dd, 8.5, 5.2)	8.32 (d, 8.6)		8.14 (s)	
	8.57 (d, 5.1)	7.88 (dd, 8.5, 5.2)	8.88 (d, 9.3)		8.55 (s)	
5,7-I_2-qn	8.93 (d, 5.0)	8.14 (dd, 8.4, 5.1)	8.16 (d, 8.4)		7.99 (s)	
	8.40 (d, 5.0)	7.90 (dd, 8.6, 5.0)	8.70 (d, 8.2)		8.74 (s)	
5-NO_2-qn	9.11 (d, 4.3)	8.32 (dd, 8.9, 5.2)	8.59 (d, 8.9)		8.95 (d, 8.9)	6.73 (d, 8.9)
	8.77 (d, 4.1)	8.04 (dd, 8.9, 5.1)	9.04 (d, 8.8)		9.53 (d, 8.9)	7.77 (d, 8.8)

[a]In DMSO-d_6, except when otherwise stated.
[b]Masked by PPh_3 multiplets.
[c]In acetone-d_6.
[d]For the $ReOCl(L)_2$ complexes, the signals in the first line are assigned to the axial ligand.

shows a proximity to H-4 in the NOESY spectrum. For the 5-substituted molecules, the doublet at 7.0–7.2 ppm is assigned to H-7, by comparison with the unsubstituted rings. As expected, the remaining H-6 resonance is found to be very sensitive to the presence of the adjacent electron-attracting substituents: for instance, introducing a 5-nitro group induces a large 1.8 ppm downfield shift. In the free molecules, small couplings of 1 to 2 Hz are generally observed between nonadjacent protons on either ring. Also, in most cases, a broad resonance appears at low field for the OH proton.

In the $ReOCl_2(L)(PPh_3)$ compounds, the phosphine gives rise to ^{1}H multiplets in the 7.2–7.5 ppm range and to a ^{31}P singlet lying between –9 and –12.5 ppm, except for the 2-substituted ligands, where this signal is shifted to ca. –17 ppm. The signals for the coordinated quinolinate are listed in Table 3. Assignments in the pyridine ring are straightforward, based on multiplicity and couplings. For the phenolate ring, the lowest-field signal, whose position is very substituent-sensitive, originates from H-6. When the ring is not substituted, two of the protons are masked by those of PPh_3, and the only resolved signal at 6.6–6.8 ppm is assigned to H-7 by comparison with the 5-substituted ligands.

The $ReOCl(L)_2$ compounds exhibit two sets of ^{1}H signals, showing that the two ligands are inequivalent, in agreement with the structure (**II**) observed by Chen et al. (9) for $ReOCl(NO_2\text{-qn})(NH_2\text{-qn})$. From the COSY spectrum of $ReOCl(qn)_2$, two sets of connected H-2/H-3/H-4 signals were defined, in which the H-2 and H-4 doublets could be identified individually from their respective coupling constants. Two H-5/H-6/H-7 sets could also be assembled, but the similar coupling constants made it impossible to identify H-5 and H-7 individually at this stage. This could be done, however, from a NOESY spectrum, where each H-4 proton showed a cross peak with a proton in the other ring, which identified the latter proton as H-5 and established the connection between the H-2/H-3/H-4 and the H-5/H-6/H-7 sets belonging to the same ligand.

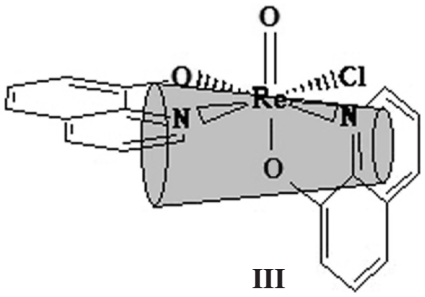


II

There is no direct evidence to associate a given complete set to either the axial or the equatorial ligand. The tentative

© 2005 NRC Canada

identification proposed in Table 3 is based on the assumption that the phenol ring signals for the axial ligand in $ReOCl(L)_2$ should be similar to those of the equally axial ligand in $ReOCl_2(L)(PPh_3)$, since this ring should be similarly influenced by the very large electronic effect of the oxo ligand via the trans O=Re-O unit and it should not be greatly affected by the anisotropy or other features of the equatorial ligands. With the assignment proposed, the average δ[axial $ReOCl(L)_2$] – δ[$ReOCl_2(L)(PPh_3)$] difference is 0.13 ppm for H-6 and –0.18 ppm for H-7, whereas these values would be 0.56 and 0.85 ppm, respectively, for the alternate possibility. In contrast, the pyridine ring signals of these axial ligands show larger differences: 0.45 ppm for H-2, 0.29 ppm for H-3, and 0.12 ppm for H-4. Since these differences are systematically positive, they may reflect the anisotropy effect of the PPh_3 rings in $ReOCl_2(L)(PPh_3)$, which is no longer present in $ReOCl(L)_2$. Also consistent with this interpretation is the fact that the H-2 or 2-CH_3 protons of the equatorial ligand appear at a much higher field than those of the axial one. For instance, the chemical shifts of H-2 in $ReOCl(qn)_2$ are 8.27 ppm (equatorial) vs. 8.88 ppm (axial), whereas those of the 2-CH_3 groups in $ReOCl(2\text{-Me-qn})_2$ are 2.34 ppm (equatorial) vs. 3.56 ppm (axial). This could be ascribed to the fact that these protons lie in the cone of anisotropy of the axial pyridine ring (**III**). Thus, these various effects are consistent with the structure proposed for $ReOCl(L)_2$, which should be the one favored electronically, since two π-donor ligands lie trans to weakly π-accepting pyridine rings.



III

X-ray diffraction studies

The $ReOCl_2(5,7\text{-}Br_2\text{-qn})(PPh_3)$ and $ReOCl_2(2\text{-Cl-qn})(PPh_3)$ molecules are shown in Figs. 1 and 2, respectively. In both compounds, the rhenium atom has a distorted octahedral coordination, created by an oxo ligand, two chlorine atoms, a phosphine, and a *N*,*O*-coordinated quinolinate. In agreement with a general trend in mono-oxo Re(V) chemistry, the quinolinate oxygen donor lies trans to the Re=O bond, which results in the quinolinate plane being roughly parallel to the Re=O direction. The PPh_3 group is found to be cis to the nitrogen atom in the equatorial plane. This arrangement has also been reported for $ReOCl_2(5\text{-nitro-qn})(PPh_3)$ (9).

Selected distances and angles are presented in Table 4. The Re=O bond lengths (1.656(8) and 1.671(4) Å) are in good agreement with the value expected for Re(V) mono-oxo complexes (18). The trans influence of PPh_3 makes the opposite Re—Cl(1) bond 0.05 Å longer than the other in both complexes. The Re—O(2) distances (1.999(6) and 2.021(4) Å), which are ~0.1 Å longer than the typical value

Fig. 1. ORTEP drawing of the $ReOCl_2(5,7\text{-}Br_2\text{-qn})(PPh_3)$ molecule. Ellipsoids correspond to 30% probability.

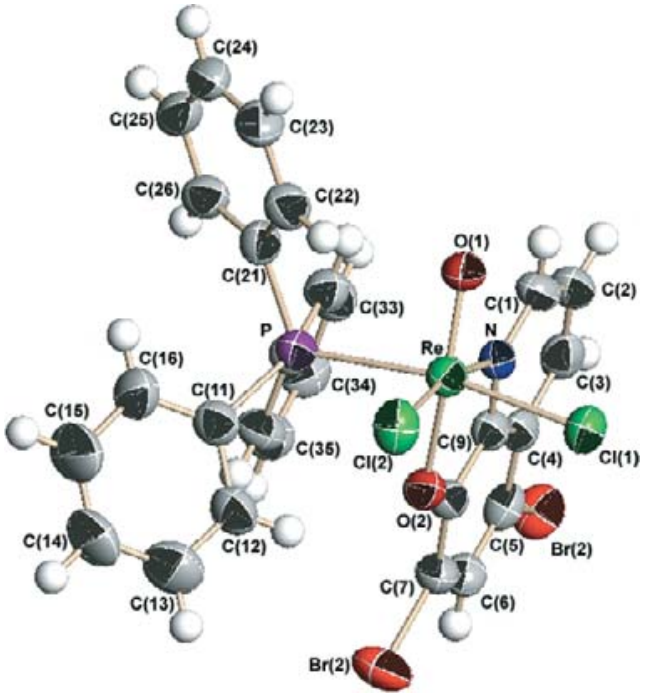
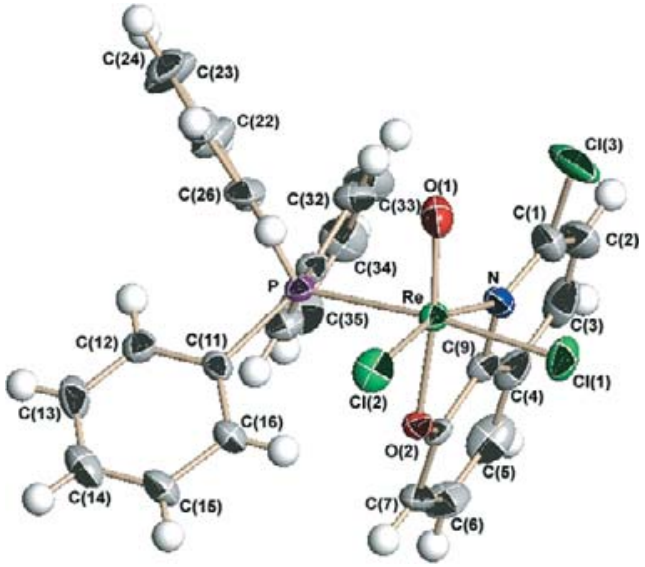


Fig. 2. ORTEP drawing of the $ReOCl_2(2\text{-}Cl_2\text{-qn})(PPh_3)$ molecule. Ellipsoids correspond to 40% probability.



for Re—OR bonds (2), reflect the constraint imposed by the five-membered chelate ring.

The oxo ligand tends to produce a general displacement of the adjacent bonds in the opposite direction, which results in the Re atom lying above the plane defined by the four equatorial donor atoms. The distances of rhenium to the $PNCl_2$ plane are 0.23 and 0.28 Å for the 5,7-Br-qn and 2-Cl-qn complexes, respectively. Additional distortion is introduced by the bidentate coordination of the quinolinate ligand, whose O(2)-Re-N bite angle is ~76°. This small angle af-

© 2005 NRC Canada

Table 4. Selected distances (Å) and angles (°) in the $ReOCl_2(L)(PPh_3)$ compounds.

	$ReOCl_2$(2-Cl-qn)(PPh_3)	$ReOCl_2$(5,7-Br_2-qn)(PPh_3)
Bond distances (Å)		
Re=O(1)	1.656(8)	1.671(4)
Re—O(2)	1.999(6)	2.021(4)
Re—N	2.183(8)	2.130(6)
Re—Cl(1)	2.390(2)	2.371(2)
Re—Cl(2)	2.334(2)	2.327(2)
Re—P	2.485(2)	2.469(2)
Bond angles (°)		
O(1)-Re-O(2)	163.2(3)	160.2(2)
O(1)-Re-N	93.2(3)	86.7(2)
O(2)-Re-N	76.2(3)	75.5(2)
O(1)-Re-Cl(1)	100.0(3)	99.8(2)
O(2)-Re-Cl(1)	92.5(2)	87.24(13)
N-Re-Cl(1)	87.1(2)	84.76(14)
O(1)-Re-Cl(2)	102.3(3)	105.67(17)
O(2)-Re-Cl(2)	89.5(2)	92.79(13)
N-Re-Cl(2)	164.0(2)	167.15(14)
Cl(1)-Re-Cl(2)	86.42(10)	89.59(7)
O(1)-Re-P	86.3(3)	91.18(16)
O(2)-Re-P	81.1(2)	81.86(13)
N-Re-P	91.3(2)	94.35(14)
Cl(1)-Re-P	173.58(8)	168.92(6)
Cl(2)-Re-P	93.49(8)	88.98(7)
Re-O(2)-C(6)	118.7(5)	119.4(4)
Re-N-C(1)	131.1(8)	127.2(5)
Re-N-C(5)	112.0(6)	115.4(4)

fects mainly the O(1)-Re-O(2) unit, which is definitely nonlinear: 163.2(3)° for 2-Cl-qn and 160.2(2)° for 5,7-Br_2-qn. The Re=O bond is displaced away from the chloro ligands, as evidenced from the Cl-Re=O angles (100°–106°) being systematically greater than the N-Re=O and P-Re=O angles (87°–94°).

The 2-chloro substituent enhances the distortion of the octahedron. This group further displaces the Re=O bond toward PPh_3, as evidenced from the O(1)-Re-P angle of 86.3(3)°, compared to 91.2(2)° in the 5,7-Br_2-qn complex. The angle between the Cl(2)-Re-O(1) plane and the mean plane through the quinolinate ligand increases from 10.5° for the dibromo complex to 22.2° here. The distortion is also illustrated by the sum of the deviations of the Cl, P, and N atoms from their least-squares plane: these atoms are virtually coplanar for the dibromo complex, but the mean deviation is 0.69 Å for $ReOCl_2$(2-Cl-qn)(PPh_3).

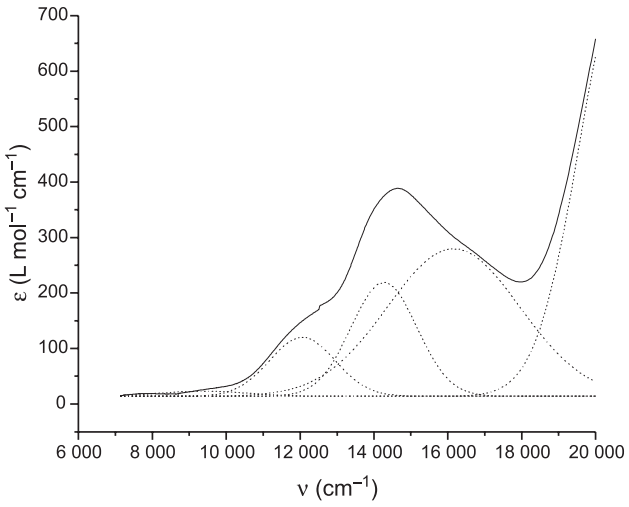
In both complexes, intramolecular π-stacking interactions exist between one of the phosphine phenyl rings (C(31)-C(36)) and the quinolinate ligand, which are roughly parallel (dihedral angles of 11.7° and 12.9° for the 5,7-Br_2-qn and 2-Cl-qn complexes, respectively) and separated by ~3.42 Å.

The molecules are packed individually in the unit cell, with normal van der Waals contacts, including some intermolecular π stacking.

UV–vis spectroscopy

The low-energy (8 000–20 000 cm^{-1}) region of the UV–vis absorption spectra was recorded for all complexes, generally in $CHCl_3$. For a few less soluble complexes, DMSO was used to improve the quality of the spectra. The DMSO solutions were stable and the spectral features were similar to those of the weaker spectra in $CHCl_3$, showing that the same species was present in both solvents. The spectra of $ReOCl_2(qn)(PPh_3)$ and $ReOCl(qn)_2$ are illustrated in Figs. 3 and 4, respectively. In each case, four individual compo-

Fig. 3. UV–vis spectra of $ReOCl_2(qn)(PPh_3)$ in DMSO (full line). Dashed lines correspond to the four components obtained by deconvolution.



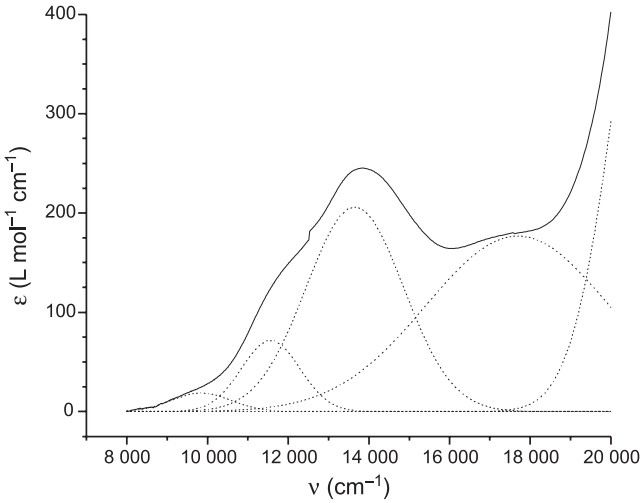
© 2005 NRC Canada

Table 5. Transition energy ($cm^{-1} \times 10^{-3}$) and absorption coefficient[a] (M^{-1} cm^{-1}, within parentheses) of the low-energy components of the electronic spectra.

	[S → T*]	[S → T**]	[S → S*]	[S → S**]
$ReOCl_2(qn)(PPh_3)$[b]	9.6 (29)	12.1 (150)	14.3 (381)	16.2 (299)
$ReOCl_2$(2-Me-qn)(PPh_3)[b]	10.0[c] (17)	12.6 (73)	14.8 (235)	16.4 (241)
$ReOCl_2$(2-Cl-qn)(PPh_3)[b]	10.9[c] (8)	12.6 (29)	14.9 (97)	16.6 (99)
$ReOCl_2$(5-Cl-qn)(PPh_3)[d]	9.8 (18)	12.1 (149)	14.3 (407)	16.3 (310)
$ReOCl_2$(5-NO_2-qn)(PPh_3)[e]	10.0[c] (22)	11.8 (195)	14.2 (544)	17.5 (430)
$ReOCl_2$(5,7-Cl_2-qn)(PPh_3)[d]	9.8 (16)	11.8 (142)	14.3 (389)	16.6 (290)
$ReOCl_2$(5,7-Br_2-qn)(PPh_3)[d]	10.0[c] (18)	11.8 (166)	14.4 (430)	16.6 (312)
$ReOCl_2$(5,7-I_2-qn)(PPh_3)[d]	10.0[c] (16)	11.8 (160)	14.2 (424)	16.5 (320)
$ReOCl(qn)_2$[d]	9.8 (24)	11.6 (120)	13.7 (243)	17.7 (181)
$ReOCl$(2-Me-qn)$_2$[d]	9.5 (38)	12.2 (185)	14.4 (441)	17.7 (360)
$ReOCl$(2-Cl-qn)$_2$[d]	—	12.5 (153)	14.6 (346)	18.3 (226)
$ReOCl$(5-Cl-qn)$_2$[d]	9.4 (6)	11.7 (51)	13.8 (111)	—
$ReOCl$(5-NO_2-qn)$_2$[d]	—	12.0[c] (230)	14.5[c] (466)	17.5[c] (970)
$ReOCl$(5,7-Cl_2-qn)$_2$[d]	—	12.0[c] (263)	14.0[c] (480)	17.5[c] (754)
$ReOCl$(5,7-Br_2-qn)$_2$[d]	—	12.0[c] (140)	14.0[c] (283)	17.0[c] (460)
$ReOCl$(5,7-I_2-qn)$_2$[d]	—	12.0[c] (433)	14.0[c] (780)	17.0[c] (1270)

[a]The ε values listed are those obtained at the indicated wavelength from the nondeconvoluted spectra.
[b]In DMSO.
[c]Peak position estimated visually.
[d]In $CHCl_3$.
[e]In CH_2Cl_2.

Fig. 4. UV–vis spectra of $ReOCl(qn)_2$ in DMSO (full line). Dashed lines correspond to the four components obtained by deconvolution.



nents were obtained by deconvolution using ORIGIN (19). The data are listed in Table 5.

Since these complexes have no symmetry, the d_{yz} and d_{xz} orbitals, which are degenerate under D_{4h} symmetry, become inequivalent. For consistency with the recent study of Da Re and Hopkins (20) on the isoelectronic oxo-Mo(IV) core, d_{yz} will be assumed to lie at lower energy than d_{xz}. The five lowest-energy electronic states expected are depicted in Fig. 5, in increasing order of energy.

Both series of complexes show a strong maximum between 13 700 and 14 900 cm^{-1}. For the $ReOCl(L)_2$ compounds, another strong peak is visible at 17 000–18 300 cm^{-1}, whereas the related band is present as an unresolved component at slightly lower energy for the $ReOCl_2(L)(PPh_3)$ compounds. These absorptions are assigned to the spin-allowed [S → S*] and [S → S**] transitions, respectively. On the low-energy side, there is a distinct dissymmetry in the main peak and a rather long tail before intensity falls off to zero. Two weak features are revealed by deconvolution, which are assigned to the two anticipated singlet–triplet transitions. These transitions being spin-forbidden, their extinction coefficients are expected to be ~10, and this is indeed the case for the first transition $(d_{xy})^2 \rightarrow (d_{xy})^1(d_{yz})^1$ [S → T*] at ~10 000 cm^{-1}. The coefficient is much higher (~100) for the second transition $(d_{xy})^2 \rightarrow (d_{xy})^1(d_{xz})^1$ [S → T**] at ~12 000 cm^{-1}, but enhanced intensity could be due to mixing between the higher-energy triplet state and the lowest-energy singlet states (20), as a result of strong spin-orbit couplings commonly found for third-row transition metals. The separations (Table 6) between the two triplet states, the two singlet states, and the second triplet – first singlet states (roughly 2000 cm^{-1}) are in good agreement with the values calculated by Da Re and Hopkins (20).

Comparison of the data within each series reveals that ring substitution does not introduce dramatic effects on the spectra: the strongly electron-attracting 5-nitro substituent seems to slightly increase the [S → S**] transition energy in the $ReOCl_2(L)(PPh_3)$ series, but the effect is modest and no recognizable trend can be detected. Thus, the HOMO–LUMO gap is not substantially affected by ligand substitution in these systems.

The spin-allowed [S → S*] and [S → S**] bands in both series are observed at somewhat lower energy than for the $ReO(OR)X_2$(dppe) compounds studied earlier, where they were found at ~16 500 and 20 000 cm^{-1}, respectively (2). This can be explained by the lower electron-donating ability

© 2005 NRC Canada

Fig. 5. Low-energy electron configurations for the Re(V) d^2 systems.

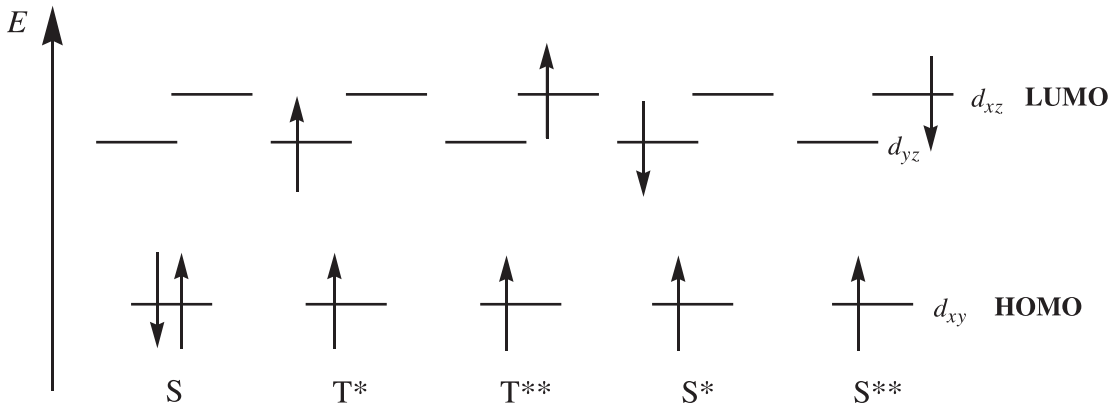


Table 6. Energy separation ($cm^{-1} \times 10^{-3}$) between the low-energy states from the electronic spectra.

	Δ[T* → T**]	Δ[S* → S**]	Δ[T** → S*]	Δ[T* → S**]
$ReOCl_2(qn)(PPh_3)$	2.5	1.9	2.2	6.6
$ReOCl_2$(2-Me-qn)(PPh_3)	2.6	1.6	2.2	6.4
$ReOCl_2$(2-Cl-qn)(PPh_3)	1.7	1.7	2.3	5.7
$ReOCl_2$(5-Cl-qn)(PPh_3)	2.3	2.0	2.2	6.5
$ReOCl_2$(5-NO_2-qn)(PPh_3)	1.8	3.3	2.4	7.5
$ReOCl_2$(5,7-Cl_2-qn)(PPh_3)	2.0	2.3	2.5	6.8
$ReOCl_2$(5,7-Br_2-qn)(PPh_3)	1.8	2.3	2.6	6.6
$ReOCl_2$(5,7-I_2-qn)(PPh_3)	1.8	2.2	2.4	6.5
$ReOCl(qn)_2$	1.8	2.3	2.1	7.9
$ReOCl$(2-Me-qn)$_2$	2.7	4.0	2.2	8.2
$ReOCl$(2-Cl-qn)$_2$	—	3.3	2.1	—
$ReOCl$(5-Cl-qn)$_2$	2.3	3.7	2.1	—
$ReOCl$(5-NO_2-qn)$_2$	—	3.0	2.5	—
$ReOCl$(5,7-Cl_2-qn)$_2$	—	3.5	2.0	—
$ReOCl$(5,7-Br_2-qn)$_2$	—	3.0	2.0	—
$ReOCl$(5,7-I_2-qn)$_2$	—	3.0	2.0	—

of the quinolinate oxygen compared to alkoxo groups, considering that donation from the ligand trans to the Re=O bond was previously identified as a very sensitive factor. However, this reduction is not large enough to bring the energies below those of the $ReOX_3$(dppe) compounds (~12 000 and ~16 400 cm^{-1}).

Concluding remarks

Homologous series of $ReOCl_2(L)(PPh_3)$ and $ReOCl(L)_2$ compounds were prepared with various 8-hydroxyquinolines bearing substituents with different steric and electronic properties. Comparisons between these related compounds allowed us to fully interpret their ^{1}H NMR spectral features. The positions of the UV–vis bands used to estimate the HOMO–LUMO gap failed to reveal a large effect of ring substitution on electronic transitions, but it confirmed that the donor ability of the ligand trans to the Re=O band plays a major role. On the other hand, the fact that the spin-forbidden singlet–triplet bands were readily observed makes these systems attractive for future in-depth spectroscopic studies to improve our understanding of the low-lying excited states and the spin-crossover processes, whose control is crucial for the eventual development of optically or magnetically tunable materials (1, 21).

Acknowledgments

We wish to thank M. Palardy for his participation in the preparative work, Dr. M. Simard and F. Bélanger-Gariépy for assistance in the interpretation of the X-ray diffraction data, and the Natural Sciences and Engineering Research Council of Canada (NSERC) for financial support.

References

1. U. Oetliker, C. Savoie, S. Stanislas, C. Reber, F. Connac, A.L. Beauchamp, F. Loiseau, and M. Dartiguenave. J. Chem. Soc. Chem. Commun. 657 (1998).
2. F. Baril-Robert and A.L. Beauchamp. Can. J. Chem. **81**, 1326 (2003).
3. G. Delapierre, J.M. Brunel, T. Constantieux, and G. Buono. Tetrahedron Asymmetry, **12**, 1345 (2001).
4. J. Chatt and G.A. Rowe. J. Chem. Soc. 4019 (1962).
5. G.R. Pettit and M.V. Kalnins. J. Org. Chem. **25**, 1365 (1960).
6. J.J. Plattner, R.D. Gless, and H. Rapoport. J. Am. Chem. Soc. **94**, 8613 (1972).

© 2005 NRC Canada

7. W.C. Fleming and G.R. Pettit. J. Org. Chem. **36**, 3490 (1971).
8. U. Mazzi, E. Roncari, R. Rossi, V. Bertolasi, O. Traverso, and L. Magon. Transition Met. Chem. **5**, 289 (1980).
9. X. Chen, F.J. Femia, J.W. Babich, and J. Zubieta. Inorg. Chim. Acta, **308**, 80 (2000).
10. SMART. Release 5.059 [computer program]. Bruker AXS Inc., Madison, Wisconsin, USA. 1999.
11. SAINT. Release 6.06 [computer program]. Bruker AXS Inc., Madison, Wisconsin, USA. 1999.
12. G.M. Sheldrick. SADABS [computer program]. Bruker AXS Inc., Madison, Wisconsin, USA. 1996.
13. G.M. Sheldrick. SHELXTL. Release 5.10 [computer program]. Bruker AXS Inc., Madison, Wisconsin, USA. 1997.
14. CAD-4. Version 5.0 [computer program]. Enraf-Nonius, Delft, The Netherlands. 1989.
15. A.L. Spek. PLATON. July 1995 version [computer program]. University of Utrecht, Utrecht, The Netherlands. 1995.
16. P. van der Sluis and A.L. Spek. Acta Crystallogr. **A46**, 194 (1990).
17. A.M. Lebuis and A.L. Beauchamp. Can. J. Chem. **71**, 441 (1993).
18. Cambridge Structural Database. Version 5.4, November 2002 release with February 2003 updates. Cambridge University, Cambridge, UK.
19. ORIGIN 6.1, 6.1052 (B232) [computer program]. OriginLab Corporation, Northampton, UK. 2000.
20. R.E. Da Re and M.D. Hopkins. Inorg. Chem. **41**, 6973 (2002).
21. C. Savoie and C. Reber. J. Am. Chem. Soc. **122**, 844 (2000).

© 2005 NRC Canada

Triazene derivatives of (1,*x*)-diazacycloalkanes. Part III. Synthesis and characterization of a series of 1,4-di[2-aryl-1-diazenyl]piperazines

Vanessa Renée Little, Reid Tingley, and Keith Vaughan

Abstract: Reaction of a series of diazonium salts with piperazine in a 2:1 molar ratio affords excellent yields of the 1,4-di-[2-aryl-1-diazenyl]piperazines (**3**), which have been characterized by IR and NMR spectroscopy. Structural characterization is supported by elemental analysis or by mass spectrometry with accurate mass measurement of the molecular ion. The protons of the piperazine ring hydrogens give rise to a sharp singlet at ca. 4 ppm in the NMR spectra, indicating that the conformational equilibrium in the piperazine ring is rapid on the NMR timescale. The four equivalent carbon atoms of the piperazine ring resonate in the range 46–48 ppm. A variable temperature NMR experiment suggests that there is restricted rotation around the N2—N3 bond of the triazene moiety in **3**. The NMR data compares favorably with previous reported data for 1-aryldiazenyl-4-methylpiperazines (**1**) and 1,4-di-(2-aryldiazen-1-yl)homopiperazines (**2b**).

Key words: triazene, piperazine, diazonium coupling, NMR.

Résumé : La réaction d'une série de sels de diazonium avec de la pipérazine dans un rapport molaire de 2 : 1 conduit, avec d'excellents rendements, à des 1,4-di-[2-aryldiazén-1-yl]pipéprazines (**3**) qui ont été caractérisées par les spectres IR et RMN. Les caractérisations des structures sont supportées par des analyses élémentaires ou par spectrométrie de masse avec des mesures précises de la masse de l'ion moléculaire. Dans le spectre RMN, les protons du noyau pipérazine se présentent sous la forme d'un singulet effilé à environ 4 ppm, ce qui suggère que l'équilibre conformationnel du cycle pipérazine est rapide par rapport à l'échelle de temps de la RMN. La résonance des quatre atomes de carbone équivalents du noyau de la pipérazine se situe entre 46 et 48 ppm. Une expérience de RMN à température variable suggère l'existence d'une rotation empêchée autour de la liaison N2—N3 de la portion triazène du composé **3**. Les données de la RMN se comparent avantageusement avec celles rapportées antérieurement pour les 1-aryldiazényl-4-méthylpipérazines (**1**) et 1,4-di-(2-aryldiazén-1-yl)homopipérazines (**2b**).

Mots clés : triazène, pipérazine, couplage de diazonium, RMN.

[Traduit par la Rédaction]

Introduction

In previous studies (1, 2), a series of 4-methyl-1-(2-aryldiazen-1-yl-)piperazines (**1**), 4-methyl-1-[aryldiazenyl]-homopiperazines (**2a**), and 1,4-di-(2-aryldiazen-1-yl) diazepanes (**2b**) were synthesized and characterized by spectroscopic measurements. In the process of characterizing these triazenes by NMR spectroscopy, the chemical shift parameters of the protons and carbons in the piperazine ring were clearly established and verified by some classical 2D NMR work. The aim of the present work was to synthesize a series of the 1,4-di-[2-aryl-1-diazenyl]piperazines (**3**) with a similar range of aryl substituents as in the previous series and to establish the spectroscopic parameters of the new series of bistriazenopiperazines (**3**). This work is an essential part of our broad-ranging study of the synthesis of triazene derivatives of (1,*x*)-diazacycloalkanes and is an essential link between the previously reported data (1, 2) and further studies of triazenes derived from several ring-substituted piperazines.

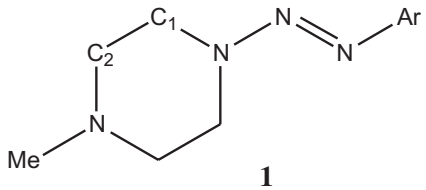
Some compounds of type **3** have been reported previously (3), but the range of aryl substituents reported excludes many of the substituents used routinely in our work. In the previous work, the range of aryl substituents was limited to the nitro, carboxyl, methyl, and halogeno groups. We have expanded the range of substituents to include the cyano, acetyl, carboxamido, sulfonamido, and alkoxycarbonyl groups. Therefore, it was essential to undertake the synthesis of the new analogues in the series **3a**–**3f**, and **3j**–**3l** inclusive, and the previously reported analogues **3g**–**3i**, **3m**, and **3n** were synthesized as part of the present study to acquire ^{13}C NMR data for the full range of compounds. In the process of repeating the literature work, it was noted that some melting points were at variance from those reported (3). These melting points have been checked assiduously and the identity of the discrepant compounds has been confirmed by elemental analysis or high-resolution mass spectrometry. It should be noted here that Butkus and co-workers (4) reported the synthesis of an analogous bistriazene (**3**, X = *p*-SO_3K) as part of a study of the anti-inflammatory activity of triazenes.

Received 21 December 2004. Published on the NRC Research Press Web site at http://canjchem.nrc.ca on 10 May 2005.

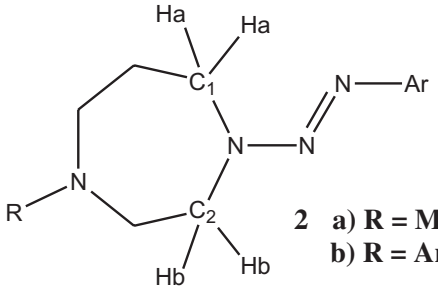
V.R. Little, R. Tingley, and K. Vaughan.[1] Department of Chemistry, Saint Mary's University, Halifax, NS B3H 3C3, Canada.

[1]Corresponding author (e-mail: keith.vaughan@smu.ca).

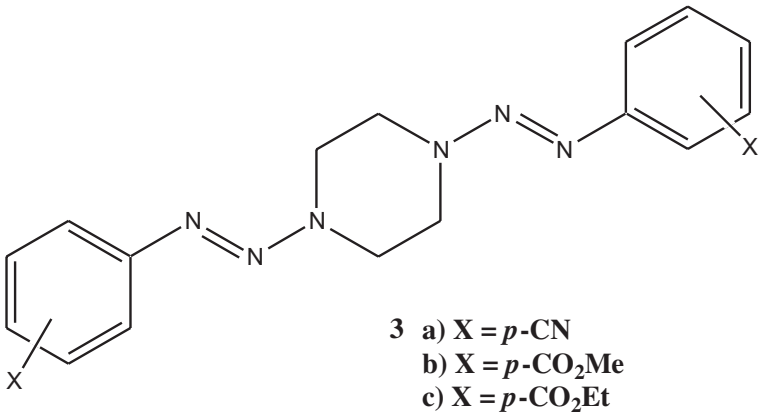
 doi: 10.1139/V05-064 © 2005 NRC Canada



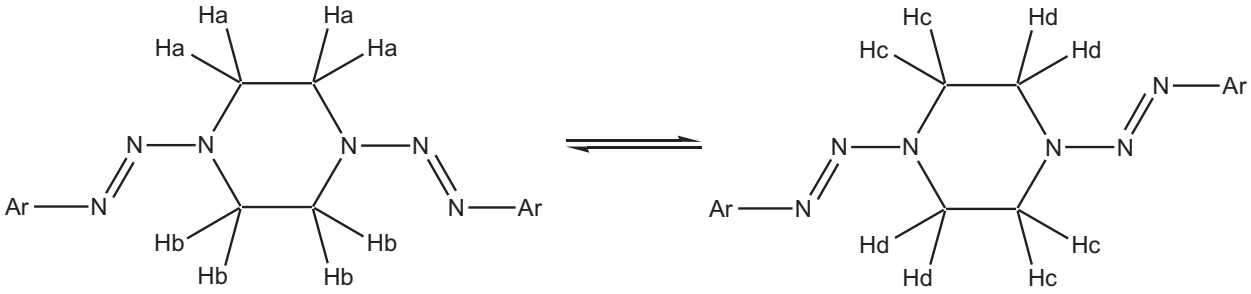
1



2 a) R = Me
b) R = Ar-N=N-



3 a) X = *p*-CN
b) X = *p*-CO_2Me
c) X = *p*-CO_2Et
d) X = *p*-$COCH_3$
e) X = *p*-$CONH_2$
f) X = *p*-SO_2NH_2
g) X = *p*-CH_3
h) X = *p*-Br
i) X = H
j) X = *o*-CN
k) X = *o*-CO_2Me
l) X = *o*-CO_2Et
m) X = *o*-CH_3
n) X = *o*-Cl



4A **4B**

Experimental

All reagents were reagent grade materials purchased from Sigma-Aldrich Canada Ltd. and were used without further purification. Melting points were determined on a Fisher-Johns melting point apparatus and are uncorrected. IR spectra were obtained using Nujol mulls or KBr discs on a Bruker Vector 22 spectrometer. ^{1}H and ^{13}C NMR spectra were obtained with either: (*i*) Bruker AC 250 MHz or 500 MHz spectrometers at the Atlantic Regional Magnetic Resonance Center at Dalhousie University; or (*ii*) the ANASAZI 60 MHz EFT spectrometer at SMU. Chemical shifts were recorded in $CDCl_3$ solutions at 20 °C (unless specified otherwise), and are relative to TMS as internal standard. Elemental analyses were performed by the Canadian Microanalytical Service Ltd., Delta, British Columbia.

© 2005 NRC Canada

Accurate mass measurements were made on a CEC 21-110B mass spectrometer operated at a mass resolution of 8000 (10% valley) by computer-controlled peak matching to appropriate PFK reference ions. Spectra were obtained using electron ionization at 70 V and a source temperature of 175 °C, with samples being introduced by means of a heatable quartz probe. The standard deviation of mass measurement was ±0.0008 amu, which is an average of 3.6 ppm over the mass range 100–300 amu.

1,4-Di-[2-aryl-1-diazenyl]-piperazines (3a–3n)

General procedure

The aromatic primary amine (0.01 mol) was dissolved in 10 mL of 3 mol/L hydrochloric acid, with the aid of heat if necessary, and the resulting solution was cooled in an ice–salt bath to 0 °C. The solution was diazotized with a solution of sodium nitrite (0.76 g, 0.011 mol) in water (10 mL) while maintaining the temperature below 5 °C, and then stirred for a further 0.5 h in the cold water. The solution was then neutralized with saturated sodium bicarbonate solution, after which the neat piperazine (0.005 mol) was added slowly to the mixture. After stirring for a further 0.5 h, the mixture was further neutralized to pH 7 with saturated sodium carbonate solution (total volume ca. 10 mL) and then left to stir until precipitation was deemed to be complete (1–3 h). The solid product was filtered under suction, dried and recrystal- from an appropriate solvent to give the following compounds.

*1,4-Di-[2-(*p*-cyanophenyl)-1-diazenyl]-piperazine (3a)*

Pale yellow needles, 91%; mp 275 to 276 °C (DMSO). IR ν_{max} (Nujol, cm^{-1}): 842, 2225. ^1H NMR (60 MHz, $CDCl_3$) δ: 4.12 (s, 8H), 7.51 (d, J = 2.4 Hz, 4H), 7.59 (d, J = 2.4 Hz, 4H). Anal. calcd. for $C_{18}H_{16}N_8$ (%): C 62.8, H 4.7, N 32.6; found: C 62.8, H 4.9, N 32.4.

p-*Methoxycarbonyl-(3b)*

Off-white needles, 100%; mp 203–206 °C (DMSO). IR ν_{max} (Nujol, cm^{-1}): 857, 1713. ^1H NMR (60 MHz, $CDCl_3$) δ: 3.90 (s, 6H, O-Me), 4.08 (s, 8H), 7.48 (d, J = 8.4 Hz, 4H), 8.04 (d, J = 8.4 Hz, 4H). HR-MS (EI) m/z calcd. for $C_{20}H_{22}N_6O_4$: 410.1702; found: 410.1692.

p-*Ethoxycarbonyl-(3c)*

Pale yellow needles, 87%; mp 172–174 °C (DMSO). IR ν_{max} (Nujol, cm^{-1}): 859, 1702. ^1H NMR (60 MHz, $CDCl_3$) δ: 1.38 (t, J = 7.0 Hz, 6H, C-Me), 4.06 (s, 8H, N-CH_2), 4.36 (q, J = 6.6 Hz, 4H, O-CH_2), 7.48 (d, J = 9 Hz, 4H), 8.05 (d, J = 9 Hz, 4H). ^{13}C NMR (15.1 MHz, $CDCl_3$) δ: 13.5 (CH_3), 45.9 (N-CH_2), 60.0 (O-CH_2), 119.8, 127.3, 129.8, 152.6 (arom.), 165.6 (C=O). HR-MS (EI) m/z calcd. for $C_{22}H_{26}N_6O_4$: 438.2015; found: 438.2019.

p-*Acetyl-(3d)*

Orange prisms, 89%; mp 239–241 °C (DMSO). IR ν_{max} (Nujol, cm^{-1}): 847, 1670. ^1H NMR (60 MHz, $CDCl_3$) δ: 2.59 (s, 6H, acetyl-Me), 4.10 (s, 8H, N-CH_2), 7.51 (d, J = 8.7 Hz, 4H), 8.0 (d, J = 8.7 Hz, 4H). ^{13}C NMR (15.1 MHz, $CDCl_3$) δ: 47.5, 121.3, 130.7. HR-MS (EI) m/z calcd. for $C_{20}H_{22}N_6O_2$: 378.1804; found: 378.1803.

p-*Carboxamido-(3e)*

Yellow solid, 100%; mp 285–287 °C (DMSO). IR ν_{max} (Nujol, cm^{-1}): 858, 1654, 3173, 3385. ^1H NMR (250 MHz, d_6-DMSO) δ: 4.09 (s, 8H), 6.77 (d, J = 9.6 Hz, 4H), 7.27 (d, J = 9.6 Hz, 4H). MS (EI) m/z (%): 77(32), 105(48), 121(100) [$C_6H_4CONH_3^+$], 148(23.5) [$NH_2COC_6H_4N_2^+$], 233(3) [$M^+ - N_2C_6H_4CONH$].

p-*Sulphonamido-(3f)*

Pale yellow solid, 60%; mp 217–223 °C (EtOH–DMSO). IR ν_{max} (Nujol, cm^{-1}): 836, 1160, 1377, 3183, 3341. ^1H NMR (60 MHz, d_6-DMSO) δ: 4.12 (s, 8H), 7.27 (d, J = 8.4 Hz, 4H), 7.82 (d, J = 8.4 Hz, 4H). MS (EI) m/z (%): 77(100), 156(25) [$C_6H_4NH_2^+$], 157(68) [$C_6H_4NH_3^+$], 170(21) [$NH_2SO_2C_6H_4N_2^+$].

p-*Tolyl-(3g)*

Short yellow needles, 89%; mp 172–174 °C (DMSO) (lit. value (3) mp 148 to 149 °C). IR ν_{max} (Nujol, cm^{-1}): 821. ^1H NMR (60 MHz, $CDCl_3$) δ: 2.33 (s, 6H, Ar-Me), 3.94 (s, 8H, N-CH_2), 7.1 (d, J = 8.7 Hz, 4H), 7.39 (d, J = 8.7 Hz, 4H). ^{13}C NMR (15.1 MHz, $CDCl_3$) δ: 20.6 (Ar-Me), 46.1 (N-CH_2), 120.7, 129.1, 135.9, 147.4 (arom.). HR-MS (EI) m/z calcd. for $C_{18}H_{22}N_6$: 322.1906; found: 322.1898.

p-*Bromo-(3h)*

Fine white needles, 91%; mp 199–203 °C (DMSO) (lit. value (3) mp 203 °C). IR ν_{max} (Nujol, cm^{-1}): 827. ^1H NMR (60 MHz, $CDCl_3$) δ: 4.00 (s, 8H), 7.32 (d, J = 7.2 Hz, 4H), 7.5 (d, J = 9 Hz, 4H). ^{13}C NMR (15.1 MHz, $CDCl_3$) δ: 46.5, 122.4, 131.9. Anal. calcd. for $C_{16}H_{16}Br_2N_6$ (%): C 42.5, H 3.5, N 18.6; found: C 42.3, H 3.6, N 18.1.

Phenyl-(3i, X = H)

Lustrous amber plates, 68%; mp 129 to 130 °C (ethanol) (lit. (3) mp 124 to 125 °C). IR ν_{max} (Nujol, cm^{-1}): 697. ^1H NMR (60 MHz, $CDCl_3$) δ: 3.97 (s, 8H), 7.1–7.5 (m, 10H). ^{13}C NMR (15.1 MHz, $CDCl_3$) δ: 47.7, 120.3, 126.0, 128.4, 137.3. Anal. calcd. for $C_{16}H_{18}N_6$ (%): C 65.3, H 6.1, N 28.6; found: C 65.3, H 6.2, N 28.6.

o-*Cyano-(3j)*

Pale yellow prisms, 94%; mp 190–192 °C (DMSO). IR ν_{max} (Nujol, cm^{-1}): 765, 2225. ^1H NMR (60 MHz, $CDCl_3$) δ: 4.19 (s, 8H), 7.08–7.73 (m, 8H). HR-MS (EI) m/z calcd. for $C_{18}H_{16}N_8$: 344.1498; found: 344.1492.

o-*Methoxycarbonyl-(3k)*

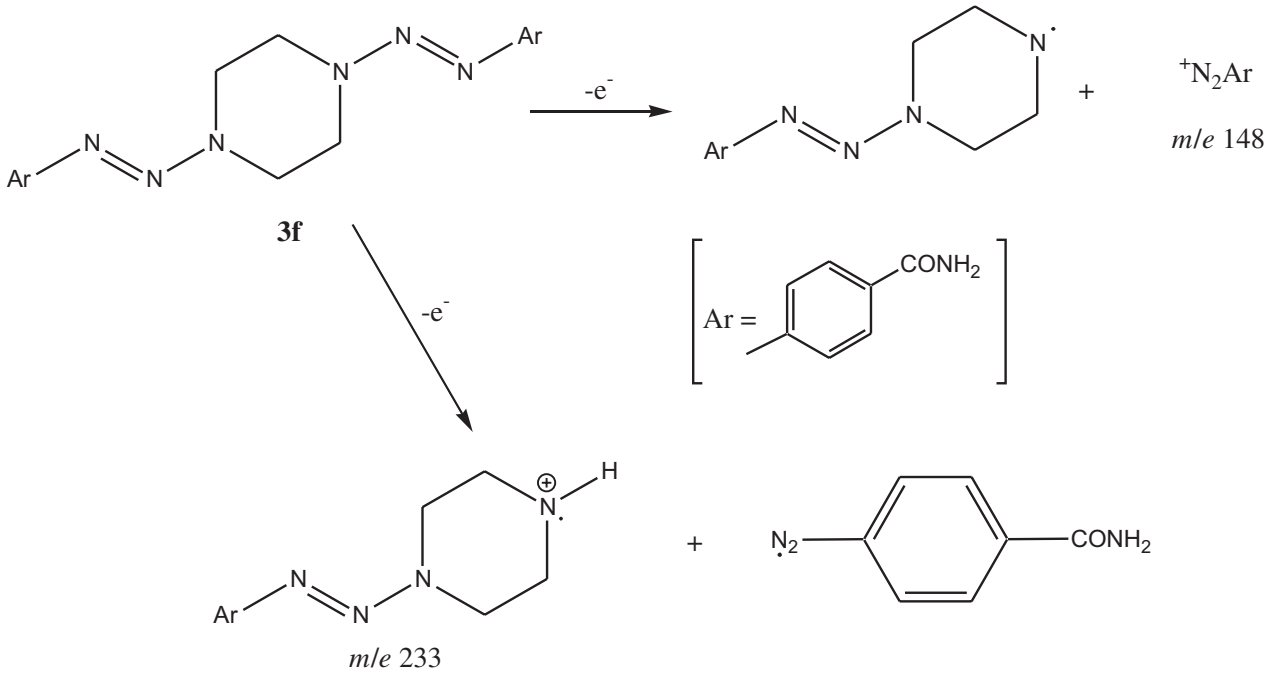
Golden oily prisms, 74%; mp 108–122 °C (ethanol). IR ν_{max} (Nujol, cm^{-1}): 765, 1715. ^1H NMR (60 MHz, $CDCl_3$) δ: 3.87 (s, 6H, O-Me), 4.03 (s, 8H, N-CH_2), 7.07–7.79 (m, 8H). ^{13}C NMR (15.1 MHz, $CDCl_3$) δ: 48.6 (N-CH_2), 53.9 (O-Me), 121.3, 127.7, 131.6, 133.7, 151.3 (aromatic), 170.0 (C=O). HR-MS (EI) m/z calcd. for $C_{20}H_{22}N_6O_4$: 410.1702; found: 410.1688.

o-*Ethoxycarbonyl-(3l)*

Golden prisms, 85%; mp 103–105 °C (ethanol). IR ν_{max} (Nujol, cm^{-1}): 764, 1703. ^1H NMR (60 MHz, $CDCl_3$) δ: 1.36 (t, J = 7.1 Hz, 6H, C-Me), 4.03 (s, 8H, N-CH_2), 4.35 (q, J = 7.1 Hz, 4H, O-CH_2), 7.07–7.79 (m, 8H). ^{13}C NMR (15.1 MHz, $CDCl_3$) δ: 15.8 (C-Me), 48.1 (N-CH_2), 62.5 (O-CH_2), 121.0, 127.5, 128.4, 131.3, 133.3, 150.7 (arom.). HR-

© 2005 NRC Canada

Fig. 1. Mass spectral fragmentation pathway of the bistriazene **3e**.



MS (EI) *m/z* calcd. for $C_{22}H_{26}N_6O_4$: 438.2015; found: 438.2010.

o-*Tolyl-(3m)*

Short off-white needles, 86%; mp 99 to 100 °C (DMSO) (lit. value (3) mp 104 to 105 °C). IR ν_{max} (Nujol, cm^{-1}): 750. ^1H NMR (60 MHz, $CDCl_3$) δ: 2.44 (s, 6H, Ar-Me), 3.99 (s, 8H, N-CH_2), 7.02–7.39 (m, 8H). ^{13}C NMR (15.1 MHz, $CDCl_3$) δ: 17.15, 46.2, 116.2, 125.9, 126.1, 130.2, 132.7, 147.5. Anal. calcd. for $C_{18}H_{22}N_6$ (%): C 67.1, H 6.8, N 26.1; found: C 66.8, H 6.8, N 26.1.

o-*Chloro-(3n)*

Off-white prisms, 76%; mp 88–90 °C (DMSO) (lit. value (3) mp 84–86 °C). IR ν_{max} (Nujol, cm^{-1}): 755. ^1H NMR (60 MHz, $CDCl_3$) δ: 4.04 (s, 8H), 7.03–7.54 (m, 8H). ^{13}C NMR (15.1 MHz, $CDCl_3$) δ: 46.25, 118.2, 126.3, 126.7, 129.4, 129.7, 146.0.

Results and discussion

Diazonium coupling with piperazine proceeded smoothly to afford the triazenes (**3a**–**3n**) in good yield ranging from 60%–100%. Percentage recovery after recrystallization ranged from 60%–89%. These bistriazenes proved to be somewhat intractable to the preferred recrystallization solvents, such as ethanol, ethyl acetate, toluene, etc., and in many cases purification was carried out by recrystallization from dimethyl sulfoxide. The melting point of the recrystallized bistriazene was sharp in most cases, but surprisingly, the melting point found in this study was in some cases different from that reported earlier by Yamarates et al. (3). These conflicting melting points have been doubly checked and the structures of the particular compounds in question have been confirmed by elemental analysis or accurate mass measurement of the molecular ions, in addition to NMR and IR spectroscopy. The IR spectra of the bistriazenes **3** have been recorded to confirm the identity of the aryl substituent (X-) and to assign the out-of-plane bending vibration as confirmation of the position of the substituent.

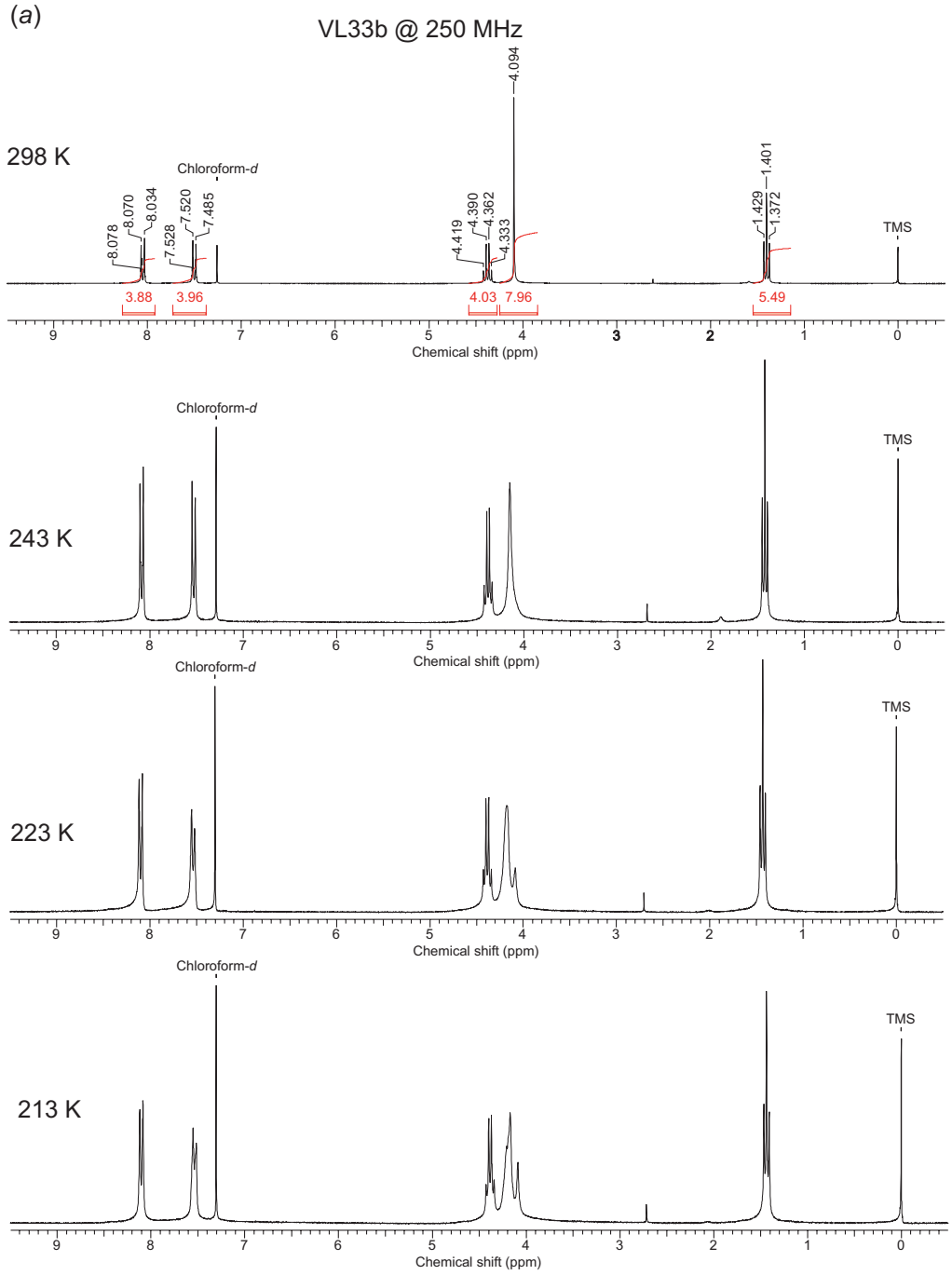
Table 1. Comparison of the ^1H and ^{13}C NMR chemical shifts in the spectra of the new bistriazenes **3** compared with the previously reported data for triazenes of type **1** (1) and the bistriazenes of type **2b** (2).

Series no.	Methylene protons of the piperazine ring (ppm)	Carbon signals of the piperazine ring carbons (ppm)
3	3.9–4.2	46–48
1	ca. 3.9	47 (C1)
2b	4.0 (Ha)	46 (C1)
	4.2 (Hb)	54 (C2)

All of the compounds in series **3** have been analyzed by ^1H NMR spectroscopy. The protons of the four equivalent methylene groups in the piperazine ring appear as a sharp singlet in the range 3.94–4.19 ppm; these spectra all show the predictable aromatic signals and the protons of the aryl substituent (if present). Although most of the new bistriazenes are only sparingly soluble in $CDCl_3$, the concentration in $CDCl_3$ was sufficient to allow recording of proton signals at 60 MHz, with the exception of the *p*-carboxamido-(**3e**) and *p*-sulfonamido-(**3f**) derivatives. These were recorded in d_6-DMSO solution. However, the low solubility of the bistriazenes limited the characterization by ^{13}C NMR to **3c**, **3d**, **3g**–**3i**, and **3k**–**3n**. Nevertheless, it is apparent that the four equivalent carbon atoms of the piperazine ring resonate in the range 46–48 ppm. The proton and carbon-13 chemical shifts in the spectra of the new bistriazenes **3** compare favorably with the previously reported data for triazenes of type **1** (1) and the bistriazenes of type **2b** (2) as shown in Table 1.

© 2005 NRC Canada

Fig. 2. (*a*) Stack plot of the variable-temperature ^{1}H NMR spectra of compound **3c** in deuteriochloroform.



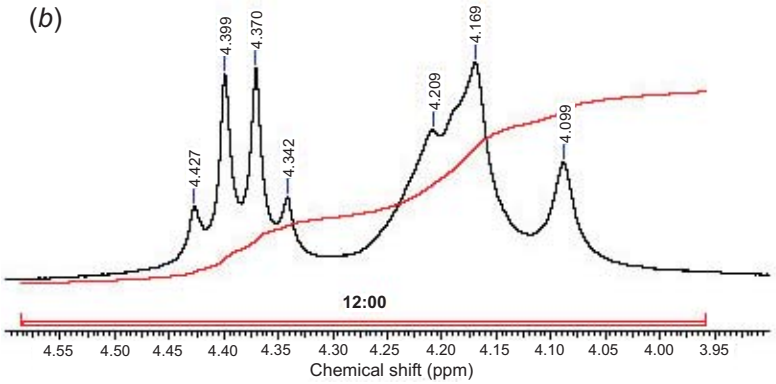
All of the new compounds in series **3** have been characterized by either elemental analysis or high resolution mass spectrometry, with the exception of **3e** and **3f**, which did not display stable molecular ions. Evidence for the structures of **3e** and **3f** was apparent from the fragmentation patterns. Thus, the mass spectrum of **3e** shows fragments at *m*/*e* 233 and 148, which are the fragments arising from cleavage of one of the N—N bonds in a triazene moiety (Fig. 1).

The simplicity of the NMR spectra of these bistriazenes **3** is a little surprising if one considers the possible conformational and rotational options available to these molecules. The sharpness of the proton and carbon signals in the ambient temperature spectra indicates that the N2—N3 bonds in the triazene moieties are not subjected to restricted rotation because of resonance, as has been observed previously with 1-aryl-3,3-dialkyltriazenes (5) and recently with 1,3-diphenyltriazenes (6); furthermore, the observation of a single sharp peak arising from the eight equivalent piperazine ring hydrogens suggests that any conformational equilibria of the piperazine ring is rapid at ambient temperature.

The next logical step in this study was to explore the VT NMR behavior of some representative examples of series **3** in solution. Compounds **3c** and **3d** were chosen on the basis of their demonstrated solubility in $CDCl_3$ at low tempera-

© 2005 NRC Canada

Fig. 2. (*b*) Detail of the ^{1}H NMR spectrum of compound **3c** at 213 K.



tures. Figure 2*a* shows a stack plot of the ^{1}H NMR spectra of **3c** down to 213 K; Fig. 2*b* is a detail of the 213 K spectrum. Most of the signals in the 213 K spectrum are sharp and unchanged with the exception of the signal at ca. 4.1 ppm, which separates into three clear lines at 4.088, 4.169, and 4.209 ppm (with the extra feature of a fourth signal as an unresolved shoulder). Clearly, there is a dynamic equilibrium occurring to create the chemical shift variance in the piperazine ring protons of the different species. There are three possible options: (*a*) equilibrium between the chair conformations of the piperazine ring; (*b*) equilibrium between species in which the N-aryldiazenylgroups occupy axial or equatorial positions; (*c*) rotational equilibrium between the rotamers **4A** and **4B**.

In light of previous work and conclusions (5) with regard to restricted rotation about the N2—N3 bond in the triazene moiety because of resonance, the third option (*c*) is the preferred explanation for the observed NMR spectrum of **3c** at 213 K. An equilibrium mixture of **4A** and **4B** would theoretically show four different proton chemical shifts in the region of the piperazine ring protons, i.e., Ha and Hb in **4A** and Hc and Hd in **4B**. This is consistent with the observed spectrum of **3c** at 213 K, if one assumes the shoulder at ca. 4.2 ppm is a real signal. The VT NMR spectrum of compound **3d** shows a similar phenomenon; the signal at 4.112 ppm resolves at 213 K into three distinct lines with a shoulder, and the aromatic signal of the H-atoms ortho to the triazenido moiety at ca. 7.5 ppm is considerably broadened.

Conclusion

The results reported here are complementary to our previous reported studies of the *N*-aryldiazenyl-*N*-methylpiperazines (**1**) (1), the *N*-aryldiazenyl-*N*-methylhomopiperazines (**2a**) (2), and the *N*,*N*-bis(aryldiazenyl-)homopiperazines (**2b**) (2). We now have a clear picture of the methodology of synthesizing these compounds and we are assembling a detailed compendium of the spectroscopic characteristics of these *N*-aryldiazenylheterocycles for future reference. This is a central part of our wider goal, which is the synthesis of new triazene derivatives of (1,*x*)-diazacycloalkanes (1, 2). Further elaboration of this goal will require exploration of the synthesis of new analogues of the bistriazene **3** with substituents in the piperazine ring, to shed light on the conformational options available to the piperazine ring. Also, we will endeavor to exploit the application of our triazenidopiperazines as triazene linkers in solid phase synthesis, an area of triazene chemistry that has recently attracted much attention (7).

Acknowledgements

The authors are grateful to the Natural Sciences and Engineering Research Council of Canada (NSERC) for a Discovery Grant to the principal author (KV) and an Undergraduate Summer Research Award (2003) to Vanessa Little. The authors thank the Faculty of Graduate Studies and Research at Saint Mary's University for a Summer Research Award (2004) to Vanessa Little. We are also grateful to the Atlantic Region Magnetic Resonance Centre at Dalhousie University for providing NMR spectra, and to Dalhousie University for providing mass spectral data. In particular, we would like to thank Dr. Bob Berno for assistance with the interpretation of the NMR spectral data, and Mr. Xiao Feng for assistance with the mass spectra.

References

1. V.R. Little and K. Vaughan. Can. J. Chem. **82**, 1294 (2004).
2. S.L. Moser and K. Vaughan. Can. J. Chem. **82**, 1725 (2004).
3. E. Yamarates, A. Disli, and Y. Yildirir. Org. Prep. Proced. Int. **31**, 429 (1999).
4. M. Kažemėkaitė, Z. Talaikytė, G. Niaura, and E. Butkus. Molecules, **7**, 706 (2002).
5. T. Axenrod, P. Mangiaracina, and P.S. Progosin. Helv. Chim. Acta, **59**, 1655 (1976).
6. M. Barra, S. Srivastava, and E. Brockman. J. Phys. Org. Chem. **17**, 1057 (2004).
7. S. Bräse, D. Enders, J. Köbberling, and F. Avemaria. Angew. Chem. Int. Ed. **37**, 3413 (1998); S. Bräse. Acc. Chem. Res. **37**, 805 (2004).

© 2005 NRC Canada

Transition metal complexes of a sterically demanding diimine ligand

Jason D. Masuda and Douglas W. Stephan

Abstract: The reaction of the metal halide with the sterically demanding ligand (i-$Pr_2C_6H_3N$)(C(Me)(NC_6H_3-i-Pr_2))$_2$ afforded the complexes (i-$Pr_2C_6H_3N$)(C(Me)(NC_6H_3-i-Pr_2))$_2MX_2$ (X = Cl, M = Fe (**2**), Co (**3**); X = Br, M = Ni (**4**), M = Cu (**5**), Zn (**6**)). The species of **2** reacts with $Li(OEt_2)B(C_6F_5)_4$ to form the yellow adduct [(i-$Pr_2C_6H_3N$)(C(Me)(NC_6H_3-i-Pr_2))$_2$Fe(μ-Cl)$_2$Li(OEt_2)$_2$][$B(C_6F_5)_4$] (**7**) while alkylation of **2** gave (i-$Pr_2C_6H_3N$)(C(Me)(NC_6H_3-i-Pr_2))$_2$FeClCH$_2$SiMe$_3$ (**8**). The species [(i-$Pr_2C_6H_3N$)(C(Me)(NC_6H_3-i-Pr_2))$_2$Ni(η^3-C_3H_5)][$B(3,5\text{-}CF_3C_6H_3)_4$] (**9**) was obtained from reaction of **1** with [(η^3-C_3H_5)NiBr]$_2$ and [Na][$B(3,5\text{-}(CF_3)_2C_6H_3)_4$] while reaction of **4** with Super-Hydride afforded (i-$Pr_2C_6H_3N$)-(C(Me)(NC_6H_3-i-Pr_2))$_2$NiH$_2$BEt_2 (**10**). X-ray data are reported for **2**–**10**. The sterically demanding nature of the ligand inhibits subsequent reactivity of these species.

Key words: sterically demanding ligands, chelate complexes, X-ray structure, diimine ligands.

Résumé : La réaction d'un halogénure métallique avec le ligand stériquement encombré (i-$Pr_2C_6H_3N$)(C(Me)(NC_6H_3-i-Pr_2))$_2$ conduit à la formation des complexes (i-$Pr_2C_6H_3N$)(C(Me)(NC_6H_3-i-Pr_2))$_2MX_2$ (X = Cl, M = Fe (**2**), Co (**3**); X = Br, M = Ni (**4**), M = Cu (**5**), Zn (**6**)). L'espèce **2** réagit avec le $Li(OEt_2)B(C_6F_5)_4$ pour former l'adduit jaune [(i-$Pr_2C_6H_3N$)(C(Me)(NC_6H_3-i-Pr_2))$_2$Fe(μ-Cl)$_2$Li(OEt_2)$_2$][$B(C_6F_5)_4$] (**7**) alors que l'alkylation du composé **2** conduit à la formation du complexe (i-$Pr_2C_6H_3N$)(C(Me)(NC_6H_3-i-Pr_2))$_2$FeClCH$_2$SiMe$_3$ (**8**). On a obtenu l'espèce (i-$Pr_2C_6H_3N$)-(C(Me)(NC_6H_3-i-Pr_2))$_2$Ni(η^3-C_3H_5)][$B(3,5\text{-}CF_3C_6H_3)_4$] (**9**) par réaction du composé **1** avec le [(η^3-C_3H_5)NiBr]$_2$ et le [Na][$B(3,5\text{-}(CF_3)_2C_6H_3)_4$] alors que la réaction du composé **4** avec le Super-Hydrure conduit à la formation du (i-$Pr_2C_6H_3N$)(C(Me)(NC_6H_3-i-Pr_2))$_2$NiH$_2$BEt_2 (**10**). On rapporte les données de diffraction des rayons X par les composés **2**–**10**. L'encombrement stérique du ligand inhibe toute réactivité subséquente de ces espèces.

Mots clés : ligands stériquement encombrés, complexes de chélates, structure par diffraction des rayons X, diimine ligands.

[Traduit par la Rédaction]

Introduction

Recently, much attention has focused on sterically demanding chelating ligands such as the neutral, diimine-based ligand ((C(Me)NC_6H_3-i-Pr_2)$_2$) and [HC(C(Me)NC_6H_3-i-Pr_2)$_2$]$^-$ (Scheme 1). Such ligands have been utilized for late transition metal olefin polymerization catalysts, as well as for the isolation of novel low-valent Al and Ga derivatives (1–4). Mindiola and co-workers (5) have used the latter ligand to isolate the first Ti–phosphinidene complex. In our labs, we have recently been probing new bulky ligands in late transition metals (6–8) and main group chemistry (9). For example, we have recently reported the use of the bulky phosphinimine–imine ligand (i-$Pr_2C_6H_3N$)C(Me)CHPPh_2-(NC_6H_3-i-Pr_2) to prepare neutral and cationic Al complexes (9), while Welch et al. (10) reported related complexes based on the ligand (i-$Pr_2C_6H_3N$)$C_6H_4PPh_2$(NC_6H_3-i-Pr_2). In recent efforts, we have also reported the synthesis of the sterically demanding *N*-aryl-imidoyl amidine ligand i-$Pr_2C_6H_3N$(C(Me)NC_6H_3-i-Pr_2)$_2$ and its use in the synthesis of Al-based alkyl and hydride cations.[2] Several previous reports have described metal complexes involving the *N*-imidoyl amidine systems (R = H) (11–19) and the related 2,2′-dipyridylamino ligand (20–34). Cotton et al. (31) serendipitously obtained [PhNCHN(Ph)CHNPh]$CoCl_2$ while the related species [(4-MePh)NCHN(4-MePh)(4-MePh)-NC]Pd(C_6F_5)$_2$ was reported by Uson et al. (33). Finally, Wilkinson and co-workers (32) characterized the species (C_5Me_5)Ir[N(2,6-MeC_6H_3)CHNRCNC_6H_3(Me)CH_2] (R = *t*-Bu, 2,6-i-PrC_6H_3). In this manuscript, we report the use of this bulky ligand i-$Pr_2C_6H_3N$(C(Me)NC_6H_3-i-Pr_2)$_2$ in the synthesis of a series of transition metal complexes. Structural studies of these complexes are presented and discussed.

Received 19 November 2004. Published on the NRC Research Press Web site at http://canjchem.nrc.ca on 14 May 2005.

J.D. Masuda and D.W. Stephan.[1] Department of Chemistry and Biochemistry, University of Windsor, Windsor, ON N9B 3P4, Canada.

[1]Corresponding author (e-mail: stephan@uwindsor.ca).

[2]J.D. Masuda and D.W. Stephan. Organometallics, submitted (2005).

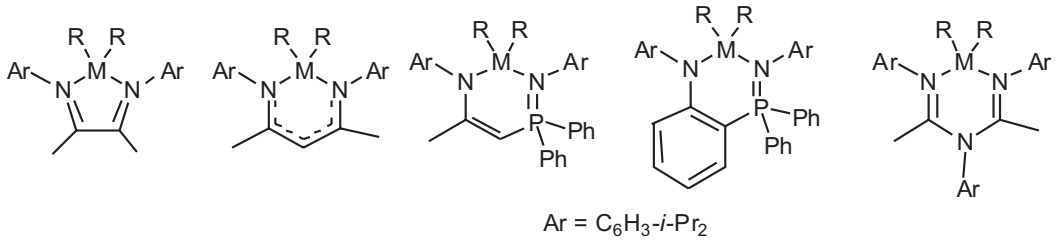
Experimental

General data

All preparations were done under an atmosphere of dry, O_2-free N_2 employing both Schlenk line techniques and a Vacuum Atmospheres inert atmosphere glovebox. Solvents were purified employing a Grubbs'-type solvent purification system manufactured by Innovative Technology. Deuterated

 doi: 10.1139/V05-057 © 2005 NRC Canada

Scheme 1. Bulking chelating ligand complexes.



solvents were purified using the appropriate techniques. All organic reagents were purified by conventional methods. ^{1}H, ^{31}P, ^{11}B, ^{19}F, and ^{13}C NMR spectra were recorded on Bruker Avance-300 and -500 spectrometers. All spectra were recorded in C_6D_6 at 25 °C unless otherwise noted. Trace amounts of protonated solvents were used as references and chemical shifts are reported relative to $SiMe_4$. ^{31}P, ^{11}B, and ^{19}F NMR spectra were referenced to external 85% H_3PO_4, $BF_3{\cdot}Et_2O$, and $CFCl_3$, respectively. Combustion analyses were done in-house employing a PerkinElmer CHN analyzer. [Na][B(3,5-$CF_3C_6H_3)_4$] was prepared as outlined (36). $LiCH_2SiMe_3$ and Super-Hydride were purchased from Aldrich Chemical Co. as solutions and crystallized. The ligand (*i*-$Pr_2C_6H_3N$)C(Me)(NC_6H_3-*i*-Pr_2)C(Me)(NC_6H_3*i*-Pr_2) (**1**) was prepared by published methods.[2]

Synthesis of (*i*-$Pr_2C_6H_3N$)(C(Me)(NC_6H_3-*i*-Pr_2))$_2MCl_2$ (M = Fe (2), Co (3))

These compounds were prepared in a similar fashion and thus one preparation is detailed. To a solution of **1** (200 mg, 0.345 mmol) in 5 mL toluene was added $FeCl_2$ (43 mg, 0.345 mmol). The mixture was heated to 110 °C for 3 days after which the insoluble, off-white $FeCl_2$ had been replaced with a yellow solid. The toluene was then removed in vacuo and the remaining solids dissolved in approximately 10 mL CH_2Cl_2. This solution was then filtered through Celite® and layered with 10 mL toluene. After several days, 213 mg of bright yellow – orange crystals were isolated. **2**: Yield: 79%; magnetic susceptibility 5.79 μ_B. Anal. calcd. for $C_{40}H_{57}N_3FeCl_2$: C 67.99, H 8.13, N 5.95; found: C 68.22, H 8.40, N 6.00. **3**: Blue crystals. Yield: 87%; magnetic susceptibility 3.35 μ_B. Anal. calcd. for $C_{40}H_{57}N_3CoCl_2$: C 67.69, H 8.09, N 5.92; found: C 67.55, H 7.84, N 5.87.

Synthesis of (*i*-$Pr_2C_6H_3N$)(C(Me)(NC_6H_3-*i*-Pr_2))$_2NiBr_2$ (4)

To a solution of **1** (1.000 g, 1.72 mmol) in 15 mL xylenes was added $NiBr_2$ (377 mg, 1.72 mmol). The mixture was heated to 140 °C for 3 days. This resulted in the formation of a purple solid suspended in a bright blue solution. The xylenes were then decanted, the solids washed with 2 × 10 mL pentane, and dried in vacuo to give 1.186 g of powder **4**. X-ray quality dark purple crystals were grown from a solution in CH_2Cl_2 layered with toluene. **4**: Yield: 86%; magnetic susceptibility 4.98 μ_B. Anal. calcd. for $C_{40}H_{57}N_3NiBr_2$: C 60.17, H 7.19, N 5.26; found: C 60.38, H 7.23, N 5.25. The decanted xylenes and pentane washings were combined and after a few weeks, a small amount of blue crystals formed. Crystallographic analysis proved this to be [CH_3C(*i*-$Pr_2C_6H_3N)_2HNiBr_3$][CH_3C(*i*-$Pr_2C_6H_3NH)_2$] resulting from a small amount of CH_3C(*i*-$Pr_2C_6H_3N)_2H$ impurity in the **1** starting material.

Synthesis of (*i*-$Pr_2C_6H_3N$)(C(Me)(NC_6H_3-*i*-Pr_2))$_2MBr_2$ (M = Cu (5), Zn (6))

These compounds were prepared in a similar fashion and thus one preparation is detailed. To a solution of **1** (100 mg, 0.172 mmol) in 5 mL THF was added 38 mg (0.172 mmol) $CuBr_2$ and the mixture was left to stir overnight, after which a copious amount of burgundy colored solids formed. The solids were filtered from the reaction mixture to give 83 mg of material. **5**: Yield: 60%; magnetic susceptibility 1.99 μ_B. X-ray quality burgundy colored crystals were grown from a hot MeCN solution slowly cooled to –35 °C. Anal. calcd. for $C_{40}H_{57}N_3CuBr_2$: C 59.81, H 7.15, N 5.23; found: C 59.43, H 7.30, N 5.15. **6**: Yield: 90%. X-ray quality colorless crystals were grown by cooling a $CHCl_3$ solution to –35 °C. ^{1}H NMR (CD_2Cl_2): 7.24–7.57 (m, 9H, *m*, *p*-Ar), 3.42 (sept, 4H, CH, $|J_{H\text{-}H}|$ = 6.9 Hz), 3.41 (sept, 2H, CH, $|J_{H\text{-}H}|$ = 6.9 Hz), 1.76 (s, 6H, Me), 1.37 (d, 12H, *i*-Pr, $|J_{H\text{-}H}|$ = 6.9 Hz), 1.30 (d, 12H, *i*-Pr, $|J_{H\text{-}H}|$ = 6.9 Hz), 1.13 (d, 12H, *i*-Pr, $|J_{H\text{-}H}|$ = 6.9 Hz). ^{13}C NMR (CD_2Cl_2): 167.8, 146.4, 141.3, 141.1, 137.2, 132.0, 127.9, 126.8, 125.5, 29.1, 28.8, 26.0, 24.8, 24.7, 24.0. Anal. calcd. for $C_{40}H_{57}N_3ZnBr_2$: C 59.67, H 7.14, N 5.22; found: C 59.26, H 7.12, N 5.12.

Synthesis of (*i*-$Pr_2C_6H_3N$)(C(Me)(NC_6H_3-*i*-Pr_2))$_2$Fe(μ-$Cl)_2Li(OEt_2)_2$][$B(C_6F_5)_4$] (7)

To a rapidly stirring suspension of **2** (100 mg, 0.142 mmol) in 5 mL toluene was added 107 mg (0.142 mmol) $Li(OEt_2)_2B(C_6F_5)_4$ in 5 mL of diethyl ether. The reaction was allowed to stir overnight after which the mixture turned from yellow-orange to a bright yellow color. Filtration of the mixture through Celite® and removal of the solvent gave a yellow oil, which crystallized upon addition of pentane. Yield: 41%; magnetic susceptibility 5.23 μ_B. X-ray quality crystals were grown by diffusion of pentane vapor into a diethyl ether – toluene solution of the material. Anal. calcd. for $C_{72}H_{77}N_3FeCl_2LiBF_{20}O$: C 56.12, H 5.03, N 2.73; found: C 56.30, H 4.73, N 2.50.

Synthesis of (*i*-$Pr_2C_6H_3N$)(C(Me)(NC_6H_3-*i*-Pr_2))$_2FeClCH_2SiMe_3$ (8)

To a rapidly stirring suspension of **2** (100 mg, 0.142 mmol) in 5 mL toluene cooled to –35 °C was added $LiCH_2SiMe_3$ (13 mg, 0.142 mmol) in 3 mL of cold toluene. The reaction was allowed to warm to 25 °C over several hours. The mixture became deep purple in color. Filtration of the mixture and cooling the filtrate to –35 °C overnight gave fine purple needles. The crystals were filtered off and washed with 2 ×

© 2005 NRC Canada

10 mL of cold pentane. Yield: 55%; magnetic susceptibility 5.61 μ_B. X-ray quality purple crystals were grown from a toluene solution layered with pentane. Anal. calcd. for $C_{44}H_{68}N_3FeSiCl$: C 69.68, H 9.03, N 5.54; found: C 70.18, H 8.56, N 6.20.

Synthesis of [(*i*-$Pr_2C_6H_3N$)(C(Me)(NC_6H_3-*i*-Pr_2))$_2$Ni(η^3-C_3H_5)][B(3,5-$(CF_3)_2C_6H_3)_4$] (9)

To a solution of **1** (100 mg, 0.174 mmol) in 8 mL CH_2Cl_2 was added $[(\eta^3\text{-}C_3H_5)NiBr]_2$ (32 mg, 0.174 mmol) and [Na][B(3,5-$(CF_3)_2C_6H_3)_4$] (155 mg, 0.174 mmol). The mixture was stirred overnight. The resulting brown solution was filtered to remove NaBr and the filtrate was cooled to –35 °C overnight to give brown crystals, which were separated from the solution by decantation and washed with 3 × 5 mL of cold pentane. Yield: 33%. ^{1}H NMR (CD_2Cl_2): 7.71 (br s, 8H, *o*-Ar_F), 7.56 (br s, 4H, *p*-Ar_F), 7.00–7.58 (m, 9H, *m*, *p*-Ar), 5.74 (dt, 1H, allyl CH, $|J_{H\text{-}H}|$ = 13.5 Hz, $|J_{H\text{-}H}|$ = 7.1 Hz), 3.69 (sept, 2H, CH, $|J_{H\text{-}H}|$ = 6.9 Hz), 3.01 (sept, 2H, CH, $|J_{H\text{-}H}|$ = 6.9 Hz), 2.87 (sept, 1H, CH, $|J_{H\text{-}H}|$ = 6.9 Hz), 2.72 (sept, 1H, CH, $|J_{H\text{-}H}|$ = 6.9 Hz), 2.16 and 2.11 (d, 2H, allyl-syn, $|J_{H\text{-}H}|$ = 13.5 Hz), 1.79 and 1.77 (d, 2H, allyl-anti, $|J_{H\text{-}H}|$ = 7.1 Hz), 1.66 (s, 6H, Me), 1.55 (d, 6H, *i*-Pr, $|J_{H\text{-}H}|$ = 6.9 Hz), 1.44 (d, 6H, *i*-Pr, $|J_{H\text{-}H}|$ = 6.9 Hz), 1.33 (d, 6H, *i*-Pr, $|J_{H\text{-}H}|$ = 6.9 Hz), 1.29 (d, 6H, *i*-Pr, $|J_{H\text{-}H}|$ = 6.9 Hz), 1.28 (d, 6H, *i*-Pr, $|J_{H\text{-}H}|$ = 6.9 Hz), 1.21 (d, 6H, *i*-Pr, $|J_{H\text{-}H}|$ = 6.9 Hz). ^{13}C NMR (CD_2Cl_2): 163.7, 162.4 (q, J_{CF} = 49 Hz), 149.4, 145.0, 149.9, 137.8, 136.9, 136.5, 135.4, 132.7, 130.6, 130.1 (br m), 129.7 (br m), 129.6, 129.3 (br m), 128.9 (br m), 128.7, 128.3, 127.3, 127.2, 127.0, 125.8, 125.5, 123.4, 119.8, 118.1 (br m), 65.6, 29.9, 29.4, 29.3, 29.1, 25.0, 24.9, 24.8, 24.2, 24.0, 23.7, 23.4, 21.7. ^{11}B NMR (CD_2Cl_2): –10.9. ^{19}F NMR (CD_2Cl_2): –63.2. Anal. calcd. for $C_{75}H_{74}N_3NiBF_{24}$: C 58.38, H 4.83, N 2.72; found: C 58.07, H 4.89, N 2.66.

Synthesis of (*i*-$Pr_2C_6H_3N$)(C(Me)(NC_6H_3-*i*-Pr_2))$_2$$NiH_2BEt_2$ (10)

To a rapidly stirring slurry of **4** (200 mg, 0.251 mmol) in 10 mL toluene was added Super-Hydride (0.551 mL, 1.0 mol/L in THF). An immediate evolution of gas was observed. The purple solution was allowed to stir for 4 h after which the solvent was removed in vacuo. The solid was dissolved in approx. 5 mL toluene, filtered through Celite®, layered with 5 mL pentane, and cooled to –35 °C overnight. The resulting brown-red crystals were separated from the solution and washed with 3 × 10 mL of cold pentane. Yield: 47%; magnetic susceptibility 1.11 μ_B. Anal. calcd. for $C_{44}H_{69}N_3NiB$: C 74.48, H 9.80, N 5.92; found: C 74.93, H 9.81, N 5.92.

X-ray data collection and reduction

Crystals were manipulated and mounted in capillaries in a glovebox, thus maintaining a dry, O_2-free environment for each crystal. Diffraction experiments were performed on a Siemens SMART System CCD diffractometer. The data were collected in a hemisphere of data in 1448 frames with 10 s exposure times. The observed extinctions were consistent with the space groups in each case. The data sets were collected ($4.5° < 2\theta < 45°$–$50.0°$). A measure of decay was obtained by recollecting the first 50 frames of each data set. The intensities of reflections within these frames showed no statistically significant change over the duration of the data collections. The data were processed using the SAINT and XPREP processing packages (37). An empirical absorption correction based on redundant data was applied to each data set. Subsequent solution and refinement was performed using the SHELXTL solution package (37).

Structure solution and refinement

Non-hydrogen atomic scattering factors were taken from the literature tabulations. The heavy atom positions were determined using direct methods employing the SHELXTL direct-methods routine. The remaining non-hydrogen atoms were located from successive difference Fourier map calculations. The refinements were carried out by using full-matrix least-squares techniques on *F*. In the final cycles of each refinement, all non-hydrogen atoms were assigned anisotropic temperature factors in the absence of disorder or insufficient data. In the latter cases, atoms were treated isotropically. C-H atom positions were calculated and allowed to ride on the carbon to which they are bonded assuming a C—H bond length of 0.95 Å. H-atom temperature factors were fixed at 1.10 times the isotropic temperature factor of the C atom to which they were bonded. The H-atom contributions were calculated, but not refined. The locations of the largest peaks in the final difference Fourier map calculation as well as the magnitude of the residual electron densities in each case were of no chemical significance. Addition details are provided in the Supplementary data.[3] See Table 1 for the crystallographic data for **2**–**10**.

Results and discussion

The reaction of the metal halide in toluene or xylenes with ligand **1** at elevated temperatures afforded the complexes (*i*-$Pr_2C_6H_3N$)(C(Me)(NC_6H_3-*i*-Pr_2))$_2$$MX_2$ (X = Cl, M = Fe (**2**), Co (**3**); X = Br, M = Ni (**4**)) in yields of 79%, 87%, and 86%, respectively (Scheme 2). In the latter case, formation of the Ni complex required the more forcing conditions of 4 days of heating in xylenes at 140 °C to form **4**. These vigorous conditions stand in stark contrast to those required for the formations of $H_2C(C(Me)NC_6H_3\text{-}i\text{-}Pr_2)_2NiBr_2$ (37) and $(C(Me)(NC_6H_3\text{-}i\text{-}Pr_2)_2)NiBr_2$ (38), which form readily at room temperature. Magnetic susceptibility measurements for **2**, **3**, and **4** gave a magnetic moment of 4.79, 3.35, and 4.98 μ_B, respectively, consistent with these formulations. In a similar fashion, the straightforward reaction of **1** with equimolar amounts of $CuBr_2$ or $ZnBr_2$ in THF at room temperature gave compounds (*i*-$Pr_2C_6H_3N$)(C(Me)(NC_6H_3*i*-Pr_2))$_2$$MBr_2$ (M = Cu (**5**), Zn (**6**)). The ^{1}H NMR spectrum of **5** gave se-

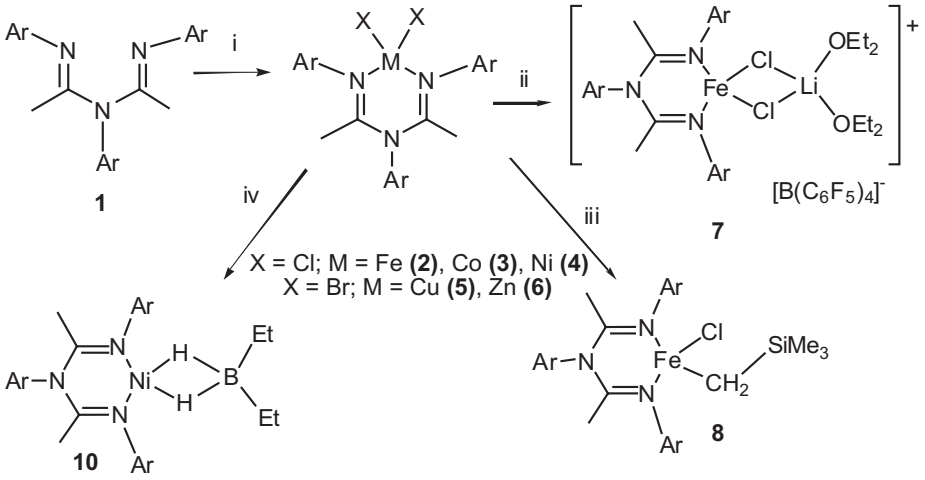
[3] Supplementary data for this article are available on the Web site or may be purchased from the Depository of Unpublished Data, Document Delivery, CISTI, National Research Council Canada, Ottawa, ON K1A 0S2, Canada. DUD 3657. For more information on obtaining material refer to http://cisti-icist.nrc-cnrc.gc.ca/irm/unpub_e.shtml. CCDC 256368–256376 contain the crystallographic data for this manuscript. These data can be obtained, free of charge, via www.ccdc.cam.ac.uk/conts/retrieving.html (or from the Cambridge Crystallographic Data Centre, 12 Union Road, Cambridge CB2 1EZ, UK; fax +44 1223 336033; or deposit@ccdc.cam.ac.uk).

© 2005 NRC Canada

Table 1. Crystallographic data.

	2·2CH_2Cl_2	**3**	**4**	**5**	**6**
Formula	$C_{42}H_{61}Cl_6FeN_3$	$C_{40}H_{57}Cl_2CoN_3$	$C_{40}H_{57}Br_2N_3Ni$	$C_{40}H_{57}Br_2CuN_3$	$C_{40}H_{57}Br_2ZnN_3$
Formula weight	876.48	709.72	798.41	803.25	805.08
Crystal System	Monoclinic	Monoclinic	Monoclinic	Triclinic	Monoclinic
Space group	$P2_1/m$	$P2_1/m$	$P2_1/n$	P-1	$P2_1/c$
a (Å)	10.369(5)	10.7514(14)	10.462(9)	10.536(6)	10.512(7)
b (Å)	19.199(9)	17.395(3)	43.18(4)	11.758(7)	43.32(3)
c (Å)	11.990(6)	11.4237(18)	18.187(16)	18.189(11)	18.257(11)
α (°)				81.676(11)	
β (°)	101.554(10)	111.716(4)	106.392(19)	74.302(10)	106.732(9)
γ (°)				67.424(12)	
V (Å^3)	2 338.5(19)	1 984.9(5)	7 882(12)	2 001(2)	7 962(9)
Z	2	2	8	2	8
d(calcd.) (g cm^{-1})	1.245	1.187	1.346	1.333	1.343
Abs. coeff. (μ, mm^{-1})	0.696	0.597	2.550	2.572	2.654
Data collected	10 074	4 578	36 954	8 599	34 217
Data $F_o^2 > 3\sigma(F_o^2)$	3 469	2 596	11 284	5 676	11 329
Variables	253	226	829	415	829
R	0.0446	0.0574	0.0536	0.0769	0.0660
Rw	0.0996	0.1477	0.1241	0.1815	0.1528
GOF	0.827	1.043	0.937	0.851	0.770

Scheme 2. Synthesis of neutral and cationic complexes: (*i*) MX_2; (*ii*) $Li[B(C_6F_5)_4]$; (*iii*) $LiCH_2SiMe_3$; (*iv*) Super-Hydride.



verely broadened lines, while the spectrum of **6** was similar to the free ligand. Magnetic susceptibility measurements of **5** gave a magnetic moment of 1.99 μ_B.

The overall geometries of the complexes **2**–**6** as determined by X-ray crystallographic studies are similar and thus only two representative ORTEP drawings are provided (Figs. 1 and 2). In all cases, the aryl rings are approximately orthogonal to the chelate plane and the metals adopt a pseudo-tetrahedral geometry. In the case of compounds **2** and **3**, the molecules crystallize such that they sit on a crystallographically imposed mirror plane bisecting the ligand and passing through the plane containing the metal atom – dichloride fragment. The key metric parameters are summarized in Table 2. The M—Cl distances in **2** and **3** and the M—Br distance in **4** increases for the Fe, Co, Ni series consistent with increasing atomic radius. The M—Br distances for **5** and **6** are longer, as expected, averaging 2.367 and 2.357 Å, respectively. The X-M-X angles found in **2**–**4** are slightly larger than the typical tetrahedral angle ranging from 116.79(8)° to 120.14(8)°. For **5** and **6**, the Br-M-Br angles were found to be 106.82(7)° and 117.80(5)°. The M—N distances fall in a narrow range between 1.959(6) and 2.096(3) Å. Similarly, the N—C distances of the imine fragments vary from 1.287(6) to 1.317(10) Å. These latter bond lengths are slightly longer than those found in the free ligand (1.272(3) and 1.269(3) Å). The ligand bite angles ranged from 84.61(15)° for the Fe species to 90.1(3)° for the Cu species. The N-M-X angles, in general, fall in the range from 101.54(12)° to 123.67(13)°; however, the largest range of thse angles was observed for **5** where the N-Cu-Br angles were found to be 132.9(2)° and 105.8(2)°. These large N-Cu-Br angles, the large bite angle, short M—N distances, and the small X-M-X angle in **5** are illustrative of the greater distortion from a tetrahedral geometry at Cu relative

© 2005 NRC Canada

Table 1 (*concluded*).

7	**8**·0.5C_6H_6	**9**·0.5C_6H_6·0.25CH_2Cl_2	**10**
$C_{72}H_{72}BCl_2F_{20}FeLiN_3O_2$	$C_{45}H_{69}Cl_3FeN_3Si$	$C_{78.25}H_{75}BCl_{0.50}F_{24}N_3Ni$	$C_{44}H_{69}BN_3Ni$
1535.83	842.32	1600.66	709.54
Triclinic	Orthorhombic	Triclinic	Triclinic
P-1	*Pnma*	*P*-1	*P*-1
15.545(3)	21.1151(12)	15.178(7)	11.861(4)
16.276(3)	19.1255(12)	16.512(7)	12.840(4)
16.461(3)	12.6066(8)	17.583(7)	16.590(5)
101.263(4)		107.375(8)	89.734(6)
92.812(4)		99.173(8)	75.663(7)
104.311(5)		97.665(9)	63.836(5)
3 937.0(13)	5 091.0(5)	4 074(3)	2 181.1(11)
2	4	2	2
1.296	1.099	1.305	1.080
0.350	0.507	0.351	0.475
19 393	24 184	17 656	6 910
11 181	3 782	11 702	4 018
883	257	929	466
0.0537	0.0473	0.1145	0.0425
0.1267	0.1195	0.3241	0.1020
0.837	1.190	1.211	0.966

Fig. 1. ORTEP of **2** or **3** (30% thermal ellipsoids are shown). Hydrogen atoms are omitted for clarity. These compounds are isomorphous.

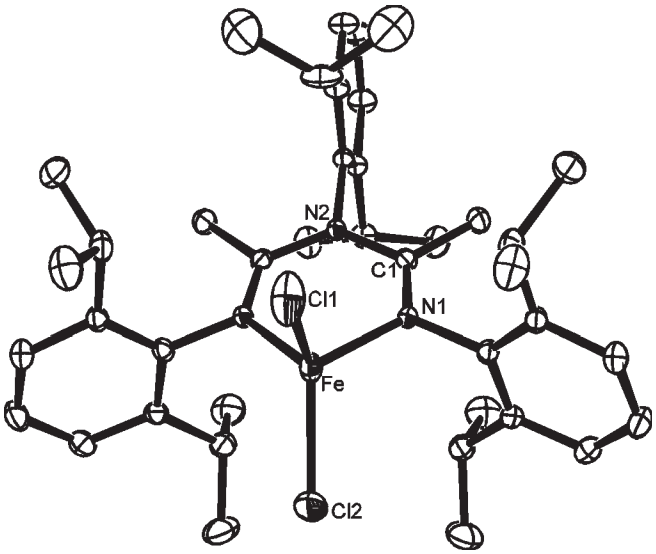
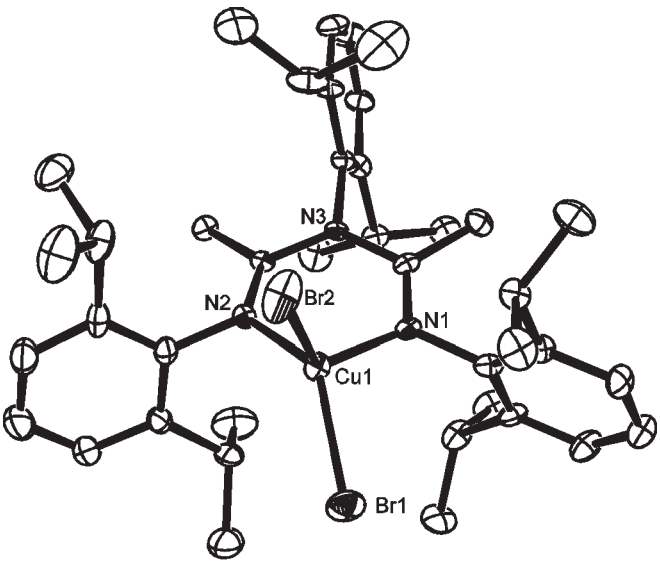


Fig. 2. ORTEP of **5** (30% thermal ellipsoids are shown). Hydrogen atoms are omitted for clarity.



to the other compounds (Fig. 2). In this case, it appears that steric crowding results in the displacement of the Cu atom out of the ligand plane, and a twisting of the $CuBr_2$ plane to minimize interactions with the bulky Ar groups.

The species **2** reacts with $Li(OEt_2)_2B(C_6F_5)_4$ to form the yellow adduct $[(i\text{-}Pr_2C_6H_3N)(C(Me)(NC_6H_3\text{-}i\text{-}Pr_2))_2Fe(\mu\text{-}Cl)_2Li(OEt_2)_2][B(C_6F_5)_4]$ (**7**) in 41% isolated yield (Scheme 2). Crystallographic characterization of **7** revealed a pseudo-tetrahedral geometry about Fe in which two chlorine atoms bridge the Fe and Li atoms (Fig. 3). The pseudo-tetrahedral coordination sphere of Li is completed by the coordination of two molecules of ether. The Fe—N distances average 2.034(4) Å, which is shorter than that observed for **2**. This is consistent with a more electron-deficient metal center as a result of the bridging of the Cl ligands to Li. This view is also consistent with the longer avg. Fe—Cl bond length of 2.2774(17) Å. A consequence of the bridging Cl atoms is also a small increase in the diimine ligand bite angle to 86.18(14)°. The Li—Cl bond lengths in **7** were found to be 2.474(10) and 2.352(11) Å, which gives rise to an Fe—Li separation of 3.163(9) Å.

Alkylation of **2** with 1 equiv. of $LiCH_2SiMe_3$ proceeds to give $(i\text{-}Pr_2C_6H_3N)(C(Me)(NC_6H_3\text{-}i\text{-}Pr_2))_2FeClCH_2SiMe_3$ (**8**) in 55% isolated yield (Scheme 2). The magnetic susceptibility of **8** was determined to be 5.61 μ_B, consistent with a high-spin Fe(II) species. X-ray structural study of **8** con-

© 2005 NRC Canada

Table 2. Metric parameters (bond distances and angles) for the complexes **2**–**6**.

Cmpd	M—X (Å)	M—N (Å)	N_M—C (Å)	N-M-N (°)	X-M-X (°)	N-M-X (°)
2	2.235(2)	2.096(3)	1.297(4)	84.61(15)	120.14(8)	110.87(9), 112.43(9)
	2.252(2)					
3	2.219(2)	1.999(3)	1.299(4)	89.78(16)	116.79(8)	108.30(10), 115.18(9)
	2.2158(17)					
4	2.328(2)	1.996(5)	1.287(6)	89.84(19)	117.93(4)	123.67(13), 114.28(12)
	2.394(2)	1.997(4)	1.290(6)			101.54(12), 104.96(12)
5	2.3455(19)	1.959(6)	1.317(10)	90.1(3)	106.82(7)	132.9(2), 105.8(2)
	2.389(2)	1.987(8)	1.296(10)			102.31(19), 119.9(2)
6	2.3416(17)	2.050(6)	1.282(8)	88.1(2)	117.80(5)	117.08(16), 112.90(17)
	2.3729(19)	2.082(6)	1.305(8)			106.96(15), 110.04(15)

Fig. 3. ORTEP of the cation of **7** (30% thermal ellipsoids are shown). Hydrogen atoms are omitted for clarity. Bond lengths (Å): Fe(1)—N(3) 2.030(4), Fe(1)—N(1) 2.034(3), Fe(1)—Cl(2) 2.2706(17), Fe(1)—Cl(1) 2.2842(17), Fe(1)—Li(1) 3.163(9), Cl(1)—Li(1) 2.474(10), Cl(2)—Li(1) 2.352(11), N(1)—C(37) 1.291(5), N(1)—C(1) 1.451(5), N(2)—C(13) 1.466(5), Li(1)—O(2) 1.943(11), Li(1)—O(1) 1.968(10). Bond angles (°): N(3)-Fe(1)-N(1) 86.18(14), N(3)-Fe(1)-Cl(2) 123.86(11), N(1)-Fe(1)-Cl(2) 114.69(11), N(3)-Fe(1)-Cl(1) 113.49(10), N(1)-Fe(1)-Cl(1) 121.78(11), Cl(2)-Fe(1)-Cl(1) 98.82(7), O(2)-Li(1)-O(1) 114.8(5), O(2)-Li(1)-Cl(2) 113.6(5), O(1)-Li(1)-Cl(2) 106.8(5), O(2)-Li(1)-Cl(1) 111.3(5), O(1)-Li(1)-Cl(1) 116.5(5).

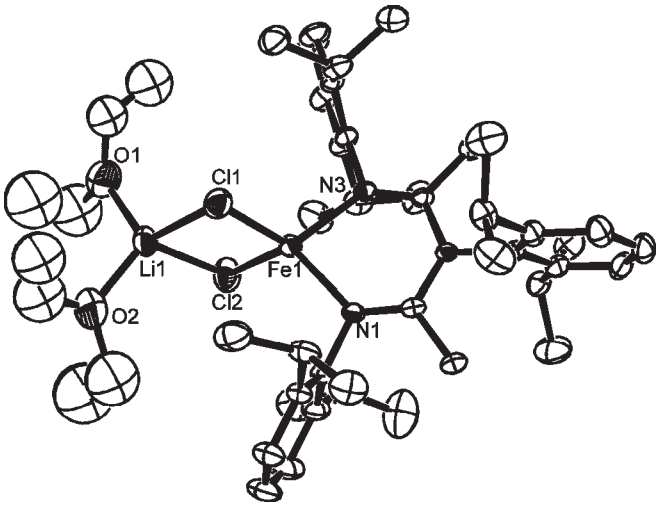
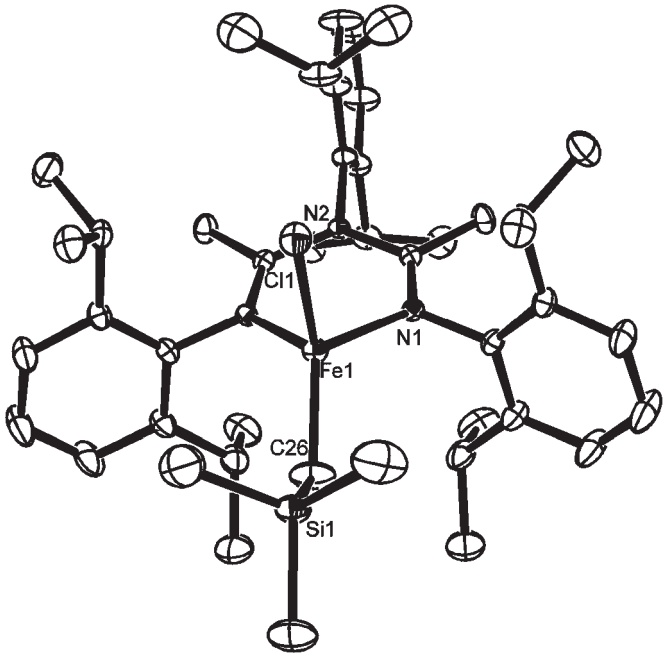


Fig. 4. ORTEP of **8** (30% thermal ellipsoids are shown). Hydrogen atoms are omitted for clarity. Bond lengths (Å): Fe(1)—C(26) 2.038(6), Fe(1)—N(1) 2.114(3), Fe(1)—Cl(1) 2.2762(15), N(1)—C(1) 1.281(4), N(1)—C(3) 1.454(4). Bond angles (°): C(26)-Fe(1)-N(1) 117.67(13), N(1)-Fe(1)-N(1) 82.99(13), C(26)-Fe(1)-Cl(1) 124.89(18), N(1)-Fe(1)-Cl(1) 102.50(7), C(1)-N(1)-Fe(1) 127.9(2).

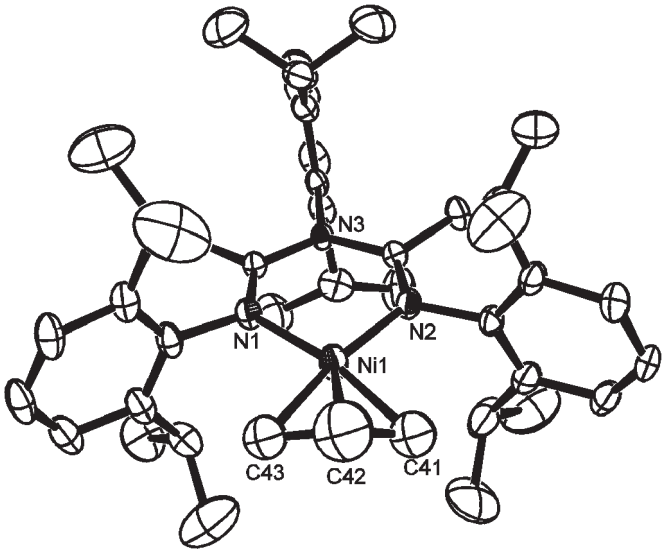


firmed the formulation, with the molecule residing on a crystallographically imposed mirror plane that bisects the ligand and passes through the pseudo-tetrahedral Fe center and the plane containing Cl and the (CH_2SiMe_3) fragment (Fig. 4). The incorporation of an electron-donating alkyl group results in the expected lengthening of the Fe—N bond length to 2.114(3) Å. Similarly the Fe—Cl distance of 2.2762(15) Å in **8** is longer than that found in **2**. The longer Fe—N distance also results in a slightly smaller ligand bite angle of 82.99(13)°. Attempts to further alkylate Fe were unsuccessful, presumably a reflection of the steric crowding about the Fe center of **8**. In addition, attempts to alkylate with MeLi or *t*-BuLi were also unsuccessful leading to apparent compound degradation.

Reactions of **1** with $[(\eta^3\text{-}C_3H_5)NiBr]_2$ and [Na][B(3,5-$(CF_3)_2C_6H_3)_4$] afforded the salt [(*i*-$Pr_2C_6H_3N$)(C(Me)-$(NC_6H_3\text{-}i\text{-}Pr_2)$)$_2$Ni($\eta^3$-$C_3H_5$)][B(3,5-$(CF_3)_2C_6H_3)_4$] (**9**) in 33% isolated yield. The ^{1}H NMR spectrum of **9** is consistent with this formulation and indicative of a η^3-bonding mode of the allyl fragment. Variable-temperature studies (–90 to 35 °C) show no change in the allyl signals, reflecting the absence of dynamic behavior. Attempts to react **9** with CO, ethylene, or $PhPH_2$ failed to show any reaction, even under forcing conditions (refluxing toluene), again reflecting the maintenance of the η^3-bonding mode of the allyl fragment. X-ray data also confirmed this binding mode (Fig. 5). The Ni—N distances in **9** were found to be 1.915(6) and 1.916(6) Å. These distances, which are shorter than those found in **4**, are con-

© 2005 NRC Canada

Fig. 5. ORTEP for the cation of **9** (30% thermal ellipsoids are shown). Hydrogen atoms are omitted for clarity. Bond lengths (Å): Ni(1)—N(1) 1.915(6), Ni(1)—N(2) 1.916(6), Ni(1)—C(42) 1.96(2), Ni(1)—C(41) 2.019(14), Ni(1)—C(43) 2.049(11), N(1)—C(3) 1.306(8), N(2)—C(1) 1.290(8). Bond angles (°): N(1)-Ni(1)-N(2) 92.1(2), N(1)-Ni(1)-C(42) 134.4(7), N(2)-Ni(1)-C(42) 131.9(7), N(1)-Ni(1)-C(41) 168.9(4), N(2)-Ni(1)-C(41) 98.1(4), C(42)-Ni(1)-C(41) 37.1(7), N(1)-Ni(1)-C(43) 97.6(4), N(2)-Ni(1)-C(43) 170.2(4), C(42)-Ni(1)-C(43) 38.5(7), C(41)-Ni(1)-C(43) 72.2(5), C(3)-N(1)-Ni(1) 127.7(4), C(41)-C(42)-C(43) 135(2).



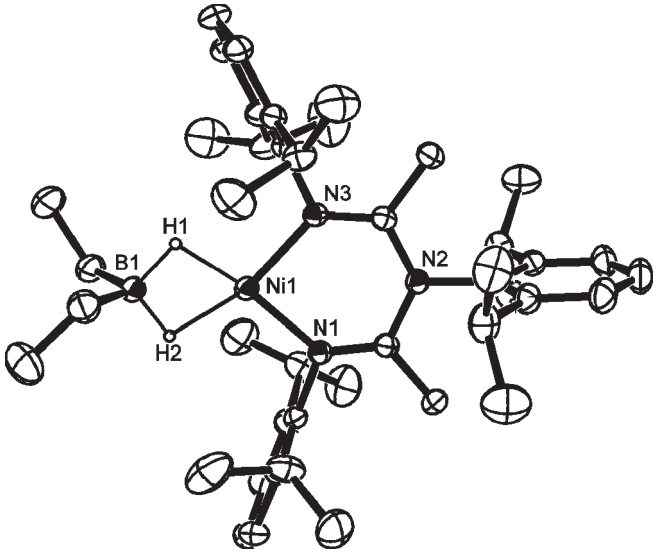
sistent with the presence of the formal positive charge. The Ni–allyl interaction results in Ni—C bond lengths of 1.96(2), 2.019(14), and 2.049(11) Å, typical of the η^3-bonding mode (39, 40).

Finally, reactions of **4** with Super-Hydride afforded brown-red crystals of the species formulated as $(i\text{-Pr}_2C_6H_3N)(C(Me)(NC_6H_3\text{-}i\text{-Pr}_2))_2NiH_2BEt_2$ (**10**) in 45% yield (Scheme 2). The magnetic susceptibility of **10** was determined to be 2.87 μ_B. X-ray data confirmed the above formulation of **10** as a formally Ni(I) species and revealed the pseudo-tetrahedral geometry about Ni in which two hydride atoms bridge the Ni and B centers (Fig. 6). The Ni—N distances average 1.947(2) Å, while the Ni—B separation is 2.165(4) Å. Location and refinement of the hydride atoms revealed an avg. Ni—H distance of 1.70(1) Å and B—H distances of 1.20(1) Å. Attempts to remove borane from **10** via reaction with BuLi were unsuccessful. Similarly, **10** proved to be unreactive with primary phosphine or phenol.

Summary

This manuscript describes the synthesis and structure of a series of transition metal complexes of the bulky *N*-aryl-imidoyl amidine ligand $(i\text{-Pr}_2C_6H_3N)(C(Me)(NC_6H_3\text{-}i\text{-Pr}_2))_2$. While a variety of complexes are readily accessible, the resulting complexes are generally robust and unreactive, principally a result of the sterically demanding nature of the ligand. As a result, we are continuing efforts to utilize this ligand to stabilize and isolate reactive transition metal fragments.

Fig. 6. ORTEP of **10** (30% thermal ellipsoids are shown). All hydrogen atoms except the bridging hydrogen atoms are omitted for clarity. Bond lengths (Å): Ni(1)—N(1) 1.946(2), Ni(1)—N(3) 1.949(2), Ni(1)—B(1) 2.165(4), B(1)—C(41) 1.600(6), B(1)—C(43) 1.616(6), N(1)—C(5) 1.456(4), N(3)—C(3) 1.305(4), N(3)—C(29) 1.447(4). Bond angles (°): N(1)-Ni(1)-N(3) 89.48(10), N(1)-Ni(1)-B(1) 138.37(13), N(3)-Ni(1)-B(1) 132.15(13), C(41)-B(1)-C(43) 114.6(3), C(41)-B(1)-Ni(1) 119.8(3), C(43)-B(1)-Ni(1) 125.5(3), C(1)-N(1)-Ni(1) 130.1(2).



Acknowledgments

Financial support from the Natural Sciences and Engineering Research Council of Canada (NSERC) and the Ontario Research and Development Challenge Fund (ORDCF) is gratefully acknowledged. JDM is grateful for the award of an Ontario Graduate Scholarship (OGS).

References

1. G.J.P. Britovsek, V.C. Gibson, and D.F. Wass. Angew. Chem. Int. Ed. **38**, 428 (1999).
2. S.D. Ittel, L.K. Johnson, and M. Brookhart. Chem. Rev. **100**, 1169 (2000).
3. C. Cui, H.W. Roesky, H.-G. Schmidt, M. Noltemeyer, H. Hao, and F. Cimpoesu. Angew. Chem. Int. Ed. **39**, 4274 (2000).
4. N.J. Hardman, R.J. Wright, A.D. Phillips, and P.P. Power. J. Am. Chem. Soc. **125**, 2667 (2003).
5. F. Basuli, B.C. Bailey, J.C. Huffman, and D.J. Mindiola. Chem. Commun. 1554 (2003).
6. K.T.K. Chan, L.P. Spencer, J.D. Masuda, J.S.J. McCahill, P. Wei, and D.W. Stephan. Organometallics, **23**, 381 (2004).
7. J.D. Masuda, P. Wei, and D.W. Stephan. Dalton Trans. 3500 (2003).
8. L.P. Spencer, R. Altwer, P. Wei, L. Gelmini, J. Gauld, and D.W. Stephan. Organometallics, **22**, 3841 (2003).
9. J.D. Masuda, D.M. Walsh, P. Wei, and D.W. Stephan. Organometallics, **23**, 1819 (2004).
10. G.C. Welch, W.E. Piers, M. Parvez, and R. McDonald. Organometallics, **23**, 1811 (2004).
11. H.C. Brown and P.D. Schuman. J. Org. Chem. **28**, 1122 (1963).
12. M. Green, S.H. Taylor, J.J. Daly, and F. Sanz. J. Chem. Soc. Chem. Commun. 361 (1974).

© 2005 NRC Canada

13. M. Bottrill, R. Goddard, M. Green, R.P. Hughes, M.K. Lloyd, S.H. Taylor, and P. Woodward. J. Chem. Soc. Dalton Trans. 1150 (1975).
14. V. Robinson, G.E. Taylor, P. Woodward, M.I. Bruce, and R.C. Wallis. J. Chem. Soc. Dalton Trans. 1169 (1981).
15. M.B. Hursthouse, M.A. Mazid, S.D. Robinson, and A. Sahajpal. J. Chem. Soc. Dalton Trans. 3615 (1994).
16. J. Barker, M. Kilner, M.M. Mahmoud, and S.C. Wallwork. J. Chem. Soc. Dalton Trans. 837 (1989).
17. D.R. Aris, J. Barker, P.R. Phillips, N.W. Alcock, and M.G.H. Wallbridge. J. Chem. Soc. Dalton Trans. 909 (1997).
18. S.V. Kryatov, M.B. Smith, E.V. Rybak-Akimova, and A.Y. Nazarenko. Chem. Commun. 1174 (2001).
19. M.N. Kopylovich, A.J.L. Pombeiro, A. Fischer, L. Kloo, and V.Y. Kukushkin. Inorg. Chem. **42**, 7239 (2003).
20. J.F. Berry, F.A. Cotton, L.M. Daniels, C.A. Murillo, and X. Wang. Inorg. Chem. **42**, 2418 (2003).
21. J.F. Berry, F.A. Cotton, P. Lei, T. Lu, and C.A. Murillo. Inorg. Chem. **42**, 3534 (2003).
22. J.F. Berry, F.A. Cotton, P. Lei, and C.A. Murillo. Inorg. Chem. **42**, 377 (2003).
23. J.F. Berry, F.A. Cotton, T. Lu, and C.A. Murillo. Inorg. Chem. **42**, 4425 (2003).
24. J.F. Berry, F.A. Cotton, T. Lu, C.A. Murillo, and X. Wang. Inorg. Chem. **42**, 3595 (2003).
25. M. Burgos, O. Crespo, M.C. Gimeno, P.G. Jones, and A. Laguna. Eur. J. Inorg. Chem. 2170 (2003).
26. Y. Kang, C. Seward, D. Song, and S. Wang. Inorg. Chem. **42**, 2789 (2003).
27. Q.-D. Liu, W.-L. Jia, G. Wu, and S. Wang. Organometallics, **22**, 3781 (2003).
28. T.-B. Tsao, G.-H. Lee, C.-Y. Yeh, and S.-M. Peng. Dalton Trans. 1465 (2003).
29. C. Tu, J. Lin, Y. Shao, and Z. Guo. Inorg. Chem. **42**, 5795 (2003).
30. T. Yajima, G. Maccarrone, M. Takani, A. Contino, G. Arena, R. Takamido, M. Hanaki, Y. Funahashi, A. Odani, and O. Yamauchi. Chem. Eur. J. **9**, 3341 (2003).
31. F.A. Cotton, L.M. Daniels, J.H. Matonic, X. Wang, and C.A. Murillo. Polyhedron, **16**, 1177 (1997).
32. A.A. Danopoulos, G. Wilkinson, T.K.N. Sweet, and M.B. Hursthouse. J. Chem. Soc. Dalton Trans. 3771 (1996).
33. R. Uson, J. Fornies, P. Espinet, and E. Lalinde. J. Organomet. Chem. **334**, 399 (1987).
34. D.N. Coventry, A.S. Batsanov, A.E. Goeta, J.A.K. Howard, and T.B. Marder. Polyhedron, **23**, 2789 (2004).
35. D.L. Reger, T.D. Wright, C.A. Little, J.J.S. Lamba, and M.D. Smith. Inorg. Chem. **40**, 3810 (2001).
36. SAINT, XPREP, and SHELXTL [computer programs]. Bruker AXS Inc., Madison, Wis. 2004.
37. J. Feldman, S.J. McLain, A. Parthasarathy, W.J. Marshall, J.C. Calabrese, and S.D. Arthur. Organometallics, **16**, 1514 (1997).
38. L.K. Johnson, C.M. Killian, and M. Brookhart. J. Am. Chem. Soc. **117**, 6414 (1995).
39. K. Landolsi, M. Rzaigui, and F. Bouachir. Tetrahedron Lett. **43**, 9463 (2002).
40. A. Mechria, C. Bavoux, and F. Bouachir. J. Organomet. Chem. **677**, 53 (2003).

© 2005 NRC Canada

Theoretical study of the reaction of titanium ion with ethane — Structure, mechanism, and potential energy surface

Dongju Zhang, Xuebing Fu, Ruoxi Wang, and Chengbu Liu

Abstract: Density functional theory in its B3LYP variant has been used to study the reaction of Ti^+ (^4F) with ethane in the gas phase. The potential energy surface corresponding to [Ti, C_2, H_6]$^+$, has been examined in detail at the B3LYP/6-311++G(3df,3pd)//B3LYP/6-311+G(d,p) level of theory. The quality of this theoretical method has been calibrated against the available thermochemical data. Three activation branches, C—H, C—C, and synchronous C—H and C—C bond activations, were proposed along the reaction coordinates, and two new mechanisms, the sequential 1,1-H_2 elimination and the concerted elimination of CH_4, were found.

Key words: Ti^+, ethane, reaction mechanism, potential energy surface, density functional theory.

Résumé : Une variante B3LYP de la théorie de la densité fonctionnelle a été utilizée pour étudier la réaction du Ti^+ (^4F) avec l'éthane en phase gazeuse. Opérant au niveau B3LYP/6-311++G(3df,3pd)//B3LYP/6-311+G(d,p) de la théorie, on a examiné en détail la surface d'énergie potentielle qui correspond à [Ti, C_2, H_6]$^+$. La qualité de cette méthode théorique a été calibrée en fonction de données thermodynamiques disponibles. On propose trois branches d'activation, C—H, C—C et des activations synchrones de liaison C—H et C—C ainsi que des coordonnées réactionnelles et on propose deux nouveaux mécanismes, l'élimination séquentielle 1,1 de H_2 et une élimination concertée de CH_4.

Mots clés : Ti^+, éthane, mécanisme réactionnel, surface d'énergie potentielle, théorie de la densité fonctionnelle.

[Traduit par la Rédaction]

Introduction

C—H and C—C bond activations of hydrocarbons at metal centers are of fundamental importance in various areas of chemical research, such as biochemistry, organometallic chemistry, and homo- and heterogeneous catalysis (1, 2). Extensive experimental studies of the reactions of first-row transition-metal ions with simple alkanes in the gas phase have been made by various techniques (1–13) since Allison et al. (14) observed in 1979 that atomic transition metal ions can activate C—C and C—H bonds in alkanes. In these reactions, the oxidative additions of C—H and C—C bonds to the metal center are two fundamental steps, from which a series of products results, such as small neutral molecules (H_2, CH_4, C_2H_4, etc.) and fragmentation ions. The general mechanisms in these reactions are shown in Scheme 1, where metal ion M^+ first inserts into a C—H or C—C bond, forming intermediate **A** or **B**. The species **A** can further rearrange into **C**, a precursor for the elimination of H_2 via a β-H shift.

As to the reactions of Ti^+ with small alkanes, detailed experimental studies have been reported by several groups during the last 20 years (7–13). On the theoretical side, several outstanding works have also been conducted in the recent years by using ab initio and density function calculations (15–19), and the relevant results have provided some important information on the potential energy surfaces (PESs). The most detailed computational results for the reaction of Ti^+ with methane have been reported by Sililia and Russo (18). However, for the reaction of Ti^+ with ethane, the detailed examination of the PES is scarce, although great effort has been devoted to its experimental research. This work aims at this gap and presents a detailed theoretical study of this reaction, including the geometries and energies of various intermediates, transition states and products, reaction mechanisms, and interesting PES properties of the [Ti, C_2, H_6]$^+$ system.

It is known that the theoretical research for the systems involving transition metals is difficult to accurately deal with in ab initio molecular orbital theory, since there are many near-degenerate electronic states in these systems. As an alternative, density functional theory (DFT) (20, 21) has recently attracted considerable attention, which has recently been widely applied to electronic structure calculations for systems that contain transition metals. The electron correlation effect in these systems is expected to play an important role in determining the geometries, energetics, and electronic configurations. The DFT method has been shown to be particularly useful and computationally efficient for systems with a relatively large number of electrons that are difficult to deal with in ab initio molecular orbital theory (22). Furthermore, the spin contamination in the Kohn–Sham single determinant reference function proved to be relatively

Received 3 January 2005. Published on the NRC Research Press Web site at http://canjchem.nrc.ca on 14 May 2005.

D.J. Zhang,[1] X.B. Fu, R.X. Wang, and C.B. Liu. College of Chemistry and Chemical Engineering, Shandong University, Jinan, Shandong 250100, P.R. China.

[1]Corresponding author: (e-mail: zhangdj@sdu.edu.cn).

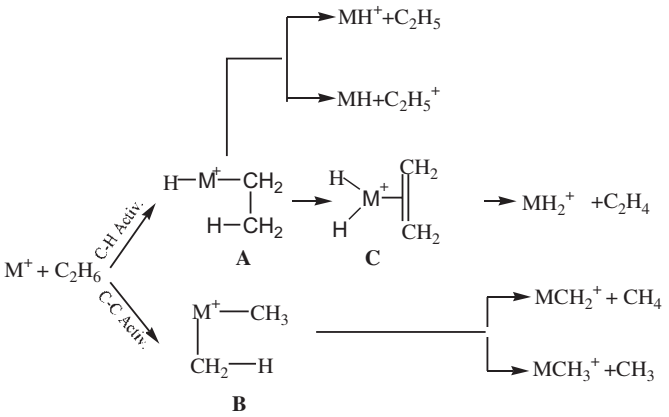
 doi: 10.1139/V05-076 © 2005 NRC Canada

Table 1. Calculated and experimental bond dissociation energies (in kcal mol^{-1}).[a]

Bond[b]	D_0[c]		Expt.[d]	Bond	D_0[c]		Expt.[e]
$^3Ti^+$-CH_3	59.7	60.1	57.5±2.8	H-H	102	104	104
$^2Ti^+$=CH_2	91.8	95.3	93.4±3.5	CH_3-H	101	101	105
$^3Ti^+$-H	47.4	47.6	54.2±2.5	C_2H_5-H	97	97	100
$^4Ti^+$-C_2H_4	34.6	35.1	34.8±2.5[f]	CH_3-CH_3	82	82	90
			≥31.8[g]				
$^3Ti^+$-C_2H_5	56.4	57.2	52.6±1.6[g]	CH_2=CH_2	168	169	174
CH_3-$^2Ti^+$-CH_3	50.5	51.0	64.6±6.0[g]				
$^4Ti^+$-C_2H_6	24.8	25.5					

[a]ZPEs have been included in the calculated BDE.
[b]The superscripts denote the spin multiplicities.
[c]The first number corresponds to the results from the B3LYP/6-311+G(d,p) level and the second number corresponds to the results from the B3LYP/6-311++G(3df,3pd) level.
[d]Reference 7.
[e]Reference 31.
[f]Reference 32.
[g]Reference 12.

Scheme 1. General mechanism for the reactions of transition metal ions with C_2H_6.



minimal. In view of the computational effectiveness and reliability of DFT, it is desirable to utilize it throughout this work.

Computational details

Density functional calculations were performed at the B3LYP/6-311+G(d,p) level (23, 24) as implemented in the GAUSSIAN 98 program (25). The stationary points on the PES of [Ti, C_2, H_6]$^+$ have been characterized as minima or first-order saddle points by evaluating their vibrational frequencies and normal modes. Intrinsic reaction coordinate (IRC) (26) calculations were performed in both directions from each transition state to further verify whether the located transition states connect the expected minima. To analyze the sensitivity of the stationary points to basis sets, the relative energies were also reevaluated using the large 6-311++G(3df,3pd) basis set based on the B3LYP/6-311+G(d,p) geometries. The stability of the wave function for symmetry breaking has been checked for each identified stationary point. The zero-point vibrational energies have been included in the reported energies.

Calibration of theoretical calculations

The B3LYP functional has shown a very promising performance for ion–ligand complexes (27–29), predicting properties such as bond dissociation energies, geometries, harmonic frequencies, and electronic details with accuracy comparable to those obtained from highly correlated wave functions based on ab initio methods. To clarify the general reliability expected from the present calculations, we compared the predicted chemical properties of several species involved in the title reaction with corresponding experimental data.

Atomic asymptote of titanium ion

We first tested the ability of the level of theory to describe low-lying states of Ti^+. Experimentally, the ground state of Ti^+ is $^4F(3d^24s^1)$, with the excited atomic state $^2F(3d^24s)$ lying just 13.2 kcal mol^{-1} higher in energy (30). In the present calculations, both the B3LYP/6-311+G(d,p) and B3LYP/6-311++G(3df,3pd)//B3LYP/6-311+G(d,p) methods predict the correct order of these two electronic states. The calculated separation values between ^4F and ^2F at the two levels of theory are almost the same, approximately 13 kcal mol^{-1}, and in good agreement with the experimental observation.

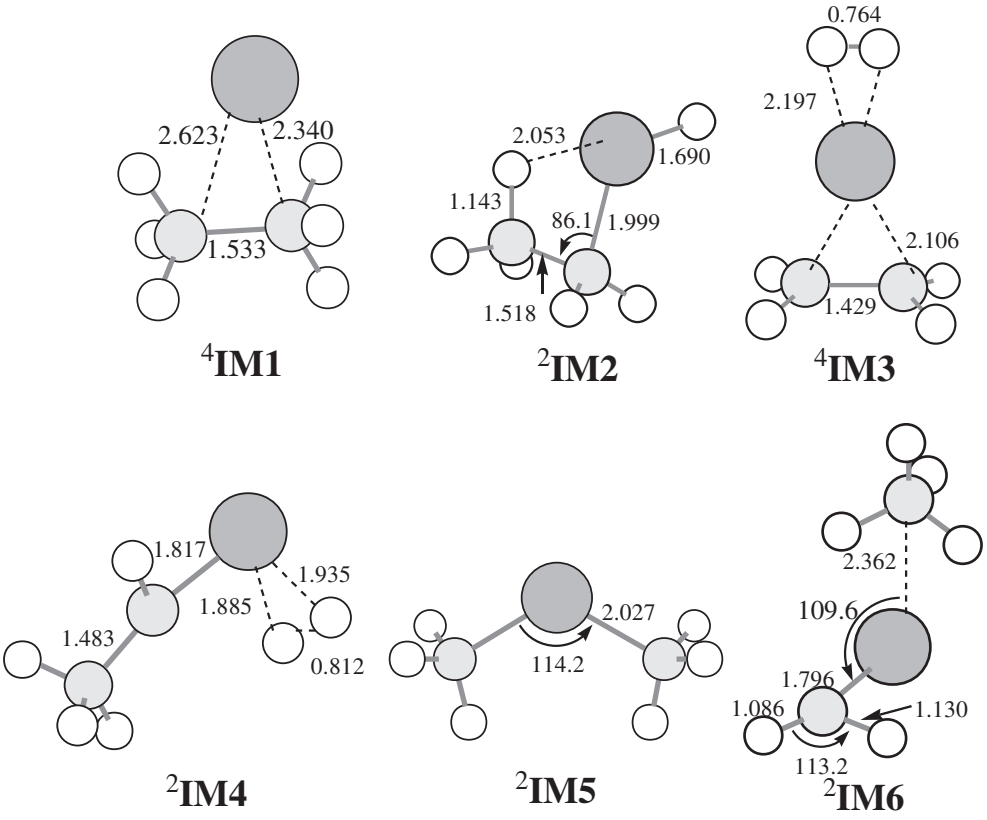
Bond dissociation energies

Table 1 compares theoretical bond dissociation energies (BDE) of several species involved in the title reaction to experimental values. To allow for a more direct comparison to the experimental values, the theoretical BDEs have been corrected to 0 K by including zero-point vibrational energy, noted as D_0. It is noted that the values obtained with the large basis set don't seem to improve the BDEs obviously, indicating that the 6-311+G(d,p) basis set is flexible enough to describe the electronic characters of the species involved in the reaction of Ti^+ with C_2H_6.

From Table 1, we found that the calculated D_0 values for the concerned species are in fairly good agreement with experimental observations. The errors introduced by the calculations are slightly more severe for the Ti^+-R species (R denotes an organic fragment) than for the simple hydrocarbon species. However, our main goals in the present work

© 2005 NRC Canada

Fig. 1. Optimized geometries (in Å and °) for the energetically most favorable intermediates on both the doublet and quartet surfaces of [Ti, C_2, H_6]$^+$ at the B3LYP/6-311+G(d,p) level. The superscripts denote the spin multiplicities.



are the examination of the detailed mechanism and the relative energies of the species involved, not the calculation of accurate bond energies. Thus, we consider that the discrepancies between the calculated results and measured values are acceptable. In addition, the reliability expected from the present theoretical level can be also estimated by comparing the expectation values of $\langle S^2 \rangle$ with the exact values of $\langle S^2 \rangle$ (0.75 for doublets, and 3.75 for quartets). We found that the spin contamination was small for all species involved.

To further clarify the general reliability of the chosen level of theory for the reactions of Ti^+ with an alkane, we first studied its reaction with methane. Table 2 compares the computed geometries and energies for the three structures involved in this reaction with early theoretical predications (18). Clearly, the present results are basically identical to the work previously published by Sicilia and Russo (18) in all essential details. This also makes us confident in using the chosen level of theory for describing the $Ti^+ + C_2H_6$ system.

The above results lead us to conclude that the level of theory used in this work is capable of describing the basic electronic characteristics of the species of interest.

Results and discussion

In terms of the mechanism proposed in Scheme 1, we designed various intermediates and transition states on the PES of [Ti, C_2, H_6]$^+$. After a careful search along both the doublet and quartet surfaces, we found two different reaction channels from those proposed in Scheme 1: one is 1,1-H_2 elimination and the other is the concerted activation of C—C and C—H bonds, which are in contrast to the general 1,2-H_2 elimination and the individual C—C and C—H bond activations, respectively.

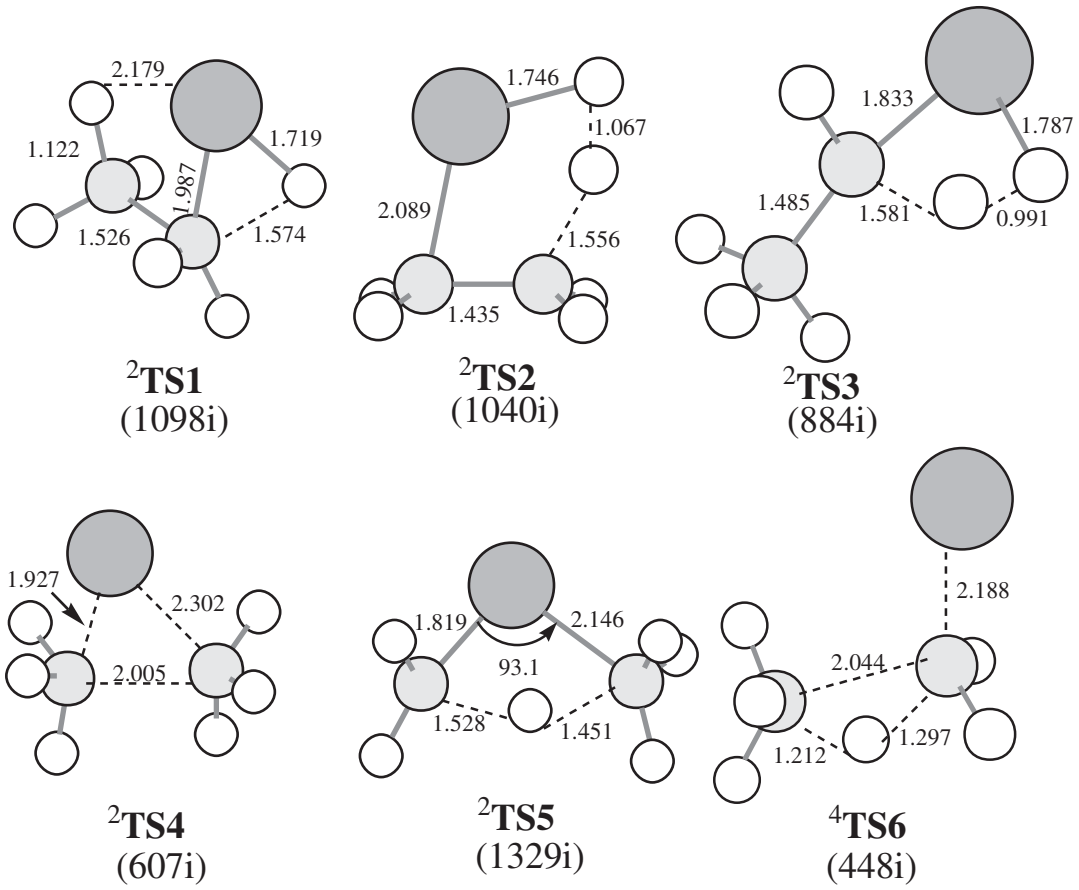
Table 2. Present and early geometries and relative energies for several species involved in the reaction of Ti^+ with CH_4.

Species	Reference 18	This work
Ti^+-CH_4	$R_{Ti\text{-}C}$ = 2.354	$R_{Ti\text{-}C}$ = 2.347
	E_{rel} = –22.21	E_{rel} = –22.0
	$R_{Ti\text{-}C}$ = 1.995	$R_{Ti\text{-}C}$ = 1.994
H-Ti^+-CH_3	$R_{Ti\text{-}H}$ = 1.676	$R_{Ti\text{-}H}$ = 1.680
	E_{rel} = –7.09	E_{rel} = –7.7
	$R_{Ti\text{-}C}$ = 1.951	$R_{Ti\text{-}C}$ = 1.942
Ti / H---CH_3	$R_{C\text{-}H}$ = 1.602	$R_{C\text{-}H}$ = 1.599
	E_{rel} = 4.39	E_{rel} = 5.1

In the present calculations, six intermediates (noted as **IM1**–**IM6**, respectively) and six first-order saddle points (noted as **TS1**–**TS6**, respectively) on each of the doublet and quartet PESs of [Ti, C_2, H_6]$^+$ have been located. We found that most of the intermediates and transition states on the doublet and quartet surfaces are geometrically very similar. Only their energetically most favorable geometries are shown in Figs. 1 and 2 for simplification, where the superscript on each species denotes the spin multiplicity. Table 3 summarizes the calculated total energies and relative ener-

© 2005 NRC Canada

Fig. 2. Optimized geometries (in Å and °) for the energetically most favorable first-order saddle points on both the doublet and quartet surfaces of [Ti, C_2, H_6]$^+$ at the B3LYP/6-311+G(d,p) level. The superscripts denote the spin multiplicities and the values in parentheses are the imaginary frequencies corresponding to the transition vectors.



gies for all species involved, including reactants, intermediates, transition states, and products at all spin states considered, at both the B3LYP/6-311+G(d,p) and B3LYP/6-311++G(3df,3pd)//B3LYP/6-311+G(d,p) levels. In the following discussion, the relative energy always involves those obtained at the latter, more accurate level.

Intermediate **IM1** is an encounter complex formed when Ti^+ (^4F) and C_2H_6 approach each other. Its ground state was located on the quartet PES and was found to more stable in energy by 26.9 kcal mol^{-1} than the isolated reactants. The corresponding doublet state is less stable by 12.3 kcal mol^{-1}. Our calculations indicate that the two Ti—C distances in ^{4}**IM1** are 2.340 and 2.623 Å, respectively, corresponding to a purely electrostatic interaction between two reactants, as is expected for a closed-shell ligand. This encounter complex is a common initial adduct to three subsequent activation branches: C—C bond activation, C—H bond activation, and synchronous C—C and C—H bond activations. In the following text, we will describe these reaction mechanisms in detail.

C—H bond activation branch

We first pay attention to the C—H bond activation branch on the PES of [Ti, C_2, H_6]$^+$. This branch starts from the initial ion–molecule complex (**IM1**). Along the reaction coordinate, it can be converted into a C—H bond inserted species **IM2**, via a C—H bond cleavage transition state (**TS1**). This C—H bond inserted species has a doublet ground state and its energy was calculated to be more stable by 17.7 kcal mol^{-1} than the reactants. This result is in good agreement with the experimental finding that the formation of this intermediate was estimated to be 18.45 ± 6.92 kcal mol^{-1} exothermic (12). Its quartet state counterpart, ^{4}**IM2** was calculated to be 27.9 kcal mol^{-1} less stable than the corresponding ground state. It should be noted that an intersystem crossing from the quartet surface over onto the doublet surface must occur to react along the ground-state surface, as the ground state of **IM1** is quartet state, while that of **IM2** is doublet. The ground state of **TS1** was also located on the doublet surface. It has C_1 symmetry and its energy was calculated to be 12.9 kcal mol^{-1} above ^{2}**IM1** with an imaginary frequency of 1098i. IRC calculations confirm that this TS is a correct, first-order saddle point for the C—H bond insertion reaction. As shown in Fig. 2, the breaking C—H bond in ^{2}**TS1** is elongated to 1.574 Å. We also attempted to optimize the quartet saddle points of the C—H bond activation, however, the initially guessed structures always collapsed into ^{4}**IM2**, indicating that the PES in this area is very flat. This may be attributed to the deficiency of the DFT method used for describing the transition states in very flat regions of PESs. To obtain more information on the quartet region, we also optimized this TS structure at the

© 2005 NRC Canada

Table 3. Electronic total energies E (hartree) and ZPE-corrected relative energies ΔE (kcal mol^{-1}) of the species involved in the reaction $Ti^+(^4F)+C_2H_6$ at the different levels.

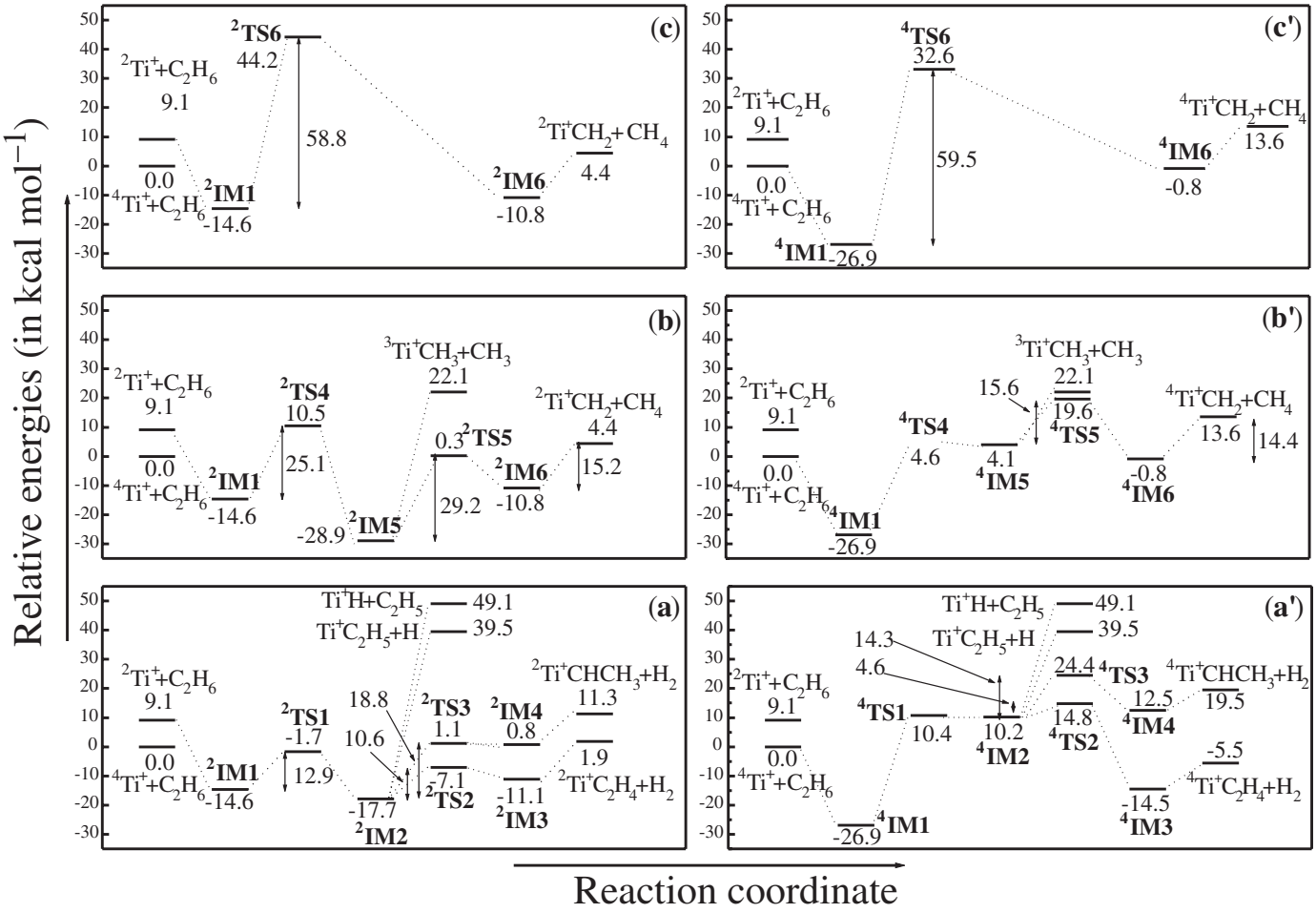
	B3LYP/6-311+G(d,p)		B3LYP/6-311++G(3df,3pd)//B3LYP/6-311+G(d,p)		
Species	E	ΔE	E	ΔE	ZPE
$Ti^+(^4F)+C_2H_6$	–928.958 044	0.00	–928.964 970	0.00	46.62
$Ti^+(^2F)+C_2H_6$	–928.943 534	9.11	–928.950 418	9.13	46.62
^{2}**IM1**	–928.979 969	–13.47	–928.988 654	–14.57	46.91
^{4}**IM1**	–928.998 238	–24.82	–929.008 426	–26.90	46.99
^{2}**IM2**	–928.978 496	–16.98	–928.986 627	–17.74	42.47
^{4}**IM2**	–928.932 254	10.97	–928.940 430	10.19	41.41
^{2}**IM3**	–928.964 772	–10.08	–928.973 329	–11.11	40.76
^{4}**IM3**	–928.970 333	–13.04	–928.979 531	–14.47	41.29
^{2}**IM4**	–928.948 115	1.17	–928.955 664	0.78	41.56
^{4}**IM4**	–928.927 236	12.92	–928.934 812	12.51	40.21
^{2}**IM5**	–928.995 099	–27.98	–929.003 551	–28.94	41.89
^{4}**IM5**	–928.940 489	5.34	–928.949 448	4.06	40.94
^{2}**IM6**	–928.967 160	–9.79	–928.975 697	–10.80	42.55
^{4}**IM6**	–928.951 196	0.12	–928.959 633	–0.83	42.44
^{2}**TS1**	–928.953 209	–0.98	–928.961 281	–1.70	42.61
^{2}**TS2**	–928.959 325	–6.09	–928.967 861	–7.10	41.33
^{4}**TS2**	–928.922 596	16.03	–928.931 454	14.82	40.41
^{2}**TS3**	–928.945 636	1.61	–928.953 362	1.10	40.44
^{4}**TS3**	–928.907 354	24.95	–928.915 087	24.44	39.76
^{2}**TS4**	–928.934 805	11.31	–928.942 981	10.53	43.35
^{2}**TS5**	–928.946 457	1.34	–928.955 112	0.26	40.69
^{4}**TS5**	–928.914 086	20.57	–928.922 503	19.64	39.61
^{2}**TS6**	–928.881 948	44.61	–928.889 529	44.20	43.48
^{4}**TS6**	–928.900 791	32.82	–928.908 093	32.58	43.51
$^2Ti^+C_2H_4+H_2$	–928.937 439	4.47	–928.948 505	1.87	38.16
$^4Ti^+C_2H_4+H_2$	–928.952 926	–4.50	–928.961 499	–5.53	38.91
$^2Ti^+CHCH_3+H_2$	–928.925 279	11.52	–928.932 532	11.30	37.58
$^4Ti^+CHCH_3+H_2$	–928.909 414	21.39	–928.919 410	19.46	37.49
$^2Ti^+CH_2+CH_4$	–928.936 277	7.66	–928.948 338	4.44	40.62
$^4Ti^+CH_2+CH_4$	–928.924 345	15.84	–928.934 848	13.59	41.31
$^3Ti^+CH_3+CH_3$	–928.910 176	20.61	–928.917 920	22.09	39.19
$^3Ti^+H+C_2H_5$	–928.868 152	49.32	–928.875 479	49.07	39.53
$^3Ti^+C_2H_5+H$	–928.882 515	40.24	–928.890 635	39.49	39.46

MP2/6-311+G(d,p) level, and indeed found a first-order saddle with a single imaginary frequency of 633i. A single-point energy calculation for this TS at the B3LYP/6-311+G(d,p)//MP2/6-311+G(d,p) level reveals its energy is only 0.2 kcal mol^{-1} above ^{4}**IM2**, confirming the very flat potential energy surface at this region. However, the TS optimization using the B3LYP/6-311+G(d,p) method starting from the MP2 saddle point leads to a continuous decrease of the imaginary frequency and converge to the quartet state of ^{4}**IM2**.

Once **IM2** is formed, it can undergo various possible production channels by decomposition or isomerization. We found that four channels are available from this intermediate along both the doublet and quartet surfaces, as shown in panels **a** and **a′** of Fig. 3, respectively. The energetically most favorable reaction path involves a β-H migration to form a product-like intermediate (**IM3**) via saddle point **TS2**. It is should be noted that **IM3** is a complex between cationic titanium-ethylene and molecular hydrogen. The ground state of this intermediate was located on its quartet surface, where H—H bond length (0.764 Å) has resembled that of free H_2 (0.742 Å). The complex differs from the generally proposed dihydrido minimum, where the metal ion has already inserted into H_2 molecule, as shown in Scheme 1. We also tried to find such a dihydrido minimum on both the doublet and quartet PESs, however, the input structures all collapsed into **IM2** or **IM3** after optimization. This behavior has also been observed in previous studies by Holthausen and co-workers (33, 34) for reactions of Fe^+ and Co^+ with ethane. IRC calculations have confirmed that the two minima (**IM2** and **IM3**) are connected by **TS2**. This TS involves a five-membered ring structure, as shown in Fig. 2. In its doublet structure (^{2}**TS2**) the breaking C—H bond is elongated to 1.556 Å and the forming H—H distance is 1.067 Å. The direct dissociation of **IM3** leads to products H_2 + $Ti(C_2H_4)^+$. This reaction channel is referred as the 1,2-H_2 elimination pathway, endothermal by 1.9 kcal mol^{-1} on the doublet surface and exothermic by 5.5 kcal mol^{-1} on the quartet surface relative to the reactants, respectively. It is the energetically most favorable reaction channel. This result is

© 2005 NRC Canada

Fig. 3. Potential energy surfaces for the reaction of Ti^+ with C_2H_6 along the reaction coordinate calculated at the B3LYP/6-311++G(3df,3dp)//B3LYP/6-311+G(d,p) level of theory for: (**a**) C—H bond activation branches on the doublet surface; (**b**) C—C bond activation branch on the doublet surface; (**c**) C—H and C—C bond concerted activation branch on the doublet surface; and (**a′**), (**b′**), (**c′**) the corresponding values on the quartet surface.



in good agreement with earlier experimental findings: i.e., only the H_2 elimination products were observed at low energies (10–13).

The second pathway from **IM2** takes some similarity to the first one mentioned previously, only the β-H migration is replaced by a α-H migration. This process involves a four-membered ring TS (**TS3**). On the doublet surface, the barrier was calculated to be 18.8 kcal mol^{-1}, higher by 8.2 kcal mol^{-1} than that of the β-H migration. The forward product of **TS3** is the intermediate **IM4**, a complex of ethylidene titanium cation with molecule hydrogen, whose dissociation also leads to the loss of H_2. This H_2 loss channel is referred to as 1,1-H_2 elimination as contrasted with the 1,2-H_2 elimination mentioned previously, which is endothermic by 11.3 kcal mol^{-1} on the doublet surface and by 19.5 kcal mol^{-1} on the quartet surface. Although this 1,1-H_2 elimination channel is energetically less favorable compared to the 1,2-H_2 elimination channel, it could be an alternative path for H_2 loss from the reaction of Ti^+ with C_2H_6 at high energy. The other two channels from **IM2** are its direct fragmentation processes by rupturing the Ti—H bond to form $TiC_2H_5^+$ + H, endothermic by 39.5 kcal mol^{-1}, or by rupturing the Ti—C bond to form TiH^+ + C_2H_5, endothermic by 49.1 kcal mol^{-1}, which is consistent with the corresponding experimentally determined threshold for this reaction (50.4 kcal mol^{-1}) (12).

C—C bond activation branch

Along the C—C bond activation branch (panels **b** and **b′** of Fig. 3), the next minimum after the initial complex **IM1** is intermediate **IM5**, a dimethyl species, in which Ti^+ has been inserted into the C—C bond. This inserted species has C_s symmetry, and as expected, its ground state is a doublet state with an energy of 28.9 kcal mol^{-1} lower than the separated reactants. The counterpart of this intermediate on the quartet surface (^{4}**IM5**) is 33.0 kcal mol^{-1} less stable. Our calculations fairly reproduce the experimental finding that this intermediate lies 28.6 ± 6.0 kcal mol^{-1} lower in energy than the Ti^+ + C_2H_6 reactants (12). Similar to the C—H bond activation branch, an intersystem crossing from the quartet surface over onto the doublet surface is expected to occur around this region. As shown in the panel **b** of Fig. 3, ^{2}**IM5** is a global minimum on the doublet surface. **IM1** and **IM5** are connected by a first-order saddle point (**TS4**), which corresponds to C—C bond activation. On the doublet surface, the activation barrier was found to be 25.1 kcal mol^{-1}. ^{2}**TS4** has C_1 symmetry, where the C—C distance is enlarged

© 2005 NRC Canada

to 2.005 Å and the two Ti—C distances are shortened to 2.302 and 1.927 Å, respectively. It is clear from these geometry parameters that ^{2}**TS4** is a three-membered ring transition state. The imaginary frequency of this TS is 607i cm^{-1}, and the corresponding transition vector indicated by the vibration analysis corresponds to the breaking of the C—C bond and the reorientation of the methyl groups. Great efforts have also been made to locate such a TS on its quartet surface using the DFT method, however, the initially guessed structures at all times converge to ^{4}**IM5**. This situation is largely similar to that found previously in the C—H bond activation branch. To estimate the barrier of C—C bond activation on the quartet surface, we optimized the structure of ^{4}**TS4** using the same method as for locating ^{4}**TS1**. Its estimated relative energy is 4.5 kcal mol^{-1} above the reactants and only 0.5 kcal mol^{-1} less stable than the corresponding intermediate ^{4}**IM5**, confirming the very flat PES around this region.

Once **IM5** is formed, it can undergo two possible production channels immediately by isomerization or decomposition. One is the process directly cleaving the Ti—C bond in **IM5**, which led to $TiCH_3^+ + CH_3$ as proposed in Scheme 1. The process was calculated to be endothermic by 22.1 kcal mol^{-1}. The other is an energetically more favorable reaction path, which involves the isomerization of **IM5** into **IM6**, via a four-center transition state (**TS5**). As shown in Fig. 2, ^{2}**TS5** is an H-migration transition state on the PES in which a hydrogen atom is migrating from a carbon atom to another one and the breaking and forming C—H bond lengths are 1.528 and 1.451 Å, respectively. The corresponding imaginary frequency is 1329i cm^{-1}. The vibration analyses have also shown that the corresponding transition vectors are completely consistent with the notion of a 1,3-H shift. The forward product of **TS5** is **IM6**, a complex between CH_4 and $TiCH_2^+$. Both the methane moiety and the titanium–carbene unit in **IM6** are only slightly distorted compared to the geometric parameters of free CH_4 and $TiCH_2^+$. The methane unit in ^{2}**IM6** coordinates to the $TiCH_2^+$ species by η^3 shape with a value of 109.6° for the C-Ti-C angle. Its energy is calculated to be 10.8 kcal mol^{-1} more stable on the doublet surface and 0.83 kcal mol^{-1} more stable on the quartet surface than the separate reactants. After **IM6** is formed, the production channel dissociating into $TiCH_2^+ + CH_4$ would be open, which requires 15.2 and 14.4 kcal mol^{-1} on the doublet and quartet surfaces, respectively, and the overall reaction $Ti^+(^4F) + C_2H_6 \rightarrow TiCH_2^+ + CH_4$ is endothermic by 4.4 kcal mol^{-1} on the doublet surface and by 13.6 kcal mol^{-1} on the quartet surface.

As shown in Fig. 3*b*, along the ground-state PES, we note that the relative energy of C—C bond activation TS, ^{2}**TS4** is 10.5 kcal mol^{-1} above the entrance channel and 12.2 kcal mol^{-1} higher than the energy of **TS1**, the C—H bond activation TS. Thus, from a purely energetic point of view, the C—C bond activation pathway is less favorable than the C—H bond activation. This is the reason why only the H_2 elimination products were observed at low energies (10–13), whereas the CH_4 elimination products were not. Our calculated barrier height for the CH_4 elimination channel (10.5 kcal mol^{-1}) is considered accurate enough in view of the good performance of the calculation method selected, although it seems to be lower than the observed threshold for the appearance of Ti^+CH_2 (22.1 ± 2.3 kcal mol^{-1}) (12), which had been noted to be an unreasonably overestimated value (12).

Concerted activation branch of C—H and C—C bonds

As indicated above, both the C—C bond and C—H bond activation mechanisms of ethane by Ti^+ are addition–elimination reactions, involving two consecutive elementary steps: the oxidative addition of Ti^+ to C-C or C-H and the following reductive elimination of small molecules. In the present calculations, however, we also found another new reaction channel for C—C bond and C—H bond activations, which is a concerted process of the C—C and C—H bond activations. On each of the doublet and quartet surfaces, a three-membered ring TS (**TS6**) has been identified as a transition structure. The ground state of this TS is located on its quartet surface, and its relative energy is 32.6 kcal mol^{-1} above the entrance channel, and the corresponding doublet state is 11.6 kcal mol^{-1} less stable. The imaginary frequency of ^{4}**TS$_6$** is 690i cm^{-1}, and its transition vector corresponds to the expected components of the reaction coordinate: the breaking of the C—C bond and migration of a H atom from one C atom to another. To confirm two minima connected by ^{4}**TS6**, a careful IRC calculation started from this TS has been performed along both "forward" and "reverse" directions. The calculated results indicate that the forward direction leads to ^{4}**IM6**, while the reverse direction leads to ^{4}**IM1**. The activation energy from ^{4}**IM1** to ^{4}**TS6** is 59.5 kcal mol^{-1}. Although this energy barrier is much higher than those of the consecutive C—C bond and C—H bond activation processes discussed previously, it could be an alternative pathway for CH_4 loss from the reaction of Ti^+ with C_2H_6 at elevated energy. The reaction processes on the doublet and quartet surfaces along the concerted activation branches are shown in panels **c** and **c′** of Fig. 3.

Summary

The gas-phase reaction of Ti^+ with C_2H_6 has been studied by using density functional theory. The reaction of Ti^+ with C_2H_6 involves two mechanisms in nature: the consecutive activation mechanism of C—C or C—H bonds and the concerted activation mechanism of C—C and C—H bonds. The PES profiles of three activation branches (C—H and C—C bond activations and concerted C—H and C—C bond activation) along the reaction coordinate have been clearly revealed. The 1,1-H_2 elimination and concerted loss of CH_4 from the reaction of Ti^+ with C_2H_6 are possible alternative pathways at elevated energy compared to the general mechanism proposed earlier. However, the activation energies of these processes are higher than the corresponding ones proposed in the general mechanisms. Our calculations provide further insight into the elementary step mechanisms of the C—C and C—H bond activations in small alkanes by metal centers.

Acknowledgments

The work described in this paper is supported by the National Science Foundation of China under grant

© 2005 NRC Canada

No. 20473047 and the Natural Science Foundation of Shandong Province under grant No. Y2002B02.

References

1. G.D. Byrd, R.C. Burnier, and B.S. Freiser. J. Am. Chem. Soc. **104**, 3565 (1982).
2. N. Aristov and P.B. Armentrout. J. Am. Chem. Soc. **108**, 1806 (1986).
3. C. Schulze, H. Schwarz, D.A. Peake, and M.L. Gross. J. Am. Chem. Soc. **109**, 2368 (1987).
4. P.A.M. van Koppen, J. Brodbelt-Lustig, M.T. Bowers, and D.V. Dearden. J. Am. Chem. Soc. **113**, 2359 (1991).
5. P.A.M. van Koppen, M.T. Bowers, E.R. Fisher, and P.B. Armentrout. J. Am. Chem. Soc. **116**, 3780 (1994).
6. P.A.M. van Koppen, M.T. Bowers, C.L. Haynes, and P.B. Armentrout. J. Am. Chem. Soc. **120**, 5704 (1998).
7. L.S. Sunderlin and P.B. Armentrout. J. Phys. Chem. **92**, 1209 (1988).
8. R. Tonkyn, M. Ronan, and J.C. Weisshaar. J. Phys. Chem. **92**, 92 (1988).
9. G.D. Byrd, R.C. Burnier, and B.S. Freiser. J. Am. Chem. Soc. **104**, 3565 (1982).
10. R. Tonkyn and J.C. Weisshaar. J. Phys. Chem. **90**, 2305 (1986).
11. M.A. Tolbert and J.L. Beauchamp. J. Am. Chem. Soc. **108**, 7509 (1986).
12. L.S. Sunderlin and P.B. Armentrout. Int. J. Mass. Spectrom. Ion Processes, **94**, 149 (1989).
13. R.S. MacTaylor, W.D. Vann, and A.W. Castleman, Jr. J. Phys. Chem. **100**, 5329 (1996).
14. J. Allison, R.B. Freas, and D.P. Ridge. J. Am. Chem. Soc. **101**, 1332 (1979).
15. C. Wang and S. Ye. Int. J. Quant. Chem. **75**, 47 (1999).
16. K. Yoshizawa, A. Suzuki, and T. Yamabe. J. Am. Chem. Soc. **121**, 5266 (1999).
17. M. Hendrickx, M. Ceulemans, K. Gong, and L. Vanquickenborne. J. Phys. Chem. A, **101**, 2465 (1997).
18. E. Sicilia and N. Russo. J. Am. Chem. Soc. **124**, 1471 (2002).
19. J. Moc, D.F. Fedorov, and M.S. Gordon. J. Chem. Phys. **112**, 10 247 (2000).
20. P. Hohenberg and W. Kohn. Phys. Rev. B, **136**, 864 (1964).
21. W. Kohn and L.J. Sham. Phys. Rev. A, **140**, 1133 (1965).
22. T. Ziegler. Chem. Rev. **91**, 651 (1991).
23. A.D. Becke. J. Chem. Phys. **98**, 5648 (1993).
24. C. Lee, W. Yang, and R.G. Parr. Phys. Rev. B, **37**, 785 (1988).
25. M.J. Frisch, G.W. Trucks, H.B. Schlegel, G.E. Scuseria, M.A. Robb, J.R. Cheeseman, V.G. Zakrzewski, J.A. Montgomery, Jr., R.E. Stratmann, J.C. Burant, S. Dapprich, J.M. Millam, A.D. Daniels, K.N. Kudin, M.C. Strain, O. Farkas, J. Tomasi, V. Barone, M. Cossi, R. Cammi, B. Mennucci, C. Pomelli, C. Adamo, S. Clifford, J. Ochterski, G.A. Petersson, P.Y. Ayala, Q. Cui, K. Morokuma, D.K. Malick, A.D. Rabuck, K. Raghavachari, J.B. Foresman, J. Cioslowski, J.V. Ortiz, A.G. Baboul, B.B. Stefanov, G. Liu, A. Liashenko, P. Piskorz, I. Komaromi, R. Gomperts, R.L. Martin, D.J. Fox, T. Keith, M.A. Al-Laham, C.Y. Peng, A. Nanayakkara, M. Challacombe, P.M.W. Gill, B. Johnson, W. Chen, M.W. Wong, J.L. Andres, C. Gonzalez, M. Head-Gordon, E.S. Replogle, and J.A. Pople. GAUSSIAN 98 [computer program]. Gaussian, Inc., Pittsburgh, Penn. 1998.
26. C. Gonzalez and H.B. Schlegel. J. Chem. Phys. **90**, 2154 (1989).
27. M. Pavlov, P.E. Siegbahn, and M. Sandstrom. J. Phys. Chem. A, **102**, 219 (1998).
28. M. Peschke, A.T. Blades, and P. Kebarle. J. Am. Chem. Soc. **122**, 1492 (2000).
29. D. Stockigt. Chem. Phys. Lett. **250**, 387 (1996).
30. J. Sugar and C. Corliss. J. Phys. Chem. Ref. Data, **14**(Suppl. 2), 1 (1985).
31. S.G. Lias, J.E. Bartmess, J.F. Liebman, J.L. Holmes, R.D. Levin, and W.G. Mallard. J. Phys. Chem. Ref. Data, **17**(Suppl. 1), 1 (1988).
32. M.R. Sievers, L.M. Jarvis, and P.B. Armentrout. J. Am. Chem. Soc. **120**, 1891 (1998).
33. M.C. Holthausen and W. Koch. J. Am. Chem. Soc. **118**, 9932 (1996).
34. M.C. Holthausen, A. Fiedler, H. Schwarrz, and W. Koch. J. Phys. Chem. **100**, 6236 (1996).

© 2005 NRC Canada

On the synthesis of new amphiphilic entities by the succinic coupling of β-cyclodextrins to calixarenes

Christopher K. Jankowski, Sébastien Arseneau, Jérome Blu, Laurent Mauclaire, and Nicolas Aychet

Abstract: Novel molecules, composed of a β-cyclodextrin coupled via a succinic diamide linker to di-*n*-octyl-calix[4]arene monocrown-6 or to biscrown-6-calix[4]arene, were synthesized by two independent routes: from mono-6′-deoxy-6′-amino-β-cyclodextrin, and from tetraaminocalix[4]arene derivatives.

Key words: β-cyclodextrin–calix[4]arene coupling, aminosuccinate-β-CD, aminosuccinate-calix[4]arene, octyloxy-calix[4]arene–monocrown-6, calix[4]arene–biscrown-6.

Résumé : La synthèse de nouvelles molécules, formées d'une β-cyclodextrine couplée à un éther di-*n*-octyl-calix[4]arène monocouronne-6 ou d'un biscouronne-6-calix[4]arène par le biais d'un diamide succinique, a été réalisée par deux voies indépendantes au départ de la mono-6′-désoxy-6′-amino-β-cyclodextrine et de dérivés du tétraaminocalix[4]arène.

Mots clés : couplage β-cyclodextrine–calix[4]arène, aminosuccinate-β-CD, aminosuccinate-calix[4]arène, octyloxy-calix[4]arène–monocouronne-6, calix[4]arène–biscouronne-6.

[Traduit par la Rédaction]

Introduction

Cyclodextrins (CD) (1, 2) and calixarenes (CAL), two important classes of compounds in inclusion chemistry, demonstrate different, but complementary affinities. Cyclodextrins are hydrophilic and amphiphilic, while calixarenes (and their crown ether derivatives) are insoluble in water (3, 4). In our search for new methods of construction of amphiphilic species from CDs, we considered the system of a CD and a CAL-crown coupled together (Fig. 1).

These new CAL-crown–CD species should demonstrate potential applications in the transport and vectorization of drugs (5–7), especially through the attachment of specific "arms"; still maintaining cage-inclusion properties (8–13), exploiting crown, calixarene, and cyclodextrin propensities to react with guest molecules, and a kind of self-organization. It is also expected that the final molecule obtained from the di-*n*-octyl-monocrown (**1**) should maintain its rigidity, in particular because of the space-oriented conformation of the calixarene crown. The second calixarene system (biscrown-6 calix[4]arene (**2**)) does in fact demonstrate greater rigidity, as well as an increased hosting capacity (two crown-6 ethers).

In our previous work (14), we reported on the successful nitration of both crown and biscrown calixarenes (Table 1). Di-*n*-octyl calix[4]arene–monocrown-6 (octMC-6) (**1**), and its biscrown analog, calix[4]arene–biscrown-6 (BC-6) (**2**), obtained by nitration with concd. HNO_3, giving up to 90% yield of crude $(NO_2)_4$octMC-6 (**4**) or $(NO_2)_4$BC-6 (**5**). In this paper, we would like to report on the synthesis of the CD–CAL-crown compounds, starting with these tetranitro derivatives **4** and **5**, and coupling them to β-CD **3** through a succinic diamide linker.

Results and discussion

In the first series, the tetranitro product **4** was reduced at high yield (>90%) with Raney nickel, giving the tetraamine $(NH_2)_4$octMC-6 (**6**). This in turn was reacted with succinic anhydride in DMF. The use of the succinyl coupling was justified by the need to create a spacer of desired length, enabling access to the amino-β-CD **8** for the coupling through an amide bond formation. This pathway has been successfully used for some hindered amines, peptides, and even small proteins (15); in the event that the coupling reaction fails, a longer linker can be used. In this case, the reaction was successful: the addition of the linker to the amino-calixarene produced (succ.-NH)$_4$octMC-6 (**9**, yield: 90%). This was then condensed with the NH_2-β-CD (**8**) prepared from β-CD by the following previously reported sequence: selective in situ supra-molecular 6-monotosylation by the inclusion method (16), conversion to its 6-azide with NaN_3, and reduction via triphenylphosphine to the amine **8** (17, 18).

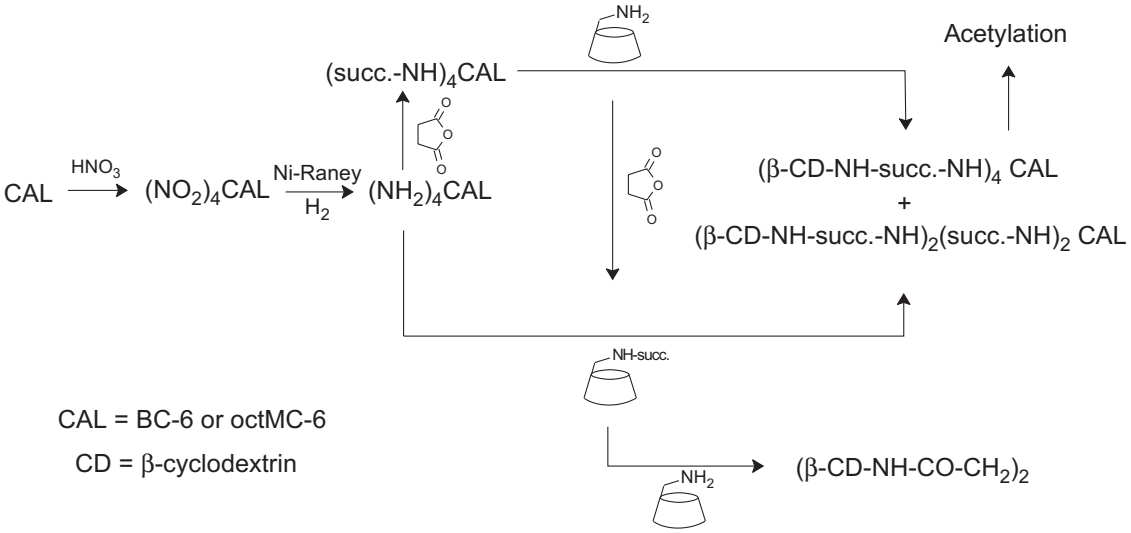
Received 17 November 2004. Published on the NRC Research Press Web site at http://canjchem.nrc.ca on 14 May 2005.

C.K. Jankowski[1] and S. Arseneau. Dept. de Chimie et Biochimie, Université de Moncton, Moncton, NB E1A 3E9, Canada.
J. Blu, L. Mauclaire, and N. Aychet. Service de Chimie Moléculaire (SCM), Département de Recherche sur l'État Condensé, les Atomes et les Molécules (DRECAM), CE de Saclay, bat 125, 91191 Gif-sur-Yvette, France.

[1]Corresponding author (e-mail: jankowc@umoncton.ca).

 doi: 10.1139/V05-070 © 2005 NRC Canada

Fig. 1. Overall scheme of the coupling reactions.



In the parallel series of the BC-6 calixarene, we produced a similar yield for the tetraamino derivative ($(NH_2)_4$BC-6, **7**) by Raney nickel reduction of the corresponding tetranitro derivative **5**, followed by obtaining the *N*-succinyl derivative **10** (yield: 87%–90%), which was condensed with NH_2-β-CD (8).

The identification of the relatively high molecular weight compounds involved in this synthetic pathway was first performed using ESI-MS then, after further purification, by NMR. The presence of crown-6 ether greatly facilitated the detection of the by-products via Cs^+ complexes, which are formed easily in the gas phase from crown-6-ether-containing compounds (19). In particular, we were able to follow the progress of the reactions by observing the presence of the stable crown–Cs^+ complex. For a second calixarene derivative (this one containing the biscrown moiety), the formation of doubly charged, two-Cs^+ cations was observed, along with the usual presence of protonation and of cationization by other alkali metal cations (20).

The NMR spectra of products recorded in solvents such as DMSO-d_6 or $CDCl_3$ displayed separate proton groups for the crown and sugar moieties, as well as for the aromatic and benzylic calixarene nuclei (21). The detailed analysis of the spectra of all molecules involved in this scheme is presented in the following sections (also see Experimental).

CD–CAL-crown coupling

Since both β-CD-amines and CAL-amines were available, as were their amino-succinates, we attempted to synthesize the (β-CD-NH-succ.-NH)$_n$-CAL via two separate methods (Fig. 1).

Condensation of amino-β-CD **8** with the tetra-*N*-succinyl derivative of octMC-6 **9** led to a mixture of products (yield: 30%). Two methods of coupling were attempted: firstly, by using the DCC or DIC coupling agents, according to the procedures developed in our laboratories (in particular with the modification of the DIC method by the addition of HOBt), and secondly, by the direct (but inefficient) coupling of the amine to the acid terminus of the mono-succinate (22).

For the octMC-6 series, analysis of the mixture of coupling products obtained via the DCC method revealed a small quantity (5%) of tetra-coupling product **12** (Table 1, n = 4, mass: 5775, detected by MALDI-TOF as MNa^+ and MK^+ ions), and a larger quantity (23%) of the diamide (n = 2, mass: 3543).

The diamides in this series were modelled: of the three isomers (cis-crown, cis-octyl, and trans), the lowest energy was calculated for the cis-crown isomer (219.87 kcal/mol), while both trans (241.90 kcal/mol) and cis-octyl (221.56 kcal/mol) isomers were more energetic. The cis-crown isomer is stabilized (relative to the trans isomer) by the hydrogen bonding between two neighboring cyclodextrin units. At this stage, we cannot confirm which of the cis (octyl and crown) or trans systems were formed.

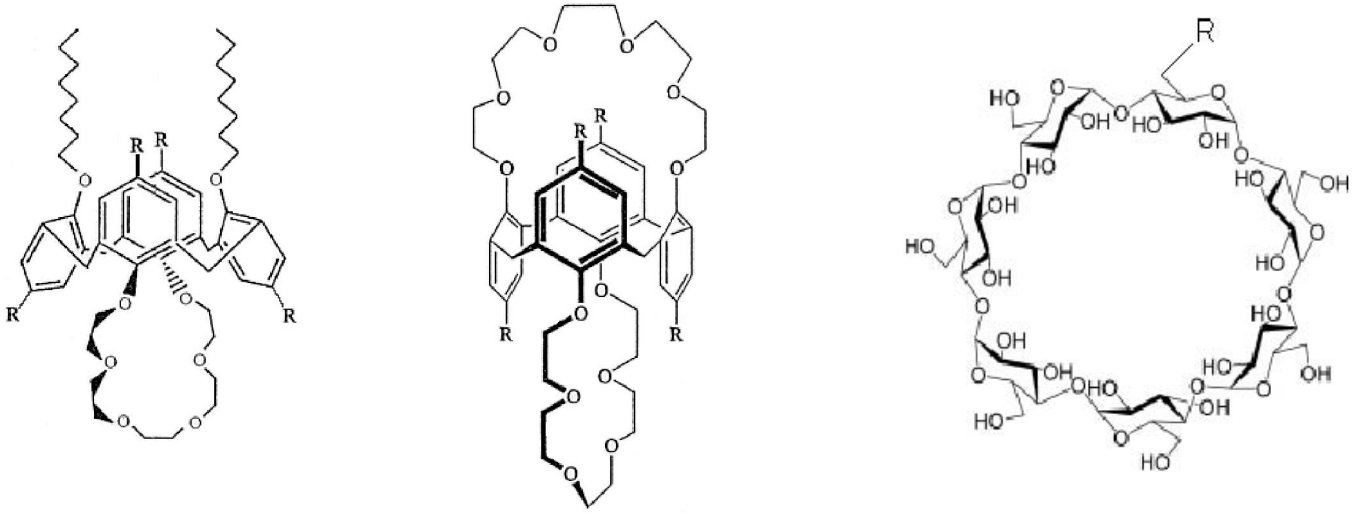
The low solubility of these compounds as well as difficulty with both their crystallization and their purification through column chromatography led us to acetylate them prior to column chromatography separation. When acetylation of the final coupling mixture involving the octMC-6 was completed, the presence of two products, the first corresponding to acetylated dicyclodextrin calixarenes **18** (23) and the second to acetylated CD-dimer **19** resulting from the earlier-mentioned coupling of the amine **8** with the (succ.-NH)-β-CD **11** was confirmed. This compound had already been characterized as a methylated derivative of (β-CD-NH-CO-CH_2)$_2$ in the previous series. The MALDI-TOF for this compound revealed, however, its incomplete acetylation. The mass observed for (Ac-β-CD-NH-succ.-NH)$_n$octMC-6 (n = 4, **18**) (peracetylated twice with acetic anhydride) was closer to that of the total *O*-acetylation of 78 of 80 hydroxyls present, and it did allow the MALDI-TOF spectrum to be recorded (target mass of 9138.6). Purification through this route did not significantly improve the quality of products obtained.

For the BC-6 series, the only β-CD-coupled products obtained were from the coupling of **10** to **8** (yield: 26%). The major components of this mixture were (β-CD-NH-succ.-NH)$_2$(succ.-NH)$_2$BC-6 (**15**, mass: 3521) and, unexpectedly, the dimer compound (β-CD-NH-CO-CH_2)$_2$ (**16**) (complete

© 2005 NRC Canada

Table 1. CAL (BC-6, octMC-6) and CD (β-cyclodextrin) derivative structures.

	Products		
R	Di-*n*-octyl monocrown	Biscrown	β-Cyclodextrin
-H	octMC-6 (**1**)	BC-6 (**2**)	—
-OH	—	—	β-CD (**3**)
-NO_2	$(NO_2)_4$octMC-6 (**4**)	$(NO_2)_4$BC-6 (**5**)	—
-NH_2	$(NH_2)_4$octMC-6 (**6**)	$(NH_2)_4$BC-6 (**7**)	NH_2-β-CD (**8**)
-NH-CO-$(CH_2)_2$-CO_2H	(succ.-NH)$_4$octMC-6 (**9**)	(succ.-NH)$_4$BC-6 (**10**)	(succ.-NH)-β-CD (**11**)
-NH-CO-$(CH_2)_2$-CO-β-CD	(β-CD-NH-succ.-NH)$_4$octMC-6 (**12**) (β-CD-NH-succ.-NH)$_2$(succ.-NH)$_2$octMC-6 (**13**) (Ac-β-CD-NH-succ.-NH)$_2$(succ.-NH)$_2$octMC-6 (**18**)	(β-CD-NH-succ.-NH)$_4$BC-6 (**14**) (β-CD-NH-succ.-NH)$_2$(succ.-NH)$_2$BC-6 (**15**)	(β-CD-NH-CO-CH_2)$_2$ (**16**) (Met-β-CD-NH-CO-CH_2)$_2$ (**17**) (Ac-β-CD-NH-CO-CH_2)$_2$ (**19**)



Note: Full compound names: 25,27-di-*n*-octyloxycalix[4]arene-26,28-crown-6 (**1**), 5,11,17,23-tetranitro-25,27-di-*n*-octyloxycalix[4]arene-26,28-crown-6 (**4**), 5,11,17,23-tetramino-25,27-di-*n*-octyloxycalix[4]arene-26,28-crown-6 (**6**), 5,11,17,23-tetra(amino-*N*-succinate)-25,27-di-*n*-octyloxycalix[4]arene-26,28-crown-6 (**9**), 5,11,17,23-*N*-[tetrakis(mono-6′-deoxy-6′-amino-cyclomaltoheptaose)yl]-tetra-*p*-amino-calix[4]arene-25,27,26,28-biscrown-6 (**14**), *N*-[bis(mono-6′-deoxy-6′-amino-cyclomaltoheptaose)yl]-*N*-[bis(amino-*N*-succinate)-tetra-*p*-amino-calix[4]arene-25,27,26,28-biscrown-6 (**15**), calix[4]arene-25,27,26,28-biscrown-6 (**2**), 5,11,17,23-tetranitro-calix[4]arene-25,27,26,28-biscrown-6 (**5**), 5,11,17,23-tetramino-calix[4]arene-25,27,26,28-biscrown-6 (**7**), 5,11,17,23-tetra(amino-*N*-succinate)-calix[4]arene-25,27,26,28-biscrown-6 (**10**), 5,11,17,23-*N*-[tetrakis(mono-6′-deoxy-6′-amino-cyclomaltoheptaose)yl]-tetra-*p*-amino-di-*n*-octyloxycalix[4]arene-26,28-crown-6 (**12**), *N*-[bis(mono-6′-deoxy-6′-amino-cyclomaltoheptaose)yl]-*N*-[bis(amino-*N*-succinate)-tetra-*p*-amino-di-*n*-octyloxycalix[4]arene-26,28-crown-6 (**13**), β-cyclodextrin (**3**), mono-6′-deoxy-6′-amino-β-cyclomaltoheptaose (**8**), mono-6′-deoxy-6′-amidosuccinyl-β-cyclomaltoheptaose (**11**), di-*N*,*N*′-[(mono-6′-deoxy-6′-amino-β-cyclomaltoheptaose)yl]succinamide (**16**), di-*N*,*N*′-[(mono-6′-deoxy-6′-amino-Met-β-cyclomaltoheptaose)yl]-succinamide (**17**), 5,11,17,23-*N*-[bis(Ac-mono-6′-deoxy-6′-amino-cyclomaltoheptaose)yl]$_2$-*N*-[bis(amino-*N*-succinate)]$_2$-tetra-*p*-amino-di-*n*-octyloxycalix[4]arene-26,28-crown-6 (**18**), di-*N*,*N*′-[(mono-6′-deoxy-6′-amino-Ac-β-cyclomaltoheptaose)yl]succinamide (**19**).

© 2005 NRC Canada

name: di-*N*,*N*′-[(mono-6′-deoxy-6′-amino-β-cyclomaltoheptaose)yl]succinamide), ratio 1:5. The coupling reaction (attempted via both the DCC and the DIC method) with **7** and **11** led only to the CD dimer resulting from the amino-β-CD and the residual succinic anhydride (total yield: 11%). To explain this result, the molecules of diamides **15** were modelled, revealing that the cis isomer was more stable (229.53 kcal/mol) than the trans isomer (256.98 kcal/mol). This is due to hydrogen bonding between the two cyclodextrin units in the cis isomer. Also, in this case, the crown-6 ring was flattened by this interaction.

A common feature of both coupling mixtures (for octMC-6 and BC-6) was (β-CD-NH-CO-CH_2)$_2$ (**16**) (24–27). Using ESI-MS, the presence of this product (mass: 2350, recorded as MNa^+ at *m*/*z* 2375) was then confirmed. The compound was compared to and characterized as its permethylated derivative **17** (mass: 2910, as MNa^+ at *m*/*z* 2933).

Initially, ESI-MS was used to identify these large molecules. In particular, the succinamides (from both sides of the synthetic scheme: amino-β-CD and amino-calixarene) showed the expected MH^+, MNa^+, and MCs^+ ions. For both series, the final coupling products were identified via MALDI-TOF.

The reversed coupling (of (succ.-NH)-β-CD (**11**) and (NH_2)$_4$octMC-6 (**6**)) produced a mixture of products with lesser yields (10%–15%). Even when the DCC method was used, the yield of cyclodextrin–calixarene coupled products was half as much.

Conclusion

The route from the amino-CAL coupled on (succ.-NH)-β-CD (**11**) gave smaller yields than the route from the tetrasuccinamido-CAL (where the linker is first fixed to the calixarene). This difference between the two coupling routes could be explained by the access to the coupling site on the bare tetraaminocalixarene being more hindered than for the equivalent site on the succinic-linked tetraaminocalixarene. The succinyl radical linked to the tetraaminocalixarene thus serves as a better spacer, which makes the coupling to NH_2-β-CD (**8**) slightly easier. This confirms the value of a longer linker for connecting with the NH_2-β-CD to realize the coupling with amino-CAL.

Another explanation for the lack of success in the formation of the coupling products in the BC-6 series is the hindrance within the BC-6 system, and (or) the stability of the tetrasuccinate (which demonstrated some hydrogen bonding between the NH and COOH groups of neighbouring systems). Molecular modelling of the succinates **9** and **10** showed that the presence of two long octyl chains disturbed the formation of this bonding relation for the octMC-6 series. In this way, the already-hindered access to the carboxylic group (even with the DCC coupling method) with the amine **8** gave lower yields because of this interaction.

The solubility of the final coupling products in most of the common organic solvents and the difficulty of separating them on a chromatographic column (because of their extreme polarity) remains a major experimental difficulty. In this respect, the use of permethylated or selectively methylated CD is a viable alternative to this route (28).

This successful assembling of calixarene to the β-CD ring, using the peptide-originated succinyl coupling via the DCC method, opens the way for further applications. For example, we can explore the connection of small peptides, and perhaps eventually use the calixarene platform with stereo-oriented amino groups to construct peptide helices (29, 30).

In particular, from the succ.-NH-calixarene in 1,3-alternate conformation we can build two double helix peptide chains, and from the cone conformation, the said self-supported quadruple helix. The certain originality of the method applied remains its versatility — if one failed to obtain the sequence from the succ.-NH-CAL route, the sequence from succ.-NH-CD could be more successful. Such an organization may afford solubilization and hosting sites affinities towards cations and neutral guests.

Experimental

Materials and methods

All chemicals used in this study were purchased from Aldrich Chemicals except the parent calixarenes bought from Acros Chemicals. The NH_2-β-CD was synthesized as described in ref. 16. The NMR spectra were recorded on Bruker 200, 300 (Chemagnetics), and 500 MHz spectrometers in DMSO-d_6, pyridine-d_5, D_2O, and $CDCl_3$ solutions as indicated. The ESI-MS spectra were recorded on a Quattro II Micromass apparatus (detailed as described in ref. 4). The MALDI-TOF spectra (UPMC, LCSOB, Paris, France) were recorded on a Voyager TM Elite, BioSpecRes Station (Applied Biosystems) with the 2550 Laser RDEHCCA method, pressure 2.71 e^{-7}, in positive ion mode, accelerating voltage 20 kV, on a DHB (dihydroxy benzoic alcohol) matrix. The molecular modelling was performed with the help of HyperChem (31).

General procedures

Nitration of octMC-6 1 and BC-6 (2)

500 mg of BC-6 (or octMC-6) were taken in 25 mL of CH_2Cl_2 in a three-necked 250 mL flask under nitrogen and continuous magnetic stirring and cooled to 0 °C. Then, 2 mL of fuming nitric acid were added and 2.5 mL of acetic anhydride with another 10 mL of CH_2Cl_2 that was added over a 15 min period. The temperature was slowly taken back to room temperature and the mixture was treated with triethylamine to alkaline pH then washed twice with 20 mL of satd. $NaHCO_3$ and NaCl. The organic layer was dried over anhydr. $MgSO_4$. After filtration and evaporation to dryness, the residue was purified on a silica gel (63–200 mesh) chromatographic column (for example with 5% MeOH in CH_2Cl_2) enabled to isolate the tetranitro compounds under constant TLC control. Yield (NMR pure compound): 75% (NO_2)$_4$octMC-6 (**4**), 55% (NO_2)$_4$BC-6 (**5**).

Tetra-p-*nitro-di*-n-*ocMC-6 (4)*

$C_{54}H_{70}N_4O_{16}$ (1031.2 g/mol), mp 184 °C. ^{1}H NMR (500 MHz, $CDCl_3$): 8.00–8.06 (8H, s, Ar*H* meta), 3.92, 4.00 (s, ArCH_2Ar), 3.73, 3.70, 3.66, 3.52, 3.50 (m, OCH_2 crown), 3.47 (octyl, H-1), 1.1–1.5 (octyl, H-2–H-7), 0.9 (octyl, H-8). ^{13}C NMR (125 MHz, $CDCl_3$): 161.5, 162.2 (Ar C-NO_2), 156.8, 156.3 (Ar C-OR), 142.1, 135.1, 122.4, 122.2 (Ar C-CH_2), 130.3, 130.0, 129.7, 125.5 (Ar C-H), 70.2–71.9 (OCH_2CH_2O crown 5C, octyl C1), 37.7, 37.2 (ArCH_2Ar),

© 2005 NRC Canada

14.0–37.0 (octyl C-2–C-8). ESI-MS *m/z* calcd.: 1054.2 (MNa^+), 1163.2 (MCs^+); found: 1053.4 (MNa^+), 1163.3 (MCs^+).

Tetra-p-*nitro-BC-6 (5)*

$C_{48}H_{56}N_4O_{20}$ (1009.0 g/mol). ^1H NMR (500 MHz, $CDCl_3$): 8.09 (s, 8H, ArH meta), 3.97 (s, 8H, ArCH_2Ar), 3.54, 3.50, 3.42, 3.41, 3.40 (m, ArCH_2Ar, OCH_2 crown). ^{13}C NMR (125 MHz, $CDCl_3$): 125.99, 134.21, 142.98, 161.52 (Ar), 69.39, 70.59, 70.66, 70.70, 70.84, 70.92, 71.03, 71.08, 71.65 (OCH_2 crown), 37.45 (ArCH_2Ar). ESI-MS *m/z* calcd.: 1032.0 (MNa^+), 1041.0 (MCs^+); found: 1031.3 (MNa^+), 1141.3 (Mcs^+).

Raney nickel reduction

300 mg of $(NO_2)_4$octMC-6 (**4**) (or $(NO_2)_4$BC-6, **5**) was taken in a three-necked 250 mL flask with 20 mL of anhydrous toluene and one spatula of Raney nickel (Aldrich 3800) and was put under nitrogen. The mixture was then connected to the hydrogen generator and put under an atmosphere of H_2 with vigorous magnetic stirring and heated to 70 °C for 3 h. The flask was transferred under nitrogen and the catalyst filtered (caution: Raney nickel with H_2 is a potential fire hazard in the lab on contact with atmospheric oxygen on dryness) on a VF4 Celite adsorbent. The toluene solution was evaporated to dryness under vacuum. Yield: 90% $(NH_2)_4$octMC-6 (**6**), 90% $(NH_2)_4$BC-6 (**7**).

Tetra-p-*amino-di*-n-*octMC-6 (6)*

$C_{54}H_{78}N_4O_8$ (911.2 g/mol), mp 160 °C. ^1H NMR (300 MHz, $CDCl_3$): 6.45 (4H, s, ArH octyl), 6.29 (4H, s, ArH crown), 3.61, 3.72, 3.80 (m, OCH_2CH_2O crown), 3.52 (2H, t, octyl H-1), 3.32 (8H, s, ArCH_2Ar), 3.30 (br, N*H*), 1.10–1.60 (m, octyl H-2–H-7), 0.8–0.9 (3H, t, octyl H-8). ^{13}C NMR (75 MHz, $CDCl_3$): 149.6 (Ar ipso octyl), 149.3 (Ar ipso crown), 140.8 (Ar para crown), 140.2 (Ar para octyl), 134.3 (Ar ortho octyl), 132.9 (Ar ortho crown), 118.4 (Ar meta crown), 117.6 (Ar meta octyl), 72.9 (C-1 octyl), 69.9–72.3 (OCH_2 crown), 36.4 (ArCH_2Ar), 22.0–32.0 (C-2–C-7 octyl), 14.3 (C-8 octyl). ESI-MS *m/z* calcd.: 1043.2 (MCs^+); found: 1043.3 (MCs^+).

Tetra-p-*amino-BC-6 (7)*

$C_{48}H_{64}N_4O_{12}$ (889.0 g/mol). ^1H NMR (300 MHz, $CDCl_3$): 6.50 (8H, s, ArH), 3.35 (8H, s, ArCH_2Ar), 3.67, 3.78, 3.86, 4.00 (m, OCH_2 crown), 3.75 (br, N*H*). ^{13}C NMR (75 MHz, $CDCl_3$): 149.2 (Ar ipso), 141.1 (Ar para), 132.9 (Ar ortho), 118.7 (Ar meta), 70.0–72.0 (OCH_2CH_2O crown), 36.3 (ArCH_2Ar). ESI-MS PI *m/z* calcd.: 1021.0 (MCs^+); found: 1021.4 (MCs^+).

Mono-6′-deoxy-6′-amino-cyclomaltoheptaose (8)

(Starting amino-CD for the reverse coupling). $C_{42}H_{71}NO_{34}$ (1133.9 g/mol), mp 190 °C. ^1H NMR (300 MHz, D_2O): 5.05–5.12 (7H, H-1 β-CD), 3.8–4.1 (H-3 β-CD amino, H-6 β-CD, H-5 β-CD, H-6 β-CD), 3.72 (dd, br, H-4 β-CD), 3.62 (t, br, H-2 β-CD), 3.53 (t), 3.22 (d, H-6′ β-CD), 2.98 (dd, H-6″ β-CD). ^{13}C NMR (75 MHz, D_2O): 102.5 (C-1), 83.5 (C-4 β-CD′), 82.0 (C-4, β-CD), 72–75 (C-2, C-3, C-5), 61.3 (C-6), 41.3 (C-NH_2). ESI-MS PI *m/z* calcd.: 1134.9 (MH^+); found: 1134.7 (MH^+).

N-*Succinylation of amines*

171 mg of (NH_2)BC-6 (or 252 mg of (NH_2)octMC-6 or 986.5 mg (NH_2)-β-CD) compound was reacted with 87 mg of succinic anhydride in 5 mL of DMF at room temperature for 12 h, then lyophilized to dryness and analyzed via ESI-MS or MALDI-TOF and NMR. Yield: 90% (succ.-NH)$_4$octMC-6 (**9**), 85% (succ.-NH)$_4$BC-6 (**10**), 90% (succ.-NH) β-CD (**11**).

(Succ.-NH)$_4$octMC-6 (9)

$C_{70}H_{94}N_4O_{20}$ (1311.5 g/mol). ^1H NMR (500 MHz, DMSO-d_6): 7.43, 7.45 (s, 8H, ArH meta), 3.0–4.0 (m, OCH_2 crown, ArCH_2Ar), 2.59, 2.62 (CH_2 succ.), 1.00–1.35 (m, octyl C-1–C-7), 0.95 (t, 3H, octyl C-8). ^{13}C NMR (125 MHz, DMSO-d_6): 174.0, 169.4, 169.0 (-CO-succ.), 152.3, 151.7, 133.9, 134.1, 133.8, 133.4, 119.6, 119.3 (Ar), 70.0, 69.9, 69.5, 68.9 (OCH_2 crown), 10.0–40.0 (ArCH_2Ar, octyl C-1–C-8), 29.38, 29.19 (CH_2 succ.), 14.20 (octyl C-8). ESI-MS *m/z* calcd.: 1443.5 (MCs^+); found: 1443.6 (MCs^+).

(Succ.-NH)$_4$BC-6 (10)

$C_{64}H_{80}N_4O_{24}$ (1289.3 g/mol). ^1H NMR (500 MHz, DMSO-d_6): 7.43 (s, 8H, ArH meta), 3.00–4.00 (m, OCH_2 crown, ArCH_2Ar), 2.50–2.60 (m, CH_2 succ.). ^{13}C NMR (125 MHz, DMSO-d_6): 173.94, 169.41 (-CO- succ.), 151.88, 133.99, 133.43, 119.41 (Ar), 69.98, 69.43, 68.95, 68.41 (OCH_2 crown), 37.88 (ArCH_2Ar), 29.07, 28.92 (CH_2 succ.). ESI-MS *m/z* calcd.: 1421.3 (MCs^+); found: 1421.4 (MCs^+).

Mono-6′-deoxy-6′-amidosuccinyl-cyclomaltoheptaose (11)

$C_{46}H_{75}NO_{37}$ (1234.1 g/mol), mp 155–159 °C. ^1H NMR (500 MHz, Pyr-d_5): 8.67 (t, 1H, NH_{CD}, $^3J_{NH\text{-}6^I}$ = 5.7 Hz), 7.4–7.9 (14 O*H*), 5.51–5.61 (6H, H-$1^{II\text{-}VII}{}_{CD}$), 5.45 (d, 1H, H-$1^I{}_{CD}$, $^3J_{1^I\text{-}2^I}$ = 3.5 Hz), 4.63–4.78 (H-$3^{II\text{-}VII}{}_{CD}$), 4.64 (H-$3^I{}_{CD}$), 4.62–4.69 (H-$6^{II\text{-}VII}{}_{CD}$), 4.31–4.57 (H-$5^{II\text{-}VII}{}_{CD}$/H-$6'^{II\text{-}VII}{}_{CD}$), 4.46 (H-$5^I{}_{CD}$), 4.04–4.27 (H-$4^{II\text{-}VII}{}_{CD}$), 4.19 (H-$6^I{}_{CD}$), 4.12 (H-$6'^I{}_{CD}$), 3.98–4.11 (H-$2^{II\text{-}VII}{}_{CD}$), 3.88 (H-$2^I{}_{CD}$), 3.87 (H-$4^I{}_{CD}$), 2.77–2.94 (4H, Hb/Hc, syst. AA′B). ^{13}C NMR (75 MHz, DMSO-d_6): 101.8 (C-1), 81.4 (C-4), 71–73 (C-2, C-3, C-5), 59.8 (C-6), 29.2–29.8 (CH_2CH_2 succ.). ESI-MS *m/z* calcd.: 1235.1 (MH^+); found: 1234.9 (MH^+).

Coupling reaction

181 mg of NH_2-β-CD (**8**) was put together with 46 mg of (succ. NH)$_4$octMC-6 (**9**) (or 45 mg of (succ. NH)$_4$BC-6 (**10**)) with the help of DCI (30 μL) and HOBt (30 mg) in 2.5 mL of DMF for over 24 h. The mixture was separated on silica gel (63–200 mesh) with 5% MeOH (in CH_2Cl_2) then with 10% MeOH (in CH_2Cl_2). Yield: 6% (β-CD-NH-succ.-NH)$_2$(succ.-NH)$_2$-BC-6 (**15**), 25% (β-CD-NH-succ-NH)$_4$octMC-6 (**12**), 5% (β-CD-NH-succ.-NH)$_2$(succ.-NH)$_2$-octMC-6 (**13**).

(β-CD-NH-succ.-NH)$_2$(succ.-NH)$_2$-octMC-6 (13)

$C_{154}H_{232}N_6O_{86}$ (3543.5 g/mol). ^1H NMR (200 MHz, DMSO-d_6): 5.10–5.30 (m, H-1, CD), 3.40–3.75 (OCH_2 crown, C-1 octyl, ArCH_2Ar, C*H* β-CD), 2.50–2.75 (CH_2, succ.), 0.85–1.50 (m, octyl). MALDI-TOF *m/z* calcd.: 3544.5 (MH^+), 3566.5 (MNa^+); found: 3543 (MH^+), 3566 (MNa^+).

(β-CD-NH-succ.-NH)$_4$-octMC-6 (12) (selected data)

$C_{238}H_{370}N_8O_{152}$ (5775.4 g/mol). Yield: total 30% (**12** and **13**). ^1H NMR (200 MHz, DMSO-d_6): 7.60 (m br, N*H*), 7.50 (m, Ar*H*), 5.10–5.30 (m, H-1, β-CD), 3.50–4.60 (m, OCH_2

© 2005 NRC Canada

crown, ArCH_2Ar, β-CD), 3.40 (m, OCH_2, octyl), 2.55–2.67 (m, CH_2 succ.), 0.90–1.40 (m, octyl). MALDI-TOF *m/z* calcd.: 5776.4 (MH^+), 5798.4 (MNa^+); found: 5775 (MH^+), 5799 (MNa^+).

(β-CD-NH-succ.-NH)$_2$(succ.-NH)$_2$-BC-6 (15) (selected data)

$C_{148}H_{218}N_6O_{90}$ (3521.3 g/mol). Yield: total 26% (6% **15** and 20% **16**). ^{1}H NMR (200 MHz, DMSO-d_6): 7.30 (Ar*H*), 5.10–5.30 (m, H-1, β-CD), 3.30–5.10 (OCH_2 crown, ArCH_2Ar, β-CD), 2.50–2.80 (m, CH_2 succ.). MALDI-TOF *m/z* calcd.: 3544.3 (MNa^+); found: 3509 (MNa^+).

(β-CD-NH-CO-CH$_2$)$_2$ (16) (selected data)

$C_{88}H_{144}N_2O_{70}$ (2350.0 g/mol). ^{1}H NMR (200 MHz, DMSO-d_6): 6.80 (m, N*H*), 5.00–5.20 (m, H-1, β-CD), 4.00–4.20 (H-6, β-CD), 3.60–4.60 (β-CD remaining protons), 3.10–3.15 (H-6, β-CD-amino), 2.49–2.53 (m, CH_2, succ.). MALDI-TOF *m/z* calcd.: 2351.0 (MH^+), 2373.0 (MNa^+); found: 2350 (MH^+), 2373 (MNa^+).

[(Acetylated-β-CD)-NH-CO-CH$_2$]$_2$ (19)

$C_{168}H_{224}N_2O_{110}$ (4031.5 g/mol). ^{1}H NMR (200 MHz, DMSO-d_6): 6.40–6.60 (m, N*H*), 6.00–6.30 (m, H-1, β-CD), 3.80–5.00 (β-CD, remaining protons), 2.56 (m, CH_2 succ.), 2.10–2.20 (CH_3-CO). MALDI-TOF *m/z* calcd.: 4070.5 (MK^+); found: 4025 (MK^+).

[(Methylated-β-CD)-NH-CO-CH$_2$]$_2$ (17)

$C_{128}H_{224}N_2O_{70}$ (2911.1 g/mol). ^{1}H NMR (200 MHz, DMSO-d_6): 6.44 (N*H*-CO), 5.09–5.14 (C*H*-O, H-1), 3.37–3.60 (H-5, H-6, H-3), 3.20 (H-2, H4), 2.57–2.66 (CH_2 succ.). ^{13}C NMR (50 MHz, DMSO-d_6): 99.2 (C-1), 170.6, 172.5 (-*C*O-), 81.9–82.4 (C-2, C-4), 76.9, 77.4 (C-3, C-6), 71.1, 71.4 (C-5, C-6′), 31.7, 21.9 (CH_2 succ.). MALDI-TOF *m/z* calcd.: 2934.1 (MNa^+); found: 2933 (MNa^+).

Acknowledgments

We are indebted to Dr. M.-R. Van Calsteren for recording some of the NMR spectra in the preliminary series of nitro crown, to Drs. D. Lesage and J.C. Tabet (Université Pierre et Marie Curie (UPMC), Jussieu), F. Libot (Faculté de Pharmacie, Université de Paris, France), and C. Hocquelet (Centre d'Études Nucléaires, Saclay (CEA)) for helpful discussion.

References

1. N. Funasaki, S. Ishikawa, and S. Neya. J. Phys. Chem. B, **108**, 9593 (2004).
2. S. Daoud-Mahammed, P. Couvreur, C. Amiel, M. Besnard, M. Appel, and R. Gref. J. Drug Deliv. Sci. Tec. **14**, 51 (2004).
3. J. Lin, C. Creminon, B. Perly, and F. Djedaïni-Pilard. J. Chem. Soc. Perkin Trans. 2, 2639 (1998).
4. J.J. Michels, J. Huskens, J.F.J. Engbersen, and D.N. Reinhoudt. Langmuir, **16**, 4864 (2000).
5. D.A. Fulton and J.F. Stoddart. Bioconjugate Chem. **12**, 655 (2001).
6. I. Higler, P. Timmerman, W. Verboom, and D.N. Reinhoudt. Eur. J. Org. Chem. 2689 (1998).
7. W. Sliwa, T. Girek, and J.J. Koziol. Curr. Org. Chem. **8**, 1445 (2004).
8. J.J. Michels, R. Fiammengo, P. Timmerman, J. Huskens, and D.N. Reinhoudt. J. Inclusion Phenom. Macrocyclic Chem. **41**, 163 (2001).
9. J.J. Michels, M.W.P.L. Baars, E.W. Meijer, J. Huskens, and D.N. Reinhoudt. J. Chem. Soc. Perkin Trans. 2, 1914 (2000).
10. Y. Liu, Y. Chen, L. Li, G. Huang, C.C. You, H.Y. Zhang, T. Wada, and Y. Inoue. J. Org. Chem. **66**, 7209 (2001).
11. N. Kuhnert and A. Le-Gesley. Chem. Commun. 2426 (2003).
12. R. Zadmard, M. Junkers, T. Schrader, T. Grawe, and A. Kraft. J. Org. Chem. **68**, 6511 (2003).
13. M.R. de Jong, J. Huskens, and D.N. Reinhoudt. Chem. Eur. J. **7**, 4164 (2001).
14. C.K. Jankowski, J.F. Dozol, F. Allain, J.C. Tabet, R. Ungaro, A. Casnati, J. Vicens, A. Asfari, and J. Boivin. Pol. J. Chem. **76**, 701 (2002).
15. C. Péan, C. Créminon, A. Wijkhuisen, J. Grassi, P. Guenot, P. Jéhan, J.P. Dalbiez, B. Perly, and F. Djedaïni-Pilard. J. Chem. Soc. Perkin Trans. 2, 853 (2000).
16. R.C. Petter, J.S. Salek, C.T. Sikorski, G. Kumaravel, and F.T. Lin. J. Am. Chem. Soc. **112**, 3860 (1990).
17. H.S. Byun, N. Zhong, and R. Bittman. Org. Synth. **77**, 225 (2000).
18. F. Djedaïni-Pilard, F. Désalos, and B. Perly. Tetrahedron Lett. **34**, 2457 (1993).
19. C.K. Jankowski, F. Allain, J.F. Dozol, H. Virelizier, J.C. Tabet, C. Moulin, and C. Lamouroux. Rapid Commun. Mass Spectrom. **17**, 1247 (2003).
20. V. Lamarre, J.F. Dozol, F. Allain, H. Virelizier, C. Moulin, C.K. Jankowski, and J.C. Tabet. ACS Symp. Vol. 757. Washington, D.C. 2000. Chap. 5. p. 55.
21. C. Lamouroux, N. Aychet, A. Lelièvre, C.K. Jankowski, and C. Moulin. Rapid Commun. Mass Spectrom. **18**, 1493 (2004).
22. A. Paquet. Can. J. Chem. **60**, 976 (1982).
23. J. Boger, R.J. Corcoran, and J.M. Lehn. Helv. Chim. Acta, **61**, 2190 (1978).
24. J.B. Harper, C.J. Easton, and S.F. Lincoln. Tetrahedron Lett. **44**, 5815 (2003).
25. J.H. Coates, C.J. Easton, S.J. van Eyk, S.F. Lincoln, B.L. May, C.B. Whalland, and M.L. Williams. J. Chem. Soc. Perkin Trans. 1, 2619 (1990).
26. H. Ikeda, Y. Horimoto, M. Nakata, and A. Ueno. Tetrahedron Lett. **41**, 6483 (2000).
27. H. Yamamura, S. Yamada, K. Kohno, N. Okuda, S. Araki, K. Kobayashi, R. Katakai, K. Kano, and M. Kawai. J. Chem. Soc. Perkin Trans. 1, 2943 (1999).
28. T. Lecourt, J.M. Mallet, and P. Sinaÿ. Tetrahedron Lett. **43**, 5533 (2002).
29. A. Sartori, A. Casnati, L. Mandolini, F. Sansone, D.N. Reinhoudt, and R. Ungaro. Tetrahedron, **59**, 5539 (2003).
30. J. Bügler, N.A.J.M. Sommerdijk, A.J.W.G. Visser, A. van Hoek, R.J.M. Nolte, J.F.J. Engbersen, and D.N. Reinhoudt. J. Am. Chem. Soc. **121**, 28 (1999).
31. HyperChem 6.03 Mm+ [computer program]. HyperCube Inc., Gainsville, Fl. 2000.

© 2005 NRC Canada

Viscosities of some tetraalkylammonium bromides in 2-ethoxyethanol at 308.15, 313.15, 318.15, and 323.15 K

Purushottam Haldar and Bijan Das

Abstract: The viscosities of the solutions of tetraethylammonium bromide (Et_4NBr), tetrapropylammonium bromide (Pr_4NBr), tetrabutylammonium bromide (Bu_4NBr), tetrapentylammonium bromide (Pen_4NBr), and tetraheptylammonium bromide (Hep_4NBr) in 2-ethoxyethanol have been reported at 308.15, 313.15, 318.15, and 323.15 K. The viscosity data have been analyzed by the Jones–Dole equation for the associated electrolytes to evaluate the viscosity *B* coefficients of the electrolytes. These data have also been analyzed by the transition-state treatment to obtain the contribution of the solutes to the free energy of activation for viscous flow of the solution. The viscosity of the solvent is found to be greatly modified by the presence of all of the tetraalkylammonium ions investigated. Moreover, the tetraalkylammonium ions are found to be unsolvated in 2-ethoxyethanol solutions, they behave neither as structure-breaker nor as structure-maker and the formation of the transition state is made less favorable in their presence.

Key words: viscosity, electrolytes, tetraalkylammonium ion, 2-ethoxyethanol, ionic contribution, solvation, transition-state treatment.

Résumé : On a mesuré les viscosités de solutions du bromure de tétraéthylammonium (Et_4NBr), du bromure de tétrapropylammonium (Pr_4NBr), du bromure de tétrabutylammonium (Bu_4NBr), du bromure de tétrapentylammonium (Pen_4NBr), et du bromure de tétraheptylammonium (Hep_4NBr) dans le 2-éthoxyéthanol, à 308,15, 313,15, 318,15 et 323,15 K. Les données de viscosité ont été analysées à l'aide de l'équation de Jones–Dole pour les électrolytes associés afin d'évaluer leurs coefficients *B* de viscosité. On a aussi analysé ces données par le traitement de l'état de transition afin de pouvoir obtenir les contributions des solutés à l'énergie libre d'activation. On a trouvé que la viscosité du solvant est grandement modifiée par la présence de chacun des ions tétraalkylammonium étudiés. Des plus, on a trouvé que les ions tétraalkylammonium ne sont pas solvatés dans les solutions de 2-éthoxyéthanol, qu'ils n'agissent ni pour briser ni pour former des structures et que la formation de l'état de transition est rendue moins favorable en raison de leur présence.

Mots clés : viscosité, électrolytes, ion tétraalkylammonium, 2-éthoxyéthanol, contribution ionique, solvatation, traitement de l'état de transition.

[Traduit par la Rédaction]

Introduction

Recently, we initiated a comprehensive program to study the solvation and association behavior of several 1:1 electrolytes in different nonaqueous solvents from the measurements of various transport, thermodynamic, and spectroscopic properties (1–5). As a part of this series of investigations, we have, very recently, reported (6, 7) the results of conductance measurements on a number of tetraalkylammonium salts, e.g., tetraethylammonium bromide (Et_4NBr), tetrapropylammonium bromide (Pr_4NBr), tetrabutylammonium bromide (Bu_4NBr), tetrapentylammonium bromide (Pen_4NBr), and tetraheptylammonium bromide (Hep_4NBr) in 2-ethoxyethanol at 308.15, 313.15, 318.15, and 323.15 K. We have now extended this work to study the viscometric behavior of these electrolyte solutions since viscometry is well-suited to provide information concerning the solvation of the ions and their effects on the structure of the solvent in the near environment of the solute particles (8–10).

Received 25 November 2004. Published on the NRC Research Press Web site at http://canjchem.nrc.ca on 18 May 2005.

P. Haldar and B. Das.[1] Department of Chemistry, North Bengal University, Darjeeling 734 430, India.

[1]Corresponding author (e-mail: bijan_dasus@yahoo.com).

Experimental

2-Ethoxyethanol (G.R.E. Merck, India) was dried with potassium carbonate and distilled twice in an all-glass distillation set immediately before use and the middle fraction was collected. The densities and viscosities of 2-ethoxyethanol at 308.15, 313.15, 318.15, and 323.15 K are reported in Table 1. The physical properties of the purified solvent are found to be in good agreement with the literature values (11–15). Also included in this table are the relative permittivities (ε) of 2-ethoxyethanol at different temperatures obtained from the literature (7, 11).

Tetraalkylammonium bromides were of purum or puriss grade (Fluka, Switzerland) and were purified as described in the literature (16). These salts were purified by recry-

 doi: 10.1139/V05-082 © 2005 NRC Canada

Table 1. Physicochemical properties of 2-ethoxyethanol at different temperatures.

T (K)	ρ_0 (g cm^{-3})		η_0 (mPa s)		
	Exptl.	Lit.	Exptl.	Lit.	ε
298.15	0.924 97	0.925 02 (11) 0.925 2 (12) 0.925 8 (13)	1.827 7	1.85 (12)	13.38
308.15	0.917 35	0.916 74 (14) 0.916 71 (15) 0.916 3 (13)	1.517 9		12.81
313.15	0.913 70		1.359 4		12.52
318.15	0.909 94		1.189 3		12.25
323.15	0.906 02		1.087 1		11.99

stallization and the higher homologues (tetrapentylammonium bromide and tetraheptylammonium bromide) were recrystallized twice to ensure maximum purity. The recrystallized salts were dried in vacuo at elevated temperatures for 12 h immediately prior to use.

The kinematic viscosities (ν) were measured by means of a suspended level Ubbelohde viscometer. The viscometer was kept in a vertical position in a water thermostat controlled to ±0.01 K. The kinematic viscosity (ν) and the absolute viscosity (η) are given by the following equations:

$$[1] \qquad \nu = Ct - K/t$$

$$[2] \qquad \eta = \nu\rho$$

where t is the efflux time, ρ is the density, and C and K are the characteristic constants of the viscometer. The values of the constants C and K, determined by using the density and the viscosity values of water and 2-methoxyethanol (17), were found to be 1.646×10^{-5} cm^2 s^{-2} and –0.023 316 47 cm^2, respectively. The calibration constants were also checked with methanol (18). The estimated error of the viscosity measurements was ±0.05%. The required densities (ρ) were measured with an Ostwald–Sprengel type pycknometer having a bulb volume of 25 cm^3 and an internal diameter of the capillary of about 0.1 cm. The relative viscosity (η_r) was obtained as the ratio of the absolute viscosity of the solution (η) to that of the pure solvent (η_0).

The solutions were prepared by mass for the viscosity runs, the molalities being converted to molarities by the use of densities. To avoid moisture pick-up, all solutions were prepared in a dehumidified room with utmost care. In all cases, the experiments were performed at least in five replicates for each solution and the results were averaged. Several independent solutions were prepared and the runs were performed to ensure the reproducibility of the results.

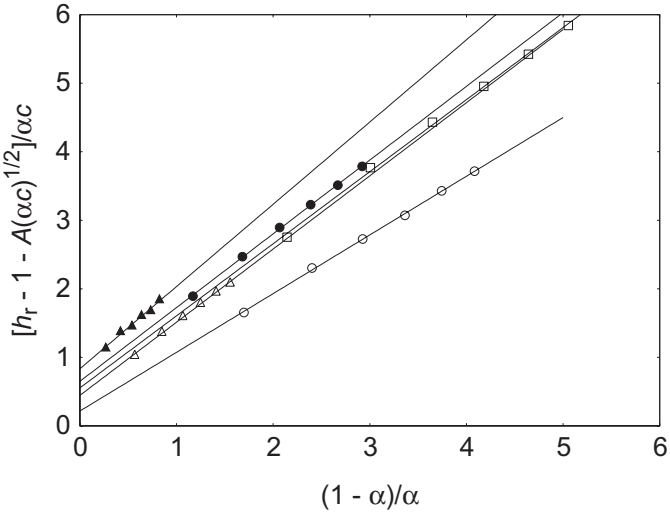
Results and discussion

The measured relative viscosities (η_r) and densities (ρ) of electrolyte solutions as functions of molar concentrations (c) at 308.15, 313.15, 318.15, and 323.15 K are given in Table 2.

The relative viscosities of the electrolytes in solution are generally analyzed by the Jones–Dole equation (19):

$$[3] \qquad \eta_r = 1 + Ac^{1/2} + Bc$$

Fig. 1. Variation of $[\eta_r - 1 - A(\alpha c)^{1/2}]/\alpha c$ against $(1 - \alpha)/\alpha$ at 308.15 K in 2-ethoxyethanol for Et_4NBr (○), Pr_4NBr (△), Bu_4NBr (□), Pen_4NBr (●), and Hep_4NBr (▲).



where A and B, the characteristic parameters for salt and solvent, depend on ion–ion and ion–solvent interactions, respectively.

As the electrolytes investigated here are found to be somewhat associated from our earlier conductivity measurements (6, 7), the viscosity data have been analyzed by the following equation (9):

$$[4] \qquad \eta_r = 1 + A(\alpha c)^{1/2} + B\alpha c + B'(1 - \alpha)c$$

Here A, B, and B' are the characteristic constants and α is the degree of dissociation of the ion pair.
Equation [4] can be rearranged to give

$$[5] \qquad \frac{[\eta_r - 1 - A(\alpha c)^{1/2}]}{\alpha c} = B + B'\left(\frac{1-\alpha}{\alpha}\right)$$

For the evaluation of B coefficients from eq. [5], plots of $[\eta_r - 1 - A(\alpha c)^{1/2}]/\alpha c$ against $(1 - \alpha)/\alpha$ were constructed. These were found to be linear in all cases. A representative plot displays the variation of $[\eta_r - 1 - A(\alpha c)^{1/2}]/\alpha c$ against $(1 - \alpha)/\alpha$ at 308.15 K (Fig. 1). The values of α were calculated from the conductance data (6, 7) using the equations described in the literature (9). The A values were calculated theoretically from the physical parameters of the solvent and the limiting ionic equivalent conductances using the Falkenhagen and Vernon equation (20):

$$[6] \qquad A = \frac{0.2577\Lambda^0}{\eta_0(\varepsilon T)^{1/2}\lambda_+^0\lambda_-^0}\left[1 - 0.6863\left(\frac{\lambda_+^0 - \lambda_-^0}{\Lambda^0}\right)^2\right]$$

where η_0 is the coefficient of viscosity of the solvent, ε is its relative permittivity, T is the temperature in absolute scale, and Λ^0, λ_+^0, and λ_-^0 are the limiting equivalent conductivities of the electrolyte, cation, and anion, respectively. The values of the A coefficients thus obtained are recorded in Table 3. These have been used for the analysis of the viscosity data. The viscosity B coefficients have also been included in Table 3.

© 2005 NRC Canada

Table 2. Molar concentrations, densities, and relative viscosities of some tetraalkylammonium bromides in 2-ethoxyethanol at 308.15, 313.15, 318.15, and 323.15 K.

c (mol dm^{-3})	ρ (g cm^{-3})	η_r	c (mol dm^{-3})	ρ (g cm^{-3})	η_r
308.15 K					
Et_4NBr			Pr_4NBr		
0.010 15	0.918 36	1.008 0	0.010 08	0.918 38	1.009 1
0.020 31	0.919 33	1.016 0	0.020 16	0.919 35	1.018 1
0.030 46	0.920 29	1.023 7	0.030 24	0.920 32	1.027 1
0.040 62	0.921 27	1.031 4	0.040 32	0.921 30	1.036 2
0.050 77	0.922 22	1.039 7	0.050 40	0.922 26	1.045 3
0.060 92	0.923 18	1.047 7	0.060 48	0.923 23	1.054 1
Bu_4NBr			Pen_4NBr		
0.009 99	0.918 42	1.010 6	0.009 96	0.918 44	1.011 1
0.019 98	0.919 39	1.021 1	0.019 92	0.919 41	1.021 4
0.029 97	0.920 37	1.031 2	0.029 88	0.920 39	1.031 7
0.039 96	0.921 36	1.041 1	0.039 84	0.921 38	1.041 8
0.049 95	0.922 33	1.051 1	0.049 80	0.922 34	1.051 8
0.059 94	0.923 31	1.061 1	0.059 76	0.923 33	1.062 1
Hep_4NBr					
0.010 12	0.918 47	1.012 8			
0.020 24	0.919 44	1.024 6			
0.030 36	0.920 43	1.034 6			
0.040 48	0.921 42	1.045 8			
0.050 60	0.922 38	1.056 1			
0.060 72	0.923 36	1.068 9			
313.15 K					
Et_4NBr			Pr_4NBr		
0.010 11	0.914 71	1.008 1	0.010 04	0.914 73	1.009 2
0.020 23	0.915 72	1.016 2	0.020 08	0.915 75	1.018 3
0.030 34	0.916 74	1.023 9	0.030 12	0.916 75	1.027 4
0.040 46	0.917 74	1.031 9	0.040 16	0.917 75	1.036 5
0.050 58	0.918 76	1.040 1	0.050 21	0.918 76	1.045 7
0.060 70	0.919 75	1.048 0	0.060 25	0.919 75	1.054 5
Bu_4NBr			Pen_4NBr		
0.009 95	0.914 75	1.010 7	0.009 92	0.914 76	1.011 2
0.019 90	0.915 77	1.021 2	0.019 84	0.915 76	1.021 6
0.029 85	0.916 76	1.031 4	0.029 76	0.916 77	1.031 9
0.039 80	0.917 78	1.041 2	0.039 68	0.917 79	1.042 1
0.049 76	0.918 78	1.051 2	0.049 61	0.918 79	1.052 1
0.059 71	0.919 79	1.061 2	0.059 35	0.919 82	1.062 1
Hep_4NBr					
0.010 08	0.914 81	1.012 9			
0.020 16	0.915 81	1.024 9			
0.030 24	0.916 82	1.036 8			
0.040 32	0.917 85	1.046 2			
0.050 38	0.918 85	1.056 6			
0.060 49	0.919 87	1.069 5			
318.15 K					
Et_4NBr			Pr_4NBr		
0.010 07	0.910 95	1.008 3	0.010 00	0.910 99	1.009 4
0.020 14	0.911 96	1.016 3	0.020 00	0.911 98	1.018 5
0.030 22	0.912 97	1.023 9	0.030 00	0.912 98	1.027 7
0.040 29	0.913 96	1.032 1	0.040 00	0.913 99	1.036 8
0.050 37	0.914 98	1.040 1	0.050 00	0.915 01	1.046 1
0.060 45	0.916 01	1.048 2	0.060 00	0.916 04	1.054 9
Bu_4NBr			Pen_4NBr		
0.009 91	0.911 01	1.010 9	0.009 88	0.911 03	1.011 5
0.019 82	0.912 01	1.021 3	0.019 76	0.912 02	1.022 0

© 2005 NRC Canada

Table 2 (*concluded*).

c (mol dm^{-3})	ρ (g cm^{-3})	η_r	c (mol dm^{-3})	ρ (g cm^{-3})	η_r
0.029 73	0.912 99	1.031 5	0.029 64	0.913 00	1.032 3
0.039 64	0.914 01	1.041 3	0.039 52	0.914 03	1.042 5
0.049 56	0.915 04	1.051 5	0.049 41	0.915 05	1.052 7
0.059 47	0.916 07	1.061 3	0.059 29	0.916 08	1.063 0
Hep_4NBr					
0.010 04	0.911 07	1.013 3			
0.020 08	0.912 07	1.025 3			
0.030 12	0.913 05	1.037 3			
0.040 16	0.914 09	1.046 8			
0.050 20	0.915 09	1.057 1			
0.060 24	0.916 12	1.069 9			
323.15 K					
Et_4NBr			Pr_4NBr		
0.010 03	0.907 03	1.008 4	0.009 96	0.907 05	1.009 5
0.020 06	0.908 02	1.016 5	0.019 91	0.908 05	1.018 7
0.030 09	0.909 05	1.024 0	0.029 87	0.909 07	1.028 0
0.040 12	0.910 04	1.032 4	0.039 83	0.910 09	1.037 1
0.050 16	0.911 07	1.040 7	0.049 80	0.911 12	1.046 5
0.060 19	0.912 08	1.048 5	0.059 75	0.912 13	1.055 4
Bu_4NBr			Pen_4NBr		
0.009 87	0.907 08	1.011 0	0.009 84	0.907 09	1.011 6
0.019 78	0.908 06	1.021 5	0.019 67	0.908 07	1.022 2
0.029 60	0.909 09	1.031 6	0.029 51	0.909 11	1.032 5
0.039 47	0.910 12	1.041 3	0.039 35	0.910 14	1.042 7
0.049 34	0.911 15	1.051 5	0.049 20	0.911 16	1.053 0
0.059 21	0.912 15	1.061 4	0.059 04	0.912 16	1.063 1
Hep_4NBr					
0.009 99	0.907 04	1.013 5			
0.019 99	0.908 12	1.025 7			
0.029 99	0.909 16	1.037 8			
0.039 99	0.910 19	1.047 4			
0.049 99	0.911 18	1.057 7			
0.059 99	0.912 21	1.070 6			

The viscosity data have also been analyzed on the basis of the transition-state treatment of the relative viscosity of electrolyte solutions, as suggested by Feakins et al. (21):

$$[7] \qquad B = \frac{\overline{V}_1^0 - \overline{V}_2^0}{1000} + \frac{\overline{V}_1^0}{1000}\left(\frac{\Delta\mu_2^{0\neq} - \Delta\mu_1^{0\neq}}{RT}\right)$$

In the above equation, $\overline{V}_1^0$ and $\overline{V}_2^0$ are the partial molar volumes of the solvent and solute, respectively. The contribution per mol of solute to the free energy of activation for viscous flow of the solution ($\Delta\mu_2^{0\neq}$) has been determined from the above relationship and is reported in Table 3. The free energy of activation per mol of the pure solvent ($\Delta\mu_1^{0\neq}$) is given by the equation:

$$[8] \qquad \Delta\mu_1^{0\neq} = \Delta G_1^{0\neq} = RT \ln\left(\frac{\eta_0 \overline{V}_1^0}{hN}\right)$$

where N is Avogadro's number and the other symbols have their usual significance.

The activation parameters for viscous flow for the electrolytes obtained from eq. [7] are given in Table 3.

The viscosity B coefficients shown in Table 3 are large and positive for all the electrolytes studied. The B values for the tetraalkylammonium bromides increase regularly as we go from tetraethylammonium bromide through tetraheptylammonium bromide. From this table, we see that $\Delta\mu_2^{0\neq}$ values for all the electrolytes are also large and positive, and they follow the same pattern as the B values.

To investigate the specific behavior of the individual ions comprising these electrolytes, it is necessary to split the viscosity B coefficients into their ionic components.

Krumgalz (22) proposed a method, to be applied for nonaqueous solvents, based on his contention that the larger tetraalkylammonium ions are essentially unsolvated in such solvents. Plots of the B coefficients of the iodides of these cations in several organic solvents against the cubes of the radii of the ions are indeed found to be linear for Bu_4N^+ and larger cations, values being known upto Hep_4N^+ (22). The intercepts of the straight lines then give the B coefficient of the counterion, iodide.

$$[9] \qquad B(R_4N^+) = B(I^-) + br^3_{R_4N^+}$$

The slope depends on the solvent and the temperature. The B coefficient of Pr_4NI may conform to the straight line ob-

© 2005 NRC Canada

Table 3. Theoretical A coefficients, the viscosity B coefficients, and the free energies of activation for viscous flow of electrolytes in 2-ethoxyethanol at 308.15, 313.15, 318.15, and 323.15 K.

Electrolyte	A ($dm^{3/2}$ $mol^{-1/2}$)	B (dm^3 mol^{-1})	$\Delta\mu_2^{0\neq}$ (kJ mol^{-1})
308.15 K			
Et_4NBr	0.0290	0.216±0.001	21.52
Pr_4NBr	0.0309	0.444±0.001	29.02
Bu_4NBr	0.0328	0.554±0.005	33.44
Pen_4NBr	0.0356	0.649±0.001	37.51
Hep_4NBr	0.0417	0.833±0.002	45.55
313.15 K			
Et_4NBr	0.0316	0.196±0.001	20.91
Pr_4NBr	0.0339	0.428±0.001	28.65
Bu_4NBr	0.0361	0.534±0.006	33.02
Pen_4NBr	0.0391	0.629±0.001	37.13
Hep_4NBr	0.0460	0.820±0.004	45.46
318.15 K			
Et_4NBr	0.0354	0.179±0.001	20.41
Pr_4NBr	0.0378	0.411±0.001	28.23
Bu_4NBr	0.0406	0.512±0.004	32.54
Pen_4NBr	0.0444	0.603±0.001	36.62
Hep_4NBr	0.0514	0.814±0.004	45.57
323.15 k			
Et_4NBr	0.0377	0.168±0.002	20.16
Pr_4NBr	0.0404	0.396±0.001	27.95
Bu_4NBr	0.0444	0.493±0.005	32.32
Pen_4NBr	0.0476	0.587±0.001	36.40
Hep_4NBr	0.0551	0.800±0.004	45.52

tained using the larger cations in some solvents and not in others, whereas the values for Et_4NI and Me_4NI generally fall below the line. Possibly, the position of these tetraalkylammonium ions are caused by the shape of these ions during the viscous flow process in 2-ethoxyethanol making a relatively smaller contribution to B values. This would result from a more compact arrangement of the alkyl groups around the central nitrogen.

Since the tetraalkylammonium ions investigated in this work are found to be unsolvated in 2-ethoxyethanol from our earlier conductivity study (6, 7), the method of Krumgalz (22) described previously should, in principle, be applicable to the present viscosity data. In fact, we obtained very good straight lines (cf. Fig. 2) for tetraalkylammonium bromides with tetrapropylammonium and larger cations when $B(R_4NBr)$ values are plotted against the cubes of the radii of the cations (r) obtained from the literature (23–25) at all temperatures investigated (Et_4NBr being an exception, B coefficients of which always fall below the lines). The ionic viscosity B coefficients obtained following the Krumgalz method (22) are given in Table 4.

The observed order of the viscosity B values for the tetraalkylammonium ions (Table 3), $Hep_4N^+ > Pen_4N^+ > Bu_4N^+ > Pr_4N^+ > Et_4N^+$ (anion being common), shows that the obstruction of the solvent viscous flow increases with an increase in the size of these species in solution. This clearly

Fig. 2. Representative plot for the variation of the viscosity B coefficient of the tetraalkylammonium bromides against the cube of the cationic radius in 2-ethoxyethanol at 308.15 K (○), 313.15 K (△), 318.15 K (□), and 323.15 K (●).

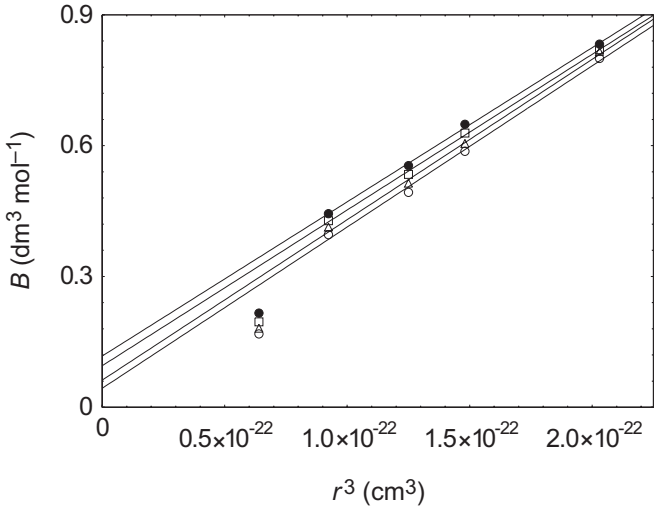


Table 4. Ionic viscositiy B coefficients and ionic free energies of activation for viscous flow in 2-ethoxyethanol at 308.15, 313.15, 318.15, and 323.15 K.

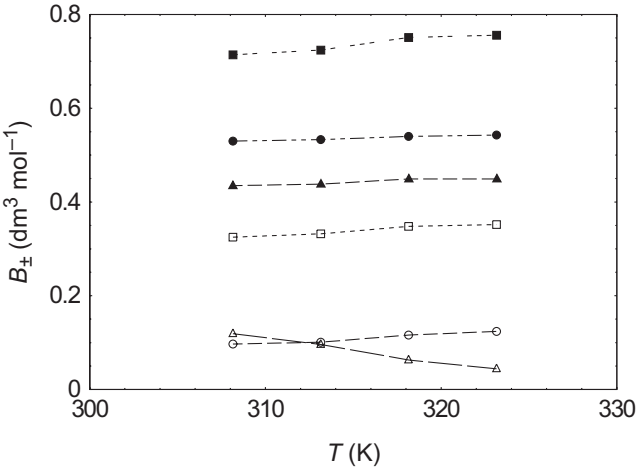
Ion	308.15 K	313.15 K	318.15 K	323.15 K
$B_\pm$ (dm^3 mol^{-1})				
Et_4N^+	0.099	0.102	0.117	0.125
Pr_4N^+	0.327	0.333	0.349	0.353
Bu_4N^+	0.437	0.439	0.450	0.450
Pen_4N^+	0.532	0.534	0.541	0.544
Hep_4N^+	0.716	0.725	0.752	0.757
Br^-	0.117	0.095	0.062	0.044
$\Delta\mu_2^{0\neq}$ (kJ mol^{-1})				
Et_4N^+	6.56	6.65	7.19	7.43
Pr_4N^+	14.06	14.39	15.01	15.22
Bu_4N^+	18.48	18.76	19.32	19.59
Pen_4N^+	22.55	22.87	23.40	23.67
Hep_4N^+	30.59	31.20	32.35	32.79
Br^-	14.96	14.26	13.22	12.73

indicates a lack of solvation of these ions in 2-ethoxyethanol solutions. Had these ions been solvated in 2-ethoxyethanol, the smaller ions with greater charge density would have been more solvated and the order of the ionic viscosity B coefficients would have been in the reverse order, which is, obviously, not the case here.

Figure 3 shows the temperature dependence of the viscosity B coefficients of the bromide and tetraalkylammonium ions in 2-ethoxyethanol. For all the ions studied, the B values are positive and their temperature coefficients are small; although positive coefficients are exhibited by the tetraalkylammonium ions, they are negligibly small. Bromide ion, however, shows a comparatively larger negative temperature coefficient. The temperature dependence of the B coefficients for the tetraalkylammonium ions in methanol, *N*-methyl-

© 2005 NRC Canada

Fig. 3. Temperature dependence of the ionic viscosity *B* coefficients in 2-ethoxyethanol for Br^- (△), Et_4N^+ (○), Pr_4N^+ (□), Bu_4N^+ (▲), Pen_4N^+ (●), and Hep_4N^+ (■).



formamide, *N*-methylpropionamide, and *N*-methylacetamide are also small (10, 26, 27), and we find the same behavior in the present solvent medium. This finding is in sharp contrast to the abnormally large temperature dependence of the *B* coefficients in water (10), and the remarkable difference can be ascribed to the extensive, hydrogen-bonded structure of water. The negligibly small d*B*/d*T* values of the tetraalkylammonium ions indicate that they behave neither as structure breaker nor as structure maker in 2-ethoxyethanol, whereas the negative d*B*/d*T* value for bromide ion in this medium demonstrates its structure-making behavior.

The ionic free energies of activation for viscous flow ($\Delta\mu_2^{0\neq}$, ion) based on a method similar to that used for the separation of the viscosity *B* coefficients have been presented in Table 4. The $\Delta\mu_2^{0\neq}$ values of the tetraalkylammonium ions are always found to be positive, thus indicating that the formation of the transition state is made less favorable in the presence of these ions. The ionic $\Delta\mu_2^{0\neq}$ values in the present series of tetraalkylammonium ions increase steadily with the formula weight of the cations (cf. Table 4); this behavior is reasonable when solvation effects are not overriding.

Acknowledgements

The authors gratefully acknowledge the financial support by the Special Assistance Programme (SAP) of the University Grants' Commission, India.

References

1. C. Guha, J.M. Chakraborty, S. Karanjai, and B. Das. J. Phys. Chem. **107**, 12 814 (2003).
2. D. Das, B. Das, and D.K. Hazra. J. Solution Chem. **32**, 77 (2003).
3. D. Das, B. Das, and D.K. Hazra. J. Solution Chem. **32**, 85 (2003).
4. J.M. Chakraborty and B. Das. Z. Phys. Chem. (Muenchen), **218**, 219 (2004).
5. D. Das, B. Das, and D.K. Hazra. J. Mol. Liq. **111**, 15 (2004).
6. P. Haldar and B. Das. Z. Phys. Chem. (Muenchen), **218**, 599 (2004).
7. P. Haldar and B. Das. Z. Phys. Chem. (Muenchen), **218**, 1129 (2004).
8. R.W. Gurney. *In* Ionic processes in solution. Dover Publications, New York. 1962.
9. J. Crudden, G.M. Delaney, D. Feakins, P.J. O'Reilley, W.E. Waghorne, and K.G. Lawrence. J. Chem. Soc. Faraday Trans. 1, **82**, 2195 (1986).
10. H.D.B. Jenkins and Y. Marcus. Chem. Rev. **95**, 2695 (1995).
11. G. Douheret and A. Pal. J. Chem. Eng. Data, **32**, 40 (1998).
12. Y. Marcus. *In* Ion solvation. John Wiley and Sons, New York. 1985.
13. M.I. Aralaguppi, C.V. Jadar, and T.M. Aminabhavi. J. Chem. Eng. Data, **42**, 301 (1997).
14. A. Pal and S. Kumar. Phys. Chem. Liq. **41**, 423 (2003).
15. G. Chandrasekhar, P. Ventatesu, and M.V. Prabhakara Rao. J. Chem. Eng. Data, **45**, 590 (2004).
16. D.F. Evans, C. Zawoyski, and R.L. Kay. J. Phys. Chem. **69**, 387 (1965).
17. B. Das and D.K. Hazra. J. Chem. Eng. Data, **38**, 361 (1993).
18. N. Saha, B. Das, and D.K. Hazra. J. Chem. Eng. Data, **40**, 1264 (1995).
19. G. Jones and M. Dole. J. Am. Chem. Soc. **51**, 2950 (1929).
20. H. Falkenhagen and E.L. Vernon. Phys. Z. **33**, 140 (1932).
21. D. Feakins, D.J. Freemantle, and K.G. Lawrence. J. Chem. Soc. Faraday Trans. 1, **70**, 795 (1974).
22. B.S. Krumgalz. J. Chem. Soc. Faraday Trans. 1, **76**, 1275 (1980).
23. P.K. Muhuri and D.K. Hazra. Z. Naturforsch A, **48a**, 523 (1993).
24. D.S. Gill and M.B. Sekhri. J. Chem. Soc. Faraday Trans. 1, **78**, 119 (1982).
25. J.F. Coetzee and G.P. Cunningham. J. Am Chem. Soc. **87**, 2529 (1965).
26. R.L. Kay, T. Vituccio, C. Zawoyski, and D.F. Evans. J. Phys. Chem. **70**, 2336 (1966).
27. R.L. Kay, C. Zawoyski, and D.F. Evans. J. Phys. Chem. **69**, 4208 (1965).

© 2005 NRC Canada

Solid lithium perchlorate as a powerful catalyst for the synthesis of β-aminoalcohols under solvent-free conditions

Najmodin Azizi and Mohammad R. Saidi

Abstract: Lithium perchlorate catalyzed the ring opening of epoxides with amines to provide the corresponding β-aminoalcohols in excellent yields with high regioselectivity. The reaction proceeds rapidly under mild and neutral conditions and worked well with primary, secondary, aliphatic, aromatic, and hindered amines in short times at room temperature, in the absence of solvent.

Key words: epoxide, lithium perchlorate, β-aminoalcohols, solvent-free.

Résumé : Le perchlorate de lithium catalyse l'ouverture de cycle des époxydes avec des amines qui conduit aux β-aminoalcools correspondants avec d'excellents rendements et une régiosélectivité élevée. La réaction se produit rapidement dans des conditions douces et neutres et elle se produit rapidement avec les amines primaires, secondaires, aliphatiques, aromatiques et empêchées, à la température ambiante et en l'absence de solvant.

Mots clés : époxyde, perchlorate de lithium, β-aminoalcools, sans solvant.

[Traduit par la Rédaction]

Introduction

β-Aminoalcohols are versatile intermediates in the synthesis of a vast variety of biologically active natural and synthetic products (1), unnatural amino acids (2), and chiral auxiliaries for asymmetric synthesis (3). The classical synthesis of β-aminoalcohols consists of heating an epoxide with an excess of amine at elevated temperatures (4). High temperatures may not be appropriate for certain functional groups. Also, a variety of air-sensitive or expensive catalysts had been reported in the literature to perform epoxide opening at room temperature. Many of these catalysts are either corrosive, or in some cases, they are being applied to aromatic amines with poor regioselectivity and with undesirable side reactions such as rearrangement and polymerization (5–7). However, there are still some limitations with the reported methods in the literature. For example, deactivated amines failed to open up the epoxides or require high temperatures. Furthermore, they require a high catalyst-to-substrate ratio, have a long reaction time, and they need volatile organic solvents that eventually results in the generation of a large amount of toxic waste. To overcome these limitations, the development of a better catalyst for the activation of epoxides, rendering them more susceptible to nucleophilic attack under a mild, efficient, and general method, is of great interest.

Received 26 July 2004. Published on the NRC Research Press Web site at http://canjchem.nrc.ca on 18 May 2005.

N. Azizi and M.R. Saidi.[1] Department of Chemistry, Sharif University of Technology, P.O. Box 11365-9516, Tehran, Iran.

[1]Corresponding author (e-mail: saidi@sharif.edu).

In recent years, to minimize the harmful organic solvents used in chemical processes, much attention has been devoted to the use of alternative media. Besides the use of supercritical fluid water and ionic liquids, the possibility of performing chemical reactions in the absence of solvent has been receiving more attention (8).

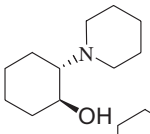
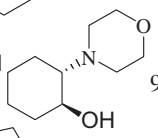
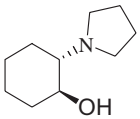
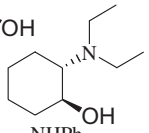
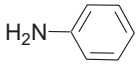
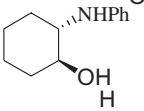
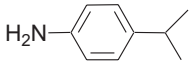
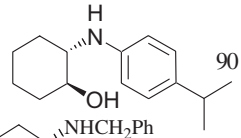
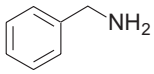
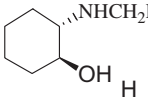
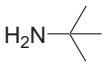
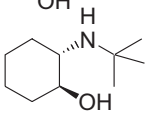
Results and discussion

Because of our interest for developing solvent-free and environmentally benign synthetic methods (9), herein, we report a more simple, general, and new catalytic route for the synthesis of β-aminoalcohols via opening of epoxides with amines under solvent-free conditions in the presence of a catalytic amount of $LiClO_4$. At first, we examined the reaction of cyclohexene oxide with aniline and 0.2 equiv. of solid $LiClO_4$ at room temperature. Complete conversion took place within 120 min, leading to quantitative yield of *trans*-2-phenyl amino cyclohexanol. This success encouraged us to exploit the generality and scope of this reaction for the opening of other epoxides with various aromatic and aliphatic amines under catalytic amounts of $LiClO_4$. The reaction proceeded well with aromatic, aliphatic, hindered, and unhindered amines. The role of $LiClO_4$ in catalyzing the opening of epoxide rings with amines maybe realized through the coordination of Li^+ with the epoxide oxygen and renders the epoxide more susceptible to nucleophilic attack by the amine, which after protonation forms the aminoalcohol (Table 1).

In the next step, we have examined various amines using styrene oxide as the unsymmetrical epoxide to investigate the regioselectivity outcome of the reaction. In all cases, the ring openings take place in highly regioselective fashion, affording the β-aminoalcohols in high yields. It should also be

 doi: 10.1139/V05-062 © 2005 NRC Canada

Table 1. β-Aminoalcohols prepared from cyclohexene oxide.

Entry	Epoxide	Amine	Product	Yield (%)[a]	Time (min)
1				93	80
2				92	40
3				94	40
4				86	80
5				95	120
6				90	120
7				90	120
8				80	120

[a]Isolated yields.

mentioned that without using solid $LiClO_4$, no reaction was observed among various amines and styrene oxide. On each occasion, the regioselectivity and the ratio of the two regioisomers were determined by ^1H NMR and by comparison with the reported value in the literature (6, 7).

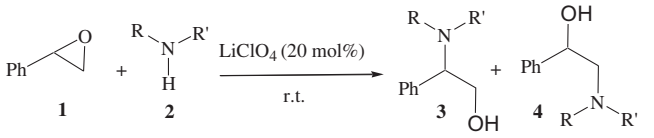
In conclusion, we have shown that $LiClO_4$ is a new, highly efficient catalyst for the opening of epoxides with amines leading to the synthesis of β-aminoalcohols. In fact, this reaction proceeds smoothly in solvent-free conditions, which is an important feature for the development of green chemistry.

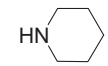
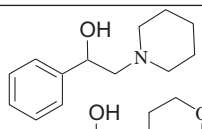
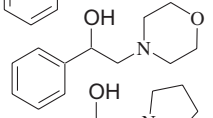
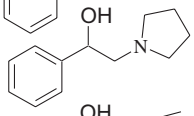
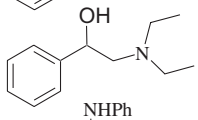
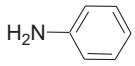
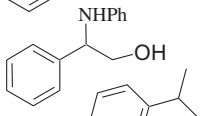
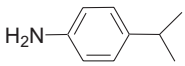
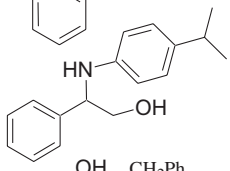
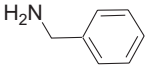
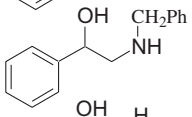
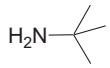
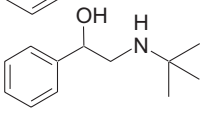
Experimental

General procedure for the preparation of β-aminoalcohols

To a mixture of epoxide (5 mmol) and amine (6 mmol) in the test tube, anhydr. $LiClO_4$ was added (0.1 g), and the mixture was stirred at room temperature for 30–180 min. When the reaction was completed, as indicated by TLC or GC, the reaction mixture was diluted with diethyl ether or ethyl acetate (15 mL) and washed with water; the organic phase was separated, dried with Na_2SO_4, and solvent was removed using a rotary evaporator. In all cases, almost pure compound was obtained. Further purification was carried out by short column chromatography on silica gel (ethyl acetate – petroleum ether). All compounds were characterized on the basis of their spectroscopic data (IR, NMR, and GC) and by comparison with those reported in the literature (Table 2).

Table 2. β-Aminoalcohols produced from styrene oxide.



Entry	Amine	Major Product	Yield[a] (%)	Ratio **3:4**	Time (min)
1			95	83:17	30
2			96	76:24	30
3			97	84:16	30
4			92	98:2	60
5			96	10:90	80
6			93	8:92	80
7			92	86:16	90
8			82	81:19	90

[a]Isolated yields.

Acknowledgments

We are grateful to the Research Council of Sharif University of Technology for financial support. We also thank Volkswagen-Stiftung, Federal Republic of Germany for financial support towards the purchase of chemicals.

References

1. (*a*) C. Bonini and G. Righi. Synthesis, 225 (1994); (*b*) V.K. Aggarwal, J.N. Harvey, and J. Richardson. J. Am. Chem. Soc. **124**, 5747 (2002); (*c*) A.K. Ghosh and Y. Wang. J. Org. Chem. **64**, 2789 (1999).
2. (*a*) D.R. Gehlert, D.J. Goldstein, and P.A. Hipskind. Ann. Rep. Med. Chem. 201 (1999); (*b*) E.J. Corey and F. Zhang. Angew. Chem. Int. Ed. **38**, 1931 (1999).
3. (*a*) P. O'Brien. Angew. Chem. Int. Ed. **38**, 326 (1999); (*b*) G. Li, H.-T. Chang, and K.B. Sharpless. Angew. Chem. Int. Ed. Engl. **35**, 451 (1996); (*c*) J. Takehra, S. Hashiguchi, A. Fujii, and R. Nayori. J. Chem. Soc. Chem. Commun. 233 (1996).

© 2005 NRC Canada

4. D.J. Ager, I. Prakash, and D.R. Schaad. Chem. Rev. **96**, 835 (1996).
5. (*a*) A.K. Chakraborti and A. Kondaskar. Tetrahedron Lett. **44**, 8315 (2003); (*b*) L.D. Pachon, P. Gamez, J.J.M. Van Brussel, and J. Reedijk. Tetrahedron Lett. **44**, 6025 (2003); (*c*) J. Iqbal and A. Pandey. Tetrahedron Lett. **31**, 575 (1990); (*d*) S. Chandrasekhar, T. Ramchander, and S.J. Prakash. Synthesis, 1817 (2000); (*e*) T. Ollevier and G. Lavie-Compin. Tetrahedron Lett. **43**, 7891 (2002); (*f*) L.R. Reddy, M.A. Reddy, N. Bhanumathi, and K.R. Roa. Synthesis, 831 (2001).
6. (*a*) M. Chini, P. Crotti, and F. Macchia. J. Org. Chem. **56**, 5939 (1991); (*b*) M. Chini, P. Crotti, and F. Macchia. Tetrahedron Lett. **31**, 4661 (1991).
7. (*a*) M.M. Mojtahedi, M.R. Saidi, and M. Bolourtchian. J. Chem. Res. S, 128 (1999); (*b*) J.S. Yadav, B.V.S. Reddy, A.K. Basak, and A. Venkat Narsaiah. Tetrahedron Lett. **44**, 1047 (2003); (*c*) A.K. Chakraborti, S. Rudrawar, and A. Kondaskar. Org. Biomol. Chem. **2**, 1277 (2004); (*d*) P.-Q. Zhao, L.-W. Xu, and C.-G. Xia. Synlett, 846 (2004); (*e*) M.M. Khodaei, A.R. Khosropour, and K. Ghozati. Tetrahedron Lett. **45**, 3525 (2004).
8. (*a*) K. Tanaka and F. Toda. Chem. Rev. **100**, 1025 (2000); (*b*) R.S. Varma. Green. Chem. 43 (1999); (*c*) J.O. Metzger. Angew. Chem. Int. Ed. **98**, 2975 (1998).
9. (*a*) N. Azizi and M.R. Saidi. Tetrahedron, **60**, 383 (2004); (*b*) N. Azizi and M.R. Saidi. Eur. J. Org. Chem. 4630 (2003).

© 2005 NRC Canada

^{29}Si NMR studies on the mechanism of dehydrocoupling of hydrosilanes with hydroxylic reagents in DMF — The role of DMF

Jerzy J. Chruściel

Abstract: Interactions of DMF with hydrosilanes were studied by ^{29}Si NMR. New resonance signals were observed in the ^{29}Si NMR spectra of $HMe_2SiOSiMe_2H$ and some (alkoxy)hydrosilanes for high ratios of concentrations [DMF]/[H-silane] at 25 °C. The intensities of new signals increased several times at –60 °C. It seems that these new resonances correspond to molecular complexes of DMF with hydrosilanes. The role of DMF in the mechanism of dehydrocoupling of hydrosilanes with hydroxylic reagents in the presence of Zn(II) and Cd(II) halides (X = Cl, Br, I) is discussed. Some common features of the reaction mechanism with the mechanism of hydride transfer from the Si—H bond to the carbenium ion are discussed.

Key words: hydrosilanes, hydroxylic reagents, reaction mechanism of dehydrocoupling in DMF, ^{29}Si NMR.

Résumé : Faisant appel à la RMN du ^{29}Si, on a étudié les interactions du DMF avec les hydrosilanes. À 25 °C et à des rapports élevés des concentrations [DMF]/[H-silane], on a observé de nouveaux signaux de résonance dans les spectres RMN du ^{29}Si du $HMe_2SiOSiMe_2H$ et de quelques (alkoxy)hydrosilanes. Les intensités des nouveaux signaux ont augmenté à quelques reprises à –60 °C. Il semble que ces nouvelles résonances correspondent à la formation de complexes moléculaires du DMF avec les hydrosilanes. On discute du rôle du DMF dans le mécanisme de déshydrocouplage des hydrosilanes avec les réactifs hydroxylés, en présence d'halogénures (X = Cl, Br, I) de Zn(II) et de Cd(II). On discute aussi de caractéristiques communes du mécanisme réactionnel avec le mécanisme de transfert d'hydrure de la liaison Si—H à l'ion carbénium.

Mots clés : hydrosilanes, réactifs hydroxylés, mécanisme de réaction du déshydrocouplage dans le DMF, RMN du ^{29}Si.

[Traduit par la Rédaction]

Introduction

A great number of publications have been devoted to the studies of the mechanism of the nucleophilic substitution of hydrogen at silicon (1–12). Dehydrocoupling reactions of hydrosilanes with nucleophilic reagents containing a hydroxyl group:

[1] $$\geq Si-H + HO-R \xrightarrow{Cat.} \geq Si-OR + H_2$$

find many practical applications, and especially in the synthesis of alkoxysilanes, acetoxysilanes, silanols, block siloxanes, and different derivatives of poly(methylsiloxanes) (13, 14). Precious contributions to acid-promoted solvolysis of hydrosilanes were made by Eaborn (2) and Nahlovský and Chvalovský (15, 16), and to the base-promoted solvolysis of hydrosilanes by Schowen and co-workers (17) and Eaborn and Jenkins (18). Reaction rates of the solvolysis of hydrosilanes strongly depend on their structure and medium effects (19–24). Usually, the reaction is catalyzed either by nucleophilic or electrophilic catalysts: bases, acids, metals, metal and tetralkylammonium salts, and metal complexes (13).

In dimethylformamide (DMF) medium, in the presence of zinc and cadmium halides as catalysts, *dehydrocoupling* of hydrosilanes with hydroxylic reagents *proceeds through a new mechanism of the nucleophilic substitution of the Si—H bond with reagents containing a hydroxyl group, because of zero order with respect to hydroxyl groups. It has been found to be first order in hydrosilanes and catalysts* (25–29). The driving force of the reaction is an electrophilic attack of active ionic forms of catalysts (Zn^{2+} or Cd^{2+}) on the hydrogen atom of the Si—H bond, as it was concluded from investigations of the effect of the common anion with the catalyst on reaction rates (29). The reaction is enthalpy-controlled. The high negative entropy of activation ($\Delta S^{\ddagger}$ = –30 to –35 eu) showed a highly complex and polar structure of the transition state (27). The low negative Hammett reaction constant (ρ = –0.12) and the low deuterium kinetic isotope effect (k_H/k_D = 1.4–1.5) suggested that the intermediate complex has an unsymmetrical nonlinear (bent) structure, and a high bond order for the Si—H (25).

Studies of DMF concentration on rates of reaction of triethylsilane with diphenylsilanediol and benzoic acid towards $ZnCl_2$ and $CdBr_2$, in solutions of DMF (n_{DMF}) with tetra-

Received 8 September 2004. Published on the NRC Research Press Web site at http://canjchem.nrc.ca on 20 May 2005.

J.J. Chruściel. Institute of Polymer and Dye Technology, Faculty of Chemistry, Technical University, 90-924 Łódź 40, Poland. (e-mail: jchrusci@p.lodz.pl).

 doi: 10.1139/V05-072 © 2005 NRC Canada

hydrofuran (THF) and 1,4-dioxane, allowed us (30) to determine the reaction order with respect to DMF, which was dependent on the concentration of DMF. At lower concentrations of DMF, $n_{DMF} = 2$ was obtained. In less polar solvents (benzene, toluene, ether, THF), even at reflux, dehydrocoupling of tertiary hydrosilanes with hydroxylic reagents doesn't take place in the presence of Zn(II) and Cd(II) halides without cocatalysis by DMF molecules.

In this paper, results of the studies of interactions of hydrosilanes with DMF by means of ^{29}Si NMR spectroscopy are presented. The role of DMF in the mechanism of dehydrocoupling of hydrosilanes with hydroxylic reagents in the presence of Zn(II) and Cd(II) halides is discussed.

Experimental

Reagents

Syntheses and purification of some hydrosilanes, diphenylsilanediol, and the purification of DMF are described elsewhere (25, 27). All hydrosilanes were dried with $MgSO_4$ or molecular sieves (4 Å) and fractionally distilled. Their purity was controlled by GC (99.9%) and NMR. Ph_2MeSiH (Gelest, Inc., Tullytown, Penn.) was fractionally distilled at a bp of 138.5 °C / 11 torr (1 torr = 133.322 4 Pa). 1,1,3,3-Tetramethyldisiloxane was prepared by a hydrolytic condensation of HMe_2SiCl in ether at 0 °C (bp 70.5–71 °C, n_D^{20} = 1.3700). The physical data for the organosilicon compounds are available from ref. 31.

NMR

^{1}H, ^{29}Si, and ^{13}C NMR spectra were recorded on Bruker MSL 300 MHz instrument, operating in the FT mode at 59.627 MHz for ^{29}Si NMR, at 300.13 MHz for ^{1}H NMR, and at 75.47 MHz for ^{13}C NMR, using 10 mm OD sample tubes with a $CDCl_3$ internal (or external) lock. Hexamethyldisiloxane was used as the external ^{29}Si NMR standard (δ = 6.98 ppm, in $CDCl_3$). ^{29}Si NMR proton-decoupled measurements were made with use of the INEPT polarization transfer microprogram and the following parameters (for most spectra): TD (time domain - computer memory used for storage of data points of a spectrum) = 32 K, AQ (acquisition time) = 0.819 s, D0 (delay between pulses) = 4.0 s (or 3.0 s). The other delay values applied were D1 = 12.0 μs, D2 = 24.0 μs, D3 = 20.0 μs, D4 = 1.0 μs, D5 = 1000.0 μs, D6 = 20.0 ms (or 4.0 ms, or 16 ms), D7 = 46.0 ms, D8 = 5.0 ms (or 1.0 ms, or 8.0 ms), D9 = 1.0 μs, D10 = 8.9 μs, D11 = 28.0 μs (or 24.0 μs), D12 = 56.0 μs (or 48.0 μs), D13 = 1.0 μs, D14 = 1.0 μs, D15 = 100.0 μs.

NMR (in $CDCl_3$, δ ppm) for $HMe_2SiOSiMe_2H$: ^{1}H NMR (in C_6D_6): 0.13 (d, 12H, J = 3.01 Hz, CH_3-Si), 4.90 (h, 2H, J = 2.78 Hz, Si-H). ^{29}Si NMR: –4.61 (s). For $(MeO)_3SiH$: bp 83.5–84.0 °C / 744 torr (1 torr = 133.322 4 Pa). ^{29}Si NMR: –54.86 (s). For $(EtO)_3SiH$: bp 131.5 °C. ^{1}H NMR: 1.25 (t, 9H, J = 7.02 Hz, CH_3), 3.85 (q, 6H, J = 7.01 Hz, CH_2O). ^{13}C NMR: 18.06 (CH_3), 58.23 (CH_2O). ^{29}Si NMR: –58.44 (s). For $(EtO)_2MeSiH$: bp 98.0–98.5 °C / 742 torr (1 torr = 133.322 4 Pa). ^{1}H NMR: 0.21 (d, 3H, J = 1.77 Hz, CH_3-Si), 1.24 (t, 6H, J = 7.00 Hz, CH_3), 3.81 (q, 4H, J = 7.00 Hz, CH_2O), 4.58 (q, 1H, J = 1.72 Hz, Si-H. ^{13}C NMR: –3.50 (CH_3-Si), 18.17 (CH_3), 59.06 (CH_2O). ^{29}Si NMR: –16.13 (s). For $(EtO)Me_2SiH$: bp 57.5 °C / 752 torr (1 torr = 133.322 4 Pa). ^{1}H NMR: 0.21 (d, 6H, J = 2.85 Hz, CH_3-Si), 1.21 (t, 3H, J = 6.98 Hz, CH_3), 3.71 (q, 2H, J = 6.99 Hz, CH_2O), 4.62 (h, J = 2.81 Hz, Si-H). ^{13}C NMR: –1.61 (CH_3-Si), 18.14 (CH_3), 59.65 (CH_2O). ^{29}Si NMR: 4.67 (s).

The ^{29}Si-NMR data for the organosilicon compounds are also accessible from ref. 32.

Results and discussion

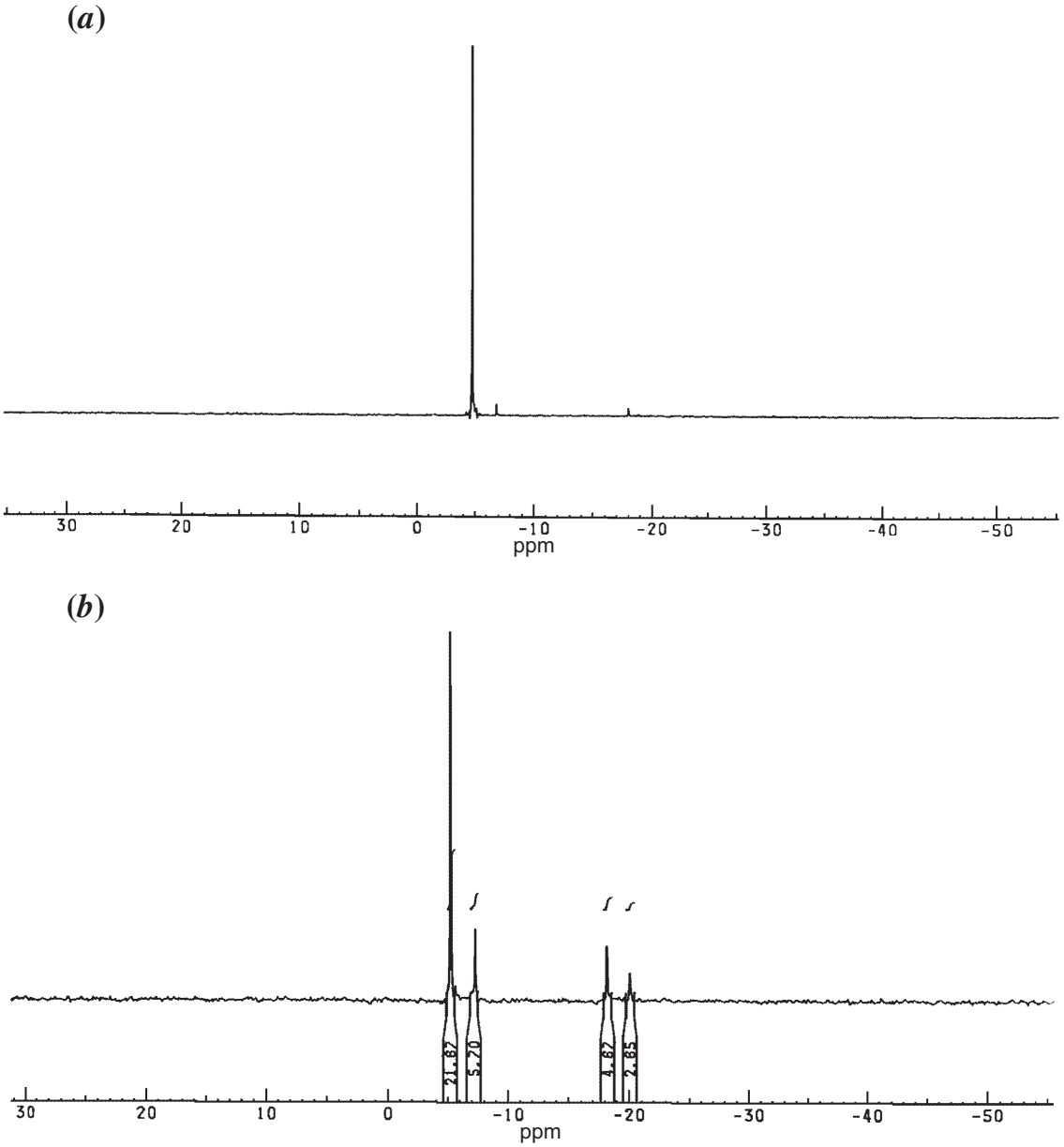
^{29}Si NMR studies

^{29}Si NMR is a very useful tool for studying the equilibria between four-coordinate silanes and higher-coordinate species in solution, as well as characterizing these compounds as penta- or hexa-coordinate silicon compounds (33, 34). According to Voronkov, such coordination of a solvent molecule to the silane takes place only when an electron-withdrawing substituent is present on the silicon atom (35–37). Five-, hexa-, and hypercoordinated silicon species were established as intermadiates in nucleophilic substitutions at silicon, in elegant and comprehensive studies, by Corriu and co-workers (6, 10, 11). Penta-coordinated silicon anions $MePhSiF_3^-$ and $Ph_3SiF_2^-$, prepared in a form of pure salts by Damrauer and Danahey (38) were found to be much more reactive toward strong nucleophiles than their tetravalent analogues (39). The temperature-dependent equilibria between tetra- and penta-coordinate forms in the compounds of the general formula o-$(Me_2NCH_2)C_6H_4SiXYZ$ were studied by West, Corriu, and co-workers (40). They concluded that the high reactivity of o-$(Me_2NCH_2)C_6H_4(C_{10}H_7)SiH_2$ with alcohols and acids was associated with intramolecular penta-coordination, which supported an earlier hypothesis that "the Si—H bond is activated toward substitution by coordinative expansion of the silicon atom". An activation of the Si—H bond by nucleophiles (e.g., in CsF-catalyzed reactions of hydrosilanes with alcohols and carbonyl compounds) is associated with coordination of the silicon atom, to give more reactive penta-coordinative species (11). The hydrogen atom has the lowest ability to penta-coordinate among functional groups at silicon (9). Five-coordinate hydrido- (41, 42) and dihydrido-silicates (43) were prepared and characterized by ^{29}Si NMR, e.g.: $HSi(OEt)_4^-K^+$, $[H_2Si(OEt)_3]^-K^+$. Five-coordinate silicon hydrides were postulated as intermediates of the reactions of trihydridosilanes with NaH, KH, and $LiAlH_4$ (44). The formation of penta-coordinated complexes of hydrosilanes containing electronegative ligands [$CF_3SO_2O^-$, 1-methylimidazole, hexamethylphosphoramid (HMPA), dimethylpropyleneurea (DMPU), EtO^-, PhO^-, and H^-) was studied by Bassindale and Jiang by means of ^{29}Si NMR spectroscopy (45). In some cases, cationic five-coordinated complexes $[Nu_2SiMe_2H]^+X^-$ (X = Cl, I, OSO_2CF_3) were isolated as pure compounds (46). Hypervalent silicon hydride compounds reacted with alcohols, water, and benzoic acid without added catalysts (47).

To confirm the presence of DMF molecules in the active complex of the reaction we have conducted studies of solutions of hydrosilanes with DMF by means of ^{29}Si NMR spectroscopy. We recorded ^{29}Si NMR spectra at different molar ratios of hydrosilanes to DMF at 25 °C and –60 °C. We did not find any evidence of a formation of molecular complexes by DMF with triorganohydrosilanes Et_3SiH, Et_2MeSiH, n-Pr_2MeSiH, t-$BuMe_2SiH$, $PhMe_2SiH$, and

© 2005 NRC Canada

Fig. 1. ^{29}Si NMR spectra of 1,1,3,3-tetramethyldisiloxane (M^H_2) and DMF in $CDCl_3$: (*a*) 0.46 cm^3 of M^H_2 and 1.60 cm^3 of DMF in 2.0 cm^3 of $CDCl_3$, at 25 °C; (*b*) 0.46 cm^3 of M^H_2 and 1.60 cm^3 of DMF in 2.0 cm^3 of $CDCl_3$, at –60 °C.



Ph_2MeSiH. No substantial changes in the chemical shifts were found in the ^{29}Si NMR spectra of their solutions in DMF, even for a large excess of DMF ([DMF]/[Si-H] ≈ 9–18) at room temperature and even at –60 °C. If such complexes are formed by alkyl(aryl)hydrosilanes in the reaction course, their concentration must be very low, but it seems to be sufficient for a promotion of their dehydrocoupling with hydroxylic reagents. According to the steady-state Bodenstein approximation (27), a concentration of the active complex doesn't need to be high. In our studies we have also used the most reactive hydrosilane towards silanols — 1,1,3,3-tetramethyldisiloxane (M^H_2, where: M^H denotes the $HMe_2SiO_{0.5}$ group). In the ^{29}Si NMR spectra of M^H_2 and DMF (in $CDCl_3$), recorded at room temperature, we have found two new singlets at about –7 ppm (δ_1) and –18 ppm (δ_2). The intensities of these new signals increased to 3.4% and 2.4%, respectively, when the molar ratio of DMF to M^H_2 increased from 1:1 to 8:1. At –60 °C, relative intensities of these signals reached 20.0% and 14.8%, respectively, for the molar ratio of DMF to M^H_2 of 8:1 (see Fig. 1 and Table 1). When the concentration of M^H_2 in the solution was doubled and the fraction of $CDCl_3$ was decreased twice, similar changes in ^{29}Si NMR spectra have been observed. In this case, high intensities of new signals at δ_1 = –7.59 ppm (20.7%) and δ_2 = –18.58 ppm (12.1%) were observed for the molar ratio 4:1 at –60 °C. At –60 °C and also at room temperature (Table 1), a third signal at δ_3 = –20.08 ppm (in expt. 6), or δ_3 = –20.70 ppm (in expt. 8), and δ_3 = –20.45 ppm (in expt. 10) was also observed in the spectra. At the lower temperature, the dielectric constant of DMF is much higher than at 25 °C (at –60 °C, ε_{DMF} = 58.3 (48)) and it can increase its ability to form complexes with hydrosilanes.

© 2005 NRC Canada

Table 1. Results of the ^{29}Si NMR studies of 1,1,3,3-tetramethyldisiloxane–DMF solutions in $CDCl_3$ at 25 °C and –60 °C.

		$HMe_2SiOSiMe_2H$		DMF					
Expt. No.	Temp. (°C)	(cm^3)	(mol)	(cm^3)	(mol)	$[(HMe_2Si)_2O]/[DMF]$	$CDCl_3$ (cm^3)	$^{29}Si^a$ (δ, ppm)	
1	25	0.46	0.002 59	—	—	∞	2.0	–4.61 (100%)	—
2	25	0.46	0.002 59	0.2	0.002 58	1:1	2.0	–4.79 (100%)	–6.93 (2.0%)
3	25	0.46	0.002 59	0.4	0.005 17	1:2	2.0	–4.95 (100%)	–7.08 (3.0%)
4	25	0.46	0.002 59	0.8	0.010 33	1:4	2.0	–4.54 (100%)	–6.67 (3.1%)
5	25	0.46	0.002 59	1.6	0.020 66	1:8	2.0	–4.77 (100%)	–6.87 (3.4%)
6	–60	0.46	0.002 59	1.6	0.020 66	1:8	2.0	–5.25 (100%)	–7.29 (20.0%)
									–20.08 (7.7%)
7	25	0.92	0.005 19	0.4	0.005 17	1:1	1.0	–5.32 (100%)	–7.95 (1.3%)
8	25	0.92	0.005 19	0.8	0.010 33	1:2	1.0	–5.54 (100%)	–7.62 (3.3%)
									–20.70 (0.74%)
9	25	0.92	0.005 19	1.6	0.020 66	1:4	1.0	–5.65 (100%)	–7.74 (3.4%)
10	–60	0.92	0.005 19	1.6	0.020 66	1:4	1.0	–5.54 (100%)	–7.59 (20.7%)
									–20.45 (2.4%)

[a]The relative intensities of the signals (singlets) are given in brackets.

Scheme 1.

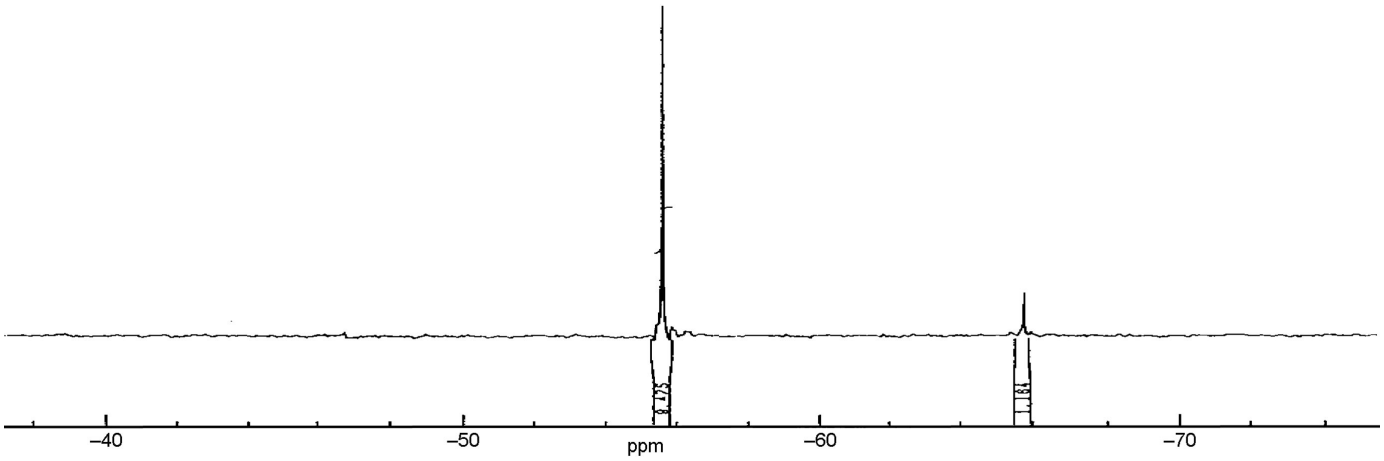
We presume that the singlets at –7 ppm (δ_1) correspond to a noncoordinated silicon atom, singlets at –18 ppm (δ_2) to the penta-coordinated silicon atom of M^H_2, and the singlets at –20 ppm (δ_3) belong to the complex of M^H_2 with two molecules of DMF (Scheme 1). The chemical shift of two magnetically equivalent silicon atoms in the molecule of $HMe_2SiOSiMe_2H$ always appears in the spectra (in $CDCl_3$) at δ_0 = –4.8 ppm.

We have also found new distinct NMR signals in the ^{29}Si NMR spectra of alkoxy-substituted hydrosilanes $(MeO)_3SiH$ (Fig. 2), $(EtO)_3SiH$, $(EtO)_2MeSiH$, and $(EtO)Me_2$-SiH, which may result from molecular complexes of the above silanes with DMF (see Table 2). (Alkoxyhydrosilanes have not been used in our kinetic studies, since ≡Si-OR groups can react with hydroxyl groups in the presence of Lewis acids (49)). For some of these silanes, we observed more than one new NMR signal. The maximum intensities of the most intensive new signals in their ^{29}Si NMR spectra recorded at –60 °C in $CDCl_3$ were as follows: 13.0% (δ_1 –65.8 ppm) for $(MeO)_3SiH$, 16.8% (δ_1 –69.1 ppm) for $(EtO)_3SiH$, 6.6% (δ_1 –26.9 ppm) for $(EtO)_2MeSiH$, and 12.7% (δ_1 –5.7 ppm) for $(EtO)Me_2SiH$. For the last three hydro(alkoxy)silanes, the intensities of these new signals were in the range 4.2%–7.6% at –60 °C when $CDCl_3$ was used as the external solvent. In the case of $(EtO)Me_2SiH$, two additional singlets at δ_2 –7.5 ppm (6.0%) and δ_2 –7.8 ppm (2.1%) were observed, and for $(EtO)_2MeSiH$ at δ_2 –43.3 ppm (1.3%) and δ_2 –50.7 ppm (1.0%). It seems that the oxygen atom of dimethyl formamide coordinates to the silicon atom of the hydrosilanes, since oxygen has a very high affinity to silicon because of (*p–d*) π conjugation. Apparently, oxygen atoms bound to silicon in M^H_2 and in hydro(alkoxy)silanes stabilize complexes of hydrosilanes with DMF. Saratov and Reikhsfeld (50) concluded that the nitrogen atom of DMF coordinates to the silicon in $PhSiH_3$, on the basis of the results of high-resolution ^{1}H NMR studies of $PhSiH_3$–DMF solutions in $CDCl_3$. The intermediacy of molecular complexes of (alkoxy)hydrosilanes with DMF and other solvents in pre-equilibriumm steps of reactions of the Si—H bond was proposed by Marciniec and Gulińska (51), on the basis of IR study of trialkoxysilane–solvent interactions.

As we can see from the NMR data, summarized in Tables 1 and 2, values of the differences ($\Delta\delta_I$) between the chemical shifts of noncomplexed hydrosilanes (δ_0) and those corresponding to the observed new signals (δ_1), $\Delta\delta_I = \delta_1 - \delta_0$, are pretty constant (~2.1 ppm for M^H_2, ~10 ppm for $(MeO)_3SiH$, ~9 ppm for $(EtO)_3SiH$ and $(EtO)_2MeSiH$, and ~8 ppm for $(EtO)Me_2SiH$), and they increased only very slightly with an increasing concentration of DMF and decreasing temperature. Also, values of $\Delta\delta_{II} = \delta_2 - \delta_0$ are constant within an experimental error (~13.3 ppm, for M^H_2; for

© 2005 NRC Canada

Fig. 2. ^{29}Si NMR spectrum of $HSi(OMe)_3$ (0.37 cm^3) and DMF (1.60 cm^3) in $CDCl_3$ (2.0 cm^3), recorded at –60 °C ([Si-H]/[DMF} = 1:8; δ (ppm): –55.60 (100%), –65.77 (13.0%)).



the (alkoxy)hydrosilanes used, more experimental data are needed).

The formation of anionic molecular complexes of $HSi(OR)_3$ (RO = EtO, PhO, *i*-PrO) with alkoxide anions (EtO^-, PhO^-, *i*-PrO^-) and H^- was proposed by Corriu and coworkers (44, 52) on the basis of their ^{29}Si NMR data (Δδ = –22 to –41 ppm). Hydrosilanes bearing strongly electronegative triflate groups at silicon form complexes with soft nucleophiles (TfO^-, NMI, HMPA, DMPU, and Et_3N). Their resonances appear at much lower frequences than those of the parent hydrosilanes (Δδ = –47 to –65 ppm). All of Corriu's and Bassindale's complexes were formed at a concentration ratio of nucleophiles to hydrosilanes of 1:1 or lower (45).

The role of DMF in the reaction mechanism

Presumably, DMF forms molecular complexes with hydrosilanes in fast reactions, prior to the formation (in the rate-determining step) of an active complex with catalysts (ZnX_2, CdX_2, X = Cl, Br, I). As a result of the interactions of DMF with the silicon atom in hydrosilanes, a polarization of the Si—H bond can be distinctly increased before it receives electrophilic assistance from the active forms of the catalysts (M^{2+}) (29), leading to the formation of the active complex.

The formation of hexa-coordinated species is consistent with the second order of dehydrocoupling with respect to DMF (30). Its molecules could neutralize a very slightly positive charge on the silicon atom in the transition state, which results from the studies of the Hammett free energy relationship (ρ = –0.12) (25). The intermediate product of the oxidative addition of the Si—H bond to M^{2+} may have a *three-centre, transition metal – hydrogen – silicon two-electron structure* (53), in which the hydride ion is replaced by the oxygen atom of the alcohol, silanol, carboxylic acid, or water in a fast consecutive step (29).

According to Baines and Eaborn (20), reactions involving the cleavage of Si—X bonds, under electrophilic conditions, consist of the electrophilic activation of a leaving group with *concerted or subsequent nucleophilic attack*. An assumption that the rate-determining step of the dehydrocoupling reaction has two stages: (1) *fast polarization of the Si—H bond, followed by* (2) *a rate-determining hydride transfer*, is also consistent with the observed formal kinetics.

It was proposed (29) that the first step of the reaction is the formation of a complex of ≡Si-H with active ionic forms of the catalysts (M^{2+}):

[2] $\equiv\overset{\delta+}{Si}-\overset{\delta-}{H} + \overset{\delta+}{M}X_2 \underset{k_{-1}}{\overset{k_1}{\rightleftharpoons}} \equiv\overset{\delta+}{Si}-\overset{\delta-}{H}\cdots\overset{\delta+}{M}X_2$

(Rate-determining step)

where M = Zn, Cd, and X = Cl, Br, I.

The slightly split silicon–hydrogen bond is completly broken in the next fast step, which might be quite complicated:

[3] $\equiv\overset{\delta+}{Si}-\overset{\delta-}{H}\cdots\overset{\delta+}{M}X_2 + HO-R \xrightarrow{k_2} \equiv Si-OR + MX_2 + H_2$

It also seems possible that the rate-determining stage (eq. [2]) could be composed of more than one step. A complexation of the Si—H bond by a catalyst could be a relatively fast process, while further rearrangement of such a complex to a three-centre transition state (A) might proceed as a rate-determining step (eq. [4]):

[4] $\equiv\overset{\delta+}{Si}-\overset{\delta-}{H}\cdots M^{2+} \underset{k_{-1}}{\overset{k_1}{\rightleftharpoons}} \left[\equiv Si\!-\!H\ (M^{2+})\right]$

(Rate-determining step) (A)

Thus, the Si—H bond may undergo a classic, fast, oxidative addition to the metal centre through the transition state (A) (eq. [5*a*]), causing a deep structural change of the hydrosilane substrate and a formation of adduct B:

[5*a*] $\left[\equiv Si\!-\!H\ (M^{2+})\right] \xrightarrow{\text{Fast}} \left[\equiv Si\ \ H\ (M^{2+})\right]$

(A) (B)

© 2005 NRC Canada

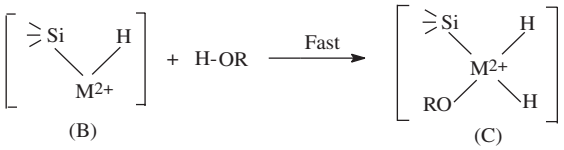
Table 2. Results of the ^{29}Si NMR studies of hydrosilanes–DMF solutions in $CDCl_3$ at 25 °C and –60 °C.

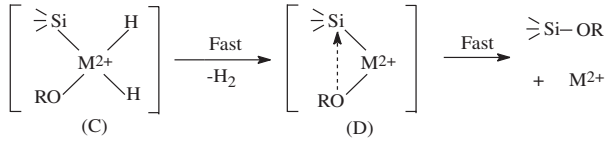
			H-silane		DMF						
Expt. No.	Temp. (°C)	Type	(cm^3)[a]	(mol)	(cm^3)	(mol)	[H-silane]/[DMF]	$CDCl_3$ (cm^3)	^{29}Si[b] (δ, ppm)		
11	25	$HSi(OMe)_3$	0.367	0.002 58	—	—	∞	2.0	–54.86 (100%)		
12	25	$HSi(OMe)_3$	0.367	0.002 58	0.2	0.002 58	1:1	2.0	–55.09 (100%)		
13	25	$HSi(OMe)_3$	0.367	0.002 58	0.4	0.005 17	1:2	2.0	–55.28 (100%)		
14	25	$HSi(OMe)_3$	0.367	0.002 58	0.8	0.010 33	1:4	2.0	–55.58 (100%)	–65.31 (2.3%)	
15	–60	$HSi(OMe)_3$	0.367	0.002 58	1.6	0.020 66	1:8	2.0	–55.93 (100%)	–65.81 (2.5%)	
					1.6	0.020 66	1:8	2.0	–55.60 (100%)	–65.77 (13.0%)	
16	25	$HSi(OEt)_3$	~0.25	~0.001 35	—	—	∞	~2.0	–58.44 (100%)		
17	25	$HSi(OEt)_3$	0.36	0.001 95	1.2	0.015 50	1:8	1.0	–59.86 (100%)	–68.81 (5.1%)	
18	–60	$HSi(OEt)_3$	0.36	0.001 95	1.2	0.015 50	1:8	1.0	–59.74 (100%)	–69.10 (16.8%)	
19	25	$HMeSi(OEt)_2$	~0.25	~0.001 54	—	—	∞	~2.0	–16.13 (100%)		
20	25	$HMeSi(OEt)_2$	0.314	0.001 94	1.2	0.015 50	1:8	1.0	–17.92 (100%)	–26.77 (1.6%)	
21	–60	$HMeSi(OEt)_2$	0.314	0.001 94	1.2	0.015 50	1:8	1.0	–17.68 (100%)	–26.85 (6.6%)	–43.32 (1.3%)
											–50.69 (1.0%)
22	25	HMe_2SiOEt	~0.25	~0.001 82	—	—	∞	~2.0	4.67 (100%)		
23	25	HMe_2SiOEt	0.267	0.001 94	1.2	0.015 50	1:8	1.0	2.87 (100%)		
24	–60	HMe_2SiOEt	0.267	0.001 94	1.2	0.015 50	1:8	1.0	2.93 (100%)	–5.72 (12.7%)	–7.46 (6.0%)
											–7.77 (2.1%)
25	25	$HSi(OEt)_3$	0.60	0.003 25	2.0	0.025 83	1:8	As external solvent	–58.68 (100%)	–67.54 (6.6%)	
26	–60	$HSi(OEt)_3$	0.60	0.003 25	2.0	0.025 83	1:8	As external solvent	–58.26 (100%)	–67.46 (7.3%)	
27	25	$HMeSi(OEt)_2$	0.523	0.003 23	2.0	0.025 83	1:8	As external solvent	–16.85 (100%)	–25.46 (2.2%)	
28	–60	$HMeSi(OEt)_2$	0.523	0.003 23	2.0	0.025 83	1:8	As external solvent	–16.28 (100%)	–25.15 (4.2%)	
29	25	HMe_2SiOEt	0.445	0.003 23	2.0	0.025 83	1:8	As external solvent	3.99 (100%)	–3.77 (4.5%)	–3.86 (2.4%)
30	–60	HMe_2SiOEt	0.445	0.003 23	2.0	0.025 83	1:8	As external solvent	4.29 (100%)	–3.71 (7.6%)	–3.82 (6.1%)

[a]Accuracy was better than ±0.005 cm^3.
[b]The relative intensities of the signals (singlets) are given in brackets.

© 2005 NRC Canada

The adduct (B) may attach a nucleophile molecule (ROH), giving adduct C:

[5*b*] 

[5*c*] 

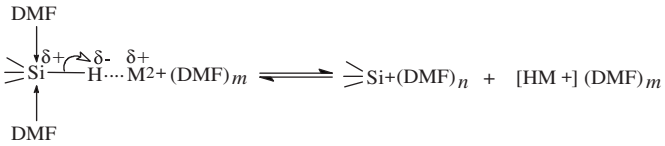
which may first undergo a reductive elimination of H_2, and subsequently, elimination of a catalyst active form (M^{2+}), through a structure (D), giving the main product of dehydrocoupling (≡Si-OR).

The participation of bishydrido complexes of Group VIII metals and other transition metals has very often been proposed in the mechanisms of reactions catalyzed by their derivatives.

Comparison of the mechanisms of dehydrocoupling and the reaction of hydrosilanes with carbenium ions

We have observed several common features for *dehydrocoupling* and the reaction of hydrosilanes with carbenium ions, however, the latter reaction occurs in weakly nucleophilic medium (54–56) with: (1) the same formal kinetics, i.e., *first reaction order with respect both to the Si-H group and the electrophilic reagent,* i.e., MX_2 (M = Zn, Cd; X = Cl, Br, I) (27), or $\equiv C^+$ (54, 56)); (2) the same values of the deuterium kinetic isotope effect (1.4–1.5) (25, 54, 56); (3) very close values of $\Delta S^{\ddagger}$ (–30 to –35 eu (27) and –25 to –28 eu (54, 56)).

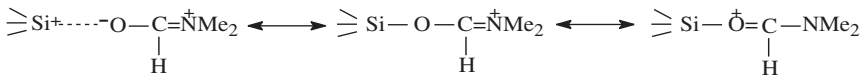
The formation of a silicocation ($\equiv Si^+$) in the rate-determining step cannot be excluded in the reaction course. We had observed an only slightly negative Hammett reaction constant (ρ = –0.12) for the dehydrocoupling process, not much different than for acid-catalyzed solvolysis of hydrosilanes (ρ = 0–0.5) (16), but still very low in comparison with ρ^* = –3.5, which was determined by Chojnowski and co-workers (54, 56) for the reaction of hydrosilanes with carbenium ions. A fast dissociation of the intermediate complex $\equiv Si\cdots H\cdots M^{2+}$ could proceed with *the formation of a silicenium cation (*$\equiv Si^+$*)*, which can be solvated by DMF:

[6] 

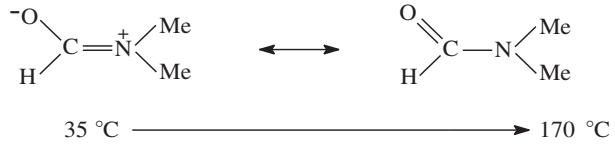
where n = 1, 2; m = 3–5 (57, 58) (here, the hydrogen atom of the Si—H bond is considered as a ligand, replacing one molecule of DMF).

The structure of $ZnCl_2$ solutions in DMF, and appropriate ionic equilibria, were studied by Ishiguro et al. (57).

The positive charge on silicon can be stabilized by a resonance:

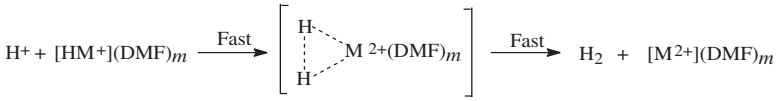
[7] 

In eq. [7], a second molecule of DMF (solvating silicenium cation), is omitted for simplicity — with two DMF molecules more resonance structures would be possible. A hindered rotation in DMF takes place at low and ambient temperature and two different ^1H NMR signals of CH_3 groups are observed, while at higher temperature both methyl protons are equivalent (59):

[8] 

Subsequently, the silicocation could be quickly attacked by the hydroxylic reagent:

[9] 

[10] 

The above mechanism is also consistent with formal kinetics. Silicenium cations are very unstable, but they can be stabilized by DMF (55), CH_2Cl_2 (57, 60), CH_3CN (61, 62), Et_2O (63), and other solvents (64). It seems that alternative to the concept of the intermediacy of the sovated $\equiv Si^+$, *the reaction could also proceed through the solvated, asymmetrical synchronous hydride transfer (SHT) transition state* because of the low value of the kinetic isotope effect (1.4–1.5). *A single electron transfer (SET) pathway* seems to be much less likely, when we consider all our eperimental results (25, 27, 29) (and especially the sensitivity of the reaction rate to steric effects (27)), and compare them with features of the SET process (54, 56).

© 2005 NRC Canada

Conclusions

1. Dehydrocoupling of tertiary hydrosilanes with hydroxylic reagents doesn't take place in the presence of Zn(II) and Cd(II) halides without cocatalysis by DMF molecules.
2. The reaction is second order with respect to DMF (30) for reactions of: (*a*) Et_3SiH with $Ph_2Si(OH)_2$, catalyzed by $ZnCl_2$, carried out at 25 °C in DMF–THF; (*b*) Et_3SiH with PhCOOH, catalyzed by $CdBr_2$, conducted at 25 °C in DMF-1,4-dioxane; and (*c*) in DMF–THF (in cases (*b*) and (*c*), only at lower concentrations of DMF.
3. New resonance signals were found in the ^{29}Si NMR spectra of solutions of $HMe_2SiOSiMe_2H$ (Fig. 1) and some (alkoxy)hydrosilanes ($(MeO)_3SiH$ (Fig. 2), $(EtO)_3SiH$, $(EtO)_2MeSiH$, and $(EtO)Me_2SiH$) in $CDCl_3$ at 25 °C and –60 °C. The intensities of these new signals were much higher at –60 °C. It seems that these new resonances correspond to molecular complexes of DMF with the hydrosilanes used. No evidence of the formation of such complexes by alkyl(aryl)-substituted tertiary hydrosilanes was found by means of ^{29}Si NMR spectroscopy. No new signals were detected in the spectra of their solutions with DMF in $CDCl_3$, neither at 25 °C nor at –60 °C.
4. Alternative mechanisms for the dehydrocoupling reaction of hydrosilanes with reagents containing hydroxyl group have been proposed. The rate-determining step of the reaction could also proceed through a three-centre transition state. Both a participation of a silicocation solvated by DMF molecules or a solvated, unsymmetrical synchronous hydride transfer (SHT) in the reaction mechanism seem to be possible as well. The single electron transfer pathway (SET) seems to be much less likely.

Acknowledgements

This paper is dedicated to the memory of Professor Zygmunt Lasocki (1921–1993), my very much respected teacher, in recognition of his precious contribution to organosilicon chemistry. The author is very grateful to Professor Julian Chojnowski (Centre of Molecular and Macromolecular Studies, Polish Academy of Sciences, Łódź) for helpful discussion. I also gratefully thank Professor Zofia M. Michalska and Dr. Krzysztof Strzelec for the gift of trimethoxysilane. This work was supported by the Polish State Committee for Scientific Research (KBN) under Research Project 1359/T09/95/08.

References

1. M.A. Brook. Silicon in organic, organometallic and polymer chemistry. J. Wiley and Sons, New York. 2000, and refs. cited therein.
2. C. Eaborn. Organosilicon compounds. Butterworth Scientific Publications, London. 1960.
3. L.H. Sommer. Stereochemistry, mechanism and silicon. McGraw-Hill, New York. 1965.
4. L.H. Sommer. Intra-Sci. Chem. Rep. **7**, 1 (1973).
5. H. Prince. Int. Rev. Sci. Inorg. Chem. Ser. One, **9**, 353 (1973).
6. R.J.P. Corriu and M. Henner. J. Organomet. Chem. **74**, 1 (1974).
7. R.J.P. Corriu and C. Guerin. J. Organomet. Chem. **198**, 231 (1980); R.J.P. Corriu and C. Guerin. Adv. Organomet. Chem. **20**, 265 (1982).
8. R.J.P. Corriu, C. Guerin, and J.J.E. Moreau. Top. Stereochem. **15**, 43 (1984).
9. R.J.P. Corriu, C. Guerin, and J.J.E. Moreau. *In* The chemistry of organic silicon compounds. *Edited by* S. Patai and Z. Rappoport. J. Wiley and Sons, New York. 1989. Chap. 4. pp. 305–370.
10. R.J.P. Corriu, C. Guerin, and J.J.E. Moreau. *In* The chemistry of organic silicon compounds. *Edited by* S. Patai and Z. Rappoport. J. Wiley and Sons, New York. 1989. Chap. 20. pp. 1241–1288.
11. C. Chuit, R.J.P. Corriu, C. Reye, and C. Young. Chem. Rev. **93**, 1371 (1993).
12. (*a*) A.R. Bassindale and P.G. Taylor. *In* The chemistry of organic silicon compounds. *Edited by* S. Patai and Z. Rappoport. J. Wiley and Sons, New York. 1989. Chap. 13. pp. 839–892; (*b*) A.R. Bassindale. *In* Organosilicon chemistry, Proceedings of the Xth International Symposium. Poznań, Poland. 15–20 August 1993. *Edited by* B. Marciniec and J. Chojnowski. Gordon and Breach Scientific Publishers, Basel, Switzerland. 1995. pp. 191–207.
13. (*a*) E. Lukevics and M. Dzintara. J. Organomet. Chem. **144**, 147 (1978); (*b*) L.D. Field, B.A. Messerle, M. Rehr, L.P. Soler, and T.W. Hambley. Organometallics, **22**, 2387 (2003).
14. (*a*) W. Noll. Chemie und Technologie der Silicone. 2 Aufl. Weinheim, Germany. 1968; (*b*) B.P.S. Chauhan and P. Boudjouk. Tetrahedron Lett. **40**, 4127 (1999); (*c*) M. Chauhan, B.P.S. Chauhan, and P. Boudjouk. Org. Lett. **2**, 1027 (2000); (*d*) B.P.S. Chauhan, T. Ready, Z. Al-Badri, and P. Boudjouk. Organometallics, **20**, 2725 (2001).
15. B. Nahlovský and V. Chvalovský. Coll. Czech. Chem. Commun. **33**, 3131 (1968).
16. B. Nahlovský and V. Chvalovský. Coll. Czech. Chem. Commun. **33**, 3391 (1968).
17. K. O'Donnel, R. Bacon, R.L. Chellappa, R.L. Schowen, and J.K. Lee. J. Am. Chem. Soc. **94**, 2500 (1972).
18. C. Eaborn and I.D. Jenkins. J. Organomet. Chem. **69**, 185 (1974).
19. F.P. Price. J. Am. Chem. Soc. **69**, 2600 (1947).
20. J.E. Baines and C. Eaborn. J. Chem. Soc. 4023 (1955).
21. J. Hetflejš and F. Mareš. Coll. Czech. Chem. Commun. **30**, 1643 (1965).
22. J. Hetflejš and F. Mareš. Coll. Czech. Chem. Commun. **31**, 586 (1966).
23. H. Gilman and G.E. Dunn. J. Am. Chem. Soc. **73**, 3404 (1951).
24. J.E. Baines and C. Eaborn. J. Chem. Soc. 1436 (1956).
25. J. Chruściel and Z. Lasocki. Main Group Met. Chem. **12**(2), 129 (1989).
26. J. Chruściel, Z. Lasocki, T. Graczyk, J. Kulpiński, and S. Piechucki. Acta Chim. Acad. Sci. Hung. **81**, 223 (1974).
27. J. Chruściel and Z. Lasocki. Pol. J. Chem. **57**, 113 (1983).
28. J. Chruściel and Z. Lasocki. Pol. J. Chem. **57**, 121 (1983).
29. J. Chruściel. Pol. J. Chem. **71**, 977 (1997); Chem. Abstr. **127**, 135 846 (1997).
30. (*a*) J. Chruściel. Xth Polish Organosilicon Symposium, Łódź, Poland. 1996. Abstracts, p. 13; (*b*) J. Chruściel. Coll. Czech. Chem. Commun. **69**, 2281 (2004).
31. V. Bažant, V. Chvalovský, and J. Rathouský. Organosilicon Compounds. Vols. 2^1 and 2^2. Publishing House of the Czechoslovak Academy of Scienes, Prague. 1965.
32. H. Marsmann. *In* Basic principles and progress Grundlagen und Fortschritte. *Edited by* P. Diehl, E.F. Fluck, and R. Korsfeld. Springer-Verlag, Berlin, Heidelberg, New York. 1981. Chap. 2. pp. 66–235.

© 2005 NRC Canada

33. E.A. Williams. *In* The chemistry of organic silicon compounds. *Edited by* S. Patai and Z. Rappoport. J. Wiley and Sons, New York. 1989. pp. 511–554.
34. C. Chuit, R.J.P. Corriu, and C. Reye. *In* Chemistry of hypervalent compounds. *Edited by* Kin-ya Akiba. Wiley-VCH, Inc., New York. 1999. Chap. 4. pp. 81–146.
35. G.I. Lebedeva and M.G. Voronkov. Izv. Akad. Nauk SSSR, 2574 (1973).
36. G.I. Lebedeva and M.G. Voronkov. Izv. Akad. Nauk. SSSR, 2597 (1973).
37. G.I. Lebedeva and M.G. Voronkov. Zh. Obshch. Khim. 2597 (1973).
38. R. Damrauer and S.E. Danahey. Organometallics, **5**, 1490 (1986).
39. R.J.P. Corriu, C. Guerin, M. Henner, and W.W.C. Wong Chi Man. Organometallics, **7**, 237 (1988).
40. B.J. Helmer, R. West, R.J.P. Corriu, M. Poirier, G. Royo, and A.D. Saxce. J. Organomet. Chem. **251**, 295 (1983).
41. B. Becker, R.J.P. Corriu, C. Guerin, M. Henner, and Q. Wang. J. Organomet. Chem. **359**, C33 (1989).
42. R.J.P. Corriu, C. Guerin, M. Henner, and Q. Wang. Organometallics, **10**, 2297 (1991).
43. R.J.P. Corriu, C. Guerin, M. Henner, and Q. Wang. Organometallics, **10**, 3574 (1991).
44. B. Becker, R.J.P. Corriu, C. Guerin, and M. Henner. J. Organomet. Chem. **369**, 147 (1989).
45. A.R. Bassindale and J. Jiang. J. Organomet. Chem. **446**, C3 (1993).
46. A.R. Bassindale and T. Stout. J. Chem. Soc. Chem. Commun. 1387 (1984).
47. M. Weinmann, O. Walter, G. Huttner, and L. Heinrich. J. Organomet. Chem. **561**, 131 (1998).
48. S.J. Bass, W.I. Nathan, R.M. Meighan, and R.H. Cole. J. Phys. Chem. **68**, 509 (1964).
49. M.B. Fromberg, E.D. Arseneva, and H.V. Aylova. Zh. Prikl. Khim. **44**, 2702 (1971).
50. I.E. Saratov and V.O. Reikhsfeld. Zh. Obshch. Khim. **36**, 1069 (1966).
51. B. Marciniec and H. Gulińska. J. Organomet. Chem. **146**, 1 (1978).
52. B. Becker, R.J.P. Corriu, C. Guerin, M. Henner, and Q. Wang. J. Organomet. Chem. **368**, C25 (1989).
53. (*a*) U. Schubert. Transition Met. Chem. **16**, 136 (1991), and refs. cited therein; (*b*) J.Y. Corey and J. Braddock-Wilking. Main Group Chem. News, **4**(3), 6 (1996).
54. J. Chojnowski, W. Fortuniak, and W. Stańczyk. J. Am. Chem. Soc. **110**, 7776 (1987).
55. J. Chojnowski and W. Stańczyk. Adv. Organomet. Chem. **30**, 243 (1990).
56. J. Chojnowski and W. Stańczyk. Main Group Chem. News, **2**(1), 6 (1994).
57. S. Ishiguro, K. Ozutsumi, and H. Ohtaki. Bull. Chem. Soc. Jpn. **60**, 531 (1987).
58. F.A. Cotton and G. Wilkinson. Advanced inorganic chemistry. 5th ed. J. Wiley and Sons, New York. 1988. pp. 607–608.
59. H. Kędziora. *In* Metody instrumentalne w analizie chemicznej i badaniach strukturalnych. *Edited by* W. Szczepaniak. A. Mickiewicz University Press, Poznań, Poland. 1984.
60. J.B. Lambert, W.J. Schulz, Jr., J.A. McConnell, and W. Schilf. J. Am. Chem. Soc. **110**, 2201 (1988).
61. S. Bahr and P. Boudjouk. 25th Silicon Symposium. Los Angeles, California. 3–4 April 1992. University of Southern California Press, Los Angeles, California. Abstracts, 83P. 1992.
62. M. Kira, T. Hino, and H. Sakurai. 25th Silicon Symposium. Los Angeles, California. 3–4 April 1992. University of Southern California Press, Los Angeles, California. Abstracts, p. 53. 1992; Chem. Lett. 153 (1993).
63. M. Kira, T. Hino, and H. Sakurai. J. Am. Chem. Soc. **114**, 6697 (1992).
64. J.B. Lambert and S. Zhang. J. Chem. Soc. 383 (1993).

© 2005 NRC Canada

RAPID COMMUNICATION / COMMUNICATION RAPIDE

Palladium-catalyzed simple and efficient hydrogenative cleavage of azo compounds using recyclable polymer-supported formate

Keelara Abiraj, Gejjalagere R. Srinivasa, and D. Channe Gowda

Abstract: Palladium-catalyzed room temperature transfer hydrogenation of azo compounds using recyclable polymer-supported formate as the hydrogen donor produces corresponding amine(s) in excellent yields (88%–98%). This method was found to be highly facile with selectivity over a number of other functional groups such as halogen, alkene, nitrile, carbonyl, amide, methoxy, and hydroxyl.

Key words: azo compounds, catalytic transfer hydrogenation, polymer-supported formate, 10% Pd-C, amines.

Résumé : L'hydrogénation par transfert, catalysée par le palladium de composés azo, et réalisée à la température ambiante en faisant appel à du formiate déposé sur un polymère recyclable comme donneur d'hydrogène, conduit à la formation des amines correspondantes avec d'excellents rendements (88 %–98 %). On a trouvé que cette méthode d'une extrême facilité présente une sélectivité par rapport à d'autres groupes fonctionnels, tels les halogènes, alcènes, nitriles, carbonyles, amides et groupes méthoxy et hydroxyles.

Mots clés : composés azo, hydrogénation par transfert catalytique, formiate déposé sur un polymère, 10 % Pd-C, amines.

[Traduit par la Rédaction]

Polymer-supported reagents, catalysts, and scavengers are now ubiquitous throughout the fields of combinatorial chemistry, organic synthesis, and catalysis (1, 2). The use of polymer-supported reagents couples the advantages of solution phase chemistry (ease of monitoring the progress of the reaction by using chromatographic and spectroscopic techniques) with those of solid phase methods (use of excess reagents and easy isolation and purification of products). The utility and power of such reagents has been exquisitely demonstrated by the groups of Ley and others in synthesizing several complex natural products by multi-step sequences requiring many different kinds of heterogenized reagents, which can be removed by simple filtration (1–3). In view of the rapid development in the field of polymer-supported chemistry over the last few years, there is a pressing need for the proper exploitation of functionalized polymer-supported reagents in organic synthesis.

Reduction of azo compounds to the corresponding amine(s) is a synthetically important transformation, both in the laboratory and in industry. Although there are a good number of methods available for the reduction of azo compounds, limitations include the use of harsh conditions and (or) costly reagents (4). In comparison with all other reduction processes, catalytic transfer hydrogenation (CTH) employing hydrogen donors, e.g., ammonium formate, is safer, cost-effective, highly selective, rapid, and environmentally friendly (5). Various CTH systems such as cyclohexene – 5% Pd on asbestos (6*a*), ammonium formate – 10% Pd-C (6*b*), ammonium formate – zinc (6*c*), ammonium formate – magnesium (6*d*), hydrazinium monoformate – zinc (6*e*), and ammonium chloride – zinc (6*f*) have been developed for the reduction of azo compounds to the corresponding amine(s). However, ammonium-formate-aided CTH systems are the most versatile and widely employed. Though efficient, these ammonium formate CTH reactions are often troublesome since ammonium formate can sublime and block the reaction apparatus. Also, the reaction leads to the release of ammonia and could create significant problems when performed on a large scale. Moreover, the use of formate salts as hydrogen donors poses complications during isolation and purification of water-soluble products. Recently, potassium formate has been used as a hydrogen donor in various transfer hydrogenation reactions (7*a*–7*c*). However, alkali metal formate salts are not recommended for CTH reactions as these hydrogen donors reduce the catalyst activity.

Desai and Danks (8*a*) and Basu et al. (8*b*) performed the transfer hydrogenation of alkenes using polymer-supported formate as the hydrogen donor in the presence of Wilkinson's catalyst or $Pd(OAc)_2$. However, it has been observed that controlling the reduction rates is difficult with these active

Received 7 October 2004. Published on the NRC Research Press Web site at http://canjchem.nrc.ca on 22 April 2005.

K. Abiraj, G.R. Srinivasa, and D.C. Gowda.[1] Department of Studies in Chemistry, University of Mysore, Manasagangotri, Mysore-570 006, Karnataka, India.

[1]Corresponding author (e-mail: dcgowda@yahoo.com).

 doi: 10.1139/V05-071 © 2005 NRC Canada

Scheme 1.

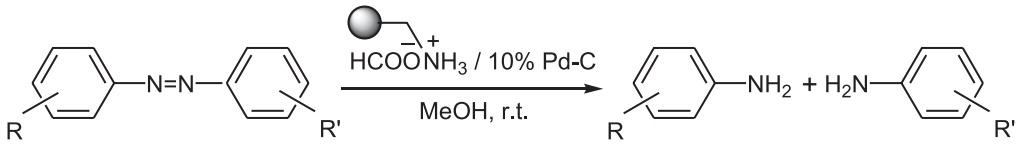
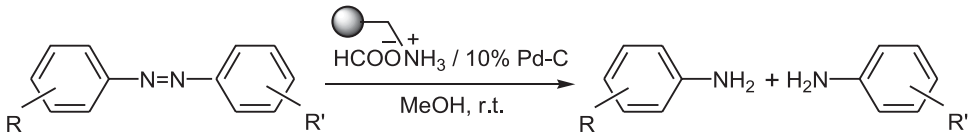


Table 1. Hydrogenative cleavage of azo compounds using polymer-supported formate and 10% Pd-C.



					Melting point (°C)	
Entry	R	R′	Time (h)	Yield (%)[a]	Found	Literature
1	H	H	2.0	98[b]	112–114	114 (11*a*)
2	4-Cl	4′-Cl	2.5	96	71	70 (11*a*)
3	2-Br	2′-Br	3.0	94[b]	98–100	99 (11*a*)
4	4-I	4′-I	2.5	95	63–65	63 (11*a*)
5	4-CH_2=CH_2	4′-CH_2=CH_2	4.0	94[c]	210–212[d]	213–214 (11*a*)
6	4-CH_2-CN	4′-CH_2-CN	5.0	90	47–49	45–48 (11*a*)
7	4-CHO	4′-CHO	3.5	93	72–74	72 (11*a*)
8	4-$COCH_3$	4′-$COCH_3$	5.0	94	105	106 (11*b*)
9	2-CH_3	2′-CH_3	3.0	96[e]	142–144	144 (11*a*)
10	4-$CONH_2$	4′-$CONH_2$	4.5	95	114–115	114 (11*a*)
11	4-OCH_3	4′-OCH_3	4.0	94[b]	57–59	57 (11*a*)
12	2-OH	2′-OH	3.5	95	173–175	174 (11*a*)
13	4-COOH	4′-COOH	4.0	96	187	188 (11*a*)
14	4-NH_2, 3-CH_3	2′-CH_3	5.0	88, 92[e]	63–65, 144	64 (11*a*), 144 (11*a*)
15	4-NH_2	H	5.0	88, 90[b]	145, 112–114	145–147 (11*b*), 114 (11*a*)

[a]Yields of isolated products.
[b]Isolated as the acetyl derivative.
[c]The spectra were compared to those of a commercial sample.
[d]Boiling point.
[e]Isolated as the benzoyl derivative.

homogeneous catalysts. On the other hand, the use of heterogeneous catalysts offers several advantages over homogeneous systems such as easy recovery and recycling of the catalyst, high selectivity, easy product isolation, and minimization of undesired toxic wastes. In this context, we probed the reduction of azo compounds employing polymer-supported formate as a hydrogen donor in the presence of 10% palladium on carbon as the heterogeneous catalyst. Our investigations revealed that the use of polymer-supported formate in conjunction with 10% Pd-C is highly efficient for the facile reduction of substituted azo compounds to the corresponding amine(s) (Scheme 1).

A wide range of structurally varied azo compounds, both symmetric and unsymmetric, underwent reduction by this procedure to furnish the corresponding amine(s). The results are summarized in Table 1. All the products were characterized by comparison of their TLC, melting points, IR and ^{1}H NMR spectra with authentic samples. The IR spectra of all the products showed a sharp doublet between 3500 and 3300 cm^{-1} ascribed for the NH_2 group and no absorption bands were noticed for the substrate azo compound (between 1630–1575 cm^{-1}) and intermediate hydrazo compound (2290–2440 cm^{-1}) clearly indicating the complete conversion of azo compounds to their corresponding amino derivate(s). Further, the appearance of a broad singlet between δ 4.5 and 6.5 owing to the NH_2 protons in the ^{1}H NMR spectra confirmed the products evidently. The reactions are, on the whole, reasonably fast and high yielding (88%–98%). It is worthwhile to note that our system selectively reduced azo compounds to the corresponding amines in the presence of other sensitive functional groups such as halogen (5*a*, 5*b*) (Table 1, entries 2–4), alkene (5*a*, 5*f*) (Table 1, entry 5), nitrile (5*a*, 5*b*) (Table 1, entry 6), and carbonyl (5*a*, 9) (Table 1, entries 7 and 8), which are susceptible to reduction under transfer hydrogenation conditions. In addition, many other functional groups such as amide, methoxy, acid, and hydroxyl are also compatible with the present system.

In the case of symmetrically substituted azo compounds,

© 2005 NRC Canada

Table 2. Recycling of polymer-supported formate for the reduction of azobenzene.

Cycle	Time (h)	Yield (%)
1	2.0	98
2	2.0	97
3	3.0	97
4	3.5	97
5	3.5	97
6	4.0	95
7	4.0	93
8	4.0	92

the separation of products from the reaction mixture is simple and involves, in most of the cases, direct removal of the catalyst and resin by filtration and evaporation of the solvent under vacuum. The crude product, so isolated, was of excellent purity for most purposes. Hence, this procedure is highly advantageous to obtain water-soluble aromatic amines in high yields (Table 1, entries 2, 8, 11–13). Further, it is noteworthy here that the polymer-supported formate was regenerated and could be reused for further hydrogenolysis process. In total, 10 successive recycle runs were possible before there was an appreciable decrease in the reaction yield (Table 2).

To obtain optimum reduction conditions, a number of trails with a range of solvents, which are commonly employed for CTH reactions, were carried out. Methanol is found to be the best one as far as the solubility of substrate and rate of reaction is concerned. To examine the effects of catalyst loading, the reduction was attempted using different ratios of catalyst and substrate. We observed the optimal ratio of catalyst to substrate to be 1:4 by weight (approximately 0.05 mmol catalyst for 1 mmol of substrate). However, the rate of reduction was significantly slower when smaller amounts of catalyst were used. During the recycle runs, another 0.025 mmol of catalyst was added after the fifth cycle to increase the rate of reduction.

The reductive cleavage of azo compounds proceeds smoothly despite the dual heterogeneity of catalyst and polymer support. The initial step in the reduction would be the formation of palladium diformate by the reaction of palladium with the formate released from the polymeric support (10*a*, 10*b*). The palladium formate can then transfer two hydrogen atoms to the azo compound. In addition to this essential feature, the polymer-supported NH_3^+ may also provide H^+ to complete the reduction process (10*c*).

In conclusion, a highly facile polymer-supported formate – 10% Pd-C system was developed for the smooth reduction of azo compounds to the corresponding amine(s). The use of polymer-supported formate combines the advantages of polymer-supported chemistry with the flexibility of the CTH technique. The advantages include a safe reaction medium, high selectivity, rapidity, ease of operation, and simple recovery of the hydrogen donor. In addition, this approach is highly helpful for the reduction of symmetric azo compounds to obtain the corresponding amines in pure form with no work-up.

Experimental

Preparation of polymer-supported formate

The aminomethyl polystyrene (Advanced Chemtech, 1% DVB cross-linked, 100–200 mesh, 2 mmol/g) was washed with an excess of a 50% solution of formic acid in dichloromethane. The resulting polymer was washed thoroughly and successively with dichloromethane and ether, and dried under vacuum. The obtained resin was used as such for the reduction.

Determination of polymer-supported formate loading

The polymer-supported formate (1 g) was placed in a manually operated solid phase vessel and washed thoroughly with dil. HCl (0.05 N). The HCl washing containing formic acid (released from the resin) was collected and diluted to 50 mL in a volumetric flask. An aliquot (10 mL) of this solution was titrated potentiometrically against a standard NaOH solution. The formate loading was calculated to be 1.92 mmol/g.

General procedure for the reduction of azo compounds

To a solution of the azo compound (1 mmol) in methanol (15 mL) taken in a horizontal solid phase vessel, polymer-supported formate (1 g) and 10% Pd-C (50 mg, 0.05 mmol) were added. The suspension was shaken well[2] for the specified time at room temperature (Table 1). After consumption of the starting material, as monitored by TLC, the reaction mixture was filtered and washed thoroughly with methanol. The combined washings and filtrate were evaporated under reduced pressure. The crude product was found to be analytically pure in most cases. Where necessary, the crude product was taken into the organic layer and washed with saturated sodium chloride. For recycling purposes, the residue containing the polymer-supported formate and the catalyst was washed thoroughly and successively with DMF, dichloromethane, a 50% solution of formic acid in dichloromethane, dichloromethane, and ether. The activated resin along with the catalyst were dried under vacuum and used as obtained for further reduction reactions.

In the case of the reduction of unsymmetrically substituted azo compounds, the crude product was subjected either to preparative TLC or to column chromatography to separate two different constituent amines.

Acknowledgements

We gratefully acknowledge financial support from the University Grants Commission, New Delhi. We also acknowledge the Council of Scientific and Industrial Research, New Delhi for a research fellowship (to KA).

[2] The reaction mixture was subjected to shaking using a manual shaker as the shaking of the polymer-supported formate instead of stirring increases its life for recycling purposes.

© 2005 NRC Canada

References

1. Leading reviews: (*a*) S.V. Ley, I.R. Baxendale, R.N. Bream, P.S. Jackson, A.G. Leach, D.A. Longbottom, M. Nesi, J.S. Scott, R.I. Storer, and S.J. Taylor. J. Chem. Soc. Perkin Trans. 1, 3815 (2000); (*b*) A. Kirschning, H. Monenschein, and R. Wittenberg. Angew. Chem. Int. Ed. **40**, 650 (2001); (*c*) S.V. Ley, I.R. Baxendale, G. Brusotti, M. Caldarelli, A. Massi, and M. Nesi. Il Farmaco, **57**, 321 (2002); (*d*) P. Hodge. Curr. Opin. Chem. Biol. **7**, 362 (2003).
2. Recent references: (*a*) G.A. Strohmeier and C.O. Kappe. Angew. Chem. Int. Ed. **43**, 621 (2004); (*b*) J. Burt, T. Dean, and S. Warriner. Chem. Commun. 454 (2004); (*c*) R.N. MacCoss, D.J. Henry, C.T. Brain, and S.V. Ley. Synlett, 675 (2004). (*d*) M.K.W. Choi and P.H. Toy. Tetrahedron, **60**, 2875 (2004), and refs. therein.
3. (*a*) I.R. Baxendale, S.V. Ley, M. Nesi, and C. Piutti. Tetrahedron, **58**, 6285 (2002), and refs. therein; (*b*) R.I. Storer, T. Takemoto, P.S. Jackson, and S.V. Ley. Angew. Chem. Int. Ed. **42**, 2521 (2003).
4. (*a*) T.L. Gilchrist. *In* Comprehensive organic synthesis. Vol. 8. *Edited by* I. Fleming. Pergamon Press, Oxford. 1991. pp. 381–402; (*b*) M.B. Smith and J. March. *In* March's advanced organic chemistry. 5th ed. John Wiley and Sons, New York. 2001.
5. (*a*) R.A.W. Johnstone, A.H. Wibly, and I.D. Entwistle. Chem. Rev. **85**, 129 (1985); (*b*) S. Ram and R.E. Ehrenkaufer. Synthesis, **1**, 91 (1988); (*c*) B. Zacharie, N. Moreau, and C. Dockendorff. J. Org. Chem. **66**, 5264 (2001); (*d*) P.G. Reddy and S. Baskaran. Tetrahedron Lett. **43**, 1919 (2002); (*e*) J.Q. Yu, H.C. Wu, C. Ramarao, J.B. Spencer, and S.V. Ley. Chem. Commun. 678 (2003); (*f*) Z. Paryzek, H. Koenig, and B. Tabaczka. Synthesis, 2023 (2003); (*g*) G.R. Srinivasa, K. Abiraj, and D.C. Gowda. Tetrahedron Lett. **44**, 5835 (2003); (*h*) K. Abiraj, G.R. Srinivasa, and D.C. Gowda. Synlett, 877 (2004).
6. (*a*) T.L. Ho and G.A. Olah. Synthesis, 167 (1977); (*b*) G.K. Jnaneshwara, A. Sudalai, and V.H. Deshpande. J. Chem. Res. (S), 160 (1998); (*c*) S. Gowda, K. Abiraj, and D.C. Gowda. Tetrahedron Lett. **43**, 1329 (2002); (*d*) K. Abiraj, S. Gowda, and D.C. Gowda. J. Chem. Res. (S), 299 (2003); (*e*) S. Gowda, K. Abiraj, and D.C. Gowda. J. Chem. Res. (S), 384 (2002); (*f*) M.B. Sridhara, G.R. Srinivasa, and D.C. Gowda. Synth. Commun. **34**, 1441 (2004).
7. (*a*) B. Basu, S. Jha, M.H.M. Bhuiyan, and P. Das. Synlett, 555 (2003); (*b*) B. Basu, M.H.M. Bhuiyan, and S. Jha. Synth. Commun. **33**, 291 (2003); (*c*) A. Arcadi, E. Bernocchi, S. Cacchi, and F. Marinelli. Synlett, 27 (1991).
8. (*a*) B. Desai and T.N. Danks. Tetrahedron Lett. **42**, 5963 (2001); (*b*) B. Basu, M.M.H. Bhuiyan, P. Das, and I. Hossain. Tetrahedron Lett. **44**, 8931 (2003).
9. S.K. Mohapatra, S.U. Sonavane, R.V. Jayaram, and P. Selvam. Org. Lett. **4**, 4297 (2002).
10. (*a*) J. Yu and J.B. Spencer. Chem. Commun. 1935 (1998); (*b*) V. Derdau. Tetrahedron Lett. **45**, 8889 (2004); (*c*) S. Rajgopal, M.K. Anwer, and A.F. Spatola. *In* Peptides: Design, synthesis, and biological activity. *Edited by* C. Basava and G.M. Anantharamaiah. Birkhauser, Boston. 1994. p. 11.
11. (*a*) A.I. Vogel. *In* Vogel's textbook of practical organic chemistry. 5th Ed. *Edited by* B.S. Furniss, A.J. Hannaford, P.W.G. Smith, and A.R. Tatchell. Addison Wesley Longman Limited, UK. 1997. p. 1298; (*b*) S. Budavari (*Editor*). The Merck index. 11th ed. Merck and Co., Inc., Rahway, New Jersey. 1989.

© 2005 NRC Canada

Oxidation of anisoles to *p*-benzoquinone monoketals catalyzed by a ruthenium complex of 1,4,7-trimethyl-1,4,7-triazacyclononane with *tert*-butyl hydroperoxide[1]

Wai-Hung Cheung, Wing-Ping Yip, Wing-Yiu Yu, and Chi-Ming Che

Abstract: A protocol based on $[Ru^{III}(Me_3tacn)(CF_3CO_2)_2(H_2O)]CF_3CO_2$ (**1**, Me_3tacn = 1,4,7-trimethyl-1,4,7-triazacyclononane) as catalyst and *tert*-butyl hydroperoxide (TBHP) as oxidant was developed for oxidation of anisoles to *p*-benzoquinone monoketals. This reaction can be formally considered as regioselective aromatic C-H oxidation. With 2-methoxyanisole as substrate, 3,4-dimethoxy-4-*tert*-butoxy-2,5-cyclohexadienone can be obtained in up to 82% yield based on 84% substrate conversion.

Key words: oxidation, quinones, *tert*-butyl hydroperoxide, ruthenium catalyst.

Résumé : Un protocole basé sur l'utilisation du $[Ru^{III}(Me_3tacn)(CF_3CO_2)_2(H_2O)]CF_3CO_2$ (**1**, Me_3tacn = 1,4,7-trimethyl-1,4,7-triazacyclononane) comme catalyseur et de l'hydroperoxyde de *tert*-butyle comme oxydant a été élaboré pour l'oxydation des anisoles menant à la formation de monocétals de *p*-benzoquinone. On peut considérer formellement cette réaction comme une oxydation C-H aromatique régiosélective. Avec le 2-méthoxyanisole comme substrat, on obtient la 3,4-diméthoxy-4-*tert*-butoxycyclohexa-2,5-diénone avec un rendement pouvant atteindre 82 %, en se basant sur un taux de conversion du substrat de 84 %.

Mots clés : oxydation, quinones, hydroperoxyde de *tert*-butyle, catalyseur de ruthénium.

[Traduit par la Rédaction]

Introduction

p-Benzoquinones constitute a key structural element in many biologically interesting natural products such as neolignans and anthraquinone antibiotics (1, 2). Stoichiometric oxidation of substituted phenols by oxidants such as ammonium cerium(IV) nitrate (3) and thallium(III) nitrate (4) represents a common approach for quinone synthesis. Similarly, quinone monoketal, which is a valuable class of synthetic intermediates, can be readily obtained through oxidation of *para*-methoxy phenols by either electrochemical (5) or chemical oxidation using hypervalent iodine reagents (6). In view of growing environmental concern, there is an upsurge of interest in developing environmentally friendly and operationally safe catalytic protocols for hydrocarbon oxidations using more tractable oxidants such as molecular oxygen, aqueous hydrogen peroxide, and *tert*-butyl hydroperoxide (TBHP) (7). However, metal-catalyzed phenol oxidations by alkyl hydroperoxides are known to give poor product selectivity because of coupling of the phenoxy radicals (8). Recently, selective oxidation of phenols by TBHP has been achieved by Murahashi et al. (9) using $Ru(PPh_3)_3Cl_2$ as catalyst, and 4-(*tert*-butyldioxy)-4-alkyl-2,5-cyclohexadienones were produced in good yields.

It is well documented that ruthenium complexes are versatile catalysts for oxidative functionalization of C=C and C—H bonds (10). Extensive studies have shown that oxo-ruthenium complexes of chelating tertiary amines are powerful oxidants for alkenes, alkynes, and alkanes (11). We previously reported the preparation and X-ray structure characterization (12*c*) of $[Ru^{III}(Me_3tacn)(CF_3CO_2)_2(H_2O)]CF_3CO_2$ (**1**, Fig. 1), which is a robust catalyst (12) for homogeneous and heterogeneous oxidation of alcohols and alkenes using TBHP as the terminal oxidant; aldehydes and (or) ketones and epoxides can be obtained in excellent yields with product turnovers >6000. As part of our continuous effort to develop

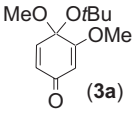
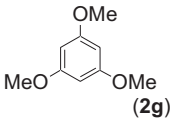
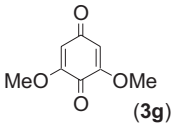
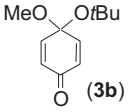
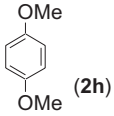
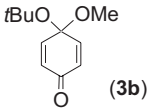
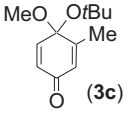
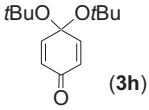
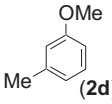
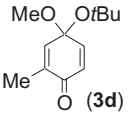
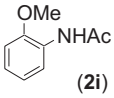
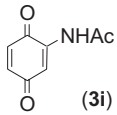
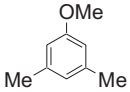
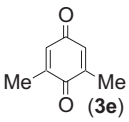
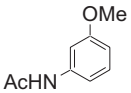
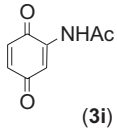
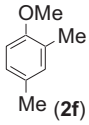
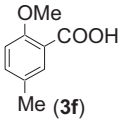
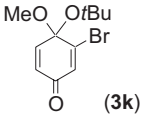
Received 9 December 2004. Published on the NRC Research Press Web site at http://canjchem.nrc.ca on 13 May 2005.

W.-H. Cheung,[2] W.-P. Yip, W.-Y. Yu,[3] and C.-M. Che.[4] Department of Chemistry and Open Laboratory of Chemical Biology of the Institute of Molecular Technology for Drug Discovery and Synthesis, The University of Hong Kong, Pokfulam Road, Hong Kong.

[1]This article is part of a Special Issue dedicated to Professor Howard Alper.
[2]Present address: Department of Surgery, 9/F, Laboratory Block, 21 Sassoon Road, Faculty of Medicine Building, The University of Hong Kong.
[3]Corresponding author (e-mail: wyyu@hku.hk).
[4]Corresponding author (e-mail: cmche@hku.hk).

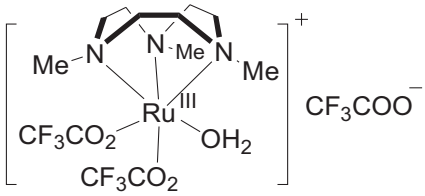
 doi: 10.1139/V05-060 © 2005 NRC Canada

Table 1. Ruthenium-catalyzed TBHP oxidation of anisoles.

Entry	Substrate	Conversion[a] (%)	Product	Yield[b] (%)	Entry	Substrate	Conversion[a] (%)	Product	Yield[b] (%)
1	 (**2a**)	46	 (**3a**)	48	7	 (**2g**)	100	 (**3g**)	76
2	 (**2b**)	84	 (**3b**)	53	8	 (**2h**)	99	 (**3b**)	32
3	 (**2c**)	100	 (**3c**)	57				 (**3h**)	19
4	 (**2d**)	95	 (**3d**)	41	9	 (**2i**)	32	 (**3i**)	12
5	 (**2e**)	100	 (**3e**)	15	10	 (**2j**)	56	 (**3i**)	20
6	 (**2f**)	45	 (**3f**)	89	11	 (**2k**)	29	 (**3k**)	15

Note: Reaction conditions (protocol I): 1:anisole:TBHP = 1:100:230, CH_2Cl_2 (5 mL), room temperature for 14 h.
[a]Substrate conversions were determined by GLC analysis.
[b]Isolated yields.

Fig. 1. Molecular structure of $[Ru^{III}(Me_3tacn)(CF_3CO_2)_2(H_2O)]$-$CF_3CO_2$.



structurally characterized ruthenium complexes for organic catalysis, we are attracted to a recent work by Hirobe and co-workers (13), which states that $[Ru^{II}(Por)(CO)]$ (Por = porphyrinato) can effect catalytic oxidation of anisoles by 2,6-dichloropyridine *N*-oxide to give *p*-benzoquinones as the major product. The transformation was proposed to occur via oxidation of an aromatic C—H bond as a principal step (13). In this work we report that complex **1** can catalyze anisole to *p*-benzoquinone monoketals with up to 90% yield using TBHP as the oxidant. Results obtained under various reaction conditions (e.g., solvent systems, temperature) and with use of various substrates will be discussed.

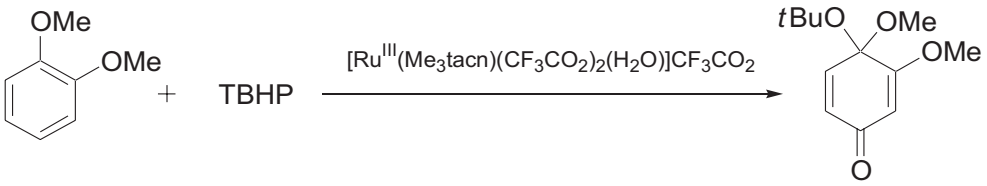
Results and discussion

At the outset, treatment of 2-methoxyanisole (**2a**, 1 mmol) with TBHP (2.3 mmol) in the presence of $[Ru^{III}(Me_3tacn)(CF_3CO_2)_2(H_2O)]CF_3CO_2$ (**1**, 1 mol%) in CH_2Cl_2 at ambient temperature for 14 h produced 3,4-dimethoxy-4-*tert*-butoxy-2,5-cyclohexadienone (**3a**) in 48% isolated yield based on 46% anisole consumption (Table 1, entry1). Other oxidants such as *m*-chloroperoxybenzoic acid, hydrogen peroxide – urea adduct, Oxone®, chloramine-T, TEMPO, and 2,6-dichloropyridine *N*-oxide have been tested for their ability to oxidize **2a**. Under our reaction conditions (i.e., **1**:**2a**:oxidant = 1:100:230 in CH_2Cl_2), formation of **3a** was not detected, and the starting anisole (>90%) was recovered. According to Murahashi et al. (9), $Ru(PPh_3)_3Cl_2$ and $RuCl_3{\cdot}H_2O$ were reported to be effective catalysts for selective phenol oxidation by TBHP to give 4-(*tert*-butyldioxy)-4-alkyl-2,5-cyclohexanedienone. In this work, when $Ru(PPh_3)_3Cl_2$ and $RuCl_3{\cdot}H_2O$ were employed as catalysts for the oxidation of **2a** using THBP as oxidant, no effective consumption of the starting anisole was observed without product **3a** being detected.

The catalytic oxidation of other anisole derivatives has been examined by employing the following reaction condi-

© 2005 NRC Canada

Table 2. Effect of various experimental parameters on the catalytic oxidation of 2-methoxyanisole.



Entry	Loading (%)	TBHP (equiv.)	Temp (°C)	Time (h)	Solvent	Yield[a] (%)	Conversion[b] (%)
1	1.0	2.3	24	14	CH_2Cl_2	48	46
2	1.0	2.3	24	14	*n*-hexane	68	9
3	1.0	2.3	24	14	*t*-BuOH	N/A	<1
4	1.0	2.3	24	14	MeOH	N/A	<1
5	1.0	2.3	24	14	1,2-DCE[c]	50	45
6	1.0	7.0	24	14	1,2-DCE	60	49
7	5.0	2.3	24	14	1,2-DCE	49	57
8	0.5	2.3	24	14	1,2-DCE	78	28
9	1.0	7.0	80	14	1,2-DCE	86	62
10	1.0	7.0	24	14	1,2-DCE	66	45
11	1.0	14.0	80	14	1,2-DCE	93	62
12[d]	1.0	3.5/3.5	80	4	MeOH/*t*-BuOH/1,2-DCE	84	82

[a]Isolated yield.
[b]The percentage of conversion was determined by GLC analysis.
[c]1,2-DCE = 1,2-dichloroethane.
[d]A dissolved mixture of complex **1** (1 mol%) in MeOH:*t*-BuOH with TBHP (3.5 mmol) was added slowly by a syringe pump (0.5 mL min^{-1}) to a solution of **2a** (1 mmol) with TBHP (3.5 mmol) in 1,2-DCE at 80 °C for 2 h. The reaction mixture was further stirred for 2 h, followed by a general work-up procedure.

tions (protocol I): **1** (1 mol%), TBHP (2.3 equiv.), and CH_2Cl_2 at room temperature. Unsubstituted anisole **2b** reacted with TBHP to afford quinone monoketal **3b** in 53% yield based on 84% conversion (Table 1, entry 2). Likewise, *ortho*- and *meta*-substituted methyl anisoles (**2c** and **2d**) were converted to their corresponding ketals in 57% and 41% yields, respectively (entries 3 and 4) under the Ru-catalyzed conditions. Yet the analogous reaction of 3,5-dimethylanisole gave quinone **3e** in 15% yield despite complete substrate conversion (entry 5). Analysis of the crude reaction mixture by ^{1}H NMR failed to identify any defined products other than **3e**. Interestingly, when 2,4-dimethylanisole (**2f**) was employed as substrate, the **1**-catalyzed TBHP reaction furnished benzoic acid **3f** as the only identifiable product in 89% yield (entry 6), presumably via benzylic C-H oxidation. Based on these findings, the **1**-catalyzed oxidation of anisoles to quinone monoketal could be regarded as a formal regioselective oxidation of the aromatic C—H bond *para* to the methoxy group.

Adopting protocol I, oxidaton of other functionalized anisoles was also explored. For example, the oxidation of 1,3,5-trimethoxybenzene was found to give dimethoxyquinone **3g** in 76% yield, without any ketal product (Table 1, entry 7). Notably, effective oxidation of 1,4-dimethoxybenzene, which does not bear any available aromatic C—H bonds, was observed under the "**1** + TBHP" conditions, and a mixture of monoketals **3b** (32%) and **3h** (19%) was obtained (entry 8).

Recently, Nicolaou et al. (14) reported a facile synthesis of aminoquinones by oxidation of anilides with hypervalent iodine reagents (Dess–Martin periodinane, DMP); aminoquinones have been shown to be valuable synthetic intermediates for polycycle constructions. In this work, we have studied the reactions of 2- and 3-methoxyanilides (**2i** and **2j**) with TBHP by employing protocol I, and the product *ortho*-aminoquinone **3i** was formed in merely 12%–20% yield (Table 1, entries 9–10). Oxidation of 2-bromoanisole also met with limited success, and the product **3k** was isolated in only 15% yield based on 29% substrate conversion (entry 11).

Having found a protocol for anisole oxidation by TBHP, we examined the effect of various experimental parameters on the efficiency of the transformation. Using **2a** as substrate, the **1**-catalyzed anisole oxidation was found to be sensitive to the solvent used. For instance, with hexane as solvent and under the reaction conditions **1**:**2a**:TBHP = 1:100:230 at room temperature for 14 h, a higher yield (68%) of **3a** was obtained, albeit with 9% conversion (Table 2, entry 2). Poor substrate conversion could be explained by the insolubility of the catalyst in hexane. Our previous results showed that **1** dissolves in alcoholic solvents such as MeOH and *t*-BuOH, leading to the formation of an alkoxyruthenium complex (12*c*). In this work, the ruthenium catalyst was found to be inactive when MeOH or *t*-BuOH was used as the solvent, and negligible substrate conversion was observed (entries 3 and 4). Compared to the case when CH_2Cl_2 was the solvent, other halogenated solvents, such as 1,2-dichloroethane, gave similar results (ca. 50% yield; 45% conversion) under identical experimental conditions (entry 5). Increasing the TBHP amount to 7.0 equiv. produced moderate improvement in product yields (60%) and substrate conversion (49%) for the **1**-catalyzed oxidation of **2a** (entry 6).

At higher catalyst loading (5.0 mol%), little improvement in the substrate conversion (57%) and product yield (49%) was observed for the **1**-catalyzed TBHP oxidation of **2a** (en-

© 2005 NRC Canada

Table 3. Catalytic oxidation of selected anisoles using protocol II.

Entry	Substrate	Product	Yield (%)[a]	Conversion (%)[b]
1	**2a**	**3a**	84	82
2	**2k**	**3k**	49	54
3	**2i**	**3i**	39	31
4	**2c**	**3c**	49	75
5	**2d**	**3d**	33	76

Note: Reaction conditions: a mixture of complex **1** (1.0 mol%) and TBHP (3.5 mmol) dissolved with MeOH-*t*-BuOH (1:1 by volume) was added slowly through a syringe pump (0.5 mL min^{-1}) over 2 h at 80 °C to a solution of the substrate (1 mmol) with TBHP (3.5 mmol). The reaction mixture was stirred for a further 2 h and quenched with sodium thiosulphate (100 mg).

[a]Isolated yield based on conversion.

[b]Conversions were determined by GLC analysis.

try 7, compare results in entry 1). However, reducing the catalyst loading to 0.5 mol% led to a higher product yield of 78% for the catalytic oxidation in spite of a 28% substrate conversion (entry 8). This finding suggests that higher catalyst loading may favor TBHP decomposition; however, the possibility of catalyst deactivation under the reaction conditions cannot be excluded.

Interestingly, when the catalytic oxidation was conducted at 80 °C (**1**:**2a**:TBHP = 1:100:700), the product ketal was obtained in 86% yield based on 62% anisole consumption (entry 9). At room temperature, the identical transformation resulted in only 45% substrate conversion and 66% yield for the formation of **3a**. Up to 93% yield of **3a** was attained when 14 equiv. TBHP was employed, though the substrate conversion remained at 62% (entry 11).

Based on the above studies, halogenated solvents are the solvents of choice for the **1**-catalyzed anisole oxidation, and an elevated temperature seems to produce high product yield and substrate conversion. While the amount of the TBHP has a moderate effect on the catalytic oxidation, low catalyst loading was found to favor high product yield. Taking these results into consideration, a modified catalytic procedure (protocol II) was developed (see experimental section for details). Complex **1** was first dissolved in an MeOH:*t*-BuOH mixture (1:1 by volume) and TBHP (3.5 equiv.). The homogenous mixture was added slowly through a syringe pump (0.5 mL min^{-1}) to a 1,2-dichloroethane solution containing **2a** (1 mmol) and TBHP (3.5 equiv.) at 80 °C. After 4 h of reaction, monoketal **3a** was obtained in 84% yield with 82% substrate conversion (entry 12). By employing protocol II and 2-bromoanisole (**2k**) as substrate, the Ru-catalyzed oxidation afforded **3k** in 49% yield based on 54% conversion (Table 3, entry 2). This result is a significant improvement when compared with the results using protocol I (yield 29%, conversion 15%; see Table 1, entry 11). As noted earlier, oxidation of 2-methoxyanilide **2i** using protocol I afforded quinone **3i** in 12% yield based on 32% conversion (Table 1, entry 9). However, when protocol II was adopted for the same reaction, a better yield of 39% for the formation of **3i** was observed, albeit with 31% conversion (Table 3, entry 3). Using protocol II, oxidation of methyl anisoles **2c** and **2d** by TBHP produced the corresponding ketals in 49% (**3c**) and 33% (**3d**) yields (Table 3, entries 4 and 5). These findings are comparable to those obtained by employing protocol I (Table 1, entries 3 and 4).

Reaction of peroxides with $[Ru^{III}(N_4)(H_2O)_2]^{3+}$ (N_4 = macrocyclic amine ligand) is known to generate oxo-ruthenium complexes (15, 16). To gain insight about the plausible reactive intermediates responsible for the **1**-catalyzed anisole oxidation by TBHP, we performed a stoichiometric reaction of a structurally defined oxo-ruthenium complex — $[Ru^{VI}(Me_3tacn)(CF_3CO_2)O_2](ClO_4)$ — with 2-methoxyanisole (**2a**). When **2a** (10 mmol) was treated with $[Ru^{VI}(Me_3tacn)(CF_3CO_2)O_2](ClO_4)$ (0.5 mmol) in degassed aqueous *tert*-butanol [*t*-BuOH:H_2O = 6:3 (by volume)] at room temperature for 16 h under an inert atmosphere, 2-methoxy-*p*-benzoquinone (**3l**) was isolated in 81% yield. The dioxoruthenium(VI) complex was reduced to $[Ru^{III}_2(Me_3tacn)(CF_3CO_2)_2(O)](ClO_4)$ in 76% yield. This finding appears to be consistent with the results reported by Hirobe and co-workers (13) that reactive oxo-ruthenium complex is an active intermediate for anisole oxidation.

Experimental section

Materials

All the solvents were distilled and dried before used. All the common laboratory reagents were used as received. $[Ru^{III}(Me_3tacn)(CF_3CO_2)_2(H_2O)]CF_3CO_2$ (**1**) was synthesized using a literature procedure (12*c*). *tert*-Butyl hydroperoxide was obtained commercially as a 70% aqueous solution, and the oxidant was pretreated according to a procedure described by Sharpless and Verhoeven (17) using 1,2-dichloroethane. The TBHP oxidant concentration was standardized by ^1H NMR (5.38 mol L^{-1} in 1,2-dichloroethane) prior to use (17).

General procedure for the catalytic oxidation of anisoles

Protocol I

A mixture of anisole (1 mmol), TBHP in 1,2-dichloroethane (0.65 mL, 2.3 equiv.), and **1** (6.3 mg, 1.0 mol%) was stirred in CH_2Cl_2 (5 mL) at room temperature for 14 h. The reaction was quenched by the addition of sodium thiosulphate (100 mg), and the mixture was analyzed by GLC to determine the substrate consumption. To isolate the reaction products, the solvent was removed by rotary evaporation, and the residue was purified by flash column chromatography using 1% ethyl acetate in *n*-hexane as eluant.

Protocol II

A mixture of complex **1** (10.6 mg, 1.6 mol%, MeOH-*t*-BuOH, 1:1 by volume, 2 mL) and TBHP (3.5 equiv.) was

© 2005 NRC Canada

added dropwise (0.5 mL min^{-1}) to a solution of 1,2-dichloroethane (2 mL) containing anisole (1 mmol) and TBHP (3.5 equiv.) at 80 °C over 2 h. The reaction mixture was stirred for an additional 2 h. The reaction was quenched by adding sodium thiosulphate (100 mg), and the substrate consumption was determined by GLC analysis. After removal of solvent by rotary evaporation, the residue was purified by flash column chromatography using 0.5%–1% ethyl acetate in *n*-hexane as eluant.

3,4-Dimethoxy-4-*tert*-butoxy-2,5-cyclohexadienone (3a)

TLC: R_f = 0.5 (30% ethyl acetate in *n*-hexane). IR (neat KBr, υ cm^{-1}): 1670, 1634, 1607. ^{1}H NMR (400 MHz, $CDCl_3$) δ_H: 6.92 (d, *J* = 10.3 Hz, 1H), 6.25 (dd, *J* = 10.3, 1.7 Hz, 1H), 5.59 (d, *J* = 1.7 Hz, 1H), 3.80 (s, 3H), 3.42 (s, 3H), 1.24 (s, 9H). ^{13}C NMR (100 MHz, $CDCl_3$) δ_c: 187.89, 169.89, 141.68, 131.41, 104.99, 98.22, 83.14, 57.71, 53.86, 26.72. EI (%): 153 ([M – O-*t*-Bu], 100). HRMS (EI) calcd. for [M – O-*t*-Bu]$^+$: 153.1552; found: 153.1554 ($C_8H_9O_3$).

4-*tert*-Butoxy-4-methoxy-2,5-cyclohexadienone (3b)

TLC: R_f = 0.6 (20% ethyl acetate in *n*-hexane as developing solvent). IR (neat KBr, υ cm^{-1}): 1644. ^{1}H NMR (400 MHz, $CDCl_3$) δ_H: 6.94 (d, *J* = 10.3 Hz, 2H), 6.26 (d, *J* = 10.3 Hz, 2H), 3.45 (s, 3H), 1.25 (s, 9H). ^{13}C NMR (100 MHz, $CDCl_3$) δ_c: 185.13, 141.39, 129.59, 95.47, 81.11, 50.75, 26.29. EI (%): 123 ([M – O-*t*-Bu], 100). HRMS (EI) calcd. for [M – O-*t*-Bu]$^+$: 123.0447; found: 123.0446 ($C_7H_7O_2$).

3-Methyl-4-*tert*-butoxy-4-methoxy-2,5-cyclohexadienone (3c)

TLC: R_f = 0.6 (30% ethyl acetate in *n*-hexane as developing solvent). IR (neat KBr, υ cm^{-1}): 1678. ^{1}H NMR (400 MHz, $CDCl_3$) δ_H: 7.14 (d, *J* = 10.4 Hz, 1H), 6.32 (d, *J* = 10.4 Hz, 1H), 6.16 (m, 1H), 3.26 (s, 3H), 2.00 (s, 3H), 1.25 (s, 9H). ^{13}C NMR (100 MHz, $CDCl_3$) δ_c: 185.48, 153.85, 143.57, 130.69, 129.52, 98.02, 81.74, 52.04, 26.72, 17.56. EI (%): 137 ([M – O-*t*-Bu], 100). HRMS (EI) calcd. for [M – O-*t*-Bu]$^+$: 137.0598; found 137.0603 ($C_8H_9O_2$).

2-Methyl-4-*tert*-butoxy-4-methoxy-2,5-cyclohexadienone (3d)

TLC: R_f = 0.6 (30% ethyl acetate in *n*-hexane as developing solvent). IR (neat KBr, υ cm^{-1}): 1651. ^{1}H NMR (400 MHz, $CDCl_3$) δ_H: 6.94 (dd, *J* = 10.3 Hz, 1H), 6.67 (m, 1H), 6.24 (d, *J* = 10.3 Hz, 1H), 3.44 (s, 3H), 1.93 (s, 3H), 1.25 (s, 9H). ^{13}C NMR (100 MHz, $CDCl_3$) δ_c: 186.20, 141.91, 137.28, 136.64, 129.86, 96.43, 81.35, 51.12, 26.74, 16.00. EI (%): 137 ([M – O-*t*-Bu], 100). HRMS (EI) calcd. for [M – O-*t*-Bu]$^+$: 137.0598; found: 137.0603 ($C_8H_9O_2$).

4,4-Di-*tert*-butoxy-2,5-cyclohexadienone (3h)

TLC: R_f = 0.7 (20% ethyl acetate in *n*-hexane as developing solvent), colorless crystal. IR (neat KBr, υ cm^{-1}): 1644. ^{1}H NMR (400 MHz, $CDCl_3$) δ_H: 7.02 (d, *J* = 10.4 Hz, 2H), 6.25 (d, *J* = 10.4 Hz, 2H), 1.26 (s, 18H). ^{13}C NMR (100 MHz, $CDCl_3$) δ_c: 185.81, 140.33, 129.67, 99.05, 81.77, 26.72. EI (%): 123 ([M – O-*t*-Bu], 100). HRMS (EI) calcd. for [M – O-*t*-Bu]$^+$: 123.0447; found: 123.0448 ($C_7H_7O_2$).

3-Bromo-4-*tert*-butoxy-4-methoxy-2,5-cyclohexadienone (3k)

TLC: R_f = 0.6 (30% ethyl acetate in *n*-hexane as developing solvent). IR (neat KBr, υ cm^{-1}): 1674. ^{1}H NMR (400 MHz, $CDCl_3$) δ_H: 7.20 (d, *J* = 10.3 Hz, 1H), 6.82 (d, *J* = 1.9 Hz, 1H), 6.40 (dd, *J* = 10.3, 1.9 Hz, 1H), 3.35 (s, 3H), 1.27 (s, 9H). ^{13}C NMR (100 MHz, $CDCl_3$) δ_c: 182.83, 143.50, 143.24, 134.98, 129.86, 96.34, 82.00, 52.07, 26.38. EI (%): 203 ([M – O-*t*-Bu], 47), 201 ([M – O-*t*-Bu], 100). HRMS (EI) calcd. for [M – O-*t*-Bu]$^+$: 200.9550; found: 200.9551 ($C_7H_6BrO_2$).

Acknowledgments

This work is supported by the Areas of Excellence Scheme (AoE/P–10/01) established under the University Grants Committee (HKSAR, China), The University of Hong Kong (University Development Fund), and the Hong Kong Research Grants Council (HKU7384/02P).

References

1. (*a*) Y. Naruta and K. Maruyama. *In* The chemistry of the quinonoid compounds. Vol. 2. Part 1. *Edited by* S. Patai and Z. Rappoport. Wiley, New York. 1988. Chap. 8. p. 241; (*b*) J.S. Swenton. *In* The chemistry of the quinonoid compounds. Vol. 2. Part 2. *Edited by* S. Patai and Z. Rappoport. Wiley, New York. 1988. Chap. 15. p. 899; (*c*) W. Oppolzer. *In* Comprehensive organic synthesis. Vol. 5. *Edited by* B.M. Trost and I. Fleming. Pergamon, Oxford. 1991. p. 315; (*d*) R.W. Sweger and A.W. Czarnik. *In* Comprehensive organic synthesis. *Edited by* B.M. Trost and I. Fleming. Vol. 5. Pergamon, Oxford. 1991. p. 551; (*e*) R.H. Thomson (*Editor*). Naturally occurring quinones IV: recent advances. 4th ed. Blackie, London. 1997. p. 746.
2. For a review see: W.M. Owton. J. Chem. Soc. Perkin Trans. 1, 2409 (1999).
3. (*a*) W. Dirckheimer and L.A. Cohen. Biochemistry, **3**, 1948 (1964); (*b*) W. Dirckheimer and L.A. Cohen. J. Am. Chem. Soc. **86**, 4388 (1964).
4. A. McKillop, D.H. Perry, M. Edwards, S. Antus, L. Farkas, M. Nogradi, and E.C. Taylor. J. Org. Chem. **41**, 282 (1976).
5. (*a*) M.G. Dolson and J.S. Swenton. J. Org. Chem. **46**, 177 (1981); (*b*) M.P. Capparelli, R.E. DeSchepper, and J.S. Swenton. J. Org. Chem. **52**, 4953 (1987); (*c*) A.J. Stern and J.S. Swenton. J. Org. Chem. **54**, 2953 (1989).
6. (*a*) A. Pelter and S. Elgendy. Tetrahedron Lett. **29**, 677 (1988); (*b*) A.E. Fleck, J.A. Hobart, and G.W. Morrow. Synth. Commun. **22**, 179 (1992); (*c*) L.A. Paquette. Encyclopedia of reagents for organic synthesis. Vol. 6. Wiley, New York. 1995. p. 1479; (*d*) S.V. Ley, A.W. Thomas, and H. Finch. J. Chem. Soc. Perkin Trans. 1, 669 (1999).
7. (*a*) G. Strukul (*Editor*). Catalytic oxidations with hydrogen peroxide as oxidant. Kluwer, Dordrecht, The Netherlands. 1992; (*b*) C.W. Jones. Applications of hydrogen peroxide and derivatives. The Royal Society of Chemistry, Cambridge. 1999.
8. (*a*) W.I. Taylor and A.R. Battersby. Oxidative coupling of phenols. Marcel Dekker, New York. 1967; (*b*) K.U. Ingold. *In* Free radicals. Vol. 1. *Edited by* J.K. Kochi. John Wiley & Sons, New York. 1973. p. 37.
9. S.-I. Murahashi, T. Naota, N. Miyaguchi, and S. Noda. J. Am. Chem. Soc. **118**, 2509 (1996).

© 2005 NRC Canada

10. (*a*) W.P. Griffith. Chem. Soc. Rev. **21**, 179 (1992); (*b*) S.V. Ley, J. Norman, W.P. Griffith, and S.P. Marsden. Synthesis, 639 (1994); (*c*) S.I. Murahashi and N. Komiya. *In* Biomimetic oxidations catalyzed by transition metal complexes. *Edited by* B. Meunier. Imperial College Press, London. 2000. p. 563.
11. (*a*) C.-M. Che and V.W.-W. Yam. Adv. Inorg. Chem. **39**, 233 (1992); (*b*) C.-M. Che and V.W.-W. Yam. Adv. Transition Met. Coord. Chem. **1**, 209 (1996); (*c*) C.-M. Che and W.-Y. Yu. Pure Appl. Chem. **71**, 281 (1999); (*d*) C.-M. Che, W.-Y. Yu, P.-M. Chan, W.-C. Cheng, S.-M. Peng, K.-C. Lau, and W.-K. Li. J. Am. Chem. Soc. **122**, 11 380 (2000).
12. (*a*) W.-C. Cheng, W.-H. Fung, W.-Y. Yu, and C.-M. Che. J. Mol. Catal. A: Chem. **113**, 311 (1996); (*b*) W.-H. Fung, W.-Y. Yu, and C.-M. Che. J. Org. Chem. **63**, 2873 (1998); (*c*) W.-H. Cheung, W.-Y. Yu, W.-P. Yip, N.-Y. Zhu, and C.-M. Che. J. Org. Chem. **67**, 7716 (2002).
13. T. Higuchi, C. Satake, and M. Hirobe. J. Am. Chem. Soc. **117**, 8879 (1995).
14. (*a*) K.C. Nicolaou, K. Sugita, P.S. Baran, and Y.-L. Zhong. Angew. Chem. Int. Ed. **40**, 207 (2001); (*b*) K.C. Nicolaou, K. Sugita, P.S. Baran, and Y.-L. Zhong. J. Am. Chem. Soc. **124**, 2221 (2002).
15. W. Adam, W.A. Herrmann, C.R. Saha-Mőller, and M. Shimizu. J. Mol. Catal. A: Chem. **97**, 15 (1995).
16. T.C.W. Mak, C.-M. Che, and K.Y. Wong. J. Chem. Soc. Chem. Commun. 986 (1985).
17. K.B. Sharpless and T.R. Verhoeven. Aldrichimica Acta, **12**(4), 201 (1979).

© 2005 NRC Canada

Synthesis of a novel photocatalyst, $ZnBiVO_4$, for the photodecomposition of H_2S[1]

B.B. Kale, Jin-Ook Baeg, Jin S. Yoo, Sang Mi Lee, Chul Wee Lee, Sang-Jin Moon, and Hyunju Chang

Abstract: A novel metal-oxide photocatalyst, $ZnBiVO_4$, was investigated for the photodecomposition of hydrogen sulfide. $ZnBiVO_4$ was prepared using the solid-state method, as well as a solution route for the first time. Oxides of zinc, bismuth, and vanadium were used for the solid-state method, whereas the respective metal salts were used as precursors for the solution route synthesis. The microstructure of the newly prepared $ZnBiVO_4$ was examined using XRD and FESEM. Tetragonal and monoclinic crystallite systems were observed in this ternary oxide system. Nanocrystalline $ZnBiVO_4$ was obtained through the solution route. The catalyst was also characterized using UV–visible diffuse reflectance spectroscopy to evaluate its band gap. Photodecomposition of H_2S using this catalyst was observed for the first time. The influence of preparation methods on the photocatalytic activity of $ZnBiVO_4$ was examined and it was observed that the $ZnBiVO_4$ prepared by the solution route led to a higher photocatalytic activity during H_2S decomposition. It is noteworthy that the hydrogen evolution was enhanced by 100% using $ZnBiVO_4$ prepared by the solution route as compared with the $ZnBiVO_4$ prepared by the solid-state method.

Key words: photocatalyst, $ZnBiVO_4$, hydrogen sulfide, metal oxide, photodecomposition.

Résumé : On a étudié le $ZnBiVO_4$, un nouvel oxyde métallique, comme photocatalyseur pour la photodécomposition du sulfure d'hydrogène. On a préparé le $ZnBiVO_4$ utilisant une voie à l'état solide et, pour la première fois, une vois en solution. Les oxydes de zinc, de bismuth et de vanadium ont été utilisés dans la méthode en phase solide alors que les sels des métaux respectifs ont été utilisés comme précurseurs pour la méthode de synthèse en solution. La microstucture du $ZnBiVO_4$, qui était préparé pour la première fois, a été caractérisée par « XRD » et « FESEM ». On a observé des de cristallisation tétragonal et monoclinique dans ce système d'oxyde ternaire. Cette voie nous a permis d'obtenir du $ZnBiVO_4$ nanocristallin. Afin d'évaluer sa bande interdite, le catalyseur a aussi été caractérisé par spectroscopie de réflectance diffuse UV–visible. La photodécomposition du sulfure d'hydrogène à l'aide de ce catalyseur a été observée pour la première fois. On a examiné l'influence des méthodes de préparation sur l'activité catalytique du $ZnBiVO_4$ et on a observé que le $ZnBiVO_4$ préparé par la voie en solution possède une activité photocatalytique supérieure pour la décomposition du H_2S. Il est remarquable que l'évolution de l'hydrogène est augmentée de 100 % dans le $ZnBiVO_4$ préparé en solution par comparaison au $ZnBiVO_4$ préparé par la méthode à l'état solide.

Mots clés : photocatalyseur, $ZnBiVO_4$, sulfure d'hydrogène, oxyde métallique, photodécomposition.

[Traduit par la Rédaction]

Introduction

Decomposition of hydrogen sulfide is of considerable interest because of its environmental hazard. The well-established Claus process is currently used for the decomposition of hydrogen sulfide (1). This conventional Claus process involves the synproportionation reaction between H_2S and SO_2, yielding elemental sulfur and water vapor. If hydrogen can be recovered from H_2S instead of oxidizing it into H_2O (Claus process), an immense amount of hydrogen can be produced (2). Photocleavage of H_2S to H_2 by semiconductor particle photocatalyst has been considered as a process that could ultimately convert solar energy into fuels. This process requires less energy than the photodecomposition of water. In this connection, recovery of H_2 from H_2S has attracted more attention because of its economic and environmental advantages. Of late, development of a photocatalyst for the photodecomposition of hydrogen sulfide and water into hydrogen has been a subject matter of immense interest, owing to the energy production and pollution abatement. Extensive work has been carried out in the development of ultraviolet-driven photocatalysts for water and H_2S

Received 29 November 2004. Published on the NRC Research Press Web site at http://canjchem.nrc.ca on 24 May 2005.

B.B. Kale. Centre For Materials For Electronics Technology (C-MET), Ministry of Information and Technology, Govt. of India, Panchawati off Pashan Road, Pune –411008, India.
J.-O. Baeg,[2] J.S. Yoo, S.M. Lee, C.W. Lee, S.-J. Moon, and H. Chang. Advanced Chemical Technology Division, Korea Research Institute of Chemical Technology, Yusong, Daejon 305–600, Republic of Korea.

[1]This article is part of a Special Issue dedicated to Professor Howard Alper.
[2]Corresponding author (e-mail: jobaeg@krict.re.kr).

 doi: 10.1139/V05-036 © 2005 NRC Canada

splitting. However, there is a demand for a highly efficient photocatalyst for the photoproduction of hydrogen. In the development of efficient photocatalyst materials, it is essential to control the band structure of the photocatalyst.

The approach for the design of the photocatalyst is classified in three ways. Approach (*a*) is the doping of foreign transition elements into active, existing photocatalysts (3–6). Especially, Ni- and Cu-doped ZnS photocatalysts show activity for H_2 evolution under visible-light irradiation even without a Pt catalyst. Many researchers have reported the doping methods for CdS, ZnS, VS, VS_4, and WO_3 (7–12). Approach (*b*) is to find materials that have a stable valence band in a more negative position than the valence band of conventional metal-oxide photocatalysts. The nitrides (Ta_3N_5), oxynitrides (TaON, $LaTiO_2N$), and oxysulfides ($Sm_2Ti_2S_2O_5$) (13–18) have been reported as active photocatalysts. Approach (*c*) involves a control of the energy structure by making solid solutions between semiconductor photocatalysts with wide and narrow band gaps. The photophysical properties and photovoltaic efficiencies of Nb_2O_5-Bi_2O_3, Ga_2O_3-In_2O_3, $SrNb_2O_7$, $Sr_2Ta_2O_7$, SnO_2-TiO_2, ZnS-CdS, CdS-CdSe, and $(AgIn)_xZn_{2(1-x)}S_2$ (19–23) have been studied extensively. Several nanocrystalline photocatalysts have been reviewed by Beydoun et al. (24), where he described the effect of nanoparticles on photocatalytic activity. Recently, CdS-TiO_2 nanocomposite film (25) has been used for the photodecomposition of H_2S. The stable and suitable metal-oxide support is lacking in this work. In the past, the research for the photodecomposition of H_2S was focused on sulfide semiconductor photocatalysts, which are unstable because of photocorrosion of the catalyst. So, there is a need to find a stable, economical, and efficient new metal-oxide photocatalyst for hydrogen production.

In view of this, we have investigated a novel photocatalyst, $ZnBiVO_4$, for the photodecomposition of H_2S for the first time. We investigated the synthesis of this catalyst by both the solid-state and the solution route. The tentative structural and morphological study was carried out using XRD and FESEM. The nanosize $ZnBiVO_4$ was obtained using the solution route. The influence of the preparation method on the activity of the photocatalyst was demonstrated. This paper describes the novelty in the synthesis of this new product, its characterization, and its photocatalytic activity.

Experimental section

Materials

To prepare $ZnBiVO_4$ by the solid-state reaction, a stoichiometric (1:0.5:0.5) mixture of ZnO, Bi_2O_3, and V_2O_3 was thoroughly ground in a mortar, and this homogeneous reaction mixture was then calcined at 670 °C for 24 h in static air and recalcined at 725 °C for 12 h. To prepare $ZnBiVO_4$ by the solution route, a stoichiometric amount of $Zn(NO_3)_2{\cdot}5H_2O$, $Bi(NO_3)_3{\cdot}6H_2O$, and ammonium metavanadate (NH_4VO_3) was dissolved in water and heated slowly at 70 °C until evaporation. The powder obtained was calcined at 180 °C for 12 h. The resulting product was washed several times with water and ethanol and then dried at 120 °C for 5 h.

Characterization

Powder X-ray diffractograms were recorded with a Model Rigaku-D/MaX-2200V X-ray diffractometer with Cu Kα radiation and an Ni filter. The surface morphology and particle size were determined using a field emission scanning electron microscope (FESEM Model JEOL-JSM6700F). Spectroscopic study of the catalyst was carried out using a UV–vis (Model SHIMADZU UV-2450 diffuse reflectance mode) spectrophotometer and a Fourier Transform Infrared Spectrophotometer (Model, JASCO 610-FTIR). Specific surface area measurements were performed using a BET Surface Area Analyzer (Model BET-MICROMERITICS ASAP-2400).

Photodecomposition of H_2S

The photocatalyst was introduced as a suspension into a cylindrical pyrex photochemical reactor with a water-cooled quartz immersion well and a thermostated water-jacket. A high-pressure mercury lamp (Hanovia) source of intensity 450 W with pyrex cut-off filter was used. At a constant temperature of 25 ± 1 °C, the vigorously stirred suspension was purged with argon for 1 h, and then hydrogen sulfide (H_2S) was bubbled through the solution for about 1 h.

Each experiment was carried out using 1 g of catalyst in 500 mL of distilled water with an H_2S flow of 10 mL/min. The excess hydrogen sulfide was trapped in an NaOH solution. The amount of evolved hydrogen was measured using a graduated gas burette and gas chromatograph (Model Shimadzu GC-14B, MS-5A column, TCD, Ar carrier).

Results and discussion

Synthesis by the solid-state method: $ZnBiVO_4$ (s-s)

$ZnBiVO_4$ has been synthesized for the first time using the solid-state route. According to the thermodynamics and the phase diagrams of the individual components (i.e., ZnO, Bi_2O_3, and V_2O_3), the reaction temperature was expected to be 1000 °C. Since the phase diagram of the V_2O_3 component system was not available in the literature, assumptions were made with the help of the V_2O_5 data. The solid solution was homogenized for 15 h in an alumina crucible at 650 °C, and the compound formed from the reactant components at 670 °C on calcination. The product obtained was crushed, homogenized in mortar, and finally recalcined at 725 °C for 12 h to obtain $ZnBiVO_4$ with good crystallinity. The composition of the final product was verified using XRD and EDS analysis. The presence of the VO_4 group was confirmed by IR spectroscopy. No weight loss or gain after reaction suggested that the stoichiometry of the product was retained.

Synthesis by the solution route: $ZnBiVO_4$ (sol)

Zinc nitrate, bismuth nitrate, and ammonium metavanadate were taken in stoichiometric quantities in aqueous medium and evaporated slowly at 70 °C until dryness. The dried powder was crushed, homogenized, and calcined at 180 °C for 12 h. Ammonium vanadate is soluble in water and forms H_3VO_4 as per the following reaction:

[1] $$H_2O + NH_4VO_3 \rightarrow NH_3 + H_3VO_4$$

© 2005 NRC Canada

During the slow evaporation, Zn and Bi ions in water were reacted with H_3VO_4 and formed $ZnBiVO_4$. The detailed mechanism of the reaction is under investigation. XRD, UV–vis (DRS), and IR spectroscopy confirmed the phase purity of the product.

X-ray analysis

Powder XRD patterns of $ZnBiVO_4$, prepared by the solid-state and the solution route, are shown in Fig. 1. The differences in the XRD patterns of $ZnBiVO_4$ (s-s) and $ZnBiVO_4$ (sol) can be judged by the existence of the peaks at $2\theta = 13°$ and the splitting peaks at $2\theta = 18.5°$, 35°, and 46°. The main (100% relative intensity) peak was obtained at $2\theta = 28.8°$ and shows the existence of the $ZnBiVO_4$ phase. From the XRD pattern, sharp peaks observed at $2\theta = 13°$ and 18.8° reveal the existence of a mixture of tetragonal and monoclinic crystal systems in $ZnBiVO_4$ (sol). In the XRD pattern of $ZnBiVO_4$ (s-s), the peak at $2\theta = 13°$ is absent and the peak at 15° is not significant (relative intensity is very low), which clearly reveals the existence of a mostly tetragonal crystal system. It also shows that the crystal system of compound $ZnBiVO_4$ is dependent on the preparation method. The XRD pattern of $ZnBiVO_4$ (s-s) shows a few unknown weak peaks, which originated from the raw materials. However, peaks pertaining to impurities or the intermediate materials were not observed in the XRD pattern of $ZnBiVO_4$ (sol). This observation indicates that $ZnBiVO_4$ (sol) is of a better quality than $ZnBiVO_4$ (s-s). The XRD pattern of $ZnBiVO_4$ (sol) shows more peak broadening because of the nanocrystalline nature of the powder. A comparison of the experimental XRD data with the XRD data of the raw materials and their related compounds showed the absence of peaks corresponding to those raw materials in the experimental XRD data. Further structural investigation of the product is in progress and will be presented in our next communication.

Powder morphology

A FESEM micrograph of $ZnBiVO_4$ (s-s) is presented in Fig. 2. Spherical and plate-like crystallites with about 0.7–2 μm particle size were observed for $ZnBiVO_4$ (s-s). The FESEM micrograph also shows considerable agglomeration of the plate-like crystallites.

Figures 3*a* and 3*b* show the FESEM pictures of $ZnBiVO_4$ (sol) at lower and higher magnifications, respectively. The particle shapes were spherical. Some of the crystals possessed plate-like morphology with a plate diameter of about 28–200 nm. The minimum size of the crystallite was observed in the range of 20–30 nm. In fact, some of the crystals were less than 20 nm and thus could not be measured by FESEM. The morphology observed for $ZnBiVO_4$ (sol) was completely different than the solid-state route sample, i.e., $ZnBiVO_4$ (s-s). Since the synthesis was carried out at a low temperature, nanocrystalline $ZnBiVO_4$ was obtained. The SEM observations are thus in agreement with our XRD results. From the SEM results it is understood that the particle size and morphology are dependent on the preparation method of the product.

Spectroscopic study

Figure 4 shows a graph of the UV–vis diffuse reflectance of (*a*) $ZnBiVO_4$ (s-s) and (*b*) $ZnBiVO_4$ (sol). The absorption

Fig. 1. XRD pattern of (*a*) $ZnBiVO_4$ (s-s) and (*b*) $ZnBiVO_4$ (sol).

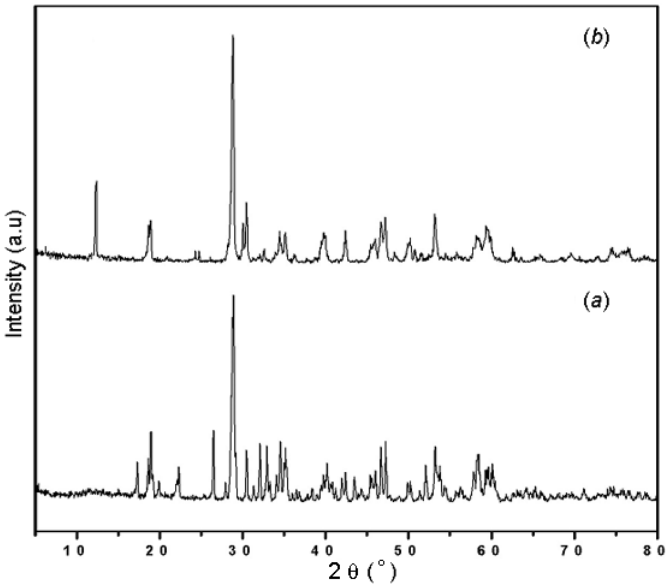
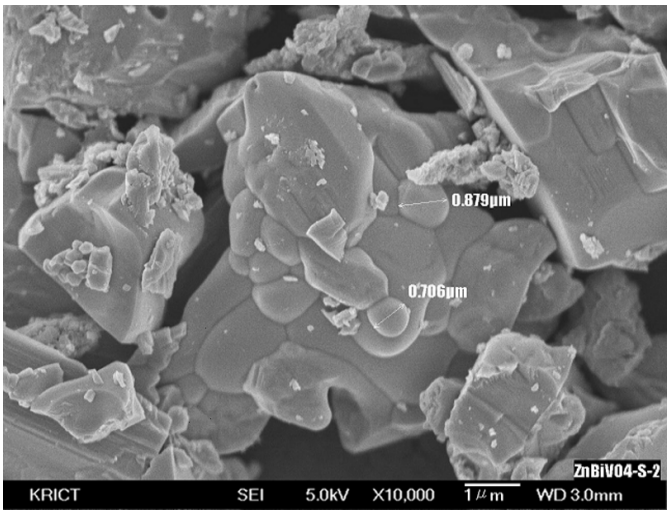


Fig. 2. FESEM micrograph of $ZnBiVO_4$ (s-s).



edge cut-off wavelengths for $ZnBiVO_4$ (s-s) and $ZnBiVO_4$ (sol) were 540 nm and 560 nm, respectively. $ZnBiVO_4$ (s-s) has a sharp absorption cut-off as compared with $ZnBiVO_4$ (sol). This implies that $ZnBiVO_4$ (s-s) is more crystalline with uniform particles, whereas $ZnBiVO_4$ (sol) has mixed crystal sizes with irregular-shaped particle morphology. These observations are in good agreement with the FESEM results. The nature of the broad steepness of the UV–vis DRS cut-off shows the nanocrystalline nature of the particle with agglomeration. Non-uniformity in particle size and shape is also one of the reasons for the broad UV cut-off of $ZnBiVO_4$. From the spectra, the estimated band gap energies (Table 1) of these materials were found to be 2.21 and 2.30 for $ZnBiVO_4$ (s-s) and $ZnBiVO_4$ (sol), respectively. The marginal difference in the band gaps shows the existence of a similar structure for both the products.

© 2005 NRC Canada

Fig. 3. FESEM micrographs of $ZnBiVO_4$ (sol).

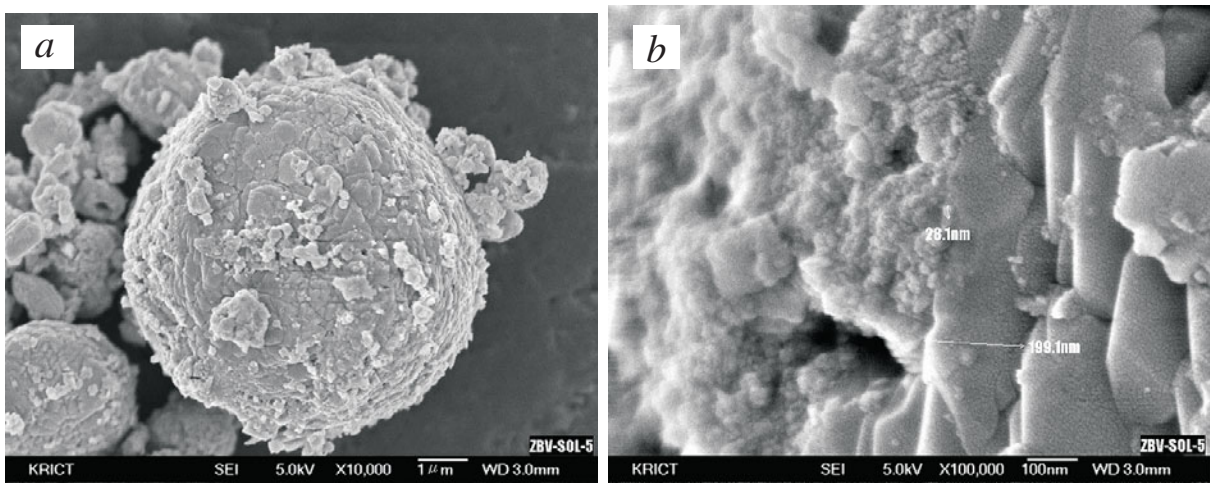


Fig. 4. UV–vis diffuse reflectance spectra of (*a*) $ZnBiVO_4$ (s-s) and (*b*) $ZnBiVO_4$ (sol).

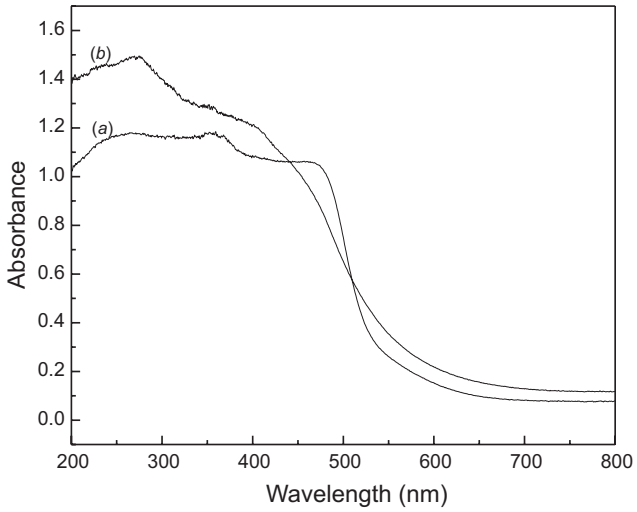


Figure 5 shows the IR spectrums of (*a*) $ZnBiVO_4$ (s-s) and (*b*) $ZnBiVO_4$ (sol). These represent a typical pattern built up by VO_4 tetrahydra (26). The absorption bands were characterized as follows: υ_1 (VO_4) and υ_3 (VO_4) = 500–900 cm^{-1} and υ_4 (VO_4) = 478 cm^{-1}. Accordingly, bands were assigned as shown in Fig. 5. A clear band centred at 734 cm^{-1} in $ZnBiVO_4$ (s-s) is the characteristic band of VO_4. This characteristic vibrational band is shifted to 743 cm^{-1} in the case of $ZnBiVO_4$ (sol). This may be because of the distortion in the metal—oxide bonds (26), which distortion indicates a monoclinic crystallite system. The bands centered at 1356 cm^{-1} and 1384 cm^{-1} are characteristic of the nitrates (present in $ZnBiVO_4$ (sol)) that originated from the starting materials. These bands were absent in the $ZnBiVO_4$ prepared by the solid-state method. A weak broad band centred at 3436 cm^{-1} was due to O–H stretching, which was present in both the samples. This O–H stretching was observed because of the adsorbed water present in the product.

The infrared spectra for the samples (*a*) $ZnBiVO_4$ (s-s) and (*b*) $ZnBiVO_4$ (sol) are similar, except for the nitrate impurity in the latter. The sample (*a*) showed other unknown weak bands, which may have originated from starting oxide materials. The absence of bands from 900–1000 cm^{-1} implies the absence of other oxygen states. The present IR data reveals that $ZnBiVO_4$ consists of tetrahedral VO_4 groups, so that the chemical structure can be described by $ZnBiVO_4$. The IR data obtained is in good agreement with our XRD observations.

Table 1. Photocatalytic activities of the $ZnBiVO_4$ photocatalyst for H_2 evolution from H_2S.

Catalyst[a]	Band gap energy (eV)	Specific surface area BET (m^2/g)	H_2 evolution rate (mL/h)
$ZnBiVO_4$ (s-s)	2.21	0.27	57
$ZnBiVO_4$ (s-s)	2.21	0.27	52[b]
$ZnBiVO_4$ (sol)	2.30	4.70	122
$ZnBiVO_4$ (sol)	2.30	4.70	104[b]

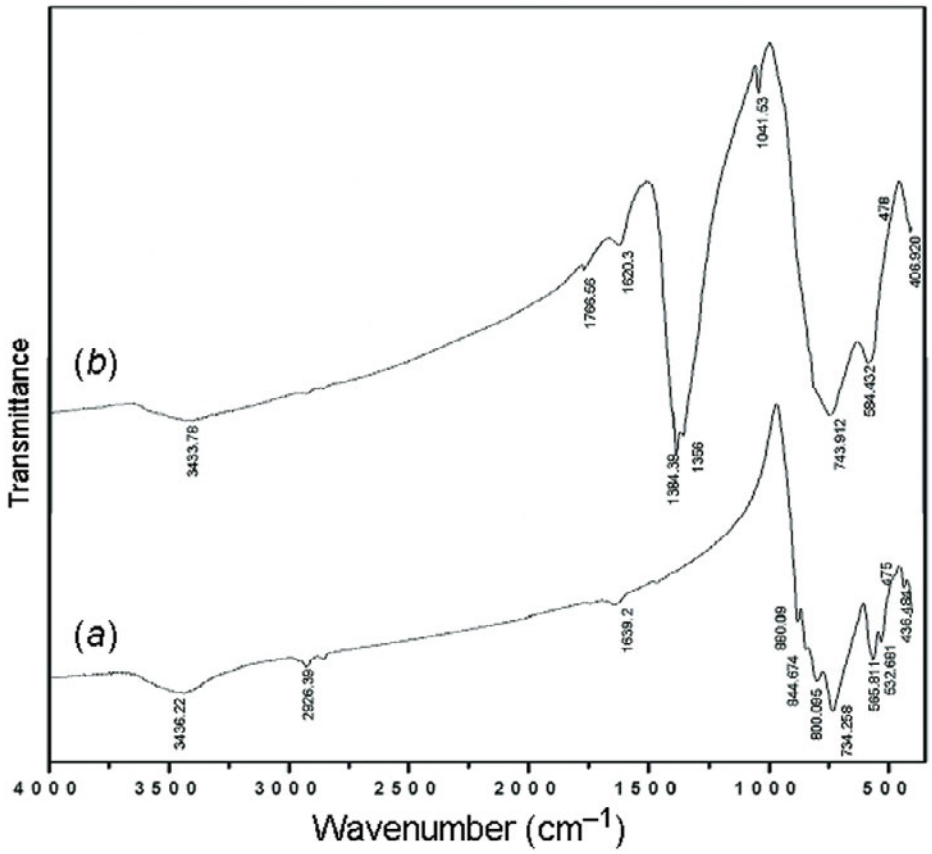
[a]Catalyst: 1.0 g, 500 mL of H_2S saturated H_2O (pH = 4.4), H_2S (10 mL/min), 450 W Hg lamp ($\lambda \geq 325$ nm).
[b]An aqueous solution of KOH (0.5 mol/L) + H_2S (pH = 8.5).

Photodecomposition of H_2S

The photocatalytic activity of the $ZnBiVO_4$ for photodecomposition of hydrogen sulfide was investigated. Different series of experiments were carried out using catalysts prepared by both the solid-state and the solution route. Table 1 shows the rates of hydrogen evolution for photocatalytic decomposition of hydrogen sulfide using $ZnBiVO_4$ (s-s) and $ZnBiVO_4$ (sol). These results reveal that the photocatalytic activity has been enhanced by almost 100% for $ZnBiVO_4$ (sol) as compared with $ZnBiVO_4$ (s-s). This enhancement in catalytic activity may be due to the nanosize particles (less than 28 nm) and high surface area of $ZnBiVO_4$ (sol). The surface area of $ZnBiVO_4$ (s-s) was 0.27 m^2/g, whereas that of $ZnBiVO_4$ (sol) was around 4.7 m^2/g (Table 1), which shows a considerable enhancement in the BET surface area in the case of the sample prepared by the solution route. This could be one of the reasons for the enhancement of the photocatalytic activity. The photodecomposition carried out at higher pH (Table 1) did not show an appreciable effect on the photocatalytic activity. A marginal decrease in activity was observed while using

© 2005 NRC Canada

Fig. 5. IR spectra of (*a*) $ZnBiVO_4$ (s-s) and (*b*) $ZnBiVO_4$ (sol).



the $ZnBiVO_4$ (sol) sample, and this may be because of the low concentration of protons at high pH (24, 27). But overall, higher photocatalytic activity was observed in the case of $ZnBiVO_4$ (sol) when compared with $ZnBiVO_4$ (s-s).

Cited literature on $BiVO_4$ (26) shows that the tetragonal $BiVO_4$ has not shown any photocatalytic activity, whereas monoclinic $BiVO_4$ showed good photocatalytic activity. The reason quoted is that the monoclinic $BiVO_4$ is greatly distorted as compared with tetragonal $BiVO_4$. A similar phenomenon is observed in $ZnBiVO_4$, where the distortion has arisen because of the $6s^2$ loan pairs of Bi^{3+}. The photocatalytic activity has been enhanced significantly in $ZnBiVO_4$ (sol), owing to distortion caused by the $6s^2$ loan pairs of Bi^{3+}. Such effects have been reported earlier (26) for the same compound with a different crystal structure. This indicates that the distortion of the metal oxygen polyhedron is an important factor affecting the photocatalytic properties. The distortion probably affects the charge separation and dislocation of photogenerated electrons and holes. The high surface area and nanosize particles also help to enhance the photocatalytic activity in $ZnBiVO_4$ (sol).

A possible reaction mechanism for the photodecomposion of H_2S is proposed as per the following scheme (28):

[2] $2H_2S \rightarrow 2HS^- + 2H^+$

[3] $2HS^- + 2h^+_{VB} \rightarrow S_2^{2-} + 2H^+$

[4] $S_2^{2-} + 2h^+_{VB} \rightarrow 2S$

[5] $4H^+ + 4e^-_{CB} \rightarrow 2H_2$

[6] $2H_2S \rightarrow 2H_2 + 2S$

According to reaction [2], the bisulfide ion and the proton are produced by the dissociation of H_2S. The photogenerated hole on the surface of the photocatalyst oxidizes the bisulfide ion to give elemental sulfur (reactions [3] and [4]). Finally, hydrogen is formed via the reduction of protons by the photogenerated electrons (reaction [5]). Reaction [6] illustrates the overall process and corresponds to the cleavage of H_2S by two photons of light, which require a Gibbs energy of 7.892 kcal/mol (29).

Summary

A new compound, $ZnBiVO_4$, for use as a photocatalyst has been synthesized by a solid-state route for the first time. A new low-temperature and ambient-pressure aqueous process has also been developed for the synthesis of $ZnBiVO_4$. The product obtained by the solid-state method (i.e., $ZnBiVO_4$ (s-s)) exhibits a tetragonal crystal structure, whereas the product obtained by the solution route (i.e., $ZnBiVO_4$ (sol)) shows a monoclinic crystal structure. The sizes of the crystallites in the product prepared by the solution route were observed to be in the range of 20–28 nm. Some of the crystals possessed plate-like morphology with plate diameter of about 28–200 nm. The photodecomposition of hydrogen sulfide for the production of hydrogen using $ZnBiVO_4$ was studied for the first time. The photocatalytic activity has been enhanced almost 100% with use of $ZnBiVO_4$ (sol) as compared with the solid-state product

© 2005 NRC Canada

$ZnBiVO_4$ (s-s). This enhancement of the photocatalytic activity was attributed to the high surface area of the nanopowder and to distortion caused by the $6s^2$ loan pairs of Bi^{3+} in $ZnBiVO_4$ (sol). This indicates that the distortion of the metal oxygen polyhedron is an important factor affecting the photocatalytic properties. The distortion probably affects the charge separation and dislocation of photogenerated electrons and holes. Further structural investigations and the detailed catalytic activity of the photocatalyst are underway.

Acknowledgements

This research paper was performed for the Hydrogen Energy R&D Center, one of the 21st Century Frontier R&D Programa, funded by the Ministry of Science and Technology of Korea. Our main author would like to thank Dr. B.K. Das, Executive Director, C-MET for his help and inspiration. We are also thankful to Brain pool scheme and KRICT management for offering support to the main author, Dr. B.B. Kale, Scientist-E, C-MET, Pune, India.

References

1. M.P. Elsner, M. Menge, C. Muller, and D.W. Agar. Catal. Today, **79**, 487 (2003).
2. C.A. Linkous, N.Z. Muradov, and S.N. Ramser. Int. J. Hydrogen Energy, **20**, 701 (1995).
3. A. Mills and S. Le Hunte. J. Photochem. Photobiol. A, **108**, 1 (1997).
4. H. Kato and A. Kudo. J. Phys. Chem. B, **106**, 5029 (2002).
5. T. Ishii, H. Kudo, and A. Kudo. J. Photochem. Photobiol. A, **163**, 181 (2004).
6. T. Ishii, H. Kato, H. Kobayashi, and A. Kudo. J. Photochem. Photobiol. A, **163**, 181 (2004).
7. S.A. Naman. Int. J. Hydrogen Energy, **22**, 783 (1997).
8. D. Park and J.O. Beag. US Patent No. 6 297 190 B1, 2 October 2001.
9. D. Park and J.O. Beag. US Patent No. 6 300 274 B1, 9 October, 2001.
10. D. Park and J.O. Beag. US Patent No. 6 447 650 B1, 10 September, 2002.
11. D. Park and J.O. Beag. US Patent No. 6 517 806 B1, 11 February, 2003.
12. H. Chang, K. Kong, Y. Choi, E. In, Y. Choi, J.O. Baeg, and S. Moon. Chem. Phys. Lett. **398**, 449 (2004).
13. A. Kudo, K. Omori, and H. Kato. J. Am. Chem. Soc. **121**, 11 459 (1999).
14. H. Tokunaga, H. Kato, and H. Kudo. Chem. Mater. **13**, 4624 (2001).
15. H. Kato, H. Kobayashi, and A. Kudo. J. Phys. Chem. **106**, 12 441 (2002).
16. A. Ishikawa, T. Takata, J. Kondo, M. Hara, K. Kobayashi, and K. Domen. J. Am. Chem. Soc. **124**, 13 547 (2002).
17. A. Kasahara, N. Nukumizu, T. Takata, J. Kondo, M. Hara, H. Kobayash, and K. Domen. J. Phys. Chem. B, **107**, 791 (2003).
18. S. Kohatani, M. Koshiko, A. Kudo, K. Tokumura, Y. Ishigaki, A. Tokumura, Y. Ishigaki, A. Toriba, K. Hayakawa, and R. Nakagaki. Appl. Catal. B, **46**, 573 (2003).
19. J. Kim, D.W. Hwang, H. Kim, S.W. Bae, S.M. Ji, and J.S. Lee. Chem. Commun. **21**, 2488 (2002).
20. H.G. Kim, D.W. Hwang, and J.S. Lee. J. Am. Chem. Soc. **126**, 8912 (2004).
21. H. Kato and A. Kudo. J. Photochem. Photobiol. A, **145**, 129 (2001).
22. M. Yoshimo, M. Kakihana, C.W. Seok, H. Kato, and A. Kudo. Chem. Mater. **14**, 3369 (2002).
23. J. Lin, J.C. Yu, D. Lo, and S.K. Lam. J. Catal. **183**, 368 (1999).
24. D. Beydoun, R. Amal, G. Low, and S. McEvoy. J. Nanopart. Res. **1**, 439 (1999).
25. W. So, K. Kim, and S. Moon. Int. J. Hydrogen Energy, **29**, 229 (2004).
26. S. Tokunaga, H. Kato, and A. Kudo. Chem. Mater. **13**, 4624 (2001).
27. J. Reber and K. Meier. J. Phys. Chem. **88**, 5903 (1984).
28. I.B. Rufus, B. Vishwanathan, V. Ramakrishnan, and J.C. Kuriacose. J. Photochem. Photobiol. A, **91**, 63 (1995).
29. R.C. Kainthla and J.O.M. Bockris. Int. J. Hydrogen Energy, **12**, 23 (1987).

© 2005 NRC Canada

Catalytic asymmetric synthesis of cyclopropylphosphonates — Catalysts' scope and reactivity[1]

André B. Charette and Jean-Emmanuel Bouchard

Abstract: The transition metal-catalyzed cyclopropanation of alkenes using α-diazomethylphosphonates leads to cyclopropylphosphonate derivatives in high yields. The reaction proceeds well with copper, rhodium, and ruthenium catalysts. The best catalysts for the enantioselective version are either Evans' Cu•bis(oxazoline) or Nishiyama's Ru•pybox.

Key words: cyclopropylphosphonic acids, copper catalysts, ruthenium catalysts, cyclopropanation, diazo reagents.

Résumé : La cyclopropanation d'alcènes impliquant la décomposition de dérivés α-diazométhylphosphonate catalysée par des métaux de transition conduit aux dérivés cyclopropylphosphonate avec de bons rendements. La réaction s'effectue efficacement avec des catalyseurs dérivés du cuivre, rhodium et ruthénium. Les meilleurs catalyseurs pour la version énantiosélective sont le Cu•bis(oxazoline) d'Evans et le Ru•pybox de Nishiyama.

Mots clés : acides cyclopropylphosphoniques, catalyseurs de cuivre, catalyseurs de ruthénium, cyclopropanation, dérivés diazoïques.

Introduction

Phosphinic acid derivatives are quite important synthetic derivatives that have been used to mimic the biological activity of phosphates and carboxylic acids (1). They have found wide applications in medicinal chemistry and agrochemical sciences. Unlike the weak phosphorus–oxygen bond in phosphates, the carbon–phosphorus bond is not easily hydrolyzed and is, therefore, unsusceptible to the action of phosphatases. Some important examples are shown in Fig. 1. Compound **1** possesses antiviral properties (2, 3), **2** is a nucleoside analog (4), and finally, fosfomycin (**3**) is a commonly used antibiotic (5).

One attractive and expedient method for the generation of enantiomerically pure cyclopropylphosphonate derivatives would be to generate them from a catalytic asymmetric addition of a suitably functionalized metal carbene to an alkene to generate the cyclopropane (Fig. 2). Given the efficiency of the analogous reaction using an ester functionality in place of the phosphonate group, one should expect excellent enantio- and diastereocontrol if the appropriately substituted precursor is used. Traditionally these compounds have been prepared by carbene chemistry (6–8), by a Michaëlis–Arbuzov reaction from a *gem*-dibromocyclopropane (9), or by an alkylation – ring closure process (10, 11).

In this paper, we report our study towards the development of an efficient synthesis of enantiomerically enriched cyclopropylphosphonates (12). Various catalysts and phosphonate esters were surveyed to optimize both the enantioselectivities and the diastereoselectivities. This work complements Simonneaux and co-workers' (13–16) recent reports on the use of ruthenium porphyrin catalysts.

Received 16 December 2004. Published on the NRC Research Press Web site at http://canjchem.nrc.ca on 2 June 2005.

This paper is dedicated to Professor Howard Alper in recognition of his many contributions to the science of organometallic chemistry and catalysis.

A.B. Charette[2] and J.-E. Bouchard. Département de chimie, Université de Montréal, P.O. Box 6128, Station Downtown, Montréal, QC H3C 3J7, Canada.

[1]This article is part of a Special Issue dedicated to Professor Howard Alper.

[2]Corresponding author (e-mail: andre.charette@umontreal.ca).

Results and discussion

Synthesis of racemic substituted cyclopropylphoshonate esters

Our first goal was to establish which were the best achiral catalysts to generate cyclopropylphosphonate derivatives (Table 1) (17). Although it is well-established that bulkier esters provide higher diastereocontrol in the cyclopropanation of alkenes using α-diazoacetate derivatives (18) and that such a trend should also be observed with the analogous phosphonate reagents, the initial catalyst calibration was done with the diethylphosphonate derivative **4**. Several catalysts were tested and, as expected, the most reactive were the rhodium-based catalysts (Table 1, entries 2–4). Copper(I) triflate was also quite effective but in all the examples, the diastereocontrol was extremely low (Table 1, entry 1). A ruthenium-based system provided a lesser reactive metal carbene, but the diastereoselectivity was much better (Table 1, entry 5).

Several alkenes were submitted to these reaction conditions using rhodium(II) pivalate and good to excellent yields

 doi: 10.1139/V05-074 © 2005 NRC Canada

Fig. 1. Examples of biologically relevant phosphonate derivatives.

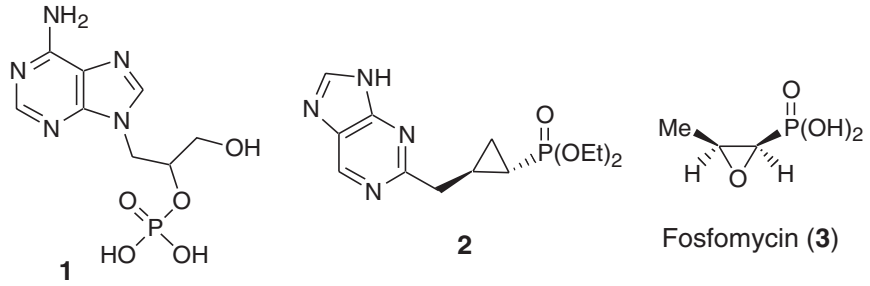


Fig. 2. Synthetic approach to cyclopropylphosphonate derivatives.

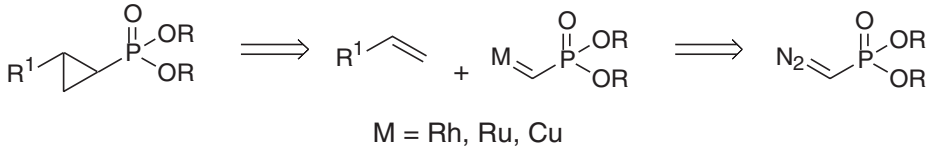
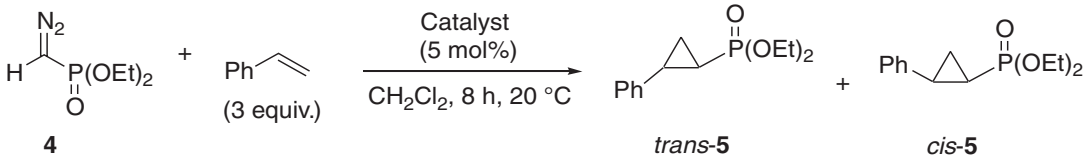


Table 1. Cyclopropanation of diethyl α-diazomethylphosphonate.



Entry	Catalyst	Ratio *trans*-**5**:*cis*-**5**	Yield (%)
1	CuOTf	50:50	77
2	$[Rh(OAc)_2]$	55:45	29
3	$[Rh(octanoate)_2]$	54:46	85
4	$[Rh(Me_3CCO_2)_2]_2$	55:45	85
5	$[RuCl_2(p\text{-cymene})]_2$	81:19	40

of the corresponding cyclopropane were obtained with mono-, di- and trisubstituted alkenes (Fig. 3). However, these reactions produced separable mixtures of the *cis*- and *trans*-cyclopropane isomers.

Enantioselective cyclopropanation — Copper-based catalysts

Although there is an extensive number of efficient copper-based catalysts for the cyclopropanation of α-diazoesters, the bis(oxazoline)-based catalysts were screened because of their accessibility and their efficiency in the cyclopropanation of mono- and disubstituted alkenes using α-diazoesters. As already highlighted by Evans et al. (19) for the cyclopropanation of α-diazoesters, the bis(oxazoline) **21** derived from *tert*-leucine provided not only the highest enantioselectivities but also the best diastereocontrol (Table 2). A similar level of enantiocontrol was also observed with the bis(oxazoline) **22** derived from serine. Increasing the steric bulk of the R groups of the phosphonate reagent led to a slightly improved diastereocontrol, but the enantioselectivities were mostly ligand-dependent. For example, the diisopropyl α-diazomethylphosphonate and the neopentyl α-diazomethylphosphonate reagents **13** and **14** led to higher diastereoselectivities, but the enantiomeric excesses of the products were similar. The scope of the reaction for the Cu·bis(oxazoline) **21** catalyzed cyclopropanation of disubstituted alkenes with diethyl α-diazomethylphosphonate is shown in Fig. 4. The general trend is that the diastereocontrol is relatively modest and the enantioselectivities are lower than those observed for the cyclopropanation of styrene. Furthermore, the cyclopropanation of 1,2-disubstituted alkenes produced the corresponding cyclopropane in modest yields and enantioselectivities.

Enantioselective cyclopropanation using ruthenium-based catalysts

Nishiyama's ruthenium catalysts (20) are among the most efficient ones for the cyclopropanation of alkenes with ethyl diazoacetate. Although the ruthenium carbene is usually less reactive than the analogous rhodium derivative, the corresponding cyclopropane is obtained with high diastereo- and enantiocontrol.

Table 3 illustrates the optimization process that led to the identification of the most efficient ligand and reagent combination. As previously reported by Nishiyama (20) for the cyclopropanation of alkenes using α-diazoesters, the ligand derived from valine was the most effective (Table 3, entry 1 vs. 2 vs. 4). Furthermore, the steric bulk of the phosphonate reagent was important in providing high diastereocontrol,

© 2005 NRC Canada

Fig. 3. Scope of the rhodium-catalyzed cyclopropanation of alkenes.

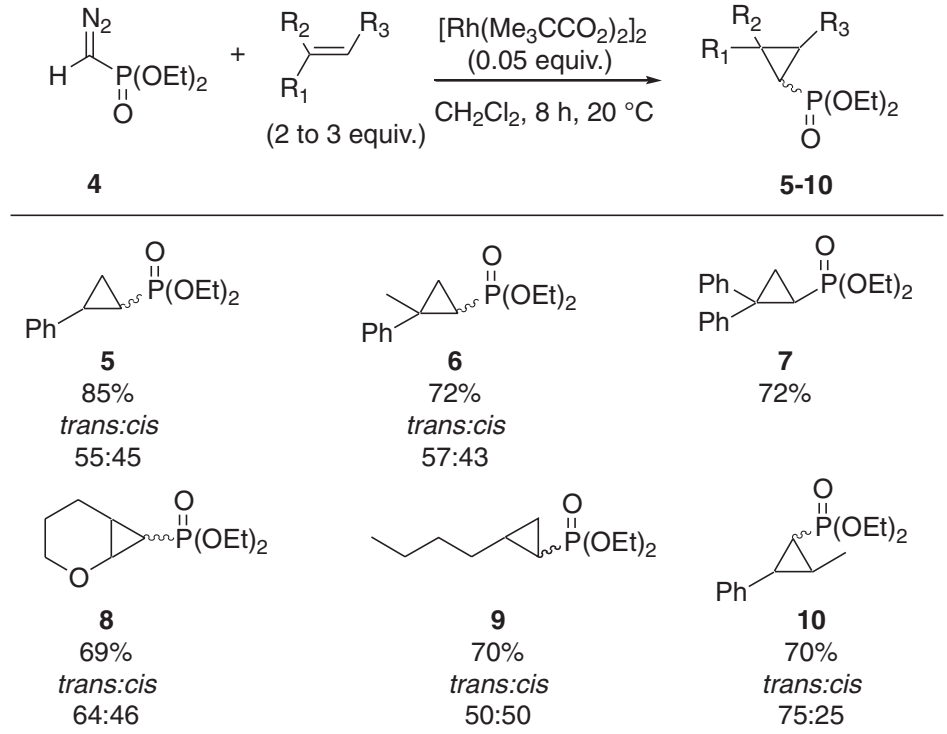
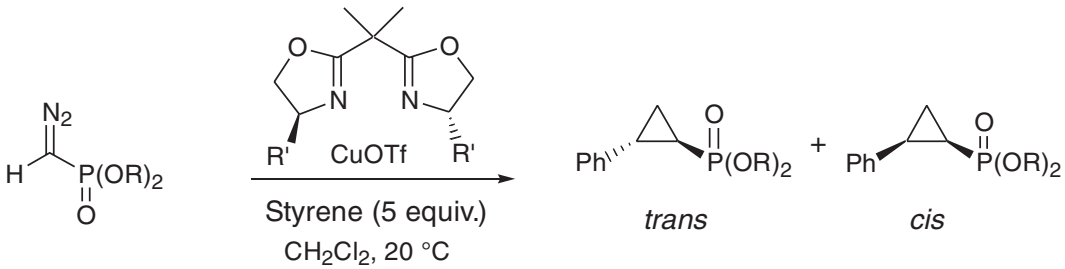


Table 2. Copper(I)-catalzyed cyclopropanation of alkenes with α-diazophosphonate reagents.



Entry	R	Ligand	Yield (%)	Product (R)	trans:cis	ee (%, trans:cis)
1	Me (**11**)	**19**	72	**15** (Me)	81:19	76:61
2	Me (**11**)	**20**	75	**15** (Me)	80:20	79:83
3	Me (**11**)	**21**	74	**15** (Me)	86:14	93:99
4	Et (**4**)	**19**	72	**5** (Et)	80:20	75:67
5	Et (**4**)	**20**	86	**5** (Et)	78:22	80:74
6	Et (**4**)	**22**	50	**5** (Et)	83:17	92:99
7	Et (**4**)	**21**	65	**5** (Et)	84:16	92:99
8	Bu (**12**)	**21**	65	**16** (Bu)	88:12	91:nd
9	*i*-Pr (**13**)	**21**	65	**17** (*i*-Pr)	90:10	92:nd
10	($CH_2C(CH_3)_3$) (**14**)	**21**	67	**18** ($CH_2C(CH_3)_3$)	92:8	92:nd

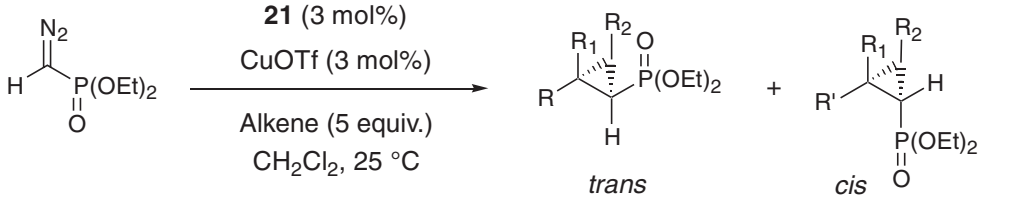
Note: nd = not determined.

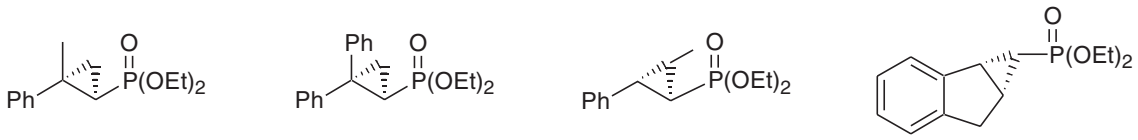
although even the diethyl derivative provided excellent diastereoselectivies (Table 3, entry 4).

The scope of the reaction is shown in Table 4. Monosubstituted alkenes led to the corresponding cyclopropane in high yield and enantiocontrol (Table 4, entries 1–3, 7). In all the reactions, the diastereoselectivity was greater than 95:5 favoring the trans isomer. The absolute stereochemistry was confirmed in one case (compound **31**) from the X-ray crystal structure (Fig. 5). 1,1-Disubstituted alkenes could also be used but the diastereocontrol was slightly lower (Table 4,

© 2005 NRC Canada

Fig. 4. Scope of the Cu·bis(oxazoline) **21** catalyzed cyclopropanation of alkenes.





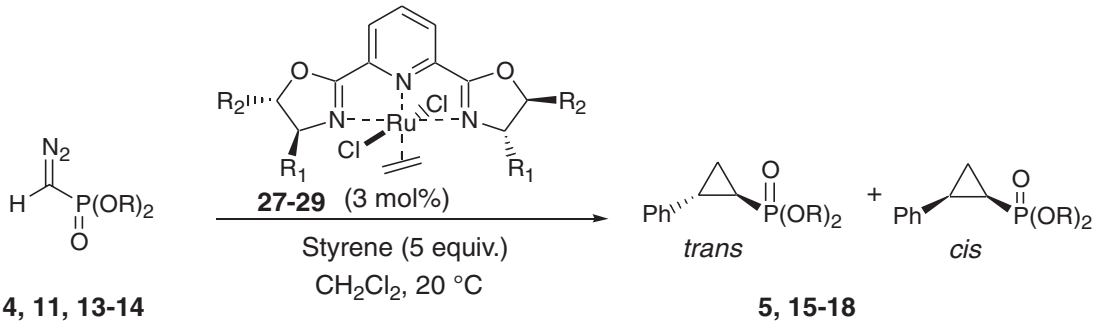
23 73% *trans/cis*: 64/36 ee *trans*: 84%

24 50% ee: 78%

25 50% *trans/cis*: 85/15 ee *trans*: 72%

26 50% *trans/cis*: 99/1 ee *trans*: 37%

Table 3. Optimization of the enantioselective cyclopropanation of alkenes using ruthenium catalysts.



Entry	R	R_1	R_2	Catalyst	Product	Yield (%)	trans:cis	ee (%, trans)
1	Et (**4**)	Me	Ph	**27**	5	68[a]	>98:2	52
2	Et (**4**)	Ph	H	**28**	5	60[a]	78:22	49
3	Me (**11**)	*i*-Pr	H	**29**	15	65	90:10	76
4	Et (**4**)	*i*-Pr	H	**29**	5	65	>98:2	96
5	*i*-Pr (**13**)	*i*-Pr	H	**29**	17	70	>98:2	96
6	$CH_2C(CH_3)_3$ (**14**)	*i*-Pr	H	**29**	18	79[a]	>98:2	96

[a]The reaction was heated under reflux.

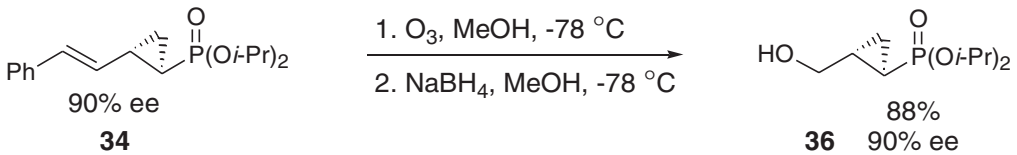
entry 4). Finally, when a diene was used, the cyclopropanation occurred at the least-hindered position (Table 4, entry 6).

It is also possible to further functionalize the cyclopropylphosphonate and to hydrolyze it to the corresponding phosphonic (21) acid. It is also possible to convert the styryl substituent into a primary alcohol through a oxidative cleavage – reduction sequence (eq. [1]).

Conclusion

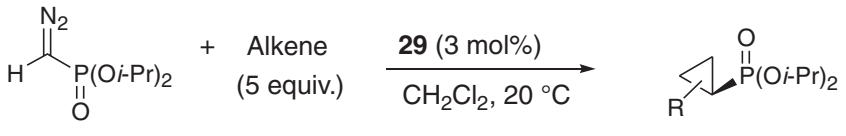
We have shown that the preparation of enantiomerically enriched cyclopropylphosphonate derivatives can easily be accomplished using the copper- or ruthenium-catalyzed decomposition of diethyl or diisopropyl α-diazomethylphosphonate. The products are usually obtained in good enantiomeric excesses and excellent diastereocontrol.

[1]

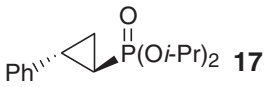
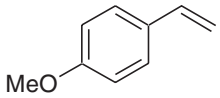
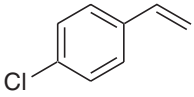
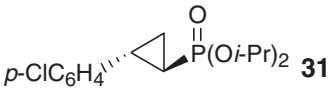
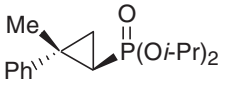
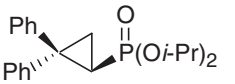
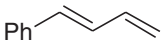
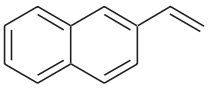


© 2005 NRC Canada

Table 4. Scope of the cyclopropanation of alkenes with Nishiyama's catalyst (20).

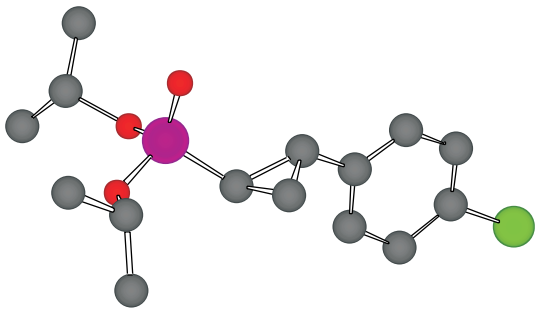


13 **17, 30-35**

Entry	Alkene	Major Product	Yield (%)	*trans*:*cis*	ee (%) *t*:*c*
1		 **17**	70	>98:2	96:—
2		 **30**	80	>98:2	94:—
3		 **31**	77	>98:2	98:—
4		 **32**	72	88:12	95:92
5		 **33**	39[a]	—	91
6		 **34**	90[a]	95:5	90:92
7		 **35**	91[a]	>98:2	97:—

[a]The reaction was heated under reflux.

Fig. 5. Chem3D® representation of X-ray structure of cyclopropylphosphonate **31**.



Experimental

(±)-Diethyl 2-phenylcyclopropylphosphonate ((±)-5) (Table 1, entry 4)

To a solution of styrene (0.154 mL, 1.35 mmol, 3 equiv.) and rhodium(II) pivalate (l4.0 mg, 0.0225 mmol, 0.05 equiv.) in dichloromethane (2.0 mL) at room temperature was added over 3 h via a syringe pump a solution of diethyl α-diazomethylphosphonate (**4**) (22) (80.0 mg, 0.449 mmol, 1 equiv.) in dichloromethane (2.0 mL). After 8 h of stirring at room temperature, the reaction mixture was concentrated under reduced pressure. The crude residue was purified by flash chromatography on silica gel using EtOAc as the eluent to give the desired compound (±)-**5** as a colorless oil (100 mg, 85%): R_f 0.40 (80% EtOAc–hexanes). IR (film, cm^{-1}): 2981, 2931, 1244, 1026, 961, 777, 699. ^{1}H NMR (300 MHz, $CDCl_3$) δ: 7.31–7.10 (m, 5H, C_6H_5), 4.12 (m, 4H, P-O-CH_2-CH_3 (trans)), 3.80 (m, 4H, P-O-CH_2-CH_3 (cis)), 2.48 (m, 1H, C_6H_5-$CH_{cycloprop}$), 1.35 (m, 1H, $CH_{2cycloprop}$), 1.30 (m, 6H, P-O-CH_2-CH_3), 1.20 (m, 1H, $CH_{2cycloprop}$), 1.14 (m, 2H, $CH_{cycloprop}$-P). ^{13}C NMR (75 MHz, $CDCl_3$) δ: 140.0, 139.97, 129.4, 129.1, 128.9, 128.5, 128.2, 127.8, 126.6, 126.5, 126.0, 63.6, 63.5, 63.4, 62.0, 61.9, 61.87, 61.8, 21.0, 20.99, 16.5, 16.4, 16.1, 13.5, 12.7, 12.6. ^{31}P NMR (160 MHz, $CDCl_3$) δ: 29.9 (trans), 28.9 (cis). Anal. calcd. for $C_{13}H_{19}O_3P$: C 61.41, H 7.53; found: C 61.06, H 7.72.

© 2005 NRC Canada

(±)-Diethyl 2-methyl-2-phenylcyclopropylphosphonate ((±)-6)

The procedure for the preparation of compound (±)-**5** was followed. Scale: rhodium(II) pivalate (14.0 mg, 0.0225 mmol, 0.05 equiv.), α-methylstyrene (0.117 mL, 0.898 mmol, 2 equiv.); diethyl α-diazomethylphosphonate (**4**) (80.0 mg, 0.449 mmol, 1 equiv.), CH_2Cl_2 (4 mL total). 80% EtOAc–hexanes was used as the eluent for the purification of the 57:43 mixture (NMR) by flash chromatography on silica gel to afford (±)-*trans*-**6** as a colorless oil (49 mg, 41%) and (±)-*cis*-**6** (37 mg, 31%) as a colorless oil. (±)-*trans*-**6**: R_f 0.37 (EtOAc). IR (film, cm^{-1}): 2981, 1245, 1058, 1027, 960, 889, 769, 701. ^1H NMR (300 MHz, $CDCl_3$) δ: 7.31–7.26 (m, 5H, C_6H_5), 4.16 (m, 1H, P-O-CH_2CH$_3$), 1.66 (s, 3H, CH_3), 1.38 (m, 8H, P-O-CH$_2$CH_3, C$H_{2cycloprop}$), 1.33 (m, 1H, C$H_{cyclopropyl}$-P). ^{13}C NMR (75 MHz, $CDCl_3$) δ: 146.3, 146.28, 128.7, 127.5, 126.7, 61.8, 61.76, 61.7, 27.6, 27.59, 22.1, 22.0, 19.8, 18.9, 18.87, 17.9, 16.8, 16.7, 16.69. ^{31}P NMR (160 MHz, $CDCl_3$) δ: 30.5. Anal. calcd. for $C_{14}H_{21}O_3P$: C 62.67, H 7.89; found: C 62.73. H 7.77. (±)-*cis*-**6**: R_f 0.25 (EtOAc). ^1H NMR (300 MHz, $CDCl_3$) δ: 7.17–7.44 (m, 5H, C_6H_5), 3.88 (m, 2H, P-O-CH_2CH$_3$), 3.70 (m, 1H, P-O-CH_2CH$_3$), 3.33 (m, 1H, P-O-CH_2CH$_3$), 1.64 (d, J = 2.4 Hz, 1H, C$H_{cycloprop}$-P), 1.60 (s, 3H, CH_3), 1.17 (m, 5H, P-O-CH$_2$CH_3, C$H_{2cycloprop}$), 0.96 (t, J = 7.1 Hz, 3H, P-O-CH$_2$CH_3). ^{13}C NMR (75 MHz, $CDCl_3$) δ: 141.96, 141.9, 129.5, 128.2, 126.9, 61.5, 61.4, 61.35, 61.35, 61.3, 29.64, 29.6, 28.24, 28.2, 21.1, 19.1, 17.4, 17.3, 16.5, 16.46, 16.4, 16.3. ^{31}P NMR (160 MHz, $CDCl_3$) δ: 27.9. HR-MS calcd. for $C_{14}H_2O_3P$ (M + H): 268.1228; found: 228.1228.

(±)-Diethyl 2,2-diphenylcyclopropylphosphonate ((±)-7)

The procedure for the preparation of compound (±)-**5** was followed. Scale: rhodium(II) pivalate (7.40 mg, 0.0121 mmol, 0.05 equiv.), 1,1-diphenylethylene (0.134 mL, 0.898 mmol, 3 equiv.), diethyl α-diazomethylphosphonate (**4**) (50.0 mg, 0.243 mmol, 1 equiv.), CH_2Cl_2 (4 mL total). Purification by flash chromatography on silica gel (80% EtOAc–hexanes) afforded (±)-**7** as a colorless oil (63 mg, 72%). R_f 0.34 (80% EtOAc–hexanes). IR (film, cm^{-1}): 2980, 1599, 1495, 1446, 1248, 1227, 1020, 953, 772, 695. ^1H NMR (300 MHz, $CDCl_3$) δ: 7.51–7.16 (m, 10H, C_6H_5), 3.95 (m, 2H, P-O-CH_2-CH$_3$), 3.76 (m, 1H, P-O-CH_2-CH$_3$), 3.50 (m, 1H, P-O-CH_2-CH$_3$), 2.03 (m, 1H, C$H_{2cycloprop}$), 1.83 (m, 1H, C$H_{2cycloprop}$), 1.57 (m, 1H, C$H_{cycloprop}$-P), 1.22 (t, J = 7.1 Hz, 3H, P-O-CH$_2$-CH_3), 1.05 (t, J = 7.1 Hz, 3H, P-O-CH$_2$-CH_3). ^{13}C NMR (75 MHz, $CDCl_3$) δ: 145.4, 145.3, 140.3, 140.26, 130.1, 128.4, 128.0, 127.91, 127.90, 126.9, 126.6, 63.6, 61.5, 61.4, 61.35, 36.7, 36.63, 21.3, 18.7, 17.9, 17.8, 16.3, 16.24, 16.2, 16.1. ^{31}P NMR (160 MHz, $CDCl_3$) δ: 27.1. HR-MS calcd. for $C_{19}H_{23}O_3P$ (M + H): 331.1463; found: 331.1457.

(±)-Diethyl 2-oxa-bicyclo[4.1.0]hept-7-ylphosphonate ((±)-8)

The procedure for the preparation of compound (±)-**5** was followed. Scale: rhodium(II) pivalate (14.0 mg, 0.0225 mmol, 0.05 equiv.), 3,4-dihydro-2*H*-pyran (0.082 mL, 0.898 mmol, 2 equiv.), diethyl α-diazomethylphosphonate (**4**) (80.0 mg, 0.449 mmol, 1 equiv.), CH_2Cl_2 (4 mL total). EtOAc was used as the eluent for the purification of the 64:46 mixture (NMR) by flash chromatography on silica gel to afford (±)-*trans*-**8** as a colorless oil (44 mg, 44%) and (±)-*cis*-**8** (25 mg, 25%) as a colorless oil. (±)-*trans*-**8**: R_f 0.21 (100% EtOAc). ^1H NMR (300 MHz, $CDCl_3$) δ: 4.15 (m, 4H, P-O-CH_2-CH$_3$), 3.85 (dt, J = 6.4, 3.1 Hz, 1H, O-C$H_{cycloprop}$), 3.75 (td, J = 10.7, 3.5 Hz, 1H, O-CH_2-CH$_2$-CH$_2$-CH$_{cycloprop}$), 3.35 (dt, J = 10.6, 2.7 Hz, 1H, O-CH_2-CH$_2$-CH$_2$-CH$_{cycloprop}$), 2.10 (m, 3H, O-CH$_2$-CH_2-CH$_2$-CH$_{cycloprop}$, O-CH$_2$-CH_2-CH$_2$-C$H_{cycloprop}$), 1.45 (m, 1H, O-CH$_2$-CH_2-CH$_2$-C$H_{cycloprop}$), 1.40 (t, J = 7.1 Hz, 1H, P-O-CH$_2$-CH_3), 0.80 (m, 1H, C$H_{cycloprop}$-P). ^{13}C NMR (75 MHz, $CDCl_3$) δ: 64.7, 61.7, 61.6, 60.9, 60.8, 53.9, 53.8, 27.0, 20.9, 17.4, 16.4, 16.3, 16.2, 15.4, 15.3, 14.8. ^{31}P NMR (160 MHz, $CDCl_3$) δ: 27.0. IR (film, cm^{-1}): 2979, 2931, 1237, 1056, 1024, 953, 806. HR-MS calcd. for $C_{10}H_{19}O_4P$ (M + H): 235.1099; found: 235.1105. (±)-*cis*-**8**: R_f 0.13 (100% EtOAc). ^1H NMR (300 MHz, $CDCl_3$) δ: 4.10 (m, 4H, P-O-CH_2-CH$_3$), 3.85 (m, 1H, O-C$H_{cycloprop}$), 3.60 (td, J = 10.9, 3.3 Hz, 1H, O-CH_2-CH$_2$-CH$_2$-CH$_{cycloprop}$), 3.35 (dt, J = 10.7, 3.1 Hz, 1H, O-CH_2-CH$_2$-CH$_2$-CH$_{cycloprop}$), 2.00 (m, 2H, CH$_2$-CH_2-CH$_2$-CH$_{cycloprop}$), 1.60 (m, 1H, O-CH$_2$-CH$_2$-CH$_2$-C$H_{cycloprop}$), 1.45 (m, 2H, O-CH$_2$-CH$_2$-CH_2-CH$_{cycloprop}$), 1.30 (t, J = 7.1 Hz, 1H, P-O-CH$_2$-CH_3), 0.90 (m, 1H, C$H_{cycloprop}$-P). ^{13}C NMR (75 MHz, $CDCl_3$) δ: 64.4, 61.9, 61.8, 61.7, 55.3, 55.2, 21.5, 19.1, 19.0, 18.1, 16.8, 16.7, 16.5, 16.4, 15.7. ^{31}P NMR (160 MHz, $CDCl_3$) δ: 28.2. IR (film, cm^{-1}): 2979, 2931, 1237, 1056, 1024, 953, 806.

(±)-Diethyl 2-butylcyclopropylphosphonate ((±)-9)

The procedure for the preparation of compound (±)-**5** was followed. Scale: rhodium(II) pivalate (14.0 mg, 0.0225 mmol, 0.05 equiv.), 1-hexene (0.116 mL, 0.898 mmol, 2 equiv.), diethyl α-diazomethylphosphonate (**4**) (80.0 mg, 0.449 mmol, 1 equiv.), CH_2Cl_2 (4 mL total). The purification of the 50:50 mixture (NMR) by flash chromatography on silica gel (80% EtOAc–hexanes) afforded (±)-*trans*-**9** as a colorless oil (42 mg, 35%) and (±)-*cis*-**9** (42 mg, 35%) as a colorless oil. (±)-*trans*-**9**: R_f 0.36 (EtOAc). ^1H NMR (300 MHz, $CDCl_3$) δ: 4.10 (m, 2H, P-O-CH_2-CH$_3$), 1.30 (m, 13H, CH$_3$-CH_2-CH_2-CH_2-C$H_{cycloprop}$, P-O-CH$_2$-CH_3), 1.00 (m, 1H, C$H_{2cycloprop}$), 0.85 (t, J = 7.0 Hz, 3H, CH_3-CH$_2$-CH$_2$-CH$_2$-CH$_{cycloprop}$), 0.60 (m, 2H, C$H_{cycloprop}$-P, CH$_{2cycloprop}$). ^{13}C NMR (75 MHz, $CDCl_3$) δ: 61.7, 61.6, 33.3, 33.27, 31.3, 22.3, 17.4, 17.3, 16.5, 16.4, 14.0, 11.9, 10.4, 10.37, 9.3. ^{31}P NMR (160 MHz, $CDCl_3$) δ: 32.3. HR-MS calcd. for $C_{11}H_{23}O_3P$ (M + H): 235.1463; found: 235.1453. (±)-*cis*-**9**: R_f 0.44 (EtOAc). IR (film, cm^{-1}): 2957, 2928, 1458, 1245, 1059, 1030, 957, 732. ^1H NMR (300 MHz, $CDCl_3$) δ: 4.10 (m, 2H, P-O-CH_2-CH$_3$), 1.70 (m, 1H, C$H_{cycloprop}$), 1.50 (m, 11H, CH$_3$-CH$_2$-CH_2-CH_2-C$H_{cycloprop}$, P-O-CH$_2$-CH_3), 1.10 (m, 2H, C$H_{2cycloprop}$), 0.90 (t, J = 7.0 Hz, 3H, CH_3-CH$_2$-CH$_2$-CH$_2$-CH$_{cycloprop}$), 0.85 (q, J = 7.0 Hz, 2H, CH$_3$-CH_2-CH$_2$-CH$_2$-CH$_{cycloprop}$). ^{13}C NMR (75 MHz, $CDCl_3$) δ: 61.4, 61.35, 61.3, 31.9, 28.5, 28.4, 22.4, 17.9, 16.5, 16.4, 16.4, 14.1, 10.9, 10.5, 10.47, 10.4, 7.9. ^{31}P NMR (160 MHz, $CDCl_3$) δ: 32.5.

(±)-Diethyl 2-methyl-3-phenylcyclopropylphosphonate ((±)-10)

The procedure for the preparation of compound (±)-**5** was followed. Scale: rhodium(II) pivalate (14.0 mg, 0.0225 mmol, 0.05 equiv.), *trans*-β-methylstyrene (0.116 mL, 0.898 mmol, 2 equiv.), diethyl α-diazomethylphosphonate (**4**) (80.0 mg,

© 2005 NRC Canada

0.449 mmol, 1 equiv.), CH_2Cl_2 (4 mL total). The purification of the 50:50 mixture (NMR) by flash chromatography on silica gel (80% EtOAc–hexanes) afforded (±)-*trans*-**10** as a colorless oil (63 mg, 53%) and (±)-*cis*-**10** (21 mg, 17%) as a colorless oil. (±)-*trans*-**10**: R_f 0.42 (EtOAc). IR (film, cm^{-1}): 2981, 2905, 1240, 1055, 1029, 963. ^1H NMR (300 MHz, $CDCl_3$) δ: 7.07–7.30 (m, 5H, C_6H_5), 4.10 (m, 4H, P-O-CH_2-CH_3), 2.35 (m, 1H, C_6H_5-$CH_{cycloprop}$), 1.85 (d, 3H, CH_3 (cis)) 1.57 (m, 1H, $CH_{cycloprop}$-P), 1.46 (d, J = 6.4 Hz, 3H, CH_3 (trans)), 1.36 (m, 6H, P-O-CH_2-CH_3), 1.20 (m, 2H, $CH_{2cycloprop}$). ^{13}C NMR (75 MHz, $CDCl_3$) δ: 140.6, 140.58, 128.5, 126.3, 125.9, 62.8, 62.7, 61.6, 61.56, 61.51, 61.4, 29.5, 29.4, 22.4, 22.3, 22.0, 19.5, 16.5, 16.46, 16.4, 16.38, 14.0, 13.9. ^{31}P NMR (160 MHz, $CDCl_3$) δ: 29.3. HR-MS calcd. for $C_{14}H_{21}O_3P$ (M + H): 268.1228; found: 268.1230.

Dineopentyl diazomethylphosphonate (14)

To a solution of dineopentyl methylphosphonate (23) (3.00 g, 12.7 mmol, 1 equiv.) in THF (125 mL) at –78 °C was added dropwise 2.5 mol/L of *n*-BuLi in hexanes (2.50 mL, 1.5 equiv.). The mixture was stirred at –78 °C for 30 min and 2,2,2-trifluoroethyltrifluoroacetate (1.90 mL, 13.9 mmol, 1.1 equiv.) was added in one portion. The reaction was stirred at –78 °C for 25 min and then warmed to room temperaure. A 10% aqueous solution of HCl (5 mL) was added and the aqueous layer was extracted with two portions of EtOAc. The combined organic layers were washed with satd. aq. $NaHCO_3$, satd. aq. NaCl, dried over Na_2SO_4, and concentrated under reduced pressure. The residue was dissolved in acetonitrile (125 mL) and *p*-acetamidobenzenesulfonyl azide (3.05 g, 12.7 mmol, 1 equiv.) was added followed by triethylamine (1.80 mL, 12.7 mmol, 1 equiv.). The reaction mixture was stirred for 12 h at room temperature and satd. aq. NH_4Cl was added. The layers were separated and the aqueous layer was washed with EtOAc. The combined organic layers were washed with satd. aq. $NaHCO_3$, satd. aq. NaCl, dried over Na_2SO_4, and concentrated under reduced pressure. The residue was dissolved in $CHCl_3$ (30 mL) and the mixture was filtered through Celite®. The filtrate was concentrated under reduced pressure and the residue was purified by flash chromatography on silica gel (30% EtOAc–hexanes) to give the desired diazo reagent **14** as a yellow oil (1.10 g, 33%). R_f 0.50 (30% EtOAc–hexanes). IR (film, cm^{-1}): 2958, 2873, 2101, 1659, 1479, 1245, 999, 874, 850, 584. ^1H NMR (300 MHz, $CDCl_3$) δ: 3.77 (d, J = 11.1 Hz, 1H, CH=N_2), 3.75 (m, 4H, P-O-CH_2), 0.96 (s, 18H, C(CH_3)$_3$). ^{13}C NMR (75 MHz, $CDCl_3$) δ: 75.75, 75.66, 32.2, 32.1, 32.06, 32.02, 26.0. ^{31}P NMR (160 MHz, $CDCl_3$) δ: 20.2. HR-MS calcd. for $C_{11}H_{23}N_2O_3P$ (M + H): 263.1511; found: 263.1513.

General procedure for the Cu·bis(oxazoline) 21 catalyzed cyclopropanation — Diethyl (1*R*,2*S*)-2-methyl-2-phenylcyclopropylphosphonate (23)

A solution of bis(oxazoline) **21** (3.70 mg, 0.0126 mmol, 0.031 equiv.) and copper(I) triflate (3.20 mg, 0.0124 mmol, 0.03 equiv.) in CH_2Cl_2 (2 mL) was stirred at room temperature for 3 h and α-methylstyrene (0.260 mL, 2.00 mmol, 5 equiv.) was added. A solution of diethyl α-diazomethylphosphonate (**4**) (73.2 mg, 0.411 mmol, 1 equiv.) in CH_2Cl_2 (2 mL) was added over 8 h via a syringe pump. The reaction was stirred for an additional 12 h at room temperature and was then concentrated under reduced pressure. The diastereomeric ratio (64:36) was determined by ^{31}P NMR of the crude reaction mixture (δ major: 30.5 and δ minor: 27.9). The crude mixture was then purified by flash chromatography on silica gel (80% EtOAc–hexanes) to give *trans*-**23** (46 mg, 47%) and *cis*-**23** (26 mg, 26%). The enantiomeric excesses (85%) were determined by SFC on a chiral stationary phase (Chiralcel OD, 1% MeOH, 1.2 mL/min: t_r (major) 19.9 min, t_r (minor), 18.1 min). *trans*-**23**: R_f 0.37 (EtOAc). IR (film, cm^{-1}): 2981, 1245, 1058, 1027, 960, 889, 769, 701. ^1H NMR (300 MHz, $CDCl_3$) δ: 7.31–7.26 (m, 5H, C_6H_5), 4.16 (m, 1H, P-O-CH_2CH_3), 1.66 (s, 3H, CH_3), 1.38 (m, 8H, P-O-CH_2CH_3, $CH_{2cycloprop}$), 1.33 (m, 1H, $CH_{cyclopropyl}$-P). ^{13}C NMR (75 MHz, $CDCl_3$) δ: 146.3, 146.28, 128.7, 127.5, 126.7, 61.8, 61.76, 61.7, 27.6, 27.59, 22.1, 22.0, 19.8, 18.9, 18.87, 17.9, 16.8, 16.7, 16.69. ^{31}P NMR (160 MHz, $CDCl_3$) δ: 30.5. Anal. calcd. for $C_{14}H_{21}O_3P$: C 62.67, H 7.89; found: C 62.73, H 7.77. *cis*-**23**: R_f 0.25 (EtOAc). ^1H NMR (300 MHz, $CDCl_3$) δ: 7.17–7.44 (m, 5H, C_6H_5), 3.88 (m, 2H, P-O-CH_2CH_3), 3.70 (m, 1H, P-O-CH_2CH_3), 3.33 (m, 1H, P-O-CH_2CH_3), 1.64 (d, J = 2.4 Hz, 1H, $CH_{cycloprop}$-P), 1.60 (s, 3H, CH_3), 1.17 (m, 5H, P-O-CH_2CH_3, $CH_{2cycloprop}$), 0.96 (t, J = 7.1 Hz, 3H, P-O-CH_2CH_3). ^{13}C NMR (75 MHz, $CDCl_3$) δ: 141.96, 141.9, 129.5, 128.2, 126.9, 61.5, 61.4, 61.35, 61.35, 61.3, 29.64, 29.6, 28.24, 28.2, 21.1, 19.1, 17.4, 17.3, 16.5, 16.46, 16.4, 16.3. ^{31}P NMR (160 MHz, $CDCl_3$) δ: 27.9. HR-MS calcd. for $C_{14}H_2O_3P$ (M + H): 268.1228; found: 228.1228.

Diethyl (1*R*)-2,2-diphenylcyclopropylphosphonate (24)

The general procedure described for the preparation of cyclopropane **23** was used on a 0.411 mmol scale. The purification was accomplished by flash chromatography on silica gel (80% EtOAc–hexanes) to give the desired cyclopropane **24** as a colorless oil (185 mg, 50%). The enantiomeric excesses (78%) was determined by SFC on a chiral stationary phase (Chiralcel OD, 1.5% MeOH, 1.0 mL/min: t_r (major) 23.9 min, t_r (minor) 18.4 min). R_f 0.34 (80% EtOAc–hexanes). IR (film, cm^{-1}): 2980, 1599, 1495, 1446, 1248, 1227, 1020, 953, 772, 695. ^1H NMR (300 MHz, $CDCl_3$) δ: 7.51–7.16 (m, 10H, C_6H_5), 3.95 (m, 2H, P-O-CH_2-CH_3), 3.76 (m, 1H, P-O-CH_2-CH_3), 3.50 (m, 1H, P-O-CH_2-CH_3), 2.03 (m, 1H, $CH_{2cycloprop}$), 1.83 (m, 1H, $CH_{2cycloprop}$), 1.57 (m, 1H, $CH_{cycloprop}$-P), 1.22 (t, J = 7.1 Hz, 3H, P-O-CH_2-CH_3), 1.05 (t, J = 7.1 Hz, 3H, P-O-CH_2-CH_3). ^{13}C NMR (75 MHz, $CDCl_3$) δ: 145.4, 145.3, 140.3, 140.26, 130.1, 128.4, 128.0, 127.91, 127.90, 126.9, 126.6, 63.6, 61.5, 61.4, 61.35, 36.7, 36.63, 21.3, 18.7, 17.9, 17.8, 16.3, 16.24, 16.2, 16.1. ^{31}P NMR (160 MHz, $CDCl_3$) δ: 27.1. HR-MS calcd. for $C_{19}H_{23}O_3P$ (M + H): 331.1463; found: 331.1457.

Diethyl (1*R*,2*S*)-2-methyl-3-phenylcyclopropylphosphonate (25)

The general procedure described for the preparation of cyclopropane **23** was used on a 0.411 mmol scale. The diastereomeric ratio (85:15) was determined by ^{31}P NMR of the crude reaction mixture (δ major: 29.3 and δ minor: 28.2). The crude mixture was then purified by flash chromatography on silica gel (60% EtOAc–hexanes) to give *trans*-**25** (128 mg, 43%) and *cis*-**25** (22 mg, 7%) as colorless oils. The

© 2005 NRC Canada

enantiomeric excesses (85%) were determined by SFC on a chiral stationary phase (Chiralcel OD, 0.8% MeOH, 1.5 mL/min: t_r (major) 24.3 min, t_r (minor) 26.9 min). *trans*-**25**: R_f 0.42 (EtOAc). IR (film, cm^{-1}): 2981, 2905, 1240, 1055, 1029, 963. ^1H NMR (300 MHz, $CDCl_3$) δ: 7.07–7.30 (m, 5H, C_6H_5), 4.10 (m, 4H, P-O-CH_2-CH_3), 2.35 (m, 1H, C_6H_5-$CH_{cycloprop}$), 1.85 (d, 3H, CH_3 (cis)) 1.57 (m, 1H, $CH_{cycloprop}$-P), 1.46 (d, J = 6.4 Hz, 3H, CH_3 (trans)), 1.36 (m, 6H, P-O-CH_2-CH_3), 1.20 (m, 2H, $CH_{2cycloprop}$). ^{13}C NMR (75 MHz, $CDCl_3$) δ: 140.6, 140.58, 128.5, 126.3, 125.9, 62.8, 62.7, 61.6, 61.56, 61.51, 61.4, 29.5, 29.4, 22.4, 22.3, 22.0, 19.5, 16.5, 16.46, 16.4, 16.38. 14.0, 13.9. ^{31}P NMR (160 MHz, $CDCl_3$) δ: 29.3. HR-MS calcd. for $C_{14}H_{21}O_3P$ (M + H): 268.1228; found: 268.1230.

General procedure for the Ru-pybox 29 catalyzed cyclopropanation — Diisopropyl (1*R*,2*S*)-2-phenylcyclopropylphosphonate (17)

To a solution of *trans*-$RuCl_2$((*S*,*S*)-*i*-Pr-pybox)(ethylene) (**29**) (5.1 mg, 0.0102 mmol, 0.03 equiv.) and styrene (0.194 mL, 1.70 mmol, 5 equiv.) in CH_2Cl_2 (2 mL) was added a solution of diisopropyl α-diazomethylphosphonate (**13**) (24) (70.0 mg, 0.340 mmol, 1 equiv.) in CH_2Cl_2 over 5 h via a syringe pump. After stirring for an additional 10 h at room temperature, the reaction mixture was concentrated under reduced pressure. The diastereomeric ratio (>98:2) was determined by ^{31}P NMR of the crude reaction product (δ major: 27.6, δ minor: 26.9). The crude residue was then purified by flash chromatography on silica gel (80% EtOAc–hexanes) to afford the desired cyclopropylphosphonate **17** as a colorless oil (67 mg, 70%). The enantiomeric excess (96%) was determined by SFC on chiral stationary phase (Chiralcel OD, 1.5% MeOH, 1.5 mL/min: t_r (major) 9.9 min, t_r (minor) 8.1 min). R_f 0.38 (EtOAc). $[\alpha]_D^{20}$ –80.0 (*c* 0.35, CH_2Cl_2). IR (film, cm^{-1}): 2978, 2933, 1732, 1385, 1243, 982, 918. ^1H NMR (300 MHz, $CDCl_3$) δ: 7.10–7.30 (m, 5H, C_6H_5), 4.71 (m, 2H, P-O-$CH(CH_3)_2$), 2.43 (m, 2H, C_6H_5-$CH_{cycloprop}$), 1.46 (m, 1H, $CH_{2cycloprop}$), 1.33 (m, 12H, P-O-$CH(CH_3)_2$), 1.20 (m, 1H, $CH_{2cycloprop}$), 1.17 (m, 1H, $CH_{cycloprop}$-P). ^{13}C NMR (75 MHz, $CDCl_3$) δ: 140.34, 140.31, 128.5, 126.4, 126.1, 70.4, 70.4, 70.38, 70.33, 24.1, 24.08, 24.04, 21.3, 21.2, 17.2, 15.2, 13.0, 12.9. ^{31}P NMR (160 MHz, $CDCl_3$) δ: 27.6. Anal. calcd. for $C_{15}H_{23}O_3P$: C 63.82, H 8.21; found: C 63.73, H 8.55.

Dineopentyl (1*R*,2*R*)-2-phenylcyclopropylphosphonate (18)

To a solution of *trans*-$RuCl_2$((*S*,*S*)-*i*-Pr-pybox)(ethylene) **(29)** (4.6 mg, 0.0915 mmol, 0.03 equiv.) and styrene (0.175 mL, 1.53 mmol, 5 equiv.) in CH_2Cl_2 (2 mL) under reflux was added a solution of dineopentyl α-diazomethylphosphonate (**14**) (80.0 mg, 0.305 mmol, 1 equiv.) in CH_2Cl_2 over 5 h via a syringe pump. After stirring for an additional 13 h under reflux, the reaction mixture was cooled to room temperaure and was concentrated under reduced pressure. The diastereomeric ratio (>98:2) was determined by ^{31}P NMR of the crude reaction product (δ major: 29.5, δ minor: 28.9). The crude residue was then purified by flash chromatography on silica gel (50% EtOAc–hexanes) to afford the desired cyclopropylphosphonate **18** as a colorless oil (81 mg, 79%). The enantiomeric excess (96%) was determined by SFC on chiral stationary phase (Chiralcel OD, 2.0% MeOH, 1.6 mL/min: t_r (major) 6.7 min, t_r (minor) 5.9 min). R_f 0.43 (50% EtOAc–hexanes). IR (film, cm^{-1}): 2957, 2871, 1246, 1062, 1008, 921, 870. ^1H NMR (300 MHz, $CDCl_3$) δ: 7.20 (m, 5H, C_6H_5), 3.70 (m, 4H, $CH_2C(CH_3)_3$), 2.50 (m, 1H, C_6H_5-$CH_{cycloprop}$), 1.55 (m, 1H, $CH_{2cycloprop}$), 1.25 (m, 1H, $CH_{cycloprop}$-P), 1.15 (m, 1H, $CH_{2cycloprop}$), 0.95 (d, J = 14.8 Hz, 18H, $CH_2C(CH_3)_3$). ^{13}C NMR (75 MHz, $CDCl_3$) δ: 140.1, 128.5, 126.5, 126.2, 75.3, 75.2, 75.1, 32.2, 32.1, 26.1, 26.0, 20.9, 15.8, 13.3, 12.4. ^{31}P NMR (160 MHz, $CDCl_3$) δ: 29.5. Anal. calcd. for $C_{19}H_{31}O_3P$: C 67.43, H 9.23; found: C 67.79, H 9.93.

Diisopropyl (1*R*,2*S*)-2-(4-methoxyphenyl)cyclopropylphosphonate (30)

The general procedure reported for compound **17** was followed using: *trans*-$RuCl_2$((*S*,*S*)-*i*-Pr-pybox)(ethylene) (**29**) (5.8 mg, 0.0116 mmol, 0.03 equiv.), 4-methoxystyrene (0.258 mL, 1.94 mmol, 5 equiv.), diisopropyl diazomethylphosphonate (**13**) (80.0 mg, 0.388 mmol, 1 equiv.). The diastereomeric ratio (>98:2) was determined by ^{31}P NMR of the crude reaction product (δ major: 28.0, δ minor: 27.9). The crude residue was then purified by flash chromatography on silica gel (80% EtOAc–hexanes) to afford the desired cyclopropylphosphonate **30** as a colorless oil (97 mg, 80%). The enantiomeric excess (94%) was determined by SFC on chiral stationary phase (Chiralcel OD, 1.0% MeOH, 1.3 mL/min: t_r (major) 23.7 min, t_r (minor) 26.1 min). R_f 0.40 (EtOAc). $[\alpha]_D^{20}$ –10.2 (*c* 1.65, CH_2Cl_2). IR (film, cm^{-1}): 2978, 2935, 1754, 1715, 1516, 1243, 979, 924, 826. ^1H NMR (300 MHz, $CDCl_3$) δ: 6.90 (m, 4H, C_6H_5), 4.70 (m, 2H, P-O-$CH(CH_3)_2$), 3.77 (s, 3H, $C_6H_5OCH_3$), 2.43 (m, 1H, C_6H_5-$CH_{cycloprop}$), 1.44 (m, 1H, $CH_{2cycloprop}$), 1.33 (m, 12H, P-O-$CH(CH_3)_2$), 1.20 (m, 1H, $CH_{2cycloprop}$), 1.14 (m, 2H, $CH_{cycloprop}$-P). ^{13}C NMR (75 MHz, $CDCl_3$) δ: 158.1, 132.2, 127.2, 113.9, 70.4, 70.3, 70.2, 70.1, 55.2, 24.1, 24.09, 24.0, 20.7, 20.6, 17.0, 14.5, 12.7, 12.6. ^{31}P NMR (160 MHz, $CDCl_3$) δ: 28.0. Anal. calcd. for $C_{16}H_{25}O_4P$: C 61.53, H 8.07; found: C 61.01, H 8.45.

Diisopropyl (1*R*,2*S*)-2-(4-chlorophenyl)cyclopropylphosphonate (31)

The general procedure reported for compound **17** was followed using: *trans*-$RuCl_2$((*S*,*S*)-*i*-Pr-pybox)(ethylene) (**29**) (5.8 mg, 0.0116 mmol, 0.03 equiv.), 4-chlorostyrene (0.233 mL, 1.94 mmol, 5 equiv.), diisopropyl diazomethylphosphonate (**13**) (80.0 mg, 0.388 mmol, 1 equiv.). The diastereomeric ratio (>98:2) was determined by ^{31}P NMR of the crude reaction product (δ major: 27.1, δ minor: 26.5). The crude residue was then purified by flash chromatography on silica gel (50% EtOAc–hexanes) to afford the desired cyclopropylphosphonate **31** as a white solid (97 mg, 80%). The enantiomeric excess (98%) was determined by SFC on chiral stationary phase (Chiralcel OD, 1.0% MeOH, 1.0 mL/min: t_r (major) 21.7 min, t_r (minor) 24.4 min); mp 58 °C. R_f 0.30 (EtOAc). $[\alpha]_D^{20}$ –88.3 (*c* 0.40, CH_2Cl_2). IR (film, cm^{-1}): 2979, 2935, 1496, 1374, 1238, 1105, 980, 923, 729. ^1H NMR (300 MHz, $CDCl_3$) δ: 7.10 (m, 4H, C_6H_5), 4.69 (m, 2H, P-O-$CH(CH_3)_2$), 2.43 (m, 2H, C_6H_5-$CH_{cycloprop}$), 1.46 (m, 1H, $CH_{2cycloprop}$), 1.33 (m, 12H, P-O-$CH(CH_3)_2$), 1.20 (m, 1H, $CH_{2cycloprop}$), 1.15 (m, 1H, $CH_{cycloprop}$-P). ^{13}C NMR (75 MHz, $CDCl_3$) δ: 138.9, 138.85, 132.0, 128.6,

© 2005 NRC Canada

127.4, 70.6, 70.4, 70.3, 24.1, 24.07, 24.02, 20.8, 20.7, 17.7, 15.1, 13.1, 13.0. ^{31}P NMR (160 MHz, $CDCl_3$) δ: 27.6. Anal. calcd. for $C_{15}H_{22}ClO_3P$: C 56.88, H 7.00; found: C 56.57, H 7.34.

Diisopropyl (1*R*,2*S*)-2-methyl-2-phenylcyclopropylphosphonate (32)

The general procedure reported for compound **17** was followed using: *trans*-$RuCl_2$((*S*,*S*)-*i*-Pr-pybox)(ethylene) (**29**) (5.1 mg, 0.0102 mmol, 0.03 equiv.), α-methylstyrene (0.221 mL, 1.70 mmol, 5 equiv.), diisopropyl diazomethylphosphonate (**13**) (70.0 mg, 0.340 mmol, 1 equiv.). The diastereomeric ratio (88:12) was determined by ^{31}P NMR of the crude reaction product (δ major: 27.6, δ minor: 26.0). The crude residue was then purified by flash chromatography on silica gel (80% EtOAc–hexanes) to afford the desired cyclopropylphosphonate *trans*-**32** (63 mg, 63%) and *cis*-**32** (9 mg, 9%) as colorless oils. The enantiomeric excesses (95% and 92%) were determined by HPLC on a chiral stationary phase. *trans*-**32**: Chiralcel AD, 98.8% hexane–isopropanol, 0.3 mL/min (t_r (major) 30.0 min, t_r (minor) 32.1 min). *cis*-**32**: Chiralcel AD, 98.8% hexane–isopropanol, 0.5 mL/min (t_r (major) 34.1 min, t_r (minor) 30.1 min). *trans*-**32**: R_f 0.45 (50% EtOAc–hexanes). $[\alpha]_D^{22}$ –59.2 (*c* 0.30, CH_2Cl_2). IR (film, cm^{-1}): 2977, 2931, 1385, 1374, 1244, 1006, 981, 891. ^{1}H NMR (300 MHz, $CDCl_3$) δ: 7.19–7.30 (m, 5H, C_6H_5), 4.75 (m, 1H, P-O-C*H*$(CH_3)_2$), 1.67 (s, 3H, CH_3), 1.37 (m, 14H, P-O-CH(CH_3)$_2$, C$H_{2cycloprop}$), 1.16 (m, 1H, C$H_{cyclopropyl}$-P). ^{13}C NMR (75 MHz, $CDCl_3$) δ: 146.4, 146.35, 128.4, 127.28, 127.27, 126.4, 69.94, 69.86, 27.5, 27.46, 27.4, 24.3, 24.2, 24.1, 24.09, 24.08, 24.0, 21.7, 21.6, 20.9, 18.9, 18.5, 18.49. ^{31}P NMR (160 MHz, $CDCl_3$) δ: 27.6. Anal. calcd. for $C_{16}H_{25}O_3P$: C 64.85, H 8.50; found: C 64.85, H 8.50. *cis*-**32**: R_f 0.39 (EtOAc). IR (film, cm^{-1}): 2978, 2933, 1732, 1385, 1243, 982, 918. ^{1}H NMR (300 MHz, $CDCl_3$) δ: 7.18–7.48 (m, 5H, C_6H_5), 4.47 (m, 1H, P-O-*CH*$(CH_3)_2$), 4.30 (m, 2H, P-O-*CH*$(CH_3)_2$), 1.63 (m, 1H, C$H_{2cycloprop}$), 1.30 (d, *J* = 2.4 Hz, 3H, CH_3), 1.17 (m, 9H, P-O-*C*H(CH_3)), 0.90 (d, *J* = 6.2 Hz, 3H, P-O-*C*H(CH_3)). ^{13}C NMR (75 MHz, $CDCl_3$) δ: 140.34, 140.31, 128.5, 126.4, 126.1, 70.4, 70.4, 70.38, 70.33, 24.1, 24.08, 24.0, 21.3, 21.2, 17.2, 15.2, 13.0, 12.9. ^{31}P NMR (160 MHz, $CDCl_3$) δ: 26.0. HR-MS calcd. for $C_{16}H_{25}O_3P$ (M + H): 297.1620; found: 297.1613.

Diisopropyl (1*R*)-2,2-diphenylcyclopropylphosphonate (33)

The general procedure reported for compound **18** was followed using: *trans*-$RuCl_2$((*S*,*S*)-*i*-Pr-pybox)(ethylene) (**29**) (5.1 mg, 0.0102 mmol, 0.03 equiv.), 1,1-diphenylethylene (0.300 mL, 1.70 mmol, 5 equiv.), diisopropyl diazomethylphosphonate (**13**) (70.0 mg, 0.340 mmol, 1 equiv.). The crude residue was then purified by flash chromatography on silica gel (50% EtOAc–hexanes) to afford the desired cyclopropylphosphonate **33** as a colorless oil (47 mg, 39%). The enantiomeric excess (91%) was determined by SFC on a chiral stationary phase (Chiralcel OD, 2.0% MeOH, 1.5 mL/min: t_r (major) 11.1 min, t_r (minor) 12.3 min). R_f 0.46 (80% EtOAc–hexanes). $[\alpha]_D^{22}$ –30.3 (*c* 0.37, CH_2Cl_2). IR (film, cm^{-1}): 2977, 1600, 1249, 980, 704. ^{1}H NMR (300 MHz, $CDCl_3$) δ: 7.15–7.52 (m, 10H, C_6H_5), 4.50 (m, 2H, P-O-C*H*$(CH_3)_2$), 2.00 (m, 1H, C$H_{2cycloprop}$), 1.75 (m, 1H, C$H_{2cycloprop}$), 1.60 (m, 1H, C$H_{cycloprop}$-P), 1.35 (m, 1H, P-O-CH(CH_3)$_2$), 1.20 (m, 8H, P-O-CH(CH_3)$_2$), 1.00 (d, 3H, P-O-CH(CH_3)$_2$). ^{13}C NMR (75 MHz, $CDCl_3$) δ: 145.7, 145.6, 140.4, 140.3, 136.5, 130.3, 127.9, 126.8, 126.5, 70.1, 69.9, 69.8, 36.9, 36.8, 24.1, 24.02, 24.00, 23.9, 23.9, 23.8, 23.6, 23.5, 22.3, 19.7, 17.9, 17.8. ^{31}P NMR (160 MHz, $CDCl_3$) δ: 25.2. HR-MS calcd. for $C_{21}H_{23}O_3P$ (M + H): 358.1698; found: 358.1684.

Diisopropyl (1*R*,2*S*)-2-[(*E*)-2-phenylvinyl]cyclopropylphosphonate (34)

The general procedure reported for compound **18** was followed using: *trans*-$RuCl_2$((*S*,*S*)-*i*-Pr-pybox)(ethylene) (**29**) (5.8 mg, 0.0116 mmol, 0.03 equiv.), (*E*)-1-phenyl-1,3-butadiene (0.253 g, 1.94 mmol, 5 equiv.), diisopropyl diazomethylphosphonate (**13**) (80.0 mg, 0.388 mmol, 1 equiv.). The diastereomeric ratio (95:5) was determined by ^{31}P NMR of the crude reaction product (δ major: 27.8, δ minor: 28.3). The crude residue was then purified by flash chromatography on silica gel (50% EtOAc–hexanes) to afford the desired cyclopropylphosphonate *trans*-**34** (103 mg, 86%) and *cis*-**34** (5 mg, 4%) as colorless oils. The enantiomeric excesses (90% and 92%) were determined by HPLC on a chiral stationary phase for *trans*-**34**: Chiralcel OD, 98% hexanes–isopropanol, 0.9 mL/min: t_r (major) 9.8 min, t_r (minor) 14.7 min) and by SFC on a chiral stationary phase for *cis*-**34**: Chiralcel OD, 2.0% MeOH, 1.6 mL/min: t_r (major) 10.7 min, t_r (minor) 9.9 min). *trans*-**34**: R_f 0.17 (50% EtOAc–hexanes). $[\alpha]_D^{20}$ –14.3 (*c* 1.60, CH_2Cl_2). IR (film, cm^{-1}): 2978, 2934, 1385, 1374, 1238, 1106, 978, 886, 746, 694. ^{1}H NMR (300 MHz, $CDCl_3$) δ: 7.16–7.35 (m, 5H, C_6H_5), 6.55 (d, *J* = 15.7 Hz, 1H, C_6H_5-C*H*=CH), 5.73 (dd, *J* = 15.7, 8.7 Hz, 1H, C_6H_5-CH=C*H*), 4.70 (m, 2H, P-O-C*H*$(CH_3)_2$), 2.15 (m, 1H, C=CH-C$H_{cyclopropyl}$), 1.34 (m, 13H, P-O-C*H*$(CH_3)_2$, C$H_{2cyclopropyl}$), 1.00 (m, 2H, C$H_{2cycloprop}$, C$H_{cycloprop}$). ^{13}C NMR (75 MHz, $CDCl_3$) δ: 137.0, 130.6, 130.57, 130.0, 128.5, 127.2, 125.8, 70.5, 70.4, 70.3, 70.2, 24.1, 24.05, 20.6, 12.9, 11.8, 11.7. ^{31}P NMR (160 MHz, $CDCl_3$) δ: 27.8. Anal. calcd. for $C_{17}H_{25}O_3P$: C 66.22, H 8.17; found: C 66.78, H 8.62. *cis*-**34**: R_f 0.28 (50% EtOAc–hexanes). ^{1}H NMR (300 MHz, $CDCl_3$) δ: 7.15–7.37 (m, 5H, C_6H_5), 6.55 (d, *J* = 15.9 Hz, 1H, C_6H_5-C*H*=CH), 6.45 (dd, *J* = 15.9, 9.6 Hz, 1H, C_6H_5-CH=C*H*), 4.70 (m, 2H, P-O-C*H*$(CH_3)_2$), 2.05 (m, C=CH-C$H_{cyclopropyl}$), 1.30 (m, 15H, P-O-CH(CH_3)$_2$, C$H_{2cycloprop}$). ^{13}C NMR (75 MHz, $CDCl_3$) δ: 137.4, 130.5, 129.5, 129.47, 128.5, 126.8, 125.9, 70.1, 70.09, 70.05, 70.0, 24.1, 24.05, 23.9, 23.88, 21.3, 21.28, 14.9, 12.3, 12.0, 11.9. ^{31}P NMR (160 MHz, $CDCl_3$) δ: 28.3. HR-MS calcd. for $C_{17}H_{25}O_3P$: 308.1541; found: 308.1549.

Diisopropyl (1*R*,2*S*)-2-(2-naphtyl)cyclopropylphosphonate (35)

The general procedure reported for compound **18** was followed using: *trans*-$RuCl_2$((*S*,*S*)-*i*-Pr-pybox)(ethylene) (**29**) (5.8 mg, 0.0116 mmol, 0.03 equiv.), 2-vinylnaphthalene (0.299 g, 1.94 mmol, 5 equiv.), diisopropyl diazomethylphosphonate (**13**) (70.0 mg, 0.340 mmol, 1 equiv.). The diastereomeric ratio (>98:2) was determined by ^{31}P NMR of the crude reaction product (δ major: 27.6, δ minor: 27.1). The crude residue was then purified by flash chromatogra-

© 2005 NRC Canada

phy on silica gel (50% EtOAc–hexanes) to afford the desired cyclopropylphosphonate **35** (116 mg, 91%) as a white solid. The enantiomeric excesses (97%) were determined by SFC on a chiral stationary phase: Chiralcel OD, 1.2% MeOH, 1.5 mL/min: t_r (major) 41.7 min, t_r (minor) 45.6 min); mp 65 °C. R_f 0.18 (50% EtOAc–hexanes). $[\alpha]_D^{20}$ –82.1 (*c* 1.00, CH_2Cl_2). IR (film, cm^{-1}): 2977, 2933, 1633, 1601, 1509, 1384, 1374, 1234, 1104, 976, 745, 729. ^{1}H NMR (300 MHz, $CDCl_3$) δ: 7.80–7.20 (m, 7H, C*H* (Napth)), 4.75 (m, 1H, P-O-C*H*$(CH_3)_2$), 2.65 (m, 1H, Napth-C$H_{cycloprop}$), 1.65 (m, 1H, CH_2), 1.35 (m, 14H, P-O-C*H*$(CH_3)_2$, C$H_{2cycloprop}$, C$H_{cycloprop}$). ^{13}C NMR (75 MHz, $CDCl_3$) δ: 137.7, 137.6, 133.3, 132.2, 128.2, 127.6, 127.3, 127.0, 126.2, 125.4, 124.9, 124.6, 124.3, 70.5, 70.5, 70.45, 70.41, 70.32, 69.7, 25.3, 24.4, 24.1, 24.0, 23.9, 23.7, 23.2, 22.8, 21.5, 17.4, 14.9, 13.0, 12.9. ^{31}P NMR (160 MHz, $CDCl_3$) δ: 27.6. HR-MS calcd. for $C_{19}H_{25}O_3P$: 332.1541; found: 332.1534.

Diisopropyl (1*R*,2*S*)-2(hydroxymethyl)cyclopropylphosphonate (36)

Ozone was bubbled through a solution of **34** (40.0 mg, 0.130 mmol, 1 equiv.) in methanol (15 mL) at –78 °C until a pale blue color persisted. Sodium borohydride (30.0 mg, 0.793 mmol, 6.1 equiv.) was then directly added and the clear solution was stirred at that temperature for 2 h. The mixture was warmed to room temperature and a satd. aq. solution of NH_4Cl was added. The mixture was concentrated under reduced pressure and the organic layer was extracted with three portions of CH_2Cl_2. The combined organic layers were dried over Na_2SO_4 and concentrated under reduced pressure. The residue was purified by flash chromatography on silica gel (95% EtOAc–hexanes) to afford the desired alcohol **36** (27.2 mg, 88%) as a colorless oil. R_f 0.13 (95% EtOAc–acetone). $[\alpha]_D^{20}$ –27.5 (*c* 0.80, CH_2Cl_2). IR (film, cm^{-1}): 3371, 2979, 2934, 1386, 1375, 1221, 982. ^{1}H NMR (300 MHz, $CDCl_3$) δ: 4.70 (m, 2H, P-O-C*H*$(CH_3)_2$), 3.55 (m, 2H, CH_2-OH) 1.75 (t, *J* = 5.8 Hz, 1H, OH), 1.60 (m, 1H, CH_2-C$H_{cycloprop}$), 1.34 (m, 12H, P-O-CH(CH_3)$_2$), 1.10 (m, 1H, C$H_{cyclopropyl}$-P), 0.80 (m, 2H, C$H_{2cycloprop}$). ^{13}C NMR (75 MHz, $CDCl_3$) δ: 70.3, 70.25, 70.2, 65.1, 65.0, 24.1, 24.0, 19.5, 19.4, 11.4, 8.8, 8.2, 8.1. ^{31}P NMR (160 MHz, $CDCl_3$) δ: 28.6. HR-MS calcd. for $C_{10}H_{21}O_4P$: 236.1177; found: 236.1174.

Acknowledgements

This work was supported by the Natural Sciences and Engineering Research Council of Canada (NSERC) and the Université de Montréal.

References

1. W.P. Malachowski and J.K. Coward. J. Org. Chem. **59**, 7625 (1994).
2. E. De Clerq, A. Holy, I. Rosenberg, T. Sakuma, J. Balzarini, and C.M. Prabhat. Nature (London), **323**, 424 (1986).
3. R. Pauwels, J. Balzarini, D. Schols, M. Baba, J. Desmyter, I. Rosenberg, A. Holy, and E. De Clercq. Antimicrob. Agents Chemother. **32**, 1025 (1988).
4. U. Groth, L. Lehmann, L. Richter, and U. Schöllkopf. Liebigs Ann. Chem. 427 (1993).
5. D. Hendlin, E.O. Stapley, M. Jackson, H. Wallick, A.K. Miller, F.J. Wolf, T.W. Miller, L. Chaiet, G.M. Kahan, E.L. Foltz, H.B. Woodruff, J.M. Mata, S. Hernandez, and S. Mochales. Science (Washington, D.C.), **166**, 122 (1969).
6. D. Seyferth, R.S. Marmor, and P. Hilbert. J. Org. Chem. **30**, 1379 (1971).
7. W.B. Motherwell and R.T. Lewis. Tetrahedron Lett. **29**, 5033 (1988).
8. C. Feasson, C. Duquenne, S. Goumain, P. Jubault, and J.C. Quirion. Org. Lett. **2**, 453 (2000).
9. T. Hirao, M. Hagihara, Y. Ohshiro, and T. Agawa. Synthesis, **36**, 60 (1984).
10. S. Hanessian, L.D. Cantin, S. Roy, D. Andreotti, and A. Gomtsyan. Tetrahedron Lett. **38**, 1103 (1997).
11. J.H. Hah and D.Y. Oh. Tetrahedron Lett. **40**, 8235 (1999).
12. Part of this work has been included in a review: H. Lebel, J.-F. Marcoux, C. Molinaro, and A.B. Charette. Chem. Rev. **103**, 977 (2003).
13. P. Le Maux, I. Abrunhosa, M. Berchel, G. Simonneaux, M. Gulea, and S. Masson. Tetrahedron: Asymmetry, **15**, 2569 (2004).
14. C. Paul-Roth, F. De Montigny, G. Rethore, G. Simonneaux, M. Gulea, and S. Masson. J. Mol. Catal. A: Chem. **201**, 79 (2003).
15. G. Simonneaux, F. De Montigny, C. Paul-Roth, M. Gulea, and S. Masson. Tetrahedron Lett. **43**, 3685 (2002).
16. Y. Ferran, P. Le Maux, and G. Simonneaux. Org. Lett. **6**, 3211 (2004).
17. H.M.L. Davies and E.G. Antoulinakis. Org. React. (N.Y.), **57**, 1 (2001).
18. M.P. Doyle, V. Bagheri, T.J. Wandless, N.K. Harn, D.A. Brinker, C.T. Eagle, and K.L. Loh. J. Am. Chem. Soc. **112**, 1906 (1990).
19. D.A. Evans, K.A. Woerpel, M.M. Hinman, and M.M. Faul. J. Am. Chem. Soc. **113**, 726 (1991).
20. H. Nishiyama, Y. Itoh, H. Matsumoto, S.-B. Park, and K. Itoh. J. Am. Chem. Soc. **116**, 2223 (1994).
21. D.W. Huchinson and G. Semple. J. Organomet. Chem. **291**, 145 (1985).
23. E. Gryszkiewicz-Trochimowski, M. Bousquet, and J. Quinchon. Bull. Soc. Chim. Fr. 1222 (1961).
24. S. Ohira. Synth. Commun. **19**, 561 (1989).

© 2005 NRC Canada

First examples of intramolecular addition of primary amidyl radicals to olefins[1]

Philippe Gaudreault, Christian Drouin, and Jean Lessard

Abstract: The first examples of intramolecular addition of primary amidyl radicals to olefins are described. Amidyl radicals were generated from *N*-(phenylthio)amides in refluxing benzene using a catalytic amount of 2,2′-azobis(isobutyronitrile) (5 mol%) and tributyltin hydride (~2.2 equiv.). The resulting yields of cyclic products ranged from 63% to 85%.

Key words: radical cyclization, amidyl radicals, nitrogen heterocycles.

Résumé : Les premiers exemples de cyclisation radicalaire impliquant un radical amidyle primaire et une oléfine sont décrits. Les radicaux amidyles sont obtenus à partir de *N*-(phénylthio)amides dans le benzène à reflux en présence d'une quantité catalytique de 2,2′-azobis(isobutyronitrile) (5 mol%) et d'hydrure de tributylétain (~2.2 équiv.). Des rendements en produits cyclisés variant de 63 % à 85 % sont obtenus.

Mots clés : cyclisation radicalaire, radicaux amidyles, hétérocycles azotés.

Introduction

Over the years, amidyl radicals have attracted continuous interest with regard to their structure (1, 2), their reactivity (3–5), and ways to generate them (3, 4). Clearly, it appears that intramolecular addition of an amidyl radical on a pendant olefin is a powerful synthetic tool for the formation of nitrogen-containing heterocycles. Numerous examples of cyclization involving secondary amidyl radicals can be found in the literature (4). However, as far as we know, there are no examples of a successful cyclization involving a primary amidyl radical (4*k*, 6), even if there are many examples of successful intermolecular additions of primary amidyl radicals to olefins (3). The main reason for the lack of data on the cyclization of primary amidyl radicals is that endeavours to prepare the usual radical precursors such as *N*-haloamides (3, 4*a*, 4*b*), *N*-(pyridine-2-thione-oxycarbonyl) amides (PTOC amides) (4*c*, 4*f*), and *N*-(ethoxythiocarbonylsulfanyl)amides (4*h*), have failed when applied to olefinic primary amides (7).[3] In the present paper, we report that *N*-(phenylthio) derivatives of olefinic primary amides can be easily prepared and that nitrogen heterocycles resulting from their radical cyclization can be obtained in good to very good yields.

The four olefinic primary amides **5**–**8** were selected as models for radical cyclization of primary amidyl radicals. They were prepared from the corresponding carboxylic acids **1**–**4** via the acid chlorides as shown in Scheme 1.[4] Carboxylic acids **1**, **2**, and **4** are commercially available and cyclohept-4-ene carboxylic acid **3** was synthesized in four steps from cyclopentanone following a method developed by Stork and Landesman (8).

Next, conversion of primary amides **5**–**8** into suitable amidyl radical precursors was examined. We found that *N*-(phenylthio)amides **9**–**12** could be easily prepared in good to very good yields (60%–84%) following a protocol developed by Esker and Newcomb (4*d*), but slightly modified, by reacting the anion of the amide with phenylsulfenyl chloride (9).[4] *N*-(Phenylthio)amides **9**–**12** were the sole amidyl precursors that could be obtained from olefinic primary amides **5**–**8**.[3]

Having the primary amidyl radical precursors in hand, intramolecular addition was next investigated. *N*-

Received 27 October 2004. Published on the NRC Research Press Web site at http://canjchem.nrc.ca on 24 May 2005.

This paper is dedicated to Howard Alper in recognition of his many achievements in chemistry.

P. Gaudreault, C. Drouin, and J. Lessard.[2] Université de Sherbrooke, Département de chimie, 2500 Boul. Université, Sherbrooke, QC J1K 2R1, Canada.

[1]This article is part of a Special Issue dedicated to Professor Howard Alper.

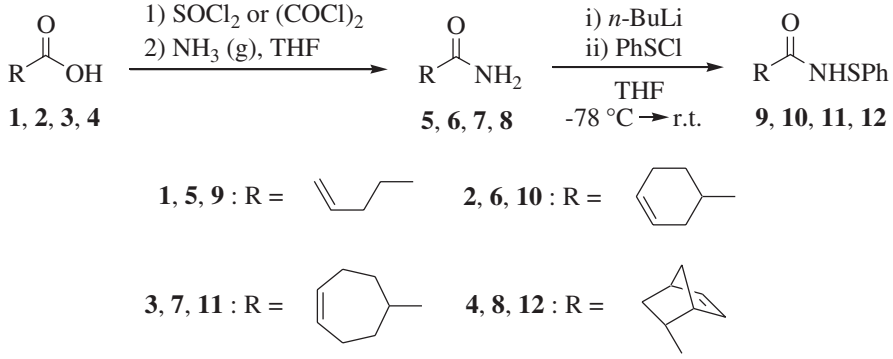
[2]Corresponding author (e-mail: Jean.Lessard@USherbrooke.ca).

[3]We tried to prepare *N*-(PTOC)amides (4*c*, 4*f*) and *N*-(ethoxythiocarbonylsulfanyl)amides (4*h*) of primary amides **5**–**7**, but all attempts were unsuccessful.

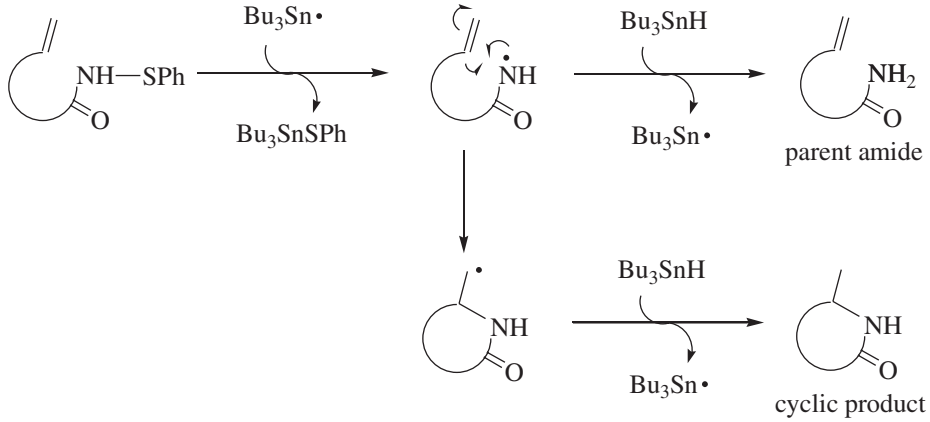
[4]Supplementary material: general procedures for the preparation of primary amides **5**–**8** and of *N*-(phenylthio)amides **9**–**12**; spectroscopic data of compounds synthesized. Supplementary data for this article are available on the Web site or may be purchased from the Depository of Unpublished Data, Document Delivery, CISTI, National Research Council Canada, Ottawa, ON K1A 0S2, Canada. DUD 3661. For more information on obtaining material refer to http://cisti-icist.nrc-cnrc.gc.ca/irm/unpub_e.shtml.

 doi: 10.1139/V05-029 © 2005 NRC Canada

Scheme 1. Preparation of primary amides and *N*-(phenylthio) derivatives.



Scheme 2. Radical chain mechanism.

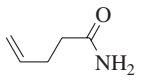
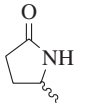
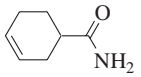
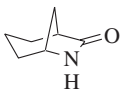
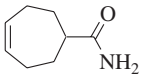
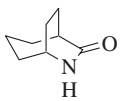
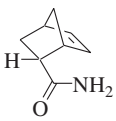
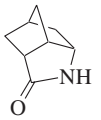


(Phenylthio)amides **9**–**12** were heated in refluxing benzene and a solution of 2,2′-azobis(isobutyronitrile) (AIBN) (5 mol%) and tributyltin hydride (~2.2 equiv.) in benzene was added. As shown in Table 1, all four models underwent radical cyclization to afford the corresponding heterocyles **13**–**16**[4] in good to very good yields (63%–85%). Interestingly, the use of less than ~2.2 equiv. of tributyltin hydride resulted in incomplete conversion of the starting olefinic *N*-(phenylthio) amide.

As expected (10), 5-*exo*-trig cyclizations were favoured over 6-*endo*-trig cyclizations for all concerned models (entries 1, 2, and 4). Also, 6-*exo*-trig cyclization occurred in good yield (71%) when this was the sole possibility (entry 3). The reactions also gave small amounts of the parent amide (8%–16% yield) as a result of the reduction of the amidyl radical by tributyltin hydride. The radical chain mechanism involved is illustrated in Scheme 2.

To the best of our knowledge, this paper reports the first examples of radical cyclizations involving a primary amidyl radical and a pendant olefin. Olefinic *N*-(phenylthio)amides were prepared in good yields (60%–84%) and used as primary amidyl radical precursors in a reaction with AIBN in catalytic amount (5 mol%) and tributyltin hydride (~2.2 equiv.), acting, respectively, as radical initiator and chain carrier. Good to very good yields of cyclization were obtained (63%–85%). Thus, it is no longer necessary to prepare an N-protected precursor and then remove the protecting group after cyclization (4*k*). Further studies are currently being conducted.

Table 1. Cyclization results.

Entry	Primary amide	*N*-(PhS)amide[a]	Cyclic product[b,c]
1	 **5**	**9** 84%	 84% **13**
2	 **6**	**10** 63%	 85% **14**
3	 **7**	**11** 64%	 71% **15**
4	 **8**	**12** 60%	 63% **16**

[a]Reaction conditions: (*i*) *n*-BuLi, (*ii*) PhSCl, THF, –78 °C → r.t.
[b]Reaction conditions: $AIBN_{cat}$–Bu_3SnH (slow addition), benzene, reflux.
[c]Yield of parent amide: 8%, 11%, 16%, and 16% in entries 1–4, respectively.

© 2005 NRC Canada

General procedure for cyclization

To a refluxing solution of *N*-(phenylthio)amide (0.5 mmol) in anhydrous and degassed benzene (20 mL) under a nitrogen atmosphere, 2,2′-azobis(isobutyronitrile) (4 mg, 0.024 mmol) and tributyltin hydride (0.28 mL, 1.0 mmol) dissolved in anhydrous and degassed benzene (10 mL) were added over 4 h. If required, a small additional amount of AIBN–Bu_3SnH in benzene was added to complete the reaction. The solvent was removed under reduced pressure and the residue was purified by flash chromatography (acetone–toluene, 2:3) monitored by GC to afford the desired lactam.

Acknowledgements

Financial support from the Natural Sciences and Engineering Research Council of Canada (NSERC) is gratefully acknowledged. We are thankful to Mr. Gaston Boulay for the mass spectral and GC–MS analyses and Mr. Dave Lee for preparing some compounds.

References

1. (*a*) R. Sutcliffe, D. Griller, J. Lessard, and K.U. Ingold. J. Am. Chem. Soc. **103**, 624 (1981); (*b*) J. Lessard, D. Griller, and K.U. Ingold. J. Am. Chem. Soc. **102**, 3262 (1980).
2. H.M. Muchall, N.H. Werstiuk, and J. Lessard. J. Mol. Struct: THEOCHEM, **469**, 135 (1999).
3. (*a*) J. Lessard, M. Mondon, and D. Touchard. Can. J. Chem. **59**, 431 (1981); (*b*) M. Mondon and J. Lessard. Can. J. Chem. **56**, 2590 (1978); (*c*) H. Driguez, J.-P. Vermes, and J. Lessard. Can. J. Chem. **56**, 119 (1978); (*d*) H. Driguez, J.M. Paton, and J. Lessard. Can. J. Chem. **55**, 700 (1977).
4. (*a*) J. Lessard, R. Côté, P. Mackiewicz, R. Furstoss, and B. Waegell. J. Org. Chem. **43**, 3750 (1978); (*b*) P. Mackiewicz, R. Furstoss, B. Waegell, R. Côté, and J. Lessard. J. Org. Chem. **43**, 3746 (1978); (*c*) J.L. Esker and M. Newcomb. J. Org. Chem. **59**, 2779 (1994); (*d*) J.L. Esker and M. Newcomb. Tetrahedron Lett. **34**, 6877 (1993); (*e*) J.L. Esker and M. Newcomb. J. Org. Chem. **58**, 4933 (1993); (*f*) J.L. Esker and M. Newcomb. Tetrahedron Lett. **33**, 5913 (1992); (*g*) M. Newcomb and J.L. Esker. Tetrahedron Lett. **32**, 1035 (1991); (*h*) F. Gagosz, C. Moutrille, and S.Z. Zard. Org. Lett. **4**, 2707 (2002); (*i*) J. Boivin, A.-C. Callier-Dublanchet, B. Quiclet-Sire, A.-M. Schiano, and S.Z. Zard. Tetrahedron, **51**, 6517 (1995); (*j*) A.-C. Callier, B. Quiclet-Sire, and S.Z. Zard. Tetrahedron Lett. **35**, 6109 (1994); (*k*) G.D. Artman III, J.H. Waldman, and S.M. Weinreb. Synthesis, **14**, 2057 (2002); (*l*) X. Lin, G.D. Artman III, D. Stien, and S.M. Weinreb. Tetrahedron, **57**, 8779 (2001).
5. J.H. Horner, O.M. Musa, A. Bouvier, and M. Newcomb. J. Am. Chem. Soc. **120**, 7738 (1998).
6. (*a*) J.L. Esker and M. Newcomb. Adv. Heterocycl. Chem. **58**, 1 (1993); (*b*) S.Z. Zard. Synlett, 1148 (1996); (*c*) A.G. Fallis and I.M. Brinza. Tetrahedron, **53**, 17 543 (1997).
7. C. Bernier. M.Sc. dissertation, Département de chimie, Université de Sherbrooke, Sherbrooke, Quebec. 1997.
8. G. Stork and H.K. Landesman. J. Am. Chem. Soc. **78**, 5129 (1956).
9. M.G.B. Drew, S.C. Ennis, J.J. Gridley, H.M.I. Osborn, and D.G. Spackman. Tetrahedron, **57**, 7919 (2001).
10. J.E. Baldwin. J. Chem. Soc. Chem. Commun. 734 (1976).

© 2005 NRC Canada

Palladium(II) complexes of bis(phosphine)monooxide and bis(phosphine)monosulphide ligands bearing *o*-*N*,*N*-dimethylanilinyl substituents[1]

Nathan D. Jones and Brian R. James

Abstract: Palladium(II) complexes of bis(phosphine)monooxide and bis(phosphine)monosulphide ligands with the general formula $Ar_2P(CH_2)_nP(E)Ar_2$ are described (n = 1 (dmapmE), E = O, S; n = 2 (dmapeE), E = O; Ar = *o*-*N*,*N*-dimethylanilinyl). The precursor, $PdCl_2$(dmapm), which exists in solution as an equilibrium mixture of the *P*,*P*- and *P*,*N*-ligated isomers, reacts with peroxides to form $PdCl_2$(*P*,*N*-dmapmO) and with sulphur to give [PdCl(*P*,*N*,*S*-dmapmS)]Cl, probably by direct oxidation of the "dangling" P atom of the *P*,*N*-isomer. $PdCl_2$(dmape), which exists in solution as a mixture of $PdCl_2$(*P*,*P*-dmape) and [PdCl(*P*,*P*,*N*-dmape)]Cl, reacts with hydroxide in H_2O–CH_2Cl_2 under argon to give the face-to-face $Pd(II)_2$ complex containing the cation $[Pd_2Cl_2(\mu\text{-}P,N:O\text{-dmapeO})_2]^{2+}$, which was isolated and crystallographically characterized as the PF_6 salt. The remarkable structure, consisting of two face-to-face Pd(II) square planes in a head-to-tail orientation, reveals a 12-membered ring containing the two non-bonded metal centres (Pd—Pd = 4.873(2) Å). The dmapmS complex shows marginal activity as a catalyst for the hydration of maleic to malic acid.

Key words: phosphine, phosphine oxide, phosphine sulphide, palladium.

Résumé : On décrit les complexes du palladium(II) de ligands bis(phosphine)monooxyde et bis(phosphine)monosulfure avec des composés de formule générale $Ar_2P(CH_2)_nP(E)Ar_2$ dans lesquels n = 1 (dmapmE), E = O, S; n = 2 (dmapeE), E = O; Ar = *o*-*N*,*N*-diméthylanilinyle. Le précurseur $PdCl_2$(dmapm), qui existe en solution sous la forme d'un mélange à l'équilibre des ligands isomères *P*,*P* et *P*,*N*, réagit avec les peroxydes pour former le $PdCl_2$(*P*,*N*-dmapmO) et avec le soufre pour donner le [PdCl(*P*,*N*,*S*-dmapmS)]Cl, probablement par une oxydation directe de l'atome de P qui se « balance » dans l'isomère *P*,*N*. Le $PdCl_2$(dmape), qui existe en solution sous la forme d'un mélange de $PdCl_2$(*P*,*P*-dmape) et de [PdCl(*P*,*P*,*N*-dmape)]Cl, réagit avec l'ion hydroxyde dans un mélange H_2O–CH_2Cl_2, sous argon, pour conduire à la formation du complexe face à face $Pd(II)_2$ contenant le cation $[Pd_2Cl_2(\mu\text{-}P,N:O\text{-dmapeO})_2]^{2+}$ qui a été isolé et caractérisé cristallographiquement sous la forme de sel de PF_6. La structure remarquable, formée de deux Pd(II) plans carrés, face à face et en position tête à queue, comporte un cycle à douze chaînons avec deux centres métalliques non liés (Pd—Pd = 4,873(2) Å). Le complexe dmapmS présente une activité marginale comme catalyseur pour l'hydratation de l'acide maléique en acide malique.

Mots clés : phosphine, oxyde de phosphine, sulfure de phosphine, palladium.

[Traduit par la Rédaction]

Introduction

Our group recently reported (1–4) on platinum(II) and palladium(II) complexes containing bis(phosphine) ligands bearing two *o*-*N*,*N*-dimethylanilinyl substituents at each P atom, including 1,1-bis(di(*o*-*N*,*N*-dimethylanilinyl)phosphino)-methane (dmapm) and 1,2-bis(di(*o*-*N*,*N*-dimethylanilinyl)-phosphino)ethane (dmape). The ligand structures, for example, are represented within complexes of formula $PdCl_2$(dmapm) and $PdCl_2$(dmape) in Schemes 1 and 2, respectively. We had designed such ligands primarily for the synthesis of water-soluble metal complexes, with one aim being to develop transition metal catalysts for olefin hydration, and indeed marginal activity for hydration of maleic to malic acid was noted for several of the complexes (4). The activity was better, for example, than that of the bridged-hydroxo complexes of the type $[(dppe)Pd(\mu\text{-}OH)]_2^{2+}$ (dppe = $Ph_2P(CH_2)_2PPh_2$) reported by Ganguly and Roundhill (5). This led us to attempts to synthesize bridged-hydroxo complexes of this type but using dmape as the bisphosphine. We thus reacted $PdCl_2$(dmape) with KOH in aqueous–CH_2Cl_2, but (to our surprise) a complex containing the bisphosphine

Received 30 November 2004. Published on the NRC Research Press Web site at http://canjchem.nrc.ca on 2 June 2005.

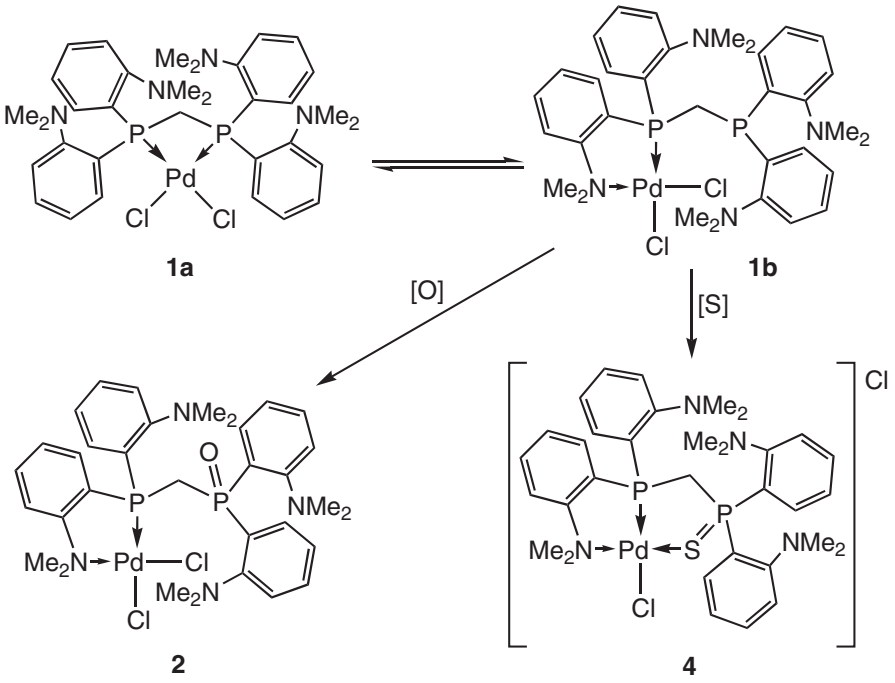
This paper is dedicated to Howard Alper, close friend and research collaborator with one of us (BRJ) and distinguished scholar.

N.D. Jones[2] and B.R. James.[3] Department of Chemistry, University of British Columbia, Vancouver, BC V6T 1Z1, Canada.

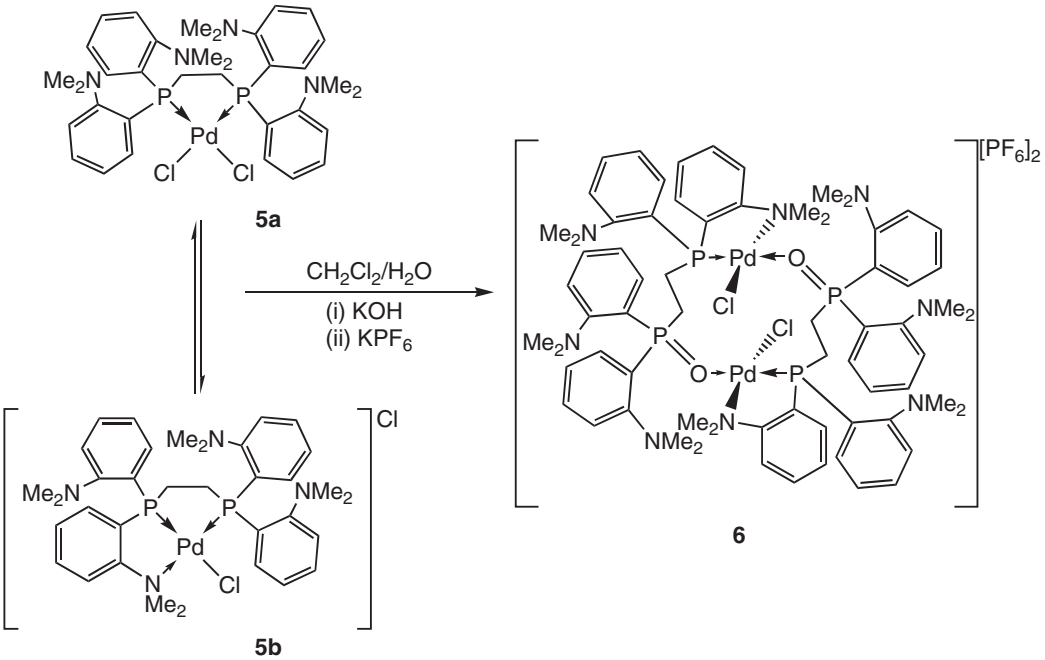
[1]This article is part of a Special Issue dedicated to Professor Howard Alper.
[2]Present address: Department of Chemistry, University of Western Ontario, London, ON N6A 5B7, Canada.
[3]Corresponding author (e-mail: brj@chem.ubc.ca).

 doi: 10.1139/V05-067 © 2005 NRC Canada

Scheme 1. Direct oxidation of one P atom of **1b** with peroxide and sulphur.



Scheme 2. Reaction of **5** with KOH in CH_2Cl_2–H_2O.



monoxide, dmapeO, was isolated, and because of the current interest in such ligands, we pursued this line of research, and the findings are reported here.

Bisphosphine monooxides (BPMOs) with the mixed P atom and O atom donors are within a class of chelating agents that, because of their potential for hemilabile coordination (6), have garnered attention in homogeneous catalysis. Transition metal complexes of such ligands have been used in a variety of catalyzed organic transformations such as hydroformylation and other carbonylation processes (7, 8), hydrosilylation (9), hydrovinylation (10), polymerization (11), and allylic alkylation (12), including asymmetric processes (9, 10, 12) Bis(phosphine)monosulphide (BPMS) complexes have also begun to attract interest and have found application in asymmetric allylic alkylation (13).

More generally, BPMO ligands can be made via metal-free organic synthesis (for example, by benzylation of a bis(tertiary phosphine) followed by basic hydrolysis of the resulting phosphonium salt) (14) or by a Pd-catalyzed process involving reaction of 1,2-bromoethane and hydroxide in a two-phase aqueous system (8). Metal-bound BPMOs may be synthesized via oxidation of a "dangling" (i.e., nonbonded)

© 2005 NRC Canada

P atom in complexes bearing polydentate ligands, exemplified in Co (15, 16), Mo (17), Rh (18), and Pd (9, 19) systems, but only in a few cases does this result in coordination of the phosphine oxide (16, 17). Less common is oxidation of a coordinated bis(phosphine) to give a BPMO in which both the P(III) atom and the O atom are bound. Examples that typically involve aerobic oxidation are those of RhCl(CO)(*P*,*P*-BINAP), which generates RhCl(CO)(*P*,*O*-BINAPO) (20), a Pd(II)-dppm species (dppm = $Ph_2PCH_2PPh_2$) that forms a Pd(II)-*P*,*O*-dppmO complex (21), and $RuCl_2$(BINAP)(N–N) complexes that give [RuCl(η^4-BINAPO)(N–N)]Cl (N–N = bipy, phen), where the BINAPO ligand is coordinated via the P(III) atom, the O atom, and two C atoms of the naphthyl ring proximate to the P(V) atom (22). An excellent introduction to the syntheses and uses of BPMOs can be found in Cyr's Ph.D. thesis (23).

This paper describes the oxidation of one P atom of $PdCl_2$(dmapm) (**1**) (3) to give $PdCl_2$(*P*,*N*-dmapmO) (**2**) and the salts [PdCl(*P*,*N*,*S*-dmapmS)]X (X = PF_6, **3**; Cl, **4**) and the similar oxidation of $PdCl_2$(dmape) (**5**) (4) to give, after anion exchange, the dipalladium complex [PdCl(μ-*P*,*N*:*O*-dmapeO)]$_2$[PF_6]$_2$ (**6**). This last reaction constitutes another example of the oxidation of a coordinated bis(phosphine) to give a complex in which both the P(III) and O atoms of the BPMO are coordinated, but it is unique in that the BPMO serves as a bridging ligand. The topic is particularly appropriate for a paper dedicated to Howard Alper because he must have experienced many times phosphine oxidation concomitant with reduction of Pd(II) to Pd(0) species, including the unwanted metal!

Experimental

Unless otherwise noted, synthetic procedures were performed using standard Schlenk techniques under an atmosphere of dry Ar or N_2. The precursors, *trans*-$PdCl_2$(PhCN)$_2$ (24), $PdCl_2$(dmapm) (**1**) (3), and $PdCl_2$(dmape) (**5**) (4), and the dmapm and dmape ligands (25) were made according to literature procedures. All other reagents were purchased from commercial sources and used as supplied. Solvents were dried over the appropriate agents and distilled under N_2 prior to use. NMR spectra were recorded in $CDCl_3$ solution on a Varian AV300 (121 MHz for ^{31}P) or AV400 (162 MHz for ^{31}P) spectrometer at 300 K. Residual solvent proton (^{1}H, relative to external $SiMe_4$ δ 0.00) and external $P(OMe)_3$ (^{31}P{^{1}H}, δ 141.00 vs. external 85% aq. H_3PO_4) were used as references. Downfield shifts were taken as positive; s = singlet, d = doublet, m = multiplet, br = broad, spt = septet, and all *J*-values are given in Hz. Conductivity measurements were obtained using a Thomas Serfass conductance bridge model RCM151B1 (Arthur H. Thomas Co. Ltd.) connected to a 3404 cell (Yellow Springs Instrument Co.); measurements were made at 25 °C using ~10^{-3} mol L^{-1} solutions of the complexes and are reported as Λ_M in Ω^{-1} mol^{-1} cm^2. Elemental analyses were conducted in the UBC Chemistry Department by Mr. Peter Borda using a Carlo Erba 1108 analyzer.

$PdCl_2$(*P*,*N*-dmapmO) (2)

This complex was prepared at room temperature either in a single phase using cumene hydroperoxide as oxidant or in a two-phase mixture using aqueous H_2O_2.

Cumene hydroperoxide

Precursor **1** was prepared in situ by the reaction of dmapm (140 mg, 0.25 mmol) and *trans*-$PdCl_2$(PhCN)$_2$ (94 mg, 0.25 mmol) in CH_2Cl_2 (10 mL), and to the yellow solution was added cumene hydroperoxide (75 μL, 0.41 mmol). The solution was stirred overnight and then reduced in vacuo to ~2 mL, when Et_2O (20 mL) was added to precipitate the yellow product, which was isolated by filtration, washed with Et_2O (3 × 3 mL), and dried under vacuum. Yield: 155 mg (84%).

H_2O_2

To a CH_2Cl_2 solution (5 mL) containing **1** (28 mg, 0.038 mmol) was added a 3% H_2O_2 (2 mL) solution. The two-phase mixture was stirred for 1 h, and the aqueous phase was removed. The volume of CH_2Cl_2 was reduced in vacuo to ~1 mL, and Et_2O (10 mL) was added to precipitate the product. Yield: 25 mg (88%). ^{1}H NMR δ: 1.7–3.3 (br, 12H, NCH_3), 2.35 (s, 3H, NCH_3), 2.51 (s, 3H, NCH_3), 3.47 (s, 3H, NCH_3), 3.70 (s, 3H, NCH_3), 4.27 (m, 1H, CH_2), 4.81 (m, 1H, CH_2), 6.8–7.9 (br m, 16H, Ar). ^{31}P{^{1}H} NMR δ: 26.2 (d, $^2J_{PP}$ = 7.0), 26.5 (d, $^2J_{PP}$ = 7.0). Λ_M (CH_2Cl_2): <1. Anal. calcd. for $C_{33}H_{42}ON_4Cl_2P_2Pd$: C 52.9, H 5.6, N 7.5; found: C 53.0, H 6.0, N 7.0.

[PdCl(*P*,*N*,*S*-dmapmS)]PF_6 (3)

To a mixture of **1** (44 mg, 0.060 mmol) and S_8 (13 mg, 0.42 mmol of S) was added 1,2-dichloroethane (5 mL), and the resulting yellow solution was refluxed for 3.5 h. The solvent was removed in vacuo, and the residue was dissolved in warm H_2O (20 mL). After filtration of the mixture through Celite 545 to remove excess S_8 and unreacted **1**, aq. KPF_6 solution (5 mL, 90 mg, 0.49 mmol) was added; this immediately precipitated a yellow-orange solid that was isolated by filtration and washed with H_2O (10 mL). Yield: 30 mg (56%). ^{1}H NMR δ: 2.15 (s, 12 H, NCH_3), 2.86 (s, 12 H, NCH_3), 4.50 (br m, 2H, CH_2), 7.30 (m, 4H, Ar), 7.46 (m, 4H, Ar), 7.57 (m, 4H, Ar), 7.87 (m, 2H, Ar), 8.50 (dd, 2H, Ar, $^2J_{HH}$ = 7.39, $^4J_{HP}$ = 15.3). ^{31}P{^{1}H} NMR δ: 37.0 (d, $^2J_{PP}$ = 33.6), 48.6 (d, $^2J_{PP}$ = 33.6), –145 (spt, $^1J_{PF}$ = 710, PF_6^-). Anal. calcd. for $C_{33}H_{42}N_4ClF_6P_3PdS$: C 45.3, H 4.8, N 6.4; found: C 45.2, H 5.0, N 6.2.

[PdCl(*P*,*N*,*S*-dmapmS)]Cl (4)

This compound was made in the same manner as outlined for **3**, except that, after the reaction of **1** (130 mg, 0.18 mmol) and S_8 (45 mg, 1.4 mmol), the reaction mixture was cooled to room temperature and then filtered through Celite 545. The filtrate volume was reduced in vacuo to ~1 mL, and Et_2O (20 mL) was added to precipitate the yellow product. Yield: 100 mg (71%). The NMR data for **4**, except for the absence of the PF_6^- resonance, are the same as for **3**. Λ_M (H_2O): 99.

[PdCl(μ-*P*,*N*:*O*-dmapeO)]$_2$[PF_6]$_2$ (6)

To a CH_2Cl_2 (10 mL) solution of **5** (30 mg, 0.041 mmol) was added aq. KOH solution (5 mL, 1 mol L^{-1}). This caused an immediate colour change in the organic layer from yellow to orange-red. The two phase mixture was stirred for 1 h at room temperature, and then the aqueous layer was removed. H_2O (5 mL) was then added to the organic layer, fol-

© 2005 NRC Canada

lowed by KPF_6 (83 mg, 0.45 mmol), and stirring was continued for 0.5 h. The aqueous layer was removed, and the CH_2Cl_2 phase was washed with H_2O (3 × 10 mL) before being filtered through Celite 545. The filtrate was reduced to dryness in vacuo, and the residue taken up in $CDCl_3$ for analysis by $^{31}P\{^1H\}$ NMR spectroscopy. About 10% of the dioxide, dmapeO$_2$ (δ_P 31.5), was apparent in the residue. A satisfactory elemental analysis was not obtained for **6**, but X-ray diffraction quality, pale yellow, irregular-shaped crystals of **6**·4$CDCl_3$ (~60% yield) were formed by slow evaporation of the $CDCl_3$ solution. $^{31}P\{^1H\}$ NMR δ: 28.1 (d, $^2J_{PP}$ = 62), 29.3 (d, $^2J_{PP}$ = 62), –145 (spt, PF_6^-, $^1J_{PF}$ = 710).

Catalytic hydration of maleic acid

Complex **4** was tested as a catalyst (at 10^{-3} mol L^{-1}) for hydration of maleic acid (0.1 mol L^{-1}) in aqueous solution at 100 °C. The experimental procedure has recently been described (4), including the determination, by ^1H NMR spectroscopy, of the conversion of the maleic acid (*cis*-$CH(CO_2H)$=$CH(CO_2H)$) to the hydration (malic acid) and isomerization (fumaric acid) products.

X-ray crystallographic analysis of complex 6

Data (see Table 1) were collected on a Siemens SMART system at 173(2) K. An initial set of cell constants was calculated from reflections harvested from three sets of 20 frames, oriented such that orthogonal wedges of reciprocal space were surveyed. This produced orientation matrices determined from 20 reflections. Final cell constants were calculated from a set of 7876 strong reflections from the actual data collection. The so-called hemisphere data collection technique, where a randomly oriented region of reciprocal space is surveyed to the extent of 1.3 hemispheres to a resolution of 0.84 Å, was used. Three major swaths of frames were collected with 0.30° steps in ω and, in case the lattice was found to be triclinic (as for **6**), additional sets of frames were collected to better model the absorption correction. The space group was determined based on systematic absences and intensity statistics (26), and a direct-methods solution provided the location of most of the non-H atoms, with several full-matrix least-squares – difference Fourier cycles locating the remaining non-H atoms. All non-H atoms were refined anistropically, and H atoms were included as riding atoms with relative isotropic displacement parameters. The structure is dimeric, with half being in the asymmetric unit that also contains one PF_6^- anion and two $CDCl_3$ molecules. Several SAME and DELU restraints were added to assist in the refinement of the solvent molecules, one of which had considerable translational motion that affected the apparent bond lengths. Complete crystallographic information is available.[4]

Table 1. Selected crystallographic data for the "half molecule" of **6**·4$CDCl_3$.

	6·4$CDCl_3$
Empirical formula	$C_{36}H_{46}Cl_7F_6N_4OP_3Pd$
Formula mass	1 112.23
Crystal size (mm^3)	0.20 × 0.10 × 0.10
Crystal system	Triclinic
Space group	$P\bar{1}$ (No. 2)
a (Å)	12.8710(3)
b (Å)	14.0672(3)
c (Å)	15.4779(4)
α (°)	72.938(1)
β (°)	68.222(1)
γ (°)	73.376(1)
Volume ($Å^3$)	2 437.8(1)
Z	2
$D_{calcd.}$ (Mg m^{-3})	1.515
Absorption coefficient (mm^{-1})	0.919
F(000)	1 124
θ range for data collection	1.45–25.00
Reflections collected	16 763
Independent reflections	8 168 (R_{int} = 0.0639)
Observed reflections	5 134 ($I > 2\sigma(I)$)
No. variables	531
Final *R* indices ($I > 2\sigma(I)$)[a]	R_1 = 0.071, wR_2 = 0.1563
R indices (all data)[b]	R_1 = 0.1179, wR_2 = 0.1768
Goodness-of-fit on F^2	0.96
Largest diff. peak and hole (e $Å^{-3}$)	1.328 and –0.90

[a] $R_1 = \Sigma||F_O| - |F_C||/\Sigma|F_O|$ (observed data).
[b] $wR_2 = (\Sigma(F_O^2 - F_C^2)^2/\Sigma w(F_O^2)^2)^{1/2}$ (all data).

Results and discussion

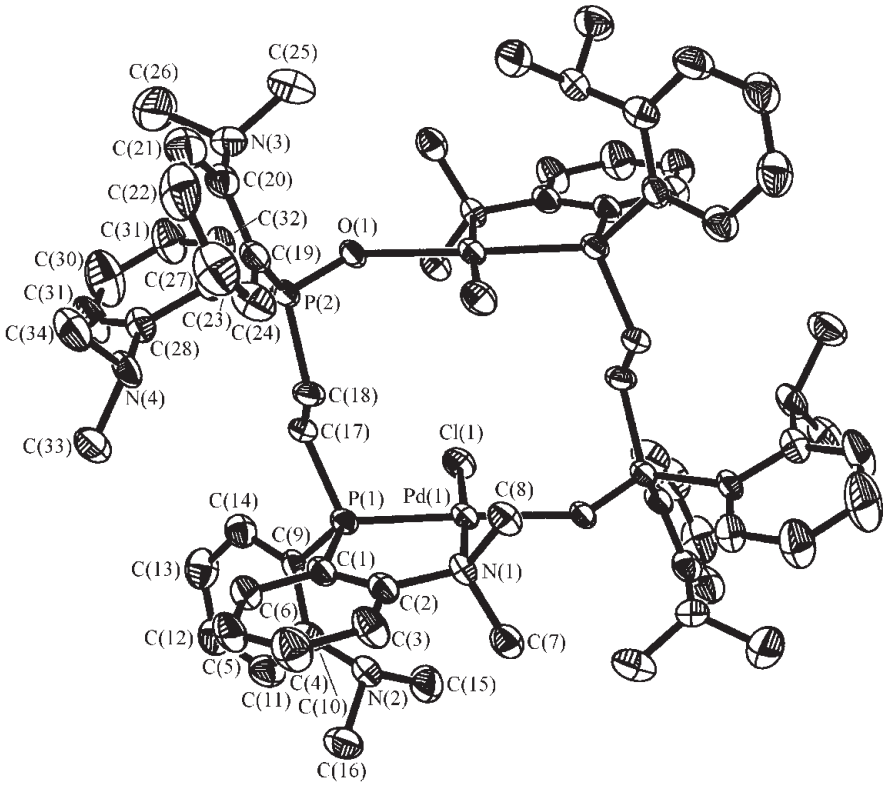
The P(III)-containing precursor $PdCl_2$(dmapm) (**1**) exists in solution as an equilibrium mixture of the neutral *P*,*P*- (**1a**) and *P*,*N*-ligated (**1b**) isomers (3), as shown in Scheme 1. Net O atom or S atom addition to **1** results in formation of BPMO and BPMS complexes: room temperature reactions with cumene hydroperoxide in CH_2Cl_2 or with H_2O_2 in CH_2Cl_2–H_2O and with S_8 in refluxing 1,2-dichloroethane cleanly give $PdCl_2$(*P*,*N*-dmapmO) (**2**) and [PdCl(*P*,*N*,*S*-dmapmS)]Cl (**4**), respectively (Scheme 1). Presumably, the oxidations occur at the free P atom of isomer **1b**. Complex **2** is a non-electrolyte in CH_2Cl_2 solution (Λ_M < 1) and does not dissolve in H_2O, while **4** dissolves in H_2O as a 1:1 electrolyte (Λ_M = 99), and the Cl^- counterion is easily exchanged for PF_6^- by reaction with KPF_6 to give [PdCl(*P*,*N*,*S*-dmapmS)]PF_6 (**3**). That the NMR data for **4** in CH_2Cl_2 are the same as those for the cation of **3** (see below) argues strongly that it is not the dissolution of **4** in water that promotes dissociation of a chloride and that **4** is ionic, unlike the neutral **2**. The softer S atom of the P=S fragment (vs. the harder O atom of P=O fragment) is apparently a sufficiently good ligand to displace a coordinated chloride in these Pd(II) systems.

We recently observed a Pt analogue of **2**, PtI_2(*P*,*N*-

[4] Supplementary data for this article are available on the Web site or may be purchased from the Depository of Unpublished Data, Document Delivery, CISTI, National Research Council Canada, Ottawa, ON K1A 0S2, Canada. DUD 3660. For more information on obtaining material refer to http://cisti-icist.nrc-cnrc.gc.ca/irm/unpub_e.shtml. CCDC 262359 contains the crystallographic data for this manuscript. These data can be obtained, free of charge, via www.ccdc.cam.ac.uk/conts/retrieving.html (or from the Cambridge Crystallographic Data Centre, 12 Union Road, Cambridge CB2 1EZ, UK; fax +44 1223 336033; or deposit@ccdc.cam.ac.uk).

© 2005 NRC Canada

Fig. 1. ORTEP representation (50% ellipsoids) of the molecular structure of the cation of **6**. H atoms are omitted for clarity.



dmapmO), that formed as an aerobic decomposition product of the heterobimetallic catalyst precursor $PtPdCl_4$(μ-*N*,*P*:*P*′,*N*′-dmapm) during the Heck coupling of PhI and styrene in DMF–H_2O with K_2CO_3 as base (1).

Unlike **1**, $PdCl_2$(dmape) (**5**) exists in CH_2Cl_2 as an equilibrium mixture of the neutral $PdCl_2$(*P*,*P*-dmape) (**5a**) and ionic [PdCl(*P*,*P*,*N*-dmape)]Cl (**5b**) isomers (4), as shown in Scheme 2. Reaction of this mixture with KOH in a biphasic H_2O–CH_2Cl_2 medium at room temperature, followed by Cl^-–PF_6^- anion exchange, gives the remarkable dipalladium complex [PdCl(μ-*P*,*N*:*O*-dmapeO)]$_2$[PF_6]$_2$ (**6**, Scheme 2). An ORTEP of the structure of the cation is shown in Fig. 1, and selected bond distances and angles appear in Table 2.

The structure of **6** consists of two face-to-face, square planar Pd(II) moieties in a head-to-tail orientation (i.e., they are related by an inversion centre that lies at the mid-point of the Pd–Pd axis). The metal centres are separated by a distance of 4.873 Å, and each is *P*,*N*-chelated by the dmape(O) and *P*,*O*-bridged to the other, thus forming a 12-membered ring containing the metal centres. The ring is flanked on either side by two $CDCl_3$ molecules (not shown in Fig. 1). The P-C-C angles in the dmape(O) ligand "backbone" (113.8° and 111.2°) are very similar to that of 110.7° found for dmape (25), indicating that the dmape(O) ligand is unstressed, with the Pd centres being too far removed from one another to interact. The Pd—P and Pd—N bond lengths (2.182 and 2.114 Å), as well as the P-Pd-N angle (87.17°), are similar to those found for **1b** (2.180 Å, 2.132 Å, and 86.10°, respectively) (4).

The bond lengths of Pd—O (2.124 Å), Pd—P (2.182 Å), and P=O (1.515 Å), and the Pd-O=P angle (137.1(3)°) in **6**, are comparable to literature data that we have found for nine

Table 2. Selected bond lengths (Å) and angles (°) for **6**·4$CDCl_3$ (esds in parentheses).

Bond distances (Å)			
Pd(1)—Cl(1)	2.296(2)	Pd(1)—N(1)	2.114(5)
Pd(1)—P(1)	2.182(2)	Pd(1)—O(1*)	2.124(4)
P(2)—O(1)	1.515(4)	Pd(1)—Pd(1*)	4.873(2)
Bond angles (°)			
P(1)-Pd(1)-N(1)	87.17(14)	Cl(1)-Pd(1)-O(1*)	95.71(13)
P(1)-Pd(1)-O(1*)	174.99(13)	Cl(1)-Pd(1)-N(1)	176.45(14)
Pd(1)-P(1)-Cl(1)	89.29(7)	N(1)-Pd(1)-O(1*)	87.8(2)
Pd(1)-P(1)-C(17)	111.2(2)	P(1)-C(17)-C(18)	113.8(5)
C(17)-C(18)-P(2)	111.2(5)	C(18)-P(2)-O(1)	108.7(3)
P(2)-O(1)-Pd(1*)	137.1(3)		

other examples of crystallographically characterized Pd(II) complexes bearing *P*,*O*-bound BPMO ligands (12, 21, 27–31), where the average Pd—O, Pd—P, and P=O distances are 2.134, 2.241, and 1.507 Å, respectively, and the average P=O-Pd angle is 125°. There is no obvious correlation between these parameters, but it is interesting to note that in all cases, including **6**, the Pd—O distance is shorter than the Pd—P distance. The Pd-O=P angle in these complexes shows a wide variation between 108° and 144°. There are also very similar crystallographic data for Pd(II) complexes *P*,*O*-bonded to heterofunctional BPMOs of the type $R_2PN(H)P(O)R_2$ (32).

Complex **6** shows some similarities to a $Pd(II)_2$ compound made recently by Leung and co-workers via a fundamentally different route (30). Their complex was synthesized by an initial [4+2] cycloaddition reaction between a Pd-coordinated

© 2005 NRC Canada

phosphole and vinyl diphenylphosphine oxide, which generated a *P*,*O*-coordinated BPMO at a Pd(II) centre. Subsequent treatment with HCl to remove an ancillary cyclometallated benzylamine ligand afforded the $Pd(II)_2$ complex containing (like **6**) two bridging BPMO ligands, the cation of which can be formulated as $[Pd_2Cl_2(\mu\text{-}P{:}O\text{-BMPO})_2(\mu\text{-Cl})]^+$. This species contains a bridging chloride that serves to complete the square planar coordination at each Pd, and thus, instead of the 12-membered ring seen in **6**, the complex contains two fused eight-membered rings (30). We are not aware of any crystallographically characterized complexes other than **6** that contain two BPMO and no other bridging ligands. The observed P=O, Pd—P, and Pd—O bond lengths and the Pd-O=P angle in **6** are very similar to those found for Leung's compound.

The $^{31}P\{^1H\}$ data (δ and *J* values) for complexes **2** and **6** and for the cation within **3** and **4** reveal the expected doublet of doublet pattern for species containing two inequivalent P atoms, but there are insufficient data to assign the respective resonances of the P(III) and P(V) centres, even with knowledge of the $^{31}P\{^1H\}$ data for the precursor complexes **1** and **5** in both their isomeric forms (see Schemes 1 and 2) (3, 4). The two doublet resonances for **2** and **6** differ by only 0.3 and 1.2 ppm, respectively, and even though there is a larger difference of 11.6 ppm for the cation, assignments still cannot be made. The lower field resonances seen for **3/4** (δ 37.0, 48.6) vs. those seen for **2** (δ 26.2, 26.5) are, however, consistent with the usual trend of deshielding with formation of five-membered ring systems of metal bisphosphine chelate complexes (33).

The ^1H NMR data for **2** and **3/4** show the resonances of the CH_2 protons as two separate multiplets for the former complex (δ 4.27, 4.81) and one broad multiplet for the latter (δ 4.50); the signal is seen at δ 2.23 as a triplet ($^2J_{HP}$ = 4.2) for free dmapm (3). Peaks for all 24 NMe protons (δ 2.68 s for free dmapm) are also seen; for **2**, there is a very broad "background" signal (δ 1.7–3.3) and four other singlets of 3H each at δ 2.35, 2.51, 3.47, and 3.70. Complex **2** is clearly fluxional, but without low temperature ^1H NMR studies, like those done for the **1a** ↔ **1b** system (Scheme 1) (3), it is difficult to assign the NMe resonances. However, based on the δ values of 3.46 and 3.79 for the methyl protons of the coordinated NMe_2 group of **1b** (3), the singlets at δ 3.47 and 3.70 likely refer to the coordinated NMe_2 group of complex **2**. Fluxionality originating from exchange of free and coordinated anilinyl groups could arise via reversible formation of a five-coordinate $PdCl_2$(*P*,*N*,*O*-dmapeO) intermediate, analogous to the associative process envisioned for such exchange within $[PtCl(P,P,N\text{-dmapcp})]^+$ via a $[PtCl(P,P,N,N\text{-dmapcp})]^+$ intermediate (4); dmapcp is similar to dmape, but in place of the $-(CH_2)_2-$ backbone the ligand has the cyclopentane $-CH(CH_2)_3CH-$ moiety. The ^1H NMR data for **6**, consisting of broad, overlapping signals, were uninformative.

The mechanism of formation of complex **6** under an anaerobic atmosphere deserves comment, as we are unaware of other systems in which a metal–BMPO complex is isolated from a metal–bisphosphine precursor in the absence of an oxidant such as oxygen or some other O atom donor. It is well known that tertiary phosphines in the presence of base act as two-electron reductants, being themselves converted to the phosphine oxide, with the two electrons commonly reducing a metal centre (see eq. [1]). Such chemistry is of key importance in the reduction of Pd(II) to Pd(0) species, particularly in a range of Pd-catalyzed coupling reactions (e.g., Heck (34), Stille (35), and Suzuki (36) reactions), aminations (37), and formation of diaryl ethers (38), where the supposed Pd(0) active catalyst is generated in situ from Pd(II) precursors. In the Heck reaction, for example, the active catalyst is often derived from a mixture of $Pd(OAc)_2$ and a phosphine, and formation of Pd(0) from this combination has been studied by Amatore et al. (39). During a study of the Pd-catalyzed carbonylation of aryl halides, Grushin and Alper (40) showed by use of a chiral phosphine that Pd(II)–PR_3 complexes are reduced by OH^- to Pd(0) species (eq. [1]) via a *cis*-hydroxo(phosphine)–Pd(II) intermediate, and not via attack at the phosphine by external hydroxide:

$$[1] \qquad [L_nPd(II)\text{-}PR_3]^{2+} + OH^- \rightarrow L_nPd(0) + O{=}PR_3 + H^+$$

where L = a general ligand. The intermediate then decomposes to Pd(0) by deprotonation and reductive elimination of phosphine oxide. Formation of **6** almost certainly occurs via such an initial reduction, following substitution of hydroxide for coordinated chloride or amine of **5a** or **5b** to give, after generation of HCl, a species such as "Pd(0)(dmapeO)". Subsequent oxidation to **6** is thought to occur via reaction with the CH_2Cl_2 solvent. Some indirect evidence for this is that **6** was not detected spectroscopically in the organic phase when the reaction of **5** with hydroxide was conducted in the absence of chlorinated solvent (for example, in H_2O–CH_3NO_2). Oxidative addition reactions of M(0)(phosphine) complexes (M = Pd, Pt) with chlorinated solvents to generate M(II)-chloro species are not uncommon (41), but further work is needed to substantiate the suggestion here.

Complex **4** was tested as a catalyst precursor for hydration of maleic to malic acid in aqueous solution at 100 °C, for comparison with corresponding, recently reported data using $PdCl_2$(dmape) (**5**) and the related [PdX(*P*,*P*,*N*-dmapcp]X complexes as catalyst precursors (4); X = Cl or I, and dmapcp is defined above. The activity of **4** is very similar to that found for [PdCl(*P*,*P*,*N*-dmapcp]Cl (4), as follows: after 24 h, 15% of the maleic acid has been converted to 7% malic acid and 8% fumaric acid, these percentages corresponding to the turn-over numbers, which are three times greater than those reported for hydration of diethylmaleate in THF–H_2O at 120 °C using $[\{Ph_2P(CH_2)_2PPh_2\}Pd(\mu\text{-}OH)]_2^{2+}$ as the catalyst precursor (5). The activity remains marginal, and indeed is comparable to that of dilute HCl for the hydration. However, HCl gives about twice as much isomerization product than do our Pd-*P*,*P*,*N* and Pd-*P*,*P*,*S* complexes (4).

Conclusions

We have demonstrated the formation of bisphosphine monoxide (BPMO) complexes of Pd(II), both by direct oxidation of a "dangling" P(III) atom and by reaction with aqueous hydroxide in a mixed solvent system, where deprotonation and reductive elimination of phosphine oxide from a *cis*-hydroxophosphine-Pd(II) intermediate is favoured. In

© 2005 NRC Canada

addition, we have shown that analogous monosulfide (BPMS) complexes can be made by the direct oxidation route.

Acknowledgements

We thank the Natural Sciences and Engineering Research Council of Canada (NSERC) for financial support of this work, the University of British Columbia for a University Graduate Fellowship (NDJ), and Dr. Victor Young (X-Ray Crystallographic Laboratory, Chemistry Department, University of Minnesota, Minneapolis, MN 55455) for determining the crystal structure of **6**·4$CDCl_3$.

References

1. N.D. Jones and B.R. James. Adv. Synth. Catal. **344**, 1126 (2002).
2. S.J.L. Foo, N.D. Jones, B.O. Patrick, and B.R. James. Chem. Commun. 988 (2003).
3. N.D. Jones, S.J.L. Foo, B.O. Patrick, and B.R. James. Inorg. Chem. **43**, 4056 (2004).
4. N.D. Jones, P. Meessen, U. Losehand, B.O. Patrick, and B.R. James. Inorg. Chem. **44**, 3290 (2005)
5. S. Ganguly and D.M. Roundhill. Organometallics, **12**, 4825 (1993).
6. (*a*) A. Bader and E. Lindner. Coord. Chem. Rev. **108**, 27 (1991); (*b*) C.S. Slone, D.A. Weinberger, and C.A. Mirkin. Prog. Inorg. Chem. **48**, 233 (1999).
7. (*a*) C.O. Abu-Gnim and I. Amer. J. Organomet. Chem. **516**, 235 (1996); (*b*) S. Gladiali, E. Aberico, S. Pulacchini, and L. Kollár. J. Mol. Catal. A: Chem. **143**, 155 (1999).
8. (*a*) V.V. Grushin. J. Am. Chem. Soc. **121**, 5831 (1999); (*b*) V. V. Grushin. Organometallics, **20**, 3950 (2001).
9. S. Gladiali, S. Pulacchini, D. Fabbri, M. Manassero, and M. Sansoni. Tetrahedron: Asymmetry, **9**, 391 (1998).
10. M. Nandi, J. Jin, and T.V. RajanBabu. J. Am. Chem. Soc. **121**, 9899 (1999).
11. I. Brassat, W. Keim, S. Killat, M. Möthrath, P. Mastorilli, C.F. Nobile, and G.P. Suranna. J. Mol. Catal. A: Chem. **157**, 41 (2000).
12. S. Gladiali, R. Taras, R.M. Ceder, M. Rocamora, G. Muller, X. Solans, and M. Font-Bardia. Tetrahedron: Asymmetry, **15**, 1477 (2004).
13. J.W. Faller, J.C. Wilt, and J. Parr. Org. Lett. **6**, 1301 (2004).
14. A.G. Abatjoglou and L. Kapicak. US Patent 4 429 161, 1984.
15. Q.-B. Bao, S.J. Landon, A.L. Rheingold, T.M. Haller, and T.B. Brill. Inorg. Chem. **24**, 900 (1985).
16. K. Heinze, G. Huttner, and L. Zsolnai. Chem. Ber. **130**, 1393 (1997).
17. T. Tanase, T. Igoshi, and Y. Yamamoto. Inorg. Chim. Acta, **256**, 61 (1997).
18. W.O. Siegl, S.J. Lapporte, and J.P. Collman. Inorg. Chem. **10**, 2158 (1971).
19. P. Sevillano, A. Habtemariam, A. Castiñeiras, M.E. Garcia, and P.J. Sadler. Polyhedron, **18**, 383 (1999).
20. K.A. Bunter, D.H. Farrar, A.J. Poë, and A. Lough. Organometallics, **21**, 3344 (2002).
21. (*a*) J. Vicente, A. Arcas, D. Bautista, and P.G. Jones. Organometallics, **16**, 2127 (1997); (*b*) J. Vicente, A. Arcas, D. Bautista, and M.C. Ramírez de Arellano. J. Organomet. Chem. **663**, 164 (2004).
22. P.W. Cyr, S.J. Rettig, B.O. Patrick, and B.R. James. Organometallics, **21**, 4672 (2002).
23. P.W. Cyr. Ph.D. dissertation, University of British Columbia, Vancouver, B.C. 2001.
24. F.R. Hartley. Organomet. Chem. Rev. (A), **6**, 119 (1970).
25. N.D. Jones, P. Meessen, M.B. Smith, U. Losehand, S.J. Rettig, B.O. Patrick, and B.R. James. Can. J. Chem. **80**, 1600 (2002).
26. Siemens Industrial Automation, Inc. SHELXTL-Plus V5.0 [computer program]. Siemens Industrial Automation, Inc., Madison, Wis. 1997.
27. N. Gül and J.H. Nelson. Tetrahedron, **56**, 71 (2000).
28. R.J. Coyle, Y.L. Slovokhotov, M.Y. Antipin, and V.V. Grushin. Polyhedron, **17**, 3059 (1998).
29. X. Morise, P. Braunstein, and R. Welter. C.R. Chim. **6**, 91 (2003).
30. T.-W. Teo, S. Selvaratnam, J.J. Vittal, and P.-H. Leung. Inorg. Chim. Acta, **352**, 213 (2003).
31. I. Brassat, U. Englert, W. Keim, D.P. Keitel, S. Killat, G.-P. Suranna, and R. Wang. Inorg. Chim. Acta, **280**, 150 (1998).
32. (*a*) A.M.Z. Slawin, J.D. Woollins, and Q. Zhang. J. Chem. Soc. Dalton Trans. 621 (2001); (*b*) M.B. Smith and A.M.Z. Slawin. Inorg. Chim. Acta, **299**, 172 (2000); (*c*) M.B. Smith, A.M.Z. Slawin, and J.D. Woollins. Polyhedron, **15**, 1579 (1996).
33. P.E. Garrou. Inorg. Chem. **14**, 1435 (1975).
34. C.B. Ziegler and R.F. Heck. J. Org. Chem. **43**, 2941 (1978).
35. J.K. Stille. Angew. Chem. Int. Ed. Engl. **25**, 508 (1986).
36. N. Miyaura and A. Suzuki. Chem. Rev. **95**, 2457 (1995).
37. (*a*) Y. Guari, G.P.F. van Strijdonck, M.D.K. Boele, J.N.H. Reek, P.C.J. Kamer, and P.W.N.M. van Leeuwen. Chem. Eur. J. **7**, 475 (2001); (*b*) M.S. Driver and J.F. Hartwig. J. Am. Chem. Soc. **118**, 7217 (1996).
38. A. Aranyos, D.W. Old, A. Kiyomori, J.P. Wolfe, J.P. Sadighi, and S.L. Buchwald. J. Am. Chem. Soc. **121**, 4369 (1999).
39. C. Amatore, A. Jutand, and M.A. M'Barki. Organometallics, **11**, 3009 (1992).
40. V.V. Grushin and H. Alper. Organometallics, **12**, 1890 (1993).
41. (*a*) L. Malatesta and C. Cariello. J. Chem. Soc. 2323 (1958); (*b*) R. McCrindle, G. Ferguson, A.J. McAlees, G.J. Arsenault, A. Gupta, and M.C. Jannings. Organometallics, **14**, 2741 (1995); (*c*) N.D. Jones. Ph.D. dissertation, University of British Columbia, Vancouver, B.C. 2001. p. 190.

© 2005 NRC Canada

Synthesis and characterization of novel polysiloxane-grafted fluoropolymers[1]

Bilal Baradie, Patricia H.M. Lai, and Molly S. Shoichet

Abstract: Fluorosilicone polymers combine the properties of both fluorocarbons and siloxanes, yielding materials with unique properties. Novel crosslinked fluorosilicone polymers were synthesized by grafting diisocyanate-terminated polydimethylsiloxane (PDMS) to hydroxyl-functionalized fluoropolymers of poly(tetrafluoroethylene-co-vinyl acetate-co-vinyl alcohol) (PTFE-VAc-VA), as confirmed by elemental bulk and surface analysis. The fluorosilicone polymers containing 34 mol% of TFE were thermally stable with a degradation temperature of 267 °C. Fluorosilicone films were found to be more hydrophobic than the parent, non-grafted fluoropolymers; dynamic advancing and receding water contact angles for PTFE-co-VAc-co-VA-g-PDMS were 104° ± 1° and 61° ± 1°, respectively, whereas for PTFE-co-VAc they were 90° ± 2° and 59° ± 2°. The combined properties of thermal stability and hydrophobicity suggest that these fluorosilicones may be useful for coating and paint applications.

Key words: fluoropolymers, fluorosilicone, polydimethylsiloxane, supercritical carbon dioxide.

Résumé : Les polymères de fluorosilicone combinent les propriétés des fluorocarbones et des siloxanes qui leur donnent des propriétés uniques. On a réalisé la synthèse de nouveaux polymères de fluorosilicones réticulés en procédant à la greffe de polydiméthylsiloxane (PDMS) se terminant par une fonction diisocyanate à des fluropolymères à fonction hydroxyle de poly(tétrafluoroéthylène-co-acétate de vinyle-co-alcool vinylique) (« PTFE-VAc-VA ») et cette synthèse a été confirmée par une analyse élémentaire globale et une analyse de surface. Les polymères de fluorosilicone comportant au moins 34 mol% de TFE sont thermiquement stables, avec une température de dégradation de 267 °C. On a trouvé que les films de fluorosilicone sont plus hydrophobes que leurs fluoropolymères parents non réticulés; les angles de contact dynamiques de l'eau qui avance ou qui se retire pour le PTFE-co-VAc-co-VA-g-PDMS sont respectivement de 104° ± 1° et 61° ± 1° alors que pour le PTFE-co-VAc, ils sont de 90° ± 2° et 59° ± 2°. Les propriétés combinées de stabilité thermique et de caractère hydrophobe suggèrent que ces fluorosilicones pourraient avoir des applications utiles pour les revêtements et la peinture.

Mots clés : fluoropolymères, fluorosilicone, polydiméthylsiloxane, dioxyde de carbone superficiel.

[Traduit par la Rédaction]

Introduction

Fluorosilicones consist of fluorocarbons and siloxanes and are generally thought of as siloxane backbone polymers with fluorocarbon pendant groups. Fluorosilicones are generally considered resilient within a working temperature range from –60 to 200 °C. They have low surface tension (2.0–2.5 μN cm^{-1}) (1), low volatility, and excellent chemical inertness, resulting in good release properties. Moreover, fluorosilicones have low glass transition temperatures (i.e., –75 °C for polymethyl-trifluoropropylsiloxane (PMTFPS)), low brittle points (i.e., of –59 °C), and do not crystallize at low temperatures (e.g., PMTFPS does not crystallize at –40 °C). Thus, fluorosilicones combine the high thermal stability and low surface tension of fluoropolymers with the high thermal stability, low adhesion, and good low-temperature flexibility of silicones (2, 3).

Fluorosilicone elastomers are used as lubricants for pumps and compressors where harsh chemical solvents are utilized. Fluorosilicone rubber is fuel resistant and, therefore, widely used in the automotive and aerospace industries to make O-rings, gaskets, washers, and sealants that are used in fuel line connections, as well as exhaust gas recirculating diaphragms for automobiles (2).

Several types of fluorosilicones have been synthesized, most of which are conceptually similar to PMTFPS — that is, with a siloxane backbone and a fluorocarbon pendant group — yet some are different. For example, Mascia et al.

Received 22 December 2004. Published on the NRC Research Press Web site at http://canjchem.nrc.ca on 2 June 2005.

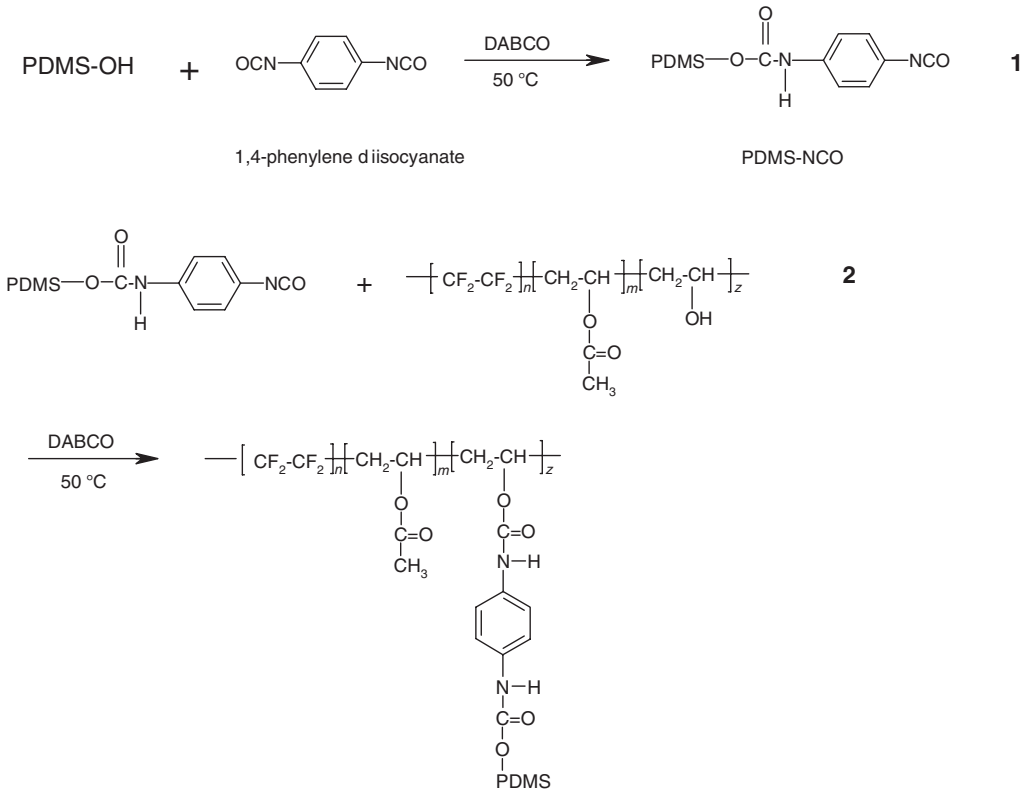
B. Baradie and P.H.M. Lai. Department of Chemical Engineering and Applied Chemistry, University of Toronto, 200 College Street, Toronto, ON M5S 3E5, Canada.

M.S. Shoichet.[2] Department of Chemical Engineering and Applied Chemistry, University of Toronto, 200 College Street, Toronto, ON M5S 3E5, Canada *and* Department of Chemistry, University of Toronto, 80 St. George Street, Toronto, ON M5S 1A1, Canada.

[1]This article is part of a Special Issue dedicated to Professor Howard Alper.
[2]Corresponding author (e-mail: molly@ecf.utoronto.ca).

 doi: 10.1139/V05-068 © 2005 NRC Canada

Scheme 1. Pre-polymer preparation and grafting reaction of PDMS-NCO onto PTFE-co-VAc-co-VA.



(4) blended poly(vinylidene fluoride) with a fluorosilicone elastomer with the thought that the vinylidene fluoride would reinforce the mechanical and thermal properties of the fluorosilicone polymer. This experimental compatibility was proven to be successful, and the polymer exhibited a peak melting temperature of approximately 120 °C (4). In a separate example, Kim et al. (5) synthesized a fluorosilicone polymer with a hydrocarbon backbone and fluorinated and siloxane pendant groups covalently bound by urethane bonds (5). Interestingly, Suzuki et al. (6) grafted polydimethylsiloxane (PDMS) onto a poly(chlorotrifluoroethylene) (CTFE) via an epoxide, yet this ether bond is non-ideal, with a low cohesion energy of 4.2 kJ mol^{-1} vs. that of a urethane bond at 36.5 kJ mol^{-1} (6, 7). In both Kim and Suzuki papers, the polymer surfaces were found to be hydrophobic. While these two systems use graft polymers as a way to achieve fluorosilicones, neither approach is ideal for thermally stable fluorosilicones because Kim's polymers have a hydrocarbon backbone and Suzuki's polymers use an ether bond for grafting. To overcome this void in thermal stability, we synthesized fluorosilicone polymers consisting of a fluorocarbon backbone and siloxane pendant groups, where urethane chemistry was utilized for the grafting.

Specifically, we investigated the use of supercritical carbon dioxide synthesized poly(tetrafluoroethylene-co-vinyl acetate) (PTFE-co-VAc) (8, 9), where the TFE-backbone polymers were found to be more thermally stable than those of CTFE and the vinyl acetate groups were hydrolyzed to vinyl alcohol (VA), yielding reactive functional groups for the covalent grafting of isocyanate-terminated PDMS. Monohydroxy- and dihydroxy-terminated PDMS were modified with 1,4-phenylene diiosocyanate, resulting in mono- and diisocyanate-terminated PDMS, respectively. As shown in Scheme 1, linear fluorosilicone polymers were synthesized by grafting monoisocyanate-terminated PDMS to PTFE-VAc-VA, whereas crosslinked fluorosilicone polymers were synthesized by grafting diisocyanate-terminated PDMS to PTFE-VAc-VA (as shown in Scheme 2). These polymers were characterized for bulk thermal stability and surface hydrophobicity of cast films.

Results and discussion

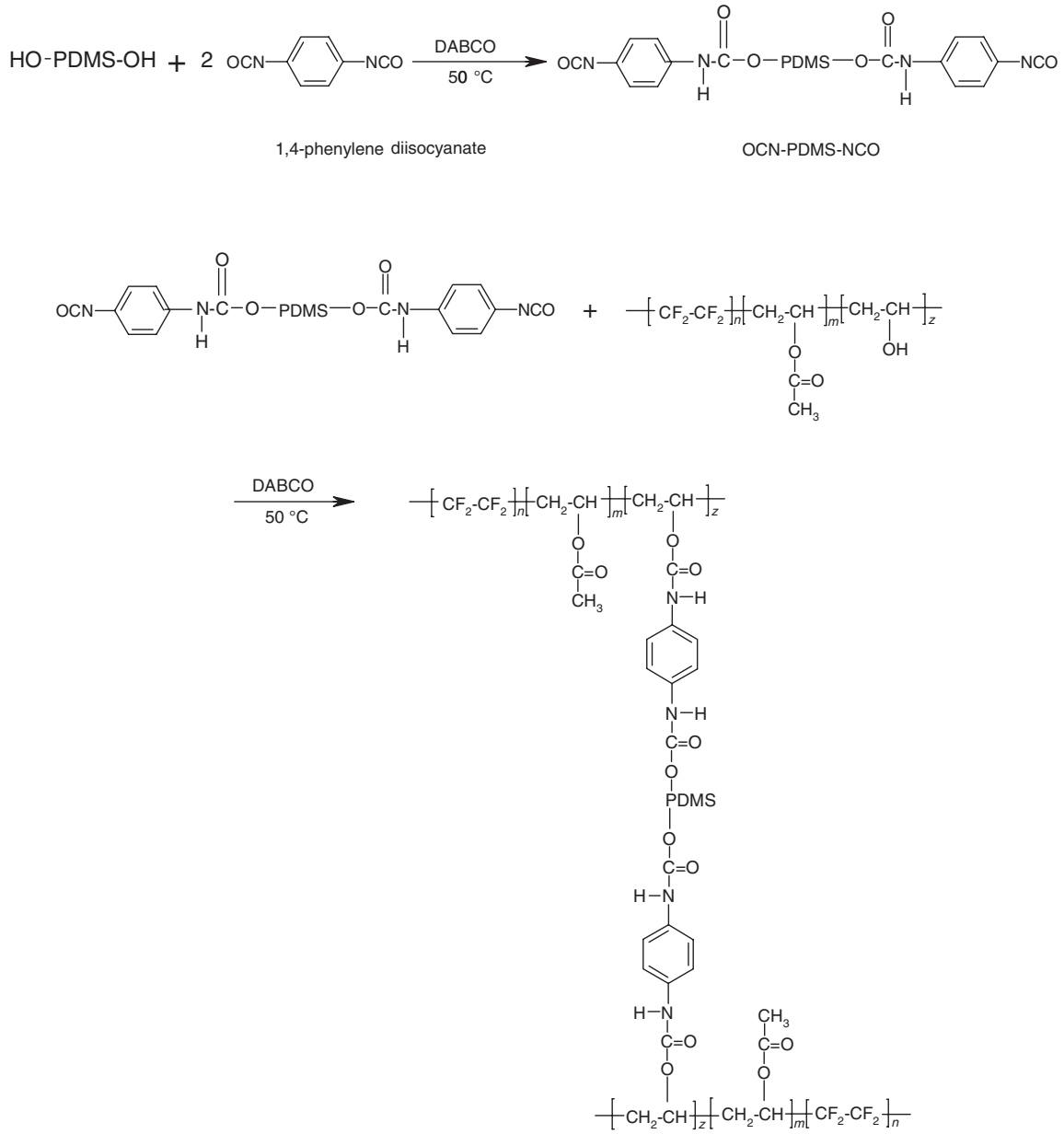
The ultimate goal of this research was to synthesize a crosslinked fluorosilicone with high thermal stability and high hydrophobicity; however, since crosslinked polymers are more difficult to analyze by, for example, ^{1}H NMR, we first synthesized linear fluorosilicones as model systems for the crosslinked polymers.

Linear fluorosilicones

PTFE-VAc was synthesized in supercritical fluid CO_2, as previously described, and found to have a linear backbone formed by hydrolysis of VAc repeats to VA (8). Three compositions of PTFE-VAc were examined for hydrolysis to PTFE-VAc-VA, each possessing TFE contents of 26 mol%, 34 mol%, and 63 mol%, respectively. However, only PTFE-VAc copolymers with TFE contents of 26 mol% and 34 mol% could be hydrolysed to PTFE-VAc-VA because of the insolubility of PTFE-VAc with 63 mol% TFE in the hydrolysis solution of THF. Thus only these two compositions were further analyzed. PDMS-isocyanate was successfully synthesized, as determined by FT-IR, which was also utilized to demonstrate the grafting of PDMS-isocyanate to

© 2005 NRC Canada

Scheme 2. Crosslinking of PTFE-co-VAc-co-VA backbone with the prepolymer NCO-PDMS-NCO.



PTFE-VAc-VA (shown in Fig. 1). The NH (3300 cm^{-1}) and C=O (1750 cm^{-1}) stretching vibrations correspond to the urethane bond, while the Si-O peak at 1260 cm^{-1} corresponds to PDMS and the CF_2 peak at 1152 cm^{-1} reflects the fluorinated backbone of PTFE-co-VAc-co-VA. The disappearance of the NCO peak at 2250 cm^{-1} indicates that the PDMS-NCO functional groups were consumed and likely grafted to the fluorinated PTFE-co-VAc-co-VA, yielding the linear fluorosilicone polymer.

The grafting reaction was confirmed by ^1H NMR, as shown in Fig. 2, where the peaks between 7.2 and 7.6 ppm correspond to phenyl protons of 1,4-phenylene diisocyanate. The three wide peaks between 5.2 and 6 ppm, as well the two peaks between 1.9 and 2.8 ppm, correspond to the methine, methyl, and methylene protons of VAc. The peak at 3.7 ppm corresponds to the N-H proton from the urethane link. The resonance peak at ~0 ppm corresponds to the methyl protons of the PDMS repeat (CH_3-Si-CH_3), and the peaks labelled (*d*) correspond to the methyl and methylene protons in the PDMS end groups, specifically the terminal butyl and ethylene groups (e.g., HO-C_2H_4-PDMS-C_4H_9) found in PDMS.

Crosslinked fluorosilicones

Surface properties

Reaction chemistries similar to those described for monoisocyanate-terminated PDMS (above) were repeated with diisocyanate-terminated PDMS with PTFE-VAc-VA, yielding crosslinked fluorosilicones. Diisocyanate-terminated PDMS 4000 and 700 were grafted to PTFE-VAc-VA, resulting in a product that possessed TFE:VAc:VA molar ratios of 34:44:22 and 26:48:26, respectively, as determined by a

© 2005 NRC Canada

Fig. 1. FT-IR spectrum of the linear PTFE-VAc-VA-g-PDMS 1100.

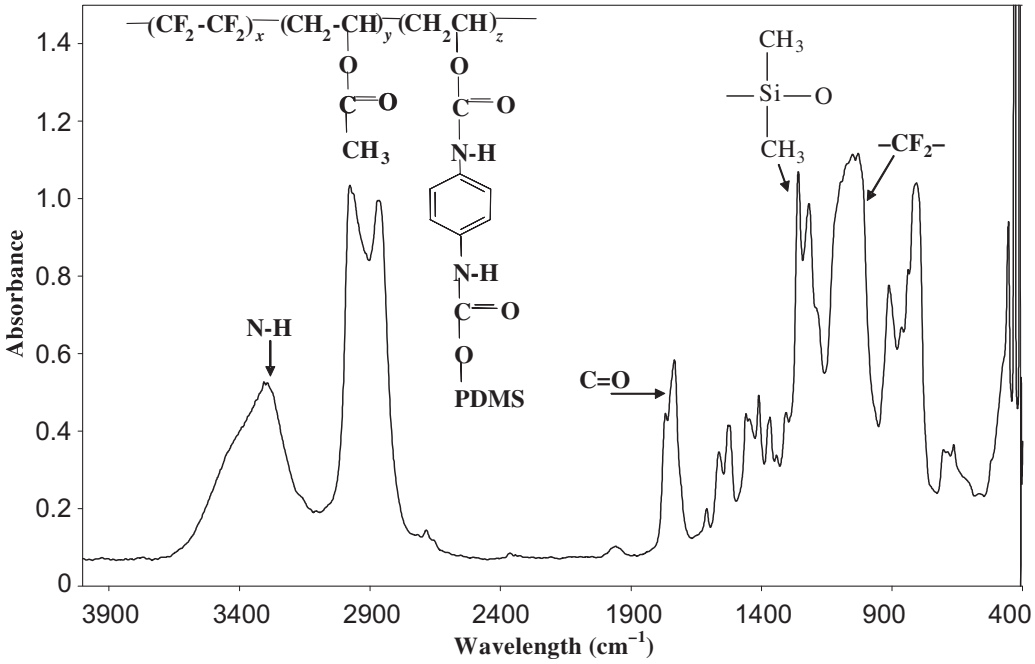
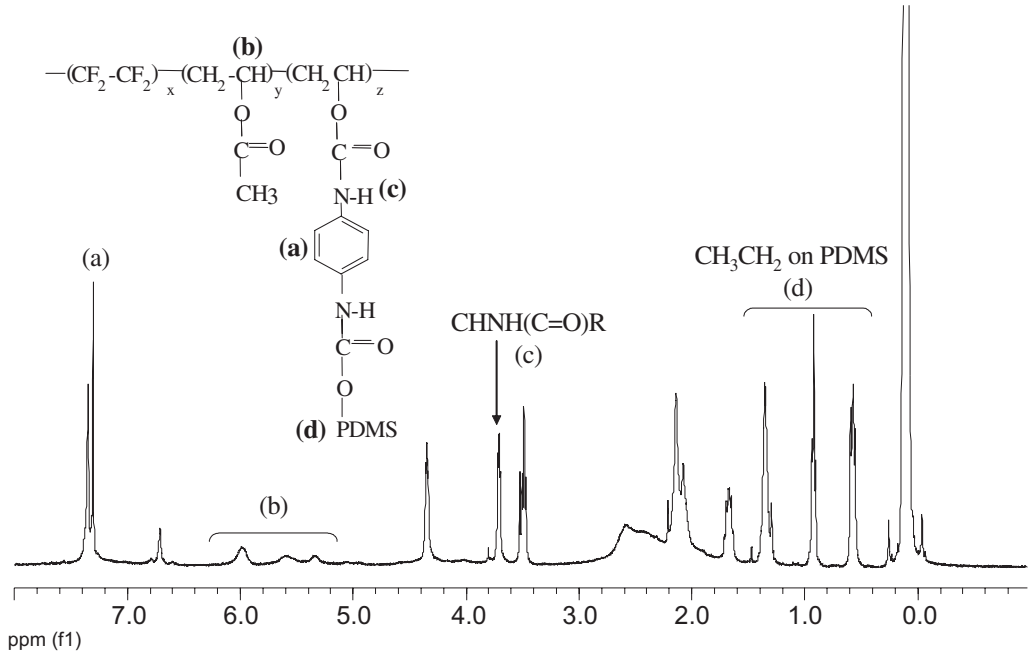


Fig. 2. ^{1}H NMR of the linear fluorosilicone polymer PTFE-VAc-VA-g-PDMS 1100.



combination of elemental analysis (for TFE:VAc molar ratio) and FT-IR (for VAc:VA molar ratio).

Films were cast from THF on glass slides, and the air–polymer surface was analyzed for hydrophobicity by dynamic advancing and receding water contact angles and for surface elemental composition by XPS. Moreover, the XPS surface composition was compared to the elemental-analysis-determined bulk composition. As shown in Table 1, PTFE-VAc-VA-g-PDMS films were hydrophobic, with greater contact angles measured for those polymers with both greater TFE molar content (i.e., 34 mol% vs. 26 mol%) and higher molar mass of PDMS (4000 vs. 700). Interestingly, the XPS elemental surface composition for both films had similar fluorine content (representative of TFE) yet different silicon content (representative of PDMS). The PDMS 4000 sample had more silicon at the surface than the PDMS 700 samples, which suggests that the greater contact angles measured reflect the greater siloxane surface composition. Interestingly, there was a surface enrichment of silicon relative to the bulk composition for both samples. Siloxane groups likely enrich the surface for several reasons, as follows: (*a*) PDMS has a lower critical surface tension (2.1 μN cm^{-1})

© 2005 NRC Canada

Table 1. Crosslinked fluorosilicones of PTFE-co-VAc-co-VA-g-PDMS: surface and bulk analysis.

			XPS (surface analysis)		Elemental analysis (bulk analysis)	
PTFE-VAc-VA mol% by elemental analysis	MW of PDMS	Advancing : receding water contact angles	F (%)	Si (%)	F (%)	Si (%)
34:44:22	4000	104°±1°:61°±1°	4.9	17.3	8.5	0.7
26:48:26	700	94°±3°:52°±3°	5.1	13	6.6	0.82

than that of either TFE (2.4 μN cm^{-1}) or that of PVAc (3.65 μN cm^{-1}) (10); (*b*) the siloxane groups have greater mobility, being pendant to the main chain, than do the TFE groups, which form the backbone, and thus PDMS groups have greater free volume of rotation and can orient themselves more easily at the air–polymer surface (11); and moreover, (*c*) polarity differences between PVAc (0.329) and PTFE (0.089) and PDMS (0.042) likely act to drive PTFE and PDMS away from each other and away from PVAc, driving PDMS to the surface and away from the bulk.

Thermal properties

Thermal stability was measured by thermogravimetric analysis (TGA) for the crosslinked PTFE-VAc-VA-g-PDMS 4000 that was most hydrophobic, and this thermal stability was compared with those of PVAc and PTFE homopolymers. The polymer films were heated from room temperature to 600 °C at a fixed heating rate of 5 °C min^{-1} in air, and mass loss vs. temperature was plotted, as shown in Fig. 3. While PTFE is clearly more stable than PTFE-VAc-VA-g-PDMS, the latter is more stable than PVAc.

To gain a greater understanding of the degradation behavior of crosslinked PTFE-VAc-VA-g-PDMS, its degradation behaviour was compared to that of PTFE and PVAc at two specific degradation temperatures, as follows: (*a*) the temperature of the initial (1%) mass loss ($T_{1\%}$) and (*b*) the temperature at 50% mass loss ($T_{50\%}$). These data are summarized in Table 2. Given that PVAc has lower $T_{1\%}$ and $T_{50\%}$ values than the PTFE-VAc-VA-g-PDMS, this suggests that TFE likely influences the decomposition temperature.

In summary, we achieved our goal of creating a thermally stable, hydrophobic fluorosilicone possessing a fluorocarbon backbone and siloxane pendant group by grafting PDMS to PTFE-VAc-VA via urethane chemistry. This chemistry may be applied to other systems, thereby extending its utility beyond the specific polymers described herein. Moreover, these fluorosilicones may be useful in coating applications where thermal stability and hydrophobicity are desirable. In ongoing studies, we are investigating other fluorosilicone systems that build on the fluorocarbon backbone and siloxane pendant chain approach.

Fig. 3. Comparison of TGA curves of mass loss vs. temperature between crosslinked (*a*) PTFE, (*b*) PTFE-VAc-VA-g-PDMS, and (*c*) PVAc.

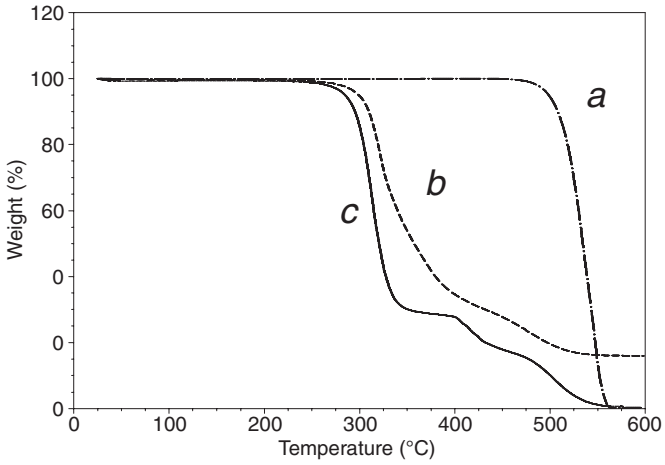


Table 2. Thermogravimetric analysis of crosslinked PTFE-VAc-VA-g-PDMS 4000 vs. PTFE and PVAc.

Polymer sample	$T_{1\%}$	$T_{50\%}$
PTFE-VAc-VA-g-PDMS	267	356
PVAc	244	319
PTFE	475	534

Experimental

General information

All chemicals were purchased from Aldrich (Ontario, Canada) and used as received unless otherwise specified. TFE was prepared by vacuum pyrolysis of PTFE (12) and stored at room temperature over *d*-limonene in a 300 mL stainless steel sample cylinder fitted with an 1800 psi (1 psi = 6.895 kPa) safety rupture disk. The *d*-limonene inhibitor was removed by inline filtration through chromatographic silica gel (200–425 mesh, Fisher Scientific, Ontario, Canada) prior to use. Monohydroxy-terminated PDMS (MW = 1000–1200 g mol^{-1}, referred to as PDMS 1100) and dihydroxy-terminated PDMS (MW = 600–850 g mol^{-1} and 3500–4500 g mol^{-1}, referred to as PDMS 700 and 4000, respectively) were used as received from Gelest Inc. (Tullytown, Pennsylvania).

All PTFE-co-VAc and PTFE-co-VAc-co-VA and PVAc were synthesized as previously reported by radical copolymerization in supercritical fluid CO_2 using diethyl peroxydicarbonate initiation (13). Water was deionized and distilled from Millipore Milli-RO 10 Plus and Milli-Q UF Plus (Bedford, Massachusetts) systems and used at 18 MΩ resistance.

Pre-polymer synthesis of PDMS-NCO and OCN-PDMS-NCO

All syntheses were anhydrous. Glassware was dried overnight in an oven at 110 °C. PDMS was purged with nitrogen gas (N_2) for at least 30 min. For the linear fluorosilicone, the NCO:OH molar ratio was 0.8:1, while it was 1:1 for the crosslinked form. DABCO was added at 1% mass fraction of all monomers. In a 50 mL round-bottom flask, 1,4-phenylene diisocyanate (PhDI) was dissolved in THF to a 50% mass fraction solution. In a 100 mL three-neck round-

© 2005 NRC Canada

bottom flask, 1,4-diazo[2,2,2]-bicyclo-octane (DABCO), PDMS, and THF were added to make a 40% mass fraction solution. Both flasks were continuously purged with N_2. THF was transferred into the flasks using a canula. The dissolved PhDI in THF was added to the flask that contained the PDMS via the canula.

Graft polymerization reaction

For both the linear and crosslinked fluorosilicone elastomers, PTFE-VAc-VA was dissolved in THF to make a 40% mass fraction solution, and it was purged under N_2 for 1 h. Under continuous stirring, the pre-polymer was added via cannula to the dissolved fluorinated polymer. For the linear form, the reaction was monitored by taking samples every 30 min for 2 h and analyzing them using FT-IR. At the end of the reaction, the graft solution was precipitated in a solution of 30% methanol and 70% distilled water. The product was washed and centrifuged in the methanol–water solution three times for 10 min. The product was then dried in the vacuum oven at 60 °C. FT-IR data of PDMS-O(CO)NH-Ph-NCO was as follows: NH (3300 cm^{-1}) and C=O (1750 cm^{-1}) correspond to the urethane bond; free isocyanate (-NCO) (2250 cm^{-1}) corresponds to the functional group at the end of the pre-polymer; and Si-O-Si (1260 cm^{-1}) corresponds to the PDMS (14).

For the crosslinked films, after the pre-polymer was completely added via cannula to the hydrolyzed polymer, the graft solution was immediately cast onto an aluminum dish. Casting of the film was performed at 40 °C. After crosslinking, all films were soaked in methanol for 3 days and then dried under vacuum at 60 °C.

Bulk characterization

Infrared spectra were recorded using the Mattson, Galaxy Series FT-IR 5000. FT-IR was used to monitor the pre-polymer and grafting reactions over time. The attenuated total reflection (ATR) FT-IR was used to analyze the crosslinked films.

Solution NMR analysis was performed using the Gemini 300 Spectrometer. ^1H and ^{19}F NMR were used to analyze the structure of the linear fluorosilicone elastomers.

Degradation and thermal stability analysis was performed using the TGA Q50 by TA Instruments. To identify the 1% mass loss temperature, the elastomer was heated from room temperature to 600 °C at 5 °C min^{-1}.

Surface characterization

Advancing and receding water contact angles were measured on air–film surfaces using a Ramé-Hart NRL telescopic goniometer equipped with a Gilmont syringe and a 22-gauge flat-tipped needle. The data presented are the average and standard deviation of at least six measurements made at different areas on the film surface. All contact angles had standard deviations of 1°–3°.

Surface elemental composition was determined by X-ray photoelectron spectroscopy (XPS, Leybold LHMax 200) using an AlK_α X-ray source at 15 kV and 25 mA emission current; data were collected at a take-off angle of 90° (between the sample plane and detector). Samples were exposed to X-ray for less than 5 min using pass energies of 192 and 42 eV for survey and C_{1s} region spectra, respectively. X-ray damage of film surfaces is negligible under these conditions, but is not negligible with longer acquisitions.

Acknowledgements

We are grateful to Peter Odell, Xerox Corporation and the Natural Sciences and Engineering Research Council of Canada (NSERC CRD program) for financial support.

References

1. C. Hepburn. Polyurethane elastomers. 2nd ed. Elsevier Applied Science Publishers Ltd., N.Y. 1992.
2. J.G. Drobny. Technology of fluoropolymers. CRC Press LLC, Florida. 2001.
3. R.E. Kirk and D.F. Othmer. Encylopedia of chemical technology: Poly(fluorosilicones). 3rd ed. Vol. 11. Wiley-Interscience, N.Y. 1980. pp. 722–729.
4. L. Mascia, S.H. Pak, and G. Caporiccio. Eur. Polym. J. **31**(5), 459 (1995).
5. D.-K. Kim, S.-B. Lee, K.-S. Doh, and Y.-W. Nam. J. Appl. Polym. Sci. **74**, 2029 (1999).
6. H. Suzuki, M. Takeish, and I. Narisawa. J. Appl. Polym. Sci. **78**, 1955 (2000).
7. C. Hepburn. Polyurethane elastomers. 2nd ed. Elsevier Applied Science Publishers Ltd., N.Y. 1992.
8. R.D. Lousenberg and M.S. Shoichet. Macromolecules, **33**, 1682 (2000).
9. B. Baradie and M.S. Shoichet. Macromolecules, **35**, 3575 (2002).
10. J. Brandrup, E.H. Immergut, and E.A. Grulke. Polymer handbook. 4th ed. John Wiley and Sons, N.Y. 1999. p. VI 521.
11. B. Baradie and M.S. Shoichet. Macromolecules. In press.
12. R.J. Hunadi and K. Baum. Synthesis, **39**, 454 (1982).
13. F. Strain, W.E. Bissinger, W.R. Dial, H. Rudoff, B.J. DeWitt, H.C. Stevens, and J.H. Langston. J. Am. Chem. Soc. **72**, 1254 (1950).
14. R.M. Silverstein. Spectrometric identification of organic compounds. 5th ed. John Wiley and Sons, Inc., Toronto. 1991.

© 2005 NRC Canada

Competing Diels–Alder intramolecular pathways from cross-conjugated trienes: Fused hydrindenones (bicyclo[4.3.0]nonenones) vs. bridged-ring (bicyclo[3.3.1]nonenones) adducts from a diene-transmissive precursor[1]

Matthew D. Clay, Ditte Riber, and Alex G. Fallis

Abstract: D-Isoascorbic acid was converted to the tetraenone **12** to examine its behaviour in the intramolecular Diels–Alder reaction with pendant dienes in a diene-transmissive environment. These studies were directed toward the synthesis of the hydrindenone nucleus via a tether-controlled Diels–Alder reaction. It was anticipated that this would lead to a diene-transmissive strategy for steroids such as Desogestrel®. In contrast to our previous studies with decalins, the dominant isomer (150 °C) was the bicyclo[3.3.1]nonadieneone adduct **23**, and none of fused adduct **27** was detected. These products were accompanied by two minor hydrindenone adducts **24** and **25**. The isomer ratio was dependent on the temperature of the reaction.

Key words: Diels–Alder, hydrindane, pentadienylation, intramolecular cycloaddition, bicyclo[3.3.1]nonenone.

Résumé : L'acide D-isoascorbique a été transformé en tétraénone **12** dans le but d'étudier son comportement dans la réaction intramoléculaire de Diels–Alder avec des dièns pendants, dans un environnement permettant une transmission. Ces études ont été dirigées vers la synthèse du noyau hydrindénone via une réaction de Diels–Alder contrôlée par une laisse. Il était prévu que cette méthode permettrait de développer une stratégie diénique permettant une transmission pour réaliser la synthèse de stéroïdes tel le Desogestrel®. Par opposition aux études antérieures réalisées dans ce laboratoire avec des décalines, l'isomère dominant (150 °C) est l'adduit bicyclo[3.3.1]nonadiénone **23** et on n'a pas détecté la présence du produit condensé **27**. Ces produits étaient accompagnés de deux adduits hydrindénones mineurs, **24** et **25**. Le rapport des isomères varie avec la température de la réaction.

Mots clés : Diels–Alder, hydrindane, pentadiénylation, cycloaddition intramoléculaire, bicyclo[3.3.1]nonénone.

[Traduit par la Rédaction]

Introduction

Despite decades of research, the total synthesis of steroid nuclei by improved strategies continues to receive considerable attention. A short synthesis of unnatural steroids, such as the oral contraceptive Desogestrel®, has proved particularly challenging (1).

Previously we reported the enantioselective synthesis of *cis*-decalins via intramolecular Diels–Alder reactions (2). These strategies employed either planar or isopropylidene tether control groups to bias the stereochemistry of the adducts. We discovered that *cis*-acetonides are preferred compared with *trans*-acetonides. The cycloadditions directed by *cis*-acetonides (**1**) occurred under milder conditions and allowed for the introduction of an inside methyl group into the decalin adducts (Scheme 1). Because of the unfavourable *trans*-geometry of the diene induced by this substituent, its introduction is often a challenge in related intermolecular cycloadditions.

We have also extended this tether control group protocol to the stereoselective construction of highly oxygenated nor-steroid and nor-triterpenoid skeletons via a diene-transmissive Diels–Alder strategy (3). A key step in our approach was the selective indium-mediated γ-pentadienylation of the appro-

Received 20 September 2004. Published on the NRC Research Press Web site at http://canjchem.nrc.ca on 14 June 2005.

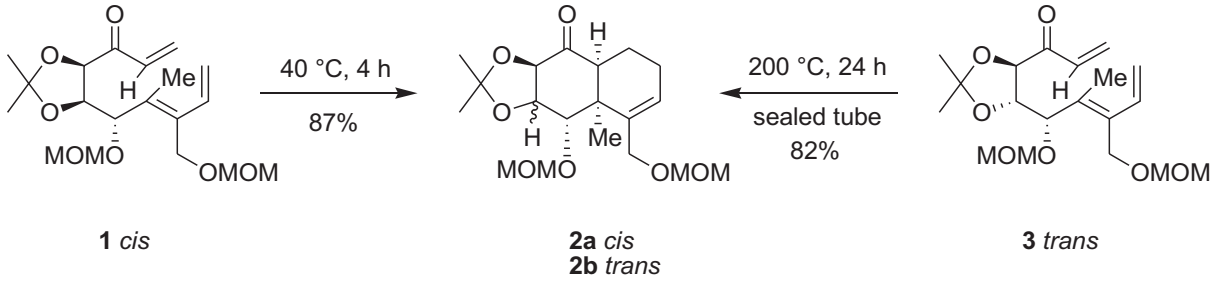
This paper is dedicated to Professor Howard Alper. Presented with respect and gratitude for his contributions to organometallic chemistry and to our friendship.

M.D. Clay, D. Riber,[2] and A.G. Fallis.[3] Department of Chemistry, University of Ottawa, 10 Marie Curie, Ottawa, ON K1N 6N5, Canada.

[1]This article is part of a Special Issue dedicated to Professor Howard Alper.
[2]Present address: Department of Chemistry, University of Aarhus, DK-8000, Aarhus, Denmark.
[3]Corresponding author (e-mail: afallis@science.uottawa.ca).

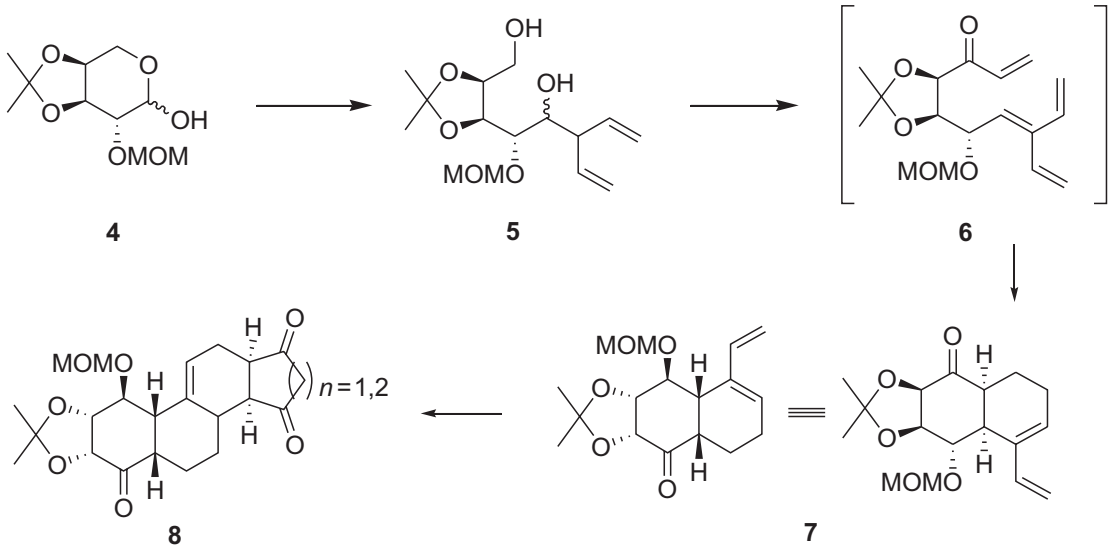
 doi: 10.1139/V05-055 © 2005 NRC Canada

Scheme 1. Cycloadditions controlled by *cis*- and *trans*-acetonides.



1 *cis* **2a** *cis* **2b** *trans* **3** *trans*

Scheme 2. A diene-transmissive Diels–Alder approach to steroids.



4 **5** **6** **7** **8**

priate aldehyde-hemiacetal **4** derived from L-arabinose. Elimination of water from the product **5**, as illustrated in Scheme 2, afforded the cross-conjugated triene **6**. Sequential cycloaddition reactions rapidly produced the tetracyclic nor-steroid or nor-terpenoid core structures **8** (4).

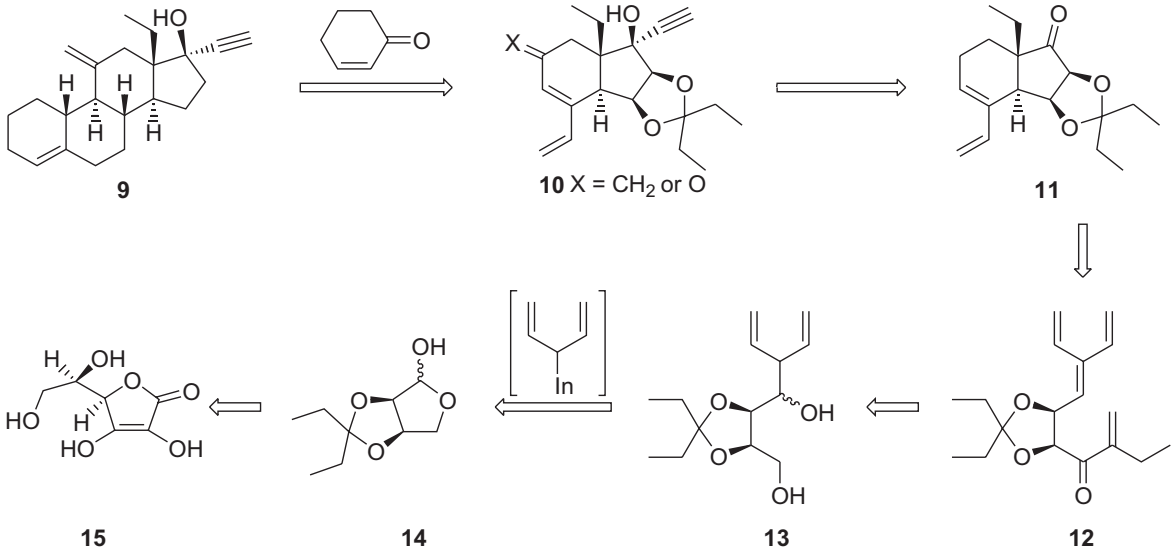
The versatility of this protocol prompted us to investigate the reverse synthetic strategy for steroids in which the hydrindane portion would be constructed first by a related tether-controlled cycloaddition reaction, followed by a second intermolecular cyclization. The challenge of efficiently and stereoselectively synthesizing the *trans*-fused hydrindane system of steroids is well recognized. Previous successful solutions have been based on an intramolecular ester enolate alkylation (5) or on the Lewis acid assisted cyclization of a suitably substituted dienone (6). Strategies involving an intramolecular Diels–Alder cyclization as the key step have also been employed (7).

To explore the feasibility of our protocol for the construction of the *trans*-fused hydrindane ring system of steroids, a widely prescribed oral contraceptive, Desogestrel® (**9**), was selected as a commercially important and challenging target. The initial industrial synthesis of Desogestrel® required 24 steps from diosgenin, the cost of which was partially offset by the potent activity of the drug (0.150 mg per pill) (8). The ethyl group at C13 of Desogestrel® is responsible for a 50-fold enhancement in activity compared with the methyl analogue. Corey et al. (1*a*) have demonstrated that this modest structural change presents a significant complication in its synthesis. In his initial synthesis, Corey surmounted this challenge by starting with the ethyl substituted Wieland–Miescher ketone (1*a*). A more recent solution employs an oxazaborolidinium-catalyzed Diels–Alder reaction as a key step (1*b*).

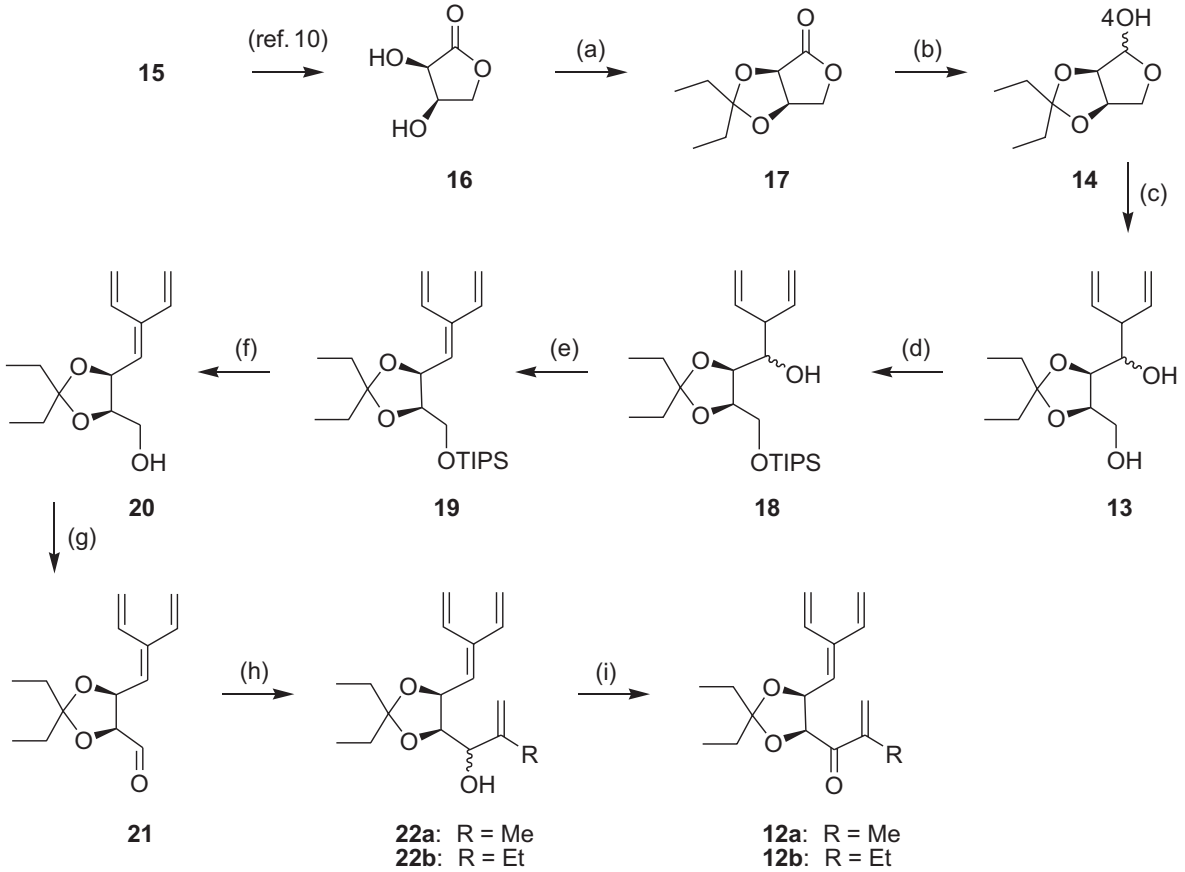
Our strategy to Desogestrel® envisaged sequential Diels–Alder cycloadditions in which the CD ring system was initially constructed via a tether-controlled intramolecular Diels–Alder reaction, followed by an intermolecular cycloaddition to provide the AB rings, as outlined retrosynthetically in Scheme 3. The AB rings of Desogestrel® (**9**) should arise from a Diels–Alder reaction of **10** (exocyclic alkene or ketone) with a suitable cyclohexanone derivative using Northrup and MacMillan's imine-catalyzed protocol (9). The hydrindane portion **11** could be generated via a tether-controlled intramolecular Diels–Alder reaction of triene **12**. An unknown variable in this approach was whether the hydrindane portion could be generated in acceptable yield and with the desired stereoselectivity, especially in view of the large number of unsaturated centers in the tetraenone. An earlier model study using an isopropylidene acetal gave poor selectivity in the Diels–Alder reaction, so we chose to protect the diol of **14** as an isopentylidene acetal. It was anticipated that the additional steric bulk of the acetal would help to differentiate the competing Diels–Alder transition states and would improve the selectivity of the initial cycloaddition. The Diels–Alder precursor **12** can be synthesized from **13**, a product arising from an indium-mediated penta-

© 2005 NRC Canada

Scheme 3. Retrosynthetic route to Desogestrel®.



Scheme 4. Synthesis of Diels–Alder precursors **12a** and **12b**.



dienylation of lactol **14**. This enantiomerically pure lactol can be easily prepared from D-isoascorbic acid (**15**).

Results and discussion

Our synthesis commenced with the known oxidative degradation of D-isoascorbic acid to generate the enantiopure *cis*-diol **16** (Scheme 4) (10). Acetalization of **16** with 3-pentanone and a catalytic amount of *p*-toluenesulfonic acid using a Dean–Stark apparatus provided *cis*-isopentylidene acetal **17** in 92% yield after distillation. Reduction of the lactone moiety with diisobutylaluminum hydride gave lactol **14** in 87% yield as a 5:1 mixture of diastereomers, epimeric at C4. Indium-mediated pentadienylation onto the aldehyde

© 2005 NRC Canada

Table 1. Summary of Diels–Alder reactions.

Entry	Conditions	Results[a]
1	Et_2AlCl, CH_2Cl_2, –78 °C (2 h) (R = Me)	Starting material
2	Et_2AlCl, CH_2Cl_2, –78 °C (30 min) to 21 °C (4 h) (R = Me)	Starting material
3	Et_2AlCl, CH_2Cl_2, –78 °C (30 min) to 42 °C (4 h) (R = Me)	Partial decomposition
4	BF_3OEt_2, CH_2Cl_2, –78 °C (4 h) (R = Me)	Starting material
5	BF_3OEt_2, CH_2Cl_2, –78 °C (30 min) to 0 °C (1 min) (R = Me)	Complete decomposition
6	HN(*i*-Pr)$_2$, $HClO_4$, H_2O, 0 °C (16 h) (R = Et)	Starting material
7	HN(*i*-Pr)$_2$, $HClO_4$, H_2O, rt (24 h) (R = Et)	Starting material
8	HN(*i*-Pr)$_2$, $HClO_4$, EtOH, 0 °C (6 h) to rt (16 h) (R = Et)	Starting material
9	HN(*i*-Pr)$_2$, $HClO_4$, EtOH, 0 °C (5 min) to 65 °C (6 h) (R = Et)	Starting material
10	*p*-TsOH, $HO(CH_2)_2OH$, PhH, 80 °C (20 h) (R = Et)	3 isomers (23:21:56)[b]
11	Toluene, 75 °C (6 days) (R = Me)	3 isomers (28:24:48)[b]
12	Toluene, 150 °C, microwave (3 h) (R = Me)	3 isomers (41:20:39)[b]
13	Toluene, 150 °C, microwave (3 h) (R = Et)	3 isomers (53:17:30)[b]

[a]Ratio determined by NMR integration.
[b]Ratio of **23**:**24**:**25**.

of the open-chain form of the lactol provided diol **13** in 82% yield as a variable mixture of diastereomers. This was inconsequential as this secondary alcohol stereocenter was removed later in the synthesis. Selective protection of the primary alcohol as a triisopropylsilyl ether provided **18** in 93% yield (as a mixture of diastereomers).

Mitsunobu-type dehydration of **18** with three equivalents each of triphenylphosphine and diethyl azodicarboxylate generated triene **19**. Interestingly, the minor isomer of **18** was resistant to dehydration. Whereas reaction of the major isomer (of the mixture) was complete within one day, dehydration of the minor isomer required three days, and often additional reagents (PPh_3 and DEAD) were required. This is likely because of steric hindrance about the reaction center caused by the isopentylidene acetal and the bulky triisopropylsilyl protecting group. Experimentally, triene **19** was isolated in 44% yield, and subsequent desilylation with tetrabutylammonium fluoride provided **20** in 82% yield. The low yield of the dehydration step was attributed to the instability of **19**, which readily decomposed during column chromatography or upon storage in a refrigerator for short periods. Thus a one-pot reaction sequence, in which **18** was first dehydrated and then desilylated to **20** without isolation of intermediate **19**, was investigated. We were gratified to achieve a higher yield of crude **20** from the one-pot procedure (~71%, compared with 36% over the two separate steps). However, **20** could not be easily separated from several impurities generated during the dehydration phase. Thus the preferred experimental method to ensure purity was the original two-step sequence.

Oxidation of the alcohol of trienol **20** also proved challenging. Oxidation occurred under a variety of conditions (e.g., Collins, Corey–Schmidt, IBX, Dess–Martin, Swern), but the product aldehyde slowly decomposed under the reaction conditions. In accord with earlier observations (11), a substantial rate enhancement occurred when water was added to the Dess–Martin oxidation of **20**. This technique pushed the oxidation to completion before noticeable decomposition of the product aldehyde had occurred and provided stable aldehyde **21** in an isolated yield of 74%. Addition of *iso*-propenyllithium or *sec*-butenyllithium (generated from the corresponding bromides via lithium–halogen exchange) to the aldehyde provided allyl alcohols **22a** and **22b**, respectively. It was subsequently discovered that addition of the Grignard reagent to the aldehyde was more efficient on larger scales and afforded **22a** and **22b** in 58% and 53% yields, respectively. Oxidation of both compounds was accomplished using the Dess–Martin periodinane–water combination (described above) and provided Diels–Alder precursors **12a** and **12b** in 78% and 72% yield, respectively.

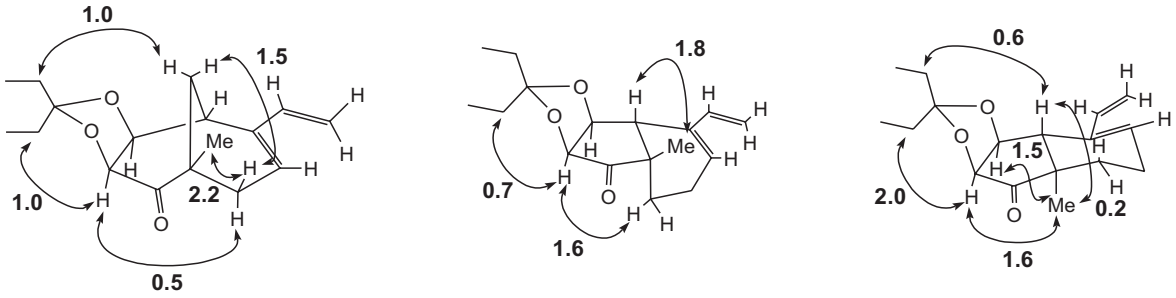
We initially attempted the Diels–Alder reaction on the simpler model system **12a** (rather than the ethyl analogue **12b**). However, once this material was consumed, subsequent reactions were conducted using **12b**. The details of these Diels–Alder studies are presented in Table 1. It was initially believed that a Lewis acid mediated cycloaddition at low temperature would provide the best selectivity. Therefore, the cycloaddition was attempted with either diethylaluminum chloride or boron trifluoride etherate as Lewis acid catalysts. However, neither gave any trace of cycloaddition products at low temperatures, and only decomposition was observed at higher temperatures (entries 1–5). In both cases, the decomposition products were not the free diol from Lewis acid assisted cleavage of the isopentylidene acetal. Apparently the increased bulk created by Lewis acid association with the carbonyl inhibits the beneficial effect anticipated from the electronic activation.

An attempt to induce the cycloaddition using a variation of MacMillan's imine-catalyzed procedure was also examined (9). Diisopropylamine was employed as the amine component, in place of the more complex amine used by MacMillan. Unfortunately, despite several attempts, no reaction or decomposition occurred, even in the presence of perchloric acid and refluxing ethanol (entries 6–9).

We next attempted the cycloaddition under thermal conditions. Heating tetraene **12a** in the microwave at 150 °C for 3 h gave a mixture of Diels–Alder adducts in 78% yield. The individual isomers were separated by preparative HPLC, and their structures and relative stereochemistry were determined by NOESY and COSY NMR experiments. The significant

© 2005 NRC Canada

Fig. 1. Significant nOe interactions in Diels–Alder adducts **23**, **24**, and **25**.



23 **24** **25**

nOe interactions are illustrated in Fig. 1. We were intrigued to find that the major isomer was the unexpected bicyclo[3.3.1]nonadieneone **23** rather than one of the anticipated hydrindenone isomers.

The highest ratio of the bicyclo[3.3.1]nonenone isomer **23** was obtained with the ethyl substrate **12b** (53:17:30, **23**:**24**:**25**) upon heating in a microwave oven at 150 °C for 3 h in toluene (entry 13). In contrast, under identical microwave conditions, the methyl substrate **12a** afforded only a slight excess of **23** (41:20:39) (entry 12). The ratio changed to favor formation of hydrindenone **25** (28:24:48) when the temperature was lowered to 75 °C. The reaction required 6 days at this temperature for completion (entry 11). In an attempt to change the electronic environment in the precursor **12b**, acetalization of the ketone of **12b** was attempted using ethylene glycol and catalytic *p*-toluenesulfonic acid in refluxing benzene (80 °C) for 20 h (entry 10). To our surprise, the acetal did not form; rather, **12b** underwent the Diels–Alder reaction to generate **25** as the major isomer in a ratio of 23:21:56 (**23**:**24**:**25**). This ratio was similar to the thermal reaction in toluene at 75 °C. The substantially shorter reaction time (20 h vs. 6 days) indicated the rate influence from ketone protonation by the *p*-toluenesulfonic acid.

Examination of the transition states in Fig. 2 suggests that formation of the desired *trans*-isomer **27** was disfavored by steric repulsion between the R group of the dienophile and the "extra" vinyl group of the diene as illustrated in **26**. This hypothesis was supported by the fact that this Diels–Alder precursor can rotate to avoid this interaction (**28**) and preferentially generate the bicyclic isomer **23**, with lesser amounts of **24** and **25**. It is also interesting that the *cis*-hydrindenone **24**, from transition state **30**, was formed in approximately the same quantity under all conditions. It was anticipated that the steric repulsion between the acetal ethyl group and the R group of the dienophile would disfavor this adduct formation. This is partly why the large isopentylidene acetal was chosen instead of the smaller isopropenyl acetal used in model studies.

General experimental

All non-aqueous reactions were performed under a positive pressure of dry nitrogen in flame-dried glassware using dry solvents. Tetrahydrofuran and diethyl ether were distilled from sodium–benzophenone. Dichloromethane, toluene, triethylamine, and methyl vinyl ketone were distilled from calcium hydride. Standard inert atmosphere techniques were employed in handling air- and moisture-sensitive reagents. *n*-BuLi solutions in hexanes from Aldrich Chemical Company (Oakville, Ont.) were titrated prior to use against diphenylacetic acid and used directly. Starting materials were purchased from Aldrich Chemical Company (Oakville, Ont.) and used without further purification unless otherwise stated.

Reactions were monitored by thin layer chromatography (TLC) using commercial aluminum-backed silica gel sheets coated with silica gel 60 F_{254} (E. Merck, Darmstad, Germany). TLC spots were developed by heating the plate after treatment with a 5% solution of ammonium molybdate in 10% aqueous sulphuric acid or a solution of $KMnO_4$ in aqueous potassium hydroxide. Room temperature corresponds to 21 °C. Anhydrous magnesium sulfate ($MgSO_4$) was used to dry solutions in organic solvents. Excess solvents were removed (concentrated) in vacuo at pressures obtained by a water or air aspirator connected to a Büchi rotary evaporator. Trace solvents were removed on a vacuum pump. Product purification by flash chromatography was performed with E. Merck Silica Gel 60 (230–400 mesh). Petroleum ether refers to a mixture of hydrocarbons with a boiling range of 30–60 °C.

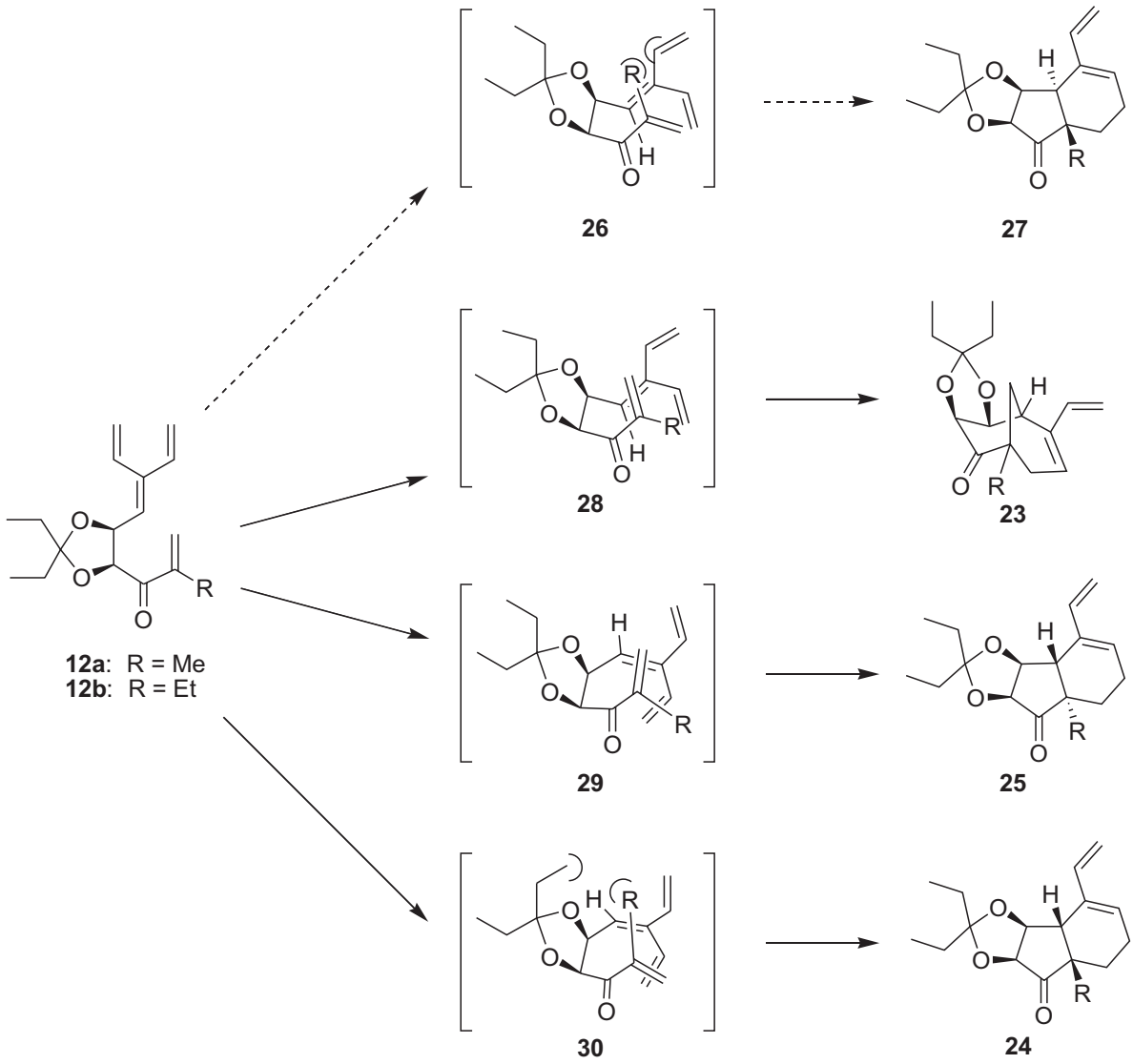
Melting points were determined with a Thomas Hoover Unit melting point apparatus and are uncorrected. Infrared (IR) spectra were obtained as neat thin films or as a solution of the sample in $CDCl_3$ or $CHCl_3$ in a sodium chloride solution cell. All IR spectra were recorded on a Bomem Michelson 100 Fourier transform infrared spectrometer (FT-IR). ^{1}H NMR (500 MHz) and ^{13}C NMR (125 MHz) spectra were run on a Brucker AMX500 spectrometer. Chemical shifts are reported downfield from tetramethylsilane (δ scale) in ppm. ^{1}H NMR data are reported as follows: chemical shift (multiplicity (s = singlet, d = doublet, t = triplet, q = quartet), coupling constants (Hz), and integration). Low-resolution mass spectroscopy (MS), using electron impact (EI), was performed on a V.G. Micromass 7070 HS mass spectrometer with an electron beam energy of 70 eV. High-resolution mass spectroscopy (HR-MS) was performed on a Kratos Concept-11A mass spectrometer with an electron beam energy of 70 eV. The purity of all title compounds was judged to be >95% as determined by a combination of ^{1}H NMR and ^{13}C NMR analyses.

3,4-Dihydroxy-dihydro-furan-2-one (16)

The title compound was prepared according to the literature procedure (10). mp 103–104 °C (lit. (10) value mp 97.5–99.5 °C). IR (neat, cm^{-1}) ν: 3421, 3281, 2989, 2922, 2867, 1773, 1154, 1105, 1031, 970. ^{1}H NMR (500 MHz,

© 2005 NRC Canada

Fig. 2. Transition states leading to various adducts.



D_2O) δ: 4.77 (d, *J* = 4.9 Hz, 1H), 4.65 (dd, *J* = 4.9, 3.0 Hz, 1H), 4.59 (dd, *J* = 10.8, 3.0 Hz, 1H), 4.43 (d, *J* = 10.8 Hz, 1H). ^{13}C NMR (125 MHz, D_2O) δ: 178.2 (C), 72.5 (CH_2), 69.2 (CH), 68.4 (CH). EI-MS *m/z* (%): 118 ([M]$^+$, 3), 73 (26), 60 (91), 56 (100), 43 (56). HR-MS calcd. for $C_4H_6O_4$ ([M]$^+$): 118.0242; found: 118.0268.

2,2-Diethyl-dihydro-furo[3,4-d][1,3]dioxol-4-one (17)

Diol **16** (14.00 g, 0.1186 mol), 3-pentanone (125 mL, 1.186 mol), and *p*-toluenesulfonic acid (2.0 g, catalytic) were dissolved in benzene (150 mL) and refluxed overnight using a Dean–Stark apparatus. The solution was then cooled to room temperature, and the majority of the solvent and excess 3-pentanone were removed by rotary evaporation at a bath temperature of ~50 °C. The remaining brown-coloured oil was distilled under aspirator pressure using a propane burner. The title compound collected as a pale brown oil (20.38 g, 92%) over a fluctuating (the aspirator pressure varied during the distillation) temperature range of 160–200 °C. IR (neat, cm^{-1}) ν: 2976, 2946, 2880, 1785, 1465, 1183, 1107, 1069, 921. ^{1}H NMR (500 MHz, C_6D_6) δ: 4.17–4.19 (m, 1H), 4.02–4.05 (m, 1H), 3.91 (d, *J* = 10.8 Hz, 1H), 3.54–3.58 (m, 1H), 1.41 (q, *J* = 7.5 Hz, 2H), 1.56 (q, *J* = 7.5 Hz, 2H), 0.75 (t, *J* = 7.5 Hz, 3H), 0.86 (t, *J* = 7.5 Hz, 3H). ^{13}C NMR (125 MHz, $CDCl_3$) δ: 174.0 (C), 117.7 (C), 75.6 (CH), 74.7 (CH), 70.3 (CH_2), 29.4 (CH_2), 29.0 (CH_2), 7.9 (CH_3), 7.0 (CH_3). EI-MS *m/z* (%): 157 ([M$^+$ – C_2H_5], 45), 57 (100), 29 (85). HR-MS calcd. for $C_7H_{11}O_4$ ([M$^+$ – C_2H_5]): 157.0501; found: 157.0492.

2,2-Diethyl-tetrahydro-furo[3,4-d][1,3]dioxol-4-ol (14)

Lactone **17** (19.0 g, 0.102 mol) was dissolved in CH_2Cl_2 (285 mL) and cooled to –78 °C. A 1.5 mol/L solution of DIBAL-H in THF (81.6 mL, 0.122 mol) was added dropwise over a period of 15 min, after which the solution was stirred for 5 h at –78 °C. The reaction was quenched at –78 °C with MeOH (16.0 mL) and brine (8.0 mL) and allowed to warm to room temperature. Ether (420 mL) and $MgSO_4$ (121 g) were then added under vigorous stirring, and stirring was continued overnight. The mixture was filtered (suction), and the filter cake was washed generously with ether (~1.0 L) in several portions until the presence of prod-

© 2005 NRC Canada

uct was no longer detected in the filtrate (use of a soxlet extractor to extract the product from the filter cake was also effective). The solvent was removed under reduced pressure to yield a colorless oil identified as a 5:1 mixture of diastereomers of the title compound (16.72 g, 87%). Major diastereomer: IR (neat, cm^{-1}) ν: 3425, 2975, 2943, 2883, 1464, 1102, 1075, 929. ^1H NMR (500 MHz, $CDCl_3$) δ: 5.38 (s, 1H), 4.79 (dd, *J* = 6.0, 3.3 Hz, 1H), 4.53 (d, *J* = 6.0 Hz, 1H), 4.03–3.92 (m, 2H), 3.18 (1H, bs), 1.65 (q, *J* = 7.5 Hz, 2H), 1.54 (q, *J* = 7.5 Hz, 2H), 0.87 (t, *J* = 7.5 Hz, 3H), 0.84 (t, *J* = 7.5 Hz, 3H). ^{13}C NMR (125 MHz, $CDCl_3$) δ: 116.5 (C), 101.9 (CH), 85.3 (CH), 80.2 (CH), 72.1 (CH_2), 29.3 (CH_2), 28.8 (CH_2), 8.3 (CH_3), 7.3 (CH_3). EI-MS *m/z* (%): 159 ([$M^+ - C_2H_5$], 64), 85 (17), 57 (100), 29 (37). HR-MS calcd. for $C_7H_{11}O_4$ ([$M^+ - C_2H_5$]): 159.0657; found: 159.0659.

1-(2,2-Diethyl-5-hydroxymethyl-[1,3]dioxolan-4-yl)-2-vinyl-but-3-en-1-ol (13)

Lactol **14** (5.00 g, 26.56 mmol) was dissolved in DMF (15 mL); the solution was cooled to 0 °C, and 5-bromo-1,3-pentadiene (15.62 g, 106.3 mmol) was added. Indium powder (100 mesh, 6.10 g, 53.13 mmol) was added to the vigorously stirred solution in small portions over a period of 55 min. The dark green mixture was then warmed to room temperature and stirred overnight. The reaction was poured into a vigorously stirred solution of ether (1000 mL) and water (3.2 mL) and stirred for a further 10 min. The mixture was then dried, filtered, and concentrated. Column chromatography (4:1, petroleum ether – ethyl acetate) yielded the title compound as a waxy solid mixture of diastereomers (5.55 g, 82%). Major diastereomer: mp 42.5–44.0 °C. IR (neat, cm^{-1}) ν: 3323, 3245, 2940, 2916, 2880, 1459, 1173, 1081, 920. ^1H NMR (500 MHz, C_6D_6) δ: 6.05–6.14 (m, 2H), 5.06–5.26 (m, 4H), 4.15–4.23 (m, 2H), 3.92 (m, 1H), 3.69–3.74 (m, 1H), 3.56–3.60 (m, 1H), 3.33–3.37 (m, 2H), 2.73 (bs, 1H), 1.57 (q, *J* = 7.5 Hz, 2H), 1.51 (q, *J* = 7.5 Hz, 2H), 0.86 (t, *J* = 7.5 Hz, 3H), 0.82 (t, *J* = 7.5 Hz, 3H). ^{13}C NMR (125 MHz, C_6D_6) δ: 139.6 (CH), 136.1 (CH), 118.4 (CH_2), 116.4 (CH_2), 112.4 (C), 78.0 (CH), 77.7 (CH), 72.7 (CH), 61.9 (CH_2), 51.4 (CH), 30.5 (CH_2), 29.4 (CH_2), 9.2 (CH_3), 8.4 (CH_3). EI-MS *m/z* (%): 227 ([$M^+ - C_2H_5$], 38), 209 (0.2), 159 (11), 87 (100), 57 (87). HR-MS calcd. for $C_{12}H_{19}O_4$ ([$M^+ - C_2H_5$]): 227.1284; found: 227.1283.

1-(2,2-Diethyl-5-triisopropylsilanyloxymethyl-[1,3]dioxolan-4-yl)-2-vinyl-but-3-en-1-ol (18)

Diol **13** (19.01 g, 74.2 mmol) was dissolved in a mixture of DMF (65 mL) and THF (200 mL) and cooled to 0 °C. Imidazole (10.12 g, 148.5 mmol) and triisopropylsilyl chloride (23.83 mL, 111.4 mmol) were added sequentially, and the solution was stirred overnight. Water was then added, and the mixture was extracted with ether. The ether extracts were washed once with saturated NH_4Cl, dried, filtered, and concentrated. Column chromatography (50:1, petroleum ether – ethyl acetate) yielded the title compound as a colorless oil (28.62 g, 93%). Major diastereomer: IR (neat, cm^{-1}) ν: 3467, 2965, 2940, 2867, 1638. ^1H NMR (500 MHz, C_6D_6) δ: 6.31–6.41 (m, 2H), 5.12–5.32 (m, 4H), 4.37–4.41 (m, 1H), 4.29–4.33 (m, 1H), 4.19 (ddd, *J* = 5.5, 2.5, 0.5 Hz, 1H), 4.00 (t, *J* = 10.2 Hz, 1H), 3.96 (dd, *J* = 3.3, 1.3 Hz, 1H), 3.73 (dd, *J* = 10.3, 3.4 Hz, 1H), 3.46 (t, *J* = 7.8 Hz, 1H), 1.64 (dq, *J* = 7.5, 1.5 Hz, 2H), 1.58 (q, *J* = 7.5 Hz, 2H), 0.92–1.00 (m, 21H), 0.93 (t, *J* = 7.5 Hz, 3H), 0.87 (t, *J* = 7.5 Hz, 3H). ^{13}C NMR (125 MHz, C_6D_6) δ: 140.5 (CH), 137.2 (CH), 117.6 (CH_2), 115.6 (CH_2), 112.5 (C), 78.6 (CH), 77.9 (CH), 72.8 (CH), 63.6 (CH), 51.9 (CH), 30.7 (CH_2), 29.4 (CH_2), 18.2_9 (CH_3), 18.2_8 (CH_3), 12.7 (CH), 12.4 (CH), 9.3 (CH_3), 8.5 (CH_3). EI-MS *m/z* (%): 383 ([$M^+ - C_2H_5$], 8), 187 (53), 131 (56), 67 (100). HR-MS calcd. for $C_{21}H_{39}O_4Si$ ([$M^+ - C_2H_5$]): 383.2618; found: 383.2628.

[2,2-Diethyl-5-(2-vinyl-buta-1,3-dienyl)-[1,3]dioxolan-4-ylmethoxy]-triisopropyl-silane (19)

Alcohol **18** (21.99 g, 53.3 mmol) was dissolved in benzene (1.20 L) and cooled to 0 °C, and PPh_3 (41.92 g, 159.8 mmol) and DEAD (25.16 mL, 159.8 mmol) were successively added. The solution was refluxed for two days and the majority of the solvent was removed in vacuo to yield a red oil. A slurry of silica gel (30:1, petroleum ether – ethyl acetate) was then added, and the mixture was quickly filtered through a thin (~7 cm) plug of silica gel to remove the majority of reaction byproducts. The silica gel plug was washed (30:1, petroleum ether – ethyl acetate) until no additional product was detected in the filtrate. The washes were combined and concentrated, and petroleum ether was added, and the triphenylphosphine oxide precipitate was filtered off and discarded. Column chromatography (100:1, petroleum ether – ethyl acetate) yielded the title compound as a colorless oil (9.36 g, 44%). Owing to the instability of the product in common NMR solvents, clean NMR spectra could not be obtained. IR (neat, cm^{-1}) ν: 3089, 2867, 2943, 2867, 1464, 1129, 1087, 939, 883. EI-MS *m/z* (%): 394 ([M]$^+$, 19), 265 (100), 108 (84). HR-MS calcd. for $C_{23}H_{42}O_3Si$ ([M]$^+$): 394.2903; found: 394.2925

[2,2-Diethyl-5-(2-vinyl-buta-1,3-dienyl)-[1,3]dioxolan-4-yl]-methanol (20)

Triene **19** (13.71 g, 34.7 mmol) was dissolved in THF (300 mL), cooled to 0 °C, and a 1.0 mol/L solution of TBAF in THF (41.7 mL, 41.7 mmol) was added dropwise over a period of 2 min. The reaction was stirred at 0 °C for 1 h. Water was added, and the reaction was extracted with ether, dried, filtered, and concentrated. Column chromatography (9:1, petroleum ether – ethyl acetate) yielded the title compound as a clear oil (6.79 g, 82%). IR (neat, cm^{-1}) ν: 3431, 3090, 2975, 2941, 2882, 1604, 1173, 1077, 1041, 927. ^1H NMR (500 MHz, C_6D_6) δ: 6.27 (dd, *J* = 17.4, 10.7 Hz, 1H), 6.23 (dd, *J* = 17.6, 11.2 Hz, 1H), 5.25 (dd, *J* = 17.4, 1.3 Hz, 1H), 5.16 (d, *J* = 17.5 Hz, 1H), 5.10 (d, *J* = 11.2 Hz, 1H), 5.02 (m, 1H), 4.96 (d, *J* = 10.7 Hz, 1H), 4.13 (dd, *J* = 11.5, 7.0 Hz, 1H), 3.47–3.57 (m, 2H), 2.16 (bs, 1H), 1.70 (q, *J* = 7.5 Hz, 2H), 1.58 (q, *J* = 7.5 Hz, 2H), 0.97 (t, *J* = 7.5 Hz, 3H), 0.86 (t, *J* = 7.5 Hz, 3H). ^{13}C NMR (125 MHz, C_6D_6) δ: 141.2 (C), 138.1 (CH), 132.2 (CH), 128.0 (CH), 119.8 (CH_2), 116.4 (CH_2), 113.1 (C), 79.9 (CH), 74.5 (CH), 62.8 (CH_2), 30.3 (CH_2), 29.5 (CH_2), 9.3 (CH_3), 8.5 (CH_3). EI-MS *m/z* (%): 238 ([M]$^+$, 4), 135 (38), 108 (38), 91 (78), 57 (100), 29 (88). HR-MS calcd. for $C_{14}H_{22}O_3$ ([M]$^+$): 238.1569; found: 238.1551.

© 2005 NRC Canada

2,2-Diethyl-5-(2-vinyl-buta-1,3-dienyl)-[1,3]dioxolane-4-carbaldehyde (21)

Triene-ol **20** (1.50 g, 6.29 mmol) was dissolved in CH_2Cl_2 (60 mL), and Dess–Martin reagent (5.45 g, 13.2 mmol) was added. The solution was stirred for 30 min at room temperature, and then water (0.113 mL, 6.29 mmol) was added. A white precipitate formed within a few minutes. After a further 15 min of stirring the reaction was quenched with a 1:1 mixture of 2 mol/L $Na_2S_2O_3$ and sat. $NaHCO_3$, and the reaction was extracted with CH_2Cl_2. The combined organics were dried, filtered, and concentrated. Column chromatography (12:1, petroleum ether – ethyl acetate) yielded the title compound as a clear oil (1.11 g, 74%). IR (neat, cm^{-1}) ν: 3093, 2976, 2942, 2884, 2812, 1736, 1464, 1172, 1075, 924. ^1H NMR (500 MHz, C_6D_6) δ: 9.45 (d, J = 3.5 Hz, 1H), 6.17 (dd, J = 17.4, 10.7 Hz, 1H), 6.16 (dd, J = 17.6, 11.2 Hz, 1H), 5.51 (d, J = 9.0 Hz, 1H), 5.22 (dd, J = 17.6, 1.9 Hz, 1H), 5.20 (dd, J = 17.4, 0.9 Hz, 1H), 5.12 (dd, J = 11.2, 1.7 Hz, 1H), 5.10 (t, J = 8.5 Hz, 1H), 4.94 (dd, J = 10.7, 0.9 Hz, 1H), 4.08 (dd, J = 8.0, 3.5 Hz, 1H), 1.75 (q, J = 7.5 Hz, 2H), 1.48 (q, J = 7.5 Hz, 2H), 0.98 (t, J = 7.5 Hz, 3H), 0.80 (t, J = 7.5 Hz, 3H). ^{13}C NMR (125 MHz, C_6D_6) δ: 199.5 (C), 142.7 (C), 137.7 (CH), 132.0 (CH), 125.7 (CH), 120.6 (CH_2), 117.2 (CH_2), 115.7 (C), 83.5 (CH), 76.2 (CH), 30.2 (CH_2), 29.5 (CH_2), 9.1 (CH_3), 8.5 (CH_3). EI-MS *m/z* (%): 207 ([$M^+ - C_2H_5$], 11), 133 (31), 99 (100), 57 (95), 29 (53). HR-MS calcd. for $C_{12}H_{15}O_3$ ([$M^+ - C_2H_5$]): 207.1021; found: 207.1016.

1-[2,2-Diethyl-5-(2-vinyl-buta-1,3-dienyl)-[1,3]dioxolan-4-yl]-2-methyl-prop-2-en-1-ol (22a)

2-Bromopropene (1.00 mL, 11.26 mmol) was dissolved in THF (10 mL) and added dropwise to a flask containing freshly washed (sequentially with 10% HCl, water, and acetone) and dried magnesium turnings (0.27 g, 11.26 mmol) in THF (10 mL). A small chip of iodine was added to initiate the Grignard reaction. When the Grignard had fully formed (as indicated by the complete consumption of Mg), 1.1 equiv. of it (13.3 mL, 7.49 mmol) was added dropwise to a solution of aldehyde **21** (1.61 g, 6.83 mmol) in THF (90 mL). The resultant pale yellow solution was stirred for 45 min. The reaction was quenched with saturated NH_4Cl, extracted with ether, dried, filtered, and concentrated. Column chromatography (30:1, petroleum ether – ethyl acetate) yielded the title compound as a waxy solid mixture of two diastereomers (1.10 g, 58%). IR (neat, both diastereomers, cm^{-1}) ν: 3422, 3089, 2973, 2941, 1648, 1460, 1172, 1073. Major diastereomer: ^1H NMR (500 MHz, C_6D_6) δ: 6.36 (dd, J = 17.3, 10.7 Hz, 1H), 6.29 (dd, J = 17.6, 11.2 Hz, 1H), 6.13 (d, J = 9.1 Hz, 1H), 5.34 (dd, J = 17.3, 1.5 Hz, 1H), 5.21 (dd, J = 17.7, 1.8 Hz, 1H), 5.14 (ddd, J = 11.2, 1.9, 0.7 Hz, 1H), 5.09 (dd, J = 9.1, 7.3 Hz, 1H), 5.01 (dd, J = 10.7, 1.5 Hz, 1H), 5.01 (quintet, J = 0.9 Hz, 1H), 4.87 (t, J = 1.5 Hz, 1H), 4.10 (dd, J = 7.9, 3.1 Hz, 1H), 2.58 (d, J = 6.9 Hz, 1H), 1.74 (q, J = 7.5 Hz, 2H), 1.73 (s, 3H), 1.58 (q, J = 7.5 Hz, 2H), 0.90 (t, J = 7.5 Hz, 3H), 0.85 (t, J = 7.5 Hz, 3H), (OH not detected). ^{13}C NMR (125 MHz, C_6D_6) δ: 146.0 (C), 141.0 (C), 138.2 (CH), 132.4 (CH), 129.1 (CH), 119.5 (CH_2), 116.5 (CH_2), 113.2 (CH_2), 112.9 (C), 80.5 (CH), 75.0 (CH), 74.1 (CH), 30.0 (CH_2), 28.8 (CH_2), 19.2 (CH_3), 9.3 (CH_3), 8.6 (CH_3). EI-MS (both diastereomers) *m/z* (%): 278 ([$M]^+$, 0.1), 249 (5), 121 (52), 105 (85), 91 (65), 57 (100), 29 (63). HR-MS calcd. for $C_{15}H_{21}O_3$ ([$M^+ - C_2H_5$]): 249.1491; found: 249.1488.

1-[2,2-Diethyl-5-(2-vinyl-buta-1,3-dienyl)-[1,3]dioxolan-4-yl]-2-methyl-propenone (12a)

Allyl alcohol **22a** (1.10 g, 3.96 mmol) was dissolved in CH_2Cl_2 (60 mL), and Dess–Martin reagent (3.35 g, 8.12 mmol) was added. The solution was stirred for 30 min at room temperature, and then water (0.071 mL, 3.96 mmol) was added. A white precipitate formed within a few minutes. After a further 15 min of stirring the reaction was quenched with a solution of 2 mol/L $Na_2S_2O_3$ and saturated $NaHCO_3$ (1:1), and the reaction was extracted with CH_2Cl_2. The solution was dried, filtered, and concentrated. Column chromatography (30:1, petroleum ether – ethyl acetate) yielded the title compound as a clear oil (0.85 g, 78%). IR (neat, cm^{-1}) ν: 3091, 2974, 2942, 2883, 1693, 1463, 1173, 1071, 1056, 930. ^1H NMR (500 MHz, C_6D_6) δ: 6.20 (dd, J = 17.6, 11.2 Hz, 1H), 6.12 (dd, J = 17.3, 10.7 Hz, 1H), 5.58 (d, J = 9.7 Hz, 1H), 5.33 (s, 1H), 5.10–5.23 (m, 6H), 4.88 (d, J = 10.7 Hz, 1H), 2.01 (qd, J = 7.5, 2.4 Hz, 2H), 1.69 (t, J = 0.6 Hz, 3H), 1.65 (q, J = 7.5 Hz, 2H), 1.13 (t, J = 7.5 Hz, 3H), 0.92 (t, J = 7.5 Hz, 3H). ^{13}C NMR (125 MHz, C_6D_6) δ: 196.5 (C), 144.9 (C), 141.3 (C), 137.7 (CH), 132.0 (CH), 127.8 (CH), 124.5 (CH_2), 119.8 (CH_2), 117.0 (CH_2), 115.3 (C), 80.3 (CH), 75.0 (CH), 30.5 (CH_2), 29.6 (CH_2), 18.3 (CH_3), 9.3 (CH_3), 8.9 (CH_3). EI-MS *m/z* (%): 276 ([$M]^+$, 0.2), 247 (11), 139 (50), 69 (100), 57 (44), 41 (58), 29 (33). HR-MS calcd. for $C_{15}H_{19}O_3$ ([$M^+ - C_2H_5$]): 247.1334; found: 247.1334.

1-[2,2-Diethyl-5-(2-vinyl-buta-1,3-dienyl)-[1,3]dioxolan-4-yl]-2-ethyl-prop-2-en-1-ol (22b)

The title compound was prepared by a method analogous to that used to prepare the methyl analogue (**22a**), except that *iso*-butenylmagnesium bromide was used as the Grignard reagent. (53% yield). IR (neat, both diastereomers, cm^{-1}) ν: 3475, 3089, 2971, 2940, 2882, 1463, 1172, 1074, 1056, 928. Major diastereomer: ^1H NMR (500 MHz, C_6D_6) δ: 6.33 (ddd, J = 17.3, 10.7, 0.6 Hz, 1H), 6.26 (dd, J = 17.5, 11.2 Hz, 1H), 6.10 (d, J = 9.1 Hz, 1H), 5.32 (dd, J = 17.4, 1.5 Hz, 1H), 5.19 (dd, J = 17.3, 1.9 Hz, 1H), 5.05–5.13 (m, 3H), 4.98 (dd, J = 10.7, 1.5 Hz, 1H), 4.89 (m, 1H), 4.21 (dd, J = 7.3, 3.9 Hz, 1H), 4.10–4.13 (m, 1H), 2.08–2.16 (m, 1H), 1.93–2.01 (m, 1H), 1.72 (q, J = 7.5 Hz, 2H), 1.57 (q, J = 7.5 Hz, 2H), 0.97 (t, J = 7.5 Hz, 3H), 0.96 (t, J = 7.5 Hz, 3H), 0.83 (t, J = 7.5 Hz, 3H) (OH not detected). ^{13}C NMR (125 MHz, C_6D_6) δ: 151.2 (C), 140.9 (C), 138.2 (CH), 132.4 (CH), 129.2 (CH), 119.4 (CH_2), 116.4 (CH_2), 112.9 (CH_2), 110.9 (C), 80.6 (CH), 75.0 (CH), 73.7 (CH), 30.1 (CH_2), 28.9 (CH_2), 25.7 (CH_2), 12.7 (CH_3), 9.3 (CH_3), 8.6 (CH_3). EI-MS (both diastereomers) *m/z* (%): 263 ([$M^+ - C_2H_5$], 3), 149 (34), 121 (54), 105 (74), 91 (61), 57 (100), 29 (79). HR-MS calcd. for $C_{16}H_{23}O_3$ ([$M^+ - C_2H_5$]): 263.1647; found: 263.1664.

1-[2,2-Diethyl-5-(2-vinyl-buta-1,3-dienyl)-[1,3]dioxolan-4-yl]-2-ethyl-propenone (12b)

The title compound was prepared by a method analogous to that used to prepare the methyl analogue (**12a**) (72%

© 2005 NRC Canada

yield). IR (neat, cm^{-1}) ν: 3091, 2973, 2940, 2882, 1692, 1463, 1173, 1078, 930. ^{1}H NMR (500 MHz, C_6D_6) δ: 6.20 (dd, *J* = 17.6, 11.2 Hz, 1H), 6.12 (ddd, *J* = 17.4, 10.7, 0.6 Hz, 1H), 5.59 (d, *J* = 9.6 Hz, 1H), 5.40 (s, 1H), 5.10–5.25 (m, 6H), 4.88 (dd, *J* = 10.6, 1.5 Hz, 1H), 2.19 (qq, *J* = 7.5, 0.8 Hz, 2H), 2.01 (dq, *J* = 7.5, 2.4 Hz, 2H), 1.65 (dq, *J* = 7.5, 1.1 Hz, 2H), 1.13 (t, *J* = 7.5 Hz, 3H), 0.92 (t, *J* = 7.5 Hz, 3H), 0.84 (t, *J* = 7.5 Hz, 3H). ^{13}C NMR (125 MHz, C_6D_6) δ: 196.2 (C), 150.5 (C), 141.2 (C), 137.8 (CH), 132.1 (CH), 127.9 (CH), 123.2 (CH_2), 119.9 (CH_2), 116.9 (CH_2), 115.2 (C), 80.2 (CH), 75.1 (CH), 30.5 (CH_2), 29.7 (CH_2), 24.9 (CH_2), 13.0 (CH_3), 9.3 (CH_3), 8.9 (CH_3). EI-MS *m/z* (%): 290 ([M]$^+$, 0.1), 261 (6), 153 (28), 83 (100), 55 (73), 29 (62). HR-MS calcd. for $C_{16}H_{21}O_3$ ([$M^+ - C_2H_5$]): 261.1491; found: 261.1508.

Diels–Alder adducts 23, 24, 25

Diels–Alder precursor **12a** (0.051 g, 0.185 mmol) was dissolved in toluene (20 mL), and the solution was purged with argon for 20 min. The solution was then placed in the microwave oven (program: 300 W power, ramp temperature to 150 °C in 15 min, then hold at 150 °C for 3 h). After allowing the reaction to cool to rt, the toluene was removed under reduced pressure. Column chromatography (20:1, petroleum ether – ethyl acetate) afforded a 41:20:39 mixture of Diels–Alder adducts (0.039 g, 78%) (Table 1, entry 12). A pure sample of each isomer was obtained by exhaustive preparative HPLC (2% hexanes in ethyl acetate; Waters Nova-Pak 19 × 300 mm silica (6 μm) column).

(1R,2S,6S,8R)-4,4-Diethyl-8-methyl-11-vinyl-3,5-dioxa-tricyclo[6.3.1.0^{2,6}]dodec-10-en-7-one (23)

T_r = 64.5 min. ^{1}H NMR (500 MHz, C_6D_6) δ: 6.08 (dd, *J* = 17.7, 10.9 Hz, 1H), 5.26 (dd, *J* = 4.3, 4.3 Hz, 1H), 5.16 (d, *J* = 17.7 Hz, 1H), 4.87 (d, *J* = 10.9 Hz, 1H), 4.49 (dt, *J* = 6.3, 2.2 Hz, 1H), 3.95 (d, *J* = 6.3 Hz, 1H), 3.00 (d, *J* = 2.2 Hz, 1H), 2.37 (dt, *J* = 13.2, 1.9 Hz, 1H), 1.96 (dd, *J* = 19.6, 4.6 Hz, 1H), 1.71 (q, *J* = 7.6 Hz, 2H), 1.65 (dd, *J* = 19.6, 1.1 Hz, 1H), 1.50 (qd, *J* = 7.6, 2.4 Hz, 1H), 1.22 (ddd, *J* = 13.2, 3.6, 1.8 Hz, 1H), 1.10 (s, 3H), 0.98 (t, *J* = 7.6 Hz, 3H), 0.81 (t, *J* = 7.6 Hz, 1H). ^{13}C NMR (125 MHz, C_6D_6) δ: 210.8 (C), 137.6 (CH), 136.9 (C), 130.2 (CH), 114.5 (C), 111.3 (CH_2), 78.8 (CH), 77.4 (CH), 43.1 (C), 38.2 (CH_2), 32.6 (CH), 30.7 (CH_2), 29.8 (CH_2), 28.5 (CH_2), 25.0 (CH_3), 8.7 (CH_3), 8.6 (CH_3). EI-MS *m/z* (%): 276 ([M]$^+$, 1), 247 (77), 191 (19), 145 (38), 119 (54), 105 (27), 91 (15), 57 (100). HR-MS calcd. for $C_{15}H_{19}O_3$ ([$M^+ - C_2H_5$]): 247.1334; found: 247.1314.

(3aS,3bR,7aS,8aS)-2,2-Diethyl-7a-methyl-4-vinyl-7,7a-dihydro-3aH-indeno[2,1-d][1,3]dioxol-8(3bH,6H,8aH)-one (24)

T_r = 70.0 min. ^{1}H NMR (500 MHz, C_6D_6) δ: 6.26 (dd, *J* = 17.7, 11.1 Hz, 1H), 5.66 (d, *J* = 17.7 Hz, 1H), 5.49 (t, *J* = 4.3 Hz, 1H), 5.06 (d, *J* = 11.1 Hz, 1H), 4.29 (dd, *J* = 6.9, 2.8 Hz, 1H), 4.23 (dd, *J* = 6.9, 0.5 Hz, 1H), 2.80 (br s, 1H), 1.65 (q, *J* = 7.5 Hz, 2H), 1.70–1.53 (m, 2H), 1.47 (q, *J* = 7.5 Hz, 2H), 1.22 (ddd, *J* = 13.0, 8.4, 5.5 Hz, 1H), 1.10 (s, 3H), 0.97–0.93 (m, 1H), 0.93 (t, *J* = 7.5 Hz, 3H), 0.81 (t, *J* = 7.5 Hz, 3H). ^{13}C NMR (125 MHz, C_6D_6) δ: 215.6 (C), 138.7 (CH), 136.0 (C), 130.0 (CH), 116.8 (C), 112.8 (CH_2), 80.7 (CH), 79.7 (CH), 48.7 (C), 46.6 (CH), 30.0 (CH_2), 29.8 (CH_2), 29.2 (CH_2), 22.0 (CH_2), 22.0 (CH_3), 8.6 (CH_3), 8.2 (CH_3). EI-MS *m/z* (%): 276 ([M]$^+$, 2), 247 (44), 191 (8), 162 (12), 145 (34), 119 (100), 105 (24), 57 (50), 43 (32). HR-MS calcd. for $C_{17}H_{24}O_3$ ([M]$^+$): 276.1725; found: 276.1748.

(3aS,3bR,7aR,8aS)-2,2-Diethyl-7a-methyl-4-vinyl-7,7a-dihydro-3aH-indeno[2,1-d][1,3]dioxol-8(3bH,6H,8aH)-one (25)

T_r = 72.0 min. ^{1}H NMR (500 MHz, C_6D_6) δ: 6.37 (ddd, *J* = 17.8, 11.5, 0.8 Hz, 1H), 5.93 (d, *J* = 17.8 Hz, 1H), 5.39 (d, *J* = 3.3 Hz, 1H), 5.06 (d, *J* = 11.5 Hz, 1H), 4.59 (ddd, *J* = 7.6, 7.6, 1.4 Hz, 1H), 4.49 (d, *J* = 7.6 Hz, 1H), 2.67 (br dd, *J* = 8.3, 2.9 Hz, 1H), 1.84–1.74 (m, 2H), 1.63 (qd, *J* = 7.6, 2.9 Hz, 2H), 1.60–1.57 (m, 1H), 1.51–1.45 (m, 1H), 1.46 (q, *J* = 7.6 Hz, 2H), 0.92 (t, *J* = 7.6 Hz, 3H), 0.81 (t, *J* = 7.6 Hz, 3H), 0.58 (s, 3H). ^{13}C NMR (125 MHz, C_6D_6) δ: 208.6 (C), 137.5 (CH), 135.4 (C), 127.9 (CH), 118.5 (C), 113.6 (CH_2), 79.9 (CH), 77.4 (CH), 51.8 (C), 50.8 (CH), 29.5 (CH_2), 29.3 (CH_2), 28.3 (CH_2), 23.4 (CH_2), 15.3 (CH_3), 8.7 (CH_3), 7.8 (CH_3). EI-MS *m/z* (%): 276 ([M]$^+$, 0.1), 247 (38), 181 (30), 145 (16), 119 (46), 99 (14), 43 (100). HR-MS calcd. for $C_{15}H_{19}O_3$ ([$M^+ - C_2H_5$]): 247.1334; found: 247.1342.

Conclusions

Twenty years ago we commented that the then-current literature indicated that, for the synthesis of bicycle[4.3.0]nonenones from intramolecular Diels–Alder reactions, the following applied: "The ring fusion is determined by a complex interplay of conformational, steric, and electronic effects that may vary independently" (12). Clearly this still applies! We have discovered that, contrary to our expectations based on studies in the decalin series, these relatively flat tetraenes follow a novel pathway in which the *trans*-adduct bicycle[4.3.0]nonenone was not generated but instead the bicyclo[3.3.1]nonenone skeleton was formed preferentially at 150 °C in toluene in a microwave oven. At lower temperatures, the fused-ring hydrindenone products dominated, but the bridged-ring product was still produced. Indeed, once we understand more about nuances that control these competing reactions it may be possible to direct the product to either the fused- or bridged-ring pathway from related tetraenes. A contributing factor to begin to achieve this control is to examine the size and nature of the R group. Unfortunately, the adduct mixture from the synthesis made further study impractical, despite the attraction of generating the steroid framework from a second cycloaddition. Possibly future investigations, with simpler and (or) sterically more demanding dienophile–diene combinations, may permit the stereoselective synthesis of functionalized hydrindanes in this manner.

Acknowledgements

We are grateful to the Natural Sciences and Engineering Research Council of Canada (NSERC) for financial support of this research. M. Clay thanks NSERC, the Ontario Graduate Scholarship Program, and the University of Ottawa for Graduate Scholarships. D. Riber thanks the University of Aarhus for a visiting fellowship. Preliminary experiments by A. Melekhov and S. Graham are also acknowledged. We

© 2005 NRC Canada

thank K. Fagnou for use of his chiral columns and the referees for their suggestions.

References

1. (*a*) E.J. Corey and A.X. Huang. J. Am. Chem. Soc. **121**, 710 (1999); (*b*) Q.-Y. Hu, P.D. Rege, and E.J. Corey. J. Am. Chem. Soc. **126**, 5984 (2004).
2. (*a*) C. Martin, N. Macintosh, N. Lamb, and A.G. Fallis. Org. Lett. **3**, 1021 (2001); (*b*) A. Melekhov, P. Forgione, S. Legoupy, and A.G. Fallis. Org. Lett. **2**, 2793 (2000); T. Wong, P.D. Wilson, S. Woo, and A.G. Fallis. Tetrahedron Lett. **38**, 7045 (1997).
3. S. Woo, S. Legoupy, S. Parra, and A.G. Fallis. Org. Lett. **1**, 1013 (1999).
4. S. Woo, N. Squires, and A.G. Fallis. Org. Lett. **1**, 573 (1999).
5. D. Kim and Y.K. Lee. Tetrahedron Lett. **32**, 6885 (1991).
6. B.B. Snider and T.C. Kirk. J. Am. Chem. Soc. **105**, 2364 (1983).
7. (*a*) S.A. Bal and P. Helquist. Tetrahedron Lett. **22**, 3933 (1981); (*b*) M.E. Jung and K.M. Halweg. Tetrahedron Lett. **22**, 3929 (1981); (*c*) J. Shiina and S. Nishiyama. Tetrahedron, **59**, 6039 (2003).
8. J. Endrikat, M. Cronin, C. Gerlinger, A. Ruebig, W. Schmidt, and B. Dusterberg. Contraception, **64**, 201 (2001).
9. A.B. Northrup and D.W.C. MacMillan. J. Am. Chem. Soc. **124**, 2458 (2002).
10. N. Cohen, B.L. Banner, A.J. Laurenzano, and L. Carozza. Org. Synth. **63**, 127 (1984).
11. S.D. Meyer and S.L. Schreiber. J. Org. Chem. **59**, 7549 (1994).
12. A.G. Fallis. Can. J. Chem. **62**, 183 (1984).

© 2005 NRC Canada

Pd(0)–PhCOOH catalyzed addition of oxygen pronucleophiles to allenes and internal alkynes[1]

Nitin T. Patil, Nirmal K. Pahadi, and Yoshinori Yamamoto

Abstract: We have developed a catalytic system that enables the addition of alcohols to allenes using a combination of 5 mol% $Pd(PPh_3)_4$ and 10 mol% benzoic acid. Likewise, the addition reaction of carboxylic acids to alkynes is described. In all cases the reaction proceeded well, giving the corresponding allylation products in good-to-high yields with high regio- and stereoselectivities.

Key words: addition, alcohols, carboxylic acids, allenes, alkynes, palladium.

Résumé : Nous avons développé un système catalytique qui utilise une combinaison de 5 mol% de $Pd(PPh_3)_4$ et de 10 mol% d'acide benzoïque et qui permet de réaliser l'addition d'alcools à des allènes. On décrit aussi la réaction d'addition d'acides carboxyliques à des alcynes. Dans tous les cas, la réaction se produit bien et conduit aux produits d'allylation correspondants avec des rendements allant de bons à élevés et avec des régio- et stéréosélectivités élevées.

Mots clés : addition, alcools, acides carboxyliques, allènes, alcynes, palladium.

[Traduit par la Rédaction]

Introduction

Transition metal catalyzed addition of nucleophiles to activated C—C bonds is one of the most important processes in organic synthesis. The addition of carbon pronucleophiles to activated C—C bonds is commonly referred to as a hydrocarbonation (1) reaction. Likewise, the addition reactions of amines and alcohols across an activated C—C bond are referred to as hydroamination (2) and hydroalkoxylation (3), respectively. All these processes are very important from the synthetic point of view because, in principle, the addition reactions can be performed with 100% atom efficiency, without any waste formation, and for this reason they fulfill the requirements of green chemistry, in contrast to substitution reactions. Although tremendous amounts of related work have been carried out in the field of hydrocarbonation and hydroamination reactions, very few reports have been found for the hydroalkoxylation and hydrocarboxylation reactions, partly because of the diminished nucleophilicity and the softer Lewis base character of oxygen nucleophiles as compared with amines.

Our interest in these type of addition reactions has prompted us to investigate a catalytic system for the addition of carbon and nitrogen pronucleophiles to allenes (2*a*, 4). As part of our ongoing interest in this area, we extended this approach to the intermolecular addition of carboxylic acids (5) to allenes (eq. [1]). In the latter case, it was found that the reaction was completed in a shorter time period (4 h), giving the allylation products in high yields with high stereo- and regioselectivity, in contrast to the previously reported cases (4) wherein the addition of carbon nucleophiles proceeded but the products were obtained in lower yields and consisted of a mixture of *E* and *Z* stereoisomers. This difference in reaction pathways in the case of carboxylic acid pronucleophiles and carbon pronucleophiles prompted us to study the catalytic system closely. To our delight, we found that, in this palladium catalyzed reaction, the addition of a catalytic amount of carboxylic acid is crucial for obtaining the allylation products in high yields and in a regio- and stereoselective manner. Our unique finding (Pd(0)–RCOOH combined catalyst) has also been successfully applied to the addition of nitrogen (6) and carbon (7) nucleophiles. However, the addition of alcohols to allenes under the newly developed procedure remains to be disclosed.

The addition of various pronucleophiles to alkynes is also a subject of interest in our laboratory (8). We recently reported a new approach for the allylation of carbon (8*a*–8*d*) and nitrogen (8*d*–8*g*) pronucleophiles with alkynes in the presence of a Pd(0)–carboxylic acid combined catalyst. Later we communicated the formal addition of alcohol to alkynes (eq. [2]) (8*h*). However, the addition of carboxylic acid to alkynes has not been addressed until now by our group. In the meantime, Zhang et al. (9) reported the addition of oxygen nucleophiles to alkynes using the catalytic system developed by us without citing our (8*h*) reference. In this paper we report, in detail, our efforts in the successful implementation of our newly developed Pd(0)–PhCOOH combined catalyst system for the addition of alcohols to

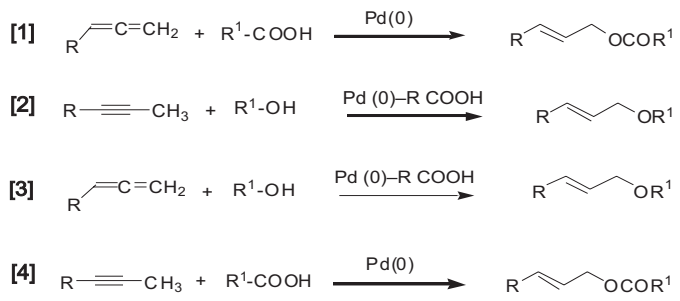
Received 17 November 2004. Published on the NRC Research Press Web site at http://canjchem.nrc.ca on 2 June 2005.

N.T. Patil, N.K. Pahadi, and Y. Yamamoto.[2] Department of Chemistry, Graduate School of Science, Tohoku University, Sendai 980-8578, Japan.

[1]This article is part of a Special Issue dedicated to Professor Howard Alper.
[2]Corresponding author (e-mail: yoshi@yamamoto1.chem.tohoku.ac.jp).

 doi: 10.1139/V05-043 © 2005 NRC Canada

allenes (eq. [3]) and the addition of carboxylic acids to alkynes in a regio- and stereoselective manner (eq. [4]).



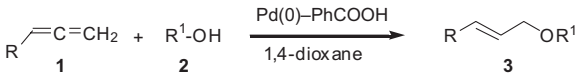
Results and discussion

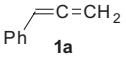
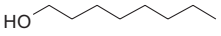
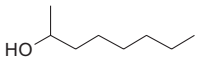
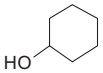
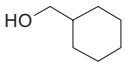
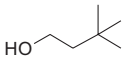
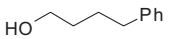
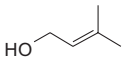
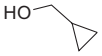
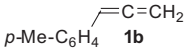
Heating a mixture of phenyl allene **1a** and acetic acid in the presence of Pd_2dba_3·$CHCl_3$ and dppf in THF at 80 °C for 4 h under argon resulted in the formation of cinnamyl acetate in 83% yield, with excellent regio- and stereoselectivity (eq. [1], R = Ph, R^1 = CH_3) (5). However, when phenyl allene was treated with carbon pronucleophiles (for instance, methylmalononitrile) under similar conditions, the reaction time was increased to 48 h (4*a*). Moreover, in most cases, the products were obtained in lower yields and consisted of a mixture of *E* and *Z* stereoisomers. At this stage the exact reason behind the superiority of the addition of carboxylic acid pronucleophiles to allenes over carbon pronucleophiles was not known. After detailed investigation into the reaction, we found that the combination of Pd(0) and carboxylic acid was best (see mechanistic part mentioned later). A dramatic change was observed when a catalytic amount of a carboxylic acid was introduced into the reaction system. The discovery of the unique role of a carboxylic acid as an additive allowed us to perform the addition of nitrogen (6) and carbon (7) nucleophiles to allenes in a highly stereo- and regioselective manner and in a shorter time. As a part of our continuing interest in this area, we then decided to study the intermolecular addition of alcohols to allenes. The results are summarized in Table 1.

Treatment of phenyl allene **1a** with benzyl alcohol **2a** under standard conditions gave the corresponding allylation product **3a** in 71% yield (entry 1). Likewise, in the hydrocarbonation (7) and hydroamination (6) of allenes, the reaction of phenyl allene **1a** with various alcohols proceeded smoothly to afford the products **3b**–**3j** in good yields (entries 2–10). Substituents such as -CH_3 and -F in the aromatic nucleus of allenes do not affect the efficiency of the reaction. Thus, when **1b** and **1c** were treated with benzyl alcohol, the corresponding allylation products **3k** and **3l** were obtained in 68% and 72% yield, respectively (entries 11 and 12).

Next, we turned our attention towards the addition of carboxylic acids to alkynes. A mixture of 1-phenyl-1-propyne (**4a**) and acetic acid (1.5 equiv.) in the presence of $Pd(PPh_3)_4$ (5 mol%) was heated in 1,4-dioxane at 100 °C for 12 h. As anticipated, the starting materials were completely consumed, giving the allylation product **6a** in 81% isolated yield as a single stereoisomer (Table 2, entry 1) (8*a*). Other acids such as 2-furoic acid (**5b**), hexanoic acid (**5c**), 1-naphthoic acid (**5d**), and 2,2-diphenylacetic acid (**5e**) reacted

Table 1. Addition of alcohols to allenes.



Entry	Allene (**1**)	Alcohol (**2**)	Product (**3**)	Yield (%)[a]
1	 **1a**	BnOH	**3a**	71
2	**1a**		**3b**	70
3	**1a**		**3c**	75
4	**1a**		**3d**	71
5	**1a**		**3e**	75
6	**1a**		**3f**	79
7	**1a**		**3g**	70
8	**1a**		**3h**	75
9	**1a**		**3i**	65
10	**1a**		**3j**	75
11	 **1b**	BnOH	**3k**	68
12	 **1c**	BnOH	**3l**	72

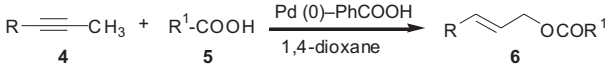
Note: All reactions were carried out as per the general procedure described in the Experimental section.
[a]Isolated yields.

well with alkyne **4a**, giving the corresponding allylation products in high yields (entries 2–5). The aryl alkynes bearing -OMe and -Cl substituents at the *para* position, **4b** and **4c**, reacted well with **5e** and **5c** to give the products **6f** and **6g**, respectively, in excellent yields (entries 6 and 7).

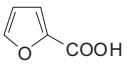
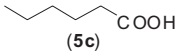
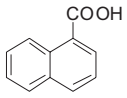
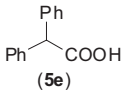
The mechanism of this reaction is presumably similar to those reported previously (8) and is shown in Fig 1. The initial step is the hydropalladation of alkynes **4** with the hydridopalladium species **8** generated from Pd(0) and benzoic acid (catalytic cycle I). The resulting vinyl palladium species **7** would produce phenyl allene **1** and the active catalyst **8** via β-elimination. Hydropalladation of **1** with **8** presumably gives the π-allylpalladium species **9**, which reacts with alcohols and carboxylic acids to give allylation products, along with the hydridopalladium species **8** (cycle II). In

© 2005 NRC Canada

Table 2. Addition of carboxylic acids to alkynes.



4 5 6

Entry	Alkyne (**4**)	R^1COOH(**5**)	Product (**6**)	Yield (%)[a]
1	**4a** R = C_6H_5	CH_3COOH (**5a**)	**6a**	81
2	**4a**	 (**5b**)	**6b**	75
3	**4a**	 (**5c**)	**6c**	90
4	**4a**	 (**5d**)	**6d**	90
5	**4a**	 (**5e**)	**6e**	83
6	**4b** R = C_6H_4-*p*-OMe	**5e**	**6f**	95
7	**4c** R = C_6H_4-*p*-Cl	**5c**	**6g**	90

Note: All reactions were carried out as per the general procedure described in the Experimental section.

[a]Isolated yields.

short, in the case of alkynes both cycles I and II operate, while in the case of allenes only cycle II operates.

In conclusion, the Pd(0)–benzoic acid catalyzed allylation of alcohols and carboxylic acids with allenes and alkynes provides a new route to allyl ethers and allyl carboxylates, respectively. Although we proposed that a role of the carboxylic acid in this catalytic system would be the formation of the hydridopalladium species (8), the precise nature and a more detailed investigation on the catalytic species should be carried out in future (10).

Experimental section

General procedure for the addition of oxygen pronucleophiles to allenes–alkynes

To a mixture of phenyl allene – 1-phenyl-1-propyne (0.4304 mmol), alcohols – carboxylic acids (0.6456 mmol), and tetrakis(triphenylphosphine)palladium (0.022 mmol) in dry 1,4-dioxane (2 mL) was added acetic acid (0.043 mmol), and the mixture was stirred at 100 °C for 12 h in a screw-capped vial. The reaction mixture was then filtered through a short silica gel column using ether as an eluent, and the filtrate was concentrated. The residue was purified by recycling preparative HPLC (LC-918), using chloroform as an eluent to give the allylated products. Structures of **3a**–**3e** (8*h*), **3g** and **3h** (8*h*), **3j** (8*h*), **6a** (9), and **6b** (11) are known in the literature. The characterization data for the newly synthesized compounds **3f**, **3i**, **3k**, **3l**, and **6c**–**6g** are given below.

3f

IR (neat) (cm^{-1}): 1615. ^1H NMR ($CDCl_3$, 400 MHz) δ: 7.40–7.20 (m, 5H), 6.60 (d, *J* = 16.1 Hz, 1H), 6.30 (dt, *J* = 16.1, 6.1 Hz, 1H), 4.13 (dd, *J* = 6.1, 1.5 Hz, 2H), 3.55 (t, *J* = 7.6 Hz, 2H), 1.58 (t, *J* = 7.6 Hz, 2H), 0.92 (s, 9H). ^{13}C NMR ($CDCl_3$, 100 MHz) δ: 136.6, 131.9, 128.4, 127.5, 126.4, 71.5, 67.8, 43.1, 29.8, 29.7. HR-MS calcd. for $C_{15}H_{22}O$ ($[M]^+$): 218.1671; found: 218.1665.

3i

IR (neat) (cm^{-1}): 1622. ^1H NMR ($CDCl_3$, 400 MHz) δ: 7.40–7.21 (m, 5H), 6.60 (d, *J* = 15.8 Hz, 1H), 6.30 (dt, *J* = 15.8, 6.01 Hz, 1H), 4.16 (dd, *J* = 6.01, 1.4 Hz, 2H), 3.33 (d, *J* = 6.8 Hz, 2H), 1.16–1.06 (m, 1H), 0.62–0.51 (m, 2H), 0.26–0.22 (m, 2H). ^{13}C NMR ($CDCl_3$, 100 MHz) δ: 136.7, 132.2, 128.4, 127.5, 126.4, 126.3, 75.1, 71.2, 10.8. HR-MS calcd. for $C_{13}H_{16}O$ ($[M]^+$): 188.1201; found: 188.1196.

3k

IR (neat) (cm^{-1}): 1606. ^1H NMR ($CDCl_3$, 400 MHz) δ: 7.35–7.01 (m, 9H), 6.55 (d, *J* = 15.8 Hz, 1H), 6.25 (dt, *J* = 15.8, 6.1 Hz, 1H), 4.5 (s, 2H), 4.15 (dd, *J* = 6.1, 1.2 Hz, 2H), 2.30 (s, 3H). ^{13}C NMR ($CDCl_3$, 100 MHz) δ: 138.2, 137.4, 133.8, 132.5, 129.2, 128.3, 127.7, 127.5, 126.3, 124.9, 72.0, 70.9, 21.3. HR-MS calcd. for $C_{17}H_{18}O$ ($[M]^+$): 238.1358; found: 238.1352.

3l

IR (neat) (cm^{-1}): 1606. ^1H NMR ($CDCl_3$, 400 MHz) δ: 7.29–7.21 (m, 7H), 6.92 (t, *J* = 8.8 Hz, 2H), 6.51 (d, *J* = 16.1 Hz, 1H), 6.11 (dt, *J* = 16.1, 5.9 Hz, 1H), 4.50 (s, 2H), 4.10 (dd, *J* = 5.9, 1.5 Hz, 2H). ^{13}C NMR ($CDCl_3$, 100 MHz) δ: 163.5, 138.1, 132.8, 131.2, 128.4, 127.9, 127.9, 127.7, 127.6, 125.7, 115.5, 72.3, 70.7. HR-MS calcd. for $C_{16}H_{15}FO$ ($[M]^+$): 242.1107; found: 242.1101.

6c

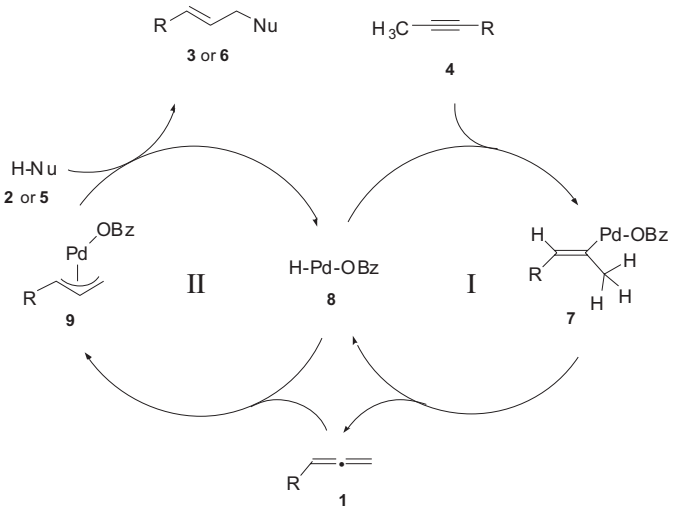
IR (neat) (cm^{-1}): 1735, 1598. ^1H NMR ($CDCl_3$, 400 MHz) δ: 7.35–7.11 (m, 5H), 6.56 (d, *J* = 15. 9 Hz, 1H), 6.20 (dt, *J* = 15.9, 6.3 Hz, 1H), 4.65 (dd, *J* = 6.3, 2.0 Hz, 2H), 2.27 (t, *J* = 7.5 Hz, 2H), 1.62–1.51 (m, 2H), 1.28–1.19 (m, 4H), 0.82 (t, *J* = 6.9 Hz, 3H). ^{13}C NMR ($CDCl_3$, 100 MHz) δ: 173.5, 136.2, 133.9, 128.5, 127.9, 126.5, 123.3, 64.8, 34.3, 31.4, 24.7, 22.4, 13.9. HR-MS calcd. for $C_{15}H_{20}O_2$ ([M + Na]): 255.1355; found: 255.1356.

6d

IR (neat) (cm^{-1}): 1708, 1620. ^1H NMR ($CDCl_3$, 400 MHz) δ: 8.51 (s, 1H), 7.96 (dd, *J* = 8.6, 1.5 Hz, 1H), 7.78 (d, *J* = 8.0 Hz, 1H), 7.70 (t, *J* = 8.32 Hz, 2H), 7.43–7.06 (m, 7H), 6.62 (d, *J* = 15.7 Hz, 1H), 6.30 (dt, *J* = 15.7, 6.3 Hz, 1H), 4.88 (dd, *J* = 6.3, 1.0 Hz, 2H). ^{13}C NMR ($CDCl_3$, 100 MHz) δ: 166.3, 136.1, 135.4, 134.2, 132.3, 130.9, 129.2, 128.6, 128.5, 128.3, 128.1, 127.9, 127.6, 127.3, 126.5, 126.4, 125.1, 123.2, 65.6. HR-MS calcd. for $C_{20}H_{16}O_2$ ([M + Na]): 311.1045; found: 311.1043.

© 2005 NRC Canada

Fig. 1. A mechanism for the addition of *O*-nucleophiles to allenes and alkynes.



6e

IR (neat) (cm^{-1}): 1732, 1598. ^1H NMR ($CDCl_3$, 400 MHz) δ: 7.27–7.15 (m, 15H), 6.49 (d, *J* = 15.9 Hz, 1H), 6.17 (dt, *J* = 15.9, 6.3 Hz, 1H), 4.50 (s, 1H), 4.72 (dd, *J* = 6.3, 1.2 Hz, 2H). ^{13}C NMR ($CDCl_3$, 100 MHz) δ: 172.1, 138.5, 136.1, 134.1, 128.6, 128.5, 128.4, 127.9, 127.2, 126.5, 122.8, 65.6, 57.1. HR-MS calcd. for $C_{23}H_{20}O_2$ ([M + Na]): 351.1354; found: 351.1356.

6f

IR (neat) (cm^{-1}): 1732, 1606. ^1H NMR ($CDCl_3$, 400 MHz) δ: 7.24–7.12 (m, 12 H), 6.72 (d, *J* = 8.8 Hz, 2H), 6.41 (d, *J* = 15.8 Hz, 1H), 6.00 (dt, *J* = 15.8, 6.6 Hz, 1H), 4.96 (s, 1H), 4.66 (dd, *J* = 6.6, 1.0 Hz, 2H), 3.64 (s, 3H). ^{13}C NMR ($CDCl_3$, 100 MHz) δ: 172.1, 159.4, 138.5, 133.9, 128.8, 128.5, 128.4, 127.7, 127.1, 120.4, 113.9, 65.9, 57.0, 55.2. HR-MS calcd. for $C_{24}H_{22}O_3$ ([M + Na]): 381.1569; found: 381.1584.

6g

IR (neat) (cm^{-1}): 1735, 1633. ^1H NMR ($CDCl_3$, 400 MHz) δ: 7.32–7.25 (m, 4H), 6.59 (d, *J* = 15.9 Hz, 1H), 6.26 (dt, *J* = 15.9, 6.3 Hz, 1H), 4.72 (dd, *J* = 6.3, 1.2 Hz, 2H), 2.35 (t, *J* = 7.6 Hz, 2H), 1.69–1.56 (m, 2H), 1.36–1.27 (m, 4H), 0.89 (t, *J* = 6.8 Hz, 3H). ^{13}C NMR ($CDCl_3$, 100 MHz) δ: 173.4, 134.7, 133.6, 132.6, 128.7, 127.7, 124.0, 64.6, 34.3, 31.4, 24.7, 22.4, 13.9. HR-MS calcd. for $C_{15}H_{19}ClO_2$ ([M + O + Na]): 305.0914; found: 305.0915.

Acknowledgements

N.T.P. thanks the Japan Society for the Promotion of Science (JSPS) for a postdoctoral research fellowship.

References

1. (*a*) Y. Yamamoto and U. Radhakrishnan. Chem. Soc. Rev. **28**, 199 (1999), and refs. therein; (*b*) I. Nakamura, G.B. Bajracharya, and Y. Yamamoto. J. Org. Chem. **68**, 2297 (2003); (*c*) B.H. Oh, I. Nakamura, and Y. Yamamoto. Tetrahedron Lett. **43**, 9625 (2002); (*d*) N. Tsukada, A. Shibuya, I. Nakamura, and Y. Yamamoto. J. Am. Chem. Soc. **119**, 8123 (1997); (*e*) N. Tsukada, A. Shibuya, I. Nakamura, H. Kitahara, and Y. Yamamoto. Tetrahedron, **55**, 8833 (1999); (*f*) A. Leitner, J. Larsen, C. Steffens, and J.F. Hartwig. J. Org. Chem. **69**, 7552 (2004).
2. (*a*) M. Meguro and Y. Yamamoto. Tetrahedron Lett. **39**, 5421 (1998); (*b*) U. Radhakrishnan, M. Al-Masum, and Y. Yamamoto. Tetrahedron Lett. **39**, 1037 (1998); (*c*) L. Besson, J. Gore, and B. Cazes. Tetrahedron Lett. **36**, 3857 (1995); (*d*) R.W. Armbruster, M.M. Morgan, J.L. Schmidt, C.M. Lau, R.M. Riley, D.L. Zabrowski, and H.A. Dieck. Organometallics, **5**, 234 (1986); (*e*) I. Nakamura, H. Itagaki, and Y. Yamamoto. J. Org. Chem. **63**, 6458 (1998); (*f*) L.B. Wolf, K.C.M.F. Tjen, F.P.J.T. Rutjes, H. Hiemstra, and H.E. Schoemaker. Tetrahedron Lett. **39**, 5081 (1998).
3. (*a*) D.R. Coulson. J. Org. Chem. **38**, 1483 (1973); (*b*) D.H. Camacho, I. Nakamura, S. Saito, and Y. Yamamoto. Angew. Chem. Int. Ed. **38**, 3365 (1999); (*c*) D.H. Camacho, I. Nakamura, S. Saito, and Y. Yamamoto. J. Org. Chem. **66**, 270 (2001), and refs. therein; (*d*) M. Utsunomiya, M. Kawatsura, and J.F. Hartwig. Angew. Chem. Int. Ed. **42**, 5865 (2003), and refs. therein.
4. For hydrocarbonation of allenes, see: (*a*) Y. Yamamoto, M. Al-Masum, and N. Asao. J. Am. Chem. Soc. **116**, 6019 (1994); (*b*) Y. Yamamoto, M. Al-Masum, and N. Fujiwara. J. Chem. Soc. Chem. Commun. 381 (1996); (*c*) Y. Yamamoto, M. Al-Masum, and A. Takeda. J. Chem. Soc. Chem. Commun. 831 (1996); (*d*) Y. Yamamoto, M. Al-Masum, N. Fujiwara, and N. Asao. Tetrahedron Lett. **36**, 2811 (1995); (*e*) Y. Yamamoto and M. Al-Masum. Synlett. 969 (1995); (*f*) M. Meguro, S. Kamijo, and Y. Yamamoto. Tetrahedron Lett. **37**, 7453 (1996); (*g*) S. Kamijo and Y. Yamamoto. Tetrahedron Lett. **40**, 1747 (1999); for a review, see: (*h*) Y. Yamamoto. Pure Appl. Chem. **68**, 9 (1996); (*i*) for a general review on palladium catalyzed reaction of allenes, see: R. Zimmer, C.U. Dinesh, E. Nandanan, and F.A. Khan. Chem. Rev. **100**, 3067 (2000).
5. M. Al-Masum and Y. Yamamoto. J. Am. Chem. Soc. **120**, 3809 (1998).
6. M. Al-Masum, M. Meguro, and Y. Yamamoto. Tetrahedron Lett. **38**, 6071 (1997).
7. N.T. Patil, N.K. Pahadi, and Y. Yamamoto. Synthesis, **12**, 2186 (2004).
8. For the references on the addition of carbon pronucleophiles to alkynes, see: (*a*) I. Kadota, A. Shibuya, Y.S. Gyoung, Y. Yamamoto. J. Am. Chem. Soc. **120**, 10 262 (1998); (*b*) N.T. Patil, I. Kadota, A. Shibuya, Y.S. Gyoung, and Y. Yamamoto. Adv. Synth. Catal. **346**, 800 (2004); (*c*) N.T. Patil and Y. Yamamoto. J. Org. Chem. **19**, 6478 (2004); (*d*) N.T. Patil, H. Wu, I. Kadota, and Y. Yamamoto. J. Org. Chem. **69**, 8745 (2004); for the references on the addition of nitrogen pronucleophiles to alkynes, see: (*e*) I. Kadota, A. Shibuya, M.L. Lutete, and Y. Yamamoto. J. Org. Chem. **64**, 4570 (1999); (*f*) M.L. Lutete, I. Kadota, A. Shibuya, and Y. Yamamoto. Heterocycles, **58**, 347 (2002); (*g*) M.L. Lutete, I. Kadota, and Y. Yamamoto. J. Am. Chem. Soc. **126**, 1622 (2004); for the reference on the addition of oxygen pronucleophiles to alkynes, see: (*h*) I. Kadota, M.L. Lutete, A. Shibuya, and Y. Yamamoto. Tetrahedron Lett. **42**, 6207 (2001); for the related reference, see: (*i*) N.T. Patil, N.F. Khan, and Y. Yamamoto. Tetrahedron Lett. **45**, 8497 (2004); (*j*) Pd catalyzed addition of acetic acid to propargylic acetate is known, see: B.M. Trost, W. Brieden, and K.H. Baringhaus. Angew. Chem. Int. Ed. Engl. **31**, 1335 (1992).

© 2005 NRC Canada

9. W. Zhang, A.R. Haight, and M.C. Hsu. Tetrahedron Lett. **43**, 6575 (2002).
10. Enhancement of reaction rates in π-allylpalladium chemistry by the use of Pd(0)–carboxylic acid combined catalytic system is also observed by other researchers, see: (*a*) B.M. Trost and F. Rise. J. Am. Chem. Soc. **109**, 3161 (1987); (*b*) B.M. Trost, C. Jakel, and B. Plietker. J. Am. Chem. Soc. **125**, 4438 (2003); (*c*) K. Manabe and S. Kobayashi. Org. Lett. **5**, 3241 (2003); (*d*) for an excellent discussion related to this topic, see: B.M. Trost. Chem. Eur. J. **4**, 2405 (1998).
11. A.S. Gajare, M.S. Shingare, V.R. Kulkarni, N.B. Barhate, and R.D. Wakharkar. Synth. Commun. **28**, 25 (1998).

© 2005 NRC Canada

A MAS NMR and DRIFT study of the Ga species in Ga/H-ZSM5 catalysts and their effect on propane ammoxidation[1]

Prem Pal, Juliette Quartararo, Sharifah B. Abd Hamid, Eric G. Derouane, Jacques C. Védrine, Pieter C.M.M. Magusin, and Bruce G. Anderson

Abstract: ^{71}Ga, ^{27}Al, and ^{29}Si MAS NMR and DRIFT spectroscopies were used to characterize the state of gallium in Ga/H-ZSM5 catalysts tested for their ability to catalyse the ammoxidation of propane. Ga species were observed in two different possible environments: octahedrally coordinated gallium in small Ga_2O_3 particles at the external surface of the zeolite crystals, octahedrally coordinated gallium in GaO(OH) or related species, and tetrahedrally coordinated gallium in cationic-exchange positions inside the zeolite. Redox (H_2–O_2) cycles promote the migration of gallium from the GaO(OH) or Ga_2O_3 species at the external surface of the zeolite crystals to cationic-exchange sites within the zeolite channels. The redox treatment definitely had a beneficial effect on its catalytic performance for the ammoxidation of propane, which is known to occur via a bifunctional mechanism. The main product was acetonitrile at high Ga and Al contents while acrylonitrile was also observed as a side product at high Ga and low Al contents.

Key words: ZSM5, MFI, in situ studies, MAS NMR, DRIFT, propane activation, ammoxidation.

Résumé : On a fait appel à la spectroscopie RMN du ^{71}Ga, ^{27}Al et ^{29}Si à l'angle magique et à la technique « DRIFT » pour caractériser l'état du gallium dans des catalyseurs de Ga/H-ZSM5 évalués pour leur habilité à catalyser l'ammonoxydation du propane. On a observé des espèces de gallium dans deux environnements possibles : gallium à coordination octaédrique dans de petites particules de Ga_2O_3, à la surface externe des cristaux de zéolite, du gallium à coordination octaédrique dans le GaO(OH) et les espèces apparentées et du gallium à coordination tétraédrique dans les positions d'échange cationique dans la zéolite. Les cycles redox (H_2–O_2) favorisent la migration du gallium des espèces GaO(OH) ou Ga_2O_3 à la surface externe des cristaux de zéolite vers les sites d'échange cationique dans les canaux internes de la zéolite. Le traitement redox est définitivement bénéfique sur la performance catalytique pour l'ammonoxydation du propane qui se produit, par un mécanisme bifonctionnel bien connu. À contenus élevés de gallium et d'aluminium, le produit principal est l'acétonitrile alors qu'il se forme de l'acrylonitrile comme sous produit lorsque les quantités de gallium sont élevées alors que celle d'aluminium sont faibles.

Mots clés : ZSM5, MF1, études in situ, RMN à l'angle magique, DRIFT, activation du propane, ammonoxydation.

[Traduit par la Rédaction]

Introduction

Ga/H-ZSM5, zeolite H-ZSM5 modified with gallium, is known to catalyse the aromatization of light alkanes (C_3, C_4) (e.g., in the CYCLAR process (1–3). The reaction mechanism is based on the bifunctional properties of the catalyst, i.e., the activation and dehydrogenation of the alkane(s) over gallium species and the conjunct polymerization (including dehydrocyclization) of the olefins over the zeolite Brønsted acid sites. Ga/H-ZSM5 catalysts were also used more recently for other reactions such as the nitro-functionalization of propane, where gallium species were found to also play a decisive role in the activation of propane (4, 5).

A detailed characterization of a Ga/H-ZSM5 catalyst (Ga = 1.3 wt%, Si/Al = 18) recently demonstrated (6, 7)

Received 28 October 2004. Published on the NRC Research Press Web site at http://canjchem.nrc.ca on 7 June 2005.

P. Pal. Catalysis Division, Indian Institute of Petroleum, Dehradun, India.
J. Quartararo. Leverhulme Centre for Innovative Catalysis, Department of Chemistry, The University of Liverpool, Liverpool L69 7ZD, UK.
S.B. Abd Hamid. Universiti Malaya Postgraduate School, Bangunan Ips 50603, Malaysia.
E.G. Derouane.[2] Universidade do Algarve, Faculdade de Ciencias e Tecnologia – Quimica (OSCAR), Campus de Gambelas, P-8000-117 Faro, Portugal.
J.C. Védrine. Laboratoire de Physico-Chimie des Surface, ENSCP, 11, Rue P. & M. Curie, F-75005, Paris, France.
P.C.M.M. Magusin and B.G. Anderson. Schuit Institute of Catalysis, Eindhoven University of Technology, Postbus 513, NL-5600 MB Eindhoven, The Netherlands.

[1]This article is part of a Special Issue dedicated to Professor Howard Alper.
[2]Corresponding author: (e-mail: derouane@ualg.pt).

 doi: 10.1139/V05-073 © 2005 NRC Canada

that, after Ga ion exchange, drying at 293 K, and calcination at 823 K, gallium was mainly present as small (about 4 to 5 nm in diameter) particles of GaO(OH) in the hydrated sample and as Ga_2O_3 in the 823 K calcined sample. In both cases, these species were found to be located at the external surface of the zeolite crystallites. TG/DSC electron microscopy with EDAX analysis and ^{27}Al and ^{29}Si MAS NMR results indicated that H_2–O_2 redox cycles at 823 K induced the migration of the gallium species into the zeolite channels (7). Gallium migration to zeolite Brønsted sites was also observed with FT IR spectroscopy for Ga/H-ZSM5 and Ga/H-MOR prepared by chemical vapour deposition (8, 9). A possible intra-zeolite Ga species, postulated as essential for the aromatization of propane on Ga/H-ZSM5, is GaO^+ located in ion-exchange positions (10), which, when hydrated, should show gallium in tetrahedral coordination.

The objectives of the present study were: (1) to obtain direct information about the nature and environment of the Ga species in Ga/H-ZSM5 zeolites following H_2–O_2 redox treatments applied during their activation by use of magic-angle spinning (MAS) ^{71}Ga, ^{27}Al, and ^{29}Si NMR spectroscopy (Ga coordination) complemented by diffuse reflectance FT IR (DRIFT) spectroscopy (Brønsted acidity); and (2) to correlate this information with their catalytic behavior for the ammoxidation of propane.

Experimental

Materials

The parent ZSM5 zeolites were obtained in the Na form from Zeolyst (Valley Forge, Penn.). Prior to modification with gallium, all samples were calcined under N_2 flow at 723 K and then in air at 823 K for 2 h to remove any organic residue possibly present in the zeolite pores. Gallium nitrate (99.9%, Aldrich) was used as a Ga^{3+} precursor for ion exchange. Four samples differing by their unit cell (uc) composition, i.e., Ga(x)ZSM5(y) with x = Ga wt% (0.4 = 0.33 Ga/uc and 1.6 = 1.32 Ga/uc) and y = Si/Al ratio (27 = 3.43 Al/uc and 150 = 0.63 Al/uc) were studied.

H-ZSM5 zeolites were obtained by suspending the Na-ZSM5 zeolites in an aqueous solution of NH_4Cl–NH_4OH (295 K, pH 9.0) followed by stirring for 2 h. The solids were filtered and thoroughly washed. The products (NH_4-ZSM5) were then calcined at 773 K to yield the H-ZSM5 zeolite precursors.

Ga/H-ZSM5 samples were prepared by stirring a known quantity of gallium nitrate solution containing a known quantity of zeolite. The mixture was refluxed for 2 h at 373 K, the solid then filtered, washed with distilled water, and dried overnight in an air oven at 383 K. Higher Ga loadings were obtained by repeating this procedure. After oven drying at 383 K, the Ga/H-ZSM5 materials were calcined at 773 K in air to yield Ga_2O_3/H-ZSM5. Gallium contents were determined by atomic absorption spectroscopic analysis.

The samples were then subjected to successive H_2–O_2 treatment cycles according to the following procedure (10). The samples were initially heated to 423 K at a heating rate of 5 K min^{-1} under a 30 mL min^{-1} flow of nitrogen in a temperature-programmed oven and maintained at that temperature for 4 h. The gas flow was then changed to air and the solids further heated to 723 K at a rate of 10 K min^{-1} and kept at that temperature for 2 h. The temperature was then further raised to 823 K at a heating rate of 20 K min^{-1}. The samples were then flushed with nitrogen for 15 min and the gas flow switched to hydrogen. After reducing the catalysts for 2 h, the gas flow was changed back to nitrogen for 30 min and then to air for 2 h. This process was repeated three times. The catalysts were then allowed to cool under a flow of air.

Microcatalytic tests

The catalytic activity of the samples before and after H_2–O_2 treatments was measured using a custom-made microcatalytic reactor (MCR) optimized to study the ammoxidation of propane. The samples, placed in a tubular reactor made of stainless steel, were contacted with the mixture of reactant gases (propane, ammonia, oxygen, and N_2 or He as inert diluent) in a down-flow direction. The inlet feed lines were maintained at 473 K using heating tape. The reactor exit gases were analyzed on line using a Varian 3400 GC equipped with three different columns. The down-stream reactor line was maintained at 523 K to avoid any condensation of the reaction products and was directly fed to the GC fitted with a 15 m capillary CP-wax 52B column and two packed columns. The capillary column was used to separate the functionalized hydrocarbons (acids, alcohols, amines, amides, nitriles, aromatics, etc.), which were detected by flame ionization (FID). The nonpolar hydrocarbons (water, CO_2, and ammonia) were separated over a Haysep C packed column and detected using a thermal conductivity detector (TCD). The permanent gases (CO and CH_4) were separated over a molecular sieve A5 packed column and detected by TCD. The gas exiting from the furnace could alternatively be bubbled into a suitable reactant for analysis of NH_3 and HCN or sampled, after passing through a cooled condenser, by mass spectrometry.

Reactant conversions and product selectivities were calculated on a carbon and a nitrogen basis. Material balance evaluations were carried out to validate the GC calibrations and the quantification of the results.

Magic-angle spinning NMR spectroscopy

^{27}Al, ^{29}Si, and ^{71}Ga NMR spectra were recorded on a Bruker DMX500 spectrometer operating at ^{27}Al, ^{29}Si, and ^{71}Ga NMR frequencies of 130.29, 99.32, and 152.48 MHz, respectively. ^{29}Si and ^{27}Al MAS NMR spectra were collected with sample spinning frequencies of 5 and 12.5 kHz, respectively. For the ^{29}Si spectra, the recycling time was 20 s and a 90° pulse of 5 μs was used (^1H decoupling field ν_{1H} = 33 kHz). ^{27}Al spectra were obtained using a MAS-synchronized echo pulse sequence (p_1–τ–p_2–τ–r_d with pulse lengths p_1 = 2.4 μs, p_2= 4.8 μs, and delays τ = 76.4 μs and r_d = 3 s). ^{71}Ga MAS NMR spectra were recorded at a sample rotation rate (ν_r) between 25 and 35 kHz by use of a MAS-synchronized echo pulse sequence p_1–τ–p_2–r_d (p_1 = 0.6 μs, p_2 = 1.2 μs, $r_d \geq 0.1$s, and $\tau = \nu_r^{-1} - p_1/2 - p_2/2$) with the signal acquisition starting 16 μs after p_2. The whole signal was Fourier transformed, followed by a first-order spectral phase correction derived from the position of the echo in the time domain.

© 2005 NRC Canada

DRIFT spectroscopy

DRIFT spectra were recorded in situ using a Nicolet Protégé 460 FT IR spectrometer equipped with a SpectraTech Collector II™ DRIFT attachment fitted with a high-temperature chamber and an MCT detector. KBr windows were used on the chamber dome. Spectra were recorded at 4 cm^{-1} resolution; 256 scans were co-added. KBr powder was used as a reference material. All DRIFT spectra (measured in absorbance units) were normalized at 1870 cm^{-1} (an overtone of the zeolite lattice mode) and then transformed using the Kubelka–Munk function assuming the reflectance of the sample was 0.9 at 5000 cm^{-1}. Helium, used for drying, was purified by flowing through moisture (Varian CP17971), oxygen (Varian CP17970), and charcoal (Varian CP17972) filters. All Ga-ZSM5 catalysts (circa 20 mg) were dried in the DRIFT cell in flowing helium (30 mL min^{-1}) by ramping the temperature from 298 to 393 K at 5 K min^{-1}, holding for 30 min, then ramping to 748 K at the same rate. DRIFT spectra were then recorded following 30 min at 748 K.

Results and discussion

Magic-angle spinning ^{29}Si, ^{27}Al, and ^{71}Ga NMR spectroscopy

The ^{29}Si MAS NMR spectra of the calcined Ga(1.6)ZSM5 samples (Fig. 1) present the typical features of zeolite ZSM5 between –109 and –118 ppm. Several resolved signals corresponding to the different crystallographic sites are observed for Ga(1.6)ZSM5(150) and an unresolved resonance for Ga(1.6)ZSM5(27) owing to the aluminium-induced lattice distortion that occurs at high Al content. A resonance was also observed at –105 ppm in the latter case, attributed to Si^{4+} in a Si [1Al,3Si] configuration. No modification of the spectra attributable to the presence of gallium was observed. The latter is not surprising as most of the Ga species in the calcined Ga-modified zeolites were previously shown to decorate the external surface of the zeolite crystals in the absence of H_2–O_2 activation (7).

^{27}Al MAS NMR spectra are shown in Fig. 2. Ga(*x*)ZSM5(27) catalysts showed two main signals at 55 ppm (framework tetrahedral Al) and at 0 ppm (extra-framework octahedral Al). For the Ga(*x*)ZSM5(150) catalysts, only the resonance of framework Al was observed at 55 ppm (spectra not shown). Following calcination, a small amount of extra-framework Al, independent of Ga loading, was detected in the Ga(*x*)ZSM5(27) catalysts (Figs. 2*a*, 2*b*). After H_2–O_2 treatment, the spectrum remained essentially unchanged for the Ga(0.4)ZSM5(27) catalyst (Fig. 2*c*) whereas substantial changes in the intensities of the resonances were observed for the Ga(1.6)ZSM5(27) catalyst (Fig. 2*d*), corresponding to about equal amounts of framework and extra-framework Al. This observation reveals that Al is extracted from the ZSM5 framework when a substantial amount of Ga is present, either because of inadvertent steaming since the redox treatment produces more water when the Ga content is higher, or because some isomorphous substitution of Al by Ga in the ZSM5 framework occurred. If the latter is the correct explanation, similar changes should also have been observed for the H_2–O_2 treated Ga(1.6)ZSM5(150) catalyst, which is not the case. Thus, the extraction of framework Al upon redox treatments is attributed to inadvertent steaming.

Fig. 1. MAS ^{29}Si NMR spectra of calcined Ga(1.6)ZSM5(150) and Ga(1.6)ZSM5(27) before H_2–O_2 treatment.

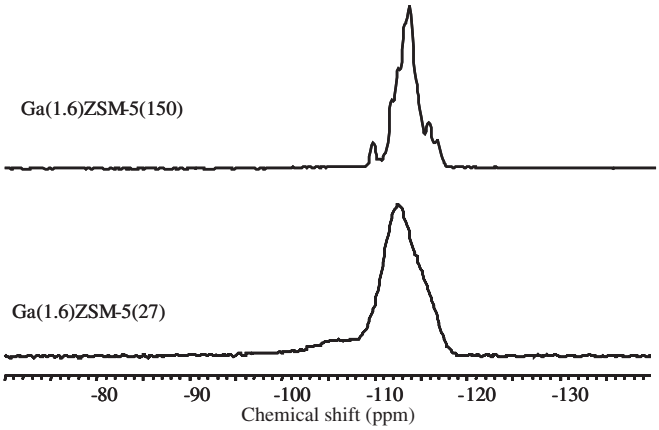
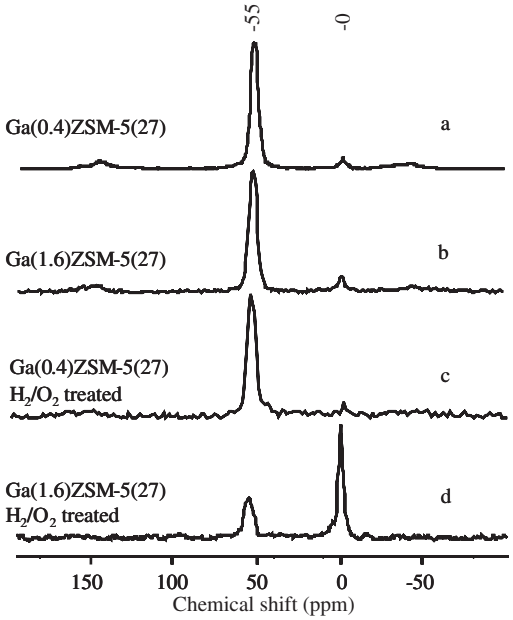


Fig. 2. MAS ^{27}Al NMR spectra of calcined (*a*, *b*) and H_2–O_2 treated (*c*, *d*) Ga(*x*)ZSM5(*y*) catalysts: *x* (Ga wt%) = 0.4 or 1.6 and *y* (Si/Al) = 27 or 150.



MAS ^{71}Ga NMR spectra for catalysts Ga(1.6)ZSM5(150), Ga(1.6)ZSM5(27), and Ga(0.4)ZSM5(27) are shown in Figs. 3 and 4. Gallium has a quadrupolar nucleus (I = 3/2) whose NMR line width is extremely sensitive to local electric field gradients. Magic-angle spinning alone does not completely remove the second-order quadrupolar line broadening, and for our catalysts, even *ultra-fast* sample rotation rates (25–35 kHz) were barely sufficient to remove the spinning sidebands from the centerband region. Further spectral improvement techniques to obtain spectra free of spinning sidebands and quadrupolar line broadening, like QPASS and MQMAS, do not work well for our zeolites with their huge ^{71}Ga quadrupolar couplings (11). The large line broadening observed in all cases probably reflects a combination of quadrupolar line broadening and chemical-shift heterogene-

© 2005 NRC Canada

Fig. 3. MAS ^{71}Ga NMR spectra of calcined Ga(1.6)ZSM5(150), Ga(1.6)ZSM5(27), and Ga(0.4)ZSM5(27) at respective sample rotation rates of 35, 30, and 30 kHz.

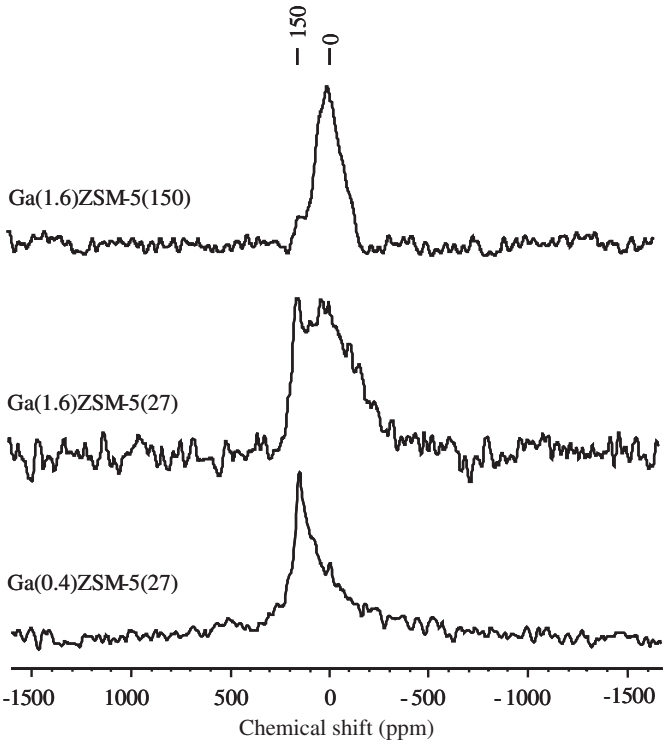
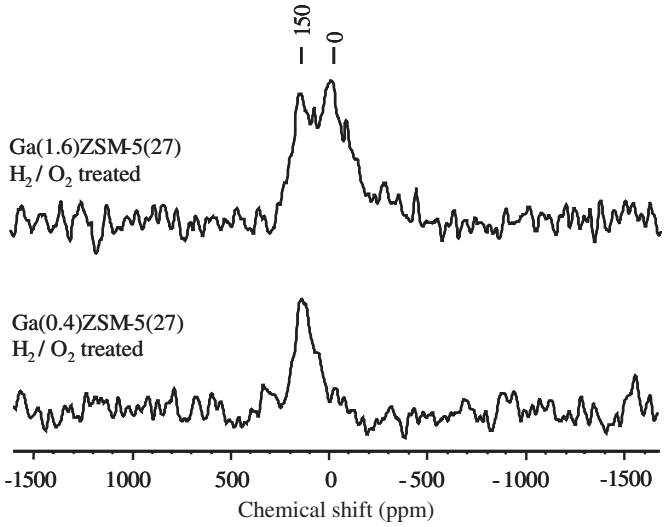


Fig. 4. MAS ^{71}Ga NMR spectra of Ga(1.6 and 0.4)ZSM5(27) after H_2–O_2 treatment at respective sample rotation rates of 35 and 25 kHz.



ity. The first arises from local electric field gradients in the partially charged zeolite structure. The second is associated with the structure differences among the various Ga species formed.

The ^{71}Ga MAS NMR spectra obtained after calcination are shown in Fig. 3. Compared to a reference spectrum of Ga_2O_3 (not shown), the spectral integrals correspond within 10%–20% to the Ga content determined by element analysis. Thus, despite the large quadrupolar line broadening, most of the Ga species is NMR-visible, indeed, and the NMR spectum is representative for the total Ga species population. The spectra differ significantly as a function of the Ga loading and the Al content in the parent zeolite. These differences are attributed to the presence of Ga species with octahedral or tetrahedral oxygen coordination. For calcined Ga(1.6)ZSM5(150) (Ga:Al ~ 2), only one resonance was observed at ~0 ppm, which is attributed to Ga octahedrally coordinated in Ga_2O_3 (12, 13). The latter observation agrees with EDX-HRTEM results showing the presence of small particles of GaO(OH) or Ga_2O_3 on the external surface of the zeolite crystallites (7). In contrast, Ga(0.4)ZSM5(27) (Ga:Al ~ 0.1) shows a single resonance at ~150 ppm assigned to tetrahedral Ga species, either in cationic-exchange positions (e.g., GaO^+ or hydrated GaO^+) or at zeolite framework sites. The ^{71}Ga NMR spectrum of the intermediate case (Ga(1.6)ZSM5(27), Ga:Al ~ 0.4) contains both signals at 150 and 0 ppm. In fact, the spectrum is well described as a superposition of the spectra of Ga(1.6)ZSM5(150) and Ga(0.4)ZSM5(27) at a normalized intensity ratio of 0.25:0.75. Comparison of the two spectra in Fig. 3 shows that the fraction of tetrahedral Ga species relative to the octahedral-Ga fraction increases with the Ga:Al ratio. This is to be expected, since a higher amount of framework Al will promote either framework substitution by Ga or Ga exchange in cationic positions. ^{71}Ga MAS NMR spectra after H_2–O_2 treatment are shown in Fig. 4 for the Ga(0.4 and 1.6)ZSM5(27) catalysts with the highest Al content and thus also the highest amount of cationic exchangeable sites. Apart from relatively minor line width changes, the spectra are similar to the corresponding spectra before the treatment. The H_2–O_2 treatment appears not to affect the overall oxygen coordination of the Ga. This is surprising because the effect of the first reductive step with H_2 is commonly believed to break up the Ga_2O_3 clusters at the external zeolite surface into smaller Ga_2O molecules, which then enter the zeolite pores. Changes in the ^{27}Al NMR spectra of Ga(1.6)ZSM5(27) showed an increase in extra-framework Al species following H_2–O_2 treatment whereas this did not occur for the Ga(0.4)ZSM5(27) catalyst (Fig. 2). Isomorphous substitution of Al by Ga in the second coordination sphere of Si within the zeolite lattice has been reported to change the ^{29}Si NMR chemical shift by 3 ppm (14), but this was not observed in our experiments. Cationic substitution as proposed earlier (10) is therefore still favored as the dominant effect although some framework substitution cannot be fully excluded.

DRIFT spectroscopy

DRIFT spectra were recorded in the hydroxyl-stretching region with IR bands being observed at 3595, 3680, and 3735 cm^{-1} corresponding to acidic hydroxyl groups (Brønsted sites), Ga-OH groups, and Si-OH groups (silanols), respectively.

The spectra observed for samples H-ZSM5(150), Ga(0.4)ZSM5(150), and Ga(1.6)ZSM5(150) following calcination are shown in Fig. 5. Whereas the intensity of the silanol band at 3735 cm^{-1} remains unaffected, the intensity of the Brønsted site band at 3595 cm^{-1} decreases and a small Ga-OH band at 3680 cm^{-1} appears as the Ga loading is increased, indicating that some protonic sites have been

© 2005 NRC Canada

Fig. 5. DRIFT spectra (T = 748 K, He flow = 30 mL min^{-1}) in the hydroxyl-stretching region of calcined (*a*) H-ZSM5(150), (*b*) Ga(0.4)ZSM5(150), and (*c*) Ga(1.6)ZSM5(150).

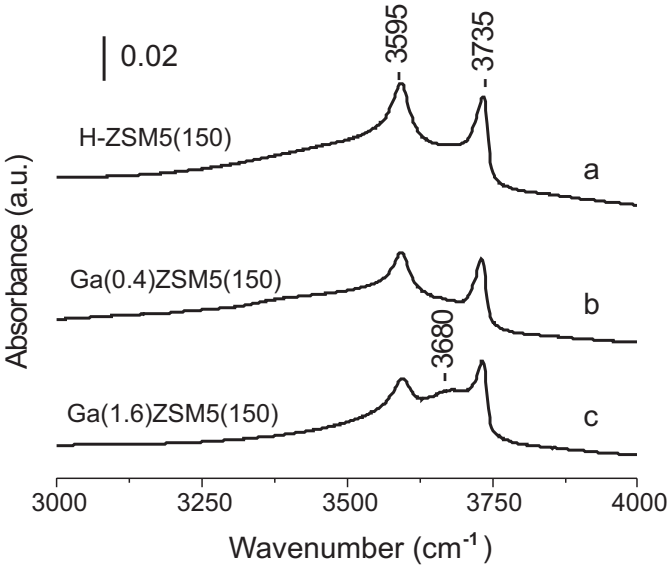
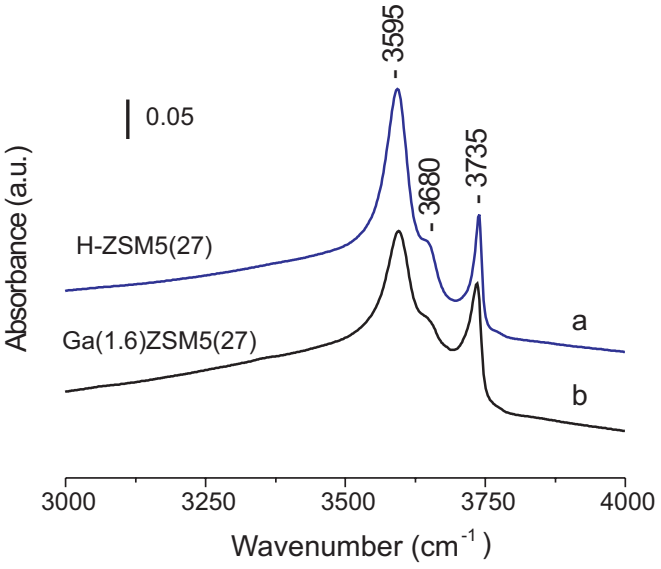


Fig. 6. DRIFT spectra (T = 748 K, He flow = 30 mL min^{-1}) in the hydroxyl-stretching region of (*a*) H-ZSM5(27) and (*b*) Ga(1.6)ZSM5(27).



exchanged by Ga species. However, given that H-ZSM5(150) contains 0.63 Al/uc and that Ga(0.4)ZSM5(150) and Ga(1.6)ZSM5(150) contain 0.33 and 1.32 Ga/uc, respectively, most of the Ga species appear not to be located at ion-exchange positions because, in that case, the Brønsted acid band at 3595 cm^{-1} should have completely disappeared for the Ga(1.6)ZSM5(150) catalyst. This is obviously not observed. Therefore, following calcination, Ga species are mostly located at the external surface of the zeolite crystals in agreement with previous observations (7) and the MAS NMR results discussed above. The Ga-OH band clearly observed for the Ga(1.6)ZSM5(150) catalyst (Fig. 5*c*) is likely to be associated with these external Ga species.

Figure 6 compares the spectra of the parent H-ZSM5(27) zeolite and of the Ga(1.6)ZSM5(27) catalyst after H_2–O_2 treatment. Again, the silanol band is not significantly affected. However, a decrease (about 30%) in the intensity of the IR band at 3595 cm^{-1} is observed and no IR band is clearly observed at 3680 cm^{-1}. These observations are consistent with the migration of Ga species from the zeolite external surface to ion-exchangeable sites within the zeolite. Indeed, the absence of a distinct IR band at 3680 cm^{-1} (Ga-OH) suggests that few Ga species are present at the surface of the zeolite crystals. As well, the decrease of the IR band at 3595 cm^{-1} is consistent with the above for Ga(1.6)ZSM5(27), the amount of Ga being 1.32/uc compared to the amount of (exchangeable) Brønsted sites of 3.43 if Ga species, as GaO^+, are in cationic-exchange positions.

In addition, a very small peak was observed at 1982 cm^{-1} for both Ga(0.4)ZSM5(27) and Ga(1.6)ZSM5(27), only after H_2–O_2 treatment. The peak was slightly larger for the higher gallium loading. Since this peak was absent in the spectra of the parent zeolite and of the calcined Ga-loaded samples, it is tentatively assigned to Ga-H groups in agreement with the frequency of Ga-H vibrations observed for gallane (Ga_2H_6) (15, 16).

Catalytic properties

The catalytic activity of the Ga/H-ZSM5 samples was evaluated for the ammoxidation of propane in a conventional fixed-bed microreactor as described above. It has been reported that propane can be activated at rather low temperatures (573–673 K) over Ga/H-ZSM5 catalysts via a protonated pseudo-cyclopropane (PPCP) intermediate that can lead to several primary products (methane, ethane, ethene, propene) as well as C1-C2 carbonium and carbenium ions (10). It was also shown that the latter species can react with various nucleophiles, e.g., CO, H_2O, and benzene (17–19). NH_3, another nucleophile, was thus another candidate expected to react with transient carbenium ions species, in the presence of oxygen, to form a C—N bond leading to acetonitrile and (or) acrylonitrile as products (16).

Figure 7 shows the influence of H_2–O_2 treatment, Ga content, and zeolite Si/Al ratio on the catalytic performance (rate in mol s^{-1} g^{-1} catalyst × 10^{-7}) of Ga(*x*)ZSM5(*y*) catalysts. Catalytic activity as well as the efficiency of the H_2–O_2 treatment increase in the order Ga(0.4)ZSM5(150) < Ga(1.6)ZSM5(150) < Ga(0.4)ZSM5(27) < Ga(1.6)ZSM5(27) as expected if the activation of propane occurs by a bifunctional mechanism, i.e., when Ga dispersion in the intracrystalline volume of the zeolite is enhanced by the redox treatments and the concentration of Brønsted acid sites is higher (lower zeolite Si/Al ratio). This observation is consistent with the findings from the ^{27}Al and ^{71}Ga MAS NMR and DRIFT results discussed above.

Table 1 shows the conversions and selectivities for the four catalysts mentioned previously, before (in parentheses) and after H_2–O_2 treatments, when the reaction is conducted at 748 K and a $GHSV_{total}$ of 1600 h^{-1} with a feed of composition C_3H_8:NH_3:O_2 = 11.5:10:22.7 (vol%). As mentioned previously, conversion increases when either the Ga or Al content increases and when the catalysts are exposed to H_2–O_2 treatment. The major products were propene (C_3^{2-}), acetonitrile (AcCN), carbon oxides (CO_x), and to a lesser ex-

© 2005 NRC Canada

Fig. 7. Catalytic activity of the Ga(*x*)ZSM5(*y*) catalysts (*x* (Ga wt%) = 0.4 or 1.6 and *y* (Si/Al) = 27 or 150) after calcination only (in grey) and after calcination and H_2–O_2 treatment (in black). The rate is expressed in 10^{-7} mol s^{-1} g^{-1} catalyst. Operating conditions were C_3H_8:NH_3:O_2 = 11.5:10:22.7 vol%, $GHSV_{total}$ = 1600 h^{-1}, *T* = 748 K.

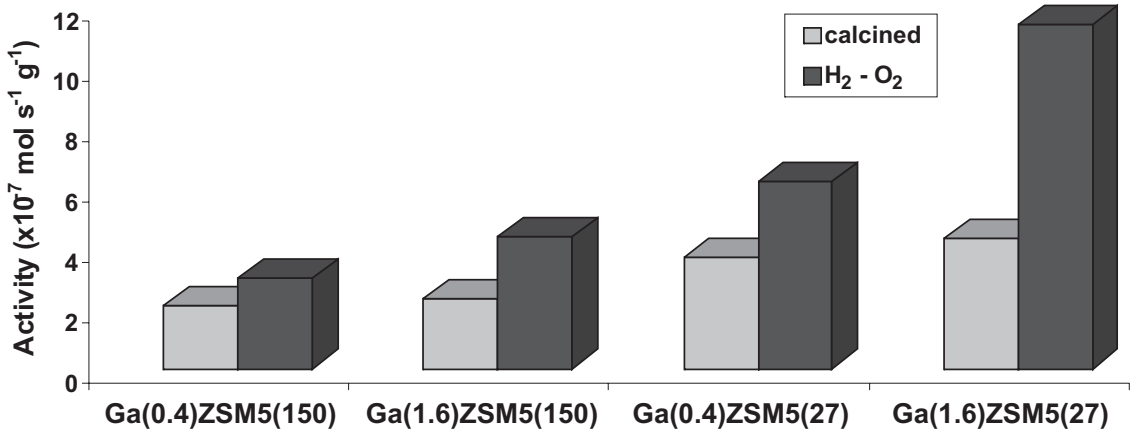


Table 1. Catalytic conversions and selectivities of different Ga(*x*)ZSM5(*y*) catalysts (*x* (Ga wt%) = 0.4 or 1.6, *y* (Si/Al) = 27 or 150) for the ammoxidation of propane without (values in parentheses) and with H_2–O_2 treatment.

		Selectivity (%)					
Catalysts	Conversion (%)	C_3^{2-}	AcCN	ACN	HCN	CO_x	ONCs
Ga(0.4)ZSM5(150)	13 (9)	36 (36)	25 (22)	7 (10)	2 (2)	23 (24)	— (6)
Ga(1.6)ZSM5(150)	18 (11)	32 (34)	26 (20)	10 (11)	3 (2)	26 (28)	— (5)
Ga(0.4)ZSM5(27)	23 (15)	29 (32)	41 (36)	1 (2)	2 (1)	25 (29)	— (1)
Ga(1.6)ZSM5(27)	41 (20)	25 (29)	47 (37)	1 (2)	2 (1)	23 (30)	— (1)

Note: Operating conditions: C_3H_8:NH_3:O_2 = 11.5:10:22.7 vol%, $GHSV_{total}$ = 1600 h^{-1}, *T* = 748 K.

tent acrylonitrile (ACN). Minor amounts of other products were also observed, namely HCN and other compounds containing N and (or) O (ONCs in Table 1). Increasing Ga and (or) Al content, as well as treatment with H_2–O_2, decreases the selectivity to propene and increases the combined selectivity to AcCN and ACN, which are final products, as expected. However, increasing the acidity of the zeolite dramatically decreases the selectivity to ACN and further promotes the formation of AcCN. As no increase in CO_x is observed, the former observation cannot be accounted for by the cracking of propene to ethylene with the C1 released fragment being oxidized. It is more likely that propene oligomers are cracked leading to a higher concentration of ethylene as an intermediate, which is obviously a precursor to AcCN.

In another study on propane oxidation to acrylic and acetic acids using MoNbSbV mixed oxides (20, 21) with low Brønsted acid site concentration and heteropolyacids (HPAs) (22) as catalysts, we observed that the reaction proceeds via two parallel pathways, one via propene leading mainly to acrylic acid and the second via isopropanol and acetone yielding mainly acetic acid. The second pathway was favoured in the presence of water and strong Brønsted acidity. As ZSM5 zeolite catalysts possess strong Brønsted acidity, it may therefore not be surprising that AcCN formation was also favored at the expense of ACN on a Ga/H-ZSM5 catalyst with higher acid site concentration. Interestingly, traces of isopropanol were also detected in the experiments reported herewith, which may further support the previous statement. Note: it was previously reported (4, 5) that Ga/H-ZSM5 catalysts were efficient for the ammoxidation of propane to acrylonitrile. It was, however, found later that the product identified as acrylonitrile in these publications was in fact acetonitrile, as mentioned in this work. The correct interpretation of the propane ammoxidation results is detailed in ref. 19.

Conclusions

^{71}Ga, ^{27}Al, and ^{29}Si MAS NMR data demonstrate that the Ga species formed by ion exchange on H-ZSM5 depend on the gallium loading and the aluminium content of the zeolite. At a low Ga:Al ratio, mainly tetrahedrally oxygen coordinated gallium is observed, probably at cation-exchange positions. At a high Ga:Al ratio, gallium is mainly present as a octahedrally oxygen coordinated species probably at the zeolite external surface of the ZSM5 zeolite crystals. DRIFT spectroscopy demonstrated that acid Brønsted sites were exchanged to a limited extent upon modification with Ga and calcination, with most of the Ga species being located at the external surface of the zeolite crystals as a result, and that indeed Ga species were present as cation-exchanged species following H_2–O_2 treatment.

The concentration of Brønsted acid sites supplied by the zeolite and its Ga content and dispersion (probably as GaO^+ species) play a direct role in the activation of propane and orient the selectivity to acetonitrile at the expense of acrylonitrile and propene at higher Al (acid site) concentration.

© 2005 NRC Canada

Gallium species working in tandem with the acidic functions of the zeolite promote the ammoxidation reaction. The results suggest that higher yields in acrylonitrile could be obtained by using Ga-modified zeolites with a higher Ga and a lower Al content.

References

1. R. Gregory and A.J. Colombos. US Patent 4 056 575, 1977, assigned to The British Petroleum Company (BP).
2. S.N. Bulford and E.E. Davies. US Patent 4 157 356, 1979, assigned to The British Petroleum Company (BP).
3. J.R. Mowry, R.F. Anderson, and J.A. Johnson. Oil Gas J. **2**, 128 (1985).
4. S.B. Abd Hamid, P. Pal, H. He, and E.G. Derouane. Catal. Today, **64**, 129 (2001).
5. S.B.D.-A. Hamid, G. Centi, P. Pal, and E.G. Derouane. Top. Catal. **15**, 161 (2001).
6. I. Nowak, J. Quartararo, E.G. Derouane, and J.C. Védrine. Stud. Surf. Sci. Catal. **145**, 201 (2003).
7. I. Novak, J. Quartararo, E.G. Derouane, and J.C. Védrine. Appl. Catal. A, **251**, 107 (2003).
8. El.-M. El-Malki, R.A. van Santen, and W.M.H. Sachtler. J. Phys. Chem. B, **103**, 4611 (1999).
9. M. Garcia-Sanchez, P.C.M.M. Magusin, E.J.M. Hensen, P.C. Thüne, X. Rozanksa, and R.A. van Santen. J. Catal. **219**, 352 (2003).
10. E.G. Derouane, S.B. Abdul Hamid, I.I. Ivanova, N. Blom, and P.-E. Højlund-Nielsen. J. Mol. Catal. **86**, 371 (1994).
11. D. Massiot, T. Vosegaard, N. Magneron, D. Trumeau, V. Montouillout, P. Berthet, T. Loiseau, and B. Bujoli. Solid State NMR, **15**, 159 (1999).
12. H. Kyung, C. Timken, and E. Oldfield. J. Am. Chem. Soc. **109**, 7669 (1987).
13. M.L. Occelli, H. Eckert, A. Wölker, and A. Auroux. Microporous Mesoporous Mater. **30**, 219 (1999).
14. M.L. Occelli, A.E. Schweiser, C. Fild, G. Shwering, H. Eckert, and A. Auroux. J. Catal. **192**, 119 (2000).
15. A.J. Downs, M.J. Goode, and C.R. Pulham. J. Am. Chem. Soc. **111**, 1936 (1989).
16. C.R. Pulham, A.J. Downs, M.J. Goode, D.W.H. Rankin, and H. Robertson. J. Am. Chem. Soc. **113**, 5149 (1991).
17. A.G. Stepanov, M.V. Luzgin, V.N. Romannikov, and K.I. Zamaraev. J. Am. Chem. Soc. **117**, 3615 (1995).
18. A.G. Stepanov, M.V. Luzgin, V.N. Romannikov, V.N. Sidelnokov, and K.I. Zamaraev. J. Catal. **164**, 411 (1996).
19. P. Pal. Ph.D. thesis, University of Liverpool, Liverpool, UK, 2001.
20. E.K. Novakova, J.C. Védrine, and E.G. Derouane. J. Catal. **211**, 226 (2002).
21. E.K. Novakova, E.G. Derouane, and J.C. Védrine. Catal. Lett. **83**, 177 (2002).
22. N. Dimitratos and J.C. Védrine. Catal. Today, **81**, 561 (2003).

© 2005 NRC Canada

Polycyclitols — Novel conduritol and carbasugar hybrids as new glycosidase inhibitors[1]

Goverdhan Mehta and Senaiar S. Ramesh

Abstract: A family of novel carbasugar analogues (bicyclitols) based on *cis*-hydrindane and *cis*-decalin frameworks has been conceptualized. These novel entities can be regarded as conduritol and carbasugar hybrids. Syntheses of these polyhydroxylated entities have been achieved in stereo- and regioselective manners, starting from the readily available Diels–Alder adducts of 5,5-dimethoxy-1,2,3,4-tetrachlorocyclopentadiene and appropriate dienophiles like cyclopentadiene or *p*-benzoquinone, that embody a masked 7-ketonorbornenone moiety. Thermally induced chelotropic elimination of CO from the appropriately functionalized 7-ketonorbornenone derivatives to deliver annulated bicyclic 1,3-cyclohexadiene derivatives was the key step in this synthetic endeavor. Further oxy-functionalization of the 1,3-cyclohexadiene moiety delivered the targeted polycyclitols. A preliminary investigation of the glycosidase inhibitory potency of these bicyclitols, identified compounds **18** and **54** as potent and selective inhibitors of α-glucosidase (yeast).

Key words: carbasugar, conduritol, glycomimics, glycosidase inhibitors.

Résumé : On a conceptualisé une nouvelle famille d'analogues de carbasucres (bicyclitols) reposant sur des squelettes de *cis*-hydrindane et de *cis*-décaline. Ces nouvelles entités peuvent être considérées comme des hybrides du conduritol et des carbasucres. Des synthèses de ces entités polyhydroxylées ont été réalisées de façons stéréo- et régiosélectives à partir d'adduits de Diels–Alder facilement accessibles du 5,5-diméthoxy-1,2,3,4-tétrachlorocyclopentadiène et de diénophiles appropriés, tels le cyclopentadiène ou la *p*-benzoquinone, qui comportent une portion 7-cétonorbornénone marquée. L'étape clé de ces synthèses implique une élimination chélotropique thermiquement induite de CO à partir des dérivés fonctionnalisés d'une façon appropriée de la 7-cétonorbornénone qui permet d'obtenir les dérivés cyclohexa-1,3-diènes bicycliques annelés. Une oxy-fonctionnalisation subséquente de la portion cyclohexa-1,3-diène conduit aux polycyclitols recherchés. Une étude préliminaire du pouvoir inhibiteur de la glycosidase de ces bicyclitols a permis d'identifier les composés **18** et **54** comme actifs et comme inhibiteurs sélectifs de l'α-glucosidase (levure).

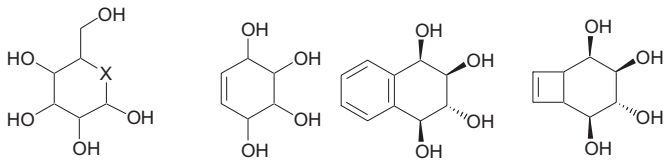
Mots clés : carbasucre, conduritol, glycomimique, inhibiteurs de la glycosidas.

[Traduit par la Rédaction]

Introduction

Glycosidases and related enzymes are crucial in many biological processes that are vital for the normal functioning of cells. Hence, inhibitors of these carbohydrate-processing enzymes have received increased attention in the past few decades from a synthetic as well as a biological activity perspective. These pursuits have been largely fuelled by the realization of their potential as therapeutic agents for the treatment of a variety of carbohydrate-mediated diseases like diabetes, cancer, AIDS, and viral infections (1, 2). The basic premise for the design of glycosidase inhibitors has been to generate transition state mimics by replacing the endocyclic oxygen atom of a monosaccahride by a carbon (carbasugar, **1**) or nitrogen atom (azasugar, **2**). The lack of a glycosidic linkage in these entities, which otherwise resemble the monosaccharides in shape, size, and functionalization, renders them hydrolytically stable. In this context, a range of carbasugars, azasugars, and their analogues, with diverse functionalization and stereochemical features have been devised, and their glycosidase inhibitory activities evaluated (1, 2). Additionally, conduritols **3** (1,2,3,4-tetrahydroxy-5-cyclohexenes) and their various derivatives have also attracted attention because of their glycosidase inhibitory properties (3). Several bicyclic and tricyclic conduritol variants like **4** and **5** have also been synthesized and evaluated for their efficacy against various glycosidases (4).

Naturally occurring alkaloids like 1-deoxynojirimycin (**6**) can be regarded as simple azasugar analogues of D-glucose and have been found to be potent inhibitors of α- and β-



1 X = CH_2
2 X = NH

3 **4** **5**

Received 30 November 2004. Published on the NRC Research Press Web site at http://canjchem.nrc.ca on 7 June 2005.

Dedicated in appreciation of the many notable contributions of Professor Howard Alper to chemistry.

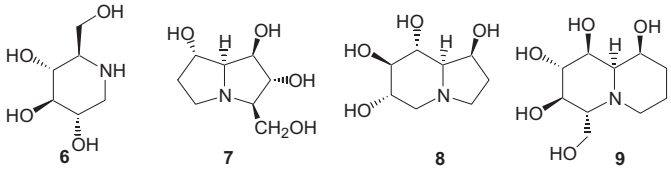
G. Mehta[2] and S.S. Ramesh. Department of Organic Chemistry, Indian Institute of Science, Bangalore 560012, India.

[1]This article is part of a Special Issue dedicated to Professor Howard Alper.

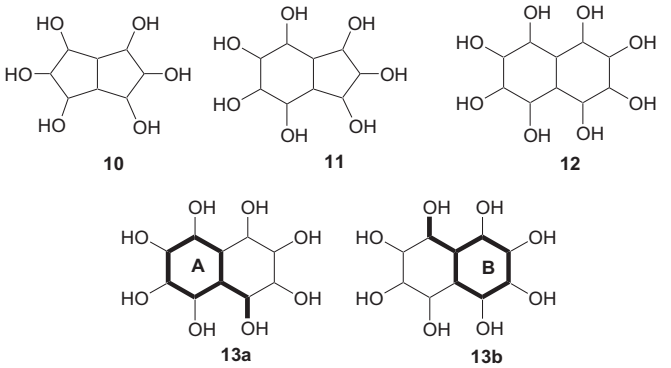
[2]Corresponding author (e-mail: gm@orgchem.iisc.ernet.in).

 doi: 10.1139/V05-032 © 2005 NRC Canada

glucosidases. Besides nojirimycins, several other mono- and bicyclic alkaloids based on polyhydroxylated pyrrolidine, piperidine, pyrrolizidine, indolizidine, and quinolizidine frameworks have also been identified as carbohydrate mimics. Typical examples include bicyclic pyrrolizidine alkaloid alexine **7**, indolizidine alkaloid castanospermine **8**, and quinolizidine alkaloid **9** (5).

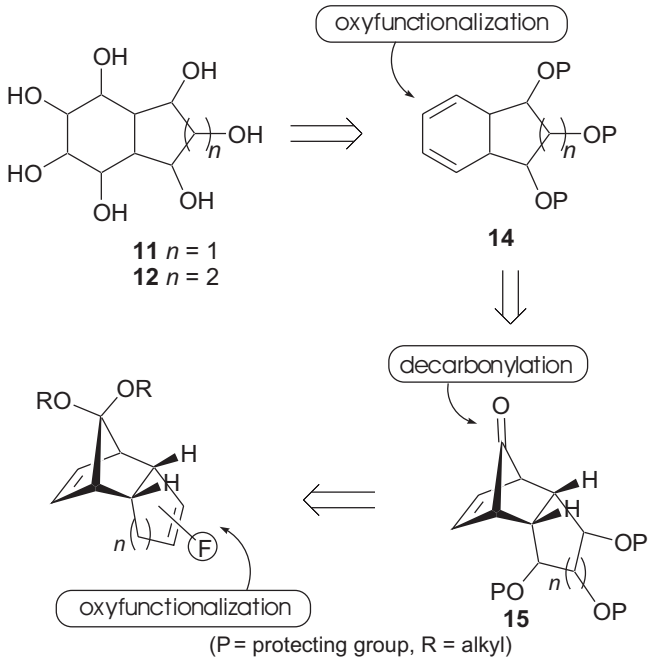


Spurred by the heightened interest in the design of potent inhibitors of glycosidases and inspired by the structures of bicyclic alkaloids **7**–**9**, we have conceived of a new family of polyhydroxylated diquinanes **10**, hydrindanes **11**, and decalins **12**, collectively termed as "polycyclitols", as potential glycomimics (6, 7). Among these bicyclitols, **11** and **12** can be considered as ring-annulated carbasugar entities and more interestingly, the decalin polyol **12** can be regarded as a hydrid of two carbasugars A and B (see bold portions in **13a** and **13b**). The presence of the additional hydroxyl groups on the annulus, it is presumed, may provide additional binding points for these analogues at the receptor site. The effect of annulation on the biological profile of biomolecules can be profound, as seen in the case of the natural glycosidase inhibitors, deoxynojirimycin **6** and castanospermine **8**. The former, a nitrogen analogue of glucose, inhibits yeast α-glucosidase, but is inactive against almond β-glucosidase. On the other hand **8**, a ring-annulated analogue of **6**, is a potent inhibitor of β-glucosidase, but exhibited no inhibition against yeast α-glucosidase (5). The bicyclitols **11** and **12** conceptualized here have a similar structural relationship to carbasugars as castanospermine **8** has to deoxynojirimycin **6**. Indeed, these bicyclitols can be visualized as the carbon analogues of castanospermine **8** and other bicyclic alkaloids exhibiting glycosidase activity. Alternatively, these novel bicyclic entities can be regarded as annulated conduritol, with **12** being a hydrid of two conduritols with shared, common ring junction carbon atoms.



Herein, we report the stereo- and regioselective synthesis of the newly conceptualized polyhydroxylated carbocyclic entities, with as many as nine (in **11**) and 10 (in **12**) stereogenic centers, starting from readily available Diels–Alder adducts, following fairly general and flexible synthetic sequences. We also report on the glycosidase inhibitory activity of the newly synthesized polycyclitols, two of which have exhibited an impressive and selective inhibition of yeast α-glucosidase.

Scheme 1. Retrosynthetic analysis of **11** and **12**.



Results and discussions

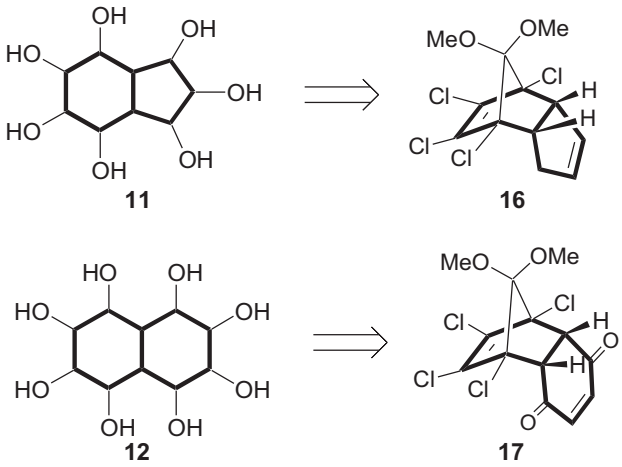
Retrosynthetic analysis

A general retrosynthetic analysis for accessing hydrindane **11** and decalin **12** based bicyclitols is depicted in Scheme 1. It was visualized that the hydroxyl group pattern on the six-membered ring could be generated through oxyfunctionalization of diene **14** (n = 1, 2), which in turn could be obtained by the thermal or photochemical decarbonylation of the 7-ketonorbornyl moiety in **15**. The precursor tricyclic ketones **15** (n = 1, 2) are readily obtainable via Diels–Alder cycloaddition between 5,5-dimethoxy-1,2,3,4-tetrachlorocyclopentadiene and an appropriate cyclic dienophile (Scheme 1).

Thus, tricyclic precursors **16** and **17** were obtained via a Diels–Alder reaction between 5,5-dimethoxy-1,2,3,4-tetrachlorocyclopentadiene and cyclopentadiene or *p*-benzoquinone, respectively. While the tricyclic endo-adduct **16** was to serve as the starting point for the hydrindane based polyols **11** (see bold portion), the benzoquinone derived Diels–Alder endo-adduct **17** was chosen as the starting material for the decalin based polyols **12** (bold portion) (Scheme 2). The main advantage in the choice of endo-adducts **16** and **17** as our basic launching pad was that their tricyclic framework built on a norbornyl matrix confers on them a topological bias towards exo-selectivity. This built-in facial bias in **16** and **17** was, therefore, expected to ensure stereoselective operations, particularly oxyfunctionalization maneuvers. The foregoing retrosynthetic analysis provided

© 2005 NRC Canada

Scheme 2.



the road map for the synthesis of the targeted new family of bicyclitols.

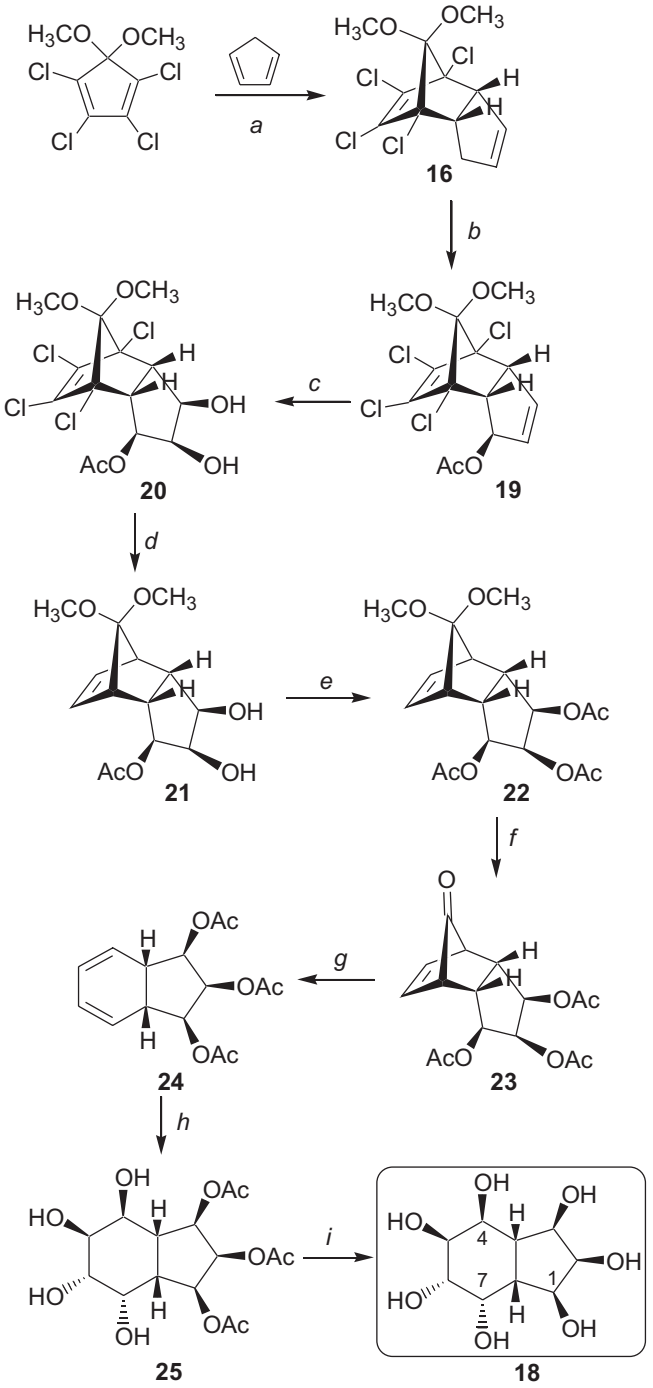
Synthesis of hydrindane based bicyclitols

The synthesis of the first galacto-configured *cis*-hydrindane-based polyol **18**, emanated from the tricyclic Diels–Alder adduct **16**, obtained by the [4 + 2] cycloaddition of 5,5,-dimethoxy-1,2,3,4-tetrachlorocyclopentadiene and cyclopentadiene (Scheme 3) (8). Adduct **16** was subjected to allylic oxidation, using in-situ-generated $Mn(OAc)_3$, to deliver the exo-acetate derivative **19** (Scheme 3) (9). The exo-acetate **19** was subjected to dihydroxylation following the Upjohn catalytic OsO_4–NMMO protocol (10) to generate diol **20**, which on reductive dehalogenation (**21**) followed by acetylation furnished the C_s-symmetric triacetate **22** (Scheme 3) (8*a*). All three acetate functionalities in **22** were cis disposed, owing to the exo-propensity of the topology of the endo-fused system **19**.

The tricyclic 7-ketal derivative **22** upon exposure to Amberlyst-15 in moist acetone, resulted in ketal deprotection and furnished the 7-ketonorbornenone derivative **23** (Scheme 3). As contemplated earlier, decarbonylation in **23** through thermal activation by heating in nitrobenzene (~160 °C) furnished the C_s-symmetric cyclohexa-1,3-diene derivative **24** in moderate yield (Scheme 3) (11). The cyclic 1,3-diene moiety in **24** was subjected to exhaustive dihydroxylation employing the catalytic OsO_4–NMMO protocol (10) to furnish a single tetrahydroxy-triacetate **25**, which was devoid of any symmetry. Loss of symmetry during the double dihydroxylation reaction on the diene secured the stereochemistry of **25**, which required the two hydroxylations on diene **24** to occur from the exo- and endo-faces, respectively, of the *cis*-hydrindane (Scheme 3). Mild base hydrolysis of triacetate **25** gave the targeted heptahydroxy bicyclitol **18**, an annulated 5a-carbagalactose derivative.

The synthesis of diastereomeric *cis*-hydrindane-based carbasugar analogue **26** started from the readily available endo-tricyclic enone **27**. Enone **27** was obtained following the protocol reported by Schuda et al. (12) involving [4 + 2] dimerization of the ethylene ketal of 2,4-cyclopentadienone and chemoselective deketalization. Enone **27** was converted to endo-allylic alcohol **28** via DIBAL-H reduction from the exo-face and the norbornene double bond was protected

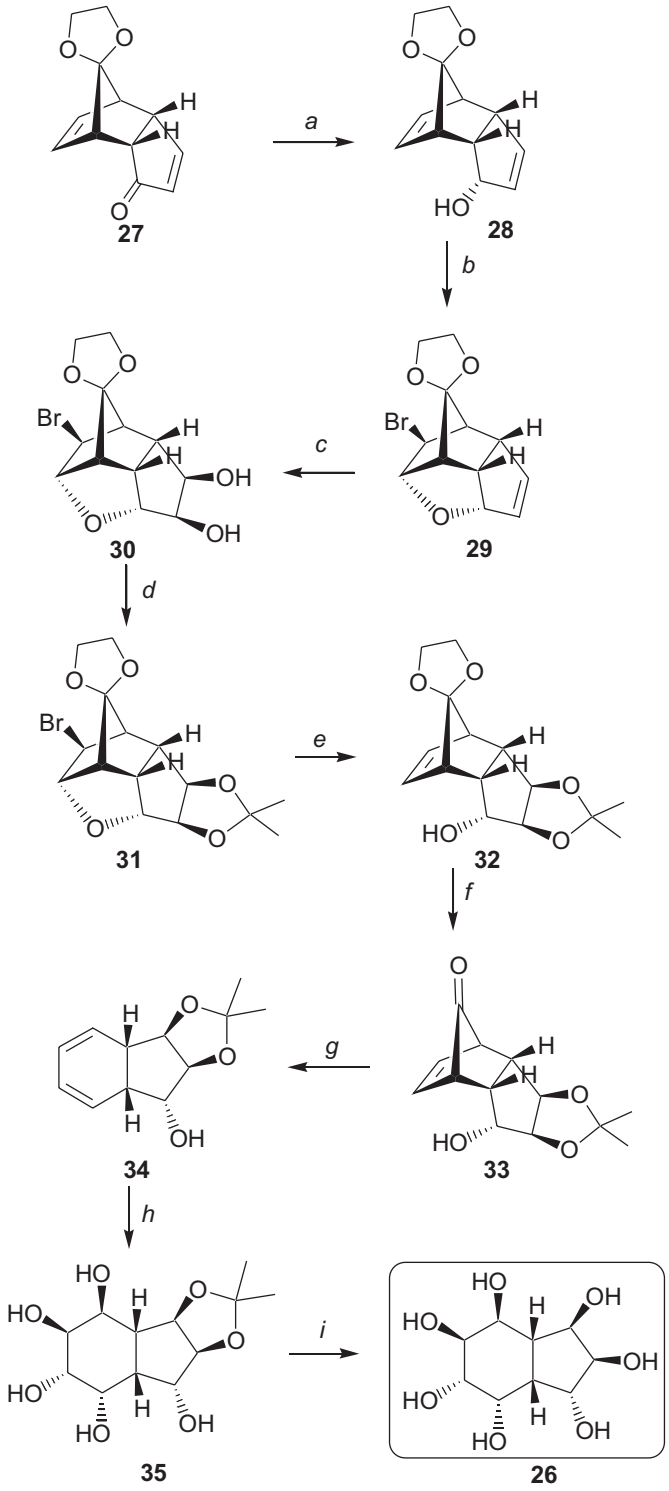
Scheme 3. Reagents and conditions: (*a*) toluene, reflux, 24 h, 70%; (*b*) $Mn(OAc)_3$, AcOH, 70 °C, 1 h, 64%; (*c*) OsO_4 (1 mol%), NMMO, Me_2CO–H_2O–*t*-BuOH (5:5:2), rt, 12 h, 80%; (*d*) Na, liq. NH_3, THF, EtOH, –33 °C, 30 min, 72%; (*e*) Ac_2O, pyridine, DMAP, CH_2Cl_2, rt, 2 h, 88%; (*f*) Amberlyst-15, acetone, rt, 1 h, 89%; (*g*) $C_6H_5NO_2$, heat, 160 °C, 2 h, 50%; (*h*) OsO_4 (1 mol%), NMMO, Me_2CO–H_2O–*t*-BuOH (5:5:2), rt, 48 h, 88%; (*i*) aq. NaOH, rt, 1 h, 60%.



through intramolecular bromoetherification to give **29** (Scheme 4). The cyclopentene double bond in **29** was stereoselectively dihydroxylated and the resulting *cis*-diol **30** was protected as acetonide **31**. The norbornene double bond

© 2005 NRC Canada

Scheme 4. Reagents and conditions: (*a*) DIBAL-H (1 mol/L in hexane), CH_2Cl_2, –78 °C, 15 min, 90%; (*b*) NBS, CH_2Cl_2, rt, 3 h, 80%; (*c*) OsO_4 (1 mol%), NMMO, Me_2CO–H_2O–*t*-BuOH, (5:5:2), rt, 12 h, 82%; (*d*) Amberlyst-15, acetone, 4 Å molecular sieves, rt, 3 h, 95%; (*e*) Zn dust, AcOH, MeOH, rt, 4 h, 85%; (*f*) Amberlyst-15, acetone, reflux, 3 h, 81%; (*g*) $C_6H_5NO_2$, 160 °C, 4 h, 67%; (*h*) OsO_4 (1 mol%), NMMO, Me_2CO–H_2O–*t*-BuOH (5:5:2), rt, 48 h, 83%; (*i*) 30% CF_3COOH, rt, 30 min, 89%.



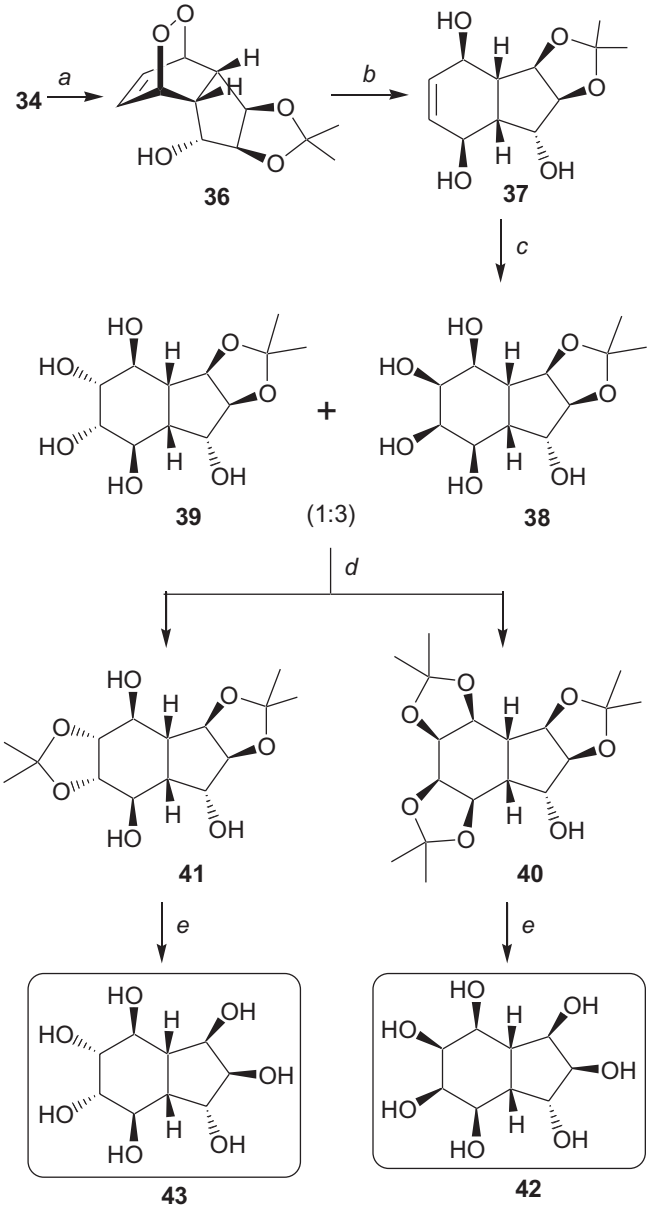
was now unmasked with Zn metal to render **32** (Scheme 4) (8*a*). The ketal moiety in **32** was carefully deprotected in the presence of Amberlyst-15 to furnish the crystalline 7-norbornenone derivative **33** (Scheme 4). Tricyclic ketone **33**, on heating in nitrobenzene (160 °C), quite readily converted to the 1,3-cyclohexadiene derivative **34** through extrusion of CO (11). At this point, it was recognized that diene **34** was well suited for generating stereochemically diverse oxygenation patterns through appropriate sequencing of the oxyfunctionalization protocol.

Towards this end, the *cis*-hydrindane diene **34** was subjected to exhaustive dihydroxylation under catalytic OsO_4 conditions to furnish the pentahydroxy compound **35** (Scheme 4). The stereochemical assignment for **35** followed from an incisive analysis of the spectral data in analogy with that of compound **25**. In addition, it is expected that the directing influence of the free α-hydroxyl group at the peri position in diene **34** would lead to the preferred stereostructure of **35**. Mild acid hydrolysis of the acetonide protecting group in **35** furnished the targeted heptahydroxylated hydrindane **26**, which was an epimer of **18** at C1. Polyol **26**, like **18**, embodies a 5a-carbagalactose moiety, with the hydroxylated carbocyclic annulation spanning the C_{5a}-C_6 atoms of the carbasugar (Scheme 4).

In another stereochemical variation in the hydroxylation pattern on the hydrindane framework, [4 + 2] cycloaddition of singlet oxygen ($^1O_2$) was effected on **34** to deliver endoperoxide **36** as the sole product in good yield with the addition of $^1O_2$ to **34** from the preferred convex face of the molecule (Scheme 5) (13). The peroxide linkage in **36** was cleanly cleaved with lithium aluminum hydride to yield the 1,4-diol derivative **37** and further dihydroxylated under the standard catalytic OsO_4 conditions to give a 3:1 mixture of tetrols **38** and **39**, respectively. All attempts to separate the mixture of tetrols at this stage were unsuccessful. At this point, we reasoned that one of the stereoisomers from the dihydroxylation should have the hydroxyl groups in an all cis orientation while the other diastereomer would have a trans–syn–trans arrangement of the hydroxyl groups on the six-membered ring. Hence, it was reasoned that the protection of the hydroxyl groups in the mixture of **38** and **39** as the corresponding acetonides, would result in the formation of a tris-acetonide derivative in the case of **38** and a bis-acetonide in the case of **39** and would thus be rendered amenable to separation. Consequently, the mixture of **38** and **39** was treated with Amberlyst-15 in acetone medium to furnish, as anticipated, tris-acetonide **40** and bis-acetonide **41**, respectively, which were then readily separable by column chromatography (Scheme 5). The major isomer **40** originates from dihydroxylation of **37** from the syn-face of allylic alcohols, an outcome that is in conflict with Kishi's rule (14) for dihydroxylation of allylic alcohols. The stereochemical outcome in this case can be attributed to the overwhelming topological preference of the *cis*-hydrindane moiety in **37** to react from the less-hindered, convex face to yield syn-dihydroxylated **38** as the major product. The acetonide deprotection in **40** and **41** in the presence of 30% trifluoroacetic acid cleanly furnished the diastereomeric heptahydroxylated hydrindanes **42** and **43**, respectively (Scheme 5). The bicyclic carbasugar analogues **42** and **43** correspond to the

© 2005 NRC Canada

Scheme 5. Reagents and conditions: (*a*) O_2, hν, methylene blue, $CHCl_3$, 20 °C, 8 h, 90%; (*b*) $LiAlH_4$, THF, rt, 1 h, 54%; (*c*) OsO_4 (1 mol%), NMMO, Me_2CO–H_2O–*t*-BuOH (5:5:2), rt, 1 h; (*d*) Amberlyst-15, acetone, 4 Å molecular sieves, followed by silica gel separation (62% for **40** and 21% for **41**); (*e*) 30% CF_3COOH, 92% for **42**, and 88% for **43**.

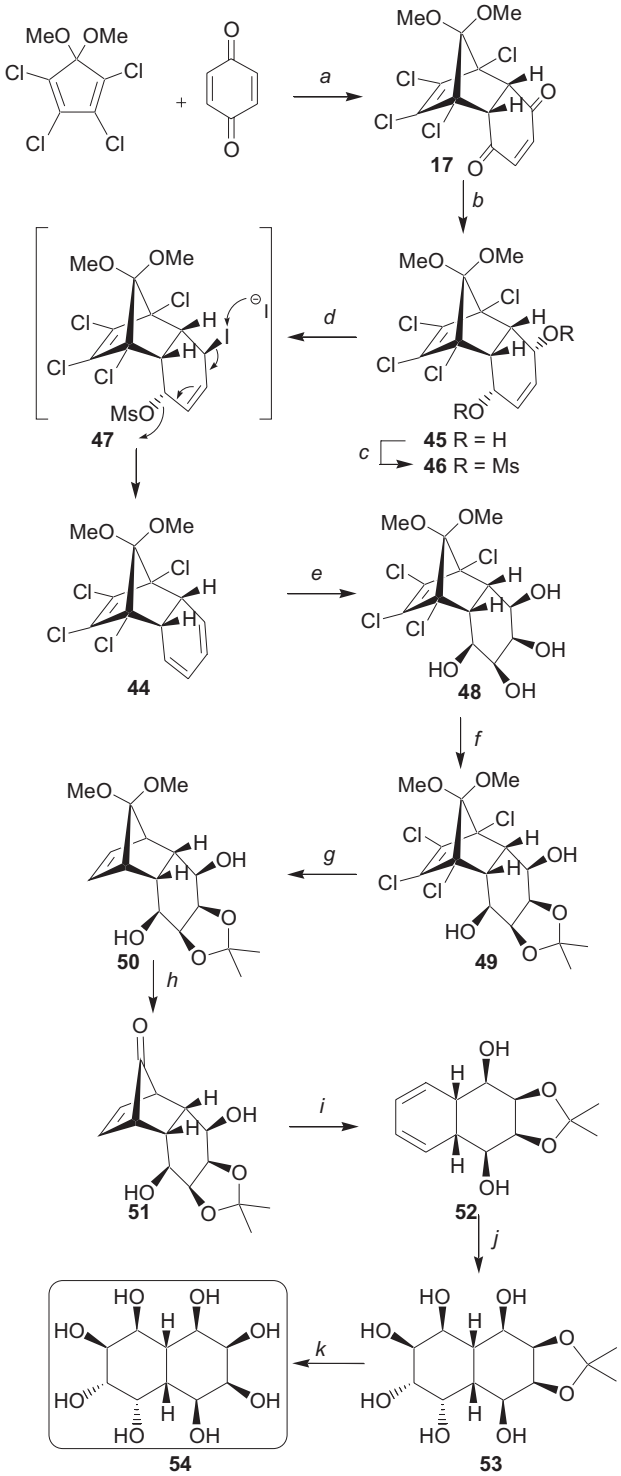


α-allopyranose and α-mannopyranose configurations, respectively.

Synthesis of *cis*-decalin-based bicyclitols

The synthetic venture towards *cis*-decalin-based carbasugar analogues of type **12** emanated from the readily available Diels–Alder adduct **17** of 5,5-dimethoxy-1,2,3,4-tetrachlorocyclopentadiene and *p*-benzoquinone (Scheme 6) (15). Tricyclic quinone **17** was elaborated to the symmetrical tricyclic diene **44** essentially following a literature procedure (16). Adduct **17** was subjected to Luche reduction ($NaBH_4$-$CeCl_3{\cdot}7H_2O$) (17) to give endo,endo-diol **45** and was further

Scheme 6. Reagents and conditions: (*a*) toluene, reflux, 24 h, 83%; (*b*) $NaBH_4$, $CeCl_3{\cdot}7H_2O$, MeOH, 0 °C, 10 min, 69%; (*c*) MsCl, pyridine, DMAP, CH_2Cl_2, rt, 24 h, 72%; (*d*) NaI, $C_2H_5COCH_3$, reflux, 8 h, 80%; (*e*) OsO_4 (1 mol%), NMMO, Me_2CO–H_2O–*t*-BuOH (5:5:2), rt, 48 h, 66%; (*f*) Amberlyst-15, acetone, 4 Å molecular sieves, rt, 3 h, 75%; (*g*) Na, liq. NH_3, THF, EtOH, –33 °C, 30 min, 49%; (*h*) Amberlyst-15, acetone, rt, 2 h, 98%; (*i*) $C_6H_5NO_2$, 160 °C, 4 h, 63%; (*j*) OsO_4 (1 mol%), NMMO, Me_2CO–H_2O–*t*-BuOH (5:5:2), rt, 48 h, 85%; (*k*) 30% CF_3COOH, rt, 30 min, 95%.



© 2005 NRC Canada

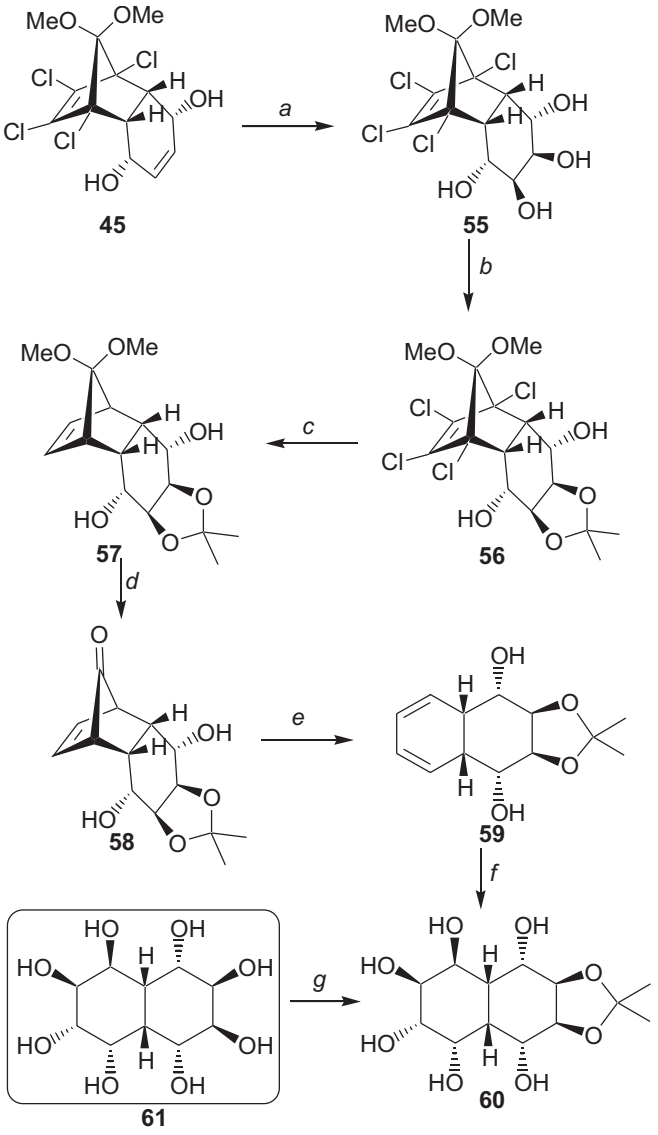
converted to dimesylate **46**, and NaI-mediated 1,4-elimination (via **47**) in **46** led to the desired C_s-symmetric tricyclic diene **44** (Scheme 6). Exhaustive catalytic-OsO_4-mediated dihydroxylation on tricyclic diene **44** furnished tetrol **48** (Scheme 6). The symmetrical nature of the ^1H and ^{13}C NMR spectra of **48** indicated an all cis relationship of the hydroxyl groups, which implied that the double dihydroxylation occurred from the exo-face of the tricyclic diene. Acetonide protection of the vicinal hydroxyl groups in tetrol **48** resulted in selective formation of the symmetrical monoacetonide **49** (Scheme 6). Acetonide **49** was subjected to reductive dechlorination in Na – liquid ammonia milieu to give the symmetrical olefin **50** in a modest yield (Scheme 6). The ketal deprotection in **50** proceeded quite uneventfully to furnish the crystalline 7-norbornenone derivative **51** in quantitative yield (Scheme 6). As contemplated earlier, thermally induced decarbonylation in tricyclic ketone **51** led to the C_s-symmetric bicyclic cyclohexadiene derivative **52** (11).

Bicyclic diene **52** was subjected to exhaustive dihydroxylation employing catalytic OsO_4 to stereoselectively furnish the hexahydroxylated decalin **53** as a single diastereomer (Scheme 6). The stereochemical assignments for **53** were done on the basis of loss of symmetry (NMR) during dihydroxylation and in analogy with earlier observations for compound **25** (see Scheme 3). The acetonide protection in **53** was relieved by exposure to 30% trifluoroacetic acid to deliver the targeted octahydroxylated decalin based carbasugar analogue **54**. Bicyclitol **54** can be regarded as embodying an α-carbagalactopyranose configuration on a *cis*-decalin framework (Scheme 6).

To generate stereochemical variations of hydroxyl groups on the decalin framework, tricyclic endo,endo-diol **45** was dihydroxylated stereoselectively to furnish tetrol **55** (Scheme 7). Dihydroxylation in **55** occurred exclusively from the convex face because of the exo-propensity of the tricyclic system built on a norbornyl scaffold, and the structure of **55** was secured on the basis of symmetry (C_s) revealed by its ^1H and ^{13}C NMR spectra. The cis-diol moiety in **55** was protected using Amberlyst-15 in acetone medium to furnish acetonide **56**. Reductive dechlorination in **56** under Birch reduction conditions delivered the C_s-symmetric olefin **57** (Scheme 7). The ketal moiety in **57** was next deprotected to unmask the carbonyl group and furnish norbornenone derivative **58** (Scheme 7). On thermal activation, tricyclic ketone **58** underwent smooth decarbonylation to furnish the C_s-symmetric bicyclic cyclohexadiene derivative **59** (Scheme 7) (11). Bicyclic diene **59** was diastereomeric with **52** (Scheme 6), and hence the protocol adopted earlier for the elaboration of **52** could be extended to diene **59** for the realization of the targeted octahydroxy polyol.

The 1,3-cyclohexadiene moiety in **59** was double dihydroxylated (OsO_4–NMMO) to furnish the hexahydroxylated *cis*-decalin derivative **60**, which was devoid of any symmetry as indicated by its NMR (^1H and ^{13}C) spectral analysis. Hence, as observed in the case of **25** and **53** (vide supra), the two sequential dihydroxylations on the diene moiety had occurred from opposite faces, thereby generating a cis–trans–cis arrangement of the hydroxyl groups in **60** (Scheme 7). The acetonide deprotection in **60** delivered octahydroxylated decalin **61**, a diastereomeric sibling of **54**.

Scheme 7. Reagents and conditions: (*a*) OsO_4 (1 mol%), NMMO, Me_2CO–H_2O–*t*-BuOH (5:5:2), rt, 1.5 h, 75%; (*b*) Amberlyst-15, acetone, 4 Å molecular sieves, rt, 1 h, 82%; (*c*) Na, liq. NH_3, THF, EtOH, –33 °C, 40 min, 88%; (*d*) Amberlyst-15, acetone, rt, 2 h, 95%; (*e*) $C_6H_5NO_2$, 160 °C, 3 h, 43%; (*f*) OsO_4 (1 mol%), NMMO, Me_2CO–H_2O–*t*-BuOH (5:5:2), rt, 48 h, 73%; (*g*) 30% CF_3COOH, rt, 30 min, 90%.



With the availability of the designer polycyclitols **18**, **26**, **42**, **43**, **54**, and **61**, our attention was turned towards the evaluation of their efficacy as glycosidase inhibitors.

Glycosidase inhibitory potencies of bicyclitols

Evaluation of the glycosidase inhibitory activity of the newly synthesized bicyclitols **18**, **26**, **42**, **43**, **54**, and **61** was carried out against various commercially available glycosidases, α-glucosidase (yeast), β-glucosidase (sweet almond), α-galactosidase (green coffee beans), β-galactosidase (*Escherichia coli*), α-mannnosidase (jack bean) and β-mannnosidase (snail acetone powder), using their corresponding *ortho*- or *para*-nitrophenylglycosides at the optimum pH and temperature for each enzyme (see Experimental) (18). All assays

© 2005 NRC Canada

were done up to 1 mmol/L concentration of the polyols. Gratifyingly, the decalin-based carbasugar analogue **54** exhibited an impressive inhibition of yeast α-glucosidase, with an inhibition constant K_i = 12 μmol/L (cf. K_i = 25 μmol/L for deoxynojirimycin). However, the same compound **54** did not show any significant inhibitory activity against almond β-glucosidase up to 1 mmol/L concentration, thus highlighting the selectivity of **54** towards α-glucosidase. To our further delight, the hydrindane-based polyol **18** exhibited a moderate and selective inhibition of yeast α-glucosidase (K_i = 84 μmol/L) but, like **54**, was totally inert to the almond β-glucosidase. Both these compounds failed to elicit any inhibition of the galactosidases and mannosidases. The other polyols **26**, **42**, **43**, and **61** failed to exhibit any significant (<1 mmol/L) inhibitory activity against the glycosidases examined. The lack of inhibitory activity of polyols **26**, **42**, **43**, and **61** when compared with their diastereomeric siblings **18** and **54**, which inhibited α-glucosidase, brings forth the effect of subtle variations in the stereochemical dispositions of the hydroxyl groups on their inhibitory potency against the carbohydrate processing enzymes. At present, the precise reasons for the selective affinity of **18** and **54** against α-glucosidase and the effect of subtle stereochemical variations on their inhibitory activity is not clear and remains a matter that still tickles our curiosity. Further investigations will hopefully illuminate this puzzling observation.

Conclusion

We have delineated a relatively short and fairly general synthetic access to novel bicyclic carbasugar analogues based on *cis*-decalin and *cis*-hydridane frameworks with as many as eight to seven hydroxyl groups, respectively. The synthetic approaches leading to secured stereochemistry at all the stereogenic centers (nine in **11** and 10 in **12**) in the bicyclitols are notable for their simplicity and stereoselectivity. The decalin-based polyol **54** and hydrindane bicyclitol **18** exhibited significant and selective inhibition of yeast α-glucosidase.

Experimental section

General

Melting points were recorded on a Büchi B-540 apparatus and are uncorrected. IR spectra were recorded on JASCO FT-IR 410 spectrometer. ^{1}H NMR spectra were recorded on a JEOL JNM-LA 300 or a Bruker AMX 400 or a Bruker DRX 500 instrument in $CDCl_3$ solutions, unless otherwise stated. Chemical shifts are reported with respect to tetramethylsilane (Me_4Si) as the internal standard (for ^{1}H NMR) and the central line (77.0 ppm) of $CDCl_3$ (for ^{13}C NMR). The chemical shifts are expressed in parts per million (δ) downfield from Me_4Si. The standard abbreviations s, d, t, q, and m refer to singlet, doublet, triplet, quartet, and multiplet, respectively. Coupling constants (*J*), whenever discernible, have been reported in Hz. Low resolution mass spectra (LR-MS) were recorded either on a Shimadzu GC–MS-QP 5050A spectrometer (EI or CI mode) or on a Q-TOF Micromass mass spectrometer. High resolution mass spectra (HR-MS) were recorded on a Q-TOF Micromass mass spectrometer. Elemental analyses were obtained on a Carlo Erba 1106 CHN analyzer. Silica gel from Acme (100–200 mesh particle size) was used for column chromatography. All moisture- and air-sensitive reactions were performed under an argon atmosphere with dry, freshly distilled solvents under anhydrous conditions using standard syringe–septum techniques. Yields reported are of isolated materials judged homogeneous by thin layer chromatography (TLC) and NMR. All solvent extracts were washed with water/brine as appropriate and dried over anhydr. Na_2SO_4 before removal of the solvent on a rotary evaporator under reduced pressure. The glycosidase enzymes and their corresponding substrates (*ortho*- or *para*-nitrophenolates) were purchased from the Sigma Chemical Company, USA.

1,7,8,9-Tetrachloro-10,10-dimethoxytricyclo[5.2.1.0^{2,6}]deca-4,8-dien-3-ylacetate (19)

Cyclopentadiene (12 g, 0.18 mol) was added to a solution of 5,5-dimethoxy-1,2,3,4-tetrachlorocyclopentadiene (50 g, 0.18 mol) in dry toluene (80 mL) and the resulting solution was refluxed for 24 h. Excess solvent was distilled off from the reaction mixture and the residue obtained was distilled under reduced pressure (130–140 °C/5 torr, 1 torr = 133.3224 Pa) to yield adduct **16** (41.6 g, 70%). To a solution of the $Mn(OAc)_2 \cdot H_2O$ (10.8 g, 44 mmol) in AcOH (40 mL) was added Ac_2O (14 mL) and the mixture was refluxed for 20 min. Solid $KMnO_4$ (1.74 g, 10.1 mmol) was carefully added and the resulting mixture was refluxed for an additional 30 min. After cooling to 70 °C, adduct **16** (12 g, 36.4 mmol) and KBr (720 mg, 6 mmol) were added and the reaction mixture was stirred at the same temperature until complete consumption of the starting material. The reaction mixture was cooled to room temperature and filtered through a Celite pad. The filtrate was extracted with hexane (3 × 100 mL) and the residue obtained after the usual work-up, was chromatographically purified on a silica gel column (5% ethyl acetate – hexane) to afford the exo-acetate **19** (9 g, 64%), mp 111 to 112 °C (lit. value (8*a*) mp 110 °C). IR (Nujol, cm^{-1}): 1740.

10,10-Dimethoxy-3,5-di(acetyloxy)tricyclo[5.2.1.0^{2,6}]dec-8-en-4-yl acetate (22)

To the solution of exo-acetate **19** (4 g, 10.3 mmol) in acetone–water–*t*-BuOH (5:5:1, 25 mL), OsO_4 (26 mg, 1 mol%), and 50% aq. NMMO solution (2.65 mL, 11.3 mmol) were added sequentially. The pale yellow reaction mixture was stirred at room temperature for 12 h prior to quenching of the reaction by addition of solid $NaHSO_3$ (1 g). The resulting mixture was filtered through a Celite pad and the filtrate was concentrated under reduced pressure to give a residue, which on chromatographic purification on a silica gel column furnished diol **20** (3.5 g, 80%). The solution of diol **20** (2.2 g, 5.2 mmol) in dry THF (25 mL) and absolute EtOH (10 mL) was added to freshly distilled liquid ammonia (250 mL) and to this solution, freshly cut pieces of sodium (1 g) were carefully added, until the blue color of the solution persisted. The reaction mixture was stirred for 15 min, prior to quenching the reaction with solid NH_4Cl (1 g). Ammonia was allowed to evaporate overnight, the residue obtained was diluted with ice-cooled water (100 mL) and extracted with ethyl acetate (3 × 100 mL). The usual work-up and evaporation of volatiles under reduced pressure fur-

© 2005 NRC Canada

nished a residue (**21**) that was dissolved in dry pyridine (10 mL), then Ac_2O (1 mL) and catalytic DMAP (100 mg) were added. The reaction mixture was stirred at room temperature for 2 h before diluting with water. The reaction mixture was extracted with CH_2Cl_2 (3 × 60 mL) and after the usual work-up was purified by silica gel column chromatography (20% ethyl acetate – hexane) to furnish triacetate **22** (1.2 g, 64%), mp 140–142 °C. IR (Nujol, cm^{-1}): 1725.

3,4,5-Tri(acetyloxy)tricyclo[5.2.1.0^{2,6}]dec-8-en-10-one (23)

A solution of ketal **22** (200 mg, 0.543 mmol) in moist acetone (8 mL) was stirred with Amberlyst-15 (~30 mg) at room temperature for 1 h. The resin was filtered through a cotton plug and the filtrate was concentrated to give a residue, which was subjected to chromatography on a silica gel column (15% ethyl acetate – hexane) to furnish ketone **23** (155 mg, 89%). IR (Nujol, cm^{-1}): 3036, 1778, 1743. ^{1}H NMR (300 MHz, $CDCl_3$) δ: 6.69 (t, J = 2.4 Hz, 2H), 5.37 (t, J = 3.4 Hz, 1H), 4.55–4.49 (m, 2H), 3.16–3.13 (m, 2H), 2.98–2.96 (m, 2H), 2.14 (s, 3H), 2.05 (s, 6H). LR-MS (CI) m/z: 323 [M^+ + 1]. Anal. calcd. for $C_{16}H_{18}O_7$: C 59.62, H 5.63; found: C 59.66, H 5.69.

1,3-Di(acetyloxy)-2,3,3a,4,5,7a-hexahydro-1*H*-2-indenyl acetate (24)

Ketone **23** (85 mg, 0.264 mmol) was heated to 160 °C in nitrobenzene solvent (2 mL) for 2 h. The reaction mixture was cooled to 80 °C and the nitrobenzene was distilled under reduced pressure. The residue obtained was chromatographed on a silica gel column (10% ethyl acetate – hexane) to deliver the crystalline cyclohexadiene triacetate **24** (39 mg, 50%), mp 198.6–199.9 °C. IR (Nujol, cm^{-1}): 1740. ^{1}H NMR (300 MHz, $CDCl_3$) δ: 5.88–5.84 (m, 2H, C=C*H*), 5.70–5.66 (m, 2H, C=C*H*), 5.25 (t, J = 4.5 Hz, 1H, C*H*OAc), 5.09–5.05 (m, 2H, C*H*OAc), 3.10 (br s, 2H), 2.09 (s, 3H, COCH_3), 2.07 (s, 6H, COCH_3). ^{13}C NMR (75 MHz, $CDCl_3$) δ: 170.1 (2C, *C*OCH$_3$), 170.0 (*C*OCH$_3$), 124.7 (2C, C=CH), 122.4 (2C, C=CH), 78.0 (2C, *C*HOAc), 69.5 (*C*HOAc), 38.9 (2C, *C*H$_{bridgehead}$), 20.7 (2C, CO*C*H$_3$), 20.6 (CO*C*H$_3$). LR-MS (EI, 70 eV) m/z: 252 [M^+ – Ac + 1]. Anal. calcd. for $C_{15}H_{18}O_6$: C 61.22, H 6.16; found: C 61.70, H 6.42.

1,3-Di(acetyloxy)-4,5,6,7-tetrahydroxyperhydro-2-indenyl acetate (25)

To a solution of diene **24** (35 mg, 0.119 mmol) in acetone–water–*t*-BuOH (5:5:2, 2 mL), catalytic OsO_4 (0.3 mg, 1 mol%) and 50% aq. NMMO (83 μL, 0.357 mmol) were sequentially added at 0 °C. The resulting pale yellow reaction mixture was stirred at room temperature for 48 h. The reaction was cooled to 0 °C, prior to quenching by addition of solid $NaHSO_3$ (10 mg). The resulting mixture was diluted with ethyl acetate (15 mL), filtered through Celite, and the filtrate was concentrated under reduced pressure. The residue obtained was subjected to silica gel column chromatography (5% methanol – ethyl acetate) to afford tetrol **25** (38 mg, 88%). IR (Nujol, cm^{-1}): 3290, 1743. ^{1}H NMR (300 MHz, D_2O) δ: 5.38 (t, J = 6.3 Hz, 1H), 5.27 (dd, J = 6.3, 1.8 Hz, 1H), 5.08 (t, J = 6.9 Hz, 1H), 3.97 (br s, 1H), 3.90 (t, J = 3.9 Hz, 1H), 3.78 (dd, J = 7.8, 3.6 Hz, 1H), 3.66 (dd, J = 8.1, 3 Hz, 1H), 2.52 (m, 1H), 2.40 (br s, 1H), 1.99 (s, 6H, COCH_3), 1.95 (s, 3H, COCH_3). ^{13}C NMR (75 MHz, D_2O) δ: 174.2 (*C*OCH$_3$), 174.1 (*C*OCH$_3$), 173.2 (*C*OCH$_3$), 75.0, 74.7, 71.7, 71.1, 70.0, 69.0, 68.6, 45.6 (CH$_{bridgehead}$), 43.5 (CH$_{bridgehead}$), 20.9 (*C*OCH$_3$), 20.8 (CO*C*H$_3$), 20.5 (CO*C*H$_3$). Anal. calcd. for $C_{15}H_{22}O_{10}$: C 49.72, H 6.12; found: C 49.53, H 6.52.

Bicyclitol 18

Tetrol **25** (22 mg, 0.061 mmol) was stirred with aq. NaOH (0.5 mol/L, 200 μL) at room temperature for 1 h and the volatiles were removed under reduced pressure. The residue obtained was dissolved in double distilled water and the solution was filtered with Dowex cation-exchange resin (50 W × 8, H^+ form). The filtrate was concentrated to furnish **18** (8 mg, 60%). ^{1}H NMR (300 MHz, D_2O) δ: 4.13 (t, J = 4.3 Hz, 1H), 3.98–3.85 (m, 4H), 3.73 (dd, J = 7.3, 4.0 Hz, 1H), 3.61 (dd, J = 7.6, 2.8 Hz, 1H), 2.21–2.08 (m, 2H). ^{13}C NMR (100 MHz, D_2O) δ: 76.4 (*C*HOH), 75.0 (*C*HOH), 74.6 (*C*HOH), 74.4 (*C*HOH), 73.1 (*C*HOH), 71.9 (*C*HOH), 71.8 (*C*HOH), 48.3 (CH$_{bridgehead}$), 47.2 (CH$_{bridgehead}$). LR-MS (CI) m/z: 237 [M^+ + 1]. Anal. calcd. for $C_9H_{16}O_7$: C 45.76, H 6.83; found: C 45.84, H 6.79.

(2*R,3*R**,7*S**,8*R**,9*S**)-5,5-Dimethylspiro[dihydro[1,3]dioxolane]-2,13-4,6-dioxatetracyclo[8.2.1.0^{2,9}.0^{3,7}]tridecen-8-ol (32)**

To a magnetically stirred solution of alcohol **28** (8) (2 g, 9.7 mmol) in CH_2Cl_2 (20 mL), NBS (2.1 g, 11.6 mmol) was added in one portion at room temperature and the resulting suspension was stirred for 3 h. Upon complete consumption of the starting material (TLC), the reaction mixture was diluted with CH_2Cl_2 (80 mL) and water (50 mL). Following the usual work-up, subsequent evaporation of the solvent gave a residue, which on chromatographic purification on a silica gel column furnished **29** (2.2 g, 80%). Osmium tetroxide (16 mg, 1 mol%) and 50% aq. NMMO (2.28 mL, 9.75 mmol) was added to a solution of bromoether **29** (1.85 g, 6.5 mmol) in an acetone–water–*t*-BuOH (5:5:2, 25 mL) solvent system, and the resulting pale yellow reaction mixture was stirred at room temperature for 12 h. The reaction mixture was cooled to ice-bath temperature, diluted with ethyl acetate (70 mL), and the osmate ester was hydrolyzed by addition of solid $NaHSO_3$ (500 mg). The solution was filtered through a Celite pad and the filtrate was concentrated under reduced pressure to furnish the crude diol **30** (1.76 g). The crude diol **30** was dissolved in dry acetone (20 mL) and Amberlyst-15 (300 mg) and powdered molecular sieves (1 g) were added. The reaction mixture was stirred for 3 h at room temperature and then was filtered through a Celite pad. The filtrate obtained on complete removal of the solvent was chromatographed on a silica gel column to furnish acetonide **31** (1.76 g, 75%). To a solution of bromoether **31** (1 g, 2.78 mmol) in MeOH (15 mL), acetic acid (0.1 mL) and Zn dust (550 mg, 8.34 m atom) were added sequentially at room temperature and the resulting suspension was stirred for 4 h. The reaction mixture was filtered through a Celite pad and the filtrate was concentrated under reduced pressure. The residue obtained was diluted with CH_2Cl_2 (60 mL) and evaporation of the solvent furnished a residue, which on purification on a silica gel column gave alcohol **32** (660 mg, 85%), mp 96 to 97 °C (lit. value (8*a*) mp 98 °C). IR (Nujol, cm^{-1}): 3400.

© 2005 NRC Canada

(2*R,3*R**,7*S**,8*R**,9*S**)-8-Hydroxy-5,5-dimethyl-4,6-dioxatetracyclo[8.2.1.0^{2,9}.0^{3,7}]tridec-11-en-13-one (33)**

Ketal **32** (350 mg, 1.24 mmol) was stirred with Amberlyst-15 (~50 mg) in moist acetone (10 mL), under reflux for 3 h. Upon complete consumption of the starting material, the reaction mixture was cooled, diluted with acetone (25 mL), and the resin was filtered through a cotton plug. The filtrate was concentrated under reduced pressure and the residue obtained was chromatographed on a silica gel column (30% ethyl acetate – hexane) to give ketone **33** (237 mg, 81%), mp 179 to 180 °C. IR (Nujol, cm^{-1}): 1771. ^{1}H NMR (300 MHz, $CDCl_3$) δ: 6.64 (m, 1H), 6.48 (m, 1H), 4.36 (dd, *J* = 9.3, 5.4 Hz, 1H), 4.10 (d, *J* = 5.4 Hz, 1H), 4.03 (t, *J* = 5.4 Hz, 1H), 3.20 (dt, *J* = 8.7, 3.9 Hz, 1H), 3.14–2.95 (m, 3H), 1.44 (s, 3H), 1.23 (s, 3H). ^{13}C NMR (75 MHz, $CDCl_3$) δ: 200.1 (C=O), 135.2 (C=*C*H), 130.3 (C=*C*H), 110.8 (C_q), 89.4 (*C*H$_{acetonide}$), 82.0 (*C*H$_{acetonide}$), 81.3 (*C*HOH), 49.2, 49.0 (CH), 47.1 (CH), 44.4 (CH), 27.9 (CH$_{3acetonide}$), 25.3 (CH$_{3acetonide}$). LR-MS (EI, 70 eV) *m*/*z*: 237 [M$^+$ + 1]. Anal. calcd. for $C_{13}H_{16}O_4$: C 66.09, H 6.83; found: C 66.46, H 7.22.

(3a*R,3b*S**,7a*R**,8*R**,8a*S**)-2,2-Dimethyl-3b,7a,8,8a-tetrahydro-3a*H*-indeno[1,2-*d*][1,3]dioxol-8-ol (34)**

A solution of ketone **33** (220 mg, 0.932 mmol) in nitrobenzene (6 mL) solvent was heated, with vigorous stirring, to 160 °C and reacted for 4 h. Upon complete consumption of the starting material (TLC), the reaction mixture was cooled to 80 °C and the solvent was distilled off under reduced pressure. The resulting dark brown residue was charged on the silica gel column and chromatographed (25% ethyl acetate – hexane) to give diene **34** (130 mg, 67%) as a white solid, mp 190.6–191.2 °C. IR (Nujol, cm^{-1}): 3470. ^{1}H NMR (300 MHz, $CDCl_3$) δ: 6.17 (dd, *J* = 9.9, 5.1 Hz, 1H, C= C*H*), 5.80 (dd, *J* = 9.9, 4.8 Hz, 2H, C= C*H*), 5.72–5.70 (m, 1H), 4.74 (d, *J* = 6.0 Hz, 1H, H$_{acetonide}$), 4.45 (d, *J* = 6 Hz, 1H, H$_{acetonide}$), 4.03 (br s, 1H, C*H*OH), 3.08–3.05 (m, 2H, H$_{bridgehead}$), 2.26 (d, *J* = 2.4 Hz, 1H, H$_{bridgehead}$), 1.42 (s, 3H), 1.31 (s, 3H). ^{13}C NMR (75 MHz, $CDCl_3$) δ: 129.2 (C=*C*H), 127.6 (C=*C*H), 123.3 (C=*C*H), 122.9 (C=*C*H), 110.4 (C_q), 87.3 (*C*H$_{acetonide}$), 83.9 (*C*H$_{acetonide}$), 79.6 (*C*HOH), 45.3 (CH), 39.6 (CH), 26.8 (CH$_{3bridgehead}$), 24.3 (CH$_{3bridgehead}$). LR-MS (EI, 70 eV) *m*/*z*: 208 [M$^+$]. Anal. calcd. for $C_{12}H_{16}O_3$: C 69.21, H 7.74; found: C 68.88, H 7.52.

(3a*R,3b*R**,4*S**,5*S**,6*S**,7*S**,7a*S**,8*R**,8a*S**)-2,2-Dimethylperhydroindeno[1,2-*d*][1,3]dioxole-4,5,6,7,8-pentaol (35)**

To a solution of diene **34** (45 mg, 0.216 mmol) in an acetone–water–*t*-BuOH (5:5:2, 4 mL) solvent system, catalytic OsO_4 (1 mol%, 0.5 mg) and 50% aq. NMMO (151 μL, 0.648 mmol) were added at 0 °C. The resulting pale yellow reaction mixture was stirred at room temperature for 48 h, before diluting with ethyl acetate (10 mL) and quenching with solid $NaHSO_3$ (10 mg). The resulting mixture was filtered through a Celite pad and the filtrate was concentrated under reduced pressure. The residue was subjected to silica gel column chromatography (5% methanol – ethyl acetate) to afford pentaol **35** (49 mg, 83%). ^{1}H NMR (300 MHz, D_2O) δ: 4.70–4.65 (m, 1H), 4.35 (dd, *J* = 6.0, 1.8 Hz, 1H), 4.06 (m, 1H), 3.98–3.93 (m, 2H), 3.69–3.58 (m, 2H), 2.59–2.51 (m, 1H, H$_{bridgehead}$), 2.41–2.37 (m, 1H, H$_{bridgehead}$), 1.32 (s, 3H), 1.20 (s, 3H). ^{13}C NMR (75 MHz, D_2O) δ: 111.0 (C_q), 87.9 (*C*H$_{acetonide}$), 83.0 (*C*H$_{acetonide}$), 77.1 (*C*HOH), 70.5, 70.4, 70.3, 69.2, 45.8, 45.6, 25.8 (C$_{bridgehead}$), 23.4 (C$_{bridgehead}$). LR-MS (EI, 70 eV) *m*/*z*: 258 [M$^+$ – H_2O].

Bicyclitol 26

Acetonide **35** (25 mg, 0.09 mmol) was stirred in 30% trifluoroacetic acid (1 mL) at room temperature for 30 min until all the starting material had been consumed. The volatiles were removed under reduced pressure to furnish polyol **26** (19 mg, 89%). ^{1}H NMR (300 MHz, D_2O) δ: 4.19–4.15 (m, 1H), 4.01–3.81 (m, 4H), 3.68–3.64 (m, 1H), 3.61–3.56 (m, 1H), 2.40–2.33 (m, 1H), 2.13–2.07 (m, 1H). ^{13}C NMR (75 MHz, D_2O) δ: 77.9, 77.2, 73.6, 72.9, 72.3, 68.4, 67.4, 45.9, 41.8. LR-MS (CI) *m*/*z*: 237 [M$^+$ + 1]. Anal. calcd. for $C_9H_{16}O_7$: C 45.76, H 6.83; found: C 45.88, H 7.32.

(2*S,3*R**,7*S**,8*R**,9*R**)-5,5-Dimethyl-4,6,11,12-tetraoxatetracyclo[8.2.2.0^{2,9}.0^{3,7}]tetradec-13-en-8-ol (36)**

A slow stream of oxygen gas was bubbled through a solution of diene **34** (60 mg, 0.288 mmol) in chloroform (6 mL), contained in a specially designed reaction flask with an outer water jacket, in the presene of methylene blue (~5 mg) as the sensitizer and under irradiation from a 500 W tungsten lamp. The temperature of the reaction mixture was maintained at 20 °C by circulating cold water through the outer jacket of the reaction flask. Upon complete consumption of the starting material (TLC, 8 h), the solvent was evaporated under reduced pressure. The residue obtained was chromatographed over a silica gel column (20% ethyl acetate – hexane) to furnish the endo-peroxide **36** (62 mg, 90%). IR (KBr, cm^{-1}): 3445. ^{1}H NMR (300 MHz, $CDCl_3$) δ: 6.78 (m, 1H, C=C*H*), 6.59 (m, 1H, C=C*H*), 4.85–4.80 (m, 2H, H$_{peroxy}$), 4.36 (dd, *J* = 9.0, 5.2 Hz, 1H, H$_{acetonide}$), 4.17 (t, *J* = 5.2 Hz, 1H, H$_{acetonide}$), 4.11 (d, *J* = 6.0 Hz, 1H), 3.33 (dt, *J* = 8.7, 4.0 Hz, 1H, H$_{bridgehead}$), 3.08 (dd, *J* = 8.7, 5.2 Hz, 1H), 1.47 (s, 3H, C*H*$_3$), 1.26 (s, 3H, C*H*$_3$). ^{13}C NMR (75 MHz, $CDCl_3$) δ: 135.3 (C=*C*H), 130.2 (C=*C*H), 111.7 (C_q), 88.0, 80.9, 79.9, 70.9 (*C*H$_{peroxy}$), 70.8 (*C*H$_{peroxy}$), 44.5, 44.0, 27.8, 25.2. LR-MS (CI) *m*/*z*: 241 [M$^+$ + 1]. Anal. calcd. for $C_{12}H_{16}O_5$: C 59.99, H 6.71; found: C 60.21, H 6.83.

(3a*R,3b*R**,4*R**,7*S**,7a*S**,8*R**,8a*S**)-2,2-Dimethyl-3b,4,7,7a,8,8a-hexahydro-3a*H*-indeno[1,2-*d*][1,3]dioxole-4,7,8-triol (37)**

$LiAlH_4$ (12 mg, 0.312 mmol) was added to a solution of the endo-peroxide **36** (50 mg, 0.208 mmol) in dry THF (6 mL) at 0 °C under an atmosphere of N_2. The resulting suspension was stirred at room temperature for 1 h, before quenching the reaction by careful addition of ethyl acetate (15 mL) followed by addition of a cold, satd. Na_2SO_4 solution (2 mL). After dilution with ethyl acetate, the aluminium salts were filtered through a Celite pad. Evaporation of the solvent under reduced pressure, after the usual work-up, gave a residue that was chromatographed over a silica gel column (60% ethyl acetate – hexane) to furnish the 1,4-diol **37** (27 mg, 54%), mp 210 to 211 °C. IR (Nujol, cm^{-1}): 3444. ^{1}H NMR (300 MHz, $CDCl_3$) δ: 5.69 (br s, 2H, C=CH), 4.71

© 2005 NRC Canada

(d, *J* = 5.7 Hz, 1H), 4.42 (d, *J* = 5.7 Hz, 1H), 4.13 (br s, 1H), 4.07 (d, *J* = 4.8 Hz, 1H), 3.81 (d, *J* = 7.8 Hz, 1H), 2.36 (m, 1H), 1.90 (t, *J* = 8.4 Hz, 1H), 1.33 (s, 3H), 1.22 (s, 3H). ^{13}C NMR (75 MHz, $CDCl_3$) δ: 133.6 (C=*C*H), 129.9 (C=*C*H), 111.5 (C_q), 86.0, 83.2, 77.7, 66.5, 62.5, 46.3, 46.1, 25.7, 23.5. LR-MS (CI) *m*/*z*: 243 [M^+ + 1]. Anal. calcd. for $C_{12}H_{18}O_5$: C 59.49, H 7.49; found: C 59.63, H 7.52.

(3a*R,3b*R**,4*S**,5*S**,6*R**,7*R**,7a*S**,8*R**,8a*S**)-2,2-Dimethylperhydroindeno[1,2-d][1,3]dioxole-4,5,6,7,8-pentaol (38) and (3a*R**,3b*R**,4*S**,5*R**,6*S**,7*R**,7a*S**,8*R**,8a*S**)-2,2-dimethylperhydroindeno[1,2-d][1,3]dioxole-4,5,6,7,8-pentaol (39)**

To a solution of diol **37** (55 mg, 0.227 mmol) in an acetone–water–*t*-BuOH (5:5:2, 5mL) solvent system, catalytic OsO_4 (0.6 mg, 1 mol%), and 50% aq. NMMO (64 μL, 0.272 mmol) were added sequentially at 0 °C and the resulting mixture was stirred at room temperature for 1 h. The reaction was quenched by addition of solid $NaHSO_3$ (10 mg), diluted with ethyl acetate (15 mL), and filtered through a Celite pad. The filtrate was concentrated under reduced pressure to yield a residue, whose ^{1}H NMR spectrum was found to be a mixture of diastereomers **38** and **39** (60 mg) in a 3:1 ratio. However, their chromatographic separation was unsuccessful and the mixture was used as such for the next step.

(3a*R,3b*S**,6a*S**,6b*S**,6*R**,9a*S**,10*R**,10a*R**,10b*R**)-2,2,5,5,8,8-Hexamethylperhydrodi[1,3]dioxolo-[4′,5′:1,2:4′,5′:6,7]indeno[4,5-*d*][1,3]dioxole-10-ol (40) and (3a*R**,3b*R**,4*S**,4a*R**,7a*S**,8*R**,8a*R**,9*R**,9a*S**)-2,2,6,6-tetramethylperhydro[1,3]dioxolo[4′,5′:1,2]indeno[5,6-*d*][1,3]dioxole-4,8,9-triol (41)**

The solution of mixture of **38** and **39** (60 mg) in dry acetone (10 mL) was treated sequentially with Amberlyst-15 resin (~5 mg) and 4 Å molecular sieves (~30 mg) and the resulting mixture was stirred at room temperature for 3 h. The reaction mixture was filtered through a Celite pad and the filtrate was concentrated under reduced pressure. The residue obtained was charged on a silica gel column and chromatographed with a 10% ethyl acetate – hexane solvent system to furnish trisacetonide **40** (48 mg, 62%). Further elution of the column with 30% ethyl acetate –hexane gave bisacetonide **41** (14 mg, 21%). Compound **40:** mp 210 to 211 °C. IR (Nujol, cm^{-1}): 3361. ^{1}H NMR (300 MHz, $CDCl_3$) δ: 4.75 (d, *J* = 6.0 Hz, 1H), 4.42 (dd, *J* = 9.6, 5.1 Hz, 2H), 4.36 (dd, *J* = 13.5, 5.1 Hz, 1H), 4.28 (dd, *J* = 6.9, 4.5 Hz, 1H), 4.08 (d, *J* = 5.1 Hz, 1H), 3.93 (t, *J* = 6.9 Hz, 1H), 2.64–2.55 (m, 2H), 1.53 (s, 3H), 1.51 (s, 3H), 1.41 (s, 3H), 1.37 (s, 3H), 1.35 (s, 3H), 1.26 (s, 3H). LR-MS (EI, 70 eV) *m*/*z*: 356 [M^+]. Compound **41**: mp 190 to 191 °C. IR (Nujol, cm^{-1}): 3372. ^{1}H NMR (300 MHz, $CDCl_3$) δ: 4.74 (br d, *J* = 5.1 Hz, 1H), 4.49 (d, *J* = 5.1 Hz, 1H), 4.41 (br d, *J* = 5.4 Hz, 1H), 4.15–4.10 (m, 2H), 4.02–3.96 (m, 1H), 3.73 (dd, *J* = 12.3, 6.9 Hz, 1H), 2.53–2.50 (m, 2H), 1.51 (s, 3H), 1.43 (s, 3H), 1.34 (s, 3H), and 1.30 (s, 3H). LR-MS (EI, 70 eV) *m*/*z*: 317 [M^+ + 1].

Bicyclitol 42

Trisacetonide **40** (35 mg, 0.098 mmol) was stirred with 30% trifluoroacetic acid (500 μL) at room temperature for 30 min. Upon complete consumption of the starting material, the volatiles were removed under reduced pressure to afford **42** (21 mg, 92%). ^{1}H NMR (300 MHz, D_2O) δ: 4.03 (dd, *J* = 6.9, 4.5 Hz, 1H), 3.89–3.85 (m, 2H), 3.74–3.70 (m, 3H), 3.62 (dd, *J* = 6.6, 3 Hz, 1H), 2.46 (dd, *J*= 14.4, 6.9 Hz, 1H), 2.11 (dd, *J* = 12.3, 6.9 Hz, 1H). ^{13}C NMR (75 MHz, D_2O) δ: 78.9, 77.6, 72.7, 72.2, 71.5, 70.8, 70.1, 47.5, 41.0. LR-MS (CI) *m*/*z*: 237 [M^+ + 1]. Anal. calcd. for $C_9H_{16}O_7$: C 45.76, H 6.83; found: C 45.53, H 6.79.

Bicyclitol 43

Bisacetonide **41** (10 mg, 0.032 mmol) was treated with 30% trifluoroacetic acid (150 μL) and the resulting biphasic mixture was stirred vigorously at room temperature for 30 min. The volatiles were removed under reduced pressure to furnish **43** (7 mg, 88%). ^{1}H NMR (300 MHz, D_2O) δ: 4.10 (t, 1H, *J* = 5.7 Hz), 4.00 (t, 1H, *J* = 5.4 Hz), 3.86 (t, *J* = 5.4 Hz, 1H), 3.83 (dd, *J* = 14, 7.2 Hz, 1H), 3.75–3.70 (m, 1H), 3.66–3.61 (m, 2H), 2.36 (dd, *J* = 15, 6.9 Hz, 1H), 1.93 (dd, *J* = 14.4, 6.9 Hz, 1H). ^{13}C NMR (75 MHz, D_2O) δ: 77.8, 77.1, 74.0, 73.2, 72.3, 72.0, 68.8, 48.6, 44.2. LR-MS (CI) *m*/*z*: 237 [M^+ + 1]. Anal. calcd. for $C_9H_{16}O_7$: C 45.76, H 6.83; found: C 45.77, H 6.98.

(2*R,3*S**,6*R**,7*S**)-1,8,9,10-Tetrachloro-11,11-dimethoxytricyclo[6.2.1.0^{2,7}]undeca-4,9-diene-3,6-diol (45)**

To a solution of 1,2,3,4-tetrachloro-5,5-dimethoxycyclopentadiene (63 mL, 0.36 mol) in dry toluene (300 mL), *p*-benzoquinone (40 g, 0.37 mol) was added and the resulting solution was refluxed for 24 h. Excess solvent was distilled off under reduced pressure and the residue obtained was recrystallized from hexane to furnish adduct **17** (110 g, 83%). Adduct **17** (10 g, 26.8 mmol) was dissolved in dry MeOH (150 mL) and to this solution at 0 °C under an inert atmosphere, $CeCl_3 \cdot 7H_2O$ (1 g, 10 mol%) and $NaBH_4$ (2 g, 53.6 mmol) were added in sequential portions. The resulting solution was stirred at the same temperature for 10 min until the starting material was completely consumed. The reaction mixture was diluted with ethyl acetate (150 mL) and quenched by the addition of water (80 mL). The organic layer was separated and after the usual work-up furnished residue **45** (6.9 g, 69%), mp 162 to 163 °C (lit. value (16) mp 167 to 168 °C). IR (Nujol, cm^{-1}): 3450.

(2*R,7*S**)-1,8,9,10-Tetrachloro-11,11-dimethoxytricyclo[6.2.1.0^{2,7}]undeca-3,5,9-triene (44)**

To a magnetically stirred solution of diol 45 (5 g, 13.3 mmol) in dry CH_2Cl_2 (25 mL), triethylamine (5.6 mL, 39.9 mmol), DMAP (162 mg, 10 mol%), and methanesulphonyl chloride (2.5 mL, 29.2 mmol) were added sequentially at 0 °C under an inert atmosphere and the resulting solution was stirred at room temperature for a further 24 h. The reaction mixture was diluted with CH_2Cl_2 (50 mL) prior to quenching the reaction by adding water (30 mL). The organic layer was separated and the aqueous layer was extracted with CH_2Cl_2 (3 × 60 mL). The residue obtained by the usual work-up was subjected to chromatographic purification on a silica gel column (35% ethyl acetate – hexane) to furnish dimesylate **46** (5.1 g, 72%). Dimesylate **46** (8.4 g, 15.7 mmol) was dissolved in 2-butanone (60 mL) and so-

© 2005 NRC Canada

dium iodide (8.2 g, 54.9 mmol) was added to this solution. The dark brown solution was then refluxed for 8 h. The reaction mixture was cooled to ice bath temperature and diluted with diethylether (100 mL) and water (80 mL). The usual work-up and evaporation of the solvent under reduced pressure gave a residue, which on purification on a silica gel column (hexane) furnished the tricyclic diene **44** (4.3 g, 80%), mp 162 to 163 °C (lit. value (16) mp 167 to 168 °C).

(2*R,3*S**,4*S**,5*R**,6*R**,7*S**)-1,8,9,10-Tetrachloro-11,11-dimethoxytricyclo[6.2.1.0^{2,7}]undec-9-ene-3,4,5,6-tetraol (48)**

A solution of diene **44** (1.2 g, 3.51 mmol) in an acetone–water–*t*-BuOH solvent system (5:5:2, 50 mL) was treated sequentially with catalytic OsO_4 (8 mg, 1 mol%) and 50% aq. NMMO (2.5 mL, 10.53 mmol). The resulting pale yellow solution was stirred vigorously at room temperature for 48 h, during which all the starting material was consumed (TLC). The reaction was quenched by addition of solid $NaHSO_3$ (500 mg), diluted with ethyl acetate (100 mL), and filtered through a Celite pad. The filtrate was concentrated under reduced pressure to give a residue, which was chromatographed on a silica gel column (70% ethyl acetate – hexane) to furnish tetrol **48** (950 mg, 66%). IR (Nujol, cm^{-1}): 3430. ^{1}H NMR (300 MHz, $CDCl_3$) δ: 3.76 (br s, 2H), 3.66 (br s, 2H), 3.63 (s, 3H), 3.56 (s, 3H), 3.14 (m, 2H). ^{13}C NMR (75 MHz, $CDCl_3$) δ: 129.7 (2C, C=*C*Cl), 111.7 (C_q), 70.7 (2C, *C*HOH), 68.0 (2C, *C*HOH), 52.8 (2C, *C*-Cl), 52.5 (2C, OMe), 51.8 (2C, CH). LR-MS (EI, 70 eV) *m*/*z*: 410 [M$^+$ + 1].

(2*R,3*S**,4*S**,8*R**,9*R**,10*S**)-1,11,12,13-Tetrachloro-14,14-dimethoxy-6,6-dimethyl-5,7-dioxatetracyclo[9.2.1.0^{2,10}.0^{4,8}]tetradec-12-ene-3,9-diol (49)**

Tetrol **48** (950 mg, 2.32 mmol) was stirred with Amberlyst-15 (~100 mg) and 4 Å molecular sieves (500 mg) in dry acetone (30 mL) at room temperature for 3 h. Upon complete consumption of the starting material, the reaction mixture was filtered through a Celite pad. The filtrate was concentrated under reduced pressure to give a residue, which was chromatographed over a short silica gel column (25% ethyl acetate – hexane) to afford acetonide **49** (783 mg, 75%), mp 180.1–181.4 °C. IR (Nujol, cm^{-1}): 3346. ^{1}H NMR (300 MHz, $CDCl_3$) δ: 4.44 (s, 2H), 3.63 (s, 3H), 3.59 (s, 3H), 3.11–3.01 (m, 2H), 2.29 (d, *J* = 6.6 Hz, 2H), 1.57 (s, 3H), 1.37 (s, 3H). LR-MS (EI, 70 eV) *m*/*z*: 451 [M$^+$ + 1]. Anal. calcd. for $C_{16}H_{20}O_6Cl_4$: C 42.69, H 4.48; found: C 42.84, H 4.80.

(2*R,3*R**,4*R**,8*S**,9*S**,10*S**)-14,14-Dimethoxy-6,6-dimethyl-5,7-dioxatetracyclo[9.2.1.0^{2,10}.0^{4,8}]tetradec-12-ene-3,9-diol (50)**

Liquid ammonia (300 mL) was distilled into a 250 mL three-necked round-bottomed flask equipped with a condenser, KOH guard tube, and septum. Acetonide **49** (10 g, 22.22 mmol) in dry THF (40 mL) and absolute EtOH (40 mL) were added to the flask. Small pieces of freshly cut sodium were introduced into the reaction mixture with stirring at –33 °C until the blue color persisted. The mixture was stirred for 30 min and solid NH_4Cl (1 g) was added. The excess ammonia was allowed to evaporate, and a cold aq. satd. NH_4Cl solution (50 mL) and water (100 mL) were added to the resulting residue, which was subsequently extracted with ethyl acetate (3 × 200 mL). Removal of the volatiles, followed by purification of the residue by silica gel column chromatography (50% ethyl acetate – hexane) gave the dechlorinated product **50** (3.4 g, 49%), mp 173–175 °C. IR (Nujol, cm^{-1}): 3460, 3380. ^{1}H NMR (300 MHz, $CDCl_3$) δ: 6.93 (s, 2H, C=C*H*), 4.38 (s, 2H), 3.24 (s, 3H), 3.17 (s, 5H), 3.05 (s, 2H), 2.60–2.50 (m, 2H), 1.91 (s, 1H), 1.88 (s, 1H), 1.53 (s, 3H), 1.35 (s, 3H). ^{13}C NMR (75 MHz, $CDCl_3$) δ: 133.8 (2C, C=*C*H), 118.9 (C_q), 110.0 (C_q), 76.6 (2C, $C_{acetonide}$), 68.8 (2C, *C*HOH), 52.0 (O*C*H$_3$), 50.0 (O*C*H$_3$), 46.8 (2C, CH), 40.4 (2C, CH), 25.9 (CH), 24.0 (CH). LR-MS (EI, 70 eV) *m*/*z*: 312 [M$^+$]. Anal. calcd. for $C_{16}H_{24}O_6$: C 61.52, H 7.74; found: C 61.83, H 7.90.

(2*R,3*R**,4*R**,8*S**,9*S**,10*S**)-3,9-Dihydroxy-6,6-dimethyl-5,7-dioxatetracyclo[9.2.1.0^{2,10}.0^{4,8}]tetradec-12-en-14-one (51)**

A solution of ketal **50** (1 g, 3.20 mmol) in moist acetone (40 mL) was stirred with Amberlyst-15 (~150 mg) at room temperature for 2 h. Upon complete consumption of the starting material, the reaction mixture was filtered through a cotton plug. The filtrate on concentration gave a solid residue, which on purification by chromatography over a short silica gel column (50% ethyl acetate – hexane) afforded ketone **51** (834 mg, 98%), mp 213–215 °C. IR (Nujol, cm^{-1}): 3270, 1777.

(3a*R,4*R**,4a*S**,8a*R**,9*S**,9a*S**)-2,2-Dimethyl-3a,4,4a,8a,9,9a-hexahydronaphtho[2,3-*d*][1,3]dioxole-4,9-diol (52)**

A solution of ketone **51** (300 mg, 1.13 mmol) in nitrobenzene (15 mL) was heated, with vigorous stirring, at 160 °C for 4 h. Upon complete consumption of the starting material (TLC), the reaction mixture was cooled to 80 °C and the solvent was distilled off under reduced pressure. The residue left behind was chromatographed over a silica gel column (30% ethyl acetate – hexane) to furnish diene **52** (169 mg, 63%) as a colorless solid, mp 189 to 190 °C. IR (KBr, cm^{-1}): 3356. ^{1}H NMR (300 MHz, $CDCl_3$) δ: 5.87–5.83 (m, 2H, C=C*H*), 5.65–5.61 (m, 2H, C=C*H*), 4.42–4.40 (m, 2H, $H_{acetonide}$), 3.74 (br s, 2H, C*H*OH), 3.00–2.98 (m, 2H, O*H*), 2.70–2.67 (m, 2H), 1.55 (s, 3H), 1.40 (s, 3H). ^{13}C NMR (75 MHz, $CDCl_3$) δ: 125.8 (2C, C=*C*H), 122.6 (2C, C=*C*H), 109.3 (C_q), 74.8 (2C, $C_{acetonide}$), 69.0 (2C, *C*HOH), 35.4 (2C, CH), 26.0 (CH), 24.4 (CH). LR-MS (EI, 70 eV) *m*/*z*: 239 [M$^+$ + 1]. Anal. calcd. for $C_{13}H_{18}O_4$: C 65.53, H 7.61; found: C 65.90, H 7.72.

(3a*R,4*R**,4a*R**,5*S**,6*S**,7*S**,8*S**,8a*S**,9*S**,9a*S**)-2,2-Dimethylperhydronaphtho[2,3-*d*][1,3]dioxole-4,5,6,7,8,9-hexol (53)**

Diene **52** (25 mg, 0.105 mmol) was treated sequentially with catalytic amounts of OsO_4 (0.2 mg, 1 mol%) and 50% aq. NMMO (54 μL, 0.231 mmol) in an acetone–water–*t*-BuOH solvent system (5:5:2, 5 mL) at 0 °C and the resulting pale yellow reaction mixture was stirred at room temperature for 48 h. The reaction mixture was cooled to 0 °C and diluted with ethyl acetate (20 mL) prior to quenching with

© 2005 NRC Canada

solid $NaHSO_3$ (10 mg). The mixture was filtered through a Celite pad and the filtrate was concentrated. The residue thus obtained was chromatographed over a silica gel column (8% methanol – ethyl acetate) to furnish hexol **53** (27 mg, 85%). IR (Nujol, cm^{-1}): 3350. ^1H NMR (300 MHz, D_2O) δ: 4.46–4.43 (m, 1H), 4.35–4.31 (m, 1H), 4.13–4.11 (br t, *J* = 3.3 Hz, 1H), 3.97 (br dd, *J* = 6.6, 2.7 Hz, 1H), 3.92 (br s, 1H), 3.85 (br dd, *J* = 12.0, 3.0 Hz, 1H), 3.71 (br dd, *J* = 8.7, 2.1 Hz, 1H), 3.64–3.61 (m, 1H), 2.21 (m, 1H), 2.06 (m, 1H), 1.39 (s, 3H), 1.26 (s, 3H). ^{13}C NMR (75 MHz, D_2O) δ: 111.1 (C_q), 77.9, 76.6, 72.8, 71.3, 70.9, 70.7, 68.4, 66.2, 40.0 (CH), 38.9 (CH), 26.2, 24.9. LR-MS (EI, 70 eV) *m*/*z*: 289 [$M^+ - H_2O + 1$]. Anal. calcd. for $C_{13}H_{22}O_8$: C 50.97, H 7.24; found: C 50.63, H 7.52.

Bicyclitol 54

Acetonide **53** (20 mg, 0.065 mmol) was stirred vigorously with 30% trifluoroacetic acid (800 μL) at room temperature for 30 min. The volatiles were removed under reduced pressure to furnish **54** (16 mg, 95%). ^1H NMR (300 MHz, D_2O) δ: 4.19 (br s, 1H), 4.00 (br s, 1H), 3.96–3.81 (series of m, 4H), 3.75–3.60 (m, 2H), 2.22–2.18 (m, 2H). ^{13}C NMR (75 MHz, D_2O) δ: 77.0, 76.7, 76.0, 74.2, 73.2, 71.2 (3C), 43.1 (CH), 40.5 (CH). LR-MS (EI, 70 eV) *m*/*z*: 264 [$M^+ - 2$]. Anal. calcd. for $C_{10}H_{18}O_8$: C 45.11, H 6.81; found: C 45.32, H 7.01.

(2*R,3*S**,4*S**,5*R**,6*S**,7*S**)-1,8,9,10-Tetrachloro-11,11-dimethoxytricyclo[6.2.1.0^{2,7}]undec-9-ene-3,4,5,6-tetrol (55)**

A solution of diol **45** (1 g, 2.66 mmol) in acetone–water–*t*-BuOH (5:5:2, 15 mL) was treated sequentially with OsO_4 (7 mg, 1 mol%) and 50% aq. NMMO (747 μL, 3.19 mmol) at 0 °C. The resulting pale yellow reaction mixture was stirred at room temperature for 1.5 h, at which point all the starting material had been consumed (TLC). The reaction mixture was cooled to 0 °C and quenched by the addition of solid $NaHSO_3$ (500 mg). The mixture was filtered through a Celite pad and the filtrate was concentrated under reduced pressure. The residue obtained was chromatographed over a silica gel column (30% ethyl acetate – hexane) to furnish **55** (817 mg, 75%). IR (Nujol, cm^{-1}): 3420, 3315, 3245. ^1H NMR (300 MHz, DMSO) δ: 3.83 (br s, 4H), 3.50 (s, 3H), 3.43 (s, 3H), 3.00 (s, 2H). ^{13}C NMR (75 MHz, DMSO) δ: 128.7 (2C, C=*C*Cl), 114.6 (C_q), 77.1 (2C, *C*-Cl), 68.4 (2C, *C*HOH), 67.3 (2C, *C*HOH), 52.4 (O*C*H_3), 51.5 (O*C*H_3), 46.2 (2C, CH). LR-MS (EI, 70 eV) *m*/*z*: 374 [$M^+ - Cl + 1$]. Anal. calcd. for $C_{13}H_{16}Cl_4O_4$: C 38.08, H 3.93; found: C 37.88, H 3.88.

(2*R,3*R**,4*S**,8*R**,9*R**,10*S**)-1,11,12,13-Tetrachloro-14,14-dimethoxy-6,6-dimethyl-5,7-dioxatetracyclo[9.2.1.0^{2,10}.0^{4,8}]tetradec-12-ene-3,9-diol (56)**

To a solution of tetrol **55** (750 mg, 1.829 mmol) in dry acetone (25 mL), Amberlyst-15 (~100 mg) and 4 Å molecular sieve powder (250 mg) were added sequentially and the resulting mixture was stirred at room temperature for 1 h. Upon complete consumption of the starting material (TLC), the reaction mixture was filtered through a Celite pad and the filtrate was concentrated under reduced pressure to give a solid residue. The residue was chromatographed over a silica gel column (6% ethyl acetate – hexane) to afford acetonide **56** (675 mg, 82%), mp 210–212 °C. IR (KBr, cm^{-1}): 3260. ^1H NMR (300 MHz, $CDCl_3$) δ: 4.43 (s, 2H, $H_{acetonide}$), 4.29 (br s, 2H, *C*HOH), 3.79 (s, 3H, O*C*H_3), 3.57 (s, 3H, O*C*H_3), 3.04 (s, 2H, $H_{bridgehead}$), 1.45 (s, 3H), 1.34 (s, 3H). ^{13}C NMR (75 MHz, $CDCl_3$) δ: 129.4 (2C, C=*C*Cl), 114.7 (C_q), 108.4 (C_q), 76.7 (2C, $C_{acetonide}$), 75.6 (2C, *C*-Cl), 65.1 (2C, *C*HOH), 53.1 (OCH_3), 51.7 (OCH_3), 46.3 (2C, *C*H), 26.1 ($CH_{3acetonide}$), 23.3 ($CH_{3acetonide}$). LR-MS (EI, 70 eV) *m*/*z*: 451 [$M^+ + 1$]. Anal. calcd. for $C_{16}H_{20}O_4Cl_6$: C 42.69, H 4.48; found: C 43.04, H 4.62.

(2*R,3*R**,4*R**,8*S**,9*R**,10*S**)-14,14-Dimethoxy-6,6-dimethyl-5,7-dioxatetracyclo[9.2.1.0^{2,10}.0^{4,8}]tetradec-12-ene-3,9-diol (57)**

Liquid ammonia (100 mL) was distilled into a three-necked round-bottomed flask equipped with a Dewar condenser, KOH guard tube, and septum. The solution of acetonide **56** (1 g, 2.22 mmol) in dry THF (10 mL) and absolute EtOH (5 mL) was added to the reaction flask. Small pieces of freshly cut sodium were introduced, with stirring, into the resulting mixture until the blue color of the solution persisted. The mixture was stirred for 40 min and quenched by addition of solid NH_4Cl (~1 g). The excess ammonia was allowed to evaporate and the residue obtained was diluted with cold aq. satd. NH_4Cl solution (20 mL) and water (50 mL). The residue, resulting from the usual work-up, was purified by silica gel column chromatography (70% ethyl acetate – hexane) to furnish the olefin diol **57** (610 mg, 88%), mp 200–202 °C. IR (Nujol, cm^{-1}): 3420, 1260. ^1H NMR (300 MHz, $CDCl_3$) δ: 6.17 (t, 2H, *J* = 3.0 Hz, C=C*H*), 3.94 (br s, 2H, $H_{acetonide}$), 3.32 (s, 3H, OCH_3), 3.13 (br s, 3H, OCH_3), 3.04 (br s, 2H, C*H*OH), 2.92 (s, 2H), 1.65 (s, 2H), 1.44 (s, 3H), 1.30 (s, 3H). ^{13}C NMR (75 MHz, $CDCl_3$) δ: 132.0 (2C, C=*C*H), 119.4 (C_q), 108.4 (C_q), 78.5 (2C, $C_{acetonide}$), 71.4 (2C, *C*HOH), 52.0 (2C, OCH_3), 49.8 (2C), 46.7 (2C), 26.7 ($CH_{3acetonide}$), 23.0. LR-MS (EI, 70 eV) *m*/*z*: 312 [M^+]. Anal. calcd. for $C_{16}H_{24}O_6$: C 61.52, H 7.74; found: C 61.90, H 7.52.

(2*R,3*R**,4*R**,8*S**,9*R**,10*S**)-3,9-Dihydroxy-6,6-dimethyl-5,7-dioxatetracyclo[9.2.1.0^{2,10}.0^{4,8}]tetradec-12-en-14-one (58)**

Ketal **57** (220 mg, 0.705 mmol) was dissolved in moist acetone (20 mL) and stirred with Amberlyst-15 resin (~50 mg) for 2 h, when all the starting material had been consumed (TLC). The reaction mixture was filtered through a Celite pad and the filtrate was concentrated under reduced pressure to give a solid residue, which was chromatographed over a silica gel column (50% ethyl acetate – hexane) to furnish the 7-ketonorbornene **58** (178 mg, 95%), mp 220–221.5 °C. IR (KBr, cm^{-1}): 3443, 1778.

(3a*R,4*S**,4a*S**,8a*R**,9*R**,9a*S**)-2,2-Dimethyl-3a,4,4a,8a,9,9a-hexahydronaphtho[2,3-*d*][1,3]dioxole-4,9-diol (59)**

A solution of ketone **58** (90 mg, 0.338 mmol) in nitrobenzene (10 mL) was heated to 160 °C, with vigorous stirring, for 3 h. Upon complete consumption of the starting material (TLC), the reaction mixture was cooled to 80 °C and the solvent was distilled off under reduced pressure. The

© 2005 NRC Canada

resulting residue was subjected to silica gel column chromatography (30% ethyl acetate – hexane) to afford diene **59** (35 mg, 43%), mp 188.5–190 °C. IR (KBr, cm^{-1}): 3321, 3034. ^1H NMR (300 MHz, $CDCl_3$) δ: 5.97–5.94 (m, 2H, C=C*H*), 5.54–5.50 (m, 2H, C=C*H*), 4.50–4.49 (m, 2H, $H_{acetonide}$), 3.86 (br s, 2H), 3.53 (d, *J* = 6.9 Hz, 2H), 3.20 (br s, 2H, $H_{bridgehead}$), 1.46 (s, 3H), 1.37 (s, 3H). ^{13}C NMR (75 MHz, $CDCl_3$) δ: 125.8 (2C, C=*C*H), 123.8 (2C, C=*C*H), 108.6 (C_q), 74.9 (2C, $C_{acetonide}$), 69.7 (2C, *C*HOH), 32.4 (2C), 26.6 ($CH_{3acetonide}$), 24.0 ($CH_{3acetonide}$). LR-MS (EI, 70 eV) *m*/*z*: 239 [M^+ + 1]. Anal. calcd. for $C_{13}H_{18}O_4$: C 65.53, H 7.61; found: C 65.90, H 7.52.

(3a*R,4*S**,4a*R**,5*S**,6*S**,7*S**,8*S**,8a*S**,9*R**,9a*S**)-2,2-Dimethylperhydronaphtho[2,3-*d*][1,3]dioxole-4,5,6,7,8,9-hexol (60)**

To a solution of diene **59** (25 mg, 0.105 mmol) in acetone–water–*t*-BuOH (5:5:2, 6 mL), catalytic amounts of OsO_4 (0.5 mg, 1 mol%) and 50% aq. NMMO (75 μL, 0.315 mmol) were sequentially added at 0 °C. The resulting pale yellow reaction mixture was stirred at room temperature for 48 h. The reaction mixture was cooled to 0 °C prior to quenching with solid $NaHSO_3$ (15 mg). The resulting mixture was diluted with ethyl acetate (20 mL), filtered through Celite, and the filtrate was concentrated under reduced pressure. The residue was subjected to silica gel column chromatography (10% methanol – ethyl acetate) to afford hexol **60** (23 mg, 73%). IR (Nujol, cm^{-1}): 3460. ^1H NMR (300 MHz, D_2O) δ: 4.27 (d, *J* = 3 Hz, 1H), 4.20 (dd, *J* = 8.4, 5.4 Hz, 1H), 4.14 (dd, *J* = 5.1, 1.2 Hz, 1H), 4.03 (t, *J* = 3 Hz, 1H), 3.97–3.92 (m, 1H), 3.86 (dd, *J* = 10.2, 3.6 Hz, 1H), 3.79 (dd, *J* = 8.4, 5.4 Hz, 1H), 3.52 (dd, *J* = 10.2, 3.3 Hz, 1H), 2.54–2.20 (m, 2H), 1.39 (s, 3H), 1.26 (s, 3H). ^{13}C NMR (75 MHz, D_2O) δ: 110.5 (C_q), 80.1 ($CH_{acetonide}$), 78.3 ($CH_{acetonide}$), 72.7, 72.3, 72.0, 71.5, 67.4, 66.4, 41.9 ($CH_{bridgehead}$), 39.3 ($CH_{bridgehead}$), 28.6, 26.6. LR-MS (EI, 70 eV) *m*/*z*: 306 [M^+]. Anal. calcd. for $C_{13}H_{22}O_8$: C 50.97, H 7.24; found: C 50.90, H 7.51.

Bicyclitol 61

Acetonide hexol **60** (14 mg, 0.046 mmol) was stirred vigorously with 30% TFA (500 μL) at room temperature for 30 min. The volatiles were removed under reduced pressure to furnish **61** (11 mg, 90%). ^1H NMR (300 MHz, D_2O) δ: 4.06 (m, 1H), 3.93 (dd, *J* = 10.5, 3.0 Hz, 1H), 3.87 (br s, 1H), 3.81 (m, 1H), 3.75 (t, *J* = 3.9 Hz, 1H), 3.73 (t, *J* = 3.0 Hz, 1H), 3.68 (t, *J* = 3.3 Hz, 1H), 3.52 (dd, *J* = 10.5, 3.0 Hz, 1H), 2.35 (dt, *J* = 6.6, 2.7 Hz, 1H), 2.28 (m, 1H). ^{13}C NMR (75 MHz, D_2O) δ: 73.6, 72.8, 71.3, 70.7, 70.4, 69.3, 69.1, 67.4, 40.2, 38.4. LR-MS (CI) *m*/*z*: 266 [M^+]. Anal. calcd. for $C_{10}H_{18}O_8$: C 45.11, H 6.81; found: C 45.45, H 7.12.

General procedure for enzymatic assays

The enzymes assayed were α-glucosidase (EC 3.2.1.20) from yeast, β-glucosidase (EC 3.2.1.21) from sweet almonds, α-galactosidase (EC 3.2.1.22) from green coffee beans, β-galactosidase (EC 3.2.1.23) from *E. coli*, α-mannnosidase (EC 3.2.1.24) from jack bean, and β-mannosidase (EC 3.2.1.25) from snail acetone powder. The substrates for the glycosidase were the corresponding *ortho*- or *para*-nitrophenylglycosides. The α-glucosidase (0.135 units/mL)[3] was assayed using *p*-nitophenyl-α-D-glucopyranoside (2.53 mmol/L) as the substrate at pH 6.8 (100 mmol/L phosphate buffer) at 37 °C, while β-glucosidase (0.133 units/mL) was assayed using *p*-nitrophenyl-β-D-glucopyranoside (2.57 mmol/L) as the substrate at pH 5.0 (10 mmol/L acetate buffer) at 37 °C. The potency of α-galactosidase (0.1 units/mL) and β-galactosidase (0.91 units/mL) was studied using *p*-nitrophenyl-α-D-galactopyranoside (2.12 mmol/L) and *o*-nitrophenyl-β-D-galactopyranoside (2.34 mmol/L) as substrate at pH 6.5 (100 mmol/L phosphate buffer) and pH 7.3 (100 mmol/L phosphate buffer) at 25 and 37 °C, respectively. The assay involving α-mannosidase (0.116 units/mL) was carried out using *p*-nitrophenyl-α-D-mannopyranoside (2.01 μmol/L) as substrate at pH 4.5 (10 mmol/L acetate buffer) at 25 °C, while β-mannosidase (0.125 units/mL) was assayed using *p*-nitrophenyl-α-D-mannopyranoside (2.15 mmol/L) as substrate at pH 4 (10 mmol/L acetate buffer) at 25 °C.

Typical assays were carried out in 1.5 mL disposable Eppendorf tubes, with the reaction volume being maintained at 200 μL. The mixture of enzyme and potential inhibitor in the optimum buffer medium was preincubated for 5 min and the reaction was initiated by adding the corresponding substrate solution (prepared in double-distilled water) to the reaction mixture. After incubation for 30 min at the optimum temperature for the enzyme, the reaction was quenched by addition of 800 μL of Na_2CO_3 buffer (400 mmol/L) solution. The enzyme activity was determined by measuring the absorption of the nitrophenolate ion released at 400 nm (in the case of *p*-nitrophenol) or 410 nm (in the case of *o*-nitrophenol). In the control experiments, the inhibitor was replaced by a corresponding buffer solution. The K_i was calculated using the Lineweaver–Burk plot.

Acknowledgements

We thank the Chemical Biology Unit of the Jawaharlal Nehru Centre for Advanced Scientific Research for financial support. High field NMR data reported here were obtained through the help of S.I.F at the Indian Institute of Science (IISc). S.S.R. thanks the Council of Scientific and Industrial Research (CSIR), India, for the award of a Research Fellowship. We appreciate the help of Dr. Utpal Tatu, Department of Biochemistry, in performing enzymatic assays.

References

1. Recent reviews: (*a*) N. Asano. Glycobiology, **13**, 93R (2003); (*b*) C.-H. Wong. Acc. Chem. Res. **32**, 376 (1999); (*c*) T.D. Heightman and A.T. Vasella. Angew. Chem. Int. Ed. **38**, 750 (1999); (*d*) P. Sears and C.-H. Wong. Angew. Chem. Int. Ed. **38**, 2300 (1999); (*e*) M. Bols. Acc. Chem. Res. **31**, 1 (1998); (*f*) S. Ogawa. *In* Carbohydrate mimics: Concepts and methods. *Edited by* Y. Chapleur. Wiley-VCH, Weinheim. 1998. p. 87; (*g*) B. Ganem. Acc. Chem. Res. **29**, 340 (1996); (*h*) S.G. Withers. Pure Appl. Chem. **67**, 1673 (1995); (*i*) G.S. Jacob. Curr. Opin. Struct. Biol. **5**, 605 (1995); (*j*) A.D. Albein. Annu. Rev. Biochem. **56**, 497 (1987).

[3] One unit of enzyme is defined as the amount that liberated 1 μmol of corresponding nitrophenol per min.

© 2005 NRC Canada

2. (*a*) A. Berecibar, C. Grandjean, and A. Siriwardena. Chem. Rev. **99**, 779 (1999); (*b*) C.R. Johnson. Acc. Chem. Res. **31**, 333 (1998); (*c*) A. Martinez-Grau and J. Marco-Contelles. Chem. Soc. Rev. **27**, 155 (1998); (*d*) Y. Landais. Chimia, **52**, 104 (1998); (*e*) T. Hudlicky, D.A. Entwistle, K.K. Pitzer, and A.J. Thorpe. Chem. Rev. **96**, 1195 (1996); (*f*) R.J. Ferrier and S. Middleton. Chem. Rev. **93**, 2779 (1993); (*g*) T. Suami. Top. Curr. Chem. **154**, 257 (1990).
3. (*a*) M.S. Gultekin, M. Celik, and M. Balci. Curr. Org. Chem. **8**, 1159 (2004); (*b*) M. Balci. Pure Appl. Chem. **69**, 97 (1997); (*c*) T. Hudlicky and J.W. Reed. *In* Advances in asymmetric synthesis. Vol. 1. JAI Press, Greenwich. 1995. p. 271; (*d*) T. Hudlicky and M. Cebulak. *In* Cyclitols and their derivatives. A handbook of physical, spectral and synthetic data. Wiley-VCH, New York. 1993; (*e*) H.A.J. Carless. Tetrahedron: Asymmetry, **3**, 795 (1992); (*f*) M. Balci, Y. Sutbeyaz, and H. Secen. Tetrahedron, **46**, 3715 (1990).
4. (*a*) M. Desjardins, M.-C. Lallemand, S. Freeman, T. Hudlicky, and K.A. Abboud. J. Chem. Soc. Perkin Trans. 1, 621 (1999); (*b*) Y. Kara, M. Balci, S.A. Bourne, and W.H. Watson. Tetrahedron Lett. **35**, 3349 (1994).
5. (*a*) N. Asano, R.J. Nash, R.J. Molyneux, and G.W.J. Fleet. Tetrahedron: Asymmetry, **11**, 1645 (2000); (*b*) A.E. Stütz. *In* Iminosugars as glycosidase inhibitors: Nojirimycin and beyond. Wiley-VCH, Weinheim. 1999; (*c*) J. Michael. Nat. Prod. Rep. **16**, 675 (1999); (*d*) A. de Raadt, C.W. Ekhart, M. Ebner, and A.E. Stütz. Top. Curr. Chem. **187**, 157 (1997); (*e*) B. Ganem. Acc. Chem. Res. **29**, 340 (1996); (*f*) G.W.J. Fleet and B. Winchester. Glycobiology, **2**, 199 (1992); (*g*) P.S. Liu, R.S. Rogers, M.S. Kang, and P.S. Sunkara. Tetrahedron Lett. **32**, 5853 (1991). (*h*) M.L. Sinnot. Chem. Rev. **90**, 1171 (1990); (*i*) G. Legler. Adv. Carbohydr. Chem. Biochem. **48**, 319 (1990).
6. The work described has already been published as preliminary communications. (*a*) G. Mehta and S.S. Ramesh. Tetrahedron Lett. **42**, 1987 (2001); (*b*) G. Mehta and S.S. Ramesh. Chem. Commun. 2429 (2000).
7. (*a*) G. Mehta and D.S. Reddy. Tetrahedron Lett. **40**, 9137 (1999); (*b*) G. Mehta, D.S. Reddy, S.S. Ramesh, and U. Tatu. Tetrahedron Lett. **40**, 9141 (1999).
8. (*a*) D.S. Reddy. Ph.D. dissertation, University of Hyderabad, Hyderabad, India. 2000; (*b*) C.A. Peri. Gazz. Chim. Ital. **85**, 1118 (1995).
9. S. Takano, M. Moriya, K. Tanaka, and K. Ogasawara. Synthesis, 687 (1994).
10. (*a*) M. Schröder. Chem. Rev. **80**, 187 (1980). (*b*) V. VanRheenen, R.C. Kelly, and D.Y. Cha. Tetrahedron Lett. **17**, 1973 (1976).
11. (*a*) E.T. McBee, W.R. Diveley, and J.E. Burch. J. Am. Chem. Soc. **77**, 385 (1955); (*b*) F.H. Allen. Chem. Rev. **45**, 309 (1945).
12. P.F. Schuda, H.L. Ammon, M.R. Heimann, and S. Battacharjee. J. Org. Chem. **47**, 3434 (1982).
13. (*a*) R. Uma. Ph.D. dissertation, University of Hyderabad, Hyderabad, India. 1999; (*b*) M. Balci. Chem. Rev. **81**, 91 (1981); (*c*) R.W. Denny and A. Nickon. *In* Organic reactions. Vol. 20. John Wiley and Sons, New York. 1973. p. 133.
14. (*a*) J.K. Cha, W.J. Christ, and Y. Kishi. Tetrahedron Lett. **37**, 3943 (1983); (*b*) W.J. Christ, J.K. Cha, and Y. Kishi. Tetrahedron Lett. **37**, 3947 (1983).
15. A.P. Marchand and T.-C. Chou. J. Chem. Soc. Perkin Trans. 1, 1948 (1973).
16. (*a*) A.P. Marchand, W.D. La Roe, G.V.M. Sharma, C.S. Suresh, and D.S. Reddy. J. Org. Chem. **51**, 1622 (1986); (*b*) T.-C. Chou and J.H. Chiou. J. Chin. Chem. Soc. (Taipei), **33**, 227 (1986).
17. J.-L. Luche. J. Am. Chem. Soc. **100**, 2226 (1978).
18. (*a*) K. Sugahara and I. Yamashina. *In* Methods in enzymology. *Edited by* C. Ginsburg. Vol. XXVIII. Part B. Academic Press, New York. 1972. p. 769; (*b*) A.L. Tarentino and F. Maley. *In* Methods in enzymology. *Edited by* C. Ginsburg. Vol. XXVIII. Part B. Academic Press, New York. 1972. p. 772; (*c*) O.P. Bail and K.M.L. Agrawal. J. Biochem. Chem. **244**, 2970 (1969); (*d*) Y.-T. Li. J. Biochem. Chem. **242**, 5474 (1969); (*e*) H. Lineweaver and D. Burk. J. Am. Chem. Soc. **56**, 658 (1934).

© 2005 NRC Canada

Oxidative addition chemistry of dimethyl(dipyridyl ketone)platinum(II)[1]

Fenbao Zhang, Michael E. Broczkowski, Michael C. Jennings, and Richard J. Puddephatt

Abstract: The dimethylplatinum(II) complex [$PtMe_2$(DPK)] (DPK = di-2-pyridyl ketone) undergoes easy oxidative addition to give platinum(IV) complexes. For example, reaction of [$PtMe_2$(DPK)] with MeI gave [$PtIMe_3$(DPK)], reaction with *N*-chlorosuccinimide in methanol gave [PtCl(OMe)Me_2(DPK)], and reaction with [$FN(CH_2CH_2)_2NCH_2Cl][BF_4]_2$ in MeCN gave [PtF(NCMe)Me_2(DPK)][BF_4]. In several cases, the ketone group of the DPK ligand took part in the reactions. For example, oxidation of [$PtMe_2$(DPK)] by air or hydrogen peroxide gave [Pt(OH)Me_2(DPKOH)] (DPKOH = κ^3-*NN′O*-(2-$C_5H_4N)_2C(OH)O$), which reacted with HCl to give [$PtClMe_2$(DPKOH)] or with excess acetyl chloride to give [$PtCl_2Me_2$(DPK)]. Reaction of [$PtMe_2$(DPK)] with methyl triflate in MeCN solution gave [$PtMe_3$(NCMe)(DPK)][OTf], which reacted with more MeOTf in the presence of base to give [$PtMe_3${DPC$(OMe)_2$}][OTf], where DPC$(OMe)_2$ = κ^3-*NN′O*-(2-$C_5H_4N)_2C(OMe)_2$. Hydrolysis of [PtF(NCMe)Me_2(DPK)][BF_4] gave [Pt{NHC(=O)Me}Me_2(DPKOH)], which crystallized in partially protonated form as an unusual supramolecular polymer [Pt{NHC(=O)Me}Me_2(DPKOH)]·0.5HBF_4.

Key words: platinum, oxidative addition, ketone, pyridyl.

Résumé : Le complexe de diméthylplatine(II) [$PtMe_2$(DPK)] (DPK = di-2-pyridyl cétone) subit une addition oxydante facile qui conduit aux complexes de platine(IV). Par exemple, la réaction du [$PtMe_2$(DPK)] avec le MeI conduit au [$PtIMe_3$(DPK)], la réaction avec le *N*-chlorosuccinimide dans le méthanol conduit à la formation du [PtCl(OMe)Me_2(DPK)] et la réaction avec du $[FH(CH_2CH_2)_2NCH_2Cl][BF_4]_2$ dans le MeCN fournit du [PtF(NCMe)Me_2(DPK)][BF_4]. Dans plusieurs cas, le groupe cétone du ligand DPK prend part aux réactions. Par exemple, l'oxydation du [$PtMe_2$(DPK)] par l'air ou le peroxyde d'hydrogène fournit du [Pt(OH)Me_2(DPKOH)] (DPKOH = κ^3-*NN′O*-(2-$C_5H_4N)_2C(OH)O$) qui, par réaction avec du HCl, conduit à la formation de [$PtClMe_2$(DPKOH)] ou, par réaction avec un excès de chlorure d'acétyle fournit du [$PtCl_2Me_2$(DPK)]. La réaction du [$PtMe_2$(DPK)] avec du triflate de méthyle dans le MeCN en solution conduit à la formation de [$PtMe_3$(NCMe)(DPK)][OTf] qui, par réaction avec un excès de MeOTf en présence de base fournit du [$PtMe_3${DPC$(OMe)_2$}][OTf] (DPC$(OMe)_2$ = κ^3-*NN′O*-(2-$C_5H_4N)_2C(OMe)_2$). L'hydrolyse du [PtF(NCMe)Me_2(DPK)][BF_4] conduit à la formation de [Pt{NHC(=O)Me}Me_2(DPKOH)] qui cristallise sous la forme partiellement protonée d'un polymère supramoléculaire inhabituel [Pt{NHC(=O)Me}Me_2(DPKOH)]·0,5HBF_4.

Mots clés : platine, addition oxydante, cétone, pyridyle.

[Traduit par la Rédaction]

Introduction

Organoplatinum(II) complexes containing nitrogen-donor ligands are known to be particularly reactive in oxidative addition reactions, and this high reactivity is important in the activation of normally inert chemical bonds (1). For example, the activation of C—H bonds in alkanes or arenes by platinum(II) complexes usually occurs by oxidative addition, and is often favoured if there are chelating diamine or diimine ligands present (2, 3).

Many studies of oxidative addition to complexes [$PtMe_2$(LL)] have been carried out using complexes with LL = 2,2′-bipyridyl or its derivatives, which give five-membered chelate rings (1). The five-membered chelate rings are usually roughly planar, but six-membered chelate rings may be significantly distorted from planarity and this can have a significant effect on reactivity (4–8). Oxidative addition reactions are particularly easy in platinum(II) complexes of the hydridotripyrazolylborate ligand and related ligands that are bidentate in platinum(II) complexes but factridentate in platinum(IV) complexes (4). The tripyrazolylborate complexes contain six-membered chelate rings (Chart 1), but the significance of this factor is difficult to determine since the transition of the ligand from bidentate to tridentate is thought to be the primary cause of the high reactivity (4). Carbon–hydrogen bond activation is easy with platinum(II) complexes of anionic β-diiminate ligands, which give six-membered chelate rings (5), or with neutral bis(azaindolyl)methane ligands, which give eight-membered chelate

Received 5 October 2004. Published on the NRC Research Press Web site at http://canjchem.nrc.ca on 8 June 2005.

Dedicated to Professor Howard Alper in recognition of his pioneering research in homogeneous catalysis.

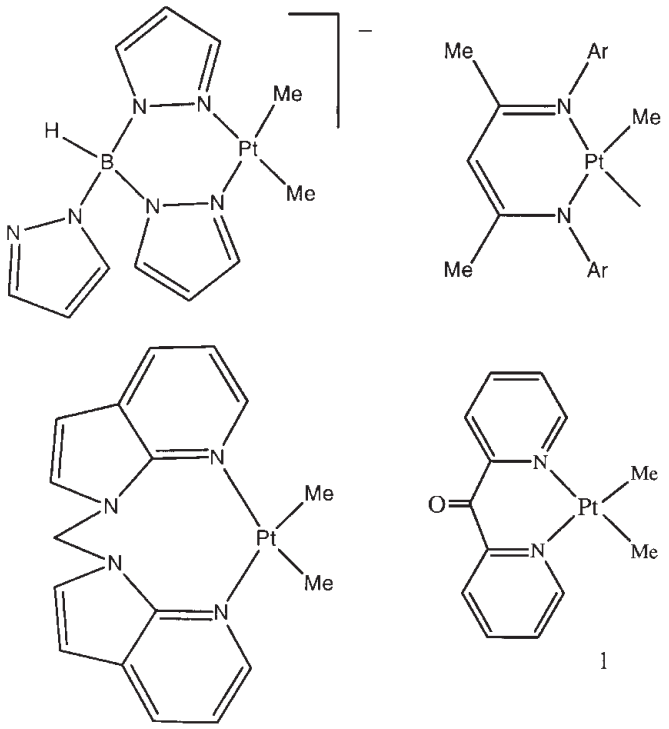
F. Zhang, M.E. Broczkowski, M.C. Jennings, and R.J. Puddephatt.[2] Department of Chemistry, University of Western Ontario, London, ON N6A 5B7, Canada.

[1]This article is part of a Special Issue dedicated to Professor Howard Alper.

[2]Corresponding author (e-mail: pudd@uwo.ca).

 doi: 10.1139/V05-028 © 2005 NRC Canada

Chart 1. Methylplatinum complexes with six- or eight-membered chelate rings.



rings (6). These intriguing results prompted this study of the oxidative addition chemistry of the dimethylplatinum(II) complex of the ligand 2,2′-dipyridyl ketone (DPK) (7, 8), as a prelude to a study of C-H activation using $[PtMe_2(DPK)]$ (**1**, Chart 1).

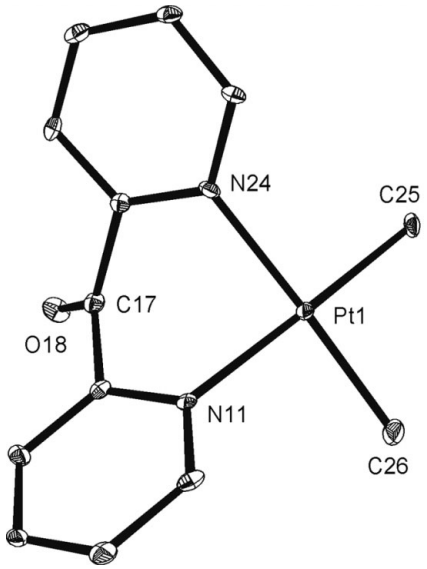
One well-known property of DPK as a ligand is that the carbonyl group is activated towards forming the hydrate $(2\text{-}C_5H_4N)_2C(OH)_2$(DPKOH$_2$) or its deprotonated form $(2\text{-}C_5H_4N)_2C(OH)O^-$(DPKOH$^-$) on coordination to transition metals. The deprotonated form DPKOH$^-$ is particularly favoured in octahedral complexes where it acts as a fac-tridentate ligand (κ^3-*NN′O*) rather than bidentate as in DPK (κ^2-*NN′*). For example, the complex $[PtCl_4(DPK)]$ is readily hydrolysed to give $[PtCl_3(DPKOH)]$ (8*a*). Although the redox chemistry of DPK complexes has been studied electrochemically, there has been little research on oxidative addition chemistry (7, 8). It was therefore of interest to investigate how the six-membered Pt(DPK) chelate ring would affect the reactivity of $[PtMe_2(DPK)]$ towards oxidative addition, and whether the carbonyl group might also be activated during oxidative addition.

Results and discussion

Platinum(II) complexes

The complex $[PtMe_2(DPK)]$ (**1**) was readily prepared by reaction of $[Pt_2Me_4(\mu\text{-}SMe_2)_2]$ (9) with the ligand DPK, and was isolated as a red solid. In the IR spectrum, the carbonyl stretching vibration occurred at ν(C=O) = 1682 cm^{-1}, unchanged from the value for free DPK. In the ^{1}H NMR spectrum, the methylplatinum resonance occurred at δ(MePt) = 0.78, with coupling ^2J(Pt-H) = 86 Hz, while the ortho pyridyl protons occurred at δ(H6) = 8.83, with coupling ^3J(Pt-H) = 26 Hz.

Fig. 1. A view of the structure of complex **1**.



The structure of complex **1** is shown in Fig. 1. It confirms the expected molecular structure, with square-planar platinum(II) having *cis*-PtC_2N_2 coordination. The angle N(11)-Pt(1)-N(24) = 87.5(2)° is only slightly different from the ideal 90° angle. The Pt—N distances (2.084(7) and 2.081(7) Å) are slightly longer than in the other reported platinum(II) complex $[Pt\{(O_2C)_2C_4H_6\}(DPK)]$, which has Pt—N = 1.999(6) and 2.002(6) Å (8*b*), as a result of the higher trans-influence of the methyl groups in complex **1**. The chelate ring is in the nonplanar boat conformation, as found for other DPK complexes (7, 8), and the angles at the ketone group are all close to the ideal 120° (C(16)-C(17)-C(19) = 118.1(6)°). The pyridyl rings are twisted out of the coordination plane of the platinum atom by 50° (N(11)-C(16)) and 44° (C(18)-N(24)), and the carbonyl carbon lies 1.67 Å out of the plane. The adoption of the boat conformation serves to minimize angle strain in the chelate ring and to minimize steric effects between the ortho hydrogen atom of each pyridyl group and the neighbouring methylplatinum group (7, 8). As the boat conformation becomes more pronounced, the angles Θ between the pyridyl groups and the coordination plane of the platinum atom, and the deviation Δ of the carbonyl carbon atom from the coordination plane, will increase. Comparative structural data for the complexes studied here are given in Table 1.

Reaction of complex **1** in benzene solution with H$[BF_4]$ gave, as a minor product only, the bis(chelate) complex $[Pt(DPK)_2][BF_4]_2$ (**2**), which formed as yellow single crystals. The crystals were insoluble in common organic solvents, so it was not possible to obtain NMR spectra. The formation of complex **2** involves some disproportionation since the precursor contains only one DPK ligand, but the overall stoichiometry was not determined. Complex **2** was characterized crystallographically and the structure is shown in Fig. 2. The platinum atom lies on an inversion centre so the two DPK ligands are identical. Each Pt(DPK) unit forms a boat conformation, very similar to the conformation in **1** (Fig. 1, Table 1), and the inversion centre defines the anti

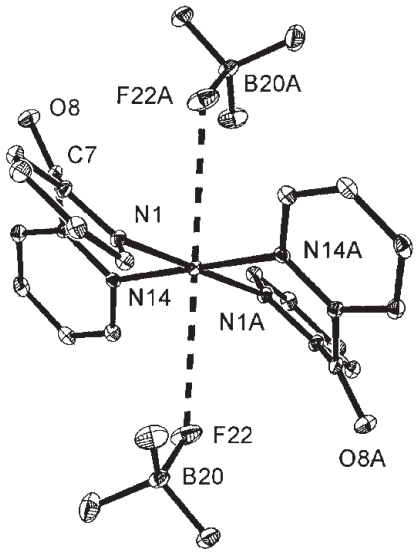
© 2005 NRC Canada

Table 1. Selected structural data for the chelate groups in the complexes.

Complex	Ligand	Pt—N (Å)	N-Pt-N (°)	C-C-C[a] (°)	Θ[b] (°)	Δ[c] (Å)
1	DPK	2.081(7), 2.084(7)	87.5(2)	118.1(6)	50, 44	1.67
2	DPK	2.014(3), 2.025(3)	88.0(1)	119.7(4)	46, 44	1.58
3	DPK	2.150(5), 2.175(6)	87.1(2)	121.1(5)	41, 36	1.48
6a	DPK	2.186(7)	85.7(4)	124(1)	38, 38	1.40
6b	DPK	2.126(8)	87.8(5)	121(1)	39, 39	1.51
9	DPK	2.13(2), 2.16(2)	84.9(6)	119(2)	50, 44	1.53
12	DPKOH	2.112(7), 2.154(9)	85.3(3)	109.4(8)	58, 57	1.89
13	DPKOH	2.156(7), 2.183(7)	83.5(2)	106.6(6)	62, 59	1.93
14	$DPC(OMe)_2$	2.146(5), 2.168(5)	85.5(2)	110.4(5)	54, 52	1.93

[a]Angle at the carbonyl carbon atom.
[b]Θ = angles between pyridyl rings and platinum plane (PtN_2C_2 atoms).
[c]Δ = distance of carbonyl carbon from the platinum plane.

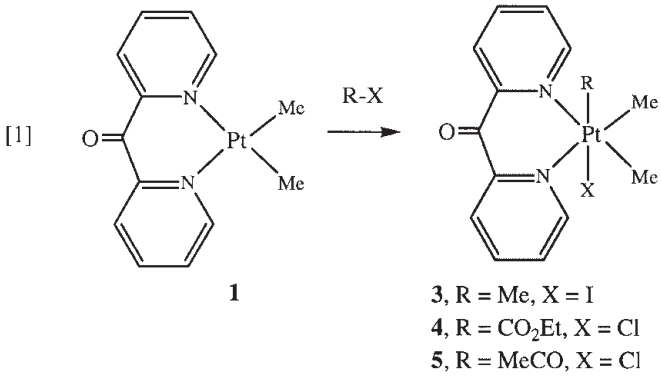
Fig. 2. A view of the structure of complex **2**, including two weakly bound tetrafluoroborate anions.



conformation of the two boats (Fig. 2). The Pt—N distances (Pt—N(1) = 2.025(3) Å, Pt—N(14) = 2.014(3) Å) are shorter than in complex **1**, as expected. The tetrafluoroborate anions lie above and below the plane of the platinum atom, with the closest Pt···F distance at Pt···F(22) = 3.14 Å, probably indicating a mostly ionic attraction.

Platinum(IV) complexes in which the DPK ligand is retained

Complex **1** reacted with organic halides (RX) according to eq. [1] to give the complexes $[PtXMe_2R(DPK)]$ (**3** (R-X = Me-I), **4** (R-X = EtO_2C-Cl), and **5** (R-X = MeC(=O)-Cl)). The complexes were characterized spectroscopically, and the structure of complex **3** was confirmed crystallographically. The IR spectrum of complex **3** contained a carbonyl band at ν(C=O) = 1687 cm^{-1} and the ^1H NMR spectrum contained two methylplatinum resonances in a 1:2 ratio for the methyl groups trans to I and N at δ(MePt) = 0.89 and 1.40 respectively, each with ^2J(Pt-Me) = 69 Hz. For each complex **3**–**5**, the pyridyl groups were equivalent and this proves the trans stereochemistry of the oxidative addition for complexes **4** and **5**. Oxidative addition of alkyl halides to platinum(II) usually occurs by the polar (S_N2) mechanism and trans addition is commonly observed (1, 10). For each complex, the ortho pyridyl protons showed coupling to platinum that was reduced compared to the value of ^3J(Pt-H6) = 26 Hz for the platinum(II) complex **1**. For example, complex **4** gave δ(H6) = 9.16, with ^3J(Pt-H6) = 15 Hz. Complexes **4** and **5** also gave the expected resonances for the carboethoxy and acetyl group, respectively.



The structure of complex **3** is shown in Fig. 3. It shows that the DPK ligand is retained in the octahedral trimethylplatinum(IV) complex and so that the carbonyl group is not directly involved in the oxidative addition reaction. The chelate ring again adopts the boat conformation, but it is flatter than in **1** or **2** (Table 1) and the carbonyl is syn to the axial methylplatinum group and anti to the iodoplatinum group. The Pt—N distances (Pt—N(1) = 2.175(6) Å, Pt—N(14) = 2.150(5) Å) are longer than in either platinum(II) complex **1** or **2** (Table 1).

Two isomeric forms of the complex $[PtCl_2Me_2(DPK)]$ (**6a** and **6b**, Chart 2) were obtained by indirect methods. Isomer **6a** was obtained by oxidation of complex **1** with hydrogen peroxide (vide infra), followed by reaction with acetyl chloride, and isomer **6b** was obtained by oxidation of complex **1** with excess *N*-chlorosuccinimide in methanol. The complexes were readily distinguished by their ^1H NMR spectra. Thus, complex **6a**, the effective product of trans oxidative addition of chlorine, gave a single methylplatinum resonance at δ = 1.77, ^2J(Pt-H) = 71 Hz, and a single set of pyridyl resonances, whereas the less symmetrical complex **6b** gave two equal intensity methylplatinum resonances at δ = 1.71, ^2J(Pt-H) = 70 Hz; δ = 1.79, ^2J(Pt-H) = 69 Hz, and two sets of pyridyl resonances. For the pyridyl resonances, those for the

© 2005 NRC Canada

Fig. 3. A view of the structure of complex **3**.

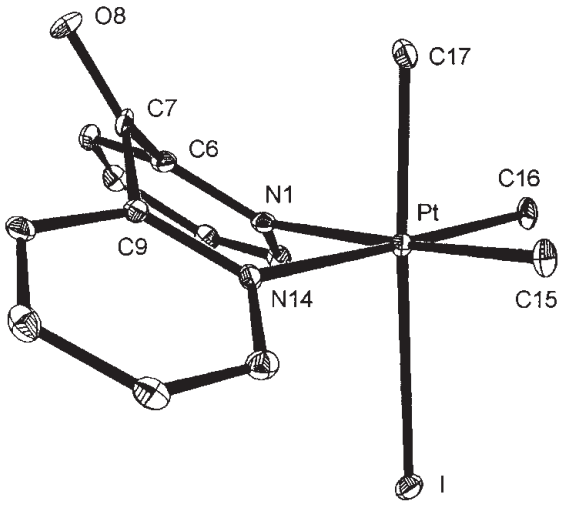
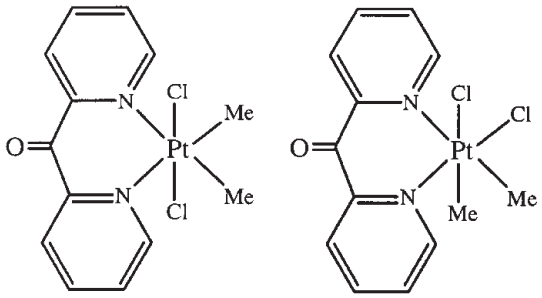


Chart 2. Isomers of complex **6**.

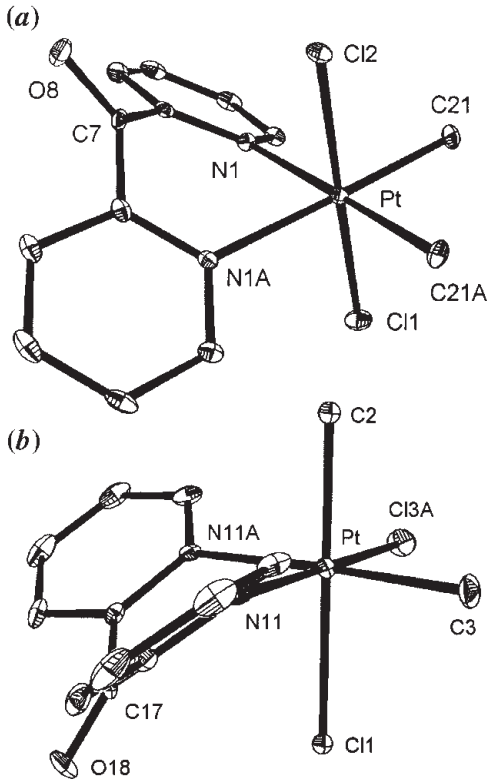


ortho protons showed very different couplings to ^{195}Pt for the pyridyl groups trans to the chloride (δ = 8.81, ^{3}J(Pt-H6) = 48 Hz) and methyl (δ = 9.10, ^{3}J(Pt-H6′) = 13 Hz).

The structures of complexes **6a** and **6b** are shown in Fig. 4. The complexes each have crystallographic mirror symmetry, and for the less symmetrical isomer **6b** this leads to a 50:50 disorder of the methyl and chloro groups trans to the DPK ligand. The axial methyl and chloro ligands were also disordered and this was modelled as a 90:10 disorder. Because of the disorder, the positions of the chlorine and methyl carbon atoms are not accurately determined, but the DPK ligand is well-defined. In **6b**, the carbonyl group is syn to the chloro ligand and anti to the axial methyl group (for the 90% occupation atoms). Since this is the opposite of the conformation for complex **3**, in which the carbonyl group is syn to the axial methyl group, we suggest that the boat conformation in complexes **3** and **6** is determined primarily by steric effects such that the carbonyl group is syn to the smaller axial ligand (Cl < Me << I). The conformation of the DPK ligand is similar in **6a** and **6b**, but the average Pt—N distance is significantly shorter in **6b** as a result of the lower trans influence of the chloride compared to the methyl (Table 1).

Several oxidation reactions of complex **1** were found to occur with the coordination of the solvent, as illustrated in Scheme 1. Thus, methyl triflate or Selectfluor® (FN-$(CH_2CH_2)_2NCH_2Cl][BF_4]_2$) in acetonitrile solution gave the acetonitrile solvate complexes, $[PtMe_3(NCMe)(DPK)]OTf$ (**7**) or $[PtFMe_2(NCMe)(DPK)][BF_4]$ (**8**) (along with $N(CH_2CH_2)_2NCH_2Cl][BF_4]$), respectively. The solvent coordination arises simply because MeCN is a better ligand for platinum(IV) than either the triflate or tetrafluoroborate anion. The presence of coordinated MeCN in **7** and **8** was proved by the presence of a singlet resonance in the ^{1}H NMR spectrum for the MeCN protons, with coupling to ^{195}Pt in complex **8** of ^{4}J(Pt-H) = 13 Hz, similar to values found in other acetonitrile complexes of platinum(IV) (3*d*, 4*g*). In addition, the ^{19}F NMR spectrum of complex **8** contained a singlet resonance for the Pt-F group at δ = 39.92, with coupling ^{1}J(Pt-F) = 1360 Hz, while the ^{1}H NMR spectrum contained a doublet resonance for the methylplatinum protons (δ(MePt) = 1.83, ^{2}J(Pt-H) = 66 Hz, ^{3}J(F-H) = 6 Hz), clearly proving the presence of the Pt-F group. The ^{195}Pt NMR spectrum contained a doublet resonance at δ(Pt) = 2114 with ^{1}J(Pt-F) = 1360 Hz, again proving the presence of a single fluoro ligand. Because complex **8** and co-product $[N(CH_2CH_2)_2NCH_2Cl][BF_4]$ had similar solubility and **8** had limited stability towards hydrolysis, it was not possible to obtain **8** in analytically pure form, but its structure is defined by the spectroscopic data.

Fig. 4. Views of the structures of the isomeric complexes **6a** and **6b**.



The reaction of complex **1** with an equimolar amount of *N*-chlorosuccinimide in methanol solution gave the chloro(methoxo)platinum(IV) complex $[PtCl(OMe)Me_2(DPK)]$ (**9**) in a similar reaction as discovered with a dimethyl-(diimine)platinum(II) complex (11). In a similar reaction, but using excess *N*-chlorosuccinimide, the dichloroplatinum(IV) complex **6b** was isolated. The formation of **6b** from initially formed complex **9** requires replacement of methoxide by chloride and stereochemical change at platinum(IV), the

© 2005 NRC Canada

Scheme 1. Reagents are: (*i*) MeOTf, MeCN; (*ii*) [FN(CH_2-CH_2)$_3$NCH_2Cl][BF_4], MeCN; (*iii*) *N*-chlorosuccinimide, MeOH.

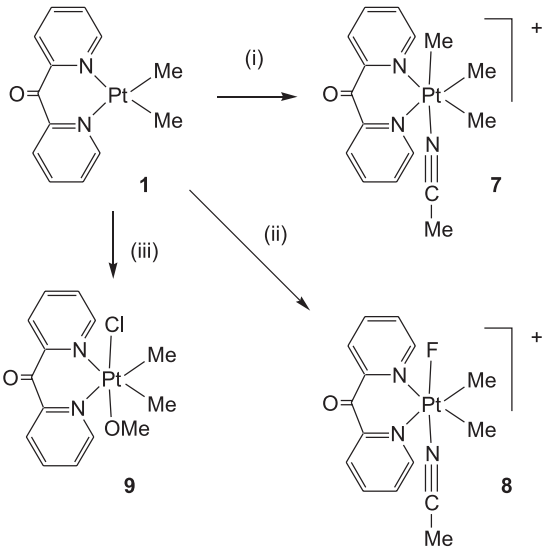
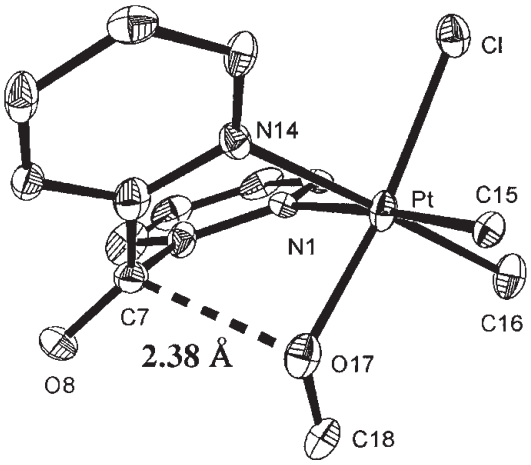


Fig. 5. A view of the structure of complex **9**, indicating the weak O···C interaction.

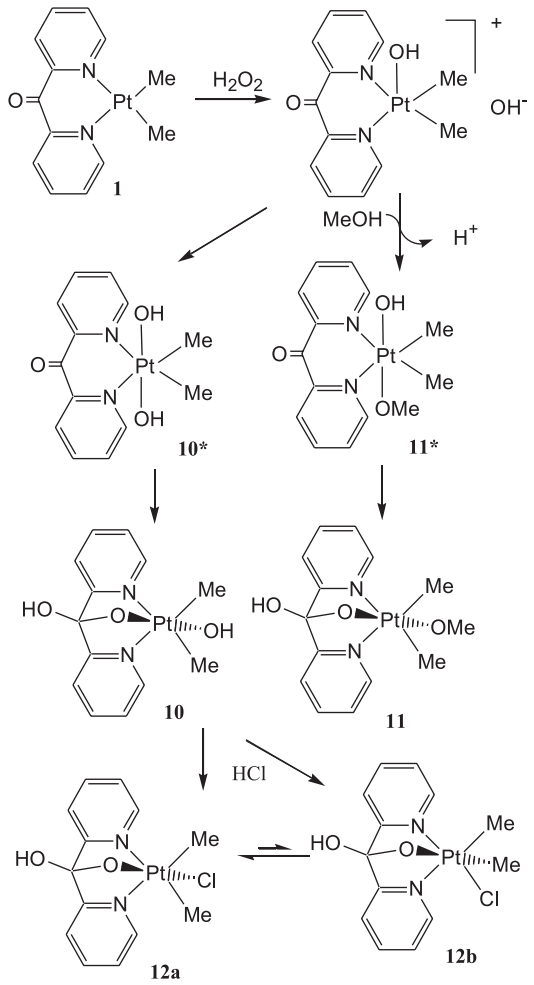


mechanism of which is unknown. The ^{1}H NMR spectrum of complex **9** gave a single methylplatinum resonance at δ = 1.53, with ^2J(Pt-H) = 72 Hz, and a methoxyplatinum resonance at δ = 2.45, with ^3J(Pt-H) = 53 Hz. A view of the structure of complex **9** is shown in Fig. 5. The DPK ligand in complex **9** is again in the boat conformation with the ketone group syn to the axial methoxide group and anti to the chloride ligand. The boat conformation is more accentuated than in the other DPK complexes of platinum(IV), as measured by the values of Θ and Δ (Table 1), and there is a short contact between the nucleophilic methoxide oxygen atom and the electrophilic carbonyl carbon atom (O(17)···C(7)= 2.38(2) Å), indicative of a secondary bonding interaction. In support, the carbonyl oxygen atom lies out of the plane defined by the atoms C(6)-C(7)-C(8) by 0.47 Å, and the sum of the bond angles at C(7) is 355°.

Platinum(IV) complexes in which the DPK ligand is modified

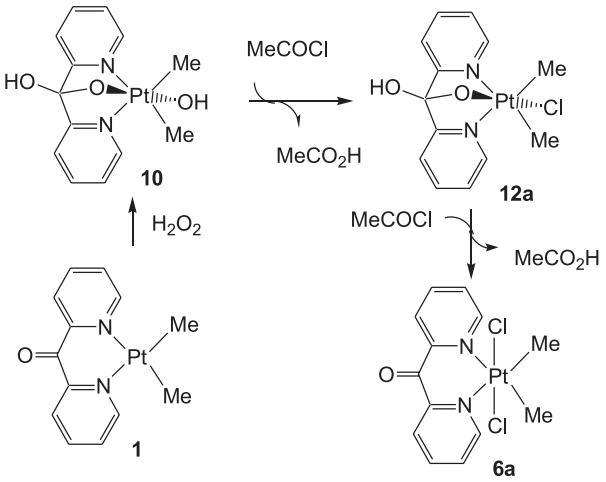
Complex **1** reacted with hydrogen peroxide in acetone solution to give [Pt(OH)Me_2(DPKOH)] (**10**) or in methanol solution to give [Pt(OMe)Me_2(DPKOH)] (**11**) (Scheme 2). These complexes did not yield crystals suitable for structure determination, so they were characterized spectroscopically. Complex **10** gave a single methylplatinum resonance in the ^{1}H NMR spectrum at δ = 1.45, ^2J(Pt-Me) = 72 Hz and a single set of pyridyl resonances, indicating the presence of a plane of symmetry between these groups. Complex **11** gave similar methylplatinum and pyridyl resonances and an additional resonance for the methoxyplatinum group at δ = 3.29, ^3J(Pt-H) = 39 Hz. In both complexes, the hydroxyl resonances were broad and did not show coupling to ^{195}Pt, perhaps indicating easy exchange, and so the NMR spectra did not distinguish unambiguously between the possible structures [Pt(OH)Me_2(DPKOH)] (**10**) or [Pt$(OH)_2Me_2$(DPK)] (**10***), or structures [Pt(OMe)Me_2(DPKOH)] (**11**) or [Pt(OH)(OMe)Me_2(DPK)] (**11***) (Scheme 2). However, in contrast to the characterized DPK complexes (vide supra), the IR spectra of complexes **10** and **11** did not contain a band owing to ν(C=O) in the region 1600–1700 cm^{-1}, indicating the absence of a carbonyl group and so supporting the proposed structures. In principle, the ^{13}C NMR spectra can distinguish between DPK and DPKOH forms, but the complexes have insufficient solubility to give good spectra. The ^{1}H NMR spectra of complex **10** were similar in dichloromethane or acetone solution and showed no sign of the pres-

Scheme 2.



© 2005 NRC Canada

Scheme 3.



ence of isomer **10*** in either case. Further support for the proposed structures of **10** and **11** is obtained from the structure determinations of the derivatives described in the following. The oxidative addition of hydrogen peroxide to complexes [$PtMe_2$(NN)] (NN = 2,2′-bipyridyl or its derivatives) is known and typically occurs by trans oxidative addition to give the corresponding derivative [$Pt(OH)_2Me_2$(NN)] (12).

The reaction of complex **1** with aqueous hydrogen peroxide followed by the addition of 1 equiv. of acetyl chloride (to produce HCl) gave the complex [$PtClMe_2$(DPKOH)] (**12**) by replacement of the hydroxide ligand by chloride (Scheme 2). Complex **12** existed very largely as the isomer **12a** with the chloro ligand trans to oxygen, but a minor amount of the isomer **12b** with the chloro ligand trans to nitrogen was also present (Scheme 2). Dissolution of isolated complex **10** in acetyl chloride led to the replacement of both the hydroxo ligand and the DPKOH hydroxyl group and gave [$PtCl_2Me_2$(DPK)] (**6a**), presumably via the formation of complex **12**. The mechanism of the formation of **6** from **12** is not known, but it clearly involves conversion of a DPKOH group to DPK (Scheme 3). Overall then, the conversion of DPK to DPKOH is shown to be reversible. The structure of complex **12** is shown in Fig. 6.

The structure of complex **12** confirms the presence of the DPKOH anion, which acts a fac-tridentate ligand for platinum(IV). There are also two methylplatinum groups and a chloroplatinum group to make up the octahedral coordination of the platinum(IV) center. There is some disorder at the Cl(1)/C(27) sites (refined as 87:13 occupation) with the chloro ligand trans or cis to oxygen. The most obvious changes in the ligand conformation compared to the DPK complexes of platinum(IV) is the accentuation of the boat conformation (Table 1) needed to form the C-O-Pt bridge. There is also a slight narrowing of the N-Pt-N angle and, of course, a change to tetrahedral stereochemistry of the former carbonyl carbon atom (C(16)-C(17)-C(20) = 109.4(8)°). The complex forms a dimer in the solid state by forming complementary O-H···O hydrogen bonds.

Another complex containing the DPKOH ligand was obtained fortuitously by hydrolysis of the complex [$PtFMe_2$(NCMe)(DPK)][BF_4] (**8**) in acetonitrile solution (Scheme 4). The product crystallized from solution and was characterized in the solid state as [$PtMe_2${NHC(=O)Me}(DPKOH)]-[$PtMe_2${NH=C(OH)Me}(DPKOH)][BF_4] (**13**) by X-ray structure determination (Fig. 7). The reaction was then monitored by ^{1}H NMR spectroscopy with hydrolysis by added D_2O. As the reaction proceeded slowly at room temperature, the MeCN resonance and the doublet MePt resonance of complex **8** (arising from the coupling ^3J(F-H)) decayed and new singlet resonances for the product grew in at δ(MePt) = 1.33, ^2J(Pt-H) = 72 Hz, and at δ(MeC) = 2.28. The rate of hydrolysis increased with the concentration of D_2O added and was typically complete in several days at room temperature. The mass spectrum, obtained either by ESI-MS in MeCN solution or EI-MS of the solid sample, contained a peak at *m/z* = 485, assigned to the cation [$PtMe_2${NH=C(OH)-Me}(DPKOH)] or its tautomeric acetamide complex form.

In the structure determination, the key hydrogen atoms were not directly located so the formulation of the product requires some explanation. There was one disordered tetrafluoroborate anion for every two platinum atoms, indicating an average charge of +0.5 for each complex, but

Fig. 6. A view of the structure of complex **12a**, showing the dimer formed by complementary hydrogen bonding between DPKOH ligands.

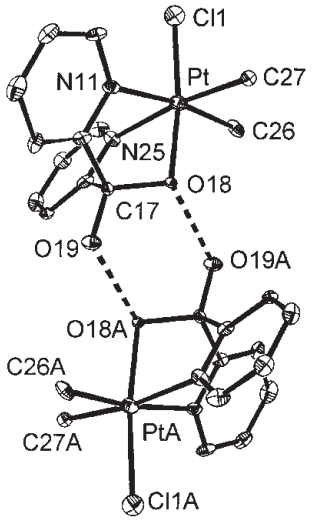
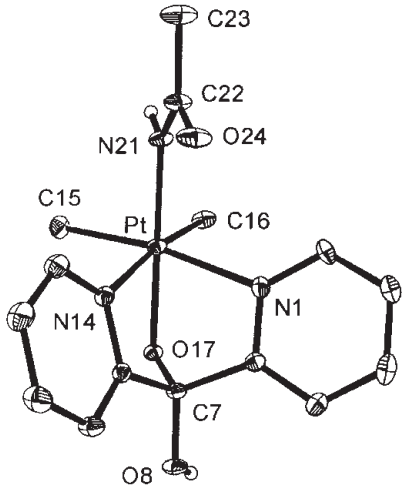


Fig. 7. A view of the molecular structure of complex **13**.



© 2005 NRC Canada

Scheme 4.

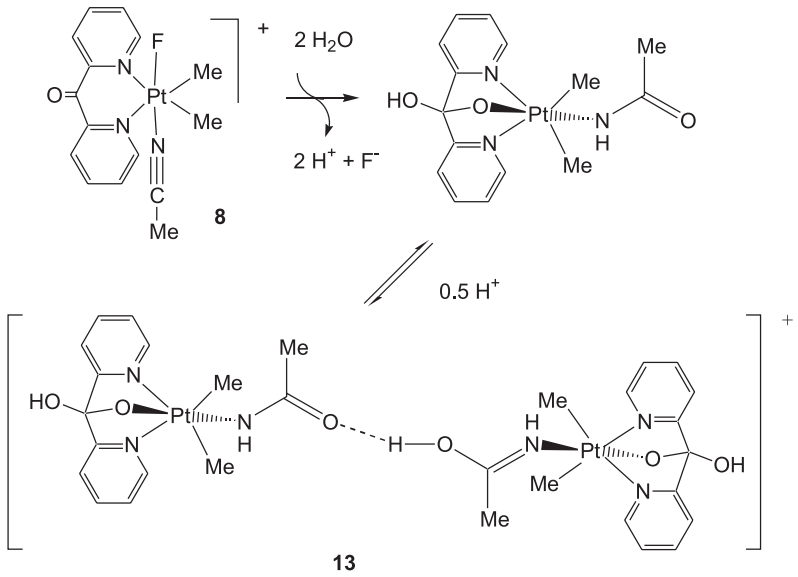
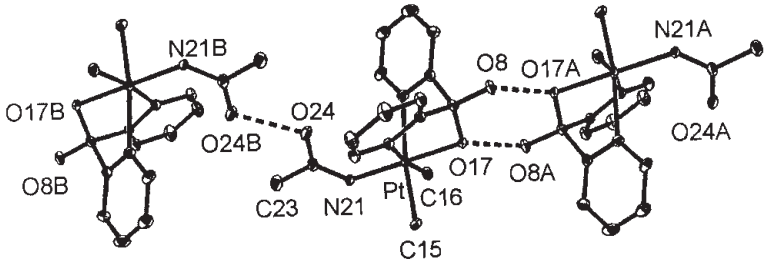


Fig. 8. A view of the supramolecular polymeric structure formed by hydrogen bonding in complex **13**.



only one unique platinum complex was present in the unit cell. The complexes self-assemble in the solid state to give a supramolecular polymer, as shown in Fig. 8. The self-assembly process has two components. Thus, each complex forms a dimer with its neighbour by complementary hydrogen bonding between DPKOH ligands (O(8)···O(17A)=O(17)···O(8A) = 2.668(7) Å), and these dimers are then linked by a strong hydrogen bond between the NHC(Me)=O···HOC(Me)=NH groups (O(24)···O(24A) = 2.42(1) Å). Since the hydrogen bond is strong and occurs between crystallographically equivalent atoms, it can be considered to be formed by the protonation of two acetamidate groups to give a rapid tautomeric equilibrium between the forms [NH-C(Me)=O···H-O-C(Me)=NH]$^-$ and [NH=C(Me)-O-H···O=C(Me)-NH]$^-$. The distances within the protonated acetamidate groups (N(21)—C(22) = 1.30(1) Å and C(22)—O(24) = 1.27(1) Å) are indicative of partial double bonds, as expected in terms of the proposed bonding scheme. There are many precedents for the hydrolysis of coordinated acetonitrile molecules to give acetamidate or acetamide complexes (13–15). For example, the complex *trans*-[Pt{NHC(=O)Me}(MeCN)$(NH_3)_2$]$^+$ is formed by partial hydrolysis of *trans*-[Pt$(MeCN)_2(NH_3)_2]^{2+}$ and has *d*(HN-C) = 1.28(2) and *d*(C=O) = 1.27(2) Å (13), while the "platinum blues" contain bridging acetamidate ligands formed by the partial hydrolysis of the acetonitrile ligands (14).

The reaction of complex **1** with excess methyl triflate in dichloromethane solution, followed by the addition of aqueous sodium hydroxide solution, gave the complex [$PtMe_3${DPC$(OMe)_2$}]OTf (**14**) containing the dimethyl ketal derivative of DPK as a fac-tridentate ligand (Scheme 5). In the ^{1}H NMR spectrum, there were two methylplatinum resonances in a 2:1 ratio for the methyl groups trans to nitrogen (δ(MePt) = 1.13, ^2J(Pt-H) = 70 Hz) and oxygen (δ(MePt) = 1.55, ^2J(Pt-H) = 83 Hz), respectively, and two equal intensity methoxy resonances for the groups coordinated (δ(MeO) = 3.43, ^3J(Pt-H) = 8 Hz) and not coordinated (δ(MeO) = 3.83) to platinum. The structure of the complex cation is shown in Fig. 9. It confirms the presence of the DPC$(OMe)_2$ ligand in a boat conformation that allows it to act as a fac-tridentate ligand. Though the hydrate DPC$(OH)_2$ and hemiketal DPC(OH)(OR) groups have been characterized in transition metal complexes, we are not aware of any other examples of ketal derivatives (7, 8).

The formation of the Pt(DPKOH) group in **10**–**13** or the Pt{DPC$(OMe)_2$} group in **14**, is likely to involve an intramolecular rearrangement of a Pt(OH)(DPK) unit at some stage, rather than the alternative external attack by hydroxide ion on the ketone group of a Pt(DPK) unit. Note in particular that the external attack mechanism in the reaction of complex **1** with hydrogen peroxide in methanol would be expected to give [Pt(OH)Me_2(DPKOMe)] and not the observed product [Pt(OMe)Me_2(DPKOH)] (**11**) (Scheme 2). The internal rearrangement mechanism involves nucleophilic attack by the oxygen atom of the PtOH group on the neigh-

© 2005 NRC Canada

Scheme 5.

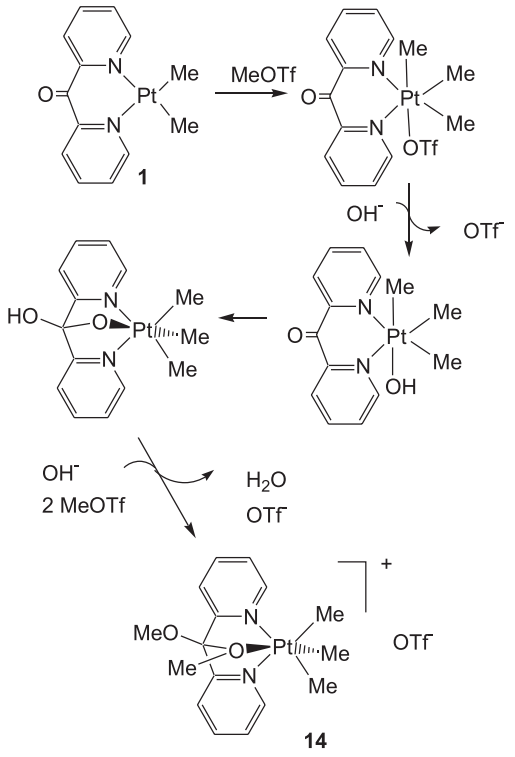
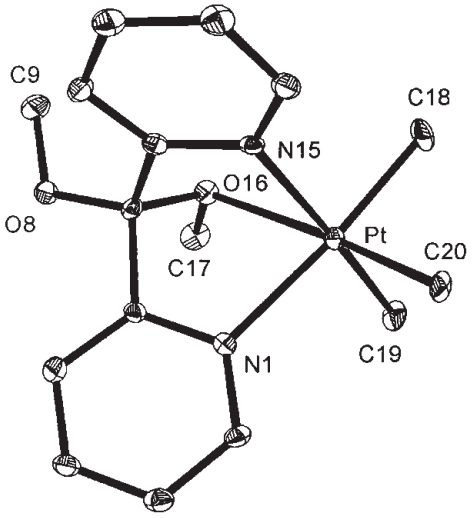


Fig. 9. A view of the structure of the cationic complex **14**.



bouring carbonyl group, as indicated in the structure of complex **9**, followed by 1,3-migration of the proton between the two oxygen atoms to give the Pt(DPKOH) group. The formation of the Pt{DPC(OMe)$_2$} group in **14** then requires initial formation of a Pt(DPKOH) group followed by deprotonation by base and methylation by methyl triflate (Scheme 5).

Experimental section

All reactions were carried under an N_2 atmosphere using standard techniques. ^{1}H NMR spectra were recorded by using a Varian Mercury or Inova 400 spectrometer, and ^{195}Pt NMR spectra were recorded by using a Varian Inova 600 spectrometer. ^{1}H NMR chemical shifts are reported relative to TMS, ^{19}F NMR chemical shifts relative to $CFCl_3$, and ^{195}Pt NMR chemical shifts relative to $[PtCl_2(SMe_2)_2]$ (16). The complex $[Pt_2Me_4(\mu\text{-}SMe_2)_2]$ was prepared as described in the literature (9).

[PtMe$_2$(DPK)] (1)

To a solution of $[Pt_2Me_4(\mu\text{-}SMe_2)_2]$ (0.25 g, 0.435 mmol) in CH_2Cl_2 (10 mL) was added a solution containing di-2-pyridyl ketone (0.16 g, 0.848 mmol) in CH_2Cl_2 (10 mL). The solution immediately turned orange and the product precipitated as dark orange solid over 30 min. The product was collected by filtration, washed with CH_2Cl_2–pentane, and dried under vacuum. Yield: 90%. IR (Nujol mull, cm^{-1}): 1682 υ(CO). ^{1}H NMR (acetone-d_6) δ: 0.78 (s, 6H, ^2J(Pt-H) = 86 Hz, Pt-Me), 7.73 (dd, 2H, ^3J(HH) = 5 Hz, 7 Hz, H5), 8.01 (d, 2H, ^3J(HH) = 7 Hz, H3), 8.24 (t, 2H, ^3J(HH) = 7 Hz, H4), 8.83 (d, 2H, ^3J(HH) = 5 Hz, ^3J(PtH) = 26 Hz, H6). ^{13}C NMR ($CDCl_3$) δ: –16.79 (s, ^1J(PtC) = 816 Hz, MePt), 125.79, 128.43, 137.53, 150.70, 153.24 (pyridyl C), 188.59 (CO). ^{195}Pt NMR ($CDCl_3$) δ: 332.8 (Pt). Anal. calcd. for $C_{13}H_{14}N_2OPt$ (%): C 38.14, H 3.45, N 6.84; found: C 38.33, H 3.21, N 6.76.

[PtIMe$_3$(DPK)] (3)

To a solution of complex **1** (0.041 g) in dry acetone (20 mL) was added excess MeI (0.05 mL). The color of the solution rapidly changed from red to yellow. After 10 min, the volume of the solution was reduced to 1 mL, and pentane (20 mL) was added to precipitate the product as a yellow solid, which was collected by filtration, washed with ether (3 × 2 mL) and pentane (3 × 8 mL), and dried under vacuum. Yield: 90%. IR (Nujol mull, cm^{-1}): 1687 υ(C=O). ^{1}H NMR (acetone-d_6) δ: 0.90 (s, 3H, ^2J(Pt-H) = 69 Hz, PtMe trans to I), 1.40 (s, 6H, ^2J(Pt-H) = 71 Hz, PtMe trans to N), 7.88 (t, 2H, ^3J(HH) = 6 Hz), 8.19 (d, ^3J(HH) = 7 Hz), 8.32 (t, 2H, ^3J(HH) = 7 Hz), 9.19 (d, 2H, ^3J(HH) = 6 Hz, ^3J(Pt-H) = 15 Hz). ^{195}Pt NMR (CD_2Cl_2) δ: 683.19 (Pt). Anal. calcd. for $C_{14}H_{17}IN_2OPt$ (%): C 30.5, H 3.11, N 5.08; found: C 31.06, H 2.99, N 5.87.

[PtClMe$_2$(CO$_2$Et)(DPK)] (4)

This was prepared similarly by reaction of excess ethyl chloroformate with a solution of complex **1** in CH_2Cl_2 for 22 h. Yield: 81%. ^{1}H NMR (CD_2Cl_2) δ: 1.07 (t, 3H, ^3J(HH) = 7 Hz, CH_3C), 1.50 (s, 6H, ^2J(Pt-H) = 71 Hz, PtMe), 3.99 (q, 2H, ^3J(HH) = 7 Hz, CH_2O), 7.68 (t, 2H, ^3J(HH) = 6 Hz), 8.10 (t, 2H, ^3J(HH) = 6 Hz), 8.22 (d, 2H, ^3J(HH) = 6 Hz), 9.16 (d, 2H, ^3J(HH) = 6 Hz, ^3J(Pt-H) = 15 Hz). EI-MS *m/z*: = 518.1 [M$^+$]. Anal. calcd. for $C_{16}H_{19}ClN_2O_3Pt$ (%): C 37.11, H 3.70, N 5.41; found: C 36.91, H 3.45, N 5.50.

[PtClMe$_2$(COMe)(DPK)] (5)

This was prepared similarly by the reaction of MeCOCl with complex **1** in acetone solution for 20 min. The product was isolated as a pale yellow solid. Yield: 78%. ^{1}H NMR (CD_2Cl_2) δ: 1.50 (s, 6H, ^2J(Pt-H) = 71 Hz, PtMe), 2.02 (s, 3H, ^3J(Pt-H) = 10 Hz, PtCOMe), 7.64 (t, 2H), 8.10 (t, 2H), 8.27 (d, 2H), 8.92 (d, 2H, ^3J(Pt-H) = 13 Hz). Anal. calcd. for

© 2005 NRC Canada

$C_{15}H_{17}ClN_2O_2Pt$: C 39.82, H 3.79, N 6.19; found: C 39.44, H 3.61, N 6.10.

[$PtCl_2Me_2$(DPK)] (6a)

To a solution of complex **1** (0.082 g) in acetone (15 mL) was added excess aq. H_2O_2 (0.1 mL, 30% solution) and then MeCOCl (36 μL). After 38 h, the product was isolated as a yellow powder. Yield: 65%. ^{1}H NMR (CD_3OD) δ: 1.77 (s, 6H, ^2J(Pt-H) = 71 Hz), 7.67 (t, 2H), 7.95 (d, 2H), 8.17 (t, 2H), 8.93 (d, 2H). Anal. calcd. for $C_{13}H_{14}Cl_2N_2OPt$ (%): C 32.51, H 2.94, N 5.83; found: C 32.41, H 2.90, N 5.81.

[$PtMe_3$(NCMe)(DPK)]OTf (7)

To a solution of complex **1** (0.41 g) in CH_3CN (20 mL) was added MeOTf (11 μL). The color of the solution immediately bleached. After 1 h, the product was isolated as an off-white powder. ^{1}H NMR (CD_3CN) δ: 0.93 (s, 3H, ^2J(Pt-H) = 75 Hz, MePt trans to NCMe), 1.11 (s, 6H, ^2J(Pt-H) = 68 Hz, MePt trans to N), 2.61 (s, 3H, PtNCMe), 7.88 (t, 2H), 8.19 (d, 2H), 8.20 (t, 2H), 8.81 (d, 2H, ^3J(Pt-H) = 16 Hz). Anal. calcd. for $C_{17}H_{20}F_3N_3O_4PtS$ (%): C 33.23, H 3.28, N 6.84; found: C 33.08, H 3.24, N 6.04.

[$PtFMe_2$(NCMe)(DPK)][BF_4] (8)

This was prepared similarly by reaction of complex **1** in MeCN solution with Selectfluor® ([$FN(CH_2CH_2)_2NCH_2Cl$]-[BF_4]$_2$). The color of the solution bleached immediately. After 30 min, the volume was reduced to 2 mL and pentane (10 mL) was added to precipitate both **8** and [$N(CH_2$-$CH_2)_2NCH_2Cl$][BF_4]. ^{1}H NMR for **8** (CD_3CN) δ: 1.83 (d, 6H, ^2J(Pt-H) = 67 Hz, ^3J(FH) = 6 Hz, PtMe), 2.69 (s, 3H, ^4J(Pt-H) = 13 Hz, PtNCMe), 7.93 (t, 2H), 8.21 (d, 2H), 8.34 (t, 2H), 8.97 (d, 2H). ^{19}F NMR (CD_3CN) δ: –151.45 (s, 4F, BF_4^-), 77.06 (br, 1F, Pt-F). At –30 °C, ^{19}F NMR (CD_3CN) δ: –146.680 (s, 4F, BF_4^-), 39.92 (s, ^1J(Pt-F) = 1360 Hz, Pt-F). EI-MS *m*/*z*: 469 [$PtFMe_2$(NCMe)(DPK)$^+$].

Attempts to grow single crystals of **8** gave instead either crystals of [$N(CH_2CH_2)_2NCH_2Cl$][BF_4] or, by hydrolysis of **8**, to crystals of the complex [$PtMe_2${NHC(=O)Me}-(DPKOH)][$PtMe_2${NH=C(OH)Me}(DPKOH)][BF_4] (**13**). ^{1}H NMR for **13** (CD_3CN) δ: 1.33 (s, 6H, ^2J(Pt-H) = 72 Hz, PtMe), 2.28 (s, 3H, MeC), 5.9, 6.4, 7.2 (br, NH, OH), 7.30 (dd, 2H, ^3J(HH) = 5, 7 Hz, H5), 7.67 (d, 2H, ^3J(HH) = 7 Hz, H3), 7.89 (t, 2H, ^3J(HH) = 7 Hz, H4), 8.47 (d, 2H, ^3J(HH) = 5 Hz, ^3J(PtH) = 12 Hz, H6). ^{19}F NMR (CD_3CN) δ: –151.45 (s, BF_4^-). EI-MS *m*/*z*: = 485 [$PtMe_2$(NHC(OH)Me)(DPKOH)$^+$].

[PtCl(OMe)Me_2(DPK)] (9)

To a solution of complex **1** (0.41 g) in MeOH (20 mL) was added a solution of *N*-chlorosuccinimide (0.14 g) in MeOH (10 mL). After 20 min, the volume was reduced to 2 mL, and pentane (10 mL) was added to precipitate the product as a yellow solid. Yield: 78%. ^{1}H NMR (CD_3OD) δ: 1.53 (s, 6H, ^2J(Pt-H) = 72 Hz, PtMe), 2.45 (s, 3H, ^3J(Pt-H) = 53 Hz, PtOMe), 7.83 (t, 2H), 8.20 (d, 2H), 8.28 (t, 2H), 8.94 (d, 2H, ^3J(Pt-H) = 12 Hz, PtNCH). Anal. calcd. for $C_{14}H_{17}ClN_2O_2Pt$ (%): C 35.34, H 3.60, N 5.89; found: C 35.75, H 3.70, N 6.27.

In a similar experiment using excess *N*-chlorosuccinimide, yellow single crystals of complex **6b** separated from the solution. ^{1}H NMR (DMSO-d_6) δ: 1.71 (s, 3H, ^2J(Pt-H) = 70 Hz, PtMe), 1.79 (s, 3H, ^2J(Pt-H) = 69 Hz, PtMe), 7.90, 8.01 (each dd, 1H, ^3J(HH) = 6, 8 Hz, H5, H5′), 8.18, 8.24 (each d, 1H, ^3J(HH) = 8 Hz, H3, H3′), 8.39, 8.43 (each t, 1H, ^3J(HH) = 8 Hz, H4, H4′), 8.81 (d, 1H, ^3J(HH) = 6 Hz, ^3J(Pt-H) = 48 Hz, H6), 9.10 (d, 1H, ^3J(HH) = 6 Hz, ^3J(Pt-H) = 13 Hz, H6′).

[Pt(OH)Me_2(DPKOH)] (10)

To a solution of complex **1** (0.41 g, 1 mmol) in acetone (25 mL) was added excess aq. H_2O_2 (0.5 mL, 30% solution). The mixture was immediately bleached. After 24 h, the product precipitated as a white solid, which was filtered, washed with pentane (3 × 5 mL), and dried under vacuum. Yield: 82%. ^{1}H NMR (CD_3COCD_3) δ: 1.45 (s, 6H, ^2J(Pt-H) = 72 Hz, PtMe), 5.55 (br, PtOH), 7.49 (t, 2H), 7.80 (d, 2H), 7.90 (t, 2H), 8.89 (d, 2H). ^{1}H NMR (CD_3CN–DMSO-d_6) δ: 1.39 (s, 6H, ^2J(Pt-H) = 73 Hz, PtMe), 3.15 (br, 1H, PtOH), 7.45 (dd, 2H, ^3J(HH) = 5, 7 Hz), 7.76 (d, 2H, ^3J(HH) = 7 Hz), 7.97 (t, 2H, ^3J(HH) = 7 Hz), 8.13 (br, 1H, PtOCOH), 8.65 (d, 2H, ^3J(HH) = 5 Hz). Anal. calcd. for $C_{13}H_{16}N_2O_3Pt$ (%): C 35.22, H 3.64, N 6.32; found: C 35.69, H 3.14, N 5.94.

[Pt(OMe)Me_2(DPKOH)] (11)

This was prepared similarly, but in methanol solution. Yield: 87%. ^{1}H NMR (CD_3OD) δ: 1.50 (s, 6H, ^2J(Pt-H) = 74 Hz, PtMe), 3.29 (s, 3H, ^3J(Pt-H) = 39 Hz, PtOMe), 4.84 (br, 1H, OH), 7.50 (t, 2H), 7.86 (d, 2H), 7.99 (t, 2H), 8.78 (d, 2H). Anal. calcd. for $C_{14}H_{18}N_2O_3Pt$ (%): C 36.76, H 3.97, N 6.12; found: C 36.67, H 3.99, N 5.84.

[PtClMe_2(DPKOH)] (12)

To a solution of complex **1** (0.04 g, 0.1 mmol) in CH_2Cl_2 (10 mL) was added aq. H_2O_2 (0.1 mmol, 30%) followed by acetyl chloride (0.1 mmol). After 30 min, the volume was reduced to 1 mL and pentane was added to precipitate the product as a yellow powder. Yield: 69%. For **12a** (ca. 90% abundance): ^{1}H NMR (CD_3CN) δ: 1.39 (s, 6H, ^2J(Pt-H) = 73 Hz, PtMe), 8.13 (s, 1H, OH), 7.45 (dd, 2H, ^3J(HH) = 5, 7 Hz, H5), 7.75 (d, 2H, ^3J(HH) = 7 Hz, H3), 7.97 (t, 2H, ^3J(HH) = 7 Hz, H4), 8.64 (d, 2H, ^3J(HH) = 5 Hz, H6). For minor isomer **12b** (ca. 10% abundance): ^{1}H NMR (CD_3CN) δ: 0.87 (s, 3H, ^2J(Pt-H) = 72 Hz, PtMe), 1.45 (s, 3H, ^2J(Pt-H) = 71 Hz, PtMe). Anal. calcd. for $C_{12}H_{13}ClN_2O_3Pt{\cdot}CH_2Cl_2$ (%): C 28.43, H 2.73, N 5.10; found: C 29.01, H 2.47, N 5.52.

[$PtMe_3${DPC$(OMe)_2$}] (14)

To a solution of complex **1** (0.041 g, 0.1 mmol) in dry CH_2Cl_2 (20 mL) was added excess MeOTf (0.01 mL). The colour of the solution immediately bleached. After 30 min, aq. NaOH (5 mL, 2 mol/L) was added. The organic layer was separated, dried with $MgSO_4$, filtered and evaporated to give the product as an off-white powder. Yield: 58%. ^{1}H NMR (CD_2Cl_2) δ: 1.13 (s, 6H, ^2J(Pt-H) = 70 Hz, PtMe), 1.55 (s, 3H, ^2J(Pt-H) = 83 Hz, PtMe), 3.43 (s, 3H, ^3J(Pt-H) = 8 Hz, PtOMe), 3.83 (s, 3H, Me, PtOCOMe), 7.72 (t, 2H, ^3J(HH) = 7 Hz), 8.08 (d, 2H, ^3J(HH) = 7 Hz), 8.23 (t, 2H, ^3J(HH) = 7 Hz), 8.55 (d, 2H, ^3J(HH) = 7 Hz, ^3J(PtH) = 14 Hz). ^{19}F NMR (CD_2Cl_2) δ: –79.362 [Otf]. Anal. calcd.

© 2005 NRC Canada

Table 2. X-ray data for the complexes.

	1	**2[BF_4]$_2$**	**3**	**6a**	**6b**	**9**	**12**	**13·0.5HBF_4·1.5MeCN**	**14[OTf]**
Formula	$C_{13}H_{14}N_2OPt$	$C_{22}H_{16}B_2F_8N_4O_2Pt$	$C_{14}H_{17}IN_2OPt$	$C_{13}H_{14}Cl_2N_2OPt$	$C_{13}H_{14}Cl_2N_2OPt$	$C_{14}H_{17}ClN_2O_2Pt$	$C_{13}H_{15}ClN_2O_2Pt$	$C_{18}H_{24}B_{0.5}F_2N_{4.5}O_3Pt$	$C_{17}H_{23}F_3N_2O_5PtS$
Fw	409.35	737.10	551.29	480.25	480.25	475.84	461.81	589.91	619.52
Temp. (K)	150(2)	150(2)	150(2)	296(2)	150(2)	150(2)	150(2)	150(2)	150(2)
λ(MoKα) (Å)	0.710 73	0.710 73	0.710 73	0.710 73	0.710 73	0.710 73	0.710 73	0.710 73	0.710 73
Crystal system	Triclinic	Monoclinic	Triclinic	Monoclinic	Monoclinic	Triclinic	Triclinic	Monoclinic	Monoclinic
Space group	*P*-1	$P2_1/n$	*P*-1	$P2_1/m$	$P2_1/m$	*P*-1	*P*-1	$P2_1/m$	$P2_1/c$
a (Å)	6.725 0(2)	8.187 0(3)	7.383 7(2)	6.679 8(3)	6.569 4(3)	7.685(2)	7.858 4(4)	7.954 1(2)	13.719 2(4)
b (Å)	8.796 2(2)	10.908 0(5)	8.897 4(2)	13.492 7(6)	13.646 9(6)	8.915(2)	8.693 9(5)	23.309(1)	13.726 7(6)
c (Å)	10.771 9(3)	12.940 7(4)	12.355 5(4)	8.274 7(2)	8.117 7(5)	12.113(2)	11.311(1)	13.206 4(5)	12.205 5(4)
α (°)	96.880(2)	90	98.401(2)	90	90	86.67(1)	81.485(2)	90	90
β (°)	93.775(2)	91.127(2)	94.574(2)	109.778	109.023(3)	81.86(1)	83.085(2)	93.181(2)	112.682(2)
γ (°)	103.901(2)	90	108.969(2)	90	90	66.071(7)	68.888(2)	90	90
Volume ($Å^3$)	611.12(3)	1 155.43(8)	752.33(4)	701.79(5)	688.02(6)	750.9(3)	711.05(8)	2 444.7(1)	2 120.8(1)
Z	2	2	2	2	2	2	2	4	4
d(calcd.) (Mg m^{-3})	2.225	2.119	2.434	2.273	2.318	2.104	2.157	1.603	1.940
Abs. coeff. (mm^{-1})	11.464	6.168	11.371	10.369	10.577	9.522	10.053	5.778	6.771
F(000)	384	704	508	452	452	452	436	1 144	1 200
No. of reflns./ind. reflns.	7142/3533	12 234/2 645	9411/4377	7395/1679	6341/1575	3023/2198	7383/2393	20 858/4 406	22 417/4 874
Abs. corr.	Integration	Integration	Integration	Integration	Integration	Integration	Integration	Integration	Integration
No. of data/restr./params.	3533/0/155	2 645/0/178	4377/0/17	1679/0/94	1575/6/96	2198/0/181	2393/2/173	4 406/33/271	4 874/0/263
*R*1, wR^2 ($I > 2\sigma(I)$)	0.048, 0.127	0.027, 0.066	0.041, 0.092	0.055, 0.145	0.054, 0.155	0.072, 0.187	0.048, 0.074	0.043, 0.103	0.043, 0.103

© 2005 NRC Canada

for $C_{17}H_{23}F_3N_2O_5PtS$ (%): C 32.96, H 3.74, N 4.52; found: C 32.66, H 3.98, N 4.19.

X-ray structure determinations

A suitable crystal was mounted on a glass fibre and data were collected by using a Nonius Kappa-CCD diffractometer. Details of the data collections and structure refinements are given in Table 2.[3]

Acknowledgments

We thank the Natural Sciences and Engineering Research Council of Canada (NSERC) for financial support. R.J.P. thanks the Government of Canada for a Canada Research Chair. We thank Dr. C.W. Kirby and Mr. D. Hairsine for assistance with the ^{195}Pt NMR and MS experiments.

References

1. L.M. Rendina and R.J. Puddephatt. Chem. Rev. **97**, 1735 (1997).
2. Reviews: (*a*) A.E. Shilov and G.B. Shul'pin. Chem. Rev. **97**, 2879 (1997); (*b*) D.E. Webster. Adv. Organomet. Chem. **15**, 147 (1997); (*c*) S.S. Stahl, J.A. Labinger, and J.E. Bercaw. Angew. Chem. Int. Ed. **37**, 2181 (1998); (*d*) A. Sen. Acc. Chem. Res. **31**, 550 (1998); (*e*) J.A. Labinger and J.E. Bercaw. Nature (London), **417**, 507 (2002); (*f*) U. Fekl and K.I. Goldberg. Adv. Inorg. Chem. **54**, 259 (2003).
3. (*a*) C.N. Iverson, C.A.G. Carter, R.T. Baker, J.D. Scollard, J.A. Labinger, and J.E. Bercaw. J. Am. Chem. Soc. **125**, 12 674 (2003); (*b*) M.P. Jensen, D.D. Wick, S. Reinartz, P.S. White, J.L. Templeton, and K.I. Goldberg. J. Am. Chem. Soc. **125**, 8614 (2003); (*c*) H.A. Zhong, J.A. Labinger, and J.E. Bercaw. J. Am. Chem. Soc. **124**, 1378 (2002); (*d*) L. Johansson, O.B. Ryan, C. Romming, and M. Tilset. J. Am. Chem. Soc. **123**, 6579 (2001).
4. (*a*) D.D. Wick and K.I. Goldberg. J. Am. Chem. Soc. **119**, 10 235 (1997); (*b*) S. Reinartz, P.S. White, M. Brookhart, and J.L. Templeton. J. Am. Chem. Soc. **124**, 7249 (2002); (*c*) C.M. Norris, S. Reinartz, P.S. White, and J.L. Templeton. Organometallics, **21**, 5649 (2002); (*d*) A.J. Canty, S.D. Fritsche, H. Jin, J. Patel, B.W. Skelton, and A.H. White. Organometallics, **16**, 2175 (1997); (*e*) A.N. Vedernikov, M. Pink, and K.G. Caulton. Inorg. Chem. **43**, 3642 (2004); (*f*) E.M. Prokopchuk, and R.J. Puddephatt. Organometallics, **22**, 787 (2003); (*g*) L. Johansson, O.B. Ryan, C. Romming, and M. Tilset. Organometallics, **17**, 3957 (2001).
5. U. Fekl, W. Kaminsky, and K.I. Goldberg. J. Am. Chem. Soc. **125**, 15 286 (2003).
6. D. Song, K. Sliwowski, J. Pang, and S. Wang. Organometallics, **21**, 4978 (2002).
7. (*a*) P.K. Byers, A.J. Canty, L.M. Engelhardt, J.M. Patrick, and A.H. White. J. Chem. Soc. Dalton Trans. 981 (1985); (*b*) I.J. Bakker, M.C. Feller, and R. Robson. J. Inorg. Nucl. Chem. **33**, 747 (1971); (*c*) B.E. Fischer and H. Sigel. J. Inorg. Nucl. Chem. **33**, 747 (1971).
8. (*a*) K.N. Crowder, S.J. Garcia, R.L. Burr, J.M. North, M.H. Wilson, B.L. Conley, P.E. Fanwick, P.S. White, K.D. Sienerth, and R.M. Granger II. Inorg. Chem. **43**, 72 (2004); (*b*) G. Annibale, L. Canovese, L. Cattalini, G. Natile, M. Biagini-Cingi, A. Manotti-Lanferdi, and A. Tiripicchio. J. Chem. Soc. Dalton Trans. 2280 (1981); (*c*) A.D.Q. Ferreira, A. Bino, and D. Gibson. Inorg. Chim. Acta, **265**, 155 (1997).
9. (*a*) J.D. Scott and R.J. Puddephatt. Organometallics, **2**, 1643 (1983); (*b*) G.S. Hill, M.J. Irwin, C.J. Levy, L.M. Rendina, and R.J. Puddephatt. Inorg. Synth. **32**, 149 (1997).
10. (*a*) F. Zhang, M.C. Jennings, and R.J. Puddephatt. Organometallics, **23**, 1396 (2004); (*b*) M. Crespo and R.J. Puddephatt. Organometallics, **6**, 2548 (1987).
11. V.V. Rostovtsev, J.A. Labinger, J.E. Bercaw, I.L. Lasseter, and K.I. Goldberg. Organometallics, **17**, 4530 (1998).
12. (*a*) K.-T. Aye, J.J. Vittal, and R.J. Puddephatt. J. Chem. Soc. Dalton Trans. 1835 (1993); (*b*) G.B. Deacon, E.T. Lawarenz, T.W. Hambley, S. Rainone, and L.K. Webster. J. Organomet. Chem. **493**, 205 (1995); (*c*) T.G. Appleton, C.J. D'Alton, J.R. Hall, M.T. Mathieson, and M.A. Williams. Can. J. Chem. **74**, 2008 (1996); (*d*) M. Rashidi, M. Nabavizadeh, R. Hakimelahi, and S. Jamali. J. Chem. Soc. Dalton Trans. 3430 (2001); (*e*) V.V. Rostovtsev, L.M. Henling, J.A. Labinger, and J.E. Bercaw. Inorg. Chem. **41**, 3608 (2002); (*f*) K. Thorshaug, I. Fjeldahl, C. Romming, and M. Tilset. J. Chem. Soc. Dalton Trans. 4051 (2003); (*g*) E.M. Prokopchuk and R.J. Puddephatt. Can. J. Chem. **81**, 476 (2003); (*h*) Y.-A. Lee, K.H. Yoo, and O.-S. Jung. Inorg. Chem. Commun. **6**, 249 (2003).
13. A. Erxleben, I. Mutikainen, and B. Lippert. J. Chem. Soc. Dalton Trans. 3667 (1994).
14. K. Sakai and K. Matsumoto. J. Am. Chem. Soc. **111**, 3074 (1989).
15. (*a*) B. Kamenar and D. Grdenic. Inorg. Chim. Acta, **3**, 25 (1969); (*b*) M.L. Schneider, G. Ferguson, and R.J. Balahura. Can. J. Chem. **51**, 2180 (1973); (*c*) C.S. Chin, D. Chong, B. Lee, H. Jeong, G. Won, Y. Do, and Y.J. Park. Organometallics, **19**, 638 (2000); (*d*) C.S. Yi, Z. He, and I.A. Guzei. Organometallics, **20**, 3641 (2001).
16. M. Rashidi, M.C. Jennings, and R.J. Puddephatt. Organometallics, **22**, 2612 (2003).

[3] Supplementary data for this article are available on the Web site or may be purchased from the Depository of Unpublished Data, Document Delivery, CISTI, National Research Council Canada, Ottawa, ON K1A 0S2, Canada. DUD 3663. For more information on obtaining material refer to http://cisti-icist.nrc-cnrc.gc.ca/irm/unpub_e.shtml. CCDC 252051–252059 contain the crystallographic data for this manuscript. These data can be obtained, free of charge, via www.ccdc.cam.ac.uk/conts/retrieving.html (Or from the Cambridge Crystallographic Data Centre, 12 Union Road, Cambridge CB2 1EZ, UK; fax +44 1223 336033; or deposit@ccdc.cam.ac.uk).

© 2005 NRC Canada

Thermally accelerated asymmetric hydrosilylations using ligated copper hydride[1]

Bruce H. Lipshutz, Bryan A. Frieman, John B. Unger, and Danielle M. Nihan

Abstract: Exposure of a variety of prochiral substrates to [(*R*)-(–)-DTBM-SEGPHOS]CuH + PMHS under microwave or conventionally heated conditions reduces reaction times for these hydrosilylations from hours to minutes without significant erosion in ee in most cases.

Key words: asymmetric hydrosilylation, copper hydride, microwave irradiation.

Résumé : Lorsqu'on soumet une variété de substrats prochiraux à l'effet combiné de [(*R*)-(–)-DTBM-SEGPHOS]CuH et du PMHS, dans des conditions de chauffage conventionnel oui par micro-ondes, on observe une réduction des temps de réaction de ces hydrosilylations qui passe d'heures à minutes sans érosion significative des ee, dans la plupart des cas.

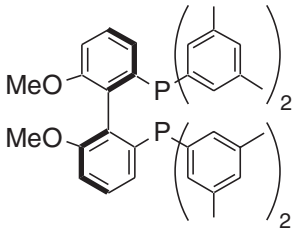
Mots clés : hydrosilylation asymétrique, hydrure de cuivre, irradiation micro-onde.

[Traduit par la Rédaction]

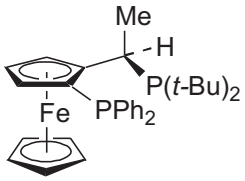
Introduction

Copper hydride (CuH) is notoriously heat sensitive (1). Complexation by ligands, usually phosphines (2), has allowed for its extensive use in synthesis at room temperature or below for effecting both 1,2- and 1,4-reductions of unsaturated carbonyl compounds (3). Since the advent of "Stryker's reagent", $[(Ph_3P)CuH]_6$, in 1988 as an especially useful reductant in synthesis (4*a*), many variations that alter the nature of the chelating phosphine (4*b*, 4*c*) have provided opportunities for utilizing CuH in an asymmetric context. Ligands such as Roche's 3,5-xylyl-MeO-BIPHEP (5) **1** and Solvias' JOSIPHOS analog (6) **2** and, in particular, Takasago's DTBM-SEGPHOS (7) **3** have spawned new technologies for controlling chirality in 1,2-reductions of aryl ketones (8*a*) and imines (8*b*), as well as 1,4-additions of hydride to acyclic (8*c*) and cyclic ketones (8*d*), enoates (8*e*), and unsaturated lactones (8*e*).

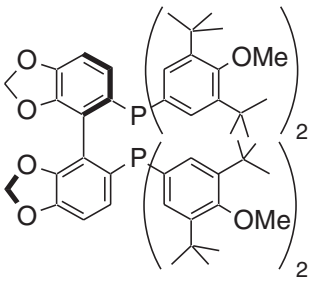
The innate bias of these ligands is remarkable, as is the reactivity they impart to CuH. In some cases, substrate-to-ligand (S:L) ratios over a hundred thousand to one have been documented (8*a*, 8*d*). In all cases reported to date, lower reaction temperatures have led to higher selectivities. Depending upon the substrate, reaction times with S:L ratios in the more convenient thousands to one range may still require hours for consumption of educt. One potential approach to increasing reaction rates is to take advantage of microwave irradiation (9). Given that this technique involves a mainly thermal component, its application to asymmetric CuH-based hydrosilylations seems counter-intuitive as the observed ees would be expected to drop. Moreover, elevated temperatures might be expected to decompose CuH at an increased pace and (or) alter ligand composition via oxidative



1
(*R*)-3,5-xyl-MeO-BIPHEP
Roche



2
(*R*)-(*S*)-PPF-P(*t*-Bu)$_2$
Solvias



3
(*R*)-(–)-DTBM-SEGPHOS
Takasago

Received 7 December 2004. Published on the NRC Research Press Web site at http://canjchem.nrc.ca on 11 June 2005.

Dedicated with warmth, admiration, and tremendous respect to Professor Howard Alper, the PI's former (undergraduate) mentor at SUNY Binghamton.

B.H. Lipshutz,[2] B.A. Frieman, J.B. Unger, and D.M. Nihan. Department of Chemistry and Biochemistry, University of California, Santa Barbara, CA 93106 USA.

[1]This article is part of a Special Issue dedicated to Professor Howard Alper.

[2]Corresponding author (e-mail: lipshutz@chem.ucsb.edu).

 doi: 10.1139/V05-083 © 2005 NRC Canada

processes due to adventitious oxygen. Notwithstanding these potential pitfalls, it seemed plausible that the overriding bias of ligands **1**–**3** and the rapidity of microwave heating could lead to fast and efficient hydrosilylations. We now report that, indeed, such ligand-accelerated reactions can be carried out in minutes under the influence of mild heating, employing either microwave irradiation or conventional means, without significant compromise in enantioselectivities.

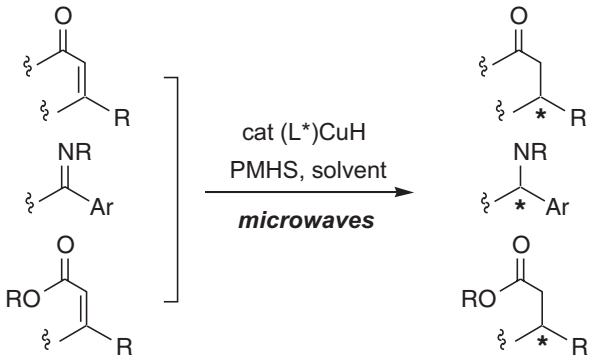
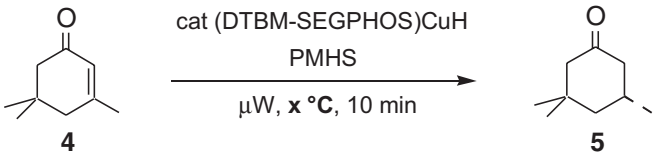


Table 1. Effect of temperature on asymmetric hydrosilylations with CuH.



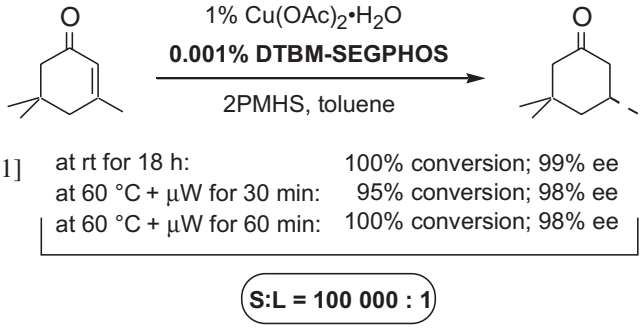
Temperature (°C)	Conversion (%)	ee (%)	
60	100	98.9	toluene
80	100	97.5	
100	73	97.2	
120	65	96.5	
80	10	86.2	CH_2Cl_2
80	70 [a]	98.0	THF
80	100	98.0	

Note: Reactions were run at an S:L ratio of 1000:1.
[a]Run for 15 min.

Results

Initial experiments were conducted on isophorone **4** employing our recently developed "Copper hydride in a Bottle",[3] where (*R*)-DTBM-SEGPHOS-chelated CuH is presumed to function as the catalytically active species. These trials were aimed at establishing a temperature at which the enone is quickly consumed. Along with this determination would also come the evaluation of reagent lifetime and the potential cost in ee. Temperatures ranging from 60 °C to 120 °C at 20° intervals were examined using a Personal Chemistry (now Biotage) Emry's Optimizer microwave instrument (Table 1). The data clearly indicate that in toluene, with increasing temperature, the extent of conversion to nonracemic adduct **5** drops significantly above 80 °C presumably because of loss of reagent (decomposition is evident). Interestingly, good selectivity even at the highest temperature remains. It is noteworthy that at 60 °C, a reaction that normally requires 3 h at room temperature can be carried out in 10 min with comparable ee. Other solvents tested at 80 °C include CH_2Cl_2 and THF. Surprisingly, the former led to only 10% conversion after 10 min (86.2% ee), while in THF the reaction was 70% complete. Extending the time of exposure to microwaves to 15 min afforded complete conversion to the product ketone in 98.0% ee.

As noted above, these reactions were run at an S:L ratio of 1000:1. We have tested the same asymmetric hydrosilylation on isophorone at the 100 000 : 1 level as well (eq. [1]). Thus, while conventionally the reduction requires ca. 18 h at room temperature to reach completion, at 60 °C in the microwave, 95% conversion is achieved within 30 min at similar concentrations. Allowing another 30 min reaction time ensures full consumption of educt. At this temperature, the ee remained at 98%.

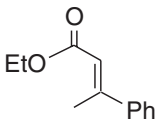
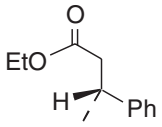
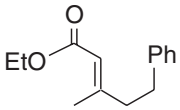
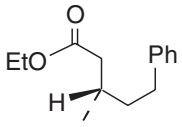
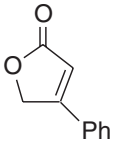
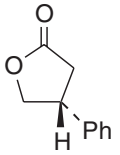
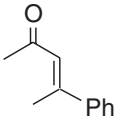
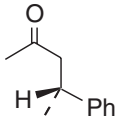
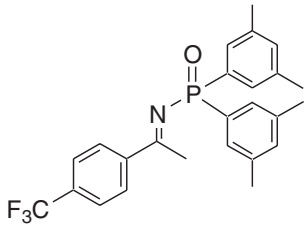
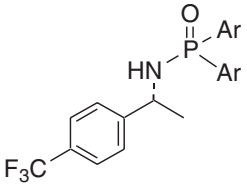


Using a microwave temperature limit of 60 °C, other substrates such as enoates, enones, an unsaturated lactone, and aryl imines were treated with cat. (DTBM-SEGPHOS)CuH–PMHS. Table 2 summarizes our observations, comparing reaction times and ees vs. those obtained previously under conventional conditions (where known). Modest erosion in observed ees at this higher temperature appears to be a consistent trend, independent of whether the nature of the addition of hydride is in the 1,4- (entries 1–4) or 1,2- (entry 5) mode. The option to switch solvents from toluene to more polar, lower boiling THF is worthy of mention and was, in fact, needed in the case of an unsaturated lactone (entry 3). Limited solubility and, hence, incomplete reaction were averted by employing ethereal media along with an 80 °C reaction temperature. This combination led smoothly and quickly to the desired nonracemic lactone in 98.6% ee, a result that compares remarkably well with the previously observed level of induction (99%) realized under conventional conditions at 0 °C (8*e*). Enone **A** (entry 4) was surprisingly unreactive to (DTBM-SEGPHOS)CuH–PMHS, returning only starting material in two separate experiments. Although WALPHOS **12** gave rise to complete conversion to keto product **B**, the ee was not particularly high. Much better results were obtained using the JOSIPHOS analog **2** as ligand for CuH (ee 93.5%). The absolute stereochemistry is indi-

[3]The experimental procedure for the preparation of "CuH in a Bottle" is available in the experimental section; B.H. Lipshutz and B.A. Frieman. Submitted.

© 2005 NRC Canada

Table 2. Asymmetric hydrosilylations with (L*)CuH under μW irradiation at 60 °C for ≤30 min (L* = a nonracemic ligand).

			Microwave reactions			Conventional reactions	
Entry	Substrate	Product	Ligand	Yield (%)[a]	ee (%)	Temp (°C), time (h)	ee (%)
1			**3**	88	97.7	rt, 5	91.0[b]
2			**3**	92	90.9	0, 4	90.0[b]
			2	31	89.6	0, 6	98.0[b]
			12	68[c]	91.6	—	—
3			**3**	94[d]	98.6	0, 3	99.0[b]
4	 **A**	 **B**	**12**	91	84.5	—	—
			2	87	93.5	—	—
5			**3**	92	95.7	rt, 17	97.3[e]

Note: Run in toluene using PMHS (2 equiv.) as stoichiometric source of hydride. All were worked up using aqueous base to hydrolyze residual silane. *t*-BuOH (1–2 equiv.) was used in each reaction to enhance the rate of (L*)CuH regeneration.

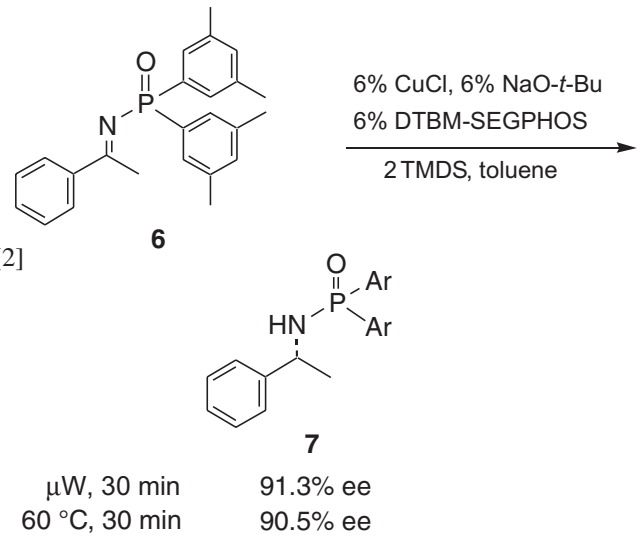
[a]Isolated, chromatographically purified materials.

[b]cf. Reference 8*e*.

[c]Conversion was 71%.

[d]Run in THF.

[e]cf. Reference 8*b*.



[2]

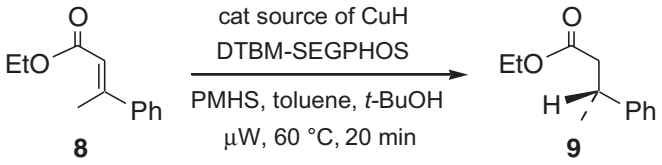
cated for known products shown in entries 1–3 and 5, while that for **B** was tentatively assigned on the basis of previous data on related enones (8*c*).

Acetophenone-derived imine **6** (eq. [2]), which, using microwave conditions at 60 °C, gave product **7** possessing an ee of 91.3%, was examined by conventional heating at 60 °C. Thus, the premixed catalyst–silane was added to a round-bottom flask, to which was added the imine immediately prior to placement in a preheated oil bath at 60 °C. After the same 30 min interval, workup and analysis by chiral HPLC indicated that the reaction had gone to completion and that the ee was 90.5%. Thus, as had been noted previously by Leadbeater and Marco (10), rapid conventional heating of reaction mixtures can on occasion give essentially the same results observed under microwave irradiation. Such appears to be the case with these asymmetric hydrosilylations when run in toluene.

Test reactions on cinnamate **8** (Table 3) were performed to assess the background reaction using Stryker's reagent as the source of CuH, rather than the in situ procedures based on

© 2005 NRC Canada

Table 3. Impact of Ph_3P on asymmetric hydrosilylations with CuH.



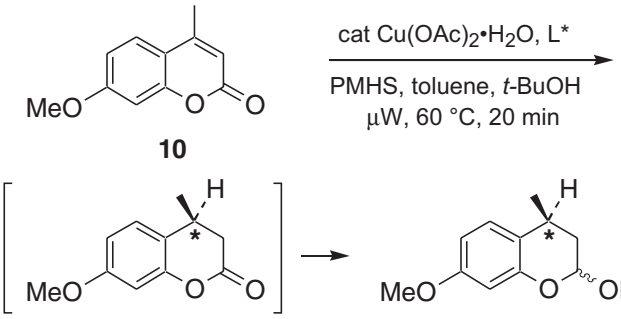
8 **9**

source of CuH	CuH : ligand : substrate	ee (%)
$Cu(OAc)_2•H_2O$	1 : 1 : 1000	97.7
$[(Ph_3P)CuH]_6$	1 : 1 : 1000	96.2
$[(Ph_3P)CuH]_6$	10 : 1 : 1000	84.5

either CuCl + NaO-*t*-Bu (11) or $Cu(OAc)_2•H_2O$ (12), which do not contain Ph_3P in solution. As illustrated, a 60 °C reaction temperature at an S:L ratio of 1000:1 causes an increase in the extent to which achiral $(Ph_3P)CuH$ competes for substrate, with the ee of product ester **9** dropping from 97.7 to 96.2. Using 1% rather than 0.1% of Stryker's reagent (i.e., an S:L = 100:1) causes a significant loss in selectivity (ee = 84.5%). Thus, as the temperature at which these asymmetric reductions are run goes up, the presence of Ph_3P should be avoided.

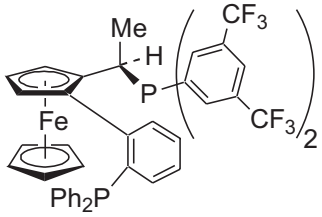
Other combinations of copper hydride and nonracemic ligands were also tested using coumarin derivative **10** (Table 4). This substitution pattern for an enoate has not previously been examined within the context of CuH-based asymmetric hydrosilylation chemistry. On first inspection, it was anticipated from prior art (8*e*) that its *Z*-cinnamate-like structure dictates that DTBM-SEGPHOS (**3**) would be the ligand of choice. When the reaction of **10** was run under conventional conditions using CuH ligated by this ligand at ambient temperature, the unexpected product of over-reduction, **11**, was obtained in 94% ee. In addition to DTBM-SEGPHOS, JOSIPHOS analog **2** and WALPHOS (**12**)[4] were screened, as were Sannicolo and co-workers's BITIANP (13) (**13**) and Boaz et al.'s BOPHOZ (14) (**14**) ligands. Unexpectedly, microwave experiments indicated that the ferrocenyl backbone common to **2** and **12** imparted the greatest enantioselectivities, significantly exceeding that observed with ligand **3**. The sense of induction for ligands **2** and **3** is the same, presumably affording the *S*-isomer from this *Z*-configured educt, while ligands **12**–**14** led to the enantiomeric product, as indicated by chiral capillary GC analyses.

Table 4. Asymmetric hydrosilylations using CuH chelated by various ligands.

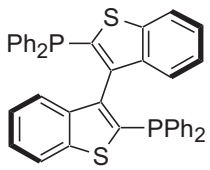


Ligand (L*)		ee (%)
(*R*)-(*S*)-PPF-P(*t*-Bu)$_2$	(**2**)	96.7
(*R*)-DTBM-SEGPHOS	(**3**)	90.0
WALPHOS	(**12**)	94.6
BITIANP	(**13**)	85.3
BOPHOZ	(**14**)	6.0

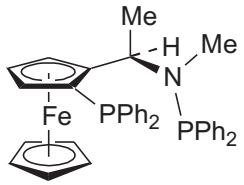
conventional reaction:
cat (DTBM-SEGPHOS)CuH
rt, 7-8 h; 94% ee



12 (*R*)-(*R*)-WALPHOS



13 *S*-(–)-BITIANP



14 (*R*)-(*S*)-BoPhoz

Discussion

Given the history of copper hydride itself, dating back to Wurtz' report in 1844 (1*a*), it is not surprising that applications of ligated CuH at elevated temperatures have not previously been considered. Chelation by modern nonracemic bidentate phosphine ligands appears to induce not only an extreme stereochemical bias in reactions of CuH, but adds an unexpected element of stability such that mild heating of reaction mixtures is well tolerated, including those that may contain only trace amounts of the reactive catalyst relative to substrate.

Our approach to heating these reactions, at least initially, was to utilize microwave irradiation. This special, highly controlled technique, when applied within the confines of the Biotage instrument,[5] was anticipated to allow for reaction temperatures above the boiling point of the solvents to be used, along with the associated elevation in pressures. From the outset, however, as illustrated by the data in Table 1, it was clear that heating beyond 80 °C, which is well

[4] (*R*)-(*R*)-$Ph_2PPhFcCHCH_3P(3,5\text{-}CF_3Ph)_2$; Available from Solvias, Basel Switzerland (SL-W001–1; CAS Reg. No. 387868–06–6; cf. http://www.solvias.com.

[5] The Personal Chemistry Emrys Optimizer has been replaced by the Biotage Initiator; cf. http://www.biotagedcg.com/DynPage.aspx?id=4193&mn1=919&mn2=1149.

© 2005 NRC Canada

below the boiling point of the reaction solvent toluene, was not viable. Nonetheless, in going from even room temperature to 60–80 °C, normal accelerations in rates were observed, while the intrinsic stereochemical bias imposed by the chelating phosphine ligand was not significantly compromised. The fact that essentially the same results (i.e., extent of conversion and observed ee; cf. eq. [2]) could be obtained by conventional heating strongly suggest that in this case, although far more convenient, microwave irradiation adds little to the chemistry. It is appreciated, however, that toluene is not likely to be the universal solvent for all substrate types. The switch to lower boiling THF would rely on the controlled temperature and pressure found under microwave conditions (cf. Table 1, last entries, and Table 2, entry 3). Although CH_2Cl_2 was surprisingly ineffective, reactions run in several other solvents that are lower boiling than toluene (bp 110 °C) can easily be envisioned to benefit from a microwave environment.

The interplay between substrate and the choice of ligand on CuH, especially under the influence of applied heat, could not have been predicted. Thus, while educt **10** had not previously been subjected to copper-hydride-based asymmetric hydrosilylation, all prior efforts on cinnamate enoates (8*e*, 15) pointed to DTBM-SEGPHOS **3** as the ligand that consistently affords extremely high levels of induction. JOSIPHOS analog **2** is also quite selective in such cases (8*e*) but typically is best utilized for β,β-*dialkyl*-substituted enoates. Thus, it was interesting to observe that both ferrocenyl-based ligand systems **2** and WALPHOS **12** led to significantly higher levels of enantioselectivity than did **3** (cf. Table 4). Curiously, the inverse of this observation, that a β,β-dialkyl-substituted enoate would best be reduced by (DTBM-SEGPHOS)CuH, as opposed to PPF-P(*t*-Bu)$_2$ **2** (cf. Table 2, entries 2 and 3), is also unexpected. These crossover results may reflect subtle changes in the degree of association of the ligand with CuH at varying temperatures, potential aggregation state issues, and (or) the likely impact of both steric and stereoelectronic factors in (L* = a nonracemic ligand)CuH that may be influential even when differences between educts are otherwise structurally quite small. Second-stage reduction, in this case of the initially formed lactone **C**, has not been observed previously with enoates or unsaturated lactones (8*e*, 15). Presumably this results from rapid quenching of the copper enolate by *t*-BuOH, followed by 1,2-reduction. None of the intermediate lactone was observed in the course of this asymmetric hydrosilylation.

What can be claimed from this study, in general, is that the increase in reaction rates gained upon mild heating to ca. 60 °C reduces the times for these asymmetric hydrosilylations to well under an hour, even where S:L ratios are in the thousands-to-one category. Several commonly studied substrate types successfully participate, and ees remain well within the synthetically useful range.

Conclusions and summary

The first study on the potential for microwave irradiation to be used to accelerate rates of asymmetric hydrosilylations by catalytic amounts of nonracemically ligated CuH is described. The results indicate that mild heating of reactions containing either complex [(*R*)-(–)-DTBM-SEGPHOS)]CuH or [(*R*)-(S)-PPF-P(*t*-Bu)$_2$]CuH via either microwave or conventional means can be tolerated and that a variety of synthetically useful 1,2- and 1,4-reductions can be realized in both good yields and excellent levels of stereoinduction.

Experimental section

General

Reactions were performed in oven-dried glassware under an argon atmosphere containing a Teflon coated stir bar and dry septum. Toluene, dichloromethane, and THF were used as is from an Innovative Technology, Inc. solvent filtration system. All commercially available reagents were distilled either from CaH_2 or molecular sieves under an inert atmosphere before use. CuCl, NaO-*t*-Bu, NaOMe, PPh_3, isophorone, and acetophenone oxime were purchased from Aldrich. Other oximes were prepared from the corresponding ketones following a literature procedure (2). Chloro bis(3,5-dimethylphenyl)phosphine was prepared according to a literature procedure (3). Phosphinylimines were prepared from the corresponding oximes by modification of a literature procedure (4). $Cu(OAc)_2 \cdot H_2O$, was purchased from Acros. Tetramethyldisiloxane was purchased from Alfa Aesar. Poly(methylhydrosiloxane) was purchased from Lancaster. Stryker's reagent was prepared by the general procedure (4). (*R*)-(–)-DTBM-SEGPHOS was generously supplied by Takasago International Corp. All microwave experiments were performed using Personal Chemistry Emry's Optimizer in 0.5–2 mL or 2–5 mL Pyrex reaction vessels that were flame dried under an argon atmosphere. Each reaction vessel contained a Teflon stir bar and a Teflon coated reaction vessel cap. Optical rotations were measured on a PerkinElmer 341 Polarimeter. HPLC analyses were performed on a Rainan Dynamax UV-1 with an HPXL solvent delivery system. GC analyses were performed on a Hewlett-Packard 6890 Series GC. GC analyses were carried out using an HP-5 capillary column (0.25 μm × 30 m; cross-linked 5% PH ME siloxane) and a time program beginning with 5 min at 50 °C, followed by a 20 °C/min ramp to 280 °C, then 20 min at this temperature. Column chromatography was performed using Davisil Grade 633 Type 60A silica gel. TLC analyses were performed on commercial Kieselgel 60 F_{254} silica gel plates. NMR spectra were obtained on Varian Inova systems using $CDCl_3$ or C_6D_6 as solvent, with proton and carbon resonances at 400 MHz and 100 MHz, respectively. FT-IR spectra were obtained on an ATI Mattson Infinity series spectrometer neat on NaCl plates or KBR pellets and are reported in cm^{-1}. Mass spectral data were acquired on a VF Autospec or an analytical VG-70-250 HF instrument.

Preparation of [(*R*)-(–)-DTBM-SEGPHOS]CuH in a Bottle (0.001 mol/L)

An oven-dried poly-coated amber glass bottle equipped with stir bar was purged under argon and brought into the glove box. $Cu(OAc)_2 \cdot H_2O$ (10 mg, 0.05 mmol) and (*R*)-DTBM-SEGPHOS (**3**, 59 mg, 0.05 mmol) were added, followed by dry toluene (44 mL), and the mixture was allowed to stir for 2 h at room temperature (rt). PMHS (6 mL) was added dropwise, and the mixture was allowed to stir for

© 2005 NRC Canada

30 min. The amber bottle was then sealed using a standard "sure–seal cap" and stored at 4 °C or rt.

(*R*)-3,3,5-Trimethylcyclohexanone (5; Table 1, entry 1)

To a 2–5 mL Emry's Optimizer glass vessel, flame dried and purged with argon, was added (DTBM-SEGPHOS)CuH in a Bottle (2 mL, 0.001 mol/L, 0.002 mmol). Isophorone (300 μL, 2 mmol) was added neat, and the reaction was immediately taken to the Emry's Optimizer. The following conditions were applied: temperature, 60 °C; time, 600 s; fixed hold time, on; sample absorption, normal; pre-stirring, 10 s. The reaction was quenched by diluting the reaction with THF (5 mL), followed by aqueous NaOH (5 mL, 3 mol/L), and the reaction was allowed to stir at rt for 2 h. The product was isolated as a colorless liquid; Chiral GC using a Chiraldex B-DM column with 75 °C isotherm showed 98.9% ee, R_t = 41.47 (minor) and 44.94 (major). The product spectral data matched previously reported spectral data (8*d*).

(*R*)-3,3,5-Trimethylcyclohexanone (temperature study; Table 1)

To a 2–5 mL Emry's Optimizer glass vessel that had been flame dried and purged with argon was added (DTBM-SEGPHOS)CuH in a Bottle (2 mL, 0.001 mol/L, 0.002 mmol). Isophorone (300 μL, 2 mmol) was added neat, and the reaction was immediately submitted to the Emry's Optimizer. The following conditions were applied: temperature, 60–120 °C; time, 600 s; fixed hold time, on; sample absorption, normal; pre-stirring, 10 s. Upon completion, the reaction was quenched by diluting with THF (5 mL) followed by aqueous NaOH (5 mL, 3 mol/L) and then allowed to stir at rt for 2 h. The product was analyzed by GC to determine the conversion; Chiral GC using a Chiraldex B-DM column with 75 °C isotherm was used to determine the ee. For the cases with dichloromethane and THF, the same protocol was used to prepare the CuH in a Bottle.

(*R*)-3,3,5-Trimethylcyclohexanone (100 000 : 1; eq. [1])

(a)

To a flame-dried, 500 mL, round-bottom flask equipped with stir bar and purged with argon was added CuCl (167.9 mg, 1.69 mmol), NaO-*t*-Bu (163 mg, 1.69 mmol), and (*R*)-DTBM-SEGPHOS (**3**, 2 mg, 1.695×10^{-3} mmol), followed by toluene (100 mL). The reaction was allowed to stir for 30 min at rt. PMHS (20.35 mL, 339.12 mmol H^-) was added dropwise via syringe and allowed to stir for 10 min. Isophorone (25.47 mL, 169.5 mmol) was then added dropwise, and the reaction was monitored by TLC. The reaction was complete in 18 h at rt, as indicated by TLC and GC.

(b)

As soon as the isophorone was added, 2 mL from the above reaction was syringed into a 2–5 mL Emry's Optimizer dry glass vessel under argon. The vessel was quickly introduced into the Emry's Optimizer, where the following reaction conditions were applied: temperature, 60 °C; time, 3600 s; fixed hold time, on; sample absorption, normal; pre-stirring, 10 s. After the 60 min reaction period, the reaction was quenched by diluting with THF (5 mL), followed by aqueous NaOH (5 mL, 3 mol/L), and was allowed to stir at rt for 2 h. The reaction was analyzed by GC to contain only product without any isophorone or byproducts; Chiral GC using a Chiraldex B-DM column with 75 °C isotherm showed 98% ee, R_t = 41.47 (minor) and 44.94 (major). The product spectral data matched previously reported spectral data (8*d*).

(*R*)-*N*-(1-Phenylethyl) bis(3,5-dimethylphenyl)phosphinamide (7; eq. [2])

CuCl (3.6 mg, 0.036 mmol), NaOMe (2.0 mg, 0.038 mmol), and (*R*)-DTBM-SEGPHOS (**3**, 42.6 mg, 0.036 mmol) were placed into a flame-dried, argon-purged round-bottom flask (RBF). Toluene (1.5 mL) was added to the RBF, and the resulting mixture was stirred at rt for 30–40 min. Meanwhile, *N*-(1-phenylethylidene) bis(3,5-dimethylphenyl)phosphinamide (75.1 mg, 0.200 mmol) was added to a 0.5–2.0 mL Emry's Optimizer glass vessel, which had been flame dried and purged with argon. *t*-BuOH (50 μL, 0.55 mmol) and toluene (450 μL) were added and allowed to stir for 5 min until the solution became homogeneous. The RBF was charged with tetramethyldisiloxane (TMDS; 0.318 mL, 1.6 mmol) and allowed to stir for 10 min. After this time, the CuH mixture (618 μL) was slowly added to the glass vessel via syringe, and the reaction was immediately taken to the Emry's Optimizer. The following conditions were applied: temperature, 60 °C; time, 1800 s; fixed hold time, on; sample absorption, normal. MeOH (1 mL) was slowly added, and after 30 min, 1 mol/L NaOH in MeOH (0.5 mL) was added. The mixture was stirred for 2–3 h, filtered through a plug of silica, and concentrated under vacuum. Purification by silica gel chromatography (10% acetone–CH_2Cl_2) gave the corresponding phosphinylamine (71 mg, 94% yield) as a white solid. HPLC analysis indicated 91.3% ee. (Daicel Chiralcel OD, hexane : isopropyl alcohol, 90:10, 1.0 mL/min, 220 nm; R_t = 5.3 min (*R*), 6.7 min (*S*)). The product spectral data matched previously reported spectral data (8*b*).

(*R*)-*N*-(1-Phenylethyl) bis(3,5-dimethylphenyl)phosphinamide, conventional heating (7; eq. [2])

CuCl (3.6 mg, 0.036 mmol), NaOMe (2.0 mg, 0.038 mmol), and (*R*)-DTBM-SEGPHOS (**3**, 42.6 mg, 0.036 mmol) were placed into a flame-dried, argon-purged round-bottom flask (RBF). Toluene (1.5 mL) was added to the RBF, and the resulting mixture was stirred at rt for 30–40 min. Meanwhile, *N*-(1-phenylethylidene) bis(3,5-dimethylphenyl)phosphinamide (75.1 mg, 0.200 mmol) was added to a 10 mL RBF, flame dried and purged with argon. *t*-BuOH (50 μL, 0.55 mmol) and toluene (450 μL) were added and allowed to stir for 5 min until the solution became homogeneous. The RBF was charged with tetramethyldisiloxane (TMDS; 0.318 mL, 1.6 mmol) and allowed to stir for 10 min. After this time, the CuH mixture (618 μL) was slowly added to the RBF via syringe, and the reaction was immediately placed into a preheated oil bath at 60 °C. After 30 min, MeOH (1 mL) was slowly added, and after 30 min, 1 mol/L NaOH in MeOH (0.5 mL) was added. The mixture was stirred for 2–3 h, filtered through a plug of silica, and concentrated under vacuum. Purification by silica gel chro-

© 2005 NRC Canada

matography (10% acetone–CH_2Cl_2) gave the corresponding phosphinylamines (70 mg, 93% yield) as a white solid. HPLC analysis indicated 90.5% ee. (Daicel Chiralcel OD, hexane : isopropyl alcohol, 90:10, 1.0 mL/min, 220 nm; R_t = 5.3 min (*R*), 6.7 min (*S*)). The product spectral data matched previously reported spectral data.

(*S*)-Ethyl 3-phenylbutanoate (9; Table 2, entry 1)

To a 2–5 mL Emry's Optimizer glass vessel, flame dried and purged with argon, was added (*E*)-ethyl 3-methyl-5-phenylpent-2-enoate (neat, 0.380 mg, 2 mmol). (DTBM-SEGPHOS)CuH in a Bottle (2 mL, 0.001 mol/L, 0.002 mmol) was added via syringe followed by *t*-BuOH (230 μL, 2.4 mmol), and the reaction was immediately taken to the Emry's Optimizer. The following conditions were applied: temperature, 60 °C; time, 1200 s; fixed hold time, on; sample absorption, normal. The TLC (9:1, hexanes:Et_2O) showed complete consumption of starting material. The reaction was quenched by diluting with THF (3 mL), followed by aqueous NaOH (2 mL, 3 mol/L), and was allowed to stir at rt for 2 h. The residue was purified by column chromatography and isolated (338 mg, 88% yield) as a clear oil; Chiral GC using a Chiraldex G-TA column with 100 °C isotherm showed 97.2% ee, R_t = 77.79 (minor) and 78.70 (major). The product spectral data matched previously reported spectral data (8*e*).

(*S*)-Ethyl 3-methyl-5-phenylpentanoate (Table 2, entry 2)

To a 25 mL round-bottom flask, flame dried and purged under argon, was added CuCl (4.2 mg, 0.042 mmol), NaO-*t*-Bu (3.7 mg, 0.039 mmol), and (*R*)-DTBM-SEGPHOS (**3**, 4.7 mg, 0.004 mmol) under an argon atmosphere. The flask was sealed with a rubber septum, and toluene (3.5 mL, dried through a column of alumina and degassed via 3 freeze–thaw cycles) was added with a dry glass syringe. The solution was stirred at rt for 45 min, at which point PMHS (0.5 mL, 0.279 mmol) was added. After 15 min of stirring, 1 mL of the solution was transferred via syringe to an Emry's Optimizer glass vial (sealed and argon purged) containing a dry stir bar and ethyl 3-methyl-5-phenylpent-2-enoate (218 mg, 1.0 mmol). *t*-BuOH (0.11 mL, 1.2 mmol) was added, and the vial was immediately taken to the Emry's Optimizer. The following conditions were applied: temperature, 60 °C; time, 1500 s; fixed hold time, on. Upon ejection of the reaction vial from the optimizer, the septum was removed and the reaction mixture poured into sat. $NaHCO_3$ (15 mL), where it was stirred for 4 h. The organic layer was extracted with diethyl ether (3 × 15 mL), washed with brine (1 × 15 mL), dried over anhydrous Na_2SO_4, and then concentrated under reduced pressure. Purification via silica gel chromatography (10 g, 2.5% Et_2O in hexanes) yielded a clear oil (206 mg, 93.6% yield). Chiral GC using a Chiraldex G-TA column with 95 °C isotherm showed 94.6% ee, R_t = 277.00 (minor) and 279.46 (major). The product spectra matched previously reported spectral data (8*e*).

(*R*)-Dihydro-4-phenyl-(3*H*)-furan-2-one (Table 2, entry 3)

A standard solution of (*R*)-(DTBM-SEGPHOS)CuH (10 mL, 0.001 mol/L) was prepared as follows: $Cu(OAc)_2 \cdot H_2O$ (2.0 mg, 0.010 mmol) and (*R*)-DTBM-SEGPHOS (11.8 mg, 0.010 mmol) were dissolved in THF (7.6 mL) and stirred at rt for 0.5 h. PMHS (2.4 mL, 40 mmol) was then added dropwise to the mixture via syringe. To a 2–5 mL Emry's Optimizer glass vessel, flame dried and purged with argon, was added 4-phenylfuran-2(5*H*)-one (80 mg, 0.50 mmol), CuH catalyst solution (0.5 mL), and *t*-BuOH (0.06 mL, 0.60 mmol). This solution was immediately transferred to the microwave and heated at 80 °C for 30 min. The reaction was quenched by diluting with ether (3 mL), followed by aqueous $NaHCO_3$ (3 mL), and then allowed to stir at rt for 0.5 h. The product lactone (75 mg, 93%) was isolated as a white solid; Chiral GC using a Chiraldex G-TA column with 160 °C isotherm showed 98.6% ee, R_t = 74.01 (minor) and 75.00 (major). The product matched previously reported spectral data (8*e*).

4-Phenylpentan-2-one (B, Table 2, entry 4)

To a 25 mL round-bottom flask, flame dried and purged under argon, was added CuCl (10 mg, 0.10 mmol), NaO-*t*-Bu (9.7 mg, 0.10 mmol), and (*R*,*S*)-PPF-P(*t*-Bu)$_2$ JOSIPHOS (5.2 mg, 0.01 mmol) under an argon atmosphere. The flask was sealed with a rubber septum and toluene (8.7 mL, dried through a column of alumina and degassed via 3 freeze–thaw cycles) was added with a dry glass syringe. The solution was stirred at rt for 45 min, at which point PMHS (1.3 mL, 0.73 mmol) was added. After 15 min of stirring, 0.87 mL of the solution was transferred via syringe to an Emry's Optimizer glass vessel (sealed and under argon) containing a dry stir bar and 4-phenylpent-3-en-2-one (**A**, 140 mg, 0.87 mmol). *t*-BuOH (0.1 mL, 1.05 mmol) was added, and the vial was immediately taken to the Emry's Optimizer. The following conditions were applied: temperature, 60 °C; time, 1500 s; fixed hold time, on. Upon ejection of the reaction vial from the optimizer, the septum was removed, and the reaction mixture poured into sat. $NaHCO_3$ (15 mL), where it was stirred for 3 h. The organic layer was extracted with diethyl ether (3 × 15 mL), washed with brine (1 × 15 mL), dried over anhydrous Na_2SO_4, and concentrated under reduced pressure. Purification via silica gel chromatography (20 g, 5% Et_2O in hexanes) yielded a clear oil (124 mg, 87% yield). Chiral GC using a Chiraldex G-TA column with 100 °C isotherm showed 93.5% ee, R_t = 51.40 (minor) and 53.00 (major). IR (neat) (cm^{-1}): 3035, 2964, 2927, 1716, 1495, 1358, 760, 700. ^1H NMR (400 MHz, $CDCl_3$) δ: 7.28–7.35 (m, 2H), 7.18–7.25 (m, 3H), 3.27–3.38 (m, 1H), 2.68 and 2.76 (dd, J = 6.4 Hz, 2H), 2.08 (s, 3H), 1.28 (d, J = 7.2 Hz, 3H). ^{13}C NMR (100 MHz, $CDCl_3$) δ: 22.17, 30.75, 35.58, 52.13, 126.48, 126.92, 128.71, 146.44, 208.08. EI-MS *m/z* (%): 162 ($[M]^+$, 52), 147(81), 119(16), 105(100), 91(47), 77(29), 51(17). HR-EI-MS calcd. for $C_{11}H_{14}O$: 162.1044; found 162.1051.

(*R*)-*N*-(1-(4-Trifluoromethylphenyl)ethyl) bis(3,5-dimethylphenyl)phosphinamide (Table 2, entry 5)

CuCl (3.6 mg, 0.036 mmol), NaOMe (2.0 mg, 0.038 mmol), and (*R*)-DTBM-SEGPHOS (**3**, 42.6 mg, 0.036 mmol) were placed into a flame-dried, argon-purged round-bottom flask (RBF). Toluene (1.5 mL) was added to the RBF, and the resulting mixture was stirred at rt for 30–40 min. Meanwhile, *N*-(1-(4-trifluoromethylphenyl)ethylidene) bis(3,5-dimethylphenyl)phosphinamide (88.6 mg, 0.20 mmol) was added to a 0.5–2.0 mL Emry's Optimizer

© 2005 NRC Canada

glass vessel, flame dried, and purged with argon. *t*-BuOH (50 μL, 0.55 mmol) and toluene (450 μL) were added and allowed to stir for 5 min until the solution became homogeneous. The RBF was charged with tetramethyldisiloxane (TMDS; 0.318 mL, 1.60 mmol) and was allowed to stir for 10 min. After 10 min, the CuH mixture (618 μL) was slowly added to the glass vessel via syringe, and the reaction was immediately taken to the Emry's Optimizer. The following conditions were applied: temperature: 60 °C; time, 1800 s; fixed hold time, on; sample absorption, normal. MeOH (1 mL) was slowly added and after 30 min 1 mol/L NaOH in MeOH (0.5 mL) was added. The mixture was stirred for 2–3 h, filtered through a plug of silica, and concentrated under vacuum. Purification by silica gel chromatography (10% acetone–CH_2Cl_2) gave the corresponding phosphinylamines (82 mg, 92% yield) as a white solid. To a solution of the phosphinyl amine was added methanol (2 mL), followed by HCl (0.5 mL, 5 mol/L in IPA) at rt, and this was allowed to stir overnight. The mixture was extracted with Et_2O (3 × 10 mL) and washed with H_2O (3 × 10 mL). To the aqueous layer containing the ammonium salt was then added NaOH (10 mL, 5 mol/L), and the product was extracted with CH_2Cl_2 (3 × 10 mL). The combined organic layers were dried over anhydrous Na_2SO_4 and evaporated in vacuo. The amine was analyzed to be 95.7% ee by Chiral GC using a Chiraldex-GTA column with 90 °C isotherm, R_t = 14.75 (*S*) and 15.21 (*R*). The product matched previously reported spectral data (8*b*).

(*S*)-Ethyl 3-phenylbutanoate (9) using 0.1% Stryker's catalyst (Table 3, entry 2)

To a 2–5 mL Emry's Optimizer glass vessel, flame dried and purged with argon, was added the (*E*)-ethyl 3-methyl-5-phenylpent-2-enoate (neat, 0.380 mg, 2 mmol). To a 10 mL round-bottom flask (RBF), flame dried and purged with argon was added (*R*)-DTBM-SEGPHOS (**3**, 2.3 mg, 0.002 mmol) and Stryker's reagent (0.6 mg, 0.002 mmol), followed by toluene (1.75 mL). The mixture was allowed to stir for 30 min. Following dropwise addition of PMHS (240 μL, 4 mmol H^-), the reaction was stirred for 20 min. The CuH was transferred via cannula into the enoate, followed by addition of *t*-BuOH (230 μL, 2.4 mmol). The reaction vessel was immediately taken to the Emry's Optimizer. The following conditions were applied: temperature, 60 °C; time, 1200 s; fixed hold time, on; sample absorption, normal. The reaction was quenched by diluting with THF (3 mL), followed by aqueous $NaHCO_3$ (2 mL), and was allowed to stir at rt for 2 h. The reaction mixture was pushed through a plug of silica to discard the ligand. Chiral GC using a Chiraldex G-TA column with 100 °C isotherm showed the titled product to have 96.2% ee, R_t = 77.79 (minor) and 78.70 (major).

(*S*)-Ethyl 3-phenylbutanoate (9) using 1% Stryker's catalyst (Table 3, entry 3)

To a 2–5 mL Emry's Optimizer glass vessel, flame dried and purged with argon, was added the (*E*)-ethyl 3-methyl-5-phenylpent-2-enoate (neat, 0.380 mg, 2 mmol). To a 10 mL RBF, flame dried and purged with argon, was added (*R*)-DTBM-SEGPHOS (**3**, 2.3 mg, 0.002 mmol) and Stryker's reagent (6.3 mg, 0.020 mmol), followed by toluene (1.75 mL). The mixture was allowed to stir for 30 min, followed by dropwise addition of PMHS (240 μL, 4 mmol H^-), and the reaction was then stirred for 20 min. The CuH was transferred via cannula into the enoate, followed by addition of *t*-BuOH (230 μL, 2.4 mmol). The reaction vessel was immediately introduced into the Emry's Optimizer. The following conditions were applied: temperature, 60 °C; time, 1200 s; fixed hold time, on; sample absorption, normal. The reaction was quenched by diluting with THF (3 mL), followed by aqueous $NaHCO_3$ (2 mL), and was allowed to stir at rt for 2 h. The reaction mixture was pushed through a plug of silica to discard the ligand. Chiral GC using a Chiraldex G-TA column with 100 °C isotherm showed the titled product to have 84.5% ee, R_t = 77.79 (minor) and 78.70 (major).

(*S*)-3,4-Dihydro-7-methoxy-4-methylchromen-2-one (11); ligand study (Table 4)

To a 2–5 mL Emry's Optimizer glass vessel, flame dried and purged with argon, was added 7-methoxy-4-methylcoumarin (neat, 190.2 mg, 1 mmol). Toluene (3 mL) was added to the coumarin followed by (*R*)-(DTBM-SEGPHOS)CuH in a Bottle (1 mL, 0.001 mol/L in PhMe, 0.001 mmol). The corresponding reagents from ligands **2**, **12**, **13**, or **14** were made as described above, followed by addition of *t*-BuOH (115 μL, 1.2 mmol). The reaction vessel was immediately taken to the Emry's Optimizer. The following conditions were applied: temperature, 60 °C; time, 1200 s; fixed hold time, on; sample absorption, normal. Each reaction (all of which went to completion) was quenched by diluting with THF (3 mL), followed by aqueous $NaHCO_3$ (2 mL), and was allowed to stir at rt for 2 h. The residue was pushed through a plug of silica and analyzed by chiral GC, and the product showed the ees listed in Table 4, which were found using a Chiraldex-GTA column with 120 °C isotherm, R_t = 114.85 (minor) and 115.31 (major). Product **11** is extremely unstable and is a mixture of cis and trans isomers at rt, as described by Goldsmith et al. (16). ^{1}H NMR (400 MHz, C_6D_6) δ: 6.99–6.97 (m, 1H), 6.68–6.63 (m, 1H), 6.60–6.56 (m, 1H), 5.24 (dt, *J* = 2.5, 6.8 Hz, 1H), 3.34 (s, 3H), 3.01 (tq, *J* = 6.8, 7.1 Hz, 1H), 2.43 (d, *J* = 7.1 Hz, 2H), 1.05 (d, *J* = 6.8 Hz, 3H). ^{13}C NMR (100 MHz, C_6D_6) δ: 160.50, 153.52, 108.25, 108.08, 102.76, 102.56, 92.07, 55.16, 36.51, 24.16, 20.81. EI-MS *m*/*z* (%): 194 ($[M]^+$, 40), 179(21), 177(73), 151(100), 89(58), 61(54), 43(48). HR-EI-MS *m*/*z* calcd. for $C_{11}H_{14}O_3$: 194.0941; found: 194.0943.

Acknowledgements

We are indebted to Biotage, Amgen, the National Science Foundation (NSF), and the University of California, Santa Barbara (UCSB) for financial assistance in making our purchase of an Emry's Optimizer possible. We warmly thank the NSF for financial support and Takasago, Solvias, and Roche for their most generous gifts of their ligands used in this study.

References

1. (*a*) A. Wurtz. Ann. Chim. Phys. **11**, 250 (1844); (*b*) H. Muller and A.J. Bradley. J. Chem. Soc. 1669 (1926).

© 2005 NRC Canada

2. J.A. Dilts and D.F. Shriver. J. Am. Chem. Soc. **91**, 4088 (1969); more recently, NH carbene ligands have been found to stabilize CuH for use in synthesis, cf.: H. Kaur, F.K. Zinn, E.D. Stevens, and S.P. Nolan. Organometallics, **23**, 1157 (2004); V. Jurkauskas, J.P. Sadighi, and S.L. Buchwald. Organic Lett. **5**, 2417 (2003); see also: N.P. Mankad, D.S. Laitar, and J.P. Sadighi. Organometallics, **23**, 3369 (2004).
3. B.H. Lipshutz. *In* Modern organocopper chemistry. *Edited by* N. Krause. Wiley-VCH, Weinheim. 2002. pp. 167–187.
4. (*a*) W.S. Mahoney, D.M. Brestensky, and J.M. Stryker. J. Am. Chem. Soc. **110**, 291 (1988); P. Chiu. Synthesis, **13**, 2210 (2004); (*b*) J.-X. Chen, J.F. Daeuble, and J.M. Stryker. Tetrahedron, **56**, 2789 (2000); (*c*) J.-X. Chen, J.F. Daeuble, D.M. Brestensky, and J.M. Stryker. Tetrahedron, **56**, 2153 (2000); (*d*) J.M. Stryker, W.S. Mahoney, J.F. Daeuble, and D.M. Brestensky. *In* Catalysis in organic synthesis. *Edited by* W.E. Pascoe. Marcel Dekker, New York. 1992. pp. 29–44.
5. (*a*) R. Schmid, E.A. Broger, M. Cereghetti, Y. Crameri, J. Foricher, M. Lalonde, R.K. Muller, M. Scalone, G. Schoettel, and U. Zutter. Pure. Appl. Chem. **68**, 131 (1996); (*b*) R. Schmid, J. Foricher, M. Cereghetti, and P. Schonholzer. Helv. Chim. Acta, **74**, 370 (1991).
6. H.-U. Blaser, W. Brieden, B. Pugin, F. Spindler, M. Studer, and A. Togni. Top. Catal. **19**, 3 (2002).
7. T. Saito, T. Yokozawa, T. Ishizaki, T. Moroi, N. Sayo, T. Miura, and H. Kumobayashi. Adv. Synth. Catal. **343**, 264 (2001).
8. (*a*) B.H. Lipshutz, K. Noson, W. Chrisman, and A. Lower. J. Am. Chem. Soc. **125**, 8779 (2003); (*b*) B.H. Lipshutz and H. Shimizu. Angew. Chem. Int. Ed. **42**, 2227 (2004); (*c*) B.H. Lipshutz and J.M. Servesko. Angew. Chem. Int. Ed. **41**, 4789 (2003); (*d*) B.H. Lipshutz, J.M. Servesko, T.B. Peterson, P.P. Papa, and A.L. Lover. Organic Lett. **6**, 1273 (2004); (*e*) B.H. Lipshutz, J.M. Servesko, and B.R. Taft. J. Am. Chem. Soc. **126**, 8352 (2004).
9. (*a*) J.P. Tierney and P. Lidstrom (*Editors*). Microwave assisted organic synthesis. Blackwell Publishing, Uppsala, Sweden. 2005; (*b*) A.K. Bose, M.S. Manhas, S.N. Ganguly, A.H. Sharma, and B.K. Banik. Synthesis, 1578 (2002).
10. N.E. Leadbeater and M. Marco. J. Org. Chem. **68**, 888 (2003).
11. D.H. Appella, Y. Moritani, R. Shintani, E.M. Ferreira, and S.L. Buchwald. J. Am. Chem. Soc. **121**, 9473 (1999).
12. (*a*) D. Lee and J. Yun. Tetrahedron Lett. **45**, 5415 (2004); (*b*) M.P. Rainka, Y. Aye, and S.L. Buchwald. Proc. Natl. Acad. Sci. U.S.A. **101**, 5821 (2004).
13. (*a*) T. Benincori, E. Cesarotti, O. Piccolo, and F. Sannicolo. J. Org. Chem. **65**, 2043 (2000); (*b*) T. Benincori, E. Brenna, F. Sannicolo, L. Trimarco, P. Antognazza, E. Cesarotti, F. Demartin, and T. Pilati. J. Org. Chem. **61**, 6244 (1996).
14. N.W. Boaz, S.D. Dedenham, E.B. Mackenzie, and S.E. Large. Org. Lett. **4**, 2421 (2002).
15. (*a*) D.H. Appella, Y. Moritani, R. Shintani, E.M. Ferreira, and S.L. Buchwald. J. Am. Chem. Soc. **121**, 9473 (1999); (*b*) G. Hughes, M. Kimura, and S.L. Buchwald. J. Am. Chem. Soc. **125**, 11 253 (2003).
16. D.J. Goldsmith, D.C. Liotta, M. Volmer, W. Hoekstra, and L. Waykole. Tetrahedron, **41**, 4873 (1985).

© 2005 NRC Canada

A practical guide to arylbiguanides — Synthesis and structural characterization[1]

Olivier LeBel, Thierry Maris, Hugues Duval, and James D. Wuest

Abstract: Monohydrochloride salts of diverse 1-arylbiguanides and 1,5-diarylbiguanides were synthesized by the reaction of anilinium chlorides with dicyandiamide or sodium dicyanamide, and the biguanidinium chlorides were converted into the corresponding biguanides by deprotonation with methanolic $NaOCH_3$. The resulting biguanides and their salts were fully characterized by spectroscopic methods, and the structures of representative compounds were determined by X-ray crystallography.

Key words: biguanide, biguanidinium, synthesis, structure, hydrogen bonds, noncovalent interactions, supramolecular chemistry.

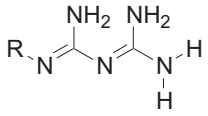
Résumé : On a effectué la synthèse de monochlorhydrates de divers 1-arylbiguanides et de 1,5-diarylbiguanides en faisant réagir des chlorures d'anilinium avec du dicyandiamide ou du dicyanamidure de sodium. Les chlorures de biguanidium ont été transformés en biguanides correspondants par déprotonation avec une solution méthanolique de $NaOCH_3$. Les biguanides correspondants et leurs sels ont été complètement caractérisés par des méthodes spectroscopiques et les structures de composés représentatifs ont été déterminées par diffraction des rayons X.

Mots clés : biguanide, biguanidinium, synthèse, structure, liaisons hydrogène, interactions non covalentes, chimie supramoléculaire.

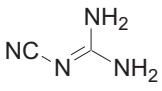
[Traduit par la Rédaction]

Introduction

The general class of compounds called biguanides has been known for more than 100 years (1–3). An early method for preparing salts of biguanide itself (**1**) was reported in 1892 by Bamberger and Dieckmann (4), who heated dicyandiamide (**2**) with ammonium chloride and then isolated the product by forming an intermediate biguanide-copper (II) complex.[4] Since then, biguanides have proven to be broadly useful. In medicine, they have important applications as antiseptics (5), antimalarials (6, 7), serotoninergic antagonists (8), antitumoral agents (9), and hypoglycemic agents (10, 11). In addition, the ability of biguanides to chelate metals has been widely used in coordination chemistry since the initial observations of Bamberger and Dieckmann (1, 3). Moreover, biguanides are strong bases (12, 13), and they are also valuable precursors for synthesizing a wide range of heterocyclic compounds (2, 14). Of special interest among the heterocyclic derivatives of biguanides are aminotriazines, which are themselves an extremely useful family of compounds. For example, they are widely used in supramolecular chemistry because they incorporate a characteristic pattern of multiple sites that can donate or accept hydrogen bonds, thereby directing molecular recognition and association. In particular, recent applications of aminotriazines in crystal engineering have highlighted their ability to direct crystallization by self-associating according to reliable hydrogen-bonding motifs (15, 16).



1 (R = H)
3 (R = Ph)
13 (R = CH_2CH_2Ph)



2

Our motivation for studying substituted biguanides stems from their potential as precursors of novel aminotriazines and from the possibility that the multiple sites of hydrogen bonding in the biguanides themselves may make them valuable components in supramolecular assembly. Unfortunately, despite the demonstrated utility of biguanides and the likelihood of new applications, few detailed syntheses and structural characterizations have been previously reported, and information about 1-aryl- and 1,5-diarylbiguanides remains

Received 23 December 2004. Published on the NRC Research Press Web site at http://canjchem.nrc.ca on 11 June 2005.

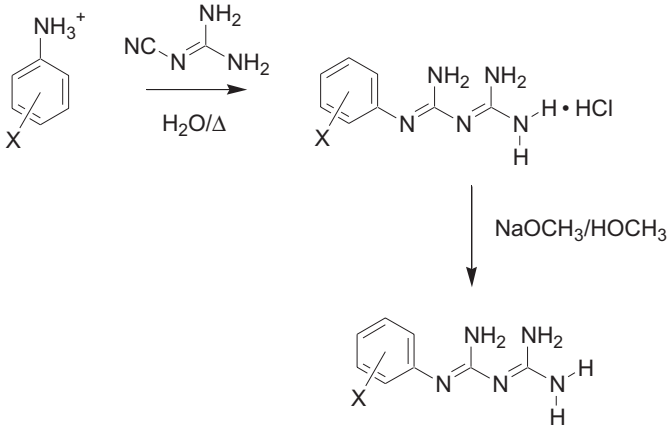
Dedicated with respect and affection to Professor Howard Alper for his friendship, wise counsel, pioneering research, and tireless service to Canadian chemistry.

O. LeBel,[2] T. Maris, H. Duval, and J.D. Wuest.[3]
Département de Chimie, Université de Montréal, Montréal, QC H3C 3J7, Canada.

[1]This article is part of a Special Issue dedicated to Professor Howard Alper.
[2]Fellow of the Ministère de l'Éducation du Québec (2002–2004).
[3]Corresponding author (e-mail: james.d.wuest@umontreal.ca).
[4]For the sake of simplicity, biguanides, dicyandiamide, and related compounds are normally represented in this paper as single tautomers.

 doi: 10.1139/V05-093 © 2005 NRC Canada

Scheme 1.

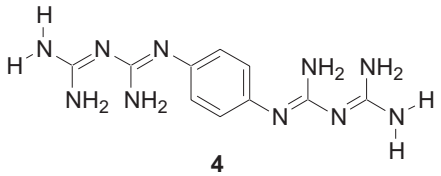


particularly sparse (17–38). To supply missing data and give other researchers a practical guide to the field, we report here the synthesis and full characterization of a series of arylbiguanides, along with crystal structures of representative compounds.

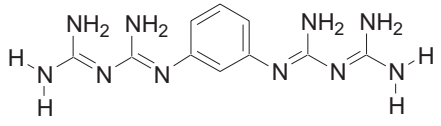
Results and discussion

Synthesis of 1-arylbiguanides

To synthesize monosubstituted 1-arylbiguanides, we used a modification of a procedure reported in a 1946 patent by Curd and Rose (23), who heated anilinium salts with dicyandiamide in water (Scheme 1). The hydrochloride salts of the arylbiguanides generally crystallize from the reaction mixture in good yield and in high purity, and they can be deprotonated with methanolic sodium methoxide in nearly quantitative yield. Detailed procedures for making 1-phenylbiguanide (**3**) and its hydrochloride salt by these methods are provided in the Experimental section, and other aryl-substituted derivatives can be made in the same way. When 1,4- or 1,3-phenylenediamine dihydrochloride reacted under these conditions with 2 equiv. of dicyandiamide, the corresponding bis(biguanide) (**4** or **5**) was obtained after deprotonation (39), whereas 1,2-phenylenediamine dihydrochloride gave 2-guanidinobenzimidazole (40).



4

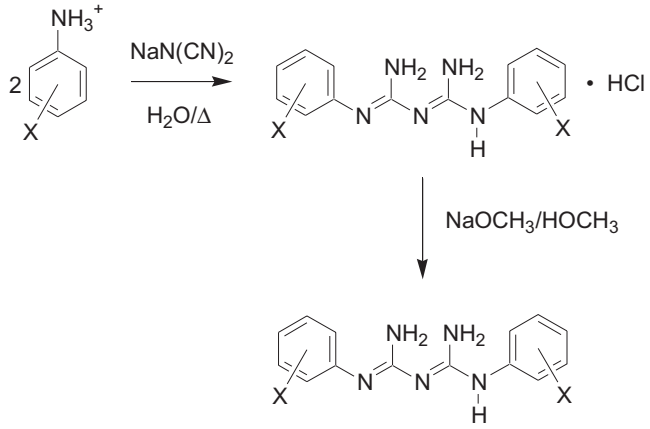


5

Synthesis of 1,5-diarylbiguanides

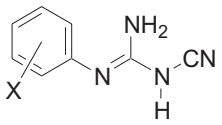
1,5-Diarylbiguanides **6a–6j** could be synthesized in good yield by a one-pot procedure based on a method reported by Neelakantan (22), in which 2 equiv. of an anilinium chloride

Scheme 2.



6a (X = X' = H)
6b (X = X' = 2-CH_3)
6c (X = X' = 3-CH_3)
6d (X = X' = 4-CH_3)
6e (X = X' = 4-OCH_3)
6f (X = X' = 4-CN)
6g (X = X' = 2-Br)
6h (X = X' = 4-Br)
6i (X = X' = 3,5-CH_3)
6j (X = X' = 2,4,6-CH_3)

are added to sodium dicyanamide in boiling water (Scheme 2). In the case of anilines with low solubility in water, the reaction can be performed in ethanol or in water–ethanol mixtures. Of all anilines tested, only 4-nitroaniline failed to give the desired product, presumably because its basicity and nucleophilicity are too low. A monosubstituted aryldicyandiamide (**7**) typically precipitated at an initial stage of each reaction, but the intermediate was eventually converted into the desired diarylbiguanide as its hydrochloride salt. It is possible to isolate the intermediate monoaryldicyandiamides and use them to synthesize unsymmetric 1,5-diarylbiguanides. For example, phenyldicyandiamide (**7**, X = H) was obtained in this way in 87% yield.



7

After the reaction of 2 equiv. of an anilinium chloride with sodium dicyanamide, the crude product typically consisted of the desired diarylbiguanide hydrochloride along with small amounts of the intermediate monoaryldicyandiamide. This impurity could be removed by dissolving the product in a small volume of DMF and then precipitating the biguanide hydrochloride by the addition of toluene. The resulting product normally required no further purification, but it could be recrystallized from hot water. Pure samples of the corresponding free base could be obtained in nearly quanti-

© 2005 NRC Canada

tative yield by treating the salt with methanolic sodium hydroxide.

Spectroscopic characterization of arylbiguanides

Arylbiguanides typically have poor solubility in organic solvents and water, and DMSO-d_6 proved to be best suited for obtaining NMR spectra of most of the compounds synthesized. The -NH and -NH_2 protons in these compounds generally show broad, poorly resolved peaks in the range δ 5–9. However, the corresponding monohydrochloride salts produce spectra in which the -NH and -NH_2 signals are better resolved and easier to identify. In the salts, the aryl -NH protons tend to give rise to a singlet near δ 9 to 10, and -NH_2 groups yield signals in the range δ 7 to 8.

To assess the possible importance of slow interconversion of tautomers or slow rotations around C—N bonds, ^{1}H NMR spectra of 1,5-diphenylbiguanide (**6a**) and its hydrochloride salt were recorded in DMSO-d_6 at temperatures ranging from 298 to 378 K (see Supplementary material).[5] The spectra of both compounds are indeed temperature-dependent and become better resolved at higher temperatures, possibly because rotations or tautomeric interconversions are accelerated. Partial decomposition was noted in spectra of the free base recorded at higher temperatures.

In general, the hydrochloride salts of both 1-arylbiguanides and 1,5-diarylbiguanides gave well-resolved ^{13}C NMR spectra in DMSO-d_6 at 298 K. The biguanide carbons have characteristic chemical shifts in the range δ 155–165. In contrast, the ^{13}C NMR spectra of the corresponding free bases are less easy to analyze, and broad signals are often observed for the biguanide carbons.

FT-IR spectra of arylbiguanides and their monohydrochloride salts in KBr both show multiple strong broad bands in the range 2900–3300 cm^{-1}. In addition, the free bases exhibit a pair of sharper but weaker bands near 3440 and 3350 cm^{-1}, presumably owing to -NH_2 groups. In both the free bases and salts, strong C=N stretching bands normally appear near 1640–1610 cm^{-1}.

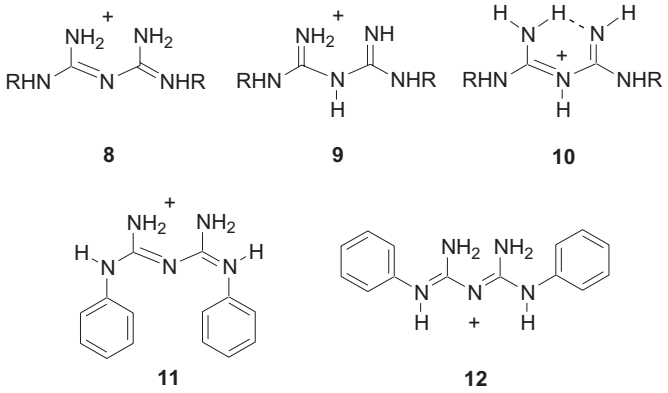
FAB and MAB mass spectra proved to be useful for characterizing arylbiguanides, and $[M + H]^+$ is typically the peak of highest intensity. Diagnostic fragments usually include $[M + H - NH_3]^+$, $[M + H - ArNH_2]^+$, $[M + H - ArNHCN]^+$, and $[M + H - ArN{=}C(NH_2)_2]^+$.

Crystal structures of 1,5-diphenylbiguanide (6a) and its monohydrochloride salt

Few structures of simple biguanidinium salts or biguanides have been reported (25–38), and in none of these cases have aryl groups been present at positions 1 and 5. As a result, we elected to determine the structures of 1,5-diphenylbiguanide (**6a**) and its monohydrochloride salt. The salt crystallized from hot water in the monoclinic space group $P2_1/n$ (Table 1).[5] The structure was determined by X-ray diffraction, and views of a single biguanidinium cation are shown in Fig. 1. The narrow range of guanidinium C—N bond lengths (1.343–1.394 Å) provides evidence of extensive delocalization, although the structure is not fully symmetric. It is noteworthy that the cation can be represented by localized structure **8** and its resonance hybrids, whereas alternatives in which the central nitrogen atom is protonated (**9**) or an intramolecular hydrogen bond is formed (**10**) are not favored in the solid state. Similar observations have been made in all previous structural studies of biguanidinium cations (25, 26, 28–34, 36–38), so protonation of biguanides to give struc-

Table 1. Crystallographic data for the hydrochloride salt of 1,5-diphenylbiguanide (**6a**·HCl) and for 1,5-diphenylbiguanide (**6a**).

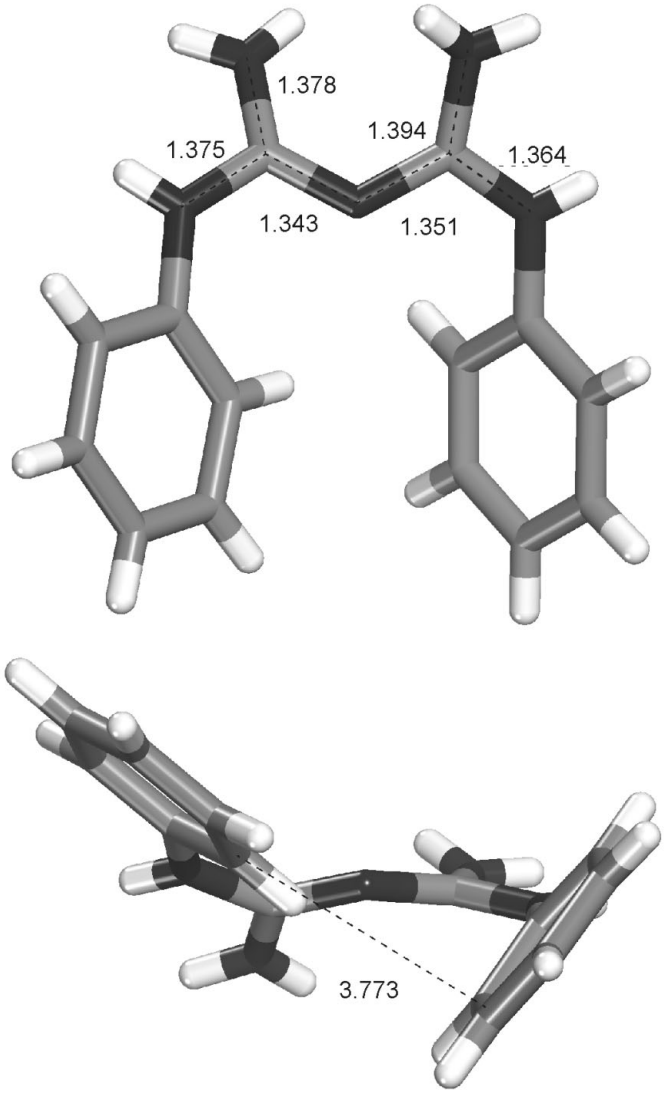
Compound	**6a**·HCl	**6a**
T (K)	293	100
λ (Å)	1.541 78 (CuKα)	1.541 78 (CuKα)
Formula	$C_{14}H_{16}ClN_5$	$C_{14}H_{15}N_5$
Fw	289.77	253.31
F(000)	608	536
Crystal system	Monoclinic	Monoclinic
Z	4	4
d (g cm^{-3})	1.146	1.308
μ (mm^{-1})	1.994	0.663
Space group	$P2_1/n$	Pc
a (Å)	9.627(5)	9.031 7(3)
b (Å)	4.975 1(5)	6.394 5(2)
c (Å)	35.253 3(5)	22.587 4(8)
α (°)	90	90
β (°)	95.79(2)°	99.588(2)°
γ (°)	90°	90°
Volume (Å^3)	1679.9(9)	1286.27(7)
θ max (°)	66.4	71.9
h, k, l max	11, 5, 41	11, 7, 27
Unique	2854	2530
Observed ($I > 2\sigma$(I))	2025	1570
R_1	0.058 7	0.067 3
$wR2$	0.179 0	0.152 5
$R1$ (all data)	0.067 6	0.074 5
$wR2$ (all data)	0.187 4	0.155 1
Diff. peak and hole (e/Å^3)	0.325/–0.273	0.321/–0.327
GoF	1.069	1.024



[5] Supplementary data for this article are available on the Web site or may be purchased from the Depository of Unpublished Data, Document Delivery, CISTI, National Research Council Canada, Ottawa, ON K1A 0S2, Canada. DUD 3662. For more information on obtaining material refer to http://cisti-icist.nrc-cnrc.gc.ca/irm/unpub_e.shtml. CCDC 258751–258752 contain the crystallographic data for this manuscript. These data can be obtained, free of charge, via www.ccdc.cam.ac.uk/conts/retrieving.html (or from the Cambridge Crystallographic Data Centre, 12 Union Road, Cambridge CB2 1EZ, UK; fax +44 1223 336033; or deposit@ccdc.cam.ac.uk).

© 2005 NRC Canada

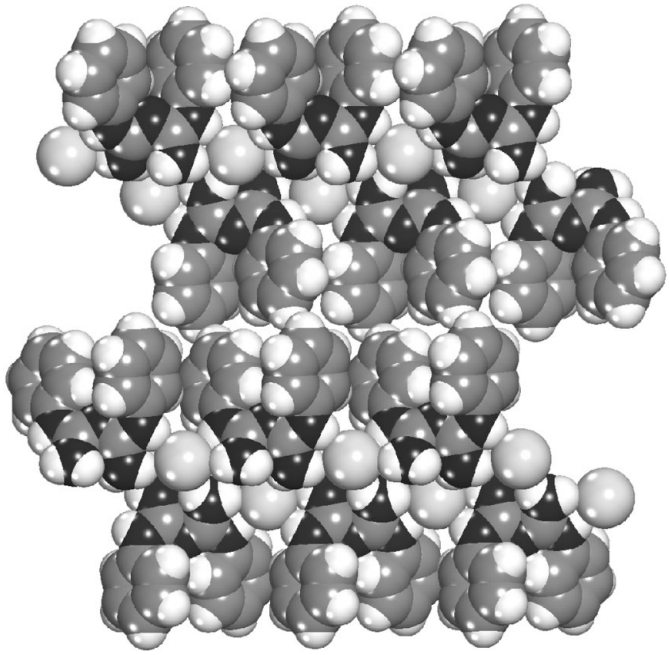
Fig. 1. Two views of the structure of individual biguanidinium cations in the crystals of the hydrochloride salt of 1,5-diphenylbiguanide (**6a**·HCl) grown from water. Hydrogen atoms appear in white, carbon atoms in gray, and nitrogen atoms in black. The upper view provides C—N bond lengths, and the lower view shows the intramolecular C-H···π interaction (broken line) present in the biguanidinium ion. All bond lengths are in Å (with standard deviations provided in the Supplementary material),[5] and the shortest C—C distance between the phenyl rings is used to define the aromatic interaction.



ture **8** appears to be a fundamental preference, both in the solid state and in solution (2).

The two guanidinium subunits that can be considered to make up the biguanidinium cation lie in two distinct planes that form an angle of 22.8(4)°. The nonplanarity of the biguanidinium core presumably reduces allylic strain while permitting a significant degree of conjugation. Again, similar observations have been made in all previous structural studies of biguanidinium salts, so nonplanarity of the

Fig. 2. View along the *b* axis of the structure of the crystals of the hydrochloride salt of 1,5-diphenylbiguanide (**6a**·HCl) grown from water. The image reveals bilayers with an ionic core and a hydrophobic exterior. The view shows a 3 × 1 × 1 array of unit cells with atoms represented by spheres of van der Waals radii. Hydrogen atoms appear in white, chlorine atoms in light gray, carbon atoms in dark gray, and nitrogen atoms in black.



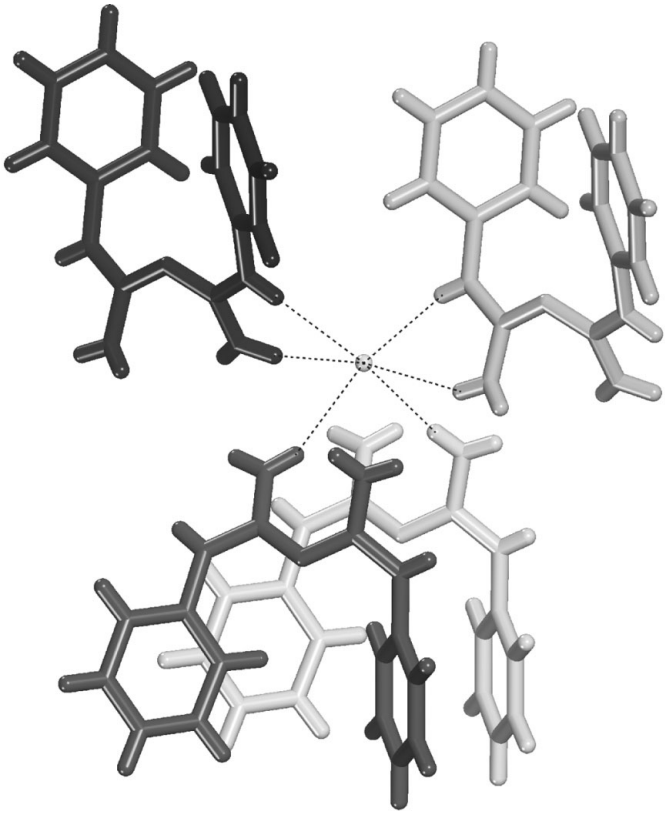
biguanidinium core appears to be a universal characteristic. The two phenyl rings are tilted from the guanidinium planes by angles of 52.4(1)° and 39.5(1)°, and together they form an angle of 88.8(1)°, thereby permitting an intramolecular C-H···π interaction in which the shortest C—C distance is 3.773 Å (Fig. 1). This may explain why the 1,5-diphenylbiguanidinium cation adopts the compact conformation represented by structure **11**, rather than extended conformation **12**.

The crystal structure of diphenylbiguanidinium salt **6a**·HCl is closed-packed (Fig. 2) and can be considered to consist of bilayers, with hydrophilic biguanidium cations and chloride anions occupying the core and hydrophobic phenyl groups forming the exterior.[6] The bilayers then stack along the *c* axis. Within the core of each bilayer, the principal interactions are hydrogen bonds and ionic attractions between biguanidinium and chloride. The biguanidinium ions do not interact directly with each other by forming hydrogen bonds. The absence of inter-cationic hydrogen bonds has been noted in most other biguanidinium salts (28, 29, 31, 34, 36–38), but they are nevertheless present in certain cases (25, 26, 32). Each chloride ion accepts a total of six hydrogen bonds from four neighboring biguanidinium cations (Fig. 3), two of which chelate chloride by donating two hydrogen bonds and two of which each contribute a single hydrogen bond. In turn, each biguanidinium cation forms hydrogen bonds with a total of four neighboring chloride ions, of which two are chelated and the others each accept a

[6] A similar bilayer organization has been noted in the structure of the monohydrochloride salt of phenformin (**13**) (32).

© 2005 NRC Canada

Fig. 3. View of the structure of the crystals of the hydrochloride salt of 1,5-diphenylbiguanide (**6a**·HCl) showing how each chloride anion is surrounded by four biguanidinium cations and accepts six ionic N-H···Cl hydrogen bonds (broken lines). Two biguanidinium cations chelate chloride and two donate single hydrogen bonds.



single hydrogen bond. Similar interactions between biguanidinium ions and halide have been observed previously (25, 28, 31, 34, 36–38). In addition, the phenyl groups of each biguanidinium cation engage in multiple aromatic contacts or interactions with phenyl groups provided by neighboring cations (Fig. 4). In total, each biguanidinium cation has four face-to-face and six edge-to-face aromatic contacts with six neighbors.

The corresponding free base (1,5-diphenylbiguanide (**6a**)) crystallized from hot ethanol in the monoclinic space group *Pc*, and one of two symmetry-independent molecules in the unit cell is shown in Fig. 5.[5] The other molecule is closely similar and is not illustrated. Unlike the twisted biguanidinium cation, the biguanide unit has a roughly planar geometry, maintained by an intramolecular N-H···N hydrogen bond (2.06(1) Å). Similar features appear in all previous structural studies of biguanides (27, 33, 34), so a nearly planar geometry and an intramolecular hydrogen bond appear to be fundamental preferences. The C—N bond lengths within the biguanide unit range from 1.294(8) to 1.406(8) Å, suggesting significant delocalization of C—N single and double bonds, but slightly less than in the corresponding biguanidinium salt. Unlike the salt, free base **6a** favors a conformation in which no intramolecular aromatic interactions are present.

Like the corresponding biguanidinium salt, biguanide **6a** forms a closed-packed layered structure consisting of alternating hydrophobic and hydrophilic domains (Fig. 6). In the free base **6a**, however, the neutral biguanide units interact directly by hydrogen bonding. Each molecule donates two hydrogen bonds to one neighbor and accepts two hydrogen bonds from another, thereby forming a corrugated ribbon (Fig. 7). Similar intermolecular hydrogen bonding has been previously observed in the structures of biguanide (**1**) and 1-phenylbiguanide (**3**) (27, 33, 34). Curiously, the donor sites that form the shortest intermolecular hydrogen bonds are the $-NH_2$ groups already involved as donors in intramolecular hydrogen bonding. As expected, one of the acceptor sites is the unprotonated central nitrogen atom in each biguanide unit. The other acceptor site is the nitrogen atom of the $-NH_2$ group not involved in intramolecular hydrogen bonding, which forms the longest C—N bond in the biguanide unit (1.406 Å).

Individual corrugated ribbons formed by intermolecular hydrogen bonding form face-to-face aromatic interactions and stack along the *ab* diagonal to create layers (Fig. 8*a*). Stacking of the layers along the *c* axis then permits the formation of multiple C-H···π interactions (Fig. 8*b*), with the shortest C—C distances ranging from 3.600 to 3.764 Å.

Conclusions

Biguanides are an intrinsically interesting class of compounds with many known or potential applications. Despite these attractive properties, biguanides remain poorly studied. Few detailed procedures for their synthesis have been published, and full spectroscopic characterizations and structural studies are rare. As a practical guide to assist other researchers interested in using biguanides, we have summarized our experience with 1-arylbiguanides, 1,5-diarylbiguanides, and their monohydrochloride salts. Various substituted derivatives can be synthesized in good yields and high purity by simple methods based on published procedures, and these compounds can be fully characterized by standard spectroscopic methods. Structural analyses of representative compounds by X-ray diffraction confirm that arylbiguanides and their salts can form networks held together by characteristic patterns of hydrogen bonds. As a result, arylbiguanides and their salts show promise as components in supramolecular construction.

Experimental

Anilines were purified by recrystallization or distillation prior to use. All other reagents were commercial products that were used without further purification. All NMR spectra were recorded at 298 K unless noted otherwise. Mass spectra are provided only for the neutral biguanides.

1-Phenylbiguanide (3·HCl)

In a 2 L round-bottomed flask equipped with a magnetic stirrer, aniline (91.3 mL, 93.3 g, 1.00 mol) was added to aq. HCl (1 L, 1 mol/L), and the mixture was stirred until it became homogeneous. Dicyandiamide (84.1 g, 1.00 mol) was then added, and the mixture was heated at reflux with constant stirring for 12 h. The mixture was cooled to 25 °C, and

© 2005 NRC Canada

Fig. 4. View along the *c* axis of the layered structure of the crystals of the hydrochloride salt of 1,5-diphenylbiguanide (**6a**·HCl) showing multiple intermolecular aromatic interactions (broken lines) within a single layer. Hydrogen atoms appear in white, carbon atoms in gray, and nitrogen atoms in black. Each biguanidinium cation has four face-to-face and six edge-to-face aromatic contacts with six neighbors, as well as one intramolecular edge-to-face interaction (not marked by a broken line). The shortest C—C distances between phenyl rings are shown in Å.

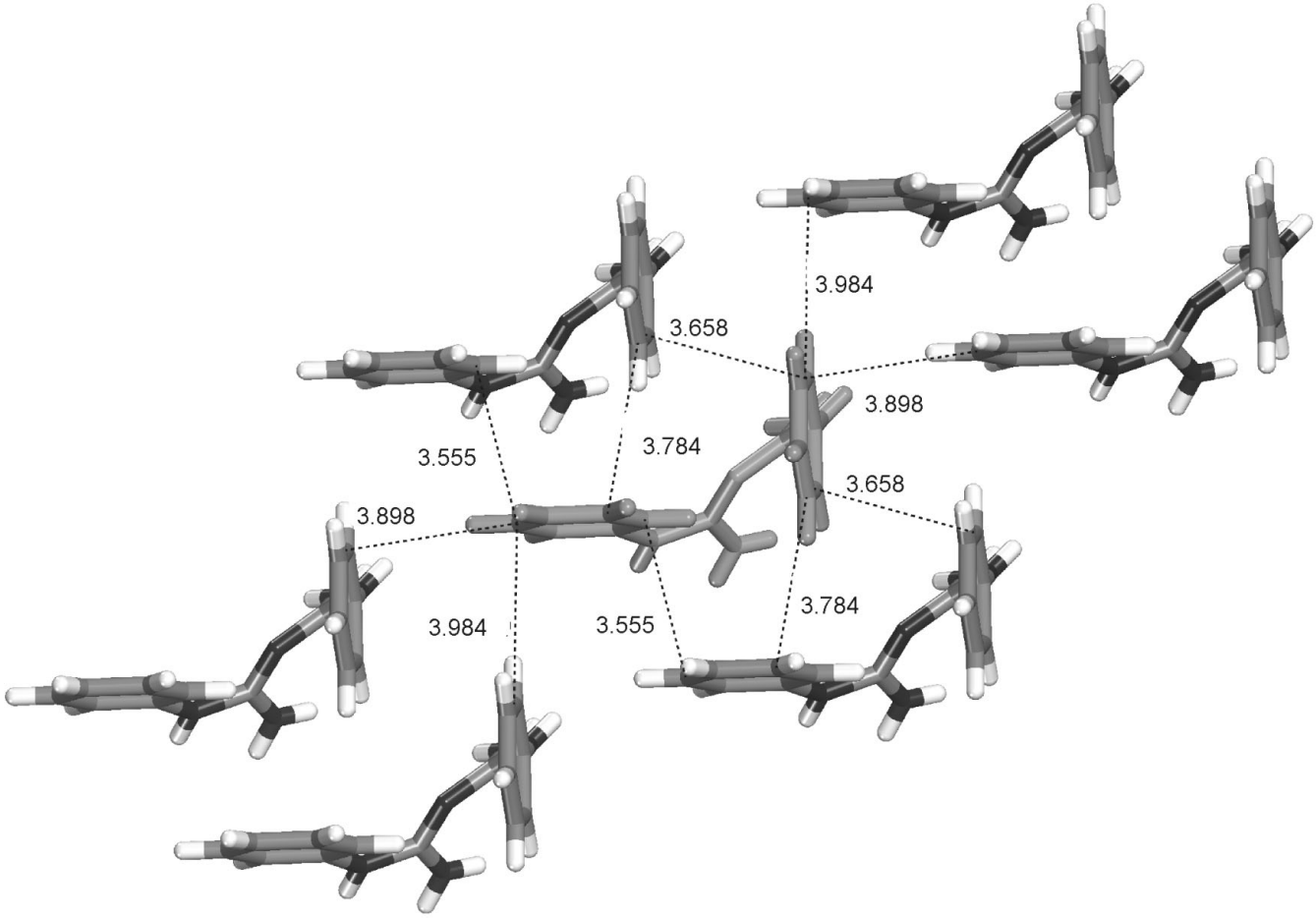
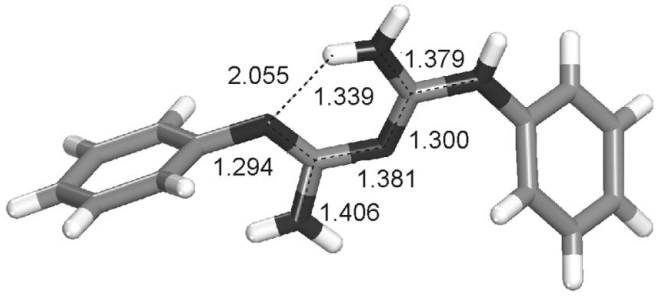


Fig. 5. View of the structure of the crystals of 1,5-diphenylbiguanide (**6a**) grown from ethanol. Hydrogen atoms appear in white, carbon atoms in gray, and nitrogen atoms in black. The intramolecular N-H···N hydrogen bond is represented by a broken line and bond lengths are shown in Å, with standard deviations provided in the Supplementary material.[5]



the resulting colorless crystals were separated by filtration and washed with THF, hexane, and acetone to yield an initial crop of 1-phenylbiguanide (**3**) monohydrochloride (159 g). Concentration of the filtrate followed by crystallization and filtration provided an additional crop of product, giving a total yield of 181 g (0.839 mol, 84%), mp 244 to 245 °C. IR (KBr, cm^{-1}): 3301 (s), 3168 (s), 1643 (s), 1604 (s), 1557 (s), 1529 (s), 1490 (s), 1455 (m), 1373 (m), 1287 (m), 1252 (w), 1075 (m). ^{1}H NMR (300 MHz, DMSO-d_6) δ: 9.96 (s, 1H), 7.42 (s, 4H), 7.38 (d, ^3J = 8 Hz, 2H), 7.27 (t, ^3J = 8 Hz, 2H), 7.15 (s, 2H), 7.02 (t, ^3J = 8 Hz, 1H). ^{13}C NMR (75 MHz, DMSO-d_6) δ: 162.1, 156.1, 139.5, 129.5, 124.1, 121.6. Anal. calcd. for $C_8H_{12}ClN_5$: C 44.97, H 5.66, N 32.78; found: C 44.84, H 5.71, N 32.58.

1-Phenylbiguanide (3)

In a 1 L round-bottomed flask equipped with a magnetic stirrer, 1-phenylbiguanide (**3**) monohydrochloride (214 g, 1.00 mol) was added to a mixture of methanol (200 mL) and methanolic $NaOCH_3$ (230 mL, 25% by weight, 1.0 mol). The resulting mixture was then stirred at 25 °C for 1 h. Suspended NaCl was separated by filtration, and solvent was removed from the filtrate by evaporation under reduced pressure. The gummy residue was triturated with hot ethanol (600 mL), and undissolved solids were removed by filtration. The filtrate was concentrated to 150 mL by partial evaporation under reduced pressure, and then hexane was

© 2005 NRC Canada

Fig. 6. View along the *a* axis of the structure of the crystals of 1,5-diphenylbiguanide (**6a**) grown from ethanol. The image reveals bilayers with a hydrophilic core and a hydrophobic exterior. The view shows a 1 × 3 × 2 array of unit cells with atoms represented by spheres of van der Waals radii. Hydrogen atoms appear in white, carbon atoms in dark gray, and nitrogen atoms in black.

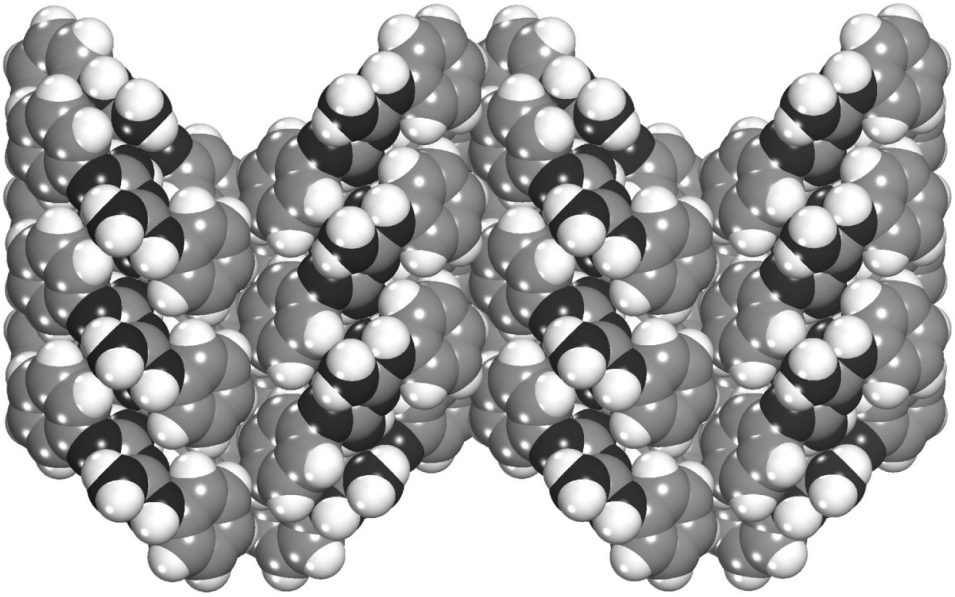
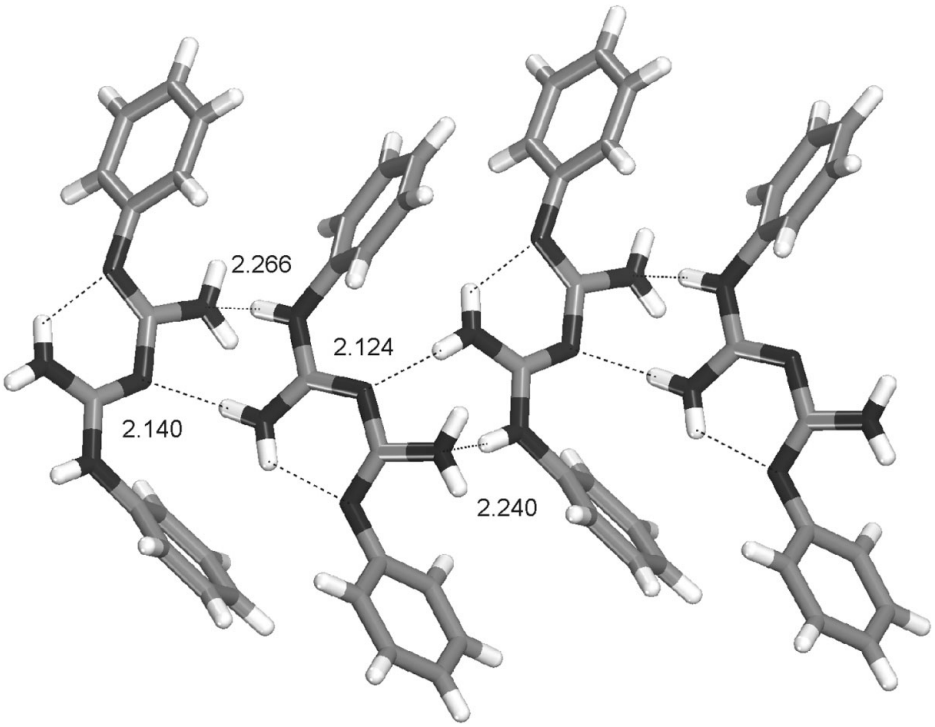


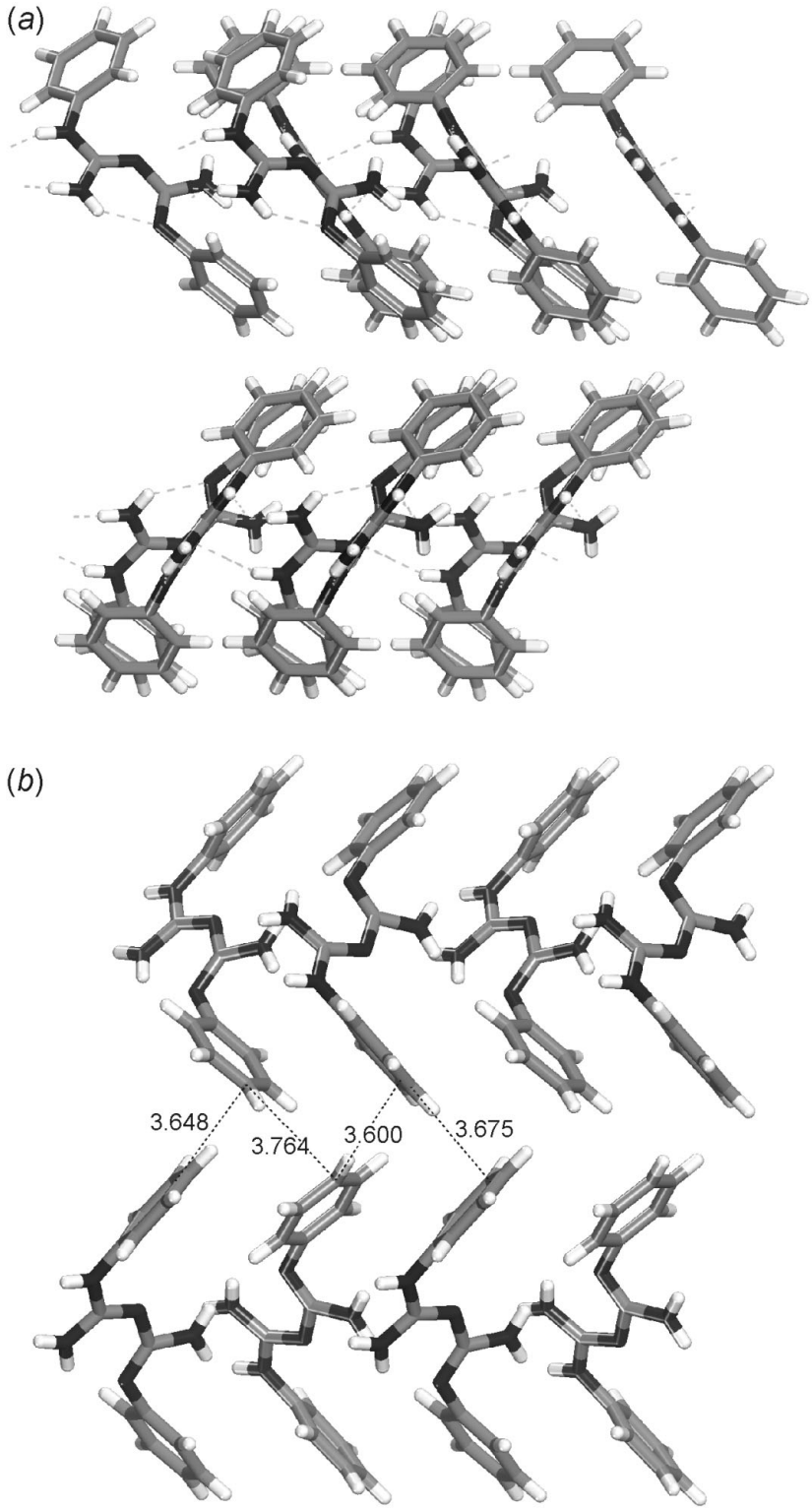
Fig. 7. View along the *ab* diagonal of the structure of 1,5-diphenylbiguanide (**6a**) showing inter- and intramolecular hydrogen bonds. The hydrogen bonds are represented by broken lines and lengths are shown in Å, with standard deviations provided in the Supplementary material.[5] Hydrogen atoms appear in white, carbon atoms in gray, and nitrogen atoms in black. Each molecule donates two hydrogen bonds to one neighbor and accepts two hydrogen bonds from another, thereby forming a corrugated ribbon.



added to precipitate the desired product, which was separated by filtration and dried under reduced pressure. This yielded pure 1-phenylbiguanide (**3**) as a colorless solid (168 g, 0.948 mol, 95%), mp 138 to 139 °C. IR (KBr, cm^{-1}): 3428 (w), 3375 (m), 3324 (m), 3153 (m), 2988 (m), 1665 (s), 1603 (s), 1555 (s), 1482 (m), 1445 (w), 1387 (m), 1363 (m), 1247 (m), 1071 (w), 756 (w), 695 (m). ^{1}H NMR (300 MHz, DMSO-d_6) δ: 7.20 (t, ^3J = 7.6 Hz, 2H), 6.85 (t,

© 2005 NRC Canada

Fig. 8. (*a*) View along the *ab* diagonal of the structure of 1,5-diphenylbiguanide (**6a**) showing how individual corrugated ribbons formed by intermolecular hydrogen bonding (broken lines) form face-to-face aromatic interactions and stack to create layers. Hydrogen atoms appear in white, carbon atoms in gray, and nitrogen atoms in black. (*b*) View along the *b* axis, showing multiple C-H···π interactions between layers. The shortest C—C distances between phenyl rings (shown in Å) are used to define the aromatic interactions.



^3J = 7.6 Hz, 1H), 6.80 (d, ^3J = 7.6 Hz, 2H), 6.70 (bs, 4H), 4.92 (bs, 2H). ^{13}C NMR (75 MHz, DMSO-d_6) δ: 160.2, 158.7, 151.7, 129.8, 123.7, 121.5. MAB-HR-MS (N_2) calcd. for $C_8H_{11}N_5$ *m/e*: 177.1014; found: 177.1022. Anal. calcd. for $C_6H_{11}N_5 \cdot 1/8H_2O$: C 53.54, H 6.32, N 39.02; found: C 53.58, H 6.30, N 39.03.

© 2005 NRC Canada

1,4-Phenylenebis(biguanide) (4·2HCl)

In a 250 mL round-bottomed flask equipped with a magnetic stirrer, 1,4-phenylenediamine (5.24 g, 48.5 mmol) was added to aq. HCl (96 mL, 1.0 mol/L, 96 mmol). Dicyandiamide (8.15 g, 96.9 mol) was then added, and the mixture was heated at reflux for 3 h. Solvent was then removed by evaporation under reduced pressure, and the residual oil was triturated with hot ethanol. The resulting solid was separated by filtration, washed with hot ethanol, and crystallized from water–acetone. The crystals were separated by filtration, washed with acetone, and dried under reduced pressure to provide pure 1,4-phenylenebis(biguanide) (**4**) dihydrochloride (10.3 g, 29.5 mmol, 61%) as a colorless solid, mp 254 to 255 °C (lit. value (39) mp 270–278 °C (dec.)). IR (KBr, cm^{-1}): 3428 (m), 3302 (s), 3186 (s), 3153 (s), 1632 (s), 1547 (s), 1497 (s), 1415 (s), 1377 (m), 1295 (w), 1240 (m), 1017 (m), 826 (m), 717 (m). ^{1}H NMR (300 MHz, DMSO-d_6) δ: 9.74 (s, 2H), 7.26 (s, 12H), 7.04 (s, 4H). ^{13}C NMR (75 MHz, DMSO-d_6) δ: 161.8, 156.4, 135.1, 122.4. Anal. calcd. for $C_{10}H_{18}Cl_2N_{10}$·1/4H_2O: C 33.95, H 5.27, N 39.60; found: C 34.17, H 5.56, N 39.60.

1,3-Phenylenebis(biguanide) (5·2HCl)

Applied to 1,3-phenylenediamine (5.24 g, 48.5 mmol), the preceding method gave pure 1,3-phenylenebis(biguanide) (**5**) dihydrochloride (8.59 g, 24.6 mmol, 51%) as a colorless solid, mp 220 to 221 °C. IR (KBr, m^{-1}): 3313 (s), 3148 (s), 1654 (s), 1544 (s), 1454 (m), 1382 (m), 1278 (w), 1193 (w), 1083 (w), 1045 (w), 920 (w), 780 (w), 733 (w). ^{1}H NMR (300 MHz, DMSO-d_6) δ: 9.78 (s, 2H), 7.34 (s, 8H), 7.21–7.08 (m, 4H), 7.05 (s, 4H). ^{13}C NMR (75 MHz, DMSO-d_6) δ: 162.0, 156.0, 139.8, 129.6, 116.7, 114.0. Anal. calcd. for $C_{10}H_{18}Cl_2N_{10}$: C 34.39, H 5.20; found: C 34.27, H 5.59.

1,4-Phenylenebis(biguanide) (4)

In a 100 mL round-bottomed flask equipped with a magnetic stirrer, the dihydrochloride of 1,4-phenylenebis(biguanide) (**4**, 1.05 g, 3.01 mmol) was added to a mixture of methanol (20 mL) and methanolic $NaOCH_3$ (1.6 mL, 25% by weight, 7.0 mmol). The resulting mixture was stirred at 25 °C for 1 h. The precipitate was separated by filtration, washed with cold water (10 mL) and ethanol (10 mL), and dried under reduced pressure to give pure 1,4-phenylenebis(biguanide) (**4**, 0.741 g, 2.68 mmol, 89%) as a colorless solid, mp 218 to 219 °C (lit. value (39) mp 218 to 219 °C (dec.)). IR (KBr, cm^{-1}): 3467 (m), 3434 (m), 3357 (m), 3329 (m), 3159 (m), 1641 (s), 1614 (s), 1548 (s), 1520 (s), 1493 (s), 1399 (s), 1378 (s), 1242 (s), 1090 (w), 883 (m), 840 (w), 758 (w), 722 (w). ^{1}H NMR (300 MHz, D_2O) δ: 6.86 (s, 4H). ^{13}C NMR (75 MHz, D_2O) δ: 159.8, 159.4, 142.0, 124.8. FAB-MS (3-nitrobenzyl alcohol) *m/e*: 277. FAB-HR-MS (3-nitrobenzyl alcohol) calcd. for $C_{10}H_{17}N_{10}$ *m/e*: 277.1638; found: 277.1649. Anal. calcd. for $C_{10}H_{16}N_{10}$·H_2O: C 40.81, H 6.16, N 47.59; found: C 40.68, H 6.19, N 47.17.

1,3-Phenylenebis(biguanide) (5)

Applied to the dihydrochloride of 1,3-diphenylenebis(biguanide) (**5**), the preceding method gave pure 1,3-phenylenebis(biguanide) (**5**) as a colorless solid, mp 206 °C (dec.). IR (KBr, cm^{-1}): 3479 (m), 3428 (m), 3335 (m), 3109 (m), 1610 (s), 1517 (s), 1470 (s), 1369 (s), 1284 (m), 1186 (m). ^{1}H NMR (300 MHz, D_2O) δ: 7.15 (t, ^3J = 7.8 Hz, 1H), 6.57 (dd, ^4J = 2.1 Hz, ^3J = 7.8 Hz, 2H), 6.46 (t, ^3J = 2.1 Hz, 1H). ^{13}C NMR (75 MHz, D_2O) δ: 159.7, 159.1, 148.3, 130.8, 118.6, 118.3. FAB-MS (3-nitrobenzyl alcohol) *m/e*: 277, 218. TOF-HR-MS calcd. for $C_{10}H_{17}N_{10}$ *m/e*: 277.1632; found: 277.1631. Anal. calcd. for $C_{10}H_{16}N_{10}$·1.5H_2O: C 39.60, H 6.31; found: C 39.79, H 5.97.

1,5-Diphenylbiguanide (6a·HCl)

In a 250 mL round-bottomed flask equipped with a magnetic stirrer, aniline (9.31 g, 100 mmol) was added to aq. HCl (100 mL, 1 mol/L, 100 mmol). The mixture was stirred until it became homogeneous. Sodium dicyanamide (4.45 g, 50.0 mol) was then added and the mixture was heated at reflux. Within 1 h, phenyldicyandiamide (**7**, X = H) had precipitated from the mixture and heating was continued. After a total of 12 h, the mixture was cooled to 25 °C, and the precipitate was separated by filtration, washed with water, and dried under reduced pressure. The solid was dissolved in hot DMF (20 mL) and toluene (150 mL) was then added, causing the formation of a gel-like precipitate. The precipitate was separated by filtration and washed successively with toluene, hexane, and water. The product could be used without further treatment, but further purification could be achieved by crystallization from hot water, which provided the monohydrochloride of 1,5-diphenylbiguanide (**6a**, 10.1 g, 34.9 mmol, 70%) as a colorless solid, mp 230–232 °C (lit. value (41) mp 232 °C; lit. value (22) mp 220 °C). IR (KBr, cm^{-1}): 3401 (w), 3307 (m), 3181 (w), 3120 (w), 1629 (m), 1602 (m), 1577 (m), 1519 (s), 1489 (m), 1445 (m), 1382 (w), 1245 (w), 754 (w), 732 (w), 688 (w). ^{1}H NMR (300 MHz, DMSO-d_6) δ: 9.90 (s, 2H), 7.44 (s, 4H), 7.29 (m, 8H), 7.08 (m, 2H). ^{13}C NMR (75 MHz, DMSO-d_6) δ: 157.7, 138.8, 129.7, 125.0, 122.4. Anal. calcd. for $C_{14}H_{16}ClN_5$: C 58.03, H 5.57, N 24.17; found: C 57.94, H 5.67, N 24.20.

The monohydrochloride salts of 1,5-bis(2-methylphenyl)biguanide (**6b**), 1,5-bis(3-methylphenyl)biguanide (**6c**), 1,5-bis(4-methylphenyl)biguanide (**6d**) (41), 1,5-bis(4-methoxyphenyl)biguanide (**6e**) (41, 42), 1,5-bis(4-cyanophenyl)biguanide (**6f**), 1,5-bis(2-bromophenyl)biguanide (**6g**), 1,5-bis(4-bromophenyl)biguanide (**6h**) (42), 1,5-bis(3,5-dimethylphenyl)biguanide (**6i**), and 1,5-bis(2,4,6-trimethylphenyl)biguanide (**6j**) were prepared in the same way. Yields, melting points, spectroscopic data, and elemental analyses are provided in the Supplementary material.[5]

1,5-Diphenylbiguanide (6a)

In a 200 mL round-bottomed flask equipped with a magnetic stirrer, the monohydrochloride of 1,5-diphenylbiguanide (8.69 g, 30.0 mmol) was added to a mixture of methanol (60 mL) and methanolic $NaOCH_3$ (8.2 mL, 25% by weight, 36 mmol). The mixture was stirred at 25 °C for 1 h and then water was added. The resulting precipitate was separated by filtration, washed with water, and dried under reduced pressure to give 1,5-diphenylbiguanide (**6a**, 7.30 g, 28.8 mmol, 96%) as a colorless solid, mp 147 to 148 °C (dec.) (lit. value (41) mp 145 to 146 °C). IR (KBr, cm^{-1}): 3439 (m), 3351 (m), 3214 (m), 3071 (m), 1621 (s), 1593 (m), 1544 (s), 1522 (s), 1495 (m), 1481 (m), 1443 (m), 1380 (m), 1349 (s), 1289 (w), 1231 (s), 1155 (w), 1067 (w), 757 (m), 738 (m), 716 (m), 688 (m), 611 (m). ^{1}H NMR

© 2005 NRC Canada

(400 MHz, DMSO-d_6) δ: 7.24 (m, 8H), 6.93 (m, 2H), 9–5 (bs, 5H). ^{13}C NMR (75 MHz, DMSO-d_6) δ: 156.6, 146.0, 129.7, 122.3. FAB-MS (3-nitrobenzyl alcohol) *m/e*: 254, 237, 161, 136, 119. FAB-HR-MS (3-nitrobenzyl alcohol) calcd. for $C_{14}H_{16}N_5$: 254.1406; found: 254.1402. Anal. calcd. for $C_{14}H_{15}N_5$: C 66.38, H 5.97, N 27.65; found: C 66.41, H 6.05, N 27.80.

1,5-Bis(2-methylphenyl)biguanide (**6b**), 1,5-bis(3-methylphenyl)biguanide (**6c**), 1,5-bis(4-methylphenyl)biguanide (**6d**) (41), 1,5-bis(4-methoxyphenyl)biguanide (**6e**), 1,5-bis(4-cyanophenyl)biguanide (**6f**) (43), bis(2-bromophenyl)biguanide (**6g**), 1,5-bis(4-bromophenyl)biguanide (**6h**), 1,5-bis(3,5-dimethylphenyl)biguanide (**6i**), and 1,5-bis(2,4,6-trimethylphenyl)biguanide (**6j**) were prepared in similar yields in the same way. Yields, melting points, spectroscopic data, and elemental analyses are provided in the Supplementary material.[5]

Phenyldicyandiamide (7, X = H)

In a 100 mL round-bottomed flask equipped with a magnetic stirrer, aniline (2.45 g, 26.3 mmol) was added to aq. HCl (25 mL, 1 mol/L, 25 mmol) and the mixture was stirred until it became homogeneous. Sodium dicyanamide (2.23 g, 25.0 mmol) was then added and the mixture was heated at reflux for 2 h with constant stirring. During this period the product precipitated, and it was separated by filtration and recrystallized from CH_3CH_2OH to give pure phenyldicyandiamide (**7**, X = H; 3.49 g, 21.8 mol, 87%) as a colorless solid, mp 197 to 198 °C (lit. value (41) mp 196 to 197 °C). IR (KBr, cm^{-1}): 3407 (m), 3319 (m), 3215 (m), 3154 (m), 2973 (m), 2176 (s), 2143 (m), 1660 (m), 1608 (m), 1585 (s), 1555 (s), 1495 (s), 1449 (m), 1393 (s), 1298 (m), 1208 (m), 1065 (m), 1051 (s), 895 (w), 744 (m), 714 (m), 686 (w), 637 (w). ^{1}H NMR (300 MHz, DMSO-d_6) δ: 9.03 (s, 1H), 7.35 (d, ^3J = 8.4 Hz, 2H), 7.30 (t, ^3J = 7.0 Hz, 2H), 7.07 (t, ^3J = 7.0 Hz, 1H), 6.98 (s, 2H). ^{13}C NMR (75 MHz, DMSO-d_6) δ: 160.4, 138.8, 129.7, 124.6, 122.2, 118.1. MAB-HR-MS (N_2) calcd. for $C_8H_8N_4$ *m/e*: 160.0749; found: 160.0750. Anal. calcd. for $C_8H_8N_4$: C 59.99, H 5.03, N 34.98; found: C 60.07, H 5.13, N 35.20.

X-ray crystallographic studies

The structures were solved by direct methods using SHELXS-97 (44) and refined with SHELXL-97 (45). All non-hydrogen atoms were refined anisotropically. Hydrogen atoms were refined as riding atoms. They were located by a difference Fourier map for compound **6a**·HCl, whereas they were placed in ideal positions for compound **6a**.

Crystallization of compounds 6a and 6a·HCl

Single crystals of compound **6a**·HCl suitable for analysis by X-ray diffraction were grown from hot water, and crystals of free base **6a** were grown from hot ethanol.

Acknowledgments

We are grateful to the Natural Sciences and Engineering Research Council of Canada (NSERC), the Ministère de l'Éducation du Québec, the Canada Foundation for Innovation, the Canada Research Chairs Program, and Merck Frosst for financial support.

In addition, we thank Professor Jurgen Sygusch for providing access to a Bruker SMART 6000 CCD diffractometer equipped with a rotating anode.

References

1. P. Hubberstey and U. Suksangpanya. Struct. Bond. **111**, 33 (2004).
2. F. Kurzer and E.D. Pitchfork. Fortschr. Chem. Forsch. **10**, 375 (1968).
3. P. Ray. Chem. Rev. **61**, 313 (1961).
4. E. Bamberger and W. Dieckmann. Ber. **25**, 543 (1892).
5. H. Tsubouchi, K. Ohguro, K. Yasumura, H. Ishikawa, and M. Kikuchi. Bioorg. Med. Chem. Lett. **7**, 1721 (1997).
6. D. Sweeney, M.L. Raymer, and T.D. Lockwood. Biochem. Pharm. **66**, 663 (2003).
7. F.L. Rose. J. Chem. Soc. 2770 (1951).
8. R.A. Glennon, M.K. Daoud, M. Dukat, M. Teitler, K. Herrick-Davis, A. Purohit, and H. Syed. Bioorg. Med. Chem. **11**, 4449 (2003).
9. Z. Brzozowski, F. Sączewski, and M. Gdaniec. Eur. J. Med. Chem. **35**, 1053 (2000).
10. R.S. Hundal and S.E. Inzucchi. Drugs, **63**, 1879 (2003).
11. K.H. Slotta and R. Tschesche. Ber. **62B**, 1398 (1929).
12. B. Kovačević and Z.B. Maksić. Org. Lett. **3**, 1523 (2001).
13. I. Kaljurand, T. Rodima, I. Leito, I.A. Koppel, and R. Schwesinger. J. Org. Chem. **65**, 6202 (2000).
14. C.G. Overberger, F.W. Michelotti, and P.M. Carabateas. J. Am. Chem. Soc. **79**, 941 (1957).
15. D. Laliberté, T. Maris, and J.D. Wuest. J. Org. Chem. **69**, 1776 (2004).
16. J.H. Fournier, T. Maris, and J.D. Wuest. J. Org. Chem. **69**, 1762 (2004).
17. S. Mayer, D.M. Daigle, E.D. Brown, J. Khatri, and M.G. Organ. J. Comb. Chem. **6**, 776 (2004).
18. S.N. Holter and W.C. Fernelius. Inorg. Synth. **7**, 58 (1963).
19. D. Karipides and W.C. Fernelius. Inorg. Synth. **7**, 56 (1963).
20. K. Shirai and K. Sugino. J. Org. Chem. **25**, 1045 (1960).
21. S.L. Shapiro, V.A. Parrino, E. Rogow, and L. Freedman. J. Am. Chem. Soc. **81**, 3725 (1959).
22. L. Neelakantan. J. Org. Chem. **22**, 1587 (1957).
23. F.H.S. Curd and F.L. Rose. UK Patent 581 346, 1946.
24. B. Clement and U. Girreser. Magn. Reson. Chem. **37**, 662 (1999).
25. G. López-Olvera and M. Soriano-García. Anal. Sci.: X-ray Struct. Anal. [online], **20**, x151 (2004).
26. A. Martin, A.A. Pinkerton, and A. Schiemann. Acta Crystallogr. Sect. C, **C52**, 966 (1996).
27. A. Dalpiaz, V. Ferretti, P. Gilli, and V. Bertolasi. Acta Crystallogr. Sect. C, **B52**, 509 (1996).
28. M. Hariharan, S.S. Rajan, and R. Srinivasan. Acta Crystallogr. Sect. C, **C45**, 911 (1989).
29. J.M. Amigó, J.M. Martínez-Calatayud, A. Cantarero, and T. Debaerdemaeker. Acta Crystallogr. Sect. C, **C44**, 1452 (1988).
30. J.M. Amigó, J. Martínez-Calatayud, and T. Debaerdemaeker. Bull. Soc. Chim. Belg. **94**, 119 (1985).
31. C.J. Brown and L. Sengier. Acta Crystallogr. Sect. C, **C40**, 1294 (1984).
32. C. Herrnstadt, D. Mootz, and H. Wunderlich. J. Chem. Soc. Perkin Trans. 2, 735 (1979).
33. A.A. Pinkerton and D. Schwarzenbach. J. Chem. Soc. Dalton Trans. 989 (1978).
34. S.R. Ernst. Acta Crystallogr. Sect. B, **B33**, 237 (1977).
35. S.R. Ernst and F.W. Cagle, Jr. Acta Crystallogr. Sect. B, **B33**, 235 (1977).

© 2005 NRC Canada

36. R. Handa and N.N. Saha. Acta Crystallogr. Sect. B, **B29**, 554 (1973).
37. R. Handa and N.N. Saha. J. Cryst. Mol. Struct. **1**, 235 (1971).
38. C.J. Brown. J. Chem. Soc. A, 60 (1967).
39. S.R. Safir, S. Kushner, L.M. Brancone, and Y. Subbarow. J. Org. Chem. **13**, 924 (1948).
40. F.E. King, R.M. Acheson, and P.C. Spensley. J. Chem. Soc. 1366 (1948).
41. F.H.S. Curd and F.L. Rose. J. Chem. Soc. 729 (1946).
42. A.B. Sen and P.R. Singh. J. Indian Chem. Soc. **39**, 41 (1962).
43. J.N. Ashley, S.S. Berg, and R.D. MacDonald. J. Chem. Soc. 4525 (1960).
44. G.M. Sheldrick. SHELXS-97. University of Göttingen, Göttingen, Germany. 1997.
45. G.M. Sheldrick. SHELXL-97. University of Göttingen, Göttingen, Germany. 1997.

© 2005 NRC Canada

Kinetics and mechanism of dealkylation of coordinated isocyanide in $Fe(PMe_3)_2(t\text{-}BuNC)_3$[1]

Christine L. Tennent and William D. Jones

Abstract: The zerovalent iron complex $Fe(PMe_3)_2(t\text{-}BuNC)_3$ undergoes thermal cleavage of the C—N bond to give $Fe(PMe_3)_2(t\text{-}BuNC)_2(H)(CN)$ and isobutylene. The reaction follows first order kinetics, and addition of the hydrogen-atom donor 1,4-cyclohexadiene leads to the preferential formation of isobutane rather than isobutylene. Mechanistic studies are consistent with a rate determining homolysis of the C—N bond, giving rise to *tert*-butyl radicals.

Key words: iron, isocyanide, elimination, C—N cleavage.

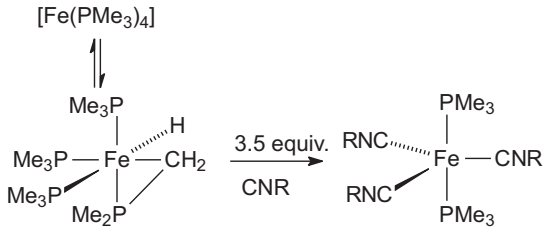
Résumé : Le complexe ferrique zérovalent, $Fe(PMe_3)_2(t\text{-}BuNC)_3$, subit un clivage thermique de la liaison C—N et génère le $Fe(PMe_3)_2(t\text{-}BuNC)_2(H)(CN)$ et l'isobutylène. La réaction suit une cinétique du premier ordre, et l'addition du cyclohexadiène-1,4 comme source d'hydrogène mène à la formation préférentielle de l'isobutane plutôt que l'isobutylene. Les modèles mécanistes sont conformes à l'homolyse cinétiquement déterminante de la liaison C—N menant à la formation de radicaux de *tert*-butyl.

Mots clés : fer, isocyanure, élimination, clivage de la liaison C—N.

Introduction

Rathke and Muetterties (1) and Klein and co-workers (2), in independent studies, reported the synthesis of the complex $[Fe(PMe_3)_4]$, which was found to be in equilibrium with the intramolecular oxidative addition adduct $Fe(\eta_2\text{-}PMe_2CH_2)(PMe_3)_3H$. The reaction of this complex with σ-donor ligands and oxidative addition substrates gave evidence of this facile equilibrium (3). The preparation and structural examination of a series of low-valent iron phosphine isocyanide complexes using the above mentioned reactive iron species has been reported by our laboratory by the reaction of this reactive species with a variety of isocyanides (eq. [1]) (4). This article addresses the C—N cleavage reaction that is seen in one of these derivatives, $Fe(PMe_3)_2(t\text{-}BuNC)_3$ (**1**).

[1]



R = Me, Et, *i*-Pr, *t*-Bu, CH_2CMe_3, Ph, 2,6-xylyl

Several isocyanides were used, and all of the resulting complexes were found to be extremely air sensitive. Most of the complexes were found to be moderately thermally stable at room temperature. Stability was found to decrease in the sequence 2,6-xylyl > Ph > CH_2CMe_3 > *t*-Bu > Me > > *i*-Pr > Et. The reaction of the isocyanides where R = *i*-Pr and Et did not give an isolable crystalline product. The complex $Fe(PMe_3)_2(t\text{-}BuNC)_3$ could be isolated as a yellow crystalline solid, but was found to decompose at 25 °C over several days.

All of these complexes have similar ^1H NMR spectra with resonances for three equivalent isocyanide ligands and a pseudotriplet (5) for the two equivalent trimethylphosphine ligands. This suggests a trigonal-bipyramidal geometry, which was confirmed by X-ray crystallography for R = CH_2CMe_3, Ph, and 2,6-xylyl. An interesting observation is the severe bending of the C-N-C linkage in each of these complexes (Table 1). The general tendancy is for two of the isocyanides to display a higher degree of bending than the third. In the case of phenyl isocyanide, crystal packing forces one isocyanide ligand to be crystallographically linear and the remaining two ligands must then take up the excess metal electron density by π-back-bonding, resulting in the bent C-N-C. The other isocyanide complexes listed in Table 1 also show this pattern. The trimethylphosphine ligands always occupy the axial positions.

Benzene solutions of the $Fe(PMe_3)_2(CNR)_3$ complexes, when treated with the corresponding free isocyanide at 25 °C, were found to be in equilibrium with their mono- and disubstituted complexes (eq. [2]). The equilibrium constants

Received 15 September 2004. Published on the NRC Research Press Web site at http://canjchem.nrc.ca on 7 June 2005.

Submitted for publication in a special issue to honour the career contributions of Professor Howard Alper.

C.L. Tennent and W.D. Jones.[2] Department of Chemistry, University of Rochester, Rochester, NY 14627 USA.

[1]This article is part of a Special Issue dedicated to Professor Howard Alper.

[2]Corresponding author (e-mail: jones@chem.rochester.edu).

 doi: 10.1139/V05-023 © 2005 NRC Canada

Table 1. C-N-C bond angles in iron isocyanide complexes (4).

Molecule	Angle C-N-C (°)
$Fe(PMe_3)_2(CNCH_2CMe_3)_3$	140, 146, 166
$Fe(PMe_3)_2(CNPh)_3$	131.8, 131.8, 180
$Fe(PMe_3)_2$(CN-2,6-xylyl)$_3$	147.7, 149.8, 161.3
$Fe(PMe_3)$(CN-2,6-xylyl)$_4$	174.5, 167.9, 166.7, 145.1

were found by comparison of the ^{1}H NMR integrations of the free and coordinated isocyanide and PMe_3 resonances. For R = *tert*-butyl, K_1 = 0.035(5) and K_2 = 0.0079(24). The equilibria for the other isocyanides were similar.

[2] $Fe(PMe_3)_2(CNR)_3 \underset{-PMe_3}{\overset{K_1 \ +CNR}{\rightleftharpoons}} Fe(PMe_3)(CNR)_4 \underset{K_2 \ -PMe_3}{\overset{+CNR}{\rightleftharpoons}} Fe(CNR)_5$

Irridation of a benzene solution of $Fe(PMe_3)_2(CNCH_2CMe_3)_3$ in the presence of excess PMe_3 resulted in the formation of a new species assigned the formula $Fe(PMe_3)_4(CNCH_2CMe_3)$ based on the ^{1}H NMR spectrum and the couplings observed (eq. [3]). All PMe_3 ligands were equivalent, suggesting the d^8 complex is fluxional.

[3] $Fe(PMe_3)_2(CNR)_3 \xrightarrow[PMe_3]{h\nu} Fe(PMe_3)_4(CNR)$

R = CH_2CMe_3

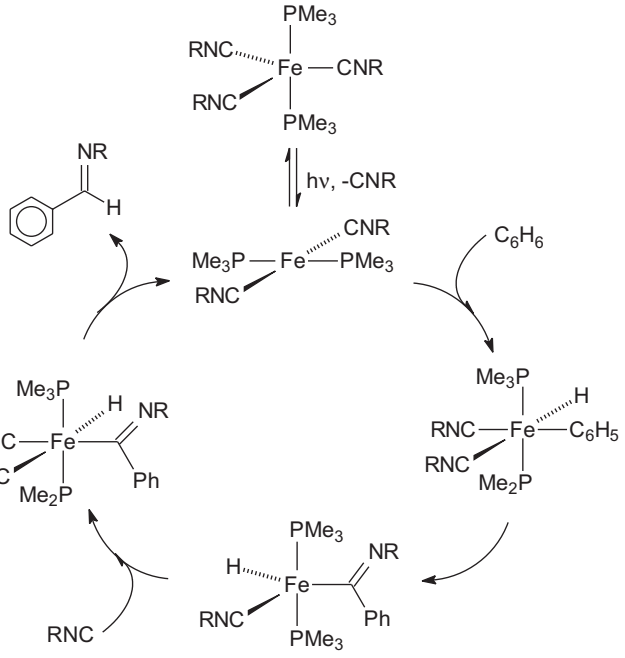
Dilute benzene solutions of $Fe(PMe_3)_2(CNCH_2CMe_3)_3$ upon irradiation gave the isocyanide insertion product, aldimine $PhCH{=}NCH_2CMe_3$, and $Fe(PMe_3)_3(CNCH_2CMe_3)_2$ (6). The reaction was found to be catalytic in iron when low concentrations of isocyanide are present. The two photochemical reactions of the neopentylisocyanide complex suggest the photochemical labilization of the isocyanide ligand. The proposed mechanism for the isocyanide insertion is shown in Scheme 1.

Results

Thermal reaction of $Fe(PMe_3)_2$(*t*-BuNC)$_3$

A benzene-d_6 solution of $Fe(PMe_3)_2$(*t*-BuNC)$_3$ (**1**), upon heating at 60 °C for 24 h, showed a gradual bleaching of its yellow color accompanied by a change in the ^{1}H NMR spectrum. A decrease of the resonances of **1** at δ 1.26 (s, 27H) and 1.55 (pseudo t, *J* = 4 Hz, 18H) was observed, while new resonances for $Fe(PMe_3)_2$(*t*-BuNC)$_2$(H)(CN) (**2**) as well as free isobutylene (δ 4.73, m, 1H; 1.58, m, 6H) appeared (eq. [4]). Cis and trans isomers of **2** are observed in a 10:1 ratio. The ratio is invariant over time. The resonances for the cis isomer appear at δ 1.51 (pseudo t, *J* = 4 Hz, 18H), 1.10 (s, 9H), 0.97 (s, 9H), and –10.6 (t, *J* = 56 Hz, 1H) while the resonances for the trans isomer are observed at δ 1.48 (pseudo t, *J* = 4 Hz, 18H), 1.06 (s, 18H), and –13.8 (t, *J* = 44 Hz, 1H). In a reaction run at room temperature over several months, only *cis*-**2** was seen. Heating the solution to 60 °C led to an equilibration with *trans*-**2**, indicating that *cis*-**2** is the initial kinetic product of the reaction. The reaction is quantitative as judged by ^{1}H NMR spectroscopy.

Scheme 1. Mechanism for isocyanide insertion.



[4] $\underset{\textbf{1}}{t\text{-BuNC}(PMe_3)_3Fe\text{—}CN\text{-}t\text{-Bu}} \xrightarrow{\triangle} \underset{\textbf{2}}{t\text{-BuNC}(Me_3P)_2(H)Fe\text{—}CN} + \underset{}{CH_2{=}C(Me)_2}$

10 : 1, *cis* : *trans*

It has been observed that at room temperature in the solid state, **1** will also react thermally to give **2**. After several months, approximately 10% of **2** had formed. Analysis for isobutylene was not done. If the material is kept at low temperatures (<20 °C), no significant formation of **2** is observed.

Kinetics of the reaction of $Fe(PMe_3)_2$(*t*-BuNC)$_3$

UV–vis spectroscopy was found to be a convenient method for determining the rate of the isocyanide cleavage reaction. The UV–vis spectrum of **1** had two broad but well defined maxima at 309 and 390 nm, which, upon thermolysis (formation of **2**), decrease to baseline. The band at 390 nm was used for kinetic studies, as it was farthest from the large solvent absorption.

The effect of concentration of **1** on the rate of the reaction was examined in the range of $1 \times 10^{-4} - 9 \times 10^{-4}$ mol/L, as indicated in Table 2. The rate constant was found to be independent of [**1**], although a rather large variation (10%) in k_{obs} was observed (k_{obs} = 4.2 (0.4) $\times 10^{-5}$ s^{-1}).

© 2005 NRC Canada

Table 2. Kinetics data for elimination of isobutylene from **1** at 67 °C.

[**1**] (mmol/L)	[PMe_3] (mol/L)	Solvent	$k_{obs} \times 10^5$ (s^{-1})
0.11	0	Iso-octane	4.7(0.03)
0.20	0	Iso-octane	5.1(0.02)
0.25	0	Iso-octane	3.9(0.01)
0.42	0	Iso-octane	4.6(0.007)
0.56	0	Iso-octane	4.2(0.009)
0.57	0	Iso-octane	3.7(0.004)
0.63	0	Iso-octane	4.8(0.004)
0.67	0	Iso-octane	3.8(0.005)
0.68	0	Iso-octane	3.7(0.003)
0.69	0	Iso-octane	4.4(0.002)
0.70	0	Iso-octane	4.0(0.003)
0.72	0	Iso-octane	3.9(0.002)
0.76	0	Iso-octane	4.7(0.008)
0.77	0	Iso-octane	4.2(0.009)
0.82	0	Iso-octane	3.7(0.004)
0.91	0	Iso-octane	4.5(0.02)
1.4	0.014	Iso-octane	4.2(0.2)*
1.2	0.03	Iso-octane	4.7(0.1)*
1.2	0.06	Iso-octane	4.9(0.1)*
1.1	0.11	Iso-octane	4.9(0.2)*
0.97	0.97	Iso-octane	4.9(0.2)*
0.55	0	Iso-octane	4.2(4)*
0.43	0	Benzene	10.7(0.01)
0.91	0	THF	10.7(0.02)
0.98	0	DMSO	30.6(0.10)

Note: * = standard deviation for multiple runs. All others are first order fits for single determination.

The rate of the reaction was measured for temperatures ranging from 50 to 85 °C. An Eyring plot of these results gave $\Delta H^{\ddagger}$ = 26(1) kcal/mol and $\Delta S^{\ddagger}$ = 15(3) eu (Fig. 1). The value of 26(1) kcal/mol for the bond breakage of the C—N bond of coordinated isocyanide is not surprising considering the high stability of the -CN ligand that remains intact.

The rate of isobutylene elimination was examined in both low polarity (iso-octane) and high polarity (DMSO) solvents. The same reaction products were observed in each solvent. The resulting k_{obs} were found to be 4.2×10^{-5} and 30.6×10^{-5} s^{-1}, respectively, indicating only a small solvent effect (7×) on the rate of the reaction.

The effect of added PMe_3 on the rate of the reaction was also examined. Solutions of **1** containing trimethylphosphine in concentrations ranging from 0 to 0.97 mol/L were employed. The rates of disappearance of **1** were found to be comparable, within experimental error (Table 2). One interesting observation was that additions of small amounts of trimethylphosphine to the reaction resulted in smaller standard deviations in the k_{obs} than found using no trimethylphosphine.

Several benzene-d_6 solutions of **1** were made with varying amounts of the radical trap 1,4-cyclohexadiene. The samples were examined by ^{1}H NMR spectroscopy after heating at 67 °C for 24 h, showing the formation of both isobutylene and isobutane, plus benzene and **2**. The ratio of isobutane to isobutylene is given in Table 3 for various diene concentrations. Once again, the scatter in the data is large, but a general trend can be noted. As the amount of added 1,4-cyclohexadiene was increased, more isobutane was produced relative to isobutylene.

Fig. 1. Eyring plot for the elimination of isobutylene from $Fe(PMe_3)_2(t\text{-BuNC})_3$.

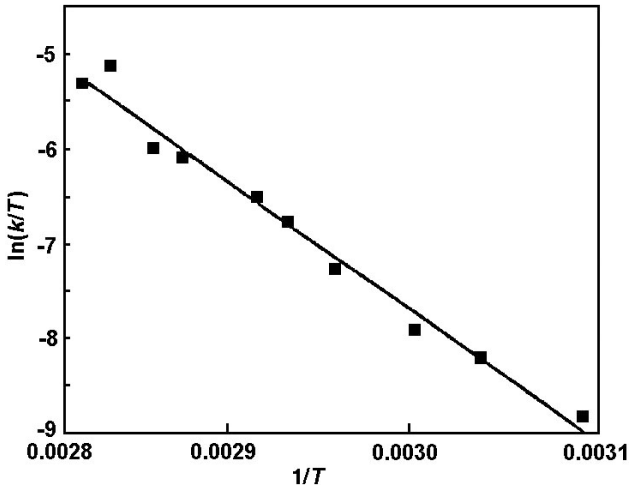


Table 3. Radical trap data for elimination of isobutylene from **1**.

[1,4-Cyclohexadiene] (mol/L)	Solvent	Isobutane/ isobutylene
0.2	Benzene	0.75
0.3	Benzene	1.04
0.3	Benzene	0.51
0.4	Benzene	0.80
0.4	Benzene	0.80
0.6	Benzene	1.32
0.6	Benzene	0.82
0.6	Benzene	0.89
0.7	Benzene	0.96
2.0	Benzene	3.54
2.0	Benzene	3.17
10.6	1,4-Cyclohexadiene	3.54

In an attempt to determine if a solvent cage reaction was occurring, a sample was made in neat 1,4-cyclohexadiene. Samples of **1** in benzene or neat 1,4-cyclohexadiene were made as described in the Experimental section. The volatiles from the samples after heating for 14 h at 67 °C were examined by ^{1}H NMR spectroscopy. The benzene samples showed the trend previously observed; that is, an increase in [1,4-cyclohexadiene] gave a decrease in the amount of isobutylene produced. However, the sample made in neat 1,4-cyclohexadiene gave approximately 25% isobutylene (see Table 3).

The partially labeled compound $Fe(PMe_3)_2[CNC(CH_3)(CD_3)_2]_3$ was synthesized to measure the kinetic isotope effect of C—H vs. C—D elimination. Benzene solutions containing $Fe(PMe_3)_2(t\text{-BuNC-}d_6)_3$ were heated for 24 h at 67 °C in resealable NMR tubes. The reaction was complete after 24 h. The volatiles from the samples were then analyzed by GC–MS using low ionizing voltages to determine the ratio of d_6 to d_5 isobutylene, which was found to be 0.56(0.01). The statistically corrected isotope effect k_H/k_D is

© 2005 NRC Canada

Scheme 2. Proposed mechanisms for C—N cleavage in **1**.

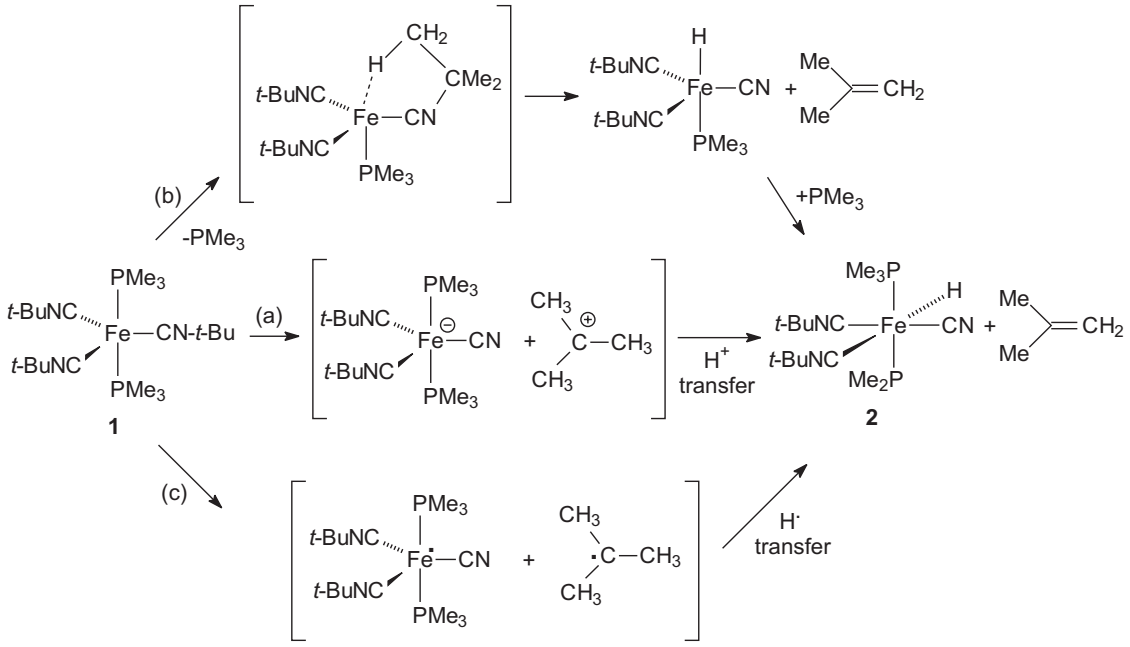
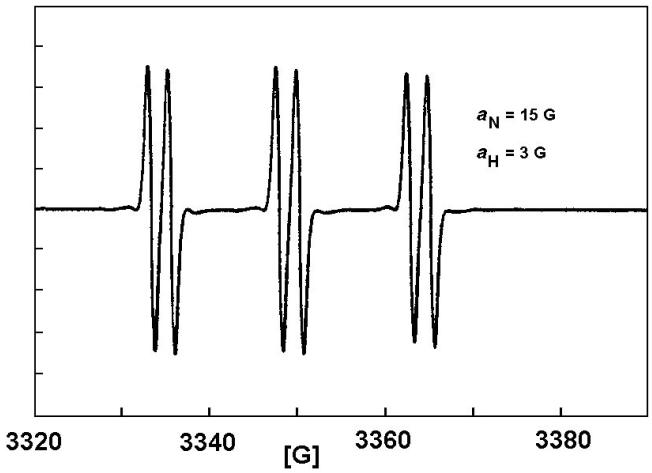


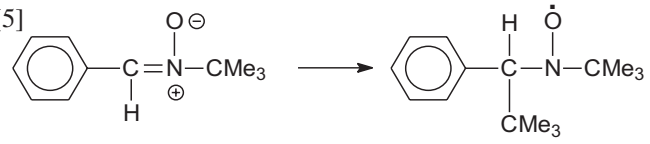
Fig. 2. ESR spectrum upon addition of *N-tert*-butyl-α-phenylnitrone (PBN) to a sample of **1** in benzene.



therefore 1.12. The overall k_{obs} for the reaction was observed to be approximately the same as for the nondeuterated material.

Addition of *N-tert*-butyl-α-phenylnitrone (PBN) to a sample of **1** in benzene showed an immediate ESR signal (Fig. 2). The signal intensity increased after heating, giving a strong triplet of doublets with a_H = 3 G and a_N = 15 G. These coupling values are reasonable for a *tert*-butyl radical coupled with PBN (eq. [5]) (7).

[5]



+ $Fe(PMe_3)_2(t\text{-BuNC})_3$

Discussion

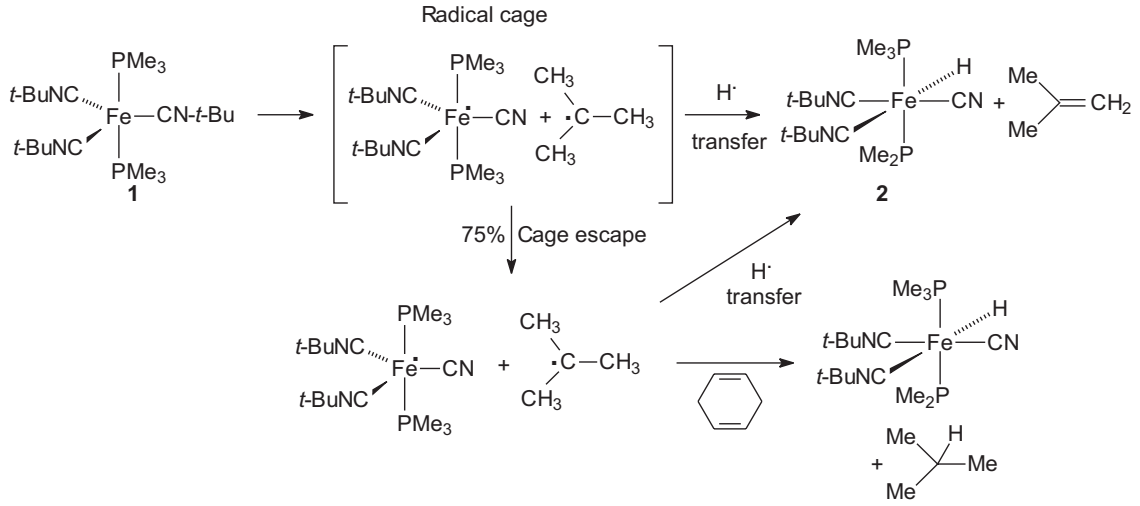
The thermal reaction of $Fe(PMe_3)_2(t\text{-BuNC})_3$ (**1**) gives the products $Fe(PMe_3)_2(t\text{-BuNC})_2(H)(CN)$ (**2**) and free isobutylene in quantitative yield. This reaction formally involves the δ-elimination of the isocyanide C—H bond and cleavage of the isocyanide C—N bond to produce the observed olefin and the metal cyano hydride. Several mechanisms were considered for this elimination reaction (Scheme 2).

One could envision that thermal reaction of **1** leads to the formation of a *tert*-butyl carbonium ion intermediate that could then act as a proton donor towards the metal anion (Scheme 2*a*). Precedence for this pathway exists in the literature on *tert*-butyl isocyanide (8). The lack of a strong dependence of the rate of the reaction on solvent polarity, however, argues against this pathway. Solvent effects on ionic reaction rates are typically on the order of three to six orders of magnitude difference (9). The effect on the thermal reaction in this case was only a sevenfold difference.

A second possible mechanism would involve intramolecular elimination (Scheme 2*b*). If an intramolecular mechanism were occurring during the thermal reaction of **1**, trimethyl phosphine dissociation would be required as the initial step to generate a vacant site. The unsaturation at the metal center would allow coordination of a terminal hydrogen of the isocyanide (agostic interaction). Olefin elimination and recoordination of the trimethyl phosphine would result in **1** and isobutylene. One concern regarding this mechanism is the strain needed to achieve the appropriate geometry for agostic hydrogen coordination to the metal center. Earlier X-ray structural studies of **1** and similar iron complexes reported the C-N-C linkage to be bent (~130°). It is not clear if this deviation from linearity would be sufficient to allow hydrogen coordination. The observation that the rate of the reaction is insensitive to added PMe_3 at concentrations up to 1 mol/L argues against this pathway, al-

© 2005 NRC Canada

Scheme 3. Radical mechanism for C—N cleavage in **1**.



though rate determining PMe_3 loss in the first step would give first order kinetics.

A third mechanism would involve the homolytic cleavage of the N—C single bond in complex **1**, which would result in a 17-electron iron(I) species and a *tert*-butyl radical (Scheme 2*c*). The *tert*-butyl radical would act as a good hydrogen atom donor to the iron(I) complex, directly giving the cyano hydride product **2** and isobutylene.

Several lines of evidence point towards a radical mechanism. First, isobutane formation from the reaction of **1** in the presence of 1,4-cyclohexadiene reveals the intermediacy of *tert*-butyl radicals. 1,4-Cyclohexadiene could act as a hydrogen atom donor towards both *tert*-butyl radicals and the 17-electron metal complex to give isobutane and **2** (plus benzene). As the concentration of the hydrogen donor increases, the amount of isobutane also goes up since competitive reaction of the *tert*-butyl radicals with the Fe(I) intermediate becomes less important (Scheme 3). The small amount of isobutylene still observed in the presence of neat 1,4-cyclohexadiene suggests the possibility that some reaction occurs within the solvent cage. The limiting observation of 25% (minimum) isobutylene suggests that at least 1/4 of the radical pairs react within the cage. Though *tert*-butyl radical coupling to form isobutane and isobutylene is highly favored, none was observed. This may be because of the high reactivity of the 17-electron iron complex, which would be in excess after one pair of *tert*-butyl radicals coupled.

The appearance of an intense ESR signal when a benzene solution of **1** was treated with excess PBN also suggests a radical mechanism. A sample of *tert*-butyl isocyanide and PBN in benzene gave no apparent ESR signal. No ESR signal was observed when a benzene solution of $Fe(PMe_3)_2(CNCH_2CMe_3)_3$ and PBN was examined. This was significant since the neopentylisocyanide complex is known to be thermally stable and does not undergo the dealkylation observed with **1**. As a side note, the addition of the spin trap 2-methyl-2-nitrosopropane dimer to benzene solutions of **1** or $Fe(PMe_3)_2(CNCH_2CMe_3)_3$ gave ESR signals in both cases, though the intensity of the signal was smaller. It is likely that these trapped radicals were formed as a result of direct reaction of the metal complexes with the added spin trap, which is a common problem with ESR spin traps.

The isotope effect measured for the hydrogen abstraction reaction that is proposed to occur in the thermal rearrangement of **1**, where the hydrogen or deuterium atom is attached in an equivalent place in the same molecule, is commonly known as a competitive intramolecular isotope effect (10). The small isotope effect observed for this reaction may be due to a small zero point energy difference between the two reactant-like transition states of this exothermic reaction step (11).

The cleavage of isocyanide C—N single bonds by transition metals, while not unprecedented, is fairly rare. Lippard and co-workers reported the dealkylation of $[M(t\text{-BuNC})_7]^{2+}$ (M = Mo, W) in refluxing ethanol in low yield (12). Although the fate of the *tert*-butyl group was not determined, it was proposed to have formed either *tert*-butyl alcohol or isobutylene. Tschugaeff and Teearu reported the formation of $Pt(t\text{-BuNC})_2(CN)_2$ upon dissolving $[Pt(t\text{-BuNC})_4]^{2+}$ in methanol (13). Earlier work in our group also showed that coordination of *t*-BuNC to $[Ru(dmpe)_2]$ leads to the formation of $Ru(dmpe)_2(H)(CN)$, $Ru(dmpe)_2(CN)_2$, isobutylene, and isobutane (14). In none of these cases was the mechanism examined in detail.

Conclusions

The thermal reaction of **1** to eliminate isobutylene and form **2** has been found to proceed by the homolytic cleavage of the *N*-*t*-Bu bond, producing a free *tert*-butyl radical and a 17-electron Fe(I) complex. The transfer of H· from the *t*-Bu radical to the metal complex gives the observed products. The observation of at least 25% isobutylene (based on the amount of **2** formed) regardless of the amount of hydrogen atom donor present suggests that a minimum of one fourth of the radical reaction occurs in the radical cage.

Experimental

The solvents THF, DMSO, diethyl ether, tetraglyme, and benzene were distilled from dark purple solutions of sodium benzophenone ketyl under a nitrogen atmosphere. Iso-octane was dried by refluxing with sodium under nitrogen for 48 h. All compounds were handled in a Vacuum Atmospheres Dri-

© 2005 NRC Canada

Lab. All NMR samples were made using resealable or sealed NMR tubes that were prepared and degassed on a high vacuum line. The UV–vis samples were run under nitrogen in a 1 cm path length quartz cell equipped with a Teflon adaptor. The ESR samples were run in new NMR tubes capped with septa. *tert*-Butyl isocyanide and 1,4-cyclohexadiene were purchased from Aldrich Chemical Company and vacuum distilled before use. Trimethylphosphine was purchased from Strem Chemical Company and used as received. The Grignard MeMgI in diethyl ether (3 mol/L), 2-methyl-2-nitropropane dimer, and *N*-*tert*-butyl-α-phenylnitrone (PBN) were purchased from Aldrich Chemical Co. and used as received. $Fe(PMe_3)_2(t\text{-}BuNC)_3$ was prepared as previously described (4).

NMR spectra were obtained on a Bruker AMX-400 instrument. NMR chemical shifts are reported in units of δ vs. residual benzene protons (δ 7.15 for ^1H; 128.0 for ^{13}C). UV–vis spectra were obtained on an HP 8452A diode array spectrophotometer, and kinetics data were processed using HP 89531A MS DOS UV–vis operating software. Gas chromatography – mass spectrometry were obtained using an HP 5890 series II instrument equipped with a 30 m Carbowax column at 50 °C and an ionizing voltage of 10 eV to ensure only parent ion detection. Infrared data were obtained using a Bruker ESP300 IR spectrometer.

Thermal reaction of $Fe(PMe_3)_2(t\text{-}BuNC)_3$ (1)

A solution of $Fe(PMe_3)_2(t\text{-}BuNC)_3$ in C_6D_6 (10 mg in 0.6 mL) was placed in a resealable NMR tube and heated at 60 °C. Periodic examination of the reaction by ^1H NMR spectroscopy for 24 h showed the disappearance of **1** and the formation of two new products identified as *cis*-**2** and *trans*-**2** in a 10:1 ratio, along with isobutylene (δ 4.72, m, 2H; 1.58, m, 6H).

$Fe(PMe_3)_2$(t-BuNC)$_3$ (1)

^1H NMR (C_6D_6) δ: 1.264 (s, 27H), 1.547 (pseudo t, J = 3.7 Hz, 18H). ^{13}C NMR (C_6D_6) δ: 20.69 (t, J = 12 Hz), 31.49 (s), 54.18 (s), 208.10 (t, J = 33 Hz). ^{31}P NMR (C_6D_6) δ: 42.08 (s).

$Fe(PMe_3)_2$(t-BuNC)$_2$(H)(CN) (2)

^1H NMR (C_6D_6) (*cis*-**2**) δ: 1.51 (pseudo t, J = 4 Hz, 18H), 1.10 (s, 18H), –10.61 (t, J = 56 Hz, 1H); (*trans*-**2**) δ: 1.48 (pseudo t, J = 4 Hz, 18H), 1.06 (s, 18H), –13.78 (t, J = 44 Hz, 1H). ^{13}C NMR (C_6D_6) (*cis*-**2**) δ: 55.03 (s), 0.88 (s), 30.64 (s), 20.81 (t, J = 12 Hz). ^{31}P NMR (C_6D_6) (*cis*-**2**) δ: 29.97 (s); (*trans*-**2**) δ: 27.43 (s). Anal. calcd.: C 50.88, H 9.29, N 10.47; found: C 50.67, H 9.16, N 10.40.

Kinetics determinations

The solvent used for all UV–vis kinetics runs was dry iso-octane, chosen because of its high boiling point and low vapor pressure. A 1 cm quartz cuvette directly attached to a Teflon adaptor allowed the very air sensitive samples to be run on the bench top at a range of temperatures (50–85 °C). All of the UV–vis samples were prepared in the drybox and run under nitrogen. A UV–vis spectrum of **1** showed two broad bands at 309 and 390 nm. The band at 390 nm was used for the kinetic measurements as it was isolated from the solvent and product absorptions. A stock solution of **1** (0.0114 mol/L) was prepared, and dilutions were made to determine the molar extinction from a Beer's law plot (ε = 2180 M^{-1} cm^{-1}).

Concentration and solvent effects

Solutions of **1** from 1×10^{-4} – 9×10^{-4} mol/L were prepared by the following procedure: In a drybox, approximately 0.1–1.0 mg of **1** was placed into a 1 cm quartz cuvette and ~2 mL iso-octane was pipetted in. The resulting solution was mixed, and the cuvette was placed in a thermostated cell holder. Following an equilibration period of 10 min, the kinetics were followed by monitoring the absorption at 390 nm for 20 h. The initial absorbance of each run was used to calculate the concentration of **1** using Beer's law. The absorbance followed a first order decay, and the k_{obs} for each run was determined using the HP software. Similar runs were made by dissolving samples of **1** in THF, DMSO, and benzene.

Effect of excess PMe_3

Samples were made from a stock solution prepared by dissolving 15 mg of **1** into a 25 mL volumetric flask, adding 10 mL iso-octane and the appropriate amount of PMe_3, and filling to the final volume with iso-octane. Aliquots of the stock solution were pipetted into the cell for kinetic runs, and the stock solution was stored in a freezer between runs.

Reaction of 1 with 1,4-cyclohexadiene

A total of eight samples of **1** containing various amounts of 1,4-cyclohexadiene in benzene were prepared as follows: Benzene-d_6 solutions containing 10 mg of **1** were placed in resealable NMR tubes. Care was taken to add known amounts of C_6D_6 solvent to each. 1,4-Cyclohexadiene was added via syringe. The samples were degassed on the vacuum line, and the concentration of 1,4-cyclohexadiene was determined by comparison of the area of the CH_2 resonance at δ 5.60 to the area of the *tert*-butyl resonance (δ 1.26) of **1** immediately following sample preparation. ^1H NMR spectra were recorded after heating at 67 °C for 25 h. The amount of isobutylene formed was determined by comparing the area of the CH_2 resonance of isobutylene (δ 4.73) to the area of the hydride resonance (δ –10.6). The reaction was complete after 24 h of heating (~6 half-lives).

Samples were also prepared by dissolving 10 mg **1** in neat 1,4-cyclohexadiene. After heating at 67 °C for 24 h, the volatiles were vacuum transferred to resealable NMR tubes and examined by ^1H NMR spectroscopy. The amount of isobutane to isobutylene was determined by comparison of the integrated area of isobutane (δ 0.86, CH_3) to isobutylene (δ 4.73, CH_2).

ESR studies

A concentrated sample of **1** (15 mg) in benzene (0.3 mL) was made in an NMR tube. An excess of *N*-*tert*-butyl-α-phenylnitrone (~20 mg) was added, and the ESR was run initially and after heating at 60 °C for 24 h. The signal increased in intensity after heating but was otherwise unchanged. A triplet of doublets was observed with a_H = 3 G and a_N = 15 G. The same general procedure was used when preparing the samples containing *tert*-butylisocyanide plus PBN, PBN alone, $Fe(PMe_3)_2(CNCH_2CMe_3)_3$ plus PBN, and

© 2005 NRC Canada

$Fe(PMe_3)_2(CNCH_2CMe_3)_3$ plus nitrone dimer using benzene as the solvent.

Preparation of *tert*-butylisocyanide-d_6

The preparation of *tert*-butylisocyanide-d_6 was accomplished in 3 steps using known reactions. The first step was the synthesis of *tert*-butanol-d_6 from acetone-d_6 by a Grignard reaction (15). Into a 1000 mL round bottom flask fitted with a septum and a 50 mL addition funnel was placed 3 mol/L CH_3MgI in ether (220 mL, 0.66 mol) and 250 mL of diethyl ether. The solution was cooled to 0 °C under a nitrogen atmosphere, and acetone-d_6 (40 mL, 0.49 mol) was slowly added to the ether solution. The flask was allowed to warm to room temperature and was stirred overnight under nitrogen. After 18 h, the solution was again placed in an ice bath, and 50 mL of 10% HCl (aq) was slowly added to neutralize the excess MeMgI. The solution was warmed to room temperature, and the *tert*-butanol-d_6 was extracted from the aqueous layer using 3 × 50 mL aliquots of diethyl ether. The ether was removed from the combined extracts, giving *tert*-butanol-d_6 (15.8 g, 0.20 mol, 35% yield). ^1H NMR (C_6D_6) δ: 1.06 (s). Overnight reaction is required to give reasonable yields.

The second step was the formation of *tert*-butylformamide-d_6 from the *tert*-butanol-d_6 via a Ritter reaction (16). Caution must be taken in this step because of the formation of HCN. In a 250 mL Erlenmeyer flask, *tert*-butanol-d_6 (15.8 g, 0.20 mol) and potassium cyanide (15 g, 0.23 mol) were dissolved in 25 mL acetic acid. A solution of 25 mL H_2SO_4 and 25 mL acetic acid was added dropwise over a period of 2 h to the solution, keeping the temperature below 60 °C. The mixture was allowed to stir overnight at room temperature. After 16 h, the mixture was poured into 500 mL of ice water. The solution was placed in an ice bath, and 15% KOH (aq) was added slowly until the acid was neutralized. The pH was checked using litmus paper. The *tert*-butylformamide-d_6 was extracted using 5 × 100 mL portions of diethyl ether. The ether was dried over potassium carbonate overnight and then removed by distillation. Fractional distillation gave *tert*-butylformamide-d_6 (5.9 g, 0.06 mol, 30% yield). bp 200 °C. ^1H NMR (C_6D_6) δ: 0.89 (s), 1.19 (s). GC-MS (10 eV) *m/z*: 107 ($[M]^+$), 92 ($[M^+ - CH_3]$), 89 ($[M^+ - CD_3]$).

The final step was the dehydration of the formamide using $POCl_3$ (17). Into a 250 mL round bottom flask equipped with a 10 mL addition funnel, condenser, and a mechanical stirrer was placed *tert*-butylformamide-d_6 (5.9 g, 0.06 mol), pyridine (30 mL, 0.37 mol), and 100 mL diethyl ether. The solution was cooled to 0 °C in an ice bath. $POCl_3$ (7 mL, 0.09 mol) was placed into the addition funnel. After purging with nitrogen for 10 min, the $POCl_3$ was slowly added. Care must be taken to ensure rapid stirring during the addition. The solution was allowed to warm to room temperature and then refluxed for 1 h. The flask was again placed in an ice bath and distilled water was added to neutralize the excess $POCl_3$ and dissolve the salts that formed. The organic layer was separated from the aqueous layer, and the aqueous layer was washed with ether (5 × 50 mL). The combined organic layers were dried over magnesium sulfate. The ether was removed by distillation and *tert*-butylisocyanide was obtained by vacuum distillation (0.5 mL, 0.005 mol, 8% yield). ^1H NMR (C_6D_6) δ: 0.87 (t, J = 4 Hz). GC-MS (10 eV) *m/z*: 89 ($[M]^+$), 74 ($[M^+ - CH_3]$), 71 ($[M^+ - CD_3]$), 63 ($[M^+ - CN]$).

Preparation of $Fe(PMe_3)_2(t\text{-BuNC-}d_6)_3$

The synthesis was the same as described previously (4) for the protio isocyanide complex, using $FeCl_2$ (0.14 g), Mg (0.08 g), and PMe_3 (103 mmHg (1 mmHg = 133.322 Pa), 300 K, 1.056 L) in THF (50 mL) and adding 0.30 mL *t*-BuNC-d_6.

Isotope effect determinations

The determination of the isotope effect was accomplished using three separate samples prepared in resealable NMR tubes. A benzene solution of 20 mg $Fe(PMe_3)_2(t\text{-BuNC-}d_6)_3$ was heated at 67 °C for 24 h. The volatiles were vacuum distilled from the NMR tube to a two-neck flask equipped with an adapter and a septum. The benzene solutions were analyzed by GC–MS using the conditions stated above to determine the ratio of d_6:d_5 isobutylene. The three samples showed ratios of 0.56 (0.01), 0.55 (0.02), and 0.56 (0.01).

Acknowledgement

The US Department of Energy, Grant FG02–86ER13569 are gratefully acknowledged for their support of this work.

References

1. J.W. Rathke and E.L. Muetterties. J. Am. Chem. Soc. **97**, 3272 (1975).
2. (*a*) H.H. Karsch, H.F. Klein, and H. Schmidbaur. Chem. Ber. **110**, 2200 (1977); (*b*) H.H. Karsch. Inorg. Synth. **20**, 69 (1977); (*c*) H.H. Karsch, H.F. Klein, and H. Schmidbaur. Angew. Chem. Int. Ed. Engl. **14**, 637 (1975).
3. (*a*) H.H. Karsch. Chem. Ber. **110**, 2213 (1977); (*b*) H.H. Karsch. Chem. Ber. **110**, 2699 (1977); (*c*) H.H. Karsch. Chem. Ber. **110**, 2712 (1977).
4. W.D. Jones, G.P. Foster, and J.M. Putinas. Inorg. Chem. **26**, 2120 (1987).
5. The observed pseudotriplet arises from what has been referred to as an $AX_9A'X'_9$ system, see: C.P. Casey, J.M. O'Conner, W.D. Jones, and K.J. Haller. Organometallics, **2**, 535 (1983).
6. W.D. Jones, G.P. Foster, and J.M. Putinas. J. Am. Chem. Soc. **7**, 2124 (1987).
7. (*a*) E.G. Janzen and B.J. Blackburn. J. Am. Chem. Soc. **90**, 5909 (1968); (*b*) E.G. Janzen and B.J. Blackburn. J. Am. Chem. Soc. **91**, 4481 (1969); (*c*) E.G. Janzen and C.A. Evans. J. Am. Chem. Soc. **97**, 205 (1975).
8. (*a*) E. Grunwald and S. Winstein. J. Am. Chem. Soc. **70**, 846 (1948); (*b*) J. Burgess. J. Chem. Soc. A, 2114 (1970); (*c*) J. Burgess. Pure Appl. Chem. **63**, 1677 (1991).
9. K. Wiberg. Chem. Rev. **55**, 713 (1955).
10. J.M. Nicovich, C.A. van Dijk, K.D. Kreutter, and P.H. Wine. J. Phys. Chem. **95**, 9890 (1991).
11. W.H. Saunders and A.F. Cockerill (*Editors*). Mechanisms of elimination reactions. Wiley, New York. 1973. p. 1073, and refs. therein.
12. C.M. Giamdomenico, L.H. Hanau, and S.J. Lippard. J. Organomet. Chem. **1**, 142 (1982).
13. L. Tschugaeff and P. Teearu. Chem. Ber. **47**, 2643 (1914).
14. W.D. Jones and W.P. Kosar. Organometallics, **5**, 1823 (1986).

© 2005 NRC Canada

15. Kharasch and Reinmuth (*Editors*). Grignard reactions of non-metallic substances. Prentice-Hall Inc., New York. 1954. p. 325.
16. J. Ritter and J. Kalish. J. Am. Chem. Soc. **70**, 4058 (1948).
17. I. Ugi (*Editor*). Organic syntheses. Coll. Vol. V. John Wiley and Sons, Inc., New York. 1973. p. 300.

© 2005 NRC Canada

Phosphino-indenyl complexes of nickel(II)[1]

Laurent F. Groux, Francine Bélanger-Gariépy, and Davit Zargarian

Abstract: The BH_3-protected phosphinoindenyl ligand indenyl$(CH_2)_2PPh_2{\cdot}BH_3$ was used in the preparation of ($\eta^{5/3}$:η^0-indenyl$(CH_2)_2PPh_2{\cdot}BH_3$)Ni(PPh_3)Cl, which has been characterized by NMR spectroscopy and X-ray diffraction studies. On the other hand, all attempts at preparing the closely related complex ($\eta^{5/3}$:η^1-indenyl$(CH_2)_2PPh_2$)NiCl, in which the tethered phosphine moiety is coordinated to the Ni centre, were unsuccessful. One of these unsuccessful attempts yielded instead the novel indenyl-PCP pincer complex {κ^P,κ^C,κ^P-1,3-$(CH_2CH_2PPh_2)_2$-2-indenyl}NiCl, which has been characterized by X-ray diffraction studies.

Key words: indenyl complexes, tethered phosphines, PCP pincer complexes.

Résumé : Le ligand protégé indenyl$(CH_2)_2PPh_2{\cdot}BH_3$ a permis la préparation du composé ($\eta^{5/3}$:η^0-indenyl$(CH_2)_2$-$PPh_2{\cdot}BH_3$)Ni(PPh_3)Cl. Ce dernier a été complètement caractérisé par la spectroscopie RMN et études cristallographiques. Toutes les tentatives de préparer et isoler le complexe ($\eta^{5/3}$:η^1-indenyl$(CH_2)_2PPh_2$)NiCl ont échoué. En revanche, nous avons obtenu lors d'une de ces tentatives un nouveau complexe inattendu; une étude cristallographique a démontré que ce dernier était un complexe de type « pincer » PCP-indényle, soit {κ^P,κ^C,κ^P-1,3-$(CH_2CH_2PPh_2)_2$-2-indenyl}NiCl.

Mots clés : complexes d'indényle, phosphines attachées, complexe de type « pincer » PCP.

Introduction

Previous studies have shown that the complexes (Ind)Ni(PR_3)X (Ind = indenyl and its substituted derivatives; R = Ph, Me, Cy; X = Cl, Me, CC-Ph, etc.) (1) are active precatalysts for the oligo- and polymerization of alkenes (2), alkynes (3), and $PhSiH_3$ (4) and the hydrosilylation of olefins and ketones (5). The available mechanistic evidence indicates that the steric and (or) electronic properties of the phosphine ligand and its relative lability influence the rates of these reactions and the catalytic activities. Thus, the PMe_3 derivatives are much more active than their PPh_3 analogues in the polymerization of ethylene (2*a*) and $PhSiH_3$ (4), whereas the opposite order of reactivity is found in the hydrosilylation reactions (5).

To examine further the influence of phosphines on the above reactions, we considered studying a series of complexes featuring ligands of the type Ind^PR_2, with ^ representing a side chain connecting the PR_2 and Ind moieties. Our reasoning was that since the chelating phosphine moiety in (Ind^PR_2)NiX should be less prone to dissociation, studying the reactivities of such complexes should allow a direct measure of the impact of phosphine lability on the reactivities of this family of complexes. A search of the literature showed that complexes bearing the analogous Cp^PR_2 ligands are known for many transition metals (except those of group 10) (6), whereas complexes of Ind^PR_2 ligands are known only for Cr (7), Ru (8), Rh (9), and Ir (9*b*). Therefore, we set out to prepare (Ind^PR_2)NiX and probe the influence of the chelating PR_2 moiety on reactivities. The present report describes our attempts to prepare the complex ($\eta^{5/3}$:η^1-Ind$CH_2CH_2PPh_2$)NiCl.

Results and discussion

The ligand Ind$(CH_2)_2PPh_2$ (**1**) was prepared by slightly modified versions of previously reported procedures (10, 11), consisting of (*a*) successive nucleophilic displacements of Cl^- in $ClCH_2CH_2Cl$ by $[PPh_2]^-$ and $[Ind]^-$ or (*b*) the reductive cleavage of spiro(cyclopropane-1,1′-indene) (12) by $[PPh_2]^-$ (Scheme 1). Crude samples of **1** obtained from these routes were reacted with $BH_3{\cdot}THF$ to protect the phosphine moiety from oxidation; pure samples of Ind$(CH_2)_2PPh_2{\cdot}BH_3$ (**1**·BH_3) were then isolated by flash chromatography and completely characterized by NMR and X-ray diffraction studies (13). Treatment of **1**·BH_3 with H^+, followed by neutralization with Na_2CO_3, removed the protecting group and gave pure samples of **1**, which were used in subsequent experiments. Alternatively, crude samples of **1** were used in a few instances for the preparation of the target complex; for this purpose, route (*b*) proved more convenient because the in situ generated anion $[Ind(CH_2)_2PPh_2]^-$ obviated the need for an additional deprotonation step.

Received 1 December 2004. Published on the NRC Research Press Web site at http://canjchem.nrc.ca on 9 June 2005.

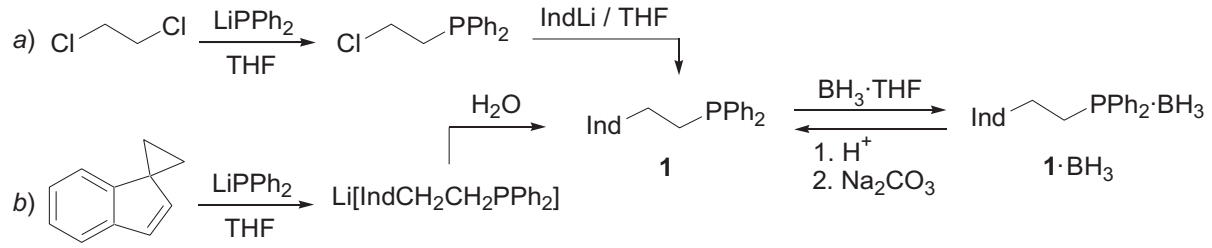
This contribution is dedicated to Professor H. Alper in recognition of his seminal contributions to organometallic catalysis.

L.F. Groux, F. Bélanger-Gariépy, and D. Zargarian.[2] Département de chimie, Université de Montréal, Montréal, QC H3C 3J7, Canada.

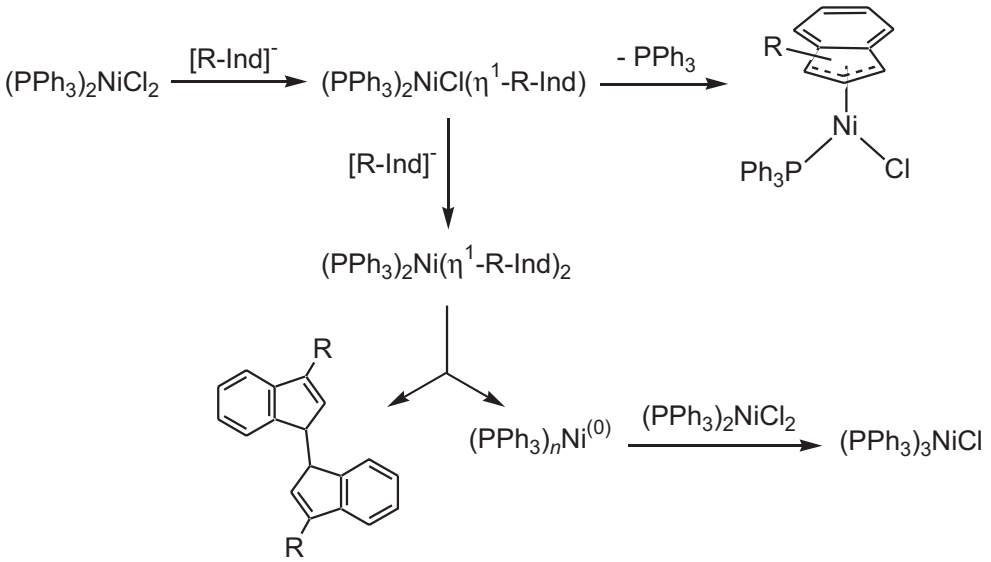
[1]This article is part of a Special Issue dedicated to Professor Howard Alper.
[2]Corresponding author (e-mail: zargarian.davit@umontreal.ca).

 doi: 10.1139/V05-079 © 2005 NRC Canada

Scheme 1.



Scheme 2.



The main synthetic route used for the attempted synthesis of the target complex was based on the procedure used for the preparation of IndNi(PR_3)Cl (14). Thus, ligand **1** was deprotonated with BuLi and added to an Et_2O suspension of Ni(PPh_3)$_2Cl_2$. This addition changed the forest-green colour of the initial mixture to dark red, the typical colour of IndNi(PR_3)Cl; shortly thereafter, however, the reaction mixture turned beige-brown and a beige solid precipitated, implying the onset of a decomposition process. The $^{31}P\{^1H\}$ NMR spectrum of the filtrate obtained from filtration of the final mixture showed that the reaction had produced a number of phosphine-containing species,[3] while the observation of several broad signals in the ^1H NMR spectrum indicated that one or more paramagnetic species had also formed. The ^1H NMR spectrum of the beige solid obtained from the filtration also showed broad and featureless signals. Cooling the beige filtrate yielded yellow crystals that were identified as the Ni(I) complex (PPh_3)$_3$NiCl (15). The formation of this species has been observed in previous studies (16) and signals a side reaction involving the nickel-catalyzed coupling of two indenyl ligands (Scheme 2).

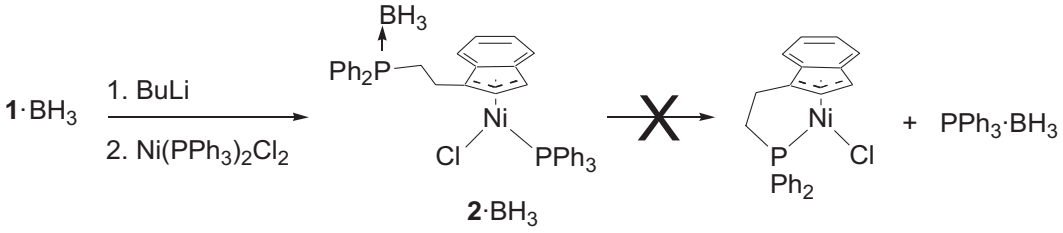
The above procedure was repeated several times under different reaction conditions (e.g., solvent, temperature, order of mixing, source of nickel, etc.), but no set of conditions allowed the successful isolation of ($\eta^{5/3}$:η^1-IndCH_2CH_2-PPh_2)NiCl. The precise reasons for the failure to obtain our target complex are not known; we speculate, however, that the dark-red species formed during the initial stages of these reactions is an intermediate species such as ($\eta^{5/3}$:η^0-Ind-$CH_2CH_2PPh_2$)Ni(PPh_3)Cl, **2**. The apparent instability of this species is in contrast to the stability of the analogous complexes ($\eta^{5/3}$:η^0-Ind^NR_2)Ni(PPh_3)Cl, which have been synthesized successfully (2*c*, 17). The discrepancy in the stabilities of these complexes leads us to suspect that the pitfall of our synthetic approach lies with the incompatible intramolecular interaction of the chelating phosphine moiety with the Ni centre.

The above hypothesis was borne out by the finding that the above-proposed intermediate is indefinitely stable when the PPh_2 moiety is coordinated by BH_3. Thus, using the BH_3-protected ligand **1**·BH_3 in our syntheses allowed the successful isolation of the complex ($\eta^{3/5}$:η^0-IndCH_2CH_2-PPh_2·BH_3)Ni(PPh_3)Cl, **2**·BH_3 (Scheme 3). The structure proposed for this complex was corroborated by the NMR spectra, as follows. For instance, the $^{31}P\{^1H\}$ NMR spectrum of **2**·BH_3 showed a sharp singlet at 29.9 ppm (parts per million), attributed to the Ni-PPh_3 moiety; for comparison, the corresponding signal in (Ind-$CH_2CH_2NMe_2$)Ni(PPh_3)Cl

[3] The $^{31}P\{^1H\}$ NMR spectrum (C_6D_6) displayed the following signals: 44.6, 33.6, 33.3, 32.8, 32.5, 30.3, 30.1, 29.9, 29.4, 29.1, 24.4 (O=PPh_3), 20.7, 3.2, –4.9 (free PPh_3). The signals displayed in the corresponding spectrum in $CDCl_3$ were as follows: 58.7, 57.9, 55.9, 34.2, 33.6, 32.5, 30.2, 29.5 (O=PPh_3), 24.8, 23.3, 21.6, 20.2, –3.5, –4.8 (free PPh_3), –14.0, –15.0.

© 2005 NRC Canada

Scheme 3.



Scheme 4.

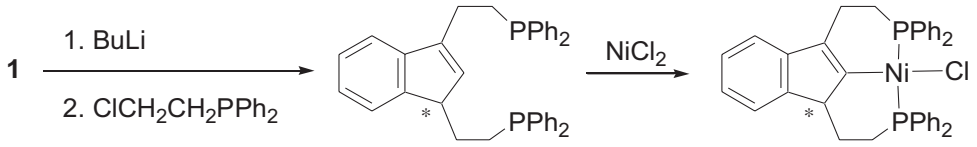
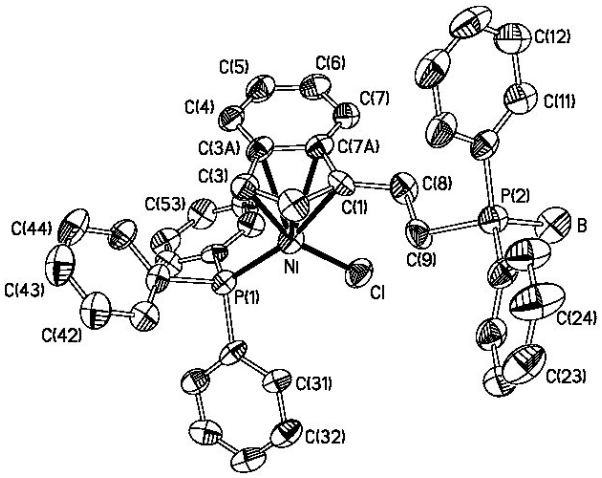


Fig. 1. ORTEP plot of **2**·BH_3. Hydrogen atoms have been omitted for clarity. Selected distances (Å) and angles (°): Ni—Cl 2.143(7), Ni—C2 2.054(6), Ni—C3 2.031(7), Ni—C3A 2.321(7), Ni—C7A 2.365(8), Ni—P1 2.179(3), Ni—Cl 2.170(2), C1—C2 1.435(8), C2—C3 1.419(8), C3—C3A 1.397(9), C3A—C7A 1.439(9), C7A—C1 1.462(8), P2—B 1.912(8); C1-Ni-P1 164.0(2), C3-Ni-C1 160.0(2), P1-Ni-C1 101.09(9), C1-Ni-C1 94.7(2), P1-Ni-C3 98.0(2), C1-Ni-C3 66.0(3).



resonates at 30.8 ppm (see ref. 17*a*). In addition, we observed a peak at 17.5 ppm that was broadened as a result of coupling to the quadrupolar ^{11}B nucleus (cf. **1**·BH_3: 16.6 ppm). The ^1H NMR spectrum contained a broad singlet at ca. 1.2 ppm assigned to BH_3, in addition to the characteristic signals for the Ind protons (e.g., a signal at ca. 3.5 ppm assigned to H3). The unequivocal confirmation of the proposed structure was furnished by the results of X-ray diffraction studies, described below.

Complex **2**·BH_3 adopts virtually the same structure as many of the previously reported Ni-indenyl complexes (1). The coordination geometry around Ni (Fig. 1) can be described as a distorted square-planar geometry with the indenyl ligand perpendicular to the coordination plane. The tethered Ph_2P·BH_3 moiety points away from the metal centre, and the absence of any P–Ni interaction results in a virtually unchanged P—BH_3 distance (1.912(3) Å in **2**·BH_3 vs. 1.923(3) Å in **1**·BH_3). The Ind hapticity is distorted toward an unsymmetrical, trihapto mode, as reflected in the following structural parameters: (*i*) the Ni—C3a and Ni—C7a bond distances (avg. 2.34 Å) are much longer than the Ni—C1 and Ni—C3 distances (avg. 2.08 Å); (*ii*) the Ni—C1 distance (ca. 2.14 Å) is significantly longer than the Ni—C3 distance (ca. 2.03 Å); (*iii*) the slip parameters[4] Δ(M—C) (0.26 Å), HA (ca. 8.7°), and FA (ca. 8.3°) are in the expected range for η^5/η^3-Ind ligands (18). This type of "slippage" is attributed to (*a*) the tendency of Ni(II) to avoid an 18-electron configuration and (*b*) the different trans influences of PPh_3 and Cl ligands, respectively (1).

With complex **2**·BH_3 at hand, we attempted to prepare **2** by thermally inducing the transfer of BH_3 from the tethered PPh_2 moiety to the PPh_3 ligand and the subsequent elimination of Ph_3P·BH_3; unfortunately, however, no BH_3-exchange was observed between the phosphine moieties. On the other hand, direct deprotection of the tethered PPh_2 moiety by amines led instead to decomposition. It appears, therefore, that the target complex ($\eta^{5/3}$:η^1-Ind$CH_2CH_2PPh_2$)NiCl is inherently unstable. Although modeling studies do not support the hypothesis that this instability is caused by the CH_2CH_2 tether, future attempts will investigate the feasibility of preparing analogous complexes bearing longer side chains.

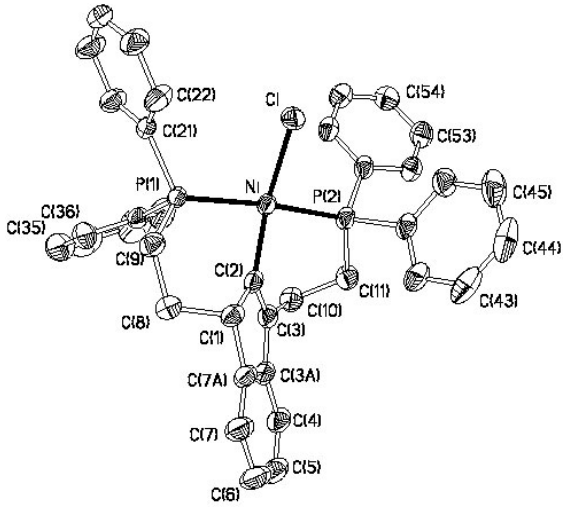
A new PCP–Ni complex

One of the attempts to synthesize the target complex resulted in the unexpected formation of a Ni complex bearing the new ligand Ph_2P^Ind^PPh_2, shown in Scheme 4. Thus, reacting $NiCl_2$ with a crude batch of **1**, prepared according to route (*a*) in Scheme 1, gave a red mixture that yielded a small quantity of red crystals identified by X-ray diffraction studies as the novel pincer complex (PCP-Ind($(CH_2)_2$-$PPh_2)_2$)NiCl, **3**. The $^{31}P\{^1H\}$ NMR spectrum of **3** showed two AB doublets displaying large coupling constants ($^2J_{P\text{-}P}$ =

[4] These slip parameters are defined as follows: ΔM—C = 1/2[(M—C3a + M—C7a) – (M—C1 + M—C3)]; HA is the angle between the planes formed by the atoms C(1), C(2), C(3) and C(1), C(3), C(3a), C(7a); FA is the angle between the planes formed by the atoms C(1), C(2), C(3) and C(3a), C(4), C(5), C(6), C(7), and C(7a).

© 2005 NRC Canada

Fig. 2. ORTEP plot of **3**. Hydrogen atoms and disordered solvent have been omitted for clarity. Selected distances (Å) and angles (°): Ni—Cl 2.2086(12), Ni—P1 2.1772(10), Ni—P2 2.2146(9), Ni—C2 1.888(3), C1—C2 1.525(4), C2—C3 1.360(4), C3—C3A 1.457(4), C3A—C7A 1.391(5), C1—C7A 1.522(4); C1-Ni-P1 98.32(4), C1-Ni-P2 91.95(4), C2-Ni-P1 85.08(9), C2-Ni-P2 88.96(9), C1-Ni-C2 162.46(9), P1-Ni-P2 163.64(3).



330 Hz), indicative of inequivalent trans phosphine moieties. The ^{1}H NMR spectrum displayed a broad singlet at ca. 3.6 ppm, which was assigned to H1, in addition to a number of multiplets in the aromatic and aliphatic regions; the latter are assigned to the chemically inequivalent[5] protons on the ethyl side chains.

X-ray diffraction studies showed that the coordination geometry around the Ni centre in **3** is slightly distorted square planar (Fig. 2), the main source of distortion arising from inter-ligand angles of ca. 163° for the trans ligands and 98°–85° for the cis ligands. Two trans coordination sites are occupied by the PPh_2 moieties, which form unequal Ni—P bond lengths (ca. 2.177 and 2.215 Å). The presence of an asymmetric centre at C1 results in the formation of two enantiomers, but the molecule crystallizes in the centrosymmetric space group $P\bar{1}$ because these enantiomers exist in a racemic mixture.

The most novel feature of complex **3** is the 2-indenyl ligand that is η^1-bonded to Ni via C2 (Ni—C(sp^2) = 1.89 Å). The localized nature of bonding within the 5-membered ring portion of the Ind ligand is evident from the much longer bond lengths for C1—C2 (1.525(4) Å), C7a—C1 (1.522(4) Å), and C3—C3a (1.457(4) Å) compared with C2—C3 (1.360(4) Å). We believe that **3** is the first isolated η^1-indenyl nickel complex and one of very few 2-η^1-indenyl complexes ever reported (19). The unanticipated formation of this compound likely results from the side reactions shown in Scheme 4: a small amount of deprotonated **1** reacts with a second equivalent of $ClCH_2CH_2PPh_2$ to give the doubly functionalized indene, 1,3-$(CH_2CH_2PPh_2)_2$IndH; the latter then reacts with $NiCl_2$ by C-H activation at the 2-position to give **3**.

Pincer compounds have attracted much attention recently owing to the many interesting reactions they promote and (or) catalyze (20), including alkane dehydrogenations (21), ketone hydrogenations (22), Heck coupling (23), olefin aminations (24), etc. (25). Most pincer complexes have a C_2 symmetric skeleton based on an *ortho*,*ortho*-disubstituted aryl ring, a 1,5-disubstituted pentyl chain, or a 1,3-disubstituted Cp moiety; what sets complex **3** apart is the presence of an optically active centre at C1. Efforts are underway to develop a reliable and high-yielding synthetic route for ligands of the type R_2P^Ind^PR_2 and their complexes. The reactivities of these complexes will then be investigated with a view to exploiting the optically active character of this type of PCP complex.

Concluding remarks

The results described in this paper indicate that ($\eta^{3/5}$:η^0-$IndCH_2CH_2PPh_2$·BH_3)$Ni(PPh_3)Cl$ owes its stability to the protection of the PPh_2 moiety by BH_3, because all attempts at preparing the original target complex wherein PPh_2 is coordinated to the Ni centre led to decomposition. We conclude, therefore, that tethering the phosphine moiety to the Ind ligand has a destabilizing effect on the complexes $IndNi(PR_3)Cl$. In contrast, many related complexes are stable and isolable (e.g., (η^5:η^1-Ind^PPh_2)$Rh^I(CO)$ (9), (η^5:η^1-Ind^PPh_2)Rh^{III}(C(=O)R)X (R = Me, Et; X = Br, I) (26), and (η^5:η^1-Ind^PR_2)Cr(X)Cl (X = Cl, Me) (7)), implying that the chelation of the tethered phosphine is not inherently destabilizing in all cases. It remains to be seen whether Ni complexes of Ind^PR_2 bearing longer tethers will be stable to isolation.

Experimental

General considerations

All manipulations were performed under an inert atmosphere of N_2 using standard Schlenk techniques and a drybox. Dry, oxygen-free solvents were employed throughout. Ind$(CH_2)_2PPh_3$ (**1**) has been prepared according to modified procedures (11, 12). All other reagents used in the experiments were obtained from commercial sources and used as received. The NMR spectra were recorded on a Bruker AMXR400 spectrometer (^{1}H (400 MHz), ^{13}C{^{1}H} (100.56 MHz), and ^{31}P{^{1}H} (161.92 MHz)).

Preparation of 2·BH_3

BuLi (0.47 mL of a 2.5 mol/L solution in hexane) was added to a solution of **1**·BH_3 (400 mg, 1.17 mmol) in Et_2O (200 mL) and stirred for 2 h. This solution was then added dropwise to a suspension of $Ni(PPh_3)_2Cl_2$ (1.48 g, 2.27 mmol) in Et_2O (50 mL), whereupon the solution turned dark red immediately. The mixture was evaporated, and the residues were dissolved in CH_2Cl_2 (30 mL); diluting this solution with hexane (120 mL) and storing the mixture at –20 °C gave a dark red solid precipitate (450 mg, 55% yield). ^{1}H NMR ($CDCl_3$): 7.9–7.2 (PPh_3 and PPh_2), 7.16 (t, $^3J_{H\text{-}H}$ = 7.4 Hz, H6), 7.09 (d, $^3J_{H\text{-}H}$ = 8.0 Hz, H7), 6.91 (t, $^3J_{H\text{-}H}$ = 7.3 Hz, H5), 6.56 (d, $^3J_{H\text{-}H}$ = 3.0 Hz, H2), 6.08 (d,

[5] The rigid geometry imposed by the chelating PPh_2 moieties and the presence of an asymmetric centre at C1 render the methylene protons diastereotopic.

© 2005 NRC Canada

Table 1. Crystal data, data collection, and structure refinement of **2** and **3**.

	2	**3**
Formula	$C_{41}H_{38}BP_2ClNi$	$C_{37}H_{33}P_2ClNi{\cdot}CH_2Cl_2$
Color and habit	Dark red block	Red plate
Dimensions (mm^3)	0.31×0.19×0.04	0.37×0.31×0.14
Symmetry	Triclinic	Triclinic
Space group	$P\bar{1}$	$P\bar{1}$
a (Å)	8.952(5)	10.741(4)
b (Å)	13.245(9)	12.875(3)
c (Å)	15.670(8)	14.361(6)
α (°)	84.66(4)	65.63(3)
β (°)	74.67(4)	73.92(3)
γ (°)	81.02(5)	77.76(2)
Volume ($Å^3$)	1767.3(18)	1727.4(10)
Z	2	2
D_{calcd} (g cm^{-1})	1.311 0	1.382
Diffractometer	Nonius CAD-4	Nonius CAD-4
Temp (K)	293(2)	293(2)
λ (Cu Kα) (Å)	1.541 78	1.540 56
μ (mm^{-1})	2.548	4.015
Scan type	ω/2θ scan	ω/2θ scan
θ_{max} (°)	70.00	69.81
h,k,l range	$-10 \le h \le 10$ $-16 \le k \le 16$ $-19 \le l \le 19$	$-13 \le h \le 13$ $-15 \le k \le 15$ $-17 \le l \le 17$
Reflections used ($I > 2\sigma(I)$)	6688	4815
$R[F^2 > 2\sigma(F^2)]$, $wR(F^2)$	0.050 2, 0.100 9	0.043 2, 0.111 5
GoF	0.860	0.938

$^3J_{H\text{-}H}$ = 7.7 Hz, H4), 3.49 (m, H3), 3.01 and 2.56 (m, CH_2), 2.18 and 2.03 (m, CH_2), 1.26 (br, BH_3). $^{13}C\{^1H\}$ NMR ($CDCl_3$): 139.7 (d), 138.6 (d), 137.6 (d), 137.6, 137.1, 136.9, 136.8, 136.1, 134.6, 134.5, 134.0 (d), 132.4 and 132.3 (C5 and C6), 123.6 and 122.7 (C4 and C7), 115.0 (m, C1), 107.5 (C2), 68.2 (C3), 22.1 (d, $^1J_{C\text{-}P}$ = 45 Hz, CH_2P), 20.0 (ind-C). $^{31}P\{^1H\}$ NMR ($CDCl_3$): 29.9 (s, PPh_3), 17.1 (br, PPh_2BH_3). Anal. calcd.: C 70.59, H 5.49; found: C 70.22, H 5.55.

Crystal structure determinations[6]

Dark red crystals of **2**·BH_3 and red crystals of **3** were obtained from CH_2Cl_2–hexane solutions kept at –20 °C. The crystal data for **2**·BH_3 and **3** were collected on a Nonius CAD-4 diffractometer with graphite-monochromated Cu Kα radiation at 223(2) K using the CAD-4 software (27). Refinement of the cell parameters was done with the CAD-4 software, while the data reduction used NRC-2 and NRC-2A (28). Both structures were solved by direct methods using SHELXS97 (29) and difmap synthesis (SHELXL96) (30). The refinements were done on F^2 by full-matrix least squares. All non-hydrogen atoms were refined anisotropically, while the hydrogens (isotropic) were constrained to the parent atom using a riding model. Crystal data and experimental details for **2**·BH_3 and **3** are listed in Table 1, and selected bond distances and angles are given in the figure captions.

Acknowledgements

We gratefully acknowledge the Natural Sciences and Engineering Research Council of Canada (NSERC), le fond FCAR of Quebec, and Université de Montréal for financial support. Christophe Valla is thanked for contributing to the preparation of complex **3**.

References

1. D. Zargarian. Coord. Chem. Rev. **233–234**, 157 (2002).
2. (*a*) M.A. Dubois, R. Wang, D. Zargarian, J. Tian, R. Vollmerhaus, Z. Li, and S. Collins. Organometallics, **20**, 663 (2001); (*b*) L.F. Groux, D. Zargarian, L.C. Simon, and J.B.P. Soares. J. Mol. Catal. A, **193**, 51 (2003); (*c*) L.F. Groux and D. Zargarian. Organometallics, **22**, 4759 (2003).
3. R. Wang, F. Bélanger-Gariépy, and D. Zargarian. Organometallics, **18**, 5548 (1999).
4. (*a*) F.-G. Fontaine and D. Zargarian. Organometallics, **21**, 401 (2002); (*b*) F.-G. Fontaine and D. Zargarian. J. Am. Chem. Soc. **126**, 8786 (2004).

[6] Supplementary data for this article are available on the Web site or may be purchased from the Depository of Unpublished Data, Document Delivery, CISTI, National Research Council Canada, Ottawa, ON K1A 0S2, Canada. DUD 3676. For more information on obtaining material refer to http://cisti-icist.nrc-cnrc.gc.ca/irm/unpub_e.shtml. CCDC 269091 and 269092 contain the crystallographic data for this manuscript. These data can be obtained, free of charge, via www.ccdc.cam.ac.uk/conts/retrieving.html (or from the Cambridge Crystallographic Data Centre, 12 Union Road, Cambridge CB2 1EZ, UK; fax +44 1223 336033; or deposit@ccdc.cam.ac.uk).

© 2005 NRC Canada

5. F.-G. Fontaine, R.-V. Nguyen, and D. Zargarian. Can. J. Chem. **81**, 1299 (2003).
6. H. Butenschoen. Chem. Rev. **100**, 1527 (2000).
7. (*a*) A. Döhring, V.R. Jensen, P.W. Jolly, W. Thiel, and J.C. Weber. Organometallics, **20**, 2234 (2001); (*b*) P.W. Jolly, A. Döhring, and J.C. Weber. Patent WO 01002323, 2001.
8. R.J. Whitby. Patent WO 03013724, 2003.
9. (*a*) Y. Kataoka, Y. Nakagawa, A. Shibahara, T. Yamagata, K. Mashima, and K. Tani. Organometallics, **23**, 2095 (2004), and refs. therein; (*b*) Y. Kataoka, Y. Nakagawa, A. Shibahara, Y. Saito, T. Yamagata, and K. Tani. Organometallics, **17**, 4338 (1998); (*c*) D.C. Brookings, S.A. Harrison, R.J. Whitby, B. Crombie, and R.V.H. Jones. Organometallics, **20**, 4574 (2001).
10. C. Charrier and F. Mathey. J. Organomet. Chem. **170**, C41 (1979).
11. Y. Kataoka, Y. Saito, A. Shibahara, and K. Tani. Chem. Lett. 621 (1997).
12. Spirocyclic indenes can be prepared through various routes, e.g., T. Kauffmann, K. Bergus, A. Rensing, and J. Ennen. Chem. Ber. **118**, 3737 (1985), including the base-induced ring-closing reaction of $IndCH_2CH_2Br$.
13. L.F. Groux and D. Zargarian. Acta Crystallogr. Sect. C, **C56**, e366 (2000).
14. (*a*) T.A. Huber, M. Bayrakdarian, S. Dion, I. Dubuc, F. Bélanger-Gariépy, and D. Zargarian. Organometallics, **16**, 5811 (1997); (*b*) F.-G. Fontaine, M.-A. Dubois, and D. Zargarian. Organometallics, **20**, 5156 (2001).
15. The unit cell parameters of a single crystal matched those previously reported for this compound: J.M. Cassidy and K.H. Whitmire. Acta Crystallogr. Sect. C, **C47**, 2094 (1991).
16. T.A. Huber, F. Bélanger-Gariépy, and D. Zargarian. Organometallics, **14**, 4997 (1995).
17. (*a*) L.F. Groux, F. Bélanger-Gariépy, D. Zargarian, and R. Vollmerhaus. Organometallics, **19**, 1507 (2000); (*b*) L.F. Groux and D. Zargarian. Organometallics, **20**, 3811 (2001); (*c*) L.F. Groux and D. Zargarian. Organometallics, **22**, 3124 (2003).
18. For a detailed discussion of slip parameters in various Ind complexes, see: (*a*) R.T. Baker and T.H. Tulip. Organometallics, **5**, 839 (1986); (*b*) S.A. Westcott, A. Kakkar, G. Stringer, N.J. Taylor, and T.B. Marder. J. Organomet. Chem. **394**, 777 (1990).
19. For a comprehensive review on η^1-indenyl complexes, see: M. Stradiotto and M.J. McGlinchey. Coord. Chem. Rev. **219–221**, 311 (2001).
20. For recent reviews on preparation and reactivities of pincer complexes, see: (*a*) M. Albrecht and G. van Koten. Angew. Chem. Int. Ed. **40**, 3750 (2001); (*b*) M.E. van der Boom and D. Milstein. Chem. Rev. **103**, 1759 (2003); (*c*) J.T. Singleton. Tetrahedron, **59**, 1837 (2003).
21. (*a*) S. Niu and M.B. Hall. J. Am. Chem. Soc. **121**, 3992 (1999); (*b*) M. Gupta, C. Hagen, W.C. Kaska, R.E. Cramer, and C.M. Jensen. J. Am. Chem. Soc. **119**, 840 (1999); (*c*) M. Gupta, C. Hagen, R.J. Flesher, W.C. Kaska, and C.M. Jensen. Chem. Commun. 2083 (1996); (*d*) D.W. Lee, W.C. Kaska, and C.M. Jensen. Organometallics, **17**, 5731 (1998); (*e*) M. Gupta, W.C. Kaska, and C.M. Jensen. Chem. Commun. 461 (1997); (*f*) F. Liu and A.S. Goldman. Chem. Commun. 655 (1999); (*g*) F. Liu, E.B. Pack, B. Singh, C.M. Jensen, and A.S. Goldman. J. Am. Chem. Soc. **121**, 4086 (1999); (*h*) C.M. Jensen. Chem. Commun. 2443 (1999).
23. P. Dani, T. Karlen, R.A. Gossage, S. Gladiali, and G. van Koten. Angew. Chem. Int. Ed. **39**, 743 (2000).
23. D. Morales-Morales, C. Grause, K. Kasaoka, R. Redon, R.E. Cramer, and C.M. Jensen. Inorg. Chim. Acta, **958**, 300 (2000).
24. A.L. Seligson and W.C. Trogler. Organometallics, **12**, 744 (1993).
25. (*a*) L.P. Barthel-Rosa, V.J. Catalano, K. Maitra, and J.H. Nelson. Organometallics, **15**, 3924 (1996); (*b*) L.P. Barthel-Rosa, V.J. Catalano, and J.H. Nelson. Chem. Commun. 1629 (1995); (*c*) M.D. Fryzuk, S.S.H. Mao, M.J. Zaworotko, and L.R. MacGillivary. J. Am. Chem. Soc. **115**, 5336 (1993).
26. Y. Kataoka, Y. Iwato, T. Yamagata, and K. Tani. Organometallics, **18**, 5423 (1999).
27. Enraf-Nonius. CAD-4 Software. Version 5.0 [computer program]. Enraf-Nonius, Delft, The Netherlands. 1989.
28. E.J. Gabe, Y. Le Page, J.-P. Charlant, F.L. Lee, and P.S. White. J. Appl. Crystallogr. **22**, 384 (1989).
29. G.M. Sheldrick. SHELXS. Program for the solution of crystal structures [computer program]. University of Goettingen, Germany. 1997.
30. G.M. Sheldrick. SHELXL. Program for the refinement of crystal structures [computer program]. University of Goettingen, Germany. 1996.

© 2005 NRC Canada

Activation of chlorobenzene with Ni(0) *N*,*N*-chelates — A remarkably profound effect of a minuscule change in ligand structure[1]

William J. Marshall and Vladimir V. Grushin

Abstract: Activation of the C—Cl bond of chlorbenzene with [$(COD)_2$Ni] and a bidentate *N*,*N*-ligand such as *N*,*N*,*N*′,*N*′-tetramethylethylenediamine (tmeda) and 2,2′-bipyridyl (bipy) has been reported to produce σ-phenyl complexes [(tmeda)Ni(Ph)Cl] (**1**) and [(bipy)Ni(Ph)Cl], respectively. However, in sharp contrast, we found that similar reactions involving almost the identical ligands *N*,*N*,*N*′,*N*′-tetraethylethylenediamine (teeda) and 6,6′-dimethyl-2,2′-bipyridyl (6,6′-Me_2bipy) resulted in homocoupling and the formation of non-organometallic dichlorocomplexes [(teeda)$NiCl_2$] and [(6,6′-Me_2bipy)$NiCl_2$]. The latter two compounds and **1** were characterized by single-crystal X-ray diffraction data. The remarkable change in the reaction outcome points to its extremely high sensitivity to minor alterations in the structure of the stabilizing *N*,*N*-ligand. In contrast, analogous reactions of [$Pd(dba)_2$] with PhI in the presence of teeda or 1,2-dipiperidinoethane (dpe) produced the expected σ-phenyl complexes [(teeda)Pd(Ph)I] and [(dpe)Pd(Ph)I], much like the previously reported reaction with tmeda.

Key words: C-Cl activation, zerovalent nickel complexes, *N*,*N*-ligands, oxidative addition, homocoupling, X-ray analysis.

Résumé : Il a été rapporté antérieurement que l'activation de la liaison C—Cl du chlorobenzène à l'aide de [$(COD)_2$Ni] et d'un ligand *N*,*N* bidentate, tel la *N*,*N*,*N*′,*N*′-tétraméthyléthylènediamine (tmeda) ou le 2,2′-bipyridyle (bipy), conduit à la formation de complexes σ-phényles, tels le [(tmeda)Ni(Ph)Cl] (**1**) et le [(bipy)Ni(Ph)Cl] respectivement. Les observations faites dans ce travail contrastent fortement avec ces résultats alors que des réactions semblables impliquant les ligands très semblables *N*,*N*,*N*′,*N*′-tétraéthyléthylènediamine (teeda) et 6,6′-diméthyl-2,2′-bipyridyle (6,6′-Me_2bipy) conduisent à un homocouplage et à la formation des dichlorocomplexes non-organométalliques [(teeda)$NiCl_2$] et [(6,6′-Me_2bipy)$NiCl_2$]. Ces deux derniers complexes et le composé **1** ont été examinés par diffraction des rayons X sur un cristal unique. Les changements remarquables observés dans les résultats de ces réactions indiquent qu'ils sont extrêmement sensibles à des changements mineurs dans la structure du ligand *N*,*N* stabilisateur. Au contraire, les réactions analogues du [$Pd(dba)_2$] avec le PhI en présence de teeda ou de 1,2-dipipéridinoéthane (dpe) ont conduit aux complexes σ-phényles attendus [(teeda)Pd(Ph)I] et [(dpe)Pd(Ph)I], tel qu'il avait été observé antérieurement dans les réactions avec le tmeda.

Mots clés : activation de la liaison C-Cl, complexes zérovalent du nickel, ligands *N*,*N*, addition oxydante, homocouplage, analyse de diffraction des rayons X.

[Traduit par la Rédaction]

Introduction

Catalysis with metal complexes is the primary tool for solving the problem of the notoriously low reactivity of non-activated (1, 2) haloarenes toward nucleophiles. Considerable progress (3–16) has been made in the development of catalytic transformations of aryl halides and triflates, Ar–X (X = Cl, Br, I, OTf), such as Kumada, Suzuki–Miyaura (11), and Negishi (12) coupling, the Mizoroki–Heck olefin arylation (13), and various carbonylation, amination (14, 15), and cyanation (16) reactions. Palladium tertiary phosphine complexes are most often used as catalysts for these reactions. Some bidentate nitrogen (17) and *N*-heterocyclic carbene (18–21) ligands have recently been offered as an alternative to organic phosphines for Pd catalysis. While in general tertiary amines are poorly efficient stabilizing ligands in Pd catalysis, the recently reported $Pd(OAc)_2$–Dabco catalytic system demonstrates high efficiency in Suzuki–Miyaura coupling (22).

Nickel, a metal that is considerably less costly than palladium, is also often used for cross-coupling reactions of haloarenes. The Ar—X bond is activated by Ni(0) more easily than by Pd(0), as illustrated by the chemistry of poorly

Received 5 October 2004. Published on the NRC Research Press Web site at http://canjchem.nrc.ca on 14 June 2005.

Dedicated to Professor Howard Alper.

W.J. Marshall and V.V. Grushin.[2] Central Research and Development, E.I. DuPont de Nemours and Co., Inc.,[3] Experimental Station, Wilmington, DE 19880-0328, USA.

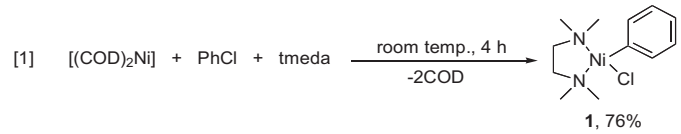
[1]This article is part of a Special Issue dedicated to Professor Howard Alper.
[2]Corresponding author (e-mail: vlad.grushin-1@usa.dupont.com).
[3]Contribution No. 8578.

 doi: 10.1139/V05-022 © 2005 NRC Canada

reactive chloroarenes (6, 23). However, oxidative addition of the Ar—X bond to Ni(0), the first key step of the catalytic loop, is often complicated, especially for X = I and Br, by radical processes (6, 24, 25) and homocoupling, also known as the Semmelhack reaction (8, 26, 27). We were interested in the oxidative addition of chloroarenes to Ni(0) stabilized with diamine ligands, to explore the possibility of using such systems as catalysts for carbon–heteroatom bond formation.

Results and discussion

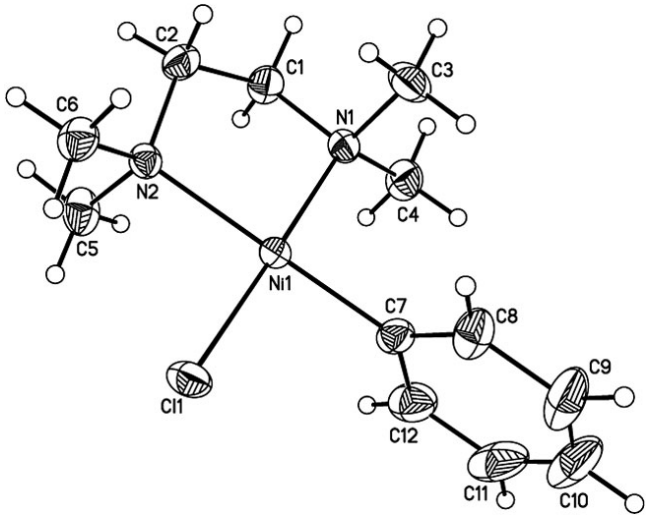
In 1987, Wenschuh and Zimmering (28) reported the formation of [(tmeda)Ni(Ph)Cl] (**1**) (tmeda = *N*,*N*,*N*′,*N*′-tetramethylethylenediamine) in 76% isolated yield upon oxidative addition of PhCl to [$(COD)_2$Ni] (COD = 1,5-cyclooctadiene) in the presence of tmeda at room temperature (eq. [1]).



No characterization of **1** was presented in the article (28), although SO_2 insertion into the Ni—C bond was later reported by the same group (29). Having prepared orange-yellow **1** in 70%–89% yield via the Wenschuh–Zimmering procedure, we attempted characterization of this complex. The composition of **1** was confirmed by satisfactory C, H, N microanalysis data. It was found that **1** is insoluble in alkanes, benzene, toluene, and ether, and slightly soluble in THF (28). Although **1** is easily soluble in CH_2Cl_2 and 1,2-dichloroethane (dce), these chlorinated solvents decompose **1** even at room temperature within a few minutes (CH_2Cl_2) or several hours (dce). We succeeded in obtaining ^{1}H and ^{13}C NMR data for **1** in dce-d_4. At room temperature, the ^{1}H NMR spectrum of **1** exhibited three sharp aromatic resonances at 6.6 (1H, *p*-Ph), 6.7 (2H, *m*-Ph), and 7.5 (2H, *o*-Ph) ppm along with a broadened multiplet at 2.0–2.7 ppm from the aliphatic protons. The ^{13}C NMR spectrum recorded at 20 °C displayed two signals from the methyl groups (47.1 and 49.3 ppm), two methylene resonances (56.9 and 61.1 ppm), and four aromatic peaks (121.4, 124.5, 136.8, and 147.5 ppm). The aromatic lines were sharp, whereas considerable line broadening ($\Delta\nu_{1/2}$ = 15–20 Hz) was observed for the methyl and methylene resonances. The latter sharpened to $\Delta\nu_{1/2}$ = 10 Hz upon cooling to 10 °C, indicating that some exchange processes were occurring. Although studying these dynamic processes was beyond the scope of our work, the ambient temperature NMR spectra were fully consistent with the structural formula of **1** as shown in eq. [1].

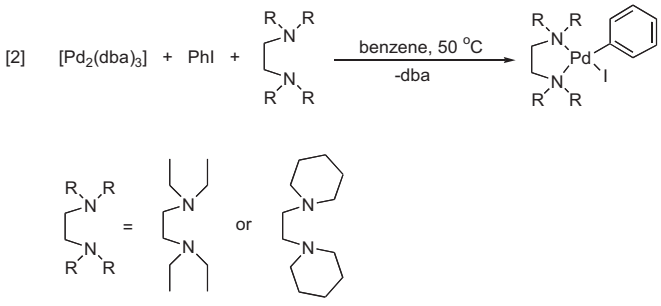
X-ray quality crystals of **1** were obtained from dce–hexanes. Two polymorphic crystalline forms of **1** were observed, thin needles (major) and irregular blocks (minor). Both forms were analyzed by X-ray diffraction. The structure of **1** determined for the thin needle polymorph (*C*2/*c*, *a* = 22.96(2) Å, *b* = 7.828(8) Å, *c* = 16.56(1) Å, β = 115.04(4)°) was of poor quality due to its small crystal size. A good quality X-ray structure of **1** (Fig. 1) was obtained for one of the irregular block crystallites. The molecule of **1** is square-planar, as expected from a diamagnetic (see the NMR data above) Ni(II) complex. In accord with trans-influence considerations, the Ni—N bond trans to Ph (2.053(1) Å) is longer than that trans to Cl (1.971(1) Å). The aromatic ring is orthogonal to the coordination plane of the complex, as in the closely related structure [(tmeda)Pd(Ph)I] (30).

Fig. 1. An ORTEP drawing of **1** with thermal ellipsoids drawn to the 50% probability level. Selected bond distances (Å) and angles (°): Ni(1)—C(7) 1.891(2), Ni(1)—N(1) 1.971(1), Ni(1)—N(2) 2.053(1), Ni(1)—Cl(1) 2.184(1); C(7)-Ni(1)-N(1) 92.61(6), C(7)-Ni(1)-N(2) 179.33(6), N(1)-Ni(1)-N(2) 86.72(5), C(7)-Ni(1)-Cl(1) 88.49(5), N(1)-Ni(1)-Cl(1) 178.80(4), N(2)-Ni(1)-Cl(1) 92.17(3).



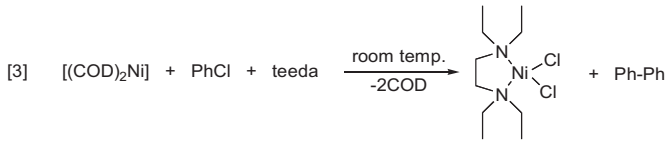
The aforementioned decomposition of **1** in chlorinated solvents was found to produce pale green crystals, which we identified by X-ray analysis as [$(tmeda)_3Ni_3(\mu\text{-}Cl)_3(\mu^3\text{-}Cl)(\mu^3\text{-}OH)]^+Cl^-$ whose X-ray structure has been reported previously (31, 32). Because **1** was handled under rigorously anhydrous conditions, the source of OH for the trinuclear complex was probably the surface of the glass.

Although the structure of **1** was established, the complex was of limited further use for stoichiometric and catalytic studies because of its poor solubility. It was then reasoned that the teeda analogue of **1** ([(teeda)Ni(Ph)Cl], teeda = *N*,*N*,*N*′,*N*′-tetraethylethylenediamnie), should be more readily soluble in organic solvents and hence suitable for further studies. Indeed, the closely related Pd complexes [(teeda)Pd(Ph)I] and [(dpe)Pd(Ph)I] (dpe = 1,2-dipiperidinoethane) were prepared (eq. [2]) by the procedure reported (30) for [(tmeda)Pd(Ph)I] and were found to be more soluble than the latter.



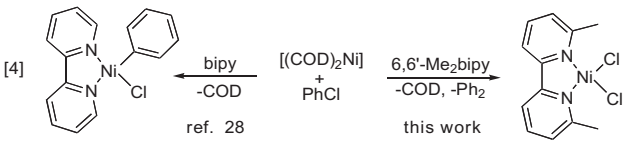
© 2005 NRC Canada

Surprisingly, however, the reaction of $[(COD)_2Ni]$ with PhCl in the presence of teeda did not afford [(teeda)Ni(Ph)Cl], but rather Semmelhack-type coupling occurred to produce deep-purple, paramagnetic $[(teeda)NiCl_2]$ (eq. [3]).



The structure of the complex $[(teeda)NiCl_2]$ was established by X-ray analysis, showing tetrahedral coordination geometry around Ni (Fig. 2). In accord with the tetrahedral structure, two broad lines at 7.5 and 11.9 ppm were observed in the ^1H NMR spectrum of paramagnetic $[(teeda)NiCl_2]$ in benzene-d_6.

Considering the minor change in the structures of tmeda and teeda, the difference in the outcomes of the two reactions (eqs. [1] and [3]) is remarkable. The tmeda vs. teeda case, however, is not unique. While it has been reported (28) that the reaction of $[(COD)_2Ni]$ with 2,2′-bipyridyl (bipy) and PhCl leads to a nickel aryl ([(bipy)Ni(Ph)Cl]), we found that 6,6′-dimethyl-2,2′-bipyridyl (6,6′-Me_2bipy) produces the paramagnetic inorganic dichloride $[(6,6'\text{-}Me_2bipy)NiCl_2]$ under similar conditions (eq. [4] and Fig. 3). No *N*-chelated Ni complexes were formed when $[(COD)_2Ni]$ was reacted with PhCl and *N*,*N*,*N*′,*N*′-tetraisopropylethylenediamine (tipeda). Considering the well-known low nucleophilicity of sterically hindered Hunig's base (i-Pr_2NEt), this observation is not surprising. Nonetheless, a simple high-yield preparation of tipeda is presented in the Experimental section.



At this point, it is unclear if the change in the reaction paths when going from tmeda to teeda or from bipy to 6,6′-Me_2bipy is largely due to electronic or steric (33) factors, or a combination of both. While considerable progress has been made in understanding the mechanisms of Semmelhack homocoupling of aryl halides (25, 27, 34), the results reported by different groups are not completely without controversy (34). The first step of the process is oxidative addition of Ar–X to Ni(0) to produce an aryl Ni(II) halide complex. Since chloroarenes are known to be almost unreactive toward $[(COD)_2Ni]$ (26), a bidentate *N*-ligand should displace at least one COD in $[(COD)_2Ni]$ before oxidative addition of PhCl can occur. As described by Tsou and Kochi (25) and discussed, most recently, in detail in an excellent review by Nelson and Crouch (34), an intermediate Ni(III) aryl species might play a key role in the homocoupling reaction. Aryl transfer from Ar–Ni(III) to Ar–Ni(II), possibly via a bridging intermediate, would produce a diaryl Ni(III) species that leads to biaryl upon C–C reductive elimination. Such Ar–Ni(III) species are more likely to emerge when more electron-rich teeda (vs. tmeda) and 6,6′-Me_2bipy (vs. bipy) are employed. On the other hand, one may not rule out the solubility factor, i.e., it is conceivable that the poorly soluble tmeda derivative **1** precipitates out immediately upon formation, whereas its more soluble teeda analogue may undergo further transformations in solution.

Fig. 2. An ORTEP drawing of $[(teeda)NiCl_2]$ with thermal ellipsoids drawn to the 50% probability level. Selected bond distances (Å) and angles (°): Ni(1)—N(1) 2.050(2), Ni(1)—N(2) 2.059(2), Ni(1)—Cl(1) 2.232(1), Ni(1)—Cl(2) 2.232(1); N(1)-Ni(1)-N(2) 89.32(6), N(1)-Ni(1)-Cl(1) 107.12(4), N(2)-Ni(1)-Cl(1) 110.87(5), N(1)-Ni(1)-Cl(2) 110.60(5), N(2)-Ni(1)-Cl(2) 106.14(4), Cl(1)-Ni(1)-Cl(2) 126.50(2).

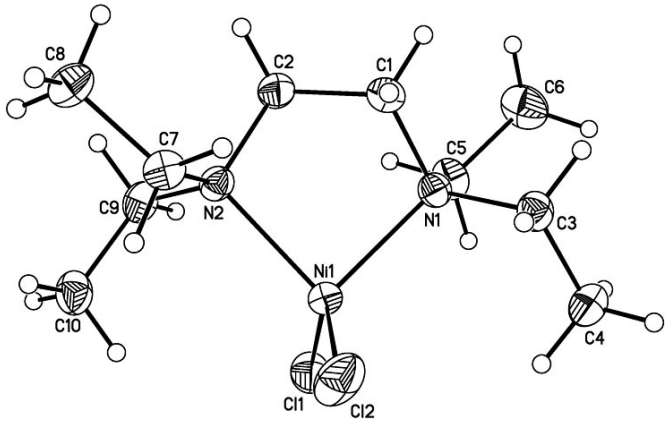
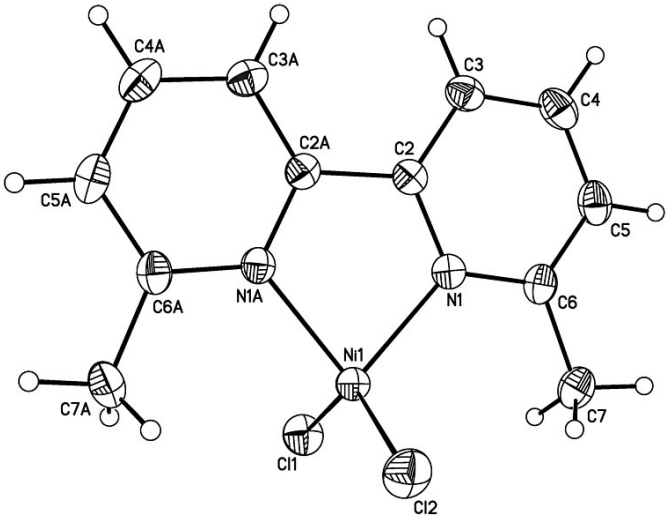


Fig. 3. An ORTEP drawing of $[(6,6'\text{-}Me_2bipy)NiCl_2]$ with thermal ellipsoids drawn to the 50% probability level. Selected bond distances (Å) and angles (°): Ni(1)—N(1) 1.985(1), Ni(1)—N(1A) 1.985(1), Ni(1)—Cl(2) 2.211(1), Ni(1)—Cl(1) 2.218(1); N(1)-Ni(1)-N(1A) 82.76(7), N(1)-Ni(1)-Cl(2) 109.05(4), N(1A)-Ni(1)-Cl(2) 109.05(4), N(1)-Ni(1)-Cl(1) 105.80(4), N(1A)-Ni(1)-Cl(1) 105.81(4), Cl(2)-Ni(1)-Cl(1) 132.93(3).



In conclusion, we have demonstrated that Ph–Cl activation by Ni(0) stabilized with *N*-chelating ligands does not

© 2005 NRC Canada

necessarily form a σ-phenyl Ni species as the final product, but can also result in homocoupling and formation of the corresponding dichloro complex. The outcome of such reactions is remarkably sensitive to even small changes in the structure of the stabilizing *N*,*N*-ligand, as illustrated by the differing behavior of the tmeda and teeda systems. These observations might be important for the design of reactions of haloarenes, catalyzed by Ni *N*,*N*-chelate complexes.

Experimental

Materials and instruments

All manipulations with Ni complexes were conducted in a glovebox under N_2. All chemicals were purchased from Aldrich, Acros Organics, and Strem Chemical Companies. The diamines were distilled from CaH_2 under N_2 prior to use. Both [$(COD)_2$Ni] and 6,6′-Me_2bipy were used as received. All solvents were purified and (or) dried by standard techniques and stored over freshly activated molecular sieves (4 Å) in the glovebox. NMR spectra were obtained with Bruker Avance DPX 300 and DRX 400 instruments. A Bruker Smart 1 K CCD system was used for single crystal X-ray diffraction studies. Microanalyses were performed by Micro-Analysis, Inc., Wilmington, Delaware, USA.

Synthesis of [(tmeda)Ni(Ph)Cl] (1)

A slight modification of the reported procedure (28) was used. A solution of tmeda (0.28 mL) in chlorobenzene (2 mL) was added to [$(COD)_2$Ni] (0.42 g), and the mixture was stirred at room temperature for 6 h. Hexanes (10 mL) were added and the mixture was left at room temperature overnight. The orange-yellow precipitate was separated by filtration, thoroughly washed with hexanes, and dried under vacuum. The yield of **1** was 0.39 g (89%). ^{1}H NMR (1,2-dichloroethane-d_4, 20 °C) δ: 2.0–2.7 (m, 16H, CH_3 and CH_2), 6.6 (1H, *p*-Ph), 6.7 (2H, *m*-Ph), 7.5 (2H, *o*-Ph). ^{13}C NMR (1,2-dichloroethane-d_4, 20 °C) δ: 47.1 (br), 49.3 (br), 56.9 (br), 61.1 (br), 121.4, 124.5, 136.8, 147.5. Anal. calcd. for $C_{12}H_{21}ClN_2Ni$ (%): C 50.1, H 7.4, N 9.7; found: C 49.9, H 7.0, N 9.7.

Preparation of [(teeda)Pd(Ph)I]

Under N_2, a stirring mixture of $Pd(dba)_2$ (1.00 g), teeda (0.39 g), iodobenzene (0.51 g), and benzene (25 mL) was slowly heated to 50 °C and kept at that temperature for 15 min. The greenish reaction mixture was filtered through Celite®, which was then washed with benzene (2 × 10 mL). After the combined filtrate and washings were evaporated, the residue was washed with ether (3 × 10 mL) to remove dba. Recrystallization of the orange residue from dichloromethane–ether produced 0.30 g (36%) of [(teeda)Pd(Ph)I] as a pale yellow crystalline solid. ^{1}H NMR (dichloromethane-d_2, 20 °C) δ: 1.4 (t, J = 7.1 Hz, 6H, CH_3), 1.5 (t, J = 7.1 Hz, 6H, CH_3), 2.7 (m, 6H, CH_2), 2.8 (m, 2H, CH_2), 3.0 (m, 2H, CH_2), 3.2 (m, 2H, CH_2), 6.7 (m, 1H, *p*-Ph), 6.9 (m, 2H, *m*-Ph), 7.3 (m, 2H, *o*-Ph). Anal. calcd. for $C_{16}H_{29}IN_2Pd$ (%): C 39.8, H 6.0, N 5.8; found: C 39.7, H 6.0, N 5.7.

Preparation of [(dpe)Pd(Ph)I]

Under N_2, a stirring mixture of $Pd(dba)_2$ (1.00 g), dpe (0.44 g), iodobenzene (0.51 g), and benzene (25 mL) was slowly heated to 50 °C and kept at that temperature for 15 min. The greenish reaction mixture was filtered through Celite®, which was then washed with benzene (2 × 10 mL). After the combined filtrate and washings were evaporated, the residue was washed with ether (3 × 10 mL) to remove dba. Recrystallization of the residue from dichloromethane–ether produced 0.40 g (46%) of [(dpe)Pd(Ph)I] as "copper" orange flakes. ^{1}H NMR (dichloromethane-d_2, 20 °C) δ: 1.0–1.8 (m, CH_2), 2.7–3.1 (m, CH_2), 3.8 (m, CH_2), 6.8 (m, 1H, *p*-Ph), 6.9 (m, 2H, *m*-Ph), 7.3 (m, 2H, *o*-Ph). Anal. calcd. for $C_{18}H_{29}IN_2Pd$ (%): C 42.7, H 5.8, N 5.5; found: C 42.3, H 5.7, N 5.4.

Preparation of [(teeda)$NiCl_2$]

A solution of teeda (1.00 g) in chlorobenzene (2 mL) was added to [$(COD)_2$Ni] (1.22 g), and the mixture was stirred at room temperature overnight. Hexanes (8 mL) were added. After 30 min, the deep-purple solid was separated by filtration, washed with hexanes (4 × 10 mL), and dried under vacuum. The yield was 0.89 g (66%). Anal. calcd. for $C_{10}H_{24}Cl_2N_2Ni$ (%): C 39.8, H 8.0, N 9.3; found: C 39.8, H 7.3, N 9.2. X-ray quality crystals were grown from dichloromethane–hexanes.

Preparation of [(6,6′-Me_2bipy)$NiCl_2$]

A mixture of 6,6′-Me_2bipy (0.50 g), [$(COD)_2$Ni] (0.70 g), and chlorobenzene (6 mL) was stirred at room temperature for 1 day. A green color emerged immediately upon mixing the reagents, which then turned dark-blue within seconds, and finally light-purple. The light-purple solid was separated by filtration, washed with chlorobenzene (2 × 2 mL) and hexanes (2 × 3 mL), and dried under vacuum. The yield was 0.79 g (99%). Anal. calcd. for $C_{12}H_{12}Cl_2N_2Ni$ (%): C 45.9, H 3.8, N 8.9; found: C 46.0, H 3.7, N 8.7. X-ray quality crystals were grown from hot 1,2-dichloroethane.

Synthesis of *N*,*N*,*N*′,*N*′-tetraisopropylethylenediamine (tipeda)

In air, a mixture of 2-iodopropane (20 mL), ethylenediamine (1.1 mL), and potassium carbonate (9.2 g) was stirred under reflux for 58 h. The tan liquid phase was separated from the solids, which were then thoroughly washed with ether (10 × 5 mL). The mother liquor and the washings were combined, evaporated, and the residue distilled under vacuum (86–98 °C at 9.5 mm Hg, (1 mm Hg = 133.322 4 Pa) to produce 3.32 g (87%) of spectroscopically pure tipeda. ^{1}H NMR (benzene-d_6, 20 °C) δ: 1.1 (t, J = 6.6 Hz, 24H, CH_3), 2.7 (s, 4H, CH_2), 3.1 (heptet, J = 6.6 Hz, 4H, CH). ^{13}C NMR (benzene-d_6, 20 °C) δ: 21.4, 48.1, 49.4.

Crystallographic studies

All crystallographic data were collected using a Bruker Smart 1 K CCD system equipped with Mo Kα radiation at –100 °C. The structures were solved using direct methods and refined with the SHELXTL program suite (35). Scattering factors were obtained from the *International Tables for X-ray Crystallography* (36). Additional data and refinement

© 2005 NRC Canada

Table 1. Crystallographic data for [(tmeda)Ni(Ph)Cl] (**1**), [(teeda)$NiCl_2$], and [(6,6′-Me_2bipy)$NiCl_2$].

	[(tmeda)Ni(Ph)Cl] (**1**)	[(teeda)$NiCl_2$]	[(6,6′-Me_2bipy)$NiCl_2$]
Empirical formula	$C_{12}H_{21}ClN_2Ni$	$C_{10}H_{24}Cl_2N_2Ni$	$C_{12}H_{12}Cl_2N_2Ni$
FW	287.47	301.92	313.85
Crystal color, form	Gold, plate	Purple, irreg. block	Red-orange, irreg. block
Crystal system	Monoclinic	Orthorhombic	Orthorhombic
Space group	*P*2(1)/*c*	*Pna*2(1)	*Pnma*
Unit cell dimensions			
a (Å)	11.0284(4)	14.7179(14)	14.594(2)
b (Å)	12.2967(5)	12.3740(12)	11.1805(15)
c (Å)	11.4778(4)	7.7454(7)	7.8560(11)
α (°)	90	90	90
β (°)	118.629(1)	90	90
γ (°)	90	90	90
V (Å^3)	1 366.24(9)	1 410.6(2)	1 281.9(3)
Z	4	4	4
Density (g cm^{-3})	1.398	1.422	1.626
Abs. μ (mm^{-1})	1.592	1.728	1.907
F(000)	608	640	640
Crystal size (mm^3)	0.22 × 0.08 × 0.04	0.45 × 0.42 × 0.24	0.35 × 0.35 × 0.32
Temp (°C)	–100	–100	–100
Scan mode	ω	ω	ω
Detector	Bruker CCD	Bruker CCD	Bruker CCD
θ_{max} (°)	28.3	28.26	28.29
No. obsrvd. reflections	10 437	7 106	10 052
No. uniq. reflections	3 392	2 146	1 589
R_{merge}	0.0251	0.0173	0.0258
No. of parameters	149	141	83
S^a	0.989	1.071	1.003
R indices [$I > 2\sigma(I)$]^b	$wR_2 = 0.0590$, $R_1 = 0.0244$	$wR_2 = 0.0446$, $R_1 = 0.0178$	$wR_2 = 0.0639$, $R_1 = 0.0238$
R indices (all data)^b	$wR_2 = 0.0618$, $R_1 = 0.0330$	$wR_2 = 0.0456$, $R_1 = 0.0189$	$wR_2 = 0.0664$, $R_1 = 0.0272$
Max diff. peak, hole (e Å^{-3})	0.358, –0.236	0.201, –0.239	0.383, –0.240

^{a}GoF = $S = \{\sum[w(F_o^2 - F_c^2)^2]/(n-p)\}^{1/2}$, where *n* is the number of reflections and *p* is the total number of refined parameters.
$^b R_1 = \sum(|F_o| - |F_c|)/\sum|F_o|$, $wR_2 = \{\sum w(F_o^2 - F_c^2)^2]/\sum w[(F_o^2)^2]\}^{1/2}$ (sometimes denoted as R_w2).

details are presented in Table 1. The crystal structures have been deposited as supplementary material.[4]

References

1. J. Miller. Aromatic nucleophilic substitution. Elsevier, London. 1968.
2. F. Terrier. Nucleophilic aromatic displacement: The influence of the nitro group. VCH, New York. 1991.
3. F. Diederich and P.J. Stang (*Editors*). Metal-catalyzed cross-coupling reactions. Wiley-VCH, New York. 1998.
4. E.-I. Negishi (*Editor*). Handbook of organopalladium chemistry for organic synthesis. Vols. 1 and 2. Wiley, Hoboken, New Jersey. 2002.
5. D. Baranano, G. Mann, and J.F. Hartwig. Curr. Org. Chem. **1**, 287 (1997).
6. V.V. Grushin and H. Alper. Top. Organomet. Chem. **3**, 193 (1999).
7. G. Poli, G. Giambastiani, and A. Heumann. Tetrahedron, **56**, 5959 (2000).
8. J. Hassan, M. Sevignon, C. Gozzi, E. Schulz, and M. Lemaire. Chem. Rev. **102**, 1359 (2002).
9. A.F. Littkle and G.C. Fu. Angew. Chem. Int. Ed. **41**, 4176 (2002).
10. K. Tamao and N. Miyaura. Top. Curr. Chem. **219**, 1 (2002).
11. N. Miyaura and A. Suzuki. Chem. Rev. **95**, 2457 (1995).
12. G. Lessene. Aust. J. Chem. **57**, 107 (2004).
13. I.P. Beletskaya and A.V. Cheprakov. Chem. Rev. **100**, 3009 (2000).
14. A.R. Muci and S.L. Buchwald. Top. Curr. Chem. **219**, 131 (2002).
15. J.F. Hartwig. Angew. Chem. Int. Ed. **37**, 2046 (1998).
16. M. Sundermeier, A. Zapf, and M. Beller. Eur. J. Inorg. Chem. 3513 (2003).
17. C.J. Elsevier. Coord. Chem. Rev. **185–186**, 809 (1999).
18. A.C. Hillier, G.A. Grasa, M.S. Viciu, H.M. Lee, C. Yang, and S.P. Nolan. J. Organomet. Chem. **653**, 69 (2002).

[4] Supplementary data for this article are available on the Web site or may be purchased from the Depository of Unpublished Data, Document Delivery, CISTI, National Research Council Canada, Ottawa, ON K1A 0S2, Canada. DUD 3677. For more information on obtaining material refer to http://cisti-icist.nrc-cnrc.gc.ca/irm/unpub_e.shtml. CCDC 251780 (**1**), 251779 ([(teeda)$NiCl_2$)], and 251778 ([(6,6′-Me_2bipy)$NiCl_2$]) contain the crystallographic data for this manuscript. These data can be obtained, free of charge, via www.ccdc.cam.ac.uk/conts/retrieving.html (Or from the Cambridge Crystallographic Data Centre, 12 Union Road, Cambridge CB2 1EZ, UK; fax +44 1223 336033; or deposit@ccdc.cam.ac.uk).

© 2005 NRC Canada

19. W.A. Herrmann. Angew. Chem. Int. Ed. **41**, 1290 (2002).
20. W.A. Herrmann, K. Ofele, D. von Preysing, and S.K. Schneider. J. Organomet. Chem. **687**, 229 (2003).
21. K.J. Cavell and D.S. McGuinness. Coord. Chem. Rev. **248**, 671 (2004).
22. J.-H. Li and W.-J. Liu. Org. Lett. **6**, 2809 (2004).
23. V.V. Grushin and H. Alper. Chem. Rev. **94**, 1047 (1994).
24. M. Foa and L. Cassar. J. Chem. Soc. Dalton Trans. 2572 (1975).
25. T.T. Tsou and J.K. Kochi. J. Am. Chem. Soc. **101**, 6319 (1979); J. Am. Chem. Soc. **101**, 7547 (1979).
26. M.F. Semmelhack, P.M. Helquist, and L.D. Jones. J. Am. Chem. Soc. **93**, 5908 (1971).
27. C. Amatore and A. Jutand. Organometallics, **7**, 2203 (1988).
28. E. Wenschuh and R. Zimmering. Z. Chem. **27**, 448 (1987).
29. E. Wenschuh and R. Zimmering. Z. Chem. **28**, 190 (1988).
30. B.A. Markies, A.J. Canty, W. de Graaf, J. Boersma, M.D. Janssen, M.P. Hogerheide, W.J.J. Smeets, A.L. Spek, and G. van Koten. J. Organomet. Chem. **482**, 191 (1994).
31. U. Turpeinen and A. Pajunen. Finn. Chem. Lett. 6 (1976).
32. D.A. Handley, P.B. Hitchcock, and G.J. Leigh. Inorg. Chim. Acta, **314**, 1 (2001).
33. G.R. Newkome, F.R. Fronczek, V.K. Gupta, W.E. Puckett, D.C. Pantaleo, and G.E. Kiefer. J. Am. Chem. Soc. **104**, 1782 (1982).
34. T.D. Nelson and R.D. Crouch. Org. React. (N.Y.), **63**, 265 (2004).
35. G.M. Sheldrick. SHELXTL, An integrated system for solving, refining, and displaying crystal structures from diffraction data. Version 5.1 [computer program]. Bruker AXS, Inc., Madison, Wisconsin. 1998.
36. A.J.C. Wilson (*Editor*). International tables for crystallography (Corrected reprint). Vol. C. Kluwer Academic Publishers, Dordrecht, the Netherlands. 1995.

© 2005 NRC Canada

An alternative convergent synthesis of silole-core dendrimers[1]

Takanobu Sanji, Hiroyuki Ishiwata, Tomoyoshi Kaizuka, Masato Tanaka, Hideki Sakurai, Ritsuko Nagahata, and Kazuhiko Takeuchi

Abstract: Silole-core dendrimers having benzyl-ether-type dendron units in the periphery are readily synthesized by the Ni-catalyzed reaction of benzyloxy-substituted diphenylacetylenes with 1,1,2,2-tetramethyldisilane.

Key words: silole, dendrimer, nickel-catalyzed reaction, convergent synthesis.

Résumé : La synthèse de dendrimères à coeur de silole possédant des dendrones de type éther benzylique à la périphérie peut être réalisée facilement en faisant appel à la réaction du 1,1,2,2-tétraméthyldisilane avec des diphénylacétylènes substitués par un groupe benzyloxy, catalysée par du nickel.

Mots clés : silole, dendrimère, réaction catalysée par le nickel, synthèse convergente.

[Traduit par la Rédaction]

Introduction

Dendrimers are a unique class of macromolecules having highly ordered, three-dimensional, and tree-like structures, and they have great potential as building blocks for the construction of functional materials (1). They are generally synthesized by "divergent" or "convergent" approaches. The divergent approach initiates growth at the core, and the generation grows outward by repetition of coupling and activation steps. The convergent method, on the other hand, propagates inward by coupling the focal point of the dendrons to the core. The convergent synthesis allows control over the number and location of functional moieties in the resultant dendrimers. This is a useful and important feature in molecular design. Indeed, quite a few reports on the derivatization of dendrimers have addressed chemical modification of the core and (or) peripheral moieties for a variety of fundamental studies and applications (2).

Recently, many groups reported accelerated approaches that combine the convergent and divergent strategies to reduce the number of tedious and iterative synthetic steps (3). In view of the synthetic improvement of the convergent approach, one-step synthesis of dendrimers, involving simultaneous construction of the core by the reaction of starting materials with the appropriate dendron units, appears promising as compared with the conventional convergent synthesis involving installation of the core in the final step. Hecht and Fréchet (4) reported the cobalt-catalyzed [2+2+2] cyclotrimerization of dendritically substituted alkynes to produce benzene-core dendrimers. This approach successfully yielded highly compact cores. Dehaen and co-workers (5) reported the synthesis of poly(1,2,3-triazolylmethyl)benzene cores via 1,3-dipolar cycloaddition reaction between poly(azidomethyl)benzenes and dendritically disubstituted acetylenedicarboxylates. Sharpless and co-workers (6) and Fokin and co-workers (7) also recently reported, on the basis of their "click chemistry" approach (6), an efficient route to triazole dendrimers by Cu(I)-catalyzed reaction of azides with alkynes (7).

Siloles and silacyclopentadienes have attracted great interest over the past decade because of their unique photophysical and electronic properties (8) and potential applications as organic electroluminescent (EL) devices (9). The silole has a relatively low LUMO energy level, due to the σ^*–π^* conjugation, in comparison with its carbon analogue, cyclopentadiene. Recently, several reports have addressed synthesis of siloles with a variety of substituent groups (10) and silole-based polymers (11). The silole-core dendrimer systems are envisioned to constitute an interesting class of macromolecule because the silole incorporated at the core acts as a functional conjugated unit and the dendritic framework provides for a site-isolation of chromophores, a light-harvesting antenna, and an energy-transfer interaction (12).

In 1972, Kumada and co-workers (13) reported the nickel-catalyzed reaction of 1,1,2,2-tetramethyldisilane and disubstituted acetylenic compounds to give siloles in good yields

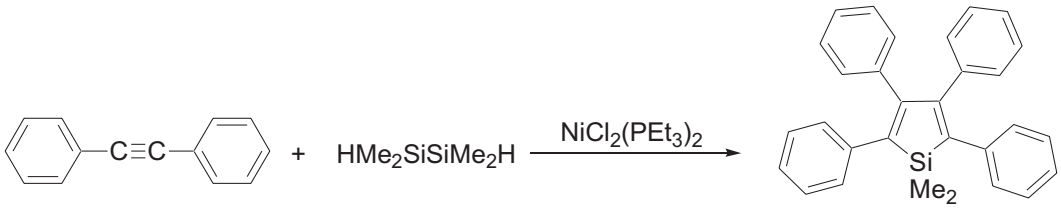
Received 12 January 2005. Published on the NRC Research Press Web site at http://canjchem.nrc.ca on 14 June 2005.

T. Sanji,[2] H. Ishiwata, T. Kaizuka, and M. Tanaka.[2] Chemical Resources Laboratory, Tokyo Institute of Technology, 4259 Nagatsuta, Midori-ku, Yokohama 226-8503, Japan.
H. Sakurai. Department of Pure and Applied Chemistry, Tokyo University of Science, Noda, Chiba 278-8510, Japan.
R. Nagahata and K. Takeuchi. National Institute of Advanced Industrial Science and Technology (AIST), Tsukuba Central 5, 1-1-1 Higashi, Tsukuba 305-8565, Japan.

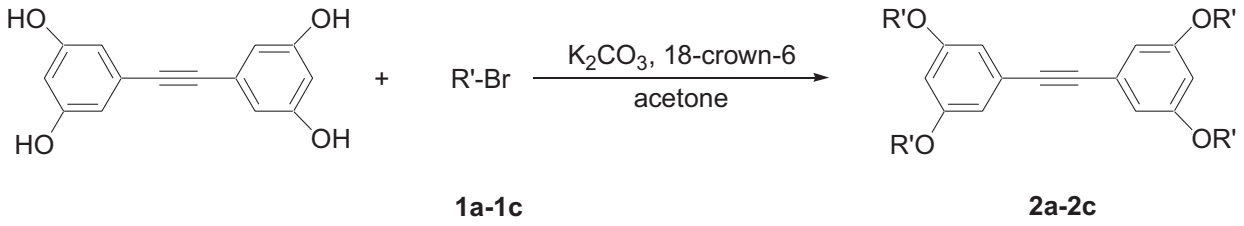
[1]This article is part of a Special Issue dedicated to Professor Howard Alper.
[2]Corresponding authors (e-mail: sanji@res.titech.ac.jp; m.tanaka@res.titech.ac.jp).

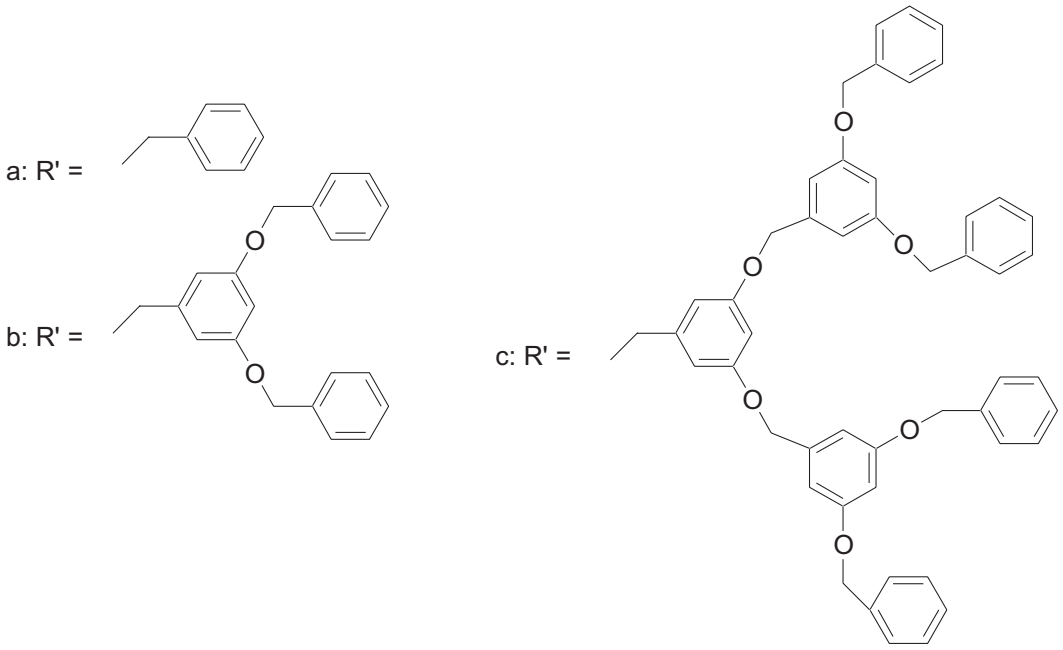
 doi: 10.1139/V05-081 © 2005 NRC Canada

Scheme 1.



Scheme 2.





(Scheme 1). The reaction is envisioned to proceed with the involvement of an intermediate nickel-silylene complex and its addition to acetylenes. We have found that this reaction works well with heavy acetylenes bearing dendritic substituents, affording silole-core dendrimers. This paper discloses a facile one-pot synthesis of silole-core dendrimers by the alternative convergent method.

Results and discussion

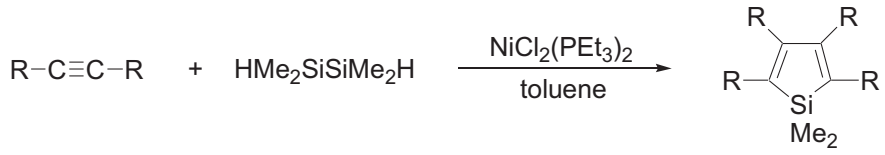
Our synthetic strategy for the silole-core dendrimers is based on the nickel-catalyzed reaction of 1,1,2,2-tetramethyldisilane with disubstituted alkynes, which has proved to work well for dendritic alkynes affording silole-core dendrimers.

The alkynes with poly(benzyl ether) dendrons, **2a**–**2c**, were prepared by the convergent method as shown in Scheme 2. 1,2-Bis(3,5-dihydroxyphenyl)acetylene was readily prepared by deprotection of 1,2-bis(3,5-dimethoxyphenyl)acetylene with boron tribromide. The benzyl ether-type dendritic bromides **1b** and **1c** were obtained according to the previously reported procedures (14). The reaction of bromides **1a**–**1c** (4 equiv.) with 1,2-bis(3,5-dihydroxydiphenyl)acetylene (1 equiv.) in the presence of potassium carbonate and 18-crown-6 proceeded smoothly to give the acetylenes with poly(benzyl ether) dendrons **2a**–**2c**. Table 1 lists the results. The dendritic acetylenes **2a**–**2c** were obtained in good yields even for the higher generation substrates (91%, 62%, and 79%, respectively). The ^{1}H and ^{13}C NMR spectra of **2a**–**2c** showed the high molecular symmetry in these products and conformed to the proposed structures. FAB mass or MALDI-TOF mass spectra were also consistent with the dendritic structures.

Next, the dendritic alkynes **2a**–**2c** were treated with 1,1,2,2-tetramethyldisilane in the presence of $NiCl_2(PEt_3)_2$

© 2005 NRC Canada

Scheme 3.



2a-2c **3a-3c**

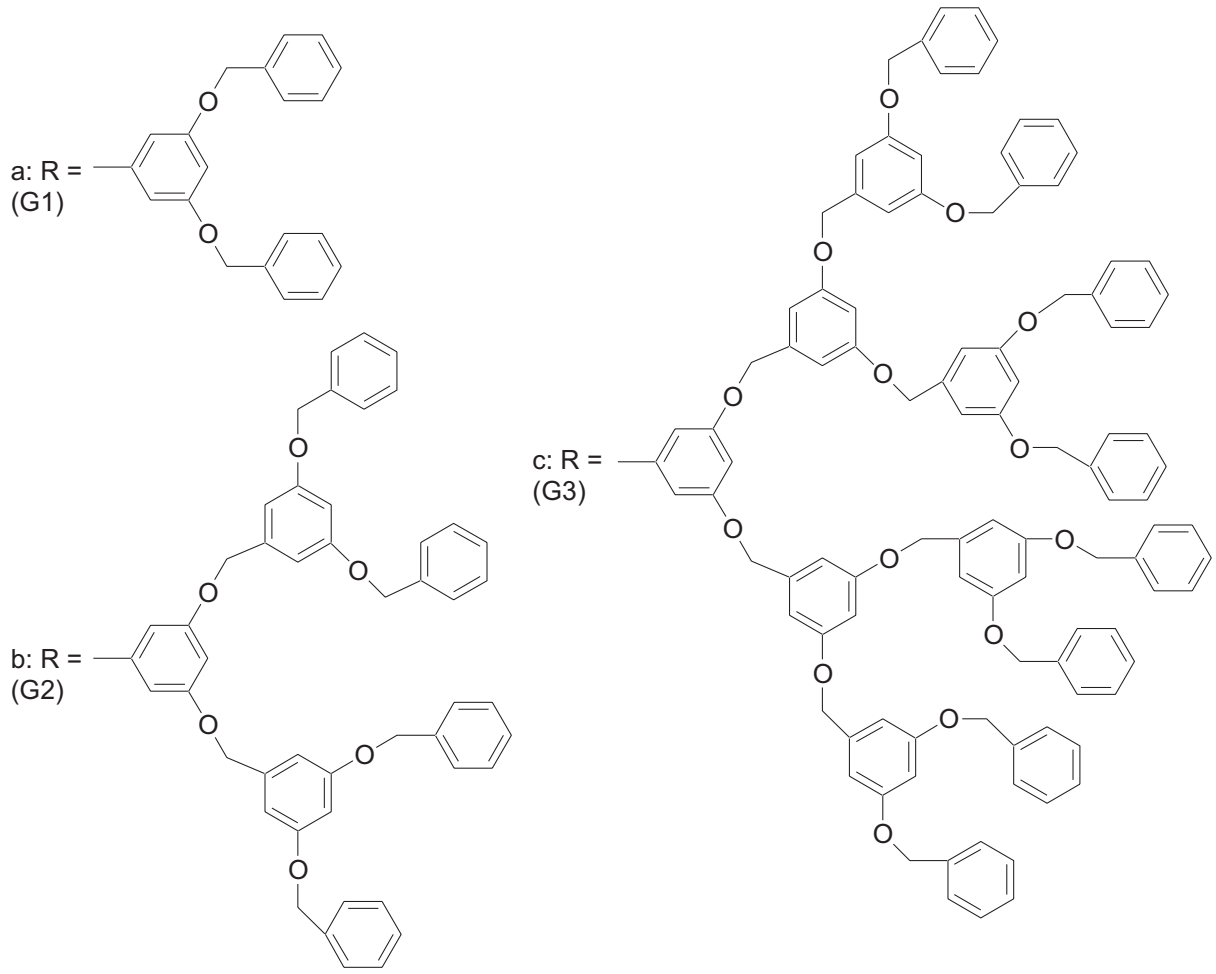


Table 1. Synthesis of dendritic acetylene **2a**–**2c** and silole-core dendrimers **3a**–**3c**.

	2	**3**		
Compound (G*n*)	Yield (%)	Time (h)	Amount of cat. (mol%)	Yield (%)
a (G1)	91	20	3	50
b (G2)	62	44	3	47
c (G3)	79	136	10	13

Note: G*n* = generation number; cat. = catalyst.

(3 mol%) in refluxing toluene (Scheme 3). The reaction, monitored by TLC, was continued until the disappearance of the starting alkynes. The results are also listed in Table 1, which shows that even though longer times are required to complete the reaction, as the generation of the desired dendrimers grows, the silole-forming reaction proceeds satisfactorily. Thus, silole-core dendrimers **3a** and **3b** were obtained in 50% (20 h) and 47% (44 h) yields, respectively. These yields are comparable to that of parent 1,1-dimethyl-2,3,4,5-tetraphenylsilole prepared from diphenylacetylene and tetramethyldisilane under the same conditions (53%, 16 h).[3] However, for the even higher generation dendrimer **3c**, the yield decreased to 13%, even after prolonged heating

[3] 1,1-Dimethyl-2,3,4,5-tetraphenylsilole was prepared as a reference compound by the nickel-catalyzed reaction of 1,1,2,2-tetramethyldisilane and diphenylacetylene. NMR data for 1,1-dimethyl-2,3,4,5-tetraphenylsilole: ^{1}H NMR (300 MHz, acetone-d_6) δ: 7.13–6.95 (m, 16H, Ph), 6.94–6.81 (m, 4H, Ph), 0.41 (s, 6H, SiCH_3). ^{13}C NMR (75 MHz, acetone-d_6) δ: 154.9 (Ph_4C_4Si), 142.6 (Ph_4C_4Si), 140.6, 139.8, 130.7, 129.5, 128.8, 128.3, 127.1, 126.5, –4.0 (SiCH_3). ^{29}Si NMR (60 MHz, acetone-d_6) δ: 8.2.

© 2005 NRC Canada

(136 h) using an increased amount of the catalyst (10 mol%). This is clearly suggestive of steric crowding around the core hindering the reaction at the higher generation. In addition, the reaction became less clean, although **3c** could be readily isolated and purified by column chromatography, as in the other cases.

Silole-core dendrimers **3a**–**3c** were fully characterized by a variety of spectroscopic techniques. The GPC analysis confirmed their monodispersity. The FAB or MALDI-TOF mass spectra showed peaks for *m*/*z* 1264 ($[M + H]^+$), 2984.5 ($[M + Na]^+$), and 6465.0 ($[M + Ag]^+$), associated with **3a**–**3c**, respectively. The ^1H and ^{13}C NMR spectra displayed the signals of methyl on the silole ring at the core along with those of the benzyl ether units (15).[3] In the ^{29}Si NMR spectra, the signals assigned to Si–Me on the silole ring core were observed at about 8 ppm for these dendrimers. All these spectral observations support the structure of the silole-core dendrimers.

In conclusion, we have prepared silole-core dendrimers by the nickel-catalyzed reaction of tetramethyldisilane and dendritic acetylenes containing poly(benzyl ether) units through the third generation. This synthetic procedure demonstrates the alternative convergent approach via a one-pot synthesis of the core, for the construction of a precise macromolecular structure. To the best of our knowledge, these are the first examples of silole-core dendrimers. The photophysical properties of the dendrimers will be reported in a forthcoming paper.

Experimental

Measurements

^1H, ^{13}C, and ^{29}Si NMR spectra were recorded on a Bruker DPX 300 FT-NMR spectrometer at 300, 75.4, and 59.6 MHz, respectively. The ^1H and ^{13}C chemical shifts were referenced to solvent residues (^1H, δ = 7.24 ppm; ^{13}C, δ = 77.0 ppm for $CDCl_3$). The ^{29}Si chemical shift was referenced to external Me_4Si (0 ppm). Mass spectra were measured by matrix-assisted laser desorption ionization time-of-flight (MALDI-TOF) technique on a Bruker reflex III. Gel permeation chromatography (GPC) was performed on a Shimadzu LC 10 HPLC equipped with PL-gel mixed-C columns calibrated with polystyrene standards.

Materials

All solvents and reagents were of reagent quality, purchased from commercial sources and used without further purification, unless otherwise noted below. Toluene was dried and distilled from sodium–benzophenone just before use. Acetone was distilled from calcium hydride. 1,2-Bis(3,5-dihydroxyphenyl)acetylene (16) and poly(benzyl ether)-dendritic bromides (14) were prepared according to the previously reported procedures.

General procedure for synthesis of poly(benzyl ether)-type dendritic acetylenes (2a–2c)

A mixture of an appropriate dendritic bromide (4 equiv.), 1,2-bis(3,5-dihydroxydiphenyl)acetylene (1 equiv.), K_2CO_3 (6 equiv.), and 18-crown-6 (0.4 equiv.) in acetone (10–100 mL) was heated under reflux under nitrogen (24–132 h). After the mixture was cooled to room temperature, water (30 mL) was added to the mixture, and then the mixture was extracted with CH_2Cl_2 (20–100 mL × 3). The combined organic layer was washed successively with water, sat. NH_4Cl solution, and sat. NaCl solution and evaporated after being dried over anhydrous $MgSO_4$. The residue was chromatographed over silica gel to give the corresponding poly(benzyl ether)-type dendritic acetylene (**2a**–**2c**).

2a

This was prepared by the reaction of 1,2-bis(3,5-dihydroxyphenyl)acetylene and benzyl bromide **1a** and purified from silica gel column chromatography with CH_2Cl_2 to give **2a** as a pale yellow solid. Yield 91%; mp 149–151 °C. ^1H NMR (300 MHz, $CDCl_3$) δ: 7.44–7.33 (m, 20H, Ar*H*), 6.80 (d, 4H, *J* = 2.2 Hz, Ar*H*), 6.63 (t, 2H, *J* = 2.2 Hz, Ar*H*), 5.04 (s, 8H, -C*H*$_2$O-). ^{13}C NMR (75 MHz, $CDCl_3$) δ: 159.7, 136.6, 128.6, 128.0, 127.5, 124.4, 110.6, 103.5, 89.0 (-*C*≡C-), 70.1 (-*C*H$_2$O-). MS (FAB) *m*/*z*: 603 ($[M + H]^+$). Anal. calcd. for $C_{42}H_{34}O_4$: C 83.70, H 5.69; found: C 83.94, H 6.00.

2b

This was prepared by the reaction of 1,2-bis(3,5-dihydroxyphenyl)acetylene and **1b** and purified from silica gel column chromatography with CH_2Cl_2 to give **2b** as a pale yellow solid. Yield 62%; mp 150–154 °C. ^1H NMR (300 MHz, $CDCl_3$) δ: 7.43–7.30 (m, 40H, Ar*H*), 6.78 (d, 4H, *J* = 2.2 Hz, Ar*H*), 6.68 (d, 8H, *J* = 2.2 Hz, Ar*H*), 6.58 (m, 6H, Ar*H*), 5.02 (s, 16H, -C*H*$_2$O-), 4.99 (s, 8H, -C*H*$_2$O-). ^{13}C NMR (75 MHz, $CDCl_3$) δ: 160.1, 159.6, 139.0, 136.7, 128.6, 128.0, 127.5, 124.4, 110.6, 106.3, 103.4, 101.6, 89.1 (-*C*≡C-), 70.1 (-*C*H$_2$O-), 70.0 (-*C*H$_2$O-). MS (FAB) *m*/*z*: 1451 ($[M]^+$). Anal. calcd. for $C_{98}H_{82}O_{12}$: C 81.08, H 5.69, O 13.23; found: C 80.98, H 5.93, O 13.01.

2c

This was prepared by the reaction of 1,2-bis(3,5-dihydroxyphenyl)acetylene and **2c** and purified from silica gel column chromatography with CH_2Cl_2–hexane (1:1) to give **2c** as a pale yellow solid. Yield 62%; mp 59–61 °C. ^1H NMR (300 MHz, $CDCl_3$) δ: 7.41–7.27 (m, 80H, Ar*H*), 6.80 (d, 4H, *J* = 2.1 Hz, Ar*H*), 6.68–6.65 (m, 24H, Ar*H*), 6.62 (t, 2H, *J* = 2.0 Hz, Ar*H*), 6.57–6.55 (m, 12H, Ar*H*), 5.00 (s, 32H, -C*H*$_2$O-), 4.95–4.93 (m, 24H, -C*H*$_2$O-). ^{13}C NMR (75 MHz, $CDCl_3$) δ: 160.1, 160.0, 159.6, 139.1, 138.9, 136.7, 128.5, 127.9, 127.5, 124.4, 110.6, 106.4, 106.3, 101.5, 89.1 (-*C*≡C-), 70.0 (-*C*H$_2$O-), 69.9 (-*C*H$_2$O-). MS (MALDI-TOF) *m*/*z*: 3172.5 ($[M + Na]^+$). Anal. calcd. for $C_{210}H_{178}O_{28}$: C 80.08, H 5.70, O 14.22; found: C 80.01, H 5.79, O 14.39.

Synthesis of silole-core dendrimer 3a

A mixture of **2a** (250 mg, 0.42 mmol), 1,1,2,2-tetramethyldisilane (72 mg, 0.60 mmol), and $Ni(PEt_3)_2Cl_2$ (4 mg, 0.01 mmol) in toluene (10 mL) was heated under reflux for 20 h under nitrogen. The mixture was cooled to room temperature and evaporated. The residue was chromatographed over silica gel with toluene–hexane (3:1) to give **3a** (130 mg, 0.103 mmol) as a greenish-yellow glass. Yield 50%. ^1H NMR (300 MHz, acetone-d_6) δ: 7.38–7.20 (m, 40H, Ar*H*), 6.46–6.44 (m, 4H, Ar*H*), 6.35 (d, 4H, *J* = 2.2 Hz, Ar*H*), 6.32 (d, 4H, *J* = 2.2 Hz, Ar*H*), 5.00 (s, 8H,

© 2005 NRC Canada

-CH_2O-), 4.89 (s, 8H, -CH_2O-), 0.37 (s, 6H, Si-CH_3). ^{13}C NMR (75 MHz, acetone-d_6) δ: 160.6, 160.5, 154.9 (Ar$_4$*C*$_4$Si), 142.3 (Ar$_4$*C*$_4$Si), 142.1, 138.3, 138.1, 129.22, 129.18, 128.51, 128.47, 128.3, 128.2, 128.1, 109.8, 108.6, 101.8, 101.4, 70.7 (-*C*H$_2$O-), 70.4 (-*C*H$_2$O-), –3.7 (Si-*C*H$_3$). ^{29}Si NMR (60 MHz, acetone-d_6) δ: 8.1. MS (FAB) *m*/*z*: 1264 ([M + H]$^+$). Anal. calcd. for $C_{86}H_{74}O_8Si$: C 81.74, H 5.90; found: C 81.58, H 6.15.

Synthesis of silole-core dendrimer 3b

A mixture of **2b** (502 mg, 0.34 mmol), 1,1,2,2-tetramethyldisilane (72 mg, 0.60 mmol), and Ni(PEt$_3$)$_2$Cl$_2$ (4 mg, 0.01 mmol) in toluene (10 mL) was heated under reflux for 44 h under nitrogen. The mixture was cooled to room temperature and evaporated. The residue was chromatographed over silica gel with toluene–hexane (10:1) to give **3b** (240 mg, 0.081 mmol) as a greenish-yellow glass. Yield 47%. ^{1}H NMR (300 MHz, acetone-d_6) δ: 7.38–7.23 (m, 80H, Ar*H*), 6.65–6.40 (m, 36H, Ar*H*), 5.02–4.74 (m, 48H, -CH_2O-), 0.41 (s, 6H, SiCH_3). ^{13}C NMR (75 MHz, acetone-d_6) δ: 160.92, 160.88, 160.7, 160.4, 154.8 (Ar$_4$*C*$_4$Si), 142.4 (Ar$_4$*C*$_4$Si), 142.0, 141.8, 140.6, 140.3, 138.1, 138.0, 129.17, 129.13, 128.53, 128.49, 128.4, 128.1, 108.7, 106.9, 102.1, 101.9, 70.8 (-*C*H$_2$O-), 70.4 (-*C*H$_2$O-), 70.3 (-*C*H$_2$O-), –3.4 (Si-*C*H$_3$). ^{29}Si NMR (60 MHz, acetone-d_6) δ: 8.1. MS (MALDI-TOF) *m*/*z*: 2984.5 ([M + Na]$^+$). Anal. calcd. for $C_{198}H_{170}O_{24}Si$: C 80.30, H 5.79; found: C 79.91, H 5.95.

Synthesis of silole-core dendrimer 3c

A mixture of **2c** (501 mg, 0.16 mmol), 1,1,2,2-tetramethyldisilane (38 mg, 0.32 mmol), and Ni(PEt$_3$)$_2$Cl$_2$ (6 mg, 0.016 mmol) in toluene (5 mL) was heated under reflux for 136 h under nitrogen. The mixture was cooled to room temperature and evaporated. The residue was chromatographed over silica gel with CH_2Cl_2–hexane (2:1) to give **3c** (68 mg, 0.011 mmol) as a greenish-yellow glass. Yield 13%. ^{1}H NMR (300 MHz, acetone-d_6) δ: 7.32–7.20 (m, 160H, Ar*H*), 6.68–6.36 (m, 84H, Ar*H*), 4.92–4.64 (m, 112H, -CH_2O-), 0.38 (s, 6H, Si-CH_3). ^{13}C NMR (75 MHz, acetone-d_6) δ: 160.9, 160.8, 140.5, 140.4, 138.0, 129.2, 128.5, 128.4, 107.2, 106.8, 102.0, 70.4 (-*C*H$_2$O-). ^{29}Si NMR (60 MHz, acetone-d_6) δ: 7.9. MS (MALDI-TOF) *m*/*z*: 6465.0 ([M + Ag]$^+$). Anal. calcd. for $C_{422}H_{362}O_{56}Si$: C 79.73, H 5.74; found: C 79.90, H 6.09.

Acknowledgements

This work was partially supported by CREST (Core Research for Evolutional Science and Technology) of JST (Japan Science and Technology Agency). We also thank the Ministry of Education, Culture, Sports, Science, and Technology of Japan (No. 16685004).

References

1. Recent reviews, see: (*a*) S.M. Grayson and J.M.J. Fréchet. Chem. Rev. **101**, 3819 (2001); (*b*) G.R. Newkome, E. He, and C.N. Moorefield. Chem. Rev. **99**, 1689 (1999).
2. (*a*) A. Adronov and J.M.J. Fréchet. Chem. Commun. 1701 (2000); (*b*) D.W. Brousmiche, J.M. Serin, J.M.J. Fréchet, G.S. He, T.-C. Lin, S.J. Chung, and P.N. Prasad. J. Am. Chem. Soc. **125**, 1448 (2003); (*c*) M. Cotlet, R. Gronheid, S. Habuchi, A. Stefan, A. Barbafina, K. Müllen, J. Hofkens, and F.C.D. Schryver. J. Am. Chem. Soc. **125**, 13 609 (2003); (*d*) P.-W. Wang, Y.-J. Liu, C. Devadoss, P. Bharathi, and J.S. Moore. Adv. Mater. **8**, 237 (1996); (*e*) A.W. Freeman, S.C. Koene, P.R.L. Malenfant, M.E. Thompson, and J.M.J. Fréchet. J. Am. Chem. Soc. **122**, 12 385 (2000); (*f*) P. Furuta, J. Brooks, M.E. Thompson, and J.M.J Fréchet. J. Am. Chem. Soc. **123**, 13 165 (2003); (*g*) C.C. Knok and M.S. Wong. Macromolecules, **34**, 6821 (2001); (*h*) S.-C. Lo, N.A.H. Male, J.P.J. Markham, S.W. Magennis, P.L. Burn, O.V. Salata, and I.D.W. Samuel. Adv. Mater. **14**, 975 (2002); (*i*) J.P.J. Markham, S.-C. Lo, S.W. Magennis, P.L. Burn, and I.D.W. Samuel. Appl. Phys. Lett. **80**, 2645 (2002).
3. (*a*) A.W. Freeman, L.A.J. Chrisstoffels, and J.M.J. Fréchet. J. Org. Chem. **65**, 7612 (2000); (*b*) B. Forier and W. Dehaen. Tetrahedron, **55**, 9829 (1999).
4. S. Hecht and J.M.J. Fréchet. J. Am. Chem. Soc. **121**, 4084 (1999).
5. G.V. Wuytswinkel, B. Verheyde, F. Compernolle, S. Toppet, and W. Dehaen. J. Chem. Soc. Perkin Trans. 1, 1337 (2000).
6. H.C. Kolb, M.G. Finn, and K.B. Sharpless. Angew. Chem. Int. Ed. **40**, 2004 (2001).
7. P. Wu, A.K. Feldman, A.K. Nugent, C.J. Hawker, A. Scheel, B. Voit, J. Pyun, J.M.J. Fréchet, K.B. Sharpless, and V.V. Fokin. Angew. Chem. Int. Ed. **43**, 3928 (2004).
8. (*a*) J. Dubac, A. Laporterie, and G. Manuel. Chem. Rev. **90**, 215 (1990); (*b*) J. Dubac, C. Guerin, and P. Meunier. The chemistry of organic silicon compounds. Vol. 2. *Edited by* Z. Rappoport and Y. Apeloig. John Wiley and Sons, New York. 1999. Chap. 34; (*c*) S. Yamaguchi and K. Tamao. Bull. Chem. Soc. Jpn. **69**, 2327 (1996).
9. K. Tamao, M. Uchida, T. Izumizawa, K. Furukawa, and S. Yamaguchi. J. Am. Chem. Soc. **118**, 11 974 (1996).
10. (*a*) S. Yamaguchi, C. Xu, and K. Tamao. J. Am. Chem. Soc. **125**, 13 662 (2003); (*b*) S. Yamaguchi, T. Endo, M. Uchida, T. Izumizawa, K. Furukawa, and K. Tamao. Chem. Eur. J. **6**, 1683 (2000); (*c*) S. Yamaguchi and K. Tamao. J. Chem. Soc. Dalton Trans. 3693 (1998); (*d*) A.J. Boydston, Y. Yin, and B.J. Pagenkopf. J. Am. Chem. Soc. **126**, 3724 (2004); (*e*) J. Ohshita, H. Kai, A. Takata, T. Iida, A. Kunai, N. Ohta, K. Komaguchi, M. Shiotani, A. Adachi, K. Sakamaki, and K. Okita. Organometallics, **20**, 4800 (2000); (*f*) K.-H. Lee, J. Ohshita, and A. Kunai. Organometallics, **23**, 5365 (2004); (*g*) J. Luo, Z. Xie, W.Y. Lam, L. Chang, H. Chen, C. Qiu, H.S. Kwok, X. Zhan, Y. Zhu, and B.Z. Tang. Chem. Commun. 1740 (2001); (*h*) J. Chen, C.C. Law, J.W.Y. Lam, Y. Dong, S.M.F. Lo, I.D. Williams, D. Zhu, and B.Z. Tang. Chem. Mater. **15**, 1535 (2003); (*i*) T. Lee, I. Jung, K.-H. Song, H. Lee, J. Choi, K. Lee, B.J. Lee, J. Park, C. Lee, S.O. Kang, and J. Ko. Organometallics, **23**, 5280 (2004); (*j*) H. Sohn, M.J. Sailor, D. Magde, and W.C. Trogler. J. Am. Chem. Soc. **15**, 3496 (2003).
11. (*a*) S. Yamaguchi, R.-Z. Jin, and K. Tamao. J. Am. Chem. Soc. **121**, 2937 (1999); (*b*) H. Sohn, R.R. Huddleston, D.P. Powell, and R. West. J. Am. Chem. Soc. **121**, 2935 (1999); (*c*) T. Sanji, T. Sakai, C. Kabuto, and H. Sakurai. J. Am. Chem. Soc. **120**, 4552 (1998); (*d*) J. Chen, Z. Xie, J.W.Y. Lam, C.C.W. Law, and B.Z. Tang. Macromolecules, **36**, 1108 (2003); (*e*) G. Zhang, J. Ma, and Y. Jiang. Macromolecules, **36**, 2130 (2003).
12. (*a*) D.-L. Jiang and T. Aida. J. Am. Chem. Soc. **120**, 10 895 (1998); (*b*) T. Sato, D.-L. Jing, and T. Aida. J. Am. Chem. Soc. **121**, 10 658 (1999); (*c*) M.S. Choi, T. Aida, T. Yamazaki, and I. Yamazaki. Chem. Eur. J. **8**, 2667 (2002); (*d*) C.

© 2005 NRC Canada

Devadoss, P. Bharathi, and J.S. Moore. J. Am. Chem. Soc. **118**, 9635 (1996).
13. H. Okinoshima, K. Yamamoto, and M. Kumada. J. Am. Chem. Soc. **94**, 9263 (1972).
14. C. Hawker and J.M.J. Fréchet. J. Am. Chem. Soc. **112**, 7638 (1990).
15. B.Z. Tang, X. Zhan, G. Yu, P.P.S. Lee, Y. Liu, and D. Zhu. J. Mater. Chem. **11**, 2974 (2001).
16. J. Docherty and C.-C. Tsai. PCT Int. Appl. WO 02/13764 A2, 2002.

© 2005 NRC Canada

Activation and cleavage of alkynes by the dinuclear tantalum complexes $([NPN]Ta)_2(\mu\text{-}H)_4$ and $([NPN]Ta)_2(\mu\text{-}\eta^1{:}\eta^2\text{-}N_2)(\mu\text{-}H)_2$ (where NPN = $PhP(CH_2SiMe_2NPh)_2$)[1]

Michael P. Shaver, Samuel A. Johnson, and Michael D. Fryzuk

Abstract: Reaction of phenylacetylene with the dinuclear tetrahydride complex $([NPN]Ta)_2(\mu\text{-}H)_4$ gives the product $([NPN]Ta)_2(\mu\text{-}PhCCH)(\mu\text{-}H)_2$ (where NPN is $PhP(CH_2SiMe_2NPh)_2$). Activation of other terminal alkynes by $([NPN]Ta)_2(\mu\text{-}H)_4$ accesses $([NPN]Ta)_2(\mu\text{-}RCCH)(\mu\text{-}H)_2$ (R = *n*-Pr, *t*-Bu). Crystallographic analysis of the R = Ph derivative showed it to be a bis(μ-alkylidene) bound asymmetrically to the two tantalum centres. Storage of solutions of $([NPN]Ta)_2(\mu\text{-}PhCCH)(\mu\text{-}H)_2$ under vacuum promotes the loss of H_2 and cleavage of the C—C bond to give a bis(μ-alkylidyne) complex, $([NPN]Ta)_2(\mu\text{-}CPh)(\mu\text{-}CH)$. Addition of diphenylacetylene did not give the desired $([NPN]Ta)_2(\mu\text{-}CPh)_2$, but rather promotes a complex decomposition of the supporting [NPN] ligands. Reaction of phenylacetylene with the dinitrogen complex $([NPN]Ta)_2(\mu\text{-}\eta^1{:}\eta^2\text{-}N_2)(\mu\text{-}H)_2$ results in the dissociation of the bound dinitrogen and the formation of $([NPN]Ta)_2(\mu\text{-}PhCCH)(\mu\text{-}H)_2$, which is identical to that derived from the reaction with the dinuclear tetrahydride.

Key words: tantalum, alkyne, alkylidene, alkylidyne, amidodiphosphine, dinuclear hydride dinitrogen, activation of small molecules.

Résumé : La réaction du phénylacétylène avec le complexe tétrahydrure dinucléaire $([NPN]Ta)_2(\mu\text{-}H)_4$ conduit au produit $([NPN]Ta)_2(\mu\text{-}PhCCH)(\mu\text{-}H)_2$ dans lesquels NPN = $PhP(CH_2SiMe_2NPh)_2$. L'activation d'autres alcynes terminaux par du $([NPN]Ta)_2(\mu\text{-}H)_4$ permet d'accéder aux composés $([NPN]Ta)_2(\mu\text{-}RCCH)(\mu\text{-}H)_2$ dans lesquels R = *n*-propyle et *t*-butyle. Une analyse cristallographique du dérivé avec R = Ph montre qu'il s'agit d'un bis(μ-alkylidène) lié d'une façon asymétrique aux deux centres de tantale. L'entreposage de solutions de $([NPN]Ta)_2(\mu\text{-}PhCCH)(\mu\text{-}H)_2$ sous vide facilite la perte de H_2 et le clivage de la liaison C—C pour conduire à la formation d'un complexe bis(μ-alkylidyne), $([NPN]Ta)_2(\mu\text{-}CPh)(\mu\text{-}CH)$. L'addition de diphénylacétylène n'a pas conduit au $([NPN]Ta)_2(\mu\text{-}CPh)_2$ attendu, mais a plutôt favorisé une décomposition complexe des ligands supports [NPN]. La réaction du phéhylacétylène avec le complexe de diazote $([NPN]Ta)_2(\mu\text{-}\eta^1{:}\eta^2\text{-}N_2)(\mu\text{-}H)_2$ conduit à une dissociation du diazote lié et à la formation de $([NPN]Ta)_2(\mu\text{-}PhCCH)(\mu\text{-}H)_2$ identique à celui obtenu par réaction avec le tétrahydrure dinucléaire.

Mots clés : tantale, alcyne, alkylidène, alkylidyne, amidodiphosphine, hydrure de diazote dinucléaire, activation de petites molécules.

[Traduit par la Rédaction]

Introduction

To cleave an element–element triple bond as found in dinitrogen (N≡N) and alkynes (RC≡CR′) formally requires the addition of six electrons. Such cleavage processes are critical to the alkyne metathesis process (1) and could be an important method to convert molecular nitrogen into higher value organic materials (2). There are a number of recent studies that have detailed cleavage of N_2 using group 5 (3–5) and group 6 (6–8) derivatives to generate metal nitride species. While the product nitrides are generally extremely stable, further functionalization of the molybdenum nitride $N{\equiv}Mo(N[Ar]\text{-}t\text{-}Bu)_3$, formed from $Mo(N[Ar]\text{-}t\text{-}Bu)_3$ and N_2, has recently been reported (9). With regard to alkyne metathesis, the prototypical reactions involve group 6 alkoxide systems, typically $RC{\equiv}W(O\text{-}t\text{-}Bu)_3$ (1), and related Mo derivatives (10), along with a variety of in-situ-generated active catalysts (11). Although the cleavage of dinitrogen and alkynes occurs via quite different mechanisms, it is remarkable that very similar systems are found for both processes albeit with quite distinct ancillary ligand sets.

A somewhat related outcome has been reported (12) for the reaction of alkynes with the dinuclear tungsten(III) hydride derivative, $[silox]_2HW{\equiv}WH[silox]_2$. In this case, a sta-

Received 8 November 2004. Published on the NRC Research Press Web site at http://canjchem.nrc.ca on 14 June 2005.

Dedicated to Howard Alper for his outstanding contributions in organometallic chemistry.

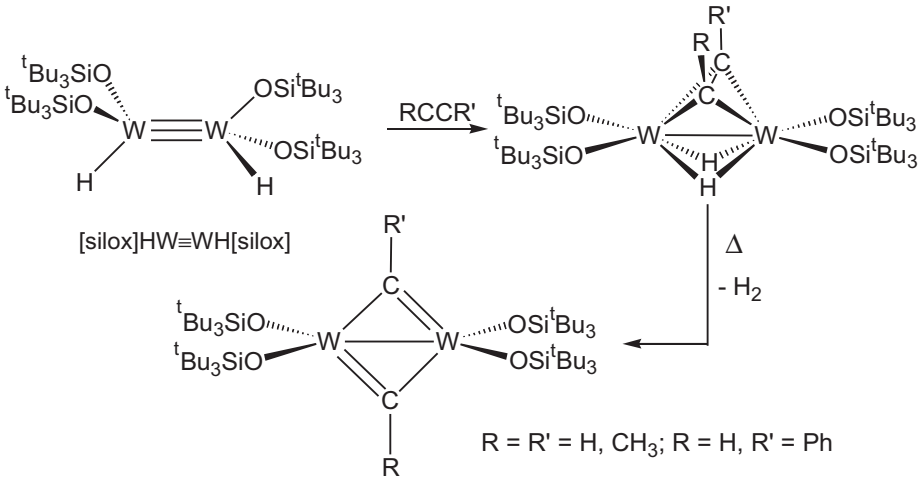
M.P. Shaver, S.A. Johnson, and M.D. Fryzuk.[2] Department of Chemistry, The University of British Columbia, 2036 Main Mall, Vancouver, BC V6T 1Z1, Canada.

[1]This article is part of a Special Issue dedicated to Professor Howard Alper.

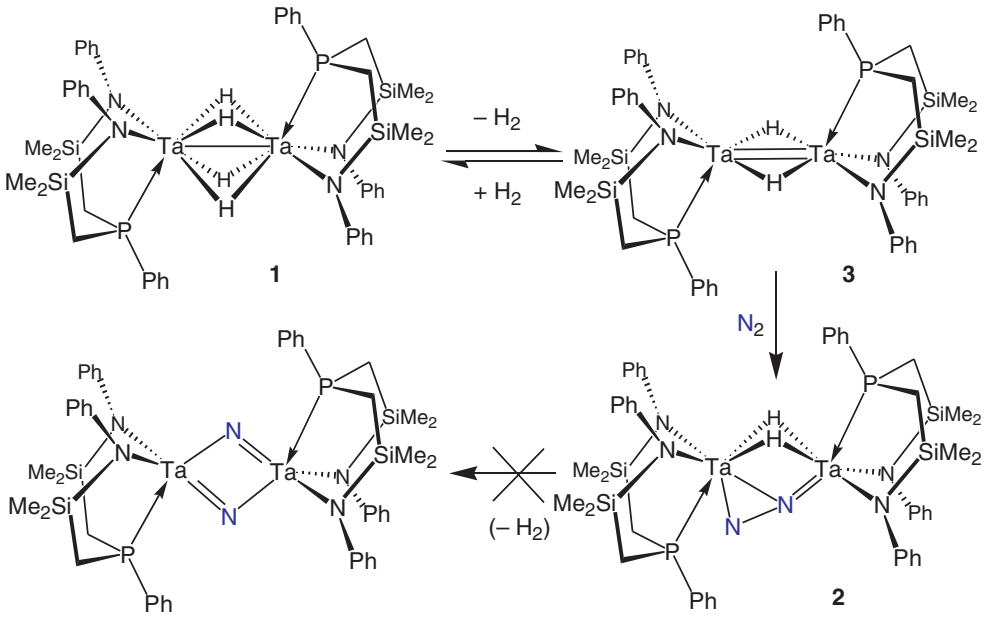
[2]Corresponding author (e-mail: fryzuk@chem.ubc.ca).

 doi: 10.1139/V05-034 © 2005 NRC Canada

Scheme 1.



Scheme 2.



ble intermediate having the formula $([silox]_2W)_2(\mu\text{-}\eta^2\text{:}\eta^2\text{-}RCCR')(\mu\text{-}H)_2$ is formed and contains an activated bridging alkyne unit, which is subsequently cleaved by loss of H_2 to generate a ditungsten species with bridging alkylidyne units (Scheme 1); the starting dinuclear hydride does not react with N_2.

We have previously reported that the ditantalum tetrahydride complex $([NPN]Ta)_2(\mu\text{-}H)_4$ (**1**) (where NPN = $PhP(CH_2SiMe_2NPh)_2$) can activate dinitrogen to generate $([NPN]Ta)_2(\mu\text{-}\eta^1\text{:}\eta^2\text{-}N_2)(\mu\text{-}H)_2$ (**2**) via loss of H_2 (13). Although cleavage of coordinated N_2 in **2** is not directly observed, subsequent reaction of **2** with boranes and silanes does result in both cleavage and functionalization of the dinitrogen moiety (14, 15). Given the analogy described previously for cleavage of N_2 and alkynes with group 6 systems, we examined the reaction of the group 5 dinuclear tetrahydride **1** with alkynes to determine if both alkynes and N_2 could be activated using the same metal with the same ligand set. In this paper, we report both activation and cleavage of terminal alkynes using both the tetrahydride (**1**) and the dinitrogen complex (**2**) as starting materials. In addition, we also describe the reaction of diphenylacetylene with **1** that results in a completely different kind of product.

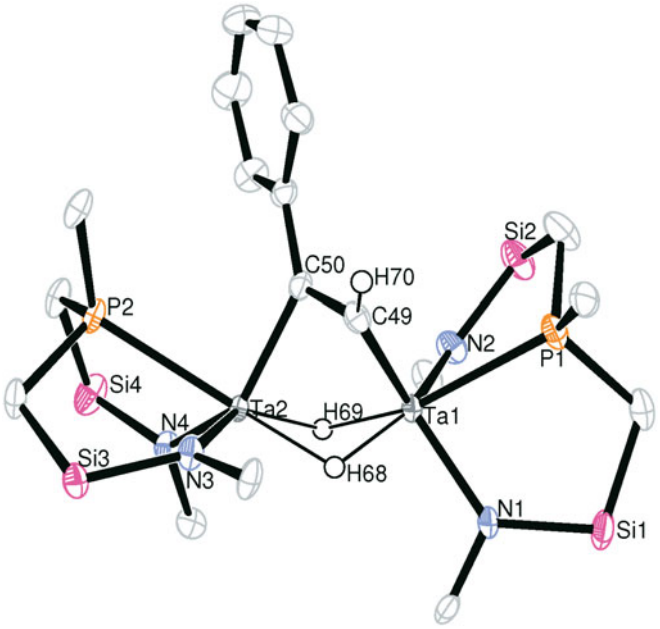
Results and discussion

The tetrahydride derivative **1** is formally a d^1–d^1 dinuclear system. It reacts with substrates by loss of H_2 to generate the reactive, unobserved d^2–d^2 dihydride $([NPN]Ta)_2(\mu\text{-}H)_2$ (**3**), a species with a Ta=Ta double bond. With N_2, only four electrons are involved in the formation of **2** (Scheme 2) (13), although if H_2 could be eliminated, the total number of electrons available would be six, ideal for cleavage of both N_2 and alkynes.

The reaction of PhC≡CH with **1** results in the formation of a new complex that displays two resonances in the ^{31}P

© 2005 NRC Canada

Fig. 1. ORTEP drawing (spheroids at 50% probability) of $([NPN]Ta)_2(\mu\text{-PhCCH})(\mu\text{-H})_2$ (**4**). Silyl methyl and phenyl ring carbons other than ipso and methine carbons have been omitted for clarity. Hydrides H68, H69, and terminal proton H70 were located in the diffraction pattern and refined isotropically.



NMR spectrum, at δ 18.1 and 20.0 ppm. In addition, there are two multiplets in the ^{1}H NMR spectrum at 13.14 and 11.65 ppm, which can be assigned to two bridging hydrides that are coupled to each other, as well as to both ligand ^{31}P nuclei. A third resonance at 11.72 ppm is coupled only to a single ^{31}P environment, with a J_{HP} value of 11.8 Hz, and corresponds to the terminal proton of the intact, coordinated phenylacetylene unit. Resonances due to eight silyl methyl environments are observed, consistent with a molecule of C_1 symmetry. On the basis of this information, the product of this reaction has the formula, $([NPN]Ta)_2(\mu\text{-PhCCH})(\mu\text{-H})_2$ (**4**).

Crystals of **4** were examined using X-ray diffraction; the solid-state molecular structure of complex **4** is shown in Fig. 1. Relevant bond lengths and angles are listed in Table 1 and crystallographic data are located in Table 2. The X-ray structure of complex **4** displays a highly unsymmetrical bonding of the phenylacetylene moiety. The Ta(1)—C(49) bond length of 2.061(4) Å is much shorter than the Ta(2)—C(49) distance of 2.511(4) Å. Likewise, the Ta(2)—C(50) bond length of 2.055(4) Å is much shorter than the Ta(1)—C(50) distance of 2.526(4) Å. A similar bonding mode was observed in $[(THF)Cl_2Ta]_2(\mu\text{-}\eta^2\text{:}\eta^2\text{-}t\text{-BuCC-}t\text{-Bu})(\mu\text{-Cl})_2$ (16). In this latter example, the asymmetry was attributed to steric factors. The differences in Ta—C bond lengths in $[(THF)Cl_2Ta]_2(\mu\text{-}\eta^2\text{:}\eta^2\text{-}t\text{-BuCC-}t\text{-Bu})(\mu\text{-Cl})_2$ are not as large (2.214(11) vs. 2.416(11) Å), corresponding to a twist of only 7° from a perfectly perpendicular projection of the acetylene C—C bond upon the Ta-Ta axis. In complex **4**, the projection of the C(49)—C(50) bond on Ta(1)—Ta(2) is closer to 45° away from a perpendicular arrangement of these two units, and is difficult to attribute to steric factors. The Ta(1)—C(49) and Ta(2)—C(50) distances are considerably shorter than that expected for Ta—C single bonds, and are similar to the Ta=C bond lengths found in tantalum alkylidene complexes. The bonding of phenylacetylene in **4** can, therefore, be viewed as a bis(μ-alkylidene) as is depicted in eq. [1]. The sum of the bond angles Ta(2)-C(50)-C(51), Ta(2)-C(50)-C(49), and C(49)-C(50)-C(51) is 356.5(10)°; the geometry at C(50) is essentially trigonal planar, as antic-

Table 1. Selected bond distances (Å), angles (°), and dihedral angles (°) for $([NPN]Ta)_2(\mu\text{-PhCCH})(\mu\text{-H})_2$ (**4**).

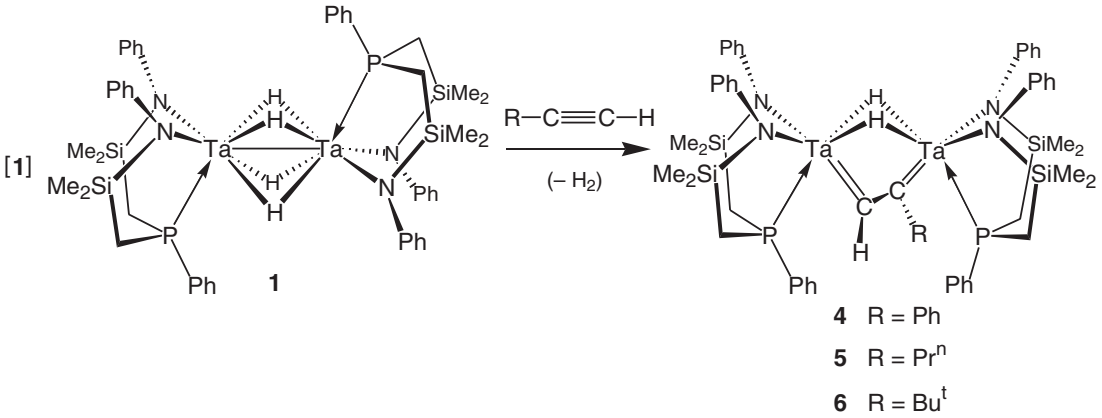
Bond lengths (Å)	
C(49)—C(50)	1.397(6)
Ta(1)—C(49)	2.061(4)
Ta(2)—C(49)	2.511(4)
Ta(1)—C(50)	2.526(4)
Ta(2)—C(50)	2.055(4)
Ta(1)—Ta(2)	2.6905(2)
Ta(1)—N(1)	2.085(3)
Ta(1)—N(2)	2.091(4)
Ta(1)—P(1)	2.583(1)
Ta(2)—N(3)	2.090(4)
Ta(2)—N(4)	2.076(3)
Ta(2)—P(2)	2.619(1)
Bond angles (°)	
P(1)-Ta(1)-C(49)	80.9(1)
N(1)-Ta(1)-C(49)	128.2(2)
N(2)-Ta(1)-C(49)	112.7(2)
P(1)-Ta(1)-C(50)	101.8(1)
N(1)-Ta(1)-C(50)	158.5(1)
N(2)-Ta(1)-C(50)	91.1(1)
P(2)-Ta(2)-C(50)	85.7(1)
N(3)-Ta(2)-C(50)	109.8(2)
N(4)-Ta(2)-C(50)	125.7(2)
P(2)-Ta(2)-C(49)	106.2(1)
N(3)-Ta(2)-C(49)	88.1(1)
N(4)-Ta(2)-C(49)	156.3(1)
Ta(2)-C(50)-C(51)	138.6(3)
Ta(2)-C(50)-C(49)	91.3(3)
C(49)-C(50)-C(51)	126.6(4)
Ta(2)-Ta(1)-P(1)	143.04(3)
Ta(2)-Ta(1)-N(1)	122.5(1)
Ta(2)-Ta(1)-N(2)	113.5(1)
Ta(2)-Ta(1)-C(49)	62.2(1)
Ta(1)-Ta(2)-P(2)	148.31(3)
Ta(1)-Ta(2)-N(3)	111.53(9)
Ta(1)-Ta(2)-N(4)	121.6(1)
Ta(1)-Ta(2)-C(50)	62.6(1)
P(1)-Ta(1)-N(1)	79.9(1)
P(1)-Ta(1)-N(2)	79.4(1)
N(1)-Ta(1)-N(2)	110.1(2)
P(2)-Ta(2)-N(3)	77.6(1)
P(2)-Ta(2)-N(4)	76.1(1)
N(3)-Ta(2)-N(4)	115.1(1)
Ta(1)-C(49)-C(50)	91.8(3)
Ta(1)-C(49)-C(50)-C(51)	–132.2(4)
P(1)-Ta(1)-Ta(2)-P(2)	36.44(7)
Ta(1)-C(49)-C(50)-Ta(2)	65.5(2)

© 2005 NRC Canada

Table 2. Crystallographic data for structures **4** and **8**.

Complex	**4**	**8**
CCDC registry	254538	254539
Empirical formula	$C_{56}H_{70}N_4P_2Si_4Ta_2$	$C_{59}H_{71}N_4P_2Si_4Ta_2$
Formula weight	1 335.38	1 372.40
Space group	*P*-1	*P*-1
Crystal system	Triclinic	Triclinic
a–*c* (Å)	11.953(2), 12.409(2), 20.487(2)	11.424(1), 12.453(2), 23.760(1)
α, β, and γ (°)	80.039(2), 88.882(3), 74.025(3)	70.66(3), 73.14(3), 72.50(3)
V (Å^3)	2 876.1(6)	2 972.9(4)
Z	2	2
$D_{calcd.}$ (g cm^{-3})	1.54	1.54
μ (Mo Kα) (cm^{-1})	39.74	38.52
T (K)	173±1	173±1
2θ range (°)	55.8	55.76
Total reflections	24 498	27 096
Unique reflections	10 910	12 280
Parameters	625	649
R_1[a]	0.054	0.0332
R_w[b]	0.087	0.0657
Goodness of fit	1.30	1.155

[a] $R_1 = \Sigma(|F_o| - |F_c|)/\Sigma|F_o|$.
[b] $R_w = [\Sigma(w(|F_o^2| - |F_c^2|)^2/\Sigma(w|F_o^2|^2)]^{1/2}$.



ipated for an alkylidene carbon. The C(49)—C(50) distance is 1.397(6) Å, which is intermediate between typical single and double C—C bond lengths. In a mononuclear tantalum alkyne complex that was also described as a bis(μ-alkylidene), a slightly shorter alkyne C—C bond length of 1.329(6) Å was reported (17).

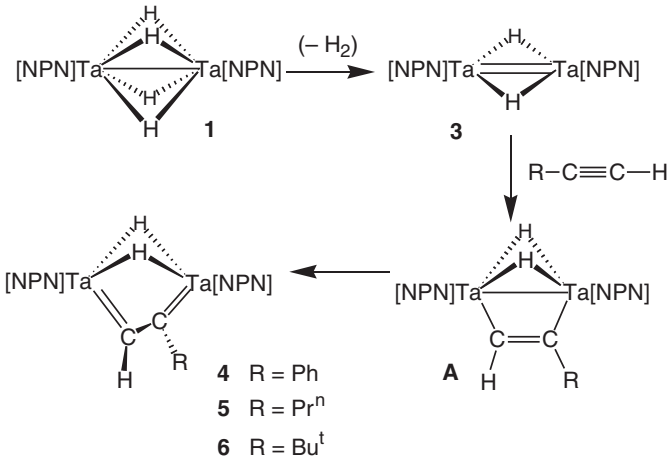
The outcome is identical for the reaction of **1** with other terminal alkynes such as *n*-PrC≡CH and *t*-BuC≡CH to produce **5** and **6**, respectively (eq. [1]). These products are readily characterized by multinuclear NMR spectroscopy. Each product exhibits two ^{31}P chemical shifts; 11.91 and 12.48 ppm for **5**, and 6.10 and 9.17 ppm for **6**. Similarly, each has a distinctive hydride region, with two asymmetric, bridging tantalum hydrides. The hydride resonances in complexes **5** and **6** do not exhibit clear AMXY patterns as in **4**, instead they appear as complicated multiplets at 11.03 and 11.56 ppm for **5**, and at 11.51 and 12.08 ppm for **6**. In each case, ^{13}C NMR studies support the assignment of products as bis(μ-alkylidene) type species as the individual alkylidene carbons can be assigned to resonances in the region 205–220 ppm. Unfortunately, attempts to characterize these products by crystallographic techniques were unsuccessful. The reaction of the dinitrogen complex **2** with terminal alkynes also produces the identical products via loss of N_2; the yields via the reaction of the tetrahydride **1** are slightly higher.

As already mentioned, the likely pathway for the formation of these products is via initial loss of H_2 to generate the coordinatively unsaturated, highly reactive dihydride **3**. A possible intermediate before formation of the bis(μ-alkylidene) species is the ditantalocyclobutene species **A** formed via a parallel approach of the terminal alkyne to the Ta=Ta double bond (18); rearrangement of **A** to the bis(μ-alkylidene) requires further reduction of the bridging alkyne moiety by the remaining Ta—Ta bond (Scheme 3).

Storing solutions of **4** under vacuum leads to the quantitative formation of a symmetrical product as evidenced by a singlet at 11.5 ppm in the ^{31}P NMR spectrum. The two downfield resonances at 11.65 and 13.14 ppm, owing to the bridging hydrides in **4**, have disappeared and the alkyne pro-

© 2005 NRC Canada

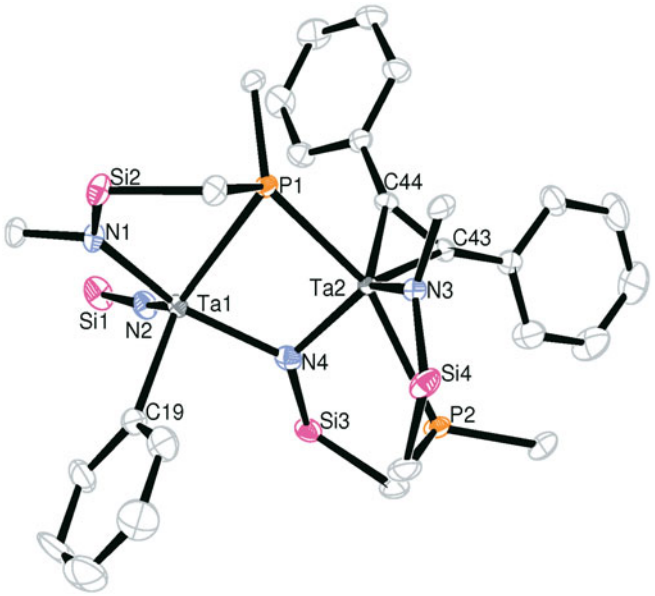
Scheme 3.



ton resonance has shifted from 11.72 to 4.95 ppm. Evidence of a symmetrical product is also seen in the reduction in the number of silyl methyl resonances from eight to four. In analogy to the W[silox] system shown in Scheme 1 (12), loss of H_2 could provide the final two electrons required to cleave the remaining C—C bond in **4** and generate a bis(μ-alkylidyne) complex. ^{13}C NMR experiments reveal that the alkylidene carbon resonances at 224.2 and 224.3 ppm in **4** have disappeared and have been replaced by two new resonances at 308.8 and 311.2 ppm, all of which support this cleavage process and the formation of $([NPN]Ta)_2(\mu\text{-}CH)(\mu\text{-}CPh)$ (**7**), as shown in eq. [2]. Unfortunately, numerous attempts to obtain X-ray quality crystals have failed; nevertheless, the analogy to the W[silox] system, the high symmetry of the product, and the ^{13}C NMR data are compelling.

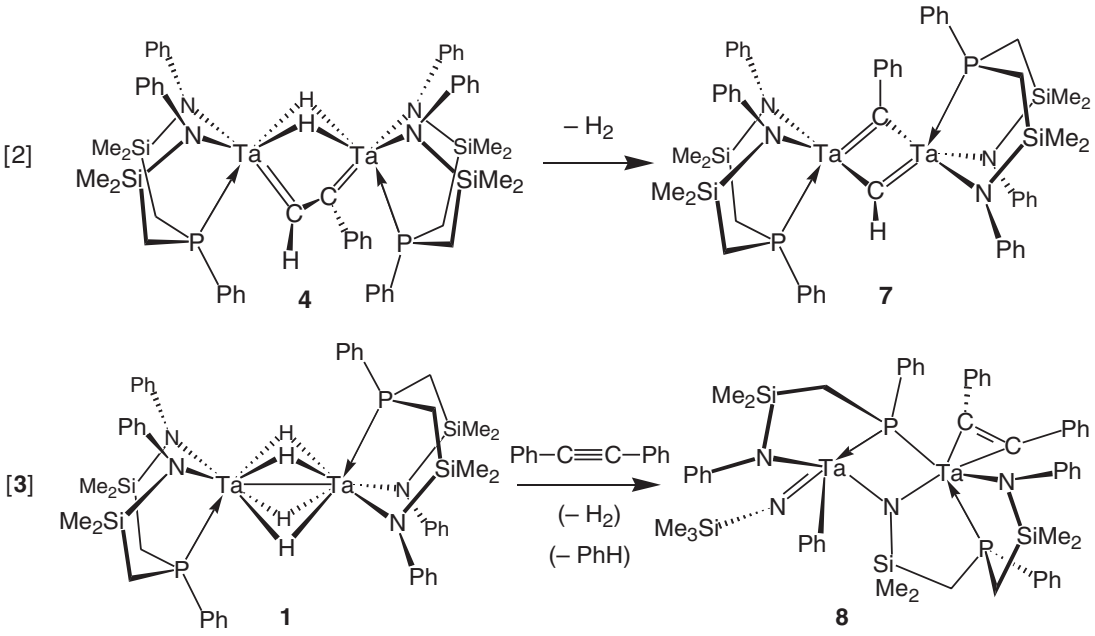
To extend this reaction further, the addition of diphenylacetylene (PhC≡CPh) to the tetrahydride **1** was examined in an effort to generate the symmetrical bis(μ-alkylidyne) $([NPN]Ta)_2(\mu\text{-}CPh)_2$; however, a completely different outcome ensued. The reaction was quite slow as evidenced by

Fig. 2. ORTEP drawing (spheroids at 50% probability) of product of $([NPN]Ta)_2(\mu\text{-}H)_4$ and PhC≡CPh (**8**). Ligand silyl methyl and phenyl ring carbons other than ipso positions have been omitted for clarity.



the slow change in colour from a purple to orange solution over a 24 h period. The NMR spectrum of the resulting isolated product indicated vastly increased complexity and loss of symmetry, not at all consistent with the desired bis(μ-alkylidyne) outcome. For example, instead of observing two singlets for the silyl methyl resonances, seven peaks were observed with different integrations. Fortunately, a single crystal X-ray diffraction study provided the identity of this unsymmetrical product, as shown in Fig. 2; a schematic of this reaction outcome is given in eq. [3].

What is most evident is that each ancillary [NPN] ligand has fractured in a unique way. One ligand has degraded through scission of a N—C bond to give a bridging imide



© 2005 NRC Canada

ligand and an η^1-phenyl ring. The other ligand has undergone P—C bond cleavage producing a new terminal trimethylsilyl-imido group that has lost its phenyl substituent and a bridging phosphide. Diphenylacetylene has been incorporated in an η^2-manner and is bound to one tantalum centre. The asymmetrical unit also contained a half equivalent of co-crystallized benzene. The bridging imide and phosphide ligands are bound asymmetrically. N(4)—Ta(1) and N(4)—Ta(2) distances are 2.121(4) and 1.961(4) Å, respectively, while P(1)—Ta(1) and P(1)—Ta(2) interatomic distances of 2.7563(11) and 2.4555(11) Å exhibit an even stronger asymmetry. Tantalum carbon bond lengths are typical: Ta(1)—C(19), Ta(2)—C(43), and Ta(2)—C(44) distances are 2.190(4), 2.124(4), and 2.129(4) Å, respectively. The C(43)—C(44) distance in the coordinated alkyne is lengthened to 1.313(6) Å and can be considered a C=C bond. For reference, the molecular structure of Ta($OC_6H_3Ph_2$-2,6)$_2$(η^2-EtCCEt)Cl(PMe_3) has a C=C distance of 1.291(6) Å, and Ta—C distances of 2.045(3) and 2.092(4) Å (19). The terminal imido ligand has a much shorter bond length with the metal centre than these tantalum amides; the Ta(1)—N(2) interatomic distance is 1.782(4) Å. These and other selected bond lengths and angles for **8** are located in Table 3 while the corresponding crystallographic data[3] can be found in Table 2.

^{1}H and ^{31}P NMR data are consistent with the product assignment. Integration of the complicated aryl region indicates that seven phenyl ring systems are present in the final complex. Seven silyl methyl resonances are also present, six of which integrate to 3H with one at 0.22 ppm that integrates to 9H. Isotopic labeling studies, tracked by the addition of diphenylacetylene to ([NPN]Ta)$_2$(μ-D)$_4$ (d_4-**1**), show clean deuterium incorporation only into the imine silylmethyl resonances. Addition of other internal alkynes (*t*-BuC≡C-*t*-Bu, *n*-BuC≡C-*n*-Bu) to the tetrahydride **1** also appears to promote ligand decomposition, although no characterizable products could be cleanly isolated. The formation of **8** is yet another example of the fragile nature of the [NPN] ligand (3, 14, 20, 21).

A mechanistic proposal for this transformation is challenging. The alkyne is presumably too bulky and thus cannot react with the dihydride intermediate in the same manner as terminal alkynes (Scheme 3), and this results in the ligand undergoing a series of oxidative cleavage and rearrangement processes. Speculation beyond such obvious statements is not useful.

Table 3. Selected bond distances (Å) and angles (°) for **8**.

Bond lengths (Å)	
Ta(1)—N(1)	2.042(4)
Ta(1)—N(2)	1.782(4)
Ta(1)—C(19)	2.190(4)
Ta(1)—N(4)	2.121(4)
Ta(1)—P(1)	2.7563(11)
Ta(2)—P(1)	2.4555(11)
Ta(2)—N(4)	1.961(4)
Ta(2)—P(2)	2.6068(11)
Ta(2)—N(3)	2.084(3)
Ta(2)—C(43)	2.124(4)
Ta(2)—C(44)	2.129(4)
C(43)—C(44)	1.313(6)
Bond angles (°)	
Ta(1)-P(1)-Ta(2)	79.38(3)
Ta(1)-N(4)-Ta(2)	109.57(17)
Ta(2)-C(43)-C(44)	72.2(2)
Ta(2)-C(44)-C(43)	71.8(2)
N(2)-Ta(1)-N(1)	103.41(16)
N(2)-Ta(1)-N(4)	104.13(16)
N(1)-Ta(1)-N(4)	150.98(14)
N(2)-Ta(1)-C(19)	105.43(17)
N(1)-Ta(1)-C(19)	92.58(15)
N(4)-Ta(1)-C(19)	88.23(15)
N(2)-Ta(1)-P(1)	128.07(11)
N(1)-Ta(1)-P(1)	76.35(10)
N(4)-Ta(1)-P(1)	126.50(13)
C(19)-Ta(1)-P(1)	126.50(13)
N(4)-Ta(2)-N(3)	123.76(13)
N(4)-Ta(2)-C(43)	112.13(15)
N(3)-Ta(2)-C(43)	116.58(14)
C(44)-Ta(2)-C(43)	35.97(15)
N(4)-Ta(2)-P(1)	91.04(11)
N(3)-Ta(2)-P(1)	89.24(10)
C(43)-Ta(2)-P(1)	118.67(11)
N(4)-Ta(2)-P(2)	77.36(11)
N(3)-Ta(2)-P(2)	76.71(10)
C(43)-Ta(2)-P(2)	89.49(11)
P(1)-Ta(2)-P(2)	151.84(3)

Concluding remarks

The dinuclear tetrahydride ([NPN]Ta)$_2$(μ-H)$_4$ (**1**) activates terminal alkynes in a manner that is reminiscent of the activation of molecular nitrogen. In both cases, unsymmetrical bridging modes are observed in which considerable bond activation has occurred. In the case of terminal acetylenes, the adduct is best described as a bis(μ-alkylidene), wherein the original C≡C triple bond has been reduced to a C—C bond. The same bis(μ-alkylidene) product is observed when phenylacetylene is added to the dinitrogen complex ([NPN]Ta)$_2$(μ-η^1:η^2-N_2)(μ-H)$_2$ (**2**) and suggests the intermediacy of a common species in the formation of ([NPN]Ta)$_2$(μ-PhCCH)(μ-H)$_2$ (**4**), likely the d^2–d^2 dinuclear dihydride ([NPN]Ta)$_2$(μ-H)$_2$ (**3**). Upon standing, **4** loses H_2 under vacuum, which results in the cleavage of the C≡C bond to give a bis(μ-alkylidyne) complex, ([NPN]Ta)$_2$(μ-CPh)(μ-CH) (**7**). This represents a formal reduction of the C≡C triple bond by six electrons, supplied by the d^2–d^2

[3] Supplementary data for this article are available on the Web site or may be purchased from the Depository of Unpublished Data, Document Delivery, CISTI, National Research Council Canada, Ottawa, ON K1A 0S2, Canada. DUD 3664. For more information on obtaining material refer to http://cisti-icist.nrc-cnrc.gc.ca/irm/unpub_e.shtml. CCDC 254538 and 254539 contain the crystallographic data for this manuscript. These data can be obtained, free of charge, via www.ccdc.cam.ac.uk/conts/retrieving.html (Or from the Cambridge Crystallographic Data Centre, 12 Union Road, Cambridge CB2 1EZ, UK; fax +44 1223 336033; or deposit@ccdc.cam.ac.uk).

© 2005 NRC Canada

dihydride **3** coupled with loss of H_2. Attempts to extend this activation process to internal alkynes were not successful, likely because of increased steric effects in the substrates. In the case of diphenylacetylene, ancillary ligand degradation and rearrangement were observed.

Experimental

General considerations

Unless otherwise stated, all manipulations were performed under an inert atmosphere of dry, oxygen-free dinitrogen or argon by means of standard Schlenk or glovebox techniques. Where choice of atmosphere affects reaction outcomes, the distinction between dinitrogen and argon use will be made. Anhydrous hexanes and toluene were purchased from Aldrich, sparged with dinitrogen, and passed through activated alumina and Ridox catalyst columns under a positive pressure of nitrogen prior to use (22). Anhydrous pentane, benzene, tetrahydrofuran, and diethylether were purchased from Aldrich, sparged with dinitrogen, and passed through an Innovative Technologies Pure-Solv 400 solvent purification system. All organic solvents were tested by addition of a toluene solution of sodium benzophenone ketyl prior to use to ensure the absence of oxygen and water. Alternatively, anhydrous diethylether was stored over sieves and distilled from sodium benzophenone ketyl under argon. Tetrahydrofuran was refluxed over CaH_2 prior to distillation from sodium benzophenone ketyl under argon, and pentane was stored over sieves and distilled from sodium benzophenone ketyl solubilized by tetraglyme under argon prior to storage over a potassium mirror. Nitrogen gas was dried and deoxygenated by passage through a column containing activated molecular sieves and MnO. Deuterated benzene was dried by heating at reflux with a sodium–potassium alloy in a sealed vessel under partial pressure, then trap-to-trap distilled, and freeze–pump–thaw degassed three times. Unless otherwise stated, ^{1}H, ^{31}P, ^{1}H{^{31}P}, and ^{31}P{^{1}H} NMR spectra were recorded on a Bruker AMX-500 instrument with a 5 mm BBI probe operating at 500.1 MHz for ^{1}H. ^{1}H NMR spectra were referenced to residual protons in C_6D_5H (δ 7.15 ppm) with respect to tetramethylsilane at δ 0.0 ppm. ^{31}P NMR spectra were referenced to either external or internal $P(OMe)_3$ (δ 141.0 ppm with respect to 85% H_3PO_4 at δ 0.0 ppm). Elemental analyses were performed by Mr. P. Borda and M. Lakha of the Department of Chemistry, University of British Columbia. Complexes $([NPN]Ta)_2(\mu\text{-}H)_4$, $([NPN]Ta)_2(\mu\text{-}D)_4$, and $([NPN]Ta)_2(\mu\text{-}\eta^1\text{:}\eta^2\text{-}N_2)(\mu\text{-}H)_2$ were prepared following literature procedures (13). PhC≡CH, *t*-uC≡CH, *n*-PrC≡CH, and PhC≡CPh were purchased from Aldrich and purified by standard procedures prior to use.

Preparation of $([NPN]Ta)_2(\mu\text{-PhCCH})(\mu\text{-}H)_2$ (4), $([NPN]Ta)_2(\mu\text{-}n\text{-PrCCH})(\mu\text{-}H)_2$ (5), and $([NPN]Ta)_2(\mu\text{-}t\text{-BuCCH})(\mu\text{-}H)_2$ (6)

A solution of $([NPN]Ta)_2(\mu\text{-}H)_4$ (500 mg, 0.405 mmol) in 20 mL Et_2O under argon was prepared in a vessel equipped with a Kontes valve. The neat alkyne RCCH (0.405 mol) was added to the flask via microsyringe, the vessel was sealed, and its contents stirred for 6 h. A colour change from deep purple to brown was observed, along with the evolution of a gas. Removal of solvent in vacuo left a dark brown solid. This solid was triturated with pentane and dried under vacuum to afford $([NPN]Ta)_2(\mu\text{-PhCCH})(\mu\text{-}H)_2$ (**4**), $([NPN]Ta)_2(\mu\text{-}n\text{-PrCCH})(\mu\text{-}H)_2$ (**5**), and $([NPN]Ta)_2(\mu\text{-}t\text{-BuCCH})(\mu\text{-}H)_2$ (**6**) in 92%, 80%, and 88% yields.

4: ^{1}H NMR (C_6D_6, 25 °C, 500 MHz) δ: –0.74, –0.48, –0.24, 0.00, 0.01, 0.09, 0.32, 0.64 (s, 24H, SiCH_3), 0.87–1.49 (m, 8H, PCH_2Si), 6.59–7.79 (m, 35H, NPh-*H*, PPh-*H*, CPh-*H*), 11.65 (d of d of d, 1H, $^2J_{HH}$ = 16.8 Hz, $^2J_{HP}$ = 5.5 Hz, $^2J_{HP}$ = 30.0 Hz, Ta*H*Ta), 11.72 (d, 1H, $^3J_{HP}$ = 11.8 Hz, PhCC*H*), 13.14 (d of d of d, 1H, $^2J_{HH}$ = 16.8 Hz, $^2J_{HP}$ = 5.9 Hz, $^2J_{HP}$ = 31.8 Hz, Ta*H*Ta). ^{13}C NMR (C_6D_6, 25 °C, selected resonances) δ: 224.2 and 224.3 (TaH*CC*Ph). ^{31}P NMR (C_6D_6, 25 °C, 202.5 MHz) δ: 18.14 (s), 20.01 (s). Anal. calcd. for $C_{56}H_{70}N_6P_2Si_4Ta_2$: C 50.37, H 5.28, N 4.20; found: C 50.24, H 5.50, N 4.26.

5: ^{1}H NMR (C_6D_6, 25 °C, 500 MHz) δ: –0.20, –0.12, 0.06, 0.10, 0.15, 0.29, 0.31, 0.33 (s, 24H, SiCH_3), 0.46–1.61 (m, 13H, $CH_2CH_2CH_3$, PCH_2Si), 3.08 (br, 2H, TaCCH_2), 6.51–7.75 (m, 30H, NPh-*H*, PPh-*H*), 10.84 (d of d, 1H, $^3J_{HP}$ = 14.5, 20.5 Hz, CH_2CC*H*), 11.03 (d of d of d, 1H, Ta*H*Ta), 11.56 (m, 1H, Ta*H*Ta). ^{13}C NMR (C_6D_6, 25 °C, selected resonances) δ: 212.9 and 214.3 (TaH*CC*C). ^{31}P NMR (C_6D_6, 25 °C, 202.5 MHz) δ: 11.91 (d, J_{PP} = 4 Hz), 12.48 (d, J_{PP} = 4 Hz).

6: ^{1}H NMR (C_6D_6, 25 °C, 500 MHz) δ: –0.14, –0.11, 0.01, 0.06, 0.18, 0.19, 0.26, 0.34 (s, 24H, SiCH_3), 0.58–1.70 (m, 8H, PCH_2Si), 1.45 (s, 9H, C(CH_3)$_3$), 6.44–7.89 (m, 30H, NPh-*H*, PPh-*H*), 11.09 (d, 1H, J_{HP} = 12.6 Hz, ^{t}BuCC*H*), 11.51 (m, 1H, Ta*H*Ta), 12.08 (m, 1H, Ta*H*Ta). ^{13}C NMR (C_6D_6, 25 °C, selected resonances) δ: 205.5 and 205.3 (TaH*CC*C). ^{31}P NMR (C_6D_6, 25 °C, 202.5 MHz) δ: 6.10 (s), 9.17 (s).

Alternative preparation of $([NPN]Ta)_2(\mu\text{-PhCCH})(\mu\text{-}H)_2$ (4)

Phenylacetylene (0.0656 g, 0.642 mmol) was added to a solution of $([NPN]Ta)_2(\mu\text{-}\eta^1\text{:}\eta^2\text{-}N_2)(\mu\text{-}H)_2$ (0.810 g, 0.642 mmol) in toluene. The solution underwent a noticeable colour change to a darker brown. The solution was stirred for 24 h to ensure complete reaction and then evaporated to dryness. The product was washed with pentanes and dried under vacuum to yield **4** as a dark brown powder in 83% yield.

Preparation of $([NPN]Ta)_2(\mu\text{-CH})(\mu\text{-CPh})$ (7)

$([NPN]Ta)_2(\mu\text{-PhCCH})(\mu\text{-}H)_2$ (250 mg) was dissolved in 20 mL Et_2O in a vessel equipped with a Kontes valve. The contents of the flask were frozen, and the vessel was evacuated. The brown solution was warmed to room temperature and stirred for 12 h prompting a distinct lightening in the solution colour. Removal of volatiles in vacuo gave a light brown solid. Washing this solid with hexanes afforded $([NPN]Ta)_2(\mu\text{-CH})(\mu\text{-CPh})$ in 75% yield. ^{1}H NMR (C_6D_6, 25 °C, 500 MHz) δ: 0.01, 0.10, 0.21, 0.33 (s, 24H, SiCH_3), 1.22 (m, 8H, PCH_2Si), 4.95 (s, 1H, Ta-C*H*), 6.62–7.37 (m, 35H, NPh-*H*, PPh-*H*, CPh-*H*). ^{13}C NMR (C_6D_6, 25 °C, selected resonances) δ: 308.8 and 311.2 (s, Ta-*C*-Ta). ^{31}P NMR (C_6D_6, 25 °C, 202.5 MHz) δ: 11.5 (s).

Preparation of 8 via addition of PhC≡CPh to $([NPN]Ta)_2(\mu\text{-}H)_4$

A solution of $([NPN]Ta)_2(\mu\text{-}H)_4$ (500 mg, 0.405 mmol) in

© 2005 NRC Canada

20 mL Et_2O under argon was prepared in a vessel equipped with a Kontes valve. A solution of diphenylacetylene (72.2 mg, 0.405 mol) in Et_2O (1 mL) was added to the flask via syringe, the vessel sealed, and its contents stirred. A slow colour change from deep purple to orange was observed, along with the evolution of a gas. After 24 h, removal of solvent in vacuo left an orange solid. This solid was triturated with pentane and dried under vacuum to afford **8** as an orange powder in 72% yield. Crystals of this product were grown from a saturated benzene solution. ^{1}H NMR (C_6D_6, 25 °C, 500 MHz) δ: –0.72 (s, 3H, SiCH_3), –0.01 (s, 3H, SiCH_3), 0.02 (s, 3H, SiCH_3), 0.03 (s, 3H, SiCH_3), 0.22 (s, 9H, Si(CH_3)$_3$), 0.50 (s, 3H, SiCH_3), 0.84 (s, 3H, SiCH_3), 1.36–2.10 (m, 6H, PCH_2Si), 6.69–8.09 (m, 35H, NPh-*H*, PPh-*H*, TaPh-*H*, CPh-*H*). ^{31}P NMR (C_6D_6, 25 °C, 202.5 MHz) δ: 13.36 (d, $^2J_{PP}$ = 141 Hz), 130.61 (d, $^2J_{PP}$ = 141 Hz). Anal. calcd. for $C_{60}H_{84}N_4P_2Si_4Ta_2$: C 51.57, H 6.06, N 4.01; found: C 51.90, H 6.39, N 3.70.

Addition of PhC≡CPh to ([NPN]Ta)$_2$(μ-D)$_4$

The experiment was conducted analogously to the preparation of **8** above via the addition of diphenylacetylene (72.2 mg, 0.405 mol) to the dinuclear tetradeuteride ([NPN]Ta)$_2$(μ-D)$_4$ (501.6 mg, 0.405 mmol). Characterization of the crude orange powder by ^{1}H and ^{31}P NMR spectroscopy showed identical resonances to **8**, except where indicated. ^{1}H NMR (C_6D_6, 25 °C, 500 MHz) δ: 0.23 (m, 8H, Si(CH_3)$_2$(CH_2D)).

X-ray crystal structure experimental information

Suitable crystals were selected and coated in Paratone-N oil or an acceptable substitute under an inert atmosphere. Crystals were then mounted on a glass fiber external to the glovebox environment. All measurements were made on a Rigaku/ADSC CCD area detector with graphite monochromated Mo-Kα radiation. The structure for compound **2** was collected and solved by Dr. Brian Patrick. The structure for compound **7** was collected with the assistance of Mr. Chris Carmichael and solved by the author (M.P.S). The data were collected at a temperature of –100 ± 1 °C. The data were processed using the d*TREK program (23) in the CrystalClear software package (version 1.3.5), and corrected for Lorentz and polarization effects, and absorption. Neutral atom scattering factors for all non-hydrogen atoms were taken from Cromer and Waber (24). Anomalous dispersion effects were included in Fcalc (25). The structures were solved by direct methods using SIR92 (26) or SIR2002 (27) and expanded using Fourier techniques. All non-hydrogen atoms were refined anisotropically using SHELXL-97 (28). When hydrogen atom locations were important in determining compound composition or connectivity, hydrogen atoms were located and refined isotropically. Otherwise, hydrogen atoms were included in fixed positions. Their positional parameters were calculated with fixed C—H bond distances of 0.99 Å for sp^2 C, 0.98 Å for sp^3 C, and 0.95 Å for aromatic *sp* C, with U_{iso} set to 1.2 times the U_{eq} values of the attached *sp* or sp^2 C and 1.5 times the U_{eq} value of the attached sp^3 C atoms. Methyl hydrogen torsion angles were determined from electron density. Structure solution and refinements were conducted using the WinGX software package (version 1.64.05) (29).

Acknowledgements

We thank the Natural Sciences and Engineering Research Council of Canada (NSERC) for funding (Discovery Grant to M.D.F. and a PGS B Scholarship to M.P.S.). M.P.S. was also supported by a Killam Predoctoral Fellowship and a Li Tse Fong Fellowship. Thanks are also extended to Mr. Chris Carmichael and Dr. Brian Patrick for collection of X-ray data and for assistance in preparing solutions.

References

1. M.L. Listemann and R.R. Schrock. Organometallics, **4**, 74 (1985).
2. M.P. Shaver and M.D. Fryzuk. Adv. Synth. Catal. **345**, 1061 (2003).
3. M.D. Fryzuk, C.M. Kozak, M.R. Bowdridge, B.O. Patrick, and S.J. Rettig. J. Am. Chem. Soc. **124**, 8389 (2002).
4. A. Caselli, E. Solari, R. Scopelliti, C. Floriani, N. Re, C. Rizzolo, and A. Chiesi-Villa. J. Am. Chem. Soc. **122**, 3652 (2000).
5. G.K.B. Clentsmith and F.G.H. Cloke. J. Am. Chem. Soc. **121**, 10 444 (1999).
6. D.J. Mindiola, K. Meyer, J.-P.F. Cherry, T.A. Baker, and C.C. Cummins. Organometallics, **19**, 1622 (2000).
7. C.E. LaPlaza and C.C. Cummins. Science (Washington, D.C.), **268**, 861 (1995).
8. C.E. LaPlaza, M.J.A. Johnson, J.C. Peters, A.L. Odom, E. Kim, C.C. Cummins, G.N. George, and I.J. Pickering. J. Am. Chem. Soc. **118**, 8623 (1996).
9. H. Henderickx, G. Kwakkenbos, A. Peters, J. van der Spoel, and K. de Vries. Chem. Commun. 2050 (2003).
10. Y.-C. Tsai, P.L. Diaconescu, and C.C. Cummins. Organometallics, **19**, 5260 (2000).
11. U.H.F. Bunz. Acc. Chem. Res. **34**, 998 (2001).
12. R.L.M. Chamberlin, D.C. Rosenfeld, P.T. Wolczanski, and E. Lobkovsky. Organometallics, **21**, 2724 (2002).
13. M.D. Fryzuk, S.A. Johnson, B.O. Patrick, A. Albinati, S.A. Mason, and T.F. Koetzle. J. Am. Chem. Soc. **123**, 3960 (2001).
14. M.D. Fryzuk, B.A. MacKay, S.A. Johnson, and B.O. Patrick. Angew. Chem. Int. Ed. **41**, 3709 (2002).
15. M.D. Fryzuk, B.A. MacKay, and B.O. Patrick. J. Am. Chem. Soc. **125**, 3234 (2003).
16. F.A. Cotton and W.T. Hall. Inorg. Chem. **19**, 2354 (1980).
17. F.A. Cotton and W.T. Hall. J. Am. Chem. Soc. **101**, 5094 (1979).
18. K.I. Goldberg, D.M. Hoffman, and R. Hoffmann. Inorg. Chem. **21**, 3863 (1982).
19. D.R. Mulford, J.R. Clark, S.W. Schweiger, P.E. Fanwick, and I.P. Rothwell. Organometallics, **18**, 4448 (1999).
20. M.D. Fryzuk, M.P. Shaver, and B.O. Patrick. Inorg. Chim. Acta, **350**, 293 (2003).
21. M.P. Shaver, R.K. Thomson, B.O. Patrick, and M.D. Fryzuk. Can. J. Chem. **81**, 1431 (2003).
22. A.B. Pangborn, M.A. Giardello, R.H. Grubbs, R.K. Rosen, and F.J. Timmers. Organometallics, **15**, 1518 (1996).
23. J.W. Pflugrath. Acta Crystallogr. **D55**, 1718 (1999).
24. D.T. Cromer and J.T. Waber. International tables for X-ray crystallography. Vol. IV. Kynoch Press, Birmingham, UK. 1974.
25. J.A. Ibers and W.C. Hamilton. Acta Crystallogr. **17**, 781 (1964).
26. A. Altomare, M.C. Burla, M. Camalli, G. Cascarano, C. Giacovazzo, A. Guagliardi, and G. Polidori. J. Appl. Crystallogr. **26**, 343 (1993).

© 2005 NRC Canada

27. M.C. Burla, M. Camalli, G.L. Carrozzini, G.L. Cascarano, C. Giacovazzo, G. Polidori, and R. Spagna. J. Appl. Crystallogr. **36**, 1103 (2003).
28. G. M. Sheldrick. SHELXL-97 [computer program]. Programs for crystal structure analysis. University of Göttingen, Göttingen, Germany. 1997.
29. L.J. Farrugia. J. Appl. Crystallogr. **32**, 837 (1999).

© 2005 NRC Canada

Synthesis and catalysed hydroboration of styryl sulfonamides[1]

Natalie A. Wynberg, Lisa J. Leger, Maren L. Conrad, Christopher M. Vogels, Andreas Decken, Stephen J. Duffy, and Stephen A. Westcott

Abstract: We have prepared the aryl sulfonamides 4,4′-R-$C_6H_4SO_2NHC_6H_4CH{=}CH_2$ (R = CH_3, **1a**; NO_2, **1b**) by addition of 2 equiv. of 4-vinylaniline to the corresponding sulfonyl chlorides. The disulfonamides 4,4,4′-(R-$C_6H_4SO_2)_2$-$NC_6H_4CH{=}CH_2$ (R = CH_3, **2a**; NO_2, **2b**) were also prepared using 4-vinylaniline and 2 equiv. of the sulfonyl chlorides in the presence of DMAP. Although hydroborations of sulfanilamide derivatives **1** suffered from competing hydrogenation reactions, judicious choice of the transition metal catalyst gave selective formation of either the primary or secondary boronate esters in hydroborations of **2a**.

Key words: boronate esters, catalysed hydroborations, sulfanilamides, vinylaniline.

Résumé : On a préparé les aryl sulfonamides, 4,4′-R-$C_6H_4SO_2NHC_6H_4CH{=}CH_2$ (R = CH_3, **1a**; NO_2, **1b**) par l'addition de deux équivalents de 4-vinylaniline aux chlorures de sulfonyle correspondants. On a aussi préparé les disulfonamides 4,4,4′-(R-$C_6H_4SO_2)_2NC_6H_4CH{=}CH_2$ (R = CH_3, **2a**; NO_2, **2b**) à partir de la 4-vinylaniline et de deux équivalents de chlorures de sulfonyle, en présence de DMAP. Quoique les réactions d'hydroboration des dérivés sulfanilamides **1** soient en compétition avec les réactions d'hydrogénation, un choix judicieux d'un catalyseur à base d'un métal de transition permet d'obtenir la formation sélective des boronates soit primaires ou secondaires lors des hydroborations du composé **2a**.

Mots clés : esters de l'acide boronique, hydroborations catalysées, sulfanilamides, vinylaniline.

[Traduit par la Rédaction]

Introduction

The hydroboration of alkenes and alkynes, which constitutes the addition of a B—H bond across a carbon—carbon multiple bond, is a remarkably important reaction in organic synthesis (1). Although simple boron hydride reagents such as borane ($H_3B{\cdot}X$, where X is a Lewis base) and 9-borabicyclo[3.3.1]nonane react readily with alkenes at room temperature, hydroborations with catecholborane (HBcat, cat = 1,2-$O_2C_6H_4$) generally require elevated temperatures. The discovery that transition metals can be used to catalyse the addition of HBcat to substrates has become an important and well-established technique in organic synthesis (2–6). These reactions can have regio-, chemo-, or stereoselectivities complementary, or more remarkably, opposite to those from products obtained via the uncatalysed variant. For example, hydroborations of styrenes ($ArCH{=}CH_2$) with HBcat proceed to give selectively either the expected primary boronate ester ($ArCH_2CH_2Bcat$) or the secondary boronate ester ($ArCH(Bcat)CH_3$), depending upon the choice of catalyst used to affect this transformation (Scheme 1) (3). Rhodium-catalysed hydroborations are the most common and synthetically useful of these reactions. They are believed to proceed via initial oxidative addition of HBcat (7), followed by coordination of the alkene to the metal centre with subsequent insertion of the alkene into either the Rh—H (8) or the Rh—B bond (9) and reductive elimination to yield the desired product (10). The unusual secondary boronate ester product is believed to arise when the metal centre can best stabilize a benzylic intermediate during the catalytic cycle.

Although a considerable amount of research has focused on the catalysed hydroboration of simple unsaturated hydrocarbon systems, much less is known about analogous reactions with heteroatom-containing substrates (3, 11–17). For instance, catalysed hydroborations of pyrrolidinyl amides with HBcat gave, after oxidation, *syn* 1,3-hydroxy amides with high levels of regio- and stereochemical control (18). The remarkable selectivities observed in these reactions are believed to arise from a directing effect of the amide moiety. As part of our ongoing investigation into generating biologically active boron compounds (19) and, in an effort to expand the scope of metal-catalysed hydroborations, we de-

Received 10 December 2004. Published on the NRC Research Press Web site at http://canjchem.nrc.ca on 8 June 2005.

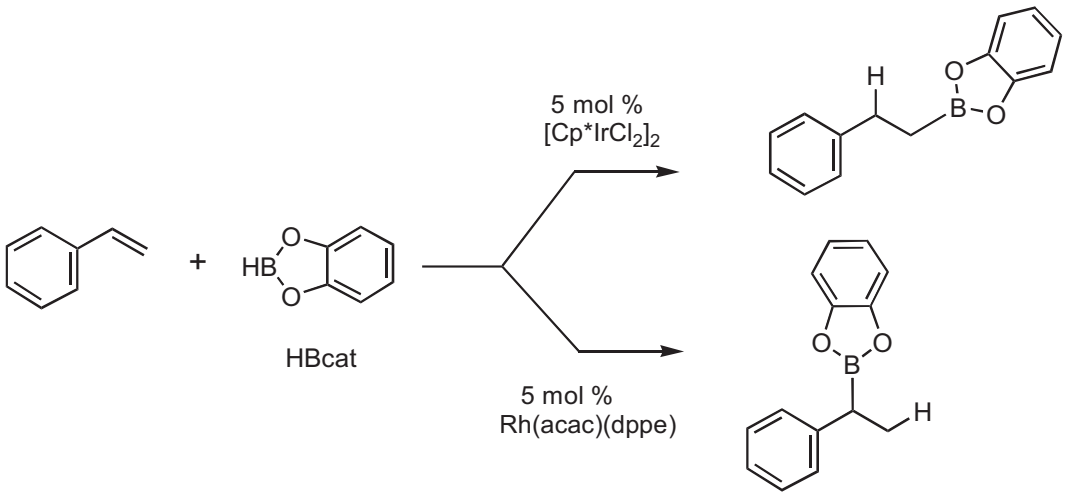
Dedicated to Professor Howard Alper in recognition of his outstanding contributions in catalysis.

N.A. Wynberg, L.J. Leger, M.L. Conrad, C.M. Vogels, S.J. Duffy, and S.A. Westcott.[2] Department of Chemistry, Mount Allison University, Sackville, NB E4L 1G8, Canada.
A. Decken.[3] Department of Chemistry, University of New Brunswick, Fredericton, NB E3B 5A3, Canada.

[1]This article is part of a Special Issue dedicated to Professor Howard Alper.
[2]Corresponding author (e-mail: swestcott@mta.ca).
[3]Corresponding author (crystallography) (e-mail: adecken@unb.ca).

 doi: 10.1139/V05-078 © 2005 NRC Canada

Scheme 1.



cided to examine the synthesis and hydroboration of sulfanilamide derivatives containing a pendant styryl moiety. Initial results are presented herein.

Experimental

Materials and methods

Reagents and solvents used were obtained from Aldrich Chemicals. $RhCl(PPh_3)_3$ (20), $Rh(acac)(coe)_2$ (21), and $[Cp^*IrCl_2]_2$ (22) were prepared as described elsewhere. NMR spectra were recorded on a JEOL JNM-GSX270 FT NMR spectrometer. ^{1}H NMR chemical shifts are reported in parts per million (ppm) and are referenced to residual protons in deuterated solvent at 270 MHz. ^{11}B NMR chemical shifts are referenced to external $BF_3{\cdot}OEt_2$ at 87 MHz. ^{13}C NMR chemical shifts are referenced to solvent carbon resonances as internal standards at 68 MHz. Multiplicities are reported as singlet (s), doublet (d), triplet (t), quartet (q), multiplet (m), broad (br), and overlapping (ov). Infrared spectra were obtained using a Mattson Genesis II FT-IR spectrometer and are reported in cm^{-1}. Melting points were measured uncorrected with a Mel-Temp apparatus. GC-MS analyses were conducted using a Varian Saturn 2000 GC/MS/MS coupled to a CP-3800 GC. The GC was equipped with both the 1177 injection port with a CP-8410 liquid autoinjector connected to an SPB-1 (Supelco) fused silica column (30 m × 0.25 mm i.d. × 0.25 μm) and the 1079 solid injector chromatoprobe, attached to a 50 cm transfer line. The GC-MS spectrometer is controlled by the Saturn Workstation software, Version 5.51.

Synthesis

General synthesis of 1a and 1b

Under an atmosphere of dinitrogen, an Et_2O (2 mL) solution of 4-vinylaniline (2 equiv.) was added dropwise to a stirred Et_2O (5 mL) solution of the appropriate sulfonyl chloride. The mixture was allowed to stir for 18 h, at which point the resulting solid was removed by filtration and the filtrate stored at –30 °C for 2 days. Any subsequent precipitate was also removed by filtration and discarded. Compounds **1a** and **1b** were recovered upon removal of solvent under vacuum and washed with hexane (3 × 3 mL).

Compound 1a

Yield: 70%, mp 80–82 °C. ^{1}H NMR ($CDCl_3$) δ: 7.65 (d, J = 8 Hz, 2H, Ar), 7.26 (d, J = 8 Hz, 2H, Ar), 7.21 (d, J = 8 Hz, 2H, Ar), 7.01 (d, J = 8 Hz, 2H, Ar), 6.76 (br s, 1H, N*H*), 6.60 (d of d, J = 18, 10 Hz, 1H, C*H*=CH_2), 5.64 (d, J = 18 Hz, 1H, CH=C*H*H), 5.18 (d, J = 10 Hz, 1H, CH=CH*H*), 2.36 (s, 3H, CH_3). ^{13}C NMR ($CDCl_3$) δ: 144.0, 136.1, 136.0, 135.9, 134.9, 129.7, 127.3, 127.2, 121.7, 113.8, 21.6. IR (Nujol): 3271, 2943, 2922, 1597, 1508, 1392, 1333, 1159, 1090, 906, 814, 681, 492. EI-MS *m*/*z* (relative intensity): 273 (73, $[M]^+$), 155 (5), 118 (100), 91 (58).

Compound 1b

Yield: 60%, mp 182–184 °C. ^{1}H NMR (DMSO-d_6) δ: 10.68 (br s, 1H, N*H*), 8.37 (d, J = 8 Hz, 2H, Ar), 7.99 (d, J = 8 Hz, 2H, Ar), 7.36 (d, J = 8 Hz, 2H, Ar), 7.08 (d, J = 8 Hz, 2H, Ar), 6.58 (d of d, J = 18, 10 Hz, 1H, C*H*=CH_2), 5.71 (d, J = 18 Hz, 1H, CH=C*H*H), 5.17 (d, J = 10 Hz, 1H, CH=CH*H*). ^{13}C NMR (DMSO-d_6) δ: 150.4, 145.4, 137.0, 136.3, 134.3, 128.8, 127.7, 125.2, 121.2, 114.4. IR (Nujol): 3224, 2935, 2912, 1606, 1527, 1348, 1165, 1086, 924, 854, 735, 604, 542. EI-MS *m*/*z* (relative intensity): 304 (41, $[M]^+$), 118 (100).

Reaction of 1a with 1 equiv. of HBcat in the presence of $RhCl(PPh_3)_3$

Under an atmosphere of dinitrogen, a 0.5 mL C_6D_6 solution of HBcat (1 equiv.) was added to a mixture of **1a** and $RhCl(PPh_3)_3$ (0.05 equiv.) in 0.5 mL of C_6D_6. The reaction was allowed to proceed for 4 h, at which point NMR spectroscopic data was collected. ^{1}H NMR δ: 7.92 (d, J = 8 Hz, 2H, Ar), 7.00 (d, J = 8 Hz, 2H, Ar), 6.96–6.82 (ov m, 4H, Ar and Bcat), 6.70–6.64 (ov m, 4H, Ar and Bcat), 2.31 (q, J = 8 Hz, 2H, CH_2CH_3), 1.82 (s, 3H, CH_3), 0.94 (t, J = 8 Hz, 3H, CH_2CH_3). ^{11}B NMR δ: 24.8 ($ArSO_2N(Bcat)CH_2CH_3$).

Reaction of 1b with 1 equiv. of HBcat in the presence of $RhCl(PPh_3)_3$

Under an atmosphere of dinitrogen, a 0.5 mL $CDCl_3$ solu-

© 2005 NRC Canada

tion of HBcat (1 equiv.) was added to a suspension of **1b** and $RhCl(PPh_3)_3$ (0.05 equiv.) in 0.5 mL of $CDCl_3$. The reaction was allowed to proceed for 18 h, at which point spectroscopic NMR data of the resulting hydrogenation product ($ArN(Bcat)CH_2CH_3$, 98% by NMR spectroscopy) was collected. ^{1}H NMR δ: 8.21 (d, *J* = 8 Hz, 2H, Ar), 7.93 (d, *J* = 8 Hz, 2H, Ar), 7.24–7.04 (ov m, 8H, Ar and Bcat), 2.56 (q, *J* = 8 Hz, 2H, CH_2CH_3), 1.16 (t, *J* = 8 Hz, 3H, CH_2CH_3). ^{11}B NMR δ: 24.5 ($ArN(Bcat)CH_2CH_3$).

General synthesis of 2a and 2b

Under an atmosphere of dinitrogen, a toluene (2 mL) solution of 4-vinylaniline was added dropwise to a stirred toluene (5 mL) mixture of the appropriate sulfonyl chloride (2.5 equiv.) and 4-DMAP (2.5 equiv.). The mixture was heated at reflux for 2 days, at which point solvent was removed under vacuum, and the resultant white solid was washed with Et_2O (3 × 5 mL). The filtrate was collected, and the Et_2O was removed under vacuum. The resulting solid was then washed with EtOH (4 × 5 mL) to afford **2**.

Compound 2a

Yield: 70%, mp 176–178 °C. ^{1}H NMR ($CDCl_3$) δ: 7.81 (d, *J* = 8 Hz, 4H, Ar), 7.36 (d, *J* = 8 Hz, 2H, Ar), 7.32 (d, *J* = 8 Hz, 4H, Ar), 6.97 (d, *J* = 8 Hz, 2H, Ar), 6.69 (d of d, *J* = 18, 10 Hz, 1H, CH=CH_2), 5.77 (d, *J* = 18 Hz, 1H, CH=C*H*H), 5.33 (d, *J* = 10 Hz, 1H, CH=CH*H*), 2.45 (s, 6H, CH_3). ^{13}C NMR ($CDCl_3$) δ: 145.1, 139.5, 136.7, 135.8, 133.6, 131.7, 129.7, 128.7, 127.0, 116.1, 21.8. IR (Nujol): 2970, 2951, 1595, 1462, 1377, 1167, 908, 806, 661, 550, 488. EI-MS *m*/*z* (relative intensity): 427 (98, $[M]^+$), 272 (53), 208 (100), 155 (13), 118 (16), 91 (20).

Compound 2b

Yield: 55%, mp 274 to 275 °C. ^{1}H NMR (DMSO-d_6) δ: 8.51 (d, *J* = 8 Hz, 4H, Ar), 8.12 (d, *J* = 8 Hz, 4H, Ar), 7.59 (d, *J* = 8 Hz, 2H, Ar), 7.10 (d, *J* = 8 Hz, 2H, Ar), 6.80 (d of d, *J* = 18, 10 Hz, 1H, CH=CH_2), 5.96 (d, *J* = 18 Hz, 1H, CH=C*H*H), 5.42 (d, *J* = 10 Hz, 1H, CH=CH*H*). ^{13}C NMR (DMSO-d_6) δ: 151.5, 143.6, 140.3, 135.8, 132.2, 132.1, 130.4, 128.1, 125.6, 117.9. IR (Nujol): 2935, 2902, 2863, 1710, 1531, 1462, 1377, 1169, 1082, 960, 920, 852, 733, 642, 602, 552. EI-MS *m*/*z* (relative intensity): 489 (2, $[M]^+$), 304 (57), 273 (3), 118 (100).

General procedure for the hydroboration of compounds 3 and 4

Under an atmosphere of dinitrogen, 1 equiv. of catecholborane in 0.5 mL of $CDCl_3$ was added to a 0.5 mL $CDCl_3$ solution of the appropriate catalyst and substrate. The reactions were allowed to proceed for 18 h, at which point NMR data were collected. Compounds **3** and **4** were isolated by recrystallization from a solution of $CDCl_3$:hexane (1:2) stored at –30 °C.

Compound 3

^{1}H NMR ($CDCl_3$) δ: 7.79 (d, *J* = 8 Hz, 4H, Ar), 7.29 (d, *J* = 8 Hz, 4H, Ar), 7.25–7.20 (ov m, 4H, Ar and Bcat), 7.08 (2nd order m, 2H, Bcat), 6.92 (d, *J* = 8 Hz, 2H, Ar), 2.99 (t, *J* = 8 Hz, 2H, CH_2CH_2Bcat), 2.44 (s, 6H, CH_3), 1.66 (t, *J* = 8 Hz, 2H, CH_2CH_2Bcat). ^{13}C NMR ($CDCl_3$) δ: 148.2, 146.0, 145.0, 136.8, 132.2, 131.5, 129.6, 128.8, 128.7, 122.7, 112.4, 29.4, 21.8, 12.1 (br, *C*-B). ^{11}B NMR ($CDCl_3$) δ: 34.8. EI-MS *m*/*z* (relative intensity): 547 (12, $[M]^+$), 429 (100), 273 (68), 155 (8), 118 (33).

Compound 4

^{1}H NMR ($CDCl_3$) δ: 7.81 (d, *J* = 8 Hz, 4H, Ar), 7.31 (d, *J* = 8 Hz, 4H, Ar), 7.30 (d, *J* = 8 Hz, 2H, Ar), 7.22 (2nd order m, 2H, Bcat), 7.09 (2nd order m, 2H, Bcat), 6.96 (d, *J* = 8 Hz, 2H, Ar), 3.01 (q, *J* = 8 Hz, 1H, $CH(Bcat)CH_3$), 2.45 (s, 6H, CH_3), 1.58 (d, *J* = 8 Hz, 3H, $CH(Bcat)CH_3$). ^{13}C NMR ($CDCl_3$) δ: 148.2, 145.7, 145.0, 136.9, 132.0, 131.6, 129.6, 128.7, 128.6, 122.9, 112.6, 24.8 (br, *C*-B), 21.8, 16.6. ^{11}B NMR ($CDCl_3$) δ: 34.1. EI-MS *m*/*z* (relative intensity): 547 (2, $[M]^+$), 428 (18), 246 (100), 155 (8), 118 (16).

X-ray data

Crystals of **3** were grown by slow evaporation using $CHCl_3$ at –30 °C. Crystals were coated with Paratone-N oil, mounted using a glass fibre, and frozen in the cold nitrogen stream of the goniometer. A hemisphere of data was collected on a Bruker AXS P4/SMART 1000 diffractometer using ω and θ scans with a scan width of 0.3° and with 90 s exposure times. The detector distance was 6 cm. The crystal was twinned, and the orientation matrixes for two components were determined (23, 24), and the data were reduced (25). The structure was solved by direct methods and refined by full-matrix least squares on F^2 (SHELXTL) (26) using all reflections. One of the ethyl linkages was disordered, and the site occupancy was determined using an isotropic model as 0.7 (C(41)—C(42)) and 0.3 (C(41′)—C(42′)) and was fixed in subsequent refinement cycles. All non-hydrogen atoms were refined anisotropically. Hydrogen atoms were included in calculated positions and refined using a riding model.

Results and discussion

N-Aryl sulfonamides are an important class of compounds, particularly in pharmaceutical research (27), where a number of these compounds have been reported to act as class III antiarrhythmic agents (28), non-nucleotide reverse transcriptase inhibitors (29), and as HIV-1 protease inhibitors (30). We have recently undertaken a study to investigate the synthesis and biological activity of novel borosulfonamides (31, 32). Interest in compounds containing boronic acids ($RB(OH)_2$) or boronate esters ($RB(OR')_2$) arises from their remarkable versatility in organic synthesis (33), as well as from their potent biological activities (34–42). For instance, the boron compounds boromycin and aplasmomycin are powerful antibiotics, and *L*-4-borono-phenylalanine has found significant application in boron neutron capture therapy for the treatment of certain cancers (43). These properties, along with their ability to transport water-insoluble reagents through membranes (44), make boronate ester compounds useful carrier ligands for biologically active compounds.

In this study, we have prepared the novel aryl sulfonamides 4,4′-R-$C_6H_4SO_2NHC_6H_4CH$=CH_2 (R = CH_3, **1a**; NO_2, **1b**) (Fig. 1) by addition of 2 equiv. of 4-vinylaniline to the corresponding sulfonyl chlorides. Varying the physical

© 2005 NRC Canada

Scheme 2.

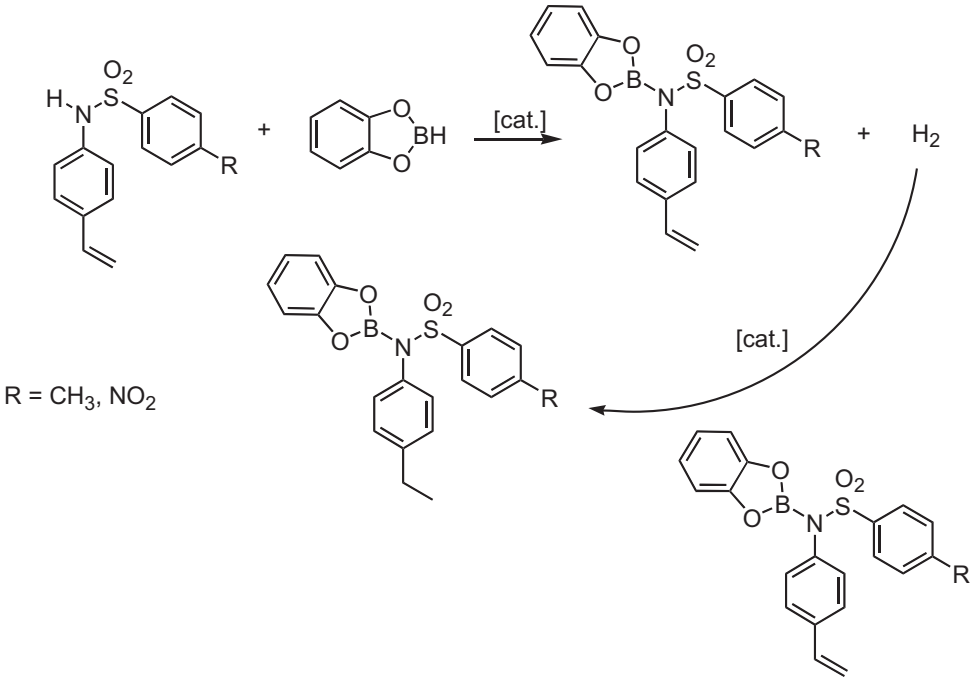
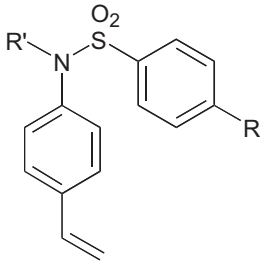


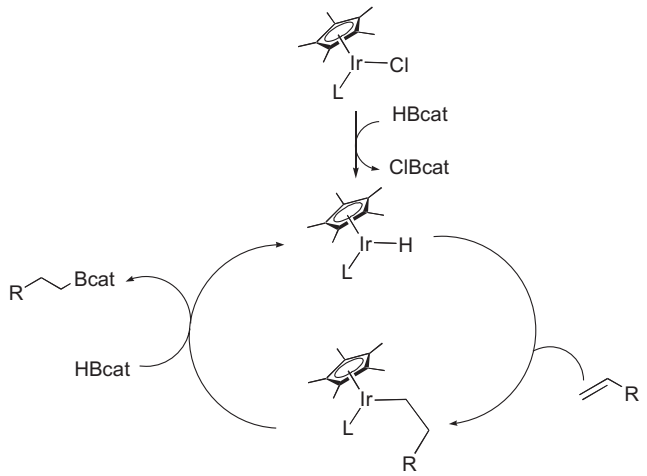
Fig. 1. Styryl sulfanilamides.



1a: R = CH_3, R' = H
1b: R = NO_2, R' = H
2a: R = CH_3, R' =4-$SO_2C_6H_4CH_3$
2b: R = NO_2, R' =4-$SO_2C_6H_4NO_2$

and electronic properties of the sulfonyl chlorides will allow for the general synthesis of a wide variety of styryl sulfanilamide derivatives. Unfortunately, we have found that metal-catalysed addition of 1.1 equiv. of HBcat to styryl sulfonamides **1a** and **1b** gave significant amounts (>95% by ^{1}H NMR spectroscopy) of hydrogenation products R-$C_6H_4SO_2N$(Bcat)$C_6H_4CH_2CH_3$ (R = CH_3 or NO_2). These products presumably arise as a result of an initial interaction of the borane with the sulfonamide N—H bond to generate a new N—Bcat bond while liberating dihydrogen, which can subsequently add to the styryl group in the presence of a catalyst (Scheme 2). Indeed, a new N—B resonance is observed in the ^{11}B NMR spectra at 25 ppm. Furthermore, reactions with excess HBcat gave a complicated mixture of products arising from competing hydrogenation and (or) hydroboration reactions, regardless of the catalyst used to affect these transformations. We therefore investigated the analogous reactions of sulfonamides **2**, which do not contain an active N—H bond.

Scheme 3.



The novel disulfonamides 4,4,4′-(R-$C_6H_4SO_2)_2NC_6H_4$-CH=CH_2 (R = CH_3, **2a**; NO_2, **2b**) could be prepared in moderate to good yields using 4-vinylaniline and 2.5 equiv. of the sulfonyl chlorides in the presence of excess DMAP. However, the introduction of a second nitrobenzene group in **2b** made this sulfonamide derivative insoluble in non-coordinating organic solvents, and as a result, hydroboration studies could not be conducted on this substrate. Addition of HBcat to **2a** using the iridium catalyst [Cp*$IrCl_2]_2$ (45) proceeded smoothly to give the expected primary boronate ester product **3** in high yields (by multinuclear NMR spectroscopy), along with minor amounts (<5%) of the corresponding hydrogenation product. A small amount of hydrogenated alkene, arising from the degradation of HBcat, is almost always observed in reactions using a late metal catalyst (46). Although it is possible that reactions using this catalyst precursor proceed via an oxidative addition mechanism, similar

© 2005 NRC Canada

Scheme 4.

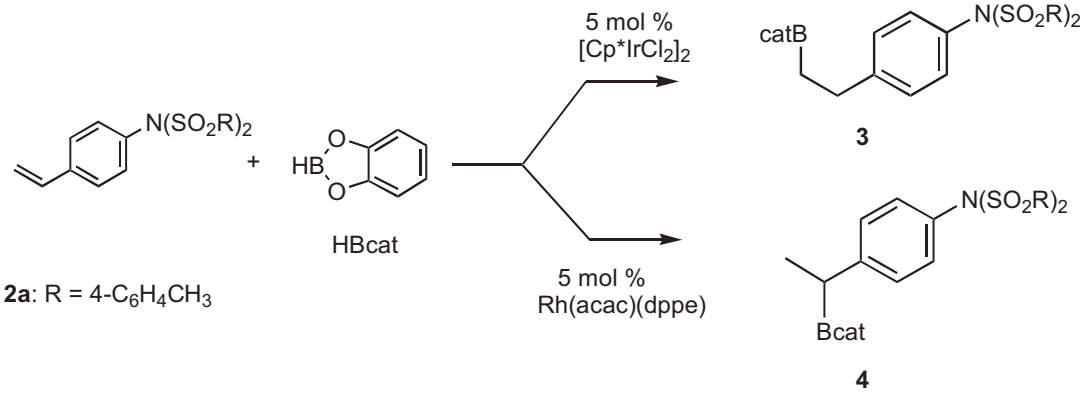
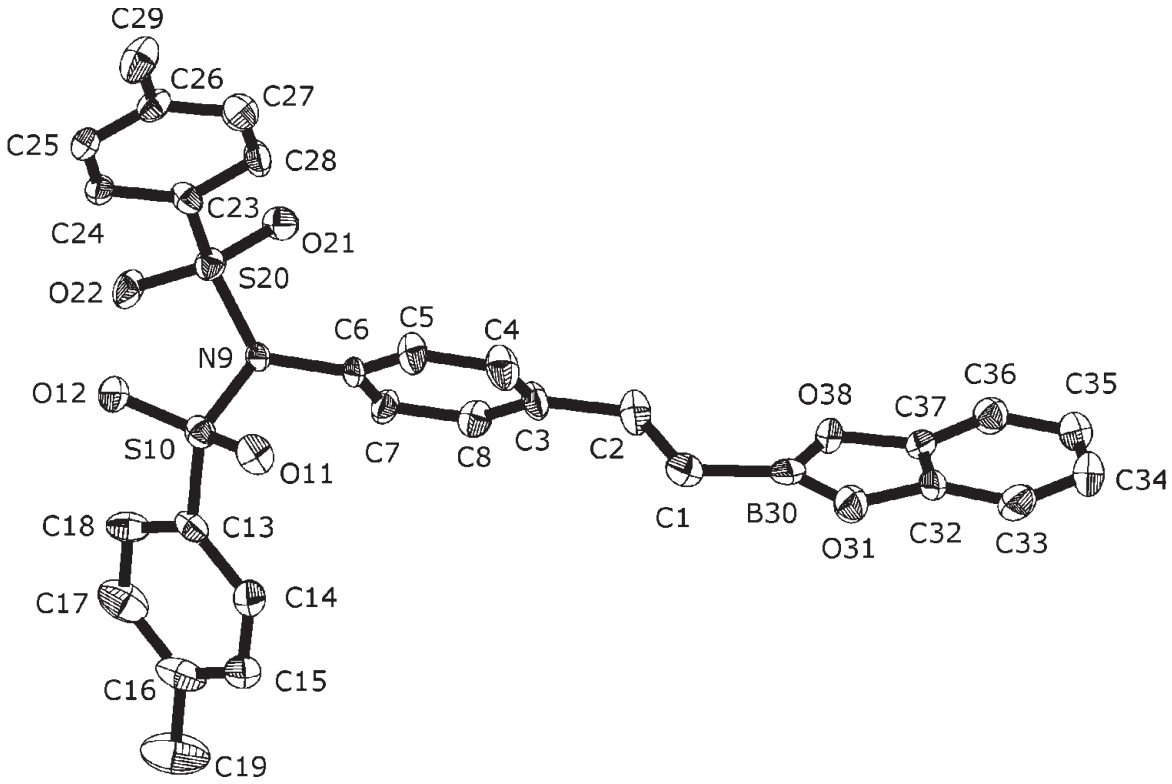


Fig. 2. Molecular structure of **3** with displacement ellipsoids drawn at the 30% probability level. Solvent molecule and hydrogen atoms omitted for clarity.



to those purported for reactions using rhodium-based catalysts, it is also possible that these reactions may be occurring via a σ-bond metathesis pathway to give **3** (Scheme 3). This reaction could proceed via initial metathesis of an Ir—Cl bond with HBcat to give a transient iridium hydride species. The formation of Ir-H species in hydroborations using HBcat has been reported previously (45). Subsequent insertion of the alkene into the Ir—H bond, followed by a σ-bond metathesis with HBcat would give the primary boronate ester while regenerating the active Ir-H catalyst. A similar mechanism has been proposed for reactions of HBcat using early metal and lanthanide catalysts (47). The iridium-catalysed hydroboration of alkenes using pinacolborane is also known to give the corresponding primary boronate ester products (48, 49).

Selective formation of the unusual secondary boronate ester **4** could be achieved in these reactions using either $RhCl(PPh_3)_3$ or Rh(acac)(dppe) (acac = acetylacetonato, dppe = 1,2-bis(diphenylphosphino)ethane) as the catalyst precursor (Scheme 4). The latter is a very active and selective catalyst precursor for a wide range of alkenes, where the resting state of the catalytically active species is the zwitterionic complex, Rh(dppe)(η^6-catBcat) (50). Compounds **3** and **4** have been characterized using a number of physical techniques, including multinuclear NMR spectroscopy. A broad peak at approximately δ 30 ppm in the ^{11}B NMR spectra is

© 2005 NRC Canada

Table 1. Crystallographic data collection parameters for **3**.

Complex	**3**
Formula	$C_{28}H_{26}BNO_6S_2 \cdot 1/2CHCl_3$
Formula mass	607.11
Crystal system	Triclinic
Space group	$P\bar{1}$
a (Å)	8.291 5(12)
b (Å)	18.403(3)
c (Å)	19.051(3)
α (°)	80.093(2)
β (°)	87.942(2)
γ (°)	84.195(2)
V (Å^3)	2 848.5(7)
Z	4
ρ_{calcd} (mg m^{-3})	1.416
Crystal size (mm^3)	0.4 × 0.075 × 0.050
Temperature (K)	173(1)
Radiation	Mo Kα (λ = 0.710 73)
μ (mm^{-1})	0.372
Total reflections	18 974
Total unique reflections	18 974
No. of variables	752
Theta range (°)	1.43–25.00
Largest difference peak and hole (e Å^{-3})	1.104 and –0.725
S (GoF) on F^2	0.835
R_1[a] ($I > 2\sigma(I)$)	0.056 9
wR_2[b] (all data)	0.143 5

[a] $R_1 = \Sigma||F_o| - |F_c||/\Sigma|F_o|$.
[b] $wR_2 = (\Sigma[w(F_o^2 - F_c^2)^2]/\Sigma[wF_o^4])^{1/2}$, where $w = 1/[\sigma^2(F_o^2) + (0.0638P)^2]$, where $P = (\max(F_o^2, 0) + 2F_c^2)/3$.

Table 2. Selected bond lengths (Å) and angles (°) for **3**.

Bond lengths (Å)	
C(1)—C(2)	1.517(5)
C(1)—B(30)	1.562(6)
N(9)—S(10)	1.687(3)
N(9)—S(20)	1.688(3)
S(10)—O(12)	1.423(2)
S(10)—O(11)	1.434(2)
S(10)—C(13)	1.752(3)
S(20)—O(21)	1.432(2)
S(20)—O(22)	1.435(2)
S(20)—C(23)	1.756(3)
B(30)—O(31)	1.389(5)
B(30)—O(38)	1.402(5)
O(31)—C(32)	1.383(4)
O(38)—C(37)	1.399(4)
Bond angles (°)	
C(6)-N(9)-S(10)	117.4(2)
C(6)-N(9)-S(20)	120.1(2)
S(10)-N(9)-S(20)	122.46(16)
O(12)-S(10)-O(11)	119.98(15)
O(12)-S(10)-N(9)	106.00(15)
O(11)-S(10)-N(9)	106.47(15)
O(12)-S(10)-C(13)	109.98(15)
O(11)-S(10)-C(13)	108.24(16)
N(9)-S(10)-C(13)	105.14(16)
O(21)-S(20)-O(22)	119.64(17)
O(21)-S(20)-N(9)	104.04(14)
O(22)-S(20)-N(9)	108.98(14)
O(21)-S(20)-C(23)	109.36(15)
O(22)-S(20)-C(23)	109.81(16)
N(9)-S(20)-C(23)	103.72(16)
O(31)-B(30)-O(38)	111.2(3)
O(31)-B(30)-C(1)	125.9(4)
O(38)-B(30)-C(1)	122.8(4)
C(32)-O(31)-B(30)	104.7(3)
C(2)-C(1)-B(30)	113.4(4)

observed for both sulfonamides, indicating that the boron atom lies in a three-coordinate C-Bcat environment (51). Compound **3** has also been characterized by a single crystal diffraction study, and the molecular structure is shown in Fig. 2;[4] crystallographic data are given in Table 1, and selected bond distances and angles are shown in Table 2. The B—O bond distances (avg. = 1.3955(5) Å) are also typical for three-coordinate Bcat groups (52–55) and are significantly shorter than those observed in chelate complexes with diphenylborinic acid (ca. 1.5 Å), where the boron atom is four coordinate (56).

In summary, we have prepared novel sulfanilamide derivatives containing styryl groups and have examined metal-catalysed hydroborations of these substrates using HBcat. Judicious choice of the catalyst precursor used to affect these transformations allows for the selective generation of either the primary or secondary boronate ester. Preliminary work has shown that these reactions are general, as analogous compounds could be obtained in metal-catalysed hydroborations of thiophene sulfonamide derivatives. Future work will investigate the potential biological activities of a wide range of novel styryl sulfonamides and the corresponding boron-containing derivatives, the results of which will be presented in due course.

Acknowledgements

Thanks are gratefully extended to the American Chemical Society – Petroleum Research Fund (Grant #37824-B1), Canada Research Chairs Programme, Canadian Foundation for Innovation – Atlantic Innovation Fund, Natural Sciences and Engineering Research Council of Canada (NSERC), and Mount Allison University for financial support. We also thank Dan Durant and Roger Smith for their expert technical assistance and anonymous reviewers for helpful comments.

[4] Supplementary data for this article are available on the Web site or may be purchased from the Depository of Unpublished Data, Document Delivery, CISTI, National Research Council Canada, Ottawa, ON K1A 0S2, Canada. DUD 3675. For more information on obtaining material refer to http://cisti-icist.nrc-cnrc.gc.ca/irm/unpub_e.shtml. CCDC 256413 contains the crystallographic data for this manuscript. These data can be obtained, free of charge, via www.ccdc.cam.ac.uk/conts/retrieving.html (or from the Cambridge Crystallographic Data Centre, 12 Union Road, Cambridge CB2 1EZ, UK; fax +44 1223 336033; or deposit@ccdc.cam.ac.uk).

© 2005 NRC Canada

References

1. H.C. Brown, G.W. Kramer, A.B. Levy, and M.M. Midland. Organic syntheses via boranes. Wiley-Interscience, New York. 1975.
2. D. Männig and H. Nöth. Angew. Chem. Int. Ed. Engl. **24**, 878 (1985).
3. For excellent reviews on the metal-catalysed hydroboration reaction, see: (*a*) I. Beletskaya and A. Pelter. Tetrahedron, **53**, 4957 (1997); (*b*) C.M. Crudden and D. Edwards. Eur. J. Org. Chem. 4695 (2003), and refs. therein.
4. D.E. Kadlecek, P.J. Carroll, and L.G. Sneddon. J. Am. Chem. Soc. **122**, 10 868 (2000).
5. S. Demay, F. Volant, and P. Knochel. Angew. Chem. Int. Ed. **40**, 1235 (2001).
6. C. Widauer, H. Grützmacher, and T. Ziegler. Organometallics, **19**, 2097 (2000).
7. H. Kono, K. Ito, and Y. Nagai. Chem. Lett. 1095 (1975).
8. A.E. Dorigo and P. von Ragué Schleyer. Angew. Chem. Int. Ed. Engl. **34**, 115 (1995).
9. D.G. Musaev, A.M. Mebel, and K. Morokuma. J. Am. Chem. Soc. **116**, 10 693 (1994).
10. X. Huang and Z. Lin. Computational modeling of homogeneous catalysis. *Edited by* F. Maseras and A. Lledos. Kluwer Academic, Amsterdam. 2002. pp. 189–212.
11. P.V. Ramachandran, M.P. Jennings, and H.C. Brown. Org. Lett. **1**, 1399 (1999).
12. C.M. Vogels, P.E. O'Connor, T.E. Phillips, K.J. Watson, M.P. Shaver, P.G. Hayes, and S.A. Westcott. Can. J. Chem. **79**, 1898 (2001).
13. P.V. Ramachandran and M.P. Jennings. Chem. Commun. 386 (2002).
14. I. Pergament and M. Srebnik. Tetrahedron Lett. **42**, 8059 (2001).
15. I. Pergament and M. Srebnik. Org. Lett. **3**, 217 (2001).
16. C.A.G. Carter, C.M. Vogels, D.J. Harrison, M.K.J. Gagnon, D.W. Norman, R.F. Langler, R.T. Baker, and S.A. Westcott. Organometallics, **20**, 2130 (2001).
17. X.-L. Hou, D.-G. Hong, G.-B. Rong, Y.-L. Guo, and L.-X. Dai. Tetrahedron Lett. **34**, 8513 (1993).
18. D.A. Evans and G.C. Fu. J. Org. Chem. **55**, 5678 (1990).
19. A.M. Irving, C.M. Vogels, L.G. Nikolcheva, J.P. Edwards, X-F. He, M.G. Hamilton, M.O. Baerlocher, F.J. Baerlocher, A. Decken, and S.A. Westcott. New J. Chem. **27**, 1419 (2003).
20. J.A. Osborn, F.H. Jardine, J.F. Young, and G. Wilkinson. J. Chem. Soc. A, 1711 (1966).
21. J.M. Burke, R.B. Coapes, A.E. Goeta, J.A.K. Howard, T.B. Marder, E.G. Robins, and S.A. Westcott. J. Organomet. Chem. **649**, 199 (2002).
22. R.G. Ball, W.A.G. Graham, D.M. Heinekey, J.K. Hoyano, A.D. McMaster, B.M. Mattson, and S.T. Michel. Inorg. Chem. **29**, 2023 (1990).
23. Bruker AXS, Inc. GEMINI 1.0 [computer program]. Bruker AXS, Inc., Madison, Wis. 1999.
24. Bruker AXS, Inc. RLATT 2.72 [computer program]. Bruker AXS, Inc., Madison, Wis. 1999.
25. Bruker AXS, Inc. SAINT 6.02 [computer program]. Bruker AXS, Inc., Madison, Wis. 1997–1999.
26. Bruker AXS, Inc. SHELXTL 6.14 [computer program]. Bruker AXS, Inc., Madison, Wis. 2000–2003.
27. H. He and Y.-J. Wu. Tetrahedron Lett. **44**, 3385 (2003).
28. J.B. Hester, J.K. Gibson, M.G. Cimini, D.E. Emmert, P.K. Locker, S.C. Perricone, L.L. Skaletzky, J.K. Sykes, and B.E. West. J. Med. Chem. **34**, 308 (1991).
29. D.L. Romero, R.A. Morge, M.J. Genin, C. Biles, M. Busso, L. Resnick, I.W. Althaus, F. Reusser, R.C. Thomas, and W.G. Tarpley. J. Med. Chem. **36**, 1505 (1993).
30. S.R. Turner, J.W. Strohbach, R.A. Tommasi, P.A. Aristoff, P.D. Johnson, H.I. Skulnick, L.A. Dolak, E.P. Seest, P.K. Tomich, M.J. Bohanon, M.M. Horng, J.C. Lynn, K.-T. Chong, R.R. Hinshaw, K.D. Watenpaugh, M.N. Janakiraman, and S. Thaisrivongs. J. Med. Chem. **41**, 3467 (1998).
31. X.-F. He, H. Zhang, C.M. Vogels, A. Decken, and S.A. Westcott. Heteroat. Chem. **15**, 369 (2004).
32. M.G. Hamilton, C.E. Hughes, A.M. Irving, C.M. Vogels, and S.A. Westcott. J. Organomet. Chem. **680**, 143 (2003).
33. N. Miyaura and A. Suzuki. Chem. Rev. **95**, 2457 (1995).
34. C. Morin. Tetrahedron, **50**, 12 521 (1994).
35. R. Smoum, A. Rubinstein, and M. Srebnik. Bioorg. Chem. **31**, 464 (2003).
36. S. Jagannathan, T.P. Forsyth, and C.A. Kettner. J. Org. Chem. **66**, 6375 (2001).
37. W. Yang, X. Gao, and B. Wang. Med. Res. Rev. **23**, 346 (2003).
38. V.M. Dembitsky and M. Srebnik. Tetrahedron, **59**, 579 (2003), and refs. therein.
39. S.K. Kumar, E. Hager, C. Pettit, H. Gurulingappa, N.E. Davidson, and S.R. Khan. J. Med. Chem. **46**, 2813 (2003).
40. C.W. Gray, Jr., B.T. Walker, R.A. Foley, and T.A. Houston. Tetrahedron Lett. **44**, 3309 (2003).
41. B. Carboni and L. Monnier. Tetrahedron, **55**, 1197 (1999).
42. E. Cama, D.M. Colleluori, F.A. Emig, H. Shin, S.W. Kim, N.N. Kim, A.M. Traish, D.E. Ash, and D.W. Christianson. Biochemistry, **42**, 8445 (2003).
43. A.H. Soloway, W. Tjarks, B.A. Barnum, F.-G. Rong, R.F. Barth, I.M. Codogni, and J.G. Wilson. Chem. Rev. **98**, 1515 (1998).
44. P.R. Westmark and B.D. Smith. J. Am. Chem. Soc. **116**, 9343 (1994).
45. S.A. Westcott, T.B. Marder, R.T. Baker, and J.C. Calabrese. Can. J. Chem. **71**, 930 (1993).
46. S.A. Westcott, H.P. Blom, T.B. Marder, and R.T. Baker. Inorg. Chem. **32**, 2175 (1993).
47. K.N. Harrison and T.J. Marks. J. Am. Chem. Soc. **114**, 9220 (1992).
48. C.M. Crudden, Y.B. Hleba, and A.C. Chen. J. Am. Chem. Soc. **126**, 9200 (2004).
49. Y. Yamamoto, R. Fujikawa, T. Unemoto, and N. Miyaura. Tetrahedron, **60**, 10 695 (2004).
50. S.A. Westcott, H.P. Blom, T.B. Marder, and R.T. Baker. J. Am. Chem. Soc. **114**, 8863 (1992).
51. H. Nöth and B. Wrackmeyer. Nuclear magnetic resonance spectroscopy of boron compounds. Springer-Verlag, Berlin. 1978.
52. C.M. Vogels, L.G. Nikolcheva, D.W. Norman, H.A. Spinney, A. Decken, M.O. Baerlocher, F.J. Baerlocher, and S.A. Westcott. Can. J. Chem. **79**, 1115 (2001), and refs. therein.
53. R.B. Coapes, F.E.S. Souza, M.A. Fox, A.S. Batsanov, A.E. Goeta, D.S. Yufit, M.A. Leech, J.A.K. Howard, A.J. Scott, W. Clegg, and T.B. Marder. J. Chem. Soc. Dalton Trans. 1201 (2001).
54. W. Clegg, M.R.J. Elsegood, F.J. Lawlor, N.C. Norman, N.L. Pickett, E.G. Robbins, A.J. Scott, P. Nguyen, N.J. Taylor, and T.B. Marder. Inorg. Chem. **37**, 5289 (1998).
55. P. Nguyen, R.B. Coapes, A.D. Woodward, N.J. Taylor, J.M. Burke, J.A.K. Howard, and T.B. Marder. J. Organomet. Chem. **652**, 77 (2002).
56. J. Grünefeld, W. Kliegel, S.J. Rettig, and J. Trotter. Can. J. Chem. **77**, 439 (1999).

© 2005 NRC Canada

Coordination polymers with Co(II) sulfate layers linked by alkanediamines of varying chain length[1]

J.N. Behera and C.N.R. Rao

Abstract: Coordination polymers of the general formula $Co[HN(CH_2)_nNH]SO_4$ possessing layers formed by CoO_4N_2 octahedra and SO_4 tetrahedra have been synthesized under solvothermal conditions. The layers, linked by diaminoalkanes, cause apertures of varying widths, which are determined by the chain length of the amine. These materials appear to possess weak ferromagnetic interaction at low temperatures.

Key words: coordination polymers, cobalt sulfate, solvothermal synthesis.

Résumé : Opérant dans des conditions solvothermiques, on a réalisé la synthèse de polymères de coordination de formule générale $Co[HN(CH_2)_nNH]SO_4$ possédant des couches formées d'octaèdres CoO_4N_2 et de tétraèdres SO_4. Les couches sont reliées par des diaminoalcanes qui provoquent des ouvertures de grandeurs variables déterminées par la longueur de la chaîne amine. À basses températures, ces matériaux semblent posséder de faibles interactions ferromagnétiques.

Mots clés : polymères de coordination, sulfate de cobalt, synthèse solvothermique.

[Traduit par la Rédaction]

Introduction

Metal-organic frameworks possess not only fascinating architectures but also give rise to materials with potential applications. Thus, hybrid materials constructed from V–Co–P–O layers comprise both left- and right-handed helical chains in the same compound (1), while in the porous extended 4,4′-bipyridyl network with Ni they exhibit a railroad 1D motif (2). In the coordination network of $[Co(bix)_2(H_2O)_2](SO_4)\cdot 7H_2O$, ribbons of rings catenated to a 3D single frame produce an open channel with nanoporous behavior (3). A metal-organic structure involving a benzene dicarboxylate of zinc is found to store hydrogen (4). Some coordination polymers and metal-organics exhibit interesting magnetic properties as well. For example, an organo-pillared octahedral cobalt sulfate is porous and metamagnetic (5). Benzene-1,2,3-tricarboxylates of cobalt possessing arrays of Δ-chains exhibit unusual magnetic properties (6). Infinite $^2[Co(ox)(bpy)]$ with a two-dimensional layered network shows canted antiferromagnetism (7). The chemistry of metal carboxylates with open architectures and porous coordination polymers has recently been reviewed (8). We have been interested in synthesizing coordination polymers of transition metals with alkanediamines acting as ligands as well as spacers between the layers. In this article, we describe the synthesis and structure of a family of three-dimensional coordination polymers of Co(II) of the general formula $[Co(HN(CH_2)_nNH)SO_4]$ (n = 3–6), obtained under mild solvothermal conditions wherein the Co(II) sulfate layers are linked by diaminoalkanes of differing chain lengths.

Experimental section

Synthesis and characterization

Compounds **I**–**IV** were synthesized under mild solvothermal conditions. In a typical synthesis, 0.237 g of $CoCl_2\cdot 6H_2O$ was dissolved in 4.6 mL of ethylene glycol and 0.9 mL of water with constant stirring. To this mixture, 0.22 mL of sulfuric acid (98%) and 0.45 mL of 1,3-diamino propane for **I**, 0.6 mL of 1,4-diamino butane for **II**, 0.7 mL of 1,5-diamino pentane for **III**, and 0.697 g of hexamethylene diamine for **IV** were added and the mixture was stirred for 1 h. The final mixture with the molar composition of $CoCl_2\cdot 6H_2O : H_2SO_4 : [H_2N\text{-}(CH_2)_n\text{-}NH_2] :$ ethylene glycol : H_2O of 1:4:6:50:50 at an initial pH of 8 was transferred into a 23 mL PTFE-lined acid digestion bomb and heated at 180 °C for 4 days. The products containing pink colored hexagonal plate-shaped crystals (yield 70% with respect to Co) were filtered and washed with ethanol. The compounds were characterized by single crystal X-ray diffraction, powder X-ray diffraction (XRD), thermogravimetric analysis (TGA), energy dispersive X-ray analysis (EDAX), elemental CNH analysis, and IR

Received 4 September 2004. Published on the NRC Research Press Web site at http://canjchem.nrc.ca on 11 June 2005.

Dedicated to Professor Howard Alper.

J.N. Behera and C.N.R. Rao.[2] Chemistry and Physics of Materials Unit, Jawaharlal Nehru Centre for Advanced Scientific Research, Jakkur P.O., Bangalore 560064, India, and Solid State and Structural Chemistry Unit, Indian Institute of Science, Bangalore 560012, India.

[1]This article is part of a Special Issue dedicated to Professor Howard Alper.
[2]Corresponding author: (e-mail: cnrrao@jncasr.ac.in).

 doi: 10.1139/V05-024 © 2005 NRC Canada

Table 1. Crystal data and structure refinement parameters for compounds **I–IV**.

	I	**II**	**III**	**IV**
Empirical formula	$C_3H_8CoN_2O_4S$	$C_4H_{10}CoN_2O_4S$	$C_5H_{12}CoN_2O_4S$	$C_6H_{14}CoN_2O_4S$
Formula mass	227.11	241.13	255.16	269.18
Crystal system	Orthorhombic (57)	Orthorhombic (57)	Orthorhombic (57)	Orthorhombic (57)
Space group	*Pbcm*	*Pbcm*	*Pbcm*	*Pbcm*
Crystal size (mm^3)	0.15 × 0.10 × 0.10	0.18 × 0.14 × 0.12	0.21 × 0.16 × 0.12	0.23 × 0.18 × 0.12
a (Å)	4.813 6(2)	4.814 4(10)	4.805 5(4)	4.808 7(5)
b (Å)	9.829 9(4)	9.847 59(10)	9.836 9(8)	9.839 3(9)
c (Å)	16.154 7(7)	18.306 1(4)	20.288(2)	22.413(2)
α = β = γ (°)	90	90	90	90
Volume ($Å^3$)	764.40(6)	867.89(3)	959.05(14)	1060.5(2)
Z	4	4	4	4
T (°C)	20	20	20	20
λ (MoKα) (Å)	0.710 73	0.710 73	0.710 73	0.710 73
ρ_{calcd} (g cm^{-3})	1.973	1.845	1.767	1.686
μ (mm^{-1})	2.486	2.195	1.992	1.806
θ range (°)	2.52–23.24	2.23–23.25	2.01–23.23	1.82–23.25
Total data	2832	3276	3518	4042
Unique data	574	648	713	792
R ($I > 2\sigma(I)$)	R_1 = 0.037 0, wR_2 = 0.089 2	R_1 = 0.027 9, wR_2 = 0.074 0	R_1 = 0.032 8, wR_2 = 0.082 9	R_1 = 0.027 4, wR_2 = 0.072 6
R (all data)	$R_1{}^a$ = 0.047 1, $wR_2{}^b$ = 0.093 2	$R_1{}^a$ = 0.029 3, $wR_2{}^b$ = 0.074 8	$R_1{}^a$ = 0.037 4, $wR_2{}^b$ = 0.087 2	$R_1{}^a$ = 0.032 9, $wR_2{}^b$ = 0.075 1

[a] $R_1 = \sum |F_0| - |F_c|$.

[b] $wR_2 = \{[w(F_0^2 - F_c^2)^2]/[w(F_0^2)^2]\}^{1/2}$ where $w = 1/[\sigma^2(F_0)^2 + (aP)^2 + bP]$, $P = [F_0^2 + 2F_c^2]/3$ and where $a = 0.0512$ and $b = 0.8435$ for **I**, $a = 0.0409$ and $b = 0.9971$ for **II**, $a = 0.0476$ and $b = 1.5251$ for **III**, and $a = 0.0523$ and $b = 0.8435$ for **IV**.

spectroscopy. Magnetic measurements on powdered samples of **I** and **IV** were performed over a 2–300 K temperature range using a Quantum design SQUID magnetometer.

EDAX analysis indicated the ratio of Co and S to be 1:1 in **I–IV** in accordance with the formula. The C, N, and H analysis (in wt%): calcd. for **I**: C 15.8, N 12.3, H 3.6; found: C 15.03, N 12.2, H 4.7; calcd. for **II**: C 19.9, N 11.6, H 4.2; found: C 19.5, N 11.4, H 4.9; calcd. for **III**: C 23.5, N 10.97, H 4.74; found: C 23.1, N 10.8, H 5.2; calcd. for **IV**: C 26.74, N 10.4, H 5.24; found: C 26.5, N 10.2, H 5.5, were in agreement with the formulae, $[Co(C_3N_2H_8)SO_4]$, $[Co(C_4N_2H_{10})SO_4]$, $[Co(C_5N_2H_{12})\ SO_4]$, and $[Co\ (C_6N_2H_{14})\ SO_4]$, respectively, as derived from crystallography.

IR spectra showed the characteristic bands for amine and sulfate moieties. The bending and stretching modes of the methylene group were observed at 1463, 1408, and 2889 cm^{-1}, and the N–H stretching band at 3276 cm^{-1}. The SO_4 bands were at 1122 (asymmetric stretch), 980 (symmetric stretch), and 662 cm^{-1} (bending).

The TGA curves (N_2 atmosphere) of **I–IV** exhibited remarkable thermal stability showing no weight losses up to 300 °C but then two major weight losses, consistent with the molecular formulae, were observed. The first weight loss at around 350 °C corresponds to the loss of diamine while the second weight losses occur at around 600 °C in **I** and **II**, and at around 800 °C in **III** and **IV** corresponding to decomposition of sulfate. The total weight loss obtained was 67%, 69%, 73%, and 71% between 120 and 800 °C in **I–IV**, respectively. The final product contained a mixture of CoO and Co_3O_4 (JCPDS file card Nos. 09-0402 and 09-0418, respectively).

Single crystal structure determination

Single crystal data were collected on a Siemens SMART-CCD diffractometer (graphite-monochromated MoKα radiation, λ = 0.710 73 Å (*T* = 298 K)). An absorption correction based on symmetry-equivalent reflections was applied using the Siemens area detector absorption (SADABS) program (9). The structure was solved by direct methods using SHELXS-86 (10) and difference Fourier synthesis. The direct methods solution readily revealed the heavy atom positions (Co and S) and facilitated the identification of the other fragments (O, C, and N) from difference Fourier maps. The last cycles of refinement included atomic positions for all the atoms, anisotropic thermal parameters for the non-hydrogen atoms, and isotropic thermal parameters for all hydrogen atoms. Full-matrix least-squares structure refinement against $|F^2|$ was carried out using the SHELXTL-PLUS (11) package of programs. Details of the final refinement are given in Table 1 along with the crystal data.[3] The atomic coordinates and equivalent isotropic displacement parameters for **I** are given in Table 2. We have not given the atomic co-

[3] Supplementary data for this article are available on the Web site or may be purchased from the Depository of Unpublished Data, Document Delivery, CISTI, National Research Council Canada, Ottawa, ON K1A 0S2, Canada. DUD 3678. For more information on obtaining material refer to http://cisti-icist.nrc-cnrc.gc.ca/irm/unpub_e.shtml. CCDC 242447–242450 contain the crystallographic data for this manuscript. These data can be obtained, free of charge, via www.ccdc.cam.ac.uk/conts/retrieving.html (Or from the Cambridge Crystallographic Data Centre, 12 Union Road, Cambridge CB2 1EZ, UK; fax +44 1223 336033; or deposit@ccdc.cam.ac.uk).

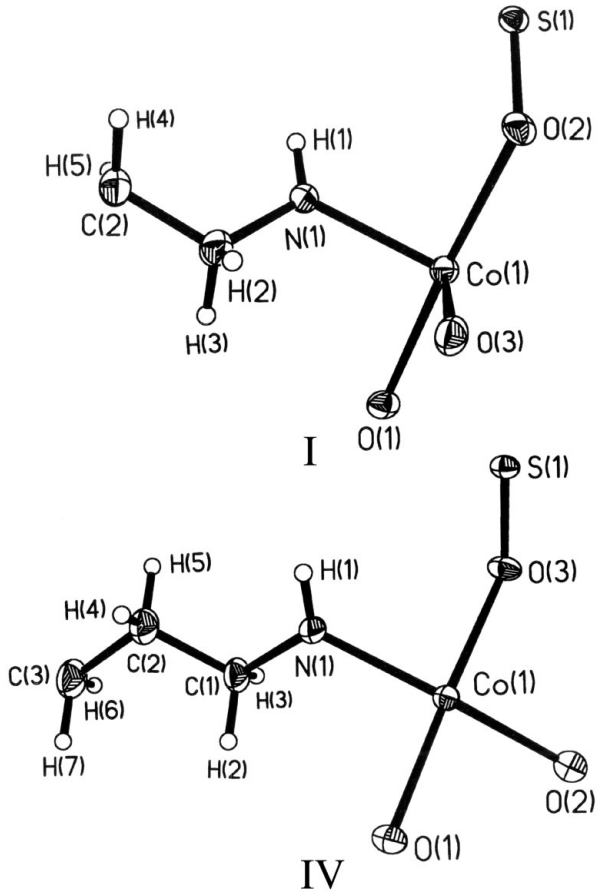
© 2005 NRC Canada

Table 2. Atomic coordinates and equivalent isotropic displacement parameters (U(eq)) for compound **I** ([$Co(C_3N_2H_8)$]).

Atom	x	y	z	U(eq) (Å)
Co(1)	1684(2)	4094(1)	2500	18(1)
S(1)	–4073(3)	6025(2)	2500	18(1)
N(1)	–454(8)	3353(4)	3537(2)	24(1)
O(1)	4635(8)	2510(4)	2500	23(1)
O(2)	–1029(9)	5830(4)	2500	24(1)
O(3)	4615(6)	5381(3)	3232(2)	26(1)
C(1)	1112(10)	3009(5)	4287(3)	29(1)
C(2)	–632(14)	2500	5000	29(2)

Note: All atomic coordinate numbers listed for x, y, and z are $\times 10^4$.

Fig. 1. ORTEP plots of [$Co(C_3N_2H_8)(SO_4)$] (**I**) and [$Co(C_6N_2H_{14})(SO_4)$] (**IV**). The asymmetric units are labeled. Thermal ellipsoids are given at 50% probability.



ordinates of **II**–**IV** in view of their structural similarity. The powder X-ray diffraction pattern of the compounds was in good agreement with the simulated pattern generated from the single crystal XRD data, indicating the phase purity of the compounds.

Results and discussion

Compounds of the general formula, $Co(HN(CH_2)_nNH)SO_4$, where n = 3 (**I**), 4 (**II**), 5 (**III**), and 6 (**IV**), were synthesized under solvothermal conditions by the reaction of $CoCl_2 \cdot 6H_2O$ with the diaminoalkane and H_2SO_4. The pink colored crystals obtained as products were investigated by X-ray crystallography. Compounds **I**–**IV** are isostructural and therefore belong to the orthorhombic crystal system (space group *Pbcm*), with comparable a and b parameters while the c parameter increases with n or the chain length of the diamine. In Fig. 1, the asymmetric units of **I** and **IV** are given. The asymmetric units of these compounds consist of one cobalt atom, one sulfur atom, four oxygen atoms, and one diamine moiety, with the metal atom in a distorted octahedral geometry. Each metal ion center is coordinated by four oxygens from three different sulfate groups and by two nitrogen atoms from two different amine units. The sulfur atom makes four S–O–Co linkages by sharing both edges and corners with the metal atom. In Table 3, we have listed

Table 3. Selected bond distances and angles in **I**.

Moiety	Distance (Å)	Moiety	Angle (°)
Co(1)—N(1)[a]	2.097(4)	O(2)-Co(1)-O(3)	86.22(13)
Co(1)—N(1)	2.097(4)	N(1)[a]-Co(1)-O(3)[a]	94.80(13)
Co(1)—O(1)	2.108(4)	N(1)-Co(1)-O(3)[a]	158.38(13)
Co(1)—O(2)	2.149(4)	O(1)-Co(1)-O(3)[a]	89.56(12)
Co(1)—O(3)	2.234(3)	O(2)-Co(1)-O(3)[a]	86.22(13)
Co(1)—O(3)[a]	2.234(3)	O(3)-Co(1)-O(3)[a]	63.9(2)
S(1)—O(2)	1.478(5)	O(2)-S(1)-O(3)[b]	111.5(2)
S(1)—O(3)[b]	1.482(3)	O(2)-S(1)-O(3)[c]	111.5(2)
S(1)—O(3)[c]	1.482(3)	O(3)[b]-S(1)-O(3)[c]	105.8(3)
S(1)—O(1)[d]	1.485(4)	O(2)-S(1)-O(1)[d]	108.0(2)
N(1)—C(1)	1.466(6)	O(3)[b]-S(1)-O(1)[d]	110.0(2)
N(1)—H(1)	0.86	C(1)-N(1)-Co(1)	119.2(3)
O(1)—S(1)[e]	1.485(4)	C(1)-N(1)-H(1)	120.4(2)
O(3)—S(1)[f]	1.482(3)	Co(1)-N(1)-H(1)	120.39(10)
C(1)—C(2)	1.510(6)	S(1)[e]-O(1)-Co(1)	127.1(2)
C(1)—H(2)	0.97	S(1)-O(2)-Co(1)	134.9(3)
C(1)—H(3)	0.97	S(1)[f]-O(3)-Co(1)	95.1(2)
C(2)—C(1)[g]	1.510(6)	N(1)-C(1)-C(2)	114.9(4)
C(2)—H(5)	0.97	N(1)-C(1)-H(2)	108.6(2)
C(2)—H(4)	0.97	C(2)-C(1)-H(2)	108.6(2)
		N(1)-C(1)-H(3)	108.6(2)
		C(2)-C(1)-H(3)	108.6(2)
		H(2)-C(1)-H(3)	107.5
		C(1)-C(2)-C(1)[g]	112.4(5)
		C(1)-C(2)-H(5)	109.1(2)
		C(1)[g]-C(2)-H(5)	109.1(2)
		C(1)-C(2)-H(4)	109.1(2)
		H(5)-C(2)-H(4)	107.8
		N(1)[a]-Co(1)-N(1)	106.1(2)
		N(1)-Co(1)-O(1)	94.25(12)
		N(1)-Co(1)-O(2)	88.73(12)
		O(1)-Co(1)-O(2)	175.0(2)
		N(1)[a]-Co(1)-O(3)	158.38(13)
		N(1)-Co(1)-O(3)	94.80(13)
		O(1)-Co(1)-O(3)	89.56(12)

[a]No. 1: x, y, $-z + 1/2$.
[b]No. 2: $x - 1$, y, $-z + 1/2$.
[c]No. 3: $x - 1$, y, z.
[d]No. 4: $-x$, $y + 1/2$, $-z + 1/2$.
[e]No. 5: $-x$, $y - 1/2$, $-z + 1/2$.
[f]No. 6: $x + 1$, y, z.
[g]No. 7: x, $-y + 1/2$, $-z + 1$.

© 2005 NRC Canada

Fig. 2. (*a*) Layer in the *ab* plane of **I–IV**, formed by CoN_2O_4 octahedra and SO_4 tetrahedra, showing the presence of six-membered apertures. (*b*) View of the infinite three-dimensional framework in **I** along the *a* axis showing the apertures.

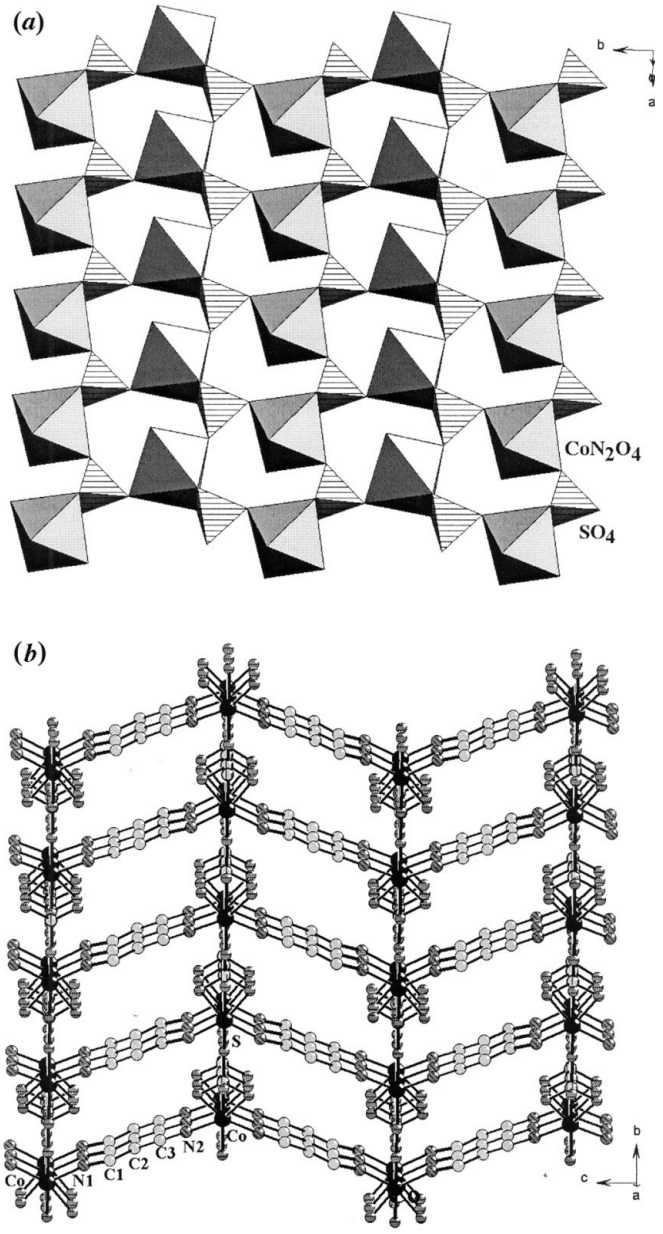
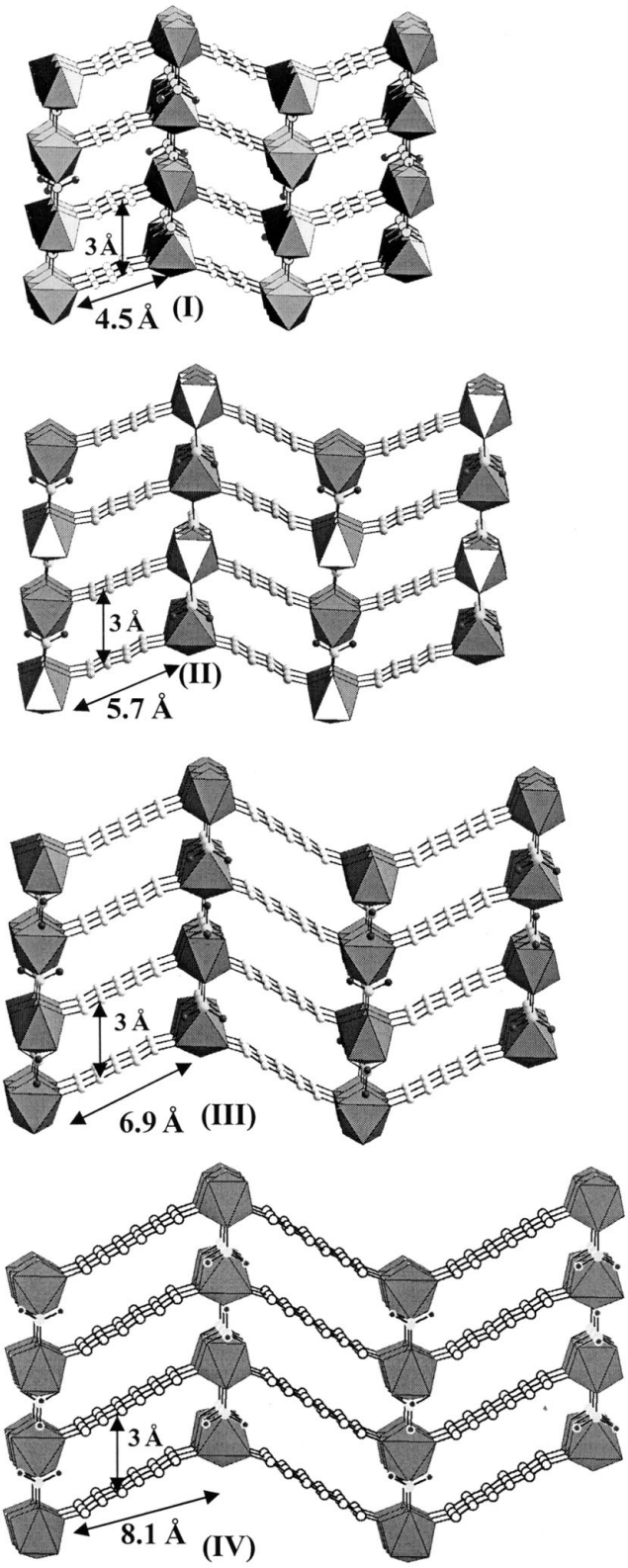


Fig. 3. Layers in **I–IV** showing the variation in aperture size with chain length for the diamine.

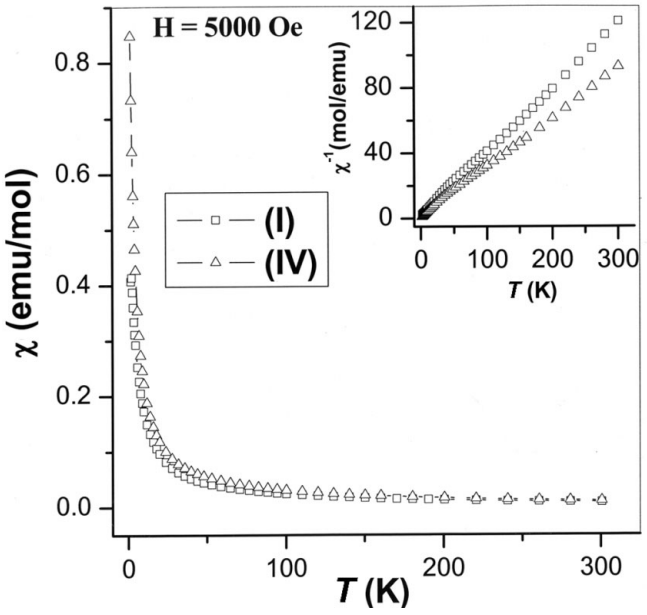


the important structural parameters for **I**, the crucial distances being the same in compounds **II–IV**. The Co—O/N bond distances are in the range 2.097(4)–2.234(3) Å. The trans N/O-Co-O/N bond angles are in the range 158.38(13)–175.0(2)° (avg. 166.7°) and the cis N/O-Co-O/N bond angles are in the range 86.22(13)–106.1(2)° (avg. 92.2°). The average S—O distance in the sulfate unit is 1.481 Å. Bond valence sum calculations (12) indicate that the oxidation states for Co and S are +2 and +6, respectively.

The structures of **I–IV** involve a three-dimensional coordinated network consisting of CoO_4N_2 octahedra and SO_4 tetrahedra sharing both the edges and vertices as shown in Fig. 2. Each sulfate unit shares an edge and two corners with three neighboring cobalt centers to form a two-dimensional sheet resulting in the formation of six-membered apertures along the *ab* plane. The layers are linked by the diamine

© 2005 NRC Canada

Fig. 4. Temperature variation of the magnetic susceptibility (χ) of **I** and **IV**. Inset shows the temperature variation of the inverse susceptibility (χ_M^{-1}).

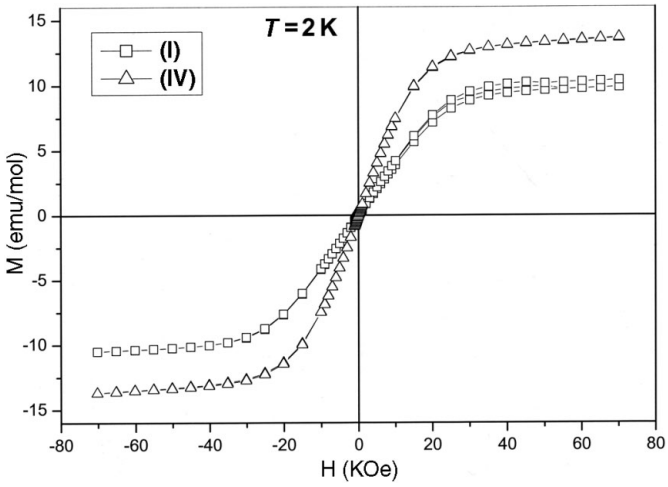


along the *c* axis to form an infinite three-dimensional (3D) coordinate network. The 3D network possesses channels along both the *a* and *b* axes. The bridged Co—Co distances are 8.6, 9.9, 11.2, and 12.5 Å in **I**, **II**, **III**, and **IV**, respectively. The estimated sizes of the aperture (excluding the van derWaals radii of the surrounding atoms) are 3 × 4.5, 3 × 5.7, 3 × 6.9, and 3 × 8.1 $Å^2$ in **I**, **II**, **III**, and **IV**, respectively. The aperture size is determined by the length of the diamine chain (Fig. 3). Calculations using SQUEEZE from the PLATON (13) package, however, gave the percentage of filled space to be 72%, 71%, 71%, and 70%, respectively in **I**–**IV**.

It is instructive to compare the structures of **I**–**IV** with the structures of $Co_4(SO_4)(OH)_6(H_2NC_2H_4NH_2)_{0.5}{\cdot}3H_2O$ (5) and $Co_4(SO_4)(OH)_6(C_6N_2H_{12})_{0.5}{\cdot}H_2O$ (14). In the last two compounds, tetrahedral–octahedral–tetrahedral (T–O–T) cobalt hydroxide layers are connected to one another by en/DABCO pillars through tetrahedral Co ions, with the sulfate group projecting into the interlayer gallery. In **I**–**IV**, however, we have layers of $CoN_2(SO_4)$ connected to each other by diamines through octahedral cobalt(II) ions.

In Fig. 4, we show the temperature variation of both the magnetic susceptibility and the inverse susceptibility of two typical compounds, **I** and **IV,** corresponding to the extremes in the diamine chain lengths. Extrapolation of the inverse susceptibility data at high temperatures gives paramagnetic Curie temperatures (θ_p) of 10 and –16 K for **I** and **IV**, respectively. The effective magnetic moment per cobalt atom is around 4.8 μ_B, a value comparable to that in other Co^{2+} compounds (15). The M–H curves (M = magnetization, H = applied field), (Fig. 5) at low temperatures do not show hysteresis but show a sigmoidal variation with saturation, similar to other cobalt compounds with weak ferromagnetic interactions (16). We are, therefore, inclined to consider **I**–**IV** as being weakly ferromagnetic in nature at low temperatures, the interaction being confined to the Co(II) sulfate layers.

Fig. 5. Isothermal M–H cycles of **I** and **IV** at 2 K.



Conclusions

In conclusion, four isostructural coordination polymers of Co(II), wherein the layers formed by CoN_2O_4 octahedra and SO_4 tetrahedra are linked by diaminoalkanes, have been synthesized and characterized. The diamine acts not only as a ligand but also as a spacer between the layers. A comparable case, in the literature, is that of 3D α,ω-dicarboxylate Mn(II) compounds where the interlayer spacing was varied by the alkyl chain length in the dicarboxylate (17). This family of coordination polymers also demonstrates how simple networks formed by transition metal polyhedra and sulfate tetrahedra can yield novel architectures.

Acknowledgements

The authors thank Dr. K.V. Gopalkrishnan of the Tata Institute of Fundamental Research (TIFR) for help with the magnetic measurements and J.N. Behera thanks the Council for Scientific and Industrial Research (CSIR), India for a fellowship.

References

1. Z. Shi, S. Feng, S. Gao, L. Zhang, G. Yang, and J. Hua. Angew. Chem. Int. Ed. **39**, 2325 (2000).
2. O.M. Yaghi, H. Li, and T.L. Groy. Inorg. Chem. **36**, 4292 (1997).
3. L. Carlucci, G. Ciani, and D.M. Proserpio. Chem. Commun. (Cambridge), 380 (2004).
4. (*a*) H. Li, M. Eddaoudi, M. O'Keeffe, and O.M. Yaghi. Nature (London), **402**, 276 (1999); (*b*) N.L. Rosi, J. Eckert, M. Eddaoudi, D.T. Vodak, J. Kim, M. O'Keeffe, and O.M. Yaghi. Science, **300**, 1127 (2003).
5. A. Rujiwatra, C.J. Kepert, and M.J. Rosseinsky. Chem. Commun. (Cambridge), 2307 (1999).
6. S.O.H. Gutschke, D.J. Price, A.K. Powell, and P.T. Wood. Angew. Chem. Int. Ed. **40**, 1920 (2001).
7. J.Y. Lu, M.A. Lawandy, J. Li, T. Yuen, and C.L. Lin. Inorg. Chem. **38**, 2695 (1999).

© 2005 NRC Canada

8. (*a*) C.N.R. Rao, S. Natarajan, and R. Vaidhyanathan. Angew. Chem. Int. Ed. **43**, 1466 (2004); (*b*) S. Kitagawa, R. Kitaura, and S.-I. Noro. Angew. Chem. Int. Ed. **43**, 2334 (2004).
9. G.M. Sheldrick. SADABS [computer program]. University of Göttingen, Göttingen, Germany. 1994.
10. (*a*) G.M. Sheldrick. SHELXS-86 [computer program]. University of Göttingen, Göttingen, Germany. 1986; (*b*) G.M. Sheldrick. Acta Crystallogr. Sect. A, **46**, 467 (1990).
11. G.M. Sheldrick. SHELXTL-PLUS [computer program]. University of Göttingen, Göttingen, Germany. 1993.
12. I.D. Brown and D. Altermatt. Acta Crystallogr. Sect. B, **B47**, 244 (1985).
13. A.L. Spek. Acta Crystallogr. Sect. A, **A46**, C34 (1990).
14. A. Rujiwatra, C.J. Kepert, J.B. Claridge, M.J. Rosseinsky, H. Kumagai, and M. Kurmoo. J. Am. Chem. Soc. **123**, 10 584 (2001).
15. (*a*) C. Livage, C. Egger, and G. Ferey. Chem. Mater. **11**, 1546 (1999); (*b*) L.-S. Long, X.-M. Chen, M.-L. Tong, Z.-G. Sun, Y.-P. Ren, R.-B. Huang, and L.-S. Zheng. J. Chem. Soc. Dalton Trans. 2888 (2001); (*c*) J.N. Behera, G. Paul, A. Choudhury, and C.N.R. Rao. Chem. Commun. (Cambridge), 456 (2004).
16. H.-L. Sun, S. Gao, B.-Q. Ma, and G. Su. Inorg. Chem. **42**, 5399 (2003).
17. Y.J. Kim, E.W. Lee, and D.-Y. Jung. Chem. Mater. **13**, 2684 (2001).

© 2005 NRC Canada

Palladium-catalyzed asymmetric cyclocarbonylation of allyl naphthols[1]

Giuseppe Vasapollo and Giuseppe Mele

Abstract: The asymmetric cyclocarbonylation reaction of allyl naphthol catalyzed by palladium complexes and chiral phosphine is reported. The reaction was performed under *syn*-gas conditions at relatively mild experimental conditions (80–100 °C, 300–600 psi (1 psi = 6.895 kPa)) in CH_2Cl_2 as the solvent.

Key words: enantioselective, carbonylation, cyclocarbonylation, lactones, palladium acetate.

Résumé : On a réalisé la réaction de cyclocarbonylation asymétrique de l'allylnaphtol catalysée par des complexes du palladium et une phosphine chirale. La réaction a été effectuée dans des conditions *syn*-gaz, en utilisant le dichlorométhane comme solvant et des conditions expérimentales relativement douces (80 à 100 °C, 300 à 600 psi (1 psi = 6,895 kPa)).

Mots clés : énantiosélective, carbonylation, cyclocarbonylation, lactones, acétate de palladium.

[Traduit par la Rédaction]

Introduction

The synthesis of optically active compounds including lactones and lactams is of great interest because of their biological properties (anti-inflammatory, analgesic, etc.). These molecules often exhibit higher biological activity in one enantiomeric form and asymmetric synthesis still represents an important method for the synthesis of chiral compounds.

Numerous strategies to pursue this goal have been developed over the last years, and transition-metal-catalyzed reactions in particular (hydrogenation, carbon—carbon bond forming, hydrosilation, carbonylation) are the most investigated, providing efficient entries to a variety of useful functionalized heterocyclic compounds (such as lactones, lactams, and pyrrolidinones) and achieving at the same time relatively high enantioselectivity (1).

A large variety of transition-metal-catalyzed cyclocarbonylation reactions of alcohols or phenols to lactones have been reported in the literature (2); on the contrary, only a few examples of enantioselective lactonization have been reported.

Alper and co-workers, pioneers of enantioselective cyclocarbonylation chemistry, have extensively studied the palladium-catalyzed cyclocarbonylation of allylic nonaromatic alcohols and have developed the first enantioselective variant of this reaction using commercially available chiral bisphosphine ligands, obtaining reasonable ees. For example, treatment of but-2-en-1-ol with carbon monoxide, oxygen, copper(II) chloride, and HCl in THF containing palladium chloride and polyleucine as chiral ligand afforded (*R*)-α-methy-γ-butyrolactone in 61% enantiomeric excess (ee). (*L*)-Diethyl tartrate and (*R*)- and (*S*)-bis(diphenylphosphino)-1,1′ binaphthyl (BINAP) have also been used as chiral ligands but gave low yields of optically active lactones (Scheme 1) (3).

Alper and co-workers have demonstrated that the commercially available chiral reagents diethyltartrate and poly-L-leucine were useful chiral ligands for the preparation of optically active lactones. This study represents the first example of the use of poly-α-amino acids as added chiral ligands in homogeneous catalysis. Other studies on asymmetric carbonylation reactions reported in the literature are, however, restricted to β-substituted allylic alcohols with dialkyl substitution at the α position (geminal dialkyl effect) (Scheme 2). For example, the cyclocarbonylation reaction of allylic alcohols catalyzed by palladium complexes and BICP [(2*R*,2′*R*)-bis[bis-(phenyl)phosphino]-(1*R*,1′*R*)-dicyclopentane or Xyl-BICP [(2*R*,2′*R*)-bis[bis-(3,5-dimethylphenyl)phosphino]-(1*R*,1′*R*)-dicyclopentane (Fig. 1) as ligands proceeded with good enantiomeric excess (4).

A major advance in these studies was the development of the first highly enantioselective cyclocarbonylation of β,γ-substituted allylic alcohols bearing geminal dialkyl substituents in the α-position (Scheme 3), which significantly increases the scope and synthetic utility of the asymmetric carbonylation reaction (5).

Received 15 December 2004. Published on the NRC Research Press Web site at http://canjchem.nrc.ca on 16 June 2005.

This paper is dedicated to honour the career contribution of Professor Howard Alper. He made a great contribution in catalysis, organometallic, and organic chemistry. His impact on the national and international chemistry community was also significant. We learned so much from him.

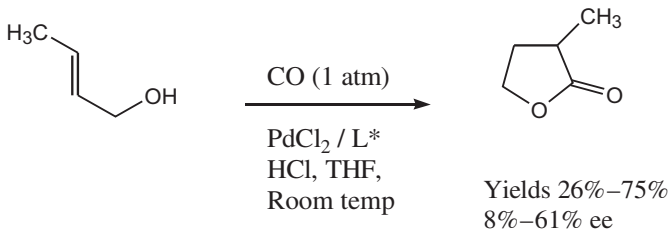
G. Vasapollo[2] and G. Mele. Dipartimento di Ingegneria dell'Innovazione, Università di Lecce, Via Arnesano 73100 Lecce, Italy.

[1]This article is part of a Special Issue dedicated to Professor Howard Alper.

[2]Corresponding author (e-mail: giuseppe.vasapollo@unile.it).

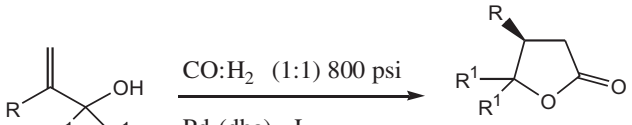
 doi: 10.1139/V05-075 © 2005 NRC Canada

Scheme 1.



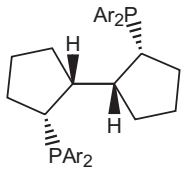
Yields 26%–75%
8%–61% ee

Scheme 2.



Yields 51%–95%
49%–97% ee

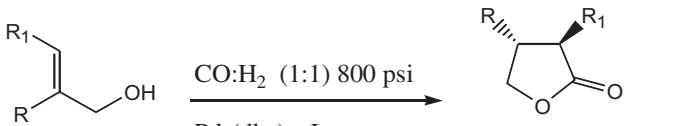
Fig. 1. BICP and Xyl-BICP ligands.



L_1: BICP Ar = Ph

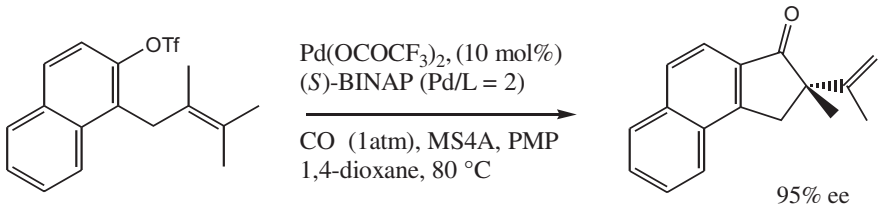
L_2: Xyl-BICP Ar 3,5-dimethyl phenyl

Scheme 3.



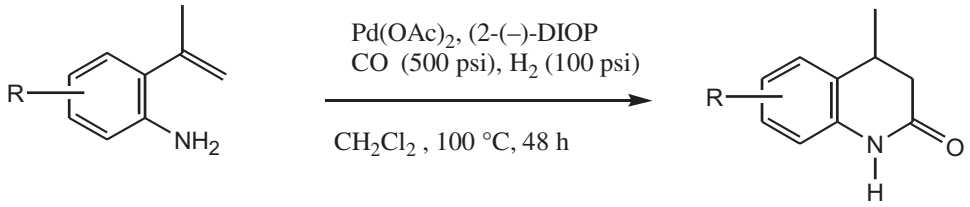
Yields 51%–95%
45%–98% ee

Scheme 4.



95% ee

Scheme 5.



9 examples

Other examples include the catalytic system $Pd(OCOCF_3)_2$–(*S*)-BINAP, which has been used to enhance the asymmetric carbonylative cyclization of prochiral *o*-allylaryl triflates and 2-allylalkenyl triflates and to produce high yields of enantiomerically enriched cyclopentenones (up to 96% ee) (Scheme 4) (6).

The asymmetric cyclocarbonylation of 2-vinylaniline derivatives catalyzed by palladium acetate and 2(–)-DIOP produced 3,4-dihydro-4-methyl-2(1*H*)-quinolin-2-ones in up to 54% ee (Scheme 5) (7).

Iridium salts in the presence of chiral diphosphine were also able to catalyze (with high enantioselectivity) intra- and intermolecular Pauson–Khand type reactions, producing various chiral cyclic enones in high enantiomeric excesses (8). So, whilst the cyclocarbonylation of unsaturated alcohols catalyzed by transition metals is well known, few examples of the asymmetric synthesis of fused aromatic ring lactones are reported (9).

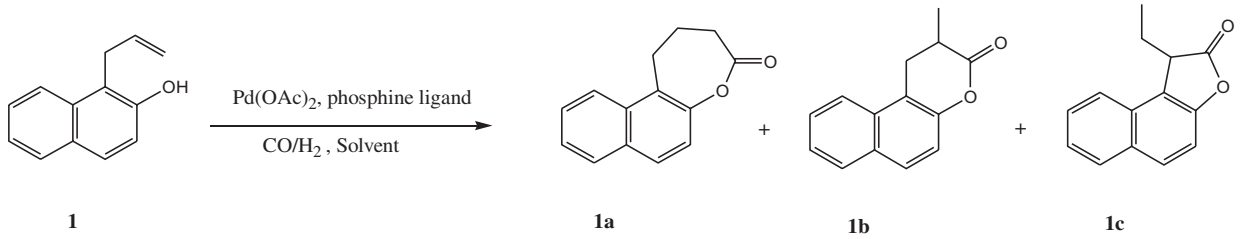
Several of us have recently reported the regioselective cyclocarbonylation of 2-allyl phenols by palladium catalysts (10), leading to five-, six-, or seven-membered lactones (Scheme 6). In this case the selectivity strongly depended on the nature of the catalyst, the solvent, and the $CO:H_2$ ratio. For example, the regioselective cyclocarbonylation of 2-allyl phenols using palladium acetate, dppb, and dichoromethane as the solvent led predominantly to six-membered ring lactones (10).

In this study we have examined the feasibility of the asymmetric cyclocarbonylation, observing that a stereogenic center can be formed during the six- and five-membered ring lactone formation if the reaction is performed in the presence of a chiral ligand.

In continuation of our previous work in this field we now wish to report our preliminary results on the regioselective and enantioselective synthesis of optically active compounds using palladium acetate and chiral phosphine ligands.

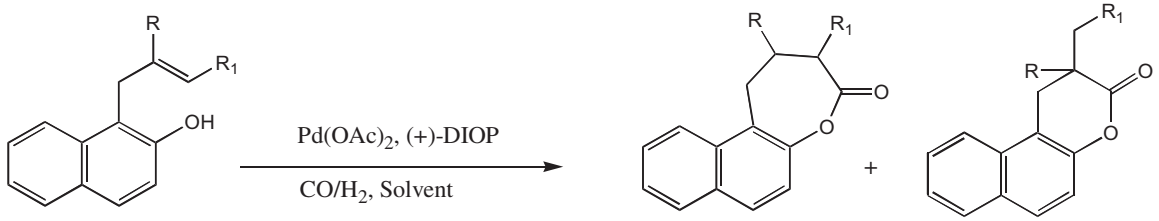
© 2005 NRC Canada

Scheme 6.



1 **1a** **1b** **1c**

Scheme 7.



1–3 **1a–3a** **1b–3b**

1: R=R$_1$=H, **2**: R=CH$_3$, R$_1$=H; **3**: R=H, R$_1$=CH$_3$

Table 1. Cyclocarbonylation reactions of substrates **1–3** with Pd(OAc)$_2$-(+)-DIOP.

Entry	Substrate	T (°C)	P_{CO} (psi)	P_{H_2} (psi)	Solvent	Time (h)	Conversion (%)	Product distibution		ee
1[a]	**1**	60	500	100	CH_2Cl_2	72	8	**1a** (83)	**1b** (17)	64
2[a]	**1**	70	500	100	CH_2Cl_2	24	33	**1a** (82)	**1b** (18)	63
3	**1**	80	500	100	CH_2Cl_2	24	90	**1a** (80)	**1b** (20)	61
4	**1**	100	500	100	CH_2Cl_2	24	92	**1a** (77)	**1b** (23)	30
5	**1**	100	500	100	Toluene	24	92	**1a** (54)	**1b** (46)	12
6	**1**	80	500	100	Hexane	24	3	**1a** (15)	**1b** (<5%)	—
7	**1**	80	500	100	DME	24	5	**1a** (68)	**1b** (32)	—
8	**2**	80	300	300	Toluene	24	90	**2a** (95)	**2b** (5)	15[b]
9	**2**	80	500	100	CH_2Cl_2	24	50	**2a** (40)	**2b** (60)	15[b]
10	**3**	80	300	300	Toluene	24	90	**3a** (95)	**3b** (5)	12[c]
11	**3**	80	500	100	CH_2Cl_2	24	45	**3a** (80)	**3b** (20)	10[c]

Note: Reaction conditions: Substrate (1.0 mmol); Pd(OAc)$_2$ (0.1 mmol); (+)-DIOP (0.15 mmol); solvent (5 mL). The autoclave was purged three times with CO and pressurized with CO and H_2. The reaction mixture was heated under stirring at 70–100 °C (oil bath temperature). Enantiomeric excesses (%) were determined by HPLC using a Chiralcel OB-H column (length 25 cm, ϕ = 0.45 cm); eluent: ethanol (9%) in hexane; flow of 0.5 mL/min. 1 psi = 6.895 kPa.

[a]The reactions reported in entries 1 and 2 have been scaled up three and two times, respectively, to obtain **1b** in a great enough amount for it to be analytically determined by HPLC.

[b]Refers to **2a**.

[c]Refers to **3a**.

We describe here the asymmetric cyclocarbonylation reaction of allyl naphthols under *syn*-gas conditions for the formation of fused-ring lactones.

Results and discussion

The asymmetric cyclocarbonylation reaction of the allylnaphthol derivatives **1–3** using Pd(II)-(+)-DIOP as a homogeneous catalytic system is shown in Scheme 7.

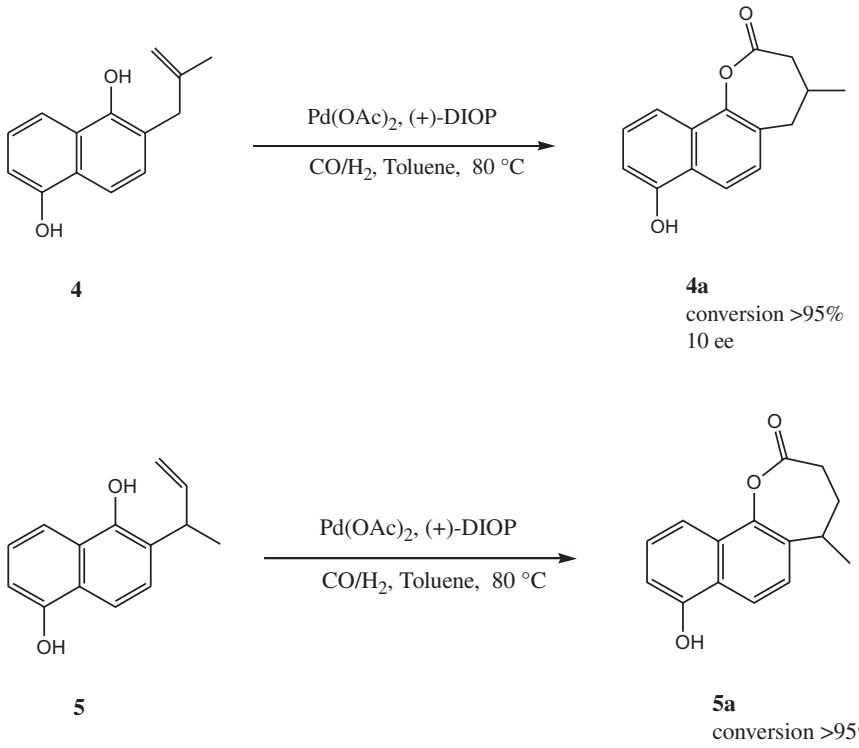
The reaction conditions used previously in our study of the palladium-catalyzed cyclocarbonylation of allyl phenol were employed in the present case. For example, allyl naphthol, **1**, reacts with CO and H_2 in the presence of 10% Pd(OAc)$_2$ and (+)-DIOP in CH_2Cl_2 at 100 °C to give seven- and six-membered ring lactones **1a** and **1b** in good yields. CH_2Cl_2 was used as a solvent because, as reported previously, the formation of the six-membered ring was favored with this solvent.

The enantiomeric excesses of the chiral cyclocarbonylation products induced by the chiral ligand were found to depend on the reaction conditions (see Table 1).

The catalyst for the enantioselective cyclocarbonylation was prepared in situ by treatment of palladium acetate with chiral phosphine ligand in CH_2Cl_2 at room temperature, and

© 2005 NRC Canada

Scheme 8.



the resulting mixture was used for cyclocarbonylation under CO and H_2.

As previously reported, allyl naphthol, **1**, reacted with CO and H_2 in the presence of 10% $Pd(OAc)_2$ and phosphine ligand at 100 °C to give seven- and six-membered ring lactones **1a** and **1b** in 90% isolated yields (Scheme 6); small amounts of five-membered-ring lactone were also obtained.

Because the phosphine units of (+)-DIOP are structurally very similar to that of dppb (used as a ligand for the palladium-catalyzed cyclocarbonylation reaction), we can predict that (+)-DIOP or similar chiral ligands would exhibit significant chiral discrimination in the palladium-catalyzed reaction. Therefore, when the reaction was carried out in the presence of a chiral phosphine such as (+)-DIOP, 90% of **1** was converted into **1a** and **1b** with distributions of 80% and 20%, respectively (Table 1, entry 3). The enantiomeric excess of **1b** (61%) was determined by HPLC analysis using a chiral stationary phase column.

Several other chiral ligands, such as (–)-bppm (98% yield, 9% ee), (+)-Binap (43% yield, 7% ee), and *R*,*R*-BDP (20% yield, 6% ee), were inferior to (+)-DIOP in terms of yields and enantioselectivity. When the reaction was performed at different temperatures, the chemical yield changed significantly, along with the enantiomeric excess (see Table 1). For example, when the reaction was performed at 70 °C and 80 °C, the conversion was 33% and 90%, respectively, while the enantiomeric excesses were 63% and 61%, respectively. At 100 °C, the chemical conversion increased but the enantiomeric excess dropped to 30%. At 60 °C, the conversion obtained was 8%, while the enantiomeric excess was 64%. The product distribution remains almost constant regardless of temperature. Although 60 °C is the best temperature for better enantiomeric excess (Table 1, entry 1), a low chemical conversion is observed at this temperature. The influence of the $CO:H_2$ ratio was not investigated because, as reported in the previous work, a $CO:H_2$ ratio of 5:1 and dichoromethane as a solvent are the best conditions for the preparation of the desired chiral six-membered ring lactone.

The cyclocarbonylation reactions of **2** and **3** afforded, respectively, lactones **2a** and **3a** in moderate enantiomeric excess. In this case, the moderate influence of the solvent on the enantioselectivity may be ascribed to the presence of methyl groups as substituents in the double bond of the allylic moiety. However, as observed in the previous work, seven-membered ring lactones were always formed (10) as the main product when toluene was used as the solvent.

High conversion into the seven-membered ring lactone, **4a**, with moderate enantiomeric excess was also observed when 2-(2-methyl-allyl)-naphthalene-1,5-diol (**4**) was used as the starting material; no enantiodiscrimination in the carbonylation products of **5** was observed (Scheme 8).

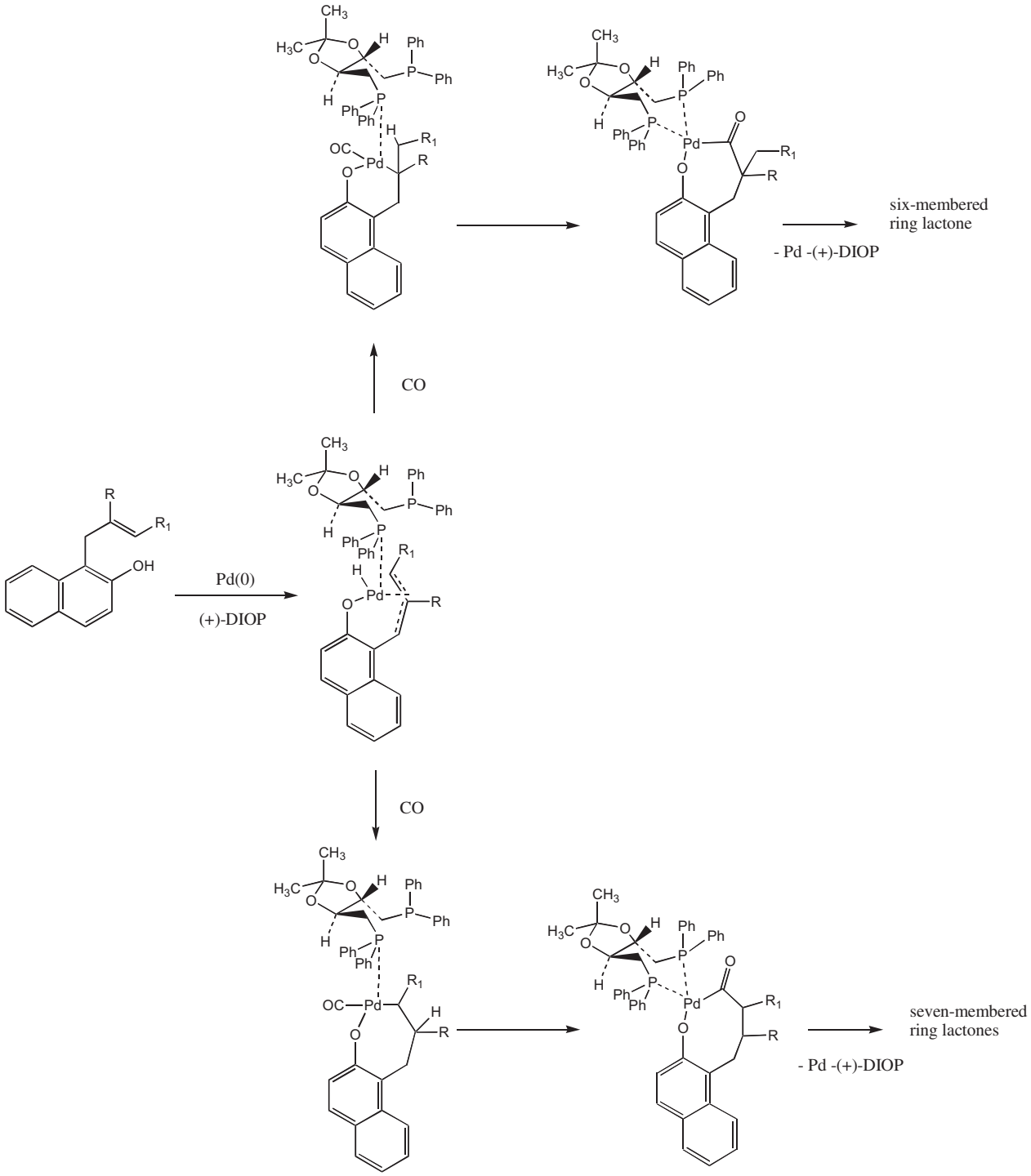
Proposed mechanism

According to that mechanism reported by Alper and coworkers (9–11), different pathways are possible for the formation of differently sized lactones (six- or seven-membered ring). These are depicted in Scheme 9. Firstly, there is an oxidative addition of Pd(0) into the O—H bond to produce a palladium hydride. Subsequently, the olefin coordinates to Pd, which also binds the chiral ligand, (+)-DIOP. Intramolecular hydropalladation, followed by coordination and insertion of carbon monoxide into the Pd—C bond, followed by reductive elimination has been hypothesized to justify the formation of different lactones with the regeneration of the catalysts.

In the light of these considerations, the enantiodiscrimination step could be either the enantioselective intramolecular

© 2005 NRC Canada

Scheme 9.



hydropalladation or the enantioselective coordination and insertion of carbon monoxide.

The catalytic reactivity observed for the Pd-catalyzed cyclocarbonylation with a 1,4-bisphosphine ligand is associated with a relatively flexible ligand–metal seven-membered ring chelate.

The higher enantiomeric excesses observed in the formation of the six-membered ring could be due to the closer distance of the chiral phosphine ligand to the metal centre.

The lower ees observed in the formation of seven-membered ring lactones could also be due to the steric hindrance of methyl groups.

Experimental section

Materials and measurements

Most chemicals were used as obtained from commercial sources. $Pd(OAc)_2$ and (+)-DIOP are commercial available,

© 2005 NRC Canada

while the allyl naphthol derivatives were prepared according to literature procedures (12). CH_2Cl_2 was dried, distilled, stored, and handled under nitrogen.

Melting points were taken on an electro thermal apparatus. ^1H and ^{13}C NMR spectra were recorded on a Bruker AC-200 at room temperature, and chemical shifts are reported relative to Me_4Si. IR and MS spectra were performed, respectively, on an FT-IR Jasco or IR Perkin Elmer 683 and on a Hewlett-Packard GC/Mass MSD 5971 instrument. The enantiomeric excesses were determined by HPLC, using a Chiralcel OB-H column (length 25 cm, $\phi = 0.45$ cm), with ethanol (9%) in hexane as the eluent, using a flow of 0.5 mL/min.

General procedure for the cyclocarbonylation reactions

Palladium acetate (0.10 mmol) and (+)-DIOP (0.15 mmol) were dissolved in 5 mL of dry CH_2Cl_2, and the allyl naphthol derivative (1.00 mmol) was added. The autoclave was purged three times with CO and pressurized with CO and H_2. The reaction mixture was heated with stirring for 24 h at 80–100 °C (oil bath temperature). The reaction mixture was cooled to room temperature, the solution was concentrated, and the residue was extracted with ether. The lactones were purified by chromatography using petroleum ether and diethyl ether as eluant.

Lactone **1a** is a known compound, and the spectral data are in accord with the literature data (9).

Selected data for isolated compounds

Compound 1b

mp 65 to 66 °C. FT-IR (neat, cm^{-1}): 1766, 1227, 1149. ^1H NMR ($CDCl_3$) δ: 7.92 (d, J = 8.4 Hz, 1H), 7.87 (d, J = 8.2 Hz, 1H), 7.79 (d, J = 8.9 Hz, 1H), 7.60 (t, J = 8.3 Hz, 1H), 7.49 (t, J = 8.2 Hz, 1H), 7.25 (d, J = 8.9 Hz, 1H), 3.54 (dd, J = 6.0, 15.5 Hz, 1H), 3.06–2.89 (m, 2H), 1.50 (d, J = 6.6 Hz, 3H). ^{13}C NMR ($CDCl_3$) δ: 171.5, 149.3, 131.0, 130.7, 128.8, 128.7, 127.0, 125.0, 124.7, 122.7, 117.2, 33.6, 27.9, 15.6. EI-MS *m/z* (%): 212 ($[M]^+$, 100), 197 (15), 184 (34), 169 (85), 169 (85), 169 (85), 128 (40). Anal. calcd: C 79.50, H 5.70; found: C 79.49, H 5.60.

$(1b)_a$

HPLC (Chiralcel OB-H) column; eluent: ethanol (9%) in hexane; flow of 0.5 mL/min. Retention time 31.21 min.

$(1b)_b$

HPLC (Chiralcel OB-H) column; eluent: ethanol (9%) in hexane; flow of 0.5 mL/min. Retention time 32.79 min (main enantiomer).

Compound 4a

mp 142–144 °C. FT-IR (neat, cm^{-1}): 3590, 1755, 1390, 1135. ^1H NMR ($CDCl_3$) δ: 8.02 (d, J = 8.3 Hz, 1H), 7.72 (d, J = 8.4 Hz, 1H), 7.40–7.26 (m, 2H), 6.84 (d, J = 7.4 Hz, 1H), 5.5 (s, broad, 1H), 3.17–3.08 (m, 1H), 2.80–2.53 (m, 3H), 2.20–2.11 (m, 1H), 1.13 (d, J = 6.6 Hz, 3H). ^{13}C NMR ($CDCl_3$) δ: 171.9, 151.7, 146.3, 126.9, 126.8, 126.7, 125.1, 125.0, 119.5, 113.8, 109.0, 38.9, 36.3, 35.0, 20.6. EI-MS *m/z* (%): 242 ($[M]^+$, 63), 173 (100), 115 (19). Anal. calcd: C 74.36, H 5.82; found: C 74.09, H 5.79.

d-(4a)

HPLC (Chiralcel OB-H) column; eluent: ethanol (9%) in hexane; flow of 0.5 mL/min. $[\alpha]_D^{20}$ = –6.6 ($CHCl_3$). Retention time 42.36 min.

l-(4a)

HPLC (Chiralcel OB-H) column; eluent: ethanol (9%) in hexane; flow of 0.5 mL/min. $[\alpha]_D^{20}$ = –6.6 ($CHCl_3$). Retention time 44.89 min.

Compound 5a

mp 50 °C (decomposes). FT-IR (neat, cm^{-1}): 3590, 1735, 1390, 1155. ^1H NMR ($CDCl_3$) δ: 8.09 (d, J = 8.3 Hz, 1H), 7.76 (d, J = 8.8 Hz, 1H), 7.44–7.30 (m, 2H), 6.84 (d, J = 7.4 Hz, 1H), 5.47 (s, broad, 1H), 3.50–3.41 (m, 1H), 2.56–2.09 (m, 3H), 1.86–1.72 (m, 1H), 1.48 (d, J = 6.8 Hz, 3H). ^{13}C NMR ($CDCl_3$) δ: 172.1, 151.4, 146.2, 129.5, 126.8, 126.7, 124.5, 122.0, 119.7, 114.2, 108.9, 35.8, 31.6, 31.5, 17.6. EI-MS *m/z* (%): 242 ($[M]^+$, 60), 187 (100), 115 (7). Anal. calcd: C 74.36, H 5.82; found: C 73.98, H 5.20.

Conclusions

In summary, we have reported the asymmetric cyclocarbonylation of allyl naphthol catalyzed by palladium and chiral phosphine. Use of a lower temperature for the reaction in CH_2Cl_2 gives the seven-membered, rather than the six-membered, ring tricyclic lactones and increases the ees. The reaction was performed under H_2 (100 psi (1 psi = 6.895 kPa)) and CO (500 psi) at 80 °C; when CH_2Cl_2 was used as the solvent, the formation of the six-membered ring lactone was favored, and higher ees were obtained. We have reported the first example of an enantioselective cyclocarbonylation reaction for the synthesis of seven-membered ring lactones, although with low ees.

Acknowledgements

This work is partially supported by the University of Lecce (Fondi MPI 60%) and Consorzio INCA-Venezia (Progetto 5, Cluster 11-A, Legge 488).

References

1. (*a*) M.P. Doyle. Catalytic asymmetric synthesis. 2nd ed. *Edited by* I. Ojima. Wiley-VCH Publishers, New York. 2000; (*b*) R. Noyori. Asymmetric catalysis in organic synthesis. Wiley, New York. 1994; (*c*) G.Q. Lin, Y.M. Li, and A.S.C. Chan. Principles and applications of asymmetric synthesis. Wiley, New York. 2001.
2. (*a*) Y. Tamaru, M. Hojo, and Z.I. Yoshida. J. Org. Chem. **56**, 1099 (1991); (*b*) C. Copéret, T. Sugihara, G. Wu, I. Shimayama, and E.I. Negishi. J. Am. Chem. Soc. **117**, 3422 (1995); (*c*) M. Wang, S. Calet, and H. Alper. J. Org. Chem. **54**, 20 (1989); (*d*) T.F. Murray, E.G. Samsel, V. Varma, and J.R. Norton. J. Am. Chem. Soc. **103**, 7520 (1981); (*e*) A. Bonardi, M. Costa, B. Gabriele, G. Salerno, and G.P. Chiusoli. Tetrahedron Lett. **36**, 7495 (1995); (*f*) W.Y. Yu and H. Alper. J. Org. Chem. **62**, 5684 (1997); (*g*) B. Gabriele, G. Salerno, F. De Pascali, M. Costa, and G.P. Chiusoli. J. Chem. Soc. Perkin Trans. 1, 147 (1997); (*h*) K. Tezuka, Y. Ishizaki, and Y. Inoue. J. Mol. Catal. A: Chem. **129**, 199 (1998); (*i*) B. Gabriele, G. Salerno, M. Costa, and G.P. Chiusoli. Tetrahedron Lett. **40**,

© 2005 NRC Canada

989 (1999); (*j*) Y. Sakurai, S. Sakaguchi, and Y. Ishii. Tetrahedron Lett. **40**, 1701 (1999); (*k*) A. Acardi, S. Cacchi, G. Fabrizi, and L. Moro. Eur. J. Org. Chem. 1137 (1999); (*l*) F.L. Quing and Z.X. Jang. Tetrahedron Lett. **42**, 9051 (2001); (*m*) B. Gabriele, G. Salerno, L. Veltri, M. Costa, and C. Massera. Eur. J. Org. Chem. 4607 (2001); (*n*) G. Battistuzzi, S. Cacchi, G. Fabrizi, F. Marinelli, and L.M. Parisi. Org. Lett. **4**, 1355 (2002); (*o*) C.S. Consorti, G. Ebeling, and J. Dupont. Tetrahedron Lett. **43**, 753 (2002); (*p*) B. El Ali and H. Alper. Synlett, 161 (2000); (*q*) D. Zagarian and H. Alper. Organometallics, **12**, 712 (1993); (*r*) B. Gabriele, G. Salerno, F. De Pascali, M. Costa, and G.P. Chiusoli. J. Chem. Soc. Perkin Trans. 1, 147 (1997); (*s*) G. Vasapollo, A. Scarpa, G. Mele, L. Ronzini, and B. El Ali. Appl. Organomet. Chem. **14**, 739 (2000); (*t*) L. Troisi, G. Vasapollo, B. El Ali, G. Mele, S. Florio, and V. Capriati. Tetrahedron Lett. **40**, 1771 (1999); (*u*) R. Amorati, O.A. Attanasi, B. El Ali, P. Filippone, G. Mele, J. Spadavecchia, and G. Vasapollo. Synthesis, **18**, 2749 (2002); (*v*) A. Maffei, G. Mele, G. Ciccarella, G. Vasapollo, C. Crisafulli, S. Scirè, and L. La Mantia. Appl. Organomet. Chem. **16**, 543 (2002); (*w*) G. Vasapollo and G. Mele. Targets Heterocycl. Sys. **6**, 197 (2002); (*x*) A. Maffei, G. Mele, G. Vasapollo, and R. Del Sole. Appl. Organomet. Chem. **16**, 543 (2003); (*y*) G. Mele, G. Vasapollo, and B. El Ali. J. Mol. Catal. A: Chem. **204**–**205**, 97 (2003).

3. H. Alper and N. Hamel. J. Chem. Soc. Chem. Commun. 135 (1990).
4. P. Cao and X. Zhang. J. Am. Chem. Soc. **121**, 7708 (1999).
5. M. Brunner and H. Alper. J. Org. Chem. **62**, 7565 (1997).
6. T. Hayashi, J. Tang, and K. Kato. Org. Lett. **1**, 1487 (1999).
7. K. Okuro, H. Kai, and H. Alper. Tetrahedron Asymmetry, **8**, 2307 (1997).
8. T. Shibata and K. Takagi. J. Am. Chem. Soc. **122**, 9852 (2000).
9. C. Dong and H. Alper. J. Org. Chem. **69**, 5011 (2004).
10. B. El Ali, K. Okuro, G. Vasapollo, and H. Alper. J. Am. Chem. Soc. **118**, 4264 (1996).
11. C. Dong and H. Alper. Tetrahedron: Asymmetry, **15**, 35 (2004).
12. S.G. Rhoads and N.R. Raulins. Org. React. (N.Y.), 22, **1** (1974).

© 2005 NRC Canada

Recent advances in cyclohydrocarbonylation reactions[1]

Wen-Hua Chiou, Seung-Yub Lee, and Iwao Ojima

Abstract: This article describes recent advances in the cyclohydrocarbonylation reactions catalyzed by transition-metal complexes and their applications in organic synthesis as a review covering the relevant literature up to the middle of 2004. The reactions are categorized into four types, i.e., intramolecular amidocarbonylation reactions, intramolecular aminocarbonylation reactions, cyclohydrocarbonylation reactions involving carbon–nucleophiles, and other cyclohydrocarbonylation reactions. Cyclohydrocarbonylation reactions provide efficient routes to various monocyclic, bicyclic, and polycyclic compounds as a one-step cascade process or a one-pot process. Reaction mechanisms for these cascade processes are discussed as needed for clarification. The heterocyclic and carbocyclic compounds, thus obtained, can be further transformed to specific targets. Examples of such applications are also discussed.

Key words: catalysis, cyclohydrocarbonylation, hydroformylation, amidocarbonylation, cyclization, regioselectivity, aldehydes, regioselective, cascade, heterocycles, rhodium.

Résumé : Cet article de revue couvre la littérature appropriée jusqu'au milieu de l'année 2004 et décrit les progrès récents réalisés dans les réactions de cyclohydrocarbonylation catalysées par des complexes de métaux de transition et leurs applications en synthèse organique. Les réactions sont divisées en quatre groupes, soit les réactions d'amidocarbonylation intramoléculaire, les réactions d'aminocarbonylation intramoléculaire, les réactions de cyclohydrocarbonylation impliquant une liaison carbone–nucléophile et les autres réactions de cyclohydrocarbonylation. Les réactions de cyclohydrocarbonylation fournissent des voies efficaces conduisant à divers composés monocycliques, bicycliques et polycycliques par des processus en cascade d'une étape ou monotopiques. On discute des mécanismes réactionnels de ces processus en cascade lorsque cela est nécessaire pour clarifier la situation. Les composés hétérocycliques ou carbocycliques ainsi obtenus peuvent ensuite être encore transformés en cibles spécifiques. On discute aussi de quelques exemples de telles applications.

Mots clés : catalyse, cyclohydrocarbonylation, hydroformylation, amidocarbonylation, cyclisation, régiosélectivité, aldéhydes, régiosélectif, cascade, hétérocycles, rhodium.

[Traduit par la Rédaction]

Introduction

The development of highly efficient catalytic processes for the synthesis of natural and unnatural compounds of biological interest or as useful intermediates for the construction of functional materials is a central focus in modern organic synthesis. One of the most productive approaches to the development of such methodologies is to apply transition metal catalyzed cyclization reactions to transform simple starting materials to monocyclic, bicyclic, and polycyclic compounds that can be further elaborated into specific targets.

Among these catalytic cyclization reactions, cyclohydrocarbonylation of functionalized alkenes catalyzed mainly by Rh or Co complexes provides powerful catalytic processes for the synthesis of heterocycles as well as carbocycles (1–5). Cyclohydrocarbonylation is an intramolecular cascade process, consisting of the hydroformylation of a functionalized alkene to form an aldehyde intermediate, followed by the addition of a nucleophile in the same molecule to the aldehyde, leading to the formation of the corresponding cyclization product(s). As a variant, the cyclohydrocarbonylation also includes an intramolecular cascade process involving the hydrocarbonylation of an functional alkene, generating an acyl–metal intermediate, which undergoes intramolecular nucleophilic substitution to give the corresponding cyclic carbonyl compounds. Amide, amine, and hydroxyl groups as well as carbon–nucleophiles are representative functional groups in the alkene substrates in these processes. The cyclohydrocarbonylation reaction has been incorporated into more sophisticated cascade processes, forming bicyclic and polycyclic compounds in one-step or one-pot. This article describes recent advances in the cyclohydrocarbonylation reactions and their applications to organic synthesis as a re-

Received 17 November 2004. Published on the NRC Research Press Web site at http://canjchem.nrc.ca on 16 June 2005.

This article is dedicated to Professor Howard Alper for his outstanding contributions to the advancement of homogeneous catalysis, organometallic chemistry, and synthetic organic chemistry over the last four decades.

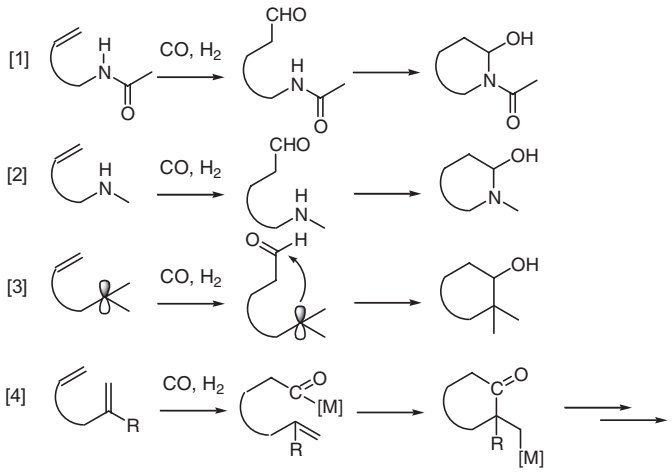
W.-H. Chiou, S.-Y. Lee, and I. Ojima.[2] Department of Chemistry, State University of New York at Stony Brook, Stony Brook, NY 11794-3400, USA.

[1]This article is part of a Special Issue dedicated to Professor Howard Alper.

[2]Corresponding author (e-mail: iojima@notes.cc.sunysb.edu).

 doi: 10.1139/V05-035 © 2005 NRC Canada

Scheme 1.



view covering the relevant literature up to the middle of 2004.

In this article, the cyclohydrocarbonylation reactions are categorized into four types as illustrated in Scheme 1, i.e., intramolecular amidocarbonylation reactions (eq. [1], Scheme 1), intramolecular aminocarbonylation reactions (eq. [2], Scheme 1), cyclohydrocarbonylation reactions involving carbon-nucleophiles (eq. [3], Scheme 1), and other cyclohydrocarbonylation reactions (eq. [4], Scheme 1).

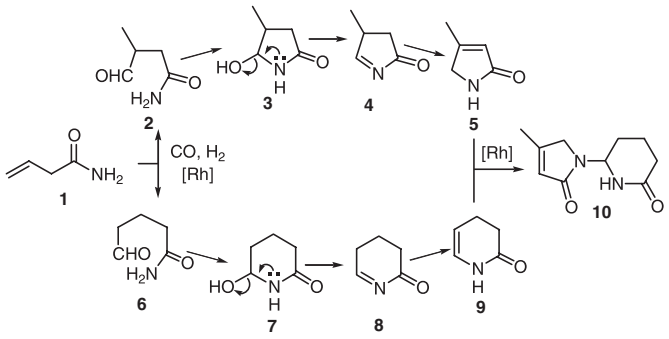
Intramolecular amidocarbonylation reactions

"Amidocarbonylation" is defined as a process involving the hydroformylation of an alkene, followed by the reaction of the resulting aldehyde with an amide or a carbamante. The intramolecular version of this process affords the corresponding nitrogen–heterocycles. For example, the intramolecular amidocarbonylation of but-3-enamide (**1**) catalyzed by $RhCl(PPh_3)_3$, $RhCl(CO)(PPh_3)_2$, or $Rh_4(CO)_{12}$ at 80–100 °C and at 82 atm (1 atm = 101.325 kPa) of "syngas" ($CO:H_2$ = 1:1 or 3:1) gives a mixture of 4-methyl-3-pyrrolin-2-one (**5**), 3,4-dihydro-2-pyridone (**9**), and 6-(4-methyl-3-pyrrolin-2-on-1-yl)-2-piperidone (**10**) (Scheme 2) (6, 7). It is reasonable to assume that **5** and **9** are formed via the intramolecular cyclization of 4-formylbutanamide (**2**) and 5-formylbutamide (**6**), respectively, whereas **10** arises from the cross coupling of **5** and **9** as illustrated in Scheme 2.

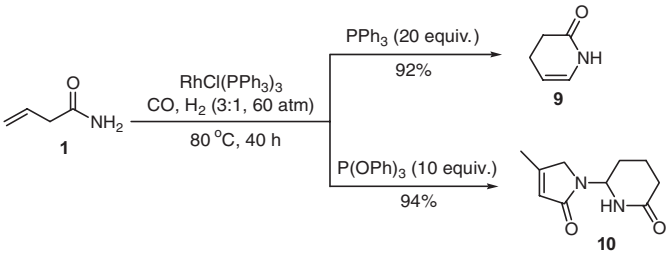
It is noteworthy that the highly selective synthesis of **9** or **10** is achieved simply by a proper choice of a phosphorus ligand to be used. As Scheme 3 shows, dihydropyridinone **9** is obtained in 92% yield by using $RhCl(PPh_3)_3$-PPh_3 (20 equiv.), whereas the reaction catalyzed by $RhCl(PPh_3)_3$-$P(OPh)_3$ (10 equiv.) affords the heterodimer **10** in 94% yield. The latter reaction is claimed to be the first example of the transition metal catalyzed cross coupling between an enamide and an amide (Scheme 3) (7).

In the case of pent-4-enamide (**11**), the reaction catalyzed by $RhCl(PPh_3)_3$ affords 4-methyl-3,4-dihydro-2-pyridone (**15**) exclusively (Scheme 4). No seven-membered ring lactam is formed even in the presence of a large excess of PPh_3 (6, 7). It has been shown that the phosphine–Rh com-

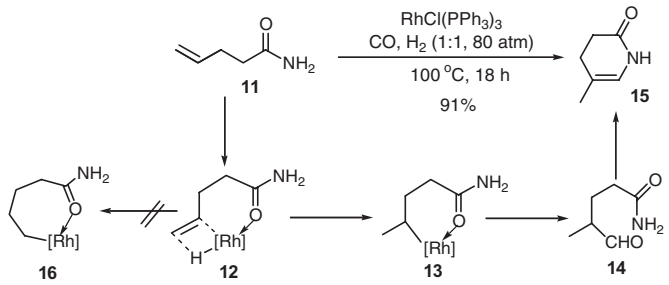
Scheme 2.



Scheme 3. Note: 1 atm = 101.325 kPa.



Scheme 4. Note: 1 atm = 101.325 kPa.



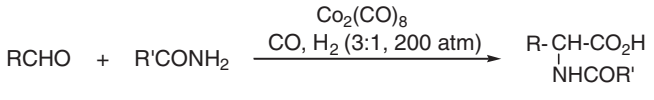
plex catalyzed hydroformylation of 1-alkenes usually gives linear aldehydes as major products (1, 2). Thus, the observed result indicates that branched aldehyde **14** is exclusively formed through a strong, amide-directed chelation control (6–11) that favors the branched alkyl–[Rh] complex **13** over the linear alkyl–[Rh] complex **16**. Then, complex **13** leads to the formation of branched aldehyde **14**, followed by cyclization to **15**.

The "Wakamatsu reaction", wherein an aldehyde is transformed to the corresponding *N*-acyl-α-amino acid through the reaction with an amide and syngas catalyzed by $Co_2(CO)_8$, was extensively studied in the 1970s (Scheme 5) (12). This unique amidocarbonylation process including double CO incorporation is applicable to the synthesis of cyclic *N*-acyl-α-amino acids (11, 13–16). For instance, the reaction of homoallylic amide **20** catalyzed by $Co_2(CO)_8$ at 100 °C and 100 atm (1 atm = 101.325 kPa) ($CO:H_2$ = 1:1) gives *N*-acylpipecolic acid (**21**) in one step (Scheme 6) (15).

The amide-directed cyclohydrocarbonylation of *N*-alkenylamides has been successfully applied to the syntheses of a variety of bicyclic nitrogen–heterocycles such as **23** and **26** (Scheme 7) (1, 8). Treatment of the resulting crude products with trifluoroacetic acid (TFA) affords enamide **24** and **27** in 86% and 92% yields, respectively.

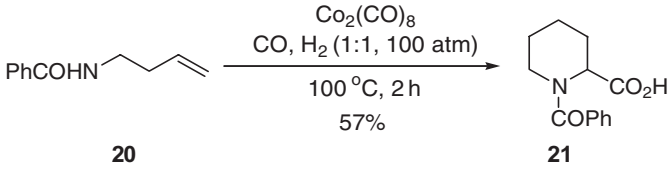
© 2005 NRC Canada

Scheme 5. Note: 1 atm = 101.325 kPa.

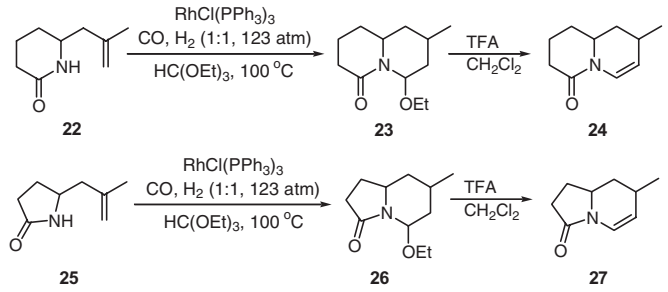


R	R'	Temp (°C)	*t* (min)	Solvent	Yield (%)
Me	Me	120	60	Dioxane	23
Me_2CH	Me	140	70	Dioxane	35
Bn	$C_{11}H_{23}$	120	15	EtOAc	40

Scheme 6. Note: 1 atm = 101.325 kPa.



Scheme 7. Note: 1 atm = 101.325 kPa.

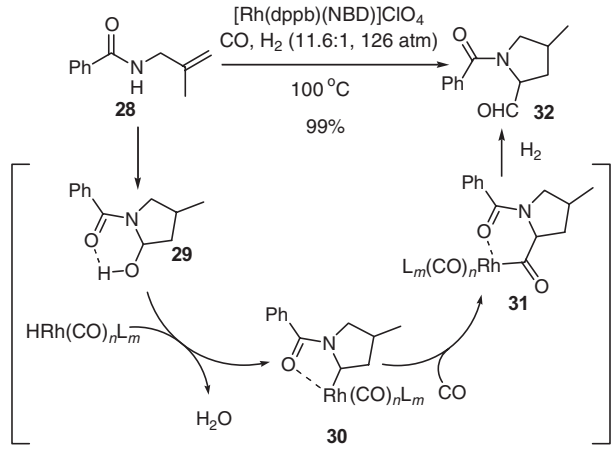


The Rh-catalyzed sequential double carbonylation of *N*-(2-methyl-2-propenyl)benzamide (**28**) gives *N*-benzoyl-2-formylpyrrolidine (**32**) (Scheme 8) (8, 9, 17). In this process, the hemiamidal **29** arising from the regioselective intramolecular amidocarbonylation of **28** is converted to alkyl–[Rh] complex **30**, and the subsequent insertion of CO gives acyl–[Rh] complex **31**. An oxidative addition of molecular hydrogen, followed by reductive elimination affords **32**.

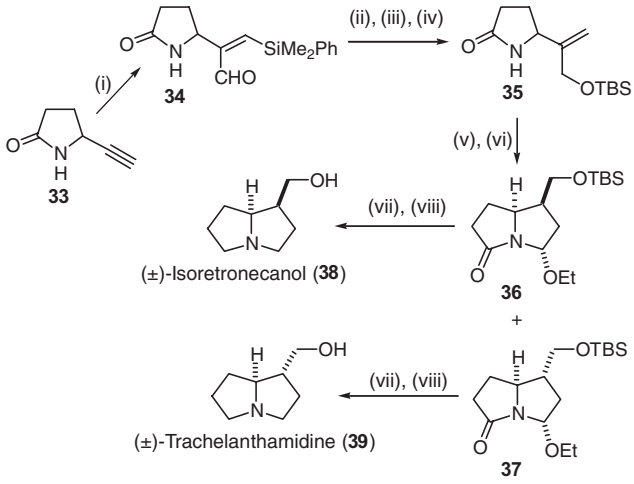
A combination of intermolecular silylformylation and amidocarbonylation provides an efficient route to pyrrolizidine alkaloids (18, 19). The regio- and diastereoselective Rh-catalyzed silylformylation of 5-ethynyl-2-pyrrolidinone (**33**) affords (*Z*)-**34** in excellent yield. Subsequent reduction and protodesilylation, followed by protection of the hydroxyl group as *tert*-butyldimethylsilyl (TBS) ether gives **35**. Cycloydrocarbonylation of **35** catalyzed by $HRh(CO)(PPh_3)_3$ affords a diastereoisomeric mixture (syn:anti = 2:1) of bicyclic products **36** and **37**, which are readily separable by flash chromatography. Removal of the silyl protecting group and reduction of both the amidal and amido group gives (±)-isoretronecanol (**38**) and (±)-trachelanthamidine (**39**), respectively (Scheme 9) (18, 19).

The combination of $Rh(acac)(CO)_2$ and a diphosphite ligand (BIPHEPHOS (21)) is an excellent catalyst system for the linear-selective hydroformylation of a wide range of alkenes (1, 19–22). This catalyst system has been successfully applied to the cyclohydrocarbonylation reactions of alkenamides and alkenylamines, which are employed in the

Scheme 8. Note: 1 atm = 101.325 kPa.



Scheme 9. Reaction conditions: (*i*) $HSiMe_2Ph$, CO (20 atm, 1 atm = 101.325 kPa), $Rh(acac)(CO)_2$, RT, 98%; (*ii*) $NaBH_4$, 0 °C, 100%; (*iii*) TsH, MeCN (2% H_2O), 75%; (*iv*) TBS-Cl, imidazole, 98%; (*v*) CO, H_2, $HRh(CO)(PPh_3)_3$, $HC(OEt)_3$, 72% (syn:anti = 2:1); (*vi*) SiO_2 column; (*vii*) *n*-Bu_4NF, RT, 96%; (*viii*) $LiAlH_4$, 65%–70%.



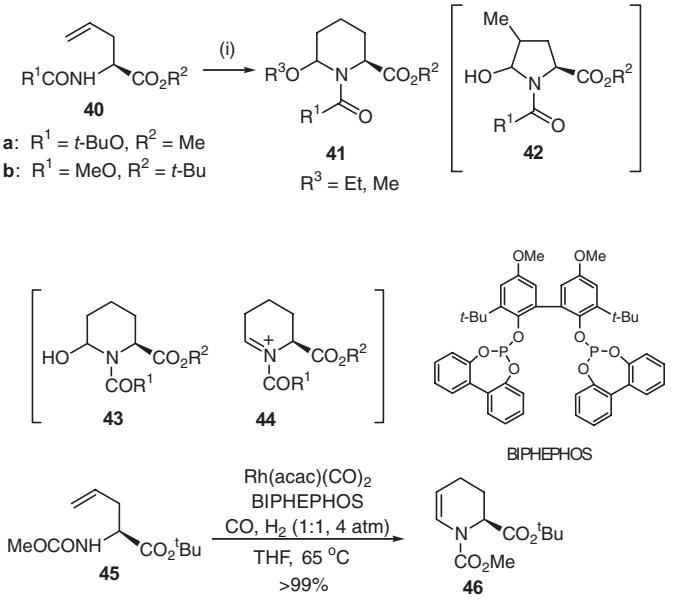
key steps for the syntheses of piperidine (23–25), indolizidine, and pyrrolizidine alkaloids (22).

Cyclohydrocarbonylation of *N*-carbalkoxyallylglycinate (**40**) catalyzed by $Rh(acac)(CO)_2$–BIPHEPHOS in an alcohol solvent gives 1-carbalkoxy-6-alkoxypipecolate (**41**) in quantitative yield (Scheme 10) (25). In this reaction, the use of the BIPHEPHOS ligand is essential for the exclusive formation of the piperidine ring via a linear aldehyde intermediate. When the same reaction is carried out using a classical catalyst, such as $HRh(CO)(PPh_3)_3$ in the presence of a large excess of PPh_3 (20 equiv.), a 1:1 mixture of regioisomers **41** and **42** is formed.

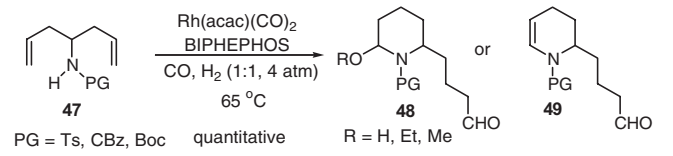
This process includes the extremely linear-selective hydroformylation of an olefin moiety, generating the corresponding terminal aldehyde, followed by the formations of hemiamidal **43** and then acyliminium ion **44**. Addition of an alcohol to the acyliminium ion intermediate **44** gives **41**. When the reaction of **45** is performed in an aprotic solvent such as THF, toluene, hexane, ethyl acetate, etc., 5,6-

© 2005 NRC Canada

Scheme 10. Reaction conditions: (*i*) Rh(acac)$(CO)_2$BIPHEPHOS, CO, H_2 (1:1, 4 atm, 1 atm = 101.325 kPa), R_3OH, 65 °C, quantitative.



Scheme 11. Note: 1 atm = 101.325 kPa.



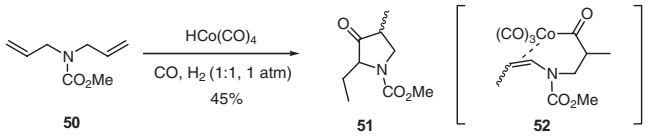
didehydropipecolate (**46**) is obtained in 99% yield via deprotonation and double bond migration of the common acyliminium ion intermediate **44** (Scheme 10) (25).

The cyclohydrocarbonylation of 4-tosylamino-1,6-heptadiene (**47**) catalyzed by Rh(acac)$(CO)_2$–BIPHEPHOS in THF gives *N*-tosyl-2-hydroxypiperidine (**48**) (R = H) and (or) *N*-tosyl-5,6-didehydropiperidine (**49**), depending on the duration of the reaction (Scheme 11) (24). When the reaction is stopped after 2 h, **48** is quantitatively formed as the sole product, but a prolonged reaction time (18 h) gives **49** exclusively in quantitative yield. This strongly indicates that the hemiamidal **48** is the precursor of the acyliminium ion intermediate similar to **44**. When the reaction is carried out in ethanol, *N*-tosyl-2-ethoxylpiperidine aldehyde (**48**) (R = Et or Me) is obtained in quantitative yield. As protecting groups for the amine moiety, carbobenzoxy (Cbz) and *tert*-butoxycarbonyl (*t*-Boc) groups are employed in addition to the tosyl group. 2-Alkoxypiperidine aldehyde (**48**) (R = Et, Me) and 5,6-didehydropiperidine aldehyde (**49**) serve as useful intermediates for the syntheses of various piperidine and indolizine alkaloids.

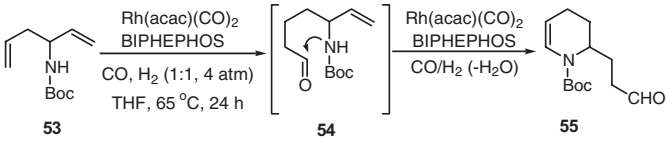
The reaction of **50** catalyzed by $HCo(CO)_4$ under the ambient pressure of CO and H_2 (1:1) gives 2-ethyl-4-methyl-3-pyrrolidinone (**51**) in 45% yield via acyl–[Co] species **52** in which an olefin isomerization takes place prior to carbocyclization (Scheme 12) (26).

The reaction of unsymmetrical amidodiene **53** catalyzed by the Rh–BIPHEPHOS complex gives dehydropiperidine

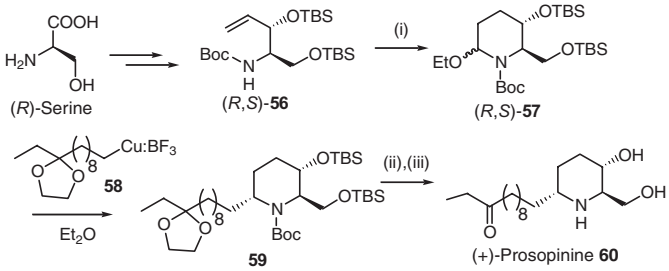
Scheme 12. Note: 1 atm = 101.325 kPa.



Scheme 13. Note: 1 atm = 101.325 kPa.



Scheme 14. Reaction conditions: (*i*) Rh(acac)$(CO)_2$ (1 mol%), BIPHEPHOS (2 mol%), CO, H_2 (1:1, 4 atm, 1 atm = 101.325 kPa), 92%; (*ii*) *n*-Bu_4NF, THF; (*iii*) TFA, CH_2Cl_2.



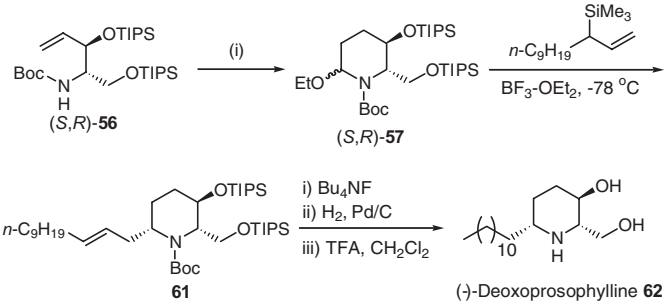
aldehyde (**55**) as the sole product, i.e., no pyrroline is formed (Scheme 13) (27). The fact that no pyrroline is formed indicates that this reaction is extremely site- and regioselective in that the hydroformylation takes place at the homoallylic olefin moiety exclusively, only yielding the linear aldehyde intermediate **54**.

A short total synthesis of (+)-prosopinine (**60**) from (*R*)-serine is achieved via cyclohydrocarbonylation catalyzed by the Rh–BIPHEPHOS complex for the construction of the key piperidine ring (2*R*,3*S*)-**57** (Scheme 14) (28). The resulting (2*R*,3*S*)-**57** is converted to (+)-prosopinine (**60**) via the nucleophilic displacement of the ethoxy group with organocopper reagent **58**. A similar strategy is used for the total synthesis of (–)-deoxoprosophylline (**62**), featuring the cyclohydrocarbonylation of (2*S*,3*R*)-**57** derived from (*S*)-serine as the key step. The C-6 side chain is introduced by a Lewis acid promoted allylsilane addition to (2*S*,3*R*)-**57** via the acyliminium ion intermediate to secure the required 2,6-cis stereochemistry of the target molecule (Scheme 15).

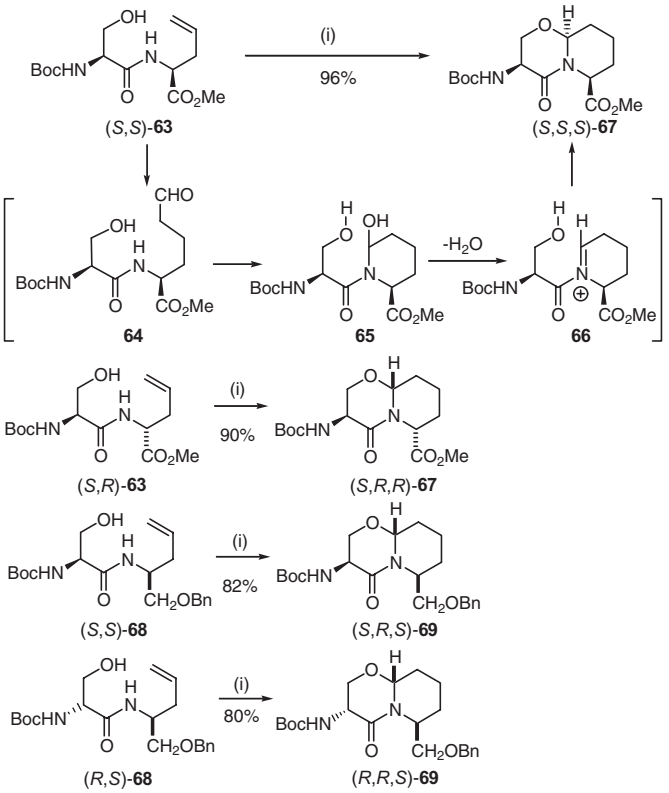
The Rh–BIPHEPHOS catalyzed cyclohydrocarbonylation has also been successfully applied to the rapid synthesis of a variety of 1-azabicyclo[X.Y.0]alkane amino acids, which serve as conformationally restricted dipeptide surrogates for enzyme inhibitors and receptor antagonists, directly from dehydrodipeptide substrates (Scheme 16) (29). Reaction of (*S*,*S*)-*N*-Boc-serinylallylglycinate ((*S*,*S*)-**63**) under the standard cyclohydrocarbonylation conditions gives 5-oxa-1-azabicyclo[4.4.0]decanecarboxylate ((*S*,*S*,*S*)-**67**) in excellent yield. This reaction includes an extremely selective hydroformylation to form linear aldehyde **64**, followed by the formation of hemiamidal **65**. Subsequent generation of acyliminium ion **66** and intramolecular nucleophilic addition

© 2005 NRC Canada

Scheme 15. Reactions conditions: (*i*) Rh(acac)$(CO)_2$ (1mol%), BIPHEPHOS (2 mol%), CO, H_2 (1:1, 4 atm, 1 atm = 101.325 kPa), EtOH, 65 °C, 96%.

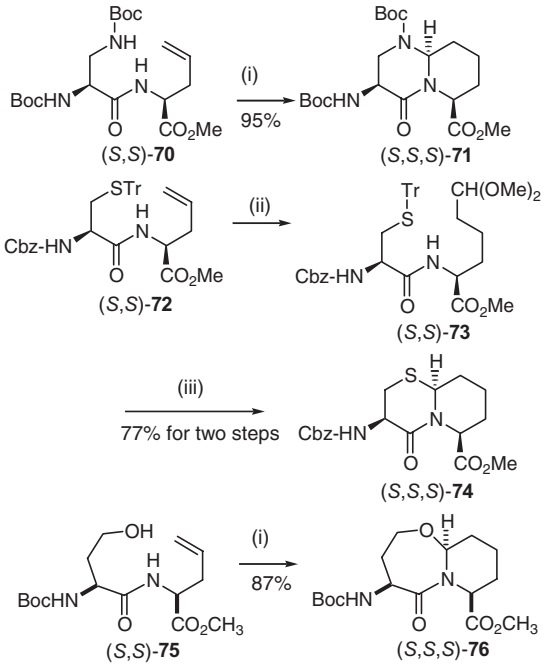


Scheme 16. Reaction conditions: (*i*) Rh(acac)$(CO)_2$ (2 mol%), BIPHEPHOS (4 mol%), CO, H_2 (1:1, 4 atm, 1 atm = 101.325 kPa), PTSA (10 mol%), toluene, 65 °C, 20 h.



of the hydroxyl group of the serine moiety yields (*S*,*S*,*S*)-**67** with excellent diastereoselectivity at C-6 (Scheme 16) (30). The reaction of the other diasteromer ((*S*,*R*)-**63**) gives (*S*,*R*,*R*)-**67** as the single product in 90% yield. Thus, the C-10 position appears to be the stereogenic center in these reactions. The stereochemistry at the C-6 position, however, is also dependent on the nature of the C-10 substituent. For example, the reaction of (*S*,*S*)-**68**, bearing a CH_2OBn group in place of a CO_2Me group at C-10, gives (*S*,*R*,*S*)-**69**, in which the absolute configuration at C-6 is *R*. In the same manner, the reaction of (*R*,*S*)-**68**, gives (*R*,*R*,*S*)-**69**, i.e., the absolute configuration at C-6 is *R* as well. The results confirm that the C-10 position is the stereogenic center in this process, but also indicate that the stereoelectronic nature of the C-10

Scheme 17. Reaction conditions: (*i*) Rh(acac)$(CO)_2$ (2 mol%), BIPHEPHOS (4 mol%), CO, H_2 (1:1, 4 atm, 1 atm = 101.325 kPa), PTSA (10 mol%), toluene, 65 °C, 20 h; (*ii*) Rh(acac)$(CO)_2$ (2 mol%), BIPHEPHOS (4 mol%), CO, H_2 (1:1, 4 atm, 1 atm = 101.325 kPa), MeOH, 65 °C, 20 h; (*iii*) TFA (cat), CH_2Cl_2.



substituent governs the diastereoface selection in the cyclization step (30).

In a similar manner, the reaction of (*S*,*S*)-**70** bearing a β-aminoalanine residue in place of the serine residue, proceeds efficiently in the presence of *p*-toluenesulfonic acid (PTSA) to give (*S*,*S*,*S*)-**71** as the single product in 95% yield (Scheme 17) (29). It should be noted that no 1-azabicyclo[4.3.0] product is formed in spite of the fact that either Boc-amino group in the β-aminoalanine residue could react with the acyliminium intermediate. In the case of a dipeptide substrate bearing a cysteine residue, an *S*-trityl derivative ((*S*,*S*,*S*)-**72**) has been used. Since the thiol group is protected, a spontaneous cyclization cannot take place. Thus, the reaction of (*S*,*S*,*S*)-**72** is carried out in MeOH to trap the resulting aldehyde moiety by converting it in situ to the corresponding acetal (*S*,*S*)-**73** (Scheme 17). The subsequent deprotection–cyclization with a catalytic amount of TFA afforded (*S*,*S*,*S*)-**74** in 77% isolated yield for two steps in one pot (Scheme 17) (29).

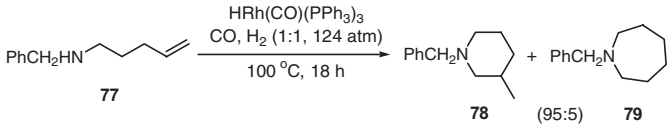
The reaction is readily applicable for the construction of 1-azabicyclo[5.4.0] system. Thus, the reaction of (*S*,*S*)-**75** under the standard conditions affords (*S*,*S*,*S*)-**76** in 87% yield (Scheme 17) (30). The stereocontrol at the C-6 position is governed by the C-10 ester group in accordance with the general mechanism proposed for this cascade process (vide supra).

Intramolcular aminocarbonylation reactions

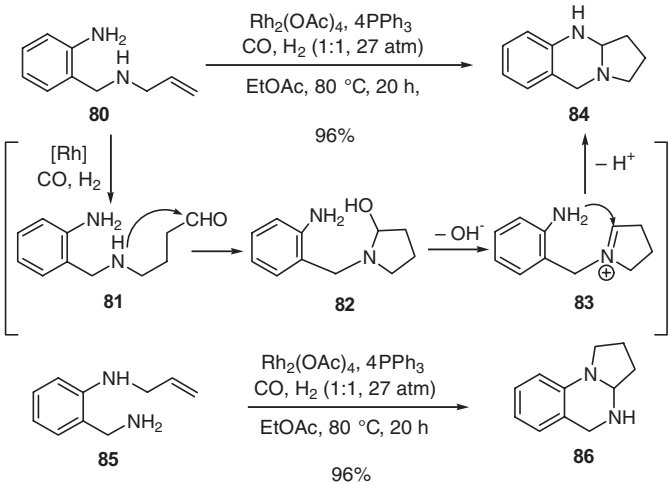
"Aminocarbonylation" is defined as a process involving the hydroformylation of an alkene, followed by the reaction

© 2005 NRC Canada

Scheme 18. Note: 1 atm = 101.325 kPa.



Scheme 19. Note: 1 atm = 101.325 kPa.



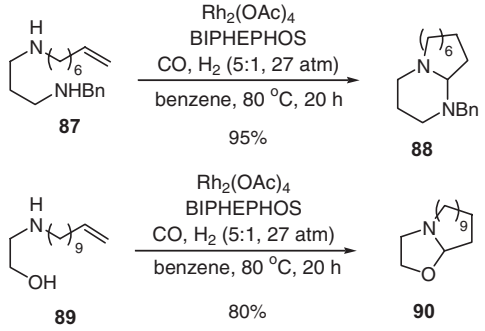
of the resulting aldehyde with an amine. In a manner similar to the amidocarbonylation discussed previously, the intramolecular version of aminocarbonylation provides unique and efficient routes to various nitrogen–heterocycles.

Cyclohydrocarbonylation of 5-benzylaminopentene (**77**) catalyzed by $HRh(CO)(PPh_3)_3$ at 100 °C and 124 atm (1 atm = 101.325 kPa) of syngas ($CO:H_2$ = 1:1) leads to the regioselective formation of piperidine **78** and a small amount of azepane **79** (Scheme 18) (31). The regioselectivity-determining step in this reaction is the hydroformylation of the olefin moiety of **77**, which strongly favors the formation of the corresponding branched aldehyde. This regioselectivity is opposite to that for the reaction of the usual alkenes. This indicates the presence of a strong amine-directed chelation control (1, 2), which is very similar to the amide-directed chelation control mentioned in the preceding section. The branched aldehyde, thus formed, undergoes intramolecular reductive amination to give **78**.

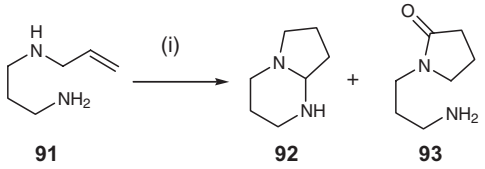
A rapid synthesis of a quinazoline skeleton has been developed by means of the Rh-catalyzed cascade cyclization of diaminoalkenes via intramolecular aminocarbonylation (32, 33). The cyclohydrocarbonylation of 2-(*N*-allylaminomethyl)aniline (**80**) gives quinazoline **84** in excellent yield through the highly linear-selective hydroformylation of **80**, followed by the sequential formations of hemiaminal **82** and iminium ion **83** as intermediates and then the subsequent intramolecular amine addition (Scheme 19) (32). In the same manner, the reaction of *N*-allyl-2-aminomethylaniline (**85**) affords **86** in 96% yield (33).

The same type of cascade cyclization has been applied to the one-step synthesis of fused azabicyclic compounds with medium to large-membered rings (Scheme 20) (34). For example, the reaction of alkenyldiamine **87** catalyzed by $Rh_2(OAc)_4$–BIPHEPHOS at 80 °C and 27 atm (1 atm = 101.325 kPa) of syngas ($CO:H_2$ = 5:1) gives diazabicyclo-[8.4.0]tetradecane (**88**) in 95% yield. In the same manner, the reaction of alkenylaminoalcohol **89** affords oxazabicyclo[11.3.0]hexadecane (**90**) in 80% yield.

Scheme 20. Note: 1 atm = 101.325 kPa.



Scheme 21. Reaction conditions: (*i*) $Rh_2(OAc)_4$, (0.5 mol%), ligands (2 mol%), CO, H_2 (27 atm, 1 atm = 101.325 kPa), C_6H_6 (0.26 mol/L), 80 °C, 20 h.



Entry	Ligand	$CO:H_2$	Product ratio[a]	
			92	**93**
1	PPh_3	1:1	40	60
2	PPh_3	1:9	95	5
3	PPh_3	9:1	10	90
4	$P(OPh)_3$	1:1	50	50
5	$P(O\text{-}o\text{-}Tol)_3$	1:1	25	75
6	$P(O\text{-}Cy)_3$	1:1	80	20
7	$P(o\text{-}Tol)_3$	1:1	15	85
8	$P(n\text{-}Bu)_3$	1:1	95	5
9	PCy_3	1:1	85	15
10	BIPHEPHOS	1:1	100	0

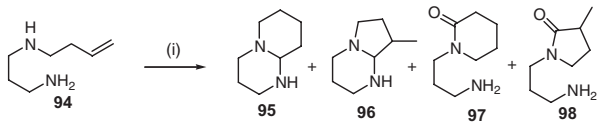
[a] Determined by ^{13}C-NMR.

Cyclohydrocarbonylation of *N*-allylpropanediamine (**91**) catalyzed by $Rh_2(OAc)_4$ in benzene at 80 °C and 27 atm (1 atm = 101.325 kPa) of syngas ($CO:H_2$ = 1:1) gives a 2:3 mixture of 1,5-diazabicyclo[4.3.0]nonane (**92**) and *N*-aminopropylpyrrolidinone (**93**, Scheme 21, entry 1) (35). The product ratio is highly dependent on the syngas composition as well as the nature of the ligand used. Thus, the higher hydrogen pressure (e.g., $CO:H_2$ = 1:9) dramatically increases the yield of **92** (Scheme 21, entry 2), while the higher CO pressure (e.g., $CO:H_2$ = 9:1) favors the formation of **93** (Scheme 21, entry 3). The higher basicity of the ligand used appears to favor the formation of **92** (Scheme 21, entries 8 and 9), but the steric factor is also playing an important role. Thus, the use of $P(O\text{-}o\text{-}Tol)_3$ leads to the predominant formation of **93**. The use of BIPHEPHOS affords only **92** in quantitative yield (Scheme 21, entry 10), which provides synthetic usefulness to this cyclohydrocarbonylation process.

In a similar manner, the reaction of *N*-homoallylpropanediamine (**94**) gives the corresponding 1,5-diazabicyclo-[4.4.0]decane) (**95**) (exclusively with the use of $Rh_2(OAc)_4$–

© 2005 NRC Canada

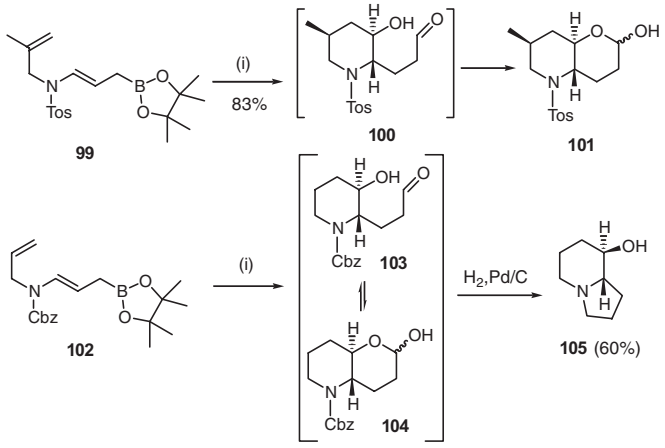
Scheme 22. Reactions conditions: (*i*) $Rh_2(OAc)_4$ (0.5 mol%), ligands (2 mol%), C_6H_6 (0.26 mol/L), 80 °C, 20 h.



Entry	Ligand	Ratio CO:H_2 (27 atm)	Product ratio[a] (95+96):(97+98)	(95:96)	(97:98)
1	BIPHEPHOS	1:1	100: 0	100: 0	—
2	BIPHEPHOS	1:9	100: 0	>95: <5	—
3	BIPHEPHOS	9:1	100: 0	100: 0	—
4	$P(OPh)_3$	1:1	75:25	85: 15	(25: 75)
5	PPh_3	1:9	>95:<5	70: 30	—
6	PPh_3	1:1	60:40	85: 15	(25: 75)
7	PPh_3	9:1	20:80	>95: <5	(55: 45)
8	$P(o\text{-Tol})_3$	1:1	5:95	95: 5	(30: 70)
9	$P(n\text{-Bu})_3$	1:1	>95:<5	75: 25	—
10	PCy_3	1:1	>95:<5	65: 35	—

[a] Determined by ^{13}C-NMR.

Scheme 23. Reaction conditions: (*i*) Rh(acac)$(CO)_2$, BIPHEPHOS, CO, H_2 (1:1, 5 atm, 1 atm = 101.325 kPa), 60 °C.

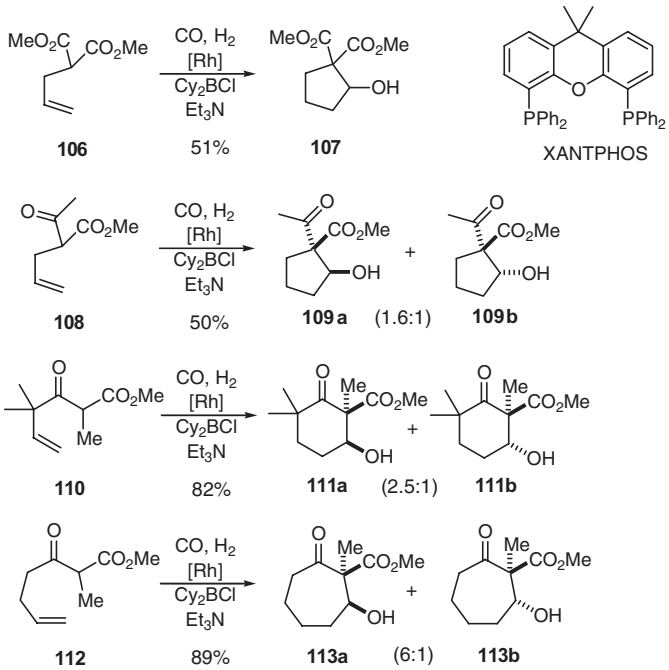


BIPHEPHOS as the catalyst and syngas with equal pressures of CO and H_2 (Scheme 22, entry 1)) (35). Since the use of BIPHEPHOS as the ligand strongly drives the reaction to linear-selective hydrocarbonylation, the ratio of CO and H_2 does not affect the product ratio (Scheme 22, entries 2 and 3). For other ligands, however, clear effects of the partial pressure of CO (or H_2) as well as the nature of ligands on the product ratio is observed in a manner similar to the reaction of **91** mentioned previously. It is interesting to note that the regioselectivity of the cyclohydrocarbonylation leading to the formation of **95** and **96** is linear selective in all cases examined, while the branched product **98** is favorable in the side reaction (Scheme 22, entries 4, 6, and 8).

Cyclohydrocarbonylation reactions involving carbon–nucleophiles

The cascade hydroformylation–allylboration–hydroformylation of (*E*)-aminoallylborate (**99**) catalyzed by Rh(acac)$(CO)_2$–BIPHEPHOS affords oxazabicyclic lactol **101** via linear aldehyde **100** in 83% yield (Scheme 23) (36). The regioselective hydroformylation of γ-amidoallylboronate (**102**) gives linear aldehyde **103**, which spontaneously cyclizes to give an equilibrium mixture of aldehyde **103** and lactol **104**. Removal of the Cbz group by hydrogenolysis initiates another cascade process, i.e., amination–hydrogenation, affording indolizidine **105** in 60% overall yield (Scheme 23) (36–38).

Scheme 24. Reaction conditions: Rh(acac)$(CO)_2$ (0.9 mol%), XANTPHOS (1.8 mol%), CO, H_2 (1:1, 60 atm, 1 atm = 101.325 kPa), Cy_2BCl (1.05 equiv.), Et_3N, CH_2Cl_2, 80 °C.

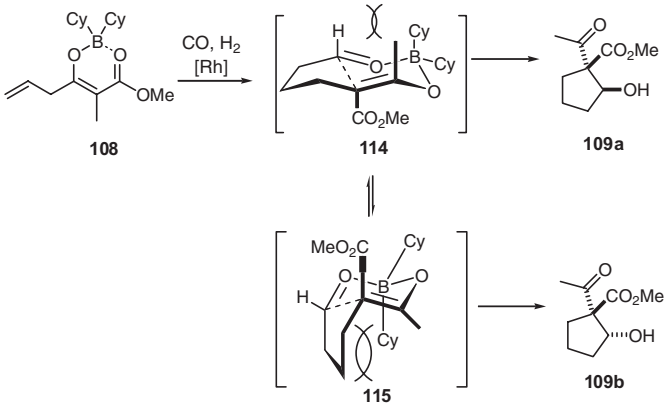


The Rh–XANPHOS catalyzed reactions of allylmalonate (**106**), 2-allylacetoacetate (**108**), 2-(3-butenoyl)propanoate (**110**), and 2-(4-pentenoyl)propanoate (**112**) with syngas in the presence of Cy_2BCl and triethylamine gave the corresponding cycloalkanols, **109**, **111**, and **113**, in fairly good to high yields (Scheme 24) (39). The cycloalkanols, **109**, **111**, and **113**, thus formed, possess a quaternary carbon center next to the hydroxyl group in a molecule, and would serve as useful polyfunctionalized synthetic intermediates in organic synthesis. The observed diastereoselectivity in these reactions can be accommodated by taking into account the relative extent of 1,3-diaxial interactions in the bicyclic transition states, involving a chair structure, e.g., **114** and **115**, for the preferential formation of **109a** (Scheme 25) (39).

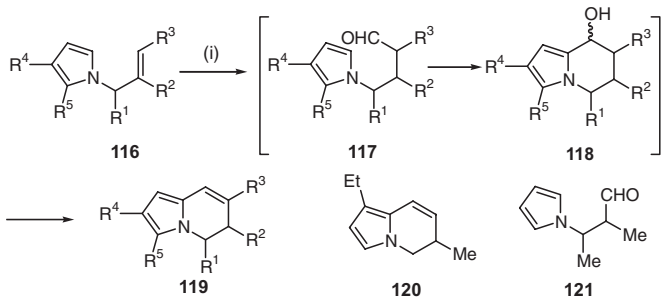
Cyclohydrocarbonylation of 1-allylpyrroles (**116a**–**116d**) catalyzed by $Rh_4(CO)_{12}$ at 100 °C and at 100 atm (1 atm = 101.325 kPa) of syngas ($CO:H_2$ = 1:1) gave the corresponding 5,6-dihydroindolizines (**119a**–**119d**) in good yield and excellent regioselectivity (Scheme 26) (40). This reaction proceeds through a cascade hydroformylation–cyclization–dehydration sequence (Scheme 26). Exclusive introduction of a formyl group at the terminal position of a gem-disubstituted olefin or at the carbon α to a phenyl group is typical for Rh-catalyzed hydroformylation reactions. However, in the reaction of **116e**, which has an unsubstituted terminal vinyl group (i.e., $R^2 = R^3 = H$), a mixture of the linear and branched aldehydes is formed, which are converted to

© 2005 NRC Canada

Scheme 25.



Scheme 26. Reaction conditions: (*i*) $Rh_4(CO)_{12}$ (0.25 mol%), CO, H_2 (1:1, 100 atm, 1 atm = 101.325 kPa), 100 °C, toluene (0.4 mol/L).



R^1	R^2	R^3	R^4	R^5	Product	Yield (%)[a]
H	Me	H	H	H	**119a**	75
H	H	Ph	H	H	**119b**	80
H	Me	H	H	Et	**119c**	72
H	Me	H	Et	H	**119d**, **120** (9:1)	75
Me	H	H	H	H	**119e, 121** (59:41)	62

[a] Isolated yield.

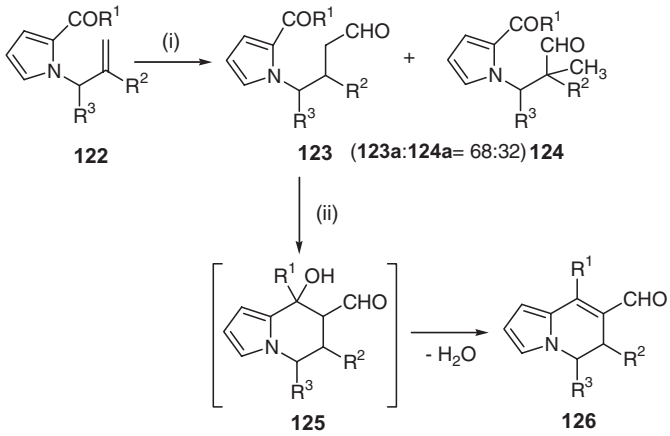
119e and **121**, respectively, in a 59:41 ratio (Scheme 26) (40).

In a similar manner, the cyclohydrocarbonylation of *N*-1-allyl-2-formylpyrroles (**122a**–**122c**) affords 7-formyl-5,6-dihydroindozilines (**126a**–**126c**) in good yield through a one-pot cascade hydroformylation – aldol condensation process (Scheme 27) (41). In this process, the crude hydroformylation product **122** is treated with a base in a one-pot process to give the final product (**126**).

Other cyclohydrocarbonylation reactions

Reaction of 3,3-disubstituted-1,4-pentadiene (**127**) with a primary amine under cyclohydrocarbonylation conditions gives cyclopenta[*b*]pyrrole (**131**) as the predominant product accompanied by a small amount of cyclopentanone (**130**) (Scheme 29) (42). This unique reaction is proposed to proceed through a cascade hydrocarbonylation–carbonylation process. The first hydrocarbonylation of **127** and the subsequent carbocyclization forms cyclopenatonylmethyl–Rh complex **128**. If **128** immediately reacts with molecular hydrogen, 2-methylcyclopentanone (**130**) is formed. However, if CO insertion takes place faster than the hydrogenolysis, cyclopentanoylacetyl–Rh complex **129** is generated, which undergoes the "Paal–Knorr" condensation (43) with a primary amine to yield cyclopenta[*b*]pyrrole (**131**).

Scheme 27. Reactions conditions: (*i*) $Rh_4(CO)_{12}$ (0.25 mol%), CO, H_2 (1:1, 100 atm, 1 atm = 101.325 kPa), 100 °C, toluene (0.4 mol/L), 0.5–2 h; (*ii*) 100 °C under N_2 for 70 h (R^1 = H) or EtONa–EtOH for 5 min (R^1 = Me).



	R^1	R^2	R^3	Product	Yield (%)[a]
a	H	H	Me	**126a**	60
b	H	Me	H	**126b**	75
c	Me	Me	H	**126c**	75

[a] Isolated yield.

Cyclohydrocarbonylation of propargylamine **132** catalyzed by $Rh_2(OAc)_4$-PPh_3 gives a mixture of pyrrole **133** (70%), pyrrolidine **134** (20%), and a small amount of lactone **135** through a deamination–cyclocarbonylation process (Scheme 29) (44).

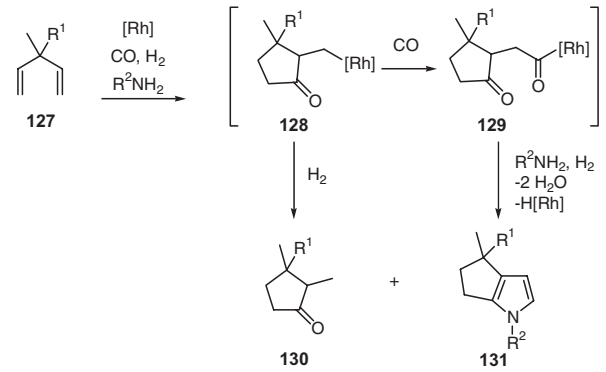
Hydroformylation of phenylacetylene **136** in the presence of *n*-hexylamine (**137**) catalyzed by $[Rh(COD)]^+[(\eta^6\text{-}C_6H_5BPh_3)]^-$ at 100 °C and at 100 atm (1 atm = 101.325 kPa) of syngas (CO:H_2 = 1:1) gives the corresponding 2-pyrrolidone (**140**). However, the reaction suffers from competing side reactions such as furanone formation and hydrogenation of allylamine intermediate **139** (Scheme 30) (45).

Cyclohydrocarbonylation of 3-TMS-propargyl alcohols cleanly gives the corresponding 2(5*H*)-furanones (**142**). For instance, the reaction of **141** catalyzed by $Rh_4(CO)_{12}$ gives spirobicyclic furanone **142** almost exclusively in 97% yield (Scheme 31) (46).

Furanones **145** or **146** can also be synthesized through the cyclohydrocarbonylation of ynones **144** catalyzed by $[Rh(COD)]^+[(\eta^6\text{-}C_6H_5BPh_3)]^-$–$P(OPh)_3$ (47). The reaction requires a total pressure of 20–40 atm (1 atm = 101.325 kPa) with an increased CO:H_2 ratio (up to 11:1) to prevent undesirable reductions. The nature of the substituent of the alkyne

© 2005 NRC Canada

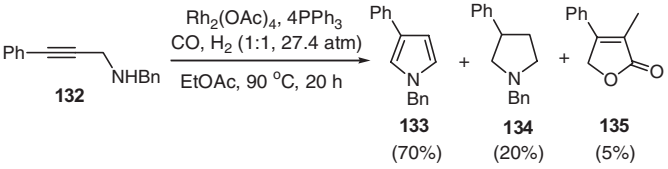
Scheme 28. Reaction conditions: (*i*) $[Rh(cod)Cl]_2$ (0.5 mol%), CO, H_2 (1:1, 100 atm, 1 atm = 101.325 kPa), dioxane (0.48–0.59 mol/L), 120 °C, 70 h.



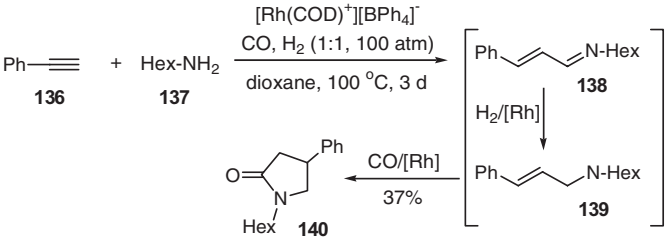
Entry	R^1	R^2	CO:H_2 (atm)	Time (h)	Yield (%)[a] 131	130
	-Me	*n*-Bu	50:50	70	54 (17)	<2
b	-Me	*i*-Pr	50:50	70	38 (21)	8
a	-Me	Bn	50:50	70	54 (30)	7
d	-Me	(R)-MeCHPh	50:50	40	47 (26)	—
e	-Me	*p*-MeO-C_6H_4	50:50	70	31 (17)	17
f	-$CH(OH)CH_3$	Bn	85:15	40	(40)	—
g	-CH_2CH_2OH	Bn	85:15	70	(20)	—

[a] GC yield. The value in parenthesis is isolated yield.

Scheme 29. Note: 1 atm = 101.325 kPa.



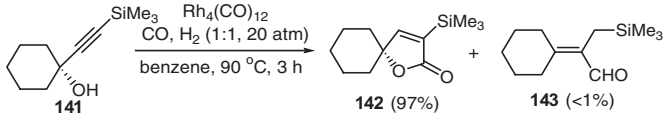
Scheme 30. Note: 1 atm = 101.325 kPa.



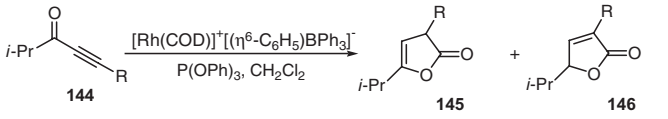
moiety has significant influence on the regioselectivity of the reaction. For example, the reactions of **144a**, **144c**, and **144d** afford corresponding **145a**, **145c**, and **145d**, while the reaction of **144b** gives **146b** in high yields (Scheme 32) (47).

A proposed mechanism for this transformation is illustrated in Scheme 33. Complexation of **144** to the [Rh]-H species forms intermediate **147**. The acetylene moiety of **147** undergoes a stereoselective intramolecular insertion into the [Rh]—H bond to give **148**. Two pathways are possible for the generation of key intermediate **153** from **148**, i.e., (*i*) through CO insertion to **149**, followed by rearrangement to zwitterionic ketene **150** and the subsequent cyclization to

Scheme 31. Note: 1 atm = 101.325 kPa.



Scheme 32. Note: 1 atm = 101.325 kPa.

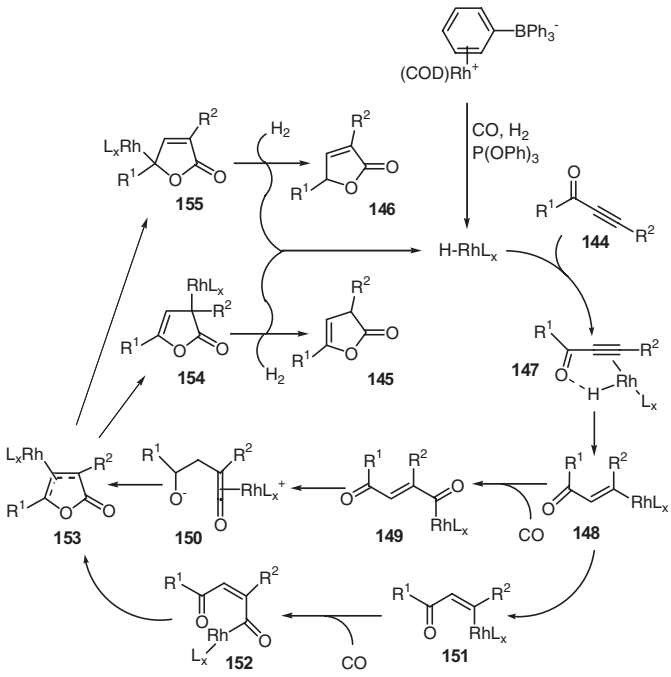


	R	CO (atm)	H_2 (atm)	Temp. (°C)	Time, (h)	Yield (%)[a] 145	146
a	*n*-Bu	38.5	3.5	90	36	88	—
b	Ph	38.5	3.5	120	24	—	88
c	C(Me)=CH_2	17.5	3.5	70	24	71	—
d	CH_2OMe	17.5	3.5	70	24	92[b]	—

[a] Isolated yield.

[b] R = Me in the product.

Scheme 33.



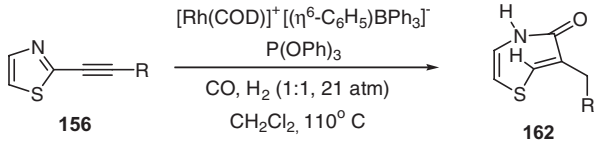
153, or (*ii*) through isomerization to **151** followed by CO insertion to **152** and subsequent cyclization to **153**. Then, intermediate **153** gives furanonyl–[Rh] complexes **154** and **155**, which afford **145** and **146**, respectively, through oxidative addition of molecular hydrogen to the [Rh] moiety followed by reductive elimination (47).

2-Alkynylthiazoles (**156**) undergo unique cyclohydrocarbonylation involving ring expansion catalyzed by $[Rh(COD)]^+[(\eta^6\text{-}C_6H_5BPh_3)]^-$ to give 2*Z*,6*E*-4*H*-[1,4]thiazepin-5-ones (**162**) (Scheme 34) (48).

A possible mechanism for this unique transformation is shown in Scheme 35 (48). The insertion of the alkyne moiety of **156** into the [Rh]—H bond of the active catalyst species [Rh]-H gives **157** regioselecively. The regioselectivity is

© 2005 NRC Canada

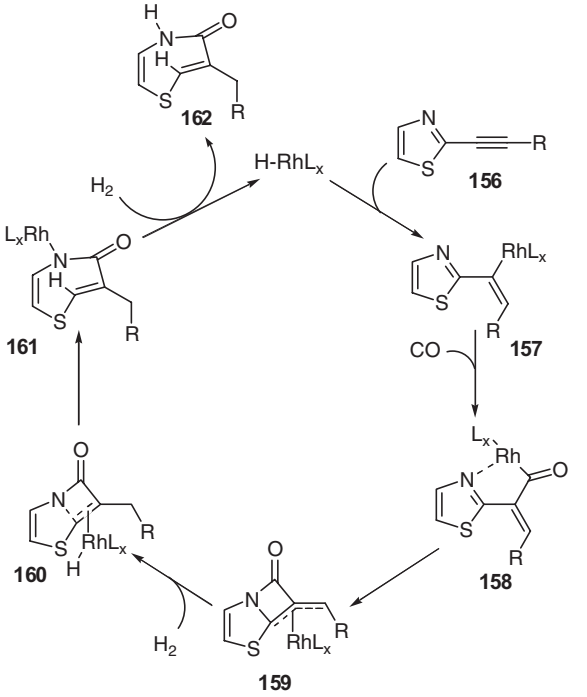
Scheme 34. Note: 1 atm = 101.325 kPa.



R	Time (h)	Yield (%)[a]
n-Bu	24	86
Ph	18	90
$C(CH_3)=CH_2$	24	72
CH_2OCH_3	24	74

[a] Isolated yield.

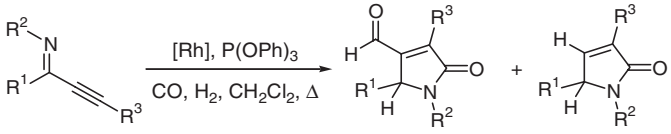
Scheme 35.



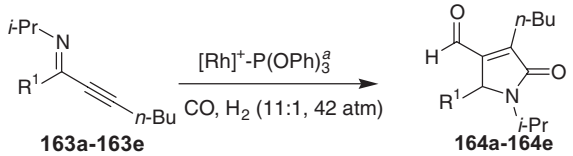
attributed to heteroatom–[Rh] interactions. The CO insertion to intermediate **157** forms acyl–[Rh] intermediate **158** in which the nitrogen atom coordinates to [Rh]. Reductive elimination and [Rh] shift gives the π-allyl–[Rh] complex with a penem skeleton **159**. Oxidative addition of molecular hydrogen, followed by a H shift affords the π-olefin–[Rh] intermediate **160**. Ring opening of **160** via formal σ-bond metathesis between the [Rh]—H and the N—C bonds yield N-[Rh]–thiazepinone complex **161**. Subsequent oxidative addition of molecular hydrogen to **161**, followed by reductive elimination gives thiazepinone **162** and regenerates the active catalyst species [Rh]-H.

Another variant of cyclohydrocarbonylation has been reported for the reaction of alkynylimines with syngas (49). The cyclohydrocarbonylation of alkynylimines **163** catalyzed by $[\eta^6\text{-}C_6H_5BPh_3]^-[Rh(1,5\text{-}COD)]^+$–$P(OPh)_3$ affords the corresponding 4-formylpyrrolinones **164** through a cascade carbonylation–hydroformylation process (Scheme 36) (49). However, this reaction is accompanied by the formation of pyrrolinone **165** as well as polymeric side products, depending on the reaction conditions, especially the pressure of syngas. The optimized conditions are at 70–100 °C and at 42 atm (1 atm = 101.325 kPa) of syngas ($CO:H_2$ = 5:1 ~ 11:1), which predominantly gave **164**. When **163j**–**163m**, bearing a phenyl group conjugated to the imine moiety, were used as the substrate, a double bond migration from the $\Delta^{3,4}$ position to the $\Delta^{4,5}$ position takes place to yield **164j**–**164m** in which the double bond is conjugated to the phenyl group

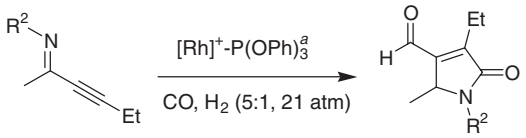
Scheme 36.



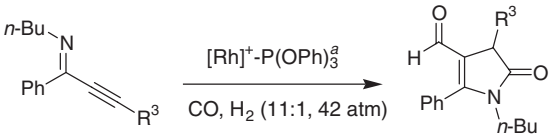
Scheme 37. Note: 1 atm = 101.325 kPa.



	R^1	Temp (°C)	Time (h)	Yield (%)[b]
a	C_6H_5-	90	24	80
b	4-MeC_6H_4-	90	24	81
c	4-$MeOC_6H_4$-	90	24	78
d	4-ClC_6H_4-	90	36	72
e	β-naphthyl	90	36	75



	R^2	Temp (°C)	Time (h)	Yield (%)[b]
f	*n*-Bu	100	18	82
g	*i*-Pr	100	24	79
h	Cy	100	36	80
i	Ph	100	18	75



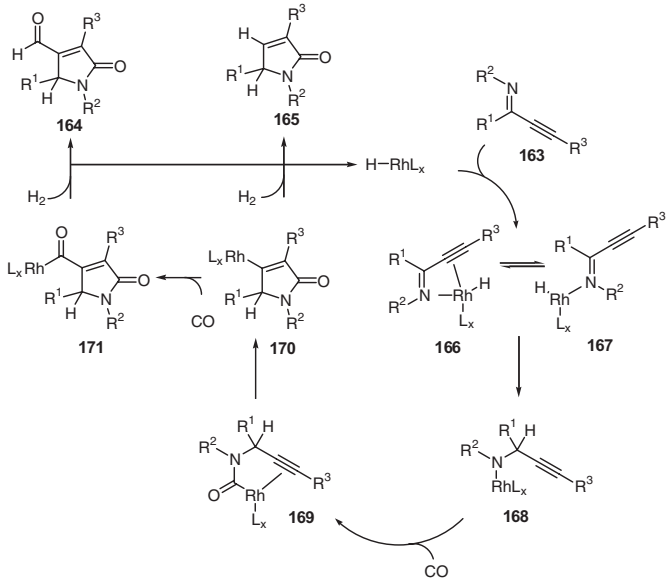
	R^3	Temp (°C)	Time (h)	Yield (%)[b]
j	*n*-Bu	90	24	80
k	*i*-Pr	90	24	75
l	CH_2-Cy	90	24	79
m	*t*-Bu	90	24	No reaction

[a] $Rh(COD)^+(\eta^6\text{-}C_6H_5BPh_3)^-$ (2 mol%), $P(OPh)_3$ (8 mol%), CO, H_2, CH_2Cl_2 (0.15 mol/L).

[b] Isolated yield.

© 2005 NRC Canada

Scheme 38.



at C-5 as shown in the third equation of Scheme 37. Relatively bulky substiuents at the acetylene moiety of **163**, e.g., isopropyl and cyclohexylmethyl, are tolerated in this reaction, but the introduction of a *tert*-butyl group to this position (see **163m** in the third equation of Scheme 37) shuts down the reaction.

A proposed mechanism for this process is illustrated in Scheme 38 (49). The imine nitrogen of **163** coordinates to the active catalyst species ([Rh]-H) to form **166** or **167** (these two intermediates are probably in equilibrium). A subsequent hydride shift to the carbon of the imine moiety gives alkynylamino–Rh complex **168**, which is further converted to alkynylamido–Rh complex **169** by CO insertion. Then, the endo-carboyclization of **169** gives pyrrolinon-4-yl–Rh complex **170**, to which the oxidative addition of molecular hydrogen and the subsequent reductive elimination take place to yield **165**, or the CO insertion occurs to form pyrrolinone-4-carbonyl–Rh complex **171**. Finally, 4-formylpyrrolinone (**164**) is yielded and the active catalyst species is regenerated through the reaction of **171** with molecular hydrogen.

In summary, recent advances in the transition metal catalyzed cyclohydrocarbonylation reactions are described. A variety of cyclohydrocarbonylation processes provide efficient and versatile methods for the construction of monocyclic, bicyclic, and polycyclic heterocycles as well as carboncycles, starting from readily accessible materials. It is noteworthy that many of the cyclohydrocarbonylation reactions can be performed under the mild conditions and low pressure of syngas, which may add more value to these processes as useful synthetic methods. The authors hope that this review encourages many synthetic chemists to explore new and creative applications of cyclohydrocarbonylation reactions in organic synthesis.

Acknowledgements

The authors would like to thank the National Science Foundation and the National Institutes of Health (NIGMS) for their generous support for their research in this area.

References

1. I. Ojima, C.-Y. Tsai, M. Tzamarioudaki, and D. Bonafoux. *In* Organic reactions. Vol. 56. *Edited by* L.E. Overman. John Wiley and Sons, New York. 2000. pp. 1–354.
2. B. Breit and W. Seiche. Synthesis, **1**, 1 (2001).
3. P. Eilbracht, L. Bärfacker, C. Buss, C. Hollmann, B.E. Kitsos-Rzychon, C.L. Kranemann, T. Rische, R. Roggenbuck, and A. Schmidt. Chem. Rev. **99**, 3329 (1999).
4. I. Ojima, D. Bonafoux, and S.-Y. Lee. *In* Encyclopedia of catalysis. Vol. 2. *Edited by* I.T. Horvath. John Wiley and Sons, Inc., Hoboken, New Jersey. 2003. pp. 706–766.
5. L.F. Tietze. Chem. Rev. **96**, 115 (1996).
6. I. Ojima and A. Korda. Tetrahedron Lett. **30**, 6283 (1989).
7. I. Ojima, A. Korda, and W.R. Shay. J. Org. Chem. **56**, 2024 (1991).
8. I. Ojima and Z. Zhang. J. Organomet. Chem. **417**, 253 (1991).
9. I. Ojima and Z. Zhang. J. Org. Chem. **53**, 4422 (1988).
10. Y. Becker, A. Eisenstadt, and J.K. Stille. J. Org. Chem. **45**, 2145 (1980).
11. K. Izawa, S. Nishi, and S. Asada. J. Mol. Catal. **41**, 135 (1987).
12. H. Wakamatsu, J. Uda, and N. Yamakami. J. Chem. Soc. Chem. Commun. 1540 (1971).
13. Y. Amino and K. Izawa. Bull. Chem. Soc. Jpn. **64**, 613 (1991).
14. Y. Amino, S. Nishi, and K. Izawa. Bull. Chem. Soc. Jpn. **64**, 620 (1991).
15. K. Izawa. J. Synth. Org. Chem. Jpn. **46**, 218 (1988).
16. K. Izawa. PETROTECH, **12**, 24 (1989).
17. J. Collin. Bull. Soc. Chim. Fr. **6**, 976 (1988).
18. M. Eguchi, Q. Zeng, A. Korda, and I. Ojima. Tetrahedron Lett. **34**, 915 (1993).
19. I. Ojima, R.J. Donovan, M. Eguchi, W.R. Shay, P. Ingallina, A. Korda, and Q.P. Zeng. Tetrahedron, **49**, 5431 (1993).
20. E. Billig, A.G. Abatjoglou, and D. Bryant. US Patent 4 769 498, 1988.
21. G.D. Cuny and S.L. Buchwald. J. Am. Chem. Soc. **115**, 2066 (1993).
22. G.D. Cuny and S.L. Buchwald. Synlett, 519 (1995).
23. I. Ojima and E.S. Vidal. J. Org. Chem. **63**, 7999 (1998).
24. I. Ojima, D.M. Iula, and M. Tzamarioudaki. Tetrahedron Lett. **39**, 4599 (1998).
25. I. Ojima, M. Tzamarioudaki, and M. Eguchi. J. Org. Chem. **60**, 7078 (1995).
26. M.E. Garst and D. Lukton. J. Org. Chem. **46**, 4433 (1981).
27. I. Ojima, D.M. Iula, and M. Tzamarioudaki. Tetrahedron Lett. **39**, 4599 (1998).
28. I. Ojima and E.S. Vidal. J. Org. Chem. **63**, 7999 (1998).
29. N. Mizutani, W.-H. Chiou, and I. Ojima. Org. Lett. **4**, 4575 (2002).
30. W.-H. Chiou and I. Ojima. Abstracts of papers, 228th ACS National Meeting, Philadelphia, Penn., 22–26 August 2004, ORGN 144, 2004.
31. Z. Zhang and I. Ojima. J. Organomet. Chem. **454**, 281 (1993).
32. E.M. Campi, J. Habsuda, W.R. Jackson, C.A.M. Jonasson, and Q.J. McCubbin. Aust. J. Chem. **48**, 2023 (1995).
33. E.M. Campi, W.R. Jackson, Q.J. McCubbin, and A.E. Trnacek. Aust. J. Chem. **47**, 1061 (1994).
34. D.J. Bergmann, E.M. Campi, W.R. Jackson, and A.F. Patti. Chem. Commun. 1279 (1999).

© 2005 NRC Canada

35. D.J. Bergmann, E.M. Campi, W.R. Jackson, Q.J. McCubbin, and A.F. Patti. Tetrahedron, **53**, 17449 (1997).
36. R.W. Hoffmann and D. Brückner. New J. Chem. **25**, 369 (2001).
37. R.W. Hoffmann, D. Brückner, and V.J. Gerusz. Heterocycles, **52**, 121 (2000).
38. R.W. Hoffmann, J. Krüger, and D. Brückner. New J. Chem. **25**, 102 (2001).
39. M.D. Keränen and P. Eilbracht. Org. Biomol. Chem. **2**, 1688 (2004).
40. R. Settambolo, A. Caiazzo, and R. Lazzaroni. Tetrahedron Lett. **42**, 4045 (2001).
41. R. Settambolo, S. Miniati, and R. Lazzaroni. Synth. Commun. **33**, 2953 (2003).
42. C.L. Kranemann, B.E. Kitsos-Rzychon, and P. Eilbracht. Tetrahedron, **55**, 4721 (1999).
43. A.R. Katrizky. Handbook of heterocyclic chemistry. Pergamon Press, New York. 1985.
44. E.M. Campi, G.D. Fallon, W.R. Jackson, and Y. Nilsson. Aust. J. Chem. **42**, 1167 (1992).
45. L. Bäffacker, C. Hollmann, and P. Eilbracht. Tetrahedron, **54**, 4493 (1998).
46. Y. Fukuta, I. Matsuda, and K. Itoh. Tetrahedron Lett. **42**, 1301 (2001).
47. B.G. Van den Hoven, B. El Ali, and H. Alper. J. Org. Chem. **65**, 4131 (2000).
48. B.G. Van den Hoven and H. Alper. J. Am. Chem. Soc. **123**, 1017 (2001).
49. B.G. Van den Hoven and H. Alper. J. Am. Chem. Soc. **123**, 10 214 (2001).

© 2005 NRC Canada

Efficient synthesis of the nonamannoside residue of high mannose glycoproteins[1]

Lu Jiang and Tak Hang Chan

Abstract: An efficient synthesis of the nonamannoside residue **1** of high mannose glycoproteins was achieved using an oligomer-supported solution synthesis with low-molecular-weight polyethylene glycol as the anchor. The synthesis required only five coupling steps from only two monosaccharide building blocks with an overall yield of 12%.

Key words: nonamannoside, oligosaccharide synthesis, soluble polymer support synthesis, glycoproteins.

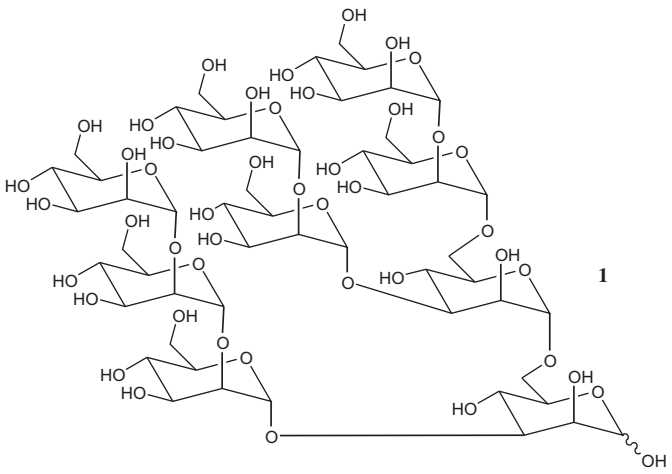
Résumé : On a réalisé une synthèse efficace de la portion nonamannoside **1** des glycoprotéines à haute teneur en mannose en faisant appel à une méthode de synthèse en solution, supportée par un oligomère, dans laquelle du polyéthylène glycol de faible poids moléculaire sert d'ancre. La synthèse qui a été effectuée avec un rendement global de 12 % ne comporte que cinq étapes de couplage qui n'utilisent que deux monosaccharides comme blocs de synthèse.

Mots clés : nonamannoside, synthèse d'oligosaccharide, synthèse sur un support de polymère soluble, glycoprotéines.

[Traduit par la Rédaction]

Introduction

The branched chain nonasaccharide **1**, Man_9, plays an essential role in the biosynthesis and processing of N-linked glycoproteins. Through the dolichol pathway, the oligosaccharide core with the composition $GlcNAc_2Man_9Glc_3$ is transferred to a polypeptide chain. The glucose and some of the mannose residues are then trimmed, and other carbohydrate residues are added by various processing enzymes to give diverse N-linked glycoproteins (1). The completed glycoproteins are targeted for secretion, incorporation into cellular organelles, or insertion into cell membranes. For membrane-bound glycoproteins, the carbohydrate moieties have been implicated in many cell–cell recognition processes, such as adhesion and infection (2). In this connection, it is interesting to note that nonasaccharide **1** is present on the conserved V3 loop of glycoprotein (Gp) 120 of the viral coat of HIV-1 (3). Gp120 plays an important role in the HIV infection of cells, being responsible for the attachment and penetration of cells to be infected, and is thus a target for immunotherapy or vaccine development. Indeed, antibodies directed against the mannose residues of HIV-1 glycoprotein Gp120 in vitro have been developed (4). Because of these considerations, nonasaccharide **1** presents itself as an attractive synthetic target, and several syntheses of the nonasaccharide structure have been described in the literature. Fraser-Reid and co-workers (5) and Ley and co-workers (6) used a highly convergent block synthesis approach to prepare a highly protected derivative of **1** (5) or its methyl and 8-(methoxycarbonyl)octyl glycoside derivatives (6). More recently, Seeberger and co-workers reported a linear synthesis of the pentyl glycoside derivative of **1** (7). Even though **1** itself was not synthesized, the total chemical synthesis of $Man_9GlcNAc_2$ was recently accomplished by Danishefsky and co-workers as part of their effort to prepare artificial HIV vaccines (8).



1

It is generally recognized that the synthesis of complex oligosaccharides is a matter of considerable challenge and a subject of extensive contemporary research attention. In addition to the classical solution synthesis, some of the current methods developed for the synthesis of oligosaccharides have involved the use of solid phase, which can now be automated (9), or high-molecular-weight polymer supported solution-phase synthesis, which facilitates separation and purification of the intermediates (10). Despite this recent progress in the solid-phase and polymer-supported solution synthesis of oligosaccharides, many issues remain to be ad-

Received 22 November 2004. Published on the NRC Research Press Web site at http://canjchem.nrc.ca on 16 June 2005.

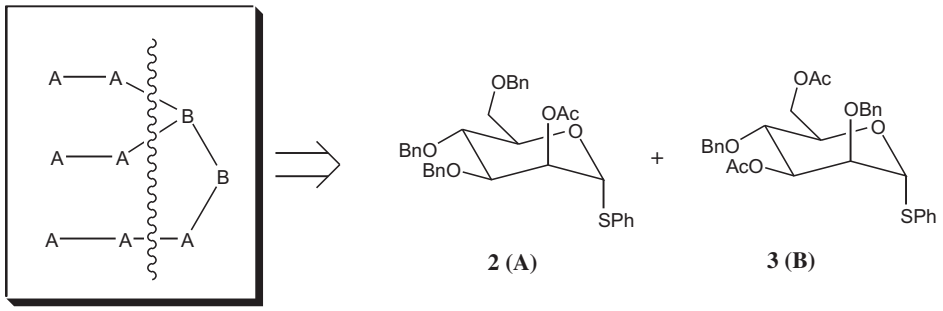
L. Jiang and T.H. Chan.[2] Department of Chemistry, McGill University, Montreal, QC H3A 2K6, Canada.

[1]This article is part of a Special Issue dedicated to Professor Howard Alper.

[2]Corresponding author (e-mail: tak-hang.chan@mcgill.ca).

 doi: 10.1139/V05-066 © 2005 NRC Canada

Scheme 1. Building blocks A and B for the synthesis of nonamannoside **1**.



1 **2 (A)** **3 (B)**

dressed. To make enough of the complex oligosaccharides for biological evaluation, one major obstacle is the scale of the synthesis. Loading of both solid-phase resins and high-molecular-weight poly(ethylene glycol)s are inherently limited. Although there is no limit on how much compound can be used in the conventional solution synthesis, the involvement of column chromatography during the separation process is a major bottleneck. To overcome the purification problem and to develop a method that can enable the synthesis of complex oligosaccharides on a large scale, we employed low-molecular-weight poly(ethylene glycol) methyl ethers (MPEG, average MW = 550, n = ca. 8–20) as polar tags for solution synthesis of oligosaccharides (11). The use of low-molecular-weight MPEGs as polar tags retains the normal advantages of polymer-supported solution synthesis of oligosaccharides, such as the following: (*i*) the MPEG-linker and its bonded synthons are completely soluble in the normal reaction solvents, and the efficiency of the various steps follows that expected of solution chemistry; and (*ii*) the reaction can be monitored readily by the conventional arsenal of spectroscopic techniques. Furthermore, purification of the MPEG-linker and its derivatives by fast column chromatography on silica gel 60 (230–400 mesh, E. Merck) is facilitated by the fact that even in neat ethyl acetate, the MPEG conjugates remain on the baseline while the much less polar by-products move rapidly through the column. Changing the eluent to dichloromethane–methanol (4:1) or to ethyl acetate – methanol (4:1) allows quick elution of the MPEG derivatives, free of silica gel contamination.

Results and discussions

General strategy

In classic oligosaccharide synthesis, to make the purification and identification of the intermediates easier as well as to maximize the overall yield, highly convergent synthetic strategies are generally desired. However, the less common linear strategy offers more advantages in the case of **1**, which is illustrated in Scheme 1. One can easily assemble the Manα1-2Man (A-A) linkage using compound **2** (representing A) (12), with the phenylthio moiety as the potential glycosyl donor. Compound **3** (representing B) (13), on the other hand, with the regioselectively available 3,6 diol moiety, can serve as the potential glycosyl acceptor to give the branched structure. Furthermore, to make the synthesis efficient, we chose to first construct the B-B-A fragment. It was anticipated that once this trisaccharide core was reached, only two triple glycosylations with **2** were needed for the construction of nonamannoside **1**.

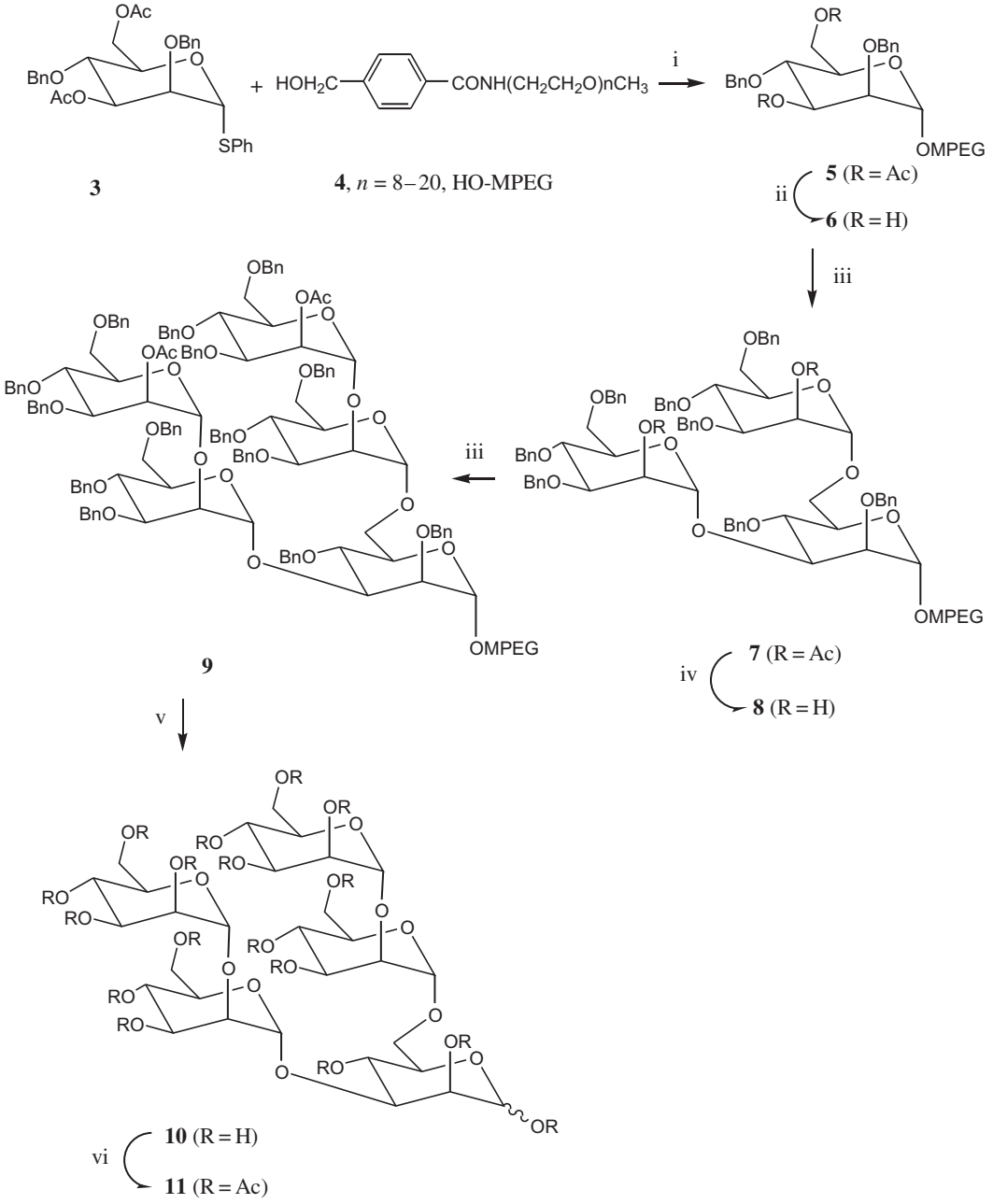
Using regioselective acylation and regioselective reductive ring opening of benzylidene acetals methods previously reported by us, compound **3** was readily obtained from methyl α-D-mannopyranoside in high overall yield (13). Coupling of **3** with the poly(ethylene glycol) linker **4**, using the combination of *N*-iodosuccinimide and trimethylsilyl triflate (NIS–Me_3SiOTf) (14), went smoothly and gave compound **5** in almost quantitative yield. Purification of the product **5** employing flash column chromatography was facilitated by the use of low-molecular-weight poly(ethylene glycol) methyl ether (MPEG) as the polar tag. The excess reagents in the reaction mixtures were readily separated from the oligomer-bonded product. The two acetyl groups of **5** were then removed by base treatment to yield the diol **6**. Double glycosylation of **6** with 3.0 equiv. of the donor **2** was carried out with NIS–TMSOTf as the promoter to afford the MPEG-trisaccharide **7**. The amount of the Lewis acid (TMSOTf) used in the glycosylation was quite critical. When less than 0.8 equiv. of TMSOTf was employed in the coupling reaction, formation of 1,2-orthoacetates resulted. The success of the double glycosylation in **7** was evidenced by the fact that its ^{1}H-^{1}H COSY NMR spectrum showed the two new anomeric protons at 5.19 and 4.97 ppm (parts per million). Incorporation of the two new mannopyranoside units was also confirmed by the ^{1}H-^{13}C HMQC NMR spectrum, revealing the existence of three anomeric cross peaks. Repetition of the deacetylation step and double glycosylation with glycosyl donor **2** gave the protected MPEG-pentasaccharide **9** through the formation of MPEG-trisaccharide diol **8**. Progress of the assembly was readily monitored by ^{1}H NMR spectroscopy, and the chemical shifts of protons and carbons could be assigned by 2D ^{1}H-^{1}H COSY and ^{1}H-^{13}C HMQC NMR spectroscopy. Hydrogenolysis of **9** over Pd–C in acetic acid released the pentasaccharide **10** from the polar tag smoothly. Purification and characterization of **10** were achieved by conversion to the peracetate derivative **11** (as a mixture of α- and β-anomers) (Scheme 2). The overall yield of the peracetylated pentamannopyranoside **11** was found to be 19% based on the starting **4**. Compound **11** was characterized by electrospray mass spectrometry, ^{1}H NMR, and ^{13}C NMR.

Synthesis of the nonamannoside 1 via triple glycosylation (Scheme 3)

Having established the feasibility and efficiency of the

© 2005 NRC Canada

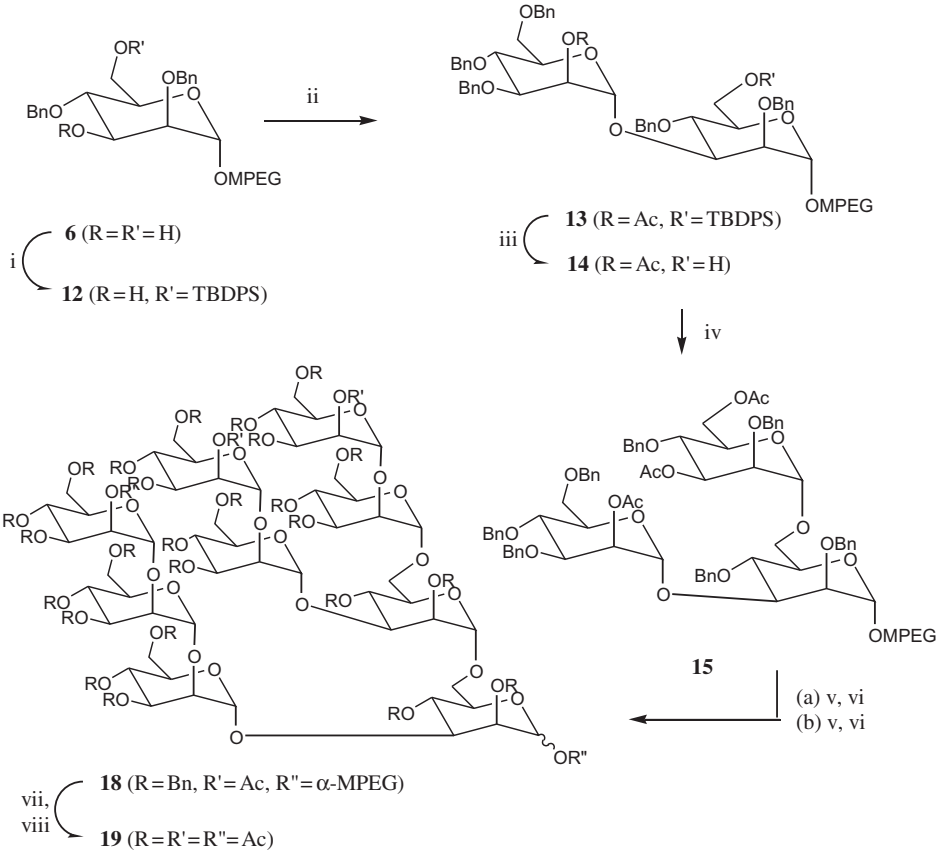
Scheme 2. Reagents and conditions: (*i*) 2.0 equiv. of thiomannoside **3**, 2.2 equiv. of NIS, 0.8 equiv. of TMSOTf, 4 Å molecular sieves, CH_2Cl_2, 0 °C to rt, 4 h; (*ii*) K_2CO_3, wet MeOH, 4 h; (*iii*) 3.0 equiv. of thiomannoside **2**, 3.3 equiv. of NIS, 0.8 equiv. of TMSOTf, 4 Å molecular sieves, CH_2Cl_2, 0 °C to rt, 4 h; (*iv*) NaOMe, MeOH, CH_2Cl_2, 12 h; (*v*) 50 psi H_2, 10% Pd–C, CH_3COOH, 5 days; (*vi*) Ac_2O, Py, DMAP, 48 h.



solution phase chemistry, attention was then turned to the construction of the complex nonamannoside residue **1** (Scheme 3). This required the differentiation of the 3- and 6-hydroxyl functions of **6**. The primary hydroxyl group in the MPEG-monosaccharide diol **6** was selectively protected by the *tert*-butyldiphenylsilyl (TBDPS) group (15), and then the partially protected **12** was glycosylated with phenyl 2-*O*-acetyl-1-thio-3,4,6-tri-*O*-benzyl-α-D-mannopyranoside (**2**) to yield the MPEG-disaccharide **13**. Removal of the silicon protecting group gave the MPEG-bound acceptor **14**, which was glycosylated with donor **3** to form MPEG-trisaccharide **15**. To avoid using TBAF (whose ammonium cation may cause problems during chromatographic separation) in the desilylation step, dilute HF was employed in the desilylation of **15** to give **16**. As anticipated, the triple glycosylation of MPEG-trisaccharide triol **16** with 4.5 equiv. of the thiomannoside **2** went smoothly to furnish the MPEG-bound hexasaccharide **17**, the ^1H and ^{13}C NMR spectra of which exhibited the anticipated three acetate peaks. The ^1H-^{13}C HMQC NMR spectrum of **17** also revealed the presence of six anomeric cross peaks. Reiteration of the deacetylation and the triple glycosylation steps gave the protected MPEG-nonasaccharide **18**. It is worth mentioning that the MPEG-bound hexasaccharides and nonasaccharide can be more

© 2005 NRC Canada

Scheme 3. Reagents and conditions: (*i*) 2.0 equiv. of *t*-$BuPh_2SiCl$, 2.0 equiv. of DMAP, CH_2Cl_2, rt, 24 h; (*ii*) 2.0 equiv. of thiomannoside **2**, 2.2 equiv. of NIS, 0.8 equiv. of TMSOTf, 4 Å molecular sieves, CH_2Cl_2, 0 °C to rt, 4 h; (*iii*) 5% HF in MeOH, 3 days; (*iv*) 2.0 equiv. of thiomannoside **3**, 2.2 equiv. of NIS, 0.8 equiv. of TMSOTf, 4 Å molecular sieves, CH_2Cl_2, 0 °C to rt, 4 h; (*v*) NaOMe, MeOH, CH_2Cl_2, 12 h; (*vi*) 4.5 equiv. of thiomannoside **2**, 4.8 equiv. of NIS, 0.8 equiv. of TMSOTf, 4 Å molecular sieves, CH_2Cl_2, 0 °C to rt, 4 h; (*vii*) 1000 psi H_2, 20% $Pd(OH)_2$–C, MeOH, 7 days; (*viii*) Ac_2O, Py, DMAP, 48 h.



easily washed out from silica gel columns than the MPEG-bound smaller saccharides, probably because of the fact that the hydrophobic portions of the MPEG-bound larger saccharides reduced the affinity of the MPEG-saccharides towards silica gel.

The final debenzylation of **18** turned out to be somewhat troublesome, in that hydrogenolysis over Pd–C in various media did not proceed even after prolonged exposure. Eventually, hydrogenolysis of **18** over Pearlman's catalyst in methanol under high pressure (1000 psi (1 psi = 6.895 kPa)) for seven days released the nonasaccharide from the MPEG oligomer. The nonamannoside was characterized as its α- and β-peracetate derivative (**19**, ca. 12% overall yield from **4**), whose electrospray mass spectrum was consistent with the expected structure. The experimental spectrum matched the theoretical spectrum created by isotopic modeling (Fig. 1). Furthermore, the ^1H-^{13}C HMQC spectrum (Fig. 2) also provided confirmation of the structure of **19** by revealing the presence of the cross peaks of nine anomeric centers.

Conclusions

In summary, a chemical synthesis of the nonamannoside residue of a highly branched mannose-type oligosaccharide present on the viral coat of HIV-1 has been achieved from only two monosaccharide building blocks (**2** and **3**). The use of low-molecular-weight MPEG aided considerably in the purification of the intermediates and in the analyses of the progress of the assembly with the use of conventional spectroscopic techniques. It should be noted that besides these advantages, this methodology also gives access to large-scale synthesis. In the present case, over 300 mg of final product **19** was obtained, and it is conceivable to work on even larger scale synthesis. This synthesis demonstrates that solution synthesis using a low-molecular-weight poly(ethylene glycol) as a polar tag to aid separation is a useful tool for the rapid and efficient preparation of complex oligosaccharides. The ability to introduce two or three saccharide units via double or triple glycosylation in one operation is particularly remarkable. On the other hand, the approach does have some limitations. Since no chromatography was used throughout the synthesis, all glycosylated products, both alpha and beta, would be accumulated. For glycosylation reactions that are not highly stereoselective, this would inevitably lead to an intractable mixture of final compounds. Another potential problem is the difficulty of the hydrogenation step in the final release of the oligosaccharide from the PEG support. This may be due to the presence of sulfur-containing contaminants that would have been removed normally in sequentially purified solution chemistry.

© 2005 NRC Canada

Fig. 1. (*a*) Theoretical spectrum created by isotopic modeling for sodium adduct of **19**; (*b*) experimental spectrum of **19**.

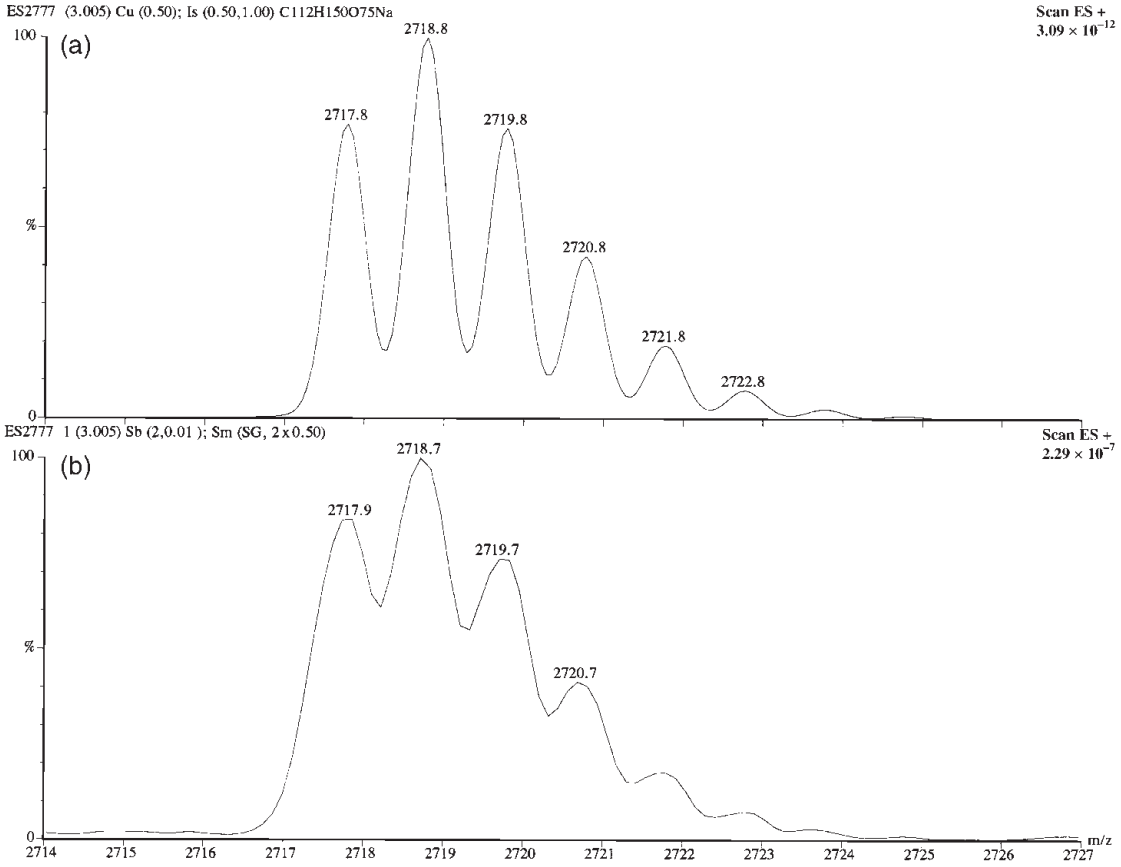
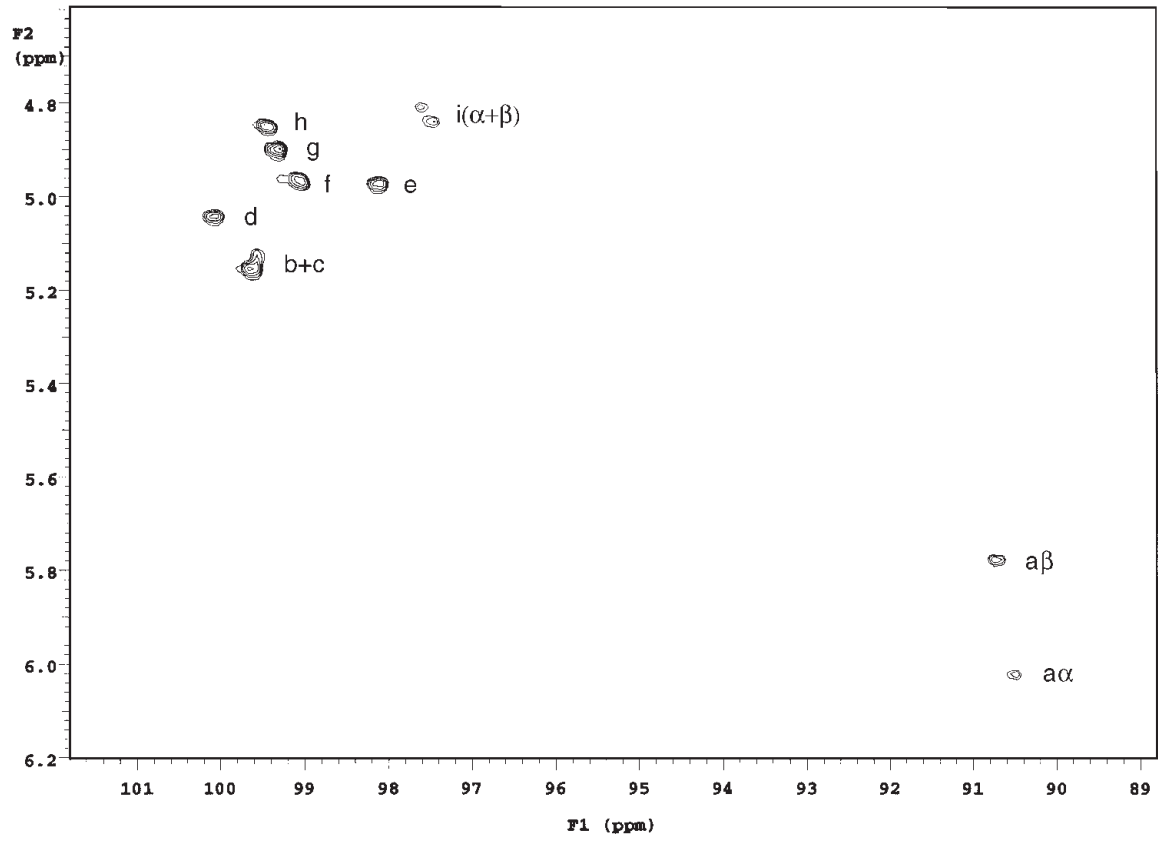


Fig. 2. Anomeric region of the ^{1}H-^{13}C HMQC NMR spectrum of **19**.



© 2005 NRC Canada

Experimental

General

^{1}H and ^{13}C NMR spectra were recorded at 500 and 125 MHz, respectively, and the chemical shifts are reported in parts per million on the δ scale relative to $CDCl_3$ (δ 7.24 ppm) for ^{1}H NMR and $CDCl_3$ (δ 77.0 ppm) for ^{13}C NMR. Solvents and reagents were used as received from commercial sources. Analytical thin-layer chromatography (TLC) was performed using E. Merck silica gel 60 F-254 polyester-backed plates (250 μm thick). Compounds **2** and **3** were prepared according to literature procedures (12, 13). Poly(ethylene glycol) methyl ether 550 (average MW = 550, n = 8–20) was purchased from Aldrich.

Preparation of compound 4

Me(OCH$_2$CH$_2$)$_n$OMs

Poly(ethylene glycol) methyl ether 550 (12.54 g, 20.0 mmol OH) was dissolved in CH_2Cl_2 (20 mL) and NEt_3 (10 mL). Methanesulfonyl chloride (8.02 g, 5.5 mL, 70 mmol) was added at 0 °C. Upon removal of the ice bath right after completion of the addition, the reaction mixture was allowed to warm up to room temperature slowly and kept for 4 h. Chloroform and an aqueous $NaHCO_3$ solution were then added to quench the reaction. After it was washed with 5% HCl solution (1 × 100 mL), saturated $NaHCO_3$ solution (1 × 100 mL), and brine (1 × 100 mL), the organic layer was dried over anhydrous Na_2SO_4 and evaporated to dryness under reduced pressure. A clear light yellow liquid (13.9 g, 98.5%) was obtained after drying on a high vacuum pump. ^{1}H NMR (500 MHz, $CDCl_3$) δ: 4.36 (2H, t, 4.5 Hz, C*H*$_2$OSO$_2$), 3.74 (2H, t, 4.5 Hz, C*H*$_2$CH$_2$OSO$_2$), 3.64–3.61 (48H, m, PEG), 3.54–3.51 (2H, m), 3.36 (3H, s, C*H*$_3$O), 3.06 (3H, s, C*H*$_3$SO$_3$).

Me(OCH$_2$CH$_2$)$_n$N$_3$

The mesylate obtained above (13.9 g) and sodium azide (4.55 g, 70 mmol) were dissolved in DMF (50 mL), and the reaction mixture was heated at 80 °C for 5 h. Water was added after DMF was removed under reduced pressure. The aqueous solution was extracted with chloroform (3 × 50 mL), and the organic layer was washed with brine and then dried over anhydrous Na_2SO_4. Evaporation of the organic layer to dryness under reduced pressure left a darker liquid (12.2 g, 95%). ^{1}H NMR (500 MHz, $CDCl_3$) δ: 3.66–3.61 (50H, m, PEG), 3.53 (2H, t, 2.4 Hz, OC*H*$_2$CH$_2$N$_3$), 3.36 (2H, t, 2.4 Hz, OCH$_2$C*H*$_2$N$_3$), 3.35 (3H, s, C*H*$_3$O).

Me(OCH$_2$CH$_2$)$_n$NH$_2$

A mixture of the azide (12.2 g), 10% Pd–C (0.8 g), and methanol (40 mL) was stirred under 40 psi H_2 for 3 h at room temperature. The solution was filtered, and the Pd–C was washed with methanol. The filtrate was evaporated to dryness under reduced pressure to give a clear light reddish liquid (11.7 g, 100%). ^{1}H NMR (500 MHz, $CDCl_3$) δ: 3.62–3.58 (48H, m, PEG), 3.50 (2H, m), 3.47 (2H, t, 5.2 Hz, OC*H*$_2$CH$_2$NH$_2$), 3.34 (3H, s, C*H*$_3$O), 2.81 (2H, t, 5.5 Hz, OCH$_2$C*H*$_2$NH$_2$).

Me(OCH$_2$CH$_2$)$_n$NHCOPhCH$_2$Cl

A mixture of the amine (5.5 g) obtained above, dicyclohexylcarbodiimide (3.1 g, 15 mmol), 4-chloromethylbenzoic acid (2.2 g, 13 mmol), CH_2Cl_2 (20 mL), and a catalytic amount of DMAP was stirred at room temperature overnight. Water was added after removing CH_2Cl_2 under reduced pressure. The precipitate dicyclohexylurea was filtered, and the aqueous solution was extracted with chloroform (3 × 20 mL). The organic layer was washed with an aqueous $NaHCO_3$ solution and brine and then dried over anhydrous Na_2SO_4. The product was obtained, after solvent removal, as a sticky light-yellow liquid (6.6 g, 96%). ^{1}H NMR (500 MHz, $CDCl_3$) δ: 7.80 (2H, d, 7.6 Hz, Ar-*H*), 7.43 (2H, d, 7.6 Hz, Ar-*H*), 6.90 (1H, s (br), PhCON*H*), 4.59 (2H, s, ClC*H*$_2$Ph), 3.70–3.50 (54H, m, PEG), 3.36 (3H, s, C*H*$_3$O).

Me(OCH$_2$CH$_2$)$_n$NHCOPhCH$_2$OH (4)

A mixture of the chloromethylbenzamide (4.3 g), Ag_2CO_3 (1.6 g, 5.8 mmol), $AgClO_4$ (0.1 g), and water (25 mL) was stirred at room temperature for two days. The reaction mixture was first filtered through celite and then extracted with chloroform (3 × 20 mL). The organic layer was dried over anhydrous Na_2SO_4 and evaporated to dryness under reduced pressure to give a dark syrup, which still contained the silver salts. The syrup was dissolved in a small quantity of ethyl acetate and added onto the top of a silica gel column for flash column chromatography. Elution with ethyl acetate – methanol (4:1 and 3:1, 150 mL each) gave **4** (4.0 g, 95%) as a sticky light-yellow liquid. ^{1}H NMR (500 MHz, $CDCl_3$) δ: 7.79 (2H, d, 7.6 Hz, Ar-*H*), 7.39 (2H, d, 7.6 Hz, Ar-*H*), 7.06 (1H, s (br), PhCON*H*), 4.70 (2H, d, 4.1 Hz, PhC*H*$_2$OH), 3.70–3.40 (54H, m, PEG), 3.35 (3H, s, C*H*$_3$O), 2.61 (1H, s (br), CH$_2$O*H*).

Protocol for the solution-phase glycosylations

After thiomannoside **2** (or **3**) (2.0 mmol) and an MPEG-acceptor (1 mmol) were co-distillated with toluene 5 times under reduced pressure, dry 4 Å molecular sieve powder (1 g/g reactant) and dichloromethane (2.5 mL/g reactant) were added into the flask. The mixture was stirred for 10–15 min under Ar and then cooled to 0 °C, followed by the addition of NIS. The color of the reaction mixture turned pink immediately as a 2 mol/L solution of TMSOTf (0.8 mmol) in dichloromethane was syringed into the flask slowly. Upon removal of the ice bath right after completion of the addition, the reaction mixture was allowed to warm to room temperature slowly and kept for 2 h. Chloroform and an aqueous $NaHCO_3$ solution were added to quench the reaction, followed by filtration of the mixture through a pad of celite to remove the molecular sieve powder. After having been washed with an aqueous $Na_2S_2O_3$ solution and brine, the organic layer was dried over anhydrous Na_2SO_4 and evaporated to dryness under reduced pressure. The resulting syrup was dissolved in a small amount of ethyl acetate and put onto the top of a silica gel column (15 times weight of the syrup) for flash column chromatography. Gradient elution with hexanes – ethyl acetate (2:1, 1:1, 1:2, 1:4, and neat EtOAc, 50 mL each) removed the side products, and further elution with ethyl acetate – methanol (4:1 and 3:1, 150 mL each) gave the MPEG–sugar conjugate.

© 2005 NRC Canada

Protocol for the deacetylation with K_2CO_3

Potassium carbonate was added to a stirred solution of MPEG–sugar in wet methanol, and the reaction was monitored by ^{1}H NMR spectroscopy. Upon completion of the deacetylation, as indicated by the disappearance of the acetyl peak (or peaks) in the ^{1}H NMR spectrum, the methanol was evaporated under reduced pressure, and brine was added. After the aqueous solution was extracted with chloroform (3 × 50 mL), the organic layer was dried over anhydrous Na_2SO_4 and evaporated to dryness under reduced pressure. Purification of the MPEG-bound products by chromatographic separation procedure was the same as described above.

Protocol for the deacetylation with NaOMe

The procedure was essentially the same as above, except that sodium methoxide was used as the base and methanol–dichloromethane (1:2) was the solvent.

MPEG-Man36OAc (5)

Colorless syrup. ^{1}H NMR (500 MHz, $CDCl_3$) δ: 7.80 (2H, d, 7.1 Hz, Ar-*H*), 7.57–7.27 (12H, m, Ar-*H*), 6.78 (1H, s (br), PhCON*H*), 5.26 (1H, dd, 3.4 and 9.0 Hz, *H*-3), 4.86 (1H, d, 2.0 Hz, *H*-1), 4.71 (1H, d, 12.4 Hz, PhCH_2), 4.67 (1H, d, 11.2 Hz, PhCH_2), 4.60 (1H, d, 12.2 Hz, PhCH_2), 4.55 (1H, d, 11.2 Hz, PhCH_2), 4.52 (1H, d, 12.2 Hz, PhCH_2), 4.51 (1H, d, 12.4 Hz, PhCH_2), 4.29 (2H, m, *H*-6a, *H*-6b), 3.93 (1H, dd, 9.3 and 9.8 Hz, *H*-4), 3.89 (1H, dd, 2.0 and 3.4 Hz, *H*-2), 3.70–3.46 (m, *H*-5, *H*-6, and PEG), 3.35 (1H, s, OCH_3), 2.06 (3H, s, CH_3CO), 1.97 (3H, s, CH_3CO).

MPEG-Man36OH (6)

Colorless syrup. ^{1}H NMR (500 MHz, $CDCl_3$) δ: 7.78 (2H, d, 8.3 Hz, Ar-*H*), 7.36–7.30 (12H, m, Ar-*H*), 6.84 (1H, s (br), PhCON*H*), 4.91 (1H, d, 1.0 Hz, *H*-1), 4.90 (1H, d, 12.4 Hz, PhCH_2), 4.72 (1H, d, 12.0 Hz, PhCH_2), 4.69 (1H, d, 12.2 Hz, PhCH_2), 4.67 (1H, d, 11.0 Hz, PhCH_2), 4.59 (1H, d, 11.8 Hz, PhCH_2), 4.49 (1H, d, 12.0 Hz, PhCH_2), 4.04 (1H, m, *H*-3), 3.57–3.52 (m, *H*-2, *H*-4, *H*-5, *H*-6a, *H*-6b, and PEG), 3.37 (3H, s, OCH_3), 2.34 (1H, d, 9.0 Hz, C_3-O*H*), 1.96 (1H, s (br), C_6-O*H*).

MPEG-TrimandiOAc (7)

Colorless syrup. ^{1}H NMR (500 MHz, $CDCl_3$) δ: 7.83 (2H, s (br), Ar-*H*), 7.38–7.20 (m, Ar-*H*), 6.78 (1H, s (br), PhCON*H*), 5.49 (1H, m (br), *H*-2a), 5.47 (1H, m (br), *H*-2b), 5.19 (1H, s (br), *H*-1a), 4.97 (1H, s (br), *H*-1b), 4.86 (2H, d, 10.7 Hz, PhCH_2), 4.83 (1H, s (br), *H*-1c), 4.74 (1H, d, 11.0 Hz, PhCH_2), 4.66–4.58 (m, PhCH_2), 4.48–4.36 (m, PhCH_2), 4.18–3.34 (m), 2.14 (3H, s, CH_3CO), 2.08 (3H, s, CH_3CO).

MPEG-TrimandiOH (8)

Colorless syrup. ^{1}H NMR (500 MHz, $CDCl_3$) δ: 7.67 (2H, d, 7.8 Hz, Ar-*H*), 7.34–7.12 (m, Ar-*H*), 6.77 (1H, s (br), PhCON*H*), 5.23 (1H, s (br), *H*-1a), 5.06 (1H, s (br), *H*-1b), 4.83 (1H, d, 10.8 Hz, PhCH_2), 4.82 (1H, d, 12.2 Hz, PhCH_2), 4.80 (1H, s (br), *H*-1c), 4.70–4.38 (m, PhCH_2), 4.16 (1H, dd, 1.0 and 9.0 Hz, *H*-3c), 4.08 (1H, s (br), *H*-2b), 4.02 (1H, s (br), *H*-2a), 3.99–3.48 (m), 3.37 (3H, s, OCH_3), 2.42 (1H, s (br), C_{2a}-O*H*), 2.38 (1H, s (br), C_{2b}-O*H*).

MPEG-PentamandiOAc (9)

Colorless syrup. ^{1}H NMR (500 MHz, $CDCl_3$) δ: 7.71 (2H, s (br), Ar-*H*), 7.38–7.08 (m, Ar-*H*), 6.55 (1H, s (br), PhCON*H*), 5.50 (2H, m (br), *H*-2a and *H*-2b), 5.19 (1H, s (br), *H*-1a), 5.05 (1H, s (br), *H*-1b), 5.03 (1H, s (br), *H*-1c), 4.93 (1H, s (br), *H*-1d), 4.86–4.22 (m, *H*-1e and PhCH_2), 4.06–3.46 (m), 3.36 (3H, s, OCH_3), 2.10 (3H, s, CH_3CO), 2.08 (3H, s, CH_3CO).

Pentamannoside peracetate (11)

A mixture of **9** (from 1 mmol of **4**) and 10% Pd–C (0.5 g) in acetic acid (40 mL) was stirred under 50 psi H_2 for 5 days at room temperature. The solution was filtered, and the 10% Pd–C was washed with methanol (2 × 10 mL). After the filtrate was evaporated under reduced pressure to afford clear syrup, acetic anhydride (15 mL), pyridine (25 mL), and a catalytic amount of DMAP (50 mg) were added. The mixture was stirred at room temperature for two days, and usual work-up gave a glassy solid, which was subject to flash column chromatography over silica gel (40 g, EtOAc–hexanes 2:1) to afford the peracetylated pentasaccharide **11** (a mixture of α- and β-anomers) in 19% yield (285 mg) based on **4**. Colorless glassy solid. R_f = 0.30 (5:2 EtOAc–hexanes). ^{1}H NMR (500 MHz, $CDCl_3$) δ: 6.01 (d, 1.7 Hz, *H*-1aα), 5.76 (d, 1.0 Hz, *H*-1aβ), 5.46 (dd, 1.0 and 2.1 Hz, *H*-2aβ), 5.38–5.15 (m), 5.12 (d, 1.7 Hz, *H*-1bα), 5.10–5.07 (m), 4.92 (d, 1.0 Hz, *H*-1cβ), 4.89 (d, 1.5 Hz, *H*-1cα), 4.88 (d, 1.0 Hz, *H*-1dβ), 4.86 (d, 1.5 Hz, *H*-1dα), 4.82 (d, 1.5 Hz, *H*-1eα), 4.80 (d, 1.0 Hz, *H*-1eβ), 4.22–3.51 (m), 2.19 (s, CH_3CO), 2.14 (s, CH_3CO), 2.13 (s, CH_3CO), 2.12 (s, CH_3CO), 2.11 (s, CH_3CO), 2.10 (s, CH_3CO), 2.09 (s, CH_3CO), 2.08 (s, CH_3CO), 2.05 (s, CH_3CO), 2.04 (s, CH_3CO), 2.03 (s, CH_3CO), 2.02 (s, CH_3CO), 2.01 (s, CH_3CO), 1.97 (s, CH_3CO). ^{13}C NMR (125 MHz, $CDCl_3$) δ: 170.7, 170.6, 170.4, 170.2, 170.1, 170.0, 169.9, 169.7, 169.6, 169.5, 169.4, 169.3, 169.2, 167.7, 99.7, 99.6, 99.4, 99.0, 98.2, 90.5, 90.2, 77.8, 74.3, 71.0, 69.6, 69.5, 69.4, 69.3, 69.2, 69.0, 68.4, 68.2, 68.1, 66.8, 66.1, 66.0, 65.6, 65.3, 62.3, 62.1, 61.9, 61.8, 21.1, 20.9, 20.8, 20.7, 20.6, 20.5, 20.4, 20.3. ES-MS calcd. for $C_{64}H_{86}O_{43}Na$ ([M + Na]$^+$): 1565.4; found: 1565.6. The experimental spectrum matches the theoretical spectrum calculated by isotopic modeling.

MPEG-Man3OH6OTBDPS (12)

MPEG derivative **6** (1 mmol) and DMAP (2 mmol) were dissolved in CH_2Cl_2 (15 mmol). *tert*-Butyldiphenylsilyl chloride (2 mmol) was added, and the reaction mixtures were stirred at room temperature for 24 h. After it was washed with a 1 mol/L HCl solution (2 × 75 mL), the organic layer was dried over anhydrous Na_2SO_4 and loaded onto the top of a silica gel column (15 times weight of compound **6**) for flash column chromatography. Gradient elution with hexanes – ethyl acetate (2:1, 1:1, 1:2, 1:4, and neat EtOAc, 50 mL each) removed the side products, and further elution with ethyl acetate – methanol (4:1 and 3:1, 150 mL each) gave the MPEG–sugar conjugate as colorless syrup. ^{1}H NMR (500 MHz, $CDCl_3$) δ: 7.76 (2H, d, 7.1 Hz, Ar-*H*), 7.74 (2H, d, 7.1 Hz, Ar-*H*), 7.71 (2H, d, 7.1 Hz, Ar-*H*), 7.44–7.19 (18H, m, Ar-*H*), 6.83 (1H, s (br), PhCON*H*), 4.97 (1H, d, <1.0 Hz, *H*-1), 4.88 (1H, d, 11.0 Hz, PhCH_2), 4.73 (1H, d, 12.4 Hz, PhCH_2), 4.71 (1H, d, 11.8 Hz, PhCH_2),

© 2005 NRC Canada

4.61 (1H, d, 11.9 Hz, PhCH_2), 4.58 (1H, d, 11.0 Hz, PhCH_2), 4.48 (1H, d, 12.4 Hz, PhCH_2), 4.05 (1H, ddd, 3.4, 9.0, and 9.5 Hz, *H*-3), 3.94 (2H, m, *H*-6a and *H*-6b), 3.80–3.77 (2H, m, *H*-2, and *H*-4), 3.70–3.52 (m, *H*-5 and PEG), 3.37 (3H, s, OCH_3), 2.43 (1H, d, 9.5 Hz, C_3-O*H*), 1.06 (9H, s, $(CH_3)_3CPh_2Si$).

MPEG-Diman6OTBDPS (13)

Colorless syrup. ^{1}H NMR (500 MHz, $CDCl_3$) δ: 7.71 (4H, d, 7.8 Hz, Ar-*H*), 7.67 (2H, d, 8.1 Hz, Ar-*H*), 7.42–7.12 (m, Ar-*H*), 6.83 (1H, s (br), PhCON*H*), 5.48 (1H, dd, 1.0 and 1.9 Hz, *H*-2a), 5.18 (1H, d, <1.0 Hz, *H*-1a), 4.85 (1H, d, <1.0 Hz, *H*-1b), 4.84 (1H, d, 11.0 Hz, PhCH_2), 4.72 (1H, d, 10.5 Hz, PhCH_2), 4.66–4.56 (m, PhCH_2), 4.53 (1H, d, 11.0 Hz, PhCH_2), 4.46–4.40 (m, PhCH_2), 4.16 (1H, dd, 3.0 and 9.3 Hz, *H*-3b), 4.06–3.79 (m), 3.70–3.50 (m, PEG), 3.35 (3H, s, OCH_3), 2.08 (3H, s, CH_3CO), 1.03 (9H, s, $(CH_3)_3CPh_2Si$).

MPEG-Diman6OH (14)

A mixture of compound **13** (1 mmol), 40% HF (4 mL), and methanol (25 mL) was stirred at room temperature for three days. Methanol was removed under reduced pressure, and the residue syrup was loaded onto the top of a silica gel column (15 times weight of compound **13**) for flash column chromatography. Gradient elution with hexanes – ethyl acetate (2:1, 1:1, 1:2, 1:4, and neat EtOAc, 50 mL each) removed the side products, and further elution with ethyl acetate – methanol (4:1 and 3:1, 150 mL each) gave the MPEG–sugar conjugate **14** as colorless syrup. ^{1}H NMR (500 MHz, $CDCl_3$) δ: 7.72 (2H, d, 8.3 Hz, Ar-*H*), 7.35–7.14 (m, Ar-*H*), 6.76 (1H, s (br), PhCON*H*), 5.49 (1H, dd, 1.0 and 1.9 Hz, *H*-2a), 5.22 (1H, d, <1.0 Hz, *H*-1a), 4.87 (1H, d, 11.0 Hz, PhCH_2), 4.82 (1H, d, <1.0 Hz, *H*-1b), 4.80 (1H, d, 11.0 Hz, PhCH_2), 4.67–4.55 (m, PhCH_2), 4.48–4.43 (m, PhC*H*), 4.20 (1H, dd, 2.7 and 9.3 Hz, *H*-3b), 4.01–3.53 (m), 3.37 (3H, s, OCH_3), 2.10 (3H, s, CH_3CO).

MPEG-TrimantriOAc (15)

Colorless syrup. ^{1}H NMR (500 MHz, $CDCl_3$) δ: 7.64 (2H, d, 8.1 Hz, Ar-*H*), 7.34–7.13 (m, Ar-*H*), 6.68 (1H, s (br), PhCON*H*), 5.49 (1H, dd, 1.0 and 1.9 Hz, *H*-2a), 5.32 (1H, dd, 2.0 and 8.0 Hz, *H*-3b), 5.21 (1H, d, 1.0 Hz, *H*-1a), 5.07 (1H, d, 1.0 Hz, *H*-1b), 4.86 (1H, d, 11.0 Hz, PhCH_2), 4.83 (1H, d, 10.6 Hz, PhCH_2), 4.75 (1H, d, 1.0 Hz, *H*-1c), 4.70–4.38 (m, PhCH_2), 4.36–3.52 (m), 3.37 (3H, s, OCH_3), 2.08 (3H, s, CH_3CO), 2.03 (3H, s, CH_3CO), 1.98 (3H, s, CH_3CO).

MPEG-TrimantriOH (16)

Colorless syrup. ^{1}H NMR (500 MHz, $CDCl_3$) δ: 7.66 (2H, d, 8.1 Hz, Ar-*H*), 7.36–7.16 (m, Ar-*H*), 6.70 (1H, s (br), PhCON*H*), 5.24 (1H, d, <1.0 Hz, *H*-1a), 5.08 (1H, d, <1.0 Hz, *H*-1b), 4.92 (1H, d, 11.2 Hz, PhCH_2), 4.82 (1H, d, 11.0 Hz, PhCH_2), 4.78 (1H, d, <1.0 Hz, *H*-1c), 4.73 (1H, d, 11.0 Hz, PhCH_2), 4.66–4.38 (m, PhCH_2), 4.18 (1H, dd, 2.9 and 9.5 Hz, *H*-3c), 4.02–3.52 (m), 3.37 (3H, s, OCH_3), 2.34 (1H, s (br), RO*H*), 1.94 (1H, t (br), C_6-O*H*).

MPEG-HexamantriOAc (17)

Colorless syrup. ^{1}H NMR (500 MHz, $CDCl_3$) δ: 7.57 (2H, d, 7.6 Hz, Ar-*H*), 7.34–7.16 (m, Ar-*H*), 6.63 (1H, s (br), PhCON*H*), 5.49 (3H, m (br), *H*-2a, *H*-2b, and *H*-2c), 5.22 (1H, d, <1.0 Hz, *H*-1a), 5.13 (1H, d, <1.0 Hz, *H*-1b), 5.02 (1H, d, <1.0 Hz, *H*-1c), 4.98 (1H, d, <1.0 Hz, *H*-1d), 4.95 (1H, d, <1.0 Hz, *H*-1e), 4.86–4.34 (m, *H*-1f and PhCH_2), 4.28–3.49 (m), 3.37 (3H, s, OCH_3), 2.11 (3H, s, CH_3CO), 2.09 (3H, s, CH_3CO), 2.02 (3H, s, CH_3CO).

MPEG-NonamantriOAc (18)

Colorless syrup. ^{1}H NMR (500 MHz, $CDCl_3$) δ: 7.50 (2H, d, 8.1 Hz, Ar-*H*), 7.36–7.05 (m, Ar-*H*), 6.45 (1H, s (br), PhCON*H*), 5.53 (1H, m (br), *H*-2a), 5.51 (1H, m (br), *H*-2b), 5.48 (1H, m (br), *H*-2c), 5.25 (1H, d, <1.0 Hz, *H*-1a), 5.18 (1H, d, <1.0 Hz, *H*-1b), 5.14 (1H, d, <1.0 Hz, *H*-1c), 5.09 (1H, d, <1.0 Hz, *H*-1d), 5.04 (2H, m (br), *H*-1e and *H*-1f), 4.97 (1H, d, <1.0 Hz, *H*-1g), 4.94 (1H, d, <1.0 Hz, *H*-1h), 4.86–3.52 (m, *H*-1i, PhCH_2 and PEG), 3.37 (3H, s, OCH_3), 2.10 (6H, s, CH_3CO), 2.05 (3H, s, CH_3CO).

Nonamannoside peracetate (19)

A mixture of **18** (from 1 mmol of **4**) and 20% $Pd(OH)_2$–C (Pearlman's catalyst, 2 g) in methanol (60 mL) was stirred under 1000 psi H_2 for 7 days at room temperature. The usual work-up and acetylation sequence gave a glassy solid, which was subject to dry flash-column chromatography over TLC-grade silica gel (average particle size 2–25 μm, 25 g, EtOAc) to afford the peracetylated nonasaccharide **19** (322 mg as a mixture of α- and β-anomers, 12% yield based on **4**) as colorless glassy solid. R_f = 0.59 (neat EtOAc). ^{1}H NMR (500 MHz, $CDCl_3$) δ: 6.02 (d, 2.0 Hz, *H*-1aα), 5.78 (d, 1.2 Hz, *H*-1aβ), 5.49 (dd, 1.2 and 3.4 Hz, *H*-2aβ), 5.41–5.21 (m), 5.16–5.12 (m), 5.04 (d, 1.7 Hz, d, 1.7 Hz, *H*-1dα and *H*-1dβ), 4.97 (d, 1.7 Hz, *H*-1e), 4.96 (d, 1.7 Hz, d, 2.0 Hz, *H*-1fα and *H*-1fβ), 4.90 (d, 2.0 Hz, d, 2.2 Hz, *H*-1gα and *H*-1gβ), 4.85 (d, 2.2 Hz, d, 2.4 Hz, *H*-1hα and *H*-1hβ), 4.84 and 4.81 (d, 2.0 Hz, d, 2.0 Hz, *H*-1iα and *H*-1iβ), 4.24–3.47 (m), 2.24 (s, CH_3CO), 2.20 (s, CH_3CO), 2.15 (s, CH_3CO), 2.14 (s, CH_3CO), 2.13 (s, CH_3CO), 2.12 (s, CH_3CO), 2.11 (s, CH_3CO), 2.10 (s, CH_3CO), 2.09 (s, CH_3CO), 2.08 (s, CH_3CO), 2.07 (s, CH_3CO), 2.06 (s, CH_3CO), 2.05 (s, CH_3CO), 2.04 (s, CH_3CO), 2.03 (s, CH_3CO), 2.02 (s, CH_3CO), 2.01 (s, CH_3CO), 2.00 (s, CH_3CO), 1.99 (s, CH_3CO). ^{13}C NMR (125 MHz, $CDCl_3$) δ: 170.9, 170.8, 170.7, 170.6, 170.5, 170.4, 170.3, 170.2, 169.9, 169.8, 169.7, 169.6, 169.5, 169.4, 169.3, 168.4, 167.9, 100.1, 99.6, 99.5, 99.4, 99.3, 99.1, 98.1, 97.6, 97.5, 90.7, 90.5, 78.0, 77.8, 77.7, 77.6, 77.5, 77.4, 77.2, 77.1, 75.6, 74.2, 74.0, 73.2, 71.7, 70.5, 70.4, 70.1, 70.0, 69.7, 69.6, 69.5, 69.4, 69.3, 69.2, 69.1, 68.6, 68.5, 68.3, 68.2, 67.4, 67.3, 66.4, 66.3, 66.2, 66.1, 65.8, 65.7, 65.5, 65.4, 65.3, 65.2, 62.4, 62.3, 62.2, 62.1, 62.0, 61.9, 61.8, 61.6, 61.5, 20.8, 20.7, 20.6, 20.5, 20.4, 20.3. ES-MS calcd. for $C_{112}H_{150}O_{75}Na$ ($[M + Na]^+$): 2717.8; found: 2717.8. The experimental spectrum matches the theoretical spectrum calculated by isotopic modeling.

Acknowledgment

We thank the Natural Sciences and Engineering Research Council of Canada (NSERC) for financial support of this research.

© 2005 NRC Canada

References

1. R. Kornfeld and S. Kornfeld. Annu. Rev. Biochem. **54**, 631 (1985).
2. A. Varki. Glycobiology, **3**, 97 (1993).
3. (*a*) G.J. LaRosa, J.P. Davide, K. Weinhold, J.A. Waterbury, A.T. Profy, J.A. Lewis, A.J. Langlois, G.R. Dreesman, R.N. Boswell, P. Shadduck, L.H. Holley, M. Karplus, D.P. Bolognesi, T.J. Matthews, E.A. Emini, and S.D. Putney. Science (Washington, D.C.), **249**, 932 (1990); (*b*) C.K. Leonard, M.W. Spellman, L. Riddle, R.J. Harris, J. Thomas, and T.J. Gregory. J. Biol. Chem. **265**, 10 373 (1990).
4. (*a*) W.E.G. Müller, H.C. Schröder, P. Reuter, A. Maidhof, G. Uhlenbruch, and I. Winkler. AIDS, **4**, 159 (1990); (*b*) D.A. Calarese, C.N. Scanlan, M.B. Zwick, S. Deechongkit, Y. Mimura, R. Kunert, P. Zhu, M.R. Wormald, R.L. Stanfield, K.H. Roux, J.W. Kelly, P.M. Rudd, R.A. Dwek, H. Katinger, D.R. Burton, and I.A. Wilson. Science, **300**, 2065 (2003).
5. J.R. Merritt, E. Naisang, and B. Fraser-Reid. J. Org. Chem. **59**, 4443 (1994).
6. (*a*) P. Grice, S.V. Ley, J. Pietruszka, and H.W.M. Priepke. Angew. Chem. Int. Ed. Engl. **35**, 197 (1996); (*b*) P. Grice, S.V. Ley, J. Pietruszka, H.M.I. Osborn, H.W.M. Priepke, and S.L. Warriner. Chem. Eur. J. **3**, 431 (1997).
7. D.M. Ratner, O.J. Plante, and P.H. Seeberger. Eur. J. Org. Chem. 826 (2002).
8. X. Geng, V.Y. Dudkin, M. Mandal, and S.J. Danishefsky. Angew. Chem. Int. Ed. **43**, 2562 (2004).
9. (*a*) P.H. Seeberger and S.J. Danishefsky. Acc. Chem. Res. **31**, 685 (1998); (*b*) O.J. Plante, E.R. Palmacci, and P.H. Seeberger. Science, **291**, 1523 (2001); (*c*) P. Sears and C.-H. Wong. Science, **291**, 2344 (2001); (*d*) K.R. Love and P.H. Seeberger. Angew. Chem. Int. Ed. **43**, 602 (2004).
10. (*a*) S.P. Douglas, D.M. Whitfield, and J.J. Krepinsky. J. Am. Chem. Soc. **113**, 5095 (1991); (*b*) S.P. Douglas, D.M. Whitfield, and J.J. Krepinsky. J. Am. Chem. Soc. **117**, 2116 (1995); (*c*) Y. Ito, O. Kanie, and T. Ogawa. Angew. Chem. Int. Ed. Engl. **35**, 2510 (1996); (*d*) P. Wentworth and K.D. Janda. Chem. Commun. 1918 (1999).
11. L. Jiang, R.C. Hartley, and T.H. Chan. Chem. Commun. 2193 (1996).
12. Y.M. Zhang, J.-M. Mallet, and P. Sinaÿ. Carbohydr. Res. **236**, 73 (1992).
13. (*a*) L. Jiang and T.H. Chan. J. Org. Chem. **63**, 6035 (1998); (*b*) L. Jiang and T.H. Chan. Tetrahedron Lett. **39**, 355 (1998).
14. P. Konradsson, D.R. Mootoo, R.E. McDevitt, and B. Fraser-Reid. Chem. Commun. 270 (1990).
15. S. Hanessian and P. Lavallee. Can. J. Chem. **53**, 2975 (1975).

© 2005 NRC Canada

Oppenauer-type oxidation of secondary alcohols catalyzed by homogeneous water-soluble complexes[1]

Abdelaziz Nait Ajjou and Jean-Louis Pinet

Abstract: The catalytic system composed of $[Ir(COD)Cl]_2$, 2,2′-biquinoline-4,4′-dicarboxylic acid dipotassium salt (BQC), and sodium carbonate is highly efficient for the selective oxidation of benzylic, 1-heteroaromatic, aliphatic, and allylic secondary alcohols using catalyst:substrate ratios ranging from 0.4% to 2.5%. Sterically hindered allylic alcohols undergo selectively good conversions to the corresponding enones, while unhindered ones are completely isomerized to saturated ketones. Mercury tests indicate that the catalytic process is likely homogeneous. The mechanism proposed for this Oppenauer-type oxidation including the isomerization process is based on iridium-alkoxide species.

Key words: Oppenauer oxidation, water, catalysis, isomerization, secondary alcohols.

Résumé : Le système catalytique composé de $[Ir(COD)Cl]_2$, 2,2′-biquinoléine-4,4′-dicarboxylate de potassium (BQC), et du carbonate de sodium est très efficace pour l'oxydation sélective des alcools secondaires benzyliques, 1-hétéroaromatiques, aliphatiques, et allyliques en cétones correspondantes en utilisant des quantités du catalyseur allant de 0,4 % à 2,5 %, par rapport aux substrats. Les alcools allyliques encombrés sont transformés, sélectivement, en énones correspondantes, alors que les alcools non-encombrés sont complètement isomérisés en cétones saturées. Les tests avec le mercure indiquent que le processus catalytique est, probablement, homogène. Le mécanisme proposé pour cette oxydation de type Oppenauer ainsi que pour l'isomérisation des alcools allyliques est basé sur la formation de l'espèce iridium-alkoxyde.

Mots clés : oxydation d'Oppenauer, eau, catalyse, isomérisation, alcools secondaires.

Introduction

The oxidation of alcohols to the corresponding aldehydes and ketones is one of the most fundamental and indispensable reactions in organic synthesis (1). For such transformations, the use of stoichiometric amounts of harmful inorganic oxidants, mainly chromium (VI) reagents, remains widespread (2). As a consequence for the increasing demand for efficient, cleaner, and environmentally friendly methods (3), numerous catalytic methods using small amounts of metallic derivatives and clean oxidants have been developed (4). Unfortunately, most of these catalytic transformations are accomplished in costly and toxic organic solvents. Furthermore, in the homogeneous processes, separation of the catalysts from the reaction products and their quantitative recovery in an active form are still the most important goals but practical problems remain. To overcome these disadvantages, aqueous organometallic catalysis has, recently, emerged as a very useful alternative technology (5). The water-soluble catalyst that operates and resides in water is, easily, separated from the reaction products by simple decantation. In addition, the products are not contaminated with traces of metal catalyst, and the use of organic solvents, such as benzene and chlorinated hydrocarbons is circumvented. Despite the obvious economical and ecological advantages of aqueous-phase catalysis, very few water-soluble catalysts have been reported for the oxidation of alcohols in water (6).

Oppenauer oxidation is an elegant and highly selective process for the oxidation of secondary alcohols to the corresponding ketones, with aluminum alkoxides (7). It can be carried out under mild conditions, and is compatible with many functional groups such as carbon–carbon double and triple bonds, halogens, amino groups, aldehydes, or sulphur atom-containing groups. The advantages of Oppenauer oxidation have led to the development of more efficient methods based on modified aluminum alkoxides (8) and the use of transition-metal complexes as catalysts (9).

In the past few years, we have developed different catalytic transformations in water including the hydration of nitriles to the corresponding amides catalyzed by $[Rh(COD)Cl]_2$–$P(m\text{-}C_6H_4SO_3Na)_3$ (TPPTS) (10), organic solvent-free oxidation of alcohols with *tert*-butyl hydroperoxide catalyzed by water-soluble copper complexes (11), and transfer hydrogenation of aldehydes and ketones with isopropanol catalyzed by water-soluble rhodium complexes (12). In the present work, we describe the results for the hydrogen transfer oxidation (Oppenauer-type oxidation) of secondary alcohols with acetone, as the oxidant, catalyzed

Received 30 November 2004. Published on the NRC Research Press Web site at http://canjchem.nrc.ca on 14 June 2005.

This paper is dedicated to Professor Howard Alper, a trailblazer in catalysis.

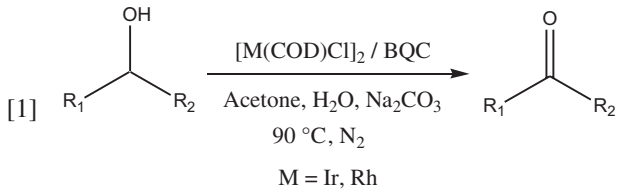
A. Nait Ajjou[2] and J.-L. Pinet. Department of Chemistry and Biochemistry, University of Moncton, Moncton, NB E1A 3E9, Canada.

[1]This article is part of a Special Issue dedicated to Professor Howard Alper.

[2]Corresponding author (e-mail: naitaja@umoncton.ca).

 doi: 10.1139/V05-037 © 2005 NRC Canada

by water-soluble iridium and rhodium complexes containing 2,2′-biquinoline-4,4′-dicarboxylic acid dipotassium salt (BQC) (eq. [1]). Some preliminary results have been published in a communication where we have reported the first example of a water-soluble transition-metal catalyst for Oppenauer-type oxidation of secondary alcohols with acetone (13).



[1]

Results and discussion

A number of catalytic systems based on different catalyst precursors and the water-soluble ligand P(*m*-$C_6H_4SO_3Na)_3$ (TPPTS) or BQC were tested for the oxidation of 1-phenylethanol, which was chosen as the model substrate. The first experiments showed that the presence of the catalyst precursor, together with acetone and sodium carbonate is required to achieve oxidation of 1-phenylethanol. While $RuCl_3 \cdot xH_2O$ and $PdCl_2(PhCN)_2$ exhibited no catalytic activity, $[Rh(COD)Cl]_2$ and $[Ir(COD)Cl]_2$ gave rise to active water-soluble systems (Table 1). The results in Table 1 indicate that the least active catalytic systems were provided by TPPTS (Table 1, entries 1 and 4). Nevertheless, we recently reported that $[Rh(COD)Cl]_2$–TPPTS was found to be quite an effective catalyst for transfer hydrogenation of aldehydes and ketones with isopropanol, under basic conditions (12). Treatment of 1-phenylethanol (2.5 mmol) in the presence of Na_2CO_3 (2.5 mmol), with catalytic amounts of $[Rh(COD)Cl]_2$ (0.01 mmol) and BQC (0.15 mmol) in a deoxygenated mixture of water (10 mL) and acetone (5 mL) at 90 °C afforded, selectively, acetophenone in 15% yield after 2 h (Table 1, entry 2). Increasing the reaction time to 17 h lead to a 57% yield (Table 1, entry 3). Remarkably, when $[Rh(COD)Cl]_2$ was substituted for its iridium analog much more active catalyst was generated. Indeed, acetophenone was obtained in 82% and 98% yields, respectively, after 2 and 4 h (Table 1, entries 5 and 6). This catalytic system has been shown to be much less active than $[Rh(COD)Cl]_2$–TPPTS for transfer hydrogenation of carbonyl groups with *i*-PrOH (12). In aqueous-phase catalysis, the most important aspects are product separation as well as catalyst recovery and recycling in further experiments. The durability of the $[Ir(COD)Cl]_2$–BQC system was tested by carrying out three consecutive cycles with the same catalyst aqueous solution, carefully separated from the organic phase under a nitrogen atmosphere at the end of each run (Table 1, entries 6–8). Only a slight decrease in catalytic activity was observed among each of the three recycling experiments demonstrating the continuing viability of the catalyst. It is relevant to point out that no metallic iridium formation was observed after the reactions and the aqueous phases remained as clear-brown solutions, indicating that there was no decomposition of the catalyst. Analysis of the organic phases, which remained clear, by atomic absorption indicated that acetophenone was extracted without leaching of the catalyst. When the oxidation was performed with $[Ir(COD)Cl]_2$ alone or in combination with 2,2′-biquinoline (BQ) in acetone containing only 0.5% water very low yields were obtained (Table 1, entries 9 and 10). Addition of water (10 mL) increased the rate of oxidation and acetophenone was isolated in 39% yield (Table 1, entry 11). An analogous positive effect of water on the rate of this homogeneous Oppenauer-type oxidation has already been observed for $RuCl_2(PPh_3)_3$ (9*a*). These results, which demonstrate the superiority of aqueous-phase catalysis over the homogeneous one in this Oppenauer-type oxidation, are even more interesting since BQC is cheaper than BQ.[3]

Table 1. Oxidation of 1-phenylethanol by acetone catalyzed with various catalytic systems.[a]

Entry	Catalyst precursor	Ligand	Time (h)	Yield (%)[b]
1	$[Rh(COD)Cl]_2$	TPPTS	2	7
2	$[Rh(COD)Cl]_2$	BQC	2	15
3	$[Rh(COD)Cl]_2$	BQC	17	57
4	$[Ir(COD)Cl]_2$	TPPTS	2	9
5	$[Ir(COD)Cl]_2$	BQC	2	82
6	$[Ir(COD)Cl]_2$	BQC	4	98[c]
7[d]	$[Ir(COD)Cl]_2$	BQC	4	82
8[e]	$[Ir(COD)Cl]_2$	BQC	4	68
9[f]	$[Ir(COD)Cl]_2$	—	4	5
10[g]	$[Ir(COD)Cl]_2$	BQ	4	4
11[h]	$[Ir(COD)Cl]_2$	BQ	4	39

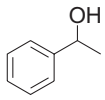
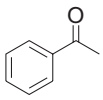
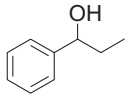
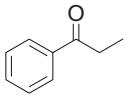
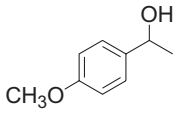
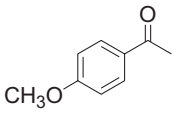
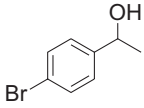
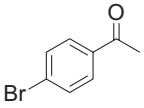
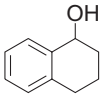
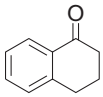
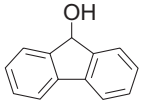
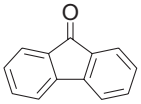
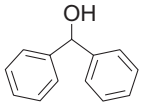
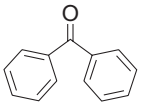
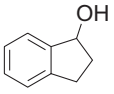
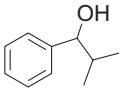
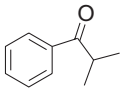
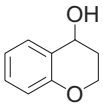
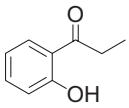
[a]Reaction conditions: 1-phenylethanol (2.5 mmol), $[M(COD)Cl]_2$ (0.01 mmol), ligand (0.15 mmol), Na_2CO_3 (2.5 mmol), water (10 mL), acetone (5 mL), 90 °C, N_2.
[b]Yields refer to isolated ketones.
[c]Full conversion of the substrate was obtained.
[d]Second cycle of entry 6.
[e]Third cycle of entry 6.
[f]Reaction conditions: 1-phenylethanol (2.5 mmol), $[Ir(COD)Cl]_2$ (0.01 mmol), Na_2CO_3 (2.5 mmol), acetone (10 mL), 90 °C, N_2.
[g]The reaction conditions are the same as in entry 9 except that BQ (0.15 mmol) was added to the mixture.
[h]The reaction conditions are the same as in entry 10 except that water (10 mL) was added to the mixture.

To demonstrate the synthetic utility and to explore the scope and limitations of the $[Ir(COD)Cl]_2$–BQC system, a range of different alcohols were subjected to oxidation by acetone in a series of batch autoclave experiments. A variety of benzylic secondary alcohols were smoothly and selectively oxidized in very high yields, with full conversions in some cases within 4 h (Table 2, entries 1–7). Under the same reaction conditions, 1-indanol led to 1-indanone with only a 53% yield. A better result was obtained by increasing the reaction time to 17 h (Table 2, entry 8). With a sterically encumbered alcohol, namely 2-methyl-1-phenyl-1-propanol, a 58% yield was achieved, while the substrate was sluggishly oxidized after 4 h (Table 2, entry 9). A special situation was observed in the case of 4-chromanol, which underwent, in addition to an oxidation of the benzylic alcohol, a hydrogenolysis of the ArO—CH_2 (Ar is the aromatic ring) bond

[3]BQC and BQ cost $4166.70 and $5854.12CAN per mol, respectively, from the Aldrich Chemical Co.

© 2005 NRC Canada

Table 2. Oxidation of different benzylic alcohols by acetone using water-soluble $[Ir(COD)Cl]_2$–BQC as the catalyst.[a]

Run	Substrate	Time (h)	Product	Yield (%)[b]
1		4		98[c]
2		4		80
3		4		96[c]
4		4		90
5		4		97[c]
6		4		96[c]
7		4		90
8		4 (17)		53 (70)
9		4 (17)		32 (58)
10		4		99

[a]Reaction conditions: substrate (2.5 mmol), $[Ir(COD)Cl]_2$ (0.01 mmol), BQC (0.15 mmol), Na_2CO_3 (2.5 mmol), water (10 mL), acetone (5 mL), 90 °C, N_2.
[b]Yields refer to isolated ketones.
[c]Full conversion of the substrate was obtained.

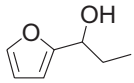
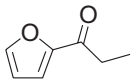
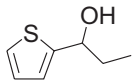
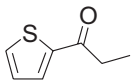
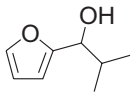
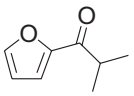
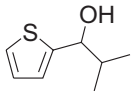
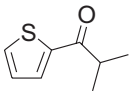
leading to *ortho*-hydroxypropiophenone as the sole product (Table 2, entry 10). When the reaction was performed in the absence of acetone the same product was obtained and no 4-chromanone was detected. These results indicate that the production of *ortho*-hydroxypropiophenone from 4-chromanol is, probably due to an intramolecular transfer hydrogenolysis. The catalytic process is envisioned as a reaction between 4-chromanol and the water-soluble iridium system resulting in an iridium alkoxide complex, which, in turn, undergoes β-hydride elimination to produce a η^2-ketone hydride species, where the 4-chromanone is still coordinated to the iridium. The transfer of iridium hydride to the methylene group of $ArO–CH_2$ of the coordinated 4-chromanone (intramolecular 1,3-hydride shift) leads to an iridium *ortho*-propionylphenoxide complex. Protonation with another 4-chromanol molecule liberates *ortho*-hydroxypropiophenone and regenerates the iridium alkoxide species. The transfer of hydride to $ArO–CH_3$ did not occur in the case of 1-(4-methoxyphenyl)ethanol (Table 2, entry 3) since the methoxy group is located far from the metal hydride core.

To explore substrate scope further, we tested the efficiency of the $[Ir(COD)Cl]_2$–BQC system to oxidize secondary 1-heteroaryl alcohols (Table 3). Good to excellent yields were obtained in all cases, although the reaction time was extended to 17 h for the oxidation of 1-(2-furyl)-2-methyl-1-propanol and the thienyl analog, which gave, respectively, 74% and 65% yields (Table 3, entries 3 and 4). The sluggishness in these two cases is attributed to steric hindrance from the isopropyl group.

The reaction was, also, extended to a variety of secondary

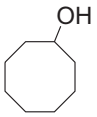
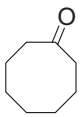
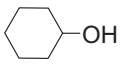
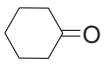
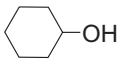
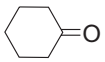
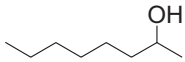
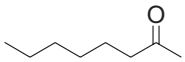
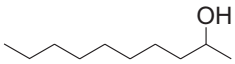
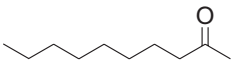
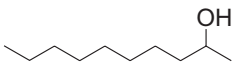
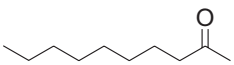
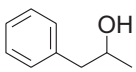
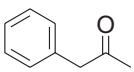
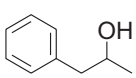
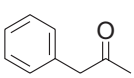
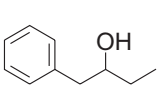
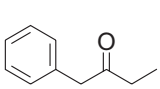
© 2005 NRC Canada

Table 3. Oxidation of different 1-heteroaryl alcohols by acetone using water-soluble $[Ir(COD)Cl]_2$–BQC as the catalyst.[a]

Run	Substrate	Time (h)	Product	Yield (%)[b]
1		4 (17)		87 (87)
2		4 (17)		88 (90)
3		4 (17)		66 (74)
4		4 (17)		48 (65)

[a]Reaction conditions: substrate (2.5 mmol), $[Ir(COD)Cl]_2$ (0.01 mmol), BQC (0.15 mmol), Na_2CO_3 (2.5 mmol), water (10 mL), acetone (5 mL), 90 °C, N_2.
[b]Yields refer to isolated ketones.

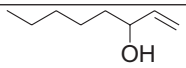
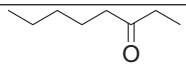
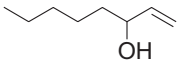
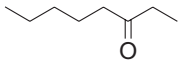
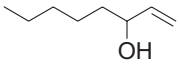
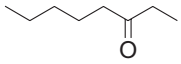
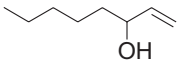
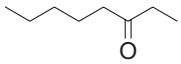
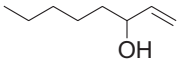
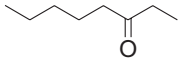
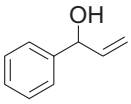
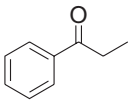
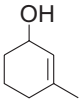
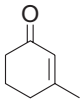
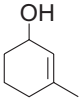
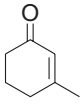
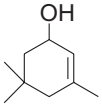
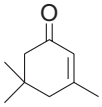
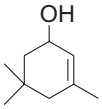
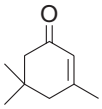
Table 4. Oxidation of different aliphatic alcohols by acetone using water-soluble $[Ir(COD)Cl]_2$–BQC as the catalyst.[a]

Run	Substrate	Time (h)	Product	Yield (%)[b]
1		4		76
2		4 (17)		15 (25)
3[c]		17		80
4		4 (17)		21 (31)
5		4 (17)		21 (30)
6[c]		17		91
7		4		23
8[c]		17		80
9[c]		20		72

[a]Unless stated otherwise, the reaction conditions are: substrate (2.5 mmol), $[Ir(COD)Cl]_2$ (0.01 mmol), BQC (0.15 mmol), Na_2CO_3 (2.5 mmol), water (10 mL), acetone (5 mL), 90 °C, N_2.
[b]Yields refer to isolated ketones.
[c]Substrate (1 mmol), $[Ir(COD)Cl]_2$ (0.025 mmol), and BQC (0.375 mmol).

© 2005 NRC Canada

Table 5. Oxidation of different allylic alcohols by acetone using various water-soluble catalysts.[a]

Run	Substrate	Catalyst	Time (h)	Product	Yield (%)[b]
1		$[Ir(COD)Cl]_2$–BQC	1		100
2		$[Ir(COD)Cl]_2$–TPPTS	4		100
3		$PtCl_2(COD)$–BQC	4		98
4		$PdCl_2(PhCN)_2$–BQC	4		100
5		$[Rh(COD)Cl]_2$–BQC	4		100
6		$[Ir(COD)Cl]_2$–BQC	1.5		100
7		$[Ir(COD)Cl]_2$–BQC	17		50
8[c]		$[Ir(COD)Cl]_2$–BQC	17		100
9		$[Ir(COD)Cl]_2$–BQC	17		13
10[c]		$[Ir(COD)Cl]_2$–BQC	17		100

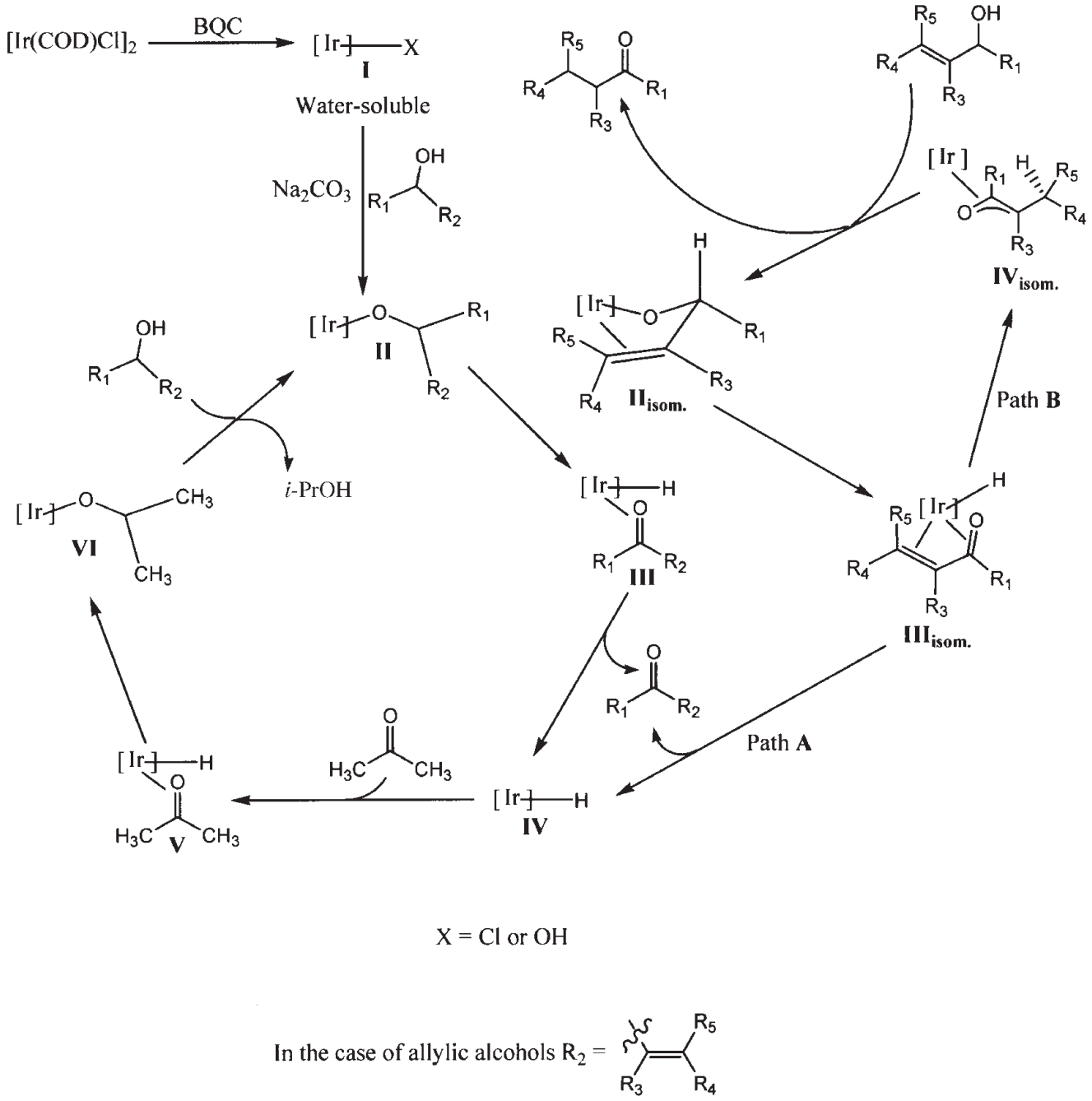
[a]Unless stated otherwise, the reaction conditions are: substrate (2.5 mmol), $[Ir(COD)Cl]_2$ (0.01 mmol), BQC (0.15 mmol), Na_2CO_3 (0.5 mmol), water (10 mL), acetone (5 mL), 90 °C, N_2.
[b]Yields were estimated by ^1H NMR.
[c]Substrate (1 mmol), $[Ir(COD)Cl]_2$ (0.025 mmol), and BQC (0.375 mmol).

aliphatic alcohols (Table 4). However, these inactivated alcohols proved to be sluggish substrates under our standard conditions, and only poor yields were obtained. Fortunately, a higher catalyst:substrate ratio (2.5 mol%) and longer reaction times greatly improve the yields (Table 4, entries 3, 6, 8, and 9). Remarkably, cyclooctanol showed a higher reactivity than cyclohexanol and the former was oxidized in 76% yield with only 0.4 mol% of $[Ir(COD)Cl]_2$ after 4 h (Table 4, entry 1).

To investigate the extent of $[Ir(COD)Cl]_2$–BQC oxidation, different allylic alcohols have been studied (Table 5). The oxidation of 1-octen-3-ol afforded 3-octanone as the sole product after only 1 h of reaction time (Table 5, entry 1). The reaction performed in the absence of acetone led to the same result after 4 h. However, this reaction was not optimized. The isomerization of allylic alcohols to saturated carbonyl compounds is an important reaction in organic chemistry that still suffers from several drawbacks (14). Surprisingly, the water-soluble catalytic systems reported for the isomerization of allylic alcohols are rare, despite their synthetic utility (15). Thus, other water-soluble catalysts were tested for the oxidation of 1-octen-3-ol (Table 5, entries 2–5). Excellent to full conversions to the isomerization product were obtained except in the case of $RuCl_3$–BQC, which is inactive. Although these reactions were not optimized, the result obtained with $[Ir(COD)Cl]_2$–BQC is promising since its catalytic frequency for the isomerization of 1-octen-3-ol (125 h^{-1} at 90 °C) is slightly better than the reported activities for other water-soluble catalysts based on $[RuCl_2(\eta^6\text{-arene})\{P(CH_2OH)_3\}]$ (4–67 h^{-1} at 75 °C) (15*a*), $Rh_2(SO_4)_3$ (30 h^{-1} at 80 °C) (15*b*), $RhCl_3$ (60 h^{-1} at 70 °C) (15*b*), and $(COD)RhCl(PAr_3)$ (15–48 h^{-1} at 104 °C) (15*c*). We are currently continuing to investigate the isomerization of allylic alcohols in the aqueous phase. The oxidation of 1-

© 2005 NRC Canada

Scheme 1. Proposed mechanism for the Oppenauer-type oxidation and isomerization of allylic alcohols.



phenyl-2-propen-1-ol, under the same conditions, also gave propiophenone as the isomerization product, with full conversion (Table 5, entry 6), whereas cyclic allylic alcohols are, surprisingly, oxidized to their corresponding unsaturated ketones albeit in low yields (Table 5, entries 7 and 9). Fortunately, under the conditions used for the oxidation of aliphatic alcohols (Table 4, entry 3), isophorol and 3-methyl-2-cyclohexenol were fully converted to their corresponding unsaturated ketones (Table 5, entries 8 and 10). Bäckvall and co-workers (9*a*) have also reported that 1-octen-3-ol was isomerized under their reaction conditions to 3-octanone using ruthenium complexes, while 2-cyclohexenol was converted to an unsaturated ketone.

Although the structure of the water-soluble active complex is not identified, a rational mechanism for this Oppenauer-type oxidation, including the isomerization process, is presented in Scheme 1.

Since no iridium mirror (black metallic iridium) was observed after the reactions and the aqueous phases remained as clear-brown solutions, we carried out mercury poisoning experiments (see the Experimental section) to rule out the possibility of catalysis by colloidal metal. Mercury poisoning is a well-known and widely used test to distinguish between heterogeneous and homogeneous processes (16). The addition of a large excess of mercury(0) (Hg:Ir molar ratio of 872) with vigorous stirring did not suppress the catalysis.

© 2005 NRC Canada

Table 6. Oxidation of 1-phenylethanol by acetone catalyzed by water-soluble $[Ir(COD)Cl]_2$–BQC using different amounts of Na_2CO_3.[a]

Run	Na_2CO_3 (mmol)	Yield (%)[b]
1	0	0
2	0.25	88
3	0.5	98
4	1	100
5	1.5	100
6	2	100
7	2.5	100

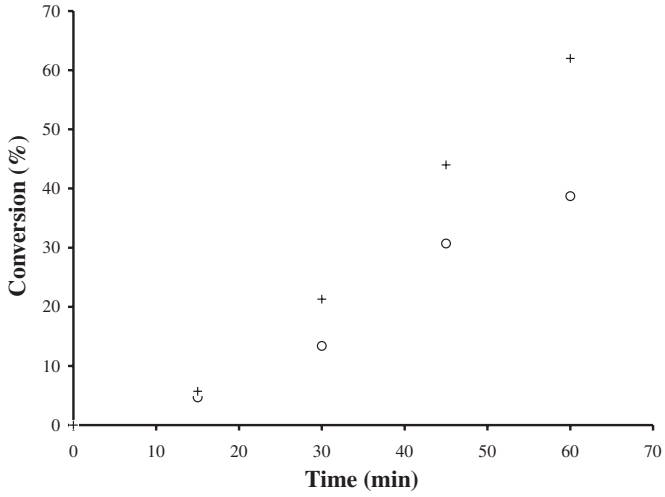
[a]Reaction conditions: substrate (2.5 mmol), $[Ir(COD)Cl]_2$ (0.01 mmol), BQC (0.15 mmol), Na_2CO_3 (0–2.5 mmol), water (10 mL), acetone (5 mL), 90 °C, N_2, 4 h.

[b]Yields were estimated by ^1H NMR.

These results suggest that nanoparticles are not the key species in the present system and that the process is likely homogeneous.

The first step of the proposed mechanism would involve the formation of iridium alkoxide **II** (9*a*, 17). Stoichiometric amounts of Na_2CO_3 were used in our experiments. However, oxidation of 1-phenylethanol with smaller amounts of Na_2CO_3 also gave excellent results (Table 6). When the reaction was performed in the absence of base, its remarkable effect was particularly noticeable because no reaction occurred (Table 6, entry 1). This effect of base in Oppenauer-type oxidations has been observed in previous reports (9*a*, 9*b*). Consequently, the primary role of the base is to facilitate formation of iridium alkoxide complex **II**. This latter species can undergo β-hydride elimination of the coordinated alkoxide to produce the desired ketone and iridium hydride species **IV**, via complex **III** where the ketone is still coordinated to the metal (η^2-ketone ligand). β-hydride elimination from metal alkoxides has been observed (17, 18) and proposed for hydrogen transfer reactions (9*a*, 19). In our case, the production of *ortho*-hydroxypropiophenone from 4-chromanol is in agreement with the formation of complex **III**. Comparison of the oxidation rates for $PhCH(OH)CH_3$ and $PhCD(OH)CH_3$, under the same conditions (Fig. 1), indicates that the rate-limiting step does not involve β-hydride elimination from **II** since the isotope effect is low (k_H/k_D = 1.2). The reaction of acetone with **IV** would produce complex **V**, which leads to iridium isopropoxide **VI** by insertion of acetone into the Ir—H bond. An exchange of alkoxy moiety would regenerate species **II** and liberate isopropanol. In the case of allylic alcohols, an additional pathway for the isomerization process is proposed. Three mechanisms have been proposed for transition metal catalyzed isomerization of allylic alcohols. The first one involves a π-allyl metal hydride complex (20), while a second one is based on metal hydride addition–elimination (21). A third mechanism, suggested by Trost and Kulawiec (22), involves the coordination of allylic alcohol as a bidentate ligand and the formation of metal alkoxide species. Our results from oxidation with $[Ir(COD)Cl]_2$–BQC (Table 5) are consistent with the alkoxide mechanism. Thus, in the case of allylic alcohols, **II** is reorganised as $\mathbf{II_{isom.}}$ to allow the coordination of Ir with R_2 (R_2 is an olefinic moiety). $\mathbf{II_{isom.}}$ undergoes β-hydride elimination to produce the enone hydride species $\mathbf{III_{isom.}}$. This latter is expected to evolve in two different ways depending on the steric requirements of the enone. In the case of bulky substrates such as isophorol, $\mathbf{III_{isom.}}$ releases the enone through path **A** and follows the catalytic cycle for the Oppenauer-type oxidation. This is in agreement with previous reports regarding the isomerization of allylic alcohols catalyzed by ruthenium complexes (21, 22). The steric unhindered enones, on the other hand, are not released and allow $\mathbf{III_{isom.}}$ to rearrange to π-oxallyl species $\mathbf{IV_{isom.}}$ through path **B**. Protonation with another allylic alcohol molecule liberates the saturated ketone and regenerates the initial species $\mathbf{II_{isom.}}$.

Fig. 1. Oxidation profiles of $PhCH(OH)CH_3$ (+) and $PhCD(OH)CH_3$ (o). Substrate (2.5 mmol), $[Ir(COD)Cl]_2$ (0.01 mmol), BQC (0.15 mmol), Na_2CO_3 (2.5 mmol), water (10 mL), acetone (5 mL), 90 °C, N_2.



Summary

In conclusion, the system composed of $[Ir(COD)Cl]_2$ and the cheap water-soluble ligand BQC is a new and highly efficient catalyst for Oppenauer-type oxidation of benzylic, 1-heteroaromatic, aliphatic, and allylic secondary alcohols. The system showed much better activity than the water-insoluble analogs. The catalytic process is likely homogeneous and the mechanism proposed for this Oppenauer-type oxidation including the isomerization process is based on iridium-alkoxide species.

Experimental

Materials and instruments

All the substrates, BQ, and BQC were purchased from Aldrich Chemical Co. and used without further purification. $[Rh(COD)Cl]_2$, $RuCl_3{\cdot}xH_2O$, $PdCl_2(PhCN)_2$, and $[Ir(COD)Cl]_2$ were acquired from Strem Chemical Co.

TPPTS was prepared according to the literature method (23) and $PhCD(OH)CH_3$ was prepared using $LiAlD_4$ (24).

Routine NMR measurements were performed on a Bruker AC-200 spectrometer at 200 MHz and 50 MHz, respectively, for ^1H and ^{13}C, using tetramethylsilane (TMS) as an internal standard and $CDCl_3$ as the solvent.

© 2005 NRC Canada

Typical procedure for this Oppenauer type oxidation with acetone

In the glass liner of a 45 mL autoclave, under an atmosphere of nitrogen, $[Ir(COD)Cl]_2$ (0.01 mmol), BQC (0.15 mmol), and Na_2CO_3 (2.5 mmol) were dissolved in degassed water (10 mL) at room temperature. Next a solution of the substrate (2.5 mmol) in degassed acetone (5 mL) was introduced. The autoclave, was then flushed several times with 80 psi (1 psi = 6.894 757 kPa) of N_2 and then placed in an oil bath at 90 °C for the required reaction time. The autoclave was cooled to room temperature and the mixture was extracted three times with degassed diethyl ether (20 mL). The combined organic layers were dried ($MgSO_4$), evaporated to dryness, and then analyzed by TLC and ^1H and ^{13}C NMR. Literature data and (or) authentic samples were used for comparison. The ^1H NMR spectra for all samples showed the presence of remaining substrate (where the conversions were not complete), the product, and small amounts of 4-hydroxy-4-methyl-2-pentanone formed by aldol condensation of acetone. In the case of isolated yields, the ketones were purified using column chromatography with ethyl acetate – petroleum ether (5:95) as the eluent.

The recycled aqueous phase obtained, after removal of solvents under a nitrogen atmosphere, was reused with only a fresh charge of solution consisting of the alcohol (2.5 mmol) in degassed acetone (5 mL).

Mercury poisoning experiments

Three experiments were performed to determine the effect of mercury (0) on the reaction.

A solution of $[Ir(COD)Cl]_2$ (13.4 mg, 0.02 mmol) and BQC (0.3 mmol, 142 mg) in water (20 mL) was stirred in the presence of excess mercury (7 g, 34.9 mmol, ca. 872 equiv.) for 24 h. The solution was decanted from the mercury and divided into two equal parts, which were used for the Oppenauer-type oxidation of 1-phenylethanol for 4 h. After 1 h of reaction time, one autoclave was cooled to room temperature, vented, and opened under a nitrogen atmosphere. Next 3.5 g of Hg(0) was added to the clear-brown catalytically active solution and the autoclave was then purged with nitrogen, resealed, and stirred for 30 min. The mixture was then heated at 90 °C for the remaining reaction time. The two experiments showed the same excellent catalytic activity.

A third experiment was done just to confirm the previous ones. In this experiment, the oxidation was initiated in the presence of excess Hg(0) (872 equiv.). The result was identical to the previous ones.

These experiments indicate that Hg(0) does not react with the precatalyst $[Ir(COD)Cl]_2$ and that the process is likely homogeneous.

Acknowledgements

We are grateful to the Natural Sciences and Engineering Research Council of Canada (NSERC) and to the Faculté des études supérieures et de la recherche (FESR) of the University of Moncton for financial support of this research.

References

1. For reviews on oxidations, see: (*a*) R.A. Sheldon and J.K. Kochi. *In* Metal-catalyzed oxidations of organic compounds. Academic Press, New York. 1981; (*b*) S.V. Ley, J. Norman, W.P. Griffith, and P. Marsden. Synthesis, 639 (1994); (*c*) M. Hudlicky. Oxidations in organic chemistry. American Chemical Society, Washington, D.C. 1990.
2. G. Cainelli and G. Cardillo. Chromium oxidations in organic chemistry. Springer, Berlin. 1984.
3. (*a*) A.R. Sheldon. J. Chem. Technol. Biotechnol. **68**, 381 (1997); (*b*) A.R. Sheldon. CHEMTECH, **21**, 566 (1991); (*c*) J. Muzart. Chem. Rev. **92**, 113 (1992).
4. (*a*) S. Aït-Mohand, F. Hénin, and J. Muzart. Tetrahedron Lett. **36**, 2473 (1995); (*b*) J. Muzart, A. Nait Ajjou, and S. Aït-Mohand. Tetrahedron Lett. **35**, 1989 (1994); (*c*) A. Riahi, F. Hénin, and J. Muzart. Tetrahedron Lett. **40**, 2303 (1999); (*d*) S.I. Murahashi, T. Naota, Y. Oda, and N. Hirai. Synlett, 733 (1995); (*e*) A.R. Sheldon, I.W.C.E. Arends, and A. Dijksman. Catal. Today, **57**, 157 (2000); (*f*) N.B. Barhate, M. Sasidharan, A. Sudalai, and R.D. Wakharkar. Tetrahedron Lett. **37**, 2067 (1996); (*g*) E.I. Markó, P.R. Giles, M. Tsukazaki, I. Chellé-Regnaut, A. Gautier, S.M. Brown, and C.J. Urch. J. Org. Chem. **64**, 2433 (1999).
5. (*a*) B. Cornils. Org. Process Res. Dev. **2**, 121 (1998); (*b*) B. Cornils and W.A. Herrmann. Applied homogeneous catalysis with organometallic compounds. Vol. 2. VCH, Weinheim, Germany. 1996; (*c*) W.A. Herrmann and C.W. Kohlpainter. Angew. Chem. Int. Ed. Engl. **32**, 1524 (1993); (*d*) F. Ungváry. Coord. Chem. Rev. **160**, 123 (1997); (*e*) F. Joó and Á. Kathó. J. Mol. Catal. **116**, 3 (1997); (*f*) A. Nait Ajjou and H. Alper. J. Am. Chem. Soc. **120**, 1466 (1998); (*g*) W.A. Herrmann, J.A. Kulpe, J. Kellner, H. Riepl, H. Bahrmann, and W. Konkol. Angew. Chem. Int. Ed. Engl. **29**, 391 (1990); (*h*) C. Mercier and P. Chabardes. Pure Appl. Chem. **66**, 1509 (1994); (*I*) C. Mercier, G. Mignani, M. Aufrand, and G. Allmang. Tetrahedron Lett. **32**, 1433 (1991); (*j*) G. Papadogianakis and R.A. Sheldon. New J. Chem. **20**, 175 (1996); (*k*) B. Cornils and E. Wiebus. CHEMTECH, **25**, 33 (1995).
6. (*a*) G.-J. ten Brink, I.W.C.E. Arends, and R.A. Sheldon. Science, **287**, 1636 (2000); (*b*) K. Sato, M. Aoki, J. Takagi, and R. Noyori. J. Am. Chem. Soc. **119**, 12 386 (1997).
7. (*a*) C.F. de Graauw, J.A. Peters, H. van Bekkum, and J. Huskens. Synthesis, 1007 (1994); (*b*) C. Djerassi. Org. React. **6**, 207 (1951); (*c*) R.V. Oppenauer. Recl. Trav. Chim. Pays–Bas, **56**, 137 (1937).
8 (*a*) T. Ooi, H. Otsuka, T. Miura, H. Ichikawa, and K. Maruoka. Org. Lett. **4**, 2669 (2002); (*b*) K.G. Akamanchi and B.A. Chaudhari. Tetrahedron Lett. **38**, 6925 (1997).
9. (*a*) M.L.S. Almeida, M. Beller, G.-Z. Wang, and J.E. Bäckvall. Chem. Eur. J. **2**, 1533 (1996); (*b*) S. Gauthier, R. Scopelliti, and K. Severin. Organometallics, **23**, 3769 (2004); (*c*) K.-I. Fujita, S. Furukawa, and R. Yamaguchi. J. Organomet. Chem. **649**, 289 (2002).
10. M.-C.K.-B. Djoman and A. Nait Ajjou. Tetrahedron Lett. **41**, 4845 (2000).
11. G. Ferguson and A. Nait Ajjou. Tetrahedron Lett. **44**, 9139 (2003).
12. A. Nait Ajjou and J.-L. Pinet. J. Mol. Catal. A: Chem. **214**, 203 (2004).
13. A. Nait Ajjou. Tetrahedron Lett. **42**, 13 (2001).
14. (*a*) R. Uma, C. Crévisy, and R. Crée. Chem. Rev. **103**, 27 (2003); (*b*) R.C. van der Drift, E. Bouwman, and E. Drent. J. Organomet. Chem. **650**, 1 (2002).

© 2005 NRC Canada

15. (*a*) V. Cadierno, P. Crochet, S.E. García-Garrido, and J. Gimeno. Dalton Trans. 3635 (2004); (*b*) C. de Bellfon, S. Caravieilhes, E.G. Kuntz. C.R. Acad. Sci. Ser. IIc: Chim. **3**, 607 (2000); (*c*) H. Schumann, V. Ravindar, L. Meltser, W. Baidossi, Y. Sasson, and J. Blum. J. Mol. Catal. A: Chem. **118**, 55 (1997); (*d*) C. Bianchini, A. Meli, and W. Oberhauser. New J. Chem. **25**, 11 (2001); (*e*) H. Bricout, E. Monflier, J.-F. Carpentier, and A. Mortreux. Eur. J. Inorg. Chem. 1739 (1998).
16. J.A. Widegren and R.G. Finke. J. Mol. Catal. A: Chem. **198**, 317 (2003).
17. H.E. Bryndza and W. Tam. Chem. Rev. **88**, 1163 (1988).
18. (*a*) O. Blum and D. Milstein. J. Organomet. Chem. **593–594**, 479 (2000); (*b*) O. Blum and D. Milstein. Angew. Chem. Int. Ed. Engl. **34**, 229 (1995); (*c*) O. Blum and D. Milstein. J. Am. Chem. Soc. **117**, 4582 (1995); (*d*) D. Milstein. J. Am. Chem. Soc. **108**, 3525 (1986); (*e*) H.E. Bryndza, J.C. Calabrese, M. Marsi, D.C. Roe, W. Tam, and J.E. Bercaw. J. Am. Chem. Soc. **108**, 4805 (1986).
19. (*a*) Y.R.S. Laxmi and J.E. Bäckvall. Chem. Commun. 611 (2000); (*b*) A. Aranyos, G. Csjernyik, J. Szabó, and J.E. Bäckvall. Chem. Commun. 351 (1999).
20. (*a*) S.H. Bergens and B. Bosnich. J. Am. Chem. Soc. **113**, 958 (1991); (*b*) H. Alper and K. Hachem. J. Org. Chem. **45**, 2269 (1980).
21. D.V. McGrath and R.H. Grubbs. Organometallics, **13**, 224 (1994).
22. (*a*) B.M. Trost and R.J. Kulawiec. J. Am. Chem. Soc. **115**, 2027 (1993); (*b*) B.M. Trost and R.J. Kulawiec. Tetrahedron Lett. **32**, 3039 (1991).
23. W.A. Herrmann, G.P. Albanese, R.B. Manetsberger, P. Lappe, and H. Bahrmann. Angew. Chem. Int. Ed. Engl. **34**, 811 (1995).
24. G. Rothenberg, L. Feldberg, H. Wiener, and Y. Sasson. J. Chem. Soc. Perkin Trans. 2, 2429 (1998).

© 2005 NRC Canada

Synthesis of acetylenic ketones by a Pd-catalyzed carbonylative three-component coupling reaction in [bmim]PF_6[1]

Takahide Fukuyama, Ryo Yamaura, and Ilhyong Ryu

Abstract: A carbonylative three-component coupling reaction of aryl iodides with terminal alkynes catalyzed by $PdCl_2(PPh_3)_2$ was carried out using an ionic liquid, [bmim]PF_6, as the reaction medium, which resulted in good yields of α,β-acetylenic ketones. The low-viscosity ionic liquid, [bmim]NTf_2, was not suitable for this reaction, since the background Sonogashira coupling reaction, a competing reaction, also proceeded.

Key words: carbonylation, palladium, three-component coupling, ionic liquid, α,β-acetylenic ketones.

Résumé : Nous avons procédé à la préparation, avec de bons rendements, de cétones α,β-acétyléniques. Pour cela, nous avons réalisé une réaction de couplage à trois composants, catalysée par le $PdCl_2(PPh_3)_2$ et réalisée dans un milieu liquide ionique formé de [bmim]PF_6, conduisant à la carbonylation des iodures d'aryles. La faible viscosité du liquide ionique [bmim]NTf_2 n'est pas appropriée pour cette réaction puisque la réaction de couplage de Sonogashira qui est en compétition avec se produit.

Mots clés : carbonylation, palladium, couplage à trois composants, liquide ionique, cétone α,β-acétylénique.

[Traduit par la Rédaction]

Introduction

α,β-Acetylenic ketones are useful intermediates for the synthesis of a variety of important heterocyclic and biologically active compounds (1). While traditional approaches to the synthesis of acetylenic ketones relied on the coupling of a carboxylic acid chloride with a metal acetylide, recent methods have employed Pd- and (or) Cu-catalyzed coupling reactions of acid halides and terminal alkynes (eq. [1]) (2). The carbonylative three-component coupling reaction of aryl halides with terminal alkynes has also been reported (eq. [2]) (3). Kobayashi and Tanaka (3*a*) reported that a three-component coupling reaction of aryl halides with terminal alkynes and CO can be achieved when $PdCl_2$(dppf) is used as a catalyst and Et_3N as a solvent. Alper and coworkers (3*b*) reported that the dimeric palladium hydroxide $[(Ph_3P)Pd(Ph)(\mu\text{-}OH)]_2$ functions as an efficient catalyst for a similar three-component coupling reaction. Mohamed Ahmed and Mori (3*c*) recently reported on a three-component coupling using $PdCl_2(PPh_3)_2$ as the catalyst and aqueous NH_3 (2 equiv.) as a base with THF as the solvent.

Received 9 December 2004. Published on the NRC Research Press Web site http://canjchem.nrc.ca on 23 June 2005.

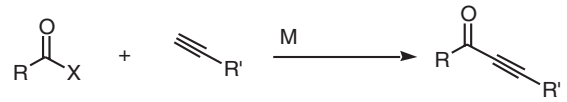
This paper is dedicated to Professor Howard Alper.

T. Fukuyama, R. Yamaura, and I. Ryu.[2] Department of Chemistry, Graduate School of Sciences, Osaka Prefecture University, Sakai, Osaka 599-8531, Japan.

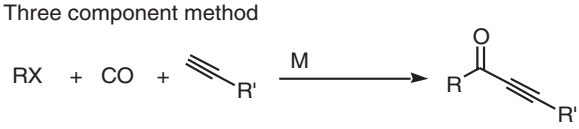
[1]This article is part of a Special Issue dedicated to Professor Howard Alper.

[2]Corresponding author (e-mail: ryu@c.s.osakafu-u.ac.jp).

Two component method

[1] 

Three component method

[2] 

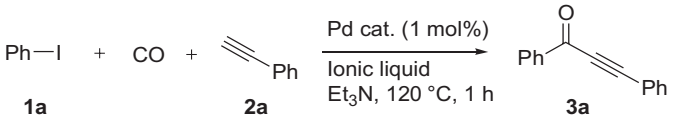
In recent years, ionic liquids have attracted broad attention in organic synthesis as alternatives to volatile organic solvents (4), and we previously reported that the Pd-catalyzed coupling reaction of aryl iodides with terminal alkynes — the Sonogashira coupling reaction — proceeds effectively in an ionic liquid, 1-butyl-3-methylimidazolium hexafluorophosphate ([bmim]PF_6), without the need for a copper co-catalyst (5). We also reported that a low-viscosity ionic liquid, [bmim]NTf_2, is an excellent reaction medium for Pd-catalyzed Mizoroki–Heck, Suzuki–Miyaura, and Stille coupling reactions (6). Herein we report on the carbonylative three-component coupling reaction of an aryl iodide with terminal alkynes, which proceeds smoothly when [bmim]PF_6 is used as the reaction medium (7).

Results and discussion

When iodobenzene (**1a**) was treated with phenylacetylene (**2a**, 1.2 equiv.) and pressurized CO (20 atm (1 atm = 101.325 kPa)) in the presence of 1 mol% $PdCl_2(PPh_3)_2$ and Et_3N (3.6 equiv.) in [bmim]PF_6 at 120 °C for 1 h, the reac-

 doi: 10.1139/V05-031 © 2005 NRC Canada

Table 1. Pd-catalyzed carbonylative coupling reaction of **1a** with **2a**.



1a **2a** **3a**

Entry	Pd	CO (atm)	Et_3N (equiv.)	Ionic liquid	Yield (%)[a,b]
1	$PdCl_2(PPh_3)_2$	20	3.6	[bmim]PF_6	82
2	$PdCl_2(PPh_3)_2$	20	3.6	[bmim]NTf_2	58 (24)
3	$PdCl_2$	20	3.6	[bmim]PF_6	60
4	$PdCl_2(CH_3CN)_2$	20	3.6	[bmim]PF_6	62
5	$Pd(OAc)_2$	20	3.6	[bmim]PF_6	60
6	$Pd(PPh_3)_4$	20	3.6	[bmim]PF_6	63 (13)
7[c]	$PdCl_2(PPh_3)_2$	20	2.0	[bmim]PF_6	48
8	$PdCl_2(PPh_3)_2$	10	3.6	[bmim]PF_6	52 (21)

Note: Reaction conditions: **1a** (1 mmol), **2a** (1.2 mmol), Pd-catalyst (1 mol%), ionic liquid (3 mL), 120 °C, 1 h.
[a]Isolated yields by chromatography on SiO_2.
[b]Yield of diphenylacetylene is shown in parentheses.
[c]Reaction was carried out for 2 h.

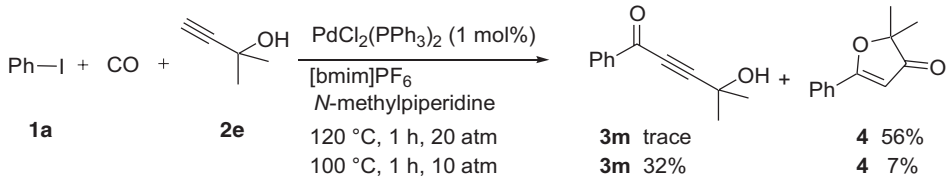
tion proceeded smoothly to give the acetylenic ketone **3a** in 82% yield (Table 1, entry 1). The reaction was clean, and diphenylacetylene, the noncarbonylated product of the Sonogashira coupling reaction, was not observed. Mohamed Ahmed and Mori (3*c*) previously reported that the reaction proceeded smoothly with aqueous NH_3 as a base. However, when aqueous NH_3 was used as a base in the present system, Michael addition of NH_3 to **3a** became a major reaction course. We also examined a low-viscosity ionic liquid, [bmim]NTf_2 (6); however, in this case, the background Sonogashira coupling reaction competed under the conditions employed (entry 2). Reactions using other Pd(II) complexes such as $PdCl_2$, $PdCl_2(CH_3CN)_2$, and $Pd(OAc)_2$ were sluggish, and significant amounts of unreacted **1a** were recovered (entries 3–5). When $Pd(PPh_3)_4$ was used as the catalyst, the Sonogashira coupling reaction competed, giving diphenylacetylene (entry 6). Reducing the amount of amine from 3.6 equiv. to 2 equiv. resulted in lower conversions even when the reaction time was prolonged (2 h) (entry 7). When the reaction was carried out at reduced CO pressure (10 atm), the Sonogashira coupling reaction competed again (entry 8).

Some results for reactions in which various aryl iodides and terminal alkynes were used are shown in Table 2. The reaction of substituted aryl iodides gave the corresponding acetylenic ketones in good yields (entries 1–6). Iodobenzenes containing a halogen atom (Br, Cl, or F) at the 4-position gave the coupling products, with the halogen atoms intact (entries 4–6). The reaction of 1-iodonaphthalene (**1h**) and 2-iodothiophene (**1i**) with **2a** also gave carbonylated products **3h** and **3i**, respectively (entries 7 and 8). Both *p*-acetylphenylacetylene and *p*-methoxyphenylacetylene could be used in this reaction (entries 9 and 10). The reaction of *tert*-butylacetylene (**2d**) gave the coupling product **3l** in relatively low yield, but when *N*-methylpiperidine was employed as a base, the yield was increased to 76% (entry 11).

When the reaction of **1a** with 2-methyl-3-butyne-2-ol (**2e**) was carried out using *N*-methylpiperidine as the base, 3-furanone **4** was obtained as the major product (eq. [3]) (8). An experiment using milder reaction conditions (100 °C, 10 atm) gave a mixture of acetylenic ketone **3m** and **4**. When the isolated **3m** was exposed to the same reaction system, furanone **4** was formed, suggesting that the initially formed **3m** served as the precursor for **4** (9).

It is well known that imidazolium-based ionic liquids react with Pd complexes to give Pd *N*-heterocyclic carbene complexes, which are thought to be the key catalyst species in many reactions in which a Pd–ionic liquid system is used (10). This may also be true for the present system, since the Pd carbene complex (which contains one imidazolylidene, one triphenylphosphine, and two chlorine ligands (6)) readily catalyzed the reaction of **1a** with **2a** to give **3a** in 73% yield (eq. [4]). We also investigated the reusability of the catalyst and the reaction medium for this reaction system. Both the catalyst and the reaction medium can be reused but with a slight decrease in efficiency (Scheme 1).

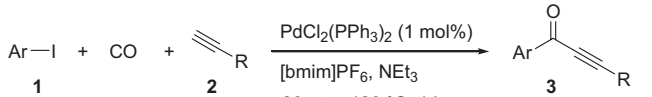
[3]

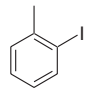
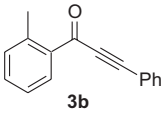
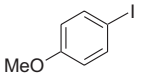
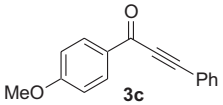
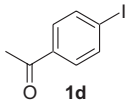
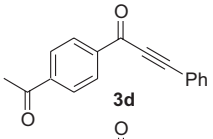
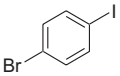
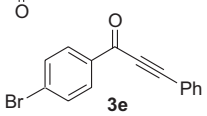
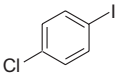
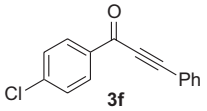
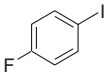
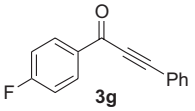
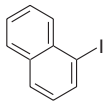
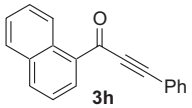
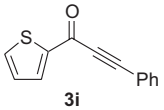
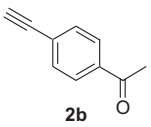
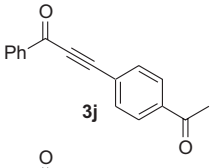
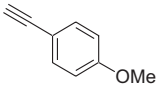
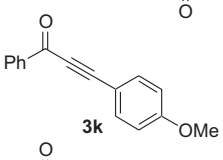
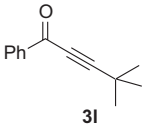


1a **2e**

© 2005 NRC Canada

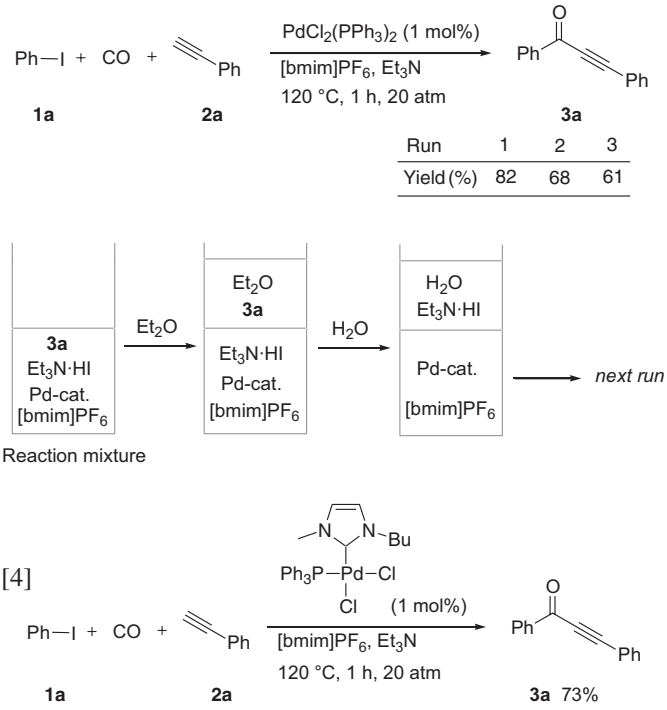
Table 2. $PdCl_2(PPh_3)_2$-catalyzed carbonylative coupling reaction of aryl iodides with terminal alkynes in $[bmim]PF_6$.



Entry	Ar—I **1**	Alkyne **2**	Product **3**	Yield (%)[a]
1	 **1b**	 **2a**	 **3b**	82
2	 **1c**	**2a**	 **3c**	82
3	 **1d**	**2a**	 **3d**	78
4	 **1e**	**2a**	 **3e**	76
5	 **1f**	**2a**	 **3f**	79
6	 **1g**	**2a**	 **3g**	81
7[b]	 **1h**	**2a**	 **3h**	78
8	 **1i**	**2a**	 **3i**	78
9[b]	Ph—I **1a**	 **2b**	 **3j**	80
10	**1a**	 **2c**	 **3k**	80
11[c]	**1a**	 **2d**	 **3l**	76

Note: Reaction conditions: **1** (1 mmol), **2** (1.2 mmol), $PdCl_2(PPh_3)_2$ (1 mol%), $[bmim]PF_6$ (3 mL), Et_3N (3.6 mmol) 120 °C, 1 h.
[a]Isolated yields after chromatography on SiO_2.
[b]Reaction carried out under 30 atm of CO.
[c]*N*-Methylpiperidine was used as the base.

Scheme 1. Recycling of the Pd catalyst and $[bmim]PF_6$ and workup process (1 atm = 101.325 kPa).



[4]

Conclusions

The findings herein show that when using $[bmim]PF_6$ as a reaction medium, the Pd-catalyzed carbonylative three-component coupling reaction of aryl iodides with terminal alkynes proceeds efficiently to give α,β-acetylenic ketones in good yields. The low-viscosity ionic liquid, $[bmim]NTf_2$, which is an excellent reaction medium for typical Pd-catalyzed coupling reactions, is not suitable for the present reaction because of the competing Sonogashira coupling reaction.

Experimental section

General information

^1H NMR spectra were recorded on a JEOL JMN-AL400 (400 MHz) spectrometer in $CDCl_3$. Chemical shifts are reported in parts per million (δ) downfield from internal tetramethylsilane. ^{13}C NMR spectra were recorded with a JEOL JMN-AL400 (100 MHz). Infrared spectra were obtained on a JASCO FT/IR-4100 spectrometer; absorptions are reported in reciprocal centimeters. Mass spectra were obtained on a Shimadzu GCMS-QP 5050A instrument. High resolution mass spectra were recorded with a JEOL MS700 spectrometer. Coupling products were purified by flash chromatography on silica gel (nacalai tesque, Silica Gel 60, 230–400 mesh) and, if necessary, were further purified by recycling preparative HPLC (JAI LC-908) equipped with a GPC column and using $CHCl_3$ as eluant. All products, except for **3j**, were known compounds and were identified by comparison with literature data.

© 2005 NRC Canada

Typical procedure for the $PdCl_2(PPh_3)_2$-catalyzed three-component coupling reaction

A magnetic stirring bar, [bmim]PF_6 (3 mL), $PdCl_2(PPh_3)_2$ (0.01 mmol, 7 mg), iodobenzene (**1a**) (1 mmol, 204 mg), Et_3N (3.6 mmol, 0.5 mL), and phenylacetylene **2a** (1.2 mmol, 122 g) were placed in a 50 mL stainless autoclave lined with a glass liner. The autoclave was closed, purged three times with 10 atm of carbon monoxide, pressurized to 20 atm with CO, and then heated at 120 °C for 1 h. Excess CO was discharged at room temperature. The product was extracted from the reaction mixture by the addition of Et_2O (5 mL), followed by decantation of the ether solution of the product. This was repeated an additional four times. The residue was purified by flash chromatography on silica gel (eluant hexane : EtOAc = 10:1) to give 166 mg (82%) of **3a**.

Recycling of Pd catalyst and [bmim]PF_6

After the reaction, the product was extracted from the reaction mixture with Et_2O (5 × 5 mL), and ammonium salts were removed by extraction with water (5 × 5 mL). Both the Et_2O and water were degassed by N_2 bubbling prior to use. Excess Et_2O and water were removed under reduced pressure, and the remaining ionic liquid layer, containing the Pd catalyst, was used in the next run.

1,3-Diphenyl-2-propynone (3a) (3b)

A white solid. mp 46–48 °C (lit. (3*b*) value mp 46 to 47 °C). IR (KBr) (cm^{-1}): 2199, 1641. ^1H NMR (400 MHz, $CDCl_3$) δ: 7.40–7.44 (m, 2H), 7.46–7.54 (m, 3H), 7.61–7.65 (m, 1H), 7.67–7.71 (m, 2H), 8.20–8.25 (m, 2H). ^{13}C NMR (100 MHz, $CDCl_3$) δ: 86.80, 93.01, 119.98, 128.52, 129.44, 130.70, 132.94, 134.01, 136.77, 177.86. EI-MS *m/z* (rel intensity): 206 ($[M]^+$, 45), 178 (100), 129 (46), 51 (23).

1-(2-Tolyl)-3-phenyl-2-propynone (3b) (11)

A colorless oil. IR (neat) (cm^{-1}): 2197, 1638. ^1H NMR (400 MHz, $CDCl_3$) δ: 2.67 (s, 3H), 7.25–7.30 (m, 1H), 7.36–7.48 (m, 5H), 7.64–7.68 (m, 2H), 8.28–8.32 (m, 1H). ^{13}C NMR (100 MHz, $CDCl_3$) δ: 21.81, 88.28, 91.65, 120.18, 125.77, 128.50, 130.45, 132.03, 132.75, 133.03, 135.55, 140.28, 179.54. EI-MS *m/z* (rel intensity): 220 ($[M]^+$, 26), 219 (100), 191 (72), 189 (21), 131 (23), 91 (21). HR-MS (EI) *m/z* calcd. for $C_{16}H_{12}O$: 220.0888 ($[M]^+$); found: 220.0894.

1-(4-Metoxyphenyl)-3-phenyl-2-propynone (3c) (3b)

A white solid. mp 96–98 °C (lit. (3*b*) value mp 97 to 98 °C). IR (KBr) (cm^{-1}): 2199, 1630. ^1H NMR (400 MHz, $CDCl_3$) δ: 3.89 (s, 3H), 6.96–7.00 (m, 2H), 7.39–7.43 (m, 2H), 7.45–7.50 (m, 1H), 7.65–7.69 (m, 2H), 8.16–8.21 (m, 3H). ^{13}C NMR (100 MHz, $CDCl_3$) δ: 55.38, 86.74, 92.09, 113.71, 120.08, 128.47, 130.04, 130.43, 131.73, 132.73, 164.30, 176.37. EI-MS *m/z* (rel intensity): 236 ($[M]^+$, 79), 209 (20), 208 (100), 193 (95), 165 (53), 129 (42), 75 (20).

1-[4-(1-Oxoethyl)phenyl]-3-phenyl-2-propynone (3d) (3c)

A white solid. mp 101 to 102 °C (lit. (3*c*) value mp 103 to 104 °C). IR (KBr) (cm^{-1}): 2197, 1684, 1634. ^1H NMR (400 MHz, $CDCl_3$) δ: 2.66 (s, 3H), 7.42–7.46 (m, 2H), 7.49–7.53 (m, 1H), 7.69–7.72 (m, 2H), 8.06–8.10 (m, 2H), 8.28–8.32 (m, 2H). ^{13}C NMR (100 MHz, $CDCl_3$) δ: 26.79, 86.64, 94.11, 119.55, 128.28, 128.62, 129.50, 130.98, 133.01, 139.61, 140.62, 176.87, 197.20. EI-MS *m/z* (rel intensity): 248 ($[M]^+$, 67), 233 (100), 205 (34), 177 (20), 176 (33), 129 (71), 103 (27), 75 (28).

1-(4-Bromophenyl)-3-phenyl-2-propynone (3e) (3b)

A white solid. mp 106 to 107 °C (lit. (3*b*) value mp 106 to 107 °C). IR (KBr) (cm^{-1}): 2199, 1651. ^1H NMR (400 MHz, $CDCl_3$) δ: 7.41–7.46 (m, 2H), 7.48–7.52 (m, 1H), 7.65–7.69 (m, 4H), 8.06–8.09 (m, 2H). ^{13}C NMR (100 MHz, $CDCl_3$) δ: 86.68, 93.78, 119.94, 128.83, 129.65, 131.01, 131.08, 132.07, 133.20, 135.77, 176.85. EI-MS *m/z* (rel intensity): 285 ($[M]^+$, 41), 284 (40), 258 (54), 256 (57), 176 (41), 129 (100), 88 (32), 75 (37), 51 (20).

1-(4-Chlorophenyl)-3-phenyl-2-propynone (3f) (3b)

A white solid. mp 104 to 105 °C (lit. (3*b*) value mp 104 °C). IR (KBr) (cm^{-1}): 2199, 1654. ^1H NMR (400 MHz, $CDCl_3$) δ: 7.40–7.45 (m, 2H), 7.46–7.52 (m, 3H), 7.66–7.69 (m, 2H), 8.13–8.16 (m, 2H). ^{13}C NMR (100 MHz, $CDCl_3$) δ: 86.68, 93.69, 119.98, 129.04, 129.07, 130.93, 131.05, 133.16, 135.41, 140.76, 176.66. EI-MS *m/z* (rel intensity): 240 ($[M]^+$, 55), 214 (31), 212 (100), 176 (33), 129 (83), 75 (43), 51 (21).

1-(4-Fluorophenyl)-3-phenyl-2-propynone (3g) (12)

A white solid. mp 100–102 °C. IR (KBr) (cm^{-1}): 2206, 1634. ^1H NMR (400 MHz, $CDCl_3$) δ: 7.15–7.21 (m, 2H), 7.40–7.45 (m, 2H), 7.47–7.51 (m, 1H), 7.66–7.69 (m, 2H), 8.22–8.27 (m, 2H). ^{13}C NMR (100 MHz, $CDCl_3$) δ: 86.68, 93.45, 115.97 (J = 22.1 Hz), 120.03, 128.81, 131.01, 132.32 (J = 9.6 Hz), 133.15, 133.49, 166.53 (J = 257.2 Hz), 176.45. EI-MS *m/z* (rel intensity): 224 ($[M]^+$, 41), 196 (100), 129 (52), 75 (23).

1-(1-Naphthyl)-3-phenyl-2-propynone (3h) (2c)

A white solid. mp 94 to 95 °C (lit. (2*c*) value mp 95 °C). IR (KBr) (cm^{-1}): 2195, 1634. ^1H NMR (400 MHz, $CDCl_3$) δ: 7.40–7.44 (m, 2H), 7.46–7.50 (m, 1H), 7.56–7.62 (m, 2H), 7.66–7.72 (m, 3H), 7.90–7.93 (m, 1H), 8.08–8.12 (m, 1H), 8.63–8.66 (m, 1H), 9.21–9.25 (m, 1H). ^{13}C NMR (100 MHz, $CDCl_3$) δ: 88.63, 91.82, 120.44, 124.60, 126.10, 126.88, 128.78, 129.07, 130.74, 130.84, 133.02, 133.05, 133.97, 134.69, 135.25, 179.83. EI-MS *m/z* (rel intensity): 256 ($[M]^+$, 100), 228 (50), 226 (47), 202 (21), 129 (35), 114 (35), 113 (33), 101 (15), 75 (21), 51 (21).

3-Phenyl-1-(2-thiophenyl)-2-propynone (3i) (13)

A colorless oil. IR (neat) (cm^{-1}): 2199, 1616. ^1H NMR (400 MHz, $CDCl_3$) δ: 7.17–7.20 (m, 2H), 7.40–7.44 (m, 2H), 7.46–7.51 (m, 1H), 7.64–7.68 (m, 2H), 7.72–7.74 (m, 1H), 8.00–8.02 (m, 1H). ^{13}C NMR (100 MHz, $CDCl_3$) δ: 86.34, 91.61, 119.71, 128.25, 128.56, 130.74, 132.87, 135.00, 135.18, 144.74, 169.60. EI-MS *m/z* (rel intensity): 212 ($[M]^+$, 46), 184 (100), 129 (26).

3-[4-(1-Oxoethyl)phenyl]-1-phenyl-2-propynone (3j)

A white solid. mp 115 to 116 °C. IR (KBr) (cm^{-1}): 2202, 1684, 1642. ^1H NMR (400 MHz, $CDCl_3$) δ: 2.64 (s, 3H), 7.51–7.56 (m, 2H), 7.63–7.68 (m, 1H), 7.76–7.79 (m, 2H), 7.98–8.02 (m, 2H), 8.20–8.23 (m, 2H). ^{13}C NMR (100 MHz, $CDCl_3$) δ: 26.75, 88.80, 91.23, 124.71, 128.45, 128.81,

© 2005 NRC Canada

129.65, 133.14, 134.49, 136.66, 138.15, 177.71, 197.08. EI-MS *m/z* (rel intensity): 248 ([M]$^+$, 72), 233 (100), 205 (53), 177 (22), 176 (48), 88 (20). HR-MS (EI) *m/z* calcd. for $C_{16}H_{12}O$: 248.0837 ([M]$^+$); found: 248.0839.

3-(4-Metoxyphenyl)-1-phenyl-2-propynone (3k) (2c)

A white solid. mp 77–79 °C (lit. (2*c*) value mp 81 to 82 °C). IR (KBr) (cm^{-1}): 2189, 1600. ^{1}H NMR (400 MHz, $CDCl_3$) δ: 3.86 (s, 3H), 6.92–6.94 (m, 2H), 7.48–7.53 (m, 2H), 7.60–7.66 (m, 3H), 8.20–8.24 (m, 2H). ^{13}C NMR (100 MHz, $CDCl_3$) δ: 55.50, 86.99, 94.45, 111.92, 114.54, 128.66, 129.54, 134.00, 135.21, 137.13, 161.85, 178.08. EI-MS *m/z* (rel intensity): 236 ([M]$^+$, 100), 208 (53), 193 (58), 165 (31), 159 (94), 77 (20), 51 (20).

4,4-Dimethyl-1-phenyl-2-pentyn-1-one (3l) (3b)

A colorless oil. IR (neat) (cm^{-1}): 2211, 1649. ^{1}H NMR (400 MHz, $CDCl_3$) δ: 1.38 (s, 9H), 7.44–7.52 (m, 2H), 7.56–7.62 (m, 1H), 8.10–8.14 (m, 2H). ^{13}C NMR (100 MHz, $CDCl_3$) δ: 28.13, 30.26, 78.19, 104.04, 128.55, 129.58, 133.90, 137.09, 178.44. EI-MS *m/z* (rel intensity): 186 ([M]$^+$, 25), 143 (50), 128 (30), 105 (100), 77 (35), 51 (22).

4-Hydroxy-4-methyl-1-phenyl-2-pentyn-1-one (3m) (3b)

A colorless oil. IR (neat) (cm^{-1}): 2212, 1645. ^{1}H NMR (400 MHz, $CDCl_3$) δ: 1.67 (s, 6H), 7.46–7.51 (m, 2H), 7.59–7.64 (m, 1H), 8.10–8.14 (m, 2H). ^{13}C NMR (100 MHz, $CDCl_3$) δ: 30.69, 65.22, 79.81, 98.27, 128.55, 129.58, 134.22, 136.41, 178.02. EI-MS *m/z* (rel intensity): 188 ([M]$^+$, 8), 173 (100), 145 (22), 105 (27), 95 (22), 77 (44), 53 (70), 51 (33).

2,2-Dimethyl-5-phenyl-3(2H)-furanone (4) (14)

A yellow oil. IR (neat) (cm^{-1}): 3103, 1694. ^{1}H NMR (400 MHz, $CDCl_3$) δ: 1.48 (s, 6H), 5.96 (s, 1H), 7.45–7.50 (m, 2H), 7.52–7.56 (m, 1H), 7.80–7.85 (m, 2H). ^{13}C NMR (100 MHz, $CDCl_3$) δ: 23.22, 88.99, 98.61, 127.22, 128.89, 129.20, 132.67, 183.49, 206.99. EI-MS *m/z* (rel intensity): 188 ([M]$^+$, 20), 102 (100).

Acknowledgment

IR thanks a Grant-in-Aid for Scientific Research on Priority Areas (A) "Reaction Control of Dynamic Complexes" from the Ministry of Education, Culture, Sports, Science and Technology, Japan, for financial support. This work was supported, in part, by a Dainippon Ink and Chemicals Inc. Award in Synthetic Organic Chemistry, Japan, granted to TF. This work was financially supported by the Highly Efficient Micro Chemical Process Technology Project of NEDO.

References

1. (*a*) A.V. Kel′in, A.W. Sromek, and V. Gevorgyan. J. Am. Chem. Soc. **123**, 2074 (2001); (*b*) A.V. Kel′in and V. Gevorgyan. J. Org. Chem. **67**, 95 (2002); (*c*) D.B. Grotjahn, S. Van, D. Combs, D.A. Lev, C. Schneider, M. Rideout, C. Meyer, G. Hernandez, and L. Mejorado. J. Org. Chem. **67**, 9200 (2002); (*d*) A.S. Karpov and T.J.J. Muller. Org. Lett. **5**, 3451 (2003); (*e*) M.M. Midland and N.H. Nguyen. J. Org. Chem. **46**, 4107 (1981); (*f*) D.R. Williams, M.G. Fromhold, and J.D. Earley. Org. Lett. **3**, 2721 (2001); (*g*) J. Aiguade, J. Hao, and C.J. Forsyth. Org. Lett. **3**, 979 (2001); (*h*) S. Aoki, K. Matsui, H. Wei, N. Murakami, and M. Kobayashi. Tetrahedron, **58**, 5417 (2002); (*i*) F.A.J. Kerdesky, S.P. Schmidt, and D.W. Brooks. J. Org. Chem. **58**, 3516 (1993).
2. For Pd–Cu catalyst: (*a*) Y. Tohda, K. Sonogashira, and N. Hagihara. Synthesis, 777 (1977); (*b*) J. Yin, X.-J. Wang, Y. Liang, X. Wu, B. Chen, and Y. Ma. Synthesis, **3**, 331 (2004); (*c*) L. Chen and C.-J. Li. Org. Lett. **6**, 3151 (2004); for Pd catalyst: (*d*) D.A. Alonso, C. Nájera, and M.C. Pacheco. J. Org. Chem. **69**, 1615 (2004); for Cu catalyst: (*e*) C. Chowdhury, N.G. Kundu, and G. Nitya. Tetrahedron, **55**, 7011 (1999); (*f*) W.P. Gallagher and R.E. Maleczka, Jr. J. Org. Chem. **68**, 6775 (2003).
3. (*a*) T. Kobayashi and M. Tanaka. J. Chem. Soc. Chem. Commun. 333 (1981); (*b*) L. Delaude, A.M. Masdeu, and H. Alper. Synthesis, 1149 (1994); (*c*) M.S. Mohamed Ahmed and A. Mori. Org. Lett. **5**, 3057 (2003).
4. (*a*) T. Welton. Chem. Rev. **99**, 2071 (1999); (*b*) P. Wasserscheid and W. Keim. Angew. Chem. Int. Ed. **39**, 3772 (2000); (*c*) C.M. Gordon. Appl. Catal. A, **222**, 101 (2001); (*d*) J. Dupont, R.F. de Souza, and P.A.Z. Suarez. Chem. Rev. **102**, 3667 (2002); (*e*) T. Fukuyama and I. Ryu. J. Synth. Org. Chem. Jpn. **63**, 503 (2005).
5. T. Fukuyama, M. Shinmen, S. Nishitani, M. Sato, and I. Ryu. Org. Lett. **4**, 1691 (2002).
6. S. Liu, T. Fukuyama, M. Sato, and I. Ryu. Synlett, 1814 (2004).
7. For examples of carbonylation reaction in ionic liquids, see: (*a*) E. Mizushima, T. Hayashi, and M. Tanaka. Green Chem. **3**, 76 (2001); (*b*) K. Qiao and Y.Q. Deng. New J. Chem. **26**, 667 (2002); (*c*) C. Hardacre, J.D. Holbrey, S.P. Katdare, and K.R. Seddon. Green Chem. **4**, 143 (2002).
8. It was reported that a transition metal catalyzed reaction of **1a**, CO, and **2e** in the presence of CO_2 gave furanone **4**, see: Y. Inoue, K. Ohuchi, I.-F. Yen, and S. Imaizumi. Bull. Chem. Soc. Jpn. **62**, 3518 (1989).
9. For similar transformation, see: (*a*) H. Saimoto, M. Shinoda, S. Matsubara, K. Oshima, T. Hiyama, and H. Nozaki. Bull. Chem. Soc. Jpn. **56**, 3088 (1983); (*b*) K.-W. Lee, Y.H. Choi, Y.H. Joo, J.K. Kim, S.S. Shin, Y.J. Byun, Y. Kim, and S. Chung. Bioorg. Med. Chem. **10**, 1137 (2002).
10. (*a*) L. Xu, W. Chen, and J. Xiao. Organometallics, **19**, 1123 (2000); (*b*) F. McLachlan, C.J. Mathews, P.J. Smith, and T. Welton. Organometallics, **22**, 5350 (2003); also see reviews on C-C coupling reactions catalyzed by Pd *N*-heterocyclic carbene complex: (*c*) W.A. Herrmann, K. Öfele, D. Von Preysing, and S.K. Schneider. J. Organomet. Chem. **687**, 229 (2003); (*d*) A.C. Hillier, G.A. Grasa, M.S. Viciu, H.M. Lee, C. Yang, and S.P. Nolan. J. Organomet. Chem. **653**, 69 (2002).
11. A. Arcadi, S. Cacchi, F. Marinelli, P. Pace, and G. Sanzi. Synlett, 823 (1995).
12. M. Reisser and G. Maas. J. Org. Chem. **69**, 4913 (2004).
13. S.-K. Kang, K.-H. Lim, P.-S. Ho, and W.-Y. Kim. Synthesis, 874 (1997).
14. A.B. Smith III, P.A Levenberg, P.J. Jerris, R.M Scarborough, Jr., and P.M. Wovkulich. J. Am. Chem. Soc. **103**, 1501 (1981).

© 2005 NRC Canada

Double elimination protocol for the synthesis of arylene ethynylenes containing heteroaromatic rings[1]

Akihiro Orita, Fangguo Ye, Govindarajulu Babu, Tomohiro Ikemoto, and Junzo Otera

Abstract: The double elimination reaction of β-substituted sulfones offers a versatile strategy for synthesis of arylene ethynylene kits containing heteroaromatic rings. A sequence of aldol reaction between α-sulfonyl carbanion and aldehyde, trapping the resulting aldolate to give β-substituted sulfone, and double elimination of this intermediate can be integrated in one pot. This protocol allows thiophene, pyridine, and ferrocene units to be accommodated in phenylene ethynylene arrays.

Key words: arylene–ethynylenes, heteroaromatic rings, ferrocene, double elimination, sulfones.

Résumé : La réaction de double élimination des sulfones β-substituées offre une possibilité de stratégie versatile pour la synthèse de trousses d'arylène éthynylène contenant des noyaux hétéroatomiques. Une séquence de réaction impliquant une réaction aldolique entre un carbanion α-sulfonyle et un aldéhyde, le piégeage de l'aldolate qui en résulte qui conduit à une sulfone β-substituée et la double élimination de cet intermédiaire peut être intégrée dans un système monotopique. Ce protocole permet d'accommoder des unités thiophène, pyridine et ferrocène dans des arrangements phénylène éthynylène.

Mots clés : arylène–éthynylènes, noyaux hétéroatomiques, ferrocène, double élimination, sulfones.

[Traduit par la Rédaction]

Introduction

The synthesis of arylene ethynylene molecular wires is the focus of current extensive research in view of developing new materials for molecular electronic devices (1). In addition to simple arylene ethynylenes that are only composed of hydrocarbon aromatics, incorporation of heteroaromatic rings into these arrays is of great promise for imparting novel functions. For example, attachment of thiophene will induce alterations of electronic and optical properties by purturbing π-electron delocalization in arylene ethynylene conjugated systems. In fact, a considerable number of oligomers or polymers are known in which thiophene and acetylene units are directly assembled (2), yet some examples are known for the integration of phenylene ethynylene and thiophene pieces (3). Pyridine derivatives are another class of blocks to be built in. Besides changing electronic properties, pyridine can serve as a ligand for metal complexes, giving rise to unique structures that are otherwise difficult to attain (4). Utilization of ferrocene is also intriguing from the electrochemical point of view, and redox profiles of some ferrocene-containing arylene ethynylenes were reported (5).

Notably, almost all of the above compounds were framed with recourse to iterative Sonogashira couplings (6). This method, though being highly versatile, suffers from some drawbacks: products are colored and occasionally contaminated by Pd or Cu catalysts residues. In this context, we advanced a double elimination protocol of β-substituted sulfones as the alternative, which is essentially free from these drawbacks, to allow us to synthesize a variety of phenylene ethynylenes (7). Herein, we report that the double elimination reaction works nicely with heteroaromatic substrates as well as resulting in the convenient synthesis of arylene ethynylenes containing such heteroaromatic rings as described previously.

Received 2 December 2004. Published on the NRC Research Press Web site at http://canjchem.nrc.ca on 18 June 2005.

Dedicated to Professor Howard Alper in recognition of his great contribution to chemistry and the chemical community.

A. Orita, F. Ye, G. Babu, T. Ikemoto, and J. Otera.[2] Department of Applied Chemistry, Okayama University of Science, Ridai-cho, Okayama 700-0005, Japan.

[1]This article is part of a Special Issue dedicated to Professor Howard Alper.

[2]Corresponding author (e-mail: otera@high.ous.ac.jp).

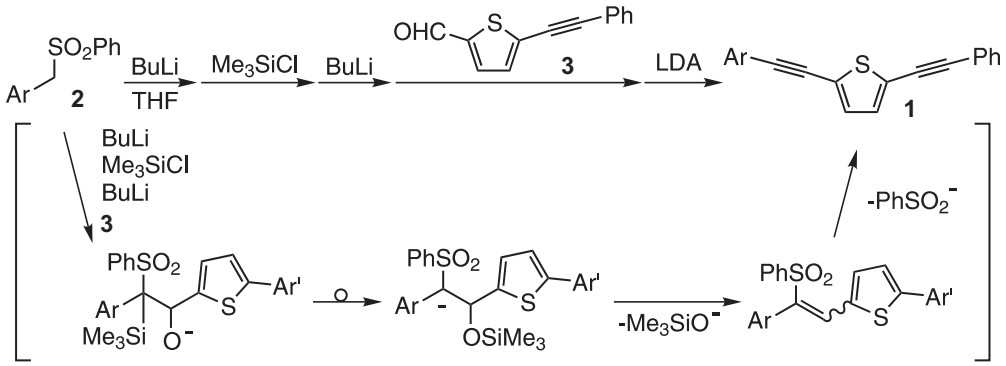
Results and discussion

Thiophene-containing arylene ethynylenes

2,5-Bis(arylethynyl)thiophenes (**1**) were readily obtained by the double elimination method using benzyl sulfone derivatives **2** and 2-formyl-5-phenylethynylthiophene (**3**) (Scheme 1). In this procedure, the following operations were sequentially conducted in one pot without the isolation of any intermediates: (1) lithiation of **2** with BuLi; (2) silylation of the resulting anion with TMSCl; (3) lithiation of the silylated sulfone with BuLi; (4) aldol-type addition of the resulting anion to **3** followed by Peterson-type elimination;

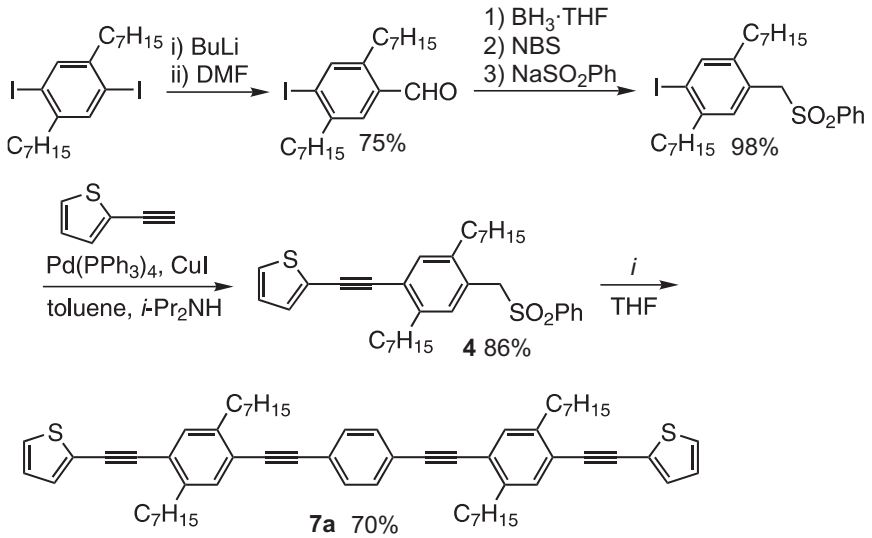
 doi: 10.1139/V05-038 © 2005 NRC Canada

Scheme 1.



Entry	Ar	Product (yield)
1	Ph (**2a**)	**1a** (**77%**)
2	*p*-MeC_6H_4 (**2b**)	**1b** (**67%**)
3	*m*-$MeOC_6H_4$ (**2c**)	**1c** (**76%**)
4	*p*-$MeOC_6H_4$ (**2d**)	**1d** (**64%**)
5	2-Naphthyl (**2e**)	**1e** (**72%**)

Scheme 2. Reagents: (*i*) BuLi – terephthalaldehyde (**6a**) – $ClP(O)(OEt)_2$ – *t*-BuOK.



and (5) conversion of the resulting vinyl sulfone to **1**. No serious problems were encountered by the use of the thienyl aldehyde in place of simple aromatic aldehydes and a variety of thiophene derivatives substituted unsymmetrically at the 2,5-positions were accessible. The overall yields through the four consecutive reactions (silylation, aldol, Peterson and final elimination reactions) were excellent (64%–77%) indicating that each reaction proceeded in more than 90% yield on average.

As shown in Schemes 2 and 3, the thiophene stoppers were installed. Reaction of thiophene-terminated building block **4** with terephthalaldehyde (**6a**) or a longer dialdehyde (**5b**) furnished **7a** and **7b** in satisfactory yields.

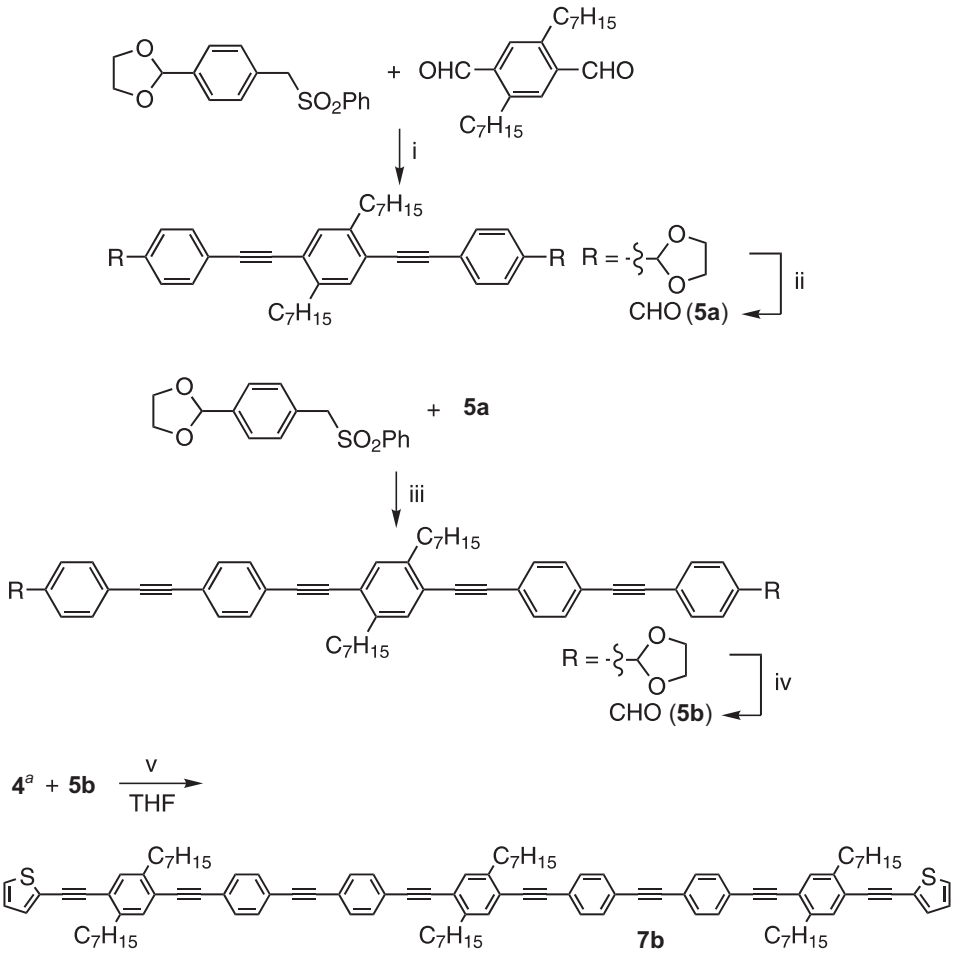
Pyridine-containing arylene ethynylenes (8)

The synthesis of some simple pyridine-containing arylene ethynylenes is illustrated in Scheme 4. First, 2-pyridylmethyl sulfone (**8**) was coupled with benzaldehyde (**9**) to give the desired product **10** in 84% yield. An alternative combination of benzyl sulfone (**2a**) and 2-pyridylcarboxaldehyde (**11**) also produced **10** in 76% yield. Dialdehydes were employable as well. Treatment of **2a** with 2,6-pyridinedicarboxaldehyde (**12**) afforded the desired diyne **13**, and enantiopure dialdehyde **14** reacted with **8** to provide tetrayne **15**.

This technology was applied to synthesize chiral arylene ethynylene (**16**), which had been found to form a unique double helicate **A** upon complexation with copper(I) and silver(I) salts (Fig. 1) (9). Previously, this compound was synthesized by Sonogashira coupling, yet iteration of Sonogashira coupling resulted in coloration of the product and required repeated operations of column chromatography for purification. Two alternative routes are possible for construction of **16** as shown in Fig. 1: connection between two pyridine rings (route A) or between the phenyl and pyridine rings (route B). However, it soon turned out that route A was not feasible because a model reaction between **8** and **11** did

© 2005 NRC Canada

Scheme 3. Reagents: (*i*) BuLi–aldehyde–ClP(O)(OEt)$_2$–*t*-BuOK (80%); (*ii*) *p*-TSA, THF, water (quant.); (*iii*) BuLi–**5a**–ClP(O)(OEt)$_2$–*t*-BuOK (81%); (*iv*) *p*-TSA, THF, water (quant.); (*v*) BuLi–**5b**–ClP(O)(OEt)$_2$–*t*-BuOK (65%). [a]See Scheme 2.



not proceed smoothly to afford only a trace amount of the desired dipyridylacetylene.[3] In sharp contrast to this disappointing result, acetylene formation was effected by use of sulfone **17** and benzaldehyde (**9**), though in a modest yield (Scheme 5). However, use of sulfoximine in place of the sulfone improved the yield: reaction between sulfoximine **19** and aldehyde **20** proceeded smoothly to give **18** in 83% yield. These results prompted us to employ route B (Scheme 6). The procedure for requisite disulfoximine **21** was already reported (7*c*), and pyridylcarboxaldehyde **22** was obtained according to the procedure shown in Scheme 7. The aldol-type coupling between **21** and **22** followed by double elimination furnished **16** in 53% yield. Notably, the product thus obtained suffered no coloration to enable facile purification by column chromatography. When the corresponding disulfone was employed instead of **21**, the desired product **16** was only obtained in 30% yield.

Ferrocene-containing arylene ethynylenes

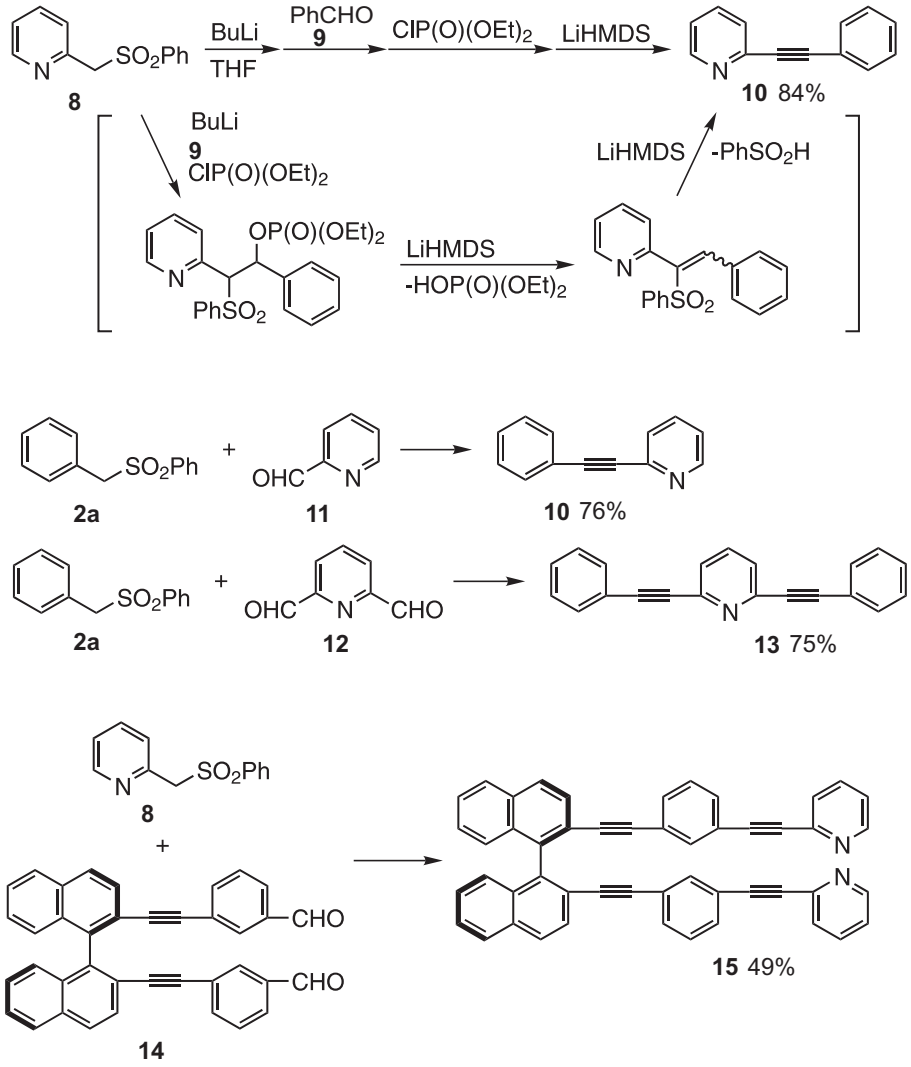
The double elimination method also led us to join phenylene ethynylene backbones to ferrocene termini. Those having symmetrical structures (**23** and **24**) are illustrated in Fig. 2. The synthetic strategy for these compounds are based on the use of ferrocene-containing benzyl sulfone (**25**), which was prepared as shown in Scheme 8. Coupling of **25a** and **25b** with **6a** afforded **23a** and **23b** in excellent yields (90% and 81%, respectively) (Table 1, entries 1 and 2). Use of **26** as a dialdehyde component led to **23c** (Table 1, entry 3). Combination of **25b** with **5a** and **5b** furnished longer molecular wires (**24a** and **24b**) in satisfactory yields (Table 1, entries 4 and 5). Quite naturally, exposure of *meta*- and *ortho*-phthalaldehydes (**6b** and **6c**) to **25a** provided the corresponding bent molecules, **27** and **28** (Table 1, entries 6 and 7).

Compounds with unsymmetrical structures were also accessible (Scheme 9). Coupling of **25a** with aldehyde **29** furnished **30** in 91% yield. Finally, an arylene ethynylene motif end-capped with both ferrocene and thiophene **31** was constructed (10). Thiophene-containing benzyl sulfone **4** was treated with 1.1 equiv. of BuLi and the resulting anion was exposed to 1.5 equiv. of **6a**. The monoaldol product was trapped with benzoyl chloride to give benzoate **32**. It is crucial to stop the reaction at this stage although the yield is not satisfactory. If more base was used to obtain the monovinyl sulfone or monoacetylene derivative directly, the remaining aldehyde was attacked and the reaction mixture became messy. Then, coupling of **32** with **25b** successfully provided **31** in 75% yield.

[3] It is not clear at present why the reaction between pyridylmethyl sulfone and formylpyridine was unsuccessful.

© 2005 NRC Canada

Scheme 4.



Conclusion

The double elimination protocol has now proved to be versatile for the synthesis of a variety of arylene ethynylenes containing heteroaromatic rings. The compounds thus obtained are potentially useful as liquid crystals, chemical sensors, electroluminescent materials, molecular wires, etc. In addition to the facileness of synthetic procedure, it is of great significance in a practical sense that the product obtained by this protocol is free from transition metal catalyst residues, which inevitably contaminate the Sonogashira coupling products. We hope, therefore that our methodology will serve in the synthesis of a wide range of arylene ethynylene molecular wires.

Experimental section

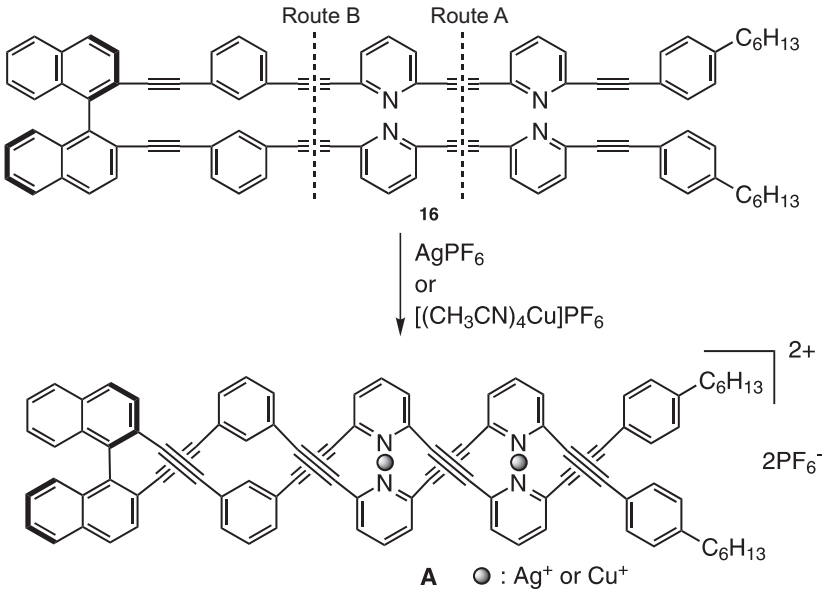
General remarks

All reactions were carried out under an atmosphere of nitrogen with freshly distilled solvents, unless otherwise noted. Tetrahydrofuran (THF) was distilled from sodium–benzophenone. Other solvents such as toluene, diisopropylamine, and methanol were distilled from CaH_2. BuLi in hexanes was purchased from Aldrich and titrated before use by the Gilman method (11). LiHMDS (lithium hexamethyldisilazide) in THF solution was purchased and used without titration. LDA (lithium diisopropylamide) was prepared prior to use from freshly distilled diisopropylamine and BuLi–hexane solution in THF. $Pd(PPh_3)_4$ was prepared according to the reported method (12). Silica gel (Daiso gel IR-60) was used for column chromatography. NMR spectra were recorded at 25 °C on JEOL Lambda 300 and JEOL Lambda 500 instruments and calibrated with tetramethylsilane (TMS) as an internal reference. Elemental analyses were performed on a PerkinElmer PE 2400.

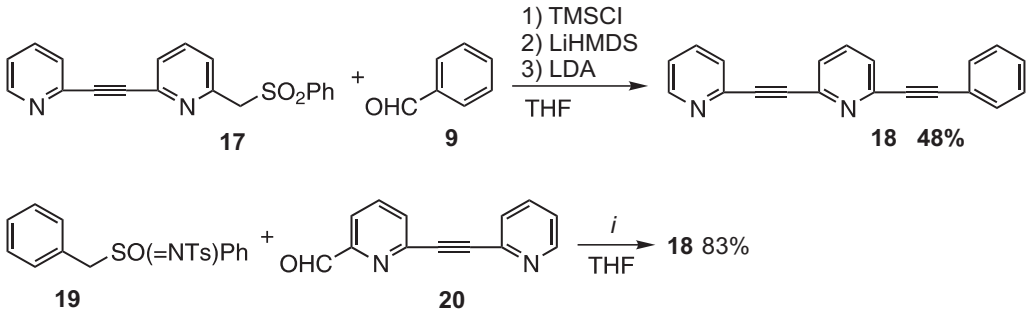
Starting compounds **6a**–**6c**, **9**, **11**, and **12** were commercially available, and sulfones **2a**–**2e** were prepared from the corresponding arylmethyl bromides. Sulfones **4** were prepared from Sonogashira coupling between 2-ethynylthiophene and 2,5-diheptyl-4-iodobenzyl phenyl sulfone (**33b**), and sulfones **25a** and **25b** were prepared from the reaction of ethynylferrocene with 2,5-dimethyl-4-iodobenzyl phenyl sulfone (**33a**) and **33b**, respectively. Dialdehyde **5a** was pre-

© 2005 NRC Canada

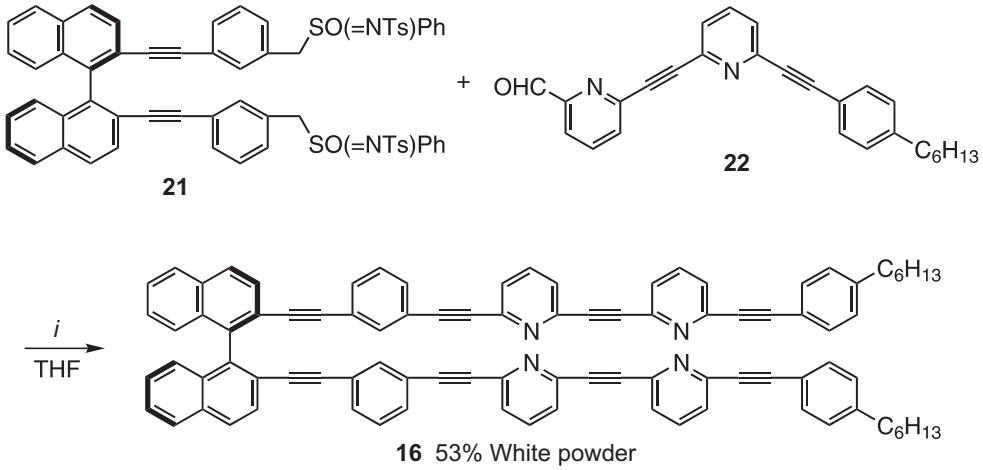
Fig. 1. Double helicate formation by complexation of **16** with Ag(I) or Cu(I).



Scheme 5.



Scheme 6. Reagents: (*i*) BuLi–**22**–$ClP(O)(OEt)_2$–LiHMDS.

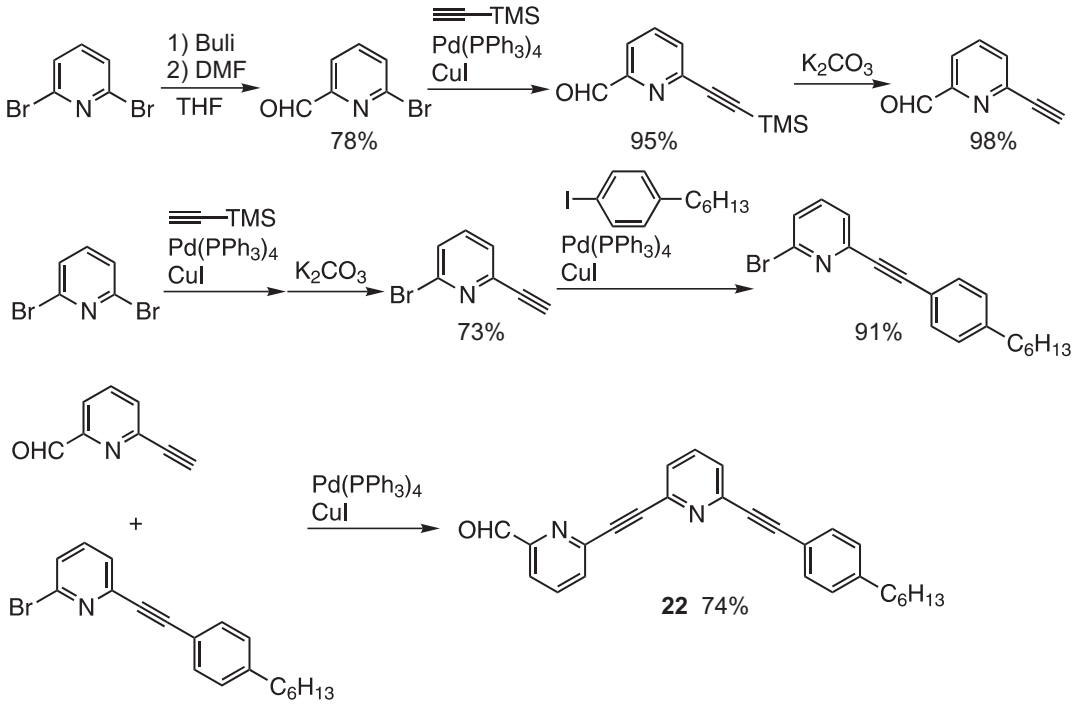


pared by hydrolysis of **36a**, which had been derived from the reaction of 2,5-diheptylbenzene-1,4-dialdehyde (**34**) with 4-(1,3-dioxolan-2-yl)benzyl phenyl sulfone (**35**). Dialdehyde **5b** was prepared similarly from the reaction of **5a** with **35**.

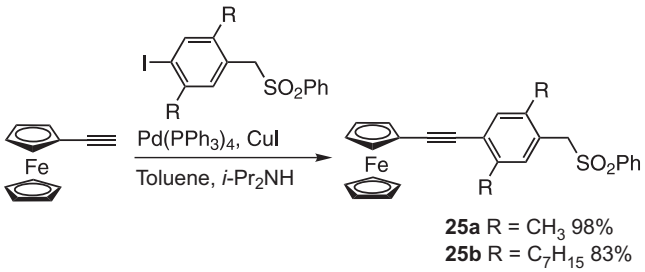
Dialdehydes **14** (7*c*), **21** (7*c*), and sulfone **8** (13) were prepared according to the reported procedure. Sulfoximine **19** was prepared from benzyl phenyl sulfide according to the reported method (7*c*).

© 2005 NRC Canada

Scheme 7.



Scheme 8.



Syntheses of **2a**–**2e**, **17**, **19**, **20**, **26**, **33a**, **33b**, **34**, and **35** are described in the Supporting information.[4]

2-Formyl-5-(phenylethynyl)thiophene (3)

Phenylacetylene (571.8 mg, 5.6 mmol) was added to a suspension of CuI (38.1 mg, 0.20 mmol), $Pd(PPh_3)_4$ (231.2 mg, 0.20 mmol), and 2-bromo-5-formylthiophene (764.4 mg, 4.0 mmol) in toluene (20 mL) and diisopropylamine (5 mL), and the mixture was stirred at r.t. for 13 h. After the usual work up with ethyl acetate and aq. NH_4Cl, drying over $MgSO_4$, and evaporation, the residue was subjected to column chromatography on silica gel to furnish **3** in a pure form (602.9 mg, 71%).

3

^{1}H NMR (500 MHz, $CDCl_3$) δ: 7.32 (d, J = 4.0 Hz, 1H), 7.36–7.42 (m, 3H), 7.54–7.56 (m, 2H), 7.67 (d, J = 4.0 Hz, 1H), 9.87 (s, 1H). ^{13}C NMR (125 MHz, $CDCl_3$) δ: 82.0, 97.9, 121.9, 128.5, 129.4, 131.7, 132.5, 132.9, 136.1, 143.8, 182.4.

Preparation of 1a through double elimination of β-substituted sulfone derived from the reaction of 2a with 3 (representative)

To a THF solution (2 mL) of benzyl phenyl sulfone **2a** (46.5 mg, 0.20 mmol) was added a hexane solution of BuLi (1.60 mol/L, 0.13 mL, 0.21 mmol) at –78 °C, and the mixture was stirred for 0.5 h. TMSCl (25.4 μL, 0.20 mmol) was added at –78 °C, and the mixture was stirred for 1.0 h. A hexane solution of BuLi (1.60 mol/L, 0.13 mL, 0.21 mmol) was added at –78 °C, and the mixture was stirred for 0.5 h. A toluene solution (10 mL) of 5-(phenylethynyl)thiophene-2-carbaldehyde (**3**) (50.9 mg, 0.24 mmol) was added at –78 °C, and the mixture was stirred at r.t. for 2 h. A THF–hexane solution of LDA (1.0 mol/L, 0.6 mL, 0.6 mmol) was added at –78 °C, and the mixture was stirred for 0.5 h. After the usual work up with ethyl acetate and aq. NH_4Cl, drying over $MgSO_4$, and evaporation, the residue was subjected to column chromatography on silica gel to furnish **1a** in a pure form (44.0 mg, 77%).

2,5-Bis(phenylethynyl)thiophene (1a) (14)

^{1}H NMR (500 MHz, $CDCl_3$) δ: 7.16 (s, 2H), 7.32–7.39 (m, 6H), 7.49–7.56 (m, 4H). ^{13}C NMR (125 MHz, $CDCl_3$) δ: 82.3, 94.1, 122.6, 124.6, 128.4, 128.7, 131.5, 131.8.

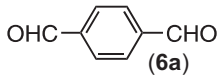
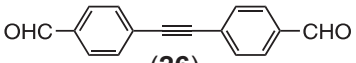
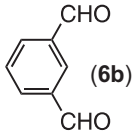
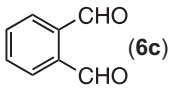
2-Phenylethynyl-5-(*p*-tolylethynyl)thiophene (1b)

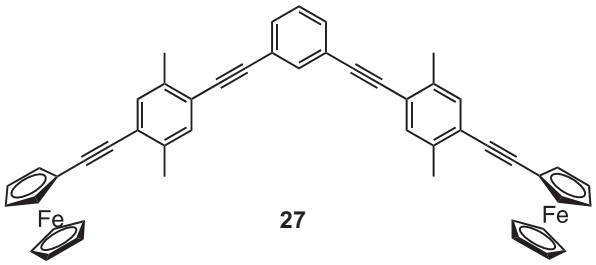
Yield: 67%. mp 103 to 104 °C. ^{1}H NMR (500 MHz, $CDCl_3$) δ: 2.37 (s, 3H), 7.13–7.17 (m, 4H), 7.34–7.36 (m, 3H), 7.41 (d, J = 7.9 Hz, 2H), 7.50–7.54 (m, 2H). ^{13}C NMR (125 MHz, $CDCl_3$) δ: 21.6, 81.7, 82.4, 93.9, 94.3, 119.5, 122.6, 124.4, 124.9, 128.4, 128.6, 129.2, 131.4, 131.5,

[4] Supplementary data for this article are available on the Web site or may be purchased from the Depository of Unpublished Data, Document Delivery, CISTI, National Research Council Canada, Ottawa, ON K1A 0S2, Canada. DUD 3680. For more information on obtaining material refer to http://cisti-icist.nrc-cnrc.gc.ca/irm/unpub_e.shtml.

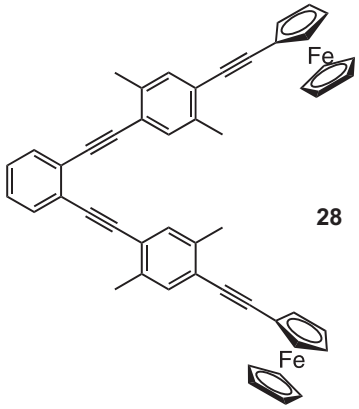
© 2005 NRC Canada

Table 1. Results of the reactions between sulfones and dicarboxyaldehydes.

Entry	Sulfone	Dicarboxaldehyde	Product	Yield (%)
1	**25a**	 (**6a**)	**23a**	90
2	**25b**	**6a**	**23b**	81
3	**25b**	 (**26**)	**23c**	76
4	**25b**	**5a**	**24a**	80
5	**25b**	**5b**	**24b**	77
6	**25a**	 (**6b**)	**27**	67
7	**25a**	 (**6c**)	**28**	52



27



28

131.6, 131.8, 138.9. Elemental anal. calcd. for $C_{21}H_{14}S$ (%): C 84.53, H 4.73; found: C 84.47, H 4.59.

2-(3-Methoxyphenyl)ethynyl-5-(phenylethynyl)thiophene (1c)

Yield: 76%. ^{1}H NMR (500 MHz, $CDCl_3$) δ: 3.82 (s, 3H), 6.90–6.92 (m, 1H), 7.05 (s, 1H), 7.11–7.19 (m, 3H), 7.24–7.28 (m, 1H), 7.33–7.39 (m, 3H), 7.49–7.56 (m, 2H). ^{13}C NMR (125 MHz, $CDCl_3$) δ: 55.3, 82.1, 82.3, 94.0, 94.1, 115.4, 116.1, 122.6, 123.5, 124.1, 124.5, 124.7, 128.4, 128.7, 129.5, 131.5, 131.8, 131.9, 159.3. Elemental anal. calcd. for $C_{21}H_{14}OS$ (%): C 80.22, H 4.49; found: C 80.05, H 4.30.

2-(4-Methoxyphenyl)ethynyl-5-(phenylethynyl)thiophene (1d)

Yield: 64%. ^{1}H NMR (500 MHz, $CDCl_3$) δ: 3.83 (s, 3H), 6.87–6.90 (m, 2H), 7.11–7.15 (m, 2H), 7.31–7.39 (m, 3H), 7.44–7.49 (m, 2H), 7.50–7.56 (m, 2H). ^{13}C NMR (125 MHz, $CDCl_3$) δ: 55.3, 81.0, 82.3, 93.9, 94.2, 114.0, 114.7, 122.7, 124.1, 125.1, 128.4, 128.6, 131.4, 131.8, 132.9, 133.1, 156.0. Elemental anal. calcd. for $C_{21}H_{14}OS$ (%): C 80.22, H 4.49; found: C 79.98, H 4.36.

2-(Naphthalen-2-yl)ethynyl-5-(phenylethynyl)thiophene (1e)

Yield: 72%. ^{1}H NMR (500 MHz, $CDCl_3$) δ: 7.17–7.21 (m, 2H), 7.34–7.37 (m, 3H), 7.49–7.57 (m, 5H), 7.80–7.85 (m,

© 2005 NRC Canada

Scheme 9. Reagents: (*i*) BuLi–**29**–ClP(O)(OEt)$_2$–LiHMDS; (*ii*) BuLi–**6a**–PhCOCl; (*iii*) BuLi–**32**–ClP(O)(OEt)$_2$–*t*-BuOK.

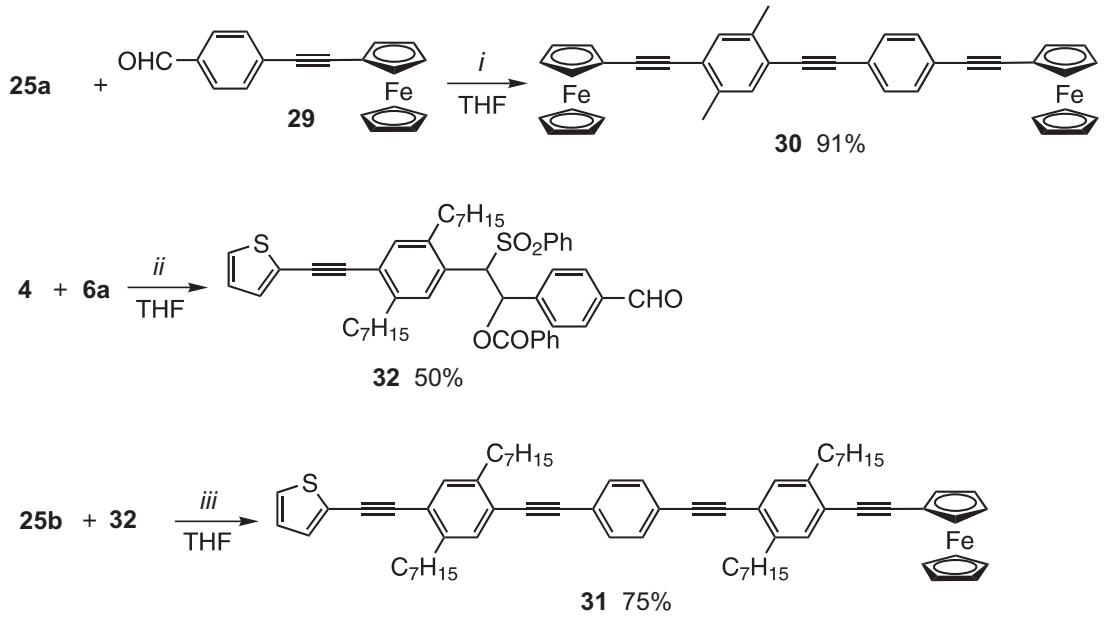
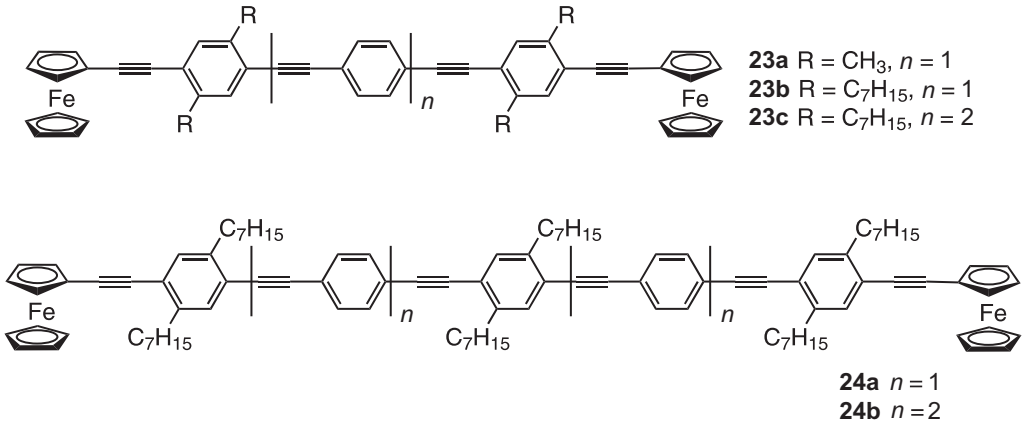


Fig. 2. Structures of phenylene–ethynylenes having ferrocenes at both terminals **23a**–**23c** and **24a** and **24b**.



3H), 8.05 (s, 1H). ^{13}C NMR (125 MHz, $CDCl_3$) δ: 82.3, 82.7, 94.2, 94.6, 119.9, 122.6, 124.7, 124.8, 126.7, 126.9, 127.8, 127.9, 128.0, 128.1, 128.4, 128.7, 131.5, 131.6, 131.8, 131.9, 133.0. HR-MS *m/z* calcd. for $C_{24}H_{14}S$: 334.0816; found: 334.0790.

2,5-Diheptyl-4-(thienylethynyl)benzyl phenyl sulfone (4)

Ethynylthiophene (119.0 mg, 1.1 mmol) was added to a suspension of CuI (9.5 mg, 0.05 mmol), $Pd(PPh_3)_4$ (57.8 mg, 0.05 mmol) and **33b** (554.6 mg, 1.0 mmol) in toluene (10 mL) and diisopropylamine (1.0 mL). The mixture was stirred at 60 °C for 3 h. After the usual work up with CH_2Cl_2 and aq. NH_4Cl, drying over $MgSO_4$, and evaporation, the residue was subjected to column chromatography on silica gel to furnish **4** in a pure form (460.0 mg, 86%).

4

^{1}H NMR (500 MHz, $CDCl_3$) δ: 0.86–0.90 (m, 6H), 1.25–1.33 (m, 16H), 1.38–1.44 (m, 2H), 1.49–1.54 (m, 2H), 2.32 (t, *J* = 8.1 Hz, 2H), 2.65 (t, *J* = 8.0 Hz, 2H), 4.37 (s, 2H), 6.83 (s, 1H), 7.01–7.03 (m, 1H), 7.24–7.26 (m, 2H), 7.29–7.31 (m, 1H), 7.46 (d, *J* = 7.8 Hz, 2H), 7.60–7.66 (m, 3H). ^{13}C NMR (125 MHz, $CDCl_3$) δ: 14.1, 14.2, 22.6, 22.7, 29.1, 29.2, 29.4, 29.5, 30.6, 30.7, 31.7, 31.8, 31.9, 34.0, 59.5, 86.5, 91.7, 122.9, 123.3, 126.3, 127.1, 127.3, 128.7, 128.9, 131.7, 132.2, 132.6, 133.7, 138.0, 140.2, 142.3.

Dialdehyde **5a** was prepared by the hydrolysis of **36a**, which had been derived from the reaction of **34** with **35**. Dialdehyde **5b** was prepared similarly from the reaction of **5a** with **35**.

1,4-Bis[4-(1,3-dioxolan-2-yl)phenyl]ethynyl-2,5-dihepthylbenzene (36a)

To a THF solution (10 mL) of **35** (289.1 mg, 0.95 mmol) was added a hexane solution of BuLi (1.60 mol/L, 0.60 mL, 0.96 mmol) at –78 °C, and the mixture was stirred for 0.5 h. A THF solution (3 mL) of 2,5-diheptylbenzene-1,4-dialdehyde (142.1 mg, 0.43 mmol) was added at –78 °C, and the mixture was stirred for 1.0 h. To the mixture was added $Cl(O)P(OEt)_2$ (0.14 mL, 0.95 mmol) at –78 °C, and the mix-

© 2005 NRC Canada

ture was stirred at r.t. for 1 h. *t*-BuOK (964.9 mg, 8.6 mmol) was added at –78 °C, and the mixture was stirred at r.t. for 1 h. After the usual work up with ethyl acetate and aq. NH_4Cl, drying over $MgSO_4$, and evaporation, the residue was subjected to column chromatography on silica gel to furnish **36a** in a pure form (223.5 mg, 84%).

36a

^{1}H NMR (500 MHz, $CDCl_3$) δ: 0.85–0.88 (m, 6H), 1.27–1.39 (m, 16H), 1.66–1.70 (m, 4H), 2.80 (t, *J* = 7.8 Hz, 4H), 4.04–4.15 (m, 8H), 5.84 (s, 2H), 7.36 (s, 2H), 7.46–7.55 (m, 8H).

1,4-Bis{4-[4-(1,3-dioxolan-2-yl)phenylethynyl]phenylethynyl}-2,5-diheptylbenzene (36b)

^{1}H NMR (500 MHz, $CDCl_3$) δ: 0.86–0.89 (m, 6H), 1.28–1.43 (m, 16H), 1.67–1.73 (m, 4H), 2.81 (t, *J* = 7.8 Hz, 4H), 4.02–4.17 (m, 8H), 5.83 (s, 2H), 7.37 (s, 2H), 7.47–7.57 (m, 16H). ^{13}C NMR (125 MHz, $CDCl_3$) δ: 14.1, 22.7, 29.2, 29.5, 30.7, 31.8, 34.1, 65.3, 89.6, 90.4, 91.0, 93.7, 103.3, 122.5, 122.9, 123.4, 123.9, 126.5, 131.4, 131.4, 131.6, 132.4, 138.1, 142.3.

1,4-Bis(4-formylphenyl)ethynyl-2,5-diheptylbenzene (5a)

Diacetal **36a** (445.5 mg, 0.72 mmol) and *p*-toluenesulfonic acid monohydrate (13.3 mg, 0.07 mmol) were dissolved in a mixture of THF (8 mL), acetone (4 mL), and water (4 mL), and the mixture was stirred at 50 °C for 14 h. After the usual work up with ethyl acetate and aq. $NaHCO_3$, drying over $MgSO_4$, and evaporation, the residue was subjected to column chromatography on silica gel to furnish **5a** in a pure form (374.5 mg, 98%).

5a

^{1}H NMR (500 MHz, $CDCl_3$) δ: 0.85–0.88 (m, 6H), 1.28–1.43 (m, 16H), 1.68–1.72 (m, 4H), 2.82 (t, *J* = 7.8 Hz, 4H), 7.41 (s, 2H), 7.67 (t, *J* = 7.9 Hz, 4H), 7.89 (d, *J* = 8.2 Hz, 4H), 10.04 (s, 2H). ^{13}C NMR (125 MHz, $CDCl_3$) δ: 14.1, 22.7, 29.2, 29.5, 30.7, 31.8, 34.1, 92.3, 93.3, 122.5, 129.6, 129.7, 132.0, 132.6, 135.4, 142.7, 191.4.

1,4-Bis[4-(4-formylphenylethynyl)phenylethynyl]-2,5-diheptylbenzene (5b)

^{1}H NMR (500 MHz, $CDCl_3$) δ: 0.86–0.89 (m, 6H), 1.28–1.43 (m, 16H), 1.67–1.74 (m, 4H), 2.81 (t, *J* = 7.8 Hz, 4H), 7.38 (s, 2H), 7.54 (td, *J* = 11.4, 5.8 Hz, 8H), 7.69 (d, *J* = 8.3 Hz, 4H), 7.88 (d, *J* = 8.3 Hz, 4H), 10.03 (s, 2H). ^{13}C NMR (125 MHz, $CDCl_3$) δ: 14.1, 22.7, 29.2, 29.5, 30.7, 31.8, 34.1, 90.3, 90.7, 93.1, 93.6, 122.2, 122.5, 124.0, 129.3, 129.6, 131.5, 131.8, 132.1, 132.4, 135.5, 142.4, 191.4.

Preparation of thiophene-containing phenylene ethynylene 7a (representative)

To a THF solution (10 mL) of **4** (112.3 mg, 0.21 mmol) was added a hexane solution of BuLi (1.6 mol/L, 0.14 mL, 0.22 mmol) at –78 °C, and the solution was stirred for 5 min. A THF solution (3 mL) of terephthalaldehyde (13.4 mg, 0.10 mmol) was added, and the mixture was stirred for 1 h. To the mixture was added $ClP(O)(OEt)_2$ (32 μL, 0.22 mmol) at –78 °C, and the mixture was stirred at r.t. for 1 h. *t*-BuOK (224.4 mg, 2.0 mmol) was added at –78 °C, and the mixture was stirred at r.t. for 2 h. After the usual work up with CH_2Cl_2 – aq. NH_4Cl, the organic layer was dried over $MgSO_4$. After evaporation, the crude product was subjected to column chromatography on silica gel to afford **7a** in a pure form (61.8 mg, 70%).

1,4-Bis[2,5-diheptyl-4-(2-thienylethynyl)phenylethynyl]benzene (7a)

^{1}H NMR (500 MHz, $CDCl_3$) δ: 0.86–0.89 (m, 12H), 1.25–1.42 (m, 32H), 1.65–1.73 (m, 8H), 2.75–2.82 (m, 8H), 7.02 (dd, *J* = 4.9, 3.7 Hz, 2H), 7.27 (dd, *J* = 3.5, 0.8 Hz, 2H), 7.30 (dd, *J* = 5.2, 0.8 Hz, 2H), 7.50 (s, 4H), 7.35 (s, 2H), 7.36 (s, 2H). ^{13}C NMR (125 MHz, $CDCl_3$) δ: 14.0, 14.1, 22.7, 29.1, 29.2, 29.5 (2C), 30.6, 30.7, 31.8 (2C), 34.1, 87.2, 90.4, 92.2, 93.7, 122.3, 122.4, 123.2, 123.5, 127.2, 127.3, 131.4, 131.6, 132.0, 132.3, 142.2, 142.3. Elemental anal. calcd. for $C_{62}H_{74}S_2$ (%): C 84.30, H 8.44; found: C 84.14, H 8.50.

1,4-Bis(4-{4-[2,5-diheptyl-4-(2-thienylethynyl)phenylethynyl]phenylethynyl}phenylethynyl)-2,5-diheptylbenzene (7b)

Yield: 65%. ^{1}H NMR (500 MHz, $CDCl_3$) δ: 0.86–0.89 (m, 18H), 1.25–1.43 (m, 48H), 1.65–1.74 (m, 12H), 2.75–2.83 (m, 12H), 7.02 (dd, *J* = 5.0, 3.5 Hz, 2H), 7.27 (dd, *J* = 5.2, 3.7 Hz, 2H), 7.30 (dd, *J* = 5.2, 1.3 Hz, 2H), 7.35 (s, 2H), 7.36 (s, 2H), 7.37 (s, 2H), 7.49–7.53 (m, 16H). ^{13}C NMR (125 MHz, $CDCl_3$) δ: 14.1, 22.7, 29.2 (2C), 29.5 (2C), 30.6, 30.7, 31.8, 34.1, 87.2, 90.5 (2C), 91.0, 91.1, 92.2, 93.7, 93.8, 122.4, 122.5 (2C), 122.8 (2C), 123.5 (2C), 127.2, 127.3, 131.4 (2C), 131.6 (2C), 132.0, 132.4 (2C), 142.2, 142.3 (2C). Elemental anal. calcd. for $C_{108}H_{118}S_2$ (%): C 87.63, H 8.04; found: C 87.44, H 8.12.

Preparation of pyridine-containing phenylene ethynylene 10 (representative)

To a THF solution (6 mL) of 2-pyridylmethyl sulfone **8** (233.3 mg, 1.0 mmol) was added a hexane solution of BuLi (1.29 mol/L, 0.93 mL, 1.2 mmol) at –78 °C, and the mixture was stirred for 0.5 h. A THF solution (2 mL) of benzaldehyde (95.5 mg, 0.90 mmol) was added at –78 °C, and the mixture was stirred for 1 h. After $ClP(O)(OEt)_2$ (0.174 mL, 1.20 mmol) had been added at –78 °C, the mixture was stirred at r.t. for 2 h. After a THF solution of lithium hexamethyldisilazide (1.0 mol/L, 10.0 mL, 10.0 mmol) had been added at –78 °C, the mixture was stirred at –78 °C for 1 h and at r.t. for 1 h. After the usual work up with aq. NH_4Cl – EtOAc, the combined organic layer was washed with brine and dried over anhydr. $MgSO_4$. After evaporation, the residue was subjected to column chromatography on silica gel to give **10** in a pure form (135.8 mg, 84%).

2-(Phenylethynyl)pyridine (10) (15)

^{1}H NMR (300 MHz, $CDCl_3$) δ: 7.39 (m, 3H), 7.25 (dt, *J* = 4.8, 1.2 Hz, 1H), 7.54 (td, *J* = 7.8, 0.9 Hz, 1H), 7.62 (m, 2H), 7.71 (dt, *J* = 7.8, 1.8 Hz, 1H), 8.63 (dd, *J* = 4.8, 0.6 Hz, 1H). ^{13}C NMR (75 MHz, $CDCl_3$) δ: 88.5, 89.1, 122.1, 122.6, 127.0, 128.2, 128.8, 131.9, 136.0, 143.3, 149.9.

2,6-Bis(phenylethynyl)pyridine (13) (16)

^{1}H NMR (500 MHz, $CDCl_3$) δ: 7.37 (m, 6H), 7.48 (d, *J* = 4.5 Hz, 2H), 7.61 (m, 4H), 7.69 (t, *J* = 4.5 Hz, 1H). ^{13}C

© 2005 NRC Canada

NMR (125 MHz, $CDCl_3$) δ: 88.2, 89.5, 122.0, 126.1, 128.3, 129.0, 132.0, 136.3, 143.7.

2,2′-Bis[3-(2-pyridylethynyl)phenylethynyl]-1,1′-binaphthyl (15)

^{1}H NMR (500 MHz, $CDCl_3$) δ: 6.72 (d, *J* = 7.8 Hz, 1H), 7.00 (s, 1H), 7.10 (t, *J* = 7.5 Hz, 1H), 7.25 (m, 1H), 7.38 (m, 3H), 7.53 (m, 2H), 7.70 (dt, *J* = 7.5, 0.9 Hz, 1H), 7.79 (d, *J* = 5.1 Hz, 1H), 8.02 (dd, *J* = 7.5, 5.1 Hz, 2H), 8.63 (d, *J* = 2.4 Hz, 1H). ^{13}C NMR (125 MHz, $CDCl_3$) δ: 88.2, 88.7, 90.1, 92.5, 121.3, 122.1, 122.8, 123.5, 126.5, 126.6, 126.8, 127.1, 128.0, 128.1, 131.2, 131.6, 132.5, 133.0, 134.4, 136.1, 140.3, 143.1, 149.9.

2-Phenylethynyl-6-(2-pyridylethynyl)pyridine (18)

^{1}H NMR (500 MHz, $CDCl_3$) δ: 7.28–7.33 (m, 1H), 7.34–7.43 (m, 3H), 7.52–7.56 (m, 1H), 7.57–7.68 (m, 4H), 7.70–7.76 (m, 2H), 8.60–8.73 (m, 1H). ^{13}C NMR (125 MHz, $CDCl_3$) δ: 87.4, 88.0, 88.1, 89.8, 122.0, 123.5, 126.7, 126.8, 127.8, 128.4, 129.1, 132.1, 136.3, 136.6, 142.5, 143.0, 143.9, 150.1. HR-MS *m*/*z* calcd. for $C_{20}H_{12}N_2$: 280.1000; found: 280.1033.

2-Formyl-6-[6-(4-hexylphenylethynyl)pyridn-2-ylethynyl]pyridine (22)

To a suspension of CuI (28.6 mg, 0.15 mmol), $Pd(PPh_3)_4$ (173.3 mg, 0.15 mmol), and **24** (1.027 g, 3 mmol) in toluene (20 mL) and diisopropylamine (2 mL) was added 2-formyl-6-ethynylpyridine (**23**) (472.1 mg, 3.6 mmol). The mixture was stirred at 40 °C for 12 h. After filtration, the usual work up with CH_2Cl_2 and aq. NH_4Cl, drying over $MgSO_4$, and evaporation, the residue was subjected to column chromatography on silica gel to furnish **22** in a pure form (871.3 mg, 74%).

22

^{1}H NMR (300 MHz, $CDCl_3$) δ: 0.86–0.88 (m, 3H), 1.30–1.50 (m, 6H), 1.59–1.65 (m, 2H), 2.62 (t, *J* = 7.7 Hz, 2H), 7.18 (d, *J* = 8.0 Hz, 2H), 7.51–8.00 (m, 8H), 10.10 (s, 1H). ^{13}C NMR (75 MHz, $CDCl_3$) δ: 14.0, 22.5, 28.9, 31.1, 31.6, 35.9, 86.8, 87.5, 88.7, 90.5, 118.9, 121.0, 126.6, 127.1, 128.5, 131.7, 132.0, 136.5, 137.5, 142.4, 143.1, 144.3, 144.6, 153.0, 192.7.

Preparation of 2,5-dimethyl-4-(ferrocenylethynyl)benzyl phenyl sulfone (25a) (representative)

To a toluene solution (10 mL) of CuI (9.5 mg, 0.05 mmol), $Pd(PPh_3)_4$ (57.8 mg, 0.05 mmol), **33a** (386.3 mg, 1.0 mmol), and diisopropylamine (1.0 mL) was added ferrocenylacetylene (231.1 mg, 1.1 mmol) at r.t. After the mixture had been heated at 60 °C for 3 h, the mixture was filtered. After the usual work up with CH_2Cl_2 – aq. NH_4Cl, the combined organic layer was washed with brine and dried over $MgSO_4$. After evaporation, the residude was subjected to column chromatography on silica gel to afford **25a** in a pure form (459.0 mg, 98%).

25a

^{1}H NMR (500 MHz, $CDCl_3$) δ: 2.01 (s, 3H), 2.35 (s, 3H), 4.24 (s, 5H), 4.25 (t, *J* = 1.8 Hz, 2H), 4.33 (s, 2H), 4.49 (t, *J* = 1.7 Hz, 2H), 6.86 (s, 1H), 7.20 (s, 1H), 7.49 (d, *J* = 7.9 Hz, 2H), 7.62–7.68 (m, 3H). ^{13}C NMR (125 MHz, $CDCl_3$) δ: 18.6, 20.1, 59.9, 65.1, 68.9, 69.9, 71.4, 84.0, 93.1, 124.3, 125.8, 128.7, 128.9, 132.9, 133.5, 133.8, 135.3, 137.3, 138.2.

2,5-Diheptyl-4-(ferrocenylethynyl)benzyl phenyl sulfone (25b)

^{1}H NMR (500 MHz, $CDCl_3$) δ: 0.87–0.91 (m, 6H), 1.26–1.41 (m, 18H), 1.54 (m, 2H), 2.32 (t, *J* = 8.1 Hz, 2H), 2.66 (t, *J* = 7.9 Hz, 2H), 4.24 (s, 5H), 4.26 (t, *J* = 1.8 Hz, 2H), 4.36 (s, 2H), 4.49 (t, *J* = 1.8 Hz, 2H), 6.80 (s, 1H), 7.21 (s, 1H), 7.47 (d, *J* = 7.8 Hz, 2H), 7.60–7.66 (m, 3H). ^{13}C NMR (125 MHz, $CDCl_3$) δ: 14.0, 14.1, 22.5, 22.6, 29.0, 29.1, 29.4, 29.5, 30.5, 30.6, 31.7, 31.8, 34.1, 59.4, 65.2, 68.8, 69.8, 71.2, 84.1, 92.3, 123.7, 125.3, 128.6, 128.8, 132.1, 132.5, 133.6, 138.1, 140.0, 141.8.

Preparation of ferrocene containing phenylene ethynylene 23a (representative)

To a THF solution (10 mL) of **25a** (98.4 mg, 0.21 mmol) was added a hexane solution of BuLi (1.60 mol/L, 0.14 mL, 0.23 mmol) at –78 °C, and the mixture was stirred for 5 min. A THF solution (3 mL) of terephthalaldehyde (13.4 mg, 0.10 mmol) was added at –78 °C, and the mixture was stirred for 1 h. After $ClP(O)(OEt)_2$ (32 μL, 0.22 mmol) had been added at –78 °C, the mixture was stirred at r.t. for 1 h. After *t*-BuOK (224 mg, 2.0 mmol) had been added at –78 °C, the mixture was stirred at r.t. for 2 h. After the usual work up with aq. NH_4Cl – CH_2Cl_2, the combined organic layer was washed with brine and dried over anhydr. $MgSO_4$. After evaporation, the residue was subjected to column chromatography on silica gel to give **23a** in a pure form (83.4 mg, 90%).

1,4-Bis[2,5-dimethyl-4-(ferrocenylethynyl)phenylethynyl]benzene (23a)

^{1}H NMR (500 MHz, CD_2Cl_2) δ: 2.45 (s, 6H), 2.47 (s, 6H), 4.25 (s, 10H), 4.28 (t, *J* = 1.7 Hz, 4H), 4.52 (t, *J* = 1.8 Hz, 4H), 7.33 (s, 2H), 7.38 (s, 2H), 7.54 (s, 4H). ^{13}C NMR (125 MHz, CD_2Cl_2) δ: 20.2, 20.3, 65.5, 69.2, 70.4, 71.8, 84.6, 90.7, 94.3, 94.4, 122.2, 123.6, 124.4, 131.8, 132.6, 132.9, 137.4, 137.8. Elemental anal. calcd. for $C_{50}H_{38}Fe_2$ (%): C 80.02, H 5.10; found: C 79.75, H 4.88.

1,4-Bis[2,5-diheptyl-4-(ferrocenylethynyl)phenylethynyl]benzene (23b)

^{1}H NMR (500 MHz, $CDCl_3$) δ: 0.86–0.91 (m, 12H), 1.28–1.45 (m, 32H), 1.66–1.74 (m, 8H), 2.76–2.81 (m, 8H), 4.25 (s, 10H), 4.26 (t, *J* = 1.7 Hz, 4H), 4.51 (t, *J* = 1.8 Hz, 4H), 7.31 (s, 2H), 7.35 (s, 2H), 7.50 (s, 4H). ^{13}C NMR (125 MHz, $CDCl_3$) δ: 14.1, 14.2, 22.6, 22.7, 29.2, 29.3, 29.6, 29.7, 30.7, 30.8, 31.8, 31.9, 34.2, 34.3, 65.4, 68.9, 69.9, 71.3, 84.6, 90.6, 93.2, 93.4, 121.5, 123.3, 123.5, 131.4, 132.0, 132.3, 141.8, 142.3. Elemental anal. calcd. for $C_{74}H_{86}Fe_2$ (%): C 81.75, H 7.97; found: C 81.46, H 7.86.

1,2-Bis{4-[2,5-diheptyl-4-(ferrocenylethynyl)phenylethynyl]phenyl}ethyne (23c)

^{1}H NMR (500 MHz, $CDCl_3$) δ: 0.86–0.91 (m, 12H), 1.28–1.47 (m, 32H), 1.67–1.73 (m, 8H), 2.76–2.81 (m, 8H), 4.26 (s, 10H), 4.27 (t, *J* = 1.7 Hz, 4H), 4.51 (t, *J* = 1.7 Hz, 4H),

© 2005 NRC Canada

7.35 (s, 2H), 7.50 (d, J = 8.3 Hz, 4H), 7.53 (d, J = 8.6 Hz, 4H). ^{13}C NMR (125 MHz, $CDCl_3$) δ: 14.1, 14.2, 22.6, 22.7, 29.2, 29.3, 29.6, 29.7, 30.6, 30.7, 31.8, 31.9, 34.2, 34.3, 65.5, 69.0, 70.0, 71.4, 84.7, 90.7, 91.2, 93.2, 93.3, 121.5, 122.7, 123.5, 123.6, 131.4, 131.6, 132.0, 132.3, 141.9, 142.3. Elemental anal. calcd. for $C_{82}H_{90}Fe_2$ (%): C 82.95, H 7.64; found: C 82.87, H 7.65.

1,4-Bis{4-[2,5-diheptyl-4-(ferrocenylethynyl)phenylethynyl]phenylethynyl}-2,5-diheptylbenzene (24a)

^{1}H NMR (500 MHz, $CDCl_3$) δ: 0.86–0.91 (m, 18H), 1.25–1.41 (m, 48H), 1.67–1.74 (m, 12H), 2.77–2.83 (m, 12H), 4.25 (s, 10H), 4.26 (t, J = 1.5 Hz, 4H), 4.50 (t, J = 2.0 Hz, 4H), 7.32 (s, 2H), 7.35 (s, 2H), 7.38 (s, 2H), 7.51 (s, 8H). ^{13}C NMR (125 MHz, $CDCl_3$) δ: 14.0, 14.1, 22.6, 22.7, 29.2, 29.3, 29.5, 29.6, 29.7, 30.7, 30.8, 31.8 (2C), 31.9, 34.1, 34.2, 34.2, 65.4, 68.9, 69.9, 71.3, 84.7, 90.3, 90.6, 93.2, 93.3, 93.8, 121.5, 122.5, 123.1, 123.4, 123.5, 131.3, 131.4, 132.0, 132.3, 132.4, 141.8, 142.2, 142.3. Elemental anal. calcd. for $C_{104}H_{122}Fe_2$ (%): C 84.18, H 8.29; found: C 83.83, H 8.35.

1,4-Bis(4-{4-[2,5-diheptyl-4-(ferrocenylethynyl)phenylethynyl] phenylethynyl}phenylethynyl)-2,5-diheptylbenzene (24b)

^{1}H NMR (500 MHz, $CDCl_3$) δ: 0.86–0.91 (m, 18H), 1.29–1.41 (m, 48H), 1.66–1.72 (m, 12H), 2.76–2.83 (m, 12H), 4.25 (s, 10H), 4.26 (t, J = 1.7 Hz, 4H), 4.51 (t, J = 2.0 Hz, 4H), 7.31 (s, 2H), 7.35 (s, 2H), 7.38 (s, 2H), 7.49–7.51 (m, 16H). ^{13}C NMR (125 MHz, $CDCl_3$) δ: 14.1, 14.2, 22.6, 22.7, 29.2, 29.3, 29.5, 29.6, 29.7, 30.6, 30.7, 31.8 (2C), 31.9, 34.1, 34.2, 34.3, 65.4, 68.9, 69.9, 71.4, 84.7, 90.5, 90.5, 91.0, 91.1, 93.2, 93.3, 93.7, 121.5, 122.5, 122.7, 122.8, 123.4, 123.5, 123.6, 131.3, 131.4, 131.5, 131.6, 132.0, 132.3, 132.4, 141.8, 142.2, 142.3. Elemental anal. calcd. for $C_{120}H_{130}Fe_2$ (%): C 85.59, H 7.78; found: C 85.48, H 7.89.

1,3-Bis[2,5-dimethyl-4-(ferrocenylethynyl)phenylethynyl]benzene (27)

^{1}H NMR (500 MHz, CD_2Cl_2) δ: 2.37 (s, 6H), 2.40 (s, 6H), 4.17 (s, 10H), 4.20 (t, J = 1.5 Hz, 4H), 4.43 (t, J = 1.7 Hz, 4H), 7.25 (s, 2H), 7.28–7.32 (m, 3H), 7.44 (dd, J = 6.4, 1.4 Hz, 2H), 7.63 (s, 1H). ^{13}C NMR (125 MHz, CD_2Cl_2) δ: 20.2, 20.3, 65.5, 69.4, 70.4, 71.8, 84.6, 89.3, 93.6, 94.3, 122.2, 124.2, 124.4, 129.0, 131.5, 132.6, 132.9, 134.5, 137.4, 137.8. Elemental anal. calcd. for $C_{50}H_{38}Fe_2$ (%): C 80.02, H 5.10; found: C 79.92, H 5.38.

1,2-Bis[2,5-dimethyl-4-(ferrocenylethynyl)phenylethynyl]benzene (28)

^{1}H NMR (500 MHz, CD_2Cl_2) δ: 2.42 (s, 6H), 2.45 (s, 6H), 4.25 (s, 10H), 4.26 (t, J = 1.7 Hz, 4H), 4.51 (t, J = 1.7 Hz, 4H), 7.31–7.33 (m, 4H), 7.38 (s, 2H), 7.56–7.59 (m, 2H). ^{13}C NMR (125 MHz, CD_2Cl_2) δ: 20.0, 20.1, 65.3, 68.9, 70.0, 71.4, 84.6, 92.6, 93.2, 93.8, 122.2, 123.8, 125.7, 128.0, 132.0, 132.3, 136.8, 137.4. Elemental anal. calcd. for $C_{50}H_{38}Fe_2$ (%): C 80.02, H 5.10; found: C 79.92, H 5.07.

4-(Ferrocenylethynyl)benzaldehyde (29)

To a toluene solution (10 mL) of CuI (5.7 mg, 0.03 mmol), $Pd(PPh_3)_4$ (34.7 mg, 0.03 mmol), 4-iodobenzaldehyde (139.2 mg, 0.60 mmol), and diisopropylamine (1.0 mL) was added ferrocenylacetylene (131.7 mg, 0.63 mmol) at r.t. After the mixture had been heated at 60 °C for 3 h, the mixture was filtered. After the usual work up with CH_2Cl_2 – aq. NH_4Cl, the combined organic layer was washed with brine and dried over $MgSO_4$. After evaporation, the residue was subjected to column chromatography on silica gel to afford **29** in a pure form (184.7 mg, 98%).

29

^{1}H NMR (500 MHz, $CDCl_3$) δ: 4.26 (s, 5H), 4.30 (t, J = 1.7 Hz, 2H), 4.54 (t, J = 1.8 Hz, 2H), 7.62 (d, J = 8.3 Hz, 2H), 7.84 (d, J = 8.3 Hz, 2H), 10.00 (s, 1H). ^{13}C NMR (500 MHz, $CDCl_3$) δ: 64.1, 69.3, 70.1, 71.7, 85.2, 93.6, 129.6, 130.4, 131.7, 134.8, 191.5.

1,4-Dimethyl-2-(ferrocenylethynyl)-5-[4-(ferrocenylethynyl)phenylethynyl]benzene (30)

^{1}H NMR (500 MHz, $CDCl_3$) δ: 2.36 (s, 3H), 2.39 (s, 3H), 4.16 (s, 5H), 4.17 (s, 5H), 4.19–4.21 (m, 4H), 4.43–4.44 (m, 4H), 7.24 (s, 1H), 7.29 (s, 1H), 7.38 (d, J = 8.3 Hz, 2H), 7.42 (d, J = 8.0 Hz, 2H). ^{13}C NMR (125 MHz, $CDCl_3$) δ: 20.2, 20.3, 65.2, 65.5, 69.4, 69.5, 70.3, 70.4, 71.7, 71.8, 84.7, 85.6, 90.3, 91.0, 94.3, 94.4, 122.3, 122.8, 124.2, 124.3, 131.6, 131.7, 132.6, 132.8, 137.4, 137.7. Elemental anal. calcd. for $C_{40}H_{30}Fe_2$ (%): C 77.20, H 4.86; found: C 76.85, H 5.03.

Preparation of 1-(4-formylphenyl)-2-[2,5-diheptyl-4-(2-thienylethynyl)phenyl]-2-(phenylsulfonyl)ethyl benzoate (32)

To a THF solution (5 mL) of **4** (107.0 mg, 0.20 mmol) was added a hexane solution of BuLi (1.60 mol/L, 0.14 mL, 0.23 mmol) at –78 °C, and the mixture was stirred for 5 min. A THF solution (3 mL) of **6a** (40.2 mg, 0.30 mmol) was added at –78 °C, and the mixture was stirred for 1 h. After benzoyl chloride (39.4 mg, 0.28 mmol) had been added at –78 °C, the mixture was stirred at –78 °C for 0.5 h and at r.t. for 2 h. After the usual work up with aq. NH_4Cl – AcOEt, the combined organic layer was washed with brine and dried over anhydr. $MgSO_4$. After evaporation, the residue was subjected to column chromatography on silica gel to give **32** in a pure form (77.3 mg, 50%).

32

^{1}H NMR (300 MHz, CD_2Cl_2) δ: 0.87–1.43 (m, 24H), 1.66–1.69 (m, 2H), 1.97–2.13 (m, 2H), 2.79–2.84 (m, 2H), 5.19 (d, J = 10.1 Hz, 1H), 6.90–6.93 (m, 2H), 7.00–7.03 (m, 1H), 7.23–7.31 (m, 4H), 7.36–7.46 (m, 5H), 7.56–7.66 (m, 6H), 8.02–8.05 (m, 2H), 9.86 (s, 1H). ^{13}C NMR (125 MHz, CD_2Cl_2) δ: 14.07, 14.11, 22.61, 22.68, 29.08, 29.22, 29.46, 29.55, 29.88, 31.01, 31.68, 31.73, 31.92, 34.30, 68.75, 75.31, 86.84, 91.39, 123.04, 123.21, 127.16, 127.51, 127.70, 127.93, 128.40, 128.66, 129.18, 129.50, 129.54, 130.07, 131.78, 132.60, 133.46, 133.47, 136.12, 139.28, 139.58, 142.63, 143.54, 164.92, 191.31.

Preparation of 1-[2,5-diheptyl-4-(ferrocenylethynyl)phenylethynyl]-4-[2,5-diheptyl-4-(2-thienylethynyl)phenylethynyl]benzene (31)

To a THF solution (10 mL) of **25b** (91.7 mg, 0.14 mmol) was added a hexane solution of BuLi (1.60 mol/L, 0.10 mL,

© 2005 NRC Canada

0.16 mmol) at –78 °C, and the mixture was stirred for 5 min. A THF solution (3 mL) of **32** (92.8 mg, 0.12 mmol) was added at –78 °C, and the mixture was stirred for 1 h. After $ClP(O)(OEt)_2$ (20 μL, 0.14 mmol) had been added at –78 °C, the mixture was stirred at r.t. for 1 h. After *t*-BuOK (269.3 mg, 2.4 mmol) had been added at –78 °C, the mixture was stirred at r.t. for 2 h. After the usual work up with aq. NH_4Cl – CH_2Cl_2, the combined organic layer was washed with brine and dried over anhydr. $MgSO_4$. After evaporation, the residue was subjected to column chromatography on silica gel to give **31** in a pure form (88.7 mg, 75%).

31

^{1}H NMR (500 MHz, $CDCl_3$) δ: 0.86–0.91 (m, 12H), 1.28–1.46 (m, 32H), 1.65–1.75 (m, 8H), 2.75–2.82 (m, 8H), 4.25 (s, 5H), 4.26 (t, *J* = 1.8 Hz, 2H), 4.50 (t, *J* = 1.8 Hz, 2H), 7.03 (dd, *J* = 5.2, 3.7 Hz, 1H), 7.27 (dd, *J* = 3.7, 0.9 Hz, 1H), 7.30–7.31 (m, 2H), 7.35 (s, 2H), 7.36 (m, 2H), 7.50 (s, 4H). ^{13}C NMR (125 MHz, $CDCl_3$) δ: 14.1 (3C), 22.7 (2C), 29.2 (3C), 29.3, 29.5 (2C), 29.6, 29.7, 30.7 (3C), 31.8 (2C), 31.9, 34.1, 34.2, 34.3, 65.4, 68.9, 69.9, 71.3, 84.7, 87.2, 90.4, 90.6, 92.2, 93.2, 93.4, 93.8, 121.5, 122.4, 122.5, 123.1, 123.4, 123.5 (2C), 127.1, 127.3, 131.3, 131.4, 131.6, 132.0, 132.2, 132.3, 141.8, 142.2, 142.3 (2C). Elemental anal. calcd. for $C_{68}H_{80}FeS$ (%): C 82.89, H 8.18; found: C 82.50, H 8.32.

References

1. (*a*) J.M. Tour. Chem. Rev. **96**, 537 (1996); (*b*) J.M. Tour. Acc. Chem. Res. **33**, 791 (2000); (*c*) D.T. McQuade, A.E. Pullen, and T.M. Swager. Chem. Rev. **100**, 2537 (2000); (*d*) T. Yamamoto. Synlett, 425 (2003).
2. For recent representative papers, see: (*a*) G. Li, T. Wang, A. Schulz, S. Bhasale, M. Lauer, P. Espindola, J. Heinz, and J.-H. Fuhrhop. Chem. Commun. 552 (2004); (*b*) G. Fuhrmann, T. Debaerdemaeker, and P. Bäuerle. Chem. Commun. 948 (2003); (*c*) T. Kaieda, S. Kobatake, H. Miyasaka, M. Murakami, N. Iwai, Y. Nagata, A. Itaya, and M. Irie. J. Am. Chem. Soc. **124**, 2015 (2002); (*d*) K. Inouchi, S. Kobashi, K. Takimiya, Y. Aso, and T. Otsubo. Org. Lett. **4**, 2533 (2002); (*e*) T.M. Pappenfus and K.R. Mann. Org. Lett. **4**, 3043 (2002); (*f*) J. Li, L. Liao, Y. Pang, and M.V. Russo. Organometallics, **20**, 4360 (2001); (*g*) S. Fraysse, C. Coudret, and J.-P. Launay. Tetrahedron Lett. **39**, 7873 (1998).
3. (*a*) J.G. Rodrígues, A. Lafuente, L. Rubio, and J. Esquivias. Tetrahedron Lett. **45**, 7061 (2004); (*b*) J.G. Rodríguez, A. Lafuente, and L. Rubio. Tetrahedron Lett. **45**, 5685 (2004); (*c*) M. Mayor and C. Didschies. Angew. Chem. Int. Ed. **42**, 3176 (2003); (*d*) S. Destri, W. Porzio, I.A. Khotina, C. Botta, and R. Consonni. Polym. Sci. Ser. A, **43**, 1899 (2001); (*e*) I.-Y. Wu, J.T. Lin, Ch.S. Li, W.C. Wang, T.H. Huang, Y.S. Wen, T. Chow, and Ch. Tsai. Tetrahedron, **55**, 13 973 (1999); (*f*) A. Abbotto, S. Bradamante, A. Facchetti, and G.A. Pagani. J. Org. Chem. **62**, 5755 (1997); (*g*) K. Sanechika, T. Yamamoto, and A. Yamamoto. Bull. Chem. Soc. Jpn. **57**, 752 (1984).
4. For recent representative papers, see: (*a*) T. Kawano, T. Kato, C.-X. Du, and I. Ueda. Bull. Chem. Soc. Jpn. **76**, 709 (2003), and their relevant studies; (*b*) T. Yamamoto, A.M. Arif, and P.J. Stang. J. Am. Chem. Soc. **125**, 12 309 (2003), and their relevant studies; (*c*) A.N. Khlobystov, M.T. Brett, A.J. Blake, N.R. Champness, P.M.W. Gill, D.P. O'Neill, S.J. Teat, C. Wilson, and M. Schröder. J. Am. Chem. Soc. **125**, 6753 (2003); (*d*) S.-S. Sun and A.J. Lees. J. Am. Chem. Soc. **122**, 8956 (2000); (*e*) P.N.W. Baxter. J. Org. Chem. **65**, 1257 (2000); (*f*) N.R. Champness, A.N. Khlobystov, A.G. Majuga, M. Schruoder, and N.V. Zyk. Tetrahedron Lett. **40**, 5413 (1999); (*g*) K.T. Potts, C.P. Horwitz, A. Fessak, K.M. Keshavarz, K.E. Nash, and P.J. Toscano. J. Am. Chem. Soc. **115**, 1044 (1993). It should be noted that arylene ethynylenes with other nitrogen aromatics such as bipyridyl, terpyridyl, etc., are not included herein. For reviews of these compounds, see: A. Harrimann and R. Ziessel. Chem. Commun. 1707 (1996), and ref. 1*d*.
5. For a review and recent papers, see: (*a*) T. Yamamoto, T. Morikita, T. Maruyama, K. Kubota, and M. Katada. Macromolecules, **30**, 5390 (1997); (*b*) N.J. Long and C.K. Williams. Angew. Chem. Int. Ed. **42**, 2586 (2003); (*c*) U. Siemeling, J. Vor der Brüggen, U. Vorfeld, B. Neumann, A. Stammler, H.-G. Stammler, A. Brockhinke, R. Plessow, P. Zanello, F. Laschi, F. Fabrizi de Biani, M. Fantani, S. Steenken, M. Stapper, and G. Gurzadyan. Chem. Eur. J. **9**, 2819 (2003); (*d*) K.H.H. Fabian, H.-J. Lindner, N. Nimmerfroh, and K. Hafner. Angew. Chem. Int. Ed. **40**, 3402 (2001); (*e*) S. Creager, C.J. Yu, C. Bamdad, S. O'Connor, T. MacLean, E. Lam, Y. Chong, G.T. Olsen, J. Luo, M. Gozin, and J.F. Kayyem. J. Am. Chem. Soc. **121**, 1059 (1999); (*f*) C.J. Yu, Y. Chong, J.F. Kayyem, and M. Gozin. J. Org. Chem. **64**, 2070 (1999); (*g*) R.P. Hsung, C.E.D. Chidsey, and L.R. Sita. Organometallics, **14**, 4808 (1995).
6. (*a*) K. Sonogashira, Y. Tohda, and N. Hagihara. Tetrahedron Lett. 4467 (1975); (*b*) Y. Tohda, K. Sonogashira, and N. Hagihara. Synthesis, 777 (1977); (*c*) S. Takahashi, Y. Kuroyama, K. Sonogashira, and N. Hagihara. Synthesis, 627 (1980).
7. (*a*) D.-L. An, T. Nakano, A. Orita, and J. Otera. Angew. Chem. Int. Ed. **41**, 171 (2002); (*b*) A. Orita, D. Hasegawa, T. Nakano, and J. Otera. Chem. Eur. J. **8**, 2000 (2002); (*c*) A. Orita, D. Hasegawa, D.-L. An, T. Nakano, J. Yaruva, N. Ma, and J. Otera. Chem. Eur. J. **8**, 2005 (2002); (*d*) F. Ye, A. Orita, A. Doumoto, and J. Otera. Tetrahedron, **59**, 5635 (2003); (*e*) A. Orita, F. Ye, A. Doumoto, and J. Otera. Adv. Synth. Catal. **346**, 767 (2004).
8. For a preliminary report, see: A. Orita, T. Nakano, T. Yokoyama, G. Babu, and J. Otera. Chem. Lett. **33**, 1298 (2004).
9. A. Orita, T. Nakano, D.-L. An, K. Tanikawa, K. Wakamatsu, and J. Otera. J. Am. Chem. Soc. **126**, 10 389 (2004).
10. For thienylene acetylenes with metallocene termini, see: S. Schouteeten, J.-P. Tranchier, F. Rose-Munch, E. Rose, and A. Auffrant. Organometallics, **23**, 4308 (2004), and refs. therein.
11. H. Gilman and F.K. Cartledge. J. Organomet. Chem. **2**, 447 (1967).
12. D.R. Coulson. Inorg. Synth. **13**, 121 (1972).
13. (*a*) S. Golding, A.R. Katritzky, and H.Z. Kucharska, J. Chem. Soc. 3090 (1965); (*b*) B.M. Trost and R. Braslau. J. Org. Chem. **53**, 532 (1988).
14. K. Sanechika, T. Yamamoto, and A. Yamamoto. Bull. Chem. Soc. Jpn. **57**, 752 (1984).
15. Y. Nishihara, K. Ikegashira, K. Hirabayashi, J. Ando, A. Mori, and T. Hiyama. J. Org. Chem. **65**, 1780 (2000).
16. M.A. Pena, I. Perez, J.P. Sestelo, and L.A. Sarandeses. Chem. Commun. 2246 (2002).

© 2005 NRC Canada

Studies towards the total synthesis of ouabagenin[1]

Ling Chen and Pierre Deslongchamps

Abstract: An anionic cyclization strategy developed in our laboratory was used to produce a versatile and convergent synthesis of an advanced tetracyclic intermediate for the construction of ouabagenin and closely related analogs.

Key words: organic chemistry, synthesis, cycloaddition, polycyclization, Michael reaction, Diels–Alder reaction, steroids, oubain, ouabagenin, natural products.

Résumé : L'utilisation d'une réaction de cyclisation anionique développée dans nos laboratoires a permis d'élaborer une route convergente et versatile d'un intermédiaire tétracyclique pour la synthèse de la ouabagénine et ses dérivés.

Mots clés : chimie organique, synthèse, cycloaddition, polycyclisation, reaction Michaël, reaction Diels–Alder, stéroïdes, ouabaïne, ouabagénine, produits naturels.

Introduction

Ouabain (**1a**), a cardioactive glycoside, was isolated from the bark of the African ouabio tree (*Acokanthera ouabio*) by Arnaud in 1888 (1). A similar compound was also isolated from bovine and other mammalian sources and it has since been established that the endogenous and the plant-derived ouabain are in fact one and the same (2). Ouabagenin (**1b**), the aglycone of ouabain, was isolated for the first time in 1942 by Mannich and Siewert (3), who proposed a structure for the aglycone, and therefore the structure for ouabain as well, which was later proven by Florey and Ehrenstein (4).

In 1988, a stereocontrolled approach to access 14-hydroxy steroid skeletons was reported by our research group (5). Under basic conditions, an α,β-unsaturated β′-ketoester can react with a γ,δ-unsaturated β-ketoester (a Nazarov intermediate)[3] to afford a tetracylic compound in good yield and with excellent diastereoselectivity. This reaction is believed to go through a cascade of anionic cyclization and aldol condensation known as anionic polycyclization, and would provide a very efficient way to construct highly oxygenated polycyclic compounds such as ouabagenin.

There are many examples in the recent literature of studies towards the total synthesis of ouabagenin by various methods from the groups of Overman (6) and Jung (7). Herein we report some of our recent efforts at completing this challenging total synthesis. In 2002, our group reported an important development for the asymmetric synthesis of ouabagenin via anionic cyclization. The reaction of an α,β-unsaturated β′-ketoester **2** with Nazarov intermediate **3** afforded, after decarboxylation and aldol condensation, steroid **6** with great control of stereochemistry (Scheme 1) (8). These reactions, which led to the stereoselective generation of five contiguous chiral centres, have laid a solid foundation for the asymmetric total synthesis of ouabain or its aglycone ouabagenin. The issues that remained unaddressed were the methods of introduction of the 3- and 5-OH groups, deoxygenation of the 7 position, synthesis of the butenolide (for which there are excellent known methods in the literature (9)), along with some relatively straight forward functional group transformations.

To achieve the total synthesis of **1b** via the previously stated strategy it was important to obtain an A-ring precursor (α,β-unsaturated β′-ketoester) that would give comparable selectivity to that obtained with **2** but with a better handle for the introduction of the 3- and 5-OH groups. With this goal in mind, we envisioned the potential use of compounds **A1–A3** (Scheme 2). A-ring precursors **A1** and **A2** could be subjected to ozonolysis with concomitant Baeyer–Villager oxidation to obtain the protected 3-OH group, thus relying solely on an enone derived from the C-7 ketone as a handle to introduce the 5-OH as illustrated. Alternatively, the use of **A3** would allow for reduction of an analogous enone to fragment the ketal, affording a chiral allylic alcohol at C-3, which would offer a variety of options for the introduction of the C-5 OH.

Received 2 November 2004. Published on the NRC Research Press Web site at http://canjchem.nrc.ca on 23 June 2005.

L. Chen and P. Deslongchamps.[2] Laboratoire de synthèse organique, Département de chimie, Institut de Pharmacologie de Sherbrooke, Université de Sherbrooke, 3001, 12e Avenue nord, Sherbrooke, QC J1H 5N4, Canada.

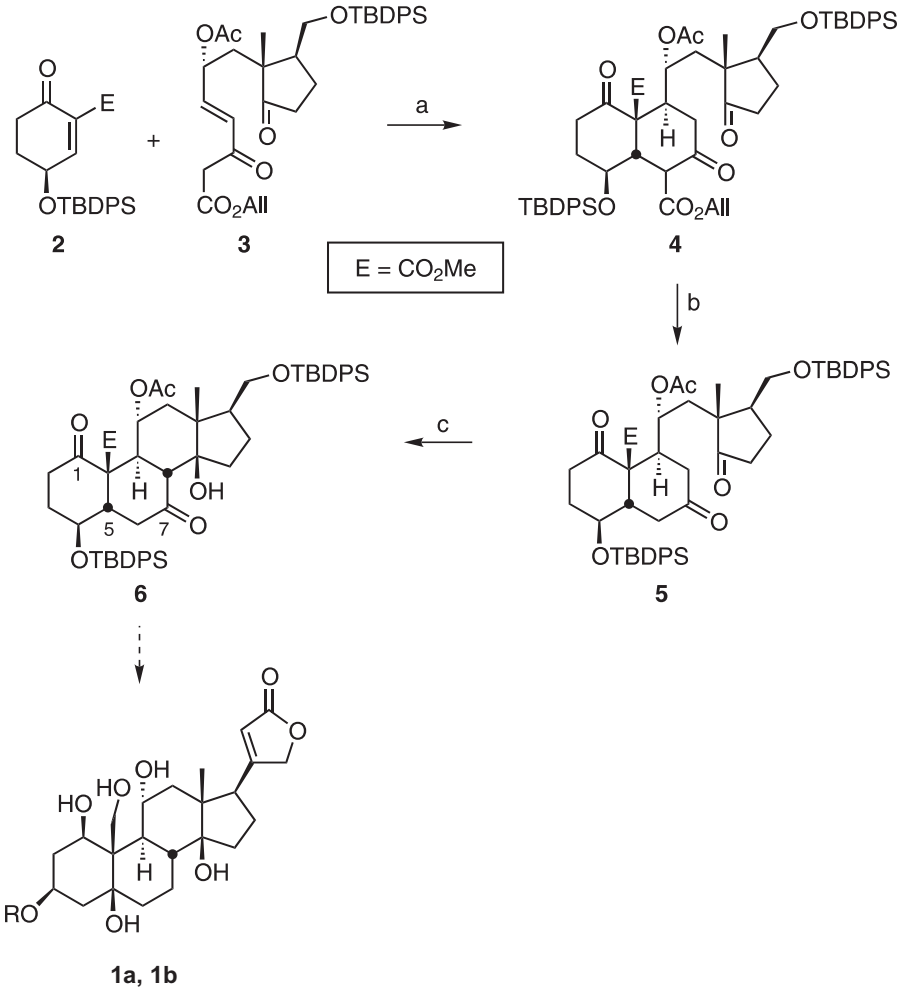
[1]This article is part of a Special Issue dedicated to Professor Howard Alper.

[2]Corresponding author (e-mail: Pierre.Deslongchamps@USherbrooke.ca).

[3]These γ,δ-unsaturated β-ketoesters were originally studied by Ivan Nikolaevich Nazarov (1906–1957) in tandem Michael–aldol reactions to form bicycles. We have named these compounds Nazarov intermediates in homage to his work. A representative example available in english is: I.N. Nazarov and S.I. Zav'yalov. Zh. Obshch. Khim. **25**, 477 (1955).

 doi: 10.1139/V05-042 © 2005 NRC Canada

Scheme 1. (*a*) Cs_2CO_3, CH_2Cl_2, r.t., 61%; (*b*) $Pd(PPh_3)_4$, morpholine, THF, r.t., 71%; (*c*) KHMDS, THF, reflux, 71%. **1a** (R = α-L-rhamnosyl (ouabain)); **1b** (R = H (ouabagenin)).



Results and discussion

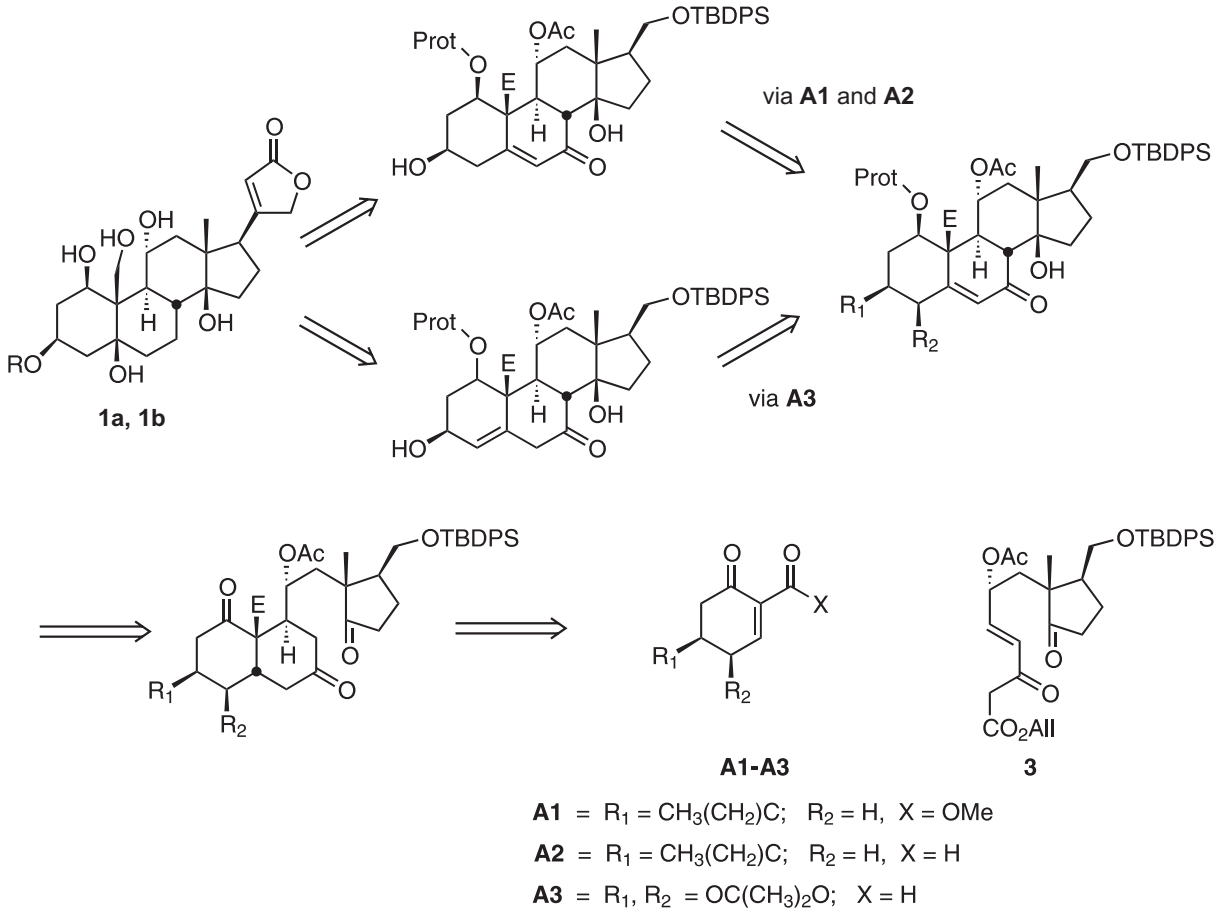
With the above synthetic strategy in mind, we proceeded to synthesize the three targeted ring-A precursors proposed above. Ring **A1** was prepared as described in the literature (10). Ring **A2** was prepared from acid **7**, an intermediate in the synthesis of **A1** (Scheme 3). Compound **7** was first converted to the corresponding Weinreb amide (11), which was then treated with methyl magnesium bromide to afford methyl ketone **8** in 80% overall yield (12). Deprotection of the acetal followed by acidic cyclization gave the cyclohexenone **9** in 62% overall yield (13). The Baylis–Hillman reaction between **9** and formaldehyde was used to introduce the hydroxylmethyl group. This β-hydroxy ketone **10** can be furnished in 54% yield. The hydroxyl group in **10** was then oxidized with Dess–Martin periodinane (14) to afford the desired aldehyde (**A2**) in 83% yield. Ring **A2** proved to be very unstable and was prepared immediately before use in the next step.

The synthesis of **A3**, with its 3,4-hydroxyl groups protected as an acetonide for potential reductive fragmentation to the allylic alcohol, began from 2-deoxy-D-ribose (Scheme 4). The sugar was converted to the lactone (**11**) according to the procedure in the literature (15). The lactone ring was opened with isopropyl magnesium chloride (16) and *N*,*O*-dimethylhydroxyamine to give Weinreb amide **12** in 86% yield. The hydroxyl group of **12** was oxidized by the Swern method (17) to afford aldehyde **13** in 75% yield. The optimum yield for the Wittig reaction (92%) was obtained with $MePPh_3Br$ and slightly less than 1 equiv. of potassium bistrimethylsilylamide (KHMDS). The Weinreb amide (**14**) was then reduced to the aldehyde (**15**) by diisobutylaluminum hydride (DIBAL-H) in 92% yield. The lithium dianion of 2-bromoallylic alcohol (18) was added to the aldehyde to afford the ring-closing metathesis (RCM) precursor **16** in 98% yield. The ring-closing metathesis reaction went smoothly using Grubb's second generation catalyst (19) to deliver cyclohexene **17** in 73% yield. Oxidation of the diol to the desired ketone aldehyde was effected by using 3 equiv. of Dess–Martin periodinane to afford **A3** in 80% yield.

With the three A-ring precursors (**A1**–**A3**) in hand, their reactions with Nazarov intermediate **3** were investigated. The preliminary results are summarized in Table 1. When ring **A1** was allowed to react with Nazarov intermediate **3** in the presence of 2 equiv. of cesium carbonate (Table 1, entry 1), all starting material was consumed after 10 h by ^1H NMR (by TLC, the products overlapped with **3**), but the desired anionic cyclization adduct (**18**) was only isolated in 7%

© 2005 NRC Canada

Scheme 2.



A1 = $R_1 = CH_3(CH_2)C$; $R_2 = H$, X = OMe

A2 = $R_1 = CH_3(CH_2)C$; $R_2 = H$, X = H

A3 = $R_1, R_2 = OC(CH_3)_2O$; X = H

yield with other unwanted products. From the previous result, it was clear that **A1** was not a good choice for the synthesis.

As expected, the reaction between ring **A2** and Nazarov intermediate **3** (Table 1, entry 2) was much faster than with **A1** owing to the more electron-withdrawing nature of the aldehyde with respect to the ester. After 2 h, the starting materials could not be detected by ^{1}H NMR. The desired anionic cyclization adduct (**19**) was isolated in 22% yield, along with another diastereomer in 24% yield (stereochemistry not determined). When subjected to the decarboxylation conditions, anionic cyclization adduct **19** gave compound **20** in 72% yield.

Finally, the anionic cyclization between ring **A3** and **3** was studied. Based on the previous work in our group (20), a catalytic amount of cesium carbonate was used to avoid the decomposition of **A3**. To our surprise, the only compound isolated appeared to be a mono-Michael addition product[4] and treating this crude product with 1 equiv. of cesium carbonate, produced the anionic cyclization adduct **21** in 36% overall yield (Scheme 5). The anionic cyclization reaction between ring **A3** and **3** was then repeated using 2 equiv. of cesium carbonate (as in the cases of the previous A-ring precursors) to afford the desired anionic cyclization product **21** in 78% yield with excellent stereoselectivity. These results suggest the possibility that the reaction could proceed via a double Michael process instead of a concerted anionic cyclization. After decarboxylation of **21**, compound **22** was obtained in 95% yield as a single diastereomer.

Based on the preliminary results from the above studies, we decided to advance on the total synthesis of ouabagenin with **A3**. The next step was to selectively reduce the aldehyde in compound **22**. This could be achieved by either $LiAlH(OCEt_3)_3$ (21) or $LiAlH(O\text{-}t\text{-}Bu)_3$. The best yield was obtained when the reaction was quenched with 5% acetic acid to afford compound **23** in 99% yield.[5]

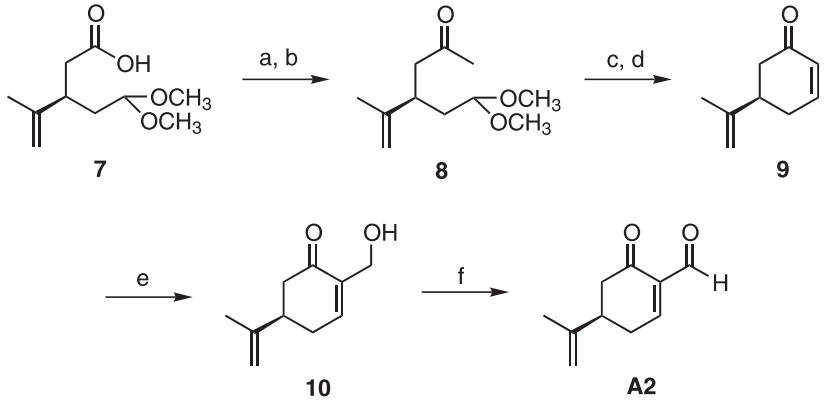
The hydroxyl group in **23** was protected as a 2-(trimethylsilyl)ethoxymethyl ether (SEM) ether (22). The intramolecular aldol condensation was examined on **24** to complete the steroid skeleton of ouabagenin. Several differ-

[4] The mono-Michael product was isolated as a continually equilibrating mixture of diastereomers and keto–enol tautomers owing to the β-ketoester and was therefore very difficult to completely characterize. Its structure was proposed based on the complex ^{1}H NMR spectra of this mixture (not given) and its subsequent reaction with Cs_2CO_3 to give the fully cyclized product (**22**), which was, after decarboxylation, identical to that obtained via the one-step reaction. Based on these results, we feel that the assignment of the structure of a single Michael addition product to compound **23** is a strong possibility, but certainly not an absolute.

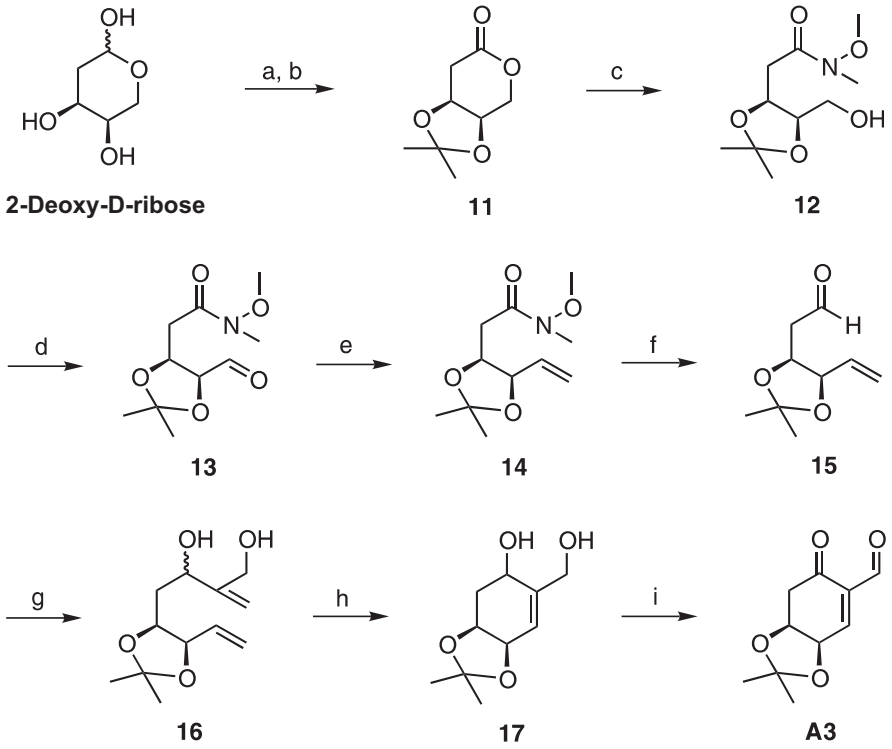
[5] Significantly lower yields were obtained when the reactions were quenched with aqueous ammonium chloride or HCl solutions or with water alone.

© 2005 NRC Canada

Scheme 3. (*a*) (*i*) Im_2CO, DCM; (*ii*) MeONHMe·HCl, NEt_3; (*b*) MeMgBr, THF, 0 °C, 80% for two steps; (*c*) 66% aq. AcOH, 40 °C; (*d*) PTSA, toluene, 100 °C, 62% for two steps; (*e*) 37% HCHO, DMAP, THF, 54%; (*f*) Dess–Martin periodinane, DCM, 83%.



Scheme 4. (*a*) 2-Methoxypropene, PPTS, AcOEt, 70%; (*b*) Br_2, $CaCO_3$, CH_3CN–H_2O (5:1), 88%; (*c*) *i*-PrMgCl, MeNHOMe·HCl, THF, –20 °C, 86%; (*d*) $(COCl)_2$, DMSO, *i*-Pr_2NEt, DCM, –78 °C, 75%; (*e*) $MePPH_3Br$, KHMDS in toluene, THF, 0 °C, 92%; (*f*) DIBAL-H in toluene, THF, –78 °C, 92%; (*g*) *t*-BuLi in pentane, CH_2CBrCH_2OH, Et_2O, 0 °C, 98%; (*h*) Grubb's second generation catalyst, DCM, 40 °C, 73%; (*i*) Dess–Martin periodinane, DCM, 80%.



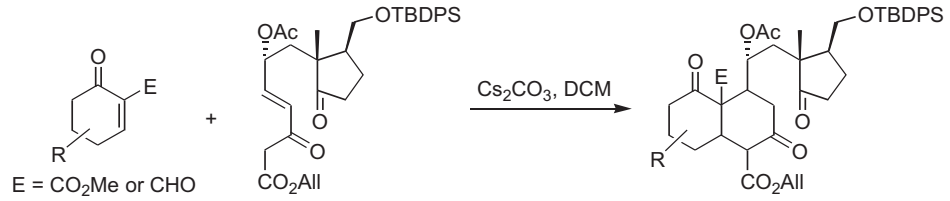
ent bases were used, however, either product **25** or **26** resulting from β elimination was obtained under the conditions shown in Table 2. By TLC, it appeared that the elimination occurred before the desired aldol.

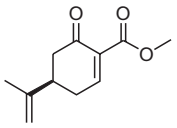
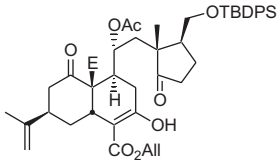
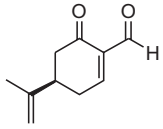
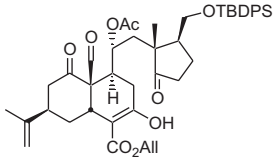
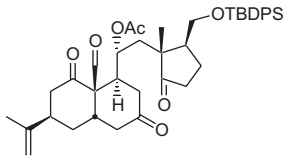
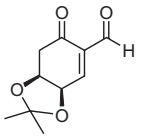
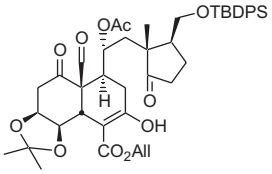
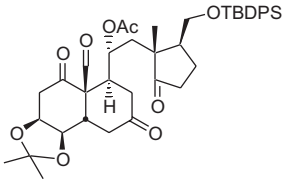
To circumvent the undesired β elimination, we proceeded to reduce the carbonyl group at C-1 before attempting the aldol. The selective reduction of the C-1 carbonyl group was effected via a hydroxyl group directed reduction with $Me_4NBH(OAc)_3$ (23), thus avoiding reduction of the other two ketones, which were less hindered and would react more rapidly with conventional reducing agents to afford compound **27** in 96% yield (Scheme 6). Unfortunately, this directed reduction allowed access to only the undesired α-OH at the 1 position, but we were confident that this could be easily corrected through a later oxidation–reduction sequence on the tetracycle. Thus, this diol (**27**) was protected as an acetonide at which point the aldol condensation of **28** went smoothly, giving the desired product **29** in 86% yield.

At this point, our efforts were directed towards the installation of a hydroxyl group at C-5. As per our original plan, this would be carried out via the reductive fragmentation of the 7,5-enone. Several conditions were examined in attempt to introduce the 5,6-double bond directly in compound **29**. Unfortunately, SeO_2 with catalytic acetic acid, SeO_2 in pyridine, 2,3-dichloro-5,6-dicyano-1,4-benzoquinone (DDQ) in benzene, and 2-iodoxybenzoic acid (IBX) in dimethylsulfoxide

© 2005 NRC Canada

Table 1. Preliminary results of the reactions between A ring units and **3**.



Entry	A ring units	Anionic cyclization (yield)[a]	Decarboxylation (yield)[a]
1	 **A1**	 **18** (7%)[b]	
2	 **A2**	 **19** (22%)[c]	 **20** (72%)
3	 **A3**	 **21** (78%)	 **22** (95%)

[a]Isolated yield.
[b]Along with three unidentified compounds.
[c]Along with 24% of an unidentified diastereomer.

(DMSO) gave no reaction at all. Trapping **29** as a *tert*-butyldimethylsilyl (TBS), enol ether **30** (24) and oxidation with $Pd(OAc)_2$ (25) over the course of 4 days allowed access to the desired enone, but in poor yield and with epimerization of the C-8 position. Fortunately, treatment of **30** with PhSeCl afforded phenyl selenide **31** in 71% yield (26). Oxidative elimination of **31** with hydrogen peroxide produced the desired compound **32** in 57% yield.

With compound **32** in hand, the reductive elimination was attempted to remove the C-4 alkoxy group and introduce the targeted allylic alcohol. In the presence of a catalytic amount of acetic acid, **32** was treated with zinc dust in ethanol at reflux (27). The desired product **33** was obtained in 32% yield, along with compound **29** in 29% yield. Compound **29**, which could be recycled, was obtained by the simple reduction of the double bond without the expected elimination.

Further optimization of this reaction is still required before undertaking the endgame of the synthesis, but we feel that we have in hand a viable method for the synthesis of a steroidal tetracycle with appropriate handles to complete the total synthesis of ouabagenin (**1b**) or closely related analogues for a structure activity relationship study.

Experimental

General

All the reactions were performed under a N_2 atmosphere with oven-dried glassware when necessary. Solvents were distilled and dried according to standard procedures. Analytical TLC was performed on precoated glass plates (0.25 mm) with silica gel 60F-250 (Merck). Flash chromatography was performed with 230–400 mesh gel 60 (Merck). ^1H and ^{13}C NMR spectra were recorded on a Brüker AC-300 and are referenced with respect to the residual signals of the solvent; they are described using standard abbreviations. IR spectra were recorded on a PerkinElmer 1600 FT-IR. Mass spectra were recorded on a ZAB-1F micromass spectrometer.

β-Hydroxyketone (10)

To a solution of **9** (20 mg, 0.147 mmol) in THF (0.25 mL) was added 37% HCHO (66 μL, 0.88 mmol) and *N,N*-dimethylaminopyridine (DMAP) (3.6 mg, 0.029 mmol). The mixture was stirred at 60 °C for 16 h. It was directly purified by preparative TLC (silica gel, hexanes – ethyl acetate

© 2005 NRC Canada

Scheme 5. (*a*) Cs_2CO_3 (0.2 equiv.), DCM, r.t. 2 h then Cs_2CO_3 (1.0 equiv.), DCM, r.t. 1 h, 36%; (*b*) Cs_2CO_3 (2.0 equiv.), DCM, r.t. 2 h, 60%; (*c*) $Pd(PPh_3)_4$, morpholine, THF, r.t., 95%; (*d*) $LiAlH(O\text{-}t\text{-}Bu)_3$, THF, –78 °C or $LiAlH(OCEt_3)_3$, THF, 0 °C; (*e*) SemCl, Imidazole, DCM, 71%.

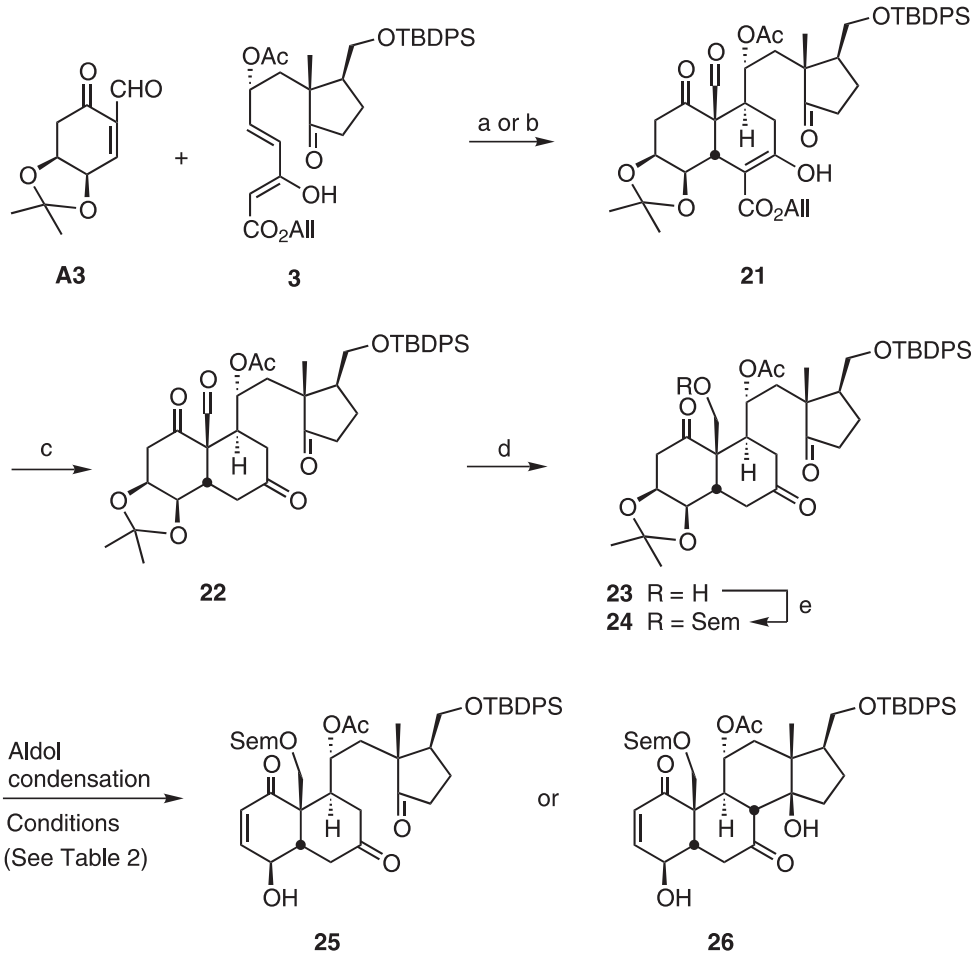


Table 2. Results of attempted aldol reactions.

Entry	Reagent	Solvent	Temp.	Product (yield, %)
1	Cs_2CO_3	CH_3CN	Reflux	**26** (18)
2	Piperidine–AcOH	Benzene	r.t.	**25** (20)
3	DBU	Benzene	Reflux	**25** (95)
4	KHMDS	THF	Reflux	**26** (22)

(Hex:EA = 1:1)) to afford **10** (13 mg, 54%) as a colourless oil. $[\alpha]_D^{20}$ –35.3 (*c* 1.62, $CHCl_3$). IR (neat, cm^{-1}) ν: 3416, 3083, 2920, 1668, 1434, 1384, 904. ^1H NMR (300 MHz, $CDCl_3$) δ: 6.94 (1H, m), 4.80 (1H, br s), 4.74 (1H, br s), 4.24 (2H, br s), 2.75–2.26 (5H, m), 1.73 (3H, s). ^{13}C NMR (75 MHz, $CDCl_3$) δ: 200.24, 146.2, 146.0, 138.0, 110.8, 61.6, 43.1, 42.0, 30.8, 20.4. EI-MS (70 eV) *m/e*: 166 (M^+), 97 (100%). HR-MS calcd. for $C_{10}H_{14}O_2$: 166.0994; found: 166.0991.

α,β-Unsaturated-β′-ketoaldehyde (A2)

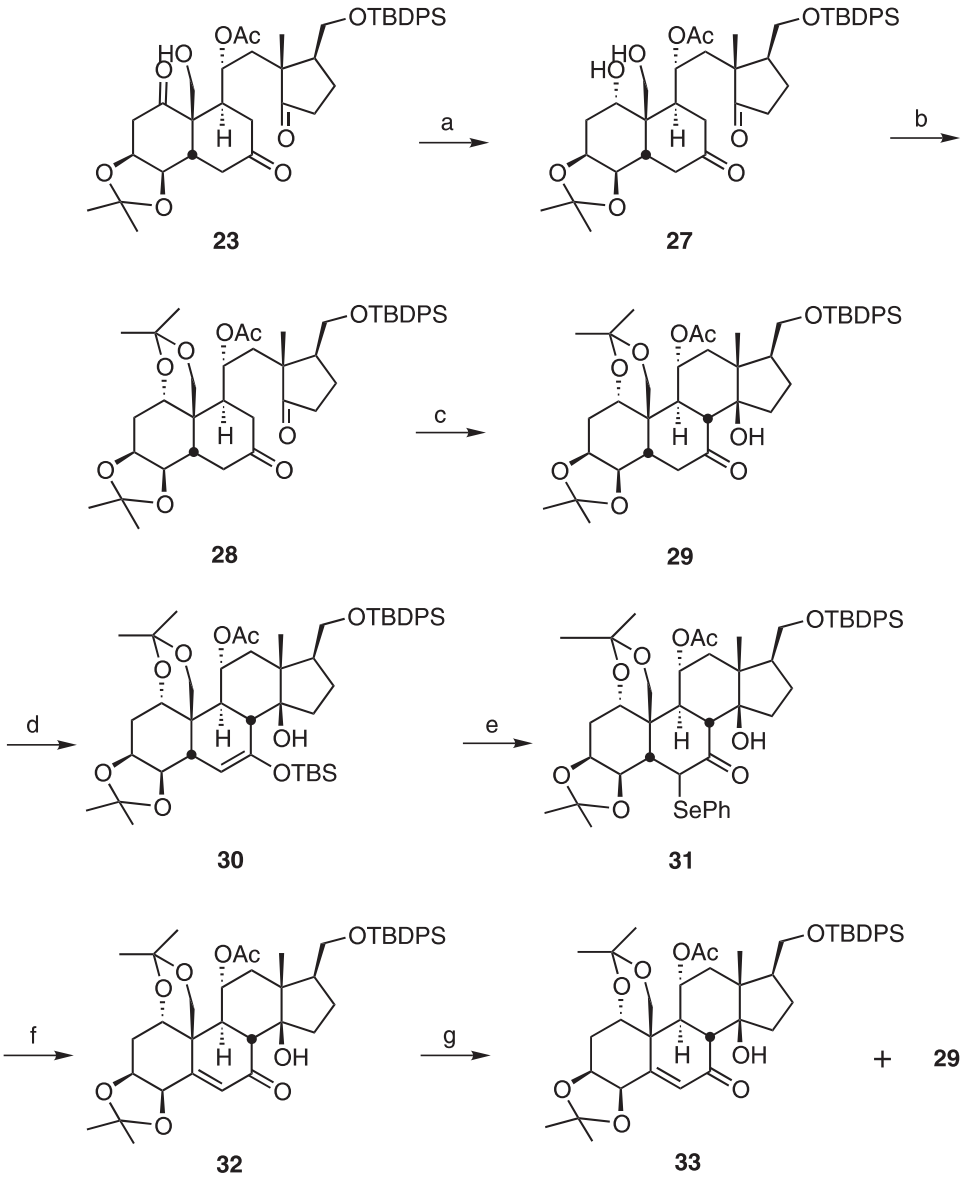
To a solution of **10** (14.3 mg, 0.036 mmol) in dichloromethane (DCM) (1 mL) was added Dess–Martin periodinane (54.7 mg, 0.129 mmol). The mixture was stirred at room temperature (r.t.) for 1 h. After removal of solvent in vacuo, the residue was purified by flash chromatography (silica gel, Hex:EA = 1:1 with 1% acetic acid (AcOH)) to give ring **A2** (11.7 mg, 83%) as a yellowish oil, which is very unstable and should be used immediately for the next step. ^1H NMR (300 MHz, $CDCl_3$) δ: 10.07 (1H, s), 7.82 (1H, dd, *J* = 2.6, 5.6 Hz), 4.90 (1H, br s), 4.81 (1H, br s), 2.80–2.43 (5H, m), 1.76 (3H, s).

Weinreb amide (12)

To a suspension of **11** (0.89 g, 5.17 mmol) and *N*,*O*-dimethylhydroxylamine (0.80 g, 8.00 mmol) in THF (10 mL) was added dropwise a 2 mol/L solution of *i*-PrMgCl in THF (10.8 mL, 21.7 mmol) at –20 °C. The reaction was stirred at –20 °C for 20 min. Aqueous (aq.) NH_4Cl solution (12 mL, satd. NH_4Cl – H_2O = 1:1) was added to quench the reaction. It was extracted with a mixture of ether and DCM (1:1, 5 × 20 mL), the combined organic layers were dried over $MgSO_4$ and concentrated. The residue was purified by flash column chromatography (silica gel, EA) to give **12** (1.04 g, 86%) as a colourless oil. $[\alpha]_D^{20}$ +33.0 (*c* 0.26, $CHCl_3$). IR (thin film, cm^{-1}) ν: 3444, 1659, 1644, 1633. ^1H NMR (300 MHz, $CDCl_3$) δ: 4.66 (1H, dt, *J* = 5.9, 8.1 Hz), 4.31 (1H, t, *J* = 5.5 Hz), 3.70 (3H, s), 3.63 (2H, br

© 2005 NRC Canada

Scheme 6. (*a*) $Me_4NBH(OAc)_3$, CH_3CN–AcOH, –20 to 0 °C, 96%; (*b*) 2-dimethoxypropane, CSA (cat.), acetone, 97%; (*c*) KHMDS in toluene, THF, 86%; (*d*) TBSOTf, Et_3N, DCM, –78 °C to r.t., 91%; (*e*) PhSeCl, 2,6-di-*tert*-butylpyridine, DCM, 9 h, 71%; (*f*) H_2O_2, DCM, 1 h, 57%; (*g*) Zn, AcOH, EtOH.



d), 3.18 (3H, s), 2.94 (1H, dd, *J* = 5.3, 16.9 Hz), 2.77 (1H, dd, *J* = 8.5, 16.8 Hz), 2.58 (1H, br s), 1.45 (3H, s), 1.36 (3H, s). ^{13}C NMR (75 MHz, $CDCl_3$) δ: 171.8, 107.7, 77.4, 73.2, 61.3, 61.1, 32.5, 32.0, 27.8, 25.1. EI-MS (70 eV) *m/e*: 218 ($M^+ - CH_3$), 144 (100%). HR-MS calcd. for $C_9H_{16}NO_5$ ($M^+ - CH_3$): 218.1028; found: 218.1024.

Aldehyde (13)

To a solution of $(COCl)_2$ (0.084 mL, 0.96 mmol) in DCM (3.0 mL) at –78 °C DMSO was added dropwise (0.148 mL, 2.09 mmol). It was then stirred for 10 min. To this mixture a solution of **12** was added dropwise (204 mg, 0.870 mmol) in DCM (1.0 mL) at –78 °C. The mixture was stirred for 30 min before diisopropylethylamine (DIPEA) (0.364 mL, 2.09 mmol) was added. It was stirred at r.t. for 15 min. Water (3 mL) was added to quench the reaction. After stirring for 5 min, the organic layer was separated. The aqueous layer was extracted with DCM (4 × 5 mL). The combined organic layers were dried over $MgSO_4$ and concentrated. The residue was purified by flash column chromatography (silica gel, EA) to afford **13** (150 mg, 75%) as a white solid. Mp: 57–59 °C. $[\alpha]_D^{20}$ +14.1 (*c* 2.29, $CHCl_3$). IR (thin film, cm^{-1}) ν: 1742, 1668, 1644. ^{1}H NMR (300 MHz, $CDCl_3$) δ: 9.69 (1H, dd, *J* = 0.5, 2.2 Hz), 4.81 (1H, q, *J* = 7.0 Hz), 4.53 (1H, dd, *J* = 2.3, 7.1 Hz), 3.67 (3H, s), 3.18 (3H, s), 2.90 (1H, dd, *J* = 6.7, 16.9 Hz), 2.67 (1H, dd, *J* = 7.2, 16.8 Hz), 1.56 (3H, s), 1.43 (3H, s). ^{13}C NMR (75 MHz, $CDCl_3$) δ: 202.4, 170.4, 110.3, 81.3, 74.2, 61.3, 32.4, 32.0, 27.4, 25.3. EI-MS (70 eV) *m/e*: 216 ($M^+ - CH_3$), 144 (100%); HR-MS calcd. for $C_9H_{14}NO_5$ ($M^+ - CH_3$): 216.0875; found: 216.0872.

Weinreb amide (14)

CH_3PPh_3Br (6.10 g, 17.1 mmol) was dried under vacuum at 110 °C for 2 h then cooled to r.t. THF (33 mL) was

© 2005 NRC Canada

added. To this suspension at 0 °C was slowly added KHMDS (0.5 mol/L in toluene, 27.0 mL, 13.5 mmol) with vigorous stirring. After addition, the temperature was raised to r.t. and the mixture was stirred for 30 min. It was cooled to –78 °C and a solution of **13** (3.29 g, 14.2 mmol) in THF (33 mL) was transferred into the above suspension by cannula. The mixture was stirred at 0 °C for 1 h. Satd. aq. NH_4Cl (0.35 mL) was added to quench the reaction. Pentane (132 mL) was added to precipitate the $POPh_3$. After filtration, the filtrate was concentrated in vacuo. The residue was purified by flash column chromatography (silica gel, Hex:EA = 1:2) to afford **14** (3.00 g, 92%) as a colourless oil. $[\alpha]_D^{20}$ –3.5 (*c* 3.33, $CHCl_3$). IR (thin film, cm^{-1}) ν: 2986, 2937, 1666, 1380, 1046. ^1H NMR (300 MHz, $CDCl_3$) δ: 5.81–5.70 (1H, m), 5.30–5.18 (2H, m), 4.73–4.64 (2H, m), 3.65 (3H, s), 3.14 (3H, s), 2.78 (1H, dd, *J* = 6.3, 16.7 Hz), 2.50 (1H, dd, *J* = 6.5, 16.6 Hz), 1.47 (3H, s), 1.36 (3H, s). ^{13}C NMR (75 MHz, $CDCl_3$) δ: 171.4, 134.0, 118.3, 108.4, 79.0, 74.3, 61.3, 33.4, 32.0, 27.9, 25.3. EI-MS (70 eV) *m/e*: 229 (M^+), 83 (100%). HR-MS calcd. for $C_{11}H_{19}NO_4$: 229.1314; found: 229.1319.

Aldehyde (15)

To a solution of **14** (1.24 g, 5.41 mmol) in THF (40 mL) was added 1.5 mol/L DIBAL-H in toluene (7.2 mL, 10.8 mmol) at –78 °C and the mixture was stirred at this temperature for 1 h. Acetone (0.6 mL) was added to consume the excess DIBAL-H and it was stirred for 5 min. The reaction solution was transferred to a mixture of 0.5 mol/L aq. tartaric acid and hexane (108 mL : 108 mL) by cannula, then it was vigorously stirred for 30 min. The organic phase was separated and washed with 45 mL of water and brine, respectively. The combined aqueous phase was extracted with 100 mL of 25% DCM in pentane. The combined organic phase was dried over Na_2SO_4 and concentrated in vacuo. The residue was purified by flash column chromatography (silica gel, Hex:EA = 2:1) to afford **15** (0.85 g, 92%) as a clear oil. $[\alpha]_D^{20}$ –16.1 (*c* 1.68, $CHCl_3$). IR (thin film, cm^{-1}) ν: 3085, 2988, 2937, 2733, 1728, 1645, 1372, 1249, 1217, 1167, 1050, 1004, 933, 869. ^1H NMR (300 MHz, $CDCl_3$) δ: 9.68 (1H, br s), 5.71–5.60 (1H, m), 5.30–5.16 (2H, m), 4.65–4.59 (2H, m), 2.67–2.58 (1H, m), 2.52–2.44 (1H, m), 1.43 (3H, s), 1.31 (3H, s). ^{13}C NMR (75 MHz, $CDCl_3$) δ: 199.9, 133.4, 118.8, 108.7, 78.6, 72.9, 45.1, 27.8, 25.3.

RCM precursor (16)

To a solution of 2-bromoallylic alcohol (6.37 g, 46.5 mmol) in ether (154 mL) was slowly added a solution of 1.47 mol/L *t*-BuLi in pentane (79 mL, 0.116 mol) at −78 °C. It was quickly warmed to 0 °C and stirred at this temperature for 4 h. **15** (2.64 g, 15.5 mmol) in ether (21 mL) was added to this mixture at –78 °C, then it was stirred at 0 °C for 30 min. MeOH (4.4 mL) was added to quench the reaction, followed by water (110 mL). The mixture was stirred for 10 min. The organic layer was separated and the aqueous layer was extracted with DCM (4 × 100 mL). The combined organic phase was dried over $MgSO_4$ and concentrated in vacuo. The residue was purified by flash column chromatography (silica gel, Hex:EA = 1:2) to give **16** (3.48 g, 98%) as a colourless oil. IR (thin film, cm^{-1}) ν: 3418, 2987, 2932, 1372, 1218, 1044. ^1H NMR (300 MHz, $CDCl_3$) two isomers δ: 9.68 (1H, br s), 5.71–5.60 (1H, m), 5.30–5.16 (2H, m), 4.65–4.59 (2H, m), 2.67–2.58 (1H, m), 2.52–2.44 (1H, m), 1.43 (3H, s), 1.31 (3H, s). ^{13}C NMR (75 MHz, $CDCl_3$) two isomers δ: 150.1, 149.2, 133.9, 133.6, 119.0, 118.6, 112.7, 112.0, 109.1, 79.7, 78.0, 74.8, 74.1, 70.9, 64.2, 64.1, 36.7, 36.1, 28.1, 28.0, 25.6, 25.5. EI-MS (70 eV) *m/e*: 213 ($M^+ - CH_3$), 83 (100%). HR-MS calcd. for $C_{11}H_{17}O_4$ ($M^+ - CH_3$): 213.1127; found: 213.1131.

Cyclohexene (17)

A solution of **16** (617 mg, 2.70 mmol) in DCM (30 mL) was degassed. To this solution was added Grubb's second generation catalyst (229 mg, 0.27 mmol). The mixture was stirred at 40 °C overnight. After removal of the solvent in vacuo, the residue was purified by flash column chromatography (silica gel, 1% MeOH in EA) to afford **17** (395 mg, 73%) as a green oil. Conformer **a**: ^1H NMR (300 MHz, $CDCl_3$) δ: 5.67 (1H, dd, *J* = 1.3, 2.9 Hz), 4.57–4.51 (1H, m), 4.50–4.48 (1H, m), 4.29–4.23 (2H, m), 4.15–4.09 (1H, m), 2.46 (1H, ddd, *J* = 2.7, 3.8, 15.2 Hz), 2.01 (1H, ddd, *J* = 2.3, 4.5, 15.2 Hz), 1.45 (3H, s), 1.37 (3H, s). ^{13}C NMR (75 MHz, $CDCl_3$) δ: 140.6, 122.6, 109.6, 72.8, 72.5, 65.3, 64.0, 31.9, 28.3, 26.5. Conformer **b**: IR (thin film, cm^{-1}) ν: 3418, 2987, 2932, 1372, 1218, 1044. ^1H NMR (300 MHz, $CDCl_3$) δ: 5.69 (1H, br s), 4.55–4.53 (2H, m), 4.50–4.45 (1H, m), 4.33–4.22 (2H, m), 2.39 (1H, dt, *J* = 4.9, 13.8 Hz), 1.85 (1H, ddd, *J* = 3.2, 8.7, 13.8 Hz), 1.36 (6H, s). ^{13}C NMR (75 MHz, $CDCl_3$) δ: 142.2, 123.7, 108.6, 72.2, 71.6, 65.5, 65.3, 35.1, 27.8, 26.1. EI-MS (70 eV) *m/e*: 185 ($M^+ - CH_3$), 95 (100%). HR-MS calcd. for $C_9H_{13}O_4$ ($M^+ - CH_3$): 185.0814; found: 185.0808.

α,β-Unsaturated-β′-ketoaldehyde (A3)

To a solution of **17** (715 mg, 3.57 mmol) in DCM (75 mL) was added Dess–Martin periodinane (4.54 g, 10.7 mmol). The mixture was stirred at r.t. for 1 h. It was filtered through a short pad of silica gel (about 5 g), and washed with a mixture of hexane, ethyl acetate, and AcOH (50:50:1). The filtrate was concentrated in vacuo and the residue was purified by flash column chromatography (silica gel, Hex:EA:AcOH = 50:50:1) to afford **A3** (560 mg, 80%) as a colourless oil, which is not stable and should be used directly in the next step. ^1H NMR (300 MHz, $CDCl_3$) δ: 10.1 (1H, br s), 7.30 (1H, dd, *J* = 2.2, 2.5 Hz), 4.89 (1H, dd, *J* = 4.8, 2.7 Hz), 4.70 (1H, m), 3.04 (1H, dd, *J* = 2.7, 7.6 Hz), 2.80 (1H, dd, *J* = 3.7, 7.5 Hz), 1.38 (3H, s), 1.29 (3H, s). ^{13}C NMR (75 MHz, $CDCl_3$) δ: 193.9, 188.9, 150.3, 128.9, 110.4, 73.1, 71.1, 39.3, 27.8, 26.3.

Anionic cyclization adduct (18)

To a solution of **3** (29.4 mg, 0.0486 mmol) in DCM (1 mL) was added Cs_2CO_3 (31.7 mg, 0.0972 mmol). The mixture was stirred at r.t. for 10 min. A solution of **A1** (19.0 mg, 0.0972 mmol) in DCM (1.0 mL) was added to the above mixture over 10 min. The reaction mixture was stirred at r.t. for 10 h. It was then filtered through a pad of Celite® and washed with DCM. After removal of the solvent in vacuo, the residue was purified by flash column chromatography (silica gel, Hex:EA = 4:1) to afford **29** (2.8 mg, 7.2%) as a colourless oil. ^1H NMR (300 MHz, $CDCl_3$) δ: 12.09 (1H, s), 7.70–7.63 (4H, m), 7.42–7.38 (6H, m), 5.92

© 2005 NRC Canada

(1H, m), 5.53 (1H, m), 5.35–5.24 (2H, m), 4.93 (1H, s), 4.84 (1H, s), 4.68 (2H, m), 3.84–3.62 (2H, m), 3.60 (3H, s), 1.84 (3H, s), 1.05 (9H, s), 0.87 (3H, s).

Anionic cyclization adduct (19)

To a solution of **3** (36 mg, 0.059 mmol) in DCM (1 mL) was added Cs_2CO_3 (40 mg, 0.122 mmol). The mixture was stirred at r.t. for 10 min. A solution of aldehyde (14 mg, 0.085 mmol) in DCM (1 mL) was added to the above mixture over 10 min. The reaction mixture was stirred at r.t. for 2 h. It was then filtered through a pad of Celite® and washed with DCM. After removal of the solvent in vacuo, the residue was purified by flash column chromatography (silica gel, Hex:EA = 2:1) to afford an unidentified isomer (11.2 mg) and **19** (10.3 mg, 22%) as a colourless oil. ^{1}H NMR (300 MHz, $CDCl_3$) δ: 12.17 (1H, s), 9.29 (1H, d, *J* = 2.0 Hz), 7.70–7.68 (4H, m), 7.43–7.39 (6H, m), 5.99–5.86 (1H, m), 5.36–5.27 (3H, m), 4.95 (1H, s), 4.85 (1H, s), 4.72 (1H, dd, *J* = 6.0, 13.0 Hz), 4.62 (1H, dd, *J* = 6.0, 13.0 Hz), 3.74 (1H, dd, *J* = 5.7, 10.3 Hz), 3.63 (1H, dd, *J* = 6.5, 10.3 Hz), 3.26 (1H, dd, *J* = 3.5, 11.9 Hz), 2.96 (1H, dd, *J* = 6.5, 14.3 Hz), 2.84–2.49 (5H, m), 2.39–1.90 (7H, m), 1.88 (3H, s), 1.84 (1H, d, *J* = 1.4 Hz), 1.77 (3H, s), 1.66 (1H, m), 1.07 (9H, s), 0.87 (3H, s). ^{13}C NMR (75 MHz, $CDCl_3$) δ: 221.9, 210.2, 198.6, 172.1, 170.7, 170.3, 145.3, 135.6, 133.3, 133.2, 131.5, 129.7, 127.7, 119.4, 113.3, 98.3, 69.8, 65.6, 64.2, 63.5, 49.2, 43.6, 42.2, 40.7, 38.5, 37.5, 36.5, 33.1, 30.5, 29.1, 26.9, 22.4, 22.2, 20.9, 19.5, 19.2.

Triketone (20)

To a solution of **19** (10.3 mg, 0.0134 mmol) in THF (1.5 mL) was added $Pd(PPh_3)_4$ (ca. 1 mg) and morphiline (6.5 μL, 0.0745 mmol). The reaction mixture was stirred at r.t. for 4 h. After removal of the solvent in vacuo, the residue was purified by flash column chromatography (silica gel, Hex:EA = 7:3) to afford **20** (6.6 mg, 72%) as a colourless oil. IR (thin film, cm^{-1}) ν: 2931, 2127, 1742, 1428, 1373, 1230, 1112, 910, 823, 736, 704. ^{1}H NMR (300 MHz, $CDCl_3$) δ: 9.70 (1H, s), 7.70–7.65 (4H, m), 7.43–7.39 (6H, m), 5.20 (1H, dd, *J* = 6.7, 8.7 Hz), 4.89 (1H, s), 4.76 (1H, s), 3.72 (1H, dd, *J* = 6.6, 10.4 Hz), 3.67 (1H, dd, *J* = 6.6, 10.4 Hz), 2.98 (1H, q, *J* = 7.2 Hz), 2.90 (1H, m), 2.79 (1H, dd, *J* = 5.6, 14.0 Hz), 2.67 (1H, m), 2.53–1.94 (11H, m), 1.89 (3H, s), 1.76 (1H, m), 1.71 (3H, s), 1.59–1.46 (2H, m), 1.07 (9H, s), 0.87 (3H, s). ^{13}C NMR (75 MHz, $CDCl_3$) δ: 221.7, 208.4, 207.7, 199.7, 170.4, 145.4, 135.63, 135.55, 133.3, 133.17, 129.8, 127.8, 112.5, 77.2, 69.7, 65.0, 64.3, 49.4, 43.5, 43.1, 42.8, 42.3, 40.7, 40.3, 39.4, 36.5, 35.3, 30.1, 26.9, 22.1, 21.4, 21.0, 19.2, 19.0.

Anionic cyclization adduct (21)

To a solution of **3** (57 mg, 0.094 mmol) in DCM (4 mL) was added Cs_2CO_3 (61 mg, 0.187 mmol). The mixture was stirred at r.t. for 10 min. A solution of **A3** (38 mg, 0.19 mmol) in DCM (2.0 mL) was added into this mixture over 10 min. The reaction mixture was stirred at r.t. for 2 h. It was then filtered through a pad of Celite® and washed with DCM. After removal of the solvent in vacuo, the residue was purified by flash column chromatography (silica gel, Hex:EA = 2:1) to afford **21** (58 mg, 77%) as a white foam. Mp: 57–59 °C. $[\alpha]_D^{20}$ +30.4 (*c* 0.51, $CHCl_3$). IR (thin film, cm^{-1}) ν: 2934, 2859, 1746, 1732, 1711, 1659, 1651, 1230. ^{1}H NMR (300 MHz, $CDCl_3$) δ: 12.3 (1H, s), 9.40 (1H, d, *J* = 1.8 Hz), 7.70–7.66 (4H, m), 7.43–7.38 (6H, m), 5.98–5.84 (1H, m), 5.49 (1H, t, *J* = 8.8 Hz), 5.36–5.23 (2H, m), 4.78–4.61 (2H, m), 4.53 (1H, t, *J* = 5.0 Hz), 4.29 (1H, dd, *J* = 5.2, 8.0 Hz), 3.68 (2H, ddd, *J* = 6.4, 10.3, 13.5 Hz), 3.58 (1H, d, *J* = 8.0 Hz), 3.08 (1H, dd, *J* = 6.1, 16.2 Hz), 2.75 (1H, dd, *J* = 1.4, 16.2 Hz), 2.68–2.54 (2H, m, H-17), 2.44–2.05 (5H, m), 1.95 (1H, dd, *J* = 9.9, 14.9 Hz), 1.82 (3H, s), 1.76 (1H, dd, *J* = 1.3, 14.9 Hz), 1.55–1.48 (1H, m), 1.46 (3H, s), 1.32 (3H, s), 1.07 (9H, s), 0.86 (3H, s). ^{13}C NMR (75 MHz, $CDCl_3$) δ: 222.1, 207.3, 197.4, 172.3, 170.6, 169.8, 135.6, 135.6, 133.3, 133.1, 131.7, 129.8, 129.7, 127.8, 127.8, 119.0, 109.5, 97.7, 78.1, 73.7, 70.0, 65.7, 64.3, 61.2, 49.3, 43.1, 40.6, 40.1, 39.8, 38.0, 36.5, 30.1, 27.8, 26.9, 25.7, 22.2, 20.7, 19.7, 19.2. CI-MS *m/e*: 818 (M + NH_4^+). HR-MS calcd. for $C_{45}H_{60}NO_{11}Si$ (M + NH_4^+): 818.3935; found: 818.3948.

Triketone (22)

To a solution of **21** (190 mg, 0.237 mmol) in THF was added $Pd(PPh_3)_4$ (13.7 mg, 0.012 mmol) and morphiline (0.103 mL, 1.19 mmol). The reaction mixture was stirred at r.t. for 5 min at which time the reaction was complete by TLC. After removal of the solvent in vacuo, the residue was purified by flash column chromatography (silica gel, Hex:EA = 1:1) to afford **22** (146 mg, 86%) as a white solid. Mp: 139–142 °C. $[\alpha]_D^{20}$ +16.7 (*c* 0.33, $CHCl_3$). IR (thin film, cm^{-1}) ν: 2932, 2859, 1738, 1731, 1714, 1471, 1428, 1372, 1223, 1112. ^{1}H NMR (300 MHz, $CDCl_3$) δ: 9.94 (1H, s), 7.68–7.59 (4H, m), 7.48–7.36 (6H, m), 5.39 (1H, dd, *J* = 5.8, 9.0 Hz), 4.57 (1H, m), 4.08 (1H, dd, *J* = 5.5, 6.8 Hz), 3.69 (2H, ddd, *J* = 6.7, 10.5, 16.9 Hz), 3.08–2.98 (2H, m), 2.69 (1H, dd, *J* = 1.8, 15.8 Hz), 2.54–2.43 (4H, m), 2.38–2.25 (3H, m), 2.17–2.07 (2H, m), 1.96 (1H, dd, *J* = 10.3, 15.1 Hz), 1.89 (3H, s), 1.60–1.43 (2H, m), 1.38 (3H, s), 1.31 (3H, s), 1.07 (9H, s), 0.85 (3H, s). ^{13}C NMR (75 MHz, $CDCl_3$) δ: 221.5, 206.4, 206.3, 200.6, 170.2, 135.6, 135.5, 133.3, 133.2, 129.8, 127.8, 109.6, 74.0, 74.0, 69.3, 64.4, 59.8, 49.2, 43.8, 43.3, 40.6, 39.5, 39.1, 39.0, 38.9, 36.4, 27.4, 26.9, 25.6, 22.2, 20.9, 19.2, 18.7. EI-MS *m/e*: 701 (M^+ – CH_3), 495 (100%). HR-MS calcd. for $C_{40}H_{49}O_9Si$ (M^+ – CH_3): 701.3146; found: 701.3140.

Alcohol (23)

To a solution of **22** (35.7 mg, 0.0498 mmol) in THF (2.0 mL) at –78 °C was slowly added $LiAlH[OC(C_2H_5)_3]_3$ (0.50 mol/L in THF, 0.130 mL, 0.0650 mmol). The temperature was raised to 0 °C and the mixture was stirred at this temperature for 1 h. Ether (5.0 mL) was added to dilute the reaction solution, then 5% aq. AcOH (4.0 mL) was added to quench the reaction. The mixture was stirred for 15 min. It was extracted with ether (3 × 10 mL), the combined organic layers were washed with satd. $NaHCO_3$ (4.0 mL) and brine (4.0 mL), and dried over $MgSO_4$. After removal of the solvent in vacuo, the residue was purified by flash column chromatography (silica gel, Hex:EA = 1:1 with 0.5% MeOH) to afford **23** (35.6 mg, 99%) as a colourless oil. ^{1}H NMR (300 MHz, $CDCl_3$) at least two conformations in $CDCl_3$ δ: 7.72–7.59 (4H, m), 7.47–7.37 (6H, m), 5.20 (0.4H, t, *J* = 9.2 Hz), 4.91 (0.6H, t, *J* = 8.8 Hz), 4.56–4.50 (1H, m),

© 2005 NRC Canada

4.18–3.71 (5H, m), 3.41 (0.6H, m), 3.21–3.03 (1H, m), 2.86–1.86 (13H, m), 1.83 (1.8H, s), 1.77 (1.2H, s), 1.42 (1.2H, s), 1.40 (1.8H, s), 1.33 (1.2H, s), 1.30 (1.8H, s), 1.09 (3.6H, s), 1.07 (5.4H, s), 0.98 (1.2H, s), 0.86 (1.8H, s).

SEM ether (24)

To a solution of **23** (45 mg, 0.0626 mmol) in DCM (2.5 mL) was added DIPEA (0.164 mL, 0.939 mmol). The solution cooled to 0 °C and 2-(trimethylsilyl)ethoxychloromethyl ether (SEMCl) (0.133 mL, 0.751 mmol) was added dropwise. The mixture was stirred at r.t. for 16 h. It was diluted with DCM (30 mL) and washed with satd. $NaHCO_3$ (5.0 mL). The aqueous layer was extracted with DCM (2 × 10 mL). The combined organic layers were washed with satd. $NaHCO_3$ and brine (5.0 mL each) and dried over $MgSO_4$ and concentrated in vacuo. The residue was purified by flash column chromatography (silica gel, Hex:EA = 2:1) to afford **24** (37.5 mg, 71%) as a white foam. Mp: 48–51 °C. $[\alpha]_D^{20}$ –6.1 (*c* 1.0, $CHCl_3$). IR (thin film, cm^{-1}) ν: 2955, 1742, 1715, 1240, 1112, 1059, 835, 704. ^1H NMR (300 MHz, $CDCl_3$) δ: 7.68–7.61 (4H, m), 7.46–7.36 (6H, m), 4.97 (1H, dd, *J* = 6.1, 9.3 Hz), 4.58 (2H, s), 4.50 (1H, dd, *J* = 5.7, 9.9 Hz), 4.02 (1H, dd, *J* = 5.7, 9.4 Hz), 3.95 (1H, d, *J* = 9.9 Hz), 3.70 (3H, ddd + d, *J* = 6.7, 10.5, 16.9 Hz and *J* = 9.6 Hz), 3.54 (2H, m), 3.08 (1H, dd, *J* = 6.0, 16.2 Hz), 2.75–2.54 (4H, m), 2.50–2.02 (7H, m), 1.84 (3H, s), 1.83 (1H, m), 1.61–1.54 (2H, m), 1.42 (3H, s), 1.30 (3H, s), 1.06 (9H, s), 0.95–0.85 (2H, m), 0.89 (3H, s), 0.00 (9H, s). ^{13}C NMR (75 MHz, $CDCl_3$) δ: 221.5, 208.0, 207.3, 170.5, 135.6, 135.5, 133.3, 133.2, 129.8, 127.8, 108.9, 95.3, 74.5, 73.1, 69.4, 65.6, 65.3, 64.4, 51.3, 49.1, 43.8, 43.8, 42.0, 40.8, 40.3, 39.6, 39.3, 38.6, 36.4, 27.9, 26.9, 25.5, 22.3, 20.9, 19.3, 18.9, 18.0, –1.4. CI-MS *m/e*: 866 ($M + NH_4^+$), 849 (MH^+). HR-MS calcd. for $C_{47}H_{69}O_{10}Si_2$ (MH^+): 849.4429; found: 849.4414.

Enone (25)

To a solution of **24** (7.1 mg, 0.008 36 mmol) in benzene (1.0 mL) was added 1,8-diazabicyclo[5.4.0]undecene (DBU) (0.62 µL, 0.00418 mmol). The mixture was heated to reflux for 4 h. After removal of the solvent in vacuo, the residue was purified by flash column chromatography (silica gel, Hex:EA = 1:1) to afford **25** (6.3 mg, 95%) as a colourless oil. $[\alpha]_D^{20}$ –33.4 (*c* 0.44, $CHCl_3$). IR (thin film, cm^{-1}) ν: 3444, 2955, 1739, 1682, 1470, 1428, 1372, 1248, 1112, 1058. ^1H NMR (300 MHz, $CDCl_3$) δ: 7.68–7.63 (4H, m), 7.46–7.36 (6H, m), 6.67 (1H, dd, *J* = 2.1, 10.3 Hz), 6.02 (1H, dd, *J* = 2.0, 10.3 Hz), 4.95 (1H, dd, *J* = 4.2, 10.9 Hz), 4.60 (2H, s), 4.19 (1H, d, *J* = 9.6 Hz), 4.10 (1H, m), 3.78–3.62 (3H, m), 3.60–3.48 (2H, m), 2.85 (1H, m), 2.73 (1H, br d, *J* = 15.3 Hz), 2.53 (1H, dd, *J* = 5.3, 15.5 Hz), 2.46–1.99 (7H, m), 1.86 (3H, s), 1.84 (1H, dd, *J* = 10.6, 14.8 Hz), 1.56–1.52 (1H, m), 1.46 (1H, d, *J* = 14.2 Hz), 1.09 (9H, s), 0.97–0.84 (2H, m), 0.89 (3H, s), 0.01 (9H, s). ^{13}C NMR (75 MHz, $CDCl_3$) δ: 221.4, 208.5, 198.2, 170.4, 147.2, 135.6, 133.4, 133.2, 129.85, 129.80, 128.5, 127.8, 95.3, 69.2, 67.2, 65.6, 64.4, 64.1, 52.1, 49.2, 45.4, 43.8, 42.3, 40.0, 38.8, 38.6, 36.4, 26.9, 22.2, 21.0, 19.3, 18.8, 18.0, –1.4. EI-MS *m/e*: 733 ($M^+ - C_4H_9$), 199 (100%). HR-MS calcd. for $C_{40}H_{53}O_9Si_2$ ($M^+ - C_4H_9$): 733.3228; found: 733.3242.

Enone (26)

To a solution of **24** (15.3 mg, 18 µmol) in THF (1.8 mL) was added KHMDS (0.5 mol/L in toluene, 18 µL, 9.0 µmol). The mixture was heated to reflux for 30 min. It was filtered through a pad of silica gel and washed with EA. The filtrate was concentrated in vacuo and the residue was purified by flash column chromatography (silica gel, Hex:EA = 16:9) to give **26** as a colourless oil (4.3 mg, 28%) along with an unidentified by-product (4.1 mg). $[\alpha]_D^{20}$ –45.8 (*c* 0.61, $CHCl_3$). IR (thin film, cm^{-1}) ν: 3466, 3071, 2956, 1747, 1693, 1471, 1428, 1378, 1231, 1112, 1036. ^1H NMR (300 MHz, $CDCl_3$) δ: 7.66–7.62 (4H, m), 7.42–7.36 (6H, m), 6.68 (1H, dd, *J* = 2.0, 10.3 Hz), 6.01 (1H, dd, *J* = 2.2, 10.3 Hz), 4.92 (1H, dt, *J* = 4.6, 11.0 Hz), 4.74 (1H, d, *J* = 16.7 Hz), 4.67 (1H, d, *J* = 16.7 Hz), 4.26 (1H, d, *J* = 9.8 Hz), 4.17 (1H, m), 3.99 (1H, d, *J* = 9.8 Hz), 3.78–3.54 (5H, m), 2.89–2.64 (4H, m), 2.42 (1H, dd, *J* = 11.0, 13.1 Hz), 2.17–2.04 (1H, m), 1.95–1.56 (5H, m), 1.88 (3H, s), 1.16–1.08 (3H, m), 1.03 (9H, s), 0.99 (3H, s), 0.02 (9H, s). ^{13}C NMR (75 MHz, $CDCl_3$) δ: 211.5, 198.4, 169.5, 146.0, 135.6, 133.9, 129.5, 128.6, 127.6, 95.5, 82.0, 67.7, 67.2, 66.4, 65.6, 63.8, 52.9, 51.9, 50.9, 47.1, 46.3, 44.4, 43.8, 40.1, 32.6, 26.9, 24.5, 20.6, 19.2, 18.1, 15.4, –1.4. EI-MS *m/e*: 791 (MH^+), 327 (100%). HR-MS calcd. for $C_{44}H_{63}O_9Si_2$ (MH^+): 791.4010; found: 791.3997.

Diol (27)

To a stirred solution of glacial AcOH (0.5 mL) was added $Me_4NHB(OAc)_3$ (76 mg, 0.29 mmol) in two batches. It was stirred at r.t. for 1.5 h and then cooled to 0 °C. It was transferred to a solution of **23** (20.8 mg, 0.029 mmol) in CH_3CN at 5 °C by cannula. The mixture was stirred at 5 °C for 3 h before the temperature was raised to 0 °C and stirred at 0 °C for 16 h. MeOH (0.10 mL) was added to quench the reaction. The solvent was removed in vacuo. The residue was diluted with DCM (15 mL) and washed with satd. $NaHCO_3$ (5.0 mL). The aqueous layer was extracted with DCM (2 × 5.0 mL). The combined organic layers were dried over $MgSO_4$ and concentrated in vacuo. The residue was purified by flash column chromatography (silica gel, Hex:EA = 1:1 with 0.5% MeOH) to afford **27** (17.3 mg, 96%) as a white solid, along with the recovered starting material (2.8 mg, 87% conversion (conv.)). Mp: 85–88 °C. IR (thin film, cm^{-1}) ν: 3453, 2933, 1730, 1428, 1371, 1244, 1112, 911, 733. ^1H NMR (300 MHz, $CDCl_3$) at least two conformations in $CDCl_3$ δ: 7.69–7.61 (4H, m), 7.48–7.36 (6H, m), 5.75 (0.56H, d, *J* = 10.5 Hz), 5.46 (0.45H, d, *J* = 11.2 Hz), 4.34–3.42 (7H, m), 2.80–1.98 (12H, m), 1.96 (3H, s), 1.94 (3H, s), 1.92–1.53 (4H, m), 1.45 (1.5H, s), 1.40 (1.8H, s), 1.31 (1.4H, s), 1.28 (1.3H, s), 1.27 (1.3H, s), 1.06 (4.5H, s), 1.05 (4.5H, s), 0.89 (2.3H, s), 0.85 (1.2H, s). ^{13}C NMR (75 MHz, $CDCl_3$) at least two conformations in $CDCl_3$ δ: 221.8, 210.4, 171.4, 135.6, 133.5, 133.3, 129.8, 129.7, 127.9, 127.8, 127.7, 79.2, 78.1, 75.4, 74.3, 72.7, 72.0, 71.1, 70.5, 70.1, 69.9, 68.4, 64.4, 64.1, 63.3, 62.2, 48.7, 44.9, 44.6, 44.2, 44.0, 43.1, 42.9, 40.6, 40.4, 40.0, 37.9, 37.5, 37.4, 37.1, 36.9, 36.7, 34.3, 34.0, 33.6, 32.8, 31.8, 31.4, 28.3, 28.1, 26.9, 25.9, 22.9, 22.6, 22.3, 21.3, 19.3, 18.3, 18.2. EI-MS *m/e*: 702 ($M^+ - H_2O$), 84 (100%). HR-MS calcd. for $C_{41}H_{54}O_8Si$ ($M^+ - H_2O$): 702.3588; found: 702.3596.

© 2005 NRC Canada

Diacetonide (28)

To a solution of **27** (348 mg, 0.483 mmol) in acetone (6.0 mL) was added DMP (1.2 mL, 9.76 mmol) and CSA (11.2 mg, 0.0483 mmol). The mixture was stirred at r.t. for 1 h. Satd. $NaHCO_3$ (20 mL) was added to quench the reaction. It was extracted with ethyl acetate (1 × 50 mL, 2 × 20 mL). The combined organic layers were washed with water and brine (15 mL each) and dried over $MgSO_4$. After concentration in vacuo, the residue was purified by flash column chromatography (silica gel, Hex:EA = 2:1) to afford **28** (342 mg, 93%) as a colourless oil. $[\alpha]_D^{20}$ +11.0 (*c* 1.36, $CHCl_3$). IR (thin film, cm^{-1}) ν: 2933, 2252, 1732, 1463, 1428, 1372, 1242, 1112, 912, 734, 704. ^1H NMR (300 MHz, $CDCl_3$) δ: 7.65–7.61 (4H, m), 7.41–7.36 (6H, m), 5.63 (1H, dt, *J* = 2.5, 11.7 Hz), 4.39 (1H, t, *J* = 4.3 Hz), 4.29 (1H, dd, *J* = 4.4, 12.8 Hz), 4.12 (1H, d, *J* = 12.4 Hz), 3.83 (1H, dd, *J* = 4.9, 10.2 Hz), 3.66 (1H, d, *J* = 12.4 Hz), 3.61–3.57 (2H, m), 2.82 (1H, m), 2.58–2.28 (6H, m), 2.21–1.96 (5H, m), 1.93 (3H, s), 1.96–1.92 (1H, m), 1.75–1.63 (2H, m), 1.49 (3H, s), 1.43 (3H, s), 1.29 (6H, s), 1.05 (9H, s), 0.90 (3H, s). ^{13}C NMR (75 MHz, $CDCl_3$) δ: 221.9, 209.1, 170.3, 135.7, 133.5, 133.3, 129.8, 127.8, 127.7, 108.2, 99.3, 75.0, 73.2, 71.8, 70.6, 64.8, 64.4, 48.9, 46.6, 45.5, 40.2, 39.2, 37.9, 37.8, 36.3, 34.2, 29.4, 28.4, 27.2, 26.9, 25.9, 22.6, 21.5, 19.3, 18.9. EI-MS *m/e*: 745 ($M^+ - CH_3$), 703 ($M^+ - C_4H_9$), 199 (100%). HR-MS calcd. for $C_{43}H_{57}O_9Si$ ($M^+ - CH_3$): 745.3772; found: 745.3787.

Aldol adduct (29)

To a solution of **28** (180 mg, 0.237 mmol) in THF (22 mL) was added KHMDS (0.5 mol/L in toluene, 0.24 mL, 0.120 mmol). The mixture was heated to reflux while stirring for 20 min. The reaction was monitored by TLC. Upon completion, the reaction was cooled to r.t. aq. NH_4Cl (25 mL, satd. NH_4Cl – water = 1:1) was added to quench the reaction. It was extracted with ethyl acetate (1 × 30 mL, 2 × 20 mL). The combined organic layers were washed with water and brine (15 mL each) and dried over $MgSO_4$. After removal of the solvent in vacuo, the residue was purified by flash column chromatography (silica gel, Hex:EA = 7:3) to give **29** (154 mg, 86%) as a colourless oil. $[\alpha]_D^{20}$ –6.5 (*c* 0.83, $CHCl_3$). IR (thin film, cm^{-1}) ν: 3534, 2933, 1732, 1699, 1472, 1428, 1383, 1249, 1112, 1045. ^1H NMR (300 MHz, $CDCl_3$) δ: 7.67–7.63 (4H, m), 7.44–7.33 (6H, m), 5.54 (1H, dt, *J* = 5.4, 9.8 Hz), 4.48–4.41 (2H, m), 4.29 (1H, dd, *J* = 4.1, 12.7 Hz), 3.81–6.61 (4H, m), 3.51 (1H, s), 2.81 (1H, d, *J* = 12.3 Hz), 2.69 (1H, m), 2.55 (1H, dd, *J* = 1.7, 15.5 Hz), 2.29–2.01 (5H, m), 1.96 (3H, s), 1.92–1.75 (5H, m), 1.49 (3H, s), 1.46 (3H, s), 1.35 (3H, s), 1.33 (3H, s), 1.19 (1H, dd, *J* = 10.3, 13.7 Hz), 1.03 (9H, s), 0.99 (3H, s). ^{13}C NMR (75 MHz, $CDCl_3$) δ: 211.2, 170.2, 135.6, 134.0, 129.5, 127.6, 108.3, 99.6, 81.8, 75.1, 73.3, 70.9, 69.9, 66.6, 66.3, 52.0, 50.8, 46.4, 45.9, 42.4, 40.5, 40.0, 38.1, 33.6, 28.5, 28.1, 27.7, 26.9, 26.0, 24.4, 21.8, 19.2, 18.7, 15.3. EI-MS *m/e*: 745 ($M^+ - CH_3$), 199 (100%). HR-MS calcd. for $C_{43}H_{57}O_9Si$ ($M^+ - CH_3$): 745.3772; found: 745.3779.

Silylenol ether (30)

To a solution of **29** (276 mg, 0.36 mmol) in DCM (12 mL) was added triethylamine (1.52 mL, 10.9 mmol) and then *tert*-butyldimethylsilyltrifluoromethanesulfonate (TBSOTf) (1.67 mL, 7.25 mmol) at 8 °C. The mixture was stirred at this temperature for 20 min then the temperature was raised to r.t. The mixture was then stirred at r.t. for 3 h. 2-Propanol (0.50 mL) was added at 0 °C to consume the excess TBSOTf. After stirring at r.t. for 10 min, satd. $NaHCO_3$ (80 mL) was added. The mixture was extracted with ethyl acetate (2 × 100 mL). The combined organic layers were dried over Na_2SO_4 and concentrated. The residue was purified by flash column chromatography (silica gel, Hex:EA = 9:1 to 1:1) to give recovered **29** (80 mg, 71% (conv.) and **30** (225 mg, 100% based on recovered starting material (borsm)) as a colourless oil. $[\alpha]_D^{20}$ +2.8 (*c* 0.21, $CHCl_3$). IR (neat, cm^{-1}) ν: 3523, 3049, 2930, 2858, 1739, 1666, 1471, 1428, 1368, 1247, 1189, 1112, 1045, 866, 838, 759, 704. ^1H NMR (300 MHz, $CDCl_3$) δ: 7.66–7.63 (4H, m), 7.44–7.34 (6H, m), 5.72 (1H, m), 5.09 (1H, dd, *J* = 1.2, 6.6 Hz), 4.45 (1H, t, *J* = 3.7 Hz), 4.37 (1H, s, OH), 4.22 (1H, dd, *J* = 4.1, 12.8 Hz), 3.99 (1H, d, *J* = 12.2 Hz), 3.88 (1H, dd, *J* = 5.1, 8.7 Hz), 3.68 (1H, *J* = 5.2, 9.9 Hz), 3.57 (1H, dd, *J* = 7.2, 9.8 Hz), 3.45 (1H, d, *J* = 12.3 Hz), 2.71 (1H, m), 2.36 (1H, d, *J* = 11.8 Hz), 2.23–1.94 (5H, m), 1.89 (3H, s), 1.85–1.82 (1H, m), 1.74–1.60 (5H, m), 1.53 (3H, s), 1.46 (3H, s), 1.37 (3H, s), 1.35 (3H, s), 1.04 (9H, s), 0.91 (9H, s), 0.83 (3H, s), 0.23 (3H, s), 0.20 (3H, s). ^{13}C NMR (75 MHz, $CDCl_3$) δ: 170.0, 151.2, 135.6, 133.9, 129.53, 129.50, 127.6, 108.5, 106.3, 99.7, 83.5, 80.7, 73.7, 71.5, 70.7, 68.1, 65.2, 50.3, 46.0, 45.8, 44.6, 38.7, 37.2, 36.8, 36.0, 28.6, 28.5, 27.3, 26.9, 26.3, 26.1, 25.9, 21.6, 19.2, 18.8, 17.5, –3.8, –4.7. EI-MS *m/e*: 859 ($M^+ - CH_3$), 817 ($M^+ - C_4H_9$), 699 (100%). HR-MS calcd. for $C_{49}H_{71}O_9Si$ ($M^+ - CH_3$): 859.4636; found: 859.4648.

Phenylselenide (31)

To a solution of **30** (236 mg, 0.270 mmol) in DCM (20 mL) was added 2,6-di-*tert*-butylpyridine (0.21 mL, 1.48 mmol) and PhSeCl (258 mg, 1.35 mmol). The mixture was stirred at r.t. for 9 h. It was diluted with ether (100 mL) and washed with satd. $NaHCO_3$ (2 × 20 mL) and brine (20 mL). The combined aqueous layers were extracted with ether (20 mL) and the organic layer was washed with brine (10 mL). The combined organic layers were dried over Na_2SO_4 and concentrated in vacuo. The residue was purified by flash column chromatography (silica gel, Hex:EA = 4:1) to afford **30** (34 mg, 86% conv.) and **31** (150 mg, 71% borsm) as a colourless oil. $[\alpha]_D^{20}$ –33.3 (*c* 0.45, $CHCl_3$). IR (thin film, cm^{-1}) ν: 3561, 2978, 2875, 1736, 1702, 1467, 1230, 1093, 723, 649. ^1H NMR (300 MHz, $CDCl_3$) δ: 7.67–7.63 (4H, m), 7.54–7.52 (2H, m), 7.43–7.27 (9H, m), 5.63 (1H, dt, *J* = 5.6, 10.0 Hz), 4.77 (1H, d, *J* = 12.6 Hz), 4.40 (1H, m), 4.30 (1H, dd, *J* = 3.9, 12.6 Hz), 3.98 (1H, d, *J* = 1.2 Hz), 3.92 (1H, d, *J* = 12.6 Hz), 3.80 (1H, m), 3.70 (1H, m), 3.62 (1H, dd, *J* = 5.0, 9.8 Hz), 3.50 (1H, d, *J* = 13.6 Hz), 3.36 (1H, s), 2.66 (1H, m), 2.21–1.97 (6H, m), 1.96 (3H, s), 1.93–1.75 (4H, m), 1.53 (3H, s), 1.49 (3H, s), 1.36 (3H, s), 1.32 (3H, s), 1.26 (1H, m), 1.04 (12H, s), 0.93–0.86 (1H, m). ^{13}C NMR (75 MHz, $CDCl_3$) δ: 207.8, 170.1, 135.6, 135.2, 134.1, 129.43, 129.35, 129.1, 129.0, 127.5, 108.4, 99.3, 81.8, 76.3, 73.2, 70.5, 70.1, 67.3, 66.6, 51.2, 51.0, 49.6, 47.2, 46.3, 42.2, 41.2, 39.0, 33.5, 28.42, 28.38, 27.4, 26.9, 26.1, 24.5, 21.8, 19.2, 18.4, 15.2. EI-MS *m/e*:

© 2005 NRC Canada

898 ($M^+ - H_2O$), 369 (100%). HR-MS calcd. for $C_{50}H_{62}O_8SiSe$ ($M^+ - H_2O$): 898.3379; found: 898.3366.

Enone (32)

To a solution of **31** (107 mg, 0.117 mmol) in DCM (12 mL) was added H_2O_2 (12 mL) at 0 °C. The mixture was stirred at r.t. for 1 h. It was diluted with ice water and extracted with DCM. The combined organic layers were washed with water and brine then dried over Na_2SO_4. After removing the solvent in vacuo, the residue was purified by flash column chromatography to afford **32** (36.1 mg, 57% borsm) as a colourless oil. $[\alpha]_D^{20}$ –40.0 (*c* 0.82, $CHCl_3$). IR (thin film, cm^{-1}) ν: 3479, 2932, 2858, 1731, 1652, 1463, 1250, 1086. ^1H NMR (300 MHz, $CDCl_3$) δ: 7.69–7.60 (4H, m), 7.45–7.32 (6H, m), 5.97 (1H, s), 5.51 (1H, dt, *J* = 5.5, 10.3 Hz), 4.79 (1H, dd, *J* = 1.8, 12.7 Hz), 4.61–4.55 (2H, m), 4.47 (1H, s), 4.15 (1H, d, *J* = 12.3 Hz), 3.89 (1H, d, *J* = 12.4 Hz), 3.68 (1H, m), 3.10 (1H, d, *J* = 12.9 Hz), 2.29 (2H, m), 2.06–1.93 (2H, m), 1.92 (3H, s), 1.91–1.70 (4H, m), 1.57 (3H, s), 1.54 (3H, s), 1.38 (6H, s), 1.34–1.05 (2H, m), 1.03 (12H, s). ^{13}C NMR (75 MHz, $CDCl_3$) δ: 204.8, 169.9, 160.5, 135.5, 134.2, 131.7, 129.4, 127.5, 109.8, 101.2, 83.0, 76.7, 74.7, 70.7, 67.3, 66.8, 66.7, 51.4, 49.9, 46.8, 42.8, 42.7, 33.1, 31.2, 28.5, 26.9, 24.7, 23.7, 21.5, 19.2, 19.1, 15.4. EI-MS *m/e*: 743 ($M^+ - CH_3$), 701 ($M^+ - C_4H_9$), 485 (100%). HR-MS calcd. for $C_{43}H_{55}O_9Si$ ($M^+ - CH_3$): 743.3615; found: 743.3623.

Allylic alcohol (33)

A mixture of **32** (10.5 mg, 0.0138 mmol), Zn dust (18.1 mg, 0.277 mmol), AcOH (0.0158 mL, 0.277 mmol), and EtOH (0.58 mL) in a sealed tube was heated to 80 °C for 2 h. More Zn dust (82 mg) was added, and the reaction was heated to reflux for another 2 h. After cooling the reaction mixture to r.t., it was diluted with ethyl acetate and filtered through a pad of Celite®. After removal of the solvent, the residue was purified by flash column chromatography (silica gel, Hex:EA = 4:1) to afford **33** (3.0 mg, 29%) and **29** (3.1 mg, 32%) as colourless oils. $[\alpha]_D^{20}$ −46.4 (*c* 0.28, $CHCl_3$). IR (thin film, cm^{-1}) ν: 3541, 3417, 2929, 2857, 1732, 1714, 1462, 1428, 1384, 1362, 1251, 1113, 1046, 758, 703. ^1H NMR (300 MHz, $CDCl_3$) δ: 7.68–7.61 (4H, m), 7.44–7.33 (6H, m), 5.74 (1H, m), 5.65 (1H, dt, *J* = 5.3, 9.4 Hz), 5.29 (1H, m), 4.51 (1H, d, *J* = 12.6 Hz), 4.28 (1H, dd, *J* = 5.4, 11.2 Hz), 3.92 (1H, d, *J* = 12.7 Hz), 3.72 (1H, dd, *J* = 5.3, 9.9 Hz), 3.65 (1H, dd, *J* = 6.8, 9.9 Hz), 3.36 (1H, s), 2.75 (1H, d, *J* = 13.6 Hz), 2.68 (1H, m), 2.54–2.39 (2H, m), 2.28–2.13 (2H, m), 1.98 (3H, s), 1.97–1.69 (4H, m), 1.50 (3H, s), 1.39 (3H, s), 1.35–1.22 (3H, m), 1.03 (9H, s), 1.00 (3H, s), 0.87 (1H, m). ^{13}C NMR (75 MHz, $CDCl_3$) δ: 211.1, 170.3, 135.6, 133.9, 129.5, 128.6, 127.7, 127.6, 99.5, 81.6, 77.2, 73.0, 69.6, 66.1, 65.9, 51.6, 50.7, 46.3, 45.0, 43.8, 42.3, 40.1, 37.4, 33.7, 29.7, 28.1, 28.0, 26.9, 24.4, 22.0, 19.2, 18.9, 15.5. EI-MS *m/e*: 671, 653, 569, 511, 493, 295, 199 (100%). HR-MS calcd. for $C_{40}H_{51}O_7Si$ ($M^+ - OCH_3$): 671.3404; found: 671.3400.

Acknowledgements

The research chair in organic chemistry granted to Pr. Pierre Deslongchamps by BioChem Pharma Inc. and financial support from the Natural Sciences and Engineering Research Council of Canada (NSERC) are highly appreciated. We thank Dr. Andrew Corbett for his assistance in the preparation of this manuscript.

References

1. (*a*) L.F. Fieser and M. Fieser. *In* Steroids. Reinhold, New York. 1959. Chap. 20; (*b*) A. Arnaud. Compt. Rend. **106**, 1011 (1888); **107**, 1162 (1888).
2. (*a*) A. Kawamura, J. Guo, Y. Itagaki, C. Bell, Y. Wang, H.T. Garner, S. Magil, R.T. Gallagher, N. Berova, and K. Nakanishi. Proc. Natl. Acad. Sci. U.S.A. **96**, 6654 (1999); (*b*) A. Kawamura, J. Guo, F. Maggiali, N. Berova, and K. Nakanishi. Pure Appl. Chem. **71**, 1643 (1999).
3. C. Mannich and G. Siewert. Ber. **75**, 737; **75**, 750 (1942).
4. K. Florey and M. Ehrenstein. J. Org. Chem. **19**, 1174 (1954).
5. (*a*) J.-F. Lavallée and P. Deslongchamps. Tetrahedron Lett. **29**, 6033 (1988); (*b*) R. Ruel and P. Deslongchamps. Tetrahedron Lett. **31**, 3961 (1990); (*c*) R. Ruel and P. Deslongchamps. Can. J. Chem. **68**, 1917 (1990); (*d*) R. Ruel and P. Deslongchamps. Can. J. Chem. **70**, 1939 (1992); (*e*) D. Chapdelaine, J. Belzile, and P. Deslongchamps. J. Org. Chem. **67**, 5669 (2002); (*f*) S. Trudeau and P. Deslongchamps. J. Org. Chem. **69**, 832 (2004).
6. (*a*) S. Laschat, F. Narjes, and L.E. Overman. Tetrahedron, **50**, 347 (1994); (*b*) W. Deng, M.S. Jensen, L.E. Overman, P.V. Rucker, and J.-P. Vionnet. J. Org. Chem. **61**, 6760 (1996); (*c*) P.V. Rucker and L.E. Overman. Tetrahedron Lett. **39**, 4643 (1998); (*d*) J.H. Hynes, L.E. Overman, T. Nasser, and P.V. Rucker. Tetrahedron Lett. **39**, 4647 (1998); (*e*) L.E. Overman and P.V. Rucker. Heterocycles, **52**, 1297 (2000).
7. (*a*) M.E. Jung and P. Davidov. Angew. Chem. Int. Ed. **41**, 4125 (2002); (*b*) M.E. Jung and G. Piizzi. J. Org. Chem. **68**, 2572 (2003); (*c*) M.E. Jung and G. Piizzi. Org. Lett. **5**, 137 (2003).
8. Z. Yang, D. Shannon, V.-L. Truong, and P. Deslongchamps. Org. Lett. **4**, 4693 (2002).
9. G. Stork, F. West, H.Y. Lee, R.C.A. Isaacs, and S. Manabe. J. Am. Chem. Soc. **18**, 10 660 (1996).
10. J.-F. Lavallée, C. Spino, R. Ruel, K.T. Hogan, and P. Deslongchamps. Can. J. Chem. **70**, 1406 (1992).
11. A. Toro, P. Nowak, and P. Deslongchamps. J. Am. Chem. Soc. **122**, 4526 (2000).
12. S. Nahm and S.M. Weinreb. Tetrahedron Lett. **22**, 3815 (1981).
13. J. Chen and J.N. Marx. Tetrahedron Lett. **38**, 1889 (1997).
14. D.B. Dess and J.C. Martin. J. Org. Chem. **48**, 4156 (1983).
15. (*a*) E.J. Corey, A. Marfat, G. Goto, and F. Brion. J. Am. Chem. Soc. **102**, 7895 (1980); (*b*) J.S. Yadav and P. Vadapalli. Tetrahedron Lett. **35**, 641 (1994).
16. J.M. Williams, R.B. Jobson, N. Yasuda, G. Marchesini, U.-H. Dolling, and E.J.J. Grabowski. Tetrahedron Lett. **36**, 5461 (1995).
17. For a review, see: T.T. Tidwell. Org. React. (N.Y.), **39**, 297 (1990).
18. (*a*) E.J. Corey and G.N. Widiger. J. Org. Chem. **40**, 2975 (1975); (*b*) P. Hayes and C. Maignan. Synthesis, 785 (1999); (*c*) H. Takikawa, J. Koizumi, Y. Kato, and K. Mori. J. Chem. Soc. Perkin Trans. 1, 2271 (1999).
19. J.P. Morgan and R.H. Grubbs. Org. Lett. **2**, 3153 (2000).
20. V.-L. Truong. M.Sc. dissertation, Université de Sherbrooke, Sherbrooke, Que. 2001.
21. S. Krishnamurthy. J. Org. Chem. **46**, 4628 (1981).
22. B.H. Lipshutz and J.J. Pegram. Tetrahedron Lett. **21**, 3343 (1980).
23. D.A. Evans, K.T. Chapman, and E.M. Carreira. J. Am. Chem. Soc. **110**, 3560 (1988).

© 2005 NRC Canada

24. L.N. Mander and S.P. Sethi. Tetrahedron Lett. **25**, 5953 (1984).
25. B.M. Stoltz, T. Kano, and E.J. Corey. J. Am. Chem. Soc. **122**, 9044 (2000).
26. For a review, see: H.J. Reich and S. Wollowitz. Org. React. (N.Y.), **44**, 1 (1993).
27. B.D. Roth and N.H. Roark. Tetrahedron Lett. **29**, 1255 (1988).

© 2005 NRC Canada

Palladium-catalysed synthesis of nonsymmetrically disubstituted-1,1′-biphenyls from *o*-substituted aryl iodides through aryl coupling and delayed hydrogenolysis[1]

Sara Deledda, Elena Motti, and Marta Catellani

Abstract: In the presence of $Pd(OAc)_2$ and norbornene as catalysts, two molecules of an ortho-substituted aryl iodide undergo aryl–aryl coupling to a palladium-bonded biphenylyl intermediate, which is hydrogenolyzed by benzyl alcohol to give 2,3′-disubstituted biaryl derivatives in satisfactory yields. A curious behaviour was observed with *o*-chloroiodobenzene, which gave activation of the C—Cl bond with four-membered ring formation.

Key words: biphenyls, aryl–aryl coupling, multistep reactions, palladium, palladacycles, C-H activation, catalysis.

Résumé : En présence de $Pd(OAc)_2$ et de norbornène agissant comme catalyseurs, deux molécules d'iodure d'aryle substituées en ortho subissent une réaction de couplage aryle–aryle conduisant à un intermédiaire biphénylyle lié au palladium qui peut subir une réaction d'hydrogénolyse sous l'action de l'alcool benzylique pour conduire à la formation de dérivés biaryles 2,3′-disubstitués, avec des rendements satisfaisants. On a observé un comportement bizarre avec l'*o*-chloroiodobenzène donne lieu à une activation de la liaison C—Cl avec formation d'un cycle à quatre membres.

Mots clés : biphényles, couplage aryle–aryle, réactions en plusieurs étapes, palladium, palladacyles, activation C-H, catalyse.

[Traduit par la Rédaction]

Introduction

Biphenyls are an important class of organic compounds, the biphenyl unit being the building block of several types of structures of current interest, including natural products, polymers, advanced materials, liquid crystals, ligands, and drugs (1).

The most successful catalytic methods in biphenyl synthesis are based on palladium catalysis (2–7). We used a catalytic system involving palladacycles (8–13). Different types of the latter have been extensively studied by several groups (14–17).

According to our methodology, aryl–aryl coupling through palladacycles occurs regioselectively. As shown in the simplified Scheme 1 (L = solvent or coordinating molecule), these palladacycles are formed by the reaction of an aryl iodide with palladium(0) and norbornene. In the presence of an *ortho*-R substituent (alkyl, aryl, and other functional groups), the palladacycle reacts selectively with the aryl iodide to form an sp^2–sp^2 carbon–carbon bond at the aryl site (pathway a), while the remaining norbornylpalladium bond readily deinserts norbornene to afford a biphenylylpalladium complex (18). By contrast, when the R substituent is H or a small group like F, the aryl group preferentially migrates on the norbornyl site of the palladacycle (pathway b) (18).

Causing the biphenylylpalladium complex to undergo a reaction able to liberate the organic product and palladium(0) renders the process catalytic. In this way the synthesis of a variety of interesting classes of organic compounds such as selectively substituted phenanthrenes (19), terphenyls (20), and biphenyl derivatives containing an oxoalkyl (21) or a vinyl (22) chain has been achieved.

We now report a catalytic synthesis of 2,3′-disubstituted-1,1′-biphenyls, based on the combination of the stoichiometric sequence leading to the biphenylylpalladium species with a delayed hydrogenolysis reaction.

Results and discussion

As shown in Scheme 2, two molecules of an ortho-substituted aryl iodide and one of a hydrogen donor react in the presence of $Pd(OAc)_2$ and norbornene as catalysts, and K_2CO_3 as a base in a dipolar aprotic solvent such as 1-methyl-2-pyrrolidinone (NMP) at 105 °C for 24 h to give 2,3′-disubstituted-1,1′-biphenyls (**1**).

The main difficulty for the achievement of this synthesis laid in obtaining an efficient hydrogenolysis of the

Received 8 December 2004. Published on the NRC Research Press Web site at http://canjchem.nrc.ca on 23 June 2005.

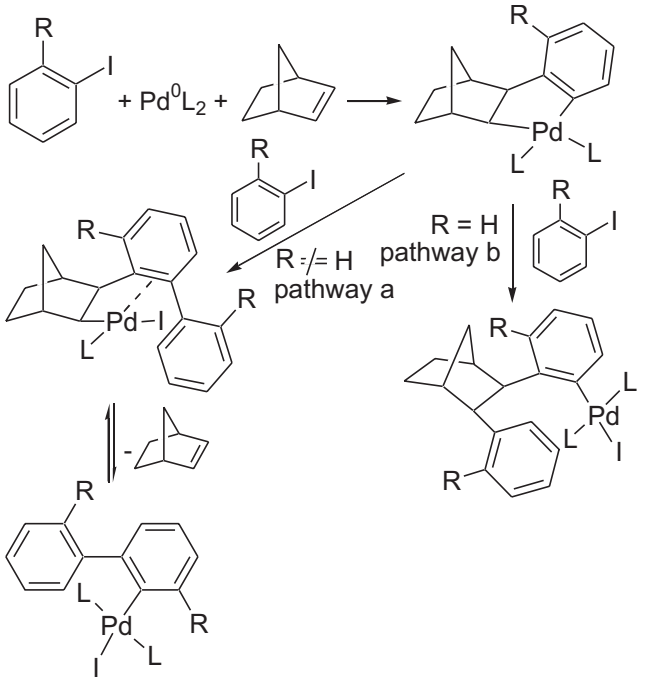
S. Deledda, E. Motti, and M. Catellani.[2] Dipartimento di Chimica Organica e Industriale and CIRCC, Parco Area delle Scienze, 17/A, 43100 Parma, Italy.

[1]This article is part of a Special Issue dedicated to Professor Howard Alper.

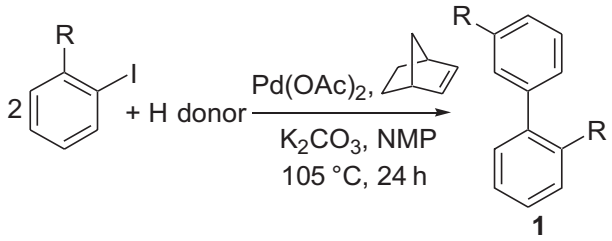
[2]Corresponding author (e-mail: marta.catellani@unipr.it).

 doi: 10.1139/V05-084 © 2005 NRC Canada

Scheme 1.



Scheme 2.



biphenylylpalladium species without interfering with the previous steps. To effect hydrogenolysis, two main methods were available: hydrogenation of the C-Pd-I bond with dihydrogen and hydrogen transfer from suitable sources. In principle, with both methods a selectivity problem could be expected since hydrogenolysis can occur at any step of the sequence. However, while hydrogenation with dihydrogen at atmospheric pressure gave a nonselective outcome, the appropriate use of the hydrogen transfer methodology led to delayed hydrogenolysis to the end of the catalytic sequence with good selectivity.

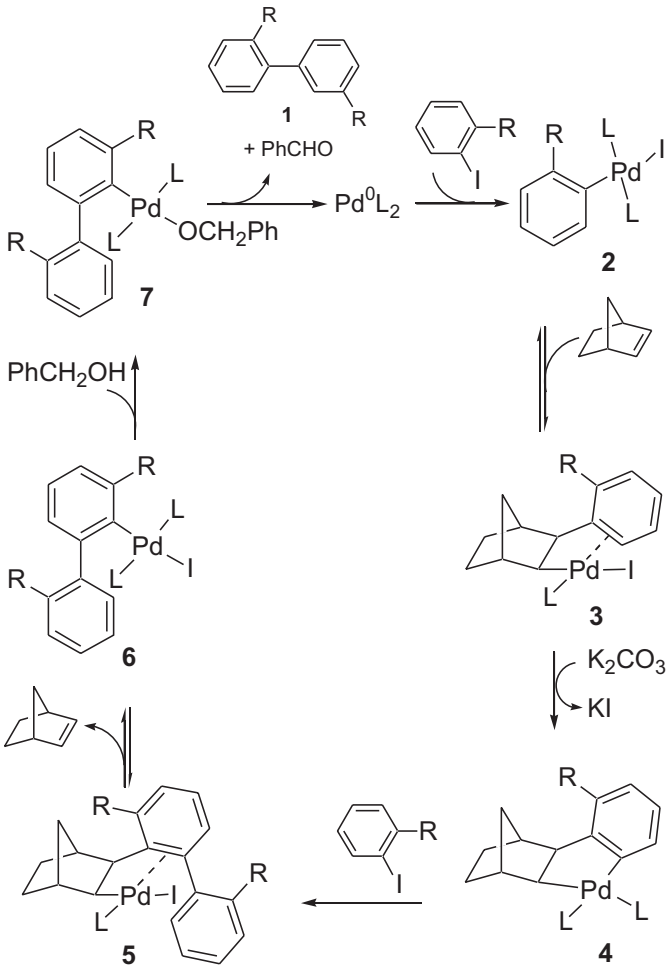
Among the combination of palladium sources, solvents, and bases examined, $Pd(OAc)_2$, NMP, and K_2CO_3 proved to be the most effective. The norbornene to aryl iodide molar ratio was found to play an important role, better results being obtained when using a ratio as low as 0.25 equiv. The reaction of *o*-isopropyliodobenzene (80 equiv.) with different hydrogen donors (80 equiv.) was thus carried out in the presence of $Pd(OAc)_2$ (1 equiv.), K_2CO_3 (160 equiv.), norbornene (20 equiv.) in NMP at 105 °C for 24 h under nitrogen. Various hydrogen donors were tested in a 1:1 molar ratio to *o*-isopropyliodobenzene as the substrate. Table 1 reports the yield of the biphenyl **1** (Scheme 2, R = *i*-Pr) obtained. Among the examined hydrogen sources, benzyl

Table 1. Reaction of *o*-*i*-propyliodobenzene and a H donor in the presence of K_2CO_3, norbornene, and $Pd(OAc)_2$.[a]

Run	Hydrogen donor	Biphenyl **1** yield (%)[b]
1	Benzyl alcohol	86
2	Benzydrol	84
3	Butanol	75
4	Isobutyl formate	72
5	Sodium formate	21
6	Water	37, 77[c]

[a]Molar ratio of the reagents *o*-*i*-propyliodobenzene : H donor : K_2CO_3 : norbornene : $Pd(OAc)_2$ = 80:80:160:20:1 at 105 °C for 24 h in NMP under nitrogen; 2×10^{-3} mmol $Pd(OAc)_2$/mL NMP.
[b]GC yield on the charged amount of the aryl iodide.
[c]Water to palladium molar ratio: 2.5×10^2.

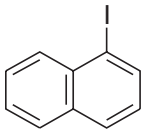
Scheme 3.



alcohol and benzhydrol appear the most effective ones (Table 1, runs 1 and 2). Butanol (Table 1, run 3) and isobutyl formate (Table 1, run 4) behave analogously affording satisfactory results, while sodium formate (23) (Table 1, run 5) gives a low yield because of the formation of products resulting from Pd-C hydrogenolysis of the intermediate complexes **3** and **4** reported in Scheme 3. Water also is effective (Table 1, run 6) but only if used in large excess (2.5×10^2 molar ratio to palladium) otherwise the reaction leads to

© 2005 NRC Canada

Table 2. Reaction of ortho-substituted aryl iodides and benzyl alcohol in the presence of K_2CO_3, norbornene, and $Pd(OAc)_2$.[a]

Run	Aryl iodide	Biphenyl **1** yield (%)[b]
1	*o*-MeC_6H_4I	72
2	*o*-EtC_6H_4I	84
3	*o*-*n*-BuC_6H_4I	79
4	*o*-*i*-PrC_6H_4I	83
5	*o*-$MeO_2CC_6H_4I$	87
6	*o*-$MeOC_6H_4I$	48
7		78

[a]Molar ratio of the reagents in the order reported in the title: 80:80:160:20:1 at 105 °C for 24 h in NMP, N_2 atmosphere; 2×10^{-3} mmol $Pd(OAc)_2$/mL NMP.
[b]Isolated yield on the charged aryl iodide. Conversion was complete.

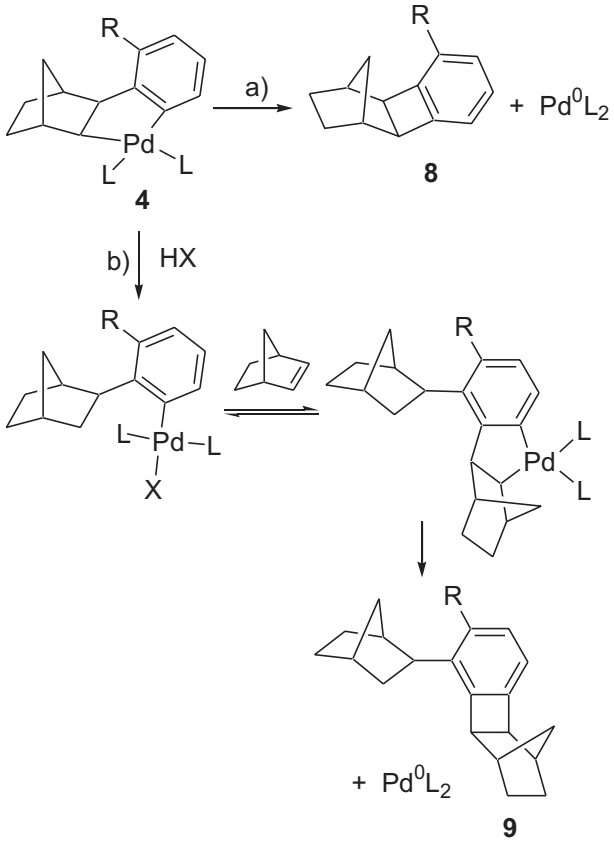
poor results. An aryl iodide to benzyl alcohol molar ratio of 1:1 was found to be optimal, an excess of benzyl alcohol being detrimental.

Scheme 3 shows the proposed reaction pathway. The catalytic cycle is initiated by the oxidative addition of the *o*-substituted aryl iodide to palladium(0) formed in situ by $Pd(OAc)_2$ reduction. Norbornene insertion into the resulting arylpalladium complex **2** occurs stereoselectively leading to the *cis*,*exo* arylnorbornylpalladium species **3** (24–28). In the presence of a base such as K_2CO_3, the open precursor undergoes ring closure to **4** (10–13) through an electrophilic aromatic substitution (11) facilitated by an η^2-interaction of palladium with one double bond of the aromatic ring (25, 28). Palladacycle formation implies activation of an usually inert aromatic C—H bond (29–31). Because of the presence of the ortho substituent in the aromatic ring of palladacycle **4**, a second molecule of aryl iodide selectively attacks the aromatic moiety of the same palladacycle **4** affording complex **5**, which deinserts norbornene with formation of the biphenylylpalladium species **6** (18). At this stage, complex **6** reacts with benzyl alcohol to give **7**, which promotes hydrogen transfer via a Pd-H intermediate to form biphenyl **1** together with palladium(0) and benzaldehyde.

Table 2 reports the results obtained carrying out the reaction with an *o*-substituted aryl iodide (80 equiv.), benzyl alcohol (80 equiv.), palladium acetate (1 equiv.), norbornene (20 equiv.), and potassium carbonate (160 equiv.) in NMP under nitrogen at 105 °C for 24 h. Satisfactory results were obtained with different primary and secondary alkyl groups as well as with electron-withdrawing substituents (Table 2, runs 1–5) while the presence of an electron-releasing group such as the methoxy one (Table 2, run 6) led only to poor results. 1-Iodonaphthalene (Table 2, run 7) behaved as an ortho-substituted arene, which is a requirement for the aryl coupling to occur, and gave acceptable yields.

By-products result from hydrogen transfer to intermediate complexes. The hydrogen donor mostly reacts with the species containing a norbornyl– rather than an aryl–palladium bond. In particular, arylnorbornylpalladium iodide **3** is readily hydrogenolysed to the corresponding arylnorbornane and

Scheme 4.



palladacycle **4**, after hydrogenolysis of the norbornylpalladium bond, inserts a new molecule of norbornene in the resulting Pd–aryl bond to form **9** according to pathway b of Scheme 4. Compound **8** also derives from palladacycle **4** as shown in Scheme 4. The steric effect of the ortho substituent favours reductive elimination to compound **8**, containing a four-membered ring (pathway a) (32), in place of the reaction with a second molecule of aryl iodide. By-products **8** and **9** were usually formed with a yield from 1% to 5%.

A 5,9-disubstituted 1,2,3,4,4a,12b-hexahydro-1,4-methanotriphenylene derivative of type **10** (33, 34), was usually formed to a large extent when the hydrogen donor became deficient owing to secondary reactions. As shown in Scheme 5, **10** derives from complex **5**, which, in the absence of an efficient terminating agent, prefers to undergo reductive elimination by ring closure instead of norbornene deinsertion.

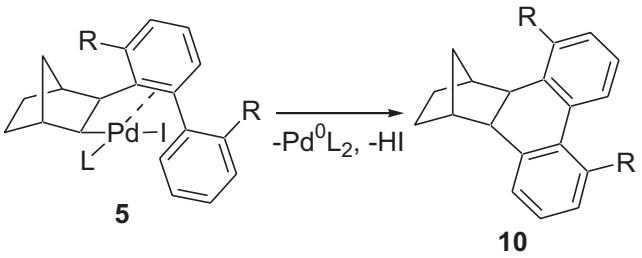
As previously reported, if R is a methyl group, two additional by-products resulting from activation of the benzylic C-H (35) were formed to a small extent (5%).

Anomalous behaviours were observed with *o*-chloro- and *o*-fluoroiodobenzene.

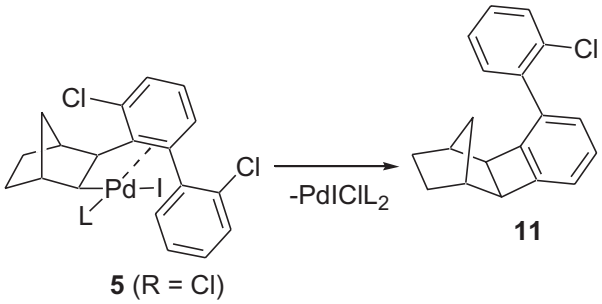
o-Chloroiodobenzene, used in a 40:1 molar ratio to palladium, gave poor conversion (28%) and only a small amount (6%) of **1** was formed. The main product was the hexahydromethanobiphenylene derivative **11** (15%), which derives from C—Cl bond activation (Scheme 6). This result is surprising not only because it implies activation of an usually inert C—Cl bond, but also because it should be regarded as involving the C—Cl bond of the norbornyl-bonded *o*-

© 2005 NRC Canada

Scheme 5.



Scheme 6.



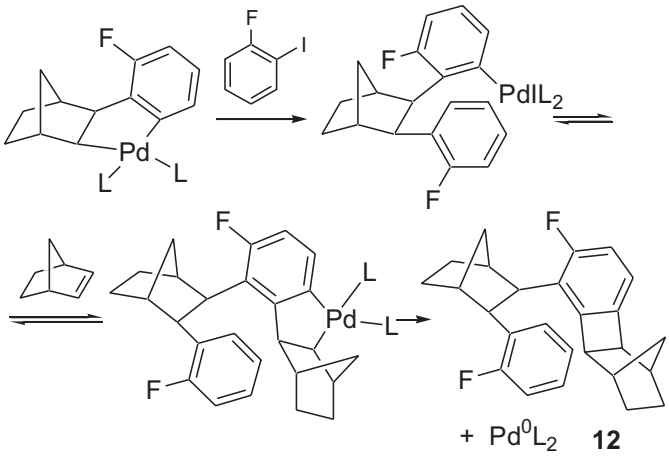
chloroaryl group of complex **5** (Scheme 6), C—Cl bond activation occurring only in the presence of a second *o*-chloroaryl unit. The alternative formation of a type **10** compound does not occur. The origin of this behaviour is probably to be attributed to a Pd-Cl interaction that favours C-Cl activation, thus preventing not only formation of a type **10** compound but also norbornene deinsertion.

As previously reported (22), the different reactivity of the F group is likely to be ascribed to the small size of the fluorine atom. The latter is not large enough to give "the ortho effect", which would cause the formation of the aryl–aryl bond of intermediate **5** by reaction of palladacycle **4** with *o*-fluoroiodobenzene (Scheme 3, R = F), and so the *ortho*-fluorophenyl group migrates to the norbornyl site of the palladacycle. Ring closure to hexahydromethanotriphenylene does not occur, however, because of the deactivation of the aromatic nucleus towards the arylpalladium electrophilic attack and norbornene is instead inserted. The reaction thus terminates with the formation of the hexahydromethanobiphenylene **12** in 67% yield, as reported in Scheme 7.

Conclusion

In conclusion, the catalytic method we have worked out offers a ready access to nonsymmetrically disubstituted biphenyls starting from two molecules of an *o*-substituted aryl iodide and represents a useful alternative to the Suzuki reaction and to other organometallic processes. The failure of *o*-fluoroiodobenzene to give the expected reaction confirms the need for a sufficiently bulky group ortho to iodobenzene, while the observation that the usually unreactive arene C—Cl bond is readily cleaved shows that competitive steps readily occur in sequential reactions when usually inert bonds are forced into the appropriate position for the interaction with the metal.

Scheme 7.



Experimental

General

All reactions were carried out under a nitrogen atmosphere, using standard Schlenk techniques. Most chemicals were obtained commercially and used as received. Compounds **1** (R = Me (36), Et (37), OMe (38), CO_2Me (39), -$(CH)_4$- (40), Cl (41)), **8** (R = Me, OMe (32), Et, *n*-Bu, *i*-Pr (42), -$(CH)_4$- (43)), **9** (R = Me, Et, *n*-Bu, *i*-Pr (20), -$(CH)_4$- (43)), and **12** (22) were previously reported. ^{1}H and ^{13}C NMR spectra were carried out in $CDCl_3$ at 20 °C using Bruker AC300 and AVANCE300 spectrometers at 300.1 and 75.4 MHz, respectively. Chemical shifts are reported in ppm using the solvent as the internal reference. The assignments of NMR resonances are based on decoupling and 2D experiments; one or more asterisks indicates interchangeable assignments. Mass spectra (EI) were recorded using a Finnigan Mat SSQ 710 spectrometer operating at 70 eV and are reported as *m*/*z* (relative intensity). IR spectra were run on a PerkinElmer 298 FT-IR spectrophotometer and are reported as wavenumbers (cm^{-1}). GC analyses were performed with a Carlo Erba HRGC 5300 instrument using a 30 m long SE-30 capillary column and a Hewlett-Packard 3394 integrator. Flash column chromatography was performed on Merck Kieselgel 60 and analytical TLC on Merck 60F_{254} plates. Melting points were determined on an Electrothermal apparatus and are uncorrected. Elemental analyses were performed with a Carlo Erba EA 1108 elemental analyser.

Reaction of *o*-substituted aryl iodides with benzyl alcohol

General procedure

A mixture of $Pd(OAc)_2$ (5 mg, 0.022 mmol), K_2CO_3 (498 mg, 3.6 mmol), the desired aryl iodide (1.8 mmol), norbornene (42 mg, 0.45 mmol), and benzyl alcohol (195 mg, 1.8 mmol) in NMP (10 mL) under nitrogen was heated at 105 °C with stirring for 24 h. The mixture was cooled to room temperature, diluted with CH_2Cl_2 (20 mL), and extracted twice with a 5% solution of H_2SO_4 (2 × 15 mL). The organic layer was washed with water (20 mL) and dried over anhydr. Na_2SO_4. The crude product was ana-

© 2005 NRC Canada

lysed by GC, GC–MS, and TLC. Products were isolated by flash column chromatography using hexane or mixtures of hexane–EtOAc as the eluents. By-product yields were determined by GC analysis.

2,3′-Dimethyl-1,1′-biphenyl (1, R = Me)

The reaction was carried out following the general procedure using 393 mg (1.8 mmol) of *o*-iodotoluene. Compound **1** (R = Me) (36) was isolated as a colourless oil in 72% yield (118 mg) by column chromatography, using hexane as the eluent. Compounds **8** (R = Me) (32) and **9** (R = Me) (20) were formed in 2% and 3% yield, respectively, together with two by-products resulting from the activation of the benzylic C—H bond (35) (2% yield each) and *exo*,*o*-tolylnorbornane (4%) (44) resulting from hydrogenolysis of complex **3** (R = Me).

2,3′-Diethyl-1,1′-biphenyl (1, R = Et)

The reaction was carried out following the general procedure using 418 mg (1.8 mmol) of *o*-ethyliodobenzene. Compound **1** (R = Et) (37) was isolated as a colourless oil in 84% yield (159 mg) by column chromatography, using hexane as the eluent. Compounds **8** (R = Et) (42) and **9** (R = Et) (20) were formed in 4% and 5% yield, respectively.

2,3′-Di*-i-*propyl-1,1′-biphenyl (1, R = i-Pr)

The reaction was carried out following the general procedure using 443 mg (1.8 mmol) of *o*-*i*-propyliodobenzene. Compound **1** (R = *i*-Pr) was isolated as a white solid in 83% yield (178 mg) by column chromatography, using hexane as the eluent. Compounds **8** (R = *i*-Pr) (42), **9** (R = *i*-Pr) (20), and **10** (R = *i*-Pr) were formed in 5%, 3%, and 2% yield, respectively.

***1** (R = i-Pr)*

^{1}H NMR δ: 7.44–7.30 (3H, m), 7.27–7.16 (4H, m), 7.13 (1H, dt, *J* = 7.4, 1.4 Hz), 3.07, 2.96 (2H, 2 hept. partly overlapping, *J* = 6.9 Hz), 1.30 (6H, d, *J* = 6.9 Hz), 1.18 (6H, d, *J* = 6.9 Hz). ^{13}C NMR δ: 148.45, 146.38, 141.98, 141.40, 129.91, 127.82, 127.52, 126.66, 125.53, 125.22, 124.82, 34.06, 29.37, 24.34, 24.02. MS *m*/*z* (%): 238 (M^+, 61), 223 (33), 195 (81), 181 (100), 179 (21), 165 (29). Anal. calcd. for $C_{18}H_{22}$: C 90.70, H 9.30; found: C 90.82, H 9.18.

5,9-Di-i-*propyl-1,2,3,4,4a,12b-hexahydro-1,4-methanotriphenylene (**10**, R = i-Pr)*

^{1}H NMR δ: 7.29–7.24 (1H, m, H8), 7.23–7.17 (3H, m, H10, H6, H7), 7.14 (1H, t, *J* = 7.5 Hz, H11), 7.03 (1H, d further split, *J* = 7.3 Hz, H12), 3.76 (1H, hept., *J* = 6.8 Hz, CH(C9)), 3.34 (1H, d, *J* = 9.4 Hz, H12b), 3.20 (1H, hept., *J* = 6.8 Hz, CH(C5)), 3.06 (1H, d, *J* = 9.4 Hz, H4a), 2.30 (1H, m, H4), 2.21 (1H, m, H1), 1.81–1.56 (4H, m, H2 exo, H3 exo, H2 endo, H3 endo), 1.53 (3H, d, *J* = 6.8 Hz, C*H*$_3$CH(C9)), 1.36 (3H, d, *J* = 6.8 Hz, C*H*$_3$CH(C5)), 1.24–1.17 (4H, m, H13 syn, C*H*$_3$CH(C5) centred at 1.21), 1.06 (3H, d, *J* = 6.8 Hz, C*H*$_3$CH(C9)), 0.96 (1H, d quintets, *J* = 10.0, 1.5 Hz, H13 anti). ^{13}C NMR δ: 147.45, 145.26, 140.04, 135.73, 133.94, 132.69, 126.99 (C8), 126.67 (C11), 125.64 (C7*), 125.19 (C12), 124.87 (C10), 124.27 (C6*), 48.57 (C1), 47.63 (C4, C12b), 42.82 (C4a), 33.77 (C13), 32.10 (C3), 30.52 (CH(C9)), 28.64 (CH(C5)), 28.28 (C2), 26.71 (*C*H$_3$CH(C9)), 24.65 (*C*H$_3$CH(C5)), 24.03 (*C*H$_3$CH(C9)), 23.57 (*C*H$_3$CH(C5)). MS *m*/*z* (%): 330 (M^+, 63), 262 (25), 245 (26), 205 (76), 203 (39), 202 (37), 179 (100). Anal. calcd. for $C_{25}H_{30}$: C 90.85, H 9.15; found: C 90.98, H 9.02.

2,3′-Di*-n-*butyl-1,1′-biphenyl (1, R = n-Bu)

The reaction was carried out following the general procedure using 469 mg (1.8 mmol) of *o*-*n*-butyliodobenzene. Compound **1** (R = *n*-Bu) was isolated as a colourless oil in 79% yield (190 mg) by column chromatography, using hexane as the eluent. Compounds **8** (R = *n*-Bu) (42) and **9** (R = *n*-Bu) (20) were formed in 4% and 3% yield, respectively.

***1** (R = n-Bu)*

^{1}H NMR δ: 7.35–7.27 (3H, m), 7.24–7.20 (2H, m), 7.19–7.09 (3H, m), 2.66 (2H, t, *J* = 7.6 Hz), 2.61–2.54 (2H, m), 1.70–1.57 (2H, m), 1.57–1.30 (6H, m), 1.30–1.09 (2H, m), 0.94 (3H, t, *J* = 7.3 Hz), 0.80 (3H, t, *J* = 7.3 Hz). ^{13}C NMR δ: 142.44, 142.03, 141.85, 140.35, 129.94, 129.40, 129.18, 127.79, 127.14, 126.77, 126.46, 125.42, 35.61, 33.65, 32.74, 22.53, 22.29, 13.96, 13.83. MS *m*/*z* (%): 266 (M^+, 39), 223 (20), 209 (22), 180 (16), 178 (16), 167 (100), 152 (10). Anal. calcd. for $C_{20}H_{26}$: C 90.19, H 9.84; found: C 90.28, H 9.75.

2,3′-Dimethoxycarbonyl-1,1′-biphenyl (1, R = CO$_2$Me)

The reaction was carried out following the general procedure using 472 mg (1.8 mmol) of methyl *o*-iodobenzoate. Compound **1** (R = CO_2Me) (39) was isolated as a solid in 87% yield (212 mg) by flash chromatography, using hexane – CH_2Cl_2 – ethyl acetate (7:2.5:0.5) as the eluent. Compounds **8** (R = CO_2Me) and **10** (R = CO_2Me) were formed in 5% and 4% yield, respectively.

***1** (R = CO$_2$Me)*

^{1}H NMR δ: 8.07–8.00 (2H, m, H4′, H2′), 7.89 (1H, dd, *J* = 7.7, 1.5 Hz, H3), 7.55 (1H, td, *J* = 7.5, 1.5 Hz, H5), 7.52–7.45 (2H, m, H5′, H6′), 7.44 (1H, td, *J* = 7.6, 1.4 Hz, H4), 7.37 (1H, dt, *J* = 7.6, 1.4 Hz, H6), 3.92 (3H, s, CO_2CH_3), 3.64 (3H, s, CO_2CH_3). ^{13}C NMR δ: 168.49 (q), 166.95 (q), 141.67 (q), 132.88 (C6′), 131.52 (C5), 130.79 (C6), 130.40 (q), 130.11 (C3), 129.99 (q), 129.43 (C2′), 128.39 (C4′), 128.00 (C5′), 127.61 (C4), 52.15 (CO_2CH_3), 51.98 (CO_2CH_3). MS *m*/*z* (%): 270 (M^+, 83), 239 (71), 207 (100), 181 (29), 180 (23), 152 (44), 151 (43), 76 (29). Anal. calcd. for $C_{16}H_{14}O_4$: C 71.10, H 5.22; found: C 71.37, H 5.19.

*5-Methoxycarbonyl-1,2,3,4,4a,8b-hexahydro-1,4-methanobiphenylene (**8**, R = CO$_2$Me)*

^{1}H NMR δ: 7.78 (1H, dd, *J* = 7.8 Hz), 7.27 (1H, dd, *J* = 7.8, 7.4 Hz), 7.15 (1H, d, *J* = 7.4 Hz), 3.39 (1H, d, *J* = 3.7 Hz), 3.20 (1H, d, *J* = 3.8 Hz), 2.48–2.43 (1H, m), 2.31–2.25 (1H, m), 1.65–1.55 (2H, m), 1.29–1.18 (1H, m), 0.97 (1H, d quintets, *J* = 10.2, 1.4 Hz), 0.78 (1H, d quintets, *J* = 10.2, 1.7 Hz). MS *m*/*z* (%): 228 (M^+, 7), 187 (100), 155 (89), 141 (26), 128 (38), 115 (22).

*5,9-Dimethoxycarbonyl-1,2,3,4,4a,12b-hexahydro-1,4-methanotriphenylene (**10**, R = CO$_2$Me)*

Mp (hexane–CH_2Cl_2, 1:1) 142 to 143 °C. IR (KBr) ν: 1735, 1712. ^{1}H NMR δ: 7.71 (1H, dd, *J* = 7.8, 1.2 Hz, H6), 7.42 (1H, dd, *J* = 7.5, 1.5 Hz, H10), 7.37–7.31 (2H, m, H8, H12), 7.25 (1H, t, *J* = 7.5 Hz, H11), 7.17 (1H, t, *J* = 7.8 Hz,

© 2005 NRC Canada

H7), 3.92 (3H, s, CH_3O_2C(C5)), 3.90 (1H, d, J = 9.9 Hz, H4a), 3.76 (3H, s, CH_3O_2C(C9)), 3.30 (1H, d, J = 9.9 Hz, H12b), 2.29 (1H, br s, H4), 2.26 (1H, br s, H1), 1.79–1.55 (4H, m, H2 exo, H3 exo, H2 endo, H3 endo), 1.29 (1H, d quintets, J = 10.2, 1.8 Hz, H13 syn), 1.02 (1H, d quintets, J = 10.2, 1.2 Hz, H13 anti). ^{13}C NMR δ: 172.13 (CO), 168.77 (CO), 140.48 (q), 139.47 (q), 132.27 (q), 132.14 (q), 131.42 (C12), 131.17 (C8), 130.96 (q), 130.32 (C6), 129.92 (q), 128.15 (C10), 127.32 (C11), 125.29 (C7), 52.30 (CH_3CO_2(C9)), 52.14 (CH_3CO_2(C5)), 49.45 (C4), 49.12 (C1), 46.60 (C12b), 42.76 (C4a), 33.57 (C13), 31.15 (C2*), 29.25 (C3*). MS *m/z* (%): 362 (M^+, 29), 295 (29), 294 (100), 293 (22), 263 (72), 204 (15), 203 (17), 176 (18). Anal. calcd. for $C_{23}H_{22}O_4$: C 76.22, H 6.12; found: C 76.02, H 6.07.

2,3′-Dimethoxy-1,1′-biphenyl (1, R = OMe)

The reaction was carried out following the general procedure using 421 mg (1.8 mmol) of 2-iodoanisole. Compound **1** (R = OMe) (38) was isolated as a colourless oil in 48% yield (93 mg) by column chromatography, using hexane – ethyl acetate (9:1) as the eluent. Compound **8** (R = OMe) (32) was formed in 2% yield. Various by-products were also isolated but not further investigated.

1,2′-Binaphthyl (1, R = -(CH)$_4$-)

The reaction was carried out following the general procedure using 457 mg (1.8 mmol) of 1-iodonaphthalene. Compound **1** (R = -$(CH)_4$-) (40) was isolated as a white solid in 78% yield (179 mg) by column chromatography, using hexane as the eluent. Compounds **8** (R = -$(CH)_4$-) and **9** (R = -$(CH)_4$-)) (43) were formed in 2% yield each.

2,3′-Dichloro-1,1′-biphenyl (1, R = Cl)

The reaction was carried out following the general procedure using 215 mg (0.9 mmol) of *o*-chloroiodobenzene. Compound **1** (R = Cl) (41) was isolated as a colourless oil in 6% yield (6 mg) by column chromatography, using hexane as the eluent together with 72% of unconverted *o*-chloroiodobenzene (155 mg) and 15% yield (19 mg) of compound **11**.

*5-(2′-Chlorophenyl)-1,2,3,4,4a,8b-hexahydro-1,4-methanobiphenylene (**11**)*

^{1}H NMR δ: 7.50–7.42 (1H, m), 7.35–7.24 (5H, m), 7.21 (1H, br d, J = 7.1 Hz), 7.01 (1H, dd, J = 7.1, 1.0 Hz), 3.26–3.19 (2H, m), 2.32–2.28 (1H, m), 2.10–2.07 (1H, m), 1.65–1.44 (2H, m), 1.28–1.05 (2H, m), 1.00–0.89 (2H, m). ^{13}C NMR δ: 146.50, 144.91, 137.89, 133.92, 132.65, 131.13, 129.72, 128.42, 128.03, 127.17, 126.44, 121.30, 50.69, 49.97, 36.61, 36.31, 32.05, 27.85, 27.67. MS *m/z* (%): 280 (M^+, 11), 241 (32), 240 (18), 239 (100), 215 (19), 204 (19), 203 (209), 202 (33). Anal. calcd. for $C_{19}H_{17}Cl$: C 81.27, H 6.10; found: C 81.42, H 6.17.

Reaction of* o-*fluoroiodobenzene

The reaction was carried out following the general procedure using 200 mg (0.9 mmol) of *o*-fluoroiodobenzene. Compound **12** (22) was isolated in 67% yield (based on norbornene, 57 mg) by column chromatography, using hexane as the eluent. Other products were isolated but not further investigated.

Acknowledgments

We gratefully acknowledge the financial support by the University of Parma and Ministero dell'Università e della Ricerca Scientifica e Tecnologica (MIUR, project No. 2003039774). Mass and NMR facilities were provided by Centro Interfacoltà di Misure dell'Università di Parma.

References

1. S.P. Stanforth. Tetrahedron, **54**, 263 (1998).
2. J.K. Stille. Angew. Chem. Int. Ed. Engl. **25**, 508 (1986).
3. A. Suzuki. *In* Handbook of organopalladium chemistry for organic synthesis. *Edited by* E.-I. Negishi. John Wiley and Sons, New York. 2002. pp. 249–262.
4. E.-I. Negishi. *In* Handbook of organopalladium chemistry for organic synthesis. *Edited by* E.-I. Negishi. John Wiley and Sons, New York. 2002. pp. 229–247.
5. J. Hassan, M. Sévignon, C. Gozzi, E. Schulz, and M. Lemaire. Chem. Rev. **102**, 1359 (2002).
6. M. Kuroboshi, Y. Waki, and H. Tanaka. J. Org. Chem. **68**, 3938 (2003).
7. S.B. Park and H. Alper. Tetrahedron Lett. **45**, 5515 (2004).
8. M. Catellani. Synlett, 298 (2003).
9. M. Catellani. *In* Palladium in organic synthesis. *Edited by* J. Tsuji. Springer, Heidelberg, Germany. 2005. pp. 21–53.
10. M. Catellani and G.P. Chiusoli. J. Organomet. Chem. **346**, C27 (1988).
11. M. Catellani and G.P. Chiusoli. J. Organomet. Chem. **425**, 151 (1992).
12. M. Catellani, B. Marmiroli, M.C. Fagnola, and D. Acquotti. J. Organomet. Chem. **507**, 157 (1996).
13. C.-H. Liu, C.-S. Li, and C.-H. Cheng. Organometallics, **13**, 18 (1994).
14. I.P. Beletskaya and A.V. Cheprakov. J. Organomet. Chem. **689**, 4055 (2004).
15. J. Cámpora, P. Palma, and E. Carmona. Coord. Chem. Rev. **193–195**, 207 (1999).
16. G. Dyker. Chem. Ber./Recl. **130**, 1567 (1997).
17. A.D. Ryabov. Chem. Rev. **90**, 403 (1990).
18. M. Catellani and E. Motti. New J. Chem. **22**, 759 (1998).
19. M. Catellani, E. Motti, and S. Baratta. Org. Lett. **3**, 3611 (2001).
20. E. Motti, A. Mignozzi, and M. Catellani. J. Mol. Catal. A: Chem. **204–205**, 115 (2003).
21. M. Catellani, S. Deledda, B. Ganchegui, F. Hénin, E. Motti, and J. Muzart. J. Organomet. Chem. **678**, 473 (2003).
22. E. Motti, G. Ippomei, S. Deledda, and M. Catellani. Synthesis, 2671 (2003).
23. R.C. Larock and P.L. Johnson. Chem. Commun. 1368 (1989).
24. H. Horino, M. Arai, and M. Inoue. Tetrahedron Lett. 647 (1974).
25. C.-S. Li, C.-H. Cheng, F.-L. Liao, and S.-L. Wang. Chem. Commun. 710 (1994).
26. B.A. Markies, P. Wijkens, H. Kooijman, A.L. Spek, J. Boersma, and G. van Koten. Chem. Commun. 1420 (1992).
27. M. Portnoy, Y. Ben-David, I. Rousso, and D. Milstein. Organometallics, **13**, 3465 (1994).
28. M. Catellani, C. Mealli, E. Motti, P. Paoli, E. Perez-Carreno, and P.S. Pregosin. J. Am. Chem. Soc. **124**, 4336 (2002).
29. G. Dyker. Angew. Chem. Int. Ed. **38**, 1699 (1999).
30. G. Karig, M.T. Moon, N. Thasana, and T. Gallagher. Org. Lett. **4**, 3115 (2002).
31. Q. Huang, A. Fazio, G. Dai, M.A. Campo, and R.C. Larock. J. Am. Chem. Soc. **126**, 7460 (2004).

© 2005 NRC Canada

32. M. Catellani and L. Ferioli. Synthesis, 769 (1996).
33. K. Albrecht, O. Reiser, M. Weber, B. Knieriem, and A. de Meijere. Tetrahedron, **50**, 383 (1994).
34. M. Catellani and G.P. Chiusoli. J. Organomet. Chem. **286**, C13 (1985).
35. M. Catellani, E. Motti, and S. Ghelli. Chem. Commun. 2003 (2000).
36. G.J. Price and A.A. Clifton. Tetrahedron Lett. **32**, 7133 (1991).
37. S.A. Deiko, A.D. Ryabov, A.K. Yatsimiriskii, and I.B. Berezin. Dokl. Chem. (Transl. of Dokl. Akad. Nauk. SSSR), **266**, 356 (1982).
38. M. Hori, T. Kataoka, H. Shimizu, M. Miyagaki, and T. Takagi. Chem. Pharm. Bull. **22**, 2030 (1974).
39. A.V. Iretskii, S.C. Sherman, M.G. White, J.C. Kenvin, and D.A. Schiraldi. J. Catal. **193**, 49 (2000).
40. L.E. Harris and E.J. Eisenbraun. J. Org. Chem. **37**, 336 (1972).
41. P. Gomes, H. Fillon, C. Gosmini, E. Labbe, and J. Perichon. Tetrahedron, **58**, 8417 (2002).
42. M. Catellani and F. Cugini. Tetrahedron, **55**, 6595 (1999).
43. M. Catellani, G.P. Chiusoli, S. Ricotti, and F. Sabini. Gazz. Chim. Ital. **115**, 685 (1985).
44. G.A. Olah, C.S. Lee, and G.K.S. Prakash. J. Org. Chem. **59**, 2590 (1994).

© 2005 NRC Canada

New pseudohalide ligands in Ru-catalyzed olefin metathesis — A robust, air-activated iminopyrrolato catalyst[1]

Samantha D. Drouin, Heather M. Foucault, Glenn P.A. Yap, and Deryn E. Fogg

Abstract: Reaction of the Grubbs catalyst $RuCl_2(PCy_3)_2(CHPh)$ (**1**) with lithium 2-[(2,6-diisopropylphenyl)imino]pyrrolide·Et_2O (LiNN′·Et_2O) gives alkylidene complex **5**, containing a chelating, σ-bound iminopyrrolato unit. The structure of **5** is confirmed by X-ray crystallography. Treatment of **5** with pyridine generates $RuCl(NN')(py)_2(CHPh)$ (**6**) via displacement of PCy_3. Complex **5** effects ring-closing metathesis in air, displaying high reactivity relative to **6**.

Key words: ruthenium, alkylidene, metathesis, pyrrolimine, iminopyrrolato.

Résumé : La réaction du catalyseur de Grubbs, $RuCl_2(PCy_3)_2(CHPh)$ (**1**) avec le dérivé 2-[(2,6-diisopropylphényl)imino]pyrrolidure·Et_2O (LiNN′·Et_2O) conduit au complexe alkylidène **5** qui contient une unité iminopyrrolato chélatant à liaison σ. La structure du composé **5** a été confirmée par diffraction des rayons X. Le traitement du complexe **5** par de la pyridine génère le produit $RuCl(NN')(py)_2(CHPh)$ (**6**) par déplacement du PCy_3. Dans l'air, le complexe **5** subit une métathèse avec fermeture de cycle en démontrant une réactivité élevée comparée à celle du composé **6**.

Mots clés : ruthénium, alkylidène, métathèse, pyrrolimine, iminopyrrolato.

[Traduit par la Rédaction]

Introduction

Ring-closing metathesis (RCM) and cross-metathesis (CM) reactions hold tremendous interest for pharmaceutical synthesis, as well as "green chemistry" initiatives aimed at transforming seed oils into α-olefin feedstocks (1). The advent of robust, functional-group tolerant ruthenium catalysts such as **1** and **2** (Fig. 1) has significantly expanded the deployment of olefin metathesis methodologies by the organic community (1). Despite important recent advances in metathesis activity (2–6), however, major issues remain to be addressed. Chief among these — particularly from the perspective of industrial deployment of RCM and CM methodologies — is the problem of short catalyst lifetimes, which increases catalyst loading requirements, as well as heavy-metal contamination of the organic products. In 2002, we reported that the chloride ligands of Grubbs-class $RuCl_2LL'(CHR)$ catalysts are implicated in catalyst deactivation, promoting dimerization to unreactive, $Ru_2(\mu\text{-}Cl)_3$ species (7, 8). We subsequently described the synthesis of highly productive "pseudohalide" catalysts **3**, in which the chloride ligands are replaced by aryloxide groups (9, 10). Among these, complex **3a** is particularly long-lived, achieving >40 000 turnovers in RCM.

The present work is directed at exploring the accessibility of Ru alkylidene complexes containing N-donor pseudohalide ligands, a broad ligand class that may offer expanded opportunities in olefin metathesis, particularly in terms of stereocontrol and anchoring. A potential limitation, however, is a tendency toward π coordination of the heterocyclic ring to give piano-stool complexes. We have previously noted the ease with which the phenoxide ligand undergoes $\sigma \rightarrow \pi$ isomerization in late transition metal complexes containing labile ancillary ligands (11, 12), and indeed one of our motivations in incorporating electron-deficient aryloxides in complexes **3** is the diminished π-donor ability of these ligands (9, 10). π-Pyrrolide complexes have ample precedent in transition metal chemistry (13–15), and the facile formation of a Ru(π-pyrrolide) complex on reaction of $RuCl_2(PPh_3)_3$ with LiC_4H_3N (Scheme 1, (16)) may reveal a similar driving force. Keshner and Basolo (13) have pointed out, however, a preference for formation of σ-pyrrole complexes, over the corresponding π-bound species, and examples of $\pi \rightarrow \sigma$ isomerization in pyrrolide complexes have also been noted (14).

Several structural features of the iminopyrrolide ligand are attractive for their potential to stabilize σ donation. These include the narrow chelate bite angle of 70°–85° (17–22); we note that chelation does *not* prevent isomerization of aryloxide ligands that form larger, seven-membered chelate rings (11, 12). The enthalpically favoured conjugation of the pyrrolide and olefinic units may also favour retention of planarity in the ligand system. Chelating mono(imino)pyrrolato

Received 3 December 2004. Published on the NRC Research Press Web site at http://canjchem.nrc.ca on 23 June 2005.

Dedicated to Professor Howard Alper in honour of his many contributions to chemistry, catalysis, and the Canadian scientific community.

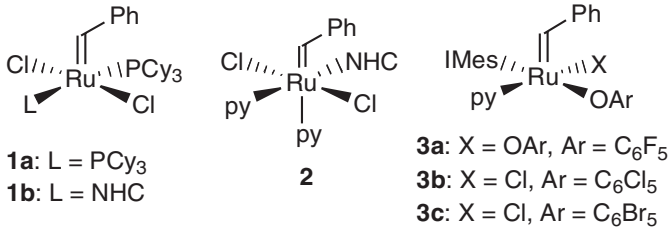
S.D. Drouin, H.M. Foucault, G.P.A. Yap, and D.E. Fogg.[2] Center for Catalysis Research and Innovation, Department of Chemistry, University of Ottawa, Ottawa, ON K1N 6N5, Canada.

[1]This article is part of a Special Issue dedicated to Professor Howard Alper.

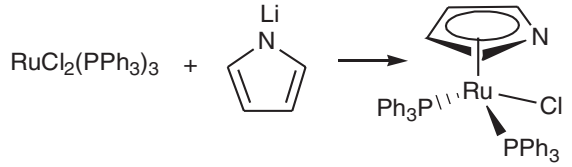
[2]Corresponding author (e-mail: dfogg@science.uottawa.ca).

 doi: 10.1139/V05-039 © 2005 NRC Canada

Fig. 1. Selected ruthenium metathesis catalysts. NHC = *N*-heterocyclic carbene; IMes = *N*,*N*′-bis(mesityl)imidazol-2-ylidene.



Scheme 1.



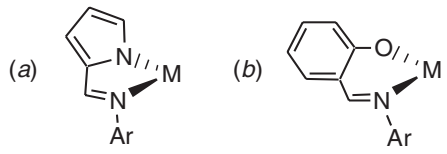
complexes have indeed been reported for a range of transition metals (17–22), including Ti complexes that prove potent polymerization catalysts (23). The ligands are attractive for their ease of access from commercially available precursors, as well as the potential for electronic and steric tuning via functionalization of the imino moiety (18). The iminopyrrolato ligand class has not previously been explored for olefin metathesis. Among existing metathesis catalysts, the closest relatives are salicylaldiminato Schiff base derivatives (24–26), which, however, form six-membered, rather than five-membered, chelate rings (Fig. 2). We now describe the synthesis of new ruthenium alkylidene complexes containing a K^2-*N*,*N*′-iminopyrrolato ligand, one of which shows impressive activity for RCM of diethyl diallylmalonate in air.

Results and discussion

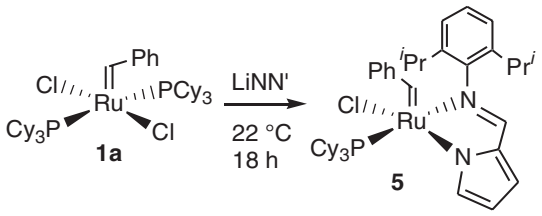
Reaction of the Grubbs catalyst **1** with 1.6 equiv. of LiNN′ in benzene effects conversion to σ-iminopyrrolide complex **5** within 18 h at room temperature (Scheme 2). Isolated yields are limited to ca. 70% by the high solubility of **5** in all solvents, including pentane. The requirement for excess LiNN′ is imposed by competing protonation to yield HNN′. Control experiments indicate that LiNN′ does not react with PCy_3 or **5** in C_6D_6, suggesting that **1** itself may be implicated in this side reaction. Complex **5** is stable in chlorinated solvents and undergoes no oxidation on exposure to air in solution for 72 h, as indicated by NMR experiments in which the alkylidene resonance for **5** is integrated against triphenylmethane as an internal standard.

Diagnostic for the presence of both the alkylidene and the PCy_3 ligand in **5** is the observation of a ^{13}C NMR doublet far downfield (303.5 ppm, $^2J_{CP}$ = 14.1 Hz), which in HMQC experiments correlates with an alkylidene doublet (δ_H 20.0 ppm, $^3J_{HP}$ = 11.6 Hz). Coupling of the alkylidene proton to phosphorus implies that the Ru=CHPh plane is oriented parallel to the Ru—P bond axis (27). A doublet is also observed for the azomethine proton (δ 7.8, d, $^4J_{HP}$ = 3.9 Hz): both of these resonances collapse to singlets in the $^1H\{^{31}P\}$ NMR spectrum. The isopropyl groups give rise to two

Fig. 2. Representative K^2-iminopyrrolato and salicylaldiminato complexes.



Scheme 2.



methine septets and four methyl doublets, implying restricted rotation about each aryl-nitrogen bond. Consistent with retention of the chelate ring, we see no coalescence of these signals, or those due to the aromatic *C*-*i*-Pr carbon nuclei (142.9, 142.0 ppm; assignment supported by HMBC correlation with isopropyl signals), up to 70 °C.

The chemical shifts of the proton and carbon nuclei in the pyrrolyl ring provide key insight into the bonding mode and hapticity of the ring, strong upfield shifts being characteristic of π-bound pyrrole (Table 1). We undertook detailed COSY, HMQC, and HMBC analysis of **5** to make unequivocal assignments, and to deconvolute the signals due to the pyrrolide ring from those due to the benzylidene or arylimine groups. Chemical shifts for the pyrrole ring protons are in good agreement with values reported for η^1-iminopyrrole complexes (17, 18, 21, 22), and are little perturbed relative to values for the parent lithium salt, consistent with σ coordination of the pyrrolide unit. The ^{13}C NMR data likewise agree with the literature values, showing little sensitivity to the identity of the metal or ancillary ligands. In comparison, the ^1H NMR resonances for the pyrrole ligand in $RuX(\eta^5\text{-}C_5H_4N)(PPh_3)_2$ (X = H, Cl) are shifted ca. 1 to 2 ppm upfield, and the ^{13}C NMR signals ca. 30 ppm upfield.

Unanswered by the NMR analysis is the question of whether the phosphine ligand is located trans to the pyrrolyl or the imine nitrogen. X-ray analysis was therefore undertaken on crystals of **5** grown from a concentrated toluene solution. An ORTEP diagram is shown in Fig. 3. The geometry at ruthenium is distorted square pyramidal, with the benzylidene ligand located in the apical site (as expected for this high trans influence ligand); consistent with the NMR data, the pyrrolyl ligand is σ-bound to the metal. The chloride and pyrrolyl nitrogen are trans-disposed in the basal plane, possibly enabling some "push–pull" interaction between the π-donor chloride ligand and the pyrrolyl group. The four basal bonds are angled toward the vacant site: the P-Ru-N(2) angle is 159.56(8)°, the N(1)-Ru-Cl angle is 164.39(8)°. As expected from the large J_{HP} value for the alkylidene ligand, the torsion angle about P-Ru-C(18)-C(24) is 129.6(3)°, resulting in a near-zero dihedral angle for P-Ru-C(18)-H_α. The bite angle of the iminopyrrolato ligand (79.04(10)°) is slightly larger than in related complexes

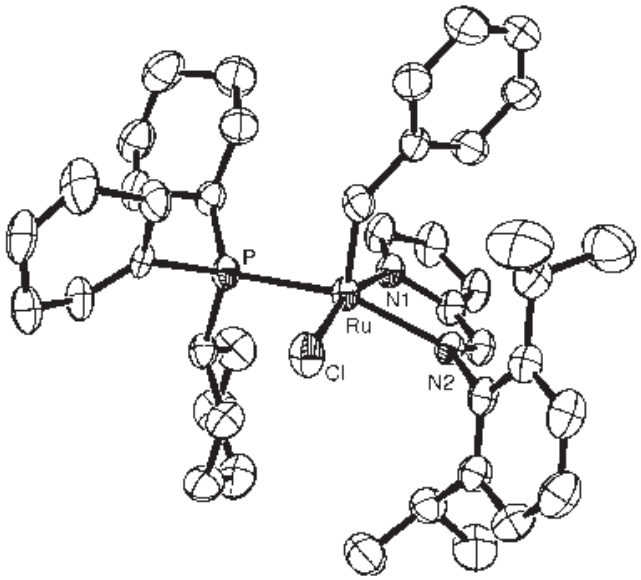
© 2005 NRC Canada

Table 1. NMR data for the pyrrolyl ligand in selected σ-iminopyrrolato and π-pyrrolyl complexes.[a]

Compound	Solvent	NMR data	Ref.
HNN′	C_6D_6	^{1}H: 6.45 (m, 1H), 6.05 (m, 2H)	28
LiNN′	C_6D_6	^{1}H: 7.15–7.2 (m, 1H), 6.89 (m, 1H), 6.42 (m, 1H)	This work
5	$CDCl_3$	^{1}H: 7.09–7.01 (m, 3H, ***H3*** + Ar), 6.51 (br, 1H, ***H5***), 6.18 (dd, ^3J = 3.9, 1.6 Hz, 1H, ***H4***); ^{13}C: 142.8 (d, $^3J_{CP}$ = 2.0 Hz, *C*2), 141.7 (s, ***C5***), 120.2 (s, ***C3***), 114.0 (s, ***C4***)	This work
6	$CDCl_3$	^{1}H: 8.59–6.91 (m, 20H, ***H3*** + Ar), 6.46 (br, 1H, ***H5***), 6.20 (m, 1H, ***H4***)	This work
$Zr(\eta^1\text{-NN}')_2(NMe_2)_2$	C_6D_6	^{1}H: 6.06 (dd, ^3J = 3.4, 1.6 Hz, 1H), 6.29 (s, 1H), 6.46 (s, 2H), 6.65 (dd, ^3J = 3.5, 1.0 Hz, 1H), 7.36 (s, 1H); ^{13}C: 113.1, 114.0, 119.5, 121.2, 147.6, 149.6	17
$Ni(\eta^1\text{-NN}')_2$	C_6D_6	^{1}H: 6.61 (m, 2H), 5.99 (m, 1H), 5.15 (m, 2H)	17
$Y(\eta^1\text{-NN}')_2[N(SiMe_3)_2]$	C_6D_6	^{1}H: 6.40 (dd, ^3J = 3.6, 2.0 Hz, 2H, ***H4***), 6.19 (br s, 2H, ***H5***), 6.63 (d, 2H, ***H3***); ^{13}C: 113.4 (***C4***), 123.7 (***C3***), 138.4 (***C5***), 141.7 (*C*2)	21
$Zn(\eta^1\text{-NN}')_2$	C_6D_6	^{1}H: 7.12 (d, ^3J = 1 Hz, 2H), 6.85–7.1 (overlaps Ar), 6.83 (^3J = 3.6, 1.0 Hz, 2H), 6.54 (dd, ^3J = 3.6, 1.7 Hz, 2H)	18
$RuH(\eta^1\text{-NN}'')(CO)(PPh_3)_2$[b]	$CDCl_3$	^{1}H: 6.68 (m, 1H), 6.59 (m, 1H), 6.38 (m, 1H)	22
$RuH(\eta^5\text{-}C_5H_4N)(PPh_3)_2$	C_6D_6	^{1}H: 5.33 (2H), 5.03 (2H); ^{13}C: 110.0, 82.0	16
$RuCl(\eta^5\text{-}C_5H_4N)(PPh_3)_2$	C_6D_6	^{1}H: 5.61 (2H), 4.24 (2H); ^{13}C: 108.4, 82.7	16

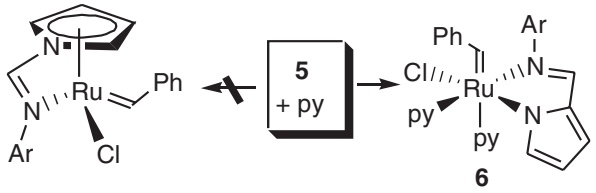
[a]Assignments (where reported) are shown in bold face.
[b]NN″ = (*R*)-2-[(1-phenylethylimino)methyl]pyrrolide.

Fig. 3. ORTEP diagram for $RuCl(NN')(PCy_3)(CHPh)$ (**5**). Thermal ellipsoids shown at 30% probability level; hydrogen atoms are omitted for clarity. Selected bond distances (Å) and angles (°): Ru—C(18) 1.828(4), Ru—P 2.3474(8), Ru—N(1) 2.065(3), Ru—N(2) 2.149(2), Ru—Cl 2.3869(8), C(18)—C(24) 1.479(5), N(2)—C(5) 1.307(4); C(18)-Ru-N(1) 98.49(13), C(18)-Ru-N(2) 105.72(12), N(1)-Ru-N(2) 79.04(10), N(1)-Ru-Cl 164.39(8), N(2)-Ru-P 159.56(8), C(18)-Ru-Cl 93.74(11), C(18)-Ru-P 94.69(10), C(24)-C(18)-Ru 134.2(2).



$(Zr(NN')_2(NMe_3)_2$ avg. 70.1° (17); $Ti[2\text{-}(PhN{=}CH)C_4H_3N]_2Cl_2$ avg. 75.9° (20)), but is considerably more acute than the O-Ru-N angle of 88.9(2)° reported for the salicylaldiminato analogue $RuCl(ON')(PCy_3)(=CHPh)$ (**4**) (ON′ = 2-(ArN=CHC_4H_3N) (24)). The sum of the bond angles around N(1) is 360°, indicating that the pyrrolyl ring remains planar. The exocyclic angle of 132.6(3)° for C(3)-C(4)-C(5) agrees with values found in previous work; this value is maintained in both free and coordinated iminopyrrolato ligands (17). The aromatic plane of the diisopropylphenyl unit is orthogonal to the chelated ring, an orientation that accommodates the steric demand of the isopropyl substituents and which is retained on dissolution, as judged from the ^{1}H NMR data above. The Ru—C(18) (alkylidene) bond distance of 1.828(4) Å is similar to that in **4** (1.850(6) Å) (24) and in $RuCl_2(PCy_3)_2(=CH\text{-}p\text{-}C_6H_4Cl)$ (1.838(3) Å) (29). The Ru—N(2) (imine) bond length of 2.149(2) Å is marginally longer than the Ru—N(1) (pyrrolyl) distance (2.065(3) Å), as found for other iminopyrrolato complexes (17, 18). Ru—Cl and Ru—P bond distances of 2.3869(8) and 2.3474(8) Å, respectively, are similar to those in **4** (2.382(2) and 2.345(2) Å) (24).

Scheme 3.



While formation of σ-pyrrolyl complex **5**, as opposed to a π-pyrrolyl piano-stool structure, tends to validate the relevance of the structural features discussed in the Introduction, we wished to examine the possibility that π → σ isomerization might simply be curbed by the low lability of the PCy_3 ligand in **5**. To probe this point, we undertook replacement of the PCy_3 ligand of **5** by a potentially more labile pyridine donor, loss of which would enable access to the three coordination sites required for π coordination of the heterocyclic ring (Scheme 3). Sequential reaction of **1** with LiNN′, fol-

© 2005 NRC Canada

Table 2. RCM of diethyl diallylmalonate catalyzed by RuCl(NN′)(PCy_3)(CHPh) (**5**) and RuCl(NN′)$(py)_2$(CHPh) (**6**).[a]

Entry	Catalyst	Additive	Time (min)	Conv. (%)[b]
1	**5**		480	100
2	**5**		1440	50[c]
3[d]	**5**		1440	45
4[d]	**5**	PCy_3[e]	1440	4
5[d]	**5**	CuCl[f]	1440	100
7	**5**	$TlPF_6$[e]	20	33
8	**5**	$TlPF_6$[g]	10	100
9[d]	**6**		1440	10
10	**6**		1440	0

[a]General conditions: reactions in air at 70 °C, 5 mol% Ru, nondegassed C_6D_6 solvent, [Ru] = 7.7 mmol/L, [substrate] = 0.154 mol/L.
[b]Determined by ^{1}H NMR analysis.
[c]Reaction in neat substrate: 13 μmol Ru in 500 μL (2.1 mmol) diethyl diallylmalonate.
[d]Performed under nitrogen in degassed C_6D_6.
[e]5.8 μmol (1 equiv. per Ru).
[f]58 μmol (10 equiv. per Ru).
[g]29 μmol (5 equiv. per Ru).

lowed by pyridine, afforded RuCl(NN′)$(py)_2$(CHPh) (**6**) as the major product, as judged by in situ NMR analysis. Complex **6** was isolated as a yellow-green microcrystalline solid; again, yields are limited (in this case to ca. 50%) by high solubility. ^{1}H and ^{13}C NMR analysis offer unequivocal evidence for retention of the σ-pyrrolide unit. Loss of phosphine is evident from the multiplicity of the signal for the alkylidene carbon (316.6 ppm), which appears as a singlet, in place of the doublet observed for **5**. The alkylidene proton gives rise to a singlet at 20.51 ppm, and the presence of two pyridine ligands is supported by integration of the aromatic region. Exposure of solid **6** to vacuum for 18 h causes ca. 10% loss of pyridine to give **7**, identified as a monopyridine species on the basis of the decrease in the integrated intensity of the aromatic signals in the ^{1}H NMR spectrum, and emergence of a new alkylidene peak at 19.70 ppm, which disappears on addition of pyridine to the sample. Similar behaviour was previously reported for **2** (2).

RCM catalysis

Complex **5** proves a robust olefin metathesis catalyst, effecting RCM of the benchmark substrate diethyl diallylmalonate at 70 °C in air, in nondistilled and nondegassed solvent (Table 2, entry 1). The reaction shows complete selectivity for RCM over intermolecular ADMET (acyclic diene metathesis) processes, even in the absence of solvent, as indicated by ^{1}H NMR analysis. A control experiment with the Grubbs catalyst **1a** resulted in ca. 30% ADMET under these conditions. As we have previously commented (30), olefin metathesis via any square-pyramidal complex in which alkylidene occupies the apical site necessitates dissociation of one of the ligands in the basal plane. Complex **5** is inactive at ambient temperature, implying that all four basal donors are rather nonlabile, a feature also exhibited by the Schiff base catalysts of type **4** (24, 25). Even at 70 °C, no exchange is observed between coordinated and free (added) PCy_3 in EXSY experiments, and the ^{1}H NMR signals for the NN′ ligand remain fully resolved, indicating retention of the chelate. Catalysis is thus presumably carried by a spectroscopically unobservable active species, as indeed also proposed for salicylaldiminato complex **4** (25). While the latter is thought to operate via decoordination of imine, we believe that **5** is activated by loss of PCy_3. Consistent with this is the inhibition of activity on addition of free PCy_3 or on use of N_2 atmosphere, but rate enhancements on addition of CuCl as a phosphine scavenger (31). Trapping of the eliminated PCy_3 as O=PCy_3, a weaker donor ligand, would account for the effect of oxygen. Ample precedent exists for the accelerating effect of oxygen in reactions catalyzed by precursors activated by phosphine loss: these include hydrogenations via $RhCl(PPh_3)_3$ (32) and *trans*-$IrCl(CO)(PPh_3)_2$ (33), and hydrosilylation via $RuCl_2(PPh_3)_3$ (34).

As an alternative to the loss of a neutral donor ligand, chloride abstraction can also create a vacant site cis to alkylidene. Addition of $TlPF_6$ dramatically increases the activity of **5**: vigorous evolution of ethylene is observed at the surface of the $TlPF_6$ granules, and RCM is complete within 10 min at 70 °C. The need for elevated temperatures in this case may reflect the poor solubility of $TlPF_6$ in C_6D_6.

The low RCM activity of pyridine complex **6** is noteworthy, given the emerging view that substitution of phosphine by pyridine enhances metathesis activity by providing a more labile "placeholder" ligand (2, 9). The effect in **6** is evidently insufficient to confer metathesis activity at room temperature. RCM via this catalyst at 70 °C in air also results in essentially zero activity, owing to rapid decomposition, as indicated by the disappearance of the alkylidene signal in the ^{1}H NMR spectrum. This observation reinforces our suggestion that the activating effect of air in RCM via **5** is due to PCy_3 oxidation. The poor performance of **6** at 70 °C under N_2 (Table 2, entries 3, 9) is more unexpected. As catalysts **5** and **6** should afford the identical active species, the difference in their performance probably reflects a shorter lifetime for the py catalyst at elevated temperatures. We speculate that the slow, reversible release of PCy_3 from **5** leaves a pool of uninitiated (pre)catalyst that functions as a reservoir, conferring activity over a longer reaction period. The weakly coordinating phosphine oxide may also play a stabilizing role.

Conclusions

The foregoing describes deployment of the iminopyrrolato group as a new pseudohalide ligand in Ru-catalyzed olefin metathesis. RuCl(NN′)(PCy_3)(CHPh) (**5**) is activated via loss of phosphine. In consequence, the catalyst achieves maximum activity in the presence of air, offering a very convenient experimental protocol for metathesis chemistry. Replacement of the PCy_3 ligand in **5** by two pyridine ligands results in a dramatic decrease in both robustness and, more surprisingly, catalytic activity. Pyridine binding is sufficiently strong that **6** is inactive for RCM at room temperature. This observation may have more fundamental implications: it raises the possibility that the apparent stability of the Ru(σ-iminopyrrolato) motif against isomerization is an artifact of the nonlability of the ancillary (PCy_3, pyridine) ligands in **5** and **6**. Indeed, this may account for the inactivity of **6** at elevated temperature, as rapid π → σ isomerization following

© 2005 NRC Canada

ligand loss could provide a facile deactivation pathway. Studies examining this possibility within iminopyrrolato complexes containing labile donor ligands are in progress and will be reported in due course.

Experimental

Synthetic operations were performed under N_2 using standard Schlenk or drybox techniques, unless otherwise stated. Catalysis was carried out under N_2 or in air. Dry, oxygen-free solvents were obtained using an Anhydrous Engineering or a Glass Contour solvent purification system and stored over Linde 4 Å molecular sieves. $CDCl_3$ and C_6D_6 were dried over activated sieves (Linde 4 Å) and degassed by consecutive freeze–pump–thaw cycles. Diethyl diallylmalonate (Aldrich) was distilled from sodium under N_2. Grubbs catalyst **1** (35), 2-[(2,6-diisopropylphenyl)imino]pyrrole (HNN′) (28), and lithium 2-[(2,6-diisopropylphenyl)imino]pyrrolide·Et_2O (LiNN′·Et_2O) (17) were prepared according to literature procedures. ^{1}H NMR analysis of the lithium salt showed reproducibly 1 mol Et_2O, indicating formation of an ether solvate.

RuCl(κ²-*C*, *N*-ArN=CHC$_4$H$_3$N)(PCy$_3$)(CHPh) (5) (Ar = 2,6-*i*-Pr$_2$C$_6$H$_3$)

A solution of **1** (0.30 g, 0.36 mmol) in 6 mL C_6H_6 was stirred as LiNN′·Et_2O (190 mg, 0.57 mmol) in 6 mL C_6H_6 was added. Complete conversion to **5** was evident after 18 h at room temperature (RT), over which time the dark purple solution turned brown. The mixture was filtered through neutral alumina and stripped of solvent. The resulting red-brown powder was extracted with pentane (5 × 3 mL) and dried under vacuum. Yield: 183 mg (66%). Low yields were incurred by the high solubility of **5** in hydrocarbon solvents, including pentane. A small amount of the product was further purified by reprecipitation from Et_2O–C_6H_6 (1:1) by addition of cold pentane. Crystals suitable for X-ray analysis were grown at RT by slow evaporation of a toluene solution. IR (Nujol, cm^{-1}): 1569 (s). ^{1}H NMR ($CDCl_3$) δ: 19.65 (d, $^3J_{HP}$ = 11.0 Hz, 1H, Ru=C*H*), 7.84 (d, $^4J_{HP}$ = 3.9 Hz, 1H, C(*H*)=N), 7.50 (t, ^3J_H = 7.3 Hz, 1H, Ph, H_{para}), 7.39 (d, ^3J_H = 7.5 Hz, 2H, Ph, H_{ortho}), 7.18 (t, ^3J_H = 7.8 Hz, 2H, Ph, H_{meta}), 7.09–7.01 (m, 3H, Ar H_3, H_4 + pyr H_3), 6.88 (m, 1H, Ar H_3), 6.51 (br, 1H, pyr H_5), 6.18 (dd, $^3J_{HH}$ = 4.0, 1.6 Hz, 1H, pyr H_4), 3.05 (sept, $^3J_{HH}$ = 6.8 Hz, 1H, C*H*Me$_2$), 2.50 (br m, 4H, C*H*Me$_2$ + 3 × Cy C*H*), 1.91–1.10 (m, 36H, 15 × CH_2 + 2 × CH_3; includes methyl doublets at 1.28 (d, $^3J_{HH}$ = 6.7 Hz) and 1.19 (d, $^3J_{HH}$ = 6.7 Hz)), 0.66 (d, $^3J_{HH}$ = 6.6 Hz, 3H, CH_3), 0.45 (d, $^3J_{HH}$ = 6.6 Hz, 3H, CH_3). ^{13}C{^{1}H} NMR ($CDCl_3$) δ: 303.7 (d, Ru=*C*, $^2J_{CP}$ = 14.1 Hz), 163.0 (s, *C*H=N), 152.6 (d, $^3J_{CP}$ = 1.7 Hz, Ph C_i), 146.1 (s, Ar C_i), 142.9 (s, Ar *C*-*i*-Pr), 142.8 (d, $^3J_{CP}$ = 2.0 Hz, pyr C_2), 142.0 (s, Ar *C*-*i*-Pr), 141.7 (s, pyr C_5), 129.3 (s, Ph, C_o), 128.93 (s, Ph, C_m or C_p), 128.88 (s, Ph, C_m or C_p), 125.8 (s, Ar, C_4), 122.5 (s, Ar, 2 × C_3), 120.2 (s, pyr C_3), 114.0 (s, pyr C_4), 33.5 (d, *C*H of Cy, $^1J_{CP}$ = 20 Hz), 30.3, 29.4, 29.3, 27.8, 27.7, 27.6, 26.8, 26.4, 25.4, 24.2, 23.3, 21.9. ^{31}P{^{1}H} NMR ($CDCl_3$) δ: 49.20 (s). Anal. calcd. for $C_{42}H_{60}ClN_2PRu$ (%): C 66.34, H 7.95; found: C 66.73, H 8.27.

RuCl(κ²-*C*, *N*-ArN=CHC$_4$H$_3$N)(py)$_2$(CHPh) (6)

A solution of **1** (0.50 g, 0.61 mmol) in C_6H_6 (5 mL) was stirred as LiNN′·Et_2O (0.32 g, 1.0 mmol) in 5 mL C_6H_6 was added. The dark purple solution was stirred at RT for 18 h, filtered through neutral alumina, stripped of solvent, and then redissolved in Et_2O–hexanes (1:1, 10 mL). Pyridine was added (2 mL, excess) and the mixture was stirred at RT for 20 h to give a yellow-green suspension. The crude product was filtered off, washed with hexanes, reprecipitated twice from CH_2Cl_2–hexanes, and washed with hexanes (10 × 3 mL). Yield of green microcrystalline **5**: 195 mg (50%). IR (Nujol, cm^{-1}): 1593 (m), 1567 (s). ^{1}H NMR ($CDCl_3$) δ: 20.51 (s, 1H, Ru=C*H*), 8.59–6.91 (m, 20H, Ar + pyr H_3), 6.46 (br s, 1H, pyr H_5), 6.20 (br s, 1H, pyr H_4), 4.41 (br m, 1H, C*H*Me$_2$), 2.83 (br m, 1H, C*H*Me$_2$), 0.99 (d, $^3J_{HH}$ = 6.0 Hz, 3H, CH_3), 0.79 (d, $^3J_{HH}$ = 6.0 Hz, 6H, 2 × CH_3), 0.62 (d, $^3J_{HH}$ = 6.0 Hz, 3H, CH_3). ^{13}C{^{1}H} NMR ($CDCl_3$) δ: 316.6 (s, Ru=*C*), 162.8, 156.9, 155.3, 154.9, 150.8, 146.6, 145.5, 143.3, 142.2, 137.0, 136.5, 136.0, 131.0, 129.8, 129.3, 126.9, 124.7, 124.2, 123.9, 123.2, 118.5, 113.0, 66.2, 27.5, 26.9, 26.5, 23.3, 22.4, 15.7. Anal. calcd. for $C_{34}H_{37}ClN_4Ru$ (%): C 63.99, H 5.84; found: C 64.27, H 6.21.

General procedure for RCM of diethyl diallylmalonate

In C$_6$D$_6$

Diethyl diallylmalonate (28 µL, 0.12 mmol) was added to a solution of Ru catalyst **5** or **6** (6 µmol) in 0.75 mL C_6D_6. Any additives were included at this point: $TlPF_6$ (10 mg, 29 µmol, 5 equiv. or 2 mg, 1 equiv.), PCy_3 (20 µL of a 0.30 mol/L solution in C_6D_6, 1 equiv.), or CuCl (6 mg, 60 µmol, 10 equiv.). The reaction was then stirred at 70 °C in an oil bath (where relevant), under an air or a N_2 atmosphere. Conversions were assessed by ^{1}H NMR analysis. The identity of the RCM product was verified by GC–MS analysis. EI-MS calcd. for $C_{11}H_{16}O_4$ $[M - H]^{+\cdot}$: 212; found: 212.

In neat substrate

Catalyst **5** (13 µmol) was added to diethyl diallylmalonate (500 µL, 2.1 mmol) in air. The reaction was stirred at 70 °C and aliquots were withdrawn periodically for ^{1}H NMR analysis.

X-ray crystallographic analysis of 5

Crystal and data collection parameters for **5** are provided in Table 3.[3] A suitable crystal was selected, mounted on a thin glass fiber using paraffin oil, and cooled to the data collection temperature. Data were collected on a Bruker AXS SMART 1 k CCD diffractometer using 0.3° ω-scans at 0°,

[3] Supplementary data for this article are available on the Web site or may be purchased from the Depository of Unpublished Data, Document Delivery, CISTI, National Research Council Canada, Ottawa, ON K1A 0S2, Canada. DUD 3682. For more information on obtaining material refer to http://cisti-icist.nrc-cnrc.gc.ca/irm/unpub_e.shtml. CCDC 257483 contains the crystallographic data for this manuscript. These data can be obtained, free of charge, via www.ccdc.cam.ac.uk/conts/retrieving.html (Or from the Cambridge Crystallographic Data Centre, 12 Union Road, Cambridge CB2 1EZ, UK; fax +44 1223 336033; or deposit@ccdc.cam.ac.uk).

© 2005 NRC Canada

Table 3. Crystal data and structure refinement for RuCl(κ²-*C*,*N*-ArN=CHC$_4$H$_3$N)(PCy$_3$)(CHPh) (**5**) (Ar = 2,6-*i*-Pr$_2$C$_6$H$_3$).

Empirical formula	$C_{42}H_{60}ClN_2PRu$
Formula weight	760.41
Temperature (K)	203(2)
Wavelength (λ)	0.710 73
Crystal system, space group	Monoclinic, *C*2/*c*
Unit cell dimensions	
a (Å)	40.258(4)
b (Å)	12.499 8(12)
c (Å)	17.707 1(16)
β (°)	115.323(2)
Volume (Å^3)	8 054.3(13)
Z, calculated density (g/cm^3)	8, 1.254
Absorption coefficient (mm^{-1})	0.525
F(000)	3216
Crystal size (mm^3)	0.20 × 0.20 × 0.10
θ range for data collection (°)	1.72–29.08
Limiting indices	$-53 \le h \le 52$, $-9 \le k \le 14$, $-23 \le l \le 15$
Reflections collected / unique	11 429 / 8 338 (R(int) = 0.020 3)
Completeness to θ = 28.65 (%)	77.3
Absorption correction	Semi-empirical from equivalents
Max and min transmission	0.949 4 and 0.902 2
Refinement method	Full-matrix, least-squares on F^2
Data / restraints / parameters	8 338 / 36 / 443
Goodness-of-fit on F^2	1.064
Final R indices ($I > 2\sigma(I)$)	R_1 = 0.044 2, wR_2 = 0.091 5
R indices (all data)	R_1 = 0.073 1, wR_2 = 0.103 8
Largest diff. peak and hole (e Å^{-3})	0.562 and –1.298

[a]Definition of R indices: $R_1 = \Sigma(F_o - F_c)/\Sigma(F_o)$; $wR_2 = [\Sigma[w(F_o^2 - F_c^2)^2]/\Sigma[w(F_o^2)^2]]^{1/2}$.

90°, and 180° in ϕ. Initial unit-cell parameters were determined from 60 data frames collected at different sections of the Ewald sphere. Semi-empirical absorption corrections based on equivalent reflections were applied (36). Systematic absences in the diffraction data are consistent with *C*2/*c* (No. 15) and *Cc* (No. 9). Solution in the centrosymmetric space group option yielded chemically reasonable and computationally stable results of refinement. The structure was solved by direct methods, completed with difference Fourier syntheses, and refined with full-matrix least-squares procedures based on F^2. One of the cyclohexyl rings in the phosphine ligand was found disordered in two conformations with an approximately 1:1 refined site occupancy distribution. Each was restrained to an ideal chair conformation, with chemically identical atoms refined with common atomic displacement parameters. All hydrogen atoms were treated as idealized contributions. All scattering factors are contained in the SHELXTL 6.12 program library (36).

Acknowledgments

This work was supported by the Natural Sciences and Engineering Research Council of Canada (NSERC), the Canada Foundation for Innovation, and the Ontario Innovation Trust.

References

1. Recent reviews: (*a*) J.C. Mol. J. Mol. Catal. A, **213**, 39 (2004); (*b*) T.M. Trnka and R.H. Grubbs. Acc. Chem. Res. **34**, 18 (2001); (*c*) A. Fürstner. Angew. Chem. Int. Ed. **39**, 3012 (2000); (*d*) A. Fürstner, L. Ackermann, B. Gabor, R. Goddard, C.W. Lehmann, R. Mynott, F. Stelzer, and O.R. Thiel. Chem. Eur. J. **7**, 3236 (2001); (*e*) J. Prunet. Angew. Chem. Int. Ed. **42**, 2826 (2003).
2. M.S. Sanford, J.A. Love, and R.H. Grubbs. Organometallics, **20**, 5314 (2001).
3. K. Grela, S. Harutyunyan, and A. Michrowska. Angew. Chem. Int. Ed. **41**, 4038 (2002).
4. A. Michrowska, R. Bujok, S. Harutyunyan, V. Sashuk, G. Dolgonos, and K. Grela. J. Am. Chem. Soc. **126**, 9318 (2004).
5. H. Wakamatsu and S. Blechert. Angew. Chem. Int. Ed. **41**, 2403 (2002).
6. P.E. Romero, W.E. Piers, and R. McDonald. Angew. Chem. Int. Ed. **43**, 6161 (2004).
7. D. Amoroso, G.P.A. Yap, and D.E. Fogg. Organometallics, **21**, 3335 (2002).
8. D. Amoroso, J.L. Snelgrove, J.C. Conrad, S.D. Drouin, G.P.A. Yap, and D.E. Fogg. Adv. Synth. Catal. **344**, 757 (2002).
9. J.C. Conrad, D. Amoroso, P. Czechura, G.P.A. Yap, and D.E. Fogg. Organometallics, **22**, 3634 (2003).
10. J.C. Conrad, H.H. Parnas, J.L. Snelgrove, and D.E. Fogg. J. Am. Chem. Soc. Accepted for publication.
11. J.L. Snelgrove, J.C. Conrad, G.P.A. Yap, and D.E. Fogg. Inorg. Chim. Acta, **345**, 268 (2003).
12. J.L. Snelgrove, J.C. Conrad, M.D. Eelman, M.M. Moriarty, G.P.A. Yap, and D.E. Fogg. Organometallics, **24**, 103 (2005).
13. D.L. Kershner and F. Basolo. Coord. Chem. Rev. **19**, 279 (1987).
14. A.P. Sadimenko, A.D. Garnovskii, and N. Retta. Coord. Chem. Rev. **126**, 237 (1993).
15. M. Rakowski DuBois. Coord. Chem. Rev. **174**, 191 (1998).
16. M. Rakowski DuBois, K.G. Parker, C. Ohman, and B.C. Noll. Organometallics, **16**, 2325 (1997).
17. D.M. Dawson, D.A. Walker, M. Thornton-Pett, and M. Bochmann. J. Chem. Soc. Dalton Trans. 459 (2000).
18. H. Hao, S. Bhandari, Y. Ding, H.W. Roesky, J. Magull, H.-G. Schmidt, M. Noltemeyer, and C. Cui. Eur. J. Inorg. Chem. 1060 (2002).
19. Y. Yoshida, J. Saito, M. Mitani, Y. Takagi, S. Matsui, S. Ishii, T. Nakano, N. Kashiwa, and T. Fujita. Chem. Commun. 1298 (2002).
20. Y. Yoshida, S. Matsui, Y. Takagi, M. Mitani, T. Nakano, H. Tanaka, N. Kashiwa, and T. Fujita. Organometallics, **20**, 4793 (2001).
21. Y. Matsuo, K. Mashima, and K. Tani. Organometallics, **20**, 3510 (2001).
22. H. Sasabe, S. Nakanishi, and T. Takata. Inorg. Chem. Commun. **6**, 1140 (2003).
23. Y. Yoshida, J. Saito, M. Mitani, Y. Takagi, S. Matsui, S.-I. Ishii, T. Nakano, N. Kashiwa, and T. Fujita. J. Chem. Soc. Chem. Commun. 1298 (2002).
24. S. Chang, L. Jones, C. Wang, L.M. Henling, and R.H. Grubbs. Organometallics, **17**, 3460 (1998).
25. B. DeClercq and F. Verpoort. Adv. Synth. Catal. **344**, 639 (2002).
26. B. DeClercq and F. Verpoort. Macromolecules, **35**, 8943 (2002).
27. P. Schwab, R.H. Grubbs, and J.W. Ziller. J. Am. Chem. Soc. **118**, 100 (1996).
28. Y. Matsuo, K. Mashima, and K. Tani. Chem. Lett. 1114 (2000).

© 2005 NRC Canada

29. P. Schwab, M.B. France, J.W. Ziller, and R.H. Grubbs. Angew. Chem. Int. Ed. Engl. **34**, 2039 (1995).
30. D.E. Fogg, D. Amoroso, S.D. Drouin, J.L. Snelgrove, and J.C. Conrad. J. Mol. Catal. A, **190**, 177 (2002).
31. E.L. Dias, S.T. Nguyen, and R.H. Grubbs. J. Am. Chem. Soc. **119**, 3887 (1997).
32. H. van Bekkum, F. van Rantwijk, and T. van de Putte. Tetrahedron Lett. 1 (1969).
33. B.R. James and N.A. Memon. Can. J. Chem. **46**, 217 (1968).
34. J. Gulinski, B.R. James, and B. Marciniec. J. Organomet. Chem. **499**, 173 (1995).
35. P. Schwab, R.H. Grubbs, and J.W. Ziller. J. Am. Chem. Soc. **118**, 100 (1996).
36. G.M. Sheldrick. SHELXTL 6.12 [computer program]. Bruker AXS, Madison, Wis. 2001.

© 2005 NRC Canada

Rhodium-catalyzed C-H–CO–olefin coupling reactions — A chelation-assisted direct carbonylation at the ortho C—H bond in the benzene ring of 2-arylpyridines[1]

Naoto Chatani, Takeshi Uemura, Taku Asaumi, Yutaka Ie, Fumitoshi Kakiuchi, and Shinji Murai

Abstract: The reaction of 2-arylpyridines with ethylene and carbon monoxide in the presence of a catalytic amount of $Rh_4(CO)_{12}$ results in selective carbonylation at the ortho C—H bond. The reaction is heavily dependent on the solvents used, with DMA (*N*,*N*-dimethylacetamide) being the solvent of choice. Steric factors are also important determinants of the efficiency of the reaction.

Key words: C—H bond activation, carbonylation, chelation, rhodium, carbon monoxide.

Résumé : La réaction des 2-arylpyridines avec l'éthylène et le monoxyde de carbone, en présence d'une quantité catalytique de $Rh_4(CO)_{12}$ conduit à une carbonylation sélection au niveau de la liaison C—H en ortho. La réaction dépend fortement de la nature du solvant utilisé et le DMA (*N*,*N*-diméthyacétamide) est le solvant de choix. Les facteurs stériques sont aussi déterminants dans l'efficacité de la réaction.

Mots clés : activation d'une liaison C—H, carbonylation, chélation, rhodium, monoxyde de carbone.

[Traduit par la Rédaction]

Introduction

The chelation-assisted cleavage of unreactive bonds has recently emerged as one of the most useful and effective methods for developing the new transition metal catalyzed reactions. Various types of catalytic reactions, such as C-H–olefin coupling (1, 2), C-H phenylation (3, 4), C-H oxidation (5), C-H silylation (6), C—C bond cleavage (7, 8), C—F bond cleavage (9), C—O bond cleavage (10), and O—H bond cleavage (11) have been reported. A variety of functional groups can be used as chelating groups, such as a carbonyl oxygen, sp^2 nitrogen, and sulfur. Various late transition metals have been used as catalysts. The methodology is also applicable to the C-H–CO–olefin coupling of nitrogen-containing compounds in which the coordination of sp^2 nitrogen of the substrates to the catalysts is a key step in the progress of the reactions (12). In most of the carbonylation reactions at C—H bonds reported thus far, only ruthenium carbonyl complexes have shown a high catalytic activity, and a rhodium carbonyl complex was also found to be fairly active. Other metals, such as Co, Pd, Ni, and Ir, were not active. However, we recently found that rhodium complexes also show a high degree of catalytic activity in C-H–CO–olefin coupling reactions of *N*-phenylimidazoles when *N*,*N*-dimethylacetamide (DMA) is used as the solvent (12*o*). This prompted us to reexamine various nitrogen-containing compounds, which are known to undergo the direct carbonylation of C—H bonds catalyzed by $Ru_3(CO)_{12}$ (12), in the $Rh_4(CO)_{12}$-catalyzed C-H–CO–olefin coupling in DMA. As expected, 2-arylpyridines were also found to undergo direct carbonylation at the ortho C—H bonds in the benzene ring in the presence of $Rh_4(CO)_{12}$. In this paper, we wish to report on the direct, Rh-catalyzed carbonylation of a C—H bond in the benzene ring of 2-arylpyridines based on chelation assistance.

Results and discussion

The reaction of 2-phenylpyridine (**1a**) was first carried out under the optimal reaction conditions employed in $Ru_3(CO)_{12}$-catalyzed carbonylation reactions, but using $Rh_4(CO)_{12}$ as the catalyst. Thus, the reaction of 2-phenylpyridine (**1a**, 2 mmol) with carbon monoxide (20 atm at room temperature (r.t.)) and ethylene (7 atm) (1 atm =

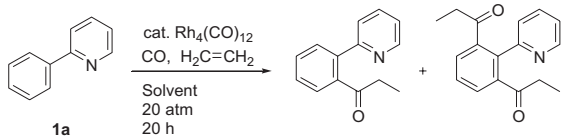
Received 2 December 2004. Published on the NRC Research Press Web site at http://canjchem.nrc.ca on 23 June 2005.

This paper is dedicated to Professor Howard Alper.

N. Chatani,[2] T. Uemura, T. Asaumi, Y. Ie,[3] F. Kakiuchi, and S. Murai. Department of Applied Chemistry, Faculty of Engineering, Osaka University, Suita, Osaka 565-0871, Japan.

[1]This article is part of a Special Issue dedicated to Professor Howard Alper.
[2]Corresponding author (e-mail: chatani@chem.eng.osaka-u.ac.jp).
[3]Present address: The Institute of Scientific and Industrial Research, Osaka University, Mihoga-oka, Ibaraki, Osaka 567-0047, Japan.

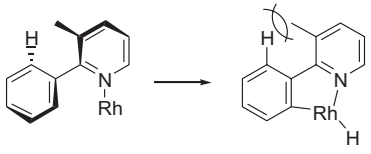
 doi: 10.1139/V05-077 © 2005 NRC Canada

[1] 

160 °C	Toluene	12%	0%	(88%)
	DMI	53%	5%	(17%)
	DMA	**57%**	**3%**	**(20%)**
180 °C	Toluene	30%	0%	(52%)
	2-Propanol	37%	0%	(62%)
	Dioxane	42%	0%	(40%)
	THF	58%	0%	(25%)
	DMA	**58%**	**1%**	**(10%)**
140 °C	DMA	42%	5%	(42%)

101.325 kPa) in the presence of $Rh_4(CO)_{12}$ (0.05 mmol) in toluene (6 mL) at 160 °C for 20 h gave 1-[2-(2-pyridinylphenyl)]-1-propanone (**2a**) in only 12% yield, along with 88% unreacted **1a** (eq. [1], the numbers in parentheses are the recoveries for the starting materials). The effect of the solvent on the carbonylation was next examined. As a result, it was found that the use of 1,3-dimethyl-2-imidazolidinone (DMI) and DMA dramatically improve the yield of **2a** to 53% and 57%, respectively. In addition to the screening of solvents, the reaction conditions were again optimized, e.g., the pressure of both CO and ethylene and the additives used, but this did not result in increased yields. It is noteworthy, however, that nearly comparable yields are obtained, even when ordinary solvents, such as dioxane and THF, are used when the reaction is carried out at an elevated temperature, such as 180 °C. At lower temperatures, such as 140 and 160 °C, DMA was the preferred solvent.

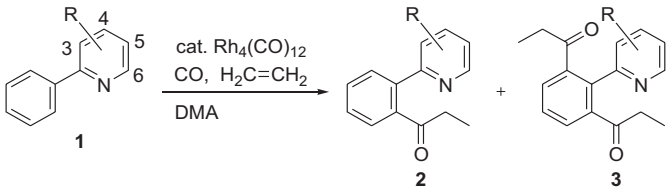
The effects of the substituent on the pyridine ring were examined (Table 1). Changing the reaction temperatures (160 and 180 °C) and reaction times (10 and 40 h) had no significant effect on the yield of **1a**. The presence of a methyl group at the 4-position and the 5-position, as in **1c** and **1d**, respectively, did not improve the product yields, although this has been reported, in some cases, to be effective (12*k*, 12*m*). However, the presence of a methyl group at the 3-position, as in **1b**, resulted in a decreased product yield because of the steric hindrance between the ortho hydrogen on the benzene ring and the methyl group on the pyridine ring in the cleavage of a C—H bond.



The reaction of **1e** led to a low conversion and gave the corresponding ketone **2e** in 16% yield even for a reaction time of 40 h because of steric hindrance around the pyridine nitrogen. This indicates that the coordination of the pyridine nitrogen to Rh is important for the carbonylation at C—H bonds to proceed with a high efficiency, as has been observed in previous Ru-catalyzed carbonylation reactions (12).

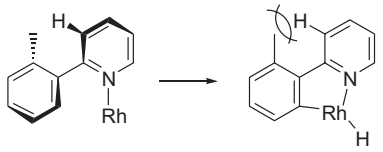
As shown in Table 2, the presence of an electron-donating group at the meta and para positions on the phenyl ring gave the corresponding ketones in moderate yields. On the other hand, the presence of a methyl group at the ortho position on the phenyl ring, as in **4a**, led to a dramatic decrease in the product yield. This is also due to steric congestion between the tolyl ring and the pyridine ring, as in the case of **1b**. A methoxy group at the ortho position, however, had no effect on the product yield. The reaction of **4f**, bearing a trifluoromethyl group, gave the corresponding carbonylation products **5f** and **6f**, albeit in low yields.

Table 1. Substituent effects on the pyridine ring.[a]



Entry	R	Conditions (°C, h)	**2** (%)[b]	**3** (%)[b]	Recovery of **1** (%)[c]
1	H(**1a**)	160, 10	62[d]	6[d]	21
2		160, 40	58[d]	4[d]	15
3		180, 10	57[d]	1[d]	11
4		180, 40	53[d]	3[d]	12
5	3-Me(**1b**)	160, 10	24[e]	0	53
6		180, 10	27[d]	0	47
7	4-Me(**1c**)	160, 10	63[f]	4[f]	20
8		180, 10	58[d]	4[d]	10
9	5-Me(**1d**)	160, 10	51[e]	6[e]	29
10		180, 10	66[f]	6[f]	11
11	6-Me(**1e**)	160, 10	11[e]	0	80
12		160, 40	16[e]	0	77
13		180, 10	7[e]	0	72

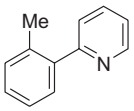
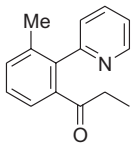
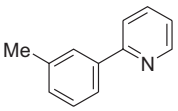
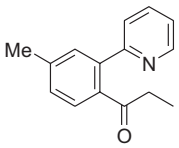
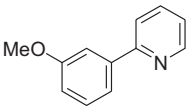
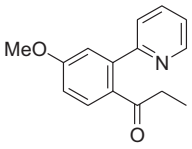
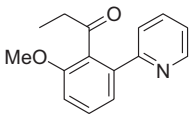
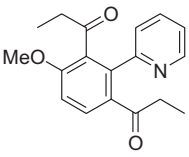
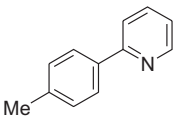
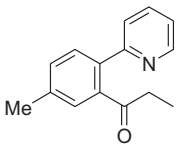
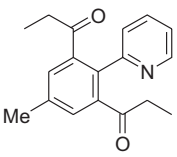
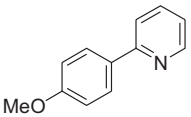
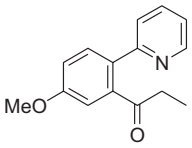
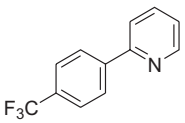
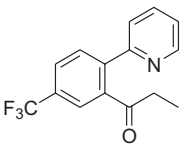
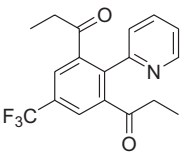
[a]Reaction conditions: 2-arylpyridine (2 mmol), ethylene (7 atm), CO (20 atm, 1 atm = 101.325 kPa), $Rh_4(CO)_{12}$ (0.05 mmol) in DMA (6 mL).
[b]Yields are based on 2-arylpyridine.
[c]Recovery of 2-arylpyridine.
[d]The ratios of **2** and **3** were determined by ^{1}H NMR.
[e]Isolated yields.
[f]The ratios of **2** and **3** were determined by GC.



In addition to the benzene ring, the carbonylation can be applied to naphthalene and thiophene rings as well. The reaction of 1-naphtylpyridine (**7**) gave the ketone in only 22% yield. On the other hand, the reaction of 2-naphtylpyridine (**9**) afforded the corresponding product **10** in good yield with a high regioselectivity. The carbonylation took place selectively at the β position. It is likely that such a dramatic difference is derived from the steric repulsion, as mentioned previously. These are in sharp contrast to the results for the $Ru_3(CO)_{12}$-catalyzed reactions of **7** and **9**, which both gave the corresponding carbonylation products **8** and **10** in 88% and 86% yields, respectively, in a $Ru_3(CO)_{12}$-catalyzed reaction (12*d*). Thiophenylpyridines **11** and **13** underwent carbonylation to give the corresponding ketones **12** and **14** in good yields. In the case of **11**, a small amount of unidentified product was also obtained as a by-product.

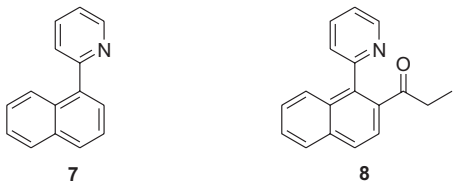
© 2005 NRC Canada

Table 2. The reaction of 2-arylpyridines with CO and ethylene.[a]

Arylpyridine	Products[b]		
 **4a**	 **5a**		
	160 °C 11% (63%)		
	180 °C 24% (46%)		
 **4b**	 **5b**		
	160 °C 75% (14%)		
	180 °C 65% (7%)		
 **4c**	 **5c**	 **5c'**	 **6c**
	160 °C 73% (**5c**/**5c'** = 73/27)[c]		7% (6%)
 **4d**	 **5d**	 **6d**	
	160 °C 59%		7% (21%)
	180 °C 72%[d]		4%[d] (12%)
 **4e**	 **5e**		
	160 °C 38% (41%)		
	180 °C 62% (15%)		
 **4f**	 **5f**	 **6f**	
	160 °C 35%[e]		1%[e] (56%)

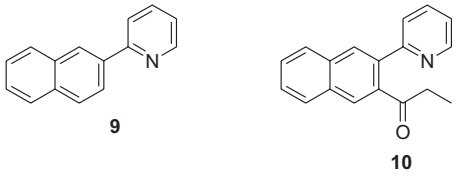
© 2005 NRC Canada

Table 2 (*concluded*).



7 **8**

160 °C 22% (53%)
180 °C 19% (37%)



9 **10**

160 °C 71% (21%)



11 **12**

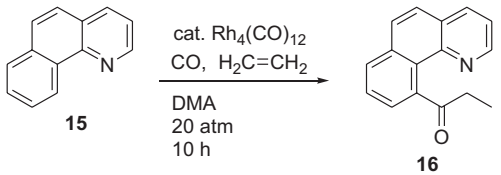
160 °C 88% (1%)



13 **14**

160 °C 87% (3%)

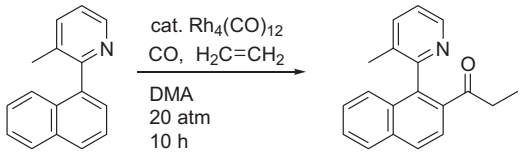
[a]Reaction conditions: 2-arylpyridine (2 mmol), ethylene (7 atm, 1 atm = 101.325 kPa), CO (20 atm, 1 atm = 101.325 kPa), $Rh_4(CO)_{12}$ (0.05 mmol) in DMA (6 mL) for 10 h.
[b]Isolated yields are based on 2-arylpyridine. The numbers in parentheses are the recoveries for 2-arylpyridine.
[c]The ratios of **5c** and **5c′** were determined by ^{1}H NMR.
[d]The ratios of **5d** and **6d** were determined by GC.
[e]The ratios of **5f** and **6f** were determined by ^{1}H NMR.

[2] 

cat. $Rh_4(CO)_{12}$, CO, $H_2C{=}CH_2$; DMA, 20 atm, 10 h

15 **16**

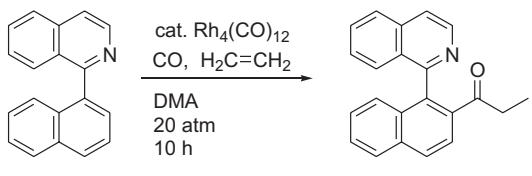
160 °C 77% (18%)

[4] 

cat. $Rh_4(CO)_{12}$, CO, $H_2C{=}CH_2$; DMA, 20 atm, 10 h

19 **20**

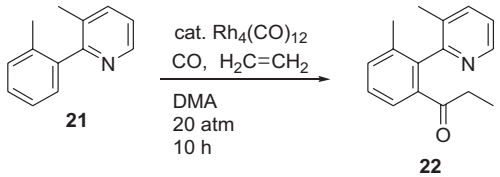
160 °C no coupling product (n.d.)

[3] 

cat. $Rh_4(CO)_{12}$, CO, $H_2C{=}CH_2$; DMA, 20 atm, 10 h

17 **18**

160 °C no coupling product (n.d.)

[5] 

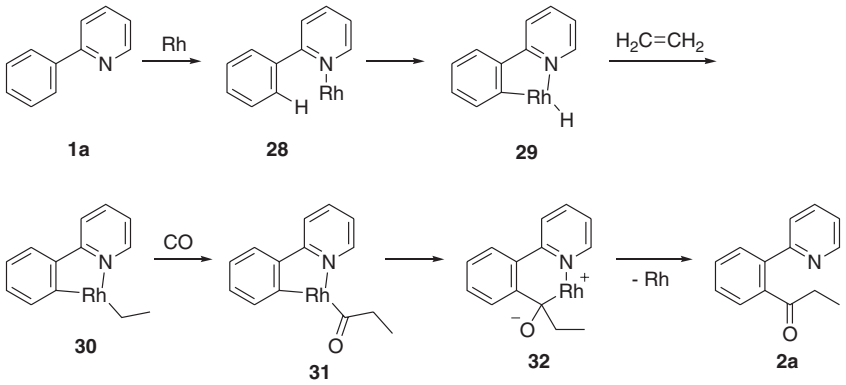
cat. $Rh_4(CO)_{12}$, CO, $H_2C{=}CH_2$; DMA, 20 atm, 10 h

21 **22**

160 °C no coupling product (n.d.)

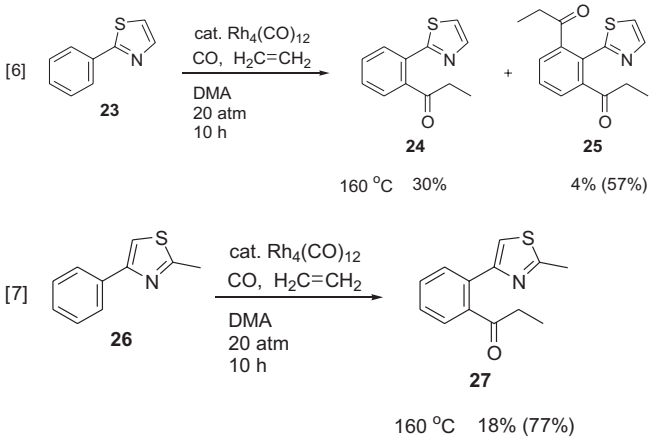
© 2005 NRC Canada

Scheme 1. A proposed reaction mechanism.



As observed in the case of **1b**, **1e**, **4e**, and **7** in the Rh-catalyzed reaction, steric factors had a dramatic effect on the progress of the reaction. To obtain information concerning the reaction mechanism and to make a comparison with the Ru-catalyzed reaction, the reaction of **15**, **17**, **19**, and **21** were conducted (eqs. [2]–[5], the numbers in parentheses are the recoveries for the starting materials). The reaction of **15** in which the sp^2 nitrogen and the C—H bond are in the same plane with CO and ethylene gave the carbonylated product **16** in high yield. Although the reaction of **17**, **19**, and **21** in the presence of $Ru_3(CO)_{12}$ proceeded,[4] the rhodium-catalyzed system did not.

A thiazole ring could also function as a directing group in the Rh-catalyzed carbonylation as shown in eqs. [6] and [7] (the numbers in parentheses are the recoveries for the starting materials).



A proposed mechanism is pictured in Scheme 1. The proposed mechanism for the Rh-catalyzed carbonylation of 2-phenylpyridine is essentially the same as that for the Ru-catalyzed reactions that have previously been reported (12*d*). The pyridine nitrogen in the substrate coordinates to the Rh, and the site-selective cleavage of the ortho C—H bond takes place to provide the Rh-H species **29**. The hydrometallation of ethylene followed by the insertion of CO gives the acyl-Rh intermediate **31** from which reductive elimination via the zwitterionic intermediate **32** affords the carbonylated product **2a**, and regenerates the active Rh species. We speculate that the coordination of the sp^2 nitrogen to Rh complexes is maintained during the reaction. In the key intermediates **29**–**31**, pyridine and the phenyl group must be coplanar. Since the presence of a substituent at the 2-position of the phenyl ring and (or) the 3-position of the pyridine ring, as in **1b**, **4a**, **7**, **17**, **19**, **21**, prevents coplanarity from being achieved, the reaction does not proceed. In contrast, coordination of the sp^2 nitrogen might not be always necessary in the Ru-catalyzed reaction. In fact, Goldman and co-workers (13) quite recently reported that coordination is not required in the C—H bond cleavage step, and that cleavage at the meta and para positions is kinetically more favorable than that at the ortho position, however the chelated ortho isomer is thermodynamically stable. On the other hand, coordination is required for the cleavage of C—H bonds and reductive elimination. This explains why the reaction is significantly affected by steric factors. The role of DMA as the solvent is not clear at the present time; one possibility is the stabilization of **32** by the polar solvent. Another possibility is the generation of rhodium nanoparticles from the rhodium cluster in DMA, which is very active.

In summary, rhodium complexes were also found to catalyze the direct carbonylation of 2-arylpyridines. The dramatic solvent effect of DMA could permit the scope of applicable substrates in carbonylation reactions to be expanded and significantly improve product yield. Detailed studies of the mechanism of this carbonylation, especially regarding the solvent effect of DMA and the difference between the Rh and Ru catalytic systems, and an examination of new types of C-H carbonylation reactions catalyzed by metal complexes other than Ru and Rh, are currently underway.

Experimental

General methods

^{1}H NMR and ^{13}C NMR spectra were recorded on a JEOL JMN-270 spectrometer in $CDCl_3$ with tetramethylsilane as the internal standard. Data are reported as follows: chemical shifts in ppm (δ), multiplicity (singlet (s), doublet (d), triplet (t), quartet (q), multiplet (m), and complex (c)), coupling

[4] The $Ru_3(CO)_{12}$-catalyzed reaction of **17** gave **20** in 54% yield along with the recovery of **17** in 44% yield (in toluene at 160 °C for 40 h). The $Ru_3(CO)_{12}$-catalyzed reaction of **19** gave **20** in 40% yield along with the recovery of **19** in 58% yield (in toluene at 160 °C for 40 h). The $Ru_3(CO)_{12}$-catalyzed reaction of **21** gave **23** in 24% yield along with the recovery of **24** in 74% yield.

© 2005 NRC Canada

constant (Hz), integration, and interpretation. IR spectra were obtained on a Hitachi 270-50 spectrometer or a Horiba FT-700 spectrometer. Mass spectra were obtained on a Shimadzu GC–MS-QP 5000 instrument with ionization voltages of 70 eV. Elemental analyses were performed by the Elemental Analysis Section of Osaka University. Analytical GC was carried out on a Shimadzu GC-14A gas chromatograph equipped with a flame ionization detector. Column chromatography was performed with SiO_2 (Merck SilicaGel 60, 230–400 mesh).

Materials

N,*N*-Dimethylacetamide (DMA) was distilled over BaO. Toluene was distilled over CaH_2. $Rh_4(CO)_{12}$ was purchased from Strem Chemicals Inc. and was used as received. $Ru_3(CO)_{12}$ was prepared from $RuCl_3 \cdot nH_2O$ and carbon monoxide according to the literature procedure (14) and used after recrystallization from hexane. 2-Phenylpyridine (**1a**), 2-(4-methylphenyl)pyridine (**1c**), and benzo[*h*]quinoline (**14**) were obtained commercially. Substituted 2-arylpyridines were obtained from the corresponding substituted arylbromides or arylboronic acids and 2-bromopyridines using the Kumada–Tamao–Corriu coupling procedure (15) or the Suzuki–Miyaura coupling procedure (16). Spectral data for known compounds have already been reported.[5,6] The purity of all known compounds was verified by ^{1}H NMR, ^{13}C NMR, and GC analyses.

General procedure for the Rh-catalyzed carbonylation reactions of 2-arylpyridines

In a 50 mL stainless autoclave were placed $Rh_4(CO)_{12}$ (37 mg, 0.05 mmol), 2-phenylpyridine (310 mg, 2 mmol), and DMA (6 mL). After flushing the system was with 10 atm (1 atm = 101.325 kPa) of ethylene three times, it was pressurized with ethylene to 7 atm and then with carbon monoxide to an additional 20 atm (1 atm = 101.325 kPa). The autoclave was then immersed in an oil bath at 160 °C. After 10 h had elapsed, it was removed from the oil bath, allowed to cool for ca. 1 h, and the gases were then released. The contents were transferred to a round-bottomed flask with EtOAc. After evaporation, the resulting residue was subjected to column chromatography on silica gel with hexane–EtOAc as the eluent to give 1-[2-(2-(pyridinyl)phenyl)]-1-propanone (**2**) (264 mg, 62% yield) and 1-[2-(3-propionyl-2-pyridinyl)phenyl]-1-propanone (**3**) (34 mg, 6% yield) as an oil.

1-[2-[2-(4-Methylpyridinyl)]phenyl]-1-propanone (2c)

Yellow oil, bp 150–155 °C (1 mmHg) (1 mmHg = 133.322 4 Pa). R_f 0.14 (hexane–EtOAc, 1:1). IR (neat): 1693, 1605. ^{1}H NMR ($CDCl_3$) δ: 1.08 (t, *J* = 7.3 Hz, 3H), 2.41 (s, 3H), 2.46 (q, *J* = 7.3 Hz, 2H), 7.06 (d, *J* = 5.0 Hz, 1H), 7.43–7.51 (c, 4H), 7.63 (d, *J* = 7.6 Hz, 1H), 8.46 (d, *J* = 5.0 Hz, 1H). ^{13}C NMR ($CDCl_3$) δ: 8.61, 21.15, 36.39, 123.13, 123.27, 127.29, 128.50, 128.73, 129.81, 138.37, 141.89, 147.83, 148.98, 157.12, 208.01. MS *m*/*z* (relative intensity, %): 225 (M^+, 0), 210 (2), 197 (16), 196 (100), 167 (15), 98 (14), 84 (21), 51 (10). Anal. calcd. for $C_{15}H_{15}NO$: C 79.97, H 6.71, N 6.22; found: C 79.80, H 6.73, N 6.27.

1-[2-[2-(5-Methylpyridinyl)]phenyl]-1-propanone (2d)

Yellow oil, bp 160 °C (1 mmHg) (1 mmHg = 133.322 4 Pa). R_f 0.20 (hexane–EtOAc, 1:1). IR (neat): 1692. ^{1}H NMR ($CDCl_3$) δ: 1.09 (t, *J* = 7.3 Hz, 3H), 2.37 (s, 3H), 2.49 (q, *J* = 7.3 Hz, 2H), 7.42–7.52 (c, 4H), 7.56 (dd, *J* = 7.9, 2.0 Hz, 1H), 7.63 (d, *J* = 7.6 Hz, 1H), 8.45 (s, 1H). ^{13}C NMR ($CDCl_3$) δ: 8.47, 17.99, 36.25, 121.46, 127.08, 128.16, 128.46, 129.65, 131.70, 137.14, 137.97, 141.55, 149.43, 154.21, 207.92. MS *m*/*z* (relative intensity, %): 225 (M^+, 0), 210 (2), 197 (15), 196 (100), 167 (13), 115 (11), 98 (14), 83 (70), 70 (13). Anal. calcd. for $C_{15}H_{15}NO$: C 79.97, H 6.71, N 6.22; found: C 79.71, H 6.73, N 6.26.

1-[2-[2-(6-Methylpyridinyl)]phenyl]-1-propanone (2e)

Yellow oil, bp 140 °C (1.5 mmHg) (1 mmHg = 133.322 4 Pa). R_f 0.54 (hexane–EtOAc, 1:1). IR (neat): 1697. ^{1}H NMR ($CDCl_3$) δ: 1.08 (t, *J* = 7.3 Hz, 3H), 2.54 (q, *J* = 7.3 Hz, 2H), 2.57 (s, 3H), 7.11 (d, *J* = 7.6 Hz, 1H), 7.40–7.52 (c, 4H), 7.63–7.69 (c, 2H). ^{13}C NMR ($CDCl_3$) δ: 8.19, 23.90, 36.03, 119.01, 121.73, 126.93, 128.29, 128.54, 129.61, 137.07, 137.91, 141.56, 156.13, 157.56, 206.11. MS *m*/*z* (relative intensity, %): 225 (M^+, 0), 197 (15), 196 (100), 153 (11). HR-MS calcd. for $C_{15}H_{15}NO$: 226.1232 (M^+ + 1); found: 226.1184.

1-[2-[2-(4-Methylpyridinyl)]-3-(1-propionyl)phenyl]-1-propanone (3c)

Brown solid. R_f 0.06 (hexane–EtOAc, 1:1). IR (KBr): 1694, 1604. ^{1}H NMR ($CDCl_3$) δ: 0.96 (t, *J* = 7.3 Hz, 6H), 2.36 (q, *J* = 7.3 Hz, 4H), 2.37 (s, 3H), 7.11 (c, 2H), 7.48–7.56 (c, 3H), 8.48 (d, *J* = 5.0 Hz, 1H). ^{13}C NMR ($CDCl_3$) δ: 8.34, 21.03, 36.16, 123.79, 125.66, 128.37, 128.61, 136.35, 142.34, 147.73, 149.33, 156.26, 207.22. MS *m*/*z* (relative intensity, %): 281 (M^+, 0), 253 (16), 252 (100), 195 (22), 167 (13). Anal. calcd. for $C_{18}H_{19}NO_2$: C 76.84, H 6.81, N 4.98; found: C 76.70, H 6.80, N 4.98.

1-[2-[2-(5-Methylpyridinyl)]-3-(1-propionyl)phenyl]-1-propanone (3d)

Brown solid, mp 90–92 °C (1 mmHg) (1 mmHg = 133.322 4 Pa). R_f 0.09 (hexane–EtOAc, 1:1). ^{1}H NMR ($CDCl_3$) δ: 0.97 (t, *J* = 7.2 Hz, 6H), 2.37 (q, *J* = 7.2 Hz, 4H), 2.38 (s, 3H), 7.19 (d, *J* = 7.8 Hz, 1H), 7.50–7.54 (c, 4H), 8.46 (s, 1H). ^{13}C NMR ($CDCl_3$) δ: 8.32, 18.31, 36.16, 124.26, 128.23, 128.59, 132.44, 136.24, 136.91, 142.32, 150.06, 153.51, 207.22. MS *m*/*z* (relative intensity, %): 281 (M^+, 0), 266 (1), 253 (19), 252 (100), 195 (21), 167 (11), 83 (15). Anal. calcd. for $C_{18}H_{19}NO_2$: C 76.84, H 6.81, N 4.98; found: C 76.61, H 6.83, N 4.91.

1-[5-Methyl-2-(2-pyridinyl)phenyl]-1-propanone (5d)

White solid, mp 115–120 °C (0.5 mmHg) (1 mmHg = 133.322 4 Pa). R_f 0.37 (hexane–EtOAc, 1:2). IR (KBr): 1690, 1591, 1430. ^{1}H NMR ($CDCl_3$) δ: 1.08 (t, *J* = 7.3 Hz, 3H), 2.42 (s, 3H), 2.48 (q, *J* = 7.3 Hz, 2H), 7.21 (ddd, *J* =

[5] For the spectral data of **2a**, **2b**, **3a**, **5a**–**5c**, **7**, **9**, **11**, and **13** see ref. 12*d*.
[6] For the spectral data of **15** see ref. 12*g*.

© 2005 NRC Canada

7.4, 4.9, 1.0 Hz, 1H), 7.23 (d, *J* = 1.0 Hz, 1H), 7.31 (dd, *J* = 7.9, 1.0 Hz, 1H), 7.55–7.60 (c, 2H), 7.74 (td, *J* = 7.9, 2.0 Hz, 1H), 8.60 (ddd, *J* = 4.9, 1.7, 1.0 Hz, 1H). ^{13}C NMR ($CDCl_3$) δ: 8.61, 21.10, 36.48, 121.89, 121.94, 127.89, 128.61, 130.48, 135.29, 136.62, 138.76, 141.83, 149.09, 157.11, 208.26. MS *m*/*z* (relative intensity, %): 225 (M^+, 1), 210 (3), 197 (14), 196 (100), 98 (10), 83 (17), 51 (12). Anal. calcd. for $C_{15}H_{15}NO$: C 79.97, H 6.71, N 6.22; found: C 79.84, H 6.74, N 6.19.

1-[5-Methoxy-2-(2-pyridinyl)phenyl]-1-propanone (5e)

Light yellow solid, mp 125–130 °C (1 mmHg) (1 mmHg = 133.322 4 Pa). R_f 0.11 (hexane–EtOAc, 1:2). IR (KBr): 1686, 1608, 1587, 1470, 1429, 1316, 1232. ^{1}H NMR ($CDCl_3$) δ: 1.09 (t, *J* = 7.3 Hz, 3H), 2.45 (q, *J* = 7.3 Hz, 2H), 3.86 (s, 3H), 6.92 (d, *J* = 2.6 Hz, 1H), 7.01 (dd, *J* = 8.6, 2.6 Hz, 1H), 7.17 (ddd, *J* = 7.6, 5.0, 1.0 Hz, 1H), 7.55 (d, *J* = 7.9 Hz, 1H), 7.61 (d, *J* = 8.6 Hz, 1H), 7.72 (td, *J* = 7.7, 1.7 Hz, 1H), 8.57 (dd, *J* = 5.0, 1.0 Hz, 1H). ^{13}C NMR ($CDCl_3$) δ: 8.57, 36.50, 55.47, 112.49, 115.36, 121.46, 121.60, 129.92, 130.40, 136.62, 143.29, 149.98, 156.64, 159.86, 207.82. MS *m*/*z* (relative intensity, %): 241 (M^+, 1), 226 (1), 213 (15), 212 (100), 197 (22), 169 (27), 141 (14), 114 (10), 63 (11), 51 (13). Anal. calcd. for $C_{15}H_{15}NO_2$: C 74.67, H 6.27, N 5.81; found: C 74.56, H 6.31, N 5.76.

1-[2-(2-Pyridinyl)-5-trifluoromethylphenyl]-1-propanone (5f)

Yellow oil, bp 160–165 °C (1 mmHg) (1 mmHg = 133.322 4 Pa). R_f 0.29 (hexane–EtOAc, 1:1). IR (neat): 1701, 1327, 1202, 1169, 1125, 1080. ^{1}H NMR ($CDCl_3$) δ: 1.11 (t, *J* = 7.3 Hz, 3H), 2.52 (q, *J* = 7.3 Hz, 2H), 7.30 (dd, *J* = 7.6, 4.6 Hz, 1H), 7.64–7.68 (c, 2H), 7.73–7.85 (c, 3H), 8.64 (d, *J* = 5.0 Hz, 1H). ^{13}C NMR ($CDCl_3$) δ: 8.09, 36.14, 122.20, 122.82, 123.50, 123.98, 126.17, 128.90, 130.30, 136.89, 141.06, 142.25, 149.00, 155.17, 206.14. MS *m*/*z* (relative intensity, %): 279 (M^+, 0), 264 (2), 251 (14), 250 (100), 153 (10). Anal. calcd. for $C_{15}H_{12}F_3NO$: C 64.52, H 4.33, N 5.02; found: C 64.40, H 4.47, N 5.06.

1-[6-Methoxy-3-(1-propionyl)-2-(2-pyridinyl)phenyl]-1-propanone (6c)

Dark brown solid, mp 148 °C (1 mmHg) (1 mmHg = 133.322 4 Pa). R_f 0.17 (hexane–EtOAc, 1:3). IR (KBr): 1690, 1587, 1564, 1477, 1415, 1291, 1233, 1185, 1136, 830. ^{1}H NMR ($CDCl_3$) δ: 0.96 (t, *J* = 7.3 Hz, 6H), 2.41 (q, *J* = 7.3 Hz, 2H), 2.54 (q, *J* = 7.3 Hz, 2H), 3.89 (s, 3H), 6.99 (d, *J* = 8.9 Hz, 1H), 7.22–7.29 (c, 2H), 7.65–7.71 (c, 2H), 8.58 (d, *J* = 4.6 Hz, 1H). ^{13}C NMR ($CDCl_3$) δ: 7.46, 8.54, 35.11, 38.21, 55.98, 110.21, 122.53, 125.05, 130.31, 132.83, 133.26, 136.06, 138.04, 149.20, 156.50, 157.32, 204.15, 207.15. MS *m*/*z* (relative intensity, %): 297 (M^+, 0), 282 (1), 269 (19), 268 (100), 153 (12), 140 (11), 120 (11). Anal. calcd. for $C_{18}H_{19}NO_3$: C 72.71, H 6.44, N 4.71; found: C 72.42, H 6.43, N 4.68.

1-[5-Methyl-3-(1-propionyl)-2-(2-pyridinyl)phenyl]-1-propanone (6d)

Brown solid, mp 74–76 °C (1 mmHg) (1 mmHg = 133.322 4 Pa). R_f 0.20 (hexane–EtOAc, 1:2). IR (KBr): 1697, 1591, 1560, 1455, 1429, 1405, 1342, 1128, 1054. ^{1}H NMR ($CDCl_3$) δ: 0.95 (t, *J* = 7.3 Hz, 6H), 2.32 (q, *J* = 7.3 Hz, 4H), 2.45 (s, 3H), 7.25–7.34 (c, 2H), 7.34 (s, 2H), 7.70 (td, *J* = 7.6, 1.6 Hz, 1H), 8.62 (d, *J* = 4.6 Hz, 1H). ^{13}C NMR ($CDCl_3$) δ: 8.32, 21.04, 36.17, 122.55, 124.78, 129.18, 133.55, 136.28, 138.69, 142.36, 149.56, 156.55, 207.35. MS *m*/*z* (relative intensity, %): 281 (M^+, 1), 253 (19), 252 (100), 195 (17), 167 (14), 166 (10), 84 (13). Anal. calcd. for $C_{18}H_{19}NO_2$: C 76.84, H 6.81, N 4.98; found: C 76.69, H 6.87, N 4.96.

10-Benzo[*h*]quinolinyl-1-propanone (16)

White solid, mp 92 to 93 °C (1 mmHg) (1 mmHg = 133.322 4 Pa). R_f 0.54 (hexane–EtOAc, 1:1). IR (KBr): 1691 s. ^{1}H NMR ($CDCl_3$) δ: 1.41 (t, *J* = 7.3 Hz, 3H), 2.60 (br, 1H), 3.08 (br, 1H), 7.47 (dd, *J* = 7.3, 0.99 Hz, 1H), 7.51 (dd, *J* = 7.9, 4.3 Hz, 1H), 7.72 (dd, *J* = 7.9, 7.3 Hz, 1H), 7.75 (d, *J* = 8.8 Hz, 1H), 7.87 (d, *J* = 8.8 Hz, 1H), 7.96 (dd, *J* = 7.9, 0.99 Hz, 1H), 8.20 (dd, *J* = 7.9, 1.8 Hz, 1H), 8.90 (dd, *J* = 4.3, 1.8 Hz, 1H). ^{13}C NMR ($CDCl_3$) δ: 8.33, 37.82, 121.70, 124.48, 125.83, 126.93, 127.73, 127.83, 127.88, 128.65, 133.82, 135.57, 141.41, 144.95, 147.67, 209.43. MS *m*/*z* (relative intensity, %): 235 (M^+, 0), 207 (16), 206 (100), 178 (31), 89 (15), 75 (18). Anal. calcd. for $C_{16}H_{13}NO$: C 81.68, H 5.57, N 5.95; found: C 81.59, H 5.61, N 5.93.

1-(1-Naphthalenyl)isoquinoline (17)

White solid, mp 116–119 °C (1 mmHg) (1 mmHg = 133.322 4 Pa). R_f 0.51 (hexane–EtOAc, 1:1). IR (KBr): 798, 775, 750. ^{1}H NMR ($CDCl_3$) δ: 7.28–7.50 (c, 4H), 7.55–7.70 (c, 4H), 7.74 (d, *J* = 5.6 Hz, 1H), 7.90–8.00 (c, 3H), 8.69 (d, *J* = 5.6 Hz, 1H). ^{13}C NMR ($CDCl_3$) δ: 120.20, 125.15, 125.89, 125.93, 126.30, 126.83, 127.15, 127.61, 127.76, 128.22, 128.24, 128.80, 130.18, 132.26, 133.66, 136.42, 136.99, 142.37, 160.44. MS *m*/*z* (relative intensity, %): 255 (M^+, 41), 254 (100), 253 (21), 127 (94), 113 (31). Anal. calcd. for $C_{19}H_{13}N$: C 89.38, H 5.13, N 5.49; found: C 89.33, H 5.24, N 5.54.

1-[2-(1-Isoquinolinyl)naphthalenyl]-1-propanone (18)

White solid, mp 135 to 136 °C (1 mmHg) (1 mmHg = 133.322 4 Pa). R_f 0.49 (hexane–EtOAc, 1:1). IR (KBr): 1682, 831. ^{1}H NMR ($CDCl_3$) δ: 0.88 (t, *J* = 7.3 Hz, 3H), 2.50 (dq, *J* = 17.8, 7.3 Hz, 1H), 2.63 (dq, *J* = 17.8, 7.3 Hz, 1H), 7.14 (d, *J* = 8.6 Hz, 1H), 7.30 (t, *J* = 7.6 Hz, 1H), 7.36–7.38 (m, 2H), 7.52 (t, *J* = 7.6 Hz, 1H), 7.65 (dt, *J* = 8.6, 4.1 Hz, 1H), 7.76 (d, *J* = 5.6 Hz, 1H), 7.89–7.96 (m, 3H), 8.05 (d, *J* = 8.6 Hz, 1H), 8.66 (d, *J* = 5.6 Hz, 1H). ^{13}C NMR ($CDCl_3$) δ: 8.10, 34.89, 120.44, 124.44, 126.96, 126.99, 127.04, 127.32, 127.49, 127.50, 127.92, 128.88, 129.04, 130.32, 132.43, 134.58, 135.86, 136.27, 136.47, 141.98, 159.74, 204.00. MS *m*/*z* (relative intensity, %): 311 (M^+, 0), 283 (30), 282 (100), 253 (22), 252 (17), 127 (84), 113 (21), 112 (14), 100 (13). HR-MS calcd. for $C_{22}H_{17}NO$: 311.1310 (M^+); found: 311.1301.

2-(1-Naphthalenyl)-3-methylpyridine (19)

White solid, mp 87 to 88 °C (1 mmHg) (1 mmHg = 133.322 4 Pa), bp 180 °C (0.7 mmHg) (1 mmHg = 133.322 4 Pa). R_f 0.49 (hexane–EtOAc, 1:1). IR (KBr): 1391, 803. ^{1}H NMR ($CDCl_3$) δ: 2.07 (s, 3H), 7.26 (dd, *J* = 7.8, 4.8 Hz, 1H), 7.37–7.57 (c, 5H), 7.64 (d, *J* = 7.6 Hz,

© 2005 NRC Canada

1H), 7.88–7.91 (c, 2H), 8.59 (d, J = 4.6 Hz, 1H). ^{13}C NMR ($CDCl_3$) δ: 19.29, 122.37, 125.18, 125.25, 125.65, 126.12, 126.22, 128.14, 128.18, 131.25, 132.39, 133.53, 137.69, 138.11, 146.71, 158.31. MS *m/z* (relative intensity, %): 219 (M^+, 34), 218 (15), 217 (16), 216 (18), 109 (33). Anal. calcd. for $C_{16}H_{13}N$: C 87.64, H 5.98, N 6.39; found: C 87.36, H 6.01, N 6.17.

1-[2-[2-(3-Methylpyridinyl)]naphthalenyl]-1-propanone (20)

White solid, mp 100–102 °C (1 mmHg) (1 mmHg = 133.322 4 Pa). R_f 0.43 (hexane–EtOAc, 1:1). IR (KBr): 1687, 806, 795. ^{1}H NMR ($CDCl_3$) δ: 1.01 (t, J = 7.3 Hz, 3H), 1.98 (s, 3H), 2.58 (dq, J = 17.8, 7.3 Hz, 1H), 2.73 (dq, J = 17.8, 7.3 Hz, 1H), 7.21–7.31 (m, 2H), 7.39 (dt, J = 7.6, 0.99 Hz, 1H), 7.52 (dt, J = 7.6, 0.99 Hz, 1H), 7.63 (d, J = 7.6 Hz, 1H), 7.79 (d, J = 8.6 Hz, 1H), 7.89 (d, J = 8.2 Hz, 1H), 7.95 (d, J = 8.6 Hz, 1H), 8.54 (d, J = 4.9 Hz, 1H). ^{13}C NMR ($CDCl_3$) δ: 8.13, 18.80, 35.07, 122.64, 124.18, 126.48, 127.02, 127.33, 128.00, 128.43, 131.44, 133.51, 134.52, 135.68, 137.21, 137.33, 146.63, 157.38, 204.78. MS *m/z* (relative intensity, %): 275 (M^+, 9), 247 (22), 246 (100), 218 (16), 217 (25), 216 (20), 123 (10), 109 (61), 108 (12), 96 (15), 95 (20). Anal. calcd. for $C_{19}H_{17}NO$: C 82.88, H 6.22, N 5.09; found: C 82.63, H 6.14, N 5.05.

3-Methyl-2-(2-methylphenyl)pyridine (21)

Colorless oil, bp 80 °C (1.6 mmHg) (1 mmHg = 133.322 4 Pa). R_f 0.43 (hexane–EtOAc, 1:1). IR (neat): 1446, 793, 758. ^{1}H NMR ($CDCl_3$) δ: 2.06 (s, 3H), 2.07 (s, 3H), 7.12–7.26 (c, 5H), 7.54 (d, J = 7.6 Hz, 1H), 8.48 (d, J = 4.3 Hz, 1H). ^{13}C NMR ($CDCl_3$) δ: 18.98, 19.30, 122.13, 125.65, 127.87, 128.40, 130.12, 131.44, 135.47, 137.66, 140.22, 146.68, 159.62. MS *m/z* (relative intensity, %): 183 (M^+, 18), 182 (44), 169 (16), 168 (100), 167 (41), 90 (55), 84 (28), 77 (13), 65 (17), 63 (18), 51 (13). Anal. calcd. for $C_{13}H_{13}N$: C 85.21, H 7.15, N 7.64; found: C 85.00, H 7.13, N 7.62.

1-[3-Methyl-2-[2-(3-methylpyridinyl)]phenyl]-1-propanone (22)

Colorless oil, bp 160 °C (0.7 mmHg) (1 mmHg = 133.322 4 Pa). R_f 0.37 (hexane–EtOAc, 1:1). IR (neat): 1695, 1450. ^{1}H NMR ($CDCl_3$) δ: 0.96 (t, J = 7.3 Hz, 3H), 1.98 (s, 3H), 2.03 (s, 3H), 2.58 (dq, J = 17.8, 7.3 Hz, 1H), 2.71 (dq, J = 17.8, 7.3 Hz, 1H), 7.18 (dd, J = 7.7, 4.9 Hz, 1H), 7.36 (t, J = 7.7 Hz, 1H), 7.40 (d, J = 8.0 Hz, 1H), 7.54–7.57 (c, 2H), 8.45 (dd, J = 4.8, 1.1 Hz, 1H). ^{13}C NMR ($CDCl_3$) δ: 8.11, 18.65, 19.33, 34.58, 122.17, 125.58, 127.72, 132.32, 133.07, 136.83, 137.13, 138.58, 138.62, 146.54, 158.58, 204.56. MS *m/z* (relative intensity, %): 239 (M^+, 1), 224 (17), 211 (21), 210 (100), 167 (17). HR-MS calcd. for $C_{16}H_{17}NO$: 239.1310 (M^+); found: 239.1313.

1-[2-(2-Thiazolyl)phenyl]-1-propanone (24)

Colorless oil, bp 116 °C (0.3 mmHg) (1 mmHg = 133.322 4 Pa). R_f 0.60 (hexane–EtOAc, 1:1). IR (neat): 1699, 1215, 764. ^{1}H NMR ($CDCl_3$) δ: 1.16 (t, J = 7.3 Hz, 3H), 2.59 (q, J = 7.3 Hz, 2H), 7.35–7.39 (c, 2H), 7.47–7.50 (c, 2H), 7.72 (m, 1H), 7.85 (d, J = 3.3 Hz, 1H). ^{13}C NMR ($CDCl_3$) δ: 8.49, 36.56, 119.82, 127.02, 129.07, 129.65, 129.79, 130.48, 141.23, 143.67, 166.06, 207.69. MS *m/z* (relative intensity, %): 217 (M^+, 0), 202 (4), 190 (7), 189 (14), 188 (100), 116 (19), 58 (31). HR-MS calcd. for $C_{12}H_{11}NOS$: 218.0640 (M^+ + 1); found: 218.0643.

1-[2-(2-Thiazolyl)-3-(1-propionyl)phenyl]-1-propanone (25)

Brown solid, mp 59 to 60 °C (1 mmHg) (1 mmHg = 133.322 4 Pa). R_f 0.43 (hexane–EtOAc, 1:1). IR (neat): 1701. ^{1}H NMR ($CDCl_3$) δ: 1.03 (t, J = 7.3 Hz, 6H), 2.45 (q, J = 7.3 Hz, 4H), 7.51 (d, J = 3.3 Hz, 1H), 7.55–7.57 (c, 3H), 7.89 (d, J = 3.3 Hz, 1H). ^{13}C NMR ($CDCl_3$) δ: 8.09, 35.96, 121.99, 128.46, 128.53, 129.59, 142.55, 143.21, 163.29, 205.78. MS *m/z* (relative intensity, %): 273 (M^+, 0), 217 (42), 189 (12), 188 (93), 160 (82), 116 (15), 77 (21), 76 (16), 58 (18), 57 (100). HR-MS calcd. for $C_{15}H_{15}NO_2S$: 274.0902 (M^+ + 1); found: 274.0909.

1-[2-[4-(2-Methylthiazolyl)phenyl]-1-propanone (27)

Colorless oil, bp 135 °C (1 mmHg) (1 mmHg = 133.322 4 Pa). R_f 0.43 (hexane–EtOAc, 2:1). IR (neat): 1688, 1492, 1442, 1410, 1344, 1206, 1164. ^{1}H NMR ($CDCl_3$) δ: 1.11 (t, J = 7.3 Hz, 3H), 2.53 (q, J = 7.3 Hz, 2H), 2.72 (s, 3H), 7.20 (s, 1H), 7.34–7.39 (c, 2H), 7.45 (ddd, J = 7.9, 0.99, 0.66 Hz, 1H), 7.65 (m, 1H). ^{13}C NMR ($CDCl_3$) δ: 8.53, 19.12, 36.47, 114.98, 126.75, 128.04, 128.61, 129.79, 132.02, 141.27, 153.56, 165.61, 208.54. MS *m/z* (relative intensity, %): 231 (M^+, 3), 203 (21), 202 (100), 161 (13), 89 (13). Anal. calcd. for $C_{13}H_{13}NOS$: C 67.50, H 5.66, N 6.06; found: C 67.37, H 5.64, N 6.06.

Acknowledgements

This work was supported, in part, by grants from the Ministry of Education, Culture, Sports, Science and Technology, Japan. T.A. acknowledges the Research Fellowships of Japan Society for the Promotion of Science for Young Scientists. Thanks are given to the Instrumental Analysis Center, Faculty of Engineering, Osaka University, for assistance in obtaining MS, HR-MS, 600 MHz NMR, and elemental analyses.

References

1. For recent reviews, see: F. Kakiuchi and S. Murai. Acc. Chem. Res. **35**, 826 (2002); F. Kakiuchi and N. Chatani. Adv. Synth. Catal. **345**, 1077 (2003); C.-H. Jun and H. Lee. Pure Appl. Chem. **76**, 577 (2004).
2. S. Ko, Y. Na, and S.-B. Chang. J. Am. Chem. Soc. **124**, 750 (2002).
3. F. Kakiuchi, S. Kan, K. Igi, N. Chatani, and S. Murai. J. Am. Chem. Soc. **125**, 1698 (2003).
4. B. Sezen, R. Franz, and D. Sames. J. Am. Chem. Soc. **124**, 13 372 (2002).
5. A.R. Dick, K.L. Hull, and M.S. Sanford. J. Am. Chem. Soc. **126**, 2300 (2004); L.V. Desai, K.L. Hull, and M.S. Sanford. J. Am. Chem. Soc. **126**, 9542 (2004).
6. F. Kakiuchi, K. Tsuchiya, M. Matsumoto, E. Mizushima, and N. Chatani. J. Am. Chem. Soc. **126**, 12 792 (2004).
7. N. Chatani, Y. Ie, F. Kakiuchi, and S. Murai. J. Am. Chem. Soc. **121**, 8645 (1999).

© 2005 NRC Canada

8. D.-Y. Lee, B.-S. Hong, E.-G. Cho, H. Lee, and C.-H. Jun. J. Am. Chem. Soc. **125**, 6372 (2003).
9. Y. Ishii, N. Chatani, S. Yorimitsu, and S. Murai. Chem. Lett. 157 (1998).
10. N. Chatani, H. Tatamidani, Y. Ie, F. Kakiuchi, and S. Murai. J. Am. Chem. Soc. **123**, 4849 (2001); F. Kakiuchi, M. Usui, S. Ueno, N. Chatani, and S. Murai. J. Am. Chem. Soc. **126**, 2706 (2004).
11. K. Yokota, H. Tatamidani, Y. Fukumoto, and N. Chatani. Org. Lett. **5**, 4329 (2003).
12. (*a*) E.J. Moore, W.R. Pretzer, T.J. O'Connell, J. Harris, L. LaBounty, L. Chou, and S.S. Grimmer. J. Am. Chem. Soc. **114**, 5888 (1992); (*b*) N. Chatani, T. Fukuyama, F. Kakiuchi, and S. Murai. J. Am. Chem. Soc. **118**, 493 (1996); (*c*) Y. Ishii, N. Chatani, F. Kakiuchi, and S. Murai. Organometallics, **16**, 3615 (1997); (*d*) N. Chatani, Y. Ie, F. Kakiuchi, and S. Murai. J. Org. Chem. **62**, 2604 (1997); (*e*) Y. Ishii, N. Chatani, F. Kakiuchi, and S. Murai. Tetrahedron Lett. **38**, 7565 (1997); (*f*) T. Fukuyama, N. Chatani, F. Kakiuchi, and S. Murai. J. Org. Chem. **62**, 5647 (1997); (*g*) N. Chatani, Y. Ishii, Y. Ie, F. Kakiuchi, and S. Murai. J. Org. Chem. **63**, 5129 (1998); (*h*) T. Fukuyama, N. Chatani, J. Tatsumi, F. Kakiuchi, and S. Murai. J. Am. Chem. Soc. **120**, 11 522 (1998); (*i*) Y. Ie, N. Chatani, T. Ogo, D.R. Marshall, T. Fukuyama, F. Kakiuchi, and S. Murai. J. Org. Chem. **65**, 1475 (2000); (*j*) N. Chatani, T. Fukuyama, H. Tatamidani, F. Kakiuchi, and S. Murai. J. Org. Chem. **65**, 4039 (2000); (*k*) N. Chatani, T. Asaumi, T. Ikeda, S. Yorimitsu, Y. Ishii, F. Kakiuchi, and S. Murai. J. Am. Chem. Soc. **122**, 12 882 (2000); (*l*) J.W. Szewczyk, R.L. Zuckerman, R.G. Bergman, and J.A. Ellman. Angew. Chem. Int. Ed. **40**, 216 (2001); (*m*) N. Chatani, S. Yorimitsu, T. Asaumi, F. Kakiuchi, and S. Murai. J. Org. Chem. **67**, 7557 (2002); (*n*) T. Asaumi, N. Chatani, T. Matsuo, F. Kakiuchi, and S. Murai. J. Org. Chem. **68**, 7538 (2003); (*o*) T. Asaumi, T. Matsuo, T. Fukuyama, Y. Ie, F. Kakiuchi, and N. Chatani. J. Org. Chem. **69**, 4433 (2004).
13. X. Zhang, M. Kanzelberger, T.J. Emge, and A.S. Goldman. J. Am. Chem. Soc. **126**, 13 192 (2004).
14. M.I. Bruce, C.M. Jensen, and N.L. Jones. Inorg. Synth. **26**, 259 (1989).
15. B.M. Holligan, J.C. Jeffery, M.K. Norgett, E. Schatz, and M.D.I. Ward. J. Chem. Soc. Dalton Trans. 3345 (1992).
16. N. Miyaura, T. Yanagi, and A. Suzuki. Synth. Commun. **11**, 513 (1981).

© 2005 NRC Canada

Oxidative carbonylation of aniline with new cobalt catalytic systems[1]

Aránzazu Orejón, Aída Castellanos, Pilar Salagre, Sergio Castillón, and Carmen Claver

Abstract: New neutral cobalt(II) complexes containing 2,9-bis(2-hydroxyphenyl)-1,10-phenanthroline and 2,9-bis(2-hydroxyphenyl)-2,2′-bipyridine ligands have been synthesized. These complexes are active catalysts in the oxidative carbonylation of aniline in 1-butanol and NaI as a promoter. The principal products obtained are *N*,*N*′-diphenylurea and 1-butyl-*N*-phenylcarbamate.

Key words: cobalt, oxidative carbonylation, aniline, *N*,*N*′-diphenylurea, 1-butyl-*N*-phenylcarbamate.

Résumé : Des complexes du cobalt(II) contenant les ligands 2,9-bis(2-hydroxyphenyl)-1,10-phénanthroline et 2,9-bis(2-hydroxyphényl)-2,2′-bipyridine ont été synthétisés. Ces complexes sont des catalyseurs actifs pour la réaction de carbonylation oxydante de l'aniline dans le 1-butanol, en utilisant le NaI comme promoteur. Les produits principaux de la réaction sont le *N*,*N*′-diphénylurée et le *N*-phenylcarbamate de 1-butyle.

Mots clés : cobalt, carbonylation oxydante, aniline, *N*,*N*′-diphénylurée, *N*-phenylcarbamate de 1-butyle.

[Traduit par la Rédaction]

Introduction

Industrially important materials, such as high-performance plastics, polyurethane elastomers, and adhesives, are usually obtained from isocyanates. The reaction of phosgene with amines is one of the most important industrial methods for the formation of isocyanates, carbamates, and ureas (1). As there are restrictions on the use of very toxic materials such as phosgene, and since large amounts of corrosive HCl are produced as a side product in the conversion of aromatic amine to isocyanate, interest has been increasing in the development of alternative methods for isocyanate production (1).

One of the proposed approaches is to first synthesize the carbamate, either by the oxidative carbonylation of amines or by the reductive carbonylation of nitro compounds in the presence of an alcohol, followed by thermal elimination of alcohol to form isocyanates (2) (Scheme 1).

The interest in developing the reductive carbonylation of nitro compounds is demonstrated by the numerous patents and papers in the literature (3). However, the commercial production of isocyanates by this route has not been industrially developed, mainly because the use of a precious metal such as palladium is necessary and also because the process involves three CO molecules and, unless CO is available at a negligible cost, the process is uneconomical.

With regard to oxidative carbonylation, several processes based on metal catalysts promoting the formation of carbamates from organic hydroxyl compounds, carbon monoxide, amines, and an oxygen-containing oxidizing agent have also been reported (4, 5). It is known that cobalt complexes are active catalysts in the oxidative carbonylation of amines. The most widely used cobalt complexes are *N*,*N*′-bis(salicylidene)ethylenediaminocobalt(II) ([Co(salen)], **1**), [Co(tetrakis-(4-methoxyphenyl)porphine)], [Co(phthalocyanine)], and [CoTTP] (TTP = mesotetraphenylporphinato dianion) (4*b*, 5). In this context, [Co(salen)] (**1**) catalyzes the oxidative carbonylation of ortho-, meta-, and para-substituted aromatic primary amines in methanol to give ureas, isocyanates, carbamates, and azo derivatives (5).

Concerning the mechanism of this reaction, it has been proposed that the oxidative reaction takes place through the formation of a superoxo complex of cobalt(III), known to be formed by coordination of the dioxygen on the [Co(salen)]-type complexes. These complexes undergo carbonylation to give the carbamoyl complexes that could be the origin of the free isocyanate or the carbamate (5).

Modification of [Co(salen)] complexes has enabled the improvement of the efficiency of many catalytic processes, but as far as we know cobalt complexes with modified salen ligands have never been studied before in the oxidative carbonylation of amines. In this paper, we study the reaction of oxidative carbonylation with salen-modified complexes such as the already known complexes **2**–**4** (6) to determine the effects in the catalytic activity of electron-donating **2** and electron-withdrawing groups **3** and **4** in the aromatic rings. We also prepared the new complexes **5** and **6** in which the

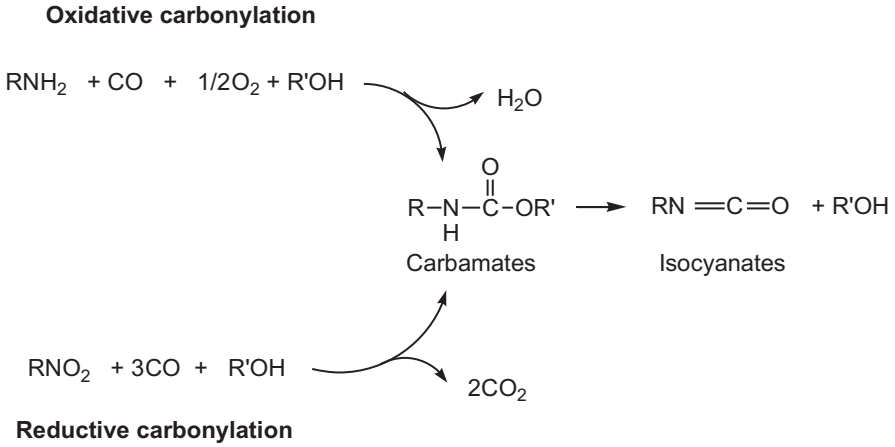
Received 27 October 2004. Published on the NRC Research Press Web site at http://canjchem.nrc.ca on 23 June 2005.

A. Orejón, A. Castellanos, P. Salagre, and C. Claver.[2] Departament de Química Física i Inorgànica, Universitat Rovira i Virgili, Marcel·lí Domingo s/n, 43007 Tarragona, Spain.
S. Castillón. Departament de Química Analítica i Orgànica, Universitat Rovira i Virgili, Marcel·lí Domingo s/n, 43007 Tarragona, Spain.

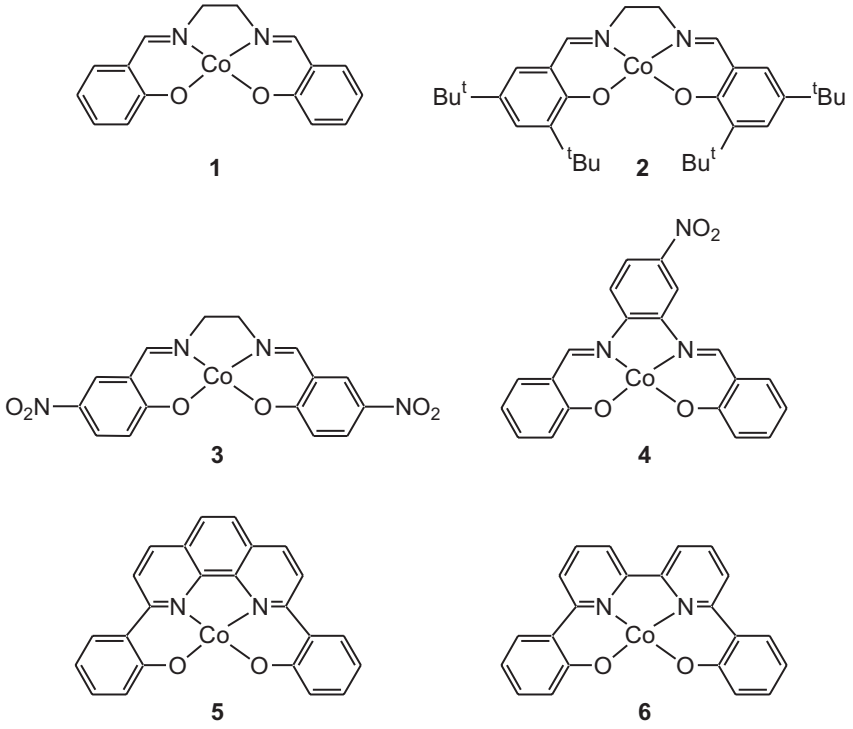
[1]This article is part of a Special Issue dedicated to Professor Howard Alper.
[2]Corresponding author (e-mail: claver@quimica.urv.es).

 doi: 10.1139/V05-080 © 2005 NRC Canada

Scheme 1. Methods for isocyanate production.



Scheme 2. Salen-modified complexes.



imine groups have been substituted by the heteroaromatic rings 2,2′-bipyridine and 1,10-phenathroline (Scheme 2).

Experimental

General procedures

All syntheses were carried out in a nitrogen atmosphere at room temperature using standard Schlenk techniques. Solvents were distilled and deoxygenated prior to use unless otherwise stated. Aniline and the catalyst *N*,*N*-bis(salicylidene)ethylenediaminocobalt(II) are commercial products. Cobalt–salen derivative complexes were synthesized according to literature procedures (6). Aniline was distilled with Na prior to use. Elemental analyses were carried out in a Carlo Erba microanalyser EA 1108. ^{1}H NMR spectra were recorded on a Varian Gemini spectrometer with a ^{1}H resonance frequency of 400 MHz.

Synthesis of the ligands

Synthesis of 2,9-bis(2-hydroxyphenyl)-1,10-phenanthroline (7)

n-Butyllithium (16.2 mL, 25.8 mmol of a 1.6 mol/L solution) was added to a stirred solution of 2-bromophenol (1.2 mL, 11.3 mmol) in 40 mL of anhydrous diethyl ether. After 24 h at room temperature, the white suspension obtained was slowly added to a warm solution (50 °C) of 1,10-phenanthroline (0.388 g, 2.15 mmol) in 25 mL of anhydrous toluene. Immediately, a red solution was formed, which was maintained at 50 °C for 48 h. The resulting brown solution was then cooled to 0 °C and slowly hydrolyzed with H_2O

© 2005 NRC Canada

(20 mL). The organic phase was separated and the aqueous phase was extracted with ethyl acetate. The organic phases were combined, 2 g of MnO_2 (Fluka No. 63548) was added, and the reaction mixture was stirred at room temperature for 24 h. After this time, the solution was dried over $MgSO_4$ for 2 h and then filtered through Celite®. The solution was evaporated to dryness with a rotatory evaporator and purified using flash chromatography with a mixture of hexane – ethyl acetate (2:1) to yield 0.253 g (33% yield) of **7** as a yellow solid. ^{1}H NMR (400 MHz, DMSO, 298 K) δ: 7.03 (td, *J* = 6.6, 1.5 Hz, 2H, arom), 7.09 (dd, *J* = 8.1, 0.9 Hz, 2H, arom), 7.42 (td, *J* = 6.9, 1.5 Hz, 2H, arom), 8.08 (s, 2H, phenanthroline), 8.28 (dd, *J* = 7.8, 1.4 Hz, 2H, arom), 8.61 (d, *J* = 8.7 Hz, 2H, phenanthroline), 8.70 (d, *J* = 8.7 Hz, 2H, phenanthroline), 13.95 (s, 2H, -OH). ^{13}C NMR (300 MHz, DMSO, 298 K) δ: 117.86, 119.16, 120.36, 121.31, 126.29, 127.38, 128.61, 132.0, 138.29, 141.57, 157.12, 159.11. FAB-MS *m*/*z*: 364.4 [M]. Elemental anal. calcd.: C 79.1, H 4.42, N 7.69; found: C 78.4, H 4.44, N 7.29.

Synthesis of 2,9-bis(2-hydroxyphenyl)-2,2′-bipyridine (8)

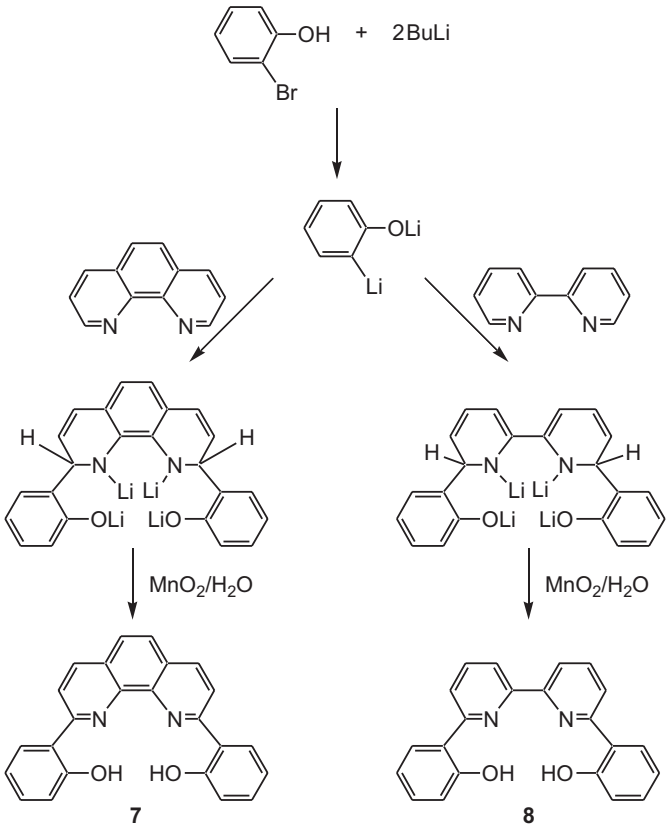
n-Butyllithium (16.2 mL, 25.8 mmol of a 1.6 mol/L solution) was added to a stirred solution of 2-bromophenol (1.2 mL, 11.3 mmol) in 40 mL of anhydrous diethyl ether. After 24 h at room temperature, the white suspension obtained was slowly added to a warm solution (50 °C) of 2,2′-bipyridine (0.35 g, 2.3 mmol) in 25 mL of anhydrous toluene. Immediately, a red solution was obtained, which was maintained at 50 °C for 48 h. The brown solution obtained was then cooled to 0 °C and hydrolyzed slowly with H_2O (20 mL). The organic phase was separated and the aqueous phase was extracted with ethyl acetate. The organic phases were combined, 2 g of MnO_2 (Fluka No. 63548) was added, and the reaction mixture was stirred at room temperature for 24 h. After this time, the solution was dried over $MgSO_4$ for 2 h and then filtered through Celite®. The solution was evaporated to dryness with a rotatory evaporator and purified using flash chromatography with a mixture of CH_2Cl_2–hexane (5:1) to yield 0.11 g (14% yield) of **8** as a yellow solid. ^{1}H NMR (400 MHz, DMSO, 298 K) δ: 6.98 (t, *J* = 7.2 Hz, 2H, arom), 7.08 (d, *J* = 8.4 Hz, 2H, arom), 7.37 (td, *J* = 7.2, 0.8 Hz, 2H, arom), 7.87 (dd, *J* = 8.0, 0.8 Hz, 2H, arom), 8.02 (m, 4H, bipyridine), 8.13 (dd, *J* = 7.2, 1.6 Hz, 2H, bipyridine), 14.20 (s, 2H, -OH). ^{13}C NMR (300 MHz, DMSO, 298 K) δ: 117.86, 119.16, 120.36, 121.31, 126.29, 127.38, 128.61, 132.0, 138.29, 141.57, 157.12, 159.11. Elemental anal. calcd.: C 77.63, H 4.74, N 8.23; found: C 77.00, H 4.78, N 7.98.

Synthesis of the neutral cobalt(II) complexes

Synthesis of 2,9-bis(2-hydroxyphenyl)-1,10-phenanthroline cobalt (5)

In a three-necked round flask equipped with a pressure-equalizing funnel and a water condenser, 2,9-bis(2-hydroxyphenyl)-1,10-phenanthroline (**7**) (0.189 g, 0.52 mmol) was dissolved in 95% ethanol (12 mL) under a nitrogen atmosphere. A solution of $Co(OAc)_2{\cdot}4H_2O$ (0.121 g, 0.486 mmol) in 3 mL of water was introduced into the pressure-equalizing funnel and added dropwise over the reluxing solution of the ligand under a nitrogen atmosphere. Initially, the solution became orange and a red precipitate started to appear. After 1 h of heating, the solution was immersed in a cold bath. The solid was filtered and washed with water and absolute ethanol. The red precipitate was dried under vacuum to yield 0.192 g (94% yield) of **5**. Elemental anal. calcd.: C 68.42, H 3.35, N 6.65; found: C 69.00, H 3.75, N 6.69.

Scheme 3. Method for the preparation of 9-bis(2-hydroxyphenyl)-1,10-phenantroline (**7**) and 2,9-bis(2-hydroxyphenyl)-2,2′-bipyridine (**8**) ligands.



Synthesis of 2,9-bis(2-hydroxyphenyl)-2,2′-bipyridine cobalt (6)

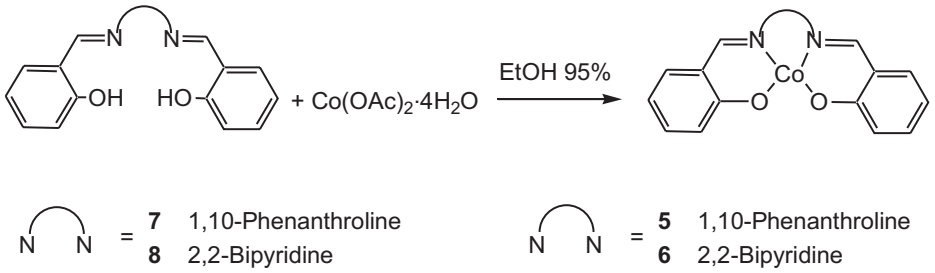
In a three-necked round flask equipped with a pressure-equalizing funnel and a water condenser, 2,9-bis(2-hydroxyphenyl)-2,2′-bipyridine (**8**) (0.04 g, 0.12 mmol) was dissolved in 95% ethanol (3 mL) under a nitrogen atmosphere. A solution of $Co(OAc)_2{\cdot}4H_2O$ (0.03 g, 0.11 mmol) in 0.6 mL of water was introduced into the pressure-equalizing funnel and added dropwise to the refluxing solution of the ligand. Initially, the solution became orange and a brown precipitate started to appear. After 1 h of heating, the solution was immersed in a cold bath. The solid was filtered, then washed with water and absolute ethanol. The brown precipitate was dried in a vacuum desiccator to yield 0.046 g (90% yield) of **6**. Elemental anal. calcd.: C 66.50, H 3.55, N 7.05; found: C 66.12, H 3.76, N 6.90.

General procedure for the oxidative carbonylation of amines

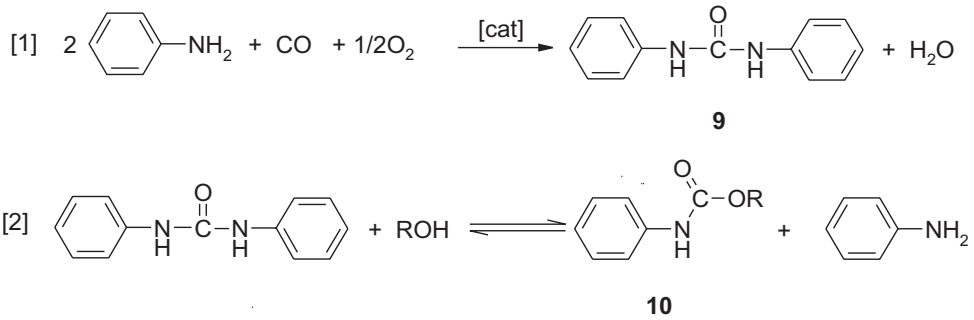
A mixture of the substrate (13.2 mmol), cobalt complex (0.25 mmol), NaI (2.72 mmol for sust/NaI = 5 or 1.89 mmol for sust/NaI = 7), and 1-butanol (20 mL) was charged in a 100 mL autoclave. The autoclave was flushed with carbon

© 2005 NRC Canada

Scheme 4. Method for the preparation of neutral(II) cobalt complexes.



Scheme 5. Oxidative carbonylation of aniline.



monoxide and pressurized to 50.1 bar (1 bar = 100 kPa), then carefully pressurized with oxygen to a total pressure of 52.7 bar (4.93% O_2–CO) (1 bar = 100 kPa). (*Caution!* Reverse addition, i.e., O_2 before CO, is dangerous). The autoclave was heated electrically to the desire temperature and stirred for 3 h. The reaction mixture was cooled to room temperature, then concentrated by rotatory evaporation. The crude material was analyzed by ^{1}H NMR in deuterated acetone.

Results and discussion

Synthesis of the ligands 9-bis(2-hydroxyphenyl)-1,10-phenanthroline (7) and 2,9-bis(2-hydroxyphenyl)-2,2′-bipyridine (8)

In this paper we prepared the ligands 9-bis(2-hydroxyphenyl)-1,10-phenanthroline (**7**) and 2,9-bis(2-hydroxyphenyl)-2,2′-bipyridine (**8**) (Scheme 3) following the method published by Burger and Baumeister (7).

This method is shown in Scheme 3. First, a solution of *n*-butyllitium (1.6 mol/L) in hexanes was added to a solution of 2-bromophenol in diethyl ether. After 12 h at room temperature, the lithium salt was obtained as a white suspension. This salt was added dropwise to a solution of 1,10-phenathroline or 2,2′-bipyridine in toluene, which was heated at 50 °C. The solution became red and after 48 h at 50 °C, hydrolysis and treatment with MnO_2 led to the isolation of the ligands. The yields were generally low, but attempts to increase them failed.

Synthesis of the neutral cobalt(II) complexes 9-bis(2-hydroxyphenyl)-1,10-phenanthrolinecobalt(II) (5) and 2,9-bis(2-hydroxyphenyl)-2,2′-bipyridinecobalt(II) (6)

Reaction of the ligands 9-bis(2-hydroxyphenyl)-1,10-phenanthroline (**7**) and 2,9-bis(2-hydroxyphenyl)-2,2′-bipyridine (**8**) with $Co(OAc)_2 \cdot 4H_2O$ in an ethanolic solution gave the 9-bis(2-hydroxyphenyl)-1,10-phenanthrolinecobalt(II) (**5**) and 2,9-bis(2-hydroxyphenyl)-2,2′-bipyridinecobalt(II) (**6**) in good yields (Scheme 4). Elemental analysis confirmed the formation of the cobalt complexes.

Oxidative carbonylation of aniline

To avoid the use of phosgene, carbamates were synthesized from the oxidative carbonylation of aniline according to the following reaction (Scheme 5), where aniline reacted catalytically with carbon monoxide and oxygen to form *N*,*N*′-diphenylurea, which further reacted to form the carbamate.

Reaction [1] (Scheme 5) is a catalytic reaction, while rxn. [2] (Scheme 5) is essentially thermal. However, the second reaction can be catalysed by Lewis acids. Although the two steps are independent, the alcoholisis of the urea to form the carbamate releases aniline, which is the starting material in the first reaction. Both reactions therefore become dependent on one another, and full conversion is achieved by an iterative process.

Therefore, at a given temperature, the reaction of the conversion of ureas into carbamates will be similar and the ratio of carbamate to urea will be an indicator of the activity of the catalysts in the oxidative carbonylation. Iodide as the additive has a beneficial effect on the reaction rate (8).

Results for the cobalt precursors **1**–**6** are summarized in Table 1. To compare the activity with other cobalt catalytic systems, the [Co(salen)] complex **1** was first used as the catalyst precursor in the oxidative carbonylation of aniline. Initially, the reaction was performed in 1-butanol at 130 °C (internal temperature of 110 °C) at 60 bar (1 bar = 100 kPa) and with NaI as the additive. Carbamate (44%) and 56% of urea were obtained with a total conversion (Table 1, entry 1). When *tert*-butyl groups were introduced into the aromatic rings of the salen ligand (precursor **2**) only the urea derivative was obtained (Table 1, entry 3). As expected, when the

© 2005 NRC Canada

Table 1. Oxidative carbonylation of aniline.[a,b]

Entry	Precursor	T/T_{int} (°C)	**9** (%)	**10** (%)
1	**1**	130/110	56	44
2	**1**	160/130	38	62
3	**2**	130/110	100	—
4	**3**	160/130	37	63
5	**4**	160/130	17	83
6	**5**	130/110	94	6
7	**5**	160/130	72	28
8	**6**	160/130	50	50

[a]0.26 mmol catalyst; 3%–5% O_2/CO; 13.2 mmol aniline; 20 mL 1-BuOH; 2.72 mmol NaI; P = 60 bar (1 bar = 100 kPa); (sust/NaI = 7, sust/cat = 50).
[b]Total conversion in 3 h.

reaction with the [Co(salen)] precursor was performed at 160 °C (internal temperature of 130 °C), the ratio of carbamate to urea increased to 62:38 (Table 1, entry 2).

To study the effect of withdrawing substituents in the ligand, we also examined the activity of complexes **3** and **4** with nitro groups in the phenyl rings of the ligand. Introducing a nitro group in the para position to the oxygen atom led to an active catalyst that provided a similar carbamate:urea ratio to the one obtained using [Co(salen)] as the catalyst precursor (Table 1, entries 2 and 4). When the nitro group was present in the ring bearing the amino groups (precursor **4**), the results were better, and 83% of the carbamate was obtained with a carbamate:urea ratio of 83:17 (Table 1, entry 5).

The cobalt precursor **5** at 130 °C (internal temperature of 110 °C) provided urea in an almost exclusive way (Table 1, entry 6), while at 160 °C the ratio of carbamate to urea increased to 28:72 (Table 1, entry 7), but this was smaller than when [Co(salen)] (**1**) was used (Table 1, entry 2), so the activity of this complex was low. Therefore, when the temperature increased, the overall yield of the process also increased, mainly because the conversion rate of urea into carbamate increased.

The cobalt compound with the bipyridine ligand **6** was also active at 160 °C (internal temperature of 130 °C) in the oxidative carbonylation of aniline. Complete conversion was obtained and the carbamate:urea ratio was 50:50 (Table 1, entry 8), i.e., the activity was higher than with complex **5**, which had a phenathroline ligand (Table 1, entry 7).

Conclusions

New cobalt catalytic systems **5** and **6** have been prepared and characterized.

Complexes **5** and **6**, together with the already known **1**–**4**, were active as catalyst precursors in the oxidative carbonylation of aniline to give *N*,*N*′-diphenylurea and carbamates.

The use of [Co(salen)] derivatives with withdrawing groups in the ligand, particularly in the case of complex **4**, led to a higher conversion into the carbamate than with complex **1**. This shows that the modification of salen complexes can be an efficient way to improve conversions in the oxidative carbonylation of amines.

References

1. Kirk-Othmer. Encyclopedia of chemical technology. Wiley-Interscience, New York. 1994; L.H. Vogt, H.M. Faigenbau, and E. Wiberley. Chem. Rev. **63**, 269 (1963).
2. S.M. Islam, D. Mal, B.K. Palit, and C.R. Saha. J. Mol. Catal. A, **142**, 169 (1999).
3. (*a*) A.M. Tafesh and J. Weiguny. Chem. Rev. **96**, 2035 (1996); (*b*) D.K. Mukherjee and C.R. Saha. J. Mol. Catal. A, **193**, 41 (2003); (*c*) J.H. Grate, D.R. Hamm, and D.H. Valentine. US Patent 4 705 883, 1987; (*d*) E. Drent and P. van Leeuwen. Eur. Patent 0 086 281 Al, 1983; (*e*) K. Sehwelick, K. Unverferth, R. Hoentsch, and M. Pfeifer. DDR Patent 121 509, 1977; (*f*) R. Rosenthol and J.G. Zajacek. US Patent 3 962 302, 1976; Chem. Abstr. **85**, 177 053a; (*g*) S. Cenini and F. Ragaini. Catalytic reductive carbonylation of organic nitro compounds. Kluwer Academic Publishers, Dordrecht, The Netherlands. 1977; (*h*) F. Paul. Coord. Chem. Rev. **203**, 269 (2000).
4. (*a*) S. Fukuoka, M. Chono, and M. Kohno. Chemtech, November 1984; (*b*) S. Fukuoka, M. Chono, and M. Kohno. J. Org. Chem. **49**, 1458 (1984); (*c*) S. Fukuoka, M. Chono, and M. Kohno. J. Chem. Soc. Chem. Commun. 399 (1984); (*d*) S. Fukukoa and M. Chono. US Patent 4 621 149, 1986; (*e*) T.W. Leung and B.D. Dombek. US Patent 5 194 660, 1993; (*f*) B.H. Lee. US Patent 0 120 140 A1, 2002.
5. (*a*) F. Benedini, M. Nali, B. Rindone, and S. Tollari. J. Mol. Catal. **34**, 155 (1986); (*b*) G. Maddinelli, M. Nali, B. Rindone, S. Tollari, S. Cenini, G. La Monica, and F. Porta. J. Mol. Catal. **39**, 71 (1987); (*c*) A. Bassoli, B. Rindone, and S. Tollari. J. Mol. Catal. **60**, 41 (1990); (*d*) E. Bolzacchini, S. Meinardi, M. Orlandi, and B. Rindone. J. Mol. Catal. A, **111**, 281 (1996).
6. (*a*) A. Pui, I. Berdan, I. Morgenstern-Badarau, A. Gref, and M. Perrée-Fauvet. Inorg. Chim. Acta, **320**, 167 (2001); (*b*) K. Bernardo, S. Leppard, A. Robert, G. Commenges, F. Dahan, and B. Meunier. Inorg. Chem. **35**, 387 (1996); (*c*) J.-E. Bäckvall, R.B. Hopkins, H. Grennberg, M.M. Mader, and A.K. Awasthi. J. Am. Chem. Soc. **112**, 5160 (1990).
7. P. Burger and J.M. Baumeister. J. Organomet. Chem. **575**, 214 (1999).
8. For a review about the role of halide additives in metal-catalyzed reactions, see: K. Fagnou and M. Lautens. Angew. Chem. Int. Ed. **41**, 26 (2002).

© 2005 NRC Canada

Hydration of the carbonyl group — Acetic acid catalysis in the co-operative mechanism[1]

Yih-Huang Hsieh, Noham Weinberg, Kiyull Yang, Chan-Kyung Kim, Zheng Shi, and Saul Wolfe

Abstract: In a co-operative reaction, solvent molecules, specifically water molecules, participate actively in the mechanism to circumvent the formation of charged intermediates. This paper extends our earlier theoretical treatment of the neutral co-operative hydration of acetone to include general acid catalysis by acetic acid. As before, the predominant neutral channel employs three catalytic water molecules. The principal acetic acid catalyzed channels employ one catalytic water molecule and, in approximately equal proportions, one or both oxygens of the carboxyl group. The theoretical rate constant for general acid catalysis is calculated to be 0.49 M^{-1} s^{-1} at 298 K. This compares to an estimated experimental value of 0.30 M^{-1} s^{-1} for acetic acid catalyzed hydration of acetone at 298 K in water solvent, determined by using the ^{18}O-isotope shift in the ^{13}C NMR spectrum of 2-^{13}C-labelled acetone as a kinetic probe. It is concluded that the notion of co-operativity can be extended to include general acid catalysis of the hydration of a carbonyl group in water solvent. This creates an obvious problem for the generally accepted view that multistep ionic mechanisms are operative in the low dielectric media that exist at the active sites of hydrolytic enzymes. The relevance of this finding to the mechanisms of action of β-lactam antibiotics has been noted.

Key words: hydration, reaction mechanism, co-operativity, general acid catalysis, ab initio, SCRF, ^{18}O-isotope shift.

Résumé : Dans une réaction coopérative, des molécules de solvants, en particulier des molécules d'eau, participent activement au mécanisme afin de contourner la formation d'intermédiaires chargés. Dans ce travail, on étend notre traitement théorique antérieur de l'hydratation coopérative neutre de l'acétone afin d'y incorporer la catalyse acide générale par l'acide acétique. Tel qu'observé antérieurement, la voie neutre prédominante fait appel à trois molécules d'eau catalytiques. Les voies principales catalysées par l'acide acétique font appel à une molécule d'eau catalytique et, dans des proportions approximativement égales, un ou les deux atomes d'oxygène du groupe carboxyle. Il a été calculé que la constante de vitesse théorique pour la catalyse acide générale est de 0,49 M^{-1} s^{-1} à 298 K. Ceci se compare à l'évaluation de la valeur expérimentale de 0,30 M^{-1} s^{-1} pour l'hydratation catalysée par l'acide acétique, à 298 K, dans l'eau comme solvant, telle que déterminée en faisant appel au déplacement chimique du ^{18}O dans les spectres RMN d'une sonde cinétique de ^{13}C d'acétone marquée au ^{13}C en position 2. On en conclut que la notion de coopération peut être étendue de façon à inclure la catalyse acide générale de l'hydratation d'un groupe carbonyle dans l'eau. Cette conclusion crée un problème évident pour la façon généralement acceptée de considérer cette réaction qui serait sensée impliquer des mécanismes ioniques par étape dans les milieux de faibles constantes diélectriques qui existent au niveau des sites actifs des enzymes hydrolytiques. On note la pertinence de ces observations sur les mécanismes d'action des antibiotiques à base de β-lactames.

Mots clés : hydratation, mécanisme réactionnel, coopération, catalyse acide générale, ab initio, SCRF, déplacement chimique du ^{18}O.

[Traduit par la Rédaction]

Received 1 November 2004. Published on the NRC Research Press Web site at http://canjchem.nrc.ca on 2 July 2005.

This paper is dedicated to Howard Alper, OC, FRSC, in recognition of his outstanding contributions to chemistry and to Canada.

Y.-H. Hsieh, N. Weinberg,[2] K. Yang,[3] C.-K. Kim,[4] Z. Shi,[5] and S. Wolfe.[6] Department of Chemistry, Simon Fraser University, Burnaby, BC V5A 1S6, Canada.

[1]This article is part of a Special Issue dedicated to Professor Howard Alper.

[2]Permanent address: Department of Chemistry, University College of the Fraser Valley, Abbotsford, BC V2S 7MA, Canada.
[3]Permanent address: Department of Chemical Education, Gyeongsang National University, Chinju 660-701, Republic of Korea.
[4]Permanent address: Department of Chemistry, Inha University, Inchon 402-751, Republic of Korea.
[5]Present address: Department of Medicine, Division of Infectious Diseases, University of British Columbia, Vancouver, BC V6T 1Z1, Canada.
[6]Corresponding author (e-mail: swolfe@sfu.ca).

 doi: 10.1139/V05-027 © 2005 NRC Canada

Introduction

Carbonyl addition reactions, of which hydration is the prototypical example, are commonly thought to be multistep processes that proceed via charged intermediates, even under strictly neutral conditions in water solvent (1), and even at the nonpolar (2) active sites of hydrolytic enzymes (3). Nonetheless, there is mounting evidence that at least some of these reactions employ water molecules and (or) other species in a cyclic, co-operative manner (4) to *avoid* the formation of charged intermediates that would have to undergo continuous solvation and desolvation as they appear and disappear.

Early experimental evidence consistent with a co-operative mechanism of hydration of a carbonyl group was provided by Bell and co-workers (5), who found the hydration kinetics of 1,3-dichloroacetone in dioxane and acetonitrile to be at least third order in water. Some of the diverse experimental studies that have followed and have been interpreted in terms of co-operative mechanisms are collected in Table 1.

These experimental findings have stimulated much theoretical research (13), and there are now numerous computational examples of co-operative processes, both in the gas phase and in water solvent. Table 2 shows some of the aqueous phase results. The experimental free energy of activation for the hydration of carbon dioxide (Table 2, entries 1 and 2) is 18.4 kcal/mol (1 cal = 4.184 J) (14).

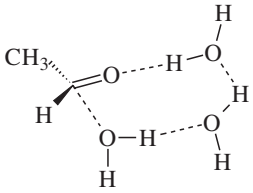
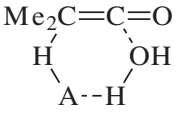
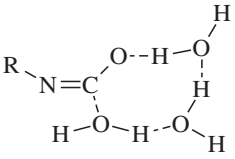
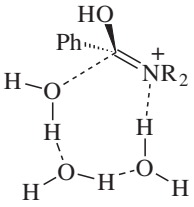
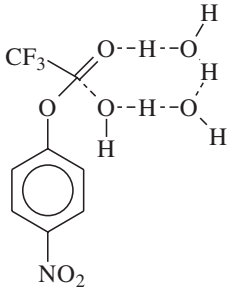
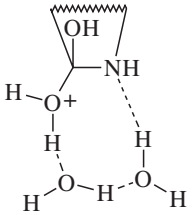
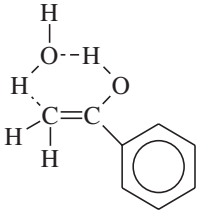
Co-operativity and the action of β-lactam antibiotics

Our interest in co-operative mechanisms began with the findings that one water molecule reduces the gas phase MP2/6-31G*//3-21G* barrier for the methanolysis of 3α-carboxypenam by 10 kcal/mol, that a second water molecule has little additional effect, and that the one-step co-operative process depicted in **1**, in which C···O and N···H bonds are formed concurrently, has a significantly lower barrier than a competing two-step process leading to a tetrahedral intermediate (18).

With the substitution of a serine side chain for methanol, and the hydroxyl groups of serine, threonine, or tyrosine for the catalytic water molecule (**1**), published 10 years ago, has recently been found[7] to resemble **2**, a portion of the complex formed when penicillin G is docked (19) to the crystal structure (20) of an exocellular penicillin-binding protein from *Streptomyces* R61, and also **3**, a portion of the complex formed upon docking (19) of penicillin G to the crystal structure (21) of the RTEM Class A β-lactamase from *Escherichia coli*. In the cases of **2** and **3**, the chemical reaction that ensues is acylation of the hydroxyl groups of Ser62 or Ser70 by the β-lactam ring. The acyl-enzyme that is formed from **2** is relatively stable (22), but the acyl-enzyme formed from **3** undergoes rapid hydrolysis, assisted by the carboxyl group of Glu166 and a water molecule that are present in the active site (23). This hydrolysis reaction and its catalysis by Glu166 and the water molecule are general to the Class A β-lactamases. As these enzymes are a major source of bacterial resistance to β-lactam antibiotics (24), the hydrolysis mechanism has received much discussion (3), most of which has been framed in terms of multistep ionic mechanisms.[8]

Because of their hydrolytic instability, acyl-enzymes of

Table 1. Experimental examples of co-operativity in carbonyl addition reactions.

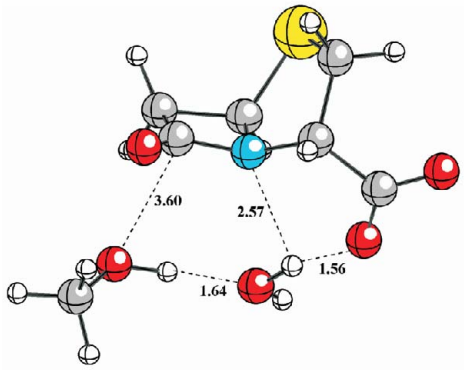
Example	Reaction	Ref.
	General acid-catalyzed, general base-catalyzed hydration of acetaldehyde	6
	General-acid catalyzed hydration of dimethyketene	7
	Hydrolysis of isocyanates	8
	Hydrolysis of benzamide in aqueous sulfuric acid	9
	Hydrolysis of *p*-nitrophenyl trifluoroacetate in aqueous acetonitrile	10
	Lactam hydrolysis in sulfuric acid	11
	Ketonization of acetophenone enol	12

[7] S. Wolfe and Z. Shi. Unpublished results.
[8] For an exception, see ref. 25.

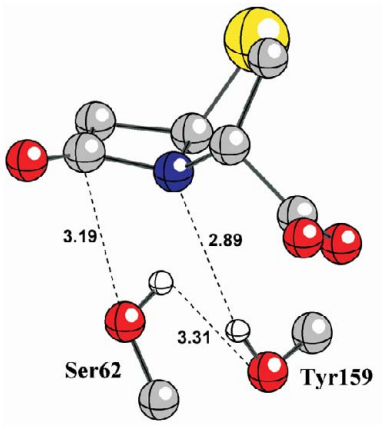
© 2005 NRC Canada

Table 2. Theoretical studies of additions to carbonyl and cognate functional groups in water solvent.

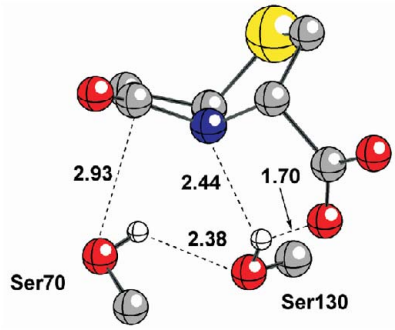
Entry	Substrate	Method/basis set	Reactant(s)	$\Delta G^{\ddagger}$ (kcal/mol)	Ref.
1	CO_2	MP4/6-31G**	H_2O	49.1±1.4	14
			$2H_2O$	21.2±1.3	
2	CO_2	6-31G**	H_2O	63.9	15
			$2H_2O$	34.4	
			$3H_2O$	31.8	
			$4H_2O$	20.8	
3	H_2NCHO	3-21G	$2H_2O$	56.7	16
4	HNCNH	MP2/6-31G**	H_2O	45.7	17
			$2H_2O$	26.4	
			$3H_2O$	15.3	
			$4H_2O$	10.4	



1



2

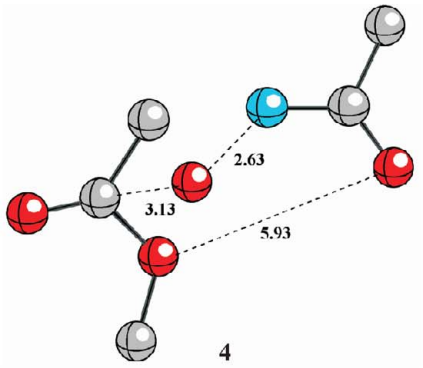


3

Class A β-lactamases have not yet submitted to crystallization. However, in an important contribution, Strynadka et al. (21) were able to obtain the crystal structure of a deacylation defective penicilloylated TEM1 enzyme in which the terminal COOH of Glu166 was replaced by the terminal $CONH_2$ of asparagine. Structures **4** and **4a** are mono and stereo views showing the C-O-C(=O)-C of the acylated serine, the CON terminus of Asn166, and the oxygen of the water molecule in this crystal structure. We comment that, if the primary amide of **4** becomes the carboxyl group of the native acyl-enzyme, the resulting structure **5**, like **1**–**3**, is poised for a co-operative one-step ester hydrolysis.

The foregoing considerations have led us to a systematic experimental and theoretical examination of co-operativity in the neutral, general, and hydronium ion catalyzed hydration of acetone, the neutral hydrolysis of methyl acetate, and the catalysis of this hydrolysis by acetic acid. In our earlier publications (26), we proposed a theoretical treatment of the co-operative aqueous neutral hydration of aldehydes and ketones, based on ab initio 3-21G calculations (27, 28) and the SCRF (self consistent reaction field) (29, 30) procedure. The treatment requires the calculation of the free energies of each of the stationary structures shown in Scheme 1 in water solvent, where RC_n is a cyclic complex of a carbonyl compound RR′C=O with n water molecules (n = 1–4), TS_n is a cyclic transition structure derived from

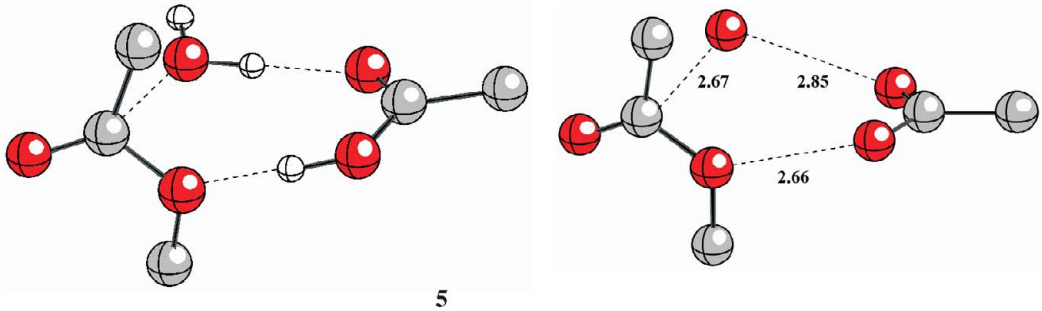
© 2005 NRC Canada



4

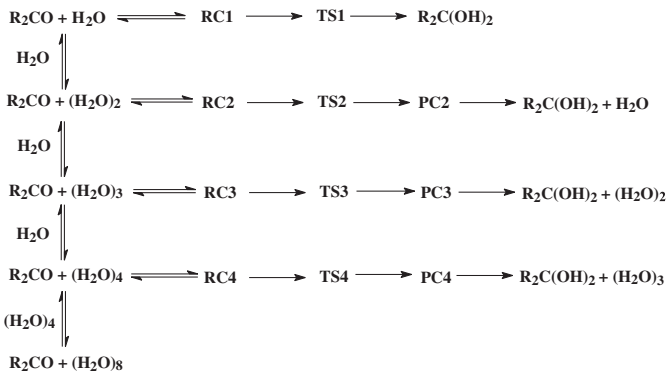


4a

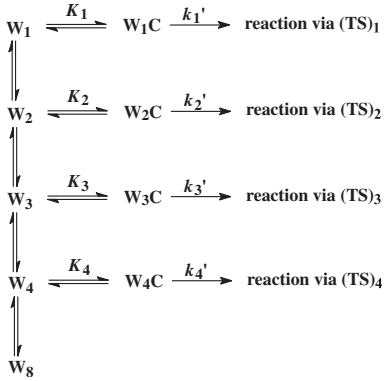


5

Scheme 1.



Scheme 2.



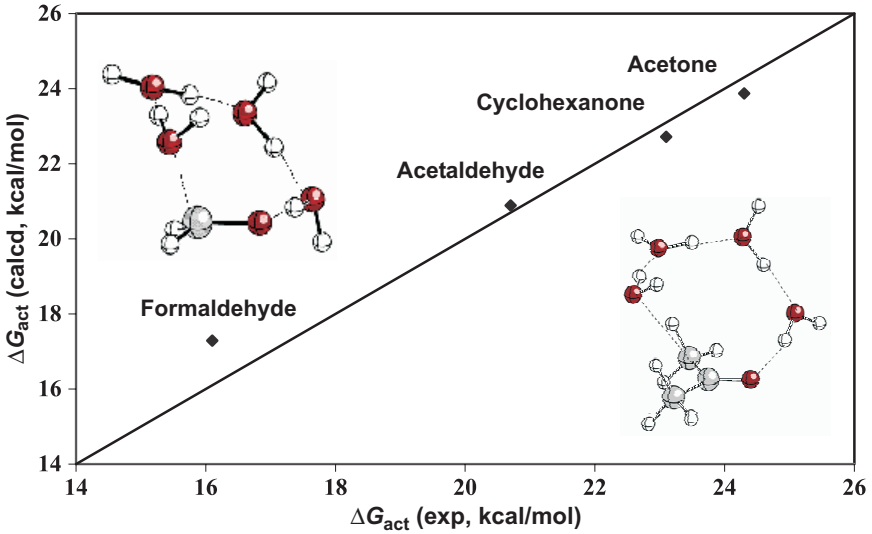
RC_n, and PC_n is a 1,1-diol, solvated by $(n - 1)$ water molecules.

The assumptions that the water clusters $(H_2O)_n$ are in rapid equilibrium with each other and with the RC_n complexes allows the hydration kinetics to be analyzed according to Scheme 2, in which C is the carbonyl compound, and this leads to eq. [1], an expression for the pseudo-first-order rate constant (k) in terms of the contributions of the individual reaction channels, and eq. [2], the theoretical free energy of activation.

$$[1] \qquad k = \frac{\boldsymbol{K_1}k'_1[\boldsymbol{W_1}] + \boldsymbol{K_2}k'_2[\boldsymbol{W_2}] + \boldsymbol{K_3}k'_3[\boldsymbol{W_3}] + \boldsymbol{K_4}k'_4[\boldsymbol{W_4}]}{1 + \boldsymbol{K_1}[\boldsymbol{W_1}] + \boldsymbol{K_2}[\boldsymbol{W_2}] + \boldsymbol{K_3}[\boldsymbol{W_3}] + \boldsymbol{K_4}[\boldsymbol{W_4}]}$$

© 2005 NRC Canada

Fig. 1. A plot of the experimental free energies of activation for the neutral aqueous hydrations of formaldehyde, acetaldehyde, acetone, and cyclohexanone vs. the theoretical free energies of activation calculated according to ref. 26*b*. The inserted structures are the formaldehyde and acetone reactant complexes.



$$[2] \qquad \Delta G^{\ddagger} = RT \ln\left(\frac{\kappa T}{h}\right) - RT \ln(k)$$

The result of this treatment is shown in Fig. 1, which compares the experimental and theoretical free energies of activation for the uncatalyzed hydrations of formaldehyde, acetaldehyde, acetone, and cyclohexanone. In each case, the principal co-operative channel, shown in Fig. 1 for formaldehyde and acetone, contains four water molecules in the cyclic complex.

To extend the theoretical treatment of acetone hydration to include catalysis by acetic acid, it is necessary to expand Scheme 1 to Scheme 3 so as to allow an acid (**A**) to complex to each of the structures of Scheme 1.

There are, however, several complications. Firstly, **A** can occupy more than one site in a complex, for example, **6a** and **6b** for **RCA1** and **7a–7d** for **RCA2**. All possible structures would have to be taken into account.

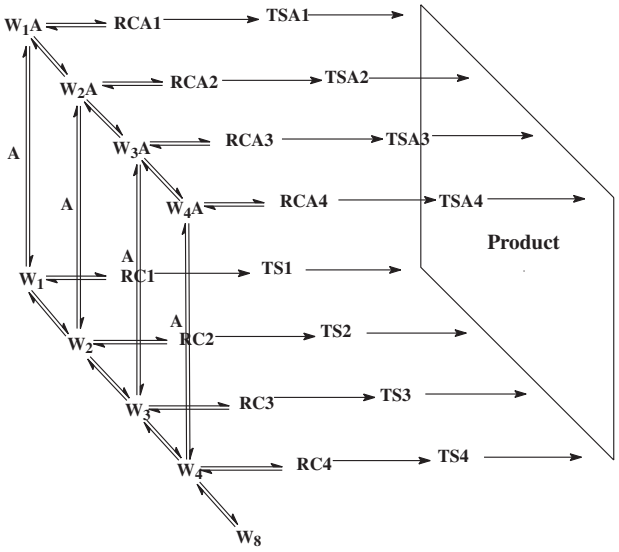
A second complication arises from basis set superposition error (BSSE) (31). When two or more molecules form a complex, the basis set that describes the complex is the combination of the basis sets of the individual molecules. Since individual reactants are described by a smaller basis than the complexes, their relative energies are artificially too high. It is, therefore, necessary to correct, the complexation energy (ΔE) by the quantity E^{BSSE} (eq. [3]), where E^{BSSE} is the basis set superposition error, $E_{\mathrm{A-B}}$ is the energy of the complex, and E_{A} and E_{B} are the energies of A and B (26*b*).

$$[3] \qquad \Delta E = E_{\mathrm{A-B}} - (E_{\mathrm{A}} + E_{\mathrm{B}}) + E^{\mathrm{BSSE}}$$

Table 3 illustrates the calculation of the BSSE correction for **8** (≡**10a**), a complex of acetic acid with two water molecules.

A third complication is that in the GAUSSIAN programme (28) the ideal gas statistical mechanical procedure is used to calculate thermodynamic parameters in the SCRF treatment.

Scheme 3.

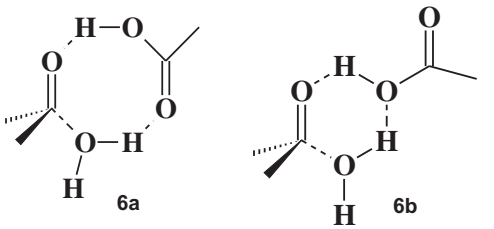


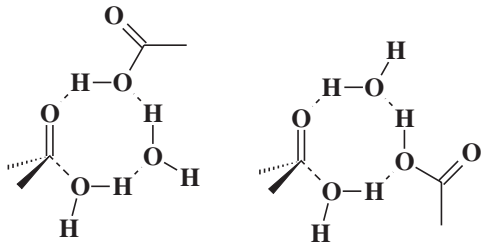
This protocol is reasonable for the description of the enthalpy of reaction in solution, but entropic effects are greatly overestimated. The reason for this is that, in the gas phase, the major contribution to the entropy change calculated for an association reaction A + B → AB arises from the loss of six degrees of freedom, representing free translations and rotations of A and B, and the conversion of these into six vibrational modes of AB. In solution, rotational and translational motions are restricted and are better described by a set of low frequency vibrations. In the simplest approximation, these vibrations can be described by a single effective frequency (ν), determined (26*b*) to be 115 cm^{-1} for the water monomer and $115(18/m)^{1/2}$ cm^{-1} for other species, where m is the mass of the species. Equation [4] gives the corrected expression for ΔG in solution. The first and second terms on the right-hand side are the BSSE-corrected enthalpy change

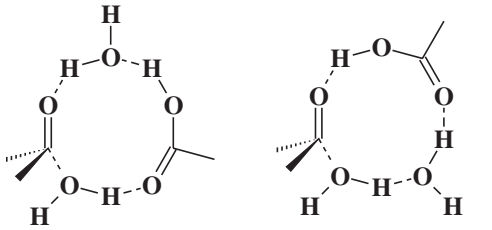
© 2005 NRC Canada

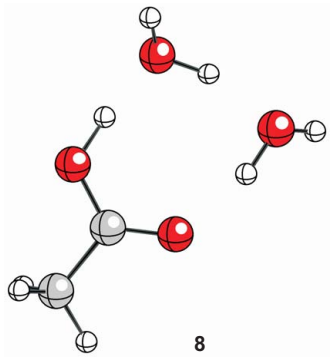
Table 3. Calculation of the BSSE for the complex **8** (≡**10a**).

Energy of acetic acid in the presence of the ghost orbitals of two water molecules	–226.836873 a.u.
Energy of acetic acid without the ghost orbitals of two water molecules	–226.529107 a.u.
Difference	4.87 kcal/mol
Energy of water dimer in the presence of the ghost orbitals of acetic acid	–151.203827 a.u.
Energy of water dimer without the ghost orbitals of acetic acid	–151.192536 a.u.
Difference	7.08 kcal/mol
BSSE	11.95 kcal/mol



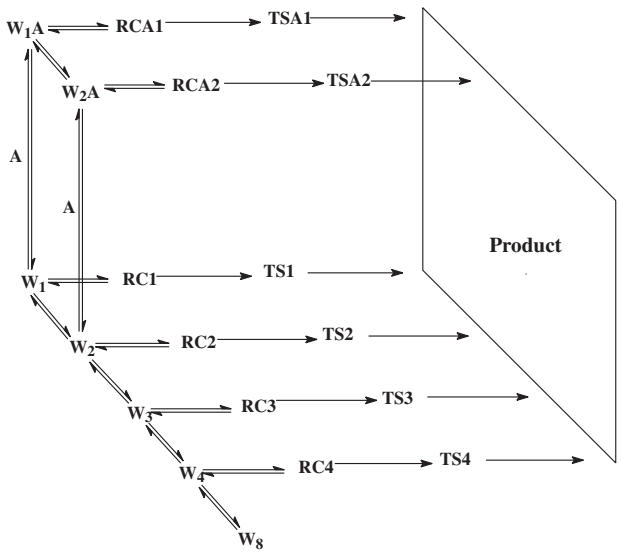






and the gas-phase vibrational entropy change calculated by the GAUSSIAN programme, and the third term is the correction for low frequency vibrations in solution.

Scheme 4.



$$[4]\qquad \Delta G_{liq} = \Delta H_{gas} - T\Delta S_{vib} - 6RT\left[\frac{\frac{h\nu}{kT}}{\exp\left(\frac{h\nu}{kT}\right)-1} - \ln\left[1-\exp\left(\frac{h\nu}{kT}\right)\right]\right]$$

Computational details

As in our previous work (26*a*, 26*b*) all calculations were performed using the 3-21G level of theory (27, 28) and the SCRF procedure (29, 30). Transition structures were located by the reaction coordinate method. Using a reactant complex as a starting point, trial values of the forming O···C=O and C=O···H bond lengths were selected, all other geometrical parameters were optimized, and the magnitudes and signs of the gradients of the two reaction coordinates were used to improve the trial values. After several such calculations, a structure close to the saddle point was reached; at this stage, a final refinement was achieved using the OPT=CALCALL option, in which force constants are calculated in every iteration. All transition structures exhibited one imaginary frequency.

For SCRF calculations, the previously optimized gas-phase structures were used to estimate the radius of the cavity, and this value was employed in the optimization. A dielectric constant of 78.5 was used to describe the water solvent.

© 2005 NRC Canada

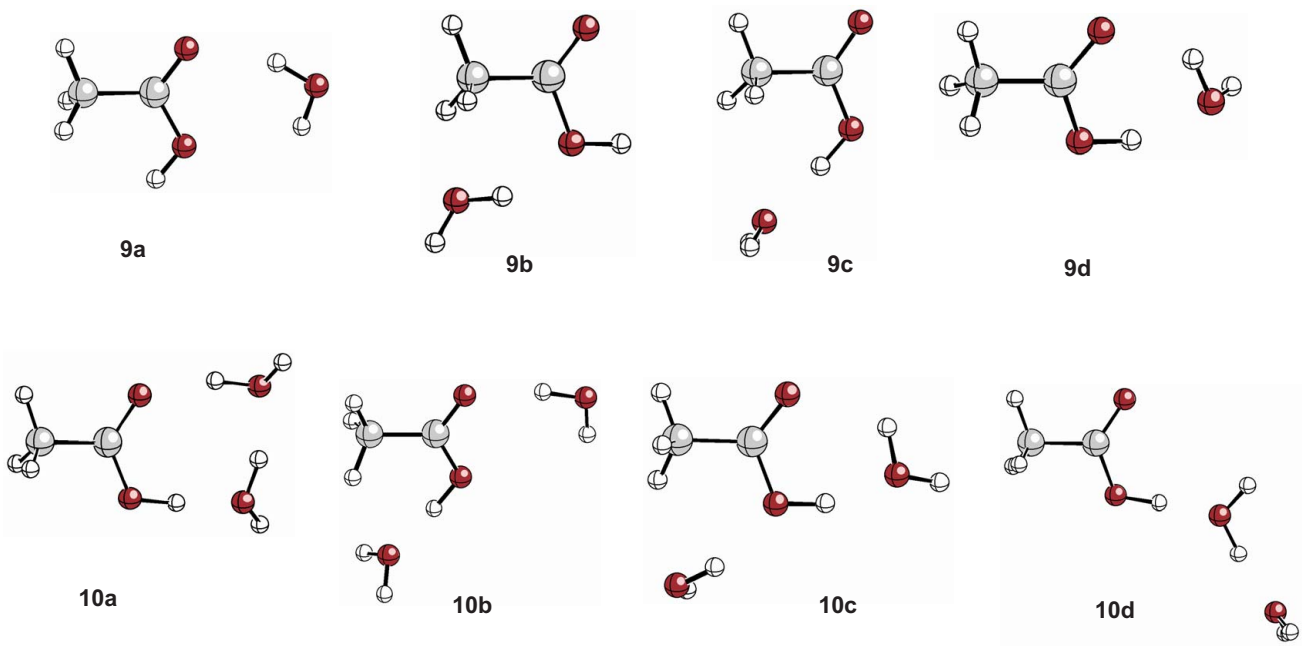


Table 4. Gibbs free energies of formation of water – acetic acid complexes (1:1) in water solvent.

Complex	ΔH (kcal/mol)	BSSE (kcal/mol)	ΔH_{corr} (kcal/mol)[a]	ΔS (cal/mol K)	ΔG (kcal/mol)
9a	–10.40	5.60	–4.80	–5.49	–3.16
9b	–8.97	7.29	–1.68	–6.49	0.26
9c	–18.69	6.92	–11.76	–6.08	–9.95
9d	–17.98	10.54	–7.44	–8.39	–4.94

[a]BSSE corrected.

Results

In an initial set of computations, the truncated Scheme 4 was employed to treat acetic acid catalysis. Structures **9a**–**9d** are the 1:1 complexes. Table 4 summarizes the data obtained for these complexes at 298 K in water solvent.

Structures **10a**–**10d** are the 2:1 complexes; Table 5 lists the ΔG values calculated for these complexes at 298 K in water solvent.

Structures **11a**–**11d** are the reactant complexes (acetone + acetic acid + $(H_2O)_n$), and **12a**–**12d** are the transition structures. Table 6 lists the ΔG and $\Delta G^{\ddagger}$ calculated at 298 K for an acetone concentration of 1.00 mol/L and an acetic acid concentration of 1.00 mmol/L. The theoretical $\Delta G^{\ddagger}$ for the neutral reaction (11.34 kcal/mol) was reported previously (26*b*).

To assess the contributions of the different pathways to the overall rate constant, it is necessary to take into account the concentrations of the different reactant complexes, and this is possible if the reasonable assumption is made that acetone, $(H_2O)_n$, acetic acid, **RCn**, and **RCAn** are in equilibrium in solution. The contributions of the different reaction channels to the overall pseudo-first-order rate constant for the acetic acid catalyzed hydration of acetone will then depend on the concentrations of **RCAn** and on the individual free energies of activation **RCAn** → **TSAn**.

This situation has been summarized in Scheme 1 for the case of neutral hydration. With the addition of the acid-catalyzed channels, Scheme 1 is expanded to Scheme 5, in which $\mathbf{W_n}$ is a water cluster, $\mathbf{WA_n}$ is a water–acid complex, K_{nn}, K_{Ann}, K'_{Ann}, K_n, and K_{nA} are equilibrium constants, and k'_n and k'_{nA} are rate constants.

Using [*S*] as the concentration of acetone and [*A*] as the concentration of acetic acid, the independent relationships among the concentrations of $(H_2O)_n$, $\mathbf{W_nA}$, **RCn**, and **RCAn** are as follows: $[\mathbf{W_2}] = K_{12}[\mathbf{W_1}]^2$, $[\mathbf{W_3}] = K_{13}[\mathbf{W_1}]^3$, $[\mathbf{W_4}] = K_{14}[\mathbf{W_1}]^4$, $[\mathbf{W_8}] = K_{18}[\mathbf{W_1}]^8$, $[\mathbf{RC1}] = K_1[\mathbf{W_1}][S]$, $[\mathbf{RC2}] = K_2[\mathbf{W_2}][S]$, $[\mathbf{RC3}] = K_3[\mathbf{W_3}][S]$, $[\mathbf{RC4}] = K_4[\mathbf{W_4}][S]$, $[\mathbf{W_1A}] = K_{A11}[\mathbf{W_1}][A]$, $[\mathbf{W_2A}] = K_{A22}[\mathbf{W_2}][A]$, $[\mathbf{RCA1}] = K_{1A}[\mathbf{W_1A}][S]$, $[\mathbf{RCA2}] = K_{2A}[\mathbf{W_2A}][S]$.

Equations [5]–[7] relate these concentrations to the analytical concentrations of water (C_W), acetone (C_S), and acetic acid (C_A).

$$[5]\quad C_W = [\mathbf{W_1}] + 2[\mathbf{W_2}] + 3[\mathbf{W_3}] + 4[\mathbf{W_4}] + 8[\mathbf{W_8}] + [\mathbf{RC_1}] + 2[\mathbf{RC_2}] + 3[\mathbf{RC_3}] + 4[\mathbf{RC_4}] + [\mathbf{W_1A}] + 2[\mathbf{W_2A}] + [\mathbf{RCA1}] + 2[\mathbf{RCA2}]$$

$$[6]\quad C_S = [S] + [\mathbf{RC1}] + [\mathbf{RC2}] + [\mathbf{RC3}] + [\mathbf{RC4}] + [\mathbf{RCA1}] + [\mathbf{RCA2}]$$

© 2005 NRC Canada

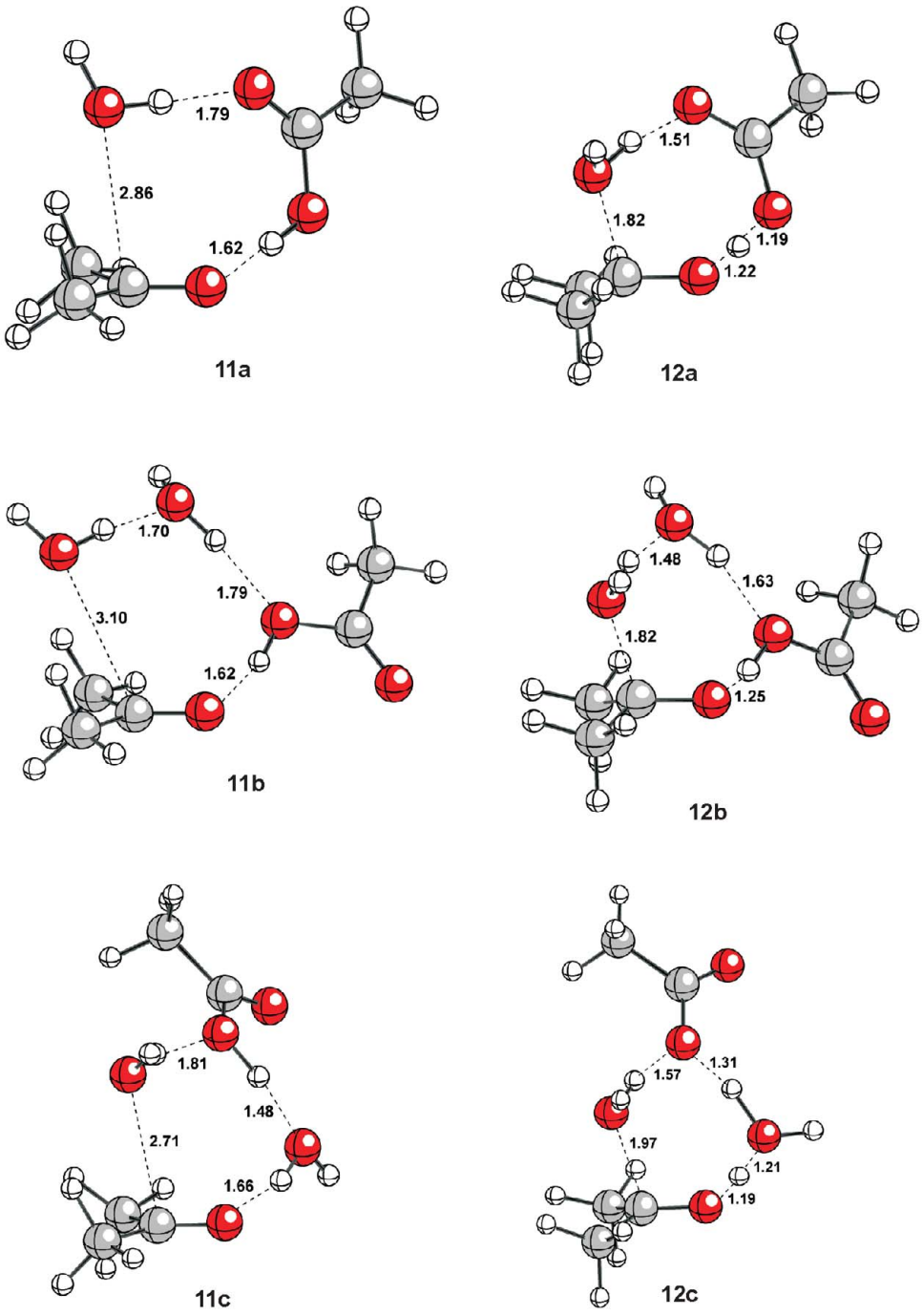


Table 5. Gibbs free energies of formation of water – acetic acid complexes (2:1) in water solvent.

Complex	ΔH (kcal/mol)	BSSE (kcal/mol)	ΔH_{corr} (kcal/mol)[a]	ΔS (cal/mol K)	ΔG (kcal/mol)
10a	–26.12	11.95[b]	–14.17	–9.52	–11.33
10b	–22.31	12.45	–9.87	–1.86	–9.31
10c	–14.71	16.47	1.76	–5.22	3.32
10d	–22.11	6.97	–15.14	0.41	–15.26

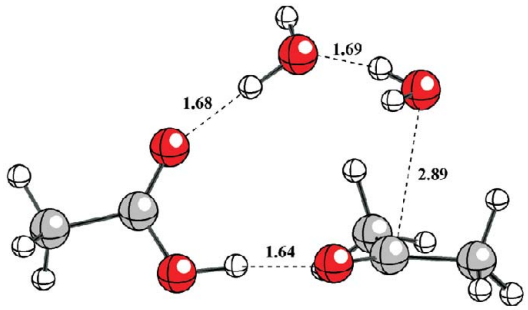
[a]BSSE corrected.
[b]See Table 3 for details of this calculation.

© 2005 NRC Canada

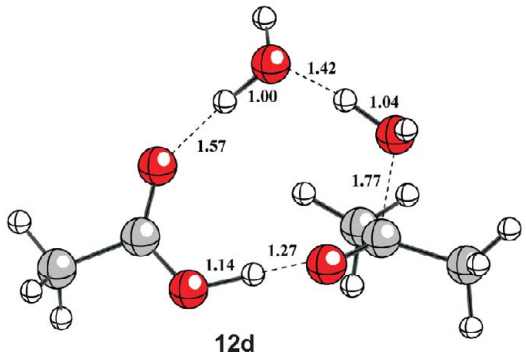
Table 6. Gibbs free energies for acetic acid catalyzed hydration of acetone via Scheme 4.

	ΔG (kcal/mol)	$\Delta G^{\ddagger}$ (kcal/mol)	ΔH (kcal/mol)	ΔH_{corr} (kcal/mol)	$\Delta H^{\ddagger}$ (kcal/mol)	BSSE (kcal/mol)	ΔS (cal/mol K)	$\Delta S^{\ddagger}$ (cal/mol K)
Complex								
RC1[a]	2.34[a]	—	—	—	—	—	—	—
RC2[a]	6.44[a]	—	—	—	—	—	—	—
RC3[a]	7.17[a]	—	—	—	—	—	—	—
RC4[a]	12.28[a]	—	—	—	—	—	—	—
11a	–6.47	—	–23.90	–7.52[b]	—	16.38	–3.51	—
11b	–4.33	—	–21.93	–4.80[b]	—	17.13	–1.58	—
11c	–0.72	—	–23.80	–1.46[b]	—	22.34	–7.32	—
11d	–3.79	—	–24.56	–5.80[b]	—	18.76	–6.76	—
Transition structure								
TS1[a]	—	45.87[a]	—	—	—	—	—	—
TS2[a]	—	21.80[a]	—	—	—	—	—	—
TS3[a]	—	12.74[a]	—	—	—	—	—	—
TS4[a]	—	11.34[a]	—	—	—	—	—	—
12a	—	10.45	—	—	6.66	—	—	–12.71
12b	—	8.14	—	—	3.65	—	—	–15.06
12c	—	11.26	—	—	6.87	—	—	–14.72
12d	—	7.74	—	—	3.00	—	—	–15.90

[a]Data from ref. 27*b*.
[b]BSSE corrected.



11d

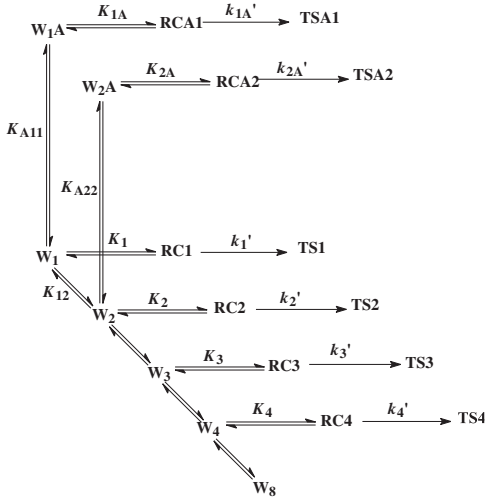


12d

[7] $$C_A = [A] + [W_1A] + [W_2A] + [RCA1] + [RCA2]$$

The concentrations of all species present in the solution were calculated to self-consistency using a water concentration of 55.5 mol/L. The calculated rate (v) is then given by

Scheme 5.



[8] $$v = \sum \{k'_n[RCn] + k'_{nA}[RCAn]\} = (k_o + k_{HA}C_A)C_S = k_{obs}C_S$$

where k_{obs} is the rate constant and contains contributions from the neutral reaction (k_o) and the acid-catalyzed reaction ($k_{HA}C_A$). Table 7 summarizes the calculated concentrations of the complexes and the contributions of the different reaction channels to the hydration of acetone at 298 K for a solution that is 1.00 mol/L in acetone and 1.00 mmol/L in acetic acid.

The principal contributors to general acid catalysis are **11b** (47.3%) and **11d** (44.7%), which exhibit $\Delta G^{\ddagger}$ = 8.14 and 7.74 kcal/mol, respectively. Minor contributors are **11a** (4.4%), which exhibits $\Delta G^{\ddagger}$ = 10.45 kcal/mol, and **RC4** (3.6%), which exhibits $\Delta G^{\ddagger}$ = 11.34 kcal/mol. Although the

© 2005 NRC Canada

Table 7. Concentrations of various complexes in acetone – acetic acid – water solution.

Species	Concentration (mol/L)	Rate constant (s^{-1})	Partial rate (M s^{-1})	Contribution (%)
$(H_2O)_1$	4.05×10^{-2}	—	—	—
$(H_2O)_2$	2.75×10^{-1}	—	—	—
$(H_2O)_3$	1.28×10^{-6}	—	—	—
$(H_2O)_4$	1.65×10^{-1}	—	—	—
$(H_2O)_8$	6.78	—	—	—
$(CH_3)_2CO$	9.99×10^{-1}	—	—	—
RC1	7.77×10^{-4}	5.99×10^{-21}	4.65×10^{-24}	0.00
RC2	5.24×10^{-6}	2.64×10^{-3}	1.38×10^{-8}	0.00
RC3	7.13×10^{-12}	1.14×10^{4}	8.13×10^{-8}	0.01
RC4	1.65×10^{-10}	1.21×10^{5}	1.99×10^{-5}	3.57
HOAc	2.90×10^{-14}	—	—	—
W_1A	1.58×10^{-7}	—	—	—
W_2A	1.00×10^{-3}	—	—	—
11a	4.51×10^{-11}	5.47×10^{5}	2.47×10^{-5}	4.41
11b	9.87×10^{-12}	2.69×10^{7}	2.65×10^{-4}	47.34
11c	4.65×10^{-14}	1.39×10^{5}	6.42×10^{-9}	0.00
11d	4.74×10^{-12}	5.26×10^{7}	2.50×10^{-4}	44.66

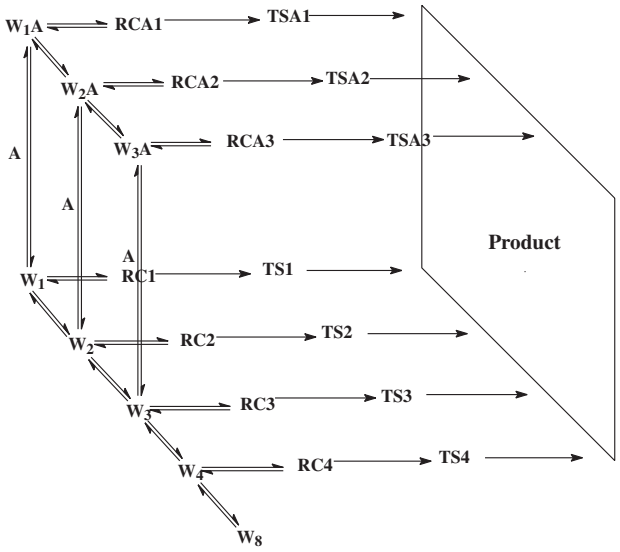
Note: Calculated rate = 5.59×10^{-4} M s^{-1}, $k_o = 2.00 \times 10^{-5}$ s^{-1}, $k_{HA} = 0.54$ M^{-1} s^{-1}.

Table 8. Gibbs free energies of formation of water – acetic acid (3:1) complexes.

Complex	ΔH (kcal/mol)	BSSE (kcal/mol)	ΔH_{corr} (kcal/mol)[a]	ΔS (cal/mol K)	ΔG (kcal/mol)
13a	–23.97	10.80	–13.17	–14.69	–8.79
13b	–27.49	11.15	–16.34	–14.72	–11.95
13c	–27.52	11.16	–16.36	–14.66	–11.99
13d	–23.02	10.84	–12.18	–18.64	–6.62
13e	–21.29	19.26	–2.03	–15.54	2.60
13f	–18.82	9.97	–8.85	–15.66	–4.18
13g	–21.62	16.32	–5.30	–17.55	–0.07
13h	–21.55	20.67	–0.88	–17.34	4.29

[a]BSSE corrected.

Scheme 6.



relative concentrations of these species (mol/L) are **11b** (1), **11d** (0.5), **11a** (4.6), and **RC4** (16.7), **11b** and **11d** make the major contributions to the overall reaction because of their lower barriers.

Scheme 4 was then expanded to Scheme 6 to incorporate an additional channel of acetic acid catalysis.

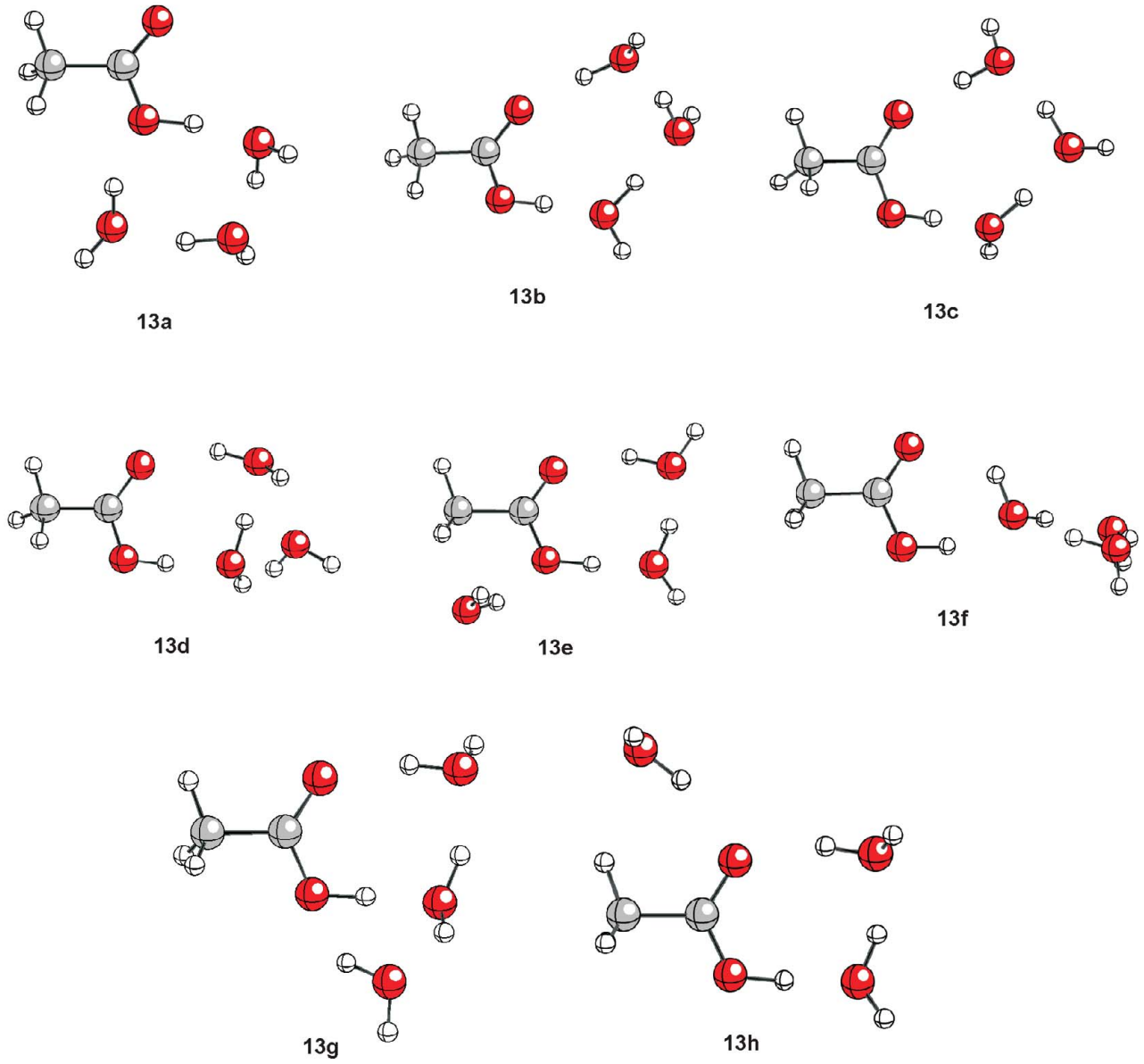
Structures **13a–13h** are the 3:1 complexes and Table 8 lists the free energies of formation of these complexes at 298 K.

Structures **14a–14f** are the reactant complexes (acetone + acetic acid + $(H_2O)_3$), and **15a–15f** are the transition structures reached from these complexes. Table 9 lists the ΔG and $\Delta G^{\ddagger}$ calculated at 298 K for an acetone concentration of 1.00 mol/L and an acetic acid concentration of 1.00 mmol/L.

Table 10 summarizes the calculated concentrations of the complexes and the contributions of the different reaction channels to the hydration of acetone at 298 K for a solution that is 1.00 mol/L in acetone and 1.00 mmol/L in acetic acid.

The resulting rate and the principal contributors to this rate are almost the same as in Scheme 4. The reason for this is that the concentrations of the six three-water molecule

© 2005 NRC Canada



complexes (**14a**–**14f**) are many orders of magnitude lower than the concentrations of the one- and two-water molecule complexes (**11a**–**11c**).

Experimental

In the presence of a general acid, the hydration of acetone can proceed with contributions from the neutral reaction (k_o), the hydronium ion catalyzed reaction ($k_H[H_3O^+]$), the co-operative acid-catalyzed reaction ($k_{HA}[HA]$), and the hydroxide ion catalyzed reaction ($k_{OH}[OH^-]$) (eq. [9]).

$$[9] \qquad k_{obs} = k_o + k_H[H_3O^+] + k_{HA}[HA] + k_{OH}[OH^-]$$

Experiments were performed at an acetic acid concentration of 0.01 mol/L in 1 mol/L acetone. At this concentration of acetic acid, [HOAc] = 9.6×10^{-3} mol/L, $[H_3O^+] = 4.1 \times 10^{-4}$ mol/L, and $[OH^-] < 10^{-10}$ mol/L (32). Since k_o is 8.9×10^{-6} s^{-1} (26*b*), eq. [9] can be truncated to

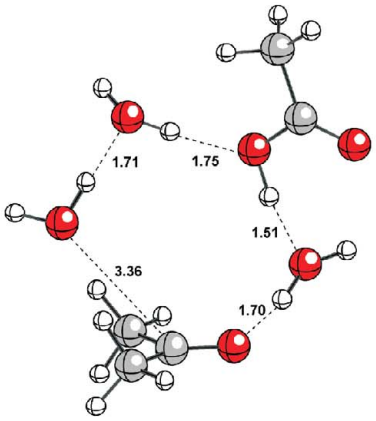
$$[10] \qquad k_{obs} \sim k_{HA}[HOAc] + k_H[H_3O^+]$$

A bulk solution of acetic acid in $H_2{}^{18}O$ was prepared by dilution of 5.00 mL of 1.000 mol/L acetic acid to 50.00 mL in H_2O and addition of 60.0 µL of this 0.100 mol/L solution to 540.0 µL of 49.1% $H_2{}^{18}O$ to give 1.00×10^{-2} mol/L [HOAc] in 44.2% enriched $H_2{}^{18}O$.

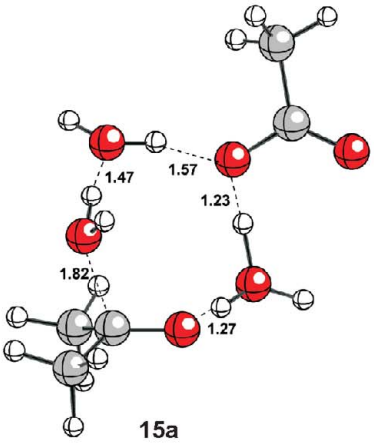
To initiate a run, 8.0 µL (6.4 µg, 0.11 µmol) of 2-^{13}C-acetone were syringed into 100 µL of the acetic acid solution in a 1 dram vial (1 fluid dram = 3.551 633 cm^3) and the reaction mixture (1.1 mol/L in acetone) was transferred immediately to a micro NMR tube maintained at 298 ± 0.1 K in the probe of a Bruker 600 AMX spectrometer operating at a frequency of 150.03 MHz. Temperature control was achieved with a Euroterm VT temperature regulator. The proton decoupled ^{13}C NMR spectrum was recorded as a single scan at appropriate intervals to obtain the peaks of $(CH_3)_2{}^{13}C={}^{16}O$ [^{16}O] and $(CH_3)_2{}^{13}C={}^{18}O$ [^{18}O], whose chemical shifts differ by 0.05 ppm (33). These spectra were integrated to obtain the [^{18}O]/[^{16}O] ratio (ρ) as a function of time.

The data were analyzed by application of version 5.1 of

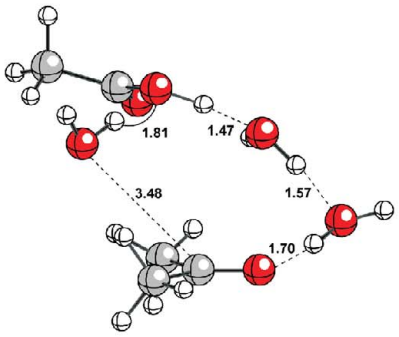
© 2005 NRC Canada



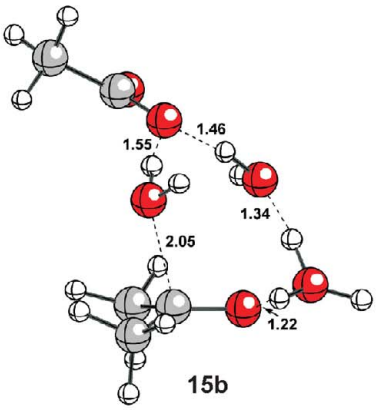
14a



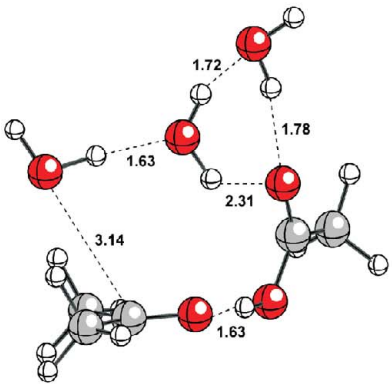
15a



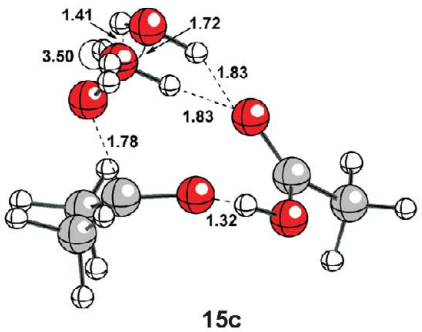
14b



15b



14c



15c

the computer programme GRAFIT, obtained from Erithacus Software Ltd., Horley, Surrey, UK, to eq. [11],

$$[11] \quad \frac{1}{1+\rho} = A\exp(-k^{t}_{obs}) + C$$

which is derived in the following manner.[9]

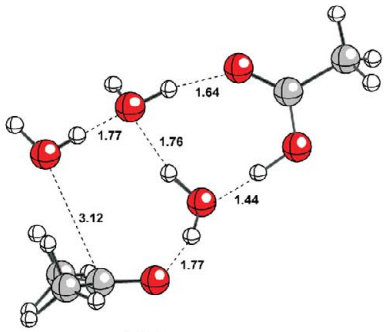
For a reaction $^{16}O \underset{k_{-1}}{\overset{k_1}{\rightleftharpoons}} {}^{18}O$, where $k_1 = k[H_2{}^{18}O]$ and $k_{-1} = k[H_2{}^{16}O]$, the time dependence of the concentration of ^{18}O is given by (34),

$$[12] \quad (k_1 + k_{-1})t = \ln\left(\frac{[^{18}O]_e}{[^{18}O]_e - [^{18}O]}\right)$$

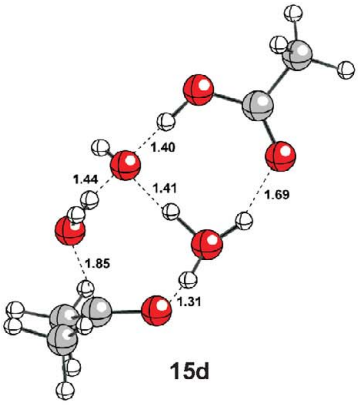
where $[^{18}O]_e$ is the concentration of ^{18}O at equilibrium. Since $[^{16}O]_o = 1$, $[^{18}O]_o = 0$, and $[^{16}O] + [^{18}O] = [^{16}O]_o = [^{16}O]_e + [^{18}O]_e = 1$, eq. [12] becomes

[9] The authors thank Professor Andrew Bennet for suggesting eq. [11], and for instruction in the use of GRAFIT.

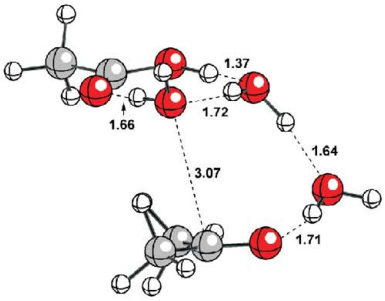
© 2005 NRC Canada



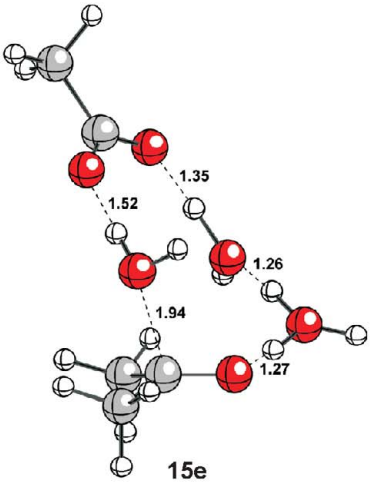
14d



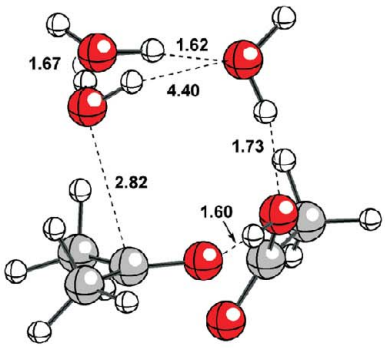
15d



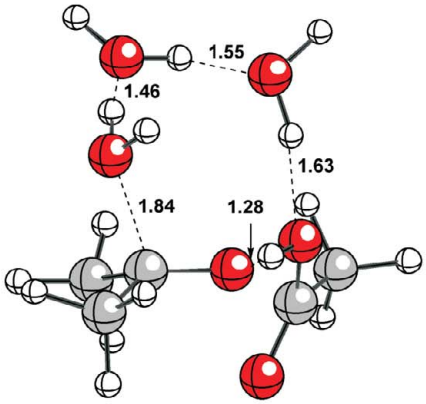
14e



15e



14f



15f

[13] $[^{18}O] = [^{18}O]_e(1 - e^{-(k_1 + k_{-1})t})$

Substitution of $[^{18}O]$ by $[^{16}O]_o - [^{16}O]$ and $[^{18}O]_e$ by $[^{16}O]_o - [^{16}O]_e$ gives

[14] $[^{16}O] = ([^{16}O]_o - [^{16}O]_e)e^{-(k_1 + k_{-1})t} + [^{16}O]_e$

Writing $\rho = [^{18}O]/[^{16}O]$, the ratio $[^{16}O]/[^{16}O]_o$ is

[15] $$\frac{[^{16}O]}{[^{16}O]_o} = \frac{1}{1+\rho}$$

Dividing eq. [14] by $[^{16}O]_o$ and substitution of eq. [15] into eq. [14] gives

[16] $$\frac{1}{1+\rho} = Ae^{-k_{obs}t} + C$$

where $A = \left(1 - \frac{[^{16}O]}{[^{16}O]_o}\right)$, $C = \frac{[^{16}O]}{[^{16}O]_o}$, and $k_{obs} = k[H_2O]$.

The results are summarized in Table 11. Figure 2 shows the result of run 1.

© 2005 NRC Canada

Table 9. Gibbs free energies for acetic acid catalyzed hydration of acetone via Scheme 6.

	ΔH (kcal/mol)	$\Delta H^{\ddagger}$ (kcal/mol)	BSSE (kcal/mol)	ΔH_{corr} (kcal/mol)[a]	ΔS (cal/mol K)	$\Delta S^{\ddagger}$ (cal/mol K)	ΔG (kcal/mol)	$\Delta G^{\ddagger}$ (kcal/mol)
Complex								
14a	–121.67	—	28.30	–93.37	–335.14	—	6.55	—
14b	–122.50	—	30.89	–91.61	–337.22	—	8.93	—
14c	–119.49	—	21.94	–97.55	–331.83	—	1.39	—
14d	–127.48	—	24.77	–102.71	–334.04	—	–3.12	—
14e	–130.03	—	26.40	–103.63	–337.22	—	–3.09	—
14f	–119.17	—	23.98	–95.19	–337.33	—	5.38	—
Transition structure								
15a	—	5.50	—	—	—	–6.24	—	7.36
15b	—	8.05	—	—	—	–5.35	—	9.65
15c	—	4.31	—	—	—	–14.40	—	8.60
15d	—	9.39	—	—	—	–17.62	—	14.64
15e	—	14.97	—	—	—	–2.66	—	15.76
15f	—	2.43	—	—	—	–10.69	—	5.62

[a]BSSE corrected.

Table 10. Concentrations of various complexes in acetone – acetic acid – water solution.

Species	Concentration (mol/L)	Rate constant (s^{-1})	Partial rate ($M\ s^{-1}$)	Contribution (%)
$(H_2O)_1$	3.37×10^{-2}	—	—	—
$(H_2O)_2$	2.75×10^{-1}	—	—	—
$(H_2O)_3$	1.31×10^{-6}	—	—	—
$(H_2O)_4$	1.66×10^{-1}	—	—	—
$(H_2O)_8$	6.78×10^{0}	—	—	—
$(CH_3)_2CO$	9.99×10^{-1}	—	—	—
RC1	7.77×10^{-4}	6.01×10^{-21}	4.66×10^{-24}	0.00
RC2	5.24×10^{-6}	2.62×10^{-3}	1.37×10^{-8}	0.00
RC3	7.24×10^{-12}	1.14×10^{4}	8.92×10^{-8}	0.02
RC4	1.65×10^{-10}	1.21×10^{5}	2.00×10^{-5}	3.89
HOAc	2.39×10^{-14}	—	—	—
W_1A	1.58×10^{-8}	—	—	—
W_2A	1.00×10^{-3}	—	—	—
W_3A	3.71×10^{-11}	—	—	—
11a	4.46×10^{-11}	5.45×10^{5}	2.43×10^{-5}	4.74
11b	9.76×10^{-12}	2.69×10^{7}	2.63×10^{-4}	51.11
11c	1.95×10^{-15}	1.39×10^{5}	2.71×10^{-10}	0.00
11d	3.93×10^{-12}	5.26×10^{7}	2.07×10^{-4}	40.24
14a	4.95×10^{-25}	1.00×10^{8}	4.96×10^{-17}	0.00
14b	8.90×10^{-27}	2.10×10^{6}	1.87×10^{-20}	0.00
14c	2.97×10^{-21}	1.24×10^{7}	3.67×10^{-14}	0.00
14d	6.05×10^{-18}	4.63×10^{2}	2.81×10^{-15}	0.00
14e	5.71×10^{-18}	7.00×10^{1}	4.00×10^{-16}	0.00
14f	3.53×10^{-24}	1.89×10^{9}	6.68×10^{-15}	0.00

Note: Calculated rate = 5.14×10^{-4} M s^{-1}, $k_o = 2.01 \times 10^{-5}$ s^{-1}, $k_{HA} = 0.49$ M^{-1} s^{-1}.

We conclude that, in the high dielectric medium provided by water solvent, acetic acid catalysis of the hydration of acetone is predominantly a co-operative, i.e., *non-ionic*, process. It is therefore necessary to reexamine the dogma (2, 3) that multistep ionic mechanisms are operative in the *low* dielectric media that exist at the active sites of hydrolytic enzymes, in particular penicillin-recognizing enzymes. Such a reexamination is the subject of a forthcoming publication in this series.[10]

Acknowledgements

The authors thank the Natural Sciences and Engineering

[10]Y.-H. Hsieh, Z. Shi, N. Weinberg, and S. Wolfe. Unpublished results.

© 2005 NRC Canada

Fig. 2. A kinetic run showing the hydration of 1 mol/L acetone at 298 K in the presence of 1×10^{-2} mol/L acetic acid (run 1 of Table 10).

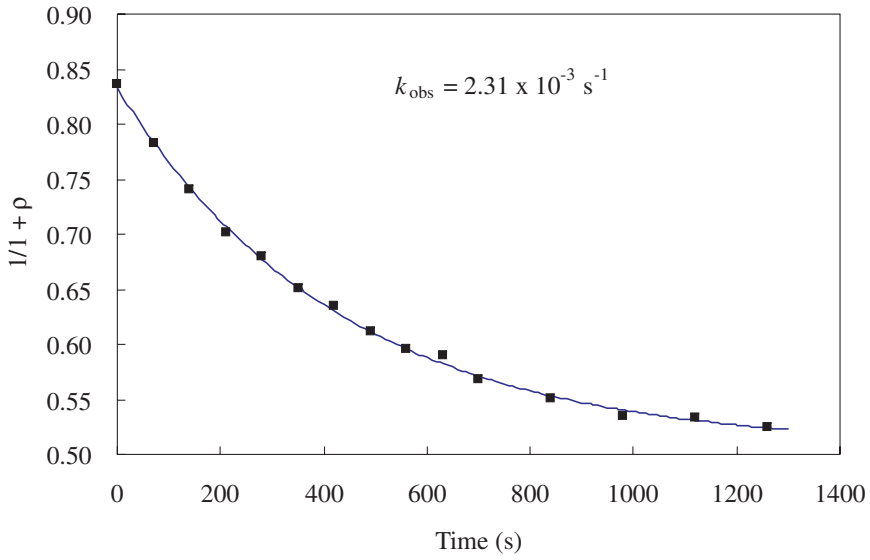


Table 11. Hydration of acetone[a] in 0.01 mol/L HOAc.

Run	k_{obs} (s^{-1})
1	2.31×10^{-3}
2	2.60×10^{-3}
3	3.19×10^{-3}
4	3.48×10^{-3}
5	3.38×10^{-3}
6	2.78×10^{-3}
Avg.	$3.0\pm0.5\times10^{-3}$

Note: $k_{HA} \leq 0.30 \pm 0.05$ M^{-1} s^{-1}[b,c] and k_{HA} theoretical = 0.49 M^{-1} s^{-1}.

[a][Acetone] = 1.1 mol/L.

[b]If $k_H[H_3O^+] << k_{HA}$[HOAc], then $k_{HA} = 0.30 \pm 0.05$ M^{-1} s^{-1}.

[c]A detailed kinetic analysis of k_{obs} vs. pH (in progress) will allow the values of k_H and k_{HA} to be assigned unambiguously.

Research Council of Canada (NSERC) for financial support and Professor Andrew Bennet for helpful discussions.

References

1. W.P. Jencks. Catalysis in chemistry and enzymology. Dover Press, New York. 1987.
2. (*a*) M.B. Swindells. Protein Sci. **4**, 93 (1995); (*b*) M. Munson, S. Balasubramanian, K.G. Fleming, A.D. Nagi, R. O'Brien, and J.M. Sturtevant. Protein Sci. **5**, 1584 (1996); (*c*) B.E. García-Moreno, J.J. Dwyer, A.G. Gittis, E.E. Lattman, D.S. Spencer, and W.E. Stites. Biophys. Chem. **64**, 211 (1997); (*d*) G.A. Lazar and T.M. Handel. Curr. Opin. Chem. Biol. **2**, 675 (1998); (*e*) G. Hummer. J. Am. Chem. Soc. **121**, 6299 (1999); (*f*) Y. Kim, H.D. Kim, and Y. Lee. J. Chem. Soc. Faraday Trans. **93**, 99 (1997); (*g*) R. Callender, D. Chen, J. Lugtenburg, C. Martin, K.W. Rhee, D. Sloan, R. Vandersteen, and K.T. Yue. Biochemistry, **27**, 3672 (1988); (*h*) R. Kanski and C.J. Murray. Tetrahedron Lett. **34**, 2263 (1993); (*i*) A.M. Silva, R.E. Cachau, H.L. Sham, and J.W. Erickson. J. Mol. Biol. **255**, 321 (1996); (*j*) C.N. Schutz and A. Warshel. Proteins: Struct. Funct. Genet. **44**, 400 (2001); (*k*) Q. Cui and M. Karplus. J. Phys. Chem. B, **106**, 1768 (2002).
3. (*a*) B. Thomas, Y. Wang, and R.L. Stein. Biochemistry, **40**, 15 811 (2001); (*b*) B. Asbóth and L. Polgár. Biochemistry, **22**, 117 (1983); (*c*) P.J. Tonge and P.R. Carey. Biochemistry, **29**, 10 723 (1990); (*d*) V. Daggett, S. Schröder, and P. Kollman. J. Am. Chem. Soc. **113**, 8926 (1991); (*e*) P.J. Tonge and P.R. Carey. Biochemistry, **31**, 9122 (1992); (*f*) A.K. Whiting and W.L. Peticolas. Biochemistry, **33**, 552 (1994); (*g*) T.K. Chang, Y. Chiang, H.-X. Guo, A.J. Kresge, L. Mathew, M.F. Powell, and J.A. Wells. J. Am. Chem. Soc. **118**, 8802 (1996); (*h*) K. Curley and R.F. Pratt. J. Am. Chem. Soc. **119**, 1529 (1997); (*i*) B.D. Wladkowski, S.A. Chenoweth, J.N. Sanders, M. Krauss, and W.J. Stevens. J. Am. Chem. Soc. **119**, 6423 (1997); (*j*) T.P. O'Connell, R.M. Day, E.V. Torchilin, W.W. Bachovchin, and J.P.G. Malthouse. Biochem. J. **326**, 861 (1997); (*k*) A. Ordentlich, D. Barak, C. Kronman, N. Ariel, Y. Segall, B. Velan, and A. Shafferman. J. Biol. Chem. **273**, 19 509 (1998); (*l*) C.-H. Hu, T. Brinck, and K. Hult. Int. J. Quant. Chem. **69**, 89 (1998); (*m*) L. Maveyraud, R.F. Pratt, and J.-P. Samama. Biochemistry, **37**, 2622 (1998); (*n*) S.R. Presnell, G.S. Patil, C. Mura, K.M. Jude, J.M. Conley, J.A. Bertrand, C.-M. Kam, J.C. Powers, and L.D. Williams. Biochemistry, **37**, 17 068 (1998); (*o*) R.S. Chittock, S. Ward, A.-S. Wilkinson, P. Caspers, B. Mensch, M.G.P. Page, and C.W. Wharton. Biochem. J. **338**, 153 (1999); (*p*) M.J. Hokenson, G.A. Cope, E.R. Lewis, K.A. Oberg, and A.L. Fink. Biochemistry, **39**, 6538 (2000); (*q*) M. Shokhen and A. Albeck. Proteins: Struct. Funct. Genet. **40**, 154 (2000); (*r*) C.C.H. Chen and O. Herzberg. Biochemistry, **40**, 2351 (2001); (*s*) P. Kusula, J. Ojala, A.-M. Lambeir, and R.K. Wierenga. Biochemistry, **41**, 15 543 (2002); (*t*) Y. Zhang, J. Kua, and J.A. McCammon. J. Am. Chem. Soc. **124**, 10 572 (2002); (*u*) M. Topf, P. Várnai, and W.G. Richards. J. Am. Chem. Soc. **124**, 14 780 (2002); (*v*) T. Ishida and S. Kato. J. Am. Chem. Soc. **125**, 12 035 (2003); (*w*) A.V. Nemukhin, I.A. Topol, and S.K. Burt. Int. J. Quant. Chem. **88**, 34 (2002); (*x*) T. Shimamura, A. Ibuka, S. Fushinobu, T. Wakagi, M. Ishiguro, Y. Ishii, and H.

© 2005 NRC Canada

Matsuzawa. J. Biol. Chem. **277**, 46 601 (2002); (*y*) Y. Zhang, J. Kua, and J.A. McCammon. J. Phys. Chem. B, **107**, 4459 (2003); (*z*) Y. Fujii, N. Okimoto, M. Hata, T. Narumi, K. Yasuoka, R. Susukita, A. Suenaga, N. Futatsugi, T. Koishi, H. Furusawa, A. Kawai, T. Ebisuzaki, S. Neya, and T. Hoshino. J. Phys. Chem. B, **107**, 10 274 (2003); (*aa*) N.R. Silvaggi, J.W. Anderson, S.R. Brinsmade, R.F. Pratt, and J.A. Kelly. Biochemistry, **42**, 1199 (2003); (*ab*) J. Fisher, J.G. Belasco, S. Khosla, and J.R. Knowles. Biochemistry, **19**, 2895 (1980); (*ac*) H. Christensen, M.T. Martin, and S.G. Waley. Biochem. J. **266**, 853 (1990); (*ad*) M.I. Page, B. Vilanova, and N.J. Layland. J. Am. Chem. Soc. **117**, 12 092 (1995); (*ae*) R.P.A. Brown, R.T. Aplin, and C.J. Schofield. Biochemistry, **35**, 12 421 (1996); (*af*) M. Coll, J. Frau, B. Vilanova, J. Donoso, F. Muñoz, and F.G. Blanco. J. Phys. Chem. A, **103**, 8879 (1999); (*ag*) M. Coll, J. Frau, B. Vilanova, J. Donoso, F. Muñoz, and F.G. Blanco. J. Phys. Chem. B, **104**, 11 389 (2000); (*ah*) N. Diaz, D. Suárez, and T.L. Sordo. J. Am. Chem. Soc. **122**, 6710 (2000); (*ai*) Y. Fujii, M. Hata, T. Hoshino, and M. Tsuda. J. Phys. Chem. B, **106**, 9687 (2002); (*aj*) E. Fonzé, M. Vanhove, G. Dive, E. Sauvage, J.-M. Frère, and P. Charlier. Biochemistry, **41**, 1877 (2002); (*ak*) N.R. Silvaggi, J.W. Anderson, S.R. Brinsmade, R.F. Pratt, and J.A. Kelly. Biochemistry, **42**, 1199 (2003); (*al*) M.I. Page and A.P. Laws. Chem. Commun. 1609 (1998); (*am*) J.J. Morris and M.I. Page. J. Chem. Soc. Perkin Trans. 2, 212 (1980); (*an*) C. Damblon, X. Raquet, L.-Y. Lian, J. Lamotte-Brasseur, E. Fonze, P. Charlier, G.C.K. Roberts, and J.-M. Frère. Proc. Natl. Acad. Sci. U.S.A. **93**, 1747 (1996); (*ao*) E.J. Lietz, H. Truher, D. Kahn, M.J. Hokenson, and A.L. Fink. Biochemistry, **39**, 4971 (2000); (*ap*) J.R. Alvarez-Idaboy, R. González-Jonte, A. Hernández-Laguna, and Y.G. Smeyers. J. Mol. Struct.: THEOCHEM, **504**, 13 (2000); (*aq*) M. Nukaga, K. Mayama, A.M. Hujer, R.A. Bonomo, and J.R. Knox. J. Mol. Biol. **328**, 289 (2003); (*ar*) M. Ishiguro and S. Imajo. J. Med. Chem. **39**, 2207 (1996); (*as*) N. Díaz, D. Suárez, T.L. Sordo, and K.M. Merz, Jr. J. Phys. Chem. B, **105**, 11 302 (2001); (*at*) R.M. Gibson, H. Christensen, and S.G. Waley. Biochem. J. **272**, 613 (1990); (*au*) J. Lamotte-Brasseur, G. Dive, O. Dideberg, P. Carlier, and J.-M. Frère. Biochem. J. **279**, 213 (1991); (*av*) I. Massova and P.A. Kollman. J. Comput. Chem. **23**, 1559 (2002); (*aw*) N.C.J. Strynadka, R. Martin, S.E. Jensen, M. Gold, and J.B. Jones. Nat. Struct. Biol. **3**, 688 (1996); (*ax*) M. Hata, Y. Fujii, M. Ishii, T. Hoshino, and M. Tsuda. Chem. Pharm. Bull. **48**, 447 (2000).

4. M. Eigen. Discuss. Faraday Soc. **39**, 7 (1965).
5. (*a*) R.P. Bell, J.P. Millington, and J.M. Pink. Proc. R. Soc. London Ser. A, **303**, 1 (1968); (*b*) R.P. Bell and J.E. Critchlow. Proc. R. Soc. London Ser. A, **325**, 35 (1971); (*c*) R.P. Bell and P.E. Sörensen. J. Chem. Soc. Perkin Trans. 2, 1740 (1972); (*d*) R.P. Bell. Adv. Phys. Org. Chem. **4**, 1 (1966).
6. Y. Pocker and J.E. Meany. J. Phys. Chem. **71**, 3113 (1967).
7. (*a*) P.J. Lillford and D.P.N. Satchell. J. Chem. Soc. B, 889 (1968); (*b*) D.P.N. Satchell and R.S. Satchell. Chem. Soc. Rev. **4**, 231 (1975); (*c*) S.H. Kabir, H.R. Seikaly, and T.T. Tidwell. J. Am. Chem. Soc. **101**, 1059 (1979).
8. G. Raspoet, M.T. Nguyen, M. McGarraghy, and A.F. Hegarty. J. Org. Chem. **63**, 6867 (1998).
9. R.A. Cox and K. Yates. Can. J. Chem. **59**, 2853 (1981).
10. K.S. Venkatasubban, M. Bush, E. Ross, M. Schultz, and O. Garza. J. Org. Chem. **63**, 6115 (1998).
11. R.A. Cox. Can. J. Chem. **76**, 649 (1998).
12. Y. Chiang, A.J. Kresge, J.A. Santaballa, and J. Wirz. J. Am. Chem. Soc. **110**, 5506 (1988).
13. (*a*) B. Jönsson, G. Karlström, H. Wennerström, S. Forsén, B. Roos, and J. Almlöf. J. Am. Chem. Soc. **99**, 4628 (1977); (*b*) E. Magid and B.O. Turbeck. Biochim. Biophys. Acta, **165**, 515 (1968); (*c*) I.H. Williams, D. Spangler, D.A. Femec, G.M. Maggiora, and R.L Schowen. J. Am. Chem. Soc. **102**, 6621 (1980); (*d*) I.H. Williams, G.M. Maggiora, and R.L. Schowen. J. Am. Chem. Soc. **102**, 7831 (1980); (*e*) I.H. Williams, D. Spangler, D.A. Femec, G.M. Maggiora, and R.L Schowen. J. Am. Chem. Soc. **105**, 31 (1983); (*f*) I.H. Williams, D. Spangler, G.M. Maggiora, and R.L. Schowen. J. Am. Chem. Soc. **107**, 7717 (1985); (*g*) C.I. Bayly and F. Grein. Can. J. Chem. **67**, 176 (1989); (*h*) J.D. Madura and W.L. Jorgensen. J. Am. Chem. Soc. **108**, 2517 (1986); (*i*) J.-Y. Liang and W.N. Lipscomb. J. Am. Chem. Soc. **108**, 5051 (1986).
14. K.M. Merz, Jr. J. Am. Chem. Soc. **112**, 7973 (1990).
15. M.T. Nguyen, G. Raspoet, L.G. Vanquickenborne, and P.T. Van Duijnen. J. Phys. Chem. A, **101**, 7379 (1997).
16. S. Antonczak, M.F. Ruiz-López, and J.L. Rivail. J. Am. Chem. Soc. **116**, 3912 (1994).
17. F. Tordini, A. Bencini, M. Bruschi, L. De Gioia, G. Zampella, and P. Fantucci. J. Phys. Chem. A, **107**, 1188 (2003).
18. S. Wolfe, C.-K. Kim, and K. Yang. Can. J. Chem. **72**, 1033 (1994).
19. G.M. Morris, D.S. Goodsell, R.S. Holliday, R. Huey, W.E. Hart, R.K. Belew, and A.J. Olson. J. Comput. Chem. **19**, 1639 (1998).
20. J.A. Kelly and A.P. Kuzin. J. Mol. Biol. **254**, 223 (1995).
21. N.C.J. Strynadka, H. Adachi, S.E. Jensen, K. Johns, A. Sielecki, C. Betzel, K. Sutok, and M.N.G. James. Nature (London), **359**, 700 (1992).
22. (*a*) J.-M. Frère and N. Joris. Crit. Rev. Microbiol. **26**, 299 (1985); (*b*) T.D.H. Bugg and C.T. Walsh. Nat. Prod. Rep. **9**, 199 (1992); (*c*) G. Seltmann. The bacterial cell wall. Springer, New York. 2002.
23. (*a*) W.A. Escobar, A.K. Tan, and A.L. Fink. Biochemistry, **30**, 10 783 (1991); (*b*) J.R. Knox and P.C. Moews. J. Mol. Biol. **220**, 435 (1991); (*c*) H. Adachi, T. Ohta, and H. Matzuzawa. J. Biol. Chem. **266**, 3186 (1991); (*d*) Y.C. Leung, C.V. Robinson, R.T. Alpin, and S.G. Waley. Biochem. J. **299**, 671 (1994); (*e*) G. Guillaume, M. Vanhove, J. Lamotte-Brasseur, P. Ledent, M. Jamin, B. Joris, and J.-M. Frère. J. Biol. Chem. **272**, 5438 (1997); (*f*) A. Matagne, J. Lamotte-Brasseur, and J.-M. Frère. Biochem. J. **330**, 581 (1998); (*g*) J.-M. Frère, A. Dubus, M. Galleni, A. Matagne, and G. Amicosante. Biochem. Soc. Trans. **27**, 58 (1999); (*h*) B. Vilanova, J. Donoso, J. Frau, and F. Muñoz. Helv. Chim. Acta, **82**, 1274 (1999); (*i*) G. Minasov, X. Wang, and B.K. Shoichet. J. Am. Chem. Soc. **124**, 5333 (2002); (*j*) J.C. Hermann, L. Ridder, A.J. Mulholland, and H.-D. Höltje. J. Am. Chem. Soc. **125**, 9590 (2003).
24. M.I. Page. The chemistry of β-lactams. Blackie Academic and Professional, New York. 1992.
25. G. Dive and D. Dehareng. Int. J. Quant. Chem. **73**, 161 (1999); M. Oliva, O. Dideberg, and M.J. Field. Proteins: Struct. Funct. Genet. **52**, 88 (2003).
26. (*a*) S. Wolfe, C.-K. Kim, K. Yang, N. Weinberg, and Z. Shi. J. Am. Chem. Soc. **117**, 4240 (1995); (*b*) S. Wolfe, Z. Shi, K. Yang, S. Ro, N. Weinberg, and C.-K. Kim. Can. J. Chem. **76**, 114 (1998).
27. W.J. Hehre, L. Radom, P.v.R. Schleyer, and J.A. Pople. Ab initio molecular orbital theory. Wiley-Interscience, New York. 1986.
28. M.J. Frisch, G.W. Trucks, H.B. Schlegel, G.E. Scuseria, M.A. Robb, J.R. Cheeseman, V.G. Zakrzewski, J.A. Montgomery, Jr., R.E. Stratmann, J.C. Burant, S. Dapprich, J.M. Millam,

© 2005 NRC Canada

A.D. Daniels, K.N. Kudin, M.C. Strain, O. Farkas, J. Tomasi, V. Barone, M. Cossi, R. Cammi, B. Mennucci, C. Pomelli, C. Adamo, S. Clifford, J. Ochterski, G.A. Petersson, P.Y. Ayala, Q. Cui, K. Morokuma, D.K. Malick, A.D. Rabuck, K. Raghavachari, J.B. Foresman, J. Cioslowski, J.V. Ortiz, B.B. Stefanov, G. Liu, A. Liashenko, P. Piskorz, I. Komaromi, R. Gomperts, R.L. Martin, D.J. Fox, T. Keith, M.A. Al-Laham, C.Y. Peng, A. Nanayakkara, C. Gonzalez, M. Challacombe, P.M.W. Gill, B. Johnson, W. Chen, M.W. Wong, J.L. Andres, M. Head-Gordon, E.S. Replogle, and J.A. Pople. GAUSSIAN 98. Revision A.6 [computer program]. Gaussian, Inc., Pittsburgh, Penn. 1998.

29. (*a*) O. Tapia and O. Goscinski. Mol. Phys. **29**, 1653 (1975); (*b*) S. Miertus, E. Scrocco, and J. Tomasi. Chem. Phys. **55**, 117 (1981); (*c*) J.L. Pascual-Ahuir, E. Silla, J. Tomasi, and R. Bonaccorsi. J. Comput. Chem. **8**, 778 (1987); (*d*) R. Bianco, G.W.A. Milne, M.C. Nicklaus, and M.J. Hodošček. J. Mol. Struct. **291**, 89 (1993); (*e*) F.J. Olivares del Valle, M.A. Aguilar, and J.C. Contador. Chem. Phys. **170**, 161 (1993); (*f*) M. Aguilar, R. Bianco, S. Miertus, M. Persico, and J. Tomasi. Chem. Phys. **174**, 397 (1993); (*g*) D.M.P. Mingos, A.L. Rohl, and J. Burgess. J. Chem. Soc. Dalton Trans. 423 (1993); (*h*) B. Honig, K. Sharp, and A.–S. Yang. J. Phys. Chem. **97**, 1101 (1993); (*i*) H.J. Kim, R. Bianco, B.J. Gertner, and J.T. Hynes. J. Phys. Chem. **97**, 1723 (1993); (*j*) M. Bachs, F.J. Luque, and M. Orozco. J. Comput. Chem. **15**, 446 (1994).
30. (*a*) M.W. Wong, K.B. Wiberg, and M.J. Frisch. J. Chem. Phys. **95**, 8991 (1991); (*b*) M.W. Wong, M.J. Frisch, and K.B. Wiberg. J. Am. Chem. Soc. **113**, 4776 (1991).
31. (*a*) S.F. Boys and F. Bernardi. Mol. Phys. **19**, 553 (1970); (*b*) O.N. Ventura, E.L. Coitiño, K. Irving, A. Iglesias, and A. LLedós. J. Mol. Struct: THEOCHEM, **210**, 427 (1990); (*c*) D.B. Cook, T.L. Sordo, and J.A. Sordo. J. Chem. Soc. Chem. Commun. 185 (1990); (*d*) P.O. Åstrand, A. Wallqvist, and G.J. Karlström. J. Phys. Chem. **95**, 6395 (1991); (*e*) R. Eggenberger, S. Gerber, H. Huber, and D. Searles. Phys. Lett. **183**, 223 (1991); (*f*) P. Valiron, A. Vibók, and I. Mayer. J. Comput. Chem. **14**, 401 (1993); (*g*) L. Turi and J.J. Dannenberg. J. Phys. Chem. **97**, 2488 (1993); (*h*) J.A. Dobado and J.M. Molina. J. Phys. Chem. **97**, 7499 (1993); (*i*) E.R. Davidson and S.J. Chakravorty. Chem. Phys. Lett. **217**, 48 (1993); (*j*) I. Mayer, A. Vibók, and P. Valiron. Chem. Phys. Lett. **230**, 35 (1994); (*k*) T. Neuheuser, B.A. Hess, C. Reutel, and E. Weber. J. Phys. Chem. **98**, 6459 (1994); (*l*) M. Kieninger, S. Suhai, and I. Mayer. Chem. Phys. Lett. **230**, 485 (1994).
32. D.D. Perrin. Ionisation constants of inorganic acids and bases in aqueous solution. Pergamon Press, New York. 1982.
33. J.M. Risley and R.L. Van Etten. J. Am. Chem. Soc. **102**, 939 (1980).
34. K.J. Laidler. Chemical kinetics. Harper and Row, New York. 1987.

© 2005 NRC Canada

Electron-rich siloxane–platinum complexes — Synthesis, structures, and reactivity[1]

Roman Goikhman, Tanya Karakuz, Linda J.W. Shimon, Gregory Leitus, and David Milstein

Abstract: New platinasiloxanes were synthesized and their reactivity was studied. Oxidative addition of $(HSiMe_2)_2O$ to $Pt(PEt_3)_3$ led to dehydrogenation and quantitative formation of the four-membered platinacyclosiloxane $[(PEt_3)_2Pt-((SiMe_2)_2O)]$ which was characterized by X-ray diffraction. This complex was stable towards non-polar substrates and aerobic conditions, but reacted readily with electrophiles and Lewis acids. Reaction with MeI resulted in ring opening, while MeOTf gave an oxonium complex, with retention of the platinacycle structure. A complex resulting from BF_3 coordination to the ring oxygen atom was also obtained. An unprecedented open-chain diplatinasiloxane containing the Pt–Si–O–Si–O–Si–Pt fragment was formed by oxidative addition of H–$SiMe_2$–O–$SiMe_2$–O–$SiMe_2$–H to $Pt(PEt_3)_3$ and it was characterized by X-ray diffraction.

Key words: cyclosiloxane, metallacycle, platinum silyl, Lewis base, oxidative addition.

Résumé : On a réalisé la synthèse de nouveaux platinasiloxanes et on en a étudié la réactivité. L'addition oxydante du $(HSiMe_2)_2O$ à du $Pt(PEt_3)_3$ conduit à une déshydrogénation et à la formation quantitative du platinacyclosiloxane à quatre chaînons $[(PEt_3)_2Pt((SiMe_2)_2O)]$ qui a été caractérisé par diffraction des rayons X. Ce complexe est stable vis-à-vis des substrats non polaires et des conditions aérobiques, mais il réagit facilement avec les électrophiles et les acides de Lewis. Sa réaction avec du MeI conduit à une ouverture de cycle, alors que sa réaction avec du MeOTf conduit à la formation d'un complexe d'oxonium, avec rétention de la structure platinacyclique. Un complexe résultant de la coordination du BF_3 à l'atome d'oxygène du cycle a aussi été obtenu. L'addition oxydante de H–$SiMe_2$–O–$SiMe_2$–O–$SiMe_2$–H à du $Pt(PEt_3)_3$ conduit d'un diplatinasiloxane à chaîne ouverte contenant le fragment Pt–Si–O–Si–O–Si–Pt inconnu jusqu'à maintenant et qui a été caractérisé par diffraction des rayons X.

Mots clés : cyclosiloxane, métallacyclique, silyle platine, base de Lewis, addition oxydante.

[Traduit par la Rédaction]

Introduction

Siloxanes are important components in the organosilicon polymer industry (1). Siloxanes bearing the terminal Si–H group are used in hydrosilylation reactions catalyzed by transition metal compounds, particularly platinum complexes (2). Moreover, symmetrical dihydridosiloxanes can form cyclic compounds with transition metal complexes (3). Such silametallacycles have attracted considerable interest because of the potential use of these species in catalytic double silylation reactions of various organic substrates to form precursors for the synthesis of functional organosilicon polymers (4). Among various silametallacycles, relatively limited information has been reported regarding the reactivity of small metallocyclosiloxanes, including Si–Si addition to carbon–carbon triple bonds using cyclic platinasiloxanes (5). An intriguing theoretical possibility for the four-membered ring metallosiloxane system is metathesis via a silanone-silylene intermediate complex. It was proposed (6) that this might involve unusual transformations at the metal center and lead to various rearrangements and oligomerization or polymerization reactions. In the present work new metallosiloxanes are described and their reactivity towards various substrates is reported for the first time.

Received 23 December 2004. Published on the NRC Research Press Web site at http://canjchem.nrc.ca on 6 July 2005.

This paper is dedicated to Professor Howard Alper in recognition of his outstanding contributions to homogeneous catalysis and organometallic chemistry.

R. Goikhman, T. Karakuz, L.J.W. Shimon, G. Leitus, and D. Milstein.[2] Department of Organic Chemistry and Unit of Chemical Research Support, The Weizmann Institute of Science, Rehovot, Israel 76100.

[1]This article is part of a Special Issue dedicated to Professor Howard Alper.

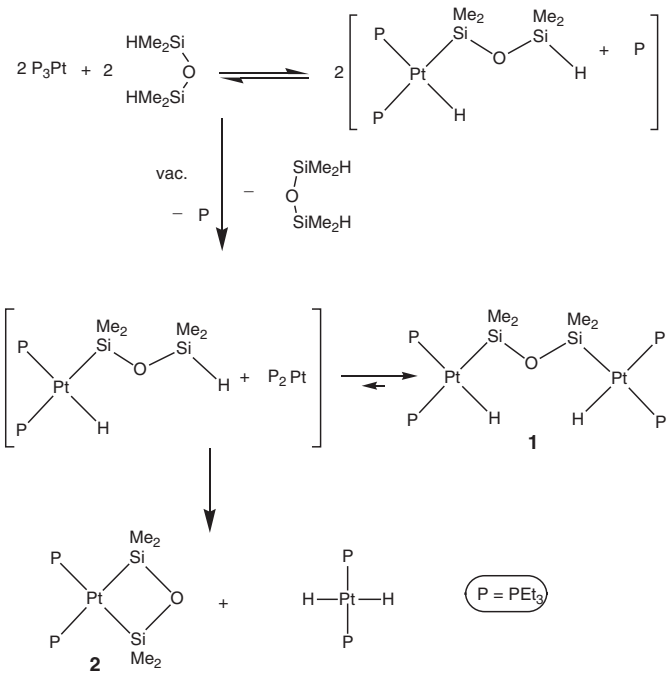
[2]Corresponding author (e-mail: david.milstein@weizmann.ac.il).

Results and discussion

Addition of $(HSiMe_2)_2O$ to $Pt(PEt_3)_3$ in pentane, followed by evaporation of the volatiles resulted in formation of a siloxane-bridged diplatinum complex *cis*-$(PEt_3)_2Pt(H)$-$SiMe_2$-O-$SiMe_2$-$Pt(H)(PEt_3)_2$ (**1**). Noteworthy, no mononuclear adduct was detected despite an initial 50% excess of the siloxane substrate. When the reaction was performed in a C_6D_6 solution, very broad peaks were observed in the ^{31}P and ^1H NMR spectra (prior to evaporation), indicating a rapid phosphine exchange process. We propose that the initial Si–H oxidative addition is reversible in the presence of free PEt_3, as previously observed by us (7). Under vacuum,

 doi: 10.1139/V05-041 © 2005 NRC Canada

Scheme 1.

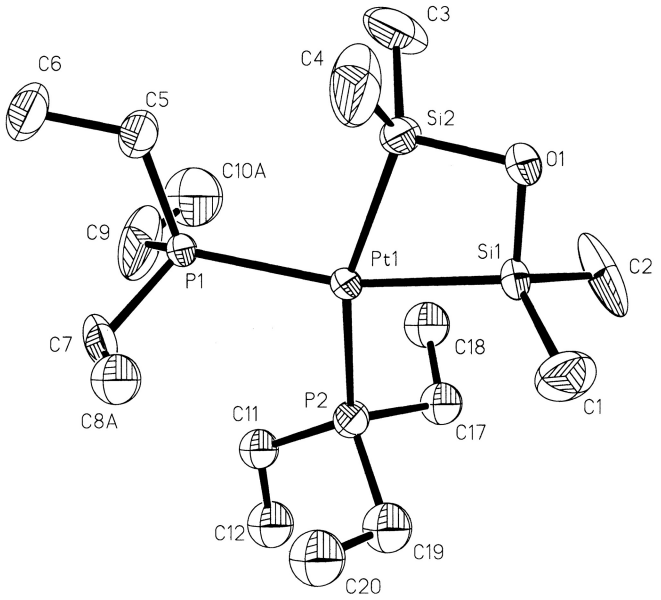


the liberated PEt_3 (together with the solvent) is removed, resulting in an equilibrium shift towards formation of the adduct. However, the vacuum conditions also promote the opposite reaction owing to the volatility of the disiloxane substrate. Phosphine deficiency makes the second Si–H addition easier, ultimately resulting in the dinuclear product **1** (Scheme 1). The latter complex slowly disproportionates at room temperature to a 1:1 mixture of the very stable new platinacycle **2** and the known dihydride *trans*-$(PEt_3)_2PtH_2$ (8) (Scheme 1).

The new compounds **1** and **2** were unambiguously characterized by multinuclear NMR spectroscopy. Complex **1** exhibits two different signals in its ^{31}P NMR spectrum with characteristic $^1J_{P,Pt}$ constants equal to 1262 Hz (P trans to Si) and 2395 Hz (P trans to H). The hydride signal appears as dd at –1.96 ppm with large $^1J_{H,Ptrans}$ and small $^1J_{H,Pcis}$ constants of 153 and 25 Hz, respectively. Integration and the lack of a Si–H peak in the ^1H NMR spectrum is consistent with the binuclear structure of **1**. We are unaware of any previously reported binuclear hydrido-disiloxane Pt complexes.

Platinacycle **2** exhibits an expected singlet with ^{195}Pt satellites ($^1J_{Pt,P}$ = 1548 Hz) in the ^{31}P NMR spectrum, the $^1J_{Pt,P}$ being similar to the $^1J_{Pt,P}$ = 1560 Hz reported for $(PhEt_2P)_2Pt((SiMe_2)_2O)$ (3*b*). The Si–Me signals in the $^1H\{^{31}P\}$ NMR and $^{13}C\{^1H\}$ NMR spectra are very characteristic, both having strong ^{195}Pt satellites with $^3J_{Pt,H}$ = 17.8 Hz, and $^2J_{Pt,C}$ = 98 Hz. For compound **1**, these constants are 24 and 151 Hz, respectively. This indicates that the Pt—Si bond is probably longer in platinacycle **2** as compared with the one in hydrido-platinum complex **1**.

Fig. 1. Perspective view (ORTEP) of **2**. Hydrogen atoms are omitted for clarity.



Similar platinacycles have been described (3).[3] ^{13}C NMR data for platinacyclosiloxanes is reported here for the first time.

Compound **2** can be obtained directly in high yield by stirring a fivefold excess of $(HSiMe_2)_2O$ with $Pt(PEt_3)_3$ in pentane overnight, and it can be easily recrystallized from pentane as colorless needles. Crystals of **2** suitable for a single crystal X-ray diffraction study were obtained from pentane solution at –30 °C. The X-ray structure of **2** is shown in Fig. 1.[3] Selected bond lengths and angles are given in Table 1. Complex **2** is the second crystallographically characterized platinacyclosiloxane (9). The structural features are similar to those reported for the analogous complex [(DPPE)Pt($(SiMe_2)_2O$)] (DPPE is bis(diphenylphosphinoethane) (9). Complex **2** exhibits a distorted square-planar structure with a very small Si-Pt-Si angle (64.4°) (65° in the DPPE analog). The Pt—Si bonds are slightly shorter than those of the DPPE analog (2.363–2.366 Å vs. 2.373–2.374 Å) probably because of steric factors. The Si-O-Si angle is also slightly smaller (97.0° vs. 97.8° in the DPPE analog). The Pt-Si-O-Si core is planar (the torsion angle for Si-Pt-Si/Si-O-Si is just 1.0°).

Complex **2** is a very stable compound and it is inert towards air and water. It is stable in the presence of a large excess of norbornene, no silylation being observed, and it does not react with nonpolar substrates such as dihydrogen and silanes. However, the platinacycle is quite a strong nucleophile and Lewis base. For example, it reacts with MeI, resulting in opening of the cycle and formation of a *trans*-$(PEt_3)_2Pt(I)(SiMe_2\text{-}O\text{-}SiMe_3)$ (**3**). The reaction proceeds overnight at room temperature in benzene. Interestingly, un-

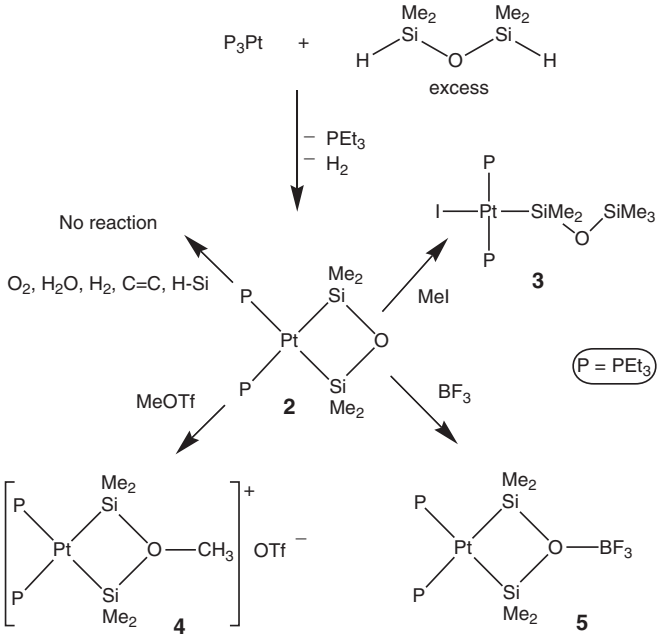
[3] Supplementary data for this article are available on the Web site or may be purchased from the Depository of Unpublished Data, Document Delivery, CISTI, National Research Council Canada, Ottawa, ON K1A 0S2, Canada. DUD 3679. For more information on obtaining material refer to http://cisti-icist.nrc-cnrc.gc.ca/irm/unpub_e.shtml. CCDC 259066 (complex **2**) and 259067 (complex **6**) contain the crystallographic data for this manuscript. These data can be obtained, free of charge, via www.ccdc.cam.ac.uk/conts/retrieving.html (Or from the Cambridge Crystallographic Data Centre, 12 Union Road, Cambridge CB2 1EZ, UK; fax +44 1223 336033; or deposit@ccdc.cam.ac.uk).

© 2005 NRC Canada

Table 1. Selected bond lengths and angles in structures **2** and **6**.

Bond lengths (Å)		Bond angles (°)	
2			
Pt(1)—P(1)	2.3291(14)	P(1)-Pt(1)-P(2)	100.04(6)
Pt(1)—P(2)	2.3461(18)	P(1)-Pt(1)-Si(2)	98.68(6)
Pt(1)—Si(1)	2.3664(15)	P(2)-Pt(1)-Si(2)	159.94(7)
Pt(1)—Si(2)	2.3631(19)	P(1)-Pt(1)-Si(1)	162.10(6)
Si(1)—O(1)	1.678(5)	P(2)-Pt(1)-Si(1)	97.62(6)
Si(2)—O(1)	1.680(4)	Si(1)-Pt(1)-Si(2)	64.24(6)
		Si(1)-O(1)-Si(2)	97.0(2)
6			
Pt(1)—P(1)	2.2948(14)	P(1)-Pt(1)-P(2)	106.20(6)
Pt(1)—P(2)	2.3406(11)	P(1)-Pt(1)-Si(1)	95.32(4)
Pt(1)—Si(1)	2.3510(11)	P(2)-Pt(1)-Si(1)	158.45(6)
Pt(1)—H(1)	1.7507	P(1)-Pt(1)-H(1)	167.3
Si(1)—O(1)	1.671(3)	P(2)-Pt(1)-H(1)	76.7
Si(2)—O(1)	1.625(3)	Si(1)-Pt(1)-H(1)	82.1
		Si(1)-O(1)-Si(2)	149.6(2)

Scheme 2.

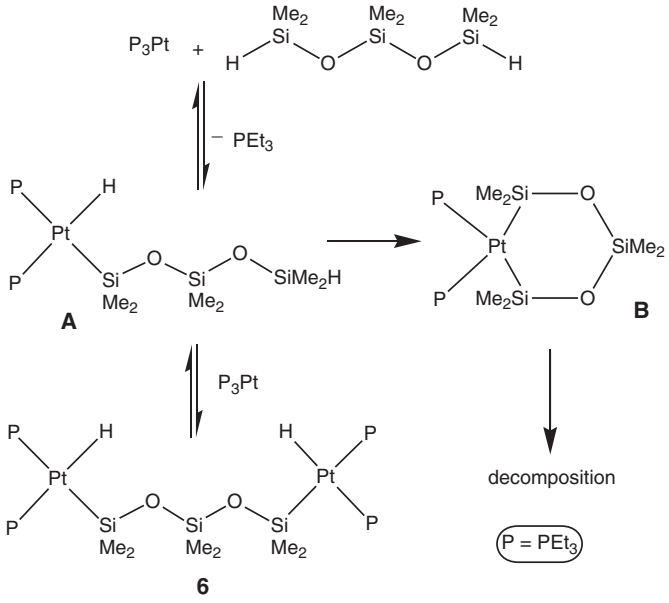


like the reaction with MeI, the reaction with MeOTf is *O*-directed, complex **2** acting as a strong Lewis base producing the cationic complex **4** (Scheme 2), which partially precipitates from benzene solution as a yellow oil.

A similar result is observed with the reagent Et_2O–BF_3. Platinacycle **2** readily abstracts BF_3 from the ether complex, producing a new complex **5** (Scheme 2). The complex is colorless and slightly less soluble in benzene than **2**, apparently becasue of a higher polarity. Scheme 2 summarizes the reactivity of complex **2**.

The reactions are easily followed by NMR spectroscopy. The ^{31}P NMR of the starting complex **2** exhibits a singlet at 18.7 ppm with a characteristic low $^1J_{Pt,P}$ = 1548 Hz. The ^{31}P NMR signal of adduct **3** appears at 16.3 ppm with $^1J_{Pt,P}$ = 2855 Hz (typical for mutually trans phosphines). Adduct **5** gives rise to a signal at 16 ppm with $^1J_{Pt,P}$ = 1705 Hz in the

Scheme 3.



^{31}P NMR spectrum. The larger coupling constant value when compared with the one observed for the starting complex **2** reflects a weakening of the (normally strong) trans influence of the Si ligand, which is affected by BF_3 binding.

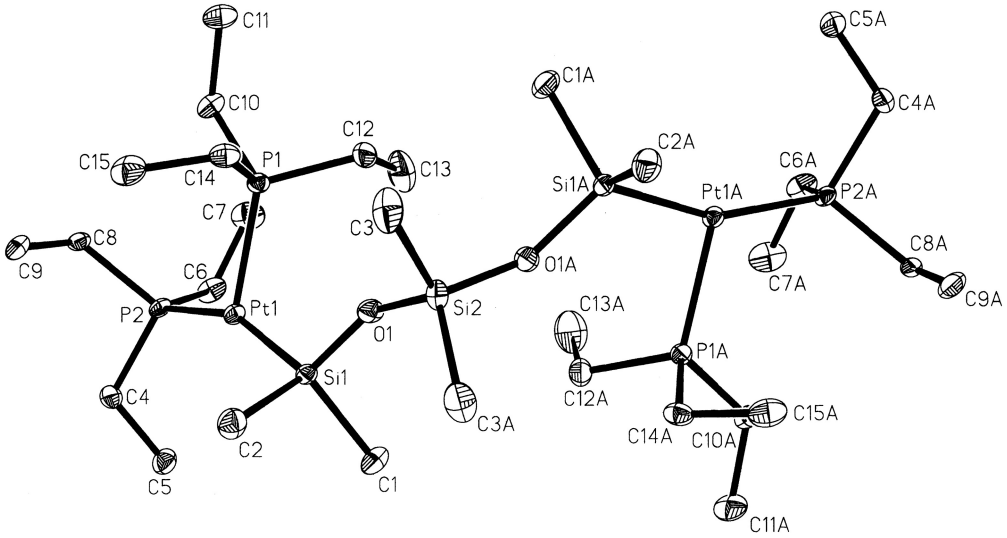
Addition of MeOTf, which results in formation of a cationic complex, causes even more dramatic changes in the NMR spectrum. Thus, the ^{31}P NMR signal of complex **4** appears at 14.8 ppm with a larger $^1J_{Pt,P}$ = 1792 Hz.

Although the reaction of BF_3 with polysiloxanes is used in polymer chemistry (10), very little is known about the reactivity of siloxanes towards BF_3. Siloxane–BF_3 adducts are unstable compounds, which either cannot be detected at all or readily decompose at room temperature to fluorosilanes (11). In particular, the adduct of BF_3 with free tetramethyldisiloxane was not observed (11*d*), but a mixture of fluorosilanes was obtained instead. Our metallosiloxane–BF_3 complex is stable at room temperature in the solid state and slowly decomposes in solution within days.

In an attempt to obtain a larger platinacycle and to compare its properties with those of **2**, the trisiloxane $HSiMe_2$-O-$SiMe_2$-O-$SiMe_2H$ was used as a substrate. Its reaction with $Pt(PEt_3)_3$ proceeds in a more complicated manner. When a stoichiometric amount of the trisiloxane was used, a mixture of two compounds was formed, and after several hours the reaction ended with the new binuclear complex **6** (Scheme 3). The product was crystallized from cold pentane and studied by X-ray crystallography (Fig. 2).[3] Selected bond lengths and angles are given in Table 1. This is a rare example of a crystallographically characterized acyclic platinasiloxane complex (12). Compound **6** exhibits the previously unreported feature of a bridging trisiloxane unit between two Pt centers. The phosphines are located cis to each other and the Pt centers exhibit a distorted square-planar structure. As expected, the Si centers are tetrahedral. The Si-O-Si angle of 149.6° is typical for long chain siloxanes, and it falls within the range of 139°–167° reported for the platinasiloxane cluster (13). The P—Pt bond lengths reflect a weaker trans-influence of the hydride ligand as com-

© 2005 NRC Canada

Fig. 2. Perspective view (ORTEP) of **6**. Hydrogen atoms are omitted for clarity.



pared with the Si ligand. Thus, P trans to Si exhibits a longer bond length (2.34 Å) than P trans to H (2.29 Å), which correlates well with the ^{31}P NMR data ($^{1}J_{P,Pt}$ is 1319 and 2366 Hz, respectively). In the Pt-Si(1)-O-Si(2) fragment, the Si(1)—O bond is considerably longer than the Si(2)—O bond (1.671 vs. 1.625 Å). There are smaller changes in the Si(1)—CH_3 vs. Si(2)—CH_3 bonds (1.884 and 1.890 Å vs. 1.874 Å), which allow us to conclude that not only steric but electronic factors as well affect the Si—O bond length. Obviously, back-donation from a Pt to Si atom lengthens the Si(1)—O bond.

Comparing the NMR data of complexes **1** and **6**, we can see that these compounds are very similar. The only noteworthy feature is that the $^{1}J_{P,Pt}$ value of P trans to Si is smaller in **1** (1262 vs. 1319 Hz in **6**), which suggests that the disiloxane ligand in **1** is bound slightly more strongly than the trisiloxane ligand in **6**. The very few crystallographically characterized Pt hydrido-silyl complexes with *cis*-phosphine geometry exhibited similar structural features (12).

Interestingly, formation of the binuclear complex **6** is also preferred over that of the mononuclear adduct, as observed in the case of disiloxane reaction with $Pt(PEt_3)_3$. A new complex, probably the mononuclear complex (compound **A** in Scheme 3) is formed initially in a mixture with dimer **6**, and then disappears upon stirring. Compound **A** was not characterized because of severe overlapping of all NMR signals with those of the starting substrate and complex **6**. Addition of 2 equiv. of Pt(0) to 1 equiv. of the trisiloxane had no obvious influence on the formation rate of dimer **6**. However, the process could be accelerated by evaporation of the liberated phosphine and by redissolving the resulting mixture.

In an attempt to prepare a six-membered cyclic platinacycle, the initial mixture of trisiloxane and $Pt(PEt_3)_3$ was heated at 45 °C for 1 h. The platinacycle (compound **B**, Scheme 3) was probably formed, as detected by ^{31}P NMR in the mixture (less than 20%), and exhibited a characteristically low $^{1}J_{Pt,P}$ = 1470 Hz. However, this cycle appears to be far less stable than the four-membered ring **2**, and decomposes during formation to an unidentified mixture (14). Prolonged stirring of **6** at room temperature gave similar results and only a small percentage of what appears to be platinacycle B was detected in the reaction mixture during decomposition of **6** (followed by NMR).

Thus, comparing the stability of the described platinasiloxanes we can conclude that: (*i*) in contrast to reported similar systems (3, 12*a*), triethylphosphine–platinum mononuclear siloxane adducts are unstable under stoichiometric reaction conditions and $(Et_3P)_2Pt(H)(SiMe_2\text{-}O\text{-}SiMe_2H)$ is far less stable than $(Et_3P)_2Pt(H)(SiMe_2\text{-}O\text{-}SiMe_2\text{-}O\text{-}SiMe_2H)$. Under analogous conditions the first species was not observed, whereas the second one was observed in the reaction mixture in its initial stages; (*ii*) the dinuclear compounds $(Et_3P)_2Pt(H)(SiMe_2\text{-}O\text{-}SiMe_2)Pt(H)(PEt_3)_2$ (**1**) and $(Et_3P)_2Pt(H)(SiMe_2\text{-}O\text{-}SiMe_2\text{-}O\text{-}SiMe_2)Pt(H)(PEt_3)_2$ (**6**) can be isolated in the solid state. They are both unstable in solution, but **1** decomposes much faster at room temperature in solution than does **6** ($t_{1/2}$ is approximately 4 h and 2 days, respectively). The initial decomposition pathways are similar and lead to mononuclear cyclization products; (*iii*) the four-membered platinacyclosiloxane **2** is a stable compound both in the solid state and in solution at room temperature, whereas the (presumed) six-membered platinacyclosiloxane B (Scheme 3) rapidly decomposes and cannot be isolated.

Overall, the reactivity of a Pt(0) complex towards Si-H containing di- and trisiloxane substrates was examined, cyclization and dimerization processes were described and discussed, reactivity of platinacycles towards various substrates was studied for the first time, and X-ray structures of platinasiloxanes were determined.

Experimental

General

All the manipulations of air- and moisture-sensitive compounds were carried out using a nitrogen-filled Vacuum Atmospheres glovebox. Solvents were purified by standard procedures, degassed, and stored over molecular sieves in the glovebox. All reagents used were of reagent grade. Commercially available 1,1,3,3-tetramethyldisiloxane was distilled prior to use while 1,1,3,3,5,5-hexamethyltrisiloxane was

© 2005 NRC Canada

used without further purification. The complex $Pt(PEt_3)_3$ was synthesized according to a literature procedure (15). NMR spectra were obtained with a Bruker AMX 400 spectrometer at ambient probe temperature in benzene-d_6 solutions unless otherwise specified.

Preparation of 1

A solution of 110 mg (0.2 mmol) of $Pt(PEt_3)_3$ in 5 mL of pentane was treated with 40 mg (53 µL, 0.3 mmol) of freshly distilled $(HSiMe_2)_2O$ and the mixture was evaporated to dryness. The residue was dissolved in pentane and kept overnight at –30 °C, resulting in the precipitation of colorless needles. The solution was decanted and the crystals were washed with 3 mL of cold pentane and dried under vacuum to afford 75 mg (75%) of **1**. The crystals contained a small amount of **2**.

NMR data for 1

$^1H\{^{31}P\}$ NMR: 1.95 (m, 12H, P-CH_2), 1.56 (m, 12H, P-CH_2), 1.04 (m, 18H, P-CH_2-CH_3), 1.03 (s, with ^{195}Pt satellites $^3J_{Pt,H}$ = 24 Hz, 12H, Si-CH_3), 0.96 (m, 18H, P-CH_2-CH_3). Methyl signals were partially overlapped. –1.96 (dd, $^2J_{H,Ptrans}$ = 153 Hz, $^2J_{H,Pcis}$ = 25 Hz, $^1J_{H,Pt}$ = 1020 Hz, 1H, Pt-H). ^{13}C NMR: 22.5 (dd, with ^{195}Pt satellites, $^1J_{C,P}$ = 22.5 Hz, $^3J_{C,P}$ = 2.4 Hz, $^2J_{C,Pt}$ = 22.1 Hz, P-CH_2), 19.6 (dd, with ^{195}Pt satellites, $^1J_{C,P}$ = 25.9 Hz, $^3J_{C,P}$ = 5.8 Hz, $^2J_{C,Pt}$ = 31.7 Hz, P-CH_2), 15.6 (dd, with ^{195}Pt satellites, $^3J_{C,Ptrans}$ = 12.5 Hz, $^3J_{C,Pcis}$ = 2.0 Hz, $^2J_{C,Pt}$ = 151 Hz, Si-CH_3), 9.2 (s, with ^{195}Pt satellites, $^3J_{C,Pt}$ = 25 Hz, P-CH_2-CH_3), and 9.0 (s, with ^{195}Pt satellites, $^3J_{C,Pt}$ = 18 Hz, P-CH_2-CH_3). ^{31}P NMR: 23.0 (d, with ^{195}Pt satellites, $^2J_{P,P}$ = 14.8 Hz, $^1J_{Pt,P}$ = 1262 Hz), 22.1 (d, with ^{195}Pt satellites, $^2J_{P,P}$ = 14.8 Hz, $^1J_{Pt,P}$ = 2395 Hz).

Preparation of 2

A solution of 275 mg (0.5 mmol) of $Pt(PEt_3)_3$ in 5 mL of pentane was treated with 335 mg (440 µL, 2.5 mmol) of $(HSiMe_2)_2O$, and the mixture was stirred at room temperature for 3 h. The color of the solution changed immediately from orange to yellowish. The solution was kept overnight at –30 °C resulting in the precipitation of colorless needles. The solution was decanted and the crystals were washed with 3 mL of cold pentane and dried under vacuum to afford 200 mg (71%) of **2**.

NMR data for 2

^1H NMR: 1.68 (m, 12H, P-CH_2), 0.95 (m, 18H, P-CH_2-CH_3), 0.82 (s, with ^{195}Pt satellites, $^3J_{Pt,H}$ = 17.8 Hz, 12H, Si-CH_3). ^{13}C NMR: 20.2 (dd, with ^{195}Pt satellites, $^1J_{C,P}$ = 13.8 Hz, $^3J_{C,P}$ = 11.4 Hz, $^2J_{C,Pt}$ = 24.5 Hz, P-CH_2), 15.6 (vt, with ^{195}Pt satellites, $^3J_{C,P}$ = 5.9 Hz, $^2J_{C,Pt}$ = 98 Hz, Si-CH_3), and 8.5 (v. quin., J = 10 Hz, P-CH_2-CH_3). ^{31}P NMR: 19.7 (s, with ^{195}Pt satellites, $^1J_{Pt,P}$ = 1548 Hz).

Preparation of 3

To a solution of 34 mg (0.06 mmol) of **2** in 0.6 mL of benzene-d_6 was added MeI (5 µL, 0.08 mmol) and the reaction was stirred at room temperature overnight, producing complex **3** quantitatively. After measuring the NMR spectrum, the solvent was evaporated to afford 40 mg (94%) of off-white compound **3**.

NMR data for 3

^1H NMR: 2.11 (m, 12H, P-CH_2), 0.97 (m, 18H, P-CH_2-CH_3), 0.56 (s, with ^{195}Pt satellites, $^3J_{Pt,H}$ = 19.9 Hz, 6H, Si-CH_3), 0.17 (s, 9H, Si-CH_3). ^{13}C NMR: 18.8 (vt, $^1J_{C,P}$ = $^3J_{C,P}$ = 17.2 Hz, P-CH_2), 11.0 (t, $^3J_{C,P}$ = 2 Hz, Si-CH_3), 8.9 (s, P-CH_2-CH_3), 2.8 (s, O-$SiMe_3$). ^{31}P NMR: 17.3 (s, with ^{195}Pt satellites, $^1J_{Pt,P}$ = 2855 Hz).

Preparation of 4

To a solution of 28 mg (0.05 mmol) of **2** in 1 mL of benzene was added methyl triflate (8 mg, 5.5 µL, 0.05 mmol) at 6 °C. Slow precipitation of a yellow oil started and after 3 h, the oil was separated from the solution. NMR measurement of a sample of the oil in C_6D_6 showed formation of compound **4** in 80% purity. Attempts to isolate complex **4** failed because of its instability.

NMR data for 4

^1H NMR: 3.5 (br., O-Me), 1.70 (m, 12H, P-CH_2), 0.84 (m, 18H, P-CH_2-CH_3), 0.37 (s, with ^{195}Pt satellites, $^3J_{Pt,H}$ = 18 Hz, 12H, Si-CH_3). ^{31}P NMR: 15.8 (s, with ^{195}Pt satellites, $^1J_{Pt,P}$ = 1792 Hz).

Preparation of 5

To a solution of 28 mg (0.05 mmol) of **2** in 1 mL of benzene-d_6 was added an Et_2O–BF_3 complex (7 mg, 0.05 mmol). NMR measurements showed immediate quantitative formation of compound **5**. Evaporation of the solvent gave 30 mg (95%) of the pure colorless complex **5**.

NMR data for 5

^1H NMR: 1.55 (m, 12H, P-CH_2), 1.01 (m, 18H, P-CH_2-CH_3), 0.82 (s, with ^{195}Pt satellites, $^3J_{Pt,H}$ = 15.4 Hz, 12H, Si-CH_3). ^{13}C NMR: 19.4 (dd, with ^{195}Pt satellites, $^1J_{C,P}$ = 14.5 Hz, $^3J_{C,P}$ = 12.8 Hz, $^2J_{C,Pt}$ = 23.8 Hz, P-CH_2), 8.2 (v. quin., J = 10 Hz, P-CH_2-CH_3), 7.3 (vt, with ^{195}Pt satellites, $^3J_{C,P}$ = 5.0 Hz, $^2J_{C,Pt}$ = 74.8 Hz, Si-CH_3). ^{19}F NMR: –142 (m). ^{31}P NMR: 17.0 (s, with ^{195}Pt satellites, $^1J_{Pt,P}$ = 1705 Hz).

Preparation of 6

To a solution of 55 mg (0.1 mmol) of $Pt(PEt_3)_3$ in 2 mL of pentane was added $HSiMe_2$-O-$SiMe_2$-O-$SiMe_2H$ (12.5 mg, 15 µL, 0.06 mmol), and the mixture was stirred for 3 h at room temperature. The resulting solution was evaporated to dryness, redissolved in 1 mL of pentane, and left in the freezer at –30 °C for 2 days, resulting in precipitation of colorless crystals. The solution was decanted and the crystals were washed with 3 mL of cold pentane and dried to afford 40 mg (65%) of **6**.

NMR data for 6

^1H NMR: 2.07 (m, 12H, P-CH_2), 1.62 (m, 12H, P-CH_2), 1.14 (m, 18H, P-CH_2-CH_3), 1.12 (s, with ^{195}Pt satellites, $^3J_{Pt,H}$ = 27.4 Hz, 12H, Si-CH_3), 1.01 (m, 18H, P-CH_2-CH_3), 0.51 (s, 6H, Si-CH_3), –2.21 (dd, $^2J_{H,Ptrans}$ = 149 Hz, $^2J_{H,Pcis}$ = 23.7 Hz, $^1J_{H,Pt}$ = 1007 Hz, 1H, Pt-H). ^{13}C NMR: 22.4 (dd, with ^{195}Pt satellites, $^1J_{C,P}$ = 19.2 Hz, $^3J_{C,P}$ = 2.4 Hz, $^2J_{C,Pt}$ = 21 Hz, P-CH_2), 19.3 (dd, with ^{195}Pt satellites, $^1J_{C,P}$ = 27 Hz, $^3J_{C,P}$ = 5.0 Hz, $^2J_{C,Pt}$ = 30 Hz, P-CH_2), 15.2 (d, with ^{195}Pt satellites, $^3J_{C,Ptrans}$ = 12 Hz, $^2J_{C,Pt}$ = 157 Hz, Si-CH_3), 9.1 (overlapped signal, P-CH_2-CH_3), 4.2 (br. s, Si-CH_3). ^{31}P NMR: 23.4 (d, with ^{195}Pt satellites, $^2J_{P,P}$ = 16.6 Hz, $^1J_{Pt,P}$ =

© 2005 NRC Canada

Table 2. Crystallographic parameters for structures **2** and **6**.

Crystal	**2**	**6**
Empirical formula	$C_{16}H_{36}O_1P_2Si_2Pt$	$C_{30}H_{80}O_2P_4P_2Si_3$
Formula mass	557.66	1071.28
Color, habit	Colorless, needles	Colorless, plates
Crystal dimensions (mm^3)	0.1 × 0.1 × 0.1	0.15 × 0.15 × 0.05
Crystal system	Monoclinic	Monoclinic
Space group	*P*2(1)*n* (No. 14)	*C*2/*c* (No. 15)
Z	4	8
a (Å)	9.980(2)	32.547(7)
b (Å)	14.401(3)	9.835(2)
c (Å)	17.505(4)	15.579(3)
α (°)	90	90
β (°)	105.21(3)	116.81(3)
γ (°)	90	90
Collection range	$-12 \le h \le 12$, $0 \le k \le 18$, $0 \le l \le 22$	$-41 \le h \le 36$, $0 \le k \le 12$, $0 \le l \le 19$
Temperature (K)	120(2)	120(2)
Volume ($Å^3$)	2 427.7(8)	4 450.9(15)
D_{calcd} (Mg m^{-3})	1.526	1.599
Radiation	MoKα (λ = 0.710 73 Å)	MoKα (λ = 0.710 73 Å)
Absorption coeff. (mm^{-1})	6.010	6.527
Absorption correlation	Integration	Integration
F(000)	1 104	2 136
θ range for data collection (°)	2.57–27.10	2.62–26.78
Observed reflections	53 657	16 955
Independent reflections	6 240 (R_{int} = 0.061)	4 992 (R_{int} = 0.055)
Data/restraints/parameters	5 355/4/205	4 716/0/195
Maximm shift/error	0.000 0	0.000 0
Goodness-of-fit on F^2	1.094	1.030
Final *R* indices ($I > 2\sigma(I)$)	R_1 = 0.039 2, wR_2 = 0.087 0	R_1 = 0.029 6, wR_2 = 0.073 1
R indices (all data)	R_1 = 0.052 3, wR_2 = 0.092 0	R_1 = 0.037 7, wR_2 = 0.076 4
Largest diff. peak and hole (e $Å^{-3}$)	2.314 and –1.303	1.355 and –1.243

1319 Hz), 22.3 (d, with ^{195}Pt satellites, $^2J_{P,P}$ = 16.6 Hz, $^1J_{Pt,P}$ = 2366 Hz).

X-ray crystal structure determination of 2

Colorless needles of complex **2** were obtained from a pentane solution at –30 °C. Crystallographic parameters are given in Table 2.

Data collection and treatment

A Nonius Kappa CCD diffractometer equipped with a MoKα graphite monochromator (λ = 0.710 73 Å) was used for X-ray measurements under the following conditions: total of 53 657 reflections collected, $-121 \le h \le 12$, $0 \le k \le 18$, $0 \le l \le 22$, frame scan width 1.0°, scan speed 1° per 60 s, typical peak mosaicity 1.336°, 6240 independent reflections (R_{int} = 0.061). The data were processed with a Denzo-Scalepack.

Solution and refinement

The structure was solved by direct methods (SHELXS-97), full-matrix least-squares refinement based on F^2 (SHELXL-97), 205 parameters with 4 restrains, final R_1 = 0.0392 (based on F^2) for data with $I > 2\sigma(I)$, and R_1 = 0.0523 on 5355 reflections, goodness-of-fit on F^2 = 1.094, and largest electron density peak = 2.314 e $Å^{-3}$.

X-ray crystal structure determination of 6

Colorless plates of complex **6** were obtained from cold pentane. Crystallographic parameters are given in Table 2.

Data collection and treatment

A Nonius Kappa CCD diffractometer equipped with a MoKα graphite monochromator (λ = 0.710 73 Å) was used for X-ray measurements under the following conditions: total of 16 955 reflections collected, $-41 \le h \le 36$, $0 \le k \le 12$, $0 \le l \le 19$, frame scan width 1.0°, scan speed 1° per 90 s, typical peak mosaicity 0.595°, 4992 independent reflections (R_{int} = 0.055). The data were processed with a Denzo-Scalepack.

Solution and refinement

The structure was solved by direct methods (SHELXS-97), full-matrix least-squares refinement based on F^2 (SHELXL-97), 195 parameters with 0 restrains, final R_1 = 0.0296 (based on F^2) for data with $I > 2\sigma(I)$, and R_1 = 0.0377 on 4716 reflections, goodness-of-fit on F^2 = 1.030, largest electron density peak = 1.355 e $Å^{-3}$.

Acknowledgments

We thank the Israel Science Foundation, Jerusalem, Israel

© 2005 NRC Canada

and The Helen and Martin Kimmel Center for Molecular Design for financial support.

References

1. R. Drake, I. McKinnon, and R. Taylor. *In* The chemistry of organic silicon compounds. *Edited by* Z. Rappoport and Y. Apeloig. J. Wiley and Sons, New York. 1998. p. 2217, and refs. therein.
2. For recent examples, see: (*a*) D.A. de Vekki and N.K. Skvortsov. Russ. J. Gen. Chem. **74**, 197 (2004); (*b*) I.E. Marko, S. Sterin, O. Buisine, G. Mignani, P. Branlard, B. Tinant, and J.-P. Declercq. Science, **298**, 204 (2002); (*c*) Scott E. Denmark and Zhigang Wang. Org. Lett. **3**, 1073 (2001).
3. (*a*) L.G. Bell, W.A. Gustavson, S. Thanedar, and M.D. Curtis. Organometallics, **2**, 740 (1983); (*b*) C. Eaborn, T.N. Metham, and A. Pidcock. J. Chem. Soc. Dalton Trans. 2212 (1975); (*c*) C. Eaborn, T.N. Metham, and A. Pidcock. J. Organomet. Chem. **63**, 107 (1973).
4. For the most recent work, see: S.T. Phan, W.C. Lim, J.S. Han, B.R. Yoo, and I.N. Jung. Organometallics, **23**, 169 (2004), and refs. therein.
5. M. Tanaka and Y. Uchimaru. Bull. Soc. Chim. Fr. **129**, 667 (1992).
6. M.D. Curtis and J. Greene. J. Am. Chem. Soc. **100**, 6362 (1978).
7. R. Goikhman, M. Aizenberg, L.J.W. Shimon, and D. Milstein. Organometallics, **22**, 4020 (2003).
8. R.S. Paonessa and W.C. Trogler. J. Am. Chem. Soc. **104**, 1138 (1982).
9. E.K. Pham and R. West. Organometallics, **9**, 1517 (1990).
10. See, for example: C. Sung, M.R. Sobarzo, and E.W. Merrill. Polymer, **31**, 556 (1990).
11. (*a*) U. Scheim, A. Porzel, and K. Ruehlmann. J. Organomet. Chem. **354**, 31 (1988); (*b*) M. Onyszchuk. Can. J. Chem. **39**, 808 (1961); (*c*) P.A. McCusker and T. Ostdick. J. Am. Chem. Soc. **81**, 5550 (1959); (*d*) H.J. Emeleus and M. Onyszchuk. J. Chem. Soc. 604 (1958).
12. (*a*) D. Chan, S.B. Duckett, S.L. Heath, I.G. Khazal, R.N. Perutz, S. Sabo-Etienne, and P.L. Timmins. Organometallics, **23**, 5744 (2004); (*b*) Y.-J. Lee, J.-D. Lee, S.-J. Kim, S. Keum, J. Ko, I.-H. Suh, M. Cheong, and S.O. Kang. Organometallics, **23**, 203 (2004); (*c*) R.S. Simons, L.M. Sanow, K.J. Galat, C.A. Tessier, and W.J. Youngs. Organometallics, **19**, 3994 (2000), and refs. therein.
13. A trinuclear cluster bearing a Pt–Si–O–Si fragment was reported by: R. Bender, P. Braunstein, S.-E. Bouaoud, N. Merabet, D. Rouag, P. Zanello, and M. Fontani. New J. Chem. **11**, 1045 (1999).
14. A non-phosphine six-membered platinacyclosiloxane was reported by: L.D. Boardman. Organometallics, **11**, 4194 (1992).
15. T. Yoshida, T. Matsuda, and S. Otsuka. Inorg. Synth. **19**, 107, (1979).

© 2005 NRC Canada

Synthesis and application of L-*N*-Boc-*N*-methyl-β-hydroxyvaline in the preparation of a depsipeptide[1]

James E. Dettwiler, Laurent Bélec, and William D. Lubell

Abstract: Enantiopure (>99% ee) L-*N*-*tert*-butyloxycarbonyl-*N*-methyl-β-hydroxyvaline (**2**) was synthesized in six steps and 43% overall yield from D-serine methyl ester (**5**). Methyl (4*S*)-*N*-(9-phenylfluoren-9-yl)-oxazolidine-4-carboxylate (**7**) was prepared in two steps and 73% yield by *N*-phenylfluorenation of **5** followed by cyclization of *N*-(PhF)amino alcohol **6** with formaldehyde and catalytic *p*-toluenesulfonic acid (PhF = 9-phenylfluoren-9-yl). The addition of MeLi to oxazolidine carboxylate **7** produced the tertiary alcohol **8** in 91% yield. Oxazolidines **8** equilibrated with oxazolidine **9** under acidic conditions. Reduction of pure **8** or the mixture of oxazolidines **8** and **9** with $NaCNBH_3$ and hydrochloric acid in anhydrous dioxane afforded *N*-methyl amino diol **11** in 86%–92% yields. Attempts to selectively oxidize *N*-(PhF)amino diol **11** were unsuccessful; however, hydrogenation of **11** in the presence of di-*tert*-butyl dicarbonate gave the corresponding *N*-(Boc)amino diol **12** in 82% yield. Selective oxidation of diol **12** was performed using a cocktail containing TEMPO free radical, $NaClO_2$, and NaOCl to give L-*N*-Boc-*N*-methyl-β-hydroxyvaline (**2**) in 87% yield. Coupling of β-hydroxyvaline **2** and (*S*)-2-hydroxy-3-methylbutanoate (**15**) was accomplished by using the methodology of Mitsunobu to provide depsipeptide Boc-(*S*)-HOMeVal-(*R*)-Hmb (**4**) for use as a building block in the synthesis of the cyclic antifungal depsipeptide aureobasidin B.

Key words: *N*-methylated amino acid, serine, depsipeptide, aureobasidin.

Résumé : La L-*N*-*tert*-butyloxycarbonyl-*N*-méthyl-β-hydroxyvaline (**2**) a été synthétisée sous sa forme énantiopure (>99 % ee) par un protocole comprenant six étapes à partir de l'ester méthylique de la D-sérine (**5**) avec un rendement total de 43 %. Le méthyle (4*S*)-*N*-(9-phénylfluoren-9-yl)-oxazolidine-4-carboxylate (**7**) a été préparé en deux étapes avec un rendement de 73 % par une *N*-phénylfluorénation de **5**, suivie par une cyclisation de l'alcool *N*-(PhF)amino **6** avec du formaldéhyde en présence catalytique d'acide *p*-toluène sulfonique (PhF = 9-phenylfluoren-9-yl). L'addition de MeLi sur l'oxazolidine carboxylate **7** a donné l'alcool tertiaire **8** avec un rendement de 91 %. L'oxazolidine **8** a équilibré avec l'oxazolidine **9** dans des conditions acides. La réaction de **8** pur ou du mélange des oxazolidines **8** et **9** avec du $NaCNBH_3$ et de l'acide chlorhydrique dans du dioxane anhydre a donné l'amino diol *N*-méthylé **11** avec des rendements de 86 % – 92 %. Les essais d'oxydation du *N*-(PhF)amino diol **11** ont échoué, cependant, le *N*-(Boc)amino diol **12** a été obtenu à partir de l'hydrogénation de **11** en présence de di-*tert*-butyle dicarbonate avec un rendement de 82 %. L'oxydation sélective du diol **12** a été effectuée avec un mélange du radical libre TEMPO, $NaClO_2$ et NaOCl pour donner la L-*N*-Boc-*N*-méthyl-β-hydroxyvaline (**2**) avec un rendement de 87 %. Le couplage entre la β-hydroxyvaline **2** et le (*S*)-2-hydroxy-3-méthylbutanoate (**15**) a été effectué avec la méthode de Mitsunobu pour donner le depsipeptide Boc-(*S*)-HOMeVal-(*R*)-Hmb (**4**) qui est un fragment pour la synthèse de l'auréoabsidine B, un depsipeptide antifongique et cyclique.

Mots clés : acide aminé *N*-méthylé, serine, depsipeptide, auréobasidine.

Introduction

L-*N*-Methyl-β-hydroxyvaline (**1**) is an important component of biologically active peptides such as the anti-HIV antibiotic luzopeptin (1) as well as members of the aureobasidin (2) family of antifungal peptides (Fig. 1). Featuring hydroxyl, amino, carboxylate, and *N*-alkyl substituents as well as a quaternary carbon, **1** is a synthetic challenge for which no efficient route presently exists. Methods to prepare L-*N*-methyl-β-hydroxyvaline (**1**) have usually required multiple steps and have often resulted in low enantiomeric purity (3–6). First synthesized in racemic form (3) and resolved, L-*N*-Boc-*N*-methyl-β-hydroxyvaline (**2**) was most recently prepared from D-*N*-Boc-serine methyl ester in eight steps with

Received 13 December 2004. Published on the NRC Research Press Web site at http://canjchem.nrc.ca on 6 July 2005.

J.E. Dettwiler, L. Bélec, and W.D. Lubell.[2] Département de Chimie, Université de Montréal, C.P. 6128, Succursale Centre Ville, Montréal, QC H3C 3J7, Canada.

[1]This article is part of a Special Issue dedicated to Professor Howard Alper.
[2]Corresponding author (e-mail: lubell@chimie.umontreal.ca).

 doi: 10.1139/V05-033 © 2005 NRC Canada

Scheme 1. Synthesis of L-*N*-*tert*-butyloxycarbonyl-*N*-methyl-β-hydroxyvaline (**2**).

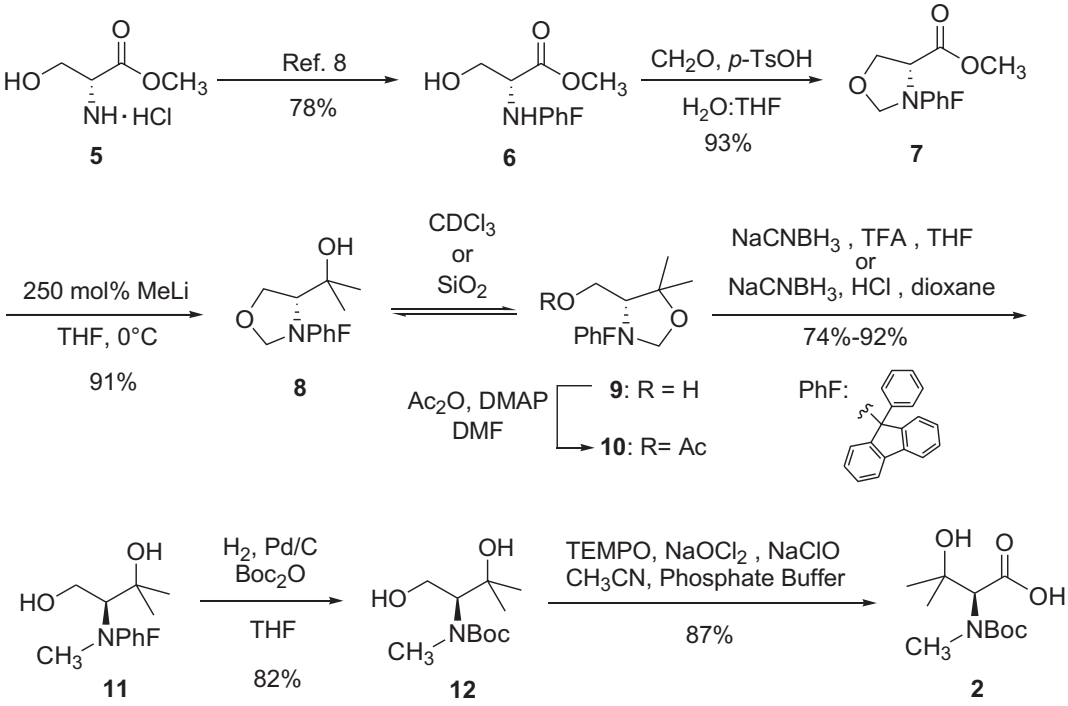
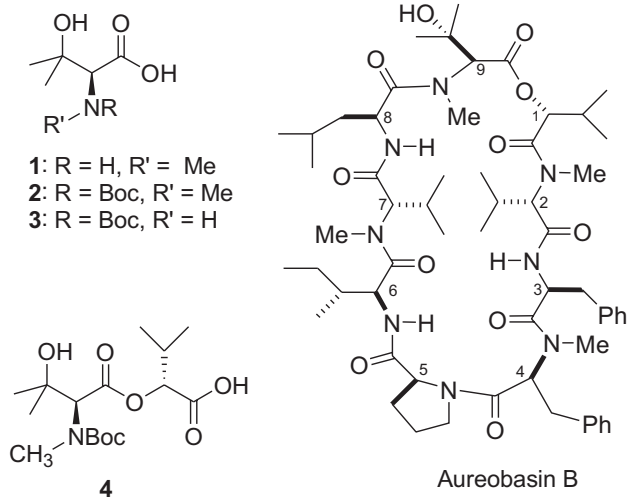


Fig. 1. L-Hydroxymethyl-*N*-methyl-β-hydroxyvaline (**1**), L-*N*-*tert*-butyloxycarbonyl-*N*-methyl-β-hydroxyvaline (**2**), L-*N*-*tert*-butyloxycarbonyl-β-hydroxyvaline (**3**), depsipeptide Boc-(*S*)-HOMeVal-(*R*)-Hmb (**4**), and aureobasidin B.



an overall yield of 66%, albeit with an enantiomeric purity of 90% (4, 5). Racemization during this synthesis was likely due to the employment of a configurationally labile α-amino aldehyde intermediate (7). Considering the requirement of enantiopure building blocks for effective peptide synthesis, alternative methodology is still necessary for synthesizing enantiopure **1** in protected form.

We have recently reported a two-step approach for synthesizing L-*N*-Boc-β-hydroxyvaline (**3**) from D-*N*-Boc-serine methyl ester (8), which involved treatment with MeMgBr followed by selective catalyzed TEMPO oxidation (9, 10) Direct *N*-methylation of L-*N*-Boc-β-hydroxyvaline (**3**) was, however, unsuccessful using various methods. Protocols using CH_3I and $(CH_3)_2SO_4$ as methylating agents in the presence of various bases (NaH, Ag_2O, Ag_2CO_3, or *n*-BuLi) were unsuccessful and either resulted in alcohol methylation or recovered starting material (11). For example, treatment of **3** with CH_3I and NaH in THF gave L-*N*-Boc-β-methoxyvaline in 65% yield. Attempts to convert **3** to an oxazolidine or oxazolidinone were also unsuccessful and resulted predominantly in recovered starting material. Instead of trying a selective *O*-protection, *N*-alkylation, and *O*-deprotection strategy, we decided to develop an alternative route to obtain L-*N*-Boc-*N*-methyl-β-hydroxyvaline (**2**) in enantiopure form (Scheme 1) (12). Our protocol involves a six-step synthesis from D-serine methyl ester (**5**) in 43% overall yield. This route employs *N*-(9-phenylfluoren-9-yl)serine methyl ester (8) as a chiral educt to deliver enantiopure **2** (>99% ee).

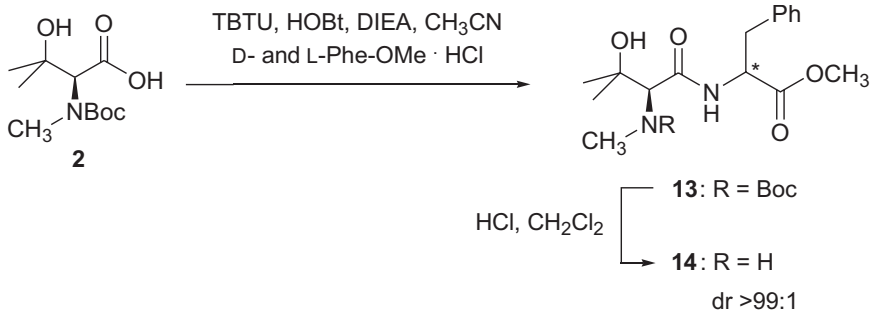
Results and discussion

The starting material D-*N*-(PhF)serine methyl ester (**6**) was synthesized according to the literature method by phenylfluorenation of D-serine methyl ester (Scheme 1) (8). Treatment of amino alcohol **6** with formaldehyde and catalytic *p*-toluenesulfonic acid in THF at room temperature afforded oxazolidine carboxylate ester **7** in 93% yield (13). The quaternary carbon was constructed using our best conditions by adding 250 mol% of MeLi to a solution of **7** in THF at 0 °C. Tertiary alcohol **8** could be isolated after filtration through a plug of silica gel; however, on prolonged exposure to silica gel, **8** equilibrated with oxazolidine primary alcohol **9**.

In chloroform, oxazolidine **8** existed in equilibrium with oxazolidine primary alcohol **9**, the latter of which could be selectively acetylated. Treatment of a 1:1 mixture of **8** and **9** with acetic anhydride and catalytic 4-dimethylaminopyridine (DMAP) in chloroform gave **8** and ester **10**. Separation of

© 2005 NRC Canada

Scheme 2. Enantiomeric purity of L-*N*-*tert*-butyloxycarbonyl-*N*-methyl-β-hydroxyvaline (**2**).



the mixture by chromatography on silica gel gave a new equilibrium and the three compounds (**8**–**10**) were isolated in pure form. In $CDCl_3$, pure **8** was found to equilibrate to a 1:1 mix of **8** and **9** after 12 h. Residual acid in chloroform may be responsible for this transformation because spectra of pure **8** and **9** could be obtained in DMSO-d_6. The assignment of the structures of oxazolidine alcohols **8** and **9** was made based on their ^{1}H NMR spectra in DMSO-d_6 in comparison to acetate **10**. Of particular note, large differences in the chemical shifts for the signals of the diastereotopic methylene and methyl protons were indicative of groups held in fixed environments by the oxazolidine ring. In the case of the primary alcohol oxazolidine **9**, the difference in the chemical shifts of the diastereotopic signals for the constrained methyl groups were larger (Δδ = 162.4 Hz) than those observed for tertiary alcohol oxazolidine **8** (Δδ = 94.6 Hz). The chemical shift differences for the diastereotopic methylene protons were greater (Δδ = 71.1 Hz) for the tertiary alcohol oxazolidine **8** relative to those of the primary alcohol oxazolidine **9** (Δδ = 26.6 Hz). Acetate **10** exhibited a similar difference in the chemical shifts of its diastereotopic methyl singlets (Δδ = 143.3 Hz) and methylene protons (Δδ = 28.2 Hz) as was seen for the primary alcohol oxazolidine **9**. Moreover, relative to the methylene signals of **9**, those for **10** were observed to be downfield shifted indicative of acylation of the primary alcohol.

The conversion of oxazolidines **8** and **9** to *N*-methyl diol **11** was accomplished by treatment with $NaCNBH_3$ under acidic conditions (13). Two conditions were tested. In the first condition, oxazolidine **8** at 0 °C was treated with $NaCNBH_3$ in anhydr. THF containing trifluoroacetic acid to give *N*-methylamino diol **11** in 74% yield after purification. In the second condition, oxazolidine **8** in 0.1 mol/L HCl in dioxane was treated with $NaCNBH_3$ to give *N*-methylamino diol **11** in 86% yield after purification. Employing these later conditions to reduce a mixture of oxazolidines **8** and **9** gave amino diol **11** in similar yield. In the ^{1}H NMR spectrum of *N*-PhF-*N*-methylamino diol **11** in $CDCl_3$, a doubling of signals was observed suggesting an equilibrium between two hydrogen-bonded forms. The doubling of signals could be avoided by recording the spectrum of **11** in deuterated methanol containing a trace of trifluoroacetic acid.

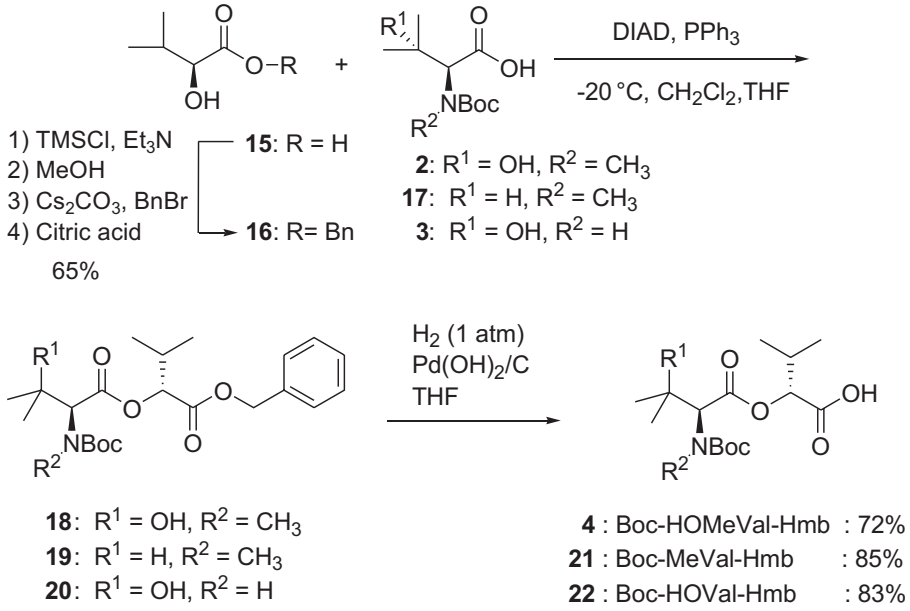
Selective oxidation of *N*-PhF-*N*-methylamino diol **11** was unsuccessful using a wide variety of oxidation methods presumably because of the oxidation of the tertiary amine. On the other hand, exchanging *N*-PhF to *N*-Boc protection could be effected by hydrogenation in the presence of di-*tert*-butyl dicarbonate and palladium hydroxide to give the *N*-(Boc)amino diol **12** in 82% yield (14). As in our synthesis of β-hydroxyvaline (10), selective primary alcohol oxidation was accomplished by treating *N*-(Boc)amino diol **12** with TEMPO (2,2,6,6-tetramethyl-1-piperidyloxy) free radical, sodium chlorite, and sodium hypochlorite in a sodium phosphate buffered acetonitrile solution (15). L-*N*-Boc-*N*-Methyl-β-hydroxyvaline (**2**) was then isolated in pure form after aqueous extraction in 87% yield.

To ascertain if any racemization had occurred during the synthesis, the enantiomeric purity of **2** was investigated by coupling to L- and D-Phe-OMe·HCl using benzotriazol-1-yl-1,1,3,3-tetramethyluronium tetrafluoroborate (TBTU) (16), 1-hydroxybenzotriazole (HOBt), and diisopropylethylamine (DIEA) in acetonitrile to produce dipeptides **13**, which existed as mixtures of carbamate isomers (Scheme 2). The *N*-Boc protecting group of the crude product was removed by bubbling a stream of HCl gas into a solution of **13** in CH_2Cl_2. The 400 MHz ^{1}H NMR spectrum of crude dipeptide (*R*)-**14** was examined during incremental additions of (*S*)-**14** in CD_3OD. Measurement of the signals for the diastereomeric methyl amine singlets at 2.52 and 2.04 ppm demonstrated dipeptide (*S*)-**14** to be of >99% diastereomeric purity. Hence, L-*N*-Boc-*N*-methyl-β-hydroxyvaline (**2**) is considered to be of the same high enantiomeric purity.

The depsipeptide Boc-(*S*)-HOMeVal-(*R*)-Hmb (**4**) was targeted to serve as a building block for the synthesis of analogs of the cyclic antifungal depsipeptide aureobasidin B (17). The preparation of depsipeptides **4**, **21**, and **22** was accomplished by the coupling of the corresponding *N*-Boc protected amino acid (**2**, **3**, and **17**) and (*S*)-2-hydroxy-3-methylbutanoic benzyl ester (**16**) using the Mitsunobu reaction, followed by benzyl ester deprotection (Scheme 3). Benzyl ester **16** was prepared from (*S*)-2-hydroxy-3-methylbutanoic acid (**15**), which was synthesized with retention of configuration via a double inversion from L-valine using the literature procedure in 52% overall yield (18). Because direct alkylation of **15** resulted in mixtures of ether and ester products, a four-step, one-pot procedure was developed to prepare the benzyl ester **16**. First, the hydroxyl and carboxylate groups were both protected with trimethylsilyl (TMS) groups. Then, the carboxylic acid was liberated selectively using MeOH and alkylated with benzyl bromide and Cs_2CO_3 to provide the silylether benzyl ester, which on treatment with citric acid gave α-hydroxy ester **16** in 65% overall yield. The conditions for formation of the depsi bonds were first optimized with Boc-MeVal (**17**) and Boc-

© 2005 NRC Canada

Scheme 3. Synthesis of the depsipeptides **4**, **21**, and **22** (1 atm = 101.325 kPa).



HOVal (**3**). Optimal conditions were then applied to Boc-HOMeVal (**2**). Formation of the depsipeptide bond was performed by an initial reaction of the secondary alcohol of **16** with triphenylphosphine and diisopropyldiazodicarboxylate (DIAD) in dichloromethane, followed by S_N2 displacement of the phosphine intermediate on addition of the *N*-Boc protected amino acid (**2**, **3**, and **17**) to form depsipeptides **18**–**20** and triphenylphosphine oxide (19). Crude depsipeptides **18**–**20** were isolated by chromatography on silica gel to remove the triphenylphosphine oxide. Hydrogenolysis by using $Pd(OH)_2$ on carbon cleaved the benzyl ester affording acids **4**, **21**, and **22**, in 72%, 85%, and 83% overall yields, respectively (14).[3]

Conclusion

Enantiopure (>99%) L-*N*-*tert*-butyloxycarbonyl-*N*-methyl-β-hydroxyvaline (**2**) was synthesized in six steps and 43% overall yield from D-serine methyl ester (**5**). Application of **2**, as well as Boc-MeVal and Boc-HOVal (**3**), in Mitsunobu reactions with (*S*)-benzyl-2-hydroxy-3-methylbutanoate (**16**) has provided three depsipeptides: Boc-(*S*)-HOMeVal-(*R*)-Hmb (**4**), Boc-(*S*)-MeVal-(*R*)-Hmb (**21**), and Boc-(*S*)-HOVal-(*R*)-Hmb (**22**). These building blocks are presently being employed in our program on antimicrobial peptide synthesis (17, 20).

Experimental section

General

For reactions performed under anhydrous conditions, glassware was either oven- or flame-dried and the reaction was run under a positive pressure of argon or nitrogen. Tetrahydrofuran (THF) was freshly distilled from sodium/benzophenone, CH_2Cl_2 from P_2O_5, dioxane from sodium. Triethylamine (Et_3N) was distilled from ninhydrin then CaH_2. The 0.2 N HCl – dioxane solution was prepared by passing a stream of HCl gas bubbles through dry dioxane and the concentration of the solution was determined by titration of 1 mL aliquots diluted with 1 mL H_2O using a 0.1 N standard NaOH solution and phenolphtalein as the indicator. Chromatography was performed using 230–400 mesh silica gel. Amines were revealed with ninhydrin on TLC plates; Boc groups were removed by dipping the plates in TFA before exposure to ninhydrin. Unless otherwise noted, ^1H and ^{13}C NMR spectra were recorded in $CDCl_3$ or CD_3OD at 300/75 or 400/100 MHz. Chemical shifts (δ) are reported in parts per million (ppm) downfield of internal tetramethylsilane ($(CH_3)_4Si$) or referenced to the residual solvent peak ($CHCl_3$ δ 7.26, 77.16 ppm; methanol δ 3.31, 49.00 ppm). Coupling constants are reported in Hz. Chemical shifts of PhF aromatic carbons are omitted for clarity in the ^{13}C NMR spectra. HR-MS (EI and FAB) were obtained by the Université de Montréal Mass Spectrometry facility. Specific rotations are reported as follows: $[\alpha]_D^{20}$, concentration (*c* in g/100 mL), and solvent. Analytical LC–MS was performed on an inverse phase column (Anal Waters C18, 250 × 4.6 mm) with a flow rate of 0.5 mL/min. A volume of 20 µL of sample with a concentration of 1 mg/mL was injected. Preparative reversed-phase HPLC was performed on an inverse phase column (Prep Prevail C18, 250 × 22 mm) with a flow rate of 15 mL/min: elution condition A, gradient 20% CH_3CN with 0.1% TFA–H_2O with 0.1% TFA to 80% CH_3CN with 0.1% TFA–H_2O with 0.1% TFA over 20 min; condition B, 70% CH_3CN with 0.1% TFA–H_2O with 0.1% TFA.

Methyl (4*S*)-*N*-(9-phenylfluoren-9-yl)-oxazolidine-4-carboxylate (7)

A solution of *N*-(PhF)serine methyl ester (**6**, 11.50 g, 32 mmol, prepared according to ref. 8), *p*-toluenesulfonic

[3] Supplementary data for this article are available on the Web site or may be purchased from the Depository of Unpublished Data, Document Delivery, CISTI, National Research Council Canada, Ottawa, ON K1A 0S2, Canada. DUD 3681. For more information on obtaining material refer to http://cisti-icist.nrc-cnrc.gc.ca/irm/unpub_e.shtml.

© 2005 NRC Canada

acid (6 mol%, 331 mg, 1.92 mmol), and a 37% aqueous formaldehyde solution (1500 mol%, 39 mL, 480 mmol) in THF (320 mL) was stirred for 24 h at room temperature, washed with a solution of satd. $NaHCO_3$ (2 × 200 mL) and brine, dried with $MgSO_4$, filtered and evaporated to a solid residue. Chromatography on silica gel using 10% EtOAc in hexanes as the eluant gave a white solid (11.05 g, 93%). TLC R_f = 0.41 (20% EtOAc in hexanes); mp 106 to 107 °C. $[\alpha]_D^{20}$ –267.3 (*c* 1.0 $CHCl_3$). ^{1}H NMR (400 MHz, $CDCl_3$) δ: 3.30 (t, 1H, *J* = 6.8), 3.54 (s, 3H), 3.61 (d, 2H), 4.73 (d, 1H, *J* = 6.4), 4.93 (d, 1H, *J* = 6.4), 7.22–7.70 (m, 13H). ^{13}C NMR (100 MHz, $CDCl_3$) δ: 52.0, 60.8, 69.1, 85.1, 119.8, 173.6. HR-MS calcd. for $C_{24}H_{22}NO_3$ ($[M + H]^+$): 372.1600; found: 372.1582.

(4*S*)-4-(1-Hydroxymethylethyl)-3-(9-phenylfluoren-9-yl)-oxazolidine (8)

To a solution of oxazolidine **7** (3.72 g, 10 mmol) in THF (182 mL) at 0 °C, a solution of 1.4 mol/L MeLi in Et_2O (250 mol%, 18 mL, 25 mmol) was added dropwise. The reaction mixture was stirred for 2 h at 0 °C and partitioned between equal volumes of EtOAc and a satd. NaH_2PO_4 solution (100 mL). The phases were separated and the aqueous phase was extracted with EtOAc (3 × 50 mL). The combined organic phase was washed with brine, dried with $MgSO_4$, filtered and evaporated to a solid residue. Chromatography on silica gel using 20% EtOAc in hexanes as the eluant provided **8** as a white solid (3.38 g, 91%). TLC R_f = 0.34 (30% AcOEt in hexanes); mp 156 to 157 °C. $[\alpha]_D^{20}$ –519.3 (*c* 0.3 DMSO). ^{1}H NMR (400 MHz, $CDCl_3$) δ: 0.91 (s, 3H), 1.05 (s, 3H), 1.95 (s, 1H), 2.49 (dd, 1H, J_1 = 3.1, J_2 = 7.5), 2.96 (t, 1H, *J* = 7.8), 3.49 (dd, 1H, J_1 = 3.1, J_2 = 8.1), 4.79 (d, 1H, *J* = 6.7), 5.10 (d, 1H, *J* = 6.7), 7.15–7.73 (m, 13H). ^{1}H NMR (400 MHz, DMSO-d_6) δ: 0.78 (s, 3H), 1.01 (s, 3H), 2.32 (dd, 1H, J_1 = 2.4, J_2 = 7.2), 2.32 (t, 1H, *J* = 7.4), 3.63 (dd, 1H, J_1 = 2.5, J_2 = 7.2), 4.13 (s, 1H), 4.71 (d, 1H, *J* = 6.3), 4.89 (d, 1H, *J* = 6.3), 7.10–7.97 (m, 13H). ^{13}C NMR (100 MHz, DMSO-d_6) δ: 26.2, 29.0, 65.2, 66.7, 71.1, 77.6, 85.5. HR-MS calcd. for $C_{25}H_{25}NO_2$ (TOF EI): 371.1885; found: 371.1886.

(4*R*)-*O*-Acetoxymethyl-5,5-dimethyl-3-(9-phenylfluoren-9-yl)-oxazolidine (10)

A solution of oxazolidine **8** (50 mg, 0.135 mmol) in $CDCl_3$ (1.4 mL) was stirred for 12 h at room temperature, treated with DMAP (10 mol%, 1.6 mg, 13.5 µmol), and dropwise with acetic anhydride (240 mol%, 42 µL, 0.324 mmol). The reaction mixture was stirred for 24 h and concentrated under reduced pressure to give a residue that was purified by chromatography on silica gel using 15% EtOAc in hexanes as the eluant. First to elute was the acetylated oxazolidine **10** as a white foam (28.0 mg, 50%). TLC R_f = 0.45 (20% AcOEt in hexanes). $[\alpha]_D^{20}$ 229.3 (*c* 0.3 DMSO). ^{1}H NMR (400 MHz, $CDCl_3$) δ: 0.70 (s, 3H), 1.15 (s, 3H), 1.87 (s, 3H), 2.30 (dd, 1H, J_1 = 4.5, J_2 = 10.3), 3.72 (dd, 1H, J_1 = 4.5, J_2 = 11.1), 3.90 (t, 1H, *J* = 10.7), 4.73 (d, 1H, *J* = 7.3), 4.88 (d, 1H, *J* = 7.3), 7.16–7.60 (m, 13H). ^{1}H NMR (300 MHz, DMSO-d_6) δ: 0.56 (s, 3H), 1.07 (s, 3H), 1.83 (s, 3H), 2.17 (dd, 1H, J_1 = 4.5, J_2 = 10.3), 3.57 (dd, 1H, J_1 = 4.5, J_2 = 11.1), 3.86 (t, 1H, *J* = 10.7), 4.65 (d, 1H, *J* = 7.2), 4.75 (d, 1H, *J* = 7.1), 7.17–7.94 (m, 13H). ^{13}C NMR (75 MHz, DMSO-d_6) δ: 20.5, 27.9, 63.4, 63.9, 76.9, 79.2, 80.9, 81.2, 169.7. HR-MS calcd. for $C_{27}H_{28}NO_3$ ($[M + H]^+$): 414.2064; found: 414.2065. Second to elute was (4*R*)-4-hydroxymethyl-5,5-dimethyl-(9-phenylfluoren-9-yl)-oxazolidine (**9**) as a white foam (12.5 mg, 25%). TLC R_f = 0.53 (30% AcOEt in hexanes). $[\alpha]_D^{20}$ 326.0 (*c* 0.2 DMSO). ^{1}H NMR (400 MHz, $CDCl_3$) δ: 0.70 (s, 3H), 1.24 (s, 3H), 2.15 (d, 1H, *J* = 4.9), 2.80 (dd, 1H, J_1 = 6.1, J_2 = 11.1), 3.20 (d, 1H, *J* = 11.0), 4.78 (d, 1H, *J* = 7.1), 4.96 (d, 1H, *J* = 7.0), 7.16–7.76 (m, 13H). ^{1}H NMR (300 MHz, DMSO-d_6) δ: 0.62 (s, 3H), 1.16 (s, 3H), 1.99 (m, 1H), 3.06 (m, 1H), 3.24 (m, 1H), 4.22 (t, 1H, *J* = 4.7), 4.59 (d, 1H, *J* = 7.0), 4.68 (d, 1H, *J* = 7.0), 7.14–7.96 (m, 13H). ^{13}C NMR (75 MHz, DMSO-d_6) δ: 20.2, 28.5, 61.6, 66.2, 77.1, 80.8, 81.6. HR-MS calcd. for $C_{25}H_{26}NO_2$ ($[M + H]^+$): 372.1958; found: 372.1961. Last to elute was oxazolidine **8** as a white foam (8.9 mg, 18%).

(2*R*)-2-*N*-(9-Phenylfluoren-9-yl)amino-3-methyl-1,3-butanediol (11)

Method 1

A solution of oxazolidine **8** (2.22 g, 6 mmol) in 0.2 mol/L HCl in dioxane (60 mL) was treated with $NaCNBH_3$ (320 mol%, 1.21 g, 19.2 mmol). The reaction mixture was stirred for 1 h at r.t.

Method 2

A solution of oxazolidine **8** (4.5 g, 14.2 mmol) and $NaCNBH_3$ (800 mol%, 4.9 g, 114 mmol) in THF (120 mL) was cooled to 0 °C and treated dropwise with trifluoroacetic acid (300 mol%, 3.3 mL, 42.6 mmol). The reaction mixture was stirred for 30 min at 0 °C. After stirring for the designated time, both reaction mixtures were washed, respectively, with a solution of satd. $NaHCO_3$ and brine, dried with $MgSO_4$, filtered and evaporated to a solid. Chromatography on silica gel using 20% EtOAc in hexanes as eluant gave a white solid (Method 1: 1.93 g, 86%; Method 2: 3.35 g, 74%). TLC R_f = 0.54 (50% AcOEt in hexanes); mp 85 to 86 °C. $[\alpha]_D^{20}$ –449.8 (*c* 1.0 MeOH). ^{1}H NMR (400 MHz, CD_3OD + TFA) δ: 0.99 (s, 3H), 1.36 (s, 3H), 2.82 (dd, 1H, J_1 = 2.0, J_2 = 5.4), 3.12 (dd, 1H, J_1 = 6.6, J_2 = 5.0), 3.15 (s, 3H), 3.42 (dd, 1H, J_1 = 3.5, J_2 = 8.1), 7.22–8.10 (m, 13H). ^{13}C NMR (100 MHz, CD_3OD) showed a mixture of conformers; the chemicals shifts are listed in order of appearance (δ): 26.8, 28.5, 29.6, 33.2, 33.4, 58.2, 60.7, 61.3, 63.0, 75.5, 76.7, 78.5, 79.1, 79.2. HR-MS calcd. for $C_{25}H_{27}NO_2$ (TOF EI): 373.2042; found: 373.2051. Employing a 1:1 mixture of oxazolidines **8** and **9** (155 mg, 0.147 mmol) using method 2 gave diol **11** in 92% yield.

(2*R*)-2-*N*-(Boc)Amino-3-methyl-1,3-butanediol (12)

A solution of diol **11** (900 mg, 2.41 mmol) and di-*tert*-butyl dicarbonate (140 mol%, 737 mg, 3.37 mmol) in THF (100 mL) was treated with palladium hydroxide on carbon (270 mg, 20 wt% in Pd) and stirred under 5 atm of hydrogen (1 atm = 101.325 kPa) for 24 h at room temperature. The catalyst was removed by filtration on Celite® and washed with THF (2 × 20 mL) and MeOH (2 × 20 mL). The combined organic phase was evaporated to a residue that was purified by chromatography on silica gel using 70% EtOAc in hexanes as the eluant. Evaporation of the ninhydrin positive fractions (visualized on TLC after treatment with TFA va-

© 2005 NRC Canada

pors) gave *N*-(Boc)amino diol **12** as a white solid (461 mg, 82%). TLC R_f = 0.49 (80% AcOEt in hexanes); mp 138 to 139 °C. $[\alpha]_D^{20}$ 37.1 (*c* 1.0 MeOH). ^{1}H NMR (400 MHz, CD_3OD) showed a 1:1.3 mixture of carbamate isomers (δ): 1.15 (s, 1.6H), [1.16 (s, 1.2H)], [1.25 (s, 1.5H)], 1.26 (s, 1.6H), 1.46 (s, 4.2H), 1.48 (s, 4.5H), [2.89 (s, 1.1H)], 2.93 (s, 1.7H), 3.83–3.92 (m, 2.5H), [4.04 (dd, 0.5H, J_1 = 4.0, J_2 = 8.0)]. ^{13}C NMR (100 MHz, CD_3OD) showed a mixture of carbamate isomers; the chemical shifts are listed in order of appearance (δ): 26.7, 27.8, 28.0, 28.3, 28.9, 57.7, 58.0, 64.8, 72.6, 72.7, 79.9, 80.1, 157.9, 158.0. HR-MS calcd. for $C_{11}H_{24}NO_4$ ([M + H]$^+$): 234.1705; found: 234.1709. Anal. calcd. for $C_{11}H_{23}NO_4$: C 56.63, H 9.94, N 6.00; found: C 56.50, H 10.28, N 5.92.

(*S*)-β-Hydroxy-*N*-(Boc)-*N*-(methyl)valine (2)

A mixture of diol **12** (278 mg, 1.19 mmol), sodium phosphate buffer (4.6 mL, 0.67 mol/L, pH 6.7), and TEMPO (10 mol%, 24 mg, 0.119 mmol) in acetonitrile (6 mL) was heated to 35 °C and treated dropwise simultaneously over 2 h (Caution! Do not mix bleach and sodium chlorite before adding to reaction mixture) (15) with a solution of sodium chlorite ($NaClO_2$, 200 mol%, 2.38 mmol, 1.2 mL of solution : 5.71 g 80% *w*/*w*, 50.5 mmol in 25 mL of water) and diluted bleach (NaOCl, 2 mol%, 0.04 mmol, 1050 µL of solution : 0.66 mL commercial bleach 10.8% *v*/*v* 25 mL of water). The mixture was stirred at 35 °C overnight, cooled to r.t., acidified with citric acid to pH 3, and extracted with EtOAc (3 × 10 mL). The organic phases were combined and evaporated. The residue was dissolved in a solution of satd. Na_2CO_3 (15 mL) and washed with EtOAc (2 × 10 mL). The aqueous phase was acidified with 1 mol/L H_3PO_4 to pH 3, saturated with NaCl, and extracted with EtOAc (3 × 15 mL). The organic phases were combined, dried with $MgSO_4$, filtered and evaporated to give an oil (256 mg, 87%). TLC R_f = 0.43 ($CHCl_3$–MeOH–AcOH, 89:10:1). $[\alpha]_D^{20}$ –34.4 (*c* 0.5 MeOH). ^{1}H NMR (400 MHz, CD_3OD) showed a 0.7:1 mixture of carbamate isomers (δ): 1.22 (s, 1.9H), [1.26 (1.2H)], [1.38 (s, 1.2H)], 1.42 (s, 1.9H), [1.46 (s, 3.6H)], 1.47 (s, 5.4H), [2.95 (s, 1.2H)], 2.96 (s, 1.8H), [4.46 (s, 0.4H)], 4.59 (s, 0.6H). ^{13}C NMR (100 MHz, CD_3OD) showed a mixture of carbamate isomers; the chemicals shifts are listed in order of appearance (δ): 26.4, 27.6, 27.9, 28.1, 33.2, 33.3, 65.3, 66.2, 72.8, 78.5, 80.5, 81.1, 156.5, 157.4, 172.2, 172.3. HR-MS calcd. for $C_{11}H_{22}NO_5$ ([M + H]$^+$): 248.1498; found: 248.1500. LC–MS: 98% purity (condition A), R_T = 14.5.

Enantiomeric purity of (*S*)-β-hydroxy-*N*-(Boc)-*N*-(methyl)valine (2)

A solution of **2** (30 mg, 0.12 mmol) in acetonitrile (1 mL) at 0 °C was treated with HOBt (100 mol%, 22 mg, 0.12 mmol) and TBTU (150 mol%, 58 mg, 0.18 mmol), stirred for 30 min, and treated with a premixed solution of (*S*)- or (*R*)-phenylalanine methyl ester hydrochloride (300 mol%, 78 mg, 0.36 mmol) and diisopropylethylamine (DIEA, 400 mol%, 0.84 µL, 0.48 mmol) in acetonitrile (1 mL) at 0 °C. The reaction mixture was stirred for 48 h at room temperature until TLC showed the complete disappearance of starting acid **2**. TLC R_f = 0.43 ($CHCl_3$–MeOH–AcOH, 89:10:1). The solvent was evaporated and the solid residue was resuspended in CH_2Cl_2 (3 mL). The organic phase was washed with an aq. satd. solution of $NaHCO_3$ (2 × 3 mL), 1 N NaH_2PO_4 (2 × 3 mL), and brine (3 mL), dried with $MgSO_4$, filtered and evaporated to a solid residue. The Boc group was subsequently removed by treating the residue in dry CH_2Cl_2 at 0 °C with a stream of HCl gas bubbles, stirring for 15 min, and concentrating the reaction mixture under reduced pressure to give a solid that was directly examined by 400 MHz ^{1}H NMR spectroscopy in CD_3OD. Measurement of the signals for the diastereomeric methyl amine singlets at 2.04 and 2.52 ppm during incremental additions of (*S*)-**14** in (*R*)-**14** demonstrated dipeptide (*R*)-**14** to be of >99% diastereomeric purity. Hence, (*S*)-β-hydroxy-*N*-(Boc)-*N*-(methyl)valine (**2**) is considered to be of the same high enantiomeric purity.

(*S*,*S*)-β-Hydroxy-*N*-(Boc)-*N*-(methyl)valinylphenylalanine methyl ester ((*S*)-13)

TLC R_f = 0.30 (30% AcOEt in hexanes). ^{1}H NMR (400 MHz, CD_3OD) showed a 1:2 mixture of carbamate isomers (δ): 1.13 (s, 3H), 1.20 (s, 3H), 1.47 (s, 9H), 2.68 (s, 2.0H), [2.71 (s, 1.1H)], 2.97 (m, 1H), 3.23 (m, 1H), [3.68 (s, 1.5H)], 3.73 (s, 3.8H), [4.44 (s, 0.28H)], 4.54 (s, 0.65H), 4.76 (dd, 1H, J_1 = 4.8, J_2 = 9.5), 7.08–7.35 (m, 5H). MS (TIC) *m*/*z*: 309.2 ([M + H]$^+$).

(*S*,*R*)-β-Hydroxy-*N*-(Boc)-*N*-(methyl)valinylphenylalanine methyl ester ((*R*)-13)

TLC R_f = 0.35 (30% AcOEt in hexanes). ^{1}H NMR (400 MHz, CD_3OD) showed a 1:2 mixture of carbamate isomers (δ): 1.08 (s, 3H), 1.15 (s, 3H), 1.46 (s, 9H), [2.70 (s, 1.1H)], 2.93 (s, 1.9H), 3.00 (m, 1H), 3.24 (m, 1H), [3.66 (s, 1.8H)], 3.72 (s, 3.6H), [4.40 (s, 0.3H)], 4.49 (s, 1H), 4.77 (dd, 0.6H, J_1 = 4.50, J_2 = 8.9), 7.01–7.34 (m, 5H). MS (TIC) *m*/*z*: 309.2 ([M + H]$^+$).

(*S*,*S*)-β-Hydroxy-*N*-(methyl)valinylphenylalanine methyl ester hydrochloride ((*S*)-14)

^{1}H NMR (400 MHz, CD_3OD) δ: 1.07 (s, 3H), 1.29 (s, 3H), 2.04 (s, 3H), 2.84 (dd, 1H, J_1 = 10.9, J_2 = 14.0), 3.17–3.23 (m, 2H), 3.58 (s, 3H), 4.82 (m, 1H), 7.14–7.20 (m, 5H).

(*S*,*R*)-β-Hydroxy-*N*-(methyl)valinylphenylalanine methyl ester hydrochloride ((*R*)-14)

^{1}H NMR (400 MHz, CD_3OD) δ: 0.84 (s, 3H), 0.87 (s, 3H), 2.52 (s, 3H), 2.83 (dd, 1H, J_1 = 11.5, J_2 = 14.2), 3.21 (m, 1H), 3.26 (dd, 1H, J_1 = 4.5, J_2 = 14.2), 3.66 (s, 3H), 4.70 (dd, 1H, J_1 = 4.5, J_2 = 11.4), 7.14–7.19 (m, 5H).

(*S*)-*N*-(Boc)-β-methoxyvaline

To a solution of (*S*)-β-hydroxy-*N*-(Boc)valine (**3**, 100 mg, 429 µmol, prepared according to ref. 10) and methyl iodide (800 mol%, 214 µL, 3.43 mmol) in THF (1.5 mL) at 0 °C, sodium hydride (60% dispersion in mineral oil, 300 mol%, 52 mg, 29 mmol) was added cautiously with gentle stirring. The suspension was stirred for 24 h, diluted with EtOAc (2 mL), treated dropwise with water to destroy the excess sodium hydride, and evaporated to an oily residue that was partitioned between ether (5 mL) and water (10 mL). The ether layer was washed with a solution of satd. $NaHCO_3$ (10 mL). The combined aqueous extracts were acidified with citric acid to pH 3 and extracted with EtOAc (3 × 10 mL).

© 2005 NRC Canada

The organic phases were combined, washed with water (2 × 10 mL), 5% aqueous sodium thiosulfate (2 × 10 mL), and water (2 × 10 mL), dried with $MgSO_4$, filtered and evaporated to give an oil that was purified by chromatography on silica gel using a mixture of $CHCl_3$, methanol, and acetic acid (94:4:1) to give an oil (69 mg, 65%). TLC R_f = 0.56 ($CHCl_3$–MeOH–AcOH, 89:10:1). $[\alpha]_D^{20}$ 9.5 (*c* 1.0 MeOH). ^{1}H NMR (400 MHz, CD_3OD) δ: 1.26 (s, 3H), 1.28 (s, 3H), 1.45 (s, 9H), 3.23 (s, 3H), 4.2 (s, 1H). ^{13}C NMR (100 MHz, CD_3OD) δ: 21.7, 21.8, 27.7, 49.0, 60.6, 76.1, 79.7, 156.8, 173.0. HR-MS calcd. for $C_{11}H_{21}NO_5Na$ ($[M + Na]^+$): 270.1312; found: 270.1319.

(*S*)-Benzyl-2-hydroxy-3-methylbutanoate (Hmb-OBn, 16)

To a solution of (*S*)-2-hydroxy-3-methylbutanoic acid (**15**, 2 g, 16.9 mmol, prepared according to ref. 18) and TMSCl (600 mol%, 8.8 mL, 101.4 mmol) in CH_2Cl_2 (170 mL) at 0 °C, Et_3N (600 mol%, 14.2 mL, 101.4 mmol) was added dropwise. The mixture was heated at reflux for 1 h, cooled to 0 °C, and treated with dry MeOH (110 mol%, 732 µL, 18.6 mmol). The reaction was stirred for 1 h at room temperature. The volatiles were removed under reduced pressure on a rotary evaporator. The residue was dissolved in acetonitrile (170 mL) and treated with anhydrous cesium carbonate (150 mol%, 8.3 g, 25.4 mmol) and benzyl bromide (500 mol%, 10 mL, 84.5 mmol), heated at reflux and stirred vigorously for 1 h, cooled to room temperature, treated with solid citric acid (1000 mol%, 32.5 g, 169 mmol), and stirred vigorously for 1 h at room temperature. The precipitate was filtered off and the filtrate was concentrated under reduced pressure. The residue was dissolved in $CHCl_3$ (150 mL), washed with a solution of satd. $NaHCO_3$ (2 × 50 mL) and brine, dried with $MgSO_4$, filtered and evaporated to a residue. Chromatography on silica gel using a gradient 20%–30% EtOAc in hexanes as the eluant and evaporation of the collected fractions provided an oil (2.3 g, 65%). TLC R_f = 0.37 (50% EtOAc in hexanes). $[\alpha]_D^{20}$ –11.3 (*c* 2.0 $CHCl_3$). ^{1}H NMR (400 MHz, $CDCl_3$) δ: 0.82 (d, 3H, *J* = 6.9), 0.98 (d, 3H, *J* = 6.9), 2.00–2.14 (m, 1H), 3.06–3.21 (m, 1H), 4.01–4.11 (m, 1H), 5.14 (d, 1H, *J* = 12.1), 5.21 (d, 1H, *J* = 12.2), 7.25–7.38 (m, 5H). ^{13}C NMR (100 MHz, $CDCl_3$) δ: 15.9, 18.7, 32.1, 67.0, 75.0, 128.3, 128.4, 128.5, 135.2, 174.7. HR-MS calcd. for $C_{12}H_{16}NO_3$ (TOF EI): 208.1099; found: 208.1098.

General procedure for the preparation of depsipeptide benzyl esters

A 0.1 mol/L solution of Hmb-OBn (**16**, 100 mmol%), Ph_3P (250 mol%), and the amino acid (Boc-HOMeVal (**2**, 100 mol%), Boc-HOVal (**3**, 150 mol%), or Boc-MeVal (**17**, 150 mol%)) in CH_2Cl_2–THF (1:1) was cooled to –20 °C, treated with diisopropyl azodicarboxylate (DIAD, 255 mol%) dropwise over 30 min, and stirred at –20 °C for 30 min. The reaction mixture was removed from the ice bath and allowed to stir at room temperature overnight. The volatiles were removed under reduced pressure on a rotary evaporator.

Boc-(*S*)-HOMeVal-(*R*)-Hmb-OBn (**18**, 169 mg) was isolated from the reaction of Hmb-OBn (**16**, 80 mg, 0.384 mmol) and Boc-HOMeVal (**2**, 91 mg, 0.384 mmol) by chromatography on silica gel using 18% EtOAc in hexanes as the eluant and directly employed in the hydrogenation step. An analytically pure sample (LC–MS: 96% purity, condition B, R_T = 23.7) was obtained by purification on RP-HPLC using condition A. TLC R_f = 0.28 (20% AcOEt in hexanes). $[\alpha]_D^{20}$ –22.2 (*c* 0.5 MeOH). ^{1}H NMR (300 MHz, CD_3OD) showed a 1:2 mixture of carbamate isomers (δ): 0.92 (d, 3H, *J* = 6.9), 0.99 (d, 3H, *J* = 6.9), [1.38 (s, 1.08H)], 1.41 (s, 1.98H), 1.22 (s, 2.01H), [1.25 (s, 1.08H)], 1.47 (s, 9H), 2.16–2.31 (m, 1H), [2.93 (s, 1.16H)], 2.94 (s, 1.96H), [4.75 (s, 0.33H)], 4.78 (s, 0.62H), 5.15 (d, 1H, *J* = 12.1), 5.21 (d, 1H, *J* = 12.1), 7.31–7.38 (m, 5H). ^{13}C NMR (75 MHz, CD_3OD) showed a mixture of carbamate isomers; the chemical shifts are listed in order of appearance (δ): 16.5, 18.1, 21.3, 26.4, 26.5, 27.6, 28.1, 30.4, 32.3, 33.3, 65.1, 65.6, 67.0, 72.5, 72.6, 77.6, 80.6, 81.0, 128.5, 128.6, 135.9, 156.5, 157.5, 196.6, 170.1. HR-MS calcd. for $C_{23}H_{36}NO_7$ ($[M + H]^+$): 438.2486; found: 438.2478.

Boc-(*S*)-MeVal-(*R*)-Hmb-OBn (**19**, 649 mg) was isolated from the reaction of Hmb-OBn (**16**, 313 mg, 1.50 mmol) and Boc-MeVal (**17**, 521 mg, 2.25 mmol) by chromatography on silica gel using 15% EtOAc in hexanes as the eluant and directly employed in the hydrogenation step. An analytically pure sample (LC–MS: 99% purity, condition A, R_T = 8.0) was obtained by purification on RP-HPLC using condition A. TLC R_f = 0.35 (10% AcOEt in hexanes). $[\alpha]_D^{20}$ –46.6 (*c* 0.5 $CHCl_3$). ^{1}H NMR (400 MHz, $CDCl_3$) showed a 1:1 mixture of carbamate isomers (δ): 0.85–0.95 (m, 6H), 0.95–1.06 (m, 6H), 1.46 (s, 9H), 2.22 (m, 2H), 2.78 (s, 1.6H), [2.83 (s, 1.4H)], [4.29 (d, 0.4H, *J* = 10.3)], 4.59 (d, 0.4H, *J* = 10.3), 4.87 (d, 1H, *J* = 4.1), 7.24–7.46 (m, 5H). ^{13}C NMR (100 MHz, $CDCl_3$) showed a mixture of carbamate isomers; the chemical shifts are listed in order of appearance (δ): 17.2, 19.0, 19.3, 20.0, 27.6, 27.8, 28.5, 30.2, 30.7, 63.1, 64.8, 66.9, 80.0, 80.3, 128.5, 128.7, 135.4, 155.8, 156.4, 169.1, 169.3, 170.8, 171.1. HR-MS calcd. for $C_{23}H_{35}NO_7$ (TOF EI): 421.2464; found: 421.2471.

Boc-(*S*)-HOVal-(*R*)-Hmb-OBn (**20**, 1.3 mg) was isolated from the reaction of Hmb-OBn (**16**, 625 mg, 3.0 mmol) and Boc-HOVal (**3**, 1050 mg, 4.5 mmol) by chromatography on silica gel using 15% EtOAc in hexanes as the eluant and directly employed in the hydrogenation step. An analytically pure sample (LC–MS: 99% purity, condition B, R_T = 16.0) was obtained by purification on RP-HPLC using condition A. TLC R_f = 0.38 (25% AcOEt in hexanes). $[\alpha]_D^{20}$ –2.8 (*c* 0.5 MeOH). ^{1}H NMR (400 MHz, CD_3OD) δ: 0.93 (d, 3H, *J* = 6.8), 0.98 (d, 3H, *J* = 6.8), 1.25 (s, 3H), 1.28 (s, 3H), 1.44 (s, 9H), 2.22 (dsept, 1H, J_1 = 4.6, J_2 = 6.8), 4.17 (s, 1H), 4.86 (d, 1H, *J* = 4.4), 5.16 (d, 1H, *J* = 12.2), 5.21 (d, 1H, *J* = 12.2), 7.28–7.40 (m, 5H). ^{13}C NMR (100 MHz, CD_3OD) δ: 16.6, 18.2, 25.8, 26.0, 27.7, 30.4, 63.1, 67.0, 71.3, 77.7, 79.8, 128.4, 128.5, 128.6, 135.9, 156.8, 169.9, 170.9. HR-MS calcd. for $C_{22}H_{33}NO_7$ ($[M + H]^+$): 424.2330; found: 424.2315.

General procedure for benzyl ester removal from depsipeptides

A 0.033 mol/L solution containing the depsipeptide benzyl ester (100 mol%) in THF was treated with palladium hydroxide on carbon (30 wt% of 20 wt% palladium (wet)), stirred under 1 atm of hydrogen for 1 h, filtered onto Celite®, and washed with THF (2×) and MeOH (2×). The filtrate was concentrated under reduce pressure to a residue that was

© 2005 NRC Canada

passed through a pad of silica gel, first using 20% EtOAc in hexanes as the eluant, then followed by 99% EtOAc containing 1% AcOH.

Boc-(S)-HOMeVal-(R)-Hmb (4)

The reaction of ester **18** (89 mg) afforded **4** as a white foam (51 mg, 72%). TLC R_f = 0.40 ($CHCl_3$–MeOH–AcOH, 89:10:1). $[\alpha]_D^{20}$ –28.2 (*c* 0.5 MeOH). ^{1}H NMR (300 MHz, CD_3OD) showed a 1:1.5 mixture of carbamate isomers (δ): 0.99 (d, 3H, *J* = 6.9), 1.03 (d, 3H, *J* = 6.9), 1.26 (d, 3H, *J* = 9.5), 1.41 (d, 3H, *J* = 8.6), 1.48 (s, H), 2.26 (dsept, 1H, J_1 = 4.0, J_2 = 6.7), [3.01 (s, 1.17H)], 3.03 (s, 1.78H), [4.75 (s, 0.37H)], 4.78 (s, 0.64H), 4.88 (d, 1H, *J* = 3.9), 4.95 (br s, 1OH). ^{13}C NMR (75 MHz, CD_3OD) showed a mixture of carbamate isomers; the chemical shifts are listed in order of appearance (δ): 16.4, 18.3, 21.1, 21.3, 26.4, 27.6, 28.1, 30.1, 32.3, 33.3, 65.2, 65.6, 69.4, 72.5, 72.7, 77.5, 78.5, 80.6, 81.0, 156.6, 157.5, 170.1, 171.5. HR-MS calcd. for $C_{16}H_{30}NO_7$ ($[M + H]^+$): 348.2017; found: 348.2016. LC–MS: 99% purity (condition A), R_T = 21.1.

Boc-(S)-MeVal-(R)-Hmb (21)

The reaction of ester **19** (250 mg) afforded **21** as an oil (167 mg, 85%). TLC R_f = 0.58 ($CHCl_3$–MeOH–AcOH, 89:10:1). $[\alpha]_D^{20}$ –75.6 (*c* 0.5 MeOH). ^{1}H NMR (300 MHz, CD_3OD) δ: 0.91 (m, 3H), 0.95–1.07 (m, 6H), 1.25 (d, 3H, *J* = 6.2), 1.45 (s, 9H), 2.13–2.33 (m, 2H), 2.84 (s, 3H), [4.27 (d, 0.43H, *J* = 10.5)], 4.45 (d, 0.45H, *J* = 10.4), 4.8 (d, 1H, *J* = 4.0), 4.84–5.00 (br s, 1OH). ^{13}C NMR (75 MHz, CD_3OD) showed a mixture of carbamate isomers; the chemical shifts are listed in order of appearance (δ): 16.5, 18.2, 18.4, 18.5, 19.3, 21.3, 27.4, 27.6, 27.8, 29.8, 30.1, 30.3, 63.6, 65.1, 69.4, 77.3, 80.5, 80.8, 156.5, 157.1, 170.9. HR-MS calcd. for $C_{16}H_{30}NO_6$ ($[M + H]^+$): 332.2073; found 332.2074. LC–MS: 97% purity (condition A), R_T = 26.0.

Boc-(S)-HOVal-(R)-Hmb (22)

The reaction of ester **20** (330 mg) afforded **22** as a white solid (224 mg, 83%). TLC R_f = 0.38 ($CHCl_3$–MeOH–AcOH, 89:10:1). $[\alpha]_D^{20}$ –29.4 (*c* 0.5 MeOH). ^{1}H NMR (400 MHz, CD_3OD) δ: 1.00 (d, *J* = 6.9, 3H), 1.03 (d, *J* = 7.0, 3H), 1.29 (s, 3H), 1.31 (s, 3H), 1.45 (s, 9H), 2.26 (dsept, J_1 = 4.1, J_2 = 6.7, 1H), 4.14 (s, 1H), 4.87 (d, *J* = 3.9, 1H). ^{13}C NMR (100 MHz, CD_3OD) δ: 14.4, 19.4, 26.9, 27.0, 28.7, 31.2, 64.2, 72.3, 78.5, 80.8, 157.8, 171.7, 173.0. HR-MS calcd. for $C_{15}H_{28}NO_7$ ($[M + H]^+$): 334.1866; found 334.1876. LC–MS: 98% purity (condition A), R_T = 18.5.

Acknowledgments

This research was supported in part by the Natural Sciences and Engineering Research Council of Canada (NSERC), the Ministère de l'Éducation du Québec, and Valorisation-Recherche Québec. We would like to thank Mr. Dalbir Sekhon for performing the LC–MS experiments.

References

1. M. Konishi, M. Ohkuma, F. Sakai, T. Tsuno, H. Koshiyama, T. Naito, and H. Kawaguchi. J. Am. Chem. Soc. **103**, 1241 (1981).
2. N. Awazu, K. Ikai, J. Yamamoto, K. Nishimura, S. Mizutani, K. Takesako, and I. Kato. J. Antibiot. **48**, 525 (1994).
3. N. Izumiya and A. Nagamatsu. J. Chem. Soc. Jpn. **72**, 336 (1951).
4. M.A. Ciufoloni and S. Swaminathan. Tetrahedron Lett. **30**, 3027 (1989).
5. M.A. Ciufoloni, D. Valognes, and N. Xi. Tetrahedron Lett. **40**, 3693 (1999).
6. C.W. Reid. M.Sc. thesis, University of Waterloo, Waterloo, Ont. 2001.
7. W.D. Lubell and H. Rapoport. J. Am. Chem. Soc. **109**, 236 (1987).
8. W.D. Lubell and H. Rapoport. J. Org. Chem. **54**, 3824 (1989).
9. J.E. Dettwiler and W.D. Lubell. Can. J. Chem. **82**, 318 (2004).
10. J.E. Dettwiler and W.D. Lubell. J. Org. Chem. **68**, 177 (2003).
11. M. Prashad, D. Har, B. Hu, H.-Y. Kim, O. Repic, and T.J. Blacklock. Org. Lett. **5**, 125 (2003), and refs. 1 and 2 cited therein.
12. J.E. Dettwiler, L. Bélec, and W.D. Lubell. *In* The 18th American Peptide Society Symposium Proceedings: Peptide revolution: Genomics, proteomics & therapeutics. Boston, Mass, 19–23 July 2003. *Edited by* M. Chorev and T.S. Sawyer. American Peptide Society. Cardiff, Calif. 2004. pp. 179–180.
13. W.D. Lubell, T.F. Jamison, and H. Rapoport. J. Org. Chem. **55**, 3511 (1990).
14. R. Sharma and W.D. Lubell. J. Org. Chem. **61**, 202 (1996).
15. M. Zhao, J. Li, E. Mano, Z. Song, D.M. Tschaen, E.J.J. Grabowski, and P.J. Reider. J. Org. Chem. **64**, 2564 (1999).
16. R. Knorr, A. Trzeciak, W. Bannwarth, and D. Gillessen. Tetrahedron Lett. **30**, 1927 (1989).
17. J.E. Dettwiler and W.D. Lubell. M.Sc. thesis, University of Montreal. Montréal, Que. 2005.
18. P. Brewster, F. Hiron, E.D. Hughes, C.K. Ingold, and P.A.D.S. Rao. Nature (London), **166**, 179 (1950).
19. O. Mitsunobu. Synthesis, 1 (1981).
20. S. Roy, H.-G. Lombart, R.E.W. Hancock, S.W. Farmer, and W.D. Lubell. J. Pept. Res. **60**, 198 (2002).

© 2005 NRC Canada

Design and synthesis of oxazolidinone ketolide antibiotic segment mimetics[1]

Stephen Hanessian and Kiran Kumar Kothakonda

Abstract: Macrolides have been modified to a large extent by structural and functional variants to expand their spectrum of activity and overcome resistance. Ketolides are new generation 14-membered ring macrolides derived by chemical modification of the readily available erythromycin A. We have designed and synthesized bicyclic oxazolidinone-δ-lactones to mimic the "left segment" periphery of ketolides.

Key words: macrolide, ketolide, 50S r-RNA, segment mimetics.

Résumé : Des macrolides ont été beaucoup modifiés par des variations de structure et de fonction afin d'élargir leur spectre d'activité et pour vaincre la résistance. Les cétolides correspondent à une nouvelle génération de macrolides à quatorze chaînons qui dérivent de modifications chimiques de l'érythromycine A qui est facilement accessible. Pour imiter le segment de gauche de la périphérie des cétolides, de nouvelles δ-lactones bicycliques de l'oxazolidinone ont été développées et synthétisées.

Mots clés : macrolide, cétolide, 50S r-ARN, imitation d'un segment.

[Traduit par la Rédaction]

Introduction

Macrolides have been used as effective antibiotics to combat infection caused by various Gram-positive bacteria such as *Staphylococcus aureus*, *Streptococcus pneumoniae*, and *Streptococcus pyogenes* for over 50 years (1). The discovery of the 14-membered macrolide erythromycin (**1**) (2) was a major breakthrough in antimicrobial research, exhibiting activity against penicillin-resistant *S. aureus*. Erythromycin has been widely prescribed for the treatment of upper and lower respiratory tract infections in children because of its excellent record of safety. However, the main disadvantage of erythromycin is its instability in the acidic medium in the stomach, which results in degradation (3). The semisynthetic macrolides such as clarithromycin (**2**) (4) and azithromycin (**3**) (5) are stable in acidic medium and also possess activity against *Haemophilus influenzae*, among other pathogenic organisms. Unfortunately, erythromycin, clarithromycin, and azithromycin are ineffective against organisms that show macrolide – lincosamide – streptogramin B (MLS_B) cross-resistance (6). As a result of extensive research aimed at discovering new analogues (7), erythromycin has been replaced to a large extent by structural and chemically modified variants such as flurithromycin, roxitromycin, and dirithromycin (8). More recently, a new class of potent antibiotics called ketolides as exemplified by telithromycin (HMR-3647) (**4**) (9) and cethromycin (ABT-773) (**5**) (10), was discovered (Fig. 1). These macrolide structures are derived from erythromycin via substantial functional modification, notably the omission of cladinose, the presence of a carbonyl group at C-3, and an oxazolidinone ring at the C-11 and (or) C-12. The presence of heterocyclic side-chain appendages on the oxazolidinones greatly enhances the antibacterial profile. Ketolides were found to be active against penicillin-resistant and erythromycin resistant *S. pneumoniae*, hence, their great potential as a new generation of macrolide antibiotics targeted to the resistant organisms.

Macrolide antibiotics exert their antibacterial action by stimulating the dissociation of peptidyl t-RNA from the bacterial ribosome during the translocation process, thereby inhibiting protein synthesis. They bind to the 2058–2062 region of 23S ribosomal RNA of the 50S ribosomal subunit in the vicinity of peptide exit channel (11).

Received 1 December 2004. Published on the NRC Research Press Web site at http://canjchem.nrc.ca on 2 July 2005.

Dedicated to Professor Howard Alper, wishing him the best in chemistry and in life.

S. Hanessian[2] and K.K. Kothakonda. Department of Chemistry, University of Montreal, P.O. Box 6128, Station Centre-Ville, Montreal, QC H3C 3J7, Canada.

[1]This article is part of a Special Issue dedicated to Professor Howard Alper.

[2]Corresponding author (e-mail: stephen.hanessian@umontreal.ca).

Results and discussion

Design

As part of a research program aimed at new antibacterial RNA-binding small molecules (12, 13), we were interested in studying the functional role of the oxazolidinone subunit spanning C-11 and C-12 in the ketolides. Recently available X-ray data on ketolides (14), and classical X-ray structural (15), and NMR studies (16) on erythromycin many years ago, have revealed the prevalence of a unique three-dimensional, crown-like conformation with the edges of hypothetical chair-like cyclohexanes (Fig. 2). A better visualization of the topology of 14-membered macrolides can be considered in conjunction with a virtual diamond lattice

 doi: 10.1139/V05-095 © 2005 NRC Canada

Fig. 1. Structure of macrolide antibiotics.

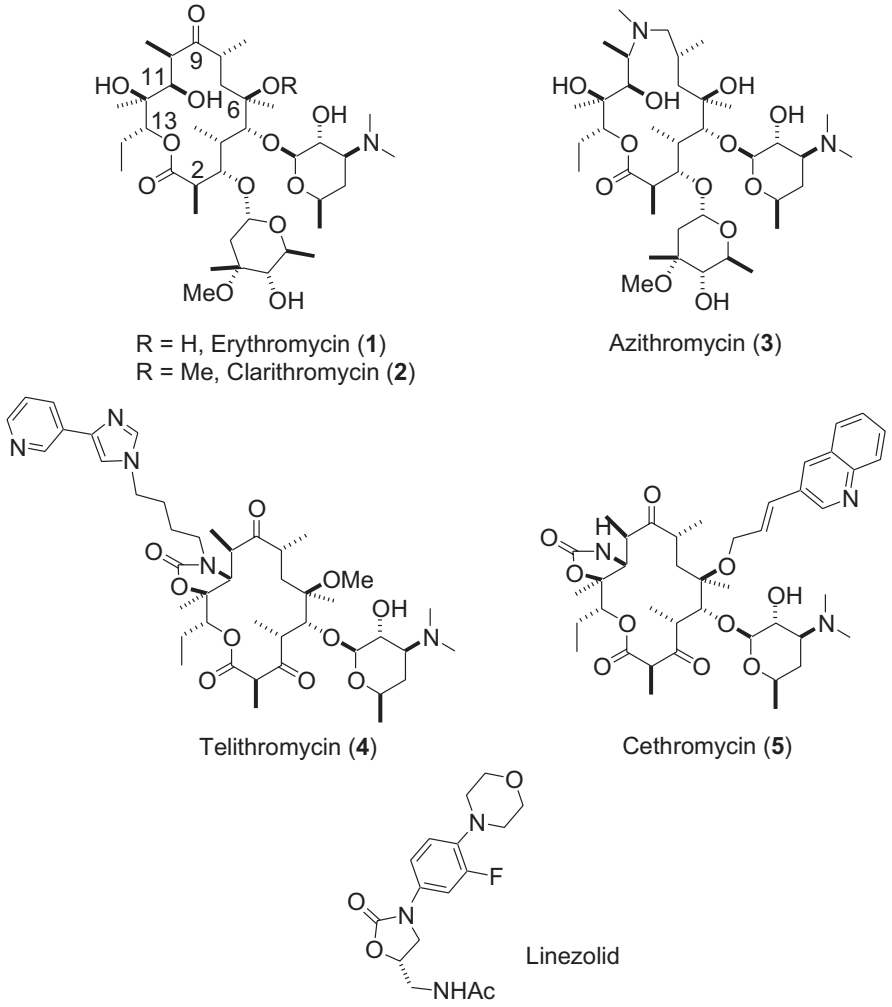
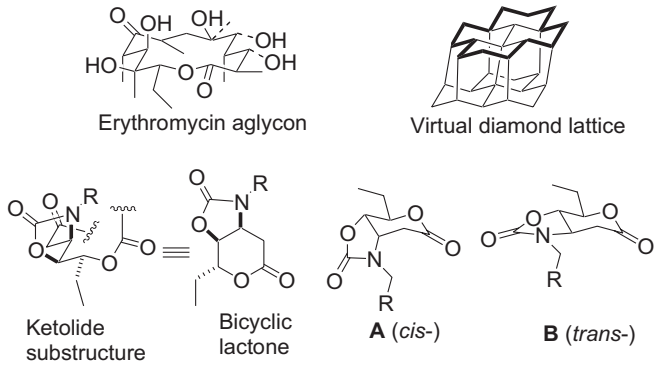


Fig. 2. Design of *cis*- and *trans*-oxazolidinone segment mimetics.



(17). We therefore hypothesized that bicyclic *cis*- and *trans*-oxazolidinone-δ-lactones represented by structures A and B could simulate the minimal spatial requirements of the ketolides "western" landscape, by occupying a corresponding region of the lattice. Although the proposed prototypes were substantially different in overall topology, and lacked the all-important desosamine sugar, compared with the ketolides, they shared a common oxazolidinone subunit. It was surmised that the diversification at nitrogen with a variety of heterocyclic side-chain appendages similar to those found in the ketolides, would prove to be an asset (18).

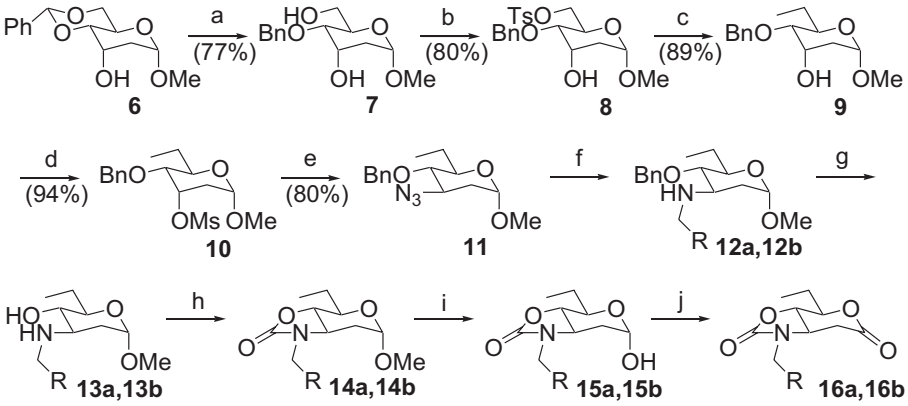
Synthesis

The synthesis of *cis*- and (or) *trans*-oxazolidinone-δ-lactones started from methyl 2-deoxy-4,6-*O*-benzylidene-α-D-*ribo*-hexopyranoside (**6**), which is readily obtained from methyl α-D-glucopyranoside (19) (Scheme 1). Regioselective reductive ring opening of the benzylidene acetal was achieved in an 85:15 ratio using LAH–$AlCl_3$ to afford **7** in 77% yield (20). Selective protection of the primary hydroxyl group with tosyl chloride gave **8**, which was treated with Me_2CuLi at –78 °C to afford the chain-extended analogue **9**. There are few reported examples of cuprate-mediated functionalizations of the terminal carbon atoms in the sugar series (21).

To obtain the *trans*-oxazolidinones, the mesylate **10** was treated with NaN_3 in refluxing DMF to give the azido analogue **11** in 80% yield. Treatment with Me_3P in THF under Staudinger (22) conditions reduced the azide to the amine, which was then subjected to reductive amination with two aldehydes using $NaCNBH_3$–AcOH in MeOH, giving **12a** and **12b** in good yields. Benzyl deprotection was achieved with 10% $Pd(OH)_2$-on-carbon in EtOAc under a hydrogen

© 2005 NRC Canada

Scheme 1. Reagents and conditions: (*a*) LAH, $AlCl_3$, CH_2Cl_2, ether, reflux, 2.5 h; (*b*) TsCl, pyridine, CH_2Cl_2, 16 h; (*c*) Me_2CuLi, ether, –78 °C to rt, 3 h; (*d*) MsCl, pyridine, 12 h; (*e*) NaN_3, DMF, 160 °C, 1.5 h; (*f*) (*i*) Me_3P, THF, H_2O, reflux, 40 min; (*ii*) R-CHO, MeOH, AcOH, $NaCNBH_3$, 12 h; (*g*) H_2, 10% $Pd(OH)_2$-C, EtOH, 14 h; (*h*) CDI, Et_3N, CH_2Cl_2, 5 h; (*i*) 6 N HCl, dioxane, 1 h; (*j*) PCC, 4 Å molecular sieves, CH_2Cl_2, 4 h.



a) R = $Ph(CH_2)_2$ **b**) R = $CH_3(CH_2)_5$

atmosphere to obtain **13a** and **13b**. Treatment with carbonyl diimidazole (23) in Et_3N gave the required oxazolidinones **14a** and **14b**. Hydrolysis of the glycosides in 6 N HCl – dioxane gave the hemiacetals **15a** and **15b**, which were oxidized with PCC to afford the desired target *trans*-oxazolidinone lactones **16a** and **16b** in good yields.

The *cis*-oxazolidinones were prepared from the common intermediate **9** (Scheme 2). Thus, a Mitsunobu reaction with *p*-nitrobenzoic acid gave the inverted ester **17** in 78% yield (24). Saponification gave **18**, which was mesylated to give **19** and the latter was treated with catalytic 10% Pd-on-carbon under a hydrogen atmosphere affording **20**. Nucleophilic displacement with NaN_3 in DMF led to **21**, which was converted to PMB **22**. Reduction under Staudinger conditions (22) reduced the azide to the amine, which was subjected to reductive amination with various aldehydes using $NaCNBH_3$–AcOH in MeOH to obtain the corresponding amines (**23a**–**23e**) in good yields. The PMB ether group was cleaved with ceric ammonium nitrate to obtain **24a**–**24e**. Treatment of the *cis*-amino alcohols with carbonyl diimidazole (23) in Et_3N gave the intended oxazolidinones **25a**–**25e**. Cleavage of the glycosides in 6 N HCl – dioxane led to the hemiacetals **26a**–**26e**, which, upon oxidation with PCC, gave the *cis*-oxazolidinone lactones **27a**–**27e** in good yields. Single crystal X-ray structure analysis of **27a** and **27c** confirmed the stereochemistry of the *cis*-oxazolidinone ring.[3]

The bicyclic oxazolidinone lactones **16a** and **16b** and **27a**–**27e** did not inhibit the growth of *S. aureus* at minimum inhibitory concentrations of >50 μg/mL (25). Lack of inhibition in the macrolide series is generally attributed to cell penetration, efflux, resistance, and ineffective binding to the ribosomal RNA target. It is clear that the simplification of the macrolide structure of the ketolides to bicyclic lactone prototypes resulted in the loss of several important contact points with the RNA targets, without alternative compensatory binding. Such an outcome was not entirely unexpected, given the drastic departure from the traditional macrolide structure, including the omission of the desosamine glycoside. Nevertheless, it was hoped that the minimal oxazolidinone motif, harboring an optimized heterocyclic side-chain appendage (as in **27e**) would contribute to a modest level of inhibition of bacterial growth. In this context, it is of interest that simple, *N*-aryl oxazolidinones such as linezolid (Fig. 1) have emerged as a new generation of antibacterial agents (26).

In conclusion, we have synthesized a series of bicyclic δ-lactone oxazolidinones as segment mimetics of ketolides. Their lack of inhibitory activity in vitro emphasizes the importance of the macrolide structure and the desosamine unit for achieving effective binding to bacterial ribosomes.

Experimental

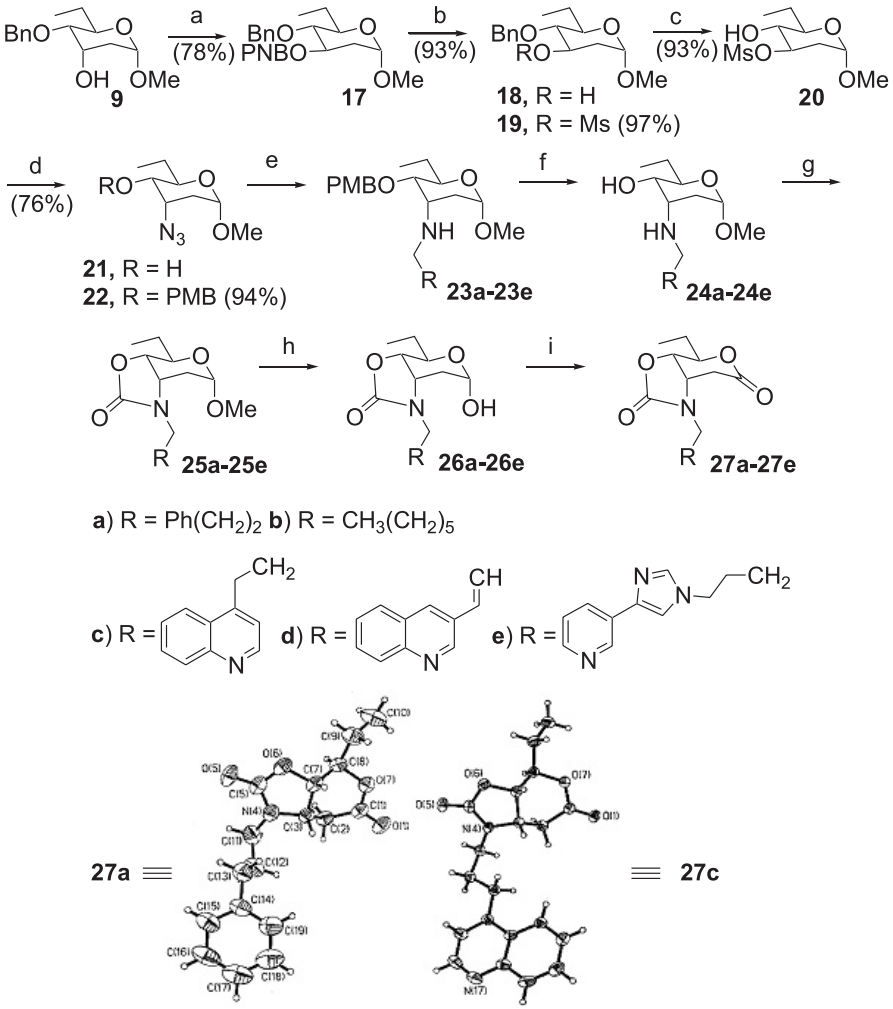
General procedure

Flash chromatography was carried out using 230–400 mesh silica gel. Mixtures of ethyl acetate and hexanes were used as the eluents, unless otherwise specified. Analytical TLC was performed on glass plates coated with a 0.02 mm layer of silica gel 60 F-254. Melting points were uncorrected. IR spectra were recorded as films. ^1H and ^{13}C NMR spectra were recorded at 300 and 400 MHz, respectively, and the chemical shifts are reported in ppm on the δ scale, with $CDCl_3$ as the reference, unless otherwise specified. MS and HR-MS spectra were recorded using electron ionization or by the FAB technique. Optical rotations were measured in $CHCl_3$ or MeOH at 23 °C. All reactions were carried out under nitrogen or argon unless otherwise specified. The –78 °C

[3] Supplementary data for this article are available on the Web site or may be purchased from the Depository of Unpublished Data, Document Delivery, CISTI, National Research Council Canada, Ottawa, ON K1A 0S2, Canada. DUD 3690. For more information on obtaining material refer to http://cisti-icist.nrc-cnrc.gc.ca/irm/unpub_e.shtml. CCDC 266401 and 266402 contain the crystallographic data for this manuscript. These data can be obtained, free of charge, via www.ccdc.cam.ac.uk/conts/retrieving.html (Or from the Cambridge Crystallographic Data Centre, 12 Union Road, Cambridge CB2 1EZ, UK; fax +44 1223 336033; or deposit@ccdc.cam.ac.uk).

© 2005 NRC Canada

Scheme 2. Reagents and conditions: (*a*) DIAD, TPP, THF, *p*-nitro benzoic acid, 12 h; (*b*) (*i*) NaOMe, MeOH, rt, 10 h; (*ii*) MsCl, pyridine, rt, 12 h; (*c*) H_2, 10% Pd-C, EtOAc, 10 h; (*d*) (*i*) NaN_3, DMF, 125 °C, 12 h; (*ii*) PMB-Br, NaH, DMF, 6 h; (*e*) (*i*) Me_3P, THF, H_2O, reflux, 40 min; (*ii*) R-CHO, MeOH, AcOH, $NaCNBH_3$, 12 h; (*f*) CAN, AcCN, H_2O, 12 h; (*g*) CDI, Et_3N, CH_2Cl_2, 5 h; (h) 6 N HCl, dioxane, 1 h; (*i*) PCC, 4 Å molecular servies, CH_2Cl_2, 4 h. (Bottom) ORTEP drawing of the X-ray crystal structures of **27a** and **27c**.



temperature is approximate, as achieved by a dry ice – acetone bath.

Methyl 4-*O*-benzyl-2-deoxy-α-D-*ribo*-hexopyranoside (7)

To a well-stirred mixture of compound **6** (5 g, 18.8 mmol), lithium aluminium hydride (1.36 g, 35.7 mmol) in ether (65 mL), and DCM (65 mL) was added aluminium chloride (3.76 g, 28.2 mmol) under reflux for 15 min and refluxing was continued for 3 h. The mixture was cooled to 0 °C, quenched with ice, filtered, and washed with EtOAc (100 mL); the filtrate was washed with brine, dried over Na_2SO_4, concentrated under vacuum, and the residue was purified by column chromatography (EtOAc–hexanes, 1:1) to give **7** as a thick syrup (3.9 g, 77%). $[\alpha]_D$ +205 (*c* 0.75, $CHCl_3$). IR (neat, cm^{-1}): 3470. ^1H NMR (400 MHz, $CDCl_3$) δ: 1.82 (m, 1H), 2.18 (dd, 1H, *J* = 1.7, 15.4 Hz), 3.38 (s, 1H), 3.42 (dd, 1H, *J* = 1.7, 11.1 Hz), 3.84 (m, 2H), 3.96 (m, 1H), 4.21 (brm, 1H), 4.56 (d, 2H, *J* = 12.5 Hz), 4.77, (d, 2H, *J* = 12.5 Hz), 4.79 (m, 1H), 7.37 (m, 5H). ^{13}C NMR (400 MHz, $CDCl_3$) δ: 35.2, 55.6, 62.8, 64.4, 66.8, 70.9, 74.7, 98.8, 128.3, 128.9, 138.2. MS calcd. for $C_{14}H_{20}NO_5$: 268.3 (M^+); found: 286.2 (M + H_2O^+).

Methyl 4-*O*-benzyl-2-deoxy-6-*O*-*p*-tolylsulfonyl-α-D-*ribo*-hexopyranoside (8)

To a solution of compound **7** (3.98 g, 14.85 mmol) in pyridine (12 mL) and DCM (40 mL) was added *p*-toluenesulfonyl chloride (2.92 g, 15.29 mmol) at 0 °C under an argon atmosphere and the solution was stirred at room temperature for 16 h. The mixture was concentrated under vacuum at low temperature, the residue was taken up in DCM (100 mL), washed with water then with brine, dried over Na_2SO_4, concentrated, and purified by column chromatography (EtOAc–hexanes, 3:7) to afford **8** (5 g, 80%). $[\alpha]_D$ +112.7 (*c* 1, $CHCl_3$). IR (neat, cm^{-1}): 3526. ^1H NMR (400 MHz, $CDCl_3$) δ: 1.82 (m, 1H), 2.15 (dd, 1H, *J* = 1.7, 15.4 Hz), 2.42 (s, 3H), 3.35 (s, 1H), 3.41 (dd, 1H, (dd, 1H, *J* = 1.7, 11.1 Hz)), 4.04 (m, 1H), 4.11 (brm, 1H), 4.22–4.36 (m, 2H), 4.44 (d, 2H, *J* = 12.5 Hz), 4.75 (m, 1H), 7.22–7.39 (m, 7H), 7.79 (d, 2H, *J* = 12.1 Hz). ^{13}C NMR (400 MHz,

© 2005 NRC Canada

$CDCl_3$) δ: 22.1, 34.9, 55.8, 64.1, 64.9, 70.1, 70.9, 74.0, 98.7, 128.3, 128.9, 130.1, 133.3, 137.7, 145.1.

Methyl 4-*O*-benzyl-2,6-dideoxy-6-*C*-methyl-α-D-*ribo*-hexopyranoside (9)

MeLi (45 mL, 1.6 mol/L in Et_2O) was added slowly to CuI (6.77 g, 35.5 mmol) in ether (180 mL) at –20 °C under an argon atmosphere and stirred at –5 °C for 20 min. Compound **8** (2.5 g, 5.93 mmol) in Et_2O (20 mL) was added to the mixture at –78 °C for 15 min and the mixture was stirred for 1 h allowing it to warm to 0 °C, then for 3 h at room temperature. The mixture was quenched with NH_4OH and NH_4Cl (1:1, 20 mL), extracted with ether (100 mL), washed with brine, dried over Na_2SO_4, and concentrated under vacuum. The residue was purified by column chromatography (EtOAc–hexanes, 2:8) to give compound **9** (1.4 g, 89%). $[\alpha]_D$ +187.2 (*c* 1, $CHCl_3$). IR (neat, cm^{-1}): 3480. ^1H NMR (400 MHz, $CDCl_3$) δ: 0.98 (t, 3H, *J* = 8.4 Hz), 1.45 (m, 1H), 1.83 (m, 1H), 1.99 (m, 1H), 2.18 (dd, 1H, *J* = 1.7, 15.4 Hz), 3.15 (dd, 1H, *J* = 1.7, 11.1 Hz), 3.37 (s, 3H), 3.82 (m, 1H), 4.22 (brs, 1H), 4.55 (d, 1H, *J* = 12.4 Hz), 4.76 (d, 1H, *J* = 12.4 Hz), 4.79 (d, 1H, *J* = 4.1 Hz), 7.23–7.38 (m, 5H). ^{13}C NMR (400 MHz, $CDCl_3$) δ: 10.1, 24.9, 35.5, 55.3, 64.4, 67.3, 70.8, 78.4, 128.1, 128.3, 128.8, 138.4. MS calcd. for $C_{15}H_{22}NO_4$: 266.3 (M^+); found: 284.2 ($M + H_2O^+$).

Methyl 4-*O*-benzyl-2,6-dideoxy-3-*O*-methanesulfonyl-6-*C*-methyl-α-D-*ribo*-hexopyranoside (10)

To a solution of compound **9** (0.33 g, 1.24 mmol) in pyridine (6 mL) was added methanesulfonyl chloride (0.24 mL, 3.1 mmol) at 0 °C and the solution was stirred for 12 h allowing it to warm to room temperature. The mixture was diluted with Et_2O (20 mL), washed sequentially with cold dilute 5% HCl, aq. 5% $NaHCO_3$ solution, water, and brine, dried over Na_2SO_4, and concentrated under vacuum. The residue was purified by column chromatography (EtOAc–hexanes, 2:8) to obtain **10** (0.4 g, 94%). $[\alpha]_D$ +177.7 (*c* 1, $CHCl_3$). IR (neat, cm^{-1}): 1346. ^1H NMR (400 MHz, $CDCl_3$) δ: 0.98 (t, 3H, *J* = 8.3 Hz), 1.21 (m, 1H), 1.93 (m, 2H), 2.37 (dd, 1H, *J* = 1.7, 15.4 Hz), 3.2 (s, 3H), 3.25 (m, 1H), 3.35 (m, 1H), 3.87 (t, 1H, *J* = 8.3 Hz), 4.51 (d, 1H, *J* = 12.4 Hz), 4.69 (m, 1H), 4.79 (d, 1H, *J* = 12.4 Hz), 5.24 (m, 1H), 7.29–7.42 (m, 5H). ^{13}C NMR (400 MHz, $CDCl_3$) δ: 9.9, 24.7, 34.8, 39.6, 55.4, 67.5, 71.8, 74.1, 76.7, 96.9, 128.5, 128.7, 128.9, 137.6.

Methyl 3-azido-4-*O*-benzyl-6-*C*-methyl-2,3,6-trideoxy-α-D-*arabino*-hexopyranoside (11)

A mixture of compound **10** (395 mg, 1.15 mmol) and NaN_3 (395 mg, 5.3 mmol) in DMF (6 mL) was heated at 160 °C for 1.5 h under an argon atmosphere. The mixture was filtered, washed with Et_2O (20 mL), concentrated, and the filtrate was purified by column chromatography (EtOAc–hexanes, 3:97) to afford **11** (264 mg, 80%). $[\alpha]_D$ +105.6 (*c* 1.1, $CHCl_3$). IR (neat, cm^{-1}): 2101. ^1H NMR (400 MHz, $CDCl_3$) δ: 1.96 (t, 1H, *J* = 8.3 Hz), 1.51 (m, 1H), 1.61 (m, 1H), 1.96 (m, 1H), 2.19 (dd, 1H, *J* = 4.1, 13.5 Hz), 3.09 (t, 1H, *J* = 11 Hz), 3.34 (s, 3H), 3.54 (m, 1H), 3.91 (m, 1H), 4.63 (d, 1H, *J* = 12.8 Hz), 4.79 (m, 1H), 4.91 (d, 1H, *J* = 12.8 Hz), 7.28–7.44 (m, 5H). ^{13}C NMR (400 MHz, $CDCl_3$) δ: 10.3, 24.9, 36.0, 54.8, 60.8, 72.3, 75.5, 82.4, 97.6, 128.4, 128.6, 128.9, 139.2.

Methyl 4-*O*-benzyl-6-*C*-methyl-3-phenylethylamino-2,3,6-trideoxy-α-D-*arabino*-hexopyranoside (12a)

To a solution of compound **11** (40 mg, 0.137 mmol) in THF was added trimethylphosphine (0.53 mL, 1 mol/L in toluene) and the solution was stirred under an argon atmosphere for 30 min. Water (16 μL) was added to the mixture and stirred under reflux condition for 45 min. The mixture was concentrated under vacuum, and the residue was dissolved in dry MeOH (3 mL) under an argon atmosphere. The requisite aldehyde (0.135 mmol) was added followed by the addition of AcOH (32 μL), and the solution was stirred. $NaCNBH_3$ (18 mg, 0.274 mmol) was added, the mixture stirred for 12 h, then concentrated under vacuum. The residue was diluted with EtOAc (10 mL), washed with 10% $NaHCO_3$ solution and brine, and the organic phase was dried over Na_2SO_4, concentrated, and then purification of the residue by column chromatography (EtOAc–hexanes, 2:3) gave **12a** (89%). $[\alpha]_D$ +53.1 (*c* 1.85, $CHCl_3$). IR (neat, cm^{-1}): 3825. ^1H NMR (400 MHz, $CDCl_3$) δ: 1.02 (t, 3H, *J* = 8.3 Hz), 1.52 (m, 2H), 1.78 (brm, 3H), 1.98 (m, 1H), 2.1 (m, 1H), 2.41–2.71 (m, 3H), 3.03 (m, 2H), 3.35 (s, 3H), 3.58 (t, 1H, *J* = 11.2 Hz), 4.59–4.69 (m, 3H), 7.11–7.39 (m, 10H). ^{13}C NMR (400 MHz, $CDCl_3$) δ: 10.4, 25.3, 32.3, 33.9, 36.0, 46.8, 54.8, 55.8, 72.3, 75.2, 84.0, 98.2, 126.2, 128.2, 128.4, 128.7, 128.8, 129.0, 138.5, 142.4. MS calcd. for $C_{24}H_{33}NO_3$: 383.5 (M^+); found: 384.4.

Methyl 4-*O*-benzyl-3-heptylamino-6-*C*-methyl-2,3,6-trideoxy-α-D-*arabino*-hexopyranoside (12b)

Following the same procedure as for compound **11** gave **12b** in 62% yield. $[\alpha]_D$ +26 (*c* 1.1, $CHCl_3$). IR (neat, cm^{-1}): 3820. ^1H NMR (400 MHz, $CDCl_3$) δ: 0.87 (m, 3H), 1.05 (m, 3H), 1.25 (brs, 6H), 1.39 (m, 2H), 1.51 (m, 2H), 1.63 (brs, 1H), 1.95 (m, 1H), 2.13 (m, 1H), 2.43 (m, 1H), 2.61 (m, 1H), 3.06 (m, 2H), 3.33 (s, 3H), 3.56 (t, 1H, *J* = 9.4 Hz), 4.61–4.75 (m, 3H), 7.29 (m, 5H). ^{13}C NMR (400 MHz, $CDCl_3$) δ: 10.4, 14.5, 23.0, 25.3, 27.7, 29.6, 30.6, 32.2, 36.0, 47.4, 54.8, 55.8, 72.3, 75.1, 84.0, 98.2, 128.2, 128.3, 129.0, 138.7. MS calcd. for $C_{22}H_{37}NO_3$: 363.5 (M^+); found: 364.3.

Methyl 6-*C*-methyl-3-phenylethylamino-2,3,6-trideoxy-α-D-*arabino*-hexopyranoside (13a)

A mixture of compound **12a** (35 mg, 0.0914 mmol) and 10% Pd $(OH)_2$-on-carbon (3 mg) in EtOAc (2 mL) was stirred under a hydrogen atmosphere for 14 h, the suspension was filtered, washed with MeOH (10 mL), concentrated, and purified by column chromatography (MeOH–EtOAc, 1:99) to afford **13a** (21 mg, 80%). $[\alpha]_D$ +17 (*c* 0.5, $CHCl_3$). IR (neat, cm^{-1}): 3860, 3720. ^1H NMR (400 MHz, $CDCl_3$) δ: 1.01 (t, 3H, *J* = 8.3 Hz), 1.42 (m, 2H), 1.94 (m, 3H), 2.09 (dd, 1H, *J* = 2 Hz), 2.56 (m, 1H), 2.69 (t, 2H, *J* = 6.9 Hz), 2.83 (m, 2H), 3.05 (t, 3H, *J* = 9.6 Hz), 3.32 (s, 3H), 3.42 (t, 1H, *J* = 11.2 Hz), 4.78 (brs, 1H), 7.19 (m, 3H), 7.29 (d, 2H, *J* = 7Hz). ^{13}C NMR (400 MHz, $CDCl_3$) δ: 10.2, 25.2, 32.1, 33.8, 35.5, 46.0, 54.8, 57.0, 73.5, 73.9, 98.5, 126.3, 128.8. MS calcd. for $C_{17}H_{27}NO_3$: 293.2 (M^+); found: 294.3.

© 2005 NRC Canada

Methyl 3-heptylamino-6-*C*-methyl-2,3,6-trideoxy-α-D-*arabino*-hexopyranoside (13b)

Following the same procedure compound as for **12b** gave **13b** as a light yellow solid (90%); mp 106 °C. $[\alpha]_D$ +78.6 (*c* 0.5, $CHCl_3$). IR (KBr, cm^{-1}): 3307. ^1H NMR (400 MHz, $CDCl_3$) δ: 0.87 (t, 3H, *J* = 5.8 Hz), 0.99 (t, 3H, *J* = 6.8 Hz), 1.26–1.48 (brm, 11H), 1.85 (m, 2H), 1.99 (m, 1H), 2.19 (m, 2H), 2.79 (q, 1H, 1H, *J* = 4.2, 8.9 Hz), 3.07 (q, 1H, *J* = 3.3, 8.9 Hz), 3.32 (s, 4H), 3.44 (t, 1H, *J* = 9.1 Hz), 3.59 (t, 1H, *J* = 9.1 Hz), 4.79 (brs, 1H). ^{13}C NMR (400 MHz, $CDCl_3$) δ: 10.1, 14.3, 22.3, 24.4, 26.5, 27.5, 29.1, 31.1, 32.1, 46.3, 54.6, 58.4, 70.1, 72.2, 96.3. MS calcd. for $C_{15}H_{31}NO_3$: 273.2 (M^+); found: 274.2.

***trans*-Oxazolidinone glycoside (14a)**

To a mixture of compound **13a** (22 mg, 0.0751 mmol) and Et_3N (0.16 mL, 1.13 mmol) in DCM (4 mL) was added carbonyl diimidazole (60 mg, 0.376 mmol) under an argon atmosphere and the mixture was stirred for 5 h at room temperature. The mixture was concentrated under vacuum and purified by column chromatography (EtOAc–hexanes, 1:9) to obtain **14a** (20 mg, 84%). $[\alpha]_D$ +96.8 (*c* 0.5, $CHCl_3$). IR (neat, cm^{-1}): 1764. ^1H NMR (400 MHz, $CDCl_3$) δ: 1.01 (t, 3H, *J* = 8.3 Hz), 1.59 (m, 1H), 1.75–2.15 (brm, 4H), 2.19 (m, 1H), 2.64 (t, 2H, *J* = 8.2 Hz), 2.83 (m, 2H), 3.19 (m, 1H), 3.33 (m, 1H), 3.39 (s, 3H), 3.59 (t, 1H, *J* = 10 Hz), 3.75 (t, 1H, *J* = 10 Hz), 3.79 (brm, 1H), 4.85 (brs, 1H), 7.19 (m, 3H), 7.26 (d, 2H, *J* = 8.3 Hz). ^{13}C NMR (400 MHz, $CDCl_3$) δ: 9.4, 25.6, 29.9, 32.1, 33.6, 35.5, 43.8, 52.3, 57.4, 73.0, 80.5, 98.3, 126.5, 128.7, 128.9, 141.6, 159.7. MS calcd. for $C_{18}H_{25}NO_4$: 319.4 (M^+); found: 320.6.

***trans*-Oxazolidinone glycoside (14b)**

Following the same procedure as for compound **13b** gave **14b** in 75% yield. $[\alpha]_D$ +86.5 (*c* 1.35, $CHCl_3$). IR (neat, cm^{-1}): 1770. ^1H NMR (400 MHz, $CDCl_3$) δ: 0.87 (m, 3H), 1.04 (m, 3H), 1.24 (brs, 8H), 1.48–1.61 (m, 3H), 1.81 (m, 2H), 2.23 (m, 1H), 3.18 (m, 2H), 3.37 (s, 3H), 3.58 (m, 1H), 3.75 (m, 1H), 3.81 (m, 1H), 4.89 (brs, 1H). ^{13}C NMR (400 MHz, $CDCl_3$) δ: 9.4, 14.5, 22.9, 25.6, 27.2, 28.2, 29.3, 32.1, 35.5, 44.0, 55.3, 57.2, 73.0, 80.5, 98.3, 159.7. MS calcd. for $C_{16}H_{29}NO_4$: 299.3 (M^+); found: 300.2.

***trans*-Oxazolidinone lactol (15a)**

To a solution of compound **14a** (20 mg, 0.063 mmol) in dioxane (2 mL) was added 6 N HCl (0.8 mL) and the mixture was stirred at room temperature for 1 h. The mixture was taken up in EtOAc (5 mL), neutralized with 10% aq. $NaHCO_3$ solution, and extracted with EtOAc (15 mL). The organic phase was washed with brine, dried over Na_2SO_4, concentrated, and the residue was purified by column chromatography (EtOAc–hexanes, 1:1) to afford **15a** (18 mg, 94%). $[\alpha]_D$ +13.6 (*c* 0.45, $CHCl_3$). IR (neat, cm^{-1}): 1718. ^1H NMR (400 MHz, $CDCl_3$) δ: 1.03 (t, 3H, *J* = 8.7 Hz), 1.41–1.71 (brm, 4H), 1.81–1.99 (m, 2H), 2.59–2.88 (m, 3H), 2.98 (m, 1H), 3.56 (m, 1H), 3.66 (m, 1H), 4.01 (t, 1H, *J* = 3.4 Hz), 4.25 (q, 1H, *J* = 9.8, 3.4 Hz), 7.19–7.29 (m, 5H), 9.89 (s, 1H). ^{13}C NMR (400 MHz, $CDCl_3$) δ: 10.0, 25.7, 29.2, 33.3, 42.3, 47.6, 51.5, 73.9, 81.1, 126.5, 128.7, 128.9, 141.5, 157.5, 199.2. MS calcd. for $C_{17}H_{23}NO_4$: 305.3 (M^+); found: 306.0.

***trans*-Oxazolidinone lactol (15b)**

Following the same procedure as for compound **14b** gave **15b** in 90% yield. $[\alpha]_D$ +9.4 (*c* 0.65, $CHCl_3$). IR (neat, cm^{-1}): 1724. ^1H NMR (400 MHz, $CDCl_3$) δ: 0.88 (t, 3H, *J* = 6.9 Hz), 1.04 (t, 3H, *J* = 7.4 Hz), 1.27 (brs, 9H), 1.42–1.63 (m, 5H), 2.78–2.98 (m, 3H), 3.46 (m, 1H), 3.68 (m, 1H), 4.02 (t, 3H, *J* = 4.7 Hz), 4.27 (q, 1H, *J* = 4.7, 6.4 Hz), 9.89 (s, 1H). ^{13}C NMR (400 MHz, $CDCl_3$) δ: 10.1, 14.5, 23.0, 25.7, 27.0, 29.3, 32.1, 42.6, 47.6, 51.5, 73.8, 81.1, 157.5, 199.6. MS calcd. for $C_{15}H_{27}NO_4$: 285.2 (M^+); found: 286.2.

***trans*-Oxazolidinone lactone (16a)**

To a mixture of compound **15a** (10 mg, 0.0328 mmol) and 4 Å molecular sieves (15 mg) in DCM (2 mL) was added pyridinium chlorochromate (11 mg, 0.0492 mmol) under an argon atmosphere and the mixture was stirred for 4 h at room temperature. After filtration and normal workup, the mixture was purified by column chromatography (EtOAc–hexanes, 4:6) to obtain compound **16a** (7 mg, 68%). $[\alpha]_D$ +49.2 (*c* 0.2, $CHCl_3$). IR (neat, cm^{-1}): 1751. ^1H NMR (400 MHz, $CDCl_3$) δ: 1.12 (t, 3H, *J* = 5.6 Hz), 1.59 (brs, 2H), 1.88 (m, 2H), 2.59 (m, 2H), 2.68–2.87 (m, 3H), 3.92 (m, 1H), 3.52 (m, 1H), 4.33 (m, 1H), 4.46 (m, 1H), 7.17–7.32 (m, 5H). ^{13}C NMR (400 MHz, $CDCl_3$) δ: 7.3, 29.3, 30.1, 33.1, 33.2, 42.3, 46.6, 52.1, 80.5, 126.6, 128.7, 128.9, 141.2, 156.5, 207.2. MS calcd. for $C_{17}H_{21}NO_4$: 303.2 (M^+); found: 304.6.

***trans*-Oxazolidinone lactone (16b)**

Following the same procedure as for compound **15b** gave **16b** in 51% yield. $[\alpha]_D$ +16.4 (*c* 0.25, $CHCl_3$). IR (neat, cm^{-1}): 1754, 1724. ^1H NMR (400 MHz, $CDCl_3$) δ: 0.86 (t, 3H, *J* = 6.9 Hz), 1.11 (t, 3H, *J* = 7.5 Hz), 1.29 (brs, 6H), 1.39–1.62 (m, 4H), 2.72 (m, 2H), 2.79–3.02 (m, 2H), 3.42 (m, 1H), 4.34 (q, 1H, *J* = 4.4, 6.9 Hz), 4.46 (m, 1H). ^{13}C NMR (400 MHz, $CDCl_3$) δ: 7.3, 14.5, 23.0, 26.9, 27.6, 30.1, 33.1, 42.7, 46.8, 52.2, 73.4, 80.6, 156.5, 207.5. MS calcd. for $C_{15}H_{25}NO_4$: 283.2 (M^+); found: 284.1.

Methyl 4-*O*-benzyl-2,6-dideoxy-6-*C*-methyl-3-*p*-nitrobenzoyl-α-D-*arabino*-hexopyranoside (17)

To a mixture of compound **9** (1.5 g, 5.64 mmol), triphenylphosphine (3.7 g, 14.1 mmol), and diisopropyl azodicarboxylate (2.8 g, 14.1 mmol) in THF (30 mL) was added *p*-nitrobenzoic acid (2.36 g, 14.1 mmol) in THF (5 mL) under an argon atmosphere at 0 °C. The mixture was stirred for 12 h at room temperature, then dilutedwith EtOAc (50 mL), washed with aq. $NaHCO_3$ and brine, dried over Na_2SO_4, and concentrated under vacuum. The residue was purified by column chromatography (EtOAc–hexanes, 5:95) to afford **17** as white solid (1.83 g, 78%); mp 70 °C. $[\alpha]_D$ –0.9 (*c* 1, $CHCl_3$). IR (KBr, cm^{-1}): 1723. ^1H NMR (400 MHz, $CDCl_3$) δ: 1.02 (t, 3H, *J* = 8.3 Hz), 1.56 (m, 1H), 1.82 (m, 1H), 1.99 (m, 1H), 2.38 (m, 1H), 3.38 (s, 3H), 3.43 (t, 1H, *J* = 9.6 Hz), 3.69 (t, 1H, *J* = 8.3 Hz), 4.65 (s, 2H), 4.81 (brs, 1H), 5.58 (m, 1H), 7.19 (s, 5H), 8.12 (d, 2H, *J* = 11 Hz), 8.25 (d, 2H, *J* = 11 Hz). ^{13}C NMR (400 MHz, $CDCl_3$) δ: 10.3, 25.1, 35.8, 54.9, 72.1, 74.1, 75.3, 81.4, 123.9, 128.0, 128.2, 128.8, 131.1, 136.1, 138.2, 150.9, 164.1. MS calcd. for $C_{22}H_{25}NO_7$: 415.2 (M^+); found: 384.3 (M^+ – OMe).

© 2005 NRC Canada

Methyl 4-*O*-benzyl-2,6-dideoxy-6-*C*-methyl-α-D-*arabino*-hexopyranoside (18)

To a solution of compound **17** (1.83 g, 4.41 mmol) in MeOH (30 mL) was added catalytic NaOMe and the mixture was stirred for 10 h at room temperature. The mixture was concentrated under reduced pressure and purified by column chromatography (EtOAc–hexanes, 1:5) to obtain **18** as white solid (1.1 g, 93%); mp 76 °C. $[\alpha]_D$ +68.6 (*c* 1, $CHCl_3$). IR (KBr, cm^{-1}): 3225. ^1H NMR (400 MHz, $CDCl_3$) δ: 1.02 (t, 3H, *J* = 7.6 Hz), 1.56 (m, 1H), 1.69 (m, 1H), 1.96 (m, 1H), 2.04–2.18 (m, 2H), 3.03 (t, 1H, *J* = 8.3 Hz), 3.33 (s, 3H), 3.49 (t, 1H, *J* = 8.4 Hz), 4.01 (m, 1H), 4.67–4.81 (m, 3H), 7.22–7.39 (m, 5H). ^{13}C NMR (400 MHz, $CDCl_3$) δ: 10.4, 25.1, 38.0, 54.8, 69.5, 72.0, 75.4, 85.0, 98.5, 128.2, 128.4, 129.1, 138.1. FAB^+ MS calcd. for $C_{15}H_{22}NO_4$: 266.2 (M^+); found: 265.1 ($M^+ - H$).

Methyl 4-*O*-benzyl-2,6-dideoxy-3-*O*-methanesulfonyl-6-*C*-methyl-α-D-*arabino*-hexopyranoside (19)

To a solution of compound **18** (0.95 g, 3.57 mmol) in pyridine (12 mL) was added methanesulfonyl chloride (0.69 mL, 8.93 mmol) at 0 °C and the mixture was stirred for 12 h allowing it to warm to room temperature. The mixture was diluted with Et_2O (20 mL), washed sequentially with cold dilute 5% HCl, aq. 5% $NaHCO_3$ solution, and water then with brine, dried over Na_2SO_4, and concentrated under vacuum. The residue was purified by column chromatography (EtOAc–hexanes, 1:4) to obtain **19** as white solid (1.2 g, 97%); mp 75 °C. $[\alpha]_D$ +98 (*c* 1, $CHCl_3$). IR (KBr, cm^{-1}): 1356. ^1H NMR (400 MHz, $CDCl_3$) δ: 1.02 (t, 3H, *J* = 8.2 Hz), 1.49 (m, 1H), 1.96 (m, 2H), 2.42 (m, 1H), 2.89 (s, 3H), 3.22–3.33 (m, 4H), 3.57 (t, 1H, *J* = 8.3 Hz), 4.67 (m, 1H), 4.78 (m, 2H), 4.91 (m, 1H), 7.22–7.39 (m, 5H). ^{13}C NMR (400 MHz, $CDCl_3$) δ: 10.3, 25.0, 37.5, 38.2, 54.9, 72.3, 75.6, 81.0, 97.8, 128.2, 128.4, 129.0, 138.0. MS calcd. for $C_{16}H_{24}O_6S$: 344.1 (M^+); found: 362.3 ($M^+ + H_2O$).

Methyl 2,6-dideoxy-3-*O*-methanesulfonyl-6-*C*-methyl-α-D-*arabino*-hexopyranoside (20)

A mixture of compound **19** (1.0 g, 2.91 mmol) and 10% Pd-on-carbon (10 mg) in EtOAc (10 mL) was stirred under a hydrogen atmosphere for 10 h; the mixture was filtered, washed with EtOAc (10 mL), concentrated, and purified by column chromatography (EtOAc–hexanes, 3:7) to afford **20** as a solid (0.69 g, 93%); mp 88 °C. $[\alpha]_D$ +65.2 (*c* 0.5, $CHCl_3$). IR (KBr, cm^{-1}): 3540. ^1H NMR (400 MHz, $CDCl_3$) δ: 1.01 (t, 3H, *J* = 6.9 Hz), 1.49 (m, 1H), 1.95 (m, 2H), 2.34 (dd, 1H, *J* = 4.8, 12.4 Hz), 3.11 (s, 3H), 3.32 (s, 3H), 3.41 (t, 1H, *J* = 8.9 Hz), 3.49 (t, 1H, *J* = 9.4 Hz), 4.80 (s, 1H), 4.91 (m, 1H). ^{13}C NMR (300 MHz, $CDCl_3$) δ: 10.1, 23.9, 36.5, 38.1, 54.8, 72.2, 73.3, 80.9, 97.5.

Methyl 3-azido-6-*C*-methyl-2,3,6-trideoxy-α-D-*ribo*-hexopyranoside (21)

A mixture of compound **20** (0.65 g, 2.56 mmol) and NaN_3 (0.97 g, 14.84 mmol) in DMF (12 mL) was heated at 125 °C for 12 h under an argon atmosphere. The mixture was filtered, washed with Et_2O (40 mL), the filtrate concentrated and purified by column chromatography (EtOAc–hexanes, 1:9) to afford **21** as a crystalline white solid (0.39 g, 76%); mp 75 °C. $[\alpha]_D$ +277.8 (*c* 0.5, $CHCl_3$). IR (KBr, cm^{-1}): 2102. ^1H NMR (300 MHz, $CDCl_3$) δ: 0.99 (t, 3H, *J* = 7.4 Hz), 1.48 (m, 1H), 1.58 (s, 1H), 1.86–2.11 (m, 2H), 2.23 (m, 1H), 3.36 (s, 3H), 3.39 (m, 1H), 3.61 (m, 1H), 4.05 (m, 1H), 4.69 (d, 1H, *J* = 4.2 Hz). ^{13}C NMR (300 MHz, $CDCl_3$) δ: 10.1, 24.1, 32.2, 55.6, 59.5, 69.4, 70.3, 96.3.

Methyl 3-azido-4-*p*-methoxybenzyl-6-*C*-methyl-2,3,6-trideoxy-α-D-*ribo*-hexopyranoside (22)

To a solution of compound **21** (190 mg, 0.946 mmol) in DMF was added 60% NaH (62 mg, 1.61 mmol) at 0 °C and the mixture was stirred for 10 min. *p*-Methoxybenzyl bromide (5.6 mL, 0.27 mol/L in toluene) was added to the mixture and the mixture stirred for 6 h allowing it to warm to room temperature. The mixture was quenched with ice, extracted with Et_2O (50 mL), washed with brine, dried over Na_2SO_4, and concentrated under vacuum. The residue was purified by column chromatography (EtOAc–hexanes, 1:9) to afford **22** (285 mg, 94%). $[\alpha]_D$ +174.8 (*c* 1.2, $CHCl_3$). IR (neat, cm^{-1}): 2099. ^1H NMR (400 MHz, $CDCl_3$) δ: 0.97 (t, 3H, *J* = 7.4 Hz), 1.36 (m, 1H), 1.93 (m, 2H), 2.09 (dd, 1H, *J* = 2.3, 4.9 Hz), 3.29 (dd, 1H, *J* = 3.5, 9.4 Hz), 3.36 (s, 3H), 3.81 (s, 3H), 3.87 (t, 1H, *J* = 7.1 Hz), 4.02 (m, 1H), 4.47 (d, 1H, *J* = 11.3 Hz), 4.62 (m, 2H), 6.89 (d, 2H, *J* = 8.4 Hz), 7.29 (d, 2H, *J* = 8.4 Hz). ^{13}C NMR (400 MHz, $CDCl_3$) δ: 10.1, 24.6, 33.6, 55.6, 68.1, 71.6, 78.2, 97.0, 114.3, 130.2.

Methyl 4-*p*-methoxybenzyl-6-*C*-methyl-3-phenylethylamino-2,3,6-trideoxy-α-D-*ribo*-hexopyranoside (23a)

To a solution of compound **22** (46 mg, 0.144 mmol) in THF was added trimethylphosphine (0.55 mL, 1 mol/L in toluene) and the mixture was stirred under an argon atmosphere for 30 min. Water (25 μL) was added to the mixture and it was stirred under reflux conditions for 45 min. The mixture was concentrated under vacuum and dried properly. The residue was diluted with dry MeOH (3 mL) under an argon atmosphere, the requisite aldehyde (0.14 mmol) was added, followed by the addition of AcOH (32 μL), then the mixture was stirred for 1 h. $NaCNBH_3$ (18 mg, 0.287 mmol) was added and the mixture stirred for 12 h at room temperature. The mixture was concentrated under vacuum, diluted with EtOAc (10 mL), washed with 10% $NaHCO_3$ and brine, the organic phase was dried over Na_2SO_4, concentrated under vacuum, and the residue was purified by column chromatography (EtOAc–hexanes, 1:1) to afford **23a** (79%). $[\alpha]_D$ +134 (*c* 1, $CHCl_3$). IR (neat, cm^{-1}): 3309. ^1H NMR (400 MHz, $CDCl_3$) δ: 0.97 (t, 3H, *J* = 7.4 Hz), 1.35 (m, 2H), 1.84 (m, 2H), 2.04 (m, 3H), 2.64 (m, 2H), 2.81 (m, 1H), 2.91 (m, 1H), 3.20 (m, 1H), 3.32 (m, 1H), 3.37 (s, 3H), 3.68 (m, 1H), 3.79 (m, 3H), 4.52 (m, 2H), 4.69 (m, 1H), 6.88 (d, 2H, *J* = 8.1 Hz), 7.19 (t, 3H, *J* = 7.6 Hz), 7.35 (d, 4H, *J* = 8.1 Hz). ^{13}C NMR (400 MHz, $CDCl_3$) δ: 9.9, 24.9, 29.8, 30.8, 33.4, 47.3, 53.6, 55.7, 68.9, 72.1, 97.8, 114.3, 126.6, 128.8, 128.9, 130.5, 141.3, 159.9. MS calcd. for $C_{25}H_{35}NO_4$: 413.3 (M^+); found: 414.4.

Methyl 3-heptylamino-4-*p*-methoxybenzyl-6-*C*-methyl-2,3,6-trideoxy-α-D-*ribo*-hexopyranoside (23b)

Following the same procedure as for compound **22** gave **23b** in 65% yield. $[\alpha]_D$ +118 (*c* 1, $CHCl_3$). IR (neat, cm^{-1}): 3219. ^1H NMR (400 MHz, $CDCl_3$) δ: 0.91 (t, 3H, *J* =

© 2005 NRC Canada

7.4 Hz), 0.98 (t, 3H, *J* = 7.4 Hz), 1.31 (brm, 10H), 1.63 (m, 2H), 1.85 (m, 2H), 2.13 (m, 1H), 2.94 (m, 2H), 3.24–3.42 (m, 5H), 3.69 (t, 1H, *J* = 7.3 Hz), 3.82 (s, 3H), 4.59 (m, 2H), 4.74 (brs, 1H), 6.88 (d, 2H, *J* = 8.3 Hz), 7.33 (d, 2H, *J* = 8.3 Hz). ^{13}C NMR (400 MHz, $CDCl_3$) δ: 9.3, 13.9, 22.4, 24.3, 26.5, 28.7, 29.6, 31.5, 46.9, 53.2, 55.2, 68.1, 71.6, 97.0, 113.9, 128.9, 130.1, 159.5. MS calcd. for $C_{23}H_{39}NO_4$: 393.3 (M^+); found: 394.4.

Methyl 3-(4-quinolinyl)propylamino-4-*p*-methoxybenzyl-6-*C*-methyl-2,3,6-trideoxy-α-D-*ribo*-hexopyranoside (23c)

Following the same procedure as for compound **22** gave **23c** in 76% yield. $[\alpha]_D$ +78.7 (*c* 1.9, $CHCl_3$). IR (neat, cm^{-1}): 3350. ^{1}H NMR (400 MHz, $CDCl_3$) δ: 0.98 (t, 3H, *J* = 7.4 Hz), 1.25 (m, 1H), 1.41 (m, 1H), 1.84 (m, 1H), 2.01 (m, 3H), 2.72 (m, 1H), 2.84 (m, 1H), 3.03 (m, 1H), 3.13 (m, 2H), 3.25 (dd, 1H, *J* = 3.8, 8.4 Hz), 3.38 (s, 3H), 3.75–3.83 (m, 4H), 4.52 (m, 2H), 4.67 (m, 1H), 6.83 (m, 2H), 7.22 (m, 3H), 7.56 (t, 1H, *J* = 8.1 Hz), 7.67 (t, 1H, *J* = 8.1 Hz), 8.05 (d, 1H, *J* = 8.3 Hz), 8.11 (d, 1H, *J* = 8.3 Hz), 8.79 (d, 1H, *J* = 4.4 Hz). ^{13}C NMR (400 MHz, $CDCl_3$) δ: 10.2, 24.9, 30.0, 30.4, 32.5, 47.8, 52.6, 55.6, 55.7, 69.5, 71.2, 98.4, 114.3, 121.1, 124.0, 126.8, 127.9, 129.5, 130.0, 130.5, 148.4, 148.7, 150.7, 159.7. MS calcd. for $C_{28}H_{36}N_2O_4$: 464.3 (M^+); found: 465.5.

Methyl 3-(3-quinolinyl)-*E*-propenylamino-4-*p*-methoxybenzyl-6-*C*-methyl-2,3,6-trideoxy-α-D-*ribo*-hexopyranoside (23d)

Following the same procedure as for compound **22** gave **23d** in 70% yield. $[\alpha]_D$ +49.9 (*c* 1.1, $CHCl_3$). IR (neat, cm^{-1}): 3413. ^{1}H NMR (400 MHz, $CDCl_3$) δ: 0.99 (t, 3H, *J* = 9.4 Hz), 1.37 (m, 1H), 1.86 (m, 2H), 2.06 (m, 1H), 3.29 (m, 1H), 3.41 (s, 3H), 2.91 (m, 1H), 3.20 (m, 1H), 3.32 (m, 1H), 3.37 (s, 3H), 3.59–3.91 (m, 6H), 4.51–4.85 (m, 4H), 6.84 (m, 3H), 7.29 (m, 3H), 7.53 (m, 1H), 7.67 (t, 1H, *J* = 9.7 Hz), 7.78 (m, 1H), 8.02 (m, 2H), 8.88 (s, 1H). MS calcd. for $C_{28}H_{34}N_2O_4$: 462.3 (M^+); found: 342.1 (M^+ – PMB).

Methyl 3-[4-(3-pyridinyl)-1-imidazolyl)butylamino-4-*p*-methoxybenzyl-6-*C*-methyl-2,3,6-trideoxy-α-D-*ribo*-hexopyranoside (23e)

Following the same procedure as for compound **22** gave **23e** in 80% yield. $[\alpha]_D$ +71.5 (*c* 0.2, MeOH). IR (neat, cm^{-1}): 3360. ^{1}H NMR (400 MHz, CD_3OD) δ: 0.98 (t, 3H, *J* = 7.8 Hz), 1.46 (m, 1H), 1.58 (m, 2H), 1.73–1.86 (m, 3H), 2.01 (m, 1H), 2.67 (m, 1H), 2.81 (m, 1H), 3.33 (m, 5H), 3.77 (s, 3H), 3.79 (m, 1H), 4.10 (t, 1H, *J* = 7.1 Hz), 4.54 (m, 2H), 4.69 (brs, 1H), 6.87 (d, 2H, *J* = 8.1 Hz), 7.27 (d, 2H, *J* = 8.1 Hz), 7.43 (m, 1H), 7.68 (s, 1H), 7.79 (s, 1H), 8.15 (q, 1H, *J* = 2.1, 8.6 Hz), 8.39 (m, 1H), 8.91 (s, 1H). ^{13}C NMR (400 MHz, CD_3OD) δ: 9.1, 15.7, 16.4, 24.3, 28.2, 46.7, 47.0, 52.6, 54.5, 54.7, 69.7, 71.1, 76.0, 97.8, 113.8, 117.1, 124.4, 130.0, 130.9, 133.0, 138.2, 138.8, 145.6, 147.0, 160.0. MS calcd. for $C_{28}H_{38}N_4O_4$: 494.3 (M^+); found: 495.4.

Methyl 6-*C*-methyl-3-phenylethylamino-2,3,6-trideoxy-α-D-*ribo*-hexopyranoside (24a)

To a solution of compound **23a** (30 mg, 0.073 mmol) in AcCN and water (2 mL, 9:1) was added ammonium cerium(IV) nitrate (151 mg, 0.277 mmol) and the mixture was vigorously stirred for 12 h at room temperature. The mixture was diluted with EtOAc (10 mL), washed with aq. 5% $NaHCO_3$ and then with brine, dried over Na_2SO_4, and concentrated under vacuum. The residue was purified by column chromatography (MeOH–EtOAc, 1:99) to afford **24a** (19 mg, 89%). $[\alpha]_D$ +123.1 (*c* 0.8, $CHCl_3$). IR (neat, cm^{-1}): 3342, 3233. ^{1}H NMR (400 MHz, $CDCl_3$) δ: 1.02 (t, 3H, *J* = 9.5 Hz), 1.42 (m, 1H), 1.77 (m, 1H), 1.84 (m, 2H), 1.98 (m, 1H), 2.14 (dd, 1H, *J* = 2.1, 13.4 Hz), 2.48 (m, 1H), 2.66 (m, 2H), 2.85 (m, 2H), 3.24 (m, 1H), 3.38 (m, 4H), 4.74 (m, 1H), 7.18–7.34 (m, 5H). ^{13}C NMR (400 MHz, $CDCl_3$) δ: 10.3, 25.2, 31.6, 31.7, 33.7, 47.5, 55.3, 55.4, 68.7, 70.3, 98.5, 126.3, 128.8, 142.2. MS calcd. for $C_{17}H_{27}NO_3$: 293.2 (M^+); found: 294.2.

Methyl 3-heptylamino-6-*C*-methyl-2,3,6-trideoxy-α-D-*ribo*-hexopyranoside (24b)

Following the same procedure as for compound **23b** gave **24b** in 75% yield. $[\alpha]_D$ +74.1 (*c* 1.5, $CHCl_3$). IR (neat, cm^{-1}): 3339. ^{1}H NMR (400 MHz, $CDCl_3$) δ: 0.89 (t, 3H, *J* = 7.2 Hz), 0.99 (t, 3H, *J* = 7.1 Hz), 1.31 (brm, 8H), 1.44 (m, 3H), 1.74 (m, 1H), 1.97 (m, 1H), 2.14 (dd, 1H, *J* = 1.5, 13.2 Hz), 2.38 (m, 1H), 2.71–2.84 (m, 2H), 3.18 (m, 1H), 3.21–3.37 (m, 4H), 4.72 (brs, 1H). ^{13}C NMR (400 MHz, $CDCl_3$) δ: 10.4, 14.5, 23.1, 25.2, 27.5, 29.6, 30.1, 31.7, 32.3, 48.5, 55.0, 55.2, 68.7, 70.4, 98.6. MS calcd. for $C_{15}H_{31}NO_3$: 273.2 (M^+); found: 274.2.

Methyl 3-(4-quinolinyl)propylamino-6-*C*-methyl-2,3,6-trideoxy-α-D-*ribo*-hexopyranoside (24c)

Following the same procedure as for compound **23c** gave **24c** in 83% yield. $[\alpha]_D$ +36.9 (*c* 1.6, $CHCl_3$). IR (neat, cm^{-1}): 3340. ^{1}H NMR (400 MHz, $CDCl_3$) δ: 1.01 (t, 3H, *J* = 7.4 Hz), 1.29 (m, 1H), 1.42 (m, 1H), 1.78 (m, 1H), 1.97 (m, 2H), 2.17 (m, 1H), 2.57 (m, 1H), 2.79 (brs, 1H), 2.98 (m, 2H), 3.17 (t, 1H, *J* = 7.8 Hz), 3.22–3.35 (m, 4H), 4.75 (brs, 1H), 7.24 (d, 3.2H), 7.58 (t, 1H, *J* = 7.3 Hz), 7.70 (t, 1H, *J* = 7.3 Hz), 8.05 (d, 1H, *J* = 8.4 Hz), 8.12 (d, 1H, *J* = 8.4 Hz), 8.82 (d, 1H, *J* = 4.3 Hz). ^{13}C NMR (400 MHz, $CDCl_3$) δ: 10.3, 25.2, 30.0, 30.1, 31.0, 31.9, 48.1, 55.2, 68.7, 70.4, 98.7, 121.2, 123.9, 126.8, 127.9, 129.5, 130.0, 130.6, 148.4, 148.7, 150.5. MS calcd. for $C_{20}H_{28}N_2O_3$: 344.4 (M^+); found: 345.3.

Methyl 3-(3-quinolinyl)-*E*-propenylamino-6-*C*-methyl-2,3,6-trideoxy-α-D-*ribo*-hexopyranoside (24d)

Following the same procedure as for compound **23d** gave **24d** in 72% yield. $[\alpha]_D$ +89.8 (*c* 0.5, $CHCl_3$). IR (neat, cm^{-1}): 3351. ^{1}H NMR (400 MHz, $CDCl_3$) δ: 0.99 (t, 3H, *J* = 7.2 Hz), 1.24 (m, 1H), 1.47 (m, 1H), 1.83 (d, 1H, *J* = 14.3 Hz), 1.99 (m, 1H), 2.21 (d, 1H, *J* = 14.3 Hz), 3.18 (m, 1H), 3.37 (s, 3H), 3.42 (m, 1H), 3.59 (m, 1H), 3.83 (m, 1H), 4.82 (brs, 1H), 6.59 (m, 1H), 6.79 (d, 1H, *J* = 15.2 Hz), 7.51 (t, 1H, *J* = 8.2 Hz), 7.69 (t, 1H, *J* = 8.2 Hz), 7.79 (d, 1H, *J* = 7.6 Hz), 8.05 (m, 2H), 8.99 (s, 1H). MS calcd. for $C_{20}H_{26}N_2O_3$: 342.2 (M^+); found: 343.2.

Methyl 3-[4-(3-pyridinyl)-1-imidazolyl)butylamino-6-*C*-methyl-2,3,6-trideoxy-α-D-*ribo*-hexopyranoside (24e)

Following the same procedure as for compound **23e** gave

© 2005 NRC Canada

24e in 90% yield. $[\alpha]_D$ +19.5 (*c* 1.5, MeOH). IR (neat, cm^{-1}): 3200. ^1H NMR (400 MHz, CD_3OD) δ: 1.01 (t, 3H, *J* = 7.2 Hz), 1.42 (m, 1H), 1.64–2.01 (brm, 6H), 2.22 (dd, 1H, *J* = 2.1, 8.2 Hz), 3.12 (m, 1H), 3.11 (m, 1H), 3.29 (s, 3H), 3.52 (m, 1H), 3.62 (m, 2H), 4.19 (m, 2H), 4.79 (brs, 1H), 7.48 (m, 1H), 7.79 (s, 1H), 7.99 (s, 1H), 8.21 (m, 1H), 8.41 (m, 1H), 8.94 (s, 1H). ^{13}C NMR (400 MHz, CD_3OD) δ: 9.0, 22.9, 24.6, 28.7, 46.0, 47.0, 54.3, 56.5, 66.9, 69.8, 97.0, 117.9, 124.9, 134.0, 138.7, 144.9, 146.7. MS calcd. for $C_{20}H_{30}N_2O_3$: 374.2 (M^+); found: 375.3.

***cis*-Oxazolidinone glycoside (25a)**

To a mixture of compound **24a** (16 mg, 0.0546 mmol) and Et_3N (0.12 mL, 0.82 mmol) in DCM (3 mL) was added carbonyldiimidazole (45 mg, 0.273 mmol) under an argon atmosphere and the mixture was stirred for 5 h at room temperature. The mixture was concentrated under vacuum and purified by column chromatography (EtOAc–hexanes, 1:4) to obtain **25a** (20 mg, 91%). $[\alpha]_D$ +128.6 (*c* 1, $CHCl_3$). IR (neat, cm^{-1}): 1752. ^1H NMR (400 MHz, $CDCl_3$) δ: 1.02 (t, 3H, *J* = 8.3 Hz), 1.54 (m, 1H), 1.72 (m, 1H), 1.83 (m, 4H), 2.14 (m, 1H), 2.63 (t, 1H, *J* = 8.4 Hz), 3.06 (m, 1H), 3.38 (s, 3H), 3.56 (m, 1H), 3.65 (m, 1H), 4.11 (t, 1H, *J* = 8.3 Hz), 4.72 (t, 1H, *J* = 6.9 Hz), 7.12–7.34 (m, 5H). ^{13}C NMR (400 MHz, $CDCl_3$) δ: 10.2, 26.7, 29.5, 30.0, 33.5, 51.3, 55.4, 69.4, 74.5, 97.3, 126.5, 128.7, 128.9, 141.6, 158.0. MS calcd. for $C_{18}H_{25}NO_4$: 319.2 (M^+); found: 320.2.

***cis*-Oxazolidinone glycoside (25b)**

Following the same procedure as for compound **24b** gave **25b** in 90% yield. $[\alpha]_D$ +127.8 (*c* 0.6, $CHCl_3$). IR (neat, cm^{-1}): 1751. ^1H NMR (400 MHz, $CDCl_3$) δ: 0.83 (t, 3H, *J* = 6.7 Hz), 1.05 (t, 3H, *J* = 6.7 Hz), 1.30 (brm, 8H), 1.57 (m, 3H), 1.81 (m, 2H), 2.24 (m, 1H), 2.98 (m, 1H), 3.39 (s, 3H), 3.47 (m, 1H), 3.67 (m, 1H), 3.82 (q, 1H, *J* = 7.2, 14.5 Hz), 4.18 (t, 1H, *J* = 8.2 Hz), 4.74 (t, 1H, *J* = 6.6 Hz). ^{13}C NMR (400 MHz, $CDCl_3$) δ: 10.2, 14.5, 23.0, 26.7, 27.1, 27.9, 29.3, 30.0, 32.1, 42.4, 51.2, 55.4, 69.5, 74.5, 97.4, 158.0. MS calcd. for $C_{16}H_{29}NO_4$: 299.2 (M^+); found: 300.2.

***cis*-Oxazolidinone glycoside (25c)**

Following the same procedure as for compound **24c** gave **25c** in 68% yield. $[\alpha]_D$ +108.2 (*c* 1.2, $CHCl_3$). IR (neat, cm^{-1}): 1751. ^1H NMR (400 MHz, $CDCl_3$) δ: 1.02 (t, 3H, *J* = 7.4 Hz), 1.27 (m, 1H), 1.57 (m, 1H), 1.81 (m, 2H), 2.04 (m, 1H), 2.18 (m, 1H), 3.12 (t, 2H, *J* = 6.9 Hz), 3.21 (m, 1H), 3.36 (s, 3H), 3.58 (m, 1H), 3.68 (m, 1H), 3.81 (m, 1H), 4.15 (t, 1H, *J* = 8.3 Hz), 4.71 (t, 1H, *J* = 5.6 Hz), 7.27 (d, 1H, *J* = 3.2 Hz), 7.59 (t, 1H, *J* = 8.1 Hz), 7.73 (t, 1H, *J* = 8.1 Hz), 8.01 (d, 1H, *J* = 8.5 Hz), 8.13 (d, 1H, *J* = 8.5 Hz), 8.82 (d, 1H, *J* = 4.3 Hz). ^{13}C NMR (400 MHz, $CDCl_3$) δ: 10.2, 26.6, 28.1, 29.6, 30.0, 42.4, 51.5, 69.2, 74.5, 97.1, 121.1, 123.7, 127.1, 127.8, 129.7, 130.0, 130.8, 147.5, 148.7, 150.6, 158.2. MS calcd. for $C_{27}H_{26}N_2O_4$: 370.2 (M^+); found: 371.2.

***cis*-Oxazolidinone glycoside (25d)**

Following the same procedure as for compound **24d** gave **25d** in 65% yield. $[\alpha]_D$ +39.8 (*c* 0.45, $CHCl_3$). IR (neat, cm^{-1}): 1747. ^1H NMR (400 MHz, $CDCl_3$) δ: 1.03 (t, 3H, *J* = 7.4 Hz), 1.59 (m, 1H), 1.84 (m, 2H), 2.28 (m, 1H), 3.42 (s, 3H), 3.78 (t, 1H, *J* = 8.9 Hz), 3.95 (m, 2H), 4.25 (t, 1H, *J* = 8.7 Hz), 4.39 (dd, 1H, *J* = 1.9, 13.2 Hz), 4.78 (brs, 1H), 6.42 (m, 1H), 6.79 (d, 1H, *J* = 15.2 Hz), 7.59 (t, 1H, *J* = 8.2 Hz), 7.79 (t, 1H, *J* = 8.2 Hz), 7.85 (d, 1H, *J* = 7.6 Hz), 8.18 (m, 2H), 8.99 (s, 1H). ^{13}C NMR (400 MHz, $CDCl_3$) δ: 10.2, 26.6, 29.9, 30.1, 44.9, 46.2, 51.5, 55.5, 69.1, 74.6, 77.7, 97.2, 127.5, 128.2, 128.4, 129.7, 130.8, 134.7, 146.5, 148.0, 157.9. MS calcd. for $C_{21}H_{24}N_2O_4$: 368.2 (M^+); found: 369.2.

***cis*-Oxazolidinone glycoside (25e)**

Following the same procedure as for compound **24e** gave **25e** in 75% yield. $[\alpha]_D$ +31.3 (*c* 1, MeOH). IR (neat, cm^{-1}): 1745. ^1H NMR (400 MHz, $CDCl_3$) δ: 1.01 (t, 3H, *J* = 7.5 Hz), 1.59 (m, 3H), 1.81 (m, 2H), 1.89 (m, 2H), 2.19 (m, 1H), 3.14 (m, 2H), 3.39 (s, 3H), 3.64 (m, 1H), 3.78 (m, 1H), 4.05 (t, 2H, *J* = 6.9 Hz), 4.17 (t, 1H, *J* = 8.6 Hz), 4.71 (t, 1H, *J* = 5.9 Hz), 7.31 (m, 1H), 7.55 (s, 1H), 7.92 (m, 1H), 8.09 (dd, 1H, *J* = 1.7, 7.9 Hz), 8.47 (m, 1H), 8.98 (s, 1H). ^{13}C NMR (400 MHz, CD_3OD) δ: 9.1, 24.4, 26.2, 28.0, 29.2, 41.3, 46.8, 51.5, 54.3, 69.0, 74.8, 97.4, 117.2, 120.9, 124.4, 131.0, 133.0, 135.1, 138.2, 138.9, 145.6, 147.0, 159.2. MS calcd. for $C_{21}H_{28}N_4O_4$: 400.2 (M^+); found: 401.3.

***cis*-Oxazolidinone lactol (26a)**

To a solution of compound **25a** (14 mg, 0.0438 mmol) in dioxane (2 mL) was added 6 N HCl (0.7 mL) and the mixture was stirred at room temperature for 1 h. The mixture was taken up in EtOAc (5 mL), neutralized with 10% $NaHCO_3$, extracted with EtOAc (15 mL), and the organic phase was washed with brine, dried over Na_2SO_4, concentrated and the residue was purified by column chromatography (EtOAc–hexanes, 1:1) to afford **26a** (11 mg, 84%). $[\alpha]_D$ +68.7 (*c* 0.75, $CHCl_3$). IR (neat, cm^{-1}): 3398, 1733. ^1H NMR (300 MHz, $CDCl_3$) δ: 0.99 (t, 3H, *J* = 9.6 Hz), 1.51 (m, 1H), 1.58–1.98 (m, 4H), 2.01–2.33 (m, 1H), 2.64 (t, 2H, *J* = 9.4 Hz), 3.08 (m, 1H), 3.38–3.78 (m, 2H), 3.79–4.27 (m, 2H), 5.05–5.29 (m, 1H), 7.14–7.35 (m, 5H). ^{13}C NMR (300 MHz, $CDCl_3$) δ: 9.8, 9.9, 26.5, 26.6, 29.3, 29.5, 30.1, 30.8, 31.5, 33.5, 42.3, 42.4, 51.3, 52.6, 69.9, 72.9, 74.5, 75.2, 90.9, 92.3, 126.5, 126.6, 128.7, 128.9, 130.0, 141.4, 141.5, 157.9, 158.4. MS calcd. for $C_{17}H_{23}NO_4$: 302.2 (M^+); found: 306.2.

***cis*-Oxazolidinone lactol (26b)**

Following the same procedure as for compound **25b** gave **26b** in 73% yield. $[\alpha]_D$ +80.8 (*c* 0.65, $CHCl_3$). IR (neat, cm^{-1}): 1739. ^1H NMR (400 MHz, $CDCl_3$) δ: 0.84 (t, 3H, *J* = 7.2 Hz), 0.99 (t, 3H, *J* = 7.3 Hz), 1.28 (m, 8H), 1.51 (m, 3H), 1.61–1.97 (m, 3H), 2.06–2.37 (m, 1H), 2.91–3.53 (m, 3H), 3.81 (m, 1H), 4.21 (t, 1H, *J* = 11.1 Hz), 5.09–5.29 (m, 1H). ^{13}C NMR (400 MHz, $CDCl_3$) δ: 9.8, 9.9, 14.5, 23.0, 26.5, 26.6, 27.0, 27.6, 27.9, 29.3, 30.9, 31.5, 32.1, 42.5, 51.2, 52.5, 69.9, 72.8, 74.5, 75.3, 91.0, 92.4, 158.0, 158.4. MS calcd. for $C_{15}H_{27}NO_4$: 285.2 (M^+); found: 286.2.

***cis*-Oxazolidinone lactol (26c)**

Following the same procedure as for compound **25c** gave **26c** in 89% yield. $[\alpha]_D$ +62.8 (*c* 0.6, $CHCl_3$). IR (neat, cm^{-1}): 3368, 1748. ^1H NMR (300 MHz, $CDCl_3$) δ: 0.99 (t, 3H, *J* = 7.4 Hz), 1.24 (m, 1H), 1.57 (m, 1H), 1.72–2.28 (brm, 4H), 3.12 (m, 2H), 3.21–3.38 (m, 1H), 3.42–3.64 (m, 2H), 3.77–3.91 (m, 1H), 4.13 (m, 1H), 5.05–5.29 (m, 1H), 7.25 (m,

© 2005 NRC Canada

1H), 7.58 (m, 1H), 7.69 (t, 1H, *J* = 7.3 Hz), 8.01 (t, 1H, *J* = 7.3 Hz), 8.13 (d, 1H, *J* = 8.4 Hz), 8.77 (dd, 1H, *J* = 4.3, 15.4 Hz). ^{13}C NMR (400 MHz, $CDCl_3$) δ: 9.9, 10.0, 26.5, 26.6, 28.2, 28.3, 29.7, 29.7, 30.9, 31.8, 42.5, 42.6, 51.7, 53.3, 69.6, 73.1, 74.5, 75.3, 90.7, 92.1, 120.9, 121.1, 123.6, 123.7, 127.1, 127.8, 129.7, 129.8, 130.4, 130.5, 147.6, 147.7, 148.4, 148.5, 150.4, 150.5, 158.2, 158.7. MS calcd. for $C_{20}H_{24}N_2O_4$: 356.2 (M^+); found: 357.2.

***cis*-Oxazolidinone lactol (26d)**

Following the same procedure as for compound **25d** gave **26d** in 97% yield. $[\alpha]_D$ +29.8 (*c* 0.8, $CHCl_3$). IR (neat, cm^{-1}): 3364, 1750. ^{1}H NMR (400 MHz, $CDCl_3$) δ: 1.01 (t, 3H, *J* = 7.2 Hz), 1.61 (m, 1H), 1.79–2.08 (brm, 2H), 2.21–2.41 (m, 1H), 3.72 (m, 1H), 3.98 (m, 2H), 4.32 (m, 2H), 5.18–5.35 (m, 1H), 6.44 (m, 1H), 6.79 (d, 1H, *J* = 15.2 Hz), 7.59 (t, 1H, *J* = 8.2 Hz), 7.72 (t, 1H, *J* = 8.2 Hz), 7.82 (d, 1H, *J* = 7.6 Hz), 8.18 (m, 2H), 9.01 (s, 1H). ^{13}C NMR (400 MHz, $CDCl_3$) δ: 9.8, 9.9, 26.6, 30.1, 30.9, 31.7, 45.0, 45.1, 51.6, 53.1, 67.5, 69.5, 73.1, 74.6, 75.3, 77.6, 90.7, 92.2, 126.1, 126.9, 127.8, 129.1, 129.6, 130.4, 130.5, 133.9, 148.9, 158.9. MS calcd. for $C_{20}H_{22}N_2O_4$: 354.2 (M^+); found: 355.2.

***cis*-Oxazolidinone lactol (26e)**

Following the same procedure as for compound **25e** gave **26e** in 74% yield. $[\alpha]_D$ +27.6 (*c* 0.45, MeOH). IR (neat, cm^{-1}): 3120, 1745. ^{1}H NMR (300 MHz, CD_3OD) δ: 0.99 (t, 3H, *J* = 7.3 Hz), 1.63 (m, 5H), 1.89 (m, 2H), 2.12–2.31 (m, 1H), 3.14 (m, 1H), 3.41 (m, 2H), 3.73–3.96 (m, 1H), 4.14 (m, 2H), 4.25 (m, 1H), 4.91–5.19 (m, 1H), 7.45 (m, 1H), 7.71 (s, 1H), 7.79 (s, 1H), 8.14 (m, 1H), 8.38 (dd, 1H, *J* = 1.5, 4.9 Hz), 8.91 (s, 1H). ^{13}C NMR (400 MHz, CD_3OD) δ: 8.8, 8.9, 24.3, 24.5, 26.3, 28.0, 30.6, 31.3, 41.2, 41.3, 46.8, 51.7, 53.7, 69.3, 73.3, 75.1, 75.3, 90.3, 92.0, 117.2, 124.4, 130.9, 133.0, 138.8, 145.6, 147.0, 159.1. MS calcd. for $C_{20}H_{26}N_4O_4$: 386.2 (M^+); found: 387.3.

***cis*-Oxazolidinone lactone (27a)**

To a mixture of compound **26a** (10 mg, 0.0328 mmol) and 4 Å molecular sieves (15 mg) in DCM (2 mL) was added pyridinium chlorochromate (11 mg, 0.0492 mmol) under an argon atmosphere and the mixture was stirred for 4 h at room temperature. The mixture was filtered and processed as usual to give a residue that was purified by column chromatography (EtOAc–hexanes, 4:6) to obtain compound **27a** as a crystalline solid (9 mg, 89%); mp 93 °C. $[\alpha]_D$ +90.9 (*c* 0.65, $CHCl_3$). IR (KBr, cm^{-1}): 1749. ^{1}H NMR (400 MHz, $CDCl_3$) δ: 1.06 (t, 3H, *J* = 7.3 Hz), 1.78 (m, 1H), 1.87 (m, 3H), 2.53 (m, 1H), 2.66 (t, 1H, *J* = 7.4 Hz), 2.84 (dd, 1H, *J* = 5.2, 14.5 Hz), 3.08 (m, 1H), 3.54 (m, 1H), 4.02 (m, 1H), 4.15 (m, 1H), 4.27 (t, 1H, *J* = 9.2 Hz), 7.15–7.34 (m, 5H). ^{13}C NMR (400 MHz, $CDCl_3$) δ: 9.5, 25.6, 29.1, 33.5, 34.0, 42.6, 51.2, 71.9, 79.4, 126.8, 128.7, 129.1, 141.1, 156.4, 168.9. MS calcd. for $C_{17}H_{21}NO_4$: 303.1 (M^+); found: 304.2.

***cis*-Oxazolidinone lactone (27b)**

Following the same procedure as for compound **26b** gave **27b** in 80% yield. $[\alpha]_D$ +129 (*c* 0.3, $CHCl_3$). IR (neat, cm^{-1}): 1749. ^{1}H NMR (400 MHz, $CDCl_3$) δ: 0.84 (t, 3H, *J* = 8.2 Hz), 1.09 (t, 3H, *J* = 8.3 Hz), 1.31 (m, 8H), 1.59 (m, 2H), 1.79 (m, 1H), 1.99 (m, 1H), 2.62 (m, 1H), 3.02 (m, 1H), 3.51 (m, 1H), 4.21 (m, 2H), 4.23 (t, 1H, *J* = 9.5 Hz). ^{13}C NMR (400 MHz, $CDCl_3$) δ: 9.5, 14.5, 22.9, 25.6, 27.0, 27.6, 29.3, 32.1, 34.1, 42.8, 51.3, 71.9, 79.5, 156.5, 169.0. MS calcd. for $C_{15}H_{25}NO_4$: 283.2 (M^+); found: 284.2.

***cis*-Oxazolidinone lactone (27c)**

Following the same procedure as for compound **26c** gave **27c** in 76% yield as crystalline solid; mp 102 °C. $[\alpha]_D$ +78.9 (*c* 0.45, $CHCl_3$). IR (KBr, cm^{-1}): 1750. ^{1}H NMR (400 MHz, $CDCl_3$) δ: 1.09 (t, 3H, *J* = 7.4 Hz), 1.77 (m, 1H), 1.91–2.15 (m, 3H), 2.57 (m, 1H), 2.92 (dd, 1H, *J* = 5.6, 14.2 Hz), 3.13 (t, 3H, *J* = 7.8 Hz), 3.21 (m, 1H), 3.62 (m, 1H), 4.06 (m, 1H), 4.18 (m, 1H), 4.38 (t, 3H, *J* = 8.9 Hz), 7.26 (d, 1H, *J* = 3.9 Hz), 7.59 (t, 1H, *J* = 7.8 Hz), 7.72 (t, 1H, *J* = 7.8 Hz), 7.98 (d, 1H, *J* = 8.3 Hz), 8.14 (d, 1H, *J* = 8.3 Hz), 8.83 (d, 1H, *J* = 4.3 Hz). ^{13}C NMR (400 MHz, $CDCl_3$) δ: 9.6, 22.1, 25.6, 27.8, 29.7, 34.1, 42.7, 51.4, 71.9, 89.6, 121.1, 123.5, 127.2, 129.8, 130.8, 146.9, 148.7, 150.6, 156.5, 168.7. MS calcd. for $C_{20}H_{22}N_2O_4$: 354.2 (M^+); found: 355.2.

***cis*-Oxazolidinone lactone (27d)**

Following the same procedure as for compound **26d** gave **27d** in 69% yield. $[\alpha]_D$ +64.3 (*c* 0.4 $CHCl_3$). IR (neat, cm^{-1}): 1749. ^{1}H NMR (400 MHz, $CDCl_3$) δ: 1.12 (t, 3H, *J* = 9.4 Hz), 1.81 (m, 1H), 2.02 (m, 1H), 2.74 (m, 1H), 3.05 (dd, 1H, *J* = 4.3, 14.5 Hz), 3.89 (m, 1H), 4.28 (m, 2H), 4.38 (dd, 1H, *J* = 4.9, 14.9 Hz), 4.53 (t, 1H, *J* = 8.9 Hz), 6.42 (m, 1H), 6.82 (d, 1H, *J* = 15.2 Hz), 7.64 (t, 1H, *J* = 8.2 Hz), 7.79 (t, 1H, *J* = 8.2 Hz), 7.88 (d, 1H, *J* = 7.6 Hz), 8.21 (m, 2H), 9.04 (s, 1H). ^{13}C NMR (400 MHz, $CDCl_3$) δ: 9.6, 25.6, 34.1, 45.4, 51.3, 72.1, 77.7, 79.5, 125.1, 217.9, 128.4, 129.4, 130.4, 132.0, 133.9, 156.4, 168.8. MS calcd. for $C_{20}H_{20}N_2O_4$: 352.1 (M^+); found: 353.2.

***cis*-Oxazolidinone lactone (27e)**

Following the same procedure as for compound **26e** gave **27e** in 65% yield. $[\alpha]_D$ +36.5 (*c* 0.2, MeOH). IR (neat, cm^{-1}): 1748. ^{1}H NMR (400 MHz, CD_3OD) δ: 1.08 (t, 3H, *J* = 6.9 Hz), 1.64 (m, 3H), 1.79 (m, 1H), 1.94 (m, 2H), 2.85 (m, 1H), 2.99 (m, 1H), 3.42 (m, 1H), 3.65 (m, 1H), 4.21 (m, 2H), 4.32–4.45 (m, 2H), 4.61 (m, 1H), 7.55 (m, 1H), 7.84 (s, 1H), 8.05 (s, 1H), 8.25 (m, 1H), 8.48 (m, 1H), 8.96 (s, 1H). ^{13}C NMR (400 MHz, CD_3OD) δ: 8.2, 24.3, 25.2, 27.8, 32.7, 41.6, 46.9, 51.7, 72.5, 79.6, 117.9, 134.1, 138.6, 144.8, 146.7, 157.9, 170.3. MS calcd. for $C_{20}H_{24}N_4O_4$: 384.2 (M^+); found: 385.3.

Acknowledgements

We thank the Natural Sciences and Engineering Research Council of Canada (NSERC) for financial assistance and Ibis therapeutics (Carlsbad, California) for financial support and antimicrobial tests. We also thank Michel Simard for the X-ray crystal structures.

References

1. (*a*) M. Gaynor and A.S. Mankin. Curr. Top. Med. Chem. **3**, 949 (2003); (*b*) D.T.W. Chu, J.J. Plattner, and L. Katz. J. Med. Chem. **39**, 5853 (1996).

© 2005 NRC Canada

2. J.M. McGuire, R.L. Bunch, R.C. Anderson, H.E. Boar, E.H. Flynn, and H.M. Powell. Antibiot. Chemother. **2**, 281 (1952).
3. P. Kurath, P.H. Jones, R.S. Egan, and T.J. Perun. Experientia, **27**, 362 (1971).
4. S. Morimoto, Y. Takahashi, Y. Watanabe, and S. Omura. J. Antibiot. **37**, 187 (1984).
5. G. Bright, A. Nagel, J. Border, K. Desai, J. Dibrino, J. Nowakowska, L. Vincent, R. Watrous, F. Sciavolino, A. English, J. Retsema, M. Anderson, L. Brennan, R. Borovoy, C. Cimchowsji, J. Faiella, D. Girard, C. Herbert, M. Manousos, and R. Mason. J. Antibiot. **41**, 1029 (1988).
6. (*a*) R. Leclereq and P. Courvalin. Antimicrob. Agents Chemother. **35**, 1267 (1991); (*b*) B. Vester and S. Douthwaite. Antimicrob. Agents Chemother. **45**, 1 (2001).
7. (*a*) R.F. Clark, Z. Ma, S. Wang, G. Griesgraber, M. Tufano, H. Yong, L. Li, X. Zhang, A.M. Nilius, D.T.W. Chu, and Y.S. Or. Bioorg. Med. Chem. Lett. **10**, 815 (2000); (*b*) T.C. Henninger, X. Xu, D. Abbanat, E.Z. Baum, B.D. Foleno, J.J. Hillard, K. Bush, D.L. Hlasta, and M.J. Macielag. Bioorg. Med. Chem. Lett. **14**, 4495 (2004).
8. T. Mazzei, E. Mini, A. Novelli, and P. Periti. J. Antimicrob. Chemother. **31** (Suppl. C), 1 (1991).
9. (*a*) F.J. Boswell, J.M. Andrews, and J.P. Ashby. J. Antimicrob. Chemother. **42**, 703 (1998); (*b*) G. Ackermann and A. Rodloff. J. Antimicrob. Chemother. **51**, 497 (2003).
10. (*a*) J.M. Andrews, T.M.A. Weller, and J.P. Ashby. J. Antimicrob. Chemother. **46**, 1017 (2000); (*b*) A.M. Nilius, M.H. Bui, and L. Almer. Antimicrob. Agents Chemother. **45**, 2163 (2001).
11. (*a*) A. Brisson-Noel, P. Trieu-Cuot, and P. Courvalin. J. Antimicrob. Chemother. **22**(Suppl. B), 13 (1988); (*b*) J.L. Hansen, J.A. Ippolito, N. Ban, P. Nissen, P.B. Moore, and T.A. Steitz. Mol. Cell, **10**, 117 (2002); (*c*) P. Nissen, J. Hansen, N. Ban, P.B. Moore, and T.A. Steitz. Science, **289**, 920 (2000); (*d*) F. Schlunzen, R. Zarivach, J. Harms, A. Tocilj, R. Albrecht, A. Yonath, and F. Franceschi. Nature (London), **413**, 814 (2001).
12. (*a*) S. Hanessian, M. Tremblay, A. Kornienko, and N. Moitessier. Tetrahedron, **57**, 3255 (2001); (*b*) B. Francois, J. Szychowski, S.S. Adhikari, K. Pachamuthu, E.E. Swayze, R.H. Griffey, M.T. Migawa, E. Westhof, and S. Hanessian. Angew. Chem. Int. Ed. **43**, 6735 (2004).
13. For reviews on RNA binding molecules, see: T. Hermann. Angew. Chem. Int. Ed. **39**, 1890 (2000).
14. (*a*) C. Agouridas, A. Denis, J.-M. Auger, Y. Benedetti, A. Bonnefoy, F. Bretin, J.-F. Chantot, A. Dussarat, C. Fromentin, S.G. D'Ambrieres, S. Lachaud, P. Laurin, O.L. Martret, V. Loyau, and N. Tessot. J. Med. Chem. **41**, 4080 (1998); (*b*) G. Griesgraber, Y.S. Or, D.T.W. Chu, A.M. Nilius, P.M. Johnson, R. Flamm, R. Henry, and J. Plattner. J. Antibiot. **49**, 465 (1996).
15. D.R. Harris, S.G. McGeachin, and H.H. Mills. Tetrahedron Lett. **11**, 679 (1965).
16. See, for example: (*a*) T.J. Perun and R.S. Egan. Tetrahedron Lett. **10**, 387 (1969); (*b*) T.J. Perun, R.S. Egan, and J.R. Martin. Tetrahedron Lett. **10**, 4501 (1969); (*c*) T.J. Perun, R.S. Egan, P.H. Jones, J.R. Martin, L.A. Mitscher, and B.J. Slater. Antimicrob. Agents Chemother. **9**, 116 (1969).
17. (*a*) W.D. Celmer. Antimicrob. Agents Chemother. 144 (1966); (*b*) J. Dale. J. Chem. Soc. 93 (1963); see also: (*c*) T.J. Perun. *In* Drug action and drug resistance in bacteria. 1. Macrolide antibiotics and lincomycin. *Edited by* S. Mitsuhashi. University Park Press, Baltimore, Maryland. 1972. p. 123.
18. S. Douthwaite and W.S. Champney. J. Antimicrob. Chemother. **48**(Topic T1), 1 (2001).
19. D.A. Prins. J. Am. Chem. Soc. **70**, 3955 (1948).
20. (*a*) A. Liptak, I. Jodal, and P. Nanasi. Carbohydr. Res. **44**, 1 (1975); (*b*) A. Liptak, J. Imre, J. Harangi, P. Nanasi, and A. Neszmelyi. Tetrahedron, **38**, 3721 (1982).
21. (*a*) J.R. Pougny. Tetrahedron Lett. **25**, 2363 (1984); (*b*) B.H. Lipshutz and S. Sengupta. Org. React. (N.Y.), **41**, 135 (1992); (*c*) S. Hanessian, B. Thavonekham, and B. DeHoff. J. Org. Chem. **54**, 5831 (1989).
22. (*a*) M. Vaultier, N. Knouz, and R. Carrie. Tetrahedron Lett. **24**, 763 (1983); (*b*) H. Staudinger and J. Meyer. Helv. Chim. Acta, **2**, 635 (1919).
23. J.S. Madalengoitia, J.J. Tepe, K.A. Werbovetz, E.K. Lehnert, and T.L. Macdonald. Bioorg. Med. Chem. **5**, 1807 (1997).
24. (*a*) D. Guianvarc'h, J.-L. Fourrey, M.-E. Tran Huu Dau, V. Guerineau, and R. Benhida. J. Org. Chem. **67**, 3724 (2002). For reviews, see: (*b*) O. Mitsunobu. Synthesis, 1 (1981); (*c*) D.C. Hughes. Org. React. (N.Y.), **42**, 335 (1992).
25. P.P. Kung, M.D. Casper, K.L. Cook, L. Wison-Lingardo, L.M. Risen, T.A. Vickers, R. Ranken, L.B. Blyn, J.R. Wyatt, P.D. Cook, and D.J. Ecker. J. Med. Chem. **42**, 4205 (1999).
26. M.R. Barbachyn and C.W. Ford. Angew. Chem. Int. Ed. **42**, 2010 (2003).

© 2005 NRC Canada

Review of gold(I) *N*-heterocyclic carbenes[1]

Ivan J.B. Lin and Chandra Sekhar Vasam

Abstract: This review presents an overview of the work on Au(I)–NHC chemistry. The efficiency of different synthetic strategies of Au(I)–NHCs is discussed. Transmetallation of Ag(I)–NHCs appears to be an easy method as compared with the others. The influence of aurophilicity "a traditional property of a Au(I) center" in making the supramolecular assemblies is also covered. The combination of the Au(I) center with NHCs has great potential in the fields of medicine, catalysis, liquid crystal, and optoelectronic.

Key words: gold–carbenes, silver–carbenes, carbene transfer, aurophilicity.

Résumé : Dans ce travail, on présente une revue des travaux effectués dans le domaine de la chimie du Au(I)–NHC. On discute de l'efficacité des diverses stratégies de synthèse des Au(I)–NHC. Par rapport à d'autres méthodes, la transmétallation des Au(I)–NHC semble la méthode la plus appropriée. On a aussi examiné l'influence du caractère aurophile, une propriété traditionnelle du centre Au(I), dans l'élaboration d'assemblages supramoléculaires. La combinaison du centre Au(I) avec des NHC possède un grand potentiel dans les domaines de la médecine, de la catalyse, des cristaux liquides et de l'optoélectronique.

Mots clés : or–carbènes, argent–carbènes, transfert de carbène, caractère aurophile.

[Traduit par la Rédaction]

Background and the scope

N-Heterocyclic carbenes (NHCs) are a novel class of electron-donating ligands, which have the advantage of forming strong metal–ligand bonds and have become universal ligands in organometallic and coordination chemistry (1). A similarity between the NHCs and phosphines in terms of their metal coordination chemistry has been proposed (2). NHCs, however, have the advantage of being easy to derivatize by varying the N- or C functionalization in the corresponding NHC precursors (3). They not only bind to many transition metals, be it in low or high oxidation states (4), but also to main group elements (5). The existence of free and stable NHC **III** (Chart 1) was initially investigated by Wanzlick et al. (6). Although a free NHC was not isolated, the predictions by Wanzlick et al. inspired the related researches.

The metal complexes with NHCs as ligands were first synthesized by Wanzlick and Öfele and co-workers (7) and later extended by Lappert and co-workers (8). It was not until the isolation of free and stable NHCs by Arduengo et al. in 1991 (9) that the chemistry of metal–NHCs was revived. Since then information about their fundamental chemical and physical properties has been obtained (10), especially, with the precursors of NHCs being the ever popular ionic liquids (11). NHCs have found tremendous application in the field of catalysis; for example, C—H activation, C—C, C—H, C—O, and C—N bond formation, and many more. Herrmann and co-workers (12) have an excellent review on the aspects of NHC complexes in catalysis. The successful application of Ru(I)–NHCs in olefin metathesis reactions and Pd(II)–NHCs in cross-coupling reactions almost revolutionized the area of catalysis. There is now significant evidence that phosphines will be supplemented, and, in part, replaced by NHCs (12). It has been described that because of the high thermal stability of the M—$C_{carbene}$ bond, excess ligand is not necessary during the catalytic reactions and orthometallation does not occur with metal–NHCs (13). NHCs as nucleophiles have a catalytic application even in nature; it was shown in the ylidene-catalyzed benzoin condensations that the vitamin B_1 enzyme cofactor thiamin, a naturally occurring thiazolium salt, plays a key role in biochemical processes (14). In recent years, the applications of metal–NHCs are being spread toward many other fields like material science (15) and medicinal chemistry (16).

The study of Au(I) complexes has received much attention lately because they have been used in pharmaceuticals (17), chemical vapour depositions (18), liquid crystals (19), and optical devices (20). Furthermore, since the discovery of the Au(I) catalyzed asymmetric aldol reaction by Ito et al. (21), the opinion in homogeneous catalysis that gold is inert and expensive has been changed. After seeing their successful role in the C—C bond formation and activation of C—C multiple bonds, the interest in gold complexes for homoge-

Received 22 November 2004. Published on the NRC Research Press Web site at http://canjchem.nrc.ca on 6 July 2005.

Dedicated to Professor Howard Alper for his contribution to the community of chemistry.

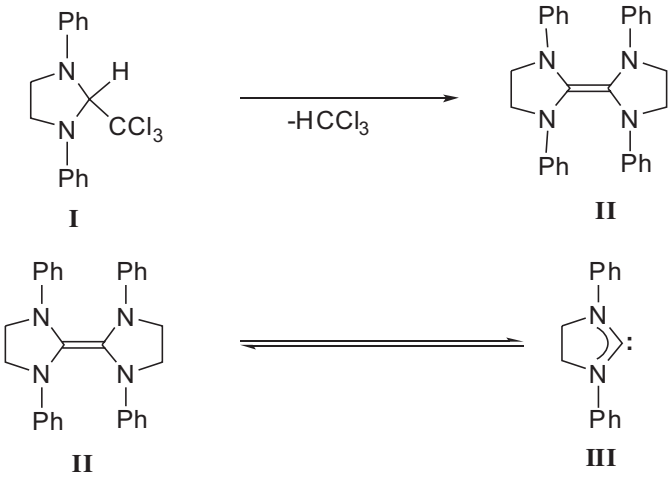
I.J.B. Lin[2] and C.S. Vasam. Department of Chemistry, National Dong Hwa University, Shou-feng, Hualien-974, Taiwan.

[1]This article is part of a Special Issue dedicated to Professor Howard Alper.

[2]Corresponding author (e-mail: ijblin@mail.ndhu.edu.tw).

 doi: 10.1139/V05-087 © 2005 NRC Canada

Chart 1. Proposed equilibrium between ene-tetramine and NHC.



neous catalysis is increasing (22). Their importance has led to a great variety of research concerning synthesis, structure, and reactivity.

Interest has also been growing in the pervasive "aurophilicity" phenomenon, i.e., the widespread observations of gold–gold interactions (closed shell d^{10}–d^{10}) in the solid phase of Au(I) complexes (23). This interaction, which has energy comparable to hydrogen bonding, may provide additional stability in the formation of supramolecules (23, 24). The aggregation is obviously dependent on the steric and electronic nature of the ligands. Much of the present basic research devoted to Au(I) complexes is aimed at the synthesis and structural characterization of new complexes to better understand the aurophilic interaction.

Despite the fact that Au(I) complexes have been investigated extensively with phosphine and thiolates, Au(I) complexes with NHCs have been less studied. The earlier information on Au(I)–NHCs, which have been known for more than a quarter century, deals only with oxidative addition reactions (25). Much effort has been diverted after the report on unexpected isolation of Au(I)–NHC by Burini and co-workers in 1989 (26). Recently, reports on antimitochondrial, antitumor (16*b*, 16*c*), antimicrobial (16*e*), and catalytic activity (27) of Au(I)–NHCs have appeared. In addition to this, as a compliment, recent investigations concerning the density functional calculations on coinage metal–NHCs including Au(I)–NHCs provide new insights into the nature of metal–NHC ligand bonding (28). Since our research interest is also confined to the synthesis and characterization of coinage metal–NHCs, we wish to present a comprehensive summary of articles that report on the synthesis, structure, and properties of Au(I)–NHC complexes and the scope for further development.

Preparation

According to the literature survey the following methods have so far been adopted to obtain Au(I)–NHC complexes: (*a*) cleavage of electron-rich olefins; (*b*) transfer of carbene from Group 6 carbonyl complexes; (*c*) reaction of azolium salts or NHCs with a Au(I) source; (*d*) protonation or alkylation of gold azolyl compounds; (*e*) transmetallation between Ag(I)–NHCs and Au(I) precursors.

Cleavage of electron-rich olefins

This strategy was introduced by Cetinkaya et al. (29) in 1974, to isolate several transition metal – NHC derivatives. The interaction between [Au(PPh_3)Cl] and electron-rich olefin based on imidazolidinylidene (**IV**) initially produced the hygroscopic Au(I)–NHC complex **1** (Scheme 1). In this way, the olefins behaved as nucleophilic NHC transfer reagents. Recently, this method was again applied during the preparation of polyimide-containing Au(I)–NHC complexes. In this reaction, the olefin (1,1,3,3-tetrakis(*p*-dimethylaminobenzyl)-2,2-biimidazolidinylidene) (**V**) and [Au(PPh_3)Cl] in refluxing toluene produced Au(I)–NHC complex **2** (Scheme 1) (30). Later, the Au(I)–NHC **2** was condensed with several aromatic dianhydrides to produce the polyimide-containing Au(I)–NHCs of type **3**. These polymers exhibited higher glass transition temperatures, better solubilities in polar solvents, higher thermal and thermo-oxidative stabilities as compared with the uncomplexed polyimides.

Transfer of carbene from Group 6 complexes

The transfer of carbene from the Group 6 complexes to other metal ions was initially studied by Fischer, and later applied by Liu's research group (31). As shown in Scheme 2, it was claimed that the interaction of different W(I)–NHCs (**VI**) with Au(SMe_2)Cl in dichloromethane gave Au(I)–NHCs **4a**–**4d**. There is no further information available on this technique.

From azolium salts or free NHCs

The Au(I)-containing metallomesogens have attracted interest in the elucidcation of the best structure – mesogenic behavior relationship. In view of the strong σ-coordination properties of NHCs and high thermal stability of their metal complexes, in 1997, we designed the first liquid crystalline compounds of Au(I)–NHCs (Chart 2) (32).

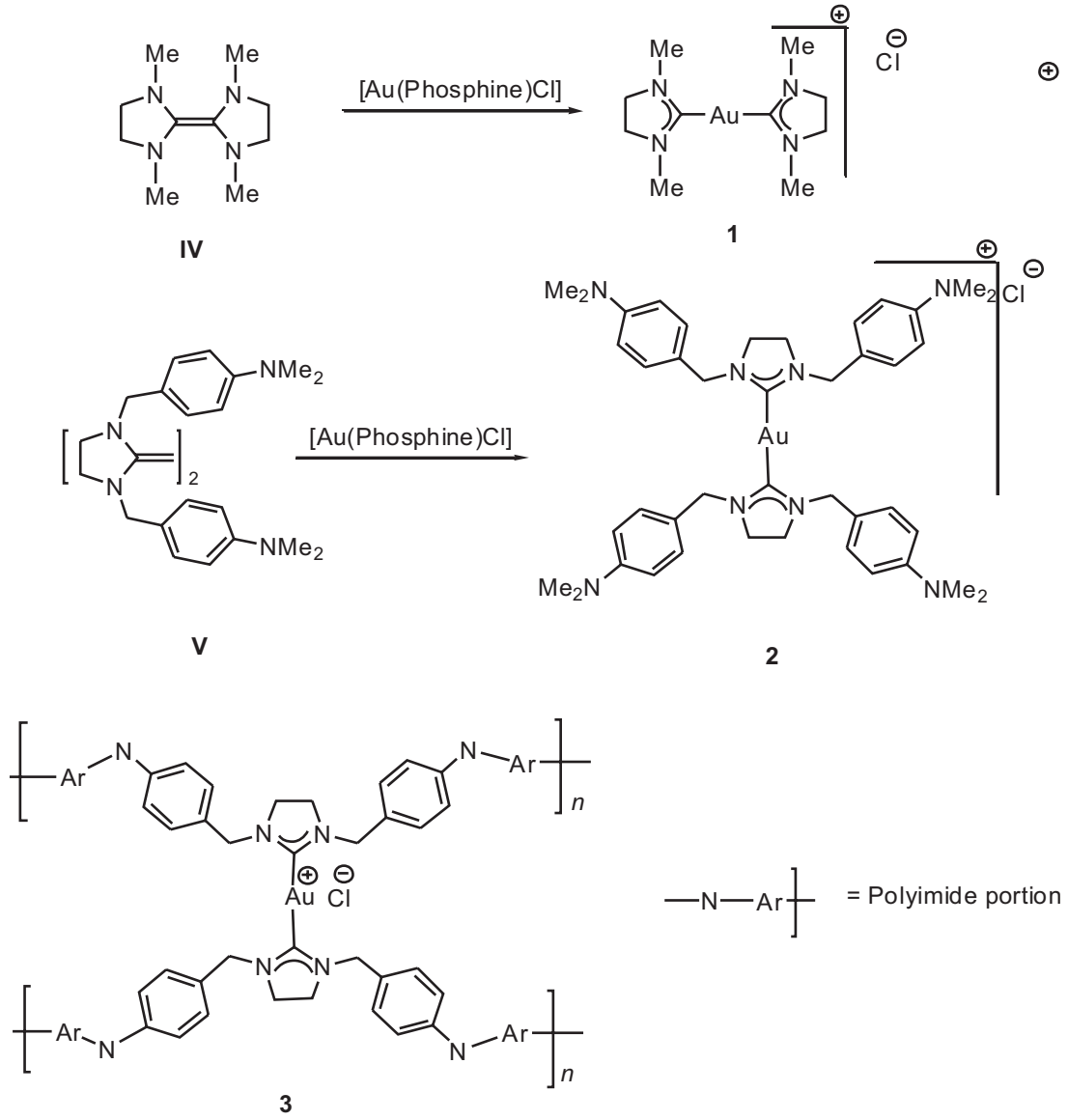
To avoid the tedious precautions required with the use of strong bases and to increase the product yields, we used the phase transfer catalysis (PTC) technique in the reaction of benzimidazolium bromide and Au(SMe_2)Cl to obtain the Au(I)–NHCs **5a**–**5c**. The crystal structure of **5c** (n = 16) revealed a head-to-tail packing with interpenetrating long alkyl chains to give a bilayer lamellar structure with Au···Au distances of ~3.6 Å. In contrast to the other Au(I) metal-containing liquid crystals (MLCs), these Au(I)–NHCs exhibited relatively low transition temperatures, broad mesophase temperature ranges, and higher thermal stabilities.

Dicationic imidazolium-linked cyclophane or cyclophane-like building units presented as one of the unusual and new classes of NHC precursors and formed thermally stable complexes with structural diversity. Considering this fact and the medicinal application of Au(I), Baker and his co-workers (33) designed Au(I)–NHCs **6**–**10** (Scheme 3), and for the first time demonstrated their antimitochondrial and antitumor activity (16*b*, 16*c*).

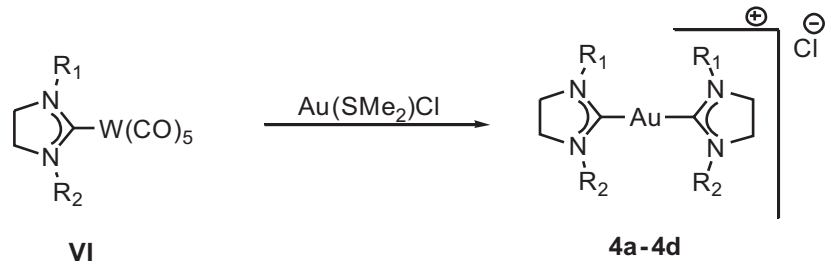
Reaction of imidazolium-linked cylcophanes with Au(SMe_2)Cl in the presence of lithium or sodium carboxylates salts was described as a useful method to obtain the Au(I)–NHCs **6**–**10** (33). However, the reported yields were

© 2005 NRC Canada

Scheme 1. Formation of Au(I)–NHCs from the olefins.



Scheme 2. Formation of Au(I)–NHCs from Group 6 complexes.



R_1, R_2 = **a)** Et, **b)** allyl, **c)** benzyl, **d)** 4-pentenyl

low when compared to the PTC technique. According to the NMR studies, those with cyclophane frameworks were rigid in solution, but the non-cyclophane analogs were fluxional. In all these dinuclear complexes, the two Au(I) centers were linked by bridging μ-dicarbene ligands. Complexes **6** and **9** displayed intra Au(I)···Au(I) interactions in the solid state. The emission spectrum of **9** in aqueous solution showed both high-energy and low-energy bands, which was attrib-

© 2005 NRC Canada

Scheme 3. Au(I) complexes of cyclophane linked NHCs.

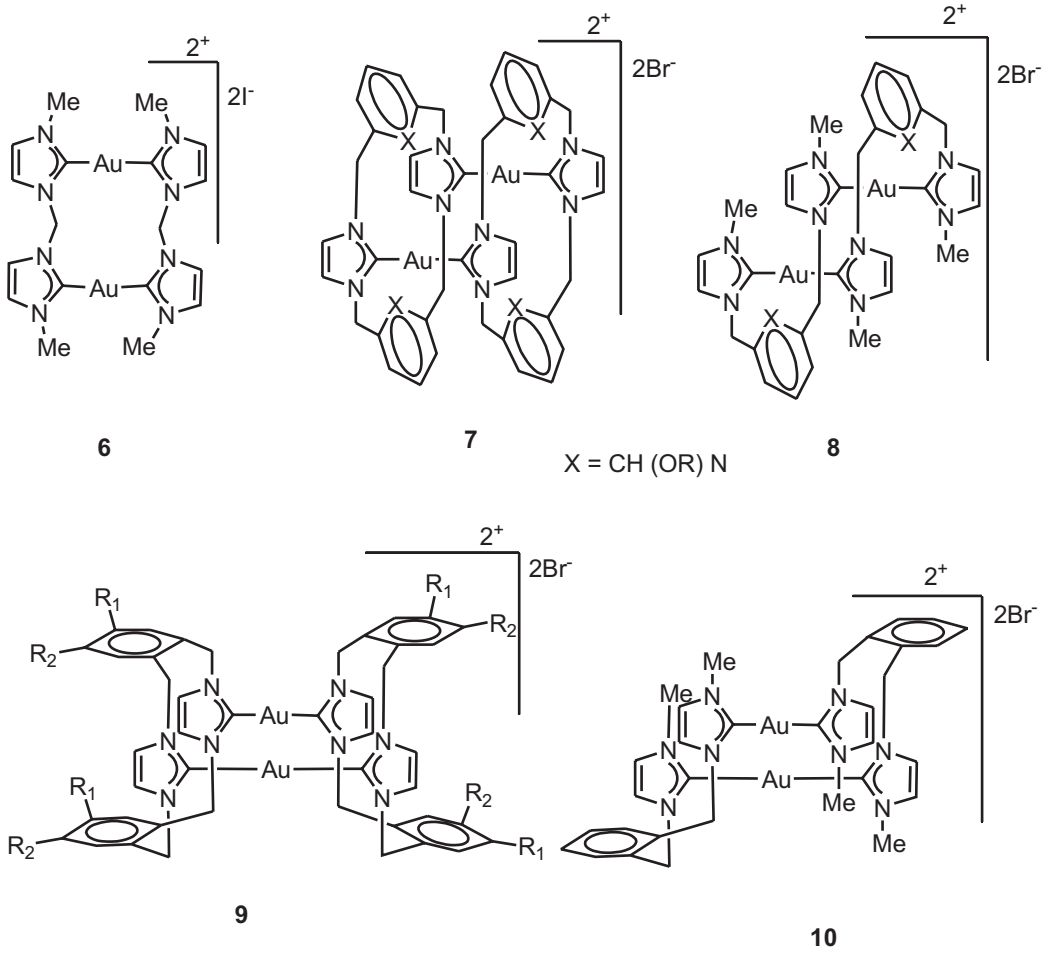
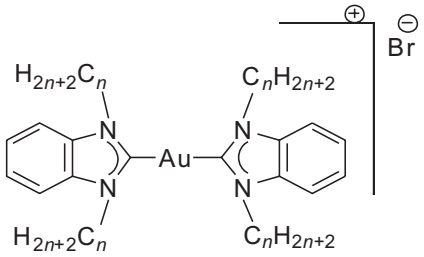


Chart. 2.



uted to arising from electronic transitions involving Au···Au interactions. The antimitochondrial activity of these lipophilic cationic Au(I)–NHCs appeared to be different from those of lipophilic cationic Au(I) complexes with phosphines (16*b*, 16*c*).

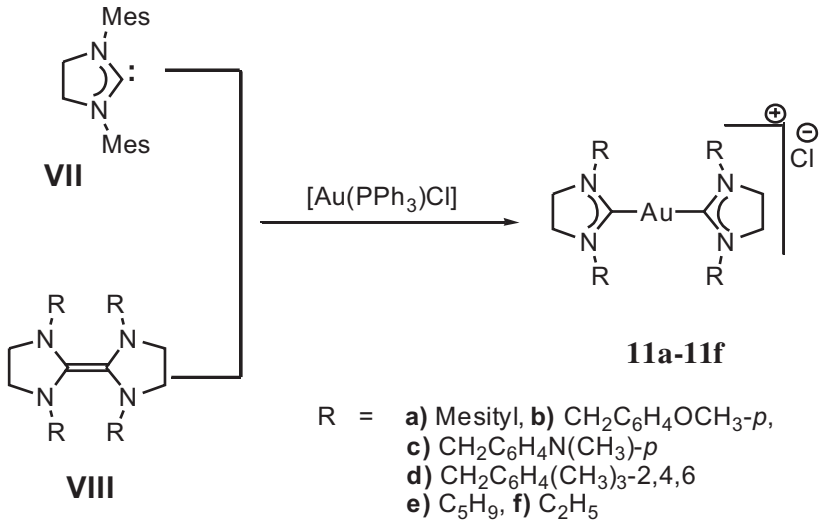
Application of Au(I)–NHCs as antimicrobial agents was described for the first time by Cetinkaya's group (16*e*). The ligand substitution reaction between [Au(PPh_3)Cl] and a free NHC (**VII**) or its dimer (**VIII**) produced the Au(I)–NHCs **11a**–**11f** (Scheme 4). The vibrational bands of NCN were observed between 1450 and 1525 cm^{-1}. The nature of the N substituents had a profound effect on the antimicrobial activity and selectivity. Complexes **11a**–**11c** showed effective biological activities.

Fehlhammer and co-workers (34) described the synthesis of the first structurally characterized tetraNHC complexes of bridging dinuclear Au(I). Interaction of the borate-bridged diNHC ligands (**IX**) with [Au(PPh_3)Cl] produced the Au(I)–NHCs **12a**–**12c** with high yields (Scheme 5). The closest approach between the two Au(I) centers of **12b** was 3.36 Å, indicating the presence of aurophilicity.

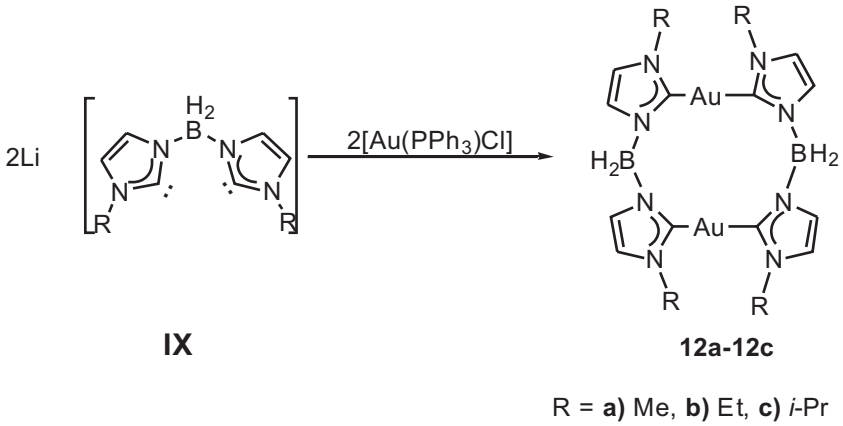
An investigation by Lock and co-workers (35) described that the reaction between tris(4,5-dimethylimidazol-2-yl)phosphine (**X**) and tetrachloroaurate did not form the targeted Au(I)–phosphine, but produced the unexpected Au(I)–NHC of type **13** instead (Scheme 6). It was suggested that the generation of NHC was possibly due to the cleavage of one of the imidazolium groups from the ligand. Structural data showed that the Au—C bond did not have much multiple-bond character. The molecules were stacked pair-wise with a short Au(I)···Au(I) interaction of about 3.37 Å. Further interpair ring π–π interactions and hydrogen bonding were also observed.

© 2005 NRC Canada

Scheme 4. Synthesis of Au(I)–NHCs **11a**–**11f** from free NHC or its dimmers.



Scheme 5. Formation of homoleptic dinuclear Au(I)–NHCs **12a**–**12c**.



Scheme 6. Unexpected formation of Au(I)–NHC **13**.

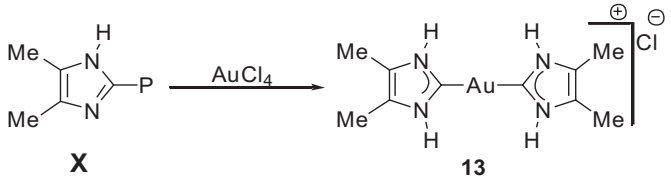
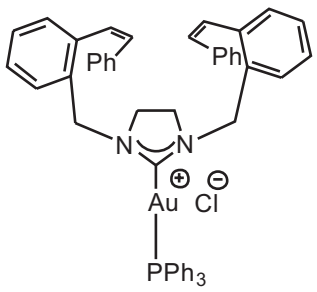


Chart 3.



The first example of a mixed phosphane–NHC–gold complex was reported by Grutzmacher's research group (Chart 3) (36). The reaction of bistropimidazolium salt, a special type of NHC precursor, with [Au(PPh$_3$)Cl] in the presence of potassium tertiarybutoxide gave complex **14**. The Au—$C_{carbene}$ bond lengths are somewhat longer than those in many other biscarbene–gold(I) complexes because of the trans influence of phosphine. Although steric congestion appears in the crystal structure, the reaction of this complex with strong acid did not lead to a replacement of the phosphine ligand, indicating the complex stability.

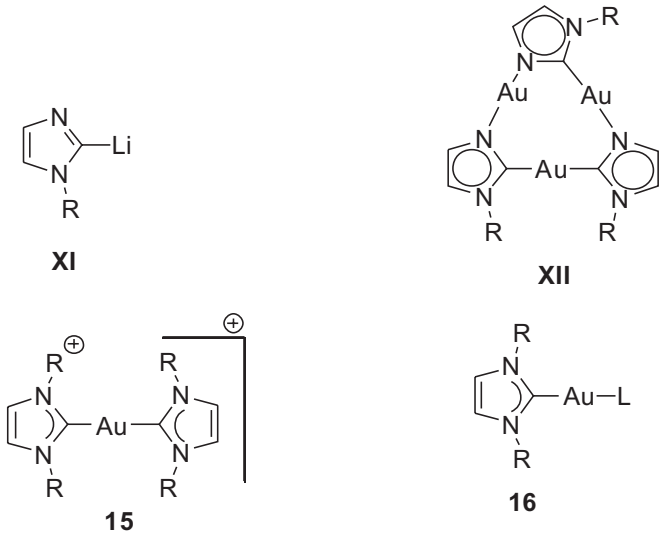
Protonation or alkylation of gold azolyl compounds

This synthetic strategy has been introduced by Burini's group (26, 37, 38) and widely applied and studied in the prolific work of Raubenheimer's group (39) to synthesize Au(I)–NHCs from the reaction of lithiated imidazoles or thiazoles with an appropriate Au(I) precursor followed by protonation or alkylation.

Firstly, we will discuss the observations by Burini and coworkers (26) during the study of the interaction of the imidazolato-N^3,C^2 ligand towards gold (Scheme 7). The unexpected isolation of a bisAu(I)–NHC of type **15** (R = benzyl) happened by the ligand substitution reaction of

© 2005 NRC Canada

Scheme 7. Au(I)–NHCs from cyclic Au(I)–imidazolate.



$(PPh_3)AuCl$ with lithiated benzylimidazolium (**XI**) in acidic media. Short Au(I)···Au(I) interactions of 3.26 Å were observed in **15** in the solid state. If the acid was not used then a cyclic trimer (**XII**) resulted. Reactions of this cyclic trimer with reagents like ClCOOEt, ClOPh, and EtI produced the mononuclear Au(I)–NHCs of type **16** and also the biscarbenes of type **15**. Crystal structures of two Au(I)–NHC-chlorides of type **16** (R_1 = benzyl, R_2 = 3-carboethoxy or 3-benzoyl, and L = Cl) showed that NHCs exhibited a stronger trans influence than the chloride. Aurophilic interactions were observed in the compound with R = benzoyl (37*a*), but not with R = carboethoxy (37*b*). According to the Mössbauer spectral data, the quadruple splitting values for the complexes of type **16** were influenced by aurophilic interactions (38).

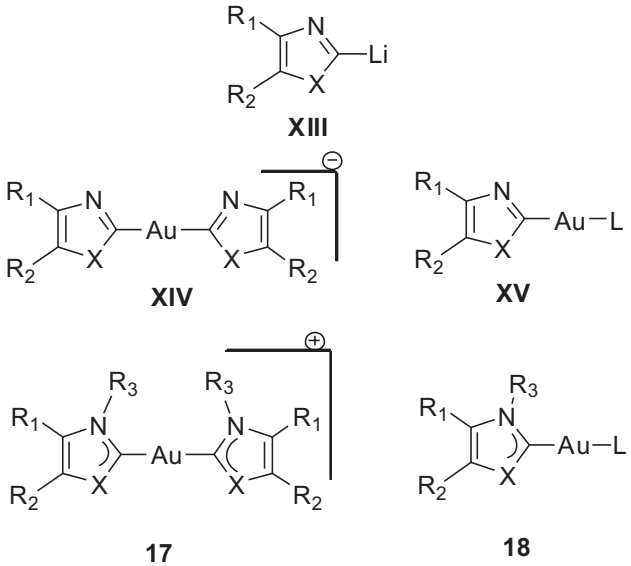
Scheme 8 gives a general overview of Raubenheimer's work to synthesize Au(I) complexes of various azolylidenes (thiazolylidene, imidazolylidene, and benzimidazolyldene) (39). The reaction between lithiated azole (**XIII**) and Au(I) sources produced the Au(I)–NHCs of type **17** and type **18** via the intermediates [Au(azolate)$_2$] (**XIV**) and [Au(azolate)L] (**XV**) (L = PPh_3, C_6F_5, azolate). Side reactions such as homoleptic rearrangement (eq. [1]) and protonation on carbon rather than nitrogen were observed.

$$[1] \qquad 2[AuL^1(L^2)] \longrightarrow [AuL^1{}_2] + [AuL^2{}_2]$$

The crystal structure of the type **17** complex (NHC = thiazolylidene, R = H) showed that the dimeric units were formed in a staggered conformation with Au(I)···Au(I) interactions of about 3.33 Å (39*d*). The crystal structure of the type **18** complex (NHC = thiazolylidene, R = H, L = thiazolate) showed a dimeric unit with the shortest Au(I)···Au(I) contacts of ~3.07 Å (39*b*). In one instance, a free imidazolium carbene (R_1 = Me, R_2 = Bu) was employed to obtain both type **17** and **18** Au(I)–NHCs (40).

Oxidative addition (Scheme 9) of halogens to Au(I)–NHCs of type **17** produced the Au(III)–NHCs of type **19** or a Au(I)–NHC of type **20** (25). Oxidative addition to the type

Scheme 8. Formation of Au(I)–NHCs derived from Au(I)–thiazolates.



18 complexes also produced the Au(I)–NHCs of type **20**, which were anticipated to form via the reductive elimination of the bisNHC–Au(III)-halide intermediate. Formation of Au(III)–(NHC)-trichloride of type **21** was observed by using excess chlorine. However, a type **21** Au(III)–NHC based on thiazolium carbene was obtained from the reaction of thiazolium bromide with $HAuCl_4$ followed by the treatment of the intermediate with a base (40). The crystal structure of chloro(imidazolylidene) gold(III) (type **19**) showed that the coordination around the gold(III) center was square-planar and the chemically equivalent ligands were trans to one another. Very little π-back donation was believed to occur. The structural analysis was further complimented by DFT calculations, where the experimentally determined bonding parameters were in good agreement with the theoretical calculations.

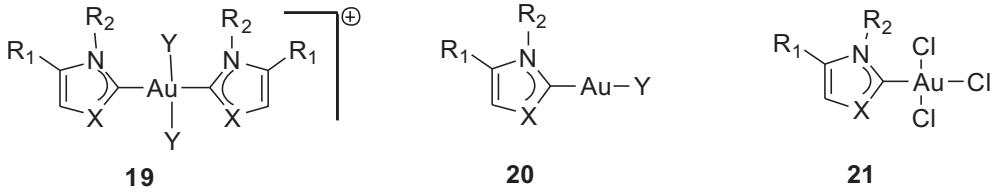
The formation of Au(I)–NHCs of type **22** and **23** were stoichiometric dependent reactions (Scheme 10). The crystal structure of **23** (X = H) revealed that the intermolecular Au(I)···Au(I) interactions were absent due to the presence of a hydrogen bonding network (41).

Transmetallation between Ag(I)–NHCs and Au(I) precursors

It is not always convenient to employ the free NHCs as they are air and moisture sensitive. It is also not that easy to selectively deprotonate imidazolium salts with strong bases, as there is a possibility of the decomposition of the imidazolium salt or the formation of side products. To avoid these difficulties, our group reported a very convenient technique in 1998 to obtain Au(I)–NHCs from Ag(I)–NHCs by carbene transfer (42, 43). Simply mixing an imidazolium salt with Ag_2O afforded a complex of Ag(I)–NHC, which was used either as isolated or generated in situ to react with Au(I) precursors by transmetallation. As both the reactants

© 2005 NRC Canada

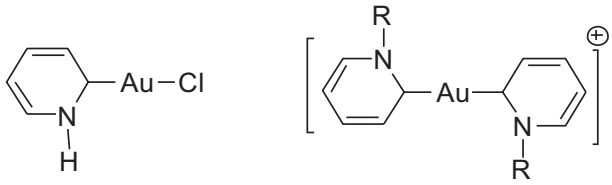
Scheme 9. Formation of Au(III)–NHCs via oxidative addition reactions.



19 **20** **21**

R_1 = Me, H; R_2 = Me, H; X = NMe, S; Y = Cl, I

Scheme 10. Au(I)–NHCs derived from lithiated pyridine.



22 **23**

R = H, Me

are air-stable, the technique of carbene transfer is regarded as a convenient entry point into metal–carbene chemistry without the need for the rigorously anaerobic conditions and additional bases to synthesize NHCs.

As shown in Scheme 11, reaction of 1,3-diethylbenzimidazolium bromide (**XVI**) with Ag_2O in dichloromethane gave an ion-pair biscarbene complex of Ag(I) (**XVII**) (42). The lack of $^{13}C^{107,109}$–Ag couplings in the ^{13}C NMR spectrum of the ion-pair compound indicated the labile nature of the Ag—$C_{carbene}$ bond and suggested an equilibrium between $[Ag(Et_2\text{-bimy})_2][AgBr_2]$ and $[Ag(Et_2\text{-bimy})Br]$ in solution. In view of this fluxional behavior, it was considered that these Ag(I)–NHCs would be efficient carbene transfer agents, and the very first time we applied this technique successfully to produce the Au(I)–NHC **24**. Similarly, reaction of $[Ag(Et_2\text{-bimy})_2][PF_6]$ (**XVIII**) with $[Au(SMe_2)Cl]$ produced a bisAu(I)–NHC complex **25**.

Later, the isolation of Au(I)-bimy carbene **26** with R = Me was reported by using the in situ generated Ag(I)-bimy carbene. The easy synthesis of $[Au(R_2\text{-bimy})Cl]$ (**24**, R = ethyl; **26**, R = methyl) allowed us to derive the Au-(R_2-bimy) core containing compounds **27**–**30** as shown in Scheme 12 (44).

Attempts to prepare the mixed-carbene compound $[Au(R_2\text{-bimy})(R'_2\text{-bimy})]PF_6$ produced a mixture of $[Au(R_2\text{-bimy})(R'_2\text{-bimy})][PF_6]$, $[Au(R_2\text{-bimy})_2][PF_6]$, and $[Au(R'_2\text{-bimy})_2][PF_6]$. Mixing the last two compounds, however, did not give the mixed-carbene compound, suggesting that the homoleptic carbene compounds were not labile. Note that analogous phosphine compounds such as [Au(phosphine)X] (X = Cl, Br, I), $[Au(phosphine)_2][PF_6]$, [Au(phosphine)(C≡CPh)], [Au(phosphine)(SR)], and $[Au(phosphine)(py)]^+$ have been reported. We also tried to synthesize $[Au(R_2\text{-bimy})(PPh_3)]^+$ without success. Reaction of $[Au(R_2\text{-bimy})Cl]$ with $AgBF_4$ followed by PPh_3 produced $[Au(PPh_3)_2]^+$ and $[Au(R_2\text{-bimy})_2]^+$ instead of the expected $[Au(R_2\text{-bimy})(PPh_3)]^+$. According to the ^1H NMR spectral results, there was no dynamic equilibrium between the monomeric and dimeric forms of these complexes as was observed in $[Au(PPh_2Me)I]$.

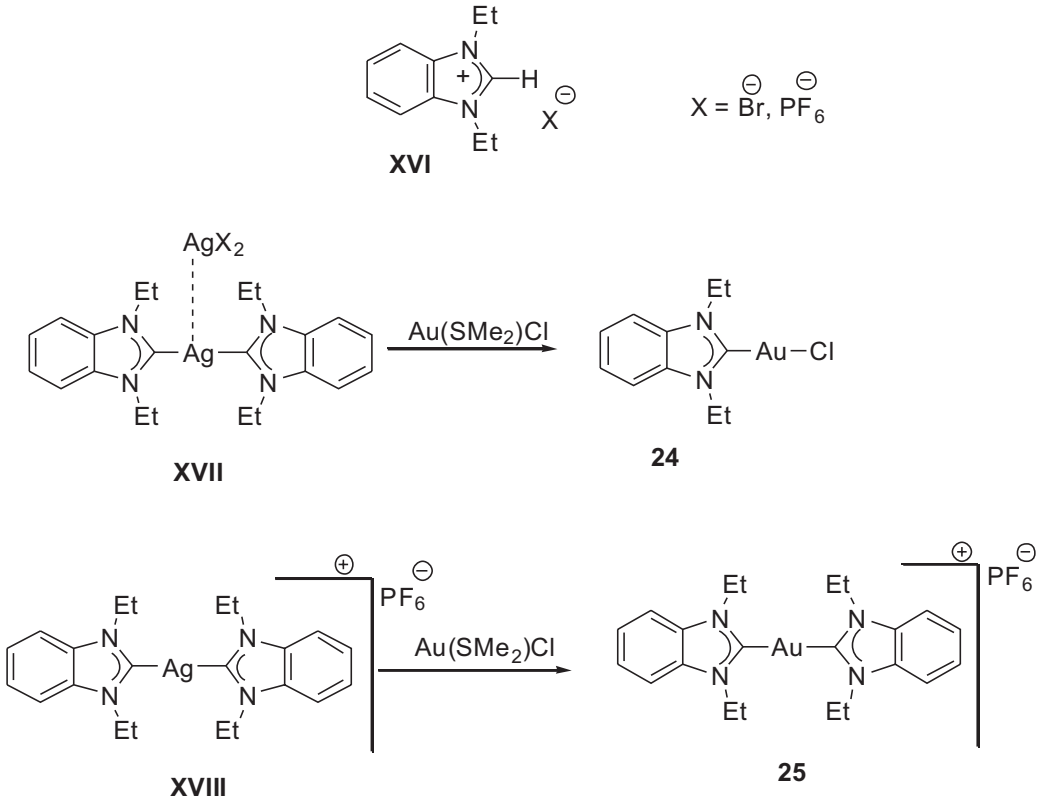
The crystal packing of $[Au(Me_2\text{-bimy})Cl]$ (**26**) exhibited both Au^I–Au^I and ring π–π type intermolecular interactions. Two linear molecules were crossed at approximately 90° with a short Au^I–Au^I contact (3.16 Å) to form a pair. Each molecule in a pair further interacted with neighboring pairs through ring π–π interactions (ring–ring distance = 3.45 Å) in a head-to-tail fashion. The molecular packing of this compound can be viewed as a polymeric chain with alternating Au(I)···Au(I) and ring–ring interactions. On the other hand, the crystal packing of [Au(Et-bimy)Cl] (**24**) showed that the oppositely oriented ethyl groups on each bimy plane allowed a columnar stacking and caused only ring π–π interactions (ring–ring distance = 3.53 Å). Each molecule interacted through the bimy ring with upper and lower bimy rings of the neighboring molecules in a head-to-tail fashion.

After the experience with Au-bimy carbenes, we intended to extend our efforts towards the imidazolium and triazolium derived carbenes (45). Our objective was to generalize the preparation method of [Au(NHC)(halide)], which appeared to be useful starting material for the synthesis of many other Au(I)–NHC core containing compounds. Another objective was to study the photophysical properties of Au(I)–NHCs, as their analogous Au(I)–phosphines have been known to display interesting luminescent properties. $[Au(Me_2\text{-azy})Cl]$ (**31** and **32**) (azy = imidazol-2-ylidene or triazol-2-ylidene) were isolated successfully by using the carbene transfer technique (Scheme 13). The crystal structures of both **31** and **32** showed that these neutral molecules were stacked to form a linear polymer with weak Au···Au interactions of 3.3–3.5 Å. Luminous carbazolate was introduced into [Au(NHC)Cl] complexes under basic PTC conditions to synthesize [Au(NHC)(cbz)] type complexes **33**–**36** (Scheme 13), which were expected to exhibit rich photophysical properties. The crystal structure of **33** showed that the imy and cbz rings were coplanar, and that two of these molecules were stacked pair-wise in a head-to-tail fashion. Cationic Au(I) complexes **37** and **38** based on Me_2-bimy and Me_2-tazy carbenes were also derived from the corresponding [Au(NHC)Cl] in acetone by reacting them with the azolium salt of $[PF_6]$ (Scheme 13). For the synthesis of mixed Au(I)–Au(III) NHC compounds, $[Au^I(R_2\text{-bimy})_2][PF_6]$ (R = Me, Et) were treated with $[(NEt_4)][Au(mnt)_2]$ (mnt = maleonitriledithiolate) to give brown $[Au^I(R_2\text{-bimy})_2][Au^{III}(mnt)_2]$ compound **39** (Scheme 13). Secondary interactions like hydrogen bonding appeared to play an important role in the crystal packing.

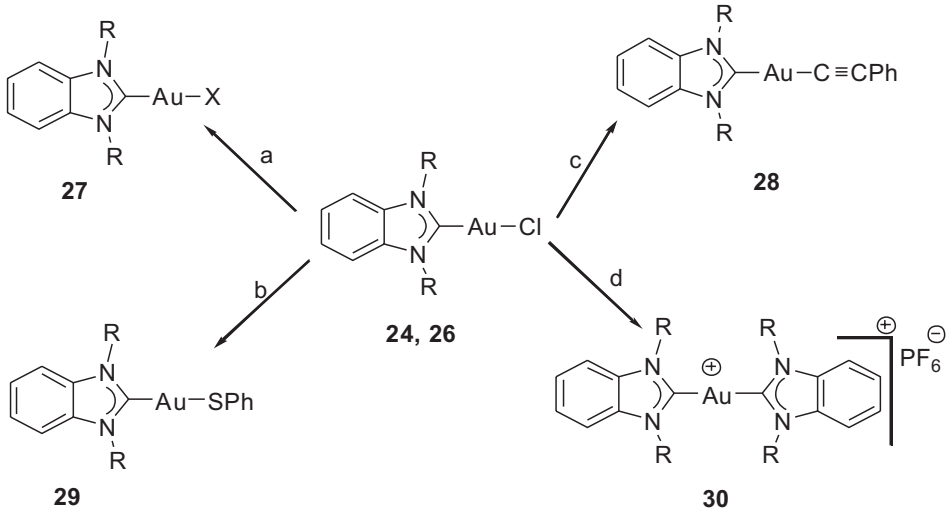
All the complexes of Schemes 12 and 13 were luminous in the solid state. In addition to the high-energy emission

© 2005 NRC Canada

Scheme 11. Formation of Au(I)–NHCs from Ag(I)–NHCs via carbene transfer.



Scheme 12. Formation of Au(I)–NHC core containing compounds.



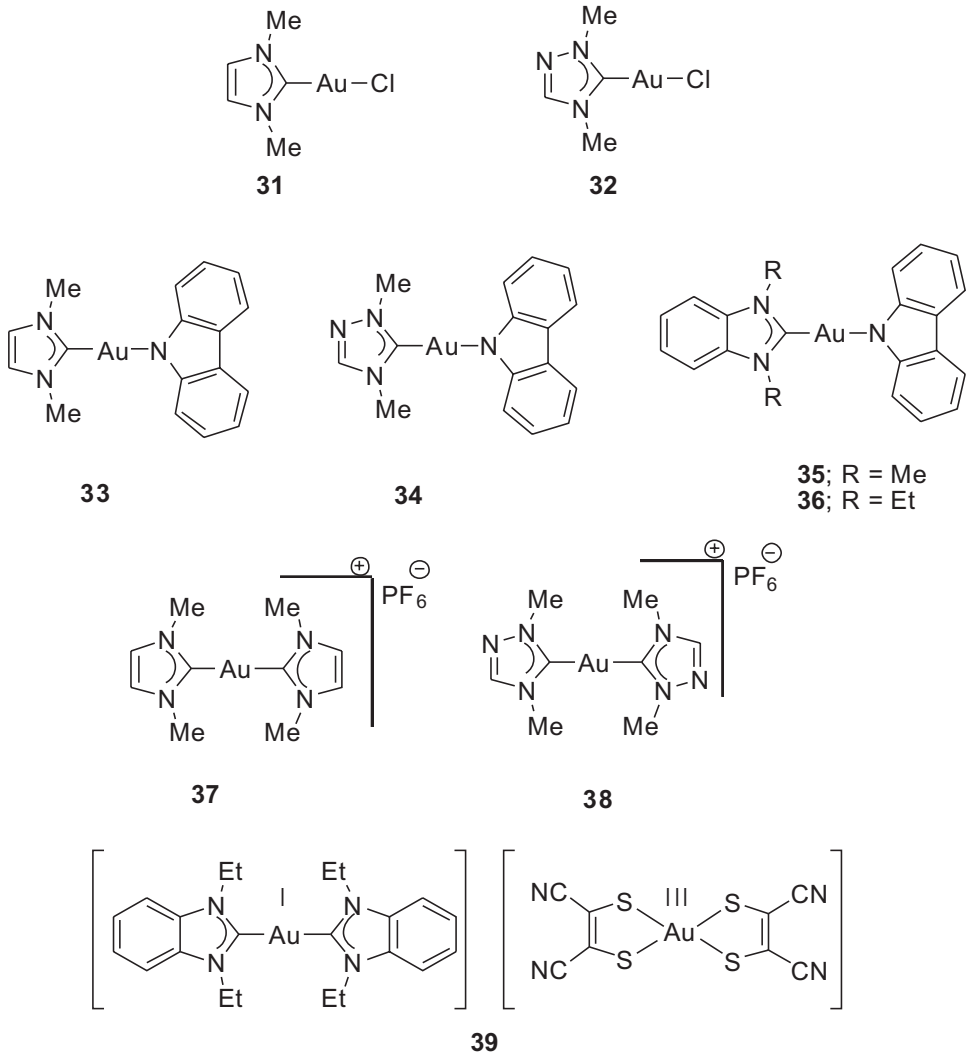
R = Et, Me: **(a)** $AgBF_4$ and KX (X = Br, I); **(b)**HSPh, KOH; **(c)** HC=CPh, K_2CO_3; **(d)** [R_2-bimyH][PF_6]

bands observed for all these carbene complexes, the [Au(NHC)Cl] complexes **26**, **31**, and **32** exhibited additional low-energy emission bands at 580–650 nm, which were attributed to Au-centered transitions involving Au···Au interactions. The [Au(NHC)(cbz)] complexes (**33**–**35**) also displayed intense low-energy emission bands at 584–592 nm with fine structures arising from carbazolate intra-ligand transitions modified by Au(I), which was also suggested by density functional calculations.

Further, the carbene transfer technique applied on the reported disilver–dicarbene complex (**XIX**) (46) also efficiently produced the corresponding digold–dicarbene

© 2005 NRC Canada

Scheme 13. Formation of [Au(NHC)(cbz)] and $[Au(NHC)_2]^+$.



complex **40** (Scheme 14).[3] Details of the reaction and structural information will be provided in future communications.

It is worth revealing that we have also reported the carbene transfer from Ag(I)–NHC (**XX** and **XXI**) of a long alkyl chain to the Au(I) center (Scheme 15) (47). Contrary to the results obtained with carbenes containing a short alkyl chain, a heteronuclear (Au_2–Ag_2) compound **41** was isolated. However, the carbene units were coordinated to the Au(I) center only; the $[Ag_2Br_4]^{2-}$ anion was intercalated between the two bisAu(I)–NHC units. It could be possible to remove the anionic unit by using appropriate methods. Instead of using the Ag–carbene transfer technique, liquid crystalline Au^I–carbene complexes (**5a**–**5c**) were best prepared by the reaction of Au^I with imidazolium salts under PTC conditions (32).

The first catalytic application of Au(I)–NHCs was explored by Herrman's group (27). As shown in Scheme 16, the carbene transfer agent (**XXII**) was treated with [Au(tht)Cl] to obtain [Au(NHC)Cl] **42**. The crystal structural parameters were found to be similar to the related Au(I)–NHCs. The NHC ligand showed significant trans influence to the Au—Cl bond length. The Au···Au separations of 4.16 Å were much longer than the van der Waals Au···Au distance of 3.6 Å.

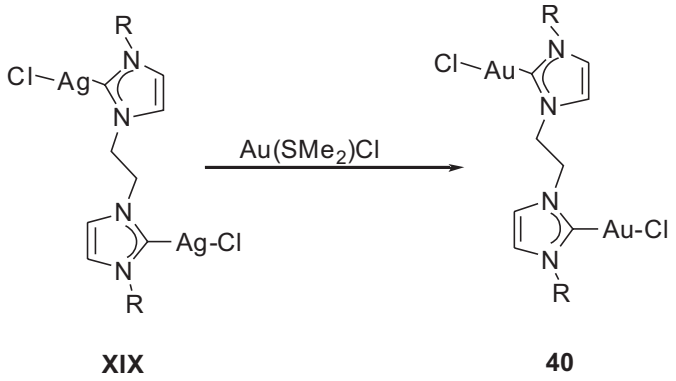
The first Au(I)–NHC containing a gold–oxygen bond (**43**) was prepared from the reaction of **42** with $AgOC(O)CH_3$ (Scheme 16). The crystal arrangement regarding the Au–NHC core was found to be similar to the parent compound. The reason for the absence of Au···Au interactions was explained on the basis of the Ahrland proposal that aurophilic interactions decrease with increasing hardness of the supporting ligands. Compound **43** was employed as the first Au(I)–NHC catalyst during the addition reaction of water to 3-hexyne. Although good results were not observed as compared to the analogous [Au(phosphane)(carboxylate)], this effort would certainly show an impact in the Au(I) based homogeneous catalysis.

Mayer and co-workers (28*a*) reported the synthesis of homoleptic trinuclear Au(I) complexes of tripodal NHC **44** via the Ag(I)–NHC route (Scheme 17). As shown in Scheme 17, carbene transfer from Ag(I)–NHC (**XXIII**) to $Au(SMe_2)Cl$ produced the corresponding isostructural

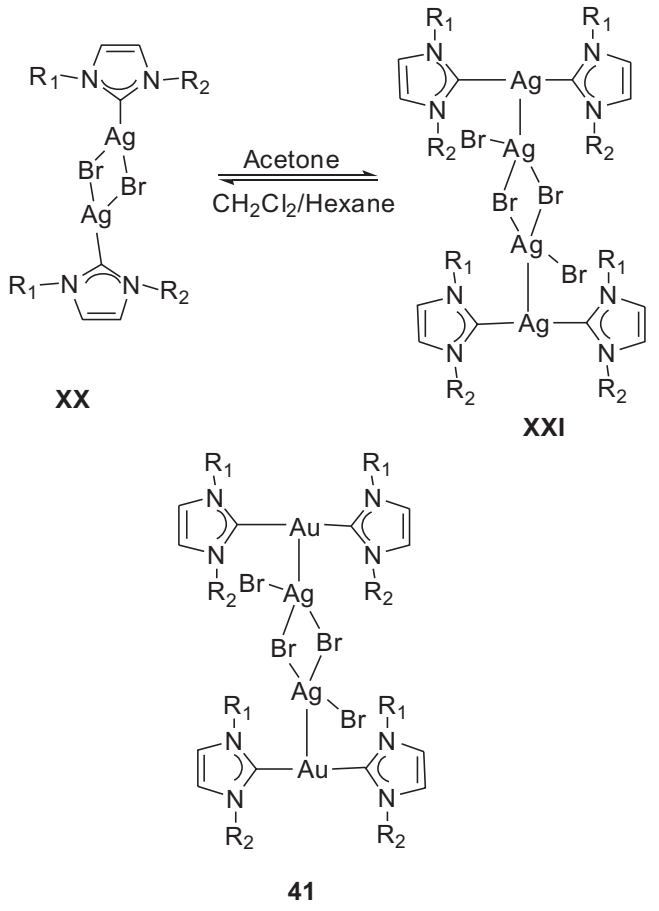
[3] Unpublished results from Professor I.J.B. Lin's research group.

© 2005 NRC Canada

Scheme 14. Formation of the digold–dicarbene complex.

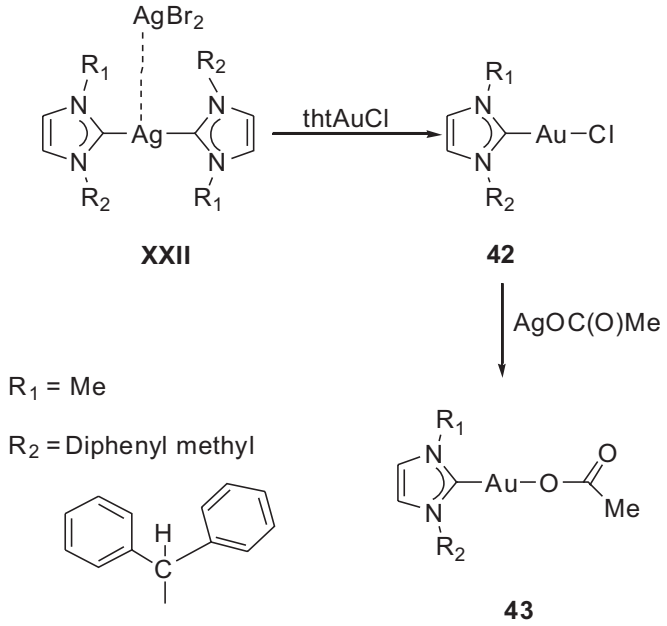


Scheme 15. Formation of the Ag_2Au_2 heterotetranuclear NHC complex.



Au(I)–NHC **44** under dry nitrogen. It was mentioned that such carbene transfer reactions performed in air produced only the imidazolium salts, and this suggested that this reaction proceeded via a free carbene intermediate as was reported for the formation of the tungsten diaminocarbene complex. The IR spectral band observed around ~1570 cm^{-1} in both the trinuclear Ag(I)–NHC and Au(I)–NHCs were ascribed for the N-C-N stretching environment. The electronic absorption spectral bands were observed between 210 and 290 nm and they proposed that they might originate from

Scheme 16. Synthesis of the first Au(I)–NHC catalyst.



ligand centered as well as ligand-to-metal and metal-to-ligand charge transfer transitions. The crystal structure of Au(I)–NHC **44** showed the nearest approach between two Au(I) centers was found to be 5.54 Å.

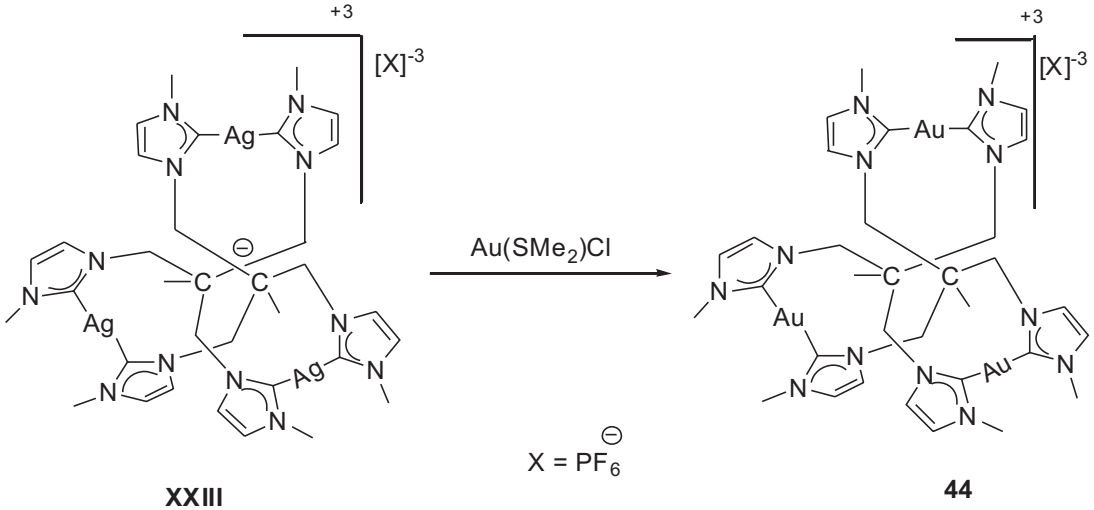
DFT studies carried on Au(I)–NHC **44** along with the parent Ag(I)–NHC and Cu(I)–NHC produced interesting results for the nature of metal–NHC bondings. Computational calculations concerning moleculear orbital interactions in these three Group 11 metal–NHCs showed a significant interaction between the metal $d(xz)$ and the $d(yz)$ orbitals and partially empty ligand π/π^* hybrid orbitals (15%–18%), and these calculations proposed that with electron-rich metal centers, π bonding could be significant (20%–30%). The elongation of C—N bond lengths in the crystal structures is consistent with the results obtained by DFT study. This phenomenon has been further supported by comparing the structural parameters of three isostructural biscarbene complexes $M(NHC)_2$ (M = I^+, Ag^+, and Ni^0).

Catalano et al. (48) reported the synthesis of Au(I) complexes with picolyl and pyridyl functionalized NHCs and extended the efforts to produce the mixed metal Ag(I)–Au(I) complexes to study the argentophilic–aurophilic interactions in the presence of functionalized NHCs (Scheme 18). Firstly, the Ag(I)–NHCs were obtained from the reaction between the pyridyl or picolyl functionalized imidazolium tetraflouroborate salt and Ag_2O. Carbene transfer performed between the Ag(I)–NHCs (**XXIV** and **XXV**) and Au(tht)Cl in dichloromethane easily produced the corresponding Au(I)–NHCs **45** and **46**. Interestingly, the Au(I)—$C_{carbene}$ bond distances in **46** were found to be slightly shorter than those observed in the corresponding parent Ag(I)–NHC. A reason owing to the smaller size of Au vs. Ag was proposed. None of these two compounds showed short aurophilic interactions.

Incorporation of additional Ag(I) atoms to **45** and **46** by treating with $AgBF_4$ resulted in two structurally different heterobimetallic complexes. Addition of $AgBF_4$ to **45** in MeCN yielded the heterotrimetallic (Ag_2Au_I) compound **47**,

© 2005 NRC Canada

Scheme 17. Formation of trinuclear Au(I)–NHC via the Ag(I)–NHC route.



in which the newly incorporated Ag^I centers were coordinated with two pyridyl side arms of the NHC fragment. Weak argentophilic–aurophilic (Ag(I)···Au(I) ~ 3.2 Å) and argentophilic–argentophilic (Ag(I)···Ag(I) ~ 3.43 Å) interactions were found in compound **47** from the X-ray crystal study. Reaction of **46** with $AgBF_4$ did not provide the expected corresponding heterotrimetallic compound, rather, an unusual helical structured heteronuclear polymer **48** was formed, as a result of the rigidity of the NHC. Formation of compound **48** was observed to be independent of reaction conditions and stoichiometry. In **48**, one of the two pyridyl groups on opposing NHCs of a Au(I)–NHC fragment was coordinating to the two alternate Ag(I) centers and formed a polymer. The Ag(I)···Au(I) separations (~2.8–2.9 Å) in **48** were found to be shorter than those in **47** (~3.2 Å) possibly owing to the strain imposed by the rigid ligand backbone of **48**.

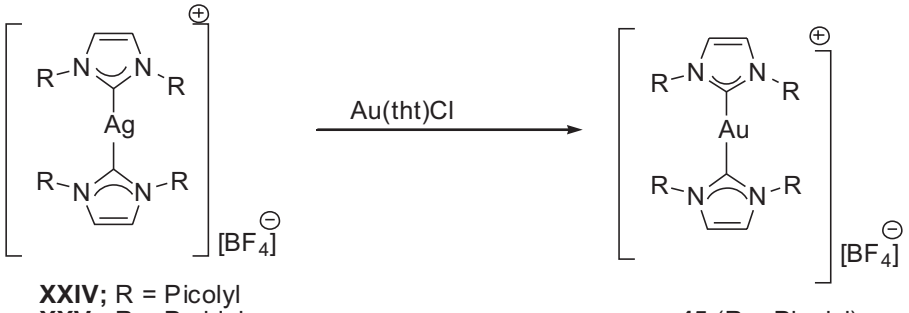
Concluding remarks

The literature survey reveals that the Au(I) metal center forms very strong bonds to NHCs. Although vast amounts of publications are not available, the reported information indicates the potential usefulness of Au(I)–NHCs in various fields. Different methods have been adopted to prepare the Au(I)–NHCs. The synthetic strategies of Au(I)–NHCs from the cleavage of electron-rich olefins or the transfer of NHC from Group 6 metal–NHCs have been less explored, probably because the starting materials are not easily accessible or the precursors are complicated. On the other hand, transmetallation of lithiated azoles followed by protonation or alkylation was applied widely as one of the easy methods in the isolation of several simple Au(I)–NHCs. It is, however, not advanced by other research groups and the validity of this method with functionalized substituents is not known. There are some Au(I)–NHCs obtained in high yields by using free NHCs, but the generation of free NHCs was hampered by the rigorous reaction conditions. Reaction of imidazolium salts with the appropriate Au(I) precursors in the presence of weak base, such as acetate salts, can also produce Au(I)–NHCs, but the yields are relatively low. On the other hand, the same kind of reaction carried out under PTC conditions produced the Au(I)–NHCs with high yields. However, much care has to be taken to remove the PTC from the final products. Carbene transfer from the Ag(I)–NHC to the Au(I) source was employed very effectively in the isolation of both simple and functionalized Au(I)–NHCs. Because the azolium salts and Ag(I)–NHCs are both air-stable, this method is recognized as a convenient entry point not only into Au(I)–NHCs, but also to other metal–NHCs. There is much evidence that the transfer of carbene from Ag(I)–NHCs to many other transition metals is particularly effective when the N-side arm contains base-sensitive functional groups. The easy synthesis of [Au(NHC)(halide)] and its high efficiency in the displacement of the halide by other ligands provides a way to the rational design of compounds containing a Au(I)–NHC core. Although anaerobic conditions are generally not necessary during the NHC transfer, the synthesis of Au(I)–NHC **44** was claimed to be carried out under a dry N_2 atmosphere to avoid the formation of imidazolium salts. These results suggest that this specific reaction proceeds via a free carbene intermediate as was observed during the synthesis of the tungsten diamino carbene complex. The carbene transfer reaction needs further study to understand the detailed mechanism.

The crystal structural study shows that in all these Au(I)–NHCs, the Au(I) center is linearly coordinated. Depending on the nature of NHCs, inter- and intramolecular aurophilic associations have been observed in several of these Au(I)–NHCs in the solid state. The aurophilic associations have been reflected in their luminescent properties in both the solid and solution state. Several other secondary interactions such as Au···H, ring π–π, and hydrogen bonding networks are also found to play an important role in the molecular assembly and properties. It is interesting to observe the mixed metal interactions, i.e., aurophilic and argentophilic interactions in the complexes of **47** and **48** with respect to the electronic and steric properties of NHCs. Computational calculations performed on Au(I)–NHCs along with other coinage metal–NHCs suggest the presence of nonnegligible π-back bonding (28) in the electron-rich metal–NHC derivatives.

© 2005 NRC Canada

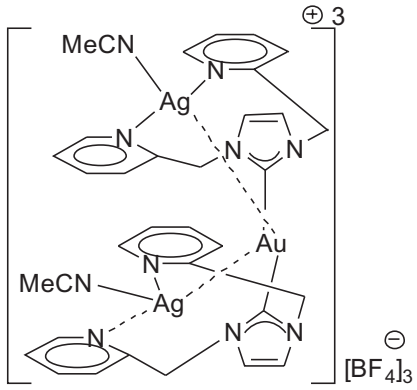
Scheme 18. Formation of Au(I)–NHCs with functionalized N substituents.



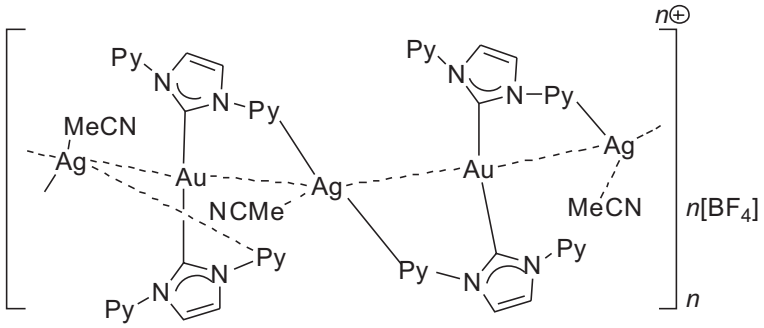
XXIV; R = Picolyl
XXV; R = Pyridyl

45 (R = Picolyl)

46 (R = Pyridyl)



47



48

Au(I)–NHCs can be applied as pharmaceuticals, homogeneous catalysts, liquid crystals, and optical devices. The performance of the Au(I)–NHCs in any application is observed to be influenced by the nature of the N substituent. The catalytic efficiency of NHC with other metal ions has already been established. In view of the facts that (*a*) gold often reacts much faster than other transition metals in the specific reactions like C—C bond formation (22), activation of C—C multiple bonds for the addition of N and O nucleophiles (22), and certain oxidations (22), (*b*) the NHC forms much stronger bonds with Au(I) than with other ligands, and (*c*) easily variable electronic or steric properties of NHCs via N- or C functionalization, we believe with certainty that the Au(I)–NHCs will show a great impact on homogeneous catalysis and other applications as mentioned previously. The generation of Au(I)–NHC polymers through short Au(I)···Au(I) interactions, their polymeric coordination mode, and photoluminescence shows the possibilities for optoelectronic and material applications. Because of the strong Au(I)—NHC bond and the linear coordination of Au(I), these complexes would be the best candidates to study the "structure – mesogenic behaviour relationship".

Acknowledgments

We thank the National Science Council (NSC) of Taiwan for providing financial assistance. The authors also thank

© 2005 NRC Canada

Dr. H.M.J. Wang for his contribution to the work of Ag– and Au(I)–NHCs.

References

1. D. Bourissou, O. Guerret, F.P. Gabbai, and G. Bertrand. Chem. Rev. **100**, 39 (2000).
2. W.A. Herrmann, M. Elisin, J. Fischer, C. Kocher, and G.R.J. Artus. Angew. Chem. Int. Ed. Engl. **34**, 2371 (1995).
3. (*a*) D.S. Clyne, J. Jin, E. Genest, J.C. Gallucci, and T.V. Rajan Babu. Org. Lett. **2**, 1125 (2000); (*b*) J.C. Garrison, R.S. Simons, J.M. Talley, C. Wesdemiotis, C.A. Tessier, and W.J. Youngs. Organometallics, **20**, 1276 (2001); (*c*) R.A. Batey, M. Shen, and A.J. Lough. Org. Lett. **4**, 1411 (2002); (*d*) A.M. Magill, D.S. McGuinness, K.J. Cavell, G.J.P. Britovsek, V.C. Gibson, A.J.P. White, D.J. Williams, A.H. White, and B.W. Skelton. J. Organomet. Chem. **617–618**, 546 (2001); (*e*) K.S. Coleman, H.T. Chamberlayne, S. Turberville, M.L.H. Green, and A.R. Cowley. Dalton Trans. 2917 (2003); (*f*) P.L. Arnold, A.C. Scarisbrick, A.J. Blake, and C. Wilson. Chem. Commun. 2340 (2001).
4. (*a*) C.D. Abernethy, G.M. Codd, M.D. Spicer, and M.K. Taylor. J. Am. Chem. Soc. **125**, 1128 (2003); (*b*) H. Braband, T.I. Zahn, and U. Abram. Inorg. Chem. **42**, 6160 (2003); (*c*) J.A. Mata, A.R. Chianese, J.R. Miecznikowski, M. Poyatos, E. Peris, J.W. Faller, and R.H. Crabtree. Organometallics, **23**, 1253 (2004); (*d*) P.L. Arnold and A.C. Scarisbrick. Organometallics, **23**, 2519 (2004).
5. W.A. Herrmann, O. Runte, and G.R.J. Artus. J. Organomet. Chem. **501**, C1–4 (1995).
6. (*a*) H.W. Wanzlick and E. Schikora. Angew. Chem. **72**, 494 (1960); (*b*) H.W. Wanzlick and H.J. Kleiner. Angew. Chem. **73**, 493 (1961); (*c*) H.W. Wanzlick, B. Lachmann, and E. Schikora. Chem. Ber. **98**, 3170 (1965).
7. (*a*) K. Öfele. J. Organomet. Chem. **12**, 42 (1968); (*b*) H.W. Wanzlick and H.J. Schönherr. Angew. Chem. **80**, 154 (1968); (*c*) H.W. Wanzlick and H.J. Schönherr. Angew. Chem. Int. Ed. Engl. **7**, 141 (1968).
8. (*a*) M.F. Lappert. J. Organomet. Chem. **100**, 139 (1975); (*b*) P.B. Hitchcock, M.F. Lappert, and P. Terreros. J. Organomet. Chem. **239**, C26 (1982); (*c*) M.J. Doyle, M.F. Lappert, P.L. Pye, and P. Terreros. J. Chem. Soc. Dalton Trans. 2355 (1984); (*d*) A.W. Coleman, P.B. Hitchcock, M.F. Lappert, R.K. Maskell, and J.H. Müller. J. Organomet. Chem. **296**, 173 (1985); (*e*) M.F. Lappert. J. Organomet. Chem. **358**, 185 (1988).
9. A.J. Arduengo, R.L Harlow, and M. Kline. J. Am. Chem. Soc. **113**, 361 (1991).
10. (*a*) A.J. Arduengo, H.V.R. Dias, R.L. Harlow, and M. Kline. J. Am. Chem. Soc. **114**, 5530 (1992); (*b*) A.J. Arduengo, J.R. Goerlich, and W.J. Marshall. J. Am. Chem. Soc. **117**, 11 027 (1995); (*c*) N. Kuhn and T. Kratz. Synthesis, 561 (1993); (*d*) D. Enders, K. Breuer, G. Raabe, J. Runsink, J.H. Teles, J.P. Melder, K. Ebel, and S. Brode. Angew. Chem. Int. Ed. Engl. **34**, 1021 (1995); (*e*) R.W. Alder, P.R. Allen, M. Murray, and G. Orpen. Angew. Chem. Int. Ed. Engl. **35**, 1121 (1996); (*f*) S. Solé, H. Gornitzka, W.W. Schoeller, D. Bourissou, and G. Bertrand. Science, **292**, 1901 (2001).
11. (*a*) D.S. McGuinness, K.J. Cavell, B.F. Yates, B.W. Skelton, and A.H. White. J. Am. Chem. Soc. **123**, 8317 (2001), and refs. therein; (*b*) T. Welton. Chem. Rev. **99**, 2071 (1999); (*c*) K.R. Seddon. Kinet. Catal. **37**, 693 (1996); (*d*) C.K. Lee, H.H. Peng, and I.J.B. Lin. Chem. Mater. **16**, 530 (2004); (*e*) R. Sheldon. Chem. Commun. 2399 (2001); (*f*) L. Xu, W. Chen, and J. Xiao. Organometallics, **19**, 1123 (2000); (*g*) P. Wasserscheid and W. Keim. Angew. Chem. Int. Ed. **39**, 3772 (2000); (*h*) J.D. Holbrey and K.R. Seddon. J. Chem. Soc. Dalton Trans. 2133 (1999); (*i*) K.J. Cavell and D.S. McGuinness. Coord. Chem. Rev. **248**, 671 (2004); (*j*) E. Peris and R.H. Crabtree. C. R. Chim. **6**, 33 (2003); (*k*) D.S. McGuinness, W. Mueller, P. Wasserscheid, K.J. Cavell, B.W. Skelton, A.H. White, and U. Englert. Organometallics, **21**, 175 (2002); (*l*) K.M. Lee, C.K. Lee, and I.J.B. Lin. Chem. Commun. **9**, 899 (1997); (*m*) C.K. Lee, H.W. Huang, and I.J.B. Lin. Chem. Commun. 1911 (2000); (*n*) K.M. Lee, H. Yi-Ting Lee, and I.J.B. Lin. J. Mater. Chem. **13**, 1079 (2003).
12. (*a*) W.A. Herrmann. Angew. Chem. Int. Ed. **41**, 1290 (2002); (*b*) W.A. Herrmann and C. Köher. Angew. Chem. **109**, 2256 (1997); (*c*) W.A. Herrmann and C. Köher. Angew. Chem. Int. Ed. Engl. **36**, 2162 (1997); (*d*) W.A. Herrmann, C. Köcher, L.J. Gooben, and G.R.J. Artus. Chem. Eur. J. **2**, 772 (1996).
13. P.E. Garrou. Chem. Rev. **85**, 171 (1985).
14. (*a*) R. Breslow. J. Am. Chem. Soc. **80**, 3719 (1958); (*b*) R. Kluger. Chem. Rev. **87**, 863 (1987).
15. (*a*) D.D. Choytun, L.D. Langlois, T.P. Johansson, C.L.B. Macdonald, G.W. Leach, N. Weinberg, and J.A.C. Clyburne. Chem. Commun. 1842 (2004); (*b*) N. Koga and H. Iwamura. *In* Carbene chemistry. From fleeting intermediates to powerful reagents. *Edited by* G. Bertrand. FontisMedia, Switzerland and Marcel Dekker, New York. 2002. p. 271; (*c*) C.K. Lee, J.C.C. Chen, K.M. Lee, C.M. Liu, and I.J.B. Lin. Chem. Mater. **11**, 1237 (1999).
16. (*a*) A. Melaiye, R.S. Simons, A. Milsted, F. Pingitore, C. Wesdemiotis, C.A. Tessier, and W.J. Youngs. J. Med. Chem. **47**, 973 (2004); (*b*) P.J. Barnard, M.V. Baker, S.J. Berners-Price, and D.A. Day. J. Inorg. Biochem. **98**, 1642 (2004); (*c*) P.J. Barnard, M.V. Baker, B.W. Skelton, A.H. White, and S.J. Berners-Price. J. Inorg. Biochem. **96**, 99 (2003); (*d*) C.A. Quezada, J.C. Garrison, M.J. Panzner, C.A. Tessier, and W.J. Youngs. Organometallics, **23**, 4846 (2004); (*e*) I. Özdemir, A. Denizci, H.T. Özturk, and B. Çetinkaya. Appl. Organometal. Chem. **18**, 318 (2004).
17. (*a*) E.R.T. Tiekink. Crit. Rev. Oncol. Hematol. **42**, 225 (2002); (*b*) C.F. Shaw III. Chem. Rev. **99**, 2589 (1999); (*c*) S.L. Best and P.J. Sadler. Gold Bull. **29**, 87 (1996); (*d*) D.H. Brown and W.E. Smith. Chem. Soc. Rev. **9**, 217 (1980); (*e*) P.J. Sadler and R.E. Sue. Metal-Based Drugs, **1**, 107 (1994); (*f*) F. Novelli, M. Recine, F. Sparatore, and C. Juliano. Farmaco, **54**, 232 (1999); (*g*) F. Caruso, M. Rossi, J. Tanski, C. Pettinari, and F. Marchetti. J. Med. Chem. **46**, 1737 (2003); (*h*) K. Nomiya, S. Takahashi, and R. Noguchi. J. Chem. Soc. Dalton Trans. 2091 (2000); (*i*) K. Nomiya, S. Yamamoto, R. Noguchi, H. Yokoyama, N.C. Kasuga, K. Ohyama, and C. Kato. J. Inorg. Biochem. **95**, 208 (2003).
18. Y.J. Chen and C.T. Yeh. J. Catal. **200**, 59 (2001).
19. P. Espinet. Gold Bull. **32**, 127 (1999).
20. J.M. Forward, J.P. Fackler, Jr., and Z. Assefa. *In* Optoelectronic properties of inorganic compounds. *Edited by* D.M. Roundhill and J.P. Fackler, Jr. Plenum Press, New York. 1999. p. 195.
21. Y. Ito, M. Sawamura, and T. Hayashi. J. Am. Chem. Soc. **108**, 6405 (1986).
22. A.S.K. Hashmi. Gold Bull. **37**, 51 (2004).
23. H. Schmidbaur. Chem. Soc. Rev. **24**, 391 (1995).
24. (*a*) S.S. Pathaneni and G.R. Desiraju. J. Chem. Soc. Dalton Trans. 319 (1993); (*b*) H. Schmidbaur, W. Graf, and G. Muller. Angew. Chem. Int. Ed. Engl. **27**, 417 (1988); (*c*) N.C. Payne, R. Ramachandran, and R. Puddephatt. Can. J. Chem. **73**, 6 (1995); (*d*) H. Schmidbaur, G. Reber, A. Schier, F.E. Wagner,

© 2005 NRC Canada

and G. Muller. Inorg. Chim. Acta, **147**, 143 (1988); (*e*) D.M.P. Mingos. J. Chem. Soc. Dalton Trans. 561 (1996); (*f*) P. Pyykko, J. Li, and N. Runeberg. Chem. Phys. Lett. **218**, 133 (1994); (*g*) J. Li and P. Pyykko. Chem. Phys. Lett. **197**, 586 (1992).
25. H.G. Raubenheimer, P.J. Olivier, L. Lindeque, M. Desmet, J. Hrušak, and G.J. Kruger. J. Organomet. Chem. **544**, 91 (1997).
26. F. Bonati, A. Burini, B.R. Pietroni, and B. Bovio. J. Organomet. Chem. **375**, 147 (1989).
27. S.K. Schneider, W.A. Herrmann, and E. Herdtweck. Z. Anorg. Allg. Chem. **629**, 2363 (2003).
28. (*a*) X. Hu, I. Castro-Rodriguez, K. Olsen, and K. Meyer. Organometallics, **23**, 755 (2004); (*b*) C. Boehme and G. Frenking. Organometallics, **17**, 5801 (1998); (*c*) D. Nemcsok, K. Wichmann, and G. Frenking. Organometallics, **23**, 3640 (2004).
29. B. Çetinkaya, P. Dixneuf, and M.F. Lappert. J. Chem. Soc. Dalton Trans. 1827 (1974).
30. T. Seckin, S. Koytepe, I. Ozdemir, and B. Çetinkaya. J. Inorg. Organomet. Polym. **13**, 9 (2003).
31. (*a*) S.T. Liu and K.R. Reddy. Chem. Soc. Rev. **28**, 315 (1999); (*b*) R.Z. Ku, J.C. Huang, J.Y. Cho, F.M. Kiang, K.R. Reddy, Y.C. Chen, K.J. Lee, J.-H. Lee, G.H. Lee, S.M. Peng, and S.T. Liu. Organometallics, **18**, 2145 (1999).
32. K.M. Lee, C.K. Lee, and I.J.B. Lin. Angew. Chem. Int. Ed. Engl. **36**, 1850 (1997).
33. P.J. Barnard, M.V. Baker, S.J. Berners-Price, B.W. Skelton, and A.H. White. Dalton Trans. 1038 (2004).
34. R. Fränkel, J. Kniczek, W. Ponikwar, H. Nöth, K. Polborn, and W.P. Fehlhammer. Inorg. Chim. Acta, **312**, 23 (2001).
35. J.F. Britten, C.J.L. Lock, and Z. Wang. Acta Crystallogr. Sect. C, **C48**, 1600 (1992).
36. C. Bohler, D. Stein, N. Donati, and H. Gruetzmacher. New J. Chem. **26**, 1291 (2002).
37. (*a*) B. Bovio, A. Burini, and B.R. Pietroni. J. Organomet. Chem. **452**, 287 (1993); (*b*) F. Bonati, A. Burini, B.R. Pietroni, and B. Bovio. J. Organomet. Chem. **408**, 271 (1991).
38. B. Bovio, S. Calogero, E.F.E. Wagner, A. Burini, and B.R. Pietroni. J. Organomet. Chem. **470**, 275 (1994).
39. (*a*) H.G. Raubenheimer, F. Scott, M. Roos, and R. Otte. Chem. Commun. 1722 (1990); (*b*) H.G. Raubenheimer, F. Scott, G.J. Kruger, J.G. Toerien, R. Otte, W. van Zyl, I. Taljaard, P. Olivier, and L. Linford. J. Chem. Soc. Dalton Trans. 2091 (1994); (*c*) H.G. Raubenheimer, L. Lindeque, and S. Cronje. J. Organomet. Chem. **511**, 177 (1996); (*d*) G.J. Kruger, P.J. Olivier, and H.G. Raubenheimer. Acta Crystallogr. Sect. C, **C52**, 1159 (1996); (*e*) G.J. Kruger, P.J. Olivier, L. Lindeque, and H.G. Raubenheimer. Acta Crystallogr. Sect. C, **C51**, 1814 (1995); (*f*) H.G. Raubenheimer, M. Desmet, and G.J. Kruger. J. Chem. Soc. Dalton Trans. 2067 (1995).
40. M. Deetlefs, H.G. Raubenheimer, and M.W. Esterhuysen. Catal. Today, **72**, 29 (2002).
41. H.G. Raubenheimer, J.G. Toerien, G.J. Kruger, R. Otte, W. van Zyl, and P. Olivier. J. Organomet. Chem. **466**, 291 (1994).
42. H.M.J. Wang and I.J.B. Lin. Organometallics, **17**, 972 (1998).
43. I.J.B. Lin and C.S. Vasam. Comments Inorg. Chem. **25**, 75 (2004).
44. H.M.J. Wang, C.Y.L. Chen, and I.J.B. Lin. Organometallics, **18**, 1216 (1999).
45. H.M.J. Wang, C.S. Vasam, T.Y.R. Tsai, S.H. Chen, A.H.H. Chang, and I.J.B. Lin. Organometallics, **24**, 486 (2005).
46. K.M. Lee, H.M.J. Wang, and I.J.B. Lin. Dalton Trans. 2852 (2002).
47. C.K. Lee, K.M. Lee, and I.J.B. Lin. Organometallics, **21**, 10 (2002).
48. V.J. Catalano, M.A. Malwitz, and A.O. Etogo. Inorg. Chem. **43**, 5714 (2004).

© 2005 NRC Canada

Microwave-accelerated, palladium-catalyzed carbonylative cyclization reactions of 2-iodophenol with alkynes — Rapid and efficient synthesis of chromen-2-one derivatives[1]

Hong Cao and Wen-Jing Xiao

Abstract: Rapid palladium-catalyzed carbonylative cyclization reactions of 2-iodophenol with various alkynes have been carried out by the use of commercially available molybdenum hexacarbonyl as a convenient and solid carbon monoxide source. The reactions were conducted at 160 °C for 30 min with microwave heating in the presence of DIEA and DMAP in 1,4-dioxane, and afford the corresponding chromen-2-one derivatives in good yields.

Key words: microwave, palladium, carbonylation, 2-iodophenol, chromen-2-one.

Résumé : Faisant appel à l'hexacarbonyle de molybdène disponible commercialement comme source solide et pratique de monoxyde de carbone, il est possible d'effectuer des réactions du 2-iodophénol avec de divers alcynes qui conduisent rapidement à des cyclisations accompagnées d'une carbonylation. Les réactions ont été en 30 min par chauffage microonde à 160 °C, en présence de DIEA et de DMAP dans le 1,4-dioxane, et elles ont conduit aux chrom-2-énones correspondantes avec de bons rendements.

Mots clés : microonde, palladium, carbonylation, 2-iodophénol, chrom-2-énone.

[Traduit par la Rédaction]

Introduction

Palladium-catalyzed carbonylative cyclizations are widely recognized as a unique, powerful, and versatile synthetic approach toward various structural cores of complex organocarbo- and heterocycles (1). Mainly because of the contributions from Alper (2), Larock (3), and Negishi (4) as well as their co-workers, the intra- and intermolecular carbo- and heteroannulations of unsaturated substrates such as alkynes, 1,2- and 1,3-dienes, vinyl cyclopropanes, homoallylic alcohols, and imines with functionally substituted aromatic or vinyl halides have been well documented in the literature (5). Although a large number of catalytic systems have been developed for the carbonylative cyclizations of a wide range of compounds, there are some limitations associated with this methodology: (1) slow reaction rate that results in long reaction time; (2) high pressure in the reaction system; and (3) less efficient utilization of toxic carbon monoxide gas. The second and third limitations are of particular concern since special gas delivery systems are needed. Therefore, the search for the improvement of carbonylation technology continues, with the goal of the development of fast, reliable, and convenient protocols. During the past 10 years, the techniques of high-throughput chemistry have been well-established and have been widely used in organic synthesis and pharmaceutical industry (6). In particular, microwave irradiation has emerged as a potential energy source for accelerated transition metal catalyzed reactions, and has proven very useful in many different applications (7). These modern methodologies offer an opportunity for the improvement of carbonylation. Consequently, Alterman and Hallberg and co-workers developed a microwave-assisted, palladium-catalyzed aminocarbonylation of aryl halides using dimethylformamide (DMF) (8) or formamide (9) as a liquid carbon monoxide source. Based on the concept that microwave-promoted thermal decomposition of metal carbonyl complexes, Larhed and co-workers reported a palldium-catalyzed carbonylation using molybdenum hexacarbonyl ($Mo(CO)_6$) as a solid carbon monoxide source (10, 11). This method, to some extent, overcomes the trouble caused by using gaseous carbon monoxide from a cylinder, and it could be suitable for high-throughput synthesis of amides and esters. Thus, Alterman and co-workers (12) subsequently explored the microwave-mediated intramolecular carbonylative cyclization reactions of bromobenzyl alcohols utilizing DMF and $Mo(CO)_6$ as two alternative CO sources.

Accordingly, we started to investigate the carbonylation reaction of 2-iodophenol with alkynes under microwave irradiation using $Mo(CO)_6$ as the CO source, and herein we

Received 13 January 2005. Published on the NRC Research Press Web site at http://canjchem.nrc.ca on 6 July 2005.

This paper is dedicated to Professor Howard Alper for his great contributions to chemistry.

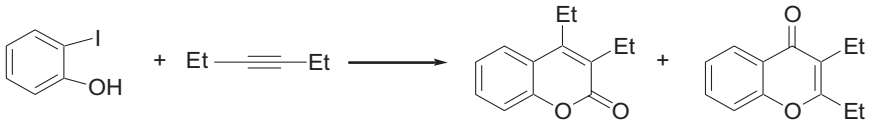
H. Cao and W.-J. Xiao.[2] The Key Laboratory of Pesticide and Chemical Biology, Ministry of Education, College of Chemistry, Central China Normal University, 152 Luoyu Road, Wuhan, Hubei 430079, China.

[1]This article is part of a Special Issue dedicated to Professor Howard Alper.

[2]Corresponding author (e-mail: wxiao@mail.ccnu.edu.cn).

 doi: 10.1139/V05-094 © 2005 NRC Canada

Table 1. Optimization of the reactions on the model reaction.[a]



1 **2a** **3a** **4a**

Entry	Catalyst	Base	Temp (°C)	Solvent	Time (min)	Yield (%)[b]	**3a**:**4a**[c]
1	$Mo(CO)_6$	DIEA	180	DMF	30	0[d]	—
2	$Pd(OAc)_2$–PPh_3	Et_2NH	160	1,4-Dioxane	30	52	1:3
3	$Pd(OAc)_2$–PPh_3	pyridine	160	1,4-Dioxane	30	43	1:3
4	$Pd(OAc)_2$–PPh_3	DIEA–DMAP[e]	180	1,4-Dioxane	30	60	1:3
5	$Pd(OAc)_2$–PPh_3	DIEA–DMAP	180	Toluene	30	59	1:3
6	$Pd(OAc)_2$–PPh_3	DIEA–DMAP	180	THF	30	54	1:3
7	$Pd(OAc)_2$–PPh_3	DIEA–DMAP	180	DMSO	30	54	1:3
8	$Pd(OAc)_2$–PPh_3	DIEA–DMAP	180	1,4-Dioxane	60	60	1:3
9	$Pd(OAc)_2$–PPh_3	DIEA–DMAP	160	1,4-Dioxane	30	74	1:3
10	$Pd(OAc)_2$–PPh_3	DIEA–DMAP	200	1,4-Dioxane	30	55	1:3

[a]Reaction conditions: 2-iodophenol (1 mmol), 3-hexyne (2 mmol), base (2–4 mmol), $Mo(CO)_6$ (0.5 mmol), $Pd(OAc)_2$ (5 mol%, 0.05 mmol), and PPh_3 (20 mol%, 0.2 mmol) in solvent (1 mL) under microwave irradiation to 60 °C for 10 min and then to a certain temperature for 30–60 min.
[b]Yield of **3a** and **4a**.
[c]Determined by ^1H NMR.
[d]Starting materials were recovered.
[e]Diisopropylethylamine (DIEA), 4-dimethylaminopyridine (DMAP).

wish to describe the first example of microwave-accelerated, palladium-catalyzed intermolecular carbonylative cyclization, resulting in chromen-2-one derivatives (eq. [1]).

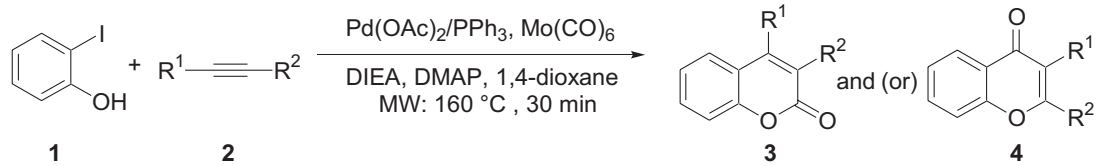
Of particular interest is the fact that some chromen-2-one derivatives possess remarkable biological activity, including anticancer and HIV-1-specific reverse transcriptase inhibitor properties (13). They are also very useful precursors of other heterocyclic compounds (14). Of the various routes to their preparation (15), the methodology presented herein is one of the most straightforward and efficient ways to afford such compounds, with small reaction scales and short reaction times.

Results and discussion

Initial studies were focused on examining the feasibility of the microwave-accelerated, intermolecular carbonylative cyclization reaction, and optimizing reaction conditions that could be applied to a variety of alkynes and 2-iodophenol. The reaction of 3-hexyne (**2a**) and 2-iodophenol (**1**) was chosen as a model reaction. On the basis of the knowledge gained from previous findings (8), DMF was initially employed as the solvent as well as a CO source. The reaction was run on a 1 mmol scale, using 5 mol% $Pd(OAc)_2$ as the catalyst, 20 mol% PPh_3 as the ligand, 2 equiv. of alkyne, and 1 equiv. of diethyl amine (DIEA) in 5 mL of DMF at 180 °C for 30 min under microwave irradiation. However, the reaction did not give the corresponding carbonylation product under these conditions. The addition of 0.5 equiv. of $Mo(CO)_6$ to the above reaction resulted in the formation of 3,4-diethyl-chromen-2-one (**3a**) and 2,3-diethyl-chromen-4-one (**4a**) in 18% and 36% isolated yields, respectively (eq. [2]). Thus, the effects of varying the base, solvent, reaction temperature, and reaction time on the model reaction were then examined.

Table 1 shows the results of the model reaction under different conditions. It was found that $Mo(CO)_6$ was not active itself as an efficient catalyst in the model reaction under mi-

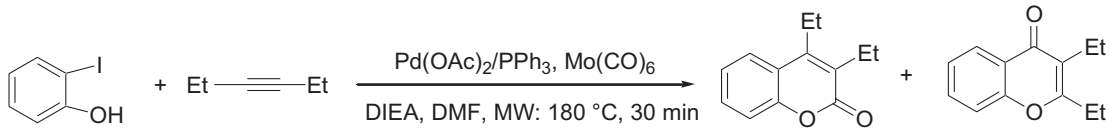
[1]



1 **2** **3** **4**

R^1, R^2 = H, alkyl or aryl

[2]



1 **2a** **3a** **4a**

18% 36%

© 2005 NRC Canada

crowave irradiation (Table 1, entry 1), while $Pd(OAc)_2$ with 4 equiv. of PPh_3 worked very well in most cases (Table 1, entries 2–10). It can be concluded from Table 1 that the reaction is significantly influenced by the solvent and base employed. For example, when *N*-ethyldiisopropylamine (DIEA) and 4-(dimethylamino)pyridine (DMAP) were used as a co-base, the reaction gave the carbonylation products in 60% isolated yield in 1,4-dioxane (Table 1, entry 4). Other solvents, such as toluene, THF, and DMSO can be employed as the solvent for the reaction, but none appears to be as good as 1,4-dioxane (Table 1, entries 5–7). In addition to DIEA–DMAP, we have examined other bases, such as diethyl amine and pyridine, for the reaction (Table 1, entries 2 and 3). The results show that both of them are inferior to DIEA–DMAP. The use of inorganic bases (K_2CO_3 or KOAc) resulted in the formation of a complicated mixture; therefore, they were ruled out for further investigation.

The reaction temperature is another critical factor for the carbonylative cyclization, with the best result being attained at 160 °C. Variations of the temperature from this value have been proven to be detrimental to the reaction. For example, increasing the temperature to 180 and 200 °C gave only 60% and 55% yields, respectively (Table 1, entries 8 and 10). Decreasing the temperature to less than 150 °C did not give any carbonylation product because $Mo(CO)_6$ could not thermally decompose to generate carbon monoxide at this temperature (16).

We did not rigorously examine the effect of the CO source on the reaction. In principle, any compounds that could liberate CO under the above conditions might be used as a CO source in the reaction. However, compared with $Cr(CO)_6$, $Fe(CO)_5$, $Co_2(CO)_8$, and $Ni(CO)_4$, $Mo(CO)_6$ was found to be the best choice for the present reaction.

Thus, the final optimized reaction conditions for the microwave-accelerated carbonylative cyclization of 2-iodophenol and 3-hexyne with $Mo(CO)_6$ as the CO source have been determined to be 1 mmol of 2-iodophenol, 2 equiv. of 3-hexyne, 0.5 equiv. of $Mo(CO)_6$, 5 mol% $Pd(OAc)_2$, 20 mol% PPh_3 in the presence of 1 equiv. of DIEA, and 1 equiv. of DMAP in 1–1.5 mL of 1,4-dioxane under microwave irradiation at 160 °C for 30 min. Using these reaction conditions, reactions of a variety of internal and terminal alkynes with 2-iodophenol were studied, and the results are summarized in Table 2.

Internal and terminal alkynes can be successfully employed in the microwave-accelerated, palladium-catalyzed carbonylative cyclization reactions with 2-iodophenol using $Mo(CO)_6$ as a solid carbon monoxide source, to give the corresponding chromenone derivatives in good isolated yields (Table 2). The regioselectivity of this reaction depends on the substrate employed. The terminal alkynes reacted with 2-iodophenol to exclusively afford the chromen-2-one derivatives in pretty good yields (Table 2, entries 3–7). Mixtures of regioisomers were obtained with modest regioselectivity when internal alkynes were applied in the reaction (Table 2, entries 1 and 2). Both the regioselectivity and the yield of the reactions of internal alkynes are affected by the steric bulk of the alkyl substituent. Increasing the size of the alkyl group from ethyl to propyl resulted in an increase in the regioselectivity (Table 2, entries 1 and 2), but a decrease in the yield of the reaction. For the reactions of terminal alkynes, in principle, they might also give two regioisomers (Scheme 1). However, during the insertion of the alkyne into the aryl–palladium bond, route a is much more favorable than route b because of the interaction of the bigger alkyl group (compare with H) with the palladium species (Scheme 1). Therefore, chromen-2-one **8**, rather than **9**, was formed as a sole product in the reaction.

The formation of two regioisomers in the reaction of internal alkynes could be rationalized according to Scheme 2. The reaction may start from the oxidative addition of 2-iodophenol to Pd(0) to form an arylpalladium complex **10**, and then both CO and the internal alkyne insert subsequently to the aryl–Pd bond to form complexes **11** and **12**, respectively. Depending on the rate difference of the insertion and (or) the stabilities of **11** and **12**, the reaction exhibits regioselectivity and eventually affords chromenones **3** and **4** in different ratios (Scheme 2).

Conclusions

In summary, this research has resulted in the first example of microwave-accelerated, palladium-catalyzed intermolecular carbonylative cyclization of 2-iodophenol and alkynes with the solid molybdenum hexacarbonyl as an efficient source of carbon monoxide. The methodology presented here is attractive because of the short reaction time, the experimental simplicity, and the fact that no external carbon monoxide needs to be added.

Experimental section

General methods

Unless otherwise noted, materials were purchased from commercial suppliers and used without further purification. Solvents and liquid organic bases were freshly distilled according to the known procedures (16). Column chromatography was performed using 200–300 mesh silica gel. IR was recorded on a PerkinElmer PE-983 IR spectrometer as KBr film with absorption in cm^{-1}. ^1H NMR spectra were recorded on Varian Mercury 400 (400 MHz) spectrometers. Chemical shifts are reported in ppm from TMS with the solvent resonance as the internal standard ($CDCl_3$: δ 7.24). Data are reported as follows: chemical shift, multiplicity (singlet (s), doublet (d), triplet (t), quartet (q), broad (br), multiplet (m)), coupling constants (Hz). ^{13}C NMR spectra were recorded on Varian Mercury 400 (100 MHz) with complete proton decoupling spectrophotometers ($CDCl_3$: δ 77.7).

All experiments were performed in a Smith Synthesizer producing controlled irradiation at 2450 MHz with a power of 0–300 W.

Typical procedure for the microwave-accelerated, palladium-catalyzed carbonylative cyclization

A 2.0–5.0 mL process vial was charged with 2-iodophenol (1 mmol) and $Pd(OAc)_2$ (0.05 mmol), PPh_3 (0.2 mmol), $Mo(CO)_6$ (0.5 mmol), alkyne (2 mmol), DIEA (1 mmol), DMAP (1 mmol), and dry 1,4-dioxane (1.0 mL). The vial was immediately capped with a Teflon septum under N_2 and irradiated with microwaves to 60 °C for 10 min, then to 160 °C for another 30 min. After cooling, the reaction mixture was filtered through a short Celite pad, and the solvent

© 2005 NRC Canada

Table 2. Microwave-accelerated, palladium-catalyzed carbonylative cyclization reactions of alkynes with 2-iodophenol using $Mo(CO)_6$ as the CO source (eq. [1]).[a]

Entry	Alkyne	Product	3:4[b]	Yield (%)
1	C_2H_5—≡—C_2H_5 **2a**	**3a** + **4a**	1:3	74
2	C_3H_7—≡—C_3H_7 **2b**	**3b** + **4b**	1:4	69
3	≡—C_3H_7 **2c**	**3c**	—	71
4	≡—C_4H_9 **2d**	**3d**	—	76
5	≡—C_5H_{11} **2e**	**3e**	—	63
6	≡—C_6H_{13} **2f**	**3f**	—	69
7	≡—C_6H_5 **2g**	**3g**	—	78

[a]Reaction conditions: 2-iodophenol (1 mmol), alkyne (2 mmol), DIEA (1 mmol), DMAP (1 mmol), $Mo(CO)_6$ (0.5 mmol), $Pd(OAc)_2$ (5 mol%, 0.05 mmol), and PPh_3 (20 mol%, 0.2 mmol) in 1,4-dioxane (1 mL) under microwave irradiation at 160 °C for 30–60 min.
[b]Determined by ^{1}H NMR (17).

was removed under reduced pressure. The residue was purified by silica gel flash chromatography to give the desired pure products.

3,4-Diethyl-chromen-2-one (3a) and 2,3-diethyl-chromen-4-one (4a) (18)

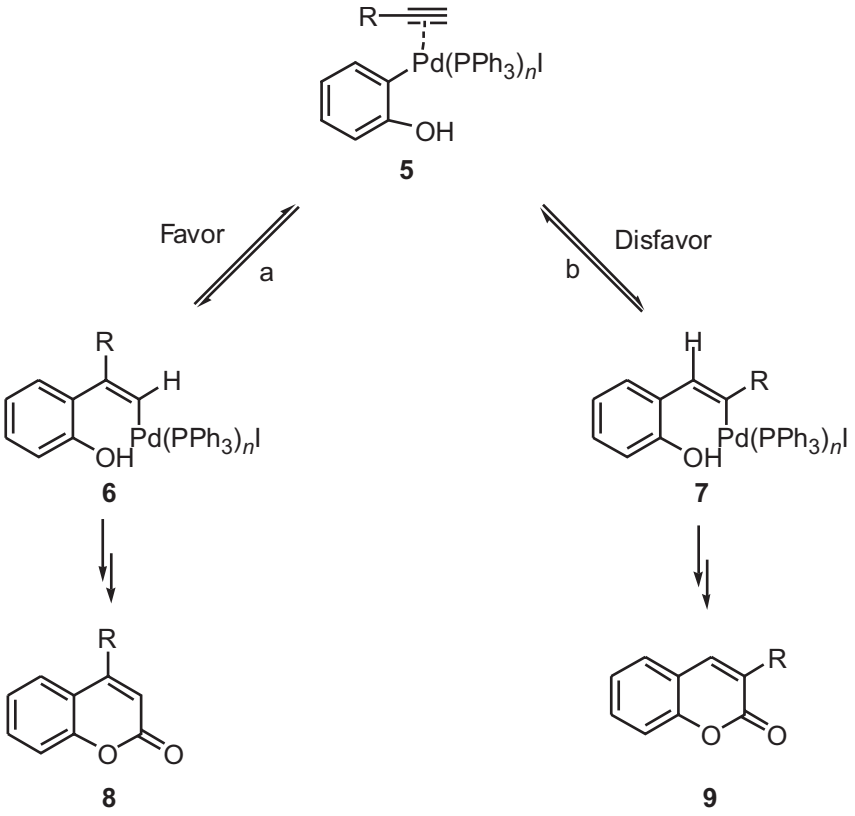
Yellow oil; a mixture of regioisomers with a ratio of 1:3. **3a**: IR (cm^{-1}): 1710. ^{1}H NMR ($CDCl_3$) δ: 7.61 (d, J = 8.0 Hz, 1/4H), 7.44 (m, 1/4H), 7.26–7.32 (m, 2 × 1/4H), 2.85 (q, J = 7.5 Hz, 2 × 1/4H), 2.67 (q, J = 7.5 Hz, 2 × 1/4H), 1.28 (t, J = 8.0 Hz, 3 × 1/4H), 1.19 (t, J = 8.0 Hz, 3 × 1/4H). **4a**: IR (cm^{-1}): 1639. ^{1}H NMR ($CDCl_3$) δ: 8.21–8.19 (d, J = 8 Hz, 3/4H), 7.63–7.61 (m, 2 × 1/4H), 7.40–7.33 (m, 3/4H), 2.76–2.73 (m, 2 × 3/4H), 2.61–2.55 (m, 2 × 3/4H), 1.36–1.34 (m, 3 × 3/4H), 1.15–1.12 (m, 3 × 3/4H). ^{13}C NMR δ: 177.1, 156.1, 132.3, 124.8, 124.7, 116.9, 26.5, 22.8, 14.8, 10.9, 10.5. MS *m/z* (rel. intensity): 202 (26, M^+).

3,4-Dipropyl-chromen-2-one (3b) and 2,3-dipropyl-chromen-4-one (4b) (18)

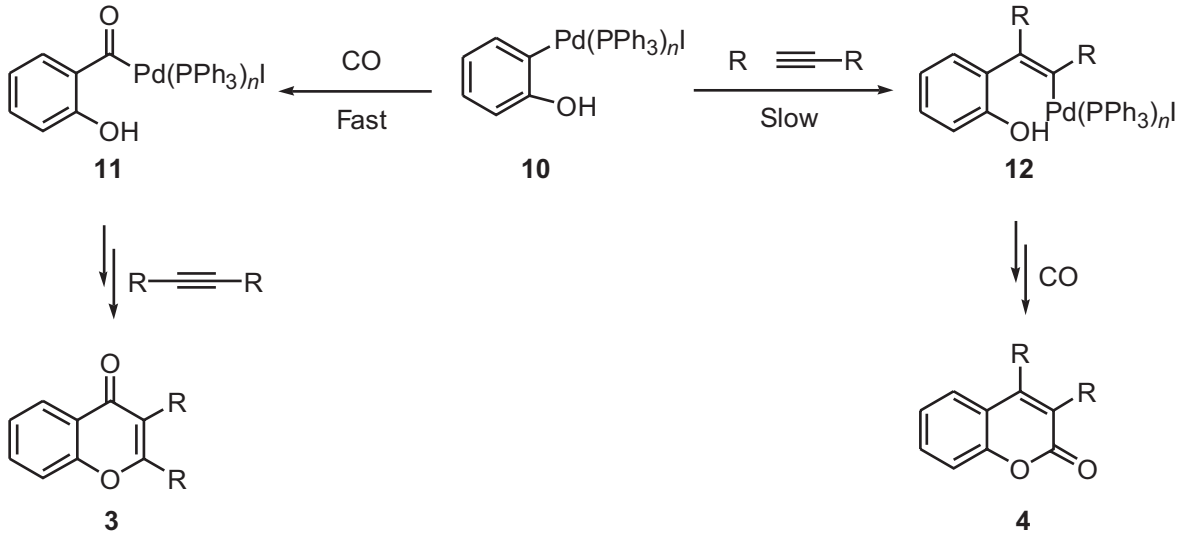
White solid; a mixture of regioisomers with a ratio of 1:4. **3b**: IR (cm^{-1}): 1716. ^{1}H NMR ($CDCl_3$) δ: 7.59 (d, J =

© 2005 NRC Canada

Scheme 1.



Scheme 2.



8.0 Hz, 1/5H), 7.45 (d, J = 8.0 Hz, 1H), 7.25–7.32 (m, 2 × 1/5H), 2.79 (m, 2 × 1/5H), 2.61 (m, 2 × 1/5H), 1.55–1.70 (m, 4 × 1/5H), 1.11 (t, J = 7.6 Hz, 3 × 1/5H), 1.03 (t, J = 7.6 Hz, 3 × 1/5H). **4b**: IR (cm^{-1}): 1639. ^1H NMR ($CDCl_3$) δ: 8.18–8.20 (d, J = 8.0 Hz, 1 × 4/5H), 7.56–7.60 (m, 2 × 4/5H), 7.34–7.37 (m, 1 × 4/5H), 2.63–2.71 (m, 2 × 4/5H), 2.50–2.59 (m, 2 × 4/5H), 1.77–1.81 (m, 2 × 4/5H, CH_2), 1.51–1.61 (m, 2 × 4/5H), 0.98–1.12 (m, 6 × 4/5H). ^{13}C NMR δ: 177.8, 155.8, 132.9, 126.3, 125.7, 124.4, 124.3, 116.8, 26.5, 22.8, 22.4, 20.9, 14.3, 14.2. MS *m*/*z* (rel. intensity): 230 (2.5, M^+).

4-Propyl-chromen-2-one (3c) (19)

Colorless oil. IR (cm^{-1}): 1720. ^1H NMR ($CDCl_3$) δ: 7.53–7.66 (m, 2H), 7.27–7.36 (m, 2H), 6.30 (s, 1H), 2.74–2.78 (m, 2H), 1.73–1.78 (m, 2H), 1.05–1.09 (t, 3H). MS *m*/*z* (rel. intensity): 189 (22, $M^+ + 1$).

4-Butyl-chromen-2-one (3d) (20)

Yellow solid. IR (cm^{-1}): 1731. ^1H NMR ($CDCl_3$) δ: 7.28–7.66 (m, 4H), 6.29 (s, 1H), 2.24–2.80 (m, 2H), 1.66–1.74 (m, 2H), 1.45–1.50 (m, 2H), 0.93–0.99 (m, 3H). MS *m*/*z* (rel. intensity): 202 (2, M^+).

© 2005 NRC Canada

4-Pentyl-chromen-2-one (3e)

Yellow solid. IR (cm^{-1}): 1717. ^1H NMR ($CDCl_3$) δ: 7.30–7.65 (m, 4H), 6.30 (s, 1H), 2.77 (t, J = 8.0 Hz, 2H), 1.69–1.73 (m, 2H), 1.38–1.44 (m, 4H), 0.93 (t, J = 8.0 Hz, 3H). ^{13}C NMR δ: 161.9, 156.3, 153.7, 131.6, 124.3, 119.3, 117.3, 113.2, 31.7, 31.5, 29.7, 27.8, 22.4, 13.9. MS *m*/*z* (rel. intensity): 216 (2, M^+).

4-Hexyl-chromen-2-one (3f)

Brown oil. IR (cm^{-1}): 1655. ^1H NMR ($CDCl_3$) δ: 7.36–8.20 (m, 4H, Ar*H*), 6.18 (s, 1H, =C*H*), 2.62 (t, J = 8.0 Hz, 2H), 1.70–1.74 (m, 2H, CH_2), 1.30–1.42 (m, 6H, 3CH_2), 0.90 (t, J = 8.0 Hz, 3H). ^{13}C NMR δ: 162.6, 156.4, 153.8, 133.4, 125.6, 124.7, 119.8, 117.9, 110.8, 34.3, 31.4, 29.7, 28.6, 22.5, 14.0. MS *m*/*z* (rel. intensity): 230 (2, M^+).

4-Phenyl-chromen-2-one (3g) (19)

Colorless oil. IR (cm^{-1}): 1645. ^1H NMR ($CDCl_3$) δ: 7.42–8.26 (m, 9H), 6.85 (s, 1H). MS *m*/*z* (rel. intensity): 222 (100, M^+).

Acknowledgments

We are grateful to the National Key Project for Basic Research of China (2004CCA00100), the Natural Science Foundation of China (20472021), the Hubei Province Science Fund for Distinguished Young Scholar (2004ABB011), and Central China Normal University, for the financial support of this research.

References

1. For reviews, see: (*a*) B. El Ali and H. Alper. *In* Transition metal catalyzed reactions. *Edited by* S.-I. Murahashi and S.G. Davies. Blackwell Science, Malden, Mass. 1999. p. 261; (*b*) R.C. Larock. J. Organomet. Chem. **576**, 111 (1999); (*c*) J. Tsuji. Palladium reagents and catalysts. Wiley, New York. 1995; (*d*) K. Khumtaveeporn and H. Alper. Acc. Chem. Res. **28**, 414 (1995).
2. (*a*) C. Dong and H. Alper. J. Org. Chem. **69**, 5011 (2004); (*b*) J.T. Lee and H. Alper. Macromolecules, **37**, 2417 (2004); (*c*) C. Larksarp, O. Sellier, and H. Alper. J. Org. Chem. **66**, 3502 (2001); (*d*) J.T. Lee, P.J. Thomas, and H. Alper. J. Org. Chem. **66**, 5424 (2001); (*e*) D.C.D. Butler, G.A. Inman, and H. Alper. J. Org. Chem. **65**, 5887 (2000); (*f*) W.-J. Xiao and H. Alper. J. Org. Chem. **64**, 9646 (1999); (*g*) C. Larksarp and H. Alper. J. Org. Chem. **63**, 6229 (1998); (*h*) H. Maas, C. Bensimon, and H. Alper. J. Org. Chem. **63**, 17 (1998); (*i*) C. Larksarp and H. Alper. J. Am. Chem. Soc. **119**, 3709 (1997); (*j*) K. Okuro and H. Alper. J. Org. Chem. **62**, 1566 (1997); (*k*) J.O. Baeg, C. Bensimon, and H. Alper. J. Am. Chem. Soc. **117**, 4700 (1995); (*l*) J.O. Baeg and H. Alper. J. Org. Chem. **57**, 157 (1992).
3. (*a*) S.V. Gagnier and R.C. Larock. J. Am. Chem. Soc. **125**, 4804 (2003); (*b*) G. Daid and R.C. Larock. Org. Lett. **4**, 193 (2002); (*c*) G. Dai and R.C. Larock. Org. Lett. **3**, 4035 (2001); (*d*) M.A. Campo and R.C. Larock. Org. Lett. **2**, 3675 (2000); (*e*) K.R. Roesch and R.C.L. Larock. Org. Lett. **1**, 553 (1999); (*f*) K.R. Roesch and R.C. Larock. J. Org. Chem. **63**, 5306 (1998); (*g*) R.C. Larock and L. Guo. Synlett, 465 (1995); (*h*) R.C. Larock, N.G. Berrios-Pena, C.A. Fried, E.K. Yum, C. Tu, and W. Leong. J. Org. Chem. **58**, 4509 (1993); (*i*) R.C. Larock, N.G. Berrios-Pena, and K. Narayanan. J. Org. Chem. **55**, 3447 (1990); (*j*) R.C. Larock and C.A. Fried. J. Am. Chem. Soc. **112**, 5882 (1990).
4. (*a*) E. Negishi, C. Coperet, S. Ma, S. Liou, and F. Liu. Chem. Rev. **96**, 635 (1996); (*b*) E. Negishi, S.M. Coperet, S. Ma, T. Mita, T. Sugihara, and J.M. Tour. J. Am. Chem. Soc. **118**, 5919 (1996); (*c*) E. Negishi, S.M. Coperet, S. Ma, T. Mita, T. Sugihara, and J.M. Tour. J. Am. Chem. Soc. **118**, 5904 (1996); (*d*) S. Ma and E. Negishi. J. Am. Chem. Soc. **117**, 6345 (1995).
5. (*a*) K. Kumar, A. Zapf, D. Michalik, A. Tillack, T. Heinrich, H. Bottcher, M. Arlt, and M. Beller. Org. Lett. **6**, 7 (2004); (*b*) B.G. Van den Hoven, B. El Ali, and H. Alper. J. Org. Chem. **65**, 4131 (2000); (*c*) S.-K. Kang and K.-J. Kim. Org. Lett. **3**, 511 (2001); (*d*) C. Ma, X.X. Liu, S. Yu, S. Zhao, and J.M. Cook. Tetrahedron Lett. **40**, 657 (1999); (*e*) M. Lautens, W. Klute, and W. Tam. Chem. Rev. **96**, 49 (1996).
6. (*a*) H. Fenniri (*Editor*). Combinatorial chemistry: A practical approach. Oxford University Press, Oxford, New York. 2000; (*b*) Curr. Opin. Chem. Biol. **4**, 243 (2000) (whole issue); (*c*) A. Lew, P.O. Krutzik, M.E. Hart, and A.R. Chamberlin. J. Comb. Chem. **4**, 95 (2002); (*d*) M. Larhed and A. Hallberg. Drug Discovery Today, **6**, 406 (2001).
7. (*a*) F. Mavandadi and P. Lidstrom. Curr. Top. Med. Chem. **4**, 773 (2004); (*b*) M. Larhed, C. Moberg, and A. Hallberg. Acc. Chem. Res. **35**, 717 (2002); (*c*) P. Lidstrom, J. Tierney, B. Wathey, and J. Westman. Tetrahedron, **47**, 9225 (2001).
8. Y. Wan, M. Alterman, M. Larhed, and A. Hallberg. J. Org. Chem. **67**, 6232 (2002).
9. Y. Wan, M. Alterman, M. Larhed, and A. Hallberg. J. Comb. Chem. **5**, 82 (2003).
10. (*a*) N.-F.K. Kaiser, A. Hallberg, and M. Larhed. J. Comb. Chem. **4**, 109 (2002); (*b*) J. Georgsson, A. Hallberg, and M. Larhed. J. Comb. Chem. **5**, 350 (2003); (*c*) J. Wannberg and M. Larhed. J. Org. Chem. **68**, 5750 (2003).
11. K. Yamazaki and Y. Kondo. J. Comb. Chem. **6**, 121 (2004).
12. X. Wu, A.K. Mahalingam, Y. Wan, and M. Alterman. Tetrahedron Lett. **45**, 4635 (2004).
13. R.D.H. Murray, J. Mendez, and S.A. Brown. The natural coumarins: Occurrence, chemistry, and biochemistry. J. Wiley, New York. 1982.
14. J.D. Hepworth. *In* Comprehensive heterocyclic chemistry. Vol. 3. *Edited by* A.R. Katritzy and C.W. Rees. Pergamon Press, Oxford. 1984. p. 737.
15. (*a*) J.R. Johnson. Org. React. (N.Y.), **1**, 210 (1942); (*b*) S. Sethna and R. Phadke. Org. React. (N.Y.), **7**, 1 (1953); (*c*) D.V. Kadnikov and R. Larock. J. Org. Chem. **68**, 9423 (2003).
16. W.L.F. Armarego and D.D. Perrin. Purifications of laboratory chemicals. Butterworth-Heinemann, Oxford. 1997.
17. V.O. Patil, S.L. Kelkar, and M.S. Waida. Indian J. Chem. Sect. B, **26**, 674 (1987).
18. D.V. Kadnikov and R.C. Larock. J. Org. Chem. **68**, 9423 (2003); J. Wu and Z. Yang. J. Org. Chem. **66**, 7875 (2001).
19. A. Alberola, B. Calvo, A.G. Ortega, M. Vicente, S. Granda, and J.V. Maelen. J. Chem. Soc. Perkin Trans. 1, 203 (1991).

© 2005 NRC Canada

Preparation, characterization, and structure of two dipyrrolide thorium homoleptic complexes — Isolation of a dipyrrolide dipotassium salt with an inverted-sandwich type of structure[1]

Arunachalampillai Athimoolam, Sandro Gambarotta, and Ilia Korobkov

Abstract: Reactions of the in-situ-generated potassium salts of the dipyrroles $(C_4H_3NH)_2C(CH_3)_2$ and of $(C_4H_3NH)_2C(CH_3)(C_6H_5)$ with $ThCl_4(DME)_2$ has afforded the corresponding homoleptic $(\{[(C_4H_3N)_2C(CH_3)_2]_3Th\}[K_2(DME)])_n$ (**1**) and $\{[(C_4H_3N)_2C(CH_3)(C_6H_5)]_3Th\}[K_2(DME)]$ (**2**). In the case of **1**, the solid state polymeric structure was elucidated by X-ray diffraction analysis. Preliminary attempts to reduce these species have so far afforded only intractable materials. Just in the case of **2**, it was possible to isolate the corresponding ligand dipotassium salt $\{(C_4H_3NH)_2C(CH_3)(C_6H_5)[K(DME)]_2\}_n$ (**3**) as the only characterizable material. This species possesses an unprecedented inversed-sandwich type of structure.

Key words: thorium, homoleptic, dipyrrolide.

Résumé : Les réactions du $ThCl_4(DME)_2$ avec des sels de potassium générés in situ des pyrroles $(C_4H_3NH)_2C(CH_3)_2$ et $(C_4H_3NH)_2C(CH_3)(C_6H_5)$ conduit à la formation des composés homoleptiques correspondants $(\{[C_4H_3N)_2C(CH_3)_2]_3Th\}[K_2(DME)])_n$ (**1**) et $\{[C_4H_3N)_2C(CH_3)(C_6H_5)]_3Th\}[K_2(DME)]$ (**2**). Dans le cas du composé **1**, on a élucidé la structure polymère de l'état solide par diffraction des rayons X. Des essais préliminaires en vue de réduire ces espèces n'ont fourni que des produits intraitables. Dans le cas du composé **2**, il a toutefois été possible d'isoler le sel dipotassique du ligand $\{(C_4H_3NH)_2C(CH_3)(C_6H_5)[K(DME)]_2\}_n$ (**3**) comme seul produit pouvant être caractérisé. Cette espèce possède une structure de type sandwich inversé, inconnue jusqu'à maintenant.

Mots clés : thorium, homoleptique, dipyrrolure.

[Traduit par la Rédaction]

Introduction

There is a revival of interest in the recent literature for the chemistry of reduced actinide complexes and in particular for the preparation of trivalent uranium derivatives (1). Recent discoveries in this direction include three cases of dinitrogen fixation (2), which have indicated that in fact these species may be versatile agents for molecular activation purposes. This has prompted a multiplication of efforts in this direction that has resulted in spectacular findings such as a unique way of reversibly bonding CO_2 (3) and the ability to coordinate a saturated hydrocarbon (4). This exciting background is obviously encouraging further efforts for the preparation and characterization of highly reduced actinide species with varied ligand systems.

Received 4 January 2005. Published on the NRC Research Press Web site at http://canjchem.nrc.ca on 13 July 2005.

A. Athimoolam, S. Gambarotta,[2] and I. Korobkov. Department of Chemistry, University of Ottawa, Ottawa, ON K1N 6N5, Canada.

[1]This article is part of a Special Issue dedicated to Professor Howard Alper.

[2]Corresponding author (e-mail: sgambaro@science.uottawa.ca).

[3]I. Korobkov, A. Arunachalampillai, and S. Gambarotta. Manuscript in preparation.

As usual, the choice of a suitable ligand system is central to the fine tuning for the control of very high reactivity. With this respect, pyrrole-based anions provide a family of ligands that has proven versatile for the stabilization of low oxidation states with a large variety of elements (5), and for sustaining a high level of reactivity with lanthanides (6) and actinides (7). Tetrapyrrolide tetra-anion complexes in particular have afforded dinitrogen labile fixation (8), reduction (9), and cleavage (10). In addition, these ligands have allowed the preparation of thorium species carrying reduced naphtalenide anions, which, in turn, work as an electronic reservoir for two-electron reduction of several substrates including solvent fragmentation (11). In other words, intact arene could be dissociated and two-electron reductions conveniently performed on a variety of substrates (11).[3] Furthermore, reduction of a trivalent uranium tetrapyrrolide derivative has provided the sole example of dinitrogen cleavage in the chemistry of *f*-block elements (10), once more reiterating the potential offered by reduced actinides for molecular activation purposes.

Dipyrrolide dianions also belong to this family of ligands and are able to stabilize low-valent *f*-block elements via clusterification that occurs by crossing σ- and π-bonding interactions with the pyrrolide rings (12). These thermally robust clusters have displayed a unique inclination towards cooperative four-electron reduction of N_2 (13). Furthermore,

 doi: 10.1139/V05-086 © 2005 NRC Canada

since a simple *bidentate* bisaryloxide complex of thorium has also afforded dinitrogen cleavage and protonation during the reduction (14), we became interested in the synthesis, characterization, and reduction of thorium complexes supported by the bidentate dipyrrolide dianions. This background has prompted us to study the chemistry of actinides supported by the dipyrrolide ligand system, which may work as a precursor towards further preparation of reduced species.

In this paper, we describe the results of our attempts.

Experimental section

All operations were performed under an inert atmosphere by using standard Schlenk techniques or inside a drybox. $ThCl_4(DME)_2$ was prepared from thorium nitrate by boiling with concd. HCl and then dehydrated with thionyl chloride, followed by recrystallization and extraction from DME. Dipyrromethanes were synthesized according to literature procedure (15). NMR spectra were recorded on a Bruker Avance 300 spectrometer. Elemental analyses were performed on a PerkinElmer 2400 CHN analyzer. Data for X-ray crystal structure determinations were obtained with a Bruker diffractometer equipped with a Smart CCD area detector. NMR spectra were recorded on a Varian AMX-300 spectrometer.

Preparation of $\{[(C_4H_3N)_2C(CH_3)_2]_3Th\}[K_2(DME)]$ (1)

A solution of the potassium salt of $(C_4H_3NH)_2C(CH_3)_2$ in THF, prepared by reacting $(C_4H_3NH)_2C(CH_3)_2$ (0.5 g, 2.9 mmol) with KH (0.23 g, 5.8 mmol) in THF, was added to a solution of $ThCl_4(DME)_2$ (0.44 g, 0.96 mmol) in THF. Stirring was continued for another 6 h. The resulting solution was evaporated to dryness and the solid residue was redissolved in DME, filtered, and layered with hexane. Colorless crystals of **1** were obtained after standing for 24 h at –35 °C (0.46 g, 53%). ^{1}H NMR (THF-d_8, 300 MHz) δ: 6.38 (d, pyrrole H, 6H), 6.04 (d, pyrrole H, 6H), 5.86 (m, pyrrole H, 6H), 3.42 (s, DME, 4H), 3.26 (s, DME, 6H), 1.56 (s, methyl, 18H). ^{13}C NMR (THF-d_8, 75.43 MHz) δ: 127.22, 126.46 (quaternary C), 124.53, 123.59, 114.81, 106.20, 104.92, 103.36, 101.60 (pyrrole C), 70.30 (DME), 56.12 (DME), 37.15 (bridging C, ligand), 31.20, 27.56 (methyl C, ligand). Elemental anal. calcd. for $C_{37}H_{46}K_2N_6O_2Th$: C 48.46, H 5.06, N 9.16; found: C 48.41, H 5.00, N 9.08.

Preparation of $\{[(C_4H_3N)_2C(CH_3)(C_6H_5)]_3Th\}[K_2(DME)]$ (2)

A solution of the potassium salt of $(C_4H_3NH)_2C(CH_3)(C_6H_5)$ in DME, prepared by reacting $(C_4H_3NH)_2C(CH_3)(C_6H_5)$ (0.5 g, 2.12 mmol) with KH (0.23 g, 5.8 mmol) in DME, was added to a solution of $ThCl_4(DME)_2$ (0.32 g, 0.71 mmol) in DME. Stirring was continued for another 6 h, after which the solution was filtered and evaporated. Analytically pure **2** was obtained upon recrystallization from the DME–hexane mixture (0.62 g, 81%). ^{1}H NMR (THF-d_8, 300 MHz) δ: 6.90 (m, phenyl H, 15H), 6.30 (t, pyrrole H, 3H), 5.89 (m, pyrrole H, 6H), 5.63 (m, pyrrole H, 6H), 5.37 (m, pyrrole H, 3H), 3.46 (s, DME, 4H), 3.29 (s, DME, 6H), 1.85 (s, methyl, 9H). ^{13}C NMR (THF-d_8, 75.43 MHz) δ: 156.49, 148.11, 144.98 (quaternary C), 127.87, 127.75, 127.34, 126.83, 126.80 (aromatic C), 125.55, 124.60, 105.20, 105.04, 103.91, 103.79, 103.72, 103.64, 103.48 (pyrrole C), 72.15 (CH_2, DME), 58.33 (CH_3, DME), 47.20 (bridging C, ligand), 30.47 (CH_3, ligand). Elemental anal. calcd. for $C_{52}H_{52}K_2N_6O_2Th$: C 56.61, H 4.75, N 7.62; found: C 56.48, H 4.71, N 7.59.

Reduction of 2 with potassium naphthalenide and isolation of $\{[(C_4H_3N)_2C(CH_3)(C_6H_5)][K(DME)]_2\}_n$ (3)

To a solution of potassium naphthalenide, prepared in situ by stirring potassium (0.04 g, 0.9 mmol) in DME (30 mL) with naphthalene (0.12 g, 0.9 mmol), compound **2** (0.5 g, 0.45 mmol) was added at –30 °C. The mixture was brought to room temperature and stirring was continued overnight. The resulting dark-red solution was filtered and concentrated to 5 mL and layered with hexane. Colorless crystals of **3** (0.13 g, 59%) were obtained along with an oily and intractable mass. Two subsequent recrystallizations of the sticky mass afforded analytically pure **3**. ^{1}H NMR ($CDCl_3$, 300 MHz) δ: 7.23 (m, phenyl H, 5H), 6.62 (dd, pyrrole H, 2H), 6.15 (t, pyrrole H, 2H), 5.93 (dd, pyrrole H, 2H), 3.25 (s, DME, 4H), 3.15 (s, DME, 6H), 2.03 (s, methyl, 3H). ^{13}C NMR ($CDCl_3$, 300 MHz) δ: 147.63, 137.65 (quaternary C), 128.53, 127.63 (aromatic C), 117.08, 108.55, 106.58 (pyrrole C), 72.17 (CH_2, DME), 59.45 (CH_3, DME), 45.06 (bridging C, ligand), 29.17 (CH_3, ligand). Elemental anal. calcd. for $C_{20}H_{24}K_2N_2O_2$: C 59.66, H 6.01, N 6.96; found: C 59.44, H 5.96, N 6.88.

X-ray crystallography

The product crystals of **1** and **3** were selected, mounted on thin glass fibers using thick paraffin oil, and cooled to the data collection temperature. Data were collected on a Bruker AXS SMART 1 k CCD diffractometer using 0.3° ω scans at 0.90 and 180 in ϕ. Initial unit-cell parameters were determined from 60 data frames collected at different sections of the Edwald sphere. Semiempirical absorption corrections based on equivalent reflections were applied (16). Systematic absences in the diffraction data sets and unit-cell parameters were consistent with *P*2(1)/*c* for **1** and *Pbca* for **3**. The structures were solved by direct methods, completed with difference Fourier syntheses, and refined with full-matrix least-squares procedures based on F^2. All hydrogens were defined with anisotropic displacement coefficients. All hydrogen atoms were treated as idealized contributions. All scattering factors are contained in several versions of the SHELTX program library with the latest used version being v. 6.12 (17). Crystallographic data and relevant bond distances and angles are reported in Tables 1 and 2, respectively.[4]

[4] Supplementary data for this article are available on the Web site or may be purchased from the Depository of Unpublished Data, Document Delivery, CISTI, National Research Council Canada, Ottawa, ON K1A 0S2, Canada. DUD 3686. For more information on obtaining material refer to http://cisti-icist.nrc-cnrc.gc.ca/irm/unpub_e.shtml. CCDC 263400 and 263401 contain the crystallographic data for this manuscript. These data can be obtained, free of charge, via www.ccdc.cam.ac.uk/conts/retrieving.html (Or from the Cambridge Crystallographic Data Centre, 12 Union Road, Cambridge CB2 1EZ, UK; fax +44 1223 336033; or deposit@ccdc.cam.ac.uk).

© 2005 NRC Canada

Table 1. Crystal data and structure analysis results.

	1	**3**
Formula	$C_{37}H_{46}K_2N_6O_2Th$	$C_{20}H_{24}K_2N_2O_2$
M_w	917.04	402.61
Crystal system	Monoclinic	Orthorhombic
Space group	*P*2(1)/*c*	*Pbca*
Z	4	8
a (Å)	11.895 2(12)	20.801(3)
b (Å)	10.999 1(11)	8.976 3(11)
c (Å)	27.777(3)	22.084(3)
α (°)	90	90
β (°)	92.901(2)	90
γ (°)	90	90
Radiation (Mo Kα)	0.710 73	0.710 73
T (K)	208(2)	208(2)
D_{calcd} (Mg m^{-3})	1.678	1.297
μ_{calcd} (mm^{-1})	4.379	0.475
F_{000}	1 816	1 696
Reflns collected/unique	20 026/7 330	15 510/2 516
R(int)	0.075 8	0.111 4
Parameters refined	433	235
R	0.055 7	0.064 6
R_w[2a]	0.123 7	0.129 9
GoF	1.040	1.026

Results and discussion

Reaction of the dipotassium salt of either dimethyl or methyl/phenyl dipyrrole with $ThCl_4(DME)_2$ afforded the corresponding $\{[(C_4H_3N)_2C(CH_3)_2]_3Th\}[K_2(DME)]$ (**1**) and $\{[(C_4H_3N)_2C(CH_3)(C_6H_5)]_3Th\}[K_2(DME)]$ (**2**). Reactions carried out with different ligand to metal stoichiometric ratios also afforded the same compounds albeit in lower yield. The NMR spectra of both complexes display similar features, thus suggesting that the two compounds might in fact be isostructural. In the case of **1**, it was possible to grow crystals of suitable quality to undertake an X-ray crystal structure determination.

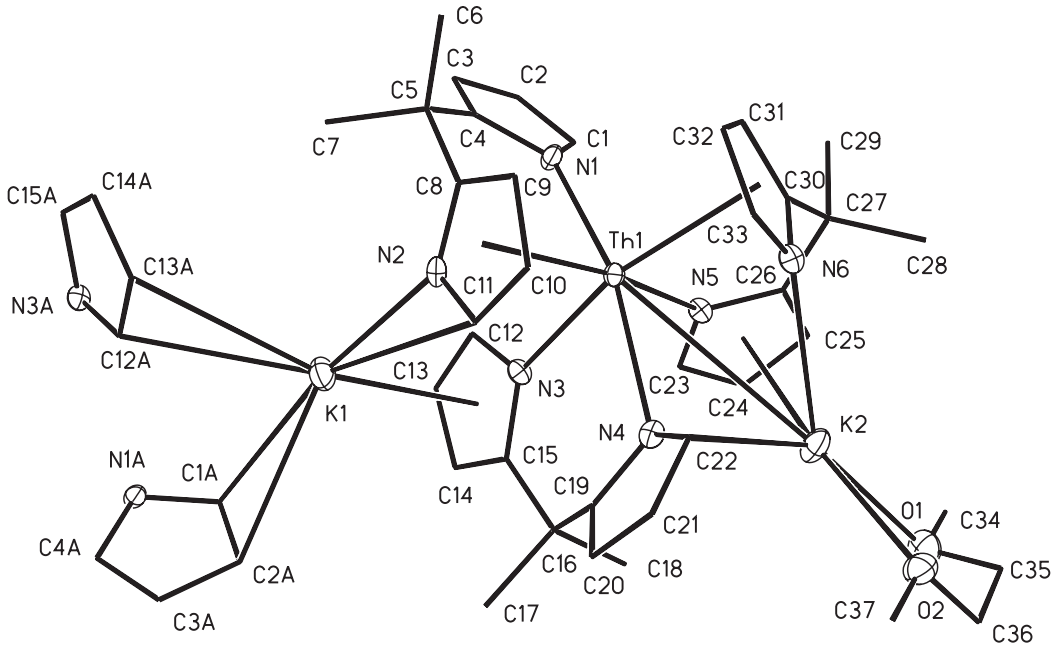
The structure of **1** consists of a thorium atom surrounded by three dipyrrolide dianions and two potassium atoms (Fig. 1). Two of the three dianions adopt the usual σ- and (or) π-bonding mode, each having one of the two rings η^5-bonded to the thorium atom (Th—N(2) = 2.787(7) Å, Th—N(6) = 2.735(7) Å, Th—C(8) = 2.907(8) Å, Th—C(9) = 3.022(8) Å, Th—C(10) = 2.975(9) Å, Th—C(11) = 2.827(9) Å, Th—C(30) = 2.903(10) Å, Th—C(31) = 3.017(10) Å, Th—C(32) = 2.996(10) Å, Th—C(33) = 2.800(9) Å), and the other that is acting as a regular N-based, σ-donor (Th—N(1) = 2.460(7) Å, Th—N(5) = 2.562(7) Å). The third ligand instead adopts the bidentate σ-bonding mode as a regular chelating diamide (Th—N(3) = 2.489(7) Å, Th—N(4) = 2.543(7) Å). Thus, the coordination geometry around each thorium atom can be described as distorted pseudo-octahedral (N(1)-Th-N(3) = 87.7(3)°, N(1)-Th-N(4) = 159.7(3)°, N(1)-Th-N(5) = 87.9(2)°, N(3)-Th-N(4) = 72.3(2)°, N(3)-Th-N(5) = 76.7(2)°, N(4)-Th-N(5) = 84.1(2)°) considering the centroids of the two π-bonded rings as occupying two cis positions of the coordination octahedron (cent-Th-cent = 107.8(3)°). The two potassium atoms that counterbalance the two negative charges of the complex have very different coordination environments. The first is partly π bonded to the pyrrole ring, which in turn is π bonded to the thorium atom (K(1)—N(2) = 2.772(8) Å, K(1)—C(11) = 3.483(11) Å), and fully π bonded to that which is σ bonded to the actinide (K(1)—N(3) = 3.140(8) Å,

Table 2. Selected bond distances (Å) and angles (°).

1		**3**	
Bond distances (Å)			
Th(1)—N(1)	2.460(7)	K(1)—N(1)	2.728(5)
Th(1)—N(3)	2.489(7)	K(1)—C(1)	2.956(6)
Th(1)—N(4)	2.543(7)	K(1)—O(1)	3.047(5)
Th(1)—N(5)	2.562(7)	K(1)—C(2)	3.105(6)
Th(1)—N(6)	2.735(7)	K(1)—N(1)	3.114(5)
Th(1)—N(2)	2.789(7)	K(1)—N(2)	3.163(5)
K(1)—N(2)	2.772(8)	K(1)—C(4)	3.300(5)
Th(1)—C(8)	2.907(8)	K(1)—C(3)	3.304(6)
Th(1)—C(9)	3.022(8)	K(2)—N(2)	2.747(5)
Th(1)—C(10)	2.975(9)	K(2)—N(1)	2.954(5)
Th(1)—C(11)	2.827(9)	K(2)—C(4)	2.993(6)
Th(1)—C(30)	2.903(10)	K(2)—C(1)	3.019(5)
Th(1)—C(31)	3.017(10)	K(2)—C(3)	3.130(6)
Th(1)—C(32)	2.996(10)	K(2)—C(2)	3.144(6)
Th(1)—C(33)	2.800(9)	K(2)—O(1A)	2.974(5)
K(1)—N(2)	2.772(8)	K(2)—O(2A)	2.681(5)
K(1)—N(3)	3.140(8)		
K(2)—O(1)	2.728(8)		
K(2)—O(2)	2.758(8)		
K(2)—N(4)	2.812(8)		
K(2)—N(5)	3.101(8)		
K(2)—N(6)	3.161(8)		
K(1)—C(12)	2.957(10)		
K(1)—C(13)	3.058(11)		
K(1)—C(14)	3.257(11)		
K(1)—C(15)	3.287(10)		
K(2)—C(23)	3.389(9)		
K(2)—C(24)	3.515(11)		
K(2)—C(25)	3.278(11)		
K(2)—C(26)	3.035(9)		
Bond angles (°)			
N(1)-Th(1)-N(3)	87.7(3)	N(1)-K(1)-O(1)	83.61(14)
N(1)-Th(1)-N(4)	159.7(3)	C(1)-K(1)-O(1)	83.72(15)
N(3)-Th(1)-N(4)	72.3(2)	O(1)-K(1)-C(2)	88.20(16)
N(1)-Th(1)-N(5)	87.9(2)	O(1)-K(1)-N(1)	105.42(13)
N(3)-Th(1)-N(5)	76.7(2)	O(1)-K(1)-N(2)	73.31(13)
N(4)-Th(1)-N(5)	84.1(2)	C(2)-K(1)-N(2)	143.15(15)
N(1)-Th(1)-N(6)	117.3(2)	N(1)-K(1)-N(2)	172.92(13)
N(3)-Th(1)-N(6)	140.0(2)	O(1)-K(1)-C(4)	123.44(14)
N(4)-Th(1)-N(6)	78.2(2)	N(2)-K(1)-C(4)	160.58(15)
N(5)-Th(1)-N(6)	73.8(2)	O(1)-K(1)-C(3)	112.74(15)
N(1)-Th(1)-N(2)	77.6(2)	N(2)-K(1)-C(3)	145.92(15)
N(3)-Th(1)-N(2)	67.6(2)	N(2)-K(2)-C(4)	63.78(15)
N(4)-Th(1)-N(2)	97.4(2)	N(2)-K(2)-C(1)	96.15(16)
N(5)-Th(1)-N(2)	141.7(2)	N(1)-K(2)-C(1)	26.35(13)
N(6)-Th(1)-N(2)	144.1(2)	N(2)-K(2)-C(3)	86.72(16)
		N(2)-K(2)-C(2)	106.13(16)

© 2005 NRC Canada

Fig. 1. Plot of **1** showing the thermal ellipsoids drawn at 30% probability level. Anisotropic ellipsoids are shown only for relevant atoms for reasons of clarity.



K(1)—C(12) = 2.957(10) Å, K(1)—C(13) = 3.058(11) Å, K(1)—C(14) = 3.257(11) Å, K(1)—C(15) = 3.287(10) Å). In addition, the partial π bonding to the rings of the dipyrrolide anion of two other identical units (K(1)—C(1A) = 3.242(10) Å, K(1)—C(2A) = 3.352(11) Å, K(1)—C(12A) = 3.150(9) Å, K(1)—C(13A) = 3.324(10) Å) assembles an infinite polymer type of structure. The second potassium is also π bonded to the ring, which is σ bonded to thorium (K(2)—N(5) = 3.101(8) Å, K(2)—C(23) = 3.389(9) Å, K(2)—C(24) = 3.515(11) Å, K(2)—C(25) = 3.278(10) Å, K(2)—C(26) = 3.035(9) Å), but also partly π bonded to a section of the ring (K(2)—N(4) = 2.812(8) Å, K(2)—C(22) = 3.212(10) Å), which, by also being σ bonded to thorium, adopts an uncommon bridging bonding mode. One molecule of coordinated DME completes the coordination sphere of this particular potassium.

The polymeric structure observed in the solid state is unlikely to be preserved in solution since the ^{1}H NMR spectrum of **1** showed only three resonances for the three protons of the pyrrolide rings. In the case of complex **2**, the pyrrolyl rings produced two well-separated resonances for the pyrrolide ring β-H atoms, probably as a result of the presence of two different substituents (i.e., methyl and phenyl) on the connecting quaternary carbon atom.

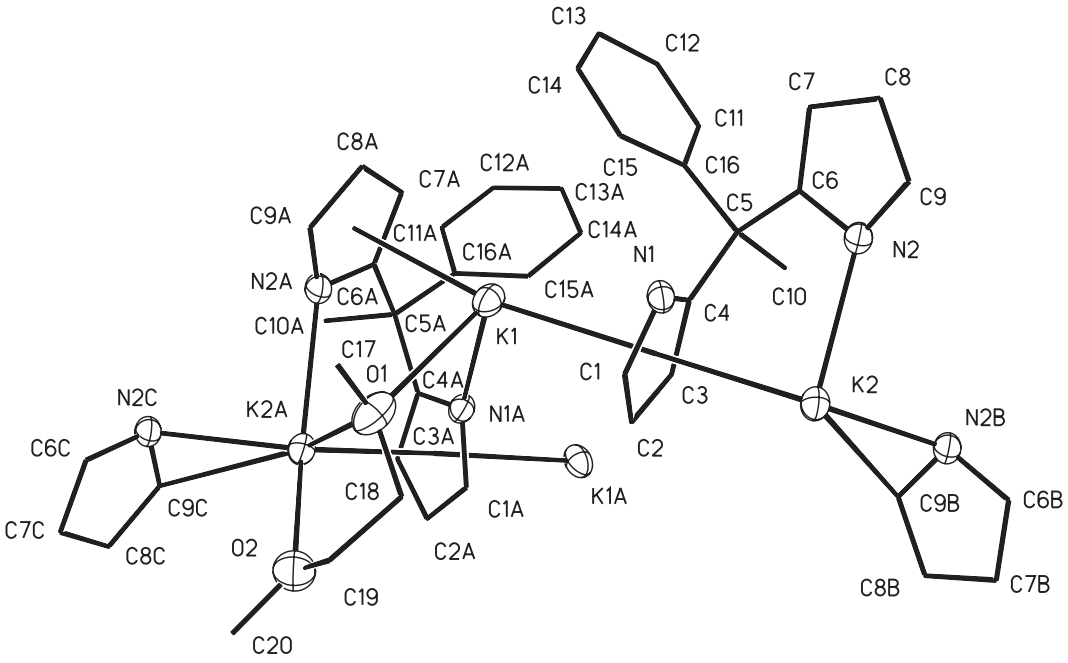
Attempts to reduce both **1** and **2** were carried out with 2 equiv. of K(naphthalenide) in DME. Both reactions gave, upon mixing, a sudden color change from dark-green to very deep-red. Unfortunately, in both cases no thorium-containing materials could be isolated. Only in the case of **2**, and after several attempts, were colorless crystals of the corresponding dipyrrolide dipotassium salt **3** isolated in crystalline form.

The structure of **3** consists of one dipyrrolide dianion surrounded by two potassium atoms (Fig. 2). A salient feature of the structure is the presence of the two metals located on the two sides of one of the two pyrrolide rings in an overall inverted-sandwich type of structure (K(1)—N(1) = 3.114(5) Å, K(1)—C(1) = 2.956(6) Å, K(1)—C(2) = 3.105(6) Å, K(1)—C(3) = 3.304(6) Å, K(1)—C(4) = 3.300(5) Å, K(2)—N(1) = 2.954(5) Å, K(2)—C(1) = 3.0191(5) Å, K(2)—C(2) = 3.144(6) Å, K(2)—C(3) = 3.130(6) Å, K(2)—C(4) = 2.993(6) Å). The coordination environments of the two alkali cations are very different. One of the two potassium atoms has its coordination sphere consisting of a σ-bonded N atom of the second dipyrrolide ring (K(2)—N(2) = 2.747(5) Å) and of another σ-bonded N atom of one identical unit. Therefore, while one of the two pyrrolide rings is used for assembling the inverted sandwich structure, the second is bridging two identical potassium atoms using the σ-bonded N atom. The π-bonded ring of the inverted sandwich structure and one coordinated molecule of DME completes the coordination sphere of this particular potassium atom (K(2A)—O(1) = 2.974(5) Å, K(2A)—O(2) = 2.681(5) Å). The coordination sphere of the other potassium atom comprises, besides the π-bonded ring of the inverted sandwich structure, the π bonding of a second ring of another unit (K(1)—N(2A) = 3.163(5) Å, K(1)—C(6A) = 3.024(6) Å, K(1)—C(7A) = 3.025(6) Å, K(1)—C(8A) = 3.152(6) Å, K(1)—C(9A) = 3.221(6) Å), which is used by the first potassium atom for σ bridging of a symmetry generated unit. The coordination sphere of the second potassium atom is completed by the σ bonding of the N atom of the ring used for the inverted sandwich structure of another unit (K(1)—N(1A) = 2.728(5) Å) and by one of the two oxygen atoms of a DME molecule (K(1)—O(1) = 3.047(5) Å), which is chelating the other potassium. All these bridging interactions generate a three-dimensional polymeric structure.

The asymmetric polymeric structure is unlikely to be preserved in solution. The NMR spectrum of **3** shows in fact only one set of pyrrolide ring H atoms appearing as a triplet for the H atom in position 4 of the ring and two well-resolved double doublets for the other two hydrogen atoms

© 2005 NRC Canada

Fig. 2. Plot of the single unit of the polymeric **3** showing the thermal ellipsoids drawn at 30% probability level. Anisotropic ellipsoids are shown only for relevant atoms for reasons of clarity.



with the correct integration ratio. This indicates that not even the inverted sandwich structure is preserved in a solution of the coordinating solvent. Unfortunately, the very poor solubility of **3** in hydrocarbon solvents has prevented the recording of spectra in a noncoordinating environment where at least some of the solid state features could be conserved.

The formation of **3** during the reduction of **2** implies dissociation of one ligand from the thorium center. This is most likely the consequence of the formation of a thorium naphthalenide complex similar to those isolated with tetrapyrrolide (11) or diphenoxide thorium complexes (14). The NMR spectra of the diamagnetic dark-red solutions showed in fact the characteristic resonances of the coordinated naphthalenide anion (11, 14). It is, therefore, most unfortunate that so far only intractable residues have been isolated in spite of reiterated attempts. Further attempts to isolate and characterize reduced dipyrrolide thorium species are in progress.

Acknowledgments

This work was supported by the Natural Sciences and Engineering Research Council of Canada (NSERC).

References

1. I. Korobkov and S. Gambarotta. Prog. Inorg. Chem. In press.
2. (*a*) P. Roussel and P. Scott. J. Am. Chem. Soc. **120**, 1070 (1998); (*b*) A.L. Odom, P.L. Arnold, and C.C. Cummins. J. Am. Chem. Soc. **120**, 5836 (1998); (*c*) F.G.N. Cloke and P.B. Hitchcock. J. Am. Chem. Soc. **124**, 9352 (2002); W.J. Evans, S.A. Kozimor, and J.W. Ziller. J. Am. Chem. Soc. **125**, 14 264 (2003).
3. I. Castro-Rodriguez, H. Nakai, L.N. Zakharov, A.L. Rheingold, and K. Meyer. Science, **305**, 1757 (2004).
4. I. Castro-Rodriguez, H. Nakai, P. Gantzel, L.N. Zakharov, A.L. Rheingold, and K. Meyer. J. Am. Chem. Soc. **125**, 15 734 (2003).
5. See, for example: (*a*) S. De Angelis, E. Solari, C. Floriani, A. Chiesi-Villa, and C. Rizzoli. J. Am. Chem. Soc. **116**, 5402 (1994); (*b*) S. De Angelis, E. Solari, C. Floriani, A. Chiesi-Villa, and C. Rizzoli. J. Am. Chem. Soc. **116**, 5691 (1994); (*c*) C. Floriani. J. Chem. Soc. Chem. Commun. 1257 (1996); (*d*) J. Jubb and S. Gambarotta. J. Am. Chem. Soc. **115**, 10 410 (1993); (*e*) J. Jubb, L. Scoles, H. Jenkins, and S. Gambarotta. Chem. Eur. J. **2**, 767 (1996); (*f*) M. Tayebani, S. Gambarotta, and G.P.A. Yap. Angew. Chem. Int. Ed. **37**, 3002 (1998).
6. (*a*) J. Jubb, S. Gambarotta, R. Duchateau, and J.H. Teuben. J. Chem. Soc. Chem. Commun. 2641 (1994); (*b*) J. Song, S. Gambarotta, Angew. Chem. Int. Ed. Engl. **34**, 2141 (1995); (*c*) T. Dubé, S. Gambarotta, and G.P.A. Yap. Angew. Chem. Int. Ed. **38**, 1432 (1999); (*d*) M. Ganesan, S. Gambarotta, and G.P.A. Yap. Angew. Chem. Int. Ed. **113**, 788 (2001); (*e*) T. Dubé, S. Gambarotta, and G.P.A. Yap. Angew. Chem. Int. Ed. **38**, 1432 (1999); (*f*) I. Korobkov, G. Aharonian, S. Gambarotta, and G.P.A. Yap. Organometallics, **21**, 4899 (2002).
7. (*a*) I. Korobkov, S. Gambarotta, and G.P.A. Yap. Organometallics, **20**, 2552 (2001); (*b*) I. Korobkov, S. Gambarotta, G.P.A. Yap, L. Thompson, and J. Hay. Organometallics, **20**, 5440 (2001).
8. J. Guan, T. Dubé, S. Gambarotta, and G.P.A. Yap. Organometallics, **19**, 4820 (2000).
9. J. Jubb and S. Gambarotta. J. Am. Chem. Soc. **116**, 4477 (1994).
10. I. Korobkov, S. Gambarotta, and G.P.A. Yap. Angew. Chem. Int. Ed. **41**, 3433 (2002).
11. I. Korobkov, S. Gambarotta, and G.P.A. Yap. Angew. Chem. Int. Ed. **42**, 814 (2003).
12. (*a*) T. Dubé, D. Freckmann, S. Conoci, S. Gambarotta, and G.P.A. Yap. Organometallics, **19**, 209 (2000); (*b*) T. Dubé, S. Conoci, S. Gambarotta, and G.P.A. Yap. Organometallics, **19**, 1182 (2000).

© 2005 NRC Canada

13. (*a*) T. Dubé, S. Conoci, S. Gambarotta, G.P.A. Yap, and G. Vasapollo. Angew. Chem. Int. Ed. **38**, 3657 (1999); (*b*) C.D. Bérubé, S. Gambarotta, and G.P.A. Yap. Organometallics, **22**, 3742 (2003); (*c*) T. Dubé, S. Conoci, S. Gambarotta, and G.P. Yap. Organometallics, **19**, 3716 (2000).
14. I. Korobkov and S. Gambarotta. Angew. Chem. Int. Ed. **42**, 4958 (2003).
15. M. Ganesan, M.P. Lalonde, S. Gambarotta, and G.P.A. Yap. Organometallics, **20**, 2443 (2001), and refs. cited therein.
16. R. Blessing. Acta Crystallogr. Sect. A, **A51**, 33 (1995).
17. G.M. Sheldrick. SHELXTL. Version 6.12 [computer program]. Bruker AXS, Madison, Wis. 2001.

© 2005 NRC Canada

Rh(I)-catalyzed cleavage of unactivated C—O bonds — Carbonylative rearrangement reactions of allenyl ethers to 2-carboalkoxy-1,3-dienes[1]

Paul A. Wender, Nicole M. Deschamps, and Robert Sun

Abstract: The initial examples of a Rh(I)-catalyzed carbonylative rearrangement reaction of allenyl ethers are described. The key reaction proceeds under remarkably mild conditions to provide good to excellent yields of 2-carboalkoxy-1,3-dienes.

Key words: carbonylative rearrangement, C-O cleavage, σ bond activation, rhodium catalysis, allenyl ethers.

Résumé : On décrit les premiers exemples de réactions, catalysées par le Rh(I), de réarrangements d'éthers allényles accompagnées d'une carbonylation. La réaction clé se produit dans des conditions particulièrement douces pour conduire à la formation de dérivés 2-carboalkoxy-1,3-dièns avec des rendements allant de bons à excellents.

Mots clés : réarrangement avec carbonylation, clivage C-O, activation d'une liaison σ, catalyse par le rhodium, éthers allényles.

[Traduit par la Rédaction]

Introduction

Metal-catalyzed σ bond activation, particularly of unreactive bonds, is an important objective in organometallic and synthetic organic chemistry (1). The ability to convert, for example, the C—O bonds in ethers and alcohols to C—C bonds without the need to prepare activated oxygen derivatives (carbonates, triflates, halogens, etc.) offers, in many situations, step-economic and strategic advantages in synthesis (2, 3). As illustrated in Scheme 1, the metal-catalyzed insertion into a C—O bond and reaction with an additional component (R″) could provide an organometallic intermediate(s) that could lead to the formation of substitution or insertion products.

Illustrative of processes that give rise to substitution products are the copper- (4), nickel- (5), palladium- (6), and zirconium-catalyzed (7) transformations of allylic ethers and allylic alcohols to the corresponding substituted alkenes with alkyl and phenyl magnesium salts and the ruthenium-catalyzed progargylation and allylation of aromatic compounds with propargylic and allylic alcohols (8). Carbonylation reactions (9) have also been achieved through metal-catalyzed cleavage of unreactive C—O bonds and the subsequent incorporation of carbon monoxide to give the corresponding insertion products. For example, cobalt- (10) and rhodium-catalyzed (11) carbonylative ring expansion reactions of unstrained cyclic ethers provide novel routes to lactones (12). Rhodium (13) and palladium (14) catalysts have been reported for the carbonylation of allylic ethers and alcohols to the corresponding esters and palladium catalysts have been reported for the carbonylation of allenyl alcohols to esters and acids (15). These carbonylation reactions often require the use of high pressures of carbon monoxide and elevated temperatures. During the course of our studies on metal-catalyzed σ bond activation, we identified a novel Rh(I)-catalyzed carbonylative rearrangement that provides for the conversion of allenyl ethers to 2-carboalkoxy-1,3-dienes. Herein, we report the initial examples of this process, which occurs under remarkably mild conditions (1 atm CO, 1 atm = 101.325 kPa) and proceeds efficiently to give a variety of 2-carboalkoxy-1,3-dienes.

At the start of this study, it was found that treatment of allenyl ether **1** with 10 mol% $[RhCl(CO)_2]_2$ in toluene at 80 °C under only 1 atm CO gave the 2-carboalkoxy-1,3-diene **2** in 77% yield (Table 1, entry 1). Investigations to determine the effects of solvent and catalyst loading on the efficiency of this carbonylative rearrangement reaction were next carried out. While the use of 1,4-dioxane as the solvent was found to have a negligible effect on the yield and reaction time (Table 1, entry 2), the use of DCE (1,2-dichloroethane) as the solvent affords a faster reaction and allows for the use of less (5 mol%) catalyst (Table 1, entries 3 and 4).

This process has thus far been shown to be unique for allenyl ethers using the above reaction conditions. Treatment of *allyl* ether **3** with 10 mol% $[RhCl(CO)_2]_2$ and CO (Scheme 2) did not provide the corresponding carbonylative rearrangement products, but instead gave a mixture of dienes

Received 30 November 2004. Published on the NRC Research Press Web site at http://canjchem.nrc.ca on 22 July 2005.

This article is dedicated to Howard Alper, an inspirational educator and scientific innovator.

P.A. Wender,[2] N.M. Deschamps, and R. Sun. Department of Chemistry, Stanford University, Stanford, California, 94305-5080, USA.

[1]This article is part of a Special Issue dedicated to Professor Howard Alper.

[2]Corresponding author (e-mail: wenderp@stanford.edu).

 doi: 10.1139/V05-085 © 2005 NRC Canada

Scheme 1. Metal-catalyzed conversion of ether C—O bonds to C—C bonds.

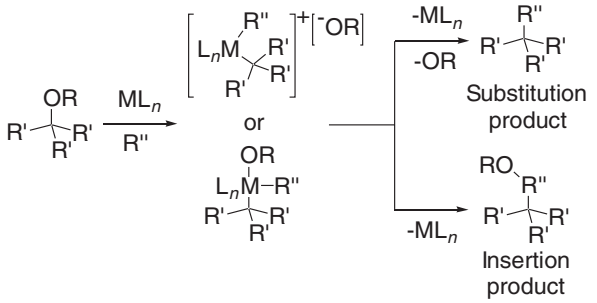
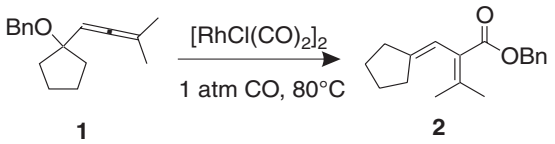


Table 1. Effect of solvent, concentration, and catalyst loading on the carbonylative rearrangement of **1**.



Entry	Solvent	Conc. (mol/L)	Cat.[a] (mol%)	Time (h)	Yield[b] (%)
1	Toluene	0.50	10	22	77
2	Dioxane	0.50	10	24	76
3	DCE	0.50	5	18	86
4	DCE	0.25	5	36	87

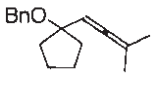
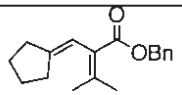
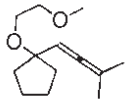
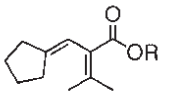
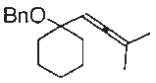
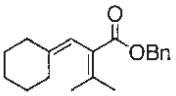
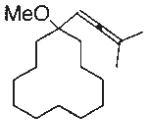
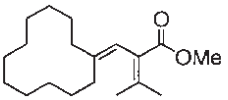
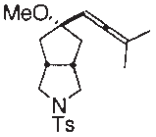
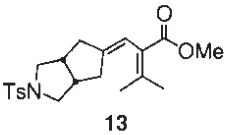
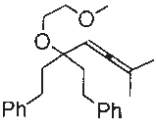
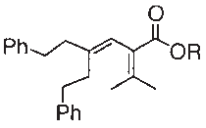
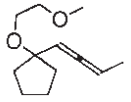
[a][RhCl(CO)$_2$]$_2$ (mol%).
[b]Isolated yield.

4. The *propargyl* ether **5** was shown to be unreactive, even after heating at 100 °C for a prolonged time (28 h).

Preliminary studies on the scope of the Rh(I)-catalyzed carbonylative rearrangement reaction were conducted. In general, the reactions proceed efficiently to provide 2-carboalkoxy-1,3-dienes in good to excellent yields. As illustrated in Table 2, the use of a methoxyethyl ether instead of a benzyl ether affords a slightly higher yield (Table 2, entries 1 and 2). The six-membered ring substrate **8** reacts more slowly than **1** and gives a somewhat lower yield of product. In contrast, the reaction of **10**, which contains a 12-membered ring, gave the corresponding 2-carboalkoxy-1,3-diene **11** in excellent yield with rates comparable to the reaction of **1**. The carbonylative rearrangement of the bicyclic heterocycle **12** gave **13** in 87% yield. Exemplifying the chemistry of these 2-carboalkoxy-1,3-dienes, **13** was converted to the spirolactone **14** in high yield upon treatment with trimethylsilyl chloride and sodium iodide (Scheme 3). The acyclic allenyl ether substrate **15** is also well-tolerated in this process, giving the 2-carboalkoxy-1,3-diene **16** in 66% yield (Table 2, entry 6). Thus far, attempts to carry out the carbonylative rearrangement reaction with allenyl ether **17** (Table 2, entry 7), which contains only one methyl group on the distal double bond of the allene, were unsuccessful.

The mechanism of the palladium-catalyzed carbonylation reaction of allenyl alcohols is proposed to involve the hydrolysis or alcoholysis of a palladium acyl species similar to that illustrated in Scheme 4 (15). We examined the effects of adding an exogenous alcohol to the Rh(I)-catalyzed reaction

Table 2. Representative carbonylative rearrangement reactions.[a]

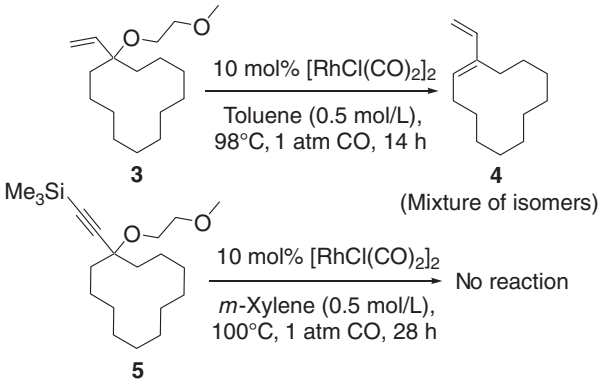
Entry	Substrate	Time (h)	Product	Yield (%)[b]
1	 **1**	18	 **2**	86
2[c]	 **6**	16	 **7**	92
3	 **8**	30	 **9**	78
4	 **10**	15	 **11**	93
5[d, e]	 **12**	24	 **13**	87
6[c, f]	 **15**	22	 **16**	66
7	 **17**	36	Decomposition	–

[a]Unless otherwise noted, reaction conditions are as follows: 5 mol% [RhCl(CO)$_2$]$_2$, DCE (0.5 mol/L), 80 °C, 1 atm CO (1 atm = 101.325 kPa).
[b]Isolated yield.
[c]R = $(CH_2)_2OCH_3$.
[d]Ts = *p*-toluenesulfonyl.
[e][RhCl(CO)$_2$]$_2$ (10 mol%), *m*-xylene (0.5 mol/L), 80 °C, 1 atm CO.
[f][RhCl(CO)$_2$]$_2$ (10 mol%), DCE (0.5 mol/L), 80 °C, 1 atm CO.

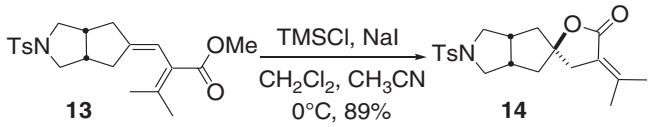
and found that crossover is observed. Thus, the addition of 10 equiv. of methoxyethanol to the reaction of **1** in DCE gave a 2:1 mixture of **2** and **7**. Similarly, the addition of 10 equiv. of benzyl alcohol to the reaction of **6** in DCE gave a 3:2 mixture of **7** and **2**. These results are consistent with the mechanistic possibilities depicted in Scheme 4. A step involving the direct reductive elimination of the acyl–alkoxy moiety from the metal, although rare (16, 17), is possible, as is the alcoholysis of the metal acyl species.

© 2005 NRC Canada

Scheme 2. Behaviour of allyl ether **3** and propargyl ether **5** in the presence of $[RhCl(CO)_2]_2$ and CO (1 atm = 101.325 kPa).



Scheme 3. Spirolactonization of 2-carboalkoxy-1,3-diene **13**.



In summary, a new Rh(I)-catalyzed carbonylative rearrangement reaction of allenyl ethers to give 2-carboalkoxy-1,3-dienes in good to excellent yields has been reported. This method allows for the selective cleavage and derivatization of allenyl ether C—O bonds under mild catalytic conditions. Further studies on the scope and mechanism of this process are ongoing.

Experimental

General methods

Elevated temperatures were maintained in a thermostat-controlled silicone oil bath. Reactions were carried out under a positive pressure of carbon monoxide from a balloon. Carbon monoxide (2.5 grade) was purchased from Praxair. $[RhCl(CO)_2]_2$ was purchased from Strem Chemicals. DCE (99+%, ACS reagent grade) was purchased from Aldrich Chemical Co. and stored over molecular sieves (4 Å). *m*-Xylene (anhydrous, 99+%, packaged in a Sure/Seal™ bottle) was purchased from Aldrich Chemical Co.

NMR spectra were measured in $CDCl_3$ on a Varian Inova 500 (^{1}H at 500 MHz, ^{13}C at 125 MHz) or Varian Mercury 400 (^{1}H at 400 MHz, ^{13}C at 100 MHz). Data for ^{1}H NMR spectra are reported as follows: chemical shift (δ ppm, referenced to solvent), multiplicity (singlet (s), doublet (d), triplet (t), doublet of doublets (dd), multiplet (m)), coupling constant (Hz), and integration. Data for ^{13}C NMR spectra are reported in terms of chemical shift (δ ppm, referenced to solvent) and quantity of carbons (if more than one). IR spectra were recorded on a PerkinElmer Spectrum BX Fourier transform spectrometer and are reported as follows: wavenumbers (cm^{-1}), description (weak (w), medium (m), strong (s)). High-resolution mass spectra (HR-MS) were recorded at the NIH regional mass spectrometry facility at the University of California, San Francisco. Elemental analyses (%C, %H) were determined by Desert Analytics, Tucson, Arizona. Melting points (uncorrected) were measured using a Unimelt capillary melting point apparatus (Arthur H. Thomas Company, 0–360 °C).

General procedure for the carbonylative rearrangement reaction

To an oven-dried 10 mm × 75 mm borosilicate glass test tube equipped with a Teflon®-coated magnetic stir bar was added the allenyl ether and $[RhCl(CO)_2]_2$ (5 mol%). DCE (volume required to give 0.5 mol/L solution of the allenyl ether) was added and the test tube was capped with a rubber septum. The resulting yellow mixture was stirred under a balloon of CO, vented to a bubbler for 5 min. This solution was then immersed into a preheated oil bath at 80 °C and was stirred under a balloon of CO until the starting material was consumed (as determined by analysis of the reaction mixture by TLC). After cooling to room temperature, the residue was purified via flash chromatography on silica gel eluting with a mixture of diethyl ether and pentane.

2-Cyclopentylidenemethyl-3-methyl-but-2-enoic acid benzyl ester (2)

Allenyl benzyl ether **1** (50 mg, 0.206 mmol) was converted to **2** (48 mg, 0.177 mmol, 86%, slightly yellow-coloured oil) using the general procedure. TLC: R_f 0.27 (hexane–Et_2O, 9:1); one spot. IR (thin film, cm^{-1}) υ: 2953 (m), 1721 (s), 1211 (s), 1147 (s), 1073 (s), 697 (m). ^{1}H NMR (500 MHz, $CDCl_3$, ppm) δ: 7.38–7.29 (m, 5H), 6.00 (s, 1H), 5.19 (s, 2H), 2.35–2.34 (m, 2H), 2.03–1.98 (m, 2H), 1.86 (s, 3H), 1.77 (s, 3H), 1.61–1.56 (m, 4H). ^{13}C NMR (125 MHz, $CDCl_3$, ppm) δ: 169.9, 147.2, 139.2, 136.0, 128.4 (2C), 128.3 (2C), 128.0, 127.5, 115.5, 66.2, 34.7, 29.5, 26.7, 25.9, 22.3, 21.4. HR-MS calcd. for $C_{18}H_{22}O_2$ (*m*/*z*): 270.1620; found: 270.1628.

2-Cyclopentylidenemethyl-3-methyl-but-2-enoic acid methoxyethyl ester (7)

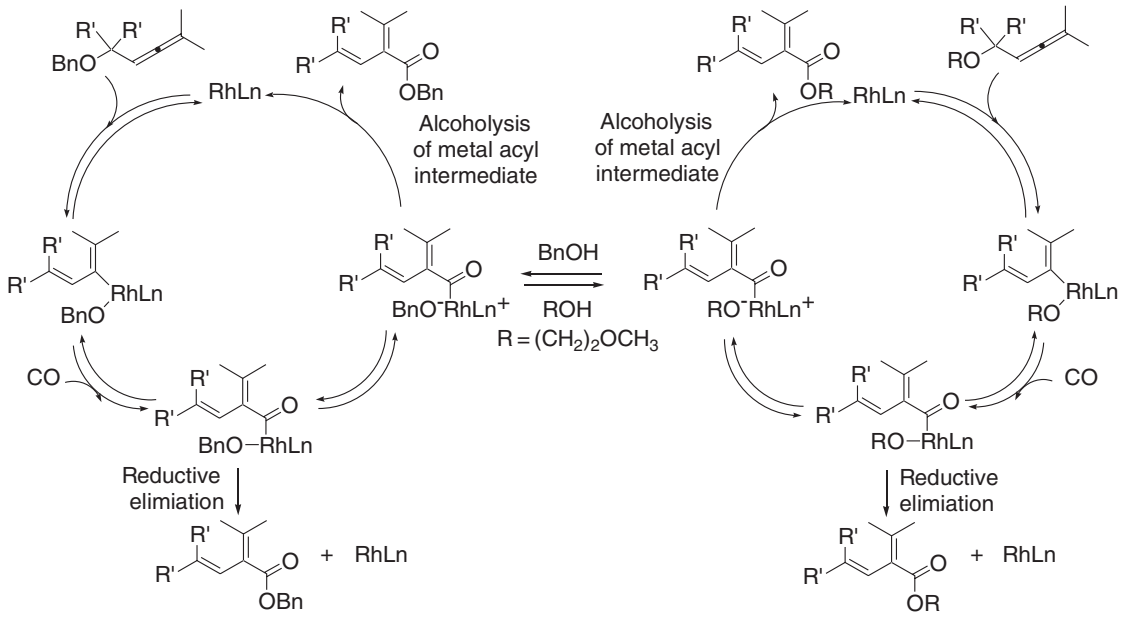
Allenyl methoxyethyl ether **6** (42 mg, 0.20 mmol) was converted to **7** (43.7 mg, 0.184 mmol, 92%, colourless oil) using the general procedure. TLC: R_f 0.12 (hexane–Et_2O, 9:1); one spot. IR (thin film, cm^{-1}) υ: 2951 (m), 1721 (s), 1617 (w), 1213 (s), 1078 (s). ^{1}H NMR (400 MHz, $CDCl_3$, ppm) δ: 4.31–4.29 (m, 2H), 3.64–3.63 (m, 2H), 3.37 (s, 3H), 2.35 (t, J = 6.8 Hz, 2H), 2.08 (t, J = 7.0 Hz, 2H), 1.88 (d, J = 0.3 Hz, 3H), 1.77 (s, 3H), 1.69–1.55 (m, 4H). ^{13}C NMR (100 MHz, $CDCl_3$, ppm) δ: 170.2, 147.1, 138.8, 127.6, 115.4, 70.3, 63.4, 58.9, 34.8, 29.4, 26.8, 25.9, 22.3, 21.3. HR-MS calcd. for $C_{14}H_{22}O_3$ (*m*/*z*): 238.1569; found: 238.1559.

2-Cyclohexylidenemethyl-3-methyl-but-2-enoic acid benzyl ester (9)

Allenyl benzyl ether **8** (52 mg, 0.203 mmol) was converted to **9** (45 mg, 0.158 mmol, 78%, slightly yellow-coloured oil) using the general procedure. TLC: R_f 0.29 (hexane–Et_2O, 9:1); one spot. IR (thin film, cm^{-1}) υ: 2928 (s), 1715 (s), 1215 (s), 1190 (m), 1065 (s), 696 (m). ^{1}H NMR (400 MHz, $CDCl_3$, ppm) δ: 7.48–7.27 (m, 5H), 5.72 (s, lH), 5.17 (s, 2H), 2.18–2.15 (m, 2H), 2.00 (d, J = 1.5 Hz, 3H), 1.96–1.93 (m, 2H), 1.76 (s, 3H), 1.58–1.50 (m, 4H), 1.44–1.40 (m, 2H). ^{13}C NMR (100 MHz, $CDCl_3$, ppm) δ: 169.0, 144.4, 143.9, 136.4, 128.4 (2C), 127.8 (3C), 125.5,

© 2005 NRC Canada

Scheme 4. Possible mechanistic pathways for the carbonylative rearrangement reaction.



117.3, 65.7, 36.6, 30.0, 28.4, 27.0, 26.5, 22.9, 22.1. HR-MS calcd. for $C_9H_{24}O_2$ (*m/z*): 284.1776; found: 284.1772. Anal. calcd. for $C_{19}H_{24}O_2$: C 80.24, H 8.51; found: C 80.38, H 8.63.

2-Cyclododecylidenemethyl-3-methyl-but-2-enoic acid methyl ester (11)

Allenyl methyl ether **10** (53 mg, 0.20 mmol) was converted to **11** (54.5 mg, 0.187 mmol, 93%, colourless oil) using the general procedure. TLC: R_f 0.34 (hexane–Et_2O, 9:1); one spot. IR (thin film, cm^{-1}) υ: 2931 (s), 1718 (s), 1217 (s), 1077 (m). ^1H NMR (400 MHz, $CDCl_3$, ppm) δ: 5.80 (s, 1H), 3.68 (s, 3H), 2.11 (td, *J* = 6.9, 1.1 Hz, 2H), 2.03 (d, *J* = 1.7 Hz, 3H), 1.92–1.89 (m, 2H), 1.74 (d, *J* = 1.1 Hz, 3H), 1.90 (t, *J* = 6.7 Hz, 2H), 1.43–1.27 (m, 14H), 1.99–1.15 (m, 2H). ^{13}C NMR (100 MHz, $CDCl_3$, ppm) δ: 169.4, 145.1, 142.4, 125.7, 121.2, 51.2, 31.1, 29.5, 24.8, 24.5, 24.21, 24.17, 24.1, 23.5, 23.4, 23.2, 23.1, 22.6, 22.1. HR-MS calcd. for $C_{19}H_{32}O_2$: 292.2402; found: 292.2405. Anal. calcd. for $C_{19}H_{32}O_2$: C 78.03, H 11.03; found: C 78.31, H 11.24.

But-2-enoic acid methyl ester (13)

Allenyl methyl ether **12** (32 mg, 0.089 mmol) was converted to **13** (30 mg, 0.077 mmol, 87%, colourless oil) using the general procedure except that *m*-xylene was used in place of DCE and 10 mol% $[RhCl(CO)_2]_2$ was used instead of 5 mol% $[RhCl(CO)_2]_2$. TLC: R_f 0.22 (hexane–EtOAc, 7:3); one spot. IR (thin film, cm^{-1}) υ: 2948 (m), 1716 (s), 1433 (m), 1345 (s), 1219 (s), 1162 (s), 665 (m). ^1H NMR (500 MHz, $CDCl_3$, ppm) δ: 7.65 (d, *J* = 8.3 Hz, 2H), 7.29 (d, *J* = 8.3 Hz, 2H), 5.86 (s, 1H), 3.66 (s, 3H), 3.31–3.26 (m, 2H), 2.92 (dd, *J* = 9.8, 4.3 Hz, 1H), 2.87 (dd, *J* = 9.8, 4.3 Hz, 1H), 2.61–2.51 (m, 3H), 2.40 (s, 3H), 2.24–2.21 (m, 1H), 2.12–2.05 (m, 1H), 1.89 (s, 3H), 1.79–1.74 (m, 1H), 1.68 (s, 3H). ^{13}C NMR (125 MHz, $CDCl_3$, ppm) δ: 169.8, 144.2, 143.4, 142.0, 133.0, 130.0 (2C), 127.6 (2C), 126.4, 117.8, 53.5, 53.3, 51.5, 42.6, 41.5, 38.7, 34.0, 22.4, 21.9, 21.5. HR-MS calcd. for $C_{21}H_{27}NO_4S$ (*m/z*): 389.1661; found: 389.1668.

Spirolactone (14)

To a solution of methyl ester **13** (20 mg, 0.051 mmol) in CH_2Cl_2 (1.2 mL) and CH_3CN (0.8 mL) at 0 °C were added NaI (78 mg, 0.51 mmol) in one portion followed by TMSCl (0.12 mL, 0.92 mmol) via syringe in one portion. The mixture was allowed to stir at 0 °C for 5 h, at which point TLC indicated the starting material was consumed. The reaction was quenched with a 1:1 mixture of satd. Na_2SO_3 and satd. $NaHCO_3$ (2.5 mL) at 0 °C (added in one portion via glass pipette). The mixture stirred at room temperature for 10 min and then was diluted with ether. The organic layer was washed with H_2O, brine, and dried over $MgSO_4$. After removal of the solvent, the residue was purified via flash chromatography on silica gel (pentane–ether (3:1), then pentane–ether (5:2)) to afford lactone **14** (17 mg, 0.045 mmol, 89%, white solid). Mp: 197.9–199.1 °C. TLC: R_f = 0.17 (hexane–EtOAc, 7:3); one spot. IR (thin film, cm^{-1}) υ: 2934 (m), 1737 (s), 1660 (m), 1331 (s), 1166 (s), 1155 (s), 1041 (s), 665 (m). ^1H NMR (500 MHz, $CDCl_3$, ppm) δ: 7.67 (d, *J* = 8.1 Hz, 2H), 7.32 (d, *J* = 8.1 Hz, 2H), 3.26 (dd, *J* = 9.6, 7.9 Hz, 2H), 2.99 (dd, *J* = 9.9, 4.3 Hz, 2H), 2.69–2.62 (m, 4H), 2.42 (s, 3H), 2.19 (s, 3H), 1.87–1.77 (m, 4H), 1.79 (s, 3H). ^{13}C NMR (125 MHz, $CDCl_3$, ppm) δ: 168.9, 150.3, 143.8, 132.3, 129.6 (2C), 127.9 (2C), 119.4, 88.4, 53.8 (2C), 43.4 (2C), 40.3 (2C), 39.0, 24.5, 21.6, 19.9. HR-MS calcd. for $C_{20}H_{25}NO_4S$ (*m/z*): 375.1504; found: 375.1509.

2-Isopropylidene-4-phenethyl-6-phenyl-hex-3-enoic acid methyl ester (16)

Allenyl methoxyethyl ether **15** (74 mg, 0.20 mmol) was converted to **16** (52 mg, 0.133 mmol, 66%, colourless oil) using the general procedure except that 10 mol% $[RhCl(CO)_2]_2$ was used instead of 5 mol% $[RhCl(CO)_2]_2$. TLC: R_f = 0.10

© 2005 NRC Canada

(hexane–EtOAc, 9:1); one spot. IR (thin film, cm^{-1}) υ: 2929 (m), 1712 (s), 1216 (s), 1080 (s), 699 (s). ^1H NMR (500 MHz, $CDCl_3$, ppm) δ: 7.29–7.23 (m, 4H), 7.21–7.13 (m, 6H), 5.81 (s, 1H), 4.23 (t, J = 4.7 Hz, 2H), 3.56 (t, J = 4.7 Hz, 2H), 3.33 (s, 3H), 2.81–2.77 (m, 2H), 2.67–2.63 (m, 2H), 2.46–2.43 (m, 2H), 2.27–2.23 (m, 2H), 1.98 (d, J = 1.5 Hz, 3H), 1.60 (s, 3H). ^{13}C NMR (125 MHz, $CDCl_3$, ppm) δ: 168.8, 144.9, 142.4, 142.1, 141.9, 128.4, 128.3, 128.3 (3C), 125.8 (4C), 125.8, 125.3, 121.9, 70.5, 63.2, 58.9, 37.9, 34.5, 33.8, 33.1, 22.7, 22.1. HR-MS calcd. for $C_{26}H_{32}O_3$: 392.2351; found: 392.2351.

Acknowledgements

This research was supported by the National Science Foundation (CHE-0131944). Fellowship support from Eli Lilly and Company (N.M.D. and R.S.) is gratefully acknowledged.

References

1. For a general review, see: S. Murai (*Editor*). Activation of unreactive bonds and organic synthesis. Springer-Verlag, Berlin, Heidelberg, New York. 1999.
2. A. Yamamoto. Adv. Organomet. Chem. **34**, 111 (1992).
3. P.A. Wender, S.T. Handy, and D.L. Wright. Chem. Ind. (London), 765 (1997).
4. A. Commerçon, M. Bourgain, M. Delaumeny, J.F. Normant, and J. Villieras. Tetrahedron Lett. **44**, 3837 (1975).
5. (*a*) C. Chuit, H. Felkin, C. Frajerman, G. Roussi, and G. Swierczewski. J. Organomet. Chem. **127**, 371 (1977); (*b*) H. Felkin, E. Jampel-Costa, and G. Swierczewski. J. Organomet. Chem. **134**, 265 (1977); (*c*) G. Consiglio, O. Piccolo, L. Toncetti, and F. Morandini. Tetrahedron, **42**, 2043 (1986).
6. T. Hayashi, M. Konishi, K. Yokota, and M. Kumada. J. Chem. Soc. Chem. Commun. **7**, 313 (1981).
7. N. Suzuki, D.Y. Kondakov, and T. Takahashi. J. Am. Chem. Soc. **115**, 8485 (1993).
8. (*a*) Y. Nishibayashi, M. Yoshikawa, Y. Inada, M. Hidai, and S. Uemura. J. Am. Chem. Soc. **124**, 11 846 (2002); (*b*) Y. Nishibayashi, Y. Inada, M. Yoshikawa, M. Hidai, and S. Uemura. Angew. Chem. Int. Ed. **42**, 1495 (2003); (*c*) G. Onodera, H. Imajima, M. Yamanashi, Y. Nishibayashi, M. Hidai, and S. Uemura. Organometallics, **23**, 5841 (2004).
9. For a general review of metal-catalyzed carbonylation reactions, see: M. Beller, B. Cornils, C.D. Frohning, and C.W. Kohlpaintner. J. Mol. Catal. A, **104**, 17 (1995).
10. W. Reppe, H. Kroper, H.J. Pistor, and O. Weissbarth. Justus Liebigs Ann. Chem. **582**, 87 (1953).
11. G. Jenner, H. Kheradmand, and A. Kiennemann. J. Organomet. Chem. **277**, 427 (1984).
12. For a review of metal-catalyzed carbonylative ring expansions, see: K. Khumtaveeporn and H. Alper. Acc. Chem. Res. **28**, 414 (1995).
13. M.-M. Barreto-Rosa, M.C. Bonnet, G. Commenges, B. Manzano, A.L. Monteiro, D. Neibecker, and I. Tkatchenko. J. Organomet. Chem. **45**, C22 (1993).
14. For representative examples and lead references, see: (*a*) J. Tsuji, J. Kiji, S. Imamura, and M. Morikawa. J. Am. Chem. Soc. **86**, 4350 (1964); (*b*) D. Medema, R. van Heiden, and C.F. Kohll. Inorg. Chim. Acta, **3**, 255 (1969); (*c*) D. Neibecker, J. Poirier, and I. Tkatchenko. J. Org. Chem. **54**, 2459 (1989); (*d*) M.C. Bonnet, J. Coombes, B. Manzano, D. Neibecker, and I. Tkatchenko. J. Mol. Catal. **52**, 263 (1989); (*e*) K. Itoh, N. Hamaguchi, M. Miura, and M. Nomura. J. Mol. Catal. **75**, 117 (1992).
15. (*a*) M.E. Piotti and H. Alper. J. Org. Chem. **59**, 1956 (1994); (*b*) K. Uemura and Y. Inoue. Appl. Organomet. Chem. **14**, 8 (2000).
16. For an example involving an acyl(alkoxy)Ir(III) complex, see: (*a*) K.A. Bernard and J.D. Atwood. Organometallics, **6**, 1133 (1987); an acyl(alkoxy)Ni(II) complex and a Pd(II) complex, see: (*b*) S. Komiya, Y. Akai, K. Tanaka, T. Yamamoto, and A. Yamamoto. Organometallics, **4**, 1130 (1985).
17. For a review of carbon–heteroatom bond-forming reductive eliminations, see: J.F. Hartwig. Acc. Chem. Res. **31**, 852 (1998).

© 2005 NRC Canada

Furoyl and thiophene carbonyl linker pyrazolyl palladium(II) complexes — Synthesis, characterization, and evaluation as ethylene oligomerization catalysts[1]

Stephen O. Ojwach, Mmboneni G. Tshivhase, Ilia A. Guzei, James Darkwa, and Selwyn F. Mapolie

Abstract: Reactions of 2-furoyl chloride and 2-thiophene carbonyl chloride with substituted pyrazoles produced the modified pyrazolyl compounds: {(3,5-Me_2pzCO)-2-C_4H_3O} (**L1**), {(3,5-Me_2pzCO)-2-C_4H_3S} (**L2**), {(3,5-*t*-Bu_2pzCO)-2-C_4H_3O} (**L3**), {(3,5-*t*-Bu_2pzCO)-2-C_4H_3S} (**L4**), {(3,5-Ph_2pzCO)-2-C_4H_3S} (**L5**), and {(pzCO)-2-C_4H_3O} (**L6**) in good yields. Reactions of these synthons with [Pd$(NCMe)_2Cl_2$] afforded the corresponding mononuclear palladium(II) complexes: [Pd(**L1**)$_2Cl_2$] (**1**), [Pd(**L2**)$_2Cl_2$] (**2**), [Pd(**L3**)$_2Cl_2$] (**3**), [Pd(**L4**)$_2Cl_2$] (**4**), [Pd(**L5**)$_2Cl_2$] (**5**), and [Pd(**L6**)$_2Cl_2$] (**6**) in moderate to high yields. All compounds synthesized were characterized by a combination of ^{1}H NMR, ^{13}C NMR, and IR spectroscopy. Compounds **L1**, **1**, and **2** were examined by single crystal X-ray crystallography. DFT theoretical studies at the B3LYP/6-31+G(*d*) level of theory with GAUSSIAN98 have been used to rationalize some of the results. When the complexes were activated with ethylaluminium dichloride ($EtAlCl_2$), they catalysed the oligomerization of ethylene to mostly C_{10} and C_{12} oligomers. Oligomer distribution greatly depends on the oligomerization conditions; for example, an increase in temperature and pressure produced a higher percentage of C_{12} compared to C_{10}.

Key words: furoyl and thiophene carbonyl linker pyrazolyl compounds, palladium complexes, ethylene oligomerization.

Résumé : Les réactions du chlorure de 2-furoyle et le chlorure de thiophène-2-carbonyle avec des pyrazoles substitués conduisent avec de bons rendements aux composés pyrazolyles modifiés: {(3,5-Me_2pzCO)-2-C_4H_3O} (**L1**), {(3,5-Me_2pzCO)-2-C_4H_3S} (**L2**), {(3,5-*t*-Bu_2pzCO)-2-C_4H_3O} (**L3**), {(3,5-*t*-Bu_2pzCO)-2-C_4H_3S} (**L4**), {(3,5-Ph_2pzCO)-2-C_4H_3S} (**L5**) et {(pzCO)-2-C_4H_3O} (**L6**). Les réactions de ces synthons avec du [Pd$(NCMe)_2Cl_2$] conduisent avec des rendements allants de modérés à élevés aux complexes mononucléaires correspondants du palladium(II): [Pd(**L1**)$_2Cl_2$] (**1**), [Pd(**L2**)$_2Cl_2$] (**2**), [Pd(**L3**)$_2Cl_2$] (**3**), [Pd(**L4**)$_2Cl_2$] (**4**), [Pd(**L5**)$_2Cl_2$] (**5**) et [Pd(**L6**)$_2Cl_2$] (**6**). Tous les composés synthétisés ont été caractérisés par une combinaison de spectroscopie infrarouge et RMN du ^{1}H et du ^{13}C. Les composés **L1**, **1** et **2** ont été examinés par diffraction des rayons X. Des études selon la théorie de la densité fonctionnelle au niveau B3LYP/6-31+G(*d*) de la théorie avec une GAUSSIAN98 ont été utilisées pour rationaliser un certain nombre de résultats. Lorsqu'ils sont activés par du dichlorure d'éthylaluminium ($EtAlCl_2$), ils catalysent l'oligomérisation de l'éthylène, principalement en oligomères en C_{10} et en C_{12}. La distribution des oligomères dépend fortement des conditions d'oligomérisation; par exemple, une augmentation de la température et de la pression conduit à des pourcentages plus élevés de produit en C_{12} par rapport à celui en C_{10}.

Mots clés : furoyle et thiophène carbonyle, lieur, composés pyrazolyles, complexes du palladium, oligomérisation de l'éthylène.

[Traduit par la Rédaction]

Introduction

Nitrogen donor compounds represent an important class of ligands in coordination chemistry. In particular, pyrazoles and pyrazolyl ligands have been widely used as terminal and bridging ligands and as precursors for various multidentate ligands in coordination chemistry (1). Indeed, the chemistry of pyrazole and pyrazolyl complexes with transition metals has been extensively reviewed (2), but despite the numerous reports on the synthesis and properties of pyrazolyl late transition metal complexes, very little is known about their catalytic activity in olefin oligomerization. Olefin oligomeri-

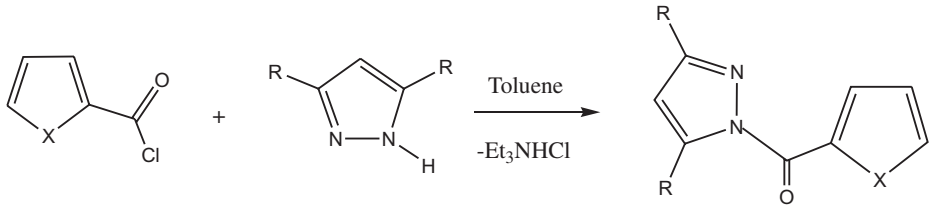
Received 9 December 2004. Published on the NRC Research Press Web site at http://canjchem.nrc.ca on 22 July 2005.

S.O. Ojwach, M.G. Tshivhase, J. Darkwa,[2] and S.F. Mapolie.[3] Department of Chemistry, University of the Western Cape, Private Bag X17, Bellville 7535, South Africa.
I.A. Guzei. Department of Chemistry, University of Wisconsin-Madison, 1101 University Avenue, Madison, WI 53706, USA.

[1]This article is part of a Special Issue dedicated to Professor Howard Alper.
[2]Corresponding author (e-mail: jdarkwa@uwc.ac.za).
[3]Corresponding author (e-mail: smapolie@uwc.ac.za).

 doi: 10.1139/V05-092 © 2005 NRC Canada

Scheme 1.



Compound	X	R	Compound	X	R
L1	O	Me	**L4**	S	^{t}Bu
L2	S	Me	**L5**	S	Ph
L3	O	^{t}Bu	**L6**	O	H

zation is typically catalysed by late transition metal complexes, particularly those of Ni(II) with P, N, and O ligands (3) because of the propensity of such reactions to undergo β-hydride elimination.

However, in the last decade it has become clear that careful tuning of ligand properties and choice of appropriate co-catalysts can lead to either oligomers or polymers after this phenomenon was first observed by Keim (4). For example, reports by Brookhart and co-workers (5) clearly demonstrate the effect of bulky substituents in pseudo axial sites in nickel catalysts. Bulky ligands block these axial sites and reduce chain transfer, whereas less bulky ligands form catalysts that produce oligomers. Another example of the role of bulky substituents on catalysts is provided by diimine–pyridine ligands. Gibson and co-workers (6) have used Fe(II) and Co(II) complexes of this ligand system, with bulky ligands, as catalysts to polymerize ethylene. However, by reducing the steric bulk of the ligand backbone, the Brookhart group found the Fe(II) catalyst to oligomerize ethylene to linear α-olefins with remarkable activity and selectivity (7).

Recently, pyrazolyl nitrogen donor ligands have been found to be tunable to produce electronic and steric effects that have resulted in the use of their late transition metal complexes as catalysts for the transformation of unsaturated hydrocarbons. The report on the polymerization of ethylene by $[\{R_2C(3\text{-}t\text{-}Bu_2pz)_2\}PdCl_2]$ (R = Me, Ph) represents one of the first examples of the use of pyrazolyl late-transition metal complexes in olefin polymerization catalysis (8). Reports by our group clearly indicate that electrophilicity of the catalyst plays a crucial role in polymer formation. We have found simple pyrazole Ni(II) and Pd(II) complexes that are good catalysts for ethylene polymerization (9), and by introducing carbonyl linkers to form benzenedicarbonyl and benzenetricarbonyl linker pyrazolyl palladium(II) complexes, catalytic activities for ethylene polymerization are significantly higher than for the analogous simple pyrazole systems (10). Steric factors also play a role (11). Our calculations of the steric encumbrance about the central metals indicate that in complex $[(3,5\text{-}t\text{-}Bu_2pz)_2PdCl_2]$ the ligands shield 92.1(3)% of the Pd surface while in $[(3,5\text{-}Mepz)_2PdCl_2]$ only 83.5(6)% of the central Pd is shielded by the coordinated moieties (12). In producing polyethylene, we have used mainly methylaluminoxane (MAO), but generally ethylaluminium halides can also activate precatalysts to polymerize ethylene (3).

In this report we describe the preparation and characterization of new furoyl and thiophene carbonyl Pd(II) complexes and their ability to catalyse ethylene oligomerization when activated by ethylaluminium dichloride ($EtAlCl_2$) as the co-catalyst. The potential for controlling the catalytic properties by varying substituents on the ligands is demonstrated by using different substituted pyrazolyl compounds. The influence of various conditions such as reaction time and temperature on the catalyst activity and selectivity in ethylene oligomerization is described.

Results and discussion

Synthesis and characterization of 2-furoyl and thiophene carbonyl pyrazolyl compounds and their palladium(II) complexes

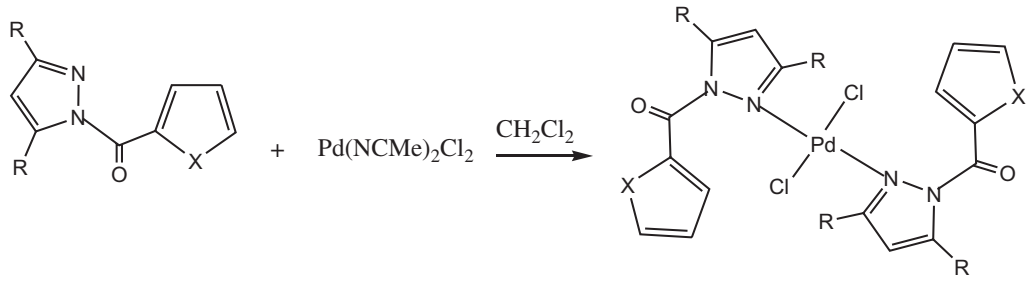
The compounds **L1**–**L6** were readily prepared from either 2-furoyl chloride or 2-thiophene carbonyl chloride and an equivalent amount of the appropriate pyrazole (Scheme 1) following the procedure previously described by us (10). The yields were moderate to high (53%–85%).

Reactions of **L1**–**L6** with $[Pd(NCMe)_2Cl_2]$ in a 2:1 ratio produced the corresponding complexes **1**–**6** (Scheme 2). While **1**–**5** were soluble in dichloromethane and could be purified by recrystallization from dichloromethane and hexane (1:1), **6** was insoluble in common organic solvents like dichloromethane, toluene, and acetonitrile. Complex **6** precipitated from the reaction mixture essentially as an analytically pure solid.

All compounds were characterized by a combination of IR, ^{1}H NMR, and ^{13}C NMR spectroscopy and elemental analyses. Structures for **L1**, **1**, and **2** were confirmed by X-ray crystallography. ^{1}H NMR spectroscopy, however, offered signals that allowed easy identification of both ligands and complexes. For example, the 3,5-disubstituted alkyl pyrazolyl compounds typically have two upfield signals for the alkyl substituents, a signal at about 6 ppm and three doublets of doublets with an AMX splitting pattern (13). As expected, the heteroatom in the linker affected the chemical shift, par-

© 2005 NRC Canada

Scheme 2.



Complex	X	R	Complex	X	R
1	O	Me	**4**	S	^{t}Bu
2	S	Me	**5**	S	Ph
3	O	^{t}Bu	**6**	O	H

ticularly those close to these atoms. Complexation of pyrazolyl compounds with Pd resulted in slight changes of the ligands NMR chemical shifts, but there were essentially no changes in the signals in the splitting patterns.

Molecular structure determination by single crystal X-ray analysis

Single crystals suitable for X-ray analysis for compound **L1**, complexes **1** and **2** were grown by slow diffusion of hexane into dichloromethane at –4 °C and used to determine their molecular structures. Crystallographic data for **L1**, **1**, and **2** are presented in Table 1 while selected bond distances and angles are tabulated in Tables 2–4, respectively. The molecular diagrams are presented in Figs. 1–3, respectively.

The solid-state conformation of **L1** is consistent with the results of the DFT studies (vide infra) of its simplified analogue pz-C(O)-C_4H_3O. In the structure of **L1**, atoms N(1) and O(1) are on the opposite sides of the N(2)—C(6) bond owing to electrostatic interactions (14) and atoms O(1) and O(2) are on the same side of the C(6)—C(7) bond. This spatial arrangement is also observed in the structure of **1**, revealing that the preferred orientation is not altered upon coordination.

The two palladium complexes **1** and **2** contain the central metal in slightly distorted square-planar arrangements. In both cases, the pyrazolyl ligands are trans to each other rendering C_i molecular symmetry. This is in line with our density functional theory studies of *trans*-$(pzH)_2PdCl_2$ (symmetry C_{2h}) and *cis*-$(pzH)_2PdCl_2$ (symmetry C_2) at the B3LYP/LANL2DZ level of theory that indicate that the trans-complex is 12.82 kcal mol^{-1} (1 cal = 4.184 J) more stable. Compounds **L1** and **L2** are not planar in their respective complexes and are monodentate with the heteroatoms sulfur and oxygen pointing away from the metal centres.

The average Pd—N bond lengths of 2.032(2) and 2.025(7) Å in complexes **1** and **2**, respectively, are statistically indistinguishable and agree well with the average Pd—N(pz) bond length of 2.06(9) Å determined by averaging 607 bonds in 229 relevant complexes reported to the Cambridge Structural Database (CSD, (15)). The Pd—Cl bond distances in **1** and **2** (2.306(9) and 2.306(3) Å, respectively) are in good agreement with the distance of 2.33(5) Å obtained by averaging 2055 Pd—Cl bonds in 1268 relevant complexes reported to the CSD.

An interesting structural aspect was revealed by examining the ligand conformations in complexes **1** and **2**. The ligands differ only by the nature of the heteroatom (sulfur vs. oxygen) in their non-pyrazole five-membered rings and one could have reasonably expected to observe very similar structures. Indeed, in both cases the heteroatom (S or O) is located on the same side of the C—C bond of the X-C-C=O link in each ligand. Recall that in free **L1** (Fig. 1), the two oxygen atoms reside on the same side of the O-C-C=O linkage. This logical result is in line with expectations, however, DFT theoretical studies of simplified analogues of the compounds **L1** and **L2** (Figs. 4 and 5) at the B3LYP/6-31+G(*d*) level of theory with GAUSSIAN98 (16) indicate that a different outcome could have been predicted. The compounds (**L1** and **L2**) can exist in several stable conformations; the two most stable are shown in Figs. 4 and 5. In the case of furoyl, the conformation in which the furan oxygen is positioned on the same side as the carbonyl oxygen in the O-C-C=O sequence is more stable. This conformation (A in Fig. 4) is observed in the crystal structures of both **L1** and **1**. On the other hand, in the case of the thiophene carbonyl compound, the other conformation (D in Fig. 5), in which the thiophene S atom is on the opposite side from the carbonyl ligand in the S-C-C=O sequence is slightly more stable. Thus, the free compound **L2** changes its conformation upon coordinating to the Pd metal centre during the formation of **2**. The activation energies for the rotation about the C—C bond of the X-C-C=O linkage are calculated to be 13.4 kcal mol^{-1} for the A to B and 7.1 kcal/mol for C to D transitions.

We have also examined the steric crowding around the Pd centres in **1** and **2** with the program SOLID-G to determine

© 2005 NRC Canada

Table 1. Crystal data and details of structure refinement for **L1**, **1**, and **2**.

Parameter	**L1**	**1**	**2**
Empirical formula	$C_{10}H_{10}N_2O_2$	$C_{20}H_{20}Cl_2N_4O_4Pd$	$C_{21}H_{22}Cl_4N_4O_2PdS_2$
Formula weight	190.2	557.7	674.75
Temperature (K)	294(2)	273(2)	100(2)
Wavelength (Å)	0.710 73	0.710 73	0.710 73
Crystal system	Monoclinic	Triclinic	Monoclinic
Space group	$P2_1/n$	$P\bar{1}$	$P2_1$
a (Å)	8.005 7(10)	7.442 2(8)	10.696(2)
b (Å)	17.761(2)	9.209 7(10)	13.332(3)
c (Å)	13.808 3(15)	15.742 2(17)	18.015(4)
α (°)	90	88.898(2)	90
β (°)	97.148(2)	88.049(2)	96.345(4)
γ (°)	90	86.608(2)	90
Volume (Å^3)	1948.2(4)	1948.2(4)	2553.1(9)
Z	8	2	4
Density (calculated, Mg m^{-3})	1.297	1.721	1.755
Absorption coefficient (mm^{-1})	0.093	1.146	1.337
F(000)	800	560	1352
Crystal size (mm^3)	0.40 × 0.20 × 0.10	0.43 × 0.32 × 0.26	0.30 × 0.20 × 0.20
θ Range for data collection (°)	1.88–26.38	2.22–26.39	1.90–28.31
Index ranges	$-10 \le h \le 9$, $-22 \le k \le 20$, $-16 \le l \le 7$	$-9 \le h \le 9$, $-11 \le k \le 11$, $-19 \le l \le 19$	$-14 \le h \le 12$, $-16 \le k \le 17$, $-23 \le l \le 20$
Reflections collected	9077	8891	16 039
Independent collections	3753 (R(int) = 0.029 6)	4401 (R(int) = 0.020 7)	10 824 (R(int) = 0.051 2)
Completeness to θ (%)	94.2	99.1	92.8
Absorption corrections	Empirical with SADABS	Empirical with SADABS	Empirical with SADABS
Max and min transmissions	0.990 8 and 0.963 9	0.754 9 and 0.638 6	0.754 9 and 0.638 6
Refinement method	Full-matrix least-squares on F^2	Full-matrix least-squares on F^2	Full-matrix least-squares on F^2
Data/restraints/parameters	3753/0/313	4401/0/287	10 829/409/622
Goodness of fit on F^2	1.025	1.063	1.045
Final R indices	$R1$ = 0.051 3, $wR2$ = 0.126 4	$R1$ = 0.027 1, $wR2$ = 0.073 7	$R1$ = 0.061 2, $wR2$ = 0.139 9
R indices (all data)	$R1$ = 0.094 8, $wR2$ = 0.145 7	$R1$ = 0.028 8, $wR2$ = 0.075 0	$R1$ = 0.069 6, $wR2$ = 0.147 9
Largest diff. peak and hole (e Å^{-3})	0.174 and –0.245	1.011 and –0.529	3.060 and –0.849

that the metal centres are shielded by the ligands to the extent of 93.1(3)% and 92.3(5)%, respectively. Since the difference between these values, determined from the crystal structures reported herein, is not statistically significant, any variation in the reactivity of these complexes towards the same reagents ought to be attributed to the differences in the electronic properties of the ligands and their conformations.

Evaluation of the complexes as catalysts for ethylene oligomerization

When complexes **1**–**5** were activated with $EtAlCl_2$, they were found to oligomerize ethylene to mainly C_{10} and C_{12}. No oligomers were obtained when controlled reactions were carried out at 25 °C and 5 atm (1 atm = 101.325 kPa) with the co-catalyst and ethylene in the absence of the complexes. Complex **6** was not evaluated because it is insoluble in toluene, the oligomerization solvent. There were a number of factors that influenced the oligomerization: First, the nature of the ligands influenced both the catalyst activity and product distribution. Complex **1**, with the furoyl linker and methyl groups, was less active (TON = 60 kg mol^{-1} Pd h^{-1}) than the analogous complex **3** with *tert*-butyl substituents (TON = 70 kg mol^{-1} Pd h^{-1}) (Table 5, entries 1 and 3). A similar trend was observed for the thiophene carbonyl analogue (Table 5, entries 2 and 5). Catalyst **5**, with the phenyl substituent on the pyrazolyl ring, was the most active.

A report by Guan and Marshall (17) on the catalytic behaviour of phosphine–imine Pd(II) complexes shows that the phenyl analogue has higher activity (TON = 17 200 kg mol^{-1} Pd h^{-1}) compared to that of the *tert*-butyl (TON = 1670 kg mol^{-1} Pd h^{-1}) and the methyl (TON = 960 kg mol^{-1} Pd h^{-1}) systems. The observed trend could be ascribed to the difference in the electronic structure of the complexes (18) where the less electron-donating phenyl group produces a more electrophilic metal centre in the catalyst. This could explain why complex **5** is the best catalyst in our study.

The nature of the linker in the ligand systems appears to have some effect on the oligomer distribution. For example, the catalysts with furoyl linkers gave higher percentages of the C_{12} than C_{10} oligomers (Table 5, entries 1 and 3) whereas the thiophene carbonyl analogues gave higher percentages of

© 2005 NRC Canada

Table 2. Selected bond lengths and angles for **L1**.

Bond lengths (Å)	
O(1)—C(6)	1.209(2)
O(2)—C(10)	1.355(3)
O(2)—C(7)	1.377(2)
N(1)—C(2)	1.311(3)
N(1)—N(2)	1.379(2)
N(2)—C(6)	1.405(2)
Bond angles (°)	
C(10)-O(2)-C(7)	105.82(18)
N(1)-N(2)-C(4)	111.88(16)
N(1)-N(2)-C(6)	120.58(16)
O(2)-C(7)-C(6)	112.40(17)
O(1)-C(6)-C(7)	122.49(18)
N(2)-C(6)-C(7)	117.53(17)

Table 3. Selected bond lengths and angles for **1**.

Bond lengths (Å)	
Pd(1)—N(1)	2.0332(15)
Pd(1)—Cl(1)	2.2993(5)
Pd(2)—N(3)	2.0300(17)
Pd(2)—Cl(2)	2.3125(5)
N(1)—C(2)	1.327(2)
N(1)—N(2)	1.388(2)
O(1)—C(6)	1.203(2)
Bond angles (°)	
N(1)-Pd(1)-N(1)	180.00(8)
N(1)-Pd(1)-Cl(1)	91.84(5)
N(1)-Pd(1)-Cl(1)	88.16(5)
N(1)-Pd(1)-Cl(1)	91.84
N(3)-Pd(2)-Cl(2)	88.84(5)
N(3)-Pd(2)-Cl(2)	91.16(5)
N(2)-C(6)-C(7)	116.36(16)

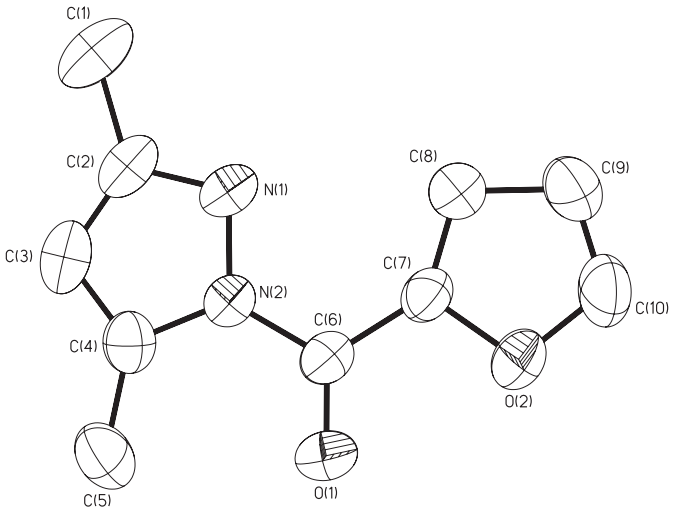
C_{10} than C_{12} (Table 5, entries 2 and 4). There was, however, no clear trend in oligomer distribution as the steric bulk of the ligands in the catalysts changed.

The co-catalyst to catalyst ratio was found to be crucial in determining activity. Complex **2** was used to establish the effective ratio for optimum activity. No activity was observed for an Al:Pd ratio below 20. This indicates that not much activation occurs below this ratio. An increase in the Al:Pd from 20 to 2000 resulted in a general increase in oligomer yield to give an optimum ratio of 1000. Above this ratio, the yield decreased (Table 6, entry 6). Catalyst **1** showed a similar trend (Table 6, entries 7–9). The co-catalyst to catalyst ratio in ethylene oligomerization catalysed by phosphinitooxazoline and pyridine Ni(II) complexes is known to increase turnover frequency from 11 600 to 49 000 mol C_2H_4 mol^{-1} Ni h^{-1} when the $EtAlCl_2$:Ni ratio is increased from 1.3 to 6 (19). Our catalyst requires much higher co-catalyst to catalyst ratio. This is probably due to the ability of the co-catalyst to interact with both the carbonyl oxygen and the heteroatom in the ligands. We found a higher Al:Pd ratio, however, resulted in an increase in the percentage of C_{10} oligomers. For instance, an Al:Pd of 50 gave 49% of C_{10} and 45% of C_{12},

Table 4. Selected bond lengths and angles for **2**.

Bond lengths (Å)	
Pd(1)—N(1A)	2.026(6)
Pd(1)—Cl(1)	2.3029(19)
Pd(2)—N(1B)	2.035(6)
Pd(1)—Cl(2)	2.3101(19)
S(14A)—C(13A)	1.694(8)
O(9A)—C(8A)	1.202(8)
N(1A)—C(2A)	1.363(8)
Bond angles (°)	
N(1A)-Pd(1)-N-(1B)	178.7(3)
N(1A)-Pd(1)-Cl(1)	88.47(5)
N(1B)-Pd(1)-Cl(1)	90.93(5)
N(1A)-Pd(1)-Cl(2)	91.29(17)
N(1C)-Pd(2)-N(1D)	179.5(3)
O(9A)-C(8A)-N(7A)	119.5(7)
O(9A)-C(8A)-C(10A)	123.4(7)

Fig. 1. ORTEP diagram of a single moiety of **L1**. Atoms are shown with 50% thermal probability ellipsoids.



while an Al:Pd of 1000 gave 66% C_{10} and 30% C_{12}. It is not clear why the changes in co-catalyst to catalyst ratio affect product distribution.

The effects of time, temperature, and pressure on ethylene oligomerization were mainly investigated using catalysts **1** and **5**. The effect of time on ethylene oligomerization activity using catalyst **1** at 25 °C, 5 atm, and an Al:Pd ratio of 500 was investigated. Longer reaction times resulted in a significant decrease in activity (Table 7). The maximum turnover number (177 kg mol^{-1} Pd h^{-1}) was obtained at 30 min (Table 7, entry 2), but at 15 min, it was evident that the process to produce the active species was still incomplete, resulting in lower yields (120 kg mol^{-1} Pd h^{-1}). The same trend was observed for catalyst **5** (Table 7, entries 5 and 6). Generally, reaction time is known to affect catalyst activity. This is usually the result of catalyst decomposition. Our catalysts appear to be stable up to about 30 min and thereafter begin to decompose, even at room temperature. A similar phenomenon is seen for ethylene oligomerization using cationic Ni(II) and Pd(II) complexes containing bidentate phen-

© 2005 NRC Canada

Fig. 2. ORTEP diagram of **1** shown with 50% probability ellipsoids. The hydrogen atoms are omitted for clarity. The complex resides on a crystallographic inversion centre.

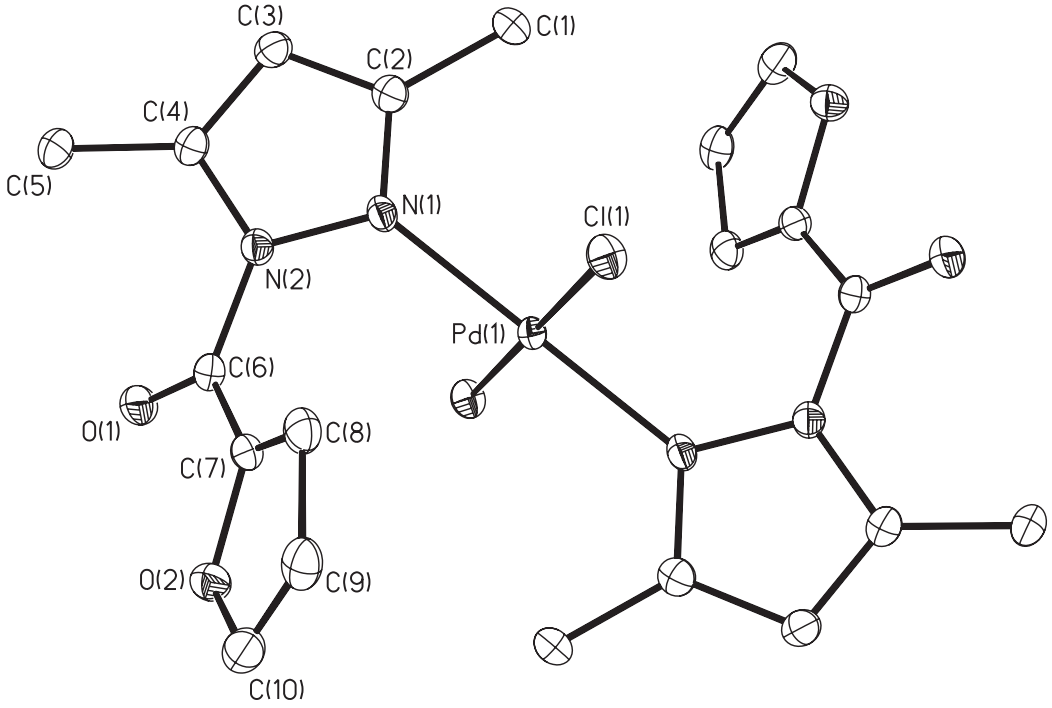
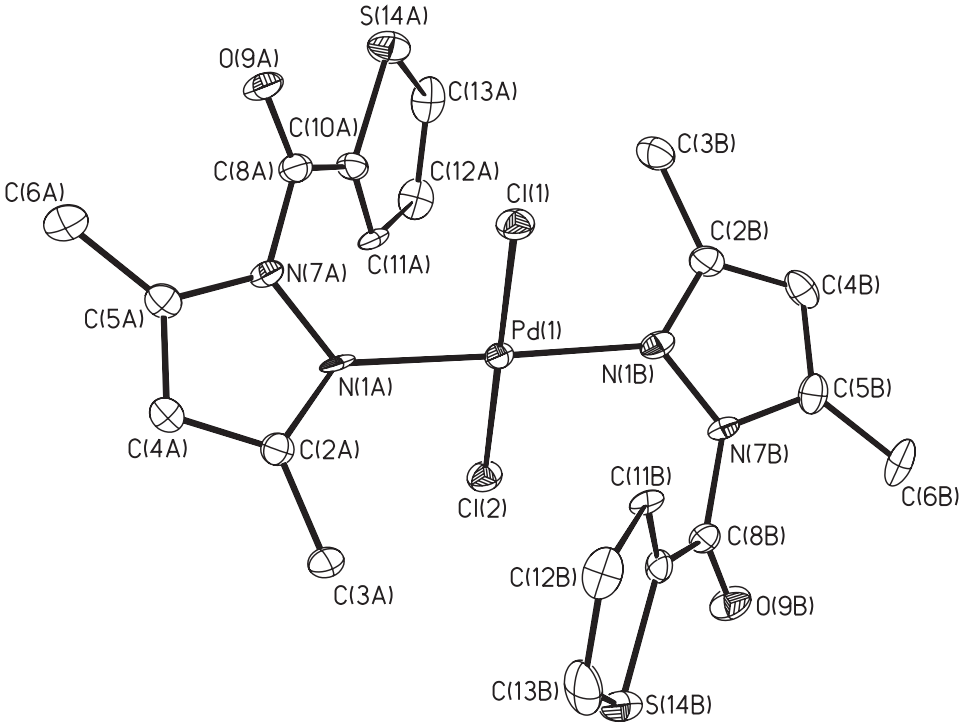


Fig. 3. ORTEP diagram of **2** drawn with 50% thermal probability ellipsoids. The hydrogen atoms have been omitted for clarity.



acyldiarylphosphine ligands (20), where TOF increases for the Pd(II) catalyst from 1.2×10^3 h^{-1} in 15 min to 5.3×10^4 h^{-1} of ethylene consumed in 1 h, but after 3 h of activity dropped to 3.3×10^4 h^{-1}, signifying some catalyst decomposition.

Reaction time was also found to have a profound effect on the nature of the oligomers produced. A higher percentage of C_{10} (77%) was obtained for the 15 min run as compared to 38% for the 2 h run (Table 7, entries 1 and 4). This indicates that oligomer molecular weight increases with time, a result of co-oligomerization of the released matured oligomers, hence, production of higher oligomers. An opposite

© 2005 NRC Canada

Table 5. Effect of the catalyst on ethylene oligomerization.[a]

		Oligomers (%)[b]				
Entry	Catalyst	C_{10}	C_{12}	C_{14+}	Yield[c] (g)	TON (kg mol^{-1} Pd h^{-1})
1	**1**	38	59	3	1.15	62
2	**2**	66	30	4	1.00	54
3	**3**	45	52	3	1.29	70
4	**4**	54	41	5	1.05	56
5	**5**	34	61	5	1.36	73
6	**5**[d]	30	64	6	2.97	124

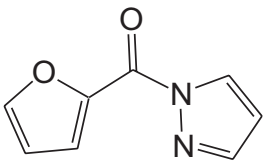
[a]Reaction conditions: solvent, toluene (50 mL); pressure 5 atm (1 atm = 101.325 kPa); temperature, 25 °C; time 2 h; amount of catalyst 9.00 μm; Al:Pd, 500; co-catalyst, $EtAlCl_2$.
[b]Product distribution determined by GC–MS.
[c]Yield of products determined by the total mass of oligomers produced after the solvent was evaporated.
[d]Al:Pd = 1000.

Table 6. Effect of co-catalyst concentration on ethylene oligomerization.[a]

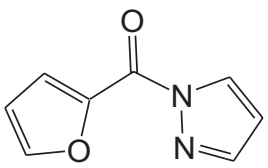
		Oligomers (%)[b]				
Entry	Al:Pd	C_{10}	C_{12}	C_{14+}	Yield[c] (g)	TON (kg mol^{-1} Pd h^{-1})
1	20	—	—	—	Trace	—
2	50	49	45	6	0.21	10
3	100	57	38	5	0.41	21
4	500	66	30	4	1.00	54
5	1000	65	30	5	1.66	94
6	2000	66	29	5	1.19	64
7	100[d]	31	65	4	1.79	30
8	500[d]	38	59	3	1.15	62
9	1000[d]	50	45	5	2.10	110

[a]Reaction conditions: solvent, toluene (50 mL); pressure 5 atm (1 atm = 101.325 kPa); temperature, 25 °C; time, 2 h; amount of catalyst, 9.00 μm; co-catalyst, $EtAlCl_2$; catalyst **2** unless stated otherwise.
[b]Product distribution determined by GC–MS.
[c]Yield of products determined by the total mass of oligomers produced after the solvent was evaporated.
[d]Catalyst **1**.

Fig. 4. The DFT studies (at the B3LYP/6-31+G(*d*) level of theory) of simplified analogues of **L1** (A and B). The more stable conformation is also observed in the solid-state structures of **L1** and **1** (1 cal = 4.184 J).

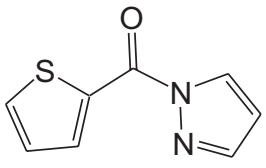


A, -2.23 kcal/mol

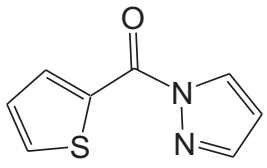


B, 0 kcal/mol

Fig. 5. The DFT studies (at the B3LYP/6-31+G(*d*) level of theory) of simplified analogues of **L2** (C and D). The less stable conformation is observed when **L2** serves as a ligand in **2** (1 cal = 4.184 J).



C, 0 kcal/mol



D, -0.43 kcal/mol

trend is seen with phosphinidine Pd(II) complexes where prolonged reaction time from 3 to 15 h resulted in reduced oligomer molecular weight from 215 to 180 (18).

An increase in temperature was found to increase the activity of catalyst **1** and a maximum activity was obtained at 60 °C (Table 7). Above 60 °C, the activity of the catalyst dropped (Table 7, entries 8 and 9), usually an indication of catalyst decomposition. This observation is consistent with Pd(II) α-diimine catalysts, which are known to decompose rapidly above 50 °C (21), and that of Guan and Salo (22) that uses bisazaferrocene Pd(II) complexes.

The influence of pressure on ethylene oligomerization is well-established, especially on catalytic activity (21). The effect of ethylene concentration on oligomerization using catalyst **1** was studied by varying the ethylene pressure from 5 to 35 atm (Table 7, entries 2, 10–12). An increase in ethylene concentration resulted in a significant increase in oligomer yield. We also observed selectivity towards higher oligomers with an increase in pressure (Table 7, entries 2 and 12). For instance, at 5 atm, 71% of C_{10} and 23% of C_{12} were produced, respectively, while at 35 atm, 48% of C_{10} and 41% of C_{12} were obtained. At high pressures, it has been postulated that ethylene co-oligomerizes with the preformed olefins resulting in a significant increase in oligomer molecular weight (3). A report on bis(salicylaldiminate)nickel catalysed

© 2005 NRC Canada

Table 7. Effect of reaction conditions on ethylene oligomerization.[a]

Entry	Temp (°C)	$P_{C_2H_4}$ (atm)	Time (min)	Oligomers (%)[b]			Yield[c] (g)	TON (kg mol^{-1} Pd h^{-1})
				C_{10}	C_{12}	C_{14+}		
1	25	5	15	77	20	3	0.28	120
2	25	5	30	71	25	4	0.82	177
3	25	5	60	58	38	4	1.27	137
4	25	5	120	38	59	3	1.30	70
5	25	5	30[d]	70	24	6	0.93	200
6	25	5	60[d]	54	41	5	1.40	151
7	40	5	30	36	61	3	1.60	345
8	60	5	30	32	64	4	4.86	1050
9	70	5	30	33	62	5	3.15	680
10	25	10	30	61	36	3	1.00	216
11	25	20	30	51	44	5	1.28	276
12	25	35	30	48	41	11	2.56	542

Note: 1 atm = 101.325 kPa.
[a]Reaction conditions: solvent, toluene (50 mL); amount of catalyst, 9.00 μm; catalyst **1** used unless stated otherwise; co-catalyst, $EtAlCl_2$; Al:Pd = 500.
[b]Product distribution determined by GC–MS.
[c]Yield of products determined by the total mass of oligomers produced after the solvent was evaporated.
[d]Catalyst **5**.

ethylene oligomerization found the C_6–C_{12} yield go up from 23% to 70% when the ethylene pressure was increased from 1 to 20 atm, but the butene content of the oligomerization product dropped from 76% to 30% (23). Our result is in line with this observation, though not as drastic.

Conclusions

Furoyl and thiophene carbonyl pyrazolyl ligands form complexes with palladium(II) that have the same structural motifs as complexes formed by simple substituted pyrazoles with palladium(II). X-ray structures of **1** and **2** confirm that in the solid state of $[Pd(L)_2Cl_2]$ a trans geometry is preferred to cis. Activation of these complexes with the alkyl aluminium compound, $EtAlCl_2$, results in active catalysts for the oligomerization of ethylene. The major oligomers produced are C_{10} and C_{12}, and no lower oligomers in the C_4–C_8 range were obtained. This shows that the catalysts favour chain propagation relative to chain termination. The activities of these palladium(II) catalysts are lower compared with the α-diimine Pd(II) complexes, possibly because of the presence of the noncoordinating donor atoms (sulfur and oxygen), which might cause catalyst deactivation by forming adducts with the aluminium co-catalyst. Thermal instability of these catalysts could also contribute to their observed low catalytic activity, as would weakly bound pyrazolyl ligands that could lead to ligand dissociation from the metal centre.

Experimental section

All ligand and complex syntheses were performed under a nitrogen atmosphere using standard Schlenk techniques. All solvents were of analytical grade and were dried and distilled prior to use. Toluene and dichloromethane were dried and distilled from sodium/benzophenone and P_2O_5, respectively. The carbonyl linkers (2-furoyl chloride and 2-thiophene carbonyl chloride) were obtained from Sigma-Aldrich and used as received. The NMR spectra were recorded on a Varian Gemini 2000 instrument (^{1}H at 200 MHz, ^{13}C at 50.3 MHz) at room temperature. The chemical shifts are reported in δ (ppm) and referenced to the residual $CHCl_3$ in the NMR solvent. Elemental analyses and IR spectroscopy were performed on a Carlo Erba NA analyzer and a PerkinElmer FT-IR Paragon 1000PC, respectively, at the Chemistry Department, University of the Western Cape.

Synthesis of the ligands and complexes

2-(3,5-Dimethylpyrazolyl-1-carbonyl)furan (L1)

To a solution of 2-furoyl chloride (2.12 g, 15.60 mmol) in toluene (40 mL) was added 3,5-dimethylpyrazole (1.49 g, 15.60 mmol) and Et_3N (2 mL). The mixture was refluxed for 24 h, filtered to remove the Et_3NHCl by-product, and the solvent removed in vacuo to give a white residue. Purification by column chromatography on silica gel with dichloromethane–hexane (1:1) as the eluent afforded a white solid. Recrystallization from CH_2Cl_2–hexane gave single crystals suitable for X-ray analysis. Yield: 2.52 g (85%). IR (Nujol, cm^{-1}) $\nu_{(C=O)}$: 1702. ^{1}H NMR ($CDCl_3$) δ: 2.29 (s, 3H, CH_3, pz), 2.62 (s, 3H, CH_3, pz), 6.02 (s, 1H, pz), 6.61 (dd, 1H, furan, $^4J_{HH}$ = 1.6 Hz, $^3J_{HH}$ = 3.6 Hz), 7.71 (dd, 1H, furan, $^4J_{HH}$ = 0.8 Hz, $^3J_{HH}$ = 3.6 Hz), 7.94 (dd, 1H, furan, $^4J_{HH}$ = 0.8 Hz, $^3J_{HH}$ = 3.8 Hz). ^{13}C{^{1}H} NMR ($CDCl_3$) δ: 13.2, 13.8, 110.4, 111.7, 123.4, 144.8, 146.9, 152.1, 156.1, 161.8. EI-MS (70 eV) *m*/*z* (%): 190 (20) [M^+], 162 (100) [$M^+ - C_2H_4$], 95 (40) [$M^+ - C_5N_2H_7$], 67 (5) [$M^+ - C_6N_2H_7CO$]. Anal. calcd. for $C_{10}H_{10}N_2O_2$ (%): C 63.25, H 5.32, N 14.71; found: C 62.76, H 4.88, N 14.49.

Compounds **L2**–**L6** were prepared following the same procedure as described for **L1**.

2-(3,5-Dimethylpyrazolyl-1-carbonyl)thiophene (L2)

Compound **L2** was synthesized using 3,5-dimethylpyrazole (1.50 g, 15.60 mmol) and 2-thiophene carbonyl chloride (2.28 g, 15.60 mmol). Yield: 2.41 g (75%). IR (Nujol, cm^{-1}) $\nu_{(C=O)}$: 1675. ^{1}H NMR ($CDCl_3$) δ: 2.32 (s, 3H, CH_3, pz), 2.63 (s, 3H, CH_3, pz), 6.03 (s, 1H, pz), 7.15 (dd, 1H, thiophene, $^4J_{HH}$ = 1.6 Hz, $^3J_{HH}$ = 4.8 Hz), 7.71 (dd, 1H,

© 2005 NRC Canada

thiophene, $^4J_{HH}$ = 1.4 Hz, $^3J_{HH}$ = 4.8 Hz), 8.34 (d, 1H, thiophene, $^4J_{HH}$ = 1.4 Hz, $^3J_{HH}$ = 4.0 Hz). $^{13}C\{^1H\}$ NMR ($CDCl_3$) δ: 13.3, 14.0, 110.8, 126.4, 127.9, 137.2, 144.5, 151.5, 156.0, 160.0. EI-MS (70 eV) *m*/*z* (%): 206 (100) [M^+], 178 (50) [$M^+ - C_2H_4$], 111 (50) [$M^+ - C_5N_2H_7$], 83 (5) [$M^+ - C_6N_2H_7$ CO]. Anal. calcd. for $C_{10}H_{10}N_2OS$ (%): C 58.32, H 4.87, N 13.65; found: C 58.15, H 4.26, N 13.68.

2-(3,5-Di*-tert-*butylpyrazolyl-1-carbonyl)furan (L3)

Compound **L3** was prepared using 2-furoyl chloride (1.42 g, 10.52 mmol) and 3,5-di-*tert*-butylpyrazole (2.90 g, 10.52 mmol). Yield: 2.31 g (80%). IR (Nujol, cm^{-1}) $\nu_{(C=O)}$: 1716. ^1H NMR ($CDCl_3$) δ: 1.35 (s, 9H, CH_3, pz), 1.46 (s, 9H, CH_3, pz), 6.18 (s, 1H, pz), 6.60 (dd, 1H, furan, $^4J_{HH}$ = 1.6 Hz, $^3J_{HH}$ = 3.4 Hz), 7.71 (dd, 1H, furan, $^4J_{HH}$ = 0.8 Hz, $^3J_{HH}$ = 1.6 Hz), 7.82 (dd, 1H, furan, $^4J_{HH}$ = 0.8 Hz, $^3J_{HH}$ = 3.8 Hz). $^{13}C\{^1H\}$ NMR ($CDCl_3$) δ: 29.0, 29.3, 31.9, 32.8, 105.5, 111.7, 123.1, 146.5, 156.1, 158.0, 161.6. EI-MS (70 eV) *m*/*z* (%): 274 (45) [M^+], 244 (30) [$M^+ - C_2H_6$], 232 (100) [$M^+ - C_3H_6$], 217 (95) [$M^+ - C_{11}N_2H_{19}$], 67 (5) [$M^+ - C_{11}N_2H_{19}CO$]. Anal. calcd. for $C_{16}H_{22}N_2O_2$ (%): C 69.82, H 8.36, N 10.18; found: C 69.77, H 8.26, N 10.02.

2-(3,5-Di*-tert-*butylpyrazolyl-1carbonyl)thiophene (L4)

Compound **L4** was prepared by reacting 3,5-di-*tert*-butylpyrazole (1.82 g, 10.34 mmol) with 2-thiophene carbonyl chloride (1.37 g, 9.35 mmol). Yield: 1.50 g (52%). IR (Nujol, cm^{-1}) $\nu_{(C=O)}$: 1686. ^1H NMR ($CDCl_3$) δ: 1.37 (s, 9H, CH3, pz), 1.46 (s, 9H, CH_3, pz), 6.17 (s, 1H, pz), 7.12 (dd, 1H, thiophene, $^4J_{HH}$ = 1.8 Hz, $^3J_{HH}$ = 5.2 Hz), 7.71 (dd, 1H, thiophene, $^4J_{HH}$ = 1.4 Hz, $^3J_{HH}$ = 5.2 Hz), 8.83 (dd, 1H, thiophene, $^4J_{HH}$ = 1.6 Hz, $^3J_{HH}$ = 4.0 Hz). $^{13}C\{^1H\}$ NMR ($CDCl_3$) δ: 28.9, 29.4, 32.1, 32.8, 106.0, 125.8, 137.2, 157.4, 159.7, 169.8. EI-MS (70 eV) *m*/*z* (%): 290 (63) [M^+], 275 (20) [$M^+ - CH_3$], 233 (65) [$M^+ - C_4H_9$], 191 (30) [$M^+ - C_7H_{15}$], 111 (100) [$M^+ - C_{11}N_2H_{19}$], 83 (5) [$M^+ - C_{11}N_2H_{19}CO$]. Anal. calcd. for $C_{16}H_{22}N_2OS$ (%): C 65.98, H 7.90, N 9.62; found: C 65.86, H 8.32, N 9.34.

2-(3,5-Diphenylpyrazolyl-1-carbonyl)thiophene (L5)

Compound **L5** was synthesized by reacting 2-thiophene carbonyl chloride (1.73 g, 11.85 mmol) and 3,5-diphenylpyrazole (2.61 g, 11.86 mmol). Yield: 3.07 g (75%). IR (Nujol, cm^{-1}) $\nu_{(C=O)}$: 1689. ^1H NMR δ: 6.61 (s, 1H, pz), 6.98 (d, 1H, thiophene, $^3J_{HH}$ = 3.6 Hz), 7.32 (m, 8H, ph), 7.63 (d, 1H, thiophene, $^3J_{HH}$ = 3.8 Hz), 7.82 (m, 2H, ph), 8.14 (d, 1H, thiophene, $^3J_{HH}$ = 3.8 Hz). $^{13}C\{^1H\}$ NMR ($CDCl_3$) δ: 109.2, 125.9, 126.5, 127.5, 128.3, 128.8, 130.6, 131.2, 133.0, 137.1, 137.9, 147.8, 153.1, 159.2. EI-MS (70 eV) *m*/*z* (%): 330 (100) [M^+], 302 (85) [$M^+ - C_2H_4$], 189 (20) [$M^+ - C_{13}H_9$], 111 (85) [$M^+ - C_{15}H_{11}N_2$], 83 (4) [$M^+ - C_{15}H_{11}N_2CO$]. Anal. calcd. for $C_{20}H_{14}N_2OS$ (%): C 72.70, H 4.27, N 8.48; found: C 72.68, H 4.05, N 8.36.

2-(Pyrazolyl-1-carbonyl) furan (L6)

Compound **L6** was prepared by reacting 2-furoyl chloride (2.97 g, 22.12 mmol) and unsubstituted pyrazole (1.50 g, 22.00 mmol). Yield: 2.40 g (75%). IR (Nujol, cm^{-1}) $\nu_{(C=O)}$: 1685. ^1H NMR ($CDCl_3$) δ: 6.50 (dd, 1H, pz, $^4J_{HH}$ = 1.4 Hz, $^3J_{HH}$ = 3.0 Hz), 6.65 (dd, 1H, furan, $^4J_{HH}$ = 1.8 Hz, $^3J_{HH}$ = 3.6 Hz), 7.78 (dd, 2H, pz, $^4J_{HH}$ = 1.6 Hz, $^3J_{HH}$ = 3.8 Hz), 8.08 (dd, 1H, furan, $^4J_{HH}$ = 0.8 Hz, $^3J_{HH}$ = 3.8 Hz), 8.44 (dd, 1H, furan, $^4J_{HH}$ = 0.8 Hz, $^3J_{HH}$ = 3.8 Hz). $^{13}C\{^1H\}$ NMR ($CDCl_3$) δ: 111.4, 117.4, 124.3, 132.6, 144.9, 145.9, 147.8, 161.8. EI-MS (70 eV) *m*/*z* (%): 162 (20) [M^+], 134 (100) [$M^+ - CN_2H_2$], 95 (40) [$M^+ - C_3N_2H_3$], 67 (5) [$M^+ - C_3N_2H_3CO$]. Anal. calcd. for $C_8H_6N_2O_2$ (%): C 59.32, H 3.72, N 17.34; found: C 58.89, H 3.35, N 16.81.

Dichloro{bis-2-(3,5-dimethylpyrazolyl-1-carbonyl)furan}palladium(II) (1)

To a solution of [$Pd(NCMe)_2Cl_2$] (0.20 g, 0.68 mmol) in dichloromethane (20 mL) was added **L1** (0.26 g, 1.43 mmol). The mixture was stirred at room temperature for 6 h and the resultant solution was concentrated in vacuo to about 10 mL. An analytically pure yellow powder was obtained upon addition of an equal volume of hexane. Yield: 0.28 g (79%). IR (Nujol, cm^{-1}) $\nu_{(C=O)}$: 1694. ^1H NMR ($CDCl_3$) δ: 2.34 (s, 6H, CH_3, pz), 2.44 (s, 6H, CH_3, pz), 6.03 (s, 2H, pz), 6.77 (d, 2H, furan, $^3J_{HH}$ = 3.6 Hz), 7.70 (d, 2H, furan, $^3J_{HH}$ = 3.6 Hz), 7.91 (d, 2H, furan, $^3J_{HH}$ = 3.6 Hz). $^{13}C\{^1H\}$ NMR ($CDCl_3$) δ: 12.8, 15.1, 110.9, 113.3, 126.8, 146.1, 147.1, 149.4, 154.8, 155.9. Anal. calcd. for $C_{20}H_{20}N_4O_4PdCl_2$ (%): C 43.09, H 3.59, N 10.05; found: C 42.57, H 3.20, N 9.65.

Complexes **2**–**4** and **6** were prepared in a similar manner as described for **1**.

Dichloro{bis-2-(3,5-dimethylpyrazolyl-1-carbonyl)thiophene}palladium(II) (2)

Complex **2** was prepared using ligand **L2** (0.50 g, 3.42 mmol) and [$PdCl_2(NCMe)_2$] (0.45 g, 1.71 mmol). Recrystallization from dichloromethane–hexane gave yellow single crystals suitable for X-ray analysis. Yield: 0.61 g (62%). IR (Nujol, cm^{-1}) $\nu_{(C=O)}$: 1688. ^1H NMR ($CDCl_3$) δ: 2.30 (s, 6H, CH_3, pz), 2.32 (s, 6H, CH_3, pz), 6.00 (s, 2H, pz), 7.29 (dd, 2H, thiophene, $^4J_{HH}$ = 1.6 Hz, $^3J_{HH}$ = 3.8 Hz), 7.73 (dd, 2H, thiophene, $^4J_{HH}$ = 1.6 Hz, $^3J_{HH}$ = 3.8 Hz), 8.02 (dd, 2H, thiophene, $^4J_{HH}$ = 6 Hz, $^3J_{HH}$ = 3.8 Hz). $^{13}C\{^1H\}$ NMR ($CDCl_3$) δ: 12.6, 14.4, 110.1, 126.4, 128.4, 136.2, 136.5, 140.1, 146.1, 155.2, 160.0. Anal. calcd. for $C_{20}H_{20}N_4O_2S_2PdCl_2$ (%): C 40.83, H 3.43, N 9.51; found: C 40.84, H 2.69, N 9.53.

Dichloro{bis-2-(3,5-di*-tert-*butylpyrazolyl-1-carbonyl)furan}palladium(II) (3)

Complex **3** was prepared using ligand **L3** (0.37 g, 1.35 mmol) and [$Pd(NCMe)_2Cl_2$] (0.18 g, 0.68 mmol). Yield: 0.25 g (52%). IR (Nujol, cm^{-1}) $\nu_{(C=O)}$: 1705. ^1H NMR ($CDCl_3$) δ: 1.32 (s, 18H, CH_3, pz), 1.46 (s, 18H, CH_3, pz), 6.17 (s, 2H, pz), 6.58 (dd, 2H, furan, $^4J_{HH}$ = 1.7 Hz, $^3J_{HH}$ = 3.6 Hz), 7.71 (dd, 2H, furan, $^4J_{HH}$ = 1.8 Hz, $^3J_{HH}$ = 3.4 Hz), 7.82 (dd, 2H, furan, $^4J_{HH}$ = 1.8 Hz, $^3J_{HH}$ = 3.4 Hz). $^{13}C\{^1H\}$ NMR ($CDCl_3$) δ: 28.8, 29.7, 30.5, 31.6, 100.1, 111.7, 119.3, 125.8, 137.2, 146.7, 156.1, 157.8. Anal. calcd. for $C_{34}H_{50}N_4O_4PdCl_6 \cdot 2CH_2Cl_2$ (%): C 45.53, H 5.58, N 6.25; found: C 46.05, H 5.03, N 6.55.

Dichloro{bis-2-(3,5-di*-tert-*butylpyrazolyl-1-carbonyl)thiophene}palladium(II) (4)

Complex **4** was prepared using ligand **L4** (0.44 g, 1.52 mmol) and [$Pd(NCMe)_2Cl_2$] (0.20 g, 0.76 mmol). Yield: 0.32 g (58%). IR (Nujol, cm^{-1}) $\nu_{(C=O)}$: 1694. ^1H NMR

© 2005 NRC Canada

($CDCl_3$) δ: 1.32 (s, 18H, CH_3, pz), 1.46 (s, 18H, CH_3, pz), 6.19 (s, 2H, pz), 7.13 (dd, 2H, thiophene, $^4J_{HH}$ = 1.6 Hz, $^3J_{HH}$ = 5.0 Hz), 7.72 (dd, 2H, thiophene, $^4J_{HH}$ = 1.2 Hz, $^3J_{HH}$ = 5.4 Hz), 8.26 (dd, 2H, thiophene, $^4J_{HH}$ = 1.6 Hz, $^3J_{HH}$ = 4.2 Hz). Anal. calcd. for $C_{32}H_{46}N_2O_2S_2PdCl_2$ (%): C 49.05, H 6.27, N 7.63; found: C 48.75, H 5.06, N 7.66.

Dichloro{bis-2-(3,5-diphenylpyrazolyl-1-carbonyl)thiophene}palladium(II) (5)

Complex **5** was synthesized by reacting **L5** (0.50 g, 1.53 mmol) and [$Pd(NCMe)_2Cl_2$] (0.20 g, 0.77 mmol). Yield: 0.23 g (37%). IR (Nujol, cm^{-1}) $\nu_{(C=O)}$: 1694. ^1H NMR ($CDCl_3$) δ: 7.20 (s, 1H, pz), 7.46 (d, 1H, thiophene, $^3J_{HH}$ = 4.0 Hz), 8.16 (m, 10H, benzene), 8.37 (d, 1H, thiophene, $^3J_{HH}$ = 3.6 Hz), 8.42 (d, 1H, thiophene, $^3J_{HH}$ = 3.8 Hz). $^{13}C\{^1H\}$ NMR ($CDCl_3$) δ: 109.2, 125.9, 126.5, 127.5, 127.7, 128.4, 128.7, 130.5, 131.2, 133.0, 137.0, 137.9, 147.8, 153.1, 158.2. Anal. calcd. for $C_{40}H_{28}N_2O_2S_2PdCl_2$ (%): C 57.32, H 4.37, N 6.63; found: C 56.82, H 4.15, N 6.16.

Dichloro{bis-2-(pyrazolyl-1-carbonyl)furan}palladium(II) (6)

To a solution of compound **L6** (0.80, 4.94 mmol) in dichloromethane (30 mL), [$Pd(NCMe)_2Cl_2$] (0.63 g, 2.47 mmol) was added. A light brown precipitate formed immediately. The resultant mixture was stirred for 3 h, filtered, and the yellow solid dried. Yield: 1.01 g (80%). IR (Nujol, cm^{-1}) $\nu_{(C=O)}$: 1712. ^1H NMR (DMSO-d_6) δ: 6.64 (dd, 2H, pz, $^4J_{HH}$ = 1.6 Hz, $^3J_{HH}$ = 3.0 Hz), 6.78 (dd, 2H, furan, $^4J_{HH}$ = 1.6 Hz, $^3J_{HH}$ = 3.6 Hz), 7.79 (dd, 4H, pz, $^4J_{HH}$ = 0.8 Hz, $^3J_{HH}$ = 3.6 Hz), 8.15 (dd, 2H, furan, $^4J_{HH}$ = 0.8 Hz, $^3J_{HH}$ = 3.0 Hz), 8.52 (dd, 2H, furan, $^4J_{HH}$ = 0.8 Hz, $^3J_{HH}$ = 1.8 Hz). $^{13}C\{^1H\}$ NMR ($CDCl_3$) δ: 106.4, 110.1, 112.2, 113.2, 117.8, 125.0, 130.5, 145.3, 147.1, 149.8, 154.3, 159.4. Anal. calcd. for $C_{16}H_{12}N_4O_4PdCl_2$ (%): C 38.31, H 2.41, N 11.17; found: C 38.06, H 2.30, N 10.33.

Ethylene oligomerization

Ethylene oligomerization was performed in a 300 mL stainless steel autoclave loaded with the respective catalyst and the appropriate amount $EtAlCl_2$ as the co-catalyst. This was carried out in a nitrogen-purged glovebox. The general procedure involved charging the autoclave with a palladium complex and $EtAlCl_2$ (25% in toluene) in 100 mL of dry toluene. The Al:Pd ratio used was between 20–2000. The autoclave was sealed, removed from the glovebox and loaded into the reactor chamber. The autoclave was flushed three times with ethylene and heated to the required temperature. The desired ethylene pressure was set and a constant flow of ethylene was maintained throughout the reaction. At the end of the reaction, an aliquot of the reaction mixture was taken for the GC analysis. The reaction was quenched by the addition of ethanol after which the solvent was removed in vacuo and the mass of the total nonvolatile products determined. Analysis of the oligomers was performed using a Finnigan-MAT GCQ GC–MS, equipped with an electron impact ionization source at 70 eV and a 30 m HP PONA capillary column with a stationary phase based on 5% poly(methylphenylsiloxane). The rate of increase in oven temperature of the GC was set at 20 °C min^{-1} and then increased by 10 °C min^{-1} until a temperature of 260 °C was reached. Under these conditions, it was possible to separate C_4 to C_{20} olefins. The retention times of the individual components were determined using standard samples of each olefin. Quantitative analysis of the olefins was done by the internal standard reference method using pentadecane as the internal reference.

X-ray crystallography

Crystal evaluation and data collection for **L1**, **1**, and **2** were performed on a Bruker CCD-1000 diffractometer with Mo Kα (λ = 0.710 73 Å) radiation and the diffractometer to crystal distance of 4.9 cm. The initial cell constants were obtained from three series of ω scans at different starting angles. The reflections were successfully indexed by an automated indexing routine built in the SMART program. The absorption correction was based on fitting a function to the empirical transmission surface as sampled by multiple equivalent measurements (24). The structures were solved by direct methods and refined by least-squares techniques using the SHELXTL program (24). All non-hydrogen atoms were refined with anisotropic displacement coefficients. All hydrogen atoms were included in the structure factor calculation at idealized positions and were allowed to ride on the neighbouring atoms with relative isotropic displacement coefficients. Additional crystallographic data for the structures are deposited with the Cambridge Crystallographic Data Centre as supplementary publication numbers CCDC 257819 (**L1**), CCDC 257820 (**1**), and CCDC 257818 (**2**).[4]

Acknowledgements

Financial support by the National Research Foundation (NRF) South Africa is highly appreciated. We thank Professor Len Barbour, University of Stellenbosch, South Africa, for solving the structure of compound **2** as a service.

References

1. (*a*) S. Trofimenko. Prog. Inorg. Chem. **34**, 115 (1986); (*b*) S. Trofimenko. Chem. Rev. **72**, 497 (1972); (*c*) Y. Sun, X. Chen, P. Cheng, S. Yan, D. Zheng Liao, and P. Wen Shen. J. Mol. Struct. **597**, 191 (2001).
2. (*a*) R. Mukherjee. Coord. Chem. Rev. **203**, 166 (2000); (*b*) S. Mecking. Coord. Chem. Rev. **203**, 325 (2000); (*c*) S. Trofimenko. Chem. Rev. **93**, 943 (1993).
3. (*a*) J. Skupinska. Chem Rev. **91**, 613 (1991); (*b*) M. Peuckert, W. Keim, S. Storp, and S.R. Weber. J. Mol. Catal. **20**, 115 (1983).
4. W. Keim. J. Mol. Catal. **52**, 19 (1989).
5. (*a*) C.M. Killian, L.K. Johnson, and M. Brookhart. Organometallics, **16**, 2005 (1997); (*b*) L.K. Johnson, C.M. Killian, and M. Brookhart. J. Am. Chem. Soc. **117**, 6414 (1995);

[4] Supplementary data for this article are available on the Web site or may be purchased from the Depository of Unpublished Data, Document Delivery, CISTI, National Research Council Canada, Ottawa, ON K1A 0S2, Canada. DUD 3687. For more information on obtaining material refer to http://cisti-icist.nrc-cnrc.gc.ca/irm/unpub_e.shtml. CCDC 257818–257820 contain the crystallographic data for this manuscript. These data can be obtained, free of charge, via www.ccdc.cam.ac.uk/conts/retrieving.html (Or from the Cambridge Crystallographic Data Centre, 12 Union Road, Cambridge CB2 1EZ, UK; fax +44 1223 336033; or deposit@ccdc.cam.ac.uk).

© 2005 NRC Canada

(*c*) S.A. Svejda, L.K. Johnson, and M. Brookhart. J. Am. Chem. Soc. **121**, 10 634 (1999).
6. G.J.P. Britovsek, S.P.D. Baugh, V.C. Gibson, and D.F. Wass. Angew. Chem. Int. Ed. **38**, 428 (1999).
7. B.L. Small and M. Brookhart. J. Am. Chem. Soc. **120**, 7143 (1998).
8. S. Tsuji, T.R. Younkin, D.C. Swenson, and R.F. Jordan. Organometallics, **18**, 4758 (1998).
9. (*a*) K. Li, J. Darkwa, I.A. Guzei, and S.F. Mapolie. J. Organomet. Chem. **660**, 108 (2002); (*b*) S.M. Nelana, J. Darkwa, I.A. Guzei, and S.F. Mapolie. J. Organomet. Chem. **689**, 1835 (2004).
10. I.A. Guzei, K. Li, G.A. Bikzhanova, J. Darkwa, and S.F. Mapolie. Dalton Trans. 715 (2003).
11. L.K. Johnson, S. Mecking, and M. Brookhart. J. Am. Chem. Soc. **118**, 11 664 (1998).
12. (*a*) I.A. Guzei and M. Wendt. SOLID-G [computer program]. Madison, Wis. 2004; (*b*) I.A. Guzei. *In* 2004 Annual Meeting of the American Crystallographic Association, 17–22 July 2004, Chicago.
13. W. Kemp. Organic spectroscopy. 3rd ed. Macmillan Education Ltd., London. 1991. p. 36.
14. I.A. Guzei, K. Li, and J. Darkwa. J. Chem. Crystallogr. **35**, 197 (2005)
15. F.H. Allen. Acta Crystallogr. Sect. B, **B58**, 380 (2002).
16. M.J. Frisch, G.W. Trucks, H.B. Schlegel, G.E. Scuseria, M.A. Robb, J.R. Cheeseman, V.G. Zakrzewski, J.A. Montgomery, Jr., R.E. Stratmann, J.C. Burant, S. Dapprich, J.M. Millam, A.D. Daniels, K.N. Kudin, M.C. Strain, O. Farkas, J. Tomasi, V. Barone, M. Cossi, R. Cammi, B. Mennucci, C. Pomelli, C. Adamo, S. Clifford, J. Ochterski, G.A Petersson, P.Y. Ayala, Q. Cui, K. Morokuma, D.K. Malick, A.D. Rabuck, K. Raghavachari, J.B. Foresman, J. Cioslowski, J.V. Ortiz, A.G. Baboul, B.B. Stefanov, G. Liu, A. Liashenko, P. Piskorz, I. Komaromi, R. Gomperts, R.L. Martin, D.J. Fox, T. Keith, M.A. Al-Laham, C.Y. Peng, A. Nanayakkara, M. Challacombe, P.M.W. Gill, B. Johnson, W. Chen, M.W. Wong, J.L. Andres, C. Gonzalez, M. Head-Gordon, E.S. Replogle, and J.A. Pople. GAUSSIAN98. Revision A9 [computer program]. Gaussian Inc., Pittsburgh, Pennsylvania. 1998.
17. Z. Guan and W.J. Marshall. Organometallics, **21**, 3580 (2002).
18. O. Daugulis, M. Brookhart, and P.S. White. Organometallics, **21**, 5935 (2002).
19. F. Speiser, P. Braunstein, L. Saussine, and R. Welter. Inorg. Chem. **43**, 1649 (2004).
20. J.M. Malinoski and M. Brookhart. Organometallics, **22**, 5324 (2003).
21. S.D. Ittel, M. Brookhart, and L.K. Johnson. Chem. Rev. **100**, 1169 (2000).
22. Z. Guan and E.V. Salo. Organometallics, **22**, 5033 (2003).
23. C. Carlini, M. Isola, V. Liuzzo, A.M.R. Galletti, and G. Sbrana. Appl. Catal. A, **231**, 307 (2002).
24. Bruker-AXS SADABS. Version 2.05 software reference manual. Bruker-AXS, Madison, Wisconsin. 2000–2004; Bruker-AXS SAINT. Version 6.22 software reference manual. Bruker-AXS, Madison, Wisconsin. 2000–2004; Bruker-AXS SHELXTL. Version 6.10 software reference manual. Bruker-AXS, Madison, Wisconsin. 2000–2004; Bruker-AXS SMART 5.622 software reference manual. Bruker-AXS, Madison, Wisconsin. 2000–2004.

© 2005 NRC Canada

Aluminium triflate as catalyst for epoxide ring-opening and esterification reactions — Mechanistic aspects[1]

Yvette M. Terblans, Johannes J. Huyser, Michelle Huyser, Michael J. Green, Desmond A. Young, and Mike S. Sibiya

Abstract: $Al(CF_3SO_3)_3$ is a highly effective catalyst for the ring opening of epoxides with methanol, as well as for the esterification of carboxylic acids with alcohols. Factors that influence the rate of the ring opening of butene oxide with methanol and the esterification of acetic acid with *n*-propanol and ethanol were investigated. It was found that low concentrations (e.g., ~5 ppm) of $Al(CF_3SO_3)_3$ catalyze the ring-opening reactions, whereas considerably higher concentrations are required for esterification reactions. Molecular modeling studies suggest that these differences can be rationalized in terms of the formation energies of the active intermediates of these reactions.

Key words: epoxide, ring opening, esterification, aluminium triflate.

Résumé : Le $Al(CF_3SO_3)_3$ est un catalyseur très efficace pour effectuer des ouvertures de cycles d'époxydes avec le méthanol ainsi que pour l'estérification d'acides carboxyliques par les alcools. On a étudié les facteurs qui influencent la vitesse d'ouverture de cycle de l'oxyde de butène par le méthanol et d'estérification de l'acide acétique par l'éthanol et le propan-1-ol. On a trouvé que, à de faibles concentrations, environ 5 ppm, le $Al(CF_3SO_3)_3$ catalyse les réactions d'ouverture de cycle alors que des concentrations beaucoup plus élevées sont nécessaires pour les réactions d'estérification. Des études de modélisation moléculaire suggèrent que ces différences peuvent être rationalisées en fonction des énergies de formation des intermédiaires actifs de ces réactions.

Mots clés : époxyde, ouverture de cycle, estérification, triflate d'aluminium.

[Traduit par la Rédaction]

Introduction

Esterification reactions between alcohols and carboxylic acids and ring-opening reactions of epoxides with alcohols have been successfully carried out for many decades. Traditionally, esterification reactions have been acid-catalyzed using mineral acids, e.g., HCl and H_2SO_4, as well as organic acids including *p*-toluene sulfonic acid and methane sulfonic acid. Epoxide ring-opening reactions can be either base- or acid-catalyzed (1).

In recent years, the use of triflate salts (also known as trifluoromethane sulfonate salts) as catalysts for both these types of reactions has become increasingly popular. Metal triflates and *N*-heterocyclic base triflates have been employed in the direct esterification of alcohols and carboxylic acids, as well as the transesterification of carboxylic acid esters and alcohols. Examples of the use of these catalysts in esterification reactions include the acylation of alcohols by anhydrides, which is catalyzed by a wide range of metal triflates (e.g., $Yb(CF_3SO_3)_3$, $Bi(CF_3SO_3)_3$, $In(CF_3SO_3)_3$, $Sc(CF_3SO_3)_3$, $Ce(CF_3SO_3)_3$) (2, 3). Rare earth triflates (lanthanide triflates), such as scandium triflate, have been successfully used to catalyze the reaction of alcohols with carboxylic anhydrides, activated esters, mixed anhydrides, acylurea, and *N*-hydroxysuccinimide at low temperatures. Reactions such as the esterification of aliphatic alcohols with carboxylic acids at room temperature and the direct polycondensation of dicarboxylic acids (succinic acids) with diols (ethylene glycol, 1,3-propanediol, and 1,4-butanediol) at 35–180 °C to synthesize polyalkylene succinates have also been reported (4). Scandium triflate has been used as a catalyst for the condensation of carboxylic acids with soluble polymers such as polyethylene glycol in toluene (5). Gadolinium triflate has been found to be a simple and efficient catalyst for the acetylation of alcohols and amines using acetic anhydride at ambient temperatures (6). Furthermore, the selective preparation of secondary esters from terminal *vic*-diols has successfully been achieved in a one-pot synthesis via the $Yb(CF_3SO_3)_3$ catalyzed formation and partial hydrolysis of cyclic orthoesters (7). *N*-Heterocyclic base triflates (e.g., diphenylammonium triflate (DPAT)) have been found to be excellent catalysts for sterically hindered esterification reactions in specific fluorous media under mild conditions using equimolar amounts of carboxylic acids and

Received 22 December 2004. Published on the NRC Research Press Web site at http://canjchem.nrc.ca on 22 July 2005.

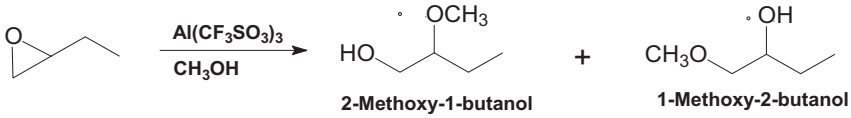
Y.M. Terblans,[2] J.J. Huyser,[3] M. Huyser, M.J. Green, D.A. Young, and M.S. Sibiya. Homogeneous Catalysis and Organic Synthesis, SASOL Technology (Pty) Ltd., Research and Development Division, SASOL, 1 Klasie Havenga Road, Sasolburg, 1947, South Africa.

[1]This article is part of a Special Issue dedicated to Professor Howard Alper.

[2]Corresponding author (e-mail: yvette.terblans@sasol.com).
[3]Corresponding author (e-mail: johan.huyser@sasol.com).

 doi: 10.1139/V05-098 © 2005 NRC Canada

Scheme 1. Ring opening of butene oxide with methanol.



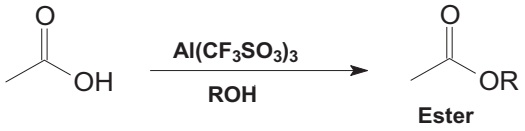
alcohols (8), as well as for the transesterification of carboxylic acid esters with a slight excess of alcohols via the use of trimethylsilyl chloride (TMSCl) as a co-catalyst (9). Other organic base triflates that have successfully been employed in esterification reactions include 4-(benzylaminocarbonyl)diphenylammonium triflate (BDPAT) (10) and polymer-supported 4-aminoforoyldiphenylammonium triflate (PS-AFDPAT) (11).

IR thermography has been used to screen the catalytic acitivity of rare earth triflates (e.g., $Eu(CF_3SO_3)_3$, $La(CF_3SO_3)_3$, $Lu(CF_3SO_3)_3$, $Nd(CF_3SO_3)_3$, $Sm(CF_3SO_3)_3$, $Sc(CF_3SO_3)_3$, $Y(CF_3SO_3)_3$, and $Ce(CF_3SO_3)_4$) for the ring opening of epoxides by alcohols as well as the Baeyer–Villiger oxidation of cyclobutanones with hydrogen peroxide. In the case of the ring opening of epoxides, scandium triflate was found to be an exceptionally active catalyst, whereas in the case of the Baeyer–Villiger oxidation, it was again the most active, followed by neodymium triflate (12). Furthermore, it has been reported that $Yb(CF_3SO_3)_3$ catalyzes intermolecular ring-opening reactions of epoxides with alcohols to give β-alkoxy alcohols in good to high yields with high regio- and stereoselectivity (13).

Aluminium triflate has been used as a catalyst in organic synthesis for reactions such as the ring opening of epoxides in the presence of alcohols or amines (14–16), Friedel–Crafts acylation and alkylation (17, 18), the epoxidation of olefins with iodosylbenzene (19), and the preparation of esters and lactones (20). It has also been used as an initiator for cationic polymerization (21) and as co-catalyst in the polymerization of olefins (22).

We now report on the considerable difference in the required concentration of $Al(CF_3SO_3)_3$ vs. $KOCH_3$ as catalysts for the ring opening of butene oxide (BuO) with methanol (MeOH) (Scheme 1) on the one hand, and the similar concentration requirements of $Al(CF_3SO_3)_3$ and *p*-TSA as catalysts for the esterification of *n*-propanol (*n*-PrOH) or ethanol (EtOH) with acetic acid (Scheme 2) on the other hand. Low $Al(CF_3SO_3)_3$ concentrations (e.g., ~5 ppm) are sufficient to obtain excellent conversions and high reaction rates when performing the ring-opening reaction of butene oxide with methanol, whereas much higher catalyst concentrations (e.g., ~1000 ppm or higher) are needed to obtain similar results for the $KOCH_3$ catalysed reactions. A related observation was that both acid (*p*-TSA) and $Al(CF_3SO_3)_3$ catalysed esterification reactions of propanol and (or) ethanol with acetic acid require similar catalyst concentrations of ~1000 ppm to get reasonable activities. A molecular modeling study was undertaken with a view to rationalizing the experimental observations and to postulate a reasonable explanation for the low levels of $Al(CF_3SO_3)_3$ needed in the ring-opening reactions. These calculations showed that ΔH_f values for the formation of the catalytically active species in the potassium methoxide and aluminium triflate catalyzed ring-opening reactions differ significantly, with ΔH_f = –3.3 kcal/mol (1 cal = 4.184 J) for the aluminium triflate reaction and ΔH_f = +12.8 kcal/mol for the potassium methoxide ring-opening reaction. It appears that the differences in catalyst concentrations required for the reactions under investigation are in line with the differences in the formation energies of the active intermediate.

Scheme 2. Esterification of acetic acid with ethanol or *n*-propanol.



ROH = CH_3CH_2OH or $CH_3CH_2CH_2OH$

Experimental

Materials

Unless otherwise stated, all chemicals used in this study were purchased from Sigma-Aldrich and used without further purification. Aluminium triflate was prepared as described in the literature (16). For the ring-opening reactions, a stock solution of 500 ppm $Al(CF_3SO_3)_3$ was prepared in methanol and the desired quantity thereof was weighed for every reaction. In the case of the esterification reactions, a fresh catalyst solution (of the desired concentration) was prepared in the alcohol substrate prior to each reaction.

Kinetic reactions

Kinetic reactions were carried out in a Parr autoclave. The catalyst concentration was varied between 0 and 10 ppm for the ring-opening reactions and between 10 and 5000 ppm for the esterification reactions. In most cases, the esterification reactions were allowed to proceed to equilibrium, since none of the reaction products (including water) were removed. Gas chromatography was performed on a Shimadzu GC-17A, equipped with a flame ionization detector and a PONA capillary column (50 m × 0.21 mm × 0.5 μm). Each sample was weighed into a GC vial and heptane was used as an internal standard.

Typical experimental procedure for the ring opening of butene oxide

Methanol (192.25 g, 6.00 mol) and butene oxide (72.11 g, 1.00 mol) were combined in a 300 mL Parr reactor. On closing, the reactor was degassed and flushed with nitrogen to remove all the air present. This flushing procedure was repeated three times.

A catalyst bomb was placed under vacuum prior to the run. The stock solution was weighed out (2.644 g, 5 ppm) and transferred via a syringe to this bomb, which was then connected to the inlet of the autoclave. A high-pressure nitrogen line was connected to the opposite side of the catalyst

© 2005 NRC Canada

bomb after which stirring of the reactor commenced. The reactor was subsequently heated to 100 °C after which the catalyst solution was discharged into the reactor and a sample taken immediately (0 min) and weighed. The sample was weighed to determine the amount removed from the reactor. Further sampling from the reactor was carried out at the following intervals; 5, 10, 15, 20, 30, 60, and 120 min, and each sample weighed. A satd. NaOH – water solution (0.5 mL) was added to all of the samples to quench the catalyst.

Typical experimental procedure for the esterification reaction between* n-*propanol and acetic acid

Acetic acid (60.10 g, 1.00 mol) and propanol (60.21 g, 1.00 mol) were combined in a 300 mL Parr reactor. The reactor was closed and heated to an operating temperature of 100 °C while stirring at 900 rpm. Upon reaching this temperature, a solution of $Al(CF_3SO_3)_3$ (0.05 g dissolved in 10.0 g of propanol, 5000 ppm) was charged into the reactor using a syringe. A sample was taken immediately and thereafter every 5 min for the first 30 min, after which samples were taken every 30 min. All samples were weighed.

Molecular modeling

All geometries were optimized with the DMol[3] DFT code in MaterialsStudio 3.0 (Accelrys, Inc.) (23) by applying the all electron nonlocal GGA/RPBE/DNP method, employing a med integration grid and 4.2 Å orbital cut-off values. All reported energies are electronic energies, which correspond to *G* at 0 K.

Results and discussion

The epoxide ring-opening and esterification reactions were probed experimentally, as well as via molecular modeling. The ring-opening reaction of butene oxide with methanol was studied at different catalyst concentrations, temperatures, and methanol – butene oxide molar ratios. For comparison, the epoxide ring opening was also carried out with a base catalyst KOMe. The esterification reaction of acetic acid with *n*-propanol and ethanol was studied at different catalyst concentrations, whereas the influence of substrate concentrations was studied by varying the ethanol – acetic acid molar ratio.

A molecular modeling study was carried out to assist in formulating a reasonable explanation for the low levels of $Al(CF_3SO_3)_3$ needed to catalyse the ring-opening reactions compared to using $KOCH_3$ as catalyst. In addition, calculations were carried out for the $Al(CF_3SO_3)_3$ and Brønsted acid catalysed esterification reactions.

Model substrates were used for the calculations to save on computational time. Propylene oxide and methanol were used as models for the ring-opening reactions and acetic acid and methanol for the esterification reactions. In the calculations involving $Al(CF_3SO_3)_3$, possible stabilization effects involving, for example, methanol coordination or other solvation effects were not taken into consideration. $KOCH_3$ was used as the model for the base-catalysed epoxide ring-opening reactions and a protonated AcOH–MeOAc complex used to describe the acid-catalysed esterification reaction.

The limited objective of these simplified modelling studies was to calculate formation energies from geometry optimizations with a view to rationalizing the experimental results rather than the more time consuming location of transition states to obtain activation energies.

Table 1. Conversion of butene oxide (mol%) at different $Al(CF_3SO_3)_3$ catalyst concentrations.

	Catalyst concentration (ppm)			
Time (min)	0	1	5	10
5	3.00	16.00	74.00	85.00
10	6.00	36.00	97.00	100.00
15	11.00	46.00	100.00	100.00
20	16.00	50.00	100.00	100.00
30	21.00	61.00	100.00	100.00
60	29.00	77.00	100.00	100.00
120	41.00	88.00	100.00	100.00

Note: T = 100 °C, MeOH:BuO = 6:1.

Table 2. Conversion of butene oxide (mol%) at different temperatures.

	Temperature (°C)			
Time (min)	60	80	100	120
5	16.05	16.68	59.18	88.80
10	36.43	54.31	94.39	100.00
15	53.47	79.95	99.55	100.00
20	69.64	81.95	100.00	100.00
30	74.33	89.17	100.00	100.00
60	88.50	93.32	100.00	100.00
120	95.86	97.15	100.00	100.00

Note: $Al(CF_3SO_3)_3$ catalyst concentration = 5 ppm, MeOH:BuO = 6:1.

Ring opening of butene oxide

The conversion of butene oxide was calculated for each reaction carried out with $Al(CF_3SO_3)_3$ and KOH as the catalyst and the data are presented in Tables 1–4. Graphs obtained from the data are shown in the Supplementary material to the publication.[4]

In the molecular modelling study, two steps in the catalytic cycle of the ring-opening reaction with $Al(CF_3SO_3)_3$ and $KOCH_3$ were considered, i.e., the ring-opening step, as well as the regeneration of the active intermediate; these steps are shown in Schemes 3 and 4.

As can be seen from the data in Table 1, butene oxide was converted to the corresponding glycol ethers with $Al(CF_3SO_3)_3$ concentrations of 10 ppm or less. When using 10 ppm of $Al(CF_3SO_3)_3$, 100% conversion was achieved within 10 min of reaction time. With a very low $Al(CF_3SO_3)_3$ concentration of 1 ppm, 88% conversion was achieved within 2 h. In all of these reactions, both isomers of the glycol ether, i.e., 1-methoxy-2-butanol and 2-methoxy-1-butanol, were formed as the main products.

[4] Supplementary data for this article are available on the Web site or may be purchased from the Depository of Unpublished Data, Document Delivery, CISTI, National Research Council Canada, Ottawa, ON K1A 0S2, Canada. DUD 3692. For more information on obtaining material refer to http://cisti-icist.nrc-cnrc.gc.ca/irm/unpub_e.shtml.

© 2005 NRC Canada

Table 3. Conversion of butene oxide (mol%) at different methanol – butene oxide ratios with $Al(CF_3SO_3)_3$.

	Methanol – butene oxide ratio					
Time (min)	4	6	8	10	12	14
5	76.69	59.18	57.44	55.53	56.75	57.03
10	100.00	94.39	96.57	96.37	96.20	92.55
15	100.00	100.00	100.00	100.00	100.00	100.00
20	100.00	100.00	100.00	100.00	100.00	100.00
30	100.00	100.00	100.00	100.00	100.00	100.00
60	100.00	100.00	100.00	100.00	100.00	100.00
120	100.00	100.00	100.00	100.00	100.00	100.00

Note: T = 100 °C, catalyst concentration = 5 ppm.

Table 4. Conversion of butene oxide (mol%) at different methanol – butene oxide ratios with KOH.

	Methanol – butene oxide ratio	
Time (min)	4	6
5	70.01	50.72
10	89.65	71.65
15	98.48	85.12
20	99.42	88.83
30	99.70	92.28
60	99.96	96.89

Note: T = 160 °C, catalyst concentration = 100 ppm.

These products were formed in a ratio of approximately 1:1, with the yield of each ranging from 40%–47%. By-products like dimers, diols, and in some instances trimers were also formed during these reactions. All products were identified using GC–MS via comparison with the literature data (16).

The effect of temperature on the ring-opening reaction of butene oxide was as expected, in that the reaction rates and conversions increased as the temperature was increased (Table 2). It was found that as the reaction temperature was increased, the formation of by-products, especially dimers and trimers, increased over time.

It is seen from the data in Table 3 that as the ratio of MeOH:BuO was increased, the rate of the reaction decreased. As the ratio was increased from 4 to 6, a decrease in the rate was clearly observed. The decrease in the rate became less as the ratio was further increased to 8. With even further increases from 8 to 14, the decrease in the rate became even less. Similarly, when KOH was used as the catalyst, it was seen that as the ratio of MeOH:BuO was increased, the rate of the reaction decreased. However, these reactions had to be carried out with higher catalyst concentrations (100 ppm KOH compared to 10 ppm $Al(CF_3SO_3)_3$) and at higher reaction temperatures (160 °C for KOH compared to 100 °C for $Al(CF_3SO_3)_3$). An explanation for this decrease in rate with an increase in MeOH:BuO ratio could be that the transfer of the $Al(CF_3SO_3)_3$ to BuO to form the active intermediate is dependant on the concentration of BuO in the reaction mixture. Since the increase in the MeOH:BuO ratio will lead to a lowering in BuO concentration, it is to be expected that a drop in rate will be seen (Scheme 3).

The mechanism of the ring-opening reaction involves the coordination of the epoxide oxygen to the aluminum, thus forming the active intermediate, a strained three-membered epoxide ring. This is seen when geometry optimized structures of a "free" epoxide are compared with those of an epoxide coordinated to the aluminum. A C—O bond lengthening from 1.44 to 1.477 Å (O—C_α) and 1.507 Å (O—C_β) is observed when Al is coordinated. Nucleophilic attack by methanol can then take place on either the C_α or C_β position. Electronic factors will favor the C_β position (the O—C_β is longer than the O—C_α bond) while steric factors will favor the C_α position (less substituted). In the case of methanol as the nucleophile, these two factors contribute equally, as is evident by the product distribution of approximately 1:1 (Scheme 5).

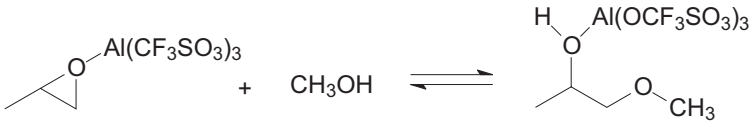
As can be expected, the formation energies for the ring-opening reactions are highly exothermic because of the release of the strained three-membered epoxide ring. In line with the Hammond postulate, it would be reasonable to assume that the activation energies for the ring-opening reactions would be low (the transition state for the ring-opening reactions should be very early and resemble the reagents because of the highly exothermic reaction). The interesting aspect about the base-catalysed ring-opening reaction is the high stability of the potassium salt of the product. The significance of this is that the regeneration of the active intermediate, $KOCH_3$, represents a highly endothermic reaction. This will explain the high levels of $KOCH_3$ necessary to obtain a reasonable rate. The ring-opening reaction itself will be facile and the rate-determining step will be the regeneration of the $KOCH_3$ species to start the catalytic cycle again (Scheme 4). The $Al(CF_3SO_3)_3$ catalysed reaction, on the other hand, does not have such a thermodynamic sink with the regeneration of the activated epoxide ring coordinated to the $Al(CF_3SO_3)_3$ being only a slightly exothermic reaction (Scheme 3). Together with the low activation energy for the ring-opening reaction, this will explain the low levels of $Al(CF_3SO_3)_3$ necessary to obtain very high rates. A reasonable explanation would then be that the difference in catalyst concentration needed for the ring-opening reaction is due to the highly endothermic and (or) unfavourable reaction for the regeneration of the $KOCH_3$ species compared to the facile reaction for the $Al(CF_3SO_3)_3$.

Esterification reaction

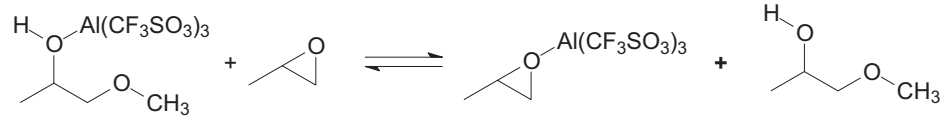
The conversion of acetic acid at different acid catalyst concentrations with *n*-propanol is shown in Table 5 and for ethanol in Table 6. The results for the variation of the acetic acid – ethanol molar ratio are shown in Table 7. Graphs ob-

© 2005 NRC Canada

Scheme 3. Formation energies for the $Al(CF_3SO_3)_3$ catalysed ring-opening reaction (1 cal = 4.184 J).



ΔH_f = -27.3 kcal/mol

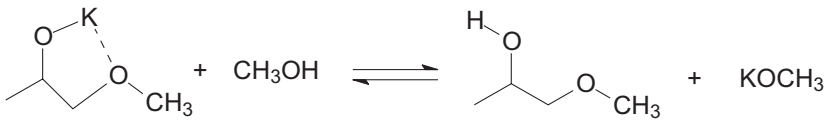


ΔH_f = -3.3 kcal/mol

Scheme 4. Formation energies for the $KOCH_3$ catalysed ring-opening reaction (1 cal = 4.184 J).

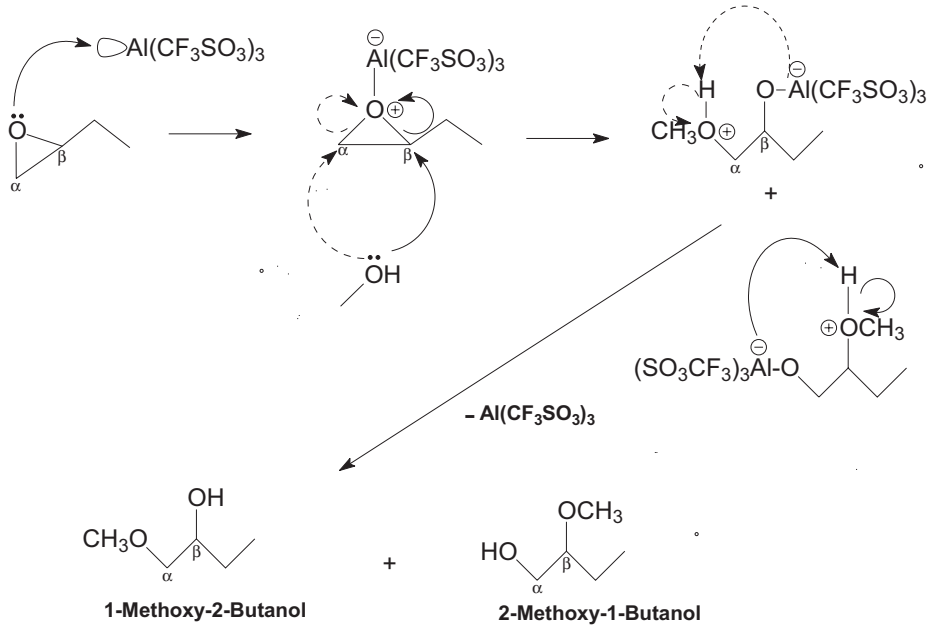


ΔH_f = -36.8 kcal/mol



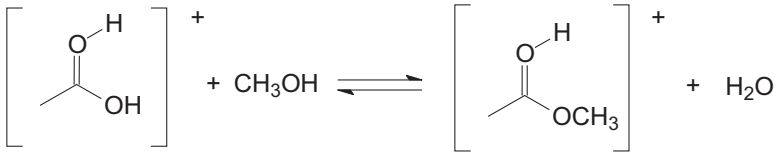
ΔH_f = 12.8 kcal/mol

Scheme 5. Reaction mechanism for butene oxide ring opening.

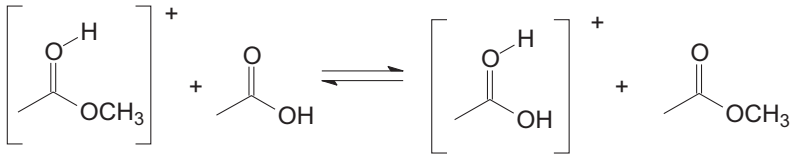


© 2005 NRC Canada

Scheme 6. Formation energies for the acid-catalysed esterification reaction (1 cal = 4.184 J).



ΔH_f = -8.8 kcal/mol



ΔH_f = -1.8 kcal/mol

Table 5. Conversion of acetic acid (mol%) at different $Al(CF_3SO_3)_3$ catalyst concentrations with *n*-propanol.

	Catalyst concentration (ppm)			
Time (min)	5000	500	100	10
10	50.73	26.73	19.17	7.38
20	57.90	35.27	22.50	8.94
30	60.78	41.18	29.79	12.12
60	66.04	—	—	—
90	—	55.94	41.82	25.84
150	66.20	60.53	51.41	33.59
210	66.6	61.21	56.92	38.64

Note: T = 100 °C, *n*-PrOH : acetic acid = 1:1.

Table 6. Conversion of acetic acid (mol%) at different $Al(CF_3SO_3)_3$ catalyst concentrations with ethanol.

	Catalyst concentration (ppm)		
Time (min)	500	100	10
30	15.72	10.75	8.72
60	30.07	20.76	19.89
120	43.37	35.44	22.69
180	53.03	48.36	26.24

Note: T = 100 °C, EtOH : acetic acid = 1:1.

tained from the data are shown in the Supplementary material[4] to the publication.

In the molecular modelling study, two steps in the catalytic cycle of the esterification reaction with $Al(CF_3SO_3)_3$ and an acid were considered, i.e., the esterification step as well as the regeneration of the active intermediate; these steps are shown in Schemes 6 and 7.

As esterification reactions are equilibrium reactions and are known to proceed very slowly in the absence of an acid catalyst (1), the addition of small quantities of the catalyst will ensure that they reach equilibrium much faster. This can clearly be seen upon comparing the data for the esterification reaction in Tables 5 and 6. It is evident that equilibrium (equilibrium conversion ≅ 66%) is reached after 1 h,

Table 7. Conversion of acetic acid (mol%) with $Al(CF_3SO_3)_3$ catalyst at different ethanol – acetic acid ratios.[a]

	Ethanol – acetic acid ratio		
Time (min)	1	4	8
5	10.02	28.47	47.82
10	15.10	34.28	57.21
15	20.22	50.65	63.04
20	25.43	55.72	71.54
25	30.05	59.94	77.67
30	32.97	64.99	84.41
60	40.07	79.65	93.20
90	45.10	85.43	97.80
120	46.21	87.46	98.68
150	49.80	90.46	98.63

Note: T = 100 °C, catalyst concentration = 5000 ppm.

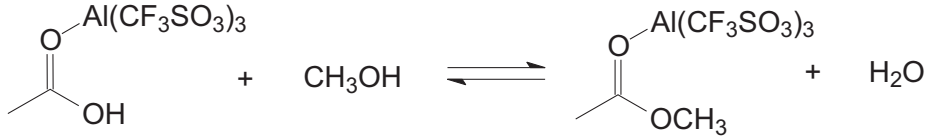
[a]These reactions were run to completion, hence the yields of ethyl acetate were ≅98%.

when using 5000 ppm of $Al(CF_3SO_3)_3$ for the esterification reaction of acetic acid and *n*-propanol. However, equilibrium is not reached for this reaction even after 210 min when using 10 ppm of the catalyst. Similar results were observed for the esterification reaction of acetic acid and ethanol when 10 ppm of catalyst is used, as equilibrium is not reached after 180 min. The main products that were formed in the esterification reactions are the corresponding esters: *n*-propyl acetate in the case of *n*-propanol and ethyl acetate in the case of ethanol. The equilibrium yields of the main products ≅64%. Some by-products were also formed in low yields; these were identified as ethers (e.g., diethyl ether or dipropyl ether) via GC–MS.

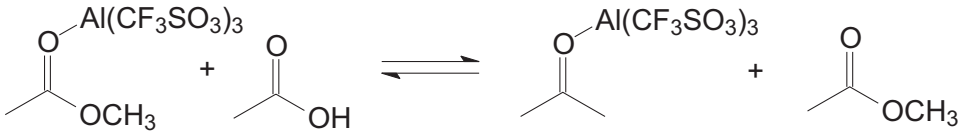
In the esterification reaction, electron density is donated from the carbonyl oxygen atom of the carboxylic acid by coordinating to the aluminum, thus forming the active intermediate. Geometry optimized structures of the free acetic acid compared to one coordinated to aluminum show the C=O bond lengthening from 1.208 to 1.245 Å. Nucleophilic attack by the methanol then takes place on the carbonyl carbon of the carboxylic acid (Scheme 8).

© 2005 NRC Canada

Scheme 7. Formation energies for the $Al(CF_3SO_3)_3$ catalysed esterification reaction (1 cal = 4.184 J).

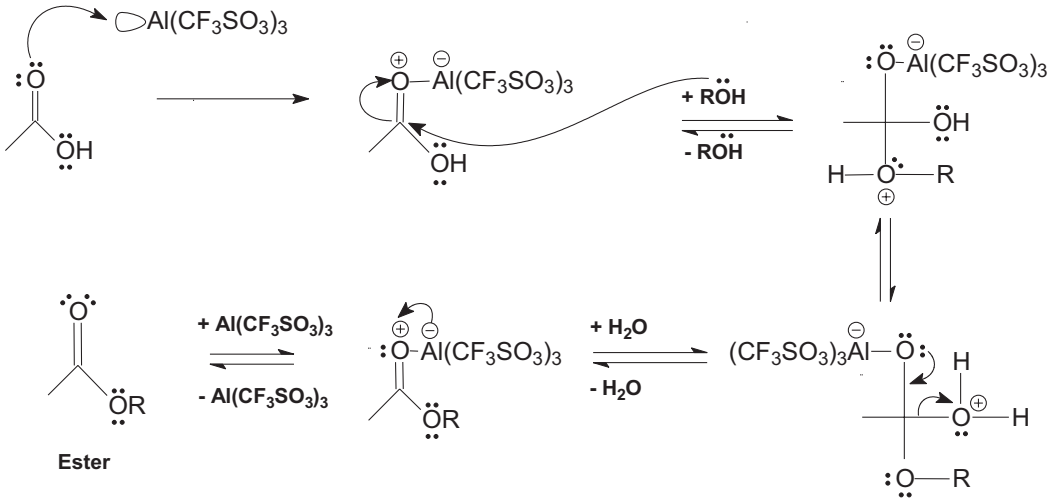


ΔH_f = -4.2 kcal/mol



ΔH_f = -2.8 kcal/mol

Scheme 8. Reaction mechanism for esterification.



Formation energies for the esterification reactions are, however, only slightly endothermic. In line with the Hammond postulate, it would thus be reasonable to assume the activation energies for the esterification reactions to be higher than those for the ring-opening reactions (ΔH_f = –4.2 kcal/mol for the esterification compared to ΔH_f = –27.3 kcal/mol for the ring-opening reaction).

Unlike the epoxide ring-opening reaction, the esterification reaction does not show any discrepancy between the $Al(CF_3SO_3)_3$ and the acid-catalysed reactions. Similar formation energies are observed for both reactions and thus similar catalyst concentrations should give similar reaction rates; this was in fact the case.[5] The only difference will be the slight variation in the energy of the transition state for the $Al(CF_3SO_3)_3$ and acid-catalysed reaction.

Conclusion

The ring-opening reaction of butene oxide with methanol is easily achieved at low concentrations (10 ppm or less) of $Al(CF_3SO_3)_3$ as the catalyst. When using 10 ppm of $Al(CF_3SO_3)_3$, 100% conversion of butene oxide is achieved within 10 min. This is, however, not the case for the $KOCH_3$ catalysed ring-opening reaction, which requires at least a 1000 ppm catalyst concentration to achieve a reasonable rate. A plausible explanation is the energy difference in the regeneration of the active intermediate that is unfavourable for the $KOCH_3$ catalysed reaction, implying the necessity of higher catalyst loading to get similar rates. Esterification of acetic acid with *n*-propanol and (or) ethanol gave similar energies for both acid and $Al(CF_3SO_3)_3$ catalysed reactions,

[5] On comparing the conversion of acetic acid using $Al(CF_3SO_3)_3$ and a conventional acid catalyst in the esterification of 1-methoxy-2-propanol with acetic acid, it was seen that the reaction rate with $Al(CF_3SO_3)_3$ was only slightly faster than that with the acid catalyst when the same catalyst concentration was used.

© 2005 NRC Canada

thus explaining the need for similar catalyst loadings to give similar rates

Acknowledgements

The authors would like to thank SASOL Technology (Pty) Ltd. for the opportunity to publish this work. Furthermore, we wish to thank our colleagues Dr. Johntho Dixon, Mr. Dave Morgan, and Dr. Matthew Overett for their inputs and suggestions during proof reading of this paper. Lastly, we also acknowledge Professor Cedric Holzapfel from the Rand Afrikaans University (RAU), Johannesburg, South Africa for his valuable comments and suggestions.

References

1. T.W. Graham Solomons. Organic chemistry. 5th ed. John Wiley and Sons Inc., New York. 1992. p. 778.
2. R. Dumeunier and I.E. Markó. Tetrahedron Lett. **45**, 4669 (2004).
3. N. Iranpoor and M. Shekarriz. Bull. Chem. Soc. Jpn. **72**, 455 (1999).
4. T. Akinori, O. Yoshika, I. Yoshitaka, I. Yoshihito, and H. Tadamichi. Macromolecules, **36**, 1772 (2003).
5. S. Chandrasekhar, S. Shameen Sultana, Ch. Narsihmulu, J.S. Yadav, R. Gree, and J.C. Guillemin. Tetrahedron Lett. **43**, 8335 (2002).
6. R. Alleti, M. Perambuduru, S. Samantha, and V.P. Reddy. J. Mol. Catal. A: Chem. **226**, 57 (2004).
7. M. Ikejiri, K. Miyashita, T. Tsunemi, and T. Imanishi. Tetrahedron Lett. **45**, 1243 (2004).
8. B. Gacem and G. Jenner. Tetrahedron Lett. **44**, 1391 (2003).
9. K. Wakasugi, T. Misaki, K. Yamada, and Y. Tanabe. Tetrahedron Lett. **41**, 5249 (2000).
10. M. Lei, C. Ma, and Y.-G. Wang. Chin. Chem. Lett. **13**, 487 (2002).
11. M. Lei, C. Ma, and Y.-G. Wang. Chin. J. Chem. **19**, 1309 (2001).
12. A. Berkessel, E. Ashkenazi, and M.R.M. Andreae. Appl. Catal. A, **254**, 27 (2003).
13. S. Kobayashi, M. Sugiura, H. Kitagawa, and W.W.-L. Lam. Chem. Rev. **102**, 2227 (2002).
14. M.J. Green. US Patent 4 605 769, 12 August 1986.
15. M.J. Green. US Patent 4 762 952, 9 August 1988.
16. D. Falgoux, D. Simoulin, and M. Pascal-Mousselard. US Patent 4 543 430, 24 September 1985.
17. G.A. Olah, O. Farroq, S.M.F. Farina, and J.A. Olah. J. Am. Chem. Soc. **110**, 2560 (1988).
18. S. Kobayashi and I. Komoto. Tetrahedron, **56**, 6463 (2000).
19. Y. Yang, F. Diederich, and J.S. Valentine. J. Am. Chem. Soc. **112**, 7826 (1990).
20. Y. Ishii and T. Nakano. EP 1078922 A1, 2001.
21. O. Farooq and W. Minn. US Patent 5 084 586, 28 January 1992.
22. S.J. Mclain and J. Feldman. WO 9803559, 29 January 1998.
23. (*a*) B. Delley. J. Chem. Phys. **92**, 508 (1990); (*b*) B. Delley. J. Chem. Phys. **100**, 6107 (1996); (*c*) B. Delley. J. Chem. Phys. **113**, 7756 (2000).

© 2005 NRC Canada

Reaction of $[Fe(CO)_4(\eta^2\text{-}Me_3SiC{\equiv}CSiMe_3)]$ with PMe_3 — CO rather than alkyne substitution[1]

James N.L. Dennett, Michael J. Ferguson, Robert McDonald, and Josef Takats

Abstract: Reaction of $[Fe(CO)_4(\eta^2\text{-BTMSA})]$ (**1**) (BTMSA = $Me_3SiCCSiMe_3$) with trimethylphosphine proceeds by stepwise loss of CO ligands yielding $[Fe(CO)_3(PMe_3)(\eta^2\text{-BTMSA})]$ (**2**) and $[Fe(CO)_2(PMe_3)_2(\eta^2\text{-BTMSA})]$ (**3**), respectively. This demonstrates the CO dissociative nature of substitution in **1** toward PMe_3, as established in analogous $M(CO)_4(\eta^2\text{-alkyne})$ (M = Fe, Ru, Os) compounds. The structures of all three compounds have been determined by X-ray crystallography to assess the effect of CO substitution by PMe_3 on the metal–alkyne bonding in these molecules.

Key words: iron, carbonyl, alkyne, substitution, phosphine, steric effects.

Résumé : La réaction du $[Fe(CO)_4(\eta^2\text{-BTMSA})]$ (**1**) (BTMSA = $Me_3SiCCSiMe_3$) avec la triméthylphosphine se produit avec des pertes successives de ligands CO qui conduisent respectivement aux complexes $[Fe(CO)_3(PMe_3)(\eta^2\text{-BTMSA})]$ (**2**) et $[Fe(CO)_2(PMe_3)_2(\eta^2\text{-BTMSA})]$ (**3**). Ces résultats confirment la nature dissociative du CO qui permet de le substituer dans le composé **1** par des groupes PMe_3, tel qu'il avait été établi avec les analogues $M(CO)_4(\eta^2\text{-alcyne})$ (M = Fe, Ru, Os). Les structures des trois composés ont été déterminées par cristallographie aux rayons X afin d'évaluer l'effet de la substitution du CO par un PMe_3 sur la liaison métal–alcyne de ces molécules.

Mots clés : fer, carbonyle, alcyne, substitution, phosphine, effets stériques.

[Traduit par la Rédaction]

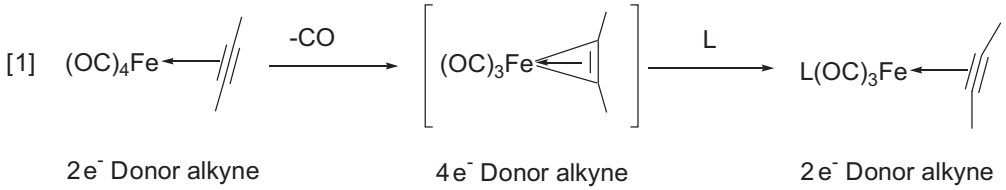
Introduction

Work from our laboratories (1) has conclusively demonstrated the intermediacy of $[Fe(CO)_4(\eta^2\text{-alkyne})]$ species in the iron carbonyl mediated alkyne–CO coupling reactions first investigated by Wender and co-workers (2) and Hübel and co-workers (3). We have also shown that the spectacular enhancement of CO lability toward substitution in these, and ruthenium and osmium analogues, was due to the ability of the alkyne ligand to act as a four-electron donor and hence stabilize the CO-dissociated intermediate in the reaction (4) (eq. [1]).

Thus, it seemed surprising that $[Fe(CO)_4(\eta^2\text{-BTMSA})]$ (**1**), the first well-characterized simple iron–carbonyl–alkyne, reported by Pannell and Crawford (5) more than 30 years ago, reacted with PPh_3 to give only bis(triphenyl)phosphine tricarbonyl iron ($Fe(CO)_3(PPh_3)_2$, eq. [2]) without any evidence of $[Fe(CO)_3(PPh_3)(\eta^2\text{-BTMSA})]$. This despite the fact that the mass spectrum of the molecule showed stepwise loss of CO groups from the parent molecular ion and carbonyl-free $Fe(BTMSA)^+$ as the base ion fragment indicating that, under mass spectrometry conditions, the Fe–BTMSA bonding is stronger than that of Fe–CO (5).

$$[2]\qquad [Fe(CO)_4(BTMSA)] + 2PPh_3 \rightarrow [Fe(CO)_3(PPh_3)_2] + CO + BTMSA$$

In view of our demonstration that substitution reactions of $[Fe(CO)_4(\eta^2\text{-alkyne})]$ compounds proceed by initial CO loss, the failure to detect BTMSA-containing products by Pannell and Crawford may have been due to the bulky nature of the PPh_3 ligand, which promotes loss of the also bulky BTMSA



Received 23 August 2004. Published on the NRC Research Press Web site at http://canjchem.nrc.ca on 22 July 2005.

This paper is dedicated to Howard Alper for his outstanding contributions and exemplary service to the Canadian chemistry community.

J.N.L. Dennett and J. Takats.[2] Department of Chemistry, University of Alberta, Edmonton, AB T6G 2G2, Canada.
M.J. Ferguson and R. McDonald. Department of Chemistry, X-Ray Crystallography Laboratory, University of Alberta, Edmonton, AB T6G 2G2, Canada.

[1]This article is part of a Special Issue dedicated to Professor Howard Alper.
[2]Corresponding author (e-mail: joe.takats@ualberta.ca).

 doi: 10.1139/V05-097 © 2005 NRC Canada

moiety from the putative $[Fe(CO)_3(PPh_3)(\eta^2\text{-BTMSA})]$ initial product via addition of the second PPh_3 ligand.

To test this hypothesis, the reaction of **1** with the sterically less-demanding PMe_3 was investigated and we report here that the substitution reaction does indeed proceed by stepwise loss of CO to yield $[Fe(CO)_3(PMe_3)(\eta^2\text{-BTMSA})]$ (**2**) and $[Fe(CO)_2(PMe_3)_2(\eta^2\text{-BTMSA})]$ (**3**), respectively.

Experimental section

All reactions were carried out using standard Schlenk techniques under a dry and oxygen-free nitrogen atmosphere. Hydrocarbon solvents were dried over CaH_2 and distilled under nitrogen using normal procedures prior to use. $[Fe(CO)_4(\eta^2\text{-BTMSA})]$ (**1**) was prepared as described in the literature (5). Carbon-13 carbon monoxide (Isotec, Inc.) and trimethylphosphine (Aldrich) were used as supplied. IR solution spectra (KBr cell) were recorded on a Bomem MB-100 FT IR spectrometer. NMR samples were prepared under a nitrogen atmosphere. NMR spectra were recorded on a Bruker AM-400 MHz operating at 400 MHz for ^1H, 161.9 MHz for ^{31}P, and 100.6 MHz for ^{13}C NMR nuclei. Elemental analyses were performed by the Microanalytical Laboratory, Department of Chemistry, University of Alberta. Electron impact (EI) mass spectra were recorded on a AEI/Kratos MS 50 spectrometer.

Preparation of $[Fe(CO)_3(PMe_3)(\eta^2\text{-BTMSA})]$ (2)

Trimethylphosphine (24.6 μL, 0.238 mmol) was added to a hexane solution (25 mL) of $[Fe(CO)_4(\eta^2\text{-BTMSA})]$ (**1**, 64.0 mg, 0.189 mmol) at 10 °C and the solution stirred for 5 h. The solvent was removed in vacuo at –20 °C. The yellow residue was dissolved in pentane and the solution filtered, concentrated, and cooled to –80 °C. Yellow crystals of $[Fe(CO)_3(PMe_3)(\eta^2\text{-BTMSA})]$ (**2**, 56.0 mg) were obtained in 76.6% yield. IR (*n*-pentane, cm^{-1}): υ_{CO} 2018 (s), 1949 (s), 1920 (s); $\upsilon_{C\equiv C}$ 1823 (w/br). ^1H NMR (CD_2Cl_2, –70 °C) δ: 1.01 (d, $^2J_{PH}$ = 8 Hz, 9H, $P(CH_3)_3$), 0.22 (s/br, 18H, $Si(CH_3)_3$). $^{13}C\{^1H\}$ NMR (CD_2Cl_2, –70 °C) δ: 220.9 (d, $^2J_{CP}$ = 35 Hz, $2CO_{eq}$), 214.6 (d, $^2J_{CP}$ = 59 Hz, CO_{ax}), 99.5 (s, $CSiMe_3$), 16.5 (d, $^1J_{CP}$ = 28 Hz, $P(CH_3)$), –0.3 (s, $Si(CH_3)$). $^{31}P\{^1H\}$ NMR (CD_2Cl_2, room temperature (r.t.)) δ: 22.4 (s). MS (EI, 16 eV) *m/z*: 386 (M^+), 302 (M^+ – 3CO). Anal. calcd. for $C_{14}H_{27}FeO_3P_1Si_2$ (%): C 43.52, H 7.00; found: C 43.23, H 7.09.

$[Fe(^{13}CO)_3(PMe_3)(\eta^2\text{-BTMSA})]$ (2*)

$[Fe(^{13}CO)_3(PMe_3)(\eta^2\text{-BTMSA})]$ (**2***) was prepared by the same procedure using $[Fe(^{13}CO)_4(\eta^2\text{-BTMSA})]$ (**1***) as the starting material. IR (*n*-pentane, cm^{-1}): υ_{CO} 1971 (s), 1902 (s), 1875 (s); $\upsilon_{C\equiv C}$ 1822 (w/br).

Preparations of $[Fe(CO)_2(PMe_3)_2(\eta^2\text{-BTMSA})]$ (3)

Method 1

Trimethylphosphine (2 equiv., 36.0 μL, 0.348 mmol) was added to a hexane solution (25 mL) of $[Fe(CO)_4(\eta^2\text{-BTMSA})]$ (**1**, 59.0 mg, 0.175 mmol) at r.t. and the solution stirred for 2 h. The solvent was removed in vacuo at 0 °C. The yellow residue was dissolved in pentane and the solution filtered, concentrated, and cooled to –80 °C. Yellow-orange crystals of $[Fe(CO)_2(PMe_3)_2(\eta^2\text{-BTMSA})]$ (**3**, 31.5 mg, 41.6%) were formed, which proved suitable for an X-ray crystallographic study.

Method 2

Trimethylphosphine (3.4 μL, 0.033 mmol) was added to a hexane solution (5 mL) of $[Fe(CO)_3(PMe_3)(\eta^2\text{-BTMSA})]$ (**2**, 12.5 mg, 0.0324 mmol) at r.t. and the solution stirred for 2 h. The solvent was removed in vacuo at r.t. The residue was dissolved in pentane and the solution filtered, concentrated, and cooled to –80 °C. Yellow-orange crystals of $[Fe(CO)_2(PMe_3)_2(\eta^2\text{-BTMSA})]$ (**3**, 5.0 mg) were obtained in 35% yield.

Method 3

Excess trimethylphosphine (50.0 μL, 0.483 mmol) was added to a hexane solution (10 mL) of $[Fe(CO)_4(\eta^2\text{-BTMSA})]$ (**1**, 39.0 mg, 0.115 mmol) at r.t. and the solution stirred for 3 h. The solvent was removed in vacuo at r.t. The yellow residue was dissolved in pentane and the solution filtered, concentrated, and cooled to –80 °C. Yellow-orange crystals of $[Fe(CO)_2(PMe_3)_2(\eta^2\text{-BTMSA})]$ (**3**, 30.0 mg) were obtained in 59.9% yield. IR (*n*-pentane, cm^{-1}): υ_{CO} 1930 (m), 1868 (s); $\upsilon_{C\equiv C}$ 1774 (w). ^1H NMR (CD_2Cl_2, r.t.) δ: 1.05 (vt, apparent J_{PH} = 3.7 Hz, 18H, $P(CH_3)_3$), 0.28 (s/br, 18H, $Si(CH_3)_3$). $^{13}C\{^1H\}$ NMR (CD_2Cl_2, r.t.) δ: 225.0 (s/br, *C*O), 116.3 (s, $CSiMe_3$), 18.6 (vt, apparent J_{PC} = 12.5 Hz, $P(CH_3)$), 1.7 (s, $Si(CH_3)$). $^{31}P\{^1H\}$ NMR (CD_2Cl_2, r.t.) δ: 26.6 (s). MS (EI, 16 eV) *m/z*: 434 (M^+), 302 (M^+ – 2CO – PMe_3). Anal. calcd. for $C_{16}H_{36}FeO_2P_2Si_2$ (%): C 44.24, H 8.35; found: C 44.25, H 8.41.

$[Fe(^{13}CO)_2(PMe_3)_2(\eta^2\text{-BTMSA})]$ (3*)

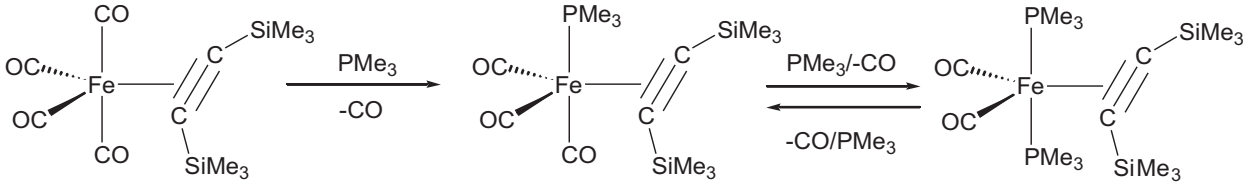
$[Fe(^{13}CO)_2(PMe_3)_2(\eta^2\text{-BTMSA})]$ (**3***) was prepared by method 1 using $[Fe(^{13}CO)_4(\eta^2\text{-BTMSA})]$ (**1***) as the starting material. IR (*n*-pentane, cm^{-1}): υ_{CO} 1888 (m), 1824 (s); $\upsilon_{C\equiv C}$ 1771 (w). ^1H NMR (CD_2Cl_2, –80 °C) δ: 0.95 (vt, apparent J_{PH} = 3.7 Hz, 18H, $P(CH_3)_3$), 0.18 (s, 18H, $Si(CH_3)_3$). $^{13}C\{^1H\}$ NMR (CD_2Cl_2, –80 °C) δ: 224.7 (t, $^2J_{CP}$ = 31 Hz, *C*O), 114.0 (s, $CSiMe_3$), 17.8 (vt, apparent J_{PC} = 12.5 Hz, $P(CH_3)$), 1.0 (s, $Si(CH_3)$). $^{31}P\{^1H\}$ NMR (CD_2Cl_2, –80 °C) δ: 29.2 (t, $^2J_{CP}$ = 31 Hz). MS (EI, 16 eV) *m/z*: 436 (M^+); estimated ratios: $[Fe(^{13}CO)_2(PMe_3)_2(\eta^2\text{-BTMSA})]$ 75%, $[Fe(^{13}CO)(^{12}CO)(PMe_3)_2(\eta^2\text{-BTMSA})]$ 25%.

Preparation of $[Fe(^{13}CO)_4(\eta^2\text{-BTMSA})]$ (1*)

$[Fe(^{13}CO)_4(\eta^2\text{-BTMSA})]$ (**1***) was prepared by stirring a hexane (20 mL) solution of $[Fe(CO)_4(\eta^2\text{-BTMSA})]$ (**1**, 191.5 mg, 0.567 mmol) in a 100 mL round-bottomed flask, under an atmosphere of ^{13}CO (approx. 3.23 mmol) for 2 days. The solvent was removed in vacuo at –20 °C. The yellow residue was dissolved in pentane and the solution filtered, concentrated, and cooled to –80 °C. Yellow crystals of $[Fe(^{13}CO)_4(\eta^2\text{-BTMSA})]$ (**1***, 125.5 mg) were obtained in 64.8% yield. IR (*n*-pentane, cm^{-1}): υ_{CO} 2029 (w), 1958 (vs), 1924 (s); $\upsilon_{C\equiv C}$ 1873 (w) (for comparison, **1**: IR (*n*-pentane, cm^{-1}): υ_{CO} 2077 (w), 2001 (vs), 1968 (s); $\upsilon_{C\equiv C}$ 1874 (w)).

© 2005 NRC Canada

Scheme 1.



1 **2** **3**

Reaction of [Fe(CO)$_4$(η^2-BTMSA)] (1) with CO

Carbon monoxide was bubbled through a pentane (10 mL) solution of [Fe(CO)$_4$(η^2-BTMSA)] (**1**) overnight (11 h). No change was observed in the solution or the IR spectrum over this period.

Reaction of [Fe(CO)$_2$(PMe$_3$)$_2$(η^2-BTMSA)] (3) with CO

A pentane (10 mL) solution of [Fe(CO)$_2$(PMe$_3$)$_2$(η^2-BTMSA)] (**3**, 10.5 mg, 0.0242 mmol) was frozen, degassed, and allowed to warm to –80 °C. The flask was then backfilled with CO via a CO line. The CO line was fitted with an oil bubbler, which maintained a constant pressure of CO (ca. 1 atm, 1 atm = 101.325 kPa). The solution was allowed to warm slowly to r.t. and the reaction monitored by IR spectroscopy. After 6 h, the reaction solution reached r.t. and contained mainly **2**, with small amounts of **3** and [Fe(CO)$_3$(PMe$_3$)$_2$] (**4**) (IR (*n*-pentane, cm^{-1}): υ_{CO} 1880 (s); compared to **4**: IR (CH_2Cl_2, cm^{-1}): υ_{CO} 1863 (s) (6)). On stirring for a further 1.5 h, the proportion of **2** and **4** to **3** continued to rise. Longer reaction times led to minor changes in the IR spectrum, but the identities of the new species were difficult to ascertain with confidence.

Reaction of [Fe(^{13}CO)$_2$(PMe$_3$)$_2$(η^2-BTMSA)] (3*) with ^{13}CO

A pentane (10 mL) solution of [Fe(^{13}CO)$_2$(PMe$_3$)$_2$(η^2-BTMSA)] (**3***) (10.0 mg, 0.0229 mmol) was frozen, degassed, and backfilled with ^{13}CO at –80 °C. The flask was then sealed. The solution was allowed to warm slowly to r.t. and the reaction monitored by IR spectroscopy. After 6 h, the reaction solution reached r.t. and contained mainly **2*** with a trace of **3***. On stirring for a further 1.5 h, [Fe(^{13}CO)$_3$(PMe$_3$)$_2$] (**4***) (IR (*n*-pentane, cm^{-1}): υ_{CO} 1835 (s); compared to **4**: IR (CH_2Cl_2, cm^{-1}): υ_{CO} 1863 (s) (6)) was also detected.

Reaction of [Fe(CO)$_4$(η^2-BTMSA)] (1) with triphenylphosphine–tricyclohexylphosphine

To a cooled (–70 °C) solution of **1** was added equimolar quantities of PPh_3 (in CH_2Cl_2) or PCy_3 (in hexane). Progress of the reaction was monitored by IR spectroscopy as the solution was slowly allowed to warm to r.t. (ca. 7 h). In the case of PPh_3, no other product but starting material **1** and [Fe(CO)$_3$(PPh$_3$)$_2$] (7*a*) (IR (CH_2Cl_2, cm^{-1}): υ_{CO} 1881 (s)) could be detected. With PCy_3, in addition to **1** and [Fe(CO)$_3$(PCy$_3$)$_2$] (7*b*) (IR (CH_2Cl_2, cm^{-1}): υ_{CO} 1850 (s)), bands at 2045 (m), 1969 (w), and 1930 (s) (cm^{-1} in *n*-hexane) were observed also.

Crystal structure determinations

Yellow crystals of **1** and **2** and yellow–orange crystals of **3** were obtained by cooling pentane solutions to –80 °C. Data were collected on a Bruker PLATFORM/SMART 1000 CCD diffractometer using Mo Kα radiation at –80 °C. For a summary of the crystal data X-ray collection data see Table 1. The structures of **1**–**3** are shown in Fig. 1.[3]

Results and discussion

Synthesis and characterization

Reaction of [Fe(CO)$_4$(η^2-BTMSA)] (**1**) with 1 equiv. of trimethylphosphine gave the monophosphine substituted [Fe(CO)$_3$(PMe$_3$)(η^2-BTMSA)] (**2**) in good yield (76%) (Scheme 1). The disubstituted [Fe(CO)$_2$(PMe$_3$)$_2$(η^2-BTMSA)] (**3**) could be prepared either by reaction of **1** with 2 or more equiv. of trimethylphosphine or by reaction of **2** with 1 or more equiv. of trimethylphosphine. The formation of **3** from **2** could be reversed by placing a pentane solution of **3** under an atmosphere of carbon monoxide. However, longer reaction time (6 h) resulted in the loss of BTMSA and formation of [Fe(CO)$_3$(PMe$_3$)$_2$] (**4**). It should also be noted that **1** does not lose BTMSA to form [Fe(CO)$_5$] under carbon monoxide overnight.

Compound **1** undergoes facile carbonyl ligand exchange. Placing a hexane solution of **1** under ^{13}CO readily gave ^{13}CO enriched **1***. Subsequent reactions with PMe_3 allowed the preparation of ^{13}CO enriched samples of **2*** and **3***.

Complex **2** was fully characterized by IR and NMR (^{1}H, ^{31}P{^{1}H}, and ^{13}C{^{1}H}) spectroscopy, mass spectrometry, and elemental analysis, the data comparing well with similar complexes prepared in this laboratory (8). Three IR active carbonyl stretching bands are expected on the basis of the C_s symmetry of **2** and are seen at 2018 (s), 1949 (s), and 1920 (s) cm^{-1}. Another IR band is seen at 1822 cm^{-1} owing to the coordinated alkyne. The identity of this last band is corroborated by comparing the IR spectra of **2** and **2***, in which, unlike the carbonyl stretching frequencies, it remains unchanged. The ^{13}C{^{1}H} NMR spectrum of **2** shows two carbonyl resonances in a 2:1 ratio at δ 220.9 (d, $^2J_{CP}$ = 35 Hz, 2CO_{eq}) and 214.6 (d, $^2J_{CP}$ = 59 Hz, CO_{ax}). The coupling constants to phosphorus confirm the geometry of **2**, with a larger trans phosphorus–carbon coupling to one carbonyl

[3] Supplementary data for this article are available on the Web site or may be purchased from the Depository of Unpublished Data, Document Delivery, CISTI, National Research Council Canada, Ottawa, ON K1A 0S2, Canada. DUD 3691. For more information on obtaining material refer to http://cisti-icist.nrc-cnrc.gc.ca/irm/unpub_e.shtml. CCDC 247947–247949 contain the crystallographic data for this manuscript. These data can be obtained, free of charge, via www.ccdc.cam.ac.uk/conts/retrieving.html (Or from the Cambridge Crystallographic Data Centre, 12 Union Road, Cambridge CB2 1EZ, UK; fax +44 1223 336033; or deposit@ccdc.cam.ac.uk).

© 2005 NRC Canada

Table 1. Crystallographic experimental details for compounds **1**–**3**.

	1	**2**	**3**
Formula	$C_{12}H_{18}FeO_4Si_2$	$C_{14}H_{27}FeO_3PSi_2$	$C_{16}H_{36}FeO_2P_2Si_2$
Formula weight	338.29	386.36	434.42
Crystal dimensions (mm^3)	0.71 × 0.60 × 0.14	0.31 × 0.26 × 0.09	0.34 × 0.30 × 0.11
Crystal system	Monoclinic	Orthorhombic	Monoclinic
Space group	$P2_1/c$ (No. 14)	$P2_12_12_1$ (No. 19)	$P2_1/c$ (No. 14)
Unit cell parameters			
a (Å)	25.275 (11)[a]	9.333 5 (6)[b]	12.454 (4)[c]
b (Å)	9.905 (4)	14.410 2 (9)	9.799 (3)
c (Å)	14.794 (6)	16.083 9 (10)	20.099 (6)
β (°)	106.088 (9)		92.222 (6)
V ($Å^3$)	3 559 (3)	2 163.2 (2)	2 451.1 (12)
Z	8	4	4
$\rho_{calcd.}$ (g cm^{-3})	1.263	1.186	1.177
μ (mm^{-1})	0.987	0.887	0.849
Data collection and refinement conditions			
Diffractometer	Bruker PLATFORM/SMART 1000 CCD[d]		
Radiation (λ, Å)	Graphite-monochromated Mo Kα (0.710 73)		
Temperature (°C)	–80	–80	–80
Scan type	ω scans (0.2°, 20 s exposures)		
Data collection 2θ limit (°)	53.04	52.80	52.86
Total data collected	19 399 (–19 ≤ h ≤ 31, –12 ≤ k ≤ 12, –18 ≤ l ≤ 18)	12 283 (–11 ≤ h ≤ 11, –18 ≤ k ≤ 18, –12 ≤ l ≤ 20)	12 373 (–15 ≤ h ≤ 15, –11 ≤ k ≤ 12, –25 ≤ l ≤16)
No. of ind. rflns.	7 249 (R_{int} = 0.077 2)	4 427 (R_{int} = 0.040 0)	4 995 (R_{int} = 0.045 7)
No. of obsd rflns. (NO)	4 888 ($F_o^2 \geq 2\sigma(F_o^2)$)	3 870 ($F_o^2 \geq 2\sigma(F_o^2)$)	3 733 ($F_o^2 \geq 2\sigma(F_o^2)$)
Structure solution method	Patterson search/structure expansion (DIRDIF-96[e])		
Refinement method	Full-matrix least-squares on F^2 (SHELXL-93[f])		
Abs. Corr. method	Multiscan (SADABS)	Multiscan (SADABS)	Multiscan (SADABS)
Range of transn. factors	0.874 2 – 0.540 9	0.924 5 – 0.770 6	0.912 4 – 0.761 2
Data/restraints/params.	7 249 ($F_o^2 \geq -3\sigma(F_o^2)$) / 0 / 343	4 427 ($F_o^2 \geq -3\sigma(F_o^2)$) / 0 / 191	4 995 ($F_o^2 \geq -3\sigma(F_o^2)$) / 0 / 208
Flack absolute structure parameter[g]		0.440 (15)	
Goodness-of-fit (S)[h]	1.039 ($F_o^2 \geq -3\sigma(F_o^2)$)	1.037 ($F_o^2 \geq -3\sigma(F_o^2)$)	1.028 ($F_o^2 \geq -3\sigma(F_o^2)$)
Final R indices[i]			
R_1 ($F_o^2 \geq 2\sigma(F_o^2)$)	0.077 1	0.034 3	0.052 0
wR_2 ($F_o^2 \geq -3\sigma(F_o^2)$)	0.202 6	0.077 1	0.143 0
Largest difference peak and hole (e $Å^{-3}$)	1.766 and –0.589	0.367 and –0.172	1.407 and –0.995

[a]Obtained from least-squares refinement of 7107 centered reflections.
[b]Obtained from least-squares refinement of 8165 centered reflections.
[c]Obtained from least-squares refinement of 8013 centered reflections.
[d]Programs for diffractometer operation, data collection, data reduction, and absorption correction were those supplied by Bruker.
[e]Reference 13.
[f]Reference 14.
[g]Reference 15. The Flack parameter will refine to a value near zero if the structure is in the correct configuration and will refine to a value near one for the inverted configuration. The value observed herein is indicative of racemic twinning, and was accomodated during the refinement (using the SHELXL-93 TWIN instruction (see footnote *d*)).
[h]$S = [\Sigma w(F_o^2 - F_c^2)^2/(n-p)]^{1/2}$ (n = number of data, p = number of parameters varied, $w = [\sigma^2(F_o^2) + (a_0P)^2]^{-1}$ where $P = [\mathrm{Max}(F_o^2, 0) + 2F_c^2]/3$ and a_0 is adjusted as suggested by the refinement program (for **1**, a_0 = 0.1126; for **2**, a_0 = 0.0402; for **3**, a_0 = 0.0929).
[i]$R_1 = \Sigma\|F_o|-|F_c\|/\Sigma|F_o|$; $wR_2 = [\Sigma w(F_o^2 - F_c^2)^2/\Sigma w(F_o^4)]^{1/2}$.

and a smaller coupling to the equatorial carbonyls. Crystals of **2** suitable for an X-ray crystallographic study were obtained through the cooling (–80 °C) of a saturated pentane solution of **2**. The study is detailed in the following text.

Complex **3** was also fully characterized by IR and NMR (^1H, $^{31}P\{^1H\}$, and $^{13}C\{^1H\}$) spectroscopy, mass spectrometry, and elemental analysis. The data compare well with similar complexes prepared in this laboratory and elsewhere (9), and with the analogous $Fe(CO)_2(PEt_3)_2$(η-BTMSA) prepared by a very different route (9*b*). The IR spectrum shows two carbonyl stretching bands at 1930 (m) and 1823 (s) cm^{-1}, consistent with the C_{2v} molecular symmetry. In addition to the carbonyl stretches a band at 1774 cm^{-1} is observed owing to the bound alkyne. The $^{13}C\{^1H\}$ NMR spectrum of **3*** shows a resonance at δ 224.7 (t, $^2J_{CP}$ = 31 Hz) for the two equivalent carbonyl carbons. The observation of virtual triplets for the PMe_3 carbons and hydrogens confirm the trans-diaxial disposition of these ligands (10). The single ^{31}P

© 2005 NRC Canada

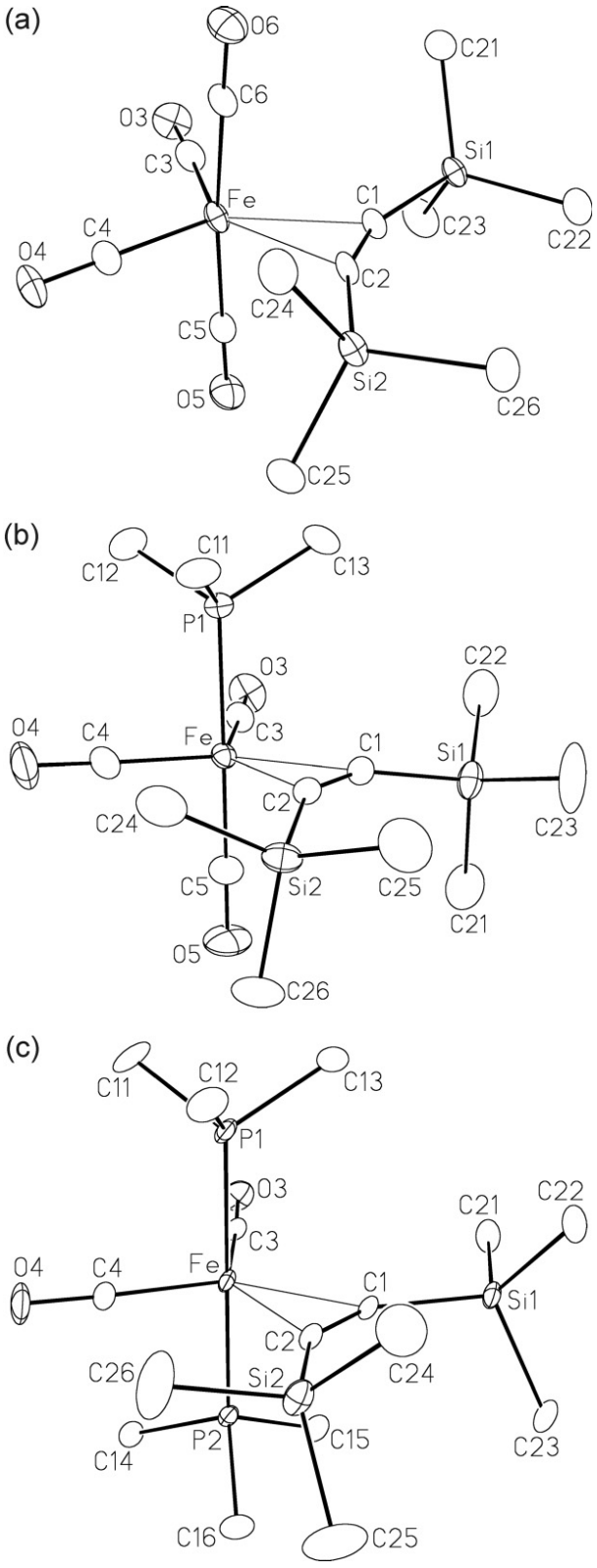


Fig. 1. Perspective views of: (*a*) one of the two crystallographically independent molecules of $[Fe(CO)_4\{\eta^2\text{-}C(SiMe_3)C(SiMe_3)\}]$ (**1**) (molecule 1) showing the atom labelling scheme; (*b*) $[Fe(CO)_3(PMe_3)\{\eta^2\text{-}C(SiMe_3)C(SiMe_3)\}]$ (**2**); and (*c*) $[Fe(CO)_2(PMe_3)_2\{\eta^2\text{-}C(SiMe_3)C(SiMe_3)\}]$ (**3**). Non-hydrogen atoms are represented by Gaussian ellipsoids at the 20% probability level. Hydrogen atoms are not shown.

resonance owing to the two equivalent PMe_3 ligands in **3*** is observed at δ 29.2 as a triplet with an inner doublet (the triplet dominant) because of incomplete ^{13}CO enrichment. It was not possible to reliably integrate the two multiplets to determine the extent of enrichment, but from the mass spectrum of the compound, we estimate a 3:1 ratio between the di- and mono-^{13}CO material. Crystals of **3** suitable for an X-ray crystallographic study were obtained by cooling (–80 °C) a saturated pentane solution of **2**. The study is detailed in the following text.

Having established that substitution of **1** also proceeds by initial CO dissociation with production of the mono- and bisphosphine alkyne carbonyls **2** and **3**, it was of interest to reinvestigate the reaction with bulky phosphines to see whether analogues of **2** and (or) **3** could be isolated or at least spectroscopically detected.

The only isolable products from the reaction of **1** with triphenylphosphine and tricyclohexylphosphine were the known compounds $[Fe(CO)_3(PPh_3)_2]$ and $[Fe(CO)_3(PCy_3)_2]$, respectively (7). Although IR monitoring of the PCy_3 reaction in hexane, where the CO stretching bands are narrow and sharp, revealed additional CO bands at 2045, 1969, and 1930 cm^{-1}, the alkyne region remained ambiguous. In the absence of additional data and no isolated product, the origin of these bands is uncertain, but most probably due to advantageous $Fe(CO)_4(PCy_3)$ (11).

Solid state structures of compounds 1–3

To corroborate the structural assignments and to assess the effect of CO substitution by PMe_3 on the metal–alkyne bonding in this series, the solid structure of the previously reported **1** was also determined by X-ray crystallography. Perspective views of the structures of compounds **1**–**3** are shown in Fig. 1 and selected bond lengths and angles are given in Table 2. All three compounds have a trigonal bipyramidal arrangement of ligands, with the bis(trimethylsilyl)acetylene and two carbonyl ligands occupying the trigonal plane. The solid state structure of **1** shows that the axial carbonyl ligands are bent towards the alkyne with C-Fe-C bond angles (for the two chemically equivalent, yet crystallographically different molecules) of 174.3(2)° and 174.5(2)°. A similar situation is seen in the solid state structure of $[Os(CO)_4(\eta^2\text{-BTMSA})]$ (**5**) (12).

As noted previously and in the Experimental section, the unit cell of **1** contains two chemically equivalent, but crystallographically independent molecules. As a consequence, in the following discussion, average values will be used for discussion and comparison.

The two incoming trimethylphosphine ligands sequentially occupy the axial positions: one in **2** and both in compound **3**. The substitution of the first axial π-acidic CO ligand by the σ-donating trimethylphosphine has the expected effect of shortening the metal–carbonyl bond distance trans to it (Fe—C5 = 1.780(3) Å in **2** compared to 1.827(9) Å for the axial Fe—C5/C6 bond distances in **1**). The differences between Fe—CO_{eq} distances are hardly significant. However, there is a significant effect on the metal–alkyne

© 2005 NRC Canada

Table 2. (*a*) Bond lengths and (*b*) angles for [$Fe(CO)_4\{\eta^2$-$C(SiMe_3)C(SiMe_3)\}$] (**1**).

(*a*) Selected interatomic distances (Å).				
	1		**2**	**3**
	Molecule 1	Molecule 2		
Fe—C1	2.175(5)	2.173(5)	2.117(3)	2.108(3)
Fe—C2	2.167(5)	2.173(5)	2.120(3)	2.112(3)
Fe—C3	1.808(6)	1.795(6)	1.774(3)	1.756(3)
Fe—C4	1.802(5)	1.797(5)	1.760(3)	1.758(4)
Fe—C5/P2	1.824(6)	1.812(6)	1.780(3)	2.2253(10)
Fe—C6/P1	1.835(6)	1.836(6)	2.2539(7)	2.2224(10)
C1—C2	1.242(6)	1.258(7)	1.252(4)	1.262(5)
(*b*) Selected interatomic angles (°).				
	1		**2**	**3**
	Molecule 1	Molecule 2		
C3-Fe-C4	114.0(2)	113.4(2)	113.49(15)	110.18(15)
C5/P2-Fe-C6/P1	174.3(2)	174.5(2)	179.03(12)	175.29(4)
Si1-C1-C2	158.5(4)	159.5(4)	151.2(2)	147.2(3)
Si2-C2-C1	160.1(4)	162.1(4)	150.6(2)	146.3(3)

bonds, with a decrease in the iron–carbon distances between **1** and **2** (2.172(5) Å in **1** and 2.119(3) Å in **2**). The shortening of these bonds shows that the alkyne also benefits from the increased electron density on the metal, with increased π backdonation from iron into the alkyne $\pi_\parallel$* orbitals. The C≡C-Si bond angles also decrease from 160.1(6)° in **1** to 150.9(3)° for **2** as the metal–alkyne bonding develops greater metallacyclopropene character.

In compound **3**, the second phosphine occupies the second axial position, trans to the other phosphine. The effect of the second phosphine on the metal–ligand bonding is slighter than that of the first. All of the relevant bond lengths in **3** are comparable to those in **2**.[4] However, the C≡C-Si bond angles decrease slighty from 150.9(3)° in **2** to 146.8(5)° for **3**, illustrating again the increasing metallacyclopropene character of the metal–alkyne bonding. It may be that the anticipated increase is attenuated by the increased four-electron repulsion between filled Fe d_π and $\pi_\perp$ BTMSA orbitals as a result of the absence of π-acidic CO in **3** along the apical positions, which could drain some electron density from the later.

It should be noted that the increased back-bonding ability, and hence increased metallacyclopropene character in the series **1** < **2** < **3**, is not reflected in a similar reduction in the BTMSA C≡C bond distance. Indeed the C1—C2 distance remains virtually unchanged: 1.250(7) Å (**1**), 1.252(4) Å (**2**), and 1.262(5) Å (**3**). A more sensitive probe is needed to gauge the changes in the C≡C bond strength. Such a probe is the C≡C stretching frequency, which decreases in the expected order: **1** (1873 cm^{-1}) > **2** (1823 cm^{-1}) > **3** (1774 cm^{-1}), the difference an almost constant 50 cm^{-1}.

Conclusion

We have demonstrated that ligand substitution in [$Fe(CO)_4(\eta^2$-BTMSA)] (**1**) proceeds by initial CO loss as in other Group 8 [$M(CO)_4(\eta^2$-alkyne)] compounds. However, the nature of the isolated products is strongly influenced by steric and electronic factors. Thus, while reaction of **1** with PMe_3 allowed isolation of [$Fe(CO)_3(PMe_3)(\eta^2$-BTMSA)] (**2**) and [$Fe(CO)_2(PMe_3)_2(\eta^2$-BTMSA)] (**3**), the bulky PPh_3 and PCy_3 ligands led only to [$Fe(CO)_3(PR_3)_2$]. Clearly steric repulsion between bulky phosphine and BTMSA ligands in the putative [$Fe(CO)_3(PR_3)(\eta^2$-BTMSA)] intermediate results in rapid loss of the BTMSA ligand and formation of [$Fe(CO)_3(PR_3)_2$].[5] That electronic factors can also influence the outcome of the substitution is evidenced from the reaction of **3** with CO. Long-term reaction time leads to formation of [$Fe(CO)_3(PMe_3)_2$] via loss of BTMSA. This is presumably the result of four-electron repulsion between the electron-rich Fe centre and the filled $\pi_\perp$ of the BTMSA ligand, which labilizes the alkyne ligand. Replacing BTMSA with strongly π-acidic alkyne HFB ($CF_3C{\equiv}CCF_3$) reduces this four-electron repulsion and both [$Fe(CO)_2(PR_3)_2(\eta^2$-HFB)] (R = Me and Ph) are resistant to HFB loss. Furthermore, reaction of [$Fe(CO)_4(\eta^2$-HFB)] with bulky phosphine ligands, including PCy_3, leads not to HFB, but further CO loss and formation of the interesting [$Fe(CO)_2(PR_3)(\eta^2$-HFB)] compounds that contain a four-electron alkyne ligand (8*b*).

Acknowledgements

We wish to thank the reviewers for their constructive com-

[4] The metrical parameters of **3** are very similar to those of the analogous $Fe(CO)_2(PEt_3)_2$(BTMSA) (9); the one exception is the C-C-Si angle (141.9(5)°) compared to 146.8(5)° in **3**.

[5] The detection of $Fe(CO)_4(PCy_3)$ in the reaction of **1** with PCy_3 may signal the existence of a minor parallel reaction path of alkyne dissociation. We have observed such an outcome with the exceedingly thermolabile $Ru(CO)_4(\eta^2$-BTMSA), which is unstable above –25 °C in solution and rapidly forms $Ru_3(CO)_{12}$ (12). The clean conversion of **1** to **2**, with no observable $Fe(CO)_4(PMe_3)$, and overnight stability of **1** under a CO atmosphere, indicate that CO loss is the predominant mode of reactivity of compound **1**.

© 2005 NRC Canada

ments. We are grateful to the Natural Sciences and Engineering Research Council of Canada (NSERC) and the University of Alberta for financial support, and Dr. Gong Kiel for technical assistance.

References

1. J. Cooke and J. Takats. J. Am. Chem. Soc. **119**, 11 088 (1997).
2. H.W. Sternberg, R. Markby, and I. Wender. J. Am. Chem. Soc. **80**, 1009 (1958).
3. (*a*) W. Hübel, H. Braye, A. Clauss, E. Weiss, U. Krüerke, D.A. Brown, G.S.D. King, and C. Hoogzand. J. Inorg. Nucl. Chem. **9**, 204 (1959); (*b*) W. Hübel and H. Braye. J. Inorg. Nucl. Chem. **10**, 250 (1959); (*c*) W. Hübel. *In* Organic synthesis via metal carbonyls. Vol. 1. *Edited by* I. Wender and P. Pino. Wiley-Interscience, New York. 1968. p. 273.
4. J. Pearson, J. Cooke, J. Takats, and R.B. Jordan. J. Am. Chem. Soc. **120**, 1434 (1998).
5. K.H. Pannell and G.M. Crawford. J. Coord. Chem. **2**, 251 (1973).
6. M.J. Therien and W.C. Trogler. Inorg. Synth. **28**, 173 (1990).
7. (*a*) S.W. Blanch, A.M. Bond, and R. Colton. Inorg. Chem. **20**, 755 (1981); (*b*) L. Song and W.C. Trogler. J. Am. Chem. Soc. **114**, 3355 (1992).
8. (*a*) T.-F. Mao, Z. Zhang, J. Washington, J. Takats, and R.B. Jordan. Organometallics, **18**, 2331 (1999); (*b*) Q. Major. Ph.D. thesis, University of Alberta, Edmonton, Alberta. 2003.
9. (*a*) M. Barron, N.L. Cromhout, A.R. Manning, and J.F. Gallagher. J. Chem. Soc. Dalton Trans. 1352 (2001), and refs. therein; (*b*) C. Gauss, D. Vaglini, and H. Berke. Chem. Ber. **130**, 183 (1997).
10. (*a*) R.K. Harris. Can. J. Chem. **42**, 2275 (1964); (*b*) R.H. Crabtree. The organometallic chemistry of transition metals. John Wiley and Sons, New York. 2001. p. 260.
11. (*a*) M.O. Albers and N.J. Coville. J. Organomet. Chem. **217**, 385 (1981); (*b*) W. Strohmeier and F.J. Muller. Chem. Ber. **102**, 2619 (1969).
12. R.G. Ball, M.R. Burke, and J. Takats. Organometallics, **6**, 198 (1987).
13. P.T. Beurskens, G. Beurskens, W.P. Bosman, R. de Gelder, S. Garcia Granda, R.O. Gould, R. Israel, and J.M.M. Smits. The DIRDIF-96 program system [computer program]. Crystallography Laboratory, University of Nijmegen, Nijmegen, The Netherlands. 1996.
14. G.M. Sheldrick. SHELXL-93 [computer program]. University of Göttingen, Göttingen, Germany. 1993.
15. H.D. Flack. Acta Crystallogr. Sect. A. **A39**, 876 (1983).

© 2005 NRC Canada

Use of fluorescent probes to determine catalytic chain length in chemically amplified resists[1]

Mathieu Frenette, Marius Gabriel Ivan, and J.C. Scaiano

Abstract: Acid-catalyzed deprotection of *tert*-butoxycarbonyl (*t*-Boc) pendant groups present in a polymer film is one of the most common chemical reactions in photolithography. We present here a novel method to determine the catalytic chain length of this reaction under different development conditions. We demonstrate this in model PMMA thin films containing triphenylsulphonium triflate as a photoacid generator, acid sensor coumarin 6, *t*-Boc protected coumarin 4, and base 2-piperidin-1-yl-ethanol (2-PE). Deprotection of the *t*-Boc group, catalyzed by the photogenerated acid, during the post-exposure bake leads to formation of coumarin 4, a strongly fluorescent molecule whose concentration is monitored using fluorescence. We take advantage of the change in the emission spectra of coumarin 6 upon protonation to monitor acid formation. To quantify the amount of acid, an acid–base titration is done in the polymer film using 2-PE. Knowing the amount of deprotected probe and the amount of acid, we are able to calculate the number of moles of deprotected C4-*t*-Boc per mol of acid, which is the actual catalytic chain length.

Key words: photolithography, chemical amplification, catalytic chain length, fluorescent sensors, photoacid generator.

Résumé : La déprotection acidocatalysée des groupes pendants *tert*-butoxycarbonyles (*t*-Boc) présents dans un film de polymère est une des réactions chimiques les plus communes en photolithographie. Dans ce travail, on présente une nouvelle méthode pour déterminer la longueur de la chaîne catalytique de cette réaction dans diverses conditions de développement. Ceci est démontré dans des films minces modèles de PMMA contenant du triflate de triphénylsulfonium comme générateur photoacide, le détecteur d'acide coumarine 6, la coumarine 4 portant un groupe protecteur *t*-Boc et la base 2-pipéridin-1-yl-éthanol (2-PE). La déprotection du groupe *t*-Boc, catalysée par l'acide photogénéré au cours de la cuisson suivant l'exposition, conduit à la formation de la coumarine 4, une molécule fortement fluorescente dont on peut déterminer la concentration par fluorescence. On tire avantage du changement dans le spectre d'émission de la coumarine 6 lors de la protonation pour déceler la formation d'acide. Afin de quantifier la quantité d'acide, on réalise un titrage acide–base dans le film de polymère à l'aide du 2-PE. Connaissant la quantité de sonde déprotonée et la quantité d'acide, il est possible de calculer le nombre de moles de C4-*t*-Boc déprotégé par mol d'acide, ce qui correspond à la longueur de la chaîne catalytique.

Mots clés : photolithographie, amplification chimique, longueur d'une chaîne catalytique, détecteurs fluorescents, générateur photoacide.

[Traduit par la Rédaction]

Introduction

The introduction of chemically amplified resists in the early 1980s radically changed resist chemistry and made possible many of the advances in lithography of the last two decades. The chemistry was largely developed by Ito, Fréchet, Willson, and co-workers (1–3). The key concept is that a hydrophobic acid-sensitive group can be deprotected to a base soluble structure in a catalytic process mediated by Brønsted acids. One of the common reactions, particularly applied in 248 nm lithography, is deprotection of the *tert*-butoxycarbonyl (*t*-Boc) group to yield phenol-derived materials, e.g., Scheme 1.

The regeneration of the proton in the last stage of Scheme 1 is responsible for the catalytic nature of the process. The number of *t*-Boc groups deprotected by one proton gives the catalytic chain length. The acid is normally produced by photolysis of a photoacid generator (PAG). Numerous PAGs have been developed in the last two decades, capable of accommodating the speed, spectral and chemical characteristics required by various resists, as the wavelengths in use have become shorter to accommodate the demand for smaller lithographic features.

In the past, our research group and others have used fluorescent probes to monitor photoacid generation (4–6) and *t*-Boc deprotection (7–9) in polymer films. Beyond its excellent sensitivity, fluorescence lends itself readily to imaging applications, and particularly in lithography, to the examination of latent images before processing (such as post-

Received 13 December 2004. Published on the NRC Research Press Web site at http://canjchem.nrc.ca on 22 July 2005.

This paper is dedicated to Howard Alper in recognition of his many achievements in chemistry.

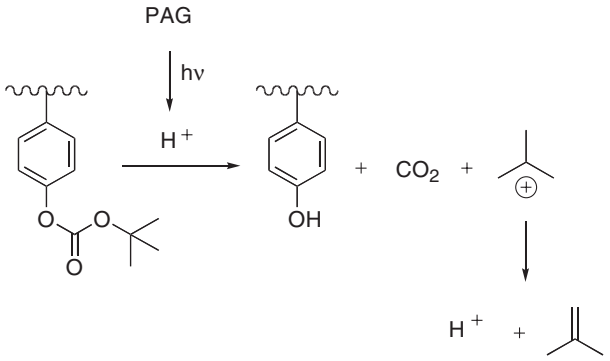
M. Frenette, M.G. Ivan, and J.C. Scaiano.[2] Department of Chemistry, Center for Catalysis Research and Innovation, University of Ottawa, 10 Marie-Curie, Ottawa, ON K1N 6N5, Canada.

[1]This article is part of a Special Issue dedicated to Professor Howard Alper.

[2]Corresponding author (e-mail: tito@photo.chem.uottawa.ca).

 doi: 10.1139/V05-090 © 2005 NRC Canada

Scheme 1. Acid-catalyzed deprotection of *t*-Boc protected phenols.



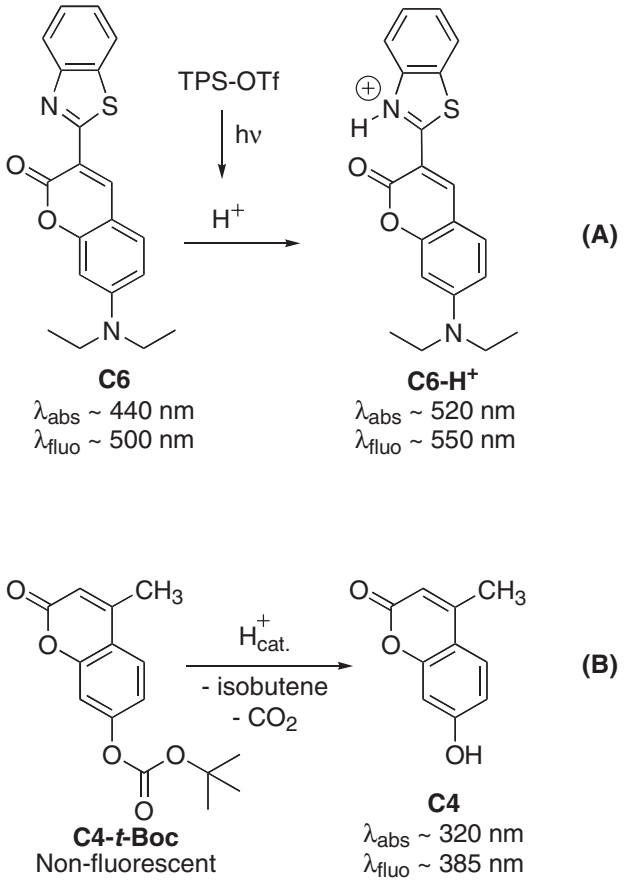
exposure bake and developing) takes place (10, 11). This is particularly important as feature size decreases, and problems such as acid diffusion are a likely candidate for loss of image integrity (12).

In this paper we develop a novel methodology based on fluorescent sensors, previously used for imaging purposes, to quantify an important parameter in chemically amplified resists: the catalytic chain length of *t*-Boc deprotection.

Determining the chain length for Scheme 1 requires knowledge of the efficiency of deprotection for a given concentration of acid. For the results to be meaningful, they need to be determined in thin polymer films and under exposure conditions similar to those employed in lithographic applications. In practice this means independently measuring proton generation and deprotection yields; a few reports in the literature generally use IR spectroscopy for the latter, since the carbonyl function (at around 1760 cm^{-1}) bleaches in the deprotection reaction. Reported catalytic chain lengths are in the range of ~100 (13) to 1000 (14) depending on the reaction conditions.

Two different coumarin dyes have been used (Scheme 2). Coumarin 6 (C6) is a convenient tool to determine acid yields since it dramatically changes its absorption and emission properties upon protonation. In this case, we have developed a titration approach that allows easy end-point determinations in thin films (vide infra). For the deprotection yields, the fluorescent 7-hydroxy-4-methylcoumarin (C4) was modified to yield the nonfluorescent 7-(*tert*-butoxycarbonyloxy)-4-methylcoumarin (C4-*t*-Boc). As deprotection occurs, C4 is released, with a concomitant increase in fluorescence.

Scheme 2. (A)"Prefluorescent" probes used to quantify acid formation, and (B) *t*-Boc deprotection. See the Supplemental information[3] for the absorbance and fluorescence spectra of the probes.



Experimental section

Materials

7-*tert*-Butoxycarbonyloxy-4-methylcoumarin (C4-*t*-Boc) was readily prepared from 7-hydroxycoumarin (C4) and di-*tert*-butyl-dicarbonate as previously described (9). Triphenyl sulfonium triflate (TPS-OTf) was a generous gift from Rohm and Haas Electronic Materials and used as received. Poly(methyl methacrylate) (PMMA, MW ~ 1.0×10^6, M_W/M_N ~ 1.10) was purchased from Polysciences, Inc. 2-Heptanone (99%) and 2-piperidin-1-yl-ethanol (2-PE, 99%) were purchased from Aldrich and used as received. Coumarin 6 (C6, 98%) was obtained from Aldrich and used as received.

Determination of catalytic chain length

All thin polymer films were spin coated on 1 inch (1 inch = 25.4 mm) quartz disks (Esco Products) at 3000 rpm for 20 s from polymer solutions previously filtered through 0.45 μm filters (Whatman Puradisk® 13 mm PTFE syringe filter). A post-application bake for 60 s on a metal plate contained in an oven at 90 °C was then performed to remove the residual solvent. Immediately after any baking, the quartz disks were rapidly cooled to room temperature on a metallic surface. The PMMA films obtained were 854 ± 14 nm thick as measured using a TFA-11CT thin film analyzer from Luzchem Research. Following post-application baking, the films were irradiated for up to 100 s in a Hybrid Technology Group exposure tool, model 64-10X, equipped with a 249 (±5) nm filter. The exposure spectral power dis-

[3] Supplementary data for this article are available on the Web site or may be purchased from the Depository of Unpublished Data, Document Delivery, CISTI, National Research Council Canada, Ottawa, ON K1A 0S2, Canada. DUD 3688. For more information on obtaining material refer to http://cisti-icist.nrc-cnrc.gc.ca/irm/unpub_e.shtml.

© 2005 NRC Canada

tribution was determined using a Luzchem SPR-1 spectroradiometer.

A stock polymer solution (PMMA stock) consisting of a 15:85 weight ratio of PMMA to 2-heptanone was used to prepare all solutions. Fluorescence measurements were done using a front face setup in a LS-50 PerkinElmer luminescence spectrometer.

Quantification of *t*-Boc group deprotection

In these experiments, a solution of C4-*t*-Boc (10% of the dry polymer weight) and TPS-OTf (3% of the dry polymer weight) dissolved in the PMMA stock was freshly prepared before each experiment to prevent the eventual thermal degradation of TPS-OTf or C4-*t*-Boc. The films were prepared as described in the previous section and immediately following UV exposure they were subject to a post-exposure bake (PEB) to minimize acid neutralization with air-borne bases (15). The PEB step was conducted either in the oven or using the temperature-controlled hotplate from a Luzchem TFA-11CT instrument. A new film was used for each individual data point; this probably accounts for some of the dispersion observed in our measurements.

The extent of C4-*t*-Boc deprotection was quantified by measuring the fluorescence of C4, i.e., deprotected C4-*t*-Boc, by exciting at 320 nm and monitoring emission at 385 nm. The fluorescence intensity was assumed to be proportional to C4 concentration in the range measured. A near-plateau in fluorescence intensity was found in all experiments, taken as 100% deprotection (vide infra). This enabled the quantification of *t*-Boc deprotection from fluorescence intensity data, scaled to the near-plateau slope, as a function of exposure time. A correlation between exposure time and acid yield, thus allowing catalytic chain length calculations, is described in the following.

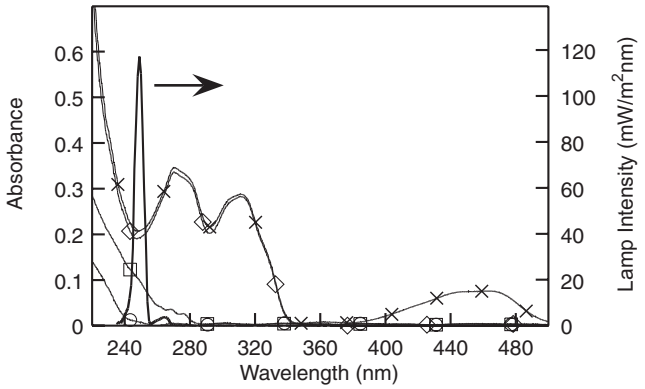
Acid quantification

The amount of acid generated during irradiation was quantified by "*in polymer*" titration experiments using 2-PE as the strong base (16) and C6 as the indicator. C6, a weak base, fluoresces green when neutral and red when protonated (4), thus giving a clear end point for acid neutralization of 2-PE.

The polymer solutions used for acid quantification were made by directly adding C6 (0.5% of the dry polymer weight) and 2-PE (as molar ratios of TPS-OTf, ranging from 0.0 to 0.5) to the solution used for *t*-Boc quantification (vide supra). The film developing procedure for acid quantification is identical to *t*-Boc quantification. It was found that acid neutralization by the bases, 2-PE and C6, in PMMA films occurs very slowly at room temperature. A PEB (90 °C in the oven for 60 s) in all acid quantification experiments corrected this lag in acid neutralization.

The presence of protonated C6 (i.e., C6-H^+) after exposure was measured by exciting at 510 nm, where C4 does not absorb. The fluorescence intensity decreased to baseline levels as the concentration of 2-PE in the casting solutions increased. Separate linear fits of the fluorescence intensity at 550 against of 2-PE concentration for both decreasing and baseline regions intersect at the neutralization point, thus providing a readily accessible end point. A correlation between exposure time and acid yield is constructed from neutralization point measurements at different exposure times (vide infra).

Fig. 1. The UV–vis absorption of typical PMMA thin films containing various additives. Legend: TPS-OTf = 3 wt.%, C4-*t*-Boc = 10 wt.%, and C6 = 0.5 wt.% of the dry PMMA weight, e.g., 3 wt.% would mean 3 g for 100 g of dry PMMA. PMMA (○), PMMA + TPS-OTf (□), PMMA + TPS-OTf + C4-*t*-Boc (◇), PMMA + TPS-OTf + C4-*t*-Boc + C6 (×). The scale on the right corresponds to the exposure tool spectrum.



Results

The objective of the present work is to establish a new useful methodology for the determination of the amplification chain length for *t*-Boc deprotection under typical lithographic conditions. An important requirement for these studies is the correct matching of absorbances at 249 nm, the exposure wavelength. The absorption spectra of typical samples, averaged over three films, as well as the exposure dose profile are shown in Fig. 1. All measurements were carried out in PMMA films, spin-coated from 2-heptanone containing 15 wt.% PMMA and various other components. The films had approximately the same thickness (vide supra).

The rest of this section is divided according to the two types of measurements carried out: quantification of acid generation by titration using C6 as the indicator and removal of *t*-Boc protecting groups.

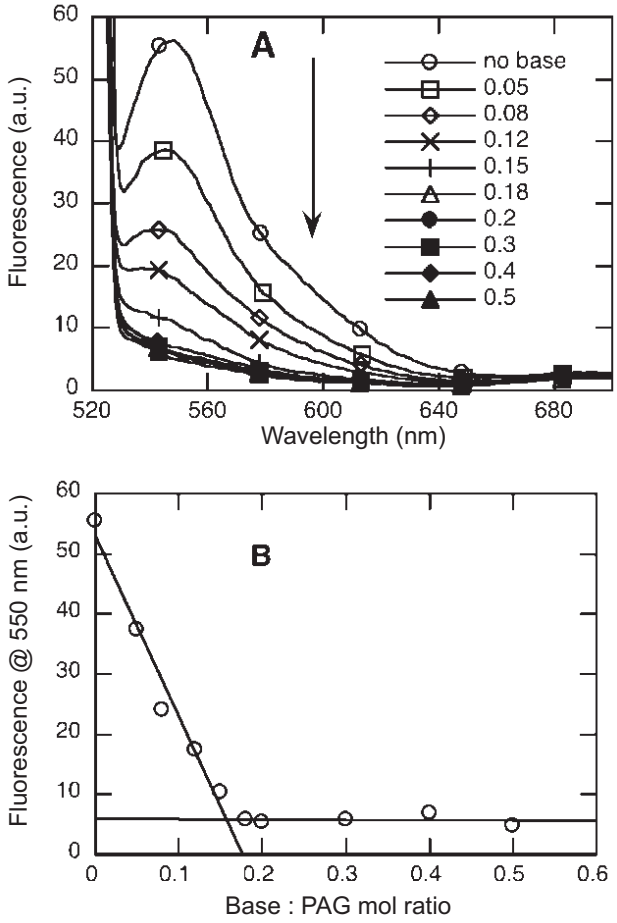
Acid quantification

Under the conditions of Fig. 1, from the fraction of light absorbed by the resist film at 249 nm, the following absorption distribution was calculated: TPS-OTf absorbs 44.1% while C4-*t*-Boc and C6 absorb 44.3% and 7.7%, respectively.

The titration strategy relies on the quantitative addition of small and variable amounts of 2-PE, acting as the strong base, at a constant concentration of TPS-OTf. The base (2-PE) does not show significant absorption at 249 nm. Figure 2A shows the decrease in fluorescence as different amounts of base are used for a series of samples exposed for 20 s. The fluorescence spectra were obtained using 510 nm excitation, a wavelength where the neutral C6 does not absorb. Figure 2B shows the C6-H^+ fluorescence intensity at 550 nm (C4 does not fluoresce at this wavelength). By detecting the ratio of base to PAG where the onset of fluores-

© 2005 NRC Canada

Fig. 2. Typical in-polymer titration experiment. (A) Fluorescence spectra (λ_{exc} = 510 nm) of C6-H^+ in PMMA, 3 wt.% TPS-OTf, and 2-PE in a different molar ratio to TPS-OTf (see legend inset in the figure), after 20 s of exposure. (B) Fluorescence intensity measured at 550 nm as a function of base to PAG mol ratio, i.e., 2-PE:TPS-OTf.

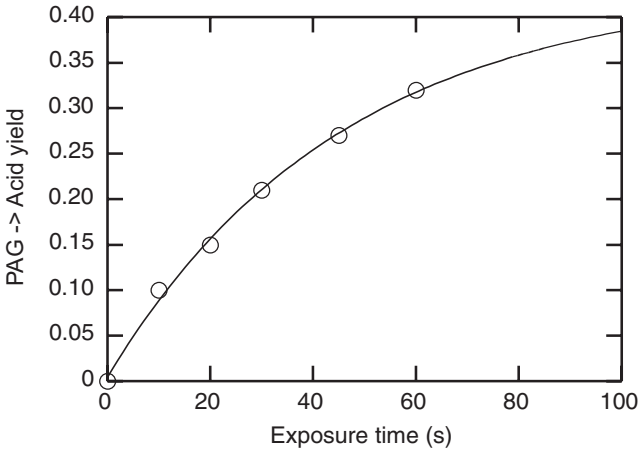


cence occurs, it is possible to evaluate the amount of acid generated for a given 249 nm exposure time.

We note that after exposure at 249 nm the samples were subject to a PEB for 60 s at 90 °C. This PEB had two purposes. First, to match the protocol used in the deprotection studies (vide infra), and the second and most important, to speed up the diffusion of H^+, because in PMMA films acid diffusion leading to protonation of C6 can take over 1 h at room temperature, while at 90 °C this process is complete in less than 1 min. Control experiments show that the presence of C4-*t*-Boc (added for absorbance matching) does not interfere with these experiments; clearly, both 2-PE and C6 are sufficiently strong bases that no deprotection occurs if base is present.

Similar results can be obtained for various irradiation times, and from these data a plot of acid yield as a function of exposure time can be constructed. It should be noted that this plot is specific for a given PAG and light intensity and for a constant fraction of the incident light absorbed by the PAG (Fig. 3).

Fig. 3. Yields of H^+ from TPS-OTf (3 wt.%) in PMMA films as a function of the exposure time at 249 nm shown as a fraction of molar PAG loading.



Deprotection studies

The PEB of samples containing C4-*t*-Boc, but with no added base, led to deprotection (Scheme 2, rxn. B) and an increase in fluorescence at ~385 nm as the highly fluorescent C4 is formed. The deprotection of C4-*t*-Boc as a function of exposure time is illustrated in Fig. 4 for a 60 s PEB. Fluorescence measurements were taken at room temperature following rapid cooling of the sample on a metal surface.

Our experiments were performed using an aluminum plate for PEB, held in an oven at 90 °C; that is, not only the surface, but also the air surrounding the sample were at 90 °C. This is not common practice in industry, where a 90 °C bake usually means that the sample is placed on a surface held at 90 °C, but exposed also at room temperature on the film side of the sample. A comparison of both conditions is shown in Fig. 4B. Clearly, the real temperature of the sample is lower in the open bake, i.e., hotplate, normally used in industry. The scatter in plots of this type (Fig. 4B) likely results from the fact that each point is the measurement of a separate exposure and PEB on a different film (the same applies to the plot in Fig. 2B).

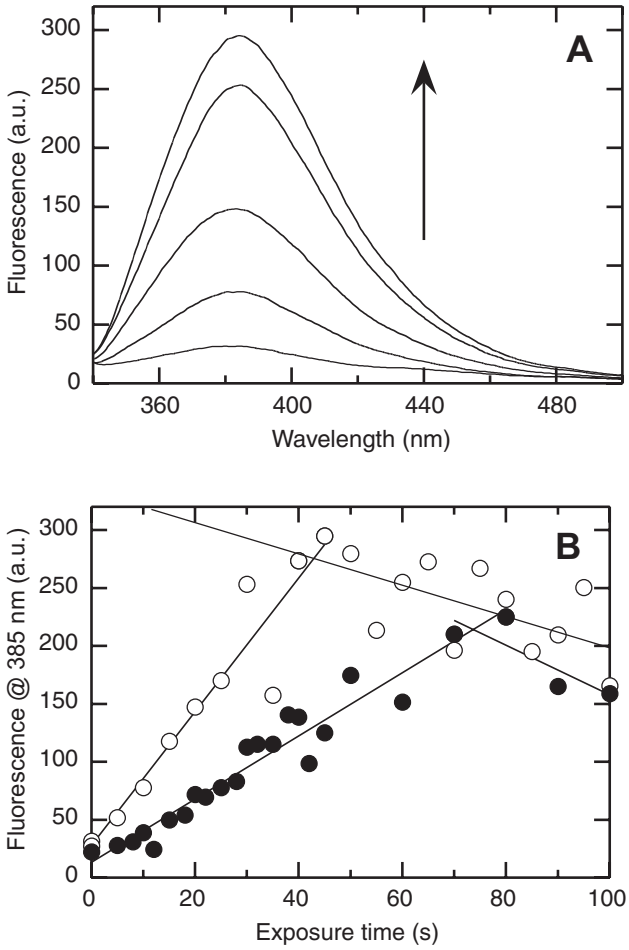
Increasing fluorescence intensity was also recorded with increasing PEB time, although the dependence is not linear; for example, between 30 and 90 s, the amount of C4 formed does not triple, but only increases by about 70%.

Discussion

Deprotection is assumed complete when the near-plateau region of plots such as those shown in Fig. 4B is attained. This assumption is based on thermogravimetric analysis (TGA) previously reported for C4-*t*-Boc (9) and the study of *t*-Boc deprotection using IR spectroscopy, which shows a complete disappearance of the *t*-Boc signal under similar conditions (14, 16). Fluorescence calibration curves using known amounts of C4 were attempted, but this methodology was not successful. For example, in equimolar concentrations with similar development conditions, the fluorescence of films containing C4 was less intense than those containing C4-*t*-Boc (following complete deprotection). The lower fluo-

© 2005 NRC Canada

Fig. 4. (A) Increase in fluorescence intensity (λ_{exc} = 320 nm) owing to the formation of C4 (i.e., deprotected C4-*t*-Boc) with increasing exposure time: (from bottom) 0, 10, 20, 30, and 45 s. PEB is constant in this case, i.e., oven baked at 90 °C for 60 s. (B) Fluorescence intensity (λ_{mon} = 385 nm) as a function of exposure time comparing oven (○) and hotplate (●) PEB, both at 90 °C for 60 s.



rescence intensity of C4 (cf. deprotected C4-*t*-Boc) may be a result of C4 clusters forming in PMMA after spin coating from solution. It would appear that aggregation can be prevented by in situ production of the dye.

Plots such as those shown in Fig. 4B normally show a small depletion slope after the anticipated plateau region is reached. This may result from the acid that negatively affects the efficiency of C4 fluorescence (17), or simply that once deprotected, the C4 molecules aggregate to less fluorescent clusters. Nonetheless, linear fits were successfully applied to the depleting plateau as well as the increasing fluorescent region. Consequently, the intercept of the two linear fits is the shortest exposure time leading to complete deprotection (see Table 1). The correlation between exposure time and acid yield (see Fig. 3) allowed the determination of the catalytic chain lengths at the onset of complete deprotection, also tabulated in Table 1.

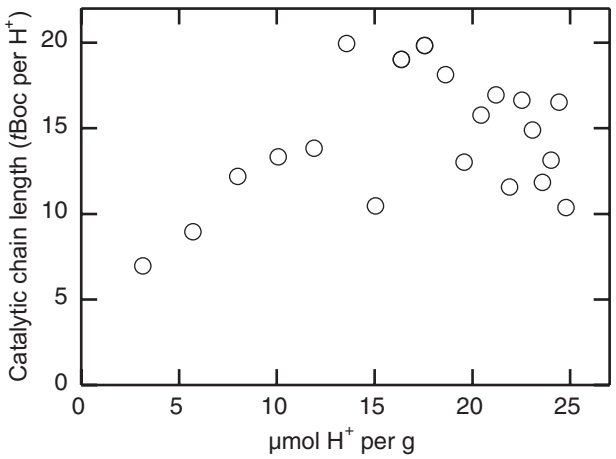
These catalytic chain lengths are low when compared with previously reported values, some of which are as high as 1000 *t*-Boc cleavages per proton (14). This is expected when

Table 1. Acid-catalyzed *t*-Boc deprotection chain lengths at the onset of 100% efficiency for different PEB conditions.[a]

PEB conditions (s)	Exposure time (s) for titration end point[b]	Catalytic chain length
30[c]	50	17
60[c]	43	19
90[c]	33	22
60[d]	74	14

[a]Errors estimated as ±20%.
[b]Exposure time required to reach the near-plateau region.
[c]In an oven at 90 °C.
[d]On a hotplate at 90 °C.

Fig. 5. Catalytic chain length for the deprotection of C4-*t*-Boc as a function of the amount of acid present.



considering the differences between the systems studied. Most importantly, the *t*-Boc groups in our experiments are very dilute in comparison to the density of the protecting groups found in actual polymer resists. Approximately 3.3% of the sample weight is *t*-Boc in our system, the remainder is mainly inert PMMA, well below its T_g, while in actual polymer resists the protecting group can account for as much as 45% of the total sample weight. In our case this means the protons have to migrate through PMMA to continue the catalytic deprotection process, obviously lowering the chain length.

While the chain lengths are quite different, it is still possible to compare acid diffusion in both systems. Assuming spherical diffusion of acid and a matrix density of 1.15 g/mL (same as bulk PMMA), we can calculate an average proton diffusion radius of 27 Å to deprotect 19 groups, i.e., after a 60 s PEB at 90 °C in an oven. A value of approximately 50 Å was reported when a proton deprotects 1000 units of poly(4-*tert*-butoxycarbonyloxystyrene) (14), i.e., of the same order of magnitude as our results. Interestingly, these diffusion radii (3–5 nm) are within an order of magnitude of the anticipated feature sizes in the near future (30–90 nm).

It is also possible to plot catalytic chain length at varying acid concentrations (Fig. 5) with the following data analysis: CCL = (*t*-Boc:PAG)($\varphi_{t\text{-Boc}}/\varphi_{acid}$), where CCL is the catalytic chain length in mol of *t*-Boc deprotected per mol of photogenerated acid, *t*-Boc:PAG is the initial molar ratio of C4-*t*-Boc to PAG (TPS-OTf in our case), $\varphi_{t\text{-Boc}}$ is the

© 2005 NRC Canada

deprotection efficiency calculated from fluorescence intensity data (scaled to the near-plateau slope, see Fig. 4B), and φ_{acid} is the acid conversion efficiency from the PAG (see Fig. 3).

It is useful to see the efficiency of deprotection when either the proton or *t*-Boc is the limiting reagent. A small decrease in catalytic chain length after quantitative *t*-Boc deprotection is expected since the number of events is held constant while the catalyst concentration is increased; this decrease is apparent at proton yields above 15 μmol/g, even if the dispersion of the data tends to mask this effect. The more interesting result happens when the acid is the limiting reagent. In this case, one might expect the catalytic chain length to be equal, or even higher, than the conditions when total deprotection is first achieved, i.e., as we approach the intercept in Fig. 4B. While the data is accompanied by a considerable uncertainty, there is a clear increase in catalytic chain length from the lower acid concentrations to the point of quantitative *t*-Boc cleavage. This lower chain length when *t*-Boc groups are in excess is counterintuitive; the proton has the "choice" of more *t*-Boc groups to deprotect without competition from other acids in these conditions.

We propose that the unusual increase in catalytic chain length at low acid concentrations in Fig. 5 is due to base contamination. The presence of air-borne base is common in chemistry laboratories, and is frequently a problem in industries employing microlithography based on PAGs (1, 2). Thus, some acid is used in a sacrificial manner to neutralize unwanted base. At low acid concentrations this has significant impact on the chain length, while at high acid concentrations the amount of sacrificial acid used is too small to impact on the overall result.

Conclusion

A novel method was developed to measure catalytic chain lengths for *t*-Boc deprotection in polymer films using fluorescent probes for both acid and deprotection yields. We used fluorescence, a very sensitive spectroscopic technique, as a tool to characterize the processes occurring in the polymer film. C6 and C4-*t*-Boc proved to be excellent probes, with considerable shifts in their absorbance and fluorescence spectra after protonation and deprotection, respectively, thus allowing easy monitoring; further, the emission spectra of these two probes are very distinct, readily allowing selective monitoring. The lower catalytic chain lengths obtained in this study apply to the low concentration of *t*-Boc group in the film. The protocol developed will be examined further and applied to resists containing polymers with pendant *t*-Boc protected groups. For the catalytic chain length, we obtained values in the 14–22 range depending on the PEB conditions.

Acknowledgements

Thanks are due to the Natural Sciences and Engineering Research Council of Canada (NSERC) and to Rohm and Hass Electronic Materials for generous financial support.

References

1. H. Ito, C.G. Willson, and J.M.J. Fréchet. Symp. VLSI Technol. **260**, 262 (1982).
2. H. Ito. J. Polym. Sci. Part A: Polym. Chem. **41**, 3863 (2003).
3. S.A. MacDonald, C.G. Willson, and J.M.J. Fréchet. Acc. Chem. Res. **27**, 151 (1994).
4. J.C. Scaiano, M. Laferriere, M.G. Ivan, and G.T. Taylor. Macromolecules, **36**, 6692 (2003).
5. M.D. Mason, K. Ray, R.D. Grober, G. Pohlers, and J. Cameron. Phys. Rev. Lett. **93**, 073004-1 (2004).
6. G. Pohlers, J.C. Scaiano, and R. Sinta. Chem. Mater. **9**, 3222 (1997).
7. N.C. Yang, H.W. Choi, J.K. Lee, J.I. Hwang, and D.H. Suh. Chem. Lett. **8**, 824 (2002).
8. J.-H. Yoo, S.-Y. Kim, I. Cho, J.-M. Kim, K.-D. Ahn, and J.-H. Lee. Polym. Commun. **45**, 5391 (2004).
9. M. Frenette, C. Coenjarts, and J.C. Scaiano. Macromol. Rapid Commun. **25**, 1628 (2004).
10. P.M. Dentinger, B. Lu, J.W. Taylor, S.J. Bukofsky, G.D. Feke, D. Hessman, and R.D. Grober. J. Vac. Sci. Technol. B, **16**, 3767 (1998).
11. G.D. Feke, D. Hessman, R.D. Grober, B. Lu, and G.T. Taylor. J. Vac. Sci. Technol. B, **18**, 136 (2000).
12. S.J. Bukofsky, G.D. Feke, Q. Wu, and R.D. Grober. Appl. Phys. Lett. **73**, 408 (1998).
13. T.U.L. Schlegel, H. Shiraishi, N. Hayashi, and T. Iwayanagi. Chem. Mater. **2**, 299 (1990).
14. U.S.D. McKean and S.A. MacDonald. J. Polym. Sci. Part A: Polym. Chem. **27**, 3927 (1989).
15. S.A. MacDonald, W.D. Hinsberg, H.R. Wendt, N.J. Clecak, C.G. Willson, and C.D. Snyder. Chem. Mater. **5**, 348 (1993).
16. A.R. Pawloski and P.F. Nealey. Chem. Mater. **14**, 4192 (2002).
17. S.G. Schulman and L.S. Rosenberg. J. Phys. Chem. **83**, 447 (1979).

© 2005 NRC Canada

Metal-catalysed tandem metathesis–hydrogenation reactions for the synthesis of carba analogues of cyclic peptides[1]

Amanda N. Whelan, Jomana Elaridi, Roger J. Mulder, Andrea J. Robinson, and W. Roy Jackson

Abstract: Dicarba cyclic peptide analogues of the cystine-containing octapeptides octreotide, lanreotide, and vapreotide, all known somatostatin analogues, have been synthesized via an on-resin homogeneous metal-catalysed sequence involving ruthenium-catalysed ring-closing metathesis followed by rhodium-catalysed hydrogenation.

Key words: dicarba-analogues of cystine-containing peptides, octreotide, vapreotide, and lanreotide; tandem ring-closing metathesis and hydrogenation.

Résumé : Des peptides cycliques dicarbonés analogues de la cystine contenant les octapeptides octréotide, lanréotide et vapréotide, tous connus comme étant des analogues de la somatostatine, ont été synthétisés sur résine via une série de catalyses homogènes impliquant une métathèse de fermeture de cycle catalysée par du ruthénium et une hydrogénation catalysée par du rhodium.

Mots clés : analogues dicarbonés de la cystine contenant des peptides, octréotide, vapréotide et lanréotide; réaction tandem de fermeture de cycle par métathèse et hydrogénation.

Introduction

Cystine bridges are common structural motifs in naturally occurring cyclic peptides. In some cases, as in spiruchostatin A (1), the disulphide bridge acts as a reactive functional group undergoing reduction within the cell to release metal-chelating thiol groups (2, 3). In many other cases, however, the cystine bridge serves only a skeletal, structural role, maintaining secondary and tertiary structure and may be replaced with a nonreducible structural mimic without significantly affecting biological activity (4). Indeed, thioether linkages (-S–CH_2-) (5) and the all carbon (-CH_2–CH_2-) bridge (6) have both been successfully implemented as cystine (-S–S-) isosteres producing peptides with enhanced biostability.

The cyclic peptide octreotide **1a** (7), a synthetic analogue of the tetradecapeptide somatostatin, has one cystine bridge that is remote from the receptor binding site. When labelled with ^{111}In, it is marketed as OctreoScan® (8) and used for the imaging of neuroendocrine tumours (9). It has also been conjugated with ^{123}I, ^{64}Cu, and ^{99m}Tc (10). The ^{99m}Tc radionuclide possesses a convenient physical half life ($t_{1/2}$ = 6 min), an attractive radiation profile, is inexpensive, and readily available as pertechnate ($^{99m}TcO_4^-$).[3] Incorporation of this isotope into cystine-containing peptides, however, is often complicated by the need for a reductive step to generate Tc^{5+} for stable chelate formation (11). In the case of octreotide, a concomitant reduction of the disulphide bridge opens the cyclic peptide and results in the loss of receptor binding affinity (12). This problem is not exclusive to octreotide and also occurs during the Tc labelling of other cyclic peptides containing cystine bridges, including the octreotide analogues lanreotide **2a** and vapreotide **3a**. Given the high desirability to label these peptides with technetium, the replacement of the reductively labile disulphide bridge with a carbon-based manifold has been investigated leading to the dicarba analogues **1b**, **2b**, and **3b**. This structural alteration would be inert to cellular reductases and also with-

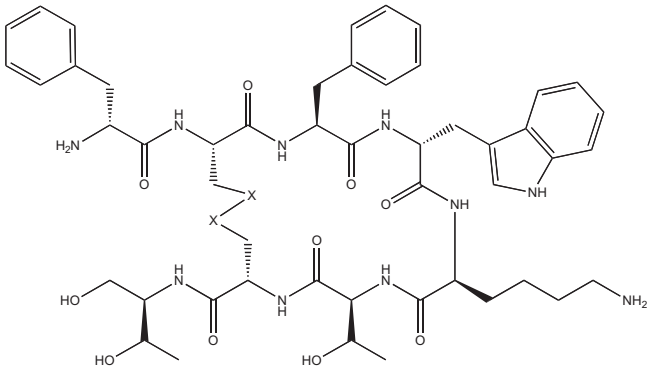
Received 14 December 2004. Published on the NRC Research Press Web site at http://canjchem.nrc.ca on 22 July 2005.

Dedicated to Professor Howard Alper in recognition of his major contribution to metal-catalysed reactions in organic synthesis.

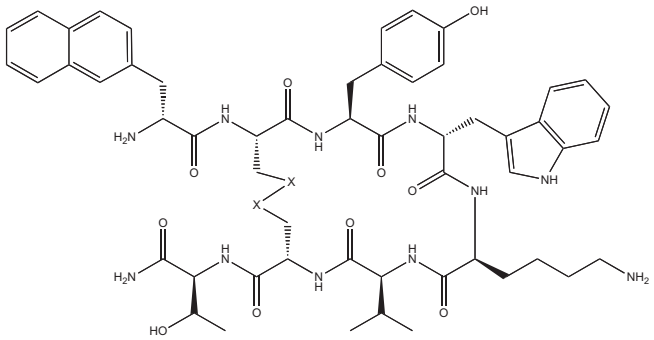
A.N. Whelan. School of Chemistry, Monash University, Clayton, VIC 3800, Australia and CSIRO Molecular Science, Bag 10, Clayton South, VIC 3169, Australia.
J. Elaridi and A.J. Robinson. School of Chemistry, Monash University, Clayton, VIC 3800, Australia.
R.J. Mulder. CSIRO Molecular Science, Bag 10, Clayton South, VIC 3169, Australia.
W.R. Jackson.[2] Centre for Green Chemistry, Monash University, Clayton, VIC 3800, Australia.

[1]This article is part of a Special Issue dedicated to Professor Howard Alper.
[2]Corresponding author (e-mail: Roy.Jackson@sci.monash.edu.au).
[3]^{99m}Tc has superior nuclear characteristics for imaging ($t_{1/2}$ = 6.02 h and monoenergetic emission 141 keV), while ^{188}Re physical characteristics are ideal for therapy ($t_{1/2}$ = 16.9 h and β-emission 2.11 MeV).

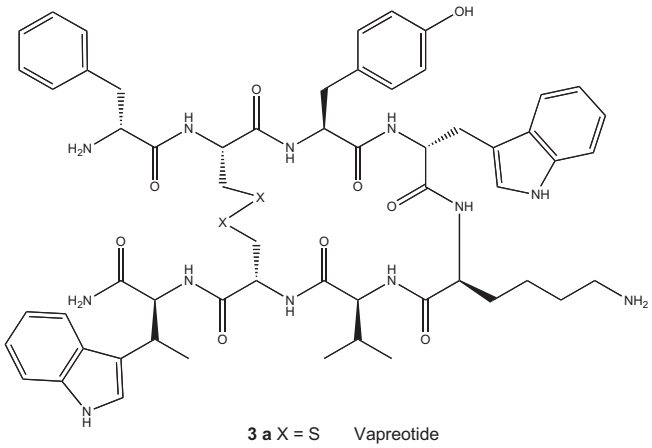
 doi: 10.1139/V05-100 © 2005 NRC Canada



1 a X = S Octreotide
1 b X = CH_2 Dicarba octreotide analogue



2 a X = S Lanreotide
2 b X = CH_2 Dicarba lanreotide analogue

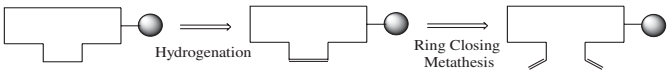


3 a X = S Vapreotide
3 b X = CH_2 Dicarba vapreotide analogue

stand chemical reducing agents, such as stannous chloride, used in the preparation of Tc-labelled radiopharmaceuticals.

A highly generic, on-resin, tandem-homogeneous catalysis strategy has been devised, which involves: (*i*) construction of the linear peptide sequence replacing cysteine residues with allyl glycine; (*ii*) Ru(II)-catalysed metathesis of the allyl groups to affect carbocycle formation; and (*iii*) Rh(I)-catalysed homogeneous reduction of the newly formed olefin to yield the desired sp^3-hybridized bridge (13) (Scheme 1).

Scheme 1.



Grubbs catalysts (14) have previously been used to facilitate the formation of cyclic peptides via metathesis (15), but only Vederas and co-workers (16), in a recent paper targeting oxytocin, have used bis(allyl glycine) containing peptides to form dicarba mimics of the cystine bridge. We believe that the protocol outlined in this paper demonstrates some clear advantages over the previously published method. It is also highly generic and can be applied to any peptide containing a cystine bridge.

Results and discussion

Synthesis of linear peptides

The protocol described utilizes the non-proteinaceous amino acid allyl glycine, which we have previously reported can be conveniently generated in both enantiomeric forms, via Rh(I)-catalysed hydrogenation of α-*N*-acyl dienamides with excellent stereoselectivity (95% ee) and yield (90%) (17). It is also commercially available, albeit at high cost.

The synthesis of dicarba-octreotide analogue **1b** also requires a second non-proteinaceous residue, Fmoc-protected threoninol. This residue is readily formed by the reduction of the protected amino acid threonine to the corresponding alcohol, although it is also commercially available. The resultant diol is functionalized as the *p*-carboxybenzaldehyde acetal in preparation for attachment to the resin.

The linear peptide precursor of the dicarba-octreotide analogue was synthesized on Rink amide resin using a modified solid-phase protocol described by Hsieh and co-workers (18). The above described acetal is attached to the resin using the coupling reagents DIC and HOBt to give **4**. The remaining sequence was constructed manually using standard solid-phase peptide synthesis techniques, utilizing Fmoc-protected amino acids and the coupling reagents HATU and NMM (Scheme 2). Intermediates were carried through without purification or characterization up to the octapeptide **5**. A sample of the linear peptide was obtained by cleavage from the resin and was determined to be of >95% purity by reverse-phase analytical chromatography and had the required molecular mass by mass spectral analysis.

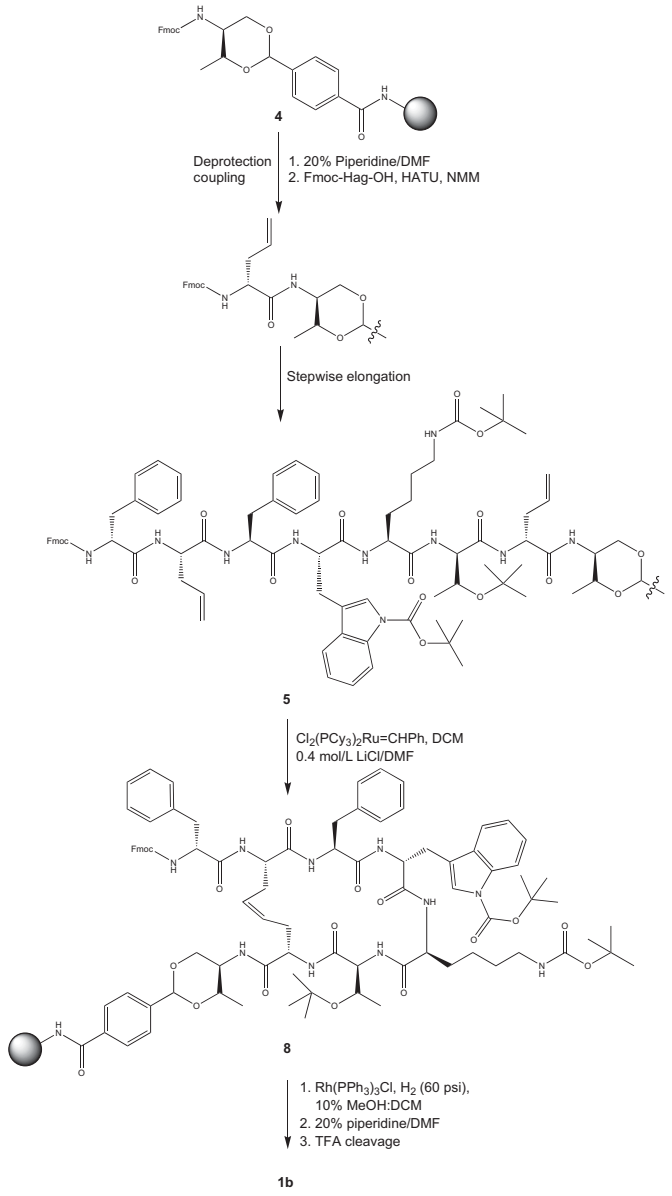
The resin-bound linear peptide precursors for the synthesis of dicarba-analogues of lanreotide **2b** and vapreotide **3b** were also prepared on Rink amide resin (Scheme 3). Use of this resin allowed the direct generation of the required C-terminal amide found in **2b** and **3b** upon acid cleavage from the resin. All couplings were accomplished utilizing HATU and NMM. After complete sequence construction, a small sample was cleaved from the resin and the presence of the desired peptide was confirmed by mass spectral analysis.

Cyclisation by ring-closing metathesis of the linear peptides

Ring-closing metathesis was carried out using the resin-attached linear peptides **5–7** to eliminate any potential problems arising from dimerization and (or) poor peptide solubility.

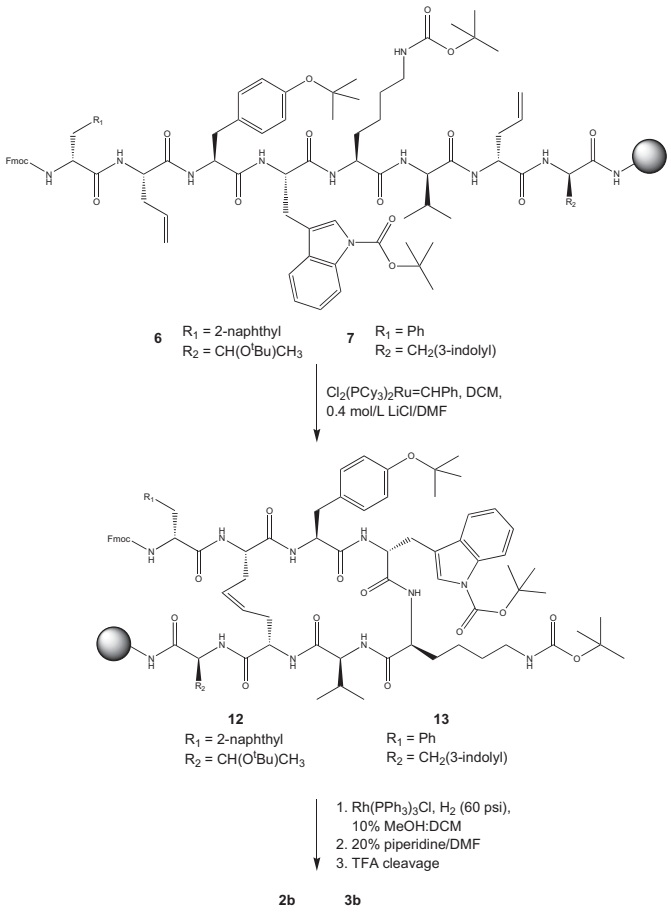
© 2005 NRC Canada

Scheme 2.

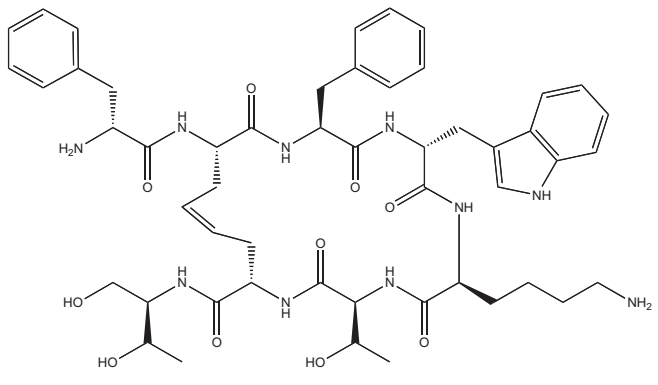


Exposure of the fully protected allyl glycine containing octreotide sequence **5** to the ruthenium benzylidene complex $Cl_2(PCy_3)_2Ru$=CHPh (Grubbs catalyst) (14) resulted in formation of the carbocycle **8** in 65% yield[4] (Scheme 2). It was necessary to react the peptide whilst fully protected as it was found that exposed amino and carboxylate groups prevented metathesis, in agreement with previous observations with other systems (19). To prevent aggregation of the resin-tethered peptide during the metathesis reaction, it was vital that a salt be added, in this case a solution of lithium chloride in DMF. Also essential for complete reaction were extended reaction times; reaction times less than 48 h yielded a significant amount of starting material. Significantly, no oligomerization or dimerization by acyclic diene metathesis (ADMET) (20) was observed.

Scheme 3.



On completion of the metathesis, an aliquot of peptide was cleaved from the resin for analysis. Analytical LC–MS analysis of the cleaved material revealed one major product with molecular mass consistent with that of **9** and a pure sample (>98%) was obtained in 46% yield after purification by preparative HPLC.



9

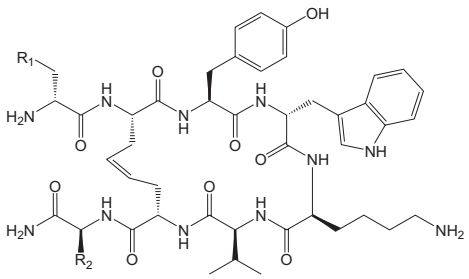
The geometry of the newly formed olefinic bond of **9** was investigated by NMR spectroscopy. The olefinic protons are represented in the ^{1}H NMR spectrum by a broad and ill-

[4] Yields of peptides were determined after cleavage of the peptide from the resin and calculated using an average peptide loading of 0.71 mmol/g of resin.

© 2005 NRC Canada

resolved signal, centred on 5.38 ppm, which integrates to two hydrogens. COSY and TOCSY experiments correlated this signal to both methylene groups adjacent to the newly formed carbon–carbon double bond (2.20/2.36 and 2.27 ppm). Whilst coupling constants could not be accurately extracted from the one-dimensional ^{1}H NMR spectrum or from the phase-sensitive COSY spectrum, simulation[5] of the NMR signals using the estimates of the coupling constants from these spectra indicates that the newly formed olefin is cis in geometry. The simulated spectrum that achieved very good similarity with the experimental data was obtained using a vicinal olefinic coupling constant of 10.2 Hz, which is consistent with the cis geometry. Good agreement between the simulated and experimental spectra could not be achieved using values of 14–19 Hz, which would be consistent with a trans double bond.

Cyclisation of the resin-attached dicarba-lanreotide **6** and dicarba-vapreotide **7** precursors proceeded via the same technique as described above (Scheme 3). The reactions did, however, require longer reaction times, with both reactions reaching completion after 96 h. In each case, mass spectral analysis of the Fmoc- and resin-cleaved peptides showed only the desired product and no remaining linear precursor or higher oligomers. Preparative HPLC of the crude unsaturated cyclic peptides **10** and **11** resulted in high purity material albeit at reduced yield. The lanreotide **10** and vapreotide **11** analogues were subsequently isolated in 25% and 2% yield with 98.6% and 99.2% purity, respectively.



10 R_1 = 2-naphthyl, R_2 = CH(OH)CH$_3$ **11** R_1 = Ph, R_2 = CH$_2$(3-indolyl)

Reduction of olefinic dicarba-peptides

Reduction of the newly installed olefinic bond is necessary to complete the synthesis of the dicarba analogues of octreotide **1b**, lanreotide **2b**, and vapreotide **3b**. A homogeneous hydrogenation catalyst, the Rh(I)-based Wilkinson's catalyst, was chosen to facilitate the reduction of the resin-bound material. This catalyst was chosen for its ease of use and facile removal from resin-bound peptides.

Reduction in dichloromethane alone, a solvent preferred for efficient swelling of the Rink amide resin but non-ideal for hydrogenation, was found to be exceptionally slow and often incomplete. The addition of a coordinating solvent subsequently enabled quantitative reduction (21). Traditional hydrogenation solvents such as methanol have very poor resin-swelling abilities, resulting in limited availability of reactive sites. Rh(I)-catalysed hydrogenation in 10% methanol – dichloromethane was investigated and this system was found to effect quantitative reduction at room temperature under mild hydrogen pressure (60 psi, 1 psi = 6.894 757 kPa). The peptide **1b** was purified using reverse-phase preparative chromatography to give material of >98.9% purity in 26% isolated yield and characterized using mass spectrometry and ^{1}H NMR spectroscopy.

Table 1. ^{1}H NMR chemical shifts (ppm) of dicarba-octreotide analogue **1b** (500.13 MHz, DMSO-d_6).

	NH	α-H	β-H	Others
D-Phe[1]	7.59	4.30	2.90, 2.75	H2, H6 7.62
				H3, H5 7.35
				H4 7.27
Hag[2]	8.09	4.29	1.05, 1.05	γ-H 4.05
Phe[3]	7.80	4.61	2.68, 2.80	H2, H6 7.81
				H3, H5 7.60
				H4 7.28
D-Trp[4]	8.49	4.28	3.05, 2.82	H2 8.51
				H4 7.05
				H5 7.50
				H6 7.32
				H7 6.95
Lys[5]	8.23	4.08	1.61, 1.61	γ-H 0.95, 0.95
				δ-H 1.45, 1.45
				ε-H 2.60, 2.60
Thr[6]	7.74	4.02	4.88	γ-H 1.08
Hag[7]	7.66	4.22	1.58	γ-H 4.10
Thr(ol)[8]	7.15	3.58	3.82	γ-H 0.95
				δ-H 2.62

The hydrogenation conditions established for the resin-tethered octreotide analogue were then applied to the olefinic dicarba analogues of lanreotide **12** and vapreotide **13** yielding the saturated carbocycles **2b** and **3b** as indicated by MS and NMR (Scheme 3). Preparative HPLC again gave significantly reduced mass recoveries of highly pure materials, 4% and 20% yields, respectively, for **2b** and **3b**, with purities of >97%.

Molecular modelling studies of carbocycle **1b** (22) based on X-ray diffraction data of octreotide (23) suggests that the structural modification should not significantly perturb the Phe^7-D-Trp^8-Lys^9-Thr^{10} binding domain and hence somatostatin receptor affinity. A detailed NMR study is in progress and ^{1}H chemical shifts for **1b** and its unsaturated analogue **9** are summarized in Tables 1 and 2, respectively. ^{1}H NMR data for the dicarba-lanreotide **2b** is shown in Table 3. The preliminary data suggests the presence of a β-turn, in agreement with the results of molecular modelling studies.

Competitive binding experiments of the six dicarba analogues **1b**–**3b** and **9**–**11** against ^{111}In-DOTA-octreotate for the sst2-expressing AR42J cell membranes is currently being investigated. Further work will involve testing the binding affinity of the new dicarba somatostatin analogues for other somatostatin receptor sub-types and the effect of conjugating bifunctional ligands on their affinity.

[5] Simulation was performed using Bruker-Biospin's NMR-Sim® v3.5. Spectral simulations were performed using the same acquisition and processing parameters that were used to acquire the original data.

© 2005 NRC Canada

Table 2. ^{1}H NMR chemical shifts (ppm) of unsaturated dicarba-octreotide analogue **9** (500.13 MHz, DMSO-d_6).

	NH	α-H	β-H	Others[a]
D-Phe[1]	7.37	4.41	2.71, 3.02	H2, H6
				H3, H5
				H4
Hag[2]	8.43	4.71	2.20, 2.36	γ-H 5.38
Phe[3]	8.05	4.62	2.76, 2.76	H2, H6
				H3, H5
				H4
D-Trp[4]	8.57	4.35	2.79, 3.03	H2
				H4
				H5
				H6
				H7
Lys[5]	8.60	4.02	0.96, 0.96	γ-H 1.42, 1.42
				δ-H 1.70, 1.70
				ε-H 2.63, 2.63
Thr[6]	7.71	4.29	3.99, 3.99	γ-H 1.04
Hag[7]	7.82	4.59	2.27, 2.27	γ-H 5.38
Thr(ol)[8]	7.37	3.97	3.65, 3.65	γ-H 1.07
				δ-H 3.37, 3.49

[a]Signal overlap prohibits unambiguous assignment of aromatic protons.

Table 3. ^{1}H NMR chemical shifts (ppm) of dicarba-lanreotide analogue **2b** (500.13 MHz, DMSO-d_6).

	NH	α-H	β-H	Others
D-β-Nal[1]	7.67	4.43	2.93, 3.12	H1 7.73
				H3 7.43
				H4 7.74
				H5 7.81
				H6 7.38
				H7 7.32
				H8 7.85
Hag[2]	8.12	4.28	1.05, 1.05	γ-H 1.34, 1.34
Tyr[3]	7.81	4.54	2.55, 2.69	H2, H6 6.70, 6.70
				H3, H5 6.48, 6.48
D-Trp[4]	8.38	4.31	2.85, 3.06	H2 7.78
				H4 7.51
				H5 6.97
				H6 7.04
				H7 7.29
Lys[5]	7.92	4.16	1.61, 1.61	γ-H 1.06, 1.06
				δ-H 1.40, 1.40
				ε-H 2.67, 2.67
Val[6]	7.65	3.98	1.96	γ-H 0.88, 0.88
Hag[7]	7.95	4.31	1.05, 1.05	δ-H 1.63, 1.63
Thr[8]	7.41	4.83	4.11	γ-H 0.99

Conclusion

The methodology described in this paper is a highly efficient, generic, on-resin route to carbon-based somatostatin mimics, which could find wide-spread use in peptidomimetic research. Our group is currently applying this methodology to other peptides, particularly cystine-containing cyclic peptides.

Experimental

Instrumentation and general procedures

^{1}H and ^{13}C NMR spectra were recorded on a Bruker DPX300 spectrometer operating at 300.13 MHz (^{1}H) and 75.48 MHz (^{13}C).

The NMR spectra of the peptides were recorded in DMSO-d_6 (referenced to δ_H 2.49 ppm) at 298 K using a Bruker DRX500 spectrometer at 500.13 MHz for ^{1}H using a 5 mm inverse-detection ^{1}H–^{13}C–^{15}N TXI probe with z gradients. Pulse sequences are from the Bruker XWIN-NMR v3.5 library. Chemical shift data were derived from a combination of the COSY45, COSY, and TOCSY experiments. Assignments were made using standard peptide NMR assignment techniques (24).

The two-dimensional COSY45 experiments were performed in magnitude mode using gradient selection and a 45° pulse: 4096 points in t_2 and 512 points in t_1 were acquired with 16 scans per t_1 point and a 0.8 s relaxation delay between scans. The spectral width was 6000 Hz in both dimensions. 2048 Points in t_2 and zero-filling to 1024 points in t_1 were used. An unshifted sine-bell window function was applied in both dimensions prior to Fourier transformation.

The two-dimensional COSY experiments were performed in phase-sensitive mode using echo/antiecho–TPPI gradient selection: 4096 points in t_2 and 512 points in t_1 were acquired with 64 scans per t_1 point and a 0.8 s relaxation delay between scans. The spectral width was 6000 Hz in both dimensions. Zero-filling to 4096 points in t_2 and forward linear prediction to 1024 points and zero-filling to 4096 points in t_1 were used. An unshifted sine-bell window function was applied in both dimensions prior to Fourier transformation.

The two-dimensional TOCSY experiments were performed in phase-sensitive mode using echo/antiecho–TPPI gradient selection: 4096 points in t_2 and 512 points in t_1 were acquired with 32 scans per t_1 point and a 0.8 s relaxation delay between scans. The spectral width was 6000 Hz in both dimensions. The TOCSY mixing time was 120 ms. 2048 Points in t_2 and zero-filling to 1024 points in t_1 were used. A π/4-shifted, sine-squared-bell window function was applied in both dimensions prior to Fourier transformation.

The two-dimensional NOESY experiments were performed in phase-sensitive mode using States gradient selection: 4096 points in t_2 and 512 points in t_1 were acquired with 64 scans per t_1 point and a 0.8 s relaxation delay between scans. The spectral width was 6000 Hz in both dimensions. The NOESY mixing time was 400 ms. 2048 Points in t_2 and zero-filling to 1024 points in t_1 were used. An exponential window function of 3.0 Hz was applied in the t_2 dimension and a π/4-shifted, sine-squared-bell window function was applied in the t_1 dimension prior to Fourier transformation.

Positive electrospray mass spectral data were obtained on a VG Platform mass spectrometer using a cone voltage of 50 V.

Analytical HPLC spectra were recorded on a Waters Alliance 2695 Separations Module equipped with a Waters PDA 2996 detector monitoring 190–300 nm. Components were separated on either an Altima 150 mm × 4.6 mm C18 5 μm

© 2005 NRC Canada

Table 4. Data for cyclic peptide analogues.

No.	Molecular formula	Exact mass	*m/z* (Pos. ion) obtained	Retention time (min)[a]	% Yield	% Purity
9	$C_{51}H_{68}N_{10}O_{10}$	980.51	981.2	30.10	46	98.9
1b	$C_{51}H_{70}N_{10}O_{10}$	982.53	983.6	33.37	23	98.8
10	$C_{56}H_{70}N_{11}O_{10}$	1057.54	1058.6	46.00	25	98.6
2b	$C_{56}H_{72}N_{11}O_{10}$	1059.55	1060.3	43.25	4	97.0
11	$C_{59}H_{71}N_{11}O_{10}$	1093.54	1094.5	11.42	2	99.2
3b	$C_{59}H_{73}N_{11}O_{10}$	1095.55	1096.4	39.50	20	99.6

[a]Preparative HPLC.

packed column or a Waters 50 mm × 4.6 mm Xterra C18 2.5 μm packed column. Purification via preparative HPLC was achieved using a Shimadzu LC-4A with an SPD-2AS detector (227 nm) and a C18 Altima 250 mm × 22 nm 5 μm packed column.

Solvents were purified, dried, and degassed according to standard procedures. Degassed methanol and dichloromethane were used in hydrogenation reactions. Deuterated chloroform was used as supplied by Merck. Deuterated dimethylsulphoxide (99.96% D, DLM-34) was used as supplied by Cambridge Isotope Laboratories. Chemical reagents, including amino acids, were purchased from Sigma-Aldrich, AusPep, or GL Biochem and were used without further purification. Catalysts were used as received from Strem chemicals. Grubbs catalyst refers to bis(tricyclohexylphosphine)benzylidene ruthenium dichloride. Wilkinson's catalyst refers to chlorotris(triphenylphosphine)rhodium(I). All ruthenium-catalysed metathesis reactions were performed using standard Schlenk techniques under an atmosphere of nitrogen. In all rhodium-phosphine hydrogenations, high purity (<10 ppm of oxygen) hydrogen and argon (supplied by BOC gases) were used and purified by passage through a series of traps to remove water, oxygen, and hydrocarbons.

Synthesis of the linear peptides

Fmoc-L-threoninol p-*carboxybenzacetal*

Fmoc-threoninol (1.0 g, 3.05 mmol), *p*-carboxybenzaldehyde (0.5 g, 3.36 mmol), and a catalytic amount of *p*-toluenesulphonic acid were suspended in dry toluene (70 mL) and stirred at reflux for 20 h using a Dean–Stark apparatus. The solvent was removed under reduced pressure to yield a clear yellow oil, which was extracted into dichloromethane and washed with water and saturated sodium chloride and dried over sodium sulphate. Purification of the yellow oil by flash chromatography (SiO_2, dichloromethane – ethyl acetate, 3:1) yielded the desired acetal (0.71 g, 51%), mp 86–88 °C (lit. value (18) mp 86–88 °C). ^{1}H NMR (300 MHz, $CDCl_3$) δ: 1.29 (d, *J* = 6.4 Hz, 3H, C*H*$_3$), 3.73 (dd, *J* = 10.1, 1.6 Hz, 1H, NHCHC*H*(H)), 4.11–4.27 (m, 4H, C*H*CH$_3$, C*H*$_2$OCO, and NHCHCH(*H*)), 4.51–4.38 (m, 2H, H9 and NHC*H*), 5.57 (d, *J* = 9.9 Hz, 1H, N*H*), 5.65 (s, 1H, OC*H*O), 7.32 (t, *J* = 7.4 Hz, 2H, H2, H7), 7.40 (t, *J* = 7.6 Hz, 2H, H3, H6), 7.62 (d, 2H, *J* = 7.2 Hz, H2′, H6′), 7.63 (d, *J* = 8.4 Hz, 2H, H3′, H5′), 7.77 (d, *J* = 7.3 Hz, 2H, H1, H8), 8.14 (d, *J* = 8.3 Hz, 2H, H4, H5), 10.05 (s, 1H, COO*H*). ^{13}C NMR (75 MHz, DMSO-d_6) δ: 17.78 (*C*H$_3$), 47.45 (C9), 48.90 (NH*C*H), 67.12 (NHCH*C*H$_2$), 72.00 (*C*H$_2$OCO), 75.61 (CHCH$_3$), 100.84 (O*C*HO), 120.07 (C3, C6), 124.74 (C2′, C6′), 126.21 (C2, C7), 127.11 (C4, C5), 127.77 (C1, C8), 129.83 (C4′), 130.30 (C3′, C5′), 141.31 (C4a, C4b), 143.82 (C1′), 143.85 (C8a, C9a), 156.52 (*C*O), 170.94 (*C*OOH). MS (ESI$^+$, DCM–MeOH) *m/z*: 350.2 (M + Na$^+$), $C_{19}H_{21}NO_4Na$.

Peptide synthesis

Linear peptides were synthesized using manual solid-phase peptide synthesis techniques on Rink amide resin, utilizing 3 equiv. each of 9-fluorenylmethoxycarbonyl (Fmoc) protected amino acids and the coupling reagent HATU (*O*-(7-azabenzotriazol-1-yl)-*N*,*N*,*N*′,*N*′-tetramethyluronium hexafluorophosphate) and 6 equiv. of NMM (4-methyl morpholine). Fmoc-L-threoninol *p*-carboxybenzacetal was coupled directly to the resin in the synthesis of **5** using 3 equiv. each of the coupling reagents DIC (diisopropylcarbodiimide) and HOBt (1-hydroxybenzotriazole), as well as 3 equiv. of the acetal.

Upon completion of the synthesis of the linear Fmoc-protected octapeptide, a resin aliquot was removed and the peptide cleaved from the resin with trifluoroacetic acid (9 mL) containing the scavengers ethanedithiol (0.25 mL), thioanisole (0.5 mL), and phenol (0.79 g), as well as water (0.25 mL). The filtrate was concentrated by application of high pressure air. The peptide was precipitated by the addition of ice cold diethyl ether and was extracted into a 50% aqueous solution of acetonitrile and lyophilized to give a white solid that was characterized by mass spectral analysis.

General procedure for ring-closing metathesis

A Schlenk flask was charged with resin-tethered peptide (50–200 mg) to which dry dichloromethane (20 mL) and degassed 0.4 mol/L lithium chloride in dimethylformamide (1 mL) were added and the resin allowed to swell for 1 h before addition of a solution of Grubbs catalyst (20 mol%) in dry dichloromethane. The suspended resin was stirred at 50 °C for a prescribed period of time (48–96 h) and collected via filtration, washed with dichloromethane, dimethylformamide, and methanol, and finally dried in vacuo. An aliquot of the resin was removed and the peptide cleaved from the resin as described previously.

The peptide was purified using preparative reverse-phase high performance liquid chromatography (RP-HPLC) (20%–100% aqueous acetonitrile with 0.1% TFA over 2 h, 10 mL/min). Fractions were collected, lyophilized, and analysed by analytical HPLC, NMR, and mass spectral analysis (Table 4).

© 2005 NRC Canada

General procedure for hydrogenation

A Fischer–Porter tube was charged in a drybox with resin-tethered peptide (50–200 mg), Wilkinson's catalyst (1–5 mg), dry and deoxygenated dichloromethane (9 mL), and dry and deoxygenated methanol (1 mL). The line and reaction vessel were degassed with three vacuum–argon cycles each before the tube was pressurised to 60 psi of hydrogen. The reaction was stirred gently at room temperature overnight. The resin was collected via filtration and washed with dichloromethane, dimethylformamide, and finally methanol, before being allowed to dry in vacuo. An aliquot of the resin was removed and the peptide cleaved from the resin as described previously.

The peptide was purified using preparative reverse-phase HPLC (20%–100% aqueous acetonitrile with 0.1% TFA over 2 h, 10 mL/min). Individual fractions were collected, lyophilized, and analysed by analytical HPLC, NMR, and mass spectral analysis (Table 4). ^{1}H NMR data for dicarba octreotide **1b**, unsaturated dicarba octreotide **9**, and dicarba lanreotide **2b** are reported in Tables 1–3.

Acknowledgements

The authors would like to acknowledge funding from an Australian Postgraduate Award (awarded to ANW), as well as CSIRO and ANSIE grants. Further thanks go to Noel Hart and Stuart Littler for assistance in purification of the peptides.

References

1. K. Shin-ya, Y. Masuoka, A. Nagai, K. Furihata, K. Nagai, K. Suzuki, Y. Hayakawa, and Y. Seto. Tetrahedron Lett. **42**, 41 (2001).
2. A. Yurek-George, F. Habens, M. Brimmell, G. Packham, and A. Ganesan. J. Am. Chem. Soc. **126**, 1030 (2004).
3. R. Furumai, A. Matsuyama, N. Kobashi, K.-H. Lee, N. Nishiyama, H. Nakajima, A. Tanaka, Y. Komatsu, N. Nishino, M. Yoshida, and S. Horinouchi. Cancer Res. **62**, 4916 (2002).
4. P. Grieco, P. Campiglia, I. Gomez-Monterrey, T. Lama, and E. Novellino. Synlett, **14**, 2216 (2003), and refs. cited therein.
5. (*a*) P. Campiglia, I. Gomez-Monterrey, L. Longobardo, T. Lama, E. Novellino, and P. Grieco. Tetrahedron Lett. **45**, 1453 (2004), and refs. cited therein; (*b*) X. Zhu and R.R. Schmidt. Eur. J. Org. Chem. 4069 (2003), and refs. cited therein.
6. (*a*) R.F. Nutt, R.G. Strachan, D.F. Veber, and F.W.J. Holly. J. Org. Chem. **45**, 3078 (1980); (*b*) K. Undheim, J. Efskind, and G. Beate Hoven. Pure Appl. Chem. **75**, 279 (2003).
7. W. Bauer, U. Briner, W. Doepfner, R. Haller, R. Huguenin, P. Marbach, T.J. Petcher, and J. Pless. J. Life Sci. **31**, 1133 (1982).
8. D.A. Pearson, J. Lister-James, W.J. McBride, D.M. Wilson, L.J. Martel, E.R. Civitello, J.E. Taylor, B.R. Moyer, and R.T. Dean. J. Med. Chem. **39**, 1361 (1996).
9. (*a*) E.P. Krenning, D.J. Kwekkeboom, W.H. Bakker, W.A.P. Breeman, P.M. Kooji, H.Y. Oei, M. van Hagen, P.T.E. Postema, M. de Jong, J.C. Reubi, T.J. Visser, A.E.M. Reijs, L.J. Hofland, J.W. Koper, and S.W. Lamberts. Eur. J. Nucl. Med. **20**, 716 (1993); (*b*) W.H. Bakker, R. Albert, C. Bruns, W.A.P. Breeman, L.J. Hofland, P. Marbach, J. Pless, D. Pralet, B. Stolz, J.W. Koper, S.W.J. Lamberts, T.J. Visser, and E.P. Krenning. Life Sci. **49**, 1583 (1991).
10. J.S. Lewis, M.R. Lewis, A. Srinivasan, M.A. Schmidt, J. Wang, and C.J.J. Anderson. J. Med. Chem. **42**, 1341 (1999).
11. (*a*) T. Maina, B. Nock, A. Nikolopoulou, P. Sotiriou, G. Loudos, D. Maintas, P. Cordopatis, and E. Choitellis. Eur. J. Nucl. Med. **29**, 742 (2002); (*b*) J. Fichna and A. Janecka. Bioconjugate Chem. **14**, 3 (2003).
12. (*a*) H. Kolan, J. Li, and M.L. Thakur. Peptide Res. **9**, 144 (1996); (*b*) J.K. Amartey. Nucl. Med. Biol. **20**, 539 (1993).
13. A.N. Whelan, J. Elaridi, M. Harte, S.V. Smith, W.R. Jackson, and A.J. Robinson. Tetrahedron Lett. **45**, 9545 (2004).
14. S.T. Nguyen, L.K. Johnson, R.H. Grubbs, and J.W. Ziller. J. Am. Chem. Soc. **114**, 9858 (1992).
15. (*a*) H. Kessler and N. Schmiedeberg. Org. Lett. **4**, 59 (2002); (*b*) J.F. Reichwein, C. Versuluis, and R.M.J. Liskamp. J. Org. Chem. **65**, 6187 (2000); (*c*) T.D. Clark and M.R. Ghadiri. J. Am. Chem Soc. **117**, 12 364 (1995); (*d*) S.J. Miller and R.H. Grubbs. J. Am. Chem. Soc. **117**, 5855 (1995); (*e*) E.N. Prabhakaran, V. Rajesh, S. Dubey, and J. Iqbal. Tetrahedron Lett. **42**, 339 (2001); (*f*) H.E. Blackwell, J.D. Sadowsky, R.J. Howard, J.N. Samson, J.A. Chao, W.E. Steinmetz, D.J. O'Leary, and R.H. Grubbs. J. Org. Chem. **66**, 5291 (2001).
16. J.L. Stymiest, B.F. Mitchell, S. Wong, and J.C. Vederas. Org. Lett. **5**, 47 (2003).
17. E. Teoh, E.M. Campi, W.R. Jackson, and A.J. Robinson. Chem. Commun. 978 (2002).
18. H.P. Hsieh, Y.T. Wu, S.T. Chen, and K.T. Wang. Bioorg. Med. Chem. **7**, 1797 (1999).
19. Intolerance of catalysts to basic functionality has been previously reported. (*a*) S. Kotha, N. Sreenivasachary, K. Mohanraja, and S. Durani. Bioorg. Med. Chem. Lett. **11**, 1421 (2001); (*b*) R.H. Grubbs and S. Chang. Tetrahedron, **54**, 4413 (1998); (*c*) T.M. Trnka and R.H. Grubbs. Acc. Chem. Res. **34**, 18 (2001); (*d*) M.S. Sanford, J.A. Love, and R.H. Grubbs. J. Am. Chem. Soc. **123**, 6543 (2003).
20. M.R. Buchmeiser. Chem. Rev. **100**, 1565 (2000).
21. R. Santini, M.C. Griffith, and M. Qi. Tetrahedron Lett. **39**, 8951 (1998). Incompatible resin–solvent pairing can lead to poor reaction site availability and diminished reaction rates. Rink amide resin swells poorly in methanol, but exhibits high swell in chlorinated solvents.
22. The unit cell of octreotide reveals the flexibility of the peptide backbone and contains three individual molecules of the peptide. Only one molecule (Molecule II) possesses the rotomer conformation believed to be associated with biological activity. This molecule was modelled using Insight II with the Discover Minimization Module [computer program]. Vol. 2002. Accelerys, San Diego, Calif. 1996.
23. E. Pohl, A. Heine, and G.M. Sheldrick. Acta Crystallogr. Sect. D, **D51**, 48 (1995).
24. K. Wüthrich. NMR of proteins and nucleic acids. John Wiley and Sons, New York. 1986.

© 2005 NRC Canada

Alkylcobalt carbonyls. Part XIV.[1] Generation of chiral conformations by centers of chirality in organocobalt complexes[2]

Claudia Zucchi, Davide Turrini, Roland Boese, Lajos Bencze, Robert Kurdi, Luciano Caglioti, and Gyula Pályi

Abstract: $R^1OC(O)CH_2Co(CO)_3PR^2_3$ complexes (**3**), (R^1 = **S**-EtOC(O)CH(CH_3), R^2 = Ph, **a**; R^1 = (1**S**,2**R**,5**S**)-2-isopropyl-5-methylcyclohexyl, R^2 = Ph, **b**; R^1 = (1**R**,2**S**,5**R**)-2-isopropyl-5-methylcyclohexyl, R^2 = Ph, **c**; R^1 = isopropyl, R^2_3 = Ph_2{(1**S**,2**S**,5**R**)-2-isopropyl-5-methylcyclohexyl}, **d**) were prepared and characterized by analyses including IR, ^{1}H-, ^{13}C{^{1}H}-, and ^{31}P{^{1}H} NMR spectra as well as by X-ray diffraction structure determination. Principles of self-organization of chiral conformations were deduced from the structural data.

Key words: alkylcobalt carbonyls, cooperative phenomena, intramolecular, chirality, conformations.

Résumé : On a préparé les complexes $R^1OC(O)CH_2Co(CO)_3PR^2_3$ (**3**) (R^1 = **S**-EtOC(O)CH(CH_3), R^2 = Ph, **a**; R^1 = (1**S**,2**R**,5**S**)-2-isopropyl-5-méthylcyclohexyl, R^2 = Ph, **b**; R^1 = (1**R**,2**S**,5**R**)-2-isopropyl-5-méthylcyclohexyl, R^2 = Ph, **c**; R^1 = isopropyl et R^2_3 = Ph_2{(1**S**,2**S**,5**R**)-2-isopropyl-5-méthylcyclohexyl}, **d**) et on les a caractérisés par des analyses, incluant l'IR, la spectroscopie RMN du ^{1}H, ^{13}C{^{1}H} et du ^{31}P{^{1}H} ainsi que la diffraction des rayons X. On a déduit les principes de l'autoorganisation des conformations chirales à partir des données de structure.

Mots clés : carbonyles d'alkylcobalt, phénomène coopératif, intramoléculaire, chiralité, conformations.

[Traduit par la Rédaction]

Introduction

Alkyl- and acylcobalt carbonyls are key intermediates of C—C bond couplings involving CO (carbonylations). The interest in these compounds goes back more than a half century into the already legendary times of Roelen, Reppe, Hieber, and Heck (2–5). Beyond practical reasons relevant to great industrial processes, these compounds and their transformations represent highly interesting preparative and theoretical challenges, met by scientists such as Cotton, Markó, and Hoffman in the 1960s and 1970s (6–9). The fact that these intermediates remain not only interesting, but also *actual in the 21st century* is in great part due to the exceptionally rich, many-sided contribution of Howard Alper (10, 11), inventor and very successful practitioner of the combination of phase-transfer catalysis with transition-metal catalysis (PTC–TM).

One of the open questions of the chemistry of alkyl- and acylcobalt carbonyls is the "fine structure" of intramolecular interactions leading to the development of chiral and (or) diastereomeric conformations, which are primarily responsible for the transfer of chiral information from one ligand ("auxiliary") to the other ("substrate"). We prepared and analyzed a number of relevant alkylcobalt carbonyls in the last decade from this viewpoint (1, 12, 13), studying mostly chiral interactions among achiral fragments of these molecules. The results of these studies and some observations with molecules containing a center of chirality either in racemic (12*e*) or in enantiopure (12*a*, 12*d*, 12*g*) form indicated that a systematic study, based on X-ray structure deter-

Received 12 October 2004. Published on the NRC Research Press Web site at http://canjchem.nrc.ca on 22 July 2005.

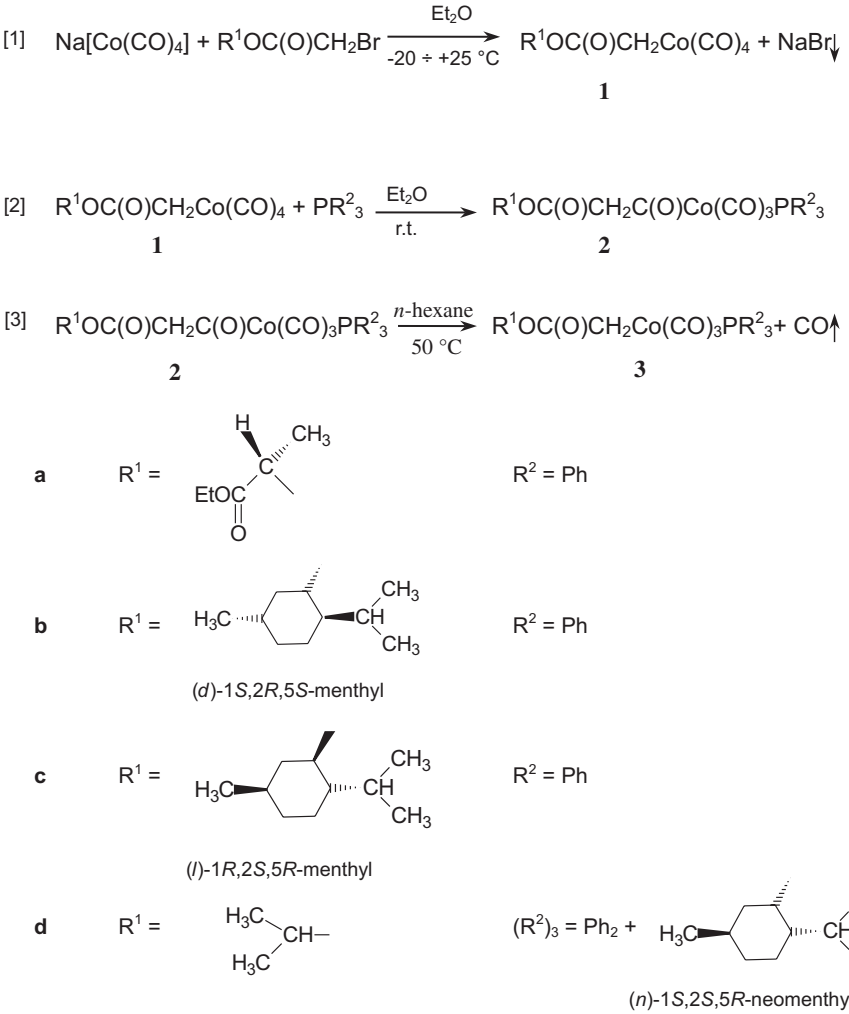
This paper is dedicated to Professor Howard Alper, pioneer of the combination of phase-transfer catalysis with transition-metal catalysts and good friend of the authors.

C. Zucchi, D. Turrini, and G. Pályi.[3] Department of Chemistry, University of Modena and Reggio Emilia, Via Campi 183, I-41100 Modena, Italy.
R. Boese. Institute of Inorganic Chemistry, University of Essen, Universitätsstrasse 5-7, D-45117 Essen, Germany.
L. Bencze and R. Kurdi. Müller Laboratory, Department of Organic Chemistry, University of Veszprém, Egyetem-u.6, H-8200 Veszprém, Hungary.
L. Caglioti. Department of Chemistry and Technology of Biologically Active Compounds, University "La Sapienza" Roma, P.zale A Moro 5, I-00185 Roma, Italy.

[1]For part XIII, see ref. 1.
[2]This article is part of a Special Issue dedicated to Professor Howard Alper.
[3]Corresponding author (e-mail: palyi@unimo.it).

 doi: 10.1139/V05-105 © 2005 NRC Canada

Scheme 1.



minations, will provide additional elements for completing the picture of the intramolecular transfer of chirality. We present here detailed analysis of four alkylcobalt carbonyl complexes of this kind.

Experimental

All operations were performed according to the standard Schlenk techniques (14).

Starting materials were of commercial origin, with the exception of *S*-2-bromoacetoxypropionic acid ethyl ester (15), the bromoacetate of *d*-menthol ((1**S**,2**R**,5**S**)-2-isopropyl-5-methylcyclohexanol) and l-(*o*)-menthol ((1**R**,2**S**,5**R**)-2-isopropyl-5-methylcyclo-hexanol) (16), as well as of dicobalt octacarbonyl (17), which were prepared according to published procedures.

IR spectra were recorded with a Bruker FT-IR IFS 113 V spectrometer, ^{1}H-, ^{13}C{^{1}H}-, and ^{31}P{^{1}H} NMR spectra were recorded with Bruker DPX-200 and AMX-400 instruments.

The X-ray diffraction experiments were performed using a Siemens P4 X-ray four circle diffractometer with Mo Kα radiation at room temperature (r.t.). The SHELXTL-Plus program and SGI IRIS Indigo computer were used for calculations. Atomic scattering factors were taken from SHELXTL and the literature (18), as well as the correction for anomalous dispersion (19).

The alkylcobalt tricarbonyl *tert*–phosphine complexes **3a**–**3d** were prepared according to variants of the procedures described in a published method (20) (Scheme 1): (1) using ion metathesis; (2) ligand-promoted carbonylation; and (3) thermal decarbonylation steps in a one-pot mode.

Preparation of (S)-EtOC(O)C(H)(CH$_3$)OC(O)CH$_2$Co(CO)$_3$PPh$_3$ (3)

A solution of Na[Co(CO)$_4$] (2.00 mmol, prepared by Na–Hg reduction of $Co_2(CO)_8$, 342 mg, 1.00 mmol) in 30 mL of dry Et_2O was filtered into a 100 mL Schlenk vessel, under an Ar atmosphere. This solution was cooled to –30 °C, and then, while stirred *S*-2-bromoacetoxypropionic acid ethyl ester (478 mg, 2.00 mmol) was added at once. Immediately after this, the formation of a white precipitate (NaBr) started and the (originally colorless) solution turned gradually yellow then brown. The stirring was continued for 2 h at –30 °C and then the reaction mixture was left to warm to room temperature (r.t.). At r.t., the stirring was continued for an additional 1 h. After this period, a liquid sample was taken for spectroscopic analysis. The IR ν(CO) spectrum showed the

© 2005 NRC Canada

Table 1. IR ν (CO) data (*n*-hexane, cm^{-1}), ^1H and $^{13}C\{^1H\}$ NMR spectra ($CDCl_3$, δ (ppm), *J* (Hz)) of complexes **1**.

Compd.	IR	^1H NMR	^{13}C NMR
1a (^1H- and ^{13}C NMR in C_6D_6)	2113 (m), 2045 (vs), 2025 (vs), 1759 (w), 1722 (w)	5.00 (q, 1H, *J* = 7.12, C(6)*H*), 4.21 (q, 2H, *J* = 7.12, C(10)H_2), 2.23 (s, 2H, C(4)H_2), 1.48 (d, 3H, *J* = 7.12, C(7)H_3), 1.28 (t, 3H, *J* = 7.12, C(11)H_3)	198.4 (*C*Ocoord.), 180.2 (*C*(5)O), 171.4 (*C*(8)O), 68.1 (*C*(6)H), 60.7 (*C*(10)H_2), 15.1 (*C*(11)H_3), 14.0 (*C*(7)H_3), 8.1 (*C*(4)H_2)
1b	2111 (m), 2045 (s), 2036 (vs), 2028 (vs), 1710 (w)	4.70 (m, 1H, OC(6)*H*), 2.17 (s, 2H, C(4)H_2), 1.47–0.87 (m, C*H*, CH_2), 0.89 (d, 6H, 2CH_3), 0.77 (d, 3H, CH_3)	196.4 (*C*Ocoord.), 177.6 (*C*(5)O), 74.0 (O*C*H_2), 68.6 (O*C*H), 46.8, 40.3, 34.2, 31.3, 26.1, 23.3, 21.8, 20.6, 16.1 (*C*H, *C*H_2, *C*H_3), 8.0 (*C*(4)H_2)
1c	2111 (m), 2045 (s), 2036 (vs), 2028 (vs), 1710 (w)	4.83 (m, 1H, OC(6)*H*), 2.17 (s, 2H, C(4)H_2), 1.47–0.86 (m, C*H*, CH_2), 0.89 (d, 6H, 2CH_3), 0.78 (d, 3H, CH_3)	196.4 (*C*Ocoord.), 177.6 (*C*(5)O), 74.0 (O*C*H_2), 68.6 (O*C*H), 46.8, 40.3, 34.2, 31.3, 26.1, 23.3, 21.8, 20.6, 16.1, (*C*H, *C*H_2, *C*H_3), 8.0 (*C*(4)H_2)
1d	2111 (m), 2046 (s), 2036 (vs), 2027 (vs), 1710 (w)	4.96 (sept, 1H, *J* = 6.4, C(7)*H*), 2.19 (s, 2H, C(4)H_2), 1.24 (d, 6H, *J* = 6.4, C(8)H_3 and C(9)H_3)	196.2 (*C*Ocoord.), 177.5 (*C*(5)O), 67.5 (*C*(7)H), 21.4 (*C*(8)H_3 and *C*(9)H_3), 8.0 (*C*(4)H_2)

Table 2. Elemental analyses of complexes **3**.

			Composition (%)	
Compd.	Formula	Mol. weight	Found	Calcd.
3a	$C_{28}H_{26}O_7CoP$	564.32	C 59.7, H 4.7	C 59.59, H 4.64
3b	$C_{33}H_{36}O_5CoP$	602.52	C 65.8, H 6.1 Co 10.0, P 5.1	C 65.78, H 6.02 Co 9.78, P 5.14
3c	$C_{33}H_{36}O_5CoP$	602.52	C 66.1, H 6.2	C 65.78, H 6.02
3d	$C_{30}H_{38}O_5CoP$	559.43	C 63.4, H 6.9	C 63.38, H 6.74

complete disappearance of the strong, broad band of $[Co(CO)_4]^-$ at ~1900 cm^{-1} and the emergence of a new band system compatible with an $XCo(CO)_4$ type complex (1, 7, 11, 12, 20, 21). This complex was characterized as $R^1OC(O)CH_2Co(CO)_4$ (R^1 = EtOC(O)CH(CH_3)-) (**1a**) on the basis of its IR and NMR spectra (Table 1). Complex **1** was not isolated.

The reaction mixture was then filtered and to the filtrate, with stirring at r.t. and under an Ar atmosphere, $P(C_6H_5)_3$ (525 mg, 2.00 mmol) was added in one portion. The stirring was then continued for an additional 8 h, and after 2 h the color of the brown solution turned gradually light yellow and gas evolution (CO) was observed. After this period, a sample was taken, which was analyzed by IR spectroscopy, conducted in the CO stretching range (2200–1600 cm^{-1}). The only detectable metal carbonyl species showed a ν(CO) band system characteristic for an $XCo(CO)_3L$ type complex (12, 20–22), and it was attributed[4] to $R^1OC(O)CH_2Co(CO)_3PPh_3$ (**3a**). Then the reaction mixture was filtered and the solvent was evaporated at r.t. under reduced pressure. The crude product (673 mg, 60.9%) was then recrystallized from diethyl ether – *n*-hexane (liquid diffusion) providing light yellow crystals (473 mg, 42.8%). Complexes **3b**–**3d** were prepared similarly. The products **3** were characterized by elemental analyses (Table 2), IR, ^1H-, $^{13}C\{^1H\}$-, and $^{31}P\{^1H\}$ NMR (Table 3), and X-ray diffraction (Tables 4 and 5).[5]

Results and discussion

In the mononuclear series, complexes of the $ROC(O)CH_2Co(CO)_3PPh_3$ (**3**) type, with R = achiral alkyl

[4] Supplementary data for this article are available on the Web site or may be purchased from the Depository of Unpublished Data, Document Delivery, CISTI, National Research Council Canada, Ottawa, ON K1A 0S2, Canada. DUD 3699. For more information on obtaining material refer to http://cisti-icist.nrc-cnrc.gc.ca/irm/unpub_e.shtml. CCDC 222027–222030 contain the crystallographic data for this manuscript. These data can be obtained, free of charge, via www.ccdc.cam.ac.uk/conts/retrieving.html (Or from the Cambridge Crystallographic Data Centre, 12 Union Road, Cambridge CB2 1EZ, UK; fax +44 1223 336033; or deposit@ccdc.cam.ac.uk).

[5] Spectroscopic and (or) preparative identification of the supposed (12, 20) acyl-type intermediate **2** (Scheme 1) was beyond the scope of the present study.

© 2005 NRC Canada

Table 3. IR ν (CO) (*n*-hexane, cm^{-1}), ^1H- and $^{13}C\{^1H\}$ NMR (δ (ppm), *J* (Hz)) data of complexes **3**.

		^1H NMR		$^{13}C\{^1H\}$ NMR ($J_{C\text{-}P}$)	
Compd.	IR	$CDCl_3$	$(CD_3)_2CO$	$CDCl_3$	$(CD_3)_2CO$
3a	2052 (vw), 1982 (s), 1971 (s), 1754 (w), 1705 (w)	7.58–7.55 (m, C*H* arom.), 4.93 (q, 1H, *J* = 7.12, C(6)*H*), 4.17 (q, 2H, *J* = 7.12, C(10)H_2), 2.23 (d, $^3J_{Hp}$ = 3.34 C(4)H), 1.42 (d, 3H, *J* = 7.12, C(7)*H*), 1.26 (t, 3H, *J* = 7.12, C(11)*H*)	7.58–7.56 (m, C*H* arom.), 4.93 (q, 1H, *J* = 7.03, C(6)*H*), 4.17 (q, 2H, *J* = 7.104, C(10)H_2), 2.20 (dd, $^2J_{HH}$ = 6.91, $^3J_{Hp}$ = 2.91, C(4)H^a), 2.14 (dd, $^2J_{HH}$ = 6.91, $^3J_{Hp}$ = 2.91, C(4)H^b), 1.42 (d, 3H, *J* = 7.03, C(7)*H*), 1.246 (t, 3H, *J* = 7.104, C(11)*H*)	198.4 (d, 22.25, *C*O coord.), 180.1 (*C*(5)O), 171.4 (*C*(8)O), 133.0 (d, 47.87), 132.9 (d, 10.91), 130.9 (d, 2.36), 128.7 (d, 10.55, C_6H_5 in PPh_3), 68.1 (*C*(6)H), 60.7 (*C*(10)H_2), 16.8 (*C*(11)H_3), 14.0 (*C*(7)H_3), 4.1 (d, 16.06, *C*(4)H_2)	199.6 (d, 24.34, *C*O coord.), 179.7 (*C*(5)O), 171.8 (*C*(8)O), 134.4 (d, 48.96), 133.7 (d, 11.32), 132.2 (d, 2.64), 129.5 (d, 11.14, C_6H_5 in PPh_3), 68.8 (C(6)H), 61.1 (C(10)H_2), 17.1 (*C*(11)H_3), 14.4 (*C*(7)H_3), 4.6 (d, 16.14, *C*(4)H_2)
3b and **3c**	2050 (vw), 1984 (s), 1975 (s), 1702 (w)	7.67–7.58, 7.46–7.38 (m, C*H*arom.), 4.68 (m, C*H*), 2.21 (dd, $^2J_{HH}$ = 7.13, $^3J_{Hp}$ = 3.16, C(4)H^a), 2.17 (dd, $^2J_{HH}$ = 7.13, $^3J_{Hp}$ = 3.16, C(4)H^b), 2.10–0.71 (m, C*H*, CH_2), 0.86 (d, $^3J_{HH}$ = 6.80, CH_3), 0.80 (d, $^3J_{HH}$ = 7.00, CH_3), 0.73 (d, $^3J_{HH}$ = 6.80, CH_3)	7.67–7.58, 7.46–7.38 (m, C*H* arom.), 4.66 (m C*H*), 2.16 (dd, $^2J_{HH}$ = 6.99, $^3J_{Hp}$ = 3.07, C(4)H^a), 2.13 (dd, $^2J_{HH}$ = 6.99, $^3J_{Hp}$ = 3.07, C(4)H^b), 2.12–0.81 (m, C*H*, CH_2), 0.94 (d, $^3J_{HH}$ = 6.55, CH_3), 0.90 (d, $^3J_{HH}$ = 7.05, CH_3), 0.80 (d, $^3J_{HH}$ = 6.95, CH_3)	199.2 (d, 21.54, *C*Ocoord.), 180.7 (*C*(5)O), 133.6 (d, 46.28), 133.3 (d, 11.07), 131.3 (d, 2.01), 129.1 (d, 11.07, C_6H_5 in PPh_3), 73.2 (O*C*H), 47.6, 41.0, 34.8, 31.7, 26.5, 23.8, 22.3, 21.3, 16.7 (*C*H, CH_2, CH_3), 6.1 (d, 17.054, CH_2-Co)	200.4 (d, 22.46, *C*Ocoord.), 180.0 (d, 1.84, *C*(5)O), 134.5 (d, 46.90), 134.2 (d, 10.76), 132.6 (d, 2.48), 130.3 (d, 10.64, C_6H_5 in PPh_3), 73.4 (O*C*H), 48.5, 42.0, 35.5, 32.6, 27.2, 24.5, 22.9, 21.6, 17.0 (*C*H, CH_2, CH_3), 6.4 (d, 16.56, CH_2-Co
3d	2046 (vw), 1981 (s), 1966 (s), 1706 (w)	7.37–6.94 (m, C*H* arom.), 5.17 (sept., *J* = 6.4, C(7)*H*), 2.10 (d, $^3J_{HP}$ = 2.8, C(4)H_2), 1.22 (d, *J* = 6.4, C(8)H_3 and C(9)H_3)	—[a]	—[a]	—[a]

[a]Decomposed during data acquisition.

© 2005 NRC Canada

Table 4. Experimental parameters of the X-ray diffraction of compounds **3**.

Compound	**3a**	**3b**	**3c**	**3d**
Empirical formula	$C_{28}H_{26}CoO_7P$	$C_{33}H_{36}CoO_5P$	$C_{33}H_{36}CoO_5P$	$C_{30}H_{38}CoO_5P$
Formula weight	564.32	602.52	602.52	559.43
Temp. of data collection	r.t.	120 (K)	120 (K)	r.t.
Wavelength (Å)	0.710 69	0.710 69	0.710 69	0.710 69
Crystal system, space group	Orthorhombic, $P2_12_12_1$	Orthorhombic, $P2_1$	Orthorhombic, $P2_1$	Orthorhombic, $P2_12_12_1$
Unit cell dimensions				
a (Å)	10.874(1)	11.386(2)	11.386(2)	12.001(2)
b (Å)	12.331(1)	16.015(3)	16.015(3)	12.440(1)
c (Å)	20.905(3)	17.697(3)	17.697(3)	20.408(2)
α (°)	90	90	90	90
β (°)	90	105.33(1)	105.33(1)	90
γ (°)	90	90	90	90
Volume (Å^3)	2802.9(5)	3112.1(5)	3112.2(9)	3046.8(6)
Z	4	4	4	4
Calculated density (Mg/m^3)	1.342	1.286	1.286	1.239
Absorption coefficient (mm^{-1})	0.71	0.64	0.64	0.65
Crystal size (mm^3)	0.51 × 0.36 × 0.23	0.39 × 0.31 × 0.23	0.37 × 0.28 × 0.19	0.49 × 0.31 × 0.28
Θ range for data collection (°)	$3 \le 2\Theta \le 50$	$3 \le 2\Theta \le 45$	$3 \le 2\Theta \le 48$	$3 \le 2\Theta \le 60$
Refl. collected / unique	4101 / 4938	4989 / 6103	8425 / 7418	5668 / 3550
Abs., ext. correction	No	No	No	No
No. of parameters refined	361	667	677	318
Largest diff. peak and hole (e Å^{-3})	0.39 and –0.26	0.81 and –0.54	0.60 and –0.44	0.43 and –0.35
Final R indices ($I > 2\sigma(I)$)	0.035 1	0.056 9	0.033 5	0.047 0
R indices (all data)	R_w = 0.035 6	R_w = 0.056 6	R_w = 0.034 0	R_w = 0.046 4
Instrument	Nicolet R3m/V	Nicolet R3m/V	Nicolet R3m/V	Nicolet R3m/V
Program and computer	SHELXTL-PLUS, Micro VAX II	SHELXTL-PLUS, Micro VAX II	SHELXTL-PLUS, Micro VAX II	SHELXTL-PLUS, Micro VAX II

Note: The absolute structure was established by refining η: η = 1.0356(32) (**3a**), η = 1.122(60) (**3b**), η = 1.039(27) (**3c**), η = 0.991(49) (**3d**). See: D. Rogers. Acta Crystallogr. Sect. A, **A37**, 734 (1981).

(12*f*, 12*h*, 12*i*), (racemic) *sec*-butyl (12*e*) and glucosyl groups (12*g*) were studied previously. The particular self-organization of these complexes is due to the concerted rotation of more groups around some single bonds, which opens relatively low activation energy paths (12*i*). As a consequence of this situation, transmission of chiral information though the achiral fragments of these molecules was observed. These (thermal) processes are *reversible* and *free of errors*, therefore always yielding racemates. The cooperation of the forces governing these self-organization processes results in concerted intramolecular displacements, very similar to movements in mechanical clockworks (Scheme 2). Experience with the (*R*,*S*)*s*-Bu (12*e*) and glucosyl (12*g*) derivatives indicated that the study of complexes with centers of chirality in the molecule may lead to interesting new effects (not necessarily the "expected" ones). This experience was the basis of the selection of the structures investigated in the present work: thus, compounds with (*i*) a flexible ester "alkyl" group with polar fragments and one center of chirality (**3a**); (*ii*) flexible apolar (not too bulky) alkyl groups with more (three) stereogenic units (**3b**, **3c**); and (*iii*) a (configurationally) chiral group in the phosphine ligand (**3d**), were chosen.

The preparative access to these molecules was developed on the basis of earlier experience with similar compounds (12, 20), using a one-pot variant, without isolation or detailed characterization of intermediates **1** and **2**. High yields of complexes **3** were obtained without attempt at optimization of the yield. No cobalt carbonyl species other than complexes **3** were detected after rxns. [1]–[3] were completed (Scheme 1). Spectroscopic analysis of the reaction mixture during the reaction and immediately after did not reveal isomers (equatorial?) other than the ones later characterized in the end-products **3a**–**3d** (cf. refs. 1, 7, 20, 21). X-ray crystal and molecular structure determination was performed for all **3a**–**3d** complexes.

The overall molecular structures of complexes **3** show a trigonal bipyramidal array with the non-carbonyl ligands in axial (trans) positions and the carbonyls in a slightly bent equatorial plane, turning its concave face toward the alkyl ligand. This picture is similar to the geometry of several other $XCo(CO)_3L$ type complexes (1, 12, 20–22). The preferential development of the trans-(bis-axial)-trigonal bipyramidal geometry in complexes **3** is a fortunate circumstance for the analysis of the mechanisms of the interaction of the conformations of ligands in the two opposite positions on the metal.

The crystal lattices of complexes **3a** and **3d** contain only one conformer of the complex (both are $P2_12_12_1$ phases), while **3b** and **3c** both form a $P2_1$ phase, with two independent molecules (each) in these lattices. All complexes contain four molecules in the elementary cell.

A comparison of the behavior of complexes **3a** and **3d** with that of the **3**, R = achiral alkyl (12*h*) (*R*,*S*)*s*-Bu (12*e*) and glucosyl (12*g*) derivatives, gives a strong indication for the supposition that the "racemates" of the conformational

© 2005 NRC Canada

Table 5. Selected bond length (Å) and bond angle (°) values for compounds **3**.

	3a	3b	3c	3d
Bond lengths (Å)				
Co—P	2.207(1)	2.213(3)	2.215(1)	2.239(1)
Co—C(1)	1.782(4)	1.776(10)	1.791(5)	1.778(5)
Co—C(2)	1.792(4)	1.789(9)	1.779(4)	1.786(5)
Co—C(3)	1.773(4)	1.802(10)	1.827(3)	1.779(5)
Co—C(4)	2.078(3)	2.088(10)	2.077(5)	2.078(4)
C(1)—O(1)	1.137(5)	1.149(12)	1.146(6)	1.138(6)
C(2)—O(2)	1.123(5)	1.144(11)	1.148(5)	1.132(7)
C(3)—O(3)	1.132(5)	1.126(12)	1.132(6)	1.141(6)
C(4)—C(5)	1.467(4)	1.496(14)	1.495(7)	1.472(8)
C(5)—O(5)	1.207(5)	1.175(12)	1.198(6)	1.218(7)
C(5)—O(6)	1.353(5)	1.379(10)	1.368(5)	1.333(7)
O(6)—C(6)	1.433(5)	1.453(11)	1.449(5)	
P—C(16)	1.828(3)	1.826(6)	1.827(3)	1.859(4)
P—C(22)	1.831(3)	1.822(5)	1.816(3)	1.834(3)
P—C(28)	1.823(3)	1.819(6)	1.827(3)	1.834(3)
Co′—P′		2.209(3)	2.208(2)	
Co′—C(1′)		1.799(10)	1.803(5)	
Co′—C(2′)		1.792(8)	1.795(4)	
Co′—C(3′)		1.783(10)	1.790(5)	
Co′—C(4′)		2.065(11)	2.080(5)	
Bond angles (°)				
P-Co-C(1)	93.7(1)	92.8(4)	92.7(2)	92.0(2)
P-Co-C(2)	90.1(1)	90.1(4)	90.4(2)	95.5(2)
P-Co-C(3)	93.5(1)	93.4(3)	93.6(2)	91.0(1)
C(1)-Co-C(2)	118.4(2)	119.6(5)	120.7(2)	116.5(2)
C(1)-Co-C(3)	116.6(2)	114.2(4)	113.8(2)	120.5(3)
C(2)-Co-C(3)	124.5(2)	125.8(4)	125.1(2)	122.4(3)
P-Co-C(4)	179.1(1)	176.8(2)	177.0(1)	175.4(2)
C(1)-Co-C(4)	87.0(1)	87.8(4)	87.2(2)	85.0(2)
C(2)-Co-C(4)	89.0(2)	87.0(4)	87.0(2)	89.0(2)
C(3)-Co-C(4)	86.8(2)	89.2(4)	89.2(2)	87.6(2)
Co-P-C(16)	115.7(1)	114.9(2)	115.0(1)	112.8(1)
Co-P-C(22)	114.8(1)	113.6(2)	114.1(1)	109.9(1)
Co-P-C(28)	114.2(1)	113.7(2)	113.7(1)	116.0(1)

isomers of the ester and phosphine groups are "resolved" by the introduction of permanent centers of chirality into the ligands. This, however, *does not lead necessarily* to the formation of only one isomer (conformer). If the steric conditions permit, additional (diastereomeric) forms develop, as in the case of the two menthylester derivatives **3b** and **3c**. The loss of helicity in the phosphine ligand at the glucosyl derivative (12*g*) as well as the development of the two diastereomers (each) in the menthylester complexes **3b** and **3c** indicates that the presence of more centers of configurational chirality does not necessarily promote the formation of the "most chiral" product. This is a problem that one encounters in preparative (empirical) attempts in terms of observing the more or less "efficiency" of additives used for the induction of chirality.

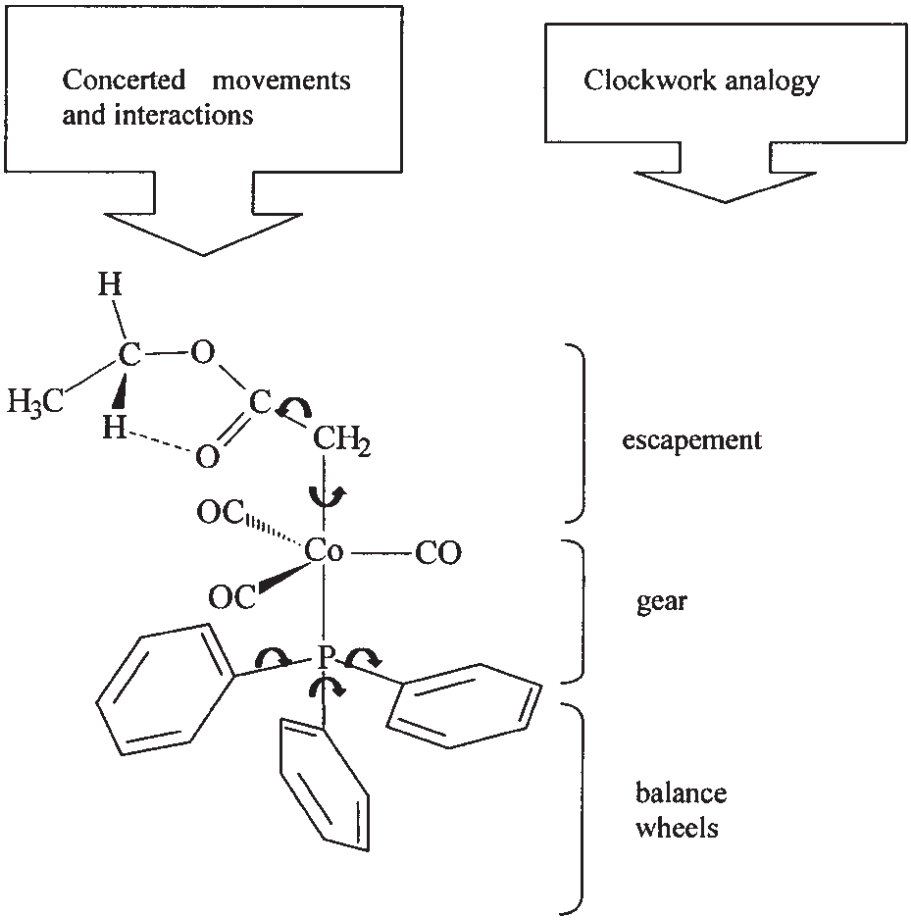
The individual features of the structural details of complexes **3a**–**3d** require some comments.

The structure of complex **3a** (Fig. 1) is primarily characterized by the remarkable nonequivalence of the (ligand) carbonyl angles OC-Co-CO: 125.8°, 118.0°, 115.5°. The broadest of these angles is certainly due to the bulkiness of the organic ligand, which is organized in a very particular manner. First of all, it is to be noted that in this long, flexible organic ligand, with six σ bonds that could generate several new conformers, *only one conformer* develops in the $P2_12_12_1$ phase. This conformer is characterized by a very symmetric orientation with respect to the rest of the molecule, as it can be seen through the dihedral angle between the main axis of the "lactic acid" fragment and the anti-CO ligand: –178.3° (almost a straight line!). The other interesting feature is the short (ester) carbonyl-O vs. α-(alkyl)C distance (C10-O8, 269.4 pm) indicative for the formation of the C(sp^3)H vs. > C=O hydrogen bond, similarly as has been found with other derivatives **3** with (ester)-α-CH groups (12*e*, 12*g*, 12*h*). The H bridging generates a *new center of chirality* on C10 (Fig. 1). It is a highly interesting feature of this structure that the new center of chirality on C10 is generated only in one enantiomeric form ("**R**"). The phosphine ligand in complex **3a** shows only one helical conformation (**M**), where the phenyl ring orientations are somewhat different from those observed at the achiral alkyl (12*h*) and *s*-Bu (12*e*) derivatives. The difference is mostly in the orientation of the C16–C21 ring, which is more "steep" than usual. This can be caused by an additional H-bridge interaction between the C17 and O8 atoms (C17—O8 distance 269 pm, C17-H17-O8 angle 152.2°), which may be one of the factors contributing to the stabilization of the astonishingly selective organization of the conformation in the ester fragment of complex **3a**. An additional "through-space" intramolecular interaction can be identified between the C5 and the Co atoms. This "enforced" interaction (distance 293.9 pm) renders the C5 atom tetracoordinated, with four different substituents (Co, O5, O6, C4) and, therefore, generates a new center of chirality on this atom. Since in the $P2_12_12_1$ phase, the C5,O5,O6 carboxyl group turns only its si face towards the Co atom, the new center of chirality will be (with quantitative enantioselectivity) of **S** configuration. This kind of intramolecular interaction (23) was detected by X-ray structural studies in some analogous molecules (12, 20*a*) as well as analyzed by MO calculations (23*c*, 23*f*) that showed that a considerable electron density transfer occurs between the C5,O5,O6 and the Co atoms. These particular interactions lead to a dramatic diminution of the number of "statistically" possible conformers. Regarding only **P** and **M** for the PPh_3 ligand, si or re (turned towards Co) for the C5-centered ester group, as well as **R** or **S** for the C10 atom, this gives eight combinations and *only one* (12.5%) in 100% enantiomeric yield, gets realized under the influence of the permanent **S** configuration on C6 with the aid of the supramolecular forces.

The considerations described earlier in this paper on the structure of complex **3a** are reflecting the situation in the condensed $P2_12_12_1$ phase. Since most of the reactions where alkylcobalt carbonyls are important intermediates are displayed in solution or vapor phase (9), we made an attempt at exploring whether the highly interesting structural features observed in the crystalline phase are to be taken into account in the solution and (or) gas phase. The results are not conclusive: (*a*) the IR ν(CO) frequencies of both "organic" carbonyl groups observed in apolar solvents (Table 3) are compatible with C-H···O and =O···C interactions; (*b*) the

© 2005 NRC Canada

Scheme 2.



ABX type signal observed (in acetone-d_6) for the CH_2 group directly bonded to the Co atom in the ^{1}H NMR spectrum may represent an additional proof for the "survival" of the chiral conformation detected in the crystalline phase, but because of a center of chirality on C6 this may (even: should) have (also) intrinsic reasons; (*c*) the ^{1}H NMR spectrum of protons on C10 and the ^{13}C NMR signal of the coordinated carbonyls are indicating free rotation (at least on the NMR timescale at r.t.).

The X-ray structure of the menthylester complexes **3b** and **3c** provided an entirely new and highly interesting picture. This is characterized by the fact that both compounds (in the $P2_1$ phase) appear as pairs of diastereomers, each of which are characterized by the different orientations of the 5-methyl group (farther from ↑ or closer to ↓ the Co atom, or ↑↓: the 5-Me group of the menthyl fragment lies in or farther away from the equatorial plane) as well as by *enantiomeric configurations* developing in the rest of the molecules (Fig. 2). The four combinations found experimentally in the crystalline phase are **L**↑*re***P**, **L**↓*si***M**, and **D**↓*re***P**, **D**↑*si***M**, while the other 12 combinations are completely lacking. This is the first instance when diastereomer pairs are found to form the unit cells of compounds **3**.

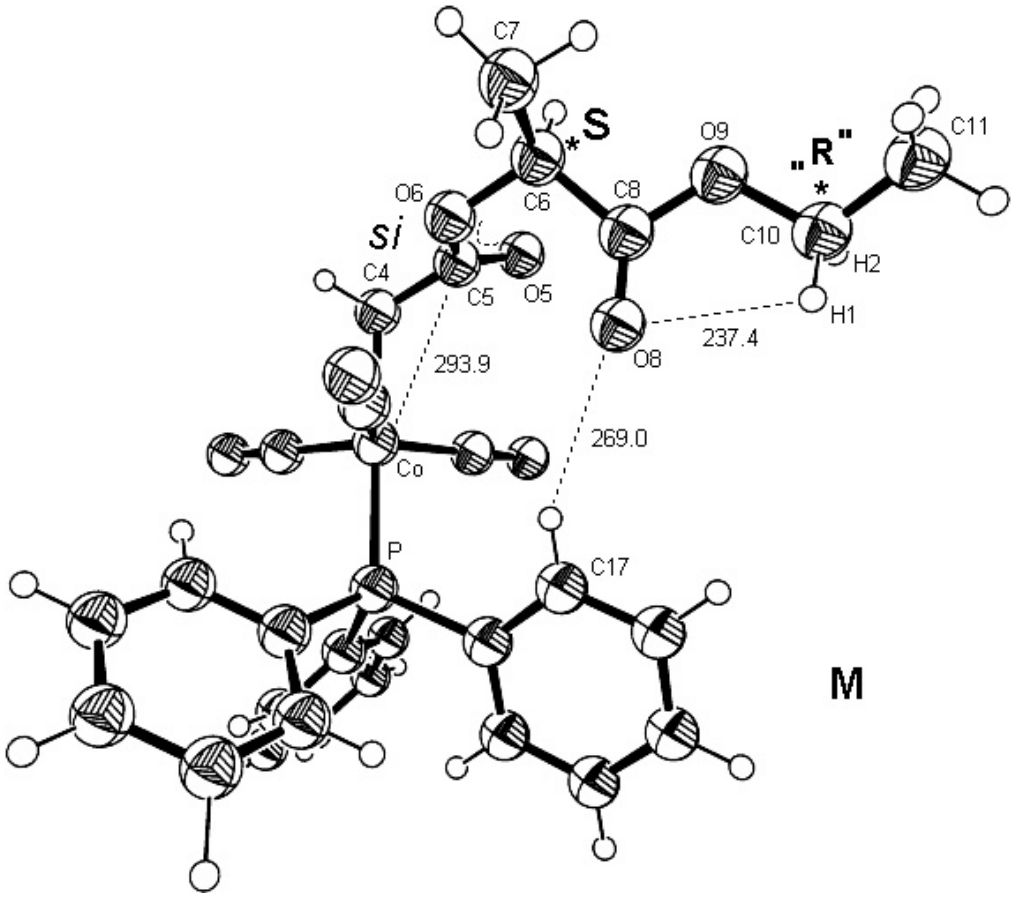
One of the most interesting features of these structures is the fact that *each of the enantiomers appear separately in different crystals*: e.g., the chiral **L**↑*re***P** molecule is in the elementary cell of **3c** while its enantiomer **D**↑*si***M** is in the lattice of complex **3b**.

Both complexes **3b** and **3c** develop H bonding between the alkyl-α-H atom and the O sp^2 atom of the carboxyl group. The five-membered, H-bonded, nonplanar rings thus formed show enantiomeric configurations characterized by exactly the same bond lengths and angles and equal dihedral angles (with opposite signs) as shown in Fig. 3 and Table 6. Since the C6 atom in the menthyl group is already chiral, the H bonding does not generate a new center of chirality as it was observed at the "outer" ester group of complex **3a** (this work) as well as at the ethyl and *n*-propylester derivatives in earlier studies (12*h*, 12*i*). It is worth noting that the distances and angles around the C-H···O bridge show an *excellent agreement among the enantiomers in different crystals* (Table 6).

The "enforced" vicinity of the carboxylic C5 and the Co, i.e., the Co···C5 (O5,O6) coordination reproduces the C5—Co distances rather efficiently (**3b** 296.2 pm, **3c** 296.9 pm). This effect generates new centers of chirality on C5 (*si*→**S** and *re*→**R**) and on the Co atom. The chiral perturbation of the metal atom is reflected also in the low-energy CD bands of complexes **3c** and **3d** (12*a*). The ABX type signal of the α-CH_2 groups in the ^{1}H NMR spectra of these complexes provide important hints at the survival of the supramolecular effects also in the solution phase.

© 2005 NRC Canada

Fig. 1. Thermal ellipsoids are shown at the 90% probability level for the X-ray crystal structure of complex **3a**.



Compound **3d** was synthesized to test the effect of a chiral organic rest in the phosphine ligand. The X-ray structure of complex **3d** shows a bis-axial tbp overall geometry, which is similar to the previous complexes **3a**–**3c** (see also refs. 12*c*–12*j*, 21*b*–12*e*, 22). In the chiral $P2_12_12_1$ phase, the elementary cells contain four *identical* chiral molecules **3d** (Fig. 4). These are characterized by the following structural features: (*a*) the autosolvation-type (23) interaction between the carboxyl-C sp^2 atom and the Co seems to be justified again by the relatively short C5—Co distance (295.1 pm). The carboxyl group is turned with its re side towards the Co atom, and acquires **R** configuration by its interaction with the metal; (*b*) the bulky neo-menthyl group has heavily distorted the structure of the phosphine ligand, especially the arrangement of the two phenyl blades with their corresponding torsion angles of –72.5° and –12.6°. The helicity is nearly collapsed, but it is still possible to assign the **P** configuration and the average of the corresponding dihedral angles is about the ideal value (–46.5°). This *re***P** configuration is the "diastereomer" of the triphenyl phosphine analogue (12*c*) (*si***P**, *re***M**, Fig. 4); (*c*) one of the (O)C-Co-C(O) angles opens up to 123.6° to accommodate a bulky menthyl group, and capitalizing on the occasion, the ester group also organizes itself into this segment, eclipsing with the menthyl group. The two isopropyl groups are found in surprisingly close vicinity to each other; (*d*) the chiral alkyl (neomenthyl) group introduced into the phosphine ligand is inducing the inversion of the coordinated ester fragment from si to re and achieving a 100% enantioselection with respect to the possible stereoisomers; (*e*) similarly to other esters containing an α-CH unit (**3b** and **3c**, refs. 12*e*, 12*i*), H bonding between the C7 and O5 atoms can be identified; (*f*) the fundamental difference between the conformations of complexes **3b** and **3c** vs. complex **3d** is rooted in the difference between the rotational freedoms of the (otherwise very similar) organic groups bearing central chirality in **3b** and **3c** with respect to **3d**.

Most of our earlier studies on the mechanism of the intramolecular transfer of chiral information concerned the recognition and self-organization of conformationally invertible stereogenic units. The origin and the major driving force of these phenomena are the new co-ordination type of the prochiral ester group of the compounds **3** that may be influenced significantly by the structure of the corresponding alkoxide group. The stereoselectivity of the self-organization of these compounds may be fundamentally enhanced by the introduction of a permanent configurational chirality in the alkoxide group. The behavior of compound **3a**, as well as of (**R**, **S**)*s*-BuOC(O)CH_2Co$(CO)_3PPh_3$ (12*e*), shows clearly that *only one center of configurational chirality is sufficient* to generate the lowest possible number (one) of chiral conformations. Some sort of the combined effect of the various structural characteristics is transferred from the ester group to the trans axial ligand determining its energetically most favorable helical configuration. Due to this combined steric effect, more centers of chirality, as in the case of compounds

© 2005 NRC Canada

Fig. 2. Thermal ellipsoids are shown at the 90% probability level for the diastereomers of complex **3c**.

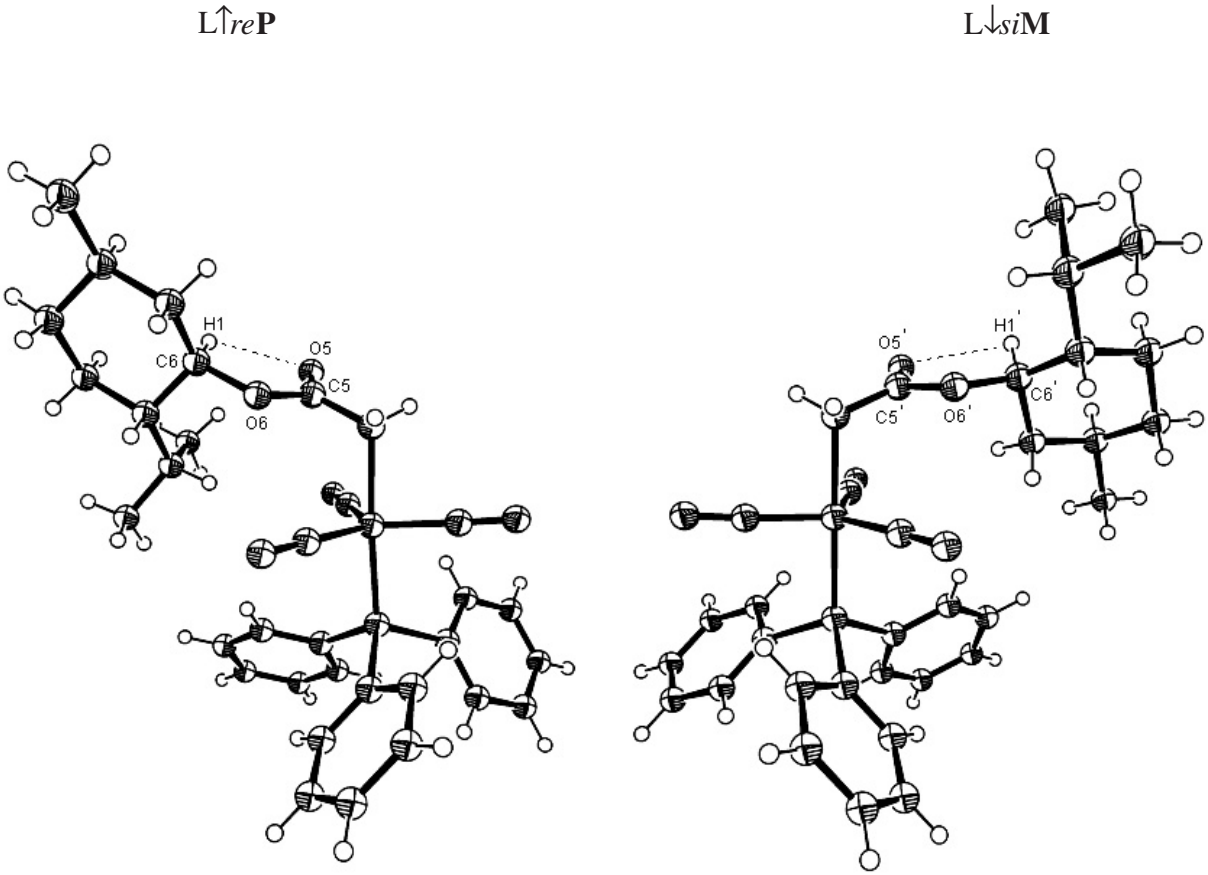
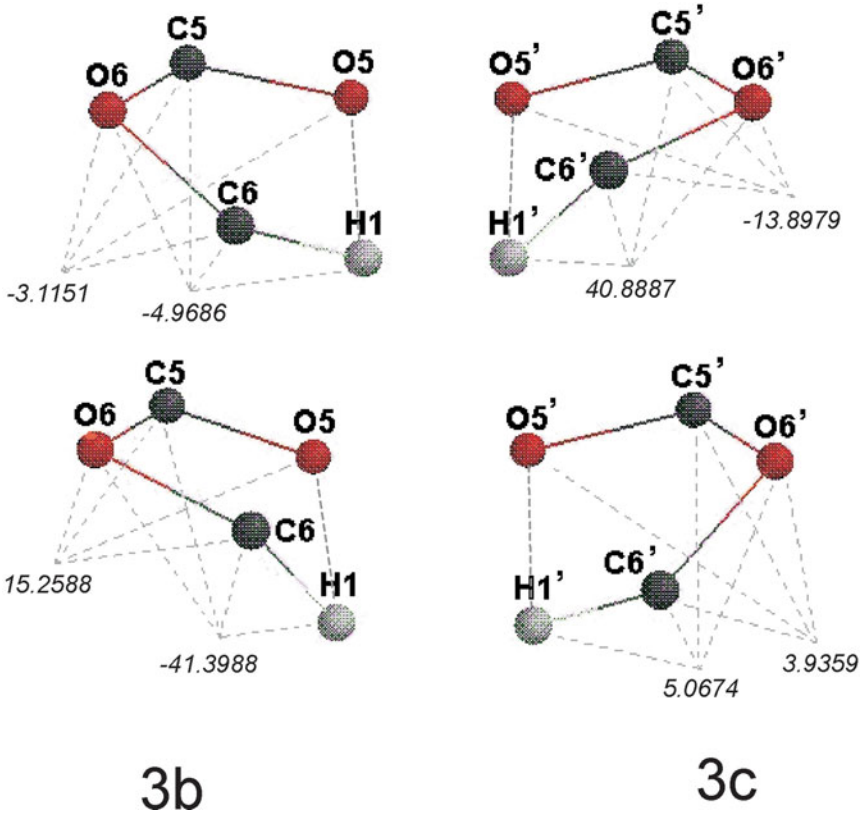


Fig. 3. Enantiomeric conformations in different crystals. Comparison of the conformations of the H-bonded rings in complexes **3b** and **3c**.



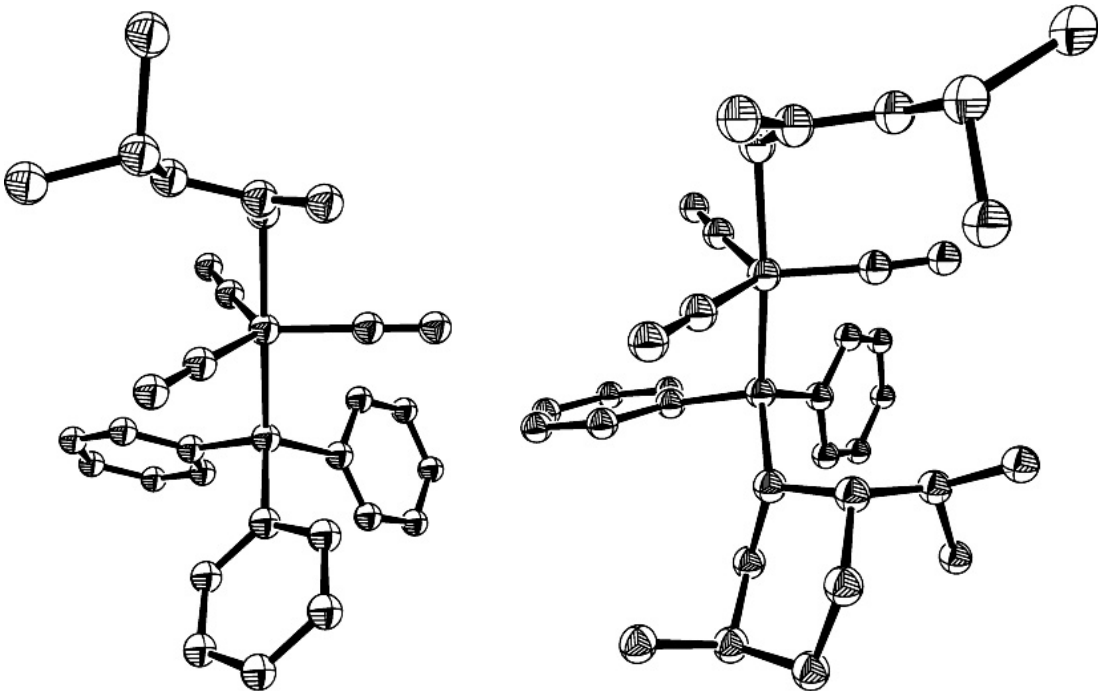
© 2005 NRC Canada

Table 6. Selected geometric data of menthyloxycarbonylmethyl-cobalt-tricarbonyl-triphenylphosphine complexes (**3b**, **3c**).

	L↑*re*(**R**)**P**	L↓*si*(**S**)**M**	D↓*re*(**R**)**P**	D↑*si*(**S**)**M**
3b				
Co-C-C=O (°)	–94	89.3	–89.9	93.3
Ester ring				
α-H···O= (pm)	230.6	239.4	239.8	229.1
α-C···O= (pm)	273.0	269.2	269.6	272.7
H···O=C (°)	82.4	80.9	80	82.5
C-H···O= (°)	105.9	97.4	97.5	106.7
3c				
O=C-O-C (°)	–3.1	–13.9	15.3	4.9
C-O-C-H (°)	–5	40.9	–41.5	4.1
O-C-H···O= (°)	6.5	–32	33.6	–6.5
H···O=C-O (°)	4.7	–3.0	1.9	–5.9
O=C···C-H (°)	–7.4	26.7	–26.4	8.1
C-H···O=C (°)	–8.1	27.2	–26.7	8.9
Co-C···C_5-C_{Me} (°)	127	9	–9.3	–127.9

Note: Sources: X-ray files for L-menthyl- and D-menthyl- (L: 1*R*,2*S*,5*R*; D: 1*S*, 2*R*, 5*S*). ↓,↑: the 5-Me group of the menthyl fragment lies in or farther away from the equatorial plane.

Fig. 4. Comparison of the structures of complexes **3d** and *i*-PrOC(O)$CH_2Co(CO)_3PPh_3$ (12*c*).



3b and **3c**, do not necessarily lead to the development of "more chiral" conformations. Even more, under certain conditions (e.g., steric repulsion) may produce "less chiral" states, as was recently observed with the glucose ester derived analogue of complexes **3** (12*g*). Now, this time we demonstrate that introducing a chiral hydrocarbon group into one of the distant trans axial positions, the chiral induction is efficiently channeled through the molecule to the other axial ligand.

The result is convincing: the intramolecular transmission of the chiral information is a two-way process and provides an easily accessible model of the transition state and for the mechanism of chiral phosphine induced, metal-catalyzed asymmetric syntheses.

The results described in this paper and in some previous reports (12) seem to support our initial hopes that a systematic study of the development of chiral conformations in transition-metal complexes might produce some useful principles for the "engineering" of sufficient systems for enantioselective catalysis. We believe, in this respect, it is not enough to develop chiral ligands, but it is also necessary to study the active complex(es) of the catalytic cycle. Our groups are working on the analysis of additional suitable models in this respect.

© 2005 NRC Canada

Acknowledgements

We acknowledge financial support of this work by the Italian Ministry of the University and Research (MURST ex60%), the Italian National Research Council (CNR, Rome), the Hungarian OTKA program (contract nos.: T-016326 and T035221). The preparation of *S*-2-bromoacetoxypropionic acid ethyl ester is gratefully acknowledged to Professor G. Frater (Dübendorf, CH). A valuable exchange of ideas during a very pleasant collaboration in the field of alkylcobalt carbonyls (see refs. 1, 11*l*, 12*j*) is thankfully acknowledged to Professor H. Alper (Ottawa, Ontario, Canada).

References

1. C. Zucchi, A. Cornia, R. Boese, E. Kleinpeter, H. Alper, and G. Pályi. J. Organomet. Chem. **586**, 61 (1999).
2. (*a*) O. Roelen. German Patent 849.548, 1939; Chem. Zentralbl. **124**, 927 (1953); (*b*) O. Hecht, H. Kroper, O. Roelen, P. Kurtz, O. Bayer, and O. Nicodemus. FIAT Rev. Ger. Sci. **35**, 1 (1948).
3. W. Reppe. FIAT Rev. Ger. Sci. **36**, 1 (1939/1946).
4. W. Hieber, O. Vohler, and G. Braun. Z. Naturforsch. B, **13b**, 192 (1958).
5. R.F. Heck and D.S. Breslow. J. Am. Chem. Soc. **84**, 2499 (1962).
6. F. Calderazzo and F.A. Cotton. Inorg. Chem. **1**, 30 (1962); Chim. Ind. (Milan), **46**, 1165 (1964).
7. (*a*) L. Markó, G. Bor, G. Almásy, and P. Szabó. Brennst. Chem. **44**, 184 (1963); (*b*) Z. Nagy-Magos, G. Bor, and L. Markó. J. Organomet. Chem. **14**, 205 (1968).
8. H. Berke and R. Hoffmann. J. Am. Chem. Soc. **100**, 7224 (1978).
9. Reviews: (*a*) V. Galamb and G. Pályi. Coord. Chem. Rev. **59**, 203 (1984); (*b*) I. Kovács and F. Ungváry. Coord. Chem. Rev. **161**, 1 (1997).
10. Reviews: (*a*) H. Alper. Fundam. Res. Homogen. Catal. **4**, 79 (1984); (*b*) H. Alper. Pure Appl. Chem. **60**, 35 (1988); (*c*) H. Alper. Aldrichimica Acta, **24**, 3 (1991); (*d*) V.V. Grushin and H. Alper. Chem. Rev. **94**, 1047 (1994); (*e*) K. Khumtaveeporn and H. Alper. Acc. Chem. Res. **28**, 414 (1995); (*f*) Y. Goldberg and H. Alper. *In* Applied homogeneous catalysis with organometallic compounds. 1st ed. *Edited by* B. Cornils and W.A. Herrmann. Wiley-VCH, Weinheim, Germany. 1996. pp. 844–865; 2nd ed. Vol. 2. 2002. pp. 953–974.
11. Selected original references (dealing with Co catalysis): (*a*) H. Alper and H. des Abbayes. J. Organomet. Chem. **134**, C11 (1977); (*b*) S. Gambarotta and H. Alper. J. Organomet. Chem. **212**, C23 (1981); (*c*) D. Roberto and H. Alper. J. Chem. Soc. Chem. Commun. 212 (1987); (*d*) S. Calet, H. Alper, J.F. Petrignani, and H. Arzoumanian. Organometallics, **6**, 1625 (1987); (*e*) H. Alper and F. Sibtain. J. Org. Chem. **53**, 3306 (1988); (*f*) G. Vasapollo and H. Alper. Tetrahedron Lett. **29**, 5113 (1988); (*g*) H. Alper and S. Calet. Tetrahedron Lett. **29**, 1763 (1988); (*h*) D. Roberto and H. Alper. J. Am. Chem. Soc. **111**, 7539 (1989); (*i*) D. Roberto and H. Alper. Organometallics, **9**, 1245 (1990); (*j*) H. Alper, A. Eisenstat, and N. Satyanarayana. J. Am. Chem. Soc. **112**, 7060 (1990); (*k*) M. de Wang and H. Alper. J. Organomet. Chem. **451**, 169 (1993); (*l*) C. Zucchi, G. Pályi, V. Galamb, E. Sámpár-Szerencsés, L. Markó, P. Li, and H. Alper. Organometallics, **15**, 3222 (1996); (*m*) M.E. Piotti and H. Alper. J. Am. Chem. Soc. **118**, 111 (1996); (*n*) P. Davoli, I. Moretti, F. Prati, and H. Alper. J. Org. Chem. **64**, 518 (1999); (*o*) J.T. Lee, P.J. Thomas, and H. Alper. J. Org. Chem. **66**, 5424 (2001).
12. (*a*) V. Galamb, G. Pályi, and M. Kajtár. Inorg. Chim. Acta, **55**, L113 (1981); (*b*) G. Pályi, C. Zucchi, T. Bartik, and R. Boese. *In* 1st J. Organomet. Chem. Conf., 4 and 5 November 1993, München, Germany, Abstr. p. 183; (*c*) G. Pályi, C. Zucchi, T. Bartik, T. Herbrich, C. Kriebel, R. Boese, A. Sorkau, and G. Fráter. Atti Accad. Sci. Ist. Bologna Cl. Sci. Fis. Rend. **281**, 159 (1992/1993); (*d*) G. Pályi, K. Alberts, T. Bartik, R. Boese, G. Fráter, T. Herbrich, A. Herfurth, C. Kriebel, A. Sorkau, C.M. Tschoerner, and C. Zucchi. Organometallics, **15**, 3253 (1996); (*e*) M.J. Szabó, R.K. Szilágyi, L. Bencze, R. Boese, L. Caglioti, C. Zucchi, and G. Pályi. Enantiomer, **5**, 549 (2000); (*f*) L. Bencze, R. Boese, G. Pályi, M.J. Szabó, R.K. Szilágyi, and C. Zucchi. Magy. Kem. Lapja, **56**, 215 (2001); (*g*) C. Zucchi, S. Tiddia, R. Boese, C.M. Tschoerner, L. Bencze, and G. Pályi. Chirality, **13**, 458 (2001); (*h*) C. Zucchi, R. Boese, K. Alberts, T. Herbrich, G. Tóth, L. Bencze, and G. Pályi. Eur. J. Inorg. Chem. 2297 (2001); (*i*) L. Bencze, R.K. Szilágyi, M.J. Szabó, R. Boese, C. Zucchi, and G. Pályi. *In* Fundamentals of life. *Edited by* G. Pályi, C. Zucchi, and L. Caglioti. Elsevier and Accademia Nazionale di Scienze Lettere e Arti (Modena, Italy), Paris. 2002. pp. 451–471; (*j*) H. Alper, L. Bencze, R. Boese, L. Caglioti, R. Kurdi, G. Pályi, S. Tiddia, D. Turrini, and C. Zucchi. J. Mol. Catal. A: Chem. **204–205**, 227 (2003).
13. Reviews: (*a*) G. Pályi, L. Bencze, K. Micskei, and C. Zucchi. Atti Mem. Accad. Naz. Sci. Lett. Arti Modena, **317**, 457 (2001); (*b*) L. Bencze, G. Pályi, and R. Kurdi. NATO Sci. Ser. II Math. Phys. Chem. **116**, 343 (2003) (Metal-ligand interactions); (*c*) L. Bencze, C. Zucchi, L. Caglioti, and G. Pályi. *In* Progress in biological chirality. *Edited by* G. Pályi, C. Zucchi, and L. Caglioti. Elsevier, Oxford, UK. 2004. pp. 29–37.
14. D.F. Shriver and M.A. Drezdzon. Manipulation of air sensitive compounds. 2nd ed. Wiley, New York. 1986.
15. D. Streinz, B. Koutek, and D. Saman. Synlett, 809 (2001).
16. I.T. Harrison and S. Harrison. Compendium of organic synthetic methods. Vol. 1. Wiley and Sons, New York. 1971. p. 272.
17. P. Szabó, L. Markó, and G. Bor. Chem. Tech. (Berlin), **13**, 549 (1961).
18. D.T. Cromer and J.B. Mann. Acta Crystallogr. Sect. A, **24A**, 321 (1968).
19. $\Delta f'$, $\Delta f''$ from: D.T. Cromer and D. Liberman. J. Chem. Phys. **53**, 1891 (1970).
20. (*a*) V. Galamb, G. Pályi, F. Cser, M.G. Furmanova, and Y.T. Struchkov. J. Organomet. Chem. **209**, 183 (1981); (*b*) V. Galamb and G. Pályi. *In* Organometallic syntheses. Vol. 3. *Edited by* J.J. Eisch and R.B. King. Elsevier, Amsterdam. 1986. pp. 142–146.
21. (*a*) G. Bor. Inorg. Chim. Acta, **1**, 81 (1967); (*b*) V. Galamb and G. Pályi. J. Chem. Soc. Chem. Commun. 487 (1982); (*c*) V. Galamb, G. Pályi, F. Ungváry, L. Markó, R. Boese, and G. Schmid. J. Am. Chem. Soc. **108**, 3344 (1986); (*d*) V. Galamb, G. Pályi, R. Boese, and G. Schmid. Organometallics, **6**, 861 (1987); (*e*) J. Somlyai-Haász, F. Haász, V. Galamb, A. Benedetti, C. Zucchi, G. Pályi, T. Krümmling, B. Happ, and T. Bartik. J. Organomet. Chem. **419**, 205 (1991).
22. (*a*) M. Tasi and G. Pályi. Organometallics, **4**, 1523 (1985); (*b*) M. Röper and C. Krüger. J. Organomet. Chem. **339**, 159 (1988); (*c*) T. Bartik, T. Krümmling, C. Krüger, L. Markó, R. Boese, G. Schmid, P. Vivarelli, and G. Pályi. J. Organomet. Chem. **421**, 323 (1991).
23. (*a*) G. Pályi and G. Váradi. J. Organomet. Chem. **86**, 119 (1975); (*b*) G. Pályi. Transition Met. Chem. (Dordrecht, Neth.), **2**, 273 (1977); (*c*) G. Pályi, M. Kovács-Toplak, and G. Váradi. Atti Accad. Sci. Ist. Bologna Cl. Sci. Fis. Rend. **266**, 139 (1978); (*d*) M. Kajtár, J. Kajtár-Miklós, G. Váradi, I.T.

© 2005 NRC Canada

Horváth, C. Zucchi, and G. Pályi. Ital. Phys. Soc. Conf. Proc. **48**, 219 (1994) (Non-linear dynamics); (*e*) M. Kajtár, J. Kajtár-Miklós, G. Giacomelli, G. Gaál, G. Váradi, I.T. Horváth, C. Zucchi, and G. Pályi. Tetrahedron: Asymmetry, **6**, 2177 (1995); (*f*) L. Bencze, M.J. Szabó, R.K. Szilágyi, and G. Pályi. *In* NATO ASI: Metal-ligand interactions in chemistry, physics and biology, 1–12 September 1998, Cetraro, Italy. Abstract: p. 33.

© 2005 NRC Canada

Synthesis and reactivity of the macrobicyclic complexes (1,5,8,12-tetraaza-17-oxabicyclo[10.5.2]-nonadecane)cobalt(III) perchlorate ($[Co(L_1)(ClO_4)](ClO_4)_2$), [(chloro(1,4,8,11-tetraaza-17-oxabicyclo-[9.5.3]nonadecane)cobalt(III) perchlorate ($[Co(L_2)(Cl)](ClO_4)_2$), (4,8-dimethyl-1,4,8,11-tetraaza-17-oxabicyclo[9.5.3]nonadecane)cobalt(III) perchlorate ($[Co(L_3)(ClO_4)](ClO_4)_2$), and (5,8-dimethyl-1,5,8,12-tetraaza-17-oxabicyclo[10.5.2]nonadecane)cobalt(III) perchlorate ($[Co(L_4)(ClO_4)](ClO_4)_2$) — Crystal structure of the L_2 complex[1]

Theo Rodopoulos, Koji Ishihara, Mary Rodopoulos, M.J. Zaworotko, M. Maeder, and A. McAuley

Abstract: The potentially penta-coordinating ligands L_2 and L_3 have been synthesized by reaction of the 10-membered macrocycle 1,5-diaza-8-oxacyclodecane with either 1,9-dichloro-3,7-diazanonane-2,8-dione, and subsequent reduction of the diamide (**3**), or with 1,9-dichloro-3,7-(dimethyl)diazanonane-2,8-dione and reduction (L_3). A similar procedure is outlined for the dimethylated macrobicycle (L_4), based on the corresponding nine-membered 1,4-diaza-7-oxacyclononane. The Co(III) complexes of these ligands and of 1,5,8,12-tetraaza-17-oxabicyclo[10.5.2]nonadecane (L_1) have been prepared. Spectrophotometric determinations on the L_1 complex ion confirm the presence of two hydrogen ion related equilibria, one of which ($pK = 2.2 \pm 0.2$) is associated with the proposed replacement of the apical ether oxygen by a water molecule that is bound to the metal centre and hydrogen bonded to the ether. The species derived from L_1 and L_2 exhibit remarkable kinetic stability. Studies on the anation of the $[Co(L_1)(H_2O)](ClO_4)_3$ with chloride ions in acidic media are consistent with the reaction of both the proton-related complex and the $[Co(L_1)(H_2O)]^{3+}$ ion. Whilst complex ions containing two secondary NH groups maintain the metal–ion coordination in strongly acidic media, corresponding species with ligands containing all four tertiary amine sites are subject to attack by protons leading to a relatively facile demetallation of the complexes. The latter finding is supported by kinetic studies and mass spectrometric fragmentation patterns of the ions.

Key words: cobalt(III), macrobicycle, hydrolysis, anation, spectroscopic analysis.

Résumé : Les ligands L_2 et L_3 qui pourraient donner lieu à une pentacoordination ont été synthétisés en faisant appel à la réaction du macrocycle à dix chaînons 1,5-diaza-8-oxacyclodécane avec la 1,9-dichloro-3,7-diazanonane-2,8-dione

Received 3 December 2004. Published on the NRC Research Press Web site at http://canjchem.nrc.ca on 23 July 2005. Reposted on the Web site with correction on 16 August 2005.

It is a pleasure to recognize the many contributions to chemistry in Canada by colleague and friend Howard Alper.

T. Rodopoulos. CSIRO, Clayton, Victoria 3169, Australia.
K. Ishihara. Department of Chemistry, Waseda University, Shinjuku-ku, Tokyo 169-8555, Japan.
M. Rodopoulos. Department of Chemistry, University of South Florida, Tampa, FL 33620, USA.
M.J. Zaworotko. Institute of Drug Technology, Boronia, Victoria 3155, Australia.
M. Maeder. Chemistry Department, University of Newcastle, Callaghan 2308, Australia.
A. McAuley.[2] Chemistry Department, University of Victoria, Victoria, BC V8W 3V6, Canada.

[1]This article is part of a Special Issue dedicated to Professor Howard Alper.
[2]Corresponding author (e-mail: amcauley@uvic.ca).

 doi: 10.1139/V05-089 © 2005 NRC Canada

et réduction subséquente du diamide cyclique (**3**) ou avec la 1,9-dichloro-3,7-(diméthyl)diazanonane-2,8-dione suivie d'une réduction (L_3). On décrit une méthode semblable pour le macrobicycle diméthylé (L_4) qui est basée sur le composé à neuf chaînons 1,4-diaza-7-oxacyclononane. On a préparé les complexes du cobalt(III) avec ces ligands et avec le 1,5,8,12-tétraaza-17-oxabicyclo[10.5.2]nonadécane (L_1). Des déterminations spectrophotométriques sur le complexe L_1 confirment la présence de deux équilibres apparentés des ions hydrogènes, dont l'un (pK = 2,2 ± 0,2) est associé au remplacement proposé de l'oxygène de l'éther apical par une molécule d'eau qui est liée au centre métallique et relié à l'éther par une liaison hydrogène. Les espèces qui dérivent des ligands L_1 et L_2 présentent une stabilité cinétique remarquable. Des études d'anation du $[Co(L_1)(H_2O)](ClO_4)_3$ avec des ions chlorures en milieu acide sont en accord avec une réaction du complexe lié par un proton et l'ion $[Co(L_1)(H_2O)]^{3+}$. Alors que les ions complexes comportant deux groupes NH secondaires maintiennent la coordination métal–ion en milieu fortement acide, les espèces correspondantes comportant des ligands sur chacun des quatre sites amines tertiaires sont sujettes à des attaques par des protons ce qui conduit à une démétallation relativement facile des complexes. Cette dernière observation est supportée par des études cinétiques et par les patrons de fragmentation en spectrométrie de masse des ions.

Mots clés : cobalt(III), macrobicycle, hydrolyse, anation, analyse spectroscopique.

[Traduit par la Rédaction]

Introduction

The synthesis of novel macrocyclic and polymacrocyclic ligands and the significant thermodynamic and kinetic stability imparted by them upon metal ion complexation has been a feature of interest for over two decades (1–5). Such species are now found in a variety of chemistries from competitive anion binding sites (6), multimacrocyclic luminescent arrays (7), and polynuclear complexes of pendant-arm ligands with unusual spin states (8). Reports from previous investigations from this laboratory have described macrobicyclic systems involving five-coordinate Cu(II) complexes (9) and six-coordinate Ni(II) (10, 11) species of L_1 and L_2, where, in the latter, the d^8 ion, being octahedral, exhibits a single substitution site. Such species exhibit extraordinary kinetic stability, with no detectable decomposition over days even in strongly acidic (4 mol/L) media. In addition, spectroscopic observations are consistent with the formation of nickel(III) species of sufficient lifetimes to permit kinetic measurements not only of redox reactions (12), but also, in some instances, the Ni(III) ions formed are sufficiently stable kinetically to permit rate studies of substitution by chloride (13). Hydrogen-ion dependences in these investigations are consistent with an unusually strongly acidic proton-related equilibrium associated with the ether linkage (13, 14). In this paper, we present the results of comparable studies of analogous cobalt(III) complexes where the d^6 ion imparts much greater kinetic stability than the nickel(III) ion, providing an opportunity to examine not only kinetic features, but also to spectroscopically identify species involved in the various proton-related equilibria. Included are kinetic observations involving a tetra-*N*-substituted macrobicycle where the stability in acidic media is diminished owing to protonation at the *N*-methyl tertiary amines competing with the complexation at the metal centre.

Experimental

The literature method was used to prepare 17-oxa-1,5,8,12-tetraazabicyclo[10.5.2]nonadecane (L_1) (11). The ligands 17-oxa-1,4,8,11-tetraazabicyclo[9.5.3]nonadecane (L_2), 4,8-dimethyl-1,4,8,11-tetraaza-17-oxabicyclo[9.5.3]nonadecane (L_3), and 5,8-dimethyl-1,5,8,12-tetraaza-17-oxabicyclo-[10.5.2]nonadecane (L_4) were synthesized as indicated in the following. Acetonitrile (Caledon) was fractionally distilled from CaH_2 and stored under nitrogen. Water, with a specific resistance of >15 MΩ cm was prepared using a MilliQ-Reagent system. $Co(ClO_4)_2{\cdot}6H_2O$ was synthesized from $CoCO_3{\cdot}xH_2O$ (Aldrich) through reaction with the stoichiometric amount of $HClO_4$. The perchlorate salt was recrystallized three times from water, dried under high vacuum for 48 h at room temperature, and stored over $CaSO_4$ in a desiccator. Ethanol (Commercial Alcohols, 100%), activated charcoal (Sigma, 250–350 mesh), $HClO_4$ (Allied Chemicals, 70% assay), HCl (Anachemia, 36.5%–38.0% assay), $NaClO_4{\cdot}H_2O$ (Fisher Scientific), NaOH (BDH), PbO_2 (BDH), D_2O (Cambridge Isotope Laboratories), and CD_3CN (Cambridge Isotope Laboratories) were all used as purchased. Mass spectra were recorded on a Kratos Concept mass spectrometer in the LSI-MS mode. The matrix employed in all cases was *m*-nitrobenzyl alcohol. Bruker WM-250 and AC-300 NMR spectrometers were used to record the ^1H and ^{13}C NMR spectra. ^{13}C NMR chemical shifts are referenced to the residual methyl carbon in incompletely deuterated CD_3CN (δ (CH_3CN) = 1.30 ppm) and ^1H NMR chemical shifts to the residual protons in incompletely deuterated D_2O (δ (H_2O) = 4.70 ppm). Elemental analyses were performed by Canadian Microanalytical Services, Vancouver, British Columbia, Canada.

Synthesis

(1,5,8,12-Tetraaza-17-oxabicyclo[10.5.2]nonadecane)cobalt(III) perchlorate ($[Co(L_1)(ClO_4)](ClO_4)_2$)

Ligand L_1 (0.299 g, 1.106 mmol) was dissolved in dry, distilled acetonitrile (30 cm^3) and an equivalent of cobalt(II) perchlorate hexahydrate (0.405 g, 1.106 mmol) was added with stirring. The solution was acidified to approximately pH 3 with $HClO_4$ and an excess of lead(II) oxide (0.400 g, 1.672 mmol) added. Upon bubbling the mixture with air overnight, a maroon solution was obtained. The mixture was centrifuged and the excess solid lead(II) oxide filtered leaving the maroon-coloured solution. Concentration of the filtrate to approximately 10 cm^3 and cooling in an ice bath resulted in the precipitation of a red solid. Crystallization of the complex was achieved by redissolution of the solid in the minimum amount of acetonitrile and allowing the solution to

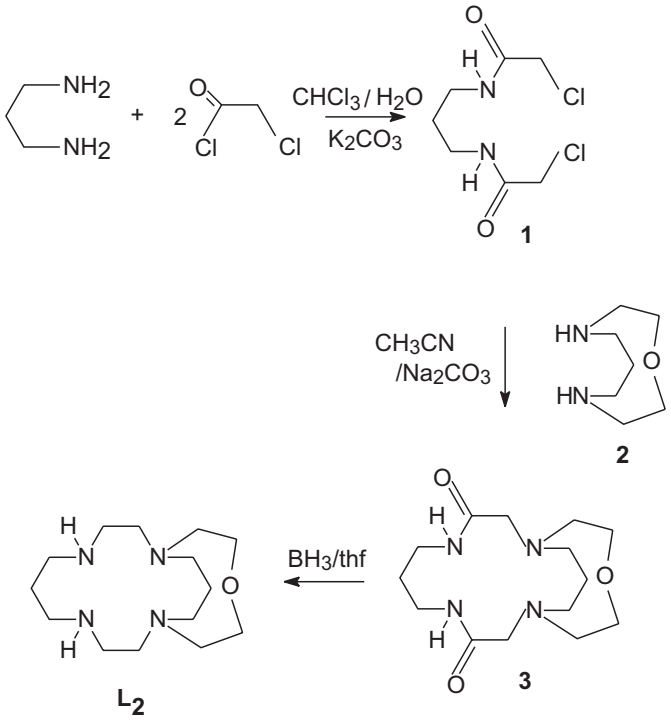
© 2005 NRC Canada

evaporate slowly. Yield: 0.165 g (24%). ^{13}C NMR (D_2O): 75.7 (-*C*H_2-O-), 61.4, 58.0, 55.3, 53.2, 46.9 (-*C*H_2-N-), 24.45 (-C-*C*H_2-C-). Anal. calcd. for $[Co(C_{14}H_{30}N_4O)(ClO_4)](ClO_4)_2$ (%): C 26.79, H 4.82, N 8.93; found: C 26.77, H 4.87, N 9.54.

17-Oxa-1,4,8,11-tetraazabicyclo[9.5.3]nonadecane (L_2)

The synthesis was carried out as shown in Scheme 1.

Scheme 1.



1,9-Dichloro-3,7-diaza-nonane-2,8 dione (1)

Propylenediamine (4.88 g, 0.0567 mol) was added under constant stirring to a mixture of $CHCl_3$ (69 mL) and H_2O (34 mL) and cooled in an ice bath. A mixture of chloroacetyl chloride (13.9 mL, 0.172 mol) in $CHCl_3$ (86 mL) and K_2CO_3 (22.36 g, 0.162 mol) in water (860 mL) were added simultaneously under a nitrogen atmosphere over a 1 h period. The reaction mixture was stirred at room temperature for a further 2 h. The $CHCl_3$ layer was separated, washed with water (2 × 100 mL), and dried over $MgSO_4$. Removal of solvent yielded a colourless oil that was dried in vacuo overnight. Upon addition of CCl_4 and cooling overnight, a white solid precipitated. Filtration and concentration of the solution followed by a further addition of CCl_4 afforded a second crop of material. The diamide (**1**) was dried under vacuum. Yield: 9.01 g, 70%. The material was used as such. ^{1}H NMR (D_2O): 7.2 (N-*H*), 4.1 (-C*H*$_2$-C(O)-), 3.4 (C*H*$_2$-NH), 1.8 (-C-C*H*$_2$-C-). ^{13}C NMR ($CDCl_3$): 170.1 (-*C*=O), 42.7 (*C*H_2-NH), 37.4 (-*C*H_2-C(O)-), 27.9 (-C-*C*H_2-C-). ^{13}C NMR (D_2O): 169.7 (-*C*=O), 42.2 (*C*H_2-NH), 37.0 (-*C*H_2-C(O)-), 27.5 (-C-*C*H_2-C-).

Cyclization with the free macrocycle, 1,5-diaza-8-oxacyclodecane (**2**), was carried out in basic acetonitrile. Doubly distilled acetonitrile (2.5 L) was placed in a 5 L four-necked flask fitted with a stirring attachment and a condenser and two septa for syringes. A stream of N_2 was attached and Na_2CO_3 (2.402 g, 22.66 mmol, 3.16 equiv.) was added to the bulk CH_3CN. The macrocycle **2** (1.036 g, 7.183 mmol) was dissolved in 200 mL of dry CH_3CN. Diamide **1** showed limited solubility in acetonitrile and only 0.408 g (1.797 mmol) was dissolved in 50 mL of solvent. The CH_3CN–Na_2CO_3 solution was heated to reflux and 50 mL each of the reactant solutions **1** and **2** were added slowly (four portions) over a period of 40 h. Reflux was continued for another 24 h. After filtration of the Na_2CO_3, the acetonitrile was removed in vacuo leaving a yellow, quasi-crystalline solid. Dissolution in $CHCl_3$ removed the residual amounts of diamide impurity yielding a yellow crystalline solid **3**. Yield: 2.07 g, 96%. ^{13}C NMR ($CDCl_3$): 174.8 (-*C*=O), 66.7 (*C*H_2-O-), 62.1, 57.4, 55.9 (*C*H_2-N), 37.4 (-*C*H_2-CH$_2$-NH-), 29.8, 27.7 (-C-*C*H_2-C-). MS: 299 $(M + 1)^+$.

The fully saturated macrocycle (**L_2**) was prepared by addition of a solution of BH_3·THF (100 mL) to a solution of **3** (1.002 g, 3.358 mmol) in dry THF (30 mL) and refluxing for 24 h. After cooling to room temperature, excess borane was destroyed with water. Upon removal of the solvent under vacuum, the white solid formed was treated with 6 mol/L HCl and refluxed for 3 h. Upon cooling, basification with KOH pellets to pH 14 and extraction with $CHCl_3$, the solution was dried, filtered, and the solvent removed, yielding a slightly yellow oil. Yield: 0.742 g, 82%. ^{13}C NMR ($CDCl_3$): 73.6 (-*C*H_2-O), 58.5, 58.1, 56.9 (*C*H_2-N), 47.8, 47.3 (-*C*H_2-*C*H_2-NH-), 28.2, 28.1 (-C-*C*H_2-C-).

[(Chloro)(1,4,8,11-tetraaza-17-oxabicyclo[9.5.3]nonadecane)cobalt(III)] perchlorate ([Co(L_2)(Cl)](ClO_4)$_2$)

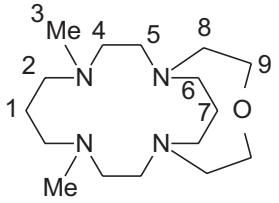
An aqueous solution of cobalt(II) perchlorate hexahydrate (0.134 g, 0.366 mmol) was added to a refluxing ethanol–H_2O (4:1, 30 cm^3) solution of the ligand L_2 (0.099 g, 0.366 mmol). The resulting solution turned green almost instantaneously. A catalytic amount of activated charcoal was then added and the solution refluxed for 2 h. After cooling, air was bubbled through the mixture for several hours yielding a purplish-red solution. The charcoal was filtered off and the solvent removed under reduced pressure. An aqueous solution of the crude complex was purified by passage down a Dowex 50W-x8 (50–100 mesh) exchange column. The complex was eluted with 6 mol/L HCl and the eluate evaporated to dryness, leaving a green solid, which was recrystallized from a hot aq. 0.2 mol/L $NaClO_4$ (10 cm^3) solution, collected, washed with ethanol and diethyl ether, and air dried. Yield: 0.082 g, 40%. ^{13}C NMR (D_2O): 82.4 (-*C*H_2-O-), 67.4, 58.7, 58.0, 52.7, 50.1 (-*C*H_2-N-), 27.8, 24.0 (-C-*C*H_2-C-). Anal. calcd. for $[Co(C_{14}H_{30}N_4O)(Cl)](ClO_4)_2$·$H_2O$ (%): C 28.91, H 5.54, N 9.63; found: C 28.94, H 5.24, N 9.64.

Neutralizing an aqueous solution of the monochloride complex with 0.1 mol/L NaOH solution resulted in a colour change from green to orange-red. Leaving the solution open to the atmosphere to allow the solvent to evaporate slowly yielded the purple perchlorate complex, $[Co(L_2)(ClO_4)](ClO_4)_2$, which was filtered out, washed with ethanol, and air dried.

4,8-Dimethyl-1,4,8,11-tetraaza-17-oxabicyclo[9.5.3]nonadecane (L_3)

The ligand, with no ionizable protons, was prepared in a manner similar to that shown for L_2 (Scheme 1, vide supra). *N*,*N*′-Dimethylpropylenediamine (5 g, 0.0489 mol) was added

© 2005 NRC Canada



L3

under constant stirring to a mixture of $CHCl_3$ (69 mL) and H_2O (34 mL) and cooled in an ice bath. A mixture of chloroacetyl chloride (22.11 g, 0.1957 mol) in $CHCl_3$ (86 mL) and K_2CO_3 (22.36 g, 0.162 mol) in water (860 mL) was added simultaneously under a nitrogen atmosphere over a 1 h period. The reaction mixture was stirred at room temperature for a further 2 h. The $CHCl_3$ layer was separated, washed with water (2 × 100 mL), and dried over $MgSO_4$. Removal of the solvent yielded a colourless oil that was dried in vacuo overnight. Upon addition of CCl_4 and cooling overnight, a white solid precipitated. Filtration and concentration of the filtrate followed by a further addition of CCl_4 afforded a second crop of material. The diamide **4** was washed with ethanol and dried. Yield: 9.5 g, 76%. The NMR spectrum showed the presence of several isomers. ^{13}C NMR ($CDCl_3$): 166.2, 166.7 (-*C*=O), 45.7, 45.6 (*C*H_2-NMe), 41.0, 41.4, 41.6 (-*C*H_2-C(O)-), 24.3, 26.6 (-C-*C*H_2-C-).

To a solution of the bis(chloro)diamide **4** (1.718 g, 6.73 mmol), in dry distilled CH_3CN (200 mL), was added sodium iodide (5.548 g, 37.01 mmol). The macrocycle **2** (0.971 g, 6.73 mmol) was dissolved in dry distilled CH_3CN (200 mL) and solutions of the reagents **4** and **2** were added very slowly (over a 24 h period) under N_2 in 50 mL batches to a refluxing solution of dry distilled acetonitrile (2.5 L) containing Na_2CO_3 (9.415 g, 88.83 mmol). Heating of the mixture, now orange coloured, was continued for a further 10 h, and the mixture was cooled overnight. Filtration under nitrogen, removal of the solvent, and addition of $CHCl_3$ (250 mL) yielded an orange solution and an off-white solid. After washing with water and further addition of $CHCl_3$, the solution was dried (Na_2SO_4), filtered, and the solvent removed yielding an orange-brown oil that was dried under high vacuum overnight. The cyclised diamide, 4,8-dimethyl-1,4,8,11-tetraaza-17-oxabicyclo[9.5.3]nonadecane-2,9-dione (**5**), solidified as a yellow, crispy honeycomb that was quite hygroscopic. Yield: 2.0 g, 90%. MS: 327 $(M + 1)^+$.

The crude diamide **5** (2.5 g, 10.46 mmol) was transferred to a 1 L flask using dry, freshly distilled THF (170 mL). After addition of the BH_3·THF complex (340 mL, 1 mol/L), the solution was refluxed for 24 h and cooled to room temperature. The solution was cooled in ice water to quench the remaining borane. Evaporation to dryness in vacuo gave a cream-coloured solid to which was added 6 mol/L HCl (140 mL), and this solution was heated to reflux for 3 h. Cooling in ice followed by the addition of KOH pellets to pH ~ 14 and extraction with $CHCl_3$, and filtration, gave a pale-yellow solution of the macrobicycle $\mathbf{L_3}$. Upon drying under high vacuum, a yellow oil formed. The product after work-up (1.944 g, 85%) was observed to be a mixture. Purification was achieved by preparation of the corresponding copper(II) complex[3] (0.642 g) followed by decomplexation of the metal ion by use of Na_2S (9). The final yield of $\mathbf{L_3}$ was 0.426 g (21% from macrocycle **2**). ^{13}C NMR ($CDCl_3$): 72.1 (*C*H_2-O), 56.6, 56.2, 56.0, 55.5, 54.7 (*C*H_2-N), 43.2 (N-*C*H_3), 26.6, 25.8 (CH_2-*C*H_2-CH_2). MS: 298 (M^+), 299 $(M + 1)^+$, 327 $(M + 29)^+$.

4,8-Dimethyl-1,4,8,11-tetraaza-17-oxabicyclo[9.5.3]nonadecane-cobalt(III) perchlorate ($[Co(L_3)(ClO_4)](ClO_4)_2$)

The ligand $\mathbf{L_3}$ (0.132 g, 0.442 mmol) was dissolved in an ethanol–water mixture (48 mL : 12 mL) and heated to reflux. An aqueous solution of $Co(ClO_4)_2$·$6H_2O$ (0.162 g, 0.442 mmol) was added and the solution turned a yellow-green colour. Several grams of activated charcoal were introduced and the solution was refluxed for 2 h. Air bubbling of the cooled solution (5 h) followed by filtration yielded a pink-red solution. After removal of the residual ethanol and addition of 1 drop of concd. $HClO_4$, the solution was left to crystallize at 4 °C overnight. The crystals were washed with ethanol, ether, and air dried. Yield: 0.106 g, 37%. ^{13}C NMR (D_2O): 66.9 (*C*H_2-O), 60.9, 55.0, 54.6, 52.3, 51.7 (*C*H_2-N), 39.0 (N-*C*H_3), 19.7 (CH_2-*C*H_2-CH_2). It appears that there is overlap of the methylene peaks, since only eight and not nine signals were observed. MS (negative ion): 654.05 $([Co(L_3)(ClO_4)](ClO_4)_2]^-$. UV–vis ($\lambda_{max}$, nm): 232 ($\varepsilon$ = 5380 $(mol/L)^{-1}$ cm^{-1}) and 516 (ε = 17 $(mol/L)^{-1}$ cm^{-1}).

The isomeric macrobicyclic ligand, 5,8-dimethyl-1,5,8,12-tetraaza-17-oxabicyclo[10.5.2]nonadecane ($\mathbf{L_4}$), was prepared[4] in a manner similar to that outlined previously using *N*,*N*′-dimethylethylenediamine and 3-chloropropionyl chloride as initial reactants. Further reaction of the resultant bis(chloro)diamide with the macrocycle 1,4-diaza-7-oxacyclononane yielded the bicyclic diamide that upon reduction, as described previously, yielded ligand L_4. For the Co(III) complex $[Co(L_4)(Cl)](ClO_4)_2$ calcd. (%): C 32.48, H 5.79, N 9.47; found: C 32.87, H 5.84, N 9.57. UV–vis (λ_{max}, nm): 461 (ε = 16 $(mol/L)^{-1}$ cm^{-1}).

Caution! Transition-metal perchlorates are known to be hazardous and must be treated with care, especially in the presence of organic solvents.

Crystallography

$[Co(L_2)(Cl)](ClO_4)_2$

X-ray quality crystals were grown by slow evaporation of an aqueous solution containing the complex and $NaClO_4$. The experimental parameters for the complex are listed in Table 1.

A crystal of dimensions 0.10 mm × 0.15 mm × 0.40 mm was mounted in a glass Lindemann tube and optically centred in an Enraf-Nonius CAD-4 diffractometer employing graphite-monochromated MoKα radiation. The unit cell was refined by using 24 reflections in the 2θ range 25°–33°. The diffraction data were collected using the ω/2θ scan mode. A total of 3554 reflections were collected. The structure solution and refinement were completed using the PC version of

[3] T. Rodopoulos. Unpublished observations.
[4] M. Rodopoulos. Unpublished observations.

© 2005 NRC Canada

Table 1. Experimental crystallographic data for $[Co(L_2)Cl](ClO_4)_2$.

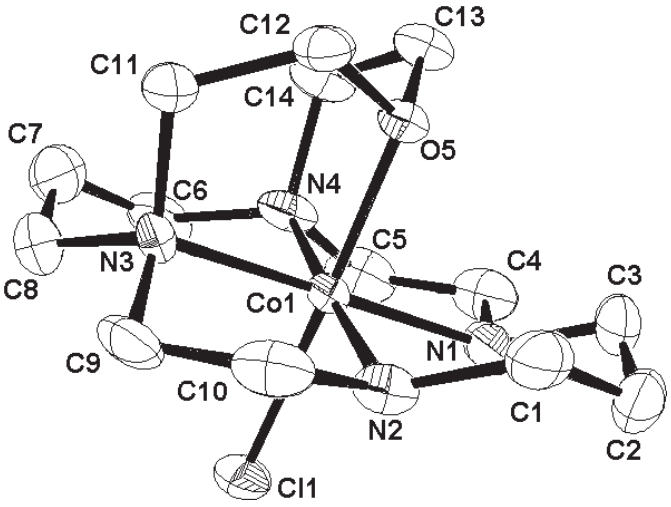
Formula	$CoC_{14}H_{30}N_4O_9Cl_3$
Formula mass	563.7
Crystal colour	Green
Crystal system	Monoclinic
Space group	$P2_1/n$
Cell dimensions	
a (Å)	9.8483(7)
b (Å)	13.1344(9)
c (Å)	16.6774(12)
α (°)	90
β (°)	90.6830(10)
γ (°)	90
$D_{calcd.}$ (Mg m^{-3})	1.707
V (A^3)	2194.0(7)
Z	4
F(000)	1168
λ (Å)	0.7093
μ (mm^{-1})	1.2
Cryst. dim. (mm^3)	0.10 × 0.15 × 0.40
Transmis. factors	0.839–0.999
2θ Range (°)	25–33
No. refls. meas.	3554
No. unique refls.	3432
No. refls. with $I_{net} > 3.00\sigma(I_{net})$	1740
R (F_0)	0.062
R_w	0.061

the NRCVAX system (15–18). Of the 3432 unique reflections observed, 1740 reflections with $I_{net} > 3.00\sigma(I_{net})$ were included in the final least-squares refinement for 61 atoms and 280 parameters. Absorption corrections were made and all non-hydrogen atoms were refined anisotropically. Min and max transmission factors were estimated to be 0.839 and 0.999, respectively. All hydrogen atoms were placed in calculated positions ($D_{C\text{-}H}$ = 1.08 Å), and were given isotropic thermal parameters based upon the atom to which they were bonded. The refinement converged with a max shift to estimated standard deviation (esd) of 0.009 in the final cycle, and a maximum peak of 0.640 e Å^{-3} at an $R(F_0)$ value of 0.062 (R_w = 0.061).

UV–vis (pK_a measurements)

UV–vis spectra were recorded on a Varian Cary 5 spectrophotometer. Small increments of NaOH solutions (varying concentrations) were added with a Gilson Pipetman P200 micropipette to approximately 1 mol/L $HClO_4$ solutions of the cobalt(III) complexes in quartz UV–vis cuvettes. The pH of the solutions was measured after each addition of base with a Fisher glass electrode connected to a Fisher Scientific Accumet pH meter 915 followed by the immediate recording of their UV–vis spectra. Measurements were made over the pH range 0.5–10.

Fig. 1. ORTEP diagram of the $[Co(L_2)(Cl)]^{2+}$ ion with 25% thermal ellipsoids.



Kinetic studies

Anation reactions of $[Co(L_1)(H_2O)](ClO_4)_3$ with chloride ions under pseudo-first-order conditions were followed at 25–40 °C using a Shimadzu UV-160A spectrophotometer at 240 nm. The rates of anation were determined by reaction with a series of LiCl solutions ranging in concentrations of 50–400 molar excess. The experiments were carried out at eight different $HClO_4$ concentrations between 0.11 and 0.96 mol/L (I = 1.0 mol/L, $LiClO_4$). Prior to mixing, the solutions were pre-equilibrated at the required temperature and were controlled to within ±0.1 °C. A minimum of three kinetic runs was collected for each pair of solutions, prior to signal averaging with kinetic analysis by nonlinear, least-squares fitting methods.

Although metal–ion complexes of ligands L_1 and L_2 were shown to be kinetically stable, with no detectable decomposition in 1 mol/L media over a >24 h period, the complexes incorporating L_3 and L_4, if left overnight in 1 mol/L acidic media, exhibited complete decomposition. Studies on $[Co(L_3)(ClO_4)](ClO_4)_2$ were undertaken at 25 °C at 232 nm where the rates of absorbance decrease over a range of acidities confirmed the acid dependence.

Results

Molecular structure

An ORTEP of the structure of the $[Co(L_2)Cl]^{2+}$ ion is shown in Fig. 1. Collection details are provided in Table 1 and selected bond lengths and bond angles are provided in Table 2. Atomic coordinates are shown in Table S1.[5] The geometry at the cobalt metal centre is only slightly distorted from an ideal octahedron expected for a d^6 ion, with the L_2 ligand occupying five of the coordination sites and a chloride ion the sixth site. The macrobicyclic ligand L_2 can be

[5] Supplementary data for this article are available on the Web site or may be purchased from the Depository of Unpublished Data, Document Delivery, CISTI, National Research Council Canada, Ottawa, ON K1A 0S2, Canada. DUD 3689. For more information on obtaining material refer to http://cisti-icist.nrc-cnrc.gc.ca/irm/unpub_e.shtml. CCDC 256926 contains the crystallographic data for this manuscript. These data can be obtained, free of charge, via www.ccdc.cam.ac.uk/conts/retrieving.html (Or from the Cambridge Crystallographic Data Centre, 12 Union Road, Cambridge CB2 1EZ, UK; fax +44 1223 336033; or deposit@ccdc.cam.ac.uk).

© 2005 NRC Canada

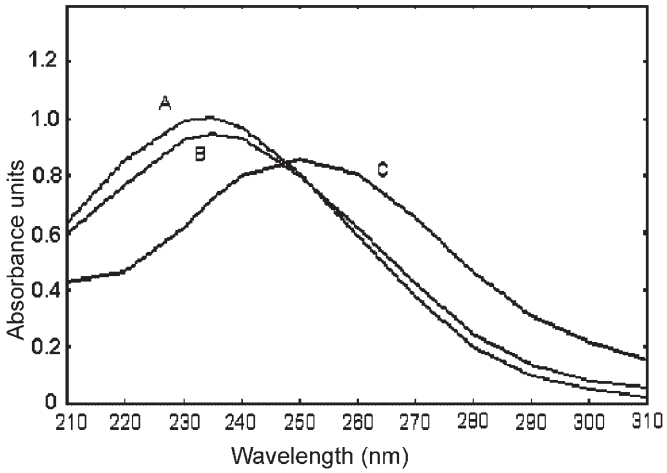
Table 2. Selected interatomic distances (Å)[a] and bond angles (°)[a] for $[Co(L_2)Cl](ClO_4)_2$.

Bond distances (Å)	
Co(1)—Cl(1)	2.219(3)
Co(1)—O(1)	1.924(6)
Co(1)—N(1)	1.979(9)
Co(1)—N(2)	2.007(9)
Co(1)—N(3)	1.949(9)
Co(1)—N(4)	1.978(8)
Bond angles (°)	
Cl(1)-Co(1)-O(1)	178.53(22)
Cl(1)-Co(1)-N(1)	92.5(3)
Cl(1)-Co(1)-N(2)	92.4(3)
Cl(1)-Co(1)-N(3)	88.4(3)
Cl(1)-Co(1)-N(4)	88.3(3)
O(1)-Co(1)-N(1)	86.3(3)
O(1)-Co(1)-N(2)	86.9(3)
O(1)-Co(1)-N(3)	92.8(3)
O(1)-Co(1)-N(4)	92.6(3)
N(1)-Co(1)-N(2)	96.5(5)
N(1)-Co(1)-N(3)	177.0(5)
N(1)-Co(1)-N(4)	87.5(4)
N(2)-Co(1)-N(3)	86.4(5)
N(2)-Co(1)-N(4)	176.0(5)
N(3)-Co(1)-N(4)	89.7(4)

[a]Estimated standard deviations are given in parentheses.

envisaged as the fusion of a 10-membered cyclodecane ring with a 14-membered cyclotetradecane ring. The cyclam ring in L_2 adopts a trans-III configuration according to the terminology of Bosnich et al. (19). Numerous studies have illustrated that for complexes of this type, the trans-III configuration is lowest in energy. In contrast to $[Co(L_2)(Cl)]^{2+}$, the trans-I configuration is adopted by ligands in the macrobicyclic ions $[Cu(L_1)]^{2+}$ and $[Ni(L_1)(ClO_4)]^{2+}$ and in the complexes of the analogous thioether ligand (1,5,8,12-tetraaza-17-thiabicyclo[10.5.2]nonadecane) (L_5) (10). Species such as $[Co(L_5)CH_3CN]^{3+}$ also incorporate nine-membered cyclononane and 14-membered cyclotetradecane rings. In effect, the only structural difference between L_2 and L_n, (where n = 1 or 5), other than the type of apical donor atom, is the placement of the five-membered apical bridge. The trans-III configuration results in a greater ability of the ether oxygen in the decane ring of L_2 to reach over and better encapsulate the axial site. The bond to the apical oxygen is quite strong with Co(1)—O(1) = 1.924(6) Å and is significantly shorter than the Co—S distance (2.206 Å) in $[Co(L_5)(CH_3CN)]^{3+}$,[6] which displays strain owing to the isomeric ligand structure. Furthermore, the Co(1)—Cl(1) bond length is 2.219(3) Å, which is similar to the Co—Cl distance (2.246 Å) observed in the crystal structure of $[Co(daptacn)(Cl)]^{2+}$ (20), where daptacn is the pentaaza ligand 1,4-di(3-aminopropyl)-1,4,7-triazacyclononane. In the latter complex ion, and in the corresponding system, 1,4,7-tri(3-aminopropyl)-1,4,7-triazacyclononane (21), there is a slight distinction between the Co—N(*tert*) and Co—N(*sec*) bond distances, with the former being slightly greater as expected owing to increased steric repulsion at the tertiary nitrogens. However, in contrast with the relatively more open species above, in the present complex, the distances are much more similar, probably owing to the constraints imposed by the macrobicyclic ligand.

Fig. 2. Spectra of the individual cobalt(III) ions. A = $[CoHL_1(OH_2)]^{4+}$; B = $[CoL_1(OH_2)]^{3+}$; C = $[CoL_1(OH)]^{2+}$.



Equilibrium studies

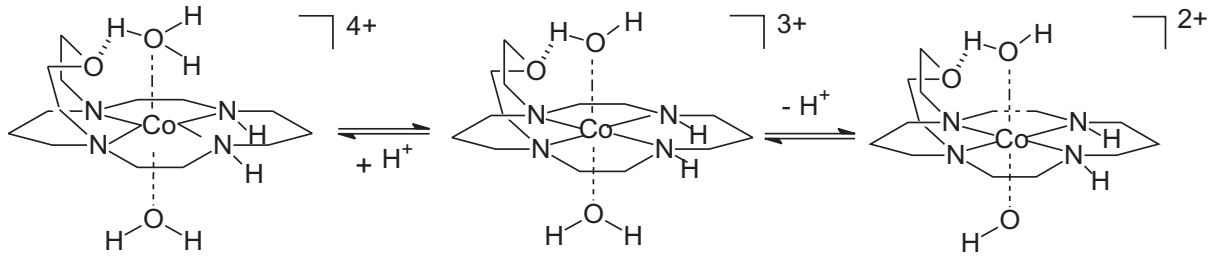
In the case of the ion $[Co(L_1)(ClO_4)]^{2+}$, spectra were measured over the pH range 0.872–9.92. The spectra showed the presence of more than one ion equilibrium (Figs. S1 and S2).[5] Measurements made at 10 nm intervals over the range 210–310 nm were analysed by a second-order global analysis procedure (22) developed to examine the existence of differing, but spectroscopically similar, species in titrations of this kind that result in an inability to reliably fit a reasonable model to the data. The EQUISPEC program (22) permits a number of titrations with differing initial concentrations of the equilibrium partners to be analysed simultaneously. The result is the determination of not only profiles for each reagent, but also the pK for each equilibrium observed. By use of the data shown in Fig. S1,[5] the absorption spectra of three species have been determined and are presented in Fig. 2. The concentration profiles and extent of agreement between observed and calculated spectra are presented in Figs. S3 and S4.[5] It was observed that there is no change in the UV–vis spectrum over 24 h under conditions of 1 mol/L $[H^+]$. Although there is maintenance of the Co–ether O linkage in the solid state, it is considered that in solution the bond dissociates and the presence of the lone pair on this oxygen provides a template for formation of a hydrogen bond as shown in Scheme 2. In increasingly basic conditions, there is loss of the protonated solvent and, at higher pH, the release of the proton from the trans aqua group with a significant change in the spectrum. The pK values associated with these equilibria are 2.2 ± 0.2 and 4.2 ± 0.2, respectively.

An alternative scheme could be envisaged in which there is retention of the Co—O (ether) bond and the site of the solvated H^+ interaction would be the remaining lone pair on

[6]K.R. Coulter. Unpublished observations.

© 2005 NRC Canada

Scheme 2.



the oxygen. It is not possible to exclude the latter, but the bond formation with the O atom to the Co(III) may be weak in this case.

The value for the first pK is higher than that (0.65) for the corresponding strongly oxidizing Ni(III) species (14). However, the second pK, not observed in the Ni(III) system owing to decomposition, is similar to that for other *trans* aquotetramminecobalt(III) species (23, 24).

Similar results on the cobalt(III) complex of the dimethylated ligand L_3 showed two spectroscopic changes, the first over the range pH 0.58–0.67, and a second more clearly defined change with pK ~ 1. For the corresponding complex of L_4, only a single pK ~1.05 is defined. In both cases, however, there is acid decomposition of the complexes owing to the protonation at the tertiary amines (vide infra).

Kinetic measurements

Anation reactions

Substitution reaction kinetics were investigated at 40 °C with chloride concentrations of approximately 50–400 times in excess halide. The rate data for the $[Co(L_1)(H_2O)]^{3+}$ reaction, obtained at 280 nm, are tabulated in Table S2.[5] In general, the scatter of individual values for k_{obs} was in the order of ±5%. The observed first-order rate constants (k_{obs}) vary linearly with chloride concentration. However, the intercepts and slope of each curve vary roughly inversely with $[H^+]$. No evidence was observed for a second substitution step in the anation.

A mechanistic scheme that accounts for the observed acid dependence is described in Scheme 3, where (neglecting all charges) CoHL and CoL represent the complex ions $[CoL(OH_3)(OH_2)]^{4+}$ and $[CoL(OH_2)_2]^{3+}$, and CoHLCl and CoLCl, the corresponding chloro complexes.

The observed rate constant derived from this equilibrium set may be represented as:

$$[1] \qquad k_{obs} = (k_1[H^+] + k_2K_a)[Cl^-]/(K_a + [H^+]) + (k_{-1}[H^+] + k_{-2}K_b)/(K_b + [H^+])$$

As can be seen from eq. [1], approximate inverse proton dependences are predicted for both the intercepts and slopes of plots of k_{obs} vs. $[Cl^-]$ (eq. [1]). A plot of slope(K_a + $[H^+]$) vs. $[H^+]$ is shown in Fig. 3 and, using the K_a value (6.3 × 10^{-3} mol/L) obtained previously, the rate constants derived are k_1 = 0.053 ± 0.002 $(mol/L)^{-1}$ s^{-1} and k_2 = 3.8 ± 1.0 $(mol/L)^{-1}$ s^{-1}. However, the plots of intercepts (K_b + $[H^+]$) vs. $[H^+]$ show a slope of zero or are slightly negative

Scheme 3.

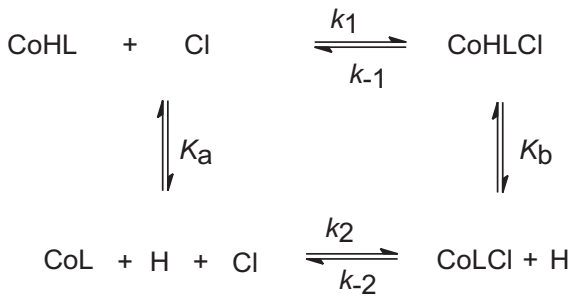
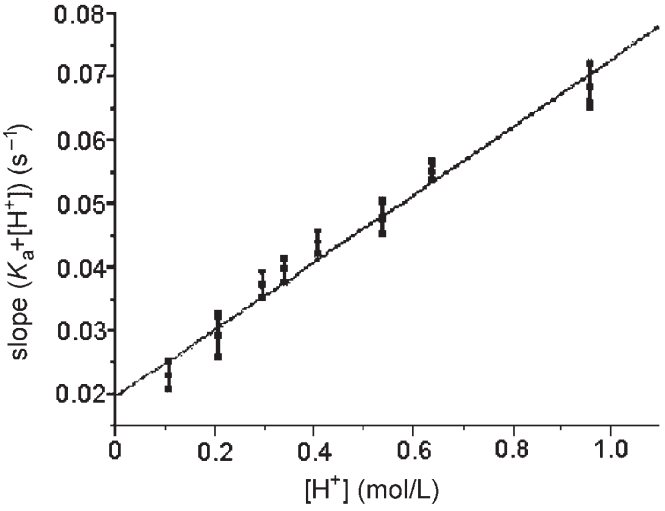


Fig. 3. Plot of slope (K_a + $[H^+]$) vs. $[H^+]$ (eq. [1]).

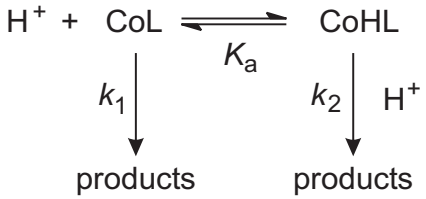


(k_{-1} not statistically discernible), with intercept $k_{-2}K_b$ = 10.4 ± 1.3 × 10^{-5} s^{-1}. Assuming K_a ~ K_b, then, at 40 °C, k_{-2} = 1.6 × 10^{-2} s^{-1} and K_2 = 230 ± 60 mol/L. Comparison with the analogous Ni(III) systems at 25 °C k_1 = 142 $(mol/L)^{-1}$ s^{-1} and k_2 = 1400 ± 300 $(mol/L)^{-1}$ s^{-1} (14) indicates, as expected, a significantly slower process for the d^6 ion.

Decomposition of $[Co(L_3)(ClO_4)](ClO_4)_2$ in acidic media

Although complexes of L_1 and L_2 appeared indefinitely stable, those incorporating the dimethylated ligands decomposed much more readily. Kinetic studies were made at 25 °C (I = 1.0 mol/L) over a range of acid concentrations using absorbance changes at 223 nm. The results are presented in Table S3[5] and are consistent with the reaction scheme (charges omitted):

© 2005 NRC Canada



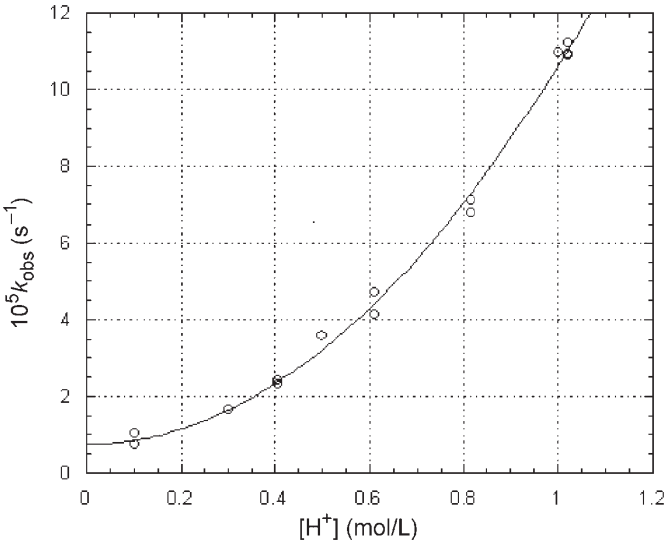
for which the observed rate constant may be written in the form: $k_{obs}([H^+] + K_a) = k_1K_a + k_2[H^+]^2$. The data are presented in Fig. 4 and the individual rate constants (derived using the value of $K_a = 0.7$ derived spectroscopically) are consistent with the reaction not only of the neutral species, but also the protonated ion. The increased rate is attributed to protonation at the tertiary nitrogen atoms, leading to a reduction in the macrocyclic coordination and eventual release of the metal ion. A similar considerable increase in lability over the unsubstituted complex has been observed previously for the Ni(II) tetramethyl-cyclam ion (25).

Confirmation of the locus of reaction is provided by a comparison of the NMR spectra in neutral and acidic media. The ^{13}C NMR spectrum of $[Co(L_3)(ClO_4)](ClO_4)_2$ in D_2O–CD_3CN is highly symmetrical with only eight distinct lines exhibited (Table S4).[5] Thus, the complex in solution possesses a time-averaged C_2 axis of symmetry. Addition of a few drops of perchloric acid to the NMR tube containing such a solution (pH ~ 0) resulted in the initial precipitation of the purple complex. However, upon allowing the solution to stand overnight, dissolution occurred with loss of colour. The resultant spectrum reflects a high-symmetry species where significant chemical shifts are seen at atoms C5, C6, and C3 when compared to the Co(III) spectrum (at pH 7), and additional shifts compared to the free ligand noted at C9 and C1 were consistent with demetallation and protonation of the ligand. Bencini et al. (26) observed a similar downfield shift by the resonances of the carbon atoms adjacent to methyl centres upon protonation of the ligand 4,10-dimethyl-1,4,7,10-tetraazabicyclo[5.5.2]tetradecane.

Mass spectroscopy

Characterization by LSI-MS indentified both positively and negatively charged ions, providing informative similarities and differences. In the positive-ion spectra of $[Co(L_1)(ClO_4)](ClO_4)_2$, $[Co(L_2)(ClO_4)](ClO_4)_2$, and $[Co(L_3)(ClO_4)](ClO_4)_2$ (see Table S5)[5], there was no evidence for the pseudo-molecular ion $[M + H^+]^+$ where $M = [Co(L_n)(ClO_4)](ClO_4)_2$. The geometric isomers $[Co(L_n)(ClO_4)](ClO_4)_2$ ($n = 1$ or 2) gave almost identical positive-ion mass spectra with the highest ion observed at 428 ($[Co(L_n)(ClO_4)]^+$) owing to the inital loss of two outer-sphere perchlorate ions with the next highest ion at 328 being due to the subsequent loss of neutral $HClO_4$ ($[Co^{II}(H_{-1}L_n)]^+$). There is no evidence for any Co(III) fragments in either decay. In contrast, for the molecule $[Co(L_3)(ClO_4)](ClO_4)_2$, while a similar initial loss of two perchlorate ions to give a $[Co^{II}(L_3)(ClO_4)]^+$ fragment at 456 is observed, there is also a fragment at 355, $[Co(H_{-2}L_3)]^+$, in which the cobalt centre remains in the +3 oxidation state. Thus, in the same spectrum, there is evidence for cobalt in both the +2 and +3 oxidation states. The only other significant fragment observed at 299 is assignable to the protonated free ligand HL_3^+. No extrusion of the metal centre was observed in the positive-ion mode spectra of the cobalt(III) complexes with ligands L_1 or L_2.

Fig. 4. Rate constants for the decomposition of $[Co(III)(L_3))OH_2)]^{3+}$ in acidic media. Curve fit: $10^5k_1 = 1.1 \pm 0.11$ s^{-1}; $10^5k_2 = 9.9 \pm 0.2$ M^{-1} s^{-1}.



In the negative-ion spectra (Table S5),[5] there is strong evidence for the molecular ion $[M]^-$. This is the result of the reduction to Co(II) and maintenance of the outer sphere perchlorates. Again, the geometric isomers $[Co(L_1)(ClO_4)](ClO_4)_2$ and $[Co(L_2)(ClO_4)](ClO_4)_2$ gave almost identical mass spectra. Other than $[M]^-$, the only other significant fragment observed was at 526 due to the loss of neutral $HClO_4$. As seen in the positive-ion spectrum for $[Co(L_3)(ClO_4)](ClO_4)_2$, the negative-ion spectrum also exhibited fragments with removal of the metal ion. Ions at 597 and 497 correspond to $[(H_2L_3)(ClO_4)_3]^-$ and $[(HL_3)(ClO_4)_2]^-$, respectively. However, there is evidence for cobalt(I) as the fragment at 355 corresponds to $[Co(H_{-2}L_3)]^-$. The differences in mass spectra reflect the kinetic stabilities and reactivities of the methylated and non-methylated complexes. From Table S5,[5] it can be seen that $[Co(L_2)(ClO_4)](ClO_4)_2$ and the chloro-related complex$[Co(L_2)(Cl)](ClO_4)_2$ gave very similar negative-ion mass spectra when the loss of either $HClO_4$ or HCl from $[M]^-$ is taken into account.

In summary, the Co(III) complexes with ligands L_1 and L_2 are kinetically more stable than their Ni(III) analogues, but exhibit similar proton-related equilibria that are exhibited in the kinetic analysis. Whilst the species with secondary NH groups maintain macrocyclic coordination in acidic media, those incorporating all four tertiary nitrogens are subject to attack by protons leading to an unexpectedly ready demetallation of the complexes, a feature also observed in the mass spectroscopic fragmentation of the complexes.

Acknowledgements

We thank the Natural Sciences and Engineering Research Council of Canada (NSERC) and the University of Victoria for support. TR acknowledges the tenure of an NSERC In-

© 2005 NRC Canada

ternational Post-doctoral Fellowship, and KI, sabbatical assistance from Waseda University.

References

1. G.A. Melson (*Editor*). Coordination chemistry of macrocyclic compounds. Plenum Press, New York. 1979.
2. I. Bertini, I.H.B. Gray, S.J. Lippard, and J.S. Valentine (*Editors*). Bioinorganic chemistry. University Science Books, Mill Valley, California. 1994.
3. R.W. Hay. Bio-inorganic chemistry. Ellis Horwood Limited, Chichester, UK. 1984.
4. L. Lindoy. The chemistry of macrocyclic ligand complexes. University Press, Cambridge, UK. 1989.
5. A.I. Ingham, M. Rodopoulos, K.R. Coulter, T. Rodopoulos, S. Subramanian, and A. McAuley. Coord. Chem. Rev. **233–234**, 255 (2002).
6. C. Bazzicalupi, A. Bencini, A. Bianchi, M. Cecchi, B. Escuder, V. Fusi, E. Garcia-España, C. Giorgi, S.V. Luis, C. Maccagni, V. Marcellino, P. Paoletti, and B. Valtancoli. J. Am. Chem. Soc. **121**, 6807 (1999).
7. D.P. Arnold and J. Blok. Coord. Chem. Rev. **248**, 299 (2004).
8. V. Pavlishchuk, F. Birkelbach, T. Weyhermüller, K. Wieghardt, and P. Chaudhuri. Inorg. Chem. **41**, 4405 (2002).
9. D.G. Fortier and A. McAuley. J. Am. Chem. Soc. **112**, 2640 (1990).
10. D.G. Fortier and A. McAuley. Inorg. Chem. **28**, 655 (1989).
11. K.A. Beveridge, A. McAuley, and C. Xu. Inorg. Chem. **30**, 2074 (1991).
12. A. McAuley, D.G. Fortier, D.H. Macartney, T.W. Whitcombe, and C. Xu. J. Chem. Soc. Dalton Trans. 2017 (1994).
13. M. Rodopoulos, T. Rodopoulos, J.N. Bridson, L.I. Elving, S.J. Rettig, and A. McAuley. Inorg. Chem. **40**, 2737 (2001).
14. A.M. Ingham, C. Xu, T.W. Whitcombe, C. Xu, J.N. Bridson, and A. McAuley. Can. J. Chem. **80**, 155 (2002).
15. E.J. Gabe, Y. LePage, J.-P. Charland, F.L. Lee, and P.S. White. J. Appl. Chem. **22**, 384 (1989).
16. Scattering factors from Vol. 4: J.A. Ibers and W.C. Hamilton (*Editors*). International tables for X-ray crystallography. Vol. IV. Kynoch Press, Birmingham, UK. 1974.
17. C.K. Johnson. ORTEP Technical Report ORNL-5138, Oak Ridge, Tenn. 1976.
18. G.M. Sheldrick. SHELX [computer program]. University of Göttingen, Göttingen, Germany. 1986 and 1990.
19. B. Bosnich, C.K. Poon, and M.L. Tobe. Inorg. Chem. **4**, 1102 (1965).
20. D.G. Fortier and A. McAuley. J. Chem. Soc. Dalton Trans. 101 (1991).
21. G.W. Bushnell, D.G. Fortier, and A. McAuley. Inorg. Chem. **27**, 2626 (1988).
22. R.M. Dyson, S. Kaderli, G.A. Lawrence, M. Maeder, and A.D. Zuberbühler. Anal. Chim. Acta, **353**, 381 (1997).
23. P.M. Brown and G.M. Harris. Inorg. Chem. **7**, 1872 (1968).
24. J. Bjerrum and S.E. Rasmussen. Acta Chem. Scand. **6**, 1265 (1952).
25. F. Wagner and E.K. Barefield. Inorg. Chem. **12**, 2435 (1973).
26. A. Bencini, A. Bianchi, A. Borselli, M. Ciampolini, P. Dapporto, E. Garcia-España, M. Micheloni, P. Paoli, J.A. Ramirez, and B. Valtancoli. Inorg. Chem. **28**, 4279 (1989).

© 2005 NRC Canada

Ruthenium catalyzed asymmetric hydrogenation of α- and β-keto esters in ionic liquids using chiral P-Phos ligand[1]

Kim Hung Lam, Lijin Xu, Lichun Feng, Jiwu Ruan, Qinghua Fan, and Albert S.C. Chan

Abstract: Chiral dipyridylphosphine ligand P-Phos was used in the Ru catalyzed asymmetric hydrogenation of α- and β-keto esters in room temperature ionic liquids (RTILs) with high conversions and good to excellent enantioselectivities. The catalyst was recycled by simple extraction and reused five times without loss of activity and enantioselectivity.

Key words: ruthenium, asymmetric hydrogenation, keto ester, ionic liquids, P-Phos.

Résumé : On a utilisé le ligand chiral dipyridylphosphine (P-Phos) dans l'hydrogénation asymétrique d'α- et de β-céto esters, catalysée par des complexes du ruthénium, à la température ambiante, dans des liquides ioniques, avec des degrés de conversion élevés et des énantiosélectivités allant de bonnes à excellentes. Le catalyseur peut être recyclé par simple extraction et peut être réutilisé jusqu'à cinq fois sans perte d'activité ou d'énantiosélectivité.

Mots clés : ruthénium, hydrogénation asymétrique, céto ester, liquides ioniques, P-Phos.

[Traduit par la Rédaction]

Introduction

Transition-metal-catalyzed asymmetric hydrogenation has become one of the most powerful tools for the preparation of optically active compounds in organic synthesis, and high activity and enantioselectivity have been observed using Rh, Ru, and Ir complexes with chiral phosphine, phosphite, or phosphoramidite as the ligand (1, 2). However, the industrial application of asymmetric hydrogenation has been hindered by the difficulty in the separation and recycling of the expensive chiral catalyst as well as the toxicity of the trace amounts of metal contaminants in the product. Immobilization of these catalysts offers an attractive solution to these problems (3). Recently, room temperature ionic liquids (RTILs) such as those based on imidazolium salts have attracted a great deal of interest because of their potential as a means to immobilize and to facilitate the recycling of transition-metal catalysts (4). A series of prochiral olefins, ketones, and imines have been successfully hydrogenated in ionic liquids, and the results were comparable to or even better than those obtained in common organic solvents (5–14). In most cases, the organic products could be easily separated via extraction with less polar solvents and the ionic liquid phase containing the active catalyst could be readily reused several times without significant loss of catalytic activity. However, recycling and reuse of the catalyst in ionic liquids has been problematic because of the leaching and (or) unstability of the catalyst. Recently, to overcome these obstacles, the attachment of the polar groups to the chiral phosphine ligands has been introduced (9–11). The synthesis of these modified ligands is tedious and much synthetic effort is required. It is highly desirable to develop efficient hydrogenation processes in ionic liquids with easily accessible ligands.

We have recently developed pyridyl-phosphine ligands, namely P-Phos and its derivatives, and have used them in transition-metal-catalyzed enantioselective hydrogenation of olefins and ketones to provide the desired products with high yields and excellent ees (15). In our pursuit of the immobilization and recycling of chiral catalysts in asymmetric hydrogenation (16), we have found that it is possible to replace the commonly used organic solvents with ionic liquids in the Ru-(P-Phos) catalyzed asymmetric hydrogenation of keto esters with retained enantioselectivity and catalytic activity. The use of ionic liquids allows easy isolation of the pure product and efficient recovery and reuse of the catalyst.

Results and discussion

The asymmetric catalytic hydrogenation of α-keto esters

Received 4 January 2005. Published on the NRC Research Press Web site at http://canjchem.nrc.ca on 25 July 2005.

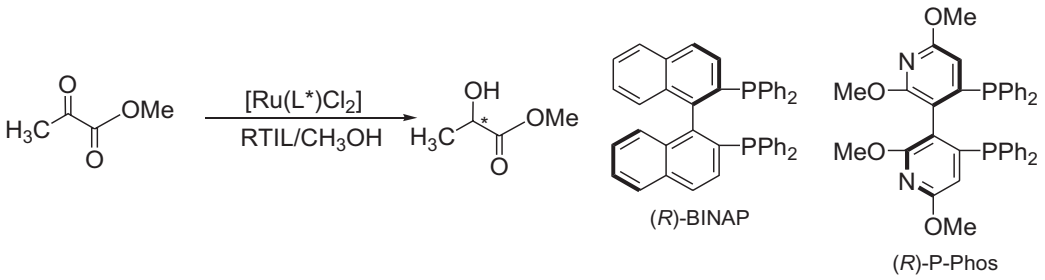
K.H. Lam, L. Xu, L. Feng, J. Ruan, and A.S.C. Chan.[2] Open Laboratory of Chirotechnology of the Institute of Molecular Technology for Drug Discovery and Synthesis and Department of Applied Biology and Chemical Technology, the Hong Kong Polytechnic University, Hong Kong, China.
Q. Fan. Institute of Chemistry, The Chinese Academy of Sciences, Beijing 100080, China.

[1]This article is part of a Special Issue dedicated to Professor Howard Alper.

[2]Corresponding author (e-mail: bcachan@polyu.edu.hk).

 doi: 10.1139/V05-102 © 2005 NRC Canada

Table 1. Asymmetric hydrogenation of methyl pyruvate in ionic liquids.[a]



L*	Solvent	ee (%)[b]	Conv. (%)[c]
(*R*)-P-Phos	[bmim][BF_4]–MeOH	83	95
(*R*)-P-Phos	[bmim][PF_6]–MeOH	86	73
(*R*)-P-Phos	MeOH	88	97
(*R*)-BINAP	[bmim][BF_4]–MeOH	55	98
(*R*)-BINAP	[bmim][PF_6]–MeOH	81	98
(*R*)-BINAP	MeOH	83	90

[a]All reactions were carried out with 1 mol% catalyst under 1000 psi H_2 in a 50:50 mixture of RTIL and MeOH at room temperature for 20 h.
[b]The ee values (%) were determined by GC on a Cyclosil-B (J & W Scientific) 30 m × 0.25 mm × 0.25 μm column.
[c]The conversions were determined by ^{1}H NMR analysis.

provides a convenient way to prepare chiral α-hydroxyl esters, and high enantioselectivities and conversions have been achieved in common organic solvents (1, 2). However, there is no report on the asymmetric hydrogenation of α-keto esters in ionic liquids. To determine whether the catalytic asymmetric hydrogenation of α-keto esters could occur in ionic liquids, we first examined the hydrogenation of methyl pyruvate in 1-butyl-3-methylimidazolium tetrafluoroborate ([bmim][BF_4]) and 1-butyl-3-methylimidazolium hexafluorophosphate ([bmim][PF_6]) using [Ru((*R*)-P-Phos)Cl_2] as the catalyst. For comparison, we also tested the catalytic performance of the extensively used chiral ligand BINAP in ionic liquids. Our results indicated that the hydrogenation in pure ionic liquids was very sluggish with very low conversions (5% and 10% in [bmim][BF_4] and [bmim][PF_6], respectively) after 20 h. In view of the significant co-solvent effect of alcohol in asymmetric hydrogenation in ionic liquids (4), we used an equal volume of MeOH as a co-solvent. As shown in Table 1, high enantioselectivities could be obtained with Ru-P-Phos in both [bmim][BF_4] and [bmim][PF_6] and the results were comparable to the ee values achieved in MeOH. The enantioselectivity was insensitive to the nature of the ionic liquids. However, the reaction in [bmim][PF_6] was slower, and only 73% conversion was achieved after 20 h while nearly complete conversion was observed in [bmim][BF_4]. In contrast, lower enantioselectivities were observed in Ru-BINAP catalyzed hydrogenation, though nearly complete conversions were attained in both ionic liquids. With the BINAP ligand, the enantioselectivity was quite dependent on the nature of the ionic liquids. As shown in Table 1, 81% ee was obtained in [bmim][BF_4] while only 55% enantioselectivity was obtained in [bmim][PF_6]. It was notable that P-Phos performed better than BINAP in ionic liquids, which may be related to the dipyridyl backbone of P-Phos.

The hydrogenation was extended to other α-keto esters and low to high enantioselectivities were observed. Low enantioselectivities and conversions were observed in the hydrogenation of ketopantolactone in both ionic liquids (Table 2, entries 1 and 2). Moderate enantioselectivities and low conversions were obtained with ethyl 2-oxo-4-phenylbutyrate as a substrate (Table 2, entries 3 and 4). High ee values but low conversions were attained in the hydrogenation of methyl benzoylformate (Table 2, entries 5 and 6). The hydrogenation of ethyl benzoylformate only led to low conversions and low enantioselectivities (Table 2, entries 7 and 8).

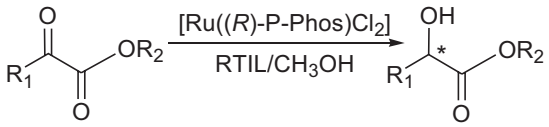
The asymmetric hydrogenation of β-keto esters has been previously studied in ionic liquids using modified BINAP ligands and the results are comparable to or better than those obtained in common organic solvents (9, 10). In this study, we examined the capability of [Ru((*R*)-P-Phos)Cl_2] in the asymmetric hydrogenation of β-keto esters in ionic liquids and the results are summarized in Table 3. The hydrogenation of methyl acetoacetate in a mixture of equal volumes of ionic liquid ([bmim][BF_4] or [bmim][PF_6]) and MeOH was first examined. After stirring at room temperature for 20 h, the reaction led to full conversion and higher than 99% ee. As shown in Table 3, the reaction was also conducted using (*R*)-BINAP as the ligand in both ionic liquids. Again, excellent conversions and enantioselectivites were achieved in both ionic liquids.

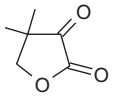
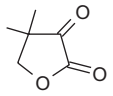
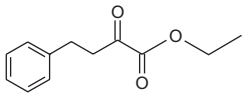
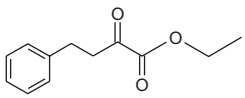
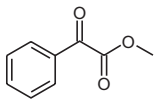
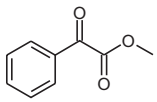
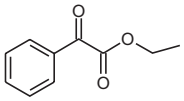
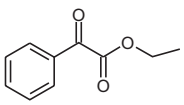
The results of the asymmetric hydrogenation of other β-keto esters are summarized in Table 4. High enantioselectivities (97%–99%) and high conversions (92% to >99%) were obtained for ethyl acetoacetate and *tert*-butyl acetoacetate (Table 4, entries 1–4). It should be pointed out that these results favorably compare with those obtained in common organic solvents. However, when R^1 was switched to other electronegative groups, both the enantioselectivity and the conversion declined (Table 4, entries 5–8). The Ru-P-Phos catalyst showed higher activity in [bmim][PF_6], but it gave better enantioselectivity in [bmim][BF_4].

The recyclability of the Ru-P-Phos catalyst in RTILs was explored using methyl acetoacetate as the model substrate.

© 2005 NRC Canada

Table 2. Asymmetric hydrogenation of α-keto esters in ionic liquids.[a]



Entry	Substrate	RTIL	ee (%)[b]	Conv. (%)[c]
1		[bmim][BF_4]	47	34
2		[bmim][PF_6]	60	46
3		[bmim][BF_4]	74	37
4		[bmim][PF_6]	76	63
5		[bmim][BF_4]	90	18
6		[bmim][PF_6]	93	65
7		[bmim][BF_4]	55	26
8		[bmim][PF_6]	38	20

[a]All reactions were carried out with 1 mol% catalyst under 1000 psi H_2 in a 50:50 mixture of RTIL and methanol at room temperature for 20 h.

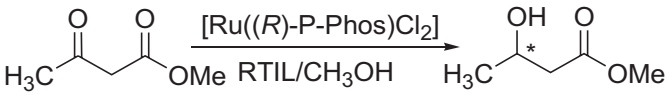
[b]The ee values (%) were determined by GC on a Cyclosil-B (J & W Scientific) 30 m × 0.25 mm × 0.25 μm column.

[c]The conversions were determined by ^{1}H NMR analysis.

Upon completion of the reaction, the methanol was evaporated in vacuo, and the product was extracted with degassed hexane. The RTIL phase was washed twice with hexane. The combined extracts were used for analysis. The RTIL phase was recharged with methyl acetoacetate and MeOH, and then subjected to hydrogenation again under the same conditions. As shown in Table 5, the Ru-P-Phos could be reused and recycled in both ionic liquids, but the results differ considerably. In [bmim][BF_4]–MeOH, the level of enantioselectivity could be reasonably maintained for nine runs, but the activity deteriorated from the second run, and the subsequent runs led to a significant drop in activity. However, in

© 2005 NRC Canada

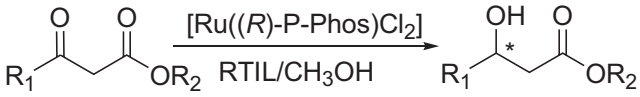
Table 3. Asymmetric hydrogenation of methyl acetoacetate in ionic liquids.[a]

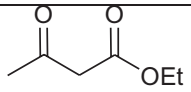
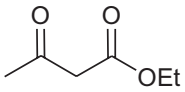
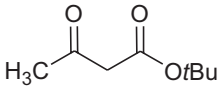
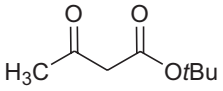
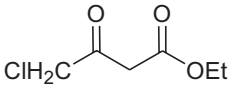
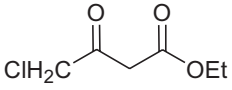
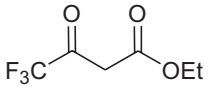
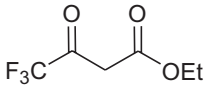


L*	RTIL	ee (%)[b]	Conv. (%)[c]
(*R*)-P-Phos	[bmim][BF_4]	>99	>99
(*R*)-P-Phos	[bmim][PF_6]	98	>99
(*R*)-BINAP	[bmim][BF_4]	>99	>99
(*R*)-BINAP	[bmim][PF_6]	>99	>99

[a]All reactions were carried out with 1 mol% catalyst under 1000 psi H_2 in a 50:50 mixture of RTIL and MeOH at room temperature for 20 h.
[b]The ee values (%) were determined by GC on a Supelco γ-Dex 225 column.
[c]The conversions were determined by ^{1}H NMR analysis.

Table 4. Asymmetric hydrogenation of β-keto esters in ionic liquids.[a]



Entry	Substrate	RTIL	ee (%)[b]	Conv. (%)[c]
1		[bmim][BF_4]	>99	>99
2		[bmim][PF_6]	97	>99
3		[bmim][BF_4]	>99	86
4		[bmim][PF_6]	>99	92
5		[bmim][BF_4]	54	91
6		[bmim][PF_6]	58	93
7		[bmim][BF_4]	50	21
8		[bmim][PF_6]	21	78

[a]All reactions were carried out with 1 mol% catalyst under 1000 psi H_2 in a 50:50 mixture of RTIL and MeOH at room temperature for 20 h.
[b]The ee values (%) were determined by GC on a Supelco γ-Dex 225 column.
[c]The conversions were determined by ^{1}H NMR analysis.

© 2005 NRC Canada

Table 5. Recycling and reuse of Ru-(*R*)-P-Phos catalyst for asymmetric hydrogenation of methyl actoacetate in ionic liquids.[a]

Entry	RTIL	Run	ee[b] (%)	Conv.[c] (%)
1	[bmim][BF_4]	1	>99	>99
2	[bmim][BF_4]	2	98	87
3	[bmim][BF_4]	3	97	78
4	[bmim][BF_4]	4	96	71
5	[bmim][BF_4]	5	95	62
6	[bmim][BF_4]	6	95	56
7	[bmim][BF_4]	7	93	52
8	[bmim][BF_4]	8	94	33
9	[bmim][BF_4]	9	94	39
10	[bmim][PF_6]	1	98	>99
11	[bmim][PF_6]	2	98	99
12	[bmim][PF_6]	3	97	96
13	[bmim][PF_6]	4	97	96
14	[bmim][PF_6]	5	96	93
15	[bmim][PF_6]	6	96	86
16	[bmim][PF_6]	7	96	78
17	[bmim][PF_6]	8	94	57
18	[bmim][PF_6]	9	94	49

[a]All the reactions were carried out with 1 mol% catalyst under 1000 psi H_2 in a 50:50 mixture of RTIL and MeOH at room temperature for 20 h.
[b]The ee values (%) were determined by GC on a Supelco γ-Dex 225 column.
[c]The conversions were determined by ^{1}H NMR analysis.

the case of [bmim][PF_6], good activity and excellent enantioselectivity were retained in the first five runs of the hydrogenation reactions.

Conclusion

We have developed an efficient Ru-P-Phos catalyst for the asymmetric hydrogenation of α- and β-keto esters in RTILs with high conversions and ee values up to >99%. The catalyst was recycled and reused with the reasonable retention of activity and enantioselectivity.

Experimental

General information

All manipulations with air-sensitive reagents were carried out under a dry nitrogen atmosphere using standard Schlenk techniques or in a nitrogen-filled MBRAUN Lab Master 130 glovebox. The hydrogenation reactions were performed in a stainless-steel autoclave from the Parr company.[bmim][BF_4] and [bmim][PF_6] were prepared according to the literature method (17). Following vacuum drying at 80 °C for 8 h, the ionic liquid was stored under nitrogen at ambient temperature. Optically pure P-Phos and [Ru((*R*)-P-Phos)Cl_2] were synthesized based on our previous reports (14). Other chemicals were purchased and were used as received. The solvents were dried prior to use via standard procedures. The ^{1}H NMR spectra were recorded on a Varian AS 500 spectrometer in ppm with reference to the TMS internal standard in $CDCl_3$.

Typical procedure for asymmetric hydrogenation

A mixture of [bmim][BF_4] (0.5 mL) and MeOH (0.5 mL) was added into a glass-lined stainless-steel autoclave containing methyl acetoacetate (26.7 mg, 0.23 mmol) and [Ru((*R*)-P-Phos)Cl_2] (18.8 mg, 0.023 mmol) in a drybox under a nitrogen atmosphere. After purging the autoclave with hydrogen gas several times, the final pressure of the hydrogen was adjusted to 1000 psi (1 psi = 6.894 757 kPa), and the reaction mixture was stirred at room temperature. After 20 h, the hydrogen gas was released, and the product was extracted with hexane and passed through a small column of silica gel. The organic volatiles were removed under reduced pressure to obtain the desired product. The conversion was then assessed based on the ^{1}H NMR analysis, while the ee value was determined by GLC using a chiral column.

Acknowledgements

We thank the University Grants Committee Area of Excellence Scheme in Hong Kong (Project No. AoE/P-10/01), the Hong Kong Polytechnic University Area of Strategic Development Fund, and the National Natural Science Foundation of China (No. 20418002) for financial support.

References

1. (*a*) R. Noyori. Asymmetric catalysis in organic synthesis. Wiley, New York. 1994; (*b*) E.N. Jacobsen, A. Pfaltz, and H. Yamamoto (*Editors*). Comprehensive asymmetric catalysis. Springer, Berlin. 1999; (*c*) I. Ojima (*Editor*). Catalytic asymmetric synthesis. Wiley-VCH, New York. 2000; (*d*) G. Lin, Y. Li, and A.S.C. Chan (*Editors*). Principles and applications of asymmetric synthesis. Wiley, New York. 2001.
2. (*a*) H.U. Blaser, C. Malan, B. Pugin, F. Spindler, H. Steiner, and M. Studer. Adv. Synth. Catal. **345**, 103 (2003); (*b*) W. Tang and X. Zhang. Chem. Rev. **103**, 3029 (2003).
3. Q. Fan and A.S.C. Chan. Chem. Rev. **102**, 3385 (2002).
4. (*a*) C.E. Song. Chem. Commun. 1033 (2004); (*b*) C. Baudequin, J. Baudoux, J. Levillain, D. Cahard, A. Gaumon, and J. Plaquevent. Tetrahedron: Asymmetry, **14**, 3081 (2003); (*c*) P. Wasserscheid and T. Welton (*Editors*). Ionic liquids in synthesis. Wiley-VCH, Weinheim. 2003; (*d*) J. Dupont, R.F. de Souza, and P.A.Z. Suarez. Chem. Rev. **102**, 2002 (3367); (*e*) C.C. Tzschucke, C. Markert, M. Bannwarth, S. Roller, A. Hebel, and R. Haag. Angew. Chem. Int. Ed. **41**, 3694 (2002).
5. Y. Chauvin, L. Mussmann, and H. Olivier. Angew. Chem. Int. Ed. Engl. **34**, 2698 (1995).
6. (*a*) A.L. Monteiro, F.K. Zinn, R.F. de Souza, and J. Dupont. Tetrahedron: Asymmetry, **8**, 177 (1997); (*b*) A. Berger, R.F. de Souza, M.R. Delgado, and J. Dupont. Tetrahedron: Asymmetry, **12**, 1825 (2001).
7. S. Guernik, A. Wolfson, M. Herskowitz, N. Greenspoon, and S. Geresh. Chem. Commun. 2314 (2001).
8. (*a*) R.A. Brown, P. Pollet, E. McKoon, C.A. Eckert, C.L. Liotta, and P.G. Jessop. J. Am. Chem. Soc. **123**, 1254 (2001); (*b*) P.G. Jessop, R.R. Stanley, R.A. Brown, C.A. Eckert, C.L. Liotta, T.T. Ngo, and P. Pollet. Green Chem. **5**, 3 (2003).
9. (*a*) H.L. Ngo, A. Hu, and W. Lin. Chem. Commun. 1912 (2003); (*b*) A. Hu, H.L. Ngo, and W. Lin. Angew. Chem. Int. Ed. **43**, 2501 (2004).
10. M. Berhod, J. Joerger, G. Mignani, M. Vaultier, and M. Lemaire. Tetrahedron: Asymmetry, **15**, 2219 (2004).

© 2005 NRC Canada

11. S. Lee, Y. Zhang, J. Piao, H. Yoon, C. Song, J. Choi, and J. Hong. Chem. Commun. 2624 (2003).
12. Y. Zhu, K. Carpenter, C. Ching, S. Bahnmueller, P. Chan, V.S. Srid, W.K. Leong, and M.F. Hawthrone. Angew. Chem. Int. Ed. **42**, 3792 (2003).
13. B. Pugin, M. Studer, E. Kuesters, G. Sedelmeier, and X. Feng. Adv. Synth. Catal. **346**, 1481 (2004).
14. M. Solinas, A. Pfaltz, P. Giorgio, and W. Leitner. J. Am. Chem. Soc. **126**, 16 142 (2004).
15. (*a*) C.C. Pai, C.W. Lin, C.C. Lin, C.C. Chen, and A.S.C. Chan. J. Am. Chem. Soc. **122**, 11 513 (2000); (*b*) J. Wu, H. Chen, Z. Zhou, C.H. Yeung, and A.S.C. Chan. Synlett, 1050 (2001); (*c*) J. Wu, H. Chen, W.H. Kwok, R. Guo, Z. Zhou, C.H. Yeung, and A.S.C. Chan. J. Org. Chem. **67**, 7908 (2002); (*d*) J. Wu, X. Chen, R. Guo, C.H. Yeung, and A.S.C. Chan. J. Org. Chem. **68**, 2490 (2003); (*e*) J. Wu, J. Ji, R. Guo, C.H. Yeung, and A.S.C. Chan. Chem. Eur. J. **9**, 2963 (2003).
16. (*a*) Q. Fan, Y. Li, and A.S.C. Chan. Chem. Rev. **102**, 3385 (2002); (*b*) Q. Fan, C. Ren, C.-H. Yeung, W. Hu, and A.S.C. Chan. J. Am. Chem. Soc. **121**, 7407 (1999); (*c*) Q. Fan, Y. Chen, X. Chen, D. Jiang, F. Xi, and A.S.C. Chan. Chem. Commun. 789 (2000); (*d*) Q. Fan, G. Deng, C. Lin, and A.S.C. Chan. Tetrahedron: Asymmetry, **12**, 1241 (2000); (*e*) G. Deng, Q. Fan, X. Chen, D. Liu, and A.S.C. Chan. Chem. Commun. 1570 (2002); (*f*) B. Yi, Q. Fan, G. Deng, Y. Li, L. Qiu, and A.S.C. Chan. Org. Lett. **6**, 1361 (2004).
17. J.D. Holbrey and K.R. Seddon. J. Chem. Soc. Dalton Trans. 2133 (1999).

© 2005 NRC Canada

Efficient ruthenium catalyzed transfer hydrogenation of functionalized imines by isopropanol under controlled microwave heating[1]

Joseph S.M. Samec, Laetitia Mony, and Jan-E. Bäckvall

Abstract: Transfer hydrogenation of various functionalized imines by isopropanol catalyzed by $[Ru(CO)_2(Ph_4C_4CO)]_2$ (**3**) has been studied. The use of either an oil bath or controlled microwave heating in toluene led to an efficient procedure with high turnover frequencies and the product amines were obtained in high yields. An advantage with catalyst **3** over the conventional $[Ru_2(CO)_4(\mu\text{-}H)(Ph_4C_4COHOCC_4Ph_4)]$ (**1**) is the absence of an initiation period, which results in a faster reaction with **3** as compared to **1**.

Key words: transfer hydrogenation, ruthenium, imines, microwave.

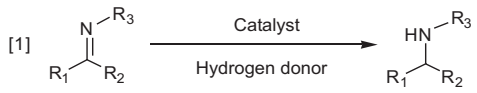
Résumé : On a étudié la réaction de transfert d'hydrogène, catalysée par le $[Ru(CO)_2(Ph_4C_4CO)]_2$ (**3**), de l'isopropanol vers diverses imines fonctionnalisées. L'utilisation d'un bain d'huile ou d'un chauffage par micro-ondes contrôlé dans le toluène conduit à une méthode efficace impliquant des fréquences élevées de renouvellement et à des rendements élevés en amines. Par rapport au catalyseur conventionnel $[Ru_2(CO)_4(\mu\text{-}H)(Ph_4C_4COHOCC_4Ph_4)]$ (**1**), le catalyseur (**3**) ne présente pas de période d'initiation et il en résulte des vitesses de réaction plus rapides avec **3** par comparaison avec **1**.

Mots clés : hydrogénation par transfert, ruthénium, imines, micro-onde.

[Traduit par la Rédaction]

Introduction

The reduction of imines to amines is an important transformation in organic synthesis since amines are useful building blocks for pharmaceuticals and other biologically active compounds. In situ reduction of imines generated by the reaction of ketones with an amine (reductive amination) is a commonly used procedure (1). Although the latter protocol works fine in many systems with various reducing agents (2), it is often associated with low selectivity. Direct reduction of imines can be carried out with hydride reagents (3) or with catalytic hydrogenation (4). More recently, transfer hydrogenation has been reported as a viable alternative for reduction of imines (eq. [1]) (5). The advantage of the latter procedure is that the use of hydrogen gas is avoided and that, e.g., isopropanol can be used as the hydrogen source. The acetone thus produced is readily removed by distillation. The transfer hydrogenation protocol also shows a higher functional group tolerance compared to hydride reagents.



Several transition-metal complexes are known to catalyze the transformation in eq. [1] with isopropanol or formic acid as the hydrogen donor (6–8). Dimeric catalyst **1** (9) (Scheme 1), which has frequently been employed in various hydrogen transfer reactions (10, 11), was recently successfully used in our group for the transfer hydrogenation of imines (8). Catalyst **1** is in equilibrium with monomers **2** and **A** (Scheme 1). The monomer **2** is able to hydrogenate a hydrogen acceptor, e.g., an imine, whereas the monomer **A** can dehydrogenate a hydrogen donor, e.g., isopropanol. These processes interconvert **2** and **A**. We recently showed that the hydrogen transfer from **2** to a ketimine occurs in a stepwise manner (12).

The active monomers **2** and **A** involved in the catalytic hydrogen transfer of imines can also be generated from the dimeric catalyst **3** (13). In the present work we studied the use of catalyst precursor **3** in the hydrogen transfer of functionalized imines.

The use of microwaves to accelerate catalytic reactions has recently attracted attention (14, 15). With the employment of microwaves, the reaction times can be reduced considerably and this is of great use when a larger number of compounds are required (e.g., for screening). In this work we have used microwave heating to lower the catalyst load-

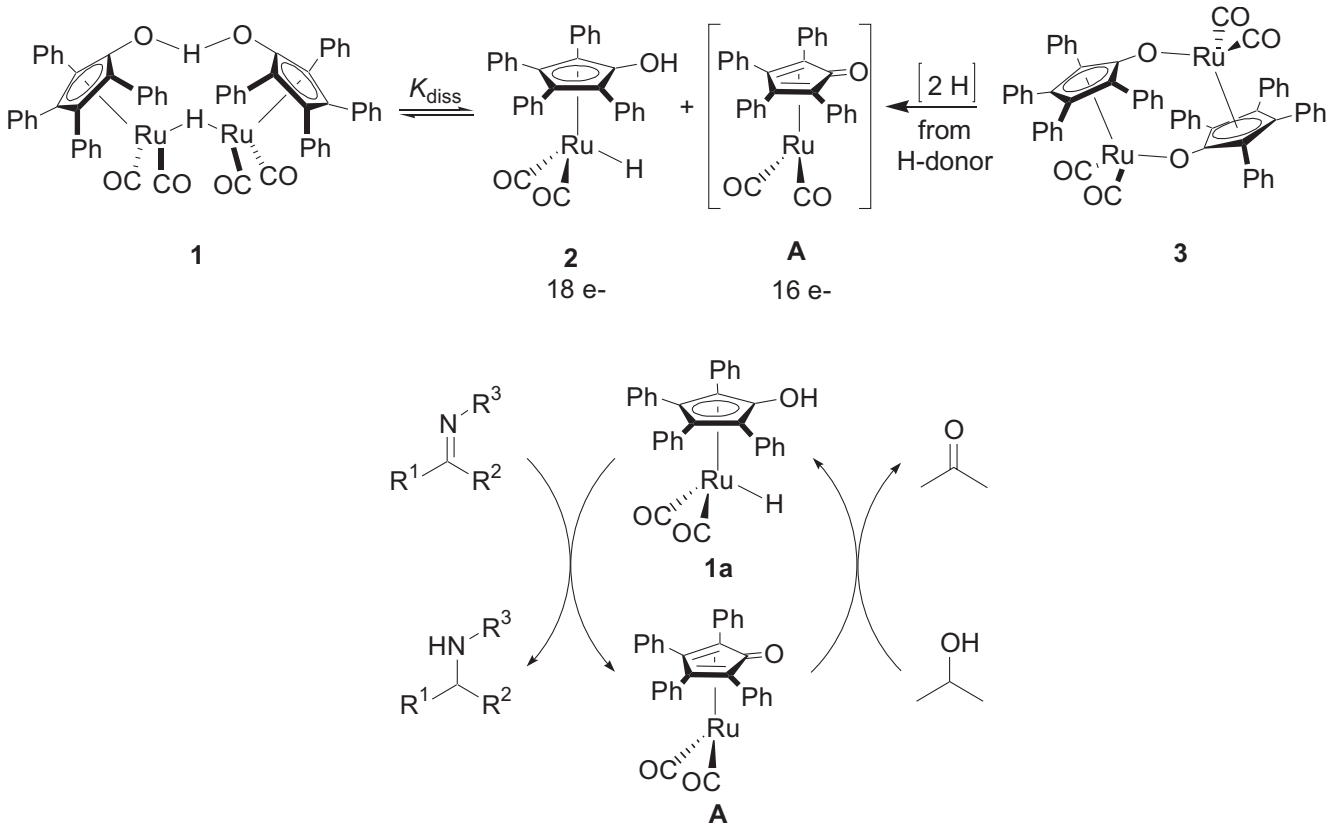
Received 4 January 2005. Published on the NRC Research Press Web site at http://canjchem.nrc.ca on 27 July 2005.

J.S.M. Samec, L. Mony, and J.-E. Bäckvall.[2] Department of Organic Chemistry, Arrhenius Laboratory, Stockholm University, SE-106 91 Stockholm, Sweden.

[1]This article is part of a Special Issue dedicated to Professor Howard Alper.
[2]Corresponding author (e-mail: jeb@organ.su.se).

 doi: 10.1139/V05-103 © 2005 NRC Canada

Scheme 1.



ing and reduce reaction times in the transfer hydrogenation of imines to amines with catalyst **3**.

Results and discussion

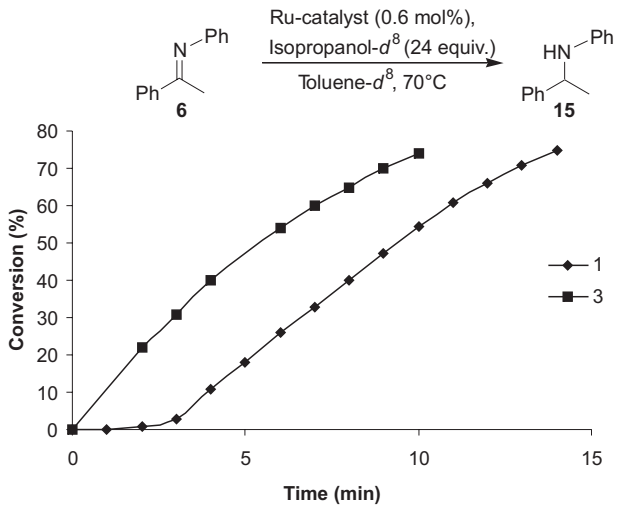
A few procedures for transfer hydrogenation of imines to amines have previously been reported in the literature (6–8). With the objective being to develop a more practical and useful procedure for ruthenium catalyzed transfer hydrogenation of imines by isopropanol, we decided to study the effects of catalyst precursor and temperature.

Choice of the catalyst precursor

Complexes **1** and **3** are catalyst precursors for the hydrogen donor **2** and hydrogen acceptor **A**. To compare **1** and **3** as catalyst precursors they were prepared according to a procedure described by Casey et al. (13). Tetraphenylcyclopentadienone and $Ru_3(CO)_{12}$ were refluxed in MeOH to give the Shvo dimer **1** or in heptane to give **3** (Scheme 2). The products were collected by filtration and recrystallized to give **1** and **3**, respectively, in high yields (~90%).

Initial experiments run in an oil bath at 110 °C revealed that catalyst **3** was more efficient than catalyst **1** in the transfer hydrogenation of imines and gave shorter reaction times. To obtain a more detailed comparison between the two catalyst precursors we studied their kinetics in the transfer hydrogenation of imine **6**. Thus, the transfer hydrogenation of imine **6** by isopropanol-d_8 in toluene-d_8 catalyzed by **1** or **3** was monitored by ^{1}H NMR at 70 °C.[3] The results are shown in Fig. 1. From these results, it is evident that catalyst precursor **1** has an initiation period of several minutes, whereas catalyst precursor **3** is active immediately and results in 23% conversion after 2 min. The time to reach 75% conversion was 14 and 10 min for **1** and **3**, respectively. During the first

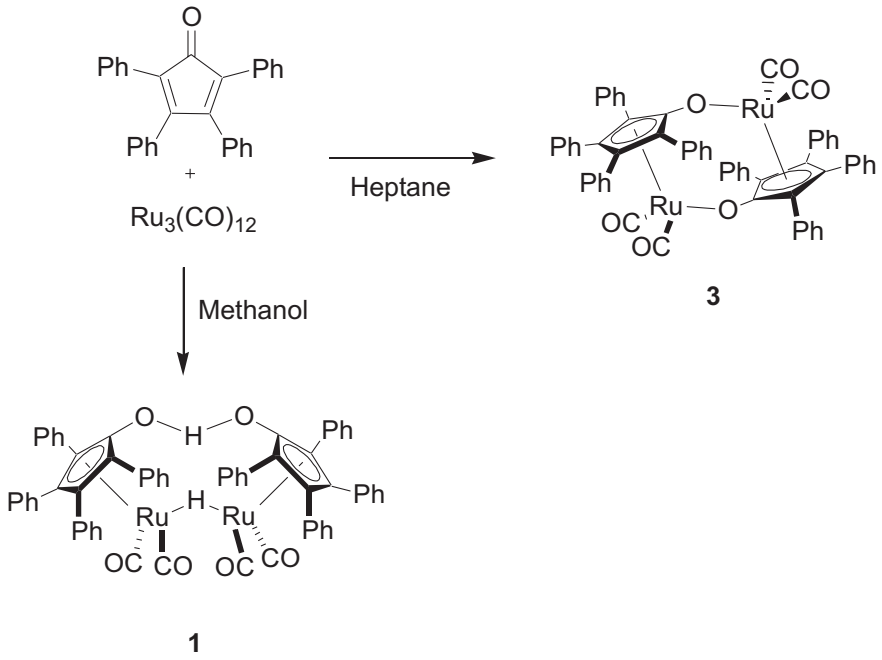
Fig. 1. Comparison between precatalysts **1** and **3** in the transfer hydrogenation of imine **6** in toluene-d_8 at 70 °C with isopropanol-d_8 using 0.6 mol% catalyst. The conversion was measured by ^{1}H NMR.



[3] Due to the low boiling point of isopropanol, the reactions were run at 70 °C to prevent overpressure in the NMR tube.

© 2005 NRC Canada

Scheme 2.



2 min, the turnover frequency (TOF) was <30 h^{-1} for **1** (<15 h^{-1} per ruthenium atom), whereas it was 1150 h^{-1} for **3** (575 h^{-1} per ruthenium atom). Because of the higher efficiency of **3** over **1**, the former catalyst was chosen for further studies.

Transfer hydrogenation of imines under thermal heating

In our previously reported procedure for transfer hydrogenation of various imines by **1** using 24 equiv. of wet isopropanol in benzene at 70 °C, electron-deficient imines had long reaction times (8). For increased efficiency, it was desirable to shorten the reaction times and also to lower the catalyst loading. An increase in temperature would lead to shorter reaction times but it may also decrease the selectivity. With the aim to increase the efficiency of the reaction, the transfer hydrogenation of model substrate **6** by catalyst precursor **3** in isopropanol–toluene at 110 °C was studied. The increase in temperature led to an efficient transfer hydrogenation of **6** where the catalyst loading could be decreased 10 times compared to our previous study (8). This prompted us to study the electron-deficient imine **11**, which required 8 h at 70 °C in benzene. In the present system, imine **11** had reached full conversion within an hour with the same catalyst loading. The present system can also transfer hydrogenate the very electron-deficient imine **14** bearing a pyridyl group. To further extend this protocol and make it an attractive alternative in organic synthesis, we decided to study the transfer hydrogenation of imines having functional groups that make them difficult to reduce to amines. It was found that the present procedure tolerates various functional groups such as esters, amines, ethers, acetals, and olefins (Table 1, entries 2–5, 7, and 8). In conventional reductions using metal hydrides, the workup protocol includes tedious extractions in the presence of strong acids and (or) bases, which not only lowers the yield of the reactions, but also lowers the functional group tolerance. In the present procedure, the only workup is the removal of the solvents. The products are then readily purified by distillation giving the amines in high yield. For example, reduction of imines with either an ester or an acetal functionality, which may cause problems in metal hydride reductions (either during the reaction or in work up) proceeded smoothly with the present method (Table 1, entries 2, 3, and 7).

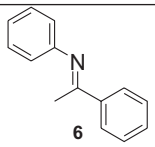
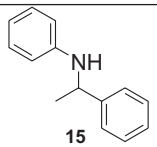
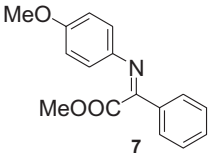
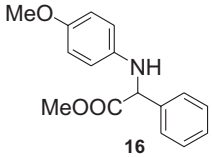
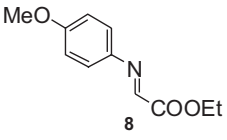
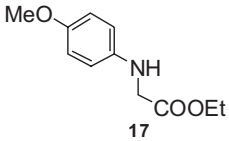
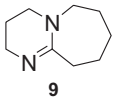
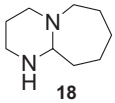
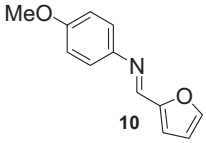
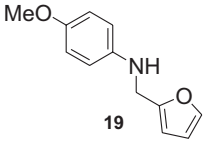
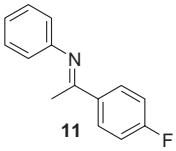
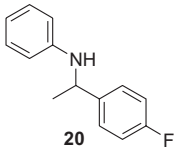
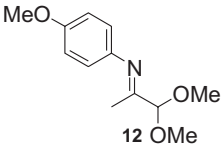
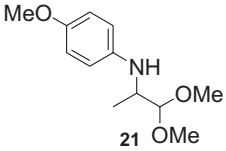
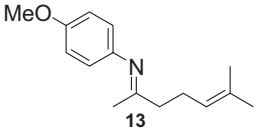
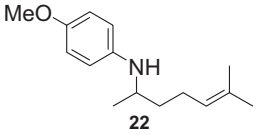
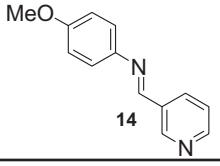
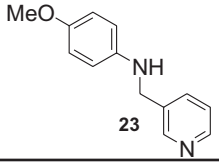
Transfer hydrogenation under controlled microwave heating

Recently, we showed that the hydrogen transfer from the active catalyst **2** to the imine is not concerted as previously proposed (13), but stepwise (12). In the latter study, we found that microwave irradiation was superior to conventional oil bath heating for the generation of the active species **2** from precursor **3** in a H_2 atmosphere (Scheme 3). Where conventional oil bath heating took several hours and with unsatisfactory results, the microwave-promoted generation of active species **2** was very efficient. Active species **2** can be generated in a minute at 180 °C using microwave irradiation, but with somewhat unreliable results. We found that decreasing the temperature to 120 °C and prolonging the reaction time to 20 min resulted in complete conversion of **3** to **2** with full reproducibility (12).

Initial attempts to perform transfer hydrogenation of imine **6** by precursor **3** in isopropanol and toluene with microwave irradiation gave unreliable results. For example, when imine **6** was run with low catalyst loading (0.03–0.06 mol%) at 110 °C, the results were difficult to reproduce. Increasing the catalyst loading slightly (to 0.1 mol%) gave a smooth transfer hydrogenation of imine **6** to amine **15** within 20 min (Table 2, entry 1). Next, it was of interest to find out if functionalized imines tolerate the transfer hydrogenation with microwave irradiation. We were pleased to find that employing microwave irradiation improved the reduction in most cases even though there were two exceptions: imines **6** and **7** (Table 2, entries 1 and 2) needed

© 2005 NRC Canada

Table 1. Transfer hydrogenation of different amines by wet isopropanol in toluene using **3**.[a]

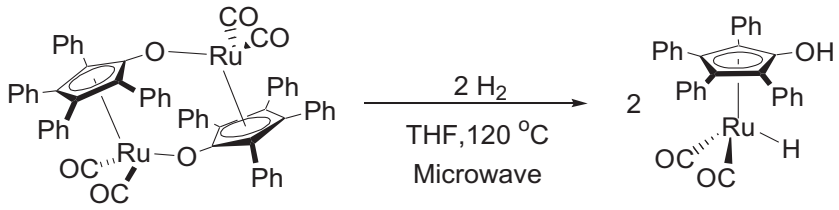
Entry	Imine	Amine	Catalyst loading (mol%)	Time (min)	Yield (%)[b]
1	 **6**	 **15**	0.03	90	93
2	 **7**	 **16**	0.06	60	93
3	 **8**	 **17**	0.06	60	95
4	 **9**	 **18**	0.3	60	>99[c]
5	 **10**	 **19**	0.3	150	97
6	 **11**	 **20**	1	60	>99[c]
7	 **12**	 **21**	3	60	95
8	 **13**	 **22**	3	60	96
9	 **14**	 **23**	3	240	96

[a]The reactions were carried out using imine (1.0 mmol), catalyst **3** (0.003–0.03 mmol), and isopropanol (24 mmol, 1.85 mL) in toluene (3.15 mL) at 110 °C. Full conversion was measured by ^{1}H NMR.
[b]Isolated yield unless otherwise noted.
[c]Yield determined by ^{1}H NMR.

higher catalyst loading in the microwave-assisted transfer hydrogenation than by conventional heating. Except for these examples, the general trend was shorter reaction times (10–20 min) and lower catalyst loading (0.1–0.5 mol%). For example, imine **10**, which needed 0.3 mol% of the catalyst and 150 min using oil bath heating, was finished within 20 min with only 0.1 mol% of the catalyst (Table 2, entry 4). This is an increase of >20 times in efficiency. Imines **12** and **13**, which needed 3 mol% of catalyst loading and 60 min with conventional oil bath heating, only needed 0.5 mol% of the catalyst and were over within 10 min in the microwave-assisted transfer hydrogenation (Table 2, entries 5 and 6). With these two imines, the efficiency is increased by a factor of 36 times. With microwave irradiation, the reaction time was reduced 12 times (from 240 to 20 min) for the electron-deficient imine **14** (Table 2, entry 7).

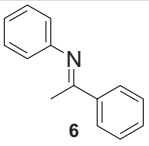
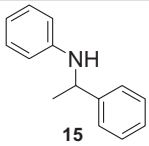
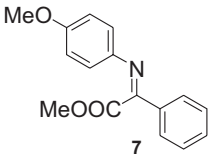
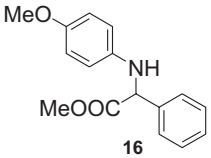
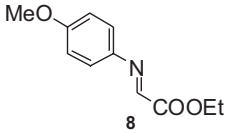
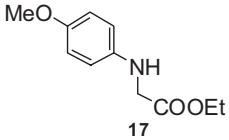
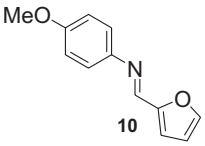
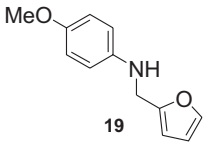
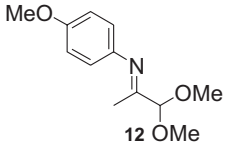
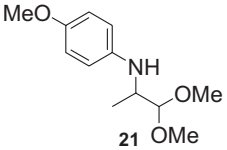
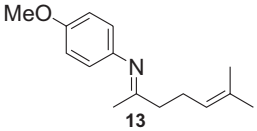
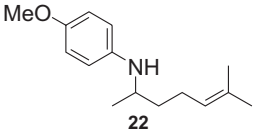
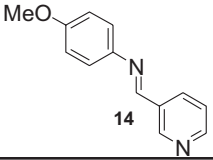
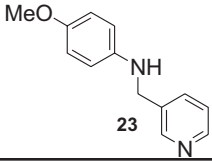
© 2005 NRC Canada

Scheme 3.



3

Table 2. Transfer hydrogenation of functionalized imines by **3** in wet isopropanol – toluene using microwave irradiation.[a]

Entry	Imine	Amine	Catalyst loading (mol%)	Time (min)	Yield[b]
1	 **6**	 **15**	0.1	20	98
2	 **7**	 **16**	0.5	20	99
3	 **8**	 **17**	0.5	10	99
4	 **10**	 **19**	0.1	20	94
5	 **12**	 **21**	0.5	10	98
6	 **13**	 **22**	0.5	10	95
7	 **14**	 **23**	3	20	98

[a]The reactions were run using imine (0.3 mmol), **3** (0.0003–0.009 mmol), toluene (1.9 mL), isopropanol (1.1 mL) under microwave irradiation for 20 min (110 °C, 2 bar (1 bar = 100 kPa)).
[b]The yield was determined by ^{1}H NMR.

Conclusions

We have developed an efficient transfer hydrogenation protocol for imines. Imines bearing acid-or base-labile functional groups, not compatible with conventional metal hydride reduction, are readily reduced with low catalyst loading and short reaction times to give high yields of the corresponding amines. The use of controlled microwave ir-

© 2005 NRC Canada

radiation led to an efficient procedure where most imines were reduced in greater than 90% yield within 20 min employing 0.1–0.5 mol% of catalyst. This procedure should be a useful complement to existing methods for the reduction of imines to amines.

Experimental section

General methods

^{1}H (400 or 300 MHz) and ^{13}C (100 or 75 MHz) NMR spectra were recorded on a Varian Mercury spectrometer. Chemical shifts (δ) are reported in ppm, using residual solvent as the internal standard, and coupling constants (*J*) are given in Hz. Unless otherwise noted, all materials were obtained from commercial suppliers and used without further purification. Toluene was distilled from sodium benzophenone and isopropanol was distilled from CaO before use. All other chemicals were used as received. Short-path distillations were conducted in a Büchi glass oven B-580. Elemental analyses were performed by Analytische Laboratorien, Lindlar, Germany. Ruthenium complexes **1** and **3** were made according to literature procedures (13).

N-Phenyl-(1-phenylethylidene)amine (6)

This compound was made according to literature procedure (8).

N-(4-Methoxyphenylimino)phenylacetic acid methyl ester (7)

Anisidine (2.46 g, 20 mmol), methylphenyl glyoxylate (13 g, 80 mmol), activated molecular sieves (4 Å, 7 g), and toluene (10 mL) were added to a round-bottomed flask and stirred at room temperature overnight. The reaction mixture was filtered through Celite, the filtrate evaporated, and the crude product was precipitated from CH_2Cl_2–pentane. Yield: 3 g (50%) of yellow-brownish crystals. ^{1}H NMR (400 Hz, $CDCl_3$, 25 °C) δ: 3.69, (s, 3H, $COOCH_3$), 3.81 (s, 3H, OCH_3), 6.87–6.96 (m, 2H, aryl of *p*-methoxyphenyl), 6.97–7.01 (m, 2H, aryl of *p*-methoxyphenyl), 7.45–7.50 (m, 3H, phenyl), 7.84–7.86 (m, 2H, phenyl). ^{13}C NMR (100 Hz, $CDCl_3$, 25 °C) δ: 51.9 (CH_3 of ester), 55.4 (OCH_3), 114.2 (aryl of *p*-methoxyphenyl), 121.1 (aryl of *p*-methoxyphenyl), 127.8 (phenyl), 128.7 (phenyl), 131.5 (phenyl), 134.1 (phenyl), 143.1 (aryl of *p*-methoxyphenyl), 157.3 (aryl of *p*-methoxyphenyl), 159.1 (C=N), 166.1 (C=O).

Ethyl [*N*-(*p*-Methoxyphenyl)imino]acetate (8)

Anisidine (2.46 g, 20 mmol), ethyl glyoxalate (4 mL, 30 mmol), activated molecular sieves (4 Å, 7 g), and benzene (5 mL) were added to a round-bottomed flask and stirred at room temperature overnight. Spectral data were in accordance with those previously reported in the literature (16).

N-[1-(2-Furyl)methylidene]-*N*-(4-methoxyphenyl)amine (10)

Anisidine (2.46 g, 20 mmol), furfural (2.4 g, 25 mmol), activated molecular sieves (4 Å, 7 g), and benzene (5 mL) were added to a round-bottomed flask and stirred at room temperature overnight. The reaction mixture was filtered through Celite, the filtrate evaporated, and the crude product was precipitated from CH_2Cl_2–pentane to yield 2.6 g (55%) of white crystals. Spectral data were in accordance with those previously reported in the literature (17).

N-Phenyl-[1-(4-fluorophenyl)ethylidene]amine (11)

The title compound was made according to the literature procedure (8).

(2,2-Dimethoxy-1-methylethylidene)-(4-methoxyphenyl)-amine (12)

Anisidine (2.47 g, 20 mmol), dimethoxy acetone (3.94 g, 30 mmol), activated molecular sieves (4 Å, 7 g), and benzene (10 mL) were added to a round-bottomed flask and stirred at room temperature overnight. Yield: 4 g (90%) of a colorless oil. ^{1}H NMR (400 Hz, $CDCl_3$, 25 °C) δ: 1.83 (s, 3H, CH_3), 3.49 (s, 6H, OCH_3), 3.80 (s, 3H, OCH_3), 4.65 (s, 1H, CH), 6.72 (m, 2H, aryl of *p*-methoxyphenyl), 6.88 (m, 2H, aryl of *p*-methoxyphenyl). ^{13}C NMR (100 Hz, $CDCl_3$, 25 °C) δ: 13.9 (CH_3), 55.1 (OCH_3), 55.4 (OCH_3), 107.6 (CH), 114.2 (aryl of *p*-methoxyphenyl), 120.7 (aryl of *p*-methoxyphenyl), 142.9 (aryl of *p*-methoxyphenyl), 156.3 (C=N), 168.2 (aryl of *p*-methoxyphenyl). Elemental anal. calcd. for $C_{12}H_{17}NO_3$ (223.27) (%): C 64.55, H 7.68, N 6.28; found: C 64.32, H 7.56, N 6.41.

N-(6-Methyl-2-hept-5-enylidene)-4-anisidine (13)

Anisidine (2.47 g, 20 mmol), 6-methyl-5-hepten-2-one (3 mL, 20 mmol), activated molecular sieves (4 Å, 7 g), and benzene (10 mL) were added to a round-bottomed flask and stirred at room temperature overnight. Yield: 2.74 g (59%) of a yellow oil. Spectral data were in accordance with those previously reported in the literature (18).

N-(4-Methoxyphenyl)-*N*-[(*E*)-1-(3-pyridyl)methylidene]amine (14)

Anisidine (2.46 g, 20 mmol), 3-pyridinecarboxaldehyde (2.67 g, 25 mmol), activated molecular sieves (4 Å, 7 g), and benzene (5 mL) were added to a round-bottomed flask and stirred at room temperature overnight. The reaction mixture was filtered through Celite and the filtrate was evaporated. The starting material was removed by bulb-to-bulb distillation (120 °C, 1 mbar, 1 bar = 100 kPa) and the product was subsequently distilled (160 °C, 1 mbar). Yield: 3.8 g (90%) of yellow crystals. Spectral data were in accordance with those previously reported in the literature (17).

Screening catalysts

Catalyst **1** (1 mg, 1 μmol) or **3** (1 mg, 1 μmol) dissolved in toluene-d_8 (0.48 mL) was added to imine **6** (0.15 mmol) in a vial. The mixture was transferred to a NMR tube and isopropanol-d_8 (0.28 mL, 3.7 mmol) was added. The NMR tube was subsequently shaken and inserted into a prewarmed (70 °C) spectrometer. After initial locking and shimming (~2 min), acquisitions were acquired every minute. The reactions were followed by ^{1}H NMR to ~75% conversion following the appearance of the methyl group of the amine at δ 1.48 and the disappearance of the methyl group of the imine at δ 2.24.

© 2005 NRC Canada

General procedure for the transfer hydrogenation under thermal heating — *N*-Phenyl-1-phenylethylamine (15)

In a typical experiment, imine **6** (0.195 g, 1.0 mmol), catalyst **3** (0.33 mg, 0.3 μmol), toluene (3.15 mL), isopropanol (1.84 mL, 24.0 mmol), and water (42 μL, 1% w/w) were added to a 10 mL Schlenk tube and heated to 110 °C for 90 min. Solvents were evaporated in vacuo and the product was purified by distillation (250 °C, 0.5 mbar) to afford amine **15** (0.182 g, 93%). Spectral data were in accordance with those previously reported in the literature (19).

(4-Methoxyphenylamino)phenylacetic acid methyl ester (16)

The general procedure was followed by using imine **7** (1.9 mmol, 0.5 g), **3** (1.1 μmol, 1 mg), toluene (8 mL), and wet isopropanol (3.5 mL, 48.0 mmol). The product was distilled (250 °C, 0.5 mbar) to afford amine **16** (0.48 g, 93%). Spectral data were in accordance with those previously reported in the literature (20).

***N*-(4-Methoxyphenyl)glycine ethyl ester (17)**

The general procedure was followed by using imine **8** (0.21 g, 1.0 mmol) and **3** (0.65 mg, 0.6 μmol). The product was bulb-to-bulb distilled (200 °C, 0.5 mbar) to afford amine **17** (0.199 g, 95%). ^{1}H NMR (400 Hz, $CDCl_3$, 25 °C) δ: 1.27 (t, 3H, J = 7.1 Hz, CH_3), 3.74 (s, 3H, OCH_3), 3.86 (s, 2H, CH_2), 4.23 (q, 2H, J = 7.1 Hz, CH_2), 6.57–6.60 (m, 2H, aryl of *p*-methoxyphenyl), 6.77–6.81 (m, 2H, aryl of *p*-methoxyphenyl). ^{13}C NMR (100 Hz, $CDCl_3$, 25 °C) δ: 14.4 (CH_3), 47.0 (CH), 55.9 (OCH_3), 61.4 (OCH_3), 114.6 (aryl of *p*-methoxyphenyl), 115.1 (aryl of *p*-methoxyphenyl), 141.5 (aryl of *p*-methoxyphenyl), 152.8 (aryl of *p*-methoxyphenyl), 171.6 (C=O of ester).

Decahydropyrimido[1,2-α]azepine (18)

Imine **9** (0.3 mmol, 45 μL), **3** (0.92 μmol, 1 mg), toluene-d_8 (0.95 mL), and isopropanol-d_8 (0.55 mL, 7.2 mmol) were added to a 10 mL Schlenk tube and heated to 70 °C for 60 min. According to the ^{1}H NMR there was full conversion. The spectral data were in accordance with those previously reported in the literature (21).

Furan-2-ylmethyl(4-methoxyphenyl)amine (19)

The general procedure was followed using imine **10** (0.171 g, 1.0 mmol) and **3** (2.8 μmol, 3 mg). The product was bulb-to-bulb distilled (250 °C, 0.5 mbar) to afford amine **19** (0.167 g, 97%). The spectral data were in accordance with those previously reported in the literature (17).

***N*-Phenyl-1-(4-fluorophenyl)ethylamine (20)**

The general procedure was followed using imine **11** (64 mg, 0.3 mmol) and catalyst **3** (3.2 mg, 3 μmol), isopropanol (0.55 mL, 7.2 mmol), and 0.95 mL of toluene. After 1 h, the sample was cooled down and analyzed by ^{1}H NMR. Conversion was >99%. Spectral data were in accordance to those previously reported in the literature (8).

***N*-(2,2-Dimethoxy-1-methylethyl)-4-methoxyphenyl)amine (21)**

The general procedure was followed by using imine **12** (0.223 g, 1.0 mmol) and **3** (33 mg, 30 μmol). The product was bulb-to-bulb distilled (250 °C, 0.5 mbar) to afford amine **21** (0.202 g, 95%). ^{1}H NMR (400 Hz, $CDCl_3$, 25 °C) δ: 1.15 (d, 2H, J = 6.6 Hz, CH_3), 3.44 (s, 3H, OCH_3), 3.47 (s, OCH_3), 3.53–3.56 (m, 1H, CH), 3.74 (s, 3H, OCH_3 of *p*-methoxyphenyl), 4.27 (d, 1H, J = 3.8 Hz, acetal), 6.60–6.62 (m, 2H, aryl of *p*-methoxyphenyl), 6.76–6.78 (m, 2H, aryl of *p*-methoxyphenyl). ^{13}C NMR (100 Hz, $CDCl_3$, 25 °C) δ: 14.6 (CH_3), 51.6 (CH), 55.5 (OCH_3), 55.7 (OCH_3), 56.5 (OCH_3), 107.1 (CH), 114.9 (aryl of *p*-methoxyphenyl), 115.2 (aryl of *p*-methoxyphenyl), 141.3 (aryl of *p*-methoxyphenyl), 152.2 (aryl of *p*-methoxyphenyl). Elemental anal. calcd. for $C_{12}H_{19}NO_3$ (225.29) (%): C 63.97, H 8.50, N 6.22; found: C 63.74, H 8.39, N 6.35.

***N*-(6-Methyl-2-hept-6-enyl)-4-methoxyaniline (22)**

The general procedure was followed using imine **13** (0.136 g, 1.0 mmol) and **3** (22.5 mg, 20.8 μmol). The product was bulb-to-bulb distilled (250 °C, 0.5 mbar) to afford amine **22** (0.147 g, 96%). Spectral data were in accordance to those previously reported in the literature (18).

4-(Methoxyphenyl)pyridin-3-ylmethylamine (23)

The general procedure was followed using imine **14** (0.212 g, 1.0 mmol) and **3** (33 mg, 30 μmol). The product was bulb-to-bulb distilled (250 °C, 0.5 mbar) to afford amine **23** (205.9 mg, 96%). ^{1}H NMR (400 Hz, $CDCl_3$, 25 °C) δ: 3.74 (s, 3H, OCH_3 *p*-methoxyphenyl), 4.32 (s, 2H, CH_2), 6.58–6.61 (m, 2H, aryl of *p*-methoxyphenyl), 6.76–6.79 (m, 2H, aryl of *p*-methoxyphenyl), 7.26–7.29 (m, 1H, pyridyl), 7.71–7.73 (m, 1H, pyridyl), 8.51–8.52 (m, 1H, pyridyl), 8.62–8.63 (m, 1H, pyridyl). ^{13}C NMR (100 Hz, $CDCl_3$, 25 °C) δ: 46.7 (CH_2), 55.8 (OCH_3), 114.5 (aryl of *p*-methoxyphenyl), 114.9 (aryl of *p*-methoxyphenyl), 122.3 (pyridyl), 134.6 (pyridyl), 141.7 (aryl of *p*-methoxyphenyl), 148.5 (pyridyl), 149.0 (pyridyl), 154.9 (aryl of *p*-methoxyphenyl). Elemental anal. calcd. for $C_{13}H_{14}N_2O$ (214.27) (%): C 72.87, H 6.59, N 13.08; found: C 73.11, H 6.72, N 13.21.

General procedure for the transfer hydrogenation of imines under controlled microwave heating — *N*-Phenyl-1-phenylethylamine (15)

In a typical experiment, imine **6** (58.6 mg, 0.3 mmol), **3** (0.3 mg, 0.3 μmol), toluene (1.9 mL), isopropanol (1.1 mL), and water (25 μL, 1%) were charged into a Pyrex tube (5 mL) fitted with a screw cap with a silicone–teflon septum (Personal Chemistry AB, Uppsala, Sweden). The septum was closed and the vessel inserted into a microwave oven. The microwave was run for 20 min (110 °C, 2 bar). The solvents were evaporated, $CDCl_3$ (0.7 mL) was added, and the solution was transferred to an NMR tube and analyzed by ^{1}H NMR, which showed 98% yield integrating the doublet at δ 1.48 (CH_3) of the amine and the singlet at δ 2.24 (CH_3) of the imine.

Amines **16**–**23** were prepared from the corresponding imines (0.3 mmol) according to the general procedure for

© 2005 NRC Canada

transfer hydrogenation under microwave heating using **3** (0.3–9 μmol). The results are given in Table 2.[4]

Acknowledgments

We thank the Swedish Research Council for financial support. Laetitia Mony thanks the Ecole Normale Supérieure for financial support.

References

1. R.O. Hutchins and M.K. Hutchins. *In* Comprehensive organic synthesis. Vol. 8. *Edited by* B.M. Trost and I. Fleming. Pergamon, Oxford. 1991. pp. 25–78.
2. R.C. Larock. Comprehensive organic transformations. WCH, New York. 1989. p. 421.
3. K.A. Schellenberg. J. Org. Chem. **28**, 3259 (1963).
4. (*a*) F. Spindler and H.-U. Blaser. *In* Transition metals for organic synthesis. Vol. 2. *Edited by* M. Beller and C. Bolm. Wiley-VCH, Weinheim, Germany. 2004. p. 113; (*b*) P.N. Rylander. *In* Hydrogenation methods. Academic Press, New York. 1985. p. 82.
5. S. Gladiali and E. Alberico. *In* Transition metals for organic synthesis. Vol. 2. *Edited by* M. Beller and C. Bolm. Wiley-VCH, Weinheim, Germany. 2004. p. 145.
6. (*a*) G.-Z. Wang and J.-E. Bäckvall. J. Chem. Soc. Chem. Commun. 980 (1992); (*b*) S. Bhaduri, N. Sapre, K. Sharma, P.G. Jones, and G. Carpenter. J. Chem. Soc. Dalton Trans. 1305 (1990); (*c*) H.A. Brune, J. Unsin, R. Hemmer, and M. Reichhardt. J. Organomet. Chem. **369**, 335 (1989); (*d*) Y. Watanabe, Y. Tsuji, H. Ige, Y. Ohsugi, and T. Ohta. J. Org. Chem. **49**, 3359 (1984); (*e*) F. Martinelli, G. Mestroni, A. Camus, and G. Zassinovich. J. Organomet. Chem. **220**, 383 (1981); (*f*) R. Grigg, T.R.B. Mitchell, and N. Tongpenyai. Synthesis, 442 (1981).
7. (*a*) N. Uematsu, A. Fujii, S. Hashiguchi, T. Ikariya, and R. Noyori. J. Am. Chem. Soc. **118**, 4916 (1996); (*b*) J. Mao and D.C. Baker. Org. Lett. **1**, 841 (1999).
8. J.S.M. Samec and J.-E. Bäckvall. Chem. Eur. J. **8**, 2955 (2002).
9. Y. Blum, D. Czarkie, Y. Rahamim, and Y. Shvo. Organometallics, **4**, 1459 (1985).
10. (*a*) N. Menashe and Y. Shvo. Organometallics, **10**, 3885 (1991); (*b*) M.L.S. Almeida, M. Beller, G.-Z. Wang, and J.-E. Bäckvall. Chem. Eur. J. **2**, 1533 (1996); (*c*) G. Csjernyik, A.H. Éll, L. Fadini, B. Pugin, and J.-E. Bäckvall. J. Org. Chem. **67**, 1657 (2002); (*d*) J.H. Choi, N. Kim, Y.J. Shin, J.H. Park, and J. Park. Tetrahedron Lett. **45**, 4607 (2004).
11. For the use of **1** as a hydrogen transfer catalyst in racemization, see: (*a*) O. Pàmies and J.-E. Bäckvall. Chem. Rev. **103**, 3247 (2003); (*b*) M.J. Kim, Y. Ahn, and J. Park. Curr. Opin. Biotechnol. **13**, 578 (2002).
12. J.S.M. Samec, A.H. Éll, and J.-E. Bäckvall. Chem. Commun. 2748 (2004).
13. C.P. Casey, S.W. Singer, D.R. Powell, R.K. Hayashi, and M. Kavana. J. Am. Chem. Soc. **123**, 1090 (2001)
14. (*a*) M. Larhed, C. Moberg, and A. Hallberg. Acc. Chem. Res. **35**, 717 (2002); (*b*) A. Svennebring, P. Nilsson, and M. Larhed. J. Org. Chem. **69**, 3345 (2004); (*c*) P.-A. Enquist, P. Nilsson, and M. Larhed. Org. Lett. **5**, 4875 (2003).
15. P. Lidström, J. Tierney, B. Wathey, and J. Westman. Tetrahedron, **57**, 9225 (2001).
16. Y. Niwa and M. Shimizu. J. Am. Chem. Soc. **125**, 3720 (2003).
17. I. Ojima, I. Habus, M. Zhao, M. Zucco, Y.H. Park, C.M. Sun, and T. Brigaud. Tetrahedron, **48**, 6985 (1992).
18. M.C. Hansen and S.L. Buchwald. Org. Lett. **2**, 713 (2000).
19. T. Kawakami, T. Sugimoto, I. Shibata, A. Baba, H. Matsuda, and N. Sonoda. J. Org. Chem. **60**, 2677 (1995).
20. E. Aller, R.T. Buck, M.J. Drysdale, L. Ferris, D. Haigh, C.J. Moody, N.D. Pearson, and J.B. Sanghera. J. Chem. Soc. Perkin Trans. 1, 2879 (1996).
21. D.A. Jeyaraj, K.K. Kapoor, V.K. Yadav, H.M. Gauniyal, and M. Parvez. J. Org. Chem. **63**, 287 (1998).

[4] Supplementary data for this article are available on the Web site or may be purchased from the Depository of Unpublished Data, Document Delivery, CISTI, National Research Council Canada, Ottawa, ON K1A 0S2, Canada. DUD 3697. For more information on obtaining material refer to http://cisti-icist.nrc-cnrc.gc.ca/irm/unpub_e.shtml.

© 2005 NRC Canada

β Elimination of a phosphonate group from an alkoxyl radical — Intramolecular acylation using acylphosphonate derivatives as carbonyl group acceptors[1]

Chang Ho Cho and Sunggak Kim

Abstract: The possibility of β elimination of a phosphonate group in radical reactions was studied. The facile β elimination of the phosphonate group from an alkoxyl radical was observed for the first time, whereas the β elimination of the phosphonate group from an aminyl and an alkyl radical did not occur. On the basis of our findings, the use of an acylphosphonate as a carbonyl group radical acceptor was investigated. Radical cyclization of the acylphosphonate in the presence of hexamethylditin in benzene at 300 nm for 2 h gave a cyclopentanone or a cyclohexanone derivative in good yield without the formation of a direct reduction product. The reaction can be carried out in the presence of a catalytic amount of hexamethylditin (0.2 equiv.) under similar conditions. In addition, an alkyl phosphonothiolformate group can act as an alkylthiocarbonyl group equivalent radical acceptor, providing ready access to a thiolactone synthesis.

Key words: radical, β elimination, acylation, cyclization, acylphosphonate.

Résumé : On a étudié la possibilité d'une élimination β d'un groupe phosphonate au cours de réactions radicalaires. On a observé pour la première fois une élimination β facile d'un groupe phosphonate à partir d'un radical alkoxyle alors qu'il ne se produit pas d'élimination β d'un groupe phosphonate à partir d'un radical aminyle ou d'un radical alkyle. Sur la base de ces observations, on a étudié l'utilisation d'un acylphosphonate comme groupe carbonyle accepteur de radical. La cyclisation radicalaire de l'acylphosphonate, en présence d'hexaméthyldiétain, dans le benzène, à 300 nm, pendant deux heures, conduit à la formation d'une cyclopentanone ou d'une cyclohexanone, avec un bon rendement, sans formation d'un produit de réduction directe. Il est possible d'effectuer la réaction dans des conditions semblables, en présence d'une quantité catalytique d'hexaméthyldiétain (0,2 équiv.). De plus, un groupe phosphonothiolformiate d'alkyle peut agir comme groupe alkylthiocarbonyle équivalent à l'accepteur radicalaire et fournir ainsi un accès facile à une synthèse de thiolactone.

Mots clés : radical, β élimination, acylation, cyclisation, acylphosphonate.

[Traduit par la Rédaction]

Introduction

The carbonyl group is one of the central functional groups in organic chemistry and can be readily prepared by treatment of carboxylic acid derivatives with organometallic compounds (1). However, the radical version of this conventional acylation reaction has not been successful to date because additions of alkyl radicals to C=O bonds are extremely difficult owing to the high π-bond strengths of C=O bonds (2, 3). Since β fragmentations of alkoxyl radicals are much faster than the additions of alkyl radicals to carbonyl groups, it is anticipated that carbonyl group derivatives cannot be used effectively as radical acceptors to achieve radical-mediated acylations. Thus, a limited number of carbonyl group radical acceptors has been utilized in intramolecular acylations and includes acyl sulfides, acyl selenides (4), and acylgermanes (5, 6). It is noteworthy that a mixed carboxylic phosphonic anhydride is a good radical acceptor in radical cyclizations but fails to function as the carbonyl group acceptor because the β fragmentation of the alkoxyl radical cleaves the carbon–carbon bond rather than the carbon–oxygen bond, as shown in Scheme 1 (7). In addition, several indirect approaches using a nitrile (8) and an oxime ether group have been developed (9, 10). In the case of intermolecular acylation, the use of carbonyl group derivatives as acceptors is uncommon and only several intermolecular radical carboxylations have been reported (11). We developed highly efficient indirect acylation approaches using sulfonyl oxime ethers (10). This indirect approach is at-

Received 20 December 2004. Published on the NRC Research Press Web site at http://canjchem.nrc.ca on 27 July 2005.

Dedicated to Professor Howard Alper in recognition of his outstanding contribution to organic chemistry.

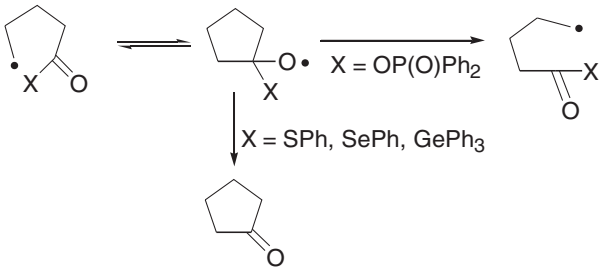
C.H. Cho and S. Kim.[2] Center for Molecular Design and Synthesis and Department of Chemistry, School of Molecular Science (BK21), Korea Advanced Institute of Science and Technology, Daejeon 305-701, Korea.

[1]This article is part of a Special Issue dedicated to Professor Howard Alper.

[2]Corresponding author (e-mail: skim@kaist.ac.kr).

 doi: 10.1139/V05-099 © 2005 NRC Canada

Scheme 1. Intramolecular acylation approach.



tractive since the carbonyl group can be easily generated by oxidative cleavage or by hydrolysis.

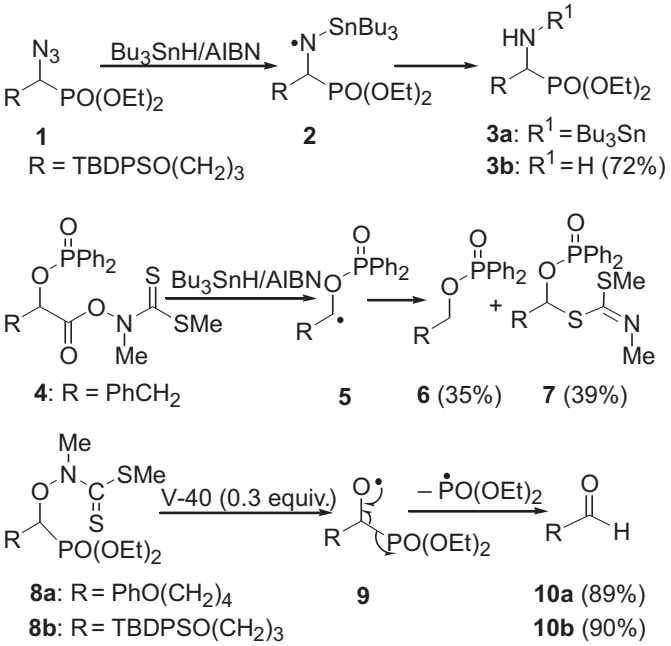
In connection with our continued interest on radical acylation, we have searched for other efficient carbonyl group radical acceptors and investigated the possibility of using a phosphonate as a leaving group in radical reactions (12).

Results and discussion

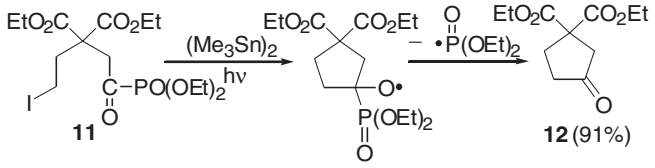
The β elimination of organophosphorous groups has not been well-studied and several reports have appeared only in recent years. The β elimination of a phosphinate group was observed during a rearomatization process (13). The β elimination of a diphenylphosphinoyl group has been known in radical allylation (14) and in tandem radical reactions involving cyclization and the subsequent β elimination of the diphenylphosphinoyl group (15).

The ease of β elimination generally depends on the nature of the π bond formed and the strength of the σ bond broken. Thus, it is expected that the β elimination would be easier when the π bond formed is stronger (16). Based on this rationale, we initially studied the β elimination of a diethyl phosphonate group from an aminyl radical (Scheme 2). When azidophosphonate **1** was treated with Bu_3SnH–AIBN in refluxing benzene for 2 h (17), **3b** was isolated in 72% yield, clearly indicating that the β elimination of the phosphonate group from the aminyl radical in radical intermediate **2** did not occur, probably because of the relatively weak π-bond strength of C=N bonds. Thus, our attention was given next to the formation of a carbonyl bond as a result of the β elimination of the phosphonate group, and we studied the possibility of β elimination of the diethyl phosphonate group from the alkyl radical using thiohydroxamate ester **4** (18). Radical reaction of **4** with Bu_3SnH–AIBN in refluxing benzene for 4 h afforded a mixture of **6** and **7** roughly in an equal ratio without the β elimination of the phosphonate group. Apparently, the phosphorous–oxygen bond in radical intermediate **5** is strong and did not undergo cleavage. Thus, **5** reacted with Bu_3SnH and the starting thiohydroxamate ester **4** to afford a mixture of **6** and **7**, respectively. Finally, the β elimination of a phosphonate group from the alkoxyl radical was examined. As shown in Scheme 2, when **8a** was treated with V-40 (1,1′-azobis(cyclohexane-1-carbonitrile)) as initiator in chlorobenzene for 3 h (19), aldehyde **10a** was isolated in 89% yield. A similar result was obtained with **8b**. Evidently, the β elimination is energetically favorable because of the formation of a strong carbonyl bond along with cleavage of a relatively weak carbon–phosphorous bond.

Scheme 2. β Elimination of a diethyl phosphonate group.



Scheme 3. Radical cyclization of an acylphosphonate.

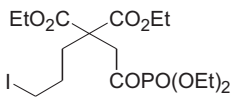
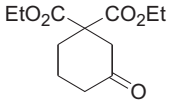
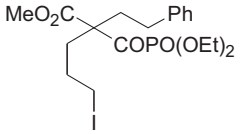
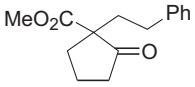
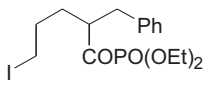
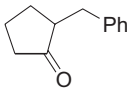
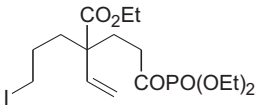
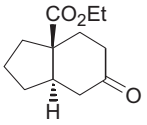
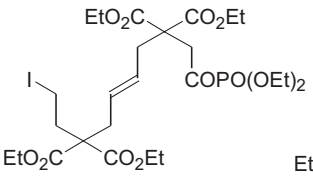
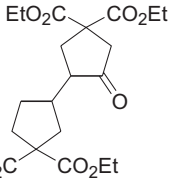
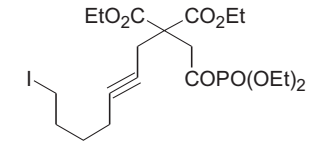
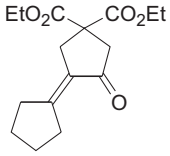


Based on our findings, we studied the feasibility of using an acylphosphonate as a carbonyl group radical acceptor in intramolecular radical acylations (Scheme 3) (12). Acyl and bis(acyl)phosphine oxides have been employed as photochemical sources of acyl radicals for use as initiators in polymerization reactions (20). Also, acylphosphonates were used as acylating agents of alcohols, amines, and enolates (21). Acyldiethylphosphonates were conveniently prepared by treatment of acid chlorides with triethyl phosphite in dichloromethane at room temperature and were quite stable to silica gel column chromatographic purification (22). Radical cyclization of acylphosphonate **11** in the presence of hexamethylditin at 300 nm (1.1 equiv.) for 2 h in benzene gave cyclopentanone **12** in 91% yield without the formation of the direct reduction product. The reaction can be carried out in the presence of a catalytic amount of hexamethylditin (0.2 equiv.) to afford **12** in 88% yield under similar conditions because the initially generated phosphonate radical reacts with an alkyl iodide to generate an alkyl radical. Thus, the remaining reactions were carried out in benzene using 0.2 equiv. of hexamethylditin at 300 nm for 3 to 4 h.

Table 1 summarizes the experimental results and illustrates the efficiency of the acylphosphonates as the carbonyl group radical acceptor. The reaction was normally clean, yielding the corresponding cyclopentanones and cyclohexanones in high yield. For most of the cases observed in this study, there was no indication of the presence of the direct reduction product and other side products. Tandem radical

© 2005 NRC Canada

Table 1. Radical cyclization of acylphosphonates.[a]

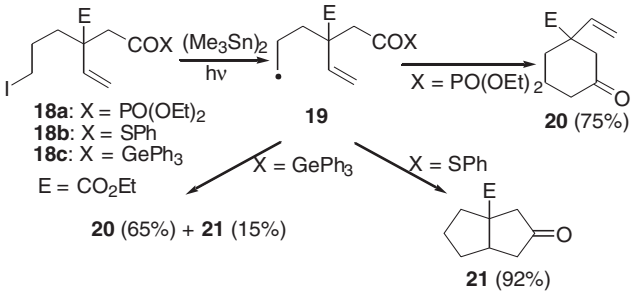
Entry	Substrate	Product	Yield (%)[b]
1			71 (82)[c]
2			61
3			72
4			69
5			79[d]
6			77

[a]The reaction was carried out with 0.2 equiv. of $(Me_3Sn)_2$ in benzene at 300 nm for 2 h.
[b]The yield was not optimized.
[c]$(Me_3Sn)_2$ (1.1 equiv.).
[d]Stereochemistry of starting material is *E* only. Diastereomeric mixture (1.2:1) of the product.

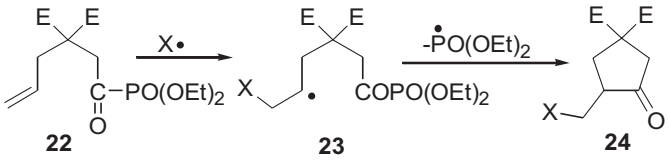
cyclizations worked equally well. Not only alkyl radicals but also alkenyl radicals reacted with acylphosphonates to give cyclopentanone derivatives (Table 1, entries 4–6).

It is noteworthy that reaction of **13a** under similar conditions gave cyclohexanone **16** as a sole product, whereas **13b**, using a thioester as acceptor, gave a mixture of **16** and **17b** in 46% and 33% yield, respectively (4) (eq. [1]). Apparently, the latter is formed as a result of the formation of stable radical intermediate **15b** owing to the facile β fragmentation of the alkoxyl radical **14b**. The result obtained here clearly indicates that the β elimination of the phosphonate group in **9** is very fast and highly efficient. Even more exciting results were obtained with **18** (Scheme 4). When **18a** was treated with hexamethylditin (0.2 equiv.) at 300 nm for 2 h, gratifyingly, **20** was obtained exclusively, whereas **21** was reported to be a sole product from the radical reaction of acyl sulfide **18b** (4). Apparently, 6-exo ring closure to the acylphosphonate group is much faster than 5-exo ring closure to the C=C bond, whereas 5-exo ring closure to the C=C bond is much faster than 6-exo ring closure to the thioester group. To strengthen the efficiency of the acylphosphonate, a comparative experiment was also carried out with acylgermane **18c**. Irradiation of a benzene solution of **18c** in the presence of hexamethylditin (0.2 equiv.) at 300 nm for 3 h afforded a 65:15 mixture of **20** and **21**, indicating higher reactivity of the acylphosphonate relative to the acylgermane as the carbonyl group radical acceptor. Since an approximate rate constant for 5-exo cyclization of a primary alkyl radical to an acylgermane is known to be 7×10^6 s^{-1} (5*c*), the approximate rate constant for the same cyclization to the acylphosphonate would be 3×10^7 s^{-1}. Apparently, the acylphosphonate is regarded as the most reactive among previously reported carbonyl group acceptors.

Scheme 4. Comparative studies of an acyl sulfide, an acylgermane, and an acylphosphonate.

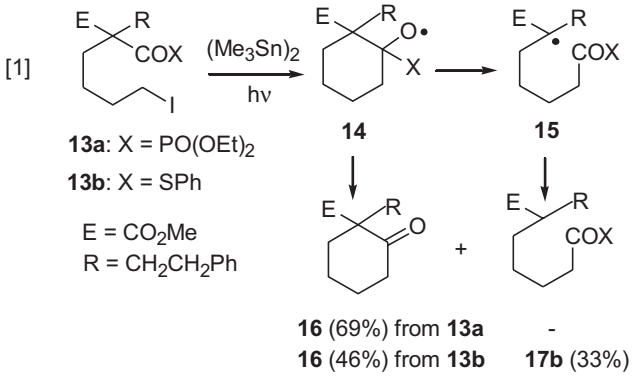


Scheme 5. Radical addition and cyclization of an acylphosphonate.



Based on the highly efficient and fast addition of the alkyl radical onto the acylphosphonate, we next studied sequential radical reactions involving intermolecular radical addition to the alkenyl and the alkynyl bond and subsequent cyclization (Scheme 5). This approach provides a ready access to β-functionalized cyclopentanones and cyclohexanones (23). Addition of a phenylsulfanyl radical and a phenylsulfonyl radical to an alkenyl group in **22** was followed by cyclization to afford cyclopentanone **24** along with the generation of the diethyl phosphonate radical for the chain propagation. Similarly, various electrophilic alkyl radicals from activated olefins bearing α-electron-withdrawing groups reacted smoothly with **22** to yield **24** in high yields. Appar-

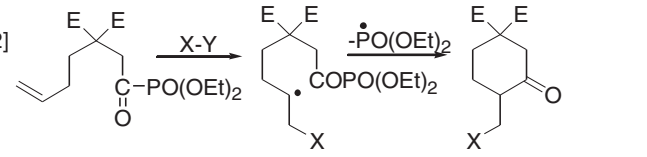
[1]



© 2005 NRC Canada

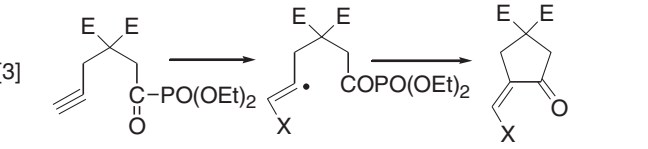
ently, the fast addition of the alkyl radical to the acylphosphonate obviates the problem of the quenching of radical intermediate **23** by the alkyl iodide prior to the cyclization. The experimental results are summarized in Table 2. The present approach can be applied to the formation of cyclohexanone derivatives (eq. [2]). Treatment of **25** with ethyl iodoacetate and hexamethylditin (0.2 equiv.) in benzene at 300 nm for 5 h afforded **26a** in 86% yield. A similar result was obtained with iodomethyl phenyl sulfone under the same conditions. Furthermore, the present approach can be applied to alkynyl-acylphosphonate **27**. When **27** was reacted with thiophenol and phenylsulfonyl bromide in the presence of AIBN in refluxing benzene for 3 h, the desired products **28a** and **28b** were obtained in 86% and 90% yield, respectively (eq. [3]).

[2]



25 X-Y: $EtOOCCH_2I$, $PhSO_2CH_2I$ **26a**: X = CH_2COOEt (86%) **26b**: X = CH_2SO_2Ph (85%)

[3]

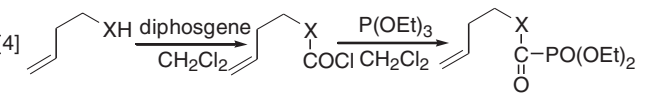


27 PhSH/AIBN **28a**: X = SPh: *E*/*Z* = 1:12, 86%

$PhSO_2Br$/AIBN **28b**: X = SO_2Ph: *E*/*Z* = 1:32, 90%

We next studied several interesting variations using a phosphonoformate and a phosphonothiolformate as radical acceptors to explore whether the present acylation could be further extended to the synthesis of lactone **31a** and thiolactone **31b**, respectively, via intermediate **30** (Scheme 6). Diethylphosphonoformate **29a** was prepared by the treatment of chloroformate **33a** with triethyl phosphite in dichloromethane at room temperature for 2 h (eq. [4]). **29a** was purified by passing it through a short column of silica gel. Similarly, diethylphosphonothiolformate **29b** was prepared from **32b** by a two-step procedure (24). Treatment of **32b** with diphosgene afforded **33b**, which was further treated with triethyl phosphite to give alkyl phosphonothiolformate **29b** in 75% yield.

[4]

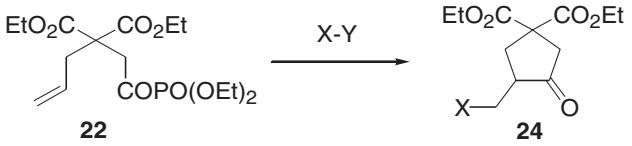


32a: X = O **32b**: X = S **33** **29a** (83%) **29b** (75%)

Reaction of **29a** with phenylsulfonyl bromide in the presence of AIBN (0.2 equiv.) in benzene at 80 °C for 6 h did not afford lactone **35** but gave addition product **36a** in 84% yield (eq. [5]). When the reaction was carried out with ethyl iodoacetate and hexamethylditin at 300 nm, a similar result was obtained, yielding **36b** in 88% yield. It is evident that intermediate radical **34** underwent bromine and iodine atom transfer rather than cyclization. To enforce the cyclization of **36a**, the solution of **36a** was irradiated at 300 nm in the presence of hexamethylditin, but lactone **35** was not formed. The failure of the cyclization may be due to the unfavorable *E*-conformation of **34** and (or) the low reactivity of the alkoxycarbonyl group as a radical acceptor. Since the differences in energy are generally smaller for the *E* and *Z* conformations in thiol esters than for the corresponding carboxylic esters (25), radical cyclization of **29b** was studied. Irradiation of a benzene solution of **29b**, ethyl iodoacetate, and hexamethylditin (0.5 equiv.) at 300 nm for 3 h afforded a mixture of addition product **38** and thiolactone **39** in 15% and 42% yield, respectively (eq. [6]). Furthermore, reaction of **38** in the presence of hexamethylditin at 300 nm for 3 h gave thiolactone **39** in 88% yield. From the results obtained here, two features are noteworthy. The addition of an alkyl radical onto the phosphonothiolformate group occurred smoothly, and the diethyl phosphonate group was eliminated preferentially relative to the alkylthio group.

In conclusion, we have shown the facile β elimination of a phosphonate group from an alkoxyl radical and its application to intramolecular acylation approach, in which we demonstrated that the acylphosphonate was a highly efficient carbonyl group radical acceptor and more reactive than the previously known acyl sulfide and acylgermane. In addition, an alkyl phosphonothiolformate group can act as an

Table 2. Radical addition and cyclization of acylphosphonates.

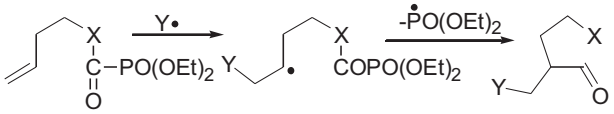


22 **24**

X-Y	Condition[a]	Time (h)	Yield (%)
PhS-H	A	10	89
$(TMS)_3Si$-H	A	2	75
$PhSO_2$-Br	A	2	90
C_6F_{13}-I	B	5	85
$EtOOCCH_2$-I	B	5	78
$EtOOCCH_2$-SC(=S)OEt	B	5	75
$PhSO_2CH_2$-I	B	5	72
$NCCH_2$-I	B	5	73

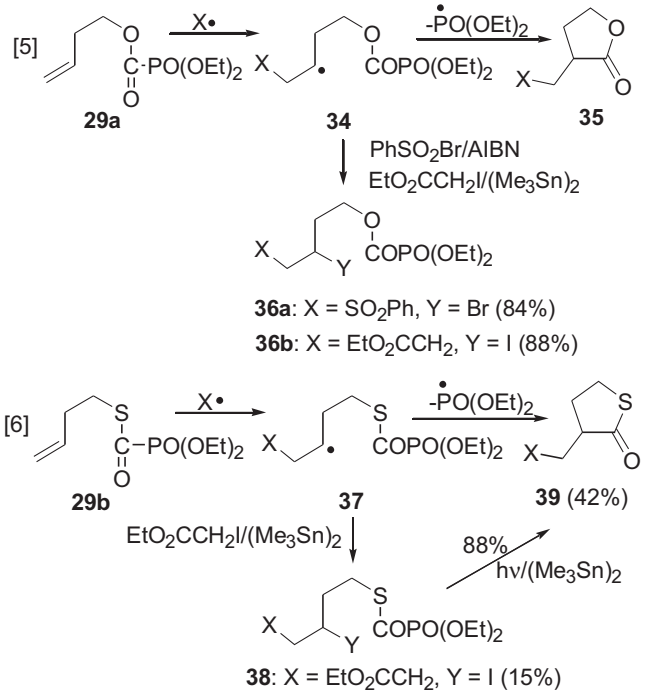
[a]Method A: AIBN, C_6H_6, reflux; Method B: 0.2 equiv. of $(Me_3Sn)_2$, C_6H_6, *hν* = 300 nm.

Scheme 6. Radical addition and cyclization of phosphonoformate and phosphonothiolformate.



29a: X = O **29b**: X = S **30** **31**

© 2005 NRC Canada



alkylthiocarbonyl group equivalent radical acceptor, providing a ready access to a thiolactone synthesis.[3]

Acknowledgments

We thank the Center for Molecular Design and Synthesis (CMDS) and Brain Korea 21 Project for financial support.

References

1. (*a*) B.T. O'Neill. *In* Comprehensive organic synthesis. Vol. 1. *Edited by* B.M. Trost and I. Fleming. Pergamon Press, New York. 1991. pp. 397; (*b*) R.C. Larock. *In* Comprehensive organic transformations. VCH Publishers, Inc., New York. 1989. p. 681; (*c*) M. Jorgensen. Org. React. (N.Y.), **18**, 1 (1970).
2. (*a*) R. Walton and B. Fraser-Reid. J. Am. Chem. Soc. **113**, 5791 (1991); (*b*) A.L.J. Beckwith and B.P. Hay. J. Am. Chem. Soc. **111**, 2674 (1989); (*c*) A.L.J. Beckwith and B.P. Hay. J. Am. Chem. Soc. **111**, 230 (1989).
3. S. Kim. Adv. Synth. Catal. **346**, 19 (2004).
4. S. Kim and S.Y. Jon. Chem. Commun. 1335 (1996).
5. (*a*) D.P. Curran, U. Diederichsen, and M. Palovich. J. Am. Chem. Soc. **119**, 4797 (1997); (*b*) U. Diederichsen and D.P. Curran. J. Organomet. Chem. **531**, 9 (1997); (*c*) D.P. Curran and M. Palovich. Synlett, 631 (1992); (*d*) D.P. Curran and H. Liu. J. Org. Chem. **56**, 3463 (1991); (*e*) S. Kiyooka, Y. Kaneko, H. Matsue, M. Hamada, and R. Fujiyama. J. Org. Chem. **55**, 5562 (1990).
6. For other carbonyl equivalent radical acceptors, see: (*a*) U. Iserloh and D.P. Curran. J. Org. Chem. **63**, 4711 (1998); (*b*) S. Kim, I.Y. Lee, J.-Y. Yoon, and D.H. Oh. J. Am. Chem. Soc. **118**, 5138 (1996); (*c*) D.L.J. Clive, P.L. Beaulieu, and L. Set. J. Org. Chem. **49**, 1313 (1984); (*d*) W.G. Bentrude and K.R. Darnall. J. Am. Chem. Soc. **90**, 3588 (1968).
7. S. Kim, S.Y. Jon, J.Y. Do, H.J. Song, and S.S. Kim. Tetrahedron Lett. **41**, 8127 (2000).
8. (*a*) D.L.J. Clive, P.L. Beaulieu, and L. Set. J. Org. Chem. **49**, 1313 (1984); (*b*) D. Griller, P. Schmid, and K.U. Ingold. Can. J. Chem. **57**, 831 (1979).
9. U. Iserloh and D.P. Curran. J. Org. Chem. **63**, 4711 (1998).
10. (*a*) S. Kim, I.Y. Lee, J.-Y. Yoon, and D.H. Oh. J. Am. Chem. Soc. **118**, 5138 (1996); (*b*) S. Kim and J.-Y. Yoon. J. Am. Chem. Soc. **119**, 5982 (1997); (*c*) S. Kim and J.-Y. Yoon. Synlett, 475 (1997); (*d*) S. Kim and C.J. Lim. Bull. Korean Chem. Soc. **24**, 1219 (2003).
11. (*a*) M.S. Kharasch, S.S. Kane, and H.C. Brown. J. Am. Chem. Soc. **64**, 1621 (1942); (*b*) M.S. Kharasch and H.C. Brown. J. Am. Chem. Soc. **64**, 329 (1942); (*c*) S. Kim and S.Y. Jon. Chem. Commun. 815 (1998); (*d*) S. Kim and S.Y. Jon. Tetrahedron Lett. **39**, 7317 (1998).
12. For a preliminary report, see: S. Kim, C.H. Cho, and C.J. Lim. J. Am. Chem. Soc. **125**, 9574 (2003).
13. (*a*) D.L.J. Clive and S. Kang. J. Org. Chem. **66**, 6083 (2001); (*b*) D.L.J. Clive and S. Kang. Tetrahedron Lett. **41**, 1315 (2000).
14. G. Ouvry. Ph.D. thesis, Ecole Polytechnique, Palaiseau, France. 12 December 2002.
15. D. Leca, L. Fensterbank, E. Lacote, and M. Malacria. Angew. Chem. Int. Ed. **43**, 4220 (2004).
16. (*a*) S. Kim and J.H. Cheong. Chem. Commun. 1143 (1998); (*b*) S. Kim, K.H. Kim, and J.R. Cho. Tetrahedron Lett. **38**, 3915 (1997).
17. S. Kim, G.H. Joe, and J.Y. Do. J. Am. Chem. Soc. **115**, 3328 (1993).
18. (*a*) S. Kim, C.J. Lim, S.-E. Song, and H.-Y. Kang. Chem. Commun. 1410 (2001); (*b*) S.G. Lee, C.J. Lim, and S. Kim. Bull. Korean Chem. Soc. **25**, 1611 (2004).
19. S. Kim, C.J. Lim, S.-E. Song, and H.-Y. Kang. Synlett, 688 (2001).
20. (*a*) A. Kajiwara, Y. Konishi, Y. Morishima, W. Schnabel, K. Kuwata, and M. Kamachi. Macromolecules, **26**, 1656 (1993); (*b*) S. Jockusch, I.V. Koptyug, P.F. McGarry, G.W. Sluggett, N.J. Turro, and D.M. Watkins. J. Am. Chem. Soc. **119**, 11 495 (1997); (*c*) M.T.L. Rees, G.T. Russell, M.D. Zammit, and T.P. Davis. Macromolecules, **31**, 1763 (1998).
21. (*a*) M. Sekine, M. Satoh, H. Yamagata, and T. Hata. J. Org. Chem. **45**, 4162 (1980); (*b*) M. Sekine, A. Kume, and T. Hata. Tetrahedron Lett. **22**, 3617 (1981); (*c*) M. Sekine, A. Kume, M. Nakajima, and T. Hata. Chem. Lett. 1087 (1981).
22. (*a*) K. Terauchi and H. Sakurai. Bull. Chem. Soc. Jpn. **43**, 883 (1970); (*b*) E. Breuer, R. Karaman, and A. Goldblum. J. Chem. Soc. Perkin Trans. 2, 2029 (1988); (*c*) M. Sprecher and D. Kost. J. Am. Chem. Soc. **116**, 1016 (1994).
23. (*a*) O. Miyata and T. Naito. C. R. Acad. Sci. IIc: Chim. **4**, 401 (2001); (*b*) O. Miyata, K. Muroya, T. Kobayashi, R. Yamanaka, S. Kajisa, J. Koide, and T. Naito. Tetrahedron, **58**, 4459 (2002).
24. C.J. Salomon and E. Breuer. Synlett, 815 (2000).
25. D.M. Pawar, A.A. Khalil, D.R. Hooks, K. Collins, T. Elliott, J. Stafford, L. Smith, and E.A. Noe. J. Am. Chem. Soc. **120**, 2108 (1998).

[3] Supplementary data for this article are available on the Web site or may be purchased from the Depository of Unpublished Data, Document Delivery, CISTI, National Research Council Canada, Ottawa, ON K1A 0S2, Canada. DUD 3693. For more information on obtaining material refer to http://cisti-icist.nrc-cnrc.gc.ca/irm/unpub_e.shtml.

© 2005 NRC Canada

Coordination chemistry of the tetrakis(2-hydroxyphenyl)ethene support mimic — Polymetallic magnesium, aluminum, and titanium derivatives[1]

Udo H. Verkerk, Robert McDonald, and Jeffrey M. Stryker

Abstract: The crystal structures of magnesium, aluminum, and titanium coordination complexes of the structurally preorganized tetrakis(2-hydroxyphenyl)ethene are reported. As a result of the absence of steric shielding and the conformational flexibility of the ligand, pseudo-dimeric complexes are formed instead of crown- or raft-like compounds. The unsubstituted tetrakis(2-hydroxyphenyl)ethene ligand thus emulates the complexation characteristics of the sterically open calix[4]arene system.

Key words: coordination chemistry, polymetallic, titanium complexes, magnesium complexes, aluminum complexes, tetrakis(2-hydroxyphenyl)ethene ligands, crystal structures.

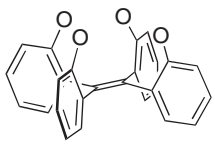
Résumé : On a déterminé les structures cristallines de complexes de coordination de tétrakis(2-hydroxyphényl)éthène structuralement préorganisés avec du magnésium, de l'aluminium et du titane. En raison de l'absence de protection stérique et de flexibilité conformationnelle du ligand, il y a formation de complexes pseudodimères au lieu de composés en forme de couronnes ou de bateau. Le ligand non substitué tétrakis(2-hydroxyphényl)éthène émule donc les caractéristiques de complexation du système calix[4]arène stériquement ouvert.

Mots clés : chimie de coordination, polymétallique, complexes du titane, complexes du magnésium, complexes de l'aluminium, ligands tétrakis(2-hydroxyphényl)éthène, structures cristallines.

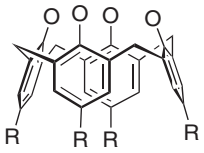
[Traduit par la Rédaction]

Introduction

The recently introduced tetrakis(2-hydroxyphenyl)ethene ligand **I** (1), a topologically unique analogue of calix[4]arene **II** (2), should by virtue of the constrained arrangement of four phenol groups be useful for modeling the coordination chemistry of an oxo surface. As reported for various calix[4]arenes (2*b*, 3), such an arrangement imposes unique reactivity on complexed metals (3) and could act as an additive (4) or model (3*c*) for heterogeneous supports as used in industrial polymerization catalysis (5). Here we report the crystal structures of magnesium, aluminum, and titanium complexes formed by coordination to tetrakis(2-hydroxyphenyl)ethene.



I



II

Results and discussion

Whereas the reaction of tetrakis(2-hydroxyphenyl)ethene (**1**) with Et_3Al in pentane yields the hydrocarbon soluble, crown-like compound **2**, the reaction of the tetraarylethene with Et_2AlCl generates a pentane insoluble precipitate, presumably the result of predominant intermolecular association (Scheme 1). The addition of THF as a stronger coordinating solvent discourages intermolecular coordination and improves the solubility, allowing isolation of tetrametallic aluminum complex **3** after crystallization from THF–toluene. Compound **3** shows, in the centrosymmetric crystal structure (Fig. 1), two pentacoordinate aluminum centers as part of a Al_2O_2 four-membered ring and two pentacoordinate ethylaluminum chloride fragments sandwiched in between two highly distorted tetraphenylethene ligands. The observed Al2—O4 bond length in the peripheral pentacoordinate fragment Al2 (Table 1) is within the range observed for alumi-

Received 3 December 2004. Published on the NRC Research Press Web site at http://canjchem.nrc.ca on 28 July 2005.

Dedicated to Professor Howard Alper for his many and unique contributions to transition-metal catalysis and his extraordinary service to the field of chemistry in Canada.

U.H. Verkerk and J.M. Stryker.[2] Department of Chemistry, University of Alberta, 11227 Saskatchewan Drive NW, Edmonton, AB T6G 2G2, Canada.
R. McDonald. X-Ray Crystallography Laboratory, Department of Chemistry, University of Alberta, 11227 Saskatchewan Drive NW, Edmonton, AB T6G 2G2, Canada.

[1]This article is part of a Special Issue dedicated to Professor Howard Alper.

[2]Corresponding author (e-mail: jeff.stryker@ualberta.ca).

 doi: 10.1139/V05-108 © 2005 NRC Canada

Scheme 1.

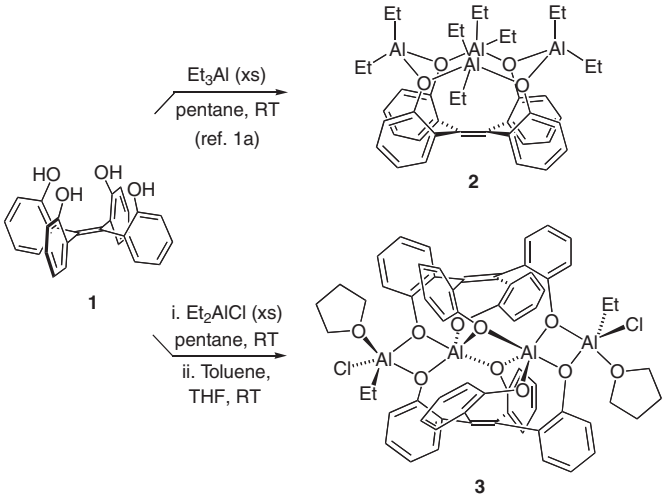
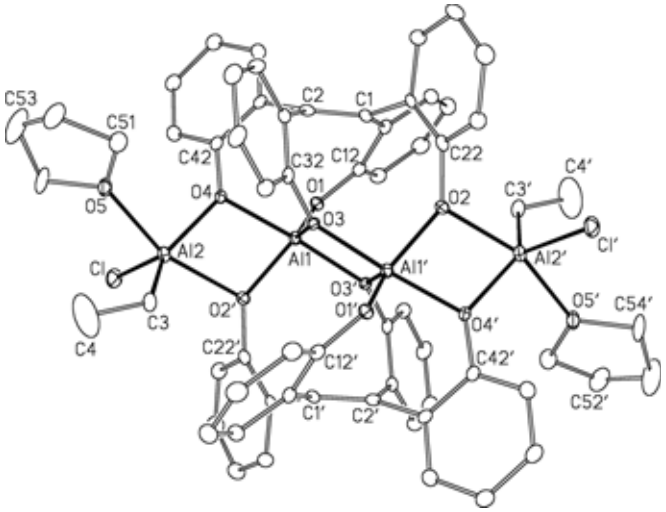


Fig. 1. Perspective view (ORTEP) of compound **3** showing the atom labeling scheme. Hydrogen atoms have been omitted for clarity. Primed atoms are related to the unprimed ones via the crystallographic inversion center (0,0,0).



num phenoxides (lit. (6, 7) value 1.79–1.895 Å), as are the Al2—Cl (lit. (6) value 2.104–2.199 Å) and Al2—C3 (lit. (6) value 1.946–1.994 Å) bond lengths. The axial Al2—O bonds are considerably longer (avg. 2.045 Å). The varying bond angles O_{eq}-Al2-O_{eq} (see Supplementary information),[3] and the O5-Al2-O2′ bond angle of 160.64(16)° (Table 1) indicate a distorted trigonal bipyramidal geometry. These features are repeated in the pentacoordinate fragment around Al1, with longer O_{axial}—Al (avg. 1.909 Å) compared to the $O_{equatorial}$—Al (avg. 1.801 Å) bond lengths (see Table 1). The observed range of O4-Al1-O1, O2′, and O3 angles (78.19–93.70°, Table 1), and the O4-Al1-O3′ angle (169.21(16)°) again indicate a significantly distorted trigonal bipyramidal geometry.

Table 1. Key bond lengths (Å), angles (°), and dihedral angles (°) for aluminum complex **3**.

Bond lengths (Å)	
Al1—O1	1.741(4)
Al1—O3	1.860(3)
Al1—O4	1.923(3)
Al2—O4	1.844(4)
Al2—Cl	2.166(2)
Al1—O2′	1.802(4)
Al1—O3′	1.895(3)
Al2—O2′	2.080(4)
Al2—O5	2.010(4)
Al2—C3	1.959(6)
Bond angles (°)	
O1-Al1-O4	93.47(16)
O3-Al1-O4	93.70(15)
O2′-Al1-O4	78.19(15)
O4-Al1-O3′	169.21(16)
O5-Al2-O2	160.64(16)
Tetrakis(2-phenoxy)ethene ligand dihedral angles (°)	
C2-C1-C11-C16	135.9(5)
C11-C1-C2-C41	–14.4(8)
C21-C1-C2-C31	–24.4(7)

The tetrakis(2-phenoxy)ethene ligand itself is highly distorted in the crystal structure (Fig. 2), with three phenoxy groups coordinating to Al1 and the other phenoxy group coordinating to Al1′. One of the phenoxy groups (O1) coordinated to Al1 is angled in towards the plane of the ethene bond (dihedral angle C2-C1-C11-C16: 135.9°) to bring that group into an equatorial binding position. This position resembles one of the transition states for the rotational isomerization of the tetraarylethene aryl ring (8). Simultaneously, the geminal phenoxy O2 is rotated outward into a position that allows the bridging of Al1′ and Al2′. As a result, the double bond is twisted between 14° and 24° to accommodate the metal binding (Table 1).

It is of interest to compare the observed bonding with that of the previously reported aluminum-fused bis-*p*-*tert*-butylcalix[4]arene (7). This structure was obtained by the reaction of the corresponding calix[4]arene with the tertiary amine adduct of aluminum hydride, and shows a sandwich ligand arrangement around a Al_2O_2 core similar to the crystal structure reported here. The calix[4]arene ligands, however, are only slightly distorted, presumably a function of the markedly different topology inherent to the [4]cyclophane structure. In contrast to the tetrakis(2-hydroxyphenyl)ethene derived complex, one calix[4]arene ligand binds all four phenoxy groups to a single, distorted, pentacoordinate aluminum atom.

The reaction of tetrakis(2-hydroxyphenyl)ethene with methylmagnesium chloride is of interest because it may be possible to isolate discrete, raft-like, magnesium complexes

[3] Supplementary data for this article are available on the Web site or may be purchased from the Depository of Unpublished Data, Document Delivery, CISTI, National Research Council Canada, Ottawa, ON K1A 0S2, Canada. DUD 4001. For more information on obtaining material refer to http://cisti-icist.nrc-cnrc.gc.ca/irm/unpub_e.shtml. CCDC 263379–263381 contain the crystallographic data for this manuscript. These data can be obtained, free of charge, via www.ccdc.cam.ac.uk/conts/retrieving.html (Or from the Cambridge Crystallographic Data Centre, 12 Union Road, Cambridge CB2 1EZ, UK; fax +44 1223 336033; or deposit@ccdc.cam.ac.uk).

© 2005 NRC Canada

Fig. 2. Alternate view of compound **3** from "above" the tetrakis(2-phenoxy)ethane ligand showing the variation in twisting of the phenyl rings.

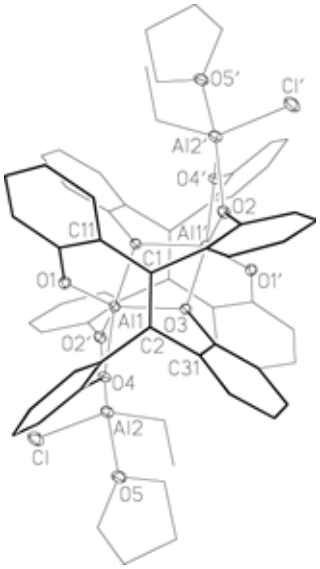
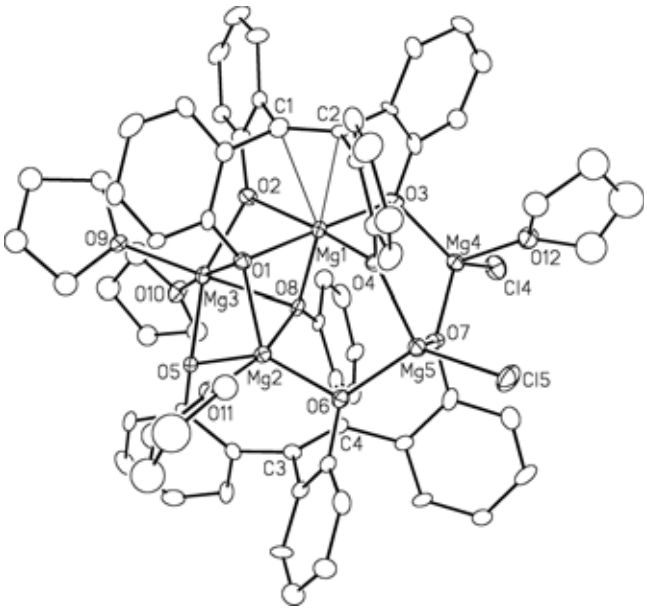


Fig. 3. Perspective view (ORTEP) of compound **4** showing the atom labeling scheme. Hydrogen atoms have been omitted for clarity. A weak interaction between Mg1 and the C1=C2 double bond is indicated by the thin Mg1-C1 and Mg1-C2 lines.



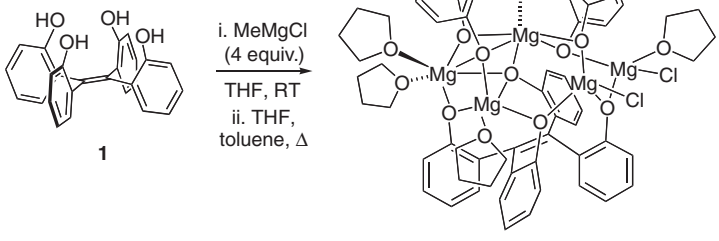
that could be used to introduce transition metals on the magnesium oxide like layer and study the catalytic behavior of such bimetallic heterogeneous catalyst models. However, even in the strongly coordinating solvent THF, the reaction between the Grignard reagent and tetrakis(2-hydroxyphenyl)ethene yields only sparingly soluble material, from which the unusual polymagnesiated complex **4** could be isolated by crystallization from hot THF – toluene (eq. [1]).

The crystal structure of compound **4** shows a sandwich of five magnesium atoms, with coordination numbers ranging from four to six, arrayed between two tetrakis(phenoxy)ethene molecules (Fig. 3). Such an arrangement minimizes intermolecular interactions and accommodates saturating the coordination demands of the magnesium cations; as a result, the cluster shows significant solubility. Unfortunately, the crystallographic analysis is hindered by the weak data set obtained and by the limited number of previously reported aryloxymagnesium solid-state structures (9).

In the crystal structure, Mg4 and Mg5 (Fig. 4) are four coordinate with a distorted tetrahedral geometry according to the wide range of O-Mg-Cl and O-Mg-O angles (see Supplementary information).[3] The observed Mg—O (avg. 1.97 Å), and Mg—Cl (avg. 2.27 Å) bond lengths are comparable to published bond lengths for Mg—μ-O (1.93–1.98 Å) and Mg—Cl (2.27 Å) in tetracoordinate magnesium structures (9). The Mg–THF coordination, Mg4—O12, with a bond length of 2.031(4) Å, also follows observations in the literature (9*e*). Pentacoordinate Mg2 has a distorted trigonal bipyramidal coordination with O_{eq}-Mg-O_{ax} angles ranging from 80.1° to 102.5°, and an O_{eq}-Mg-O_{eq} range of 90.6°–143.1° (see Supplementary information).[3] The Mg—O bond lengths are irregular, but more or less follow the behavior of metal alkoxides (9*e*): as the degree of bridging by an oxygen increases, so does the Mg—O bond length (Mg2—O1, Mg2—O8 > Mg2—O5, Mg2—O6; Table 2). Within the observed range, the Mg2—O8 bond length (2.241(12) Å) is much larger than the Mg2—O1 bond length (2.020(12) Å). This may be a ligand imposed effect or, possibly, a consequence of crystal packing forces. The observed Mg—O_{THF} bond length falls within the reported range of Mg–ether bonds (2.033–2.232 Å) (9*d*).

In the crystal structure, two hexacoordinate magnesium atoms are also present, Mg1 and Mg3 (Fig. 5), with a wide range of bond lengths (Mg—O: 1.973(12)–2.317(11) Å, lit. (9) value 2.0379–2.244 Å) and bond angles (O-Mg-O, cis: 77.6(4)°–106.7(5)°, lit. (9) value 78.4°–85.5°; see Supplementary information).[3] No π complexes of an olefin with Mg are known, but the data presented here do not support a definitive Mg–ethene interaction. First, the shortest Mg1—C

[1]



1 **4**

© 2005 NRC Canada

Fig. 4. Alternate view of compound **4**, omitting thermal ellipsoids for the carbon atoms, emphasizing the coordination environment for Mg2, Mg4, and Mg5.

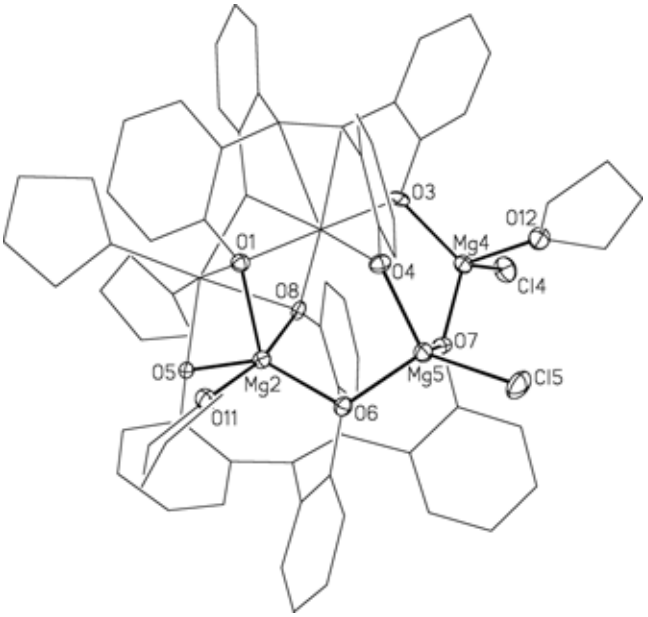
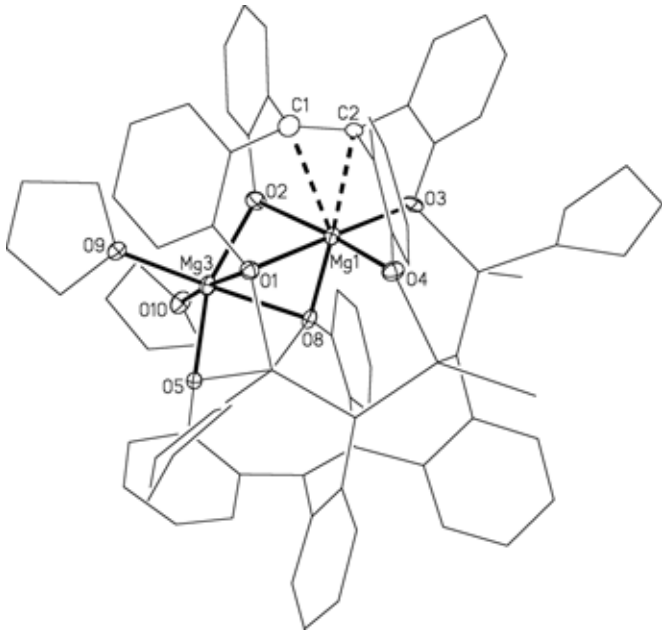


Table 2. Key bond lengths (Å), angles (°), and dihedral angles (°) for magnesium complex **4**.

Mg1, Mg3 (hexacoordinated) bond lengths (Å)	
C1—Mg1	2.530(17)
C2—Mg1	2.514(17)
Mg2 (pentacoordinated) bond lengths (Å)	
Mg2—O1	2.020(12)
Mg2—O6	1.994(11)
Mg2—O11	2.069(13)
Mg2—O5	1.994(11)
Mg2—O8	2.241(12)
Mg4, Mg5 (tetracoordinated) bond lengths (Å)	
Mg4—O12	2.031(13)
Tetrakis(2-phenoxy)ethene ligands dihedral angles (°)	
C51-C3-C4-C71	–154(16)
C51-C3-C4-C81	21(3)
C1-C2-C31-C36	97(2)
C1-C2-C41-C42	94(2)
C3-C4-C71-C76	61(2)
C3-C4-C81-C82	74(2)
C11-C1-C2-C41	–1(3)
C61-C3-C4-C71	18(3)
C61-C3-C4-C81	–166.6(16)
C2-C1-C21-C22	107(2)
C2-C1-C11-C16	103.3(19)
C4-C3-C51-C56	82(2)
C4-C3-C61-C62	58(2)

distance (2.514(17) Å) is well beyond the Mg—C bond distances observed for an alkyne complex (10*d*), although within the range of Mg—(π-C) bonds observed for magnesium-cyclopentadienyl interactions (10*a*–10*c*). Secondly, the position of the Mg relative to a plane defined by O1-O2-O3-O4 is 0.1 Å *further away* from the ethene bond.

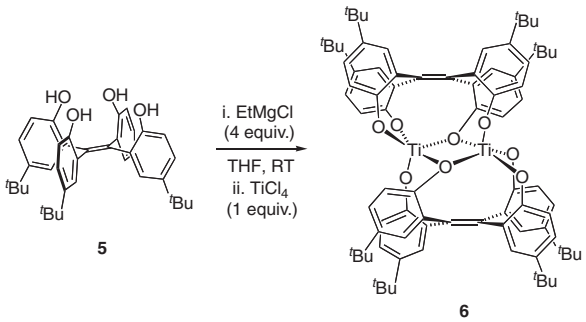
Fig. 5. Alternate view of compound **4**, omitting thermal ellipsoids for the carbon atoms, emphasizing the coordination environment for Mg1 and Mg3. A weak interaction between Mg1 and the C1, C2 double bond is indicated by dashed lines. The distance between Mg1 and the center of the C1, C2 double bond is 2.432 Å.



The tetraarylethene framework involved in bonding to Mg1 shows minimal distortion of the C1—C2 ethene bond, with phenyl ring – ethene bond dihedral angles ranging from 94° to 107° (Table 2) and Mg1—O bond lengths ranging from 1.973(12) to 2.120(11) Å (see Supplementary information).[3] The second tetraarylethene moiety centered around C3—C4 shows a distorted double bond and an irregular phenyl ring twist motif (Table 2). As observed for the aluminum compound, the metal coordination preferences appear to dictate the ligand geometry and binding.

The direct approach to forming Mg–Ti bimetallic procatalysts was attempted by using nonheterogeneous conditions for in situ generation of the magnesium salt of the more soluble ligand tetrakis(2-hydroxy-5-*tert*-butylphenyl)ethene (**5**) (1*a*). Thus, the magnesium salt was generated in THF, followed by the addition of $TiCl_4$ (eq. [2]). Unfortunately, crystallization did not result in isolation of a bimetallic Ti–Mg compound, producing instead a homobimetallic titanitum complex. The crystal structure of dititanium complex **6** is quite similar to the aluminum and magnesium sandwich complexes **3** and **4** (Fig. 6). Trapped

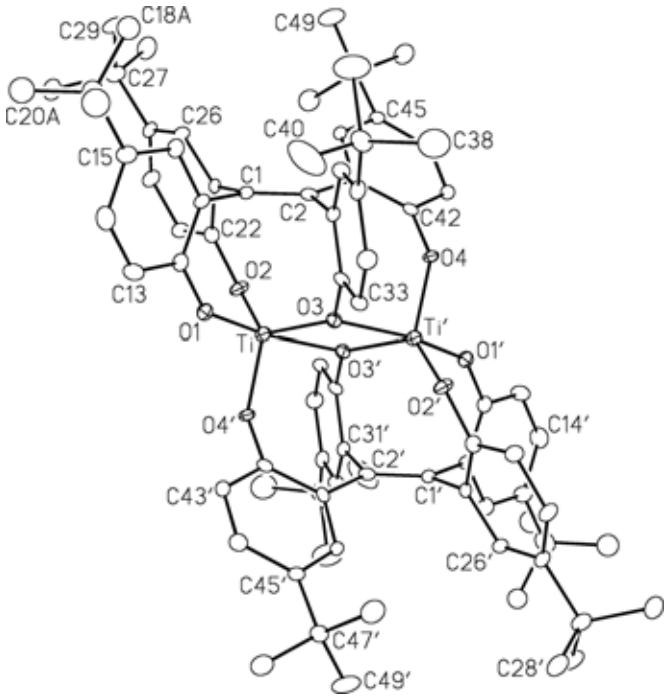
[2]



5 **6**

© 2005 NRC Canada

Fig. 6. Perspective view (ORTEP) of compound **6** showing the atom labeling scheme. Hydrogen atoms are not shown. Primed atoms are related to unprimed ones via the crystallographic inversion center (0, 0, 0) at the center of the molecule.



between two tetraarylethene units are two titanium atoms in a centrosymmetric arrangement. No coordinating solvent molecules or magnesium chloride fragments are present. The observed Ti—O bond lengths are within the expected range (lit. (11, 12) value 1.809–1.937 Å, Table 3), except for the Ti—O3′ bond length (2.122(4) Å), which is significantly longer. If four coordination is assumed, the Ti—O1, O2, O4′, and O3 bond lengths should be approximately the same, which is the case. However, the observed bond angles of O1-Ti-O3 (93.93°) and O2-Ti-O3 (128.11°) show significant deviations from true tetrahedral geometry. The deviation could be due to ligand-imposed restrictions on the O2-Ti-O3 angle, given that the O2 and O3 are positioned across the ethene bond, but this argument does not appear to apply to the O1-Ti-O3 angle. If instead a pentacoordinate titanium is assumed, the variation in the Ti—O_{axial} and Ti—$O_{equatorial}$ bond lengths become apparent, as well as the irregularity of O_{eq}-Ti-O_{eq} and O_{eq}-Ti-O_{ax} bond angles (see Table 3). On this basis, the metals in complex **6** may best be considered five-coordinate, albeit distorted. The dilemma with regard to coordination of the titanium atoms is similar to that reported for a *p-tert*-butylcalix[4]arene titanium complex (12). This structure, obtained from the reaction of $Ti(NMe_2)_4$ with *p-tert*-butylcalix[4]arene, shows two tetracoordinated titanium atoms between two calix[4]arene ligands. The authors opted for tetracoordination on the basis of a weak Ti—O bridging interaction (2.473 Å), a significantly longer bond than that observed for Ti—O3′ in complex **6** (2.122(4) Å) (Table 3).

The tetraarylethene framework also shows distortion in the planarity of the ethene bond, with a dihedral angle range of 7.6°–10.6°. Three of the phenyl ring – ethene bond dihedral angles fall in the range of 76°–88°, the fourth ring is significantly tilted towards the ethene bond plane with a dihedral angle of 37° (Table 3). A similar combination of a single phenyl ring and double bond torque is also observed in aluminum complex **3**.

Table 3. Key bond lengths (Å), angles (°), and dihedral angles (°) for titanium complex **6**.

Bond lengths (Å)	
Ti—O1	1.812(4)
Ti—O2	1.806(4)
Ti—O4′	1.813(4)
Ti—O3	1.934(4)
Ti—O3′	2.122(4)
Bond angles (°)	
O1-Ti-O3	93.93(19)
O1-Ti-O4′	102.43(19)
O1-Ti-O3′	166.14(19)
O2-Ti-O3	128.11(18)
O2-Ti-O4′	112.12(19)
O3-Ti-O4′	112.53(18)
Tetrakis(2-phenoxy)ethene ligands dihedral angles (°)	
C11-C1-C2-C41	–172.5(5)
C11-C1-C2-C31	7.6(8)
C1-C2-C41-C46	36.8(8)
C1-C2-C31-C32	88.1(7)
C21-C1-C2-C31	–169.3(6)
C21-C1-C2-C41	10.6(10)
C2-C1-C21-C22	76.2(8)
C2-C1-C11-C16	95.1(7)

Conclusion

In all cases reported here, ligand dimers surrounding a set of metal atoms rather than raft-like surface analogues are isolated. In this way, intermolecular interactions are minimized to produce the solubility required for crystallization. The tetrakis(2-aryloxy)ethene ligands incorporated in these structures show a surprising flexibility in both ethene bond torsion and aryl ring twist. Taken together, the limited solubility of the initially obtained metal–ligand complexes, the preferential formation of pseudo-dimeric products, and the pronounced deformation of the ligand geometry all suggest that modification of the ligand system (1*b*) is required to prevent indiscriminate ligand–metal interactions. The results of such ligand modifications on the ligand–metal coordination will be reported in forthcoming publications.

Experimental

Reagents and solvents

All solvents were distilled from appropriate drying agents under nitrogen. The tetrakis(2-hydroxyaryl)ethene ligands were prepared by published procedures (1).

General methods

All manipulations were carried out in oven-dried glassware, under a dry and oxygen-free nitrogen atmosphere using a Vacuum Atmospheres drybox. Spectroscopic and elemental analyses to establish the identity and purity of bulk samples were severely constrained by a combination of very

© 2005 NRC Canada

Table 4. Crystallographic experimental details.

Crystal	Complex **3**	Complex **4**	Complex **6**
Empirical formula	$C_{78}H_{74}Al_4Cl_2O_{10}$	$C_{77}H_{76}Cl_2Mg_5O_{12.5}$	$C_{98}H_{112}O_8Ti_2$
Formula mass	1350.19	1 393.83	1513.68
Crystal habit	Colorless, block	Colorless, block	Plates, red-brown
Crystal dimensions (mm^3)	0.27 × 0.23 × 0.21	0.19 × 0.10 × 0.09	0.20 × 0.08 × 0.06
Crystal system	Triclinic	Orthorhombic	Monoclinic
Space group	$P\bar{1}$ (No. 2)	$Pna2_1$ (No. 33)	$P2_1/c$ (No. 14)
Z	1	4	2
Unit cell parameters			
a (Å)	12.184 0 (13)	24.781 2 (16)	12.325 6 (16)
b (Å)	12.890 7 (18)	20.720 9 (16)	23.396 (3)
c (Å)	13.556 8 (13)	14.849 5 (11)	15.248 4 (17)
α (°)	66.485 (9)		
β (°)	87.343 (8)		107.982 (3)
γ (°)	62.822 (9)		
Collection ranges	$-14 \le h \le 0$,	$-27 \le h \le 31$,	$-15 \le h \le 15$,
	$-13 \le k \le 12$,	$-25 \le k \le 25$,	$-29 \le k \le 29$,
	$-16 \le l \le 16$	$-17 \le l \le 18$	$-15 \le l \le 19$
Temperature (K)	213	193	193
Volume ($Å^3$)	1712.6 (3)	7 625.1 (10)	4182.4 (9)
$D_{calcd.}$ (g cm^{-3})	1.309	1.214	1.202
Diffractometer	Siemens P4/RA	Bruker P4/RA/SMART 1000 CCD	Bruker P4/RA/SMART 1000 CCD
Radiation (λ, Å)	Graphite-monochromated Mo Kα (0.710 73)	Graphite-monochromated Mo Kα (0.710 73)	Graphite-monochromated Mo Kα (0.710 73)
Scan type		φ Rotations (0.3°) / ω scans (0.3°) (30 s exposures)	φ Rotations (0.3°) / ω scans (0.3°) (30 s exposures)
Absorption coeff. (μ, mm^{-1})	0.207	0.185	0.248
Absorption correction	Semi-empirical (ψ scans)	Multi-scan (SADABS)	Multi-scan (SADABS)
Data collection 2θ limit (°)	50.00	52.80	52.88
Observed reflections (*NO*)	3333 ($F_o^2 \ge 2\sigma(F_o^2)$)	4 463 ($F_o^2 \ge 2\sigma(F_o^2)$)	2426 ($F_o^2 \ge 2\sigma(F_o^2)$)
Independent reflections	5519 (R_{int} = 0.040 7)	15 313 (R_{int} = 0.256 3)	8559 (R_{int} = 0.241 6)
Data/restraints/parameters	5519 ($F_o^2 \ge -3\sigma(F_o^2)$) / 6 / 386	15 313 ($F_o^2 \ge -3\sigma(F_o^2)$) / 10 / 784	8559 ($F_o^2 \ge -3\sigma(F_o^2)$) / 6 / 436
Goodness-of-fit (*S*)	1.013 ($F_o^2 \ge -3\sigma(F_o^2)$)	0.887 ($F_o^2 \ge -3\sigma(F_o^2)$)	0.812 ($F_o^2 \ge -3\sigma$ (F_o^2))
Final R indices	R_1 [$F_o^2 \ge 2\sigma(F_o^2)$] = 0.074 7,	R_1 [$F_o^2 \ge 2\sigma(F_o^2)$] = 0.086 4,	R_1 [$F_o^2 \ge 2\sigma(F_o^2)$] = 0.072 5,
	wR_2 [$F_o^2 \ge -3\sigma(F_o^2)$] = 0.182 0	wR_2 [$F_o^2 \ge -3\sigma(F_o^2)$] = 0.282 8	wR_2 [$F_o^2 \ge -3\sigma(F_o^2)$] = 0.180 5
Largest difference peak and hole (e $Å^{-3}$)	0.749 and –0.569	0.811 and –0.382	0.498 and –0.586

low solubility (complexes **3** and **4**) and systematic inconsistencies in the analytical data obtained from combustion elemental analyses. The latter may arise either from bulk heterogeneity or from incomplete combustion (presumably a consequence of metal oxide formation), difficulties common to the coordination complexes of highly electrophilic metals. To some extent, such problems mirror those identified in the coordination chemistry of the calix[4]arenes.

Tetraaluminum complex 3

To a stirred suspension of 37 mg (0.1 mmol) tetrakis(2-hydroxyphenyl)ethene in 10 mL pentane was added 245 mg (0.5 mmol) Et_2AlCl as a 25 wt% solution in toluene diluted in 5 mL pentane. A bright yellow suspension formed. No ethane formation was observed. After stirring overnight, the solvent was removed under vacuum and the remaining residue resuspended in pentane. After removal of the pentane by decanting, a solid was obtained that, after crystallization from toluene at –30 °C in a glovebox freezer, yielded crystals of insufficient quality and size. This material was redissolved in toluene with the addition of a small amount of THF, from which crystals of sufficient quality for X-ray diffraction were obtained at –30 °C.

Polymagnesium complex 4

A solution of 0.12 g (0.3 mmol) of tetrakis(2-hydroxyphenyl)ethene in 12 mL THF was added to 0.5 mL (1.2 mmol) of a rapidly stirred solution of 3 mol/L methylmagnesium chloride solution in Et_2O. After 12 h at room temperature, the solvents were removed under vacuum and the resulting solid resuspended in a small amount of THF. After removal of soluble by-products by decanting, the remaining solid was dissolved in a minimum of boiling THF. After addition of toluene, crystals of sufficient quality for an X-ray diffraction study were obtained by leaving the solution undisturbed at room temperature for several days.

© 2005 NRC Canada

Dititanium complex 6

A solution of 0.12 g (0.2 mmol) of tetrakis(2-hydroxy-5-*tert*-butyl-phenyl)ethene in 10 mL of THF was slowly added to a stirred THF solution (10 mL) of EtMgCl (70 mg, 0.8 mmol). After stirring for 1 h at room temperature, a solution of 65 mg (0.2 mmol) $TiCl_4$·2THF dissolved in 3 mL THF was added. After stirring for 12 h at room temperature, the solution was reduced in vacuo to 5 mL and 20 mL pentane was added. The precipitate obtained was isolated from the supernatant by decanting and washed with and additional 20 mL of pentane. The solid was extracted with 40 mL of toluene and the resulting deep red solution reduced in vacuo to 5 mL. Crystals of sufficient quality for an X-ray diffraction study were obtained after repeated recrystallizations from toluene at –30 °C.

X-ray crystallographic analysis

Crystals obtained as described were mounted on a glass fiber from a pool of Paratone-N and immediately placed under a cold nitrogen stream and mounted on the diffractometer. Diffraction data were collected on Siemens P4/RA (compound **3**) or Bruker P4/RA/SMART 1000 CCD (compounds **4** and **6**) using Mo Kα radiation (Table 4); details are reported as Supplementary information.[3] For compound **3**, unit cell parameters were obtained from least-squares refinement of 44 reflections with $22.0° < 2\theta < 24.8°$. Unit cell parameters for compounds **4** and **6** were obtained from least-squares refinement of 5270 and 3028 centered reflections, respectively. The data for compound **3** were semi-empirically corrected for absorption. The data for compounds **4** and **6** were absorption corrected using the SADABS procedure (15). The structures of compounds **3** and **6** were solved using the SHELXS-86 program (13), the refinement method was a full-matrix least-squares on F^2 using the program SHELXL-93 (14). For compound **3**, distances involving the methyl carbons of the inversion-disordered solvent toluene molecules were given fixed idealized values. For compound **6**, the methyl carbon positions of the disordered solvent toluene molecule were refined in idealized positions by fixing $d(C_{methyl}—C_{ipso})$ = 1.54 Å and $d(C_{methyl}\cdots C_{ortho})$ = 2.54 Å. The toluene ring carbons were refined as idealized hexagons with d(C—C) = 1.39 Å. For compound **4**, the structure solution program used was a DIRDIF-96 (16) and the refinement program SHELXL-93 (14). An idealized geometry was imposed upon the solvent THF. Full details of the crystal structure determinations are included as Supplementary information.[3]

Acknowledgement

Financial support from NOVA Chemicals Corporation and the Natural Sciences and Engineering Research Council of Canada (NSERC, CRD and CRO grant programs) is gratefully acknowledged.

References

1. (*a*) U.H. Verkerk, M. Fujita, T.L. Dzwiniel, R. McDonald, and J.M. Stryker. J. Am. Chem. Soc. **124**, 9988 (2002); (*b*) M. Fujita, G. Qi, U.H. Verkerk, T.L. Dzwiniel, R. McDonald, and J.M. Stryker. Org. Lett. **6**, 2653 (2004).
2. (*a*) C.D. Gutsche. Calixarenes. Royal Society of Chemistry, Cambridge, UK. 1989; (*b*) Z. Asfari, V. Böhmer, J. Harrowfield, and J. Vicens (*Editors*). Calixarenes 2001. Kluwer Academic, Dordrecht, The Netherlands. 2001.
3. (*a*) D.M. Roundhill. Prog. Inorg. Chem. 533 (1995); (*b*) C. Wieser, C.B. Dieleman, and D. Matt. Coord. Chem. Rev. **165**, 93 (1997); (*c*) C. Floriani and R. Floriani-Moro. Adv. Organomet. Chem. **47**, 167 (2001); (*d*) F.T. Ladipo, V. Sarveswaran, J.V. Kingston, R.A. Huyck, S.Y. Bylikin, S.D. Carr, R. Watts, and S. Parkin. J. Organomet. Chem. **689**, 502 (2004).
4. R.A. Kemp, D.S. Brown, M. Lattman, and J. Li. J. Mol. Catal. A: Chem. **149**, 125 (1999).
5. (*a*) P. Pino and R. Mülhaupt. Angew. Chem. Int. Ed. Engl. **19**, 857 (1980); (*b*) E. Albizzati, U. Giannini, G. Collina, L. Noristi, and L. Resconi. *In* Polypropylene handbook: Polymerization, characterization, properties, applications. *Edited by* E.P. Moore. Hanser Publications, New York. 1996. pp. 11–111.
6. (*a*) M.D. Healy, D.A. Wierda, and A.R. Barron. Organometallics, **7**, 2543 (1988); (*b*) B. Cetinkaya, P.B. Hitchcock, H.A. Jasim, M.F. Lappert, and H.D. Williams. Polyhedron, **9**, 239 (1990); (*c*) R. Kumar, M.L. Sierra, V.S. de Mel, and J.P. Oliver. Organometallics, **9**, 484 (1990); (*d*) R.C. Mehrotra and A.K. Rai. Polyhedron, **10**, 1967 (1991); (*e*) M.D. Healy, J.W. Ziller, and A.R. Barron. Organometallics, **11**, 3041 (1992).
7. J.L. Atwood, S.G. Bott, C. Jones, and C.L. Raston. J. Chem. Soc. Chem. Commun. 1349 (1992).
8. (*a*) R. Willem, H. Pepermans, K. Hallenga, M. Gielen, R. Dams, and H.J. Geise. J. Org. Chem. **48**, 1890 (1983); (*b*) Z. Rappoport and S.E. Biali. Acc. Chem. Res. **30**, 307 (1997).
9. (*a*) H.L. Uhm. *In* Handbook of Grignard reagents. *Edited by* G.S. Rakita. Marcel Dekker, New York. 1996. Chap. 9; (*b*) C.A. Zechmann, T.J. Boyle, M.A. Rodriguez, and R.A. Kemp. Polyhedron, **19**, 2557 (2000); (*c*) P. Sobota, J. Utko, K. Sztajnowska, J. Ejfler, and L.B. Jerzykiewicz. Inorg. Chem. **39**, 235 (2000); (*d*) G. Guillemot, E. Solari, C. Rizzoli, and C. Floriani. Chem. Eur. J. **8**, 2072 (2002); (*e*) K.W. Henderson, G.W. Honeyman, A.R. Kennedy, R.E. Mulvey, J.A. Parkinson, and D.C. Sherrington. J. Chem. Soc. Dalton Trans. 1365 (2003).
10. (*a*) J.L. Atwood and K.D. Smith. J. Am. Chem. Soc. **96**, 994 (1974); (*b*) P. Jutzi. Adv. Organomet. Chem. **26**, 217 (1975); (*c*) C. Johnson, J. Toney, and G.D. Stucky. J. Organomet. Chem. **40**, C11 (1975); (*d*) S.I. Troyanov, V. Varga, and K. Mach. Organometallics, **12**, 2820 (1993).
11. (*a*) S.G. Bott, A.W. Coleman, and J.L. Atwood. J. Chem. Soc. Chem. Commun. 610 (1986); (*b*) A.G. Orpen, L. Brammer, F.H. Allen, O. Kennard, D.G. Watson, and R. Taylor. J. Chem Soc. Dalton Trans. S1 (1989); (*c*) W. Clegg, M.R.J. Elsegood, S.J. Teat, C. Redshaw, and V.C. Gibson. J. Chem. Soc. Dalton Trans. 3037 (1998).
12. M.M. Olmstead, G. Sigel, H. Hope, X. Xu, and P.P. Power. J. Am. Chem. Soc. **107**, 8087 (1985).
13. G.M. Sheldrick. Acta Crystallogr. Sect. A, **A46**, 467 (1990).
14. G.M. Sheldrick. SHELXL-93 [computer program]. University of Göttingen, Göttingen, Germany. 1993.
15. G.M. Sheldrick. SADABS [computer program]. University of Göttingen, Göttingen, Germany. 1996.
16. P.T. Beurskens, G. Beurskens, W.P. Bosman, R. de Gelder, S. Garcia Granda, R.O. Gould, R. Israel, and J.M.M. Smits. The DIRDIF-96 program system. Crystallography Laboratory, University of Nijmegen, Nijmegen, The Netherlands. 1996.

© 2005 NRC Canada

Synthesis and conformational analysis of disaccharide analogues containing disulfide and selenosulfide functionalities in the interglycosidic linkages[1]

Nagasree Chakka, Blair D. Johnston, and B. Mario Pinto

Abstract: The synthesis of novel disaccharides containing disulfide (methyl-4-*S*-(β-D-galactopyranosyl-1′-thio)-4-thio-α-D-glucopyranoside (**1**)) and selenosulfide (methyl-4-*Se*-(β-D-galactopyranosyl-1′-thio)-4-seleno-α-D-glucopyranoside (**2**)) functionalities in the interglycosidic linkages is described. The synthetic strategy relied on the reaction of a β-glycosylthiosulfonate with a carbohydrate thiol or selenol nucleophile. The resulting protected β-dihetero-linked disaccharides were deprotected to give the target compounds. The conformational preferences of these dihetero analogues were inferred from NOESY experiments and line-broadening effects in variable-temperature NMR spectra, and are rationalized in terms of molecular orbital theory. Low-energy conformations of these compounds can populate regions of conformational space not usually occupied by β-linked disaccharides, and offer the possibility for presentation of novel ligand topographies.

Key words: disaccharides, disulfides, selenosulfides, interglycosidic linkages, conformations, MO explanation.

Résumé : On décrit la synthèse de nouveaux disaccharides comportant des fonctionnalités disulfure (4-*S*-(β-D-galactopyranosyl-1′-thio)-4-thio-α-D-glucopyranoside de méthyle (**1**)) et sélénosulfure (4-*Se*-(β-D-galactopyranosyl-1′-thio)-4-séléno-α-D-glucopyranoside de méthyle (**2**)) dans les liaisons interglycosidiques. La stratégie de synthèse se base sur la réaction d'un β-glycosylthiosulfonate avec un carbohydrate comportant un nucléophile thiol ou sélénol. Les disaccharides protégés à liaison β-dihétéro ont été déprotégés pour fournit les composés cibles. Les préférences conformationnelles de ces analogues dihétéro ont été déduites d'expériences « NEOSY » et d'effets d'élargissement de bande dans les spectres de RMN à température variable et elles sont rationalisées en fonction de la théorie des orbitales moléculaires. Les conformations de basse énergie de ces composés occuper des régions de l'espace conformationnel qui ne sont généralement pas occupés par des disaccharides à liaisons β et elles offrent la possibilité de présenter de nouvelles topographies pour les ligands.

Mots clés : disaccharides, disulfures, sélénosulfures, liaisons interglycosidiques, conformations, explication d'orbitales moléculaires.

[Traduit par la Rédaction]

Introduction

Carbohydrates and carbohydrate mimetics are essential tools for the investigation of a variety of biological functions that are mediated by carbohydrate recognition events (1, 2). Furthermore, some of these compounds are known to be therapeutic agents (3–7). It is therefore of interest to examine novel types of carbohydrate derivatives or mimetics to expand the collection of potential drug candidates. The next level of carbohydrate mimetic design should include the potential for presentation of different conformational families on the potential energy surface. Such an approach should provide access to an alternative selection of ligand topographies that might have advantages in drug design.

In general, the conformational preferences about glycosidic linkages in oligosaccharides can be described by the ϕ and ψ torsional angles, as shown in Fig. 1. Excursions about the ψ torsional angles in α- and β-glycosides are pronounced, and are dictated by the exact steric requirements about a particular glycosidic linkage (8). However, the preferences about the ϕ torsional angle are much more restricted by the endo- (9) and exo- (10) anomeric effect. Thus, the preferences in α-glycosides are largely restricted to a ϕ_H gauche+ conformation, whereas those in β-glycosides are re-

Received 4 October 2004. Published on the NRC Research Press Web site at http://canjchem.nrc.ca on 10 August 2005.

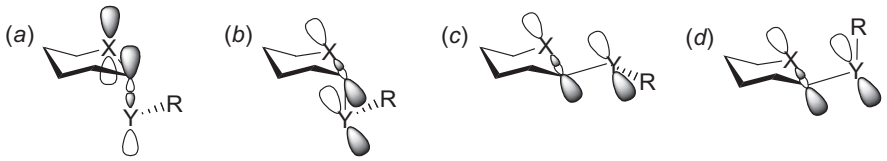
Dedicated to Howard Alper for his contributions to chemistry.

N. Chakka, B.D. Johnston, and B.M. Pinto.[2] Department of Chemistry, Simon Fraser University, Burnaby, BC V5A 1S6, Canada.

[1]This article is part of a Special Issue dedicated to Professor Howard Alper.
[2]Corresponding author (e-mail: bpinto@sfu.ca).

 doi: 10.1139/V05-107 © 2005 NRC Canada

Fig. 1. Stabilizing orbital interactions associated with (*a*) the endo-anomeric effect and (*b*), (*c*), (*d*) the exo-anomeric effect.



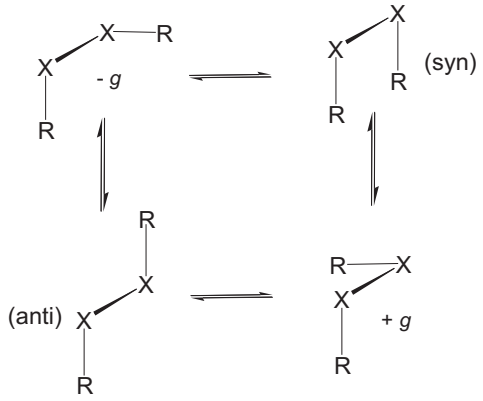
stricted to the ϕ_H gauche– conformation, dictated by the exo-anomeric effect (see structures *b* and *c* in Fig. 1), other conformations about the exocyclic C–O linkage being minimally populated (11).

Thus far, carbohydrate heteroanalogues have been used to advantage to gain access to alternative conformational preferences. For example, disaccharides containing 5-thio sugars, i.e., a sulfur atom in the ring, with different heteroatoms in the interglycosidic linkage, show population of conformations with different ϕ torsional angles (12), and thiooligosaccharides, i.e., those containing a sulfur atom in the interglycosidic linkage, e.g., thiocellobiose, show variations in both ϕ and ψ angles (13). Similarly, the pseudodisaccharide moiety in the tetrasaccharide dihydroglucoacarbose, containing a nitrogen atom in an α-glycosidic linkage, also displays variations in the ψ angle when free in solution (14). However, examples of β-glycosides containing ϕ angles that differ from the gauche conformation shown, e.g., a ϕ_H anti conformation (structure *d* in Fig. 1), have been elusive (15). It is worthy of note that the ϕ_H anti conformation will still permit operation of the exo-anomeric effect, i.e., the $n_Y \rightarrow \sigma^*_{C-X}$ stabilizing orbital interaction.

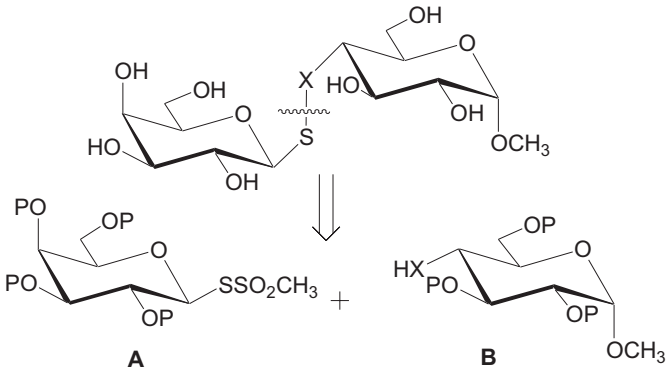
We were intrigued by the reported conformational preferences of oligosaccharides containing dihetero functionalities in the interglycosidic linkage, for example, those about the N–O glycosidic linkage in the naturally occurring calicheamycins (16), a family of enediyne antitumor antibiotics. These newly discovered compounds with unusual molecular structure have striking biological activity. This unusual N–O linkage has attracted the attention of several groups, and disaccharide mimics wherein two monosaccharide units are linked by a N—O bond have recently been reported (17–19). We propose here to investigate the corresponding compounds containing the S–S and S–Se functionalities in the glycosidic linkages.

Fraser et al. (20) have reported a variable-temperature NMR study of the effects of substitution on the barriers to rotation about the sulfur–sulfur bond in acyclic disulfides, and proposed that interconversion between the preferred ground-state enantiomeric +*g* and –*g* conformations proceeds by way of either syn or anti transition states (Fig. 2). A study of the influence of structure on the height of the interconversion barrier for a series of different R groups showed that the syn transition state, previously assumed to be less stable, was actually of lower energy than the anti transition state. The barrier to rotation about the S—S bond was found to increase from E_a = 7.0 to E_a = 9.4 kcal/mol with an increase in substituent size. The apparent steric rate retardation was explained in terms of a strong preference for the syn over the anti transition state. However, Jorgensen and Snyder (21) concluded on the basis of molecular mechanics calculations on dialkyl disulfides that rotation proceeds by way of an anti transition state. Although syn/anti

Fig. 2. Interconversion between preferred ground-state conformations.



Scheme 1.



X = S for disulfide **1**

X = Se for selenosulfide **2**

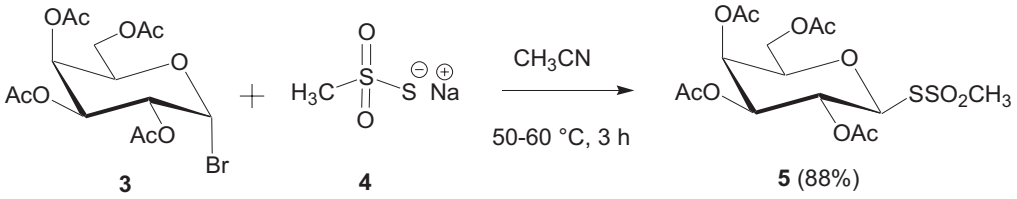
P = protecting group

barriers for simple, uncongested disulfides (e.g., HSSH and CH_3SSCH_3) have been computed at various levels of sophistication (22), the anti energy maximum was always lower than the syn energy maximum. Our own previous study of restricted rotation in hindered dichalcogenides showed that diselenides and ditellurides exhibit similar conformational preferences to disulfides (23).

We chose to examine in detail the conformational preferences in β-linked disaccharides containing disulfide and selenosulfide moieties in the interglycosidic linkage and report herein that these compounds take up the nomal ϕ_H gauche+ conformation about the C-1′—S bond but exhibit restricted rotation about the S—X bond and preferentially populate either the (+*g*) or the (–*g*) conformation about this linkage. Szilágyi et al. (24) and Davis et al. (25) have separately reported the syntheses of symmetric, nonreducing di-

© 2005 NRC Canada

Scheme 2.



saccharides containing interglycosidic (1→1′) disulfide linkages; these compounds also display unusual conformational preferences. In addition, the syntheses of monosaccharides containing sulfenamide aglycons have been described recently (26).

Results and discussion

Synthesis

Retrosynthetic analysis of the target compounds showed that they could be synthesized by the coupling reaction of monosaccharide **A** (a glycosylthio donor) with a monosaccharide **B** containing an appropriate nucleophile at C-4 (Scheme 1).

The synthesis of the glycosyl donor **5** was first attempted by the reaction of acetobromogalactopyranose **3** with sodium thiomesylate **4** (27, 28) in ethanol, as described for the corresponding glucose derivative (29). No desired product was observed even after refluxing. A similar result was obtained when DMF was used as the solvent. However, the displacement reaction proceeded smoothly in acetonitrile at room temperature, to give thiomesylate **5** (Scheme 2).

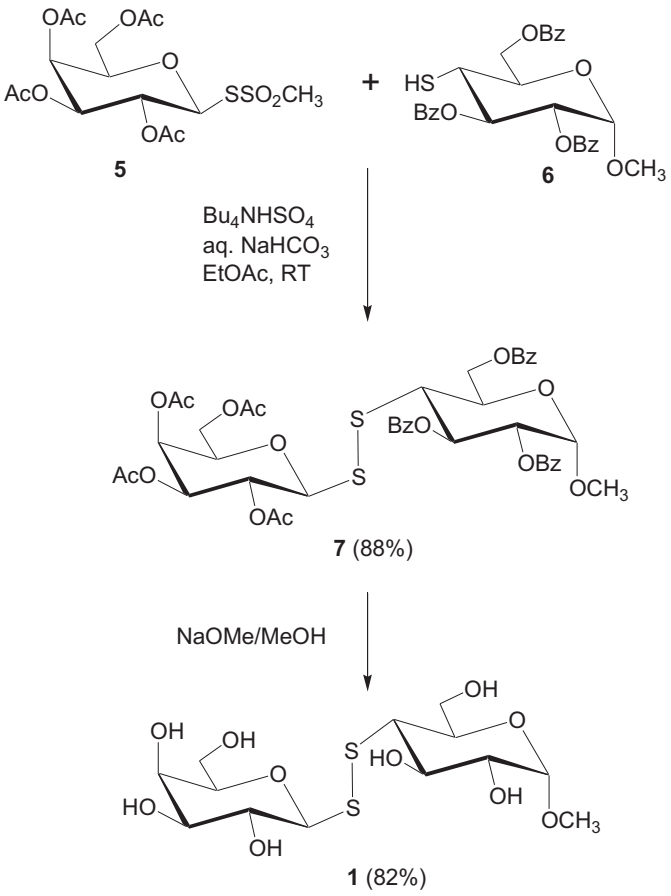
The coupling reaction of thiomesylate **5** with thiol **6** (30) in the presence of a phase-transfer catalyst (tetrabutylammonium hydrogensulfate) and saturated aqueous sodium bicarbonate in EtOAc at room temperature gave the (1′→4) disulfide **7** in excellent yield (Scheme 3). Methanolysis then afforded the target disulfide **1**.

Analogously, the coupling reaction of thiomesylate **5** with selenol **8** (31) gave selenosulfide **9**, (4→4′) diselenide **10** being formed as an oxidative by-product. The target selenosulfide **2** was obtained by deprotection of compound **9** by methanolysis. Similarly, diselenide **11** was obtained by deprotection of (4→4′) diselenide **10** under Zemplén conditions (Scheme 4).

Conformational analysis

The conformational preferences of compounds **7** and **9** may be defined in terms of the φ, ψ, and ω angles shown in Fig. 3. These preferences were probed by means of ^{1}H NMR spectroscopy. The NOESY spectrum for each compound showed cross peaks for H-3/H-1′, H-3/H-5′, and OCH_3/H-5′, in addition to the cross peaks generally expected for the two monosaccharide units. COSY-type cross peaks for strongly coupled resonances could be distinguished from true NOESY correlations by their anti-phase character. The specific NOESY cross peaks suggest that the disaccharides have a preferred –gauche (–*g*) conformation about the ψ angle, although the ω angle could not be defined explicitly with the limited number of observed NOE cross peaks (Fig. 3). A more rigorous analysis by computational methods in the absence of experimental data did not seem warranted for the purposes of this study. Inspection of molecular models suggested that the observed NOEs would be consistent with a conformation in which the $C_1'SXC4$ (X = S, Se) torsion angle is about –60° (Fig. 3). Our assignment of conformational preferences is consistent with those reported by Szilágyi et al. (24) for 1→1′-linked disaccharides containing a disulfide moiety in the interglycosidic linkage.

Scheme 3.



The ^{1}H NMR spectra for compounds **7** and **9** in deuterated toluene showed broad resonances for H-1′, H-5′, H-6A′, and H-6B′ in ring **A**, suggesting that there is exchange on the NMR timescale between conformations in the intermediate exchange regime at room temperature. Heating the samples to about 350 K led to sharp NMR signals, as indicated in Fig. 4 for the case of **7**. As the temperature was lowered below room temperature, the spectra showed coalescence behaviour and eventually, below 200 K, resolution into resonances for two separate conformers at the slow-exchange limit. The ratio of the major conformer to the minor conformer was 3:1 based on integrations of the separate H-4

© 2005 NRC Canada

Scheme 4.

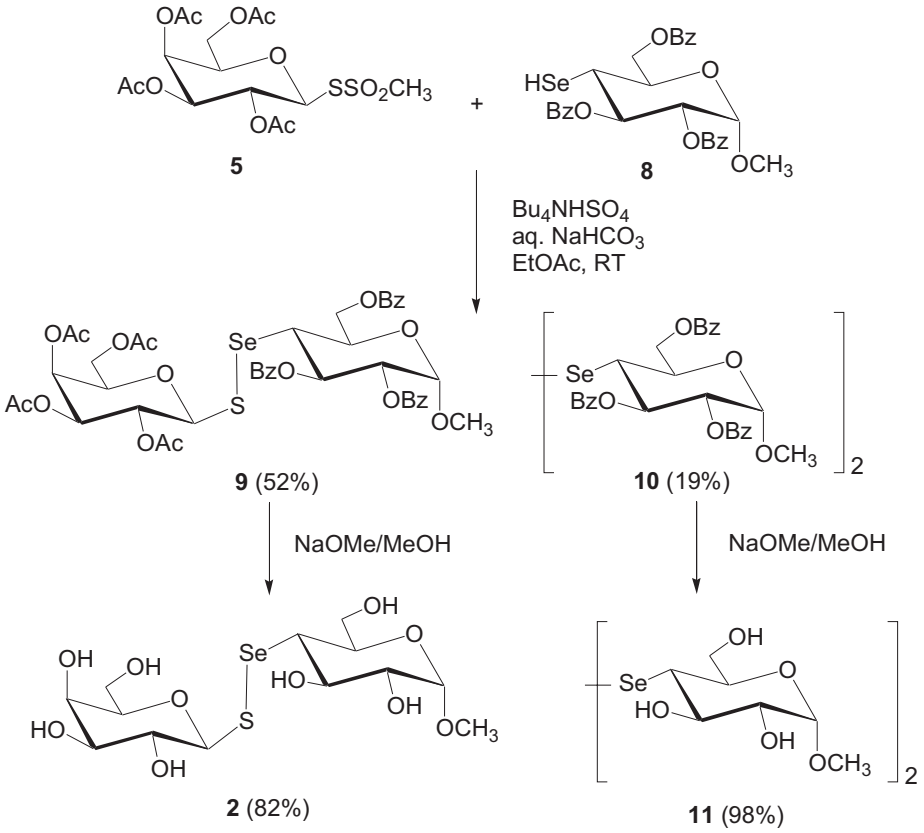
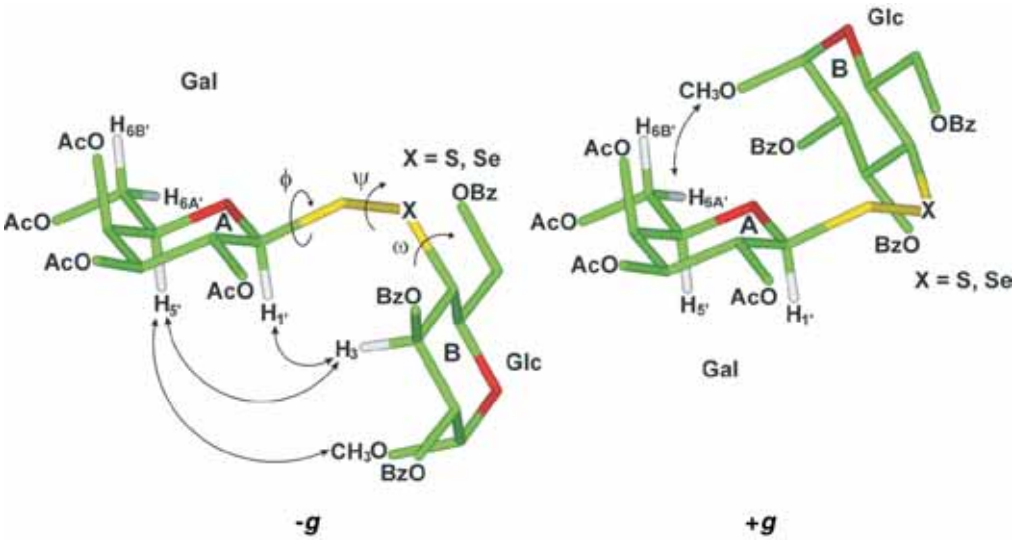


Fig. 3. Preferred conformations of compounds **7** and **9**.



resonances at δ 2.95 and δ 2.45 in the spectrum recorded at 193 K (Fig. 4). Based on these variable-temperature NMR results, we conclude that a second conformation, namely the +gauche (+*g*) conformation (Fig. 3) is also populated. Broadening of the H-1′ and H-5′ signals can then be accounted for by the proximity of ring **B** to ring **A**, in the (–*g*) conformation, where ring **B** is under ring **A**, and broadening of the H-6′ signal by the proximity of the two rings in the (+*g*) conformation, where ring **B** is above ring **A** (Fig. 3). The observations of weak OCH_3/H-6′ correlations in the NOESY spectra lend additional support to the importance of the (+*g*) conformation about the S—X bond in these compounds.

The NOESY spectra for target compounds **1** and **2** showed cross peaks for OCH_3 with the H-5′/H-6′ multiplet. However, the high degree of spectral overlap did not permit unambiguous assignment of the other signals. It seems reasonable that compounds **1** and **2** will have similar

© 2005 NRC Canada

Fig. 4. Variable-temperature ^{1}H NMR spectra of compound **7** in toluene-d_8.

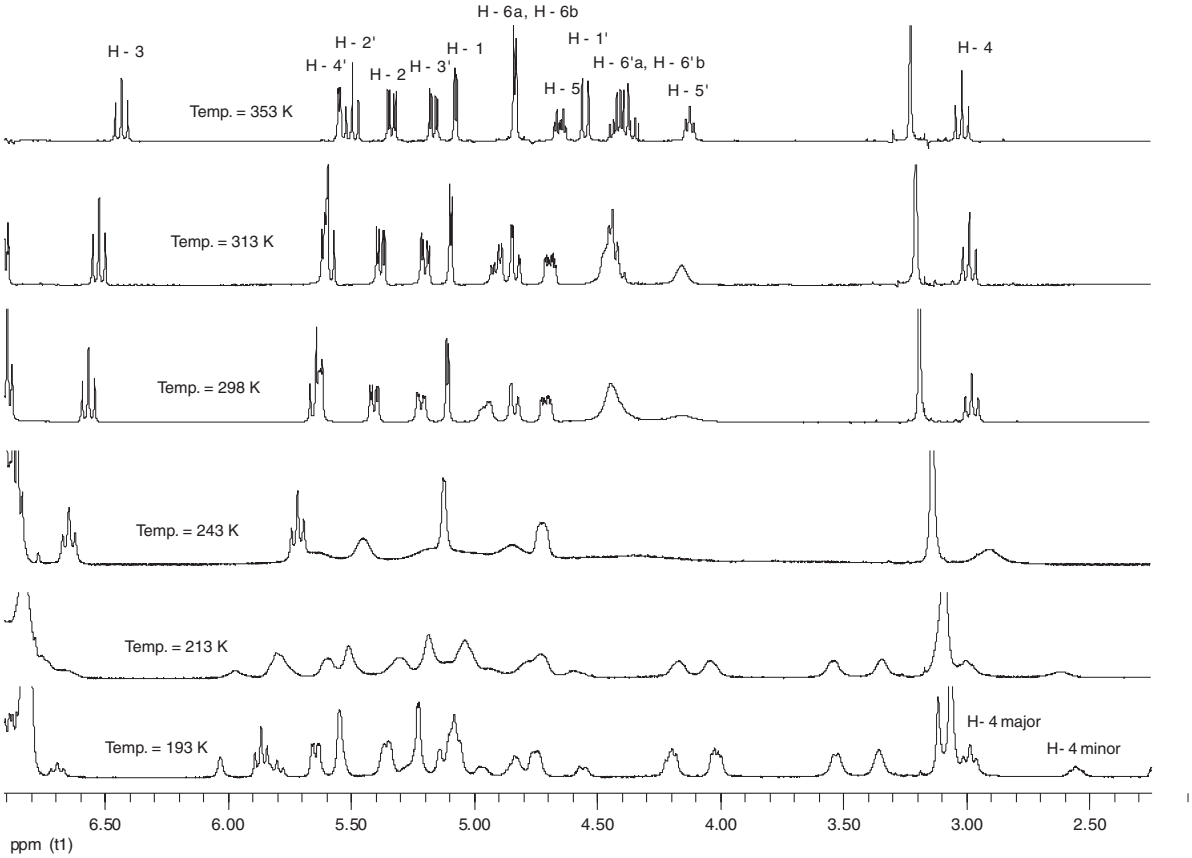
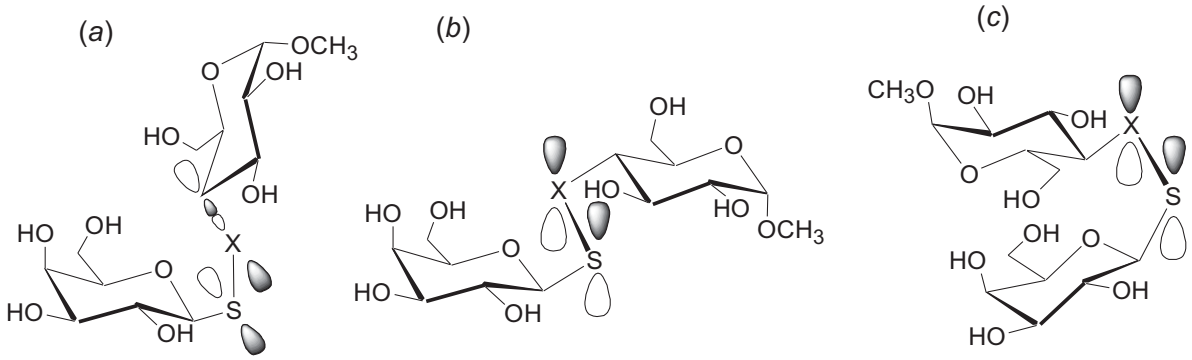


Fig. 5. Fragment molecular orbital interactions in compounds **1** and **2** (X = S, Se).



conformational preferences as their protected precursors. However, in these cases, no significant line-broadening effects were observed at room temperature, indicating that the barrier to rotation about the S—X (X = S, Se) bond is less than in the corresponding protected compounds.

The gauche conformational preferences about the S—S and S—Se bonds are consistent with arguments based on perturbational molecular orbital theory. Thus, an anti or syn preference is disfavored based on a 4e repulsive interaction between the 3*p* orbitals on the sulfur atom with either the S (3*p*) or Se (4*p*) orbital on the adjacent atom (Figs. 5*b*, 5*c*) (32). In contrast, the gauche conformations (e.g., Fig. 5*a*) permit a 2e stabilizing $n_S \rightarrow \sigma^*_{X-C}$ hyperconjugative interaction.

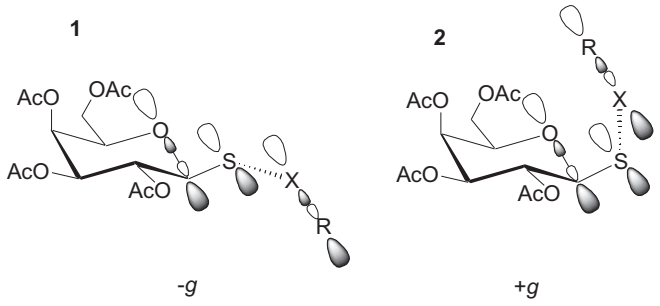
Interestingly, both (+*g*) and (–*g*) conformations also permit expression of the $n_S \rightarrow \sigma^*_{C1-O5\,Gal}$ exo-anomeric interaction (Fig. 6). These two conformations are therefore stabilized by both the exo-anomeric effect and the hyperconjugative interactions associated with the RS–SR′ and RS—SeR′ linkages (Fig. 6). Importantly, the (+*g*) conformation (Fig. 6*b*) places the glucose ring above the galactose ring in a manner similar to the elusive ϕ_H anti conformation in β-linked disaccharides while the (–*g*) conformation places the two sugar rings in a similar orientation to that observed for ordinary disaccharides.

Conclusions

Disaccharide analogues in which the interglycosidic linkage is either a disulfide or selenosulfide moiety have been

© 2005 NRC Canada

Fig. 6. Combined exo-anomeric $n_S \rightarrow \sigma^*_{C\text{-}1\text{-}O\text{-}5}$ and $n_S \rightarrow \sigma^*_{X\text{-}R}$ interactions (X = S, Se).



synthesized. The compounds display interesting conformational preferences, as determined by NOE spectroscopy and line-broadening effects. These preferences are consistent with the operation of the destabilizing and stabilizing orbital interactions associated with the RS–SR′ and RS–SeR′ linkages as well as with the stabilizing $n_S \rightarrow \sigma^*_{C\text{-}1'\text{–}O\text{-}5'}$ exo-anomeric orbital interaction. The conformational preferences suggest a means of expanding the repertoire of carbohydrate topographies for use as biological probes.

Experimental section

General

Melting points were determined on a Fisher-Johns melting point apparatus and are uncorrected. Optical rotations were measured with a Rudolph Research Autopol II automatic polarimeter. ^{1}H NMR and ^{13}C NMR spectra were recorded on a Bruker AMX-400 NMR spectrometer at 400.13 MHz and 100.6 MHz for proton and carbon, respectively. Chemical shifts are given in ppm downfield from TMS for those spectra measured in $CDCl_3$, CD_3OD, $(CH_3)_2CO$, or toluene-d_8 and from 2,2-dimethyl-2-silapentane-5-sulfonate (DSS) for those spectra measured in D_2O. Chemical shifts and coupling constants were obtained from a first-order analysis of the spectra. All assignments were confirmed with the aid of two-dimensional ^{1}H/^{1}H (COSYDFPT), ^{1}H/^{13}C (INVBTP), ^{1}H (NOESYTP), and ^{1}H (MLEVTP) experiments using standard Bruker pulse programs. Processing of the spectra was performed with standard UXNMR (Bruker) and WINNMR software. Zero filling of the acquired data (512 t_1 values and 2 K data points in t_2) led to a final data matrix of 1 K × 1 K ($F_1 \times F_2$) data points. MALDI-TOF mass spectra were obtained for samples dispersed in a 2,5-dihydroxybenzoic acid matrix using a PerSeptive Biosystems Voyager-DE instrument. Analytical TLC was performed on aluminum plates precoated with Merck silica gel 60F-254 as the adsorbent. The developed plates were air-dried, exposed to UV light and (or) sprayed with a solution containing 1% $Ce(SO_4)_2$ and 1.5% molybdic acid in 10% aq. H_2SO_4 and heated. Compounds were purified by flash column chromatography on Kieselgel 60 (230–400 mesh). Solvents were distilled before use and were dried, as necessary. Solvents were evaporated under reduced pressure and below 50 °C.

2,3,4,6-Tetra-*O*-acetyl-β-D-galactopyranosyl methanethiosulfonate (5)

Acetobromogalactose **3** (1.00 g, 2.43 mmol) was added to a solution of sodium methanethiosulfonate **4** (0.38 g, 2.84 mmol) in acetonitrile (25 mL) at room temperature under nitrogen. The temperature was then slowly raised to 50–60 °C and the reaction mixture was stirred for 3 h until TLC showed completion of the reaction. The suspension was cooled and the solvent was removed. The residue was purified by chromatography on silica gel, (EtOAc–hexane, 7:12) to give the title compound as a white solid (0.95 g, 88%); mp 124–126 °C. $[\alpha]_D^{23}$ +3 (*c* 1.9, $CHCl_3$). ^{1}H NMR (400 MHz, acetone-d_6) δ: 5.50 (1H, dd, $J_{3,4}$ = 3.5 Hz, $J_{4,5}$ = 1.0 Hz, H-4), 5.47 (1H, d, $J_{1,2}$ = 10.4 Hz, H-1), 5.39 (1H, dd, $J_{2,3}$ = 9.9 Hz, H-3), 5.19 (1H, dd, H-2), 4.44 (1H, ddd, H-5), 4.22 (1H, dd, $J_{5,6a}$ = 4.4 Hz, $J_{6a,6b}$ = 11.6 Hz, H-6a), 4.13 (1H, dd, $J_{5,6b}$ = 8.0 Hz, H-6b), 3.56 (3H, s, SSO_2CH_3), 2.15–1.92 (12H, 4s, 4 × OAc). ^{13}C NMR (400 MHz, $CDCl_3$) δ: 170.17–169.69 (CO, 4 × OAc), 86.98 (C-1), 75.37 (C-5), 71.33 (C-3), 67.07 (C-4), 65.79 (C-2), 61.86 (C-6), 52.76 (SSO_2CH_3), 20.62–20.47 (Me, 4 × OAc). Anal. calcd. for $C_{15}H_{22}O_{11}S_2$: C 40.72, H 5.01; found: C 41.01, H 5.05.

Methyl 2,3,6-tri-*O*-benzoyl-4-*S*-(2′,3′,4′,6′-tetra-*O*-acetyl-β-D-galactopyranosyl-1′-thio)-4-thio-α-D-glucopyranoside (7)

To a mixture of thiosulfonate **5** (2.14 g, 4.8 mmol) and thiol **6** (2.75 g, 5.1 mmol) in EtOAc (58 mL) was added phase-transfer catalyst, tetrabutylammonium hydrogensulfate (2.16 g, 6.4 mmol), and saturated aqueous sodium hydrogencarbonate (13 mL). The reaction mixture was stirred at room temperature under nitrogen for 18 h and then diluted with EtOAc (100 mL). The organic layer was then washed with saturated sodium chloride solution (2 × 30 mL) followed by water (2 × 30 mL). The organic layer was dried over anhydrous sodium sulfate and evaporated. The crude product was purified by column chromatography (EtOAc–hexane, 1:2). The title compound **7** was obtained as an amorphous white solid (3.97 g, 88%). $[\alpha]_D^{23}$ –30.3 (*c* 3.5, $CHCl_3$). ^{1}H NMR (400 MHz, $CDCl_3$) δ: 8.09–7.94 (6H, 3d, 3 × OBz ortho Hs), 7.64–7.34 (9H, m, 3 × OBz meta + para H), 6.23 (1H, dd, $J_{2,3}$ = 9.6 Hz, $J_{3,4}$ = 10.4 Hz, H-3), 5.50 (1H, d, $J_{3',4'}$ = 3.4 Hz, $J_{4',5'} \approx 0.0$ Hz, H-4′), 5.31 (1H, dd, $J_{1',2'}$ = 10.0 Hz, H-2′), 5.20 (1H, dd, $J_{1,2}$ = 3.6 Hz, H-2), 5.17 (1H, d, H-1), 5.13 (1H, dd, $J_{2',3'}$ = 10.1 Hz, H-3′), 4.82 (1H, broad dd, $J_{5,6a}$ = 4.0 Hz, $J_{6a,6b}$ = 12.1 Hz, H-6a), 4.73 (1H, dd, $J_{5,6b}$ = 2.1 Hz, H-6b), 4.53–4.51 (2H, m, H-1′, H-5), 4.44–4.27 (3H, m, H-5′, H-6a′, H-6b′), 3.48 (3H, s, OMe), 3.11 (1H, dd, $J_{4,5}$ = 10.4 Hz, H-4), 2.20–1.99 (12H, 4s, 4 × OAc). ^{13}C NMR (400 MHz, $CDCl_3$) δ: 170.38–169.42 (CO, 4 × OAc), 166.17–165.72 (CO, 3 × OBz), 133.29–128.36 (15C, Ph), 97.18 (C-1), 89.50 (br, C-1′), 74.51 (C-5′), 73.35 (C-2), 71.81 (C-3′), 69.62 (br, C-3), 67.58 (C-5), 66.87 (2C, C-2′, C-4′), 63.56 (C-6), 60.35 (C-6′), 55.67 (OMe), 47.91 (C-4), 20.72–20.56 (Me, 4 × OAc). MALDI-TOF-MS calcd. for $C_{42}H_{44}O_{17}S_2$: 884.20; found: 907.07 $(M + Na)^+$. Anal. calcd. for $C_{42}H_{44}O_{17}S_2$: C 57.01, H 5.01; found: C 57.28, H 5.08.

Methyl-4-*S*-(β-D-galactopyranosyl-1′-thio)-4-thio-α-D-glucopyranoside (1)

The blocked disulfide **7** (1.06 g, 1.19 mmol) was treated with 1 mol/L methanolic sodium methoxide (4 mL) at room temperature for 10 min in dry methanol (40 mL). The reaction mixture was then neutralized to pH 6.4 with Rexyn 101

© 2005 NRC Canada

H^+. The neutralized solution was filtered and evaporated to dryness in vacuo to give a white solid. The crude product was purified by column chromatography on silica gel (EtOAc–methanol–water, 6:3:1) to give the title compound as a white crystalline solid (0.39 g, 82%); mp 151–153 °C (EtOH). $[\alpha]_D^{23}$ –100 (*c* 1.15, D_2O). ^1H NMR (400 MHz, D_2O) δ: 4.81 (1H, d, $J_{1,2}$ = 3.7 Hz, H-1), 4.36 (1H, d, $J_{1',2'}$ = 9.5 Hz, H-1′), 4.07 (1H, dd, $J_{2,3} \approx J_{3,4} \approx$ 9.9 Hz, H-3), 4.00–3.94 (4H, m, H-4′, H-5′, H-6a, H-6b), 3.77 (1H, dd, $J_{2',3'}$ = 9.6 Hz, H-2′), 3.76 (1H, dd, $J_{5,6a}$ = 6.9 Hz, $J_{6a,6b}$ = 12.2 Hz, H-6a′), 3.73–3.66 (3H, m, H-5, H-3′, H-6b′), 3.62 (1H, dd, H-2), 3.40 (3H, s, OMe), 2.65 (1H, dd, $J_{4,5}$ = 10.2 Hz, H-4). ^{13}C NMR (400 MHz, D_2O) δ: 102.06 (C-1), 91.84 (C-1′), 82.23 (C-5′), 76.53 (C-3′), 75.18 (C-2), 73.77 (C-4′), 71.22 (C-5), 71.09 (C-2′), 70.52 (C-3), 64.22 (C-6′), 63.96 (C-6), 57.84 (OMe), 52.61 (C-4). MALDI-TOF-MS calcd. for $C_{13}H_{24}O_{10}S_2$: 404.1; found: 427.3 $(M + Na)^+$. Anal. calcd. for $C_{13}H_{24}O_{10}S_2$: C 38.61, H 5.98; found: C 38.55, H 6.00.

Methyl 2,3,6-tri-*O*-benzoyl-4-*Se*-(2′,3′,4′,6′-tetra-*O*-acetyl-β-D-galactopyranosyl-1′-thio)-4-seleno-α-D-glucopyranoside (9) and methyl 2,3,6-tri-*O*-benzoyl-4-seleno-α-D-glucopyranoside diselenide (10)

To a mixture of thiosulfonate **5** (2.20 g, 4.98 mmol) and selenol **8** (3.68 g, 6.29 mmol) in EtOAc (55 mL) was added phase-transfer catalyst, tetrabutylammonium hydrogensulfate (2.56 g, 7.5 mmol), and saturated aqueous sodium hydrogencarbonate (40 mL). The reaction mixture was stirred at room temperature under nitrogen overnight and diluted with EtOAc (150 mL). The organic layer was then washed with saturated sodium chloride solution (2 × 50 mL) followed by water (2 × 100 mL). The organic layer was dried over anhydrous sodium sulfate and evaporated. The crude product was then purified by column chromatography on silica gel (EtOAc–hexane, 1:2.5). The title compound **9** was obtained as a colorless amorphous solid (2.4 g, 52%) and the protected (4→4′) diselenide **10**, a by-product, was obtained as a yellow solid (1.43 g, 38% with respect to selenol **8**). Compound **9**: $[\alpha]_D^{23}$ +66 (*c* 0.5, $CHCl_3$). ^1H NMR (400 MHz, $CDCl_3$) δ: 8.10–7.94 (6H, 3d, 3 × OBz ortho H), 7.62–7.32 (9H, m, 3 × OBz meta + para H), 6.21 (1H, dd, $J_{2,3}$ = 9.2 Hz, $J_{3,4}$ = 10.7 Hz, H-3), 5.51 (1H, d, $J_{3',4'}$ = 3.4 Hz, $J_{4',5'}$ = 0.0 Hz, H-4′), 5.30 (1H, dd, $J_{1',2'}$ = 10.0 Hz, H-2′), 5.22 (1H, dd, $J_{1,2}$ = 3.6 Hz, H-2), 5.20 (1H, d, H-1), 5.13 (1H, dd, $J_{2',3'}$ = 10.0 Hz, H-3′), 4.89 (1H, broad dd, $J_{6a,6b}$ = 12.1 Hz, H-6a), 4.73 (1H, dd, $J_{5,6b}$ = 2.0 Hz, H-6b), 4.65 (1H, broad d, H-1′), 4.57 (1H, ddd, H-5), 4.40–4.28 (3H, br m, H-5′, H-6a′, H-6b′), 3.48 (3H, s, OMe), 3.30 (1H, dd, H-4), 2.21, 2.02, 2.00, 1.99 (12H, 4s, 4 × OAc). ^{13}C NMR (400 MHz, $CDCl_3$) δ: 170.45–169.54 (CO, 4 × OAc), 166.20, 165.81, 165.57 (CO, 3 × OBz), 133.29–128.37 (18C, 3 × Ph), 97.35 (C-1), 87.0 (C-1′), 74.60 (C-5′), 73.35 (C-2), 71.77 (C-3′), 69.86 (C-3), 68.26 (C-5), 66.85 (C-2′,4′), 64.39 (C-6), 60.36 (C-6′), 55.69 (OMe), 42.60 (C-4), 20.80–20.60 (Me, 4 × OAc). MALDI-TOF-MS calcd. for $C_{42}H_{44}O_{17}SSe$: 932.1; found: 955.5 $(M + Na)^+$. Anal. calcd. for $C_{42}H_{44}O_{17}SSe$: C 54.14, H 4.76; found: C 54.03, H 4.90. Compound **10**: This product was found to have identical physical constants and NMR data to those previously reported (31).

Methyl-4-*Se*-(β-D-galactopyranosyl-1′-thio)-4-seleno-α-D-glucopyranoside (2)

The blocked selenosulfide **9** (2.0 g, 2.15 mmol) was treated with 1 mol/L methanolic sodium methoxide (6 mL) at room temperature for 1 h in dry methanol (80 mL). The reaction mixture was then adjusted to pH 6.4 with Rexyn 101 H^+. The solution was filtered and evaporated to dryness in vacuo to give a white solid. The crude product was purified by column chromatography on silica gel (EtOAc–methanol–water, 6:3:1); the title compound was obtained as a white crystalline solid (0.75 g, 77%); mp 122–124 °C (EtOH). $[\alpha]_D^{23}$ –114 (*c* 2.75, D_2O). ^1H NMR (400 MHz, D_2O) δ: 4.63 (1H, d, $J_{1,2}$ = 3.7 Hz, H-1), 4.37 (1H, d, $J_{1',2'}$ = 8.3 Hz, H-1′), 4.03 (1H, dd, $J_{2,3} \approx J_{3,4}$ = 9.6 Hz, H-3), 4.01–3.93 (4H, m, H-5, H-4′, H-6a, H-6b), 3.79–3.65 (5H, m, H-5′, H-6a′, H-6b′, H-2′, H-3′), 3.62 (1H, dd, H-2), 3.39 (3H, s, OMe), 2.94–2.83 (1H, second order multiplet, H-4). ^{13}C NMR (400 MHz, D_2O) δ: 102.15 (C-1), 90.56 (C-1′), 82.20 (C-5′), 76.39 (C-3′), 75.19 (C-2), 74.31 (C-4′), 72.68 (C-5), 71.39 (C-2′), 71.11 (C-3), 64.94 (C-6′), 63.94 (C-6), 57.87 (OMe), 48.62 (C-4). MALDI-TOF-MS calcd. for $C_{13}H_{24}O_{10}SSe$: 452.0; found: 475.1 $(M + Na)^+$. Anal. calcd. for $C_{13}H_{24}O_{10}SSe$: C 34.59, H 5.36; found: C 34.27, H 5.50.

Methyl 4-seleno-β-D-glucopyranoside diselenide (11)

The protected (4→4′) diselenide **10** (0.725 g, 0.62 mmol) was treated with 1 mol/L methanolic sodium methoxide (4 mL) at room temperature for 2.5 h in dry methanol (40 mL). The reaction mixture was then neutralized to pH 6.2 with Rexyn 101 H^+. The neutralized solution was filtered and evaporated to dryness in vacuo to give a yellow solid. The crude product was purified by column chromatography on silica gel (EtOAc–methanol–water, 6:3:1) to give the title compound as a yellow crystalline solid (0.31 g, 98%); mp 95–97 °C. $[\alpha]_D^{21}$ –77 (*c* 0.4, D_2O). ^1H NMR (400 MHz, D_2O) δ: 4.83 (1H, d, $J_{1,2}$ = 3.4 Hz, H-1), 3.99 (2H, d, H-6a, H-6b), 3.85 (1H, dd, $J_{2,3}$ = 9.7 Hz, H-3), 3.72 (1H, ddd, $J_{5,6a}$ = 2.9 Hz, H-5), 3.64 (1H, dd, H-2), 3.78 (3H, s, OCH_3), 2.85 (1H, dd, $J_{3,4}$ = 10.7 Hz, H-4). MALDI-TOF-MS calcd. for $C_{14}H_{26}O_{10}Se_2$: 514.0; found: 537.2 $(M + Na)^+$. Anal. calcd. for $C_{14}H_{26}O_{10}Se_2$: C 32.82, H 5.12; found: C 33.09, H 5.37.

Acknowledgment

We are grateful to the Natural Sciences and Engineering Research Council of Canada (NSERC) for financial support.

References

1. A. Varki, R. Cummings, J. Esko, H. Freeze, G. Hart, and J. Marth (*Editors*). Essentials of glycobiology. Cold Spring Harbor Laboratory Press, Cold Spring Harbor, New York. 1999.
2. M.E. Taylor and K. Drickamer. Introduction to glycobiology. Oxford University Press, New York. 2003.
3. A. Helenius and M. Aebi. Science, **291**, 2364 (2001).
4. (*a*) R.A. Dwek, T.D. Butters, F.M. Platt, and N. Zitzmann. Nature Rev. Drug Discovery, **1**, 65 (2002); (*b*) R.A. Dwek. Chem. Rev. **96**, 683 (1996).
5. V.H. Lillelund, H.H. Jensen, X. Liang, and M. Bols. Chem. Rev. **102**, 515 (2002).
6. N. Asano. Glycobiology, **13**, 93R (2003).

© 2005 NRC Canada

7. T.A. Houston and J.T. Blanchfield. Mini-Rev. Med. Chem. **3**, 669 (2003).
8. E.F. Hounsell. Prog. Nucl. Magn. Reson. Spectrosc. **27**, 445 (1995).
9. J.-P. Praly and R.U. Lemieux. Can. J. Chem. **65**, 213 (1987).
10. R.U. Lemieux and S. Koto. Tetrahedron, **30**, 1933 (1974).
11. I. Tvaroska and T. Bleha. Adv. Carbohydr. Chem. Biochem. **47**, 45 (1989).
12. T. Weimar, U.C. Kreis, J.S. Andrews, and B.M. Pinto. Carbohydr. Res. **315**, 222 (1999).
13. (*a*) E. Montero, M. Vallmitjana, J.A. Perez-Pons, E. Querol, J. Jimenez-Barbero, and F.J. Canada. FEBS Lett. **421**, 243 (1998); (*b*) B. Aguilera, J. Jimenez-Barbero, and A. Fernandez-Mayoralas. Carbohydr. Res. **308**, 19 (1998); (*c*) K. Bock, J.O. Duus, and S. Refn. Carbohydr. Res. **253**, 51 (1994).
14. K. Bock, M. Meldal, and S. Refn. Carbohydr. Res. **221**, 1 (1991).
15. L. Schleifer, H. Senderowitz, P. Aped, E. Tartakovsky, and B. Fuchs. Carbohydr. Res. **206**, 21 (1990).
16. A.L. Smith and K.C. Nicolaou. J. Med. Chem. **39**, 2103 (1996).
17. O. Renaudet and P. Dumy. Tetrahedron Lett. **42**, 7575 (2001).
18. O. Renaudet and P. Dumy. Tetrahedron, **58**, 2127 (2002).
19. M. Hornyak, F. Sztaricskai, I.F. Pelyvas, and G. Batta. Carbohydr. Res. **338**, 1787 (2003).
20. R.R. Fraser, G. Boussard, J.K. Saunders, J.B. Lambert, and C.E. Mixan. J. Am. Chem. Soc. **93**, 3822 (1971).
21. F. Jorgensen and J.P. Snyder. Tetrahedron, **35**, 1399 (1979).
22. N.L. Allinger, M.J. Hickey, and J. Kao. J. Am. Chem. Soc. **98**, 2741 (1976).
23. B.M. Pinto, R.Y.N. Leung, and R.D Sharma. Magn. Reson. Chem. **26**, 729 (1988).
24. L. Szilágyi, T.-Z. Illyés, and P. Herczegh. Tetrahedron Lett. **42**, 3901 (2001).
25. B.G. Davis, S.J. Ward, and P.M. Rendle. Chem. Commun. 189 (2001).
26. T.-Z. Illyés, D. Molnar-Gabor, and L. Szilágyi. Carbohydr. Res. **339**, 1561 (2004).
27. B.G. Davis, M.A.T. Maughan, M.P. Green, A. Ullman, and J.B. Jones. Tetrahedron: Asymmetry, **11**, 245 (2000).
28. L. Field and J.W. McFarland. J. Am. Chem. Soc. **75**, 5582 (1953).
29. J.D. Macke and L. Field. J. Org. Chem. **53**, 396 (1988).
30. L.A. Reed and L. Goodman. Carbohydr. Res. **94**, 91 (1981).
31. S. Mehta, J.S. Andrews, B. Svensson, and B.M. Pinto. J. Am. Chem. Soc. **117**, 9783 (1995).
32. T.A. Albright, J.K. Burdett, and M.H. Whangbo. Orbital interactions in chemistry. Wiley, New York. 1985.

© 2005 NRC Canada

Direct synthesis of unprotected α-amino acids via allylation of hydroxyglycine[1]

Masaharu Sugiura, Chieko Mori, Keiichi Hirano, and Shū Kobayashi

Abstract: Hydroxyglycine, the ammonia adduct of glyoxylic acid, was found to react with various allylboronates in the presence of triethylamine in methanol to give unprotected α-amino acids directly with high stereoselectivity. For instance, the reactions with (*E*)- and (*Z*)-crotylboronates afforded the corresponding anti- and syn-crotylated products (isoleucine and alloisoleucine after hydrogenation) with high diastereoselectivity, respectively. Interestingly, it was found that isomerization of the products (γ-adducts to α-adducts) occurred under the reaction conditions in some cases. Control experiments have suggested that the isomerization took place via 2-aza (or azonia) Cope rearrangement of imines derived from γ-adducts and glyoxylic acid.

Key words: hydroxyglycine, glyoxylic acid, allylboronates, α-amino acids, allylglycines, isoleucine, alloisoleucine, stereoselective reactions, isomerization, 2-aza (azonia) Cope rearrangement.

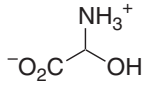
Résumé : On a trouvé que l'hydroxyglycine, le produit d'addition de l'ammoniac sur l'acide glyoxylique, réagit avec divers allylboronates, en présence de triéthylamine dans le méthanol, pour conduire directement à la formation d'acides α-aminés non protégés, avec une stéréosélectivité élevée. Par exemple, les réactions des (*E*)- et (*Z*)-crotylboronates conduisent respectivement aux produits anticrotylés et syncrotylés correspondants (isoleucine et alloisoleucine après hydrogénation) avec des diastéréosélectivités élevées. Fait intéressant, on a trouvé que, dans les conditions expérimentales et pour quelques cas, il se produit une isomérisation des produits (adduits γ en adduits α). Des expériences de contrôle ont suggéré que l'isomérisation se produit par un réarrangement 2-aza (ou azonia) de Cope des imines dérivées d'adduits γ et de l'acide glyoxylique.

Mots clés : hydroxyglycine, acide glyoxylique, allyboronates, acides α-aminés, allylglycines, isoleucine, alloisoleucine, réactions stéréosélectives, isomérisation, réarrangement 2-aza (ou azonia) de Cope.

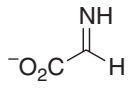
[Traduit par la Rédaction]

Introduction

Hydroxyglycine (**1**), which is obtained as a zwitterionic solid under the isoelectronic conditions (pH ca. 6), is an equimolar adduct of glyoxylic acid and ammonia (1). It readily decomposes to glyoxylic acid in an aqueous media at pH < 6, while it oligomerizes via iminoacetate **2** (an assumed intermediate) at pH > 6. These compounds attracted us because we recently found that three-component reactions (α-aminoallylation) of glyoxylic acid (other aldehydes as well), ammonia, and allylboronates proceeded smoothly to afford allylglycines (homoallylic primary amines) in high yields (2). In these reactions, both **1** and **2** are supposed to serve as intermediates. However, despite their potential utility as intermediates for direct synthesis of *unprotected* α-amino acids, **1** and **2** have been barely utilized in organic synthesis (3). Herein, we report that nucleophilic addition of allylboronates to hydroxyglycine **1** provides an efficient, stereoselective route to unprotected allylglycines.



1



2

Results and discussion

Initial attempts were made for allylation of hydroxyglycine **1** with allylboronate **3a** (4*a*). First, the effect of varying solvents was investigated by simply mixing **1** and **3a** (1.2 equiv.) in a solvent at 0 °C to room temperature (rt) for 15–18 h (Table 1, entries 1–6). Protic solvents (ethanol, methanol, and water) were found to be effective (Table 1, entries 1–3), whereas less polar solvents (toluene, THF, and acetonitrile) were much inferior (Table 1, entries 4–6). The reaction mixtures were suspensions in these solvents except for in water because of the low solubility of **1**. Among the solvents tested, methanol gave the highest yield and chemoselectivity (amine **4a** vs. alcohol **5a**) (Table 1, entry 2). To improve the yield, further optimization of the conditions were performed choosing methanol as a solvent. A longer reaction time (72 h) or a higher temperature (50 °C) dramatically improved the yield (Table 1, entries 7 and 8). It is also

Received 13 December 2004. Published on the NRC Research Press Web site at http://canjchem.nrc.ca on 16 August 2005.

This paper is dedicated to Professor Howard Alper for his great contributions to the fields of catalysis, organometallic, and organic chemistry.

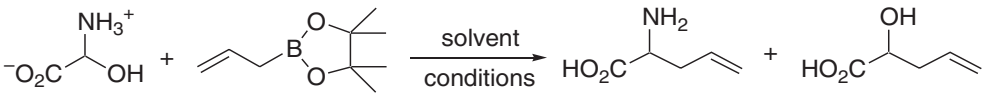
M. Sugiura, C. Mori, K. Hirano, and S. Kobayashi.[2]
Graduate School of Pharmaceutical Sciences, The University of Tokyo, Hongo, Bunkyo-ku, Tokyo 113-0033, Japan.

[1]This article is part of a Special Issue dedicated to Professor Howard Alper.

[2]Corresponding author (e-mail: skobayas@mol.f.u-tokyo.ac.jp).

 doi: 10.1139/V05-096 © 2005 NRC Canada

Table 1. Allylation of hydroxyglycine (**1**) with allylboronate **3a**.



1 **3a** (1.2 equiv.) **4a** **5a**

Entry	Solvent	Conditions	Yield (%) **4a**[a]	**5a**[b]
1	EtOH	rt, 18 h	27	5
2	MeOH	rt, 18 h	42[c]	3
3	H_2O	rt, 18 h	39	67[d]
4	Toluene	rt, 18 h	2	Trace
5	THF	0 °C, 15 h	0	0
6	CH_3CN	rt, 18 h	0	0
7	MeOH	rt, 72 h	73	nd
8	MeOH	50 °C, 18 h	84	nd
9	MeOH	Et_3N (20 mol%), rt, 18 h	90[c]	nd

Note: nd = not detected.
[a]Isolated yield.
[b]Estimated by ^{1}H NMR analysis of the crude product on the basis of the isolated yield of **4**.
[c]Average of two trials.
[d]Supposed to include an experimental error on integration of the ^{1}H NMR spectrum.

noteworthy that only allylated amine **4a** was obtained exclusively in these entries. Furthermore, a catalytic amount of triethylamine (20 mol%) was found to accelerate the reaction showing the highest yield and selectivity of **4a** (Table 1, entry 9). It is presumable that the base promotes formation of an active intermediate, iminoacetate **2** from **1**.

With the optimal conditions in hand, we then investigated reactions of **1** with various allylboronates **3** (4*b*–4*d*) (Table 2). Methallyboronate **3b** afforded the corresponding adduct **4b** in high yield (Table 2, entry 1). Triethylamine (1 equiv.) was used in this case to facilitate the desired reaction.[3] Significantly, (*Z*)-crotylboronate ((*Z*)-**3c**) provided syn-crotylated product (*syn*-**4c**) exclusively (>99% syn) along with a small amount of α-adduct (*Z*)-**4c′**, while anti-adduct (*anti*-**4c**) was obtained from (*E*)-crotylboronate ((*E*)-**3c**) in good yield with excellent selectivity (97% anti, Table 2, entries 2 and 3). In the later case, a very small amount of α-adduct **4c′** was yielded. Direct treatment of hydrogen (1 atm, 1 atm = 101.325 kPa) and Pd/C in the same pot successfully converted syn- and anti-adducts (*syn*- and *anti*-**4c**) to alloisoleucine (75%) and isoleucine (82%), respectively (Scheme 1). On the other hand, reactions of **1** with (*E*)-cinnamylboronate **3d** and cyclohexenylboronate **3e** provided **4d** and **4e**, respectively, in high yield with high diastereoselectivities (Table 2, entries 4 and 5). In the former case, 1 equiv. of triethylamine was effective to suppress formation of α-adduct **4d′**. Sterically more demanding prenylboronate **3f** also reacted with **1** in the presence of 2 equiv. of triethylamine to afford a mixture of the desired allylated product **4f** and α-adduct **4f′** (85:15) in high yield (Table 2, entry 6).

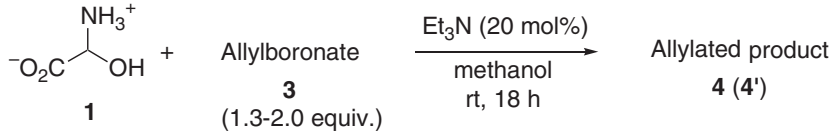
We were then interested in the mechanism of the formation of α-adduct **4′**. It was found that the formation of α-adduct **4′** became prominent when the reaction mixtures were concentrated with heating before purification. In the reaction of **1** with **3f**, for example, this manipulation led to only formation of **4f′**. In contrast, the formation of **4′** was suppressed to a large extent when the reaction mixture was directly purified by ion exchange resin (Dowex 50W-X2). Addition of a stoichiometric amount of triethylamine in allylations was also effective to suppress the formation of **4′** (vide supra). These observations indicated that some impurity involved in the reaction mixture promoted the isomerization on heating. We speculated that glyoxylic acid (or hydroxyglycine) formed an imine with allylated product **4**, which could undergo 2-aza (or azonia) Cope rearrangement leading to the isomerization (Scheme 2) (5, 6). To prove this hypothesis, purified *syn*- and *anti*-**4c** were treated with glyoxylic acid (0.1 equiv.) in D_2O at 50 °C (Fig. 1). Monitoring by ^{1}H NMR spectroscopy clearly showed gradual isomerization of *syn*- and *anti*-**4c** to α-adduct **4c′** (first order in [**4c**]; $t_{1/2}$ = 78 min for *syn*-**4c**, 34 min for *anti*-**4c**), whereas no isomerization was observed in the absence of glyoxylic acid.

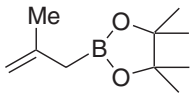
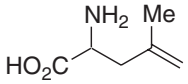
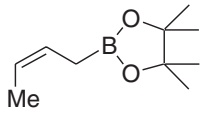
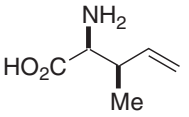
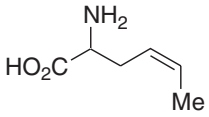
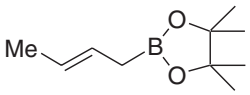
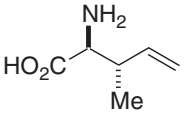
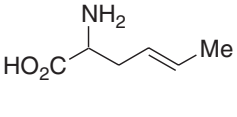
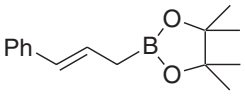
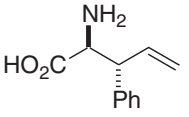
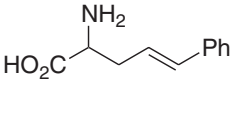
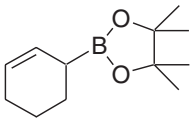
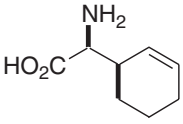
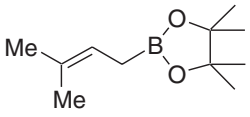
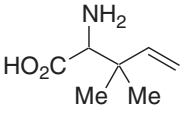
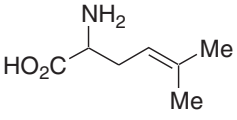
It should also be noted that (*Z*)-**4c′** was predominantly obtained from *syn*-**4c**, whereas *anti*-**4c** gave (*E*)-**4c′** with high selectivity (also see the Experimental section). Chair-like transition states **TS-*syn*** with the pseudo-axial methyl group[4] and **TS-*anti*** with the pseudo-equatorial methyl group could account for the observed stereochemical outcomes (Scheme 3). We also found that the rate of the isomerization of *anti*-**4c** to (*E*)-**4c′** was faster than that of *syn*-**4c** to (*Z*)-

[3] When a catalytic amount of triethylamine was used, an unidentified product was obtained along with **4b**. The ^{1}H and ^{13}C NMR spectra of this by-product suggested a Prins-type cyclization product. Further structural elucidation is now in progress.
[4] The preference of the equatorial CO_2H group might be ascribed to the acid–base interaction of the CO_2H group with the imino nitrogen.

© 2005 NRC Canada

Table 2. Allylation of hydroxyglycine (**1**) with various allylboronates **3**.



Entry	Allylboronate	Yield (%)[a]	Allylated products	4/4'[b]
1[c]	 **3b**	81	 **4b** 2-Amino-4-methyl-pent-4-enoic acid	—
2	 (*Z*)-**3c** (>95% *Z*)	73	 *syn*-**4c** (>99% syn) +  **4c'** (77% *Z*)	95/5
3	 (*E*)-**3c** (>95% *E*)	66	 *anti*-**4c** (97% anti) +  **4c'** (>97% *E*)	98/2
4[c]	 **3d** (>99% *E*)	93	 **4d** (>99% anti) +  **4d'** (>99% *E*)	93/7
5	 **3e**	88	 **4e** (>99% syn)	—
6[d,e]	 **3f**	92	 **4f** +  **4f'**	85/15

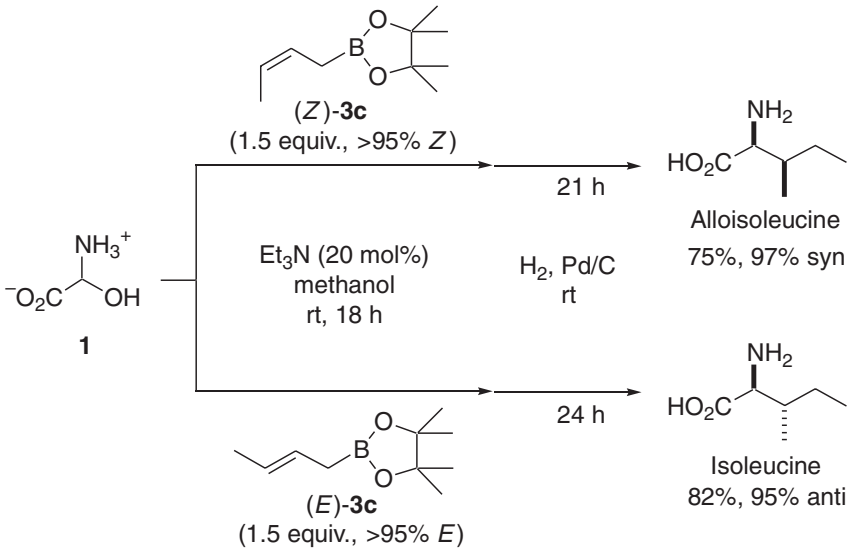
[a]Combined yields of **4** and **4′**.
[b]Determined by ^{1}H NMR analyses.
[c]Triethylamine (1 equiv.) was used.
[d]Triethylamine (2 equiv.) was used.
[e]The reaction was conducted for 6 h.

4c′. This rate difference would be ascribed to the fact that **TS-*anti*** is more stable than **TS-*syn*** because of the number of pseudo-equatorial substituents. In addition, the higher isomerization tendency of **4f** could be explained by the mechanism via 2-aza (or azonia) Cope rearrangement in which the equilibrium favors release of the steric hindrance to the more stable trisubstituted alkene **4f′**.

In summary, we have demonstrated that hydroxyglycine (**1**), the ammonia adduct of glyoxylic acid, reacts with various allylboronates in the presence of a tertiary amine to give

© 2005 NRC Canada

Scheme 1. Stereoselective synthesis of alloisoleucine and isoleucine.



Scheme 2. Assumed mechanism for isomerization via 2-aza Cope rearrangement.

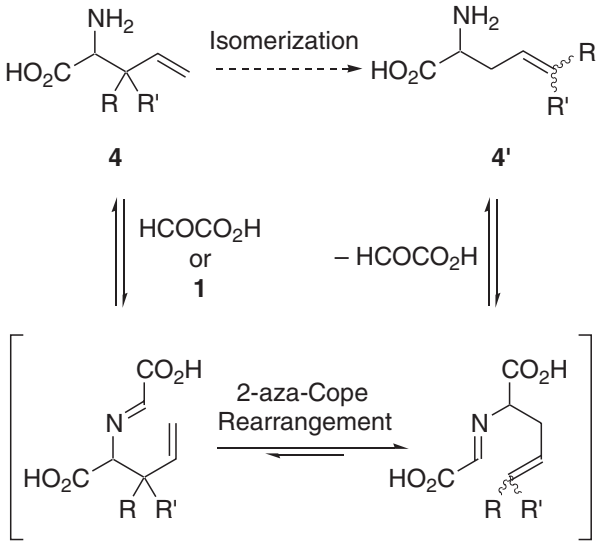
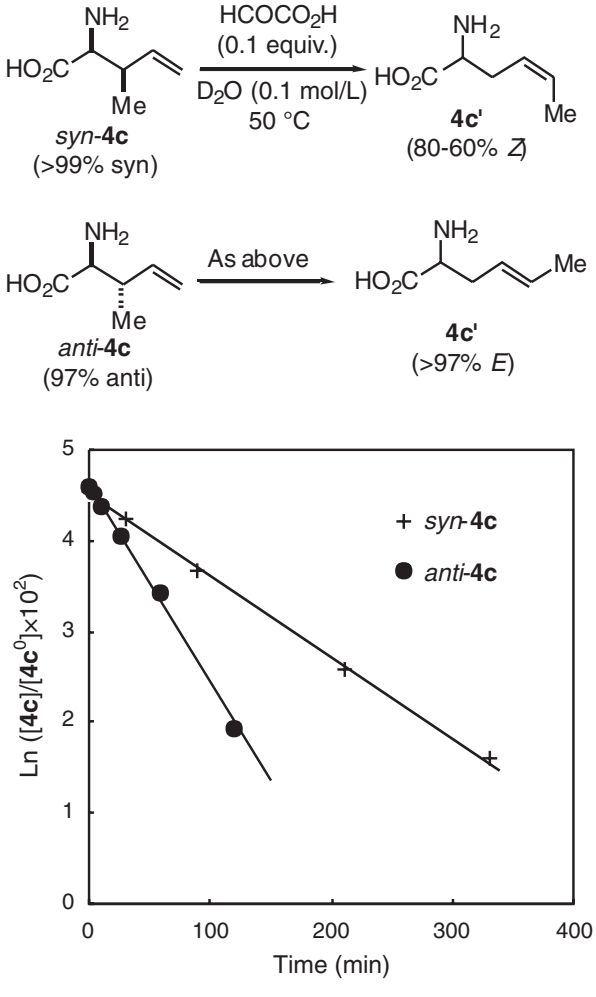


Fig. 1. Isomerization of *syn*- and *anti*-**4c**.



the corresponding unprotected α-amino acids directly. Reactions with γ-substituted allylboronates showed high diastereoselectivity, while isomerization of γ-adducts to α-adducts was accompanied to some extent. Further studies regarding its application to asymmetric synthesis are now in progress.

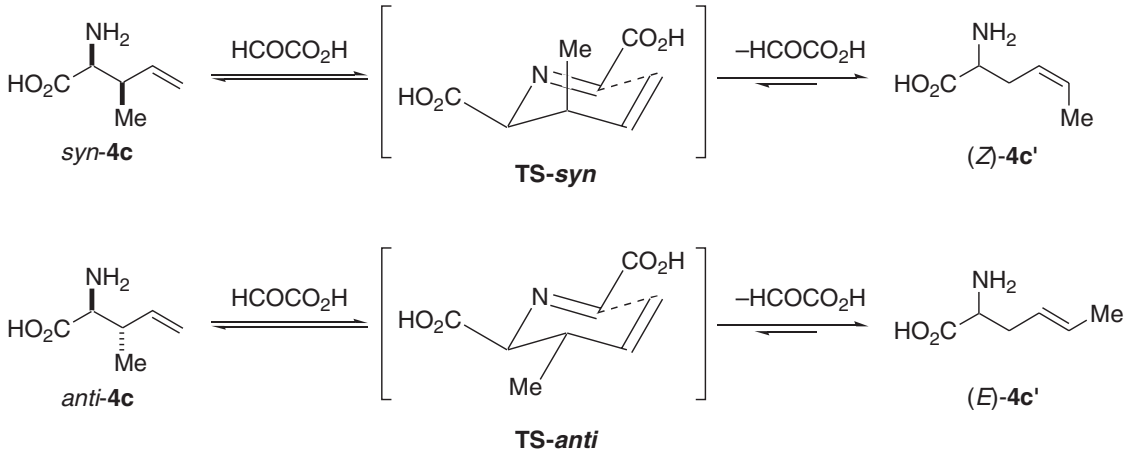
Experimental section

General methods

Melting points (mp) are uncorrected. ^{1}H and ^{13}C NMR spectra were recorded on JEOL ECX-400 or ECX-600 spectrometers in D_2O. 1,4-Dioxane served as the internal standard (δ 3.75 ppm for ^{1}H NMR and δ 67.19 ppm for ^{13}C NMR). High-resolution electrospray ionization mass spectra (HR-ESI-MS) were measured with a Bruker Daltonics BioTOF II mass spectrometer. Methanol was distilled from magnesium–iodine and stored over 3 Å MS. Purified water was employed for work-up and purification. All other solvents were purified based on standard procedures. Hydroxyglycine (**1**) (1) and allylboronates **3a**–**3f** (4) were prepared according to literature procedures.

© 2005 NRC Canada

Scheme 3. Chair-like transition state models for 2-aza Cope rearrangement.



General procedure for allylation of hydroxyglycine

Under an argon atmosphere, to a suspension of hydroxyglycine (**1**) (45.5 mg, 0.5 mmol) in dry methanol (2 mL), were added allylboronate **3** (1.2–2.0 equiv.) and triethylamine (0.1–2.0 equiv.) successively at ambient temperature. The mixture was stirred at that temperature for the indicated time, diluted with water, and charged on a cationic ion exchange resin column (Dowex 50W-X2, 50–100 mesh, H^+ form; ca. 5 g/wet) with water. After washing with a sufficient amount of water, α-amino acid **4** was eluted with 1.0 mol/L aqueous ammonia (fractions were checked by 0.1 wt% ninhydrine in acetone–water (4:1)), and concentrated to dryness.

Physical data of allylglycines

2-Aminopent-4-enoic acid (4a)

See ref. 2.

2-Amino-4-methylpent-4-enoic acid (4b)

mp 228–231 °C. ^{1}H NMR (400 MHz) δ: 5.00 (s, 1H), 4.90 (s, 1H), 3.85 (dd, *J* = 9.6, 4.6 Hz, 1H), 2.68 (dd, *J* = 14.7, 4.6 Hz, 1H), 2.50 (dd, *J* = 14.7, 9.6 Hz, 1H), 1.77 (s, 3H). ^{13}C NMR (100 MHz) δ: 175.2, 140.7, 116.0, 53.2, 39.7, 21.3. HR-ESI-MS calcd. for $C_6H_{12}NO_2$: 130.0863 (M + H^+); found: 130.0867.

syn-*2-Amino-3-methylpent-4-enoic acid (*syn-*4c)*

mp 224–227 °C. ^{1}H NMR (400 MHz) δ: 5.84 (ddd, *J* = 17.9, 10.1, 6.4 Hz, 1H), 5.26 (d, *J* = 10.1 Hz, 1H), 5.25 (d, *J* = 17.9 Hz, 1H), 3.76 (d, *J* = 4.1 Hz, 1H), 2.94–2.82 (m, 1H), 1.10 (d, *J* = 6.9 Hz, 3H). ^{13}C NMR (100 MHz) δ: 174.0, 138.2, 118.2, 59.0, 38.4, 13.6. HR-ESI-MS calcd. for $C_6H_{12}NO_2$: 130.0863 (M + H^+); found: 130.0866.

anti-*2-Amino-3-methylpent-4-enoic acid (*anti-*4c)*

mp 220–223 °C. ^{1}H NMR (400 MHz) δ: 5.75 (ddd, *J* = 17.4, 10.1, 7.3 Hz, 1H), 5.25 (d, *J* = 17.4 Hz, 1H), 5.24 (d, *J* = 10.1 Hz, 1H), 3.61 (d, *J* = 5.5 Hz, 1H), 2.87–2.74 (m, 1H), 1.16 (d, *J* = 7.3 Hz, 3H). ^{13}C NMR (100 MHz) δ: 174.4, 137.3, 118.8, 59.8, 39.1, 16.0. HR-ESI-MS calcd. for $C_6H_{12}NO_2$: 130.0863 (M + H^+); found: 130.0862.

2-Aminohex-4-enoic acid (4c′)

^{1}H NMR (400 MHz) (*E*-isomer) δ: 5.74 (dqt, *J* = 15.1, 6.4, 1.4 Hz, 1H), 5.38 (dtq, *J* = 15.1, 7.3, 1.8 Hz, 1H), 3.83 (dd, *J* = 6.7, 5.3 Hz, 1H), 2.67–2.49 (m, 2H), 1.67 (d, *J* = 6.4 Hz, 3H); (*Z*-isomer, a representative signal) δ: 1.63 (d, *J* = 6.9 Hz, 3H).

anti-*2-Amino-3-phenylpent-4-enoic acid (4d) and (*E*)-2-amino-5-phenylpent-4-enoic acid (4d′) (4d:4d′ = 93:7)*

mp 172–176 °C. ^{1}H NMR (400 MHz) δ: 7.52–7.28 (m, 5.00H), 6.65 (d, *J* = 15.6 Hz, 0.07H), 6.29–6.14 (m, 1.00H), 5.36 (d, *J* = 17.4 Hz, 0.93H), 5.34 (d, *J* = 10.1 Hz, 0.93H), 3.98 (d, *J* = 7.8 Hz, 0.93H), 3.91–3.83 (m, 1.00H), 2.89–2.71 (m, 0.14H). For **4d**: ^{13}C NMR (150 MHz) δ: 173.6, 139.2, 135.3, 129.8, 128.54, 128.47, 120.6, 60.0, 51.8; for **4d′**: (distinguishable signals) δ: 174.7, 137.2, 129.5, 127.0, 123.6, 54.9, 34.7. HR-ESI-MS calcd. for $C_{11}H_{14}NO_2$: 192.1019 (M + H^+); found: 192.1021.

syn-*Aminocyclohex-2-enyl-acetic acid (4e)*

mp 233–236 °C. ^{1}H NMR (400 MHz) δ: 6.07–5.96 (m, 1H), 5.54 (d, *J* = 10.1 Hz, 1H), 3.78 (d, *J* = 4.1 Hz, 1H), 2.94–2.80 (m, 1H), 2.08–1.90 (m, 2H), 1.85–1.74 (m, 1H), 1.72–1.61 (m, 1H), 1.60–1.46 (m, 1H), 1.40–1.25 (m, 1H). ^{13}C NMR (100 MHz) δ: 174.4, 133.7, 126.1, 58.9, 37.1, 24.8, 23.2, 21.6. HR-ESI-MS calcd. for $C_8H_{14}NO_2$: 156.1019 (M + H^+); found: 156.1015.

2-Amino-3,3-dimethylpent-4-enoic acid (4f)

mp 212–216 °C. ^{1}H NMR (400 MHz) δ: 5.86 (dd, *J* = 17.4, 11.0 Hz, 1H), 5.24 (d, *J* = 11.0 Hz, 1H), 5.21 (d, *J* = 17.4 Hz, 1H), 3.52 (s, 1H), 1.21 (s, 3H), 1.14 (s, 3H). ^{13}C NMR (100 MHz) δ: 173.4, 143.0, 116.0, 62.9, 38.8, 25.0, 22.0. HR-ESI-MS calcd. for $C_7H_{14}NO_2$: 144.1019 (M + H^+); found: 144.1020 (checked as an 85:15 mixture of **4f** and **4f′**).

2-Amino-5-methylhex-4-enoic acid (4f′)

mp 198–202 °C. ^{1}H NMR (400 MHz) δ: 5.10 (t, *J* = 7.8 Hz, 1H), 3.74 (t, *J* = 6.0 Hz, 1H), 2.68–2.50 (m, 2H), 1.74 (s, 3H), 1.65 (s, 3H). ^{13}C NMR (100 MHz) δ: 175.1, 139.6, 116.7, 55.3, 29.7, 25.7, 17.7. HR-ESI-MS calcd. for $C_7H_{14}NO_2$: 144.1019 (M + H^+); found: 144.1021.

© 2005 NRC Canada

Table 3. Isomerization of *syn*-**4c**.

Time (min)	*syn*-**4c**:**4c′**	*E*:*Z* ratio of **4c′**
0	94:6	20:80
30	70:30	33:67
90	39:61	37:63
210	13:87	40:60
330	5:95	38:62

Table 4. Isomerization of *anti*-**4c**.

Time (min)	*anti*-**4c**:**4c′**	*E*:*Z* ratio of **4c′**
0	98:2	>97:<3
4	93:7	>97:<3
10	81:19	>97:<3
28	57:43	>97:<3
59	31:69	>97:<3
120	7:93	>97:<3
180	3:97	>97:<3

(±)-Alloisoleucine and (±)-isoleucine

Prepared according to the reported method (2).

Monitoring isomerization of 4c to 4c′ by ^{1}H NMR spectroscopy

A solution of *syn*- or *anti*-**4c** (7.7 mg, 0.06 mmol including a small amount of **4c′**) in deuterium oxide (0.6 mL) in a NMR sample tube was heated at 50 °C for 1 h and checked by ^{1}H NMR spectroscopy. No isomerization between **4c** and **4c′** was observed. Then, glyoxylic acid (0.1 equiv., 60 µL of a 0.1 mol/L solution in deuterated oxide) was added to the solution. The mixture was heated at 50 °C and monitored by ^{1}H NMR spectroscopy intermittently. Gradual changes of the **4c**:**4c′** ratio was observed as shown in Tables 3 and 4 (see also Fig. 1). Epimerization between *syn*- and *anti*-**4c** was not observed during the reaction.

Acknowledgements

This work was partially supported by CREST (Core Research for Evolutional Science and Technology), SORST (Solution Oriented Research for Science and Technology), ERATO (Exploratory Research for Advanced Technology), the Japan Science and Technology Agency (JST), and a Grant-in-Aid for Scientific Research from the Japan Society of the Promotion of Science (JSPS).

References

1. A. Hoefnagel, H. van Bekkum, and J.A. Peters. J. Org. Chem. **57**, 3916 (1992).
2. M. Sugiura, K. Hirano, and S. Kobayashi. J. Am. Chem. Soc. **126**, 7182 (2004).
3. Synthesis of 1,2-dihydro-4-phenylquinazoline-2-carboxylic acids from hydroxyglycine and 2-aminobenzophenones was reported, though no carbon–carbon bond formation is involved in this reaction, see: A. Hoefnagel, H. van Koningsveld, F. van Meurs, J.A. Peters, A. Sinnema, and H. van Bekkum. Tetrahedron, **49**, 6899 (1993).
4. (*a*) W.R. Roush and A.E. Walts. Tetrahedron Lett. **26**, 3427 (1985); (*b*) W.R. Roush, M.A. Adam, A.E. Walts, and D.J. Harris. J. Am. Chem. Soc. **108**, 3422 (1986); (*c*) R.W. Hoffmann, W. Ladner, and K. Ditrich. Liebigs Ann. Chem. 883 (1989); (*d*) M. Murata, S. Watanabe, and Y. Masuda. Tetrahedron Lett. **41**, 5877 (2000).
5. Several examples of 2-aza (or azonia) Cope rearrangement have been reported: (*a*) R.M. Horowitz and T.A. Geissman. J. Am. Chem. Soc. **72**, 1518 (1950); (*b*) L.E. Overman and M. Kakimoto. J. Am. Chem. Soc. **101**, 1310 (1979), and refs. cited therein; See also a review: (*c*) N.M. Przheval'skii and I.I. Grandberg. Usp. Khim. **56**, 814 (1987).
6. Related isomerization of homoallylic alcohols via 2-oxonia Cope rearrangement has been reported, see: (*a*) S. Sumida, M. Ohga, J. Mitani, and J. Nokami. J. Am. Chem. Soc. **122**, 1310 (2000); (*b*) J. Nokami, L. Anthony, and S. Sumida. Chem. Eur. J. **6**, 2909 (2000); (*c*) K.-T. Tan, S.-S. Chng, H.-S. Cheng, and T.-P. Loh. J. Am. Chem. Soc. **125**, 2958 (2003).

© 2005 NRC Canada

Synthesis, structure determination, and hydroformylation activity of *N*-heterocyclic carbene complexes of rhodium[1]

Austin C. Chen, Daryl P. Allen, Cathleen M. Crudden, Ruiyao Wang, and Andreas Decken

Abstract: The effect of ancillary phosphine ligands on the structure and hydroformylation activity of Rh-*N*-heterocyclic carbene complexes of type [Rh(IMes)(PR_3)(CO)Cl] and [Rh(SIMes)(PR_3)(CO)Cl] is described. Very high selectivities for the branched isomer (>95:5) were obtained in the hydroformylation of vinylarenes in all cases except for R = OPh. The new complexes were characterized spectroscopically and by X-ray crystallography.

Key words: hydroformylation, rhodium, *N*-heterocyclic carbene, IMes.

Résumé : On décrit l'effet des ligands phosphines d'appoint sur la structure et l'activité d'hydroformylation de carbènes complexes Rh-*H*-hétérocyclique, du type [Rh(IMes)(PR_3)(CO)Cl] et [Rh(SIMes)(PR_3)(CO)Cl]. Dans tous les cas excepté celui où R = OPh, des sélectivités très élevées de l'isomère ramifié (>95 : 5) ont été obtenues lors de l'hydroformylation de vinylarènes. Les nouveaux complexes ont été caractérisés par spectroscopie et par diffraction des rayons X.

Mots clés : hydroformylation, rhodium, carbène *N*-hétérocyclique, IMes.

[Traduit par la Rédaction]

Introduction

The hydroformylation of alkenes is among the most important and well-studied catalytic reactions. First discovered in 1938 by Otto Roelen, the reaction adds the elements of hydrogen and carbon monoxide across carbon–carbon multiple bonds (1). Industrially, the hydroformylation reaction is employed for the production of 5–10 billion tons of aldehydes and alcohols yearly (2). The largest single product from this reaction is 2-ethylhexanol, a precursor to phthalate ester plasticizers (Scheme 1). For major industrial applications, the desired product in the hydroformylation of propene is the linear isomer (3).

The process is run commercially with homogeneous Rh catalysts in the presence of large excesses of phosphine, usually greater than 0.3 mol/L, which translates to 8%–50% of the total solution by weight. Such excesses of phosphine are required because under carbon monoxide pressure, the catalyst is in equilibrium with di- and tricarbonyl species that have a lower selectivity for the linear isomer (eq. [1]) (4). In addition, degradation of the phosphine occurs by oxidative addition of Rh into the P—C bond (5). Ultimately, this process leads to an erosion of selectivity because the degraded phosphines give lower selectivity, and more importantly, inactive Rh dimers can form that decrease the overall efficiency of the catalyst.

With vinylarenes as the substrates, the branched isomer is the target since the hydroformylated product can be converted into the corresponding 2-aryl propionic acid by a simple oxidation (eq. [2]) (6). High-branched selectivity can often be obtained depending on the choice of catalyst and ligand. Since the analgesic activity of 2-arylpropionic acids is ascribed solely to the S enantiomer, the asymmetric hydroformylation of vinylarenes has also been developed (7). However, ibuprofen, one of the largest volume nonsteroidal anti-inflammatory drugs (NSAIDs), is sold as a

[1] $$HRh(CO)_3(PPh_3) \underset{CO}{\overset{PPh_3}{\rightleftharpoons}} HRh(CO)_2(PPh_3)_2 \underset{CO}{\overset{PPh_3}{\rightleftharpoons}} HRh(CO)(PPh_3)_3$$

Received 25 October 2004. Published on the NRC Research Press Web site at http://canjchem.nrc.ca on 20 August 2005.

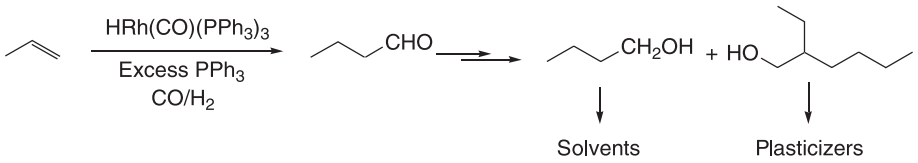
This paper is dedicated to Howard Alper, scientist and mentor.

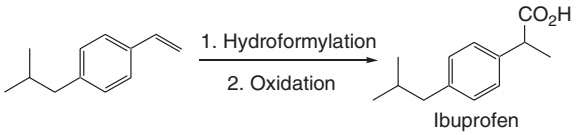
A.C. Chen,[2] D.P. Allen, C.M. Crudden,[3] and R. Wang.[4] Department of Chemistry, Queen's University, 90 Queen's Crescent, Kingston, ON K7L 3N6, Canada.
A. Decken.[4] Department of Chemistry, University of New Brunswick, P.O. Box 45222, Fredericton, NB E3B 6E2, Canada.

[1]This article is part of a Special Issue dedicated to Professor Howard Alper.
[2]Present address: Merck Frosst Centre for Therapeutic Research, Merck Frosst Canada Ltd., 16711 Trans Canada Highway, Kirkland, QC H9H 3L1, Canada.
[3]Corresponding author (e-mail: cruddenc@chem.queensu.ca).
[4]Corresponding authors for crystallography (e-mail: rwang@chem.queensu.ca and adecken@unb.ca).

 doi: 10.1139/V05-106 © 2005 NRC Canada

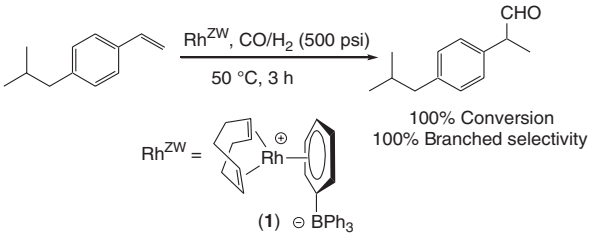
Scheme 1. Hydroformylation of propylene to produce commodity chemicals.



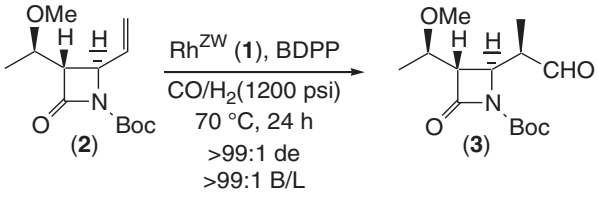
[2] 

racemate because of the presence of an inverting enzyme in the body that converts the inactive R enantiomer into the S (8). Naproxen, another large volume drug in this class, is sold in enantiomerically pure form, but the final step in the commercial process is a dynamic kinetic resolution (9). Therefore, an efficient, racemic hydroformylation that provides the branched isomer as the major product could be a viable method for the synthesis of ibuprofen or naproxen.

Several catalysts have been examined for the branched selective hydroformylation of vinylarenes, with one of the most effective being a zwitterionic catalyst (**1**) developed by Alper and Amer (10) (eq. [3]). This catalyst promotes the highly selective hydroformylation of vinylarenes at moderate pressures of carbon monoxide and hydrogen. In the hydroformylation of *p*-isobutylstyrene, the precursor to ibuprofen is obtained in 100% conversion after 3 h, with no detectable linear aldehyde.

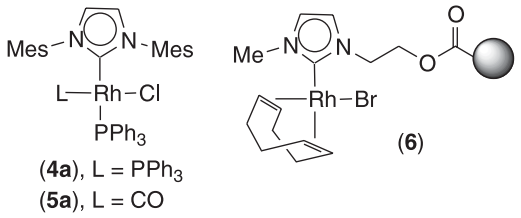
[3] 

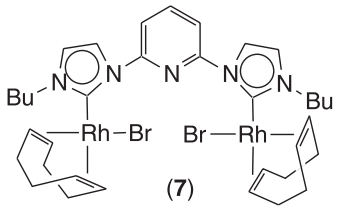
In addition to the hydroformylation of vinylarenes, a variety of functionalized alkenes react with high levels of selectivity using catalyst **1** (11). As shown in eq. [4], densely functionalized 4-vinyl β-lactam substrates such as **2** can be hydroformylated with high levels of regio- and stereocontrol using catalyst **1**. The product (**3**) can be easily elaborated into 1-methylcarbapenem antibiotics.

[4] 

Transition-metal complexes of *N*-heterocyclic carbenes (NHCs) have received considerable attention of late, particularly in coupling reactions (12, 13) and metathesis chemistry (14). Despite the importance of the hydroformylation reaction, and the significant number of Rh–NHC complexes that were prepared in the early 1980s by Lappert and co-workers (15), very little work has been done on the catalytic activity of NHC-ligated complexes in the hydroformylation reaction. This is somewhat remarkable since the professed strength of the metal–carbene bond (16) would prevent the type of dissociative equilibria that is problematic in Rh–phosphine complexes. Furthermore, breakdown of the carbene ligand is not anticipated to occur to the same extent as it occurs with phosphine complexes. However, it should be noted that examples have been reported in which carbene complexes breakdown under catalytic conditions (17).

Chart 1. *N*-Heterocyclic carbene-based hydroformylation catalysts.





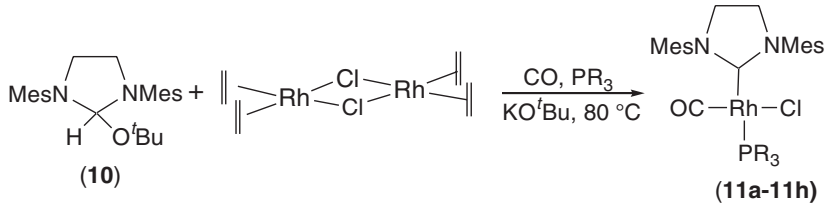
In addition to our recent report of Rh–NHC catalysts **4a** and **5a** (Chart 1) for the hydroformylation of vinylarenes (18), we are aware of only two other published reports of NHC complexes that are catalytically active in the hydroformylation reaction. Weberskirch and co-workers (19) have described a Rh catalyst immobilized on a hydrophilic polymer (**6**) for the hydroformylation of 1-octene and Fernandez and co-workers (20) have prepared a bimetallic Rh carbene (**7**) that is active in the hydroformylation of styrene (Chart 1). A cobalt–carbene complex has been prepared by Van Rensburg et al. (21), but it showed no hydroformylation activity.

Results and discussion

The first complex that we examined in the hydroformylation of vinylarenes was **4a** ([ClRh(IMes)(PPh_3)$_2$]), a direct analog of Wilkinson's catalyst (**8**) ([ClRh(PPh_3)$_3$]), which was prepared in 87% yield by reaction between free IMes (**9**, 1,3-bis(2,4,6-trimethylphenyl)imidazol-2-ylidene) and **8** (eq. [5]). Since this species was highly air sensitive and somewhat difficult to handle, we employed its carbonyl derivative **5** ([ClRh(IMes)(CO)(PPh_3)]) in hydroformylation

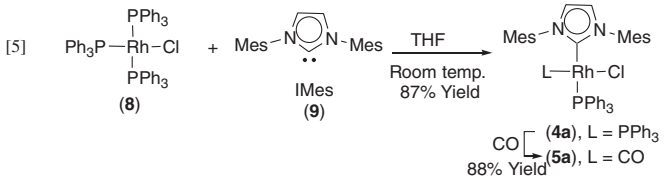
© 2005 NRC Canada

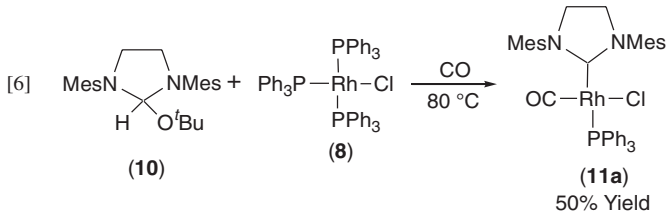
Table 1. Synthesis of rhodium–carbene complexes **11a**–**11h**.

[7] 

Complex	Phosphine	Carbene	Isolated yield (%)[a]
5a[b]	PPh_3	IMes	88
11a	PPh_3	SIMes	86
11b	$P(OPh)_3$	SIMes	77
11c	$P(p\text{-}OMePh)_3$	SIMes	64
11d	$P(p\text{-}FPh)_3$	SIMes	63
11e	Ph-DBP[c]	SIMes	57
11f	$P(furyl)_3$	SIMes	31
11g	PCy_3	SIMes	29
11h	$P(o\text{-}tolyl)_3$	SIMes	31

[a]Isolated after chromatography on silica gel.
[b]Note that the IMes complex **5a** was prepared by the two-step route shown in eq. [5].
[c]Ph-DBP stands for phenyldibenzophosphole.

[5] 

[6] 

studies. This species was readily prepared by passing a stream of carbon monoxide through a solution of **4a**, providing **5a** in 88% yield.

The resulting lime-yellow complex (**5a**) was highly stable, and could be handled in air and even purified by silica gel chromatography. The ^{31}P NMR spectrum of **5a** contained one phosphine doublet at 31.7 ppm, with a ^{31}P–^{103}Rh coupling constant of 115 Hz, consistent with a phosphine ligand trans to the carbene ligand (22). X-ray quality crystals were obtained by slow diffusion of hexanes into a solution of **5a** in THF.[5]

Since Grubbs' catalyst is more active when prepared with the saturated carbene SIMes (1,3-dimesitylimidazolin-2-ylidene) than IMes itself, we attempted to prepare a Rh complex of this carbene using the in situ protocol described by Morgan and Grubbs (23). To generate the free carbene from *tert*-butanol adduct **10**, heating to 80 °C is required. Unfortunately, treatment of Wilkinson's catalyst (**8**) with **10** at this temperature gave none of the desired complex. Subsequent studies from our group have shown that complexes of the type $[ClRh(NHC)(PR_3)_2]$ have limited thermal stability, and thus it was likely that the desired complex was decomposing under the reaction conditions. However, when this reaction was carried out under an atmosphere of carbon monoxide, the desired carbene complex was isolated in 50% yield as bright yellow bricks (eq. [6]).

To prepare a variety of carbene complexes from a common rhodium source, $[Rh(CH_2{=}CH_2)_2Cl]_2$ was examined as an alternative to Wilkinson's type complexes. Treatment of this species with **10** in the presence of 1 equiv. of phosphine and 1 atm of CO (1 atm = 101.325 kPa) gave the desired complex **11a** in 85% isolated yield (Table 1). This procedure was effective for a variety of different complexes **11a**–**11h** in moderate to good yield (eq. [7], Table 1). In those cases where decreased yield is observed, biscarbene and bisphosphine complexes were invariably observed. However, the high air and moisture stability of the complexes **11a**–**11h** permitted their facile separation from these species by column chromatography. After chromatographic purification, crystallization from dichloromethane–pentane mixtures provided X-ray quality crystals in all cases except for **11c** and **11d**. The crystal structures of complexes **11a** and **11b** and **11e**–**11h** are shown in Figs. 1–6, and the crystallographic data summarized in Tables 2–5.

As previously observed in the crystal structure of **5a**, complexes **11a**–**11h** are square-planar about rhodium, with the Cl and CO ligands in a trans orientation as would be expected. Table 4 describes the key bond lengths and angles,

[5]Note that the original crystal structure reported in ref. 18 was carried out at room temperature. For comparison's sake, we have performed a new crystal structure determination at –93 °C.

© 2005 NRC Canada

Fig. 1. X-ray crystallographic structure of compound **11a**.

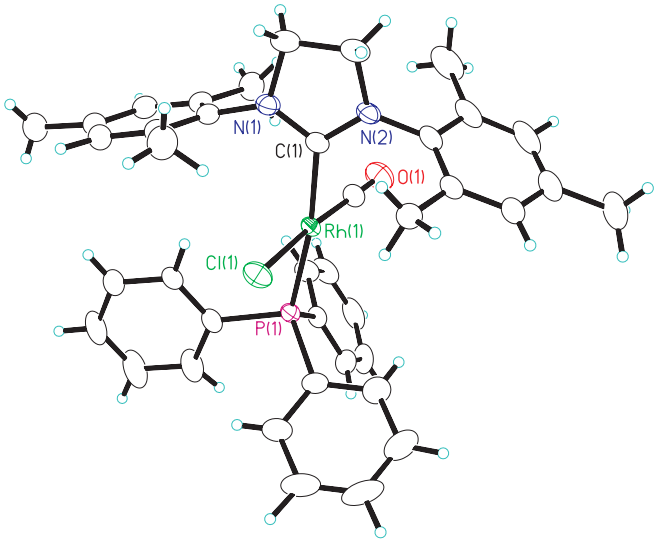
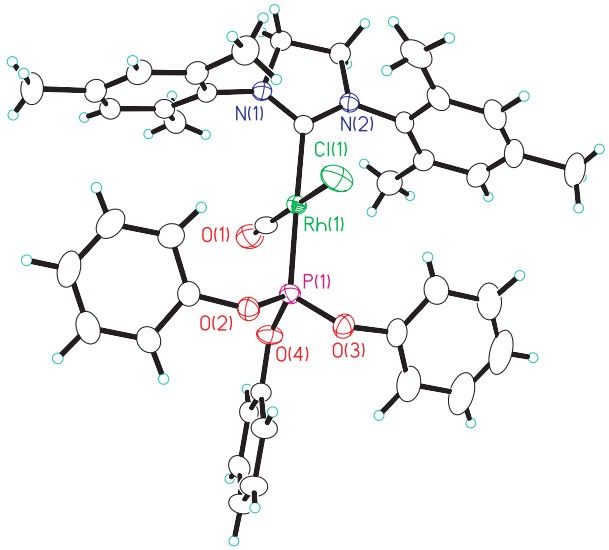


Fig. 2. X-ray crystallographic structure of compound **11b**.

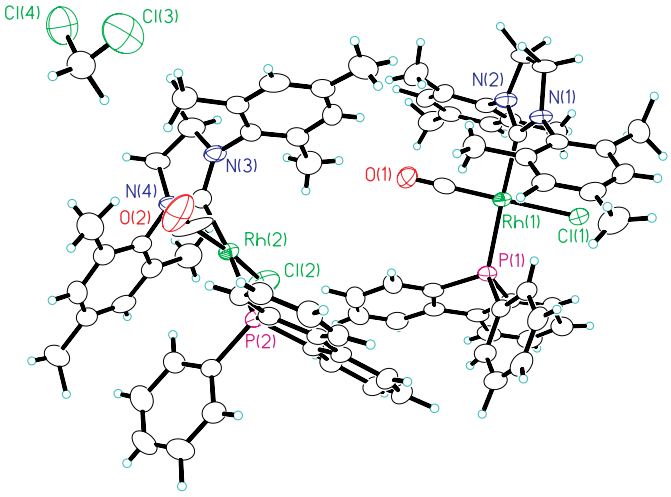


respectively, for carbene complexes **4a** (24), **5a**, and **11a**, along with data for the all phosphine derivatives **8** (25) and **12** ([ClRh(CO)(PPh_3)$_2$]) (26). All compounds are approximately square-planar around Rh, with the sums of the bond angles around Rh equaling approximately 360°. The most distorted is the IMes bisphosphine complex **4a**. In this case, the sum of the angles on the side of the phosphines (C_{NHC}-Rh-PPh_3 and Ph_3P-Rh-PPh_3) is 194.7(15)°, which is significantly greater than 180°. The chloro side of the molecule compensates for this with both angles being acute, and adding up to 165.9(15)°. Replacing the phosphine cis to the IMes with a CO ligand as in compound **5a** relieves the steric strain considerably such that the sum of the angles on the CO side of the molecule is very close to 180° (184.1(2)° in one molecule and 176.1(9)° in the other molecule in the crystal structure). SIMes derivative **11a** and phosphine carbonyl species **12** all have similar bond angles, but Wilkinson's catalyst **8** (25) is also significantly distorted. Thus, it is likely the presence of two *cis*-phosphines that leads to the distortion from ideal geometry.

The Rh–carbene bond length is similar in the SIMes, IMes, and CO derivatives, but interestingly the Rh—CO bond length is quite short in IMes complex **5a** (1.706(5) Å), especially compared with **11a** and **12** (26) at 1.8126(17) and 1.810(7) Å, respectively. However, in this case, the crystals were found to be disordered with 50% occupancy of the Cl and CO ligands,[6] and if one examines the other molecule in the crystal structure, the Rh—CO bond length is quite long at 1.828(7) Å. Thus, packing effects obviously cannot be ignored and the length of the Rh—CO bond should not be over interpreted.

The shortest Rh—P bond is found for **5a** at 2.2988(7) Å. The Rh—P bonds are shorter in all the carbene complexes compared with the phosphine complexes **8** and **12**, although the differences are not large. Rh—Cl bonds again show similarities among NHC complexes and bisphosphine complexes, being approximately 2.39 Å in the former and 2.37 Å in the latter.

Fig. 3. X-ray crystallographic structure of compound **11e** showing both independent molecules in the crystal structure.



In Table 5, the crystallographic data of other SIMes carbonyl derivatives are collected along with data for **5a**. All the complexes are square-planar, with little distortion as evidenced by the sum of the bond angles in many cases being close to 180°. The C(2)-Rh-P tensor is most linear for phosphite complex **11b** compared with all of the other complexes (179.19(4)°). With the exception of **5a** and **11e**, which are composed of two independent molecules in the crystal structure, the Rh—CO bond length is longest for **11b** (1.856(2) Å), which is reasonable since the phosphite ligand likely accepts some of the electron density from Rh, resulting in less backbonding to the CO ligand. The Rh—CO bond length is the shortest for complexes **11g** and **11h**, which have relatively bulky phosphine ligands (P(*o*-tolyl)$_3$ and PCy_3). Interestingly, the two orientations of the molecules in the crystal structures of **5a** and **11e** sport one very short (1.706(5) and 1.793(5) Å) and one very long (1.828(7)

[6] Note that this was the case in two separate crystal structure determinations on different batches of **5a**.

© 2005 NRC Canada

Fig. 4. X-ray crystallographic structure of compound **11f** showing the two independent molecules in the crystal structure.

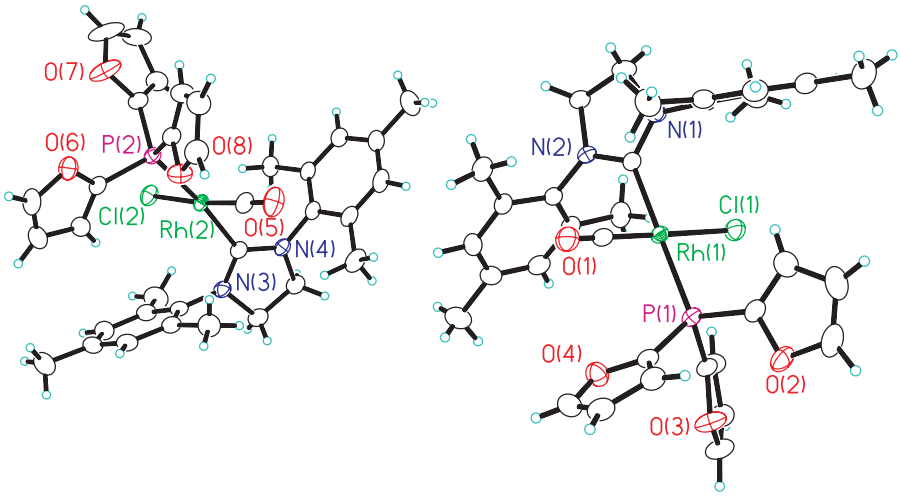


Fig. 5. X-ray crystallographic structure of compound **11g**.

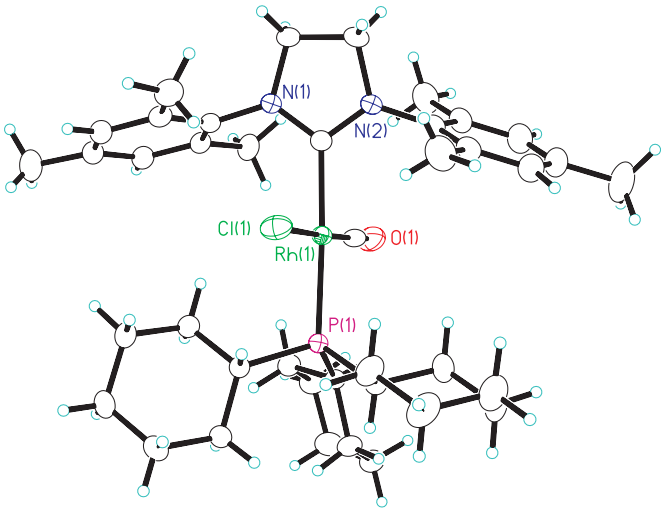
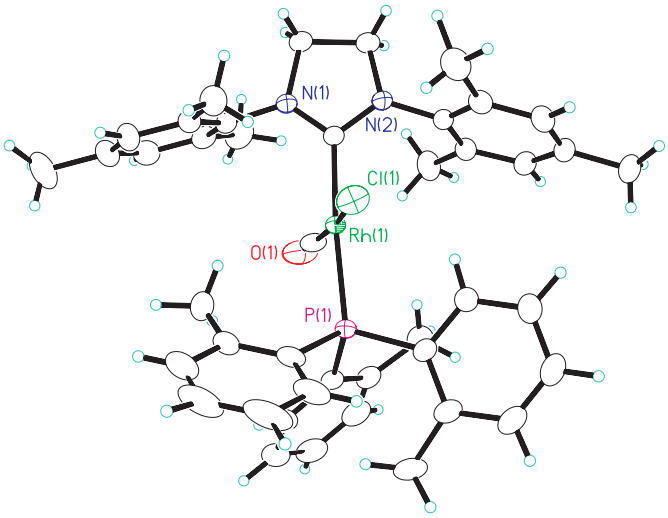


Fig. 6. X-ray crystallographic structure of compound **11h**.



and 1.931(8) Å) Rh—CO bond. However, compound **11f**, which is also composed of two individual orientations, has relatively similar bond lengths: 1.8106(17) and 1.8075(17) Å.

The IR frequencies for key stretches in complexes **11a**–**11h** and **5a** are compiled in Table 6 (27). The carbonyl IR frequency for **12** ([ClRh(PPh_3)$_2$(CO)]) is 1980 cm^{-1} (27*c*), which is significantly higher than that of the SIMes derivative [ClRh(SIMes)(PPh_3)(CO)] **11a** (1954 cm^{-1}) and IMes derivative **5a** (1944 cm^{-1}). This implies that backbonding is more significant in the *N*-heterocyclic carbene complexes, which would be expected since carbenes are better donors than phosphines. Interestingly, the carbonyl stretch of IMes derivative **5a** is lower than that of the SIMes derivative, which is contrary to what would be expected since SIMes is believed to be a stronger donor than IMes, although the difference is small (28). Within the SIMes derivatives, the lowest stretch comes from the most electron-rich phosphine complex **11g** (PCy_3) at 1940 cm^{-1}), while the highest is for triphenylphosphite derivative **11b** (1976 cm^{-1}), consistent with the decreased back donation into the CO ligand for the phosphite derivative.

NMR data for the NHC–Rh complexes are also compiled in Table 6. As expected, the ^{31}P NMR spectra display a simple doublet from coupling to ^{103}Rh. The ^{13}C NMR data show little variation in the carbon monoxide resonance, even compared to **12**, where the CO resonates at 187.4 ppm (27*c*). However, there is a significant difference of 27.4 ppm between the NHC resonance for the carbon bound to Rh in the IMes derivative **5a** and the same carbon in SIMes complex **11a** (Table 6, entries 1 and 2). The IMes ligand resonates at 184.1 ppm, while the SIMes derivatives are all around 211 ppm. Although large, this difference tracks extremely well with the observed difference in the chemical shifts of the free carbenes, where SIMes is 24 ppm downfield of IMes (SIMes 243.8 ppm, IMes 219.7 ppm) (29). The position of the carbene carbon resonance is quite sensitive to electronics, as this carbon appears at 197.14 ppm in ClRh(IMes)(PPh_3)$_2$ (**4a**) and is shifted a remarkable 13 ppm

© 2005 NRC Canada

Table 2. Crystallographic data for **5a**, **11a**, **11b**, and **11e**.

	5a	**11a**	**11b**	**11e**
Empirical formula	$C_{40}H_{39}ClN_2OPRh$	$C_{40}H_{41}ClN_2OPRh$	$C_{40}H_{41}ClN_2O_4PRh$	$C_{40}H_{39}N_2OPClRh{\cdot}0.5CH_2Cl_2$
Formula weight	733.06	735.08	783.08	775.53
Crystal system	Monoclinic	Monoclinic	Monoclinic	Monoclinic
Space group	$P2_1/c$	$P2_1/n$	$P2_1/n$	$P2_1/n$
Unit cell dimensions				
a (Å)	17.698(7)	9.5449(5)	10.6810(5)	21.994(4)
b (Å)	13.592(5)	17.4887(10)	15.0618(7)	14.847(3)
c (Å)	14.851(5)	21.2791(12)	23.9284(11)	23.653(4)
α (°)	90	90	90	90
β (°)	93.356(6)	93.7350(10)	101.9110(10)	109.268(4)
γ (°)	90	90	90	90
Volume (Å^3)	3 566(2)	3 544.5(3)	3 766.6(3)	7 291(2)
Z	4	4	4	8
Density (calcd.) (Mg/m^3)	1.365	1.377	1.381	1.413
Crystal size (mm^3)	0.5 × 0.2 × 0.1	0.10 × 0.37 × 0.40	0.175 × 0.25 × 0.375	0.050 × 0.175 × 0.325
F(000)	1 512	1 520	1 616	3 192
Reflections collected	23 770	38 753	41 479	47 155
Independent reflections	8 366 (R_{int} = 0.0239)	12 744 (R_{int} = 0.0449)	13 557 (R_{int} = 0.0207)	12 849 (R_{int} = 0.1147)
Data/restraints/parameters	8 366/0/598	12 744/0/579	13 557/0/603	12 849/0/1 176
Final R indices ($I > 2\sigma(I)$)	R_1 = 0.0270,	R_1 = 0.0323,	R_1 = 0.0341,	R_1 = 0.0487,
	wR_2 = 0.0553	wR_2 = 0.0824	wR_2 = 0.0949	wR_2 = 0.1082
R indices (all data)	R_1 = 0.0434,	R_1 = 0.0446,	R_1 = 0.0451,	R_1 = 0.0803,
	wR_2 = 0.0588	wR_2 = 0.0872	wR_2 = 0.0989	wR_2 = 0.1131
Goodness-of-fit on F^2	0.942	1.001	1.068	0.911
θ Range for data collection (°)	1.15–28.31	1.51–32.50	1.61–32.50	1.54–25.00
Absorption coefficient (mm^{-1})	0.632	0.636	0.609	0.693
Largest diff. peak and hole (e Å^{-3})	0.522 and –0.596	1.515 and –0.612	2.053 and –0.392	1.466 and –0.852

upfield by replacing one phosphine with a carbonyl ligand. Since the two downfield resonances in **5a** are very close to each other, a derivative of **5a** in which the carbene carbon was labeled with ^{13}C was prepared by treating ^{13}C-labeled **4a** with carbon monoxide.[7,8] This allowed us to assign the resonance at 184.1 ppm to the carbene carbon. As expected, both the NHC and CO resonances appeared as doublets of doublets because of the one-bond coupling to Rh and two-bond coupling to the phosphine.

Hydroformylation activity

Carbene complexes **4a** and **5a** were both examined in the hydroformylation of styrene as shown in Table 7. Wilkinson's catalyst itself (**8**) gives only 35% conversion after 19 h at 60 °C, with a poor branched to linear ratio of 87:13 (Table 7, entry 1). Replacing one phosphine with IMes (catalyst **4a**) results in significantly higher selectivity for the branched isomer (96:4), and approximately twice the conversion (Table 7, entry 2). The carbon monoxide derivative (**5a**) reacted with equally high selectivity, but to retain the activity, an equimolar amount of triphenyl phosphine was added (Table 7, entry 4). The reason for this is currently under investigation, but may have to do with the requirement for more than one phosphine on Rh in the key catalytic species, as in eq. [1]. Interestingly, compound **12** ([Rh(CO)-$PPh_3)_2$Cl]) displayed decreased regioselectivity and poor conversion, even in the presence of added phosphine (Table 7, entry 7), illustrating that the improved activity and selectivity are due to the carbene ligand. Under optimized conditions, a variety of vinylarenes were hydroformylated with complex **5a** in high yield and high selectivity (Table 7, entries 8–11).

The effect of varying the nature of the phosphine and the carbene was then examined as shown in Table 8 (31). On changing the catalyst from the unsaturated IMes derivative to the saturated SIMes catalyst, the turnover frequency doubled while the selectivity for the branched isomer stayed the same. Electron-donating substituents at the para position of the phosphine such as in compound **11c** (Table 8, entry 4) had little effect on the rate or the branched selectivity. Sterically hindered phosphines such as tricyclohexylphosphine and P(o–tolyl)$_3$ gave decreased selectivity for the branched isomer and decreased rates (Table 8, entries 8 and 9). The worst ligand in terms of rate and selectivity is triphenyl phosphite **11b** (Table 8, entry 3). Phenyl-dibenzophosphole also displayed decreased activity and somewhat diminished selectivity. In terms of rate, the best catalyst was

[7] This species was prepared for another project in collaboration with Jason Clyburne, starting with ^{13}C-labeled imidazolium chloride: C.M. Crudden, D.P. Allen, J.A.C. Clyburne, and T. Ramnial. Manuscript in preparation.

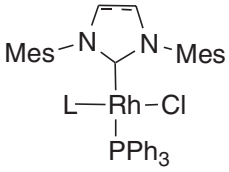
[8] In the case of the SIMes derivatives, the assignment was made based on the coupling constants to Rh and to the adjacent phosphine, which are very similar in magnitude to those reported for **12** ([ClRh($PPh_3)_2$CO]), δ 187.4 ppm, $^1J_{C\text{-}Rh}$ = 73 Hz, $^2J_{C\text{-}P}$ = 16 Hz (27).

© 2005 NRC Canada

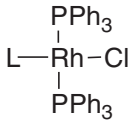
Table 3. Crystallographic data for **11f–11h**.

	11f	**11g**	**11h**
Empirical formula	$C_{34}H_{35}ClN_2O_4PRh$	$C_{40}H_{59}ClN_2OPRh$	$C_{43}H_{47}ClN_2OPRh$
Formula weight	704.97	753.22	777.16
Crystal system	Monoclinic	Monoclinic	Monoclinic
Space group	$P2_1/c$	$P2_1/c$	$P2_1/c$
Unit cell dimensions			
a (Å)	16.2872(7)	18.8173(18)	10.4520(5)
b (Å)	22.3885(10)	13.5796(12)	22.9109(11)
c (Å)	17.6696(8)	15.2781(14)	17.0653(8)
α (°)	90	90	90
β (°)	91.0470(10)	98.644(2)	105.8270(10)
γ (°)	90	90	90
Volume (Å^3)	6442.1(5)	3859.7(6)	3931.6(3)
Z	8	4	4
Density (calcd.) (Mg/m^3)	1.454	1.296	1.313
Crystal size (mm^3)	0.025 × 0.20 × 0.50	0.025 × 0.525 × 0.525	0.25 × 0.50 × 0.55
F(000)	2 896	1 592	1 616
Reflections collected	71 269	41 549	43 618
Independent reflections	23 209 (R_{int} = 0.0279)	13 837, (R_{int} = 0.0444)	14 143 (R_{int} = 0.0182)
Data/restraints/parameters	23 213/0/1 055	13 837/0/665	14 143/0/630
Final R indices ($I > 2\sigma(I)$)	R_1 = 0.0293, wR_2 = 0.0631	R_1 = 0.0365, wR_2 = 0.0800	R_1 = 0.0278, wR_2 = 0.0747
R indices (all data)	R_1 = 0.0523, wR_2 = 0.0673	R_1 = 0.0681, wR_2 = 0.0872	R_1 = 0.0362, wR_2 = 0.0780
Goodness-of-fit on F^2	0.914	0.930	1.084
θ Range for data collection (°)	1.47–32.50	1.86–32.50	1.53–32.50
Absorption coefficient (mm^{-1})	0.703	0.585	0.577
Largest diff. peak and hole (e Å^{-3})	0.980 and –0.337	1.610 and –0.449	1.000 and –0.469

Table 4. Crystallographic data of rhodium–carbene and phosphine complexes.



4a, NHC = IMes, L = PPh_3
5a, NHC = IMes, L = CO
11a, NHC = SIMes, L = CO



8, L = PPh_3
12, L = CO

Complex	Bond angles (°)		Bond lengths (Å)				
	Sum of angles[a]	C_{NHC}-Rh-P_{trans}	Rh—C_{NHC}	Rh—C_{CO}	Rh—P_{cis}[b]	Rh—P_{trans}[b]	Rh—Cl
4a (24)	194.7(15)/165.9(13)	164.10(4)	2.0527(14)	—	2.3053(4)	2.2158(4)	2.3941(4)
5a	184.1(2)/176.1(9)[c,d]	173.88(5)	2.0498(18)	1.706(5) (1.828(7))[c]	2.2988(7)	—	2.398(3) (2.398(2))[c]
11a	182.8(6)/177.9(14)	172.05(4)	2.0526(14)	1.8126(17)	2.3080(4)	—	2.3888(4)
8 (25)	194.1(2)/169.8(1)[e]	159.1(2)[e,f]	—	—	2.304(4) (2.338(4))[g]	2.225(4)	2.404(4)
12 (26)	183.6(2)/176.5(1)	176.0(1)[f]	—	1.810(7)	2.327(1) (2.324(1))[g]	—	2.371(2)

[a]NHC-Rh-L plus L-Rh-PPh_3 or Ph_3P-Rh-L plus L-Rh-PPh_3 is given first followed by the sum of the angles on the other side of the molecule.
[b]Trans or cis to Cl.
[c]**5a** was obtained with 50% occupancy in the Cl/CO sites, so values for each molecule in the crystal are given.
[d]The sum of the angles in the second molecule is 176/184.2.
[e]Values are only given for the orange allotrope. See ref. 25 for the red allotrope.
[f]P-Rh-P angle.
[g]Rh—P bond length for the second phosphine cis to chlorine.

© 2005 NRC Canada

Table 5. Crystallographic data for rhodium–carbene complexes with different phosphines.

		Bond angles (°)		Bond lengths (Å)		
Complex	Phosphine	Sum of angles[a]	C_{NHC}-Rh-P	Rh—C_{NHC}	Rh—C_{CO}	Rh—P
5a	PPh_3	184.1(2)/176.1(9)	173.88(5)	2.0498(18)	1.706(5)[b] (1.828(7))	2.2988(7)
11a	PPh_3	182.8(6)/177.9(14)	172.06(4)	2.0523(14)	1.8125(17)	2.3079(4)
11b	$P(OPh)_3$	180.4(6)/179.7(16)	179.19(4)	2.0800(14)	1.856(2)	2.2402(4)
11e[c]	Ph-DBP	181.7(18)/178.3(12)[c] (180.7(19)/178.9(13))	175.78(13) (175.05(13))	2.057(4) (2.057(4))	1.793(5) (1.931(8))	2.3065(12) (2.3250(12))
11f[c]	$P(furyl)_3$	179.4(6)/180.5(14)[c] (180.4(6)/180.3(14))	178.77(4) (173.26(4))	2.0605(14) (2.0593(15))	1.8106(17) (1.8075(17))	2.2806(4) (2.2889(4))
11g	PCy_3	183.5(7)/176.5(18)	176.31(5)	2.0479(17)	1.811(2)	2.3312(5)
11h	$P(o\text{-tolyl})_3$	180.8(5)/179.8(12)	175.56(3)	2.0465(11)	1.8287(18)	2.3363(3)

[a]NHC-Rh-L plus L-Rh-PPh_3 given first followed by the sum of the angles on the other side of the molecule.
[b]**5a** was obtained with 50% occupancy in the Cl/CO sites, so values for each molecule in the crystal are given.
[c]**11e** and **11f** had two independent molecules in the crystal structure and so values are given for each individual molecule in the crystal.

Table 6. Spectroscopic data of the rhodium–carbene complexes.

			^{31}P NMR		^{13}C NMR	
Complex	Phosphine	IR (ν_{CO}, cm^{-1})	δ(ppm)	$J_{P\text{-}Rh}$ (Hz)	δ_{NHC} (ppm)[a]	δ_{CO} (ppm)
5a	PPh_3	1944	31.7	115.0	184.1	187.2
11a	PPh_3	1954	31.2	114.5	211.5	187.3
11b	$P(OPh)_3$	1976	122.2	196.0	209.4	184.5
11c	$P(p\text{-}OMePh)_3$	1954	26.7	111.6	211.7	187.2
11d	$P(p\text{-}FPh)_3$	1954	29.0	112.6	210.9	187.2
11e	Ph-DBP	1954	20.9	108.1	210.6	187.4
11f	$P(furyl)_3$	1969	–24.5	114.5	209.7	185.7
11g	PCy_3	1940	38.4	109.0	213.8	187.5
11h	$P(o\text{-tolyl})_3$	1956	26.0	90.0	211.6	187.9
12 (27, 31)	PPh_3	1980	29.1	124.0	n.a.	187.4

Note: n.a. = not applicable.
[a]Carbene carbon bound to Rh.

the trifuryl phosphine, although the regioselectivity was somewhat eroded.[9]

Several additives were examined for their effect on the reaction, with triethyl amine displaying the most dramatic effects. As shown in Table 9, the addition of triethyl amine increased the turnover frequencies for the hydroformylation by an order of magnitude in some cases, without any erosion in the branched to linear selectivity for most of the catalysts (compare to Table 8). Phosphite derivative **11b**, the phenyldibenzophosphole complex **11e**, and the two bulky phosphines **11g** and **11h** showed only marginal improvements upon the addition of triethylamine. It is likely that the accelerating effect of triethylamine is caused by removal of the chloride from the catalyst as HCl, a reaction that is accelerated by base (32). The reason that this effect is more dramatic with some of the catalysts is not clear yet, but may be due to the relative rates of reductive elimination of HCl. The catalysts that showed the lowest response to the addition of triethyl amine are also those with more electron-rich phosphines. These might be expected to undergo reductive elimination more slowly. It is possible that pretreament of the catalyst with triethylamine prior to the reaction would be a more effective strategy in these cases, an approach currently being investigated in our laboratories.

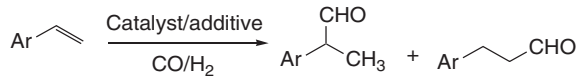
Interestingly, the hydroformylation of styrene with complex **11h** in the presence of triethylamine gave a considerable amount of the reduced alcohol along with the expected aldehyde. The ratio of alcohol to aldehyde was 63:37. This is the only time reduction was observed to accompany hydroformylation and is somewhat unusual since reducing ability is usually attributed to cobalt catalysts, not rhodium.

In conclusion, we have successfully prepared a variety of rhodium *N*-heterocyclic carbene complexes, which are capable of hydroformylating vinylarenes with high selectivity for the branched isomer. The IMes and SIMes complexes are more active than the corresponding all-phosphine derivatives, and SIMes-based catalysts appear to be twice as active as IMes derivatives. The addition of triethylamine causes an order of magnitude increase in rate, probably by promoting reductive elimination of HCl. Current work in our group is di-

[9]Note that in this case some decrease was observed in the turnover frequency with time so it is not clear how stable the catalyst is throughout the reaction conditions.

© 2005 NRC Canada

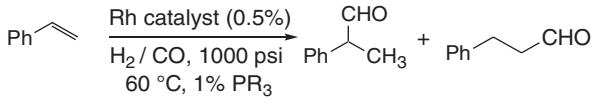
Table 7. Hydroformylation of vinylarenes with various catalysts.

[8] 

Entry	Ar	Catalyst	Additive	Conversion (%)[a]	Yield (%)[b]	B:L ratio[c]
1	Ph	**8**	None	35	—	87:13
2	Ph	**4a**	None	78	—	96:4
3	Ph	**5a**	None	38	—	94:6
4	Ph	**5a**	1 equiv. PPh_3	74	—	96:4
5	Ph	**5a**	2 equiv. PPh_3	79	—	96:4
6	Ph	**5a**	10 equiv. PPh_3	80	—	96:4
7	Ph	**12**	2 equiv. PPh_3	27	—	88:12
8	*p*-MePh	**5a**	2 equiv. PPh_3	—	96	96:4
9	*p*-ClPh	**5a**	2 equiv. PPh_3	—	94	97:3
10	*p*-MeOPh	**5a**	2 equiv. PPh_3	—	98	95:5
11	*p*-*i*-BuPh	**5a**	2 equiv. PPh_3	—	93	96:4

[a]At 0.5% catalyst loading after 19 h at 60 °C under an 1000 psi (1:1) atmosphere of CO and H_2 (1 psi = 6.894 757 kPa).
[b]Isolated yield at 1% catalyst loading.
[c]Branched-to-linear ratio elucidated from ^{1}H NMR analysis of the crude mixture.

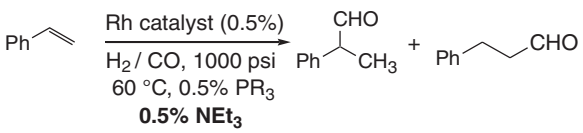
Table 8. Hydroformylation of styrene with rhodium–carbene catalysts.[a]

[9] 

Entry	Catalyst	Phosphine	TOF[b]	B:L ratio[c]
1	**5a**	PPh_3	8[d]	96:4
2	**11a**	PPh_3	14	94:6
3	**11b**	$P(OPh)_3$	0.5	65:35
4	**11c**	$P(p\text{-MeOPh})_3$	13	96:4
5	**11d**	$P(p\text{-FPh})_3$	31	95:5
6	**11e**	Ph-DBP	3	93:7
7	**11f**	$P(furyl)_3$	44[d]	91:9
8	**11g**	PCy_3	2	84:16
9	**11h**	$P(o\text{-tolyl})_3$	3	91:9

[a]At 0.5% catalyst loading (with 1% phosphine additive) at 60 °C under a 1000 psi (1:1) atmosphere of CO and H_2 (1 psi = 6.894 757 kPa).
[b]TOF = turnover frequency, measured at 25%–50% conversion unless otherwise noted.
[c]Branched-to-linear ratio determined by ^{1}H NMR analysis of the crude mixture.
[d]Measured at 70% conversion.

Table 9. Effect of added triethyl amine on the hydroformylation ability of Rh–carbene catalysts.[a]

[10] 

Entry	Catalyst	Phosphine	TOF[b]	B:L ratio[c]
1	**11a**	PPh_3	120	94:6
2	**11b**	$P(OPh)_3$	14	68:32
3	**11c**	$P(p\text{-MeOPh})_3$	121	96:4
4	**11d**	$P(p\text{-FPh})_3$	125	95:5
5	**11e**	Ph-DBP	9	94:6
6	**11f**	$P(furyl)_3$	113[d]	91:9
7	**11g**	PCy_3	n.r.[e]	—
8	**11h**	$P(o\text{-tolyl})_3$	12	94:6[f]

Note: n.r. = no reaction.
[a]Reaction stopped after 1 h unless otherwise noted.
[b]Turnover frequency.
[c]Estimated by ^{1}H NMR of crude reaction mixture.
[d]Measured after 30 min.
[e]After 1 h.
[f]Note that in this case the reduced alcohol was also observed. See text.

rected towards the de novo synthesis of a rhodium hydride carbene complex to obviate the need for the addition of NEt_3.

Experimental

General experimental

NMR spectra were recorded on an XL-200 (^{1}H at 200 MHz), a Varian Unity-400 (^{1}H at 400 MHz, ^{13}C at 100 MHz, ^{19}F at 376 MHz, and ^{31}P at 162 MHz), or a Bruker Avance 500 (^{1}H at 500 MHz, ^{13}C at 125 MHz) spectrometer in deuterated chloroform ($CDCl_3$) containing 0.03% TMS unless otherwise noted. ^{1}H NMR chemical shifts are reported in ppm relative to TMS (0.0 ppm) or $CHCl_3$ (7.26 ppm). ^{13}C NMR chemical shifts are reported in ppm relative to $CDCl_3$ (77.0 ppm). ^{19}F NMR chemical shifts are reported in ppm relative to the external standard $C_6H_5CF_3$ (–63.73 ppm). ^{31}P NMR chemical shifts are recorded in ppm relative to the external standard H_3PO_4 (0.0 ppm). Multiplicities are reported as broad (br), singlet (s), doublet (d), triplet (t), quartet (q), and multiplet (m),

© 2005 NRC Canada

along with integration (for ^{1}H NMR) and coupling constants (Hz). IR spectra were obtained with a Bruker IFS25 spectrometer as thin films on NaCl discs or as KBr pellets. Peaks are reported in cm^{-1} with relative intensities indicated (strong (s), medium (m), weak (w)). Mass spectra from UNB were recorded on a Kratos Concept 1H double-focusing mass spectrometer with 8 kV accelerating and 70 eV ionizing voltages. The spectrometer was calibrated against perfluorokerosene and has a resolution of 7000. Data are reported as *m*/*e* with intensities relative to the base peak. Mass spectra were recorded at Queen's University on an Applied Biosystems/MDS Sciex QSTAR XL Q-TOF mass spectrometer (Toronto, Ontario) equipped with an electrospray source. The sample was infused in a 1:1 mixture of CH_2Cl_2 and dried CH_3NO_2 at a flow rate of 6 μL/min. The spectrometer was internally calibrated and run in positive mode.

Solvents were dried and distilled under an inert atmosphere from the drying agents listed (33) — pentane, hexane, benzene, and toluene from sodium metal; acetonitrile, dichloromethane, and triethylamine from calcium hydride; diethyl ether and THF from sodium wire and benzophenone ketyl; DME from LAH; and acetone from $KMnO_4$. When necessary, solvents were purged of oxygen just prior to use by either flushing with argon or using repeated freeze–pump–thaw cycles.

With the exception of *p*-isobutylstyrene, which was prepared in three steps using a literature procedure (34), all other vinylarenes were purchased from commercial sources. Prior to use, they were distilled under a partial vacuum of argon and percolated through a column of dry, neutral alumina. *N*,*N*′-Bis(2,4,6-trimethylphenyl amino)ethane (35) and rhodium complexes $Rh(PPh_3)_3Cl$ (36) and $[Rh(C_2H_4)_2Cl]_2$ (37) were prepared according to literature procedures. Phosphine ligand Ph–DBP (38) was donated by Melanie Neil of Frank Bottomley's group. Triphenylphosphine was recrystallized from boiling ethanol and stored under argon. Technical grade chloromethyl methyl ether was distilled under argon and stored in a Schlenk flask.

Crystals of **5a** were grown by slow diffusion of hexane into a saturated solution of the complex in THF. A crystal of **5a** (colorless, plate-shaped, size 0.5 mm × 0.2 mm × 0.1 mm) was very quickly mounted on a glass fiber with grease. Data collection was performed at Queen's University on a Bruker SMART CCD 1000 X-ray diffractometer with graphite-monochromated Mo K radiation (λ = 0.710 73 Å), operating at 50 kV and 30 mA over 2θ ranges of 2.30°~56.62° at –93 °C controlled with a Crysostream Controller 700. No significant decay was observed during the data collection. Data were processed on a Pentium PC using the Bruker AXS Windows NT software package (version 5.10) (39). Neutral atom-scattering factors were taken from Cromer and Waber (40). The raw intensity data were converted (including corrections for scan speed, background, and Lorentz and polarization effects) to structure amplitudes and their esds using the program SAINT-Plus (39), which corrects for *L*p and decay. Empirical absorption corrections were applied using the program SADABS (41). The structure was solved and refined by using SHELXTL (39). The compound crystallized in the monoclinic space group $P2_1/c$, based on the systematic absences, *E* statistics, and successful refinement of the structure. The structure was solved by direct methods. Full-matrix least-square refinements minimizing the function $\Sigma w(F_o^2 - F_c^2)^2$ were applied to the compound. All non-hydrogen atoms were refined anisotropically. All hydrogen atoms were located gradually from the difference Fourier map and their contributions were included in the structure factor calculations.

Both Cl^- and CO have two positions (Cl(1A), C(22A), and O(1A) or Cl(1B), C(22B), and O(1B)) with 50% occupancy on each position. The two positions are not stereotically equal and, thus the two bonds Rh(1)—C(22A) and Rh(1)—C(22B) are of different lengths (1.828(7) and 1.706(5) Å, respectively). Convergence to final $R_1 = 0.0270$ and $wR_2 = 0.0553$ by using 8366 independent reflections and 589 parameters was achieved,[10] with the largest residual peak and hole to be 0.522 and –0.258 e/Å^3, respectively. Atomic coordinates, thermal parameters, and bond lengths and angles have been deposited as supporting information.[11]

Crystals of **11a**, **11b**, and **11e**–**11h** were grown by crystallization from a dichloromethane–pentane mixture. Single crystals were coated with Paratone-N oil, mounted using a glass fibre, and frozen in the cold nitrogen stream of the goniometer. A hemisphere of data was collected at UNB on a Bruker AXS P4/SMART 1000 diffractometer using ω and θ scans with a scan width of 0.3° and 10–40 s exposure times (**11a** 30 s exposure time, **11b** 20 s, **11e** 30 s, **11f** 40 s, **11g** 30 s, **11h** 10 s). The detector distance was 4 cm (**11a**–**11d** and **11f**–**11h**) or 5 cm (**11e**). The data were reduced (SAINT) (42) and corrected for absorption (SADABS) (41). The structures were solved by direct methods and refined by full-matrix least-squares on F^2(SHELXTL) (43). All non-hydrogen atoms were refined anisotropically. Hydrogen atoms were located in Fourier difference maps and refined isotropically. Crystallographic data are summarized in Tables 2–4 and atomic coordinates, thermal parameters, and bond lengths and angles have been deposited as supporting information.[11]

Synthesis of catalysts

Chloro rhodium 1,3-bis(2,4,6-trimethylphenyl)imidazol-2-ylidene carbonyl triphenylphosphine (ClRh(IMes)(CO)(PPh$_3$), 5a)

In a 100 mL Schlenk flask, under an argon purge, was weighed catalyst **4a** (201.9 mg, 0.21 mmol). To the vessel was then added 25 mL of freshly deoxygenated THF. Through this yellow solution was bubbled a gentle stream of CO at ambient temperature for 2 h. The resulting homogeneous solution was then concentrated on the Schlenk line to afford a pale yellow foam. The foam was redissolved in a minimum amount of dichloromethane and triturated with

[10] $R_1 = \Sigma||F_o| - |F_c||/\Sigma|F_o|$, $wR_2 = \{\Sigma[w(F_o^2 - F_c^2)^2]/\Sigma[w(F_o^2)^2]\}^{1/2}$ ($w = 1/[\sigma^2(F_o^2) + (0.0266P)^2]$, where $P = [\max(F_o^2, 0) + 2F_c^2]/3$).

[11] Supplementary data for this article are available on the Web site or may be purchased from the Depository of Unpublished Data, Document Delivery, CISTI, National Research Council Canada, Ottawa, ON K1A 0S2, Canada. DUD 4002. For more information on obtaining material refer to http://cisti-icist.nrc-cnrc.gc.ca/irm/unpub_e.shtml. CCDC 271302–271307 contain the crystallographic data for this manuscript. These data can be obtained, free of charge, via www.ccdc.cam.ac.uk/conts/retrieving.html (Or from the Cambridge Crystallographic Data Centre, 12 Union Road, Cambridge CB2 1EZ, UK; fax +44 1223 336033; or deposit@ccdc.cam.ac.uk).

© 2005 NRC Canada

pentane (20 mL) under a vigorous argon purge. The resulting pentane suspension was then Schlenk filtered. The pale lime-yellow powder thus obtained was washed with additional pentane (3 × 10 mL) and dried under vacuum for 4 h. From this crude product, 129.9 mg (88% yield) of X-ray quality crystals of catalyst **5a** were grown (THF–hexane); mp 258–263 °C. IR (KBr pellet) ν: 2950 (m), 2884 (m), 1944 (s), 1680 (m), 1529 (s), 1475 (m), 1446 (m), 1355 (m), 1268 (s), 1188 (m), 1102 (s), 1080 (m), 845 (m), 788 (m), 691 (m). ^{1}H NMR (400 MHz, $CDCl_3$) δ: 7.2–7.4 (m, 15H), 7.09 (s, 2H), 7.02 (s, br, 4H), 2.42 (s, 6H), 2.26 (s, br, 12H). $^{13}C\{^1H\}$ NMR (100 MHz, $CDCl_3$) δ: 187.15 (dd, *J* = 77.8, 16.6 Hz), 184.14 (dd, *J* = 123.4, 47.5 Hz), 138.3, 136.3, 134.7 (d, *J* = 11.1 Hz), 134.4, 134.3 (d, *J* = 40.6 Hz), 129.4 (d, *J* = 1.3 Hz), 128.9, 127.5 (d, *J* = 9.6 Hz), 122.9 (d, *J* = 3.2 Hz), 21.3, 18.9 (br). $^{31}P\{^1H\}$ NMR (162 MHz, $CDCl_3$) δ: 31.7 (d, *J* = 115 Hz). HR-TOF-MS *m/z*: 771.1180 $[M + K]^+$ calcd. for: 771.1167 ($C_{40}H_{39}N_2OPClRhK$); 697.1555 $[M - Cl]^+$, calcd. for: 697.1825 ($C_{40}H_{39}N_2OPRh$).

1,3-Dimesityl-4,5-dihydroimidazolium tetrafluoroborate (SIMesHBF$_4$, 13)

Into a 25 mL round-bottomed flask (RBF) were weighed *N*,*N*′-bis(2,4,6-trimethylphenylamino)ethane (3.91 g, 13 mmol) and ammonium tetrafluoroborate (1.36 g, 13 mmol). The resulting mixture was vigorously stirred in vacuo for 20 min. Then, the vessel was refilled with argon and triethylorthoformate (2.16 mL, 13 mmol) was added. After the attachment of an oven-dried reflux condenser, the reaction mixture was heated to 120 °C for 2 h. The resulting mixture, a white solid residue immersed in a dark oily liquid, was separated from its volatiles (ethanol and unreacted triethylorthoformate) in vacuo. The resulting residue was thoroughly triturated in 20 mL of dichloromethane and filtered. The insoluble ammonium tetrafluoroborate was washed with dichloromethane (2 × 5 mL) and the combined filtrate was then added slowly to 100 mL of rapidly swirled pentane. The pentane precipitated powder was thoroughly triturated and then harvested by filtration. The white powder was washed with pentane (3 × 25 mL) and dried in vacuo to yield 3.80 g (74% yield) of imidazolium salt **13** with spectroscopic properties consistent with those found in the literature (44).

Preparation of chloro rhodium 1,3-bis(2,4,6-trimethylphenyl)-4,5-dihydroimidazol-2-ylidene carbonyl triphenylphosphine (ClRh(SIMes)(CO)(PPh$_3$), 11a) from ClRh(PPh$_3$)$_3$

Into a 100 mL Schlenk flask was suspended the dihydroimidazolium salt **13** (0.278 g, 0.70 mmol) in 10 mL of deoxygenated THF. To this suspension was then added potassium *tert*-butoxide (0.70 mL of a 1.0 mol/L THF solution, 0.70 mmol) at room temperature, during which **13** dissolved to give a cloudy yellow solution. After 1 h of stirring, the reaction mixture was transferred via a cannula into another Schlenk flask containing a suspension of $Rh(PPh_3)_3Cl$ (0.463 g, 0.50 mmol) in deoxygenated benzene (20 mL). A stream of CO was then bubbled into the purple suspension for 15 min at room temperature before an oven-dried reflux condenser was attached. The flow of CO was stopped and the vessel was sealed. The resulting mixture was then heated to 80 °C for 1 h, at which point the reaction was complete as indicated by ^{31}P NMR. The volatiles were removed in vacuo and the resulting residue was triturated with pentane (150 mL). The bright yellow powder was then filtered, dissolved in dichloromethane (50 mL), and filtered through a bed of silica gel. The filtrate, when concentrated, revealed a yellow microcrystalline solid from which 0.18 g (50% yield) of X-ray quality crystals of **11a** were grown (dichloromethane–pentane).

Preparation of 11a (second route)

In a 100 mL Schlenk flask was prepared, as before, the protected carbene precursor **10** (0.70 mmol) in THF (10 mL) from the tetrafluoroborate salt **13** (0.276 g, 0.70 mmol) and potassium *tert*-butoxide (0.70 mL of a 1.0 mol/L THF solution, 0.70 mmol). Concurrently, in another Schlenk flask, was suspended $[Rh(C_2H_4)Cl]_2$ (0.097 g, 0.25 mmol) and triphenylphosphine (0.183 g, 0.70 mmol) in 20 mL of deoxygenated benzene. The resulting orange suspension was first stirred under a CO atmosphere for 15 min before the carbene precursor **10** was added via a cannula. Then, under a CO purge, an oven-dried reflux condenser was rapidly attached and the reaction mixture was heated to 80 °C for 2 h. After this period of reflux, the CO flow was stopped and the yellow homogeneous solution was allowed to cool to ambient temperature overnight. Concentration of the reaction mixture in vacuo followed by flash chromatography (silica gel, dichloromethane) afforded catalyst **11a** as a yellow microcrystalline solid from which 0.315 g (86% yield) of X-ray quality crystals were grown (dichloromethane–pentane); mp 228–232 °C. IR (NaCl) ν: 2958 (m), 1954 (s), 1684 (m), 1654 (m), 1538 (m), 1478 (m), 1434 (m), 1376 (m), 1266 (s), 1186 (m), 1090 (m), 1024 (m), 908 (m), 848 (m), 740 (m), 696 (m), 636 (m). ^{1}H NMR (400 MHz, $CDCl_3$) δ: 7.18–7.34 (m, 15H), 7.01 (s, 4H), 4.06 (s, br, 2H), 4.00 (s, br, 2H), 2.55 (s, br, 6H), 2.45 (s, br, 6H), 2.41 (s, 6H). $^{13}C\{^1H\}$ NMR (100 MHz, $CDCl_3$) δ: 211.50 (d, *J* = 115.9, 44.4 Hz), 187.25 (dd, *J* = 77.8, 17.1 Hz), 138.0 (br), 137.4, 136.8, 134.7 (d, *J* = 11.9 Hz), 134.2 (d, *J* = 40.6 Hz), 129.4 (br), 129.2, 128.9 (br), 127.5 (d, *J* = 9.6 Hz), 51.39, 51.36, 21.2, 19.6 (br), 18.5 (br). $^{31}P\{^1H\}$ NMR (162 MHz, $CDCl_3$) δ: 31.2 (d, *J* = 114.5 Hz). HR-TOF-MS *m/z*: 773.1337 $[M + K]^+$, calcd. for: 773.1322 ($C_{40}H_{41}N_2OPClRhK$); 699.2011 $[M - Cl]^+$, calcd. for: 699.2028 ($C_{40}H_{41}N_2OPRh$).

Preparation of chloro rhodium 1,3-bis(2,4,6-trimethylphenyl)-4,5-dihydroimidazol-2-ylidene carbonyl triphenylphosphite (ClRh(SIMes)(CO)(P(OPh)$_3$), 11b)

*Preparation of catalyst **11b** (route two)*

Following the procedure outlined for the synthesis of catalyst **11a**, tetrafluoroborate salt **13** (0.28 g, 0.70 mmol), potassium *tert*-butoxide (0.70 mL of a 1.0 mol/L THF solution, 0.70 mmol), $[Rh(C_2H_4)Cl]_2$ (0.097 g, 0.25 mmol), and triphenylphosphite (0.22 g, 0.70 mmol) were reacted to give, after purification by way of chromatography (silica gel, pentane–dichloromethane (1:4)) and crystallization (dichloromethane–pentane), 0.30 g (77% yield) of complex **11b**. IR (NaCl) ν: 2916 (s), 1976 (s), 1588 (s), 1486 (s), 1450 (s), 1384 (m), 1296 (m), 1266 (s), 1222 (m), 1194 (s), 1164 (s), 1068 (m), 1024 (s), 966 (m), 908 (s), 856 (s), 776 (s), 732 (m), 688 (m), 622 (m). ^{1}H NMR (400 MHz, $CDCl_3$) δ: 7.03–7.14 (m, 15H), 6.88 (s, 4H), 3.89 (s, br, 4H), 2.36 (s, 6H), 2.30 (s, br, 12H). $^{13}C\{^1H\}$ NMR (100 MHz, $CDCl_3$) δ:

© 2005 NRC Canada

209.4 (dd, J = 180.9, 42.2 Hz), 184.5 (dd, J = 77.3, 19.9 Hz), 151.2 (d, J = 4.0 Hz), 137.3, 135.7, 129.8, 129.3 (br), 129.0, 128.6, 123.9, 121.1 (d, J = 5.5 Hz), 51.6 (br), 21.2, 19.3 (br). $^{31}P\{^1H\}$ NMR (162 MHz, $CDCl_3$) δ: 122.2 (d, J = 196.0 Hz).

*Preparation of chloro rhodium 1,3-bis(2,4,6-trimethylphenyl)-4,5-dihydroimidazol-2-ylidene carbonyl tris(**p**-methoxyphenyl)phosphine (ClRh(SIMes)(CO)(P(**p**-MeOPh)$_3$), 11c)*

*Preparation of catalyst **11c** (route two)*

Following the procedure outlined for the synthesis of catalyst **11a**, tetrafluoroborate salt **13** (0.28 g, 0.70 mmol), potassium *tert*-butoxide (0.70 mL of a 1.0 mol/L THF solution, 0.70 mmol), $[Rh(C_2H_4)Cl]_2$ (0.097 g, 0.25 mmol), and tris(*p*-methoxy)phosphine (0.25 g, 0.70 mmol) were reacted to give, after purification by way of chromatography (silica gel, pentane–dichloromethane (1:5)) and crystallization (dichloromethane–pentane), 0.27 g (64% yield) of complex **11c**; mp 218–220 °C. IR (NaCl) ν: 2958 (s), 2916 (s), 1954 (s), 1596 (s), 1566 (s), 1500 (s), 1486 (s), 1434 (m), 1288 (m), 1252 (s), 1178 (s), 1098 (s), 1032 (s), 848 (m), 826 (s), 798 (s), 732 (s), 702 (m), 636 (m). ^1H NMR (400 MHz, $CDCl_3$) δ: 7.19 (m, 6H), 6.98 (s, 4H), 6.69 (m, 6H), 4.03 (s, br, 2H), 3.96 (s, br, 2H), 3.75 (s, 9H), 2.54 (s, br, 6H), 2.42 (s, br, 6H), 2.38 (s, 6H). $^{13}C\{^1H\}$ NMR (100 MHz, $CDCl_3$) δ: 211.7 (d, J = 119.0, 40.3 Hz), 187.3 (dd, J = 79.4, 17.6 Hz), 160.2, 138.1 (br), 137.3, 136.5, 135.9 (d, J = 13.5 Hz), 129.4 (br), 128.9 (br), 126.0 (d, J = 44.7 Hz), 113.1 (d, J = 11.1 Hz), 55.0, 51.4, 51.3, 21.2, 19.6 (br), 18.4 (br). $^{31}P\{^1H\}$ NMR (162 MHz, $CDCl_3$) δ: 26.7 (d, J = 111.6 Hz). HR-TOF-MS *m*/*z*: 863.1654 $[M + K]^+$, calcd. for: 863.1614 ($C_{43}H_{47}N_2OPClRhK$); 789.2328 $[M - Cl]^+$, calcd. for: 789.2357 ($C_{43}H_{47}N_2OPRh$).

*Preparation of chloro rhodium 1,3-bis(2,4,6-trimethylphenyl)-4,5-dihydroimidazol-2-ylidene carbonyl tris(**p**-fluorophenyl)phosphine (ClRh(SIMes)(CO)(P(**p**-FPh)$_3$), 11d)*

Following the procedure outlined for the synthesis of catalyst **11a** tetrafluoroborate salt **13** (0.28 g, 0.70 mmol), potassium *tert*-butoxide (0.70 mL of a 1.0 mol/L THF solution, 0.70 mmol), $[Rh(C_2H_4)Cl]_2$ (0.097 g, 0.25 mmol), and tris(*p*-fluorophenyl)phosphine (0.22 g, 0.70 mmol) were reacted to give, after purification by way of chromatography (silica gel, pentane–dichloromethane (4:1)), 0.25 g (63% yield) of complex **11d**; mp 204–210 °C. IR (NaCl) ν: 2916 (m), 1954 (s), 1588 (s), 1494 (s), 1442 (m), 1390 (m), 1266 (s), 1230 (s), 1164 (s), 1090 (m), 1010 (m), 908 (m), 826 (s), 732 (m), 636 (m). ^1H NMR (400 MHz, $CDCl_3$) δ: 7.21–7.28 (m, 6H), 6.99 (s, 4H), 6.88 (m, 6H), 4.04 (s, br, 2H), 3.99 (s, br, 2H), 2.51 (s, br, 6H), 2.41 (s, br, 6H), 2.38 (s, 6H). $^{13}C\{^1H\}$ NMR (100 MHz, $CDCl_3$) δ: 210.9 (dd, J = 115.5, 43.0 Hz), 187.2 (dd, J = 77.4, 17.5 Hz), 163.8 (d, J = 248.7 Hz), 138.3 (br), 137.9, 136.8 (dd, J = 13.6, 8.0 Hz), 136.6, 136.3 (d, J = 14.0, 10.0 Hz), 136.0 (br), 130.1, 129.7 (br), 129.2 (br), 115.3 (dd, J = 21.7, 11.1 Hz), 51.7, 21.5, 19.8 (br), 18.8 (br). ^{19}F NMR (376 MHz, $CDCl_3$) δ: –110.6. $^{31}P\{^1H\}$ NMR (162 MHz, $CDCl_3$) δ: 29.0 (d, J = 112.6 Hz). HR-TOF-MS *m*/*z*: 827.1054 $[M + K]^+$, calcd. for: 827.1070 ($C_{40}H_{38}N_2PF_3OClRhK$); 753.1728 $[M - Cl]^+$, calcd. for: 753.1732 ($C_{40}H_{38}N_2PF_3ORh$).

Preparation of chloro rhodium 1,3-bis(2,4,6-trimethylphenyl)-4,5-dihydroimidazol-2-ylidene carbonyl phenyldibenzophosphole (ClRh(SIMes)(CO)(Ph-DBP), 11e)

Following the procedure outlined for the synthesis of catalyst **11a**, tetrafluoroborate salt **13** (0.28 g, 0.70 mmol), potassium *tert*-butoxide (0.70 mL of a 1.0 mol/L THF solution, 0.70 mmol), $[Rh(C_2H_4)Cl]_2$ (0.097 g, 0.25 mmol), and phenyl-dibenzophosphole (Ph-DBP) (0.18 g, 0.70 mmol) were reacted to give, after purification by way of chromatography (silica gel, pentane–dichloromethane (1:5)) and crystallization (dichloromethane–pentane), 0.21 g (57% yield) of complex **11e**; mp (dec) 272–278 °C. IR (NaCl) ν: 2916 (m), 1954 (s), 1604 (m), 1478 (s), 1434 (s), 1376 (m), 1258 (s), 1178 (m), 1128 (m), 1090 (m), 1024 (s), 914 (s), 848 (s), 724 (m), 688 (m), 636 (m). ^1H NMR (400 MHz, $CDCl_3$) δ: 7.90 (t, J = 7.8 Hz, 2H), 7.68 (d, J = 8.0 Hz, 2H), 7.33 (d, J = 8.0 Hz, 2H), 6.99~7.20 (m, 7H), 6.97 (s, 4H), 4.05 (s, br, 4H), 2.53 (s, br, 12H), 2.31 (s, 6H). $^{13}C\{^1H\}$ NMR (100 MHz, $CDCl_3$) δ: 210.64 (d, J = 115.2, 45.1 Hz), 187.4 (dd, J = 77.8, 17.6 Hz), 142.4 (d, J = 8.0 Hz), 138.6 (d, J = 43.9 Hz), 137.6, 136.3, 134.5 (d, J = 40.6 Hz), 134.2 (d, J = 13.5 Hz), 132.1 (d, J = 13.6 Hz), 130.0, 129.5, 129.4 (br), 127.5 (d, J = 9.6 Hz), 120.8 (d, J = 4.8 Hz), 51.4, 21.1, 19.1 (br). $^{31}P\{^1H\}$ NMR (162 MHz, $CDCl_3$) δ: 20.9 (d, J = 108.1 Hz). HR-TOF-MS *m*/*z*: 771.1180 $[M + K]^+$, calcd. for: 771.1173 ($C_{40}H_{39}N_2OPClRhK$); 697.1855 $[M - Cl]^+$, calcd. for: 697.1869 ($C_{40}H_{39}N_2OPRh$).

Preparation of chloro rhodium 1,3-bis(2,4,6-trimethylphenyl)-4,5-dihydroimidazol-2-ylidene carbonyl tris(2-furyl)phosphine (ClRh(SIMes)(CO)(P(furyl)$_3$), 11f)

Following the procedure outlined for the synthesis of catalyst **11a**, tetrafluoroborate salt **13** (0.28 g, 0.70 mmol), potassium *tert*-butoxide (0.70 mL of a 1.0 mol/L THF solution, 0.70 mmol), $[Rh(C_2H_4)Cl]_2$ (0.097 g, 0.25 mmol), and tris(2-furyl)phosphine (0.16 g, 0.70 mmol) were reacted to give, after purification by way of chromatography (silica gel, gradient elution, 1:4 to 1:20 pentane–dichloromethane) and crystallization (dichloromethane–pentane), 0.11 g (31% yield) of complex **11f**. IR (NaCl) ν: 2916 (s), 1969 (s), 1684 (m), 1654 (m), 1486 (s), 1442 (s), 1368 (m), 1296 (m), 1266 (s), 1216 (m), 1164 (m), 1120 (s), 1002 (s), 908 (m), 886 (m), 848 (m), 746 (s), 636 (m). ^1H NMR (400 MHz, $CDCl_3$) δ: 7.53 (m, 3H), 6.99 (s, 4H), 6.58 (m, 3H), 6.26 (m, 3H), 4.02 (s, br, 4H), 2.50 (s, br, 12H), 2.35 (s, 6H). $^{13}C\{^1H\}$ NMR (100 MHz, $CDCl_3$) δ: 209.7 (d, J = 124.4 Hz), 185.7 (dd, J = 76.5, 18.4 Hz), 147.3 (d, J = 4.8 Hz), 145.4 (d, J = 61.4 Hz), 137.8, 136.2, 129.5 (br), 124.1 (d, J = 23.2 Hz), 110.6 (d, J = 8.0 Hz), 51.5, 51.4, 21.1, 19.6 (br), 18.5 (br). $^{31}P\{^1H\}$ NMR (162 MHz, $CDCl_3$) δ: –24.5 (d, J = 114.5 Hz).

Preparation of chloro rhodium 1,3-bis(2,4,6-trimethylphenyl)-4,5-dihydroimidazol-2-ylidene carbonyl tricyclohexylphosphine (ClRh(SIMes)(CO)(PCy$_3$), 11g)

Following the procedure outlined for the synthesis of catalyst **11a**, tetrafluoroborate salt **13** (0.28 g, 0.70 mmol), potassium *tert*-butoxide (0.70 mL of a 1.0 mol/L THF solution, 0.70 mmol), $[Rh(C_2H_4)Cl]_2$ (0.097 g, 0.25 mmol), and

© 2005 NRC Canada

tricyclohexylphosphine (0.20 g, 0.70 mmol) were reacted to give, after purification by way of column chromatography (silica gel, pentane–dichloromethane (1:2)) and crystallization (dichloromethane–pentane), 0.11 g (29% yield) of complex **11g**. IR (NaCl) ν: 2916 (s), 2854 (s), 1940 (s), 1478 (s), 1442 (s), 1376 (m), 1288 (m), 1258 (s), 1170 (m), 1002 (m), 892 (m), 848 (s), 740 (s), 636 (m). ^{1}H NMR (400 MHz, $CDCl_3$) δ: 6.92 (s, 4H), 4.04 (s, br, 2H), 3.96 (s, br, 2H), 2.53 (s, 6H), 2.41 (s, 6H), 2.38 (s, 6H), 1.93 (dd, br, *J* = 21.6, 11.6 Hz, 3H), 1.61 (m, br, 12H), 1.23 (m, br, 6H), 1.10 (m, br, 12 H). ^{13}C{^{1}H} NMR (100 MHz, $CDCl_3$) δ: 213.8 (dd, *J* = 110.0, 49.0 Hz), 187.5 (dd, *J* = 75.0, 17.0 Hz), 138.0 (br), 137.2, 136.6, 135.6 (br), 129.1 (br), 128.6 (br), 51.2 (br), 33.0 (d, *J* = 19.9 Hz), 29.8, 27.6 (d, *J* = 9.6 Hz), 21.0, 19.5 (br), 18.6 (br). ^{31}P{^{1}H} NMR (162 MHz, $CDCl_3$) δ: 38.4 (d, *J* = 109.0 Hz).

Preparation of chloro rhodium 1,3-bis(2,4,6-trimethylphenyl)-4,5-dihydroimidazol-2-ylidene carbonyl tri-o-tolylphosphine (ClRh(SIMes)(CO)(P(o-tolyl)$_3$), 11h)

Following the procedure outlined for the synthesis of catalyst **11a**, tetrafluoroborate salt **13** (0.28 g, 0.70 mmol), potassium *tert*-butoxide (0.70 mL of a 1.0 mol/L THF solution, 0.70 mmol), $[Rh(C_2H_4)Cl]_2$ (0.097 g, 0.25 mmol), and tris(*o*-tolyl)phosphine (0.21 g, 0.70 mmol) were reacted to give, after purification by way of chromatography (silica gel, dichloromethane) and crystallization (dichloromethane–pentane), 0.12 g (31% yield) of complex **11h**. IR (NaCl) ν: 2906 (m), 1956 (s), 1584 (m), 1482 (s), 1438 (s), 1380 (m), 1262 (s), 1174 (m), 1130 (m), 1028 (m), 904 (s), 852 (s), 802 (m), 758 (s), 728 (s), 640 (m). ^{1}H NMR (400 MHz, CD_2Cl_2) δ: 7.24 (t, br, *J* = 7.2 Hz, 3H), 7.06 (s, br, 4H), 6.98 (m, br, 9H), 4.07 (s, br, 2H), 3.98 (s, br, 2H), 2.47 (s, br, 6H), 2.36 (s, br, 12H), 1.86 (s, br, 9H). ^{13}C{^{1}H} NMR (100 MHz, $CDCl_3$) δ: 211.6 (dd, *J* = 116.0, 46.0 Hz), 188.0 (dd, *J* = 85.0, 16.5 Hz), 143.4 (br), 138.5 (br), 138.1, 137.0, 136.5 (br), 131.7, 131.6, 130.1 (br), 129.8 (br), 129.3 (br), 125.4, 125.3, 51.8 (br), 23.4 (br), 21.4, 19.7 (br), 18.7 (br). ^{31}P{^{1}H} NMR (162 MHz, $CDCl_3$) δ: 26.0 (d, br, *J* = 90.0 Hz).

Representative hydroformylation experiment

Preparation of (±)-2-phenylpropanal

A glass liner was charged with catalyst **5a** (5.8 mg, 0.0079 mmol), triphenylphosphine (4.2 mg, 0.016 mmol), and dried benzene (5 mL). The resulting pale yellow solution was stirred under a static argon atmosphere for 10 min before the liner was inserted into the autoclave. To minimize liner movement and to facilitate heat transfer, benzene (3 mL) was also added between the liner and the autoclave's inner surface. Rapidly, the gauge and gauge block assemblies were attached to the autoclave. The system was filled and flushed three times with CO before it was finally pressurized to 500 psi (1 psi = 6.894 757 kPa). Then, the autoclave was charged with 500 psi of H_2, bringing the total pressure to 1000 psi. Finally, the autoclave was placed in the centre of an oil bath preheated to 60 °C on an efficient heater-stirrer. After 19 h, the autoclave was removed from the oil bath and cooled in an ice bath for 45 min. The excess gases were then discharged and the apparatus disassembled. The contents in the liner were transferred to a RBF and carefully concentrated in vacuo to approximately 0.5 mL in volume. The conversion was then determined by ^{1}H NMR with a known amount of hexamethylbenzene as the internal standard.

Acknowledgements

The Natural Sciences and Engineering Research Council of Canada (NSERC) is gratefully acknowledged for support of this research in terms of equipment and operating grants to CMC, and postgraduate scholarships to ACC and DPA. The Canada Foundation for Innovation is also thanked for funding this research. UNB is thanked for providing Wiesner Awards to ACC and DPA, and for a Magee Third Century award to DPA. BioChem Pharma is also thanked for a scholarship to ACC.

References

1. O. Roelen. German Patent 849 548, 1938.
2. P.J. Chenier. Survey of industrial chemistry. 2nd ed. VCH, Weinheim, Germany. 1992.
3. (*a*) I. Ojima, C.Y. Tsai, M. Tzamarioudaki, and D. Bonafoux. Org. React. (N.Y.), **56**, 1 (2000); (*b*) H.M. Colquhoun, D.J. Thompson, and M.V. Twigg. Carbonylation: Direct synthesis of carbonyl compounds. Plenum Press, New York. 1991; (*c*) L.A. van der Veen, M.D.K. Boele, F.R. Bregman, P.C.J. Kamer, P.W.N.M. van Leeuwen, K. Goubitz, J. Fraanje, H. Schenk, and C. Bo. J. Am. Chem. Soc. **120**, 11 616 (1998); (*d*) M. Kranenburg, Y.E.M. van der Burgt, P.C.J. Kamer, P.W.N.M. van Leeuwen, K. Goubitz, and J. Fraanje. Organometallics, **14**, 3081 (1995); (*e*) C.P. Casey and G.T. Whiteker. Isr. J. Chem. **30**, 299 (1990); (*f*) C.P. Casey, E.L. Paulsen, E.W. Beuttenmueller, B.R. Proft, L.M. Petrovich, B.A. Matter, and D.R. Powell. J. Am. Chem. Soc. **119**, 11 817 (1997); (*g*) J.M. Brown and A.G. Kent. J. Chem. Soc. Perkin Trans. 2, 1597 (1987).
4. R.L Pruett and J.A. Smith. J. Org. Chem. **34**, 327 (1969).
5. (*a*) A.G. Abatjoglou, E. Billig, and D.R. Bryant. Organometallics, **3**, 923 (1984); (*b*) M. Lewin, Z. Aizenshtat, and J. Blum. J. Organomet. Chem. **184**, 255 (1980); (*c*) P.E. Garrou. Chem. Rev. **85**, 171 (1985); (*d*) A.J. Carty. Pure Appl. Chem. **54**, 113 (1982).
6. (*a*) J.M. Brown, S.J. Cook, and R. Khan. Tetrahedron, **42**, 5105 (1986); (*b*) J.-P. Rieu, A. Bouchelere, H. Cousse, and G. Mouzin. Tetrahedron, **42**, 4095 (1986).
7. (*a*) N. Sakai, K. Nozaki, and H. Takaya. J. Chem. Soc. Chem. Commun. 395 (1994); (*b*) N. Sakai, S. Mano, K. Nozaki, and H. Takaya. J. Am. Chem. Soc. **115**, 7033 (1993); (*c*) T. Horiuchi, T. Ohta, E. Shirakawa, K. Nozaki, and H. Takaya. J. Org. Chem. **62**, 4285 (1997); (*d*) G.J.H. Buisman, P.C.J. Kamer, and P.W.N.M. van Leeuwen. Tetrahedron: Asymmetry, **4**, 1625 (1993); (*e*) G.J.H. Buisman, M.E. Martin, E.J. Vos, A. Klootwijk, P.C.J. Kamer, and P.W.N.M. van Leeuwen. Tetrahedron: Asymmetry, **6**, 719 (1995).
8. D.G. Kaiser, G.J. Vangiessen, R.J. Reischer, and W.J. Wechter. J. Pharm. Sci. **65**, 269 (1976).
9. P.J. Harrington and E. Lodewijk. Org. Process Res. Devel. **1**, 72 (1997).
10. H. Alper and I. Amer. J. Am. Chem. Soc. **112**, 3674 (1990).
11. (*a*) J.Q. Zhou and H. Alper. J. Chem. Soc. Chem. Commun. 233 (1993); (*b*) H. Alper and J.Q. Zhou. J. Org. Chem. **57**, 3729 (1992); (*c*) J.Q. Zhou and H. Alper. J. Org. Chem. **57**,

© 2005 NRC Canada

3328 (1996); (*d*) H. Alper and J.Q. Zhou. J. Chem. Soc. Chem. Commun. 316 (1993); (*e*) C.M. Crudden and H. Alper. J. Org. Chem. **59**, 3091 (1994).

12. (*a*) T. Weskamp, W.C. Schattenmann, M. Spiegler, and W.A. Herrmann. Angew. Chem. Int. Ed. **37**, 2490 (1998); (*b*) W.A. Herrmann. Angew. Chem. Int. Ed. **41**, 1290 (2002), and refs. therein; (*c*) T. Weskamp, F.J. Kohl, W. Hieringer, D. Gleich, and W.A. Herrmann. Angew. Chem. Int. Ed. **38**, 2416 (1999); (*d*) L. Ackermann, A. Furstner, T. Weskamp, F.J. Kohl, and W.A. Herrmann. Tetrahedron Lett. **40**, 4787 (1999); (*e*) W.A. Herrmann, M. Elison, J. Fischer, C. Kocher, and G.R.J. Artus. Angew. Chem. Int. Ed. Engl. **34**, 2371 (1995); (*f*) W.A. Herrmann, K. Öfele, D.v. Preysing, and S.K. Schneider. J. Organomet. Chem. **687**, 229 (2003), and refs. cited therein; (*g*) W.A. Herrmann, C.-P. Reisinger, and M. Spiegler. J. Organomet. Chem. **557**, 93 (1998); (*h*) C.W.K. Gstöttmayr, V.P.W. Böhm, E. Herdtweck, M. Grosche, and W.A. Herrmann. Angew. Chem. Int. Ed. **41**, 1363 (2002).
13. For applications to the Suzuki–Miyaura reaction, see: (*a*) G. Altenhoff, R. Goddard, C.W. Lehmann, and F. Glorius. Angew. Chem. Int. Ed. **42**, 3690 (2003); (*b*) C. Zhang, J. Huang, M.L. Trudell, and S.P. Nolan. J. Org. Chem. **64**, 3804 (1999); (*c*) A. Fürstner and A. Leitner. Synlett, **2**, 290 (2001); (*d*) for the Sonogashira coupling, see: M. Eckhardt and G.C. Fu. J. Am. Chem. Soc. **125**, 13 642 (2003); (*e*) for the Kumada coupling, see: A.C. Frisch, F. Rataboul, A. Zapf, and M. Beller. J. Organomet. Chem. **687**, 403 (2003). For aminations of aromatic halides, see: (*f*) S.R. Stauffer, S. Lee, J.P. Stambuli, S.I. Hauck, and J.F. Hartwig. Org. Lett. **2**, 1423 (2000); (*g*) M.S. Viciu, R.A. Kelly III, E.D. Stevens, F. Naud, M. Studer, and S.P. Nolan. Org. Lett. **5**, 1479 (2003); (*h*) J. Cheng and M.L. Trudell. Org. Lett. **3**, 1371 (2001); (*i*) J. Huang, G. Grasa, and S.P. Nolan. Org. Lett. **1**, 1307 (1999); (*j*) B. Gradel, E. Brenner, R. Schneider, and Y. Fort. Tetrahedron Lett. **42**, 5689 (2001).
14. (*a*) M. Scholl, T.M. Trnka, J.P. Morgan, and R.H. Grubbs. Tetrahedron Lett. **40**, 2247 (1999); (*b*) M. Scholl, S. Ding, C.W. Lee, and R.H. Grubbs. Org. Lett. **1**, 953 (1999); (*c*) M.S. Sanford, J.A. Love, and R.H. Grubbs. J. Am. Chem. Soc. **123**, 6543 (2001); (*d*) T.M. Trnka, J.P. Morgan, M.S. Sanford, T.E. Wilhelm, M. Scholl, T. Choi, S. Ding, M.W. Day, and R.H. Grubbs. J. Am. Chem. Soc. **125**, 2546 (2003); (*e*) J.A. Love, M.S. Sanford, M.W. Day, and R.H. Grubbs. J. Am. Chem. Soc. **125**, 10 103 (2003); (*f*) T.J. Seiders, D.W. Williams, and R.H. Grubbs. Org. Lett. **3**, 3225 (2001).
15. (*a*) D.J. Cardin, B. Cetinkaya, and M.F. Lappert. Chem. Rev. **72**, 545 (1972); (*b*) M.J. Doyle and M.F. Lappert. J. Chem. Soc. Chem. Commun. 679 (1974); (*c*) M.J. Doyle, M.F. Lappert, G.M. McLaughlin, and J. McMeeking. J. Chem. Soc. Dalton Trans. 1494 (1974); 1591 (1974); (*d*) P.B. Hitchchock, M.F. Lappert, and P.L. Pye. J. Chem. Soc. Dalton Trans. 2160 (1977); (*e*) M.J. Doyle, M.F. Lappert, P.L. Pye, and P. Terreros. J. Chem. Soc. Dalton Trans. 2355 (1984); (*f*) A.W. Coleman, P.B. Hitchcock, M.F. Lappert, R.K. Maskell, and J.H. Muller. J. Organomet. Chem. **296**, 173 (1985); (*g*) M.F. Lappert. J. Organomet. Chem. **358**, 185 (1988); (*h*) B. Cetinkaya, P.B. Hitchcock, M.F. Lappert, D.B. Shaw, K. Spyropoulos, and N.J.W. Warhurst. J. Organomet. Chem. **459**, 311 (1993); (*i*) E. Cetinkaya, P.B. Hitchcock, H. Kucukbay, M.F. Lappert, and S. Al-Juaid. J. Organomet. Chem. **481**, 89 (1994).
16. J. Huang, H.J. Schanz, E.D. Stevens, and S.P. Nolan. Organometallics, **18**, 2370 (1999).
17. (*a*) C.M. Crudden and D.P. Allen. Coord. Chem. Rev. **248**, 2247 (2004); (*b*) D. Allen, C.M. Crudden, L.A. Calhoun, and R. Wang. J. Organomet. Chem. **689**, 3203 (2004); (*c*) D.S. McGuinness, M.J. Green, K.J. Cavell, B.W. Skelton, and A.H. White. J. Organomet. Chem. **565**, 165 (1998); (*d*) D.S. McGuinness, N. Saendig, B.F. Yates, and K.J. Cavell. J. Am. Chem. Soc. **123**, 4029 (2001); (*e*) D.S. McGuinness, K.J. Cavell, B.W. Skelton, and A.H. White. Organometallics, **18**, 1596 (1999); (*f*) D.S. McGuinness and K.J. Cavell. Organometallics, **19**, 4918 (2000); (*g*) S. Caddick, F.G.N. Cloke, P.B. Hitchcock, J. Leonard, A.K. de K. Lewis, D. McKerrecher, and L.R. Titcomb. Organometallics, **21**, 4318 (2002); (*h*) W.J. Marshall and V.V. Grushin. Organometallics, **22**, 1591 (2003); (*i*) R.F.R. Jazzar, S.A. Macgregor, M.F. Mahon, S.P. Richards, and M.K. Whittlesey. J. Am. Chem. Soc. **124**, 4944 (2002); (*j*) M.J. Chilvers, R.F.R. Jazzar, M.F. Mahon, and M.K. Whittlesey. Adv. Synth. Catal. **345**, 1111 (2003); (*k*) A.K. de K. Lewis, S. Caddick, F.G.N. Cloke, N.C. Billingham, P.B. Hitchcock, and J. Leonard. J. Am. Chem. Soc. **125**, 10 066 (2003).
18. A.C. Chen, L. Ren, A. Decken, and C.M. Crudden. Organometallics, **19**, 3459 (2000).
19. M.T. Zarka, M. Bortenschlager, K. Wurst, O. Nuyken, and R. Weberskirch. Organometallics, **23**, 4817 (2004).
20. M. Poyatos, P. Uriz, J.A. Mata, C. Claver, E. Fernandez, and E. Peris. Organometallics, **22**, 440 (2003).
21. H. van Rensburg, R.P. Tooze, D.F. Foster, and A.M.Z. Slawin. Inorg. Chem. **43**, 2468 (2004).
22. M.J. Doyle, M.F. Lappert, P.L. Pye, and P. Terreros. J. Chem. Soc. Dalton Trans. 2355 (1984).
23. J.P. Morgan and R.H. Grubbs. Org. Lett. **2**, 3153 (2000).
24. G.A. Grasa, Z. Moore, K.L. Martin, E.D. Stevens, S.P. Nolan, V. Paquet, and H. Lebel. J. Organomet. Chem. **658**, 126 (2002).
25. M.J. Bennett and P.B. Donaldson. Inorg. Chem. **16**, 655 (1971).
26. A. Cerioiti, G. Ciani, and A. Sironi. J. Organomet. Chem. **247**, 345 (1983).
27. For other studies of NHC carbonyl complexes, see: (*a*) K. Denk, P. Sirsch, and W.A. Herrmann. J. Organomet. Chem. **649**, 219 (2002); (*b*) M.-T. Lee and C.-H. Hu. Organometallics, **23**, 976 (2004); (*c*) L.S. Bresler, N.A. Buzina, Yu.S. Varshavsky, N.V. Kiseleva, and T.G. Cherkasova. J. Organomet. Chem. **171**, 229 (1979).
28. A.C. Hillier, W.J. Sommer, B.S. Yong, J.L. Petersen, L. Cavallo, and S.P. Nolan. Organometallics, **22**, 4322 (2003).
29. A.J. Arduengo III, R. Krafczyk, R. Schmulzler, H.A. Craig, J.R. Goerlich, W.J. Marshall, and M. Unverzagt. Tetrahedron, **55**, 14 523 (1999).
30. T.H. Brown and P.J. Green. J. Am. Chem. Soc. **92**, 2359 (1970).
31. It should be noted that the use of chloro complexes is not optimal for the hydroformylation reaction since chloride can inhibit the hydroformylation reaction: F.H. Jardine, J.A. Osborn, and G. Wilkinson. Chem. Ind. (London), **13**, 560 (1965); J.A. Osborn, G. Wilkinson, and J.F. Young. J. Chem. Soc. Chem. Commun. 17 (1965). We are currently preparing NHC analogs of $HRh(CO)(PPh_3)_3$, which will be tested in the hydroformylation of vinylarenes and related substrates.
32. I.D. Hills and G.C. Fu. J. Am. Chem. Soc. **126**, 13 178 (2004).
33. W.L.F. Amarego and D.D. Perrin. Purification of laboratory chemicals. 4th ed. Butterworth-Heinemann, Oxford, UK. 1996.
34. G. Parrinello and J.K. Stille. J. Am. Chem. Soc. **109**, 7122 (1987).
35. A.J. Arduengo III, R. Krafczyk, R. Schmutzler, H.A. Craig,

© 2005 NRC Canada

J.R. Goerlich, W.J. Marshall, and M. Unverzagt. Tetrahedron, **55**, 14 523 (1999).
36. It is necessary to recrystallize Wilkinson's catalyst from ethanol in the presence of excess triphenylphosphine prior to use. See: J.A. Osborn and G. Wilkinson. Inorg. Synth. **10**, 67 (1967).
37. A. van der Ent and A.L. Onderdelinden. Inorg. Synth. **27**, 92 (1981).
38. A. Affandi, R. Green, B. Hsieh, M. Holt, and E. Alyla. Synth. React. Inorg. Met. Org. Chem. **17**, 307 (1987).
39. Bruker AXS Inc. Crystal structure analysis package. Version 5.10 (SMART NT (Version 5.053), SAINT-Plus (Version 6.01), SHELXTL (Version 5.1)) [computer programs]. Bruker AXS Inc., Madison, Wis. 1999.
40. D.T. Cromer and J.T. Waber. International tables for X-ray crystallography. Vol. 4. Kynoch Press, Birmingham, UK. 1974. Table 2.2 A.
41. G. Sheldrick. SADABS [computer program]. Bruker AXS Inc., Madison, Wis. 1999.
42. Bruker AXS Inc. SAINT. Version 6.02 [computer program]. Bruker AXS Inc., Madison, Wis. 1999.
43. G. Sheldrick. SHELXTL. Version 5.1 [computer program]. Bruker AXS Inc., Madison, Wis. 1997.
44. M. Scholl, S. Ding, C.W. Lee, and R.H. Grubbs. Org. Lett. **1**, 953 (1999).

© 2005 NRC Canada

Synthesis, thermal, electrochemical, and photophysical characterization of 1,5-bis(diarylamino)naphthalene derivatives as potential hole transport OLED materials[1]

Jingning Shan, Glenn P.A. Yap, and Darrin S. Richeson

Abstract: Novel 1,5-bis(diarylamino)naphthalene derivatives (**1**–**9**), which have potential as hole-transporting materials for electroluminescent devices, were obtained through palladium-catalyzed coupling of diarylamines and 1,5-dibromonaphthalene. The thermal, electrochemical, and photophysical properties of these compounds were examined and the effects of the *N*-aryl substituents on these properties were investigated. These materials possess glass transition temperatures (T_g) that range from 70–131 °C and these values are related to the identity of the aryl substituents. Cyclic voltammetric measurements demonstrated that these compounds possess two reversible oxidation processes and were further used to estimate the HOMO energy levels of these materials by comparison with the ferrocene/ferrocenium couple. The intramolecular charge mobility, as gauged by the difference between the two oxidation potentials, indicates that compounds **1**–**8** have a similar degree of delocalization as *meta*-diaminobenzene derivatives while that of **9** is similar to **TPD**. Compounds **1**–**9** emit in the blue-green region and optical absorption and emission data for these materials can be rationalized in terms of the electronic donating properties of the aryl substituents. This data when combined with the electrochemically determined HOMO energies allowed estimation of the LUMO energy levels.

Key words: hole transport materials, diaminonaphthalene, thermal analysis, palladium-catalyzed arylation.

Résumé : Faisant appel à un couplage catalysé par le palladium de diarylamines et de 1,5-dibromonaphtalène, on a préparé des 1,5-bis(diarylamino)naphtalènes (**1**–**9**), qui ont le potentiel de transporter des trous pour les appareils électroluminescents. On en a examiné les propriétés thermiques, électrochimiques et photophysiques et on a étudié les effets des substituants *N*-aryles sur ces propriétés. Ces matériaux possèdent des températures de transition de verre (T_g) qui s'étalent de 70 à 131 °C et on a pu établir une corrélation entre cette propriété et l'identité des substituants aryles. Des mesures de voltampérométrie cyclique démontrent que ces composés possèdent deux processus d'oxydations réversibles qui ont, de plus, été utilisées pour évaluer les niveaux d'énergie de l'orbitale moléculaire haute occupée de ces composés par comparaison avec le couple ferrocène/ferrocénium. La mobilité de la charge intramoléculaire, telle qu'évaluée par la différence entre les deux potentiels d'oxydation, indique que les composés **1**–**8** possèdent un degré de délocalisation semblable à celui des dérivés du *méta*-diaminobenzène alors que celle du composé **9** est semblable à celle du **TDP**. Les composés **1**–**9** émettent dans la région du bleu-vert et les données d'absorption et émission optique de ces composés peuvent être rationalisées en termes du caractère électrodonneur des substituants aryles. Lorsque ces données sont combinées avec les énergies de l'orbitale moléculaire haute occupée déterminée électrochimiquement, il est possible d'évaluer les niveaux d'énergie de l'orbitale moléculaire basse vacante.

Mots clés : matériaux pouvant transporter des trous, diaminonaphtalène, analyse thermique, arylation catalysée par le palladium.

[Traduit par la Rédaction]

Introduction

Polyaromatic amines have been essential components in molecular electroluminescent (EL) devices beginning with the first report of a two-layer organic light-emitting diode (OLED) (1, 2). Generally the amine assumes the role of the hole transport (HT) material in such devices (3, 4). Aromatic diamine derivatives and in particular *N*,*N*,*N*′,*N*′-tetraaryl-(1,1′-biphenyl)-4,4′-diamines remain synthetic targets for HT materials because of the ease with which they form

Received 25 November 2004. Published on the NRC Research Press Web site at http://canjchem.nrc.ca on 20 August 2005.

Dedicated to Professor Howard Alper.

J. Shan, G.P.A. Yap, and D.S. Richeson.[2] Department of Chemistry and the Center for Catalysis Research and Innovation, University of Ottawa, Ottawa, ON K1N 6N5, Canada.

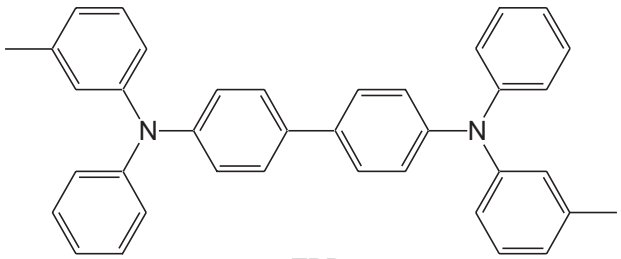
[1]This article is part of a Special Issue dedicated to Professor Howard Alper.

[2]Corresponding author (e-mail: darrin@science.uottawa.ca).

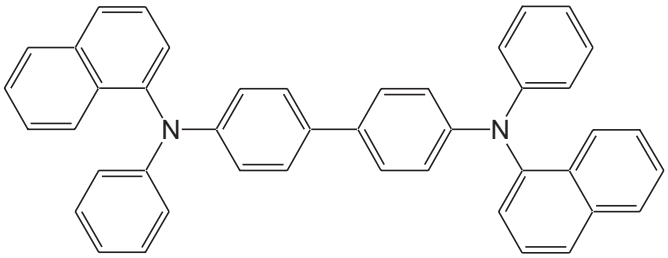
 doi: 10.1139/V05-101 © 2005 NRC Canada

amorphous thin films, their high hole mobility, and suitable HOMO energy level (5–8).

Benchmark compounds in this field are represented by *N*,*N*′-diphenyl-*N*,*N*′-di(*m*-tolyl)benzidine (**TPD**) and *N*,*N*′-bis(1-naphthyl)-*N*,*N*′-diphenyl-benzidine (**NPD**). Establishing relationships between the molecular structure of these and related compounds and their physical characteristics such as oxidation potential (9, 10), solid-state structures (11, 12), reorganization energy upon charge transfer (13–15), and environmental stability is of considerable interest, as each of these properties will influence the hole transport performance of the compound in a device.



TPD



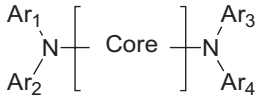
NPD

The hole transport in these materials has associated with it a reorganization energy (λ) that is related to the geometric rearrangments between the neutral and radical cation states (e.g., **TPD** and **TPD**$^+$). In the case of diamines with a biphenyl core such as **TPD** and **NPD**, the torsion angle between the two rings of the biphenyl bridges changes between the neutral and the cation radical and this has been ascribed to be the major barrier to electron exchange between these two species (13). Minimizing this reorganization term is one factor that may lead to improved hole mobility.

One of the chief failure modes for OLEDs is thermal instability in the molecular thin films, and in most devices, the HT component has the lowest thermal stability. Thermal stresses are inherent in device operation or can arise in the operating environment and can lead to significant expansion of the material or crystallization of the HT material. Furthermore, poor lifetimes for devices operated near room temperature have been attributed in part to thermal instabilities of the amorphous organic layers, which has been correlated with low glass transition temperatures (T_g) (2, 4, 16). For example, the T_g of tris(8-hydroxyquinolinato)aluminum (Alq), a common electron transport (ET) material, is 175 °C while those for **TPD** and **NPD** are reported to be 65 and 95 °C, respectively (17).

A major objective in developing new HT materials is the improvement of their thermal properties without sacrificing the advantageous properties exhibited by compounds such as **TPD** and **NPD**. A variety of approaches have been undertaken to improve the performance features of the HT component in EL devices, many of which center around core modifications to the generic diamine represented in Chart 1 (3, 6, 18–25). In addition to variation of the core structure, the aryl groups have been modified to produce symmetric (17–20) and asymmetric compounds (21, 24). Among the improved properties that have been observed in these examples are increased thermal stability and novel emission properties (20, 21, 26–29). Certainly, further development of related species could have significant device implications.

Chart 1.



Ar = aromatic groups

Herein we report our results for potential HT materials designed around the 1,5-diaminonaphthalene structure and an examination of the effects of variations of the aromatic substituents in these species. Only one example of an HT material designed around the naphthyl core has been reported and this compound displayed improved thermal properties as well as potential as a blue light-emitting material (30). In this case, the implementation of a fused aromatic core will remove the torsional freedom of the biphenyl core. In addition to characterizing the thermal behavior of these new diamines, we present their electronic spectra and electrochemical properties for comparison with **TPD**. Our synthetic methodology exploited the versatile and efficient palladium catalyzed amine arylation reactions pioneered by Buchwald and co-workers (31, 32) and Hartwig (33, 34).

Experimental section

General information

All reactions were carried out under a nitrogen atmosphere using standard Schlenk techniques. Aryl amines, aryl bromides, diphenylamine, tris(dibenzylidineacetone)dipalladium ($Pd_2(dba)_3$), *rac*-2,2′-bis(diphenylphosphino)-1,1′-binaphthyl (BINAP), and sodium *tert*-butoxide were purchased from the Aldrich Chemical Company and used without further purification. Tri-*tert*-butylphosphine was purchased from Strem Chemicals. 1,5-Dibromonaphthalene was synthesized from 1,5-diaminonaphthalene according to literature procedures (35). Toluene was purified by passage through a column of activated alumina using an apparatus from Anhydrous Engineering. Dichloromethane was freshly distilled under nitrogen using CaH_2 as the dessicant.

Reactions were monitored using Silica gel 60 F_{254} TLC aluminum sheets by UV lamp and (or) GC–MS using a mass selective detector from Agilent GC systems 6890 series with an HP-5 capillary column (cross-linked 5% PH ME siloxane).

^{1}H NMR spectra were collected on a Varian Gemini-200 or a Bruker 300 MHz spectrometer using the residual protons of the deuterated solvent for reference. The overlapping ^{13}C peaks were identified through ^{13}C DEPT and ^{1}H^{13}C HMQC analysis on a Bruker 300 MHz spectrometer. Electron impact mass spectra (EI-MS) were recorded on a Kratos

© 2005 NRC Canada

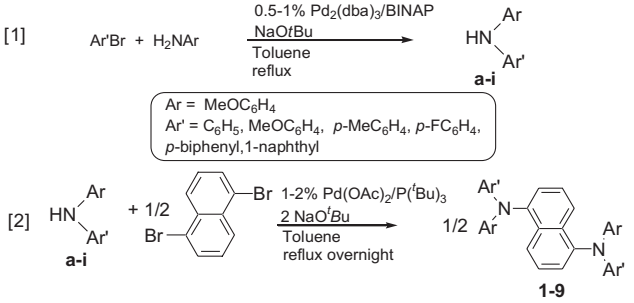
Concept IIH instrument using electron ionization at 70 eV. High resolution mass spectra (HR-MS) were obtained at the University of Ottawa on a Kratos Concept IIH instrument using electron ionization at 70 eV, acceleration 8 KV, and resolution 7 000 – 10 000. The glass transition temperatures and melting points were measured using a TA 2010 differential scanning calorimeter (DSC) instrument. Heating rates of 5–20 °C/min were employed for these measurements. UV spectra were recorded in CH_2Cl_2 on a Varian Cary spectrophotometer. Steady-state fluorescence spectroscopy was carried out using a Photon Technology International version 1.2 X luminescence spectrometer with the same cuvette used for UV–vis spectra. Fluorescence quantum efficiency (Φ_f) of the compounds was determined by comparing with that of Coumarin-102 (Φ_f = 0.93 in ethanol) (36) in CH_2Cl_2 solution. Cyclic voltammograms (CV) were obtained using a Hokuto Denko HA501 potentiostat connected to a Hokuto Denko HB105 programmable function generator. A Nicolet 310 oscilloscope was used to follow the in situ CV scans. A freshly polished Pt wire and Pt plate were used as working and counter electrode, respectively. A silver wire was employed as pseudo-reference electrode. All solutions were prepared in millimolar concentrations in dry CH_2Cl_2, which was freshly distilled from CaH_2. Tetrabutyl ammonium hexafluorophosphate (TBAHFP) was used as the supporting electrolyte with a concentration of 0.1 mol/L. The electrochemical cell was degassed with nitrogen prior to analysis and was maintained under a nitrogen atmosphere during the potential scans. At the end of each set of CV scans, ferrocene (Cp_2Fe) was added to the solution and another potential scan was performed to provide the redox potential for the Cp_2Fe/Cp_2Fe^+ couple.

Compounds **a**–**h** were prepared via Pd catalyzed coupling of arylbromides and arylamines according to eq. [1] in Scheme 1. The general procedure for the synthesis of diarylamines followed that reported in the literature with details provided in the Electronic supplementary information (37, 38).[3]

General procedure for the synthesis of diaminonaphthalene derivatives

The general procedure for the synthesis of 1,5-diaminonaphthalene derivatives (**1**–**9**) according to eq. [2] in Scheme 1 was modified from the literature (39). In a drybox, a Schlenk flask was charged with toluene, 1,5-dibromonaphthalene, and 2.2 equiv. of the appropriate diarylamines (**a**–**i**). To this solution was added 1% to 2% $Pd(OAc)_2/P(t\text{-}Bu)_3$ (ligand/Pd = 1) and 2.8 equiv. of NaO-*t*-Bu. The reaction mixture changed from orange to dark black over the first few seconds. The flask was sealed, removed from the drybox, and was heated at 120 °C overnight. The reaction was then cooled to room temperature, filtered, and the residue was washed with ethylacetate and combined with the toluene. The solvents were then removed by vacuum evaporation and the residue was dissolved in $CHCl_3$. Column chromatography was used to purify the product using $CHCl_3$ as the eluent. Collection of the product was monitored by TLC and all fractions were combined at the end of the separation procedure. The solvents were removed under vacuum to yield pure compounds.

Scheme 1.



1,5-Bis(di-*p*-methoxyphenylamino)naphthalene (1)

Yield: 50%. ^{1}H NMR ($CDCl_3$) δ: 3.79 (s, 12H), 6.64–6.80 (m, 8H), 6.91 (d, 8H), 7.08–7.30 (m, 4H), 7.84 (d, 2H). ^{13}C NMR ($CDCl_3$) δ: 55.48, 114.41, 121.98, 123.44, 126.12, 126.25, 132.82, 142.98, 144.92, 154.54. *m*/*z*: 582 (M^+). HR-MS (*m*/*z*) calcd. for $C_{38}H_{34}N_2O_4$: 582.2519; found: 582.2530.

1,5-Bis(*p*-methoxyphenylphenylamino)naphthalene (2)

Yield: 75%. ^{1}H NMR ($CDCl_3$) δ: 3.76 (s, 6H), 6.7–6.9 (m, 9H), 7.0–7.4 (m, 13H), 7.87 (d, 2H). ^{13}C NMR ($CDCl_3$) δ: 55.46, 114.55, 119.84, 120.26, 122.43, 125.38, 126.56, 126.95, 128.93, 133.06, 141.55, 144.30, 149.5, 155.49. *m*/*z*: 522 (M^+). HR-MS (*m*/*z*) calcd. for $C_{36}H_{30}N_2O_2$: 522.2307; found: 522.2328.

1,5-Bis(*p*-methoxyphenyltolylamino)naphthalene (3)

Yield: 80%. ^{1}H NMR ($CDCl_3$) δ: 2.28 (s, 6H), 3.77 (s, 6H), 6.81 (t, 8H), 7.02 (t, 8H), 7.16–7.34 (m, 4H), 7.88 (d, 2H). ^{13}C NMR ($CDCl_3$) δ: 20.62, 55.46, 114.45, 120.77, 122.20, 124.59, 126.39, 126.58, 129.55, 130.11, 133.00, 142.18, 144.61, 147.05, 155.03. *m*/*z*: 550 (M^+). HR-MS (*m*/*z*) calcd. for $C_{38}H_{34}N_2O_2$: 550.2620; found: 550.2642.

1,5-Bis(*p*-methoxyphenyl-*p*-fluorophenylamino)naphthalene (4)

Yield: 78%. ^{1}H NMR ($CDCl_3$) δ: 3.76 (s, 6H), 6.72–7.32 (m, 20H), 7.82 (d, 2H). ^{13}C NMR ($CDCl_3$) δ: 55.48, 114.64, 115.63 ($J_{C\text{-}F}$ = 22.6 Hz), 122.15 ($J_{C\text{-}F}$ = 5.0 Hz), 122.22, 124.60, 126.49, 126.54, 132.84, 142.11, 144.59, 145.70, 155.33, 157.58 ($J_{C\text{-}F}$ = 240.2 Hz). *m*/*z*: 558 (M^+). HR-MS (*m*/*z*) calcd. for $C_{36}H_{28}F_2N_2O_2$: 558.2119; found: 558.2101.

1,5-Bis(*p*-methoxyphenyl-*p*-propylphenylamino)naphthalene (5)

Yield: 66%. ^{1}H NMR ($CDCl_3$) δ: 0.92 (t, 6H), 1.57 (m, 4H), 2.47 (t, 4H), 3.76 (s, 6H), 6.75–6.83 (m, 8H), 6.95–7.04 (M, 8H), 7.19–7.30 (m, 4H), 7.86 (d, 2H). ^{13}C NMR

[3] Supplementary data for this article are available on the Web site or may be purchased from the Depository of Unpublished Data, Document Delivery, CISTI, National Research Council Canada, Ottawa, ON K1A 0S2, Canada. DUD 3696. For more information on obtaining material refer to http://cisti-icist.nrc-cnrc.gc.ca/irm/unpub_e.shtml. CCDC 242552 and 242553 contain the crystallographic data for this manuscript. These data can be obtained, free of charge, via www.ccdc.cam.ac.uk/conts/retrieving.html (Or from the Cambridge Crystallographic Data Centre, 12 Union Road, Cambridge CB2 1EZ, UK; fax +44 1223 336033; or deposit@ccdc.cam.ac.uk).

© 2005 NRC Canada

Table 1. Crystal data and structure refinement for compounds **3** and **5**.

Compound	**3**	**5**
Empirical formula	$C_{38}H_{34}N_2O_2$	$C_{42}H_{42}N_2O_2$
Formula weight	550.67	606.78
Temperature (K)	203(2)	203(2)
Wavelength (Å)	0.710 73	0.710 73
Crystal system	Monoclinic	Monoclinic
Space group	*P*2(1)/*c*	*P*2(1)/*c*
Unit cell dimensions		
a (Å)	8.114(2)	14.394 6(19)
b (Å)	16.800(5)	11.688 2(16)
c (Å)	11.090(3)	21.188(3)
β (°)	95.361(5)	109.706(3)
V (Å^3)	1505.1(7)	3356.1(8)
Z	2	4
Final *R* indices ($I > 2\sigma(I)$)	R_1 = 0.085 8, wR_2 = 0.197 0	R_1 = 0.079 2, wR_2 = 0.148 4

($CDCl_3$) δ: 13.91, 24.62, 37.30, 55.45, 114.45, 120.50, 122.27, 124.65, 126.40, 126.68, 128.89, 133.07, 134.99, 142.12, 144.59, 147.21, 155.03. *m*/*z*: 606 (M^+). HR-MS (*m*/*z*) calcd. for $C_{42}H_{42}N_2O_2$: 606.3246; found: 606.3229.

1,5-Bis(*p*-methoxyphenyl-*p*-biphenylamino)naphthalene (6)

Yield: 50%. ^{1}H NMR ($CDCl_3$) δ: 3.78 (s, 6H), 6.78–7.58 (m, 30H), 7.92 (d, 2H). ^{13}C NMR ($CDCl_3$) δ: 55.47, 114.64, 119.74, 122.58, 125.64, 126.45, 126.70 (two overlapping singlets), 127.08, 127.55, 128.66, 132.82, 133.07, 140.79, 141.25, 144.14, 148.81, 155.51. *m*/*z*: 674 (M^+). HR-MS (*m*/*z*) calcd. for $C_{48}H_{38}N_2O_2$: 674.2933; found: 674.2908.

1,5-Bis(*p*-methoxyphenyl-1-naphthylamino)naphthalene (7)

Yield: 80%. ^{1}H NMR (C_6D_6) δ: 3.20 (s, 6H), 6.54 (d, 4H), 6.72–7.22 (m, 16H), 7.44 (d, 2H), 7.63 (d, 2H), 8.25 (d, 2H), 8.41 (d, 2H). ^{13}C NMR (C_6D_6) δ: 54.82, 114.88, 121.75, 123.85, 124.51, 124.92, 125.04, 125.16, 126.24, 126.43, 126.59, 127.12, 128.80, 130.35, 132.50, 135.83, 144.88, 146.34, 147.13, 155.29. *m*/*z*: 622 (M^+). HR-MS (*m*/*z*) calcd. for $C_{44}H_{34}N_2O_2$: 622.2620; found: 622.2647.

1,5-Bis(di-*m*-methoxyphenylamino)naphthalene (8)

Yield: 50%. ^{1}H NMR ($CDCl_3$) δ: 3.61 (s, 3H), 3.68 (s, 3H), 6.15 (t, 1H), 6.18 (d, 1H), 6.33 (d, 1H), 6.82–7.33 (m, 14H), 7.96 (d, 2H). ^{13}C NMR ($CDCl_3$) δ: 54.99, 55.61, 103.82, 104.02, 110.55, 112.79, 121.26, 122.81, 125.99, 126.13, 126.26, 128.76, 129.10, 132.86, 135.95, 143.78, 150.78, 155.31, 160.12. *m*/*z*: 582 (M^+). HR-MS (*m*/*z*) calcd. for $C_{38}H_{34}N_2O_4$: 582.2519; found: 582.2509.

1,5-Bis(diphenylamino)naphthalene (9)

Yield: 52%. ^{1}H NMR ($CDCl_3$) δ: 6.90–7.31 (m, 24H), 7.88 (d, 2H). ^{13}C NMR ($CDCl_3$) δ: 121.71, 121.95, 122.69, 126.73, 127.52, 129.09, 133.24, 144.00, 148.50. *m*/*z*: 462 (M^+). HR-MS (*m*/*z*): calcd. for $C_{34}H_{26}N_2$: 462.2096; found: 462.2109.

Structural determination for compounds 3 and 5

Single crystals were mounted on thin glass fibers using viscous oil and then cooled to the data collection temperature. Crystal data and details of the measurements are summarized in Table 1. Data were collected on a Bruker AX SMART 1 k CCD diffractometer using 0.3° ω scans at 0°, 90°, and 180° in ϕ. Unit-cell parameters were determined from 60 data frames collected at different sections of the Ewald sphere. Semi-empirical absorption corrections based on equivalent reflections were applied. The structures were solved by direct methods, completed with difference Fourier syntheses, and refined with full-matrix least-squares procedures based on F^2. All non-hydrogen atoms were refined with anisotropic displacement parameters. All hydrogen atoms were treated as idealized contributions. All scattering factors and anomalous dispersion factors are contained in the SHELXTL 5.1 program library (40).

Results and discussion

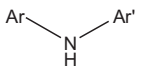
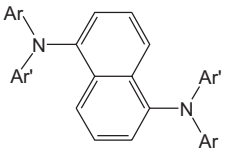
Synthesis of naphthalene diamines

Our strategy for preparing new aromatic amines possessing a naphthyl core (**1**–**9**) is outlined with eqs. [1] and [2] in Scheme 1. Diarylamines (**a**–**i**) were either first prepared via Pd catalyzed coupling of arylbromide and arylamine (**a**–**h**) (37, 38) or purchased (**i**). A $Pd(OAc)_2/P(t\text{-}Bu)_3$ catalyst system was then employed for the coupling reactions between 1,5-dibromonaphthalene and diarylamines (39). We also explored an alternative route based on the coupling of 1,5-diaminonaphthalene with aryl halides. This proved to be unsatisfactory and only led to products with a single arylation of each nitrogen center as the major products. The synthesis of a related diamine, 1,5-bis[*N*-(1-naphthyl)-*N*-phenyl]naphthalene diamine (**NND**) was recently reported via a modified Ullman condensation of 1,5-diiodonaphthalene and naphthylphenylamine, however, no details for this transformation were reported (30).

The naphthyl core diamines presented in Table 2 were isolated in good yields and were fully characterized by ^{1}H and ^{13}C NMR and HR-MS. The versatility of this method provides an avenue to invoke a wide range of amine substituent variation including electron-donating and electron-withdrawing groups. The molecular structures of two of these diamines, compounds **3** and **5**, were definitively established using single crystal X-ray diffraction analysis (Table 1). The structures of **3** and **5** are presented in Figs. 1 and 2, respectively, and selected bond distances and angles are provided in Ta-

© 2005 NRC Canada

Table 2. Summary of the synthesis and thermal properties of HN(Ar)Ar′ and 1,5-bis(diarylamino)naphthalenes shown in Scheme 1.

 (% Yield)	 (% Yield) $T_g/T_m/T_c$
HN(*p*-$C_6H_4OMe)_2$ **a** (78)	**1** (50) (Ar = Ar' = *p*-C_6H_4OMe) 76/216/143 °C
N(C_6H_4OMe)(C_6H_5) **b** (80)	**2** (75) (Ar = *p*-C_6H_4OMe, Ar' = C_6H_5) 70/230/145 °C
HN(C_6H_4OMe)(C_6H_4Me) **c** (70)	**3** (80) (Ar = *p*-C_6H_4OMe, Ar' = C_6H_4Me) 82/249/103 °C
HN(C_6H_4OMe)(C_6H_4F) **d** (84)	**4** (78) (Ar = *p*-C_6H_4OMe, Ar' = C_6H_4F) 73/192/138 °C
HN(C_6H_4OMe)(C_6H_4Pr) **e** (86)	**5** (66) (Ar = *p*-C_6H_4OMe, Ar' = C_6H_4Pr) 51/187/126 °C
HN(C_6H_4OMe)(4,4'-biphenyl) **f** (50)	**6** (50) (Ar = *p*-C_6H_4OMe, Ar' = 4,4'-bipheny) 116/283/200 °C
HN(C_6H_4OMe)(1-naphthyl) **g** (50)	**7** (80) (Ar = *p*-C_6H_4OMe, Ar' = 1-naphthyl) 131/220/NO °C[a]
HN(m-$MeOC_6H_4)_2$ **h** (40)	**8** (50) (Ar = Ar' = *m*-C_6H_4OMe) 72/220/NO °C[a]
HN($C_6H_5)_2$ **i**	**9** (52) (Ar = Ar' = C_6H_5) 83/244/NO °C[a]
TPD	65/175/167 °C

[a]NO = not observed.

ble 3. Both species display planar nitrogen centers with propeller-like arrangement of the three aromatic groups on each nitrogen. In **3**, the N—$C_{naphthyl}$ distance (N(1)—C(1) = 1.462(3) Å) is longer than the corresponding distances for the outer aryl groups (N(1)—C(18) = 1.416(6) Å and N(1)—C(11) = 1.449(6) Å). In contrast, although the longest N—C distance in compound **5** is to the naphthyl core, the C—N distances in this compound span a narrower range from 1.423(4) to 1.435(4) Å. These trends in C—N distance are opposite to those observed for **TPD** and for *N*,*N*′-diphenyl-*N*,*N*′-bis(2,4-dimethylphenyl)-(1,1′-biphenyl)-4,4′-diamine, where the N—$C_{biphenyl}$ distances are the shortest distances with values of 1.411(5) and 1.415(5) Å, respectively (7, 8). There are no unusual C—C bond lengths within the peripheral or core aryl groups.

Thermal properties

To be of practical consideration for OLED fabrication, the diamines **1**–**9** should form stable glasses. This general feature of materials for OLED construction avoids problems associated with grain boundaries in polycrystalline materials and provides for a high degree of uniformity within thin films. Associated with this amorphous state is a characteristic temperature (or temperature range) where the glassy and amorphous state of the material begins to soften and flow, which is referred to as the glass transition temperature (T_g). Above T_g, materials tend to crystallize generating grain boundaries and causing nonuniform thin films (17). The kinetics of the crystallization process will dictate whether or not a T_g is observed. Generally, large, globular, and rigid molecules or asymmetric molecules with high molecular masses and without strong intermolecular forces have high T_g values (17, 41). Such general features favor a high energy for the reorganization – molecular reorientation of the amorphous phase into a crystalline material. Strong intermolecular forces may favor organization of the molecules as they cool below their melting points, which, in turn, encourage crystallization at the expense of glass formation.

A typical DSC for the naphthalene diamines is shown in Fig. 3. The initial temperature scan of compound **3** shows a

© 2005 NRC Canada

Fig. 1. Molecular structure and atom numbering scheme for **3**. Hydrogen atoms have been omitted for clarity.

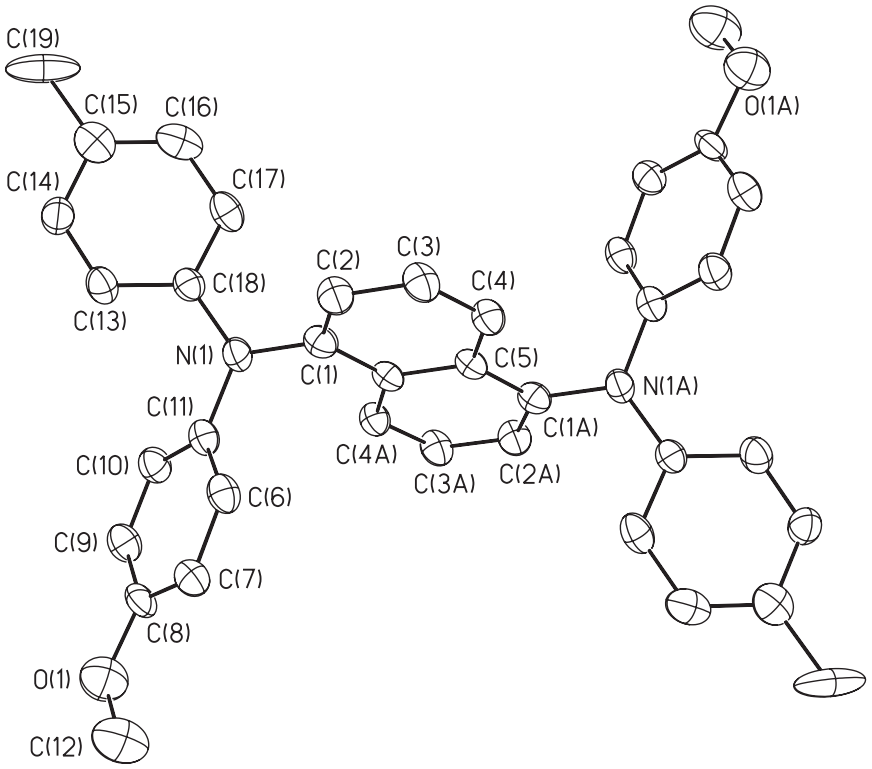
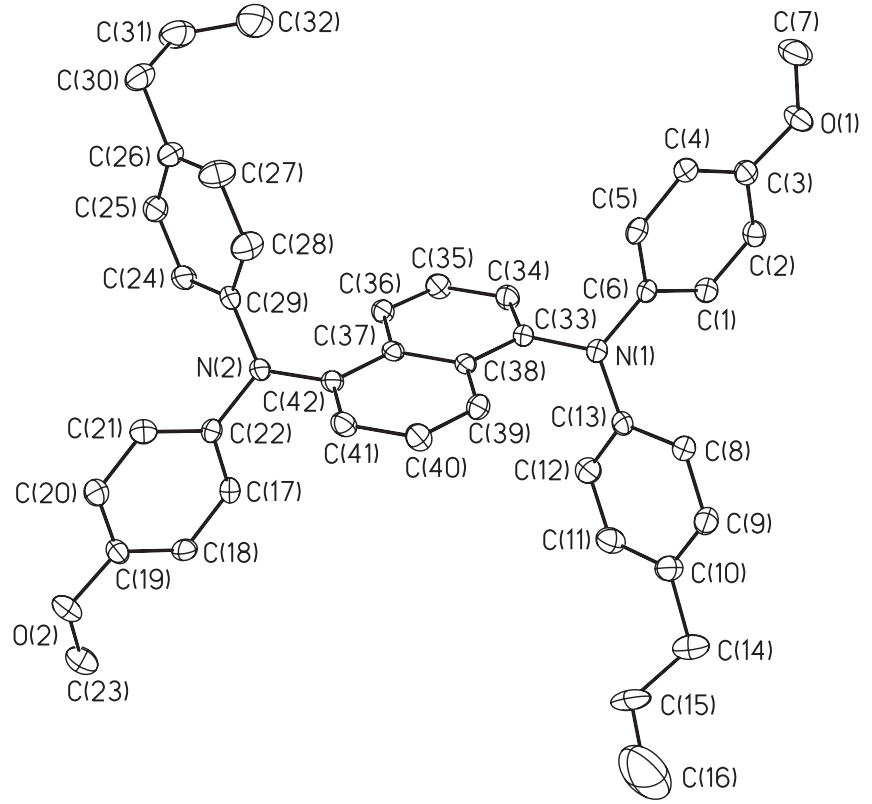


Fig. 2. Molecular structure and atom numbering scheme for **5**. Hydrogen atoms have been omitted for clarity.



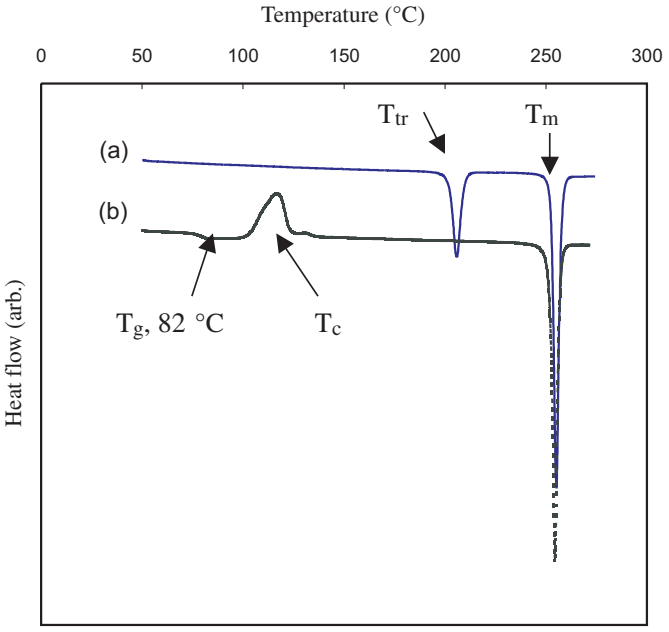
crystalline phase transition (T_{tr} = 200 °C) and a melting point (T_m) at 249 °C. This sample was then allowed to cool to room temperature and heated a second time. This temperature scan displayed the glass transition (T_g) at 82 °C. Continuing to heat this sample revealed an exotherm at 103 °C, which was associated with crystallization. Finally, the sam-

© 2005 NRC Canada

Table 3. Selected bond lengths (Å) and angles (°) for compounds **3** and **5**.

Compound **3**		Compound **5**	
Bond distances (Å)			
N(1)—C(18)	1.416(6)	N(1)—C(13)	1.423(4)
N(1)—C(11)	1.449(6)	N(1)—C(6)	1.427(4)
N(1)—C(1)	1.462(3)	N(1)—C(33)	1.429(4)
		N(2)—C(29)	1.423(4)
		N(2)—C(22)	1.429(4)
		N(2)—C(42)	1.435(4)
Bond angles (°)			
C(18)-N(1)-C(11)	123.3(4)	C(13)-N(1)-C(6)	120.7(3)
C(18)-N(1)-C(1)	118.5(4)	C(13)-N(1)-C(33)	119.1(3)
C(11)-N(1)-C(1)	116.5(4)	C(6)-N(1)-C(33)	117.5(3)
		C(29)-N(2)-C(22)	119.0(3)
		C(29)-N(2)-C(42)	118.4(3)
		C(22)-N(2)-C(42)	116.7(3)
Torsion angles (°)			
C(11)-N(1)-C(1)-C(2)	108.57	C(6)-N(1)-C(33)-C(34)	50.12

Fig. 3. DSC of compound **3**. Heating rate of 20 °C/min. Curve (*a*) corresponds to first heating and curve (*b*) corresponds to second heating.



ple was observed to melt at T_m. Similar DSC measurements allowed the determination of the T_g and T_m values of diamines **1–9** and these results are presented in Table 2. For comparison, the corresponding values for **TPD** are included in this table.

Figure 4 displays the DSC data for compound **6**. In the first run, compound **6** exhibits a coupled endothermic and exothermic phase transition prior to melting at 283 °C. This type of transition has been attributed to polymorphism of the crystalline materials (42). After the compound was flash cooled in liquid nitrogen to form the glassy state, the sample was subjected to a second heating cycle that allowed observation of the T_g (116 °C) and T_c (185 °C). Following this second run, the compound was allowed to cool under ambient conditions to room temperature, and a third heating cycle was initiated. This run was stopped prior to melting. The purpose of this heating cycle was to anneal the sample into a crystalline phase. The fourth heating cycle confirmed that **6** was again a crystalline sample in that no T_g was observed but T_m was clearly seen. The data presented in Fig. 4 demonstrates that the rate of sample cooling of **6** has no effect on the T_g values, but it will effect T_c. For example, T_c is observed at 185 °C for the compound cooled in the liquid nitrogen, while T_c is 200 °C for the compound cooled under ambient conditions.

As summarized in Table 4, compounds **1–9** possess melting points from 187–283 °C, which all exceed that of **TPD** at 175 °C. With the exception of **5**, diamines **1–9** have higher T_g values than **TPD** and in two cases surpass this value by more than 50 °C. We attribute the low T_g that was observed for **5** to the fact that it possesses a *n*-propyl group, a feature that makes it unique among these compounds and likely reduces the overall rigidity of this compound. The highest T_g values were observed for compounds **6** and **7**, which have extended aromatic substituents. The 4,4′-biphenyl and 1-naphthyl groups increase both the molecular weight and the rigidity of **6** and **7**. The remaining compounds have T_g values that fall within the narrow range of 70–83 °C. Compound **9** possesses N-substituents that are simple phenyl rings and it exhibited a slightly higher T_g of 83 °C compared with the substituted aromatic analogues. This suggests that there is little gain in thermal properties by using simple methoxy, methyl, or fluoro substituents on the aromatic groups in these systems.

Electrochemistry

In a simple OLED, emission arises from the recombination of electrons originating in the ET layer with holes that are transported in the HT material. This combination can occur in either of the two layers and for charge transfer across the ET/HT interface some degree of HOMO and (or) LUMO matching is required. Matching of the HOMO level of the

© 2005 NRC Canada

Fig. 4. DSC curves for compound **6** under various heating and cooling conditions as described in the text. The five heating cycles are sequentially labeled a–e. Scan rate of 20 °C/min.

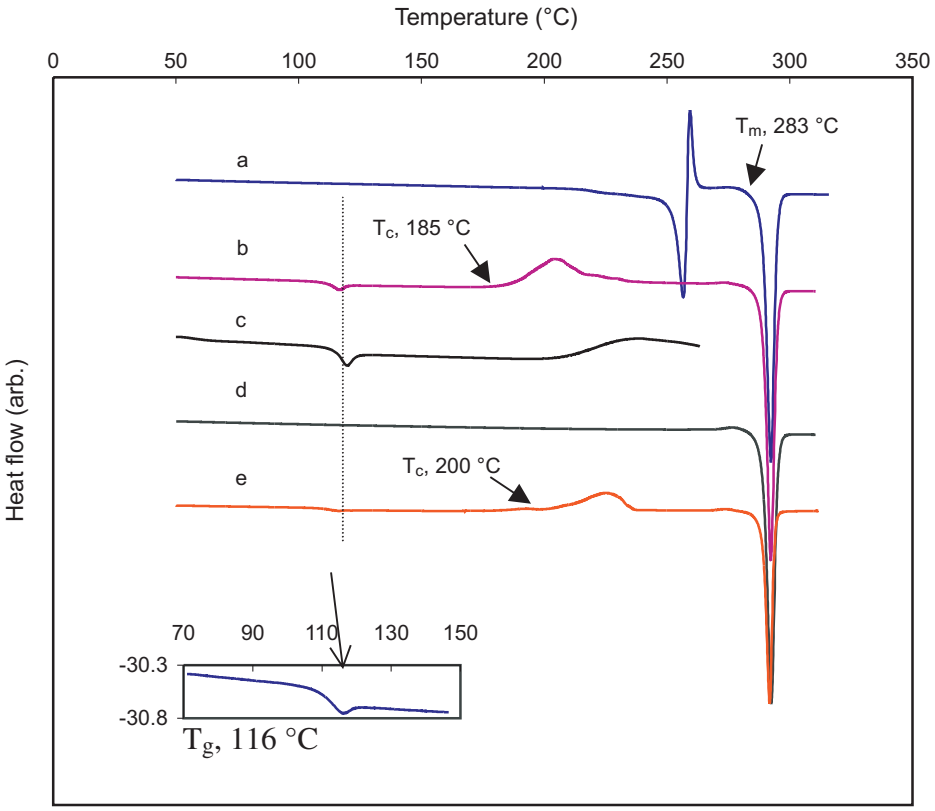


Table 4. Summary of electrochemical and spectroscopic data for naphthyl core diamines.

Compound	ΔE_{oxid} [a] (mV)	ΔE_p [b] (V)	Absorption (λ_{max}, nm)	Emission (λ_{emi}, nm)	Energy gap[c] (nm)	(Φ_f)[d]	HOMO[e] (eV)	LUMO[f] (eV)
1	145	0.081	375	500	433	0.18	5.10	2.24
2	130	0.160	372	475	421	0.19	5.11	2.16
3	144	0.091	376	480	425	0.22	5.14	2.22
4	140	0.135	370	476	420	0.20	5.15	2.20
5	140	0.123	379	480	429	0.20	5.09	2.20
6	121	0.106	375	475	425	0.19	5.16	2.24
7	160	0.125	375	465	410	0.08	5.14	2.11
8	169	0.202	361	441	395	0.46	5.24	2.10
9	255	0.210	362	441	401	0.48	5.31	2.22
TPD	220	0.127	350	404	385	NA[g]	5.08	1.86

[a]Potential difference between first and second oxidations.
[b]Potential difference between the $Cp_2Fe^{+/0}$ and diamine$^{+/0}$ couples.
[c]Estimated from the intersection of the normalized absorption and emission graph.
[d]Relative to Coumarin 102.
[e]HOMO = (4.8 + ΔE_p) eV.
[f]LUMO = HOMO – energy gap (eV).
[g]NA = not available.

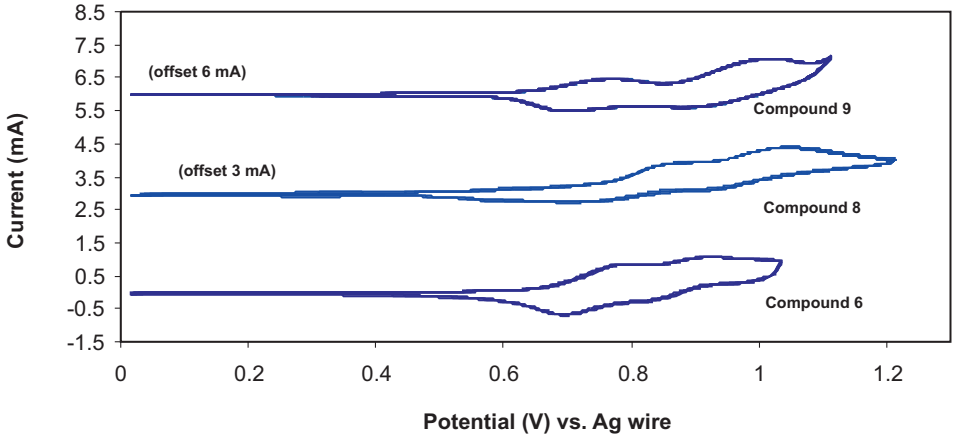
HT layer and that of the cathode is also important in EL device engineering. An electrochemical method based on cyclic voltammetry was used to estimate the HOMO energies of the naphthalene diamines **1**–**9** and to examine their electrochemical stability (43, 44).

Cyclic voltammetric scans were recorded under a N_2 atmosphere in CH_2Cl_2 solvent with a Ag wire pseudo-reference electrode and with TBAHFP as the supporting electrolyte. At the end of each set of scans, Cp_2Fe was added to the solution and another potential scan was performed that provided a reference potential for the Cp_2Fe/Cp_2Fe^+ couple as a calibration standard.

Over the positive potential scan range (0 to ~1.5 V), compounds **1**–**9** exhibited two reversible oxidation waves (examples are shown in Fig. 5). If the potential scan is extended to more positive potentials (~2 V), irreversible oxidation processes were also observed for all the compounds with the exception of **8**. The two reversible oxidation peaks in the CV

© 2005 NRC Canada

Fig. 5. CV scans of compounds **6**, **8**, and **9** at 100 mV/s in CH_2Cl_2 with 0.05 mol/L TBAHP under N_2. Five scans are shown.



curves can be ascribed to one-electron oxidation processes of the two amine centers. The first oxidation process corresponds to the HOMO energy level of the diamine and correlates directly to the energy required for hole generation and transport in the HT layer. The $E_{1/2}$ value of the diamine/diamine$^+$ couple relative to the $E_{1/2}$ value for the Cp_2Fe/Cp_2Fe^+ couple was used to estimate the HOMO energy levels for compounds **1**–**9**. The established value of the ferrocene HOMO energy level of 4.8 eV was added to the difference in the two oxidation potentials to obtain the diamine HOMO energy values and the results of these calculations are summarized in Table 4 (43, 44).

The extent of intramolecular charge mobility can be estimated by the difference between the first and second oxidation events for each of the diamines (ΔE_{oxid}). In the case of a large degree of charge delocalization, the first positive charge should have a pronounced effect on the second nitrogen center making it more difficult to oxidize and leading to a large difference in the two oxidation potentials. On the other hand, if the two charges are isolated from each other, only one oxidation couple would be observed. For example, **TPD** shows a potential gap of 220 mV indicating electronic communication between the two nitrogens after the first oxidation. Aromatic di- and triamines in which the N centers are bridged by a single phenyl group with a para or ortho disposition often exhibit even larger potential gaps in the range 330–530 mV (45–48). In contrast, the corresponding values for *meta*-diaminobenzene derivatives are smaller at 161–191 mV, presumably reflecting a low degree of conjugation between the two N centers (49). A similar lack of charge delocalization is observed for compounds **1**–**8**. Except for compound **9** (ΔE_{oxid} = 255 mV), the diaminonapthalene compounds **1**–**8** exhibit small ΔE_{oxid} values (121–169 mV).

The reproducibility of the voltammetric behavior over multiple potential scan cycles demonstrates the stability of these materials to the repeated redox steps they would experience in a device. When only the first two oxidation waves were scanned, compounds **1**–**9** showed reproducible CV behavior for at least five scan cycles as shown in the Fig. 5. With a wider potential range, compounds **1**–**7** continued to exhibit superimposible CV curves for at least five scan cycles. However, scanning of **8** and **9** over this wider potential range that included the third, irreversible oxidation process led to changes in the voltammograms. We attribute this instability to the deposition of the oxidized species onto the electrodes. In fact, during the CV scans for **9** a brown film was observed on the working Pt electrode, while for compound **8** a green precipitate was observed in the solution near the working electrode. These precipitates were not observed if the potential range did not extend beyond the second oxidation peak. The identity of these new species that are produced upon extensive oxidation of **8** and **9** has not been established, but the fact that this observation is associated with N-substitutents that do not have para substitution suggests that there may be a reaction of the oxidized species on the *N*-phenyl ring.

Electronic spectra

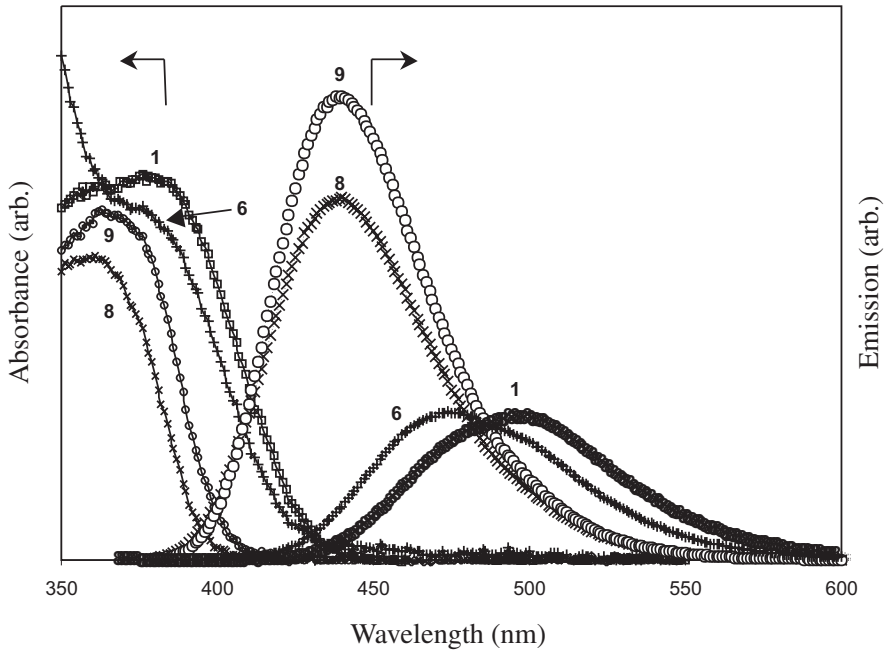
The naphthalene diamines **1**–**9** are white, yellow, or pale orange solids and they possess well-separated absorption and emission maxima with the later appearing in the blue to green region of the spectrum. The UV–vis absorption and emission spectra for these compounds is summarized in Table 4, and typical spectra for compounds **1**, **6**, **8**, and **9** are shown in Fig. 6. Except for compound **6**, these compounds exhibit a single λ_{max} in their absorption spectra. In the case of **6**, the value of λ_{max} was taken from the shoulder at 375 nm (Fig. 6). The HOMO–LUMO gap energy was also estimated from these spectra and is included in Table 4 (21, 22).

The absorption maximum for **TPD** at 350 nm has been assigned to an $n \rightarrow \pi^*$ electronic transition that is due to electron transfer from a nitrogen lone pair to the π^* orbital of the biphenyl group (41). We assign the λ_{max} absorption values for **1**–**9** as arising from a similar $n \rightarrow \pi^*$ electron transition with the π^* orbital residing on the naphthalene moiety. In the case of **6**, we propose that the rising absorption below 375 nm is a result of another $n \rightarrow \pi^*$ electron transition involving the nitrogen lone pair and the π^* orbital of the biphenyl group.

In comparison with compound **9**, all of the para-substituted phenyl compounds (**1**–**7**) exhibit a bathochromic shift in both absorption and emission, which can be ascribed to the electron-donating properties of the aromatic substituents. The electron-donating properties of the methoxy substituents appear to overwhelm the electron-withdrawing effects of the fluoro (**4**), phenyl (**6**), and naphthyl groups (**7**).

© 2005 NRC Canada

Fig. 6. UV–vis absorption (left) and emission (right) spectra for compounds **1** (□), **6** (+), **8** (×), and **9** (○).



As a result, compound **1** displays the largest red shift for emission and Stokes shift.

Generally, the HT materials in an OLED are not used as the source of emission. This is due to the fact the hole mobility is much faster than electron mobility, and as a result, the charge recombination usually occurs in the ET layer and this is where the emission arises. However, if the difference of HOMO energy levels between HT and ET is large enough and the difference in LUMO energy levels is small, holes will be blocked within the HT layer. As a result, emission could arise in the HT layer and there are recent reports of diamine-based HT materials functioning in the role of emitter hosts and as emission sources (20, 26, 29, 50). The emission properties of HT materials, both the emission wavelength (λ_{emi}) and quantum efficiency (Φ_f) provide important performance criteria for OLED fabrication. The values of Φ_f for diamines **1**–**9** were measured in CH_2Cl_2 relative to Coumarin 102 as a standard (36) and the results are presented Table 4.

Compounds **1**–**9** fall into two groups based on their Φ_f values. In particular, the Φ_f values for **8** and **9** are identical and more than twice those of the other diamines. Furthermore, **8** and **9** have identical values for their absorption and emission maxima. This phenomenon can be ascribed to the electron-donating properties of the substituents on the *N*-aryl groups. Since the transition is $n \rightarrow \pi^*$ in the diamines, the electron-rich amines that possess electron-donating groups at the para position of the aryl substituents (i.e., **1**–**7**) will display higher energies for the nonbonding HOMO electrons relative to those amines that do not have such groups (i.e., **8** and **9**). The result will be a reduced HOMO–LUMO gap and a smaller energy difference between the singlet and triplet states, which in turn allows for increased rate of intersystem crossing and a reduction in the Φ_f (51).

Estimates for the diamine LUMO energy levels were obtained by subtracting the HOMO energy values determined electrochemically from the HOMO–LUMO energy gap that was obtained from the absorption and emission spectra. With this method we can then compare the relative energy levels of the naphthyl core diamine compounds. From the data, we can see that meta-substituted **8** and unsubstituted **9** have the largest HOMO values, while all of the para-substituted compounds have similar HOMO values. These two groupings of HOMO energies are consistent with a HOMO that is predominantly the nonbonding electrons localized on the nitrogen centers. Furthermore, the very similar values of the LUMO energies for all of the compounds are also in harmony with a naphthalene core localized π^* orbital. The overall effects of the aryl substituents provides direction for orbital level tuning of these and related materials for the matching of the energy levels between the charge transport layers that is required for successful OLED fabrication.

Conclusions

Pd catalyzed coupling reactions have been used to synthesize a series of naphthyl core diamines with the general formula 1,5-$[Ar(Ar')N]_2C_{10}H_6$ (Ar = $MeOC_6H_4$; Ar′ = C_6H_5, $MeOC_6H_4$, *p*-MeC_6H_4, *p*-FC_6H_4, *p*-PhC_6H_4, 1-naphthyl) and the characterization of these species points to their potential as optoelectronic materials. We have examined the thermal, electrochemical, and photophysical properties of these materials. By varying the aryl groups, we have demonstrated the features that lead to the best thermal stability. All of these materials show enhanced glass forming ability and thermal stability compared to **TPD**. The relative HOMO and LUMO levels for these materials, important parameters for the design of efficient OLEDs, were assessed through electrochemical and spectroscopic measurements. Compounds **1**–**9** have the potential to function as hole transport materials and they emit in the blue to green color range. We are currently

© 2005 NRC Canada

investigating the transport properties of these materials and their use as HT materials in OLEDs.

References

1. C.W. Tang and S.A. Vanslyke. Appl. Phys. Lett. **51**, 913 (1987).
2. C.W. Tang, S.A. Vanslyke, and C.H. Chen. J. Appl. Phys. **65**, 3610 (1989).
3. L.S. Hung and C.H. Chen. Mater. Sci. Eng. R. **39**, 143 (2002).
4. M. Stolka, J.F. Yanus, and D.M. Pai. J. Phys. Chem. **88**, 4707 (1984).
5. R. Dale, R. Meyer, N. Jubran, Z. Tokarski, R. Moudry, and K. Law. J. Electroanal. Chem. **567**, 19 (2004).
6. R.D. Hreha, C.P. George, A. Haldi, B. Domercq, M. Malagoli, S. Barlow, J.L. Bredas, B. Kippelen, and S.R. Marder. Adv. Funct. Mater. **13**, 967 (2003).
7. A.R. Kennedy, W.E. Smith, D.R. Tackley, W.I.F. David, K. Shankland, B. Brown, and S.J. Teat. J. Mater. Chem. **12**, 168 (2002).
8. P.J. Low, M.A.J. Paterson, H. Puschmann, A.E. Goeta, J.A.K. Howard, C. Lambert, J.C. Cherryman, D.R. Tackley, S. Leeming, and B. Brown. Chem. Eur. J. **10**, 83 (2004).
9. J. Cornil, N.E. Gruhn, D.A. dos Santos, M. Malagoli, P.A. Lee, S. Barlow, S. Thayumanavan, S.R. Marder, N.R. Armstrong, and J.L. Bredas. J. Phys. Chem. A, **105**, 5206 (2001).
10. E. Bellmann, S.E. Shaheen, R.H. Grubbs, S.R. Marder, B. Kippelen, and N. Peyghambarian. Chem. Mater. **11**, 399 (1999).
11. J. Cornil, D. Beljonne, J.P. Calbert, and J.L. Bredas. Adv. Mater. **13**, 1053 (2001).
12. M. Malagoli, M. Manoharan, B. Kippelen, and J.L. Bredas. Chem. Phys. Lett. **354**, 283 (2002).
13. M. Malagoli and J.L. Bredas. Chem. Phys. Lett. **327**, 13 (2000).
14. N.E. Gruhn, D.A. da Silva, T.G. Bill, M. Malagoli, V. Coropceanu, A. Kahn, and J.L. Bredas. J. Am. Chem. Soc. **124**, 7918 (2002).
15. K. Sakanoue, M. Motoda, M. Sugimoto, and S. Sakaki. J. Phys. Chem. A, **103**, 5551 (1999).
16. C. Adachi, T. Tsutsui, and S. Saito. Appl. Phys. Lett. **56**, 799 (1990).
17. K. Naito and A. Miura. J. Phys. Chem. **97**, 6240 (1993).
18. J. Salbeck, N. Yu, J. Bauer, F. Weissortel, and H. Bestgen. Synth. Met. **91**, 209 (1997).
19. J. Salbeck, F. Weissortel, and J. Bauer. Macromol. Symp. **125**, 121 (1998).
20. K.R.J. Thomas, J.T. Lin, Y.T. Tao, and C.W. Ko. Adv. Mater. **12**, 1949 (2000).
21. K.R.J. Thomas, J.T. Lin, Y.T. Tao, and C.W. Ko. J. Am. Chem. Soc. **123**, 9404 (2001).
22. M.X. Yu, J.P. Duan, C.H. Lin, C.H. Cheng, and Y.T. Tao. Chem. Mater. **14**, 3958 (2002).
23. K. Danel, T.H. Huang, J.T. Lin, Y.T. Tao, and C.H. Chuen. Chem. Mater. **14**, 3860 (2002).
24. S. Toguchi, Y. Morioka, H. Ishikawa, A. Oda, and E. Hasegawa. Synth. Met. **111**, 57 (2000).
25. T.H. Huang, J.T. Lin, Y.T. Tao, and C.H. Chuen. Chem. Mater. **15**, 4854 (2003).
26. S. Tokito, K. Noda, H. Fujikawa, Y. Taga, M. Kimura, K. Shimada, and Y. Sawaki. Appl. Phys. Lett. **77**, 160 (2000).
27. X.C. Li, Y.Q. Liu, M.S. Liu, and A.K.Y. Jen. Chem. Mater. **11**, 1568 (1999).
28. Y. Shirota, K. Okumoto, and H. Inada. Synth. Met. **111**, 387 (2000).
29. K. Okumoto and Y. Shirota. Appl. Phys. Lett. **79**, 1231 (2001).
30. Y. Qiu, J. Qiao, Y. Gao, D. Zhang, and L. Wang. Synth. Met. **129**, 25 (2002).
31. A.R. Muci and S.L. Buchwald. Top. Curr. Chem. **219**, 131 (2002).
32. J.P. Wolfe, S. Wagaw, J.F. Marcoux, and S.L. Buchwald. Acc. Chem. Res. **31**, 805 (1998).
33. J.F. Hartwig. *In* Handbook of organopalladium chemistry for organic synthesis. Vol. 1. *Edited by* E. Negishi. Wiley Interscience, New York. 2002. p. 1051.
34. J.F. Hartwig. Acc. Chem. Res. **31**, 852 (1998).
35. H.O. House, W.J. Campbell, and D.G. Koepsell. J. Org. Chem. **37**, 1003 (1972).
36. J. Stampf, S. Tasch, G. Leising, and U. Scherf. Synth. Met. **71**, 2125 (1995).
37. J.P. Wolfe, H. Tomori, J.P. Sadighi, J.J. Yin, and S.L. Buchwald. J. Org. Chem. **65**, 1158 (2000).
38. J.P. Wolfe and S.L. Buchwald. J. Org. Chem. **65**, 1144 (2000).
39. J.F. Hartwig, M. Kawatsura, S.I. Hauck, K.H. Shaughnessy, and L.M. Alcazar-Roman. J. Org. Chem. **64**, 5575 (1999).
40. G.M. Sheldrick. SHELXTL 5.1 [computer program]. Bruker–AXS, Madison, Wis. 2001.
41. B.E. Koene, D.E. Loy, and M.E. Thompson. Chem. Mater. **10**, 2235 (1998).
42. M. Cölle, J. Gmeiner, W. Milius, H. Hillebrecht, and W. Brütting. Adv. Funct. Mater. **13**, 108 (2003).
43. J. Pommerehne, H. Vestweber, W. Guss, R.F. Mahrt, H. Bassler, M. Porsch, and J. Daub. Adv. Mater. **7**, 551 (1995).
44. M. Thelakkat and H.W. Schmidt. Adv. Mater. **10**, 219 (1998).
45. M.J. Plater and T. Jackson. J. Chem. Soc. Perkin Trans. 1, 2548 (2001).
46. S. Sasaki and M. Iyoda. Chem. Lett. 1011 (1995).
47. S. Dapperheld, E. Steckhan, K.H.G. Brinkhaus, and T. Esch. Chem. Ber. **124**, 2557 (1991).
48. Y. Shirota, T. Kobata, and N. Noma. Chem. Lett. 1145 (1989).
49. M. Yano, K. Sato, D. Shiomi, A. Ichimura, K. Abe, T. Takui, and K. Itoh. Tetrahedron Lett. **37**, 9207 (1996).
50. W.L. Li, Z.Q. Gao, Z.Y. Hong, C.S. Lee, and S.T. Lee. Synth. Met. **111**, 53 (2000).
51. N.J. Turro. Modern molecular photochemistry. University Press, Menlo Park, Calif. 1978.

© 2005 NRC Canada

Effect of charge and surface area on the cytotoxicity of cationic metallointercalation reagents[1]

Gavin L. Edwards, David St.C. Black, Glen B. Deacon, and Laurence P.G. Wakelin

Abstract: Reaction of a series of nitrogen donor ligands (1-phenylpyrazoles, 2-phenylpyridine, benzo[*h*]quinoline, 1-(2′-pyridyl)indole, 1-phenylindazole, and 2-phenylindazole) with palladium(II) and platinum(II) salts gave complexes where ortho-metallation had occurred resulting in bidentate binding to the metal centres through N and C atoms. These cyclometallated products were isolated as μ-chloro dimers. Subsequent treatment of these μ-chloro dimers with chelating diamines such as 1,2-ethanediamine converted them into 14 cationic (1+) complexes. Analogous coordination mixed ligand complexes (charge 2+) were prepared by reaction of dichloro(1,2-ethanediamine-*N*,*N*′)palladium(II) with aromatic diamines such as 2-(1′-pyrazolyl)pyridine, 2,2′-bipyridine, and 1,10-phenanthroline. The complexes exhibited growth inhibitory activity against L1210 mouse leukæmia cells in vitro over a wide concentration range; in general, the cyclometallated complexes were more active than the mixed ligand complexes, although one cyclometallated organoplatinum complex was less active than the mixed ligand analogue. Substitution around the periphery of the aromatic ligands also resulted in increased activity. One complex, derived from 1-(2′-pyridyl)indole, was tested in vivo and showed no significant antitumour inhibition against P388 leukæmia at doses below toxic levels.

Key words: anticancer, metallointercalator, cyclometallation, palladium, platinum, cytotoxicity.

Résumé : La réaction d'une série de ligands donneurs d'azote (1-phénylpyrazoles, 2-phénylpyridine, benzo[*h*]quinoléine, 1-(2′-pyridyl)indole, 1-phénylindazole et 2-phénylindazole) avec des sels de palladium(II) et de platine(II) conduit à la formation de complexes dans lesquels il s'est produit une ortho-métallation qui résulte en une liaison bidentate avec les centres métalliques par le biais des atomes de N et de C. On a isolé ces produits sous la forme de dimères μ-chloro et un traitement subséquent de ces dimères avec des diamines qui peuvent agir comme agent chélatant, telles l'éthane-1,2-diamine, a permis de les transformer en quatorze complexes cationiques (1+). On a préparé des complexes analogues avec des ligands à coordination mixte (charge 2+) en faisant réagir du dichloro(éthane-1,2-diamine-*N*,*N*′)palladium(II) avec des diamines aromatiques, telle la 2-(1′-pyrazolyl)pyridine, la 2,2′-bipyridine et la 1,10-phénanthroline. Dans des essais in vitro, ces complexes présentent, sur large plage de concentration, une activité inhibitrice de la croissance des cellules de la lignée L1210 de la leucémie de la souris; en général, les complexes cyclométallés sont plus actifs que les complexes de ligands mixtes, même si un complexe organique cyclométallé du platine est moins actif que l'analogue avec un ligand mixte. Une substitution autour de la périphérie des ligands aromatiques conduit aussi à une augmentation de l'activité. Un complexe, celui dérivé du 1-(2′-pyridyl)indole, a été évalué in vivo et, à des doses inférieures aux niveaux toxiques, il ne présente aucune activité d'inhibition antitumorale contre la leucémie P388.

Mots clés : anticancéreux, intercalation métallique, cyclométallation, palladium, platine, cytotoxicité.

[Traduit par la Rédaction]

Introduction

Cancer, as a group of diseases, ultimately kills one-quarter of the human population. The quest for new and effective chemotherapeutic agents to combat cancers has led to tremendous activity; however, until relatively recently, the use of heavy metals has attracted only sporadic interest. The serendipitous discovery by Rosenberg et al. (1) that *cis*-

Received 7 December 2004. Published on the NRC Research Press Web site at http://canjchem.nrc.ca on 25 August 2005.

It is a pleasure to honour Howard Alper's very significant contributions both to chemistry and to the chemical profession.

G.L. Edwards and D.St.C. Black.[2] School of Chemistry, University of New South Wales, Sydney, New South Wales, Australia, 2052.
G.B. Deacon. School of Chemistry, Monash University, Victoria, Australia, 3800.
L.P.G. Wakelin. Department of Physiology and Pharmacology, School of Medical Sciences, University of New South Wales, Sydney, New South Wales, Australia, 2052.

[1]This article is part of a Special Issue dedicated to Professor Howard Alper.
[2]Corresponding author (e-mail: d.black@unsw.edu.au).

 doi: 10.1139/V05-110 © 2005 NRC Canada

Table 1. Products of cyclometallation reactions.

Ligand	Abbreviation	Metal	Complex	Yield (%)
1-Phenylpyrazole (**1**)	Hpzph	Pd	**3**	99
2-Phenylpyridine (**2**)	Hpyph	Pd	**4**	96
2-Phenylpyridine (**2**)	Hpyph	Pt	**5**	65
1-(2′-pyridyl)indole (**6**)	Hpyin	Pd	**10**	97
1-Phenyl-1*H*-indazole (**7**)	H-1phiz	Pd	**11**	99
2-Phenyl-2*H*-indazole (**8**)	H-2phiz	Pd	**12**	98
Benzo[*h*]quinoline (**9**)	Hbq	Pd	**13**	92
3,5-Dimethyl-1-phenylpyrazole (**14**)	Hdmpzph	Pd	**15**	45

diamminedichloroplatinum(II) (cisplatin) inhibited cell division in *Escherichia coli*, and the subsequent establishment that a range of platinum complexes inhibited the development of sarcoma 180 and leukæmia L1210 in mice (2), led not only to the introduction of cisplatin as a clinically efficacious agent against testicular and ovarian cancers in 1978 (3), but also to the rekindling of interest in metal-based therapies (4, 5). While the clinical effectiveness of cisplatin against human malignancies, both as a single agent and in combination therapy, has had a major impact on cancer treatment, its therapeutic usefulness has been offset by a range of toxic side effects. The combination of good activity, dose-limiting side effects, and the disadvantage that some tumours acquire resistance to the drug, has stimulated research into second and third generation platinum drugs (6, 7).

While the anticancer activity of cisplatin has been attributed to the formation of bifunctional adducts with DNA, especially guanine–guanine crosslinks (6), pioneering work initiated by Lippard and co-workers (8) utilized another aspect of the chemistry of platinum(II) — its ability to act as a square-planar template to impart planarity on ligands such as 2,2′-bipyridine (bpy). While these complexes would have been predicted to have negligible anticancer activity based on observations gleaned from cisplatin and its analogues, the synthesis of planar, kinetically inert metal complexes provided a new mechanism of action namely, intercalation. In particular, Lippard used platinum(II) as a framework to force the aromatic rings of ligands such as bpy and 2,2′:6′,2″-terpyridine (terpy) into a coplanar arrangement, providing a flat aromatic surface capable of intercalation into DNA. However, despite extensive studies on the interactions of these materials with isolated nucleic acids or synthetic polynucleotides (9, 10), until recently there have been relatively few reports of the biological activity of square-planar platinum(II) or palladium(II) metallointercalators (11, 12).

The work initiated by Lippard and co-workers (8) provided the basis for the design of a range of complexes as potential new anticancer agents. Based on the metallointercalation model, a potential intercalator (13) should incorporate a kinetically inert metal with square-planar geometry, and it should fix aromatic, multidentate ligands in a coplanar array. Central to our strategy was the use of bidentate, nonlabile cyclometallated ligands to stabilize the complex and suppress dissociation of the intercalating aromatic ligand from the metal centre in vivo. Analogous mixed ligand coordination compounds with nitrogen donor ligands would provide contrasts to determine the importance of intercalator charge. Most metal complexes with anticancer activity are based on platinum, and to date analogous palladium complexes have shown marginal in vivo activity at best. While some palladium complexes have shown promising activity in vitro (12) or in animal models (6), they have not made a successful transition to clinical usefulness; the poor activity could be attributed to the higher reactivity of palladium species towards ligand displacement reactions. In this study drugs were designed where covalent binding to DNA is not expected and, as the coordination chemistries of platinum(II) and palladium(II) are similar, both metals should provide suitable frameworks upon which to build intercalating complexes. In a following paper we report the activity of a range of monofunctional cyclometallated platinum(II) and palladium(II) complexes (14).

Results and discussion

Cyclometallation reactions

Reactions of nitrogen donor ligands such as 1-phenylpyrazole (Hpzph) (**1**) (15) and 2-phenylpyridine (Hpyph) (**2**) (16) with palladium(II) salts to give cyclometallated complexes (referred to herein as cyclopalladated complexes) have been well-documented. While we have previously shown that the cyclopalladation of these ligands occurs readily providing products **3** and **4** in near-quantitative yields (Table 1), the analogous reaction of **2** with a platinum(II) salt (cycloplatination) requires more forcing conditions and gives only a moderate (65%) yield of the μ-chloro dimer **5** (17) (Fig. 1). Although the dimeric complexes are insoluble or very sparingly soluble in most solvents, they dissolve with reaction in dimethyl sulfoxide. An examination of the ^{1}H NMR spectra recorded in ($^2H_6$)dimethyl sulfoxide ($(CD_3)_2SO$) indicated the loss of one aryl proton, in agreement with the cyclometallated structures. An alternative confirmation that cyclometallation had taken place was obtained in many cases by addition of one drop of ($^2H_5$)pyridine (py-d_5) to a suspension of the dimers in $CDCl_3$; the complexes dissolved with reaction to give monomers where loss of one proton was evident and shielding of the proton ortho to the site of metallation was observed as a result of its proximity to the pyridine ligand (Fig. 1) (17).

Variation of the aromatic ligand could provide increased surface area for the planar intercalator possibly resulting in enhanced DNA binding, and it was shown that 1-(2′-pyridyl)indole (Hpyin) (**6**), 1-phenylindazole (H-1phiz) (**7**), 2-phenylindazole (H-2phiz) (**8**) (18), and benzo[*h*]quinoline (Hbq) (**9**) (19) could be cyclopalladated with $Na_2[PdCl_4]$ in near-quantitative yields giving μ-chloro dimers **10**–**13** on heating of the reaction mixtures for up to 24 h (Table 1,

© 2005 NRC Canada

Fig. 1. Cyclometallation reaction and product of bridge cleavage with py-d_5.

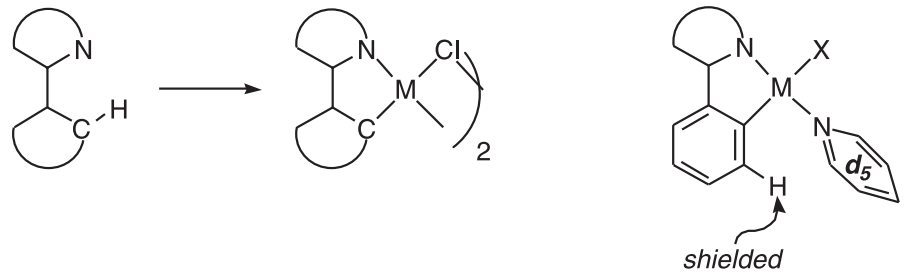


Fig. 2. Ligands and abbreviations with positions of metallation indicated.

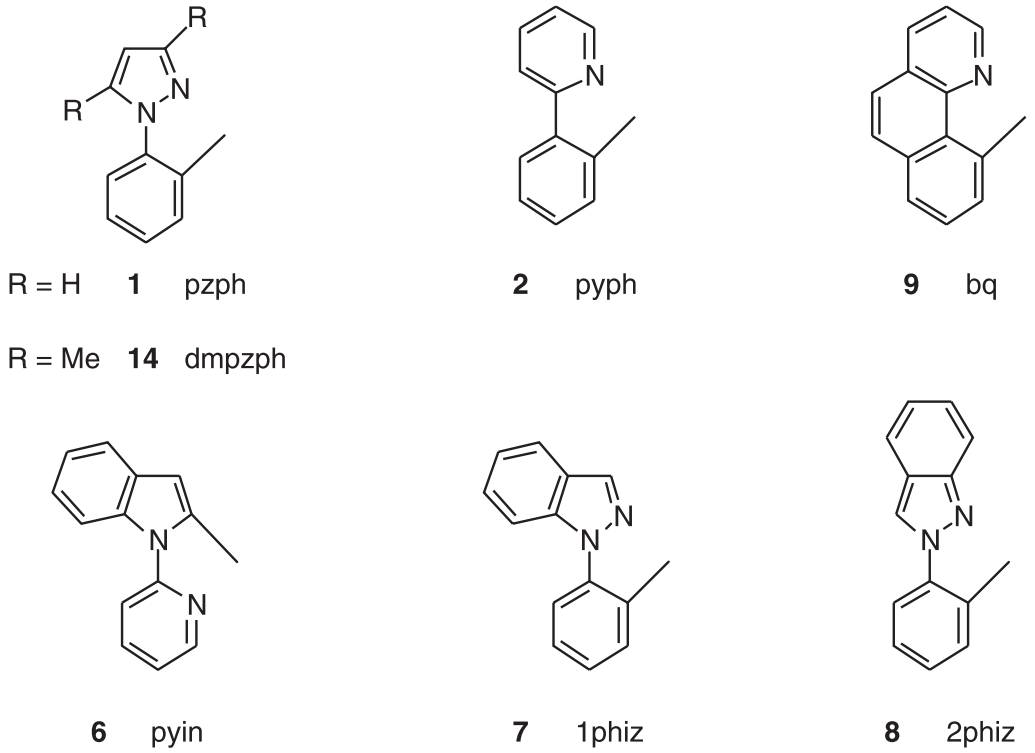


Fig. 2). Nonoyama and Nakajima (20) have recently reported the cyclometallation of **6** in moderate yield with palladium(II) acetate in boiling acetonitrile. Attempted cyclometallation of **6** with $Na_2[PdCl_4]$ at room temperature gave a mixture of the cyclometallated dimer **10** and a non-metallated coordination complex, as shown by a complex ^{1}H NMR spectrum in $(CD_3)_2SO$, where evidence for non-metallated ligand (indole H3 was noted as a doublet at δ 6.76 ppm, J = 3.5 Hz) was observed. A terminal ν(Pd–Cl) corresponding to the coordination complex was also observed at 343 cm^{-1} in the far-IR region, suggesting trans stereochemistry. No attempt was made to separate the mixture into its components. In several cases throughout this work, metathesis of the complexes with LiBr in acetone or dimethyl sulfoxide assisted interpretation of the far-IR spectra (17).

Cyclometallation of 3,5-dimethyl-1-phenylpyrazole (Hdmpzph) (**14**) using $K_2[PdCl_4]$ in boiling aqueous methanol gave a mixture of cyclometallated product **15** and coordination complex **16** (Fig. 3), at variance with earlier reports by Trofimenko and Vaughan (21) that cyclometallation was achieved quantitatively. Extended heating only increased the yield of the desired product **15** marginally. The products could be separated by extraction of coordination complex **16** into boiling dichloromethane. While the insoluble cyclometallated dimer **15** was contaminated with a small amount of palladium metal, it was of sufficient purity for further use. Analytically pure material could be obtained by precipitation of the dimer from a filtered solution of *N*,*N*-dimethylformamide (DMF) by the addition of methanol. Coordination complex **16** was identified as the cis stereoisomer by observation of two terminal ν(Pd–Cl) bands in the far-IR spectrum at 362 and 321 cm^{-1}; while approximately 10% of a second component was observed in the ^{1}H NMR spectrum, it was not determined whether this was due to a small amount of the trans isomer, or restricted rotation of the pyrazole ligands within the complex on the ^{1}H NMR timescale resulting in detection of syn and anti rotamers of complex **16**. All attempts to convert coordination complex **16** into cyclometallated dimer **15** were unsuccessful.

The ligand 1-methyl-3,5-diphenylpyrazole (**17**) is potentially able to form a five-membered chelate ring by metal-

© 2005 NRC Canada

Fig. 3. Products from cyclometallation of 3,5-dimethyl-1-phenylpyrazole (**14**).

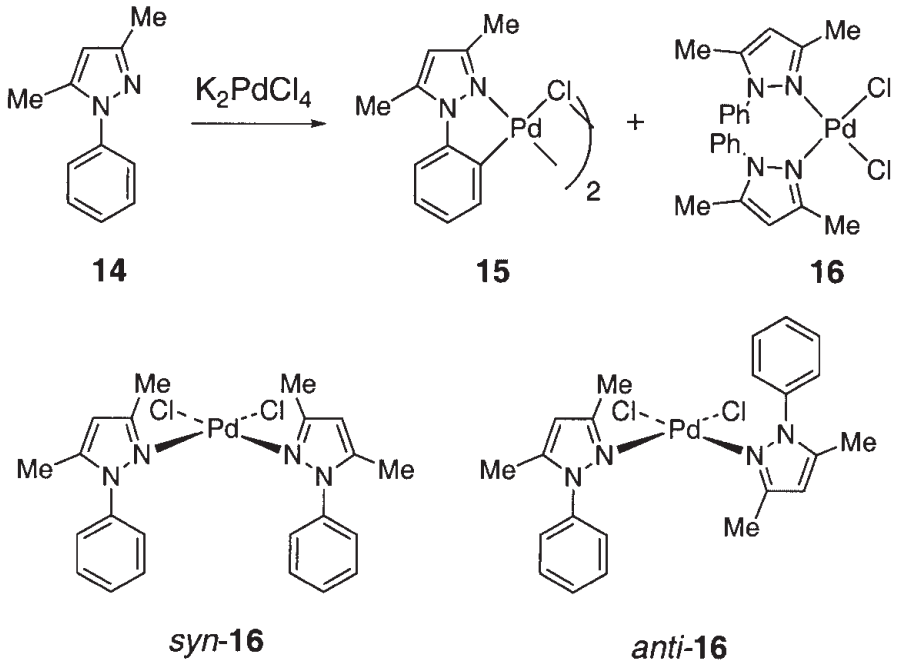
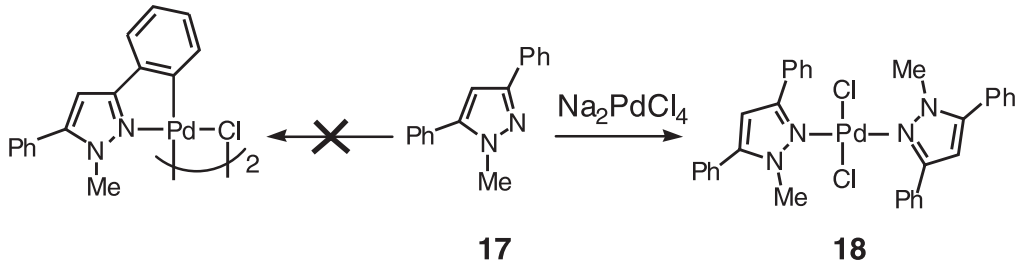


Fig. 4. Attempt to cyclometallate 1-methyl-3,5-diphenylpyrazole (**17**).



lation onto an ortho carbon of the 3-phenyl ring; this would provide an intercalator of comparable size but different geometry to other phenylpyrazoles (Fig. 4). Heating the ligand with $Na_2[PdCl_4]$ in methanol only gave the coordination complex $PdCl_2L_2$ (**18**) (22); a single ν(Pd–Cl) was observed in the far-IR spectrum at 349 cm^{-1} suggesting formation of the trans stereoisomer, and the ^1H NMR spectrum indicated that the product was a 15:1 mixture of two components, which Alonso et al. (22) have suggested results from restricted rotation about the Pd—N bonds. It is noteworthy that pyrazole **17** gives the trans stereoisomer **18**, whereas pyrazole **14** gives mainly the cis isomer **16**, despite both reaction mixtures being heated for comparable periods.

Preparation of cationic complexes

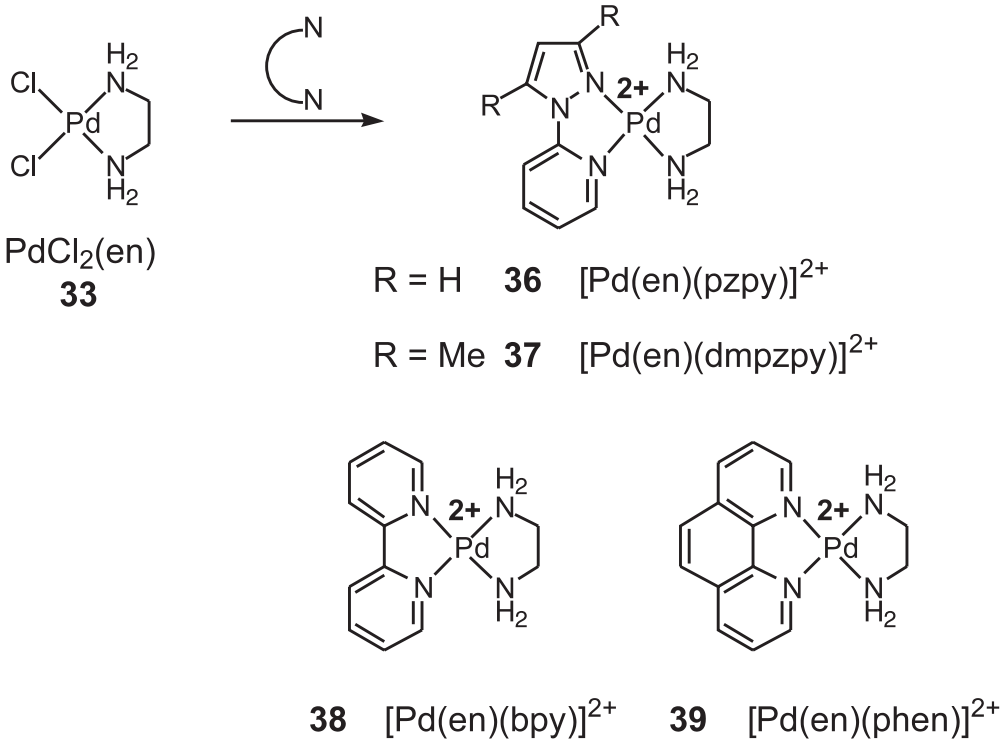
Addition of a bidentate diamine to the appropriate μ-chloro dimers gave the desired cationic complexes as water- and alcohol-soluble products (Table 2), which could be purified by precipitation of the complexes from alcoholic or aqueous alcoholic solution by the addition of ether. Diamine ligands chosen for study included 1,2-ethanediamine (en), 1,3-propanediamine (trimethylenediamine, tn), and *cis*- and *trans*-cyclohexanediamine (chxn). Biological and clinical studies of platinum complexes of chxn have been extensive (6, 7); in general, complexes of *trans*-chxn are more active than their *cis*-chxn analogues (6, 23), and complexes prepared from *R*,*R*-chxn are more active than those containing *S*,*S*-chxn (23). The oxalate-containing complex oxaliplatin ($Pt(C_2O_4)$(*R*,*R*-chxn)) in combination with 5-fluorouracil is emerging as a major therapy for colorectal cancer (24). In

Table 2. Cationic cyclometallated complexes.

Cyclometallated ligand	Metal	Diamine	Compound	Yield (%)
pzph	Pd	en	**19**	59
pzph	Pd	*cis*-chxn	**20**	65
pzph	Pd	*trans*-chxn	**21**	67
pyph	Pd	en	**22**	85
pyph	Pd	tn	**23**	79
pyph	Pd	*cis*-chxn	**24**	62
pyph	Pd	*trans*-chxn	**25**	80
pyph	Pt	en	**26**	75
dmpzph	Pd	en	**27**	70
dmpzph	Pd	tn	**28**	74
bq	Pd	en	**29**	69
pyin	Pd	en	**30**	67
1phiz	Pd	en	**31**	80
2phiz	Pd	en	**32**	78

© 2005 NRC Canada

Fig. 5. Mixed ligand complexes isolated as dichloride salts.



this study, complexes of *cis*- and racemic *trans*-chxn were prepared for biological testing.

Several of the complexes were isolated as hydrates; attempted drying at elevated temperature led to partial decomposition and drying at ambient temperature failed to remove the water of crystallization. In general, while the IR spectra of the complexes usually showed several absorptions of medium to strong intensity in the range 3000–3300 cm^{-1}, which could be attributed to the N–H stretching frequencies of the coordinated diamine ligands; absorptions at higher frequencies (3300–3500 cm^{-1}) were only observed for the hydrated complexes and were assigned to water of crystallization. Examination of the far-IR spectra of the complexes supported the assigned chelate structures as no strong absorptions between 240 and 360 cm^{-1}, which might be attributed to ν(M-Cl), were observed.

In the ^1H NMR spectra of the complexes, two distinct NH_2 signals were observed that can be attributed to a nonequivalence of the NH_2 groups as a result of the different trans carbon and nitrogen ligands. It is interesting that, for the platinum complex **26**, $^2J_{Pt,H}$ was only resolved in the signal for the downfield (6.15 ppm) NH_2 group; mere broadening of the other signal (5.44 ppm) was observed. The poly(methylene) bridges in the en and tn complexes were observed as broad signals. Coordination of chxn to a metal constrains the ligand to adopt specific conformations and, as a result, further resolution of the cyclohexyl amine protons was observed. The rigidity of the chelate ring constrains the protons on each nitrogen to lie in pseudoaxial and pseudoequatorial environments; as a result, up to four distinct exchangeable signals were observed for the chxn complexes.

The cyclometallation reaction gives complexes with anionic carbon σ-donor ligands and the overall charge on the resulting cationic complexes is therefore one less than the corresponding Pt(II) complexes $[Pt(en)(bpy)]^{2+}$ and $[Pt(en)(phen)]^{2+}$. A range of nonmetallated, cationic complexes analogous to these classical coordination compounds was also prepared to determine the relationship of intercalator charge to biological activity. Comparison of the activities of the palladium(II) complexes with those reported for the corresponding platinum(II) complexes could allow an assessment of the relationship between metal and activity.

Synthesis of the mixed complexes was achieved by reaction of $PdCl_2(en)$ **33** with the appropriate bidentate aromatic ligand (pyrazolylpyridines **34** and **35**, bpy, and phen) by an adaptation of the method of Watt and Carter (25); the mixed ligand complexes **36–39** (Fig. 5) were isolated in moderate to good yields. The alternative approach, where en was added to Pd complexes of the bidentate aromatic ligands, led to partial displacement of the ligand from the metal with $[Pd(en)_2]Cl_2$ being isolated instead. Some hydration of the mixed ligand complexes was evident from the microanalytical data, and this was confirmed by observation of ν(O-H) in the range 3300–3500 cm^{-1}, as described previously. The ^1H NMR spectra of the complexes were unremarkable; whereas two signals for the coordinated NH_2 groups were observed for the cyclometallated complexes, the symmetry or pseudosymmetry of the coordination complexes caused the NH_2 groups to be chemical-shift equivalent.

In vitro and in vivo testing

The complexes were subjected to an in vitro screen for growth inhibitory activity against the murine leukæmia cell line L1210. While these tests do not discriminate between cytotoxic and cytostatic activity, they provide valuable infor-

© 2005 NRC Canada

Table 3. Growth inhibition of L1210 cells in culture.

Complex	Aromatic ligand	Diamine	Metal	Charge	IC_{50} (μmol/L)
19	pzph	en	Pd	1	63
20	pzph	*cis*-chxn	Pd	1	24
21	pzph	*trans*-chxn	Pd	1	43
22	pyph	en	Pd	1	34
23	pyph	tn	Pd	1	18
24	pyph	*cis*-chxn	Pd	1	11.5
25	pyph	*trans*-chxn	Pd	1	20.5
26	pyph	en	Pt	1	300
27	dmpzph	en	Pd	1	11
28	dmpzph	tn	Pd	1	14
29	bq	en	Pd	1	16
30	pyin	en	Pd	1	14
31	1phiz	en	Pd	1	18
32	2phiz	en	Pd	1	17
36	pzpy	en	Pd	2	230
37	dmpzpy	en	Pd	2	>200
38	bpy	en	Pd	2	60
39	phen	en	Pd	2	13
	bpy	en	Pt	2	33 (11)
	phen	en	Pt	2	2 (11)

mation about whether the complexes can affect the rate at which cells grow and divide. The complexes (drugs) were dissolved in sterile water or ethanol (for the chxn complexes) and growth inhibition experiments were conducted for a 48 h period against L1210 cell cultures, providing drug concentrations that caused a 50% inhibition of cell growth (IC_{50}) (Table 3). For comparison, it should be noted that cisplatin has an IC_{50} of 0.9 μmol/L under similar conditions.

The cationic planar complexes reported in this study caused 50% growth inhibition over a wide range of concentrations. The cyclometallated complexes (formal charge 1+) generally were more active than the dipositive coordination analogues (compare **19** with **36**, **27** with **37**, and **22** with **38**), but it should be noted that the phenanthroline complex **39** had a similar IC_{50} value (13 μmol/L) to that of the benzo[*h*]quinolinyl complex **29** (16 μmol/L). Although a variation of the intercalator charge might influence the biological activity, especially in electrostatic stabilization of an initial drug–DNA complex, the relative stabilities of the organometallic drugs in the presence of a wide range of biological ligands could also explain the observed differences. As described above, in the preparation of the cationic complexes, addition of diamines to the cyclometallated μ-chloro dimers gave the desired products cleanly, whereas addition of en to palladium complexes of bidentate heterocyclic ligands resulted in at least partial displacement of the aromatic ligand. Thus, it is proposed that the presence of the palladium–carbon σ bond appears to increase the stability of the complexes, and therefore the cyclometallated complexes would be more likely to reach their biological target intact. It is possible that the increased stability of the phenanthroline complex with respect to displacement of the ligand from the metal centre meant that its stability was similar to that of the benzo[*h*]quinolinyl complex under biological conditions, hence its activity was likewise similar.

Table 4. Antitumour testing for complex **30** against P388 leukæmia.

Dose (mg/kg/injection)	%T/C
0 (control)	100
2	110
4	111
8	110
16	0
32	0
50 (5-fluorouracil: standard)	158

In this study, a single organoplatinum cyclometallated complex $[Pt(pyph)(en)]^+$ (**26**) was prepared and its biological activity was measured (IC_{50} = 300 μmol/L); somewhat surprisingly it was almost an order of magnitude less active than $[Pt(en)(bpy)]^{2+}$ (IC_{50} = 33 μmol/L) (11). This suggests that there might be no firm correlation between platinum and palladium metallointercalators as the analogous organopalladium complex **22** $[Pd(pyph)(en)]^+$ (IC_{50} = 34 μmol/L) was *more* active than the coordination analogue **38** $[Pd(en)(bpy)]^{2+}$ (IC_{50} = 60 μmol/L).

Increased biological activity is observed with increased substitution on the planar organometallic ligand. Substitution with methyl groups or fusion of an extra benzene ring onto the planar aromatic structure, led to lower IC_{50} values. The methyl substituents may provide a steric barrier to dislodgement of an intercalated drug, accounting for the increased activity. The position of fusion of an extra aromatic ring did not seem to affect the activity greatly (compare: 1phiz **31** (18 μmol/L) and 2phiz **32** (17 μmol/L) complexes). Additional aromatic rings give a larger surface area to intercalate between the base pairs in a drug–DNA complex, and the extra aromatic ring could lead to a more stable complex as a result of an enhanced π-orbital overlap. The weakest drug–DNA complexes would be expected for complexes such as the 2-(2-pyridyl)phenyl and 1-(pyrazolyl)phenyl complexes, which have only two coplanar aromatic rings, and stronger drug–DNA adducts would be expected for larger cationic complexes. However, it is noteworthy that McFadyen et al. (11) found that a series of structurally related, cationic complexes exerted their biological activities in different ways, and it is possible that structurally similar complexes here might likewise be inhibiting cell growth by different mechanisms.

Variation of the diamine ligand also resulted in a change in biological activity. Increased bulk (chxn vs. en or tn) tended to give more active complexes, and a consistent effect was noted for the chxn complexes, where lower IC_{50} values for the *cis*-chxn complexes **20** and **24** than their trans analogues **21** and **25** were measured.

One of the more active complexes (the 1-(2-pyridyl)indolyl complex **30**) was selected for further study. Potential antitumour activity against P388 leukæmia in mice was evaluated over a range of dose levels up to a maximum tolerated dose, with results expressed (%T/C) as a ratio of mean survival times of treated animals (T) relative to control animals (C); significant antitumour activity requires %T/C values greater than 125%, and values of 0% indicate that no treated animals survived the drug regime at these dose levels. Results obtained in this screening (Table 4) indicated that the

© 2005 NRC Canada

metallointercalator showed no significant antitumour activity in vivo at doses below toxic levels.

Experimental

General procedure

Elemental analyses were performed by the Microanalytical Service, School of Chemistry, University of New South Wales. IR spectra were measured with a PerkinElmer 180 Grating IR spectrophotometer with a far-IR option, and refer to paraffin mulls of solids, measured between KBr plates (4200–380 cm^{-1}) and between polyethylene discs (550–100 cm^{-1}). Only absorptions of strong to medium intensity are reported herein. ^1H NMR spectra were recorded at 90 MHz (Bruker WH90 spectrometer), 200 MHz (Bruker AC200 spectrometer), or 300 MHz (Bruker AM300 spectrometer). Chemical shifts are reported in parts per million (ppm) downfield from tetramethylsilane (δ 0.00 ppm, referenced to $CHCl_3$ impurity in $CDCl_3$). Addition of one drop of py-d_5 to $CDCl_3$ suspensions of dimers **10**, **11**, **12**, **15**, and **18** converted the insoluble dimers into soluble monomeric complexes, which gave well-resolved spectra that integrated cleanly, providing excellent evidence for cyclometallation. Hbq (**9**), phen, bpy, *trans*-1,2-cyclohexanediamine (*trans*-chxn), en, and trimethylenediamine (tn) were obtained from the Aldrich Chemical Company and were recrystallized or distilled prior to use. *cis*-1,2-Cyclohexanediamine (*cis*-chxn) was separated from a mixture of isomers by the method of Saito and Kidani (26). 1-Phenylpyrazole (**1**) and **14** were prepared by the method of Finar and Hurlock (27). 1-(2′-Pyridyl)indole (**6**) was prepared by the method of Khan and Polya (28). 1-Phenyl-indazole (H-1phiz) (**7**) was prepared by the method of Pozharskii et al. (29), and **8** was prepared by the method of Cadogan and Mackie (30). 2-(1′-Pyrazolyl)pyridine (**34**) and 2-(3′,5′-dimethyl-1′-pyrazolyl)pyridine (**35**) were prepared by the general method of Khan and Pinto (31). Cyclopalladations of **1** to give **3** (15), of **2** to give **4** (16, 32), and of **9** to give **13** (19), and cycloplatination of **2** to give **5** (17), were carried out according to published procedures. Dichloro(1,2-ethanediamine-*N*,*N*′)palladium(II) ($PdCl_2$(en)) (**33**) was prepared by the method of McCormick et al. (33). Mixed ligand complex $[Pd(en)(phen)]Cl_2$ (**39**) (9) was prepared by the method described for complex **36** in the following section.

Preparations

Di-μ-chlorobis[1-(2′-pyridyl)indol-2-yl)-N′,C]dipalladium (10)

1-(2′-Pyridyl)indole (**6**) (1.50 g, 7.7 mmol) in methanol (20 mL) was added to a stirred solution of $Na_2[PdCl_4]$ (1.96 g, 6.7 mmol) in methanol (60 mL) under a nitrogen atmosphere. The mixture was heated under reflux for 24 h, and the resultant yellow precipitate was filtered off and washed successively with methanol and ether. A suspension of the crude product in dichloromethane (30 mL) was heated under reflux for 2 h, and then cooled to room temperature. The sparingly soluble solid was collected, washed with dichloromethane and then ether, and dried to give the μ-chloro dimer **10** as a yellow powder (2.16 g, 97%), mp 228–230 °C (dec.). A sample was recrystallized from DMF–methanol for microanalysis. IR (cm^{-1}): 1613, 1510, 1489, 1318, 1288, 1253, 1185, 745, 734, 418, 319 (Pd–Cl), 290, 240 (Pd–Cl). ^1H NMR (90 MHz, $CDCl_3$ – one drop of py-d_5) δ: 9.22 (dd, J = 5.9, 1.2 Hz, 1H, pyridyl H6), 7.91–7.07 (m, 6H, aryl), 6.89 (ddd, J = 7.4, 5.9, 1.4 Hz, 1H, pyridyl H5), 5.58 (d, J = 0.5 Hz, 1H, indolyl H3). Elemental anal. calcd. for $C_{26}H_{18}Cl_2N_4Pd_2$ (%): C 46.6, H 2.7, N 8.4; found: C 46.6, H 2.55, N 8.2.

Di-μ-chlorobis[2-(1′H-indazol-1′-yl)phenyl-N′,C]dipalladium (11)

The title compound **11** was prepared by a similar method to **10**, from **7** (0.62 g, 3.2 mmol) and $Na_2[PdCl_4]$ (0.75 g, 2.6 mmol), as a yellow powder (0.84 g, 99%), mp > 300 °C. A sample was recrystallized from DMF–methanol for microanalysis. IR (cm^{-1}): 1215, 1100, 836, 735, 722, 615, 421, 306 (Pd–Cl), 279, 230 (Pd–Cl). ^1H NMR (300 MHz, $CDCl_3$ – one drop of py-d_5) δ: 8.83 (s, 1H, indazolyl H3), 7.98 (dd, J = 8.7, 0.6 Hz, 1H, indazolyl H7), 7.79 (d, J = 8.1 Hz, 1H, aryl), 7.59 (ddd, J = 8.7, 7.1, 1.2 Hz, 1H, indazolyl H6), 7.54 (dd, J = 8.0, 1.0 Hz, 1H, aryl), 7.30 (t, J = 7.1 Hz, 1H, indazolyl H5), 7.17 (td, J = 7.7, 1.2 Hz, 1H, aryl), 6.80 (td, J = 7.6, 1.0 Hz, 1H, aryl), 6.33 (dd, J = 7.6, 1.1 Hz, 1H, phenyl H6). Elemental anal. calcd. for $C_{26}H_{18}Cl_2N_4Pd_2$ (%): C 46.6, H 2.7, N 8.4; found: C 46.5, H 2.5, N 8.45.

Di-μ-chlorobis[2-(2′H-indazol-2′-yl)phenyl-N′,C]dipalladium (12)

The title compound **12** was prepared by a similar method to **10**, from **8** (0.62 g, 3.2 mmol) and $Na_2[PdCl_4]$ (0.75 g, 2.6 mmol), as a yellow powder (0.83 g, 98%), mp > 300 °C (lit. value (18) mp > 300 °C). A sample was recrystallized from DMF–methanol for microanalysis. IR (cm^{-1}): 1627, 1519, 1489, 1352, 1071, 792, 784, 753, 745, 739, 437, 330 (Pd–Cl), 246 (Pd–Cl). ^1H NMR (300 MHz, $CDCl_3$ – one drop of py-d_5) δ: 9.01 (d, J = 8.9 Hz, 1H, indazolyl H7), 8.44 (s, 1H, indazolyl H3), 7.58 (d, J = 8.5 Hz, 1H, indazolyl H4), 7.34 (t, J = 7.4 Hz, 1H, aryl), 7.30 (dd, J = 7.9, 0.9 Hz, 1H, phenyl H3), 7.09 (t, J = 7.9 Hz, 1H, aryl), 7.03 (t, J = 7.5 Hz, 1H, aryl), 6.79 (t, J = 7.5 Hz, 1H, aryl), 6.08 (d, J = 7.6 Hz, 1H, phenyl H6). Elemental anal. calcd. for $C_{26}H_{18}Cl_2N_4Pd_2$ (%): C 46.6, H 2.7, N 8.4; found: C 46.5, H 2.7, N 8.4.

Di-μ-chlorobis[2-(3′,5′-dimethyl-1′-pyrazolyl)phenyl-N′,C]dipalladium (15)

A mixture of $K_2[PdCl_4]$ (1.50 g, 4.6 mmol) and **14** (1.00 g, 5.8 mmol) in aqueous dioxan (60 mL of 50% *v*/*v*) was stirred under a nitrogen atmosphere. A yellow precipitate separated and the mixture was stirred at room temperature for 18 h, and then heated under reflux for 36 h. The precipitate was filtered off, washed successively with methanol and ether, and dried. The product was suspended in dichloromethane (60 mL) and the suspension was heated under reflux for 6 h. The sparingly soluble solid was collected, washed with dichloromethane and ether, and dried to give the μ-chloro complex **15** as a yellow powder (0.65 g, 45% based on Pd), mp 337–339 °C (dec.). A sample was recrystallized from DMF–methanol for microanalysis. IR (cm^{-1}): 1552, 1443, 1438, 743, 738, 341 (Pd–Cl), 283, 265 (Pd–Cl). ^1H NMR (90 MHz, $(CD_3)_2SO$) δ: 7.64 (d br, J = 7.0 Hz, 1H, phenyl), 7.31–6.70 (m, 3H, phenyl), 6.21 (s, 1H,

© 2005 NRC Canada

pyrazolyl H4), 2.63 (s, 3H, Me), 2.33 (s, 3H, Me). Elemental anal. calcd. for $C_{22}H_{22}Cl_2N_4Pd_2$ (%): C 42.2, H 3.5, N 8.95; found: C 42.3, H 3.5, N 8.9.

The filtrate was evaporated to dryness and the residue was dissolved in dichloromethane and the solution filtered. On addition of hexane, dichlorobis(3,5-dimethyl-1-phenylpyrazole-N^2)palladium (**16**) separated as orange needles (0.98 g, 41% based on Pd), mp 315–317 °C (dec.) IR (cm^{-1}): 1595, 1555, 1503, 1418, 1399, 808, 764, 760, 696, 692, 565, 362 (Pd–Cl), 321 (Pd–Cl). ^{1}H NMR (90 MHz, $CDCl_3$) (major: minor components, 10:1) δ: 7.84–7.58 (m, 10H major + 10H minor, phenyl), 6.02 (s, 2H minor, H4′), 5.91 (s, 2H major, H4′), 3.05 (s, 6H minor, Me), 2.21 (s, 6H major, Me), 2.09 (s, 6H major, Me), 1.97 (s, 6H minor, Me). Elemental anal. calcd. for $C_{22}H_{24}Cl_2N_4Pd$ (%): C 50.6, H 4.6, N 10.7; found: C 50.7, H 4.6, N 10.7.

Dichlorobis(1-methyl-3,5-diphenylpyrazole-N^2)palladium (18)

1-Methyl-3,5-diphenylpyrazole (**17**) (0.22 g, 0.94 mmol) in methanol (10 mL) was added to a stirred solution of $Li_2[PdCl_4]$ (prepared from $PdCl_2$ (0.14 g, 0.79 mmol) and LiCl (0.20 g, 4.7 mmol)) in methanol (40 mL). A yellow solid separated, and the mixture was heated under reflux for 40 h under a nitrogen atmosphere. The product was filtered off and dissolved in dichloromethane, and the solution was filtered. On addition of hexane the palladium complex **18** separated as small yellow needles (0.19 g, 63%), mp 280–282 °C (dec.) (lit. value (22) mp 290–293 °C). IR (cm^{-1}): 3085, 1437, 1428, 1296, 838, 775, 766, 751, 703, 694, 681, 349 (Pd–Cl). ^{1}H NMR (300 MHz, $CDCl_3$) (major:minor components, 15:1) δ: 8.43–8.33 (m, 2H major + 2H minor, phenyl), 7.59–7.45 (m, 8H major + 8H minor, phenyl), 6.43 (s, 1H major + 1H minor, pyrazole H4), 4.80 (s, 3H minor, NMe), 4.36 (s, 3H major, NMe). Elemental anal. calcd. for $C_{32}H_{28}Cl_2N_4Pd$ (%): C 59.5, H 4.4, N 8.7; found: C 59.2, H 4.2, N 8.6.

(1,2-Ethanediamine-N,N′)[2-(1′-pyrazolyl)phenyl-N′,C]palladium(1+) chloride (19)

1,2-Ethanediamine (60 mg, 1.0 mmol) in chloroform (5 mL) was added to a stirred suspension of μ-chloro dimer **3** (0.233 g, 0.41 mmol) in chloroform (10 mL). A white powder slowly formed, and the mixture was stirred at room temperature for 12 h. The solid was filtered off, washed with chloroform, and dried. Recrystallization of the crude product from methanol–dichloromethane gave the title compound **19** as a white powder (0.166 g, 59%), mp 230 °C (dec.) (lit. value (15) mp 195 °C (dec.)). IR (cm^{-1}): 3295 (br), 3170 (br), 3105 (br), 1589, 1416, 1344, 1181, 1113, 1057, 1031, 755, 750, 612, 492, 406, 244, 192. ^{1}H NMR (300 MHz, $(CD_3)_2SO$) δ: 8.77 (d, J = 2.7 Hz, 1H, pyrazolyl H5), 7.95 (d, J = 2.2 Hz, 1H, pyrazolyl H3), 7.56 (d, J = 7.5 Hz, 1H, phenyl), 7.20–7.12 (m, 2H, phenyl), 7.00 (td, J = 7.4, 1.0 Hz, 1H, phenyl), 6.70 (t, J = 2.5 Hz, 1H, pyrazolyl H4), 5.40 (s br exch, 2H, NH_2), 4.59 (s br exch, 2H, NH_2), 2.71 (s br, C 4H, H_2CH_2). Elemental anal. calcd. for $C_{11}H_{15}ClN_4Pd$ (%): C 38.3, H 4.4, N 16.2; found: C 38.2, H 4.4, N 16.2.

(cis-1,2-Cyclohexanediamine-N,N′)[2-(1′-pyrazolyl)phenyl-N′,C]palladium(1+) chloride (20)

Freshly distilled *cis*-chxn (10 drops) was added to a stirred suspension of **3** (0.201 g, 0.35 mmol) in methanol (20 mL) and water (10 mL). The reaction mixture was warmed for 10 min and then stirred at room temperature overnight. Evaporation of the solvents gave a pale yellow solid that was recrystallized from methanol–ether to give the title compound **20** as fine colourless needles (0.183 g, 65%), mp 276–278 °C (dec.). IR (cm^{-1}): 3200, 3170 (br), 3135, 3095, 1600, 1511, 1412, 1210, 1093, 1070, 1059, 750, 741, 737, 364. ^{1}H NMR (300 MHz, $(CD_3)_2SO$) δ: 8.78 (d, J = 2.9 Hz, 1H, pyrazolyl H5), 7.93 (d, J = 2.2 Hz, 1H, pyrazolyl H3), 7.56 (dd, J = 7.8, 1.0 Hz, 1H, phenyl), 7.22 (dd, J = 7.5, 1.0 Hz, 1H, phenyl), 7.17 (td, J = 7.6, 1.0 Hz, 1H, phenyl), 7.00 (td, J = 7.4, 1.0 Hz, 1H, phenyl), 6.70 (t, J = 2.5 Hz, 1H, pyrazolyl H4), 5.59 (d br, J = 6 Hz, 1H, NH), 4.90 (dd br, J = 11, 7 Hz, 1H, NH), 4.82 (d br, J = 7 Hz, 1H, NH), 4.41 (dd br, J = 11, 7 Hz, 1H, NH), 3.04 (s br, 2H, C*H*NH_2), 1.78–1.57 (m, 6H, cyclohexyl), 1.32 (s br, 2H, cyclohexyl). Elemental anal. calcd. for $C_{15}H_{21}ClN_4Pd$ (%): C 45.1, H 5.3, N 14.0; found: C 44.9, H 5.4, N 14.0.

(trans-1,2-Cyclohexanediamine-N,N′)[2-(1′-pyrazolyl)phenyl-N′,C]palladium(1+) chloride (21)

Freshly distilled *trans*-chxn (15 drops) was added to a stirred, boiling suspension of μ-chloro dimer **3** (0.560 g, 0.95 mmol) in ethanol (70 mL) under a nitrogen atmosphere. The mixture was heated under reflux for 2 h, during which time the μ-chloro dimer dissolved. The resultant solution was filtered while hot, cooled to room temperature, and slowly diluted with ether to give the crude product. Recrystallization (twice) from ethanol–ether gave the title compound **21** as fine colourless needles (0.458 g, 67%), mp 287 to 288 °C (dec.). IR (cm^{-1}): 3195, 3150 (br), 3110, 3065, 1601, 1514, 1413, 1073, 1064, 1057, 755, 745, 738, 606, 363. ^{1}H NMR (300 MHz, $(CD_3)_2SO$) δ: 8.78 (d, J = 2.7 Hz, 1H, pyrazolyl H5), 7.96 (d, J = 2.2 Hz, 1H, pyrazolyl H3), 7.57 (dd, J = 7.3, 1.2 Hz, 1H, phenyl), 7.19–7.15 (m, 2H, phenyl), 7.01 (t, J = 7.3 Hz, 1H, phenyl), 6.70 (t, J = 2.5 Hz, 1H, pyrazolyl H4), 5.44 (d exch, J = 7 Hz, 1H, NH), 5.17 (t exch, J = 10.5 Hz, 1H, NH), 4.95 (d exch, J = 7 Hz, 1H, NH), 4.18 (t exch, J = 10.5 Hz, 1H, NH), 2.43–2.31 (m, 2H, C*H*NH_2), 1.99 (t, J = 14.7 Hz, 2H, cyclohexyl), 1.63 (d br, J = 7.6 Hz, 2H, cyclohexyl), 1.32 (sextet br, J = 10.7 Hz, 2H, cyclohexyl), 1.10 (t br, J = 10 Hz, 2H, cyclohexyl). Elemental anal. calcd. for $C_{15}H_{21}ClN_4Pd$ (%): C 45.1, H 5.3, N 14.0; found: C 45.0, H 5.3, N 13.8.

(1,2-Ethanediamine-N,N′)[2-(2′-pyridyl)phenyl-N′,C]palladium(1+) chloride (22)

This compound was prepared by the same method as complex **21** from the μ-chloro dimer **4** (0.258 g, 0.44 mmol) and 1,2-ethanediamine (0.06 g, 1.0 mmol) in methanol (10 mL). Recrystallization of the crude product from methanol–ether gave the title compound **22** as fine, pale yellow needles (0.263 g, 85%), mp 245 to 246 °C (dec.). IR (cm^{-1}): 3260 (br), 3185 (br), 3115 (br), 3090 (br), 1605, 1578, 1438, 1160, 1058, 753, 744, 341. ^{1}H NMR (300 MHz, $(CD_3)_2SO$) δ: 8.39 (d, J = 5.6 Hz, 1H, pyridyl H6), 8.10–8.06 (m, 2H, pyridyl), 7.74–7.72 (m, 1H, phenyl), 7.42–7.37 (m, 1H, aryl), 7.16–7.09 (m, 3H, aryl), 5.27 (s br exch, 2H, NH_2), 4.55 (s br exch, 2H, NH_2), 2.72 (m br, 4H, CH_2CH_2). Elemental anal. calcd. for $C_{13}H_{16}ClN_3Pd$ (%): C 43.8, H 4.5, N 11.8; found: C 43.9, H 4.6, N 11.8.

© 2005 NRC Canada

(1,3-Propanediamine*-N,N′*)[2-(2′-pyridyl)phenyl*-N′,C*]palladium(1+) chloride monohydrate (23)

This compound was prepared by the same method as complex **21** from **4** (0.217 g, 0.37 mmol) and 1,3-propanediamine (10 drops) in methanol (10 mL). Recrystallization of the crude product from methanol–ether gave the title compound **23** as pale yellow needles (0.224 g, 79%), mp 210 to 211 °C (dec.). IR (cm^{-1}): 3450 (br), 3365 (br), 3325 (br), 3240 (br), 3115 (br), 1607, 1582, 1433, 1191, 1150, 1037, 902, 755, 735. ^{1}H NMR (90 MHz, $(CD_3)_2SO$) δ: 8.41 (d, J = 5.6 Hz, 1H, pyridyl H6), 8.18–7.97 (m, 2H, aryl), 7.74–7.11 (m, 5H, aryl), 4.89 (s br exch, 2H, NH_2), 4.22 (s br exch, 2H, NH_2), 2.88–2.66 (m br, 4H, 2 × CH_2N), 1.76–1.55 (m, 2H, CH_2). Elemental anal. calcd. for $C_{14}H_{20}ClN_3OPd$ (%): C 43.3, H 5.2, N 10.8; found: C 43.3, H 5.1, N 10.8.

(*cis*-1,2-Cyclohexanediamine*-N,N′*)[2-(2′-pyridyl)phenyl*-N′,C*]palladium(1+) chloride (24)

This compound was prepared by the same method as complex **20** from **4** (0.357 g, 0.60 mmol) and *cis*-chxn (10 drops). Recrystallization of the crude product from ethanol–ether gave the title compound **24** as fine, pale yellow needles (0.308 g, 62%), mp 292 to 293 °C (dec.). IR (cm^{-1}): 3205 (br), 3175 (br), 3135, 3095 (br), 1602, 1578, 1434, 1093, 750, 730, 627, 407, 363. ^{1}H NMR (300 MHz, $(CD_3)_2SO$) δ: 8.36 (d br, J = 4.9 Hz, 1H, pyridyl H6), 8.08 (s br, 2H, aryl), 7.73 (d br, J = 6.9 Hz, 1H, aryl), 7.44–7.36 (m, 1H, aryl), 7.18–7.08 (m, 3H, aryl), 5.42 (s br exch, 1H, NH), 4.72–4.61 (m br exch, 2H, 2 × NH), 4.23 (s br exch, 1H, NH), 3.02 (s br, 2H, C*H*NH_2), 1.82–1.57 (m, 6H, cyclohexyl), 1.42–1.26 (m br, 2H, cyclohexyl). Elemental anal. calcd. for $C_{17}H_{22}ClN_3Pd$ (%): C 49.8, H 5.4, N 10.2; found: C 49.7, H 5.6, N 10.35.

(*trans*-1,2-Cyclohexanediamine*-N,N′*)[2-(2′-pyridyl)phenyl*-N′,C*]palladium(1+) chloride (25)

This compound was prepared by the same method as complex **21** from **4** (0.560 g, 0.95 mmol) and *trans*-chxn (15 drops). Recrystallization of the crude product from ethanol–ether gave the title compound **25** as fine, pale yellow needles (0.622 g, 80%), mp 350–352 °C (dec.). IR (cm^{-1}): 3210, 3175, 3085 (br), 3050 (br), 1608, 1601, 1579, 1434, 752, 732, 627, 364. ^{1}H NMR (300 MHz, $(CD_3)_2SO$) δ: 8.37 (d, J = 5.5 Hz, 1H, pyridyl H6), 8.10–8.07 (m, 2H, aryl), 7.75–7.72 (m, 1H, aryl), 7.44–7.37 (m, 1H, aryl), 7.17–7.11 (m, 3H, aryl), 5.25 (d exch, J = 6.2 Hz, 1H, NH), 5.04 (t exch, J = 10.6 Hz, 1H, NH), 4.79 (d exch, J = 6.9 Hz, 1H, NH), 4.14 (t exch, J = 10.2 Hz, 1H, NH), 2.43–2.28 (m, 2H, C*H*NH_2), 1.99 (t, J = 14.6 Hz, 2H, cyclohexyl), 1.63 (d br, J = 7.0 Hz, 2H, cyclohexyl), 1.30 (sextet br, J = 12.6 Hz, 2H, cyclohexyl), 1.11 (t br, J = 10.6 Hz, 2H, cyclohexyl). Elemental anal. calcd. for $C_{17}H_{22}ClN_3Pd$ (%): C 49.8, H 5.4, N 10.2; found: C 49.5, H 5.5, N 10.1.

(1,2-Ethanediamine*-N,N′*)[2-(2′-pyridyl)phenyl*-N′,C*]platinum(1+) chloride (26)

This compound was prepared by the same method as complex **21** from the μ-chloro dimer **5** (0.250 g, 0.32 mmol) and 1,2-ethanediamine (10 drops) in methanol (50 mL). Recrystallization of the crude product from methanol–ether gave the title compound **26** as fine yellow needles (0.216 g, 75%), mp 297 to 298 °C (dec.). IR (cm^{-1}): 3245 (br), 3170 (br), 3095 (br), 3060 (br), 1611, 1584, 1428, 1424, 1160, 1152, 1125, 1061, 754, 730, 414, 252. ^{1}H NMR (200 MHz, $(CD_3)_2SO$) δ: 8.69 (d with satellites, J = 5.6 Hz, $J_{Pt,H}$ = 27 Hz, 1H, pyridyl H6), 8.14–8.02 (m, 2H, aryl), 7.72–7.68 (m, 1H, aryl), 7.38–7.25 (m, 2H, aryl), 7.15–7.08 (m, 2H, aryl), 6.15 (s br with satellites, exch, $J_{Pt,H}$ = 46 Hz, 2H, NH_2), 5.44 (s br exch, 2H, NH_2), 2.67 (m br, 4H, CH_2CH_2). Elemental anal. calcd. for $C_{13}H_{16}ClN_3Pt$ (%): C 35.1, H 3.6, N 9.45; found: C 35.2, H 3.7, N 9.2.

[2-(3′,5′-Dimethyl-1′-pyrazolyl)phenyl*-N′,C*](1,2-ethanediamine*-N,N′*)palladium(1+) chloride monohydrate (27)

This compound was prepared by the same method as complex **21** from **15** (0.23 g, 0.37 mmol) and 1,2-ethanediamine (45 mg, 0.75 mmol) in methanol (10 mL). Recrystallization of the crude product from methanol–ether gave the title compound **27** as fine colourless needles (0.20 g, 70%), mp 250 °C (dec.). IR (cm^{-1}): 3420 (br), 3310, 3290, 3210 (br), 3160, 3120 (br), 3085 (br), 3030, 1554, 1440, 1424, 1184, 1164, 1136, 1102, 1083, 1061, 776, 484, 411, 238, 186. ^{1}H NMR (300 MHz, $(CD_3)_2SO$) δ: 7.37 (dd, J = 7.3, 0.8 Hz, 1H, phenyl), 7.15 (td, J = 7.6, 1.3 Hz, 1H, phenyl), 7.07 (dd, J = 7.6, 1.3 Hz, 1H, phenyl), 6.97 (td, J = 7.4, 0.8 Hz, 1H, phenyl), 6.27 (s, 1H, pyrazolyl H4), 5.34 (s br exch, 2H, NH_2), 4.52 (s br exch, 2H, NH_2), 2.67 (s br, 4H, CH_2CH_2), 2.66 (s, 3H, 5′-Me), 2.22 (s, 3H, 3′-Me). Elemental anal. calcd. for $C_{13}H_{21}ClN_4OPd$ (%): C 39.9, H 5.4, N 14.3; found: C 39.5, H 5.5, N 14.2.

[2-(3′,5′-Dimethyl-1′-pyrazolyl)phenyl*-N′,C*](1,3-propanediamine*-N,N′*)palladium(1+) chloride hemihydrate (28)

This compound was prepared by the same method as complex **21** from **15** (0.158 g, 0.25 mmol) and 1,3-propanediamine (10 drops) in methanol (10 mL). Recrystallization of the crude product from ethanol–ether gave the title compound **28** as fine colourless needles (0.148 g, 74%), mp 201 to 202 °C (dec.). IR (cm^{-1}): 3440 (br), 3270 (br), 3240 (br), 3165, 3145, 3050, 1550, 1440, 1422, 1186, 1175, 1165, 1160, 1037, 1028, 927, 794, 746, 479. ^{1}H NMR (90 MHz, $(CD_3)_2SO$) δ: 7.42–7.06 (m, 4H, phenyl), 6.25 (s, 1H, pyrazolyl H4), 4.90 (s br exch, 2H, NH_2), 4.07 (s br exch, 2H, NH_2), 2.75 (s br, 4H, 2 × CH_2N), 2.65 (s, 3H, 5′-Me), 2.33 (s, 3H, 3′-Me), 1.78–1.58 (m, 2H, CH_2). Elemental anal. calcd. for $C_{14}H_{22}ClN_4O_{0.5}Pd$ (%): C 42.4, H 5.6, N 14.1; found: C 42.5, H 5.6, N 14.1.

(Benzo[*h*]quinolin-10-yl*-N′,C*)(1,2-ethanediamine*-N,N′*)palladium(1+) chloride (29)

This compound was prepared by the same method as complex **21** from the μ-chloro dimer **13** (0.157 g, 0.25 mmol) and 1,2-ethanediamine (5 drops) in methanol (10 mL). Recrystallization of the crude product from methanol–ether gave the title compound **29** as small yellow prisms (0.128 g, 69%), mp 215–220 °C (dec.). IR (cm^{-1}): 3205 (br), 3165 (br), 3120, 3080, 1405, 1058, 848, 714, 482. ^{1}H NMR (300 MHz, $(CD_3)_2SO$) δ: 8.75 (dd, J = 5.2, 0.9 Hz, 1H, H2), 8.69 (d, J = 8.1 Hz, 1H, H4), 7.92 (d, J = 8.8 Hz, 1H, aryl), 7.84 (d, J = 8.8 Hz, 1H, aryl), 7.78 (dd, J = 8.1, 5.2 Hz, 1H, H3), 7.72 (d, J = 7.8 Hz, 1H, aryl), 7.50 (t, J = 7.5 Hz, 1H, H8), 7.36 (d, J = 7.0 Hz, 1H, aryl), 5.49 (s br exch, 2H, NH_2), 4.69 (s br exch, 2H, NH_2), 2.82–2.78 (m br, 4H,

© 2005 NRC Canada

CH_2CH_2). Elemental anal. calcd. for $C_{15}H_{16}ClN_3Pd$ (%): C 47.4, H 4.2, N 11.05; found: C 47.3, H 4.2, N 11.0.

(1,2-Ethanediamine-*N,N′*)(1-(2′-pyridyl)indol-2-yl-*N′,C*)palladium(1+) chloride dihydrate (30)

This compound was prepared by the same method as complex **21** from the μ-chloro dimer **10** (0.244 g, 0.36 mmol) and 1,2-ethanediamine (5 drops) in ethanol (15 mL) and water (4 mL). Recrystallization by slow addition of ether to a solution of the crude product in ethanol–water (90% *v*/*v*) gave the title compound **30** as cream-coloured needles (0.211 g, 67%), mp 223–225 °C (dec.). IR (cm^{-1}): 3460 (br), 3355 (br), 3295 (br), 3230 (br), 3140 (br), 1611, 1595, 1510, 1490, 1146, 1061, 777, 754, 731, 420. ^1H NMR (300 MHz, $(CD_3)_2SO$) δ: 8.31 (d, *J* = 5.6 Hz, 1H, pyridyl H6), 8.19–8.15 (m, 2H, aryl), 8.01–7.98 (m, 1H, aryl), 7.49–7.46 (m, 1H, aryl), 7.25–7.13 (m, 3H, aryl), 6.35 (s, 1H, indolyl H3), 5.46 (s br exch, 2H, NH_2), 4.80 (s br exch, 2H, NH_2), 2.78 (s br, 2H, CH_2), 2.70 (s br, 2H, CH_2). Elemental anal. calcd. for $C_{15}H_{21}ClN_4O_2Pd$ (%): C 41.8, H 4.9, N 13.0; found: C 41.8, H 4.6, N 13.05.

(1,2-Ethanediamine-*N,N′*)(2-(1′*H*-indazol-1′-yl)phenyl-*N′,C*)palladium(1+) chloride sesquihydrate (31)

This compound was prepared by the same method as complex **21** from the μ-chloro dimer **11** (0.127 g, 0.19 mmol) and 1,2-ethanediamine (10 drops) in methanol (10 mL). Recrystallization of the crude product from ethanol–ether gave the title compound **31** as colourless microcrystals (0.128 g, 80%), mp 242 °C (dec.). IR: A satisfactory paraffin mull could not be prepared. ^1H NMR (300 MHz, $(CD_3)_2SO$) δ: 8.76 (s, 1H, indazolyl H3), 8.41 (d, *J* = 8.6 Hz, 1H, aryl), 8.05 (d, *J* = 8.2 Hz, 1H, aryl), 7.90 (d, *J* = 7.7 Hz, 1H, aryl), 7.76–7.72 (m, 1H, aryl), 7.43 (t, *J* = 7.5 Hz, 1H, aryl), 7.26 (td, *J* = 7.7, 1.1 Hz, 1H, aryl), 7.20 (dd, *J* = 7.5, 1.1 Hz, 1H, aryl), 7.01 (t, *J* = 7.4 Hz, 1H, aryl), 5.49 (s br exch, 2H, NH_2), 4.72 (s br exch, 2H, NH_2), 2.77 (s br, 4H, CH_2CH_2). Elemental anal. calcd. for $C_{15}H_{20}ClN_4O_{1.5}Pd$ (%): C 42.7, H 4.8, N 13.3; found: C 42.65, H 4.6, N 13.4.

(1,2-Ethanediamine-*N,N′*)(2-(2′*H*-indazol-2′-yl)phenyl-*N′,C*)palladium(1+) chloride monohydrate (32)

This compound was prepared by the same method as complex **21** from the μ-chloro dimer **12** (0.120 g, 0.18 mmol) and 1,2-ethanediamine (10 drops) in methanol (10 mL). Recrystallization of the crude product from ethanol–ether gave the title compound **32** as fine, off-white needles (0.115 g, 78%), mp 271 to 272 °C (dec.). IR: 3460 (br), 3330 (br), 3245 (br), 3200, 3105 (br), 3070, 1929, 1520, 1444, 1282, 1056, 1050, 748, 729. ^1H NMR (300 MHz, $(CD_3)_2SO$) δ: 9.51 (s, 1H, indazolyl H3), 7.89 (d, *J* = 8.4 Hz, 1H, aryl), 7.87 (d, *J* = 7.7 Hz, 1H, aryl), 7.56–7.51 (m, 1H, aryl), 7.42 (d, *J* = 8.8 Hz, 1H, aryl), 7.30–7.25 (m, 2H, aryl), 7.22 (d, *J* = 7.2 Hz, 1H, aryl), 7.14 (t, *J* = 7.3 Hz, 1H, aryl), 5.54 (s br exch, 2H, NH_2), 5.00 (s br exch, 2H, NH_2), 2.75 (s br, 4H, CH_2CH_2). Elemental anal. calcd. for $C_{15}H_{19}ClN_4OPd$ (%): C 43.6, H 4.6, N 13.6; found: C 43.6, H 4.5, N 13.8.

(1,2-Ethanediamine-*N,N′*)[2-(1′-pyrazolyl)pyridine-*N,N′*]palladium(2+) dichloride dihydrate (36)

2-(1′-Pyrazolyl)pyridine (**34**) (0.37 g, 2.5 mmol) in methanol (40 mL) was added to a stirred suspension of $PdCl_2$(en) (0.60 g, 2.5 mmol) in water (50 mL) and the reaction mixture was heated under reflux for 24 h. During this time the orange solid dissolved to give a pale yellow solution. After being cooled to room temperature, the solution was filtered and the solvent removed. The crude product was dissolved in water (5 mL) and the solution was filtered and diluted with ethanol. On the addition of ether, the title compound **36** separated as fine, pale yellow needles (0.62 g, 59%), mp 328 °C (dec.). IR (cm^{-1}): 3420 (br), 3185, 3110, 3060, 1609, 1591, 1493, 1407, 1136, 1074, 1053, 784, 596. ^1H NMR (90 MHz, $(CD_3)_2SO$) δ: 8.62 (dd, *J* = 2.5, 0.5 Hz, 1H, pyrazolyl H5), 8.48 (dt, *J* = 4.9, 1.8 Hz, 1H, pyridyl H6), 8.03–7.94 (m, 2H, pyridyl H3 and H4), 7.83 (dd, *J* = 1.8, 0.5 Hz, 1H, pyrazolyl H3), 7.36 (ddd, *J* = 6.2, 4.9, 2.3 Hz, 1H, pyridyl H5), 6.58 (dd, *J* = 2.5, 1.8 Hz, 1H, pyrazolyl H4), 4.89 (s br exch, 4H, 2 × NH_2), 2.34 (s br, 4H, CH_2CH_2). Elemental anal. calcd. for $C_{10}H_{19}Cl_2N_5O_2Pd$ (%): C 28.7, H 4.6, N 16.7; found: C 28.5, H 4.4, N 17.1.

Heating a mixture of 1,2-ethanediamine (2.5 mL of a 0.03 g/mL solution in methanol, 1.2 mmol) and dichloro[2-(1′-pyrazolyl)pyridine-*N*,*N*′]palladium (34) (0.21 g, 0.7 mmol) in methanol (20 mL) and water (5 mL) gave, on addition of ether, a white solid that was identified as bis(1,2-ethanediamine-*N*,*N*′)palladium(2+) dichloride (35) (0.129 g, 69%), mp 245 °C (dec.). IR (cm^{-1}): 3195, 3150, 3060, 3020, 1606, 1599, 1318, 1274, 1136, 1126, 1058, 468, 370, 290. ^1H NMR (90 MHz, D_2O) δ: 2.75 (s br, 8H, CH_2CH_2).

[2-(3′,5′-Dimethyl-1′-pyrazolyl)pyridine-*N,N′*](1,2-ethanediamine-*N,N′*)palladium(2+) dichloride dihydrate (37)

This compound was prepared from 2-(3′,5′-dimethyl-1′-pyrazolyl)pyridine (**35**) (0.100 g, 0.58 mmol) in methanol (10 mL) and $PdCl_2$(en) (0.139 g, 0.59 mmol) in water (10 mL) as described for compound **36**. The crude product was dissolved in methanol–water (85% *v*/*v*) and ether was added slowly to give the title compound **37** as fine, pale yellow needles (0.182 g, 71%); mp 301 to 302 °C (dec.). IR (cm^{-1}): 3420 (br), 3370 (br), 3210, 3125, 3060, 1610, 1560, 1491, 1420, 1139, 1067, 1064, 773, 590. ^1H NMR (300 MHz, $(CD_3)_2SO$) δ: 8.44 (ddd, *J* = 4.9, 1.5, 0.8 Hz, 1H, pyridyl H6), 7.93 (ddd, *J* = 8.5, 7.1, 1.5 Hz, 1H, pyridyl H4), 7.79 (dd, *J* = 8.5, 0.9 Hz, 1H, pyridyl H3), 7.30 (ddd, *J* = 7.1, 4.9, 0.9 Hz, 1H, pyridyl H5), 6.11 (s, 1H, pyrazolyl H4), 4.89 (s br exch, 4H, 2 × NH_2), 2.57 (s, 3H, 5′-Me), 2.32 (s br, 4H, CH_2CH_2), 2.20 (s, 3H, 3′-Me). Elemental anal. calcd. for $C_{12}H_{23}Cl_2N_5O_2Pd$ (%): C 32.3, H 5.2, N 15.7; found: C 32.35, H 4.95, N 15.8.

(2,2′-Bipyridine-*N,N′*)(1,2-ethanediamine-*N,N′*)palladium(2+) dichloride sesquihydrate (38)

This compound was prepared from 2,2′-bipyridine (0.228 g, 1.5 mmol) in methanol (15 mL) and $PdCl_2$(en) (0.283 g, 1.2 mmol) in water (5 mL) as described for compound **36**. The crude product was dissolved in methanol and dichloromethane was added slowly to give the title compound **38** as small, pale yellow needles (0.388 g, 77%); mp > 270 °C (dec.). A sample was recrystallized from ethanol (95%) for microanalysis. IR (cm^{-1}): 3420 (br), 3150 (br), 3115, 3080, 3050, 3020, 1607, 1601, 1560, 1473, 1172, 770, 722, 580. ^1H NMR (300 MHz, $(CD_3)_2SO$) δ: 8.70 (d, *J* = 8.1 Hz, 2H, 2 × pyridyl H3), 8.53 (d, *J* = 5.6 Hz, 2H, 2 × pyridyl H6), 8.45 (t, *J* = 7.8 Hz, 2H, 2 × pyridyl H4), 7.89

© 2005 NRC Canada

(t, J = 6.6 Hz, 2H, 2 × pyridyl H5), 6.47 (s br exch, 4H, 2 × NH_2), 2.78 (s br, 4H, CH_2CH_2). Elemental anal. calcd. for $C_{12}H_{19}Cl_2N_4O_{1.5}Pd$ (%): C 34.3, H 4.55, N 13.3; found: C 34.25, H 4.3, N 13.3.

Growth inhibition of murine leukæmia L1210 cells in vitro (continuous exposure)

This procedure was adapted from the method of McFadyen et al. (11). Mouse lymphoid leukæmia L1210 cells in in vitro culture were grown on Minimum Essential Medium (Flow Laboratories, USA) supplemented with 15% foetal calf serum, glutamine (2 mmol/L), and gentamycin (2 mg/100 mL). Cells were incubated without agitation in a 5% O_2 – 10% CO_2 atmosphere at 37 °C and, under these conditions, the average doubling time was approximately 12 h. The drugs were dissolved in the appropriate sterile solvent (water or ethanol) and serial dilutions of the stock solution were made using the same solvent. Aliquots of the drug solutions (40 μL) were dispensed into 2 mL of medium containing approximately 5×10^4 cells/mL. Control cultures received the same volume of sterile solvent, and assays were conducted in duplicate for each drug concentration. After incubation at 37 °C for 48 h, cells were counted using a Coulter particle counter (Model ZM, Coulter Electronics Ltd., Luton, UK) with the lower (10) and upper (99) thresholds set to include all particles above 8 μm in diameter (the normal L1210 cell diameter is approximately 11 μm). Cell growth as a percentage of control cultures was plotted against drug concentration and the IC_{50} concentration (the concentration of drug required to effect 50% growth inhibition) was determined. Assays were repeated at least once and IC_{50} values quoted are the means of these determinations.

Antitumour testing was carried out by the method described by McFadyen et al. (11).

Acknowledgments

This work was initiated during the tenure of a grant from the Anti-Cancer Council of Victoria and was supported by the Australian Research Council. The authors would also like to thank Johnson Matthey Chemicals Ltd., UK, for the generous loan of platinum and palladium precursors. We would also like to thank Dr. Ian A.G. Roos for helpful discussions, and Virginia A. Leopold, Experimental Chemotherapy Unit, Cancer Institute, Melbourne, Victoria Australia, for assistance with the biological testing.

References

1. B. Rosenberg, L. Van Camp, and T. Krigas. Nature (London), **205**, 698 (1965).
2. B. Rosenberg, L. Van Camp, J.E. Trosko, and V.H. Mansour. Nature (London), **222**, 385 (1969).
3. M.J. Cleare and P.C. Hydes. *In* Metal ions in biological systems. Vol. 11. *Edited by* H. Sigel. Marcel Dekker, New York. 1980. Chap. 1.
4. Z. Guo and P.J. Sadler. Angew. Chem. Int. Ed. **38**, 1512 (1999).
5. P. Yang and M. Guo. Coord. Chem. Rev. **185–186**, 189 (1999).
6. T.W. Hambley. Coord. Chem. Rev. **166**, 181 (1997).
7. E. Wong and C.M. Giandomenico. Chem. Rev. **99**, 2451 (1999).
8. K.W. Jennette, S.J. Lippard, G.A. Vassiliades, and W.R. Bauer. Proc. Natl. Acad. Sci. U.S.A. **71**, 3839 (1974); S.J. Lippard. Acc. Chem. Res. **11**, 211 (1978).
9. J.G. Collins, R.M. Rixon, and J.R. Aldrich-Wright. Inorg. Chem. **39**, 4377 (2000).
10. M. Cusumano and A. Giannetto. J. Inorg. Biochem. **65**, 137 (1997).
11. W.D. McFadyen, L.P.G. Wakelin, I.A.G. Roos, and V.A. Leopold. J. Med. Chem. **28**, 1113 (1985).
12. G. Zhao, H. Sun, H. Lin, S. Zhu, X. Su, and Y. Chen. J. Inorg. Biochem. **72**, 173 (1998).
13. L.S. Lerman. J. Mol. Biol. **3**, 18 (1961); M.J. Waring. Ann. Rev. Biochem. **50**, 159 (1981).
14. G.L. Edwards, D.St.C. Black, G.B. Deacon, and L.P.G. Wakelin. Can. J. Chem. **83**, 980 (2005).
15. M. Nonoyama and H. Takayanagi. Trans. Met. Chem. **1**, 10 (1975/1976).
16. A. Kasahara. Bull. Chem. Soc. Jpn. **41**, 1272 (1968).
17. D.St.C. Black, G.B. Deacon, and G.L. Edwards. Aust. J. Chem. **47**, 217 (1994).
18. G.B. Caygill and P.J. Steel. J. Organomet. Chem. **327**, 115 (1987).
19. G.E. Hartwell, R.V. Lawrence, and M.J. Smas. Chem. Commun. 912 (1970).
20. M. Nonoyama and K. Nakajima. Polyhedron, **17**, 1 (1998).
21. S. Trofimenko and L.G. Vaughan. US Patent 3 718 488, 1973; S. Trofimenko, US Patent 3 876 675, 1975.
22. M.T. Alonso, O. Juanes, J. de Mendoza, and J.C. Rodríguez-Ubis. J. Organomet. Chem. **430**, 335 (1992).
23. J.F. Vollano, S. Al-Baker, J.C. Dabrowiak, and J.E. Schurig. J. Med. Chem. **30**, 716 (1987); W.K. Anderson, D.A. Quagliato, R.D. Haugwitz, V.L. Narayanan, and M.K. Wolpert-DeFilippes. Cancer Treat. Rep. **70**, 997 (1986).
24. S. Mani, M.A. Graham, D.B. Bregman, P. Ivy, and S.G. Chaney. Cancer Invest. **20**, 246 (2002); D. Simpson, C. Dunn, M. Curran, and K.L. Goa. Drugs, **63**, 2127 (2003).
25. G.W. Watt and D.H. Carter. J. Inorg. Nucl. Chem. **31**, 1863 (1969).
26. R. Saito and Y. Kidani. Chem. Lett. 123 (1976).
27. I.L. Finar and R.J. Hurlock. J. Chem. Soc. 3024 (1957).
28. M.A. Khan and J.B. Polya. J. Chem. Soc. (C), 85 (1970).
29. A.F. Pozharskii, B.K. Martsokha, and A.M. Simonov. J. Gen. Chem. **33**, 994 (1963).
30. J.I.G. Cadogan and R.K. Mackie. Org. Synth. Coll. **5**, 941 (1973).
31. M.A. Khan and A.A.A. Pinto. Monatsh. Chem. **111**, 883 (1980).
32. M.A Gutierrez, G.R. Newkome, and J. Selbin. J. Organomet. Chem. **202**, 341 (1980).
33. B.J. McCormick, E.N. Jaynes, Jr., and R.I. Kaplan. Inorg. Synth. **13**, 216 (1972).
34. J. Elguero, A. Guerrero, F. Goméz de la Torre, A. de la Hoz, F.A. Jalón, B.R. Manzano, and A Rodríguez. New J. Chem. **25**, 1050 (2001).
35. G.W. Watt and D.S. Klett. Inorg. Chem. **5**, 1278 (1966); D.B. Powell and N. Sheppard. Spectrochim. Acta, **17**, 68 (1961).

© 2005 NRC Canada

In vitro and in vivo studies of neutral cyclometallated complexes against murine leukæmias[1]

Gavin L. Edwards, David St.C. Black, Glen B. Deacon, and Laurence P.G. Wakelin

Abstract: Cyclometallated μ-halogeno dimers derived from nitrogen donor ligands (1-phenylpyrazoles, 2-phenylpyridine, and 1-(2′-pyridyl)indole) were treated with unidentate nitrogen and phosphorus donor ligands to give a series of neutral monomeric palladium(II) and platinum(II) complexes. An initial prescreen of the complexes against the mouse lymphoid leukæmia cell line L1210 indicated that the complexes exhibited growth inhibitory activity over a relatively wide concentration range. Two factors that gave rise to increased activity were steric hindrance about the metal centre resulting from hindered ligands such as 2,6-dimethylpyridine, or the presence of a phosphorus donor ligand. Little correlation between palladium and platinum complexes was noted. Four complexes were selected for further in vivo study and, while none of the palladium complexes showed more than marginal activity against P388 leukæmia at doses below toxic levels, one platinum complex with a hindered metal centre did display significant antitumour activity against this model.

Key words: cyclometallation, palladium, platinum, cytotoxicity, anticancer.

Résumé : Des dimères μ-halogéno cyclométallés dérivés de ligands donneurs d'azote (1-phénylpyrazoles, 2-phénylpyridine, 1-(2′-pyridyl)indole) ont été traités avec des ligands donneurs unidentates d'azote et de phosphore pour conduire à la formation d'une série de complexes monomères neutres du palladium(II) et du platine(II). Un préfiltrate de l'activité de ces complexes contre la lignée L1210 de cellules de leucémie lymphoïde de la souris ont montré qu'ils présentent une activité inhibitrice de la croissance sur une grande plage de concentration. Il y a deux facteurs qui provoquent une augmentation de l'activité, l'empêchement stérique autour du centre métallique résultant de la présence de ligands encombrés comme la 2,6-diméthylpyridine et la présence d'un ligand donneur de phosphore. On n'a pas noté de corrélation entre le palladium et le platine. Quatre complexes ont été sélectionnés pour des études in vivo ultérieures et, même si aucun des complexes du palladium n'a montré plus qu'une activité marginale contre la leucémie P388 à des doses inférieures aux degrés toxiques, un des complexes du platine avec un centre métallique encombré a présenté une activité antitumorale significative contre ce modèle.

Mots clés : cyclométallation, palladium, platine, cytotoxicité, anticancéreux.

[Traduit par la Rédaction]

Introduction

Throughout history heavy metals have been used as therapeutic agents (1); mercury was once used as a treatment for syphilis (2), and arsenic compounds have been used for over 2000 years (3). In modern times, heavy metals fell out of favour and until relatively recently they have been largely ignored as starting points for rational drug design. Rosenberg et al. (4) changed the face of modern chemotherapy with their observation of the antiproliferative activity of *cis*-diamminedichloroplatinum(II) (cisplatin) and their subsequent discovery of the anticancer properties of a range of

Received 17 December 2004. Published on the NRC Research Press Web site at http://canjchem.nrc.ca on 25 August 2005.

It is a pleasure to honour Howard Alper's very significant contributions both to chemistry and to the chemical profession.

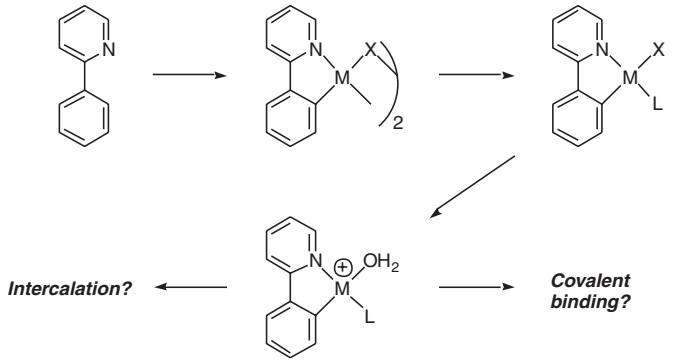
There once was a Canuck called Howard,
Over other chemists he towered,
His group in fine fettle,
Used many a metal,
Leaving the science empowered.

G.L. Edwards and D.St.C. Black.[2] School of Chemistry, University of New South Wales, Sydney, New South Wales, Australia, 2052.
G.B. Deacon. School of Chemistry, Monash University, Victoria, Australia, 3800.
L.P.G. Wakelin. Department of Physiology and Pharmacology, School of Medical Sciences, University of New South Wales, Sydney, New South Wales, Australia, 2052.

[1]This article is part of a Special Issue dedicated to Professor Howard Alper.
[2]Corresponding author (e-mail: d.black@unsw.edu.au).

 doi: 10.1139/V05-109 © 2005 NRC Canada

Fig. 1. Potential mechanisms of action.



platinum complexes (5), resulting in the introduction of cisplatin into the clinic in 1978 (6).

The development of second and third generation platinum drugs has followed in an attempt to broaden the spectrum of activity, overcome resistance, and obviate toxic side effects. Some general principles emerged as a guide to the design of new bioactive platinum containing therapeutics, and several useful platinum based anticancer drugs were developed as a result (6, 7). Active agents are neutral platinum(II) or (IV) complexes, normally containing two kinetically inert ligands that should be primary amines or ammonia, and also containing two labile anionic ligands in a cis configuration to enable bidentate binding to the heterocyclic bases of the target DNA (7). Complexes containing aromatic amines such as pyridine, monohalo complexes ("monofunctional" complexes), and those with trans stereochemistry, were generally inactive, although there have been some notable exceptions (7–9), and there remains significant scope for the development of more varied platinum containing structures (10) as drugs.

The formation of bifunctional lesions upon the binding of cisplatin to DNA has been linked to its activity, and studies on the relatively small number of monofunctional platinum complexes — those with a single labile ligand — have reinforced the notion that bifunctional binding is necessary for activity. Interesting exceptions are found in a new class of organoamidoplatinum(II) complexes that are monofunctional and have *trans*-amine ligands, yet possess excellent activity across in vitro, cellular, and animal studies (11). However, many monofunctional platinum complexes studied to date have been charged and therefore issues such as membrane permeability may influence the biological activity of these complexes adversely (7). As a part of a programme investigating nitrogen directed metallations (12, 13), we sought to develop a series of neutral cyclometallated complexes as potential monofunctional DNA binding agents (Fig. 1). Cyclometallation of ligands such as 2-phenylpyridine gives μ-halogeno dimers, which, upon cleavage with appropriate unidentate ligands, provide neutral monomeric complexes. These complexes could act as monofunctional DNA binding agents where, in the low chloride concentration of intracellular fluid, aquation would lead to a reactive cationic species. While the aquated complex could bind covalently to DNA, another possible interaction would be intercalation of the planar chromophore into the DNA double helix, in a similar manner to metallointercalation reagents studied by Lippard (14), Barton and co-workers (15), and others (16, 17). Recent reports on highly cytotoxic cyclometallated complexes by Kodaka and co-workers (18), Navarro-Ranninger and co-workers (19), and Ma and Che (20) have prompted us to publish our findings on a range of mononuclear platinum(II) and palladium(II) complexes that exhibit significant activity against murine leukæmia L1210 in vitro with a notable effect shown by complexes containing bulky ligands. This correlates with the recently discovered activity of the crowded complex *cis*-amminedichloro(2-methylpyridine)platinum(II) AMD473 (ZD0473) (21), which has progressed to phase III clinical trials (10). In the preceding paper (22), we have also reported our results on the synthesis and biological activity of a series of cationic metallointercalation complexes, many of which incorporate a cyclometallated chromophore.

Fig. 2. Ligands and abbreviations with positions of metallation indicated.

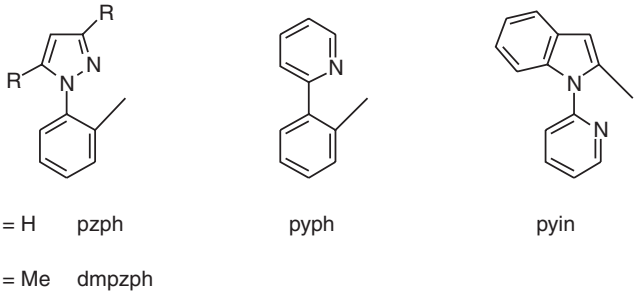


Table 1. Cyclometallated dimers.

Compound	Aromatic ligand N–C	Metal	Halogen	Yield (%)
1	pyph	Pd	Cl	89
2	pyph	Pd	Br	73
3	pyph	Pd	I	71
4	pyph	Pt	Cl	65
5	pyph	Pt	Br	62
6	pzph	Pd	Cl	99
7	pzph	Pd	Br	79
8	pzph	Pd	I	76
9	dmpzph	Pd	Cl	45
10	pyin	Pd	Cl	97

Results and discussion

Synthesis of metal complexes

Preparation of the required ligands (Fig. 2) and the subsequent cyclometallation reactions to provide μ-chloro dimers **1** (23), **4** (12), **6** (24), **9** (22), and **10** (22) (Table 1) have been described previously. While the nature of the halide was of little importance for the cationic metallointercalators where the halide would merely act as a counterion, variation between coordinated chloride, bromide, and iodide could be crucial for increased activity in the series of neutral complexes, and therefore several μ-chloro dimers were converted to the corresponding bromo and iodo derivatives **2** (12), **3** (12), **5** (12), **7** (24), and **8** (12) (Table 1) by metathesis reactions with the appropriate lithium halide as described previously (12). The structures were confirmed by elemental analysis, far-IR, and ^{1}H NMR spectroscopy. ^{1}H NMR analy-

© 2005 NRC Canada

Table 2. Monomeric complexes and growth inhibition of L1210 cells in vitro.

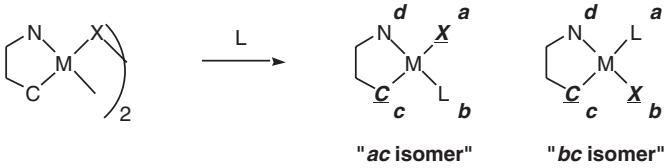
Complex	Aromatic ligand	Metal	"a" Ligand[a] (trans to C)	"b" Ligand[a] (trans to N)	IC_{50} (μmol/L)
11 (12)	pyph	Pd	Cl	py-d_5	11
12 (12)	pyph	Pd	Br	py-d_5	12
13 (12)	pyph	Pd	I	py-d_5	12
14	pyph	Pd	Cl	blut	11
15 (12)	pyph	Pd	Cl	alut	1.2
16	pyph	Pd	Cl	NH_3	12
17	pyph	Pd	Cl	$MeNH_2$	10
18	pyph	Pd	Cl	*t*-$BuNH_2$	14
19	pyph	Pd	Cl	PPh_3	1.8
20	pyph	Pd	Cl	$P(OMe)_3$	1.1
21	pyph	Pt	Cl	py	5.0
22 (12)	pyph	Pt	Cl	py-d_5	5.8
23 (12)	pyph	Pt	Cl	2phpy	3.2
24 (12)	pyph	Pt	Cl	alut	1.5
25 (12)	pyph	Pt	Cl	*S*-dmso	15
26	pyph	Pt	Cl	PPh_3	10
27 (12)	pyph	Pt	alut	Cl	19
28 (12)	pyph	Pt	alut	Br	11
29 (24)	pzph	Pd	Cl	py	52
30 (12)	pzph	Pd	Br	py-d_5	61
31 (12)	pzph	Pd	I	py-d_5	45
32	pzph	Pd	Cl	pic	34
33 (12)	pzph	Pd	Cl	alut	6.4
34	dmpzph	Pd	Cl	alut	3.0
35	pyin	Pd	Cl	py-d_5	7.7
36	pyin	Pd	Cl	$P(OMe)_3$	1.2

[a]Key to unidentate ligands: pyridine (py), perdeuteropyridine (py-d_5), β-lutidine (3,5-dimethylpyridine) (blut), α-lutidine (2,6-dimethylpyridine) (alut), 2-phenylpyridine (2phpy), dimethylsulfoxide coordinated through sulfur (*S*-dmso), α-picoline (2-methylpyridine) (pic).

sis of the dimers proved difficult because of their extremely low solubility in common solvents, and therefore the μ-halogeno dimers were converted to the monomers by the addition of a drop of ($^2H_5$)pyridine (py-d_5) to a suspension in $CDCl_3$ providing the monomeric complexes in solution; loss of one proton confirmed that cyclometallation had taken place, and observation of a single set of resonances demonstrated that metathesis was complete (12).

Synthesis of the monomeric complexes **11**–**36** (Table 2) was effected by treatment of a suspension of a μ-halogeno dimer in dichloromethane or acetone with a unidentate ligand (L) to give clear solutions; the products usually separated as microcrystalline solids upon the addition of hexane or pentane. The palladium dimers reacted quite rapidly; by comparison, cleavage of the platinum–halogen bridge appeared to be much slower. The complexes were stable at room temperature and the platinum complexes could be recrystallized from hot solvents, however attempts to recrystallize the analogous palladium complexes (where L = nitrogen donor ligands) at elevated temperatures led to dissociation of the ligand L and reformation of the μ-halogeno dimers. Thus, these palladium complexes were purified by dissolution in an appropriate solvent at room temperature and reprecipitation upon the addition of hexane or pentane. Far-IR and ^1H NMR spectroscopy as well as microanalysis established the identity and purity of our products. Any attempts to heat the palladium complexes — to speed drying, measure melting points, or volatilize the complexes for mass spectrometric analysis — led to quantitative loss of the unidentate ligand. This may explain the discrepancy between the observed (mp 155 °C (dec.)) and reported (24) (mp 200 °C (dec.)) melting points for compound **29**: a significant difference in the rate of heating could mean that a larger proportion of one sample may have degraded before reaching the melting (decomposition) point. Pérez et al. (25) have recently determined the activation energy for the decomposition of this class of complexes by this pathway as 90–100 kJ mol^{-1}.

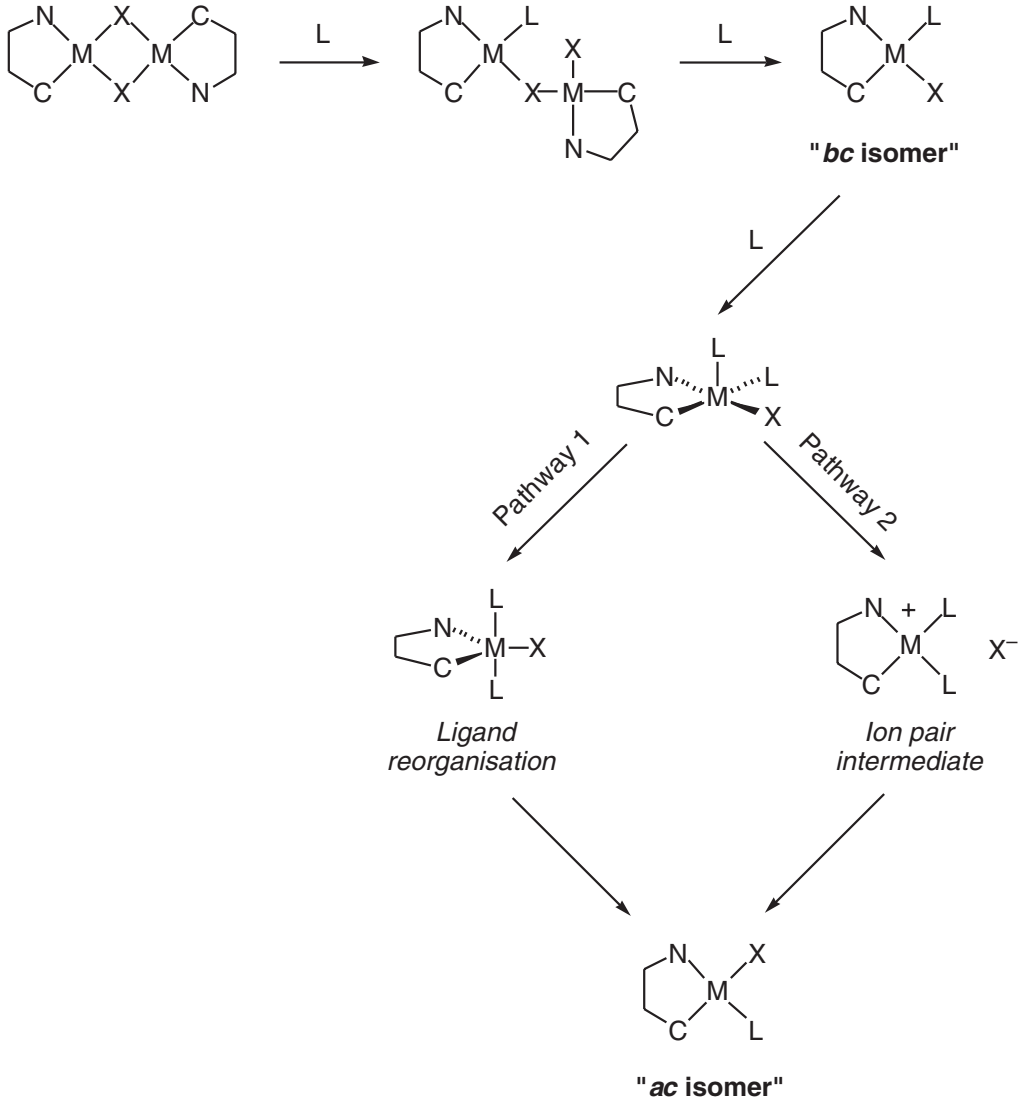
Fig. 3. Possible products of bridge cleavage.



While the bridge cleavage reactions can, in principle, produce two isomeric products (Fig. 3) — one, with the halogen

© 2005 NRC Canada

Fig. 4. Mechanism for isomerization of the *bc* isomer to the *ac* isomer (adapted from ref. 12).



ligand trans to the carbon donor (the *ac* isomer)[3] and the other with the unidentate ligand L trans to the carbon donor ligand (the *bc* isomer) — the palladium complexes and many of the platinum complexes were isolated as the *ac* isomers exclusively. In these reactions, the strong kinetic trans effect of the σ-carbon ligand means that the first bond in the bridge to be cleaved is that trans to the aryl substituent. Thus, the initial (kinetic) product from bridge cleavage should be the *bc* isomer (Fig. 4). Subsequent rearrangement of this kinetic product could occur either via formation of a five-coordinate transition state with accompanying ligand reorganisation (Pathway 1), or formal formation of a square-planar ion pair as an intermediate (Pathway 2). The subsequent conversion of this ionic intermediate to the neutral complex would be governed by the strong kinetic trans effect of the σ-carbon ligand, leading to selective cleavage of the C—L bond trans to the aryl group. In all cases, the palladium complexes are sufficiently reactive and only the thermodynamically favoured *ac* isomers are observed. Platinum(II) complexes are less labile and, if there is sufficient steric hindrance around the metal centre (2,6-dimethylpyridine ligands introduce hindrance above and below the metal), the kinetic *bc* product can be isolated. Other platinum complexes are isolated as the *ac* products. A fuller mechanistic discussion and supporting experimental evidence has been published previously (12).

In all cases, the structures and stereochemistry of the monomeric products were confirmed by spectroscopic analysis. Comparison between the far-IR spectra of analogous complexes below 300 cm^{-1} often allowed assignment of the palladium–halogen stretching frequencies and these values were used as a guide to the assignment of ν(Pd–X) for other neutral monomeric species. The relatively low frequencies observed for most ν(Pd–X) (for example, palladium–chlorine stretching frequencies were observed in the range 230 to ≈260 cm^{-1}, while ν(Pd–Br) was approximately 160 cm^{-1}, and ν(Pd–I) was in the range 120–140 cm^{-1}) (12) were indicative that the halogen ligand is trans to an σ-carbon donor

[3] The *ac*/*bc* nomenclature system was adopted in our previous report (12) to simplify the discussion of stereochemistry: all *ac* complexes have the halide trans to the carbon donor ligand and all *bc* complexes have the halide cis to the carbon donor ligand.

© 2005 NRC Canada

of strong trans influence (26); this confirmed that the complexes had *ac* stereochemistry. Structural assignments for the platinum complexes were discussed in the mechanistic report (12).

The ^{1}H NMR spectra of the complexes likewise confirmed the assigned structures, where several features were noteworthy. Coordination of unidentate pyridine ligands results in deshielding of the α-pyridyl protons (27) or the α substituents; for example, 2,6-dimethyl substituents move downfield by about 0.7 ppm on coordination. Presumably, this effect is a combination of the inductive nature of the metal as well as the through-space paramagnetic anisotropy of the metal atom (28). As described previously (12), strong shielding of the proton ortho to the site of metallation (H_{ortho}) was observed where L is a pyridine ligand, owing to the proximity of the proton to the adjacent orthogonal pyridine ring. Greater shielding with increased α substitution on the pyridine nucleus indicates that the α-methyl groups restrict rotation about the Pd—N bond and thus prevent rotation of the ring current associated with the unidentate ligand away from H_{ortho}. While ammine and primary amine ligands (complexes **16**–**18**) produced no noticeable effect on H_{ortho} (the proton ortho to the C—M bond), deshielding of the pyridyl H6 in the cyclometallated ligand of 2-pyridylphenyl complexes was observed, consistent with coordination to the metal and also with the through-space paramagnetic anisotropy of the adjacent halide ligand.

Palladium complexes **19**, **20**, and **36** containing triphenylphosphine and trimethyl phosphite ligands were more stable than those with nitrogen donor ligands. They could be recrystallized from hot solvents without reverting to the dimeric precursors, and mass spectra could also be measured. Numerous absorptions because of the triphenylphosphine ligand were observed in the far-IR spectra of complexes **19** and **26**; the most distinctive of these were several bands in the regions 400–460 cm^{-1} and 490–550 cm^{-1} (29). In the ^{1}H NMR spectra of the complexes, several ^{31}P–^{1}H and ^{195}Pt–^{1}H couplings were observed. In the triphenylphosphine complexes **19** and **26**, the phenyl protons H5 and H6 were both shielded by the ring currents of the adjacent P–Ph groups, confirming the *ac* stereochemistry. In the low-field region of the ^{1}H NMR spectrum of complex **26**, the signal owing to the pyridyl H6 proton is observed as a distorted triplet with fine coupling and ^{195}Pt satellites. Although exact coupling constants could not be assigned, it is apparent that $J_{5,6} \approx J_{P,H6} \approx$ 4.5–5.5 Hz. The estimated $J_{Pt,H6}$ of 27 Hz is lower than observed for other platinum complexes (27) as a result of the strong trans influence of the *trans*-phosphine ligand. Platinum-195 coupling to phenyl H6 (56 Hz) is comparable with literature values (24), and ^{31}P–^{1}H coupling to pyridyl H6 is also similar to published results (30).

In vitro and in vivo testing

Most metal complexes with anticancer activity are based on platinum; while the coordination chemistry of platinum(II) and palladium(II) are similar, many palladium complexes show moderate in vivo activity at best (7). Although some palladium complexes have shown promising activity in vitro (31) or in animal models (22), to date they have not made a successful transition to clinical trials (7). However, the possibility of covalent or intercalative mechanisms of action for this class of compounds suggested that the monofunctional palladium complexes were worthy of study.

The complexes were subjected to an in vitro prescreen for growth inhibitory activity against the murine leukæmia cell line L1210, as described in the preceding paper (22). As the complexes are neutral, water proved to be an unsuitable solvent for preparation of stock solutions or for serial dilutions, and therefore ethanol, ethanol – dimethyl sulfoxide, or dimethyl sulfoxide were used. Serial dilutions of stock solutions were made using ethanol without precipitation. It is desirable that the complexes retain their structures in solution prior to the addition of the drug to the cell culture, and ^{1}H NMR spectroscopy was employed to examine the behaviour of selected complexes in solution. The spectrum of the 2,6-dimethylpyridine complex **15** in perdeuteromethanol was unchanged after the solution was allowed to stand at room temperature for 3 days, and the spectrum was well-resolved with the exception of a broadened signal corresponding to a single proton at low field that could be assigned as pyridyl H6 for the cyclometallated ligand. The observed broadening of this signal could result from weak axial association and exchange of CD_3OD ligands, or from reversible displacement of the chloride ligand; the chemical shift of this pyridyl H6 correlates with a coordinated ligand and therefore the cyclometallated ligand is essentially unaffected. The 2,6-dimethylpyridine ligand also remains complexed to the metal centre. The ^{1}H NMR spectra of monomeric py-d_5 complexes **11**–**13** in perdeuterodimethylsulfoxide ($(CD_3)_2SO$) were broadened by comparison with the spectra recorded in $CDCl_3$ (12), however the spectra of the three complexes in $(CD_3)_2SO$ were clearly different from one another, and the observation of signals at low field (above 9 ppm, pyridyl H6) and at high field (below 6.1 ppm, phenyl H6) indicates that a significant concentration of unchanged complex exists in solution and the clear differences indicated that the halogen had not been displaced.

The results of growth inhibition experiments against L1210 cells in vitro, expressed as drug concentrations that caused a 50% inhibition of cell growth (IC_{50}), are given in Table 2. For comparison, cisplatin has an IC_{50} of 0.9 μmol/L under similar conditions.

Antitumour screening of simple analogues of cisplatin ($Pt(NH_3)_2X_2$) has indicated that there is a strong relationship between the halide leaving group X and biological activity, where antitumour activity generally decreases with larger halogens (32). In this study, results for complexes **11**–**13** and **29**–**31** suggest that changing halogen has no significant effect on the biological activity of the organopalladium complexes in vitro. Either aquation of the labile palladium complexes (or displacement of the halogen by other ligands) occurs and therefore the drugs are converted to the same active intermediates, or reaction of the Pd—X bond is not crucial for activity. Two platinum complexes with *bc* stereochemistry were also evaluated and the bromo complex **28** was almost twice as active as the chloro complex **27**; while a definitive statement concerning trends cannot be made based on two results, it does appear as though the bulkier halides lead to more active complexes.

The unidentate ligand (L) is observed to play an important role in the biological activity of these drugs. Small amine ligands such as NH_3 (complex **16**), $MeNH_2$ (**17**), and *t*-

© 2005 NRC Canada

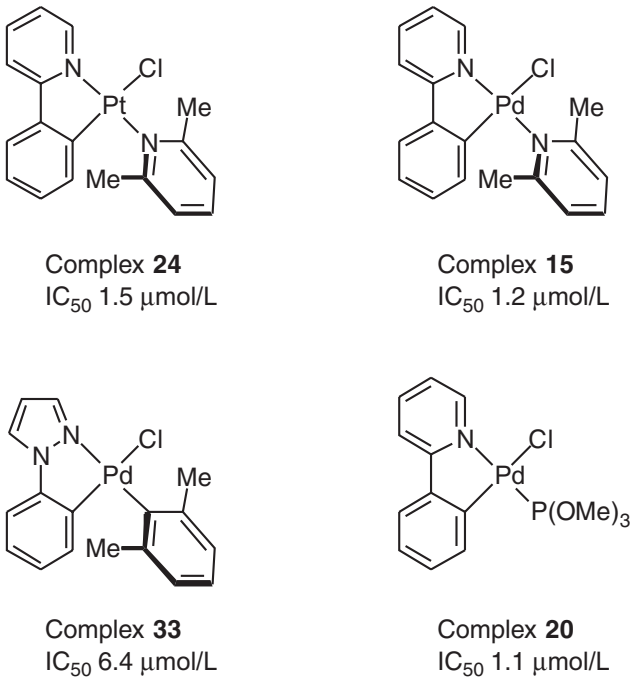
$BuNH_2$ (**18**), and unsubstituted pyridine ligands (**11** and **29**) cause 50% growth inhibition at similar concentrations. Use of pyridine (platinum complex **21**) or py-d_5 (**22**) has no significant effect on activity, suggesting that reaction of the coordinated unidentate ligand is not involved in the modes of action of the drugs. A pyridine ligand that is substituted away from the metal–nitrogen bond (the 3,5-dimethylpyridine ligand (blut), complex **14**) does not affect the biological activity compared to the unsubstituted analogue. However and notably, introduction of steric crowding around the metal ion with successive α substituents on the pyridine rings (compare complexes **29**, **32**, and **33**, or **11** and **15**) leads to greatly enhanced activity. The mechanism of action of this class of compounds is not clear, but the poor activity of free 2,6-dimethylpyridine (IC_{50} > 200 μmol/L) indicates that the enhanced biological activity is not due to the unidentate ligands following release from the metal. In fact, for good activity it appears as though the neutral ligand L must remain coordinated to the metal.

The introduction of α substituents on the unidentate pyridine ligands (L) gives increased steric hindrance around the metal, and interactions between the α-methyl groups and the bidentate organometallic ligand would cause the ligand L to lie approximately orthogonal to the coordination plane of the metal. These α-methyl substituents would hinder the formation of a trigonal bipyramidal intermediate, and therefore impede substitution by an associative mechanism. This effect is similar to that observed for the sterically hindered α-picoline platinum complex, AMD473 (ZD0473) (8, 21), however, in the case of the palladium complexes reported herein two α-methyl substituents are required before significant enhancement of activity is noted. Whether, in the case of drugs reported in this study, the enhanced activity with extra α substituents on L is due to slower displacement of the halide ligand (X) or of the unidentate ligand (L), is unclear.

Complexes with unidentate phosphorus donor ligands in general effect growth inhibition at relatively low concentrations with some complexes showing IC_{50} values approaching that of cisplatin. The phosphorus donor ligands L give stable complexes where L is not readily displaced, and the trimethyl phosphite ligands (complexes **20** and **36**) would introduce negligible steric hindrance around the metal and therefore $P(OCH_3)_3$ would not impede substitution at the metal centre by an associative mechanism. Thus, if the mechanism of action of these complexes is similar to that for the nitrogen donor ligands, then slow or negligible displacement of the unidentate ligand is indicated as an important event for activity. This can be achieved by either steric or coordinative stabilization of the complexes with respect to substitution. Another alternative is that the antiproliferative effects could arise from localized release of the phosphine/phosphite ligands within the cells; the lower activity observed for platinum complex **26** (IC_{50} = 10 μmol/L) compared to its palladium analogue **19** (IC_{50} = 1.8 μmol/L) could reflect the greater lability of the palladium complex and the faster release of bioactive phosphine ligands (33).

The nature of the cyclometallated ligand also appears to be crucial for activity. If an intercalative mode of binding is implicated in the mechanism of action, increased surface area should result in higher activity. Pyrazolylphenyl ligands gave complexes that generally caused growth inhibition at relatively high concentrations, but addition of methyl groups produced a more active drug (compare pzph complex **33** (IC_{50} = 6.4 μmol/L) with dmpzph complex **34** (IC_{50} = 3.0 μmol/L)). Likewise, fusion of an extra benzene ring (compare pyin complex **35** (IC_{50} = 7.7 μmol/L) with pzph complex **29** (IC_{50} = 52 μmol/L)) resulted in enhanced activity. These factors are consistent with an intercalative mechanism.

Fig. 5. Complexes selected for in vivo testing against P388 leukæmia (in vitro IC_{50} vs. L1210 given for comparison).



Insufficient platinum complexes have been prepared in this study for clear trends to become evident, however, a comparison of the *ac* (complexes **22**–**24**, for instance) and *bc* (**27** and **28**) complexes suggests that the thermodynamically favoured *ac* complexes are likely to be more active. Further work is needed to confirm this observation. Additionally, it is apparent that there is not necessarily any firm correlation between the palladium and the platinum complexes; in some cases, the platinum complexes are more active than the palladium analogues (compare **22** (Pt) with **11** (Pd)), while in others the palladium complex was more active (compare **26** (Pt) with **19** (Pd)), and the key 2,6-dimethylpyridine complexes (compare **24** (Pt) with **15** (Pd)) have similar activities.

Four of the more active complexes (Fig. 5) were selected for evaluation of potential antitumour activity against P388 leukæmia in mice. The drugs were tested over a range of dose levels with results expressed as a ratio of mean survival times of treated animals (T) relative to controls (C). Significant antitumour activity is indicated by a %T/C greater than 125%. A %T/C of 0% indicates that none of the treated animals survived as a result of the toxicity of the drug at that dose level. Results are shown in Tables 3*a* and 3*b*; the anticancer agent 5-fluorouracil (5-FU) is used for comparison. Platinum complex **24** showed significant activity (%T/C 138%) against P388 leukæmia at 80 mg/kg. Complex **15**, its

© 2005 NRC Canada

Table 3. Antitumour testing against P388 leukæmia.

(*a*)

Dose (mg/kg/injection)	%T/C Complex **24**	Dose (mg/kg/injection)	%T/C Complex **20**
0 (Control)	100	0 (Control)	100
10	114	2	99
20	108	4	101
40	105	8	108
80	138	16	84
160	58	32	0
50 (5-FU: standard)	168	50 (5-FU: standard)	158

(*b*)

	%T/C	
Dose (mg/kg/injection)	Complex **15**	Complex **33**
0	100	100
25	110	116
50	116	116
100	118	120
200	116	97
400	126	0
50 (5-FU: standard)	162	162

palladium analogue, demonstrated only marginal activity (%T/C 126%) at the highest dose level of 400 mg/kg despite showing almost identical activity against L1210 in vitro. Pyrazolylphenyl complex **33** achieved a %T/C of 120% at doses of 100 mg/kg before toxicity then became evident. Finally, trimethyl phosphite complex **20**, while being highly active in vitro, showed no antitumour activity in vivo, and was toxic at relatively low doses with no treated animals surviving doses of 16 mg/kg or higher. Among the palladium complexes chosen for study, only marginal antitumour activity was observed at best. The very high dose levels required to demonstrate activity, and the possibility that complexes such as **15** may be approaching limiting toxicity, indicated that further testing of those complexes was not warranted.

On the other hand, platinum complex **24** has steric bulk around the metal centre in a similar manner to the clinically active 2-methylpyridine containing complex AMD473 (21), and the results obtained in this study for this complex **24** are encouraging (%T/C 138% at 80 mg/kg). In light of Kodaka and co-workers' recent reports (18, 34) of the promising activity against a cisplatin resistant mouse sarcoma 180 cell line of platinum complex **23** previously prepared in our laboratories (12), extension into the platinum series focussing on systems with bulky ligands is being investigated further.

Experimental

General procedure

General experimental details, including instrumental specifications and in vitro and in vivo biological testing protocols, have been described previously (22). Mass spectra were obtained on a VG Micromass 7070F spectrometer at 70 eV, samples being introduced by direct evaporation. Where relevant, the listed value is the most intense peak (^{195}Pt, ^{231}(PtCl), ^{106}Pd, ^{143}(PdCl)) of a cluster with the correct isotope pattern. Cyclometallated dimers **1** (23), **2**–**5** (12), **6** and **7** (24), **8** (12), and **9** and **10** (22) were prepared by published procedures, and monomeric complexes **11**–**13**, **15**, **22**–**25**, **27**–**31**, and **33** were prepared by the procedures referred to in Table 2. Unidentate ligands (2-methylpyridine, 2-phenylpyridine, 2,6-dimethylpyridine, 3,5-dimethylpyridine, triphenylphosphine, and trimethyl phosphite) were obtained from the Aldrich Chemical Company and were recrystallized or distilled prior to use. ($^2H_5$)Pyridine (py-d_5) (Aldrich Gold Label) was used without further purification. Solvents and organic reagents were purified by established methods.

Preparations

General method

The appropriate unidentate ligand was added to a stirred suspension of the μ-halogeno dimer in dichloromethane or acetone. The mixture was stirred at room temperature until the reaction was complete (this was indicated when the solid had dissolved completely). Hexane or pentane was added to precipitate the crude product, which was filtered off and washed with hexane or pentane. The solid was dissolved in a polar solvent (dichloromethane or acetone) at room temperature, and the solution was filtered. Slow addition of hexane or pentane gave the monomeric complex as a microcrystalline solid, which was dried at room temperature.

a-*Chloro*-b-*(3″,5″-dimethylpyridine*-N″)-dc-*[2-(2′-pyridyl)-phenyl*-N′,C]*palladium (14)*

This compound was prepared from μ-chloro dimer **1** (0.359 g, 0.61 mmol) and 3,5-dimethylpyridine (10 drops) in acetone (15 mL). Recrystallization of the crude product from acetone–hexane at room temperature gave the title compound **14** as a pale yellow microcrystalline solid (0.399 g, 82%); mp 204 to 205 °C. IR (cm^{-1}): 1606, 1595, 1578, 1568, 1437, 1422, 1275, 1157, 857, 854, 790, 766, 756, 731,

© 2005 NRC Canada

699, 410, 323, 300, 238 ν(Pd–Cl). ^{1}H NMR (90 MHz, $CDCl_3$) δ: 9.45 (d, J = 5.6 Hz, 1H, pyridyl H6′), 8.59 (s br, 2H, pyridyl H3″ and H5″), 7.90–6.85 (m, 7H, aryl), 6.18 (dd, J = 7.3, 1.5 Hz, 1H, phenyl H6), 2.35 (s, 6H, 2 × Me). Elemental anal. calcd. for $C_{18}H_{17}ClN_2Pd$ (%): C 53.6, H 4.25, N 6.95; found: C 54.0, H 4.3, N 6.8.

b-*Ammine*-a-*chloro*-dc-*[2-(2′-pyridyl)phenyl*-N′,C*]palladium (16)

A solution of anhydrous ammonia in methanol was added dropwise to a stirred suspension of **1** (0.116 g, 0.20 mmol) in dichloromethane (5 mL) until a colourless solution resulted. Hexane was added to give a white solid, which was filtered off and washed with hexane. The crude product gradually became yellow on standing in air. Recrystallization twice from dichloromethane–ether at room temperature gave the title compound **16** (35) as small, bright yellow needles (0.090 g, 73%); mp > 300 °C. IR (cm^{-1}): 3315 (br), 3210 (br), 3045, 3040, 1606, 1579, 1437, 1421, 1204, 1182, 1166, 1156, 1022, 738, 722, 404, 230 ν(Pd–Cl). ^{1}H NMR (90 MHz, $CDCl_3$) δ: 9.05 (d, J = 5.0 Hz, 1H, pyridyl H6), 7.68–6.71 (m, 7H, aryl), 2.86 (s br, 3H, NH_3). Elemental anal. calcd. for $C_{11}H_{11}ClN_2Pd$ (%): C 42.2, H 3.5, N 8.95; found: C 42.3, H 3.5, N 8.8.

a-*Chloro*-b-*(methylamine)*-dc-*[2-(2′-pyridyl)phenyl*-N′,C*]-palladium (17)

This compound was prepared by the general method by the addition of anhydrous methylamine (as a solution in dichloromethane) to **1** (0.153 g, 0.26 mmol) in dichloromethane (2 mL). Recrystallization of the crude product from dichloromethane–hexane at room temperature gave the title compound **17** as fine yellow needles (0.139 g, 82%); mp 205 °C (dec.). IR (cm^{-1}): 3295 (br), 3220 (br), 3150, 1605, 1588, 1582, 1437, 1424, 1161, 1156, 1030, 748, 727, 406, 243 ν(Pd–Cl) or 215 ν(Pd–Cl) (either assignment possible). ^{1}H NMR (300 MHz, $CDCl_3$) δ: 8.98 (dd, J = 5.7, 1.2 Hz, 1H, pyridyl H6), 7.62 (td, J = 7.8, 1.6 Hz, 1H, aryl), 7.36 (d, J = 8.0 Hz, 1H, pyridyl H3), 7.21–7.18 (m, 1H, aryl), 7.01–6.38 (m, 4H, aryl), 3.34 (m br exch, 2H, NH_2), 2.82 (t (s after exch), J = 6.6 Hz, 3H, Me). Elemental anal. calcd. for $C_{12}H_{13}ClN_2Pd$ (%): C 44.1, H 4.0, N 8.6; found: C 44.2, H 4.0, N 8.6.

b-*(*tert*-Butylamine)*-a-*chloro*-dc-*[2-(2′-pyridyl)phenyl*-N′,C*]-palladium (18)

This compound was prepared from **1** (0.255 g, 0.43 mmol) and *tert*-butylamine (10 drops) in dichloromethane (4 mL). Recrystallization of the crude product from dichloromethane–hexane at room temperature gave the title compound **18** as pale yellow microcrystals (0.256 g, 81%); mp > 290 °C. IR (cm^{-1}): 3275 (br), 3220 (br), 3140, 1606, 1588, 1578, 1439, 1426, 1160, 1149, 1030, 749, 733, 413, 227 ν(Pd–Cl). ^{1}H NMR (300 MHz, $CDCl_3$) δ: 9.31 (dd, J = 5.7, 1.0 Hz, 1H, pyridyl H6), 7.74 (td, J = 7.8, 1.6 Hz, 1H, aryl), 7.54 (d, J = 7.9 Hz, 1H, pyridyl H3), 7.36 (dd, J = 7.2, 1.8 Hz, 1H, aryl), 7.09 (ddd, J = 7.4, 5.7, 1.3 Hz, 1H, pyridyl H5), 7.06–6.92 (m, 3H, aryl), 3.41 (s br exch, 2H, NH_2), 1.51 (s, 9H, CMe_3). Elemental anal. calcd. for $C_{15}H_{19}ClN_2Pd$ (%): C 48.8, H 5.2, N 7.6; found: C 48.7, H 5.1, N 7.4.

a-*Chloro*-dc-*[2-(2′-pyridyl)phenyl*-N′,C*]-b-*(triphenylphosphine)palladium (19)

This compound was prepared from **1** (0.156 g, 0.26 mmol) and triphenylphosphine (0.140 g, 0.53 mmol) in dichloromethane (16 mL). Recrystallization of the crude product from dichloromethane–hexane gave the title compound **19** (34) as small pale yellow prisms (0.242 g, 82%); mp 211–214 °C (dec.). IR (cm^{-1}): 1602, 1579, 1566, 1439, 1434, 1426, 1423, 1313, 1100, 1093, 1018, 750, 745, 731, 705, 695, 689, 628, 531, 513, 501, 498, 310, 244 ν(Pd–Cl). ^{1}H NMR (300 MHz, $CDCl_3$) δ: 9.64 (dddd, J = 5.4, 1.0, 0.6 Hz, $J_{P,H}$ = 3.7 Hz, 1H, pyridyl H6), 7.86–7.73 (m, 8H, aryl), 7.52 (d, J = 7.9 Hz, 1H, aryl), 7.47–7.33 (m, 9H, aryl), 7.26–7.21 (m, 1H, aryl), 6.98–6.92 (m, 1H, aryl), 6.57–6.48 (m, 2H, H5 and H6). Elemental anal. calcd. for $C_{29}H_{23}ClNPPd$ (%): C 62.4, H 4.15, N 2.5; found: C 62.2, H 3.9, N 2.8.

a-*Chloro*-dc-*[2-(2′-pyridyl)phenyl*-N′,C*]-b-*(trimethyl phosphite)palladium (20)

This compound was prepared from **1** (0.116 g, 0.20 mmol) and trimethyl phosphite (0.049 g, 0.40 mmol) in dichloromethane (6 mL). Recrystallization of the crude product from cyclohexane gave the title compound **20** as fine, pale yellow needles (0.121 g, 74%), mp 139 to 140 °C. IR (cm^{-1}): 1604, 1578, 1436, 1427, 1012, 810, 801, 770, 764, 740, 544, 285, 238 ν(Pd–Cl). ^{1}H NMR (300 MHz, $CDCl_3$) δ: 9.48 (dddd, J = 5.7, 1.0, 0.7 Hz, $J_{P,H}$ = 4.9 Hz, 1H, pyridyl H6), 7.85 (td, J = 7.7, 1.6 Hz, 1H, aryl), 7.74 (d, J = 8.2 Hz, 1H, pyridyl H3), 7.62 (td, J = 7.2, 1.5 Hz, 1H, aryl), 7.58 (d, J = 8.0 Hz, 1H, aryl), 7.28–7.09 (m, 3H, aryl), 3.89 (d, $J_{P,H}$ = 12.8 Hz, 9H, $P(OMe)_3$). Mass spectrum m/z (%): 421 (M^+, 1.1), 384 ($C_{14}H_{17}NO_3PPd^+$, 0.1), 369 ($C_{13}H_{14}NO_3PPd^+$, 0.2), 297 ($C_{11}H_8ClNPd^+$, 0.2), 278 ($C_{11}H_{10}NOPd^+$, 22), 260 ($C_{11}H_8NPd^+$, 2.3). Elemental anal. calcd. for $C_{14}H_{17}ClNO_3PPd$ (%): C 40.0, H 4.1, N 3.3; found: C 40.1, H 4.1, N 3.3.

a-*Chloro*-b-*(pyridine*-N″)-dc-*[2-(2′-pyridyl)phenyl*-N′,C*]-platinum (21)

This compound was prepared by the general method by the addition of pyridine (5 drops) to the μ-chloro dimer **4** (0.21 g, 0.27 mmol) in dichloromethane (15 mL). Recrystallization of the crude product from dichloromethane–pentane gave the title compound **21** as small yellow needles (0.25 g, 99%). ^{1}H NMR (200 MHz, $CDCl_3$) δ: 9.70 (dd with satellites, J = 5.1, 1.6 Hz, $J_{Pt,H}$ = 39 Hz, 1H, pyridyl H6′), 9.01 (dt with satellites, J = 5.1, 1.4 Hz, $J_{Pt,H}$ = 46 Hz, 2H, pyridyl H2″ and H6″), 7.95–7.79 (m, 2H, aryl), 7.66 (d with satellites, J = 8 Hz, $J_{Pt,H}$ = 9 Hz, 1H, pyridyl H3′), 7.51–7.41 (m, 3H, aryl), 7.19–7.07 (m, 2H, aryl), 6.98 (td with unresolved satellites, J = 7.4, 1.4 Hz, 1H, phenyl H5), 6.36 (dd with satellites, J = 7.5, 0.9 Hz, $J_{Pt,H}$ = 48 Hz, 1H, phenyl H6). Mass spectrum (%): m/z 464 (M^+, 6), 428 ($C_{16}H_{13}N_2Pt^+$, 1), 385 ($C_{11}H_8ClNPt^+$, 8), 348 ($C_{11}H_7NPt^+$, 9), 321 ($C_{10}H_6Pt^+$, 2). This compound is the py analogue of py-d_5 complex **22** and full analytical data for **22** has been previously reported (12).

a-*Chloro*-dc-*[2-(2′-pyridyl)phenyl*-N′,C*]-b-*(triphenylphosphine)platinum (26)

This compound was prepared from **4** (0.232 g, 0.30 mmol) and triphenylphosphine (0.200 g, 0.76 mmol) in dichloromethane (50 mL). Recrystallization of the crude product

© 2005 NRC Canada

from dichloromethane–pentane gave the title compound **26** as yellow needles (0.195 g, 50%); mp 305–307 °C (dec.). IR (cm^{-1}): 1605, 1583, 1439, 1436, 1425, 1100, 1096, 750, 746, 731, 706, 702, 695, 690, 542, 519, 505, 300, 284 ν(Pt–Cl). ^1H NMR (300 MHz, $CDCl_3$) δ: 9.90–9.87 (m with satellites, $J_{Pt,H} \approx 27$ Hz, 1H, pyridyl H6), 7.89–7.76 (m, 8H, aryl), 7.52 (J = 7.8, 1.4 Hz, 1H, aryl), 7.46–7.33 (m, 9H, aryl), 7.29 (qt, J = 7.1, 6.0, 1.5 Hz, $J_{P,H}$ = 1.5 Hz, 1H, pyridyl H5), 6.95 (td, J = 7.5, 1.2 Hz, 1H, aryl), 6.67 (ddd with satellites, J = 7.9, 0.9 Hz, $J_{P,H}$ = 3.3 Hz, $J_{Pt,H}$ = 56 Hz, 1H, phenyl H6), 6.52 (td with unresolved satellites, J = 7.6, 1.4 Hz, 1H, phenyl H5). Mass spectrum *m/z* (%): 647 (M^+, 14), 611 ($C_{29}H_{23}NPPt^+$, 3). Elemental anal. calcd. for $C_{29}H_{23}ClNPPt$ (%): C 53.8, H 3.6, N 2.2; found: C 53.6, H 3.5, N 2.1.

a-*Chloro*-dc-*[2-(1′-pyrazolyl)phenyl*-N′,C*]-b-*(pyridine*-N″)-*palladium–dichloromethane (2/1) (29)

This compound was prepared from the μ-chloro dimer **6** (0.110 g, 0.19 mmol) and pyridine (0.033 g, 0.42 mmol) in dichloromethane (2 mL). Recrystallization of the crude product from dichloromethane–hexane at room temperature gave the title compound **29** (24) as colourless plates (0.131 g, 83%); mp 155 °C (dec.) (lit. value (24) mp 200 °C (dec.)). IR (cm^{-1}): 3095, 3085, 1446, 1416, 1408, 1398, 1345, 1205, 1080, 757, 734, 692, 252 ν(Pd–Cl) (lit. value (24) ν(Pd–Cl) 254 cm^{-1}). ^1H NMR (90 MHz, $CDCl_3$) δ: 8.95 (d, J = 5.0 Hz, 2H, pyridyl H2 and H6), 8.19 (d, J = 2.0 Hz, 1H, pyrazolyl H3), 7.95–7.82 (m, 2H, aryl), 7.47 (t, J_{av} = 6.9 Hz, 2H, pyridyl H3 and H5), 7.14–6.81 (m, 3H, aryl), 6.46 (t, J = 2.5 Hz, 1H, pyrazolyl H4), 6.30 (d, J = 7.6 Hz, 1H, phenyl H6), 5.29 (s, 1H, 0.5 CH_2Cl_2). Elemental anal. calcd. for $C_{14.5}H_{13}Cl_2N_3Pd$ (%): C 42.8, H 3.2, N 10.3; found: C 42.95, H 3.0, N 10.4.

a-*Chloro*-b-*(2″-methylpyridine*-N″)-dc-*[2-(1′-pyrazolyl)-phenyl*-N′,C*]palladium (32)

This compound was prepared from **6** (0.130 g, 0.23 mmol) and 2-methylpyridine (5 drops) in dichloromethane (5 mL). Recrystallization of the crude product from dichloromethane–hexane at room temperature gave the title compound **32** as colourless microcrystals (0.105 g, 61%); mp 210 to 211 °C (dec.). IR (cm^{-1}): 3130, 1605, 1512, 1441, 1424, 1410, 1396, 1341, 1288, 1105, 1072, 1052, 1025, 775, 752, 746, 310, 258 ν(Pd–Cl). ^1H NMR (90 MHz, $CDCl_3$) δ: 8.97 (d, J = 5.5 Hz, 1H, pyridyl H6), 8.18 (d, J = 2.1 Hz, 1H, pyrazolyl H3), 7.94 (d, J = 2.9 Hz, 1H, pyrazolyl H5), 7.79 (td, J = 7.6, 1.4 Hz, 1H, aryl), 7.48–6.70 (m, 5H, aryl), 6.48 (t, J = 2.5 Hz, 1H, pyrazolyl H4), 5.98 (d, J = 7.3 Hz, 1H, phenyl H6), 3.12 (s, 3H, Me). Elemental anal. calcd. for $C_{15}H_{14}ClN_3Pd$ (%): C 47.6, H 3.7, N 11.1; found: C 47.4, H 3.7, N 11.2.

a-*Chloro*-b-*(2″,6″-dimethylpyridine*-N″)-dc-*[2-(3′,5′-dimethyl-1′-pyrazolyl)phenyl*-N′,C*]-palladium (34)

This compound was prepared from the μ-chloro dimer **9** (0.180 g, 0.29 mmol) and 2,6-dimethylpyridine (5 drops) in dichloromethane (10 mL). Recrystallization of the crude product from dichloromethane–hexane at room temperature gave the title compound **34** as fine, colourless needles (0.114 g, 47%); mp > 300 °C. IR (cm^{-1}): 1603, 1580, 1568, 1551, 1440, 1422, 1400, 1392, 1028, 795, 786, 761, 749, 299, 263 ν(Pd–Cl). ^1H NMR (90 MHz, $CDCl_3$) δ: 7.67 (J = 7.1 Hz, 1H, pyridyl H4), 7.26–7.17 (m, 3H, aryl), 7.03 (td, J = 7.5, 1.5 Hz, 1H, aryl), 6.66 (td, J = 7.4, 1.5 Hz, 1H, aryl), 5.98 (s, 1H, pyrazolyl H4), 5.70 (d, J = 7.6 Hz, 1H, phenyl H6), 3.20 (s, 6H, 2″- and 6″-Me), 2.76 (s, 3H, pyrazolyl Me), 2.64 (s, 3H, pyrazolyl Me). Elemental anal. calcd. for $C_{18}H_{20}ClN_3Pd$ (%): C 51.45, H 4.8, N 10.0; found: C 51.2, H 4.9, N 9.8.

a-*Chloro*-b-*[($^2H_5$)pyridine*-N″]-dc-*[1-(2′-pyridyl)indol-2-yl*-N′,C*]palladium (35)

This compound was prepared from the μ-chloro dimer **10** (0.281 g, 0.42 mmol) and ($^2H_5$)pyridine (10 drops) in dichloromethane (5 mL). The crude product was dissolved in dichloromethane and the resulting solution was filtered and diluted with ether. On addition of hexane, the title compound **35** separated as small yellow prisms (0.232 g, 66%); mp 236–238 °C (dec.). IR (cm^{-1}): 2290 ν(C–D), 1612, 1598, 1563, 1510, 1496, 1448, 1322, 1318, 1290, 1258, 1189, 1147, 1085, 777, 756, 742, 740, 728, 616, 538, 530, 304, 240 ν(Pd–Cl). ^1H NMR (300 MHz, $CDCl_3$) δ: 9.25 (dd, J = 5.7, 1.7 Hz, 1H, pyridyl H6), 7.86 (ddd, J = 8.5, 7.3, 1.7 Hz, 1H, aryl), 7.69–7.65 (m, 2H, aryl), 7.37–7.34 (m, 1H, aryl), 7.16 (td, J = 7.3, 1.6 Hz, 1H, aryl), 7.12 (td, J = 7.2, 1.2 Hz, 1H, aryl), 6.95 (ddd, J = 7.2, 5.7, 1.1 Hz, 1H, pyridyl H5), 5.61 (d, J = 0.7 Hz, 1H, indolyl H3). Elemental anal. calcd. for $C_{18}H_9(^2H_5)ClN_3Pd$ (%): C 51.6, H 3.5, N 10.0; found: C 51.2, H 3.2, N 9.7.

a-*Chloro*-dc-*[1-(2′-pyridyl)indol-2-yl*-N′,C*]-b-*(trimethyl phosphite)palladium (36)

This compound was prepared from **10** (0.209 g, 0.31 mmol) and trimethyl phosphite (0.087 g, 0.70 mmol) in dichloromethane (8 mL). Recrystallization of the crude product from cyclohexane gave the title compound **36** as lustrous yellow plates (0.222 g, 78%); mp 168 to 169 °C. IR (cm^{-1}): 1607, 1596, 1506, 1323, 1293, 1261, 1181, 1166, 1151, 1071, 1065, 1004, 826, 808, 768, 763, 746, 740, 730, 613, 546, 537, 274, 236 ν(Pd–Cl). ^1H NMR (300 MHz, $CDCl_3$) δ: 9.28 (dddd, J = 5.8, 1.7, 0.7 Hz, $J_{P,H}$ = 5.1 Hz, 1H, pyridyl H6), 7.94 (ddd, J = 8.6, 7.1, 1.8 Hz, 1H, aryl), 7.85 (dt, J = 7.5, 1.0 Hz, 1H, pyridyl H3), 7.76–7.73 (m, 1H, aryl), 7.53–7.50 (m, 1H, aryl), 7.23–7.14 (m, 2H, aryl), 7.08 (dddd, J = 7.1, 5.8, 1.3 Hz, $J_{P,H}$ = 2.0 Hz, 1H, pyridyl H5), 6.68 (d, $J_{P,H}$ = 2.3 Hz, 1H, indolyl H3), 3.93 (d, $J_{P,H}$ = 13.1 Hz, 9H, $P(OMe)_3$). Mass spectrum *m/z* (%): 460 (M^+, 7.5), 423 ($C_{16}H_{18}N_2O_3PPd^+$, 0.5), 408 ($C_{15}H_{15}N_2O_3PPd^+$, 0.4), 364 ($C_{14}H_{14}N_2O_3Pd^+$, 0.5), 336 ($C_{13}H_9ClN_2Pd^+$, 3.4), 317 ($C_{13}H_{11}N_2OPd^+$, 57), 299 ($C_{13}H_9N_2Pd^+$, 3). Elemental anal. calcd. for $C_{16}H_{18}ClN_2O_3PPd$ (%): C 41.85, H 3.95, N 6.1; found: C 41.9, H 4.0, N 6.3.

Acknowledgments

This work was initiated during the tenure of a grant from the Anti-Cancer Council of Victoria, and was supported by the Australian Research Council. The authors would also like to thank Johnson Matthey Chemicals Ltd., UK, for the generous loan of platinum and palladium precursors. We would also like to thank Dr. Ian A.G. Roos for helpful discussions, and Virginia A. Leopold and Dr. Lorraine Webster,

© 2005 NRC Canada

Experimental Chemotherapy and Pharmacology Unit, Cancer Institute, Melbourne, Victoria Australia, for assistance with the biological testing.

References

1. C. Orvig and M.J. Abrams. Chem. Rev. **99**, 2201 (1999).
2. H.E. Howard-Lock and C.J.L. Lock. *In* Comprehensive coordination chemistry. Vol. 6. *Edited by* G. Wilkinson, R.D. Gillard, and J.A. McCleverty. Pergamon, Oxford, UK. 1987. p. 755.
3. K.H. Antman. Oncologist, **6**(Suppl. 2), 1 (2001).
4. B. Rosenberg, L. Van Camp, and T. Krigas. Nature (London), **205**, 698 (1965).
5. B. Rosenberg, L. Van Camp, J.E. Trosko, and V.H. Mansour. Nature (London), **222**, 385 (1969).
6. M.J. Cleare and P.C. Hydes. *In* Metal ions in biological systems. Vol. 11. *Edited by* H. Sigel. Marcel Dekker, New York. 1980. Chap. 1
7. T.W. Hambley. Coord. Chem. Rev. **166**, 181 (1997).
8. E. Wong and C.M. Giandomenico. Chem. Rev. **99**, 2451 (1999).
9. G. Natile and M. Coluccia. Coord. Chem. Rev. **216–217**, 383 (2001).
10. M.A. Jakupec, M. Galanski, and B.K. Keppler. Rev. Physiol. Biochem. Pharmacol. **146**, 1 (2003).
11. T. Talarico, D.R. Phillips, G.B. Deacon, S. Rainone, and L.K. Webster. Invest. New Drugs, **17**, 1 (1999).
12. D.St.C. Black, G.B. Deacon, and G.L. Edwards. Aust. J. Chem. **47**, 217 (1994).
13. D.St.C. Black, G.B. Deacon, G.L. Edwards, and B.M. Gatehouse. Aust. J. Chem. **46**, 1323, (1993).
14. S.J. Lippard. Acc. Chem. Res. **11**, 211 (1978).
15. K.E. Erkkila, D.T. Odom, and J.K. Barton. Chem. Rev. **99**, 2777 (1999).
16. W.D. McFadyen, L.P.G. Wakelin, I.A.G. Roos, and V.A. Leopold. J. Med. Chem. **28**, 1113 (1985).
17. J.G. Collins, R.M. Rixon, and J.R. Aldrich-Wright. Inorg. Chem. **39**, 4377 (2000); M. Cusumano and A. Giannetto. J. Inorg. Biochem. **65**, 137 (1997).
18. T. Okada, I.M. El-Mehasseb, M. Kodaka, T. Tomohiro, K.-i. Okamoto, and H. Okuno. J. Med. Chem. **44**, 4661 (2001).
19. F. Zamora, V.M. González, J.M. Pérez, J.R. Masaguer, C. Alonso, and C. Navarro-Ranninger. Appl. Organomet. Chem. **11**, 491 (1997); **11**, 659 (1997).
20. D.-L. Ma and C.-M. Che. Chem. Eur. J. **9**, 6133 (2003), and refs. therein.
21. Y. Chen, Z. Guo, S. Parsons, and P.J. Sadler. Chem. Eur. J. **4**, 672 (1998).
22. G.L. Edwards, D.St.C. Black, G.B. Deacon, and L.P.G. Wakelin. Can. J. Chem. **83**, 969 (2005).
23. A. Kasahara. Bull. Chem. Soc. Jpn. **41**, 1272 (1968).
24. M. Nonoyama and H. Takayanagi. Trans. Met. Chem. **1**, 10 (1975/1976).
25. J. Pérez, G. Sánchez, J. García, J.L. Serrano, and G. López. J. Therm. Anal. Calorim. **66**, 361 (2001).
26. T.G. Appleton, H.C. Clark, and L.E. Manzer. Coord. Chem. Rev. **10**, 335 (1973).
27. C. Tessier and F.D. Rochon. Inorg. Chim. Acta, **295**, 25 (1999).
28. A.J. Deeming, I.P. Rothwell, M.B. Hursthouse, and L. New. J. Chem. Soc. Dalton Trans. 1490 (1978).
29. K. Shobatake, C. Postmus, J.R. Ferraro, and K. Nakamoto. Appl. Spectrosc. **23**, 12 (1969); G.B. Deacon and J.H.S. Green. Spectrochim. Acta Sect. A, **24A**, 845 (1968).
30. G.E. Hartwell, R.V. Lawrence, and M.J. Smas. Chem. Commun. 912 (1970).
31. J.D. Higgins III, L. Neely, and S. Fricker. J. Inorg. Biochem. **49**, 149 (1993).
32. M.J. Cleare. J. Clin. Hematol. Oncol. **7**, 1 (1977); M.J. Cleare. Coord. Chem. Rev. **12**, 349 (1974).
33. The authors wish to thank one referee for this suggestion. See: S.J. Berners-Price and P.J. Sadler. Struct. Bonding, **70**, 27 (1988).
34. I.M. El-Mehasseb, M. Kodaka, T. Okada, T. Tomohiro, K.-i. Okamoto, and H. Okuno. J. Inorg. Biochem. **84**, 157 (2001).
35. M.A. Gutierrez, G.R. Newkome, and J. Selbin. J. Organomet. Chem. **202**, 341 (1980).

© 2005 NRC Canada

Synthesis of *N*-substituted isoindolinones via a palladium catalysed three-component carbonylation – amination – Michael addition cascade[1]

Ronald Grigg, Xinjie Gai, Tossapol Khamnaen, Shuleewan Rajviroongit, Visuvanathar Sridharan, Lixin Zhang, Simon Collard, and Ann Keep

Abstract: We herein describe a novel palladium catalysed three-component cascade process involving carbonylation of an aryl iodide to generate an acyl palladium(II) species that is intercepted by a primary aliphatic or aromatic amine, amide, or sulfonamide followed by intramolecular Michael addition to furnish *N*-substituted isoindolinones in good yield. Overall, the cascade results in the formation of one C—C and two C—N bonds, one ring and one stereocentre.

Key words: isoindolinone, palladium, cascade, amidation, sulfonamidation.

Résumé : On décrit un nouveau processus en cascade, à trois composants et catalysé par le palladium qui permet de procéder à la carbonylation d'un iodure d'aryle pour générer une espèce palladium(II) acyle qui peut être interceptée par une amine, un amide ou un sulfonamide primaire, aliphatique ou aromatique, suivie d'une addition intramoléculaire de Michael qui permet d'obtenir des isoindolinones *N*-substituées avec de bons rendements. La cascade globale conduit à la formation d'une liaison C—C et de deux liaisons C—N, d'un cycle et d'un stéréocentre.

Mots clés : isoindolinone, palladium, cascade, amidation, sulfonamidation.

[Traduit par la Rédaction]

Introduction

Nitrogen heterocycles containing isoindolinone skeletons have attracted much interest in recent years owing to their biological activity. *N*-Substituted isoindolinones of general structure **1** (Fig. 1) possess anxiolytic activity and are of interest as sedatives, hypnotics, and muscle relaxants (1). Typical examples are the anxiolytics pazinaclone (**2**), pagoclone (**3**) (Aventis/Pfizer, phase III clinical trials) (2), and the anxiolytic and anticonvulsant zopiclone (**4**) (3, 4). The isoindolinone moiety also features in anti-cancer drug candidates including protein kinase inhibitors.

Current syntheses of isoindolinones are often unsatisfactory because of severe reaction conditions (5–7), substituent restrictions (8–10), multi-step protocols, or even product purification difficulties (11–13). We earlier described a simple one-step process for the synthesis of *N*-substituted isoindolones (14) from *o*-phthalaldehyde that did not access 1(3)-substituted derivatives. Naming and numbering of isoindolones using ACD/I-Lab version 8.0 software results in interchange of the 1- and 3-positions depending upon the 1(3)-substituent. This simple protocol was subsequently extended by others (15, 16) for accessing more complex polysubstituted isoindolinones (17–22). Additionally, we have described a range of catalytic processes that exploit the versatility of carbon monoxide and allene as powerful relay switches in palladium catalysed cyclisation – anion capture cascades (23). Our ongoing interest in designing palladium catalysed atmospheric pressure carbonylation processes in a tactical combination with core reactions led us to explore combinations with Michael addition processes as a novel approach to isoindolinone derivatives (Scheme 1) (24). Alter-

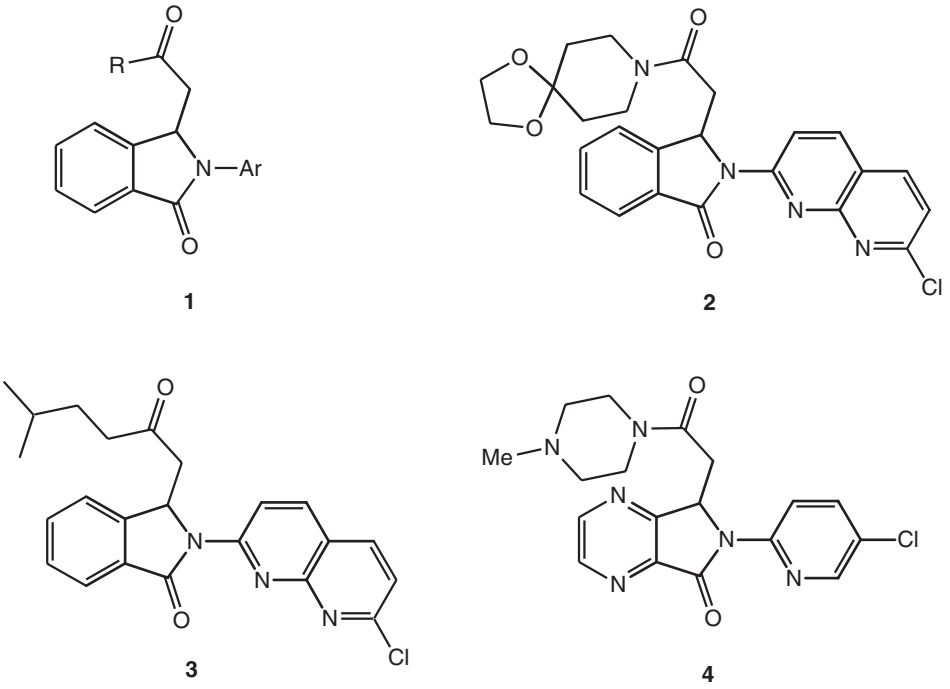
Received 7 January 2005. Published on the NRC Research Press Web site at http://canjchem.nrc.ca on 27 August 2005.

R. Grigg,[2] X. Gai, V. Sridharan, and L. Zhang. Molecular Innovation Diversity and Automated Synthesis (MIDAS) Centre, School of Chemistry, Leeds University, Leeds LS2 9JT, UK.
T. Khamnaen. Molecular Innovation Diversity and Automated Synthesis (MIDAS) Centre, School of Chemistry, Leeds University, Leeds LS2 9JT, UK and Department of Chemistry, Faculty of Science, Mahidol University, Rama VI Road, Rajthevee, Bangkok 10400, Thailand.
S. Rajviroongit. Department of Chemistry, Faculty of Science, Mahidol University, Rama VI Road, Rajthevee, Bangkok 10400, Thailand.
S. Collard and A. Keep. Johnson Matthey, Orchard Road, Royston, Herts SG8 5HE, UK.

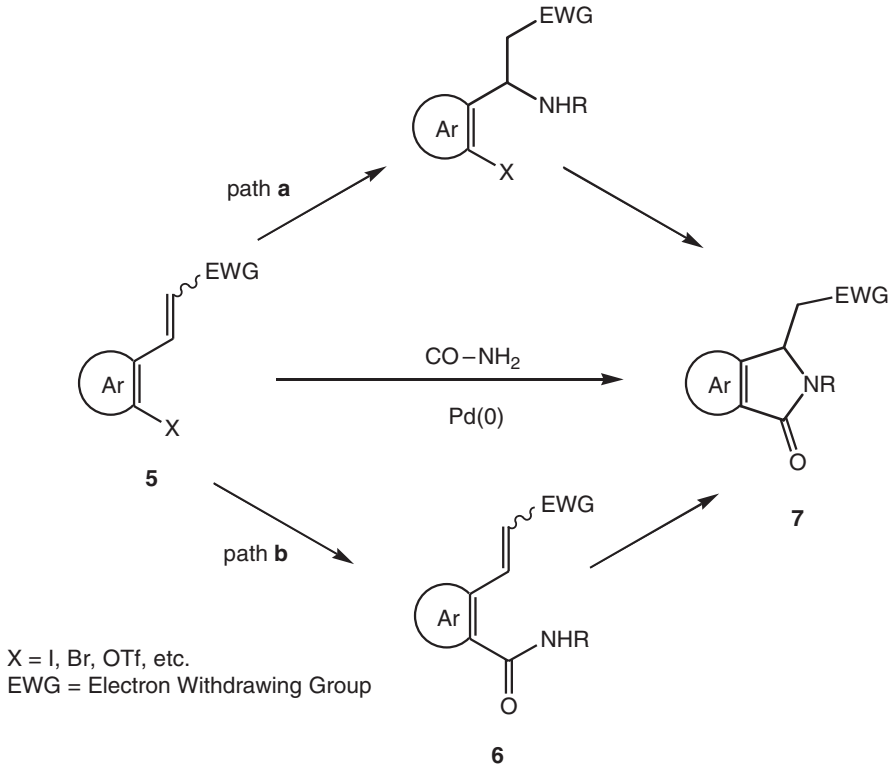
[1]This article is part of a Special Issue dedicated to Professor Howard Alper.
[2]Corresponding author (e-mail: r.grigg@chem.leeds.ac.uk).

 doi: 10.1139/V05-111 © 2005 NRC Canada

Fig. 1. Examples of biologically active *N*-substituted isoindolinones.



Scheme 1. R = alkyl, aryl, heteroaryl, amido, sulphonamido.



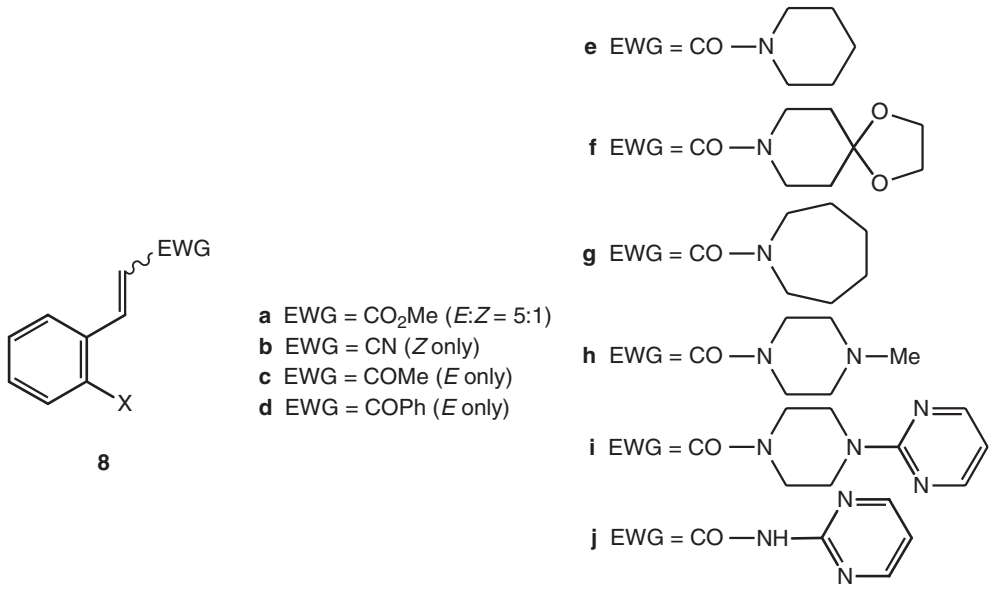
native catalytic approaches to isoindolinones involving inter- or intramolecular carbopalladation of imines have been reported by Cho et al. in a series of papers (25–30).

Results and discussion

Recently, we reported palladium catalysed three-component cascade allenylation – amination – Michael addition furnishing 4-methylene-tetrahydroisoquinolines and 4-methylene-tetrahydronaphthalenes (31), which utilized **5** as key substrates. We therefore initially selected **8a**–**8d** (Fig. 2) as the prototypical dual aryl iodide – Michael acceptors, but using carbon monoxide, instead of allene, to evaluate the novel Scheme 1 three-component cascade. Subsequently, the in-

© 2005 NRC Canada

Fig. 2. Prototypical dual aryl iodide – Michael acceptors.



vestigation was extended to the particular biologically important heterocyclic amides **8e**–**8j** (Fig. 2) as the electron-withdrawing group in the Michael acceptor. Compounds of type **8a**–**8j** could react with carbon monoxide (1 atm, 1 atm = 101.325 kPa) and a primary amine in the presence of palladium(0) to afford *N*-substituted isoindolinones via either path **a** or path **b** (Scheme 1). In path **a**, carbon monoxide insertion is followed by amination to give the amide **6**, which subsequently undergoes intramolecular Michael addition to afford *N*-substituted isoindolinones **7**. In path **b**, the order of events, beginning with an intermolecular Michael addition, is reversed.

Arylamine nucleophiles

Compounds **8a** and **8b** reacted with carbon monoxide, a primary aromatic or heteroaromatic amine, $Pd(OAc)_2$ (10 mol%) and PPh_3 (20 mol%) and Cs_2CO_3 in toluene at 90 °C over 24 h to afford isoindolinones **9**–**12** in good yield (Table 1, entries 1–4). The reactivity of aniline nucleophiles (Table 1, entries 1–3) with different para substituents showed that the more nucleophilic *p*-anisidine (Table 1, entry 2) afforded **10a** in 90% yield, whereas *p*-(trifluoromethyl)aniline (Table 1, entry 3), a weaker nucleophile, gave **11a** in 68% yield under the same reaction conditions. However, 2-aminothiazole required 48 h under the same reaction conditions for complete conversion to **12a** (73%) (Table 1, entry 4). In the cases of the use of 2- and 4-aminopyridines (Table 1, entries 5 and 6), a catalyst system comprising Pd_2dba_3 (2.5 mol%) and tris(2-furyl)phosphine (10 mol%) was utilized to provide the corresponding isoindolinones **13** and **14** in excellent yield, whilst bicyclic heteroaromatic amines in the presence of a modified catalyst system consisting of $Pd(PPh_3)_2Cl_2$ (2 mol%) and TFP (12 mol%) afforded isoindolinone **15e** (86%) (Table 1, entry 7). The pK_as of the nucleophiles (Table 1) fall into two groups. Those (Table 1, entries 1–3) involving protonation at the NH_2 group and those (Table 1, entries 4–8) involving protonation on sp^2 N centres in the heterocyclic rings. It is likely that in all cases, except perhaps entry 3, that the reactive nucleophiles are not the neutral species (vide infra).

Note that for all isoindolones where the electron-withdrawing group (EWG) is CN or CO_2Me naming and (or) numbering is as shown by **9a** and **9b** (Table 1). When EWG is a ketone, amide, or 2-pyridyl, the numbering is as shown by **13e** (Table 1).

Aliphatic amine nucleophiles

The cascade successfully incorporated primary aliphatic amines furnishing **16**–**21** (Table 2, entries 1–6). We briefly studied the diastereoselectivity of the Michael addition reaction with (*R*)-(+)-α-methylbenzylamine (Table 2, entries 7 and 8), which afforded a 1:1.75 and a 2:3 diastereomeric mixture of **22a** and **22b**, respectively. *S*-Alanine methyl ester similarly afforded **23a** as an 1:1 diastereomer mixture. In a case of **23a**, 2 mol equiv. of amine and increasing the reaction time to 48 h were required for complete conversion, probably owing to competitive self-condensation of the amino acid ester (diketopiperazine formation). Thus, under our standard conditions there is little inherent diastereoselectivity.

Unexpectedly, Michael acceptor **8**, where EWG = NO_2, failed to furnish the cascade product with benzylamine using the same catalyst system possibly owing to its instability under the reaction conditions.

Amide and sulfonamide nucleophiles

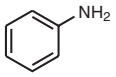
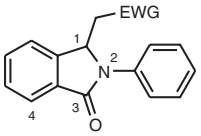
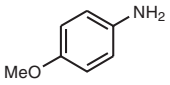
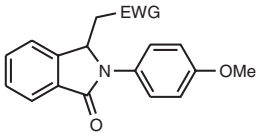
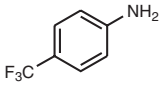
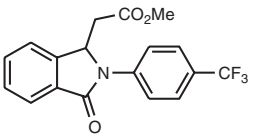
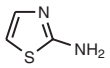
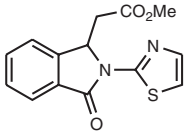
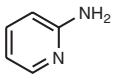
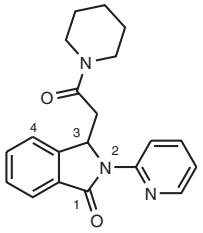
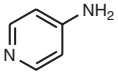
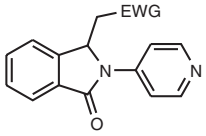
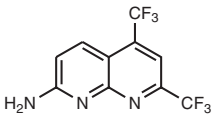
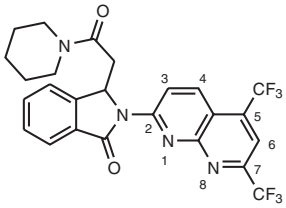
Amides and sulfonamides were also successfully used as nucleophiles in the above cascades (Table 3). When trifluoroacetamide was utilized as a nucleophile, hydrolysis occurred furnishing NH amide **25e** in good yield (Table 3, entry 2). This opens up a significant number of further synthetic opportunities.

2-Vinylpyridine as a Michael acceptor

It is well-known that 2-vinylpyridines can function as Michael acceptors (32) and this prompted the evaluation of **8k**

© 2005 NRC Canada

Table 1. Three-component carbonylation – amination – Michael addition cascades employing primary aromatic amines.[a–c]

Entry	Aryl iodide	Nucleophile (pKa)[d]	Product	Yield (%)[e]	
1	**8a**	 (4.61)		**9a**	75
	8b			**9b**	65
2	**8a**	 (5.21)		**10a**	90
	8b			**10b**	79
3	**8a**	 (2.77)		**11a**	68
4	**8a**	 (5.42)		**12a**	73[f]
5	**8e**	 (6.67)		**13e**	86
	8e			**14e**	92
	8f			**14f**	99
6	**8g**	 (9.26)		**14g**	89
	8i			**14i**	88
	8j			**14j**	58
7	**8e**	 (2.35)		**15e**	86

Note: EWG = electron-withdrawing group.

[a]Entries 1–4: primary amine (1.2 mol equiv.), $Pd(OAc)_2$ (10 mol%), PPh_3 (20 mol%), Cs_2CO_3 (2 mol equiv.), toluene, 90 °C, 24 h.

[b]Entries 5–6: primary amine (1.2 mol equiv.), Pd_2dba_3 (2.5 mol%), TFP (10 mol%), Cs_2CO_3 (2 mol equiv.), toluene, 90 °C, 18 h.

[c]Entry 7: primary amine (1.2 mol equiv.), $Pd(PPh_3)_2Cl_2$ (2 mol%), TFP (12 mol%), Cs_2CO_3 (2 mol equiv.), toluene, 110 °C, 18 h.

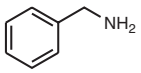
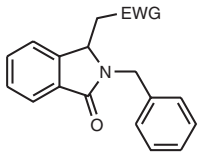
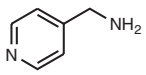
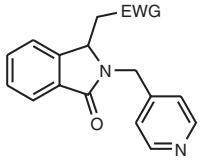
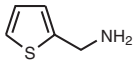
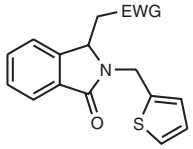
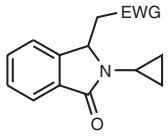
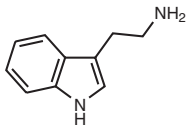
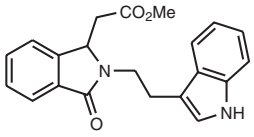
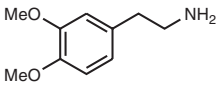
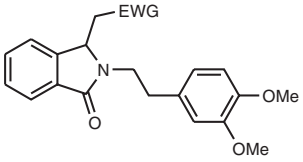
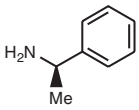
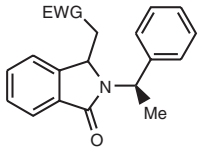
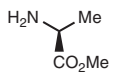
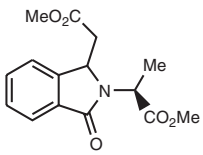
[d]Calculated using ACD/I-Lab version 8.0 software.

[e]Isolated yield.

[f]Reaction time 48 h.

© 2005 NRC Canada

Table 2. Three-component carbonylation – amination – Michael addition cascades employing achiral and chiral primary aliphatic amines.[a–c]

Entry	Aryl iodide	Nucleophile	Product	Yield (%)[d]	
1	**8a**			**16a**	91
	8b			**16b**	69
	8c			**16c**	61
	8d			**16d**	70
2	**8a**			**17a**	95
	8b			**17b**	88
3	**8a**			**18a**	87
	8b			**18b**	77
	8c			**18c**	55
	8d			**18d**	55
4	**8a**			**19a**	79
	8b			**19b**	52
5	**8a**			**20a**	69
6	**8e**			**21e**	85
	8h			**21h**	96
7	**8a**			**22a**	74
	8b			**22b**	77
8	**8a**			**23a**	63

Note: EWG = electron-withdrawing group.

[a]Entries 1–5, 7, and 8: primary amine (1.2 mol equiv.), $Pd(OAc)_2$ (10 mol%), PPh_3 (20 mol%), Cs_2CO_3 (2 mol equiv.), toluene, 90 °C, 24 h.

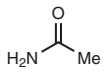
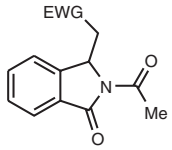
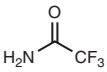
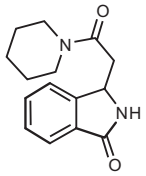
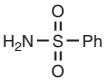
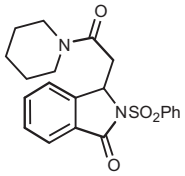
[b]Entry 6: primary amine (1.2 mol equiv.), $Pd(PPh_3)_2Cl_2$ (2 mol%), TFP (12 mol%), Cs_2CO_3 (2 mol equiv.), toluene, 110 °C, 18 h.

[c]Entries 7 and 8: amine (2 mol equiv.), reaction time 48 h.

[d]Isolated yield.

© 2005 NRC Canada

Table 3. Three-component carbonylation – amination – Michael addition cascades employing amide and sulphonamide nucleophiles.[a]

Entry	Aryl iodide	Nucleophile	Product	Yield (%)[b]
1	**8e**			**24e** 62
	8f			**24f** 52
2	**8e**			**25e** 60
3	**8e**			**26e** 56

Note: EWG = electron-withdrawing group.
[a]Primary amine (1.2 mol equiv.), $Pd(PPh_3)_2Cl_2$ (2 mol%), TFP (12 mol%), Cs_2CO_3 (2 mol equiv.), toluene, 110 °C, 18 h.
[b]Isolated yield.

in our three-component cascade using alkyl-, aryl-, and heteroarylamines (Table 4). For these cascades, we used our cyclopalladated catalyst **27** (5 mol%), which is known to form Pd nanoparticles rapidly in the presence of carbon monoxide (33*a*). The corresponding isoinolinones **28–33** were obtained in good yield in all cases.

Mechanism

We have only very briefly probed the mechanism of the reaction. A control experiment in which carbon monoxide was omitted as the reagent and benzylamine used as the nucleophile was carried out, but no Michael adduct resulting from the reaction of **8a** with benzylamine was detected under the standard reaction conditions. Intermediates were detected in a study of a related reaction by our group (33*b*). It is inherently unlikely that with such a disparate collection of *N*-nucleophiles that the mechanism is identical in every case. Rather, one would expect that the reactive nucleophiles in the case of the aryl and heteroarylamines and the amides and sulfonamides are the *N*-deprotonated species, whilst in the case of the aliphatic amines the neutral species are involved. Our control experiment is supportive of path **a** rather than path **b** (Scheme 1), but clearly a more detailed study is indicated before drawing any firm conclusions.

Summary

N-Substituted isoindolinones have been successfully synthesized via a novel palladium catalysed three-component carbonylation – amination – intramolecular Michael addition cascade process. The reaction tolerates a wide variety of *N*-nucleophiles and delivers a diverse range of isoindolinones. Overall, the cascade results in the formation of one C—C and two C—N bonds, one ring and one stereocentre.

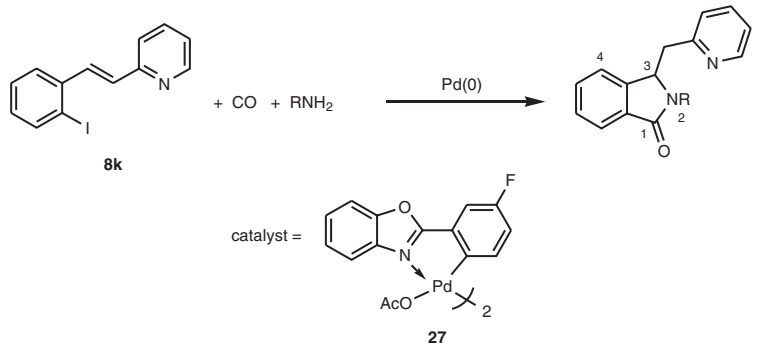
Experimental

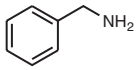
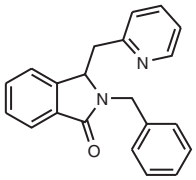
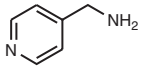
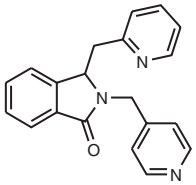
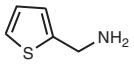
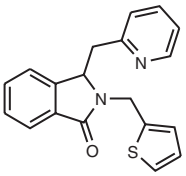
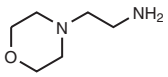
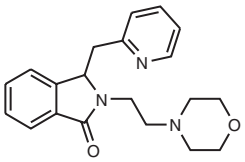
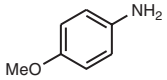
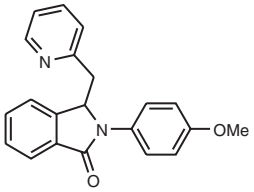
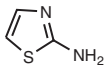
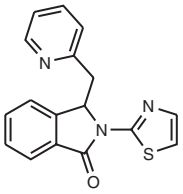
Melting points were determined on a Reichert hot-stage apparatus and are uncorrected. IR spectra were recorded on a Nicolet Magna FT-IR 560 spectrometer (to prepare samples for IR, a small amount of sample was dissolved in dichloromethane, transferred onto a germanium plate, and left to evaporate to provide a film). NMR spectra were recorded at 250 MHz on a Bruker AC 250 spectrometer, at 300 MHz on a Bruker DPX 300 spectrometer, and at 500 MHz on a Bruker DRX 500 spectrometer. Unless otherwise specified, deuteriochloroform was used as the solvent with tetramethylsilane (TMS) as the internal standard. Chemical shifts are given in parts per million (ppm, δ) downfield from TMS and the coupling constants are given in Hertz (Hz). The splitting patterns are designed as singlet (s), doublet (d), triplet (t), quartet (q), multiplet (m), and double doublet (dd). The mass spectral mode of ionization is EI unless otherwise stated. EI and FAB were obtained using a VG-Autospec operating at 70 eV. ES were obtained on a LCT Micromass (TOF). Accurate molecular weights were determined using perfluorotributylamine or polyethylenimine as an internal standard at Leeds University or from the EPSRC Swansea Mass Spectroscopy Service. Microanalyses were obtained using a Carlo Erba MOD 11016 elemental analyser. Flash column chromatography was performed using silica gel 60 (Merck 9385, 230–400 mesh).

Commercially available reagents and solvents were used without further purification. The term ether refers to diethyl

© 2005 NRC Canada

Table 4. Three-component carbonylation – amination – Michael addition cascades of the 2-vinyl pyridine Michael acceptor **8k**.[a]



Entry	Nucleophile	Product	Yield (%)[b]	
1			**28**	64
2			**29**	70
3			**30**	74
4			**31**	64
5			**32**	67
6			**33**	72

Note: R = alkyl, aryl, heteroaryl.
[a]Primary amine (1.2 mol equiv.), catalyst **27** (5 mol%), Cs_2CO_3 (2 mol equiv.), toluene, 95 °C, 48 h.
[b]Isolated yield.

© 2005 NRC Canada

ether and petroleum ether refers to the fraction with a boiling point of 40–60 °C.

General procedure A

Michael acceptor **8** (1 mmol), *N*-nucleophile (1.2 mmol), $Pd(OAc)_2$ (0.022 g, 0.1 mmol), PPh_3 (0.052, 0.2 mmol), and Cs_2CO_3 (0.650 g, 2 mmol) were mixed in dry toluene (10 mL). Carbon monoxide was then introduced through a balloon and the mixture heated with stirring at 90 °C for 24 h, cooled to room temperature, filtered to remove inorganic materials, and concentrated in vacuo. The crude product was purified by flash column chromatography.

General procedure B

Michael acceptor **8** (0.5 mmol), *N*-nucleophile (0.6 mmol), $Pd(OAc)_2$ (0.011 g, 0.05 mmol), PPh_3 (0.026, 0.1 mmol), and Cs_2CO_3 (0.325 g, 1 mmol) were mixed in dry toluene (6 mL). Carbon monoxide was then introduced through a balloon and the mixture heated with stirring at 95 °C for 48 h. Work-up was as for general procedure A.

General procedure C

As for general procedure A, but with Pd_2dba_3 (0.024 g, 0.025 mmol) and TFP (0.025 g, 0.1 mmol) as the catalyst precursors and heating at 90 °C for 18 h.

General procedure D

As for general procedure A, but with $Pd(PPh)_3Cl_2$ (0.014 g, 0.02 mmol) and TFP (0.029 g, 0.12 mmol) as the catalyst precursors, dry dioxane as the solvent, and heating under reflux for 18 h.

General procedure E

As for general procedure A, but with precatalyst **27** (0.02 g, 0.025 mmol).

Methyl (3-oxo-2-phenyl-2,3-dihydro-1*H*-isoindol-1-yl)acetate (9a)

Prepared according to general procedure A employing **8a** (0.288 g, 1 mmol) and aniline (0.111 g, 1.2 mmol). Column chromatography of the crude product eluting with 3:7 *v*/*v* ethyl acetate – petroleum ether afforded the product (0.208 g, 75%) as colourless needles, mp 121 to 122 °C. IR (cm^{-1}): 2951, 1736, 1697, 1649, 1597, 1498, 1456, 1379. ^1H NMR ($CDCl_3$, 250 MHz) δ: 2.50 (dd, 1H, *J* = 16.3, 8.5 Hz, C*H*HCO), 2.95 (dd, 1H, *J* = 16.3, 4.5 Hz, CH*H*CO), 3.64 (s, 3H, OMe), 5.60 (dd, 1H, *J* = 8.5, 4.5 Hz, NCH), 7.26 (m, 1H, ArH), 7.60–7.43 (m, 7H, ArH), 7.90 (d, 1H, *J* = 7.5 Hz, Ar 4-H). ^{13}C NMR ($CDCl_3$, 62.5 MHz) δ: 37.8, 52.4, 57.9, 123.0, 124.2, 124.6, 126.3, 129.3, 129.7, 132.2, 132.8, 136.8, 144.6, 167.2, 171.2. ES-MS *m*/*z* (%): 304 ([MNa^+], 100). Anal. calcd. for $C_{17}H_{15}NO_3$: C 72.60, H 5.40, N 5.00; found: C 72.55, H 5.40, N 4.85.

3-Oxo-2-phenyl-2,3-dihydro-1*H*-isoindol-1-yl)acetonitrile (9b)

Prepared according to general procedure B employing **8b** (0.255 g, 1 mmol) and aniline (0.111 g, 1.2 mmol), catalyst **27** (0.040 g, 0.05 mmol), and cesium carbonate (0.65 g, 2 mmol) in dry toluene (12 mL). Column chromatography of the crude product eluting with 2:3 *v*/*v* ethyl acetate – petroleum ether afforded the product (0.16 g, 65%) as colourless needles, mp 183 to 184 °C. IR (cm^{-1}): 1683, 1496, 1391, 1214. ^1H NMR ($CDCl_3$, 250 MHz) δ: 2.69 (dd, 1H, *J* = 16.8, 7.2 Hz, C*H*HCN), 3.02 (dd, 1H, *J* = 16.8, 3.3 Hz, CH*H*CN), 5.35 (dd, 1H, *J* = 6.9, 3.3 Hz, NCH), 7.2–7.35 (m, 1H, ArH), 7.45–7.75 (m, 6H, ArH), 7.98 (dd, 1H, *J* = 7.2, 1.0 Hz, Ar 4-H). ^{13}C NMR ($CDCl_3$, 62.5 MHz) δ: 22.3, 55.9, 115.4, 115.8, 122.8, 124.4, 125.1, 127.1, 130.1, 130.3, 132.4, 133.3, 136.0, 142.1, 167.0. MS *m*/*z* (%): 248 ([M^+], 22), 208 (100), 77 (37). Anal. calcd. for $C_{16}H_{12}N_2O$: C 77.25, H 5.05, N 11.10; found: C 77.40, H 4.85, N 11.25.

Methyl [2-(4-methoxyphenyl)-3-oxo-2,3-dihydro-1*H*-isoindol-1-yl]acetate (10a)

Prepared according to general procedure A employing **8a** (0.288 g, 1 mmol) and *p*-anisidine (0.147 g, 1.2 mmol). Column chromatography of the crude product eluting with 2:3 *v*/*v* ethyl acetate – petroleum ether afforded the product (0.279 g, 90%) as colourless needles, mp 97–99 °C. IR (cm^{-1}): 2952, 1735, 1694, 1613, 1512, 1467, 1438, 1386. ^1H NMR ($CDCl_3$, 250 MHz) δ: 2.50 (dd, 1H, *J* = 16.0, 8.5 Hz, C*H*HCO), 2.90 (dd, 1H, *J* = 16.0, 4.5 Hz, CH*H*CO), 3.62 (s, 3H, OMe), 3.83 (s, 3H, OMe), 5.50 (dd, 1H, *J* = 8.5, 4.5 Hz, NCH), 6.98 (d, 2H, *J* = 6.8 Hz, ArH), 7.43 (d, 2H, *J* = 6.8 Hz, ArH), 7.52–7.60 (m, 3H, ArH), 7.92 (d, 1H, *J* = 7.5 Hz, Ar 4-H). ^{13}C NMR ($CDCl_3$, 62.5 MHz) δ: 38.1, 52.4, 55.9, 58.5, 115.0, 122.9, 124.6, 126.5, 129.3, 129.5, 132.3, 132.6, 144.6, 158.3, 167.3, 171.3. ES-MS *m*/*z* (%): 334 ([MNa^+], 100). Anal. calcd. for $C_{18}H_{17}NO_3$: C 69.45, H 5.55, N 4.50; found: C 69.55, H 5.80, N 4.35.

[2-(Methoxyphenyl)-3-oxo-2,3-dihydro-1*H*-isoindol-1-yl)acetonitrile (10b)

Prepared according to general procedure B employing **8b** (0.13 g, 0.5 mmol) and *p*-anisidine (0.074 g, 0.6 mmol). Column chromatography of the crude product eluting with 2:3 *v*/*v* ethyl acetate – petroleum ether afforded the product (0.11 g, 79%) as colourless needles, mp 197–199 °C. IR (cm^{-1}): 1695, 1513, 1387, 1248. ^1H NMR ($CDCl_3$, 250 MHz) δ: 2.67 (dd, 1H, *J* = 16.8, 7.2 Hz, C*H*HCN), 3.0 (dd, 1H, *J* = 16.8, 3.4 Hz, CH*H*CN), 3.84 (s, 3H, OMe), 5.25 (dd, 1H, *J* = 7.2, 3.3 Hz, NCH), 7.0, 7.39 (2 × d, 2 × 2H, *J* = 9.0 Hz, ArH), 7.3–7.5 (m, 3H, ArH), 7.97 (dd, 1H, *J* = 7.1, 1.3 Hz, Ar 4-H). ^{13}C NMR ($CDCl_3$, 62.5 MHz) δ: 22.4, 55.9, 57.6, 115.4, 115.9, 122.8, 125.0, 126.6, 128.6, 130.2, 132.4, 133.1, 142.2, 158.8, 167.0. ES-MS *m*/*z* (%): 301 ([MNa^+], 100). Anal. calcd. for $C_{17}H_{14}N_2O_2$: C 73.30, H 5.00, N 10.05; found: C 73.10, H 5.10, N 10.15.

Methyl {3-oxo-2-[4-(trifluoromethyl)phenyl]-2,3-dihydro-1*H*-isoindol-1-yl}acetate (11a)

Prepared according to general procedure A employing **8a** (0.288 g, 1 mmol) and *p*-(trifluoromethyl)aniline (0.193 g, 1.2 mmol). Column chromatography of the crude product eluting with 3:7 *v*/*v* ethyl acetate – pentane afforded the product (0.237 g, 68%) as colourless needles, mp 156–158 °C. IR (cm^{-1}): 2955, 1736, 1705, 1612, 1520, 1469, 1438, 1375. ^1H NMR ($CDCl_3$, 250 MHz) δ: 2.50 (dd, 1H, *J* = 16.3, 8.8 Hz, C*H*HCO), 2.98 (dd, 1H, *J* = 16.3, 3.8 Hz, CH*H*CO), 3.67 (s, 3H, OMe), 5.67 (dd, 1H, *J* = 8.8, 3.8 Hz, NCH), 7.52–7.80 (m, 7H, ArH), 7.93 (dd, 1H, *J* = 8.3,

© 2005 NRC Canada

7.5 Hz, Ar 4-H). ^{13}C NMR ($CDCl_3$, 62.5 MHz) δ: 38.1, 52.6, 57.4, 123.0, 123.1, 124.9, 126.7, 126.8, 126.9, 129.6, 129.7, 131.7, 133.3, 140.1, 144.4, 167.4, 171.0. FAB-MS *m/z* (%): 350 ([MH$^+$], 100). Anal. calcd. for $C_{18}H_{14}F_3NO_3$: C 61.85, H 4.05, N 4.00; found: C 61.65, H 4.00, N 4.05.

Methyl [3-oxo-2-(1,3-thiazol-2-yl)-2,3-dihydro-1*H*-isoindol-1-yl]acetate (12a)

Prepared according to general procedure A employing **8a** (0.288 g, 1 mmol) and 2-aminothiazole (0.120 g, 1.2 mmol). Column chromatography of the crude product eluting with 2:3 *v/v* ethyl acetate – pentane afforded the product (209 mg, 73%) as pale yellow needles, mp 150 to 151 °C. IR (cm^{-1}): 2951, 1733, 1706, 1616, 1595, 1505, 1466, 1437, 1411, 1369. ^{1}H NMR ($CDCl_3$, 250 MHz) δ: 2.85 (dd, 1H, *J* = 16.3, 8.8 Hz, C*H*HCO), 3.69 (s, 3H, OMe), 3.78 (dd, 1H, *J* = 16.3, 3.5 Hz, CH*H*CO), 5.78 (dd, 1H, *J* = 8.8, 3.5 Hz, NCH), 7.06 (d, 1H, *J* = 3.5 Hz, thiazolyl 5-H), 7.54 (d, 1H, *J* = 3.5 Hz, thiazolyl 4-H), 7.63–7.66 (m, 3H, ArH), 7.95 (dd, 1H, *J* = 7.5, 1.0 Hz, Ar 4-H). ^{13}C NMR ($CDCl_3$, 62.5 MHz) δ: 37.4, 52.4, 58.6, 114.2, 123.5, 124.9, 129.6, 130.4, 134.0, 138.3, 144.5, 157.4, 166.5, 171.1. ES-MS *m/z* (%): 311 ([MNa$^+$], 100). Anal. calcd. for $C_{14}H_{12}N_2O_3S$: C 58.30, H 4.20, N 9.70, S 11.10; found: C 58.35, H 4.35, N 9.80, S 10.95.

3-(2-Oxo-2-piperidin-1-ylethyl)-2-pyridin-2-ylisoindolin-1-one (13e)

Prepared according to general procedure D employing **8e** (0.341 g, 1.0 mmol) and 2-aminopyridine (0.113 g, 1.2 mmol). Column chromatography of the crude product eluting with 4:1 *v/v* ethyl acetate – hexane afforded the product (0.288 g, 86%) as a pale yellow gum. IR (cm^{-1}): 2250, 1693, 1468, 1403, 1210, 1107, 1030, 960. ^{1}H NMR ($CDCl_3$, 300 MHz) δ: 1.42–1.61 (m, 6H, $CH_2CH_2CH_2CH_2CH_2$), 2.38 (dd, 1H, *J* = 15.2, 9.9 Hz, C*H*HCO), 3.34 (m, 2H, NCH_2), 3.55 (dd, 1H, *J* = 15.2, 3.0 Hz, CH*H*CO), 3.64 (m, 2H, NCH_2), 6.14 (dd, 1H, *J* = 9.9, 3.0 Hz, NCH), 7.07 (m, 1H, ArH), 7.50 (t, 1H, *J* = 7.3 Hz, ArH), 7.59 (t, 1H, *J* = 7.4 Hz, ArH), 7.77 (m, 2H, pyridyl H), 7.92 (d, 1H, *J* = 7.3 Hz, Ar 7-H), 8.43 (dd, 1H, *J* = 4.1, 0.8 Hz, pyridyl 4-H), 8.60 (d, 1H, *J* = 8.4 Hz, pyridyl 6-H). ^{13}C NMR ($CDCl_3$, 75 MHz) δ: 24.9, 26.0, 26.9, 37.9, 43.3, 47.0, 57.7, 115.9, 119.8, 124.4, 128.9, 131.9, 133.3, 138.3, 146.4, 148.2, 151.4, 168.2, 168.7. MS *m/z* (%): 336 ([MH$^+$], 100), 251 (68), 223 (20), 209 (71). Anal. calcd. for $C_{20}H_{21}N_3O_2$: C 71.60, H 6.30, N 12.50; found: C 71.80, H 6.30, N 12.45.

3-(2-Oxo-2-piperidin-1-ylethyl)-2-pyridin-4-ylisoindolin-1-one (14e)

Prepared according to general procedure D employing **8e** (0.341 g, 1.0 mmol) and 4-aminopyridine (0.113 g, 1.2 mmol). Column chromatography of the crude product eluting with 4:1 *v/v* ethyl acetate – hexane afforded the product (0.308 g, 92%) as a colourless viscous oil. IR (cm^{-1}): 1701, 1656, 1504, 1454, 1380, 1210. ^{1}H NMR ($CDCl_3$, 300 MHz) δ: 1.42 (m, 2H, $CH_2CH_2CH_2CH_2CH_2$), 1.61 (m, 4H, $CH_2CH_2CH_2CH_2CH_2$), 2.49 (dd, 1H, *J* = 16.2, 9.7 Hz, C*H*HCO), 3.01 (dd, 1H, *J* = 16.2, 2.8 Hz, CH*H*CO), 3.14–3.28 (m, 2H, NCH_2), 3.58–3.75 (m, 2H, NCH_2), 5.96 (dd, 1H, *J* = 9.7, 2.7 Hz, NCH), 7.54 (dt, 1H, *J* = 7.2, 1.4 Hz, ArH), 7.60–7.69 (m, 2H, ArH), 7.77 (d, 2H, *J* = 4.8 Hz, pyridyl 3- and 5-H), 7.94 (dd, 1H, *J* = 7.5, 1.0 Hz, Ar 7-H), 8.64 (d, 2H, *J* = 4.8 Hz, pyridyl 2- and 6-H). ^{13}C NMR ($CDCl_3$, 75 MHz) δ: 24.7, 26.0, 26.8, 36.8, 43.5, 47.0, 57.1, 115.2, 123.9, 124.8, 129.4, 131.2, 133.7, 144.6, 145.9, 151.3, 167.7, 168.0. ES-MS *m/z* (%): 358 ([MNa$^+$], 100). Anal. calcd. for $C_{20}H_{21}N_3O_2$: C 71.6, H 6.3, N 12.5; found: C 71.3, H 6.35, N 12.75.

3-[2-(1,4-Dioxa-8-azaspiro[4,5]dec-8-yl)-2-oxoethyl]-2-pyridin-4-ylisoindolin-1-one (14f)

Prepared according to general procedure D employing **8f** (0.399 g, 1 mmol) and 4-aminopyridine (0.113 g, 1.2 mmol). Column chromatography of the crude product eluting with 4:1 *v/v* ethyl acetate – hexane afforded the product (0.390 g, 99%) as a pale yellow gum. IR (cm^{-1}): 1701, 1656, 1504, 1454, 1380. ^{1}H NMR ($CDCl_3$, 300 MHz) δ: 1.55 (m, 2H, NCH_2CH_2), 1.73 (m, 2H, NCH_2CH_2), 2.50 (dd, 1H, *J* = 16.2, 9.8 Hz, C*H*HCO), 3.05 (dd, 1H, *J* = 16.2, 2.6 Hz, CH*H*CO), 3.27–3.40 (m, 2H, NCH_2CH_2), 3.69–3.77 (m, 2H, NCH_2CH_2), 3.94–4.01 (m, 4H, OCH_2CH_2O), 5.94 (dd, 1H, *J* = 9.8, 2.6 Hz, NCH), 7.52–7.60 (m, 1H, ArH), 7.62–7.66 (m, 2H, ArH), 7.76 (d, 2H, *J* = 6.2 Hz, pyridyl 3- and 5-H), 7.94 (d, 1H, *J* = 7.5 Hz, Ar 7-H), 8.65 (d, 2H, *J* = 6.2 Hz, pyridyl 2- and 6-H). ^{13}C NMR ($CDCl_3$, 75 MHz) δ: 32.2, 35.9, 36.8, 40.6, 43.9, 57.0, 64.9, 106.9, 115.2, 123.8, 124.8, 129.5, 131.2, 133.8, 144.5, 145.8, 151.4, 167.9, 168.0. MS *m/z* (%): 394 ([MNa$^+$], 100), 225 (23), 211 (32), 186 (44), 144 (82), 95 (69), 80 (51). Anal. calcd. for $C_{22}H_{23}N_3O_4$: C 67.20, H 5.90, N 10.70; found: C 67.00, H 5.90, N 10.80.

3-(2-Azepan-1-yl-2-oxoethyl)-2-pyridin-4-ylisoindolin-1-one (14g)

Prepared according to general procedure D employing **8g** (0.355 g, 1 mmol) and 4-aminopyridine (0.113 g, 1.2 mmol). Column chromatography of the crude product eluting with 4:1 *v/v* ethyl acetate – hexane afforded the product (0.310 g, 89%) as a pale yellow gum. IR (cm^{-1}): 1701, 1656, 1504, 1454, 1380. ^{1}H NMR ($CDCl_3$, 300 MHz) δ: 1.21–1.50 (m, 6H, azepyl H), 1.71–1.83 (m, 2H, azepyl H), 2.47 (dd, 1H, *J* = 16.1, 9.6 Hz, C*H*HCO), 3.05 (dd, 1H, *J* = 16.1, 3.0 Hz, CH*H*CO), 3.14–3.32 (m, 2H, NCH_2), 3.50–3.58 and 3.67–3.76 (2 × m, 2 × 1H, NCH_2), 5.97 (dd, 1H, *J* = 9.6, 3.0 Hz, NCH), 7.51–7.67 (m, 3H, ArH), 7.78 (d, 2H, *J* = 4.8 Hz, pyridyl 3- and 5-H), 7.95 (d, 1H, *J* = 7.5 Hz, Ar 7-H), 8.64 (d, *J* = 4.8 Hz, pyridyl 2- and 6-H). ^{13}C NMR ($CDCl_3$, 75 MHz) δ: 27.2, 27.3, 27.9, 29.2, 37.2, 46.7, 48.2, 57.2, 115.2, 123.8, 124.8, 129.4, 131.2, 133.7, 144.6, 146.0, 151.3, 168.0, 169.2. MS *m/z* (%): 50 ([MH$^+$], 100), 273 (11), 159 (18), 142 (67), 120 (22), 95 (100), 80 (73). Anal. calcd. for $C_{21}H_{23}N_3O_2$: C 72.20, H 6.80, N 12.10; found: C 72.20, H 6.60, N 12.00.

3-[2-Oxo-2-(4-pyrimidin-2-ylpiperazin-1-yl)ethyl]-2-pyridin-4-ylisoindolin-1-one (14i)

Prepared according to general procedure D employing **8i** (0.420 g, 1 mmol) and 4-aminopyridine (0.113 g, 1.2 mmol). Column chromatography of the crude product eluting with 4:1 *v/v* ethyl acetate – hexane afforded the product (0.363 g, 88%) as a pale brown gum. IR (cm^{-1}): 1701, 1656, 1504, 1454, 1380, 1210. ^{1}H NMR ($CDCl_3$, 300 MHz) δ: 2.55 (dd,

© 2005 NRC Canada

1H, *J* = 16.2, 9.0 Hz, C*H*HCO), 3.09 (dd, 1H, *J* = 16.2, 2.8 Hz, CH*H*CO), 3.70–3.93 (m, 6H, piperazyl H), 5.98 (dd, 1H, *J* = 9.0, 2.8 Hz, NCH), 6.56 (m, 2H, piperazyl H), 7.28–7.69 (m, 3H, ArH), 7.77 (d, 2H, *J* = 6.0 Hz, pyridyl 3- and 5-H), 7.96 (d, 1H, *J* = 7.4 Hz, Ar 7-H), 8.33 (m, 3H, pyrimidyl H), 8.65 (d, 2H, *J* = 6.0 Hz, pyridyl 2- and 6-H). ^{13}C NMR ($CDCl_3$, 75 MHz) δ: 37.0, 42.2, 43.8, 43.9, 45.6, 57.0, 111.1, 115.2, 123.8, 124.9, 129.5, 131.2, 133.8, 144.5, 145.7, 151.4, 161.7, 161.8, 167.9, 168.4. MS *m*/*z* (%): 415 ([MH$^+$], 98), 207 (50), 165 (100), 134 (18), 95 (78), 80 (51). Anal. calcd. for $C_{23}H_{22}N_6O_2$: C 66.65, H 5.35, N 20.30; found: C 66.70, H 5.45, N 20.60.

3-[2-Oxo-(2-aminopyrimidin-2-yl)ethyl]-2-pyridin-4-ylisoindolin-1-one (14j)

Prepared according to general procedure D employing **8j** (0.351 g, 1 mmol) and 4-aminopyridine (0.113 g, 1.2 mmol). Column chromatography of the crude product eluting with 4:1 *v*/*v* ethyl acetate – hexane afforded the product (0.199 g, 58%) as a pale yellow gum. IR (cm^{-1}): 1699, 1651, 1500, 1455, 1379. ^{1}H NMR ($CDCl_3$, 300 MHz) δ: 2.46 (dd, 1H, *J* = 15.6, 9.5 Hz, C*H*HCO), 3.29 (dd, 1H, *J* = 15.6, 3.1 Hz, CH*H*CO), 5.87 (dd, 1H, *J* = 9.5, 3.1 Hz, NCH), 7.08 (d, 2H, *J* = 6.3 Hz, pyridyl 3- and 6-H), 7.52–7.64 (m, 3H, ArH), 7.75 (m, 3H, pyrimidyl H), 8.17 (d, 1H, *J* = 8.4 Hz, Ar 7-H), 8.45 (bs, 1H, NH), 8.63 (d, 2H, *J* = 6.3 Hz, pyridyl 2- and 6-H). ^{13}C NMR ($CDCl_3$, 75 MHz) δ: 0.9, 56.5, 114.6, 115.3, 120.8, 123.3, 125.1, 129.7, 132.2, 133.9, 139.1, 144.3, 145.0, 148.3, 151.1, 151.4, 167.6, 168.6. MS *m*/*z* (%): 345 ([MH$^+$], 6), 207 (22), 165 (17), 144 (23), 137 (48), 94 (78), 80 (38). Anal. calcd. for $C_{20}H_{16}N_4O_2$: C 69.80, H 4.70, N 16.30; found: C 69.50, H 4.75, N 16.10.

2-[5,7-Bis(trifluoromethyl)-1,8-naphthyridin-2-yl]-3-(2-oxo-2-piperidin-1-ylethyl)isoindolin-1-one (15e)

Prepared according to general procedure D employing **8e** (0.341 g, 1.0 mmol) and 7-amino-2,4-bis(trifluromethyl)-1,8-napthyridine (0.232 g, 1.2 mmol). Column chromatography of the crude product eluting with 4:1 *v*/*v* ethyl acetate – hexane afforded the product (0.449 g, 86%) as a colourless, viscous oil. IR (cm^{-1}): 1710, 1650, 1505, 1445, 1382. ^{1}H NMR ($CDCl_3$, 300 MHz) δ: 1.49–1.69 (m, 6H, piperidyl H), 2.67 (dd, 1H, *J* = 14.5, 9.3 Hz, C*H*HCO), 3.57–3.71 (m, 4H, piperidyl H), 3.82 (dd, 1H, *J* = 14.5, 3.2 Hz, CH*H*CO), 6.15 (dd, 1H, *J* = 9.3, 3.2 Hz, NCH), 7.55 (t, 1H, *J* = 7.4 Hz, ArH), 7.68 (m, 1H, ArH), 7.74 (d, 1H, *J* = 7.6 Hz, ArH), 7.97 (d, 1H, *J* = 7.6 Hz, Ar 7-H), 8.00 (s, 1H, napthyridyl 6-H), 8.60 (d, 1H, *J* = 9.4 Hz, napthyridyl 3-H), 9.26 (d, 1H, *J* = 9.4 Hz, napthyridyl 4-H). ^{13}C NMR ($CDCl_3$, 75 MHz) δ: 24.9, 26.1, 26.9, 37.6, 43.4, 47.6, 58.2, 113.7, 119.7, 124.5, 125.0, 129.3, 130.9, 134.4, 135.4, 146.2, 155.3, 168.0, 169.1. ES-MS *m*/*z* (%): 421 ([MH$^+$], 100). Anal. calcd. for $C_{23}H_{21}ClN_4O_2$: C 65.65, H 5.05, Cl 8.40, N 13.30; found: C 65.60, H 5.20, Cl 8.25, N 13.05.

Methyl (2-benzyl-3-oxo-2,3-dihydro-1*H*-isoindol-1-yl)acetate (16a)

Prepared according to general procedure A employing **8a** (0.288 g, 1 mmol) and benzylamine (0.128 g, 1.2 mmol). Column chromatography of the crude product eluting with 2:3 *v*/*v* ethyl acetate – pentane afforded the product (0.268 g, 91%) as colourless prisms, mp 92–94 °C. IR (cm^{-1}): 2951, 1736, 1690, 1617, 1495, 1469, 1435, 1408, 1360. ^{1}H NMR ($CDCl_3$, 250 MHz) δ: 2.85 (dd, 1H, *J* = 16.3, 7.3 Hz, C*H*HCO), 2.86 (dd, 1H, *J* = 16.3, 5.5 Hz, CH*H*CO), 3.63 (s, 3H, OMe), 4.43 (d, 1H, *J* = 15.5 Hz, NC*H*HPh), 4.83 (dd, 1H, *J* = 7.3, 5.5 Hz, NCH), 5.20 (d, 1H, *J* = 15.5 Hz, NCH*H*Ph), 7.25–7.31 (m, 5H, ArH), 7.40–7.54 (m, 3H, ArH), 7.95 (d, 1H, *J* = 7.5 Hz, Ar 4-H). ^{13}C NMR ($CDCl_3$, 62.5 MHz) δ: 37.8, 44.7, 52.4, 56.5, 122.8, 124.3, 128.0, 128.3, 129.0, 129.2, 132.1, 133.3, 137.4, 145.2, 168.8, 171.1. FAB-MS *m*/*z* (%): 296 ([MH$^+$], 100). Anal. calcd. for $C_{18}H_{17}NO_3$: C 73.20, H 5.80, N 4.75; found: C 73.00, H 5.85, N 4.60.

(2-Benzyl-3-oxo-2,3-dihydro-1*H*-isoindol-1-yl)acetonitrile (16b)

Prepared according to general procedure B employing **8b** (0.13 g, 0.5 mmol) and benzylamine (0.064 g, 0.6 mmol). Column chromatography of the crude product eluting with 2:3 *v*/*v* ethyl acetate – petroleum ether afforded the product (0.09 g, 69%) as colourless needles, mp 104–106 °C. IR (cm^{-1}): 2248, 1689, 1469, 1405. ^{1}H NMR ($CDCl_3$, 250 MHz) δ: 2.72 (dd, 1H, *J* = 16.9, 6.6 Hz, C*H*HCO), 2.93 (dd, 1H, *J* = 16.9, 4.4 Hz, CH*H*CO), 4.42 (d, 1H, *J* = 15.4 Hz, NC*H*HPh), 4.56 (dd, 1H, *J* = 6.5, 4.4 Hz, NCH), 5.29 (d, 1H, *J* = 15.4 Hz, NCH*H*Ph), 7.29–7.35 (m, 5H, ArH), 7.56–7.61 (m, 3H, ArH), 7.95 (dd, 1H, *J* = 8.0, 1.5 Hz, Ar 4-H). ^{13}C NMR ($CDCl_3$, 62.5 MHz) δ: 22.1, 44.7, 55.3, 116.1, 122.7, 124.8, 128.4, 128.5, 129.5, 129.9, 132.1, 132.8, 136.6, 142.9, 168.6. MS *m*/*z* (%): 262 ([MH$^+$], 100), 222 (51), 91 (100). Anal. calcd. for $C_{17}H_{14}N_2O$: C 77.85, H 5.30, N 10.70; found: C 77.60, H 5.45, N 10.80.

2-Benzyl-3-(2-oxopropyl)isoindolin-1-one (16c)

Prepared according to general procedure B employing **8c** (0.15 g, 0.5 mmol) and benzylamine (0.064 g, 0.6 mmol). Column chromatography of the crude product eluting with 2:3 *v*/*v* ethyl acetate – petroleum ether afforded the product (0.085 g, 61%) as colourless prisms, mp 87–89 °C. IR (cm^{-1}): 1717, 1687, 1469, 1408, 1362, 1160. ^{1}H NMR ($CDCl_3$, 250 MHz) δ: 2.50 (s, 3H, Me), 2.68 (dd, 1H, *J* = 17.8, 6.3 Hz, C*H*HCO), 2.89 (dd, 1H, *J* = 17.8, 5.9 Hz, CH*H*CO), 4.62, 4.89 (2 × d, 2 × 1H, *J* = 15.4 Hz, NCH_2Ph), 5.03 (dd, 1H, *J* = 6.3, 5.9 Hz, NCH), 7.25–7.30 (m, 5H, ArH), 7.35 (dd, 1H, *J* = 7.3, 0.7 Hz, ArH), 7.50 (m, 2H, ArH), 7.90 (dd, 1H, *J* = 7.5, 1.2 Hz, Ar 7-H). ^{13}C NMR ($CDCl_3$, 62.5 MHz) δ: 30.8, 45.2, 47.1, 55.9, 122.8, 124.3, 127.9, 128.3, 128.9, 129.1, 132.1, 132.3, 137.6, 145.9, 168.9, 206. ES-MS *m*/*z* (%): 280 ([MH$^+$], 100). Anal. calcd. for $C_{18}H_{17}NO_2$: C 77.40, H 6.10, N 5.00; found: C 77.30, H 6.15, N 4.95.

2-Benzyl-3-(2-oxo-2-phenylethyl)isoindolin-1-one (16d)

Prepared according to general procedure B employing **8d** (0.167 g, 0.5 mmol) and benzylamine (0.064 g, 0.6 mmol). Column chromatography of the crude product eluting with 2:3 *v*/*v* ethyl acetate – petroleum ether afforded the product (0.12 g, 70%) as colourless prisms, mp 97 to 98 °C. IR (cm^{-1}): 1683, 1596, 1448, 1408, 1211, 988. ^{1}H NMR ($CDCl_3$, 250 MHz) δ: 3.14 (dd, 1H, *J* = 17.6, 7.2 Hz, C*H*HCO), 3.47 (dd, 1H, *J* = 17.6, 5.3 Hz, CH*H*CO), 4.53, 5.06 (2 × d, 2 × 1H, *J* = 15.3 Hz, NCH_2Ph), 5.24 (dd, 1H, *J* = 7.2, 5.3 Hz,

© 2005 NRC Canada

NCH), 7.15–7.25 (m, 5H, ArH), 7.35–7.50 (m, 6H, ArH), 7.56 (t, 1H, *J* = 7.0 Hz, ArH), 7.79 (dd, 2H, *J* = 8.1, 0.9 Hz, ArH), 7.91 (d, 1H, *J* = 8.5 Hz, Ar 7-H). ^{13}C NMR ($CDCl_3$, 62.5 MHz) δ: 42.5, 45.0, 56.3, 123.3, 124.3, 127.9, 128.4, 128.5, 128.8, 129.1, 132.1, 132.3, 134.0, 136.6, 137.5, 146.3, 168.9, 196.0. ES-MS *m*/*z* (%): 364 ([MNa$^+$], 100). Anal. calcd. for $C_{23}H_{19}NO_2$: C 80.90, H 5.55, N 4.10; found: C 80.70, H 5.60, N 4.10.

Methyl [3-oxo-2-(pyridin-4-ylmethyl)-2,3-dihydro-1*H*-isoindol-1-yl]acetate (17a)

Prepared according to general procedure A employing **8a** (0.288 g, 1 mmol) and *p*-(aminomethyl)pyridine (0.129 g, 1.2 mmol). Column chromatography of the crude product eluting with 4:1 *v*/*v* ethyl acetate – petroleum ether afforded the product (0.275 g, 93%) as pale yellow needles, mp 148 to 149 °C. IR (cm^{-1}): 2952, 1734, 1689, 1601, 1563, 1494, 1469, 1435, 1409, 1364. ^{1}H NMR ($CDCl_3$, 250 MHz) δ: 2.73 (dd, 2H, *J* = 6.3, 4.3 Hz, CH_2CO), 3.61 (s, 3H, OMe), 4.55 (d, 1H, *J* = 16.3 Hz, NC*H*HAr), 4.91 (t, 1H, *J* = 6.3 Hz, NCH), 5.08 (d, 1H, *J* = 16.3 Hz, NCH*H*Ar), 7.18 (d, 2H, *J* = 4.5 Hz, pyridyl 3- and 5-H), 7.28–7.59 (m, 3H, ArH), 7.90 (dd, 1H, *J* = 7.5, 1.0 Hz, Ar 4-H), 8.55 (d, 2H, *J* = 4.5 Hz, pyridyl 2- and 6-H). ^{13}C NMR ($CDCl_3$, 62.5 MHz) δ: 38.2, 44.1, 52.6, 57.0, 122.8, 122.9, 124.5, 129.3, 131.5, 132.7, 145.0, 146.4, 150.6, 169.1, 171.0. ES-MS *m*/*z* (%): 319 ([MNa$^+$], 100). Anal. calcd. for $C_{17}H_{16}N_2O_3$: C 68.90, H 5.45, N 9.45; found: C 68.75, H 5.40, N 9.45.

[3-Oxo-2-(pyridin-4-ylmethyl)-2,3-dihydro-1*H*-isoindol-1-yl]acetonitrile (17b)

Prepared according to general procedure A employing **8b** (0.255 g, 1 mmol) and 4-aminomethylpyridine (0.13 g, 1.2 mmol) and heating at 95 °C for 48 h. Column chromatography of the crude product eluting with 4:1 *v*/*v* ethyl acetate – petroleum ether afforded the product (0.23 g, 88%) as colourless prisms, mp 147 to 148 °C. IR (cm^{-1}): 2251, 1690, 1602, 1469, 1406. ^{1}H NMR ($CDCl_3$, 250 MHz) δ: 2.80 (dd, 1H, *J* = 16.9, 5.9 Hz, C*H*HCN), 2.92 (dd, 1H, *J* = 16.9, 4.9 Hz, CH*H*CN), 4.52 (d, 1H, *J* = 16.2 Hz, NC*H*HAr), 4.64 (dd, 1H, *J* = 5.4, 4.9 Hz, NCH), 5.23 (d, 1H, *J* = 16.2 Hz, NCH*H*Ar), 7.23 (d, 2H, *J* = 5.0 Hz, pyridyl 3- and 5-H), 7.55–7.68 (m, 3H, ArH), 7.93 (dd, 1H, *J* = 8.2, 1.3 Hz, Ar 4-H), 8.57 (d, 2H, *J* = 5.0 Hz, pyridyl 2- and 6-H). ^{13}C NMR ($CDCl_3$, 62.5 MHz) δ: 22.4, 43.8, 55.8, 115.9, 122.8, 122.9, 124.9, 130.2, 131.5, 133.2, 142.8, 145.7, 150.8, 168.8. MS *m*/*z* (%): 263 ([M$^+$], 41), 223 (100), 92 (87). Anal. calcd. for $C_{16}H_{13}N_3O$: C 73.00, H 4.90, N 16.00; found: C 72.70, H 5.05, N 16.15.

Methyl [3-oxo-2-(thien-2-ylmethyl)-2,3-dihydro-1*H*-isoindol-1-yl]acetate (18a)

Prepared according to general procedure A employing **8a** (0.288 g, 1 mmol) and 2-(aminomethyl)thiophene (0.135 g, 1.2 mmol). Column chromatography of the crude product eluting with 3:7 *v*/*v* ethyl acetate – pentane afforded the product (0.261 g, 87%) as pale yellow needles, mp 148 to 149 °C. IR (cm^{-1}): 2950, 1734, 1690, 1617, 1500, 1469, 1436, 1406, 1366. ^{1}H NMR ($CDCl_3$, 250 MHz) δ: 2.69 (dd, 1H, *J* = 16.0, 6.8 Hz, C*H*HCO), 2.92 (dd, 1H, *J* = 16.0, 5.5 Hz, CH*H*CO), 3.66 (s, 3H, OMe), 4.58 (d, 1H, *J* = 16.0 Hz, NC*H*HAr), 4.92 (dd, 1H, *J* = 6.8, 5.5 Hz, NCH), 5.32 (d, 1H, *J* = 16.0 Hz, NCH*H*Ar), 6.91 (dd, 1H, *J* = 5.3, 3.5 Hz, thienyl 4-H), 7.01 (dd, 1H, *J* = 3.5, 1.3 Hz, thienyl 3-H), 7.18 (dd, 1H, *J* = 5.3, 1.3 Hz, thienyl 5-H), 7.41–7.51 (m, 3H, ArH), 7.83 (dd, 1H, *J* = 7.5, 1.0 Hz, Ar 4-H). ^{13}C NMR ($CDCl_3$, 62.5 MHz) δ: 37.7, 39.3, 52.5, 56.2, 122.9, 124.2, 126.0, 127.0, 127.3, 129.0, 131.9, 132.4, 139.9, 145.2, 168.4, 171.1. MS *m*/*z* (%): 301 ([M$^+$], 44), 228 (47), 97 (100). Anal. calcd. for $C_{16}H_{15}NO_3S$: C 63.75, H 5.00, N 4.65, S 10.65; found: C 63.50, H 4.90, N 4.80, S 10.60.

[3-Oxo-2-(thien-2-ylmethyl)-2,3-dihydro-1*H*-isoindol-1-yl]acetonitrile (18b)

Prepared according to general procedure A employing **8b** (0.255 g, 1 mmol) and 2-aminomethylthiophene (0.135 g, 1.2 mmol) and heating at 95 °C for 48 h. Column chromatography of the crude product eluting with 2:3 *v*/*v* ethyl acetate – petroleum ether afforded the product (0.22 g, 82%) as colourless needles, mp 129–131 °C. IR (cm^{-1}): 2251, 1690, 1469, 1405. ^{1}H NMR ($CDCl_3$, 250 MHz) δ: 2.82 (dd, 1H, *J* = 16.5, 6.5 Hz, C*H*HCN), 2.99 (dd, 1H, *J* = 16.9, 4.5 Hz, CH*H*CN), 4.55 (d, 1H, *J* = 15.8 Hz, NC*H*HAr), 4.67 (dd, 1H, *J* = 6.5, 4.5 Hz, NCH), 5.43 (d, 1H, *J* = 15.8 Hz, NCH*H*Ar), 6.96 (dd, 1H, *J* = 5.1, 3.5 Hz, thienyl 4-H), 7.07 (d, 1H, *J* = 3.5 Hz, thienyl 3-H), 7.25 (dd, 1H, *J* = 5.1, 1.2 Hz, thienyl 5-H), 7.55–7.65 (m, 3H, ArH), 7.91 (dd, 1H, *J* = 7.9, 1.3 Hz, Ar 4-H). ^{13}C NMR ($CDCl_3$, 62.5 MHz) δ: 22.2, 39.3, 55.1, 116.2, 122.8, 124.8, 126.6, 127.6, 129.9, 131.8, 132.9, 138.9, 142.9, 168.2. MS *m*/*z* (%): 268 ([M$^+$], 44), 228 (24), 97 (100). Anal. calcd. for $C_{15}H_{12}N_2OS$: C 67.10, H 4.50, N 10.50, S 11.90; found: C 66.90, H 4.50, N 10.60, S 11.90.

3-(2-Oxopropyl)-2-(thien-2-ylmethyl)isoindolin-1-one (18c)

Prepared according to general procedure A employing **8c** (0.272 g, 1 mmol) and 2-aminomethylthiophene (0.135 g, 1.2 mmol) and heating at 95 °C for 48 h. Column chromatography of the crude product eluting with 2:3 *v*/*v* ethyl acetate – petroleum ether afforded the product (0.095 g, 55%) as colourless prisms, mp 74–77 °C. IR (cm^{-1}): 1716, 1686, 1407, 1365. ^{1}H NMR ($CDCl_3$, 250 MHz) δ: 2.48 (s, 3H, Me), 2.76 (dd, 1H, *J* = 17.9, 6.4 Hz, C*H*HCO), 2.99 (dd, 1H, *J* = 17.9, 5.8 Hz, CH*H*CO), 5.03, 5.13 (2 × d, 2 × 1H, *J* = 15.6 Hz, NCH_2Ar), 5.11 (dd, 1H, *J* = 6.4, 5.8 Hz, NCH), 6.92 (dd, 1H, *J* = 5.0, 3.5 Hz, thienyl 4-H), 6.94 (dd, 1H, *J* = 3.5, 1.3 Hz, thienyl 5-H), 7.21 (dd, 1H, *J* = 5.0, 1.3 Hz, thienyl 3-H), 7.37 (dd, 1H, *J* = 7.1, 0.8 Hz, ArH), 7.46 (td, 1H, *J* = 6.9, 1.1 Hz, ArH), 7.53 (td, 1H, *J* = 7.5, 1.6 Hz, ArH), 7.86 (dd, 1H, *J* = 7.8, 1.2 Hz, Ar 7-H). ^{13}C NMR ($CDCl_3$, 62.5 MHz) δ: 30.9, 39.9, 47.2, 55.7, 122.9, 124.3, 126.0, 127.0, 127.2, 128.9, 121.9, 132.4, 140.2, 145.9, 168.6, 207.0. MS *m*/*z* (%): 285 ([M$^+$], 14), 227 (66), 146 (39), 131 (37), 97 (100), 43 (67). Anal. calcd. for $C_{16}H_{15}NO_2S{\cdot}0.25H_2O$: C 66.30, H 5.35, N 4.85; found: C 66.60, H 5.20, N 5.00.

3-(2-Oxo-2-phenylethyl)-2-(thien-2-ylmethyl)isoindolin-1-one (18d)

Prepared according to general procedure B employing **8d**

© 2005 NRC Canada

(0.167 g, 0.5 mmol) and 2-aminomethylthiophene (0.068 g, 0.6 mmol). Column chromatography of the crude product eluting with 2:3 *v*/*v* ethyl acetate – petroleum ether afforded the product (0.095 g, 55%) as colourless prisms, mp 99 to 100 °C. IR (cm^{-1}): 1684, 1406, 1211, 987. ^1H NMR ($CDCl_3$, 250 MHz) δ: 3.24 (dd, 1H, *J* = 17.7, 6.8 Hz, C*H*HCO), 3.55 (dd, 1H, *J* = 17.7, 5.5 Hz, CH*H*CO), 4.68, 5.21 (2 × d, 2 × 1H, *J* = 15.6 Hz, NCH_2Ar), 5.33 (dd, 1H, *J* = 6.8, 5.5 Hz, NCH), 6.82 (dd, 1H, *J* = 5.1, 3.4 Hz, thienyl 4-H), 6.96 (d, 1H, *J* = 3.4 Hz, thienyl 5-H), 7.13 (d, 1H, *J* = 5.1 Hz, thienyl 3-H), 7.38–7.49 (m, 5H, ArH), 7.58 (t, 1H, *J* = 7.0 Hz, ArH), 7.85–7.89 (m, 3H, ArH). ^{13}C NMR ($CDCl_3$, 62.5 MHz) δ: 39.8, 42.7, 56.0, 123.3, 124.3, 126.0, 127.2, 127.2, 128.5, 128.9, 129.2, 132.0, 132.4, 134.2, 136.6, 140.0, 146.3, 168.6, 198.0. ES-MS *m*/*z* (%): 370 ([MNa^+], 100). Anal. calcd. for $C_{21}H_{17}NO_2S$: C 72.60, H 4.90, N 4.00, S 9.20; found: C 72.40, H 4.90, N 4.00, S 9.00.

Methyl (2-cyclopropyl-3-oxo-2,3-dihydro-1*H*-isoindol-1-yl)acetate (19a)

Prepared according to general procedure A employing **8a** (0.288 g, 1 mmol) and cyclopropylamine (0.206 mL, 3 mmol). Column chromatography of the crude product eluting with 1:1 *v*/*v* ethyl acetate – pentane afforded the product (0.181 g, 74%) as a pale yellow oil. IR (cm^{-1}): 2952, 1735, 1694, 1614, 1468, 1436, 1404, 1370. ^1H NMR ($CDCl_3$, 250 MHz) δ: 0.80–1.10 (m, 4H, 2 × cyclopropyl CH_2), 2.66 (m, 1H, cyclopropyl CH), 2.67 (dd, 1H, *J* = 15.6, 8.0 Hz, C*H*HCO), 3.11 (dd, 1H, *J* = 15.6, 5.0 Hz, CH*H*CO), 3.74 (s, 3H, OMe), 4.83 (dd, 1H, *J* = 8.0, 5.0 Hz, NCH), 7.43–7.53 (m, 3H, ArH), 7.8 (dd, 1H, *J* = 7.5, 6.8 Hz, Ar 4-H). ^{13}C NMR ($CDCl_3$, 62.5 MHz) δ: 5.3, 8.2, 23.3, 39.3, 52.5, 58.2, 122.8, 124.0, 129.0, 132.2, 132.6, 144.7, 169.3, 171.4. FAB-MS *m*/*z* (%): 246 ([MH^+], 100). Anal. calcd. for $C_{14}H_{15}NO_3$: C 68.55, H 6.15, N 5.70; found: C 68.30, H 6.40, N 5.50.

2-(Cyclopropyl)-3-oxo-2,3-dihydro-1*H*-isoindol-1-yl)acetonitrile (19b)

Prepared according to general procedure B employing **8b** (0.255 g, 1 mmol) and cyclopropylamine (0.206 mL, 3 mmol) and heating at 95 °C for 48 h. Column chromatography of the crude product eluting with 2:3 *v*/*v* ethyl acetate – petroleum ether afforded the product (0.11 g, 52%) as a pale yellow oil. IR (cm^{-1}): 2250, 1693, 1468, 1403, 1210, 1107, 1030, 960. ^1H NMR ($CDCl_3$, 250 MHz) δ: 0.81–1.18 (m, 4H, 2 × cyclopropyl CH_2), 2.70 (m, 1H, cyclopropyl CH), 2.89 (dd, 1H, *J* = 16.8, 7.2 Hz, C*H*HCN), 3.10 (dd, 1H, *J* = 16.8, 4.4 Hz, CH*H*CN), 4.63 (dd, 1H, *J* = 7.2, 4.4 Hz, NCH), 7.32–7.75 (m, 3H, ArH), 7.85 (dd, 1H, *J* = 7.3, 1.1 Hz, Ar 4-H). ^{13}C NMR ($CDCl_3$, 62.5 MHz) δ: 5.3, 8.3, 22.6, 23.3, 57.3, 116.3, 122.7, 124.5, 129.9, 132.6, 132.7, 142.5, 169.1. MS *m*/*z* (%): 212 ([M^+], 32), 172 (100), 128 (31), 102 (30), 89 (37), 77 (43), 41 (53). Anal. calcd. for $C_{13}H_{12}N_2O{\cdot}H_2O$: C 71.90, H 5.75, N 12.90; found: C 71.60, H 6.05, N 13.20.

Methyl {2-[(2-1*H*-indazol-3-yl)ethyl]-3-oxo-2,3-dihydro-1*H*-isoindol-1-yl}acetate (20a)

Prepared according to general procedure A employing **8a** (0.288 g, 1 mmol) and tryptamine (0.192 g, 1.2 mmol). Column chromatography of the crude product eluting with 1:1 *v*/*v* ethyl acetate – pentane afforded the product (0.241 g, 69%) as a yellow oil. IR (cm^{-1}): 3293, 2950, 1733, 1676, 1619, 1513, 1469, 1455, 1436, 1415, 1364. ^1H NMR ($CDCl_3$, 250 MHz) δ: 2.57 (dd, 1H, *J* = 16.3, 7.0 Hz, C*H*HCO), 2.80 (dd, 1H, *J* = 16.3, 5.5 Hz, CH*H*CO), 3.12 (m, 2H, NCH_2CH_2Ar), 3.64 (s, 3H, OMe), 4.29, 4.45 (2 × m, 2 × 1H, NCH_2CH_2Ar), 4.87 (dd, 1H, *J* = 7.0, 5.5 Hz, NCH), 6.98 (d, 1H, *J* = 2.3 Hz, ArH), 7.11–7.14 (m, 2H, ArH), 7.30–7.49 (m, 3H, ArH), 7.67 (m, 1H, ArH), 7.82 (d, 1H, *J* = 1.3 Hz, Ar 4-H), 8.78 (bs, 1H, NH). ^{13}C NMR ($CDCl_3$, 62.5 MHz) δ: 24.8, 37.7, 41.4, 52.6, 56.9, 111.9, 112.7, 119.0, 119.7, 122.3, 122.7, 122.8, 124.0, 127.7, 129.0, 132.2, 132.4, 136.8, 145.2, 168.8, 171.4. ES-MS *m*/*z* (%): 349 ([MH^+], 100). Anal. calcd. for $C_{21}H_{20}N_2O_3$: C 72.40, H 5.80, N 8.05; found: C 72.10, H 5.90, N 7.85.

2-[2-(3,4-Dimethoxyphenyl)ethyl]-3-(2-oxo-2-piperidin-1-ylethyl)isoindolin-1-one (21e)

Prepared according to general procedure D employing **8e** (0.341 g, 1 mmol) and 2-(3,4-dimethoxyphenyl)ethylamine (0.217 g, 1.2 mmol). Column chromatography of the crude product eluting with 4:1 *v*/*v* ethyl acetate – hexane afforded the product (0.358 g, 85%) as a brown gum. IR (cm^{-1}): 1699, 1650, 1510, 1450, 1382, 1210. ^1H NMR ($CDCl_3$, 300 MHz) δ: 1.28–1.89 (m, 6H, piperidyl H), 2.44 (dd, 1H, *J* = 16.1, 7.1 Hz, C*H*HCO), 2.68 (dd, 1H, *J* = 16.1, 5.7 Hz, CH*H*CO), 2.94 (m, 2H), 3.23 (t, 2H, *J* = 5.5 Hz, NCH_2CH_2Ar), 3.40 (m, 1H, piperidyl H), 3.65 (t, 2H, *J* = 5.5 Hz, NCH_2CH_2Ar), 3.82, 3.84 (2 × s, 2 × 3H, 2 × OMe), 4.11 (m, 3H, piperidyl H), 5.19 (dd, 1H, *J* = 7.1, 5.7 Hz, NCH), 6.77–6.83 (m, 3H, ArH), 7.43–7.52 (m, 3H, ArH), 7.85 (d, 1H, *J* = 7.1 Hz, Ar 7-H). ^{13}C NMR ($CDCl_3$, 75 MHz) δ: 24.8, 26.0, 26.8, 34.4, 37.3, 43.3, 47.0, 56.2, 57.4, 111.5, 112.5, 121.3, 123.4, 123.7, 131.9, 132.4, 146.4, 147.9, 149.2, 168.2, 168.8. MS *m*/*z* (%): 423 ([MH^+], 100), 271 (5), 164 (40), 146 (6). HR-MS calcd. for $C_{25}H_{30}N_2O_4+H^+$: 423.2284; found: 423.2281.

2-[2-(3,4-Dimethoxyphenyl)ethyl]-3-[2-(4-methylpiperazin-1-yl)-2-oxoethyl]isoindolin-1-one (21h)

Prepared according to general procedure D employing **8h** (0.356 g, 1 mmol) and 2-(3,4-dimethoxyphenyl)ethylamine (0.217 g, 1.2 mmol). Column chromatography of the crude product eluting with 4:1 *v*/*v* ethyl acetate – hexane afforded the product (0.419 g, 96%) as a brown gum. IR (cm^{-1}): 1708, 1656, 1500, 1444, 1382, 1200. ^1H NMR ($CDCl_3$, 300 MHz) δ: 2.29 (s, 3H, NMe), 2.30–2.40 (m, 6H, piperidyl H), 2.43 (dd, 1H, *J* = 16.2, 7.4 Hz, C*H*HCO), 2.69 (dd, 1H, *J* = 16.2, 5.5 Hz, CH*H*CO), 2.69 (m, 2H, NCH_2CH_2Ar), 3.28 (m, 2H, piperidyl H), 3.42 (m, 1H, piperidyl H), 3.67–3.88 (m, 2H, NCH_2CH_2Ar), 3.81, 3.84 (2 × s, 2 × 3H, 2 × OMe), 4.09 (m, 1H, piperidyl H), 5.15 (dd, 1H, *J* = 7.2, 5.5 Hz, NCH), 6.73–6.79 (m, 3H, ArH), 7.43–7.52 (m, 3H, ArH), 7.85 (d, 1H, *J* = 6.7 Hz, Ar 7-H). ^{13}C NMR ($CDCl_3$, 75 MHz) δ: 34.4, 37.1, 42.2, 43.4, 45.7, 46.3, 55.0, 55.3, 56.2, 56.3, 57.4, 111.6, 112.5, 121.3, 123.4, 123.9, 128.8, 131.9, 132.0, 132.4, 146.2, 147.9, 149.2, 168.5, 168.8. MS *m*/*z* (%): 438 ([MH^+], 100), 286 (3), 164 (32), 99(7). HR-MS calcd. for $C_{25}H_{31}N_3O_4+H^+$: 438.2393; found: 438.2393.

© 2005 NRC Canada

Methyl {3-oxo-2-[(1*R*)-1-phenylethyl]-2,3-dihydro-1*H*-isoindol-1-yl}acetate (22a)

Prepared according to general procedure A employing **8a** (0.288 g, 1 mmol) and (*R*)-(+)-α-methylbenzylamine (0.145 g, 1.2 mmol). Column chromatography of the crude product eluting with 2:3 *v*/*v* ethyl acetate – pentane afforded a 1:1.75 inseparable diastereomeric product mixture (0.217 g, 74% combined yield) as a pale yellow oil. IR (cm^{-1}): 2951, 1735, 1686, 1615, 1494, 1468, 1436, 1398. ^1H NMR spectra of both isomers were assigned from the mixture of diastereomers. Diastereomer 1 (minor): ^1H NMR ($CDCl_3$, 250 MHz) δ: 1.80 (d, 3H, *J* = 7.3 Hz, Me), 2.15 (dd, 1H, *J* = 16.8, 8.3 Hz, C*H*HCO), 2.55 (dd, 1H, *J* = 16.8, 4.3 Hz, CH*H*CO), 3.56 (s, 3H, OMe), 5.10 (dd, 1H, *J* = 8.3, 4.3 Hz, N*CH*CH_2), 5.73 (q, 1H, *J* = 7.3 Hz, N*CH*Me), 7.27–7.36 (m, 5H, ArH), 7.42–7.52 (m, 3H, ArH), 7.87 (dd, 1H, *J* = 8.0, 7.0 Hz, Ar 4-H). Diastereomer 2 (major): ^1H NMR ($CDCl_3$, 250 MHz) δ: 1.80 (d, 3H, *J* = 7.3 Hz, Me), 2.55 (dd, 1H, *J* = 16.3, 12.3 Hz, C*H*HCO), 2.97 (dd, 1H, *J* = 16.3, 4.0 Hz, CH*H*CO), 3.59 (s, 3H, OMe), 4.68 (dd, 1H, *J* = 12.3, 4.0 Hz, N*CH*CH_2), 5.54 (q, 1H, *J* = 7.3 Hz, N*CH*Me), 7.27–7.36 (m, 5H, ArH), 7.42–7.52 (m, 3H, ArH), 7.87 (dd, 1H, *J* = 8.0, 7.0 Hz, Ar 4-H). ES-MS (isomer mixture) *m*/*z* (%): 332 ([MNa^+], 100). Anal. calcd. for $C_{19}H_{19}NO_3$: C 73.75, H 6.20, N 4.55; found (isomer mixture): C 73.70, H 6.30, N 4.35.

{3-Oxo-2-[(1*R*)-1-phenylethyl]-2,3-dihydro-1*H*-isoindol-1-yl}acetonitrile (22b)

Prepared according to general procedure A employing **8b** (0.255 g, 1 mmol) and (*R*)-(+)-α-methylbenzylamine (0.145 g, 1.2 mmol) and heating at 95 °C for 48 h. Column chromatography of the crude product eluting with 2:3 *v*/*v* ethyl acetate – petroleum ether afforded a 2:3 separable diastereomeric mixture the product (0.212 g, 77% combined yield). Diastereomer 1 (major): colourless prisms, mp 89–94 °C. $[\alpha]_D$ +145.6 (0.71, $CHCl_3$). IR (cm^{-1}) ν: 1685, 1468, 1395, 1218. ^1H NMR ($CDCl_3$, 250 MHz) δ: 1.75 (d, 3H, *J* = 7.2 Hz, Me), 1.99 (dd, 1H, *J* = 16.8, 7.5 Hz, C*H*HCN), 2.51 (dd, 1H, *J* = 16.8, 3.5 Hz, CH*H*CN), 4.81 (dd, 1H, *J* = 7.5, 3.5 Hz, N*CH*CH_2), 5.83 (q, 1H, *J* = 7.2 Hz, N*CH*Me), 7.36–7.44 (m, 3H, ArH), 7.51 (m, 2H, ArH), 7.61 (m, 3H, ArH), 7.94 (d, 1H, *J* = 6.7 Hz, Ar 4-H). ^{13}C NMR ($CDCl_3$, 62.5 MHz) δ: 17.1, 23.4, 49.5, 54.3, 116.2, 122.6, 124.7, 127.7, 128.6, 129.4, 129.9, 132.1, 132.8, 140.7, 143.4, 168.9. MS *m*/*z* (%): 276 ([M^+], 49), 261 (27), 158 (48), 132 (53), 105 (100), 77 (72), 51 (32). HR-MS calcd. for $C_{18}H_{16}N_2O$: 277.1341; found: 277.1338. Anal. calcd. for $C_{18}H_{16}N_2O$: C 78.20, H 5.80, N 10.15; found: C 77.80, H 5.90, N 10.25. Diastereomer 2 (minor): colourless prisms, mp 123–127 °C. $[\alpha]_D$ +70 (0.86, $CHCl_3$). IR (cm^{-1}): 1685, 1468, 1395, 1218. ^1H NMR ($CDCl_3$, 250 MHz) δ: 1.82 (d, 3H, *J* = 7.2 Hz, Me), 2.76 (dd, 1H, *J* = 16.8, 6.5 Hz, C*H*HCN), 2.94 (dd, 1H, *J* = 16.8, 3.4 Hz, CH*H*CN), 4.36 (dd, 1H, *J* = 6.5, 3.4 Hz, N*CH*CH_2), 5.74 (q, 1H, *J* = 7.2 Hz, N*CH*Me), 7.34–7.40 (m, 5H, ArH), 7.48 (m, 1H, ArH), 7.56 (m, 1H, ArH), 7.91 (d, 1H, *J* = 6.6 Hz, Ar 4-H). ^{13}C NMR ($CDCl_3$, 62.5 MHz) δ: 18.8, 23.9, 51.2, 55.2, 115.9, 122.4, 124.6, 127.9, 128.6, 129.5, 129.9, 132.3, 132.7, 139.4, 143.0, 168.8. MS *m*/*z* (%): 276 ([M^+], 58), 261 (38), 158 (42), 132 (57), 105 (100), 77 (64). Anal. calcd. for $C_{18}H_{16}N_2O$: C 78.20, H 5.80, N 10.15; found: C 78.00, H 6.10, N 10.10.

Methyl (2*S*)-2-[(2-methoxy-2-oxoethyl)-3-oxo-1,3-dihydro-2*H*-isoindol-1-yl]propanoate (23a)

Prepared according to general procedure A employing **8a** (0.288 g, 1 mmol) and *S*-alanine methyl ester hydrochloride (0.279 g, 2 mmol) and heating at 90 °C for 48 h. Column chromatography of the crude product eluting with 3:2 *v*/*v* ethyl acetate – pentane afforded a 1:1 inseparable diastereomeric mixture of the product (0.185 g, 63%) as a yellow oil. IR (cm^{-1}): 2952, 1738, 1693, 1617, 1469, 1436, 1416, 1353. ^1H NMR spectra of both isomers were assigned from the mixture of diastereomers. Diastereomer 1: ^1H NMR ($CDCl_3$, 250 MHz) δ: 1.62 (d, *J* = 7.5 Hz, 3H, Me), 2.62 (m, 1H, C*H*HCO), 2.99 (m, 1H, CH*H*CO), 3.71 (s, 3H, OMe), 3.75 (s, 3H, OMe), 4.64 (m, 1H, N*CH*CH_2), 5.10 (m, 1H, NCH), 7.41–7.59 (m, 3H, ArH), 7.83 (m, 1H, Ar 4-H). Diastereomer 2: ^1H NMR ($CDCl_3$, 250 MHz) δ: 1.67 (d, *J* = 7.5 Hz, 3H, Me), 2.79 (m, 1H, C*H*HCO), 3.02 (m, 1H, CH*H*CO), 3.75 (s, 6H, 2 × OMe), 4.91 (m, 1H, N*CH*CH_2), 5.10 (m, 1H, NCH), 7.41–7.59 (m, 3H, ArH), 7.83 (m, 1H, Ar 4-H). ES-MS (isomer mixture) *m*/*z* (%): 314 ([MNa^+], 100). Anal. calcd. for $C_{15}H_{17}NO_5$: C 61.85, H 5.90, N 4.80; found (isomer mixture): C 62.15, H 6.05, N 4.70.

2-Acetyl-3-(2-oxo-2-piperidin-1-ylethyl)isoindolin-1-one (24e)

Prepared according to general procedure D employing **8e** (0.341 g, 1.0 mmol) and acetamide (0.072 g, 1.2 mmol). Column chromatography of the crude product eluting with 4:1 *v*/*v* ethyl acetate – hexane afforded the product (0.186 g, 62%) as colourless prisms, mp 107–109 °C. IR (cm^{-1}): 2995, 1700, 1648, 1500, 1450, 1382. ^1H NMR ($CDCl_3$, 300 MHz) δ: 1.48–1.67 (m, 6H, piperidyl H), 2.44 (dd, 1H, *J* = 15.5, 9.7 Hz, C*H*HCO), 2.68 (s, 3H, Me), 3.31–3.38 (m, 2H, piperidyl H), 3.51 (dd, 1H, *J* = 15.5, 2.7 Hz, CH*H*CO), 3.53–3.67 (m, 2H, piperidyl H), 5.68 (dd, 1H, *J* = 9.7, 2.7 Hz, NCH), 7.50 (t, 1H, *J* = 7.4 Hz, ArH), 7.63 (dt, 1H, *J* = 7.7, 1.1 Hz, ArH), 7.74 (d, 1H, *J* = 7.7 Hz, ArH), 7.80 (d, 1H, *J* = 7.6 Hz, Ar 7-H). ^{13}C NMR ($CDCl_3$, 75 MHz) δ: 24.8, 26.0, 26.1, 37.6, 43.2, 46.9, 57.0, 124.9, 125.3, 129.3, 130.3, 134.8, 146.8, 167.9, 168.3, 171.6. ES-MS *m*/*z* (%): 301 ([MH^+], 100). Anal. calcd. for $C_{17}H_{20}N_2O_3$: C 68.00, H 6.70, N 9.35; found: C 68.30, H 6.55, N 9.40.

2-Acetyl-3-[2-(1,4-dioxa-8-azaspiro[4.5]dec-8-yl)-2-oxoethyl]isoindolin-1-one (24f)

Prepared according to general procedure D employing **8f** (0.399 g, 1 mmol) and acetamide (0.072 g, 1.2 mmol). Column chromatography of the crude product eluting with 4:1 *v*/*v* ethyl acetate – hexane afforded the product (0.186 g, 52%) as colourless needles, mp 145–147 °C. IR (cm^{-1}): 2990, 1690, 1648, 1500, 1456, 1382. ^1H NMR ($CDCl_3$, 300 MHz) δ: 1.61–1.73 (m, 4H, 2 × NCH_2CH_2), 2.48 (dd, 1H, *J* = 15.6, 9.7 Hz, C*H*HCO), 2.68 (s, 3H), 3.47–3.51 (m, 4H, 2 × NCH_2CH_2), 3.54 (dd, 1H, *J* = 15.6, 2.7 Hz, CH*H*CO), 3.72–3.77 (m, 4H, 2 × OCH_2), 5.68 (dd, 1H, *J* = 9.7, 2.7 Hz,), 7.51 (dt, 1H, *J* = 7.4, 0.7 Hz, ArH), 7.64 (dt,

© 2005 NRC Canada

1H, *J* = 7.4, 1.2 Hz, ArH), 7.72 (d, 1H, *J* = 7.4 Hz, ArH), 7.90 (d, 1H, *J* = 7.6 Hz, Ar 7-H). ^{13}C NMR ($CDCl_3$, 75 MHz) δ: 35.2, 35.9, 37.5, 40.3, 43.9, 57.0, 64.9, 107.1, 124.8, 125.4, 129.4, 130.4, 134.8, 146.7, 168.0, 168.3, 171.6. ES-MS *m/z* (%): 359 ([MH$^+$], 100). Anal. calcd. for $C_{19}H_{22}N_2O_5$: C 63.70, H 6.20, N 7.80; found: C 63.50, H 6.25, N 7.65.

3-(2-Oxo-2-piperidin-1-ylethyl)isoindolin-1-one (25e)

Prepared according to general procedure D employing **8e** (0.341 g, 1.0 mmol) and 1,1,1-trifluoroacetamide (0.136 g, 1.2 mmol). Column chromatography of the crude product eluting with 4:1 *v/v* ethyl acetate – hexane afforded the product (0.155 g, 60%) as a pale yellow gum. IR (cm^{-1}): 2991, 1700, 1648, 1498, 1445, 1382. ^{1}H NMR ($CDCl_3$, 300 MHz) δ: 1.43–1.66 (m, 6H, piperidyl H), 2.38 (dd, 1H, *J* = 16.5, 10.8 Hz, C*H*HCO), 3.06 (dd, 1H, *J* = 16.5, 2.9 Hz, CH*H*CO), 3.33 (m, 2H, piperidyl H), 3.44–3.69 (m, 2H, piperidyl H), 5.03 (dd, 1H, *J* = 10.8, 2.9 Hz, NCH), 7.02 (bs, 1H, NH), 7.42–7.52 (m, 2H, ArH), 7.57 (t, 1H, *J* = 7.2 Hz, ArH), 7.87 (d, 1H, *J* = 7.4 Hz, Ar 7-H). ^{13}C NMR ($CDCl_3$, 75 MHz) δ: 24.8, 25.9, 26.7, 37.4, 43.2, 46.8, 53.8, 122.7, 124.5, 128.8, 132.1, 132.4, 146.8, 168.6, 170.1. ES-MS *m/z* (%): 259 ([MH$^+$], 100). Anal. calcd. for $C_{15}H_{18}N_2O_2$: C 69.75, H 7.00, N 10.85; found: C 69.90, H 7.20, N 10.65.

3-(2-Oxo-2-piperidin-1ylethyl)-2-(phenylsulfonyl)isoindolin-1-one (26e)

Prepared according to general procedure D employing **8e** (0.341 g, 1 mmol) and benzenesulfonamide (0.188 g, 1.2 mmol). Column chromatography of the crude product eluting with 4:1 *v/v* ethyl acetate – hexane afforded the product (0.223 g, 56%) as colourless needles, mp 190–192 °C. IR (cm^{-1}): 2995, 1710, 1667, 1498, 1450, 1380. ^{1}H NMR ($CDCl_3$, 300 MHz) δ: 1.52–1.70 (m, 6H, piperidyl H), 2.69 (dd, 1H, *J* = 16.0, 9.9 Hz, C*H*HCO), 3.30–3.42 (m, 2H, piperidyl H), 3.57–3.72 (m, 2H, piperidyl H), 3.80 (dd, 1H, *J* = 16.0, 2.6 Hz, CH*H*CO), 5.81 (dd, 1H, *J* = 9.9, 2.6 Hz, NCH), 7.44 (t, 1H, *J* = 7.5 Hz, ArH), 7.50–7.65 (m, 5H, ArH), 7.70 (d, 1H, *J* = 7.8 Hz, ArH), 7.77 (d, 1H, *J* = 7.7 Hz, ArH), 8.12 (dd, 1H, *J* = 8.5, 1.3 Hz, Ar 7-H). ^{13}C NMR ($CDCl_3$, 75 MHz) δ: 24.8, 26.0, 26.8, 39.8, 43.3, 47.0, 60.2, 124.9, 125.2, 128.6, 129.4, 129.5, 134.5, 134.8, 138.8, 147.1, 167.1, 167.7. ES-MS *m/z* (%): 399 ([MH$^+$], 100). Anal. calcd. for $C_{21}H_{22}N_2O_4$: C 63.30, H 5.60, N 6.90; found: C 63.25, H 5.60, N 6.90.

2-Benzyl-3-pyridin-2-ylmethylisoindolin-1-one (28)

Prepared according to general procedure E employing **8k** (0.15 g, 0.5 mmol) and benzylamine (0.064 g, 0.6 mmol). Column chromatography of the crude product eluting with 1:2 *v/v* ethyl acetate – petroleum ether afforded the product (0.10 g, 64%) as colourless prisms, mp 118 to 119 °C. IR (cm^{-1}): 1685, 1590, 1469, 1436. ^{1}H NMR ($CDCl_3$, 250 MHz) δ: 3.10 (dd, 1H, *J* = 14.0, 7.1 Hz, NCHC*H*HAr), 3.41 (dd, 1H, *J* = 14.0, 5.3 Hz, NCHCH*H*Ar), 4.37 (d, 1H, *J* = 15.3 Hz, NC*H*HPh), 5.00 (dd, 1H, *J* = 7.1, 5.3 Hz, NCH), 5.27 (d, 1H, *J* = 15.3 Hz, NCH*H*Ph), 6.81 (m, 1H, pyridyl 3-H), 6.97 (m, 1H, pyridyl 5-H), 7.15–7.30 (m, 6H, ArH), 7.40–7.50 (m, 3H, pyridyl 6-H and 2 × ArH), 7.85 (m, 1H, Ar 7-H), 8.53 (m, 1H, pyridyl 4-H). ^{13}C NMR ($CDCl_3$, 62.5 MHz) δ: 44.4, 44.8, 59.2, 122.4, 123.1, 124.2, 124.5, 127.8, 128.3, 128.6, 129.1, 131.7, 132.4, 136.7, 137.7, 145.6, 149.8, 157.0, 168.9. ES-MS *m/z* (%): 315 ([MH$^+$], 100). Anal. calcd. for $C_{21}H_{18}N_2O$: C 80.20, H 5.75, N 8.90; found: C 80.00, H 5.85, N 8.90.

2-Pyridin-4-ylmethyl-3-pyridin-2-ylmethylisoindolin-1-one (29)

Prepared according to general procedure E employing **8k** (0.15 g, 0.5 mmol) and 4-aminomethylpyridine (0.065 g, 0.6 mmol). Column chromatography of the crude product eluting with ethyl acetate afforded the product (0.11 g, 70%) as a colourless oil. IR (cm^{-1}): 1689, 1600, 1470, 1436, 1412. ^{1}H NMR ($CDCl_3$, 250 MHz) δ: 3.50 (dd, 1H, *J* = 14.2, 6.6 Hz, NCHC*H*HAr), 3.31 (dd, 1H, *J* = 14.2, 6.0 Hz, NCHCH*H*Ar), 4.45, 5.10 (2 × d, 2 × 1H, *J* = 16.0 Hz, NCH_2Ar), 5.14 (dd, 1H, *J* = 6.6, 6.0 Hz, NCH), 6.83 (m, 1H, pyridyl 3-H), 7.04 (m, 1H, pyridyl 5-H), 7.05 (d, 2H, *J* = 5.5 Hz, pyridyl 3′- and 5′-H), 7.18 (m, 1H, pyridyl 4-H), 7.44–7.45 (m, 3H, ArH), 7.88 (m, 1H, Ar 7-H), 8.48 (d, 2H, *J* = 5.5 Hz, pyridyl 2′- and 6′-H), 8.54 (m, 1H, pyridyl 4-H). ^{13}C NMR ($CDCl_3$, 62.5 MHz) δ: 41.7, 44.2, 59.7, 122.6, 122.9, 123.1, 124.3, 124.5, 128.8, 131.7, 132.1, 136.9, 145.7, 146.8, 149.9, 150.3, 156.7, 169.2. MS *m/z* (%): 316 ([MH$^+$], 100), 200 (48), 151 (91). HR-MS calcd. for $C_{20}H_{18}N_3O$+H$^+$: 316.1444; found: 316.1446.

3-Pyridin-2-ylmethyl-2-thiophen-2-ylmethylisoindolin-1-one (30)

Prepared according to general procedure E employing **8k** (0.15 g, 0.5 mmol) and 2-aminomethylthiophene (0.068 g, 0.6 mmol). Column chromatography of the crude product eluting with 1:2 *v/v* ethyl acetate – petroleum ether afforded the product (0.12 g, 74%) as colourless prisms, mp 124 to 125 °C. IR (cm^{-1}): 1688, 1591, 1469, 1436, 1408. ^{1}H NMR ($CDCl_3$, 250 MHz) δ: 3.21 (dd, 1H, *J* = 14.0, 6.9 Hz, NCHC*H*HAr), 3.45 (dd, 1H, *J* = 14.0, 5.4 Hz, NCHCH*H*Ar), 4.54, 5.38 (d, 1H, *J* = 15.7 Hz, NC*H*HAr), 5.10 (dd, 1H, *J* = 6.9, 5.4 Hz, NCH), 5.38 (d, 1H, *J* = 15.7 Hz, NCH*H*Ar), 6.86 (d, 1H, *J* = 7.7 Hz, thienyl 4-H), 6.89–6.95 (m, 2H, ArH), 7.00–7.05 (m, 1H, thienyl 3-H), 7.15–7.20 (m, 2H, ArH), 7.35–7.45 (m, 2H, ArH), 7.51 (dt, 1H, *J* = 7.7, 1.8 Hz, thienyl 5-H), 7.77–7.83 (m, 1H, Ar 7-H), 8.57 (d, 1H, *J* = 4.5 Hz, pyridyl 4-H). ^{13}C NMR ($CDCl_3$, 62.5 MHz) δ: 39.5, 41.4, 59.1, 122.5, 123.1, 124.2, 124.5, 125.8, 126.9, 127.2, 128.6, 131.8, 132.3, 136.8, 140.1, 145.6, 149.9, 157.0, 168.5. ES-MS *m/z* (%): 321 ([MH$^+$], 100). Anal. calcd. for $C_{19}H_{16}N_2OS$: C 71.20, H 5.05, N 8.75, S 10.00; found: C 71.10, H 5.15, N 8.65, S 9.80.

2-(2-Morpholin-4-ylethyl)-3-pyridin-2-ylmethylisoindolin-1-one (31)

Prepared according to general procedure E employing **8k** (0.15 g, 0.5 mmol) and 2-morpholin-4-ylethylamine (0.079 g, 0.6 mmol). Column chromatography of the crude product eluting with ethyl acetate afforded the product (0.11 g, 64%) as a colourless oil. IR (cm^{-1}): 1684, 1652, 1470, 1434, 1310, 1116, 861, 775. ^{1}H NMR ($CDCl_3$, 250 MHz) δ: 2.47 (t, 4H, *J* = 4.1 Hz, $NCH_2CH_2N(CH_2)_2$), 2.59 (t, 4H, *J* = 4.1 Hz,

© 2005 NRC Canada

$NCH_2CH_2N(CH_2)_2$), 3.05 (dd, 1H, J = 13.9, 7.5 Hz, NCHC*H*HAr), 3.29 (dt, 2H, J = 14.3, 6.3 Hz, $NCH_2CH_2N(CH_2)_2$), 3.47 (dd, 1H, J = 13.9, 5.2 Hz, NCHCH*H*Ar), 3.66 (t, 4H, J = 4.5 Hz, CH_2OCH_2), 4.17 (dt, 2H, J = 14.3, 6.7 Hz, $NCH_2CH_2N(CH_2)_2$), 5.32 (dd, 1H, J = 7.5, 5.2 Hz, NCH), 6.93–6.97 (m, 2H, ArH), 7.19 (dd, 1H, J = 7.1, 5.0 Hz, ArH), 7.38–7.45 (m, 2H, ArH), 7.57 (dt, 1H, J = 7.6, 1.9 Hz, ArH), 7.76–7.82 (m, 1H, Ar 7-H), 8.59 (d, 1H, J = 4.1 Hz, pyridyl 4-H). ^{13}C NMR ($CDCl_3$, 62.5 MHz) δ: 37.6, 41.5, 54.1, 57.2, 59.9, 67.4, 122.5, 122.9, 123.9, 124.6, 128.5, 131.5, 132.6, 136.8, 145.9, 149.9, 157.3, 168.7. ES-MS *m*/*z* (%): 338 ([MH^+], 100). HR-MS calcd. for $C_{20}H_{24}N_3O_2$+H^+: 338.1863; found: 338.1859.

2-(4-Methoxyphenyl)-3-pyridin-2-ylmethylisoindolin-1-one (32)

Prepared according to general procedure E employing **8k** (0.15 g, 0.5 mmol) and *p*-anisidine (0.074 g, 0.6 mmol). Column chromatography of the crude product eluting with 1:2 *v*/*v* ethyl acetate – petroleum ether afforded the product (0.11 g, 67%) as colourless prisms, mp 127–129 °C. IR (cm^{-1}): 1685, 1512, 1472, 1457, 1387, 1247. ^{1}H NMR ($CDCl_3$, 250 MHz) δ: 2.83 (dd, 1H, J = 13.9, 8.6 Hz, C*H*HAr), 3.46 (dd, 1H, J = 13.9, 4.8 Hz, CH*H*Ar), 3.82 (s, 3H, OMe), 5.77 (dd, 1H, J = 8.6, 4.8 Hz, NCH), 6.85 (m, 2H, ArH), 6.95 (d, 2H, J = 9.0 Hz, ArH), 7.41 (m, 1H, ArH), 7.43–7.45 (m, 3H, ArH), 7.53 (d, 2H, J = 9.0 Hz, ArH), 7.90 (m, 1H, Ar 7-H), 8.55 (m, 1H, pyridyl 4-H). ^{13}C NMR ($CDCl_3$, 62.5 MHz) δ: 41.8, 55.9, 61.3, 114.8, 122.3, 123.2, 124.4, 124.9, 125.8, 128.8, 130.4, 131.9, 132.5, 136.7, 145.1, 149.9, 157.4, 157.8, 167.4. ES-MS *m*/*z* (%): 331 ([MH^+], 100). Anal. calcd. for $C_{21}H_{18}N_2O_2$: C 76.35, H 5.50, N 8.50; found: C 76.10, H 5.40, N 8.30.

3-Pyridin-2-ylmethyl-2-thiazol-2-ylisoindolin-1-one (33)

Prepared according to general procedure E employing **8k** (0.15 g, 0.5 mmol) and 2-aminothiazole (0.06 g, 0.6 mmol) and the reaction heated at 95 °C for 96 h. Column chromatography of the crude product eluting with 3:2 *v*/*v* ethyl acetate – petroleum ether afforded the product (0.11 g, 72%) as pale yellow prisms, mp 141 to 142 °C. IR (cm^{-1}): 1702, 1591, 1505, 1465, 1435, 1368, 1276, 1212, 1134. ^{1}H NMR ($CDCl_3$, 250 MHz) δ: 2.31 (dd, 1H, J = 13.5, 8.5 Hz, C*H*HAr), 3.20 (dd, 1H, J = 13.5, 3.4 Hz, CH*H*Ar), 5.01 (dd, 1H, J = 8.5, 3.4 Hz, NCH), 6.93 (d, 1H, J = 7.7 Hz, thiazolyl 5-H), 7.02 (d, 1H, J = 7.0 Hz, thiazolyl 4-H), 7.03–7.10 (m, 2H, ArH), 7.44–7.52 (m, 3H, ArH), 7.62 (d, 1H, J = 3.6 Hz, ArH), 7.85 (m, 1H, Ar 7-H), 8.50 (m, 1H, pyridyl 4-H). ^{13}C NMR ($CDCl_3$, 62.5 MHz) δ: 40.7, 61.9, 114.0, 122.3, 123.8, 124.6, 129.0, 130.4, 132.3, 136.6, 138.5, 145.7, 149.8, 156.9, 157.6, 166.7. ES-MS *m*/*z* (%): 308 ([MH^+], 100). Anal. calcd. for $C_{17}H_{13}N_3OS$: C 66.40, H 4.25, N 13.65, S 10.40; found: C 66.20, H 4.15, N 13.75, S 10.30.

Acknowledgements

We thank Johnson Matthey, Leeds University, the Thailand Research Fund (TRF) of the Royal Golden Jubilee project, and the Thailand Postgraduate Education and Research in Chemistry (PERCH) Fund for support.

References

1. I. Takahashi, T. Kawakami, E. Hirano, H. Yokota, and H. Kitajima. Synlett, 353 (1996).
2. L.A. Sorbera, P.A. Leeson, J. Silvestre, and J. Castaner. Drugs Future, **26**, 651 (2001).
3. M. Anzini, A. Capelli, S. Vomero, G. Giorgi, T. Langer, G. Bruni, M.K. Rome, and A.S. Basile. J. Med. Chem. **36**, 4275 (1996).
4. V. Gotar, R. Limeres, R. Garcia, M. Bayod, and R. Bliveva. Tetrahedron: Asymmetry, **8**, 995 (1997).
5. C.J.M. Stirling. J. Chem. Soc. 255 (1960).
6. F.M. Rowe, E. Levin, A.C. Burns, J.S.H. Davies, and W. Tepper. J. Chem. Soc. 690 (1926).
7. S.C. Shim, L.H. Jiang, D.Y. Lee, C.S. Cho, and S. Chan. Bull. Korean Chem. Soc. **16**, 1064 (1995).
8. S. Murahashi. J. Am. Chem. Soc. **77**, 63 (1955).
9. A. Rosenthal and M.R.S. Weir. J. Org. Chem. **28**, 3025 (1963).
10. T.M.V.D. Pinho e Melo, C.I.A. Santos, A.M.dA. Rocha Gonsalves, J.A. Paixão, and A.M. Beja. Tetrahedron, **60**, 3949 (2004).
11. J. Clayden and C.J. Menet. Tetrahedron Lett. **44**, 3059 (2003).
12. Z. Guo and A.G. Schultz. J. Org. Chem. **66**, 2154 (2001).
13. I. Azumaya, H. Kagechika, Y. Fujiwara, M. Itoh, K. Yamaguchi, and K. Shudo. J. Am. Chem. Soc. **113**, 2833 (1991).
14. R. Grigg, H.Q.N. Gunaratre, and V. Sridharan. Chem. Commun. 1183 (1985).
15. S.M. Allin, D.G. Vaidya, M.I. Page, A.M.Z. Slawin, and T.S. Smith. Tetrahedron Lett. **41**, 2219 (2000).
16. C.J. Northfield, M.I. Page, and A.M. Slawin. J. Chem. Soc. Perkin Trans. 1, 2843 (2000).
17. R. Grigg, V. Sridharan, P. Stevenson, and T. Worakun. J. Chem. Soc. Chem. Commun. 1697 (1986).
18. R. Grigg, V. Sridharan, P. Stevenson, and S. Sukirthalingam. Tetrahedron, **45**, 3557 (1989).
19. R. Grigg, V. Sridharan, P. Stevenson, S. Sukirthalingam, and T. Worakun. Tetrahedron, **46**, 4003 (1990).
20. R. Grigg, M.J. Dorrity, J.F. Malone, V. Sridharan, and S. Sukirthalingam. Tetrahedron Lett. **31**, 1343 (1990).
21. R. Grigg, M.J. Dorrity, J.F. Malone, T. Mongkolaussavaratana, W.D.J.A. Norbert, and V. Sridharan. Tetrahedron Lett. **31**, 3075 (1990).
22. R. Grigg, W.S. MacLachlan, D.T. MacPherson, V. Sridharan, S. Suganthan, M. Thornton-Pett, and J. Zhang. Tetrahedron, **56**, 6585 (2000).
23. R. Grigg and V. Sridharan. J. Organomet. Chem. **576**, 65 (1999).
24. X. Gai, R. Grigg, T. Khamnaen, S. Rajviroongit, V. Sridharan, L. Zhang, S. Collard, and A. Keep. Tetrahedron Lett. **44**, 7441 (2003).
25. C.S. Cho, H.S. Shim, H.J. Choi, T.J. Kim, and S.C. Shim. Synth. Commun. **32**, 1821 (2002).
26. C.S. Cho, H.S. Shim, H.J. Choi, T.J. Kim, S.C. Shim, and M.C. Kim. Tetrahedron Lett. **41**, 3891 (2000).
27. C.S. Cho, J.H. Jiang, D.Y. Lee, and S.C. Shim. Bull. Korean Chem. Soc. **17**, 1095 (1996).
28. C.S. Cho, J.H. Jiang, D.Y. Lee, S.C. Shim, H.S. Lee, and S.D. Cho. J. Heterocycl. Chem. **34**, 1371 (1997).
29. C.S. Cho, X. Wu, L.H. Jiang, S.C. Shim, H.J. Choi, and T.J. Kim. J. Heterocycl. Chem. **35**, 265 (1998).

© 2005 NRC Canada

30. C.S. Cho, X. Wu, L.H. Jiang, S.C. Shim, and H.R. Kim. J. Heterocycl. Chem. **36**, 297 (1999).
31. X. Gai, R. Grigg, I. Köppen, J. Marchbank, and V. Sridharan. Tetrahedron Lett. **44**, 7445 (2003).
32. M. Abou-Gharbia, U.R. Patel, M.B. Webb, J.A. Moyer, T.H. Andree, and E.A. Muth. J. Med. Chem. **30**, 1818 (1987).
33. (*a*) R. Grigg, L. Zhang, S. Collard, P. Ellis, and A. Keep. J. Organomet. Chem. **689**, 170 (2004); (*b*) R. Grigg, L. Zhang, S. Collard, and A. Keep. Tetrahedron Lett. **44**, 6979 (2003).

© 2005 NRC Canada

Pauson–Khand reactions in water[1]

Marie E. Krafft, James A. Wright, and Llorente V.R. Boñaga

Abstract: We have investigated the cobalt mediated Pauson–Khand (PK) reaction in water. In the presence of detergents and surfactants, $Co_2(CO)_8$ and $Co_4(CO)_{12}$ are effective under aqueous-phase, thermal PK reactions. In a water–Triton®X-100 medium, $Co_4(CO)_{12}$ is catalytically active. Further, dicobalthexacarbonyl complexes of alkynes and enynes undergo effective cyclization under thermal (70 °C) and NMO-promoted conditions. The oxidative nature of the latter conditions inhibits the reductive PK reaction. In all protocols, moderate to excellent yields of the cycloadducts are obtained. Substrates that are prone to hydrolysis, such as acetals, highly activated carboxylic acid derivatives, and those bearing propargylic heteroatom groups are tolerated under appropriate conditions. Finally, the more challenging intermolecular cycloadditions can also be easily achieved under aqueous conditions.

Key words: alkyne, cycloaddition, green chemistry, Pauson–Khand reaction, water.

Résumé : On a étudié la réaction de Pauson–Khand (PK) catalysée par le cobalt et effectuée dans l'eau. En présence de détergents et d'agents de surface, le $Co_2(CO)_8$ et le $Co_4(CO)_{12}$ sont efficaces pour les réactions de PK thermiques, effectuées en phase aqueuse. Dans un milieu d'eau et de Triton®X-100, le $Co_4(CO)_{12}$ est catalytiquement actif. De plus, les complexes du dicobalthexacarbonyle des alcynes et des énynes subissent une cyclisation effective dans des conditions thermiques (70 °C) catalysées par NMO. Dans tous les protocoles et dans des conditions appropriées, des rendements allant de modérés à excellents ont été obtenus. Les substrats sujets à une hydrolyse, tels les acétals, les dérivés hautement activés d'acides carboxyliques et ceux portant des groupes propargyliques avec hétéroatomes sont tolérés. Enfin, dans des conditions aqueuses, il est possible de réaliser les cycloadditions intermoléculaires présentant les plus grands défis.

Mots clés : alcyne, cycloaddition, chimie verte, réaction de Pauson–Khand, eau.

[Traduit par la Rédaction]

Introduction

Organometallic reactions conducted in nonorganic solvents, such as water (1), ionic liquids (2), and supercritical fluids (3) have become increasingly more relevant (4); the Pauson–Khand (PK) and the PK-type reactions are no exception to this (5). These reactions are the widely studied approaches to cyclopentenones, which incorporate two unsaturated components with a carbonyl unit in a transition-metal-mediated [2 + 2 + 1] cycloaddition process (Scheme 1, eq. [1]). To date, this transformation can be derived from a reaction of alkynes with alkenes (5), allenes (6), or dienes (7), and can also be promoted by complexes of titanium, zirconium, molybdenum, tungsten, iron, ruthenium, rhodium, nickel, iridium and cobalt (5).

The use of water as an alternative solvent is most attractive for practical reasons. However, the poor solubility of the reactants, such as organic compounds and metal complexes, in water results in problems associated with phase separation and inefficient mixing of reactants (1*c*). Instability and reduced reactivity of reactants also pose a problem. The solubility issue has been addressed by taking advantage of the solubilizing properties of organic co-solvents and surfactants, and (or) employing hydrophilic ligand auxiliaries and heterogenous or homogeneous catalysts (1).

Relatively few studies have focused on aqueous-phase PK reactions. Quite understandably, this is owing to the presumed sensitivity of the cobalt carbonyl complexes toward water, such that early work concentrated only on supercritical fluids (3) and ionic liquids (8). Interestingly, water was used as additive in a $Co_2(CO)_8$-catalyzed thermal protocol in toluene (9), and was also found to accelerate the thermally promoted cyclizations of cobalt carbonyl complexes of enynes (10). In the context of green chemistry (4), Chung and co-workers first described the use of water as solvent in PK reactions promoted by colloidal cobalt nanoparticles, in the presence of sodium dodecyl sulfate (11). More recently, Kakiuchi and co-workers developed an effective $[RhCl(cod)]_2$-catalyzed PK-type reaction in water employing a water-soluble phosphine salt, triphenylphosphane-3,3′,3″-trisulfonic acid trisodium salt, in addition to 1,3-bis(diphenylphosphanyl)propane (12). Chung and co-workers also developed an asymmetric version of the $[RhCl(cod)]_2$-catalyzed PK-type reaction in aqueous media (13).

We describe in this report the first comprehensive studies on the cobalt-promoted PK reaction in water. The reactivity

Received 16 November 2004. Published on the NRC Research Press Web site at http://canjchem.nrc.ca on 26 August 2005.

Dedicated to Professor Howard Alper for his exemplary work in organometallic chemistry.

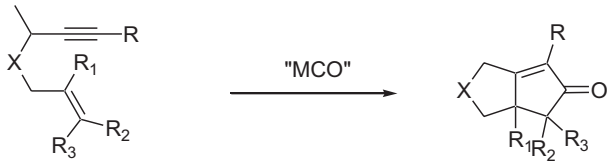
M.E. Krafft,[2] J.A. Wright, and L.V.R. Boñaga. Department of Chemistry and Biochemistry, The Florida State University, Tallahassee, FL 32306-4390, USA.

[1]This article is part of a Special Issue dedicated to professor Howard Alper.

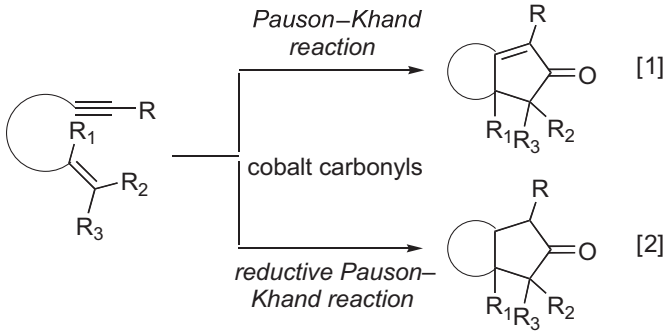
[2]Corresponding author (e-mail: mek@chem.fsu.edu).

 doi: 10.1139/V05-112 © 2005 NRC Canada

Scheme 1. The Pauson–Khand and the Pauson–Khand-type reactions.



X = C, N, O, S, Si
R = H, alkyl, aryl, SiR_3
R_1 = H, alkyl
R_2 = R_3 = H, alkyl (alkene); =CHR (allene); CH_2C=CHR (diene)
"MCO" = carbonyl complexes of Ti, Zr, Mo, W, Fe, Ru, Rh, Ni, Ir, Co



of dicobalthexacarbonyl complexes of alkynes and enynes, as well as uncomplexed enynes, with $Co_2(CO)_8$ and $Co_4(CO)_{12}$ in water, and the effectiveness of surfactants and detergents were examined. The scope and limitations of these methods, in terms of substrate compatibility and reactivity, and reaction conditions (thermal and oxidative promotions) were also explored.

Results and discussion

Reactivity of dodecacarbonyltetracobalt in water (14)

There has been a limited amount of exploration on the use of $Co_4(CO)_{12}$ in organometallic reactions despite its greater stability towards air oxidation than the congeneric $Co_2(CO)_8$ (15, 16). The dinuclear complex has been widely used in the Pauson–Khand (5) and Nicholas reactions (17), conversions of aziridine to β-lactams (18), 1-(1-alkynyl)cyclopropanols to cyclopentenones (19), enones to ketones (20), and in a tandem cycloaddition reaction (21). We discovered the reactivity of $Co_4(CO)_{12}$ in the PK reaction under mild reaction conditions and reported its mechanistic implications in the related reactivity of $Co_2(CO)_8$ (22, 23). Early studies demonstrated that $Co_4(CO)_{12}$ catalyzed the PK reaction under elevated temperatures and CO pressures to presumably favor the formation of $Co_2(CO)_8$, the accepted precatalyst of the reaction (23). We became interested in pursuing the synthetic potential of this cobalt cluster, and found that it can also induce a reductive PK reaction (eq. [2]) and reductive cyclization of specific types of enynes (24). These results further led us to examine its reactivity towards alkynes under aqueous conditions since the reactivity of $Co_4(CO)_{12}$ with alkynes in water was unknown. Additionally, $Co_4(CO)_{12}$ catalyzed PK reactions in aqueous media are significant from the practical standpoint. We reported the unprecedented reactivity of $Co_4(CO)_{12}$ with alkynes (22), and more importantly, its catalytic activity in water in the presence of additives that subsequently lead to the development of a mild and simple aqueous-phase $Co_4(CO)_{12}$ catalyzed PK reaction protocol (14).

Stoichiometric amounts of $Co_4(CO)_{12}$ were used in our initial studies (eq. [1], Table 1, reaction condition I). Based on literature precedents we focused on surfactants and detergents as additives in our aqueous-phase PK reactions.[3] We found that the cationic micelle-forming surfactant cetyltrimethylammonium bromide (CTAB)[4] worked as a general surfactant for our aqueous reactions (vide infra). We were gratified to find that $Co_4(CO)_{12}$ is active in a water–CTAB media allowing enynes that typically undergo PK reactions conducted in organic solvents to smoothly undergo cyclization (Table 1, condition I). 1,6-Enynes bearing an internal alkyne and either a terminal alkene (Table 1, entries 1–3, 8 and 9) or a disubstituted alkene (Table 1, entries 13 and 14) easily underwent cyclization. A 1,7-enyne also uneventfully underwent the PK reaction (Table 1, entry 16). A particular exception, however, is evident in the unsuccessful cyclization of substrates bearing the hydrolyzable ester and amide groups (Table 1, entries 11 and 12). In contrast, substrates possessing heteroatoms in the tether proved to be stable to hydrogenolysis under these conditions (Table 1, entries 8 and 9 vs. 11 and 12).

We next examined the corresponding reactions of enynes using catalytic amounts of $Co_4(CO)_{12}$, initially screening its catalytic activity in water or a water–alcohol mixture, with and without additives (Table 2). Cyclization of enyne **2** in water alone, using only 10% of $Co_4(CO)_{12}$, under a blanket of carbon monoxide is inefficient, providing only a modest yield of the cycloadduct **18** and unreacted **2** (Table 2, entry 1). Similar low efficiencies were observed in cyclizations conducted in water–alcohol and water–THF mixtures (Table 2, entries 2–4). Addition of triphenylphosphane-3,3,3-trisulfonic acid trisodium salt (TPPTS)[5] or cyclohexylamine (10, 25) to PK reactions in a water–methanol solvent system only resulted in the isolation of unreacted enyne as the major product after the reactions (Table 2, entries 5 and 6). Incomplete conversions were noted in aqueous reactions carried out with additives, such as TPPTS, tetrabutylammonium

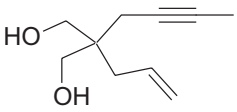
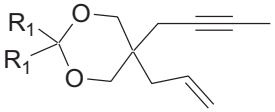
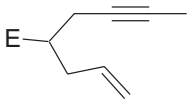
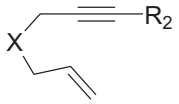
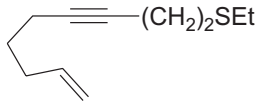
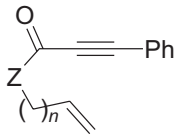
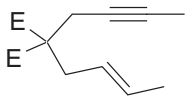
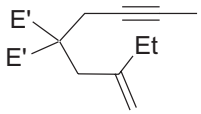
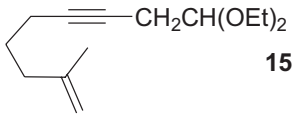
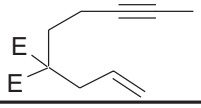
[3] Surfactants and detergents are amphiphiles (molecules carrying a hydrophilic headgroup and a hydrophobic tail) and are surface-active agents, which assemble in aqueous or nonpolar media. They aggregate to form supramolecular assemblies in a colloidal dimension, such as micelles, vesicles, and related species. Surfactants are adsorbed at the interfaces of aqueous and organic two-phase systems resulting in reduced interfacial tension. The very high polarity gradient between surface and core causes micelles to enclose organic species out of the surrounding aqueous phase. The encapsulation of reactants in micelles often enhances or inhibits the reaction rates (1*a*). "Detergent" is often used interchangeably with "surfactant"; detergent is a substance capable of cleaning, and contains, inter alia, surfactants (1*a*).

[4] CTAB: $[CH_3(CH_2)_{15}N(CH_3)_3][Br]$.

[5] TPPTS, with all three aromatic rings of triphenylphosphine sulfonated, is water-soluble. Metal compounds with this ligand are also water-soluble.

© 2005 NRC Canada

Table 1. Intramolecular Pauson–Khand reactions in water (cf. eq. [1]).

Entry	Enyne substrates			Cycloadduct	Yield (%)[a] Reaction conditions			
					I	II	III	IV
1		**1**	R = Me	**17**	82	79	83	83
2		**2**	R = *n*Pr	**18**	81	80	85	83
3		**3**	R = Ph	**19**	78	85	88	73
4		**4**		**20**	_	_	65	_
5		**5**	R_1 = Me	**21**	_	82	40	81
6		**6**	R_1 = nC_5H_{11}	**22**	_	_	58	_
7		**7**		**23**	_	78	78	80
8		**8**	X = O, R_2 = Ph	**24**	36	70	74	74
9		**9**	X = NTs, R_2 = *n*Pr	**25**	57	84	_	88
10		**10**		**26**	_	68	_	_
11		**11**	Z = NH, *n* = 1	**27**	0	73	_	0
12		**12**	Z = O, *n* = 2	**28**	0	80	_	0
13		**13**		**29**[b]	34	_	_	86
14		**14**		**30**	60	86	_	91
15		**15**		**31**	_	70	_	_
16		**16**		**32**	73	76	65	76

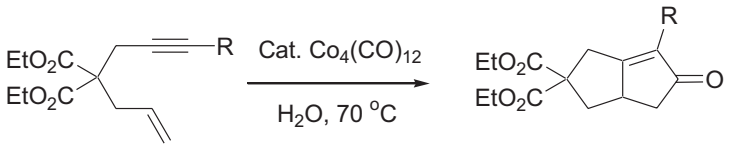
Note: I: 1 mol equiv. $Co_4(CO)_{12}$, 0.6 mol equiv. CTAB, water, 70 °C, ca. 18 h. II: 20 mol% $Co_4(CO)_{12}$, 0.5 mol equiv. Triton®X–100, water 70 °C, CO atm in a resealable tube, ca. 18 h. III: 1 mol equiv. $Co_2(CO)_8$, 0.6 mol equiv. CTAB, water, 70 °C, ca. 18 h. IV: 1 mol equiv. $Co_2(CO)_8$, 0.5 mol equiv. Triton®X-100, water, 6 mol equiv. NMO·H_2O, rt, 6 h. For conditions III and IV, the cobalt complexes were prepared from the enyne and $Co_2(CO)_8$ prior to cycloaddition. E = CO_2Et; E′ = CO_2Me.

[a]Isolated yields from reaction conditions III and IV are for two steps (preparation of the alkyne dicobalthexacarbonyl complex and the PK reaction).

[b]Exo cycloadduct.

© 2005 NRC Canada

Table 2. Optimization of the thermally promoted, $Co_4(CO)_{12}$ catalyzed PK reaction in water.[a]



R = *n*Pr, **2**
R = Ph, **3**

R = *n*Pr, **18**
R = Ph, **19**

Entry	Enyne	Solvent[b]	$Co_4(CO)_{12}$ (mol%)	Additive (mol equiv.)	Yield (%) **2**	**18**	**3**	**19**
1	**2**	H_2O	10	_	5	35		
2	**2**	H_2O–MeOH	10	_	_	45		
3	**2**	H_2O–*i*PrOH	10	_	35	41		
4	**2**	H_2O–THF	10	_	44	10		
5	**2**	H_2O–MeOH	10	TPPTS (0.3)	62	0		
6	**2**	H_2O-MeOH	10	$CyNH_2$ (0.5)	38	13		
7	**2**	H_2O	10	TPPTS (0.3)	19	22		
8	**2**	H_2O	10	*n*Bu_4NBr (0.2)	32	28		
9	**2**	H_2O	10	Fisher detergent[c]	15	64		
10	**2**	H_2O	20	CTAB (0.5)	_	64		
11	**3**	H_2O	10	Tween 40 (0.5)			_	54
12	**3**	H_2O	20	Tween 40 (0.5)			_	59
13	**3**	H_2O	20	Triton X®-100 (0.5)			_	67

[a]Reactions were conducted at concentrations of 0.05 mol/L (relative to enyne **2** or **3**) in the appropriate solvent at 70 °C under a CO atmosphere, and were complete in 12–15 h. Entry 10: 0.10 mol/L; entries 11–13: 1 mol/L.
[b]Entries 2–6: 1:1 (*v*/*v*) solvent mixture.
[c]Solution (20% (*w*/*v*)) in water.

bromide, and Fisher detergent[3] (Table 2, entries 7–9). Ultimately, CTAB, Tween 40, and polyoxyethylene(10) isooctylcyclohexyl ether, Triton® X-100, all led to relatively efficient catalytic activity of $Co_4(CO)_{12}$ in PK reactions in water (Table 2, entries 10–13).

To explore the generality of the catalytic activity of $Co_4(CO)_{12}$, we surveyed the cyclizations of various enynes in water with the aid of Triton® X-100 (eq. [1], Table 1, condition II). Efficient cyclization was achieved with enynes that typically undergo PK reactions in organic solvents. Our studies focused on the behavior of substrates that are potentially unsuitable for aqueous conditions due to their proclivity to hydrolyze, and revealed noteworthy results. The acetal moieties in enynes **5** and **15** were stable in this aqueous medium. Reaction of the dicobalthexacarbonyl complex of **5** in water using Brij 35 or the anionic surfactant cetyltrimethylammonium hydrogen sulfate (CTAHS)[3] as additives led to cycloadducts with hydrolyzed acetal groups (vide infra). Successful cyclizations of **8** and **9** are also striking since hydrogenolysis of the heteroatom group in the propargylic position could potentially occur. In fact, this has been observed as a side reaction in PK reactions conducted even in organic solvents (26*a*, 26*e*). These types of substrates (**8** and **9**) underwent substantial hydrogenolysis (~50%) under $Co_4(CO)_{12}$ mediated cycloadditions in DME, even in the presence of only 20 equiv. of water (26*b*). Enyne **10**, which is devoid of substitution on the tether and thus lacking Thorpe–Ingold assistance in the cyclization, cleanly underwent PK reaction. Successful reaction of enynes **11** and **12** is particularly impressive since activated carboxylic acid derivatives can easily be hydrolyzed, and the chemical reactivity of electron-deficient alkynes is unpredictable in the PK reaction (27). It is worth nothing that the corresponding reactions of **11** and **12** using stoichiometric $Co_4(CO)_{12}$ in the water–CTAB medium failed (Table 1, condition I). We showed in our earlier work that cyclizations of substrates bearing alkynes substituted with electron-withdrawing groups, such as **11** and **12**, occur in low to modest yields in organic solvents (27). While the thermally promoted PK reaction of **11** (toluene, 70 °C, 3 days) gave a 15% yield of cycloadduct **27**, the NMO-promoted variant (CH_2Cl_2, rt) gave a 59% yield of **27** (cf. Table 1, entry 11) (27). Enynes **12** and **16**

© 2005 NRC Canada

also provide examples of successful PK reactions of 1,7-enynes providing the bicyclononenones. Substrates **14** and **15** bearing an internal alkyne and a disubstituted alkene smoothly cyclized, furnishing highly substituted bicyclooctenone adducts. These results illustrate the catalytic efficiency of $Co_4(CO)_{12}$ in promoting the PK reaction of various types of enynes in water, by taking advantage of the micellar properties of Triton®X-100 (Table 1, condition II).

We also addressed the issue of realizing a carbon-monoxide-free, $Co_4(CO)_{12}$ catalyzed PK reaction (12). However, a slight decrease in the yield of cycloadducts from reactions conducted under an argon atmosphere was noted. PK cyclization of enynes **2** and **3** in the water–Triton®X-100 medium using 20 mol% of $Co_4(CO)_{12}$ gave rise to 70% and 59% yields of bicyclooctenones **18** and **19**, respectively (cf. Table 1, condition II). Nevertheless, these results show the potential of the aqueous protocol in the absence of carbon monoxide and warrant further studies.

Reactivity of dicobalthexacarbonyl–alkyne complexes in water (28)

The ease with which dicobalthexacarbonyl complexed enynes undergo PK reactions in water was also studied. We prepared the dicobalthexacarbonyl complexes of several enynes and surveyed their thermal reactions in water with different additives (Table 3). Use of CTAB (Table 3, entries 4, 8, and 11) and Tween 40 (Table 3, entries 2 and 5) as additives with preformed enyne–$Co_2(CO)_6$ complexes resulted in consistently efficient aqueous PK reactions. PK cyclization of the cobalt carbonyl complex of **2** using tris[2-(2-methoxyethoxy)ethyl]amine (TDA-1)[6] and castor oil were a little inferior when compared to the use of CTAB as an additive (Table 3, entry 8 vs. 6 and 7). Use of the surfactants Brij 35 (Table 3, entry 9) and CTAHS (Table 3, entry 10) led to the hydrolysis of the acetal group. Under both conditions, reactions of the dicobalthexacarbonyl complex of acetal **5** provided the bishydroxyl bearing cycloadduct **20**, which is also derived from the reaction of diol **4**. We then examined the cyclization efficiencies of a series of dicobalthexacarbonyl complexed enynes in water using CTAB as the additive (eq. [1], Table 1, condition III). As expected, results showed a similar general trend as the reactions conducted according to conditions I and II (Table 1).

Reactivity of dicobalthexacarbonyl–alkyne complexes with NMO in water (29)

Using NMO as a reaction promoter, we also explored the cyclization efficiencies of enynes with internal alkynes and with various substitution patterns in the alkene component (eq. [1], Table 1, condition IV). As anticipated, these substrates underwent PK cyclizations efficiently resulting in good to excellent yields of PK reaction cycloadducts. Table 1 further shows that the yields in the NMO-promoted cyclizations are comparable to or better than the yields derived from the thermally promoted variant (70 °C, Table 1, condition III). In both cases, enynes that undergo PK reactions conducted in organic solvents also cyclized smoothly. 1,6-Enynes with a terminal alkene, and an alkyne component bearing alkyl (Table 1, entries 1, 2, 5, and 7) and aryl groups (Table 1, entries 3 and 8), underwent efficient cylization. Substitution on both alkene and alkyne moieties is well tolerated, e.g., Table 1, entry 1 vs. 13 (cf. entry 14). Groups prone to undergo hydrolysis, such as an acetal (Table 1, entry 5) and propargylic heteroatom groups (Table 1, entries 8 and 9), are stable under these aqueous conditions. However, the amide and ester moieties were hydrolyzed under these reaction conditions (Table 1, condition IV, entries 11 and 12, cf. conditions I and II). Cyclization of a 1,7 enyne occurred smoothly as well (Table 1, entry 16).

We further noted several interesting observations in the cyclizations of enyne **2** while probing the manner of preparation of the alkyne cobalt complex and the amount and source of NMO. The cobalt complex of enyne **2** can alternatively be prepared directly in the reaction media, i.e., by treatment of the enyne with $Co_2(CO)_8$ in the water-Triton®X-100 mixture. Synthesis of the cobalt enyne complex in this manner (1.5 h) and subsequent addition of crystalline NMO·H_2O (6 mol equiv.) gave 80% of adduct **18** after 6 h (cf. Table 1, entry 2, condition IV). Commercially available NMO (6 mol equiv., 50% in water) or only 3 mol equiv. of crystalline NMO·H_2O can also be used in the reaction, providing 68% and 76% of enone **18**, respectively (cf. Table 1, entry 2, condition IV).

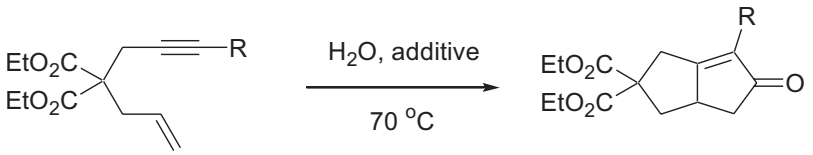
Previously developed stoichiometric and catalytic thermal PK reaction procedures proceed efficiently under aqueous conditions, but are limited to enyne substrates bearing internal alkynes (vide supra). Enynes containing terminal alkynes gave rise to bicyclooctanones (eq. [2]), either as a side product (11) or the exclusive product (14, 28). These thermal conditions, either stoichiometric or catalytic in the cobalt carbonyl complex, are conducive to reductive PK reaction to give ketones (eq. [2]) (24). We proposed earlier that residual cobalt carbonyl complexes from PK reactions utilizing $Co_2(CO)_8$, $Co_4(CO)_{12}$, and enyne–$Co_2(CO)_6$ complexes may react with a proton source, such as aqueous and alcoholic solvents, to form $HCo(CO)_4$ (24*a*). A metal hydride transfer from the hydridocobalt complex can effect a 1,4-reduction of the enone generated in the PK reaction. We also found that unsubstituted bicyclooctenones, derived from 1,6-enynes with terminal alkynes (via eq. [1]), are prone to this secondary process. We became interested in the behavior of enynes bearing terminal alkynes towards PK reaction (eq. [1]) or reductive PK reaction (eq. [2]) in water, most importantly in the inhibition of the reductive PK reaction as a side reaction.

Results revealed that the reductive PK reaction was preferred in aqueous reactions using stoichiometric amounts of $Co_4(CO)_{12}$ leading to the favored formation of bicyclooctanones instead (eq. [2], Table 4). In our control experiments, we learned that thermal cyclization of an enyne bearing a terminal alkyne such as **33** primarily furnished bicyclooctanone **37**, along with the bicyclooctenone **35**, in water as the solvent (Table 4, entry 1). The nature of the additive, i.e., Triton®X-100 and CTAB (Table 4, entry 4 vs. 6) and quantity (Table 4, entries 2–5) did not prevent the occurrence of reductive PK reaction, i.e., the reaction depicted in eq. [1] is

[6] TDA-1 ($N(CH_2CH_2OCH_2CH_2OCH_3)_3$) is a very hydrophilic phase-transfer catalyst, which is most useful for solubilizing solid salts. It also forms complexes with some metal carbonyls (1*a*).

© 2005 NRC Canada

Table 3. Optimization of the thermally promoted PK reaction of enyne–$Co_2(CO)_6$ complexes in water.[a,b]

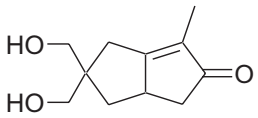


R = Me, **1**
R = *n*Pr, **2**

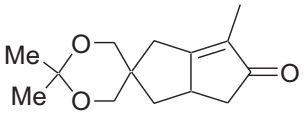
R = Me, **17**
R = *n*Pr, **18**

Entry	Enyne	Additive (mol equiv.)	Yield (%) 17	18	21
1	**1**	Brij 35 (0.6)	74		
2	**1**	Tween 40 (0.6)	74		
3	**1**	CTAHS (0.6)	82		
4	**1**	CTAB (0.6)	83		
5	**2**	Tween 40 (0.5)		76	
6	**2**	Castor Oil (1 mL)		71	
7	**2**	TDA-1 (0.5 mL)		65	
8	**2**	CTAB (0.6)		85	
9	**5**	Brij 35 (0.6)			4 (56)[c]
10	**5**	CTAHS (0.6)			0 (64)[c]
11	**5**	CTAB (0.6)			65

[a]Reactions were conducted at concentrations of 0.05 mol/L in water at 70 °C under a nitrogen atmosphere and were complete in 18 h. Enynes were first converted to the corresponding dicobalthexacarbonyl complexes.
[b]Entries 5 and 6: 3.0 mol/L reaction concentrations; entry 7: 0.8 mol/L reaction concentration.



20



21

less favored than in eq. [2]. Understandably, the amount of the cobalt cluster affected the efficiency of cycloaddition and the extent of the reductive PK reaction (Table 4, entry 2 vs. 4 and 3 vs. 5) (24*a*).

Preformed dicobalthexacarbonyl complexes of substrates bearing a terminal alkyne behaved as expected under thermal conditions, undergoing inefficient PK reactions in water (28). Use of additives such as cyclodextrins β-CD and γ-CD (30), Triton®X-100, and Triton®X-100 (reduced form) did not significantly improve the reaction efficiency in water and in a water–methanol system. In these reactions, up to 10% of saturated bicyclooctanones was observed as a side product.[7]

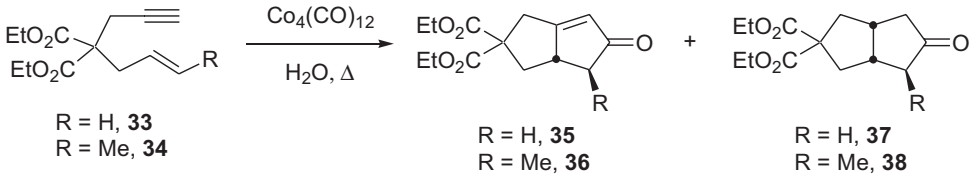
We were however delighted to discover that when NMO was used as promoter, room-temperature cyclization of the dicobalthexacarbonyl enyne complex of **39** furnished 74% of the bicyclooctenone **40** (eq. [3]) (31). This result is particularly striking since the corresponding bicyclooctanone was not observed. In contrast, Me_3NO promoted cyclization of complex **39** in dichloromethane under an argon atmosphere (–78 °C to rt) furnished an 82% yield of a 4:1 mixture of bicyclooctenone **40** and the corresponding bicyclooctanone (31*b*). The oxidative nature and (or) the ambient temperature of these present reaction conditions have apparently prevented the occurrence of the reductive PK reaction. Further, NMO is water-soluble, thus is advantageous in promoting the PK reaction in water.

The behavior of various terminal alkynes in the NMO promoted PK reaction was examined to gain a sense of the scope and limitations of this important observation. Results indeed show that enynes with terminal alkynes generally underwent the PK reaction smoothly, providing good yields of enones (eq. [1], Table 5). Substitution on the alkene moiety

[7]We inadvertently overlooked the formation of by-products from reductive PK reaction in our preliminary communication (28).

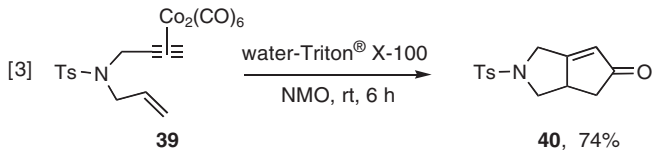
© 2005 NRC Canada

Table 4. Thermally promoted, $Co_4(CO)_{12}$ mediated PK reaction of enynes bearing terminal alkynes in water.[a]



Entry	Enyne	Additive (mol equiv.)	$Co_4(CO)_{12}$ (mol equiv.)	Yield (%) 35	37	38
1	**33**	_	1	5	21	
2	**33**	Triton X®-100 (1)	1	0	46	
3	**33**	Triton X®-100 (2)	1	16	28	
4	**33**	Triton X®-100 (1)	2	0	59	
5	**33**	Triton X®-100 (2)	2	0	61	
6	**33**	CTAB (1)	2	0	66	
7	**34**	Triton X®-100 (2)	2			46

[a]Reactions were conducted at concentrations of 0.05 mol/L (relative to enyne) in water at 70 °C under a nitrogen atmosphere and were complete in 18 h.



(Table 5, entry 1 vs. 6) and a longer tether length (Table 5, entries 6 and 7) are tolerated. As a comparison, the thermal version was also conducted and showed the significant formation (up to 46%) of the reductive PK reaction adduct (Table 5, entries 2, 3 and 5).

Cyclization of the dicobalthexacarbonyl complex of enyne **33** under various thermal conditions deserves comment. In a water – sodium dodecyl sulfate medium and using colloidal cobalt nanoparticles as the catalyst (20 atm CO (1 atm = 101.325 kPa), 130 °C), a significant amount of the bicyclooctanone (24%), in addition to enone **35** (71%), was observed (11). In the presence of either catalytic or stoichiometric amounts of $Co_4(CO)_{12}$, thermally promoted reaction of the complex of **33** in water with additives, such as Triton®X-100 and CTAB exclusively provided the corresponding bicyclooctanone (Table 4). It also gave 80% of bicyclooctanone **34**, when it was treated with an equivalent of $Co_2(CO)_8$ and 20 mol equiv. of water in refluxing DME (26*b*).

The room temperature, NMO promoted PK reaction proceeds efficiently in the water–Triton®X-100 medium (Table 1, condition IV), and is as efficient as the thermal reaction in the water–CTAB medium (Table 1, condition III). This procedure is particularly useful for the PK reactions of enynes bearing terminal alkynes because of the inhibition of further 1,4-reduction of the enone (cf. eq. [2]). Substrates that possess acetals prone to undergo hydrolysis are stable under these aqueous conditions.

Intermolecular PK reactions in water

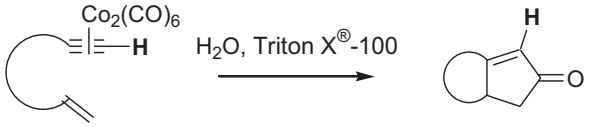
We were also interested in the application of several aqueous protocols to the intermolecular PK reaction (6) (Table 6). We felt that the challenging intermolecular nature of such reactions under aqueous conditions deserved study. Results showed that both strained and unstrained alkenes reacted with alkynes to provide good yields of PK reaction cycloadducts. The good results observed in the intermolecular PK cyclization of a less reactive alkene, such as 1-nonene, under three different sets of aqueous conditions is particularly worth emphasizing. As expected, the regiochemical outcomes parallel that observed in adducts generated from intermolecular reactions conducted in organic solvents (26*a*).

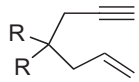
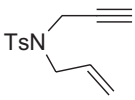
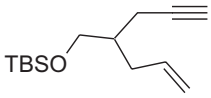
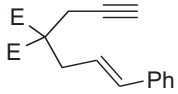
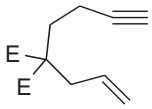
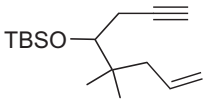
Summary and conclusions

We have studied the PK reaction under aqueous conditions, where we have focused on the (*a*) reactivity of $Co_2(CO)_8$ and $Co_4(CO)_{12}$ towards alkynes, (*b*) determination of optimal aqueous conditions, (*c*) compatibility of the PK reaction with various detergents and surfactants, and (*d*) stability of the substrates. In the presence of detergents and surfactants, such as Triton®X-100 and CTAB, PK reactions of enynes in water were efficiently promoted by $Co_2(CO)_8$ and $Co_4(CO)_{12}$ at 70 °C. A desirable catalytic protocol was developed using $Co_4(CO)_{12}$, which further delineated the unprecedented reactivity of the cobalt cluster under aqueous conditions. We have noted however that these thermal aqueous procedures were only suitable for enynes with internal alkynes. Enynes with terminal alkynes underwent the reductive PK reaction providing bicyclooctanones. Gratifyingly, this problem was avoided by promoting the aqueous PK reaction with NMO. Lastly, our studies have defined the type of enyne substrates that are compatible with water, and

© 2005 NRC Canada

Table 5. NMO and thermally promoted PK reaction of substrates bearing terminal alkynes in water.



Entry	Substrate(s)[a]		PK reaction adduct	Yield (%)[b] NMO[c]	Yield (%)[b] Δ[d]
1		**33**	**35**	72 (5)	–
2	R = $CH_2OC_6H_{13}$	**41**	**43**	73	30 (46)
3	R = CH_2OBn	**42**	**44**	70	40 (26)
4		**39**	**40**	74	–
5		**45**	**49**	61 (13)	52 (23)
6		**46**	**50**	71[e]	–
7		**47**	**51**	63	–
8		**48**	**52**	75[f]	–

[a]As alkyne dicobalthexacarbonyl complexes.
[b]Reported yields are for two steps (preparation of the alkyne dicobalthexacarbonyl complex and the PK reaction). Numbers in parenthesis are isolated yields of the corresponding bicyclooctanones.
[c]Water, 0.5 mol equiv. Triton®X-100, 5 mol equiv. NMO, rt, 6 h.
[d]Water, 0.5 mol equiv. Triton®X-100, 70 °C, 6 h.
[e]Exo cycloadduct.
[f]Diastereomeric ratio (1:1); E = CO_2Et.

illustrated various examples of successful intermolecular reactions.

Experimental section

General procedure

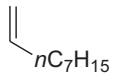
$Co_4(CO)_{12}$ and $Co_2(CO)_8$ were purchased from Strem Chemicals Co. and used without further purification. Brij 35, *n*-Bu_4NBr, castor oil, β- and γ-CD, CTAB, CTAHS, $CyNH_2$, Fisher detergent, TDA-1, TPPTS, Triton®X-100, Triton® X-100 (reduced form), and Tween 40 were purchased from commercial suppliers and used as received. Distilled deionized water was used for these reactions. Base-washed glassware was also used.

Reaction condition I

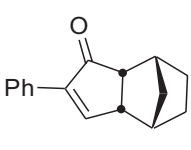
To a round-bottomed flask containing enyne **1** (83 mg, 0.329 mmol) and $Co_4(CO)_{12}$ (188 mg, 0.329 mmol) was added CTAB (72 mg, 0.197 mmol) followed by water (4 mL). The reaction mixture was then placed under an atmosphere of nitrogen and heated at 70 °C for 18 h. Upon completion of the reaction, the mixture was filtered through paper on a Büchner funnel, extracted with ethyl acetate, dried over $MgSO_4$, and filtered through a short pad of Celite.

© 2005 NRC Canada

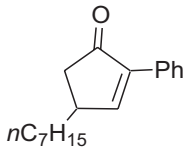
Table 6. Representative intermolecular PK reactions in water.

Entry	Alkyne[a]	Alkene[b]	Reaction condition[c]	PK reaction adduct	Yield (%)[d]
1	Ph—		I	**53**	64
2			II		70
3			III		62
4			IV		63
5	Ph—		I	**54/55**	13 (1:1)
6			II		54 (1:1)
7			III		67 (1:1)
8			IV		72 (1:1)

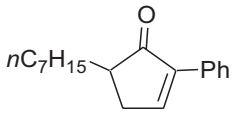
[a]As alkyne dicobalthexacarbonyl complexes (conditions III and IV, see Table 1).
[b]Five mol equiv.
[c]See Table 1 for conditions.
[d]Reported yields for conditions III and IV are for two steps (preparation of the alkyne dicobalthexacarbonyl complex and the PK reaction).



53



54



55

Subsequent concentration and purification by flash column chromatography (SiO_2, 25% EtOAc in hexanes) provided 75 mg of enone **17** (82% yield).

Reaction condition II

To a resealable tube containing enyne **3** (90 mg, 0.28 mmol), $Co_4(CO)_{12}$ (32 mg, 0.57 mmol, 20 mol%), and Triton®X-100 (91 mg, 0.14 mmol, 0.5 mol equiv.) was added water (1 mL). Carbon monoxide was then bubbled through the mixture (1 to 2 min), the tube was then sealed, and the reaction mixture was heated at 70 °C. Upon completion of the reaction (6–18 h), the mixture was filtered through a filter paper on a Büchner funnel, extracted with EtOAc, dried over $MgSO_4$, and filtered through a short pad of Celite. Subsequent concentration, followed by purification by flash column chromatography (SiO_2, 20% EtOAc in hexanes) provided 83 mg of enone **19** (85% yield).

Synthesis of dicobalthexacarbonyl complexes of alkynes and enynes

To a solution of enyne **3** (85 mg, 0.30 mmol) in CH_2Cl_2 (1 mL) was added $Co_2(CO)_8$ (114 mg, 0.332 mmol). The reaction mixture was then stirred at room temperature under N_2 for 1 h or until complex formation was complete. Concentration under reduced pressure provided the corresponding enyne–$Co_2(CO)_6$ complex in quantitative yield. These organocobalt complexes can alternatively be prepared by treating the enyne with $Co_2(CO)_8$ in a water–Triton®X-100 mixture. These complexes were then subjected immediately to reaction conditions III and IV.

Reaction condition III

To a round-bottomed flask containing the enyne–$Co_2(CO)_6$ complex of **2** (0.31 mmol) was added water (3 mL), followed by CTAB (67 mg, 0.18 mmol) and a small amount of Celite. The reaction mixture was then placed under an atmosphere of nitrogen and heated at 70 °C. Upon completion of the reaction (6–18 h), the mixture was filtered through a filter paper on a Büchner funnel, extracted with diethyl ether, and dried over $MgSO_4$. Subsequent concentration and purification by flash column chromatography (SiO_2, 25% EtOAc in hexanes) afforded 80 mg of enone **18** (85% yield). In some cases, a small amount of Celite was added into these reaction mixtures to facilitate stirring and to adsorb cobalt residues after the reaction. Insignificant differences in the yields were observed when Celite was not added to the reaction mixture.

Reaction condition IV

To a round-bottomed flask containing the enyne–$Co_2(CO)_6$ complex of **13** (0.285 mmol) was added Triton®X-100 (91 mg, 0.14 mmol), water (1 mL), and $NMO{\cdot}H_2O$ (235 mg, 1.7 mmol). The reaction mixture was then placed under an atmosphere of nitrogen and stirred at rt for 6 h. Upon completion of the reaction, the mixture was filtered through paper on a Büchner funnel, extracted with EtOAc, and dried over $MgSO_4$. Subsequent concentration and purifi-

© 2005 NRC Canada

cation by flash column chromatography (SiO_2, 25% EtOAc in hexanes) afforded 72 mg of enone **29** (86% yield).

The following compounds were previously reported and characterized: **3**, **13**, **19**, **29**, **42**, **44**, and **51**, (ref. 24); **2**, **9**, **10**, **18**, **25**, **26**, **33**, **35**, **47**–**49**, **52**, **53**, **56**, and **57** (ref. 25); **4**–**7**, **16**, **20**–**23**, **30**, and **32** (ref. 28); **11**, **12**, **27**, and **28** (ref. 27); **1** and **17** (ref. 32); **54** and **55** (ref. 33).

Enyne 41

^{1}H NMR ($CDCl_3$, 500 MHz) δ: 5.81 (ddt, J = 16.8, 10.1, 7.4 Hz, 1H, CH_2CH=CH_2), 5.08 (dm, J = 16.8 Hz, 1H, CH_2CH=CHH), 5.05 (dm, J = 10.1 Hz, 1H, CH_2CH=CHH), 3.38 (t, J = 6.7 Hz, 4H, 2 × ($CH_3(CH_2)_4CH_2OCH_2$)), 3.28 (AB, J_{AB} = 9.4 Hz, 2H, $CH_3(CH_2)_4CH_2OCH_2$), 3.24 (AB, J_{AB} = 9.4 Hz, 2H, $CH_3(CH_2)_4CH_2OCH_2$), 2.21 (d, J = 2.7 Hz, 2H, CH_2CCH), 2.17 (d, J = 7.4 Hz, 2H, CH_2CH=CH_2), 1.94 (t, J = 2.7 Hz, 1H, CH_2CCH), 1.46–1.60 (m, 4H, 2 × ($CH_3(CH_2)_3CH_2CH_2OCH_2$)), 1.22–1.40 (m, 12H, 2 × ($CH_3(CH_2)_3(CH_2)_2OCH_2$)), 0.88 (t, J = 7.4 Hz, 6H, 2 × ($CH_3(CH_2)_5OCH_2$)). ^{13}C NMR ($CDCl_3$, 75 MHz) δ: 134.14, 117.67, 81.50, 71.88, 71.27, 69.68, 41.60, 36.07, 31.45, 29.36, 25.62, 22.40, 21.84, 13.78. IR (cm^{-1}): 3312, 3076, 2956, 2930, 2860, 2796, 1638, 1482, 1466, 1458, 1438, 1376, 1112, 1002, 916. Anal. calcd. for $C_{21}H_{38}O_2$: C 78.20, H 11.87; found: C 78.44, H 11.99.

Enone 43

^{1}H NMR ($CDCl_3$, 500 MHz) δ: 5.84 (br s, 1H, CH_2C=CHC=O), 3.44 (obscured t, J = 6.6 Hz, 2H, $CH_3(CH_2)_4CH_2OCH_2C$), 3.42 (obscured AB, J_{AB} = 8.7 Hz, 1H, $CH_3(CH_2)_5OCHHC$), 3.39 (obscured AB, J_{AB} = 8.7 Hz, 1H, $CH_3(CH_2)_5OCHHC$), 3.37 (obscured t, J = 6.6 Hz, 2H, $CH_3(CH_2)_4CH_2OCH_2C$), 3.25 (AB, J_{AB} = 8.7 Hz, 1H, $CH_3(CH_2)_5OCHHC$), 3.20 (AB, J_{AB} = 8.7 Hz, 1H, $CH_3(CH_2)_5OCHHC$), 3.12 (m, 1H, CH_2CHCH_2C=O), 2.59 (dd, J = 18.1, 6.6 Hz, 1H, $CH_2CHCHHC$=O), 2.53 (br s, 2H, CH_2C=CHC=O), 2.11 (dd, J = 12.6, 8.7 Hz, 1H, $CHHCH$-CH_2C=O), 2.03 (dd, J = 18.1, 2.9 Hz, 1H, $CH_2CHCHHC$=O), 1.45–1.62 (m, 4H, 2 × ($CH_3(CH_2)_3CH_2CH_2OCH_2C$)), 1.18–1.40 (m, 12H, 2 × ($CH_3(CH_2)_3CH_2CH_2OCH_2C$)), 1.07 (dd, J = 12.8, 12.8 Hz, 1H, $CHHCHCH_2C$=O), 0.88 (t, J = 7.0 Hz, 6H, 2 × ($CH_3(CH_2)_5OCH_2C$)). ^{13}C NMR ($CDCl_3$, 75 MHz) δ: 211.04, 190.34, 124.43, 75.05, 74.75, 71.28, 71.19, 49.55, 44.25, 42.48, 37.34, 33.95, 31.29, 31.27, 29.20, 29.08, 25.52, 25.44, 22.24, 13.64. IR (cm^{-1}): 2931, 2857, 2793, 1713, 1634, 1483, 1466, 1412, 1377, 1294, 1259, 1220, 1201, 1170, 1111, 900, 831. Anal. calcd. for $C_{22}H_{38}O_3$: C 75.38, H 10.93; found: C 75.39, H 11.00.

Acknowledgments

We thank the National Science Foundation and the MDS Research Foundation for the generous financial support of this work.

References

1. (*a*) B. Cornils and W.A. Herrmann (*Editors*). Aqueous-phase organometallic catalysis. Wiley-VCH, Weinheim, Germany. 1998; (*b*) C.J. Li and T.H. Chan. Organic reactions in aqueous media. John Wiley and Sons, New York. 1997. p. 115; (*c*) U.M. Lindström. Chem. Rev. **102**, 2751 (2002).
2. (*a*) C.E. Song. Chem. Commun. 1033 (2004); (*b*) J.H. Davis, Jr. and P.A Fox. Chem. Commun. 1209 (2003); (*c*) H. Zhao and S.V. Malhotra. Aldrichimica Acta, **35**, 75 (2002); (*d*) R. Sheldon. Chem. Commun. 2399 (2001).
3. (*a*) 2.5 mol% $Co_2(CO)_8$, P_{CO_2} = 112 atm (37 °C), P_{CO} = 30 atm, 90 °C, 24 h: N. Jeong, S.H. Hwang, Y.W. Lee, and J.S. Lim. J. Am. Chem. Soc. **119**, 10 549 (1997); (*b*) $Co_4(CO)_{11}P(OPh)_3$, 5 atm CO, 110 atm ethylene, 34–85 °C, 24 h: N. Jeong and S.H. Hwang. Angew. Chem. Int. Ed. **39**, 636 (2000).
4. Development of cost-effective, safe, and environmentally benign organic processes has been an increasing research focus. (*a*) P. Tundo and P.T. Anastas. Green chemistry: Challenging perpectives. Oxford University Press, Oxford. 2000; (*b*) P.T. Anastas and J.C. Warner. Green chemistry: Theory and practice. Oxford University Press, Oxford. 1998.
5. For recent reviews, see: (*a*) J. Blanco-Urgoiti, L. Añorbe, L. Perez-Serrano, G. Dominguez, and J. Perez-Castells. Chem. Soc. Rev. **33**, 32 (2004); (*b*) S.E. Gibson and A. Stevenazzi. Angew. Chem. Int. Ed. **42**, 1800 (2003); (*c*) K.M. Brummond and J.L. Kent. Tetrahedron, **56**, 3263 (2000).
6. (*a*) B. Alcaide and P. Almendros. Eur. J. Org. Chem. 3377 (2004); (*b*) K.M. Brummond, H. Chen, K.D. Fisher, A.D. Kerekes, B. Rickards, P.C. Sill, and S.J. Geib. Org. Lett. **4**, 1931 (2002); (*c*) K.M. Brummond. *In* Advances in cycloaddition chemistry. Vol 6. *Edited by* M. Harmata. JAI Press Inc., Greenwich, Connecticut. 1999. p. 211.
7. P.A. Wender, N.M. Deschamps, and G.G. Gamber. Angew. Chem. Int. Ed. **42**, 1853 (2004).
8. A. Becheanu and S. Laschat. Synlett, 1865 (2002).
9. 4 mol% of water, 10 mol% $Co_2(CO)_8$, toluene, 7 atm CO, 120 °C, 10 h: T. Sugihara and M. Yamaguchi. Synlett, 1384 (1998).
10. 1,4-dioxane and 2 mol/L aq. NH_4OH (1:3, *v*/*v*): T. Sugihara, M. Yamada, H. Ban, M. Yamaguchi, and C. Kaneko. Angew. Chem. Int. Ed. Engl. **36**, 2801 (1997).
11. Stabilized cobalt nanoparticles, water, sodium dodecyl sulfate, 20 atm CO, 130 °C, 12 h: S.U. Son, S.I. Lee, Y.K. Chung, S.W. Kim, and T. Hyeon. Org. Lett. **4**, 277 (2002).
12. 5 mol% $[RhCl(cod)]_2$, 10 mol% dppp, 10 mol% TPPTS, 2 mol equiv. SDS, water, 100 °C, nitrogen, 2–12 h: F. Koji, T. Morimoto, K. Tsutsumi, and K. Kakiuchi. Angew. Chem. Int. Ed. **42**, 2409 (2003).
13. 3 mol% $[Rh(cod)Cl]_2$, 6 mol% BINAP, water–dioxane (1:1), 90 °C, 1.5 h: W.H. Suh, M. Choi, S.I. Lee, and Y.K. Chung. Synthesis, 2169 (2003).
14. For a preliminary report, see: L.V.R. Boñaga, J.A. Wright, and M.E. Krafft. Chem. Commun. 1746 (2004).
15. General review on tetranuclear clusters contains many references to $Co_4(CO)_{12}$: (*a*) P. Chini and B.T. Heaton. Top. Curr. Chem. **71**, 3 (1977). See also: (*b*) R.D.W. Kemmitt and D.R. Russell. *In* Comprehensive organometallic chemistry. Vol 5. *Edited by* E.W. Abel, F.A. Stone, and G. Wilkinson. Pergamon Press, Oxford. 1982. p. 7.
16. The use of $Co_3(CO)_9(\mu^3$-CH) in organic transformations, prepared by treating $Co_2(CO)_8$ with $CHBr_3$, has been exploited by the Sugihara laboratory. For Pauson–Khand reactions: (*a*) T. Sugihara and M. Yamaguchi. J. Am. Chem. Soc. **120**, 10 782 (1998); (*b*) T. Sugihara, M. Yamaguchi, and M. Nishizawa. Chem. Eur. J. **7**, 1589 (2001); $Co_4(CO)_{12}$ is inferior to $Co_3(CO)_9(\mu^3$-CH) in alkyne cyclotrimerizations: (*c*) T. Sugihara, A. Wakabayashi, Y. Nagai, H. Takao, H. Imagawa, and M. Nishizawa. Chem. Commun. 576 (2002). For cyclopentadienone synthesis: (*d*) T. Sugihara, A. Wakabayashi, H. Takao, H. Imagawa, and M. Nishizawa. Chem. Commun. 2456 (2001).

© 2005 NRC Canada

17. B.J. Teobald. Tetrahedron, **58**, 4133 (2002).
18. M.E. Piotti and H. Alper. J. Am. Chem. Soc. **118**, 111 (1996).
19. N. Iwasawa, T. Matsuo, M. Iwamoto, and T. Ikeno. J. Am. Chem. Soc. **120**, 3903 (1998).
20. H.-Y. Lee and M. An. Tetrahedron Lett. **44**, 2775 (2003).
21. A. Oledra, C.-J. Wu, R.J. Madhushaw, S.-L. Wang, and R.-S. Liu. J. Am. Chem. Soc. **125**, 9610 (2003).
22. M.E. Krafft and L.V.R. Boñaga. Angew. Chem. Int. Ed. **39**, 3676 (2000), and refs. cited therein.
23. $Co_4(CO)_{12}$ was initially shown to catalyze the PK reaction at 150 °C and 10 atm CO, and was believed to be detrimental to $Co_2(CO)_8$ catalysis. High temperature and pressure was supposed to drive the $Co_4(CO)_{12}$–$Co_2(CO)_8$ towards the dinuclear cobalt complex, the presumed precatalyst in the PK reaction. J.W. Kim and Y.K. Chung. Synthesis, 142 (1998). The use of $Co_4(CO)_{12}$ in the PK reaction was also briefly mentioned in a reaction using supercritical fluid (3).
24. (*a*) M.E. Krafft, L.V.R. Boñaga, J.A. Wright, and C. Hirosawa. J. Org. Chem. **67**, 1233 (2002); (*b*) S.U. Son, K.H. Park, and Y.K. Chung. Org. Lett. **4**, 3983 (2002).
25. M.E. Krafft, L.V.R. Boñaga, and C. Hirosawa. J. Org. Chem. **66**, 3004 (2001), and refs. cited therein.
26. For a review of side reactions observed under the PK reaction conditions, see: (*a*) L.V.R. Boñaga and M.E. Krafft. Tetrahedron, **60**, 9795 (2004). For specific examples, see also: (*b*) H.-Y. Lee, M. An, and J.-H. Sohn. Bull. Korean Chem. Soc. **24**, 539 (2003); (*c*) J. Cassayre and A.Z. Zard. J. Organomet. Chem. **64**, 316 (2001); (*d*) L. Pérez-Serrano, J. Blanco-Urgoiti, L. Casarrubios, G. Dominguez, and J. Pérez-Castells. J. Org. Chem. **65**, 3513 (2000); (*e*) T. Sugihara, M. Yamada, M. Yamaguchi, and M. Nishizawa. Synlett, 771 (1999).
27. M.E. Krafft, R.H. Romero, and I.L. Scott. J. Org. Chem. **57**, 5277 (1992).
28. For a preliminary communication, see: M.E. Krafft, J.A. Wright, and L.V.R. Boñaga. Tetrahedron Lett. **44**, 3417 (2003).
29. For a preliminary report, see: M.E. Krafft, J.A. Wright, and L.V.R. Boñaga. Synlett, 71 (2005).
30. Cyclodextrins (CD) are cyclic oligosaccharides consisting of six (α-CD), seven (β-CD), and eight (γ-CD) glucopyranose units and possessing both hydrophilic and hydrophobic sites. The cyclodextrin cavity is slightly apolar so that when it is occupied by polar water molecules it can be energetically unfavorable. Because of this negative interaction, the water molecules can be substituted by the less polar molecules in a host–guest manner. The cyclodextrin molecule usually can trap one guest molecule so that it can theoretically improve the normally unfavorable environment that exists with a poorly soluble molecule and the aqueous solution. The reactivity of the trapped molecule can either decreased because of stabilization or be enhanced in other cases. For a background on cyclodextrins, see: J. Szejtli. Chem. Rev. **98**, 1743 (1998).
31. (*a*) S. Shambayati, W.E. Crowe, and S.L. Schreiber. Tetrahedron Lett. **31**, 5289 (1990); (*b*) N. Jeong, Y.K. Chung, B.Y. Lee, S.H. Lee, and S.-E. Yoo. Synlett, 204 (1991).
32. T. Kondo, N. Suzuki, T. Okada, and T. Mitsudo. J. Am. Chem. Soc. **119**, 6187 (1997).
33. M. Periasamy and M.R.A. Devasagayaraj. Tetrahedron, **50**, 6955 (1994).

© 2005 NRC Canada

Surface organometallic chemistry — Carbonyl complexes of Re(I) with silanolates as models of silica anchored rhenium carbonyl species[1]

Giuseppe D'Alfonso, Claudia Dragonetti, Simona Galli, Elena Lucenti, Piero Macchi, Dominique Roberto, and Renato Ugo

Abstract: Reaction of Me_3SiONa with $[Re(CO)_5Cl]$ affords the new complex $Na[Re_2(CO)_6(\mu\text{-}OSiMe_3)_3]$, which could be generated via formation of $[Re(CO)_5OSiMe_3]$ followed by immediate reaction with Me_3SiO^-. Substitution of some CO ligands by phosphines significantly decreases the electrophilicity of the Re(I) center, and therefore hinders further attack by Me_3SiO^-. Thus, *fac*-$[Re(CO)_3(Ph_2PCH_2CH_2PPh_2)OTf]$ (OTf is the triflate anion) reacts with Me_3SiONa to give *fac*-$[Re(CO)_3(Ph_2PCH_2CH_2PPh_2)OSiMe_3]$, a molecular model of silica anchored $[Re(CO)_5OSi\equiv]$. However, substitution of only one CO by triphenylphosphine is not enough to avoid the formation of $[Re_2(CO)_6(\mu\text{-}OSiMe_3)_3]^-$. While *fac*-$[Re(CO)_3(Ph_2PCH_2CH_2PPh_2)OSiMe_3]$ is stable towards hydrolysis, $[Re_2(CO)_6(\mu\text{-}OSiMe_3)_3]^-$ is readily hydrolyzed to $[Re_2(CO)_6(\mu\text{-}OH)(\mu\text{-}OSiMe_3)_2]^-$, a molecular model of silica anchored $[Re_2(CO)_6(\mu\text{-}OH)(\mu\text{-}OSi\equiv)_2]^-$, whose structure has been determined by single crystal X-ray diffraction.

Key words: surface organometallic chemistry, rhenium, silica, silanolate, molecular model.

Résumé : La réaction de Me_3SiONa avec $[Re(CO)_5Cl]$ fournit le nouveau complexe $Na[Re_2(CO)_6(\mu\text{-}OSiMe_3)_3]$, probablement généré via la formation de $[Re(CO)_5OSiMe_3]$ suivie par une réaction immédiate avec Me_3SiO^-. La substitution de quelques CO par des phosphines diminue fortement l'électrophilicité du centre Re(I) et, par conséquent, empêche toute attaque ultérieure par Me_3SiO^-. Ainsi, *fac*-$[Re(CO)_3(Ph_2PCH_2CH_2PPh_2)OTf]$ (OTf est l'anion triflate) réagit avec Me_3SiONa pour donner *fac*-$[Re(CO)_3(Ph_2PCH_2CH_2PPh_2)OSiMe_3]$, modèle moléculaire de l'espèce ancrée à la silice $[Re(CO)_5OSi\equiv]$. Cependant la substitution d'un seul CO par la triphenylphosphine ne suffit pas à empêcher la formation de $[Re_2(CO)_6(\mu\text{-}OSiMe_3)_3]^-$. Alors que *fac*-$[Re(CO)_3(Ph_2PCH_2CH_2PPh_2)OSiMe_3]$ est stable en présence d'eau, $[Re_2(CO)_6(\mu\text{-}OSiMe_3)_3]^-$ s'hydrolyse rapidement pour donner $[Re_2(CO)_6(\mu\text{-}OH)(\mu\text{-}OSiMe_3)_2]^-$, modèle moléculaire de l'espèce ancrée à la silice $[Re_2(CO)_6(\mu\text{-}OH)(\mu\text{-}OSi\equiv)_2]^-$, dont la structure a été déterminée par diffraction des rayons X.

Mots clés : chimie organométallique de surface, rhénium, silice, silanolate, modèle moléculaire.

Introduction

Transition-metal carbonyls supported on silica are hybrid materials of interest as precursors of highly dispersed metals that may show improved or unusual catalytic properties (1). Although largely investigated in the last two decades (2), the surface organometallic chemistry between molecular metal carbonyl fragments and the surface sites is not always fully established. A recently developed way for a better understanding of the structure and reactivity of molecular metal carbonyl fragments bound to the silica surface is based on the structural and chemical characterization of metal carbonyl compounds bearing various silanolate ligands that mimic the functional groups of the silica surface. These models are a useful tool not only to understand the structural aspects of surface organometallic species, but also to clarify

Received 25 November 2004. Published on the NRC Research Press Web site at http://canjchem.nrc.ca on 7 September 2005.

In honour of Professor Howard Alper.

G. D'Alfonso, C. Dragonetti, and D. Roberto.[2] Centro di Eccellenza CIMAINA and Unità di Ricerca di Milano dell'INSTM and Dipartimento di Chimica Inorganica, Metallorganica ed Analitica dell'Università di Milano, Via Venezian, 21, 20133 Milan, Italy.
S. Galli. Dipartimento di Scienze Chimiche ed Ambientali, Università dell'Insubria, Via Valleggio, 11, 22100 Como, Italy.
E. Lucenti. Centro di Eccellenza CIMAINA and Unità di Ricerca di Milano dell'INSTM dell'Università di Milano, Via Venezian, 21, 20133 Milan, Italy and Istituto di Scienze e Tecnologie Molecolari del CNR (ISTM), via Golgi 19, 20133 Milan, Italy.
P. Macchi. Centro di Eccellenza CIMAINA and Unità di Ricerca di Milano dell'INSTM and Dipartimento di Chimica Strutturale e Stereochimica Inorganica dell'Università di Milano, via Venezian 21, 20133 Milan, Italy.
R. Ugo. Centro di Eccellenza CIMAINA and Unità di Ricerca di Milano dell'INSTM and Dipartimento di Chimica Inorganica, Metallorganica ed Analitica dell'Università di Milano, Via Venezian, 21, 20133 Milan, Italy and Istituto di Scienze e Tecnologie Molecolari del CNR (ISTM), via Golgi 19, 20133 Milan, Italy.

[1]This article is part of a Special Issue dedicated to Professor Howard Alper.
[2]Corresponding author (e-mail: dominique.roberto@unimi.it).

 doi: 10.1139/V05-104 © 2005 NRC Canada

the rather complex chemical behavior of metal carbonyl species anchored to silica (2). Many models of silica anchored carbonyl species of various noble metals (e.g., Rh (3), Os (2, 4),[3] and Ru (5)) have been synthesized, structurally characterized, and chemically investigated; however, in the case of the oxophilic metal Re, just anionic $[Re_2(CO)_6(\mu\text{-}OH)_x(\mu\text{-}OSiEt_3)_{3-x}]^-$ (x = 0, 1, or 2) (6) and neutral $[Re_2(CO)_8(\mu\text{-}H)(\mu\text{-}OSiR_2R')]$ (R = Et, Ph; R′ = Et, Ph, OH, or $OSiPh_2OH$) (7) species have been obtained and described only recently. Nevertheless, these few models cannot give a full understanding of the surface organometallic chemistry involving various rhenium carbonyl species anchored to silica. There is still a need for the synthesis and investigation of novel rhenium carbonyl species bearing silanolate ligands to fully clarify the complex surface chemistry occurring when rhenium carbonyl species such as $[Re_2(CO)_{10}]$ or $[Re(CO)_3(OH)]_4$ are chemically interacting with the silica surface. Indeed, this kind of surface organometallic chemistry is not yet well known, despite the industrial relevance of Re catalysts supported on inorganic oxides (8).

Recently, in fact, we reported that silica supported $[Re(CO)_3(OH)]_4$ is easily converted into $[Re_2(CO)_{10}]$ by reductive carbonylation under very mild conditions (1 atm CO, 1 atm = 101.325 kPa). This reaction does not occur in solution, suggesting that the silica surface plays a unique role via the formation of the surface anchored species $[Re(CO)_5OSi\equiv]$, which could also act as the intermediate in the silica mediated conversion under N_2 of $[Re_2(CO)_{10}]$ into $[Re(CO)_3(OH)]_4$ (9). Evidence for an intermediate chemically bound to the silica surface was based on IR studies and on its lack of extraction with solvents, together with its reactivity with HCl and $HReO_4$ to afford $[Re(CO)_5Cl]$ and $[Re(CO)_5OReO_3]$, respectively. This proposed surface species anchored via a Re—OSi bond to the surface is quite peculiar since carbonyl species of the type $[Re(CO)_5OR]$ have so far eluded isolation (9). Therefore, to produce additional evidence for its existence and to enlighthen its chemical behavior, we started an investigation on the synthesis and characterization of molecular models of this unusual silica anchored species.

Results and discussion

Attempts to prepare the molecular model of silica anchored $[Re(CO)_5OSi\equiv]$ by reaction of $[Re(CO)_5Cl]$ with Me_3SiONa invariably failed. The expected compound, $[Re(CO)_5OSiMe_3]$, was not obtained upon addition of Me_3SiONa to a solution of $[Re(CO)_5Cl]$ in dichloromethane (1:1 molar ratio), working under nitrogen at room temperature. Under these conditions, only some $Na[Re_2(CO)_6(\mu\text{-}OSiMe_3)_3]$ (ν(CO) = 2007 (s, br) and 1879 (vs, br) cm^{-1}) is quickly formed. With a 1.5:1 molar ratio Me_3SiONa:$[Re(CO)_5Cl]$, $Na[Re_2(CO)_6(\mu\text{-}OSiMe_3)_3]$ is quantitatively obtained (eq. [1]). Similarly, Et_3SiONa leads to the known anion $[Re_2(CO)_6(\mu\text{-}OSiEt_3)_3]^-$, previously prepared by reaction of an anisole solution of $[Re_2(CO)_6(\mu\text{-}OH)_3]^-$ with an excess of triethylsilanol at 200 °C (6).

$$[1]\qquad 2[Re(CO)_5Cl] + 3Me_3SiO^- \rightarrow [Re_2(CO)_6(\mu\text{-}OSiMe_3)_3]^- + 2Cl^- + 4CO$$

Reaction of $[Re(CO)_5Cl]$ with the anion Me_3SiO^- reasonably generates $[Re(CO)_5OSiMe_3]$ as a very reactive intermediate species, which could not be detected even by working under CO at 0 °C. This intermediate would be so reactive towards nucleophiles to react rapidly with the anion Me_3SiO^- affording, finally, by a double nucleophilic attack, $[Re_2(CO)_6(\mu\text{-}OSiMe_3)_3]^-$. Such an easy dimerization by silanolates bridging and concomitant loss of carbon monoxide, even under a CO atmosphere, suggests that the silanolate anion, as the alkoxide one (10), is an exceptionally good cis-labilizing ligand, which facilitates a further nucleophilic attack: the behavior of Me_3SiO^- towards $[Re(CO)_5Cl]$ is thus parallel to that of the structurally related alkoxide Me_3CO^- (11), despite its lower basicity. The quite high stability of the proposed silica anchored $[Re(CO)_5OSi\equiv]$ intermediate (9) can be due to the much lower nucleophilicity of surface silanols because the lack of dimerization cannot be attributed to the topological arrangement of surface silanols. In fact, we produced evidence for covalent anchoring of the dimer $[Re_2(CO)_6(\mu\text{-}OH)_3]^-$ to surface silanols (6).

It was thus clear that we could follow two strategies to obtain mononuclear Re(I) carbonyl silanolates: to decrease either the nucleophilic power of the silanolate anion or the electrophilic character of the Re(I) center. In this work we report on the results obtained by following the second option.

Substitution of some CO ligands of $[Re(CO)_5Cl]$ by phosphine ligands should decrease the electrophilicity of the Re(I) center and therefore hinder further nucleophilic attacks by Me_3SiO^- with formation of anionic dimeric species. Therefore, we treated *fac*-$[Re(CO)_3(Ph_2PCH_2CH_2PPh_2)Cl]$ with a stoichiometric amount of Me_3SiONa, at room temperature in dichloromethane. No reaction took place because of the large increase of the electronic density on the Re(I) center, as it can be inferred from the IR spectrum. This effect obviously inhibits even the first nucleophilic attack by the trimethylsilanolate anion. However, it is well-known that in Re(I) carbonyl species the triflate anion is a much better leaving group than the chloride one. Thus, we studied the reaction of *fac*-$[Re(CO)_3(Ph_2PCH_2CH_2PPh_2)OTf]$ (OTf is the triflate anion), easily obtained by reaction of AgOTf with *fac*-$[Re(CO)_3(Ph_2PCH_2CH_2PPh_2)Cl]$.

Addition of Me_3SiONa to a dichloromethane solution of *fac*-$[Re(CO)_3(Ph_2PCH_2CH_2PPh_2)OTf]$ slowly affords *fac*-$[Re(CO)_3(Ph_2PCH_2CH_2PPh_2)OSiMe_3]$. The reaction, which can be easily followed by IR and ^{31}P NMR spectroscopies (see the Experimental section), is complete in 2 days. Interestingly, although alkoxide complexes such as *fac*-$[Re(CO)_3(R'_2PCH_2CH_2PR'_2)OR]$ (R = Me, Et, or *i*-Pr; R′ = Et or Ph) were prepared by treatment of the triflate complex with the sodium salt of the appropriate primary or secondary alcohol (10, 12), it was reported that by reaction with the anion Me_3CO^-, structurally related to Me_3SiO^- but of increased nucleophilicity, the corresponding *tert*-butoxide complex was not isolated (10).

[3] E. Lucenti, F.J. Feher, and J.W. Ziller. Submitted for publication.

© 2005 NRC Canada

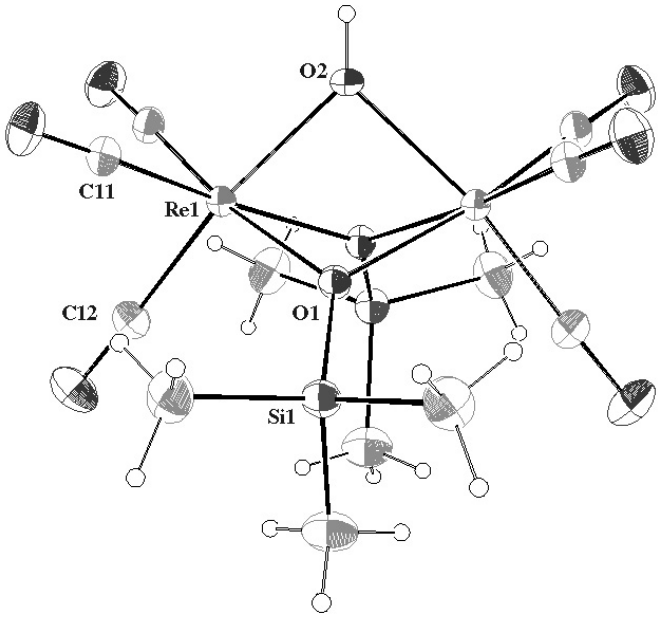
fac-$[Re(CO)_3(Ph_2PCH_2CH_2PPh_2)OSiMe_3]$ reacts readily with HCl(aq) to give *fac*-$[Re(CO)_3(Ph_2PCH_2CH_2PPh_2)Cl]$, a behavior that mimics the formation of $[Re(CO)_5Cl]$ by treatment of the proposed silica anchored $[Re(CO)_5OSi\equiv]$ species with HCl(aq). As a matter of fact, it was already reported that addition of gaseous HCl to the related alkoxide complex *fac*-$[Re(CO)_3(Et_2PCH_2CH_2PEt_2)OEt]$ results in a similar cleavage of the metal–oxygen bond with formation of the corresponding chloride (13).

It appears that the balance of the electron density on the rhenium atom is of paramount relevance for the stabilization of monomeric silanolate complexes. Indeed, by decreasing the electronic density on the rhenium center, such as when replacing a chelating diphosphine with one triphenylphosphine as in *cis*-$[Re(CO)_4(PPh_3)OTf]$, reaction with the anion Me_3SiO^- still gives $[Re_2(CO)_6(\mu\text{-}OSiMe_3)_3]^-$ with release of CO and even PPh_3, as evidenced by ^{29}Si and ^{31}P NMR spectroscopy, also when working at 0 °C (see the Experimental section). This latter result suggests that the coordination to rhenium of only one phosphorous donor atom is not sufficient to avoid aggregation by bridging silanolates when working in the normal range of temperatures between 0 and 25 °C.

It is worth pointing out that the Re-$OSiMe_3$ bond in *fac*-$[Re(CO)_3(Ph_2PCH_2CH_2PPh_2)OSiMe_3]$ is quite stable to hydrolysis in the presence of water at room temperature, as in some other neutral rhenium silanolate models such as $[Re_2(CO)_8(\mu\text{-}H)(\mu\text{-}OSiR_2R')]$ (R = Et, Ph; R′ = Et, Ph, OH, or $OSiPh_2OH$) (7), but in sharp contrast with the fast hydrolysis of anionic species such as $[Re_2(CO)_6(\mu\text{-}OH)_x(\mu\text{-}OSiEt_3)_{3-x}]^-$ (x = 0, 1, or 2) (6). Indeed, addition of a stoichiometric amount of $[NEt_4]Cl$ to an acetonitrile solution of $Na[Re_2(CO)_6(\mu\text{-}OSiMe_3)_3]$, followed by evaporation of the solvent and extraction of the organometallic anion with dry dichloromethane, afforded $[NEt_4][Re_2(CO)_6(\mu\text{-}OSiMe_3)_3]$. However, by slow crystallization from dichloromethane–*n*-pentane at –20 °C, only crystals of the product of the first step of the hydrolysis (6), namely $[NEt_4][Re_2(CO)_6(\mu\text{-}OH)(\mu\text{-}OSiMe_3)_2]$, were obtained because a partial hydrolysis arose even from very minor traces of water. The related complex $[Re_2(CO)_6(\mu\text{-}OH)(\mu\text{-}OSiEt_3)_2]^-$ has already been characterized spectroscopically (6), but has never been structurally investigated, although it is of interest as a model of the silica anchored surface species $[Re_2(CO)_6(\mu\text{-}OH)(\mu\text{-}OSi\equiv)_2]^-$ proposed to be thermally formed by condensation of $[Re_2(CO)_6(\mu\text{-}OH)_3]^-$ with surface silanols (6).

The crystal structure of $[NEt_4][Re_2(CO)_6(\mu\text{-}OH)(\mu\text{-}OSiMe_3)_2]$ (orthorhombic *Cmcm*) is composed by dimeric $[Re_2(CO)_6(\mu\text{-}OH)(\mu\text{-}OSiMe_3)_2]^-$ anionic units (Fig. 1), lying about a crystallographic *m2m* position (C_{2v}), counterbalanced by disordered tetraethylamonium cations, lying on a 2/*m* symmetry operator. Crystallographic data as well as data collection and treatment details are gathered in Table 1. A synoptic collection of bond lengths and angles is reported in Table 2. To our knowledge, this is the first example of a $[Re_2(CO)_6(\mu\text{-}OH)_x(\mu\text{-}OR)_{3-x}]^-$ structure (x = 0, 1, or 2) in which R is a silyl group. Previous characterizations regarding both homo- and hetero-bridged dimers of this kind invariably involved alkoxy or aryloxy bridges (14). Moreover, among the known X-ray structures of hetero-bridged $[Re_2(CO)_6(\mu\text{-}OH)_x(\mu\text{-}OR)_{3-x}]^-$ complexes, a well-defined

Fig. 1. ORTEP representation (at 20% probability) of $[Re_2(CO)_6(\mu\text{-}OH)(\mu\text{-}OSiMe_3)_2]^-$. The labels adopted for the structural description are depicted.



structure for the anionic dimer, as in the present case, was obtained only for the anion $[Re_2(CO)_6(\mu\text{-}OH)(\mu\text{-}OPh)_2]^-$ (14*f*), heavy disorder affecting the alkoxy groups in all the other cases (14*a*, 14*e*).

Within each $[Re_2(CO)_6(\mu\text{-}OH)(\mu\text{-}OSiMe_3)_2]^-$ dimer, the metal center, hexa-coordinated in distorted octahedral stereochemistry, is bound by three terminal carbonyl ligands, occupying facial positions, by two bridging -$OSiMe_3$ moieties and a bridging hydroxy group. The metal atom thus satisfies the valence bond electron rule without invoking a bonding metal···metal interaction, whose distance (3.111(1) Å) is anyway only slightly greater than that of 3.02 Å found in $[Re_2(CO)_{10}]$ (15), as occurs in other RO^- supported Re–Re dimers (see Table 2). Comparable Re—O(H) and Re—O(Si) bond distances (2.142(5) and 2.141(3) Å, respectively) find correspondence in similar Re-O(H)-Re and Re-O(Si)-Re bond angles (93.1(3)° and 93.2(2)°, respectively). Both independent carbonyl groups reveal almost normal features, with Re—C bond distances of 1.888(6) and 1.904(9) Å, C—O bond distances of 1.161(7) and 1.166(11) Å, and Re-C-O angles of 177.3(6)° and 176.9(9)°.

The steric hindrance of the trimethylsilanolate group seems not to induce significant molecular rearrangements: by inspecting Table 2, the major sterical effect seems to occur when PhO^- is acting as the bridge (see, in particular, the Re—O and Re···Re distances).

The dimeric $[Re_2(CO)_6(\mu\text{-}OH)(\mu\text{-}OSiMe_3)_2]^-$ units pack to generate rows parallel to **a** which stack, staggered, along **b** with minor intermolecular interactions (Fig. 2). Consecutive stacks of rows are separated, along **c**, by the counterions.

Conclusions

Due to (*i*) the high cis-labilizing effect of the silanolate ligand, (*ii*) the lability of CO ligands in "$Re(CO)_5$" and

© 2005 NRC Canada

Table 1. Crystallographic data and structure refinement parameters for compound $[NEt_4][Re_2(CO)_6(\mu\text{-}OH)(\mu\text{-}OSiMe_3)_2]$.

Empirical formula	$C_{20}H_{39}NO_9Re_2Si_2$
Formula weight (g mol^{-1})	865.96
Crystallographic system	Orthorhombic
Space group	*Cmcm*, No. 63
a (Å)	11.062(1)
b (Å)	11.887(2)
c (Å)	23.530(4)
V ($Å^3$)	3 094.1(8)
Z	4
F(000)	1604
Calculated density (Mg m^{-3})	1.859
Absorption coefficient (mm^{-1})	7.934
Temperature (K)	299
Crystal morphology	Needle
Crystal size (mm^3)	0.12 × 0.14 × 0.22
Integration range (°)	$3.5 \le 2\theta \le 61.1$
Indexes range	$-15 \le h \le 15$; $-16 \le k \le 16$; $-33 \le l \le 33$
Measured reflections	26 963
Unique reflections	2 537
Observed reflections for $I > 2\sigma(I)$	2 098
R_{int}, R_σ[a]	0.047, 0.025
Data / Restraints / Parameters	2 537 / 3 / 80
Goodness-of-fit[b]	$S(F^2)$ 1.225
Figures of merit for $I > 2\sigma(I)$[c]	$R(F)$ 0.037, $wR(F^2)$ 0.089
Figures of merit for all data	$R(F)$ 0.050, $wR(F^2)$ 0.092
Largest difference peak and hole (e $Å^{-3}$)	1.24 and –2.36

[a] $R_{int} = \Sigma|F_o^2 - F_{mean}^2|/\Sigma|F_o^2|$; $R_\sigma = \Sigma|\sigma(F_o^2)|/\Sigma|F_o^2|$.

[b] $S(F^2) = [\Sigma w(F_o^2 - F_c^2)^2/(n-p)]^{1/2}$, where n is the number of reflections, p is the number of parameters, and $w = 1/[\sigma^2(F_o^2) + (0.019P)^2 + 1.88P]$ with $P = (F_o^2 + 2F_c^2)/3$.

[c] $R(F) = \Sigma||F_o| - |F_c||/\Sigma|F_o|$ and $wR(F^2) = [\Sigma w(F_o^2 - F_c^2)^2/\Sigma wF_o^4]^{1/2}$.

"$Re(CO)_4$" moieties containing mutually trans carbonyls, and (*iii*) the strong tendency of $OSiR_3$ groups to function as bridging ligands (4*g*), the molecular model $[Re(CO)_5OSiMe_3]$ of the proposed surface species $[Re(CO)_5OSi\equiv]$ can not be obtained by reaction of $[Re(CO)_5Cl]$ with the trimethylsilanolate anion, despite the lower nucleophilicity of this latter compound when compared with alkoxy or aryloxy anions. The reaction product, under different reaction conditions, is invariably the bridged anion $[Re_2(CO)_6(\mu\text{-}OSiMe_3)_3]^-$, as it occurs with alkoxy anions (11).

Only substitution of CO groups with a chelating diphosphine to increase the electron density on the Re(I) complex enhances the stability of CO ligands and thus allows the preparation of neutral rhenium silanolate mononuclear species. Thus, the easy reaction of Me_3SiONa with *fac*-$[Re(CO)_3(Ph_2PCH_2CH_2PPh_2)OTf]$ provides a pathway to the novel complex *fac*-$[Re(CO)_3(Ph_2PCH_2CH_2PPh_2)OSiMe_3]$, characterized by an increased stability towards hydrolysis of a Re—OSi bond in sharp contrast with the easy hydrolysis of anionic species such as $[Re_2(CO)_6(\mu\text{-}OH)_x(\mu\text{-}OSiR_3)_{3-x}]^-$ (x = 0, 1, or 2; R = Me, Et) (6).

The increased stability of carbonyl ligands and the lower electrophilicity of the rhenium center, which is the origin of the stability of the monomeric silanolate complexes towards dimerization by further nucleophilic attack by the trimethylsiloxy anion, are quite dependent on the number of phosphorous donor atoms coordinated to the rhenium center. Whereas the complex *fac*-$[Re(CO)_3(Ph_2PCH_2CH_2PPh_2)OSiMe_3]$ does not react with excess Me_3SiO^-, *cis*-$[Re(CO)_4(PPh_3)OSiMe_3]$, reasonably formed as intermediate species by reaction of *cis*-$[Re(CO)_4(PPh_3)OTf]$ with Me_3SiO^-, still shows a great lability of a cis carbonyl and even a phosphine ligand giving place to $[Re_2(CO)_6(\mu\text{-}OSiMe_3)_3]^-$.

In conclusion, this work has indirectly suggested that the relative stability of the proposed "$Re(CO)_5(OSi\equiv)$" species anchored to the silica surface may be due to the extremely low nucleophilicity of the silanols of the silica surface. Therefore, work is in progress to synthesize $[Re(CO)_5OSiR_3]$ species where R_3 better represents the tetrahedral oxygen sphere of silica silanols, which, being quite acidic, display a very low basicity either as such or even as silanolates.

Experimental section

General comments

$[Re(CO)_5Cl]$ and $[Re(CO)_4Cl]_2$ were prepared according to the literature, the first complex by reaction of $[Re_2(CO)_{10}]$ (commercially available from Acros Organics) with Cl_2 (16), the second by heating under reflux a heptane solution of $[Re(CO)_5Cl]$ (17). AgOTf and Me_3SiONa (1 mol/L solution in dichloromethane) were purchased from Sigma-Aldrich. Organic solvents were freshly distilled before use (Et_2O and THF from sodium/benzophenone; CH_2Cl_2 from CaH_2). All reactions were carried out under N_2 (dried by flowing over drierite) in anhydrous conditions. Products were characterized by IR and NMR (^1H, ^{29}Si, ^{31}P) spectroscopies, by mass spectrometry, and by elemental analyses, which were carried out at the Dipartimento di Chimica Inorganica, Metallorganica ed Analitica of the Università di Milano.

Synthesis of $Na[Re_2(CO)_6(\mu\text{-}OSiMe_3)_3]$

In a typical synthesis, a solution of Me_3SiONa in CH_2Cl_2 (0.65 mL of a 1 mol/L solution) was added to a solution of $[Re(CO)_5Cl]$ (150 mg, 0.415 mmol, molar ratio $[Re(CO)_5Cl]$:Me_3SiONa = 1:1.6) in freshly distilled anhydr. CH_2Cl_2 (35 mL) under N_2 in a 100 mL two-neck round bottomed flask equipped with a magnetic stirring bar. After 24 h under stirring at room temperature, a white precipitate was present and the reaction was complete as evidenced by IR spectroscopy of the solution, which showed that no $[Re(CO)_5Cl]$ (ν(CO) in CH_2Cl_2 = 2046 (m), 1985 (s) cm^{-1}) was left. Evaporation to dryness of the solvent afforded a white residue that was dissolved in freshly distilled anhydr. THF (5 mL). Anhydr. Et_2O was slowly added to the latter solution, at ca. –5 °C (ice and salt bath), to precipitate the NaCl formed during the reaction. The solution was then separated from the precipitate using a syringe. Evaporation of the solvent followed by washing with a few mL of anhydrous pentane afforded pure $Na[Re_2(CO)_6(\mu\text{-}OSiMe_3)_3]$ as a white powder (162 mg, 0.195 mmol, 94% yield). IR (in

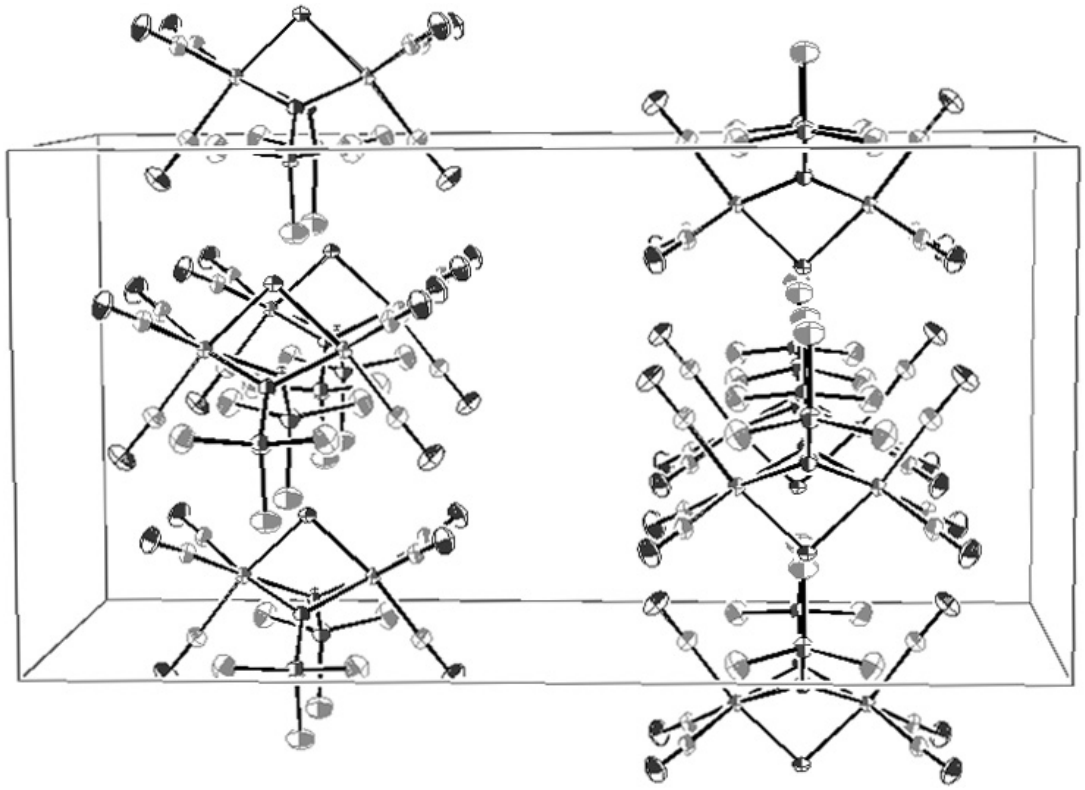
© 2005 NRC Canada

Table 2. Synoptic collection of significant geometrical parameters (distances, Å; angles, °) in the known dimeric anionic $[Re_2(CO)_6(\mu\text{-}OR)_x(\mu\text{-}OR')_y]^-$ units ($x + y = 3$).

Dimeric unit	Re···Re (Å)	Re—O(H) (Å)	Re—O (Å)	Re-O(H)-Re (°)	Re-O-Re (°)	Ref.
$[Re_2(CO)_6(\mu\text{-}OSiMe_3)_2(\mu\text{-}OH)]^-$	3.111	2.141	2.142	93.2	93.1	This work
$[Re_2(CO)_6(\mu\text{-}OMe)_x(\mu\text{-}OEt)_y]^-$[a]	3.085	n.a.	2.065	n.a.	95.65	14*a*
$[Re_2(CO)_6(\mu\text{-}OMe)_x(\mu\text{-}OEt)_y]^-$[a]	3.117	n.a.	2.123	n.a.	94.51	14*c*
			2.121		94.59	
$[Re_2(CO)_6(\mu\text{-}OPh)_3]^-$	3.154	n.a.	2.107, 2.149[b,c]	n.a.	95.65	14*b*
			2.133, 2.145[b,c]		94.98	
			2.128, 2.154[b,c]		94.89	
$[Re_2(CO)_6(\mu\text{-}OH)_3]^-$	3.103	2.063[d]	n.a.	97.55	n.a.	14*d*
		2.130[d]		93.53		
$[Re_2(CO)_6(\mu\text{-}OMe)(\mu\text{-}OEt)_2]^-$	3.117	n.a.	2.108, 2.109[b,e]	n.a.	95.32	14*e*
			2.145, 2.157[b,f]		92.86	
			2.132, 2.149[b,f]		93.46	
$[Re_2(CO)_6(\mu\text{-}OH)(\mu\text{-}OPh)_2]^-$	3.152	2.119, 2.138[b]	2.162, 2.163[b,g]	95.51	93.55	14*f*
			2.148, 2.151[b,g]		94.29	

Note: n.a. = not applicable.
[a]Severe disorder affecting the alkoxo groups impeded a definite assessment of stoichiometry.
[b]The two values on each line refer to the two independent Re atoms present.
[c]The values refer to one of the three independent phenoxy ligands.
[d]The values refer to one of the two independent hydroxy ligands.
[e]The values refer to the methoxy ligand.
[f]The values refer to one of the two independent ethoxy ligands.
[g]The values refer to one of the two independent phenoxy ligands present.

Fig. 2. ORTEP representation (at 20% probability) of the packing motif of the dimeric units in $[NEt_4][Re_2(CO)_6(\mu\text{-}OH)(\mu\text{-}OSiMe_3)_2]$ viewed down [1 0 0]. Horizontal axis, c; vertical axis, b. Disordered tetraethylammonium cations and hydrogen atoms have been omitted for clarity.



© 2005 NRC Canada

CH_2Cl_2, cm^{-1}): ν(CO) 2007 (s, br), 1879 (vs, br). ^1H NMR (in CD_3CN, ppm) δ: 0.02. ^{29}Si NMR (in CD_3CN, ppm) δ: 0.59; the ^{29}Si NMR signal of Me_3SiONa in CD_3CN lies at –13.09 ppm. In the FAB$^-$ mass spectrum, the ion peak corresponding to $[Re_2(CO)_6(\mu\text{-}OSiMe_3)_3]^-$ lies at *m/e* = 807. Elemental anal. calcd.: C 21.67, H 3.25; found: C 21.79, H 3.41.

Synthesis of $Na[Re_2(CO)_6(\mu\text{-}OSiEt_3)_3]$

Synthesis of Et_3SiONa

An excess of metallic Na (3.82 g, 166 mmol, cut in small pieces) was added to a solution of Et_3SiOH (0.98 mmol, 0.15 mL, *d* = 0.846 g/mL) in anhydr. Et_2O (15 mL) under N_2. After stirring at room temperature for ca. 4 h no more gas was evolved, the solution was separated with a syringe and evaporated to dryness affording pure Et_3SiONa. ^1H NMR (in CD_3CN, ppm) δ: 0.36 (q, 2H, CH_2), 0.93 (t, 3H, CH_3). ^{29}Si NMR (in CD_3CN, ppm) δ: –3.19.

Synthesis of $Na[Re_2(CO)_6(\mu\text{-}OSiEt_3)_3]$

A solution of Et_3SiONa in anhydr. CH_2Cl_2 (6.5 mL of a 0.0981 mol/L solution) was added to a solution of $[Re(CO)_5Cl]$ (150 mg, 0.415 mmol, molar ratio $[Re(CO)_5Cl]$:Et_3SiONa = 1:1.5) in freshly distilled anhydr. CH_2Cl_2 (35 mL) under N_2 in a 100 mL two-neck round bottomed flask equipped with a magnetic stirring bar. After 24 h under stirring at room temperature, a white precipitate was present and the reaction was complete as evidenced by IR spectroscopy of the solution. Evaporation to dryness of the solvent afforded a white residue that was dissolved in freshly distilled anhydr. THF (5 mL). Anhydr. Et_2O was slowly added to the latter solution, at –5 °C, to precipitate the NaCl formed during the reaction. The solution was then separated from the precipitate using a syringe. Evaporation of the solvent followed by washing with a few mL of anhydrous pentane (to remove traces of $Et_3SiOSiEt_3$ and Et_3SiOH) afforded the known complex $Na[Re_2(CO)_6(\mu\text{-}OSiEt_3)_3]$ (6) as a white powder (188 mg, 0.197 mmol, 95% yield).

Synthesis of *fac*-$[Re(CO)_3(Ph_2PCH_2CH_2PPh_2)OSiMe_3]$

The new complex *fac*-$[Re(CO)_3(Ph_2PCH_2CH_2PPh_2)OSiMe_3]$ was prepared from *fac*-$[Re(CO)_3(Ph_2PCH_2CH_2PPh_2)OTf]$ (12), easily obtained by the reaction of AgOTf with *fac*-$[Re(CO)_3(Ph_2PCH_2CH_2PPh_2)Cl]$ (18) recovered in quantitative yield by refluxing under N_2 for 14 h a $CHCl_3$ solution of $[Re(CO)_4Cl]_2$ (0.154 mmol) with a stoichiometric amount of $PPh_2CH_2CH_2PPh_2$ (0.308 mmol).

Thus, addition of AgOTf (19.8 mg, 0.073 mmol) to a solution of *fac*-$[Re(CO)_3(Ph_2PCH_2CH_2PPh_2)Cl]$ (54 mg, 0.077 mmol, IR (in CH_2Cl_2 cm^{-1}): ν(CO) 2034 (vs), 1954 (s), 1906 (s); ^{31}P NMR (in CD_2Cl_2, ppm) δ: 32.65) in anhydr. CH_2Cl_2 (10 mL) led to the precipitation of AgCl and the formation of *fac*-$[Re(CO)_3(Ph_2PCH_2CH_2PPh_2)OTf]$ as confirmed by IR and ^{31}P NMR spectroscopies (IR (in CH_2Cl_2, cm^{-1}): ν(CO) 2044 (vs), 1966 (s), 1919 (s); ^{31}P NMR (in CD_2Cl_2, ppm) δ: 38.68). After 2.5 h under stirring in the dark at room temperature, the reaction was complete, as evidenced by IR spectroscopy, and the solution containing *fac*-$[Re(CO)_3(Ph_2PCH_2CH_2PPh_2)OTf]$ was transferred with a syringe in a round-bottomed flask. Then Me_3SiONa (1 mol/L solution in CH_2Cl_2, 0.152 mmol, molar ratio Re:Me_3SiONa = 1:2) was added at 0 °C, and the resulting solution was stirred under nitrogen at room temperature for 48 h, evaporated to dryness, and the residue extracted with anhydrous pentane to give, after evaporation to dryness of the solvent, *fac*-$[Re(CO)_3(Ph_2PCH_2CH_2PPh_2)OSiMe_3]$ in 75% yield (43.75 mg, 0.058 mmol). IR (in CH_2Cl_2, cm^{-1}): ν(CO) 2014 (vs), 1927 (s), 1873 (s). ^1H NMR (in CD_2Cl_2, ppm) δ: –0.61 (s, 9H, $OSiMe_3$), 2.43 (m, 2H, CH_2), 3.04 (m, 2H, CH_2), 7.21–7.83 (m, 20H, $2PPh_2$). ^{31}P NMR (in CD_2Cl_2, ppm) δ: 31.36. ^{29}Si NMR (in CD_2Cl_2, ppm) δ: 6.05. Mass spectrometry (EI, *m/e*): 758 (M = Molecular ion peak), 730 [M – CO], 702 [M – 2CO], 674 [M – 3CO]. Elemental anal. calcd.: C 50.71, H 4.35; found: C 50.32, H 4.30.

Reactivity of *fac*-$[Re(CO)_3(Ph_2PCH_2CH_2PPh_2)OSiMe_3]$

Addition, at room temperature, of a drop of aq. HCl to *fac*-$[Re(CO)_3(Ph_2PCH_2CH_2PPh_2)OSiMe_3]$ (4 mg) dissolved in CH_2Cl_2 (5 mL) led to the immediate formation of *fac*-$[Re(CO)_3(Ph_2PCH_2CH_2PPh_2)Cl]$ as confirmed by IR and ^{31}P NMR spectroscopies. On the contrary, no reaction occurred upon stirring a CH_2Cl_2 solution of *fac*-$[Re(CO)_3(Ph_2PCH_2CH_2PPh_2)OSiMe_3]$ in the presence of a few drops of water for ca. 48 h at room temperature.

Reactivity of *cis*-$[Re(CO)_4(PPh_3)OTf]$ with Me_3SiONa

Addition of AgOTf (20.6 mg, 0.084 mmol) to a solution of *cis*-$[Re(CO)_4(PPh_3)Cl]$ (19) (40 mg, 0.067 mmol; IR (in CH_2Cl_2, cm^{-1}): ν(CO) 2107 (m), 2005 (vs), 1947 (s); ^{31}P NMR (in CD_2Cl_2, ppm) δ: 4.28) in anhydr. CH_2Cl_2 (8 mL), at room temperature, led to the precipitation of AgCl and the formation of *cis*-$[Re(CO)_4(PPh_3)OTf]$ as confirmed by IR and ^{31}P NMR spectroscopies (IR (in CH_2Cl_2, cm^{-1}): ν(CO) 2117 (m), 2016 (vs), 1961 (s); ^{31}P NMR (in CD_2Cl_2, ppm) δ: 11.60). After 2.5 h under stirring in the dark at room temperature, the reaction was complete, as evidenced by IR spectroscopy, and the solution containing *cis*-$[Re(CO)_4(PPh_3)OTf]$ was filtered on Celite under nitrogen. Then Me_3SiONa (1 mol/L solution in CH_2Cl_2, 0.067 mL, 0.067 mmol, molar ratio Re:Me_3SiONa = 1:1) was added, leading to the precipitation of some product. After 1.5 h, evaporation of the solvent afforded a residue that contained $Na[Re_2(CO)_6(\mu\text{-}OSiMe_3)_3]$ and free PPh_3 as evidenced by ^{29}Si NMR (signal at δ 0.59 ppm) and ^{31}P NMR (signal at δ –4.91 ppm) spectroscopy (in CD_3CN).

Formation of $[NEt_4][Re_2(CO)_6(\mu\text{-}OH)(\mu\text{-}OSiMe_3)_2]$

Addition of $[NEt_4]Cl$ (stoichiometric amount) to a solution of $Na[Re_2(CO)_6(\mu\text{-}OSiMe_3)_3]$ in acetonitrile, followed by evaporation of the solvent to dryness, extraction of the residue with CH_2Cl_2 and filtration, afforded a solution of $[NEt_4][Re_2(CO)_6(\mu\text{-}OH)(\mu\text{-}OSiMe_3)_2]$ because of the presence of traces of water. Addition of pentane to this solution led, at –20 °C, to the formation of colorless crystals of $[NEt_4][Re_2(CO)_6(\mu\text{-}OH)(\mu\text{-}OSiMe_3)_2]$ suitable for X-ray structure determination. IR (in CH_2Cl_2, cm^{-1}): ν(CO) 1995 (s, br), 1876 (vs, br). ^1H NMR (in CD_3CN, ppm) δ: 0.22 (s, 18H, $2Si(CH_3)_3$), 1.22 (t, *J* = 7.2 Hz, 12H, $4NCH_2CH_3$), 1.76 (s, 1H, O*H*), 3.18 (q, *J* = 7.2 Hz, 8H, $4NCH_2CH_3$). ^{29}Si

© 2005 NRC Canada

NMR (in CD_3CN, ppm) δ: 16.61; the ^{29}Si NMR signal of Me_3SiONa in CD_3CN lies at –13.09 ppm.

X-ray crystallography

A suitable colorless needle of $[NEt_4][Re_2(CO)_6(\mu\text{-}OH)(\mu\text{-}OSiMe_3)_2]$, obtained by slow crystallization of a CH_2Cl_2–pentane solution of $[NEt_4][Re_2(CO)_6(\mu\text{-}OSiMe_3)_3]$, was mounted in air on the glass fiber tip of a goniometer head. Data collection was performed on a Bruker Axs SMART CCD area-detector equipped with graphite-monochromatized Mo Kα radiation (λ = 0.710 73 Å), by applying the ω-scan method. 2500 frames were acquired with Δω = 0.3°, t = 25 s per frame, and sample–detector distance fixed at 3.45 cm. Data reduction within the hemisphere with 2θ < 61.2° afforded 26 963 reflections of which 2537 were unique. An empirical absorption correction was applied (20). The structure was solved by direct methods (21) and refined with full-matrix least-squares calculations on F^2 (22). Anisotropic temperature factors were assigned to all atoms but: (*i*) hydrogens, riding their parent atoms with an isotropic temperature factor arbitrarily chosen as 1.2 times that of the parent itself; and (*ii*) the nitrogen and carbon atoms of the tetraethylammonium cation. To properly describe the heavily disordered tetraethylammonium cation: (*i*) some of its carbon atoms have been "splitted" over two positions, with a fixed site occupation factor of 0.5; (*ii*) soft restraints have been imposed on its C—C bond distances (1.55 Å); (*iii*) all its carbon atoms have been given a common isotropic displacement parameter; and (*iv*) hydrogen atoms have not been assigned.[4]

Acknowledgements

DR deeply thanks her first master, Professor Howard Alper, for his magic teaching and guidance during the first years of her scientific life. We are grateful to Dr. Silvia Malaguti for NMR experiments and to Dr. Carmen Roveda, Dr. Matteo Vailati, and Dr. Virna Formaggio for some experimental help. This work was supported by the Ministero dell'Istruzione, dell'Università e della Ricerca (PRIN 2003, Research Title: Proprietà di singole molecole ed architetture molecolari funzionali supportate: caratterizzazione chimico-fisica, sviluppo di sintesi chimiche e di sistemi per l'indagine) and by the Consiglio Nazionale delle Ricerche (CNR, Roma).

References

1. For example, see the following reviews and refs. therein: (*a*) Y. Iwasawa and B.C. Gates. Chem. Tech. 173 (1989); (*b*) B.C. Gates. Catalytic chemistry. Wiley, New York. 1992; (*c*) S.L. Scott and J.M. Basset. J. Mol. Catal. **86**, 5 (1994); (*d*) R. Psaro and S. Recchia. Catal. Today. **41**, 139 (1998); (*e*) P. Braunstein and J. Rosé. *In* Metal clusters in chemistry. *Edited by* P. Braunstein, L. Oro, and P. Raithby. Wiley-VCH Verlag, Weinheim, Germany. 1999. pp. 616–665; (*f*) F. Lefebvre, J.-P. Candy, and J.-M. Basset. *In* Metal clusters in chemistry. *Edited by* P. Braunstein, L. Oro, and P. Raithby. Wiley-VCH Verlag, Weinheim, Germany. 1999. pp. 782–793.
2. (*a*) E. Lucenti, D. Roberto, and R. Ugo. Organometallics, **20**, 1725 (2001), and refs. therein; (*b*) E. Cariati, D. Roberto, R. Ugo, and E. Lucenti. Chem. Rev. **103**, 3707 (2003), and refs. therein.
3. (*a*) A. Vizi-Orosz, G. Pályi, and L. Markó. J. Organomet. Chem. **57**, 379 (1973); (*b*) G. Pályi, A. Vizi-Orosz, L. Markó, F. Marcati, and G. Bor. J. Organomet. Chem. **66**, 295 (1974); (*c*) A. Théolier, A.K. Smith, M. Leconte, J.-M. Basset, G.M. Zanderighi, R. Psaro, and R. Ugo. J. Organomet. Chem. **191**, 415 (1980); (*d*) A. Vizi-Orosz and L. Markó. Transition Met. Chem. (Dordrecht, Neth.), **7**, 216 (1982); (*e*) G. Pályi, C. Zucchi, R. Ugo, R. Psaro, A. Sironi, and A. Vizi-Orosz. J. Mol. Catal. **74**, 51 (1992); (*f*) A. Vizi-Orosz, R. Ugo, R. Psaro, A. Sironi, M. Moret, C. Zucchi, F. Ghelfi, and G. Pályi. Inorg. Chem. **33**, 4600 (1994).
4. (*a*) R. Psaro, R. Ugo, B. Besson, A.K. Smith, and J.M. Basset. J. Organomet. Chem. **213**, 215 (1981); (*b*) J. Evans and B.P. Gracey. J. Chem. Soc. Dalton Trans. 1123 (1982); (*c*) L. D'Ornelas, A. Choplin, J.M. Basset, L.Y. Hsu, and S. Shore. Nouv. J. Chim. **9**, 155 (1985); (*d*) F.J. Feher. J. Am. Chem. Soc. **108**, 3850 (1986); (*e*) F.J. Feher, S.L. Gonzales, and J.W. Ziller. Inorg. Chem. **27**, 3440 (1988); (*f*) F.J. Feher and J.F. Walzer. Inorg. Chem. **29**, 1604 (1990); (*g*) E. Lucenti, D. Roberto, C. Roveda, R. Ugo, and A. Sironi. Organometallics, **19**, 1051 (2000); (*h*) J.C. Liu, S.R. Wilson, J.R. Shapley, and F.J. Feher. Inorg. Chem. **29**, 5138 (1990).
5. J. Puga, T.P. Fehlner, B.C. Gates, D. Braga, and F. Grepioni. Inorg. Chem. **29**, 2376 (1990).
6. D. Roberto, G. D'Alfonso, R. Ugo, and M. Vailati. Organometallics, **20**, 4307 (2001).
7. G. D'Alfonso, V. Formaggio, D. Roberto, R. Ugo, E. Lucenti, and L. Carlucci. Organometallics, **22**, 3271 (2003).
8. (*a*) P.S. Kirlin and B.C. Gates. Nature (London), **325**, 38 (1987); (*b*) S.K. Purnell and B.C. Gates. J. Mol. Catal. **94**, L1 (1994).
9. G. D'Alfonso, D. Roberto, R. Ugo, C.L. Bianchi, and A. Sironi. Organometallics, **19**, 2564 (2000), and refs. therein.
10. R.D. Simpson and R.G. Bergman. Organometallics, **12**, 781 (1993).
11. A.A. Ioganson, B.V. Lokshin, E.E. Kolobova, and K.N. Anisimov. J. Gen. Chem. **20**, 20 (1974); Zh. Obshch. Khim. **44**, 23 (1974).
12. S.K. Mandal, D.M. Ho, and M. Orchin. Inorg. Chem. **30**, 2244 (1991).
13. R.D. Simpson and R.G. Bergman. Organometallics, **11**, 3980 (1992).
14. (*a*) $[NEt_4][Re_2(CO)_6(\mu\text{-}OCH_3)_3]$ (with some methoxy groups replaced by ethoxy ones): G. Ciani, A. Sironi, and A. Albinati. Gazz. Chim. Ital. **109**, 615 (1979); (*b*) $[NEt_4][Re_2(CO)_6(\mu\text{-}OPh)_3]$: T. Beringhelli, G. Ciani, G. D'Alfonso, A. Sironi, and M. Freni. J. Chem. Soc. Dalton Trans. 1507 (1985); (*c*) $[NMe_4][Re_2(CO)_6(\mu\text{-}OCH_3)_3]$: W.A. Herrmann, D. Mihalios, K. Ofele, P. Kiprof, and F. Belmedjahed. Chem. Ber. **125**, 1795 (1992); (*d*) $[NEt_4][Re_2(CO)_6(\mu\text{-}OH)_3]\cdot 2H_2O$: R. Alberto, A. Egli, U. Abram, K. Hegetschweiler, V. Gramlich, and P.A. Schubiger. J. Chem. Soc. Dalton Trans. 2815 (1994); (*e*) [N-CH_3-adamantanium]$[Re_2(CO)_6(\mu\text{-}OCH_3)(\mu\text{-}OCH_2CH_3)_2]$: N.E. Kolobova, V.I. Zdanovich, I.A. Lobanova, V.G. Andrinov,

[4] Supplementary data for this article are available on the Web site or may be purchased from the Depository of Unpublished Data, Document Delivery, CISTI, National Research Council Canada, Ottawa, ON K1A 0S2, Canada. DUD 4000. For more information on obtaining material refer to http://cisti-icist.nrc-cnrc.gc.ca/irm/unpub_e.shtml. CCDC 256488 contains the crystallographic data for this manuscript. These data can be obtained, free of charge, via www.ccdc.cam.ac.uk/conts/retrieving.html (Or from the Cambridge Crystallographic Data Centre, 12 Union Road, Cambridge CB2 1EZ, UK; fax +44 1223 336033; or deposit@ccdc.cam.ac.uk).

© 2005 NRC Canada

Yu.T. Struchkov, and P.V. Petrovskii. Bull. Acad. Sci. USSR, Div. Chem. Sci. (Engl. Transl.), **33**, 871 (1984); (*f*) $[NEt_4][Re_2(CO)_6(\mu\text{-}OH)(\mu\text{-}OPh)_2]$: C. Jiang, Y.S. Wen, L.K. Liu, A.T.S. Hor, and Y.K. Yan. Organometallics, **17**, 173 (1998).
15. L.F. Dahl, E. Ishishi, and R.E. Rundle. J. Chem. Phys. **26**, 1750 (1957).
16. S.P. Schmidt, W.C. Trogler, and F. Basolo. Inorg. Synth. **23**, 41 (1985).
17. E.W. Abel, G.B. Hargreaves, and G. Wilkinson. J. Chem. Soc. 3149 (1958).
18. J. Chatt, J.R. Dilworth, H.P. Gunz, and G.J. Leigh. J. Organomet. Chem. **64**, 245 (1974).
19. F. Zingales, U. Sartorelli, F. Canziani, and M. Raveglia. Inorg. Chem. **6**, 154 (1967).
20. G.M. Sheldrick. SADABS [computer program]. University of Göttingen, Göttingen, Germany. 1996.
21. A. Altomare, G. Cascarano, C. Giacovazzo, A. Guagliardi, A.G.G. Moliterni, M.C. Burla, G. Polidori, M. Cavalli, and R. Spagna. SIR97 [computer program]. University of Bari, Bari, Italy. 1997.
22. G.M. Sheldrick. SHELX97 [computer program]. University of Göttingen, Göttingen, Germany. 1997.

© 2005 NRC Canada

Novel nitrogen containing chelating ligands from aziridines — Preparation, coordination studies, and catalytic application in the cyclopropanation of styrene[1]

Larissa B. Krasnova and Andrei K. Yudin

Abstract: Novel ligands have been synthesized by the reaction of readily available aziridines with appropriate nitrogen based nucleophiles under mild conditions. Complexes of different stoichiometry can be readily obtained upon reaction between these ligands and the corresponding copper salts. The enantiomerically pure form of one of the ligands was obtained and applied in the styrene cyclopropanation reaction, where the copper catalyst revealed unexpectedly high diastereoselectivity in comparison with the known systems.

Key words: ligands, aziridines, cyclopropanation, copper catalysts, metal complexes.

Résumé : On a effectué la synthèse de nouveaux ligands en procédant à la réaction, dans des conditions douces, d'aziridines facilement disponibles avec des nucléophiles appropriés à base d'azote. On peut facilement obtenir des complexes de stoechiométries différentes par réaction de ces ligands avec les sels de cuivre correspondants. On a pu obtenir la forme énantiomériquement pure d'un de ces ligands et on l'a appliquée à la réaction de cyclopropanation du styrène pour laquelle le catalyseur de cuivre conduit à une diastéréosélectivité aussi haute qu'inattendue par comparaison avec les systèmes connus.

Mots clés : ligands, aziridines, cyclopropanation, catalyseurs de cuivre, complexes métalliques.

[Traduit par la Rédaction]

Introduction

Cheleating ligands based on a rigid cyclohexyl backbone have been widely used in asymmetric catalysis (1). Among them is Trost's ligand for asymmetric palladium catalyzed allylic substitution (2), alkylation of β-ketoesters (3), and addition of alcohols to vinyl epoxides (4). The salen-type ligands, which have been extensively studied by Jacobsen, were successfully applied in the epoxidation of olefins (5), asymmetric sulfoxidation (6), hetero-Diels–Alder reaction (7), ene reaction (8), asymmetric ring opening of epoxides (9), and cyclopropanation (10). Recently, a new type of *P,N*-ligands containing a cyclohexyl backbone was developed in our lab and applied in the Suzuki coupling with sterically hindered substrates (11). The relative facility of the aziridine ring opening coupled with complete trans selectivity should also make cyclohexyl aziridine a convenient precursor towards cyclohexyl-backbone-containing ligands with an anti relationship between the two nitrogen containing functional groups. The present manuscript details our explorations in this area.

Results and discussion

Our recent interest in aziridine chemistry prompted us to explore simple aziridine building blocks as precursors to new nitrogen containing ligands. The 7-azabicyclo-[4.1.0]heptane was synthesized from cyclohexyl oxide using the Staudinger reaction (Scheme 1) (12). The resulting aziridine was opened with hydrazine hydrate. The product of the reaction was characterized by NMR and was submitted to the next step without purification. The reaction with 2,4-pentanedione led to the formation of racemic pyrazole **1**. The reaction between 7-azabicyclo[4.1.0]heptane and 5-phenyltetrazole occurred under mild conditions at pH 5 (Scheme 1) giving tetrazole **2** (13).

Several chiral acids were screened to resolve the ligand **2** in enantiomerically pure form. The best results were

Received 29 April 2005. Published on the NRC Research Press Web site at http://canjchem.nrc.ca on 7 September 2005.

Dedicated to Professor Howard Alper in recognition of his contributions to chemistry.

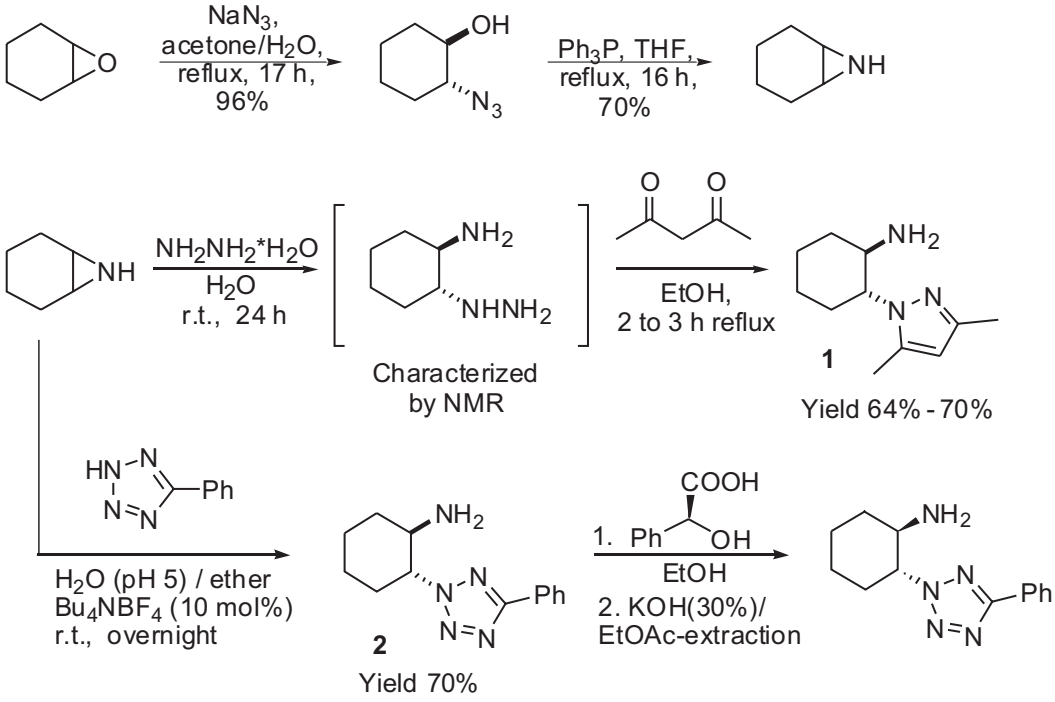
L.B. Krasnova and A.K. Yudin.[2] Davenport Building, Department of Chemistry, University of Toronto, 80 St. George Street, Toronto, ON M5S 3H6, Canada.

[1]This article is part of a Special Issue dedicated to Professor Howard Alper.

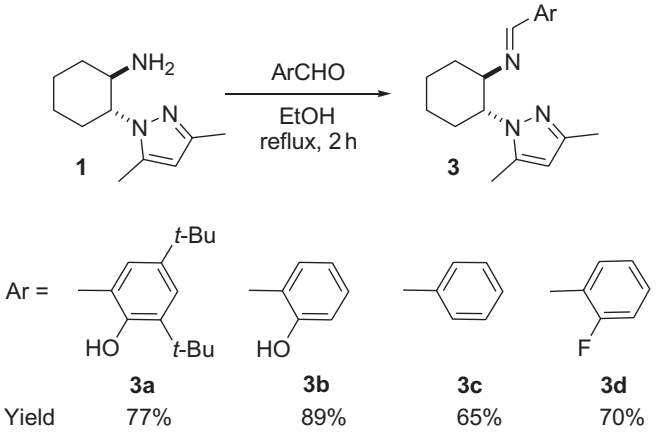
[2]Corresponding author (e-mail: ayudin@chem.utoronto.ca).

 doi: 10.1139/V05-113 © 2005 NRC Canada

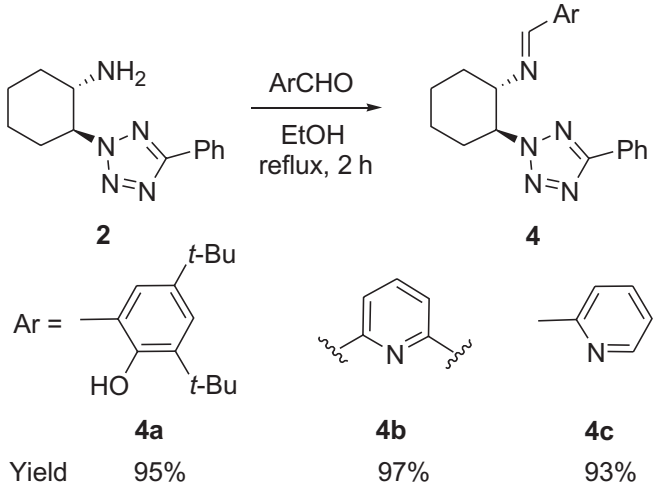
Scheme 1.



Scheme 2.



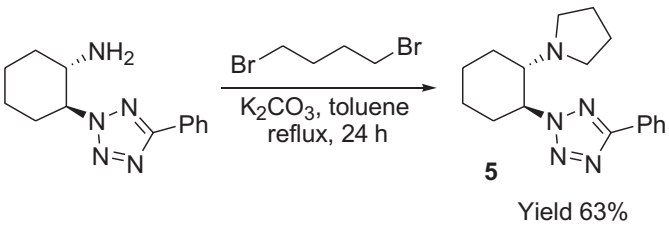
Scheme 3.



achieved with (*S*)-(–)-mandelic acid and (*S*)-(+)-camphorsulfonic acid. The enantiomeric purity was measured by ^{19}F NMR of the Mosher amide with (*R*)-(–)-MTPA.[3] The absolute stereochemistry of the amine was determined from the X-ray analysis of the diastereomeric salt obtained with (*S*)-(+)-mandelic acid. The amine **1** was resolved with D- or L-dibenzoyltartaric acid, however, we were not able to prove the absolute stereochemistry of enaniomerically pure **1**.

The corresponding imines of ligand precursor **1** were synthesized in good yields (Scheme 2). Different aromatic aldehydes were also used under similar reaction conditions to give the corresponding imines from aminotetrazole **2** (Scheme 3). The imines were synthesized in high yields. The amine **2** was found to be more stable than **1** and its derivatives and can be stored at room temperature without decomposition. In addition, tertiary amine **5** can be easily synthesized from **2** according to Scheme 4.

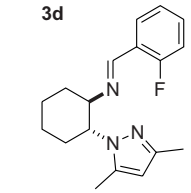
Scheme 4.



[3] The stereochemistry of the enantiomer obtained from the diastereomeric salt with (*S*)-(+)-10-camphorsulfonic acid was assigned to be opposite, since both enantiomers have different ^{19}F NMR signals in the Mosher amide with (*R*)-(+)-α-methoxy-α-(trifluoromethyl)phenyl acetic acid.

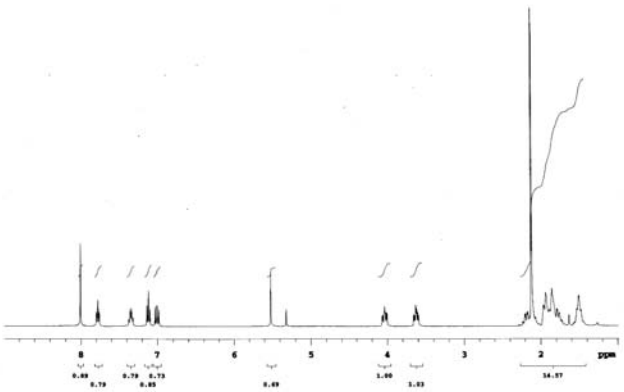
© 2005 NRC Canada

Fig. 1. ^{1}H NMR studies of Cu(I) coordination to ligand **3d**.



Shift of pyrazole and imine protons indicate coordination of Cu(I) to both pyrazole and imine functionalities.

Free ligand



Coordination to Cu(I)

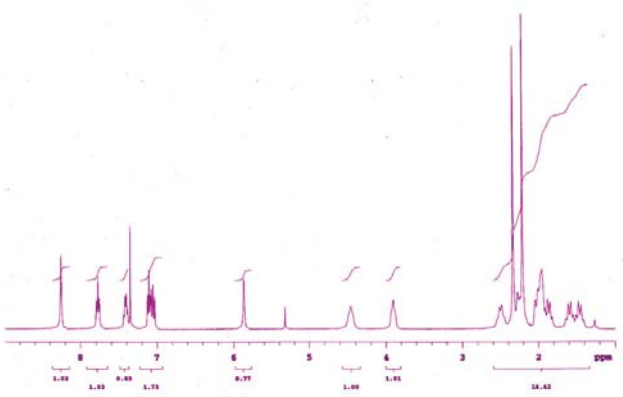
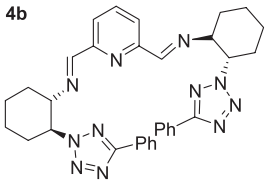
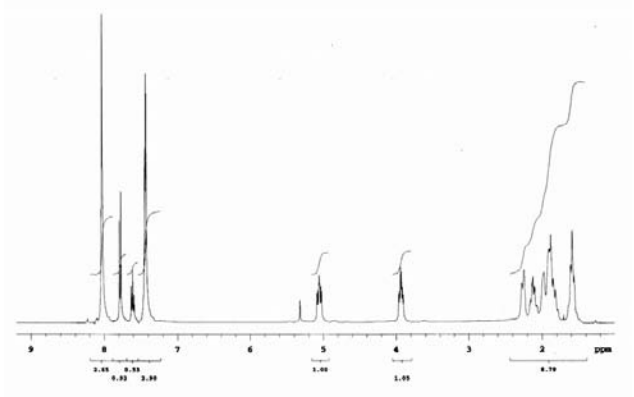


Fig. 2. ^{1}H NMR studies of Cu(I) coordination to ligand **4b**.

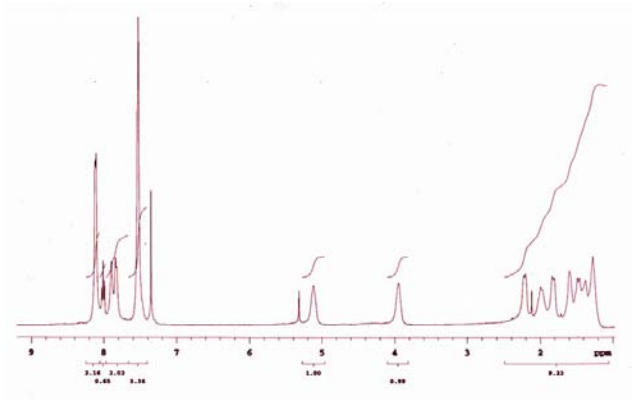


Shift of the pyridine para proton corresponds to the coordination of the metal to the pyridine ring.

Free ligand



Coordination to Cu(I)



We used ^{1}H NMR to evaluate the coordination ability of the newly synthesized ligands to transition metals. This allowed us to screen several complexes of different ligands with CuOTf·0.5C_6H_6. Coordination of the metal to the heterocycle moiety is known to induce a downfield shift of the aromatic proton signals (14). For example, ligand **3d** (Fig. 1) shows coordination to Cu(I) through the pyrazole and imine nitrogens. The imine proton shifts from 8.0 to 8.22 ppm, whereas the pyrazole proton shifts from 5.48 to 5.82 ppm. In addition, nonequivalent methyl protons of the pyrazole ring were observed in the spectrum of the Cu(I)/**3d** mixture. The other two examples did not reveal any copper coordination to the heterocycle moiety. Thus, comparison of the ^{1}H NMR of ligand **4b** with and without Cu(I) (Fig. 2) shows the downfield shift of the pyridine para proton (7.7–8.1 ppm) and corresponds to the copper coordination to the imine. This fact was also confirmed by the X-ray analysis of complex **6** (Fig. 3). No coordination between the tetrazole group and Cu(I) was observed. Importantly, the complex preserves the C_2 symmetry present in the starting material. On the other hand, mixing Cu(I) and ligand **5** showed coordination to the tertiary amine, whereas coordination to the tetrazole was not detected by ^{1}H NMR at all (Fig. 4).

No catalytic activity was observed when ligands **3a**–**3c** and **4a** were applied in asymmetric cyclopropanation according to the literature conditions (15). In light of these negative results, we were encouraged to obtain interesting data in the cyclopropanation using **4b** as the catalyst precursor (Scheme 5). The diastereoselectivity of the copper catalyzed cyclopropanation is known to mostly depend on the nature of the diazo compound ester group. The sterically bulky menthyl group usually gives the best trans:cis ratio. However, in the case of ligand **4b**, a 93:7 trans:cis ratio (determined by ^{1}H NMR) of the regioisomers was obtained even with a group as small as methyl. Unfortunately, the enantioselectivity was very low (<5%). In comparison, the background reaction without the ligand proceeds with a 57:43 trans:cis ratio. Under the same conditions, ligand **4c**

© 2005 NRC Canada

Fig. 3. X-ray structure of (*S*)-(*S*)-[2,6-di-*trans*-(5-phenyltetrazol-2-yl)cyclohexyl]pyridin-2-yl methylene-amine / Cu(I) complex (**6**).

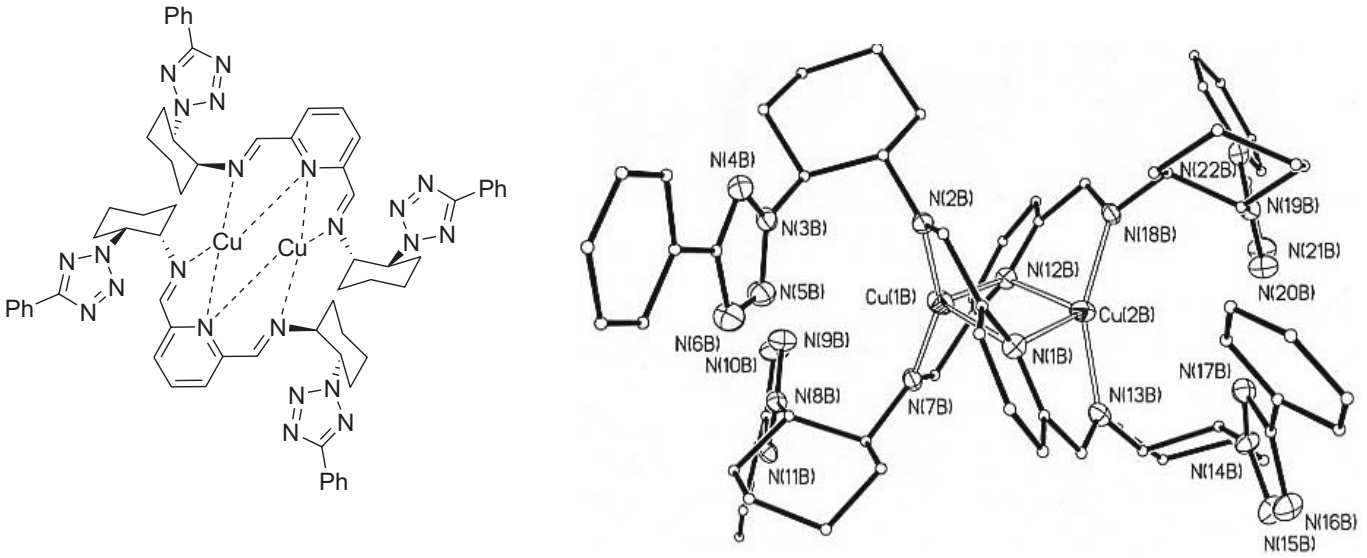
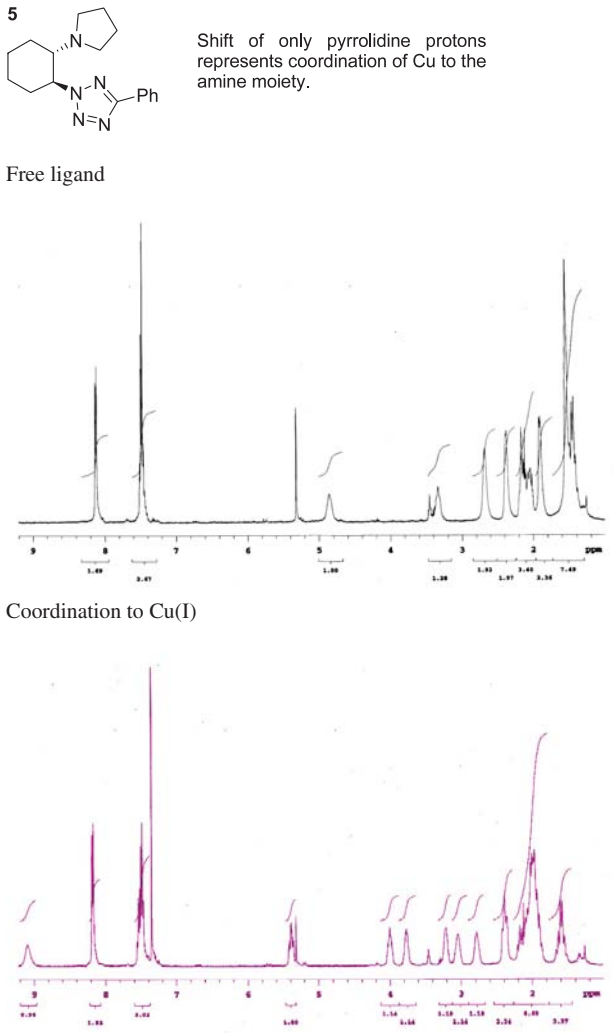


Fig. 4. ^{1}H NMR studies of Cu(I) coordination to ligand **5**.



gave lower diastereoselectivity (trans:cis ratio, 73:27). These results demonstrate that ligand **4b** gives the highest reported diastereoselectivity in cyclopropanation among the ligands synthesized to date. Unexpectedly, ruthenium, which is known to show better results with the pybox system compared to copper, showed no diastereoselectivity in the case of ligand **4b**. In comparison, diastereoselectivity as well as enantioselectivity for the cyclopropanation of styrene catalyzed by Cu(I) with a pybox-type ligand was found to be low (16).

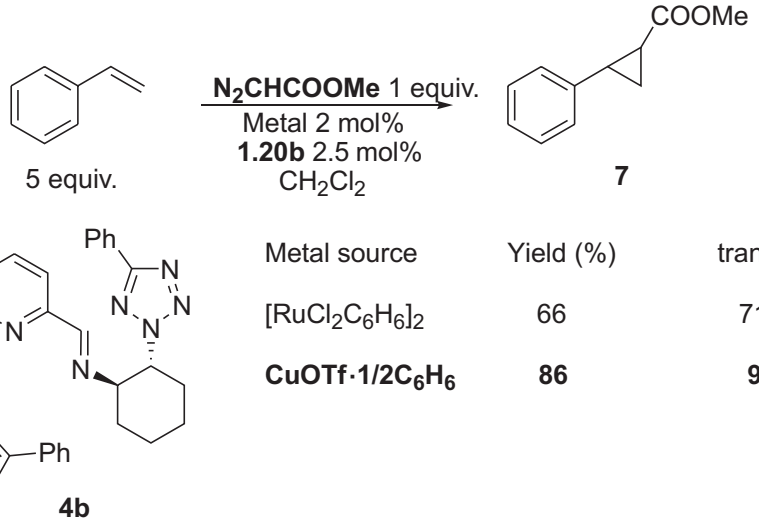
In summary, new *N*,*N*-ligands have been synthesized by the reaction of readily available cyclohexane based aziridines with appropriate nitrogen based nucleophiles under mild conditions. It was shown that Cu(I) coordinates to these ligands and, depending on modifications of the amino group, complexes of different stoichiometry can be obtained. The enantiomerically pure forms of one of the ligands were obtained and applied in the cyclopropanation reaction, where the copper catalyst revealed unexpectedly high diastereoselectivity in comparison with the ruthenium catalyst. The observed diastereoslectivity is superior to the known copper catalyzed cyclopropanation systems. The mechanistic basis for this observation is currently under scrutiny, along with attempts to find enantioselective systems in this new structural class.

Experimental section

Dichloromethane, ether, acetonitrile, toluene, and hexanes were purchased from Aldrich as "anhydrous". Tetrahydrofuran (THF) was dried over sodium benzophenone ketyl. Moisture-sensitive reactions were carried out using standard syringe–septum techniques under a nitrogen atmosphere. ^{1}H and ^{13}C NMR spectra were recorded on 300 or 400 MHz spectrometers. ^{1}H NMR spectra were referenced to residual $CHCl_3$ (δ 7.27 ppm), CH_2Cl_2 (δ 5.32 ppm), DMSO (δ 2.50 ppm), CH_3CN (δ 1.94 ppm), and benzene (δ 7.16 ppm); ^{13}C NMR spectra were referenced to $CDCl_3$ (δ 77.0 ppm), CD_2Cl_2 (δ 54.0 ppm), DMSO-d_6 (δ 99.5 ppm), CD_3CN (δ 118.7 ppm), and benzene-d_6 (δ 128.4 ppm).

© 2005 NRC Canada

Scheme 5.



Metal source	Yield (%)	trans:cis
$[RuCl_2C_6H_6]_2$	66	71:29
$CuOTf \cdot 1/2C_6H_6$	**86**	**93:7**

7-Azabicyclo[4.1.0]heptane (12)

A mixture of cyclohexene oxide (31 mL, 306 mmol) and NaN_3 (50.4 g, 775 mmol) in H_2O–acetone (1:1, 320 mL) mixture was heated to reflux for 17 h (temperature of the oil bath was 75 °C). Acetone was removed under reduced pressure and the residue extracted with Et_2O (3 × 160 mL). The combined extracts were washed with H_2O (2 × 40 mL) and dried over $MgSO_4$. After filtration, removal of the solvent yielded the azido alcohol (~93%–96% yield) as a practically pure yellow oil, which was concentrated and used in the next step without further purification. ^{1}H NMR (benzene-d_6) δ: 0.72–1.12 (m, 4H), 1.20–1.34 (m, 2H), 1.59 (m, 1H), 1.74 (m, 1H), 2.23 (s, 1H), 2.79 (m, 1H), 3.10 (m, 1H). ^{13}C NMR (benzene-d_6) δ: 24.7, 25.0, 30.7, 34.2, 67.7, 74.3.

Triphenylphosphine (77.2 g, 294 mmol) was added within 30 min to a solution of azidocyclohexanol (41.7 g, 294 mmol) in THF (250 mL) while N_2 evolved from the reaction mixture. The reaction mixture was then refluxed for 16 to 17 h. Pentane (~1 L) was added to precipitate $Ph_3P{=}O$, and the white precipitate was filtered off and the solvent was removed on a rotary evaporator (water bath 30–45 °C). The THF was distilled off at 25 mmHg (1 mmHg = 133.322 4 Pa), and the residue was again distilled at 45 °C (oil bath temperature) under vacuum (1 mmHg), collecting aziridine in the receiving flask, which was placed in a dry ice – acetone bath. 7-Azabicyclo[4.1.0]heptane (20 g, 70% yield) was obtained as a colorless oil, which solidified upon cooling at –5 °C. Storage: over KOH; bp 50 °C / 1 mmHg. ^{1}H NMR ($CDCl_3$) δ: 1.19–1.37 (m, 6H), 1.81 (m, 6H), 2.17 (m, 2H). ^{13}C NMR ($CDCl_3$) δ: 20.0, 24.5, 29.3.

***trans*-2-(3,5-Dimethyl-pyrazole-1-yl)cyclohexylamine (1)**

$NH_2NH_2 \cdot H_2O$ (490 μL, 10 mmol) was added to the 1 mol% solution of NH_4Cl in 2 mL of H_2O and 1 mL (10 mmol) of aziridine. The reaction was stirred at room temperature for several hours (24 h) and turned from a white suspension to the colorless solution. Upon completion, the reaction mixture was treated with 25–50 mL of benzene, concentrated, and dried under high vacuum. *trans*-2-Hydrazinocyclohexylamine was obtained as a colorless oil and was used without further purification in the next step. ^{1}H NMR (DMSO-d_6) δ: 1.14 (m, 4H), 1.60 (s, 2H), 1.73 (m, 1H), 1.83 (m, 2H), 2.29 (dt, J = 4.2, 10.5 Hz, 1H), 2.65 (dt, J = 4.2, 10.5 Hz, 1H), 3.56 (m, 1H). ^{13}C NMR (DMSO-d_6) δ: 24.5, 29.1, 31.6, 53.4, 63.2, 67.5.

The crude *trans*-2-hydrazinocyclohexylamine was suspended in 20 mL of ethanol and at 0 °C, 1 mL (12 mmol) of 2,4-pentadione was added dropwise and the reaction was stirred for another 30 min and then concentrated. The residue was washed with 5 mL of 30% KOH, and the water layer was extracted with EtOAc (3 × 25 mL), which was washed with brine, dried over Na_2SO_4, concentrated, and dried under the high vacuum. The product can be further purified by Kugelrohr distillation. *trans*-2-(3,5-Dimethylpyrazol-1-yl)cyclohexylamine (1.25 g, 65% yield) was obtained as a beige solid; mp 120 °C / 1 mmHg. ^{1}H NMR ($CDCl_3$) δ: 1.25–1.46 (m, 4H), 1.60–2.05 (m, 6H), 2.23 (s, 3H), 2.25 (s, 3H), 3.40 (dt, J = 5.2, 10.8 Hz, 1H), 3.59 (dt, J = 5.2, 10.8 Hz, 1H), 5.77 (s, 1H). ^{13}C NMR ($CDCl_3$) δ: 11.3, 13.8, 24.8, 25.6, 32.2, 34.6, 53.8, 64.5, 104.6, 139.5, 147.8.

***trans*-2-(5-Phenyltetrazol-2-yl)cyclohexylamine (2)**

Aziridine (1.75 mL, 17 mmol) was added to the reaction mixture containing Bu_4NBF_4 (570 mg, 1.7 mmol) and 2.5 g (17 mmol) of tetrazole in 34 mL of buffered H_2O (AcONa–AcOH, pH 5) / ether mixture (1:1). The reaction was stirred for 5 to 6 h. Completion of the reaction was confirmed by TLC (hexane–EtOAc, 8:2). The reaction was quenched with 5% NaOH and extracted with EtOAc. Combined organic extracts were washed with brine, dried over $MgSO_4$, and concentrated. The product was purified by flash chromatography on silica gel (hexane–EtOAc, 6:4 with 3 vol% of Et_3N). *trans*-2-(5-Phenyltetrazol-2-yl)cyclohexylamine (2.96 g, 70% yield) was obtained as a white solid; mp 70–72 °C. ^{1}H NMR ($CDCl_3$) δ: 1.35–1.54 (m, 4H), 1.85–2.24 (m, 4H), 3.37 (dt, J = 4.5, 11.1 Hz, 1H), 4.47 (m, 1H), 7.43–8.15 (m, 5H). ^{13}C NMR ($CDCl_3$) δ: 25.0, 25.3, 32.5, 35.0, 54.1, 71.5, 126.8, 127.6, 128.9, 130.2, 164.8.

Resolution of *trans*-2-(3,5-dimethylpyrazol-1-yl)cyclohexylamine (1) with D-(+)-dibenzoyl tartaric acid

D-(+)-Dibenzoyltartaric acid (1.5 equiv.) was added to the

© 2005 NRC Canada

solution of amine in a minimum amount of CH_2Cl_2–MeOH (9:1). The reaction was heated to dissolve the acid and then cooled to room temperature. The precipitate was filtered off and recrystallized from CH_2Cl_2–MeOH. ^{1}H NMR (DMSO-d_6) δ: 1.29–1.80 (m, 8H), 2.10 (s, 3H), 2.18 (s, 3H), 2.59 (s, 4H), 3.58 (dt, J = 4.5, 10.2 Hz, 1H), 4.97 (dt, J = 4.5, 10.2 Hz, 1H), 5.73 (s, 1H), 7.49–8.00 (m, 10H).

The precipitate was hydrolyzed with KOH, and extracted with EtOAc, dried over Na_2SO_4, and concentrated to give 184 g (48% yield) of one of the enantiomers of *trans*-2-(3,5-dimethylpyrazol-1-yl)cyclohexylamine obtained as a white solid, with 99.9% ee determined from the ^{19}F NMR of the Mosher amide (–69.55 ppm signal).

General procedure for the resolution of *trans*-2-(5-phenyltetrazol-2-yl)cyclohexylamine (2)

Racemic *trans*-2-(5-phenyltetrazol-2-yl)cyclohexylamine (4.23 g, 17.4 mmol) was dissolved in 50 mL of 95% EtOH and reacted with 0.7 equiv. (12.2 mmol) of resolving acid. In the case of mandelic acid, the precipitate was dissolved in an additional 200 mL of ethanol. The hot, clear solution was then cooled down to room temperature and a crystalline precipitate was filtered off and recrystallized from ethanol. The precipitate was hydrolyzed with KOH and the water layer was extracted with EtOAc (3 × 50 mL), dried over Na_2SO_4, and concentrated.

(*R*)-(*R*)-*trans*-2-(5-Phenyltetrazol-2-yl)cyclohexylamine (2)

(*R*)-(*R*)-*trans*-2-(5-phenyltetrazol-2-yl)cyclohexylamine (490 mg, 70% yield) was obtained through the formation of a diastereomeric salt with (*S*)-(+)-mandelic acid, followed by hydrolysis. (*R*)-(*R*)-*trans*-2-(5-Phenyltetrazol-2-yl)cyclohexylamine was isolated as a white solid with 99.9% ee, determined from the ^{19}F NMR of the Mosher amide (–69.82 ppm). Absolute stereochemistry of the amine was determined from the X-ray analysis (see Supplementary notes)[4] of the diastereomeric salt with (*S*)-(+)-mandelic acid. A sample for X-ray analysis was obtained after recrystallization from ethanol; mp 204–205.5 °C. ^{1}H NMR (DMSO-d_6) δ: 1.42 (m, 2H), 1.68–2.20 (m, 5H), 3.39 (m, 1H), 4.70 (s, 1H), 4.81 (dt, J = 4.2, 11.7 Hz, 1H), 5.20 (br s, 1H), 7.18–8.08 (m, 10H). ^{13}C NMR (DMSO-d_6) δ: 23.7, 24.0, 31.9 (d, J = 78.9 Hz), 52.9, 67.0, 72.8, 126.0, 126.1, 126.4, 126.9, 127.3, 128.9, 130.1, 141.8, 163.5, 173.9.

(*S*)-(*S*)-*trans*-2-(5-Phenyltetrazol-2-yl)cyclohexylamine (2)

(*S*)-(*S*)-*trans*-2-(5-Phenyltetrazol-2-yl)cyclohexylamine (455 mg, 65% yield) was obtained through the formation of a diastereomeric salt with (*S*)-(+)-10-camphorsulfonic acid, followed by hydrolysis. (*S*)-(*S*)-*trans*-2-(5-Phenyltetrazol-2-yl)cyclohexylamine was isolated as a white solid with 99.9% ee, determined from the ^{19}F NMR of the Mosher amide (–70.07 ppm); mp 194 °C. ^{1}H NMR (DMSO-d_6) δ: 0.73 (s, 3H), 1.03 (s, 3H), 1.26 (m, 1H), 1.40–2.30 (m, 9H), 2.38 (d, J = 15 Hz, 1H), 2.66 (m, 1H), 2.88 (d, J = 15 Hz, 1H), 3.38 (s, 3H), 3.69 (m, 1H), 5.04 (dt, J = 3.9, 11.4 Hz, 1H), 7.57 (m, 2H), 8.08 (m, 3H). ^{13}C NMR (DMSO-d_6) δ: 19.6, 20.2, 22.9, 23.6, 24.1, 26.4, 29.5, 31.5, 42.2 (d, J = 44.4 Hz), 46.7, 47.1, 52.4, 58.2, 64.3, 126.5, 127.1, 129.3, 130.7, 164.4, 216.4.

General procedure for Mosher amide synthesis (17)

Oxalyl chloride (5 μL, 0.057 mmol) was added to a stock solution of (*R*)-(+)-MTPA (2.8 mg, 0.012 mmol) in DMF (0.95 μL, 0.012 mmol) / hexane (0.5 mL) at room temperature. A white precipitate formed immediately with evolution of gas. After 1 h, the mixture was filtered and concentrated in vacuo. A solution of amine (0.01 mmol), Et_3N (4 μL, 0.03 mmol), and DMAP (small crystals, ~1 mg) in $CDCl_3$ (100 μL) was added to the residue. After 1 h, ^{1}H NMR and ^{19}F NMR of the mixture revealed the conversion into the diastereomeric Mosher amide. *N*-[*trans*-2-(3,5-Dimethylpyrazol-1-yl)-cyclohexyl]-3,3,3-trifluoro-2-methoxy-2-phenylpropionamide: ^{19}F NMR ($CDCl_3$, ppm) δ: –65.5 or –69.5. 3,3,3-Trifluoro-2-methoxy-2-phenyl-*N*-[*trans*-2-(5-phenyltetrazol-2-yl)cyclohexyl]propionamide: ^{19}F NMR ($CDCl_3$, ppm) δ: –69.8 or –70.1.

General procedure for imine synthesis (18)

A solution of the amine (1 or 2 equiv. in case **4b**) and the appropriate aromatic aldehyde (1–1.2 equiv.) in EtOH (0.1 mol/L reaction mixture) was refluxed for 2 to 3 h. The solvent was removed and pentane was added to the resulting oil. If the imine does not crystallize after 24 h at –25 °C, it can be purified by column chromatography on silica gel (eluent: hexane–EtOAc, 6:4 with 5 vol% of Et_3N) followed by crystallization from pentane or hexane.

2,4-Di-(*tert*-butyl-6-{[*trans*-2-(3,5-dimethylpyrazol-1-yl)cyclohexylimino]methyl}phenol (3a)

2,4-Di-(*tert*-butyl-6-{[*trans*-2-(3,5-dimethylpyrazol-1-yl)cyclohexylimino]methyl}phenol (36.5 mg, 77% yield) was obtained as a yellow solid after recrystallization from pentane. ^{1}H NMR ($CDCl_3$) δ: 1.26 (s, 9H), 1.41 (s, 9H), 1.46–2.24 (m, 8H), 2.09 (s, 3H), 2.19 (s, 3H), 3.67 (dt, J = 4.5, 10.8 Hz, 1H), 3.97 (m, 1H), 5.53 (s, 1H), 6.80 (d, J = 2.7 Hz, 1H), 7.30 (d, J = 2.4 Hz, 1H), 7.76 (s, 1H). ^{13}C NMR ($CDCl_3$) δ: 11.3, 14.1, 24.5, 25.8, 29.8, 31.7, 31.8, 34.4, 35.3, 61.2, 72.1, 100.1, 104.4, 117.9, 126.0, 126.7, 136.3, 139.7, 147.3, 157.8, 163.0, 166.0.

2-{[*trans*-2-(3,5-Dimethylpyrazol-1-yl)cyclohexylimino]-methyl}phenol (3b)

2-{[*trans*-2-(3,5-Dimethylpyrazol-1-yl)cyclohexylimino]-methyl}phenol (2.65 g, 89% yield) was obtained as an orange solid. ^{1}H NMR ($CDCl_3$) δ: 1.40–2.00 (m, 8H), 2.07 (s, 3H), 2.20 (s, 3H), 3.95 (dt, J = 4.2, 9.9 Hz, 1H), 3.70 (m, 1H), 5.56 (s, 1H), 6.79–7.26 (m, 4H), 7.71 (s, 1H). ^{13}C NMR ($CDCl_3$) δ: 11.1, 13.8, 24.2, 25.5, 31.4, 33.8, 60.9, 72.1, 104.4, 117.0, 118.7, 118.9, 131.6, 132.3, 140.0, 147.7, 161.1, 165.4.

[4] Supplementary data for this article are available on the Web site or may be purchased from the Depository of Unpublished Data, Document Delivery, CISTI, National Research Council Canada, Ottawa, ON K1A 0S2, Canada. DUD 4003. For more information on obtaining material refer to http://cisti-icist.nrc-cnrc.gc.ca/irm/unpub_e.shtml. CCDC 271471 contains the crystallographic data for this manuscript. These data can be obtained, free of charge, via www.ccdc.cam.ac.uk/conts/retrieving.html (Or from the Cambridge Crystallographic Data Centre, 12 Union Road, Cambridge CB2 1EZ, UK; fax +44 1223 336033; or deposit@ccdc.cam.ac.uk).

© 2005 NRC Canada

Benzylidene[*trans*-2-(3,5-dimethylpyrazol-1-yl)cyclohexyl]amide (3c)

Benzylidene[2-(3,5-dimethylpyrazol-1-yl)cyclohexyl]amide (1.69 g, 75% yield) was obtained as a yellow solid (purified by column chromatography and then recrystallized from pentane); mp 89 °C. ^{1}H NMR ($CDCl_3$) δ: 1.10–2.25 (m, 8H), 2.11 (s, 3H), 2.18 (s, 3H), 3.61 (dt, *J* = 4.5, 10.5 Hz, 1H), 4.02 (m, 1H), 5.50 (s, 1H), 7.32–7.50 (m, 5H), 7.64 (s, 1H). ^{13}C NMR ($CDCl_3$) δ: 11.5, 14.1, 24.5, 25.8, 31.4, 33.9, 60.9, 74.1, 103.9, 127.9, 128.4, 130.4, 136.4, 139.8, 147.0, 161.00.

[*trans*-2-(3,5-Dimethylpyrazol-1-yl)cyclohexyl]-(2-fluorobenzylidene)amine (3d)

[2-(3.5-Dimethylpyrazol-1-yl)cyclohexyl]-(2-fluorobenzylidene)amine (21 mg, 70% yield) was obtained as a beige solid; mp 74 °C. ^{1}H NMR ($CDCl_3$) δ: 1.40–2.40 (m, 8H), 2.16 (s, 3H), 2.21 (s, 3H), 3.70 (dt, *J* = 4.2, 10.5 Hz, 1H), 4.07 (m, 1H), 5.56 (s, 1H), 6.98–7.82 (m, 4H), 8.05 (s, 1H). ^{13}C NMR ($CDCl_3$) δ: 11.3, 13.8, 24.2, 25.6, 31.2, 33.7, 60.8, 74.4, 104.0, 115.9 (d, *J* = 84.3 Hz), 124.0, 124.3, 127.5, 132.1 (d, *J* = 34 Hz), 139.9, 147.5, 154.8, 164.0. ^{19}F NMR ($CDCl_3$) δ: –122.1 (dq, *J* = 5.7, 7.5 Hz).

(*S*)-(*S*)-2,4-Di-*tert*-butyl-6-{[*trans*-2-(5-phenyltetrazol-2-yl)cyclohexylimino]methyl}phenol (4a)

(*S*)-(*S*)-2,4-Di-*tert*-butyl-6-{[*trans*-2-(5-phenyltetrazol-2-yl)cyclohexylimino]methyl}phenol (210 mg, 95% yield) was obtained as a yellow solid after recrystallization from pentane. ^{1}H NMR ($CDCl_3$) δ: 1.18 (s, 9H), 1.28 (s, 9H), 1.48–2.34 (m, 8H), 3.91 (dt, *J* = 4.8, 10.8 Hz, 1H), 5.01 (m, 1H), 6.87 (d, *J* = 2.4 Hz, 1H), 7.30 (d, *J* = 2.4 Hz, 1H), 7.7.43–8.01 (m, 5H), 8.15 (s, 1H). ^{13}C NMR ($CDCl_3$) δ: 24.1, 24.8, 29.5, 29.6, 31.5, 31.6, 31.1, 34.2, 35.2, 68.0, 71.1, 117.7, 126.3, 127.1, 127.5, 129.0, 130.3, 136.8, 140.3, 158.0, 164.8, 166.9.

(*S*)-(*S*)-[2,6-Di-*trans*-(5-phenyltetrazol-2-yl)cyclohexyl]pyridin-2-yl methyleneamine (4b)

(*S*)-(*S*)-[2,6-Di-*trans*-(5-phenyltetrazol-2-yl)cyclohexyl]pyridin-2-yl methyleneamine (142 mg, 97% yield) was obtained as a beige solid after recrystallization from pentane. ^{1}H NMR ($CDCl_3$) δ: 1.50–2.30 (m, 8H), 3.92 (dt, *J* = 5.1, 9.9 Hz, 1H), 5.07 (m, 1H), 7.40 (m, 3H), 7.55 (t, *J* = 7.8 Hz, 0.5H), 7.77 (d, *J* = 7.8 Hz, 1H), 8.02 (m, 2H). ^{13}C NMR ($CDCl_3$) δ: 24.1, 25.1, 32.0, 33.7, 67.9, 72.2, 122.5, 126.8, 127.7, 128.7, 130.0, 136.8, 153.5, 162.2, 164.6.

(*S*)-(*S*)-[*trans*-2-(5-Phenyltetrazol-2-yl)cycloexyl]pyridin-2-yl methyleneamine (4c)

(*S*)-(*S*)-[*trans*-2-(5-Phenyltetrazol-2-yl)cyclohexyl]pyridin-2-yl methyleneamine (123 mg, 93% yield) was obtained as a pale brown solid. ^{1}H NMR ($CDCl_3$) δ: 1.50–2.30 (m, 8H), 4.00 (dt, *J* = 4.8, 10.2 Hz, 1H), 5.12 (m, 1H), 7.17–8.50 (m, 7H), 8.15 (s, 1H). ^{13}C NMR ($CDCl_3$) δ: 24.1, 25.0, 32.0, 33.6, 67.8, 72.1, 121.5, 124.8, 126.7, 127.5, 128.7, 130.0, 136.4, 149.1, 153.8, 162.4, 164.5.

5-Phenyl-2-((*R*)-(*R*)-*trans*-2-pyridin-1-ylcyclohexyl)-2*H*-tetrazole (5)

trans-2-(3,5-Dimethylpyrazol-1-yl)cyclohexylamine (100 mg, 0.411 mmol) 1,4-dibromobutane (54 μL, 0.452 mmol, 1.1 equiv.), and 68 mg (0.822 mmol, 2 equiv.) of $NaHCO_3$ in toluene (1 to 2 mL) were refluxed under N_2 with good stirring and Dean–Stark removal of water for 19–24 h (controlled by TLC). The reaction mixture was concentrated and purified by column chromatography (hexane with 5 vol% of Et_3N, then hexane–EtOAc, 6:4 with 5 vol% of Et_3N). 5-Phenyl-2-(*trans*-2-pyridin-1-ylcyclohexyl)-2*H*-tetrazole (230 mg, 77% yield) was obtained as a brown solid. ^{1}H NMR (CD_2Cl_2) δ: 1.30–2.10 (m, 6H), 1.92 (br s, 2H), 2.18 (br s, 2H), 2.39 (br s, 2H), 2.69 (br s, 2H), 3.36 (br s, 1H), 4.85 (br s, 1H), 7.40–8.20 (m, 5H). ^{13}C NMR (CD_2Cl_2) δ: 23.9, 24.8, 25.1, 25.3, 31.1, 31.8, 32.9, 47.7, 62.2, 66.1, 127.0, 128.2, 129.0, 130.1, 164.4.

General procedure for ^{1}H NMR studies

The ligand (0.02 mmol) in CD_2Cl_2 was mixed at room temperature with 0.02 mmol of $CuOTf{\cdot}0.5C_6H_6$, stirred at room temperature for 1 h, and filtered. In the case of **4b**, upon mixing in an 1:1 ratio (Cu^I/L), part of the metal complex did not dissolve. A sample of 1:2 ratio (Cu^I/L) was prepared, which showed the same ^{1}H NMR spectra as the first sample.

Cu^I coordination to 3d

^{1}H NMR (CD_2Cl_2) δ: 1.44–1.61 (m, 2H), 1.85–2.60 (m, 6H), 2.12 (s, 3H), 2.34 (s, 3H), 3.90 (br s, 1H), 4.45 (br s, 1H), 5.87 (s, 1H), 7.03–7.79 (m, 4H), 8.25 (s, 1H). ^{19}F NMR (CD_2Cl_2) δ: –122.1 (dq, *J* = 5.7, 7.5 Hz).

Cu^I coordination to 4b

The NMR sample gave red crystals of complex **1.23** after storage at room temperature for several days in an inert atmosphere upon slow addition of hexane. These sample crystals were further characterized by X-ray analysis. ^{1}H NMR (CD_2Cl_2) δ: 1.26–2.23 (m, 8H), 3.95 (br s, 1H), 5.11 (br s, 1H), 7.52 (br s, 3H), 7.85 (m, 1H), 8.01 (t, *J* = 8 Hz, 0.5H), 8.10 (m, 2H).

Cu^I coordination to 5

^{1}H NMR (CD_2Cl_2) δ: 1.50 (m, 2H), 1.86–2.20 (m, 8H), 2.39 (m, 2H), 2.78 (br s, 1H), 3.04 (br s, 1H), 3.77 (m, 1H), 4.00 (m, 1H), 5.39 (m, *J* = 4.4, 10.8 Hz, 1H), 7.50 (m, 3H), 8.17 (d, *J* = 7.2 Hz, 2H), 9.09 (br s, 1H).

General procedure for cyclopropanation

A flame-dried Schlenk flask was charged with metal precursor (2 mol%, 0.007 mol/L stock solution in CH_2Cl_2), ligand (4 mol%, 0.1 mol/L stock solution in CH_2Cl_2), and styrene (5 equiv.) and the reaction was stirred under an inert atmosphere at room temperature in approximately 1 mL of CH_2Cl_2. A solution of 1 mL (1 equiv., 1 mmol) of $N_2CHCOOMe$ in dichloromethane (1 mL) was added gradually over 8–10 h via a syringe pump and the reaction mixture was stirred for another 10–12 h. The reaction was concentrated and the product was purified by column chromatography (hexane, then hexane–EtOAc (8:2)).

2-Phenylcyclopropanecarboxylic acid methyl ester (7)

2-Phenylcyclopropanecarboxylic acid methyl ester was obtained as a colorless oil. Yield with $[RuCl_2C_6H_6]_2$ was

© 2005 NRC Canada

found to be 66% with a trans:cis ratio of 71:29 determined from ^{1}H NMR. Yield with CuOTf·0.5C_6H_6 was found to be 86% with a trans:cis ratio of 93:7 determined from ^{1}H NMR. **a**: ^{1}H NMR ($CDCl_3$) δ: 1.32 (m, 1H), 1.60 (m, 1H), 1.90 (m, 1H), 2.43 (m, 1H), 3.72 (s, 3H), 7.09–7.31 (m, 5H). **b**: ^{1}H NMR ($CDCl_3$) δ: 0.88 (m, 1H), 1.70 (m, 1H), 2.10 (m, 1H), 2.57 (m, 1H), 3.45 (s, 3H), 7.09–7.31 (m, 5H)

Acknowledgments

We thank the Natural Sciences and Engineering Research Council of Canada (NSERC), Foundation for Innovation, ORDCF, Affinium Pharmaceuticals, Amgen, and the University of Toronto for financial support.

References

1. H. Tokahashi, M. Yoshioka, M. Shibasaki, M. Ohno, N. Imai, and S. Kobayashi. Tetrahedron, **51**, 12 013 (1995); I. Ojima (*Editor*). Catalytic asymmetric synthesis. VCH, New York. 2000.
2. B.M. Trost and R.C. Bunt. Angew. Chem. Int. Ed. Engl. **35**, 99 (1996).
3. B.M. Trost, R. Radinov, and E.M. Grenzer. J. Am. Chem. Soc. **119**, 7879 (1997).
4. B.M. Trost, E.J. McEachern, and F.D. Toste. J. Am. Chem. Soc. **120**, 12 702 (1998).
5. M. Palucki, P.J. Pospisil, W. Zhang, and E.N. Jacobsen. J. Am. Chem. Soc. **116**, 9333 (1994).
6. M. Palucki, P. Hanson, and E.N. Jacobsen. Tetrahedron Lett. **33**, 7111 (1992).
7. S.E. Schaus, J. Brånalt, and E.N. Jacobsen. J. Org. Chem. **63**, 403 (1998).
8. R.T. Ruck and E.N. Jacobsen. J. Am. Chem. Soc. **124**, 2882 (2002).
9. L.E. Martinez, J.L. Leighton, D.H. Carsten, and E.N. Jacobsen. J. Am. Chem. Soc. **117**, 5897 (1995).
10. F. Fache, E. Schulz, M.L. Tommasino, and M. Lemaire. Chem. Rev. **100**, 2159 (2000).
11. A. Caiazzo, S. Dalili, and A.K. Yudin. Org. Lett. **4**, 2597 (2002).
12. J. Christoffers, Y. Schulze, and J. Pickardt. Tetrahedron, **57**, 1765 (2001).
13. H.C. Kolb, M.G. Finn, and K.B. Sharpless. Angew. Chem. Int. Ed. **40**, 2004 (2001).
14. (*a*) H. Günther. NMR spectroscopy. John Wiley and Sons, Ltd., Toronto, Ontario. 1980; (*b*) For a specific example, see: F. Tuna, J. Hamblin, A. Jackson, G. Clarkson, N.W. Alcock, and M.J. Hannon. Dalton Trans. **11**, 2141 (2003).
15. D.L. Christenson, C.J. Tokar, and W.B. Tolman. Organometallics, **14**, 2148 (1995).
16. A.D. Gupta, D. Bhuniya, and V.K. Singh. Tetrahedron, **50**, 13 725 (1994).
17. D.E. Ward and C.K. Rhee. Tetrahedron Lett. **32**, 7165 (1999).
18. M. Barz, M.U. Rauch, and W.R. Thiel. J. Chem. Soc. Dalton Trans. 1, 2155 (1997).

© 2005 NRC Canada

RAPID COMMUNICATION / COMMUNICATION RAPIDE

Anion effects in the formation of the active catalyst in the Ruhrchemie – Rhône-Poulenc aqueous biphasic hydroformylation process. Are there any?[1]

József Kovács, Ferenc Joó, and Carl D. Frohning

Abstract: The water soluble [Rh(OAc)(CO)(*m*tppms)$_2$] containing monosulfonated triphenylphosphine ligands was prepared for the first time and its hydrogenation was studied in aqueous solutions. In the presence of additional *m*tppms, the reaction yielded [RhH(CO)(*m*tppms)$_3$], a close analogue of [RhH(CO)(*m*tppts)$_3$], the immediate catalyst precursor in the Ruhrchemie – Rhône-Poulenc aqueous biphasic hydroformylation process. The extent of the [Rh(OAc)(CO)(*m*tppms)$_2$] → [RhH(CO)(*m*tppms)$_3$] transformation strongly depended on the solution pH, similar to the case of the hydrogenation of [RhCl(CO)(*m*tppms)$_2$] studied earlier. In this respect, $RhCl_3$·aq and $Rh(OAc)_3$·aq can be used equally well for the in situ preformation of [RhH(CO)(*m*tppts)$_3$], although the latter is the preferred choice in the industrial process.

Key words: rhodium, water-soluble, hydrides, sulfonated phosphines, biphasic.

Résumé : On a préparé pour la première fois les complexes [Rh(OAc)(CO)(*m*tppms)$_2$] qui sont solubles dans l'eau et qui contiennent des ligands triphénylphosphines monosulfonées et on a étudié leur hydrogénation dans des conditions aqueuses. En présence de *m*tppms additionnel, la réaction a conduit à la formation du [RhH(CO)(*m*tppms)$_3$], un analogue apparenté au [RhH(CO)(*m*tppts)$_3$], le précurseur immédiat du catalyseur utilisé dans le procédé d'hydroformylation biphasique aqueuse de la société Ruhrchemie – Rhône-Poulenc. Le degré de transformation de [Rh(OAc)(CO(*m*tppms)$_2$] → [RhH(CO)(*m*tppms)$_3$] dépend fortement du pH de la solution, ce qui est semblable à ce qui a été observé antérieurement dans le cas de l'hydrogénation du [RhCl(CO)(*m*tppms)$_2$]. À cet effet, le $RhCl_3$·aq et le $Rh(OAc)_3$·aq peuvent être utilisés aussi bien l'un que l'autre pour la préformation in situ du [RhH(CO)(*m*tppts)$_3$], même si le dernier est préféré dans le procédé industriel.

Mots clés : rhodium, soluble dans l'eau, hydrures, phosphines sulfonées, biphasique.

[Traduit par la Rédaction]

Introduction

The Ruhrchemie – Rhône-Poulenc process for the aqueous/organic biphasic hydroformylation of propene (1–3) was introduced into the industrial scene more than two decades ago. The key to the success of this process was the invention of an utterly hydrophilic, active, and stable catalyst [RhH(CO)(*m*tppts)$_3$] (*m*tppts = 3,3′,3″-phosphinetriylbenzenesulfonic acid, *meta*-trisulfonated triphenylphosphine) (4). In practice, the catalyst is *preformed* from suitable precursors, most commonly from hydrated rhodium(III) acetate and *m*tppts under synthesis gas pressure, and used without isolation (5). Under actual hydroformylation conditions, [RhH(CO)(*m*tppts)$_3$] is involved in various chemical equilib-

Received 11 January 2005. Published on the NRC Research Press Web site at http://canjchem.nrc.ca on 12 May 2005.

Dedicated to Professor Howard Alper in recognition of his outstanding achievements in organic and organometallic chemistry and catalysis.

J. Kovács. Homogeneous Catalysis Research Group, Hungarian Academy of Sciences, University of Debrecen, P.O. Box 7, 4010 Debrecen, Hungary.
F. Joó.[2] Homogeneous Catalysis Research Group, Hungarian Academy of Sciences and Institute of Physical Chemistry, University of Debrecen, P.O. Box 7, 4010 Debrecen, Hungary.
C.D. Frohning. Regnitstr. 50, 46485 Wesel, Germany.

[1]This article is part of a Special Issue dedicated to Professor Howard Alper.
[2]Corresponding author (e-mail: fjoo@delfin.unideb.hu).

 doi: 10.1139/V05-088 © 2005 NRC Canada

ria, leading to the formation of $[RhH(CO)_2(mtppts)_2]$, $[RhH(CO)_2(mtppts)]$, and $[RhH(CO)(mtppts)_2]$ (2–5). Of these compounds, $[RhH(CO)(mtppts)_2]$ is the active catalyst for the formation of linear products, and these equilibria have been studied in detail (6) to obtain optimum rate and selectivity performance of the in situ formed catalyst.

Despite the continuous research and development, a few questions with regard to the reaction mechanism still deserve scrutiny. One of these is the effect of pH on the rate of hydroformylation. It is known that an increase in pH from 5.5 to 7.5 brings about a 35% increase in the reaction rate of the hydroformylation of propene (1). A similar rate increase was observed in the reaction of octene-1 (7). Since the chemical reaction does not involve H^+ or OH^-, the answer may involve the pH-sensitivity of the formation and further equilibria of the catalytically active rhodium complexes.

Some time ago, it was shown that the hydrogenation of the related, water-soluble $[RhCl(CO)(mtppms)_2]$ complex (*m*tppms = (3-diphenylphosphino)benzenesulfonic acid, *meta*-monosulfonated triphenylphosphine) in aqueous solution was, indeed, governed by the pH (8). In the presence of excess *m*tppms and chloride, the hydrogenation of $[RhCl(CO)(mtppms)_2]$ to yield $[RhH(CO)(mtppms)_3]$ did not take place below pH 4.5 but reached 100% conversion at pH 10. Importantly, at basicities between pH 5 and 8, the conversion increased gradually with the gradual increase of pH, and that referred to a pH-dependent mobile equilibrium (eq. [1]).

$$[1] \quad [RhCl(CO)(mtppms)_2] + mtppms + H_2 = [RhH(CO)(mtppms)_3] + H^+ + Cl^-$$

Although the conditions of this model study and those of the industrial hydroformylation strongly differ, one may expect similar equilibria be involved in the pH dependence of the hydroformylation reaction. However, albeit hydrated $RhCl_3$ is a suitable starting material for the synthesis of $[RhH(CO)(mtppts)_3]$, industry prefers $Rh(OAc)_3$·aq ($OAc^- = CH_3COO^-$) for the preformation of the catalyst to avoid the presence of the strongly nucleophilic chloride (4, 5). On the contrary, the pH-static hydrogenations [8] were performed at constant ionic strength maintained by KCl. The question arose, therefore, whether it is justified to draw conclusions regarding the pH effects on the formation of $[RhH(CO)(mtppts)_3]$ based on studies of chloride-containing systems, or to put it another way, whether there is an effect of the anion of the precursor on the formation of this hydroformylation catalyst. In the following, we report the results of a pH-static hydrogenation study of $[Rh(OAc)(CO)(mtppms)_2]$ under chloride-free conditions.

Experimental

All manipulations were done under an argon or nitrogen atmosphere. All solvents were purified by distillation and carefully deaerated before use.

IR spectra were recorded on a PerkinElmer Paragon 1000 PC FT-IR spectrometer in KBr discs. ^1H and ^{31}P NMR spectra were recorded on Bruker AV 360 equipment in D_2O or $(CD_3)_2SO$ (DMSO-d_6). Chemical shifts are referenced to residual solvent peaks further referenced to external 2,2-dimethyl-2-silapentane-5-sulfonate (DSS) sodium salt (^1H) and 85% H_3PO_4 (^{31}P), respectively. Conditions of the pH-potentiometric measurements are described in detail in refs. 9 and 10.

$RhCl_3$·aq was purchased from the Pressure Chemical Co. (Pittsburgh, Pennsylvania), D_2O and DMSO-d_6 from Cambridge Isotope Laboratories, and H_2, N_2, Ar, and CO from Linde (Hungary). Other reagents were obtained from Aldrich and used without further purification. *m*tppms (Na^+-salt) (11) and $[Rh(OAc)_2]_2$·2MeOH (12) were prepared as described in the literature.

$[Rh(OAc)(CO)(mtppms)_2]$ was prepared by a modification of the literature method (13) for the synthesis of $[Rh(OAc)(CO)(PPh_3)_2]$. To a suspension of 0.1 g (0.4 mmol Rh) $[Rh(OAc)_2]_2$·2MeOH in 10 mL ethanol was added 0.25 mL of 50% HBF_4 and the solution was stirred at 60 °C for 20 h. To the resulting green solution, a solution of 640 mg (1.6 mmol) *m*tppms and 545 mg (4 mmol) $NaOAc·3H_2O$ in 10 mL ethanol was added at room temperature and the mixture was refluxed for 3 h. An orange solid separated that was filtered and washed with ethanol. This raw product ($[Rh(OAc)(mtppms)_3]$ together with inorganic impurities, NaOAc, $NaBF_4$) can be directly used for further synthesis. It was suspended in 5 mL of fresh ethanol, and bubbled with CO at room temperature, upon which the color changed gradually to orange then to yellow with dissolution of the solid. The reaction with CO overnight gave a cream-coloured precipitate. The *complex* was filtered, washed with ethanol, and dried. Weight: 300 mg (67% overall yield). IR (cm^{-1}): 1978 ν(CO), 1399 ν_s(COO), 1579 ν_{as}(COO), 1038, 1195 ν(SO_3). ^1H NMR (360 MHz, DMSO-d_6, r.t., ppm) δ: 0.67 (s, CH_3COO), 6 to 7 (m, aromatic protons). ^{31}P NMR (360 MHz, DMSO-d_6, r.t., ppm) δ: 35.3 (d, ^1J(Rh-P) = 138 Hz). Anal. calcd. (%): C 47.28, H 3.97, S 6.47; found: C 46.30, H 4.07, S 6.49.

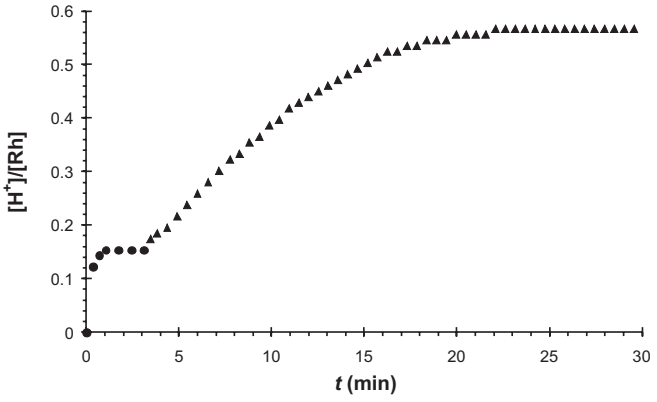
Results and discussion

$[Rh(OAc)(CO)(mtppms)_2]$ was synthesized for the first time by a modified procedure of Mitchell et al. (13) for the synthesis of $[Rh(OAc)(CO)(PPh_3)_2]$, based on the reaction of the green dirhodium(II) cation (Rh_2^{4+}) with *m*tppms) followed by carbonylation with CO. Replacement of PPh_3 with *m*tppms in the procedure described by Spencer (14) for the preparation of $[Rh(OAc)(PPh_3)_3]$ from $RhCl_3$·aq did not yield the expected acetatorhodium(I) complex, but afforded $[RhCl(mtppms)_3]$. The cream-coloured $[Rh(OAc)(CO)(mtppms)_2]$ dissolves well in water and in DMSO, but is only slightly soluble in ethanol and insoluble in apolar organic solvents. According to the IR and NMR spectra, it has a square-planar geometry with a monodentate acetato ligand (ν_{as}(COO) – ν_s(COO) = 180 cm^{-1}) (15) and with the phosphine ligands in the trans position.

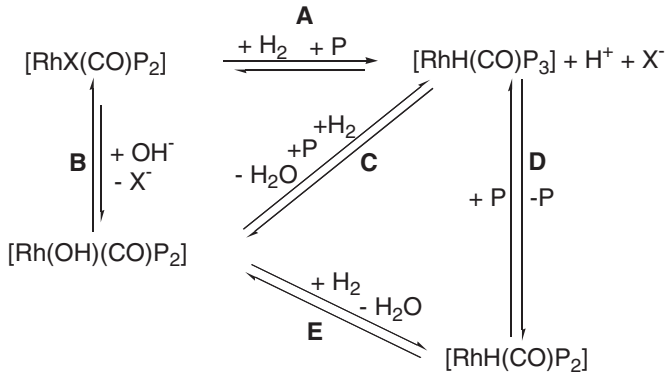
Aqueous solutions of $[Rh(OAc)(CO)(mtppms)_2]$ react with H_2 and in the presence of excess *m*tppms yield the known $[RhH(CO)(mtppms)_3]$ (8, 16). This reaction was studied in a pH-static hydrogenation apparatus as described in detail for $[RhH(CO)(mtppms)_3]$ (8). Briefly, the pH of the deoxygenated solvent (0.1 mol/L $NaClO_4$ to maintain constant ionic strength) was set to a given value in the range $4 < pH < 10$ using $HClO_4$ or KOH, and a known amount of the complex was dissolved in it under an argon atmosphere. De-

© 2005 NRC Canada

Fig. 1. Proton production upon dissolution (●) and subsequent hydrogenation (▲) of [Rh(OAc)(CO)(*m*tppms)$_2$]. [Rh] = 1.8 mmol/L, [*m*tppms] = 5.4 mmol/L, [$NaClO_4$] = 0.1 mol/L, pH = 7.0, $p(H_2)$ = 1 bar (1 bar = 100 kPa), T = room temperature.



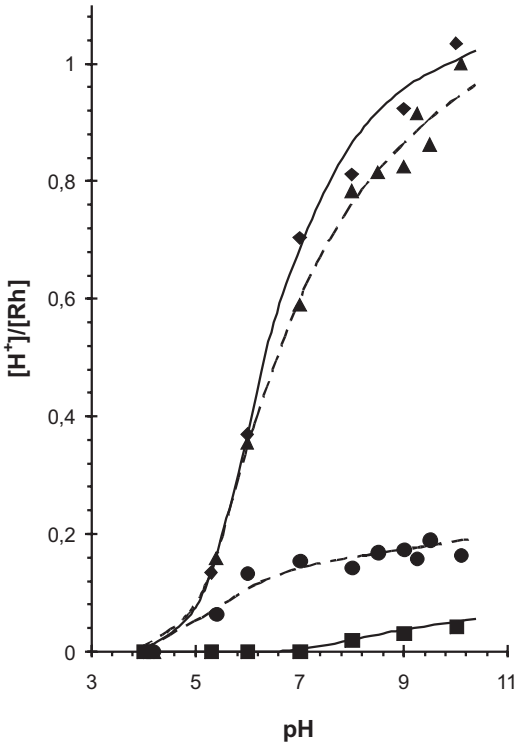
Scheme 1. Equilibria in solutions of [RhX(CO)P$_2$] (X = OAc$^-$ or Cl$^-$, P = *m*tppms) under H_2 in the presence of excess *m*tppms.



pending on the actual pH, hydrolysis of the complex to [Rh(OH)(CO)(*m*tppms)$_2$], the *m*tppts analog of which is described in ref. 17, occurred to a certain extent, resulting in proton release to the solution. However, the acid formed in this reaction was neutralized by KOH supplied by the autoburette and the pH remained constant; furthermore, the extent of hydrolysis could be calculated from the volume (amount) of KOH consumed. Figure 1 shows such a "titration curve" and the first "step" on the graph refers to the hydrolysis of the complex under an inert atmosphere (at the particular pH, i.e., 7.0 used in the experiment). Bubbling H_2 through the equilibrated solution resulted in further KOH consumption, indicating a heterolytic split of H_2 in its reaction with [Rh(OAc)(CO)(*m*tppms)$_2$] (and with [Rh(OH)(CO)(*m*tppms)$_2$] produced by the partial hydrolysis). This is the second step on Fig. 1. The reactions involved are shown on Scheme 1. Of particular interest is the fact that at this pH, the [H$^+$]/[Rh] ratio levels off at about 0.55 showing that only 55% (i.e., by far less than 100%) of all Rh reacted to yield [RhH(CO)(*m*tppms)$_3$].

Similar measurements were made at several pH values and the results are shown on Fig. 2. It is seen that [Rh(OAc)(CO)(*m*tppms)$_2$] does not react with H_2 below pH 4. However, the [H$^+$]/[Rh] ratio increases steadily with

Fig. 2. Proton production upon dissolution (●, ■) and subsequent hydrogenation (▲, ◆) of [Rh(OAc)(CO)(*m*tppms)$_2$] (●, ▲) and [RhCl(CO)(*m*tppms)$_2$] (■, ◆) at various pH. Conditions (●, ▲): [Rh] = 1.8 mmol/L, [*m*tppms] = 5.4 mmol/L, [$NaClO_4$] = 0.1 mol/L, $p(H_2)$ = 1 bar (1 bar = 100 kPa), T = room temperature; (■, ◆): [Rh] = 2.4 mmol/L, [*m*tppms] = 7.2 mmol/L, [$NaClO_4$] = 0.1 mol/L, $p(H_2)$ = 1 bar (1 bar = 100 kPa), T = 35 °C.



increasing pH showing that the reaction goes more and more extensively towards the formation of [RhH(CO)(*m*tppms)$_3$], reaching a practically complete conversion at pH 10. It is important to note that all reactions in Scheme 1 are reversible, and the pH-static hydrogenations reveal the extent to which [Rh(OAc)(CO)(*m*tppms)$_2$] (together with [Rh(OH)(CO)(*m*tppms)$_2$]) are converted to [RhH(CO)(*m*tppms)$_3$]. This extent is strongly pH dependent. Taking the closely similar chemical properties of *m*tppms and *m*tppts, we may assume that during the preformation of the catalyst in the Ruhrchemie – Rhône-Poulenc process [RhH(CO)(*m*tppts)$_3$] takes part in similar equilibria. Since [RhH(CO)(*m*tppts)$_3$] is the immediate precursor of the true hydroformylation catalysts (under syngas [RhH(CO)$_2$(*m*tppts)] and [RhH(CO)(*m*tppts)$_2$]), the actual proportion of rhodium that may enter the catalytic cycle(s) is strongly influenced by the pH, and this explains (at least in part) the higher catalytic activities observed at pH 7.5 vs. 5.5.

Data of the pH-static hydrogenation of [RhCl(CO)(*m*tppms)$_2$] are also shown in Fig. 2 for comparison. It can be concluded that there is no substantial effect of the anionic ligand (Cl$^-$ or OAc$^-$) on the pH dependence of the formation of [RhH(CO)(*m*tppms)$_3$]. In aqueous solutions, the heterolytic split of H_2 by transition metal complexes (such as shown by rxn. [1] and Scheme 1) is largely facilitated (18, 19) by the strong

© 2005 NRC Canada

hydration of the resulting H^+, $\Delta H^\circ_{hyd} = -1091$ kJ mol^{-1} (20), and the particular anion. It seems that the relatively small difference in the hydration ethalpies of Cl^- and OAc^-, –381 kJ mol^{-1} (20) and –334 kJ mol^{-1} (21), respectively, does not modify substantially the overall energy balance. The hydration enthalpy of OH^-, $\Delta H^\circ_{hyd} = -460$ kJ mol^{-1} (20), is higher than that of Cl^- and OAc^-; furthermore, formation of H_2O adds an additional driving force to reaction **E** (Scheme 1), so [Rh(OH)(CO)(*m*tppms)$_2$] is expected to react preferentially over [Rh(OAc)(CO)(*m*tppms)$_2$] and [RhCl(CO)(*m*tppms)$_2$]. Whether [RhH(CO)(*m*tppms)$_3$] (the resting state of the catalyst at high phosphine concentrations) is formed on path **A**, on path (**B** + **C**), or on path (**A** + **E** + **D**) is not known from these investigations, but its equilibrium concentration is pH-governed, independent of the way of formation. [Rh(CO)(OAc)(*m*tppms)$_2$] shows a somewhat higher tendency towards hydrolysis than [RhCl(CO)(*m*tppms)$_2$], although at room temperature, the extent of this hydrolysis does not exceed 20%.

Based on the above findings, it can be concluded that the pH of the aqueous phase has the same effect on the catalytic activity of Rh(I)-carbonyl-hydrides independent of the anion of the precursor being chloride or acetate. Nevertheless, the industrial preference for Rh(III)-acetate may be justified on other grounds, e.g., less corrosion or more favourable kinetics of the preformation of the catalyst. It is understood that the chemistry going on in the industrial hydroformylation reactor is far more complex than that described in this communication, and that the operational conditions of the Ruhrchemie – Rhône-Poulenc process for the aqueous/organic biphasic hydroformylation of propene (120 °C, 50 bar syngas (1 bar = 100 kPa)) are far from those of our measurements. This may influence the *positions* of the equilibria on Scheme 1, however, no other species were detected under pressure in case of the related *m*tppts complexes (6). Therefore, we think that the pH effects observed under more realistic hydroformylation conditions (1, 7) can also be related to the base-promoted formation of the actual hydroformylation catalysts, [RhH(CO)$_2$(*m*tppts)] and [RhH(CO)(*m*tppts)$_2$], as described previously.

Acknowledgements

This work was supported by the Hungarian National Research Foundation (OTKA F037358 to JK and T043365 to FJ) and by the European Commission (MRTN-CT-2003–503864; AQUACHEM).

References

1. B. Cornils and W.A. Herrmann (*Editors*). Aqueous phase organometallic catalysis — Concepts and applications. 2nd ed. Wiley-VCH, Weinheim, Germany. 2004.
2. J. Herwig and R. Fischer. *In* Rhodium catalyzed hydroformylation. *Edited by* P.W.N.M van Leeuwen and C. Claver. Kluwer, Dordrecht, The Netherlands. 2000. p. 189.
3. E. Kuntz. CHEMTECH, **17**, 570 (1987).
4. B. Cornils. Top. Curr. Chem. **206**, 133 (1999).
5. C.D. Frohning and C.W. Kohlpaintner. *In* Aqueous phase organometallic catalysis — Concepts and applications. 2nd ed. *Edited by* B. Cornils and W.A. Herrmann. Wiley-VCH, Weinheim, Germany. 2004. p. 377.
6. I.T. Horváth, R.V. Kastrup, A.A. Oswald, and E.J. Mozeleski. Catal. Lett. **2**, 85 (1989).
7. R.M. Deshpande, Purwanto, H. Delmas, and R.V. Chaudhari. J. Mol. Catal. A: Chem. **126**, 133 (1997).
8. F. Joó, J. Kovács, A.Cs. Bényei, L. Nádasdi, and G. Laurenczy. Chem. Eur. J. **7**, 193 (2001).
9. F. Joó, J. Kovács, A.Cs. Bényei, and Á. Kathó. Angew. Chem. Int. Ed. **37**, 969 (1998).
10. F. Joó, J. Kovács, A.Cs. Bényei, and Á. Kathó. Catal. Today **42**, 441 (1998).
11. F. Joó, J. Kovács, Á. Kathó, A.Cs. Bényei, T. Decuir, and D.J. Darensbourg. Inorg. Synth. **32**, 1 (1998).
12. G.A. Rempel, P. Legdzins, H. Smith, and G. Wilkinson. Inorg. Synth. **13**, 90 (1972).
13. R.W. Mitchell, J.D. Ruddick, and G. Wilkinson. J. Chem. Soc. A, 3224 (1971).
14. A. Spencer. J. Organometal. Chem. **93**, 389 (1975).
15. T.A. Stephenson, S.M. Morehouse, A.R. Powell, J.P. Heffner, and G. Wilkinson. J. Chem. Soc. A, 3632 (1965).
16. A.F. Borowski, D.J. Cole-Hamilton, and G. Wilkinson. Nouv. J. Chim. **2**, 137 (1978).
17. W.A. Herrmann, J.A. Kulpe, W. Konkol, and H. Bahrmann. J. Organometal. Chem. **389**, 85 (1990).
18. B.R. James. Homogeneous hydrogenation. Wiley, New York. 1973.
19. F. Joó. Aqueous organometallic catalysis. Kluwer, Dordrecht, The Netherlands. 2001.
20. D.W. Smith. J. Chem. Ed. **54**, 541 (1977).
21. E. Gallicchio, L.Y. Zhang, and R.M. Levy. J. Comput. Chem. **23**, 517 (2002).

© 2005 NRC Canada

RAPID COMMUNICATION / COMMUNICATION RAPIDE

Synthesis, characterization, and reactivity of the first hafnium alkyl complex stabilized by amidate ligands[1]

Robert K. Thomson, Brian O. Patrick, and Laurel L. Schafer

Abstract: A photo and thermally stable bis(amidate)–dibenzyl complex of Hf ($[^{DMP}(NO)^{Ph}]_2Hf(CH_2Ph)_2$(THF) (**2a**) was formed as a monosolvated THF adduct in near quantitative yield from $Hf(CH_2Ph)_4$ and *N*-2,6-dimethylphenyl(phenyl)amide (**1**). Isomerization between the THF-bound product and the THF-free product can be observed visually by the conversion from a red-orange product at low temperatures to a pale yellow product at high temperatures. Solid-state crystallographic characterization of the orange product confirmed its constitution as a monosolvated species. Kinetic parameters for the exchange of the THF moiety were determined from variable-temperature NMR experiments. The product of the hydrolysis of the Hf dibenzyl species by water was characterized by X-ray crystallography, and was found to be a rare tetrametallic Hf oxo cluster species (**3**).

Key words: hafnium, protonolysis, amidate, coordination chemistry, organometallic chemistry, exchange processes.

Résumé : Un complexe de bis(amidate)–dibenzyle de Hf ($[^{DMP}(NO)^{Ph}]_2Hf(CH_2Ph)_2$(THF) (**2a**) qui est stable à la lumière et à la chaleur a été formé comme adduit monosolvaté de THF avec un rendement presque quantitatif de $Hf(CH_2Ph)_4$ et *N*-2,6-dimethylphenyl(phenyl)amide (**1**). L'isomérisation entre le produit avec THF et le produit sans THF peut être observée visuellement par la conversion d'un produit rouge-orange aux températures basses en un produit jaune pâle aux températures élevées. La caractérisation cristallographique du produit orange à l'état solide a confirmé sa constitution comme l'espèce monosolvaté. Des paramètres cinétiques pour l'échange du THF ont été déterminés à partir d'expériences de RMN à la température variable. Le produit d'hydrolyse de l'espèce dibenzyle de Hf par l'eau a été caractérisé par cristallographie de rayons X et c'est une espèce rare d'agrégat oxotétramétallique de Hf (**3**).

Mots clés : hafnium, protonolyse, amidate, la chimie de coordination, la chimie organométallique, processus d'échange.

Introduction

Much of the recent research in Group 4 metal chemistry has involved the development of new non-cyclopentadienyl (Cp) ligands and the exploration of their reactivity (1). In recent reports from our research group, we have shown that amidate ligands are versatile ancillary ligands for Group 4 metals (2–4). The amide proligands are highly modifiable and are synthesized in a modular manner, making them attractive alternatives to Cp (Fig. 1). The amide proligands have a pK_a of approximately 15, which makes protonolysis a highly useful method of synthesizing metal complexes.

In particular, we have shown that the synthesis of bis(amidate)–bis(amido) complexes of Ti and Zr is facile and high yielding, and can be accomplished via protonolysis of commercially available tetrakisamido metal starting materials (2, 3). Since amidate ligands have been underexplored in early transition metal chemistry, there is a need to discover the general utility of these ligands to support reactive metal centers. To this end, here we report the first examples of stable bis(amidate)–dibenzyl complexes of Hf. The stability and coordination geometry of this new class of complexes has been established by X-ray crystallographic analysis as well as VT NMR spectroscopic investigations.

Received 17 November 2004. Published on the NRC Research Press Web site at http://canjchem.nrc.ca on 2 July 2005.

Dedicated to Professor Howard Alper.

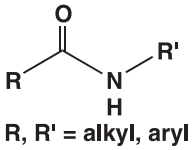
R.K. Thomson, B.O. Patrick, and L.L. Schafer.[2] University of British Columbia, Department of Chemistry, 2036 Main Mall, Vancouver, BC V6T 1Z1, Canada.

[1]This article is part of a Special Issue dedicated to Professor Howard Alper.

[2]Corresponding author (e-mail: schafer@chem.ubc.ca).

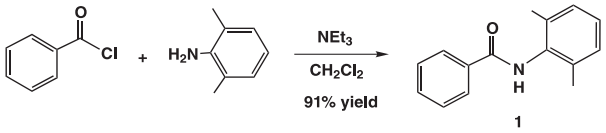
 doi: 10.1139/V05-030 © 2005 NRC Canada

Fig. 1. Amide proligand set $[^{R'}(NO)^{R}]H$.



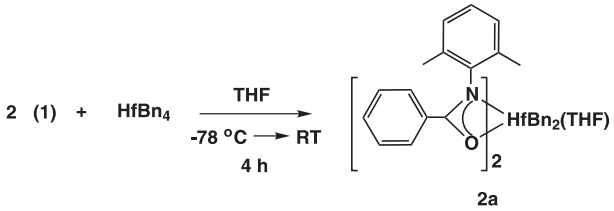
Results and discussion

Easily assembled modular ligand systems are important in expediting the discovery of catalyst systems for various organic transformations (5). Organic amides offer an easily modified scaffold for the study of ligand-based effects in their resultant transition metal complexes. A general synthetic scheme for the preparation of organic amides is shown in eq. [1]. Elimination of HCl upon reaction of an acid chloride and a primary amine results in the formation of the desired amide product in high yields (75%–95% yield). Purification of these proligands for use in metal chemistry can be accomplished by vacuum sublimation or recrystallization from an appropriate solvent. Proligand **1** (*N*-2,6-dimethylphenyl(phenyl)amide) was synthesized in excellent yield. Purification via recrystallization from $CHCl_3$ at –20 °C and

[1] 

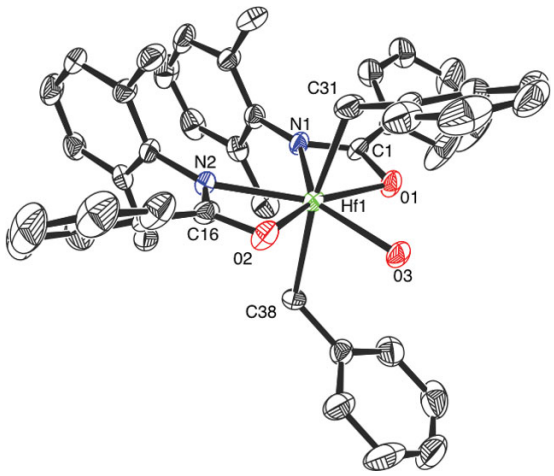
subsequent drying while heating under vacuum overnight gave pure proligand **1** in 64% yield.

Protonolysis reactions have been utilized successfully in the synthesis of amidinate (6) and guanidinate (7) complexes of the Group 4 metals. Given the structural similarity of the amidate ligand motif, protonolysis was anticipated to be an efficient route into analogous amidate complexes. The protonolysis methodology used to form this bis(amidate)–bis(alkyl) Group 4 metal complex (**2a**) was facile and high yielding (eq. [2]). Freshly prepared and recrystallized $Hf(CH_2Ph)_4$ was combined with 2 equiv. of proligand **1** ($[^{DMP}(NO)^{Ph}]H$) in a darkened Schlenk flask, which was cooled to –78 °C before introduction of THF via cannula transfer. Warming to room temperature resulted in the for-

[2] 

mation of a bright red-orange solution, which was concentrated in vacuo to give a bright orange powder in 98% crude yield. Low temperatures utilized during this process were necessary to control the rate of reaction, as reaction at room temperature results in the formation of the desired product contaminated with a homoleptic side-product. In addition, the starting material ($Hf(CH_2Ph)_4$) is well-known to exhibit a high sensitivity towards ambient visible light, and the

Fig. 2. ORTEP depiction of the solid-state molecular structure of $[^{DMP}(NO)^{Ph}]_2Hf(CH_2Ph)_2(THF)$ (**2a**) (the THF ring at O3 has been omitted for clarity).



protonolysis of the Hf—C bonds proceeds very rapidly and exothermically because of the low pK_a of the organic amide proligands.

Purification of this complex in moderate yield can be achieved by recrystallization from a concentrated solution of **2a** in hexanes, giving orange single crystals. X-ray crystallographic analysis of this complex revealed that the bis(amidate)–dibenzyl species is monosolvated by THF in the solid state, as shown in Fig. 2. Selected bond lengths and angles are found in Table 1 and crystallographic details are located in Table 2.

The solid-state structure of **2a** exhibits pseudo-C_{2v} symmetry in a slightly distorted pentagonal bipyramidal geometry. This coordination geometry has been previously observed for seven-coordinate salen complexes of Hf (8), acetylacetonato complexes of Zr (9), and structurally related monothiocarbamate and dithiocarbamate complexes of Ti (10, 11). Both amidate ligands in **2a** are found in the equatorial plane, with the O atoms nearly trans to each other at 156°. A bound THF molecule occupies the final equatorial coordination site. The plane containing Hf and the N and O donor atoms is nearly perfectly planar, with the sum of the bond angles about the Hf center being 360.2°. In the axial positions, the two benzyl groups are located 169.8° apart. As expected, the Hf1—O3 bond length of the coordinated THF (2.236 Å) is significantly longer than the Hf1—O1 and Hf1—O2 bond lengths (2.161 and 2.174 Å, respectively). Bond lengths between the amidate N atoms and the Hf center are somewhat longer than the corresponding Hf – amidate O bond lengths (Hf1—N1 = 2.265 Å, Hf1—N2 = 2.258 Å), indicating that the amidate ligands are bound in an alkoxy-imine fashion (2). Unexpected elongation of the C—N bond in the ligand backbone is also observed; however, the steric bulk at the N of the amidate ligands precludes the formation of the anticipated shorter C—N bond. This ligand binding motif has been seen previously by our group for bis(amidate)-bis(amido) complexes of Ti and Zr (2, 4). There are some variations from expected bond lengths, which may be due to the unique π-stacking interactions present between the coplanar *N*-aryl rings of the amidate ligands, whose centroids are separated by approximately 3.6 Å. Intramolecular

© 2005 NRC Canada

Table 1. Selected bond distances (Å) and angles (°) for $[^{DMP}(NO)^{Ph}]_2Hf(CH_2Ph)_2(THF)$ (**2a**).

Bond distances (Å)	
Hf(1)—O(1)	2.161(4)
Hf(1)—O(2)	2.174(4)
Hf(1)—O(3)	2.236(4)
Hf(1)—N(1)	2.258(5)
Hf(1)—N(2)	2.265(5)
Hf(1)—C(31)	2.326(6)
Hf(1)—C(38)	2.328(5)
N(1)—C(1)	1.308(7)
N(2)—C(16)	1.325(7)
O(1)—C(1)	1.303(7)
O(2)—C(16)	1.282(7)
Bond angles (°)	
O(1)-Hf(1)-N(1)	59.53(15)
O(2)-Hf(1)-N(2)	59.45(16)
N(1)-Hf(1)-N(2)	84.81(17)
O(1)-Hf(1)-O(3)	77.61(15)
O(2)-Hf(1)-O(3)	78.76(15)
C(31)-Hf(1)-C(38)	169.8(2)
N(1)-C(1)-O(1)	114.7(5)
N(2)-C(16)-O(2)	114.9(5)

Table 2. Crystallographic data and refinement details for $[^{DMP}(NO)^{Ph}]_2Hf(CH_2Ph)_2(THF)$ (**2a**).

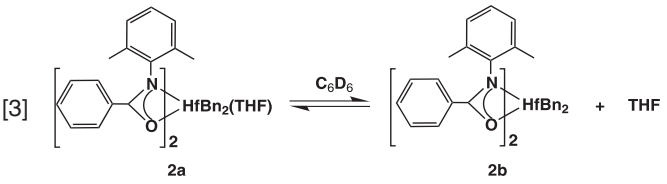
Empirical formula	$C_{48}H_{50}HfN_2O_3$
Formula weight	881.39
Crystal system	Triclinic
Space group	*P*-1
a, b, c (Å)	11.605(2), 12.207(2), 16.353(2)
α, β, γ (°)	103.027(2), 102.455(2), 106.651(3)
V (Å^3)	2 062.6(5)
Z	2
D_{calcd} (g cm^{-3})	1.419
μ (Mo Kα) (cm^{-1})	34.60
T (K)	173
2θ range (°)	55.7
Total reflections	18 282
Unique reflections	8 417
Parameters	491
R_1[a]	0.0624
R_w[a]	0.1169
Goodness-of-fit	1.153

[a] $R_1 = \Sigma||F_o| - |F_c||/\Sigma|F_o|$; $R_w = \Sigma(|F_o^2| - |F_c^2|)^2/(\Sigma w|F_o^2|^2)^{1/2}$.

monometallic π-stacking interactions of this type are rare, but the phenyl ring separation of 3.6 Å is consistent with a previously reported π-stacking interaction in a Ti – late metal bimetallic species, in which the interactions ranged between 3.51 and 3.77 Å (12). In our case, the bulky 2,6-dimethylphenyl rings orient themselves in a cis fashion in the crystal structure and are stabilized by the π interaction between them. Furthermore, the difference between the two ligand C—O, C—N bond asymmetries may be due to the slight canting of the rings to one side, resulting in more steric crowding of the C16—N2 bond than the C1—N1 bond. These observations could also be due to crystal packing effects.

^{1}H and ^{13}C NMR spectra of the recrystallized orange product indicate that the solid state C_{2v} symmetry of this species is maintained in solution at room temperature. A single resonance is seen for the aryl methyl protons at δ 2.34 ppm, and the requisite singlet for the benzylic methylene protons is present at δ 2.55 ppm. Bound THF peaks are also present at δ 1.64 and 3.83 ppm. The ^{13}C NMR spectrum showed a broadened signal at δ 81.64 ppm, which was correlated to the broadened THF OCH_2CH_2 proton signal at δ 3.83 ppm in the ^{1}H NMR spectrum by ^{1}H^{13}C HMQC. Dissolution of the orange crystals of **2a** in C_6D_6 at room temperature immediately resulted in a light orange solution. Warming of the tube resulted in a color change to pale yellow, and cooling of the tube to temperatures at or below 0 °C was accompanied by a color change to a deep orange. Given these preliminary observations, we suspected that the THF solvated complex **2a** is stable in the solid state, but undergoes exchange to the unsolvated species **2b** in solution (eq. [3]).

Variable-temperature NMR experiments were performed on the orange product **2a** to verify the THF exchange process and to determine the activation energy ($\Delta G^{\ddagger}$) and the rate of exchange (k_{solv}). The two bound THF peaks are observed to broaden in response to decreased temperature. The peak at δ 3.59 ppm is observed to broaden and split into two peaks at δ 4.12 and 3.50 ppm that sharpen at –50 °C. The coalescence temperature for these two peaks, corresponding to bound and free THF, respectively, occurs at (–25 ± 5) °C. The rate constant for the THF exchange process was calculated to be (560 ± 110) s^{-1}, and the activation energy for this process was likewise found to be (47 ± 1.5) kJ mol^{-1}.[3] To verify that the yellow product observed at higher temperatures was desolvated, this compound was isolated as a powder by removing all solvent at elevated temperatures. The ^{1}H NMR spectrum of this compound does not show the presence of any THF. Independent synthesis of the yellow product in toluene yielded material that gave identical NMR spectroscopic data as seen in the aforementioned preparation of **2b**. Ongoing investigations are focused on complete structural characterization of this complex.

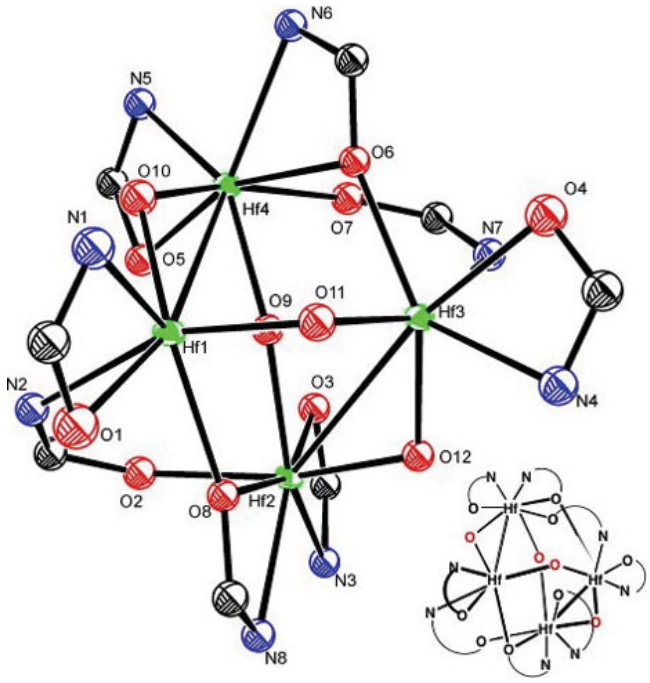
[3] 

Although complexes **2a** and **2b** are stable to ambient light and heat (prolonged heating at 80 °C resulted in slow decomposition), they are highly sensitive to moisture and can be hydrolyzed by the presence of trace amounts of H_2O. Slow hydrolysis of **2a** by reaction with adventitious water resulted in the formation of the novel tetrametallic-bridged oxo species shown in Fig. 3. Complex **3** exhibits C_2 symme-

[3] Determined by NMR methods as described in ref. 13.

© 2005 NRC Canada

Fig. 3. ORTEP representation of the solid-state molecular structure of $\{[^{DMP}(NO)^{Ph}]_2Hf(\mu\text{-}O)\}_4$ (**3**) (the aryl rings have been omitted for clarity).



try in the solid state, with two pairs of different bridging oxo ligands, depicted in Fig. 3. Selected bond lengths and angles are given in Table 3, and crystallographic data is located in Table 4. The C_2 axis is located along the vector joining O9 and O11. It can also be seen that half of the amidate ligands are bound η^2 to a single Hf center analogous to complex **2**, and the other half are bridging between two adjacent Hf atoms. This is the first example of these bulky amidate ligands adopting a bridging mode for Group 4 metals. Independent synthesis of the hydrolyzed product resulted in the formation of an insoluble white powder that has resisted recrystallization. EI-MS data of this species did not give a parent ion, however, monomeric fragments ($[^{DMP}(NO)^{Ph}]_2HfO$) and higher order fragments ($[^{DMP}(NO)^{Ph}]_3HfO$, $[^{DMP}(NO)^{Ph}]_3Hf_2O_3$), were observed, which supports the formation of a complex oligomeric structure. Due to the low solubility of this complex, full spectroscopic characterization was not possible; however, the formation of toluene was observed and interestingly, there was no evidence of free ligand in the soluble fraction. The lack of complete hydrolysis of the amidate ligands implies that the amidate–Hf bonding interactions are strong and can act as robust ancillary ligands during reactions at the metal center. We are currently taking advantage of this observed stability and are investigating a wide range of reactivity of complexes **2a** and **2b**.

Conclusion

The first amidate-stabilized Hf alkyl complex was synthesized and structurally and spectroscopically characterized. The bis(amidate)–dibenzyl Hf species (**2a**) is pentagonal bipyramidal in the solid state, with an interesting intramolecular π-stacking interaction stabilizing the complex. Monosolvation of **2a** was observed in the solid state, with

Table 3. Selected bond distances (Å) and angles (°) for $\{[^{DMP}(NO)^{Ph}]_2Hf(\mu\text{-}O)\}_4$ (**3**).

Bond distances (Å)	
Hf(1)—O(1)	2.182(3)
Hf(1)—O(8)	2.230(3)
Hf(1)—O(10)	2.000(3)
Hf(1)—O(11)	1.978(3)
Hf(1)—N(1)	2.327(4)
Hf(1)—N(2)	2.474(4)
Hf(1)—Hf(4)	3.2423(5)
Hf(2)—O(2)	2.088(3)
Hf(2)—O(3)	2.177(3)
Hf(2)—O(8)	2.259(3)
Hf(2)—O(9)	2.117(3)
Hf(2)—O(12)	1.944(3)
Hf(2)—N(3)	2.272(4)
Hf(2)—N(8)	2.341(4)
O(1)—C(1)	1.299(5)
N(1)—C(1)	1.276(5)
O(2)—C(16)	1.305(4)
N(2)—C(16)	1.300(5)
O(8)—C(106)	1.318(5)
N(8)—C(106)	1.293(6)
Bond angles (°)	
Hf(1)-O(8)-Hf(2)	103.56(11)
Hf(1)-O(10)-Hf(4)	110.40(14)
Hf(1)-O(11)-Hf(3)	113.06(15)
Hf(4)-Hf(1)-O(10)	34.27(9)
N(1)-C(1)-O(1)	115.2(4)
N(2)-C(16)-O(2)	120.9(3)
N(8)-C(106)-O(8)	112.4(4)
O(1)-Hf(1)-N(1)	57.58(13)
O(11)-Hf(1)-Hf(4)	91.31(9)

Table 4. Crystallographic data and refinement details for $\{[^{DMP}(NO)^{Ph}]_2Hf(\mu\text{-}O)\}_4$ (**3**).

Empirical formula	$C_{120}H_{112}Hf_4N_8O_{12}\cdot 3C_7H_8$
Formula weight	2 848.54
Crystal system	Triclinic
Space group	*P*-1 (No. 2)
a, b, c (Å)	14.7220(8), 20.1280(9), 22.2090(9)
α, β, γ (°)	92.02(1), 99.12(1), 109.55(1)
V (Å^3)	6 095.6(5)
Z	2
D_{calcd} (g cm^{-3})	1.552
μ (Mo Kα) (cm^{-1})	34.60
T (K)	173
2θ range (°)	55.8
Total reflections	57 074
Unique reflections	24 854
Parameters	1 472
$R_1{}^a$	0.036
$R_w{}^a$	0.079
Goodness-of-fit	1.13

$^a R_1 = \Sigma||F_o| - |F_c||/\Sigma|F_o|$; $R_w = \Sigma(|F_o^2| - |F_c^2|)^2/(\Sigma w|F_o^2|^2)^{1/2}$.

© 2005 NRC Canada

the bound THF being coordinatively labile. The rate constant for THF exchange (k_{solv}) is (560 ± 110) s^{-1}, and the activation energy ($\Delta G^{\ddagger}$) for this process is (47 ± 1.5) kJ mol^{-1}, as determined by variable-temperature NMR spectroscopic experiments. Hydrolysis of **2a** resulted in the formation of a unique tetrametallic Hf oxo cluster species, which was also crystallographically characterized. The amidate ligands in this complex survived the hydrolysis and remained bound to Hf in either a bidentate chelating mode or as a bridge between two Hf centers.

Experimental

General information

Unless otherwise stated, all reactions were carried out using standard Schlenk line and glovebox techniques, under an atmosphere of nitrogen. Tetrahydrofuran and hexanes were purified by passage through a column of activated alumina and degassed with nitrogen. C_6D_6 was degassed and dried over molecular sieves prior to use. d^8-Toluene was purified by distillation from Na, followed by degassing and storing over molecular sieves. 2,6-Dimethylaniline, benzoyl chloride, and benzylmagnesium chloride (1 mol/L in Et_2O) were purchased from Aldrich and used without further purification. $HfCl_4$ was purchased from Strem and used as received. $Hf(CH_2Ph)_4$ was synthesized according to literature procedures and purified by recrystallization at –30 °C in the dark prior to use (14). ^1H, ^{13}C, and HMQC NMR spectra were recorded on Bruker 300 MHz or 400 MHz Avance spectrometers at ambient temperature, and chemical shifts are given relative to residual solvent. Variable-temperature ^1H NMR experiments were performed on Bruker 300 MHz or 400 MHz Avance spectrometers equipped with cryoprobes. Mass spectra were recorded on a Kratos MS-50 spectrometer using an electron impact (70 eV) source. Elemental analysis and single crystal X-ray structure determinations were performed at the Department of Chemistry, University of British Columbia.[4]

$[^{DMP}(NO)^{Ph}]H$ (1)

Ligand preparation was performed on the benchtop with no further precautions. A solution of 11.5 mL (11.3 g, 92.8 mmol) of 2,6-dimethylaniline in 75 mL of CH_2Cl_2 was stirred at room temperature. To this solution was added 12.9 mL (9.40 g, 92.8 mmol) of NEt_3 via pipette over a period of 5 min. The resulting solution was allowed to stir for 1 h before cooling to –78 °C in a dry ice – isopropanol bath. Using an addition funnel, a solution of 8.25 mL (10.0 g, 71.4 mmol) of benzoyl chloride dissolved in 50 mL of CH_2Cl_2 was added dropwise to the amine solution. The resulting colorless solution was allowed to warm to room temperature over a period of 4 h. The product was washed with 1 mol/L HCl (3 × 20 mL), 1 mol/L NaOH (20 mL), and brine (20 mL). The organic fraction was dried over anhydr. $MgSO_4$, filtered, and the solvent was removed in vacuo, giving 14.6 g of the crude product as a white microcrystalline solid (91% yield). Recrystallization from $CHCl_3$ gave 10.3 g of the purified product (64% overall yield). The final product was dried by heating under vacuum overnight at 70 °C. ^1H NMR ($CDCl_3$, 25 °C, 400 MHz) δ: 2.31 (s, 6H, Ar-CH_3), 7.18–7.30 (m, 3H, Ar-*H*), 7.55 (m, 2H, Ar-*H*), 7.63–7.75 (m, 2H, Ar-*H* and N-*H*), 7.98 (d, 2H, Ar-*H*). ^{13}C NMR ($CDCl_3$, 25 °C, 100 MHz) δ: 18.35, 127.21, 127.25, 128.13, 128.58, 131.60, 133.98, 134.38, 135.57, 165.90. EI-MS *m*/*z* (%): 225 ([M^+], [$^{DMP}(NO)^{Ph}$]H, 40). Anal. calcd. for $C_{15}H_{15}NO$ (%): C 79.97, H 6.71, N 6.22; found: C 80.24, H 6.72, N 6.20.

$[^{DMP}(NO)^{Ph}]_2Hf(CH_2Ph)_2(THF)$ (2a)

In a foil-wrapped Schlenk flask, 3.50 g (6.45 mmol) of $Hf(CH_2Ph)_4$ and 2.90 g (12.90 mmol) of [$^{DMP}(NO)^{Ph}$]H (**1**) were weighed out together. The mixture of the two solids was cooled to –78 °C in a dry ice – isopropanol bath. To this mixture was added approximately 125 mL of THF via cannula while stirring vigorously. The solution was allowed to warm to room temperature while stirring overnight. Excess THF was removed from the bright red-orange solution in vacuo, resulting in the isolation of 5.60 g of the crude product as a vibrant orange solid (98% yield). The product was dissolved in approximately 150 mL of hexanes at room temperature and filtered through a fritted disk. A small amount of a pale yellow hexanes insoluble product **2b** (0.57 g, 11% yield) was collect on the frit, and the dark orange filtrate was collected and cooled to –30 °C overnight. Microcrystals of a red-orange product **2a** were obtained in 34% yield (1.96 g) in the first batch. Repeated concentration and crystallization of the mother liquor resulted in a combined yield of approximately 65% for **2a**. ^1H NMR (C_6D_6, 25 °C, 300 MHz) δ: 1.64 (m, 4H, O-(CH_2CH_2)$_2$), 2.34 (s, 12H, Ar-CH_3), 2.55 (s, 4H, Hf-CH_2Ph), 3.83 (t, 4H, O-(CH_2CH_2)$_2$), 7.05–7.15 (m, 12H total, Ar-*H*), 7.35–7.46 (m, 10H total, Ar-*H*), 7.85 (d, 4H, Ar-*H*). ^{13}C NMR (C_6D_6, 25 °C, 75 MHz) δ: 18.69, 25.75, 68.03, 81.64, 122.13, 126.03, 128.55, 128.68, 128.86, 129.08, 131.99, 132.33, 133.07, 142.07, 144.73, 179.56. EI-MS *m*/*z* (%): 719 (M^+ – THF – CH_2Ph, 100). Anal. calcd. for $C_{48}H_{50}N_2O_3Hf$ (%): C 65.41, H 5.72, N 3.18; found: C 65.15, H 6.00, N 3.54.[5]

Acknowledgments

Funding for this research was provided by the University of British Columbia (UBC) and by the Natural Sciences and Engineering Research Council of Canada (NSERC) in the

[4] Crystallographic data for compounds **2a** and **3** appear in Tables 2 and 4, respectively. All measurements were made on Rigaku/ADSC or Rigaku AFC7 CCD area detectors with graphite-monochromated Mo Kα radiation. The data were processed (15) and corrected for Lorentz and polarization effects. The structures were solved by direct methods (16) and expanded by using Fourier (17) techniques. All non-hydrogen atoms were refined with anisotropic thermal parameters. Neutral atom scattering factors and anomalous dispersion corrections were taken from the International Tables for X-ray Crystallography (18, 19). Structures are visualized as ORTEP-3 depictions (20).

[5] Supplementary data for this article are available on the Web site or may be purchased from the Depository of Unpublished Data, Document Delivery, CISTI, National Research Council Canada, Ottawa, ON K1A 0S2, Canada. DUD 3665. For more information on obtaining material refer to http://cisti-icist.nrc-cnrc.gc.ca/irm/unpub_e.shtml. CCDC 256046 and 256047 contain the crystallographic data for this manuscript. These data can be obtained, free of charge, via www.ccdc.cam.ac.uk/conts/retrieving.html (Or from the Cambridge Crystallographic Data Centre, 12 Union Road, Cambridge CB2 1EZ, UK; fax +44 1223 336033; or deposit@ccdc.cam.ac.uk).

© 2005 NRC Canada

form of a Discovery Grant to L.L.S. and a postgraduate scholarship to R.K.T.

References

1. G.J.P. Britovsek, V.C. Gibson, and D.F. Wass. Angew. Chem. Int. Ed. **38**, 428 (1999).
2. C. Li, R.K. Thomson, B. Gillon, B.O. Patrick, and L.L. Schafer. Chem. Commun. 2462 (2003).
3. Z. Zhang and L.L. Schafer. Org. Lett. **5**, 4733 (2003).
4 R.K. Thomson, F.E. Zahariev, Z. Zhang, B.O. Patrick, Y.A. Wang, L.L. Schafer. Inorg. Chem. In press.
5. R. Kempe. Angew. Chem. Int. Ed. **39**, 468 (2000).
6. J.R. Hagadorn and J. Arnold. J. Am. Chem. Soc. **118**, 893 (1996).
7. P. Bazinet, D. Wood, G.P.A. Yap, and D.S. Richeson. Inorg. Chem. **42**, 6225 (2003).
8. K. Matsumoto, A. Watanabe, T. Uchida, K. Ogi, and T. Katsuki. Tetrahedron Lett. **45**, 2385 (2004).
9. R.B. VonDreele, J.J. Stezowski, and R.C. Fay. J. Am. Chem. Soc. **93**, 2887 (1971).
10. S.L. Hawthorne and R.C. Fay. J. Am. Chem. Soc. **101**, 5268 (1979).
11. W.L. Steffen, H.K. Chun, and R.C. Fay. Inorg. Chem. **17**, 3498 (1978).
12. Q.F. Mokuolu, P.A. Duckmanton, P.B. Hitchcock, C. Wilson, A.J. Blake, L. Shukla, and J.B. Love. Dalton Trans. 1960 (2004).
13. H. Friebolin. Basic one- and two-dimensional NMR spectroscopy. 2nd ed. VCH, Toronto. 1993. pp. 287–298.
14. U. Zucchini, E. Albizzati, and U. Giannini. J. Organomet. Chem. **36**, 357 (1972).
15. Molecular Structure Corp. teXsan for Windows [computer program]. Molecular Structure Corp., The Woodlands, Texas. 1996.
16. A. Altomane, M.C. Burla, G. Cammali, M. Cascarano, C. Giacovazzo, A. Gagliardi, A.G.G. Moliterni, G. Polidoi, and A. Spagna. SIR-97 [computer program]. CNR-IRMEC, Universitario, Bari, Italy. 1999.
17. P.T. Beurkens, G. Admiraal, G. Baurskens, W.P. Bosman, R. de Gelder, R. Israel, and J.M.M. Smits. DIRDIF-94 [computer program]. University of Nijmegen, Nijmegen, The Netherlands. 1994.
18. International Union of Crystallography. International tables for X-ray crystallography. Kynoch Press, Birmingham, UK. 1974.
19. International Union of Crystallography. International tables for X-ray crystallography. Kluwer Academic, Boston, Mass. 1992.
20. L.J. Farrugia. J. Appl. Crystallogr. **30**, 565 (1997).

© 2005 NRC Canada

PREFACE / PRÉFACE

It is a great honor and privilege to contribute the preface to this special issue honouring Professor Howard Alper of the University of Ottawa. Professor Alper is among the most influential scholars in the area of chemical science of our days. He has contributed in many ways to research, education, and also scientific administration, particularly in Canada.

Professor Alper has made a number of truly outstanding contributions to homogeneous catalysis based on organometallic chemistry. His accomplishments in the broad realm of catalytic chemistry are listed in a large number of first-rate journals, but his impact on organometallic chemistry using carbon monoxide, with associated mechanistic insights, is particularly noteworthy. Among his superb contributions, one of the most significant is the ring expansion of saturated heterocyclic compounds such as aziridines and epoxides to lactams or lactones, respectively. The efficient synthesis of chiral β-lactams from racemic aziridines in the presence of (–)- or (+)-menthol is remarkable. His synthesis of tetrahydroindolizidines from piperidines is also very unique. He also discovered the Pd catalyzed cycloaddition of carbodiimides and heterocycles leading to imidazoline and pyrimidine imines. Furthermore, Alper achieved a general chiral synthesis of five-membered heterocycles by the Pd·BINAP promoted reaction of racemic aziridines and heterocumulenes. In addition, he discovered a series of regio- and stereoselective hydrocarbonylations and hydrocarboxylations of olefinic substrates under mild conditions. The highly enantioselective synthesis of naproxen and ibuprofen, very important anti-inflammatory agents, highlights the utility of his original approach to chemistry. His discovery of the double and triple carbonylation of organic compounds catalyzed by transition metals and lanthanides was a great surprise to many in the community, including ourselves. Alper was also the first to recognize the utility of zwitterionic Rh complexes for the regioselective (branched or linear) hydroformylation of olefins including α,β-unsaturated esters, vinylsilanes, unsaturated sulfones, and sulfoxides. Using this method, allyl acetate can be converted to 1,4-butanediol monoacetate.

Throughout his career, Alper developed many new reactions in homogeneous, liquid–liquid two-layer, and heterogeneous phases. Some exciting results generated from the biphasic chemistry ongoing in Alper's labs include the development of excellent methods for the dechlorination of chloroarenes aided by Pd catalysts. He also found an attractive method for the Pd – clay-catalyzed synthesis of commercially important isocyanates from nitroarenes. More recently, Alper described the ability of recyclable Rh dendrimers bound to silica- or resin-based supports to hydroformylate olefins.

Many of these discoveries were totally unexpected prior to his work. I have admired his intuitive insights that are far beyond the precise "designing" of chemical reactions. Overall, his scientific work is characterized by simplicity and sufficient practicality. Accordingly, many of his new reactions are potentially of high value to the pharmaceutical, petrochemical, and commodity chemical sectors. In fact, he has 37 patents based on his original chemistry. Professor Alper is obviously among the world-leading figures in this impor-

Il s'agit d'un grand honneur et privilège pour moi de contribuer à la préface du présent numéro spécial dédié au professeur Howard Alper, de l'Université d'Ottawa. Le professeur Alper est un des plus influents savants de notre temps dans le domaine de la chimie. Il a foncièrement transformé la recherche, l'enseignement et l'administration scientifique, particulièrement au Canada.

Nous devons au professeur Alper des contributions véritablement marquantes à la catalyse homogène organométallique. Même si ses réalisations dans le vaste secteur de la chimie catalytique sont attestées dans d'innombrables revues savantes prestigieuses, ce sont ses travaux de chimie organométallique axés sur l'usage du monoxyde de carbone dans une optique mécaniste qui ont galvanisé sa réputation. Parmi ses superbes contributions, l'une des plus notables est l'expansion du cycle des composés hétérocycliques saturés, tels que les aziridines et les époxydes pour la synthèse de lactames et de lactones respectivement. La synthèse concluante de β-lactames chiraux à partir d'aziridines sous forme racémique en présence de (–)-menthol ou de (+)-menthol est remarquable. D'ailleurs, sa synthèse de tétrahydroindolizidines à partir de pipéridines ne laisse rien à désirer. M. Alper a aussi découvert la cycloaddition catalysée par Pd de carbodiimides et d'hétérocycles conduisant à la formation des imines imidazoline et pyrimidine. Par ailleurs, il est arrivé à réaliser une synthèse chirale générale d'hétérocycles à cinq chaînes par réaction induite par Pd·BINAP des hétérocumulènes et des aziridines sous forme racémique. Il a aussi découvert une série d'hydrocarbonylations et d'hydrocarboxylations régiosélectives et stéréosélectives de substrats oléfiniques dans des conditions douces. La synthèse fortement énantiosélective du naproxène et de l'ibuprofène, deux agents anti-inflammatoires réputés, avère les vastes répercussions de sa démarche scientifique dans le domaine de la chimie. Sa découverte de la double et triple carbonylation des composés organiques catalysée par les métaux de transition et les lanthanides en a surpris plus d'un dans la collectivité, nous y compris. M. Alper a aussi été le premier chercheur à reconnaître le rôle crucial de complexes Rh zwitterioniques dans l'hydroformylation régiosélective (ramifiée ou linéaire) des oléfines, notamment des esters α,β-insaturés, des vinylsilanes, des sulfones insaturés et des sulfoxydes. Grâce à cette méthode, l'acétate d'allyle peut être converti en monoacétate de butanediol-1,4.

Au fil de sa carrière, M. Alper a défini de nombreuses nouvelles réactions en phase homogène, en phase liquide–liquide bicouche et en phase hétérogène. Parmi les fascinants résultats issus de ses expériences sur les systèmes biphasés, on remarque l'élaboration de très efficaces méthodes de déchloration des chloroarènes à l'aide de catalyseurs Pd. M. Alper a aussi trouvé une élégante méthode de synthèse catalysée par Pd – argile des isocyanates, prisés sur le marché, à partir de nitroarènes. Plus récemment, il a décrit les qualités des dendrimères Rh recyclables liés aux supports de silice ou de résine en vue de l'hydroformylation des oléfines.

Nombre de ces découvertes étaient tout à fait inattendues avant ses travaux. J'admire sa démarche intuitive qui s'écarte de la simple « orchestration » de réactions chimiques. Dans l'ensemble, ses travaux sont fondés sur la sobriété et sur l'applicabilité. Voilà pourquoi nombre des réactions qu'il a concoctées sont économiquement prometteuses pour

© 2005 NRC Canada

tant scientific realm. His seminal accomplishments have been recognized with many national and international awards that include: the Alcan Award for Inorganic Chemistry (1986, CSC), the Alfred Bader Award (1990, CSC), the Commemorative Medal from the Canadian Government (1992), the E.W.R. Steacie Award (1993, CSC), the Urgel–Archambault Prize in physical sciences and engineering (1996), the Chemical Institute of Canada Medal (1997), the Bell Canada Forum Award (1998), the NSERC Excellence in Research Award (2000), the most prestigious Gerhard Herzberg Gold Medal for Science and Engineering (2000), the President's Award (2001), and the Montreal Medal (2003). In 2001, Alper received the National Merit Award for contributions to the Life Sciences. In addition, he was given the Le Sueur Memorial Award of the Society of Chemical Industry in the UK (2002), and the award of Officer, National Order of Merit by the President of the Republic of France (2002).

It should be mentioned that Professor Alper is an outstanding "ambassador" of chemistry; he has received countless invitations from significant international conferences and academic or industrial research institutes. As such, Alper has encouraged the younger generation worldwide by not only publishing excellent papers (over 470), but also giving beautiful oral presentations in a unique lecture style. In addition, many leading scientific journals have asked Alper to put his name on their editorial boards. Furthermore, he has been heavily involved in scientific and educational administration in Canada. Most importantly, he is currently Vice-Rector (President), Research, of the University of Ottawa, and a member of the Council of the Canadian Institute for Advanced Research. Alper was named the President of the Academy of Science of the Royal Society of Canada in 2001–2003, and awarded the title of an Officer of the Order of Canada in 1999. He was elected to the European Academy of Arts, Sciences, and Humanities (1996) and the Third World Academy of Sciences (2003).

The foregoing describes only a few of Professor Alper's seminal contributions to modern science and the academic community. He has served as a vigorous and dedicated leader in the Canadian chemical community. Alper's activities encompass various roles outside the purely scientific domain. I deeply respect him as a stellar scientist, an enthusiastic educator, and an effective administrator, and also believe that such overall professional service is equally respected by the rest of the scientific community.

I have personally known Howard Alper for three decades. He is a superb scientist and an extremely warm person. Last but not least, a clever woman always exists behind a great man. Howard could be successful only with the support of his thoughtful wife, Anne, whose devotion must be deeply appreciated. I wish the Alper family continued success, health, and happiness.

Ryoji Noyori

l'industrie pharmaceutique, pétrochimique et chimique. De fait, il détient trente-sept brevets fondés sur les processus chimiques qu'il a mis en lumière. Le professeur Alper est sans contredit une des figures de proue du domaine. Ses importantes contributions ont été consacrées par de nombreux prix nationaux et internationaux dont le Prix Alcan en chimie inorganique (1986, SCC), le prix Alfred Bader (1990, SCC), la Médaille commémorative du 125^{e} anniversaire du Canada (1992), la Bourse commémorative E.W.R. (1993, SCC), le prix Urgel-Archambault en sciences physiques, mathématiques et génie (1996), la Médaille de l'Institut de chimie du Canada (1997), le prix Forum Bell Canada (1998), le prix d'excellence en recherche du CRSNG (2000), la très prestigieuse Médaille d'or Gerhard Herzberg en sciences et en génie (2000), le prix du président (2001) et la Médaille de Montréal (2003). En 2001, M. Alper a reçu le prix du mérite national pour ses contributions aux sciences de la vie. De plus, il a été primé par la Society of Chemical Industry du Royaume-Uni, qui lui a remis le prix Le Sueur Memorial Award (2002) et par le Président de la République française, qui lui a conféré le grade d'officier de l'Ordre national du Mérite (2002).

Il importe de souligner que le professeur Alper est un excellent « ambassadeur de la chimie » et qu'il a été invité à d'innombrables grandes conférences internationales et à des instituts de recherche universitaires et industriels réputés. M. Alper a inspiré une nouvelle génération de chercheurs du monde entier non seulement en signant des communications qui ont fait école (plus de 470), mais aussi en donnant des exposés oraux lumineux, dans un style bien à lui. De plus, nombreuses sont les revues savantes renommées qui ont invité M. Alper à se joindre à leur comité de rédaction. M. Alper a également touché de près à l'administration de la science et de l'enseignement au Canada. Il est d'ailleurs vice-recteur (président) à la recherche à l'Université d'Ottawa et membre du conseil d'administration de l'Institut canadien de recherches avancées. M. Alper a été le président de l'Académie des sciences de la Société royale du Canada de 2001 à 2003 et, en 1999, a été fait officier de l'Ordre du Canada. Il a été nommé membre titulaire de l'Académie européenne des arts, des sciences et des lettres (1996) et de la Third World Academy of Sciences (2003).

Ce qui précède ne constitue que quelques bribes de l'immense contribution du professeur Arper à la science contemporaine et à la collectivité universitaire. Il a été un porte-parole ardent et passionné de la collectivité de la chimie canadienne. Témoin la diversité de ses activités, l'étendue de l'influence de M. Alper n'est pas circonscrite au domaine scientifique. Je le respecte profondément sous toutes ses incarnations, soit celles de scientifique hors pair, d'enseignant enthousiaste et d'administrateur efficace, et je suis convaincu que l'impeccabilité de son service est tout autant respecté par l'ensemble de la communauté scientifique.

Je côtoie Howard Alper depuis une trentaine d'années. C'est un homme de science doué et une personne on ne peut plus affable. Cela étant, derrière tout homme remarquable se trouve une femme avertie, et Howard doit une grande partie de son succès au soutien de son attentive conjointe, Anne, dont le dévouement doit être profondément apprécié. Je souhaite beaucoup de succès, de santé et de bonheur à la famille Alper pour les années à venir.

Ryoji Noyori

© 2005 NRC Canada

TRIBUTE / HOMMAGE

It is my great pleasure to serve as co-editor of this special issue dedicated to an extraordinarily special individual, Dr. Howard Alper, Professor of Chemistry and Vice-Rector of Research at the University of Ottawa. I know Professor Alper best as the superb mentor that he was to me while I was a graduate student in his lab in the mid-1990s. During this time, I was impressed not only by his scientific insight and creativity, by his understanding of the complex factors affecting the political funding of science and superb grasp of university and scientific administration, or even by his talent as a teacher and mentor, but by his outstanding ability to excel at all three of these areas: research, administration, and education, at the same time. In my interactions with chemists around the world, I have never met someone as gifted in all of these areas as Howard Alper.

His abilities as a researcher are well-known to anyone who reads the current literature, and are beautifully summarized by the accompanying preface to this issue written by Professor Ryoji Noyori, Nobel Laureate. I was delighted by Professor Noyori's offer to pen this preface, and was reminded of the first time I met him. While a Ph.D. student in Professor Alper's lab, I had the incredible opportunity to work in Japan in the labs of Professor Shinji Murai for 3 months. During this time, Professor Murai arranged for me to visit several universities, including the University of Nagoya where I presented my Ph.D. work at one of Professor Noyori's group meetings. At the end of my presentation, Professor Noyori asked the first question. It was memorable: "How does Dr. Alper have so many unique research ideas?". Although this was and is a difficult question, I think the answer lies in his unique way of looking at science, his broad interest in all areas of chemistry and science, and his willingness to take risks. Working in his group was truly a remarkable experience.

When embarking on this issue, it was my sincere hope that the contributions would reflect the respect Howard Alper has generated throughout the international chemistry community. A quick perusal of the titles and contributors show not only the large number of people who have been influenced by his character and his chemistry, but also the breadth of his interests in science. In addition to the multitude of articles on catalysis, both heterogeneous and homogeneous, this issue contains articles describing radical chemistry, photochemistry, total synthesis, conformational analysis, materials science, sugar chemistry, peptide synthesis, and enzymology. Articles have been submitted from around the globe, representing researchers at all stages of their careers, including emeritus professors, presidents of chemical societies, and assistant professors, again illustrating the remarkable influence that Howard Alper continues to have on all generations of scientists. It has been a pleasure to compile this issue as a tribute to Professor Howard Alper, scientist, scholar, and mentor.

Cathleen M. Crudden

J'ai l'immense plaisir d'être rédactrice adjointe de ce numéro spécial consacré à une personne extraordinaire, monsieur Howard Alper, Ph.D., professeur de chimie et vice-recteur à la recherche à l'Université d'Ottawa. Pour moi, le professeur Alper représente d'abord et avant tout l'excellent mentor qui m'a accueillie dans son laboratoire au milieu des années 1990, durant mes études supérieures. À l'époque, son intuition et sa créativité sur le plan scientifique m'impressionnaient vraiment, ainsi que sa compréhension des facteurs complexes se rapportant au financement politique de la science, sans oublier son incroyable maîtrise de l'administration universitaire et scientifique, ni son talent en enseignement et en encadrement. Toutefois, ce qui m'avait vraiment renversée, c'est son exceptionnelle capacité à exceller simultanément dans les domaines suivants : la recherche, l'administration et l'éducation. Jamais au cours de mes interactions avec des chimistes partout dans le monde n'ai-je rencontré quelqu'un d'aussi talentueux dans ces trois domaines que Howard Alper.

Ses talents de chercheur, bien connus de tous ceux qui consultent la documentation courante, sont résumés de brillante façon par la préface qui accompagne ce numéro et qui a été rédigée par le professeur Ryoji Noyori, récipiendaire du prix Nobel. Par ailleurs, j'ai été ravie d'apprendre que le professeur Noyori s'est offert pour rédiger la préface, et je me suis souvenue de ma première rencontre avec lui. Lors de mes études doctorales réalisées au laboratoire du professeur Alper, j'ai eu une occasion rêvée de travailler au Japon au sein des laboratoires du professeur Shinji Murai pour une période de trois mois. Durant ce temps, le professeur Murai m'a permis de visiter plusieurs universités, y compris l'Université de Nagoya où j'ai présenté mes travaux de recherche doctorale lors d'une réunion de groupe du professeur Noyori. À la fin de ma présentation, le professeur Noyori a posé une première question qui était tout à fait mémorable : « Comment fait-il [professeur Alper] pour avoir des idées de recherches aussi uniques? ». Et même si cette question est toujours aussi difficile à répondre aujourd'hui que lors de mon exposé, je crois que la réponse réside dans son approche unique à la science, son intérêt varié pour tout ce qui traite de la chimie et de la science et sa disposition à courir des risques. Mon séjour au sein de son équipe s'est avéré une expérience très enrichissante.

Lorsque j'ai entrepris ce projet, je souhaitais sincèrement que la teneur du texte témoigne de la solide réputation que M. Alper s'est forgée au sein de la collectivité internationale. Une lecture cursive des titres et des collaborateurs révèle non seulement la portée de son talent et de ses travaux de recherche auprès de nombreux chercheurs, mais aussi l'étendue de son intérêt pour la science. Outre le grand nombre d'articles sur la catalyse hétérogène et homogène, ce numéro renferme des articles sur la chimie radicalaire, la photochimie, la synthèse totale, l'analyse conformationnelle, la science des matériaux, la sucrochimie, la synthèse peptidique et l'enzymologie. Les articles proviennent de partout dans le monde et de chercheurs à diverses étapes de leur carrière, y compris des professeurs émérites, des présidents de sociétés chimiques et des professeurs adjoints. Cela témoigne, une fois de plus, de l'importante influence que M. Alper continue d'exercer auprès de toutes les générations de scientifiques. C'est donc avec plaisir que j'ai compilé ce numéro qui rend hommage au professeur Howard Alper — scientifique, savant et mentor.

Cathleen M. Crudden

© 2005 NRC Canada

AWARD LECTURE / CONFÉRENCE D'HONNEUR

2003 Alcan Award Lecture — Roles of the adjacent metals in the coupling of methylene groups promoted by heterobinuclear complexes of Group 8 and 9 metals

Martin Cowie

Abstract: The reactivities of the heterobinuclear complexes, $[MM'(CO)_4(dppm)_2][X]$ (MM′ = RhOs, RhRu, IrRu; dppm = μ-$Ph_2PCH_2PPh_2$; X^- = BF_4^-, $CF_3SO_3^-$) with diazomethane are reported. The RhOs species reacts to give three products of methylene-group incorporation, depending on the temperature; at –80 °C the methylene bridged product, $[RhOs(CO)_4(\mu\text{-}CH_2)(dppm)_2][X]$, is formed exclusively, at ambient temperature only $[RhOs(\eta^1\text{-}C_3H_5)(CH_3)(CO)_3(dppm)_2]$-[X], having the allyl group bound to Rh and the methyl group bound to Os, is obtained, while at intermediate temperatures $[RhOs(\eta^1{:}\eta^1\text{-}C_4H_8)(CO)_3(dppm)_2][X]$, having the butanediyl fragment chelating on Os, is generated. Based on labeling studies a mechanism is proposed rationalizing formation of the different products. Under the same range of conditions the Rh/Ru and Ir/Ru species yield only the methylene bridged products, $[MM'(CO)_4(\mu\text{-}CH_2)(dppm)_2][X]$ (MM′ = RhRu, IrRu). A rationalization for the different reactivities observed and a description of the roles of the different metals in coupling of the methylene groups are presented. Attempts to model key intermediates in the methylene coupling sequence promoted by the Rh/Os complexes, through coupling of methylene groups with ethylene or alkynes, are described.

Key words: heterobinuclear, rhodium/osmium, rhodium/ruthenium, iridium/ruthenium, methylene coupling, Fischer–Tropsch, alkyne insertions, bimetallic cooperativity.

Résumé : On a étudié les réactivités des complexes hétérobinucléaires $[MM'(CO)_4(dppm)_2][X]$ (MM′ = RhOs, RhRu, IrRu; dppm = μ-$Ph_2PCH_2PPh_2$; X^- = BF_4^-, $CF_3SO_3^-$) avec le diazométhane. Suivant la température de la réaction, les espèces RhOs réagissent pour donner trois produits d'incorporation du méthylène; à –80 °C, le seul produit formé est le composé à pont méthylène, le $[RhOs(CO)_4(\mu\text{-}CH_2)(dppm)_2][X]$, à la température ambiante, le seul produit obtenu est le $[RhOs(\eta^1\text{-}C_3H_5)(CH_3)(CO)_3(dppm)_2][X]$ dans lequel le groupe allyle est lié au Rh alors que le groupe méthyle est lié au Os; aux températures intermédiaires, il y a formation du produit $[RhOs(\eta^1{:}\eta^1\text{-}C_4H_8)(CO)_3(dppm)_2][X]$ dans lequel le fragment butanediyle est lié au Os. Sur la base d'études de marquage, on propose un mécanisme pour rationaliser la formation de chacun des produits. Sous diverses conditions, les espèces Rh/Ru et Ir/Ru ne conduisent qu'à la formation des produits comportant le pont méthylène, $[MM'(CO)_4(\mu\text{-}CH_2)(dppm)_2][X]$ (MM′ = RhRu, IrRu). On présente une rationalisation des différentes réactivités observées et une description des rôles des différents métaux dans le couplage des groupes méthylènes. On décrit aussi des essais de modélisation des intermédiaires clés dans la séquence de couplage du méthylène catalysé par les complexes Rh/Os et impliquant un couplage des groupes méthylènes avec l'éthylène ou des alcynes.

Mots clés : hétérobinucléaire, rhodium/osmium, rhodium/ruthénium, iridium/ruthénium, couplage de méthylène, Fischer–Tropsch, insertions d'alcynes, coopération bimétallique.

[Traduit par la Rédaction]

Background

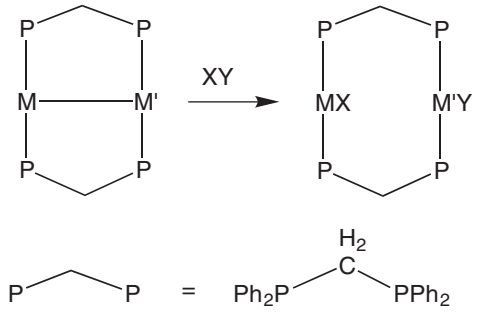
I arrived at the University of Alberta in 1976, fresh from a postdoctoral position in the group of Jim Ibers at Northwestern University, where I had become interested in the organometallic chemistry of the late transition metals. In starting an independent research program, I looked to create a niche for myself in this fascinating area. At the time, the organo-

Received 10 February 2005. Published on the NRC Research Press Web site at http://canjchem.nrc.ca on 16 August 2005. Reposted on the Web site with correction on 9 September 2005.

M. Cowie. Department of Chemistry, University of Alberta, Edmonton, AB T6G 2G2, Canada. (e–mail: martin.cowie@ualberta.ca).

 doi: 10.1139/V05-122 © 2005 NRC Canada

Chart 1.



metallic chemistry of complexes such as Wilkinson's catalyst (1) and Vaska's compound (2) was an active area of research so we decided to expand the scope of this chemistry by generating the binuclear analogues of these and related species on the assumption that the presence of the adjacent metals could give rise to significant reactivity differences compared to the mononuclear counterparts. We set out to establish whether adjacent metals could interact in a cooperative manner in the activation of organic substrates and to determine the roles of the adjacent metals in the activation process. Irrespective of how adjacent metals might cooperate in substrate activation, it certainly seemed that at a minimum the ability of substrates to bridge metals in multinuclear complexes should give rise to significant differences in reactivity compared to that of terminally bound substrates in mononuclear species.

At the time we started our work, there was already substantial interest in the chemistry of binuclear complexes (3). However, many of these complexes fragment into mononuclear species on reaction with substrates, removing any apparent advantage of having the metals initially bound together. It was immediately obvious that an appropriate bridging ligand was needed to hold the metals together, even upon cleavage of the metal–metal bond. I was fortunate at the time to be introduced to bis(diphenylphosphino)methane as a bridging ligand (commonly abbreviated as dppm) by Alan Sanger and Joel Mague, with whom I briefly collaborated (4). Dppm has an ideal bite and is flexible enough to bridge a wide range of metal–metal separations in the presence or absence of metal–metal bonds, as diagrammed in Chart 1 (ancillary ligands on M and M′ are not shown).

The study of dppm bridged complexes was an area of great interest and I found myself in the stimulating company of competitors such as Alan Balch (5), Richie Eisenberg (6), Bernard Shaw (7), Dick Puddephatt (8) (who at the time was still in Liverpool, but who was subsequently to move to London, Ontario), and Ray Haines, who studied diphosphines closely related to dppm (9). Other groups such as those of Selby Knox (10), Chuck Casey (11), Rowland Pettit (12), Luis Oro (13), and René Poilblanc (14) had similar goals related to binuclear reactivity, but did not routinely use diphosphines as bridging groups. In addition, there was substantial interest during this period in higher nuclearity clusters, which were being championed as links between classic coordination complexes and heterogeneous metal catalysts (15), and therefore could serve as valuable models for catalytic processes occurring on difficult-to-study metal surfaces. The relationship between metal surfaces and metal complexes was eloquently stated by Earl Muetterties (15*d*): "Surface chemistry is coordination chemistry. If the molecule or molecules in question are organic then the surface chemistry is organometallic chemistry".

Although it is unreasonable to expect binuclear complexes to be meaningful models for metal surfaces, they can, nonethe-less, yield valuable information on, and therefore can effectively model aspects of substrate coordination and activation at surfaces since many of the known ligand coordination modes occur in each. Furthermore, we felt that the lack of unnecessary complexity in two-metal systems made them ideal for establishing the intimate details of how adjacent metals were involved in cooperative substrate activation.

Our interests in dppm and related diphosphines, presumably like those of our closest competitors, derived from the similarities of dppm bridged complexes to the well-known mononuclear, late-metal phosphine complexes, such as those of Wilkinson and Vaska, that had played such a prominent role in studies of metal-promoted activation of small molecules (16). However, the importance of ^{31}P NMR spectroscopy in characterization of the dppm complexes was also a major reason for using this ligand. In this context, we have been extremely fortunate to have benefited greatly from the expertise in our Departmental NMR facility, supervised over most of my career, until his (early) retirement, by Tom Nakashima, and more recently by his replacement, Albin Otter.

Although our earlier work was concerned with the homobinuclear pairs of metals, Rh_2 (17) and Ir_2 (18), we eventually branched out into the mixed-metal combination, Rh/Ir (19), and realizing the potential richness of systems containing combinations of metals from different groups in the periodic table, it was not long afterwards that we began to experiment with a variety of metal combinations. Dave Antonelli, a former graduate student in my group, was instrumental in initiating this chemistry (20). It seemed clear that combining the unique properties of different metals could give rise to interesting variations in reactivity compared to either metal alone, thereby significantly extending the flexibility of the chemistry.

At this time, bimetallic catalysts were being extensively used, particularly in the petrochemical industry (21), in processes such as gasoline reforming (using Pt/Re or Pt/Ir catalysts), hydrocracking (using Ni/Mo or Ni/W), and hydrodesulfurization (using Co/Mo or Ni/Mo). This interest has continued, but in spite of their extensive use, little is understood about the roles of the different metals in these bimetallic catalysts. It seemed therefore that our interest in the reactivity of well-defined heterobinuclear complexes could shed light on the roles of adjacent metals in the activation of organic substrates.

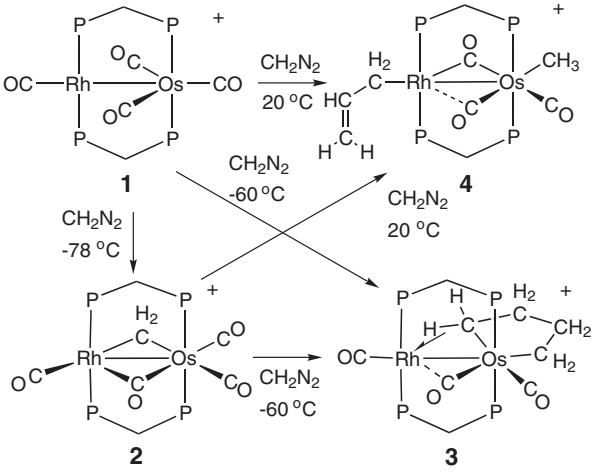
One constant throughout most of our chemistry has been the use of either Rh or Ir as one of the two metals involved, thereby introducing a site of coordinative unsaturation into the complexes. This unsaturation is pivotal in endowing these species with remarkable reactivity, even at temperatures down to –80 °C.

Fischer–Tropsch chemistry

A process that had fascinated me for years is the Fischer–Tropsch (FT) reaction (22) in which synthesis gas ($CO + H_2$)

© 2005 NRC Canada

Scheme 1.



is converted, over a Group 8 or Group 9 metal catalyst, to mixtures of alkanes, alkenes, and oxygen containing products, as outlined in the (unbalanced) eq. [1].

$$[1] \quad CO + H_2 \xrightarrow{\text{catalyst}} C_nH_{2n+2} + C_nH_{2n} + \text{oxygenates} + H_2O$$

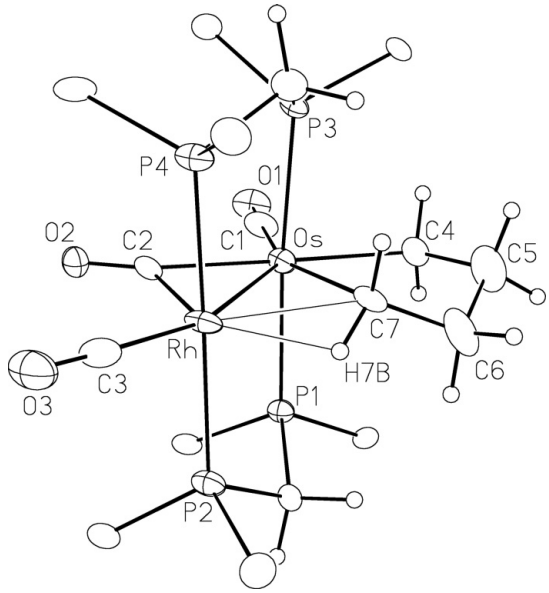
Although much remains to be learned about the mechanisms of carbon–carbon bond formation in this process, a number of proposals have been put forward, in which surface-bound methylenes play a prominent role (12*b*, 12*c*, 22*a*, 23–25). Furthermore, the observation that different metals catalyze the formation of different product distributions (26), suggested that *combinations* of metals may lead to interesting variations in product distributions. Work has been reported describing the use of the Ru/Co combination of metals as a FT catalyst (27).

Model systems

Realizing the importance of methylene fragments and the Group 8 and 9 metals in the FT process, we set out to investigate the reactivity of mixed Group 8/Group 9 metal complexes having bridging methylene groups in the aforementioned dppm bridged systems with the goal of investigating the roles of the different metals in carbon–carbon bond formation involving this C_1 fragment (28). At this time, a senior graduate student in my group, Brian Sterenberg, needing a break from writing his thesis on the organometallic chemistry of mixed Rh/Os and Rh/Ru complexes, chose to attempt the synthesis of the methylene bridged complex, $[RhOs(CO)_4(\mu\text{-}CH_2)(dppm)_2][X]$ (**2**; dppm = μ-$Ph_2PCH_2PPh_2$; X = BF_4, CF_3SO_3) by reacting one of his standard precursors, $[RhOs(CO)_4(dppm)_2][X]$ (**1**), with diazomethane at ambient temperature. Although he did not succeed in obtaining the targeted methylene bridged species, the product obtained, $[RhOs(\eta^1\text{-}CH_2CH{=}CH_2)(CH_3)(CO)_3(dppm)_2][X]$ (**4**), shown in Scheme 1, was far more interesting, having incorporated four methylene groups to give the allyl and methyl fragments, bound to the different metals.

The generation of an allyl group from methylene groups was reminiscent of one step in the proposal by Peter Maitlis and co-workers (24) for chain growth in the FT process,

Fig. 1. Perspective view of $[RhOs(\eta^1{:}\eta^1\text{-}C_4H_8)(CO)_3(dppm)_2]^+$ (**3**). Only the ipso carbons of the dppm phenyl groups are shown.



through the coupling of surface-bound vinyl and methylene groups. Both Peter and I were interested in this parallel, and I spent several enjoyable weeks over two summers in Sheffield, as part of a NATO-sponsored collaboration, discussing our mutual interests in FT chemistry with Peter, Mike Turner, and their group members. In turn, Peter and Mike visited Edmonton on separate occasions to interact with my group. In England, Peter and his wife Marion were wonderful hosts, involving me in dinner parties, the theatre, and tours through the nearby countryside. Meanwhile, Mike and members of the Maitlis group ensured that I also sampled other cultural highlights of the UK, such as football, fish and chips, hill walking, and English bitter. I still can think of few greater pleasures than enjoying fish and chips over a pint of bitter in a country pub after a vigorous walk in the British hills (except maybe if the match of the day were also playing on the telly).

Shortly after Brian graduated and left the group, another graduate student, Steve Trepanier, took up the project and succeeded in obtaining the targeted methylene bridged $[RhOs(CO)_4(\mu\text{-}CH_2)(dppm)_2][X]$ (**2**) by carrying out the reaction of **1** with diazomethane at –78 °C. He discovered that this species was stable and could be readily isolated as long as the excess diazomethane was removed at –78 °C. However, warming a mixture of **2** and diazomethane above –78 °C resulted in further reactivity. Steve found that carrying out this reaction at ambient temperature generated the aforementioned compound **4**, whereas at intermediate temperatures around –40 to –60 °C, the butanediyl product $[RhOs(\eta^1{:}\eta^1\text{-}C_4H_8)(CO)_3(dppm)_2][X]$ (**3**), shown in Scheme 1 and Fig. 1, was obtained. The finding that compounds **3** and **4** could be obtained under the respective conditions from either **1** or **2** suggested that **2** was an intermediate in the formation of both products. However, the failure of **3** and **4** to interconvert, at ambient temperature or higher, indicated that these two species are derived from **2** by independent pathways (28, 29).

© 2005 NRC Canada

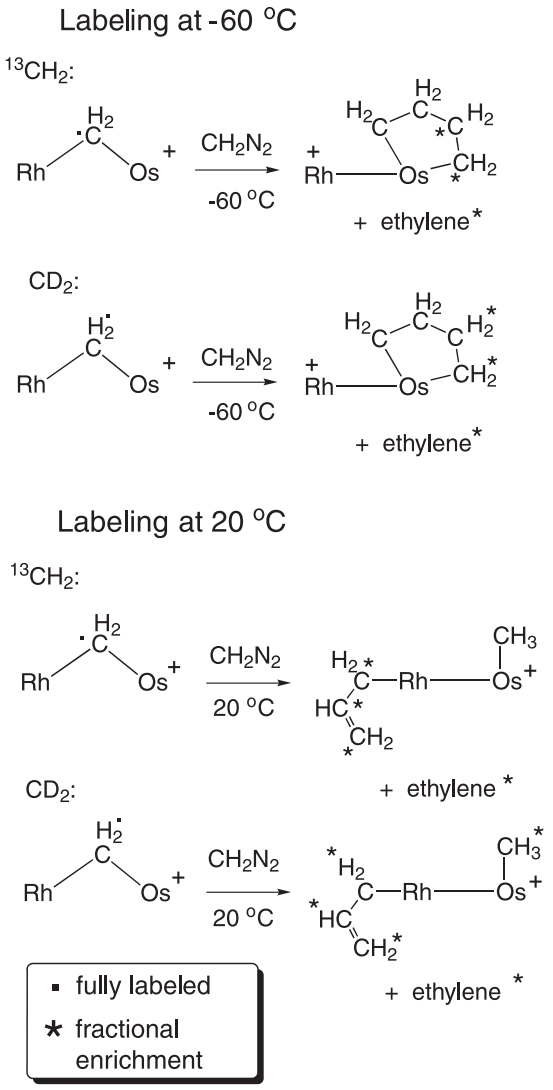
The selective transformation of diazomethane generated methylene groups into either C_3 and C_1 fragments (allyl/methyl groups) or a C_4 fragment (butanediyl group) depending on the temperature, together with ethylene in both cases, was unprecedented, and we were eager to learn more about this system. In particular, we wanted to resolve the roles of the metals in these methylene coupling reactions and to determine why termination at C_3 and C_4 species occurred, instead of generating longer C_n fragments. Furthermore, it was of interest to determine what products would be obtained using other metal combinations.

Mechanism of CH_2 incorporation

Valuable information about how methylene coupling occurred was obtained from labeling studies. Steve had subsequently prepared the $^{13}CH_2$ and the CD_2 labeled versions of **2**, and upon subsequent reaction with unlabeled diazomethane was able, using NMR spectroscopy, to track the distribution of the label through the final products. These experiments are summarized in Scheme 2 in which only the metals and hydrocarbyl groups are represented for simplicity. In the reaction carried out at between –40 and –60 °C, both the ^{13}C and the ^{2}H label occupied the two adjacent sites remote from Rh (as shown in this scheme), as well as appearing in ethylene that was also generated. However, for the allyl methyl product, the ^{13}C label appears in the three allyl carbons in a 1:2:1 intensity ratio, with no ^{13}C incorporation into the methyl ligand. In the experiments involving CD_2 labeled **2**, deuterium incorporation into all sites of the allyl and methyl groups occurred. As in the low-temperature experiment, ^{13}C and ^{2}H incorporation into free ethylene was also observed.

On the basis of these results, we suggested the mechanism of methylene incorporation outlined in Scheme 3 (in this scheme only the $^{13}CH_2$ label is tracked, and again, only the metals and hydrocarbyl groups are shown). In all cases, we propose that methylene insertion into the Rh—CH_2 bond of the bridging hydrocarbyl fragment occurs. Methylene insertion into the Rh—CH_2 bond of **2** is proposed to yield the ethylene bridged intermediate **A**, which at this stage would have the label (either ^{13}C or ^{2}H) solely in the CH_2 site adjacent to Os. Movement of a bridging ethylene group to a terminal, η^2-bound group (**B**) has been observed (30) and the well-documented, facile ethylene rotation (31) followed by regeneration of the ethylene bridged species would scramble the label over both CH_2 sites in **A***. Of course, some ethylene loss could occur from **B** accounting for the ethylene observed in these experiments, and the resulting Rh/Os containing product could regenerate compound **2** upon reaction with diazomethane. Subsequent methylene insertion into the Rh—CH_2 bond of **A*** would yield the propanediyl bridged intermediate **C** in which the label is evenly distributed between the two sites shown — the central site and the one adjacent to Os. At low temperatures, a fourth methylene group can react yielding the butanediyl bridged **D**, which can readily rearrange to the chelated product **3** by migration of the Rh bound methylene group to Os. This migration is presumably favoured by the relatively unstrained five-membered metallacycle that results, as opposed to the strained six-membered dimetallacycle of **D**. In this product,

Scheme 2.

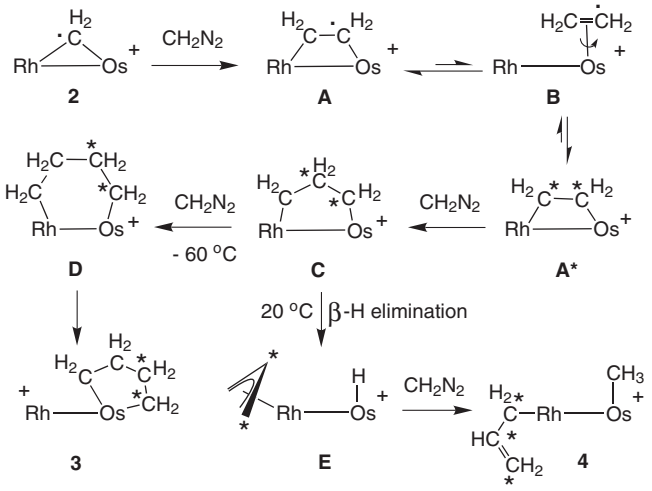


the scrambling of the label over only the two sites remote from Rh is explained by the olefin rotation process occurring in intermediate **B**, and by selective methylene insertion into the Rh—CH_2 bond of the bridging hydrocarbyl unit. Based on our assumption of diazomethane activation at Rh and subsequent insertion of the resulting methylene group into the Rh—CH_2 bond of the bridging hydrocarbyl moiety, the isomerization of **D** to **3** in which there no longer is a Rh—CH_2 bond, explains our failure to obtain hydrocarbyl fragments longer than C_4. Presumably, the lifetime of **D** is too short to allow incorporation of a fifth methylene group.

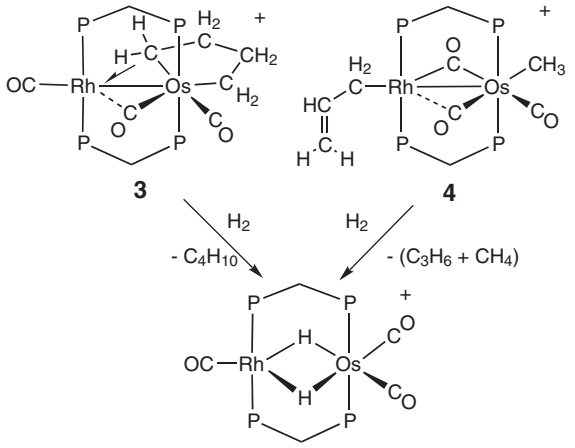
Raising the temperature to near ambient is assumed to allow the activation of a C—H bond of the central CH_2 group in intermediate **C**, leading to an allyl hydride intermediate resembling **E**, which upon reaction with an additional diazomethane molecule can yield the allyl methyl product **4**. This process begins to appear at approximately –40 °C, at which temperature **4** is a very minor product, and becomes increasingly favoured over the methylene insertion step (**C** → **D**) as the temperature is increased, such that at ambient temperature, generation of **4** occurs essentially exclusively. In the

© 2005 NRC Canada

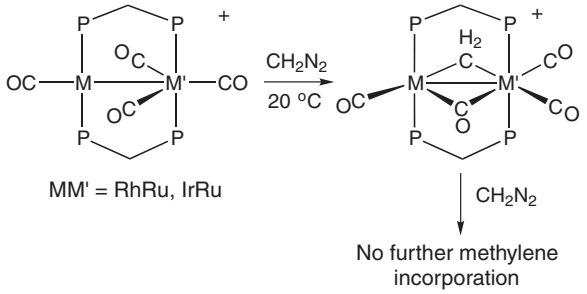
Scheme 3.



Scheme 4.



Scheme 5.



$^{13}CH_2$ labeled system the label becomes scrambled through the three positions of the allyl moiety in a 1:2:1 ratio, reflecting the equal probability of either end of the allyl unit coordinating to Rh, in the conversion of **E** to **4**, further diluting the label at both ends of this unit. We also note that slow exchange of both ends of the allyl ligand in **4** occurs in solution, representing another mechanism for scrambling of the terminal label. It is clear that the methyl group of **4** will contain no ^{13}C label since this group originates from an unlabeled methylene group. The observation of deuterium scrambling into this methyl group arises from the β-hydrogen elimination step, since the β position of intermediate **C** contains some deuterium from the previous scrambling process.

Hydrocarbons from hydrogenolysis

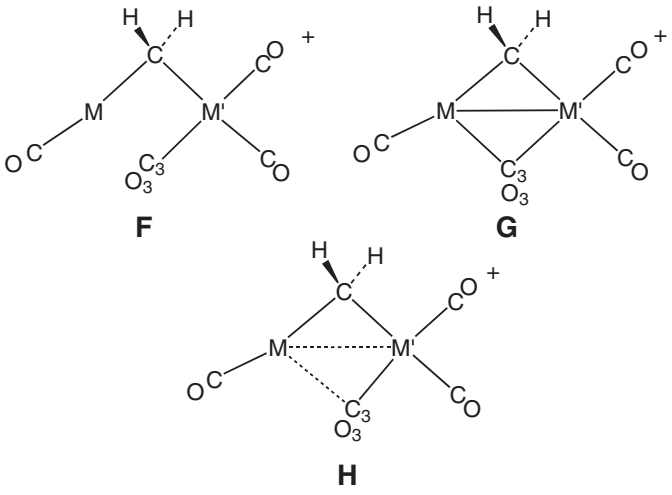
Both compounds **3** and **4** react slowly with H_2 yielding the respective products, *n*-butane or propene and methane, by hydrogenolysis of the metal–alkyl bonds, as shown in Scheme 4. In both cases, the metal-containing product is the known dihydride, $[RhOs(CO)_3(\mu\text{-}H)_2(dppm)_2][X]$, a species that can be readily converted into the precursor **1** upon addition of CO (32). This sequence allows us to construct a pseudo-catalytic cycle for the selective generation of butane or methane and propene (together with ethylene, produced in both cases) from diazomethane and hydrogen, fulfilling part of the FT sequence of conversion of methylene groups into different hydrocarbons.

Different metal combinations

The conversion of either **1** or **2** into the products **3** and **4** is accompanied by the loss of one carbonyl group, leading us to question the role of CO loss in the process and the stage at which this loss occurred. It seemed reasonable to expect that if CO loss is important in the methylene coupling process, the analogous Rh/Ru system should be more reactive owing to the greater lability of Ru compared to Os (33). Surprisingly, this has not proven to be the case. Bryan Rowsell, another graduate student in my group, established that the reaction of $[RhRu(CO)_4(dppm)_2][X]$ with diazomethane gave only the methylene bridged *tetracarbonyl* complex $[RhRu(CO)_4(\mu\text{-}CH_2)(dppm)_2][X]$(as shown in Scheme 5) even at ambient temperature (34). No carbonyl loss or further incorporation of methylene groups was observed under conditions similar to those investigated in the Rh/Os system. At the same time, Steve Trepanier and Maria Michela Dell'Anna, a visiting graduate student from Francesco Nobile's group in Bari, found that the Ir/Ru analogue also generated only the methylene bridged tetracarbonyl product (35). This contrast in reactivity compared to the Rh/Os system raised obvious questions about the lability of the carbonyl ligands in the series of compounds $[MM'(CO)_4(\mu\text{-}CH_2)(dppm)_2][X]$ (MM′ = RhRu (**5**), RhOs (**2**), IrRu (**6**)). Reflecting our crystallographic bias (originating in my previous associations with two very talented crystallographers, Mike Bennett, my Ph.D. supervisor, and Jim Ibers, my postdoctoral supervisor), we reasoned that a comparison of the solid-state structures of these three species might give clues about their reactivity differences. At the outset, three structural types could be envisioned as diagrammed in Chart 2 (dppm groups above and below the plane of the drawing are omitted for clarity). In one extreme (**F**), all carbonyls are terminally bound leaving the Group 9 metal (M) with a 16e configuration; this, in our view, was the ideal arrangement, allowing for incorporation of an additional diazomethane at the coordinatively unsaturated metal. In the other bonding extreme (**G**), one carbonyl bridges the metals leaving both metals coordinatively saturated, by virtue of this bridging carbonyl arrangement accompanied by the metal–metal

© 2005 NRC Canada

Chart 2.



bond. Also possible is the intermediate structure (**H**) in which one carbonyl is primarily bound to the Group 8 metal (M′) while involved in a weaker, semi-bridging interaction with Rh or Ir. For a species having one of the carbonyl bridged geometries to react with diazomethane at the Group 9 metal (as established in the previous labeling studies), displacement of the bridging carbonyl from this metal needs to occur, and it seems reasonable to expect that this could be more difficult in the case of the symmetrically bridged **G** in which binding to the Group 9 metal is strongest.

Structural comparisons and carbonyl lability

The structure of the Rh/Os member of this series (compound **2**) is diagrammed in Fig. 2, and a comparison of the key structural parameters of the three analogues is presented in Table 1. Referring to Chart 2, it is clear that the closer a compound resembles structure **G**, the shorter will be the metal–metal bond, the more symmetric will be the M-C(3)-O(3) and M′-C(3)-O(3) angles, and the more acute will be the C(5)-M-C(4) angle as the hybridization at M becomes perturbed by interaction with carbonyl C(3)O(3). Although it seems clear that a tendency towards extreme **G** should also be accompanied by a shortening of the M—C(3) distance, this is not observed in a comparison of these compounds for reasons that are not clear.

Superficially, all structures are similar, but a close comparison of the parameters given in Table 1 establishes that the Ir/Ru species (**6**) differs from the other two in having an essentially symmetrically bridged carbonyl, close to extreme **G**, while both the Rh/Os (**2**) and Rh/Ru (**5**) compounds have a geometry like **H** in which the bridging carbonyl tends significantly towards the semi-bridged geometry. A closer comparison of the structural parameters of compounds **2** and **5** indicates that **5** lies slightly closer to the symmetrically bridged extreme **G**. On the basis that the most reactive compound (**2**) appears to be least well-represented by extreme **G** and therefore presumably has the weakest interaction between M and C(3)O(3), we proposed that this carbonyl can be more easily displaced from this Group 9 metal upon

Fig. 2. Perspective view of $[RhOs(CO)_4(\mu\text{-}CH_2)(dppm)_2]^+$ (**2**). Only the ipso carbons of the dppm phenyl rings are shown.

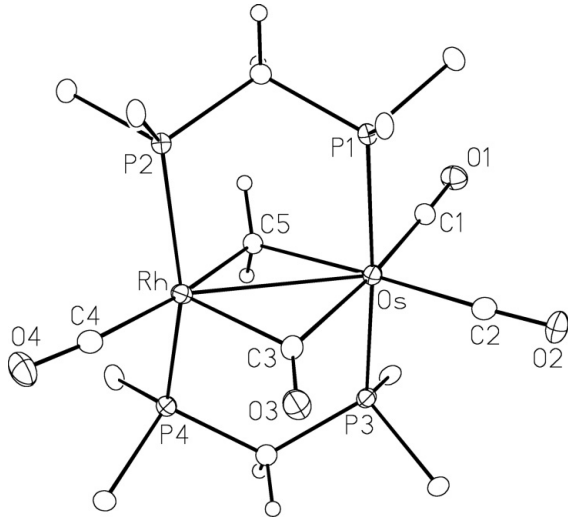


Table 1. Comparison of (*a*) bond lengths and (*b*) bond angles for the compounds $[MM'(CO)_4(\mu\text{-}CH_2)(dppm)_2][BF_4]$ (MM′ = RhOs, RhRu, IrRu).[a]

(*a*) Bond lengths (Å)			
MM′	RhOs[29]	RhRu[34]	IrRu[35]
M—M′[b]	2.9413(4)	2.9114(5)	2.8650(7)
M′—C(3)	2.157(4)	2.155(4)	2.072(8)
M—C(3)	2.027(4)	2.021(3)	2.033(8)
M′—C(5)	2.210(4)	2.213(3)	2.305(12)
M—C(5)	2.088(4)	2.089(3)	2.045(11)
(*b*) Bond angles (°)			
MM′	RhOs[29]	RhRu[34]	IrRu[35]
M′-C(3)-O(3)	141.7(3)	141.1(3)	137.1(7)
M-C(3)-O(3)	128.9(3)	130.4(3)	134.4(7)
C(5)-M-C(4)	169.1(2)	167.9(1)	161.7(5)

[a]The numbering scheme used for all compounds is that used for compound **2** in Fig. 2.
[b]M = Rh, Ir; M′ = Ru, Os.

nucleophilic attack by diazomethane at this metal, as shown in Scheme 6 (dppm groups omitted).

Support for these ideas about nucleophilic displacement of a carbonyl in the series of compounds **2**, **5**, and **6** was obtained in their reactions with trimethylphosphine. In all cases, reaction of these species with PMe_3 occurred readily, yielding the products $[MM'(PMe_3)(CO)_3(\mu\text{-}CH_2)(dppm)_2][X]$ (MM′ = RhOs, RhRu, IrRu), having a structure like that represented by **I** in Scheme 6 (Nu = PMe_3) and shown for the Ir/Ru species in Fig. 3. Furthermore, the rates of CO displacement at –25 °C at which these reactions could be conveniently monitored by NMR, was in the order: rate of **2** ≈ 30 × rate of **5** ≈ 36 × rate of **6**. These relative rates, under identical conditions, in an excess of PMe_3, are consistent with the structural trends noted above and with the argument that compound **2** having the weakest bridging carbonyl interaction with the Group 9 metal would react the fastest, while that having the strongest such interaction (**6**) would react the slowest.

© 2005 NRC Canada

Scheme 6.

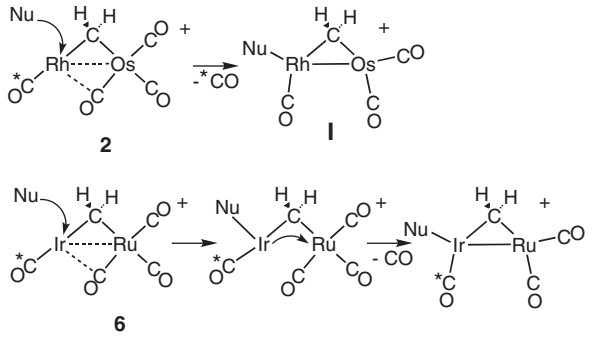
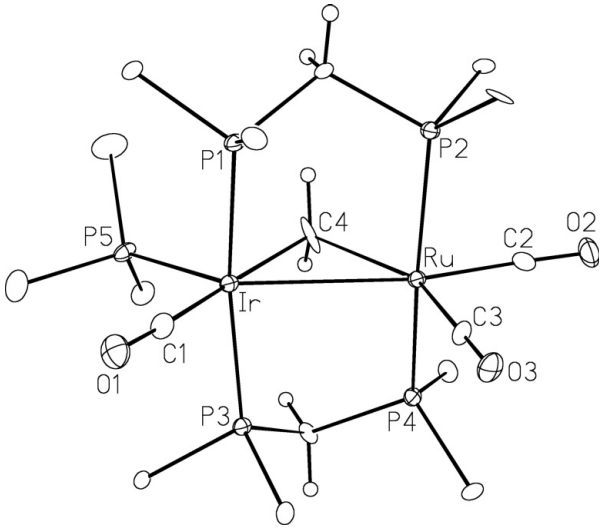


Fig. 3. Perspective view of $[IrRu(PMe_3)(CO)_3(dppm)_2]^+$. Only the ipso carbons of the dppm phenyl rings are shown.

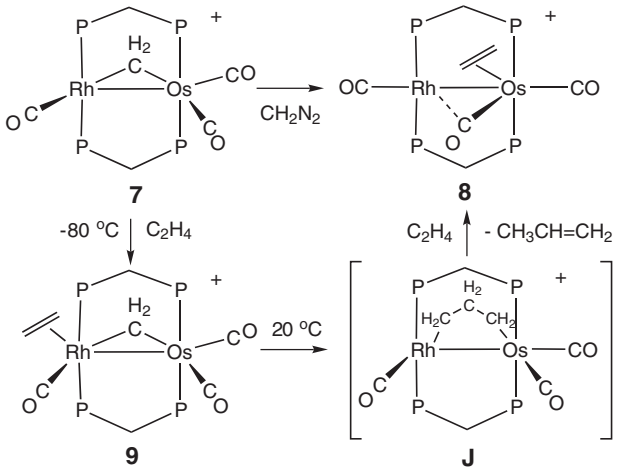


By selectively labeling the carbonyl bound to the Group 9 metal in compounds **2** and **6**, through reactions of the unlabeled precursors with ^{13}CO at –78 °C, we have been able to detect two subtly different mechanisms for carbonyl substitution by PMe_3. When the monolabeled **2** is reacted with PMe_3 at –78 °C, displacement of the labeled carbonyl occurs exclusively (see Scheme 6), indicating that for this metal combination, carbonyl substitution occurs solely at Rh. However, the Ir/Ru analogue (**6**) reacts in a binuclear fashion, with retention of the labeled CO on Ir and loss of an unlabeled Ru bound carbonyl. For the latter process, we can envision a mechanism in which nucleophilic attack at Ir is followed by dative bond formation, from Ir to Ru, which assists in displacing a carbonyl ligand from the latter. These different mechanisms can be rationalized based on the greater labilities of the second-row metals compared to their third-row congeners. As the reaction temperature is raised, carbonyl scrambling occurs in the Ir/Ru compound accompanied by some loss of labeled CO, indicating that other mechanisms become operable at higher temperatures. Unfortunately, we have not yet succeeded in selectively labeling the Rh/Ru analogue (**5**).

Carbonyl loss and methylene coupling

It seemed reasonable to assume that the reaction of **2** with diazomethane might parallel the PMe_3 reaction by loss of carbonyl to give an intermediate such as **I**, which might subsequently proceed through N_2 loss and coupling of the two methylene groups. This suggested to us that starting with the tricarbonyl analogue of **2**, namely $[RhOs(CO)_3(\mu\text{-}CH_2)(dppm)_2][X]$ (**7**), might yield either **3** or **4** under appropriate conditions, and that inducing CO loss from **5** and **6** in the presence of diazomethane might result in subsequent methylene incorporation in these species. We had presumed that the failures of **5** and **6** to react further with diazomethane had resulted because diazomethane was too weak a nucleophile to displace a carbonyl ligand in these species.

Scheme 7.

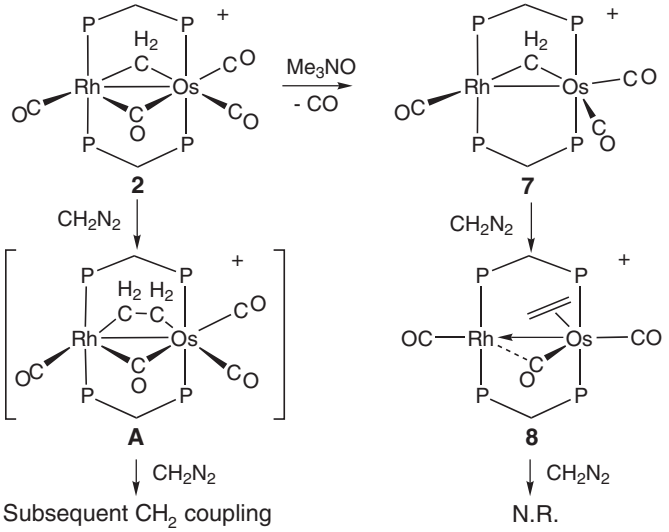


Surprisingly, Steve found that the reaction of **7** (generated by the reaction of **2** with 1 equiv. of Me_3NO) with diazomethane yielded neither **3** nor **4** over a wide temperature range, but instead yielded the ethylene adduct $[RhOs(\eta^2\text{-}C_2H_4)(CO)_3(dppm)_2]^+$ (**8**) as shown in Scheme 7. This product was shown by NMR techniques to have the ethylene group bound in an η^2 fashion to Os in a site adjacent to the bridging position between both metals (29). As such, compound **8** is similar to intermediate **B** in Scheme 3, which had been proposed as the species responsible for scrambling of the labels outlined in Scheme 2. It was puzzling therefore that the ethylene ligand in **8** did not move readily to the bridging site, resulting in subsequent methylene incorporation (as proposed in Scheme 3). Certainly, the failure of **8** to incorporate additional methylene groups is supportive of our earlier proposal that hydrocarbyl chain growth in this series arises by methylene insertion into the Rh—CH_2 bond of the *hydrocarbyl bridged* precursor.

The difference in the reactivity of the methylene bridged tetracarbonyl species **2** and its tricarbonyl analogue **7** with diazomethane is summarized in Scheme 8. Whereas the tetracarbonyl species gives rise to multiple methylene insertions yielding compounds **3** or **4**, the tricarbonyl species **7** yields only **8** with no further methylene incorporation occurring. Presumably, the additional carbonyl in intermediate **A** (of Schemes 3 and 8) is responsible for forcing the osmium bound ethylene in intermediate **B** (Scheme 3) back into the bridging site owing to steric congestion at Os. In the absence of this additional carbonyl, a terminally bound ethylene ligand, as observed in **8**, is favoured. In related chemistry, Jim Dennett, a postdoctoral fellow from Selby Knox's group, together with Steve Trepanier, have generated a series

© 2005 NRC Canada

Scheme 8.



of mono- and bisethylene analogues of **8**, all of which have been shown to contain terminally bound ethylenes and are unreactive towards additional diazomethane (29). The failure of **8** to incorporate additional methylene groups suggests that carbonyl loss does not occur until *after* incorporation of the *third* methylene group, otherwise intermediate **A**, upon loss of a carbonyl, would yield the unreactive tricarbonyl species **8**.

As noted earlier, both the Ir/Ru and Rh/Ru analogues of **2** failed to incorporate additional methylene groups, presumably because the bridging carbonyl in these species was too strongly bound to the Group 9 metal to allow its displacement by diazomethane. Clearly, generation of the tricarbonyl analogues of these methylene bridged species, which is readily achieved by reaction of the tetracarbonyl precursors with Me_3NO, and their subsequent reaction with diazomethane was of interest to help establish the role of carbonyl loss in the methylene coupling sequence. In the case of $[IrRu(CO)_3(\mu\text{-}CH_2)(dppm)_2][X]$, analogous to **7**, Maria found that reaction with diazomethane yielded the ethylene adduct $[IrRu(CO)_3(\eta^2\text{-}C_2H_4)(\mu\text{-}CH_2)(dppm)_2][X]$ in which the ethylene ligand is bound to Ir, much like the structure proposed for compound **9**, shown in Scheme 7. However, labeling studies established that the metal-bound methylene group of the precursor was *not* incorporated into the ethylene ligand (35). Presumably, the strong Ir—CH_2 bond (36) of the precursor inhibits methylene insertion into this bond, and the ethylene is generated by a mechanism different from that proposed in Scheme 3 for the Rh/Os compound. In the case of the Rh/Ru analogue, Steve observed that reaction of $[RhRu(CO)_3(\mu\text{-}CH_2)(dppm)_2][X]$ with diazomethane at −40 °C yielded $[RhRu(CO)_3(\eta^2\text{-}C_2H_4)(dppm)_2][X]$, analogous to the Rh/Os product **8** (shown in Scheme 7); this ethylene adduct was also obtained at ambient temperature, but was contaminated by several unidentified products. Also observed in solution was free ethylene. Consistent with the expected weaker binding of ethylene to Ru than to Os (33), the Rh/Ru compound was found to be much less stable than **8**, surviving only a few hours in solution compared to several days for **8**.

The C_3 bridged intermediate

Looking back at our proposal for methylene coupling (shown in Scheme 3), it is clear that the pivotal intermediate in the production of either **3** or **4** is the propanediyl bridged intermediate **C**. This species either reacts with an additional diazomethane to give the butanediyl product **3** or undergoes β-H elimination and subsequent methylene incorporation to give the allyl methyl product **4**. We therefore were interested in learning more about this important C_3 bridged species.

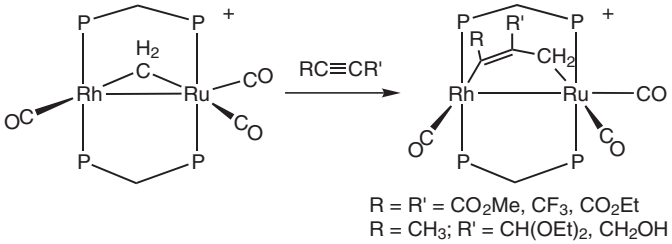
In principle, another route to such a species is through ethylene insertion into the bridging methylene group of precursors such as **2** or **7**, as has been previously documented in related compounds (37). However, at ambient temperature, Jim and Steve found that neither reaction yielded the targeted product. Whereas **2** was unreactive towards ethylene, **7** reacted readily yielding the ethylene containing product **8** (as shown in Scheme 7) together with propene. At –80 °C, the ethylene adduct $[RhOs(\eta^2\text{-}C_2H_4)(CO)_3(\mu\text{-}CH_2)(dppm)_2]^+$ (**9**) was observed in which the ethylene ligand is assumed to be bound to Rh adjacent to the bridging CH_2 group. Although the lability of this ethylene ligand in **9** made unambiguous identification of the ethylene binding site impossible, the Ir/Ru analogue noted earlier, is much less labile and was clearly shown to have the geometry proposed for **9**, having the olefin bound to the Group 9 metal, adjacent to the bridging methylene ligand (35). Warming **9** to ambient temperature results in its transformation to **8** and propene, which we assume proceeds through ethylene insertion to yield the targeted propanediyl bridged intermediate **J**, which undergoes β-H elimination to yield an unobserved allyl hydride, which reductively eliminates propene. The putative "$[RhOs(CO)_3(dppm)_2]^+$" product would then react with an additional ethylene molecule to yield **8**.

Models for the C_3 bridged intermediate

Our failure to generate a propanediyl species was hardly surprising, given the proclivity of such species to undergo β-H elimination in the presence of coordinatively unsaturated late transition metals (12*a*, 12*f*, 38). We therefore considered the possibility of generating models for the C_3 bridged intermediates utilizing unsaturated substrates that would insert into the Rh—CH_2 bond of **2** or **7** to give products without hydrogen atoms in the β position of the resulting bridging hydrocarbyl group. One obvious substrate for achieving this is an internal alkyne, and the reactivities of several of these substrates with both Rh/Os and Rh/Ru series of compounds were investigated. Todd Graham, a former graduate student and at the time a postdoctoral fellow in my group, initiated the study on the Rh/Os compounds, which was completed by Amala Chokshi, while Bryan Rowsell looked at the Rh/Ru analogues. In both pairs of metal combinations, the tetracarbonyl precursors, $[RhM(CO)_4(\mu\text{-}CH_2)(dppm)_2][X]$ either failed to react with alkynes at ambient temperature or reacted very slowly. However, in the presence of trimethylamine oxide, the resulting loss of a carbonyl ligand to give $[RhM(CO)_3(\mu\text{-}CH_2)(dppm)_2][X]$, led to immediate reaction with the alkynes investigated. In the case of the Rh/Ru system, Bryan showed that reaction with RC≡CR′ (R = R′ = CO_2Me, CO_2Et, CF_3; R = CH_3, R′ = $CH(OEt)_2$, CH_2OH) yielded the products $[RhRu(CO)_3(\mu\text{-}\eta^1\text{:}\eta^1\text{-}RC{=}C(R')CH_2)$-

© 2005 NRC Canada

Scheme 9.

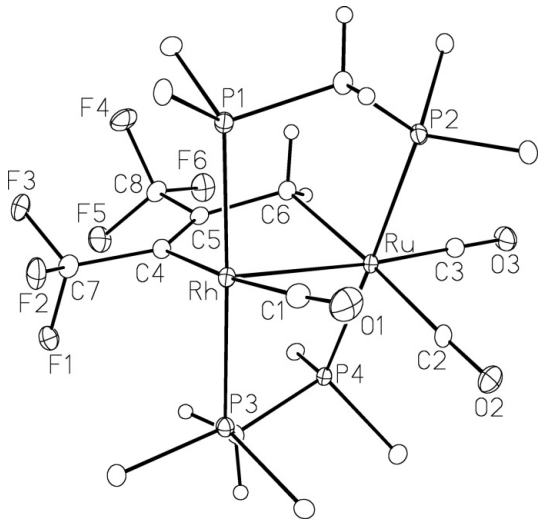


$(dppm)_2]^+$, as diagrammed in Scheme 9 (39). Todd and Amala demonstrated that the Rh/Os system reacted analogously with dimethyl acetylenedicarboxylate and hexafluorobutyne.[1] All products were found to have the targeted structure as diagrammed in Scheme 9 and shown in Fig. 4 for the hexafluorobutyne insertion product of Rh/Ru. These products are unsaturated analogues of the propanediyl bridged species (**C**) shown earlier.

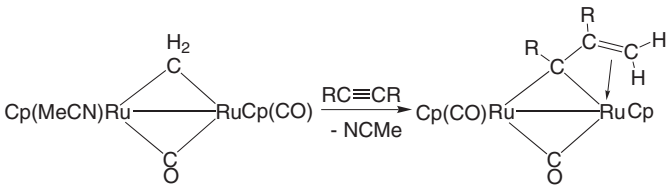
Adjacent metals in hydrocarbyl group isomerization

Although these products of alkyne insertion were the targeted species, in some ways their structures were surprising. Previous alkyne insertions into bridging methylene groups had yielded the somewhat different bridging vinylcarbene products (40) as outlined for one example (40*f*) in Scheme 10. However, this η^1:η^3 coordination mode is closely related to the η^1:η^1 mode observed by us; whereas the former functions as a 4e donor, the latter is only a 2e donor. It seemed therefore that carbonyl loss from our compounds might induce a change in the hydrocarbyl group binding mode to alleviate the resulting electron deficiency, as suggested in Scheme 10. In the case of the Rh/Os compounds, $[RhOs(CO)_3(\mu\text{-}\eta^1\text{:}\eta^1\text{-}RC{=}C(R)CH_2)(dppm)_2][CF_3SO_3]$ (R = CO_2Me, CF_3), Amala discovered that carbonyl loss was merely accompanied by coordination of the triflate anion, leaving the hydrocarbyl binding mode unchanged. In the case of the Rh/Ru compound, $[RhRu(CO)_3(\mu\text{-}\eta^1\text{:}\eta^1\text{-}(CO_2Me)C{=}C(CO_2Me)CH_2)(dppm)_2][CF_3SO_3]$, the expected transformation (Scheme 11) to give **K** again did not occur. Instead, a related species resulted from a 1,3-hydrogen shift from the methylene group to the other end of the alkenyl group, accompanied by rotation of the vinylcarbene unit such that the carbon of the former methylene group ended up in the bridging position (as shown for **L**) (39). We propose that this occurs as diagrammed in Scheme 12 in which only the metals and the bridging hydrocarbyl groups are shown. First, C—H bond activation of the Ru bound methylene group yields a product such as **M**. We propose that carbon–hydrogen activation at the end remote from Rh is made possible by the twisting of the molecule about the Rh—Ru bond (as represented in Fig. 4). This twisting brings one of the methylene hydrogens into the vicinity of Rh, facilitating activation of this group. Reductive elimination of the hydride and vinyl fragment from Rh would yield the vinylcarbene complex **N**, which can yield the final product by rotation of the carbene moiety and subsequent coordination of the olefinic group at Ru.

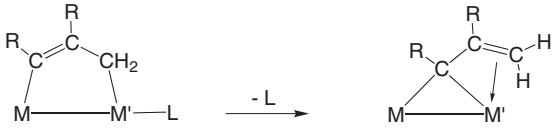
Fig. 4. Perspective view of $[RhRu(CO)_3(\mu\text{-}\eta^1\text{:}\eta^1\text{-}(CF_3)C{=}C(CF_3)CH_2)(dppm)_2]^+$. Only the ipso carbons of the dppm phenyl rings are shown.



Scheme 10.



Compare 2e donor to 4e donor:

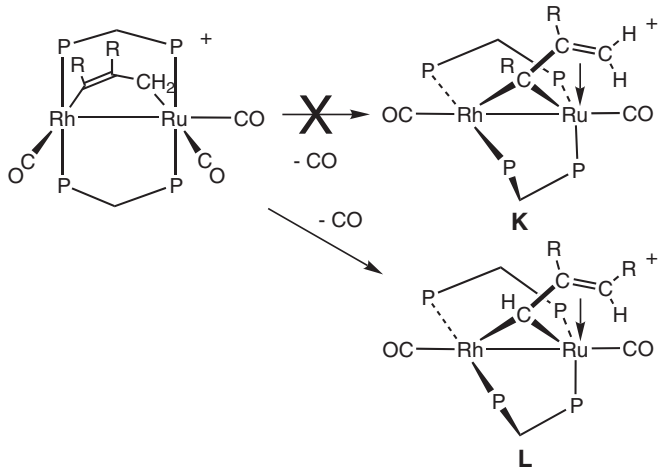


Although this isomerization of the hydrocarbyl fragment (demonstrated in Scheme 12) has no direct relevance to the methylene coupling sequence discussed throughout this paper, it certainly helps demonstrate how adjacent metals can work together to activate an organic fragment. The Ru bound methylene group is α to this metal, but is in a β position relative to the adjacent Rh centre, so facile β-H elimination can occur leading to subsequent rearrangements. This transformation also demonstrates the subtle reactivity differences that can be observed between otherwise similar pairs of metals. Therefore, carbonyl removal from the Rh/Os species results only in anion coordination, whereas the same initiation step in the Rh/Ru species leads to isomerization of the hydrocarbyl fragment. This reactivity difference is even more surprising when it is considered that the initial reactivity after carbonyl loss — either the initial C–H activation step in the Rh/Ru systems or anion coordination in the Rh/Os system — *occurs at Rh*. The subtle influence of an

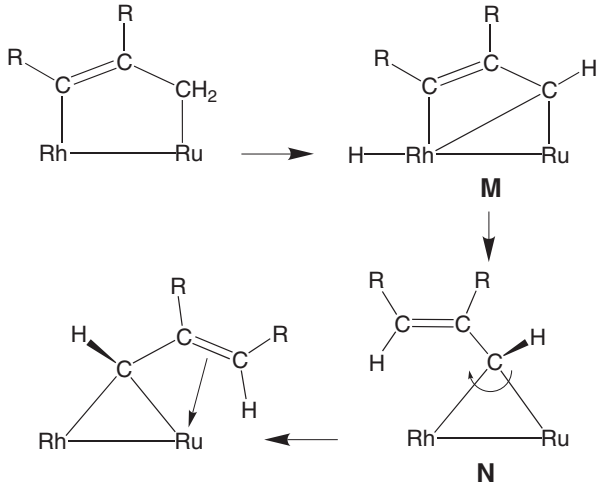
[1] J.R. Wigginton, A. Chokshi, T.W. Graham, R. McDonald, M.J. Ferguson, and M. Cowie. Submitted for publication.

© 2005 NRC Canada

Scheme 11.



Scheme 12.

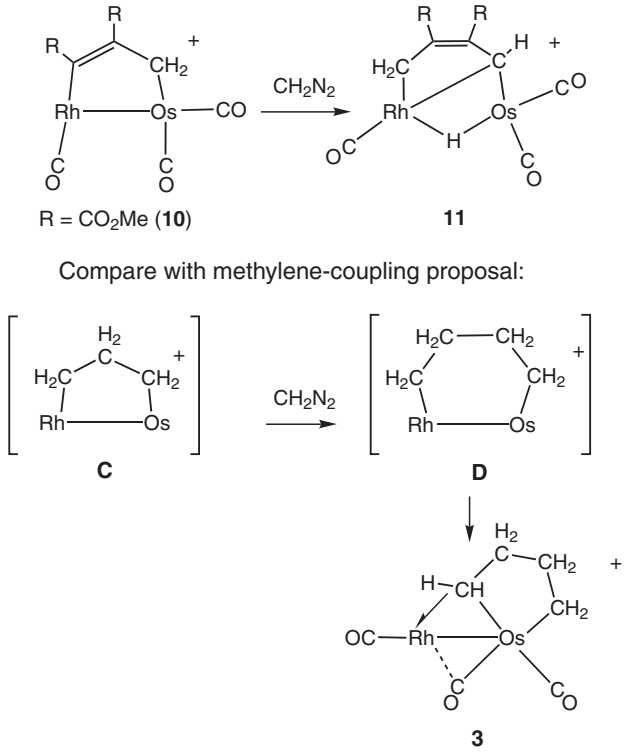


adjacent metal on the reactivity at another is an aspect that is currently not well understood.

C_3 to C_4 conversion

Irrespective of the isomerization discussed above, we were still interested in the use of species such as $[RhOs(CO)_3(\mu\text{-}\eta^1\text{:}\eta^1\text{-}RC{=}C(R)CH_2)(dppm)_2]^+$ (R = CO_2Me (**10**)), as models for the propanediyl bridged intermediates in methylene coupling reactions. Amala therefore sought to extend the above C_3 bridged fragment into C_4 or even higher fragments through reactions with diazomethane.[1] The reaction of compound **10** with diazomethane is summarized in Scheme 13 (dppm groups omitted). Significantly, this compound readily adds 1 equiv. of CH_2 to give the C_4 bridged product **11**, not unlike the C_3 to C_4 conversion proposed earlier in Scheme 3. Of some surprise is that methylene addition is accompanied by C–H cleavage of one of the methylene groups. Amala was able to establish by labeling studies that it is the original methylene group in **10** that undergoes C—H bond cleavage and not the newly added CH_2 group. The binding of both the methylene and methyne carbons to Rh is established by $^{13}C\{^1H\}$ NMR spectroscopy in which the

Scheme 13.



methylene carbon resonates at δ 70.3 showing 25 Hz coupling to Rh, while the methyne carbon appears at δ 118.3 with 16 Hz coupling to Rh. This C–H activation of a Group-8-bound methylene group by the adjacent Rh is reminiscent of the process noted earlier and shown in Scheme 12 for a related Rh/Ru complex.

In Scheme 13 is also shown a comparison with the transformation of a propanediyl group in **C** to the butanediyl product (**3**) through methylene incorporation. As shown, the immediate precursor of **3** is a butanediyl bridged species (**D**), having a structure that is not unlike that of **11**. It remains unclear why the butanediyl bridged intermediate **D** favours migration of the Rh bound end of the hydrocarbyl fragment to Os instead of the C–H activation process that yields **11**. It certainly seems clear that the putative unsaturated 2-butenediyl bridged intermediate immediately preceding **11** will experience a different strain within the dimetallacycle framework compared to that of the saturated analogue (**D**). This strain will influence, not only the tendency of the bridging group to migrate to Os to generate a more favourable five-membered ring, but also probably how close the C-H group to be activated can approach Rh. We assume here that a twisted structure as described above for the C_3 bridged species (see Fig. 4) will also be present in the C_4 bridged intermediates.

Recent results

James (Wiggy) Wigginton, a postdoctoral fellow also from Selby's group in Bristol, has recently followed up on Amala's studies in attempts to understand the subtle reactivity differences noted above for the two C_4 bridged species. He has generated a bridging "$CH_2CH_2C(R){=}CR$" group (R =

© 2005 NRC Canada

CO_2Me) by reacting the alkyne bridged complex, $[RhOs(CO)_3(\mu\text{-}RC{=}CR)(dppm)_2][X]$ (32), with 2 equiv. of diazomethane.[1] Interestingly, this species does not undergo C—H bond cleavage as diagrammed in Scheme 13 for the presumed precursor of **11**, which contains the isomeric "$CH_2C(R){=}C(R)CH_2$" fragment. Instead, it rearranges from the "C_4 bridged" structure to one in which the C_4 fragment is chelated to Os, analogous to the transformation of intermediate **D** to product **3**. The failure of a "$Rh(\mu\text{-}\eta^1{:}\eta^1\text{-}CH_2CH_2C(R){=}C(R))Os$" moiety to undergo C–H activation is certainly consistent with our proposal, described earlier, that it is a CH_2 group adjacent to either Ru or Os that is activated by Rh. Currently, we are continuing our attempts to further resolve the factors that influence the reactivity of these subtly different C_4 fragments.

In contrast to the above studies, Bryan Rowsell has established that the alkyne bridged Rh/Ru species, $[RhRu(CO)_3(\mu\text{-}RC{=}CR)(dppm)_2][X]$, appear not to give rise to CH_2 insertions into the metal–alkyne linkages (39), again demonstrating the strong tendency of the Rh/Os system to give rise to facile methylene insertions into the Rh—C bond of bridging hydrocarbyl fragments, while closely related systems containing other metal combinations are less reactive.

Wiggy and Amala have also demonstrated unusual differences in reactivity in the otherwise closely related alkyne bridged complexes, $[RhOs(CO)_3(\mu\text{-}\eta^1{:}\eta^1\text{-}RC{=}CR)(dppm)_2][X]$ (R = CO_2Me, CF_3). Whereas the first species (R = CO_2Me) reacts with diazomethane, as described previously, by the sequential insertions of *two* CH_2 groups into the Rh—alkyne bond, the second compound (R = CF_3) reacts with only a single equivalent of diazomethane to give the product of *apparent* CH_2 insertion into the *Os—alkyne* bond.[1] If this were the case, it would be the first example in our studies of preferential insertion into the Os—C bond in preference to insertion into Rh—C. However, we believe that the reaction occurs via alkyne loss at some stage followed by its insertion into the Rh—CH_2 bond of a bridging methylene group (as diagrammed earlier in Scheme 9). These observations again show that subtle changes to the system can give rise to significant reactivity differences. We need to obtain a better understanding of these effects and we are currently working towards this goal.

Concluding remarks

As noted in my introductory comments, one of our research goals has been to obtain a better understanding of the roles of adjacent metals in the activation of substrate molecules. I believe that the study presented herein achieves this goal in a number of important ways. First, we have established the importance of bridging hydrocarbyl groups in carbon–carbon bond formation while related terminally bound groups failed to lead to coupling of the hydrocarbyl fragments. The role of Rh in the Rh/Os and Rh/Ru compounds is clear; the coordinative unsaturation at this metal is pivotal in allowing initial substrate coordination at this metal followed by insertion into the adjacent Rh—C bond. Clearly, the lability of the Rh—C bond is also an important parameter, since upon substituting this metal by Ir a significantly lower tendency for insertions is observed.

The roles of the Group 8 metals in this chemistry are more subtle. In the methylene coupling sequence, we have observed the formation of C_3 and C_4 products only for the Rh/Os combination of metals. We propose that the strength of the Os–ethylene interaction seems necessary for enabling the ethylene to remain coordinated, rendering it susceptible to subsequent insertions. Although we have no direct comparison on the role played by the strength of ethylene binding upon the tendency to give increased hydrocarbyl chain length in the different metal combinations, since the Ir/Ru and Rh/Ru systems do not give chain growth under the same conditions as the Rh/Os system, we do note that the ethylene ligand in $[RhM(\eta^2\text{-}C_2H_4)(CO)_3(dppm)_2][X]$ (M = Ru, Os) is much more labile for Ru than for Os. Clearly, facile ethylene loss is not conducive to obtaining longer hydrocarbyl chain lengths.

We have also observed the subtle influence of the Group 8 metal in other ways. Although the chemistry reported is occurring primarily at Rh, the nature of this chemistry can change markedly upon changing the adjacent metal from Os to Ru. In the simple substitution reaction, for example, in which a PMe_3 group replaces a carbonyl on Rh, we might expect this to occur more readily with the Rh/Ru combination of metals (both being more labile than their third-row congeners). Instead, this combination is less labile than with Rh/Os. It is clear that in multinuclear systems, the influence of the adjacent metal, through interactions such as metal–metal bonds and involving bridging ligands, must also be considered in addition to the metal–ligand bond strengths.

An additional role of adjacent metals is observed in the facile activation of carbon–hydrogen bonds. We have observed a number of examples involving the activation of a C—H bond that is α to either Os or Ru by the adjacent Rh centre. In a metal–metal bonded binuclear species, a C—H bond that is α to one metal is β to the other, and facile torsion about the metal–metal bond seems capable of moving this C—H bond into a position that facilitates activation by the adjacent metal. Such an activation process is not possible in mononuclear systems.

As noted at several points throughout this paper, we still have a number of things to learn about the subtleties of binuclear reactivity. Nevertheless, our approach of methodically substituting the pairs of metals by their congeners appears to be useful in giving us a much improved understanding of the roles of these adjacent metals in the activation of organic substrates.

Acknowledgements

I have been fortunate in my career at the University of Alberta to have enjoyed the stimulating company of supportive colleagues such as John Bertie, Stan Brown, Bob Crawford, Bill Graham, Jeff Stryker, Rik Tykwinski, Rod Wasylishen, and (especially) Joe Takats, all of whom frequently advised me, particularly in matters related to organic chemistry or spectroscopy. I am also indebted to members of my research group over the years who were not only dedicated to the chemistry, but also helped create an enjoyable working environment. Only my diligence in checking purchase requisitions prevented one of them from owning a Porsche! In addition to the group members mentioned within this article,

© 2005 NRC Canada

I also acknowledge the following: postdoctoral fellows — Tim Southern, Ian McKeer, Barry Hames, Steve Loeb, Jimmy Ennett, Allen Hunter, Thomas Sielisch, Steve Sherlock, Pino Vasapollo, Rob Hilts, Giovanni Moro, Francoise Van Gastel, Angela Llamazares, Amjad Hussain, Li Xu, and Dusan Ristic–Petrovic; graduate students — Steve Dwight, Michele Gauthier, Ray Dickson, John Gibson, Bruce Sutherland, Brian Vaartstra, Bob McDonald, Jim Jenkins, Jianliang Xiao, Fred Antwi-Nsiah, Li-Sheng Wang, Jeff Torkelson, John Muritu, Darren George, Okemona Oke, Dusan Ristic-Petrovic, Jason Anderson, Rahul Samant, and Kyle Wells; undergraduate students — Del Permann, Judy Ulan, Rob Verhagen, Roberta Franchuk, Brian Sterenberg, Darren George, Todd Graham, Roy Park, Oliver Kuhnert, Elizabeth Fryz, Jason Anderson, John Lo, Mark Teshima, and Rahul Samant. I am also grateful to our Departmental X-ray crystallographers, Bob McDonald and Mike Ferguson, who carry out our structure determinations since we now rarely do them ourselves. Financial support from the University of Alberta, the Natural Sciences and Engineering Research Council of Canada (NSERC), NATO Science Program for a Collaborative Research Grant with Professor P.M. Maitlis (Sheffield), and Consiglio-Nazionale delle Richerche (Rome) for support of the work described herein is gratefully acknowledged.

Finally, I thank my wife, Gail, and our sons, Grahaeme, Geoff, and Andrew, for their love and support.

References

1. (*a*) J.F. Young, J.A. Osborn, F.H. Jardine, and G. Wilkinson. J. Chem. Soc. Chem. Commun. 131 (1965); (*b*) R.S. Coffey. British Patent 1 121 642, 1965; (*c*) F.H. Jardine. Prog. Inorg. Chem. **28**, 63 (1981).
2. (*a*) L. Vaska and J.W. Diluzio. J. Am. Chem. Soc. **84**, 679 (1962); (*b*) L. Vaska and J. Peone. Inorg. Synth. **15**, 64 (1974).
3. See, for example: (*a*) L.F. Dahl, C. Martell, and D.L. Wampler. J. Am. Chem. Soc. **83**, 1761 (1961); (*b*) J.A. Ibers and R.G. Snyder. Acta Crystallogr. **15**, 923 (1962); (*c*) L.F. Dahl and R.E. Rundle. Acta Crystallogr. **16**, 419 (1963); (*d*) L.F. Dahl and C.H. Wei. Acta Crystallogr. **16**, 611 (1963); (*e*) J.K. Hoyano, D.J. Patmore, and W.A.G. Graham. Inorg. Nucl. Chem. Lett. **4**, 201 (1968); (*f*) M.J. Bennett and R. Mason. J. Chem. Soc. A, 75 (1968); (*g*) J.K. Hoyano and W.A.G. Graham. J. Am. Chem. Soc. **91**, 4568 (1969); (*h*) J. Coetzer and G. Gafner. Acta Crystallogr. Sect B, **B26**, 985 (1970); (*i*) R. Whyman. J. Chem. Soc. Chem. Commun. 1194 (1970); (*j*) M.J. Bennett and P.B. Donaldson. J. Am. Chem. Soc. **93**, 3307 (1971); (*k*) A.S. Foust, W.A.G. Graham, and R.P. Stewart, Jr. J. Organomet. Chem. **54**, C22 (1973); (*l*) R.M. Kirchner, T.J. Marks, J.S. Kristoff, and J.A. Ibers. J. Am. Chem. Soc. **95**, 6602 (1973).
4. (*a*) M. Cowie, J.T. Mague, and A.R. Sanger. J. Am. Chem. Soc. **100**, 3628 (1978); (*b*) M. Cowie, S.K. Dwight, and A.R. Sanger. Inorg. Chim. Acta, **31**, L407 (1978).
5. See, for example: (*a*) A.L. Balch. J. Am. Chem. Soc. **98**, 8049 (1976); (*b*) A.L. Balch and B. Tulyathan. Inorg. Chem. **16**, 2840 (1977); (*c*) M.M. Olmstead, H. Hope, L.S. Benner, and A.L. Balch. J. Am. Chem. Soc. **99**, 5502 (1977); (*d*) L.S. Benner and A.L. Balch. J. Am. Chem. Soc. **100**, 6099 (1978); (*e*) A.L. Balch, J.W. Labadie, and G. Delker. Inorg. Chem. **18**, 1224 (1979); (*f*) A.L. Balch, L.S. Benner, and M.M. Olmstead. Inorg. Chem. **18**, 2996 (1979).
6. See, for example: (*a*) C.P. Kubiak and R. Eisenberg. J. Am. Chem. Soc. **99**, 6129 (1977); (*b*) C.P. Kubiak and R. Eisenberg. Inorg. Chem. **19**, 2726 (1980); (*c*) C.P. Kubiak, C. Woodcock, and R. Eisenberg. Inorg. Chem. **19**, 2733 (1980); (*d*) C.P. Kubiak, C. Woodcock, and R. Eisenberg. Inorg. Chem. **21**, 2119 (1982).
7. See, for example: (*a*) P.G. Pringle and B.L. Shaw. J. Chem. Soc. Chem. Commun. 581 (1982); (*b*) D.M. McEwan, P.G. Pringle, and B.L. Shaw. J. Chem. Soc. Chem. Commun. 859 (1982); (*c*) A.T. Hutton, P.G. Pringle, and B.L. Shaw. Organometallics, **2**, 1889 (1983).
8. See, for example: (*a*) M.P. Brown, R.J. Puddephatt, M. Rashidi, and K.R. Seddon. J. Chem. Soc. Dalton Trans. 516 (1978); (*b*) M.P. Brown, R.J. Puddephatt, M. Rashidi, and K.R. Seddon. J. Chem. Soc. Dalton Trans. 1540 (1979); (*c*) M.P. Brown, S.J. Cooper, A.A. Frew, L. Manojlović-Muir, K.W. Muir, R.J. Puddephatt, and M.A. Thomson. J. Organomet. Chem. **198**, C33 (1980); (*d*) S.J. Cooper, M.P. Brown, and R.J. Puddephatt. Inorg. Chem. **20**, 1374 (1981); (*e*) M.P. Brown, S.J. Cooper, A.A. Frew, L. Manojlović-Muir, K.W. Muir, R.J. Puddephatt, K.R. Seddon, and M.A. Thomson. Inorg. Chem. **20**, 1500 (1981); (*f*) M.P. Brown, S.J. Cooper, A.A. Frew, L. Manojlović-Muir, K.W. Muir, R.J. Puddephatt, and M.A.Thomson. J. Chem. Soc. Dalton Trans. 300 (1982); (*g*) R.J. Puddephatt. Chem. Soc. Rev. **12**, 98 (1983).
9. See, for example: (*a*) R.J. Haines, M. Laing, E. Meintjies, and P. Sommerville. J. Organomet. Chem. **215**, C17 (1981); (*b*) R.J. Haines, E. Meintjies, M. Laing, and P. Sommerville. J. Organomet. Chem. **216**, C19 (1981); (*c*) J.S. Field, R.J. Haines, and C.N. Sampson. J. Chem. Soc. Dalton Trans. 1933 (1987).
10. See, for example: S.A.R. Knox. J. Organomet. Chem. **400**, 255 (1990), and refs. cited therein.
11. See, for example: (*a*) C.P. Casey, P.J. Fagan, and W.H. Miles. J. Am. Chem. Soc. **104**, 1134 (1982); (*b*) C.P. Casey and P.J. Fagan. J. Am. Chem. Soc. **104**, 4950 (1982); (*c*) C.P. Casey and P.J. Fagan. J. Am. Chem. Soc. **104**, 7360 (1982); (*d*) C.P. Casey, W.H. Miles, P.J. Fagan, and K.J. Haller. Organometallics, **4**, 559 (1985).
12. See, for example: (*a*) C.E. Sumner, Jr., P.E. Riley, R.E. Davis, and R. Pettit. J. Am. Chem. Soc. **102**, 1752 (1980); (*b*) R.C. Brady III and R. Pettit. J. Am. Chem. Soc. **102**, 6181 (1980); (*c*) R.C. Brady III and R. Pettit. J. Am. Chem. Soc. **103**, 1287 (1981); (*d*) S.C. Kao, P.P.Y. Lu, and R. Pettit. Organometallics, **1**, 911 (1982); (*e*) C.E. Sumner, Jr., J.A. Collier, and R. Pettit. Organometallics, **1**, 1350 (1982); (*f*) S.C. Kao, C.H. Thiel, and R. Pettit. Organometallics, **2**, 914 (1983).
13. See, for example: (*a*) R. Usón, L.A. Oro, M.A. Ciriano, M.P. Pinillos, A. Tiripicchio, and M. Tiripicchio Camellini. J. Organomet. Chem. **205**, 247 (1981); (*b*) R. Usón, L.A. Oro, M.A. Ciriano, D. Carmona, A. Tiripicchio, and M. Tiripicchio Camellini. J. Organomet. Chem. **224**, 69 (1982); (*c*) R. Usón, L.A. Oro, M.A. Ciriano, F.J. Lohoz, and M.C. Bello. J. Organomet. Chem. **234**, 205 (1982); (*d*) L.A. Oro, D. Carmona, and J. Reedijk. Inorg. Chim. Acta, **71**, 115 (1983); (*e*) R. Usón, J. Gimeno, L.A. Oro, M.A. Aznar, and J.A. Cabeza. Polyhedron, **2**, 163 (1983).
14. See, for example (*a*) A. Maisonnat, P. Kalck, and R. Poilblanc. Inorg. Chem. **13**, 661 (1974); (*b*) A. Maisonnat, P. Kalck, and R. Poilblanc. J. Organomet. Chem. **75**, C36 (1974); (*c*) A. Maisonnat, P. Kalck, and R. Poilblanc. Inorg. Chem. **13**, 2994 (1974); (*d*) P. Kalck and R. Poilblanc. Inorg. Chem. **14**, 2779

© 2005 NRC Canada

(1975); (*e*) R. Poilblanc. J. Organomet. Chem. **94**, 241 (1975); (*f*) K. Fauvel, R. Mathieu, and R. Poilblanc. Inorg. Chem. **15**, 976 (1976); (*g*) R. Mathieu and R. Poilblanc. J. Organomet. Chem. **142**, 351 (1977); (*h*) A. Maisonnat and R. Poilblanc. J. Organomet. Chem. **160**, 307 (1978); (*i*) J.J. Bonnet, A. Thorez, A. Maisonnat, J. Gaby, and R. Poilblanc. J. Am. Chem. Soc. **101**, 5940 (1979).

15. (*a*) E.L. Muetterties. Bull. Soc. Chim. Belg. **84**, 959 (1975); (*b*) E.L. Muetterties. Science (Washington, D.C.), **196**, 839 (1977); (*c*) E.L. Muetterties. Angew. Chem. Int. Ed. Engl. **17**, 545 (1979); (*d*) E.L. Muetterties. Pure Appl. Chem. **54**, 83 (1982); (*e*) E.L. Muetterties and M.J. Krause. Angew. Chem. Int. Ed. Engl. **22**, 135 (1983).
16. F.A. Cotton, G. Wilkinson, C.A. Murillo, and M. Bochmann. Advanced inorganic chemistry. 6th ed. John Wiley and Sons Inc., New York. 1999. Chaps. 18, 21, and 22.
17. See, for example: (*a*) M. Cowie. Inorg. Chem. **18**, 286 (1979); (*b*) M. Cowie and S.K. Dwight. Inorg. Chem. **18**, 2700 (1979); (*c*) M. Cowie and S.K. Dwight. Inorg. Chem. **19**, 209 (1980); (*d*) M. Cowie and T.G. Southern. J. Organomet. Chem. **193**, C46 (1980); (*e*) M. Cowie and S.K. Dwight. J. Organomet. Chem. **214**, 233 (1981); (*f*) I.R. McKeer. Inorg. Chim. Acta, **65**, L107 (1982).
18. See, for example: (*a*) B.R. Sutherland and M. Cowie. Organometallics, **3**, 1869 (1984); (*b*) B.R. Sutherland and M. Cowie. Organometallics, **4**, 1437 (1985); (*c*) M. Cowie, G. Vasapollo, B.R. Sutherland, and J.P. Ennett. Inorg. Chem. **25**, 2648 (1986); (*d*) B.A. Vaartstra and M. Cowie. Inorg. Chem. **28**, 3138 (1989).
19. See, for example: (*a*) B.A. Vaartstra and M. Cowie. Organometallics, **8**, 2388 (1989); (*b*) R. McDonald and M. Cowie. Inorg. Chem. **29**, 1564 (1990).
20. (*a*) D.M. Antonelli and M. Cowie. Organometallics, **9**, 1818 (1990); (*b*) D.M. Antonelli and M. Cowie. Inorg. Chem. **29**, 3339 (1990); (*c*) D.M. Antonelli and M. Cowie. Inorg. Chem. **29**, 4039 (1990); (*d*) D.M. Antonelli and M. Cowie. Organometallics, **10**, 2173 (1991); (*e*) D.M. Antonelli and M. Cowie. Organometallics, **10**, 2550 (1991).
21. (*a*) D.A. Dowden. *In* Catalysis. Vol. 2. *Edited by* C. Kemball and D.A. Dowden. (Special periodical report), The Chemical Society, London. 1978. p. 1; (*b*) C.N. Satterfield. Heterogeneous catalysis in industrial practice. 2nd ed. McGraw-Hill Inc., New York. 1991. Chap. 9.
22. (*a*) P. Biloen and W.M.H. Sachtler. Adv. Catal. **30**, 165 (1981); (*b*) P.M. Maitlis, R. Quyoum, H.C. Long, and M.L. Turner. Appl. Catal. A, **186**, 363 (1999); (*c*) A.A.C.M. Beenachers. Catal. Rev. Sci. Eng. **41**, 255 (1999).
23. (*a*) F. Fischer and H. Tropsch. Brennst.–Chem. **7**, 97 (1926); (*b*) F. Fischer and H. Tropsch. Chem. Ber. **59**, 830 (1920).
24. (*a*) P.M. Maitlis, H.C. Long, R. Quyoum, M.L. Turner, and Z.-Q. Wang. Chem. Commun. 1 (1996); (*b*) H.C. Long, M.L. Turner, P. Fornasiero, J. Kaspar, M. Graziani, and P.M. Maitlis. J. Catal. **167**, 172 (1997).
25. (*a*) R. Hugues, B. Besson, P. Bussière, J.A. Dalmon, J.M. Basset, and D. Olivier. Nouv. J. Chim. **5**, 207 (1981); (*b*) M.E. Dry. Appl. Catal. A, **138**, 319 (1996).
26. M.A. Vannice. J. Catal. **37**, 449 (1975).
27. E. Iglesia, S.L. Soled, R.A. Fiato, and G.H. Via. J. Catal. **143**, 345 (1993).
28. S.J. Trepanier, B.T. Sterenberg, R. McDonald, and M. Cowie. J. Am. Chem. Soc. **121**, 2613 (1999).
29. S.J. Trepanier, J.N.L. Dennett, B.T. Sterenberg, R. McDonald, and M. Cowie. J. Am. Chem. Soc. **126**, 8046 (2004).
30. (*a*) B.R. Bender, D.L. Ramage, J.R. Norton, D.C. Wiser, and A.K. Rappé. J. Am. Chem. Soc. **119**, 5628 (1997); (*b*) B.F.G. Johnson, J. Lewis, and D.A. Pippard. J. Chem. Soc. Dalton Trans. 407 (1981).
31. J.P. Collman, L.S. Hegedus, J.R. Norton, and R.G. Finke. Principles and applications of organotransition metal chemistry. University Science Books, Mill Valley, California. 1987. pp. 523–660.
32. R.W. Hilts, R.A. Franchuk, and M. Cowie. Organometallics, **10**, 304 (1991).
33. (*a*) J.E. Huheey, E.A. Keiter, and R.L. Keiter. Inorganic chemistry: Principles of structure and reactivity. 4th ed. Harper Collins, New York. 1993. Chap. 14; (*b*) J. Li, G. Schreckenbach, and T. Ziegler. Inorg. Chem. **34**, 3245 (1995); (*c*) S.H. Liu, S.-Y. Yang, S.T. Lo, Z. Xu, W.S. Ng, T.B. Wen, Z.Y. Zhou, Z. Lin, C.P. Lau, and G. Jia. Organometallics, **20**, 4161 (2001); (*d*) M.S. Nechaev, V.M. Rayón, and G. Frenking. J. Phys. Chem. A, **108**, 3134.
34. B.D. Rowsell, S.J. Trepanier, R. Lam, R. McDonald, and M. Cowie. Organometallics, **21**, 3228 (2002).
35. M.M. Dell'Anna, S.J. Trepanier, R. McDonald, and M. Cowie. Organometallics, **20**, 88 (2001).
36. (*a*) T. Ziegler and V. Tschinke. Bonding energetics in organometallic compounds. *Edited by* T.J. Marks. American Chemical Society, Washington, D.C. 1990. Chap. 19; (*b*) T. Ziegler, V. Tschinke, and B. Ursenbach. J. Am. Chem. Soc. **109**, 4825 (1987); (*c*) P.B. Armentrout. Bonding energetics in organometallic compounds. *Edited by* T.J. Marks. American Chemical Society, Washington, D.C. 1990. Chap. 2.
37. (*a*) T.R. Howard, J.B. Lee, and R.H. Grubbs. J. Am. Chem. Soc. **102**, 6876 (1980); (*b*) J.B. Lee, G.J. Gajola, W.P. Schaefer, T.R. Howard, T. Ikariya, D.A. Straus, and R.H. Grubbs. J. Am. Chem. Soc. **103**, 7358 (1981); (*c*) K.M. Motyl, J.R. Norton, C.K. Schauer, and O.P. Anderson. J. Am. Chem. Soc. **104**, 7325 (1982).
38. K.H. Theopold and R.G. Bergman. J. Am. Chem. Soc. **103**, 2489 (1981).
39. B.D. Rowsell, R. McDonald, M.J. Ferguson, and M. Cowie. Organometallics, **22**, 2944 (2003).
40. (*a*) A.F. Dyke, S.A.R. Knox, P.J. Naish, and G.E. Taylor. J. Chem. Soc. Chem. Commun. 803 (1980); (*b*) B.J. Gracey, S.A.R. Knox, K.A. Macpherson, A.G. Orpen, and S.R. Stobart. J. Chem. Soc. Dalton Trans. 1935 (1985); (*c*) R.E. Colborn, A.F. Dyke, S.A.R. Knox, K.A. Macpherson, and A.G. Orpen. J. Organomet. Chem. **239**, C15 (1982); (*d*) P.Q. Adams, D.L. Davies, A.F. Dyke, S.A.R. Knox, K.A. Mead, and P. Woodward. J. Chem. Soc. Chem. Commun. 222 (1983); (*e*) R.E. Colborn, D.L. Davies, A.F. Dyke, S.A.R. Knox, K.A. Mead, A.G. Orpen, J.E. Guerchais, and J. Roué. J. Chem. Soc. Dalton Trans. 1799 (1989); (*f*) M.J. Fildes, S.A.R. Knox, A.G. Orpen, M.L. Turner, and M.I. Yates. J. Chem. Soc. Chem. Commun. 1680 (1989); (*g*) M. Akita, R. Hua, S. Nakanishi, M. Tanaka, and Y. Moro-oka. Organometallics, **16**, 5572 (1997); (*h*) J.N.L. Dennett. Ph.D. thesis, University of Bristol, Bristol, UK. 2000; (*i*) Y. Kaneko, T. Suzuki, K. Isobe, and P.M. Maitlis. J. Organomet. Chem. **554**, 155 (1998).

© 2005 NRC Canada

Synthesis of fused pyrazolo-, isoxazolo-, pyrimido-, and pyridopyrimidines

Herojit S. Thokchom, Anita D. Nongmeikapam, and Warjeet S. Laitonjam

Abstract: A systematic study of the synthesis of the 5,7-diaryl-4-oxo-pyrazolo[3,4-*d*]pyrimidin-6-thiones (**3**), 2-phenyl-5,7-bis(2′-methylphenyl)-4-oxo-pyrazolo[3,4-*d*]pyrimidin-6-thiones (**4b**), 2(3*H*)-3-phenyl-5,7-diaryl-4-oxo-pyrazolo[3,4-*d*]pyrimidin-6-thiones (**5**), 5,7-diaryl-4-oxo-isoxazolo[5,4-*d*]pyrimidin-6-thiones (**7**), 3,5,7-triaryl-2,3-dihydro-4-oxo-isoxazalo[5,4-*d*]pyrimidin-6-thiones (**8**), 2-amino-6,8-diaryl-5-oxo-pyrimido[4,5-*d*]pyrimidin-7-thiones (**9**), 3,4-dihydro-2-amino-4-phenyl-6,8-diaryl-5-oxo-pyrimido[4,5-*d*]pyrimidin-7-thiones (**10**), 3-cyano-6,8-diaryl-2,5-dioxo-pyrido[2,3-*d*]pyrimidin-7-thiones (**11**) from the condensation products **1** and **2**, derived from 1,3-diaryl-2-thiobarbituric acids is described.

Key words: synthesis, fused, pyrazole, isoxazole, pyrimidines.

Résumé : On décrit une étude systématique de la synthèse des 5,7-diaryl-4-oxo-pyrazolo[3,4-*d*]pyrimidin-6-thiones (**3**), 2-phényl-5,7-bis(2′-méthylphényl)-4-oxo-pyrazolo[3,4-*d*]pyrimidin-6-thiones (**4b**), 2(3*H*)-3-phényl-5,7-diaryl-4-oxo-pyrazolo[3,4-*d*]pyrimidin-6-thiones (**5**), 5,7-diaryl-4-oxo-isoxazolo[5,4-*d*]pyrimidin-6-thiones (**7**), 3,5,7-triaryl-2,3-dihydro-4-oxo-isoxazolo[5,4-*d*]pyrimidin-6-thiones (**8**), 2-amino-6,8-diaryl-5-oxo-pyrimido[4,5-*d*]pyrimidin-7-thiones (**9**), 3,4-dihydro-2-amino-4-phényl-6,8-diaryl-5-oxo-pyrimido[4,5-*d*]pyrimidin-7-thiones (**10**) et 3-cyano-6,8-diaryl-2,5-dioxo-pyrido[2,3-*d*]pyrimidin-7-thiones (**11**) à partir des produits de condensation **1** et **2** obtenus à partir des acides 1,3-diaryl-2-thiobarbituriques.

Mots clés : synthèse, condensé, pyrazole, isoxazole, pyrimides.

[Traduit par la Rédaction]

Introduction

Development of newer synthetic methods for the construction of fused heterocyclic rings of pyrimidine derivatives is a challenging task for synthetic organic chemists. It is well-known that pyrimidines either in isolated or in fused systems are associated with a number of biological activities. Moreover, the pyrimidine nucleus containing the thiouriedo linkage (-NH-C(S)-NH-) is pharmaceutically important because the development of medicines mainly arose from the heterocyclic compounds containing nitrogen and sulphur atoms (1, 2). It has been found that incorporation of various fused heterocycles into a pyrimidine nucleus enhances the biological activity (3, 4). In view of such wide applications, we have synthesized several derivatives of fused pyrimidines in maximum yields by using 1,3-diarylthiobarbituric acids. 1,3-Diarylthiobarbituric acids having an active methylene group can furnish several condensation products for easy cyclization to give various fused heterocyclic compounds of interest.

The 1,3-diarylthiobarbituric acids are among the simplest synthetic intermediates that can be easily prepared in a one-pot reaction by treating 1,3-diaryl thioureas with malonic acid in the presence of acetyl chloride. These intermediates have been extensively explored for five- and six-membered hetrocycles (5). The 1,3-diarylthiobarbituric acids undergo condensation with ethyl orthoformate and benzaldehyde to give the respective condensation products, namely, 5-ethoxymethylene-1,3-diaryl-2-thiobarbituric acids (**1**) and 5-phenylmethylene-1,3-diaryl-2-thiobarbituric acids (**2**), respectively (6). These condensation products possessing three electrophilic centers could undergo cyclocondensation with various binucleophiles to give various fused heterocycles of pyrimidine derivatives. In this paper, we report the synthesis of 4-oxo-pyrazolo[3,4-*d*]pyrimidin-6-thiones, 4-oxo-isoxazolo-[5,4-*d*]pyrimidin-6-thiones, 5-oxo-pyrimido[4,5-*d*]pyrimidin-7-thiones, and 5-oxo-pyrido[2,3-*d*]pyrimidin-7-thiones.

It is well-known that the fused heterocycles possessing the pyrazolo[3,4-*d*]pyrimidine nucleus serve as a class of compounds exhibiting a remarkable variety of biological activities (7–10). The pyrazolo[3,4-*d*]pyrimidine compounds have been found to show similar characteristics to purines, since they are isomeric structural purine analogues, which have resulted in several potent antagonists in biological systems (11, 12). It was also reported that the isoxazolo-pyrimidine derivatives exhibited antifungal, antibacterial, and many other important biological properties (13–15). The derivatives of pyrimido-pyrimidines are quite effective in the inhibition of cancer cell sickness (16), exhibition of diuretic activities (17), and also have central depressant analgesic and antiinflammatory activities (18).

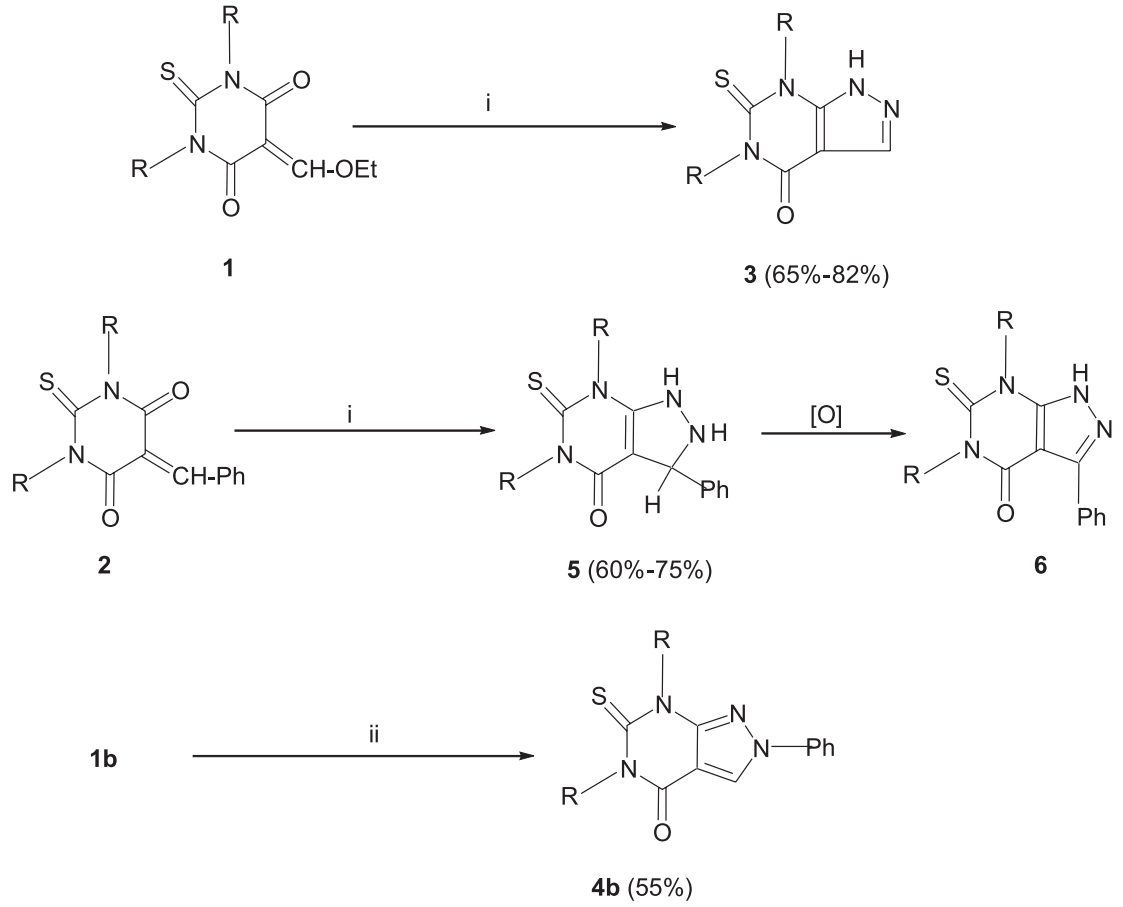
Received 12 October 2004. Published on the NRC Research Press Web site at http://canjchem.nrc.ca on 6 July 2005.

H.S. Thokchom, A.D. Nongmeikapam, and W.S. Laitonjam.[1] Department of Chemistry, Manipur University, Canchipur–795 003, Manipur, India.

[1]Corresponding author (e-mail: warjeet@yahoo.com).

 doi: 10.1139/V05-054 © 2005 NRC Canada

Scheme 1. Reagents: (*i*) N_2H_4, EtOH, AcOH; (*ii*) $PhNHNH_2$, EtOH, AcOH.



(a) R = C_6H_5
(b) R = 2-$CH_3C_6H_5$
(c) R = 3-$CH_3OC_6H_5$

Results and discussion

A number of methods for the synthesis of pyrazolo-pyrimidines have been reported (19–24), but most of the methods involved a number of steps and yields were poor. In view of this, it was considered of interest to devise a convenient route for the synthesis of such compounds. Treatment of 5-ethoxymethylene-1,3-diaryl-2-thiobarbituric acids (**1**) with hydrazine hydrate in the presence of ethanol and acetic acid gave the corresponding pyrazolo[3,4-*d*]pyrimidin-6-thiones (**3**) in 65%–82% overall yields (Scheme 1). When **1b** was treated with phenyl hydrazine in ethanol and acetic acid, 2-phenyl-5,7-bis(2′-methylphenyl)-4-oxo-pyrazolo[3,4-*d*]pyrimidin-6-thione (**4b**) was produced in 55% yield (Scheme 1). When 1,3-diaryl-5-phenyl-methylene-2-thiobarbituric acids (**2**) were refluxed with hydrazine hydrate in ethanol and acetic acid, the corresponding 2(3*H*)-3-phenyl-5,7-diaryl-4-oxo-pyrazolo[3,4-*d*]pyrimidin-6-thiones (**5**) were obtained in 60%–75% overall yields (Scheme 1). It may be noted that **5** can be further oxidized to give the respective 3-oxo-pyrazolo-[3,4-*d*]pyrimidin-6-thiones (**6**).

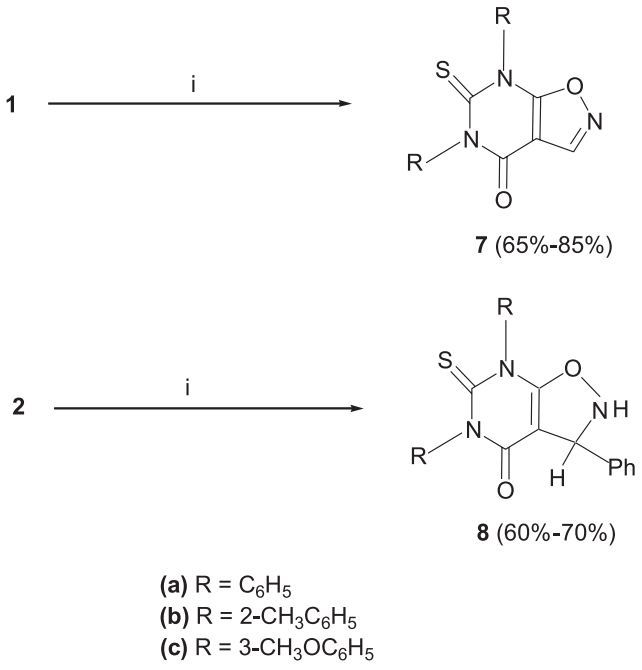
Most of the methods for the preparation of the isoxazolo[5,4-*d*]pyrimidine system are initiated from the construction of an isoxazole ring first and followed by pyrimidine ring closure (25–27). As a part of our synthetic strategy, 1,3-diarylthiobarbituric acids were used as precursors for the synthesis of various isoxazolo[5,4-*d*]pyrimidines (28). The condensation products (**1** and **2**) on treatment with hydroxylamine hydrochloride in dehydrated alcohol and acetic acid gave the respective 5,7-diaryl-4-oxo-isoxazolo[5,4-*d*]pyrimidin-6-thiones (**7**) in 65%–85% overall yields and 3,5,7-triaryl-2,3-dihydro-4-oxo-isoxazolo[5,4-*d*]pyrimidin-6-thiones (**8**) in 60%–70% overall yields (Scheme 2).

In view of the various physiological properties, and in continuation of our work on fused pyrimidine systems, we also undertook the synthesis of substituted pyrimido[4,5-*d*]pyrimidines. In most cases, the pyrimido[4,5-*d*]pyrimidines were generally prepared from derivatives of enamines (29, 30). Various substituted 2-amino-6,8-diaryl-5-oxo-pyrimido[4,5-*d*]pyrimidin-7-thiones (**9**) in 55%–75% overall yields and 3,4-dihydro-2-amino-4-phenyl-6,8-diaryl-5-oxo-pyrimido[4,5-*d*]pyrimidin-7-thiones (**10**) in 62%–75% overall yields can be synthesized by reacting the respective compounds **1** and **2** with guanidine nitrate in the presence of sodium methoxide and methanol (Scheme 3).

Very few substituted pyrido[2,3-*d*]pyrimidines were syn-

© 2005 NRC Canada

Scheme 2. Reagents: (*i*) NH_2OH, EtOH, AcOH.



thesized from 6-aminouracils (31, 32). We report the synthesis of substituted 3-cyano-6,8-diaryl-2,5-dioxo-pyrido[2,3-*d*]pyrimidin-7-thiones (**11**) from the corresponding condensation product (**1**) derived from 1,3-diarylthiobarbituric acids (Scheme 4). Thus, we are reporting the synthesis of various fused heterocycles of pyrimidine derivatives from easily available starting materials, and most of the methods used by others are found to involve a number of steps and are of poor yields.

Experimental

Melting points were determined in open capillary tubes and are uncorrected. Infrared (IR) spectra were recorded on an ATI Mattson Genesis Series FT IR spectrometer. All samples were run as a thin film (produced by evaporation of a chloroform solution) on a sodium chloride plate. Absorption maxima were recorded in wavenumbers (cm^{-1}). ^1H NMR spectra were recorded on Varian Unity 500 (500 MHz), Bruker AC-300, and Varian XL (300 MHz) spectrometers. ^{13}C NMR spectra were recorded on Bruker AC-300 and Varian XL (75 MHz) spectrometers. Residual non-deuterated solvent was used as an internal reference and all chemical shifts (δ_H and δ_C) are quoted in parts per million (ppm) downfield from tetramethylsilane (TMS). All samples were run in deutero-chloroform ($CDCl_3$) as the solvent unless otherwise stated. Mass spectra were recorded on a Kratas Concept-IS mass spectrometer coupled to a Mach 3 data system, or on a Jeol-D 300 mass spectrometer.

5,7-Diphenyl-4-oxo-pyrazolo[3,4-*d*]pyrimidin-6-thione (3a)

A mixture of **1a** (3.52 g, 0.01 mol), hydrazine hydrate (1 mL, 0.015 mol), ethanol (25 mL), and acetic acid (10 mL) was refluxed for 8 h. The reaction mixture was then concentrated, cooled, poured into ice water, and extracted with chloroform (3 × 100 mL), washed with water (3 × 100 mL), dried, and concentrated. Flash chromatography (petroleum ether – EtOAc, 4:1) gave **3a** (2.56 g, 80%) as a white-grey solid, mp 261–263 °C. IR (ν_{max}, cm^{-1}): 3340, 1660. ^1H NMR (DMSO-d_6) δ: 5.00 (1H, br s, NH), 7.10–7.70 (10H, m, aromatic), 8.35 (1H, s, -CH=N-). MS (70 eV) *m*/*z* calcd. for $C_{17}H_{12}N_4OS$: 320.0750; found: 320.0734 (M^+).

5,7-Di(2-methylphenyl)-4-oxo-pyrazolo[3,4-*d*]pyrimidin-6-thione (3b)

A mixture of **1b** (3.80 g, 0.01 mol), hydrazine hydrate (1 mL, 0.015 mol), ethanol (25 mL), and acetic acid (10 mL) was refluxed for 9 h. The solution was worked up by pouring the concentrated residue onto ice water and extracted with chloroform (3 × 100 mL), washed with water (3 × 100 mL), dried, and concentrated. The product was crystallized from ethanol to give **3b** (2.61 g, 75%) as a white solid, mp 282–284 °C. IR (ν_{max}, cm^{-1}): 3305, 1675. ^1H NMR (DMSO-d_6) δ: 2.08 (6H, s, 2 × CH_3), 5.35 (1H, br s, NH), 6.80–7.30 (8H, m, aromatic), 8.12 (1H, s, -CH=N-). MS (70 eV) *m*/*z* calcd. for $C_{19}H_{16}N_4OS$: 348.0970; found: 348.0960 (M^+).

5,7-Di(3-methoxyphenyl)-4-oxo-pyrazolo[3,4-*d*]pyrimidin-6-thione (3c)

A mixture of **1c** (4.12 g, 0.01 mol), hydrazine hydrate (1 mL, 0.015 mol), ethanol (25 mL), and acetic acid (10 mL) was refluxed for 9 h. The reaction mixture was then concentrated, cooled, poured into ice water, and extracted with chloroform (3 × 100 mL), washed with water (3 × 100 mL), dried, and concentrated. The product was crystallized from ethanol to give **3c** (3.12 g, 82%) as a white solid, mp 248–250 °C. IR (ν_{max}, cm^{-1}): 3310, 1680. ^1H NMR (DMSO-d_6) δ: 3.70 (6H, s, 2 × OCH_3), 4.75 (1H, br s, NH), 6.70–7.35 (8H, m, aromatic), 8.55 (1H, s, -CH=N-). MS (70 eV) *m*/*z* calcd. for $C_{19}H_{16}N_4O_3S$: 380.0603; found: 380.0607 (M^+).

5,7-Di(2-methylphenyl)-4-oxo-2-phenyl-pyrazolo[3,4-*d*]pyrimidin-6-thione (4b)

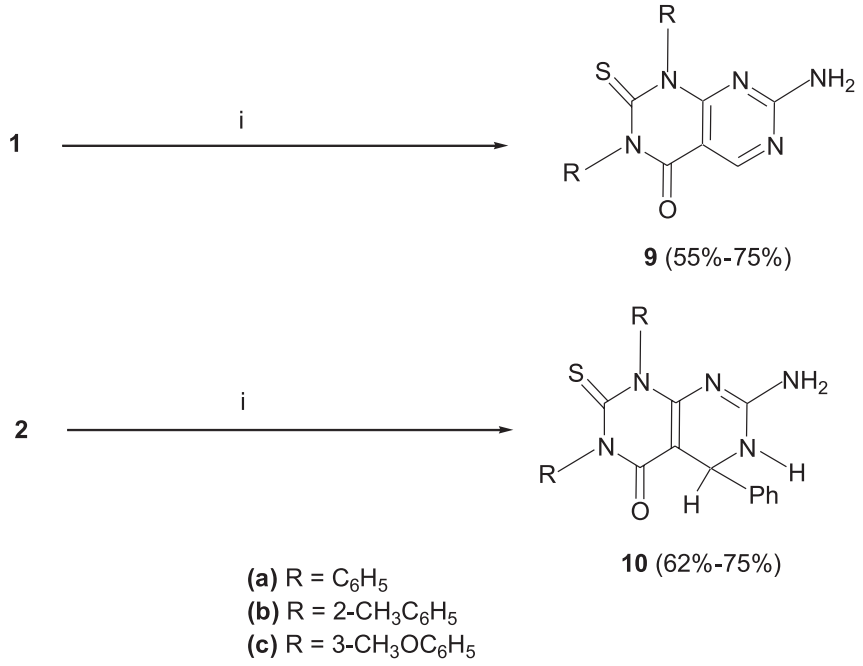
A mixture of **1b** (3.80 g, 0.01 mol), phenylhydrazine (1 mL, 0.015 mol), ethanol (25 mL), and acetic acid (10 mL) was refluxed for 6 h. The solution was worked up by pouring the concentrated residue into ice water and extracted with chloroform (3 × 100 mL), washed with water (3 × 100 mL), dried, and concentrated. The product was crystallized from ethanol to give **4b** (2.32 g, 55%) as a white solid, mp 232–234 °C. IR (ν_{max}, cm^{-1}): 2950, 1660. ^1H NMR (DMSO-d_6) δ: 2.55 (6H, s, 2 × CH_3), 7.05–7.80 (13H, m, aromatic), 8.18 (1H, s, -CH=N-). MS (70 eV) *m*/*z* calcd. for $C_{25}H_{20}N_4OS$: 424.0707; found: 424.0716 (M^+).

2(3*H*)-3,5,7-Triphenyl-2(3*H*)-4-oxo-pyrazolo[3,4-*d*]pyrimidin-6-thione (5a)

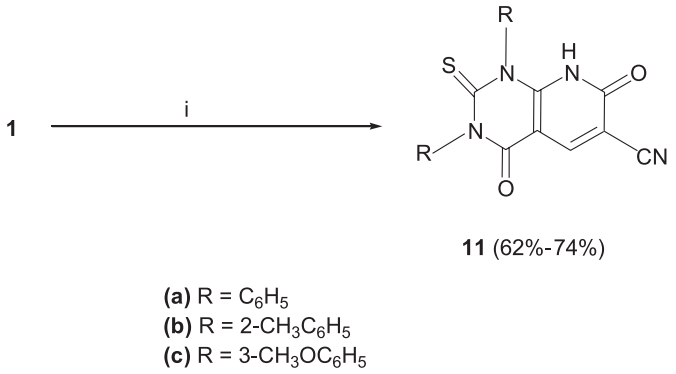
A mixture of **2a** (3.84 g, 0.01 mol), hydrazine hydrate (1 mL, 0.015 mol), ethanol (25 mL), and acetic acid (10 mL) was refluxed for 12 h. The reaction mixture was then concentrated, cooled, poured into ice water, and extracted with chloroform (3 × 100 mL), washed with water (3 × 100 mL), dried, and concentrated. Flash chromatography (petroleum ether – EtOAc, 4:1) gave **5a** (2.58 g, 65%) as a white-grey solid, mp 212–214 °C. IR (ν_{max}, cm^{-1}): 3430, 3303, 1660. ^1H

© 2005 NRC Canada

Scheme 3. Reagents: (*i*) $H_2NC(=NH)NH_2$, MeOH, NaOMe.



Scheme 4. Reagents: (*i*) $NCCH_2CONH_2$, $(CH_3)_2CHONa$, $(CH_3)_2CHOH$.



NMR (DMSO-d_6) δ: 7.05 (1H, s, H-3), 7.15–7.80 (15H, m, aromatic), 10.02 (2H, m, 2 × NH). MS (70 eV) *m/z* calcd. for $C_{23}H_{18}N_4OS$: 398.0712; found: 398.0716 (M^+).

2(3*H*)-3-Phenyl-2(3*H*)-5,7-di(2-methylphenyl)-4-oxo-pyrazolo[3,4-*d*]pyrimidin-6-thione (5b)

A mixture of **2b** (4.12 g, 0.01 mol), hydrazine hydrate (1 mL, 0.015 mol), ethanol (25 mL), and acetic acid (10 mL) was refluxed for 9 h. The reaction mixture was then concentrated, cooled, poured into ice water, and extracted with chloroform (3 × 100 mL), washed with water (3 × 100 mL), dried, and concentrated. Flash chromatography (petroleum ether – EtOAc, 4:1) gave **5b** (2.08 g, 70%) as a white solid, mp 215–217 °C. IR (ν_{max}, cm^{-1}): 3400, 3300, 1680. ^1H NMR (DMSO-d_6) δ: 2.32 (6H, s, 2 × CH_3), 6.65 (1H, s, H-3), 6.80–7.60 (13H, m, aromatic), 9.38 (2H, m, 2 × NH). MS (70 eV) *m/z* calcd. for $C_{25}H_{22}N_4OS$: 426.0249; found: 426.0254 (M^+).

2(3*H*)-3-Phenyl-2(3*H*)-5,7-di(3-methoxyphenyl)-4-oxo-pyrazolo[3,4-*d*]pyrimidin-6-thione (5c)

A mixture of **2c** (4.44 g, 0.01 mol), hydrazine hydrate (1 mL, 0.015 mol), ethanol (25 mL), and acetic acid (10 mL) was refluxed for 11 h. The reaction mixture was then concentrated, cooled, poured into ice water, and extracted with chloroform (3 × 100 mL), washed with water (3 × 100 mL), dried, and concentrated. The product was crystallized from ethanol to give **5c** (3.30 g, 72%) as a white solid, mp 235–237 °C. IR (ν_{max}, cm^{-1}): 3390, 3320, 1690. ^1H NMR (DMSO-d_6) δ: 3.30 (6H, s, 2 × OCH_3), 6.80 (1H, s, H-3), 6.95–7.80 (13H, m, aromatic), 9.68 (2H, m, 2 × NH). MS (70 eV) *m/z* calcd. for $C_{25}H_{22}N_4O_3S$: 458.0928; found: 458.0934 (M^+).

5,7-Diphenyl-4-oxo-isoxazolo[5,4-*d*]pyrimidin-6-thione (7a)

A mixture of **1a** (3.52 g, 0.01 mol), absolute ethanol (50 mL), acetic acid (10 mL), and hydroxylamine hydrochloride (1.4 g, 0.02 mol) was refluxed for 8 h and excess ethanol was distilled off under reduced pressure. The residue was poured onto crushed ice, extracted with chloroform (3 × 100 mL), washed with water (3 × 100 mL), dried (Na_2SO_4), and concentrated. Crystallization from ethanol gave **7a** (2.25g, 70%) as a white solid, mp 235 °C. IR (ν_{max}, cm^{-1}): 2980, 1670, 1210, 835, 725. ^1H NMR (DMSO-d_6) δ: 7.08–7.52 (10H, m, aromatic), 8.30 (1H, s, -CH=N-). MS (70 eV) *m/z* calcd. for $C_{17}H_{11}N_3O_2S$: 321.0762: found: 321.0754 (M^+).

5,7-Di(2-methylphenyl)-4-oxo-isoxazolo[5,4-*d*]pyrimidin-6-thione (7b)

A mixture of **1b** (3.80 g, 0.01 mol), absolute ethanol (50 mL), acetic acid (10 mL), and hydroxylamine hydrochloride (1.4 g, 0.02 mol) was refluxed for 10 h. The solution was worked up by pouring the concentrated residue into ice water, and extracted with chloroform (3 × 100 mL),

© 2005 NRC Canada

washed with water (3 × 100 mL), dried, and concentrated. The product was crystallized from ethanol to give **7b** (2.27 g, 65%) as a white solid, mp 220–222 °C. IR (ν_{max}, cm^{-1}): 3100, 1690, 1220, 840, 785. ^1H NMR (DMSO-d_6) δ: 2.10 (6H, s, 2 × CH_3), 6.80–7.80 (8H, m, aromatic), 8.20 (1H, s, -CH=N-). MS (70 eV) *m/z* calcd. for $C_{19}H_{15}N_3O_2S$: 349.0578; found: 349.0583 (M^+).

5,7-Di(3-methoxyphenyl)-4-oxo-isoxazolo[5,4-*d*]pyrimidin-6-thione (7c)

A mixture of **1c** (4.12 g, 0.01 mol), absolute ethanol (50 mL), acetic acid (10 mL), and hydroxylamine hydrochloride (1.4 g, 0.02 mol) was refluxed for 11 h. The residue was poured onto crushed ice, extracted with chloroform (3 × 100 mL), washed with water (3 × 100 mL), dried (Na_2SO_4), and concentrated. Crystallization from ethanol gave **7c** (3.24 g, 85%) as a white solid, mp 215–217 °C. IR (ν_{max}, cm^{-1}): 2900, 1680, 1240, 845, 685. ^1H NMR (DMSO-d_6) δ: 3.75 (6H, s, 2 × OCH_3), 6.70–7.50 (8H, m, aromatic), 8.15 (1H, s, -CH=N-). MS (70 eV) *m/z* calcd. for $C_{19}H_{15}N_3O_4S$: 381.0250; found: 381.0254 (M^+).

3,5,7-Triphenyl-2,3-dihydro-4-oxo-isoxazolo[5,4-*d*]pyrimidin-6-thione (8a)

A mixture of **2a** (3.84 g, 0.01 mol) and hydroxylamine hydrochloride (1.4 g, 0.02 mol) in absolute ethanol (50 mL) and acetic acid (10 mL) was refluxed for 12 h. The excess solvent was distilled off under reduced pressure and poured onto crushed ice, extracted with chloroform (3 × 100 mL), washed with water (3 × 100 mL), dried (Na_2SO_4), and concentrated to give the crude product. Crystallization from chloroform–hexane gave **8a** (2.59 g, 65%) as a reddish-yellow solid, mp 195–198 °C. IR (ν_{max}, cm^{-1}): 3430, 2975, 1660, 1210, 838, 770. ^1H NMR (DMSO-d_6) δ: 6.50 (1H, s, -3CH), 6.80–7.70 (14H, m, aromatic), 10.40 (1H, s, NH). MS (70 eV) *m/z* calcd. for $C_{23}H_{17}N_3O_2S$: 399.0444; found: 399.0458 (M^+).

3-Phenyl-5,7-di(2-methylphenyl)-2,3-dihydro-4-oxo-isoxazolo[5,4-*d*]pyrimidin-6-thione (8b)

A mixture of **2b** (4.12 g, 0.01 mol) and hydroxylamine hydrochloride (1.4 g, 0.02 mol) in absolute ethanol (50 mL) and acetic acid (10 mL) was refluxed for 10 h. The excess solvent was distilled off under reduced pressure and poured onto crushed ice, extracted with chloroform (3 × 100 mL), washed with water (3 × 100 mL), dried (Na_2SO_4), and concentrated. The product was crystallized from ethanol to give **7b** (2.69 g, 63%) as a white solid, mp 205–207 °C. IR (ν_{max}, cm^{-1}): 3400, 2960, 1670, 1240, 845, 742. ^1H NMR (DMSO-d_6) δ: 2.20 (6H, s, 2 × CH_3), 6.65 (1H, s, H-3), 6.80–7.50 (13H, m, aromatic), 10.68 (1H, s, NH). MS (70 eV) *m/z* calcd. for $C_{25}H_{21}N_3O_2S$: 427.0800; found: 427.0803 (M^+).

3-Phenyl-5,7-di(3-methoxyphenyl)-2,3-dihydro-4-oxo-isoxazolo[5,4-*d*]pyrimidin-6-thione (8c)

A mixture of **2c** (4.44 g, 0.01 mol) and hydroxylamine hydrochloride (1.4 g, 0.02 mol) in absolute ethanol (50 mL) and acetic acid (10 mL) was refluxed for 15 h. The solution was worked up by pouring the concentrated residue onto ice water, and extracted with chloroform (3 × 100 mL), washed with water (3 × 100 mL), dried, and concentrated. The product was crystallized from ethanol to give **7c** (3.58 g, 78%) as a white solid, mp 210–212 °C. IR (ν_{max}, cm^{-1}): 3390, 2980, 1680, 1240, 840, 785. ^1H NMR (DMSO-d_6) δ: 3.68 (6H, s, 2 × OCH_3), 6.30 (1H, s, H-3), 6.60–7.50 (13H, m, aromatic), 10.44 (1H, s, NH). MS (70 eV) *m/z* calcd. for $C_{25}H_{21}N_3O_4S$: 459.0342; found: 459.0347 (M^+).

2-Amino-6,8-diphenyl-5-oxo-pyrimido[4,5-*d*]pyrimidine-7-thione (9a)

The condensation product **1a** (3.52 g, 0.01 mol) in methanol (10 mL) was added to a well-stirred suspension of sodium methoxide (prepared by dissolving 0.92 g of sodium in 50 mL of methanol) and guanidine nitrate (2.57 g, 0.02 mol) and refluxed for 7 h. The solvent was removed under reduced pressure and the residue was poured onto crushed ice, extracted with chloroform (3 × 100 mL), washed with water (3 × 100 mL), dried (Na_2SO_4), and concentrated to give the crude product. Crystallization from chloroform–hexane gave **9a** (2.50 g, 72%) as a reddish-yellow solid, mp 205–208 °C. IR (ν_{max}, cm^{-1}): 3380, 3320, 3200, 1650, 1580, 845. ^1H NMR (DMSO-d_6) δ: 5.24 (2H, br s, NH_2, exchangeable with D_2O), 7.10–7.80 (11H, m, aromatic and H-4). MS (70 eV) *m/z* calcd. for $C_{18}H_{13}N_5OS$: 347.0812; found: 347.0820 (M^+).

2-Amino-6,8-di(2-methyl)phenyl-5-oxo-pyrimido[4,5-*d*]pyrimidine-7-thione (9b)

The condensation product **1b** (3.80 g, 0.01 mol) in methanol (10 mL) was added to a well-stirred suspension of sodium methoxide (prepared by dissolving 0.92 g of sodium in 50 mL of methanol) and guanidine nitrate (2.57 g, 0.02 mol) and refluxed for 12 h. The solvent was removed under reduced pressure and the residue was poured onto crushed ice, extracted with chloroform (3 × 100 mL), washed with water (3 × 100 mL), dried (Na_2SO_4), and concentrated to give the crude product. The product was crystallized from ethanol to give **9b** (2.21 g, 59%) as a yellowish solid, mp 196–198 °C. IR (ν_{max}, cm^{-1}): 3375, 3330, 3200, 1668, 1580, 804. ^1H NMR (DMSO-d_6) δ: 2.20 (6H, s, 2 × CH_3), 4.88 (2H, br s, NH_2, exchangeable with D_2O), 6.82–7.70 (9H, m, aromatic and H-4). MS (70 eV) *m/z* calcd. for $C_{20}H_{17}N_5OS$: 375.0528; found: 375.0543 (M^+).

2-Amino-6,8-di(2-methyl)phenyl-5-oxo-pyrimido[4,5-*d*]pyrimidine-7-thione (9c)

The condensation product **1c** (4.12 g, 0.01 mol) in methanol (10 mL) was added to a well-stirred suspension of sodium methoxide (prepared by dissolving 0.92 g of sodium in 50 mL of methanol) and guanidine nitrate (2.57 g, 0.02 mol) and refluxed for 8 h. The solution was worked up by pouring the concentrated residue into ice water, and extracted with chloroform (3 × 100 mL), washed with water (3 × 100 mL), dried, and concentrated. The product was crystallized from ethanol to give **9c** (3.05 g, 75%) as a pale yellowish solid, mp 225–230 °C. IR (ν_{max}, cm^{-1}): 3382, 3325, 3210, 1655, 1585, 847. ^1H NMR (DMSO-d_6) δ: 3.76 (6H, s, 2 × OCH_3), 5.15 (2H, br s, NH_2, exchangeable with D_2O), 6.75–7.50 (9H, m, aromatic and H-4). MS (70 eV) *m/z* calcd. for $C_{20}H_{17}N_5O_3S$: 407.0829; found: 407.0834 (M^+).

© 2005 NRC Canada

3(4*H*)-2-Amino-4,6,8-triphenyl-5-oxo-pyrimido[4,5-*d*]pyrimidine-7-thiones (10a)

The condensation product **2a** (3.84 g, 0.01 mol) in methanol (10 mL) was added to a well-stirred suspension of sodium methoxide (prepared by dissolving 0.92 g of sodium in 50 mL of methanol) and guanidine nitrate (2.57 g, 0.02 mol) and refluxed for 7 h. The solvent was removed under reduced pressure and the residue was poured onto crushed ice, extracted with chloroform (3 × 100 mL), washed with water (3 × 100 mL), dried (Na_2SO_4), and concentrated to give the crude product. The crude product was purified by flash chromatography (eluting with benzene–hexane, 1:2) and crystallized from chloroform–hexane to give **10a** (2.63 g, 62%) as a reddish-yellow solid, mp 215–218 °C. IR (ν_{max}, cm^{-1}): 3360, 3320, 3200, 1645, 1580, 824. ^1H NMR (DMSO-d_6) δ: 4.90 (2H, br s, NH_2, exchangeable with D_2O), 6.20 (1H, s, H-4), 6.80–7.60 (15H, m, aromatic). MS (70 eV) *m*/*z* calcd. for $C_{24}H_{19}N_5OS$: 425.0122; found: 425.0125 (M^+).

3(4*H*)-2-Amino-4-phenyl-6,8-di(2-methyl)phenyl-5-oxo-pyrimido[4,5-*d*]pyrimidine-7-thiones (10b)

The condensation product **2b** (4.12 g, 0.01 mol) in methanol (10 mL) was added to a well-stirred suspension of sodium methoxide (prepared by dissolving 0.92 g of sodium in 50 mL of methanol) and guanidine nitrate (2.57 g, 0.02 mol) and refluxed for 10 h. The reaction mixture was then concentrated, cooled, poured into ice water, and extracted with chloroform (3 × 100 mL), washed with water (3 × 100 mL), dried, and concentrated. Flash chromatography (eluting with benzene–hexane, 1:2) and crystallization from chloroform–hexane gave **10b** (2.94 g, 65%) as a yellowish solid, mp 198–202 °C. IR (ν_{max}, cm^{-1}): 3385, 3330, 3205, 1655, 1570, 438. ^1H NMR (DMSO-d_6) δ: 2.30 (6H, s, 2 × CH_3), 4.85 (2H, br s, NH_2, exchangeable with D_2O), 6.25 (1H, s, H-4), 7.00–7.75 (13H, m, aromatic). MS (70 eV) *m*/*z* calcd. for $C_{26}H_{23}N_5OS$: 453.0639; found: 453.0642 (M^+).

3(4*H*)-2-Amino-4-phenyl-6,8-di(2-methyl)phenyl-5-oxo-pyrimido[4,5-*d*]pyrimidine-7-thiones (10c)

The condensation product **2c** (4.44 g, 0.01 mol) in methanol (10 mL) was added to a well-stirred suspension of sodium methoxide (prepared by dissolving 0.92 g of sodium in 50 mL of methanol) and guanidine nitrate (2.57 g, 0.02 mol) and refluxed for 6 h. The reaction mixture was then concentrated, cooled, poured into ice water, and extracted with chloroform (3 × 100 mL), washed with water (3 × 100 mL), dried, and concentrated. Flash chromatography (eluting with benzene–hexane, 1:2) and crystallization from chloroform–hexane gave **10c** (3.49 g, 72%) as a yellowish solid, mp 225–230 °C. IR (ν_{max}, cm^{-1}): 3375, 3330, 3200, 1650, 1580, 438. ^1H NMR (DMSO-d_6) δ: 3.70 (6H, s, 2 × CH_3), 4.93 (2H, br s, NH_2, exchangeable with D_2O), 6.30 (1H, s, H-4), 6.65–7.50 (13H, m, aromatic). MS (70 eV) *m*/*z* calcd. for $C_{26}H_{23}N_5O_3S$: 485.1018; found: 485.1023 (M^+).

3-Cyano-6,8-diphenyl-2,5-dioxo-pyrido[2,3-*d*]pyrimidin-7-thione (11a)

To a solution of sodium isopropoxide (prepared by dissolving sodium (0.46 g, 0.02 mol) in propan-2-ol (70 mL)), cyanoacetamide (1.68 g, 0.02 mol) was added and the reaction mixture was stirred for 10 min. Then, **1a** (3.52 g, 0.01 mol) was added and refluxed for 8 h. Evaporation of the solvent yielded an orange sodium salt of pyridone, which was dissolved in water (25 mL) and acidified with dilute HCl (8%) to give the crude product (**11a**). The product was crystallized from acetic acid to give **11a** (2.42 g, 65%) as an yellowish solid, mp 152–154 °C. IR (ν_{max}, cm^{-1}): 3333, 2194, 1686, 813. ^1H NMR (acetone-d_6) δ: 6.22 (1H, s, H-4), 6.85–7.58 (10H, m, aromatic), 8.83 (1H, br s, NH). M.S. (70 eV) *m*/*z* calcd. for $C_{20}H_{12}N_4O_2S$: 372.0716; found: 372.0710 (M^+).

3-Cyano-6,8-di(2-methylphenyl)-2,5-dioxo-pyrido[2,3-*d*]pyrimidin-7-thione (11b)

To a solution of sodium isopropoxide (prepared by dissolving sodium (0.46 g, 0.02 mol) in propan-2-ol (70 mL)), cyanoacetamide (1.68 g, 0.02 mol) was added and the reaction mixture was stirred for 10 min. Then, **1b** (3.80 g, 0.01 mol) was added and refluxed for 10 h. The solution was worked up by pouring the concentrated residue into ice water and acidified with dilute HCl (8%) to give the crude product. Crystallization from acetic acid afforded 3-cyano-6,8-di(2-methylphenyl)-2,5-dioxo-pyrido[2,3-*d*]pyrimidin-7-thione (**11b**, 2.96 g, 74%) as a yellow solid, mp 205–207 °C. IR (ν_{max}, cm^{-1}): 3346, 2210, 1684, 784. ^1H NMR (acetone-d_6) δ: 1.95 (3H, s, CH_3), 2.30 (3H, s, CH_3), 6.12 (1H, s, H-4), 6.65–7.95 (8H, m, aromatic), 8.78 (1H, br s, NH). MS (70 eV) *m*/*z* calcd. for $C_{22}H_{16}N_4O_2S$: 400.1012; found: 400.1015 (M^+).

3-Cyano-6,8-di(2-methylphenyl)-2,5-dioxo-pyrido[2,3-*d*]pyrimidin-7-thione (11c)

To a solution of sodium isopropoxide (prepared by dissolving sodium (0.46 g, 0.02 mol) in propan-2-ol (70 mL)), cyanoacetamide (1.68 g, 0.02 mol) was added and the reaction mixture was stirred for 10 min. Then, **1c** (4.12 g, 0.01 mol) was added and refluxed for 10 h. Evaporation of the solvent yielded an orange sodium salt of pyridone, which was dissolved in water (25 mL) and acidified with dilute HCl (8%) to give the crude product. Crystallization from acetic acid afforded 3-cyano-6,8-di(2-methylphenyl)-2,5-dioxo-pyrido[2,3-*d*]pyrimidin-7-thione (**11c**, 2.67 g, 62%) as a yellow solid, mp 186–188 °C. IR (ν_{max}, cm^{-1}): 3340, 2215, 1692, 811. ^1H NMR (acetone-d_6) δ: 3.62 (6H, s, 2 × OCH_3), 6.26 (1H, s, H-4), 6.95–7.45 (8H, m, aromatic), 8.92 (1H, br s, NH). MS (70 eV) *m*/*z* calcd. for $C_{22}H_{16}N_4O_4S$: 432.0970; found: 432.0959 (M^+).

Acknowledgements

We are thankful to the Department of Chemistry, University of Manchester, UK and the Regional Sophisticated Instrumentation Center (RSIC), the Central Drug Research Institute (CDRI), Lucknow, India for the spectral data, and the Council of Scientific and Industrial Research (CSIR), New Delhi, India for the financial support.

References

1. H. Singh and L.D.S. Yadav. Agric. Biol. Chem. **40**, 759 (1976).
2. A. Omar and O.M. Aboulwafa. J. Heterocycl. Chem. **23**, 1939 (1987).

© 2005 NRC Canada

3. E.C. Taylor and H.P. Hemanta Kumar. Tetrahedron, **48**, 8089 (1992).
4. J.B. Hynes, R.F. Greatz, and W.T. Aston. J. Med. Chem. **15**, 1332 (1972).
5. V.K. Ahluwalia, H.R. Sharma, and R. Tyagi. Tetrahedron, **42**, 4045 (1986).
6. N.A. Devi and L.W. Singh. Indian J. Chem. **33B**, 7091 (1994).
7. R.K. Robins. J. Am. Chem. Soc. **78**, 784 (1956).
8. F.R. White. Cancer Chemother. Rep. **3**, 26 (1959).
9. J.L. Jun Scott and L.V. Foye. Cancer Chemother. Rep. **20**, 73 (1962).
10. R.K. Robins. J. Med. Chem. **7**, 186 (1964).
11. S. Kobayashi. Chem. Pharm. Bull. Jpn. **21**, 941 (1973).
12. J.J. Marr, R.L. Berens, D.J. Nelson, and S.W. Lason. Biochem. Pharmacol. **29**, 2397 (1980).
13. A.B. Homer. Chem. Abstr. **80**, 48 033 (1974).
14. J. Matsuda, K. Yamazaki, and K. Yamagata. Chem. Abstr. **80**, 480 319 (1974).
15. J.M. Bellary and V.V. Badiger. Indian J. Chem. **20B**, 654 (1981).
16. H. Gastpar. Chem. Abstr. **84**, 144 410 (1976).
17. A. Miyaki. Chem. Abstr. **83**, 206 197 (1975).
18. K. Nada and A. Nakagawa. Chem. Abstr. **87**, 533 (1977).
19. S. Kohra, Y. Tomonaga, and A. Hosomi. J. Heterocycl. Chem. **25**, 959 (1988).
20. R. Justoni and R. Fusco. Gazz. Chim. Ital. **68**, 66 (1938).
21. S.M. Mect and D. Werner. J. Chem. Soc. Perkin Trans. 1, 1903 (1973).
22. V. Papesch and R.M. Dodson. J. Org. Chem. **30**, 199 (1965).
23. Y. Maki, K. Izuta, and M. Suzuki. J. Chem. Soc. Chem. Commun. 1442 (1971).
24. F. Yoneda, T. Nagamatsu, and T. Nagamura. J. Chem. Soc. Perkin Trans. 1, 765 (1977).
25. E.C. Taylor and E.E. Garcia. J. Org. Chem. **29**, 2116 (1964).
26. G. Desimoni, P. Grunanger, and P. Vita Finzi. Tetrahedron, **23**, 675 (1967).
27. P. Rajagopalan and C.N. Talaty. Tetrahedron, **23**, 3541 (1967).
28. L.W. Singh and N.A. Devi. Indian J. Chem. **35B**, 478 (1996).
29. Y. Taminage, H. Okuda, and Y. Matsuda. Heterocycles, **12**, 503 (1979).
30. K. Grohe and H. Helmet. Chem. Abstr. **84**, 74 208 (1976).
31. A.D. Broom, J.L. Shin, and G.L. Anderson. J. Org. Chem. **41**, 1095 (1976).
32. P. Bhuyan, R.C. Boruah, and J.S. Sandhu. J. Org. Chem. **55**, 568 (1990).

© 2005 NRC Canada

Late metal salicylaldimine complexes derived from 5-aminosalicylic acid — Molecular structure of a zwitterionic mono Schiff base zinc complex

Tara A. Bourque, Megan E. Nelles, Teri J. Gullon, Christian N. Garon, Melissa K. Ringer, Lisa J. Leger, Jamie W. Mason, Susan L. Wheaton, Felix J. Baerlocher, Christopher M. Vogels, Andreas Decken, and Stephen A. Westcott

Abstract: Condensation of salicylaldehyde (2-$HOC_6H_4C(O)H$) with 5-aminosalicylic acid (5-$H_2NC_6H_3$-2-(OH)-CO_2H) afforded the Schiff base 2-$HOC_6H_4C(H)=NC_6H_3$-2-(OH)-5-CO_2H (**a**). Similar reactivity with 5-bromosalicylaldehyde was also observed to give 5-Br-2-$HOC_6H_3C(H)=NC_6H_3$-2-(OH)-5-CO_2H (**b**). Reaction of these salicylaldehydes with Pd(II), Cu(II), and Zn(II) salts gave the corresponding bis(*N*-arylsalicylaldiminato)metal complexes (M = Pd (**1**), Cu (**2**), Zn (**3**)). The molecular structure of the Schiff base compound **a** has been confirmed by an X-ray diffraction study. Crystals of **a** were monoclinic, space group *P*2(1)/*c*, *a* = 7.0164(7) Å, *b* = 11.0088(11) Å, *c* = 14.8980(15) Å, β = 102.917(2)°, *Z* = 4. The molecular structure of a novel zwitterionic conformer of **3a** was also characterized by an X-ray diffraction study. Crystals of **4** were monoclinic, space group *P*2(1)/*c*, *a* = 9.5284(5) Å, *b* = 19.5335(11) Å, *c* = 8.6508(5) Å, β = 90.596(1)°, *Z* = 4. All new compounds have been tested for their antifungal activity against *Aspergillus niger* and *Aspergillus flavus*.

Key words: 5-aminosalicylic acid (5-ASA), antifungal, copper, palladium, salicylaldimines, Schiff base, zinc.

Résumé : La condensation du salicylaldéhyde (2-$HOC_6H_4C(O)H$) avec l'acide 5-aminosalicylique (5-$H_2NC_6H_3$-2-(OH)-CO_2H) conduit à la formation de la base de Schiff 2-$HOC_6H_4C(H)=NC_6H_3$-2-(OH)-5-CO_2H (**a**). On a observé une réactivité semblable avec le 5-bromosalicylaldéhyde qui conduit à la formation de la 5-Br-2-$HOC_6H_3C(H)=NC_6H_3$-2-(OH)-5-CO_2H (**b**). La réaction de ces salicylaldéhydes avec des sels de Pd(II), Cu(II) et Zn(II) conduit aux complexes correspondants bis(*N*-arylsalicylaldiminato)métal (M = Pd (**1**), Cu (**2**), Zn (**3**)). La structure moléculaire de la base de Schiff **a** a été confirmée par une étude de diffraction des électrons. Les cristaux de **a** sont monocliniques, groupe d'espace *P*2(1)/*c*, avec *a* = 7,0164(7) Å, *b* = 11,0088(11) Å et *c* = 14,8980(15) Å, β = 102,917(2)° et *Z* = 4. Faisant appel à la diffraction des rayons X, on a aussi caractérisé la structure moléculaire d'un nouveau conformère zwitterionique du composé **3a**. Les cristaux de **4** sont monocliniques, groupe d'espace *P*2(1)/*c*, avec *a* = 9,5284(5) Å, *b* = 19,5335(11) Å et *c* = 8,6508(5) Å, β = 90,596(1)° et *Z* = 4. L'activité fongicide des tous les nouveaux composés a été vérifiée contre *Aspergillus niger* et *Aspergillus flavus*.

Mots clés : acide 5-aminosalicylique (5-AAS), fongicide, cuivre, palladium, salicylaldimines, base de Schiff, zinc.

[Traduit par la Rédaction]

Introduction

Inflammatory bowel disease (IBD) is a serious disorder of the lower gastrointestinal tract where tissue damage and inflammation can impair the use of the bowel (1–13). Ulcerative colitis involves inflammation of the lining of the colon while Crohn's disease affects all layers of the intestinal wall. Both disorders are chronic, progressive diseases whose etiopathogenesis is not well understood. Current therapies for treating these disorders include glucocorticoids and 5-aminosalicylic acid (5-ASA, Fig. 1*a*) derivatives. Despite the well-documented benefits of 5-ASA in the treatment of IBD, its efficacy is limited due to side effects and allergic reactions associated with its mode of delivery. For example, sulfasalazine (Fig. 1*b*) was introduced over 60 years ago and has become the most widely prescribed agent for IBD, where the pharmacological action of this compound has been attributed to 5-ASA (14). When ingested orally, 88%

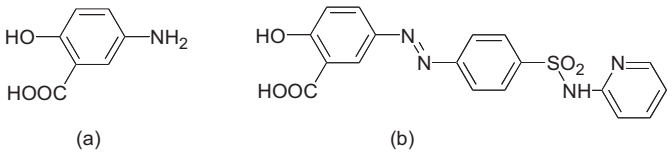
Received 31 January 2005. Published on the NRC Research Press Web site at http://canjchem.nrc.ca on 14 September 2005.

T.A. Bourque, M.E. Nelles, T.J. Gullon, C.N. Garon, M.K. Ringer, L.J. Leger, J.W. Mason, S.L. Wheaton, C.M. Vogels, and S.A. Westcott.[1] Department of Chemistry, Mount Allison University, Sackville, NB E4L 1G8, Canada.
F.J. Baerlocher. Department of Biology and Biochemistry, Mount Allison University, Sackville, NB E4L 1G7, Canada.
A. Decken.[2] Department of Chemistry, University of New Brunswick, Fredericton, NB E3B 5A3, Canada.

[1]Corresponding author (e-mail: swestcott@mta.ca).
[2]Corresponding author regarding X-ray crystallography (e-mail: adecken@unb.ca).

 doi: 10.1139/V05-091 © 2005 NRC Canada

Fig. 1. (*a*) 5-ASA and (*b*) sulfasalazine.



of the sulfasalazine reaches the colon where it is degraded by azo reductases of the colonic microflora, into 5-ASA and sulfapyridine (8). All toxic effects associated with sulfasalazine are believed to arise from the sulfapyridine and, as a result, there has been a considerable amount of research focussed on designing new prodrugs of 5-ASA with less harmful side effects.

As part of our program designing metal complexes containing biologically active ligands, we have made Schiff base metal complexes derived from 5-ASA. As an initial screen of potential biological properties, we have examined all new complexes for their ability to act as antifungal agents.

Experimental

General

Reagents and solvents used were purchased from Aldrich Chemicals. $Pd(OAc)_2$ was purchased from Precious Metals Online Ltd. (Melbourne, Australia). NMR spectra were recorded on a JEOL JNM-GSX270 FT spectrometer or a Varian Mercury Plus 200 NMR spectrometer. ^{1}H NMR chemical shifts are reported in ppm and referenced to residual solvent protons in deuterated solvent at 270 and 200 MHz, respectively. ^{13}C NMR chemical shifts are referenced to solvent carbon resonances as internal standards at 68 and 50 MHz, respectively, and are reported in ppm. Multiplicities are reported as singlet (s), doublet (d), triplet (t), multiplet (m), broad (br), and overlapping (ov). IR spectra were obtained using a Mattson Genesis II FT-IR spectrometer. Melting points were determined using a Mel-Temp apparatus and are uncorrected. Microanalyses for C, H, and N were carried out at Guelph Chemical Laboratories, Guelph, Ontario.

5-{[(1*E*)-(2-Hydroxyphenyl)methylene]amino}-2-hydroxybenzoic acid (a)

To an EtOH (10 mL) solution of 5-aminosalicylic acid (0.50 g, 3.26 mmol) was added an EtOH (5 mL) solution of salicylaldehyde (0.44 g, 3.60 mmol). The mixture was heated at reflux for 2 h to ensure completion, at which point a yellow precipitate was collected by suction filtration and washed with EtOH (3 × 5 mL) and Et_2O (3 × 10 mL). The yellow solid was then dried to afford **a** (0.63 g, 75%); mp 258–260 °C. IR (Nujol, cm^{-1}) ν: 1610 (C=N). Spectroscopic NMR data (in DMSO-d_6): ^{1}H NMR δ: 13.07 (br s, 1H, -O*H*), 8.98 (s, 1H, C(*H*)=N), 7.84 (d, *J* = 3 Hz, 1H, Ar), 7.67–7.64 (ov m, 2H, Ar), 7.39 (d of d, *J* = 8, 3 Hz, 1H, Ar), 7.06–6.94 (ov m, 3H, Ar). ^{13}C{^{1}H} NMR δ: 172.2, 162.2, 160.8, 160.7, 139.7, 133.4, 133.0, 129.1, 123.1, 119.8, 119.5, 118.6, 117.0, 114.1.

5-{[(1*E*)-(5-Bromo-2-hydroxyphenyl)methylene]amino}-2-hydroxybenzoic acid (b)

To an EtOH (10 mL) solution of 5-aminosalicylic acid (0.50 g, 3.26 mmol) was added an EtOH (5 mL) solution of 5-bromosalicylaldehyde (0.72 g, 3.58 mmol). The mixture was heated at reflux for 2 h to ensure completion, at which point a yellow precipitate was collected by suction filtration and washed with EtOH (3 × 5 mL) and Et_2O (3 × 10 mL). The pale yellow solid was then dried to afford **b** (0.93 g, 85%); mp 271 °C. IR (Nujol, cm^{-1}) ν: 1604 (C=N). Spectroscopic NMR data (in DMSO-d_6): ^{1}H NMR δ: 13.05 (br s, 1H, -O*H*), 8.94 (s, 1H, C(*H*)=N), 7.84–7.81 (ov m, 2H, Ar), 7.62 (d of d, *J* = 8, 3 Hz, 1H, Ar), 7.50 (d of d, *J* = 8, 3 Hz, 1H, Ar), 7.03 (d, *J* = 8 Hz, 1H, Ar), 6.90 (d, *J* = 8 Hz, 1H, Ar). ^{13}C{^{1}H} NMR δ: 172.2, 161.0, 160.9, 159.8, 139.8, 135.8, 134.6, 129.7, 123.3, 121.9, 119.6, 118.9, 114.2, 110.5.

Compound 1a

To an EtOH (50 mL) solution of palladium(II) acetate (0.20 g, 0.89 mmol) was added an EtOH (15 mL) solution of **a** (0.48 g, 1.87 mmol). The mixture was heated at reflux for 3 h at which point a yellow-green precipitate was collected by suction filtration and washed with cold EtOH (3 × 5 mL) and Et_2O (3 × 10 mL). The pale yellow solid was then dried to afford complex **1a** (0.47 g, 85%); mp 305 to 306 °C (decomposition). IR (Nujol, cm^{-1}) ν: 1608 (C=N). Spectroscopic NMR data (in DMSO-d_6): ^{1}H NMR δ: 8.11 (s, 2H, C(*H*)=N), 7.71 (d, *J* = 3 Hz, 2H, Ar), 7.47–7.43 (ov m, 4H, Ar), 7.17 (d of d, *J* = 8, 3 Hz, 2H, Ar), 6.99 (d, *J* = 8 Hz, 2H, Ar), 6.51 (t, *J* = 8 Hz, 2H, Ar), 6.03 (d, *J* = 8 Hz, 2H, Ar). ^{13}C{^{1}H} NMR δ: 172.1, 164.5, 164.4, 160.2, 140.8, 135.9, 135.7, 132.9, 126.2, 120.6, 120.1, 116.7, 115.4, 112.8. Anal. calcd. for $C_{28}H_{20}N_2O_8Pd$ (%): C 54.34, H 3.26, N 4.53; found: C 53.95, H 2.89, N 4.09.

Compound 1b

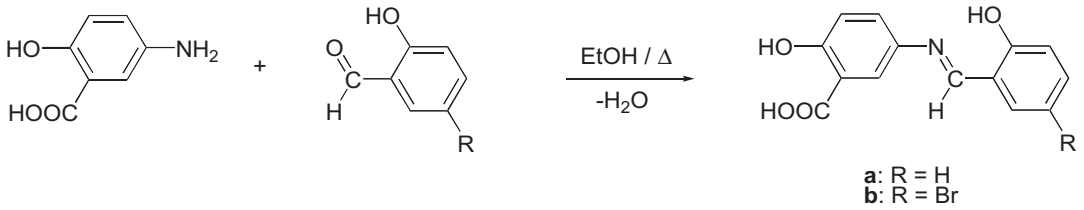
To an EtOH (40 mL) solution of palladium(II) acetate (0.15 g, 0.67 mmol) was added an EtOH (10 mL) solution of **b** (0.47 g, 1.40 mmol). The mixture was heated at reflux for 2 h at which point a yellow-green precipitate was collected by suction filtration and washed with cold EtOH (3 × 5 mL) and Et_2O (3 × 10 mL). The pale yellow solid was then dried to afford complex **1b** (0.47 g, 90%); mp 294 to 295 °C (decomposition). IR (Nujol, cm^{-1}) ν: 1603 (C=N). Spectroscopic NMR data (in DMSO-d_6): ^{1}H NMR δ: 8.09 (s, 2H, C(*H*)=N), 7.67 (d of d, *J* = 8, 3 Hz, 4H, Ar), 7.48 (d of d, *J* = 8, 3 Hz, 2H, Ar), 7.25 (d of d, *J* = 8, 3 Hz, 2H, Ar), 6.97 (d, *J* = 8 Hz, 2H, Ar), 5.93 (d, *J* = 8 Hz, 2H, Ar). ^{13}C{^{1}H} NMR δ: 172.2, 164.1, 163.4, 160.3, 140.6, 138.1, 137.2, 133.1, 126.2, 122.5, 122.4, 117.0, 112.7, 105.6. Anal. calcd. for $C_{28}H_{18}N_2Br_2O_8Pd$ (%): C 43.30, H 2.34, N 3.61; found: C 43.62, H 2.32, N 3.27.

Compound 2a

To an EtOH (50 mL) solution of copper(II) acetate (0.20 g, 1.10 mmol) was added an EtOH (15 mL) solution of **a** (0.59 g, 2.29 mmol). The mixture was heated at reflux for 3 h at which point a yellow-green precipitate was collected by suction filtration and washed with cold EtOH (3 × 5 mL) and Et_2O (3 × 10 mL). The pale yellow solid was then dried

© 2005 NRC Canada

Scheme 1. Synthesis of Schiff base compounds derived from 5-ASA.



to afford complex **2a** (0.60 g, 95%); mp 291 to 292 °C (decomposition). IR (Nujol, cm^{-1}) ν: 1608 (C=N). Anal. calcd. for $C_{28}H_{20}N_2CuO_8$ (%): C 58.38, H 3.51, N 4.86; found: C 57.74, H 3.32, N 4.75.

Compound 2b

To an EtOH (50 mL) solution of copper(II) acetate (0.20 g, 1.10 mmol) was added an EtOH (15 mL) solution of **b** (0.78 g, 2.32 mmol). The mixture was heated at reflux for 3 h at which point a yellow-green precipitate was collected by suction filtration and washed with cold EtOH (3 × 5 mL) and $CHCl_3$ (3 × 10 mL). The pale yellow solid was then dried to afford complex **2b** (0.52 g, 64%); mp 318–320 °C (decomposition). IR (Nujol, cm^{-1}) ν: 1610 (C=N). Anal. calcd. for $C_{28}H_{18}N_2Br_2CuO_8 \cdot 1.5CHCl_3$ (%): C 38.80, H 2.16, N 3.07; found: C 38.90, H 2.03, N 2.79.

Compound 3a

To an EtOH (50 mL) solution of zinc(II) acetate (0.20 g, 1.09 mmol) was added an EtOH (15 mL) solution of **a** (0.59 g, 2.29 mmol). The mixture was heated at reflux for 3 h at which point a yellow-green precipitate was collected by suction filtration and washed with cold EtOH (3 × 5 mL) and Et_2O (3 × 10 mL). The pale yellow solid was then dried to afford complex **3a** (0.60 g, 95%); mp 332–334 °C (decomposition). IR (Nujol, cm^{-1}) ν: 1608 (C=N). Spectroscopic NMR data (in DMSO-d_6): ^{1}H NMR δ: 13.36 (br s, 2H, -O*H*), 8.91 (s, 2H, C(*H*)=N), 7.79 (d, *J* = 3 Hz, 2H, Ar), 7.59 (d, *J* = 8 Hz, 2H, Ar), 7.44 (d of d, *J* = 8, 3 Hz, 2H, Ar), 7.33 (t, *J* = 8 Hz, 2H, Ar), 6.95–6.80 (ov m, 6H, Ar). ^{13}C{^{1}H} NMR δ: 173.6, 161.5, 161.1, 160.8, 139.1, 133.3, 133.0, 127.6, 123.7, 120.0, 119.6, 118.1, 117.6, 117.1. Anal. calcd. for $C_{28}H_{20}N_2O_8Zn$ (%): C 58.19, H 3.50, N 4.85; found: C 58.14, H 3.62, N 4.87.

Compound 3b

To an EtOH (50 mL) solution of zinc(II) acetate (0.20 g, 1.09 mmol) was added an EtOH (15 mL) solution of **b** (0.77 g, 2.29 mmol). The mixture was heated at reflux for 3 h at which point a yellow-green precipitate was collected by suction filtration and washed with cold EtOH (3 × 5 mL) and Et_2O (3 × 10 mL). The pale yellow solid was then dried to afford complex **3b** (0.64 g, 80%); mp 298–300 °C (decomposition). IR (Nujol, cm^{-1}) ν: 1601 (C=N). Spectroscopic NMR data (in DMSO-d_6): ^{1}H NMR δ: 13.33 (br s, 2H, -O*H*), 8.92 (s, 2H, C(*H*)=N), 7.81 (br m, 4H, Ar), 7.51–7.44 (ov m, 4H, Ar), 6.91–6.84 (ov m, 4H, Ar). ^{13}C{^{1}H} NMR δ: 173.1, 162.0, 159.9, 159.7, 138.4, 135.5, 134.5, 127.8, 123.6, 122.0, 119.6, 118.1, 118.0, 110.4. Anal. calcd. for $C_{28}H_{18}Br_2N_2O_8Zn$ (%): C 45.71, H 2.47, N 3.81; found: C 46.16, H 2.47, N 3.57.

X-ray crystallography

Crystals of **a** and **4** were grown from saturated EtOH and DMSO solutions, respectively, at 20 °C. Single crystals were coated with Paratone-N oil, mounted using a glass fibre, and frozen in the cold stream of the goniometer. A hemisphere of data was collected on a Bruker AXS P4/SMART 1000 diffractometer using ω and θ scans with a scan width of 0.3° and exposure times of 40 (**a**) and 30 s (**4**). The detector distances were 5 cm. The data were reduced (15) and corrected for absorption (16). The structures were solved by direct methods and refined by full-matrix least-squares on F^2 (17). All non-hydrogen atoms were refined anisotropically. Hydrogen atoms were placed in calculated positions and refined using a riding model (**a**) or located in Fourier difference maps and refined isotropically (**4**).

Antifungal testing

Compounds were tested for antifungal activity against pure cultures of *Aspergillus niger* and *Aspergillus flavus* supplied by Ward's Natural Science Ltd. (St. Catharines, Ontario). Cultures were maintained on Sabouraud dextrose agar. Six agar plugs (10 mm diameter) were cut from a 5–8 day old colony and homogenized in distilled, sterilized water (3 mL). From this suspension, 0.5 mL was transferred aseptically to a petri plate with Sabouraud dextrose agar (15 mL) and spread evenly over the entire surface. Each plate was provided with four evenly spaced paper disks (6 mm Fisherbrand P8 filter paper) containing the compound (100 μg). Each compound was applied to the disks as a solution (5 mg of compound per 1 mL of THF), where control disks were treated with neat THF (20 μL). Amphotericin B acted as a standard (100 μg) prepared in THF. Test plates with fungal homogenates were incubated at 20 °C for 48 h. Four replicate plates were used for each test. Antifungal activity was taken by the diameter of the clear zone surrounding the disk.

Results and discussion

Salicylaldimines

Schiff bases are remarkable compounds that have been utilized extensively in organic syntheses (18–24). For instance, a recent report describes a highly diastereo- and enantioselective asymmetric aldol reaction of glycinate Schiff bases with aldehydes (24). In this study, we have found that salicylaldehyde derivatives add to 5-aminosalicylic acid to give compounds having spectroscopic data consistent with the Schiff bases **a** and **b** (Scheme 1). As expected, a shift for the aldehyde proton from 10 to 9 ppm is observed in the ^{1}H NMR spectra and a resonance at ca. 160 ppm in the ^{13}C NMR spectra corresponds to the N=CH methine carbon. Likewise, formation of these compounds can be monitored

© 2005 NRC Canada

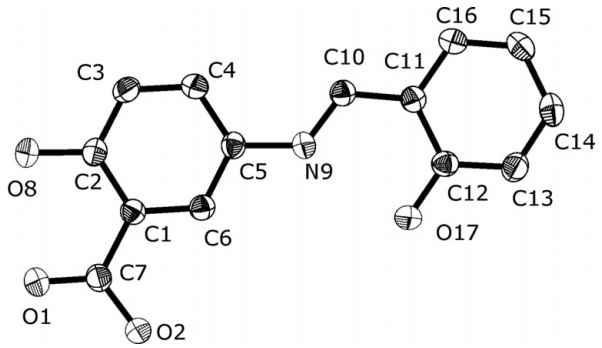
Table 1. Crystallographic data collection parameters for **a** and **4**.

Complex	**a**	**4**
Chemical formula	$C_{14}H_{11}NO_4$	$C_{16}H_{15}NO_5SZn$
Formula weight	257.26	398.72
Crystal dimensions (mm^3)	0.20 × 0.125 × 0.10	0.30 × 0.15 × 0.125
Crystal system	Monoclinic	Monoclinic
Space group	*P*2(1)/*c*	*P*2(1)/*c*
Z	4	4
a (Å)	7.016 4(7)	9.528 4(5)
b (Å)	11.008 8(11)	19.533 5(11)
c (Å)	14.898 0(15)	8.650 8(5)
β (°)	102.917(2)	90.596(1)
V ($Å^3$)	1121.63(19)	1 610.03(15)
$\rho_{calcd.}$ (Mg m^{-3})	1.517	1.645
Temperature (K)	198(1)	173(1)
Radiation	Mo Kα (λ = 0.710 73 Å)	Mo Kα (λ = 0.710 73 Å)
μ (mm^{-1})	0.113	1.681
Total reflections	7445	10 977
Total unique reflections	2484	3 617
Observed reflections ($F_o > 4\sigma(F_o)$)	2482	3 617
No. of variables	212	220
R_{int}	0.021 4	0.024 9
θ range (°)	2.32–27.48	2.09–27.48
S (GoF) on F^2	1.106	1.036
R_1 ($I > 2\sigma(I)$)[a]	0.047 9	0.031 2
wR_2 (all data)[b]	0.140 4	0.087 0
Largest diff. peak and hole (e $Å^{-3}$)	0.779 and –0.220	0.905 and –0.273

[a] $R_1 = \Sigma\|F_o| - |F_c\|/\Sigma|F_o|$.

[b] $wR_2 = (\Sigma[w(F_o^2 - F_c^2)^2]/\Sigma w[F_o^4])^{1/2}$, where $w = 1/[\sigma^2(F_o^2) + (0.0575 \cdot P)^2 + (0.2611 \cdot P)]$ (**a**) and $w = 1/[\sigma^2(F_o^2) + (0.0513 \cdot P)^2 + (0.7014 \cdot P)]$ (**4**), where $P = (\max(F_o^2, 0) + 2 \cdot F_c^2)/3$.

Fig. 2. Molecular structure of **a** with ellipsoids drawn at the 30% probability level. Hydrogen atoms omitted for clarity.



by the diagnostic C=N stretching band in the IR spectra at ca. 1620 cm^{-1} (20).

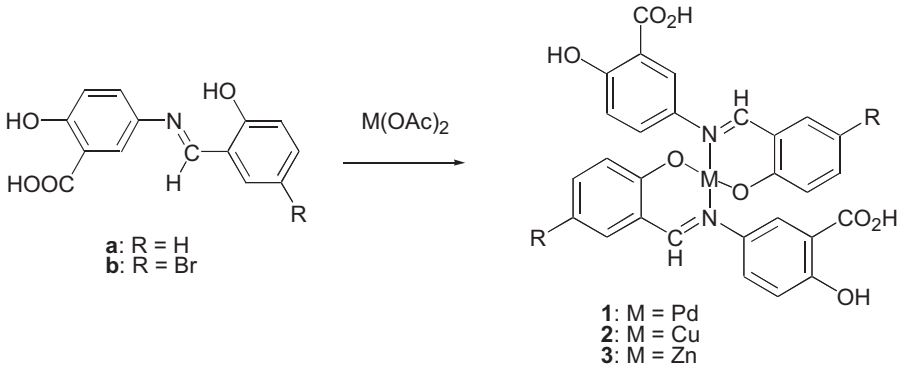
Compound **a** has also been characterized by a single crystal X-ray diffraction study, the molecular structure of which is shown in Fig. 2. Crystallographic data are provided in Table 1[3] and bond distances and angles are shown in Table 2. Structural features of **a** are similar to those reported recently for the hydroxy imide tautomer of sulfasalazine, 5-[4-[(2-pyridylideneamino)sulfonyl]phenyldiazenyl]salicylic acid (25). For instance, both molecules are almost planar as a result of extensive delocalization arising from an additional intramolecular interaction between the phenolic OH group on the 5-ASA fragment and the carboxylic acid C=O moiety (in **a**, O(8)-H(8)···O(1) = 1.622(2) Å). The imine C(10)—N(9) bond distance of 1.307(2) Å in **a** is comparable to bond lengths observed in other salicylaldimine derivatives (26). Although *N*-salicylaldimines are well-known to exist in tautomeric forms because of the intramolecular proton shift between the phenolic oxygen and the imine nitrogen (O-H···N ↔ O···H-N), no evidence for the other keto amine tautomer is present in the case of **a** (27).

Interestingly, lavendustin A, a structural derivative of compound **a**, has been reported to inhibit tyrosine kinase, an enzyme whose activity is often overexpressed in proliferative diseases (28). Compound **a** has also shown some inhibitory activity against tyrosine kinase (29). Likewise, the anti-inflammatory and antipyretic activities of Schiff bases derived from mesalazine and arylaldehydes have also been reported (30). These promising biological properties prompted

[3] Supplementary data for this article are available on the Web site or may be purchased from the Depository of Unpublished Data, Document Delivery, CISTI, National Research Council Canada, Ottawa, ON K1A 0S2, Canada. DUD 4009. For more information on obtaining material refer to http://cisti-icist.nrc-cnrc.gc.ca/irm/unpub_e.shtml. CCDC 261731 and 261732 contain the crystallographic data for this manuscript. These data can be obtained, free of charge, via www.ccdc.cam.ac.uk/conts/retrieving.html (or from the Cambridge Crystallographic Data Centre, 12 Union Road, Cambridge CB2 1EZ, UK; fax: +44 1223 336033; or deposit@ccdc.cam.ac.uk).

© 2005 NRC Canada

Scheme 2. Synthesis of metal Schiff base complexes **1**–**3**.



us to investigate the antifungal properties of late metal complexes containing these bioactive ligands.

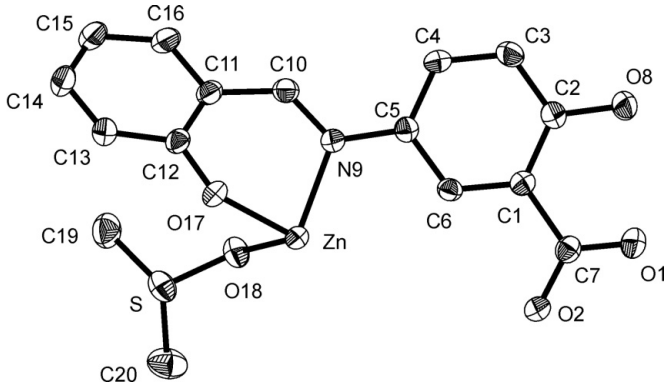
Metal complexes

Schiff bases are ubiquitous in coordination chemistry and several reviews have recently been published outlining the practical aspects and challenges associated with these complexes (31–33). As part of our investigation into designing new chelating agents from biologically active compounds, we decided to examine the synthesis, reactivity, and antifungal properties of Schiff base Pd(II), Cu(II), and Zn(II) complexes derived from 5-ASA. Related Schiff base Pd(II) complexes derived from *S*-alkyldithiocarbazates have recently shown considerable antimicrobial activity against a number of pathogenic bacteria including methicillin-resistant *Staphylococcus aureus* (MRSA) and *Bacillus subtilis* (34). Copper and zinc Schiff base complexes have also shown considerable antibacterial and antifungal activity (35, 36).

We have found that addition of **a** and **b** to $M(OAc)_2$ (M = Pd, Cu, Zn) afforded bis(salicylaldiminato)metal(II) complexes (Scheme 2, **1**–**3**) in high to excellent yields (64%–95%). Complexes **1**–**3** have been characterized by a number of physical methods. For instance, elemental analyses for paramagnetic copper complexes **2** are consistent with bis-Schiff base formulation (37). The diagnostic C=N stretching band in the FT-IR spectra has shifted from ca. 1620 cm^{-1} to ca. 1595 cm^{-1} upon coordination to the metal centre (38). Multinuclear NMR spectroscopy was also used to characterize diamagnetic palladium and zinc complexes. For instance, a significant upfield shift in the ^1H NMR spectra is observed for the imine methine proton, from ca. 9 ppm to ca. 8 ppm, upon coordination of the ligand to the d^8 metal centre in complexes **1**. Coordination to the d^{10} zinc centres resulted in only minor shifts to ca. 8.9 ppm. More notable, however, is the absence of the broad OH stretch in the FT-IR spectra when the ligands are coordinated to the metals.

Interestingly, a zwitterionic conformer of complex **3a** has been characterized by an X-ray diffraction study, the molecular structure of which is shown in Fig. 3. Crystallographic data are given in Table 1, and bond distances and angles are listed in Table 3. Attempts to grow single crystals of **3a** in DMSO resulted in the loss of one Schiff base ligand, presumably via protonation by the carboxylic acid group of the 5-ASA moiety, to give the DMSO adduct **4** shown in Fig. 3. The solvent ligand is coordinated to the hard zinc via the oxygen atom of the DMSO. The remaining coordinated Schiff

Fig. 3. The molecular structure of **4** with ellipsoids drawn at the 30% probability level. Hydrogen atoms omitted for clarity.



base ligand must be behaving as a divalent anion to balance the Zn^{2+} cation. Indeed, the carboxylic carbon–oxygen bond lengths are roughly equivalent with C(7)—O(1) (1.254(3) Å) and C(7)—O(2) (1.261(3) Å), which is consistent with a deprotonated resonance structure (39). In comparison, the analogous distances in **a** are C(7)—O(1) (1.238(2) Å) and C(7)—O(2) (1.308(2) Å), where the single C(7)—O(2) bond is clearly defined as the benzylic oxygen. In related zinc 5-ASA complexes, coordination is believed to occur through the deprotonated carboxylate group (40).

Complex **4** exists as a self-assembled polymer consisting of dimeric units where two zinc atoms are connected asymmetrically by bridging Schiff base ligands via the phenolic oxygens (Fig. 4) (Zn—O(17) = 1.980(2) Å, Zn—O(17′) = 2.139(2) Å). The dimers form a 1D polymer via the carboxylic acid group (Zn—O(2) = 1.960(2) Å), and the distorted square pyramidal environment of Zn is completed by coordination of a DMSO molecule (Zn—O(18) = 2.130(2) Å) and the imine nitrogen (Zn—N(9) = 2.048(2) Å), the latter occupying the axial position.

Although zwitterionic zinc complexes are relatively well-known (41–48), Schiff base analogues are much less common. For instance, Zn(II) complexes of the type $ZnX_2(H_2salen)$ (X = Cl, Br, I, NO_3, SO_4) containing *N*,*N*′-ethylenebis(salicylideneimine) ligands have been reported previously (49). However, in these complexes the Schiff base ligand is bound to the metal centre through the negatively charged phenolic oxygens and not the nitrogen atoms. Related copper complexes containing only one tridentate Schiff base ligand have also been reported (50, 51). Complex **4** is

© 2005 NRC Canada

Table 2. Bond lengths (Å) and angles (°) for **a**.

Bond lengths (Å)	
C(1)—C(6)	1.388(2)
C(1)—C(2)	1.408(2)
C(1)—C(7)	1.477(2)
C(2)—O(8)	1.351(2)
C(2)—C(3)	1.391(3)
C(3)—C(4)	1.373(3)
C(4)—C(5)	1.400(2)
C(5)—C(6)	1.388(2)
C(5)—N(9)	1.417(2)
C(7)—O(1)	1.238(2)
C(7)—O(2)	1.308(2)
N(9)—C(10)	1.307(2)
C(10)—C(11)	1.414(2)
C(11)—C(16)	1.412(2)
C(11)—C(12)	1.430(2)
C(12)—O(17)	1.310(2)
C(12)—C(13)	1.404(3)
C(13)—C(14)	1.372(3)
C(14)—C(15)	1.396(3)
C(15)—C(16)	1.363(3)
Bond angles (°)	
C(6)-C(1)-C(2)	119.19(16)
C(6)-C(1)-C(7)	121.21(15)
C(2)-C(1)-C(7)	119.58(16)
O(8)-C(2)-C(3)	117.92(16)
O(8)-C(2)-C(1)	122.10(16)
C(3)-C(2)-C(1)	119.98(16)
C(4)-C(3)-C(2)	120.26(17)
C(2)-C(3)-H(3)	123.2(11)
C(3)-C(4)-C(5)	120.33(17)
C(6)-C(5)-C(4)	119.64(16)
C(6)-C(5)-N(9)	117.10(15)
C(4)-C(5)-N(9)	123.25(15)
C(5)-C(6)-C(1)	120.58(16)
O(1)-C(7)-O(2)	122.87(16)
O(1)-C(7)-C(1)	121.51(16)
O(2)-C(7)-C(1)	115.60(15)
C(10)-N(9)-C(5)	127.25(15)
N(9)-C(10)-C(11)	122.31(16)
C(16)-C(11)-C(10)	120.27(16)
C(16)-C(11)-C(12)	119.12(17)
C(10)-C(11)-C(12)	120.60(16)
O(17)-C(12)-C(13)	122.42(16)
O(17)-C(12)-C(11)	119.24(16)
C(13)-C(12)-C(11)	118.34(16)
C(14)-C(13)-C(12)	120.54(18)
C(13)-C(14)-C(15)	121.36(19)
C(16)-C(15)-C(14)	119.61(18)
C(15)-C(16)-C(11)	121.02(18)

unique, however, in that it contains only one zwitterionic bidentate Schiff base ligand where the third coordination site is occupied by a solvent molecule.

Antifungal activity

As mentioned previously, the ability of metal Schiff base complexes to inhibit fungal growth is well-documented (34–

Table 3. Selected bond lengths (Å) and angles (°) for **4**.

Bond lengths (Å)	
Zn—O(2)^a	1.9598(16)
Zn—O(17)	1.9796(15)
Zn—N(9)	2.0476(18)
Zn—O(18)	2.1296(17)
Zn—O(17)^b	2.1387(16)
Zn—Zn^b	3.1381(5)
C(2)—O(8)	1.352(3)
C(5)—N(9)	1.427(3)
C(7)—O(1)	1.254(3)
C(7)—O(2)	1.261(3)
O(2)—Zn^a	1.9597(16)
N(9)—C(10)	1.295(3)
C(12)—O(17)	1.341(3)
O(17)—Zn^b	2.1387(16)
O(18)—S	1.5149(17)
S—C(20)	1.785(3)
S—C(19)	1.786(3)
Bond angles (°)	
O(2)^a-Zn-O(17)	145.61(7)
O(2)^a-Zn-N(9)	121.03(7)
O(17)-Zn-N(9)	93.03(7)
O(2)^a-Zn-O(18)	91.32(7)
O(17)-Zn-O(18)	93.35(6)
N(9)-Zn-O(18)	90.18(7)
O(2)^a-Zn-O(17)^b	89.02(7)
O(17)-Zn-O(17)^b	80.79(7)
N(9)-Zn-O(17)^b	98.26(7)
O(18)-Zn-O(17)^b	169.93(6)
O(2)^a-Zn-Zn^b	120.59(5)
O(17)-Zn-Zn^b	42.28(5)
N(9)-Zn-Zn^b	97.54(5)
O(18)-Zn-Zn^b	135.07(4)
O(17)^b-Zn-Zn^b	38.51(4)
C(6)-C(5)-N(9)	117.79(19)
C(4)-C(5)-N(9)	123.54(19)
C(7)-O(2)-Zn^a	118.25(14)
C(10)-N(9)-C(5)	120.35(19)
C(10)-N(9)-Zn	117.84(15)
C(5)-N(9)-Zn	121.61(14)
N(9)-C(10)-C(11)	126.8(2)
N(9)-C(10)-H(10)	116.6
O(17)-C(12)-C(13)	119.2(2)
O(17)-C(12)-C(11)	122.94(19)
C(12)-O(17)-Zn	118.62(13)
C(12)-O(17)-Zn^b	125.57(14)
Zn-O(17)-Zn^b	99.21(6)
S-O(18)-Zn	119.87(10)
O(18)-S-C(20)	105.27(13)
O(18)-S-C(19)	104.83(12)
C(20)-S-C(19)	98.85(14)

[a]Symmetry transformations used to generate equivalent atoms: –x, –y + 1, –z + 1.
[b]Symmetry transformations used to generate equivalent atoms: –x, –y + 1, –z.

© 2005 NRC Canada

Fig. 4. View of compound **4**, showing the polymeric nature. Thermal ellipsoids are at the 50% probability level. Hydrogen atoms and DMSO molecules have been omitted for clarity.

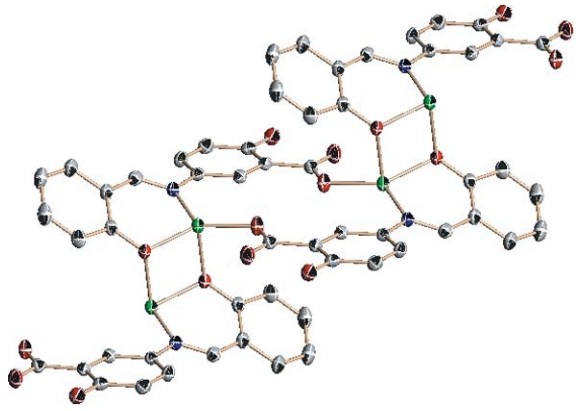


Table 4. Antifungal testing in THF at a dose of 100 μg/disk.

	Diameter of clear zone (mm)	
Compound	*Aspergillus niger*	*Aspergillus flavus*
1a	0	3
1b	3	5
2a	2	3
2b	7	8
3a	3	2
3b	6	11
Amphotericin B	18	12

36). As a result, we have carried out initial antifungal studies on all new metal 5-ASA complexes described above (52). Unfortunately, only compounds **2b** and **3b** showed any appreciable activity against both *A. niger* and *A. flavus* (Table 4). It is interesting to note that the brominated derivatives showed slightly increased activities as compared to the parent Schiff base complexes and that copper and zinc complexes were more active than the analogous palladium complexes. Further work is needed, however, to fully understand the structural activity relationships in these complexes in an effort to design a more powerful antifungal agent.

Conclusion

We have prepared salicylaldimine compounds from 5-ASA and examined their ability to chelate to metals. Pd(II), Cu(II), and Zn(II) bis(*N*-arylsalicylaldiminato) complexes have been prepared in good to excellent yields. A novel zinc complex has been structurally characterized as a mono Schiff base DMSO adduct that forms a self-assembled polymer unit. The brominated complexes all showed moderate antifungal activity against both *A. niger* and *A. flavus*.

Acknowledgments

Thanks are gratefully extended to the American Chemical Society – Petroleum Research Fund (Grant No. 37824-B1), Canada Research Chairs Programme, Canadian Foundation for Innovation – Atlantic Innovation Fund, New Brunswick Innovation Foundation (SLW), Natural Sciences and Engineering Research Council of Canada (NSERC), and Mount Allison University for financial support. We also thank Dan Durant and Roger Smith for their expert technical assistance and anonymous reviewers for helpful comments.

References

1. R.P. MacDermott. Am. J. Gastroenterol. **95**, 3343 (2000).
2. R. Wiwattanapatapee, L. Lomlin, and K. Saramunee. J. Control. Release, **88**, 1 (2003).
3. Q.X. Cai, K.J. Zhu, D. Chen, and L.P. Gao. Eur. J. Pharm. Biopharm. **55**, 203 (2003).
4. M.A. Bailey, M.J. Ingram, and D.P. Naughton. Biochem. Biophys. Res. Commun. **317**, 1155 (2004).
5. N. Zerrouk, J.M. Ginès Dorado, P. Arnaud, and C. Chemtob. Int. J. Pharm. **171**, 19 (1998).
6. Y.J. Jung, J.S. Lee, and Y.M. Kim. J. Pharm. Sci. **89**, 594 (2000).
7. S. Davaran, J. Hanaee, and A. Khosravi. J. Control. Release, **58**, 279 (1999).
8. E. Carceller, J. Salas, M. Merlos, M. Giral, R. Ferrando, I. Escamilla, J. Ramis, J. García-Rafanell, and J. Forn. J. Med. Chem. **44**, 3001 (2001).
9. A. Garjani, S. Davaran, M. Rashidi, and N. Maleki. DARU, **12**, 24 (2004).
10. B. Nigović, Z. Mandić, B. Šimunić, and I. Fistrić. J. Pharm. Biomed. Anal. **26**, 987 (2001).
11. M.K. Chourasia and S.K. Jain. J. Pharm. Pharmaceut. Sci. **6**, 33 (2003).
12. T.J. Anastasiou and K.E. Uhrich. J. Polym. Sci. Part A, **41**, 3667 (2003).
13. Y.J. Kimj, J.S. Lee, and Y.M. Kim. J. Pharm. Sci. **90**, 1767 (2001).
14. G. Jarnerot. Drugs, **37**, 73 (1989).
15. Bruker AXS, Inc. SAINT 6.02 [computer program]. Bruker AXS, Inc., Madison, Wis. 1997–1999.
16. G.M. Sheldrick. SADABS [computer program]. Bruker AXS, Inc., Madison, Wis. 1999.
17. G.M. Sheldrick. SHELXTL. Version 5.1 [computer program]. Bruker AXS, Inc., Madison, Wis. 1997.
18. H.E. Sailes, J.P. Watts, and A. Whiting. Tetrahedron Lett. **41**, 2457 (2000).
19. F. Firooznia, C. Gude, K. Chan, N. Marcopulos, and Y. Satoh. Tetrahedron Lett. **40**, 213 (1999).
20. H. Höpfl, M. Sánchez, N. Farfán, and V. Barba. Can. J. Chem. **76**, 1352 (1998).
21. M.P. Hughes and B.D. Smith. J. Org. Chem. **62**, 4492 (1997).
22. M.P. Groziak, A.D. Ganguly, and P.D. Robinson. J. Am. Chem. Soc. **116**, 7597 (1994).
23. I.B. Sivaev, A.B. Bruskin, V.V. Nesterov, M. Yu. Antipin, V.I. Bregadze, and S. Sjöberg. Inorg. Chem. **38**, 5887 (1999).
24. T. Ooi, M. Kameda, M. Tanigushi, and K. Maruoka. J. Am. Chem. Soc. **126**, 9685 (2004).
25. A.J. Blake, X. Lin, M. Schröder, C. Wilson, and R.-X. Yuan. Acta Crystallogr. Sect. C, **C60**, o226 (2004).
26. M. Sánchez, O. Sánchez, H. Höpfl, M.-E. Ochoa, D. Castillo, N. Farfán, and S. Rojas-Lima. J. Organomet. Chem. **689**, 811 (2004).
27. A. Star, I. Goldberg, and B. Fuchs. J. Organomet. Chem. **630**, 67 (2001).
28. T. Onoda, H. Iinuma, Y. Sasaki, M. Hamada, K. Isshiki, H. Naganawa, T. Takeuchi, K. Tatsuta, and K. Umezawa. J. Nat. Prod. **52**, 1252 (1989).

© 2005 NRC Canada

29. H. Chen, J. Boiziau, F. Parker, R. Maroun, B. Tocque, B.P. Roques, and C. Garbay-Jaureguiberry. J. Med. Chem. **36**, 4094 (1993).
30. P. Jayasekhar, S.B. Rao, and G. Santhakumari. Indian J. Pharm. Sci. **59**, 8 (1997).
31. C.-M. Che and J.-S. Huang. Coord. Chem. Rev. **242**, 97 (2003).
32. P.A. Vigato and S. Tamburini. Coord. Chem. Rev. **248**, 1717 (2004).
33. P.G. Cozzi. Chem. Soc. Rev. **33**, 410 (2004).
34. M. Akbar Ali, A.H. Mirza, R.J. Butcher, M.T.H. Tarafder, T.B. Keat, and A.M. Ali. J. Inorg. Biochem. **92**, 141 (2002).
35. E. Toyota, H. Sekizaki, K. Itoh, and K. Tanizawa. Chem. Pharm. Bull. **51**, 625 (2003).
36. Z.H. Chohan, H. Pervez, A. Rauf, K.M. Khan, G.M. Maharvi, and C.T. Supuran. J. Enzyme Inhib. Med. Chem. **19**, 161 (2004).
37. R.H. Holm, G.W. Everett, Jr., and A. Chakravorty. Prog. Inorg. Chem. **7**, 83 (1966).
38. J.S. Kim and B.K. Koo. Bull. Korean Chem. Soc. **13**, 507 (1992).
39. U.P. Singh, P. Babbar, and A.K. Sharma. Inorg. Chim. Acta, **358**, 271 (2005).
40. F.-L. Cui, J. Fan, W. Li, Y.-C. Fan, and Z.-D. Hu. J. Pharm. Biomed. Anal. **34**, 189 (2004).
41. X.-M. Zhang, R.-Q. Fang, H.-S. Wu, and S.W. Ng. Acta Crystallogr. Sect. E, **E60**, m941 (2004).
42. D.A. Clemente, A. Marzotto, and F. Benetollo. Polyhedron, **21**, 2161 (2002).
43. J.-P. Costes, J.-P. Laussac, and F. Nicodème. J. Chem. Soc. Dalton Trans. 2731 (2002).
44. N. Habbadi, M. Dartiguenave, L. Lamandé, M. Sanchez, M. Simard, A.L. Beauchamp, and A. Souiri. New J. Chem. 983 (1998).
45. K. Nakano, K. Nozaki, and T. Hiyama. J. Am. Chem. Soc. **125**, 5501 (2003).
46. D.J. Darensbourg, J.R. Wildeson, and J.C. Yarbrough. Organometallics, **20**, 4413 (2001).
47. S. Das, C.-H. Hung, and S. Goswami. Inorg. Chem. **42**, 5153 (2003).
48. C.C. Kwok, S.C. Yu, I.H. Sham, and C.M. Che. Chem. Commun. 2758 (2004).
49. H.A. Tajmir-Riahi. Polyhedron, **2**, 723 (1983).
50. M. Kishita, Y. Muto, and M. Kubo. Aust. J. Chem. **11**, 309 (1958).
51. M. Kubo, Y. Kuroda, M. Kishita, and Y. Muto. Aust. J. Chem. **16**, 7 (1963).
52. F.J. Baerlocher, M.O. Baerlocher, C.L. Chaulk, R.F. Langler, and S.L. MacQuarrie. Aust. J. Chem. **53**, 399 (2000).

© 2005 NRC Canada

Triazene derivatives of (1,*x*)-diazacycloalkanes. Part IV.[1] Synthesis and characterization of 1-[2-aryl-1-diazenyl]-3-(3-[2-aryl-1-diazenyl]hexahydro-1-pyrimidinylmethyl)hexahydropyrimidines and 1-(5,5-dimethyl-3-[2-aryl-1-diazenyl]hexahydro-1-pyrimidinylmethyl)-5,5-dimethyl-3-[2-aryl-1-diazenyl]hexahydropyrimidines from the reaction of diazonium salts with mixtures of formaldehyde and 1,3-diaminopropanes

Shasta Moser, Ryan Church, M. Brad Peori, and Keith Vaughan

Abstract: Two new series of bistriazenes have been synthesized from a general reaction of diazonium salts with a mixture of a propanediamine and formaldehyde. Such reaction with 1,3-diaminopropane itself affords the 1-[2-aryl-1-diazenyl]-3-(3-[2-aryl-1-diazenyl]hexahydro-1-pyrimidinylmethyl)hexahydropyrimidines (**6**). 2,2-Dimethyl-1,3-diaminopropane reacts in an analogous manner to give the 1-(5,5-dimethyl-3-[2-aryl-1-diazenyl]hexahydro-1-pyrimidinylmethyl)-5,5-dimethyl-3-[2-aryl-1-diazenyl]hexahydropyrimidines (**7**). All new compounds have been characterized by IR and NMR spectroscopy, with elemental analysis or high resolution mass spectrometry of most of the new compounds. NMR assignments have been analyzed by a series of DEPT, COSY, and HSQC experiments. One example of each series has been unequivocally characterized by X-ray crystallography. The general conclusion of this study is that alkanediamines with three carbon atoms in the spacer link between the nitrogen atoms give rise to the linear bicyclic molecules of type **18**, in contrast to the case of ethylenediamine (spacer link has two carbon atoms), which affords cage-like molecules of type **17**.

Key words: bistriazene, hexahydropyrimidine, diazonium coupling, formaldehyde, diaminopropane, nuclear magnetic resonance.

Résumé : Deux nouvelles séries de bistriazènes ont été synthétisées par une réaction générale de sels de diazonium avec un mélange de propanediamine et de formaldéhyde. Une telle réaction avec le 1,3-diaminopropane conduit à la formation de 1-[2-aryldiazén-1-yl]-3-(3-[2-aryldiazén-1-yl]hexahydropyrimidin-1-ylméthyl)hexahydropyrimidines (**6**). Le 2,2-diméthyl-1,3-diaminopropane réagit d'une façon semblable pour conduire à la formation de 1-(5,5-diméthyl-3-[2-aryldiazén-1-yl]hexahydropyrimidin-1-ylméthyl)-5,5-diméthyl-3-[2-aryldiazén-1-yl]hexahydropyrimidines (**7**). Tous les nouveaux composés ont été caractérisés par spectroscopies IR et RMN, avec analyses élémentaires ou spectrométrie de masse à haute résolution pour la plupart des nouveaux composés. Les attributions RMN ont été analysées par une séries d'expériences DEPT, COSY et HSQC. Un exemple de chacune des séries a été caractérisé sans équivoque par diffraction des rayons X. La conclusion générale de cette étude est que les alcanediamines à trois atomes de carbones peuvent être utilisées comme lien pour créer un espace entre deux atomes d'azote avec la formation des molécules bicycliques linéaires de type **18**, par opposition aux produits résultant d'une insertion d'éthylènediamine (lien pour créer un espace de deux atomes de carbone) qui conduit à la formation de molécules en forme de cage du type **17**.

Mots clés : bistriazène, hexahydropyrimidine, couplage de diazonium, formaldéhyde, diaminopropane, résonance magnétique nucléaire.

[Traduit par la Rédaction]

Received 8 April 2005. Published on the NRC Research Press Web site at http://canjchem.nrc.ca on 15 September 2005.

S. Moser, R. Church, M.B. Peori, and K. Vaughan.[2] Department of Chemistry, Saint Marys University, Halifax, NS B3H 3C3, Canada.

[1]For part III in this series, see: Can. J. Chem. **83**, 471 (2005).
[2]Corresponding author (e-mail: keith.vaughan@smu.ca).

 doi: 10.1139/V05-131 © 2005 NRC Canada

Introduction

The term "bistriazene" has been coined to describe any molecule that contains two triazene units in the same molecule, with a link or spacer in between the triazene moieties. Recent progress in the synthesis of bistriazenes has been reviewed (1). The first encounter with bistriazenes in this laboratory was serendipitous. Reaction of a series of diazonium salts with mixtures of methylamine and formaldehyde was found to afford the novel hydroxymethyltriazenes (**1**) (2). A by-product of the synthesis of **1** was later found to be the bistriazene (**2**) (3); the bistriazene of type **2** is favoured by the presence of electron-donating groups in the aryl ring of the diazonium salt. Subsequent work found that the bistriazenes of type **3** (built around a central tetraazabicyclo[3.3.3]nonane cage) were produced from the analogous reaction of diazonium salts with ammonia–formaldehyde mixtures (4). This bridged bicyclic structure was also evident in the bistriazene products (**4**) synthesized by reaction of the diazonium salts with mixtures of ethylenediamine and formaldehyde (5). However, when the latter reaction was extended to the *trans*-1,2-diaminocyclohexane–formaldehyde–diazonium salt system, a different type of bistriazene with a linear bicyclic structure, rather than a bicyclic bridged structure, was formed. This structure is exemplified by compound **5**, which has been characterized by X-ray crystallography (6).

Thus, there seems to be a cross-over in behaviour of the alkanediamine going from ethylenediamine to cyclohexanediamine, and it is an intriguing question to see how other alkanediamines react under similar conditions. In the present study, we have explored these reactions with the next higher homologue of ethylenediamine, namely 1,3-diaminopropane, and also with 2,2-dimethyl-1,3-diaminopropane, which afford linear bicyclic molecules analogous to structure **5**. The products of these reactions are seen in structures **6** (**6a**–**6l**) and **7** (**7a**–**7l**), and they have been characterized by IR, ^{1}H and ^{13}C NMR spectroscopy, and elemental analysis or high resolution ESI mass spectrometry. One example of each series has been solved unequivocally by X-ray crystallography.

Experimental

All reagents were reagent grade materials purchased from the Aldrich Chemical Co. Ltd., and were used without further purification. Melting points were determined on a Fisher-Johns melting point apparatus and are uncorrected. IR spectra were obtained using Nujol mulls on a PerkinElmer 299 spectrophotometer or with a Bruker Vector 22 spectrometer. ^{1}H and ^{13}C NMR spectra were obtained using either the Anasazi Instruments 60 MHz EFT spectrometer at Saint Mary's University, or the Bruker 250 MHz spectrophotometer at the Atlantic Regional Magnetic Resonance Centre at Dalhousie University in Halifax, Nova Scotia. Chemical shifts were recorded in $CDCl_3$ or d_6-DMSO solutions at 20 °C, and are relative to TMS internal standard. The crystal structures were determined on a Nonius Kappa CCD diffractometer with graphite monochromated Mo Kα radiation (λ = 0.7107 Å). Elemental analyses were performed by the Canadian Microanalytical Service, Ltd., Delta, British Columbia.

Accurate mass measurements were performed at the Chemistry Department MS facility at UBC, Vancouver. ESI-MS was measured on a Water/Micromass LCT. The sample was dissolved in methanol or methanol–chloroform. The solution concentration was about 50~100 μmol/L. It was infused to LCT at a flow rate of 30 μL/min. For accurate mass measurement of $(M + H)^+$, either tetralysine KKKK or angiotensin III was used as the reference compound. The mass of $(M + H)^+$ from tetralysine was used as the lock mass.

Reaction of diazonium salts with mixtures of formaldehyde and a propanediamine

General procedure

Method A

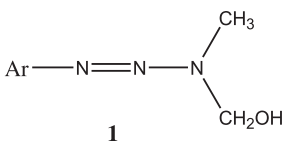
The appropriate arylamine (0.010 mol) was dissolved in 40 mL of hydrochloric acid (3 mol/L) with heating if necessary to obtain a clear solution, and then this solution was cooled in an ice–salt bath. The arylamine hydrochloride solution was diazotized at 0–5 °C with a solution of sodium nitrite (0.011 mol) in water and the resulting mixture was stirred in the cold for 0.5 h, after which any insoluble impurities were removed by vacuum filtration. The mixture was brought to pH 7 using a saturated solution of sodium bicarbonate, at which point 37% aqueous formaldehyde solution (5 mL) was added. An appropriate amount of the diaminopropane (0.010 mol) was slowly added to the solution, which was allowed to stir in the cold for a further 0.5 h. Occasionally, a slight precipitate was evident during the period of the addition, but was not removed. The mixture was then adjusted to alkaline pH with additional saturated sodium bicarbonate solution, whereupon the product precipitated out of solution. Solid precipitates were isolated by vacuum filtration and purified by recrystallization from an appropriate solvent. Oils were recovered by extraction into dichloromethane (3 × 20 mL aliquots), dried over anhydrous $MgSO_4$, and rotoevaporated under vacuum.

Method B

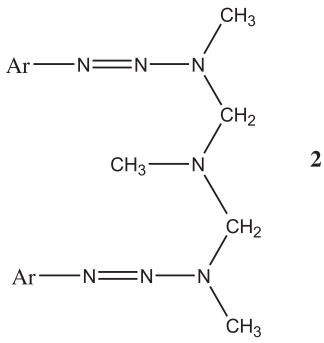
The procedure of method A was followed exactly, with the exception of the amount of formaldehyde used; a 40:1 molar ratio of formaldehyde:arylamine was used, i.e., approx 32 mL of 37% aqueous formaldehyde was added at the appropriate time.

The application of method A or B with 1,3-diaminopropane gave the following compounds of series **6**: 1-[2-(*p*-cyanophenyl)-1-diazenyl]-3-(3-[2-(*p*-cyanophenyl)-1-diazenyl]-hexahydro-1-pyrimidinylmethyl)hexahydropyrimidine (**6a**): method B, 88% yield, mp 165 to 166 °C (EtOH). IR ν_{max} (cm^{-1}): 845, 2222 (CN). Anal. calcd. for $C_{23}H_{26}N_{10}$ (%): C 62.4, H 5.9, N 31.6; found: C 62.4, H 5.6, N 31.2. 1-[2-(*p*-Nitrophenyl)-1-diazenyl]-3-(3-[2-(*p*-nitrophenyl)-1-diazenyl]hexahydro-1-pyrimidinylmethyl)hexahydropyrimidine (**6b**): method B, 87% yield, mp 170–173 °C (toluene). IR ν_{max} (cm^{-1}): 850, 1378, 1510 (NO_2). Anal. calcd. for $C_{21}H_{26}N_{10}O_4$ (%): C 52.3, H 5.4, N 29.0; found: C 52.4, H 5.4, N 28.7. 1-[2-(*p*-Methoxycarbonylphenyl)-1-diazenyl]-3-(3-[2-(*p*-methoxycarbonyl phenyl)-1-diazenyl]hexahydro-1-pyrimidinylmethyl)hexahydropyrimidine (**6c**): method A, 75% yield, method B, 55% yield, mp 95–97 °C (hexanes). IR ν_{max} (cm^{-1}): 774, 1721(C=O). HR-MS *m*/*z* calcd. for $C_{25}H_{33}N_8O_4$: 509.2625;

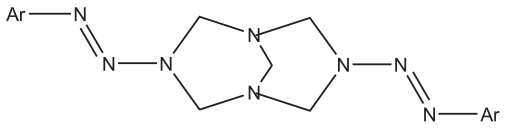
© 2005 NRC Canada



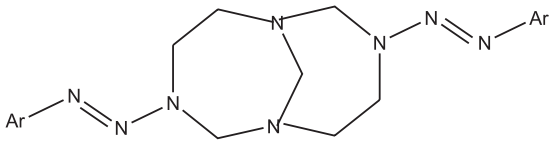
1



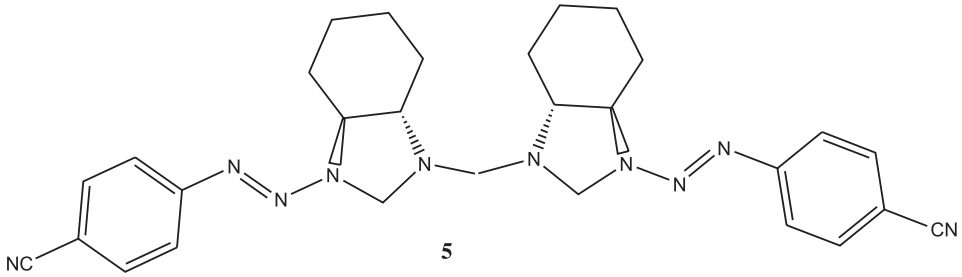
2



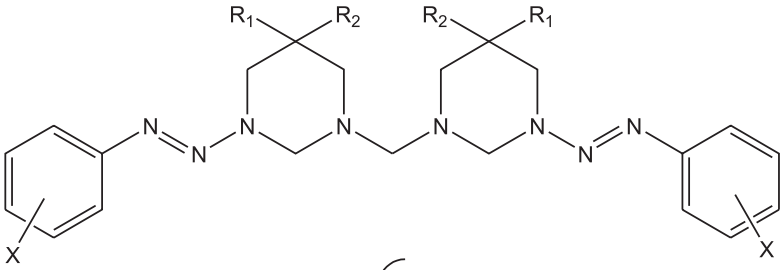
3



4



5



6 $R_1 = R_2 = H$

7 $R_1 = R_2 = Me$

a) X = *p*-CN
b) X = *p*-NO_2
c) X = *p*-CO_2Me
d) X = *p*-CO_2Et
e) X = *p*-$COCH_3$
f) X = *p*-$CONH_2$
g) X = *p*-Br
h) X = *p*-CH_3
i) X = *p*-OCH_3
j) X = H
k) X = *o*-Br
l) X = *o*-CN

© 2005 NRC Canada

Table 1. ^{1}H NMR data (ppm) in $CDCl_3$ relative to TMS for the 1-[(2-aryl-1-diazenyl]-3-(3-[2-aryl-1-diazenyl]hexahydro-1-pyrimidinylmethyl)hexahydropyrimidines (**6**).

		Aromatic	H_a,H_b	H_c,H_d	H_e,H_f	H_g,H_h	H_i,H_j	
Number	X	8H	2H	4H	4H	4H	4H	X
6a	*p*-CN	7.48 (d, *J* = 7.5 Hz), 7.59 (d, *J* = 7.5 Hz)	3.37 (s)	4.66 (s)	1.77 (br)	4.00 (t)	2.99 (t)	—
6b	*p*-NO_2	7.54 (d, *J* = 7.7 Hz), 8.22 (d, *J* = 7.6 Hz)	3.39 (s)	4.70 (s)	1.79 (br)	4.04 (t)	3.02 (t)	—
6c	*p*-CO_2Me	7.47 (d, *J* = 8.3 Hz), 8.02 (d, *J* = 8.3 Hz)	3.37 (s)	4.66 (t)	1.75 (br)	3.97 (t)	2.97 (br t)	3.90 (s)
6d	*p*-CO_2Et	7.47 (d, *J* = 8.4 Hz), 8.02 (d, *J* = 8.4 Hz)	3.365 (s)	4.65 (s)	1.75 (br)	3.97 (t, *J* = 5.5 Hz)	2.97 (t, *J* = 5.5 Hz)	1.39 (t, *J* = 7.3 Hz), 4.36 (q, *J* = 7.2 Hz)
6e	*p*-$COCH_3$	7.47 (d, *J* = 8.5 Hz), 7.92 (d, *J* = 8.8 Hz)	3.38 (s)	4.67 (s)	1.77 (br t)	4.00 (t, *J* = 5.7 Hz)	2.99 (t, *J* = 5.7 Hz)	2.59 (s)
6f	*p*-$CONH_2$	7.44 (d, *J* = 8.4 Hz), 7.93 (d, *J* = 8.4 Hz)	3.45 (s)	4.6 (br) (4.3)	1.76 (br)	3.93 (br)	2.52 (br, pent)	2.9 or 4.3
6g	*p*-Br	7.30 (d, *J* = 6.5 Hz), 7.42 (d, *J* = 6.5 Hz)	3.34 (s)	4.59 (s)	1.68–1.77 (m)	3.94 (t)	2.94 (t)	—
6h	*p*-CH_3	7.10 (d *J* = 8.7 Hz), 7.37 (d, *J* = 8.7 Hz)	3.35 (s)	4.57 (s)	1.69 (br pent)	3.87 (br t)	2.97 (br t)	2.33 (s)
6i	*p*-OCH_3	6.83 (d, *J* = 8.6 Hz), 7.42 (d, *J* = 8.7 Hz)	3.31 (s)	4.51 (s)	1.73 (br pent)	3.80 (br t)	2.87 (br t)	3.78 (s)
6j	H	7.10–7.51 (m)	3.29 (br t, *J* = 1.9 Hz)	4.55	1.64 (br pent)	3.85 (br t, *J* = 5.1 Hz)	2.86 (br t, *J* = 5.1 Hz)	—
6k	*o*-Br	6.96 (d), 7.08 (d), 7.21 (t), 7.37 (t), 7.49 (d), 7.61 (d)	3.27 (br t, *J* = 3.1 Hz)	4.56 (s)	1.67 (br)	3.91 (br t, *J* = 4.9 Hz)	2.84 (br)	—
6l	*o*-CN	7.5–8.0 (m)	3.41 (s)	4.65 (br)	1.71 (br)	4.10 (br)	3.08 (br)	—

found: 509.2624 (ESI). 1-[2-(*p*-Ethoxycarbonylphenyl)-1-diazenyl]-3-(3-[2-(*p*-ethoxycarbonylphenyl)-1-diazenyl]hexahydro-1-pyrimidinylmethyl)hexahydropyrimidine (**6d**): method B, 83% yield, *unstable solid*. IR ν_{max} (cm^{-1}): 862, 1712(C=O). 1-[2-(*p*-Acetylphenyl)-1-diazenyl]-3-(3-[2-(*p*-acetylphenyl)-1-diazenyl]hexahydro-1-pyrimidinylmethyl)hexahydropyrimidine (**6e**): method B, 69% yield, mp 108–110 °C (EtOH). IR ν_{max} (cm^{-1}): 858, 1671 (C=O). HR-MS *m*/*z* calcd. for $C_{25}H_{33}N_8O_2$: 477.2726; found: 477.2722 (ESI). 1-[2-(*p*-Carboxamidophenyl)-1-diazenyl]-3-(3-[2-(*p*-carboxamidophenyl)-1-diazenyl]hexahydro-1-pyrimidinylmethyl)hexahydropyrimidine (**6f**): method B, 64% yield, mp 153–155 °C (hexanes – ethyl acetate). IR ν_{max} (cm^{-1}): 856, 1652 (C=O). HR-MS *m*/*z* calcd. for $C_{23}H_{31}N_{10}O_2$: 479.2631; found: 479.2626. 1-[2-(*p*-Bromophenyl)-1-diazenyl]-3-(3-[2-(*p*-bromophenyl)-1-diazenyl]hexahydro-1-pyrimidinylmethyl)hexahydropyrimidine (**6g**): method B, 31% yield, mp 91 to 92 °C (EtOH). IR ν_{max} (cm^{-1}): 818. HR-MS *m*/*z* calcd. for $C_{21}H_{27}N_8$79Br_2: 549.0725; found: 549.0726 (ESI). Anal. calcd. for $C_{21}H_{26}N_8Br_2$ (%): H 4.8, N 20.3; found: H 4.6, N 19.8. 1-[2-(*p*-Tolyl)-1-diazenyl]-3-(3-[2-(*p*-tolyl)-1-diazenyl]-hexahydro-1-pyrimidinylmethyl)hexahydropyrimidine (**6h**): method B, 61% yield, mp 49–61 °C. IR ν_{max} (cm^{-1}): 823. HR-MS *m*/*z* calcd. for $C_{23}H_{33}N_8$: 421.2828; found: 421.2827 (ESI). 1-[2-(*p*-Methoxyphenyl)-1-diazenyl]-3-(3-[2-(*p*-methoxyphenyl)-1-diazenyl]hexahydro-1-pyrimidinylmethyl)hexahydropyrimidine (**6i**): method B, 21% yield, oil. IR ν_{max} (cm^{-1}): 835. 1-[2-Phenyl-1-diazenyl]-3-(3-[2-phenyl-1-diazenyl]hexahydro-1-pyrimidinylmethyl)hexahydropyrimidine (**6j**, X = H): method A, 69% yield, oil. IR ν_{max} (cm^{-1}): 771. HR-MS *m*/*z* calcd. for $C_{21}H_{29}N_8$: 393.2515; found: 393.2511 (ESI). 1-[2-(*o*-Bromophenyl)-1-diazenyl]-3-(3-[2-(*o*-bromophenyl)-1-diazenyl]hexahydro-1-pyrimidinylmethyl)hexahydropyrimidine (**6k**): method B, 87% yield, mp 45–50 °C. IR ν_{max} (cm^{-1}): 751. HR-MS *m*/*z* calcd. for $C_{21}H_{27}N_8$79Br_2: 549.0725; found: 549.0729 (ESI). 1-[2-(*o*-Cyanophenyl)-1-diazenyl]-3-(3-[2-(*o*-cyanophenyl)-1-diazenyl]hexahydro-1-pyrimidinylmethyl)hexahydropyrimidine (**6l**): method B, 26% yield, mp 78–82 °C (EtOH). IR ν_{max} (cm^{-1}): 771, 2230 (CN). HR-MS *m*/*z* calcd. for $C_{12}H_{14}N_5$: 228.1249; found 228.1244 (ESI).

^{1}H NMR spectroscopic data for compounds **6** (**6a**–**6l**) are shown in Table 1; Table 2 is a list of the ^{13}C NMR spectroscopic data for these compounds. Proton and carbon labels relevant to these tables are shown in Fig. 1.

The application of method A with 2,2-dimethyl-1,3-diaminopropane afforded the following compounds of series **7**: 1-(5,5-dimethyl-3-[2-(*p*-cyanophenyl)-1-diazenyl]hexahydro-1-pyrimidinyl-methyl)-5,5-dimethyl-3-[2-(*p*-cyanophenyl-1-diazenyl]hexahydropyrimidine (**7a**): 83% yield, mp 120–123 °C (hexanes – ethyl acetate). IR ν_{max} (cm^{-1}): 834, 852, 2222 (CN). Anal. calcd. for $C_{27}H_{34}N_{10}$ (%): C 65.1, H 6.8, N

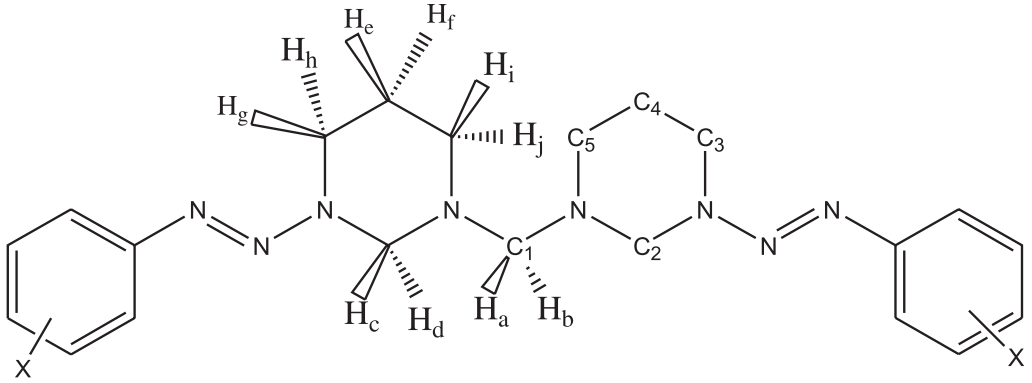
© 2005 NRC Canada

Table 2. ^{13}C NMR data in $CDCl_3$ relative to TMS for the 1-[2-aryl-1-diazenyl]-3-(3-[2-aryl-1-diazenyl]hexahydro-1-pyrimidinylmethyl)hexahydropyrimidines (**6**).

Number	X	C-1	C-2	C-3	C-4	C-5	Aromatics	X
6a	*p*-CN	67.8 (br)	71.2	44.9 (br)	22.6	50.0	119.7, 121.7, 133.5, 154.3	108.7 (CN)
6b	*p*-NO_2	70.4	(a)	44.3 (w)	21.9	49.1	120.6. 124.6, 144.7, 155.6	—
6c	*p*-CO_2Me	70.6 (68.1)	71.8 (w)	45.1 (br)	21.9	49.4	120.3, 126.9, 130.4, 154.0	166.7 (C=O), 51.7 (O-CH_3)
6d	*p*-CO_2Et	70.5 (67.8)	72.2 (w)	45.0 (br)	22.0	49.5	120.3, 127.4, 130.4, 153.9	166.2 (C=O), 60.6 (O-CH_2), 14.3 (CH_3)
6e	*p*-$COCH_3$	70.8 (67.0, br)	(a)	43.8 (br)	22.3	49.7	120.7, 129.6, 134.4, 154.3	197.3 (C=O), 26.6 (CH_3)
6g	*p*-Br	71.3 (br) (68.3, br)	73.2 (w)	45.4 (br)	22.4	50.0	119.4, 122.6, 132.2, 149.9	—
6h	*p*-CH_3	70.4 (67.6)	72.7 (w)	44.2	21.1 (20.3)	49.0	120.2, 128.7, 135.0, 147.6	21.1 (CH_3)
6i	*p*-OCH_3	68.2 (71.2)	72.5	44.8	21.7	49.6	113.9, 121.7, 144.2, 158.0	55.1 (O-CH_3)
6j	H	68.0 (70.9)	72.3 (w)	44.7	21.7	49.5	120.7, 125.9, 128.7, 150.4	—
6k	*o*-Br	70.7	71.2	45.7 (br)	22.2	49.9	119.1, 120.6, 127.3, 128.2, 133.5, 148.3	—
6l	*o*-CN	70.7 (br)	72.6	45.1 (w)	22.7 (br)	49.4 (br)	117.7, 125.7, 133.2, 152.9	107.8 (CN)

Note: not observed (a), weak signal (w), broad signal (br).

Fig. 1. Proton and carbon labels for the interpretation of the NMR spectra in Tables 1 and 2.



28.1; found: C 65.5, H 6.8, N 28.3. 1-(5,5-Dimethyl-3-[2-(*p*-nitrophenyl)-1-diazenyl]hexahydro-1-pyrimidinyl-methyl)-5,5-dimethyl-3-[2-(*p*-nitrophenyl-1-diazenyl]hexahydropyrimidine (**7b**): 29% yield, mp 130–136 °C (hexanes – ethyl acetate). IR ν_{max} (cm^{-1}): 850, 1336, 1508 (NO_2). HR-MS *m/z* calcd. for $C_{25}H_{35}N_{10}O_4$: 539.2843; found: 539.2847 (ESI). 1-(5,5-Dimethyl-3-[2-(*p*-methoxycarbonylphenyl)-1-diazenyl]-hexahydro-1-pyrimidinyl-methyl)-5,5-dimethyl-3-[2-(*p*-methoxycarbonylphenyl-1-diazenyl]-hexahydropyrimidine (**7c**): 41% yield, mp 122–124 °C (EtOH). IR ν_{max} (cm^{-1}): 856, 1711 (C=O). Anal. calcd. for $C_{29}H_{40}N_8O_4$ (%): C 61.7, H 7.1, N 19.9; found: C 61.7, H 7.06, N 19.8. 1-(5,5-Dimethyl-3-[2-(*p*-ethoxycarbonylphenyl)-1-diazenyl]hexahydro-1-pyrimidinyl-methyl)-5,5-dimethyl-3-[2-(*p*-ethoxycarbonylphenyl-1-diazenyl] hexahydropyrimidine (**7d**): 26% yield, mp 107–110 °C (ethanol – ethyl acetate). IR ν_{max} (cm^{-1}): 858, 1716(C=O). 1-(5,5-Dimethyl-3-[2-(*p*-acetylphenyl)-1-diazenyl]-hexahydro-1-pyrimidinyl-methyl)-5,5-dimethyl-3-[2-(*p*-acetylphenyl-1-diazenyl]hexahydropyrimidine (**7e**): 44% yield, mp 53–61 °C (EtOH). IR ν_{max} (cm^{-1}): 842, 1673 (C=O). 1-(5,5-Dimethyl-3-[2-(*p*-carboxamidophenyl)-1-diazenyl]hexahydro-1-pyrimidinyl-methyl)-5,5-dimethyl-3-[2-(*p*-carboxamidophenyl-1-diazenyl] hexahydropyrimidine (**7f**): 55% yield, mp 189–191 °C (EtOH – ethyl acetate). IR ν_{max} (cm^{-1}): 858, 1654 (C=O). HR-MS *m/z* calcd. for $C_{27}H_{39}N_{10}O_2$: 535.3257; found: 535.3279. 1-(5,5-Dimethyl-3-[2-(*p*-bromophenyl)-1-diazenyl]hexahydro-1-pyrimidinyl-methyl)-5,5-dimethyl-3-[2-(*p*-bromophenyl-1-diazenyl]hexahydropyrimidine (**7g**): 32% yield, mp 114–116 °C (EtOH). IR ν_{max} (cm^{-1}): 826. Anal. calcd. for $C_{25}H_{34}N_8Br_2$ (%): C 49.5, H 5.6, N 18.5, Br

© 2005 NRC Canada

Table 3. ^{1}H NMR data for the 1-(5,5-dimethyl-3-[2-aryl-1-diazenyl]hexahydro-1-pyrimidinylmethyl)-5,5-dimethyl-3-[2-aryl-1-diazenyl]hexahydropyrimidine (**7**) in $CDCl_3$.

Number	X	Aromatic	H_a,H_b	H_c,H_d	H_e,H_f	H_g,H_h	Methyls	X
7a	*p*-CN	7.48 (d, *J* = 7.5 Hz), 7.60 (d, *J* = 7.5 Hz)	3.18 (s)	4.43 (br s)	3.89 (br s)	2.51 (s)	1.02 (s)	—
7b	*p*-NO_2	6.41 (d, *J* = 8.7 Hz), 7.90 (d, *J* = 8.9 Hz)	3.20 (s)	4.45 (br s)	3.93 (br s)	2.53 (s)	1.04 (s)	—
7c	*p*-CO_2Me	7.45 (d, *J* = 7.5 Hz), 7.98 (d, *J* = 7.5 Hz)	3.16 (s)	4.45 (br s)	3.66 (br s)	2.49 (s)	1.02 (s)	3.90 (s)
7d	*p*-CO_2Et	7.45 (d, *J* = 8.6 Hz), 8.01 (d, *J* = 8.6 Hz)	3.17(s)	4.45 (br s)	3.66 (br)	2.49 (s)	1.02 (s)	1.39 (t, *J* = 7.1 Hz), 4.36 (q, *J* = 7.1 Hz)
7e	*p*-$COCH_3$	7.44 (d, *J* = 8.7 Hz), 7.88 (d, *J* = 8.3 Hz)	3.16 (s)	4.47 (s)	3.67 (s)	2.49 (s)	1.03 (s)	2.57 (s)
7f	*p*-$CONH_2$ (a)	7.42 (d, *J* = 8.5 Hz), 7.81 (d, *J* = 8.5 Hz)	3.19 (s)	4.47 (s)	3.66 (s)	2.56 (s)	0.96 (s)	—
7g	*p*-Br	7.29 (d, *J* = 8.8 Hz), 7.42 (d, *J* = 8.8 Hz)	3.13 (s)	4.40 (s)	3.60 (s)	2.46 (s)	1.00 (s)	—
7h	*p*-CH_3	7.08 (d, *J* = 8.2 Hz), 7.37 (d, *J* = 8.4 Hz)	3.13 (s)	4.30 (s)	3.57 (s)	2.45 (s)	0.99 (s)	2.33 (s)
7i	*p*-OCH_3	6.82 (d, *J* = 8.6 Hz), 7.41 (d, *J* = 9.0 Hz)	3.12 (s)	4.37 (s)	3.54 (s)	2.49 (br s)	1.00 (s)	3.80 (s)
7j	H	7.17–7.43 (m)	3.13 (s)	4.38 (s)	3.57 (s)	2.45 (s)	0.99 (s)	—
7k	*o*-Br	7.00 (t, *J* = 7.6 Hz), 7.22 (t, *J* = 7.9 Hz), 7.40 (d, *J* = 7.6 Hz), 7.56 (d, *J* = 7.9 Hz)	3.17 (s)	4.43 (br s)	3.74 (br s)	2.49 (s)	1.02 (s)	—
7l	*o*-CN	7.18 (br t), 7.66 (dt, *J* = 1.2, 7.55 Hz), 7.765 (dt, *J* = 1.2, 7.55 Hz), 7.95 (dd, *J* = 1.2, 8.1 Hz)	3.2 (br s)	4.43 (br s)	3.83 (br s)	2.50 (s)	1.02 (s)	—

Note: in d_6-DMSO (a), singlet (s), doublet (d), triplet (t), quartet (q), multiplet (m), doublet of triplets (dt), doublet of doublets (dd), broad (br).

26.3; found: C 49.5, H 5.7, N 18.3, Br 26.1. 1-(5,5-Dimethyl-3-[2-(*p*-tolyl)-1-diazenyl]hexahydro-1-pyrimidinylmethyl)-5,5-dimethyl-3-[2-(*p*-tolyl)-1-diazenyl]hexahydropyrimidine (**7h**): 65% yield, mp 39–51 °C (ethanol – ethyl acetate). IR ν_{max} (cm^{-1}): 760. HR-MS *m/z* calcd. for $C_{27}H_{41}N_8$: 477.3454; found: 477.3452 (ESI). 1-(5,5-Dimethyl-3-[2-(*p*-methoxyphenyl)-1-diazenyl]hexahydro-1-pyrimidinyl-methyl)-5,5-dimethyl-3-[2-(*p*-methoxyphenyl-1-diazenyl] hexahydropyrimidine (**7i**): 55% yield, oil. IR ν_{max} (cm^{-1}): 832. 1-(5,5-Dimethyl-3-[2-phenyl-1-diazenyl]hexahydro-1-pyrimidinyl-methyl)-5,5-dimethyl-3-[2-phenyl-1-diazenyl]hexahydropyrimidine (**7j**, X = H): 91% yield, oil. IR ν_{max} (cm^{-1}): 759. HR-MS *m/z* calcd. for $C_{25}H_{37}N_8$: 449.3141; found: 449.3145 (ESI). 1-(5,5-Dimethyl-3-[2-(*o*-bromophenyl)-1-diazenyl]-hexahydro-1-pyrimidinyl-methyl)-5,5-dimethyl-3-[2-(*o*-bromophenyl-1-diazenyl]hexahydropyrimidine (**7k**): 26% yield, mp 88–91 °C (EtOH). IR ν_{max} (cm^{-1}): 759. Anal. calcd. for $C_{25}H_{34}N_8Br_2$ (%): C 49.5, H 5.6, N 18.5, Br 26.3; found: C 49.7, H 5.6, N 18.4, Br 26.2. 1-(5,5-Dimethyl-3-[2-(*o*-cyanophenyl)-1-diazenyl]hexahydro-1-pyrimidinyl-methyl)-5,5-dimethyl-3-[2-(*o*-cyanophenyl-1-diazenyl]hexahydropyrimidine (**7l**): 22% yield, mp 171–177 °C (EtOH). IR ν_{max} (cm^{-1}): 758, 2223 (CN). HR-MS *m/z* calcd. for $C_{27}H_{35}N_{10}$: 499.3046; found 449.3040 (ESI).

^{1}H NMR spectroscopic data for compounds **7** (**7a**–**7l**) are shown in Table 3; Table 4 is a list of the ^{13}C NMR spectroscopic data for these compounds. Proton and carbon labels relevant to these tables are shown in Fig. 2.

Results and discussion

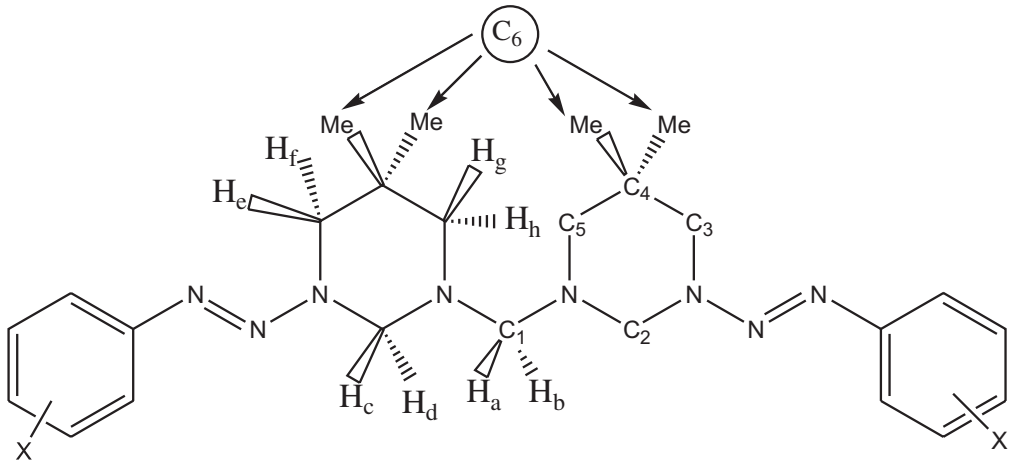
Reaction of a mixture of 1,3-diaminopropane and formaldehyde with an arene diazonium salt afforded the new bistriazene series, the 1-[2-aryl-1-diazenyl]-3-(3-[2-aryl-1-diazenyl]hexahydro-1-pyrimidinylmethyl)hexahydropyrimidines (**6a**–**6l**), in moderate to excellent yields. It should be noted at the outset that there is a wide range of stability of the compounds in this series. Some of the compounds, notably **6d** and **6i**, started to decompose within a short time of being isolated, so that characterization of these products was restricted to immediate IR and NMR spectroscopic analysis. Several of the more stable products displayed a limited shelf life when stored for a couple of years; samples that were fine powders when fresh are now glass, such as **6c** and **6e**. Others like **6b**, **6f**, and **6g** show little, if any, sign of decay. Compound **6a**, which afforded an X-ray crystallographic structure, is somewhat fickle in this regard; a crude sample that was stored for over 2 years shows signs of glassiness, whereas two purified samples of the same compound show no sign of decomposition. It is possible that the stability of

© 2005 NRC Canada

Table 4. ^{13}C NMR data for the 1-(5,5-dimethyl-3-[2-aryl-1-diazenyl]hexahydro-1-pyrimidinylmethyl)-5,5-dimethyl-3-[2-aryl-1-diazenyl]hexahydropyrimidine (**7**).

Number	X	C-1	C-2	C-3	C-4	C-5	C-6	Aromatic	X
7a	*p*-CN	70.5 (br)	72.8 (w)	52.3 (br)	31.6	61.7	24.1	118.4, 120.3, 131.9, 153.0	107.3 (CN)
7b	*p*-NO_2	70.9	73.2	53.0	32.1	62.2	24.3	120.2, 124.1, 144.4, 155.2	—
7c	*p*-CO_2Me	71.0	74.0	53.1	32.5	63.9	25.2	120.5, 127.6, 130.5, 154.1	167.2 (C=O), 51.9 (O-CH_3)
7d	*p*-CO_2Et	70.9 (w)	73.6 (w)	53.6	32.3	62.8	24.9	120.4, 127.4, 130.4, 154.0	166.0 (C=O), 60.4 (O-CH_2), 14.3 (CH_3)
7e	*p*-$COCH_3$	71.5 (br)	73.7	54.6 (br)	32.4	62.8	25.0	120.5, 129.3, 134.3, 154.1	196.5 (C=O), 26.3 (CH_3)
7f	*p*-$CONH_2$	—	—	57.3	32.3	63.4 (w)	24.9	120.5, 120.7, 128.3, 153.2	170.3 (C=O)
7g	*p*-Br	67.3 (br)	74.7	55.6	31.9	63.1	24.9	118.6, 122.0, 131.5, 149.3	—
7h	*p*-CH_3	68.0	74.2	56.3	32.1	63.0	25.3	120.6, 129.4, 135.4, 148.3	21.0 (CH_3)
7i	*p*-OCH_3	68.4	74.0	56.2	31.9	63.0	25.2	113.9, 121.7, 144.3, 158.0	55.8 (OCH_3)
7j	H	67.5 (br)	74.1 (br)	56.1	32.1	63.1	25.2	120.8, 125.9, 128.8, 150.5	—
7k	*o*-Br	71.2	74.0	53.2	32.6	63.2	25.3	118.7, 120.0, 126.7, 127.7, 133.0, 147.9	—
7l	*o*-CN	71.1 (br)	73.6 (w)	53.1	32.9	62.8	24.9	117.8, 125.5, 126.3, 133.0, 152.0, 152.8	107.8 (CN)

Fig. 2. Proton and carbon labels for the interpretation of the NMR spectra in Tables 3 and 4.

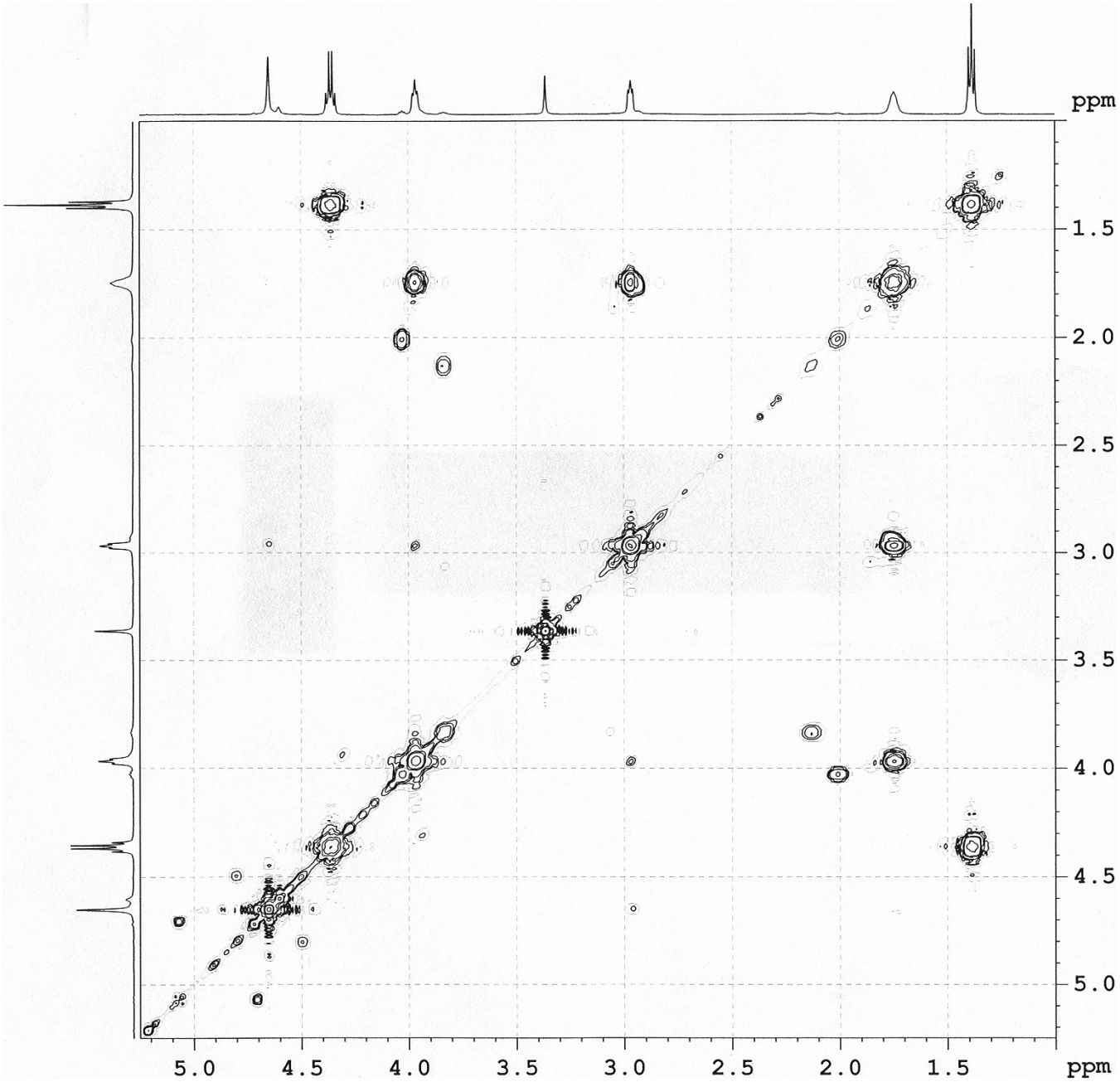


these bis(aryldiazenylhexahydropyrimidinyl)methanes is prolonged in the crystalline state compared to the amorphous state, but we have not undertaken a systematic study of this question.

In spite of these problems with handling and stability, there is no doubt that the structures of the products in series **6** are correct as described. An X-ray crystal structure of compound **6a** has been published recently (7). All compounds in series **6** have been characterized by ^{1}H NMR and, with the exception of compound **6f**, by ^{13}C NMR spectroscopy. **6f** was simply not sufficiently soluble to afford a ^{13}C spectrum. There is excellent correlation of chemical shifts throughout the series to reinforce the structural assignment. In the proton NMR spectra (Table 1), the central methylene protons (H_a and H_b), bridging the two heterocyclic rings, give rise to a singlet at ca. 3.3–3.4 ppm, with the exception of the signals in **6j** and **6k**, which appear as triplets. The small coupling constants associated with these triplets suggests that some long range coupling is responsible. A singlet methylene at ca. 4.6–4.7 ppm of twice the intensity arises from H_c and H_d attached to C-2 of the heterocyclic ring. The protons of the methylene groups H_g/H_h and H_i/H_j appear as broad triplets at ca. 4.0 and 3.0 ppm, respectively, with coupling constants around ca. 5 to 6 Hz, owing to vicinal coupling with the H_e/H_f protons of the central methylene group. The latter gives a broad signal at ca. 1.7 ppm, which is sometimes resolved into the expected pentuplet with a coupling constant of 5.5 Hz. The broadness of the signals in these spectra suggests that there is a dynamic equilibrium within the molecule, either arising from restricted rotation around the N—N bond in the triazene moieties (8) or from conformational equilibria in the heterocyclic rings. All compounds of series **6** give rise to the expected pattern of signals in the aromatic region and also show the appropriate

© 2005 NRC Canada

Fig. 3. COSY NMR spectrum of 1-[2-{*p*-ethoxycarbonylphenyl}-1-diazenyl]-3-(3-[2-{*p*-ethoxycarbonylphenyl}-1-diazenyl]hexahydro-1-pyrimidinylmethyl)hexahydropyrimidine (**6d**).



signals from the protons, if any, in the aryl substituent. The aryl substituents were also characterized by IR spectroscopic analysis.

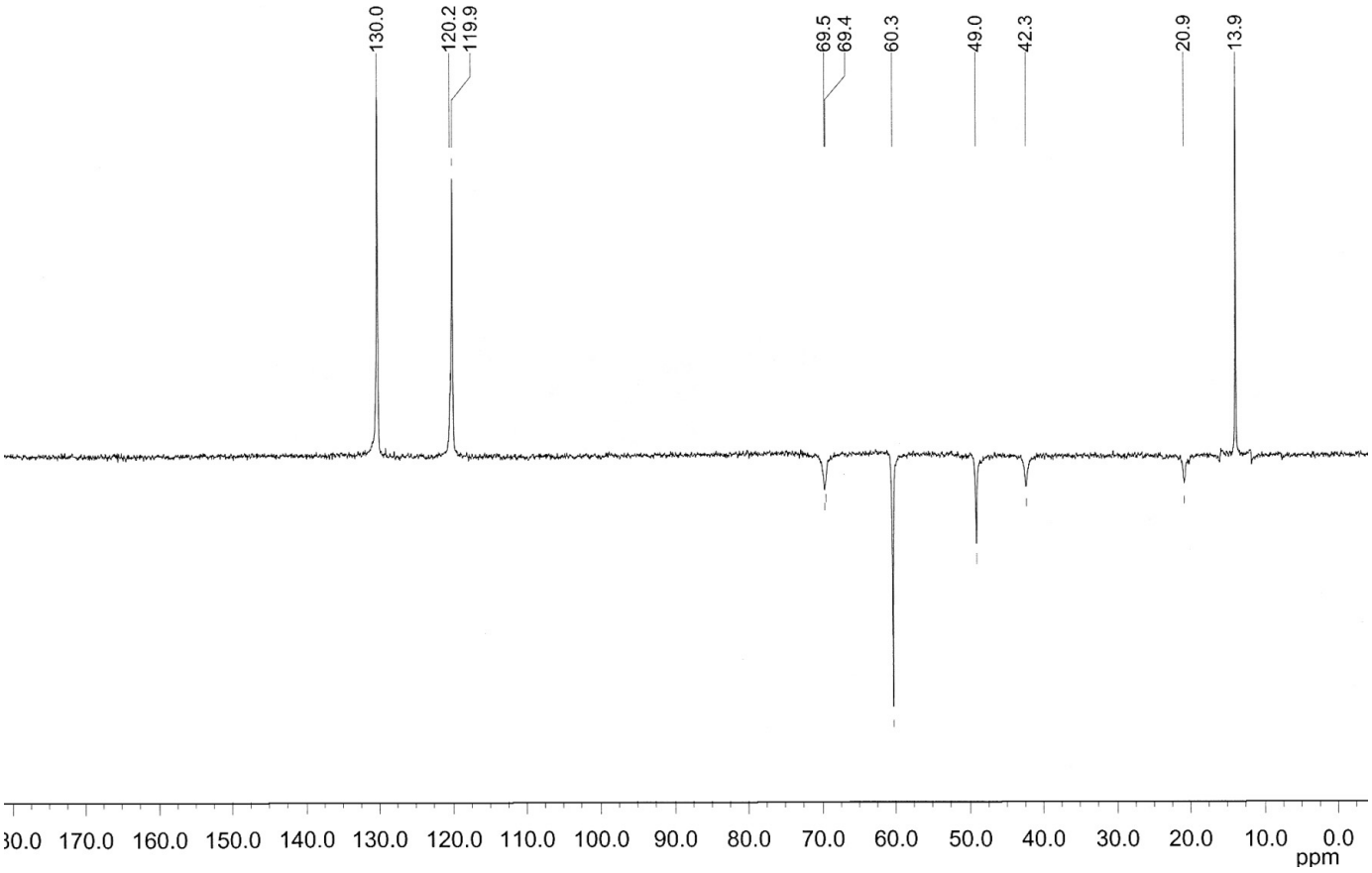
Correlation of proton NMR data and carbon NMR data was enhanced by a series of NMR experiments with the *p*-ethoxycarbonyl derivative (**6d**). Although this bistriazene was among the least stable of this series in the solid state, once it was taken up in solution in deuteriochloroform, it appeared to be reasonably stable in solution. A COSY spectrum of **6d** (Fig. 3) showed the coupling of the 1.39 and 4.36 ppm signals from the ethyl group. It also showed that the 1.75 ppm signal (assigned to H_e,H_f) is coupled both to the 2.97 ppm signal (H_i,H_j) and to the 3.97 ppm signal (H_g,H_h); there was no interaction between H_i,H_j and H_g,H_h evident in the COSY. As expected, the signals of the isolated methylene groups, H_a,H_b (3.36 ppm) and H_c,H_d (4.65 ppm) showed no interaction with other protons.

A DEPT 135 spectrum of **6d** (Fig. 4) showed first of all that the ethyl group assignments were correct with the methyl carbon at 14.3 ppm and the methylene carbon at 60.55 ppm. The DEPT spectrum also showed that the signals at 22.0, 45.0, 49.5, and 70.6 ppm arise from the methylene groups at C-4, C-3, C-5, and C-1 respectively. The signal of C-2 is not seen in the DEPT spectrum; this may be because the signal of this carbon is only barely seen in the fully decoupled ^{13}C spectrum of **6d**.

The dynamic equilibrium that causes the broadening of signals in the proton NMR spectra of **6** also caused the

© 2005 NRC Canada

Fig. 4. DEPT 135 spectrum of 1-[2-{*p*-ethoxycarbonylphenyl}-1-diazenyl]-3-(3-[2-{*p*-ethoxycarbonylphenyl}-1-diazenyl]hexahydro-1-pyrimidinylmethyl)hexahydropyrimidine (**6d**).



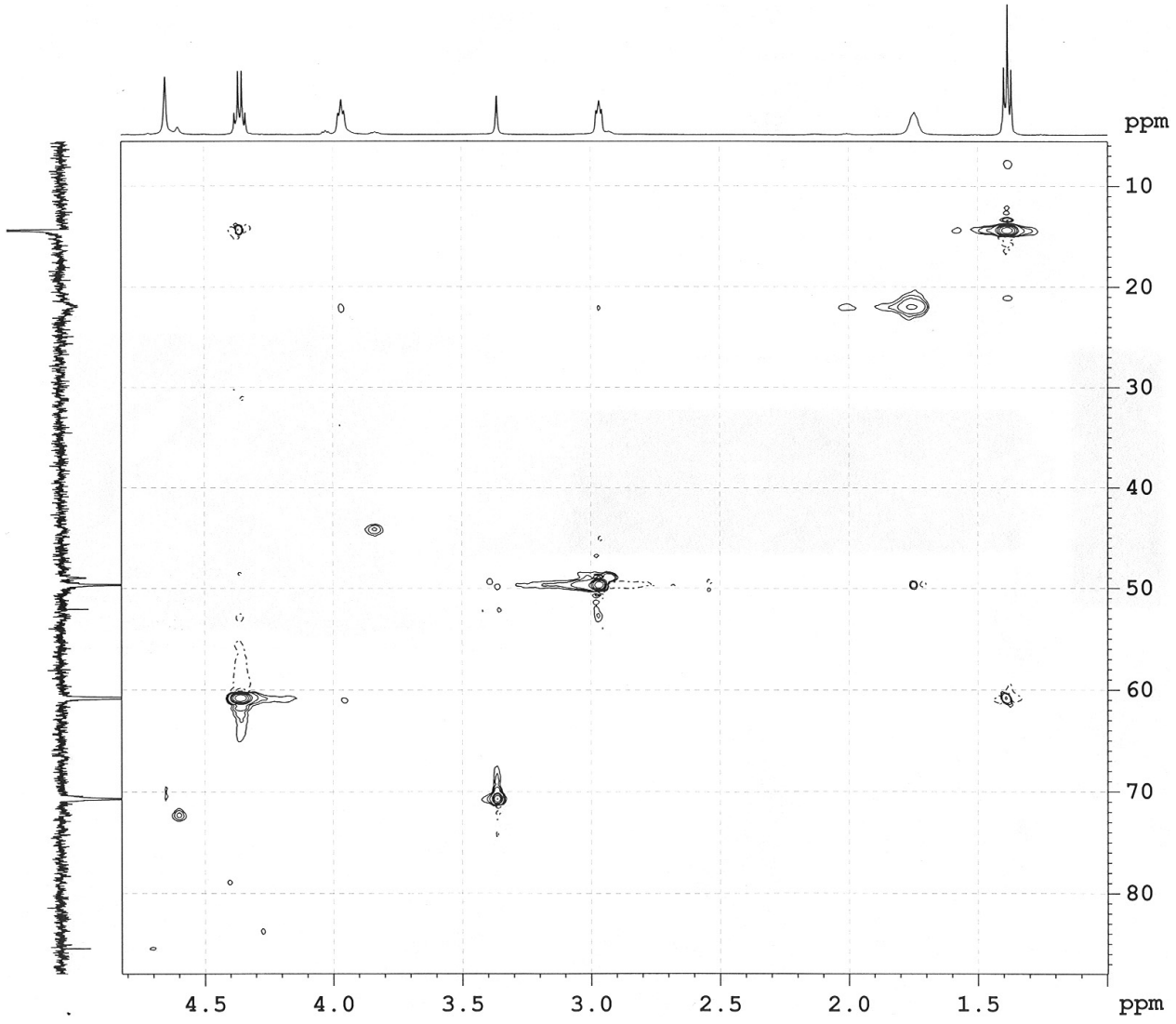
carbon-13 signals in the NMR to be significantly broadened. The assignment of the chemical shifts in the ^{13}C NMR spectra of these compounds was facilitated by the analysis of the HSQC spectrum of compound **6d** (Fig. 5), which firstly confirms the assignment of signals at 13.8 and 60.1 ppm to the ethyl group carbons in the ethoxycarbonyl substituent. The carbon signals at 21.7 (C-4), 44.6 (C-3), and 49.1 (C-5) ppm correlate with the proton signals at 1.75 (H_e,H_f), 3.97 (H_g,H_h), and 2.97 (H_i,H_j) ppm, respectively. The proton signal at 3.365 ppm, which integrates for 2H and is thereby assigned to H_a,H_b, correlates in the HSQC with the carbon signal at 70.5 ppm. The latter is therefore assigned to C-1. A weak, broad signal at 67.5 ppm in the carbon spectrum of **6d** also correlates with the proton signal at 3.365 ppm in the HSQC spectrum, suggesting that the higher field carbon signal arises from the presence of a minor isomer of **6d**. This hypothesis correlates with the general observation that the carbon signals of the compounds of series **6** are often extremely broadened because of the restricted rotation around the N—N bond in the triazene (8). The last feature of the HSQC spectrum of **6d** gives a clue to the chemical shift of the elusive carbon atom at C-2, since the proton peak at 4.65 ppm correlates with a weak carbon signal at 72.2 ppm, which is thereby assigned to C-2. Indeed, most of the compounds in series **6** do show a weak signal at ca. 72 ppm in the ^{13}C spectra.

Thus, it is possible to record and assign all of the carbon signals in these compounds (Table 2), with the exception of C-2 in compounds **6b** and **6e**. The aromatic carbon atoms give rise to the expected number of signals in the range 114–158 ppm, and the carbon atoms in the aryl substituents are all assigned. The bridging methylene carbon (C-1) is found at ca. 70 ppm, and the carbon atom at C-2 in the heterocyclic ring is universally weak in the range 71–73 ppm. The other carbons of the heterocyclic ring are found at ca. 49 to 50 ppm (C-5), ca. 44 to 45 ppm (C-3), and ca. 22 ppm (C-4). Intuitively, the lower field carbon signal at 50 ppm would be assigned to C-3 because of its proximity to the triazene moiety; however, the two-dimensional NMR spectra recorded with compound **6d** proved otherwise.

Extension of the foregoing reaction to the analogous reaction with 2,2-dimethyl-1,3-diaminopropane proved to be successful and afforded the new bistriazene series, the 1-(5,5-dimethyl-3-[2-aryl-1-diazenyl]hexahydro-1-pyrimidinylmethyl)-5,5-dimethyl-3-[2-aryl-1-diazenyl]hexahydropyrimidines (**7a**–**7l**). The compounds of series **7** displayed similar characteristics of instability as with series **6**, and the compounds of series **7** have been characterized in a parallel manner. An X-ray crystal structure of compound **7c** has been published (9), which verifies the linear bicyclic bistriazene structure for this compound and, by inference, the structures of the other compounds in this series. ^1H NMR results are listed in Table 3; the protons of the aromatic rings are as expected and the alkyl protons are all singlets. The vicinal coupling evident in series **6** is precluded by the intervention of the methyl groups attached to C-4. These methyl protons

© 2005 NRC Canada

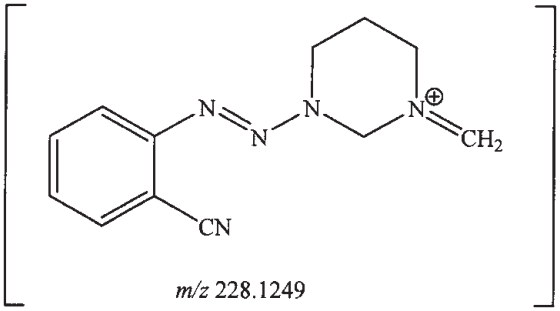
Fig. 5. HSQC spectrum of 1-[2-{*p*-ethoxycarbonylphenyl}-1-diazenyl]-3-(3-[2-{*p*-ethoxycarbonylphenyl}-1-diazenyl]hexahydro-1-pyrimidinylmethyl)hexahydropyrimidine (**6d**).



give rise to a 12 proton singlet at ca. 1 ppm. The chemical shifts of the methylene protons in compounds of series **7** are shifted a little upfield from the analogous protons in series **6**. An almost complete set of carbon-13 NMR data for the compounds of series **7** is listed in Table 4; the only signals not detected are those arising from C-1 and C-2 in compound **7f**.

The structures of the compounds in series **6** and **7** have been verified wherever possible by either elemental analysis or high resolution mass spectrometry. Only five of the 24 new compounds have *not* been analyzed in this way, owing to the stability problems described earlier. The *o*-cyano derivative (**6l**) did not show a molecular ion under EI or ESI mass spectrometry, but an accurate mass was obtained for the *m*/*z* 228 fragment shown in Fig. 6.

Fig. 6. Mass spectral fragment (*m*/*z* 228) identified in the ESI high resolution mass spectrum of compound **6l**.

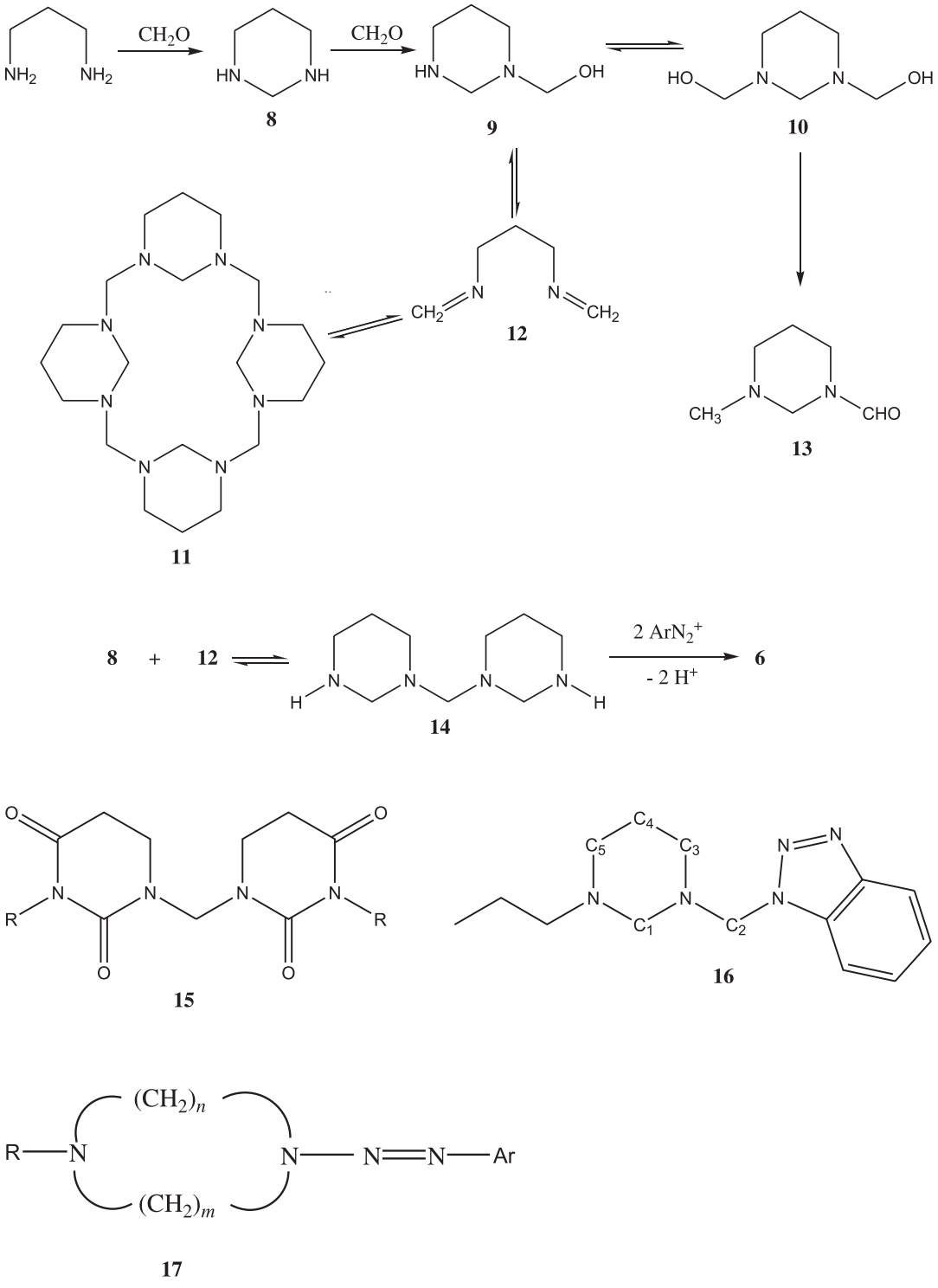


Previous studies of the propanediamine–formaldehyde reaction

An important issue regarding the synthesis of compounds of series **6** and **7** is the question of the manner of their formation. Central to this question is the previously reported work relating to the reaction of 1,3-propanediamine and formaldehyde. There is a considerable body of work on the subject of the general reaction of alkanediamines with formaldehyde, but surprisingly no one has previously investigated what happens when a diazonium salt is introduced into the mixture. Scheme 1 illustrates the structures of various

© 2005 NRC Canada

Scheme 1.



molecules that have been implicated in the reaction of 1,3-propanediamine with formaldehyde; this scheme is mainly reproduced from Dale and Sigvartsen (10). Previous work by Krassig (11) was the first to suggest that the product of the reaction of formaldehyde with propanediamine is the tetrameric compound (**11**). Later work by Evans (12) confirmed this observation, which was then reinvestigated by Bagga et al. (13), who concluded that the reaction products were more complex. However, a complete picture of the chemistry involved did not appear until the pivotal work of Dale and Sigvartsen (10), who applied NMR spectroscopy to the analysis. Surprisingly, neither the monocyclic hexahydropyrimidine (**8**) or the dimeric molecule (**14**) have been observed. The tetrameric product (**11**) is a short-term prod-

© 2005 NRC Canada

uct, whereas after long reaction times, the extremely unlikely formamide derivative (**13**) becomes the exclusive product. Krassig and Evans failed to observe this stable end product, which is formed from intermediate **10** by a novel intramolecular hydride shift (10). Because the formation of **13** requires long reaction times, it is unlikely to feature in the formation of our products **6** (or **7**). In the formation of **6**, the diamine–formaldehyde mixture is reacted immediately with the diazonium salt, so our concern is more with what happens in the early phase of the diamine formaldehyde reaction.

The simplest explanation for our observations is that the dimeric hexahydropyrimidine (**14**), formed by reaction of **8** + **12**, is trapped out by reaction with the diazonium ion to afford the bistriazene **6**. Ironically, the dimeric species (**14**) is not considered as a possible product or an intermediate by any of the previous authors. The significance of our present work could be that we have demonstrated that the dimer (**14**) must be considered as a viable intermediate in the formation of the tetramer (**11**). This observation further exemplifies the importance of diazonium coupling as a tool for trapping otherwise unstable amines from solution and identifying them. Thus, the original formation of the hydroxymethyltriazenes (**1**) (2) essentially can be interpreted as diazonium "trapping" of the unstable carbinolamine, CH_3NHCH_2OH; likewise, the formation of the bistriazene (**2**) amounts to trapping the bis(methylaminomethyl)amine, $CH_3NHCH_2N(CH_3)CH_2NHCH_3$.

Compound **11** is reported to be thermally unstable (10). The decomposition of **11** has been studied by mass spectrometry, giving evidence for formation of the bisimine (**12**) and its precursor **9**, accompanied by a much weaker (M + 1) mass from the dimeric species **14**. Although the mechanism of the decomposition of **11** is not clearly delineated, these observations do provide a clue to the observation in the present work that the bistriazenes **6** and **7** are not universally thermally stable. The instability of compounds of types **6** and **7** is also evident from attempts to record mass spectra under electron ionization conditions; no molecular ions were observed under EI, in contrast to the ESI spectra that allowed us to obtain high resolution measurement of molecular ion mass.

In searching the literature for other model compounds of hexahydropyrimidines, only a few systems were found. Habermeier and Porret (14) reported the dihydrouracil derivatives (**15**), but provided little NMR data for comparison. Katritzky et al. (15), on the other hand, reported extensive NMR data for the hexahydropyrimidine (**16**), which was obtained by reaction of benzotriazole with a mixture of *N*-propyl-1,3-propanediamine and formaldehyde in aqueous methanol. The carbon-13 assignments in **16** are 22.8 (C-4), 51.3 (C-5), 56.4 (C-3), 66.9 (C-1), and 72.8 (C-2), which agrees well with the assignments in **6** in the present work.

Conclusion

It appears now that the interaction of a diazonium salt with a mixture of formaldehyde and an alkanediamine $[NH_2(CH_2)_nNH_2]$ gives rise to two distinct types of oligomer. Bistriazenes of types **3** and **4** are examples of the bridged bicyclic bistriazene, whereas the new compounds of series **6** and **7** exemplify the linear bicyclic bistriazene. Clearly, there is a cross-over in the molecular architecture going from ethylenediamine (two-carbon spacer) to propanediamine (three-carbon spacer). This type of cross-over was also observed in the transition from ethylenediamine to cyclohexanediamine in structure **5** (6).

This paper is part IV in a series that describes the synthesis of a variety of triazenes and bistriazenes that fit the general classification of 1-aryldiazenyl-(1,*x*)-diazacycloalkanes described by the general structure **17**, where $m = 1$ or 2 and $n = 2$, 3, 4, or 5. The new compounds of series **6** and **7** fit to the general structure **17** where $m = 1$ and $n = 3$. Previously, we reported new triazenes derived from piperazine (16, 17) ($m = n = 2$) and homopiperazine (18) ($m = 2$, $n = 3$). It is worth pointing out that the hexahydropyrimidine rings in **6** and **7** represent the isomeric heterocycle to the piperazine ring system.

In future papers in this series, we will report more examples of the linear bicyclic bistriazene derived from other diamines, such as 1,4-diaminobutane, 1,3-diaminopentane, and 2-methyl-1,2-diaminopropane. Evidently, the linear bicyclic bistriazene reported here in compounds of series **6** and **7** appears to be the normal type of molecular architecture in this field of chemistry.

Acknowledgements

The authors are grateful to the Natural Sciences and Engineering Research Council of Canada (NSERC) for a Discovery Grant to the principal author (KV) and to the Faculty of Graduate Studies and Research at Saint Mary's University for a Summer Research Award (2003) to Shasta Moser. Financial support, to Ryan Church, was provided by the Student Employment Experience Program (SEEP) at Saint Mary's University. We are also grateful to the Atlantic Region Magnetic Resonance Centre at Dalhousie University for providing NMR spectra; in particular, we would like to thank Dr. Bob Berno for assistance with the interpretation of the NMR spectral data.

References

1. K. Vaughan. Org. Prep. Proced. Int. **33**, 59 (2001).
2. K. Vaughan, Y. Tang, G. Llanos, J.K. Horton, R.J. Simmonds, J.A. Hickman, and M.F.G. Stevens. J. Med. Chem. **27**, 357 (1984).
3. R.J. LaFrance, Y. Tang, K. Vaughan, and D.L. Hooper. Chem. Commun. 721 (1983).
4. R.D. Singer, K. Vaughan, and D.L. Hooper. Can. J. Chem. **64**, 1567 (1986).
5. M.B. Peori, K. Vaughan, and D.L. Hooper. J. Org. Chem. **63**, 7437 (1998).
6. J.F. Glister, K. Vaughan, and V. Bertolasi. J. Chem. Crystallogr. **34**, 175 (2004).
7. M.B. Peori, K. Vaughan, and V. Bertolasi. J. Chem. Crystallogr. **35**, 297 (2005).
8. M. Barra, S. Srivastava, and E. Brockman. J. Phys. Org. Chem. **17**, 1057 (2004).
9. S.L. Moser, V. Bertolasi, and K. Vaughan. J. Chem. Crystallogr. **35**, 307 (2005).

© 2005 NRC Canada

10. J. Dale and T. Sigvartsen. Acta Chem. Scand. **45**, 1064 (1991).
11. H. Krassig. Makromol. Chem. **17**, 77 (1955).
12. R.F. Evans. Austr. J. Chem. **20**, 1643 (1967).
13. M.M. Bagga, B. Everatt, and I.G. Hinton. J. Chem. Soc. Chem. Commun. 259 (1987).
14. J. Habermeier and D. Porret. Helv. Chim. Acta, **55**, 686 (1972).
15. A.R. Katritzky, S.K. Singh, and H.-Y. He. J. Org. Chem. **67**, 3115 (2002).
16. V.R. Little and K. Vaughan. Can. J. Chem. **82**, 1294 (2004).
17. V.R. Little, R. Tingley, and K. Vaughan. Can. J. Chem. **83**, 471 (2005).
18. S.L. Moser and K. Vaughan. Can. J. Chem. **82**, 1725 (2004).

© 2005 NRC Canada

Synthesis and preliminary bioactivity evaluation of new pregnane brassinosteroid-like compounds

Daniel G. Rivera and Francisco Coll

Abstract: Seven new pregnane compounds bearing some representative A- and B-ring brassinosteroid functions, as well as hydrogen bond donor and acceptor ones on the D ring, were efficiently synthesized. The obtained compounds did not show remarkable plant growth-promoting activity in the radish hypocotyl elongation and cotyledon expansion bioassays, however, introducing oxygen and amino functions on the D ring led to an enhancement of the bioactivity. The 16β-functionalized pregnane brassinosteroid-like compounds were slightly more active than the 16α-functionalized ones.

Key words: steroids, brassinosteroids, pregnane analogues.

Résumé : On a réalisé des synthèses efficaces de sept nouveaux dérivés du prégnane portant des fonctions représentatives des cycles A et B des brassinostéroïdes, ainsi que des fonctions pouvant donner ou accepter des liaisons hydrogènes sur le cycle D. Les composés obtenus ne présentent pas d'activité remarquable pour la promotion de la croissance dans des bioessais d'élongation de l'hypocotyle du radis et de l'expansion du cotylédon, toutefois l'introduction de fonctions oxygénées et aminées sur le cycle D conduit à une augmentation de leur bioactivité. Les composés du prégnane fonctionnalisés en 16β, de type brassinostéroïde, sont légèrement plus actifs que ceux fonctionnalisés en 16α.

Mots clés: stéroïdes, brassinostéroïdes, analogues du prégnane.

[Traduit par la Rédaction]

Introduction

Since their discovery (1), the brassinosteroids have commanded much interest in both the chemical and biological communities (2, 3) because of their extremely high plant growth-promoting activity and anti-stress effect (4). In view of their challenging steroidal structures and the presence of different stereochemical arrays of hydroxy groups, this class of plant hormones has also been the subject of elegant synthetic and biosynthetic studies (2, 3).

Nevertheless, the fascinating goal of achieving more synthetically accessible bioactive compounds continues to be a promising approach for improving the benefits of these hormones in agriculture. Thus, a highlight of this program has been the development of interesting analogues with drastic modifications either in the side chains or the ring system (3, 5–8), which has also facilitated the structure–activity relationship (SAR) studies and a thorough understanding of their mode of action (9–11).

Whereas brassinolide (**1**) is endowed with the unique feature of having a 6-oxo-7-oxa lactone function on ring B, a number of bioactive analogues bearing the 5α-hydroxyl group (e.g., **2**) have been reported and the effect of this function on the brassinosteroid-type activity is well documented (5, 12) (Fig. 1). Whilst this later function certainly does not bring out noteworthy improvements over the natural one from the biological point of view, its advantage is due to the greater synthetic accessibility starting from the readily available 5,6-epoxide derivatives (12, 13).

Additionally, despite the fact that most active natural and synthetic brassinosteroids are known to be those with campestane, ergostane, and stigmastane side chains, Kohout and co-workers have reported a set of analogues with androstane (14–16) and pregnane (17–19) side chains (e.g., **3**), some of them showing activity in the bean second internode bioassay.

Herein, we report the synthesis and a preliminary evaluation of the biological activity of seven pregnane brassinosteroid-like compounds. In connection with ongoing projects towards the development of brassinosteroid analogues, our approach was to exploit the great accessibility of the 2α,3α,5α-trihydroxy-6-oxo functionality and to introduce a variety of functions on ring D of the pregnane skeleton. The potential advantages of this approach should be realized in the further possible construction of the natural brassinosteroid side chain from 20-oxo derivatives (20), thereby achieving a striking array of structural features not found in any natural or synthetic brassinosteroid.

Results and discussion

The scope of our strategy is focused on the influence in the activity of modified D rings bearing either hydrogen

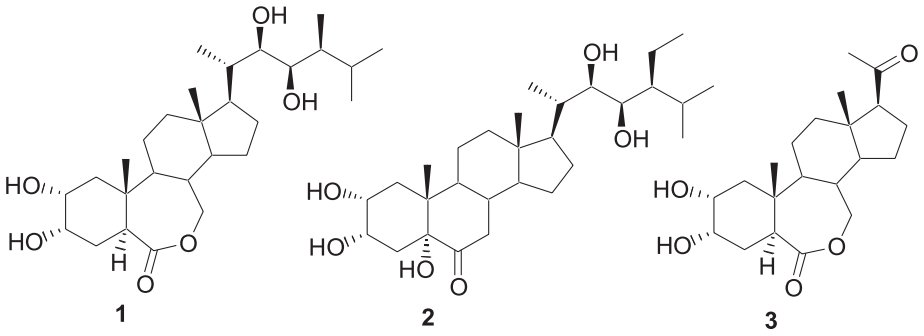
Received 23 March 2004. Published on the NRC Research Press Web site at http://canjchem.nrc.ca on 14 September 2005.

D.G. Rivera[1,2] and F. Coll. Center for Natural Products Studies, Faculty of Chemistry, University of Havana, Zapata y G, Vedado, 10400 Habana, Cuba.

[1]Present address: Institute of Plant Biochemistry, Weinberg 3, D-06120, Halle (Saale), Germany.
[2]Corresponding author (e-mail: drivera@ipb-halle.de).

 doi: 10.1139/V05-051 © 2005 NRC Canada

Fig. 1. Structures of some natural and synthetic brassinosteroids.



bond acceptors or donors. With a view toward achieving this goal, an efficient plan, which could generate A- and B-ring brassinosteroid functionalities, as well as functional and stereochemical diversity on ring D, was chosen. Moreover, encouraged by the fact that D-ring functionalized brassinosteroid analogues have not been studied, mainly because this ring is not recognized as one of the subsites of interaction in the brassinosteroid-receptor complex (11), we envisioned not only generating a set of brassinosteroid-like pregnanes, but also establishing the starting point of a more promising strategy towards D-ring functionalized brassinosteroid analogues.

Our approach for functionalizing rings A and B took advantage of the simple synthetic pathway to achieve the 5α-hydroxy-6-oxo functionality from the Δ^5 double bond via the acid-catalyzed epoxide opening (13). The attainment of the key Δ^2 double bond was accomplished by selective tosylation of the 3β-OH group and subsequent dehydrotosylation (without previous purification) to afford the precursor Δ^2-5α-hydroxy-6-oxo system. Additionally, we did not detect the formation of the 2β,3β-diol functionality by using the common osmium tetroxide – *N*-methylmorpholine *N*-oxide (NMO) procedure, which had been previously described in the osmium-catalyzed asymmetric dihydroxylation of both the Δ^2-5α-hydroxy-6-oxo and Δ^{22} systems on stigmastane analogues (12).

Scheme 1 summarizes the initial pathway to synthesize the target brassinosteroid-like compounds. Ketol **4** was obtained following a reported procedure (13) and represents the starting material of our synthetic route. The D-ring unfunctionalized analogue **7** was synthesized by a conventional procedure, which involved the reduction of the conjugated Δ^{16}-olefin by catalytic hydrogenation and the previously described method for functionalizing ring A in 46% yield from ketol **4**. The emphasized importance of this analogue is beyond its synthesis, since it is certainly necessary for SAR studies. Alternatively, the pentahydroxylated analogue **9** was obtained in good yield through the simultaneous Δ^2- and Δ^{16}-dihydroxylation processes, though several equivalents of NMO and noncatalytic amounts of OsO_4 as well as long reaction times were required because of the deactivation of the Δ^{16} double bond.

At this stage, we planned an efficient route, which avoided the use of protecting groups, and consisted of first introducing the D-ring functions and performing the Δ^2-dihydroxylation as the last step. The conjugated character of the Δ^{16} double bond allowed us to achieve this goal since precursors **10** and **11** were successfully obtained by treatment of intermediate **8** with NaOMe–MeOH and H_2O_2–NaOH–MeOH, respectively. Final dihydroxylation led to the desired analogues **12** and **13**.

As can be noted, this initial synthetic planning allowed us to only access one of the faces of ring D, since the expected stereoselectivity was achieved in the introduction of epoxy, methoxy, and hydroxy functions giving an α configuration for substituents at C-16 and C-17. Clearly, to achieve stereochemical diversity on ring D, it was critical to implement reactions that could enable us to obtain 16β-substituted pregnanes. With the 16,17-epoxide previously obtained, the oxirane ring opening was the first attempt to introduce different functionalities. However, in our hands, this system was extremely sensitive, even to mild acidic and basic conditions. Finally, this task was accomplished efficiently by performing the successful Mitsunobu reaction (21) for the epimerization of the 16α-hydroxy function, also making it possible to access nonoxygenated functions previously introduced at different sites of the steroidal moiety (22).

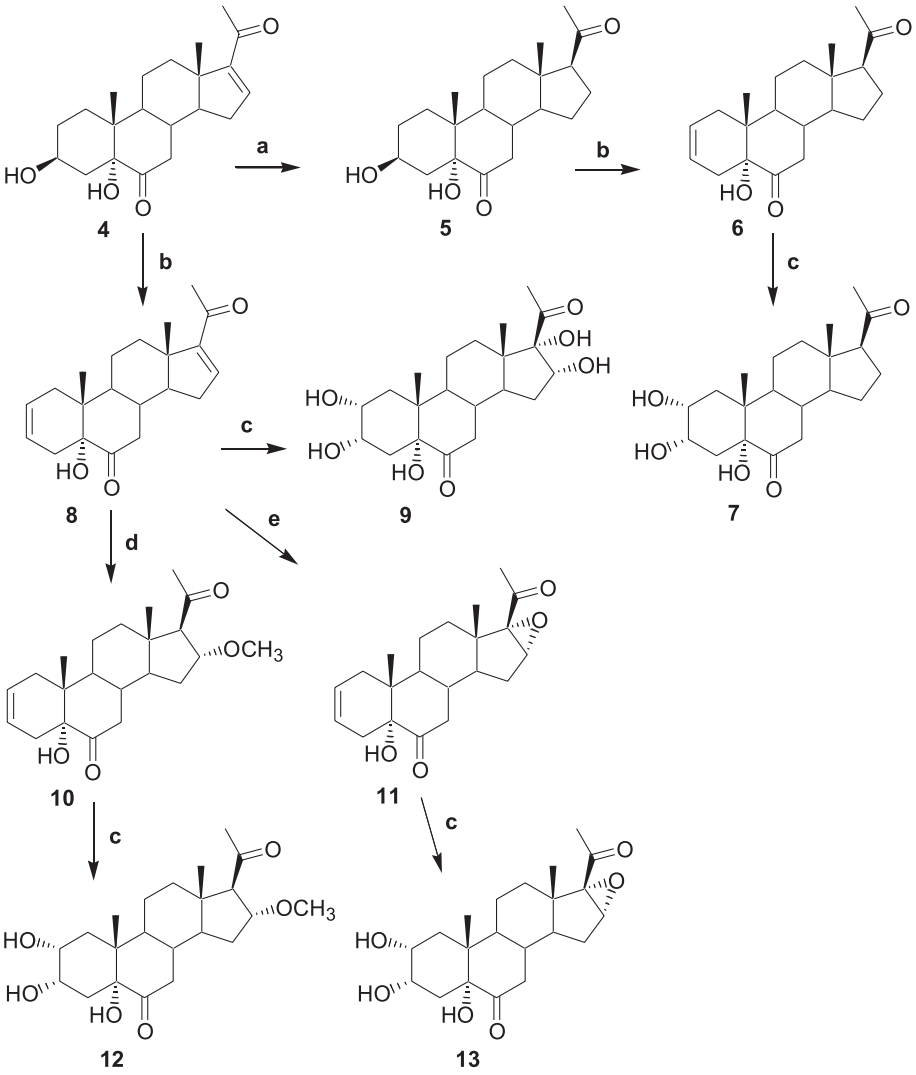
Two examples, highlighted in Scheme 2, illustrate the possibility of conveniently functionalizing the β face of ring D. Ketol **4** was initially tosylated and subsequently submitted to the Δ^{16}-dihydroxylation procedure affording the tosylate **14** in excellent overall yield. Further dehydrotosylation and selective protection of the secondary 16α-OH group with *tert*-butyldimethylsilyl (TBDMS) ether (23) gave the key intermediate **15**. The established Δ^2-dihydroxylation procedure and isopropylidene protection of the resulting diol succeeded in obtaining the acetonide **16** by using the 2,2-dimethoxypropane – pyridinium *p*-toluenesulfonate (PPTS) system without affecting the silicon protecting group (24). Selective removal of the TBDMS group (23) by using tetrabutylammonium fluoride (TBFA) gave the acetonide **17** in 33% overall yield, representing an advanced intermediate on the synthetic pathway towards the 16β-functionalized derivatives.

Epimerization of C-16 was accomplished by using the known DIAD–Ph_3P–HCO_2H system and subsequent cleavage of the 16β-formyloxy group, following a protocol already applied to a sort of equatorial hydroxyl at different sites of the steroidal moiety (5, 13, 25, 26). Final removal of the isopropylidene ketal led to the target compound **21** in 61% yield from **17**.

We were also attracted to introducing amine functions on ring D, since nitrogen-containing-brassinosteroid analogues have been previously tested and included in the currently ac-

© 2005 NRC Canada

Scheme 1. Reagents and conditions: (*a*) 10% Pd(C), MeOH; (*b*) (*i*) TsCl, Py, (*ii*) LiBr, Li_2CO_3, DMF; (*c*) OsO_4, NMO, THF–*t*-BuOH–H_2O; (*d*) NaOMe, MeOH; (*e*) NaOH, H_2O_2, MeOH, 0 °C.



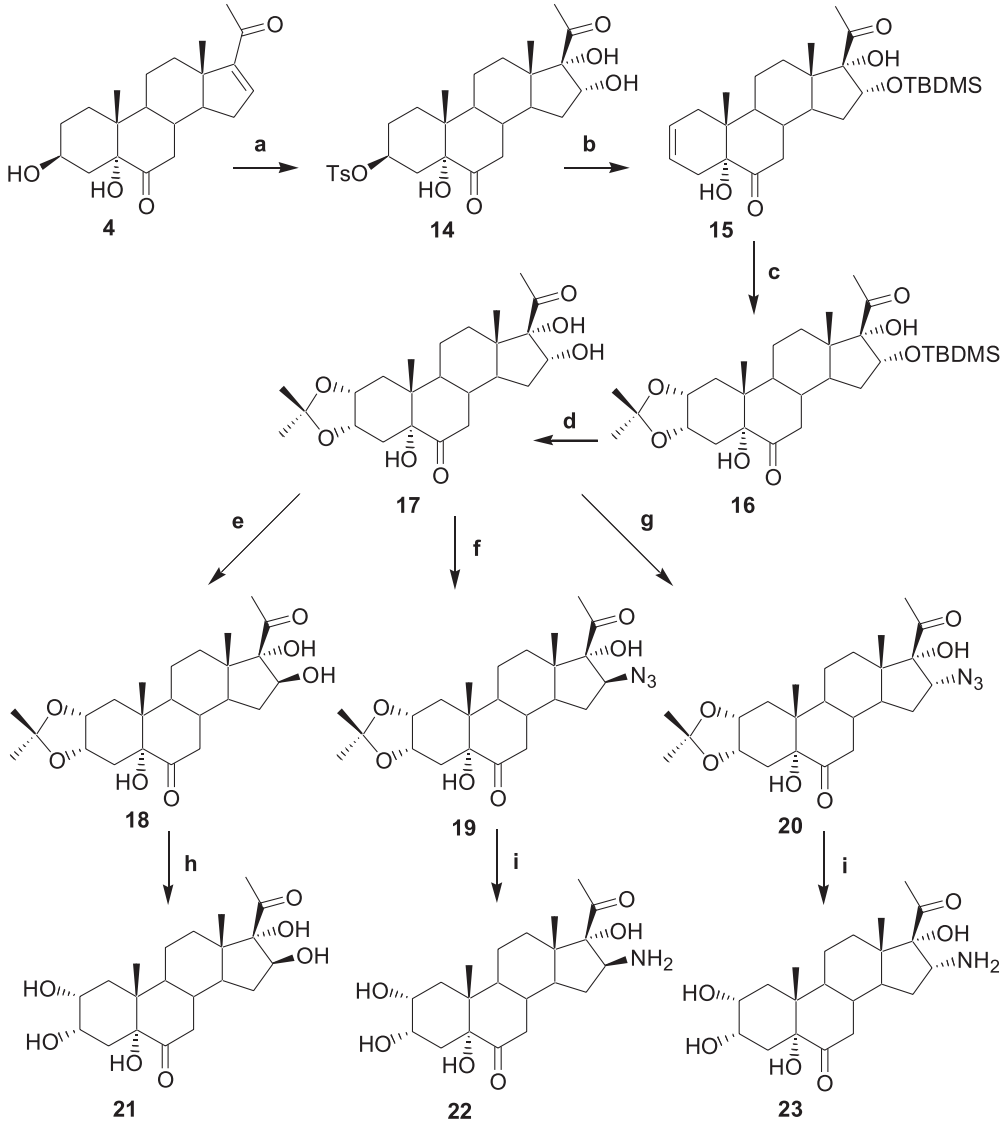
cepted SAR studies (11, 27, 28). Thus, a simple mesylation of the 16α-OH group followed by azide displacement afforded the intermediate **19**, which upon reduction of the azide group and subsequent deprotection of the 2α,3α-diol functionality led to the final 16β amino derivative **22** in 46% yield from **17**.

Evidently, synthetically challenging is the introduction of the 16α amino group from the function 16α,17α-diol of compound **17**. However, having previously established the value of the Mitsunobu reaction to access the β face of ring D, the replacement of the 16α-OH group by azide with the net retention of configuration was fulfilled by utilizing methanesulfonic acid as the acidic–nucleophilic component of the Mitsunobu reaction and consecutive azide displacement of the resulting 16β mesylate (23). The isopropylidene removal procedure used for achieving the epimer **22** similarly succeeded affording the final 16α amino derivative **23** in 36% yield from **17**. Of particular interest is the the prospect of introducing a variety of functions on ring D of pregnane brassinosteroid-like compounds. Whilst these could not be considered as brassinosteroid analogues since they lack the classical side-chain functionalities, the planning strategy used in the present work was intended to serve as the opening issue for accessing D-ring-functionalized brassinosteroid analogues. Moreover, considering that these additional D-ring functions could somehow present a high influence on the final active conformation of the hormone, the present approach might have a further outstanding impact on the present way of focussing the SAR studies.

The ^1H and ^{13}C NMR assignments of the obtained compounds were achieved by a combination of 1D and 2D experiments. The ^1H NMR features of the 2α,3α-diol functionality are usually the easiest to be assigned from the H-2 and H-3 coupling patterns even in the presence of the 5α-OH. Additionally, the stereochemistry of the functionalized carbons was unequivocally demonstrated by performing 1D NOE difference experiments, in which the enhancements on H-16, H-2, and H-3 upon irradiation of the two β-angular methyl groups CH_3-18 and CH_3-19 confirmed the α stereochemistry of the functions at these positions. The β stereochemistry of the functions at C-16 on compounds **21** and **22** was similarly demonstrated because of the lack of

© 2005 NRC Canada

Scheme 2. Reagents and conditions: (*a*) (*i*) TsCl, Py, (*ii*) OsO_4, NMO, THF–*t*-BuOH–H_2O; (*b*) (*i*) LiBr, Li_2CO_3, DMF, (*ii*) TBDMSCl, imidazole, DMF; (*c*) (*i*) OsO_4, NMO, THF–*t*-BuOH–H_2O, (*ii*) $Me_2C(OMe)_2$, PPTS, DMF; (*d*) TBFA, THF; (*e*) (*i*) HCO_2H, Ph_3P, DIAD, THF, (*ii*) $NaHCO_3$, MeOH–H_2O; (*f*) (*i*) MsCl, TEA, CH_2Cl_2, (*ii*) NaN_3, DMPU; (*g*) (*i*) $MeSO_3H$, Ph_3P, DIAD, THF, (*ii*) NaN_3, DMPU; (*h*) AcOH, MeOH–H_2O; (*i*) (*i*) H_2, PtO_2, AcOEt, (*ii*) AcOH, MeOH-H_2O. DIAD = diisopropylazodicarboxylate, DMPU = 1,3-dimethyl-3,4,5,6-tetrahydro-2(1*H*)-pyrimidonone.



enhancement on H-16 upon irradiation of CH_3-18. Interestingly, the coupling pattern of H-16 in the 16α-functionalized pregnanes showed the lack of coupling with one of the C-15 protons, suggesting a dihedral angle near 90° between H-16β and H-15α.

The growth-promoting activity was evaluated using the radish (*Raphanus sativus* L.) hypocotyl elongation and cotyledon expansion bioassays (29). Thus, the bioactivities were assessed in terms of increments of hypocotyl length or cotyledon weight with respect to the untreated control plants referred to as 100%.

As should be expected from the fact that these compounds lack the brassinosteroid functionalities in the side chain, the results of plant growth-promoting activity in the radish bioassays are far away from being considered as remarkable. However, analysis of Table 1 highlights some tendencies that might be seen as promising. Thus, all D-ring functionalized compounds were more active than the D-ring unfunctionalized pregnane **7**. Compound **22**, bearing the function 16β,17α-diol, was found to be the most active in the hypocotyl elongation bioassay.

Interestingly, the presence of hydroxy functions provoked a higher bioactivity than for epoxy and methoxy, which is in agreement with the classical behavior in bioassays reported for these functions at different sites of the steroidal moiety or the side chain. Furthermore, similar results were found in a comparison between hydroxy and amino groups at the same position, since the 16,17-dihydroxy derivatives **9** and **21** clearly were more active than the 16-amino-17-hydroxy ones (**22**, **23**). In both series of analogues, the epimerization of the function at C-16 provoked a moderate enhancement of activity either in the hypocotyl elongation or cotyledon ex-

© 2005 NRC Canada

Table 1. Results of the radish bioassays.

	Elongation of hypocotyls (%)[a]			Weight of cotyledons (%)[a]		
Compound	Conc. 0.1 ppm	Conc. 0.01 ppm	Conc. 0.001 ppm	Conc. 0.1 ppm	Conc. 0.01 ppm	Conc. 0.001 ppm
7	105±5	105±5	103±5	104±4	102±4	103±4
9	124±6	123±6	123±6	115±5	114±5	114±5
12	117±5	116±5	116±5	110±5	108±5	109±5
13	111±5	112±5	110±5	124±6	121±6	118±6
21	128±6	126±6	127±6	117±6	115±6	114±6
22	120±5	121±5	119±5	110±5	110±5	109±5
23	117±5	116±5	116±5	104±4	105±4	104±4

[a]Control experiment (untreated plants) refers to 100%.

pansion bioassays. As can be noted, the general tendency was that the tested compounds elicited higher activity in the hypocotyl elongation bioassay than in the cotyledon expansion one, with the only exception being the epoxy derivative **13**.

Conclusions

Seven new pregnane brassinosteroid-like compounds were efficiently synthesized and their plant growth-promoting activities evaluated. Either the introduction of oxygen or amino functions on ring D led to an increment in the bioactivity in the radish bioassays. Further experiments to compare the biological activity of the reported compounds with that of natural brassinosteroids are required.

Experimental

Chemistry

Melting points were determined on a Stuart Scientific apparatus and are uncorrected. IR spectra were obtained on a Nicolet 205 FT-IR spectrometer. ^{1}H NMR and ^{13}C NMR were recorded on a Bruker ACF-250 spectrometer at 250.13 and 62.9 MHz, respectively, using TMS as the internal standard. Two dimensional spectra: ^{1}H–^{1}H correlation spectroscopy (COSY), heteronuclear single-quantum coherence (HSQC), and heteronuclear multiple bond correlation (HMBC) were measured for the final compounds on a Varian INOVA-500 spectrometer operating at 499.81 MHz using the standard pulse sequences given by the manufacturer. Elemental analyses were performed with a Leco CHNS-932 instrument. Reactions were monitored by thin-layer chromatography (TLC) on precoated plates with silica gel (Merck) and spots were visualized with a 0.01 g/mL solution of vanillin in perchloric acid and subsequent heating. Flash column chromatography was performed on silica gel 60 (Merck, >230 mesh). "Usual work-up" refers to dilution with water, extraction with an organic solvent, washing the extract consecutively with 5% HCl and (or) 5% $NaHCO_3$ and brine, drying over anhydr. Na_2SO_4, and removal of the solvent under reduced pressure. The solvents were purified and dried according to recommended procedures.

3β,5-Dihydroxy-5α-pregna-6,20-dione (5)

Pd/C 10% (210 mg) was added to a solution of **4** (1.5 g, 4.3 mmol) in 80 mL of MeOH. The mixture was treated successively with hydrogen and vacuum and finally stirred under a hydrogen atmosphere for 24 h. The reaction was monitored on TLC by the absence of UV absorption. The suspended catalyst was filtered off and the resulting solution was evaporated under reduced pressure to give the ketol **5** (1.44 g, 96%); mp (MeOH) 192–195 °C. IR (KBr, cm^{-1}): 3547, 3445, 1705, 1702, 1080, 1039. ^{1}H NMR ($CDCl_3$) δ: 0.59 (s, 3H, H-18), 0.80 (s, 3H, H-19), 2.03 (s, 3H, H-21), 2.50 (t, 1H, J = 8.9 Hz, H-17α), 3.87 (br m, 1H, H-3α). ^{13}C NMR ($CDCl_3$) δ: 29.7 (C-1), 29.7 (C-2), 66.6 (C-3), 35.2 (C-4), 79.8 (C-5), 213.9 (C-6), 41.4 (C-7), 37.1 (C-8), 44.0 (C-9), 42.2 (C-10), 21.2 (C-11), 38.6 (C-12), 13.7 (C-13), 56.2 (C-14), 23.9 (C-15), 22.5 (C-16), 63.3 (C-17), 13.2 (C-18), 13.7 (C-19), 210.1 (C-20), 31.3 (C-21). Anal. calcd. for $C_{21}H_{32}O_4$: C 72.4, H 9.3; found: C 72.7, H 9.6.

5-Hydroxy-5α-pregn-2-ene-6,20-dione (6)

Tosyl chloride (1.14 g, 6 mmol) was added to a solution of ketol **5** (1.4 g, 4.0 mmol) in 50 mL of pyridine and the reaction was stirred at room temperature in the dark for 24 h. After completion as indicated by TLC, the mixture was poured into 300 mL of 10% $NaHCO_3$ and the resulting suspension was stirred for another hour and filtered under reduced pressure. The obtained tosylate was dried and dissolved in 60 mL of anhydr. DMF. Li_2CO_3 (2.2 g) and LiBr (2.5 g) were added to this solution and the resulting mixture was refluxed under a nitrogen atmosphere for 2 h, poured slowly with stirring into 300 mL of 10% HCl, and filtered under reduced pressure. The solid was washed with water, dried, and recrystallized from acetone to give the olefin **6** (1.17 g, 88%); mp (acetone) 156 to 157 °C. IR (KBr, cm^{-1}): 3550, 3020, 1705, 1702, 1086, 1048. ^{1}H NMR ($CDCl_3$) δ: 0.56 (s, 3H, H-18), 0.66 (s, 3H, H-19), 1.97 (dd, 1H, J = 12.8, 4.2 Hz, H-7β), 2.04 (s, 3H, H-21), 2.50 (t, 1H, J = 8.9 Hz, H-17α), 2.75 (t, 1H, J = 12.6 Hz, H-7α), 5.60 (m, 2H, H-3 + H-2). ^{13}C NMR ($CDCl_3$) δ: 30.0 (C-1), 125.2 (C-2), 122.4 (C-3), 34.5 (C-4), 77.7 (C-5), 211.0 (C-6), 42.2 (C-7), 36.7 (C-8), 44.9 (C-9), 42.2 (C-10), 20.7 (C-11), 38.6 (C-12), 43.7 (C-13), 56.2 (C-14), 23.9 (C-15), 22.5 (C-16), 63.3 (C-17), 13.2 (C-18), 13.7 (C-19), 210.1 (C-20), 31.3 (C-21). Anal. calcd. for $C_{21}H_{30}O_3$: C 76.3, H 9.15; found: C 76.5, H 9.1.

© 2005 NRC Canada

2α,3α,5-Trihydroxy-5α-pregnane-6,20-dione (7)

General dihydroxylation procedure

NMO (1.05 g, 9.0 mmol) and a solution of OsO_4 in *t*-BuOH (9 mL, 12.5 mg/mL) were added to a solution of **6** (1.0 g, 3.0 mmol) in 60 mL of the solvent mixture THF–*t*-BuOH–H_2O (10:10:1). The reaction was stirred under a nitrogen atmosphere at room temperature for 16 h and then treated with 50 mL of a saturated solution of Na_2SO_3. The mixture was stirred for an additional hour and concentrated to half volume. The usual work-up (AcOEt) yielded a product that was purified by flash column chromatography ($CHCl_3$–MeOH, 10:1) to give the triol **7** (884 mg, 81%); mp (heptane–acetone) 205 to 206 °C. IR (KBr, cm^{-1}): 3477, 3420, 3335, 1715, 1697, 1121, 1080, 1034. ^1H NMR ($CDCl_3$) δ: 0.56 (s, 3H, H-18), 0.73 (s, 3H, H-19), 1.97 (dd, 1H, *J* = 12.9, 4.6 Hz, H-7β), 2.04 (s, 3H, H-21), 2.50 (t, 1H, *J* = 8.9 Hz, H-17α), 2.69 (t, 1H, *J* = 12.5 Hz, H-7α), 3.78–3.84 (br m, 1H, H-2β), 4.12 (m, 1H, H-3β). ^{13}C NMR ($CDCl_3$) δ: 30.1 (C-1), 67.4 (C-2), 69.5 (C-3), 34.1 (C-4), 79.3 (C-5), 211.0 (C-6), 41.2 (C-7), 36.9 (C-8), 44.2 (C-9), 45.2 (C-10), 21.0 (C-11), 38.5 (C-12), 44.5 (C-13), 56.2 (C-14), 24.0 (C-15), 22.7 (C-16), 63.3 (C-17), 13.3 (C-18), 14.6 (C-19), 209.8 (C-20), 31.4 (C-21). Anal. calcd. for $C_{21}H_{32}O_5$: C 69.2, H 8.85; found: C 69.1, H 8.9.

5-Hydroxy-5α-pregna-2,16-diene-6,20-dione (8)

Ketol **4** (6.0 g, 17.4 mmol) was submitted to tosylation (TsCl, 3.30 g, 26.1 mmol) and subsequent dehydrotosylation (Li_2CO_3 (6.8 g), LiBr (7.2 g)) in a similar way as described in the synthesis of **6** to furnish the olefin **8** (5.32 g, 80%); mp (acetone) 157 to 158 °C. IR (KBr, cm^{-1}): 3550, 3020, 1707, 1660, 1583, 1060, 1029. ^1H NMR ($CDCl_3$) δ: 0.86 (s, 3H, H-18), 0.72 (s, 3H, H-19), 2.25 (s, 3H, H-21), 2.32 (dd, 1H, *J* = 12.6, 4.5 Hz, H-7β), 2.79 (t, 1H, *J* = 12.8 Hz, H-7α), 5.63 (m, 2H, H-3 + H-2), 6.68 (dd, 1H, *J* = 3.4, 1.8 Hz, H-16). ^{13}C NMR ($CDCl_3$) δ: 30.1 (C-1), 125.4 (C-2), 122.3 (C-3), 34.3 (C-4), 78.0 (C-5), 210.7 (C-6), 42.4 (C-7), 35.6 (C-8), 45.5 (C-9), 42.4 (C-10), 20.7 (C-11), 46.5 (C-13), 56.1 (C-14), 31.9 (C-15), 143.9 (C-16), 155.0 (C-17), 15.7 (C-18), 14.4 (C-19), 196.6 (C-20), 27.0 (C-21). Anal. calcd. for $C_{21}H_{28}O_3$: C 76.8, H 8.6; found: C 76.85, H 8.5.

2α,3α,5,16α,17α-Pentahydroxy-5α-pregna-6,20-dione (9)

Olefin **8** (500 mg, 1.5 mmol) was treated following the general dihydroxylation procedure (NMO, 1.05 mg, 9 mmol; OsO_4–*t*-BuOH, 9 mL, 12.5 mg/mL) for 48 h. Purification by flash column chromatography ($CHCl_3$–MeOH, 5:1) afforded the pentol **9** (365 mg, 65%); mp (EtOAc) 238 to 239 °C. IR (KBr, cm^{-1}): 3337, 3414, 3439, 1697, 1240, 1162, 1048. ^1H NMR (CD_3OD) δ: 0.70 (s, 3H, H-18), 0.73 (s, 3H, H-19), 2.07 (s, 3H, H-21), 2.71 (t, 1H, *J* = 12.5 Hz, H-7α), 3.74–3.82 (br m, 1H, H-2β), 4.10 (m, 1H, H-3β), 4.50 (d, 1H, *J* = 7.3 Hz, H-16β). ^{13}C NMR (CD_3OD) δ: 30.7 (C-1), 66.7 (C-2), 69.3 (C-3), 33.4 (C-4), 79.0 (C-5), 211.0 (C-6), 40.2 (C-7), 35.5 (C-8), 43.2 (C-9), 44.6 (C-10), 19.5 (C-11), 34.5 (C-12), 47.0 (C-13), 48.9 (C-14), 27.9 (C-15), 74.0 (C-16), 77.2 (C-17), 16.5 (C-18), 14.5 (C-19), 216.5 (C-20), 29.7 (C-21). Anal. calcd. for $C_{21}H_{32}O_5$: C 63.6, H 8.1; found: C 63.5, H 8.3.

5-Hydroxy-16α-methoxy-5α-pregn-2-ene-6,20-dione (10)

A freshly prepared solution of sodium (1.24 g, 54 mmol) in 30 mL of dry MeOH was added to a solution of the enone **8** (2.0 g, 5.4 mmol) in 100 mL of MeOH. The reaction mixture was stirred for 8 h under a nitrogen atmosphere, after which time TLC analysis (hexane–EtOAc, 3:1) revealed that some starting material had not been consumed. The solvent was removed under reduced preasure and the usual work-up (Et_2O) yielded a product, which was purified by flash column chromatography (hexane–EtOAc, 4:1) to furnish **10** (1.5 g, 70%); mp (acetone) 158–160 °C. IR (KBr, cm^{-1}): 3335, 3020, 1705, 1702, 1224, 1086, 1048. ^1H NMR ($CDCl_3$) δ: 0.57 (s, 3H, H-18), 0.66 (s, 3H, H-19), 2.15 (s, 3H, H-21), 2.54 (d, 1H, *J* = 6.3 Hz, H-17α), 2.75 (t, 1H, *J* = 12.5 Hz, H-7α), 4.00 (br s, 1H, OH), 3.16 (s, 3H, OCH_3), 4.29 (t, 1H, *J* = 6.5 Hz, H-16β), 5.60 (m, 2H, H-3 + H-2). ^{13}C NMR ($CDCl_3$) δ: 30.0 (C-1), 125.2 (C-2), 122.4 (C-3), 34.5 (C-4), 77.7 (C-5), 211.0 (C-6), 42.2 (C-7), 36.7 (C-8), 44.9 (C-9), 42.2 (C-10), 20.7 (C-11), 38.6 (C-12), 44.7 (C-13), 54.0 (C-14), 31.5 (C-15), 81.2 (C-16), 71.2 (C-17), 14.4 (C-18), 14.5 (C-19), 207.9 (C-20), 31.6 (C-21), 57.2 (OCH_3). Anal. calcd. for $C_{22}H_{32}O_4$: C 73.3, H 8.95; found: C 73.2, H 8.8.

2α,3α,5-Trihydroxy-16α-methoxy-5α-pregna-6,20-dione (12)

Olefin **10** (600 mg, 1.7 mmol) was treated following the general dihydroxylation procedure (NMO (596 mg, 5.1 mmol), OsO_4–*t*-BuOH (5 mL, 12.5 mg/mL)). Purification by flash column chromatography ($CHCl_3$–MeOH, 9:1) gave the triol **12** (470 mg, 72%); mp (heptane–acetone) 222–224 °C. IR (KBr, cm^{-1}): 3547, 3447, 3416, 3335, 1705, 1698, 1245, 1121, 1086. ^1H NMR ($CDCl_3$) δ: 0.56 (s, 3H, H-18), 0.72 (s, 3H, H-19), 2.15 (s, 3H, H-21), 2.54 (d, 1H, *J* = 6.3 Hz, H-17α), 2.73 (t, 1H, *J* = 12.5 Hz, H-7α), 3.17 (s, 3H, OCH_3), 3.74–3.81 (br m, 1H, H-2β), 4.09 (m, 1H, H-3β), 4.17 (br s, 1H, OH), 4.29 (t, 1H, *J* = 6.5 Hz, H-16β). ^{13}C NMR ($CDCl_3$) δ: 30.2 (C-1), 67.4 (C-2), 69.5 (C-3), 34.1 (C-4), 79.3 (C-5), 210.9 (C-6), 41.0 (C-7), 36.4 (C-8), 44.2 (C-9), 45.2 (C-10), 20.7 (C-11), 38.6 (C-12), 44.8 (C-13), 53.9 (C-14), 31.4 (C-15), 81.1 (C-16), 71.1 (C-17), 14.5 (C-18), 14.6 (C-19), 208.3 (C-20), 31.5 (C-21), 57.1 (OCH_3). Anal. calcd. for $C_{22}H_{34}O_6$: C 67.0, H 8.7; found: C 66.85, H 8.8.

16α,17α-Epoxy-5-hydroxy-5α-pregn-2-ene-6,20-dione (11)

A solution of enone **8** (2.0 g, 6 mmol) in 180 mL of MeOH was cooled to 0 °C and treated successively with 12 mL of 30% H_2O_2 and 4 mL of cold, aqueous 4 mol/L NaOH. The mixture was stirred and kept at 0–5 °C for 24 h. The reaction was monitored on TLC by the absence of UV absorption. The usual work-up (Et_2O) yielded a white crude solid, which was purified by flash column chromatography (hexane–EtOAc, 5:1) to give the epoxide **11** (1.5 g, 72%); mp (acetone) 158 to 159 °C. IR (KBr, cm^{-1}): 3550, 3020, 1705, 1700, 1092, 1036. ^1H NMR ($CDCl_3$) δ: 0.95 (s, 3H, H-18), 0.66 (s, 3H, H-19), 2.06 (s, 3H, H-21), 2.75 (t, 1H, *J* = 12.6 Hz, H-7α), 3.77 (d, 1H, *J* = 2.5 Hz, H-16β), 5.60 (m, 2H, H-3 + H-2). ^{13}C NMR ($CDCl_3$) δ: 30.0 (C-1), 125.2 (C-2), 122.4 (C-3), 34.5 (C-4), 77.7 (C-5), 211.0 (C-6), 42.2 (C-7), 36.7 (C-8), 44.9 (C-9), 42.2 (C-10), 20.7 (C-11), 38.6 (C-12), 41.6 (C-13), 44.8 (C-14), 27.3 (C-15), 60.4 (C-16), 70.8 (C-17), 15.3 (C-18), 14.0 (C-19), 205.1 (C-20), 25.9

© 2005 NRC Canada

(C-21). Anal. calcd. for $C_{21}H_{28}O_4$: C 73.2, H 8.2; found: C 73.1, H 8.3.

16α,17α-Epoxy-2α,3α,5-trihydroxy-5α-pregna-6,20-dione (13)

Olefin **11** (860 mg, 2.5 mmol) was treated following the general dihydroxylation procedure (NMO (978 mg, 7.5 mmol), OsO_4–*t*-BuOH (7 mL, 12.5 mg/mL)). Purification by flash column chromatography ($CHCl_3$–MeOH, 10:1) gave the epoxytriol **13** (766 mg, 81%); mp (heptane–acetone) 213–215 °C. IR (KBr, cm^{-1}): 3477, 3420, 3335, 1700, 1697, 1121, 1080, 1034. ^{1}H NMR ($CDCl_3$) δ: 0.95 (s, 3H, H-18), 0.73 (s, 3H, H-19), 2.06 (s, 3H, H-21), 2.70 (t, 1H, *J* = 12.5 Hz, H-7α), 3.77 (d, 1H, *J* = 2.5 Hz, H-16β), 3.78–3.84 (br m, 1H, H-2β), 4.12 (m, 1H, H-3β). ^{13}C NMR ($CDCl_3$) δ: 30.1 (C-1), 67.4 (C-2), 69.5 (C-3), 34.1 (C-4), 79.3 (C-5), 211.0 (C-6), 41.2 (C-7), 36.9 (C-8), 44.2 (C-9), 45.2 (C-10), 21.0 (C-11), 38.5 (C-12), 41.6 (C-13), 44.8 (C-14), 27.3 (C-15), 60.5 (C-16), 70.6 (C-17), 15.3 (C-18), 14.0 (C-19), 205.0 (C-20), 25.8 (C-21). Anal. calcd. for $C_{21}H_{30}O_6$: C 66.65, H 8.0; found: C 66.6, H 8.05.

5,16α,17α-Trihydroxy-3β-tosyloxy-5α-pregna-6,20-dione (14)

Tosyl chloride (6.6 g, 34.6 mmol) was added to a solution of ketol **4** (8.0 g, 23.1 mmol) in 120 mL of pyridine and the reaction was stirred at room temperature in the dark for 24 h. After completion as indicated by TLC, the mixture was poured into 500 mL of 10% $NaHCO_3$, stirred for another hour, and filtered under reduced pressure. The resulting tosylate was treated following the general dihydroxylation procedure (NMO (7.7 g, 66 mmol), OsO_4–*t*-BuOH (40 mL, 12.5 mg/mL)) for 48 h. Purification by flash column chromatography ($CHCl_3$–MeOH, 8:1) afforded the triol **14** (9.38 g, 76%); mp (AcOEt) 219 °C (decomp). IR (KBr, cm^{-1}): 3419, 3402, 1695, 1702, 1360, 1175, 1119, 1104. ^{1}H NMR ($CDCl_3$) δ: 0.70 (s, 3H, H-18), 0.76 (s, 3H, H-19), 2.05 (s, 3H, H-21), 2.41 (s, 3H, CH_3-Ts), 2.70 (t, 1H, *J* = 12.4 Hz, H-7α), 4.51 (d, 1H, *J* = 7.1 Hz, H-16β), 4.84 (br m, 1H, H-3α), 7.75 (d, 2H, *J* = 8.3 Hz, Ts), 7.30 (d, 2H, *J* = 8.5 Hz, Ts). ^{13}C NMR ($CDCl_3$) δ: 24.8 (C-1), 25.4 (C-2), 75.6.6 (C-3), 35.7 (C-4), 79.4 (C-5), 212.6 (C-6), 41.9 (C-7), 36.8 (C-8), 42.09 (C-9), 43.8 (C-10), 21.3 (C-11), 39.2 (C-12), 47.0 (C-13), 48.9 (C-14), 27.9 (C-15), 74.1 (C-16), 77.2 (C-17), 16.5 (C-18), 16.9 (C-19), 216.5 (C-20), 29.7 (C-21), 21.3 (*C*H_3-Ts), 134.2, 127.5, 129.8, 144.6 (6C-Ts). Anal. calcd. for $C_{28}H_{38}O_8S$: C 62.9, H 7.2, S 6.00; found: C 63.1, H 7.2, S 6.2.

*16α-(*tert*-Butyldimethylsilyloxy)-5,17α-dihydroxy-5α-pregn-2-ene-6,20-dione (15)*

Li_2CO_3 (12.0 g) and LiBr (14.5 g) were added to a solution of tosylate **14** (9.3 g, 17.5 mmol) in 100 mL of anhydr. DMF. The reaction mixture was refluxed under a nitrogen atmosphere for 2 h and followed by TLC until completion, then poured slowly with stirring into 600 mL of cool water, and filtered under reduced pressure. The resulting solid was washed with water, dried and dissolved in 80 mL of anhydr. DMF. TBDMSCl (2.6 g, 17.5 mmol) and imidazole (1.8 g, 26 mmol) were added to the solution and the reaction mixture was stirred under a nitrogen atmosphere for 3 h. The usual work-up ($CHCl_3$) yielded a product that was purified by flash column chromatography (hexane–AcOEt, 3:1) to give the olefin **15** (6.6 g, 79%); mp (acetone) 171–173 °C. IR (KBr, cm^{-1}): 3481, 3382, 3020, 1698, 1702, 1163, 1086, 1048. ^{1}H NMR ($CDCl_3$) δ: 0.07 (s, 3H, (CH_3)$_2$Si), 0.09 (s, 3H, (CH_3)$_2$Si), 0.69 (s, 3H, H-18), 0.66 (s, 3H, H-19), 0.92 (s, 9H, (CH_3)$_3$CSi), 2.05 (s, 3H, H-21), 4.56 (d, 1H, *J* = 7.0 Hz, H-16β), 5.63 (m, 2H, H-3 + H-2). ^{13}C NMR ($CDCl_3$) δ: 30.1 (C-1), 125.1 (C-2), 122.4 (C-3), 34.5 (C-4), 77.9 (C-5), 211.6 (C-6), 42.2 (C-7), 36.6 (C-8), 44.7 (C-9), 42.0 (C-10), 20.7 (C-11), 38.9 (C-12), 43.7 (C-13), 49.2 (C-14), 27.0 (C-15), 75.2 (C-16), 77.4 (C-17), 13.1 (C-18), 13.7 (C-19), 210.3 (C-20), 31.3 (C-21), 26.1 ((*C*H_3)$_3$CSi), 18.3 ((CH$_3$)$_3$*C*Si), –2.9 ((*C*H_3)$_2$Si). Anal. calcd. for $C_{27}H_{44}O_5Si$: C 68.0, H 9.3; found: C 68.5, H 9.5.

*16α-(*tert*-Butyldimethylsilyloxy)-5,17α-dihydroxy-2α,3α-isopropylidenedioxy-5α-pregna-6,20-dione (16)*

Olefin **15** (6.5 g, 13.6 mmol) was treated following the general dihydroxylation procedure (NMO (4.6 g, 39 mmol), OsO_4–*t*-BuOH (30 mL, 12.5 mg/mL)) until completion as indicated by TLC (minor impurities were also detectable). The usual work-up (AcOEt) afforded a product that was dried, dissolved in anhydr. DMF (150 mL), and treated with PPTS (0.8 g) and 2,2-dimethoxypropane (30 mL). Activated K_2CO_3 (500 mg) was added to the solution after 24 h, and the mixture was stirred overnight at room temperature. The usual work-up (CH_2Cl_2) yielded a product that was purified by flash column chromatography (hexane–AcOEt, 2:1) to give the colorless syrup **16** (4.93 g, 61%); mp (MeOH) 206–209 °C. IR (KBr, cm^{-1}): 3461, 1703, 1699, 1116, 1089, 1056, 1041. ^{1}H NMR ($CDCl_3$) δ: 0.08 (s, 3H, (CH_3)$_2$Si), 0.09 (s, 3H, (CH_3)$_2$Si), 0.67 (s, 3H, H-18), 0.75 (s, 3H, H-19), 0.90 (s, 9H, (CH_3)$_3$CSi), 1.47 (s, 3H, CH_3-ketal), 1.34 (s, 3H, CH_3-ketal), 2.05 (s, 3H, H-21), 4.08–4.15 (br m, 1H, H-2β), 4.31 (m, 1H, H-3β), 4.56 (d, 1H, *J* = 7.0 Hz, H-16β). ^{13}C NMR ($CDCl_3$) δ: 28.2 (C-1), 73.7 (C-2), 74.3 (C-3), 33.8 (C-4), 79.5 (C-5), 211.8 (C-6), 41.0 (C-7), 36.4 (C-8), 44.2 (C-9), 45.2 (C-10), 20.7 (C-11), 38.6 (C-12), 43.7 (C-13), 49.2 (C-14), 27.2 (C-15), 75.2 (C-16), 77.4 (C-17), 13.1 (C-18), 14.2 (C-19), 210.3 (C-20), 31.3 (C-21), 26.0 ((*C*H_3)$_3$CSi), 18.3 ((CH$_3$)$_3$*C*Si), –2.9 ((*C*H_3)$_2$Si), 108.2 (O-C-O), 26.9 + 28.4 (*C*H_3 ketal). Anal. calcd. for $C_{31}H_{54}O_7Si$: C 55.7, H 9.6, Si 4.95; found: C 55.8, H 9.7, Si 5.1.

5,16α,17α-Trihydroxy-2α,3α-isopropylidenedioxy-5α-pregna-6,20-dione (17)

TBAF (3 mL, 1 mol/L in THF) was added to a solution of acetonide **16** (4.9 g, 8.9 mmol) in anhydr. THF (100 mL). The reaction mixture was stirred under a nitrogen atmosphere for 6 h and then concentrated. The usual work-up (Et_2O) yielded the crude product in quantitative yield, which was recrystallized from MeOH to furnish the acetonide **17** (3.49 g, 90%); mp (MeOH) 211 to 212 °C. IR (KBr, cm^{-1}): 3414, 3339, 1700, 1697, 1205, 1142, 1118. ^{1}H NMR ($CDCl_3$) δ: 0.69 (s, 3H, H-18), 0.74 (s, 3H, H-19), 1.48 (s, 3H, CH_3-ketal), 1.34 (s, 3H, CH_3-ketal), 2.07 (s, 3H, H-21), 2.72 (t, 1H, *J* = 12.4 Hz, H-7α), 4.08–4.15 (br m, 1H, H-2β), 4.31 (m, 1H, H-3β), 4.50 (d, 1H, *J* = 7.3 Hz, H-16β). ^{13}C NMR ($CDCl_3$) δ: 28.4 (C-1), 73.6 (C-2), 74.0 (C-3), 33.8 (C-4), 79.4 (C-5), 211.7 (C-6), 41.0 (C-7), 36.4 (C-8), 44.2 (C-9), 45.2 (C-10), 20.5 (C-11), 34.5 (C-12), 47.0 (C-13), 48.9 (C-14), 27.9 (C-15), 74.1 (C-16), 77.2 (C-17), 16.5 (C-18),

© 2005 NRC Canada

14.7 (C-19), 216.4 (C-20), 29.8 (C-21). Anal. calcd. for $C_{24}H_{36}O_7$: C 66.0, H 8.3; found: C 66.0, H 8.25.

5,16β,17α-Trihydroxy-2α,3α-isopropylidenedioxy-5α-pregna-6,20-dione (18)

To a stirred solution of triol **17** (700 mg, 1.6 mmol), formic acid (300 μL), and triphenylphosphine (635 mg, 2.49 mmol) in THF (50 mL) was added dropwise a solution of DIAD (570 μL, 2.94 mmol) in 7 mL of THF. The reaction mixture was stirred at room temperature for 24 h, after which time TLC analysis revealed that all the starting material had been consumed. Then the volatiles were evaporated off under reduced pressure and the resultant crude was dissolved in 80 mL of a saturated solution of $NaHCO_3$ in MeOH–H_2O (4:1) and stirred for 1 h at room temperature. The usual work-up (Et_2O) yielded a crude product, which was purified by flash column chromatography (hexane–AcOEt, 3:1) to give the triol **18** (497 mg, 71%); mp (EtOH) 215 to 216 °C. IR (KBr, cm^{-1}): 3459, 3401, 3346, 1700, 1696, 1204, 1145, 1074. ^{1}H NMR ($CDCl_3$) δ: 0.77 (s, 3H, H-18), 0.74 (s, 3H, H-19), 1.47 (s, 3H, CH_3-ketal), 1.34 (s, 3H, CH_3-ketal), 2.09 (s, 3H, H-21), 4.09–4.16 (br m, 1H, H-2β), 4.32 (m, 1H, H-3β), 4.41 (dd, 1H, J = 8.1, 5.9 Hz, H-16α). ^{13}C NMR ($CDCl_3$) δ: 28.5 (C-1), 73.6 (C-2), 74.0 (C-3), 33.7 (C-4), 79.4 (C-5), 211.8 (C-6), 41.0 (C-7), 36.4 (C-8), 44.2 (C-9), 45.2 (C-10), 20.5 (C-11), 34.5 (C-12), 46.1 (C-13), 53.0 (C-14), 28.1 (C-15), 73.7 (C-16), 77.0 (C-17), 15.1 (C-18), 14.5 (C-19), 216.2 (C-20), 29.7 (C-21). Anal. calcd. for $C_{24}H_{36}O_7$: C 66.0, H 8.3; found: C 66.2, H 8.4.

2α,3α,5,16β,17α-Pentahydroxy-5α-pregna-6,20-dione (21)

Acetic acid (2 mL) was added to a solution of **18** (400 mg, 0.9 mmol) in 20 mL of the solvent mixture MeOH–H_2O (5:1) and the reaction mixture was refluxed for 1 h. The usual work-up (AcOEt) yielded a white product, which was recrystallized from AcOEt to afford the pure pentaol **21** (282 mg, 86%); mp (AcOEt) 241 to 242 °C. IR (KBr, cm^{-1}): 3447, 3421, 3329, 3301, 1701, 1697, 1240, 1162, 1186, 1048. ^{1}H NMR ($CDCl_3$) δ: 0.78 (s, 3H, H-18), 0.72 (s, 3H, H-19), 2.09 (s, 3H, H-21), 2.70 (t, 1H, J = 12.5 Hz, H-7α), 3.78–3.84 (br m, 1H, H-2β), 4.11 (m, 1H, H-3β), 4.41 (dd, 1H, J = 8.0, 5.9 Hz, H-16α). ^{13}C NMR ($CDCl_3$) δ: 30.1 (C-1), 67.4 (C-2), 69.5 (C-3), 34.1 (C-4), 79.3 (C-5), 211.0 (C-6), 41.2 (C-7), 36.9 (C-8), 44.2 (C-9), 45.2 (C-10), 21.0 (C-11), 34.5 (C-12), 46.1 (C-13), 53.4 (C-14), 28.2 (C-15), 73.8 (C-16), 77.1 (C-17), 15.0 (C-18), 14.5 (C-19), 216.2 (C-20), 29.7 (C-21). Anal. calcd. for $C_{21}H_{32}O_5$: C 63.6, H 8.1; found: C 63.5, H 8.2.

16β-Azido-5,17α-dihydroxy-2α,3α-isopropylidenedioxy-5α-pregna-6,20-dione (19)

Mesyl chloride (0.558 g, 4.9 mmol) was added dropwise to a stirred solution of acetonide **17** (1.44 g, 3.3 mmol) in dry CH_2Cl_2 (50 mL) and Et_3N (1.0 mL, 7.3 mmol) at 0 °C under a nitrogen atmosphere. The resulting suspension was stirred at this temperature for 1 h, allowed to reach room temperature, and then poured into 200 mL of 10% $NaHCO_3$. The usual work-up (CH_2Cl_2) yielded a product, which was carefully dried and dissolved in DMPU (50 mL). NaN_3 (322 mg, 4.95 mmol) was added and the resulting mixture was stirred vigorously under an argon atmosphere at 50 °C for 48 h. TLC analysis of a mini work-up revealed the formation of two products, one being the more polar and the major steroidal product. The usual work-up (EtOAc) yielded a crude product, which was purified by flash column chromatography (hexane–AcOEt, 3:1) to afford, by collection of the more hydrophilic fractions, the azide **19** (1.1 g, 73%); mp (MeOH) 207–210 °C. IR (KBr, cm^{-1}): 3335, 3322, 2091, 1702, 1698, 1168, 1110. ^{1}H NMR ($CDCl_3$) δ: 0.78 (s, 3H, H-18), 0.74 (s, 3H, H-19), 1.49 (s, 3H, CH_3-ketal), 1.34 (s, 3H, CH_3-ketal), 2.08 (s, 3H, H-21), 4.08–4.15 (br m, 1H, H-2β), 4.24 (dd, 1H, J = 8.1, 5.7 Hz, H-16α), 4.32 (m, 1H, H-3β). ^{13}C NMR ($CDCl_3$) δ: 28.5 (C-1), 73.6 (C-2), 74.1 (C-3), 33.6 (C-4), 79.5 (C-5), 212.0 (C-6), 41.0 (C-7), 36.4 (C-8), 44.1 (C-9), 45.2 (C-10), 20.5 (C-11), 34.5 (C-12), 46.1 (C-13), 53.1 (C-14), 28.0 (C-15), 68.1 (C-16), 76.5 (C-17), 15.0 (C-18), 14.6 (C-19), 216.1 (C-20), 29.8 (C-21). Anal. calcd. for $C_{24}H_{35}O_6N_3$: C 62.5, H 7.6, N 9.1; found: C 62.3, H 7.5, N 9.2.

16β-Amino-2α,3α,5,17α-tetrahydroxy-5α-pregna-6,20-dione (22)

Lindlar catalyst (200 mg) was added to a solution of azide **19** (1.0 g, 2.1 mmol) in 60 mL of absolute EtOH. The mixture was treated successively with hydrogen and vacuum and finally stirred under a hydrogen atmosphere for 36 h, when TLC analysis revealed that all the azide had been consumed. The catalyst was removed by filtration and the resulting solution was evaporated under reduced pressure to give the corresponding amine, which was dissolved in 60 mL of the solvent mixture MeOH–H_2O (5:1). Acetic acid (4 mL) was added and the reaction mixture was refluxed for 1 h. The solvent was concentrated until half volume and partitioned between 10% NaOH (200 mL) and EtOAc (300 mL). The aqueous layer was extracted successively with EtOAc (3 × 100 mL), dried over anhydr. Na_2SO_4, and concentrated under reduced pressure. Recrystallization from EtOAc gave the pure amine **22** (522 mg, 63%); mp (EtOAc) 227–230 °C. IR (KBr, cm^{-1}): 3428, 3391, 3326, 3311, 1700, 1204, 1158, 1116. ^{1}H NMR ($CDCl_3$) δ: 0.78 (s, 3H, H-18), 0.73 (s, 3H, H-19), 2.10 (s, 3H, H-21), 3.74–3.81 (br m, 1H, H-2β), 4.09 (m, 1H, H-3β), 4.17 (br s, 1H, OH), 4.33 (dd, 1H, J = 7.9, 5.9 Hz, H-16α). ^{13}C NMR ($CDCl_3$) δ: 30.2 (C-1), 67.4 (C-2), 69.5 (C-3), 34.1 (C-4), 79.3 (C-5), 210.9 (C-6), 41.0 (C-7), 36.4 (C-8), 44.2 (C-9), 45.2 (C-10), 20.7 (C-11), 35.3 (C-12), 46.1 (C-13), 53.2 (C-14), 28.2 (C-15), 73.8 (C-16), 76.9 (C-17), 15.1 (C-18), 14.5 (C-19), 216.2 (C-20), 29.8 (C-21). Anal. calcd. for $C_{21}H_{33}O_6N$: C 63.8, H 8.4, N 3.5; found: C 63.7, H 8.3, N 3.65.

16α-Azido-5,17α-dihydroxy-2α,3α-isopropylidenedioxy-5α-pregna-6,20-dione (20)

Methanesulfonic acid (570 μL, 8.8 mmol) was added to a stirred solution of acetonide **17** (1.74 g, 4.0 mmol) and triphenylphosphine (3.14 g, 12.0 mmol) in dry THF (120 mL). The temperature was raised to 40 °C and a solution of DIAD (2.33 mL, 12 mmol) in 15 mL of THF was added dropwise over a 10 min period under an argon atmosphere. The reaction mixture was stirred vigorously for 24 h at 40 °C under an argon atmosphere, and then the volatiles were evaporated off under reduced pressure. The crude product was purified by flash column chromatography to give a pure product, which was analyzed by ^{1}H NMR confirming the structure of the mesylate. This later was submitted to

© 2005 NRC Canada

azide displacement as described for the synthesis of **19**. Purification by flash column chromatography yielded the azide **20** (1.12 g, 61%); mp (MeOH) 205 to 206 °C. IR (KBr, cm^{-1}): 3368, 3312, 2091, 1701, 1162, 1130, 1058. ^1H NMR ($CDCl_3$) δ: 0.70 (s, 3H, H-18), 0.74 (s, 3H, H-19), 1.48 (s, 3H, CH_3-ketal), 1.34 (s, 3H, CH_3-ketal), 2.06 (s, 3H, H-21), 2.70 (t, 1H, J = 12.5 Hz, H-7α), 4.08–4.15 (br m, 1H, H-2β), 4.28 (d, 1H, J = 7.1 Hz, H-16β), 4.32 (m, 1H, H-3β). ^{13}C NMR ($CDCl_3$) δ: 28.5 (C-1), 73.6 (C-2), 74.1 (C-3), 33.8 (C-4), 79.6 (C-5), 211.9 (C-6), 41.0 (C-7), 36.4 (C-8), 44.2 (C-9), 45.2 (C-10), 20.5 (C-11), 34.5 (C-12), 47.1 (C-13), 48.9 (C-14), 27.7 (C-15), 67.9 (C-16), 76.3 (C-17), 16.4 (C-18), 14.7 (C-19), 216.3 (C-20), 29.8 (C-21). Anal. calcd. for $C_{24}H_{35}O_6N_3$: C 62.5, H 7.6, N 9.1; found: C 62.1, H 7.5, N 9.05.

16α-Amino-2α,3α,5,17α-tetrahydroxy-5α-pregna-6,20-dione (23)

Azide **20** (800 mg, 1.73 mmol) was treated as described in the synthesis of the amine **22**. Recrystallization from EtOAc gave the pure amine **23** (403 mg, 59%); mp (EtOAc) 229 to 230 °C. IR (KBr, cm^{-1}): 3345, 3428, 3419, 1701, 1697, 1240, 1162, 1048. ^1H NMR (CD_3OD) δ: 0.769 (s, 3H, H-18), 0.73 (s, 3H, H-19), 2.06 (s, 3H, H-21), 2.72 (t, 1H, J = 12.4 Hz, H-7α), 3.74–3.82 (br m, 1H, H-2β), 4.09 (m, 1H, H-3β), 4.39 (d, 1H, J = 7.1 Hz, H-16β). ^{13}C NMR (CD_3OD) δ: 30.5 (C-1), 66.7 (C-2), 69.3 (C-3), 33.4 (C-4), 79.4 (C-5), 211.6 (C-6), 40.2 (C-7), 35.5 (C-8), 43.2 (C-9), 44.6 (C-10), 19.5 (C-11), 34.5 (C-12), 47.0 (C-13), 48.9 (C-14), 27.9 (C-15), 73.4 (C-16), 77.0 (C-17), 16.5 (C-18), 14.5 (C-19), 216.5 (C-20), 29.8 (C-21). Anal. calcd. for $C_{21}H_{33}O_6N$: C 63.8, H 8.4, N 3.5; found: C 63.9, H 8.6, N 3.6.

Biological activity

Radish seeds (*R. sativus* L.) were germinated over wet cotton in the dark at 25 °C for 72 h. The hypocotyls (cut to 1 cm long) and the cotyledons were placed in independent plates (diameter 11 cm) over filter paper (diameter 9 cm), and 5 mL of the ethanol–water solutions containing the targets pregnane-brassinosteroid-like compounds (concentrations: 0.1–0.001 ppm) were applied over the filter paper. For control experiments, cotyledons and hypocotyls were treated with 5 mL of distilled water. After 72 h, the lengths of the hypocotyls were measured, the cotyledons were weighted, and the averages of these magnitudes were calculated. Each experiment at one concentration consisted of three different plates containing 10 hypocotyls or cotyledons per plate. Statistical analysis of the data was carried out to establish significant differences with respect to control utilizing the Duncan test as implemented in the STATGRAPHICS program.

Acknowledgments

We are grateful to Dr. Carlos. S. Pérez from the University of Havana, and Dr. Andrea Porzel from the Institute of Plant Biochemistry, Halle (Saale) Germany, for the spectroscopic measures. We also gratefully acknowledge Ing. Deysma C. Herrera for experimental assistance.

References

1. M.D. Grove, G.F. Spencer, W.K. Rohwedder, N.B. Mandava, J.F. Worley, J.D. Warthen, G.L. Steffens, J.L. Flippen-Anderson, and J.C. Cook. Nature (London), **281**, 216 (1979).
2. H.G. Cluter, T. Yokota, and G. Adam. Brassinosteroids: Chemistry, bioactivity and applications. ACS Symp. Ser. No. 474. American Chemical Society, Washington, D.C. 1991.
3. V.A. Khripach, V.N. Zhabinskii, and A.E. de Groot. Brassinosteroids: A new class of plant hormones. Academic Press, San Diego, California. 1999.
4. Y. Kamuro and S. Takatsuto. *In* Brassinosteroids. Steroidal plant hormones. *Edited by* A. Sakurai, T. Yokota, and S.D. Clouse. Springer-Verlag, Tokyo. 1999. pp. 223–241.
5. J.A. Ramirez, E.G. Gros, and L.R. Galagovsky. Tetrahedron, **56**, 6171 (2000).
6. J.A. Ramirez, O.M. Teme-Centurion, E.G. Gros, and L.R. Galagovsky. Steroids, **65**, 329 (2000).
7. M.A. Iglesias-Ateaga, R.P. Gil, C.S. Pérez, and F. Coll. J. Chem. Soc. Perkin Trans. 1, **3**, 261 (2001).
8. M.A. Iglesias-Arteaga, C.P. Martínez, and F. Coll. Steroids, **67**, 159 (2002).
9. T. Yokota and K. Mori. *In* Molecular structure and biological activity of steroids. *Edited by* M. Bohl and W.L. Duax. CRC Press, Boca Raton, Florida. 1992. pp. 317–340.
10. T.G. Back and R.P. Pharis. J. Plant Growth Regul. **22**, 350 2003.
11. C. Brosa. *In* Brassinosteroids. Steroidal plant hormones. *Edited by* A. Sakurai, T. Yokota, and S.D. Clouse. Springer-Verlag, Tokyo 1999. pp. 191–222.
12. C. Brosa, L. Soca, E. Terricabras, J.C. Ferrer, and A. Alsina. Tetrahedron, **54**, 12 337 (1998).
13. D.G. Rivera, F. Coll, and F. León. J. Chem. Res. (S), 284 (2004).
14. L. Kohout. Coll. Czech. Chem. Commun. **54**, 3348 (1989).
15. L. Kohout, H. Velgova, M. Strnad, and M. Kaminev. Coll. Czech. Chem. Commun. **52**, 476 (1987).
16. M. Strnad and L. Kohout. Plant Growth Regul. **40**, 39 (2003).
17. L. Kohout and M. Strnad. Coll. Czech. Chem. Commun. **57**, 1731 (1992).
18. L. Kohout and M. Strnad. Coll. Czech. Chem. Commun. **61**, 930 (1996).
19. L. Kohout, H. Chodounská, T. Macek, and M. Strnad. Coll. Czech. Chem. Commun. **65**, 1754 (2002).
20. T. Kametani, T. Katoh, J. Fujio, I. Nogiwa, M. Tsubuki, and T. Honda. J. Org. Chem. **53**, 1982 (1988).
21. O. Mitsunobu. Synthesis, 1 (1981).
22. A.P. Davis, S. Dresen, and L.J. Lawless. Tetrahedron Lett. **38**, 4305 (1997).
23. P.J. Kocienski. Protecting groups. Thieme-Verlag, Stuttgart, Germany. 2000. pp. 33–38.
24. T. Kitamura, M. Isobe, Y. Ichikawa, and T. Goto. J. Am. Chem. Soc. **106**, 3252 (1984).
25. A.K. Bose, B. Lal, W.A. Hoffman, and M.S. Manhas. Tetrahedron Lett. **14**, 1619 (1973).
26. A.P. Davis and J.J. Walsh. Chem. Commun. 449 (1996).
27. C. Brosa, I. Zamora, E. Terricabas, and L. Kohout. Coll. Czech. Chem. Commun. **63**, 1635 (1998).
28. C. Brosa, M. Amorós, M. Molist, and X. Hernández. Tetrahedron, **60**, 8529 (2004).
29. D.S. Lethan. *In* Biochemistry and physiology of plant growth substances. *Edited by* F. Wightman and G. Setterfield. Runge Press, Ottawa. 1968. Chap. 2.

© 2005 NRC Canada

One-step synthesis of Sb_2O_3 broom-like belts with controllable morphology

Qingrui Zhao, Xuanjun Zhang, Qing Yang, and Yi Xie

Abstract: A direct and simple surfactant- and template-free route has been developed for the controlled synthesis of Sb_2O_3 belt-like microstructures. By adjusting the reactant ratio between $SbCl_3$ and urea under solvothermal reaction conditions, broom-like belts and rods of Sb_2O_3 have been successfully prepared. X-ray powder diffraction (XRD), scanning electron microscopy (SEM), high-resolution transmission electron microscopy (HR-TEM), and X-ray photoelectron spectroscopy (XPS) has been used to characterize the phases and morphologies of the as-prepared products. A possible formation mechanism is also discussed.

Key words: antimony trioxide, solvothermal synthesis, broom-like belts.

Résumé : Une méthode simple et directe n'impliquant aucun gabarit ou agent de surface a été développée pour la synthèse contrôlée de microstructures de Sb_2O_3 en forme de ceinture. La réaction du $SbCl_3$ et de l'urée, dans des conditions solvothermiques et en ajustant le rapport des réactifs, permet de préparer avec succès des tiges et des ceintures de Sb_2O_3 en forme de balais. On a fait appel à la diffraction des rayons X par des poudres, à la microscopie électronique à balayage et la microscopie électronique en transmission à haute résolution et à la spectroscopie photoélectronique des rayons X pour caractériser les phases et les morphologies des produits tels que préparés. On discute aussi du mécanisme possible de leur formation.

Mots clés : trioxyde d'antimoine, synthèse solvothermique, ceintures en forme de balais.

[Traduit par la Rédaction]

Introduction

Recently, compounds with interesting morphologies and specific structures, especially one-dimensional (1D) nano- and microstructures, have drawn an increasing amount of attention since the discovery of carbon nanotubes (1). The unique physical and chemical properties of 1D materials have been well documented and are proposed for a wide range of potential applications in the fabrication of electroluminescent devices (2, 3), photovoltaic devices (4), and light-emitting diodes (5, 6). Consequently, considerable effort has been devoted to the synthesis of various 1D tubes and wires over the past decade. More recently nano- and microscale belts, which are distinctively different from wires and tubes, have been the subjects of intensive research since they have shown promise as new kinds of building blocks that can be integrated into electronic devices. At present, several strategies have been developed for the growth of nano- or submicroscaled belts through different growth mechanisms. These strategies include evaporation of the source compounds via a vapor–solid (VS) or vapor–liquid–solid (VLS) process (7, 8), a complex, surfactant-assisted hydrothermal route to ferromagnetic nickel nanobelts (9), and the organogel template-directed synthesis of helical titanium dioxide nanoribbons (10).

Among published reports, general strategies for the synthesis of belt-like materials involve high-temperature, template- or catalyst-based methods, and complicated processes in which impurities may be introduced. In this paper, we report a low-temperature, simple solution synthetic method to produce large-scale, single-crystalline Sb_2O_3 belts without using any catalysts or templates. This synthetic strategy will provide an effective approach to the development of 1D structures.

Sb_2O_3, which possesses many distinctive properties, has been widely used as an effective catalyst in photochemistry, either individually or combined with other oxides, and is employed as a highly efficient flame retardant (11). Recently, several groups have prepared 1D nanostructures of Sb_2O_3, such as Sb_2O_3 fibrils and tubules synthesized via a VS route (12) and nanorods via a surfactant-assisted solvothermal process (13). Additionally, with the help of a microemulsion system composed of sodium bis(2-ethylhexyl)-sulfosuccinate (AOT), water, and toluene (14) or carbon nanotube templates (15), Sb_2O_3 nanorods were also prepared. To date, there have been very few reports on the large-scale synthesis of Sb_2O_3 on a micrometer scale. In this paper, we report for the first time a facile and simple surfactant- and template-free solution route to prepare Sb_2O_3 belts with a micrometer size.

Received 9 May 2004. Published on the NRC Research Press Web site at http://canjchem.nrc.ca on 14 September 2005.

Q.R. Zhao, X.J. Zhang, Q. Yang, and Y. Xie.[1] Nano-materials and Nano-chemistry, Hefei National Laboratory for Physical Sciences at Microscale, University of Science & Technology of China, Hefei, Anhui 230026, China.

[1]Corresponding author (e-mail: yxielab@ustc.edu.cn).

 doi: 10.1139/V05-123 © 2005 NRC Canada

Experimental section

Synthesis of Sb_2O_3 broom-like belts

A total of 1 mmol $SbCl_3$ and 4 mmol of urea were dissolved in a 10 mL water–ethanol solution (1:1, *v*/*v*). The mixture was then transferred into a 15 mL Teflon-lined autoclave. The autoclave was maintained at 160 °C for 12 h and then cooled to room temperature. The light yellow powders formed were collected, washed sequentially several times with distilled water and ethanol, and then dried in vacuum at 50 °C for 6 h.

Characterization of the products

The phase of the products was determined by X-ray powder diffraction (XRD) using a Japan Rigaku D/max γA X-ray diffractometer with graphite-monochromatized Cu Kα radiation (λ = 1.541 78 Å). The scan rate of 0.05°/s was applied to record the patterns in the 2θ range of 10°~70°. The morphology and size of the as-prepared products were observed by scanning electron microscopy (SEM), performed using an X-650 scanning electron microanalyzer. High-resolution transmission electron microscopy (HR-TEM) images and selected area electron diffractions were taken using a JEOL-2010 high-resolution electron microscope with an accelerating voltage of 200 kV. X-ray photoelectron spectroscopy (XPS) was performed using an ESCALAB MKII with Mg Kα ($h\nu$ = 1253.6 eV) as the excitation source. The binding energies obtained in the XPS spectral analysis were corrected for specimen charging by referencing the C1s peak to 284.60 eV.

Results and discussion

The product was firstly characterized using XRD and a typical diffraction pattern is shown in Fig. 1. From the XRD pattern, all reflection peaks could be readily indexed to the orthorhombic phase of Sb_2O_3, with calculated lattice constants of a = 4.910 Å, b = 12.348 Å, and c = 5.329 Å, which were in good agreement with the values of the Joint Committee for Powder Diffraction Studies (JCPDS) file (No. 11-689), and no obvious impurities could be detected in the obtained pattern.

The morphology of the as-prepared product was examined using SEM. Figure 2 shows images of the Sb_2O_3 structure at different magnifications. A low-magnification image (Fig. 2*a*) displays a panorama of as-prepared belts, indicating that the Sb_2O_3 belts cluster form in a high yield, and the proportion of free-standing belts in the whole sample is under 10%. Some belts grow from the original core and extend toward different directions. Figure 2*b* reveals that the Sb_2O_3 belts are fairly straight with lengths of approximately several micrometers. The surfaces of the belts are clean with regular edges and the belts appear to have generally uniform widths over their entire length. The high-magnification images (Figs. 2*c* and 2*d*) give further details about the morphological features of the belts. From the top view (Fig. 2*c*), we can see many uniform Sb_2O_3 belts, with widths of about 3–7 μm extending in different directions, all issuing from a common center. More detail about the belts can be found in a partially magnified image (Fig. 2*d*) in which one can see that a small belt can be split from a thicker belt as indicated by the arrowhead and that the typical thickness of the products can vary from 300 to 400 nm. HR-TEM images of an individual belt (Figs. 3*a* and 3*b*) provide further insight into the fine structure of these products. The selected area electron diffraction (SAED) pattern was recorded with the electron beam perpendicular to the surface of an individual belt, as shown in Fig. 3*a*. Through careful analysis of the diffraction pattern, the spots could be readily indexed, as marked in the figure, and the [100] zone axis of the belts could be identified by diffraction of orthorhombic Sb_2O_3. These results mean that the wide surface and the narrow side surface of the belt correspond to the (010) and (100) planes, respec-

Fig. 1. XRD pattern of the broom-like belts of Sb_2O_3.

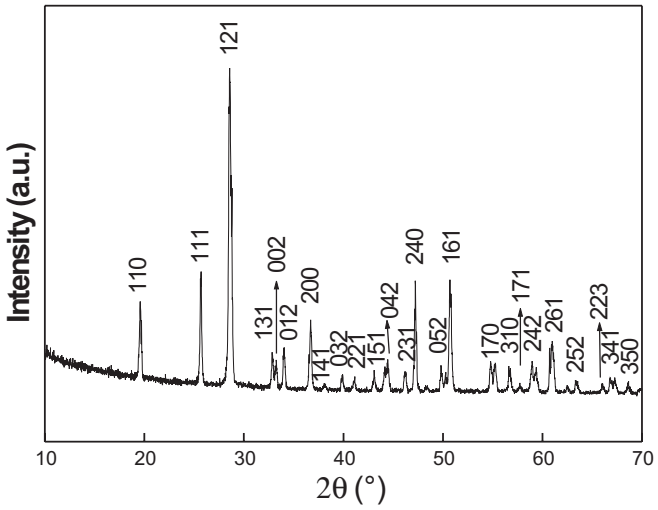
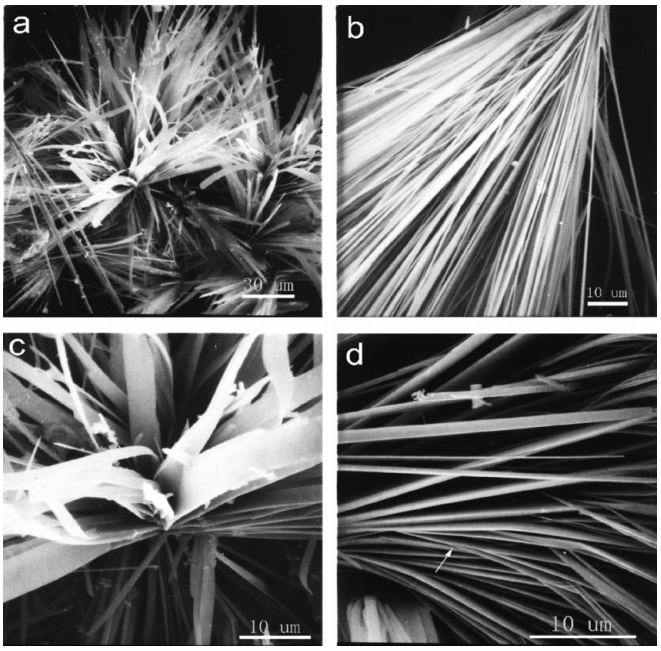
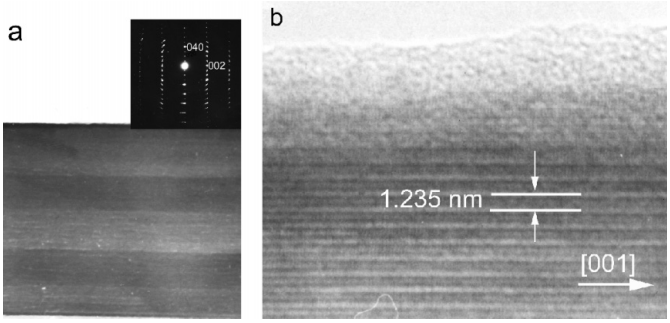


Fig. 2. Representative SEM images of Sb_2O_3 belts. (*a*) A low-magnification image showing high yield belt-like Sb_2O_3. (*b*) A medium-magnification showing broom-like belts of Sb_2O_3. (*c*) The top view showing Sb_2O_3 are uniform belts. (*d*) A high-magnification image revealing the side belts are tip-split.



© 2005 NRC Canada

Fig. 3. (*a*) HR-TEM image of an individual belt and a SAED pattern (inset) of the belt. (*b*) HR-TEM image of high quality Sb_2O_3 belts projected along the [100] zone axis.



tively. The growth of the long axis is along the [001] direction. This conclusion is supported by our subsequent HR-TEM investigation, and the image obtained is shown in Fig. 3*b*. The identified fringe spacing of 1.235 nm corresponds well with the separation between neighboring (010) lattices. We employed SAED and HR-TEM to characterize different belts, as well as different parts of the same belt. All results confirm that the belts grow along the [001] direction.

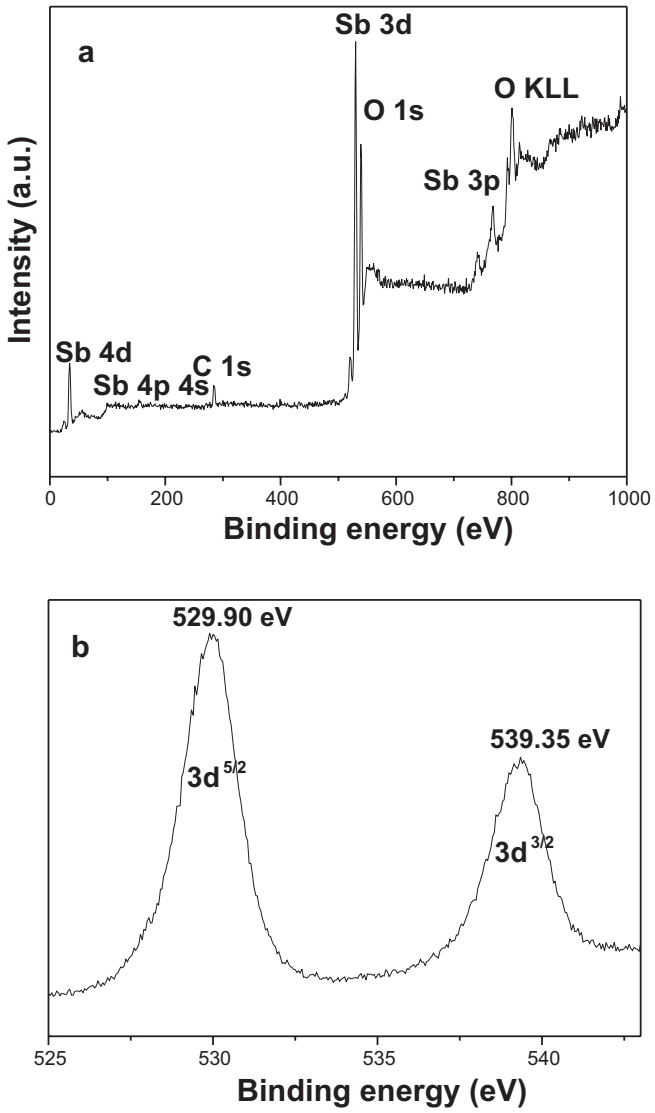
To further characterize the product, XPS was carried out to investigate the surface composition and chemical state of the broom-like Sb_2O_3 belts. Typical high-resolution spectra of Sb_2O_3 are shown in Fig. 4. Since the position of the Sb $3d^{5/2}$ binding energy is superimposed over that of the O 2p binding energy, the Sb $3d^{3/2}$ binding energy was used for characterization. Figure 3*b* shows that the strong peak centered at 539.35 eV corresponds to the Sb $3d^{3/2}$ binding energy and this coincides with the value reported in the literature (16). No obvious impurities (besides trace adsorbent O_2) could be detected in the samples. Quantification gave an atomic ratio of Sb to O elements of 0.736 based on the areas of the Sb and O peaks, respectively, including adsorbent O_2 consistent with the given stoichiometric ratio within experimental error. The valence state of the Sb ions in the product is confirmed as Sb^{3+} rather than Sb^{5+}. On the basis of the above characterizations of the XRD pattern and XPS, the as-synthesized products are pure-phase Sb_2O_3.

The whole reaction process can be formulated as follows:

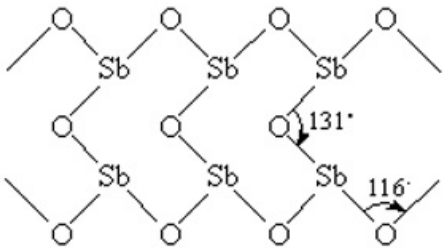
$$[1] \quad 2SbCl_3 + 3CO(NH_2)_2 + 6H_2O \longrightarrow Sb_2O_3 + 3CO_2 + 6NH_4Cl$$

To understand the observed behavior of Sb_2O_3, it is necessary to investigate its unusual crystal structure, as shown in Scheme 1. Sb_2O_3 forms in the orthorhombic system with space group *Pccn*. It has infinite double chains of corner sharing SbO_6 octahedra in a unit cell with a strong covalent bond of Sb—O and each double chain is held to the next chain only by weak Van der Waals forces. Orthorhombic structured Sb_2O_3 has a pseudo-two-dimensional structure, which is seldom found in oxides (17). This kind of molecular structure can confine and promote one-dimensional growth along one particular axis, as has been demonstrated for tungsten (18) and molybdenum trioxide nanobelts (19). In addition, one-dimensional growth occurs because the orthorhombic lattice is intrinsically anisotropic and has a unique (001) axis (20, 21). Sb and O atoms are bound in infinite pseudo-two-dimensional hexagonal sheets along the [001] direction. It is the large difference in lattice parameters between *b* and *a* and *c* in the orthorhombic Sb_2O_3 that leads to the notably different growth rates in different directions and belts with a large width-to-length ratio form come into being. It is the inherent chain type of Sb_2O_3 that could demonstrate the structure that tends to exhibit belt-like growth along the [001] direction (22, 23).

Fig. 4. XPS spectra of a Sb_2O_3 belt. (*a*) Survey spectrum. (*b*) Sb region.

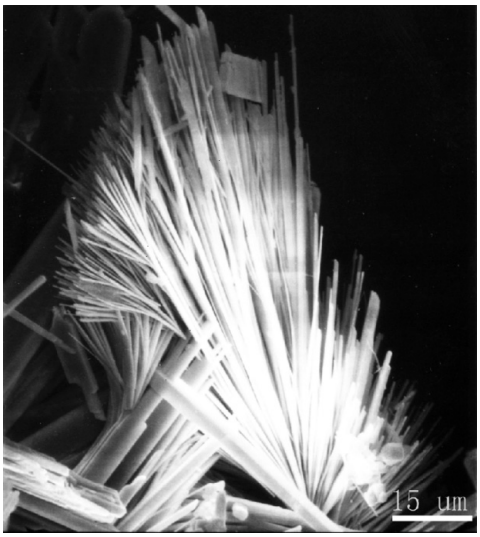


Scheme 1. Chain structure of Sb_2O_3.



© 2005 NRC Canada

Fig. **5.** SEM image of Sb_2O_3 broom-like belts at 9 h.



For a better understanding of the synthesis of Sb_2O_3 belts, we performed several experiments in which intermediates were collected at different times. In this experiment, the products with the reaction time of 3 h were removed and checked with SEM. It was found that the products were mainly slabs that exhibited nonuniform roughness. Prolonging the reaction time resulted in slabs that kept on growing along the preferred growth direction until at 9 h small Sb_2O_3 belts could be obtained in combination with some short rods, which had not been able to evolve into complete belts (Fig. 5). During the growth course from rods to belts, owing to the different growth rates at different sites, tip slipping occurred, which eventually resulted in bundle broom-like belts.

It was also found that many factors, such as temperature and molar ratio of $SbCl_3$ to urea, had a profound influence on the morphology of the product. The suitable temperature and reaction time provided a greater possibility for nucleation and growth of belt-like crystals. For example, if the reaction temperature was decreased to 80 °C, the decomposition of urea was very slow, and as a result, the nucleation and growth rate of the crystals were also very slow and the major products were solids with irregular shapes. The influence of the molar ratio between $SbCl_3$ and urea, which is a prerequisite for controlling the synthesis of Sb_2O_3 with different product morphologies, has also been investigated in some detail. If the molar ratio between $SbCl_3$ and urea was decreased to 1:1, rough irregular flakes (Fig. 6) were formed. However, when the molar ratio between $SbCl_3$ and urea was changed to 1:3 or 1:5, minor belts of Sb_2O_3 were also produced in addition to the existence of irregular particles. However, if the ratio of $SbCl_3$ to urea was increased to 1:10, short rods (Fig. 7) were formed as the final product. Therefore, it is worth pointing out that a molar ratio of 1:4 between $SbCl_3$ and urea is the optimal experimental condition to produce broom-like belts of Sb_2O_3.

Summary

In summary, broom-like belts and rods of Sb_2O_3 were successfully synthesized from $SbCl_3$ and urea via a simple mild process. If the molar ratio of $SbCl_3$ to urea is 1:4, the main products are broom-like belts of Sb_2O_3. Changing the molar ratio of $SbCl_3$ to urea to 1:10 results in the transformation of the broom-like belts to rods. Sb_2O_3 with both these morphologies may have applications in many areas. The influence of reaction temperature and reaction time on the formation of different morphologies was also investigated in detail. This synthesis route provides a simple method for preparing broom-like belts of Sb_2O_3, which could offer new opportunities for technological applications.

Fig. 6. SEM image of Sb_2O_3 with an irregular shape ($SbCl_3$:urea = 1:1).

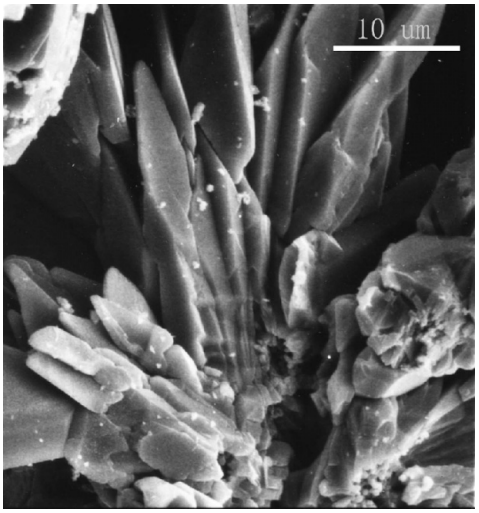
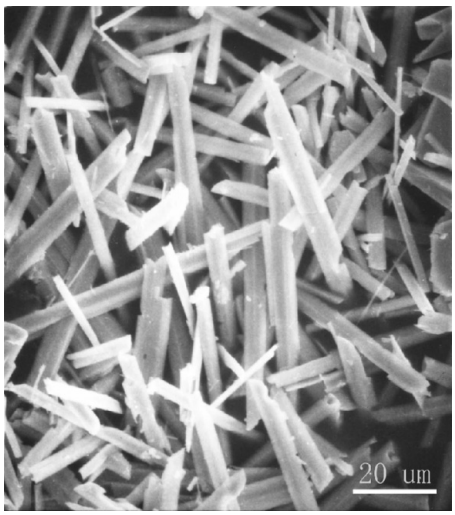


Fig. 7. SEM image of Sb_2O_3 short rods ($SbCl_3$:urea = 1:10).



Acknowledgments

This work was supported by the National Natural Science Foundation of China and the Chinese Ministry of Education.

References

1. S. Iijima. Nature (London), **354**, 56 (1991).
2. J. Hu, L.S. Li, W. Yang, L. Manna, L.W. Wang, and A.P. Alivisatos. Science, **292**, 2060 (2001).

© 2005 NRC Canada

3. A. Aoki, Y. Tamagawa, and T. Miyashita. Macromolecules, **35**, 3686 (2002).
4. A.P. Alivisatos. Science (Washington, D.C.), **271**, 933 (1996).
5. N. Tessler, V. Medvedev, M. Kazes, S. Kan, and U. Banin. Science, **295**, 1506 (2002).
6. S.W. Jung, W.I. Park, and G.C. Yi. Adv. Mater. (Weinheim Ger.), **15**, 1358 (2003).
7. Z.W. Pan, Z.R. Dai, and Z.L. Wang. Science, **291**, 1947 (2001).
8. M. Law, H. Kind, B. Messer, F. Kim, and P.D. Yang. Angew. Chem. Int. Ed. **41**, 2405 (2002).
9. Z.P. Liu, S. Li, Y. Yang, S. Peng, Z.K. Hu, and Y.T. Qian. Adv. Mater. (Weinheim Ger.), **22**, 1946 (2003).
10. J.H. Jung, H. Kobayashi, K.J.C. Van Bommel, S. Shinkai, and T. Shimizu. Chem. Mater. **14**, 1445 (2002).
11. B. Pillep, P. Behrens, U.A. Schuber, J. Spengler, and H. Konezinger. J. Phys. Chem. B, **103**, 9595 (1999).
12. C.H. Ye, G.W. Meng, L.D. Zhang, G.Z. Wang, and Y.H. Wang. Chem. Phys. Lett. **363**, 34 (2002).
13. Y.X. Zhang, G.H. Li, and L.D. Zhang. Chem. Lett. **33**, 334 (2004).
14. L. Guo, Z.H. Wu, T. Liu, W.D. Wang, and H.S. Zhu. Chem. Phys. Lett. **318**, 49 (2000).
15. S. Friedrichs, R.R. Meyer, J. Sloan, A.I. Kirkland, J.L. Hutchison, and M.L.H. Green. Chem. Commun. 929 (2001).
16. U.A. Schubert, F. Anderle, J. Spengler, J. Zuehlker, H.J. Eberle, R.K. Grasselli, and H. Knoezinger. Top. Catal. **15**, 195 (2001).
17. S.F. Xiang, X.S. Yan, T.L. Cao, and B.N. Guo. *In* Inorganic chemistry series. Vol. 4. Scientific Press, Beijing. 1998. p. 442.
18. Y.B. Li, Y. Bando, D. Golberg, and K. Kurashima. Chem. Phys. Lett. **367**, 214 (2003).
19. X.L. Lin, J.F. Liu, and Y.D. Li. Appl. Phys. Lett. **81**, 4832 (2002).
20. Z.Y. Tang, N.A. Kotov, and M. Giersig. Science, **297**, 237 (2002).
21. X.B. Cao, Y. Xie, and L.Y. Lin. J. Solid State Chem. **177**, 202 (2004).
22. X.W. Zheng, Y. Xie, L.Y. Zhu, X.C. Jiang, Y.B. Jia, W.H. Song, and Y.P. Sun. Inorg. Chem. **41**, 455 (2002).
23. B. Gates, Y.D. Yin, and Y.N. Xia. J. Am. Chem. Soc. **122**, 12 582 (2000).

© 2005 NRC Canada

Study of the nitration of di-*n*-octylcrown-6 calix[4]arene using LC–MS, NMR, and molecular modelling

C.K. Jankowski, M.-R. Van Calsteren, N. Aychet, J.F. Dozol, C. Moulin, and C. Lamouroux

Abstract: The selective HNO_3 nitration of di-*n*-octylcrown-6 calix[4]arene using different conditions, studied with LC–MS and NMR (^1H and ^{13}C) spectroscopic techniques, lead to the identification of most of the expected nitro derivative isomeric compounds. The formation of these isomers under acidic and radiolytic conditions is discussed with the help of molecular modelling.

Key words: calix crown compounds, nitration of calixarenes, NMR of isomeric nitrocalixarenes, LC–ESI-MS.

Résumé : La nitration sélective au HNO_3 du di-*n*-octylcouronne-6 calix[4]arène dans différentes conditions, étudiée par des techniques spectroscopiques de LC–MS et de RMN (^1H et ^{13}C), conduisent à l'identification de la plupart des isomères de dérivés nitro attendus. La formation de ces isomères dans des conditions acides et radiolytiques est discutée avec l'aide de la modélisation moléculaire.

Mots clés : composés calix couronne, nitration de calixarènes, RMN des nitrocalixarènes isomères, LC–ESI-MS.

Introduction

The calixarene crown compounds have their notoriety as efficient and selective extractants of several cations, for example, cesium in the presence of sodium (1) within the nuclear spent fuel reprocessing framework. Nitric acid slurries contaminated with radioactive material could be treated with calix[4]arenes derivatives in order to extract or to retain some of the radioactive cations (2).

The calix[4]arene crown-6 compounds have an exceptional capacity to bind (complex) Cs^+ cations, in particular ^{137}Cs or ^{135}Cs. Unfortunately, during this process, the aromatic ring of the calixarenes could be nitrated via the acid-catalysed or radiolytic (probably assisted by radiolysis) processes. This can decrease their extractant ability, in particular by hindering crown access to the cations, and lead to a deterioration in the performance of a calix[4]arene crown-6 based device (diaphragm) (3).

In this study, we would like to report on the nitration of di-*n*-octyl calix[4]arene crown-6 (oct-MC-6 or as used in this paper c0o0) (4)[2,3]. This compound was found to be a promising cesium extractant, combining fair stability under industrial radiolysis conditions, conformational homogeneity (1,3-alternate conformation only), and as a result of that, lipophilic octyl chains are in a preferred anti position to the crown orientation (5) (Figs. 1 and 2).

Under uncontrolled nitration conditions, such as those used during the reprocessing of nuclear fuel, several nitrations can take place. First, the nitric phase is strongly acidic and this leads to the aromatic S_E substitution of one or more of the calix[4]arene crown-6 aromatic rings. It is then foreseeable that up to eight isomeric nitrocalix[4]arene crown-6 compounds having from one to four NO_2 groups placed in the electronically favoured para position (para to the electrodonating crown or octyloxy substituents) can be obtained. Some of these isomers can also be obtained from the radical $NO_2\cdot$ reaction with the aromatic ring. Nitration of an oct-MC-6 from the crown side in particular could block access to this cavity for the Cs^+ cation and subsequently reduce the extractant capacity of the entire system.

The nitration of the benzylic methylene of the crown ether or of the octyl chain methylenes could be considered less probable and more related to the radical nitration.

These two nitrations, S_E or radical, were observed in our previous studies of a nuclear fuel solvent reprocessing cycle (tributylphosphate, TBP) (6).

Received 12 January 2005. Published on the NRC Research Press Web site at http://canjchem.nrc.ca on 15 September 2005.

C.K. Jankowski[1] and M.-R. Van Calsteren. Département de chimie et biochimie, Faculté des sciences, Université de Moncton, Moncton, NB E1A 3E9, Canada.
N. Aychet, J.F. Dozol, C. Moulin, and C. Lamouroux. DEN/DPC/SECR/LSRM, Bat. 391, Centre d'Études de Saclay, b.p. 2, 91191 Gif-sur-Yvette, France.

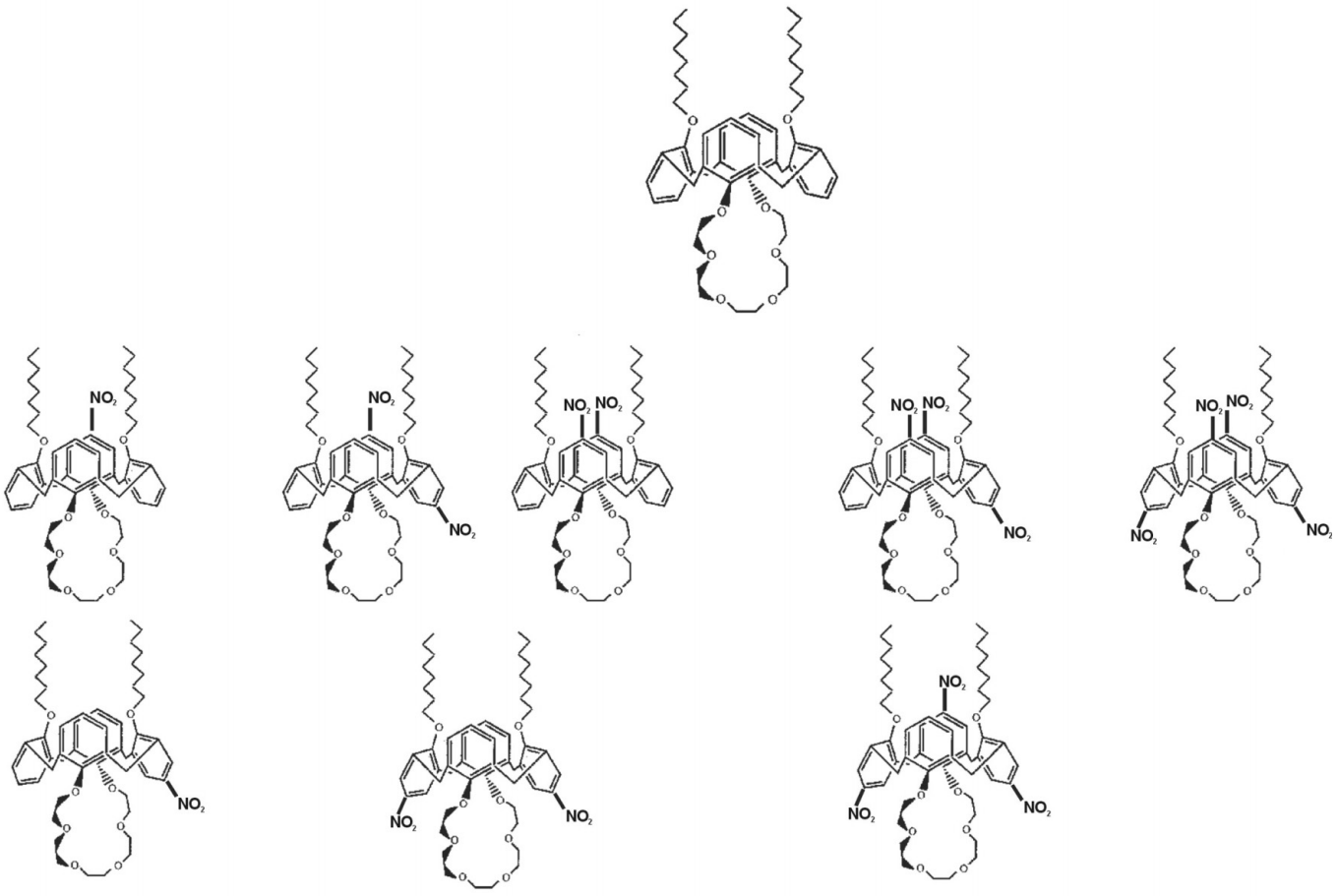
[1]Corresponding author (email: jankowc@umoncton.ca).

[2]Formal name 26,27-bis(1-octyloxy)calix[4]arene crown-6.

[3]c0o0 means – no nitro group on either the crown or octyl side; c1o1 – one nitro on each side, octyl and crown; c1o2 - one nitro on the crown side and two on the octyl side, etc.

 doi: 10.1139/V05-126 © 2005 NRC Canada

Fig. 1. Structures of calixarenes in this study. First row: oct-MC-6 (c0o0); Second row left to right: (NO_2)-oct-MC-6 (c0o1), $(NO_2)_2$-oct-MC-6 (c1o1), $(NO_2)_2$-oct-MC-6 (c0o2), $(NO_2)_3$-oct-MC-6 (c1o2), $(NO_2)_4$-oct-MC-6 (c2o2); Third row left to right: (NO_2)-oct-MC-6 (c1o0), $(NO_2)_2$-oct-MC-6 (c2o0), $(NO_2)_3$-oct-MC-6 (c2o1).



Although most similar calix[4]arene crown compounds when tested under radiolysis displayed good stability of the skeleton structure, several substitution reactions were also observed (7). During these studies, it was necessary to develop selective nitration methodology. For di-isopropyl-MC-6 and biscrown BC-6 calix[4]arenes, several nitro isomers were prepared and the structures were identified using electrospray ionization mass spectrometry (ESI-MS) (8).

In this study, while pursuing the search for selective synthesis of different nitro-oct-MC-6, a detailed study of these complex molecules with a complete assignment of their spectra was performed (Tables 1–6) by high-resolution NMR (^{1}H and ^{13}C). We also report on LC–MS use for this identification together with ESI-MS (Table 7). Finally, some mechanistic hypotheses for the formation of specific isomers were advanced with the help of molecular modelling (Table 8).

Synthesis

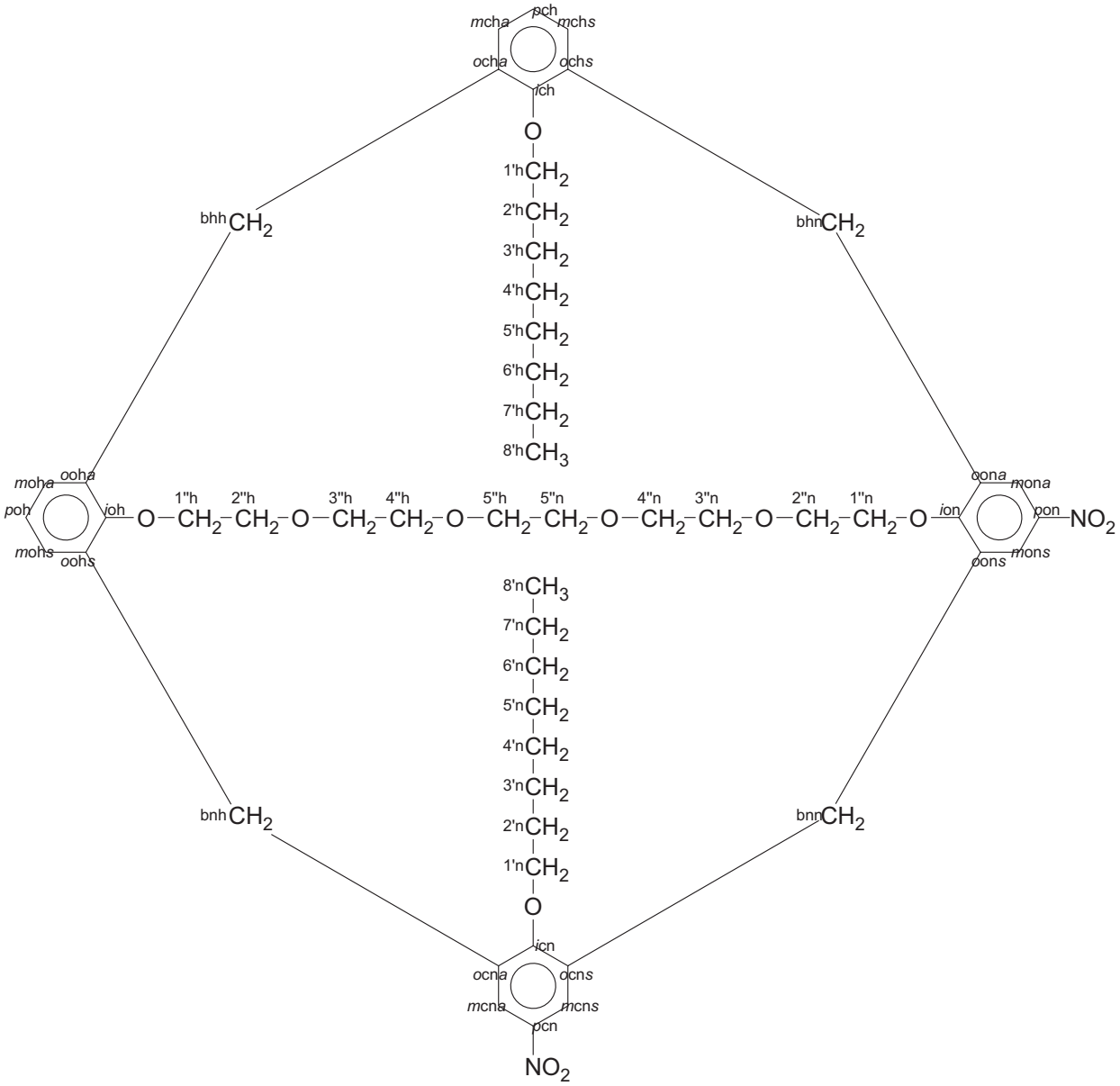
There are many methods of pernitration of activated aromatic rings. The calix[4]arene crown compounds, which formally are phenol ethers, fully maintain this capacity and react easily, despite some solubility problems showed by the parent polyphenol substrates (9). The selective nitration of similarly activated aromatic rings is a more sensitive reaction. The usual methodology applied to obtain some specific undernitrated isomers is to use the low-temperature nitration with formation of the S_E postulated intermediate NO_2^+ cation stabilized by an acetate or trifluoroacetate anion. The second approach is the use of nitrates. The most common approach, however, remains the undernitration of the substrate followed sometimes by very tedious separation of the resulting isomers. The nitration of calix[4]arene crowns under several conditions were successfully attempted by our group (8) by using seven different methods of nitration leading to the identification of almost all the possible isomeric nitro isomers of di-isopropyl calix[4]arene crown-6 and calix[4]arene biscrown-6 (Fig. 1).

The calix[4]arene studied in this paper has two *n*-octyl chains and one crown; both substituents of the calix[4]arene ring have a similar activating effect on the nitration of the molecule fixed in the 1,3-alternate conformation.

Access to specific isomers of nitro-oct-MC-6 is possible with the use of our previous methodology of low-temperature nitration. There are eight different polynitrated oct-MC-6 compounds in total: two isomeric mononitro-oct-MC-6, one with the NO_2 on the crown side (c1o0) and one on the *n*-octyl side (c0o1) of the molecule; three dinitro –

© 2005 NRC Canada

Fig. 2. Nomenclature used to report NMR data taking as an example the trans $(NO_2)_2$-oct-MC-6 (c1o1) molecule.



two cis, one with two NO_2 on the crown side (c2o0) and the other with two NO_2 on the *n*-octyl side (c0o2), and one *trans*-dinitro-oct-MC-6 having one NO_2 group on each side of the molecule (c1o1); two trinitro-oct-MC-6 (c2o1 and c1o2); and finally, one tetranitro-oct-MC-6 (c2o2).

The most challenging synthetic problem was the synthesis of specific mononitro and dinitro compounds.

The use of nitric acid at low temperature with acetic anhydride or trifluoroacetic anhydride leads to the discrete synthesis of two resulting mononitro isomers. In a second successful synthesis, we obtained two dinitro-oct-MC-6 of a total of three possible, by modification and strict control of the reaction conditions. The trinitro-oct-MC-6 was obtained as a secondary nitration product in several attempts; however, its specific synthesis from the dinitro-oct-MC-6 of known geometry was achieved only after rigorous identification of the starting dinitro-oct-MC-6 structure as c2o0. In total, six specific nitro-oct-MC-6 were synthesized and their structures established.

During this work, it was necessary to develop a reliable and fast method of identification of nitro-oct-MC-6 derivatives. This was done first by using the fast ESI-MS method on the Cs^+ spiked solution of oct-MC-6 (10–12); we have tried to cross compare the results using LC and LC–MS techniques.

In general, the more rigorous but slower method using LC needs specific standards to give a quantitative picture of the reaction. The LC method offers the possiblity of determining specific isomers.

Both techniques (MS and LC) are complementary in the synthetic framework and were constantly used in this study. However, despite all these important qualities, they do not completely identify the structure of isomeric nitro-oct-MC-6; this could only be done by the use of NMR.

© 2005 NRC Canada

Table 1. NMR data for oct-MC-6 (c0o0).

Position	δ_C (ppm)	Multiplicity	δ_H (ppm)	No. H	Multiplicity	*J* (Hz)
*i*c	156.98	Q	—			
*o*c	134.08	Q	—			
*m*c	129.63	T	7.079	4	d	7.5
*p*c	122.10[a]	T	6.825	2	t	7.5
*i*o	156.51	Q	—			
*o*o	133.74	Q	—			
*m*o	129.79	T	7.012	4	d	7.4
*p*o	122.09[a]	T	6.770	2	t	7.4
b	37.94	S	3.775	8	s	—
1′	70.64	S	3.43	4	t	7
2′	29.44[b]	S	1.23[c]		m	
3′	25.86	S	1.13	4	m	
4′	29.73[b]	S	1.3–1.2[c]		m	
5′	29.35[b]	S	1.3–1.2[c]		m	
6′	31.95	S	1.29[c]		m	
7′	22.76	S	1.33[c]		m	
8′	14.16	P	0.92	6	t	7
1″	69.88	S	3.589	4	t	6.0
2″	69.93	S	3.386	4	t	6.0
3″	71.02	S	3.492	4	m	6.1, 3.5[d]
4″	71.10	S	3.654	4	m	6.1, 3.5[d]
5″	71.23	S	3.705	4	s	—

[a,b]Assignments interchangeable.
[c]Total: 20 H.
[d]Geminal coupling ambiguous.

Table 2. NMR data for (NO_2)-oct-MC-6 crown side (c1o0).

Position	δ_C (ppm)	Multiplicity	δ_H (ppm)	No. H	Multiplicity	*J* (Hz)
*i*ch	156.74	Q	—			
*o*ch	133.51	Q	—			
*m*ch	129.75	T	7.095	2	d	7.5
*p*ch	122.38	T	6.836	1	t	7.5
*i*cn	162.78	Q	—			
*o*cn	135.51	Q	—			
*m*cn	125.19	T	8.007	2	s	—
*p*cn	142.01	Q	—			
*i*o	156.34	Q	—			
*o*oa	134.05	Q	—			
*o*os	132.23	Q	—			
*m*oa	130.47	T	7.038	2	dd	7.6, 1.7
*m*os	129.65	T	7.007	2	dd	7.7, 1.7
*p*o	122.38	T	6.792	2	t	7.7, 7.6
bh	37.81	S	3.775	4	s	—
bn	37.80	S	3.859	2	d	–15.4
		0	3.774	2	d	–15.4
1′h	70.58	S	3.44[a]		m	
2′h	29.40	S	1.21[b]		m	
3′h	25.82	S	1.13[c,d]		m	
4′h	29.71[e]	S	1.3–1.2[b]		m	
5′h	29.66[e,f]	S	1.3–1.2[b]		m	
6′h	31.92	S	1.28[b,c]		m	
7′h	22.75	S	1.34[b]		m	
8′h	14.15	P	0.91[g]		t	7
1′n	71.44	S	3.49[a]		m	
2′n	29.65[f]	S	1.35[b]		m	
3′n	25.73	S	1.17[c,d]		m	

© 2005 NRC Canada

Table 2 (*concluded*).

Position	δ_C (ppm)	Multiplicity	δ_H (ppm)	No. H	Multiplicity	*J* (Hz)
4′n	29.42[e]	S	1.3–1.2[b]		m	
5′n	29.40[e]	S	1.3–1.2[b]		m	
6′n	31.91	S	1.29[b,c]		m	
7′n	22.73	S	1.34[b]		m	
8′n	14.15	P	0.91[g]		t	7
1″	69.99	S	3.73	2	m	
		0	3.58[a]		m	
2″	69.80	S	3.37[a]		m	
3″	71.08	S	3.50[a,c]		m	
4″	70.62	S	3.58[a,c]		m	
5″	70.89	S	3.634	4	s	—

[a]Total: 18 H.
[b]Total: 20 H.
[c]From the CHORTLE experiment.
[d]Total: 4 H.
[e,f]Assignments interchangeable.
[g]Total: 6 H.

Table 3. NMR data for $(NO_2)_2$-oct-MC-6 cis crown side (c2o0).

Position	δ_C (ppm)	Multiplicity	δ_H (ppm)	No. H	Multiplicity	*J* (Hz)
*i*c	162.49	Q	—			
*o*c	135.22	Q	—			
*m*c	124.99	T	8.020	4	s	—
*p*c	142.26	Q	—			
*i*o	156.19	Q	—			
*o*o	132.60	Q	—			
*m*o	130.19	T	7.055	4	d	7.5
*p*o	122.80	T	6.849	2	t	7.5
b	37.85	S	3.914	4	d	–16.1
			3.820	4	d	–16.1
1′	71.04	S	3.48	4	m	
2′	29.64	S	1.24[a]		m	
3′	25.64	S	1.11	4	m	
4′	29.38[b]	S	1.24[a,b,c]		m	
5′	29.37[b]	S	1.27[a,b,c]		m	
6′	31.91	S	1.29[a]		m	
7′	22.74	S	1.34[a]		m	
8′	14.14	P	0.92	6	t	7
1″	69.84	S	3.662	4	t	6.2
2″	69.38	S	3.272	4	t	6.2
3″	71.38	S	3.47[c]	4	m	
4″	70.48	S	3.50[c]	4	m	
5″	70.96	S	3.554	4	s	—

[a]Total: 20 H.
[b]Assignments interchangeable.
[c]From the CHORTLE experiment.

Liquid chromatography study of nitration of oct-MC-6

The determination of postreaction mixtures of oct-MC-6 was done using a C18 or TSK-GEL Super-ODS column. Using several samples from different nitration trials, we prepared a reconstructed mixture with some spiking with pure synthetic isomers (13, 14). We were then able to identify up to six isomeric nitro-oct-MC-6 from the spent fuel samples and to separate up to seven of the eight possible isomers of the nitration reactions (Table 7). The only missing isomer, polynitro-oct-MC-6, seems to be one of the three dinitro compounds, although there was a small peak in the LC within the expected retention time area corresponding to its presence.

The detection of isomeric nitro-oct-MC-6 followed the logical trend of retention times as presented in Figs. 3–5 and Table 7. The detection of these derivatives varied according to the wavelength used. However, using the appropriate analytical grade synthetic standards, such as the starting oct-

© 2005 NRC Canada

Table 4. NMR data for (NO_2)-oct-MC-6 octyl side (c0o1).

Position	δ_C (ppm)	Multiplicity	δ_H (ppm)	Multiplicity	J (Hz)
*i*c	156.80	Q	—		
*o*ca	134.26	Q	—		
*o*cs	132.63	Q	—		
*m*ca	130.36	T	7.114	dd	7.6, 1.6
*m*cs	129.74	T	7.089	dd	7.6, 1.6
*p*c	122.42	T	6.847	t	7.6, 7.6
*i*oh	156.30	Q	—		
*o*oh	133.34	Q	—		
*m*oh	130.04	T	7.007	d	7.5
*p*oh	122.21	T	6.756	t	7.5
*i*on	161.85	Q	—		
*o*on	135.18	Q	—		
*m*on	125.50	T	7.973	s	—
*p*on	142.10	Q	—		
bh	37.71	S	3.756	s	—
bn	37.52	S	3.846	d	–15.2
			3.778	d	–15.2
1′	71.13[a]	S	3.55	m	
2′	29.41[b]	S	1.32	m	
3′	25.90	S	1.4–1.1	m	
4′	29.71[b]	S	1.4–1.1	m	
5′	29.67[b]	S	1.4–1.1	m	
6′	31.93	S	1.29	m	
7′	22.73	S	1.33	m	
8′	14.15	P	0.91	t	7
1″h	70.02	S	3.63	m	
2″h	69.97	S	3.40	t	6
3″h	71.13[a]	S	3.68[a]	m	
4″h	71.11[a]	S	3.55[a]	m	
5″h	71.31[a]	S	3.702	s	—
1″n	71.21[a]	S	3.545	s	—
2″n	70.19[a]	S	3.545	s	—
3″n	71.16[a]	S	3.63[a]	m	
4″n	71.11	S	3.47[a]	m	
5″n	71.21[a]	S	3.702	s	—

[a,b]Assignments interchangeable.

Table 5. NMR data for $(NO_2)_2$-oct-MC-6 trans (c1o1).

Position	δ_C (ppm)	Multiplicity	δ_H (ppm)	No. H	Multiplicity	J (Hz)
*i*ch	156.51	Q	—			
*o*ch*a*	133.73[a]	Q	—			
*o*ch*s*	131.97	Q	—			
*m*ch*a*	130.61	T	7.154	1	dd	7.7, 1.7
*m*ch*s*	129.84	T	7.124	1	dd	7.6, 1.7
*p*ch	122.73	T	6.875	1	t	7.7, 7.6
*i*cn	162.48	Q	—			
*o*cn*a*	135.67	Q	—			
*o*cn*s*	134.06	Q	—			
*m*cn*a*	125.85	T	8.039	1	d	2.8
*m*cn*s*	125.28	T	8.022	1	d	2.8
*p*cn	142.17[b]	Q	—			
*i*oh	156.11	Q	—			
*o*oh*a*	133.68[a]	Q	—			
*o*oh*s*	131.79	Q	—			
*m*oh*a*	130.75	T	7.039	1	dd	7.6, 1.9
*m*oh*s*	129.84	T	7.006	1	dd	7.7, 1.9

© 2005 NRC Canada

Table 5 (*concluded*).

Position	δ_C (ppm)	Multiplicity	δ_H (ppm)	No. H	Multiplicity	*J* (Hz)
*p*oh	122.46	T	6.783	1	t	7.7, 7.6
*i*on	161.63	Q	—			
*o*on*a*	135.46	Q	—			
*o*on*s*	133.66[a]	Q	—			
*m*on*a*	126.17	T	8.002	1	d	2.9
*m*on*s*	125.32	T	7.971	1	d	2.9
*p*on	142.19[b]	Q	—			
bhh	37.55	S	3.761	2	s	—
bhn	37.43	S	3.857	1	d	–14.9
			3.785	1	d	–14.9
bnh	37.52	S	3.845	1	d	–14.7
			3.776	1	d	–14.7
bnn	37.32	S	3.854	2	s	—
1′h	71.08	S	3.54[c]		m	
2′h	29.38[d,e]	S	1.30[f]		m	
3′h	25.87	S	1.18[f]		m	
4′h	29.70[e]	S	1.4–1.1[f]		m	
5′h	29.65[d,e]	S	1.4–1.1[f]		m	
6′h	31.91	S	1.29[f]		m	
7′h	22.72	S	1.33[f]		m	
8′h	14.14	P	0.92[g]		t	7
1′n	71.91	S	3.65[c]		m	
2′n	29.58[d,e]	S	1.45	2	m	
3′n	25.78	S	1.22[f]		m	
4′n	29.51[d,e]	S	1.4–1.1[f]		m	
5′n	29.32[c]	S	1.4–1.1[h]		m	
6′n	31.88	S	1.29[f]		m	
7′n	22.70	S	1.33[f]		m	
8′n	14.13	P	0.92[g]		t	7
1″h	70.21	S	3.75[c]		m	
			3.62[c]		m	
2″h	69.87	S	3.40[c]		m	
			3.33[c]		m	
3″h	71.11[h]	S	3.7–3.4[c]		m	
4″h	70.64[h]	S	3.7–3.4[c]		m	
5″h	70.89[i]	S	3.632[c]		s	—
1″n	71.33	S	3.77	1	m	
			3.57[c]		m	
2″n	69.99	S	3.61[c]		m	
3″n	71.23[h]	S	3.7–3.4[c]		m	
4″n	70.92[h,i]	S	3.7–3.4[c]		m	
5″n	70.76[i]	S	3.632[c]		s	—

[a,b]Assignments interchangeable.
[c]Total: 23 H.
[d,e]Assignments interchangeable.
[f]Total: 22 H.
[g]Total: 6 H.
[h,i]Assignments interchangeable.

MC-6 or one of the dinitro isomers $(NO_2)_2$-oct-MC-6, the mixture constituents could be quantified.

Assuming that the starting oct-MC-6 has a relative retention time of 1.00, all polynitro-oct-MC-6 derivatives followed in order; for example, mono-, di-, tri-, and finally tetranitro compounds. This detection was based on several crude nitration mixture analyses and in particular on those coming from the real-life nuclear cycle of fuel reprocessing. In this manner, we were able, for instance, to identify that only one mononitro-oct-MC-6 of two possible (Fig. 3) and one dinitro-oct-MC-6 (Fig. 4) of three isomers were present in these slurries (with trace quantities of the other isomers at an equal nitration level). Because both mononitro-oct-MC-6 were synthesized, we were able to identify which of the two was a result of radiolysis.

Curiously, in several of the synthetic mixtures obtained as a result of temperature variation during nitration, we were able to identify and confirm most of the missing or difficult to synthesize in larger quantity isomers, using the other analytical tool MS. This method is also a very reliable way to

© 2005 NRC Canada

Table 6. NMR data for $(NO_2)_3$-oct-MC-6 two crown, one octyl (c2o1).

Position	δ_C (ppm)	Multiplicity	δH (ppm)	No. H	Multiplicity	*J* (Hz)
ic	162.21	Q	—			
oca	135.43	Q	—			
ocs	134.18	Q	—			
mca	125.71	T	8.051	2	d	3.0
mcs	125.09	T	8.040	2	d	3.0
pc	142.45	Q	—			
*i*oh	156.02	Q	—			
*o*oh	132.25	Q	—			
*m*oh	130.40	T	7.055	2	d	7.5
*p*oh	122.93	T	6.848	1	t	7.5
*i*on	161.46	Q	—			
*o*on	133.80	Q	—			
*m*on	125.86	T	8.015	2	s	—
*p*on	142.48	Q	—			
bh	37.72	S	3.909	2	d	–16.1
		0	3.817	2	d	–16.1
bn	37.47	S	3.929	2	d	–16.4
		0	3.900	2	d	–16.4
1′	71.43	S	3.61	4	m	
2′	29.46	S	1.31[a]		m	
3′	25.66	S	1.17	4	m	
4′	29.57[b]	S	1.3–1.2[a]		m	
5′	29.33[b]	S	1.3–1.2[a]		m	
6′	31.86	S	1.31[a]		m	
7′	22.69	S	1.32[a]		m	
8′	14.13	P	0.92	6	t	7
1″h	69.96	S	3.652	2	t	5.7
2″h	69.41	S	3.277	2	t	5.7
3″h	71.33[c]	S	3.5–3.4[c,d]		m	
4″h	70.49[c]	S	3.5–3.4[c,d]		m	
5″h	70.88[e]	S	3.537[f]		s	—
1″n	71.24	S	3.733	2	t	5.4
2″n	69.53	S	3.501	2	t	5.4
3″n	71.50[c]	S	3.52[c]	2	t	6
4″n	70.94[c]	S	3.5–3.4[c,d]		m	
5″n	70.68[e]	S	3.537[f]		s	—

[a]Total: 20 H.
[b,c]Assignments interchangeable.
[d]Total: 6 H.
[e]Assignments interchangeable.
[f]Total: 4 H.

quantify the mixtures using the synthetic mononitro-oct-MC-6 (c1o0) isomer as a standard.

Finally, we could compare the LC method to the very efficient and fast evaluation of all oct-MC-6 derivatives using the ESI-MS technique. This comparison was necessary in order to validate and eventually extend the previous claim that the Cs^+ cationization of the crown-6 component of these compounds can be used for this purpose. When the Cs^+ solution is added to the mixture, one can quantify the nitro compounds within this narrow family with a certainty of ±3%–5% (8).

ESI-MS identification of postreaction mixtures

The obvious advantage of ESI over the other techniques remains its speed and the possibility to analyse many samples in a relatively short time using a very simple procedure.

This method, used and developed in our previous studies, is based on cationization by Cs^+ of the crown cavity. In a way, the principle of nuclear fuel reprocessing is used here in the opposite way — the Cs^+ cation is added to the solution and ESI spectra were run on such mixtures, allowing identification of the starting material as well as all the polynitrated oct-MC-6 according to their characteristic *m*/*z* ratios. This technique, however, cannot be used for the identification of isomers, since all isomers having the same mass are present as the same *m*/*z* ion. Examples of typical spectra are presented in Figs. 3 and 4 for mononitro and dinitro isomers, respectively. The presence of other oct-MC-6 cations was also detected, in particular Na^+ cationization for higher nitration level isomers, and to some extent its protonation was also observed (Fig. 5).

In particular, the ion current variation corresponding to *m*/*z* 1053 $[(NO_2)_4$-oct-MC-6 + $Na]^+$, *m*/*z* 963 $[(NO_2)_2$-oct-

© 2005 NRC Canada

Table 7. Relative LC retention time (Rt) of polynitro-oct-MC-6 detected as calixarene-Na^+ ions.

Structure	Type	Rt[a]	No. NO_2	Side
oct-MC-6	c0o0	1.00	0	—
(NO_2)-oct-MC-6	c1o0	0.90	1	Crown
(NO_2)-oct-MC-6	c0o1	0.80	1	Octyl
$(NO_2)_2$-oct-MC-6	c1o1	0.74	2	trans
$(NO_2)_2$-oct-MC-6	c2o0	0.68	2	Crown
$(NO_2)_3$-oct-MC-6	c2o1	0.59	3	Two crown, one octyl
$(NO_2)_4$-oct-MC-6	c2o2	0.31	4	Two crown, two octyl

[a]Real time of 19.66 min on TSK-GEL Super-ODS column (see Experimental).

Table 8. Molecular modelling of oct-MC-6 calixarenes.

Structure	Number of NO_2	Code[a]	Energy (kcal/mol)
oct-MC-6	0	c0o0	41.41
(NO_2)-oct-MC-6	1 crown site	c1o0	37.75
	1 octyl side	c0o1	43.17
$(NO_2)_2$-oct-MC-6	2 cis crown side	c2o0	43.17
	2 cis octyl side	c0o2	48.29
	2 trans	c1o1	41.84
$(NO_2)_3$-oct-MC-6	3 (one octyl side, two crown side)	c2o1	47.34
	3 (one crown side, two octyl side)	c1o2	53.17
$(NO_2)_4$-oct-MC-6	4	c2o2	56.69

Note: See Experimental for details. 1 cal = 4.184 J.
[a]c crown side, o octyl side; for example, c0o0 means no NO_2 group on any of two sites of the calixarene.

MC-6 + Na]$^+$, *m*/*z* 918 [(NO_2)-oct-MC-6 + Na]$^+$, and *m*/*z* 873 [oct-MC-6 + Na]$^+$ ions show that the elution order corresponds to the polarity of the compounds under the given chromatographic conditions. In such a way, the predominant mononitro isomer (NO_2)-oct-MC-6 (c1o0) was established as the main product formed in the slurries under radiolysis (also see the Supporting information).

Molecular modelling

Molecular modelling of all isomeric polynitro-oct-MC-6 was performed using the HyperChem 6 program. These calculations (Table 8) seem to indicate that if the NO_2 group is placed on the crown side, the calculated energy was lower than in the case when this group is placed on the octyloxy side. This trend was also preserved for polynitration in this family as well as for the Cs^+ cation inclusion complexes.

From the calculations, it could also be deduced that in the 1,3-alternate conformation all nitro-oct-MC-6 have the octyl chains oriented to the exterior of the molecule as well as, as already observed (4, 8, 15), the crown was not symmetrical and was bent toward one of the two aromatic rings. The Cs^+-crown complexes were found to be somewhat more stable when compared to the compounds without cations. When the nitration took place from the crown side, the products were less stable; this was also observed for the calculated Cs^+ complexes.

Modelling of the calix[4]arene crown system of the oct-MC-6 compounds was also done assuming that the 1,3-alternate conformation was replaced in the whole series by the partial cone conformation. This conformation was obtained by rotating one of the two benzene rings bearing the octyloxy substituent by 180°. In these cases, the calculated energies were situated at ca. 2 kcal/mol higher for the whole series of nitro-oct-MC-6 compounds.

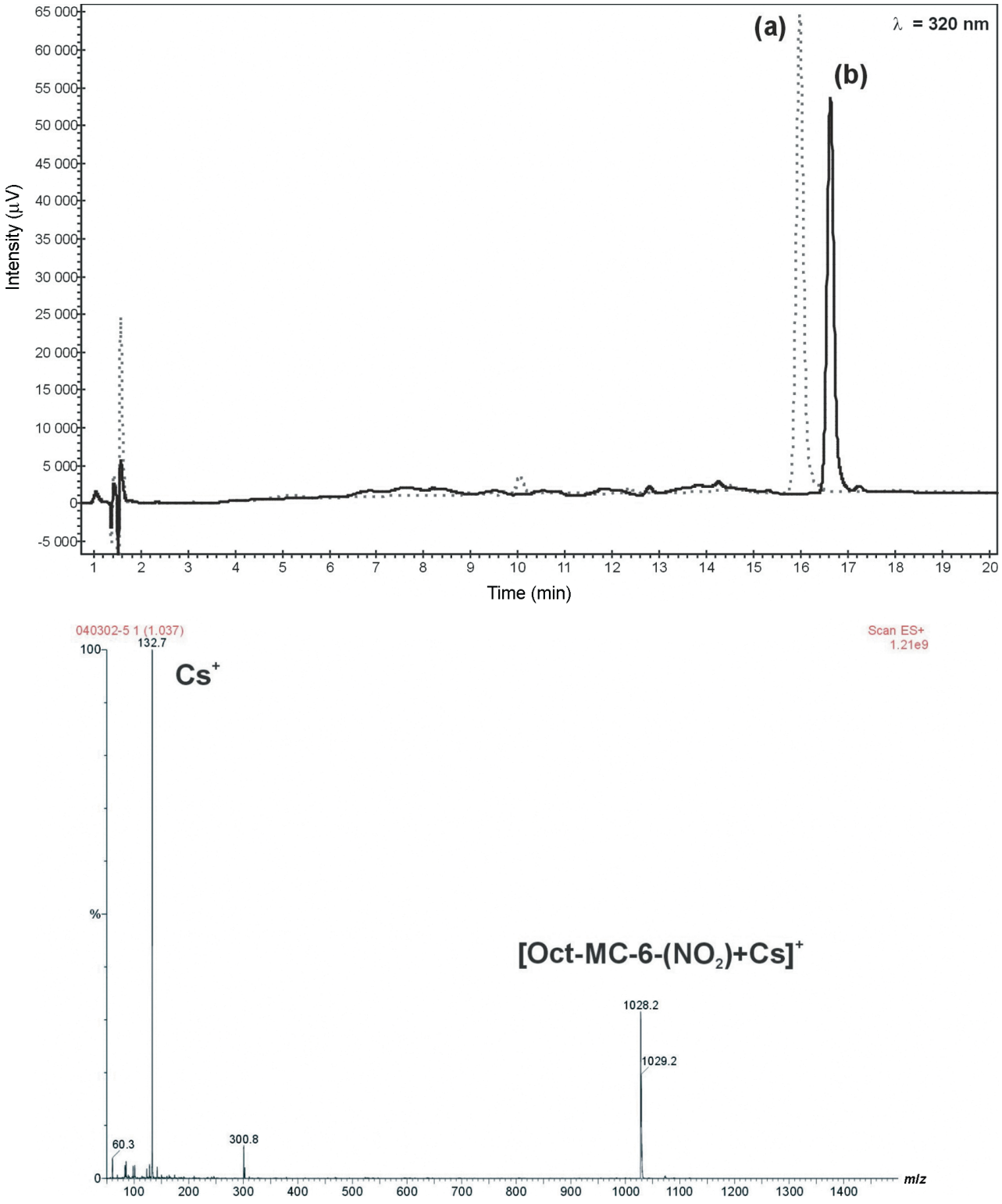
Molecular modelling was attempted to provide a mechanistic hypothesis for the formation of specific isomers according to particular mechanistic pathways. The synthesis of polynitro-oct-MC-6 was done using typical kinetically controlled S_E reaction conditions with the formation of a NO_2^+ cation intermediate, under fuel reprocessing procedures, but contact with the radioactive material could also involve the formation of a radical $NO_2\cdot$ that could subsequently result in many different nitrations. Finally, the highly acidic nitric slurries could also produce their own S_E nitration conditions. The fact that for mononitro derivatives, the lower calculated energy was found for the crown side isomer (c1o0) could indicate that this isomer is obtained from the radical rather than the S_E pathway.

NMR studies of the nitro-oct-MC-6 calixarenes

The assignment of all resolved ^1H and ^{13}C NMR signals was made using several high-resolution 2D experiments, in particular COSY, NOESY, ROESY, HETCOR, HSQC, CHORTLE, and HMBC (16–26). In the following section, we would like to comment on these interpretations, highlighting the most interesting features, and to conclude with

© 2005 NRC Canada

Fig. 3. Comparison of $[M + Cs]^+$ ion chromatogram for (NO_2)-oct-MC-6. (*a*) c0o1 (dotted line); (*b*) c1o0 (solid line).



some conformational observations (detailed spectra interpretation Tables 1–6, Fig. 2).

The molecules were considered as a collection of building blocks roughly corresponding to spectral regions: aromatic, interarylic benzyl methylene, crown, and octyl chain.

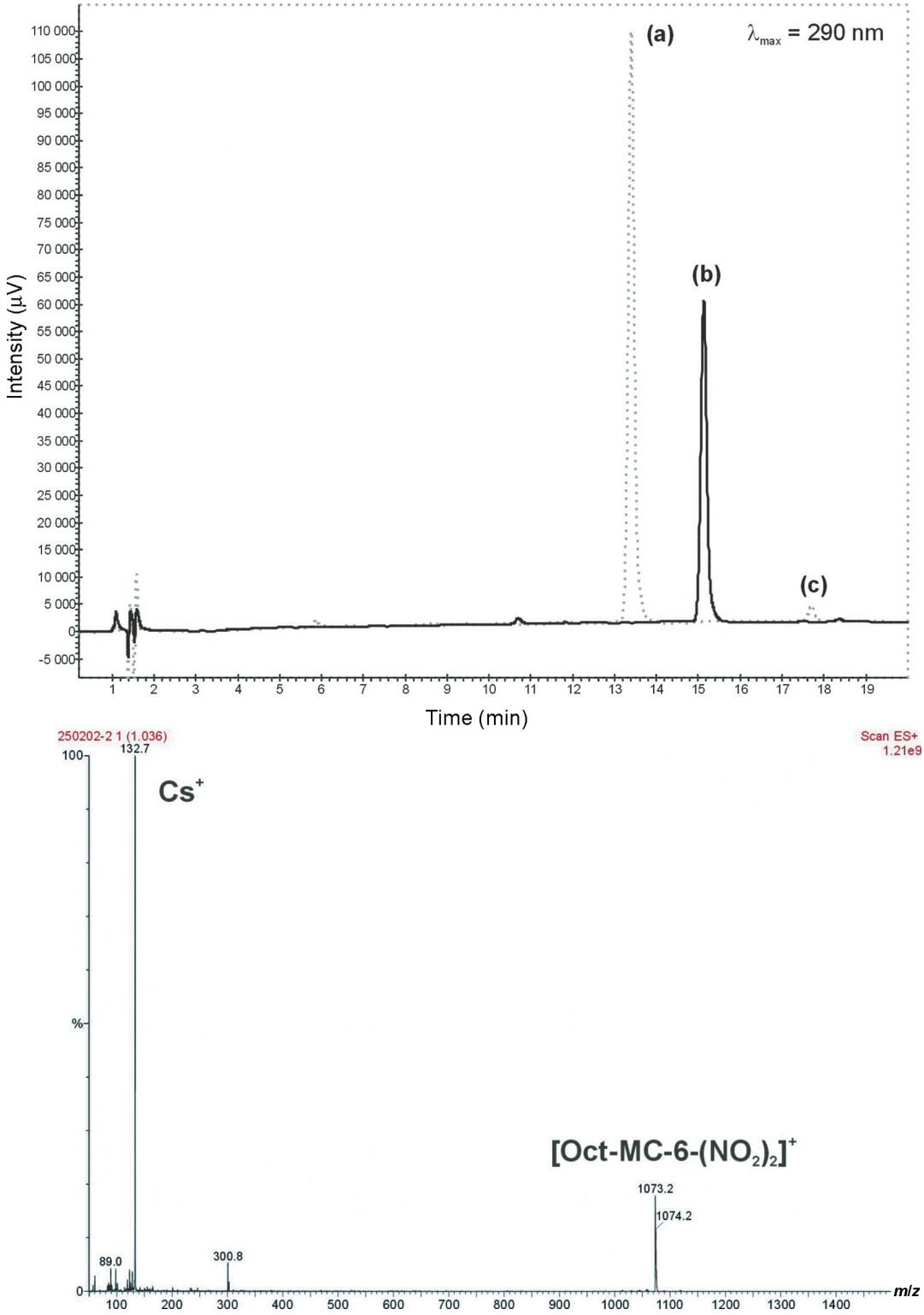
The starting oct-MC-6 (c0o0) compound was first used as a basis in determining the skeleton proton and carbon signals and was then considered as a reference when several nitro groups were added in a regiospecific way.

Nomenclature

Figure 2 displays the structure of the unsymmetrical

© 2005 NRC Canada

Fig. 4. $(NO_2)_2$-oct-MC-6 Cs^+ detection ESI (M, *m*/*z* 1073). LC profiles shown: (*a*) $(NO_2)_2$-oct-MC-6 (c1o1) (dotted line); (*b*) $(NO_2)_2$-oct-MC-6 (c2o0) (solid line); (*c*) $(NO_2)_2$-oct-MC-6 (c0o2) (dashed - traces line).

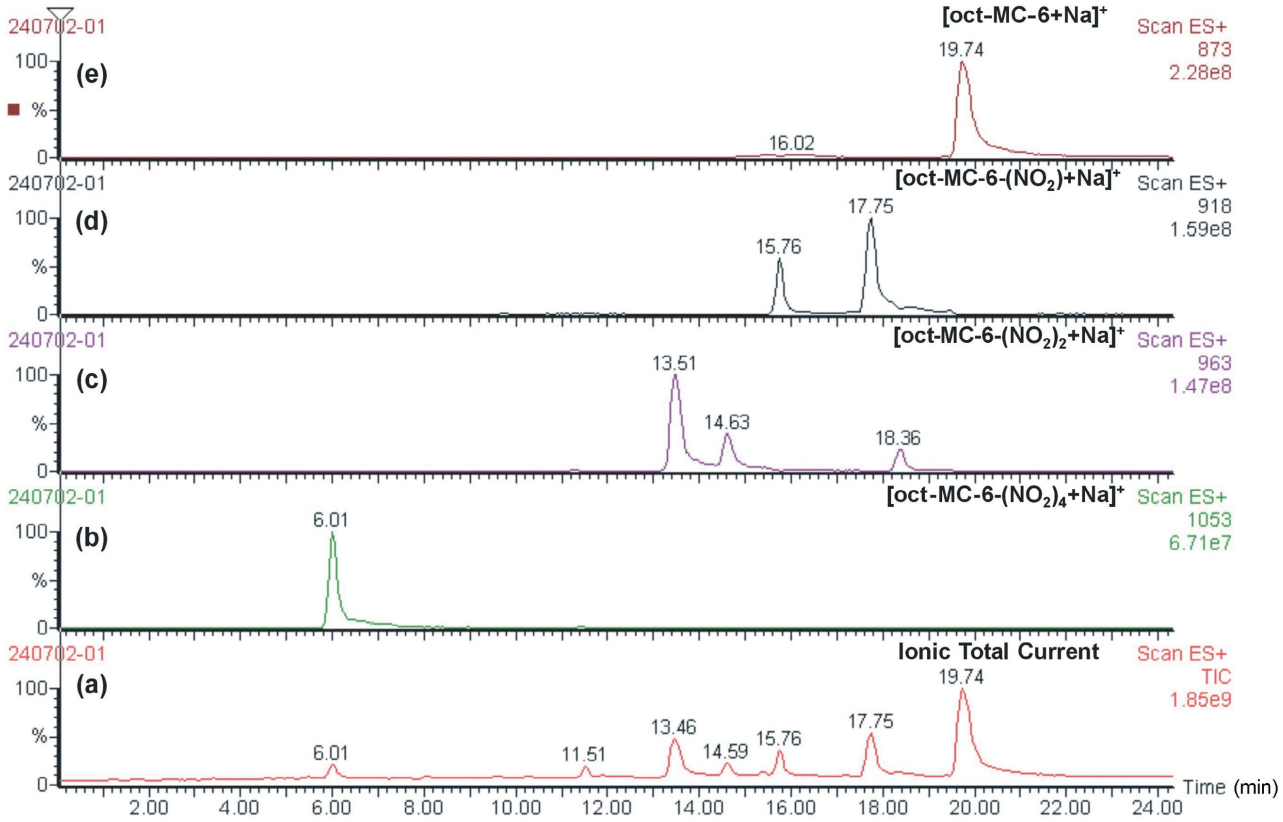


dinitro derivative $(NO_2)_2$-oct-MC-6 (c1o1), the least symmetrical of the nitrocalixarenes studied, which is used to explain the nomenclature used in this paper.

Aromatic carbons are labelled *i*, *o*, *m*, and *p* for ipso, ortho, meta, and para, respectively. The side is identified by c or o depending on whether it is crown or octyl, respectively. Then, h or n is used to identify the hydrogen or nitro substituent in the para position. Finally, *a* or *s* is used to identify whether the side is anti or syn towards an adjacent nitro substituted ring. The benzylic methylenes are labelled b followed by two letters, h or n, describing the hydrogen or nitro substituent on the adjacent aryl rings on the crown and

© 2005 NRC Canada

Fig. 5. LC–MS scan of the crude nitration of oct-MC-6. The corresponding masses of 1053 (tetranitro), 963 (dinitro), 918 (mononitro), and 873 (starting product) refer to $[M + Na]^+$ ions.



octyl sides, in that order. The octyl chain carbons are labelled 1′–8′ with h or n for the hydrogen or nitro substituent on the adjacent aromatic ring. For the crown part of the molecule, 1″–5″ are used, counting the carbons only. Again h or n represents the hydrogen or nitro substituent in the para position of the attached aryl ring.

c0o0

In the aromatic area of the proton spectrum of the parent oct-MC-6 (c0o0), we identified two spin systems of the AA′X type each composed of two meta and one para protons. The nOe effect enabled identification of the interaction between meta protons and 1′ or 1″ and 2″ protons, as well as a small interaction between *p*c and 5″, which led to the precise identification of the orientation of this aryl side toward the calixarene ring. The same system is also a primary indication of the number of nitro groups introduced on the molecule aryl rings. The benzylic methylene signal of this molecule displayed long-range coupling as well as nOe to the meta protons of the aromatic rings. The crown protons displayed two spin systems, one with full averaging corresponding to 1″ and 2″ protons, the other corresponding to 3″ and 4″ protons with only partial averaging despite some ambiguities in geminal coupling interpretation, and one singlet for two methylenes at the centre of the crown system. This observation confirmed a certain conformational flexibility of the crown, especially close to the centre. The chain protons on carbons 1′ and 2′ were assigned from their mutual coupling, H-3′ and H-6′ with the help of ^{13}C correlations, and finally the end protons on C-7′ and C-8′ from coupling to each other. Some minor discrepancies in the interpretation of the spectra of methylene proton signals by Casnati et al. (27) were corrected (Table 1).

Protonated carbons were assigned with the help of proton correlations and quarternary carbons (ipso and ortho) from long-range couplings. The distinction between carbons from the octyl or the crown sides was also made using long-range couplings. There were no problems with the assignment of the remaining methylene, crown, and chain carbons.

From the three possible isomeric dinitrocalixarene compounds, two were successfully isolated and obtained in pure form, enabling detailed interpretation of their NMR spectra (Tables 3 and 5).

c2o0

The first $(NO_2)_2$-oct-MC-6 (c2o0), having two nitro groups on the crown side (Table 3) and displaying a higher symmetry, showed in the aromatic area of its ^1H NMR spectrum one spin system of the AA′X type for the para unsubstituted aryl rings, and one singlet for two meta protons for the remaining nitro-bearing aryl ring protons. The side of substitution was unambiguously identified by nOe between given meta protons and 1′ or 1″ and 2″ protons. The interaryl methylene protons displayed a pair of geminal doublets (4H each) with some small long-range couplings and nOe to the above-mentioned meta aryl protons. The crown system ap-

© 2005 NRC Canada

peared as expected, with one singlet for four middle methylene protons and two spin systems, one with full averaging for 1″ and 2″ protons, the other ambiguous for 3″ and 4″ protons. The chain protons were assigned as in the previous case, that is H-1′ and H-2′ from mutual coupling, the second pair H-7′ and H-8′ from mutual coupling, H-3′ from its coupling to H-2′ and from ^{13}C, and H-6′ with the help of the ^{13}C correlation.

The ^{13}C spectrum was assigned according to our previous methodology: the quaternary carbons from long-range couplings, the ipso carbons from their connectivity to either 1′ octyl or 1″ crown protons. The benzylic, crown, and chain proton assignments were simplified using the same approach.

The spectra of two mononitrated oct-MC-6 isomers, one from the crown side and the second with NO_2 on the octyl chain side of the calixarene, were also assigned (Tables 2 and 4).

c1o0

First, the proton spectrum of the mononitro isomer (NO_2)-oct-MC-6 (c1o0) with the nitro group on the crown side accordingly showed two spin systems of the AA′X and ABX type (twice the integration), as well as one singlet for the remaining meta protons. The side of substitution by the NO_2 radical was identified with the help of the nOe effect between meta protons and 1′h, 1′n, or 1″ (1 of 2) and 2″ (Table 2). The methylene protons displayed one singlet (4H) and one pair of geminal doublets (2H each) with the usual long-range couplings and nOe to meta protons. The crown protons were present as two spin systems, one with no averaging corresponding to the 1″ and 2″ protons, one ambiguous for the 3″ and 4″ protons, plus one singlet for the middle two vicinal methylenes. For the chain protons, similarly to the previous compound, the pairs H-1′h and H-2′h as well as H-1′n and H-2′n were assigned from coupling to each other, then equivalent pairs of protons on C-7′ and C-8′ were assigned from their coupling to each other, whereas protons on C-3′ and C-6′ were assigned from their heterocorrelation to ^{13}C. There was a nOe effect observed between protons H-1′h and H-2′h.

In the ^{13}C spectrum, all aromatic carbons were assigned either from their proton partners for tertiary carbons or from long-range couplings for quaternary carbons. The connectivity of the ipso carbons to 1′h, 1′n, or 1″ (2 of 2) protons were observed. The methylene, crown, and chain carbons could generally be assigned without ambiguity with the help of the proton assignments as well as from long-range couplings and known chemical shifts.

c2o1

The structure of the last nitro derivative of oct-MC-6 (c2o1), the one with three nitro groups (Table 6), was assigned as the one having two nitro on the crown and one nitro on the octyl chain sides. Some important features used during the assignment of this one of two possible isomers were the following.

The aromatic region displayed one spin system of the AA′X type containing two meta and one para protons, one spin system of the AB type comprised of two meta protons (twice the integration), and one singlet for two meta protons. The crown or octyl side was identified by nOe between meta protons and 1′, 1″h and 2″h, or 1″n and 2″n. The interarylic methylene protons showed up as two pairs of geminal doublets. Again, long-range couplings and nOe were observed to nearby meta protons. For the crown portion of the molecule, four spin systems were present, two for 1″ and 2″ on each side were fully averaged, two for 3″ and 4″ on each side were ambiguous, and one singlet for 5″h/n. The chain protons were identified as described previously.

The ^{13}C spectrum was assigned as above, that is the protonated carbons from correlations to protons and the quaternary carbons from long-range correlations. There were connectivities between ipso carbons and 1′, 1″h, or 1″n. For the crown portion of the molecule, 3″ and 4″ on each side were ambiguous, and the 5″h and 5″n signals were not equivalent.

c1o1

The last dinitro-oct-MC-6 (c1o1) structure was established as the one having one nitro group on both sides of the molecule, one on the crown and one on the octyl chain sides (Table 5).

The aromatic region of the proton spectrum showed two spin systems of the ABX type containing two meta and one para protons and two spin systems of the AB type containing two meta protons. The side of substitution for each was identified by nOe between their meta protons and 1′h, 1′n, 1″h, or 1″n (1 of 2) and 2″n. Another nOe was observed between *p*ch and 5″h/n. The methylene protons appeared as two singlets (2H each) and two pairs of geminal doublets (1H each). Long-range couplings and nOe to meta proton were again observed. Four spin systems and one singlet corresponding to crown protons were found, as for the previous molecule. For the chain protons, 1′h and 2′h, 1′n and 2′n, as well as 7′h/n and 8′h/n, were assigned from their mutual coupling, whereas 3′h, 3′n, and 6′h/n were assigned from ^{13}C.

The ^{13}C spectrum was assigned as previously. In the aromatic region, para carbons on the NO_2 side were not resolved. In the crown region, 3″ and 4″ on each side were ambiguous, whereas the 5″h and 5″n signals were not equivalent.

c0o1

The second mononitro derivative (NO_2)-oct-MC-6 (c0o1) (Table 4), isolated in smaller yield, is the one with the nitro group on the octyl chain side.

The aromatic region of the ^1H NMR spectrum showed two spin systems of two meta and one para protons, one of the AA′X type, the other of the ABX type (twice the integration), and a singlet for two meta protons. The side was identified by nOe between the meta protons and 1′ or 1″h, 1″n, 2″h, and 2″n. There was also a nOe between *p*c and 5″h/n. The interarylic methylenes showed up as one singlet (4H) and a pair of geminal doublets (2H each). Long-range couplings and nOe to meta protons were again present. The crown protons appeared as three spin systems (1″h and 2″h resolved; 3″ and 4″ on each side ambiguous), a singlet with 1″n and 2″n superimposed, and a singlet for 5″h/n. The chain protons were assigned as previously.

Carbon signals were assigned as above. Connections showed up on the HMBC spectrum between ipso carbons

© 2005 NRC Canada

and 1″h and 1″n. Signals for 5″h and 5″n were not equivalent.

It is clear then that the structural difference between the two mononitro derivatives of oct-MC-6 was fully reflected by NMR, especially nOe and long-range.

Since the six compounds formed a family with zero, one, or two nitro groups on the crown side and zero or one nitro group on the octyl side, it was possible to extract substitution effects from the data.

In ^{1}H, *m*cs were shifted by 0.921 ± 0.013 ppm (N = 6) and *m*os by 0.962 ± 0.002 ppm (N = 4) with adjacent NO_2 substitution. On neighbouring rings, *m*as were always shifted more downfield (0.03–0.06 ppm) than the corresponding mss (0.00–0.03 ppm). Protons at position 5″ were shifted upfield by 0.071 ± 0.001 ppm (N = 2) with one NO_2 and by 0.158 ± 0.010 ppm (N = 2) with two NO_2s on the crown side.

In ^{13}C, *i*cs were shifted by 5.73 ± 0.05 ppm (N = 4), *i*os by 5.30 ± 0.03 ppm (N = 3), *o*cs by 1.4–2.2 ppm, and *o*os by 1.38 ± 0.12 ppm (N = 4) with para NO_2 substitution; *m*cs were shifted upfield by –4.64 ± 0.19 ppm (N = 6) and *m*os by –4.31 ± 0.01 ppm (N = 4) with adjacent para NO_2 substitution; *p*s were shifted by 19.8 ppm upon NO_2 substitution. On neighbouring rings, *i*cs were shifted downfield (0.2–0.3 ppm), *i*os upfield (–0.2 to –0.1 ppm), *o*as downfield (0.1–0.5 ppm), *o*css upfield (–1.5 to –1.0 ppm), and *o*oss upfield by –1.51 ± 0.09 ppm (N = 6); *m*cas were shifted more downfield (0.7–0.9 ppm) than the corresponding *m*css (0.10 ± 0.00 ppm (N = 4)); *m*oas were shifted downfield (0.5–0.7 ppm), *m*oss upfield (–0.4 to –0.2 ppm) and *p*s downfield (0.1–0.5 ppm). Finally, 1′′ signals were shifted by 1.3–1.4 ppm upon para NO_2 substitution on the attached ring.

The spectra of the last and least interesting polynitro derivative of oct-MC-6, the tetranitro one, $(NO_2)_4$-oct-MC-6 (c2o2), were also recorded but did not reveal any peculiarities, generally confirming the already assigned signals in the expected places (see Experimental).

Conclusion

In this study, we showed that the synthesis of specifically nitrated nitro-oct-MC-6 was possible. Specifically, the mononitration of this compound was successfully accomplished as was the production of several di- and tetranitro derivatives and, following a two-step procedure, trinitro derivatives were also obtained. The separation on a column was the key step in purification of these compounds. Refinement of the separation technique (HPLC) as well as full multidimensional NMR characterization of six of the compounds in this series was achieved. In addition, molecular modelling was used in order to rationalize the obtainment of one of two isomers of the mononitro-oct-MC-6 (c1o0) under radiolytic-mimetic conditions as being the result of radical NO_2 nitration.

All these derivatives will be used as viable standards for the quantitation of degradation products of calixarenes as well as for the evaluation of their capacity of extraction, particularly of Cs^+, during procedures for the retreatment of spent nuclear fuel.

These structure identifications meant that one of three nitro derivatives of the double nitration of oct-MC-6, the one with nitro groups on the octyl chain side, although formed and detected by LC, was present in a very small quantity in the original radiolysis mixture. Only one of the trinitro derivatives was also present in a very small quantity in a laboratory simulated *cold* nitration mixture and was formed to complete this NMR study by the mononitration at low temperature of the symmetrical dinitro isomer of the oct-MC-6 (c2o0) having both nitro groups on the crown side.

Only after the synthesis of this last standard, by the method mentioned in the previous sentence, was it possible to positively detect at least one of two trisubstituted oct-MC-6 (c1o2 or c2o1) in the LC. It also seems that the one with the lower retention time (of 8 or 10 min) corresponds to the trinitro isomer previously described (c2o1) while the second trinitro isomer (c1o2) was probably observed at ca. 10 or 12 min in two LC runs of these two mixtures (resulting from the radiolytic hot and cold synthetic cycles, respectively).

In the future, we would like to try this kind of synthesis under the newer microwave-assisted technology; the first results seem to be promising, especially from a perspective of synthesis of the other missing nitro-oct-MC-6 isomers.

Experimental

HPLC

A Bio-Tek series 525 LC system with a high-pressure binary pump, an autosampler, and a diode array detector (DAD), equipped with a 4.6 mm × 10 mm TSK-GEL Super-ODS (TosoHaas) column, 3 μm particle size, was used for the separations. The flow rate was 0.8 mL/min and the column was thermostatted at 40 °C (chosen after optimization tests between 20 and 80 °C). The injection volume was 20 μL. The DAD and ESI-MS detectors were connected in series. The column effluent was split after the DAD since the flow rate introduced into the mass spectrometer was optimum at 50 μL/min.

ESI-MS

Identification of the synthetic products was accomplished using a Quattro II triple-quadrupole mass spectrometer (Micromass, Manchester, UK) equipped with an ESI source and Mass Lynx software version 3.5. The instrumental operating parameters were as follows: capillary voltage 3.5 kV and source temperature 80 °C. Nitrogen was used as the bath and nebulization gas, and the pressure in the analyser was 3.5×10^5 mbar (1 bar = 100 kPa). The high voltage lens (counter electrode) was maintained at 600 V. The electron multiplier was fixed at 700 V. The source parameters, especially the cone voltage, were optimized at the beginning of the experiments by direct infusion of a test mixture containing $(NO_2)_x$-oct-MC-6 (with x = 0, 1, 2, 4), in that order, to obtain the best signal sensitivity, and were kept constant during all the LC–MS experiments; the cone voltage value was finally fixed at 45 V. Spectra were recorded in continuum mode by scanning the quadrupole between m/z 50–1500 with a scan time cycle of 2.1 s.

In parallel, the chromatograms were recorded at various wavelengths: at 200 nm to observe the maximum number of peaks, and at 270, 290, and 320 nm, corresponding to the maximum absorption wavelengths of oct-MC-6 (c0o0),

© 2005 NRC Canada

$(NO_2)_2$-oct-MC-6 (c2o0), and (NO_2)-oct-MC-6 (c1o0), respectively.

Selective nitration of oct-MC-6

Mononitration

A solution of 0.5 g of oct-MC-6 (c0o0) (Acros Chemicals) in 25 mL of acetic anhydride was treated with fumic nitric acid (1 equiv., 24.6 μL) in acetic anhydride (2.5 mL) and acetic acid (2.5 mL) for 45 min at –20 °C. The mixture was allowed to stand overnight, then was carefully neutralized, and purified on a SiO2 63/200 μm column with cyclohexane – ethyl acetate (8:2 or 7:3). The yield of mononitro isomers was 34%. The unreacted starting material was recovered. Two isomeric (NO_2)-oct-MC-6 were separated on similar columns.

Dinitration

Similarly, 0.5 g of oct-MC-6 (c0o0) in 25 mL of acetic anhydride was treated with 2.2 equiv. (54 μL) of nitric acid in 12.5 mL of acetic anhydride and 12.5 mL of acetic acid at –20 °C for 15 min, then for one more hour at room temperature. The yield of dinitration mixture was 54%.

Trinitration

Pure $(NO_2)_2$-oct-MC-6 (c2o0) (0.11 g) in 5 mL of acetic anhydride was treated as in the case of mononitration. $(NO_2)_3$-oct-MC-6 (c2o1) was obtained in a 12% yield.

Tetranitration

Oct-MC-6 (c0o0) (200 mg) in 10 mL of methylene chloride was treated for 5 min with 80 equiv. of fuming nitric acid in acetic anhydride (1 mL). The worst yield of pure $(NO_2)_4$-oct-MC-6 (c202) was 81%.

Molecular modelling

Molecular modelling calculations were performed with HyperChem 6 using Mm+ (Université de Moncton – U de M) in gas-phase and in solvent box (ethanol) modes. The minimization of energy was performed using the technique described in the HyperChem instruction manual and as in ref. 28. In a first phase, 1600 Polak–Ribiere iterations were applied. A small incremental energy was applied in a second phase (0.001 ps for a total of 1 ps, 370 K) for selected insertion models only. All calculated complex structures (1:1, 2:1, and 1:2 stoichiometry) and energy data are available upon request from CKJ (U de M).

$(NO_2)_4$-oct-MC-6 (c2o2) (as reference)

Yield: ≥81%, mp 184 °C. ESI-MS *m/z*: 1053.4 $[M + Na]^+$, 1163.3 $[M + Cs]^+$.

NMR

The samples were dissolved in $CDCl_3$, and TMS was used as an internal standard. High-resolution ^1H and ^{13}C NMR spectra were acquired at 25 °C on a Chemagnetics Infinity 300 spectrometer using 5 mm Nalorac probes: either *z*-gradient $^1H\{^{109}Ag–^{31}P\}$ or $^{13}C/^1H$.

A combination of 1D and 2D high-resolution NMR experiments were used to assign the ^1H and ^{13}C spectra as completely as possible. Connectivities between protons were obtained using 2D gradient-selected COSY (16). The 2D phase-sensitive NOESY (17) and ROESY (18) experiments were performed with a mixing time of 300–400 ms. The 1D ^{13}C NMR spectra were recorded with WALTZ proton decoupling (19). The multiplicity of the carbon signals was established using the 1D APT experiment (20) with an evolution time of 6.8–7.0 ms or the DEPT experiment (21) with a reading pulse of 135° and an evolution time of 3.4–3.5 ms. The 2D HETCOR (22) was performed using evolution times of 3.45 and 2.3 ms for $1/(2J_{CH})$ and $1/(3J_{CH})$, respectively. The 2D gradient-selected phase-sensitive HSQC (23) spectra were acquired with a 1.7 ms evolution time and MPF9 (24) carbon decoupling during acquisition. A higher precision in the proton dimension was obtained from the CHORTLE experiment (25) run with four increments for cosine and sine subspectra: 0.4, 1.0, 2.4, and 3.2 ms. The 2D gradient-selected magnitude HMBC (26) was run without carbon decoupling with one-bond and long-range evolution times of 3.4–3.5 and 72–83 ms, respectively.

Accurate ^1H chemical shifts and coupling constants were obtained by spectral simulation using the gNMR program from IvorySoft.

Supporting information

All other detailed spectral material is available on request from Christopher K. Jankowski (Canada).

The following LC and NMR partial spectra of compounds are available as supporting information:

LC: Fig. 6. Comparison of irradiated and synthetic samples: (*a*) Synthetic sample as per Fig. 4 (two peaks at 17.67 and 15.67 min) corresponding to mononitro (dotted line); (*b*) scan of mononitro 918 $[M + Na]^+$ of (*a*); (*c*) irradiated sample (an interesting feature is the presence of the more abundant mononitro isomer at 17.5 min but less abundant at 15.68 min); (*d*) scan of mononitro 918 $[M + Na]^+$ of (*c*).

Figure 7. LC of reconstituted mixture of all $(NO_2)_x$-oct-MC-6 isomers: (*a*) $(NO_2)_4$-oct-MC-6 (c2o2); (*b*) $(NO_2)_3$-oct-MC-6 (c2o1); (*c*) $(NO_2)_2$-oct-MC-6 (c2o0); (*d*) $(NO_2)_2$-oct-MC-6 (c1o1); (*e*) (NO_2)-oct-MC-6 (c0o1); (*f*) (NO_2)-oct-MC-6 (c1o0); (*g*) oct-MC-6 (c0o0, starting) at 18.2 traces of $(NO_2)_2$-oct-MC-6 (c0o2).

NMR partial spectra (Figs. 8–17): Figure 8. Partial NOESY spectrum of oct-MC-6 (c0o0). Figure 9. Partial HMBC spectrum of oct-MC-6 (c0o0). Figure 10. Partial ROESY spectrum $(NO_2)_2$-oct-MC-6 (c2o0). Figure 11. Partial HMBC spectrum $(NO_2)_2$-oct-MC-6 (c2o0). Figure 12. Partial (H,H) homonuclear COSY spectrum of (NO_2)-oct-MC-6 (c1o0). Figure 13. Partial HMBC spectrum (NO_2)-oct-MC-6 (c1o0). Figure 14. Partial NOESY spectrum $(NO_2)_3$-oct-MC-6 (c2o1). Figure 15. Partial HMBC spectrum $(NO_2)_3$-oct-MC-6 (c2o1). Figure 16. Partial (H,H) homonuclear COSY spectrum of $(NO_2)_2$-oct-MC-6) (c1o1). Figure 17. Partial NOESY spectrum $(NO_2)_2$-oct-MC-6 (c1o1).

Acknowledgements

The authors are indebted to G. LeClair for some molecular modelling calculations.

© 2005 NRC Canada

References

1. M. Grunder, J.F. Dozol, Z. Asfari, and J. Vicens. J. Radioanal. Nucl. Chem. **241**, 59 (1999); J.F. Dozol, V. Lamare, N. Simon, R. Ungaro, and A. Casnati, ACS Symp. Ser. **757**, 12 (2000); also see: A. Ikeba and S. Shinkai. Chem. Rev. **97**, 1713 (1997).
2. J.T. Haverlock, V.P. Bonnensen, A.R. Sachleben, and A.B. Moyer. Radiochim. Acta, **76**, 59 (1997); A.R. Sachleben, P.V. Bonnensen, T. Descaseaud, T.J. Haverlock, A. Urvoas, and B.A. Moyer. Solvent Extr. Ion Exch. **17**, 1445 (1999).
3. Z. Asfari, C. Brescot, J. Vicens, C. Hill, J.F. Dozol, J.F. Rouquette, S. Eymard, V. Lamare, and B. Tournois. Anal. Chem. **67**, 3133 (1995).
4. C. Lamouroux, N. Aychet, and C.K. Jankowski. Commissariat à l'Énergie Atomique (CEA), Direction du Cycle des Combustibles (DCC) (Note technique No. 00-43). 2002. p. 34.
5. G. Wipff and M. Lauerbach. Supramol. Chem. **6**, 187 (1995).
6. V. Bonnensen, T.J. Haverlock, N.L. Engle, R.A. Schleben, and B.A. Moyer. ACS Symp. Ser. **757**, 26 (2000); R.A. Peterson, C.L. Crawford, F.F. Fondeur, and T.L. White. ACS Symp. Ser. **757**, 45 (2000); C.V. Lamare, J.F. Dozol, F. Allain, H. Virelizier, C. Moulin, C.K. Jankowski, and J.C. Tabet. ASC Symp. Ser. **757**, 55 (2000).
7. C.K. Jankowski, F. Allain, J.F. Dozol, H. Virelizier, J.C. Tabet, C. Moulin, and C. Lamouroux. Rapid Commun. Mass Spectrom. **17**, 1247 (2003); C.K. Jankowski, F. Allain, C. Lamouroux, H. Virelizier, C. Moulin, J.C. Tabet, V. Lamare, and J.F. Dozol. Spectrosc. Lett. **36**, 327 (2003).
8. C.K. Jankowski, J.F. Dozol, F. Allain, J.C. Tabet, R. Ungaro, A. Casnati, J. Vicens, A. Asfari, and J. Boivin. Pol. J. Chem. **76**, 701 (2002).
9. V. Lamarre, C. Bressot, J.F. Dozol, J. Vicens, Z. Asfari, R. Ungaro, and A. Casnati. Sep. Sci. Technol. **32**, 175 (1997).
10. V. Lamare, J.F. Dozol, S. Fuangswasdi, F. Arnaud-Neu, P. Theury, M. Nierlich, Z. Asfari, and J. Vicens. J. Chem. Soc. Perkin Trans. 2, 271 (1999).
11. E. Ghidini, F. Ugozzoli, R. Ungaro, S. Harkema, A. Abu El-Fadl, and D.N. Reinhoud. J. Am. Chem. Soc. **112**, 6979 (1990).
12. F. Allain, H. Virelizier, C. Moulin, C.K. Jankowski, J.F. Dozol, and J.C. Tabet. Spectroscopy, **14**, 127 (2000).
13. C. Lamouroux, N. Aychet, A. Lelievre, C.K. Jankowski, and C. Moulin. Rapid Commun. Mass Spectrom. **18**, 1493 (2004).
14. A. Dodi. Analusis, **28**, 93 (2000); B. Graham, J.M. Harrofiels, and R.D. Trengove. J. Liq. Chromatogr. Relat. Technol. **41**, 1197 (1997); also see the bibliography quoted in ref. 13.
15. V. Lamare, J.F. Dozol, F. Ugozzoli, A. Casnati, and R. Ungaro. Eur. J. Org. Chem. 1559 (1998); C. Hill, J.F. Dozol, V. Lamare, H. Rouquette, S. Eymard, B. Tournois, J. Vicens, Z. Asfari, C. Bressot, R. Ungaro, and A. Casnati. J. Inclusion Phenom. Mol. Recognit. Chem. **19**, 399 (1994).
16. M. von Kienlin, C.T.W. Moonen, A. van der Toorn, and P.C.M. van Zijl. J. Magn. Reson. **93**, 423 (1991).
17. G. Bodenhausen, H. Kogler, and R.R. Ernst. J. Magn. Reson. **58**, 370 (1984).
18. A. Bax and D.G. Davis. J. Magn. Reson. **63**, 207 (1985).
19. A.J. Shaka, J. Keeler, and R. Freeman. J. Magn. Reson. **53**, 313 (1983).
20. S.L. Patt and J.N. Shoolery. J. Magn. Reson. **46**, 535 (1982).
21. D.M. Doddrell, D.T. Pegg, and M.R. Bendall. J. Magn. Reson. **48**, 323 (1982).
22. A. Bax and G.A. Morris. J. Magn. Reson. **42**, 501 (1981).
23. J. Ruiz-Cabello, G.W. Vuister, C.T.W. Moonen, P. van Gelderen, J.S. Cohen, and P.C.M. van Zijl. J. Magn. Reson. **100**, 282 (1992).
24. T. Fujiwara, T. Anai, N. Kurihara, and K. Nagayama. J. Magn. Reson. Ser. A, **104**, 103 (1993).
25. G.A. Pearson. J. Magn. Reson. **64**, 487 (1985).
26. W. Willker, D. Leibfritz, R. Kerssebaum, and W. Bermel. Magn. Reson. Chem. **31**, 287 (1993).
27. A. Casnati, A. Pochini, R. Ungaro, F. Ugozzoli, F. Arnaud, S. Fanni, M.J. Schwing, R.J.M. Egberink, F. de Jong, and D.N. Reinhoudt. J. Am. Chem. Soc. **117**, 2767 (1995).
28. B.D. Wagner, N. Stojanovic, G. LeClair, and C.K. Jankowski. J. Inclusion Phenom. Macrocyclic Chem. **48**, 275 (2003).

© 2005 NRC Canada

Spectroscopy and electrochemistry of new 6,6′-disubstituted-4,4′-bipyrimidine molybdenum(0) and tungsten(0) tetracarbonyl complexes

Elena Ioachim and Garry S. Hanan

Abstract: A new family of tetracarbonyl molybdenum(0) and tungsten(0) complexes based on new 6,6′-disubstituted-4,4′-bipyrimidine ligands was synthesized and characterized. The visible region of the absorption spectrum of each complex is dominated by a metal-to-ligand charge transfer band significantly lower in energy than the corresponding transition in 2,2′-bipyridine tetracarbonyl metal complexes. The 6,6′-substituents create a larger π-electronic system in the substituted bipyrimidines and are consequently better π acceptors than even the parent 4,4′-bipyrimidine. The absorption bands are shifted bathochromically with a decrease in solvent polarity.

Key words: molybdenum and tungsten, nitrogen ligands, tetracarbonyl metal complexes, absorption spectroscopy, electrochemistry.

Résumé : Une nouvelle famille de complexes de type tétracarbonyle de molybdène(0) et tungstène(0), à base des 4,4′-bipyrimidine substituées dans les positions-6,6′, a été synthétisée et caractérisée. Le spectre d'absorption dans la région du visible de chaque composé indique un déplacement vers le rouge pour la bande de transfert de charge métal-ligand comparé à celui du complexe tétracarbonyle de 2,2′-bipyridine. Ceci démontre une meilleure délocalisation du système π-électronique dans la bipyrimidine substituée qui rend ces ligands des meilleurs accepteurs π. Cette bande d'absorption est déplacée bathochromiquement avec la diminution de la polarité du solvant.

Mots clés : molybdenum et tungsten, ligands azotés, complexes métal-tétracarbonyle, spectroscopie d'absorption, électrochimie.

Introduction

Polypyridyl complexes of d^6 metal ions have been extensively studied over the last two decades owing to their fascinating spectroscopic, redox, and excited-state properties (1, 2). For example, α-diimine complexes of Ru(II) and Os(II) have been proposed as photosensitizers in the conversion of solar energy to chemical energy (3, 4) and have been successfully applied to the photolysis of water (5, 6). Re(I) complexes of type [(α-diimine)$Re(CO)_3$] represent another promising class of d^6 metal ion that are used in the photoreduction of CO_2 (7, 8), where the Re(I) complexes may act as both photosensitizer and homogenous catalyst.

Another class of compounds, the tetracarbonyl-diimine complexes of group 6 transitions metals (Cr, Mo, W) of type $M(CO)_4L$, also provide a unique combination of an electron-rich d^6 metal atom, stabilized by four CO ligands, and an electron-accepting diazine ligand. The growth in interest for these compounds stems not only from their role as starting materials for different classes of complexes, but also from their interesting spectroscopic properties. Thus, excitation of the metal-to-ligand charge transfer (MLCT) state can lead to CO dissociation (9), which can be used as the first step in photocatalytic cycles and photoinitiated redox processes (10).

The structural simplicity of this type of complex also makes them suitable for experimental and theoretical investigations of their MLCT transitions. It has been demonstrated that the relative position of the MLCT excited state is dependent on solvent polarity, as well as on the nature of the π-acceptor ligand (11, 12). The effect of the solvent on the electronic absorption spectra of transition-metal complexes is well recognized, and a correlation between the solvent parameters and electronic properties of this type of complex has been established (13). In addition, extensive modifications of the coordinating heterocyclic ligands can tune the ground- and excited-state properties of these complexes. Substitution on the pyridine ring (14) and replacement of the CH group by N, with the formation of a bidiazine ligand that possesses a more π-electron-deficient system (15), represent different strategies in which the photophysical properties of metal carbonyl complexes may be influenced.

In the bidiazine series (Chart 1), 4,4′-bipyrimidine (bpm) is the ligand with the lowest-lying π* orbitals, which leads to its metal complexes having the lowest energy MLCT excited states. Although this property would be favourable for the development of new red-emitting species for use in organic light-emitting diodes (16) or as biomarkers (17), no systematic study of substituted bpm complexes has been presented, even though considerable research has been done on 2,2′-bipyrimidine metal complexes (15, 18). Suitable substituents in the 6,6′ positions of bpm may yield bpm-type metal complexes that display favourable electrochemical and

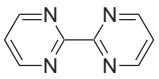
Received 24 February 2005. Published on the NRC Research Press Web site at http://canjchem.nrc.ca on 15 September 2005.

E. Ioachim and G.S. Hanan.[1] Département de Chimie, Université de Montréal, 2900 Edouard-Montpetit, Montréal, QC H3T 1J4, Canada.

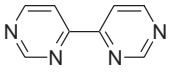
[1]Corresponding author (e-mail: garry.hanan@umontreal.ca).

 doi: 10.1139/V05-127 © 2005 NRC Canada

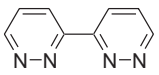
Chart 1. Possible bidiazine ligands.



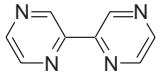
2,2'-bipyrimidine
(bpym)



4,4'-bipyrimidine
(bpm)

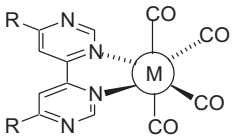


bipyridazine
(bpdz)



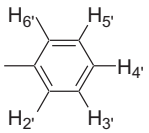
bipyrazine
(bpz)

Chart 2. The $M(CO)_4$ complexes of Mo(0) and W(0) with 6,6′-disubstituted-4,4′-bipyrimidine ligands and their ^1H NMR labels.



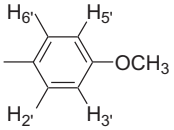
a = 6,6'-diphenyl-4,4'-bipyrimidine (dpb), R = phenyl

1a, M = Mo
2a, M = W



b = 6,6'-di(*p*-methoxyphenyl)-4,4'-bipyrimidine (dmpb), R = *p*-methoxyphenyl

1b, M = Mo
2b, M = W



photophysical properties based on even lower lying π* orbitals. In this paper, we report on the synthesis of a novel series of Mo(0) and W(0) complexes of type (*N*-*N*)$M(CO)_4$ (Chart 2), where M = Mo or W, and *N*-*N* = 6,6′-diphenyl-4,4′-bipyrimidine (dpb) (**a**) or 6,6′-bis(*p*-methoxyphenyl)-4,4′-bipyrimidine (dmpb) (**b**). The investigation of their electrochemical and spectroscopic properties will verify whether or not they are suitable candidates for incorporation into photoactive d^6 metal systems.

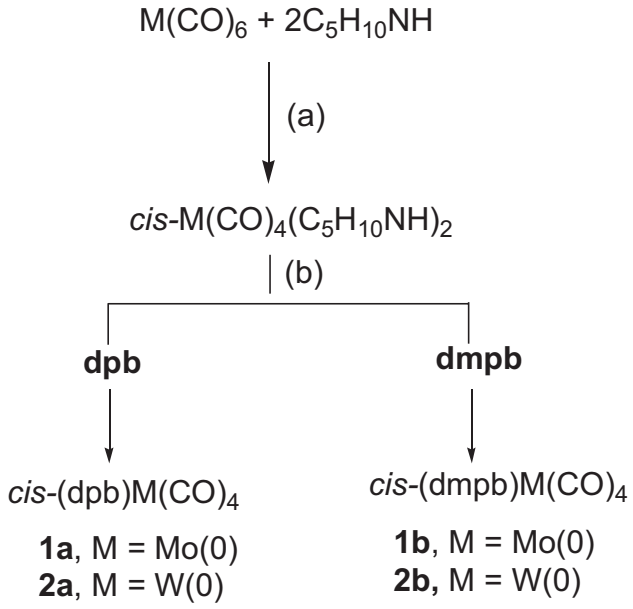
Results and discussion

Synthesis

The new (*N*-*N*)$M(CO)_4$ complexes, where M = Mo or W, were obtained via substitution reactions, as outlined in Scheme 1.

In step (*a*), the piperidine metal carbonyls were prepared in good yield by refluxing the corresponding metal hexacarbonyl complexes with a large excess of piperidine, following a previously established method (19). The *cis*-(*N*-*N*)$M(CO)_4$ compounds of Mo and W were prepared in step (*b*) in moderate yield by treating *cis*-$M(CO)_4(pip)_2$ with the appropriate bidiazine ligands in dichloromethane for 20 min at reflux. The formation of complex **1b** was monitored by recording the ^1H NMR spectra every 5 min for 1 h. During this period, new peaks, corresponding to the coordinated ligand, appeared and intensified. After about 40 min, these newly formed peaks started to lose their intensity and the original peaks for the starting material reappeared. This observation suggests that a longer reaction time leads to decomposition of the complexes. The precipitate that formed after cooling the reaction mixture overnight was recrystallized from hexane and further purified by column chromatography on silica gel in order to purify the product. Attempts to use alumina as the support for the column chromatography failed as a result of the decomposition of the compounds during the purification process.

Scheme 1. Synthesis of (*N*-*N*)$M(CO)_4$ complexes. Reagents and conditions: (*a*) toluene, 4 h, yield: 56%–64%; (*b*) 1 equiv. *N*-*N*, CH_2Cl_2, reflux 20 min, yield: 46%–71%.



NMR spectroscopy

All of the compounds were characterized by ^1H and ^{13}C NMR spectroscopy. The 400 MHZ ^1H NMR data for the Mo(0) and W(0) complexes are displayed in Table 1 and are compared with the free ligands. The numbering scheme for the ligands is presented in Chart 2. The ^1H NMR spectra show that the signal of the H_2 proton of the pyrimidine ring is deshielded with respect to the signal of the free ligand (Table 1), as well as those of the phenyl substituents of the pyrimidine rings. The protons $H_{3',5'}$ of complexes **1b** and **2b** do not follow this trend, indeed, the opposite trend is observed, these protons being slightly more shielded when compared to the free ligand. The second proton of the pyrimidine ring, H_5, is shifted to higher field in all of the complexes when compared to the free ligand. To coordinate to the metal ions, the N atoms must move from a trans to a cis geometry about the pyrimidine–pyrimidine bond. This has the effect of diminishing the deshielding effect caused by the trans arrangement of the N atoms about the interannular bond (20), which leads to an upfield shift in the H_5 protons of the complexes.

© 2005 NRC Canada

Table 1. ^{1}H NMR resonances for compounds **1a**, **1b**, **2a**, **2b**, and free ligands.

	Pyrimidine		Substituent R				
Compound	2	5	2′	3′	4′	5′	6′
a	9.42	8.93	8.27	7.58	7.58	7.58	8.27
b	9.35	8.89	8.25	7.19		7.19	8.25
(dpb)Mo(CO)$_4$ (**1a**)	9.84	8.56	8.29	7.66	7.66	7.66	8.29
(dmpb)Mo(CO)$_4$ (**1b**)	9.71	8.43	8.28	7.14		7.14	8.28
(dpb)W(CO)$_4$ (**2a**)	9.95	8.61	8.31	7.65	7.65	7.65	8.31
(dmpb)W(CO)$_4$ (**2b**)	9.82	8.48	8.26	7.13		7.13	8.26

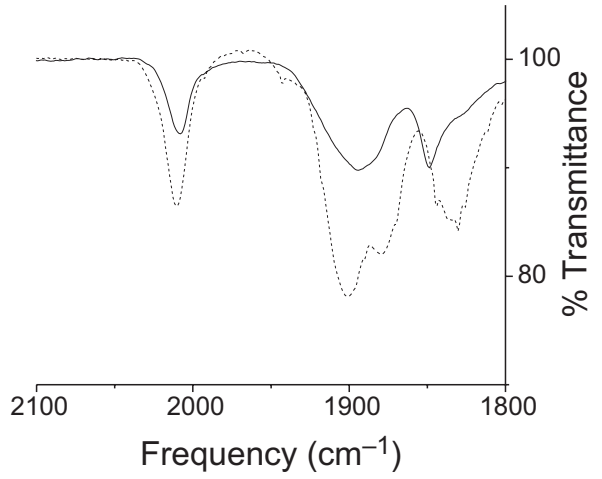
Note: $CDCl_3$ at 400 MHz, referenced to residual $CHCl_3$. See Chart 2 for ^{1}H labels.

Table 2. Carbonyl ligand stretching frequencies of (*N*-*N*)M(CO)$_4$ complexes.

Compound	ν(CO) (cm^{-1})			
(dpb)Mo(CO)$_4$ (**1a**)	2010	1901	1879	1830
(dmpb)Mo(CO)$_4$ (**1b**)	2007	1894	1880	1848
(dpb)W(CO)$_4$ (**2a**)	2009	1897	1877	1831
(dmpb)W(CO)$_4$ (**2b**)	2006	1893	1876	1846
(bpm)Mo(CO)$_4$[a]	2010	1908	1895	1850
(bpm)W(CO)$_4$[a]	2000	1900	1900	1850

Note: In KBr pellets.
[a]In THF solution from ref. 15.

Fig. 1. Infrared spectra of **1a** (dashed line) and **1b** (solid line).



Mass spectrometry

Even though the structures of the tetracarbonyl metal complexes have been confirmed by NMR spectroscopy, their matrix-assisted laser desorption–ionization (MALDI) and electron impact (EI) mass spectrometry analyses only displayed the signal corresponding to the free ligand. A possible explanation could be the low stability of these compounds under the conditions used for MALDI and EI mass spectrometry, which leads to the decomposition of the complexes. Even the milder electrospray ionization (ES) technique leads to their decomposition. Typically ES-MS requires the addition of acid to neutral complexes to generate cations. The ES-MS technique in combination with Ag^+ labeling, however, proved to be a convenient tool for the mass spectrometric characterization of this novel series of complexes. It has been demonstrated that this method is a convenient way to generate positively charged species that are sensitive to acid (21). The signals detected in the MS spectra of the complexes corresponded to the masses of the Ag^+ complexes as calculated from the chemical composition of the complexes and Ag^+. The MS spectra also contained one intense peak attributed to the ion with one less CO ligand. This fact supports the low stability of the tetracarbonyl complexes under MS conditions.

IR spectroscopy

All of the complexes that were synthesized in this study were characterized by vibrational spectroscopy in KBr. The energies for the vibrational bands are given in wavenumbers and are listed in Table 2, while the IR spectra of complexes **1a** and **1b** are illustrated in Fig. 1 for comparison. In their IR spectra, the tetracarbonyl metal complexes display four carbonyl stretching bands. The energy of these bands is shifted to slightly higher energy with the increase in π-acceptor ability of the bidiazine ligand as the better back-donation from metal to bidiazine diminishes the charge density on the metal center, which in turn diminishes the back-donation to the carbonyl groups. However, these differences in the series of bidiazine complexes are relatively small. The metal ion also has a slight effect on the energies of ν(CO), albeit a small one. The ν(CO) energies are similar to those found for Mo(bpm)(CO)$_4$ and W(bpm)(CO)$_4$ (Table 2) (15).

Electronic absorption spectra

The electronic absorption spectral data of complexes **1a** and **1b** and **2a** and **2b** in three different solvents are summarized in Table 3 and are compared to their unsubstituted bpm analogues.

The absorption spectra in the UV region display characteristic ligand-centered π–π* transitions. In the visible region, the absorption spectra of the bidiazine tetracarbonyl complexes consist of two bands. The band at lower energy has been assigned to a metal-to-ligand charge transfer d(M) → π*(bidiazine) MLCT transition. The next higher-energy band near 400 nm is also attributed to a MLCT transition, from the HOMO orbital localized on the metal center to the second SLUMO orbital of the bidiazine, by analogy with similar bidiazine-based complexes (15). In any particular solvent, the nature of the substituent on the bipyrimidine influences the position of the lowest MLCT band. Figure 2 shows the absorption spectra of (dpb)W(CO)$_4$ and

© 2005 NRC Canada

Table 3. Metal-to-ligand charge transfer absorption maxima of (*N-N*)$M(CO)_4$ complexes in three different solvents.

	Tetrahydrofuran (0.59)[a]		Chloroform (0.42)[a]		Toluene (0.30)[a]	
Compound	λ_1, nm; (ε)[b]	λ_2, nm; (ε)[b]	λ_1, nm; (ε)[b]	λ_2, nm; (ε)[b]	λ_1, nm; (ε)[b]	λ_2, nm; (ε)[b]
(dpb)$Mo(CO)_4$ (**1a**)	596 (0.8)	378 (1.5)	630 (0.2)	383 (0.5)	645 (1.1)	399 (1.3)
(dmpb)$Mo(CO)_4$ (**1b**)	587 (1.5)	381 (5.2)	604 (0.5)	390 (5.1)	610 (1.1)	385 (4.1)
(dpb)$W(CO)_4$ (**2a**)	621 (1.1)	382 (2.3)	653 (2.3)	387 (4.3)	664 (1.1)	424 (1.4)
(dmpb)$W(CO)_4$ (**2b**)	612 (1.1)	383 (3.8)	636 (0.2)	389 (1.3)	642 (0.9)	392 (2.9)
(bpm)$Mo(CO)_4$[c]	579 (3.5)	364 (3.6)			629	380
(bpm)$W(CO)_4$[c]	607 (3.6)	364 (3.7)			659	382

[a]E^*_{MLCT} derived solvent parameters from ref. 13.
[b]$\varepsilon \times 10^{-3}$ $(mol/L)^{-1}$ cm^{-1}.
[c]From ref.15.

Fig. 2. Absorption spectra at room temperature of (dpb)$W(CO)_4$ (solid line) and (dmpb)$W(CO)_4$ (dashed line) in THF solution.

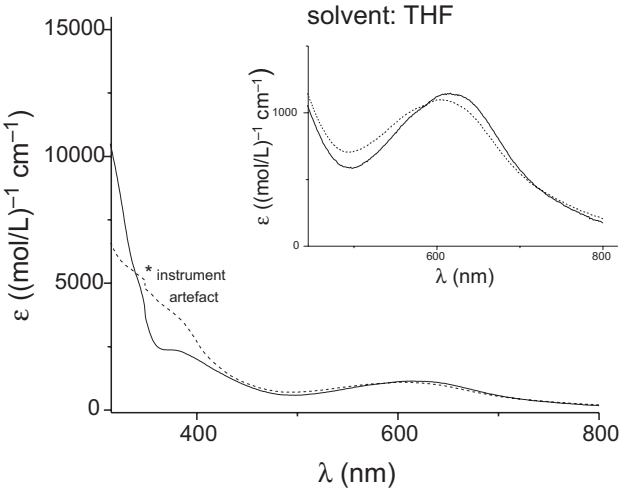
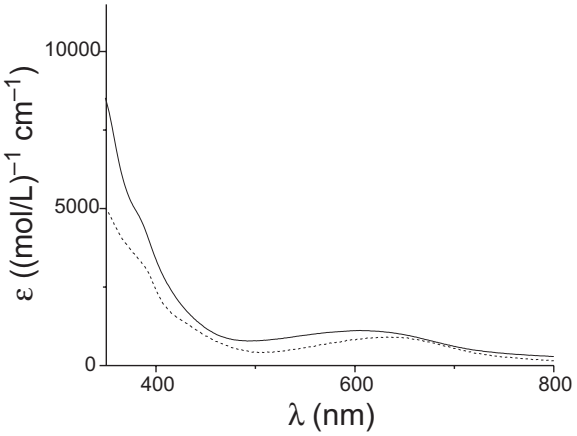


Fig. 3. Absorption spectra of (dmbp)$Mo(CO)_4$ (solid line) and (dmbp)$W(CO)_4$ (dashed line) in toluene.



(dmpb)$W(CO)_4$ in THF at room temperature. The presence of the methoxy donor group destabilizes the empty π^* orbitals of the dmpb ligand and gives rise to absorption at higher energy when compared to the dpb ligand. However, for both ligands, the corresponding Mo and W complexes present MLCT absorption bands at lower energy than the parent complexes with unsubstituted 4,4′-bipyrimidine (Table 3), for which MLCT transitions were observed at 579 nm for (bpm)$Mo(CO)_4$ and 607 nm for (bpm)$W(CO)_4$ in THF (15). This in accordance with the more extended π conjugation of the 6,6′-disubstituted-4,4′-bpm ligands and has the effect of lowering the MLCT energy in the newly prepared complexes. The planarity of the aryl substituent was demonstrated in the solid state for a tricarbonyl Re(I) complex of ligand **b**.[2] The *p*-methoxyphenyl rings were twisted with dihedral angles of 4.0° and 5.2° around the aryl-pyrimidine bond.

For a given *N-N* bidiazine ligand and solvent, the energy of the MLCT absorption follows the order Mo > W, as can be seen from the data listed in Table 3. This is exemplified in Fig. 3 for tetracarbonyls of Mo and W, with dmpb as the bidiazine ligand in toluene.

The MLCT absorption band is very sensitive to the nature of the solvent. All of the (*N-N*)$M(CO)_4$ complexes present a negative solvatochromism, translated by a shift of the MLCT absorption band to higher energy as the solvent polarity increases. The same trend has been observed for other $M(CO)_4$(α-diimine) related complexes (22, 23) and has been explained in terms of dipole moment changes between the ground and excited states (22, 24). The tetracarbonyl metal complexes are more polar in the ground state than in the excited state. Hence, the more polar solvents allow an enhanced stabilization of the ground state, which in turn leads to an increase in the transition energy. The results of correlating MLCT energies with solvent polarity are shown in Fig. 4 for the (dpb)$Mo(CO)_4$ complex in three different solvents for which the solvent parameter (E^*_{MLCT}) is included in parentheses in Table 3. The MLCT band is shifted to lower energy in going from tetrahydrofuran to toluene, along with the decrease in solvent polarity.

Electrochemistry

The electrochemical properties of the newly prepared complexes have been studied by cyclic voltammetry in acetonitrile solutions. The redox potentials are collected in Table 4 along with the corresponding redox potentials of the tetracarbonyl Mo and W complexes of bpm.

[2]E. Ioachim, E.A. Medlycott, and G.S. Hanan. Submitted for publication (2005).

© 2005 NRC Canada

Fig. 4. Absorption spectra at room temperature of (dpb)$Mo(CO)_4$ in THF (solid line), chloroform (dotted line), and toluene (dashed line).

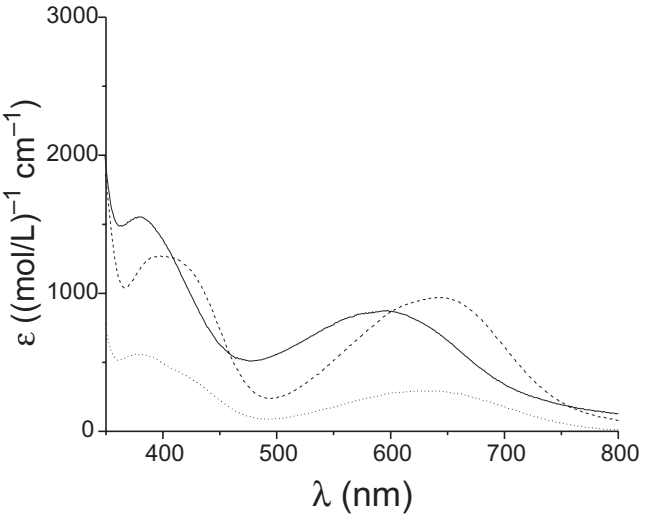


Table 4. Half-wave potentials ($E_{1/2}$) for (*N-N*)$M(CO)_4$ complexes.

Compound	$E_{1/2}$(ox)[a]	$E_{1/2}$(red)	
(dpb)$Mo(CO)_4$ (**1a**)	0.67 (irr)	–0.89 (63)	–1.48 (103)
(dmpb)$Mo(CO)_4$ (**1b**)	0.59 (irr)	–0.98 (60)	–1.55 (74)
(dpb)$W(CO)_4$ (**2a**)	0.65 (irr)	–0.83 (62)	–1.30 (68)
(dmpb)$W(CO)_4$ (**2b**)	0.58 (irr)	–0.91 (67)	–1.25 (91)
(bpm)$Mo(CO)_4$[b]	0.66 (irr)	–0.91	–1.65
(bpm)$W(CO)_4$[b]	0.64 (irr)	–0.88	–1.59

Note: From cyclic voltammetry in acetonitrile (0.1 mol/L in tetrabutylammonium perchlorate). Potentials are in volts vs. SCE, recorded at room temperature at a sweep rate of 500 mV/s. The difference between cathodic and anodic peak potentials (mV) is given in parentheses.

[a]Irreversible (irr); potential is given for the cathodic wave.

[b]In DMF solution, adjusted to acetonitrile as per ref. 15.

All of the complexes display one oxidation and two reduction processes in the potential region from +1.50 to –2.00 V. The oxidation is associated with a metal-centered process M(0) → M(I) and has proved to be irreversible in all cases, owing to the known lability of the complexes in the M(I) state with a 17-electron configuration (25). Indeed, the $Mo(CO)_4$ and $W(CO)_4$ complexes of the parent 4,4′-bipyrimidine, 3,3′-bipyridazine, 2,2′-bipyrimidine, and 2,2′-bipyrazine are also irreversible (15). The increase in π-acceptor properties of the bidiazine makes the abstraction of the electron from the metal center more difficult, and consequently, the oxidation occurs at more positive potentials for complexes **1a** and **2a** as compared to **1b** and **2b** and to the reference compounds $Mo(CO)_4$bpm and $W(CO)_4$bpm. The donating methoxyphenyl substituents of complexes **1b** and **2b** destabilize the metal-based orbitals, which facilitates the oxidation of the metal centres. The two reversible or quasi-reversible reduction waves observed in the cyclic voltammograms of all of the complexes are bidiazine centered. The reduction potentials depend on the nature of the bidiazine ligand, while the metal has just a slight influence on the reduction potentials. In the case of complexes **1b** and **2b**, the slight negative shift of the first reduction potential is due to electron donation by the methoxy groups to the bpm ligand, which raises the π* level of the coordinating diazine.

Conclusion

A number of tetracarbonyl bidiazine based complexes of Mo and W have been synthesized and characterized, and their electrochemical and photophysical properties have been investigated. It has been shown that acceptor ligands with low-lying π* levels can be used to red shift the energy of the lowest MLCT bands. (*N-N*)$M(CO)_4$ complexes show a negative solvatochromism, with a shift to lower energy of the MLCT absorption in nonpolar solvents. Electrochemical data was used to identify the lowest energy ligand acceptor. This study confirms that this new family of substituted bidiazine ligands has exceptional π-accepting properties, which bodes well for their incorporation into other transition-metal complexes. Further studies with metal carbonyls, such as the luminescent $Re(CO)_3Cl$ (α-diimine) type, and other metal complexes, such as the luminescent $M(\alpha\text{-diimine})_3^{2+}$ type, are underway and will be discussed in due course.

Experimental

Materials

All substituted bipyrimidine ligands were available in our laboratory from a previous study (26). $M(CO)_4(pip)_2$ (M = Mo or W) were synthesized according to a literature procedure (19). All metal complexes were purified by column chromatography on Kiesegel 60 (230–400 mesh) silica gel. Tetrabutylammonium hexafluorophosphate was purchased from Aldrich and purified by recrystallization from toluene–methanol. All of the solvents used for photophysical and electrochemical experiments were of spectroscopic grade. Elemental analyses were performed by Laboratoire d'Analyse Elementaire de l'Université de Montréal (Montreal, Quebec).

Instrumentation

NMR spectra were recorded in $CDCl_3$ at room temperature (rt) on a Bruker AV400 spectrometer at 400 MHz for ^{1}H NMR and at 100 MHz for ^{13}C NMR. Chemical shifts are reported in parts per million (ppm) relative to residual solvent protons (7.26 ppm for chloroform-*d*) and carbon resonance of the solvent. Routine absorption spectra were measured in deaerated tetrahydrofuran, chloroform, and toluene solutions at rt on a Cary 500i UV–vis–NIR spectrophotometer. The IR spectra were recorded as solid KBr discs on a Bio-Rad IR spectrophotometer. Electrochemistry data were collected in deaerated acetonitrile with 0.1 mol/L Bu_4NPF_6 on a BAS CV–50W voltammetric analyzer. Redox potentials were corrected by internal reference ferrocene (395 mV for acetonitrile vs. SCE).

Preparation of compounds

General procedure for the synthesis of (N-N)M(CO)$_4$ (1a and 2b)

(dpb)Mo(CO)$_4$ (1a)

A solution of 6,6′-diphenyl-4,4′-bipyrimidine (0.032 g, 1 mmol) and $Mo(CO)_3(pip)_2$ (0.039 g, 1 mmol) in dichloro-

© 2005 NRC Canada

methane was heated to reflux for 15 min. The reaction mixture was filtered through Celite followed by addition of hexane. Upon cooling, crystals formed, which were isolated by filtration. The complex was purified by column chromatography (SiO_2, ethyl acetate–hexane = 1:3). Yield: 58%. ^{1}H NMR (400 MHz, $CDCl_3$, 25 °C) δ: 9.84 (s, 2H, H_2), 8.56 (s, 2H, H_5), 8.29 (d, J = 3.5 Hz, 4H, $H_{2',6'}$), 7.66 (m, 6H, $H_{3',4',5'}$). ^{13}C NMR (75 MHz, $CDCl_3$, 25 °C) δ: 210.1, 166.2, 161.9, 161.2, 159.4, 136.9, 131.8, 129.5, 127.8, 113.9. HR-MS calcd. for $C_{24}H_{14}N_4O_4Mo$-Ag: 626.9114 [M + 1]; found: 626.9147.

*(dmpb)Mo(CO)$_4$ (**1b**)*

Yield: 51%. ^{1}H NMR (400 MHz, $CDCl_3$, 25 °C) δ: 9.71 (s, 2H, H_2), 8.43 (s, 2H, H_5), 8.28 (d, J = 8.5 Hz, 4H, $H_{2',6'}$), 7.14 (d, J = 8.5 Hz, 4H, $H_{3',5'}$), 3.93 (s, 6H, *O-Me*). ^{13}C NMR (75 MHz, $CDCl_3$, 25 °C) δ: 229, 178.8, 165.3, 162.8, 161.7, 159.3, 129.4, 129.3, 114.8, 113.0, 55.9. HR-MS calcd. for $C_{26}H_{18}N_4O_6Mo$-Ag: 686.1497 [M + 1]; found: 686.1502.

*(dpb)W(CO)$_4$ (**2a**)*

Yield: 46%. ^{1}H NMR (400 MHz, $CDCl_3$, 25 °C) δ: 9.95 (s, 2H, H_2), 8.61 (s, 2H, H_5), 8.29 (d, J = 3.5 Hz, 4H, $H_{2',6'}$), 7.66 (m, 6H, $H_{3',4',5'}$). ^{13}C NMR (75 MHz, $CDCl_3$, 25 °C) δ: 190.2, 166.2, 161.9, 161.3, 159.4, 136.8, 131.8, 129.9, 127.8, 113.9. HR-MS calcd. for $C_{24}H_{14}N_4O_4W$-Ag: 712.9570 [M + 1]; found: 712.9579.

*(dmpb)W(CO)$_4$ (**2b**)*

Yield: 71%. ^{1}H NMR (400 MHz, $CDCl_3$, 25 °C) δ: 9.82 (s, 2H, H_2), 8.48 (s, 2H, H_5), 8.26 (d, J = 8.5 Hz, 4H, $H_{2',6'}$), 7.13 (d, J = 8.5 Hz, 4H, $H_{3',5'}$), 3.96 (s, 6H, *O-Me*). ^{13}C NMR (75 MHz, $CDCl_3$, 25 °C) δ: 218.0, 190.8, 165.6, 162.8, 161.4, 159.3, 129.4, 129.3, 115.3, 114.8, 55.9. HR-MS calcd. for $C_{26}H_{18}N_4O_6W$-Ag: 772.9781 [M + 1]; found: 772.9740.

Acknowledgements

We thank the Natural Sciences and Engineering Research Council of Canada (NSERC) and l'Université de Montréal for financial support. François Baril-Robert and Alexandra Furtos are thanked for assistance with the IR and MS measurements, respectively.

References

1. (*a*) J.-P. Sauvage, J.-P. Collin, J.-C. Chambron, S. Guillerez, C. Coudret, V. Balzani, F. Barigelletti, L. De Cola, and L. Flamigni. Chem. Rev. **94**, 993 (1994); (*b*) E.A. Medlycott and G.S. Hanan. Chem. Soc. Rev. **34**, 133 (2005).
2. V. Balzani, A. Juris, M. Venturi, S. Campagna, and S. Serroni. Chem. Rev. **96**, 956 (1996).
3. R. Argazzi, C.A. Bignozzi, G.M. Hasselman, and G.J. Meyer. Inorg. Chem. **37**, 4533 (1998).
4. A. Juris, F. Barigelletti, S. Campagna, V. Balzani, P. Belser, and A. von Zelewsky. Coord. Chem. Rev. **84**, 85 (1988).
5. K. Kalyanasundaram. Coord. Chem. Rev. **46**, 159 (1982).
6. K. Kalyanasundaram, J. Kiwi, and M. Gratzel. Helv. Chim. Acta, **61**, 2720 (1978).
7. J. Hawecker, J.M. Lehn, and R. Ziessel. Helv. Chim. Acta, **69**, 1990 (1986).
8. B.P. Sullivan and T.J. Meyer. J. Chem. Soc. Chem. Commun. 1244 (1984).
9. A. Vlček, Jr. Coord. Chem. Rev. **177**, 219 (1998).
10. (*a*) I.R. Farrell, P. Matousek, and A. Vlček, Jr. J. Am. Chem. Soc. **121**, 5296 (1999); (*b*) C.A. Tolman. Chem. Soc. Rev. **1**, 337 (1972).
11. J.A. Lees and A.W. Adamson. J. Am. Chem. Soc. **102**, 6874 (1980).
12. D.M. Manuta and J.A. Lees. Inorg. Chem. **22**, 572 (1983).
13. D.M. Manuta and J.A. Lees. Inorg. Chem. **22**, 3825 (1983).
14. J.A. Connor and C. Overton. J. Organomet. Chem. **249**, 165 (1983).
15. S. Ernst and W. Kaim. J. Am. Chem. Soc. **108**, 3578 (1986).
16. S. Lamansky, P. Djurovich, D. Murphy, F. Abdel-Razzaq, H.-E. Lee, C. Adachi, P.E. Burrows, S.R. Forrest, and E.M. Thompson. J. Am. Chem. Soc. **123**, 4304 (2001).
17. G. MacDermott, S.M. Prince, A.A. Freer, A.M. Hawthornthwaite-Lawless, M.Z. Papiz, R.J. Cogdell, and N.W. Isaacs. Nature (London), **374**, 517 (1995).
18. (*a*) C. Overton and J.A. Connor. Polyhedron, **1**, 53 (1982); (*b*) A.J. Downard, I.G. Phillips, and P.J. Steel. Aust. J. Chem. **57**, 865 (2004); (*c*) W. Kaim, S. Kohlmann, A.J. Lees, T.L. Snoeck, D.J. Stufkens, and M.M. Zulu. Inorg. Chim. Acta, **210**, 159 (1993); (*d*) E.S. Dodsworth and A.B.P. Lever. Coord. Chem. Rev. **97**, 271 (1990); (*e*) A. Razakbin, J. Burgess, M. Kotowski, and R. Van Eldik. Transition Met. Chem. **12**, 230 (1987); (*f*) W. Kaim. Inorg. Chem. **23**, 3365 (1984); (*g*) W. Kaim and S. Kohlmann. Inorg. Chem. **25**, 3306 (1986); (*h*) W. Kaim and S. Kohlmann. Inorg. Chem. **26**, 68 (1987).
19. D.J. Darensbourg and R.L. Kump. Inorg. Chem. **17**, 2680 (1978).
20. (*a*) G.S. Hanan, U.S. Schubert, D. Volkmer, E. Rivière, J.-M. Lehn, N. Kyritsaka, and J. Fischer. Can. J. Chem. **75**, 169 (1997); (*b*) G.S. Hanan, J.-M. Lehn, N. Kyritsaka, and J. Fischer. J. Chem. Soc. Chem. Commun. 765 (1995); (*c*) G.S. Hanan, D. Volkmer, and J.-M. Lehn. Can. J. Chem. **82**, 1428 (2004); (*d*) G.S. Hanan, C.R. Arana, J.-M. Lehn, G. Baum, and D. Fenske. Chem. Eur. J. **2**, 1292 (1996).
21. P. Timmerman, K.A. Jilliffe, M. Crego Calama, J.-L. Weidmann, L.J. Prins, F. Cardullo, B.H.M. Snellik-Ruël, R.H. Fokkens, N.M.M. Nibbering, S. Shinkai, and D.N. Reinhoudt. Chem. Eur. J. **22**, 4104 (2000).
22. S. Ernst and W. Kaim. J. Organomet. Chem. **302**, 211 (1986).
23. I. Veroni, A. Rontoyianni, and C.A. Mitsopoulou. J. Chem. Soc. Dalton Trans. 255 (2003).
24. A. Vlček, Jr. Coord. Chem. Rev. **230**, 235 (2002).
25. J. Hanzlík, L. Pospíšil, A.A. Vlček, and M. Krejčík. J. Electroanal. Chem. **331**, 831 (1992).
26. E. Ioachim, E.A. Medlycott, M.I.J. Polson, and G.S. Hanan. Eur. J. Org. Chem. **17**, 3775 (2005).

© 2005 NRC Canada

Convenient tetrahydropyranylation of alcohols and phenols by catalytic ferric sulfate hydrate ($Fe_2(SO_4)_3 \cdot xH_2O$)

Lingjun Li, Lizhi Zhu, Xinying Zhang, Guisheng Zhang, and Guirong Qu

Abstract: Ferric sulfate hydrate ($Fe_2(SO_4)_3 \cdot xH_2O$) is found to be an efficient heterogeneous catalyst for the tetrahydropyranylation of alcohols and phenols at ambient or near ambient temperature. In addition, selective monotetrahydropyranylation of symmetrical diols is achieved under similar conditions. The deprotection of THP ether and direct transformation of THP ether to the corresponding acetate by $Fe_2(SO_4)_3 \cdot xH_2O$ is also studied. The simplicity of manipulation, mild conditions, reusable catalyst, good selectivity, and environment benign characters make this method a good alternative way for the THP protection of alcohols.

Key words: tetrahydropyranylation, selective monotetrahydropyranylation, ferric sulfate hydrate, green chemistry.

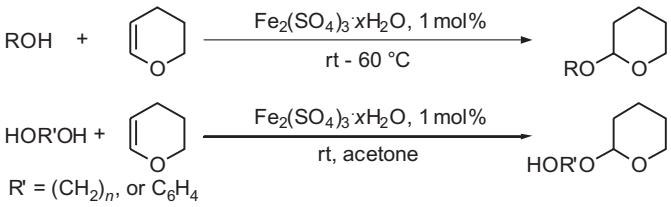
Résumé : On a trouvé que l'hydrate du sulfate ferrique [$Fe_2(SO_4)_3 \cdot xH_2O$] est un catalyseur hétérogène efficace pour la tétrahydropyranylation des alcools et des phénols à la température ambiante. De plus, dans les mêmes conditions, on peut obtenir une monotétrahydropyranylation des diols symétriques. On a aussi étudié la réaction de déprotection des éthers THP et la transformation des éthers THP en acétate correspondant à l'aide de $Fe_2(SO_4)_3 \cdot xH_2O$. La simplicité de la manipulation, les conditions douces, la possibilité de réutiliser le catalyseur, la bonne sélectivité et les caractères bénins pour l'environnement font de cette méthode une bonne méthode alternative pour la protection des alcools.

Mots clés : tétrahydropyranylation, monotétrahydropyranylation sélective, hydrate du sulfate ferrique, chimie verte.

[Traduit par la Rédaction]

The protection of hydroxyl groups is a common event in multistep organic syntheses. Among various available methods, tetrahydropyranylation is one of the most frequently employed strategies because of THP ether's stability against a wide range of strong nucleophilic or basic reagents (1). A variety of protonic acid catalysts as well as Lewis acid catalysts have been developed for tetrahydropyranylation of alcohols and phenols, such as acidic clay (1), PTSA (2), DDQ (3), $BF_3 \cdot OEt_2$ (4), triphenylphosphine hydrobromide (5), $[Ru(CH_3)_3 \cdot (triphos)](Otf)_3$ (6), I_2 (7), ionic liquid (8), LiOTf (9), $In(OTf)_3$ (10), polyaniline salt (11), and heteropolyacids (12). However, these methods require large amounts of catalysts, harsh acidic conditions, organic solvent, or solid supports, which finally result in the generation of toxic waste. Meanwhile, the selective protection of one of two identical hydroxyl groups in a symmetrical molecule is relatively limited. Previously, the selective monotetrahydropyranylation was achieved through control of the volume of solvents and usage of metallic sulfates supported on silica gel (13). Recently, I_2 under microwave-assisted (14), ionic liquid ([CnMIM][$AlCl_4$]) (15), and LiOTf in $ClCH_2CH_2Cl$ at reflux (9) have been reported for this transformation. Unfortunately, those methods do not agree with the rule of green chemistry, and involve the problems of tedious work-up procedures and expensive reagents and equipment.

Scheme 1.



In our efforts to develop clean methods for functional group transformations, it was found that $Fe_2(SO_4)_3 \cdot xH_2O$ is an efficient, operationally simple (16), and reusable catalyst for esterification and preparation of acylals (17). Herein, we disclose a mild, efficient, and fairly clean protocol for tetrahydropyranylation of a variety of alcohols and phenols using 3,4-dihydro-2*H*-pyran in the presence of a catalytic amount of $Fe_2(SO_4)_3 \cdot xH_2O$ under solvent-free conditions. Selective monotetrahydropyranylation of symmetrical diols was achieved in similar conditions (Scheme 1). The deprotection of THF ether and the direct transformation of THP

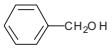
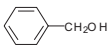
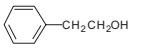
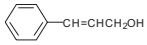
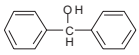
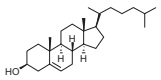
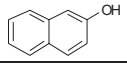
Received 26 April 2005. Published on the NRC Research Press Web site at http://canjchem.nrc.ca on 15 September 2005.

L. Li, X. Zhang, G. Zhang,[1] and G. Qu. School of Chemical and Environmental Sciences, Henan Key Laboratory for Environmental Pollution Control, Henan Normal University, Xinxiang, Henan 453007, P.R. China.
L. Zhu. Department of Biochemistry, The Ohio State University, 484 West 12th Avenue, Columbus, OH 43210, USA.

[1]Corresponding author (e-mail: zgs6668@yahoo.com).

 doi: 10.1139/V05-136 © 2005 NRC Canada

Table 1. Tetrahydropyranylation of alcohols and phenols catalyzed by $Fe_2(SO_4)_3{\cdot}xH_2O$ under solvent-free conditions.

Entry	Substrate	Temperature (°C)	Reaction time (h)	Yield (%)[a, b]
1		rt	1.0	95
2		rt	2.5	95[c]
3		rt	1.0	98
4		rt	1.0	97
5		60	1.0	82
6		60	0.5	87
7		rt	0.5	90[d]
8		60	1.5	81
9		rt	1.5	83
10		40	2.0	92[e]
11		40	2.0	90[e]

[a]Isolated yield; all products were identified by IR, ^{1}H NMR, and MS.
[b]The ratio of substrate:DHP was 1:1.2, with the addition of 1 mol% catalyst.
[c]Catalyst (0.4 mol%) is used.
[d]Excess DHP was used to dissolve the solid alcohol.
[e]Acetone was added to dissolve the solid alcohol.

ether to the corresponding acetate by $Fe_2(SO_4)_3{\cdot}xH_2O$ were also studied.

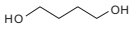
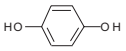
After a mixture of benzyl alcohol (10.0 mmol), 3,4-dihydro-2*H*-pyran (DHP, 1.1 mL, 12.0 mmol), and $Fe_2(SO_4)_3{\cdot}xH_2O$ (0.05 g, 0.1 mmol)[2] was stirred at ambient temperature for 1 h, the desired product, benzyl THP ether (2.21 g in 95% yield), was isolated through a short silica gel column. As shown in Table 1, with a catalytic amount of $Fe_2(SO_4)_3{\cdot}xH_2O$, a wide range of alcohols, including primary, secondary, tertiary, benzylic, and allylic alcohols as well as phenol and naphthol, undergo tetrahydropyranylation in good to excellent yields. Tetrahydropyranylation of primary alcohols was achieved at room temperature (rt) smoothly in excellent yields (Table 1, entries 1–4).[3] Secondary alcohols were protected as their THP ethers under increased temperature (Table 1, entries 5–7) with good yields. However, under these conditions without the addition of $Fe_2(SO_4)_3{\cdot}xH_2O$, no THP ether formation was observed. Carbon–carbon double bonds successfully survived the protection conditions (Table 1, entries 4 and 7). In addition, protection of a bulky molecule like diphenylmethanol (Table 1, entry 5) was achieved at 60 °C in good yield. *tert*-Butyl alcohol, which is an acid-sensitive alcohol, also undergoes tetrahydropyranylation smoothly and no dehydration was observed (Table 1, entry 8). Tetrahydropyranylation of phenolic hydroxyl groups (Table 1, entries 9–11) was

[2] $Fe_2(SO_4)_3{\cdot}xH_2O$ used in the experiments was purchased from the Beijing Chemical Factory (A.R. grade). The moles of $Fe_2(SO_4)_3{\cdot}xH_2O$ are calculated based on the formula: $M_{Fe_2(SO_4)_3{\cdot}xH_2O} = 0.5 \times (W_{Fe_2(SO_4)_3{\cdot}xH_2O} \times Fe(III)\%/55.8)$.

[3] The general procedure for tetrahydropyranylation and reuse of catalyst: benzyl alcohol (10.0 mmol), DHP (1.1 mL, 12.0 mmol), and $Fe_2(SO_4)_3{\cdot}xH_2O$ (0.05 g, 0.1 mmol) were stirred at rt. The progress of the reaction was monitored by TLC. At completion, the catalyst was moved by filtration and washed with dry acetone for further use. The filtrate was concentrated and the crude product was purified through silica gel column chromatography (petroleum ether – acetone, 125:1 *v*/*v*) to give benzyl THP ether (2.21 g, 95% yield). The product was identified by GC–MS and ^{1}H NMR and the spectroscopic data are comparable with the literature data.

© 2005 NRC Canada

Table 2. Monotetrahydropyranylation of symmetrical diols catalyzed by $Fe_2(SO_4)_3 \cdot xH_2O$ in acetone.

Entry	Substrate	Reaction time (min)	Yield (%)[a]
1		55	82
2		65	80
3		60	72[b]

[a]Isolated yield of monoTHP ether; all products were identified by IR, ^{1}H NMR, and MS.
[b]BisTHP ether (12%) was also obtained.

achieved in good yields rather than forming a complex with Fe(III) or being oxidized by Fe(III). In general, 1 mol% of $Fe_2(SO_4)_3 \cdot xH_2O$ is enough for a fairly high yield. However, with 0.4 mol% of $Fe_2(SO_4)_3 \cdot xH_2O$, the same yield was also achieved under a longer reaction period (Table 1, entry 2).

The deprotection of the THP ether by $Fe_2(SO_4)_3 \cdot xH_2O$ was then explored. It was found that the deprotection of THP ether with the presence of a catalytic amount of $Fe_2(SO_4)_3 \cdot xH_2O$ was realized successfully. For example, the THP ether (1.0 mmol) of the compounds in Table 1 (entries 1, 5, 6, 8, and 10) were treated in anhydr. MeOH (3.0 mL) with 10 mol% of $Fe_2(SO_4)_3 \cdot xH_2O$ under reflux. Once the reaction was completed (indicated by TLC), the corresponding alcohols were finally isolated in 95%, 85%, 90%, 80%, and 90% yield, respectively. Therefore, a new reagent for both THP protection and deprotection was found, which will enrich the toolbox for organic chemists.

Meanwhile, selective monotetrahydropyranylation of symmetrical diols was studied under similar reaction conditions.[4] The reaction was carried out by stirring diol (5.0 mmol), DHP (0.45 mL, 5.0 mmol), and hydrated ferric sulfate (0.025 g, 0.05 mmol) in the presence of dry acetone (1.5 mL) and the process was monitored by TLC. After completion, symmetrical diols were selectively protected as their corresponding monotetrahydropyranylated products in good yields (Table 2). It is worth noting that hydroquinone (Table 2, entry 3) was selectively protected to give the monotetrahydropyranylation product in 72% yield (along with 12% of the diprotected product), which has seldom been achieved in the literature so far.

The effects of acetone and reaction time on the yield of monoprotected diol were then investigated by taking ethylene glycol as the model substrate. As shown in Fig. 1, at the primary stage, the reaction mainly gave the monoprotected product. Even when the yield of monoether reached 82% (Fig. 1, curve 1), the yield of diprotected diol was still lower than 10% (Fig. 1, curve 3). However, the yield of diprotected product increased remarkably after this stage, which implied that optimization of the reaction time (55 min under standard reaction conditions) leads to a maximum amount of monotetrahydropyranylation output. On the other hand, it

Fig. 1. Yield vs. reaction time. Ethylene glycol (5.0 mmol), DHP (0.45 mL, 5.0 mmol), and $Fe_2(SO_4)_3 \cdot xH_2O$ (0.05 mmol) were stirred at room temperature in the presence of acetone (1.5 mL). MonoTHP ether (■), bisTHP ether (●), monoTHP ether (▲) without the addition of acetone.

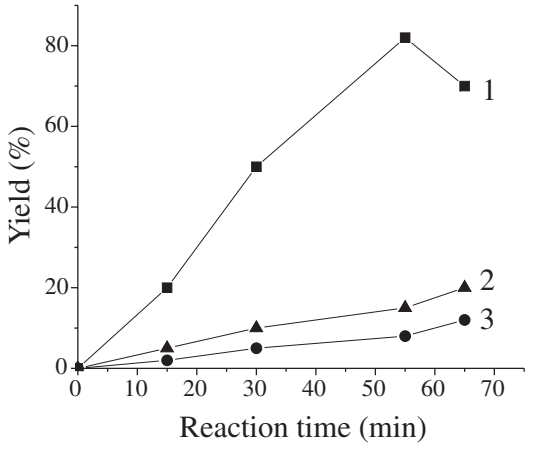


Table 3. The reusability of $Fe_2(SO_4)_3 \cdot xH_2O$ catalyzed tetrahydropyranylation.

Round	Substrate	Catalyst recovered (g)	Reaction time (min)	Yield (%)[a]
1	$C_6H_5CH_2OH$	0.025	60	95
2	$C_6H_5CH_2OH$	0.024	80	92
3	$C_6H_5CH_2OH$	0.022	110	92
4	$C_6H_5CH_2OH$	0.021	150	89

[a]Isolated yield; all the products were identified by ^{1}H NMR.

was found that the presence of a small amount of acetone facilitated the reaction procedure significantly (Fig. 1, curve 1). In fact, acetone is very helpful in making the two reagents (ethylene glycol and DHP) into a homogeneous mixture, which helps the reaction proceed more smoothly than in a heterogeneous state (Fig. 1, curve 2).

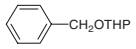
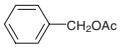
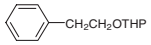
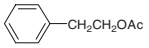
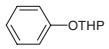
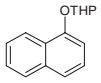
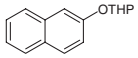
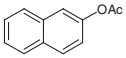
In the view of green chemistry, efficient recovery and reuse of the catalyst are highly preferred. In our process, $Fe_2(SO_4)_3 \cdot xH_2O$ was easily recovered from the reaction mixture by filtration and subsequent washing with dry acetone. The recovered catalysts were ready to be used for the next reaction cycle. For example, benzyl alcohol was protected as its THP ether by using the recovered catalyst and the yields were not significantly decreased even after three recovery cycles (Table 3). However, an increased reaction period is necessary to achieve comparable yields.

On the other hand, the development of new methods for direct transformation from one protecting group to another has been gaining importance in recent years. However, the available method for direct transformation of THP ether to the corresponding acetate is very limited (18). Two reported

[4]Typical procedure for the monotetrahydropyranylation of symmetrical diols: ethylene glycol (5.0 mmol) and DHP (0.45 mL, 5.0 mmol) in dry acetone (1.5 mL) were stirred for several minutes. Then, $Fe_2(SO_4)_3 \cdot xH_2O$ (0.025 g, 0.05 mmol) was added. After 55 min, the reaction was terminated by filtration. The filtrate was concentrated and purified through silica gel column chromatography (2:1 petroleum ether – EtOAc) to give the monoTHP product (0.60 g, 82% yield). The product was identified by GC–MS and ^{1}H NMR and the spectroscopic data are comparable with the literature data.

© 2005 NRC Canada

Table 4. On-pot conversion of THP ether to acetate.

Entry	Substrate	Time (h)	Product	Yield (%)[a]
1		3		75
2		3		82
3		1.5		80
4		2		78
5		2		77

[a]Isolated yields.

methods for this conversion utilized either harsh conditions (AcOH/AcCl) or an expensive catalyst ($TiCl_4/Ac_2O$ in anhydrous dichloromethane). In our research, we found that $Fe_2(SO_4)_3{\cdot}xH_2O$ is a good catalyst for this transformation. As shown in Table 4, the THP ethers (1 mmol) were successfully converted to the acetates in the presence of Ac_2O (2.0 equiv.) and $Fe_2(SO_4)_3{\cdot}xH_2O$ (10 mol%) in refluxing 1,2-dichloroethane (15 mL).

It was also found that the transformation was very slow at rt under solvent-free conditions. Under reflux (large excess of Ac_2O), a complex mixture was observed and no significant amount of acetate was detected. However, in refluxing $ClCH_2CH_2Cl$ the reaction processed very well. Corresponding acetates were isolated after a short reaction period. Compared with the reported methods, this protocol is much milder and the catalyst is cheaper. It is worth noting that this protocol allowed a one-pot conversion of an acid-labile protecting group to a base-labile protecting group.

In conclusion, the present method is an efficient and practical method for the tetrahydropyranylation of alcohols and phenols as well as the monotetrahydropyranylation of symmetrical diols. In addition, a practical and mild protocol is developed for direct transformation of THP ethers to their corresponding acetates. The simplicity of manipulation, mild conditions, reusable catalyst, good selectivity, and environment benign characters will make this method a good alternative way for the THP protection of alcohols. Currently, further investigations of ferric sulfate hydrate as an efficient green catalyst are underway.

Acknowledgments

This work was supported by the Natural Science Foundation of the Education Commission of Henan Province of China under grant No. 1999150027.

References

1. (*a*) T.W. Greene and P.G.M. Wuts (*Editors*). Protective groups in organic synthesis. 3rd. ed. John Wiley and Sons, New York. 1999; (*b*) S. Hoyer and P. Laszlo. Synthesis, 655 (1986); (*c*) P.J. Kocienski (*Editor*). Protecting groups. Thieme, Stuttgart. 1994.
2. M. Miyashita, A. Yoshikoshi, and P.A. Grieco. J. Org. Chem. **42**, 3772 (1977).
3. K. Tanemura, T. Horaguchi, and T. Suzuki. Bull. Chem. Soc. Jpn. **65**, 4583 (1992).
4. H. Alper and L. Dinkes. Synthesis, 81 (1972).
5. V. Bolitt, C. Mioskowski, D.S. Shin, and J.R. Falck. Tetrahedron Lett. **29**, 4583 (1988).
6. S. Ma and L.M. Venanzi. Tetrahedron Lett. **34**, 5269 (1993).
7. N. Deka and J.C. Sarma. Synth. Commun. **30**, 4435 (2000).
8. L.C. Branco and C.A.M. Afonso. Tetrahedron Lett. **57**, 4405 (2001).
9. B. Karimi and M. Jafar. Tetrahedron Lett. **43**, 5353 (2002).
10. T. Mineno. Tetrahedron Lett. **43**, 7975 (2002).
11. S. Palaniappan, M.S. Ram, and C.A. Amarnath. Green Chem. **4**, 369 (2002).
12. G.P. Romanelli, G. Baronetti, H.J. Thamas, and J.C. Autino. Tetrahedron Lett. **43**, 7589 (2002).
13. T. Nishiguchi, K. Kawamine, and T.J. Ohtsuka. J. Chem. Soc. Perkin Trans. 1, 153 (1992).
14. N. Deka and J.C. Sarma. J. Org. Chem. **66**, 1947 (2001).
15. V.V. Namboodiri and R.S. Varma. Chem. Commun. 342 (2002).
16. (*a*) G. Zhang and H. Gong. Synth. Commun. **29**, 1547 (1999); (*b*) G. Zhang. Synth. Commun. **29**, 607 (1999).
17. X. Zhang, L. Li, and G. Zhang. Green Chem. **5**, 646 (2003).
18. (*a*) M. Schwarz and R.M. Waters. Synthesis, 567 (1972); (*b*) S. Chandrasekhar, T. Ramachandar, M. Venkat Reddy, and M. Takhi. J. Org. Chem. **65**, 4729 (2000).

© 2005 NRC Canada

Characterization and identification of disintegrins in *Crotalus horridus* venom by liquid chromatography and tandem matrix-assisted laser desorption ionization – quadrupole ion trap time-of-flight (MALDI-QIT-TOF) mass spectrometry

Jacob A. Galán, Elda E. Sánchez, Sajid Bashir, and John C. Pérez

Abstract: Two disintegrins were purified from the venom of *Crotalus horridus* by multiple-dimension liquid chromatography (MDLC) (specifically C18 reverse phase (RP) high-performance liquid chromatography followed by size exclusion chromatography (SEC), and anion exchange chromatography (SCX)). Both disintegrins were subjected to mass spectrometry to determine their intact molecular mass, the number of disulfide linkages, and protein sequence, respectively. These disintegrins were named horrdistatin 1 (nominal mass, 7231 Da) and horrdistatin 2 (nominal mass, 7451 Da), and had IC_{50} (inhibitory concentrations) of 12.5 and 16.2 nmol/L (at 50%), respectively. For sequence confirmation from the C-terminal end, both disintegrins were derivatized using chemical-assisted fragmentation (CAF) and subsequently *unzipped* via collision-induced dissociation (CID) by matrix-assisted laser desorption – ionization – quadrupole ion trap time-of-flight (MALDI-QIT-TOF) mass spectrometry.

Key words: disintegrins, mass spectrometry, snake venom, Timber rattlesnake, *Crotalus horridus*.

Résumé : Deux désintégrines ont été extraites et purifiées à partir du venin de *Crotalus horridus* en faisant appel à la chromatographie liquide multidimensionnelle (CLMD) [particulièrement à la chromatographie liquide à haute performance à phase inversée (PI) C18 suivie d'une chromatographie par exclusion de taille (CET) et une chromatographie d'échange ionique (CXI)]. Les deux désintégrines ont été soumises à la spectrométrie de masse pour déterminer respectivement leur masse moléculaire intacte, le nombre de liaisons disulfures et la séquence des protéines. Ces désintégrines qui ont été dénommées respectivement horridistatine 1 (masse nominale de 7231 Da) et horridistatine 2 (masse nominale 7451 Da) présentent des concentrations inhibitrices à 50 % (IC_{50}) de 12,5 et 16,2 nmol/L. Pour confirmer la séquence à partir de l'extrémité C-terminale, on a préparé les dérivés des deux désintégrines en faisant appel à la fragmentation chimiquement assistée (FCA) et ceux-ci ont été soumis à un fractionnement par le biais d'une dissociation induite par une collision (DIC) par spectrométrie de masse à piège ionique quadripolaire avec désorption–ionisation au laser assisté d'une matrice (MALDI-QIT-TOF).

Mots clés : désintégrines, spectrométrie de masse, venin de serpent, serpent à sonnette des bois, *Crotalus horridus*.

[Traduit par la Rédaction]

Introduction

Crotalus horridus (Timber rattlesnake) is found in the central and northeastern United States. Herpetologists differ in opinion of whether the southern specimen consists of a separate subspecies, *Crotalus h. atricaudatus* (canebrake rattlesnake), or if instead it is a color variant because of geographical location (1). Due to the geographical locations of the specimens used in this study, the Natural Toxins Research Center had initially obtained them as *C. h. atricaudatus*. However, for practical purposes, the scientific name of *C. horridus* will be used.

In 1967, it was first discovered that *C. horridus* contained extremely lethal venom (2). However, prior to this discovery, *C. horridus* venom was not considered to be exceptionally toxic. The LD_{50} (lethal dose killing 50% of a population) for the venom of *C. horridus* ranged from 0.29 to 6.6 mg/kg body weight (2–4). Researchers have isolated a "canebrake toxin" from *C. horridus*, which is a two-component neurotoxin (5). Canebrake toxin is relatively homologous to phospholipase A (PLA) complex in the neurotoxins of crotoxin and Mojave toxin found in the venom of *Crotalus durissus terrificus* and *Crotalus scutulatus scutulatus*, respectively (5). *Crotalus horridus* venom is a complex mixture with the majority of molecules having pIs less than 6 (6). To date, *C. horridus* venom has been reported to have hemorrhagic,

Received 2 February 2005. Published on the NRC Research Press Web site at http://canjchem.nrc.ca on 15 September 2005.

J.A. Galán, E.E. Sánchez, and J.C. Pérez.[1] Natural Toxins Research Center (NTRC), Texas A&M University-Kingsville, 920 University Blvd., MSC 158, Kingsville, TX 78363, USA. **S. Bashir.** Chemical Biology Research Group (CBRG), Department of Chemistry, Texas A&M University-Kingsville, 920 W. Santa Gertrudis Ave., MSC 161, Kingsville, TX 78363, USA.

[1]Corresponding author (e-mail: kfjcp00@tamuk.edu).

 doi: 10.1139/V05-128 © 2005 NRC Canada

neurotoxic, myotoxic, and thrombin-like enzymes along with other proteolytic enzymes that are used in the capture and digestion of prey (4, 6–10). These snakes, like many other Viperidae species, exhibit geographical variation with respect to venom composition and lethality (11, 12).

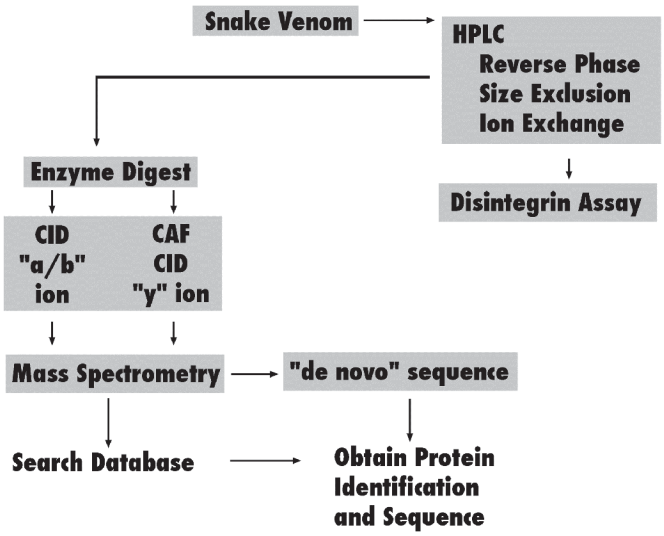
Hemorrhagins and disintegrins are only two types of many components found in snake venom that affect hemostasis and cell adhesion (13). Many disintegrins are found in snake venom as single components that are proteolytically cleaved from the class PII of snake venom metalloprotease (SVMP) or found attached to metalloproteases (*a d*isintegrin *a*nd *m*etalloprotease, ADAM) (14, 15). The first disintegrin to be discovered, trigramin, was isolated from the venom of *Trimeresurus gramineus* (16). Trigramin blocks platelet aggregation and binding of ^{125}I-fibrinogen to ADP-stimulated platelets. Trigramin also blocks the binding of the human von Willebrand factor (vWF) to the $\alpha_{IIb}\beta_3$ complex in thrombin-activated platelets (16).

Disintegrins are naturally occurring proteins many of which have been isolated from snake venom. They are low molecular weight molecules ranging from 4–21 kDa. Many disintegrins possess an "RGD loop" found at the tip of a flexible hairpin loop (17), and can be recognized by their polypeptide length and number of disulfide bonds (18). Disintegrins and disintegrin-like proteins can be categorized into five groups. Examples of the short group are eristostatin, echistatin, and ocellatusin, which have 49–51 amino acid residues along with four disulfide bonds (19, 20). The medium-sized group that includes crotatroxin, kistrin, and flavoridin has approximately 70 amino acid residues and has six disulfide bonds (21, 22). The longest group has about 84 amino acid residues and seven disulfide bonds, which include bilitoxin-1, bitistatin, bothrostatin, and salmosin3 (23). Catrocollastatin and jararhagin are two examples belonging to a fourth group, which contains approximately 100 amino acid residues with eight disulfide bonds and have a disintegrin domain of PIII-SVMP (14, 15, 24). The homo- and heterodimeric disintegrins make up a fifth group, which contains approximately 67 amino acid residues and 10 cysteines that form four intrachain disulfides and two interchain linkages (24). Today there are over 90 disintegrins that have been isolated and characterized (23). Many isolated disintegrins show homology with one another, particularly in the cysteine arrangement. Because of their affinity to bind integrins on platelets and many other cells, disintegrins could be useful therapeutic agents in thrombosis, cancer, diabetes militius, angiogenesis, and inflammation (25–29).

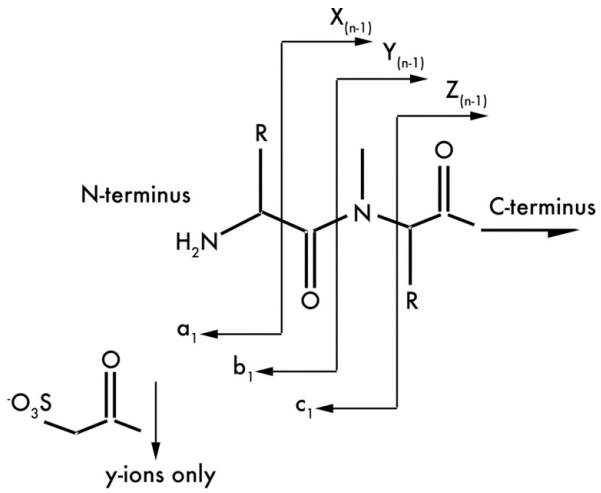
There are many snakes containing different disintegrins in their venoms (23) and Duvernoy's gland secretions (30); and hence, a need for rapid isolation and characterization is essential. Multiple-dimension liquid chromatography along with mass spectrometry is a powerful tool in allowing the separation and identification of complex protein mixtures such as those found in snake venom (31).

The aim of this study was to isolate, characterize, and determine the sequences of two closely related disintegrins using MDLC and mass spectrometry. The isolated disintegrin proteins were de novo sequenced using mass spectrometry (32). We have attempted to utilize collision-induced dissociation (33) and chemical derivatization (34) to obtain the unique primary sequence of the disintegrins (35–37). The generic scheme is illustrated in Scheme 1 whilst the specific fragmentation types and derivatization is shown in Scheme 2. This is the first report of the isolation of disintegrins from *C. horridus* venom and the subsequent de novo sequencing.

Scheme 1. The route taken for snake venom disintegrin purification, isolation, and identification.



Scheme 2. CAF derivatization and secondary y-type ions generated.



Experimental

Specimen

The *C. horridus* (Avid No. 011-522-004) and *C. horridus* (Avid No. 010-782-102) specimens were obtained in Tennessee and Texas, respectively. These snakes are currently housed at the Natural Toxins Research Center (NTRC) at Texas A&M University-Kingsville, Kingsville, Texas. The Avid No. is a nine digit code given to individual snakes at the NTRC. Additional information pertaining to this snake can be queried using the Avid No. on the NTRC's snake database found at http://ntrc.tamuk.edu (6).

© 2005 NRC Canada

Fig. 1. The complete amino acid sequence of horrdistatin 1 and 2, and the comparison with other closely related snake venom disintegrins. Shaded areas indicate similar amino acids.

```
                1_______10_______20_______30_______40_______50_______60_______70_73

Horrdistatin 1  GEECDCGSPANPCCDAATCKLRPGAQCADGLCCDQCRFIKKGTVCRPARGDWNDDTCTGQSADCPRNGL    (7231 Da, 69 aa)
Horrdistatin 2  GEECDCGSPANPCCDAATCKLRPGAQCADGLCCDQCRFIKKGTVCRPARGDWNDDTCTGQSADCPRNGLYG  (7451 Da, 71 aa)
Crotatroxin      AGEECDCGSPANPCCDAATCKLRPGAQCADGLCCDQCRFIKKGTVCRPARGDWNDDTCTGQSADCPRNGLYG  (7521 Da, 72 aa)
Lutosin        EAGEECDCGSPANPCCDAATCKLRPGAQCADGLCCDQCRFIKKGTVCRVARGDWNDDTCTGQSADCPRNGLYG  (7652 Da, 73 aa)
Viridin         AGEECDCGSPANPCCDAATCKLRPGAQCADGLCCDQCRFIKKGKICRRARGDNPDDRCTGQSADCPRNRFH   (7368 Da, 71 aa)
Cerastin       EAGEECDCGTPENPCCDAATCKLRPGAQCADGLCCDQCRFMKKGTVCRVARGDWNDDTCTGQSADCPRNGLYG  (7743 DA, 73 aa)
Molossin       EAGIECDCGSPENPCCDAATCKLRPGAQCADGLCCDQCRFIKKGKICRRARGDNPDDRCTGQSADCPRNRFHA  (7880 Da, 73 aa)
Cereberin      EAGEECDCGSPANPCCDAATCKLRPGAQCAEGLCCDQCRFIKKGKICRRARGDNPDDRCTGQSADCPRNRFH   (7781 Da, 72 aa)
```

Venom collection

Venom was extracted by allowing the snakes to bite into a parafilm stretched over a disposable plastic container. The venom samples were clarified by centrifugation (500 × g for 10 min), filtered through a 0.45 μm filter, and frozen at –90 °C until lyophilized. Venom samples were collected from the individual snakes and were fractionated and analyzed individually.

Reverse-phase chromatography C18

A total of 5 mg of venom sample was fractionated by reverse-phase high-performance liquid chromatography (HPLC). Venom was injected into a Grace Vydac® reverse phase C18 (250 mm × 4.6 mm) column. Fractions were eluted using 0.1% TFA and 80% acetonitrile in 20% of a 0.1% TFA gradient over 60 min with a flow rate of 1 mL/min. A 2487 detector was used to monitor absorbances at 280 nm. Millennium software v.4 was used to control the 1525 binary HPLC pumps and store the data. Fractions were stored at –90 °C. Protein concentrations were determined by standard methods at 280 nm. The venom fractions from both specimens were tested for inhibition of platelet aggregation. Only specimen No. 011-522-004 contained a fraction that inhibited platelet aggregation and was further purified.

Size exclusion chromatography

Fractions collected from reverse-phase C18 chromatography inhibiting platelet aggregation were further fractionated by size exclusion HPLC. Two hundred and fifty micrograms of protein were injected into a Waters Protein-Pak™ 60 (7.8 mm × 300 mm) column. The buffer used was 0.02 mol/L sodium phosphate, pH 6.2 over 60 min with a flow rate of 0.5 mL/min, and proteins were detected at 280 nm using a 484 tunable detector. Millennium software v.4 was used to control the 510 pumps and store the data. The fractions were tested for inhibition of platelet aggregation.

Anion exchange chromatography

Fractions collected on size exclusion chromatography inhibiting platelet aggregation were further fractionated by anion exchange HPLC. Two hundred micrograms of protein were injected into a Waters Protein-Pak™ DEAE 5PW (7.5 mm × 7.5 mm) column. The buffer used was 0.02 mol/L Tris-HCl, pH 8.0 over 60 min with a flow rate of 1 mL/min, and proteins were detected at 280 nm using a 484 tunable detector. Millennium software v.4 was used to control the 510 pumps and store the data. The fractions were tested for inhibition of platelet aggregation.

Inhibition of platelet aggregation

A Chronolog™ whole blood lumi-aggregometer was used to monitor platelet aggregation, by impedance, when venom samples were added. Four hundred and fifty microliters of 10% citrated human blood were incubated to 37 °C at least 5 min prior to use with equal amounts of 0.15 mol/L saline solution. Ten microliters of venom fraction were incubated with the blood sample for 2 min. An electrode was inserted in the blood sample, and 1.5 min later, 10 μL of a 1 mmol/L adenosine diphosphate (ADP) solution was added to the blood sample to promote platelet aggregation. Per cent inhibition of platelet aggregation was calculated by the following equation: $[(C - E/C)] \times 100$, where C is the units of platelet aggregation (ohms) for the control and E is the unit of platelet aggregation (ohms) for the experimental fraction.

Characterization and identification of isolated proteins

Following isolation of disintegrin-like proteins from specimen No. 011-522-004, the samples were analyzed using the Axima-QIT™ MALDI-QIT-TOF (Shimadzu Biotech USA, Columbia, Maryland). The lyophilized proteins were resuspended in 20 μL of 25 mmol/L ammonium bicarbonate. From this stock approximately 2 μL were diluted in 10 μL of 0.1% TFA followed by a zip-tip (Millipore C4 zip-tip, Billerica, Massachussetts) clean up. Samples were then mass analyzed in high mass mode for both nonreduced and reduced forms. For the digest, the lyophilized protein was resuspended (1 mg) in 100 mmol/L ammonium hydrogen carbonate, pH 7.5, and digested with trypsin (1:50 $w_{enzyme}/w_{substrate}$) for 18 h at 37 °C (38, 39). The tryptic mixture was lyophilized and resuspended in 0.1% TFA and derivatized using a CAF labeling kit accordingly (40). Prior to digestion, half the sample (10 μL) was reduced using dithiothretol (DTT, Sigma, Louis, Missouri) and alkylated using idoacetamide (Sigma). The samples were then desalted using C18 micro zip-tips. Approximately 0.5 μL of protein, or digest, was mixed with 0.5 μL of 2,5-dihydroxybenzoic acid (DHB).

The QIT was used to store and fragment the MALDI generated ions, which were mass analyzed in the TOF reflectron in positive ion selection mode. The tryptic digest samples were calibrated using peptide standard P14R (m/z 1533.86), its fragments (m/z 1339.75, 1145.65, 951.44, 757.44) and angiotension 18–39 clip (m/z 2465.20). The MS–MS spectrum was externally calibrated using the fragments from P14R (PPPPPPPPPPPPPR, m/z 1533.86). The intact proteins were externally calibrated using a protein mixture consisting of insulin oxidized B chain (m/z 3494.65), insulin

© 2005 NRC Canada

Fig. 2. Reverse phase C18 chromatography of *C. horridus* (No. 011-522-004) venom. A total of 5 mg of venom was injected into a Grace Vydac™ C18 column (4.6 mm × 150 mm). The venom was separated using 0.1% TFA with the eluting solvent of 80% acetonitrile in 0.1% TFA on a Waters HPLC system. The fractions were tested for inhibition of platelet aggregation. Fraction *9 contained disintegrin-like activity.

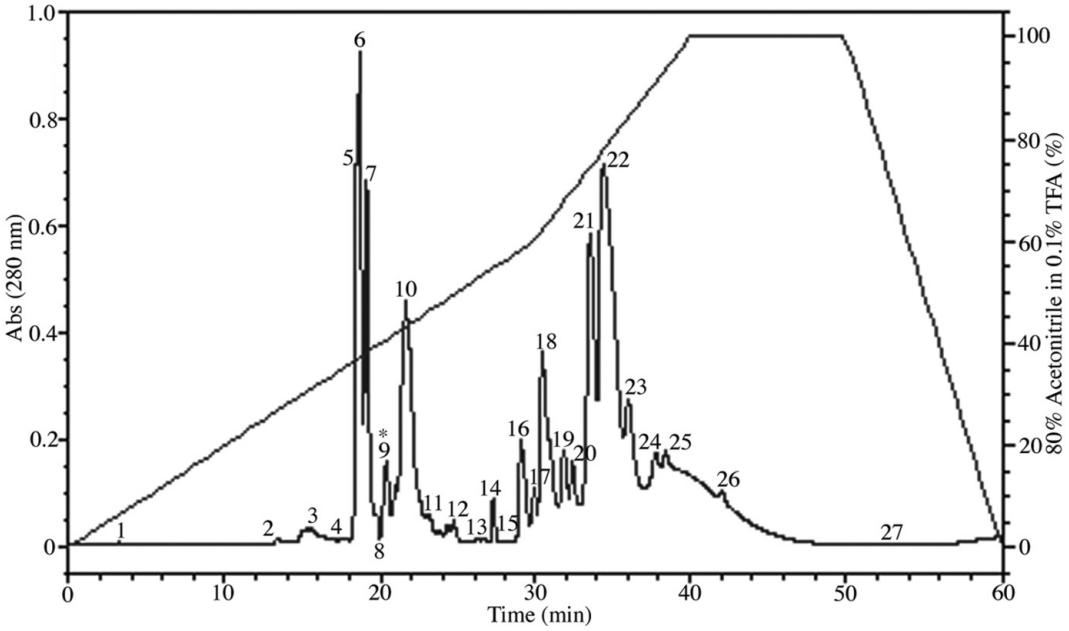
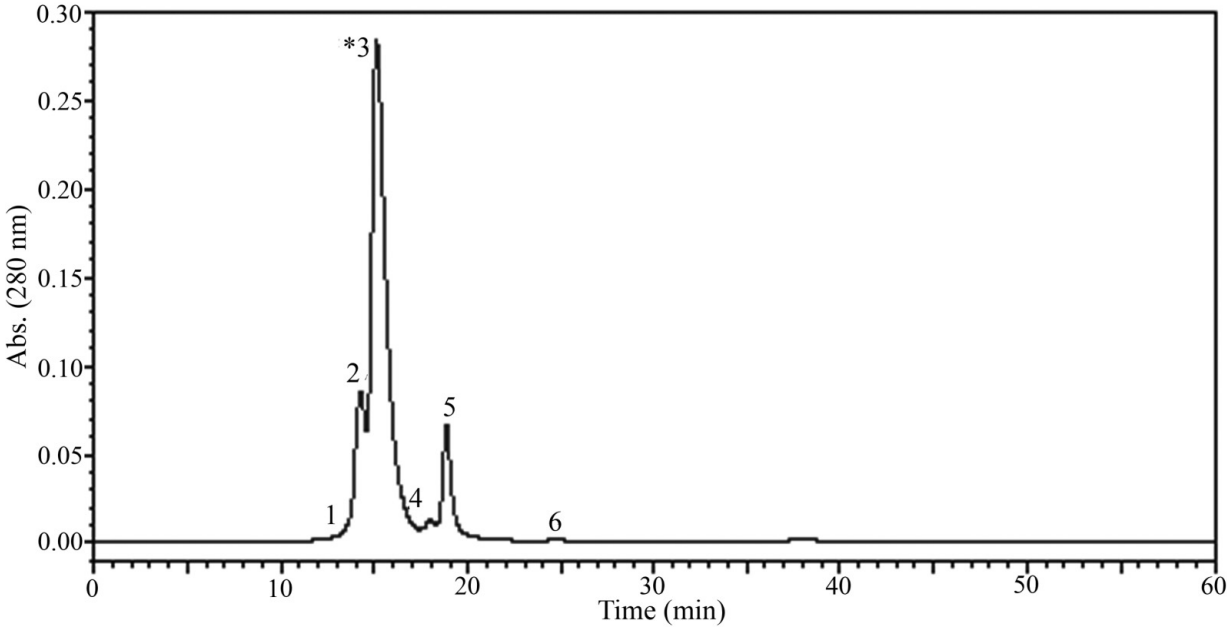


Fig. 3. Size exclusion chromatography of fraction 9 (Fig. 1). A total of 250 µg of fraction 9 was injected into a Waters ProteinPak™60 column (7.8 mm × 300 mm). The venom was separated using 0.02 mol/L sodium phosphate buffer (pH 6.2) on a Waters HPLC system. The fractions were tested for inhibition of platelet aggregation. Fraction *3 contained disintegrin-like activity.



(bovine, *m*/*z* 5730.61), and cytochrome C (equine, *m*/*z* 12 361.96). Argon was used as the collision gas for the generation of CID spectra and He was used as the cooling gas.

Database searching and amino acid sequence

The proteins digest masses-to-charge ratio's obtained from the matrix DHB were searched against a expressed sequence tag (EST) database for others (EST_{others}) at the National Center for Biotechnology Information, (NCBI, Bethesda, Maryland (http://www.ncbi.nlm.nih.gov/PMGifs/Genomes/others.html. The database can be downloaded from http://www.ncbi.nlm.nih.gov/dbEST/). The mascot and total ion scores obtained were search-parameter dependant and were stored within the data system. In the initial search, no enzyme specificity was used although carbamidomethyl (C) and (or) deamidation (NQ) were selected.

© 2005 NRC Canada

Fig. 4. Anion exchange chromatography of fraction 3 (Fig. 2). A total of 200 µg of protein was injected into a Waters Protein-Pak™ DEAE 5PW (7.5 mm × 7.5 mm) column. The venom was separated using 0.02 mol/L Tris-HCl buffer (pH 8.0) on a Waters HPLC system. The fractions were tested for inhibition of platelet aggregation. Fractions *1 and *2 contained disintegrin-like activity.

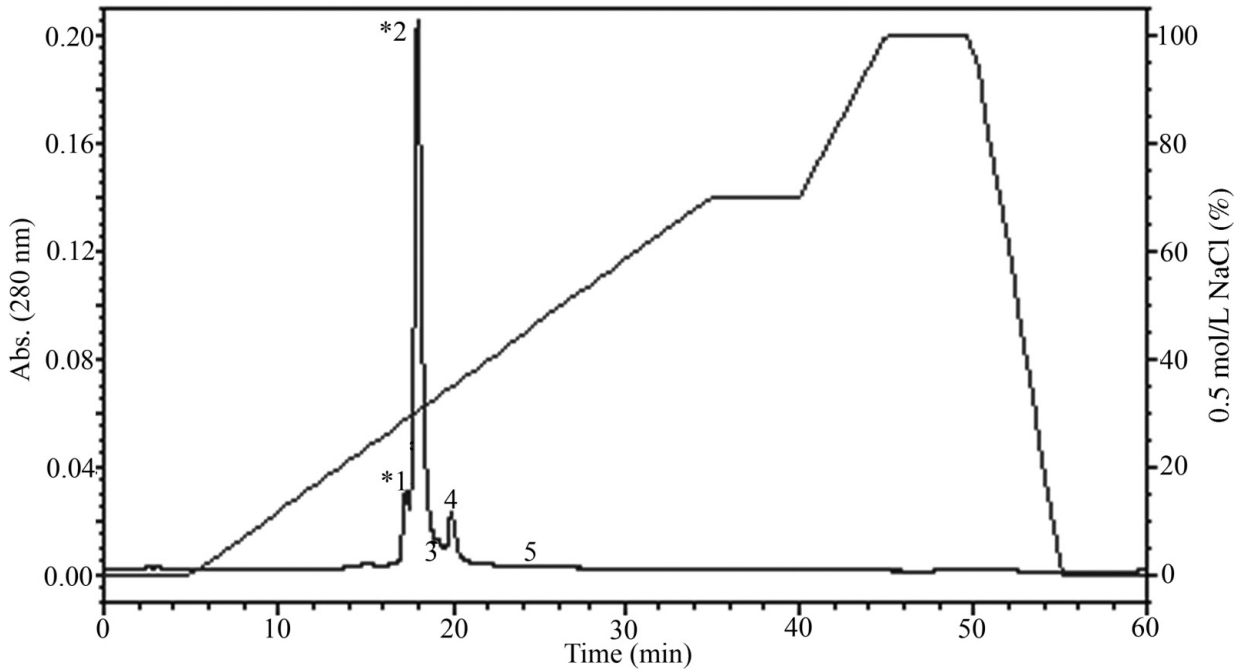
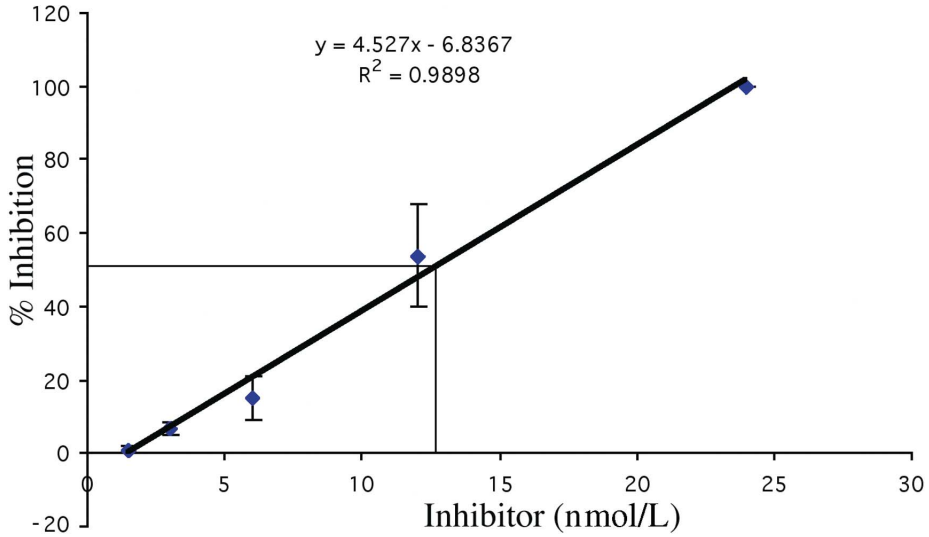


Fig. 5. The effects of horrdistatin 1 on ADP induced platelet aggregation. Various concentrations of horrdistatin 1 were preincubated with whole blood for 2 min at 37 °C prior to the addition of ADP (1 mmol/L). The IC_{50} was 12.5 nmol/L. Data was presented as the mean value of inhibition percentage to the control value. The values are in triplicate measurements and are representative of three independent experiments.



Results and discussion

In the present study, two disintegrins have been isolated and identified from the venom of one of the two Timber rattlesnakes tested. The venom of the Timber rattlesnake, like the Mojave rattlesnake, can exhibit intraspecific variation and have hemorrhagic, neurotoxic, and procoagulant enzymes (6–10). However, disintegrins have never been reported in the venom of the Timber rattlesnake. The two disintegrins isolated in this study share similar sequence homology and activity (22) with disintegrins found in the venom of other *Crotalus* species (Fig. 1).

The two disintegrins isolated by a three-step chromatography procedure (Figs. 2–4) were called horrdistatin 1 and horrdistatin 2. Both disintegrins had very similar IC_{50}s with regards to biological activity; the inhibition of ADP induced platelet aggregation. Horrdistatin 1 had an IC_{50} of 12.5 nmol/L and horrdistatin 2 had an IC_{50} of 16.2 nmol/L (Figs. 5 and 6). Following protein purification using the MDLC system, the samples were analyzed by MALDI-QIT-

© 2005 NRC Canada

Fig. 6. The effects of horrdistatin 2 on ADP induced platelet aggregation. Various concentrations of horrdistatin 2 were preincubated with whole blood for 2 min at 37 °C prior to the addition of ADP (1 mmol/L). The IC_{50} was 16.2 nmol/L. Data was presented as the mean value of inhibition percentage to the control value. The values are in triplicate measurements and are representative of three independent experiments.

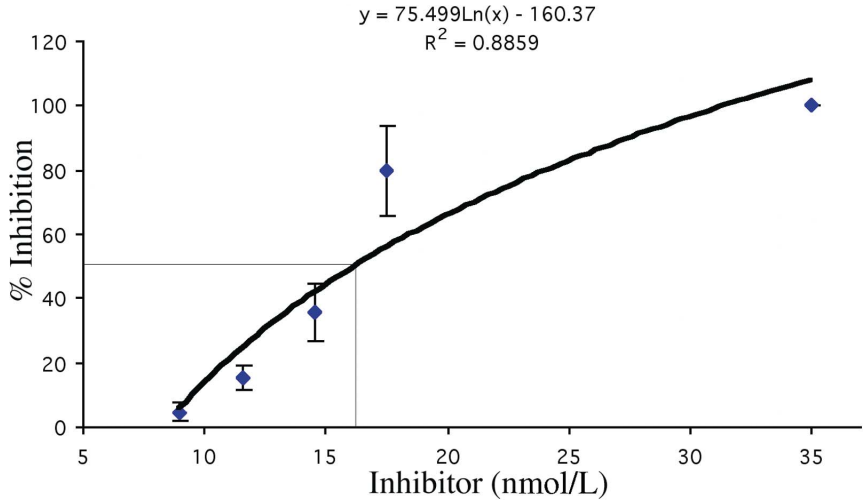
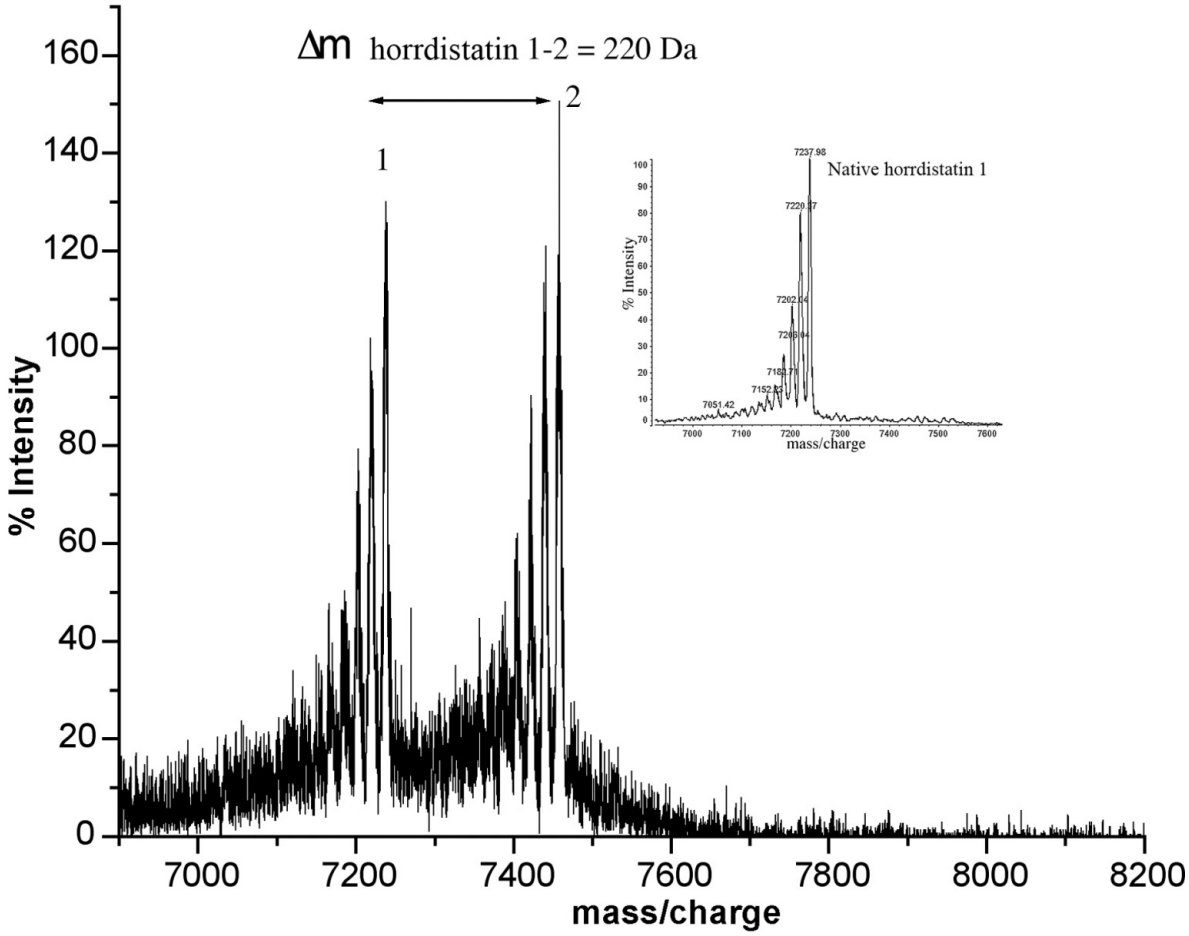
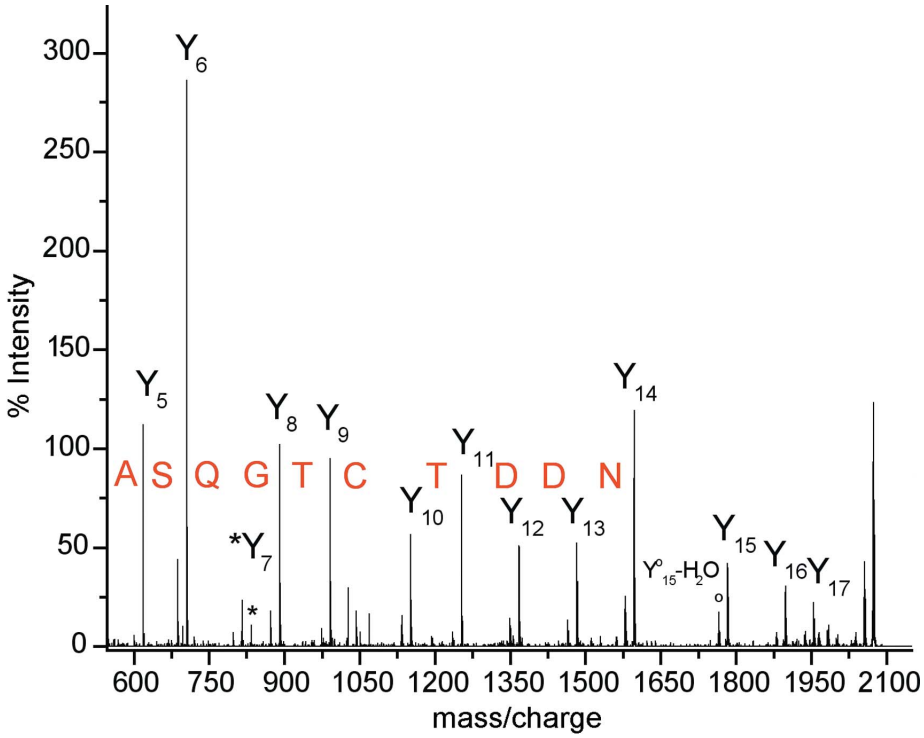


Fig. 7. MALDI-QIT-TOF mass spectrum of the isolated proteins horrdistatin 1 and 2. The samples were reduced and alkylated with DTT and iodoacetamide, respectively, and analyzed in positive mode. The insert is the corresponding mass spectrum for horrdistatin 1 (native). The mass difference between the native form and reduced form is an indicator of disulfide linkage. Note: $Exp_{measure-reduced}$ + H-H_2O = 7469 Da, calcd. 7550.4 Da, Δm = 0.6 Da, $\Delta m_{horrdistatin(nonreduced-reduced)}$ = 12 Da ~ six disulfide bonds.



© 2005 NRC Canada

Fig. 8. MALDI-CAF-CID spectrum of tryptic peptide ladder *m/z* 2090.72 from horrdistatin 1 from which the sequence could be determined. (The tryptic fragments from both proteins were compared; the common matched "paired" peptide fragments were used to generate the common sequence between the proteins, whilst the "unique" unmatched peptides were used to determine the differences between the proteins and also to confirm the assigned sequences). A tryptic fragment of *m/z* 2090.72 that could not be matched between the proteins was chemically derivatized to allow favored C-terminal fragmentation and subjected to CID fragmentation. The CAF-CID of unique peptide 2090.72 *m/z* and precursors of 1954.73 *m/z* generated "y"-type fragment ion, which were used to determine the amino acid differences between the two isolated proteins allowing the unique peptides to be "unzipped" allowing facile readout of the de novo sequence.



TOF. The nominal intact molecular mass for horrdistatin 1 was 7231 Da. The nominal intact molecular mass of horrdistatin 2 was 7469 Da with a true mass of 7451 Da (18 Da was due to hydration) resulting in a mass difference of 238 Da. A typical mass spectrum is shown in Fig. 7. Comparison of the nonreduced and reduced forms indicated a mass difference of 12 Da, revealing a high degree of disulfide cross-linking (~six disulfides), which was consistent with other known disintegrin proteins (Fig. 7).

The resulting mass sequence tags (MST) and initial peptide mass fingerprint (PMF) were jointly searched to obtain protein identities based upon sequence homology. This combined approach proved to be more successful than using PMF alone (32, 41). Almost 40% of the total protein sequence identified in this method, combined with CID, gave overall sequence coverage of 60% or more, allowing for unique identification. A CAF-CID spectrum representing horrdistatin 1 is shown in Fig. 8. Analysis of the tryptic digest in mid-mass mode between the two proteins indicated almost identical mass spectra, except horrdistatin 1 contained a fragment of mass-to-charge of 2239.88 Da that was absent from horrdistatin 2, which itself contained a tryptic fragment at mass-to-charge 2459.91 Da, which was absent in horrdistatin 1. The mass difference between these two unique tryptic fragments corresponds approximately to 220 Da, which was the mass difference between the native intact proteins (Fig. 7). The MS–MS search of the tryptic fragments (1954.74, 2036.86, and 2258.78 Da) from both proteins putatively indicated to be disintegrins similar to that of crotatroxin, a disintegrin from the Western Diamondback rattlesnake venom (Fig. 8). The difference in mass between the two proteins could be accounted for by consideration of the truncation of the former by two amino acids (deletion of the last two amino acids on the C terminus in horrdistatin 1 (Tyr-Gly)), which also accounts for the 220 Da difference in mass between the two proteins (Fig. 1). Additional MS–MS of the 2258.78 tryptic fragments indicates loss of Ala from the N terminal for both samples. The calculated mass of 7450.4 Da is in good agreement with the measured mass of 7469 Da (for the hydrated reduced form, where hydration is the inclusion of one water molecule).

Disintegrin proteins have been found in the venom of various snake species showing homology in their sequences, potencies, and their selective interactions with integrin receptors (42–45). The disintegrins, horrdistatin 1 and 2 have a high selectivity to the integrin $\alpha_{IIb}\beta_3$, which is responsible for the aggregation of platelets; and thus, could possibly have potential use in the treatment of myocardial infarctions and cerebrovascular accidents.

Acknowledgements

This research was supported by the following grants: NIH/RIMI No. 5 PMD000216-02, NIH/Viper No. 1 P40

© 2005 NRC Canada

RR018300-02, and NIH/SCORE No. 5 S06 GM008107-29. The authors are pleased to acknowledge Nora Diaz De Leon, Miguel Villegas Rocha, Lucy E. Arispe, and Arlene Velez for their technical assistance. We would also like to thank Dr. John Leszyk at the University of Massachusetts for his services.

References

1. A. Tennant. A field guide to snakes of Florida. Gulf Publishing Co., Houston, Texas. 1997. p. 219.
2. S.A. Minton. Animal toxins. Pergamon Press, New York. 1967. p. 213.
3. J.L. Glenn and R.C. Straight. Rattlesnake venoms: Their action and treatment. Merk Dekker Inc., New York. 1982. p. 3.
4. E.E. Sánchez, J.A. Galán, J.C. Perez, A. Rodríguez-Acosta, P.B. Chase, and J.C. Pérez. Toxicon, **41**, 315 (2003).
5. R.C. Straight and J.L. Glenn. Toxicon, **27**, 80 (1989).
6. J.C. Perez, M.R. McKeller, J.C. Pérez, E.E. Sánchez, and M.S. Ramírez. Toxicon, **39**, 621 (2001).
7. C.A. Bonilla. Thromb. Res. **6**, 151(1975).
8. M.A. Bober, J.L. Glenn, R.C. Straight, and C.L. Ownby. Toxicon, **26**, 665 (1988).
9. J.L. Glenn, R.C. Straight, and T.B. Wolt. Comp. Biochem. Physiol. Part C: Pharmacol. Toxicol. Endocrinol. **107C**, 337 (1994).
10. E.E. Sánchez, M.S. Ramírez, J.A. Galán, G. López, A. Rodríguez-Acosta, and J.C. Pérez. Toxicon, **41**, 315 (2003).
11. R.C. Straight, J.L. Glenn, T.B. Wolt, and M.C. Wolfe. Comp. Biochem. Physiol. Part B: Biochem. Mol. Biol. **100**, 51 (1991).
12. B.L. Adame, J.G. Soto, D.J. Secraw, J.C. Perez, J.L. Glenn, and R.C. Straight. Comp. Biochem. Physiol. Part B Biochem. Mol. Biol. **97**, 95 (1990).
13. T.F. Huang. New Taipei J. Med. **2**, 225 (2002).
14. R.M. Kini and H.J. Evans. Toxicon, **30**, 265 (1992).
15. F.S. Markland. Toxicon, **36**, 1749 (1998).
16. T.F. Huang, J.C. Holt, H. Lukasiewiecz, and S. Niewiarowski. J. Biol. Chem. **262**, 16 157 (1987).
17. V. Saudek, R.A. Atkinson, and J.T. Pelton. Biochemistry, **30**, 7369 (1991).
18. M.A. McLane, C. Marcinkiewicz, S. Vijay-Kumar, I. Wierzbicka-Patynowski, and S. Niewiarowski. Proc. Soc. Exp. Biol. Med. **219**, 109 (1998).
19. M. Bauer, Y. Sun, C. Degenhardt, and B. Kozikowski. J. Protein Chem. **12**, 759 (1993).
20. J.J. Calvete, Y. Wang, K. Mann, W. Schäfer, S. Niewiarowski, and G.J. Stewart. FEBS Lett. **309**, 316 (1992).
21. M. Adler, R.A. Lazerus, M.S. Dennis, and G. Wagner. Science (Washington, D.C.), **253**, 445 (1991).
22. R.M. Scarborough, J.W. Rose, M.A. Naughton, D.R. Phillips, L. Nannizzi, A. Arfsten, A.M. Campbell, and I.F. Charo. J. Biol. Chem. **268**, 1058 (1993).
23. M.A. McLane, E.E. Sanchez, A. Wong, C. Paquette-Straub, and J.C. Perez. Current Drug Targets Cardiovas. Haemat. Dis. **4**, 327 (2004).
24. J.J. Calvete, M. Jurgens, C. Marcinkiewicz, A. Romero, M. Schrader, and S. Niewiarowski. Biochem. J. **345**, 573 (2000).
25. E.H. Danen, C. Marcinkiewicz, and I.M. Corenelissen. Exp. Cell Res. **238**, 188 (1998).
26. C. Marcinkiewicz, J.J. Calvete, M.M. Marcinkiewicz, M. Raida, S. Vijay-Kumar, Z. Huang, R.R. Lobb, and S. Niewiarowski. J. Biol. Chem. **274**, 12 468 (1999).
27. C. Brando, C. Marcinkiewicz, B. Goldman, M.A. McLane, and S. Niewiarowski. Biochem. Biophys. Res. Commun. **267**, 413 (2000).
28. M.R. Ritter, Q. Zhou, and F.S. Markland. J. Cell Biochem. **79**, 28 (2001).
29. Q. Zhou, M.T. Nakada, C. Arnold, K.Y. Shieh, and F.S. Markland. Angiogenesis, **3**, 259 (1999).
30. S.A. Weinstein and K.V. Kardong. Toxicon, **32**, 1161 (1994).
31. B. Champluvier and M.R. Kula. Bioseparation, **2**, 343 (1992).
32. K.G. Standing. Curr. Opin. Struct. Biol. **13**, 595 (2003).
33. A.K. Shukla and J.H. Futrell. J. Mass Spectrom. **35**, 1069 (2000).
34. K.D. Roth, Z.H. Huang, N. Sadagopan, and J.T. Watson. Mass Spectrom. Rev. **17**, 255 (1998).
35. C. Cheng and M.L. Gross. Mass Spectrom. Rev. **19**, 398 (2000).
36. K. Biemann. Biomed. Environ. Mass Spectrom. **16**, 99 (1988).
37. T. Keough, R.S. Youngquist, and M.P. Lacey. Anal. Chem. **75**, 156A (2003).
38. S.P. Mackessy. J. Toxicol. Toxin Rev. **21**, 43 (2002).
39. R.M. LoPachin, R.C. Jones, T.A. Patterson, W. Slikker, and D.S. Barber. NeuroToxicology, **24**, 761 (2003).
40. P. Juarez, L. Sanz, and J.J. Calvete. Proteomics, **4**, 327 (2004).
41. J.V. Olsen and M. Mann. Proc. Natl. Acad. Sci. U.S.A. **101**, 13 417 (2004).
42. R.J. Gould, M.A. Polokoff, P.A. Friedman, T.F. Huang, J.C. Holt, J.J. Cook, and S. Niewiarowski. Proc. Soc. Exp. Biol. Med. **195**, 168 (1990).
43. R.M. Scarborough, J.W. Rose, M.A. Hsu, D.R. Phillips, V.A. Fried, A.M. Campbell, L. Nannizzi, and I.F. Charo. J. Biol. Chem. **266**, 9359 (1991).
44. E.F. Plow, T.A. Haas, L. Zhang, J. Loftus, and J.W. Smith. J. Biol. Chem. **275**, 21 785 (2000).
45. Q. Zhou, R.P. Sherwin, C. Parrish, V. Richters, S.G. Groshen, D. Tsao-Wei, and F.S. Markland. Breast Cancer Res. Treat. **61**, 249 (2000).

© 2005 NRC Canada

Role of the solvent in the oxidative process of a Hg electrode in the presence of thiopyrimidine derivatives

Souad Bakari, Marco Borsari, Maria Cannio, Giovanna Gavioli, Antonio Ranieri, Silvia Peressini, and Claudio Tavagnacco

Abstract: The electrochemical oxidation of a Hg electrode in the presence of thiopyrimidine derivatives has been investigated in a collection of organic solvents using voltammetric and polarographic techniques. Remarkable adsorption phenomena control the electrochemical process, which in all cases gives rise to a Hg(I) complex. The Laviron adsorption model is found to describe well the polarographic adsorption wave. Some correlations between adsorption parameters and solvent properties have also been observed and discussed.

Key words: polarography, voltammetry, thiopyrimidine, solvent effect, adsorption.

Résumé : On a étudié l'oxydation électrochimique d'une électrode de mercure en présence de dérivés thiopyrimidines dans divers solvants organiques, en faisant appel à des techniques polarographiques et voltampérométriques. Un phénomène remarquable d'adsorption contrôle le processus électrochimique qui, dans tous les cas donne lieu à un complexe Hg(I). On a trouvé que le modèle d'adsorption de Laviron décrit bien la vague d'adsorption polarographique. On a observé et on discute de quelques corrélations entre les paramètres d'adsorption et les propriétés du solvant.

Mots clés : polarographie, voltampérométrie, thiopyrimidine, effet de solvant, adsorption.

[Traduit par la Rédaction]

Introduction

Interest in the chemistry of thiopyrimidine derivatives arises from their involvement in some biological systems and from their potential use as anti-tumour and anti-thyroid agents (1–3). Studies have been reported concerning the electrochemistry of thiopyrimidines (4–14) in which particular attention has been focused on the reduction process in aqueous solutions. However, few data concerning the electrochemical oxidation in organic solvents are available. In dimethylformamide (DMF), adsorption phenomena are involved in the process, and the formation of a Hg(I) complex was observed (4). In this paper, polarographic and voltammetric methods have been used to characterize the electrochemical oxidation of a collection of thiopyrimidines (15, 16) on a Hg electrode in several solvents. Moreover, the role of the medium and the pyrimidine ring substituents on the adsorption processes has been emphasized. In fact, studies on electrosorption of organic molecules can provide fundamental information, which can be useful in clarifying the relation between the microstructure of the double layer in the presence of specific adsorption and the measured macro properties of the electrochemical system.

Received 12 November 2004. Published on the NRC Research Press Web site at http://canjchem.nrc.ca on 21 September 2005.

S. Bakari, M. Borsari,[1] M. Cannio, G. Gavioli, and A. Ranieri. Department of Chemistry, University of Modena and Reggio Emilia, Via Campi 183, I-41100 Modena, Italy. **S. Peressini and C. Tavagnacco.** Department of Chemical Science, University of Trieste, Via Giorgieri 1, I-34127 Trieste, Italy.

[1]Corresponding author (e-mail: borsari.marco@unimo.it).

Results and discussion

The oxidative electrochemistry of a Hg electrode in the presence of 2-thiopyrimidines, 2-thiopyrimidine (**1**), 4,6-dimethyl-2-thiopyrimidine (**2**), 1,4,6-trimethyl-2-thiopyrimidine (**3**), and 4,6-dimethyl-1-phenyl-2-thiopyrimidine (**4**), has been investigated in several solvents (DMF, DMSO, acetonitrile (ACN), EtOH, and MeOH). The observed behaviour is found to be similar to that already reported for compounds **2** and **4** in DMF (4) and is found to be independent of the nature of the solvent.

In the cyclic voltammetry (CV) curves, in fact, at a concentration (c) of thiopyrimidine higher than a critical value independent of the solvent (c_m = 2.2 ± 0.2 × 10^{-4}, 2.0 ± 0.2 × 10^{-4}, 1.9 ± 0.2 × 10^{-4}, and 0.8 ± 0.1 × 10^{-4} mol/L for compounds **1**, **2**, **3**, and **4**, respectively), two anodic peaks (A_1,A_2) and their corresponding cathodic counterparts (C_1,C_2) are present (Fig. 1A-*ii*), while at $c < c_m$ only one pair of peaks (A_1,C_1) is observed (Fig. 1A-*i*). The A_1,C_1 couple shows the characteristics of an electrochemical signal corresponding to a reversible faradic process involving the adsorption of a species involved in the electron transfer (17, 18): the peak current (i_p) remains constant at $c > c_m$ (Fig. 2) and is proportional to the scan rate (v) (Fig. 3*a*). The A_2,C_2 peaks, however, show typical *diffusion* characteristics, corresponding to a faradic process involving a species that freely

 doi: 10.1139/V05-125 © 2005 NRC Canada

Fig. 1. Cyclic voltammogram (A) and polarographic curves (B) for (*i*) 2×10^{-4} and (*ii*) 5×10^{-4} mol/L solutions of 1,4,6-trimethyl-2-thiopyrimidine in ACN. Base electrolyte 0.1 mol/L TBAP, T = 25 °C, scan rate 0.05 V s^{-1}. Wave I – adsorption signal and wave II – diffusion-controlled signal. E values are referred to the reversible redox couple cobaltocene/cobaltocinium.

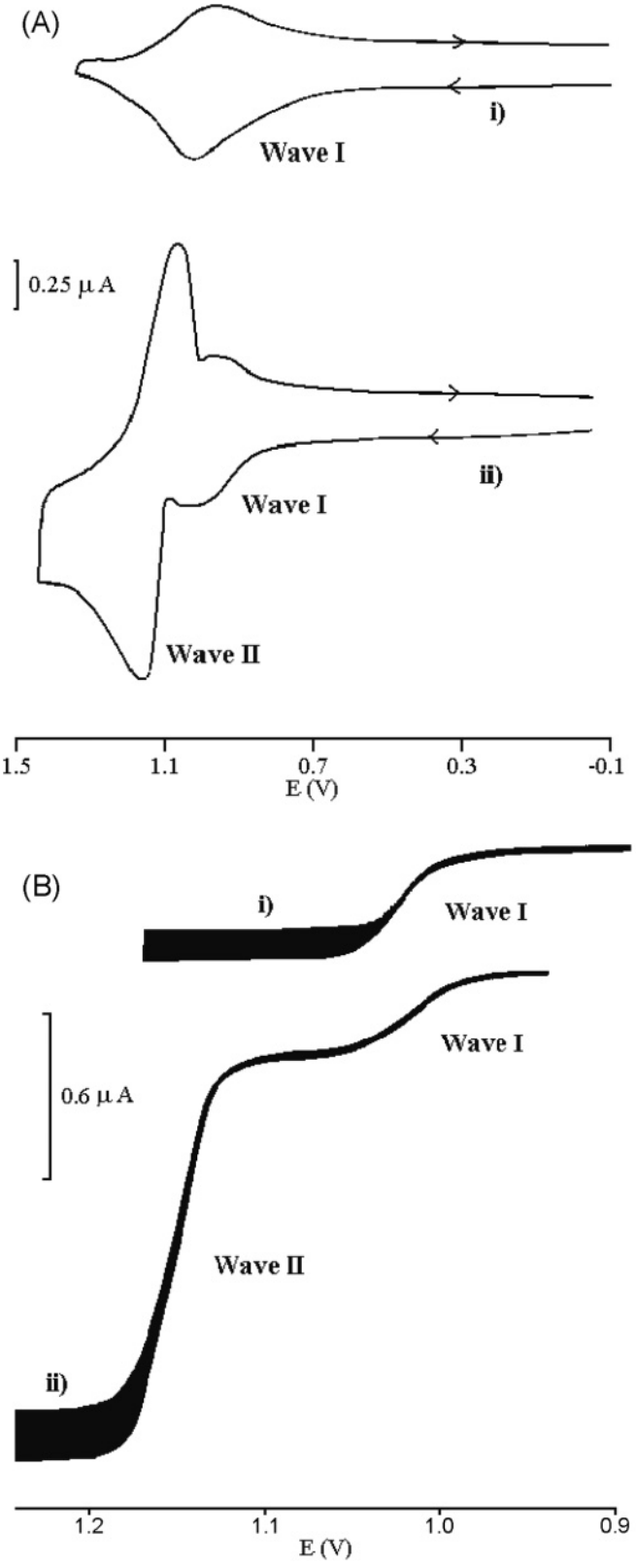
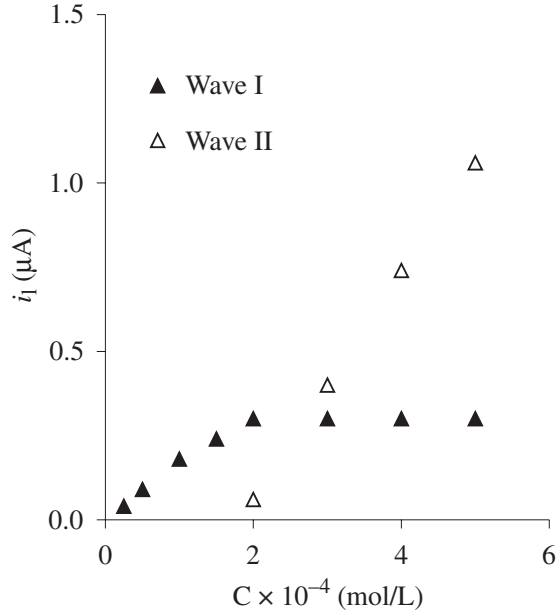


Fig. 2. Voltammetric anodic limiting current (i_l) vs. concentration (c) for 1,4,6-trimethyl-2-thiopyrimidine in ACN. Scan rate 0.05 V s^{-1}. Base electrolyte 0.1 mol/L TBAP, T = 25 °C.



diffuses toward the electrode surface: i_p is proportional to c (Fig. 2) and $v^{1/2}$ (Fig. 3*b*), but no limiting value is observed.

The polarographic behaviour strongly resembles that found using voltammetric techniques (Fig. 1B): two oxidative waves occur at $c > c_m$ (wave I and II, c_m is the same as observed in the CV measurements, Fig. 1B-*ii*), while at $c < c_m$ only one wave (wave I) is present (Fig. 1B-*i*). Wave I is the adsorption wave (17, 19). In fact, at $c < c_m$ its limiting current (i_l) is proportional to c and $t_d^{1/6}$ (t_d = dropping time), while at $c > c_m$, i_l is independent of c and proportional to $t_d^{-1/3}$ (20). Wave II (the diffusion wave) is characterized by a more positive half-wave potential ($E_{1/2}$), and its i_l value is invariably found to be proportional to c and $t_d^{1/6}$ (20). Therefore, the voltammetric and polarographic results indicate the presence of a solely electrochemical process characterized by two signals corresponding to the oxidation product in two different states, one possibly arising from diffusion in solution and the second from adsorption on the mercury surface.

Coulometry at a constant potential value (CPO) has been performed at a potential value 50 mV more positive than peak A_2, and the number of electrons involved in the oxidative process, calculated by integration of the i vs. t curves, is found to be one in all of the solvents. The product of the CPO process was separated and identified (by elemental analysis, and IR and UV spectra) as $[Hg(L)]ClO_4$ (L = compounds **1**–**4**) for all solvents.

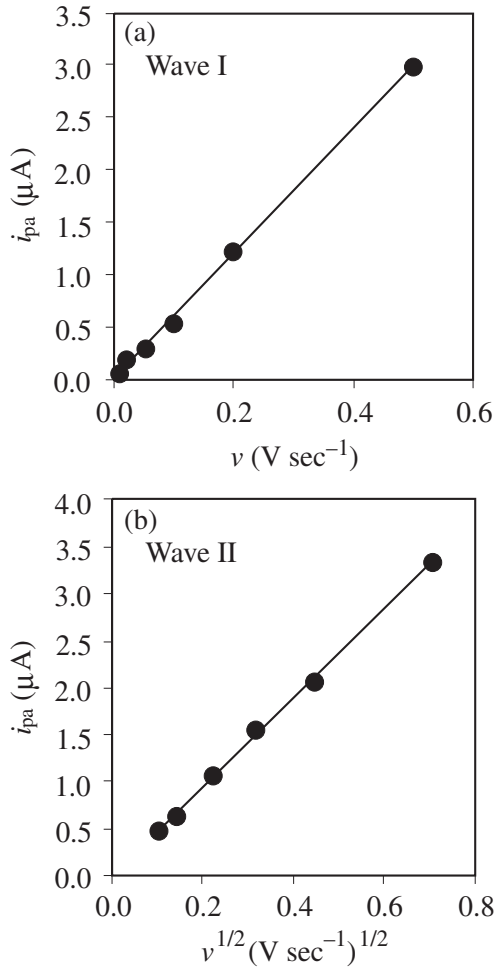
In the case of DMF, $[Hg(L)]^+$ is observed during electrolysis, but changes slowly in a mixture of Hg^{2+} into difficult to characterize complexes having a formula of $[Hg(L)_n](ClO_4)_2$ (n = 1–3). This can probably be attributed to the disproportionation of the Hg^+ complex to Hg^0 and Hg^{2+}, as is often observed for several Hg^+ compounds in DMF (21–24).

Therefore, the oxidation mechanism on the Hg electrode can be summarized as follows:

$$Hg + L = [Hg(L)]^+ + e^-$$

© 2005 NRC Canada

Fig. 3. (*a*) Plot of i_{pa} vs. v (scan rate) for wave I and (*b*) plot of i_{pa} vs. $v^{1/2}$ for wave II for a 5×10^{-4} mol/L solution of 1,4,6-trimethyl-2-thiopyrimidine in ACN. Base electrolyte 0.1 mol/L TBAP, T = 25 °C.



The observed behaviour of the CV and polarographic signals is apparently typical of reversible electrochemical processes involving a species electroactive both in solution and in adsorbed form (20). In our case, the product of the electrochemical process is the most strongly adsorbed. At low concentrations the single observed signal (a peak couple in CV) is due to an oxidative process involving dissolved thiopyrimidine, which forms a layer of adsorbed product on the electrode surface. At increasing thiopyrimidine concentrations, the current of this signal increases until a limiting value, corresponding to complete coverage of the electrode surface, is reached. Then an apparent diffusion signal appears and grows with respect to the adsorption signal, which remains constant. The diffusion signal is a result of the same faradic process as the adsorption one, but the product of the electrochemical process is not adsorbed but is free to diffuse in solution (20). The diffusion signal is characterized by a more positive potential value than the adsorption signal because adsorption of the oxidation product contributes to the free energy of the electrochemical reaction thereby making oxidation easier than in the case where the product freely diffuses (20). Such behaviour has been observed for a variety of thiols, thiourea derivatives, and thiobarbiturates (25–28), but while the origin of the first signal (adsorption) is invariably attributed to the formation of a Hg(I) compound adsorbed on the Hg surface, the origin of the second signal is not so clear. As a matter of fact, in our case it is limited by diffusion of the thiopyrimidine (at least in the concentration range examined) and gives a Hg(I) compound. Careful investigations concerning the oxidation of the Hg electrode in the presence of cysteine (26–28) in aqueous solution indicate the presence of two steps corresponding to the formation of Hg(I) and Hg(II) cysteine compounds, respectively. In particular, the first step is pH and concentration dependent, but in all cases, at concentrations higher than a critical value, it appears to involve two signals. The first one (*adsorption pre-wave*) exhibits a limited current value attributed to the inhibition effect of the adsorbed reaction product (cysteine mercurous thiolate). The second wave is attributed to the increased dissolution pressure of Hg under the adsorbed layer (26). The case of thiopyrimidine is probably not that different from cysteine, even if the presence of organic solvent renders the solubility of the Hg complex greater than that in aqueous solution, and this fact could affect the *compactness* of the adsorbed film. However, since the aim of this paper is to provide information on the characteristics of the first adsorption process on the Hg surface in the presence of different solvents, the nature of the second signal has not been investigated further.

As a matter of fact the thiopyrimidine derivatives (compounds **1**–**4**, r species) as well as the products of the oxidative process (Hg(I) complexes, p species) can be strongly adsorbed. For this reason, the polarographic adsorption wave I was analyzed in the different solvents according to the model proposed by Laviron introducing the mixed Frumkin isotherm (4, 19):

$$b_i c_i\ (0,t_d) = [\theta_i/n_i\ (1 - \theta_i - \theta_j)]\ \exp(-2a_i n_i \theta_i - 2a_{ij} n_{ij} \theta_{ij})$$

where i and j refer to the r and p species, θ is the coverage, b is the adsorption coefficient, n_i is the number of solvent molecules removed by one molecule of i, and a is the interaction parameter. The saturation value of the surface concentration of the p species ($\Gamma_{m,p}$) was determined from the polarographic adsorption current at $\theta = 1$ (17) (Table 1), while the $\Gamma_{m,r}$ for the r species was evaluated using the Korita equation (29) at $c = c_m$ (Table 1). Thus, according to Laviron (19) and Muller et al. (30–32), the following theoretical relationship between E and the current intensity (I) was used to analyze the adsorption wave:

$$E = E_{1/2} + (RT/\alpha nF)\{\ln[\Phi/2(I - \Phi)^2] + \sigma n_r G[4(\Phi - 1/2)]\}$$

where

$$\Phi = (I/I_l),\ \sigma = 0.74 D_r t_d^{1/2} c_r / \Gamma_{m,p}$$

$$G = a_{pr}(1 + 2\Gamma_{m,p}/\Gamma_{m,r}) - a_p - 2(\Gamma_{m,p}/\Gamma_{m,r})a_r$$

α is the electron transfer (ET) coefficient, F is Faraday's constant, D is the diffusion coefficient of species r, I_l is the limit current intensity, and G is the mixed Frumkin interaction parameter.

© 2005 NRC Canada

Table 1. Γ_m values ($\Gamma_m \times 10^{10}$ (mol cm^{-2})) for the compounds investigated in a collection of solvents.

	1		**2**		**3**		**4**	
Solvent	*r*	*p*	*r*	*p*	*r*	*p*	*r*	*p*
DMF	4.17	8.67	3.70	2.26	3.22	2.77	1.22	0.84
DMSO	4.21	8.69	3.78	2.26	3.31	2.78	1.24	0.85
ACN	4.32	8.71	3.82	2.29	3.33	2.78	1.25	0.86
MeOH	4.07	8.64	3.62	2.23	3.14	2.72	1.18	0.81
EtOH	4.16	8.66	3.65	2.25	3.18	2.75	1.19	0.83

Table 2. Mixed Frumkin interaction parameter values (*G*) in different solvents for the following compounds: 2-thiopyrimidine (**1**), 4,6-dimethyl-2-thiopyrimidine (**2**), 1,4,6-trimethyl-2-thiopyrimidine (**3**), and 4,6-dimethyl-1-phenyl-2-thiopyrimidine (**4**).

		G			
Solvent	$\varepsilon^{-1} \times 10^2$	**1**	**2**	**3**	**4**
DMF	2.61	–0.03	–0.29	–0.26	–0.15
DMSO	2.12	–0.02	–0.24	–0.21	–0.12
ACN	2.73	–0.04	–0.3	–0.27	–0.16
MeOH	3.03	–0.04	–0.34	–0.29	–0.17
EtOH	3.95	–0.05	–0.43	–0.4	–0.22

Note: ε = relative dielectric constant.

Therefore, a linear dependence of *E* vs. $\{\ln[I/(I_l - I)^2] + \sigma n_p G(I/I_l)\}$, i.e., *E* vs. *f*(*I*), is expected with a slope of $(RT/\alpha nF)$. The n_p value, evaluated according to Koppitz et al. (33), is found to be about 2 for all the compounds. The validity of Laviron's model is confirmed by the fact that plots of *E* vs. *f*(*I*) show a good linear shape using the *G* values reported in Table 2 (*G* = 0 corresponds to non interactive Langmuir behaviour).

The $\Gamma_{m,r}$ value can be used to evaluate the area occupied by one adsorbed molecule of each investigated thiopyrimidine on the Hg surface. The values obtained are nearly independent of the solvent and correspond to an area of 40 ± 2 Å^2 for **1**, 45 ± 2 Å^2 for **2**, 51 ± 2 Å^2 for **3**, and 135 ± 4 Å^2 for **4**. The calculated areas (Hyperchem program) for a flat orientation are 38, 41, 48, and 125 Å^2, respectively. As already proposed for **2** and **4** in DMF (4), these data suggest that all the compounds lie flat on the electrode, independent of the nature of the solvent.

A linear correlation can be observed to exist in plots of *G* vs. ε^{-1} (the dielectric constant) (Fig. 4). This kind of comparison could appear to be not completely justified on physical grounds, since *G* should be a corrective factor in the thermodynamic isotherm with respect to ideal behaviour; in spite of this, some information on the nature of the *real* behaviour of the system can be revealed by this type of procedure. *G* is somewhat directly related to the interaction energy among the adsorbed molecules, and its correlation with ε^{-1} suggests that its value is, at least partially, due to electrostatic potentials (34, 35). Since one of the adsorbed species (*r*) is neutral, the hypothesis that a partial charge could be localized on this once it is adsorbed as a result of its interaction with the Hg surface should be considered. It is also worthwhile noting that nonnegligible changes in electron density distribution have been observed when aromatic molecules are adsorbed in a planar disposition (34–36).

Fig. 4. Plot of *G* parameter vs. ε^{-1} for the compounds investigated in a collection of solvents.

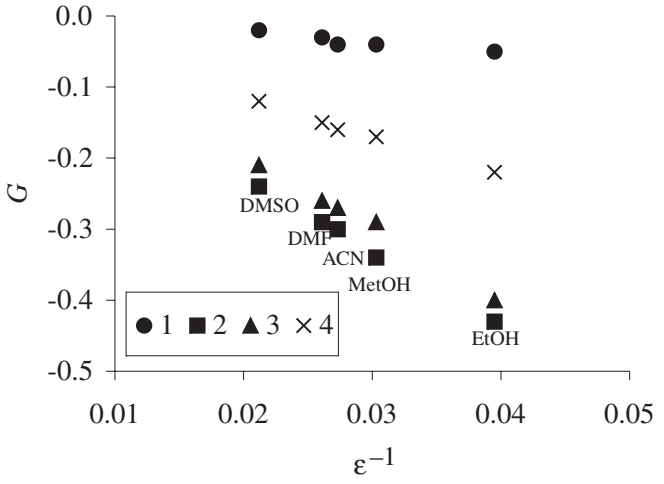
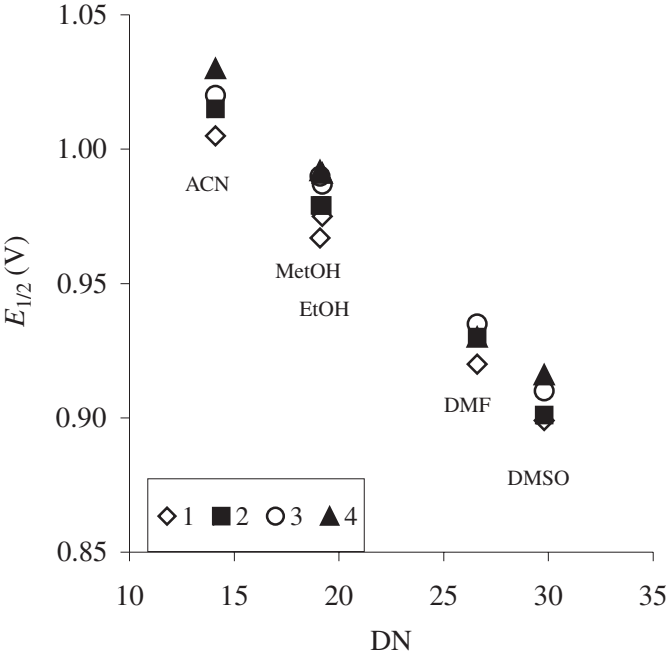


Fig. 5. Plot of $E_{1/2}$ vs. DN (donor number) for the investigated 2-thiopyrimidines in a collection of solvents. $E_{1/2}$ values are referred to the reversible redox couple cobaltocene/cobaltocinium. Base electrolyte 0.1 mol/L TBAP, *T* = 25 °C, thiopyrimidine concentration 5×10^{-4} mol/L.



Plots of $E_{1/2}$ vs. DN (donor number) for the investigated solvents show a rather good correlation for wave II (Fig. 5), while wave I appears to be almost independent of any change in DN value. This result is probably related to the nature of the electrochemical process. In fact, in an electron-transfer process the solvent interactions tend to stabilize the redox state corresponding to the form that carries the higher charge. In our case, the oxidized species, the Hg(I) complex, is the only charged form involved in the electrochemical process, and it should, therefore, interact more strongly with the solvent. Due to its positive charge, DN is the most appropriate and useful solvent index in this type of approach. Actually, the increase in DN value causes a shift in the $E_{1/2}$

© 2005 NRC Canada

values towards more negative values, according to the stabilization of the oxidized species. The low sensitivity of wave I to DN change is probably due to the relatively marginal role played by the solvent in the oxidative processes involving adsorbed species that are predominantly driven by the molecule–surface interaction.

The results indicate that the solvent characteristics affect the oxidation process of Hg in the presence of thiopyrimidines. Electrostatic repulsions among the adsorbed molecules appear to be modulated by the dielectric constant value of the solvent medium, while the disposition of the adsorbed molecules on the electrode surface is found to be independent of the nature of the solvent. The DN values play a certain role in determining the $E_{1/2}$ value and so induce a stabilization of the oxidation product.

Experimental section

All compounds were synthesized according to the literature methods (15, 16).

The electrochemical measurements were performed in dimethylformammide (DMF, Fluka), acetonitrile (ACN, Fluka), dimethylsulfoxide (DMSO, Fluka), ethanol (EtOH, Carlo Erba), and methanol (MetOH, Fluka) dried over 4 Å sieves and stored under Ar in dark bottles. Tetrabutylammonium perclorate (TBAP) (Fluka) was recrystallized from methanol and vacuum dried at 25 °C.

The concentrations of the investigated compounds ranged between 2×10^{-4} and 5×10^{-4} mol dm^{-3} in 0.1 mol dm^{-3} solutions of TBAP as the supporting electrolyte.

The polarographic and voltammetric measurements were carried out using a PAR 273 A Potenziostat–Galvanostat. The working electrode was a Metrohm 463 VA Hg stand, while a Pt ring and a $NaCl_{sat}$ calomel electrode were used as counter and reference electrode, respectively. Coulometric measurements, however, were performed using a Hg pool as the working electrode. All potentials were measured using the satd. aq. NaCl calomel electrode contained in a glass tube separated from the solution by a glass frit of medium porosity, which was located 1 mm from the tip of the working electrode to minimize the ohmic drop, and filled with the supporting electrolyte solution. To compare the results in different solvents, all the potential values were referred to the cobaltocene/cobaltocinium couple, as explicitly indicated. The measurements were all conducted at 25 ± 0.1 °C under an Ar atmosphere in a three-electrode thermostated jacket cell.

Acknowledgements

We are grateful to the Ministero dell'Istruzione, Università e Ricerca (MIUR) for financial support.

References

1. R.K. Robbins. J. Med. Chem. **7**, 186 (1964).
2. I. Vortruba, A. Holý, and K. Jošt. Collect. Czech. Chem. Commun. **39**, 364 (1974).
3. D.T. Hurst. An introduction to the chemistry and biochemistry of pyrimidines, purines and pteridines. Wiley, New York. 1980. p. 244.
4. R. Battistuzzi, M. Borsari, D. Dallari, G. Gavioli, C. Tavagnacco, and G. Costa. J. Electroanal. Chem. **368**, 227 (1994).
5. T.J. Bardes, R.R. Herr, and T. Eukoji. J. Am. Chem. Soc. **77**, 960 (1955).
6. O. Manousek and P. Zuman. Collect. Czech. Chem. Commun. **20**, 1340 (1955).
7. P. Zuman and M. Kuik. Collect. Czech. Chem. Commun. **24**, 3861 (1959).
8. G. Horn and P. Zuman. Collect. Czech. Chem. Commun. **25**, 3401 (1960).
9. W.F. Smyth, P. Zuman, and G. Svehla. J. Electroanal. Chem. **30**, 101 (1971).
10. M. Wrona and B. Czochralska. J. Electroanal. Chem. **48**, 433 (1973).
11. M. Wrona, B. Czochralska, and D. Shugar. J. Electroanal. Chem. **68**, 355 (1976).
12. M. Wrona. J. Electroanal. Chem. **104**, 243 (1979).
13. M. Wrona and M. Geller. J. Electroanal. Chem. **104**, 263 (1979).
14. A. Izquierdo, E. Bosch, and M.D. Prat. Electrochim. Acta, **27**, 1465 (1982).
15. R. Battistuzzi and G. Peyronel. Transition Met. Chem. (Weinheim, Ger.), **3**, 345 (1978).
16. R. Battistuzzi. Transition Met. Chem. (Weinheim, Ger.), **13**, 401 (1988).
17. E. Laviron. J. Electroanal. Chem. **52**, 355 (1974).
18. M. Noel, S. Chandrasekaran, and C. Ahmed Basha. J. Electroanal. Chem. **255**, 93 (1987).
19. E. Laviron. J. Electroanal. Chem. **63**, 245 (1975).
20. A.J. Bard and L.R. Faulkner. Electrochemical methods. Wiley, New York. 1980.
21. J.M. Fernández Alvarez and M.R. Smith. Analyst (Cambridge, U.K.), **114**, 1603 (1989).
22. N. Van Kiet and M. Breant. C. R. Acad. Sci. Ser. IIC, **264**, 1042 (1967).
23. C.K. Mann and K.K. Barnes. Electrochemical reactions in nonaqueous systems. *Edited by* A.J. Bard. Marcel Dekker, New York. 1970. p. 18.
24. P.K. Wrona and Z. Galus. *In* Encyclopedia of electrochemistry of the elements. Vol. IX, Part A. *Edited by* A.J. Bard. Marcel Dekker, New York. 1982. p. 22.
25. M. Brezina and P. Zuman. Polarography in medicine, biochemistry, and pharmacy. Interscience, London. 1958.
26. M. Heyrovský, P. Mader, S. Vavřička, V. Veselá, and M. Fedurco. J. Electroanal. Chem. **430**, 103 (1997).
27. M. Heyrovský and S. Vavřička. J. Electroanal. Chem. **423**, 125 (1997).
28. M. Heyrovský and S. Vavřička. Bioelectrochem. Bioenerg. **48**, 43 (1999).
29. J. Korita. Collect. Czech. Chem. Commun. **18**, 93 (1953).
30. C. Muller, J. Clorat, J.M. Felin, and J. Virgili. Collect. Czech. Chem. Commun. **49**, 481 (1984).
31. C. Muller, J. Clorat, Z. Martinez, and M. Soret. J. Electroanal. Chem. **202**, 203 (1986).
32. C. Muller, E. Valles, O. Valves, and E. Gomez. J. Electroanal. Chem. **204**, 237 (1987).
33. F.D. Koppitz, J.W. Schultze, and D. Rolle. J. Electroanal. Chem. **170**, 5 (1984).
34. D. Rolle and J.W. Schultze. J. Electroanal. Chem. **229**, 141 (1987).
35. L. Benedetti, C. Fontanesi, G. Camurri, and G. Gavioli. Collect. Czech. Chem. Commun. **56**, 750 (1991).
36. J.W. Schultze and K.J. Vetter. J. Electroanal. Chem. **44**, 63 (1973).

© 2005 NRC Canada

A mild and efficient procedure for the conversion of aromatic carboxylic esters to secondary amides

Revika Arora, Satya Paul, and Rajive Gupta

Abstract: A mild and efficient procedure has been developed for the conversion of aromatic carboxylic esters to secondary amides using reusable Zn dust with microwave heating in the presence of *N*,*N*-dimethylformamide or conventional heating by stirring in an oil bath using THF as solvent. Zn dust can be reused several times after simple washing with dil. HCl and distilled water.

Key words: aromatic carboxylic esters, aromatic primary amines, secondary amides, Zn dust, microwave activation.

Résumé : On a mis au point une méthode douce et efficace de transformer des esters d'acides carboxyliques aromatiques en amides secondaires en faisant appel à un catalyseur de Zn en poudre réutilisable, avec chauffage microonde en présence de *N*,*N*-diméthylformamide ou par chauffage conventionnel à l'aide d'un bain d'huile en utilisant du THF comme solvant. La poudre de Zn peut être réutilisée plusieurs fois après simple lavage avec de l'acide chlorhydrique dilué et de l'eau distillée.

Mots clés : esters d'acides carboxyliques aromatiques, amines primaires aromatiques, amides secondaires, poudre de Zn, activation par micro-ondes.

[Traduit par la Rédaction]

Introduction

The amide unit (1) is one of the most widely occurring functional groups as it represents a key feature in many biologically important natural and synthetic products. Numerous methods are available for the preparation of amides. These include ammonolysis of carboxylic acids and derivatives, thermal decomposition of ammonium salts of carboxylic acids, partial hydrolysis of cyanides, etc. The reaction of carboxylic acids with ammonia or amines to provide the corresponding amides is not a mild, efficient, and cost-effective method (2) as it requires the use of expensive reagents like DCC (3), Fe^{3+}-K10 montmorillonite clay (4), molecular sieves (5), silicon tetrachloride in pyridine (6), polymer-supported HOBT (7), chlorosulfonyl isocyanate (8), PCl_3 (9), etc. The other derivatives of carboxylic acids, particularly acyl halides, acid anhydrides and esters, are most commonly used. However, limitations are associated with the use of acyl halides and acid anhydrides and thus esters are preferred. Reactions of ammonia or amines with acyl halides are highly exothermic. Acid anhydrides, especially cyclic anhydrides, easily form imides with ammonia and primary amines.

Usually, reactions with esters require strongly basic catalysts and (or) high pressure. Although quite a number of methods are reported for the conversion of esters to amides (10), most of these have serious drawbacks with regard to toxicity of the reagent, particularly those involving tin compounds (10*b*, 10*c*), operational simplicity and efficiency. Thus, in recent times other approaches involving *N*-acylimidazoles (11), *N*-acylbenzotriazoles (12), and indium triiodide (13) have been demonstrated that also are not very simple and cost effective. Thus, there is a need to develop a simple, mild, cost-effective, and environment friendly procedure for the preparation of secondary amides. Some microwave-assisted synthesis of amides in the presence of strong bases has been reported (14–16).

In recent years, metal- or metal-salt-catalyzed reactions (17) are finding considerable attention because metals can be removed by simple filtration and be reused several times only by washing with suitable solvents. Among various metals, Zn dust (18) is attracting great attention because of its easy availability, inexpensiveness, and nontoxic nature. Recently, we have reported the use of reusable Zn powder for the Friedel–Crafts acylation (19), the Fries rearrangement (20), and the Williamson ether synthesis (21), and here we wish to report another successful application of Zn dust for the conversion of aromatic carboxylic esters to secondary amides by treatment with primary amines with microwave heating in the presence of *N*,*N*-dimethylformamide or conventional heating by stirring in an oil bath using THF as a solvent (Scheme 1).

Results and discussion

To demonstrate the applicability of this method, a series of secondary amides were prepared in good to excellent yields by taking various substituted methyl benzoates and aromatic primary amines using Zn dust with both microwave (MW) heating (70%–91%) or stirring in an oil bath at 70 °C using THF as the solvent (70%–84%).

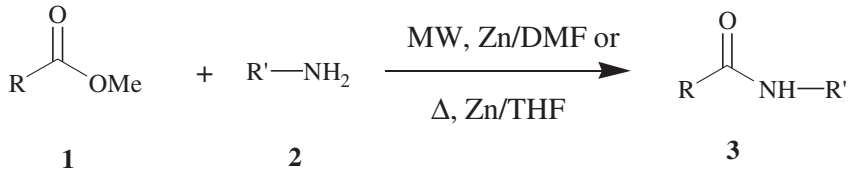
Received 28 March 2005. Published on the NRC Research Press Web site at http://canjchem.nrc.ca on 21 September 2005.

R. Arora, S. Paul,[1] and R. Gupta. Department of Chemistry, University of Jammu, Jammu-180 006, India.

[1]Corresponding author (e-mail: paul7@rediffmail.com).

 © 2005 NRC Canada

Scheme 1.



1 **2** **3**

3a. R = C_6H_5, R' = C_6H_5
3b. R = C_6H_5, R' = 4-$MeOC_6H_4$
3c. R = C_6H_5, R' = 2-$NO_2C_6H_4$
3d. R = C_6H_5, R' = 3-$NO_2C_6H_4$
3e. R = C_6H_5, R' = 4-$NO_2C_6H_4$
3f. R = $CH_2C_6H_5$, R' = C_6H_5
3g. R = $CH_2C_6H_5$, R' = 4-$MeOC_6H_4$
3h. R = $CH_2C_6H_5$, R' = 2-$NO_2C_6H_4$
3i. R = $CH_2C_6H_5$, R' = 3-$NO_2C_6H_4$
3j. R = $CH_2C_6H_5$, R' = 4-$NO_2C_6H_4$
3k. R = 4-ClC_6H_4, R' = C_6H_5
3l. R = 4-ClC_6H_4, R' = 4-$MeOC_6H_4$
3m. R = 4-ClC_6H_4, R' = 2-$NO_2C_6H_4$
3n. R = 4-ClC_6H_4, R' = 3-$NO_2C_6H_4$
3o. R = 4-ClC_6H_4, R' = 4-$NO_2C_6H_4$

Firstly, with MW heating, experimental conditions were carefully monitored to regulate the use of Zn dust, irradiation time, and power level to achieve the optimum conditions. The 1:1 ratio of an ester and amine was the most acceptable one, whereas 0.5 equiv. each of Zn dust and DMF were required to allow the reaction to proceed efficiently. The power level of 640 W was found to be the most acceptable as the low power level gave low yields along with prolonged reaction time, whereas, at a high power level, charring of the reaction mixture was observed. Further, the addition of DMF along with Zn dust in the ratio of 1:1 was very important as without DMF, the reaction did take place, but after 10 s of irradiation, the reaction became violent and charring of the reaction mixture was observed. So the role of DMF is possibly to make the reaction medium homogeneous and absorb some of the extra energy so that the reaction proceeds safely (every reaction was repeated four times to ensure that the reaction proceeds safely). Further, the amount of Zn dust to be used was examined. If a lesser amount of Zn dust was used, the product yield was low and with more amounts, the reaction became violent, which could burn the reaction mixture. The work-up procedure is simple, involving dilution with DMF and filtration followed by the addition of crushed ice.

With conventional heating (stirring in an oil bath), the optimum conditions selected are: for 5 mmol of an ester and amine each, 2.5 mmol of Zn dust, 10 mL of THF as the solvent, and 70 °C as the reaction temperature. When compared with MW heating, the yields of the products using oil-bath heating were lower and also the reaction times were longer (Table 1).

To see whether the formation of amides was catalyzed by commercially available Zn dust, the reaction of methyl benzoate (5 mmol) with aniline (5 mmol) was carried out in the absence of Zn dust with MW heating using DMF (2.5 mmol) or by stirring in an oil bath at 70 °C using THF (10 mL) as the solvent (product **3a**, Table 1). It was found that under conditions similar to those described for Zn dust, no reaction was observed on TLC (2 min under MW irradiation and 16 h in the case of oil-bath heating). Thus, Zn dust catalyzes the conversion of carboxylic esters into secondary amides.

Since the reactions were not carried out under an inert atmosphere and unpurified commercially available zinc dust was used, there may be a possibility of the formation of ZnO, which may catalyze the reaction. To see whether the reaction was catalyzed by Zn or ZnO, we carried out the reaction in the case of product **3a** using 0.5 equiv. of ZnO, instead of Zn dust, under the same conditions as described for the microwave and oil-bath heating experiments. It was found that we were not able to isolate the desired product after the final work-up (10 min under MW irradiation and 16 h using oil-bath heating). This observation clearly indicated that the formation of secondary amides was catalyzed by Zn dust.

The Zn powder can be reused six times after simple washing with diethyl ether and dilute HCl without much loss of activity, thus rendering the process more economical (Table 2).

To check the possibility of specific nonthermal MW effects for the Zn catalyzed conversion of aromatic carboxylic esters to secondary amides, we carried out the reaction of aniline with methyl benzoate (product **3a**, Table 1) using a preheated oil bath at 135 °C (temperature measured at the end of the reaction in the MW oven) for 2 min, keeping all other conditions identical as for the MW experiment. It was found that no reaction took place (TLC), although a yield of 60% was obtained when the reaction time was extended up to 12.5 h. This observation suggests that the effect of MW irradiation is not purely thermal. The results are summarized in Table 3.

Experimental

Melting points were determined on a Buchi melting point apparatus and are uncorrected. ^{1}H NMR spectra were obtained on a Bruker DPX-200 NMR spectrometer (200 MHz) in $CDCl_3$, with tetramethylsilane as the internal standard, and IR spectra were recorded using a KBr disc on a FT-Bruker Vector 22 spectrophotometer. The mass spectral data

© 2005 NRC Canada

Table 1. Synthesis of secondary amides from aromatic carboxylic esters and aromatic primary amines in the presence of Zn dust.

	MW[a]		Oil bath[b]		
Product	Time (min)	Yield[c] (%)	Time (h)	Yield[c] (%)	mp/lit. mp (°C)
3a	2	90	16	82	160–162/162 (22)
3b	1	91	12	82	152–154/154 (22)
3c	8	78	26	70	96–98/98 (22)
3d	2	90	11	84	155–157/158 (22)
3e	4	89	18	80	195–197/199 (22)
3f	6	88	15	80	113–115/117 (22)
3g	4	89	12	79	122–124/124 (23)
3h	8	70	30	64	81–84/84 (24)
3i	6	89	20	82	124 to 125[d]
3j	4	78	22	73	183 to 184[d]
3k	1	90	12	81	193–195/195 (22)
3l	1	88	6	80	153 to 154/155 (25)
3m	5	78	20	70	88–90[d]
3n	1	88	7	80	130 to 131[d]
3o	1.25	84	6	80	168 to 169/170 (26)

[a]Reactions were carried out with a pulse of 15 s (5 s cooling time) in the presence of DMF.
[b]Reactions were carried out by stirring in an oil bath at 70 °C.
[c]Isolated yield from three experimental runs.
[d]Spectral data of some compounds. **3i**: IR (ν_{max} in cm^{-1}, KBr): 3344 (NH), 1706 (C=O). ^1H NMR ($CDCl_3$) δ: 3.90 (s, 2H, CH_2), 6.90–8.30 (m, 9H, H_{arom}), 10.20 (bs, 1H, NH). *m/z* (%): 256 (0.2), 211 (8.3), 166 (1.7), 132 (4.6), 123 (8.1), 92 (100), 65 (70.9). **3j**: IR (ν_{max} in cm^{-1}, KBr): 3340 (NH), 1700 (C=O). ^1H NMR ($CDCl_3$) δ: 3.82 (s, 2H, CH_2), 6.92–8.20 (m, 9H, H_{arom}), 10.25 (bs, 1H, NH). *m/z* (%): 256 (0.4), 211 (7.2), 166 (1.3), 132 (4.2), 123 (8.3), 92 (98), 65 (68.2). **3m**: IR (ν_{max} in cm^{-1}, KBr): 3342 (NH), 1701 (C=O). ^1H NMR ($CDCl_3$) δ: 6.80–8.20 (m, 8H, H_{arom}), 10.10 (bs, 1H, NH). *m/z* (%): 279 (1.4), 156 (72.7), 139 (100), 111 (42), 92 (32.5), 65 (34.7). **3n**: IR (ν_{max} in cm^{-1}, KBr): 3340 (NH), 1702 (C=O). ^1H NMR ($CDCl_3$) δ: 6.90–8.10 (m, 8H, H_{arom}), 10.00 (bs, 1H, NH). *m/z* (%): 279 (1.3), 156 (70.2), 139 (99), 111 (44), 92 (36), 65 (32.1).

Table 2. Reuse studies of Zn dust for the synthesis of secondary amides.

	MW		Oil bath	
No. of uses	Time[a] (min)	Yield[b] (%)	Time[a] (h)	Yield[b] (%)
1	2	90	16	82
2	2.5	89	16.5	80
3	3	85	18	78
4	4.5	82	19	75
5	5	78	21.5	72
6	6	72	22	64

[a]Time at which maximum yield was obtained.
[b]Isolated yield from three experimental runs.

Table 3. Comparison of microwave activation (MW) and thermal heating (Δ) in the case of aniline (5 mmol) and methyl benzoate (5 mmol) using Zn dust (2.5 mmol) and DMF (2.5 mmol) (power = 640 W).

Method	Time (min)	Temp. (°C)[a]	Yield (%)[b]
MW	2	133–135	90
Δ	2	135	No reaction
Δ	12.5[c]	135	60

[a]The final temperature was measured by immersing the glass thermometer into the reaction mixture at the end of exposure during the MW experiment and was approximate temperature range.
[b]Isolated yield from three experimental runs.
[c]Time reported in hours.

was obtained on a JEOL JMS-D 300 spectrometer. The reactions were monitored by TLC. For the microwave irradiation experiments described in the following, a conventional (unmodified) household microwave oven equipped with a turntable was used (LG Little Chef MS 194 W operating at 2450 MHz having a maximum output of 800 W).

General procedure for the synthesis of secondary amides in the presence of Zn dust

Microwave heating approach

To a mixture of the aromatic carboxylic ester (5 mmol), the appropriate aromatic amine (5 mmol), and Zn dust (2.5 mmol) in a 50 mL borosil beaker, DMF (2.5 mmol) was added. The reaction mixture was mixed thoroughly with a glass rod (10 s) and then irradiated in a microwave oven for an appropriate time (Table 1) at 640 W. After cooling, DMF (5 mL) was added and the reaction mixture was filtered. To the filtrate, ice-cold water (100 mL) was added and the product extracted with ethyl acetate (3 × 15 mL). The combined extracts were washed with water and dried over anhydrous sodium sulfate. The product was obtained after the removal of the solvent under reduced pressure followed by crystallization from EtOAc – petroleum ether or by passing through a column of neutral alumina and elution with petroleum ether.

Oil-bath heating approach

To a mixture of the aromatic carboxylic ester (5 mmol), the appropriate aromatic amine (5 mmol), and Zn dust

© 2005 NRC Canada

(2.5 mmol) in a round-bottomed flask (50 mL), THF (10 mL) was added. The round-bottomed flask was fitted with a reflux condenser and the reaction mixture was stirred at 70 °C in an oil bath for an appropriate time (Table 1). After completion (monitored by TLC), the reaction mixture was cooled and filtered. The THF was removed under reduced pressure and the product was obtained by the same procedure as described for the MW experiment.

The structures of the products were confirmed by ^{1}H NMR, IR, mass spectral data, and by comparison with authentic samples.

Conclusion

In conclusion, we have developed an efficient procedure for the synthesis of secondary amides using Zn dust with MW heating in the presence of DMF or by stirring in an oil bath using THF as a solvent. The salient features of our method is that it is simple, rapid, economic, general, and environment friendly, and Zn dust can be reused several times without much loss of activity. This method could be a very efficient alternative to other existing methods.

Acknowledgements

The authors thank the Jammu and Kashmir State Council, the Department of Science and Technology, and the Jammu and Kashmir Government for providing financial assistance and awarding a project fellowship to Revika Arora.

References

1. W.-C. Chou, C.-W. Tan, S.-F. Chen, and H. Ku. J. Org. Chem. **63**, 10 015 (1998).
2. (*a*) J. March. *In* Advanced organic chemistry. 4th ed. John Wiley and Sons, New York. 1992. pp. 417–425; (*b*) A. Vogel. *In* Textbook of practical organic chemistry. Longman Scientific and Technical and Wiley, New York. 1989. pp. 708–710; (*c*) G.V.M. Sharma, T. Shekharam, and V. Upender. Tetrahedron, **46**, 5665 (1990).
3. S.-T. Chen, S.-H. Wu, and K.-T. Wang. Synthesis, 37 (1989).
4. K.V.N.S. Sriniwas and B. Das. J. Org. Chem. **68**, 1165 (2003).
5. J. Cossy and C. Pale-Grosdemange. Tetrahedron Lett. **30**, 2771 (1989).
6. T.-H. Chan and L.T.L. Wong. J. Org. Chem. **34**, 2766 (1969).
7. K. Dendrinos, J. Jeong, W. Huang, and A.G. Kalivretenos. Chem. Commun. 499 (1998).
8. K.S. Keshavamurthy, Y.D. Vankar, and D.N. Dhar. Synthesis, 506 (1982).
9. H.W. Grimmel, A. Guenther, and J.F. Morgan. J. Am. Chem. Soc. **68**, 539 (1946).
10. (*a*) H. Yazawa, K. Tanaka, and K. Kariyone. Tetrahedron Lett. **15**, 3995 (1974); (*b*) W.-B. Wang and E.J. Roskamp. J. Org. Chem. **57**, 6101 (1992); (*c*) W.-B. Wang, J.A. Restituyo, and E.J. Roskamp. Tetrahedron Lett. **34**, 7217 (1993).
11. (*a*) G.M. Strunz and H. Finlay. Tetrahedron, **50**, 11 113 (1994); (*b*) N. Raju, K. Ramalingam, and D.P. Nowotnik. Tetrahedron, **48**, 10 233 (1992).
12. A.R. Katritzky, H.-Y. He, and K. Suzuki. J. Org. Chem. **65**, 8210 (2000), and refs. cited therein.
13. B.C. Ranu and P. Dutta. Synth. Commun. **33**, 297 (2003).
14. R.S. Varma and K.P. Naicker. Tetrahedron Lett. **40**, 6177 (1999).
15. F.-Z. Zradni, J. Hamelin, and A. Derdour. Synth. Commun. **32**, 3525 (2002).
16. L. Perreux, A. Loupy, and M. Delmotte. Tetrahedron, **59**, 2185 (2003).
17 (*a*) J.K. Shorrock, J.H. Clark, K. Wilson, and J. Chisem. Org. Process Res. Dev. **5**, 249 (2001); (*b*) C. Baleizao, A. Corma, H. Garcia, and A. Leyva. Chem. Commun. 606 (2003); (*c*) E.B. Mobofu, J.H. Clark, and D.J. Macquarrie. Green Chem. **3**, 23 (2001).
18. (*a*) S.D. Burke and R.L. Danheiser. Handbook of reagents for organic syntheis: Oxidizing and reducing agents. John Wiley and Sons, Chichester. 1999. pp. 504–510; (*b*) M.S.R. Murty, B. Jyothirmai, P.R. Krishna, and J.S. Jadav. Synth. Commun. **33**, 2483 (2003); (*c*) J.S. Yadav, B.V.S. Reddy, G. Kondaji, R.S. Rao, and S.P. Kumar. Tetrahedron Lett. **43**, 8133 (2002); (*d*) Y. Ogawa, A. Saiga, M. Mori, T. Shibata, and K. Takegi. J. Org. Chem. **65**, 1031 (2000).
19. S. Paul, P. Nanda, R. Gupta, and A. Loupy. Synthesis, 2877 (2003).
20. S. Paul and M. Gupta. Synthesis, 1789 (2004).
21. S. Paul and M. Gupta. Tetrahedron Lett. **45**, 8825 (2004).
22. N.K. Vishnoi. *In* Advanced practical organic chemistry. 2nd ed. 1996. Vikas Publishing House Pvt. Ltd., New Delhi.
23. V. Joshi, S.S. Jalisatgi, and M.I. Hari. Indian J. Chem. Sect. B, **25B**, 83 (1986).
24. T. Jan, D. Floner, and C. Moinet. Electrochim. Acta, **42**, 2075 (1997).
25. A.F.M. Fahmy, G. Hosni, and H. Abdel Fadeel. Indian J. Chem. Sect. B, **14B**, 871 (1976).
26. A.F.M. Fahmy, N.F. Aly, and M.H. Arief. Indian J. Chem. Sect. B, **16B**, 697 (1978).

© 2005 NRC Canada

Calmodulin antagonists: Structure of *N*-(6-aminohexyl)-5-chloro-1-naphthalenesulfonamide hydrochloride (W-7) and comparison with trifluoperazine (TFP) — Calmodulin binding

Andrew Hempel, Norman Camerman, Donald Mastropaolo, and Arthur Camerman

Abstract: The crystal structure of the title compound contains one *N*-(6-aminohexyl)-5-chloro-1-naphthalenesulfonamide hydrochloride molecule in the asymmetric unit. The molecule adopts an extended conformation with a linear hexyl group. Protonation occurs at the side chain terminal nitrogen atom. Hydrophobic packing and a three-dimensional hydrogen-bond network, involving all the hydrogen atoms capable of making hydrogen-bond contacts, stabilizes the crystal structure. Due to head-to-head and tail-to-tail arrangement of these hydrophobic molecules, an unusually long cell constant (b = 61.27 Å) characterizes the crystal structure. A stereochemical comparison with trifluoperazine suggests similar calmodulin binding mechanisms.

Key words: crystal structure, stereochemistry, W-7, calmodulin binding, TFP.

Résumé : La structure cristalline du composé mentionné dans le titre contient une molécule de chlorhydrate de *N*-(6-aminohexyl)-5-chloronaphtalène-1-sulfonamide par unité asymétrique. La molécule adopte une conformation étendue avec un groupe hexyle linéaire. La protonation se produit sur l'atome d'azote de la chaîne latérale. Un empilement hydrophobe et un réseau de liaisons hydrogènes tridimensionnel impliquant tous les atomes d'hydrogène capable de faire des contacts par liaisons hydrogène stabilise la structure. En raison de l'arrangement tête-à-tête et queue-à-queue de ces molécules hydrophobes, la structure cristalline est caractérisée par une constante de cellule particulièrement longue (b = 61,27 Å). Une comparaison stéréochimique avec la trifluopérazine suggère l'existence de mécanismes de fixation semblables à ceux de la calmoduline.

Mots clés : structure cristalline, stéréochimie, W-7, fixation de calmoduline, TFP.

[Traduit par la Rédaction]

Introduction

N-(6-Aminohexyl)-5-chloro-1-naphthalenesulfonamide (W-7) (Scheme 1) belongs to a group of vasodilating agents like sphingosine, W-5, and trifluoperazine (TFP), which were noted to relax blood vessels by inhibition of calmodulin-mediated processes involving actin and myosin (1, 2). Regarded as a calmodulin (CaM) antagonist, W-7 binds directly to the active, calcium saturated ($4Ca^{2+}$) form of CaM (3). Initiation of the smooth muscle contraction is associated with Ca^{2+} binding to CaM. W-7 and other calmodulin antagonists (sphingosine, trifluoperazine, calmidazolium) effectively block Ca^{2+} elevation through interaction with calmodulin-dependent processes (2). We have performed an X-ray analysis of W-7 to determine if there are stereochemical features shared by W-7 and the known calmodulin antagonist TFP that may be responsible for their apparent similar biological activity.

Experimental

The compound was synthesized at the Department of Pharmacology, Mie University School of Medicine, Edobashi, Japan, and made available to us by Professor H. Hidaka. Crystals of W-7 suitable for X-ray analysis were obtained by very slow crystallization from 95% ethanol. A crystal of dimensions 0.40 mm × 0.27 mm × 0.22 mm was used to obtain lattice parameters and X-ray intensities. Systematic absences visible on precession photographs taken with CuKα radiation were consistent with the space group *Pbca*. The cell parameters were determined from the least-squares refinement of the angular positions of 16 high angle

Received 21 March 2005. Published on the NRC Research Press Web site at http://canjchem.nrc.ca on 21 September 2005.

A. Hempel. Biochemistry Department, University of Toronto, Toronto, ON M5S 1A8, Canada.
N. Camerman.[1] Biochemistry Department, University of Toronto, Toronto, ON M5S 1A8, Canada and Ardono Research, 341 101st Avenue SE, Bellevue, WA 98004, USA.
D. Mastropaolo and A. Camerman.[2] Ardono Research, 341 101st Avenue SE, Bellevue, WA 98004, USA.

[1]Corresponding author (e-mail: norman.camerman@utoronto.ca).
[2]Deceased.

 doi: 10.1139/V05-133 © 2005 NRC Canada

Scheme 1.

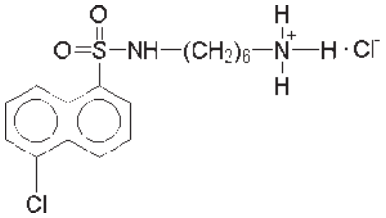


Table 1. Crystal data and details of the structure determination.

Crystal data	
Empirical formula	$C_{16}H_{21}ClN_2O_2S{\cdot}HCl$
Formula weight	377.33
Crystal system	Orthorhombic
Space group	*Pbca* (No. 61)
a, *b*, *c* (Å)	7.628(2), 61.272(9), 7.868(2)
V (Å^3)	3677.4(9)
Z	8
$D_{calcd.}$ (g/cm^3)	1.363
F(000)	1584
μ(CuKα) (mm)	4.3
Crystal size (mm^3)	0.22 × 0.27 × 0.40
Data collection	
Temperature (K)	294
Radiation (Å)	CuKα λ = 1.541 78
2Θ Min–max (°)	2.9, 130.0
Dataset	*h* = 0:8, *k* = 0:72, *l* = 0:9
Scan	Θ/2Θ
Tot. and uniq. data	3130, 3130
Observed data ($I > 2\sigma(I)$)	1916
Refinement	
Nref, Npar	3130, 215
R, *S*	0.077 6, 1.01
$w = 1/[s^2(F_o^2) + (0.1231P)^2]$	where $P = (F_o^2 + 2F_c^2)/3$
Max. and avg. shift and error	0.00, 0.00
Min and max resd. dens. (e/Å^3)	–0.48, 0.49

reflections with 40° ≤ 2Θ ≤ 60°. Intensity data were collected using a Θ ÷ 2Θ scan mode with Ni filtered CuKα radiation on a Picker FACS-1 four-circle diffractometer. The scan speed was 2°/min, and three standard reflections monitored every 100 reflections showed only random variations of 4% in intensity. A total of 3130 unique reflections within the range 3° ≤ 2Θ ≤ 130° were recorded, 1916 with $I > 2\sigma(I)$ were considered observed. The intensities were corrected for Lorentz and polarization factors and also for absorption from empirical data obtained using ϕ scan (4).

Solution and refinement of the structure

The structure was solved by direct methods and refined using SHELXS-97 and SHELXL-97 (5). The best solution E-map revealed all the atoms of the molecule heavier than hydrogen. The hydrogen atoms at N19 and N12 nitrogen atoms were found from a difference electron density map. The remaining hydrogen atoms were fitted geometrically and during the refinement were "riding" on host atoms. The final discrepancy index converged at *R* = 7.76% and *S* = 1.006 for the 1916 observed reflections. A final difference electron density map contained a featureless residual density of +0.49 and –0.48 e/Å^3. The highest residual density peaks and holes were located in the vicinity of chlorine and sulfur atoms. The data collection, solution, and refinement details are summarized in Table 1. The final positional parameters and equivalent isotropic temperature factors are listed in Table 2.

Table 2. Atomic coordinates (×10^4) and equivalent isotropic displacement parameters (Å^2 × 10^3).

Atom	*x*	*y*	*z*	U_{eq}
C-1	3 518(6)	888(1)	–1196(6)	35(1)
C-2	3 234(7)	944(1)	–2857(6)	48(1)
C-3	3 717(8)	807(1)	–4163(7)	55(2)
C-4	4 417(7)	607(1)	–3831(7)	50(1)
C-5	4 737(7)	543(1)	–2124(6)	43(1)
C-6	5 472(8)	338(1)	–1725(7)	51(1)
C-7	5 864(8)	274(1)	–110(10)	62(2)
C-8	5 470(10)	421(1)	1212(7)	57(2)
C-9	4 700(8)	616(1)	920(6)	49(1)
C-10	4 300(7)	679(1)	–762(6)	38(1)
S-11	2 901(2)	1084(1)	349(2)	43(1)
N-12	4 608(7)	1211(1)	948(6)	50(1)
C-13	5 357(8)	1393(1)	–66(7)	54(1)
C-14	7 100(10)	1459(1)	621(7)	59(2)
C-15	7 850(10)	1657(1)	–260(10)	75(2)
C-16	9 630(10)	1718(1)	510(10)	91(2)
C-17	10 570(10)	1899(1)	–370(10)	96(3)
C-18	9 860(10)	2123(1)	90(10)	82(2)
N-19	10 806(8)	2287(1)	–865(8)	81(2)
O-20	2 204(5)	973(1)	1813(4)	52(1)
O-21	1 803(5)	1241(1)	–498(5)	60(1)
Cl-22	5 933(2)	153(1)	–3356(2)	79(1)
Cl	14 859(2)	2233(1)	–227(3)	78(1)

Note: U_{eq} = 1/3(trace of the orthogonalized U_{ij} matrix).

Discussion

The molecular structure of W-7 and the atom numbering is shown in Fig. 1. The naphthalene ring system is planar within experimental error, and bond distances and angles in the molecule do not differ significantly from expected values. The aminohexyl side chain adopts a fully extended conformation, roughly perpendicular to the naphthalene plane. A difference electron density calculation clearly showed three hydrogen atoms at N19, indicating it as the protonation site. A projection of the crystal structure-packing diagram is presented in Fig. 2. The molecules are arranged in a head-to-head and tail-to-tail manner along the *b* direction. Hydrogen bonds between the amino hydrogen atoms and the chloride ions and Van der Waals and stacking π interactions hold the molecules in the crystal. The chloronaphthalene rings are stacked perpendicular to the *a* axis direction, and the aminohexyl groups form parallel chains. All the hydrogen atoms capable of participating in hydrogen bonds are involved. The details of the hydrogen bond geometry are shown in Table 3. The chloride ions are hydrogen bonded to three N19 hydrogen atoms (H19A, H19B, and H19C) involving three different W-7 molecules, with very similar geometric parameters.

© 2005 NRC Canada

Fig. 1. ORTEP-3 (16) view of the title compound showing 50% probability displacement elipsoids. H atoms are drawn as small circles of an arbitrary radius.

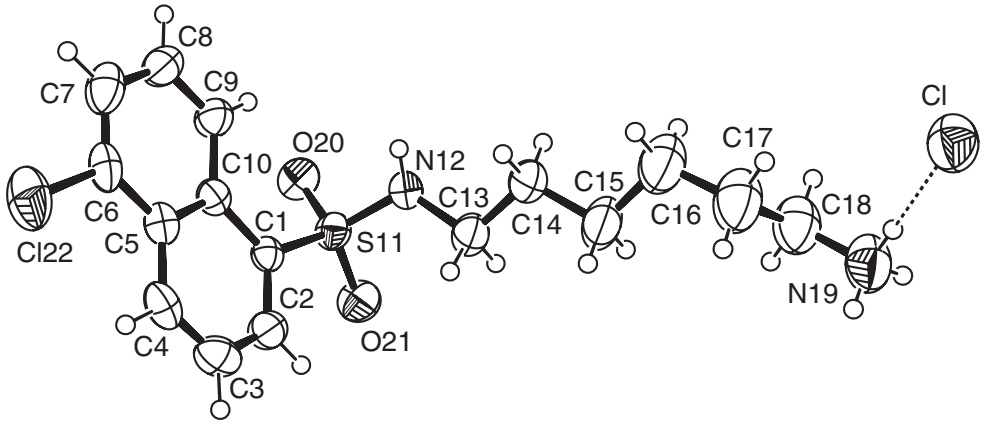


Fig. 2. ORTEP-3 view of the crystal packing diagram.

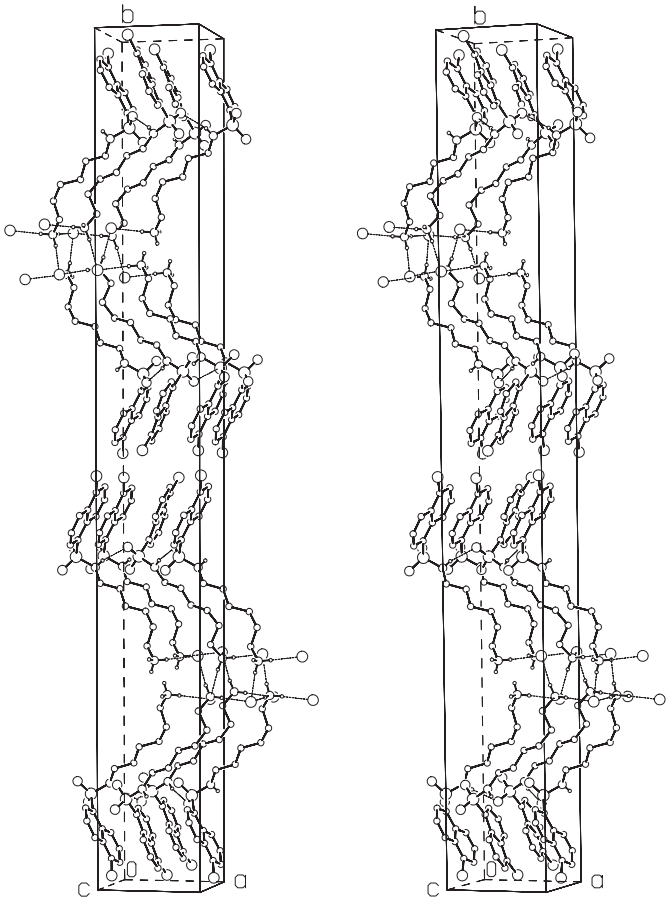


Table 3. Hydrogen bonds (Å, °).

D-H···A	D-H (Å)	H···A (Å)	D···A (Å)	∠ (°)
N12-H12···O20[a]	0.76(8)	2.27(8)	3.024(6)	174(8)
N19-H19A···Cl	0.8901	2.2610	3.149(6)	175.93
N19-H19B···Cl[b]	0.8882	2.2618	3.144(6)	172.12
N19-H19C···Cl[c]	0.8897	2.2902	3.176(7)	173.47

[a]Symmetry code: 1/2 + *x*, *y*, 1/2 – *z*.
[b]Symmetry code: –1/2 + *x*, 1/2 – *y*, – *z*.
[c]Symmetry code: –1/2 + *x*, *y*, –1/2 – *z*.

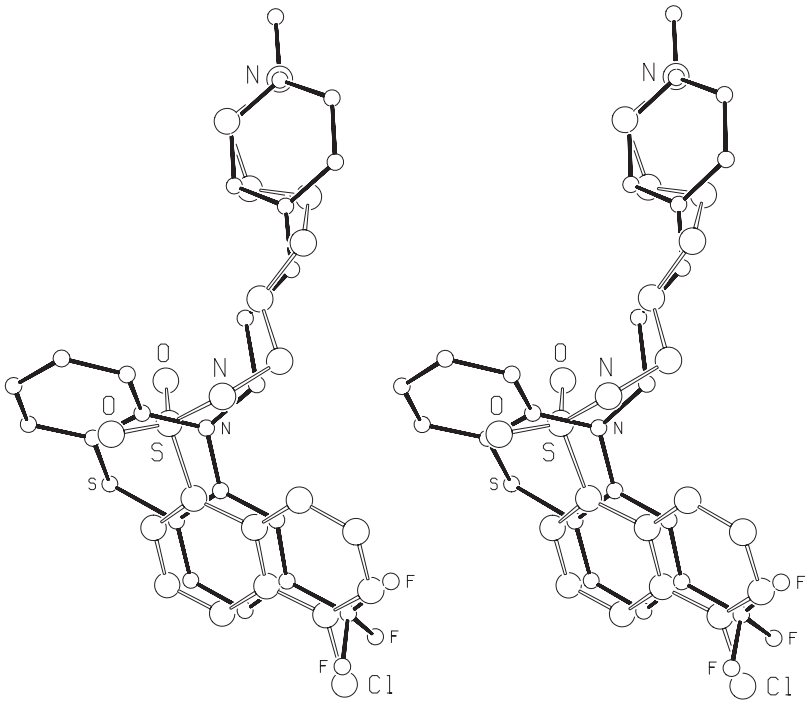
Binding of W-7 to calmodulin

Calmodulin is a small calcium binding protein with four Ca^{2+} binding sites, two in each C- and N-terminal domain. CaM antagonists like W-7, W-5, TFP, and sphingosine bind in hydrophobic patches of the protein, subsequently inhibiting CaM dependent processes of the activation of various intracellular enzymes (phosphodiesterase, myosine kinase, brain adenylate cyclase, Ca^{2+} ATPase, phosphorylase kinase). The CaM molecule was shown to possess two high-affinity apolar pockets, one of which is located in the N-terminal domain and the second, with an affinity of more than an order of magnitude higher, in the C-terminal region (6). Studies have shown that the affinity of pharmacological agents, known as calmodulin antagonists, is related to their hydrophobicity. Structure–activity relationship investigations also concluded that a positive charge at some distance from the phenothiazine moiety of TFP is essential when interacting with CaM (7). Comparative molecular modeling studies of TFP binding to calmodulin have shown the feasibility of the hydrophobic phenothiazine rings to stack against the residues in the hydrophobic cleft, while the positively charged piperazine ring nitrogen atom extends out to make contacts with negatively charged residues residing on the outer rim of the hydrophobic pocket (8).

Although chemically dissimilar to TFP, W-7 possesses certain structural features in common. The two molecules share a similar overall shape, both have hydrophobic ring systems, phenothiazine in TFP and chloronaphthalene in W-7, and the side chain of W-7 has an extended conformation, similar to that found in the crystal structure of TFP (9), with enough flexibility to adjust to the negatively charged acidic residues lining the outsides of the hydrophobic pocket of the protein. Another important feature common in both compounds is a positively charged nitrogen atom at some distance from the hydrophobic region. In W-7 the separation between the hydrophobic naphthalene moiety and the terminal positively charged atom N19 is similar to the distance from the hydrophobic phenothiazine ring to the positively charged side chain piperazine ring nitrogen in TFP, a feature that for TFP was shown to be important in binding to calmodulin (7). More recent molecular modeling studies of interactions between tamoxifen and some of its derivatives

© 2005 NRC Canada

Fig. 3. Stereoscopic comparison of stereochemistries of W-7 (large circles) and TFP (small circles) based on flexible fitting of the W-7 side chain.



with calmodulin also showed the importance, for binding, of similar structural features, i.e., a well-defined hydrophobic part and a side chain with the terminal atom capable of being protonated (10). Three crystal structure determinations of a Ca^{2+}–CaM–TFP complex have been reported: one (11) found only one TFP molecule bound to the protein in the C-terminal hydrophobic pocket, while the second (12) found four TFP molecules in the structure, the one with the highest occupancy in the same position in the C-terminal pocket but with a completely different orientation. The third determination (13) reported two TFP molecules in the complex, occupying the two best-defined sites of the four-TFP structure, but showing no evidence for TFP molecules in the other two sites. The forces responsible for binding TFP molecules to Ca^{2+}CaM are mainly hydrophobic and to a lesser degree electrostatic in nature, involving acidic side chains of CaM Glu residues and a positively charged nitrogen atom of the TFP side chain piperazine ring. Solution structure studies of a Ca^{2+}–CaM–W-7 complex determined by multidimensional NMR spectroscopy have been interpreted to indicate that the structure contains two W-7 molecules, one in each N- and C-terminal hydrophobic pocket (14). A postulated structure for W-7 in that complex has a position and ring orientation different from that of TFP, but that postulation was totally arbitrary.[3] Thus, resolution problems in the protein-inhibitor complexes result in conflicting evidence both on the numbers and positions of TFP (and, presumably, W-7) with respect to Ca^{2+}–CaM and in any relationships to W-7 binding to the protein.

A report on Ca^{2+}–CaM–W-7 solution structure studies using small-angle X-ray scattering and NMR shows that W-7 induces structural change in CaM resulting in a globular shape caused by an inter-domain compaction (15), similar to the situation observed in the Ca^{2+}–CaM–TFP crystal structure complexes (11, 12), again indicating similarities in the effects of TFP and W-7 binding to Ca^{2+}–CaM.

A flexible fitting of W-7 and TFP is presented in Fig. 3 and shows the main structural features (positively charged nitrogen atoms, chlorine atom and trifluoromethyl group, and overall stereochemistry) responsible for binding of TFP to overlap well with those of W-7. The positively charged nitrogen atom of W-7 overlaps with its counterpart in TFP, and the chlorine atom is in a very close proximity to the trifluoromethyl group of TFP. Hydrophobic rings of the two compounds also show a good overlap.

On the basis of the X-ray structure investigation of W-7 and the flexible fitting of the two substrates along with the arguments presented above, it is appropriate to conclude that the stereochemistry and the mechanism of binding of W-7 to calmodulin are likely to be similar to that of TFP.[4]

Acknowledgments

Supported by the National Cancer Institute of Canada

[3] M. Ikura. Private communication. 1999.

[4] Supplementary data for this article are available on the Web site or may be purchased from the Depository of Unpublished Data, Document Delivery, CISTI, National Research Council Canada, Ottawa, ON K1A 0S2, Canada. DUD 4013. For more information on obtaining material refer to http://cisti-icist.nrc-cnrc.gc.ca/irm/unpub_e.shtml. CCDC 260755 contains the crystallographic data for this manuscript. These data can be obtained, free of charge, via www.ccdc.cam.ac.uk/conts/retrieving.html (Or from the Cambridge Crystallographic Data Centre, 12 Union Road, Cambridge CB2 1EZ, UK; fax +44 1223 336033; or deposit@ccdc.cam.ac.uk).

© 2005 NRC Canada

with funds from the Canadian Cancer Society (NC) and by grant AI40392 from the National Institutes of Health (AC).

References

1. H. Hidaka, M. Asano, S. Iwadare, I. Matsumoto, T. Totsuka, and N. Aoki. J. Pharmacol. Exp. Ther. **207**, 8 (1978).
2. M. Sitges and B.R. Talamo. J. Neurochem. **61**, 443 (1993).
3. H. Hidaka, Y. Sasaki, T. Tanaka, T. Endo, S. Ohno, Y. Fujii, and T. Nagata. Proc. Natl. Acad. Sci. U.S.A. **78**, 4354 (1981).
4. A.C.T. North, D.C. Phillips, and F.S. Mathews. Acta Crystallogr. Sect. A, **A24**, 351 (1968).
5. G.M. Sheldrick. SHELXS 97 and SHELXL 97 [computer programs]. University of Göttingen, Göttingen, Germany. 1997.
6. P.C. Dalgarno, R.E. Klevit, B.A. Levine, G.M. Scott, R.J.P. Williams, J. Gergely, Z. Grabarek, P.C. Leavis, R.J. Grand, and W. Drabikowski. Biochim. Biophys. Acta, **791**, 164 (1984).
7. W.C. Prozialeck and B.J. Weiss. J. Pharmacol. Exp. Ther. **222**, 509 (1982).
8. N.C.J. Strynadka and M.N.G. James. Proteins, **3**, 1 (1988).
9. J.J.H. McDowell. Acta Crystallogr. Sect. B, **B36**, 2178 (1980).
10. K.J. Edwards, C.A. Laughton, and S.J. Neidle. J. Med. Chem. **35**, 2753 (1992).
11. W.J. Cook, L.J. Walter, and M.R. Walter. Biochemistry, **33**, 15 259 (1994).
12. M. Vandoselaar, R.A. Hickie, W.J. Quail, and L.T.J. Delbaere. Nat. Struct. Biol. **1**, 795 (1994).
13. B.G. Vertessy, V. Harmat, Z. Bocskei, G. Naray-Szabo, F. Orosz, and J. Ovadi. Biochemistry, **37**, 15 300 (1998).
14. M. Osawa, M.B. Swindells, J. Tanikawa, T. Tanaka, T. Mase, T. Furuja, and M. Ikura. J. Mol. Biol. **276**, 165 (1998).
15. M. Osawa, S. Kuwamoto, Y. Izumi, K.L. Yap, M. Ikura, T. Shibanuma, H. Yokokura, H. Hidaka, and N. Matsushima. FEBS Lett. **442**, 173 (1999).
16. L.J. Farrugia. J. Appl. Crystallogr. **30**, 565 (1997).

© 2005 NRC Canada

Catalyzed β scission of a carbenium ion — Mechanistic differences from varying catalyst basicity

Qingbin Li and Allan L.L. East

Abstract: The β-scission mechanism of physisorbed and chemisorbed pentenium ions, as catalyzed by $AlH_2(OH)_2^-$ and by $AlHCl_3^-$ anions, was investigated using density functional theory computations and explicit-contact modelling. A thorough search of intermediates was performed for each catalyst. On the aluminum chloride, β scission of an aliphatic, secondary carbenium ion featured chemisorbed and physisorbed ion intermediates, while on the aluminum hydroxide, β scission featured chemisorbed ions but physisorbed *neutral* species. The importance of this work is its demonstration of a qualitatively different mechanism, with qualitatively different intermediates, due only to the different basicity of the two catalysts.

Key words: C—C bond fission, β scission, carbenium ion, catalysis, mechanism.

Résumé : Faisant appel à la méthode de calculs de la théorie de la densité fonctionnelle et à la modélisation par contacts explicites, on a étudié le mécanisme de la scission β d'ions penténium physisorbés et chimisorbés, tel que catalysée par les anions $AlH_2(OH)_2^-$ et $AlHCl_3^-$. Pour chacun des catalyseurs, on a fait une étude approfondie des intermédiaires. Sur le chlorure d'aluminium, la scission β d'un ion carbénium secondaire et aliphatique implique des intermédiaires ioniques chimisorbés et physisorbés alors que sur l'hydroxyde d'aluminium, la scission β implique des ions chimisorbés, mais des espèces neutres physisorbées. L'importance de ce travail est de démontrer que, en raison seulement de différences dans les basicités des deux catalyseurs, que les réactions impliquent des mécanismes qualitativement différents avec des intermédiaires qualitativement différents.

Mots clés : fission d'une liaison C—C, scission β, ion carbénium, catalyse, mécanisme.

[Traduit par la Rédaction]

Introduction

Alkane cracking can be catalyzed by solid zeolites (aluminosilicates), chloroaluminate ionic liquids (1), and liquid superacids (2) such as $HF{\cdot}SbF_5$ and $HSO_3F{\cdot}SbF_5$ (having a great deal of ionic-liquid character). The cracking is generally performed by carbenium ions in a chain reaction (3), where the first step is hydride abstraction by a little carbenium ion to make a big carbenium ion, and the second step is β scission of the big carbenium ion, e.g.,

$$CHR_2\text{-}CH_2\text{-}C^+HR' \rightarrow C^+HR_2 + CH_2{=}CHR'$$

to create another little carbenium ion. The net result is cracking of the big alkane.

Upon closer scrutiny, the mechanism of the β-scission step must be different for different catalysts. From product distribution studies, several scientists (3–7) suggested that carbenium ion chemistry as observed in liquid superacids could be applied to the reactions on zeolites, although the product distributions were generally different. However, the direct comparison to liquid superacid chemistry was called into question by both experimental studies (8, 9) and theoretical computations (10, 11), which suggested that bound alkoxy groups (chemisorbed carbenium ions), rather than labile (physisorbed) carbenium ions, are the intermediates on zeolite surfaces (12, 13).

The success of those initial computations, combined with the belief that the differences may be due to large structural physical effects of the zeolite, pushed some computational chemists into invoking "large-scale" computational modelling in which the number of atoms in the calculation is maximized by invoking further computational approximations. Currently, however, this field is still in its infancy, limited in its accuracy by the approximations required to do large-scale modelling. A good example of this is the work of Demuth et al. (14), who modelled the isomerization of 2-pentene (actually, chemisorbed 2-pentenium ion to chemisorbed 2-methyl-1-butenium ion) in a ZSM-22 zeolite with a large-scale simulation, invoking periodic boundary conditions, the PW91 exchange functional, a plane-wave basis set, and approximate transition states. Their computations produced a physisorbed carbenium ion that would be observably stable, with barriers of 8 kcal mol^{-1} for chemisorption and 18 kcal mol^{-1} for proton transfer to the catalyst (1 cal = 4.184 J). This is in complete disagreement with in situ magic-angle-spinning nuclear magnetic resonance (MAS NMR) studies,

Received 3 May 2005. Published on the NRC Research Press Web site at http://canjchem.nrc.ca on 21 September 2005.

Q. Li and A.L.L. East.[1] Department of Chemistry and Biochemistry, University of Regina, Regina, SK S4S 0A2, Canada.

[1]Corresponding author (e-mail: Allan.East@uregina.ca).

 doi: 10.1139/V05-135 © 2005 NRC Canada

in which physisorbed nonaromatic carbenium ions have been eagerly searched for but never found (9, 15–22).

Despite the limitations on large-scale computational modelling, quantum chemical calculations are still a powerful tool in studying and understanding these molecular mechanisms. For example, the effect of the relative acidity or basicity of the catalyst upon the mechanism can be studied, without the need to invoke large-scale modelling. In 2003, our group published a theoretical study on an idealized Bronsted acid catalytic cycle for $C_6H_{14} \rightarrow C_3H_8 + C_3H_6$, using small cationic Bronsted acids in the computations (23). There we demonstrated that the existence of certain intermediates varied with the catalyst, simply because of the acidity of the catalyst. Here, we are going to show that varying catalyst basicity can change the catalyzed β-scission mechanism of $C_5H_{11}^+ \rightarrow C_2H_5^+ + C_3H_6$.

Modelling real systems is not a goal of this paper. If large-scale computational modelling of zeolites and ionic liquids could be achieved, and the results demonstrated a difference in mechanism, we would likely still be unable to state which aspect of the two catalysts is the most important one responsible for the mechanism change. Fundamental studies are required, and this is one of them. Also, we are certainly not suggesting that the change in relative basicity is the only reason for the mechanism change between zeolites and ionic liquids. We are simply providing the extremely important demonstration that relative catalyst basicity can be responsible for qualitative changes in the β-scission mechanism.

This paper is a computational chemistry study of the mechanisms, i.e., minimum energy pathways, used by the aluminum chloride $AlHCl_3^-$ and the aluminum hydroxide $AlH_2(OH)_2^-$ in performing the β scission of 2-pentenium ion into ethenium ion and propene. All the pathways start and end with covalently bound (chemisorbed) ion–catalyst complexes, as influenced by the β-scission study by Frash et al. (FKRS) (24). The initial purpose was to investigate the β scission with $AlHCl_3^-$ and compare these results to the results of FKRS who used $AlH_2(OH)_2^-$. However, it was soon discovered that the potential energy surface for the reaction on $AlH_2(OH)_2^-$ is even more complex than those reported by FKRS, and a direct comparison required a thorough investigation with one carbenium ion (2-pentenium ion), one level of theory (B3LYP/6-31G(d,p)), and the two catalyst fragments. We will compare our results with the other published computational studies of cationic β scission, which are the β-scission papers of FKRS (24) and Hay et al. (25), and the reverse β-scission (oligomerization) paper of Svelle et al. (26).

This paper is not addressed solely to those interested in the effects of varying the basicity of a catalyst. We hope it is also of interest to organic chemists interested in catalysis at the molecular level, and to surface scientists interested in the nature of physisorbed and chemisorbed states (27) on compound surfaces like metal oxides.

Methods, models, and terminology

All calculations used the semi-empirical density functional theory model called B3LYP (28, 29) with the 6-31G(d,p) orbital basis set (30). Molecular geometries and harmonic frequencies for intermediates and transition states were computed using analytic first and second derivative formulae, as are routine with most quantum chemistry codes. All reported results come from calculations with the GAUSSIAN 98 software suite (30) using the default numerical grid. In most cases, the PQS 3.0 software suite (31) was used to speed up transition-state searches because of its parallelism and because the Baker eigenvector-following algorithm (32) is not restricted to 50 variables, as it is in GAUSSIAN 98. However, because the default grid in PQS 3.0 is finer, the B3LYP energies between the two codes are not compatible, and final results were run with GAUSSIAN 98. The energies reported are not corrected for zero-point vibrational energies or thermal corrections, primarily to maintain focus on the underlying (and complicated) potential energy surface (PES).

Explicit-contact modelling was used with small catalysts. The catalysts are small for several reasons. First, this study required thorough searches of two tricky potential energy surfaces, so we wanted to compute real transition states in full-coordinate space (63 and 57 degrees of freedom, respectively), and properly verify each one by following the connections from these to the intermediates on either side; this cannot be done with larger catalyst models. Second, the 1998 FKRS study (24) with pentenium ion and $AlH_2(OH)_2^-$ was incomplete, and we wished to make use of the stationary points they had. Third, the $AlHCl_3^-$ catalyst was chosen from our exploratory ionic liquid calculations (33), which suggest that the active $Al_2Cl_7^-$ Lewis acid anion (34, 35) will create $AlHCl_3^-$ upon hydride abstraction from an alkane.

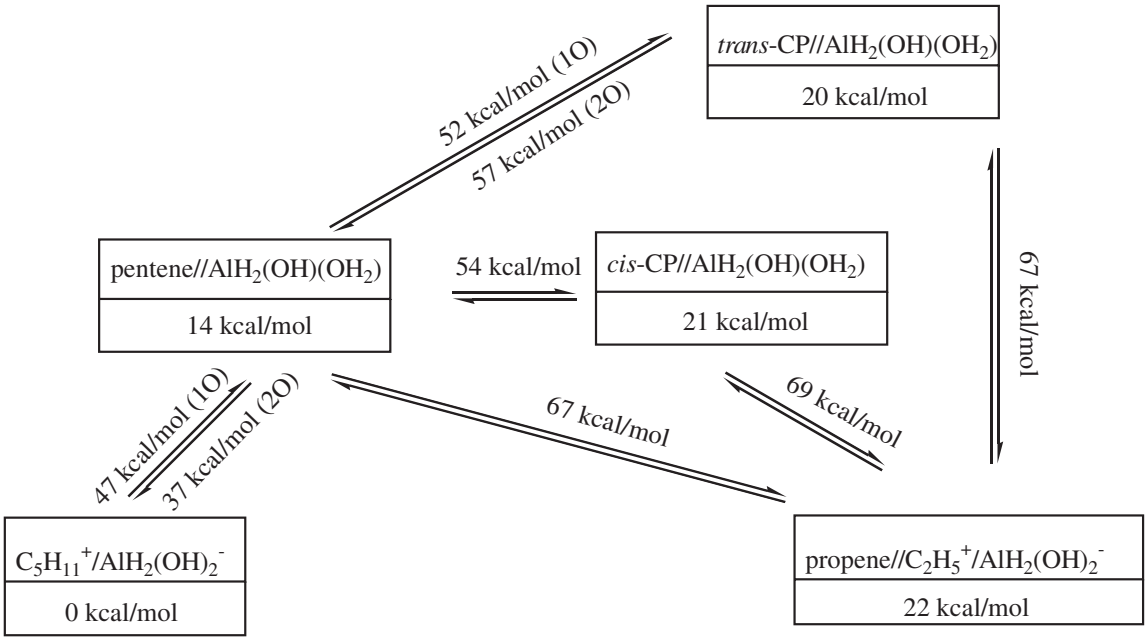
We will use the word chemisorbed to describe states in which there is a covalent bond between catalyst and reactant; this refers to states that have been variously called alkoxy, σ bonded, or alkyl silyl ether. We will use the word physisorbed to describe van der Waals neutral-pair complexes of catalyst and reactant, but also ion-pair (cation–anion, or sometimes called "zwitterionic") complexes. Some ion-pair complexes have an ionic bond strong enough to be considered chemisorbed, but in our systems the dissociation energies are much smaller because a proton transfer would occur if the molecular ions were pulled apart, resulting in neutral dissociated molecules. Although the concepts of chemisorbed and physisorbed states are taken from surface-science terminology (27), we think these states may prove to be pervasive in homogeneous as well as heterogeneous catalysis. We will use single and double slashes to denote chemisorbed and physisorbed complexes, respectively (e.g., $C_5H_{11}^+/AlHCl_3^-$ vs. $C_5H_{11}^+//AlHCl_3^-$). We will refer to the conversion from chemisorbed to physisorbed as ascension, and the opposite as descension, since the terms desorption and adsorption strictly refer to molecules leaving and approaching the surface.[2]

For most stationary points, there is more than one possible orientation of the reactant relative to the catalyst, and many possibilities were investigated. These possibilities are usually indistinguishable in energy on the scale of the reaction pathway, as will be demonstrated. Our atom-numbering con-

[2] R.A. Wolkow and G.P. Lopinski. Private communication. 2004.

© 2005 NRC Canada

Scheme 1. Overview of the B3LYP/6-31G(d,p) potential energy surface for the β scission of 2-pentenium ion on the $AlH_2(OH)_2^-$ catalyst fragment. Notation: chemisorbed (/), physisorbed (//), dimethylcyclopropane (CP). Transition-state energies are listed as well, including two values in cases where two distinct paths were found for the same step in the mechanism.



vention will be to count the carbon atoms as C1, C2, C3, C4, and C5, such that the C2 atom is initially bound to the O1 or Cl1 atom of the catalyst in the chemisorbed state.

The transition states that were located had only one imaginary vibrational frequency corresponding to the desired reaction coordinate. Each transition state was validated by two verification minimizations (to locate the two relevant intermediates) from displaced geometries on either side of the transition state. The displaced geometries for these verification runs were obtained by identifying the key internal coordinates in the crucial normal mode via the animation of the imaginary frequency, and then displacing these coordinates in both directions (minus or plus 0.03 Å for bond lengths; minus or plus 3° for angles and dihedrals).

Finally, we define some abbreviations for the rest of the article: potential energy surface (PES), dimethylcyclopropane (CP), protonated dimethylcyclopropane (PCP) (the prevalent form of a poorly solvated or gas-phase 2-pentenium ion).

Results

$AlH_2(OH)_2^-$ catalyst

Scheme 1 shows an overview of the results for the β scission of a chemisorbed 2-pentenium ion on $AlH_2(OH)_2^-$, to form a chemisorbed ethenium ion and a physisorbed propene. The only first step we could find is ascension to a physisorbed, neutral 1-pentene. After ascension, the physisorbed 1-pentene was found to be able to produce the intended products via more than one path. The direct one is Bronsted acid catalyzed β scission; the indirect paths involve Bronsted acid catalyzed isomerization of physisorbed 1-pentene to physisorbed *cis*- or *trans*-CP, followed by Bronsted acid catalyzed fission of two simultaneous C—C bonds. FKRS had presented the transition state for only the second step of one of the indirect routes (24); we believe it is the step from *trans*-CP to products.

On this PES, all the physisorbed intermediate states are neutral-pair complexes. For the various transition states, there are varying degrees of charge separation between catalyst and reactant, as caused by proton transfer. Also, as FKRS had found (24), direct β scission from a chemisorbed state is not a minimum energy pathway on this PES. We now describe the various steps on this PES in more detail.

Ascension step

Figure 1 shows the 3D images of the stationary-point geometries for three different versions of the ascension of 2-pentenium to 1-pentene on $AlH_2(OH)_2^-$. Figure 2 has sketches of the transition states that demonstrate the bond rearrangement mechanism. Table 1 provides some geometric data for the nine structures of Fig. 1 using the atom numbering of Fig. 2.

All three transition states feature partial ascension of the pentenium cation, as well as partial proton transfer from it to the catalyst anion to avoid the creation of an ion pair. In the top row path, the transferring proton goes from C1 to O1 (the single oxygen pathway, Fig. 2*a*), while in the other two paths the proton goes from C1 to O2 (the two oxygen pathways, Fig. 2*b*), and all three paths result in the coordination of the newly formed OH bond of the catalyst to the pentene double bond. The involvement of the second oxygen atom lowers the barrier height from 47 to 37 kcal mol^{-1}.

The lower two paths in Fig. 1 only differ by the conformer of the hydrocarbon; the middle path produces a gauche alkene from an all-trans alkoxy species, while the bottom path in the figure produces a *cis*-alkene from a gauche alkoxy species. While the lower two pathways are isoenergetic with this model fragment, a truer zeolite surface would probably make gauche alkoxy forms more favoured

© 2005 NRC Canada

Table 1. Selected geometry parameters (Å and °) for three different ascension paths with a zeolite fragment.[a]

	M1	TS	M2	M1	TS	M2	M1	TS	M2
	1O from trans			2O from trans			2O from gauche		
Bond lengths (Å)									
C1—C2	1.521	1.417	1.340	1.522	1.407	1.340	1.521	1.409	1.341
C2—C3	1.527	1.469	1.503	1.527	1.500	1.502	1.530	1.499	1.503
C3—C4	1.536	1.541	1.542	1.534	1.533	1.541	1.536	1.536	1.531
C2—C4	2.585	2.542	2.540	2.575	2.580	2.549	2.605	2.581	2.576
O1—C2	1.476	2.505	3.189	1.473	2.150	4.356	1.478	2.135	3.774
C1—H1	1.093	1.181	2.239	1.093	1.324	2.179	1.092	1.304	2.183
O1—H1	2.645	1.664	0.985	2.640	2.534	2.983	2.580	2.512	2.830
O2—H1	4.470	3.332	2.849	2.467	1.300	0.983	2.532	1.324	0.986
O2—H2	2.475	1.859	2.460	3.350	3.684	3.620	3.792	3.821	3.576
Bond angles (°)									
C2-C3-C4	115.1	115.2	113.1	114.6	116.6	113.8	116.3	116.5	116.2
C1-C2-C3-C4	179.1	140.1	121.3	–176.1	175.7	124.9	57.5	40.6	–2.7
C2-C3-C4-C5	173.3	175.5	173.6	–179.6	176.5	174.9	175.9	180.0	–179.2
C2-C1-H1	110.7	87.1	73.4	109.7	104.7	84.4	109.9	104.4	80.3

[a]Corresponds to the images of Fig. 1 with the atom numbering of Fig. 2. TS = transition state between two minima (MI, M2).

Fig. 1. B3LYP/6-31G(d,p) stationary points for three different ascension paths of 2-pentenium ion to pentene on $AlH_2(OH)_2^-$. The blue hydrogen is the one transferring from the pentenium ion to the catalyst. Top row: a one oxygen path. Middle row: a two oxygen path from a *trans*-pentenium ion form. Bottom row: a two oxygen path from a *gauche*-pentenium ion form.

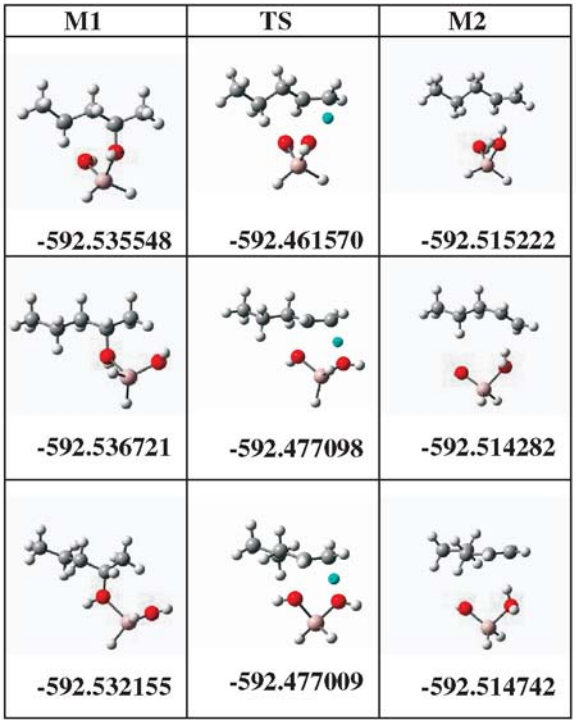
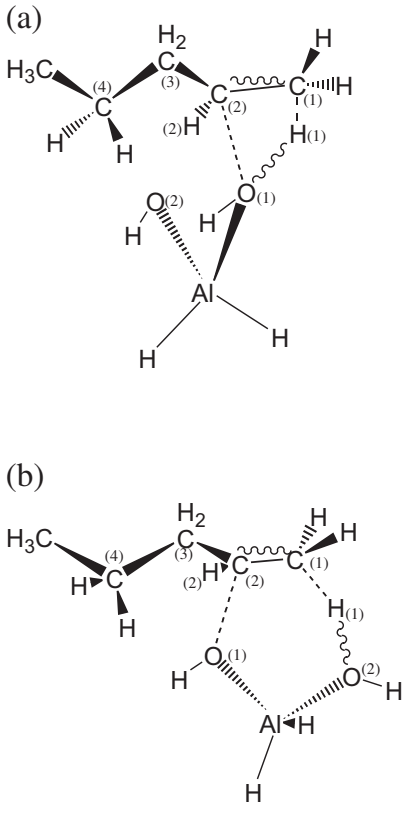


Fig. 2. Transition-state sketches for the ascension paths of 2-pentenium ion to pentene on $AlH_2(OH)_2^-$: (*a*) the single oxygen pathway; (*b*) the two oxygen pathways. The dashed lines indicate bonds in the reactant, while the squiggly lines indicate bonds in the product.



than all-trans ones. Paths involving other conformers may also exist.

Cyclization step

Figure 3 shows the 3D images of the geometries for three different versions of the isomerization of 1-pentene to CP on $AlH_2(OH)_2^-$. Figure 4 has sketches of the transition states that demonstrate the bond rearrangement mechanism. Table 2 provides some geometric data for the nine structures of Fig. 3 using the atom numbering of Fig. 4.

All three paths involve an ion-pair transition state in which the proton H1 has returned to C1 from the catalyst. However, to finish forming the cyclized intermediate, the proton H4 returns to the catalyst from C4, making this a

© 2005 NRC Canada

Table 2. Selected geometry parameters (Å and °) for three different isomerization paths with a zeolite fragment.[a]

	M1	TS	M2	M1	TS	M2	M1	TS	M2
	1O forming *cis*-CP			1O forming *trans*-CP			2O forming *trans*-CP		
Bond lengths (Å)									
C1—C2	1.341	1.463	1.516	1.341	1.463	1.517	1.340	1.462	1.519
C2—C3	1.503	1.427	1.507	1.504	1.425	1.508	1.504	1.440	1.507
C3—C4	1.541	1.627	1.508	1.544	1.633	1.506	1.542	1.584	1.508
C2—C4	2.542	2.088	1.540	2.566	2.100	1.535	2.538	1.972	1.536
O1—C2	3.213	3.050	3.139	3.219	3.050	3.124	3.226	3.483	3.995
C1—H1	2.214	1.112	1.096	2.191	1.112	1.096	2.289	1.140	1.094
O1—H1	0.986	2.006	3.036	0.986	2.003	2.863	0.985	1.756	2.936
C4—H4	1.097	1.118	2.239	1.099	1.115	2.420	1.096	1.159	2.232
O1—H4	3.184	1.996	0.982	3.327	2.036	0.979			
O2—H2	2.407	1.764	2.628	2.456	1.800	2.487			
O2—H4							2.868	1.720	0.979
O2—C4							3.728	2.869	3.167
C2—H4	2.796	2.02	2.197	2.804	2.037	2.181	2.701	1.897	2.360
Bond angles (°)									
C2-C3-C4	113.3	86.0	61.4	114.7	86.5	61.2	112.9	81.3	61.3
C1-C2-C3-C4	–121.7	–92.4	–113.0	126.0	94.7	110.6	117.9	96.7	112.3
C2-C3-C4-C5	–176.8	120.9	113.0	65.2	114.3	112.4	172.6	125.2	110.9
C2-C1-H1	76.0	105.1	111.9	76.6	105.2	112.3	72.2	108.2	110.8

[a]Corresponds to the images of Fig. 3 with the atom numbering of Fig. 4.

Fig. 3. B3LYP/6-31G(d,p) stationary points for three different isomerization paths of pentene on $AlH_2(OH)_2^-$. The blue hydrogens are the ones transferring between the hydrocarbon and the catalyst. Top row: a one oxygen path forming *cis*-dimethylpropane. Middle row: a one oxygen path forming *trans*-dimethylpropane. Bottom row: a two oxygen path forming *trans*-dimethylpropane.

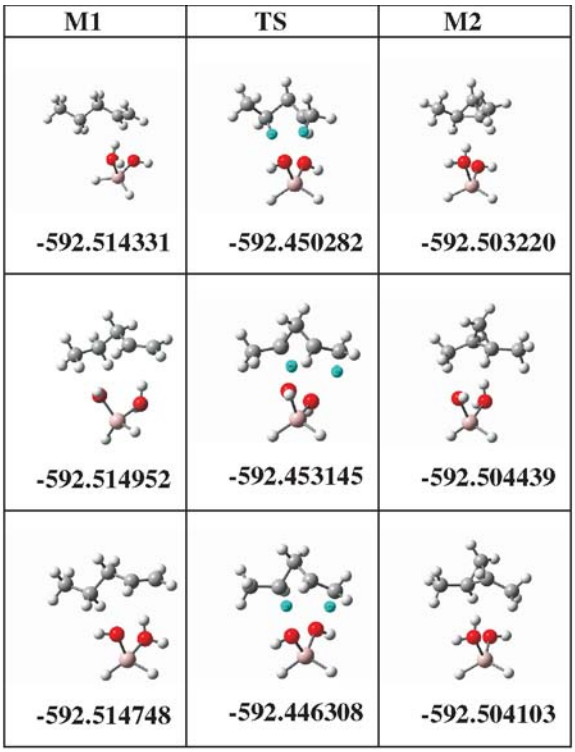
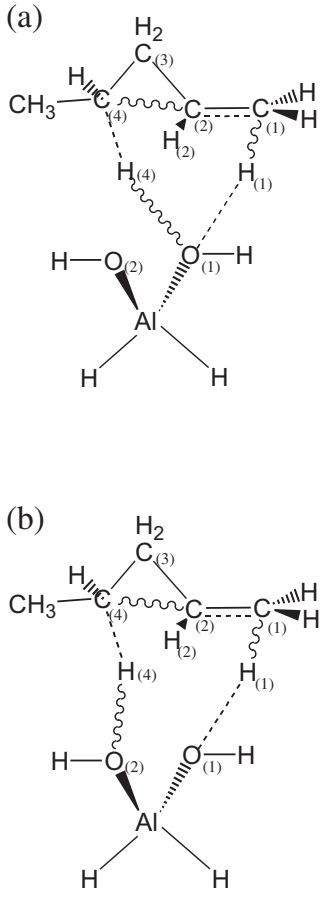
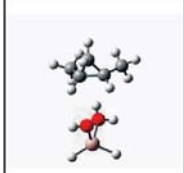
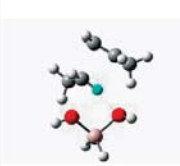
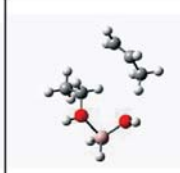
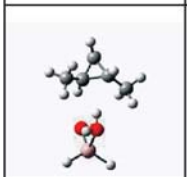
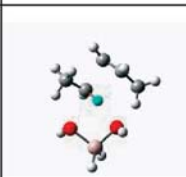
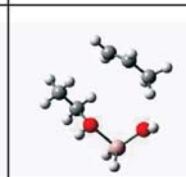
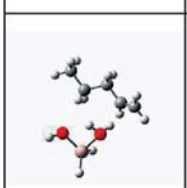
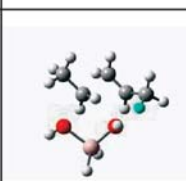


Fig. 4. Transition-state sketches for the isomerizations of pentene on $AlH_2(OH)_2^-$: (*a*) the single oxygen pathways; (*b*) the two oxygen pathway. The dashed lines indicate bonds in the reactant, while the squiggly lines indicate bonds in the product.



© 2005 NRC Canada

Fig. 5. B3LYP/6-31G(d,p) stationary points for three different scission (cracking) reactions on $AlH_2(OH)_2^-$. The blue hydrogen is the one transferring from the catalyst to the hydrocarbon. Top row: scission of *cis*-dimethylpropane. Middle row: scission of *trans*-dimethylpropane. Bottom row: scission of 1-pentene.

M1	TS	M2
		
-592.503225	-592.426301	-592.500980
		
-592.504103	-592.429541	-592.501223
		
-592.515471	-592.429249	-592.501570

double-proton transfer step. The top two paths in the figure are single oxygen pathways (Fig. 4*a*) in which departing and incoming protons use the same oxygen atom, while the bottom path is a two oxygen pathway (Fig. 4*b*). All three paths result in a newly formed OH bond on the catalyst that coordinates to the region of the two tertiary carbons C2 and C4. Unlike in the ascension step, the two oxygen path has a higher barrier than the single oxygen paths in the cyclization step, although the difference here is smaller (43 vs. 38 kcal mol^{-1}).

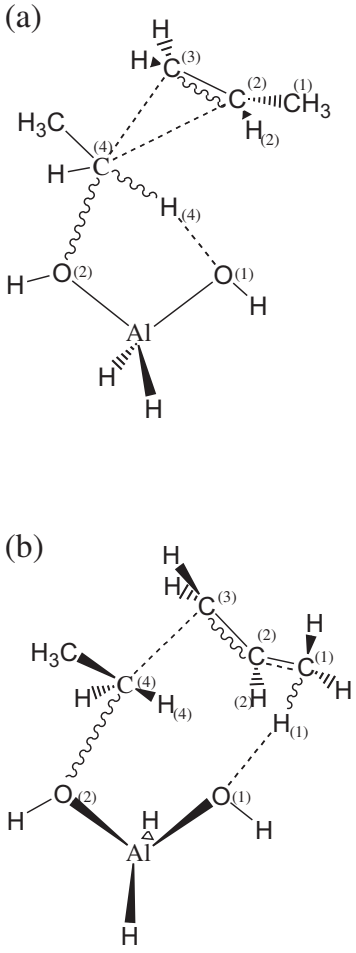
The two upper paths in Fig. 3 only differ by the conformation; the top path forms *cis*-CP from a trans-gauche pentene, while the middle path forms *trans*-CP from all-gauche pentene. Since our two oxygen pathway produced *trans*-CP, this model fragment might also produce a two oxygen pathway that forms *cis*-CP.

Scission step

Figure 5 shows the 3D images of the stationary points for three different versions of the scission step that produces chemisorbed ethenium ion and physisorbed propene. Figure 6 has sketches of the transition states that demonstrate the bond rearrangement mechanism. Table 3 provides some geometric data for the nine structures of Fig. 5, using the atom numbering of Fig. 6.

All three paths involve a transition state in which a proton has transferred from a catalyst oxygen to the hydrocarbon, and the C4 atom has migrated in an S_N2-like fashion between C3 and a second catalyst oxygen (all two oxygen pathways). In the upper two versions in Fig. 5, products are

Fig. 6. Transition-state sketches for the scission (cracking) steps on $AlH_2(OH)_2^-$: (*a*) the dimethylcyclopropane pathways; (*b*) the pentene pathway. The dashed lines indicate bonds in the reactant, while the squiggly lines indicate bonds in the product.



created from CP (Fig. 6*a*), and all the action happens at the C4 atom; it sheds its bonds to C2 and C3 and creates bonds to the Bronsted proton and a catalyst oxygen. The bottom path creates the products directly from pentene (Fig. 6*b*) by transferring the catalytic proton to C1, and allowing the C4 atom to break its bond to C3 and form its bond to the catalyst. The three transition states are very isoenergetic, lying in a 69–72 kcal mol^{-1} range relative to the products.

The two upper paths in Fig. 5 only differ by conformation; the top path starts with *cis*-CP, while the middle path starts with *trans*-CP. The three versions of the products appearing in Fig. 6 represent three different orientations of the ethyl and propene groups on the catalyst.

$AlHCl_3^-$ catalyst

Scheme 2 shows an overview of the results for the same β-scission reaction, but with $AlHCl_3^-$ as the catalyst. There are two significant differences between this PES and that from $AlH_2(OH)_2^-$ catalysis. One is the absence of minimum energy pathways involving physisorbed neutral-pair intermediates; instead, a barely stable ion-pair intermediate is seen (upper path in Scheme 2), involving a physisorbed, protonated *cis*-PCP. The second difference is that there is a

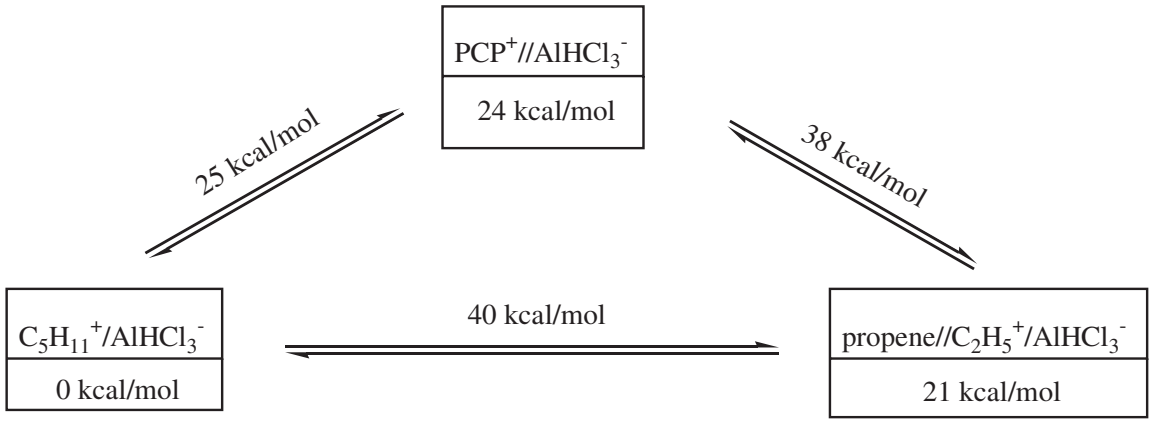
© 2005 NRC Canada

Table 3. Selected geometry parameters (Å and °) for three different scission (cracking) paths with a zeolite fragment.[a]

	M1	TS	M2	M1	TS	M2	M1	TS	M2
	Scission of *cis*-CP			Scission of *trans*-CP			Scission of 1-pentene		
Bond lengths (°)									
C1—C2	1.516	1.487	1.501	1.519	1.482	1.500	1.340	1.475	1.500
C2—C3	1.508	1.365	1.335	1.507	1.367	1.336	1.503	1.369	1.336
C3—C4	1.507	2.121	3.976	1.508	2.096	3.944	1.540	2.107	3.937
C2—C4	1.540	2.289	3.922	1.536	2.367	4.024	2.552	2.554	4.021
O1—C2	3.159	3.403	4.029	3.302	3.417	4.070	3.321	3.524	4.058
O1—C4	3.123	2.940	2.591	3.169	2.970	3.802			
C1—H1							2.165	1.115	1.098
O1—H1							0.983	1.991	2.373
C4—H4	2.185	1.094	1.089	2.232	1.092	1.091			
O1—H4	0.983	1.883	2.591	0.979	1.936	3.405			
O2—C4	3.428	2.419	1.465	3.388	2.428	1.462	3.689	2.362	1.462
Bond angles (°)									
C2-C3-C4	61.5	78.8	78.0	61.3	83.4	83.7	114.0	92.0	83.9
C1-C2-C3-C4	112.9	92.8	93.9	112.3	89.6	96.8	–131.8	–90.6	–95.2
C2-C3-C4-C5	–113.0	–118.2	–137.5	110.9	127.3	116.3	–177.8	171.1	152.2

[a]Corresponds to the images of Fig. 5 with the atom numbering of Fig. 6.

Scheme 2. Overview of the B3LYP/6-31G(d,p) potential energy surface for the β scission of 2-pentenium ion on the $AlHCl_3^-$ catalyst fragment. Notation: chemisorbed (/), physisorbed (//), protonated dimethylcyclopropane (PCP). Transition-state energies are listed as well.



direct one-step β-scission pathway from chemisorbed 2-pentenium ion. Several bombed searches suggest that a *flat*, *wide energy shelf* for PCP exists for both paths on the PES; PCP is barely stable in the upper pathway and not stable on the lower pathway.

The PES is also fairly flat in the region of neutral pair physisorbed intermediates. Here, the flat PES caused difficulties when using GAUSSIAN 98 frequency runs to verify stationary points because, in a few cases, a low-frequency mode had a frequency below the noise level of the normal mode diagonalization. This appears to be due to the coarse DFT numerical grid; when we switched to the "ultrafine" grid, we were able to definitively find four physisorbed intermediates (two ion pair and two neutral pair), and two transition states for conversion of these neutral-pair ones to ion-pair ones. In Scheme 2, the $PCP^+//AlHCl_3^-$ intermediate sits at 24 kcal mol^{-1}; the other three physisorbed minima are at 21 kcal mol^{-1} ($pentenium^+$), 21 kcal mol^{-1} (pentene), and 28 kcal mol^{-1} (CP), and the transition states are at 22 kcal mol^{-1} ($pentenium^+ \rightarrow$ pentene) and 30 kcal mol^{-1} ($PCP^+ \rightarrow$ CP). We are not presenting these results in Scheme 2 because: (*i*) no paths leading to β scission could be found from these minima; and (*ii*) they required the ultrafine grid.

In both β-scission pathways in Scheme 2, the hydrogens never leave their respective carbon partners. The C2—Cl1 and C3—C4 bonds are broken, and a C4—Cl3 bond is formed (both are two chlorine pathways). The presence of three chlorines in our catalyst model may prevent a *trans*-PCP intermediate from forming vis-à-vis the cis form.

Ascension step

We present only one path for the ascension of 2-pentenium ion on $AlHCl_3^-$; Fig. 7 shows the 3D images of its stationary-point geometries. Figure 8 has the sketch of the transition state demonstrating the "hydrogen bonds" between catalyst and reactant, and Table 4 provides some geometric data for the three structures of Fig. 7 using the atom numbering of Fig. 8.

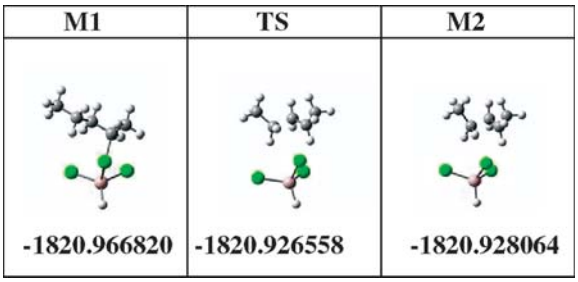
© 2005 NRC Canada

Table 4. Selected geometry parameters of the ascension of pentenium ion and two different scission (cracking) paths with an ionic liquid fragment.

	M1	TS	M2	M1	TS	M2	M1	TS	M2
	Ascension step[a]			Scission of chemisorbed pentenium ion[b]			Scission of physisorbed pentenium ion[b]		
Bond lengths (Å)									
C2—C3	1.523	1.419	1.415	1.415	1.354	1.335	1.522	1.358	1.335
C3—C4	1.533	1.648	1.64	1.638	2.418	3.756	1.534	2.359	3.765
C2—H2	2.867	2.236	1.917	1.910	2.497	3.607	2.853	2.397	3.110
C4—H2	1.097	1.096	1.113	1.114	1.082	1.089	1.096	1.083	1.089
C2—Cl1	1.917	3.306	3.442	3.450	4.046	4.874	1.917	4.163	4.720
C2—Cl2	3.697	3.398	3.411	3.412	3.879	4.299	3.713	5.872	6.370
C4—Cl3	4.710	3.660	3.584	3.578	2.565	1.869	4.846	2.653	1.872
Cl1—H2	3.792	2.946	2.565	2.544	2.770	3.122	2.919	2.539	2.920
Cl2—H1	2.827	2.471	2.523	2.518	2.999	3.497	2.836	5.506	5.954
Cl3—H3	4.399	2.781	2.820	2.798	2.594	2.386	5.832	2.639	2.364
Cl3—Al				2.187	2.275	2.483	2.137	2.268	2.492
Bond angles (°)									
C2-C3-C4	117.0	93.4	80.6	80.3	84.6	78.5	117.0	82.1	83.1
C1-C2-C3-C4	–54.4	–97.0	–96.0	–96.1	–99.0	–96.3	–53.2	–95.4	–90.7
C2-C3-C4-C5	–179.7	141.3	116.5	116.4	146.4	174.2	–179.0	–111.5	–108.0
Cl3-C4-H2				66.8	81.7	103.8			
Cl3-C4-H3				37.9	79.4	104.4			
Al-Cl3-C4				80.5	92.4	103.6	85.4	96.6	106.9

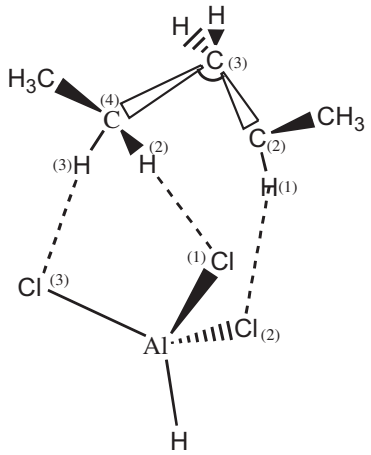
[a]Corresponds to the images of Fig. 7 with the atom numbering of Fig. 8.
[b]Corresponds to the images of Fig. 9 with the atom numbering of Fig. 10.

Fig. 7. B3LYP/6-31G(d,p) stationary points for the ascension step found on $AlHCl_3^-$.



The chemisorbed state has a C2—Cl1 distance of 1.9 Å. After ascension, the physisorbed pentenium ion has a structure that some scientists describe as an edge-protonated cyclopropane ring, where the C2, C3, C4, and H2 atoms lie nearly planar, and the C2-C3-C4 angle is acute (81°); we refer to it as PCP, to remind the reader of the analogous CP structure in the $AlH_2(OH)_2^-$ modelling. The resulting $C_5H_{11}^+$//$AlHCl_3^-$ intermediate features three H···Cl interactions in a stool-like structure in which the three catalyst chlorine atoms are coordinated with three different hydrogens near the C-C-C-H ring. These three H···Cl bond distances change from 3.8, 2.8, and 4.4 Å to 2.9, 2.5, and 2.8 Å in the transition state, and finish at 2.6, 2.5, and 2.8 Å in the stool-like structure, respectively. During this procedure, the C4—Cl3 bond distance also decreases from 4.7 to 3.6 Å, thus preparing for tight coordination in the scission step. The transition state for this endothermic step is extremely late, with the C2—Cl1 bond almost completely broken, and the closing of the C2 carbenium site to the C4 atom (actually to the C4—H2 bond) almost complete.

Fig. 8. Transition-state sketch for the ascension of pentenium ion on $AlHCl_3^-$. The dashed lines indicate coordination interactions between Cl and H in the stool-like structure of the ion-pair complex.

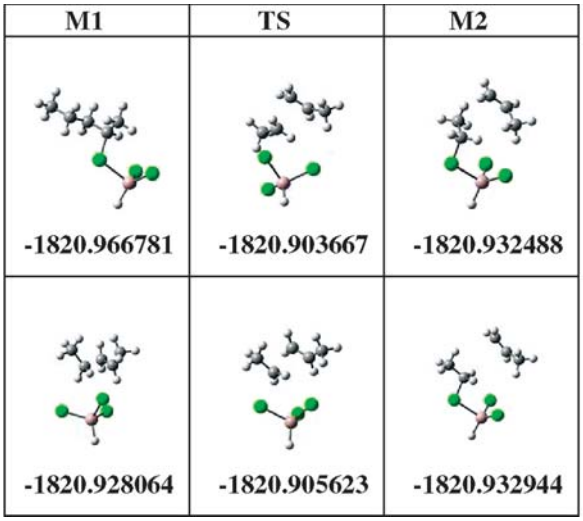


Scission step

We present two versions of the scission step that produce chemisorbed ethenium ion and physisorbed propene; Fig. 9 shows the 3D images of their stationary-point geometries. Figure 10 has the sketch of the transition states to demonstrate the bond rearrangement mechanism, and Table 4 provides some geometric data for the three structures of Fig. 9 using the atom numbering of Fig. 10.

© 2005 NRC Canada

Fig. 9. B3LYP/6-31G(d,p) stationary points for two different scission (cracking) reactions on $AlHCl_3^-$. Top row: one-step β scission of chemisorbed pentenium ion. Bottom row: scission of physisorbed pentenium ion (also called protonated dimethylcyclopropane).



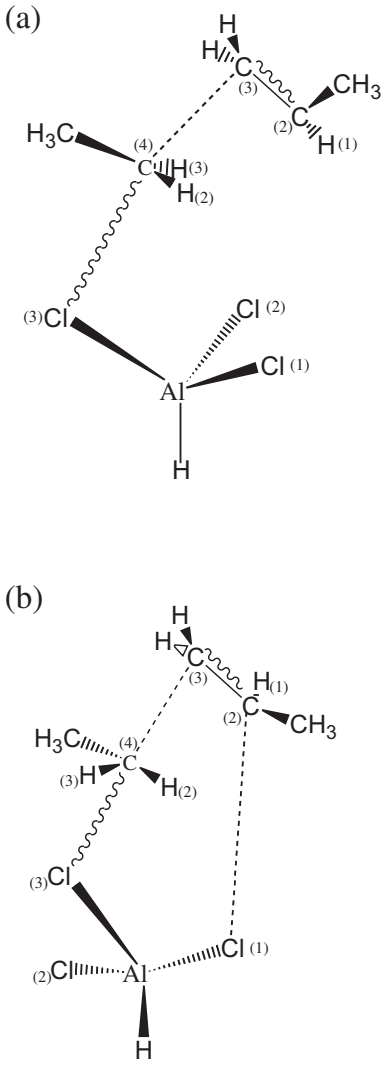
The top row of Fig. 9 shows the path for β scission directly from the chemisorbed pentenium ion, and the bottom row is the scission from the precariously stable PCP ion. Both go through very similar scission transition states in which the migrating C4 atom has moved to a spot roughly equidistant between the C3 atom it was leaving (2.4 Å) and the Cl3 atom it was approaching (2.6–2.7 Å). The C1—C2 bond changes from a single bond (1.41 Å) through the transition state (1.35 Å) to a double bond (1.33 Å). The products from these two scission-step versions differ in orientation of the ethyl and propene units relative to the catalyst, but are otherwise identical chemically.

Discussion

Visualizing and comparing the two catalyst mechanisms

The PES energetics are key to understanding the apparently dramatic qualitative differences in the β-scission mechanism on $AlHCl_3^-$ vs. $AlH_2(OH)_2^-$. To do this comparison, we chose to sketch approximate contour plots of the PES for both catalysts (Figs. 11 and 12), oriented in a common way that includes both neutral-pair and ion-pair physisorbed regions in both plots. The contours are approximate, based only on the 11 and six stationary points, respectively, of the lowest-energy paths between regions, but also guided by the nonexistence of other stationary points. For both these plots, the horizontal coordinate is a crude coordinate representing the general stepwise reaction path of ascension, isomerization, and β scission, and the vertical coordinate represents the ion-pair vs. neutral-pair nature of the physisorbed complexes (ion pair on the bottom, neutral pair on the top). The layout of this plot is rather arbitrary, but we have chosen to put the physisorbed pentene and 2-pentenium regions to the left of the CP and PCP ones because they require less geometrical rearrangement from the chemisorbed reactant state than the cyclopropanes would.

Fig. 10. Transition-state sketches for the scission (cracking) steps on $AlHCl_3^-$: (*a*) from a chemisorbed pentenium ion; (*b*) from a physisorbed protonated dimethylcyclopropane. The dashed lines indicate bonds in the reactant, while the squiggly lines indicate bonds in the product.



In Figure 11 ($AlH_2(OH)_2^-$ catalyst), although the intermediates are physisorbed neutral-pair complexes, the transitions states for the steps are more like ion-pair ones, causing the reaction paths to be curved in this plot. Without the catalyst, the steps would have much larger reaction barriers as indicated by the high walls blocking the direct routes on this plot. Each step proceeds via a significant (40–50 kcal mol^{-1}) energy barrier in the transition state before falling down into a well. This plot also helps to suggest that if the chemisorbed reactant has sufficient energy to overcome the first barrier, it might have sufficient excess energy and kinetic momentum to continue further down the channel towards complete β scission without having to fall down into either of the two potential wells for physisorbed neutral-pair intermediates.

In Fig. 12 ($AlHCl_3^-$ catalyst), the biggest difference relative to Fig. 11 is that the energies of the ion-pair intermediates (the lower half of the plot) have dropped significantly

© 2005 NRC Canada

Fig. 11. Sketch of a plausible PES for β scission of the 2-pentenium ion on the $AlH_2(OH)_2^-$ catalyst, based on B3LYP/6-31G(d,p) stationary points. Each contour represents a rise of 10 kcal mol^{-1} from dark to light (1 cal = 4.184 J). The bottom half of the figure represents ion-pair complexes, such that a vertical rise to the top half represents proton transfer to the catalyst to obtain neutral-pair complexes. Note that all four transition states have a great deal of ion-pair character, as indicated by their location in the bottom half of the diagram.

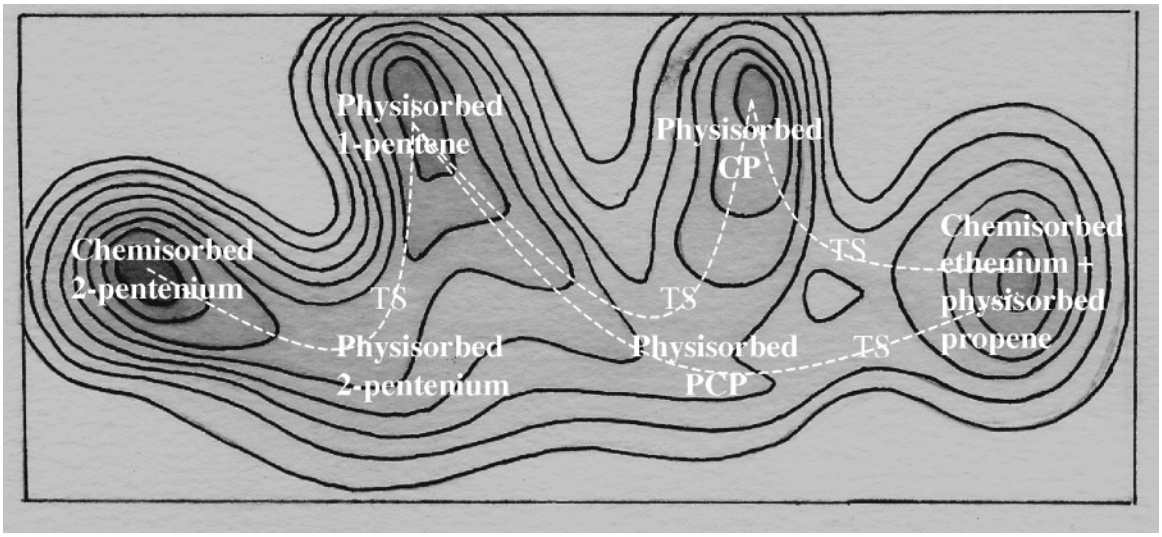
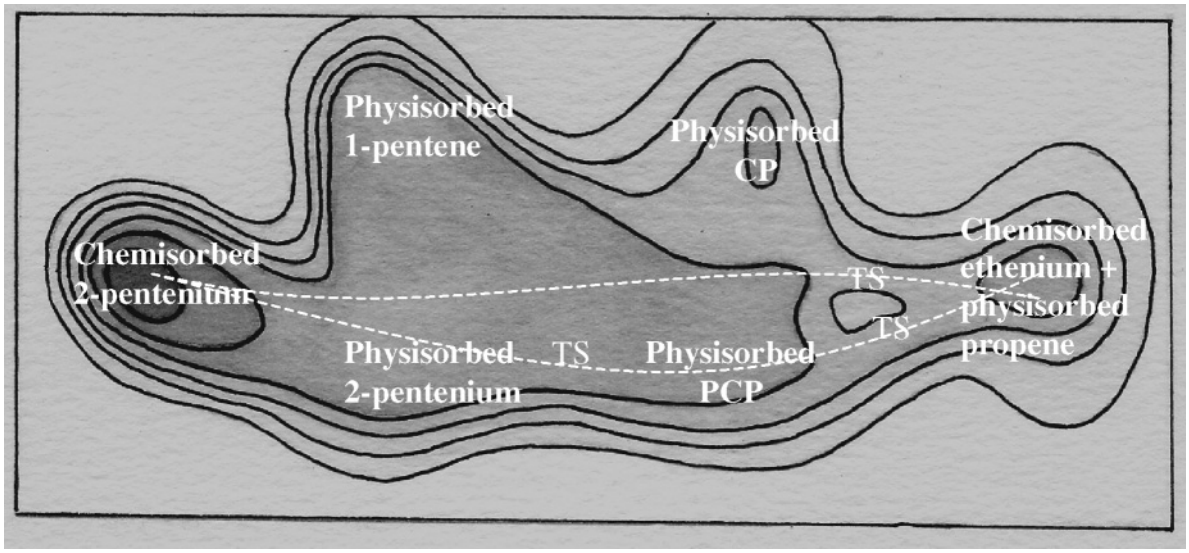


Fig. 12. Sketch of a plausible PES for β scission of the 2-pentenium ion on the $AlHCl_3^-$ catalyst, based on B3LYP/6-31G(d,p) stationary points. Each contour represents a rise of 10 kcal mol^{-1} from dark to light (1 cal = 4.184 J). The bottom half of the figure represents ion-pair complexes, such that a vertical rise to the top half represents proton transfer to the catalyst to obtain neutral-pair complexes. The minimum for the physisorbed ion-pair complex $PCP^+//AlHCl_3^-$ cannot be seen on this scale, owing to the flatness of the surface in the physisorbed regions.



relative to the neutral-pair intermediates, and so much so that the energies of ion-pair vs. neutral-pair structures have become competitive. The β-scission reaction proceeds along a wide, flat path before rising over a transition state late in the reaction.

We think these plots demonstrate that the qualitative differences between the two mechanisms are due to the lowering of the ion-pair regions of the PES relative to the neutral-pair ones, in substituting chloride for hydroxide on the catalyst. This lowering is due to the lowered proton affinity of the catalyst; we computed the proton affinities of our two catalysts with B3LYP/6-31G(d,p), and they are 338 kcal mol^{-1} for $AlH_2(OH)_2^-$ and 276 kcal mol^{-1} for $AlHCl_3^-$. For those concerned with the imbalance of the number of hydrides on each catalyst, this effect is minor; we calculated the proton affinity of $AlH_2Cl_2^-$ and obtained 285 kcal mol^{-1}. Hence, since the catalysts are virtually identical in size, the lower basicity (or proton affinity) of chlorine atoms vs. oxygen atoms is the cause of the mechanistic differences here. This demonstration of catalyst basicity effects on mecha-

© 2005 NRC Canada

nism meshes nicely with our earlier study on the protolysis of hexane (23), which demonstrated that catalyst acidity could cause qualitative differences in its mechanism.

Revisiting previous β-scission modelling work

Frash et al. (FKRS) (24) studied the β scission of chemisorbed 1-butenium and 2-pentenium ions on two model zeolite fragments, $AlH_2(OH)_2^-$ and $AlH_2(OSiH_3)_2^-$, using HF/6-31G(d) and B3LYP/6-31G(d) geometry optimizations. The B3LYP results with the $AlH_2(OH)_2^-$ fragment were the ones we took and greatly extended by adding five transition states to their one on this PES. FKRS stated that on this PES the "alkoxy" (chemisorbed) reactant first converts to a CP intermediate before performing the scission step; we have convinced ourselves that this is not correct, and that minimum energy ascension of the chemisorbed reactant leads formally to a physisorbed propene intermediate, which can then isomerize to CP or directly perform β scission itself. FKRS were likely misled by the 1-butenium PES for which they did find a transition state from the chemisorbed reactant directly to CP, but the difference may be due to the ability of 2-pentenium ion to lose a nearby methyl proton upon ascension, which 1-butenium ion cannot do. FKRS also expressed surprise that the B3LYP PES produced a two-step pathway, because their HF/6-31G(d) PES produced a one-step, direct β scission from chemisorbed 2-pentenium ion. Our Fig. 11 may help to understand the qualitative difference; it is conceivable that a different level of theory might produce a slight shift of the contours around 40 kcal mol^{-1} to produce a direct connection from chemisorbed reactant all the way to chemisorbed product. FKRS seemed to prefer the HF results over the B3LYP results, despite B3LYP being the higher level of theory; given that the difference may only be a subtle change in the PES, we suggest that the qualitative difference should not be worrisome, and that a proper description of the mechanism should include pathways connecting all four minima of Fig. 11 via carbenium ion paths.

Hay et al. (25) modelled the β-scission reaction of 2-pentenium ion with the zeolite fragment $AlH_2(OSiH_3)_2^-$, using HF/6-31G(d) optimized structures and B3LYP/6-31G(d) energies computed at the HF structures. They state the path as going from physisorbed pentene to chemisorbed 2-pentenium ion and then directly to products, in disagreement with our results. However, the direct β scission from the chemisorbed reactant does agree with the HF/6-31G(d) results of FKRS (24) with a different fragment model, and hence we merely comment that HF theory is being consistent in this matter, but that B3LYP optimizations present a different picture.

Svelle et al. (26) modelled the dimerization of linear alkenes with the zeolite fragment $Al(OH)(OSiH_3)_3^-$ (the active catalyst had an extra proton on an O atom between Al and a Si atom) using B3LYP/6-31G(d) optimizations and higher level single-point energies at these geometries. β Scission is the same reaction in the opposite direction. They refer to π and σ complexes, which in our language are physisorbed alkene and chemisorbed species, respectively. They refer to concerted vs. stepwise pathways; their stepwise hypothesis features a β-scission step between chemisorbed states, while the concerted hypothesis features a β-scission step between physisorbed states. However, despite showing figures of these hypotheses in their Results section, they admit to never finding chemi- to chemi-β-scission steps, as well as discovering some CP minima upon testing their transition states. Their results in fact agree with ours that β scission starts from various physisorbed states and not chemisorbed ones. Their finding of a β-scission step between two physisorbed states intrigued us, since we could not find such a step with our model system, so we tried some further calculations. We found that this step is unusually sensitive to the fragment model used: such a step exists for our pentene intermediate (1-pentene → propene + ethene) on the activated $Al(OH)(OSiH_3)_3^-$ fragment of Svelle et al., but not on activated $Al(OH)_4^-$ or $AlH_2(OH)_2^-$.

Chemisorbed or physisorbed reactants?

Conventional organic chemistry states that cationic β scission starts from a carbenium ion. After the initial computations of Kazansky and co-worker (10, 11), it has been assumed (12, 24) that this β scission (on a zeolite) starts with the carbenium ion in an alkoxy (chemisorbed) state. However, this is not necessarily true. Our thorough calculations with $AlH_2(OH)_2^-$ suggest that *physisorbed alkenes* can undergo β scission directly, without having to become chemisorbed ions (see Fig. 11). Furthermore, even though the β-scission step immediately results in a chemisorbed primary carbenium ion on $AlH_2(OH)_2^-$, Svelle et al. (26) with $Al(OH)(OSiH_3)_3^-$ found a β scission that resulted in physisorbed products. Hence, chemisorbed ions are not a requirement for the initial or final state in the cracking step. It might be better to think of the chemisorbed state as a "storage" state of alkenes or carbenium ions, rather than the active form of the reactant species.

Conclusions

At the B3LYP/6-31G(d,p) level of theory, catalyzed β scission of a secondary carbenium ion is qualitatively different on $AlHCl_3^-$ than it is on $AlH_2(OH)_2^-$, which is due only to the differing basicities of Cl and O atoms. On the $AlH_2(OH)_2^-$ catalyst, the stable physisorbed intermediates are neutral alkenes or alkylcyclopropanes (CP). On the less basic $AlHCl_3^-$ catalyst, however, the intermediates are protonated alkylcyclopropanes (PCP).

Although these chosen catalysts are not models of true ionic liquids or aluminosilicate zeolites, they happened to produce the same qualitative intermediates (ion pair vs. neutral pair) that are thought to exist in these two true systems.

With $AlHCl_3^-$, β scission can occur directly from the chemisorbed state, or occur via a barely stable ion-pair intermediate. With $AlH_2(OH)_2^-$, the scission step does not start from the chemisorbed state, but from physisorbed neutral-pair states, although trajectories with small excess energies and reaction momentum could achieve β scission from chemisorbed states.

Acknowledgments

This research was funded by the Natural Sciences and Engineering Research Council of Canada (NSERC) and the Canada Foundation for Innovation (CFI). The Laboratory of Computational Discovery (University of Regina, Regina,

© 2005 NRC Canada

Saskatchewan) is thanked for computational resources. D. Roettger is thanked for drawing the contour plots.

References

1. L. Xiao, K.E. Johnson, and R.G. Treble. J. Mol. Catal. A, **214**, 121 (2004).
2. G.A. Olah, Y. Halpern, J. Shen, and Y.K. Mo. J. Am. Chem. Soc. **95**, 4960 (1973).
3. Y. Zhao, G.R. Bamwenda, and B.W. Wojciechowski. J. Catal. **142**, 465 (1993).
4. W.O. Haag and R.M. Dessau. Proc. Int. Congr. Catal. 8th. **2**, 305 (1985).
5. J. Engelhardt and W.K. Hall. J. Catal. **151**, 1 (1995).
6. S.T. Sie. *In* Handbook of heterogeneous catalysis. Vol. 4. *Edited by* G. Ertl, H. Knozinger, and J. Weitkamp. VCH, Weinheim, Germany. 1997. p. 1998.
7. J.F. Haw. Phys. Chem. Chem. Phys. **4**, 5431 (2002).
8. G.M. Kramer, G.B. McVicker, and J.J. Ziemiak. J. Catal. **92**, 355 (1985).
9. J.F. Haw, B.R. Richardson, I.S. Oshiro, N.D. Lazo, and J.A. Speed. J. Am. Chem. Soc. **111**, 2052 (1989).
10. V.B. Kazansky and I.N. Senchenya. Kinet. Katal. **28**, 566 (1987).
11. V.B. Kazansky. Acc. Chem. Res. **24**, 379 (1991).
12. V.B. Kazansky. Catal. Today, **51**, 419 (1999).
13. M.V. Frash and R.A. van Santen. Top. Catal. **9**, 191 (1999).
14. T. Demuth, X. Rozanska, L. Benco, J. Hafner, R.A. van Santen, and H. Toulhoat. J. Catal. **214**, 68 (2003).
15. J.L. White, L.W. Beck, and J.F. Haw. J. Am. Chem. Soc. **114**, 6182 (1992).
16. J.B. Nicholas, T. Xu, and J.F. Haw. Top. Catal. **6**, 141 (1998).
17. W. Song, J.B. Nicholas, and J.F. Haw. J. Am. Chem. Soc. **123**, 121 (2001).
18. I.I. Ivanova, E.B. Pomakhina, A.I. Rebrov, and E.G. Derouane. Top. Catal. **6**, 49 (1998).
19. E.G. Derouane, H. He, S.B. Derouane-Abd Hamid, D. Lambert, and I. Ivanova. Catal. Lett. **58**, 1 (1999).
20. E.G. Derouane, H. He, S.B. Derouane-Abd Hamid, D. Lambert, and I. Ivanova. J. Mol. Catal. A: Chem. **158**, 5 (2000).
21. A.G. Stepanov, M.V. Luzgin, V.N. Romannikov, and K.I. Zamaraev. Catal. Lett. **24**, 271 (1994).
22. A.G. Stepanov, M.V. Luzgin, V.N. Romannikov, V.N. Sidelnikov, and E.A. Paukshtis. J. Catal. **178**, 466 (1998).
23. K.C. Hunter, C. Seitz, and A.L.L. East. J. Phys. Chem. A, **107**, 159 (2003).
24. M.V. Frash, V.B. Kazansky, A.M. Rigby, and R.A. van Santen. J. Phys. Chem. B, **102**, 2232 (1998).
25. P.J. Hay, A. Redondo, and Y. Guo. Catal. Today, **50**, 517 (1999).
26. S. Svelle, S. Kolboe, and O. Swang. J. Phys. Chem. B, **108**, 2953 (2004).
27. D.E. Brown, D.J. Moffatt, and R.A. Wolkow. Science (Washington, D.C.), **279**, 542 (1998).
28. A.D. Becke. J. Chem. Phys. **98**, 5648 (1993).
29. C. Lee, W. Yang, and R.G. Parr. Phys. Rev. B, **37**, 785 (1988).
30. M.J. Frisch, G.W. Trucks, H.B. Schlegel, G.E. Scuseria, M.A. Robb, J.R. Cheeseman, V.G. Zakrzewski, J.A. Montgomery, R.E. Stratmann, J.C. Burant, S. Dapprich, J.M. Millam, A.D. Daniels, K.N. Kudin, M.C. Strain, O. Farkas, J. Tomasi, V. Barone, M. Cossi, R. Cammi, B. Mennucci, C. Pomelli, C. Adamo, S. Clifford, J. Ochterski, G.A. Petersson, P.Y. Ayala, Q. Cui, K. Morokuma, D.K. Malick, A.D. Rabuck, K. Raghavachari, J.B. Foresman, J. Cioslowski, J.V. Ortiz, B.B. Stefanov, G. Liu, A. Liashenko, P. Piskorz, I. Komaromi, R. Gomperts, R.L. Martin, D.J. Fox, T. Keith, M.A. Al-Laham, C.Y. Peng, A. Nanayakkara, C. Gonzalez, M. Challacombe, P.M.W. Gill, B.G. Johnson, W. Chen, M.W. Wong, J.L. Andres, M. Head-Gordon, E.S. Replogle, and J.A. Pople. GAUSSIAN 98. Revision A.9 [computer program]. Gaussian, Inc., Pittsburgh, Pennsylvania. 1998.
31. PQS 3.0 [computer program]. Parallel Quantum Solutions, Fayetteville, Arkansas. 2004.
32. J. Baker. J. Comput. Chem. **7**, 385 (1986).
33. K.C. Hunter. M.Sc. thesis, University of Regina, Regina, Saskatchewan. 2002.
34. D.W. Chandler and K.E. Johnson. J. Inorg. Chem. **38**, 2050 (1999).
35. J.L. Campbell and K.E. Johnson. J. Am. Chem. Soc. **117**, 7791 (1995).

© 2005 NRC Canada

Salicylaldimine dimers derived from 2-$H_2NC_6H_4Bpin$ (pin = 1,2-$O_2C_2Me_4$)

Jonathan D. Webb, Hanni A. Darwish, Haiwen Zhang, Susan L. Wheaton, Felix J. Baerlocher, Christopher M. Vogels, Andreas Decken, and Stephen A. Westcott

Abstract: Condensation of salicylaldehyde (2-$HOC_6H_4C(O)H$) with 2-$H_2NC_6H_4Bpin$ (pin = 1,2-$O_2C_2Me_4$) afforded the macrocyclic dimer **1** with an OBOBO structural unit. Similar reactivity with substituted salicylaldehyde derivatives gave the corresponding Schiff bases **2**–**6**. Crystals of **1** were triclinic, space group *P*-1, a = 9.7915(4) Å, b = 10.8569(5) Å, c = 12.8445(6) Å, α = 102.067(1)°, β = 96.011(1)°, γ = 90.458(1)°, Z = 2. All new compounds have been tested for their antifungal activity against *Aspergillus niger* and *Aspergillus flavus*.

Key words: antifungal, boron, dehydration, heterocycles, Schiff bases.

Résumé : La condensation de l'aldéhyde salicylique (2-$HOC_6H_4C(O)H$) avec le 2-$H_2NC_6H_4Bpin$ (pin = 1,2-$O_2C_2Me_4$) conduit à la formation du dimère macrocyclique **1** qui comporte une unité structurale OBOBO. Une réactivité similaire avec des aldéhydes salicyliques substitués conduit aux bases de Schiff correspondantes, **2**–**6**. Les cristaux du composé **1** sont tricliniques, groupes d'espace *P*-1, a = 9,7915(4) Å, b = 10,8569(5) Å, c = 12,8445(6) Å, α = 102,067(1)°, β = 96,011(1)°, γ = 90,458(1)°, Z = 2. Tous les nouveaux composés ont été évalués pour leur activité antifongique contre l'*Aspergillus niger* et l'*Aspergillus flavus.*

Mots clés : antifongique, bore, déshydratation, hétérocycles, bases de Schiff.

[Traduit par la Rédaction]

Introduction

Compounds containing boronic acids [$RB(OH)_2$] or boronate esters [$RB(OR')_2$] have been used extensively as intermediates in Suzuki–Miyaura cross-coupling reactions for a variety of applications (1–11). Interest in these boron compounds also arises from their potent biological activities (12–26). For instance, aminoboronic acids are potent inhibitors of serine proteases, a diverse group of proteolytic enzymes responsible for the generation of most disease processes (13–18). The boronic acid containing inhibitor 2(*S*)-amino-6-boronohexanoic acid has also recently been shown to enhance erectile function in male rats (25). Likewise, simple aminoboronic acid derivatives are also being examined for application in boron neutron capture therapy, a binary form of cancer treatment that relies on delivering a compound containing boron-10 selectively to tumour tissues prior to irradiation by neutrons (26). With the wealth of medicinal properties associated with boron compounds, we decided to examine the reactivity of salicylaldehyde and the boronate ester aniline compound 2-(4,4,5,5-tetramethyl-[1,3,2]-dioxaborolan-2-yl)phenylamine (2-$H_2NC_6H_4Bpin$ (pin = 1,2-$O_2C_2Me_4$)). Results of our study are presented herein.

Received 18 February 2005. Published on the NRC Research Press Web site at http://canjchem.nrc.ca on 24 September 2005.

J.D. Webb, H.A. Darwish, H. Zhang, S.L. Wheaton, C.M. Vogels, and S.A. Westcott.[1] Department of Chemistry, Mount Allison University, Sackville, NB E4L 1G8, Canada.
F.J. Baerlocher. Department of Biology. Mount Allison University, Sackville, NB E4L 1G7, Canada.
A. Decken. Department of Chemistry, University of New Brunswick, Fredericton, NB E3B 5A3, Canada.

[1]Corresponding author (e-mail: swestcott@mta.ca).

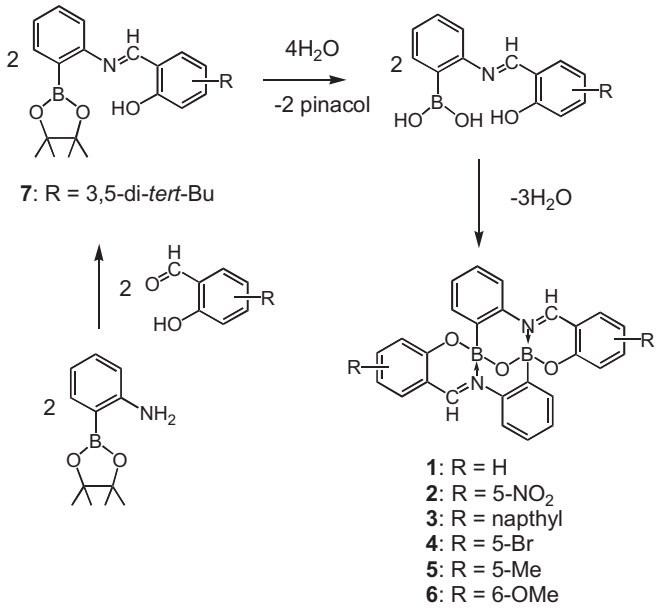
Results and discussion

Salicylaldimines are versatile intermediates in organic synthesis and have been used to prepare numerous pharmacologically important compounds (27–33). For instance, Whiting and co-workers (27) have used imines containing boronate esters to make enantio-enriched γ-phenyl-γ-amino alcohols, and Höpfl and co-workers (33) have prepared air-stable cyclophane-type macrocycles from salicylideneaminoaryl alcohols and arylboronic acids. In this study, we found that addition of the ortho-substituted aniline derivative 2-$H_2NC_6H_4Bpin$ adds to salicylaldehyde in wet ethanol to give the Schiff base dimer **1** (Fig. 1). While the imine proton is observed in the ^{1}H NMR spectra at δ 8.47 ppm, the pinacol methyl groups are absent. The diagnostic C=N stretching band is observed in the FT-IR spectra at ca. 1620 cm^{-1}, and a broad peak at δ 3.7 ppm in the ^{11}B NMR spectra indicates that the boron atom is four coordinate (34, 35).

It is possible that the formation of **1** proceeds via initial formation of a Schiff base with subsequent cleavage of the pinacol group to give the corresponding boronic acid. This transient imine could then rapidly dehydrate to form the anhydride dimer **1**. Indeed, we have found that addition of water to the aldimine derived from salicylaldehyde and 2-$H_2NC_6H_4Bpin$ (prepared in dry THF) gave **1** as the only new

 doi: 10.1139/V05-124 © 2005 NRC Canada

Fig. 1. Possible formation of Schiff base dimers.



boron containing product. Anhydride formation is also observed with substituted salicylaldehyde derivatives to give the corresponding heterocycles **2**–**6**, respectively, and similar reactivity has been reported previously for analogous Schiff bases derived from 2-aminophenol and 2-(4,4,5,5,-tetramethyl-[1,3,2]-dioxaborolan-2-yl)benzaldehyde (34). Interestingly, the reaction of 2-$H_2NC_6H_4$Bpin with 3,5-di-*tert*-butyl-2-hydroxybenzaldehyde gave the corresponding aldimine **7** as the only new boron containing compound. It is possible that the increased steric bulk of the *tert*-butyl groups inhibits the formation of the dimer.

The molecular structure of **1** is shown in Fig. 2, crystallographic data are given in Table 1, and selected bond distances and angles are shown in Table 2. The two fragments form six-membered rings and are connected via a B-O-B bridge (B(1)-O(1)-B(2) = 111.50(12)°) with average B—O bond distances of 1.429(2) Å. The B-O-B angle, however, is somewhat smaller in **1** than that observed in a related heterocycle (B-O-B bond angle is 137(3)°) prepared through a condensation reaction between 2,4-pentanedione, 2-ethanolamine, and phenylboronic acid (Fig. 3) (36). In this latter example, the B-O-B fragment is part of a flexible seven-membered ring. Interestingly, the two phenolic B—O distances in **1** are slightly longer (1.475(2) and 1.473(2) Å) than the bridged B-O-B bonds (avg. 1.429(2) Å) (33, 37–45). Similar distances and angles have been reported for other O-B-O ring systems. For instance, a monomeric boronate compound derived from a salicylideneaminoaryl alcohol and 4-nitrophenylboronic acid has distances of 1.48(1) and 1.45(1) Å for the heterocyclic and terminal B—O bonds, respectively (33). The aldimine functionality in **1** is stabilized by N→B interactions with average B—N bonds of 1.619(2) Å, which is characteristic of strong coordination (33). Similar bond distances have been reported in related oxime, salen, and salicylaldehyde derivatives (46–59).

All new compounds were tested as potential antifungal agents against *Aspergillus niger* and *Aspergillus flavus* using Amphotericin B as a control. Although we recently reported that related N_2B heterocycles are potent antifungal agents (60), compounds **1**–**6** showed only negligible activity (Table 3). The starting aniline derivative 2-$H_2NC_6H_4$Bpin showed no activity. This result is also somewhat surprising, as the corresponding aldehydes, 2-formylphenyl boronic acid (2-$HC(O)C_6H_4B(OH)_2$), and its pincaolated derivative 2-$HC(O)C_6H_4$Bpin, displayed considerable fungitoxicity against both *A. niger* and *A. flavus* (61). Further work is therefore required to design more potent fungicidal compounds containing biologically active aminoboron groups.

Conclusion

Reactions of 2-$H_2NC_6H_4$Bpin with salicylaldehydes gave novel heterocyclic dimers containing six-membered rings with a B-O-B bridge. The aldimine functionality in these dimers is stabilized by intramolecular N→B interactions. These complexes showed only negligible antifungal activity against both *A. niger* and *A. flavus*.

Experimental

General

Reagents and solvents used were purchased from Aldrich Chemicals. 2-$H_2NC_6H_4$Bpin was synthesized by modification of an established procedure (62). NMR spectra were recorded on a JEOL JNM-GSX270 FT spectrometer or a Varian Mercury Plus 200 NMR spectrometer. ^{1}H NMR chemical shifts are reported in ppm and referenced to residual solvent protons in deuterated solvent at 270 and 200 MHz, respectively. ^{13}C NMR chemical shifts are referenced to solvent carbon resonances as internal standards at 68 and 50 MHz, respectively, and are reported in ppm. ^{11}B NMR chemical shifts are reported in ppm and are referenced to BF_3·OEt_2 as an external standard at 87 MHz. Multiplicities are reported as singlet (s), doublet (d), triplet (t), multiplet (m), broad (br), and overlapping (ov). IR spectra were obtained using a Mattson Genesis II FT-IR spectrometer. Melting points were determined using a Mel-Temp apparatus and are uncorrected. Microanalyses for C, H, and N were carried out at Guelph Chemical Laboratories (Guelph, Ontario).

Compound 1

A solution of 2-$H_2NC_6H_4$Bpin (0.25 g, 1.14 mmol) in EtOH (3 mL) was added to a solution of salicylaldehyde (0.14 g, 1.14 mmol) in EtOH (3 mL) and the reaction was heated to reflux for 2 h. The reaction was stored at 5 °C, and after 18 h a precipitate was collected by suction filtration and was washed with cold EtOH (3 × 3 mL) to afford **1** (0.18 g, 75%) as a yellow solid; mp 362 to 363 °C. IR (Nujol, cm^{-1}) ν: 2931, 2870, 1620 (C=N), 1552, 1466, 1379, 1313, 1279, 1240, 1182, 1057, 1038, 987, 968, 926, 837, 764, 687, 573. Spectroscopic NMR data (in $CDCl_3$): ^{1}H δ: 8.47 (s, 2H, C*H*=N), 7.51 (t, *J* = 8 Hz, 2H, Ar), 7.43–7.40 (ov m, 4H, Ar), 7.21–7.12 (ov m, 6H, Ar), 7.04 (d, *J* = 8 Hz, 2H, Ar), 6.89 (t, *J* = 8 Hz, 2H, Ar). ^{13}C{^{1}H} δ: 160.4 (*C*=N), 154.1, 143.8, 142 (br, *C*-B), 137.8, 132.8, 132.1, 128.7, 128.6, 119.6, 118.9, 115.9, 115.6. ^{11}B{^{1}H} δ: 3.7 (br). Anal. calcd. for $C_{26}H_{18}N_2B_2O_3$·CH_3CH_2OH (%): C 70.92, H 5.11, N 5.91; found: C 70.01, H 4.99, N 5.86.

© 2005 NRC Canada

Fig. 2. The molecular structure of **1** with ellipsoids drawn at 30% probability level. Hydrogen atoms are omitted for clarity.

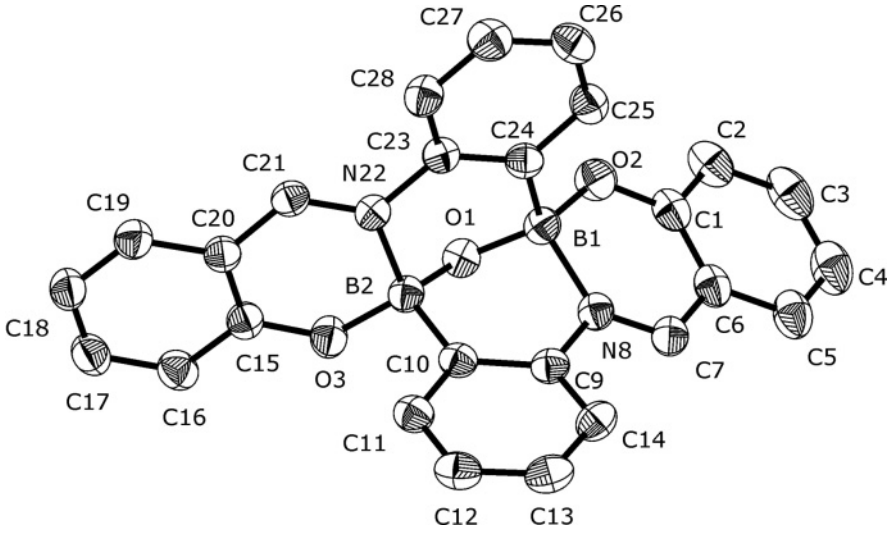


Table 1. Crystallographic data collection parameters for **1·2 EtOH**.

Complex	**1·2 EtOH**
Chemical formula	$C_{26}H_{18}B_2N_2O_3$·2EtOH
Formula mass	520.18
Crystal dimensions (mm^3)	0.075 × 0.30 × 0.40
Crystal system	Triclinic
Space group	*P*-1
Z	2
a (Å)	9.791 5(4)
b (Å)	10.856 9(5)
c (Å)	12.844 5(6)
α (°)	102.067(1)
β (°)	96.011(1)
γ (°)	90.458(1)
Volume ($Å^3$)	1327.3(1)
ρ_{calcd} (Mg m^{-3})	1.302
T (K)	198(1)
Radiation	Mo Kα (λ = 0.710 73 Å)
μ (mm^{-1})	0.087
Total reflections	9518
Total unique relections	5832
No. of variables	453
R_{int}	0.017 6
θ (°)	1.63–27.50
Goodness-of-fit on F^2	1.119
R_1[a] ($I > 2\sigma(I)$)	0.048 2
wR_2[b] (all data)	0.148 3
Largest diff. peak and hole (e $Å^{-3}$)	0.533 and –0.314

[a] $R_1 = \Sigma(|F_o| - |F_c|/\Sigma|F_o|$.
[b] $wR_2 = (\Sigma[w(F_o^2 - F_c^2)^2] / \Sigma w[F_o^4])^{1/2}$, where $w = 1/[\sigma^2(F_o^2) + (0.0735P)^2 + (0.3456P)]$, where $P = (\max(F_o^2, 0) + 2F_c^2)/3$.

Table 2. Selected bond lengths (Å) and angles (°) for **1**.

Bond lengths (Å)	
B(1)—O(1)	1.430(2)
B(1)—O(2)	1.4754(19)
B(1)—N(8)	1.617(2)
B(1)—C(24)	1.627(2)
B(2)—O(1)	1.427(2)
B(2)—O(3)	1.4732(19)
B(2)—C(10)	1.620(2)
B(2)—N(22)	1.621(2)
O(2)—C(1)	1.3315(19)
O(3)—C(15)	1.3304(18)
Bond angles (°)	
O(1)-B(1)-O(2)	111.50(12)
O(1)-B(1)-N(8)	105.92(12)
O(2)-B(1)-N(8)	108.68(12)
O(1)-B(1)-C(24)	111.43(13)
O(2)-B(1)-C(24)	110.03(12)
N(8)-B(1)-C(24)	109.15(11)
O(1)-B(2)-O(3)	109.89(12)
O(1)-B(2)-C(10)	113.01(12)
O(3)-B(2)-C(10)	111.67(13)
O(1)-B(2)-N(22)	107.03(12)
O(3)-B(2)-N(22)	109.01(12)
C(10)-B(2)-N(22)	105.99(11)
B(2)-O(1)-B(1)	111.06(11)
C(1)-O(2)-B(1)	124.99(13)
C(15)-O(3)-B(2)	124.86(12)

Compound 2

A solution of 2-$H_2NC_6H_4$Bpin (0.17 g, 0.75 mmol) in EtOH (3 mL) was added to an EtOH (3 mL) solution of 2-hydroxy-5-nitrobenzaldehyde (0.13 g, 0.75 mmol). The solution was heated at reflux for 2 h and the resultant precipitate was collected by suction filtration and was washed with EtOH (2 × 3 mL) and hexane (2 × 3 mL) to afford **2** (0.10 g, 51%) as a yellow solid; mp 360 °C. IR (Nujol, cm^{-1}) ν: 2953, 2924, 2856, 1618 (C=N), 1564, 1514, 1464, 1377, 1338, 1281, 1196, 1099, 1066, 968, 910, 839, 752. Spectroscopic NMR data (in DMSO-d_6): ^{1}H δ: 9.51 (s, 2H, C*H*=N), 8.79 (d, *J* = 3 Hz, 2H, Ar), 8.44 (d of d, *J* = 8, 3 Hz, 2H, Ar), 7.68 (d, *J* = 8 Hz, 2H, Ar), 7.34 (m, 2H, Ar), 7.25–7.14 (ov m, 6H, Ar). ^{13}C{^{1}H} δ: 164.5 (*C*=N), 155.8, 142.9, 140 (br, *C*-B), 139.8, 132.7, 132.1, 130.5, 129.7, 129.6, 119.9,

© 2005 NRC Canada

Fig. 3. The structure of a related 2,4-pentanedione phenylboronic acid derivative (36).

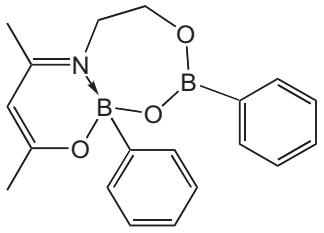


Table 3. Antifungal testing.

Compound	Dose (μg/disk)	Diameter of clear zone (mm) *Aspergillus niger*	Diameter of clear zone (mm) *Aspergillus flavus*
1	200	0	0
2	200	0	0
3	200	0	6
4	200	0	0
5	200	0	5
6	200	0	0
2-$H_2NC_6H_4$Bpin	200	0	0
Amphotericin B	200	14	11

117.7, 116.2. $^{11}B\{^1H\}$ (in THF) δ: 4.2 (br). Anal. calcd. for $C_{26}H_{16}N_4B_2O_7$ (%): C 60.27, H 3.12, N 10.82; found: C 59.86, H 3.15, N 10.23.

Compound 3

An EtOH (3 mL) solution of 2-hydroxy-1-naphthaldehyde (0.15 g, 0.87 mmol) and 2-(4,4,5,5-tetramethyl-[1,3,2]-dioxaborolan-2-yl)phenylamine (0.19 g, 0.87 mmol) in EtOH (3 mL) were mixed and heated to reflux for 2 h. After storing the solution at 5 °C for 18 h, a precipitate formed and was collected by suction filtration and was washed with EtOH (3 × 3 mL) and hexane (3 × 3 mL) to afford **3** (0.15 g, 65%) as a yellow solid; mp 370 °C. IR (Nujol, cm^{-1}) ν: 2950, 2922, 2856, 1622 (C=N), 1549, 1462, 1400, 1363, 1346, 1309, 1275, 1198, 1178, 1095, 1070, 1001, 928, 837, 748, 580. Spectroscopic NMR data (in $CDCl_3$): ^1H δ: 9.30 (s, 2H, C*H*=N), 8.15 (d, *J* = 8 Hz, 2H, Ar), 7.98 (d, *J* = 8 Hz, 2H, Ar), 7.80 (d, *J* = 8 Hz, 2H, Ar), 7.62 (t, *J* = 8 Hz, 2H, Ar), 7.46–7.39 (ov m, 6H, Ar), 7.28–7.23 (ov m, 4H, Ar), 7.14 (t, *J* = 8 Hz, 2H, Ar). $^{13}C\{^1H\}$ δ: 162.7 (*C*=N), 149.1, 144.2, 140 (br, *C*-B), 139.1, 132.8, 132.2, 129.7, 128.8, 128.7, 128.3, 127.9, 124.1, 121.5, 118.6, 115.6, 107.3. $^{11}B\{^1H\}$ δ: 3.7 (br). Anal. calcd. for $C_{34}H_{22}N_2B_2O_3 \cdot 0.5CH_3CH_2OH$ (%): C 76.26, H 4.58, N 5.08; found: C 75.75, H 3.89, N 5.10.

Compound 4

2-$H_2NC_6H_4$Bpin (0.33 g, 1.50 mmol) was dissolved in EtOH (3 mL) and added to a solution of 5-bromosalicyaldehyde (0.30 g, 1.50 mmol) in EtOH (3 mL). The reaction was heated at reflux for 2 h and the precipitate collected by suction filtration was washed with EtOH (3 × 3 mL) and hexanes (2 × 3 mL) to afford **4** (0.16 g, 36%) as a bright yellow solid; mp 376 to 377 °C. IR (Nujol, cm^{-1}) ν: 2933, 2856, 1619 (C=N), 1543, 1462, 1377, 1306, 1171, 1036, 926, 837, 733, 568. Spectroscopic NMR data (in $CDCl_3$): ^1H δ: 8.41 (s, 2H, C*H*=N), 7.58–7.54 (ov m, 4H, Ar), 7.36 (m, 2H, Ar), 7.22–7.15 (ov m, 6H, Ar), 6.95 (d, *J* = 8 Hz, 2H, Ar). $^{13}C\{^1H\}$ δ: 159.4 (*C*=N), 153.0, 143.6, 140.5, 139.4 (br, *C*-B), 133.8, 132.9, 129.4, 129.1, 121.7, 117.4, 115.9, 110.4. ^{11}B $\{^1H\}$ δ: 3.7 (br). Anal. calcd. for $C_{26}H_{16}N_2B_2Br_2O_3$ (%): C 53.30, H 2.76, N 4.78; found: C 52.99, H 2.49, N 4.85.

Compound 5

2-$H_2NC_6H_4$Bpin (0.48 g, 2.20 mmol) was dissolved in EtOH (3 mL) and added to a solution of 2-hydroxy-5-methylbenzaldehyde (0.30 g, 2.20 mmol) in EtOH (3 mL). The reaction was heated at reflux for 2 h and the precipitate collected by suction filtration was washed with EtOH (3 × 3 mL) and hexanes (2 × 3 mL) to afford **5** (0.19 g, 38%) as a bright yellow solid; mp 362 to 363 °C. IR (Nujol, cm^{-1}) ν: 2964, 2854, 1627 (C=N), 1554, 1462, 1377, 1278, 1165, 1163, 972, 832, 727. Spectroscopic NMR data (in $CDCl_3$): ^1H δ: 8.41 (s, 2H, C*H*=N), 7.40 (m, 2H, Ar), 7.30 (d, *J* = 8 Hz, 2H, Ar), 7.25–7.08 (ov m, 8H, Ar), 6.98 (d, *J*= 8 Hz, 2H, Ar), 2.32 (s, 6H, CH_3). $^{13}C\{^1H\}$ δ: 158.7 (*C*=N), 154.1, 144.0, 142.5 (br, *C*-B), 139.3, 132.9, 131.6, 128.7, 128.6, 128.1, 119.5, 115.7, 115.6, 20.5. $^{11}B\{^1H\}$ δ: 3.2 (br). Anal. calcd. for $C_{28}H_{22}N_2B_2O_3$ (%): C 73.72, H 4.87, N 6.14; found: C 73.41, H 4.43, N 5.75.

Compound 6

2-$H_2NC_6H_4$Bpin (0.43 g, 1.98 mmol) was dissolved in EtOH (3 mL) and added to a solution of *o*-vanillin (0.30 g, 1.98 mmol) in EtOH (3 mL). The reaction was heated at reflux for 3 h and the precipitate collected by suction filtration was washed with EtOH (3 × 3 mL) and hexanes (2 × 3 mL) to afford **6** (0.19 g, 39%) as a bright yellow solid; mp 338 to 339 °C. IR (Nujol, cm^{-1}) ν: 2913, 2856, 1619 (C=N), 1560, 1458, 1378, 1315, 1252, 1188, 1063, 991, 892, 808, 727. Spectroscopic NMR data (in $CDCl_3$): ^1H δ: 8.42 (s, 2H, C*H*=N), 7.41 (m, 2H, Ar), 7.16–7.00 (ov m, 10H, Ar), 6.81 (t, *J* = 8 Hz, 2H, Ar), 3.82 (s, 6H, OCH_3). $^{13}C\{^1H\}$ δ: 154.2 (*C*=N), 151.2, 150.0, 144.3, 143.5 (br, *C*-B), 133.1, 128.9, 128.6, 123.7, 119.2, 118.5, 116.2, 115.7, 56.7. $^{11}B\{^1H\}$ δ: 3.9 (br). Anal. calcd. for $C_{28}H_{22}N_2B_2O_5$ (%): C 68.89, H 4.55, N 5.74; found: C 68.47, H 4.24, N 5.40.

Compound 7

2-$H_2NC_6H_4$Bpin (0.14 g, 0.64 mmol) was dissolved in EtOH (3 mL) and added to a stirring solution of 3,5-di-*tert*-butyl-2-hydroxybenzaldehyde (0.15 g, 0.64 mmol) also in EtOH (3 mL). The reaction was heated at reflux for 3 h and the precipitate collected by suction filtration was washed with hexane (2 × 3 mL) to afford **7** (0.13 g, 46%) as a yellow solid; mp 152 to 153 °C. IR (Nujol, cm^{-1}) ν: 3206 (br, O-H), 2925, 2854, 1619 (C=N), 1592, 1564, 1460, 1377, 1352, 1317, 1274, 1169, 1144, 764, 721, 655. Spectroscopic NMR data (in $CDCl_3$): ^1H δ: 13.47 (br s, 1H, O*H*), 8.62 (s, 1H, C*H*=N), 7.86 (d, *J* = 8 Hz, 1H, Ar), 7.54–7.45 (ov m, 2H, Ar), 7.30–7.22 (ov m, 3H, Ar), 1.51 (s, 12H, $C_2O_2(CH_3)_4$), 1.37 (s, 9H, *tert*-butyl), 1.35 (s, 9H, *tert*-butyl). $^{13}C\{^1H\}$ δ: 163.1 (*C*=N), 158.2, 154.1, 140.2, 137.1, 136.5, 132.4, 127.9, 127.1, 126.5 (br, *C*-B), 126.0, 118.9, 117.4, 84.1, 35.3, 34.4, 31.8, 29.7, 25.0. $^{11}B\{^1H\}$ δ: 30.1 (br).

© 2005 NRC Canada

Antifungal testing

Compounds were tested for antifungal activity against pure cultures of *A. niger* and *A. flavus* supplied by Ward's Natural Science Ltd. (St. Catharines, Ontario). Cultures were maintained on Sabouraud dextrose agar. Six agar plugs (10 mm diameter) were cut from a 5–8 day old colony and homogenized in distilled, sterilized water (3 mL). From this suspension, 0.5 mL was transferred aseptically to a Petri plate with Sabouraud dextrose agar (15 mL) and spread evenly over the entire surface. Each plate was provided with four evenly spaced paper disks (6 mm Fisherbrand P8 filter paper) containing the compound (200 μg). Each compound was applied to the disks as a solution (5 mg compound per 0.5 mL chloroform), where control disks were treated with neat chloroform (20 μL). Amphotericin B acted as a standard. Test plates with fungal homogenates were incubated at 20 °C for 48 h. Four replicate plates were used for each test. Antifungal activity was taken by the diameter of the clear zone surrounding the disk.

X-ray crystallography

Crystals of **1·2 EtOH** were grown from an EtOH solution at 5 °C. Single crystals were mounted using a glass fibre and Paratone-N oil and frozen in the cold stream of the goniometer. Data were collected on a Bruker AXS P4/SMART 1000 diffractometer using ω and ϕ scans with a scan width of 0.3° and 40 s exposure times. The detector distance was 5 cm. The data were reduced (SAINT) (63) and corrected for absorption (SADABS) (64). The structure was solved by direct methods and refined by full-matrix least squares on F^2 (SHELXTL) (65). All non-hydrogen atoms were refined anisotropically. Hydrogen atoms were located in Fourier difference maps and refined isotropically, with the exception of the hydrogens of one of the solvent molecules, which were included in calculated positions and refined using a riding model.[2]

Acknowledgements

Thanks are gratefully extended to the Research Corporation (Cottrell College Science Award), the Natural Sciences and Engineering Research Council of Canada (NSERC), the Canada Research Chair – Atlantic Innovation Fund Programs, the University of New Brunswick, and Mount Allison University for financial support. We also thank Pfizer Inc. for a Summer Undergraduate Research Fellowship Award (HAD), Dan Shrubby Durant and Roger Smith for their expert technical assistance, and anonymous reviewers for helpful comments.

References

1. N. Miyaura and A. Suzuki. Chem. Rev. **95**, 2457 (1995).
2. B.M. Trost and M.D. Spagnol. J. Chem. Soc. Perkin Trans. 1, 2083 (1995).
3. D.M.T. Chan, K.L. Monaco, R.P. Wang, and M.P. Winters. Tetrahedron Lett. **39**, 2933 (1998).
4. B. Carboni, C. Pourbaix, F. Carreaux, H. Deleuze, and B. Maillard. Tetrahedron Lett. **40**, 7979 (1999).
5. N. Fárfan, H. Höpfl, V. Barba, M.-E. Ochoa, R. Santillan, E. Gómez, and A. Gutiérrez. J. Organomet. Chem. **581**, 70 (1999).
6. F. Minutolo and J.A. Katzenellenbogen. Organometallics, **18**, 2519 (1999).
7. D.S. Matteson. Tetrahedron, **45**, 1859 (1989).
8. N.A. Petasis and I.A. Zavialov. J. Am. Chem. Soc. **120**, 11 798 (1998).
9. R.A. Batey, D.B. MacKay, and V. Santhakumar. J. Am. Chem. Soc. **121**, 5075 (1999).
10. M. Yamamoto, M. Takeuchi, and S. Shinkai. Tetrahedron, **54**, 3125 (1998).
11. H. Eggert, J. Frederiksen, C. Morin, and J.Chr. Norrild. J. Org. Chem. **64**, 3846 (1999).
12. C. Morin. Tetrahedron, **50**, 12 521 (1994).
13. G.S. Weston, J. Blázquez, F. Baquero, and B.K. Shoichet. J. Med. Chem. **41**, 4577 (1998).
14. V.S. Stoll, B.T. Eger, R.C. Hynes, V. Martichonok, J.B. Jones, and E.F. Pai. Biochemistry, **37**, 451 (1998).
15. J. Adams, M. Behnke, S. Chen, A.A. Cruickshank, L.R. Dick, L. Grenier, J.M. Klunder, Y.-T. Ma, L. Plamondon, and R.L. Stein. Bioorg. Med. Chem. Lett. **8**, 333 (1998).
16. C. Gao, B.J. Lavey, C.L. Lo, A. Datta, P. Wentworth, Jr., and K.D. Janda. J. Am. Chem. Soc. **120**, 2211 (1998).
17. W. Han, J.C. Pelletier, L.J. Mersinger, C.A. Kettner, and C.N. Hodge. Org. Lett. **1**, 1875 (1999).
18. J.D. Cox, N.N. Kim, A.M. Traish, and D.W. Christianson. Nat. Struct. Biol. **6**, 1043 (1999).
19. V.M. Dembitsky and M. Srebnik. Tetrahedron, **59**, 579 (2003), and refs. cited therein.
20. T. Pandey and R.V. Singh. Synth. React. Inorg. Met.-Org. Chem. **30**, 855 (2000), and refs. cited therein.
21. T. Pandey and R.V. Singh. Met.-Based Drugs, **7**, 7 (2000).
22. W. Wang, X. Gao, and B. Wang. Curr. Org. Chem. **6**, 1285 (2002).
23. T.D. James, P. Linnane, and S. Shinkai. Chem. Commun. 281 (1996).
24. W. Yang, X. Gao, and B. Wang. Med. Res. Rev. **23**, 346 (2003).
25. E. Cama, D.M. Colleluori, F.A. Emig, H. Shin, S.W. Kim, N.N. Kim, A.M. Traish, D.E. Ash, and D.W. Christianson. Biochemistry, **42**, 8445 (2003).
26. G.W. Kabalka and M.-L. Yao. Tetrahedron Lett. **44**, 1879 (2003).
27. H.E. Sailes, J.P. Watts, and A. Whiting. Tetrahedron Lett. **41**, 2457 (2000).
28. F. Firooznia, C. Gude, K. Chan, N. Marcopulos, and Y. Satoh. Tetrahedron Lett. **40**, 213 (1999).
29. H. Höpfl, M. Sánchez, N. Farfán, and V. Barba. Can. J. Chem. **76**, 1352 (1998).
30. M.P. Hughes and B.D. Smith. J. Org. Chem. **62**, 4492 (1997).
31. M.P. Groziak, A.D. Ganguly, and P.D. Robinson. J. Am. Chem. Soc. **116**, 7597 (1994).
32. I.B. Sivaev, A.B. Bruskin, V.V. Nesterov, M. Yu. Antipin, V.I. Bregadze, and S. Sjöberg. Inorg. Chem. **38**, 5887 (1999).

[2] Supplementary data for this article are available on the Web site or may be purchased from the Depository of Unpublished Data, Document Delivery, CISTI, National Research Council Canada, Ottawa, ON K1A 0S2, Canada. DUD 4010. For more information on obtaining material refer to http://cisti-icist.nrc-cnrc.gc.ca/irm/unpub_e.shtml. CCDC 223549 contains the crystallographic data for this manuscript. These data can be obtained, free of charge, via www.ccdc.cam.ac.uk/conts/retrieving.html (or from the Cambridge Crystallographic Data Centre, 12 Union Road, Cambridge CB2 1EZ, UK; fax: +44 1223 336033; or deposit@ccdc.cam.ac.uk).

© 2005 NRC Canada

33. M. Sánchez, H. Höpfl, M-E. Ochoa, N. Farfán, R. Santillan, and S. Rojas-Lima. Chem. Eur. J. **8**, 612 (2002).
34. D.W. Norman, J.P. Edwards, C.M. Vogels, A. Decken, and S.A. Westcott. Can. J. Chem. **80**, 31 (2002).
35. H. Nöth and B. Wrackmeyer. Nuclear magnetic resonance spectroscopy of boron compounds. Springer-Verlag, Berlin. 1978.
36. M. Sánchez, O. Sánchez, H. Höpfl, M.-E. Ochoa, D. Castillo, N. Farfán, and S. Rojas-Lima. J. Organomet. Chem. **689**, 811 (2004).
37. Q.G. Wu, G. Wu, L. Brancaleon, and S. Wang. Organometallics, **18**, 2553 (1999).
38. Q.G. Wu, M. Esteghamatian, N.-X. Hu, Z. Popovic, G. Enright, S.R. Breeze, and S. Wang. Angew. Chem. Int. Ed. **38**, 985 (1999).
39. S.-F. Liu, C. Seward, H. Aziz, N.-X. Hu, Z. Popović, and S. Wang. Organometallics, **19**, 5709 (2000).
40. Q.G. Wu, M. Esteghamatian, N.-X. Hu, Z. Popovic, G. Enright, Y. Tao, M. D'lorio, and S. Wang. Chem. Mater. **12**, 79 (2000).
41. A. Lang, H. Nöth, and M. Schmidt. Chem. Ber. **128**, 751 (1995).
42. U. Bossek, H. Hummel, T. Weyhermüller, K. Wieghardt, S. Russell, L. van der Wolf, and U. Kolb. Angew. Chem. Int. Ed. Engl. **35**, 1552 (1996).
43. V.C. Gibson, C. Redshaw, W. Clegg, and M.R.J. Elsegood. Polyhedron, **16**, 2637 (1997).
44. R. Anulewicz-Ostrowska, S. Luliński, J. Serwatowski, and K. Suwińska. Inorg. Chem. **39**, 5763 (2000).
45. V. Barba, D. Cuacutle, R. Santillan, and N. Farfán. Can. J. Chem. **79**, 1229 (2001).
46. W. Kliegel, S.J. Rettig, and J. Trotter. Can. J. Chem. **62**, 1363 (1984).
47. P. Wei and D.A. Atwood. Inorg. Chem. **37**, 4934 (1998).
48. P. Wei, T. Keizer, and D.A. Atwood. Inorg. Chem. **38**, 3914 (1999).
49. B.N. Ghose. Synth. React. Inorg. Met.-Org. Chem. **16**, 1383 (1986).
50. H. Höpfl. J. Organomet. Chem. **581**, 129 (1999).
51. T.S. Keizer, L.J. De Pue, S. Parkin, and D.A. Atwood. Can. J. Chem. **80**, 1463 (2002).
52. N. Yalcin, A. Kenar, C. Arici, O. Atakol, and M. Tastekin. Main Group Met. Chem. **24**, 247 (2001).
53. V. Barba, G. Vargas, E. Gömez, and N. Farfán. Inorg. Chim. Acta, **311**, 133 (2000).
54. M. Sánchez, H. Höpfl, M.-E. Ochoa, N. Farfán, R. Santillan, and S. Rojas. Inorg. Chem. **40**, 6405 (2001).
55. H. Höpfl and N. Farfán. Can. J. Chem. **76**, 1853 (1998).
56. M. Sánchez, T.S. Keizer, S. Parkin, H. Höpfl, and D.A. Atwood. J. Organomet. Chem. **654**, 36 (2002).
57. V. Barba, H. Höpfl, N. Farfán, R. Santillan, H.I. Beltran, and L.S. Zamudio-Rivera. Chem. Commun. 2834 (2004).
58. G. Vargas, I. Hernández, H. Höpfl, M.-E. Ochoa, D. Castillo, N. Farfán, R. Santillan, and E. Gómez. Inorg. Chem. **43**, 8490 (2004).
59. V. Barba, A. Rodríguez, M.-E. Ochoa, R. Santillan, and N. Farfán. Inorg. Chim. Acta, **357**, 2593 (2004).
60. A.M. Irving, C.M. Vogels, L.G. Nikolcheva, J.P. Edwards, X.-F. He, M.G. Hamilton, M.O. Baerlocher, F.J. Baerlocher, A. Decken, and S.A. Westcott. New. J. Chem. **27**, 1419 (2003).
61. C.M. Vogels, L.G. Nikolcheva, D.W. Norman, H.A. Spinney, A. Decken, M.O. Baerlocher, F.J. Baerlocher, and S.A. Westcott. Can. J. Chem. **79**, 1115 (2001).
62. O. Baudoin, D. Guénard, and F. Guéritte. J. Org. Chem. **65**, 9268 (2000).
63. Bruker AXS, Inc. SAINT Version 6.02 [computer program]. Bruker AXS, Inc., Madison, Wis. 1997–1999.
64. G.M. Sheldrick. SADABS [computer program]. Bruker AXS, Inc., Madison, Wis. 1999.
65. G.M. Sheldrick. SHELXTL Version 5.1 [computer program]. Bruker AXS, Inc., Madison, Wis. 1997.

© 2005 NRC Canada

One-pot conversion of β-aminocrotononitrile to secondary enaminonitriles including chiral ones — Application to synthesis

A. Chatterjee, M. Mishra, S.K. Dutta Chowdhury, and Kumar K. Mahalanabis

Abstract: A highly efficient one-pot conversion of β-aminocrotononitrile to secondary enaminonitriles including chiral ones is described. In contrast to β-aminocrotononitrile, some of these *N*-substituted β-enaminonitriles on reacting with acid chlorides show a unique preference for C-terminal selection allowing preparation of pyrazoles without separation of regioisomers. In addition, use of secondary enaminonitriles also provided access to pyrazoles that are not obtainable with primary enaminonitriles owing to an exclusive preference for *N*-terminal selection.

Key words: β-aminocrotononitrile, *N*-substituted enaminonitriles, regioselective, pyrazoles.

Résumé : On décrit une méthode unipot très efficace de conversion du β-aminocrotononitrile en énaminonitriles secondaires, y compris ceux de nature chirale. Contrairement à ce qui est observé avec le β-aminocrotononitrile, certains de ces β-énaminonitriles *N*-substitués réagissent avec les chlorures d'acides avec une préférence unique pour la position C-terminale, ce qui permet de préparer des pyrazoles sans avoir à séparer les régioisomères. De plus, l'utilisation d'énaminonitriles secondaires permet aussi d'accéder à des pyrazoles qui ne peuvent pas être obtenus à partir de l'énaminonitrile primaire en raison de la préférence exclusive pour la sélection *N*-terminale.

Mots clés : β-aminocrotononitrile, énaminonitriles *N*-substitués, régiosélective, pyrazoles.

[Traduit par la Rédaction]

Introduction

The chemistry of β-aminocrotononitrile is well-documented (1) and continues to remain an active area for further study. For some time now we have been engaged in systematic studies on the acylation reactions of β-aminocrotononitrile (**1**) with acid chlorides in the presence of an added organic base to evaluate preferences for regioselection (2–5) and to explore the utility of the derived products for synthesis of novel heterocyclic compounds (6–9). β-Acylenaminonitriles behave as masked 1,3-diketones and are considered to be useful intermediates (10) particularly in heterocyclic chemistry (11). Results reported from this laboratory on acylation reactions of primary enaminonitriles with acid chlorides although indicating a high degree of preference for terminal selection depending on the choice of acid chlorides used, nevertheless indicate that there is room to develop new routes to ensure exclusive acylation at the C-terminal particularly in those cases where either *N*-acylation occurred or a mixture of *C*- and *N*-acylated products were obtained. To realize this objective we decided to explore secondary enaminonitriles instead of **1** in our acylation study and to observe if there was any change in preference for terminal selection with regard to **1**. This contemplated study required preparation of a large number of secondary enaminonitriles in reasonably good yields under mild conditions. Several methods of preparation of *N*-substituted enaminonitriles are reported in the literature (12–17), but most of these employed indirect methods and thus are not suitable for a preparatory scale. Dedina et al. (16) reported three different procedures for the preparation of *N*-substituted-3-aminocrotononitrile: procedure A uses a solution of enaminonitrile and an amine in ethanol in an autoclave at 130–136 °C for 5–8 h. In procedure B, a solution of HCl (6 mol/L) in ethanol was added to a dioxane solution of enaminonitrile and amine and the mixture was heated for 5 to 6 h in a pressure tube at 120–140 °C. Procedure C involves heating a mixture of enaminonitrile and amine without any solvent. In our study we observed that the use of HCl or the absence of ethyl alcohol resulted in extensive polymerization of the enaminonitrile itself and the yield of the secondary enaminonitrile was poor. For example, we obtained *N*-phenyl-β-aminocrotononitrile (**2g**) in an 87% yield when the reaction was carried out in the presence of an alcohol, whereas in the case of procedure C as described by Dedina et al. (16) the yield of **2g** was reported to be only 37%.

Lack of a general approach, consistency in yields, and inadequacies of *N*-substituent variants leave significant room for improvement in the methodology for preparation of secondary enaminonitriles notwithstanding the extensive work done by Dedina et al. (16). Herein, we report a very simple,

Received 13 December 2004. Published on the NRC Research Press Web site at http://canjchem.nrc.ca on 24 September 2005.

A. Chatterjee, M. Mishra, and K.K. Mahalanabis.[1] Department of Chemistry, Jadavpur University, Kolkata 700 032, India.
S.K. Dutta Chowdhury. Department of Chemistry, Jadavpur University, Kolkata 700 032, India, and Jogesh Chandra Chowdhury College, Kolkata 700 033, India.

[1]Corresponding author (e-mail: kkmahalanabis@yahoo.co.in).

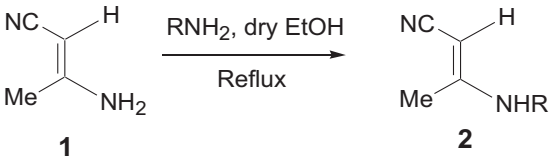
 doi: 10.1139/V05-143 © 2005 NRC Canada

Table 1. Data for prepared compounds **2a**–**2p**.

Compound	R	Yield (%)[a]	mp (°C) or bp (°C)	$[\alpha]^{25}_{D}$ (°) (*c* 0.5 in $CHCl_3$)
2a	Me	65	54 to 55 (lit. value (16) mp 54 to 55)	—
2b	CH_2Me	70	45 (lit. value (16) mp 45 to 46)	—
2c	CH_2CH_2OH	76	70 to 71	—
2d	C_6H_{11}	97	88 to 89 (lit. value (16) mp 88 to 89)	—
2e	CH_2CO_2Et	72	44 to 45	—
2f	CH_2Ph	84	81 to 82 (lit. value (16) mp 78 to 79)	—
2g	Ph	87	116 (lit. value (16) mp 116 to 117)	—
2h	*p*-MeO·C_6H_4	80	126 to 127	—
2i	*o*-Me·C_6H_4	70	65 to 66	—
2j	*p*-Me·C_6H_4	81	90 to 91	—
2k	CH(Me)Ph	95	65 to 66	+100
2l	$CH(Me)CO_2Me$	74	150–153 (0.05 mm)	–52
2m	$CH(CHMe_2)CO_2Me$	82	160–167 (0.05 mm)	–96.83
2n	$CH(CH_2CHMe_2)CO_2Me$	71	170–175 (0.05 mm)	–95.6
2o	$CH(CH_2Ph)CO_2Me$	77	220–225 (0.01 mm)	+107.42
2p	$CHCH_2$(*p*-HO·C_6H_4) CO_2Me	70	195–200 (0.01 mm)	+119.11

[a]Yields of isolated products.

Scheme 1.



1 2

direct, and highly efficient general method for the one-pot preparation of secondary enaminonitriles **2a**–**2j** including the optically active ones **2k**–**2p** by reacting **1** with amines in refluxing dry ethyl alcohol (Scheme 1, Table 1). For the preparation of *N*-methyl-β-aminocrotononitrile (**2a**) and *N*-ethyl-β-aminocrotononitrile (**2b**), methyl ammonium chloride and ethyl ammonium chloride, respectively, were used in the presence of triethyl amine.

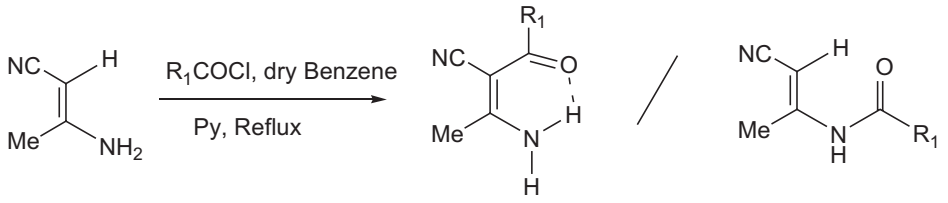
In the case of the optically active enaminonitriles **2k**–**2p**, the amino acids were first converted to their corresponding methyl ester hydrochlorides by treatment with thionyl chloride in refluxing dry methyl alcohol (18, 19). These ester hydrochlorides were then reacted with **1** in the presence of triethyl amine in refluxing ethyl alcohol. The amino acids used were (*S*)-(+)-alanine, (*S*)-(+)-leucine, (*S*)-(+)-valine, (*R*)-(+)-α-methylbenzyl amine, (*S*)-(–)-phenylalanine, and (*S*)-(–)-tyrosine. The homogeneity of the liquid products was checked by HPLC using a C-18 Bonda-pak column and a methanol–water (1:1) mixture as the mobile phase. The structures of these enaminonitriles are supported by consistent elemental and spectral analyses. Careful analysis of the ^{1}H NMR spectra of the isolated products is suggestive of the E conformation for the enaminonitriles (16). When compared with documented literature methods, the present procedure scores favorably in terms of simplicity, yields, choice of *N*-substituent variants, and purity of the products.

In our earlier investigations (5) on acylation of **1** we demonstrated that by choosing a suitable acid chloride it is possible to control the site of acylation to a large degree. β-Acylcyanoenaminonitriles thus obtained were easily converted to novel 5-substituted 1,2-azoles (8, 9). Although a high degree of success was achieved in terminal selection, there were examples where either a mixture of regioisomers or only *N*-acylated products were obtained. Since β-enaminones have proven to be valuable intermediates in the synthesis of a wide variety of heterocyclic compounds (20), we have initiated this study on the acylation reaction of secondary enaminonitriles to observe if there was any change in their preference for terminal selection when compared to primary enaminonitriles. Results obtained thus far indicate that *N*-substituted β-aminocrotononitriles show a strong preference for C-terminal selection when compared with the results obtained earlier for **1** (Scheme 2). Thus, *N*-benzyl-β-aminocrotononitrile (**2f**) on reaction with acid chlorides of benzoic acid, *o*-nitrobenzoic acid, *m*-nitrobenzoic acid, and thiophene-2-carboxylic acid afforded only *C*-acylated products in contrast to our earlier results with **1** whereby a mixture of regioisomers **3** and **4** (1:1) was obtained. The presence of compounds **3** and **4** in the reaction mixture was confirmed by ^{1}H NMR spectral analysis, and the pure regioisomers were obtained by column chromatography. A dramatic reversal of preference for site selection occurred when acylation of **2f** was carried out with isobutyryl chloride resulting in exclusive C-terminal selection. In an earlier experiment, treatment of **1** with isobutyryl chloride afforded only the *N*-acylated product, thereby precluding its use for the preparation of pyrazole (Scheme 2, Table 2). Such a strong preference by **2f** for C-terminal selection allowed us to synthesize pyrazoles that previously needed either separation of regioisomers or where the total lack of preference for C-terminal selection excluded their formation (Scheme 3, Table 3). Presently, we are working on the synthetic application of other secondary enaminonitriles including chiral ones.

Thus, easy access to secondary enaminonitriles provides a direct route for the synthesis of heterocycles that otherwise are not directly obtainable from acylation reactions of primary enaminonitriles. In addition, the availability of optically active secondary enaminonitriles is likely to provide

© 2005 NRC Canada

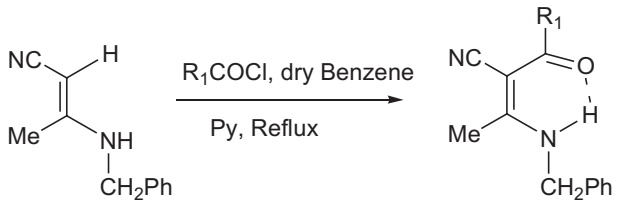
Scheme 2.



1 **3** **4**

R_1 = Ph, *o*-NO_2-C_6H_4, *m*-NO_2-C_6H_4, 2-thienyl, the product is a mixture (1:1) of **3** and **4**

R_1 = isobutyryl, the product is only **4**



2f **3a-3e**

R_1 = Ph, *o*-NO_2-C_6H_4, *m*-NO_2-C_6H_4, 2-thienyl, isobutyryl

Table 2. Data for the acylation reaction of *N*-benzyl-β-aminocrotononitrile (**2f**) and prepared compounds **3a**–**3e**.

Compound	R	R_1	mp (°C)	Yield (%)[a]
3a	CH_2Ph	Ph	84 to 85	71
3b	CH_2Ph	*o*-NO_2-C_6H_4	137 to 138	67
3c	CH_2Ph	*m*-NO_2-C_6H_4	123 to 124	70
3d	CH_2Ph	2-Thienyl	80 to 81	76
3e	CH_2Ph	Isobutyryl	88 to 89	80

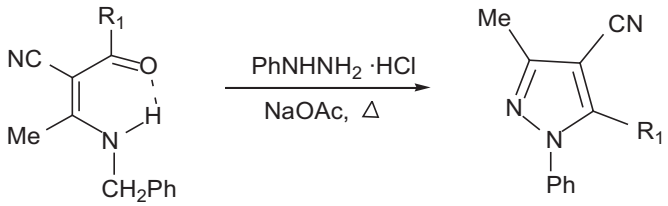
[a]Yields of isolated products.

opportunities for their utilization as chiral auxiliaries towards the synthesis of chiral heterocycles.

Experimental

Melting points were determined in open capillaries. NMR spectra were recorded using a Brucker AC-300 and (or) Brucker Avance 400 MHz spectrometer. Elemental analyses were performed using a PerkinElmer 240C elemental analyzer, mass spectra were obtained with an Hitachi RMU 6L and JMS-Ax505H mass spectrometer, and GC–MS spectra were obtained using an Agilnet 6890N. Optical rotations were measured on a Jasco Dip 360 digital polarimeter. HPLC was carried out using a Water Corporation UV detector and version 2.1 Mellenium software. UV and IR spectra were obtained using Hitachi U-2000 and Hitachi 270–30 spectrometers, respectively.

Scheme 3.



3a-3e **5a-5e**

Table 3. Data for prepared compounds **5a**–**5e**.

Compound	R_1	mp (°C)	Yield (%)[a]
5a	Ph	191 to 192	78
5b	*o*-NO_2-C_6H_4	155 to 156	67
5c	*m*-NO_2-C_6H_4	162 to 163	90
5d	2-Thienyl	204–206	67
5e	Isobutyryl	73 to 74	70

[a]Yields of isolated products.

β-Aminocrotononitrile and acid chlorides were prepared according to literature procedures in refs. 21 and 22, respectively.

General procedure

Preparation of N-substituted β-aminocrotononitriles

(*a*) A mixture of **1** (10 mmol), primary amine (10 mmol), and dry ethyl alcohol (40 mL) was refluxed for 2–5 h under dry conditions. Excess alcohol was distilled off

© 2005 NRC Canada

under reduced pressure, water was poured into the flask, and the contents were extracted with a suitable organic solvent. The organic layer was first washed with 2 N HCl, then with brine until neutral, it was then dried over anhydr. Na_2SO_4 and evaporated to dryness. Recrystallization of the crude product from a suitable solvent furnished the pure compound.

(*b*) A mixture of chiral amine (5 mmol), thionyl chloride (10 mmol), and dry methanol (15 mL) was refluxed for 2.5 h. Excess methanol and thionyl chloride were removed under reduced pressure and the residue was dried under vacuum. A solution of **1** (5 mmol) in dry ethyl alcohol (20 mL) was added to the residue with stirring at 0 °C followed by addition of triethylamine (5 mmol) in dry ethyl alcohol (5 mL). The reaction mixture was refluxed for 3 h. Following the usual work-up, purification of the crude product by column chromatography on silica gel (100–200 mesh) with 30% ethyl acetate – hexane as eluent afforded the product as a thick liquid.

Acylation reaction of *N*-benzyl-β-aminocrotononitrile with acid chlorides

The acid chloride (5 mmol) in dry benzene (10 mL) was added dropwise under ice cold conditions to a magnetically stirred solution of **2f** (5 mmol) in dry benzene (50 mL) and pyridine (15 mmol). Upon completion of the addition, stirring was continued for an additional 1 h at room temperature, and then refluxed for 3–5 h. The reaction mixture was then poured on ice water, acidified with HCl (2 N) followed by extraction with ethyl acetate (3 × 25 mL). The organic layer was then washed with a 5% $NaHCO_3$ solution followed by brine and then dried over anhydr. Na_2SO_4. Removal of the solvent afforded solid materials, which on crystallization furnished pure acylated products.

Preparation of pyrazoles

A mixture of α-cyanoenaminone (3 mmol) and phenyl hydrazine reagent (23) (9 mmol) was heated on a steam bath for 20–45 min, during which a yellow oily material separated. The reaction mixture was acidified with acetic acid (50%) followed by neutralization with solid $NaHCO_3$. It was then extracted with diethyl ether or ethyl acetate (3 × 20 mL). The organic layer was washed with brine and dried over anhydr. Na_2SO_4. The crude material obtained on removal of the solvent was purified by crystallization from a suitable solvent or by column chromatography (silica gel, 60–120 mesh, 5% ethyl acetate – petroleum ether).

Spectral data of prepared compounds 2a–2p

2a

UV (λ_{max}, EtOH, nm): 260 ($\epsilon = 1.97 \times 10^4$). IR (KBr, cm^{-1}): 3336, 2925, 2188, 1603, 1545. ^{1}H NMR ($CDCl_3$, ppm) δ: 2.12 (3H, s, =C-C*H*$_3$), 2.72 (3H, d, *J* = 5.9 Hz, NHC*H*$_3$), 3.75 (1H, s, =C*H*CN), 5.21 (1H, bs, -N*H*). MS *m*/*z*: 96 (M^+). Anal. calcd. for $C_5H_8N_2$ (%): C 62.47, H 8.39, N 29.14; found: C 62.50, H 8.36, N 29.19.

2b

UV (λ_{max}, EtOH, nm): 259 ($\epsilon = 2.08 \times 10^4$). IR (KBr, cm^{-1}): 3329, 2188, 1601, 1544, 1458. ^{1}H NMR ($CDCl_3$, ppm) δ: 1.16 (3H, t, *J* = 7.18 Hz, -CH_2CH_3), 2.04 (3H, s, C*H*$_3$), 2.93 (2H, m, C*H*$_2$CH$_3$), 3.69 (1H, s, =C*H*CN), 4.55 (1H, bs, -N*H*). ^{13}C NMR ($CDCl_3$, ppm) δ: 13.17, 19.79, 38.37, 58.69, 122.53, 160.39. MS *m*/*z*: 110 (M^+). Anal. calcd. for $C_6H_{10}N_2$ (%): C 65.42, H 9.15, N 25.43; found: C 65.46, H 9.12, N 25.47.

2c

UV (λ_{max}, EtOH, nm): 259 ($\epsilon = 1.93 \times 10^4$). IR (KBr, cm^{-1}): 3389, 2927, 2196, 1600, 1451. ^{1}H NMR ($CDCl_3$, ppm) δ: 2.01 (3H, s, -C*H*$_3$), 2.94 (2H, q, *J* = 5.6 Hz, -NHC*H*$_2$-), 3.49 (2H, q, *J* = 5.6 Hz, -C*H*$_2$OH), 3.78 (1H, s, =C*H*CN), 4.73 (1H, t, *J* = 5.6 Hz, -CH_2O*H*), 6.88 (1H, bs, -N*H*). ^{13}C NMR ($CDCl_3$, ppm) δ: 19.67, 45.90, 57.56, 58.77, 122.93, 161.18. MS *m*/*z*: 126 (M^+). Anal. calcd. for $C_6H_{10}N_2O$ (%): C 57.12, H 7.99, N 22.21; found: C 57.15, H 7.94, N 22.25.

2d

UV (λ_{max}, EtOH, nm): 263 ($\epsilon = 1.95 \times 10^4$). IR (KBr, cm^{-1}): 3307, 3073, 2931, 2855, 2185, 1595, 1548, 1446. ^{1}H NMR ($CDCl_3$, ppm) δ: 1.13–1.94 (10H, com, H atoms of cyclohexane ring), 2.08 (3H, s, =CC*H*$_3$), 3.05 (1H, tq, *J* = 4, 9 Hz, proton of cyclohexane ring α to NH), 3.79 (1H, s, =C*H*CN), 4.33 (1H, bs, -N*H*). ^{13}C NMR ($CDCl_3$, ppm) δ: 20.59, 24.54, 25.19, 32.05, 34.28, 51.72, 52.09, 59.65, 122.34, 158.67. MS *m*/*z*: 164 (M^+). Anal. calcd. for $C_{10}H_{16}N_2$ (%): C 73.12, H 9.82, N 17.06; found: C 73.17, H 9.78, N 17.10.

2e

UV (λ_{max}, EtOH, nm): 255 ($\epsilon = 2.00 \times 10^4$). IR (KBr, cm^{-1}): 3399, 3377, 3056, 2995, 2912, 2189, 1731, 1600, 1526, 1474, 1408. ^{1}H NMR ($CDCl_3$, ppm) δ: 1.09 (3H, t, *J* = 7.1 Hz, -CH_2CH_3), 1.96 (3H, s, =CC*H*$_3$), 3.53 (1H, s, =C*H*CN), 3.57 (2H, d, *J* = 5.1 Hz, -NHC*H*$_2$-), 4.05 (2H, q, -C*H*$_2$CH$_3$), 5.42 (1H, bs, -N*H*). ^{13}C NMR ($CDCl_3$, ppm) δ: 13.53, 19.14, 44.24, 60.73, 61.20, 120.92, 159.64, 168.59. MS *m*/*z*: 168 (M^+). Anal. calcd. for $C_8H_{12}N_2O_2$ (%): C 57.12, H 7.19, N 16.65; found: C 57.15, H 7.25, N 16.63.

2f

UV (λ_{max}, EtOH, nm): 272 ($\epsilon = 2.30 \times 10^4$). IR (KBr, cm^{-1}): 3304, 3088, 2192, 1594, 1560, 1492, 1446. ^{1}H NMR ($CDCl_3$, ppm) δ: 2.13 (3H, s, -C*H*$_3$), 3.86 (1H, s, =C*H*CN), 4.13 (2H, d, *J* = 5.02 Hz, -C*H*$_2$Ph), 4.64 (1H, bs, -N*H*), 7.25–7.38 (5H, m, Ar-*H*). ^{13}C NMR ($CDCl_3$, ppm) δ: 20.12, 47.46, 60.83, 121.71, 127.56, 127.90, 129.32, 136.40, 159.87. MS *m*/*z*: 172 (M^+). Anal. calcd. for $C_{11}H_{12}N_2$ (%): C 76.71, H 7.02, N 16.27; found: C 76.75, H 6.97, N 16.30.

2g

UV (λ_{max}, EtOH, nm): 288 ($\epsilon = 1.61 \times 10^4$). IR (KBr, cm^{-1}): 3266, 3125, 3058, 2199, 1612, 1586, 1542. ^{1}H NMR ($CDCl_3$, ppm) δ: 2.24 (3H, s, =CC*H*$_3$), 4.40 (1H, s, =C*H*CN), 6.13 (1H, bs, -N*H*), 7.12–7.38 (5H, m, Ar-H). ^{13}C NMR ($CDCl_3$, ppm) δ: 20.50, 64.88, 121.26, 123.85, 125.67, 129.51, 138.46, 158.29. MS *m*/*z*: 158 (M^+). Anal. calcd. for $C_{10}H_{10}N_2$ (%): C 75.92, H 6.37, N 17.71; found: C 75.96, H 6.42, N 17.67.

2h

UV (λ_{max}, EtOH, nm): 284 ($\epsilon = 1.61 \times 10^4$). IR (KBr, cm^{-1}): 3304, 3278, 2191, 1605, 1514. ^{1}H NMR ($CDCl_3$, ppm) δ: 2.22 (3H, s, =CC*H*$_3$), 3.80 (3H, s, -OC*H*$_3$), 4.12 (1H, s,

© 2005 NRC Canada

=C*H*CN), 5.94 (1H, bs, -N*H*), 6.88 and 7.06 (each 2H, d, *J* = 8.2 Hz, Ar-*H*). ^{13}C NMR ($CDCl_3$, ppm) δ: 20.21, 55.44, 63.73, 82.14, 114.32, 121.58, 126.52, 131.0, 157.81, 159.54. MS *m*/*z*: 188 (M^+). Anal. calcd. for $C_{11}H_{12}N_2O$ (%): C 70.19, H 6.43, N 14.88; found: C 70.24, H 6.39, N 14.91.

2i

UV (λ_{max}, EtOH, nm): 293 ($\epsilon = 1.93 \times 10^4$). IR (KBr, cm^{-1}): 3276, 2190, 1580, 1521, 1438. ^{1}H NMR ($CDCl_3$, ppm) δ: 2.20 (3H, s, =CC*H*$_3$), 2.24 (3H, s, -*o*-C*H*$_3$ C_6H_4), 3.81 (1H, s, =C*H*CN), 5.82 (1H, bs, -N*H*), 7.10–7.23 (4H, m, Ar-*H*). ^{13}C NMR ($CDCl_3$, ppm) δ: 17.18, 19.75, 63.89, 119.00, 126.41, 126.55, 126.67, 126.80, 126.97, 130.99, 159.90. MS *m*/*z*: 172 (M^+). Anal. calcd. for $C_{11}H_{12}N_2$ (%): C 76.75, H 7.02, N 16.27; found: C 76.79, H 6.93, N 16.21.

2j

UV (λ_{max}, EtOH, nm): 294 ($\epsilon = 1.94 \times 10^4$). IR (KBr, cm^{-1}): 3312, 2184, 1598, 1548, 1310. ^{1}H NMR ($CDCl_3$, ppm) δ: 2.21 (3H, s, =CC*H*$_3$), 2.32 (3H, s, *p*-C*H*$_3$ C_6H_4), 4.28 (1H, s, =C*H*CN), 5.96 (1H, bs, -N*H*), 6.99 and 7.14 (each 2H, d, *J* = 8.2 Hz, Ar-*H*). MS *m*/*z*: 172 (M^+, 100). Anal. calcd. for $C_{11}H_{12}N_2$ (%): C 76.75, H 7.02, N 16.27; found: C 76.81, H 7.09, N 16.32.

2k

UV (λ_{max}, EtOH, nm): 258 ($\epsilon = 2.10 \times 10^4$). IR (KBr, cm^{-1}): 3301, 3061, 2190, 1596, 1545, 1446, 1382. ^{1}H NMR ($CDCl_3$, ppm) δ: 1.45 (3H, d, *J* = 6.7 Hz, -CHC*H*$_3$), 2.11 (3H, s, -C*H*$_3$), 3.61 (1H, s, =C*H*CN), 4.28 (1H, m, *J* = 6.71 Hz, -C*H*-CH$_3$), 4.73 (1H, bs, -N*H*), 7.18–7.34 (5H, m, Ar-H). ^{13}C NMR ($CDCl_3$, ppm) δ: 20.54, 23.94, 53.61, 63.08, 121.79, 125.49, 125.67, 129.06, 142.61, 158.80. MS *m*/*z*: 186 (M^+). Anal. calcd. for $C_{12}H_{14}N_2$ (%): C 77.38, H 7.57, N 15.05; found: C 77.42, H 7.46, N 15.09.

2l

UV (λ_{max}, $CHCl_3$, nm): 257 ($\epsilon = 1.60 \times 10^4$). IR (as oil, cm^{-1}): 3322, 3076, 2956, 2850, 2199, 1740, 1607, 1546, 1454. ^{1}H NMR ($CDCl_3$, ppm) δ: 1.43 (3H, d, *J* = 6.9 Hz, -CHC*H*$_3$), 2.13 (3H, s, =CC*H*$_3$), 3.77 (1H, s, =C*H*CN), 3.78 (3H, s, -CO$_2$C*H*$_3$), 3.92 (1H, quintet, *J* = 7 Hz, -C*H*CO$_2$CH$_3$), 4.90 (1H, bs, -N*H*). ^{13}C NMR ($CDCl_3$, ppm) δ: 18.04, 20.78, 51.79, 53.14, 62.87, 121.36, 159.00, 173.33. MS *m*/*z*: 168 (M^+). Anal. calcd. for $C_8H_{12}N_2O_2$ (%): C 57.12, H 7.19, N 16.65; found: C 56.97, H 7.13, N 16.51.

2m

UV (λ_{max}, $CHCl_3$, nm): 256 ($\epsilon = 1.65 \times 10^4$). IR (as oil, cm^{-1}): 3332, 3074, 2966, 2877, 2197, 1738, 1604, 1541, 1436. ^{1}H NMR ($CDCl_3$, ppm) δ: 0.94 (3H, d, *J* = 6.75 Hz, -C*H*$_3$), 1.0 (3H, d, *J* = 6.75 Hz, -C*H*$_3$), 2.08–2.13 (1H, com, C*H*Me$_2$), 2.15 (3H, s, =CC*H*$_3$), 3.64 (1H, q, *J* = 5.8 Hz, -C*H*COOCH$_3$), 3.76 (3H, s, -CO$_2$C*H*$_3$), 3.81 (1H, s, =C*H*CN), 4.86 (1H, d, *J* = 7.2 Hz, -N*H*). ^{13}C NMR ($CDCl_3$, ppm) δ: 17.81, 18.60, 30.83, 31.75, 52.21, 61.36, 63.12, 120.99, 159.42, 171.85. MS *m*/*z*: 196 (M^+). Anal. calcd. for $C_{10}H_{16}N_2O_2$ (%): C 61.20, H 8.22, N 14.27; found: C 61.24, H 8.29, N 14.22.

2n

UV (λ_{max}, $CHCl_3$, nm): 256 ($\epsilon = 1.68 \times 10^4$). IR (as oil, cm^{-1}): 3319, 3074, 2957, 2871, 2198, 1739, 1604, 1543, 1437. ^{1}H NMR ($CDCl_3$, ppm) δ: 0.83 (3H, d, *J* = 6.2 Hz, -CHC*H*$_3$), 0.87 (3H, d, *J* = 6.2 Hz, -CHC*H*$_3$), 1.53–1.63 (3H, com, -C*H*$_2$-C*H*Me$_2$), 2.04 (3H, s, =CC*H*$_3$), 3.66 (3H, s, -CO$_2$C*H*$_3$), 3.71 (1H, s, =C*H*CN), 3.75 (1H, q, *J* = 7.3 Hz, -CHCO$_2$C*H*$_3$), 5.12 (1H, d, *J* = 7.6 Hz, -N*H*). ^{13}C NMR ($CDCl_3$, ppm) δ: 19.75, 21.75, 22.22, 24.54, 41.65, 52.82, 54.95, 62.07, 120.92, 159.69, 172.81. MS *m*/*z*: 210 (M^+). Anal. calcd. for $C_{11}H_{18}N_2O_2$ (%): C 62.83, H 8.63, N 13.32; found: C 62.90, H 8.70, N 13.38.

2o

UV (λ_{max}, $CHCl_3$, nm): 258 ($\epsilon = 2.41 \times 10^4$). IR (as oil, cm^{-1}): 3318, 3029, 3066, 2953, 2198, 1740, 1604, 1541, 1438. ^{1}H NMR ($CDCl_3$, ppm) δ: 2.09 (3H, s, =CC*H*$_3$), 3.03 (1H, dd, *J* = 5.76, 13.57 Hz, -C*H*$_2$Ph), 3.73 (3H, s, -CO$_2$CH$_3$), 3.84 (1H, s, =C*H*CN), 4.16 (1H, dt, *J* = 5.76, 6.33 Hz, -C*H*CH$_2$-), 4.77 (1H, bd, *J* = 6.33 Hz, -N*H*), 7.05–7.33 (5H, m, Ar-*H*). ^{13}C NMR ($CDCl_3$, ppm) δ: 20.03, 36.80, 52.50, 56.30, 61.80, 63.00, 120.70, 127.40, 128.60, 129.00, 134.90, 158.30, 171.30. MS *m*/*z*: 245 (MH^+). Anal. calcd. for $C_{14}H_{16}N_2O_2$ (%): C 68.83, H 6.60, N 11.46; found: C 68.93, H 6.65, N 11.41.

2p

UV (λ_{max}, $CHCl_3$, nm): 258 ($\epsilon = 1.81 \times 10^4$). IR (as oil, cm^{-1}): 3318, 3074, 2976, 2871, 2199, 1739, 1604, 1516, 1442. ^{1}H NMR ($CDCl_3$, ppm) δ: 2.09 (3H, s, =CC*H*$_3$), 2.96 (1H, dd, *J* = 5.5, 13.8 Hz, -C*H*$_2$), 3.08 (1H, dd, *J* = 5.8, 13.8 Hz, -C*H*$_2$), 3.74 (3H, s, -CO$_2$C*H*$_3$), 3.83 (1H, s, =C*H*CN), 4.07–4.15 (1H, com, -C*H*-), 4.78 (1H, bd, *J* = 6.8 Hz, -N*H*), 5.98 (1H, bs, -O*H*), 6.77 and 6.92 (each 2H, d, *J* = 8.3 Hz, Ar-*H*). ^{13}C NMR ($CDCl_3$, ppm) δ: 20.28, 36.14, 52.65, 56.76, 62.07, 111.65, 121.23, 126.36, 130.25, 145.15, 155.60, 159.34, 171.78. MS *m*/*z*: 260 (M^+). Anal. calcd. for $C_{14}H_{16}N_2O_3$ (%): C 64.60, H 6.19, N 10.76; found: C 64.72, H 6.26, N 10.71.

Spectral data of prepared compounds 3a–3e

3a

UV (λ_{max}, EtOH, nm): 321 ($\epsilon = 1.85 \times 10^4$). IR (KBr, cm^{-1}): 2198, 1608, 1465, 1321. ^{1}H NMR ($CDCl_3$, ppm) δ: 2.40 (3H, s, C*H*$_3$), 4.62 (2H, d, *J* = 5.9 Hz, C*H*$_2$Ph), 7.21–7.79 (10H, m, Ar-*H*), 12.66 (1H, bs, N*H*). ^{13}C NMR ($CDCl_3$, ppm) δ: 18.1, 48.2, 82.5, 121.3, 127.0, 127.7, 128.0, 128.3, 129.2, 131.2, 135.2, 139.1, 172.1, 192.6. MS *m*/*z*: 276 (M^+). Anal. calcd. for $C_{18}H_{16}N_2O$ (%): C 78.24, H 5.84, N 10.14; found: C 78.29, H 5.81, N 10.16.

3b

UV (λ_{max}, EtOH, nm): 310 ($\epsilon = 1.63 \times 10^4$). IR (KBr, cm^{-1}): 2199, 1605, 1584, 1473, 1316. ^{1}H NMR ($CDCl_3$, ppm) δ: 2.39 (3H, s, C*H*$_3$), 4.64 (2H, d, *J* = 6.2 Hz, C*H*$_2$Ph), 7.0–8.22 (9H, m, Ar-*H*), 11.97 (1H, bs, N*H*). ^{13}C NMR ($CDCl_3$, ppm) δ: 18.5, 48.6, 84.1, 120.0, 124.8, 127.3, 128.7, 128.8, 129.6, 130.6, 134.3, 135.3, 136.2, 146.1, 171.9, 190.7. MS *m*/*z*: 321 (M^+). Anal. calcd. for $C_{18}H_{15}N_3O_3$ (%): C 67.28, H 4.71, N 13.08; found: C 67.33, H 4.69, N 13.11.

© 2005 NRC Canada

3c

UV (λ_{max}, EtOH, nm): 324 ($\epsilon = 2.08 \times 10^4$). IR (KBr, cm^{-1}): 2200, 1601, 1528, 1461, 1317. ^1H NMR ($CDCl_3$, ppm) δ: 2.43 (3H, s, C*H*$_3$), 4.67 (2H, d, *J* = 5.9 Hz, C*H*$_2$Ph), 7.28–7.42 (5H, m, CH$_2$*Ph*), 7.60 (1H, t, *J* = 7.9 Hz, 5-H of *m*-NO$_2$-Ph ring), 8.12 (1H, d, *J* = 7.8 Hz, 6-H of *m*-NO$_2$-Ph ring), 8.30 (1H, d, *J* = 7.8 Hz, 4-H of *m*-NO$_2$-Ph ring), 8.60 (1H, s, 2-H of *m*-NO$_2$-Ph ring), 12.57 (1H, bs, N*H*). ^{13}C NMR ($CDCl_3$, ppm) δ: 18.4, 48.6, 82.6, 120.7, 123.3, 125.7, 127.4, 128.7, 129.3, 129.5, 133.6, 134.9, 140.6, 148.1, 172.8, 189.6. MS *m*/*z*: 321 (M^+). Anal. calcd. for $C_{18}H_{15}N_3O_3$ (%): C 67.28, H 4.71, N 13.08; found: C 67.32, H 4.72, N 13.10.

3d

UV (λ_{max}, EtOH, nm): 340 ($\epsilon = 1.96 \times 10^4$), 249 ($\epsilon = 1.22 \times 10^4$). IR (KBr, cm^{-1}): 2195, 1619, 1601, 1544, 1511, 1453. ^1H NMR ($CDCl_3$, ppm) δ: 2.38 (3H, s, C*H*$_3$), 4.61 (2H, d, *J* = 5.8 Hz, C*H*$_2$Ph), 7.0–8.25 (8H, m, Ar-*H*), 12.45 (1H, bs, N*H*). MS *m*/*z*: 282 (M^+). Anal. calcd. for $C_{16}H_{14}N_2OS$ (%): C 68.07, H 4.99, N 9.92; found: C 68.09, H 4.96, N 9.95.

3e

UV (λ_{max}, EtOH, nm): 304 ($\epsilon = 1.58 \times 10^4$). IR (KBr, cm^{-1}): 2192, 1623, 1574, 1468. ^1H NMR ($CDCl_3$, ppm) δ: 1.07 (3H, d, *J* = 7.1 Hz, CH(C*H*$_3$)CH$_3$), 1.14 (3H, d, *J* = 7.1 Hz, CH(CH$_3$)C*H*$_3$), 2.30 (3H, s, C*H*$_3$), 3.14 (1H, m, C*H*(CH$_3$)$_2$), 4.54 (2H, d, *J* = 6.1 Hz, C*H*$_2$Ph), 7.34 (5H, m, Ar-*H*), 12.26 (1H, bs, N*H*). ^{13}C NMR ($CDCl_3$, ppm) δ: 18.0, 19.1, 31.0, 37.8, 48.2, 82.6, 121.0, 127.2, 128.4, 129.3, 135.5, 170.8, 203.3. MS *m*/*z*: 242 (M^+). Anal. calcd. for $C_{15}H_{18}N_2O$ (%): C 74.34, H 7.49, N 11.56; found: C 74.30, H 7.52, N 11.58.

Spectral data of prepared compounds 5a–5e

5a

UV (λ_{max}, EtOH, nm): 255 ($\epsilon = 1.14 \times 10^4$). IR (KBr, cm^{-1}): 2220, 1593, 1538, 1504, 1450, 1424, 1137. ^1H NMR ($CDCl_3$, ppm) δ: 2.50 (3H, s, C*H*$_3$), 7.24–7.52 (10H, m, Ar-*H*). MS *m*/*z*: 259 (M^+). Anal. calcd. for $C_{17}H_{13}N_3$ (%): C 78.74, H 5.05, N 16.20; found: C 78.79, H 5.02, N 16.23.

5b

UV (λ_{max}, EtOH, nm): 246 ($\epsilon = 1.39 \times 10^4$). IR (KBr, cm^{-1}): 2228, 1595, 1528, 1502, 1445. ^1H NMR ($CDCl_3$, ppm) δ: 2.54 (3H, s, C*H*$_3$), 7.0–8.06 (9H, m, Ar-*H*). MS *m*/*z*: 304 (M^+). Anal. calcd. for $C_{17}H_{12}N_4O_2$ (%): C 67.10, H 3.97, N 18.41; found: C 67.18, H 3.95, N 18.45.

5c

UV (λ_{max}, EtOH, nm): 254 ($\epsilon = 1.57 \times 10^4$). IR (KBr, cm^{-1}): 2227, 1596, 1526, 1501, 1429, 1387, 1348. ^1H NMR ($CDCl_3$, ppm) δ: 2.53 (3H, s, C*H*$_3$), 7.22–8.28 (9H, m, Ar-*H*). ^{13}C NMR ($CDCl_3$, ppm) δ: 12.54, 94.60, 113.4, 123.93, 124.55, 125.30, 128.78, 129.16, 129.53, 130.21, 134.64, 138.02, 145.02, 148.36, 152.95. MS *m*/*z*: 304 (M^+). Anal. calcd. for $C_{17}H_{12}N_4O_2$ (%): C 67.10, H 3.97, N 18.41; found: C 67.17, H 3.99, N 18.44.

5d

UV (λ_{max}, EtOH, nm): 237 ($\epsilon = 0.59 \times 10^4$), 249 ($\epsilon = 1.22 \times 10^4$). IR (KBr, cm^{-1}): 2221, 1593, 1545, 1513, 1456, 1416. ^1H NMR ($CDCl_3$, ppm) δ: 2.48 (3H, s, C*H*$_3$), 6.90–7.90 (8H, m, Ar-*H*). MS *m*/*z*: 265 (M^+). Anal. calcd. for $C_{15}H_{11}N_3S$ (%): C 67.91, H 4.18, N 15.84; found: C 67.95, H 4.20, N 15.88.

5e

UV (λ_{max}, EtOH, nm): 255 ($\epsilon = 1.51 \times 10^4$). IR (KBr, cm^{-1}): 2222, 1595, 1545, 1513, 1460. ^1H NMR ($CDCl_3$, ppm) δ: 1.38 (6H, d, *J* = 7.2 Hz, (C*H*$_3$)$_2$), 2.40 (3H, s, C*H*$_3$), 3.07 (1H, heptet, *J* = 7.2 Hz, C*H*(CH$_3$)$_2$), 7.32–7.52 (5H, m, Ar-*H*). ^{13}C NMR ($CDCl_3$, ppm) δ: 12.31, 18.94, 21.43, 89.85, 114.40, 126.09, 128.22, 129.15, 138.30, 152.62, 155.57. MS *m*/*z*: 225 (M^+). Anal. calcd. for $C_{14}H_{15}N_3$ (%): C 74.64, H 6.71, N 18.65; found: C 74.69, H 6.69, N 18.63.

Acknowledgements

The authors are indebted to Dr. V.A. Snieckus, Queen's University, Kingston, Ontario and Dr. W. Froestl, Novartis Pharma AG, Basel, Switzerland for recording the NMR and MS spectra of some of the compounds. MM thanks Jadavpur University for a Senior Research Fellowship.

References

1. A.W. Erian. Chem. Rev. **93**, 1991 (1993).
2. M. Sarkar, S. Chattopadhyaya, and K.K. Mahalanabis. Indian J. Chem. Sect. B, **25B**, 1133 (1986).
3. K.K. Mahalanabis, M. Sarkar, S.K. Dutta Chowdhury, and C.R. Ghosal. Indian J. Chem. Sect. B, **41B**, 1902 (2002).
4. K.K. Mahalanabis, M. Sarkar, S.K. Dutta Chowdhury, and S. Dutta-Bose. Indian J. Chem. Sect. B, **37B**, 1234 (1998).
5. K.K. Mahalanabis, M. Sarkar, S.K. Dutta Chowdhury, and A. Chatterjee. J. Indian Chem. Soc. **80**, 1143 (2003).
6. S.K. Dutta Chowdhury, M. Sarkar, S. Roychowdhury, and K.K. Mahalanabis. Synth. Commun. **26**, 4233 (1996).
7. S.K. Dutta Chowdhury, M. Sarkar, A. Chatterjee, and K.K. Mahalanabis. Indian J. Chem. Sect. B, **42B**, 2563 (2003).
8. S.K. Dutta Chowdhury, M. Sarkar, and K.K. Mahalanabis. J. Chem. Res. Synop. **11**, 746 (2003).
9. M. Mishra, S.K. Dutta Chowdhury, and K.K. Mahalanabis. Synth. Commun. **34**, 2681, (2004).
10. C.L. Habraken and J.A. Moore. J. Org. Chem. **30**, 1892 (1965).
11. (*a*) W.S. Murphy and M. Bertrand. J. Chem. Soc. Perkin Trans. 1, 4115 (1998); (*b*) S. Krischbaum and H. Waldmann. J. Org. Chem. **63**, 4936 (1998); (*c*) A.W. Trautwein and G. Jung. Tetrahedron Lett. **39**, 8263 (1998); (*d*) N. Nishimura, Y. Koyano, M. Sugiura, and I. Maeba. Heterocycles, **51**, 803 (1999).
12. E. Meyer. J. Prakt. Chem. (Leipzig), **78**, 497 (1908).
13. E. Meyer. Chem. Zentralbl. **79**, 591 (1908).
14. J. Sander and K. Clauss. Angew. Chem. **92**, 138 (1980).
15. J.W. Pavlik and N. Kebede. J. Org. Chem. **62**, 8325 (1997).
16. J. Dedina, J. Kuthan, J. Palecek, and J. Schraml. Coll. Czech. Chem. Commun. **40**, 3476 (1975).
17. L. Rene, J. Poncet, and G. Auzou. Synthesis, 419 (1986).
18. S. Schwarz, F.M. Bumjms, and I.H. Page. J. Am. Chem. Soc. **79**, 5697 (1957).
19. H.S. Mosher, J.A. Dale, and D.L. Dull. J. Org. Chem. **34**, 2543 (1969).

© 2005 NRC Canada

20. A.R. Katritzky, Y. Fang, A. Donkor, and J. Xu. Synthesis, 2029 (2000).
21. H. Adkins and G.M. Whitman. J. Am. Chem. Soc. **64**, 150 (1942).
22. (*a*) H.C. Brown. J. Am. Chem. Soc. **60**, 1325 (1938); (*b*) E.C. Horning (*Editor*). Organic syntheses collection. Vol. 3. John Wiley and Sons Inc., New York. 1955. p. 29 and 714.
23. A.I. Vogel. *In* A textbook of practical organic chemistry. 3rd ed. ELBS and Longman, London. 1973. p. 121.

© 2005 NRC Canada

Synthesis and structure of new trichloromethyl-β-diketones — 5-Trichloromethylisoxazole and 5-isoxazolecarboxylic acid derivatives

Marcos A.P. Martins, Sergio Brondani, Victor L. Leidens, Darlene C. Flores, Sidnei Moura, Nilo Zanatta, Manfredo Hörner, and Alex F.C. Flores

Abstract: An improved method for the synthesis of a new series of trichloromethyl-β-diketones including 1,1,1-trichloropentan-2,4-dione (**2a**), 1,1,1-trichloro-3-methylhexan-2,4-dione (**2b**), 4,4,4-trichloro-1-phenylbutan-1,3-dione (**2c**), 4,4,4-trichloro-2-methyl-1-phenylbutan-1,3-dione (**2d**), 2-trichloroacetylcyclohexanone (**2e**), 4-*tert*-butylcyclohexanone (**2f**), 4-*tert*-butylcycloheptanone (**2g**), and 4-*tert*-butylcyclooctanone (**2h**) is reported. A multinuclear NMR study showed that β-dicarbonyl compounds **2b** and **2d**–**2h** are predominantly in the keto form and **2a** and **2c** are in the enol form. The trichloromethyl-β-diketones react with hydroxylamine hydrochloride leading to three sets of isoxazole derivatives.

Key words: acetals, acylation, trichloromethyl-1,3-diketones, 2-trichloroacetylcycloalkanones, isoxazoles, cyclocondensation.

Résumé : On rapporte la mise au point d'une méthode améliorée de synthèse d'une nouvelle série de trichlorométhyl-β-dicétones, dont la 1,1,1-trichloropentan-2,4-dione (**2a**), la 1,1,1-trichloro-3-méthylhexan-2,4-dione (**2b**), la 4,4,4-trichloro-1-phénylbutan-1,3-dione (**2c**), la 4,4,4-trichloro-2-méthyl-1-phénylbutan-1,3-dione (**2d**) et les 2-trichloroacétylcyclohexanone (**2e**), 4-*tert*-butylcyclohexanone (**2f**), 4-*tert*-butylcycloheptanone (**2g**) et 4-*tert*-butylcyclooctanone (**2h**). Une étude de RMN multinucléaire a permis de montrer que les composés β-dicarbonylés **2b** et **2d**–**2h** existent principalement sous la forme dicétonique alors que les produits **2a** et **2c** existent sous la forme énolique. Les trichlorométhyl-β-dicétones réagissent avec le chlorhydrate d'hydroxylamine pour conduire à trois ensembles de dérivés isoxazoles.

Mots clés : acétals, acylation, trichlorométhyl-1,3-dicétones, 2-trichloroacétylcycloalkanones, isoxazoles, cyclocondensation.

[Traduit par la Rédaction]

Introduction

An ongoing research program enabled the development of a general acetal acylation method for the synthesis of trihalomethyl-1,3-dielectrophiles and demonstrated their usefulness for the preparation of heterocycles (1–4). The easy transformation of the trichloromethyl group attached to azoles into carboxyl groups led to devoting special attention to trichloromethyl-1,3-dielectrophiles (5–7).

Although trifluoromethyl-1,3-dicarbonyl compounds are well-known (8–16), the studies on trichloromethyl-1,3-dicarbonyl analogs are scarce (17–20). The most employed method to obtain trifluoromethyl-β-diketones is acylation of enol and enolates with perfluoralkanoates (8, 11, 16). The lack of literature and data on trichloromethyl-β-diketones is due to the acylation of enolates by Claisen condensation being limited in use to obtain perchloroalkyl-β-diketones. This is a result of the lability of the perchloroalkyl groups in basic medium (21, 22).

Continuing research focus in trichloromethyl substituted 1,3-dielectrophiles and their cyclocondensations with hydroxylamine hydrochloride prompted us to perform a systematic study of the dimethoxyacetals acylation with trichloroacetyl chloride. The aim of this investigation is to report the results of the synthesis of a series of the trichloromethyl-β-diketones prepared from the reaction of dimethoxy acetals with trichloroacetyl chloride. Also discussed are ^{1}H, ^{13}C, and ^{17}O NMR data for isolated β-dicarbonyl compounds and the influence of the trichloromethyl group on the keto–enol equilibrium. In addition, we report the cyclocondensation reactions of trichloromethyl-β-dicarbonyl compounds with hydroxylamine hydrochloride for the synthesis of isoxazole derivatives and the structural study of 4-alkyl substituted 4,5-dihydroisoxazoles. ^{1}H and ^{13}C NMR and X-ray data showed that cyclocondensation was enantioselective, only one pair of enantiomers was obtained for 4-alkyl substituted 4,5-dihydroisoxazoles.

Received 27 October 2004. Published on the NRC Research Press Web site at http://canjchem.nrc.ca on 23 September 2005.

M.A.P. Martins, S. Brondani, V.L. Leidens, D.C. Flores, S. Moura, N. Zanatta, M. Hörner, and A.F.C. Flores.[1] NUQUIMHE, Departamento de Química, Universidade Federal de Santa Maria, 97.105-900 - Santa Maria, RS, Brazil.

[1]Corresponding author (e-mail: alexflores@smail.ufsm.br).

Results and discussion

Synthesis

Trichloromethyl-β-diketones

Dimethoxy ketals **1a**–**1h** were synthesized from the

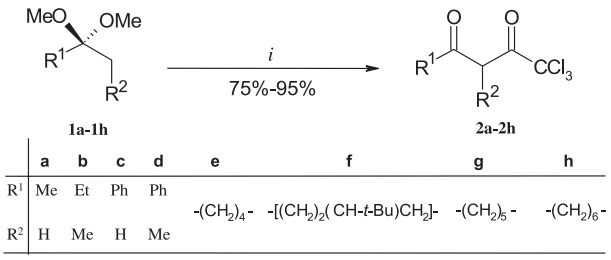
 doi: 10.1139/V05-130 © 2005 NRC Canada

Table 1. Yields, melting points, elemental analysis, and IR stretching frequencies of the β-diketones **2a**–**2h**.

Compound	Molecular formula	Yield (%)[a]	Melting point (°C)[b]	Elemental analysis[c] (calcd.) C	Elemental analysis[c] (calcd.) H	Elemental analysis[c] (found) C	Elemental analysis[c] (found) H	IR[d] $\nu_{C=O}$ C=O	IR[d] $\nu_{C=O}$ $Cl_3CC=O$
2a	$C_5H_5Cl_3O_2$	90	Oil	29.50	2.48	29.50	2.50	1595	1600
2b	$C_7H_9Cl_3O_2$	85	Oil	36.32	3.92	36.50	4.00	1700	1765
2c	$C_{10}H_7Cl_3O_2$	95	Oil	45.24	2.66	45.50	2.70	1568	1593
2d	$C_{11}H_9Cl_3O_2$	80	65–68	47.26	3.25	47.30	3.30	1670	1760
2e	$C_8H_9Cl_3O_2$	95	88–90	39.46	3.73	39.50	3.80	1709	1750
2f	$C_{12}H_{17}Cl_3O_2$	80	91–93	48.10	5.72	48.00	5.70	1713	1760
2g	$C_9H_{11}Cl_3O_2$	92	54–56	41.97	4.31	42.00	4.30	1697	1752
2h	$C_{10}H_{13}Cl_3O_2$	95	44–46	44.23	4.82	44.40	4.80	1695	1755

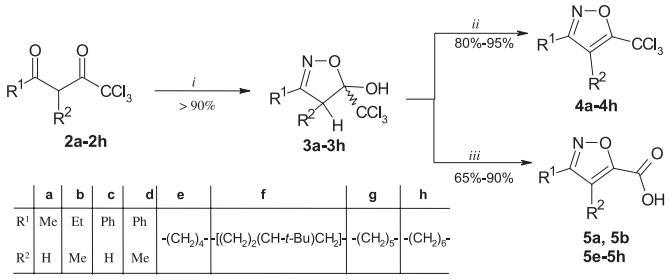
[a]Yields of isolated compounds.
[b]The melting points are uncorrected.
[c]Elemental analyses were performed on a CHNS-Vario El Elementar Analysensysteme.
[d]Film for **2a**–**2c** and KBr pellets for **2d**–**2h**.

Scheme 1.



i. $2Cl_3CCOCl$, 2Pyridine, $CHCl_3$, 0-50 °C, overnight (10-12 h), then H_2SO_4 (2 mol/L), 80 °C, 2 h.

Scheme 2.



i. $NH_2OH{\cdot}HCl$, MeOH, 40 °C, 5-8 h. *ii*. H_2SO_4 (98%), 25-30 °C, 5 h. *iii*. H_2SO_4 (85%), 75-100 °C, 8 h.

acetalization reaction of the respective ketones with trimethyl orthoformate in the presence of *p*-toluenesulfonic acid (23). The acylation of compounds **1a**–**1h** was carried out with trichloroacetyl chloride in chloroform in the presence of pyridine. The reaction was monitored by HPLC and the most satisfactory reaction time was found to be 12 h at 25–30 °C for **2a** and **2c** and 10 h at 50 °C for **2b** and **2d**–**2g**. After the acylation time had elapsed, 2 mol/L sulfuric acid was added and the mixture was stirred at 50 °C for 2 h. The trichloromethyl-β-diketones **2a**–**2h** were obtained with good yields (75%–95%) (Scheme 1). Compounds **2a**–**2c** are liquid and were purified by column chromatography with silica gel and hexane–chloroform (9:1) as the eluent. The crystalline **2d**–**2h** compounds were purified by crystallization from hexane. The yields and selected physical and spectral data for compounds **2a**–**2h** are reported in Table 1. We have the acetal acylation method as routine work for 1,1,1-trihalo-4-alkoxyalk-3-en-2-one synthesis (1–4), however, the posterior hydrolysis to the respective trichloromethyl-1,3-diketones closely with structural studies was the new contribution.

Isoxazole derivatives

The cyclization of **2a**–**2h** with hydroxylamine hydrochloride was carried out in methanol at 40 °C for 5–8 h. The products (5-hydroxy-5-trichloromethyl-4,5-dihydroisoxazoles, **3a**–**3h**) were obtained in good yields and they were dehydrated with concentrated sulfuric acid at 35 °C for 5 h to afford the corresponding 5-trichloromethylisoxazoles **4a**–**4h** in good yields (Scheme 2). However, when compounds **3a** and **3b** and **3e**–**3h** were heated at 75–100 °C for 12 h in an 85% sulfuric acid solution, respective 5-isoxazole carboxylic acids **5a** and **5b** and **5e**–**5h** were obtained with good yields. Under the same reaction conditions, compounds **3c** and **3d** were not converted to the respective carboxylic acids (6). We are able to demonstrate the effect of the substituents in the trichloromethyl hydrolysis to the carboxyl group. The 3-alkyl or 3,4-dialkyl substituted isoxazoles were suitable for conversion of the 5-trichloromethyl group to a carboxyl, however, the 3-phenyl substituted isoxazoles did not hydrolyse the 5-trichloromethyl group to a carboxyl even if a severely acidic medium was used.

Molecular structure

Trichloromethyl-β-diketones

For compounds **2a** and **2c** only one set of signals in the ^1H, ^{13}C, and ^{17}O NMR spectra was observed, which was assigned to an enol form (Tables 2 and 3). ^1H NMR spectra showed the signal of the enolic hydrogen at δ 13.0–14.0, and the chemical shifts for H-2 and C-2 are typical of vinyl moieties (δ 6.10–6.70 and δ 96.5–97.8, respectively) (see Tables 2 and 4). The IR spectra have a band at 1568–1595 cm^{-1} assigned to the absorption of the HO-C= group along with the band at 1593–1600 cm^{-1} attributed to the vibration of the C=O fragment from the trichloroacetyl group. ^{17}O NMR spectra for **2a** and **2c** showed two signals at δ 170 and δ 360,

© 2005 NRC Canada

Table 2. ^{1}H NMR[a] data for 2-trichloroacetylcycloalkanones **2a**–**2h**.

Compound	H-2 (mult., $^2J_{HH}$ Hz)	R^1 and R^2 (mult.)
2a	6.10 (s)	2.2 (s) Me, 13.9 enolic hydrogen
2b	4.50 (qu, 8.0)	2.65 (q) -CH_2-, 1.55 (d) Me, 1.08 (t) Me
2c	6.70 (s)	7.5–7.8 (m) Ar 5H, 12.5 enolic hydrogen
2d	5.4 (qu, 8.0)	7.93 (m) Ar 2H, 7.45 (m) Ar 3H, 1.45 (d) Me
2e	4.35 (dd)	2.28 (m) H-3, 1.81 (m) H-4, 2.03 (m) H-5, 2.13 (m) H-5, 2.44 (ddd) H-6a, 2.58 (ddd) H-6e
2f	4.38 (dd, 12.6, 5.2)	1.93 (dt) H-3a, 2.31 (dm) H-3e (12.6, 12.6, 12.8), 1.71 (tt) H-4a (12.6, 2.8), 1.61 (tdd) H-5a, 2.19 (dm) H-5e (12.8), 2.51 (ddd) H-6a, 2.55 (ddd) H-6e, 0.95 (s) *t*-Bu
2g	4.55 (dd, 10.0, 3.6)	1.41 (m) H-3, 1.98 (m) H-3, 1.57 (m) H-4, 1.98 (m) H-4, 2.14 (m), 1.98 (m) H-5, 1.71 (m), 1.98 (m) H-6, 2.65 (m), 2.75 (m) H-7
2h	4.70 (dd, 11.4, 3.4)	2.27 (m) H-3e, 2.08 (m) H-3, 1.58 (m) H-4, 1.80 (m), 1.65 (m) H-5, 1.65 (m), 1.30 (m) H-6, 2.07 (m), 1.92 (m) H-7, 2.54 (m), 2.75 (m) H-8

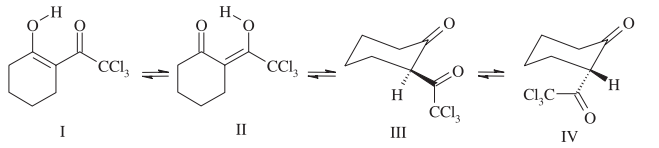
[a]^{1}H NMR spectra measured at 400 MHz in 0.01 mol/L $CDCl_3$–TMS solutions, in a Bruker DPX 400 spectrometer.

Table 3. Selected ^{1}H and ^{13}C NMR[a] data for **2e** in different solvents.

				^{13}C NMR δ			
Solvent	δ H-2	$^2J_{H\text{-}2H\text{-}ax}$ (Hz)	$^2J_{H\text{-}2H\text{-}eq}$ (Hz)	C-1	C-2	$COCCl_3$	CCl_3
$CDCl_3$	4.35	11.4	5.6	204.6	56.8	186.2	96.3
CCl_4	4.50	8.90	8.5	202.2	57.0	185.4	97.0
C_6D_6	4.00	12.10	5.5	203.3	56.8	186.4	97.0
$(CD_3)_2CO$	4.60	12.40	5.4	205.2	57.1	187.4	96.6
$(CD_3)_2SO$	4.60	12.30	5.5	205.0	57.0	187.0	97.0

[a]0.01 mol/L solutions with internal TMS, in a Bruker DPX 400 spectrometer with SF 400.13 MHz for ^{1}H and 100.62 MHz for ^{13}C.

Table 4. MO calculation data for 2-trichloroacetylcyclohexanone.



I II III IV

MO Data

E (kcal/mol)	-2141.46	-2138.33	-2143.40	-2143.29
Isomers (%)[a]	2	0	53	45

Note: The MO calculations were carried out by the AM1 semiempirical method (see Experimental).

[a]Calculated for the equilibrium at 298 K, as described in the Experimental.

characteristics for the push–pull conjugated keto–enol system (24, 25). Compounds 1,1,1-trichloropentan-2,4-dione (**2a**) and 4,4,4-trichloro-1-phenyl-butan-1,3-dione (**2c**) exhibited the same enolic trend as the fluorinated analogs 1,1,1-trifluoropentan-2,4-dione and 4,4,4-trifluoro-1-phenyl-butan-1,3-dione, respectively (26, 27) (Table 5).

The ^{1}H, ^{13}C, and ^{17}O NMR spectra for trichloromethyl-β-diketones **2b** and **2d**–**2h** showed that these compounds have an overall preference for the keto form. The chemical shift of H-2 is typical of the keto form for compounds **2b** and **2d**–**2h** at δ 4.35–5.48 (Table 2). For compounds **2e**–**2h**, the clear doublet of doublets signal and the coupling constants ($^3J_{HH}$) are consistent with pseudo-axial placement of H-2 (28). The $^{13}C\{^1H\}$ NMR spectrum for compounds **2b** and **2d**–**2h** showed only one set of peaks for each carbon. The signals in the range of δ 52–58 for C-2 confirmed the keto structure for compounds **2b** and **2d**–**2h** (Table 4). The IR spectra have a band at 1670–1713 cm^{-1} assigned to the absorption of the aromatic C=O (**2d**) and aliphatic C=O (**2b**, **2e**–**2h**) groups, along with the band at 1750–1765 cm^{-1} attributed to the vibration of the C=O fragment from the trichloroacetyl group. The ^{17}O NMR spectra for **2b** and **2d**–**2h** showed two near signals between δ 500–600, typical for nonconjugated carbonyl groups (29, 30). Therefore, the trichloroacetyl group in **2e**–**2h** strongly prefers a pseudo-equatorial position without conjugation.

The trichloromethyl-β-diketones with substituents at C-α (between the two carbonyls) prefer the keto form probably because of thermodynamic factors. Endocyclic or exocyclic enol forms increase molecular strain by planar placement of the bulky trichloroacetyl group. For these β-diketones, the keto–enol equilibrium on the NMR timescale is unlikely. Commonly simple 1,3-dicarbonyl compounds exhibit high concentrations of enol forms in solution, except if prohibitive structural factors are present. NMR data showed that 2-acetylcycloalkanones and 2-trifluoroacetylcycloalkanones are preferentially enol forms (31). These results showed that the trichloromethyl group on compounds **2b** and **2d**–**2h** (R^2 = alkyl) act like an anchor for the keto form. The ^{1}H and (or) ^{13}C NMR spectra of 2-trichloroacetylcyclohexanone (**2e**) were performed in different deuterated solvents (Table 3) without significant change to the spectral and (or) structural characteristics. The AM1 calculations performed showed that tautomer III of **2e** presents the lowest minimum energy. The calculated minimum energy values and relative % values for tautomer and (or) conformer concentrations are listed in the Table 4.

© 2005 NRC Canada

Table 5. ^{13}C and ^{17}O NMR data for trichloromethyl-β-diketones **2a**–**2h**.

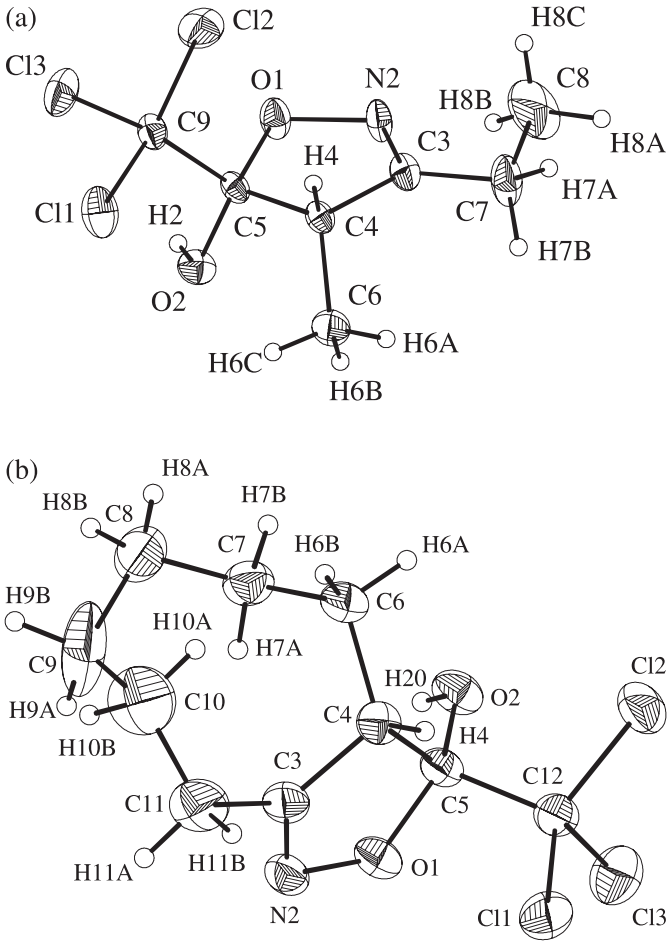
	^{13}C NMR[a]					^{17}O NMR[b] δ (*w*1/2)	
Compound	C-1	C-2	$COCCl_3$	CCl_3	R^1/R^2	C=O	$C1_3CC=O$
2a	198.7	97.8	175.9	96.8	26.9 (Me)	176 (170)	370 (230)
2b	204.1	52.1	186.7	96.0	34.0 (CH_2), 16.5 (Me-3), 7.55 (Me)	553 (410)	538 (480)
2c	181.5	96.5	175.5	95.9	136.9, 130.7, 128.1, 127.7 (Ar)	165 (170)	360 (400)
2d	188.4	52.0	187.2	94.3	143.9, 132.5, 130.6, 128.0 (Ar), 115 (Me)	550 (750)	540 (750)
2e	204.6	56.8, J_{CH} = 132	186.2	96.3	23.9, 27.2, 32.7, 41.8	557 (470)	538 (470)
2f	205.1	56.3, J_{CH} = 132	186.5	96.3	28.1, 33.8, 41.3, 46.1	570 (600)	540 (650)
2g	206.1	57.6, J_{CH} = 133	186.6	96.2	23.9, 28.5, 28.7, 30.3, 43.0	564 (470)	538 (470)
2h	207.7	55.0, J_{CH} = 130	184.4	96.3	23.8, 24.2, 24.6, 27.5, 33.4, 42.1	571 (450)	540 (510)

[a]0.01 mol/L $CDCl_3$–TMS solutions in a Bruker DPX 400 spectrometer with SF 100.62 MHz for ^{13}C.
[b]1.5 mol/L $CHCl_3$ solution, external coaxial reference capillary with H_2O in a Bruker DPX 400 spectrometer with SF 54.23 MHz for ^{17}O (locked with C_6D_6 in a 5 mm coaxial tube). For details on ^{17}O NMR see ref. 10.

5-Hydroxy-5-trichloromethyl-4,5-dihydroisoxazoles

The nonequivalence for the diastereotopic hydrogens H-4a and H-4b is well-known for 5-hydroxy-5-trichloromethyl-4,5-dihydroisoxazoles **3a** and **3c** (19, 20). The 4,5-dihydroisoxazoles substituted on position 4 have two chiral centers, the C-4 and the C-5 of the isoxazole ring. However, the ^1H NMR spectra for **3b** and **3d** showed the signal of H-4 at δ 3.70–3.73 as quartets (^3J = 8.0 Hz), and for compounds **3e**–**3h** the ^1H NMR spectra showed the H-4 signals at δ 3.15–3.77 as a doublet of doublets; the coupling constant data is consistent with the pseudo-axial position of H-4 (28). The $^{13}C\{^1H\}$ NMR spectra for compound **3** also showed one set of signals for each carbon atom (see Experimental). The presence of one set of signals indicates only one pair of enantiomers (4*R*,5*R*/4*S*,5*S* or 4*R*,5*S*/4*S*,5*R*). The X-ray diffraction for the monocrystals showed the 4*S*,5*S* configuration for **3b** and **3h**. In these compounds, the alkyl group is cis to the OH group and the bulky CCl_3 group is cis to H-4. The crystal structures of 3-ethyl-4-methyl-5-hydroxy-5-trichloromethyl-4,5-dihydroisoxazole (**3b**) and 5-trichloromethyl-3,4-hexamethylene-5-hydroxy-4,5-dihydroisoxazole (**3h**) with the atomic numbering are displayed in Fig. 1. Previous structural analyses for X-ray diffraction performed on **3e** showed the 4*R*,5*R* configuration (32). X-ray diffraction enabled us to conclude that the synthetic procedure used always furnished a pair of diastereoisomers 4*R*,5*R*/4*S*,5*S* for compounds **3b** and **3d**–**3h**. The regiochemistry of these cyclocondensation reactions was discussed in ref. 32. The NMR and selected physical data from aromatic isoxazole derivatives **4** and **5** are shown in the Experimental.

Fig. 1. ORTEP plot with atom-labeling scheme of the structure of: (*a*) 5-trichloromethyl-3-ethyl-5-hydroxy-4-methyl-4,5-dihydroisoxazol (**3b**); and (*b*) 5-trichloromethyl-5-hydroxy-3,4-hexamethylene-4,5-dihydroisoxazole (**3h**). Displacement ellipsoids at the 30% level (see Experimental).



Conclusion

In summary, this work has presented a convenient one-pot method to obtain unusual trichloromethyl-β-diketones and we have demonstrated some important features of their molecular structure. This series of trichloromethyl-β-diketones were successfully used as precursors to obtain regiospecifically new 5-trichloromethylisoxazoles and 5-isoxazole carboxylic acids.

Experimental

Unless otherwise indicated, all common reagents and solvents were used as obtained from commercial suppliers without further purification. All melting points were taken on a Reichert-Thermovar melting point microscope and are uncorrected. The ^1H and ^{13}C NMR spectra were recorded on a Bruker DPX 400 (^1H at 400.13 MHz, ^{13}C at 100.62 MHz) with 5 mm sample tubes, at 300 K, in 0.02 mol/L in $CDCl_3$–

© 2005 NRC Canada

Table 6. Crystallographic data[2] for compounds **3b** and **3h**.

Crystal data	**3b**	**3h**
Molecular formula	$C_7H_{10}Cl_3NO_2$	$C_{10}H_{14}Cl_3NO_2$
Molecular mass	246.51	286.57
Crystal color	Colorless	Colorless
Crystal size (mm^3)	0.55 × 0.25 × 0.05	0.15 × 0.20 × 0.28
Crystal class	Monoclinic	Monoclinic
Parameters of the unit cell		
a (Å)	9.9547(5)	24.667(2)
b (Å)	9.1478(5)	7.227(4)
c (Å)	11.8058(6)	18.767(3)
Volume of the unit cell (*V*, $Å^3$)	1062.12(10)	2536.9(15)
Space group	*P*21/*c*	*C*2/*c*
Number of molecules per unit cell (*Z*)	4	8
Density (*d*, g/cm^3)	1.543	1.501
Absorption coefficient (μ, mm^{-1})	0.831	0.707
Number of independent reflexions	2201	2552
Number of reflexions with $I > 2\sigma(I)$	2092	2488
Number of parameters refined	119	150
Final residual factor (*R*)	0.0492	0.0542

TMS, with a digital resolution of ±0.01 ppm. The ^{17}O NMR spectra were recorded at 54.26 MHz in 10 mm tubes, at 323 K, in 2 mol/L $CHCl_3$ solutions, with chemical shifts referenced to external H_2O (capillary coaxial tube). The spectra were recorded at natural abundance with a ring down eliminate (RIDE) sequence for suppression of acoustic ringing (31, 32). Mass spectra were registered in a HP 5973 MSD connected to a HP 6890 GC and interfaced by a Pentium PC. The GC was equipped with a split–splitless injector, autosampler, cross-linked HP-5 capillary column (30 m, 0.32 mm i.d.), and helium was used as the carrier gas. The dimethoxy ketals **1a**–**1h** were synthesized according to the literature (23) and purified by distillation.

Monocrystals of compounds **3b** and **3h** were grown from hexane. Diffraction data were collected at 293(2) K on an Enraf-Nonius CAD4 automatic four-circle diffractometer (MoKα, $2\theta_{max}$ = (3*b*), $2\theta_{max}$ = (3*h*)) (33). The structures were solved by direct methods and refined by full-matrix least-squares in anisotropic approximation. The basic crystallographic characteristics and the parameters of the refined crystal structures are cited in Table 6. Calculations were carried out using the programs ZORTEP and SHELXS-93 (34, 35).

MO calculations were performed using the Austin Model 1 (AM1) semiempirical method, implemented in the HyperChem 4.5 package (1995) (36). Geometries were completely optimized without fixing any parameter, thus bringing all geometric variables to their equilibrium values. The energy minimization protocol employs the Polak–Ribiere algorithm, which is a conjugated gradient method. Convergence to a local minimum was achieved when the energy gradient was <0.01 kcal mol^{-1} (1 cal = 4.184 J). The relative abundance of each species in equilibrium was calculated from the minimum energy associated with each compound employing the relationships: (1) $\Delta E = -RT \ln K$ (where ΔE stands for the standard energy difference between two given species, *R* is the molar gas constant expressed in units of kcal mol^{-1} K^{-1}, *T* is the absolute temperature in K, *K* is the corresponding equilibrium constant) and (2) [I] + [II] + [III] + [IV] = 100, where [I], [II], [III], and [IV] represent the percentage molar ratio of each tautomer and (or) conformer in equilibrium (Table 4). The calculations were performed using a Dell Precision 330 Pentium IV 1.4 GHz computer.

Trichloroacetylation of acetals 1a–1h

General procedure

To a stirred solution of dimethoxy acetal derivatives **1a**–**1h** (30 mmol) and pyridine (5.2 mL, 60 mmol) in chloroform (30 mL) kept at 0 °C, a solution of trichloroacetyl chloride (7.0 mL, 60 mmol) in chloroform (20 mL) was added dropwise. The mixture was stirred for 10–12 h at 25–50 °C. The mixture was quenched with a 2 mol/L sulfuric acid solution (30 mL) and stirred for 2 h at 80 °C. The organic layer was dried with sodium sulfate, the solvent was evaporated, and the products were obtained with high purity (see Table 1). The liquid compounds **2a**–**2c** were purified by column chromatography with Kieselgel 60 and hexane–chloroform (9:1) as the eluent. The crystalline compounds **2d**–**2h** were purified by recrystallization from hexane.

Synthesis of 5-trichloromethyl-4,5-dihydroisoxazoles 3a–3h

General procedure

To a stirred solution of trichloromethyl-β-diketones **2a**–**2h** (15 mmol) in methanol (5 mL), kept at 40 °C, was added

[2] Supplementary data for this article are available on the Web site or may be purchased from the Depository of Unpublished Data, Document Delivery, CISTI, National Research Council Canada, Ottawa, ON K1A 0S2, Canada. DUD 4012. For more information on obtaining material refer to http://cisti-icist.nrc-cnrc.gc.ca/irm/unpub_e.shtml. CCDC 241207 and 241208 contain the crystallographic data for this manuscript. These data can be obtained, free of charge, via www.ccdc.cam.ac.uk/conts/retrieving.html (Or from the Cambridge Crystallographic Data Centre, 12 Union Road, Cambridge CB2 1EZ, UK; fax +44 1223 336033; or deposit@ccdc.cam.ac.uk).

© 2005 NRC Canada

hydroxylamine hydrochloride (1.2 g, 16.5 mmol) in methanol (10 mL). The mixture was stirred for 10 h at 40 °C. The solvent was evaporated and the solid residue was dried under vacuum. The 3-alkyl-5-trichloromethyl-4,5-dihydroisoxazoles **3a** and **3b** and **3e**–**3h** were recrystallized from hexane. The 3-phenyl-5-trichloromethyl-4,5-dihydroisoxazoles **3c** and **3d** were recrystallized from methanol. The overall yields were higher than 90% (see Scheme 2). 5-Trichloromethyl-4,5-dihydroisoxazole compounds were fully characterized by spectroscopic methods. Data for **3a**: $C_5H_6Cl_3NO_2$, mp 125–127 °C, lit. value (19) mp 127 °C. ^{1}H NMR δ (mult., *J* Hz): 3.7 (Ha-4, d, 18.8), 3.25 (Hb-4, d, 18.8), 2.04 (Me-3, s). ^{13}C NMR δ: 156.7 (C-3), 111.0 (C-5), 101.9 (CCl_3), 47.9 (C-4). Anal. calcd.: C 27.49, H 2.77; found: C 27.30, H 2.75. **3b**: $C_7H_{10}Cl_3NO_2$, mp 140–142 °C. ^{1}H NMR δ (mult., *J* Hz): 3.73 (H-4, q, 7.6), 2.45 (CH_2, dq, J^2 = 16, J^3 = 7.6), 2.25 (CH_2, dq, J^2 = 16, J^3 = 7.6), 1.35 (Me-4, d, 7.6), 1.20 (Me, t, 7.6). ^{13}C NMR δ: 164.7 (C-3), 109.4 (C-5), 102.3 (CCl_3), 49.0 (C-4), 20.0 (CH_2), 11.45 (Me-4), 10.2 (Me). Anal. calcd.: C 34.11, H 4.10; found: C 34.00, H 4.20. **3c**: $C_{10}H_8Cl_3NO_2$, mp 155–158 °C, lit. value (38) mp 156 °C. ^{1}H NMR δ (mult., *J* Hz): 4.15 (Ha-4, d, 18.8), 3.73 (Hb-4, d, 18.8), 7.1–7.8 (Ph, m). ^{13}C NMR δ: 157.5 (C-3), 112.8 (C-5), 102.5 (CCl_3), 45.3 (C-4). Anal. calcd.: C 42.80, H 2.87; found: C 42.60, H 2.85. **3d**: $C_{11}H_{10}Cl_3NO_2$, mp 170–172 °C. ^{1}H NMR δ (mult., *J* Hz): 3.7 (H-4, q, 7.8), 2.2 (Me-4, d, 7.8), 7.0–8.0 (Ph, m). ^{13}C NMR δ: 156.7 (C-3), 111.0 (C-5), 101.9 (CCl_3), 47.9 (C-4). Anal. calcd.: C 44.85, H 3.42; found: C 45.0, H 3.5. **3e**: $C_8H_{10}Cl_3NO_2$, mp 148–150 °C, lit. value (38) mp 148–151 °C. ^{1}H NMR δ (mult., *J* Hz): 3.15 (H-4, dd, 12.6, 6.0). ^{13}C NMR δ: 161.6 (C-3), 109.0 (C-5), 102.12 (CCl_3), 52.8 (C-4). Anal. calcd.: C 37.17, H 3.90; found: C 37.2, H 3.85. **3f**: $C_{12}H_{18}Cl_3NO_2$, mp 183–186 °C. ^{1}H NMR δ (mult., *J* Hz): 3.52 (H-4, dd, 12.6, 6.0). ^{13}C NMR δ: 161.9 (C-3), 109.2 (C-5), 102.1 (CCl_3), 53.4 (C-4). Anal. calcd.: C 45.81, H 5.77; found: C 46.0, H 5.9. **3g**: $C_9H_{12}Cl_3NO_2$, mp 123–125 °C. ^{1}H NMR δ (mult., *J* Hz): 3.8 (H-4, ddt, 8.6, 4.8, 1.2). ^{13}C NMR δ: 164.8 (C-3), 109.6 (C-5), 102.2 (CCl_3), 55.9 (C-4). Anal. calcd.: C 39.66, H 4.44; found: C 40.0, H 4.5. **3h**: $C_{10}H_{14}Cl_3NO_2$, mp 118–120 °C. ^{1}H NMR δ (mult., *J* Hz): 3.7 (H-4, dd, 7.2, 4.0). ^{13}C NMR δ: 164.2 (C-3), 110.2 (C-5), 102.5 (CCl_3), 54.1 (C-4). Anal. calcd.: C 41.49, H 4.92; found: C 41.80, H 5.00.

Synthesis of 5-trichloromethylisoxazoles 4a–4h

General procedure

A mixture of 5-trichloromethyl-4,5-dihydroisoxazoles **3a**–**3h** (5 mmol) and concentrated sulfuric acid (5–10 mL) was stirred at 25–30 °C for 5 h. The mixture was slowly poured into 50 mL of ice water and the solution was extracted with chloroform (3 × 30 mL). The combined organic fractions were washed with water, dried under anhydrous sodium sulfate, and the solvent removed under vacuum. The liquid compound **4a** was purified by distillation and the liquid **4b** was purified by column chromatography with Kieselgel 60 and hexane–chloroform (9:1) as the eluent. The crystalline compounds **4c** and **4d** were purified by crystallization from methanol and crystalline **4e**–**4h** were recrystallized from hexane. 5-Trichloromethylisoxazole compounds were fully characterized by spectroscopic methods. Data for **4a**: $C_5H_4Cl_3NO$, oil. ^{1}H NMR δ (mult., *J* Hz): 7.25 (H-4, s), 2.04 (Me-3, s). ^{13}C NMR δ: 160.0 (C-3), 168.5 (C-5), 104.4 (C-4), 84.8 (CCl_3). Anal. calcd.: C 29.96, H 2.01; found: C 30.0, H 2.00. **4b**: $C_7H_8Cl_3NO$, oil. ^{1}H NMR δ (mult., *J* Hz): 2.60 (CH_2, q, 7.4), 2.30 (Me-4, s), 1.1 (Me, t, 7.4). ^{13}C NMR δ: 160.8 (C-3), 159.3 (C-5), 105.1 (C-4), 84.0 (CCl_3). Anal. calcd.: C 36.79, H 3.53; found: C 37.0, H 3.50. **4c**: $C_{10}H_6Cl_3NO$, mp 80–84 °C, lit. value (37) mp 80 to 81 °C. ^{1}H NMR δ (mult., *J* Hz): 7.41 (H-4, s), 7.20–7.85 (Ph, m). ^{13}C NMR δ: 163.5 (C-3), 169.6 (C-5), 103.2 (C-4), 85.0 (CCl_3). Anal. calcd.: C 45.75, H 2.30; found: C 46.0, H 2.50. **4d**: $C_{11}H_8Cl_3NO$, oil. ^{1}H NMR δ (mult., *J* Hz): 2.40 (Me-4, s), 7.2–7.8 (Ph, m). ^{13}C NMR δ: 162.8 (C-3), 160.2 (C-5), 105.4 (C-4), 83.6 (CCl_3). Anal. calcd.: C 47.78, H 2.92; found: C 48.0, H 3.0. **4e**: $C_8H_8Cl_3NO$, mp 174–177 °C. ^{1}H NMR δ (mult., *J* Hz): 1.7–2.0 ($(CH_2)_2$, m), 2.6–3.0 ($(CH_2)_3$, m). ^{13}C NMR δ: 161.8 (C-3), 159.9 (C-5), 112.8 (C-4), 85.9 (CCl_3). Anal. calcd.: C 39.95, H 3.35; found: C 40.4, H 3.5. **4f**: $C_{12}H_{16}Cl_3NO$, mp 79–82 °C. ^{1}H NMR δ (mult., *J* Hz): 1.3–3.1 (CH_2, m). ^{13}C NMR δ: 162.4 (C-3), 160.4 (C-5), 114.0 (C-4), 86.3 (CCl_3). Anal. calcd.: C 48.59, H 5.44; found: C 49.00, H 5.5. **4g**: $C_9H_{10}Cl_3NO$, mp 34–37 °C. ^{1}H NMR δ (mult., *J* Hz): 1.5–1.9 ($(CH_2)_3$, m), 2.7–2.95 ($(CH_2)_2$, m). ^{13}C NMR δ: 167.7 (C-3), 161.2 (C-5), 118.2 (C-4), 86.4 (CCl_3). Anal. calcd.: C 42.47, H 3.96; found: C 42.3, H 3.90. **4h**: $C_{10}H_{12}Cl_3NO$, oil, n^{20} 1.5675. ^{1}H NMR δ (mult., *J* Hz): 1.0–5.4 (-CH_2-, m). ^{13}C NMR δ: 166.4 (C-3), 161.1 (C-5), 116.0 (C-4), 86.4 (CCl_3). Anal. calcd.: C 44.72, H 4.50; found: C 44.50, H 4.50.

Synthesis of 5-carboxyisoxazoles 5a and 5b and 5e–5h

General procedure

A mixture of 5-trichloromethyl-4,5-dihydroisoxazoles **3a**–**3h** (5 mmol) and a solution of 85% sulfuric acid (5–10 mL) was stirred at 75–100 °C for 5–10 h. The mixture was slowly poured into 20 mL of ice water; the product **5** was obtained in high purity by filtration from the cold aqueous solution and washed with water. The crystalline compounds **5a** and **5b** and **5e**–**5h** were purified by recrystallization from hexane–chloroform or hexane. 5-Carboxyisoxazole compounds were fully characterized by spectroscopic methods. **5a**: $C_5H_5NO_3$, mp 210 °C, lit. value (6) mp 208–210 °C. ^{1}H NMR δ: 7.0 (H-4), 2.3 (Me-3). ^{13}C NMR δ: 158.7 (COOH), 161.5 (C-3), 161.3 (C-5), 110.3 (C-4). Anal. calcd.: C 42.23, H 3.97; found: C 42.32, H 4.02. **5b**: $C_7H_9NO_3$, mp 210 °C. ^{1}H NMR δ: 7.0 (CH_2), 2.3 (Me-4), 1.0 (Me). ^{13}C NMR δ: 158.7 (COOH), 161.5 (C-3), 161.3 (C-5), 110.3 (C-4). Anal. calcd.: C 54.19, H 5.85; found: C 54.0, H 6.0. **5e**: $C_8H_9NO_3$, mp 128–130 °C, lit. value (38) mp 128–130 °C. ^{1}H NMR δ: 1.5–1.9 $(CH_2)_2$, 2.6–2.9 $(CH_2)_2$. ^{13}C NMR δ: 152.9 (COOH), 162.1 (C-3), 160.8 (C-5), 123.2 (C-4). Anal. calcd.: C 57.48, H 5.43; found: C 57.60, H 5.5. **5f**: $C_{12}H_{17}NO_3$, mp 191–196 °C. ^{1}H NMR δ: 1.35–3.2 $(CH_2)_2$. ^{13}C NMR δ: 152.9 (COOH), 162.5 (C-3), 161.6 (C-5), 124.8 (C-4). Anal. calcd.: C 64.55, H 7.67; found: C 64.5, H 7.8. **5g**: $C_9H_{11}NO_3$, mp 132–134 °C. ^{1}H NMR δ: 1.65–1.8 $(CH_2)_2$, 1.85 (CH_2), 2.8–3.0 $(CH_2)_2$. ^{13}C NMR δ: 152.8 (COOH), 167.2 (C-3), 161.6 (C-5), 128.5 (C-4). Anal. calcd.: C 57.48, H 5.43; found: C 57.60, H 5.5. **5h**: $C_{10}H_{13}NO_3$, mp 130–

© 2005 NRC Canada

132 °C. ^{1}H NMR δ: 1.5–1.9 $(CH_2)_2$, 2.6–2.9 $(CH_2)_2$. ^{13}C NMR δ: 153.3 (COOH), 165.7 (C-3), 161.34 (C-5), 126.6 (C-4). Anal. calcd.: C 61.53, H 6.71; found: C 61.5, H 6.70.

Acknowledgements

The authors are thankful for the financial support from Fundação de Apoio à Pesquisa do Estado do Rio Grande do Sul (FAPERGS) and Conselho Nacional de Desenvolvimento Científico e Tecnológico (CNPq/PADCT III, Proj.62.0228/97-0–QEQ). Fellowships from CNPq (D.C. Flores, S. Brondani, S. Moura, V.L. Leidens, and W. Cunico) are also acknowledged.

References

1. A.F.C. Flores, S. Brondani, N. Zanatta, A. Rosa, and M.A.P. Martins. Tetrahedron Lett. **43**, 8701 (2002).
2. M.A.P. Martins, G.P. Bastos, H.G. Bonacorso, N. Zanatta, A.F.C. Flores, and G.M. Siqueira. Tetrahedron Lett. **40**, 4309 (1999).
3. H.G. Bonacorso, M.A.P. Martins, S.R.T. Bittencourt, R.V. Lourega, N. Zanatta, and A.F.C. Flores. J. Fluorine Chem. **99**, 177 (1999).
4. A.F.C. Flores, G.M. Siqueira, R. Freitag, N. Zanatta, and M.A.P. Martins. Quím. Nova, **17**, 298 (1994).
5. M.A.P. Martins, A. Sinhorin, N.E.K. Zimmermann, H.G. Bonacorso, N. Zanatta, and G.P. Bastos. Synthesis, 1959 (2001).
6. M.A.P. Martins, A.F.C. Flores, G.P. Bastos, A. Sinhorin, H.G. Bonacorso, and N. Zanatta. Tetrahedron Lett. **41**, 293 (2000).
7. M.A.P. Martins, R.A. Freitag, A. Rosa, A.F.C. Flores, N. Zanatta, and H.G. Bonacorso. J. Heterocycl. Chem. **36**, 217 (1999).
8. R. Levine, J.A. Conroy, J.T. Adams, and C.R. Hauser. J. Am. Chem. Soc. **67**, 1510 (1945).
9. A.L. Hene, M.S. Newman, L.L. Quill, and R.A. Staniforth. J. Am. Chem. Soc. **69**, 1819 (1947).
10. D.V. Sevenard, O.G. Khomutov, M.I. Kodess, K.I. Pashkevich, I. Loop, E. Lork, and G.-V. Röschenthaler. Aust. J. Chem. **54**, 157 (2001).
11. K.A.K. Ebraheem, S.T. Hamdi, and M.N. Khalaf. Can. J. Spectrosc. **26**, 225 (1981).
12. T. Ishihara, T. Seki, and T. Ando. Bull. Chem. Soc. Jpn. **55**, 3345 (1982).
13. I. Katsuyama, S. Ogawa, Y. Yamaguchi, K. Funabiki, M. Matsui, H. Muramatsu, and K. Shibata. Synthesis, 1321 (1997).
14. K.C. Joshi and V.N. Pathak. Coord. Chem. Rev. **22**, 37 (1977).
15. J.T. Welch. Tetrahedron, **43**, 3123 (1987).
16. J.D. Park, H.A. Brown, and J.R. Lacher. J. Am. Chem. Soc. **75**, 4753 (1953).
17. F. Effenberger, R. Maier, K.-H. Schönwälder, and T. Ziegler. Chem. Ber. **115**, 2766 (1982).
18. W. Spiegler and N. Götz. Synthesis, 69 (1986).
19. A. Colla, M.A.P. Martins, G. Clar, S. Krimmer, and P. Fischer. Synthesis, 483 (1991).
20. M. Hojo, R. Masuda, S. Sakaguchi, and M. Takagawa. Synthesis, 1016 (1986).
21. C. Zucco, C.F. Lima, M.C. Rezende, and R.A. Rebelo. J. Org. Chem. **52**, 5356 (1987).
22. C. Zucco, F. Nome, M.C. Rezende, and R.A. Rebelo. Synth. Commun. **17**, 1741 (1987).
23. R.A. Wohl. Synthesis, 38 (1974).
24. J. Emsley. Struct. Bonding **57**, 147 (1984).
25. A.I. Koltsov and D.Kh. Zheglova. The last NMR research in organic and polymer chemistry in Russia. *Edited by* A.I. Koltsov. Norell Press, New York. 1996.
26. A.J. Villa, C.M. Lagier, and A.C. Olivieri. Magn. Reson. Chem. **28**, 529 (1990).
27. A.I. Koltsov, A. Yu Elkin, and D. Kh. Zheglova. J. Mol. Struct. **221**, 309 (1990).
28. A. Kumar and D.W. Boykin. J. Mol. Struct. **296**, 95 (1993).
29. A.L. Baumstark, M. Dotrong, R.R. Stark, and D.W. Boykin. Tetrahedron Lett. **29**, 2143 (1988).
30. C.F.G.C. Geraldes, M.T. Barros, C.D. Maycock, and M.I. Silva. J. Mol. Struct. **238**, 335 (1990).
31. M.A.P. Martins, A.N. Zoch, N. Zanatta, and A.F.C. Flores. Spectrosc. Lett. **31**, 621 (1998).
32. M.A.P. Martins, A.F.C. Flores, R.A. Freitag, N. Zanatta, M. Hörner, and A.J. Bortoluzzi. Spectrosc. Lett. **30**, 661 (1997).
33. Enraf-Nonius. CAD4 [software manual]. Delft, The Netherlands. 1986.
34. L. Zsolnai and H. Pritzkow. ZORTEP [computer program]. University of Heidelberg, Heidelberg, Germany. 1996.
35. G.M. Sheldrick. SHELXS-97 [computer program]. University of Göttingen, Göttingen, Germany. 1997.
36. Hypercube Inc. HyperChem 6.03 package [computer program]. Hypercube Inc., Gainesville, Florida. 1999; HyperChem manual [software manual]. Computational Chemistry, Waterloo, Ontario. 1994.
37. M.A.P. Martins, G.M. Siqueira, G.P. Bastos, H.G. Bonacorso, and N. Zanatta. J. Heterocycl. Chem. **33**, 1619 (1996).
38. M.A.P. Martins, A.F.C. Flores, R.A. Freitag, and N. Zanatta. J. Heterocycl. Chem. **32**, 731 (1995).

© 2005 NRC Canada

Electron spin resonance analysis of the oxidation reactions of nitrone type spin traps with gold(III) ion

Akira Nakajima, Yuto Ueda, Nobuyuki Endoh, Kunihiko Tajima, and Keisuke Makino

Abstract: When cyclic nitrones, such as 5,5-dimethyl-1-pyrroline-*N*-oxide (DMPO), 4-phenyl-5,5-dimethyl-1-pyrroline-*N*-oxide (PDMPO), and 3,3,5,5-tetramethyl-1-pyrroline-*N*-oxide (M4PO) were mixed with hydrogen tetrachloroaurate(III), DMPOX (5,5-dimethyl-1-pyrrolid-2-one-*N*-oxyl) type free radicals appeared with the precipitation of Au(0). The reaction did not proceed with noncyclic nitrones, such as *N-tert*-butyl-α-phenyl-nitrone (PBN) and α-(4-pyridyl-1-oxide)-*N-tert*-butyl-nitrone (POBN). The order of the $HAuCl_4$ decrease was DMPO > PDMPO > M4PO. The reaction was depressed by the addition of chloride or hydroxide ions. 1-Hydroxy-5,5-dimethyl-1-pyrrolid-2-one (HDMPN), the precursor of DMPOX, was also oxidized to DMPOX by $HAuCl_4$. Every step of the gold reduction from Au(III) to Au(0) can be used for the oxidation of HDMPN to DMPOX. Based on these and previous results, the reaction was assumed to proceed by the following scheme consisting of a ligand exchange interaction of $AuCl_4^-$ with $>N^+–O^-$ in DMPO, then nucleophilic addition of a water molecule to DMPO, then the stepwise intramolecular transfer of three electrons from DMPO to Au(III), and finally the precipitation of Au(0).

Key words: ESR, nitrone, spin traps, DMPO, DMPOX, gold(III) ion.

Résumé : Lorsque des nitrones cycliques, tels que 5,5-diméthyl-1-pyrroline-*N*-oxyde (DMPO), 4-phényl-5,5-diméthyl-1-pyrroline-*N*-oxyde (PDMPO), et 3,3,5,5-tétraméthyl-1-pyrroline-*N*-oxyde (M4PO) ont été mélangés avec du tétrachloroaurate(III) d'hydrogène, des radicaux libres de type DMPOX (5,5-diméthyl-1-pyrrolidine-2-one-*N*-oxyl) apparut avec la précipitation de Au(0). La réaction ne s'est pas produite avec les nitrones non cycliques, tels que *N-tert*-butyl-α-phényl-nitrone (PBN) et α-(4-pyridyle-1-oxyde)-*N-tert*-butyl-nitrone (POBN). L'ordre de la diminution de $HAuCl_4$ était DMPO > PDMPO > M4PO. La réaction a été abaissée par l'addition d'ions chlorure ou hydroxyde. 1-Hydroxy-5,5-diméthyl-1-pyrrolidine-2-one (HDMPN), le précurseur de DMPOX, a été aussi oxydé en DMPOX par $HAuCl_4$. Chaque étape de la réduction de l'or de Au(III) à Au(0) peut être utilisée pour l'oxydation de HDMPN en DMPOX. Basée sur ceux-ci ainsi que sur les résultats précédents, la réaction a été expliquée par la combinaison supposée se composant de l'interaction d'échange du ligand de $AuCl_4^-$ avec $>N^+–O^-$ dans DMPO, de l'addition nucléophilique d'une molécule d'eau à DMPO, du transfert intramoléculaire par étape de trois électrons de DMPO à Au(III), et de la precipitation de Au(0).

Mots clés : RPE, nitrone, piège à spin, DMPO, DMPOX, ion Au(III).

Introduction

Recently, various nitrones have been used as spin traps for short-lived free radicals, such as the hydroxyl radical, in biosystems (1). However, some of these are well-known to produce free radicals not only through radical reactions but also through ionic reactions. 5,5-Dimethyl-1-pyrroline-*N*-oxide (DMPO), one of the most popular nitrone type spin traps, was oxidized to 5,5-dimethyl-1-pyrrolid-2-one-*N*-oxyl (DMPOX) by various oxidants (2–11) or through oxidative bioreactions (12–17). Similar DMPOX-type radicals were also observed for 3,3,5,5-tetramethyl-1-pyrroline-*N*-oxide (M4PO) (9, 18, 19). Makino et al. (5) reported that DMPO was oxidized to DMPOX by Fe^{3+} ion through 2-hydroxy-5,5-dimethyl-1-pyrrolidinyloxy (DMPO-OH), 2-hydroxy-5,5-dimethyl-1-pyrrolid-2-one (HDMPO), and 1-hydroxy-

Received 2 March 2005. Published on the NRC Research Press Web site at http://canjchem.nrc.ca on 24 September 2005.

A. Nakajima.[1] Section of Chemistry, Department of Medical Science, Faculty of Medicine, University of Miyazaki, Kiyotake, Miyazaki 889-1692, Japan.
Y. Ueda. Department of Psychiatry, Faculty of Medicine, University of Miyazaki, Kiyotake, Miyazaki 889-1692, Japan.
N. Endoh. The Wakasa Wan Energy Research Center, Nagatani 64-52-1, Tsuruga, Fukui 914-0192, Japan.
K. Tajima. Department of Applied Biology, Kyoto Institute of Technology, Matsugasaki, Sakyo-ku, Kyoto 606-8585, Japan.
K. Makino. International Innovation Center, Kyoto University, Yoshida, Sakyo-ku, Kyoto 606-8501, Japan.

[1]Corresponding author (e-mail: akanaka@med.miyazaki-u.ac.jp).

 doi: 10.1139/V05-132 © 2005 NRC Canada

5,5-dimethyl-1-pyrrolid-2-one (HDMPN). Tajima and coworkers (18, 19) clarified in their electrochemical study that DMPO was oxidized to DMPOX by removal of three electrons. As the use of various nitrones for spin-trapping analysis has been increased recently, further information on specificities and kinetics of the DMPOX-type radical formation for various nitrones should become very important.

Various compounds containing sulfur, such as methionine (20), are well-known to reduce the Au(III) ion to Au(0). Recently, Zou et al. (21) found that Au(III) oxidized glycine through deamination and decarboxylation with formation of glyoxylic acid, ammonium ion, formic acid, carbon dioxide, and metallic gold. These results suggest that Au(III) is one of the best oxidants for various organic compounds, and can be applied for the analysis of DMPO oxidation.

The authors, therefore, examined the interaction between Au(III) and nitrone type spin traps, such as DMPO, and found the formation of DMPOX-type free radicals. In this study, some aspects and the mechanism of the nitrone oxidation reaction with Au(III) are discussed.

Experimental

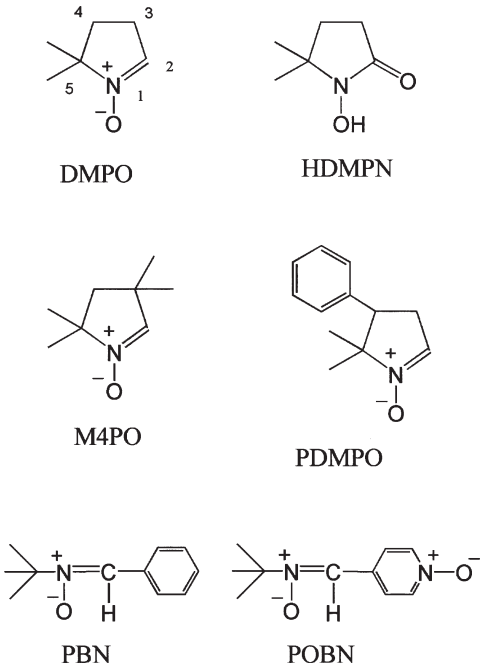
Chemicals

Hydrogen tetrachloroaurate(III) ($HAuCl_4$) dihydrate and sodium dicyanoaurate(I) were obtained from Nacarai Tesque (Kyoto, Japan). DMPO, M4PO, *N-tert*-butyl-α-phenyl-nitrone (PBN), and α-(4-pyridyl-1-oxide)-*N-tert*-butyl-nitrone (POBN) were obtained from DOJINDO Ltd. (Kumamoto, Japan). During manufacture, a purity of more than 99% was obtained by repeated vacuum distillation and was checked by gas chromatography. 4-Phenyl-5,5-dimethyl-1-pyrroline-*N*-oxide (PDMPO) was obtained from Sigma-Aldrich Japan Inc. (Tokyo, Japan). HDMPN was prepared according to the method described by Bonnett et al. (22). Molecular structures of nitrones used in this study are shown in Fig. 1. All nitrones and the HDMPN used were examined by electron spin resonance (ESR) and no radical species were observed.

ESR measurements

Forty microliters of $HAuCl_4$ solution (1.25 mmol/L) and 40 μL of nitrone solution (1.25 mmol/L) were mixed at pH 4. After aspirating the mixture into a capillary tube, its ESR spectrum was immediately recorded using an X-band ESR spectrometer (JES TE-100, JEOL Ltd., Tokyo, controlled by a WIN-RAD ESR data analyzer, Radical Research Inc., Tokyo) under the following conditions: microwave power 5 mW; microwave frequency 9.42 GHz; magnetic field 335.3 mT; field amplitude ±5 mT; field modulation 100 kHz; modulation width 0.025~0.1 mT; sweep time 1 min; and the response time was 0.1 s. The solution pH was adjusted to the desired value with 0.1 N HNO_3 and 0.1 N NaOH solutions. To avoid the photochemical reduction of Au(III), the reaction was conducted under dark conditions. To determination the radical concentration, 60 μL of the sample solutions were aspirated into capillary tubes and their ESR spectra were recorded individually. The concentration of DMPOX-type radical was calibrated by using TEMPOL as a standard, following double integration of the observed ESR signal.

Fig. 1. Molecular structure of nitrone type spin traps and HDMPN, the precursor of DMPOX.



Gold determination

Total amounts of the Au(III) species in the reaction mixture were determined by spectrophotometry using Rhodamine B (23). The resulting amounts of Au(0) in the reaction mixture were determined as follows: the precipitate was dissolved in a solution of aqua regia (HNO_3–HCl mixture of 1:3) and then the concentration of gold in the solution was determined by using an ICP quantometer (Shimadzu ICPQ-1000II).

Results

Formation of aminoxyl radicals in nitrone–$HAuCl_4$ solutions

When solutions of cyclic nitrones (1.25 mmol/L), such as DMPO, PDMPO, and M4PO, were mixed with a $HAuCl_4$ solution (1.25 mmol/L) at pH 4, ESR signals with 9, 10, and 3 lines appeared, respectively (Fig. 2). The hyperfine coupling constants, that were estimated from computer simulations, are listed in Table 1. From these values, the radicals were identified as DMPOX (5, 7, 12, 13) and 3,3,5,5-tetramethyl-1-pyrrolid-2-one-*N*-oxyl (M4POX) (9). No β proton in M4POX gave the primary nitroxide triplet without any additional hyperfine splitting. Radical species that appeared in the PDMPO–Au(III) solution gave three hyperfine coupling constants at 0.71, 0.40, and 0.30 mT. Two of these, 0.71 and 0.40 mT, are identical to the a_N and a_{3H} of DMPOX. In PDMPO, the chiral C-4 atom, which can couple with one hydrogen atom and one phenyl group, will give rise to different hyperfine coupling constants for the two β protons, and they should appear at values of 0.40 and 0.30 mT. Therefore, the resultant radical can be assigned as a DMPOX-type radical, namely 4-phenyl-5,5-dimethyl-1-pyrrolid-2-one-*N*-oxyl (PDMPOX).

© 2005 NRC Canada

Fig. 2. ESR spectra of free radicals observed in the solution mixtures containing the following nitrones: (*a*) DMPO, (*b*) PDMPO, (*c*) M4PO, (*d*) PBN, and (*e*) POBN (1.25 mmol/L) and $HAuCl_4$ (1.25 mmol/L). The microwave frequency was 9.42 GHz.

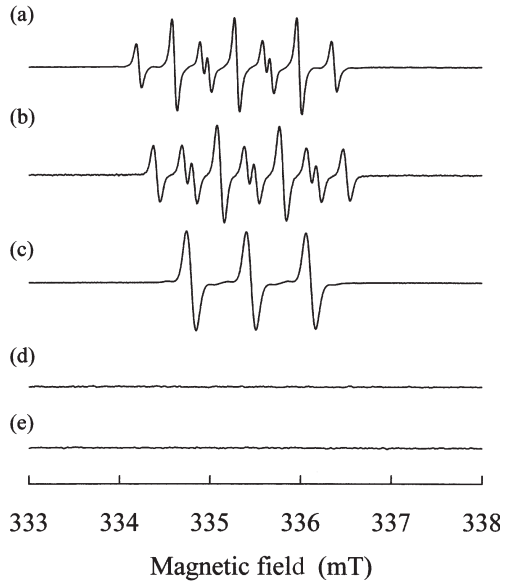


Table 1. Hyperfine coupling constants of free radicals observed in the reaction mixtures of hydrogen tetrachloroaurate(III) and cyclic nitrones, DMPO, PDMPO, and M4PO.

	Hyperfine coupling constant $A/g\beta$ (mT)	
Free radicals	a_N	a_{3H}[a]
DMPOX	0.71	0.40[b]
PDMPOX	0.71	0.40[c]
		0.30[c]
M4POX	0.67	

[a]The hyperfine coupling constant for protons combined with the C-3 atom in nitrone.
[b]Two protons combined with the C-3 atom are equivalent.
[c]Two protons combined with the C-3 atom are not equivalent to each other.

As the reaction proceeded, red-brown colored fine particles were deposited on the inner surface of the vessel. Deposited particles could be dissolved only in an aqua regia solution, and not in any other mineral acids. The resultant solution contained $AuCl_4^-$ species, which were identified by their absorbance at 322 nm (24) and by ICP quantometry. The deposited particles were thus deduced to be Au(0). These results indicate that Au(III) in the reaction mixture was reduced to Au(0) through the three-electron oxidation of nitrones to DMPOX-type free radicals. The reaction between DMPO and $HAuCl_4$ was conducted in N_2-bubbling water. No clear difference in any aspect of the reaction was observed in ordinal water. These results suggested that oxygen does not play an important role in the reaction.

In reaction mixtures of $HAuCl_4$ and noncyclic nitrones, such as PBN and POBN, no radical species, such as *N-tert*-butyl-α-phenyl-nitroxyl (PBNX) and α-(4-pyridyl-1-oxide)-*N-tert*-butyl nitroxyl (POBNX), were observed. These results indicated that the reaction proceeds only with cyclic nitrones, such as DMPO, PDMPO, and M4PO.

No ESR signal was observed for both neutral and acidic solutions of DMPO in the presence of excess amounts of sodium dicyanoaurate(I). The redox potentials are E[Au(III) – Au(0)] = +1.0, E[Au(III) – Au(I)] = +0.93, E[Au(I) – Au(0)] = +1.15 V for Cl^-, and E[Au(I) – Au(0)] = –0.61 V for CN^-. These values indicated that $Au(III)Cl_4^-$ is far more easily reduced to Au(0) than $Au(CN)_2^-$. Furthermore, CN^- in the dicyanaurate(I), being very stable under neutral conditions (β_2 = 11.23) (25), cannot be replaced with DMPO. Disproportionation of the Au(I) ion occurs only with difficulty (eq. [1]).

$$[1] \qquad 3[Au(I)L_2]^- \rightarrow [Au(III)L_4] + 2Au(0) + 2L$$

In the present system (20) disproportionation is not favourable since for L = CN^- the equilibrium constant of eq. [1] may be in the order of 10^{-25}. These results suggest that the oxidation of DMPO to DMPOX occurs only because of coupling with the three-electron reduction of Au(III) ion to Au(0).

Aspects of DMPOX-type radical formation in cyclic nitrone–$HAuCl_4$ solutions

Time course of radical formation

The time course of DMPOX-type radical formation was examined using mixtures of nitrones (1.25 mmol/L) and $HAuCl_4$ (1.25 mmol/L) at pH 4. The ESR signal intensities for all DMPOX-type radicals examined increased with time, and reached a maximum value within 20~30 min for DMPOX and PDMPOX, and more than 60 min for M4PO (Fig. 3). No other free radical species, except DMPOX-type ones, were observed for a period of 2 h after the reaction was started.

As shown in Fig. 3, the time course of DMPOX-type radical formation in these nitrones show lag phases in the first 5–10 min, which suggests complicated reaction processes. The decrease in Au(III) concentration in the reaction mixtures was fitted to eq. [2] and exhibited second-order reaction kinetics (Fig. 3),

$$[2] \qquad [Au(III)] = C/(Ckt + 1)$$

where C is the initial Au(III) concentration (1.25 mmol/L), t is time, and k is the equilibrium constant. The k values for each nitrone are listed in Table 2. As shown in Table 2, the relative order of magnitude in the rate for the initial stage of the reaction was PDMPO > DMPO >> M4PO, while for the final radical formation it was PDMPO ≥ DMPO > M4PO. In PDMPO, a weak inductive effect proceeds the reaction, while in M4PO, a couple of methyl groups at C-3 strongly hindered the reaction.

Effect of nitrone concentration

The effect of nitrone concentration on DMPOX-type radical formation was examined using a mixture of DMPO (0.5~5 mmol/L) and $HAuCl_4$ (1.25 mmol/L) at pH 3. As shown in Fig. 4, an unusual time dependency was observed for DMPOX radical formation. An anomalous increase in

© 2005 NRC Canada

Fig. 3. Time course of ESR signal intensities and Au(III) concentration in mixtures of nitrones (1.25 mmol/L) and $HAuCl_4$ (1.25 mmol/L). Closed circles are the ESR signal intensity in DMPO, closed triangles in PDMPO, and closed diamonds in M4PO solutions; open circles are the Au(III) concentration in DMPO, open triangles in PDMPO, and open diamonds in M4PO solutions. The solid lines indicate the best fitting curves using the least-squares method, while the dotted lines are those estimated using eq. [2]. Parallel experiments were conducted to determine the gold concentrations as described in the Experimental section.

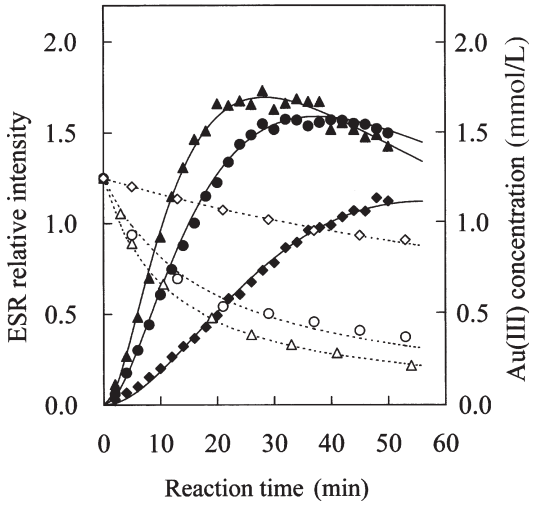


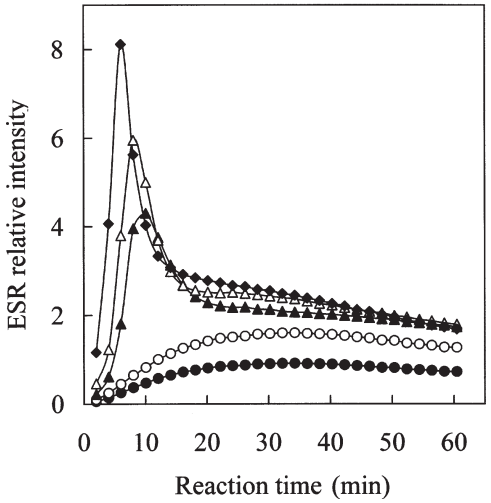
Table 2. Kinetic parameters for DMPOX-type radical formation.

Nitrone	k	Maximum amount of free radical (mmol/L)
DMPO	0.043	0.014
PDMPO	0.069	0.015
M4PO	0.0061	0.010

Note: [Au(III)] = $C/(Ckt + 1)$. The initial concentration of each nitrone was 1.25 mmol/L.

DMPOX was observed within the first 10 min of mixing DMPO (2.5~5 mmol/L) and $HAuCl_4$ (1.25 mmol/L). Twenty minutes after the reaction started, this time dependency slowed and settled down to match that of low DMPO concentrations (0.5 and 1.25 mmol/L). These results suggested that excess amounts of DMPO eliminated the DMPOX radical formed in the mixture. Thornalley et al. (14) reported a similar rapid decrease of DMPOX in *tert*-butyl hydroperoxide–methaemoglobin systems and suggested that DMPOX decomposed to various products such as 5,5-dimethyl-1-hydroxy-2-pyrrolidone (DMPOXH), 4-methyl-4-nitrosopentanoic acid (MNPA), 4-methyl-4-nitropentanoic acid (MNOPA), 4-methyl-4-nitrosobutane, and a radical species, *N*-(5,5-dimethyl-1-oxyl-pyrrolidine)-4-hydroylamino-4-methylpentane (DMPO–PNO) (26). In the present system, an ESR signal for DMPO–PNO with 18 lines characterized by a_{N1} = 1.43, a_H = 1.62, and a_{N2} = 0.42 mT was not observed under excess DMPO conditions. Furthermore, DMPOX decreased slower with small amounts of DMPO present than under excess DMPO conditions (Fig. 3). Other possibilities include the reduction of DMPOX to its hydroxyl amine or even dimerization of the DMPOX. Further precise experiments will be needed to clarify this situation. In this paper, low concentrations, such as 1.25 mmol/L of DMPO, where the anomalous increase was not observed within the first 10 min, will be adopted for the following experiments.

Fig. 4. Effect of DMPO concentration on DMPOX formation in mixtures of DMPO (0.5~5 mmol/L) and $HAuCl_4$ (1.25 mmol/L). Closed circles are 0.5 mmol/L, open circles are 1.25 mmol/L, closed triangles are 2.5 mmol/L, open triangles are 3.75 mmol/L, and closed diamonds are 5 mmol/L DMPO solutions. The solid lines indicate the best fitting curves using the least-squares method.



Effect of co-existing salts

Addition of sodium chloride to the reaction mixture markedly decreased the ESR signal intensities of DMPOX, PDMPOX, and M4POX, while no effect was observed when $NaNO_3$ was added (Fig. 5). The amount of $AuCl_4^-$ in the solutions, as depicted in Fig. 5, was calculated using the formation constants listed by Sillen and Martell (25). As shown in Fig. 5, formation of the stable complex anion, $AuCl_4^-$, suppressed the redox reaction.

Effect of solution pH

The ESR signal intensities of DMPOX-type radicals decreased below pH 1 and above pH 6 (Fig. 6) in DMPO, PDMPO, and M4PO. The ratios of chemical species, $AuCl_4^-$, $Au(OH)Cl_3^-$, $Au(OH)_2Cl_2^-$, $Au(OH)_3Cl^-$, and $Au(OH)_4^-$ calculated using the formation constants listed by Sillen and Martell (25), are also shown in Fig. 6. As shown in Fig. 6, as the ratios of $AuCl_4^-$ and $Au(OH)_4^-$ in the reaction mixture were increased, the ESR signal intensities decreased. Below pH 2, excess amounts of Cl^- stabilize the $AuCl_4^-$ ion, while above pH 7, excess amounts of OH^- stabilize the $Au(OH)_4^-$ ion. In the intermediate pH range, Cl^- ion in the complex ions were easily replaced with the OH^- ion. When DMPO exists in the solution, Cl^- ion in the complex ions were easily replaced with DMPO, in a manner similar to the reaction between thiomorpholin-3-one and $AuCl_4^-$ ion as proposed by De Filippo et al. (27). Complex formation between DMPO and the Au(III) ion will proceed via the redox reaction. These results suggest that the formation of stable com-

© 2005 NRC Canada

Fig. 5. Effect of sodium salts on ESR signal intensities in mixtures of nitrones (1.25 mmol/L), $HAuCl_4$ (1.25 mmol/L), and the desired amounts of sodium salts. The reaction time was 1 h. Closed circles are the ESR signal intensity in DMPO–NaCl solution, open circles are DMPO–$NaNO_3$, closed triangles are PDMPO–NaCl, open triangles are PDMPO–$NaNO_3$ (superimposed on open circles), closed diamonds are M4PO–NaCl, and open diamonds are M4PO–$NaNO_3$ solutions. Dotted lines indicate the ratio of [$AuCl_4^-$] calculated using the formation constants listed by Sillen and Martell (25).

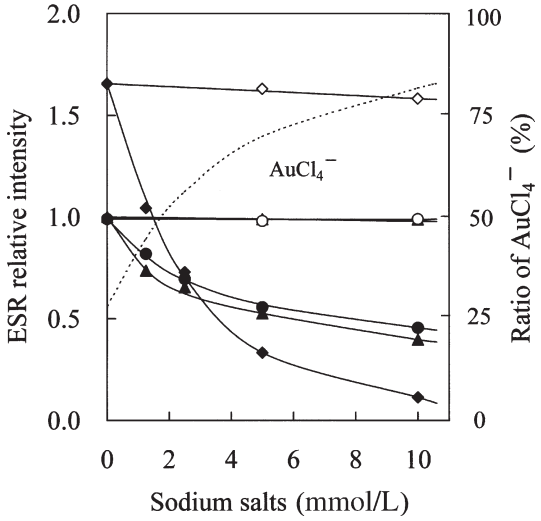
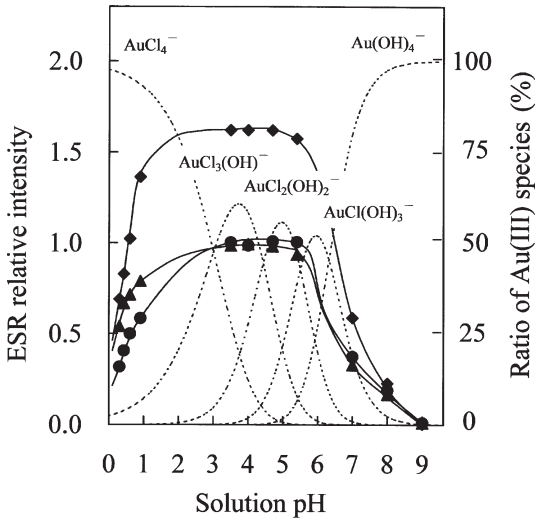


Fig. 6. Effect of solution pH on the ESR signal intensities in mixtures of nitrones (1.25 mmol/L) and $HAuCl_4$ (1.25 mmol/L). The reaction time was 1 h. Closed circles are the ESR signal intensity of DMPOX, closed triangles are PDMPOX, and closed diamonds are M4POX. Dotted lines indicate the ratios of $AuCl_4^-$, $AuCl_3(OH)^-$, $AuCl_2(OH)_2^-$, $AuCl(H)_3^-$, and $Au(OH)_4^-$ calculated as described in the caption of Fig. 5.

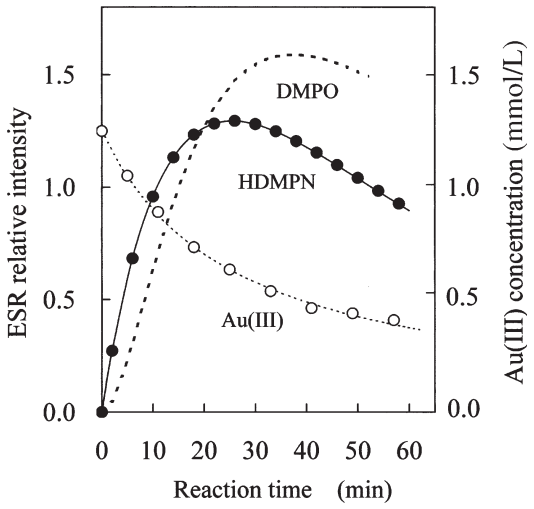


plex anions, such as $AuCl_4^-$ and $Au(OH)_4^-$, suppress the redox reaction.

Reaction of the DMPOX precursor with $HAuCl_4$

HDMPN, the precursor of DMPOX in the oxidation of DMPO by Fe^{3+} ion (5) and in the electrochemical oxidation of DMPO (18, 19), was also oxidized to DMPOX by the

Fig. 7. Time course of ESR relative intensities of DMPOX observed in the solution mixtures of $HAuCl_4$ and HDMPN. $HAuCl_4$ (1.25 mmol/L) was mixed with DMPO and HDMPN (1.25 mmol/L), respectively. Closed circles are the ESR signal intensity and open circles are the Au(III) concentration in the HDMPN–$HAuCl_4$ solution. The solid line indicates the best fitting curve using the least-squares method while the dotted line has been estimated using eq. [2]. The dashed line indicates the ESR intensity in the DMPO–$HAuCl_4$ solution. Parallel experiments were conducted to determine the gold concentrations as described in the Experimental section.

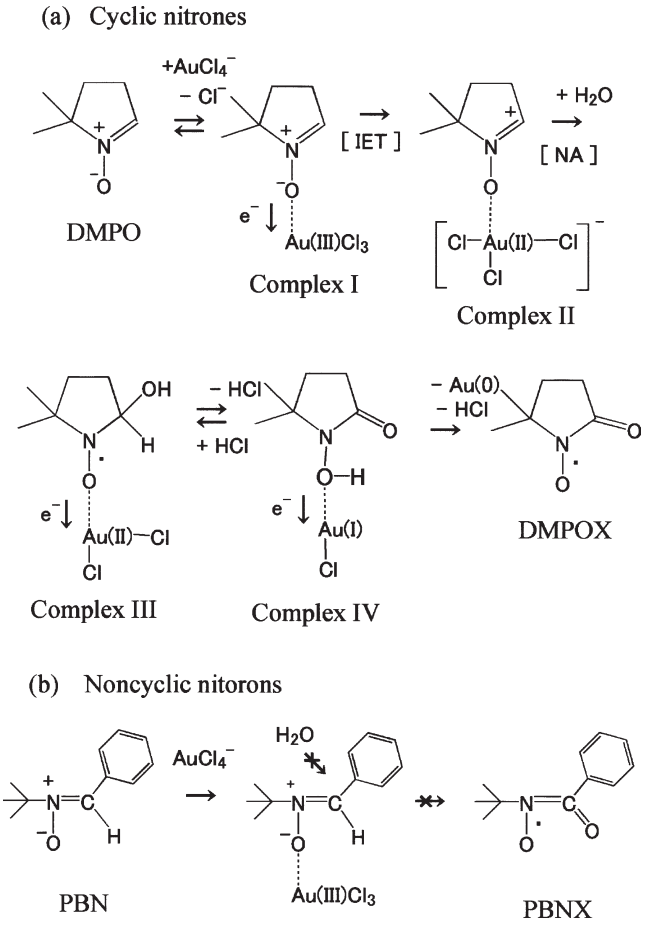


Au(III) ion. The ESR signal intensity of DMPOX in the 1:1 mixture of HDMPN and $HAuCl_4$ (1.25 mmol/L) was increased with the time course (Fig. 7). The time course of Au(III) reduction in the system was also well described by eq. [1], where $k = 0.028$ and the maximum amount of free radical was 0.012 mmol/L. Complexation between Au(III) and HDMPN is slower than that observed between Au(III) and DMPO. No precipitation of Au(0) was observed during the course of the reaction, which showed that the reduction step from Au(I) to Au(0) was not used for HDMPN oxidation in the 1:1 mixture. On the other hand, in the 3:1 mixture of HDMPN (1.25 mmol/L) and $HAuCl_4$ (0.417 mmol/L), DMPOX was formed with Au(0) precipitation, which indicated that the reduction step from Au(I) to Au(0) was coupled with HDMPN oxidation. Summarizing these results, it is proposed that the three-electron-reduction process from Au(III) to Au(0) can be coupled with the oxidation of DMPO to DMPOX.

A weak ESR signal for DMPOX was observed in a sodium dicyanoaurate(I)–HDMPN solution mixture under acidic conditions (pH 0.5), despite exhibiting no signal at neutral pH. There are two possible explanations for these results: first is the oxidation ability of Au(I) ions. Since dicyanoaurate(I) ion is very stable under neutral conditions (β_2 = 11.23) (25), HDMPN cannot form a complex with Au(I) if cyanide ions are present in the system. However, under acidic conditions, small amounts of CN^- in the dicyanoaurate(I) ion can be replaced with HDMPN, which causes transfer of an electron from Au(I) to HDMPN and DMPOX forms. Second is the disproportionation of the Au(I) ion (eq. [1]) (20). As discussed in the previous section, disproportionation is not favourable for the dicyanoaurate(I) ion

© 2005 NRC Canada

Fig. 8. Overall reaction of $HAuCl_4$ with cyclic nitrones such as (*a*) DMPO and noncyclic nitrones such as (*b*) PBN. The intramolecular electron transfer is abbreviated as IET and the nucleophilic addition as NA.



(20). These results, therefore, indicate the possibility that the reduction step from Au(I) to Au(0) was used for HDMPN oxidation.

Discussion

Cyclic nitrones, such as DMPO, PDMPO, and M4PO, were oxidized to DMPOX-type free radicals by the Au(III) ion with precipitation of Au(0). The reaction was greatly hindered by chloride ion, and was depressed in acidic and basic solutions. An assumed overall reaction scheme for the DMPO–$HAuCl_4$ system is shown in Fig. 8*a*. First, DMPO···Au(III)Cl_3 (complex I) is formed by the ligand exchange interaction between Cl^- and DMPO, in a manner similar to the formation of the Fe^{3+}–DMPO complex (5). This is followed by the intramolecular electron transfer from DMPO to Au(III)Cl_3 (complex II). The resultant complex II is then converted to complex III (DMPO-OH···Au(II)Cl_2) by the nucleophilic addition of a water molecule at the C-2 atom. The resultant complex III is converted to complex IV (HDMPN···Au(I)Cl) by the intramolecular electron transfer from DMPO-OH to Au(II)Cl_2 with the loss of HCl. Finally, complex IV is converted to DMPOX by the intramolecular electron transfer from HDMPN to Au(I)Cl and release of HCl and Au(0). Three electrons are, therefore, moved from DMPO to Au(III) through the reaction. When stable complex anions, such as $AuCl_4^-$ or $Au(OH)_4^-$ are formed by the addition of HCl, NaCl, or NaOH, the ligand exchange interaction in the first stage will be depressed. The rate of total Au(III) decrease corresponded to the increase in the ESR signal intensity of the resultant radical. Thus, the formation of complex I should be the rate-determining step in the reaction process. Two methyl groups at the C-3 atom in M4PO sterically hinder the addition of a water molecule to the C-2 atom, thereby causing the slower reaction rate. Similar kinetics for M4PO oxidation were found in the Fe^{3+}–M4PO system (27). The weak inductive effect of the 4-phenyl group in PDMPO will cause a slightly faster reaction rate than for DMPO.

In the reaction mixture of $HAuCl_4$ and noncyclic nitrones, such as PBN and POBN, no ESR signal was observed. Similar results were observed in the Fe^{3+}–PBN system and in the electrochemical redox reaction of PBN (19). These results suggest that steric hindrance of the phenyl group in PBN or the 4-pyridyl-1-oxide group in POBN inhibits the nucleophilic addition of a water molecule and chelation to the metal ion (Fig. 8*b*). Ozawa et al. (9) reported the formation of PBNX and POBNX by oxidation of PBN and POBN with the ClO_2 radical. They explained this reaction as the direct oxidation of the α-C atom in PBN and POBN by the ClO_2 radical, which is quite different from our scheme.

As discussed in the previous section, the results reported herein can be explained quite well by the proposed reaction mechanism shown in Fig. 8*a*. The reduced forms of DMPOX and HDMPN (18, 19) were also oxidized to DMPOX by reaction with 0.33 mol/L $HAuCl_4$, indicating that every step of the gold reduction, from Au(III) to Au(0), is coupled with oxidation of HDMPN and DMPO. These results suggested the possibility that HDMPN was the DMPOX precursor in our system. If the first step involved in the $HAuCl_4$–DMPO system is the ligand exchange interaction and the nucleophilic addition of a water molecule, then the reaction will proceed with a rate constant having a time dependency of $[1 - \exp(-0.043t)]$. Since the total Au(III) decrease should be caused by the ligand exchange interaction, the nucleophilic addition of a water molecule, the electron transfer, and complex III formation, then the increase in DMPOX formation should be a little bit faster than the total Au(III) decrease, namely $\exp(-0.070t)$. However, complexation between Au(III) and HDMPN is slower than that between Au(III) and DMPO. The decrease in Au(III) in the DMPO–$HAuCl_4$ solution is faster than that in the HDMPN–$HAuCl_4$ solution, while formation of DMPOX in the former solution is slower than in the latter solution. The amounts of radical formed in the system (0.014 mmol/L) (Table 2) are far smaller than the initial DMPO concentration (1.25 mmol/L), which means that the Au(III) decrease and the DMPOX formation are independent. The reaction process from DMPO to HDMPN is a little bit complicated, which causes slower DMPOX formation in the DMPO–$HAuCl_4$ solution than that in the HDMPN–$HAuCl_4$ solution.

References

1. G.R. Buettner. Free Radical Biol. Med. **3**, 259 (1987).
2. H.G. Aurich and J. Troesken. Liebigs Ann. Chem. **745**, 159 (1971).

© 2005 NRC Canada

3. C. Bernofsky, B.M.R. Bandara, and O. Hinojosa. Free Radical Biol. Med. **8**, 231 (1990).
4. X. Shi, N.S. Dalal, and K.S. Kasprzak. Arch. Biochem. Biophys. **299**, 154 (1992).
5. K. Makino, A. Hagi, H. Ide, and A. Murakami. Can. J. Chem. **70**, 2818 (1992).
6. S. Pou, L. Keaton, W. Surichamorn, P. Frigillana, and G.M. Rosen. Biochim. Biophys. Acta, **1201**, 18 (1994).
7. X. Shi, A. Lenhart, and Y. Mao. Biochem. Biophys. Res. Commun. **203**, 1515 (1994).
8. X. Shi, Y. Rojanasakul, P. Gannett, K. Liu, Y. Mao, L.N. Daniel, N. Ahmed, and U. Saffiotti. J. Inorg. Biochem. **56**, 77 (1994).
9. T. Ozawa, Y. Miura, and J. Ueda. Free Radical Biol. Med. **20**, 837 (1996).
10. S. Leonard, P.M. Gannett, Y. Rojanasakul, D. Schwegler-Berry, V. Castranova, V. Vallyathan, and X. Shi. J. Inorg. Biochem. **70**, 239 (1998).
11. L. Eberson. Acta Chem. Scand. **53**, 584 (1999).
12. A. Floyd and L.M. Soong. Biochem. Biophys. Res. Commun. **74**, 9 (1977).
13. G.M. Rosen and E.J. Rauckman. Mol. Pharmacol. **17**, 233 (1980).
14. P.J. Thornalley, R.J. Trotta, and A. Stern. Biochim. Biophys. Acta, **759**, 16 (1983).
15. G.D. Mao, P.D. Thomas, and M. Poznansky. Free Radical Biol. Med. **16**, 493 (1994).
16. W. Adam, A. Kurz, and C.R. Saha-Moller. Free Radical Biol. Med. **26**, 566 (1999).
17. S. Ohnishi, M. Murata, and S. Kawanishi. Cancer Lett. **178**, 37 (2002).
18. K. Tajima, N. Endoh, K. Kanaori, and K. Makino. *In* Modern applications of EPR/ESR from biophysics to materials science. *Edited by* C.Z. Rudowicz, K.N. Yu, and H. Hiraoka. Proceedings of the First Asia Pacific EPR/ESR Symposium, Hong Kong. 20–24 January 1997. Springer Verlag, Singapore. 1997. pp. 54–57.
19. N. Endoh, K. Kanaori, K. Tajima, and K. Makino. Magn. Reson. Med. **9**, 52 (1998).
20. R.J. Puddephatt. The chemistry of gold. Elsevier Science Publishing Company Inc., Amsterdam, The Netherlands. 1978. pp. 20–22 and 203–209.
21. J. Zou, Z. Guo, J.A. Parkinson, Y. Chen, and P.J. Sadler. J. Chem. Soc. Chem. Commun. 1359 (1999).
22. R. Bonnett, R.F.C. Brown, V.M. Clark, and I.O. Sutherland. J. Chem. Soc. Faraday Trans. 1, 2094 (1959).
23. A. Mizuike. Applied colorimetric analysis. Vol. 1. *Edited by* S. Hirano. Kyoritu Publisher, Japan. 1973. pp. 230–232.
24. R. Roulet, N.Q. Lan, W.R. Mason, and G.P. Feske, Jr. Helv. Chim. Acta, **56**, 2405 (1973).
25. L.G. Sillen and A.E. Martell. Stability constants of metal-ion complexes. Inorganic ligands. The Chemical Society, London. 1971. Suppl. 1, Part. I.
26. H.A.O. Hill and P.J. Thornalley. Inorg. Chim. Acta, **67**, L35 (1982).
27. D. De Filippo, F. Devillanova, and C. Preti. Inorg. Chim. Acta, **5**, 103 (1971).

© 2005 NRC Canada

Oxazoline chemistry. Part VIII. Synthesis and characterization of a new class of pincer ligands derived from the 2-(*o*-anilinyl)-2-oxazoline skeleton — Applications to the synthesis of group X transition metal catalysts[1]

Andreas Decken, Robert A. Gossage, and Paras N. Yadav

Abstract: The synthesis and characterization of a new and readily synthesized class of potentially anionic pincer ligands with C_1 point group symmetries is described. These materials can be made via amide coupling of a 2-(2′-anilinyl)-2-oxazoline unit with picolinic acid; the incorporation of enantiopure oxazoline fragments facilitates the construction of chiral C_1 pincers. Treatment of the free ligands with Pd metal sources leads to the formation of amido–Pd pincer complexes in good yield. One of these Pd complexes has been characterized by single crystal X-ray diffraction methods, which confirms the proposed tridentate binding mode of the ligand and the formation of an amido N—Pd bond. The metal complexes have been shown to be suitable precusors for catalytically active Pd species that are useful for C—C bond forming reactions, notably the Heck reaction under standard conditions.

Key words: oxazoline, 4,5-dihydro-2-oxazole, palladium, pincer ligand, amido, Heck reaction.

Résumé : On décrit la synthèse facile et la caractérisation d'une nouvelle classe de ligands anioniques à pinces ayant des groupes de symétrie ponctuelle C_1. Ces produits peuvent être obtenus par couplage d'amide d'une unité 2-(2′-anilinyl)-2-oxazoline avec de l'acide picolinique; l'incorporation de fragments oxazolines énantiopurs facilite la formation de ligands à pince de symétrie C_1. Le traitement des ligands libres avec des sources de palladium métallique conduit à la formation, avec de bons rendements, de complexes amido–Pd pincer. On a caractérisé un de ces complexes du Pd par diffraction des rayons X par un cristal unique et on a ainsi pu confirmer le mode de liaison tridentate du ligand et la formation d'une liaison N—Pd amido. On a montré que les complexes métalliques sont des précurseurs appropriés pour des espèces catalytiquement actives de Pd qui sont utiles dans les réactions de formation de liaisons C—C, particulièrement dans la réaction de Heck dans des conditions standards.

Mots clés : oxazoline, 4,5-dihydro-2-oxazole, palladium, ligand à pince, amido, réaction de Heck.

[Traduit par la Rédaction]

Introduction

In recent years, enantiopure (C_2 symmetric) bisoxazolines have become a popular and useful class of ligands for applications in asymmetric synthesis promoted by Lewis acids (1). Oxazolines have been shown to possess a rich transition-metal chemistry (2), and recently the oxazoline fragment has been incorporated into the design of the so-called "pincer" ligand framework. This has resulted in the accessibility of potentially anionic and C_2-symmetric pincers (3). Pincer ligands have been at the forefront of a number of areas of investigation within organometallic chemistry including dendrimer chemistry, molecular sensor technology, the study of unusual bonding motifs or metal oxidation states (e.g., Ni^{3+}), and metal-mediated catalysis (4). Despite these advances, there has been increasing interest in ligands of *lower* symmetry; this is due to the fact that in many cases superior enantioselective catalysis can be obtained from species containing such ligands (1*a*, 1*c*, 5). Herein, we report the facile syntheses of C_1-symmetric amide pincer ligands containing a chiral (or achiral) oxazoline group in addition to a secondary binding (pyridine) functionality. In addition, these amides (Fig. 1) are shown to readily deprotonate (to form anionic pincers) on reaction with Pd sources to form Pd–

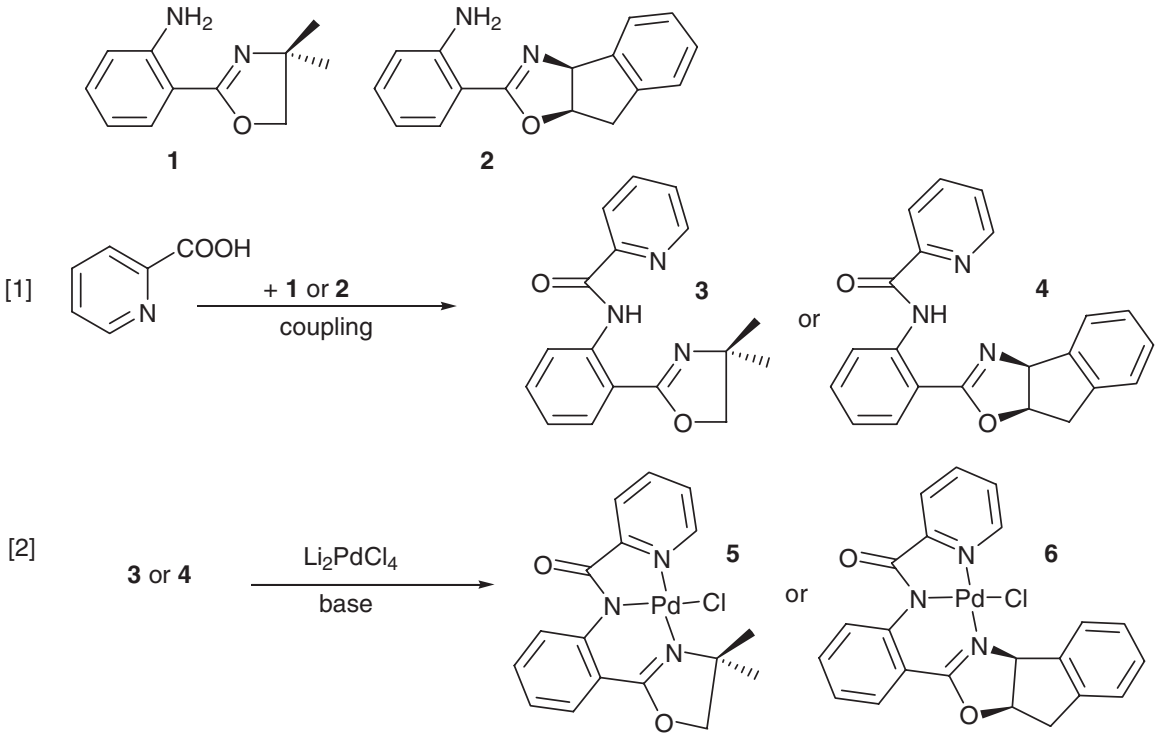
Received 3 March 2005. Published on the NRC Research Press Web site at http://canjchem.nrc.ca on 30 September 2005.

A. Decken.[2] Department of Chemistry, University of New Brunswick, Fredericton, NB E3B 6E2, Canada.
R.A. Gossage[3] **and P.N. Yadav.** The David Upton Hill Laboratories of Inorganic Chemistry, Department of Chemistry, Acadia University, 6 University Avenue, Wolfville, NS B4P 2R6, Canada.

[1]Part VII: A. Decken and R.A. Gossage. J. Inorg. Biochem. **99**, 644 (2005). This manuscript is dedicated to Professor Stephen R. Stobart on the occasion of his retirement.
[2]Corresponding author for crystallography (e-mail: adecken@unb.ca).
[3]Corresponding author (e-mail: rgossage@acadiau.ca).

 doi: 10.1139/V05-163 © 2005 NRC Canada

Fig. 1. Synthetic methodologies for the production of **3**–**6**.



amido complexes; these metal derivatives are shown to be active catalysts for the Heck reaction under standard protocols.

Results and discussion

The synthesis of amide **3** (Fig. 1) was accomplished using the in situ produced ($SOCl_2$) acid chloride (6) derivative of picolinic acid (PA), followed by the low temperature addition of readily available 4,4-dimethyl-2-(*o*-anilinyl)-2-oxazoline (**1**, Fig. 1, eq. [1]) (7). Unfortunately, yields of chiral analogue **4** were found to be variable by the above methodology, but the desired product could be reproducibly synthesized using PA and **2** under DCC–DMAP protocols (Fig. 1, eq. [1], also see Experimental section). Both **3** and **4** can thus be easily produced in large quantities (>1 g). The air-stable nature of these materials makes them easier to handle than many of the sensitive "PCP" or "pincer carbene" ligands (1). Facile ligand "tuning" (8) can be readily envisioned because of the availability of a number of analogues of **1** and **2** (7).

Palladium complexes of deprotonated **3** or **4** are formed in good yield upon treatment of (MeOH) solutions of the ligands with stoichiometric Li_2PdCl_4. These reactions lead to the isolation of solid and air-stable brown-coloured complex **5** (82%) and yellow **6** (91%), respectively (Fig. 1, eq. [2]). ^{1}H NMR data on both materials, in combination with elemental analysis, IR data, and the diamagnetic nature of both complexes, strongly suggest the formation of 1:1 adducts of the ligand fragments with Pd^{2+}. Specifically, the disappearance of the ^{1}H NMR signal assigned to the amide N-*H* proton and loss of the corresponding IR stretching frequency assigned to this group, imply the formation of complexes of the general formula $[Pd(L\text{-}H)Cl]_x$ (L = **3** or **4**, respectively). To confirm the mononuclear nature of these species, a single crystal X-ray diffraction study was carried out on a sample of complex **5**. A molecular respresentation of this material is found in Fig. 2. Crystal data can be found in Table 1; Table 2 gives a list of selected bond lengths and angles for complex **5**.

The X-ray data confirm that **5** is a monopalladium complex incorporating deprotonated **3**; bond lengths and angles are typical for a formal Pd^{2+} metal centre (1, 9). Of note is the formal amido–Pd interaction in addition to the coordination of both the pyridine and the oxazoline groups forming five- and six-membered rings, respectively; the latter functionality binds through the N atom, as expected (2). Thus, a tridenate (κN, κN′, κN″) bonding motif is presented. The coordination geometry around the Pd atom is best described as distorted square-planar in nature. Therefore, ligands such as **3** do form pincer complexes and in excellent yields.

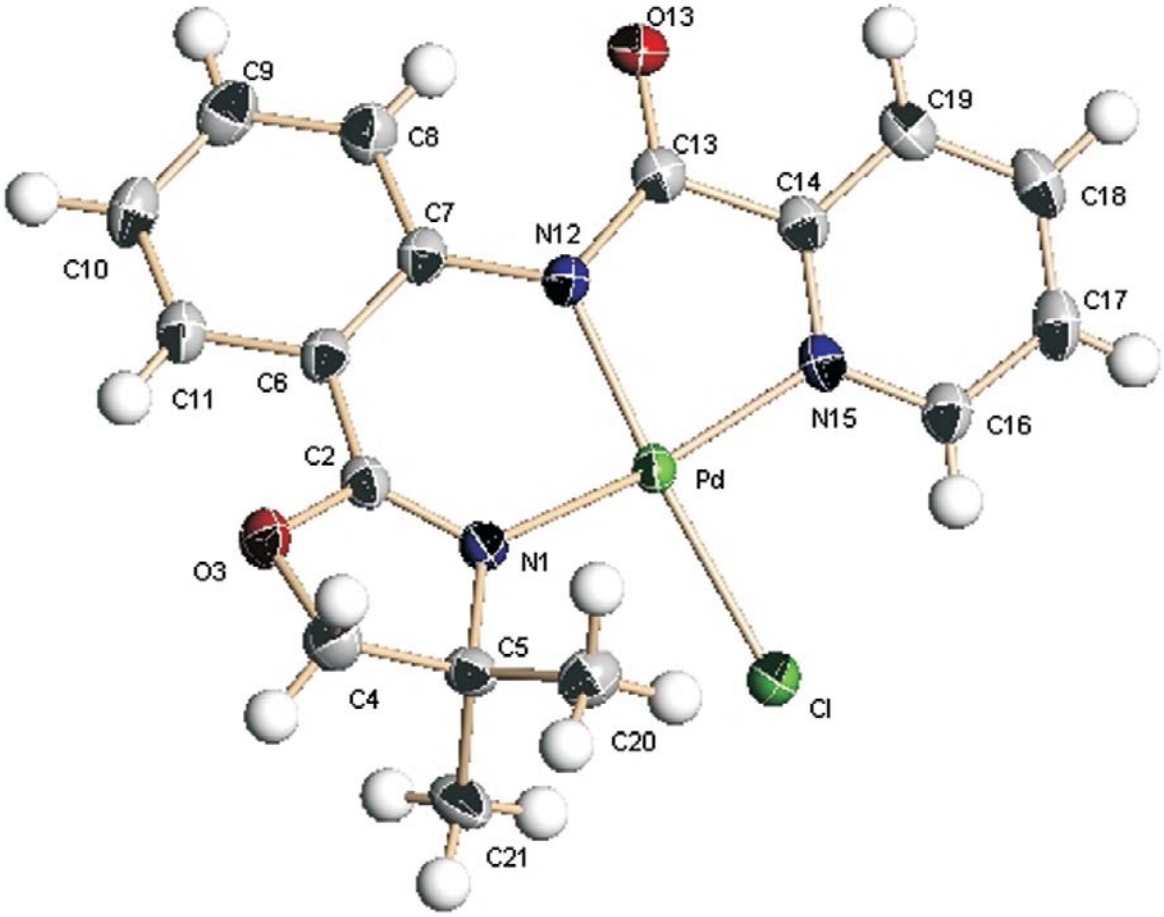
Several Pd pincer compounds are known to be active promoters of selective C—C bond formation (10). We have therefore performed some preliminary tests on complexes **5** and **6** as promoters of the Heck reaction under typical reaction conditions (9). Both complexes catalyse the regioselective coupling of iodobenzene with styrene to give high yields of *trans*-stilbene under standard protocols in the presence of base (NaOAc, see the Experimental section). Notably, these reactions were preformed *in open air* and hence these pincer catalysts appear to be highly robust (11) to the high temperature oxidizing conditions employed.

Conclusions

In conclusion, access to a new and readily synthesized class of potentially anionic pincer ligands has been realised. These compounds can be used to make catalytically active

© 2005 NRC Canada

Fig. 2. Image of the molecular structure of complex **5** showing the atomic numbering scheme. Thermal ellipsoids are at the 30% probability level.



Pd species for selective C—C bond forming reactions that can be used in the absence of inert atmosphere conditions. The investigation of other transition-metal complexes of these and related ligands, and their catalytic potentials, will be disclosed in due course.

Experimental section

General

All reactions were carried out using standard bench-top laboratory techniques using commercially available, reagent-grade solvents. ^{1}H NMR spectra were recorded from chloroform-*d* solutions at 300 MHz using a Bruker Avance 300 NMR spectrometer. Microanalyses were recorded at the analytical services department of the University of Windsor (Windsor, Ontario). IR spectra were obtained as Nujol muls using a PerkinElmer 683 IR spectrometer. Melting point data were obtained using a Mel-Temp II apparatus and reported values are uncorrected. Optical rotation measurements were made on a Bellingham + Stanley Ltd. model ADP220 polarimeter using a 1 dm path length optical cell.

Syntheses

Synthesis of 3

Thionyl chloride (5.6 g, 50 mmol) was added dropwise to a stirred and cold (0 °C) mixture of PA (6.15 g, 50 mmol) and Et_3N (7.6 g, 75 mmol) in 35 mL of CH_2Cl_2 (6). Stirring was continued for 30 min and then a suspension of **1** (7*a*) (9.5 g, 50 mmol) in 20 mL of CH_2Cl_2 was added (at 0 °C). The stirring was continued for a further 3 h as the mixture warmed to room temperature (RT); the reaction vessel was then left standing overnight. Neutralization by the addition of satd. aq. Na_2CO_3 was followed by isolation of the organic layer, which was subsequently washed with water (3 × 15 mL) and then evaporated in vacuo. The crude product thus obtained was purified by (flash) chromatography (SiO_2, 230–400 mesh) using hexanes – ethyl acetate (3:1, *v*/*v*) as the eluent (R_f = 0.50). The yellow solid *product* was thereafter isolated following solvent evaporation. Yield: 6.63 g (45%); mp 110 °C. IR (cm^{-1}): 3054 (w), 1670 (s), 1645 (s), 1583 (s), 1540 (s). ^{1}H NMR (300 MHz, $CDCl_3$) δ: 1.51 (s, 6H), 4.12 (s, 2H), 7.15 (t, 1H, *J* = 7.9 Hz), 7.47–7.58 (m, 2H), 7.87–7.95 (m, 2H), 8.30 (d, 1H, *J* = 7.9 Hz), 8.69 (d, 1H, *J* = 4.5 Hz), 9.03 (d, 1H, *J* = 8.3 Hz). Anal. calcd. for $C_{17}H_{17}N_3O_2$ (%): C 69.14, H 5.80, N 14.23; found: C 70.03, H 5.82, N 14.57.

Synthesis of 4

In a round-bottomed flask containing chilled (10 °C) CH_2Cl_2 (160 mL) was added **2** (7*a*) (2.136 g, 11.2 mmol) and PA (1.674 g, 13.6 mmol). The mixture was stirred under an inert atmosphere for 25 min at 0 °C. To this mixture was added DMAP (0.412 g, 3.2 mmol) and DCC (3.492 g,

© 2005 NRC Canada

Table 1. X-ray diffraction data for complex **5**.

Formula weight	436.18
Formula	$C_{17}H_{16}ClN_3O_2Pd$
Temperature (K)	198(1)
λ (Å)	0.710 73
Crystal system	Monoclinic
Space group	*P*2(1)/*c*
Unit cell dimensions:	
a (Å)	11.231 8(6)
b (Å)	17.399 1(10)
β (°)	95.515(1)
c (Å)	8.421 0(5)
Volume (Å^3)	1 638.04(16)
Z	4
Density (calcd., Mg/m^3)	1.769
Absorption coefficient (mm^{-1})	1.311
F(000)	872
Crystal size (mm^3)	0.40 × 0.25 × 0.20
θ Range for data collection (°)	1.82–27.50
Index ranges	$-13 \le h \le 14$, $-20 \le k \le 22$, $-10 \le l \le 10$
Reflections	11 291
Independent reflections	3 679
R(int)	0.020 6
Completeness to θ (°)	97.6% (27.50)
Absorption correction	SADABS
Refinement method	Full-matrix least-squares on F^2
Data / restraints / parameters	3 679 / 0 / 281
Goodness-of-fit on F^2	1.066
Final *R* indices ($I > 2\sigma(I)$)	
R_1	0.020 0
wR_2	0.052 3
R indices (all data)	
R_1	0.023 6
wR_2	0.054 3
Largest diff. peak and hole (e Å^{-3})	0.612 and –0.185

Note: where $wR_2 = \{\Sigma[w(F_o^2 - F_c^2)^2]/\Sigma[F_o^4]\}^{1/2}$, $R_1 = \Sigma||F_o| - |F_c||/\Sigma|F_o|$. Weight = $1/[\sigma^2(F_o^2) + (0.0303P)^2 + (0.6142P)]$, where $P = (\max(F_o^2, 0) + 2F_c^2)/3$.

16.8 mmol) and the mixture was then stirred for an additional 25 min at 0 °C. The cooling bath was removed and the solution warmed up to RT. After being stirred for 48 h, the mixture was filtered (thrice) to yield a clear filtrate. The filtrate was then washed with water (4 × 300 mL), 5% aq. HOAc (160 mL), and again with water (4 × 200 mL). The organic layer was then dried ($MgSO_4$), filtered, and then all volatile components were removed on a rotary evaporator. The crude product thus obtained was purified by flash silica gel chromatography (230–400 mesh) using hexanes – ethyl acetate (75:25, R_f = 0.61) as the eluent, following by solvent evaporation. Yield: 1.79 g (45%); mp 189 °C. $[\alpha]_D$ (300 K, *c* 0.5, CH_2Cl_2) –74°. IR (cm^{-1}): 1680 (s), 1636 (s), 1579 (s), 1520 (s). ^{1}H NMR (300 MHz, $CDCl_3$) δ: 3.45 (s, 1H), 3.54 (d, 1H, *J* = 6.7 Hz), 5.49 (m, 1H), 5.97 (d, 1H, *J* = 7.9 Hz), 7.15 (t, 1H, *J* = 8.0 Hz), 7.27 (m, 3H), 7.49–7.57 (m, 2H), 7.67 (t, 1H, *J* = 4.1 Hz), 7.90–7.95 (m, 2H), 8.31 (d, 1H, *J* = 7.8 Hz), 8.90 (d, 1H, *J* = 4.3 Hz), 9.01 (d, 1H, *J* = 8.3 Hz). Anal. calcd. for $C_{22}H_{17}N_3O_2$ (%): C 74.35, H 4.82, N 11.82; found: C 74.91, H 4.63, N 12.26.

Table 2. Selected bond lengths (Å) and angles (°) for complex **5** (esds in brackets).

Bond lengths (Å)	
Pd—N1	2.0254(14)
Pd—Cl	2.3248(5)
Pd—N12	2.0077(14)
Pd—N15	2.0236(15)
Bond angles (°)	
N1-Pd-N15	169.07(6)
Cl-Pd-N12	171.55(4)
N12-Pd-N1	90.01(6)
N12-Pd-N15	81.76(6)

Synthesis of 5

To a 10 mL solution (MeOH) of in situ formed Li_2PdCl_4 (0.5 mmol, prepared by boiling 0.088 g (0.5 mmol) of $PdCl_2$ and 0.127 g of LiCl (3 mmol)) was added **3** (0.145 g, 0.5 mmol). The mixture was stirred at RT for 48 h and the resulting brown complex isolated by filtration, washed with MeOH and ether, and then dried at 60 °C overnight. Yield: 0.179 g (82%), mp 251 to 252 °C. IR (cm^{-1}): 1646 (s), 1614 (s), 1485 (s), 520 (w), 340 (w). ^{1}H NMR (300 MHz, $CDCl_3$) δ: 1.79 (s, 6H), 4.30 (s, 2H), 7.02 (t, 1H, *J* = 7.7 Hz), 7.41–7.53 (m, 2H), 7.82 (t, 1H, *J* = 8.1 Hz), 8.04 (m, 2H), 8.49 (d, 1H, *J* = 8.6 Hz), 9.27 (d, 1H, *J* = 5.5 Hz). Anal. calcd. for $C_{17}H_{16}N_3O_2ClPd\cdot 1/2H_2O$ (%): C 45.86, H 3.85, N 9.44; found: C 45.53, H 3.64, N 9.68.

Synthesis of 6

As described above for complex **5** using Li_2PdCl_4 (0.5 mmol) and **4** (0.145 g, 0.5 mmol). Yield: 0.225 g (91%) of a yellow powder; mp > 300 °C. $[\alpha]_D$ (300 K, *c* 0.49, CH_2Cl_2) –385°. IR (cm^{-1}): 1623 (s), 1598 (s), 1482 (s), 530 (w), 335 (w). ^{1}H NMR (300 MHz, $CDCl_3$) δ: 3.50 (t, 1H, *J* = 5.1 Hz), 3.57 (s, 1H), 5.49 (m, 1H), 6.43 (d, 1H, *J* = 7.1 Hz), 6.98 (t, 1H, *J* = 8.1 Hz), 7.25–7.37 (m, 3H), 7.43–7.47 (m, 1H), 7.50–7.55 (m, 1H), 7.86 (dd, 1H, *J* = 8.1 Hz), 8.03–8.05 (m, 2H), 8.43 (d, 1H, *J* = 8.4 Hz), 8.53 (t, 1H, *J* = 5.3 Hz), 9.23 (d, 1H, *J* = 5.6 Hz). Anal. calcd. for $C_{22}H_{16}N_3O_2ClPd$ (%): C 53.25, H 3.25, N 8.47; found: C 53.68, H 3.17, N 9.25.

Catalysis

Heck coupling reactions of iodobenzene and styrene using 5 or 6[4]

Iodobenzene (25 mmol), styrene (30 mmol), *N*,*N*-dimethylformamide (25 mL), sodium acetate (30 mmol), and 0.5 mg (~1 μmol) of **5** or **6** were combined in a round-bottomed flask equipped with a reflux condenser (9). The mixture was heated, in open air, to 140–150 °C for 24 h. After cooling to RT, 0.1 L of dil. aq. HCl was added and the

[4] Nota bene: no attempt was made to optimize the reaction conditions.

© 2005 NRC Canada

organic components were extracted with ethyl acetate (3 × 100 mL). The organic layer was washed (brine) and dried (Na_2SO_4). After filtration, volatiles were removed (vacuo) and the product *trans*-stilbene (correct mp and ^{1}H NMR) was purified by flash column chromatography (hexanes–EtOAc, 9:1). Yield: 95% (using **5**); 89% (using **6**).

X-ray crystallography of complex 5[5]

Single crystals were coated with Paratone-N oil, mounted using a glass fibre, and frozen in the cold nitrogen stream of the goniometer. A hemisphere of data was collected on a Bruker AXS P4/SMART 1000 diffractometer using ω and θ scans with a scan width of 0.3° and 10 s exposure times. The detector distance was 5 cm. The data were reduced (SAINT) (12) and corrected for absorption (SADABS) (13). The structure was solved by direct methods and refined by full-matrix least-squares on F^2 (SHELXTL) (14). Hydrogen atoms were included in calculated positions and refined using a riding model.

Acknowledgements

This work has been supported by the Natural Sciences and Engineering Research Council of Canada (NSERC). Sepracor Canada Ltd. is thanked for a generous donation of chiral indanols and Johnson-Matthey, Inc. is thanked for a loan of Pd salts.

References

1. e.g.: (*a*) A. Pfaltz and W.J. Drury III. Proc. Natl. Acad. Sci. U.S.A. **101**, 5723 (2004); (*b*) J.S. Johnson and D.A. Evans. Acc. Chem. Res. **33**, 325 (2000); (*c*) G. Desimoni, G. Faiti, and P. Quadrelli. Chem. Rev. **103**, 3119 (2003).
2. (*a*) H.A. McManus and P.J. Guiry. Chem. Rev. **104**, 4151 (2004); (*b*) D. Rechavi and M. Lemaire. Chem. Rev. **102**, 3467 (2002); (*c*) M. Gómez, G. Muller, and M. Rocamora. Coord. Chem. Rev. **193–195**, 769 (1999); (*d*) T.M. Barclay, I. del Río, R.A. Gossage, and S.M. Jackson. Can. J. Chem. **81**, 1482 (2003); (*e*) A. Decken, C.R. Eisnor, R.A. Gossage, and S.M. Jackson. Inorg. Chim. Acta. In press; (*f*) D.J. Berg, C. Zhou, T.M. Barclay, X. Fei, S. Feng, K.A. Ogilvie, R.A. Gossage, B. Twamley, and M. Wood. Can. J. Chem. **83**, 449 (2005).
3. (*a*) M. Stol, D.J.M. Snelders, J.J.M. de Pater, G.P.M. van Klink, H. Kooijman, A.L. Spek, and G. van Koten. Organometallics, **24**, 743 (2005); (*b*) R.B. Bedford, C.S.J. Cazin, and D. Holder. Coord. Chem. Rev. **248**, 2283 (2004); (*c*) Y. Tsuchiya, Y. Kanazawa, T. Shiomi, K. Kobayashi, and H. Nishiyama. Synlett, 2493 (2004); (*d*) Y. Motoyama and H. Nishiyama. Synlett, 1883 (2003); (*e*) Y. Motoyama, Y. Mikami, H. Kawakami, K. Aoki, and H. Nishiyama. Organometallics, **18**, 3584 (1999); (*f*) S.E. Denmark, R.A. Stavenger, A.-M. Faucher, and J.P. Edwards. J. Org. Chem. **62**, 3375 (1997); (*g*) Y. Motoyama, H. Kawakami, K. Shimozono, K. Aoki, and H. Nishiyama. Organometallics, **21**, 3408 (2002); (*h*) J.S. Fossey and C.J. Richards. J. Organomet. Chem. **689**, 3056 (2004).
4. e.g.: (*a*) A.C. Frisch and M. Beller. Angew. Chem. Int. Ed. **44**, 674 (2005); (*b*) N. Solin, O.A. Wallner, and K.J. Szabó. Org. Lett. **7**, 689 (2005); (*c*) J. Kjellgren, H. Sundén, and K.J. Szabó. J. Am. Chem. Soc. **127**, 1787 (2005); (*d*) R. Çelenligil-Çetin, L.A. Watson, C. Guo, B.M. Foxman, and O.V. Ozerov. Organometallics, **24**, 186 (2005); (*e*) M. Albrecht and G. van Koten. Angew. Chem. Int. Ed. **40**, 3750 (2001); (*f*) X. Zhou and S.R. Stobart. Organometallics, **20**, 1898 (2001); (*g*) M.D. Fryzuk. Chem. Rec. **3**, 2 (2003); (*h*) L.P. Spenser, S. Winston, and M.D. Fryzuk. Organometallics, **23**, 3372 (2004); (*i*) M.D. Fryzuk, M.J. Petrella, R.C. Coffin, and B.O. Patrick. C.R. Chimie, **5**, 451 (2002); (*j*) M.E. van der Boom and D. Milstein. Chem. Rev. **103**, 1759 (2003); (*k*) G.R. Rosa, G. Ebeling, J. Dairpont, and A.L. Monteiro. Synthesis, 2894 (2003); (*l*) B.M. Trost. Proc. Natl. Acad. Sci. U.S.A. **101**, 5348 (2004); (*m*) S. Nemeh, R.J. Flesher, K. Gierling, C. Maichle-Mössmer, H.A. Mayer, and W.C. Kaska. Organometallics, **17**, 2003 (1998); (*n*) M.W. Haenel, S. Oevers, K. Angermund, W.C. Kaska, H.-J. Fan, and M.B. Hall. Angew. Chem. Int. Ed. **40**, 3596 (2001); (*o*) J.T. Singleton. Tetrahedron, **59**, 1837 (2003); (*p*) A.M. Winter, K. Eichele, H.-G. Mack, W.C. Kaska, and H.A. Mayer. Organometallics, **24**, 1837 (2005).
5. (*a*) R. Noyori, M. Kitamura, and T. Ohkuma. Proc. Natl. Acad. Sci. U.S.A. **101**, 5356 (2004); (*b*) X. Hu, H. Chen, and X. Zhang. Angew. Chem. Int. Ed. **38**, 3518 (1999).
6. Y.N. Belokon, N.B. Bespalova, T.D. Churkina, I. Cisařová, M.G. Ezernitskaya, S.R. Harutyunyan, R. Hrdina, H.B. Kagan, P. Kočovský, K.A. Kochetkov, O.V. Larionov, K.A. Lyssenko, M. North, M. Polášek, A.S. Peregudov, V.V. Prisyazhnyuk, and Š. Vyskočil. J. Am. Chem. Soc. **125**, 12 860 (2003).
7. (*a*) K.M. Button and R.A. Gossage. J. Heterocyclic Chem. **40**, 513 (2003); (*b*) J.T. Banks, K.M. Button, R.A. Gossage, T.D. Hamilton, and K.E. Kershaw. Heterocycles, **55**, 2251 (2001).
8. L.A. van de Kuil, H. Luitjes, D.M. Grove, J.W. Zwikker, J.G.M. van der Linden, A.M. Roelofsen, L.W. Jenneskens, W. Drenth, and G. van Koten. Organometallics, **13**, 468 (1994).
9. R.A. Gossage, H.A. Jenkins, and P.N. Yadav. Tetrahedron Lett. **45**, 7689 (2004).
10. e.g.: (*a*) A. Zapf and M. Beller. Chem. Commun. 431 (2005); (*b*) A.A.D. Tulloch, A.A. Danopoulos, G.J. Tizzard, S.J. Coles, M.B. Hursthouse, R.S. Hay-Motherwell, and W.B. Motherwell. Chem. Commun. 1270 (2001).
11. (*a*) J.A. Loch, M. Albrecht, E. Peris, J. Mata, J.W. Faller, and R.H. Crabtree. Organometallics, **21**, 700 (2002); (*b*) E. Peris, J.A. Loch, J. Mata, and R.H. Crabtree. Chem. Commun. 201 (2001); (*c*) J.G. de Vries. Can. J. Chem. **79**, 1086 (2001); (*d*) I.D. Kostas, F.J. Andreadaki, D. Kovala-Demertzi, C. Prentjas, and M.A. Demertzis. Tetrahedron Lett. **46**, 1967 (2005); (*e*) L. Botella and C. Njera. Tetrahedron, **60**, 5563 (2004); (*f*) C.-L. Chen, Y.-H. Liu, S.-M. Peng, and S.-T. Liu. Organometallics, **24**, 1075 (2005).
12. Bruker AXS, Inc. SAINT 6.02 [computer program]. Bruker AXS, Inc., Madison, Wisconsin. 1997–1999.
13. G. Sheldrick. SADABS [computer program]. Bruker AXS, Inc., Madison, Wisconsin. 1999.
14. G. Sheldrick. SHELXTL 5.1 [computer program]. Bruker AXS, Inc., Madison, Wisconsin. 1997.

[5] Supplementary data for this article are available on the Web site or may be purchased from the Depository of Unpublished Data, Document Delivery, CISTI, National Research Council Canada, Ottawa, ON K1A 0S2, Canada. DUD 4011. For more information on obtaining material refer to http://cisti-icist.nrc-cnrc.gc.ca/irm/unpub_e.shtml. CCDC 263208 contains the crystallographic data for this manuscript. These data can be obtained, free of charge, via www.ccdc.cam.ac.uk/conts/retrieving.html (Or from the Cambridge Crystallographic Data Centre, 12 Union Road, Cambridge CB2 1EZ, UK; fax +44 1223 336033; or deposit@ccdc.cam.ac.uk).

© 2005 NRC Canada

NOTE / NOTE

Induced structural changes of a supported planar bilayer after exposure to halothane — A real-time atomic force microscopy study

L.G. Shamrakov and D.T. Cramb

Abstract: Atomic force microscopy (AFM) was used to study the effect of the general anesthetic halothane on a supported DOPC phospholipid bilayer, under conditions of high anaesthetic loading. The presence of the anaesthetic in the lipid-induced restructuring of the supported bilayer, erosion of the bilayer from the mica surface, and the formation of lipid aggregates. Addition of halothane to lipid vesicles prior to adsorption on the mica surface inhibited the lysis of adsorbed vesicles and thus no planar bilayer formation was observed.

Key words: lipid bilayer restructuring, atomic force microscopy, halothane, anesthesis.

Résumé : On a fait appel à la microscopie des forces atomiques (MFA) pour étudier l'effet de l'anesthésique général, halothane sur une bicouche supportée de phospholipide DOPC, dans des conditions de charge élevée d'anesthésique. La présence de l'anesthésique dans le lipide induit une restructuration de la bicouche supportée, une érosion de la bicouche de la surface du mica et la formation d'agrégats de lipides. L'addition d'halothane aux vésicules de lipide avant l'adsorption sur la surface de mica inhibe la lyse des vésicules adsorbées et on ne peut alors observer de formation de bicouche planaire.

Mots clés : restructuration d'une bicouche de lipide, microscopie de forces atomiques, halothane, anesthésique.

[Traduit par la Rédaction]

Introduction

Although, general anaesthetics are known to have a direct interaction with biological cell membranes (1), the exact sequence of events leading to anesthetic action remains unknown at the molecular level. Presently, there is significant evidence that the targets of volatile anaesthetics are ligand-gated ion channels embedded in cell membranes (2). However, it has also been hypothesized that the interaction between anaesthetics and these ion channels occurs indirectly, via a change in the microenvironment of the phospholipid bilayer surrounding the ion channels (3). Regardless, since anaesthetic potency increases with lipophilicity, an understanding of the changes that occur within model biological membranes in the presence of anaesthetics will provide insight regarding anaesthetic mechanisms.

Received 8 February 2005. Published on the NRC Research Press Web site at http://canjchem.nrc.ca on 15 September 2005.

L.G. Shamrakov and D.T. Cramb.[1] Department of Chemistry, University of Calgary, 2500 University Dr., NW, Calgary, AB T2N 1N4, Canada.

[1]Corresponding author (e-mail: dcramb@ucalgary.ca).

A supported 1,2-dioleoyl-*sn*-glycero-3-phosphocholine (DOPC) planar bilayer is often chosen as a model biological cell membrane, because its behavior is well-characterized and membrane mimetic (4). In addition, DOPC is stable in the form of a supported planar bilayer for a period of days (5, 6), allowing for long-term observations of interactions with anaesthetics.

The anaesthetic used in this study, halothane, is an amphiphilic molecule. Fluorescent studies have indicated that halothane resides predominantly in the headgroup region of a model DOPC bilayer (5). Moreover, using atomic force microscopy (AFM) we have recently shown that halothane likely has a heterogeneous lateral distribution in gel-phase 1,2-dipalmitoyl-*sn*-glycero-3-phosphocholine (DPPC) SPBs (6). Finally, molecular dynamic simulations revealed halothane is distributed unevenly across the membrane interior (7). It is of interest how this uneven distribution affects the stability of a supported planar bilayer. One would expect uneven distribution of halothane within a supported phospholipid bilayer to decrease line tension, resulting in destabilization, and possibly restructuring of the bilayer.

Supported planar bilayer restructuring after the addition of chitosan was previously observed by Fang and Chan (8). The presence of the protein chitosan within the bilayer induced growth clusters to form within the bilayer, and aggre-

 doi: 10.1139/V05-129 © 2005 NRC Canada

gation of lipids was observed. A decrease in bilayer line tension was cited as the cause of the changes. In addition, Fang and Chan reported an erosion of fragments of the lipid membrane from the mica surface.

In the present work, magnetic A/C mode (MAC) AFM was used to examine the effect of the presence of the general anaesthetic halothane on a mica-supported planar DOPC bilayer. The halothane-induced changes in a DOPC SPB were monitored over a 22 h period.

Methods

Materials

DOPC in chloroform solution was used without further purification (Avanti Polar-lipids Inc., Alabaster, Maine). Filtered (0.1 μm pore size) ultrapure water was used for the preparation of all solutions. Freshly cleaved ASTMV-2 quality, scratch-free ruby mica (Asheville-Schoonmaker Mica Co., Newport News, Virginia) was used as the SPB substrate for imaging.

Supported DOPC bilayer in water

A 0.7 mg/mL DOPC solution was prepared in ultrapure water using the method previously described (9). Briefly, an aliquot of DOPC suspended in chloroform was transferred into a dry vessel. The solution was then dried under a stream of nitrogen to remove the chloroform. The phospholipid was then resuspended in ultrapure water and stirred for 30 min. The solution was then sonicated and stirred for successive 10 min cycles at room temperature until it became clear (Branson 1200, Dansbury, Connecticut). The solution was then filtered (0.2 μm pore size) and sonicated for 10 min prior to deposition onto the mica substrate.

Supported planar bilayers were prepared via vesicle fusion (9). DOPC solution (75 μL, 0.7 mg/mL) was deposited on unmodified, freshly cleaved mica and incubated for 45 min. The surface was then gently rinsed with ultrapure water. All bilayers were imaged in ultrapure water at room temperature.

Supported DOPC bilayer containing halothane

Halothane (60 μL) was added to the AFM cell containing a previously imaged supported DOPC bilayer and incubated at room temperature for 30 min (creating a 10% *v*/*v* solution in ultrapure water). A series of exposure times were tested. Thirty minutes was the minimum time needed to observe change, and allows imaging of further changes in bilayer structure. The liquid above the bilayer was then gently removed from the cell with a pipette, and fresh ultrapure water was immediately added to prevent drying of the sample. Under these conditions the solution would be saturated with halothane (17.5 mmol/L).

AFM imaging conditions

All imaging was done using MAC mode AFM in which a magnetically coated probe, driven by an alternating magnetic field, oscillates near its resonant frequency. This technique was chosen as it has proven to be minimally invasive to supported planar bilayers in situ (9–11). Images were obtained using a Pico SPM microscope with an AFMS-165 scanner (Molecular Imaging Inc., Phoenix, Arizona) and magnetically coated type I Maclevers® (Molecular Imaging Inc.) were used. The cantilever used had a force constant of 0.6 N/m and the tip radius of curvature was quoted as being within the range of 5–10 nm. A standard MAC mode fluid cell (Molecular Imaging Inc.) was used in all experiments.

Results and discussion

To study the effect of halothane's presence on the supported phospholipid bilayer, it was first necessary to obtain a single planar supported bilayer via vesicle fusion on the mica surface. In the absence of halothane, a uniform supported planar DOPC bilayer was observed (Fig. 1A). Viscoelasticity analysis (9) was used to confirm the presence of a single supported bilayer (data not shown).

Next, halothane was added to a preformed SPB as described in the Methods section. The addition of halothane resulted in a restructuring of the supported DOPC bilayer. Images obtained 6 h and 45 min after halothane addition to the supported planar bilayer displayed large structures, which are presumably lipid aggregates (Fig. 1B). The largest aggregate observed had a height of 100 nm and was imaged at 7 h after halothane addition. It is uncertain whether this is the maximum size of aggregate, or whether they continue to increase in size indefinitely. Control experiments where halothane was added directly to the mica surface did not produce images comparable to those with a bilayer. Further control experiments were performed where the SPB was treated in the same way as for halothane addition, with the exception that an equivalent volume of water was injected. No changes in the SPB were observed under these conditions.

Although there is no evidence that these aggregates result from uncontrolled foreign substances acting upon the bilayer, viscoelasticity analysis should provide additional insight into the nature of the aggregates, possibly confirming that they are lipid-based. Viscoelasticity (i.e., phase) images provide information about a sample's ability to dissipate energy transferred from interactions with the AFM tip. Differences in viscoelasticity result from differences in phase, and thus viscoelasticity analysis can be used to distinguish samples that are different in lipid phase. For instance, the solid mica support can be distinguished from liquid- or gel-phase SPBs. Fig. 2A displays an aggregate of interest. Topography images indicate the presence of larger entities on the mica substrate (Fig. 1A). In the corresponding viscoelasticity (i.e., phase) image, areas of only two different viscoelasticities are evident. These two represent the bilayer and the mica support. There is no phase contrast between the large aggregates (identified by a circle in Fig. 1C) and the domain that surrounds them, suggesting that the aggregates are lipid based and possibly multilamellar. The formation of these lipid aggregates could result from erosion of the lipid from the mica support and restructuring of the lipids owing to a destabilizing effect of halothane on the supported bilayer. This destabilization would result from a decrease in line tension caused by uneven distribution of halothane within the bilayer.

Significantly, we were able to monitor the spontaneous formation of a lipid aggregate at times ranging from 4 h and 25 min to 5 h after initial halothane addition (Fig. 2). The

© 2005 NRC Canada

Fig. 1. Topography image of a supported planar DOPC phospholipids bilayer (A) prior to halothane addition, and (B) 6 h and 45 min after halothane addition. Panel C is a viscoelasticity (i.e., phase) image collected simultaneously with B. Large structures present in the topography image do not appear in the viscoelasticity image, indicating the structures are lipid based.

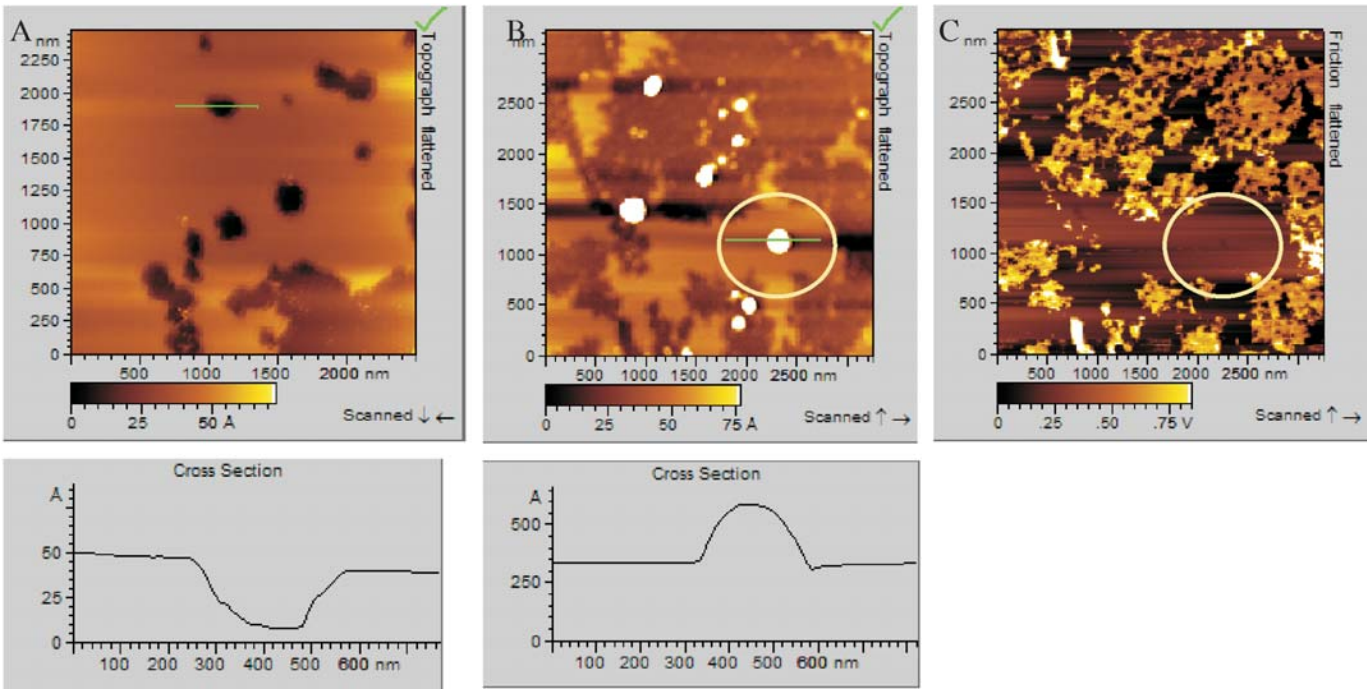
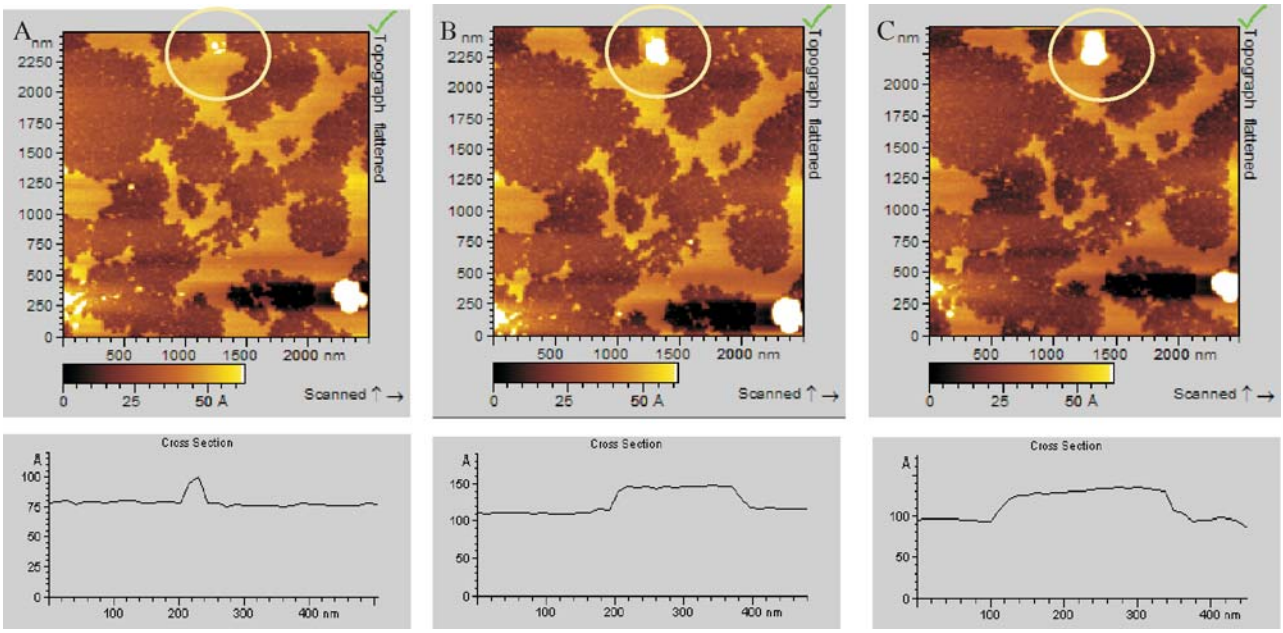


Fig. 2. DOPC supported planar bilayer (A) 4 h and 25 min after halothane addition, (B) 20 min after panel (A), (C) 35 min after panel (A). Cross-sections are taken of aggregate height relative to the supported planar bilayer.

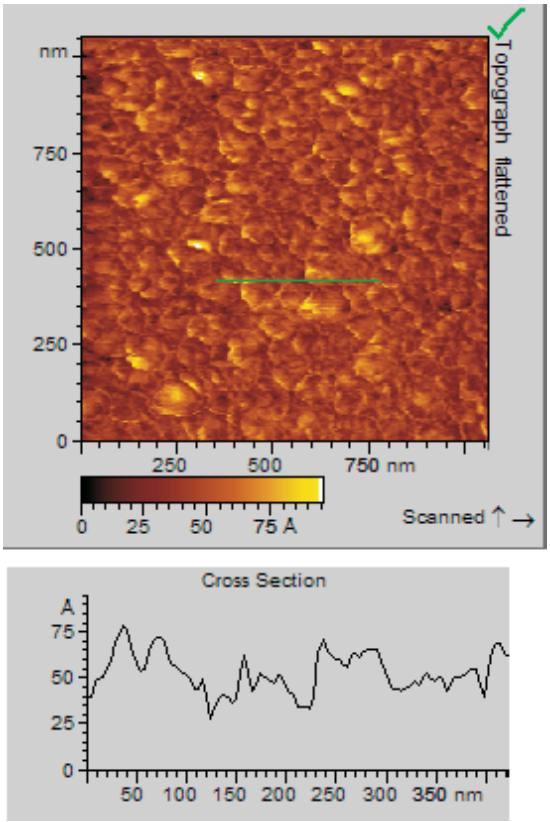


lipid aggregation observed is concluded to be solely because of the presence of halothane in the bilayer, as there is minimal perturbation of the system by the AFM probe during imaging. Moreover, a supported planar DOPC bilayer is stable in the absence of halothane over a period of up to days (6). The aggregate formation, observed after 4 h and 25 min, indicates halothane (at a high concentration regime) has a prolonged destabilizing effect on a supported phospholipid bilayer.

The results above suggest that in the presence of halothane a DOPC bilayer has a lower energy when curved rather than when planar. We postulate this is related to a ten-

© 2005 NRC Canada

Fig. 3. Topography image of DOPC vesicles deposited on a mica surface. Halothane was added to the vesicle solution prior to surface deposition. Nonuniform curved structures are evident.



dency of halothane to reside in a region of the bilayer in which the space between head groups is increased. This is supported by the observation that halothane preferentially resides in a liquid-phase bilayer compared to a gel-phase bilayer (5). To test the hypothesis that a DOPC bilayer is more stable in a curved structure in the presence of halothane, halothane-containing DOPC vesicles were deposited onto the mica surface. This yielded no bilayer formation. Nonuniformly sized curved structures were observed adsorbed to mica. These are presumably nonlysed vesicles (Fig. 3).

Taken together, these observations are consistent with halothane's uneven bilayer distribution, which destabilizes the planar structure leading to an energetically favored curved configuration. The destabilization of the bilayer in the presence of the drug, attributed to a decrease in line tension, could be the consequence of many factors. First, the presence of halothane within the bilayer likely has a detergent effect, as its shape (Fig. 4) is much different from that of the cylindrical DOPC headgroup/tail unit. Thus, insertion of halothane may disrupt the packing of individual cylindrical headgroup/tail units within the bilayer. The molecular dynamics study of halothane in uneven distribution of halothane within the bilayer could further disrupt the stability of packed lipid units within a bilayer, therefore contributing to decreased line tension and inducing further restructuring. Since this behavior was not observed in previous studies at low halothane loading conditions (approximately 0.5 mmol/L halothane solution) (5), we postulate that the destabilization is concentration dependent. Furthermore, the anaesthetic interaction with the SPB may be co-operative. Initial aggregation of the SPB appears to enhance further restructuring locally, without affecting other regions of the bilayer (Fig. 2), likely owing to co-operative localization of halothane within the bilayer. It is possible that halothane absorbs initially near the edges of bilayer patches. However, change in the thickness of the bilayer edges were not observed either in this study or in our previous work (5). The possibility of halothane co-operativity in DOPC bilayers is consistent with our observation that halothane induces fusion between large unilamellar DOPC vesicles (12).

These results are comparable to those observed by Fang and Chan (8) in their lipid-restructuring study. They reported erosion of lipid fragments from a mica surface, and restructuring of an SPB in the presence of the protein chitosan. They cited decreased line tension as the cause of the induced restructuring, which is consistent with our postulation for the anaesthetic-induced SPB changes. Our results can also be compared with those of You et al. (13) where bilayer restructuring was observed induced by the peptide saposin C. Saposin C was found to induce two changes in a gel-phase bilayer. One was the formation of elevated patches and the other thinned domains. These differences were hypothesized to result from different local concentrations of the peptide, especially along the edges of bilayer patches.

An important property of supported DOPC bilayers for analysis is their stability over long periods of time. In the absence of the anaesthetic, vesicle deposition of DOPC consistently yields a supported bilayer that remains stable for imaging over a period of days, as was observed in this study. After addition of halothane to the supported planar bilayer, we observed a restructuring of the supported planar bilayer and the formation of lipid aggregates. Although AFM is typically used to study immobile biological samples, in this study, dynamic lipid aggregation was observed.

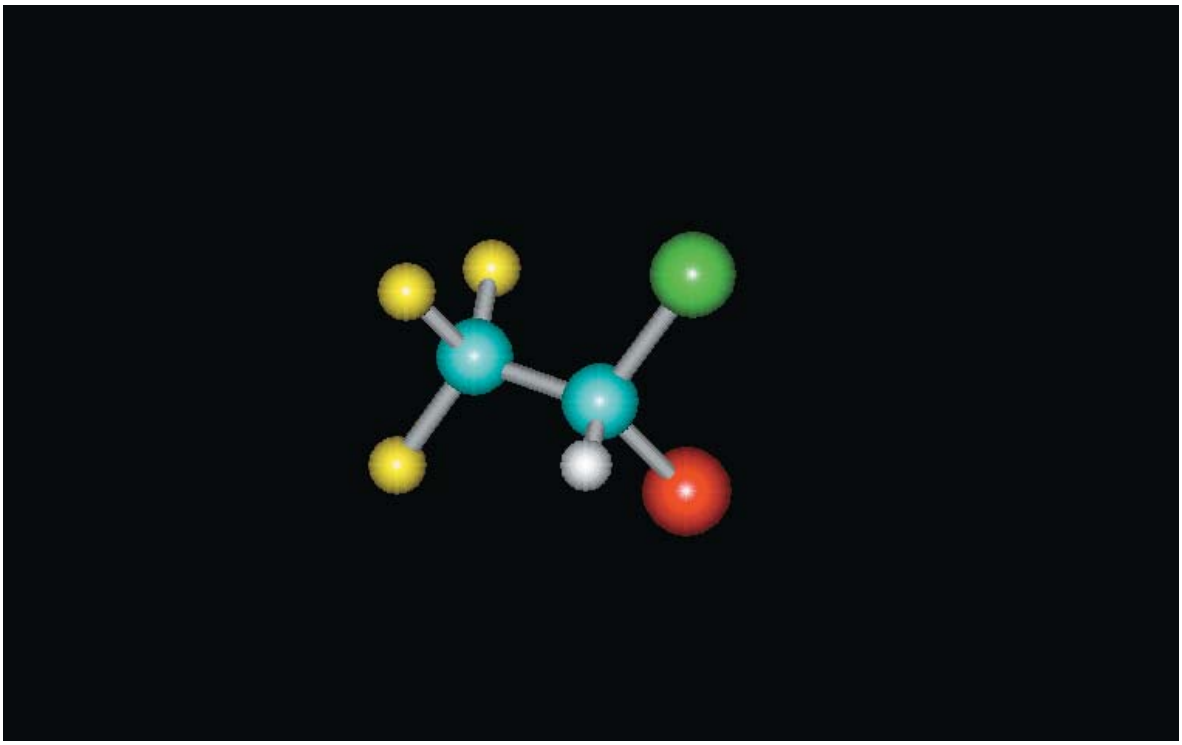
Thermodynamic theories suggest that the presence of anaesthetics within a bilayer may induce slight changes in lateral pressure that result in large conformational changes of embedded proteins (3). The lipid aggregation we observed in the present work could be due to pooling of halothane near the headgroup region. This, coupled with our fluorescence-based halothane distribution results (5), suggests that halothane may induce changes in lateral pressure gradients in phospholipid bilayers. Thus, in addition to direct anesthetic protein interactions, asymmetric anesthetic distribution may contribute to the mechanism of anesthesia. The question, then, is whether these two possible mechanisms compete or are synergistic.

Conclusion

DOPC vesicles were deposited onto a mica surface, both in the absence of the drug and after the addition of halothane. Height and viscoelasticity analysis indicate the lipid is stable in the form of a single planar bilayer in the absence of halothane. However, in the presence of the drug, a curved bilayer structure is favored. The addition of halothane to vesicles in solution followed by vesicle deposition did not yield the formation of a supported bilayer. How-

© 2005 NRC Canada

Fig. 4. Molecular model of halothane ($CF_3CHClBr$).



ever, adhesion of curved vesicles on the mica surface was observed. Together, these results indicate the destabilizing effect of halothane on a planar lipid bilayer at high anaesthetic loading regimes. To our knowledge, this is the first study to date of supported phospholipid bilayer restructuring induced by a general anaesthetic.

Acknowledgements

The authors thank the Natural Sciences and Engineering Research Council of Canada (NSERC), the Alberta Heritage Foundation for Medical Research, and the Alberta Cancer Board for financial support. Also, we thank Professor Nils Peterson (University of Western Ontario, London, Ontario) for helpful discussions.

References

1. K. Meyer. Int. Rev. Neurobiol. **27**, 1 (1985).
2. R. Eckenhoff and J. Johnasson. Pharmacol. Rev. **49**, 343 (1997).
3. R.S. Cantor. J. Phys. Chem. B, **101**, 1723 (1997).
4. Z.V. Leonenko, E. Finot, H. Ma, T.E.S. Dahms, and D.T. Cramb. Biophys. J. **86**, 3783 (2004).
5. A. Carnini, H. Phillips, L. Shamrakov, and D.T. Cramb. Can. J. Chem. **82**, 1139 (2004).
6. Z. Leonenko and D.T. Cramb. Can. J. Chem. **82**, 1128 (2004).
7. L. Koubi, M. Tarek, M.L. Klein, and D. Scharf. Biophys. J. **78**, 800 (2000).
8. N. Fang and V. Chan. Biomacromolecules, **4**, 1596 (2003).
9. Z. Leonenko, A. Carnini, and D.T. Cramb. Biochim. Biophys. Acta, **1509**, 131 (2000).
10. W. Han, S.M. Lindsay, and T. Jing. Appl. Phys. Lett. **69**, 1 (1996).
11. W. Han and S.M. Lindsay. Appl. Phys. Lett. **72**, 1656 (1998).
12. J.L. Swift, A. Carnini, T.E.S. Dahms, and D.T. Cramb. J. Phys. Chem. B, **108**, 11 133 (2004).
13. H.X. You, X. Qi, G.A. Grabowski, and L. Yu. Biophys. J. **84**, 2043 (2003).

© 2005 NRC Canada

ERRATUM / ERRATUM

Erratum: 2004 Alcan Award Lecture From dinuclear to triakontahexanuclear complexes — Adventures in supramolecular coordination chemistry

Laurence K. Thompson

Ref.: Can. J. Chem. **83**, 77–92 (2005).

In the above paper on page 78 there was an omission from the caption for Fig. 1. The correct version follows.

Fig. 1. Academic family tree and portrait of August Hofmann. The academic family tree is available from http://www.careerchem.com/GENEALOGIES/TREES/HofmannAW.pdf (p. 1; Dr. John Andraos, Department of Chemistry, York University, Toronto, Ontario). The portrait of August Hofmann is available from http://www.bioanalytical.com/info/calendar/98/12hof.htm.

Received 18 August 2005. Published on the NRC Research Press Web site at http://canjchem.nrc.ca on 30 Sepember 2005.

L.K. Thompson. Department of Chemistry, Memorial University, St. John's NL A1B 3X7, Canada. (e-mail: lthomp@mun.ca).

 doi: 10.1139/V05-213 © 2005 NRC Canada

Physical organic chemistry in Canada 1900–2005[1]

Thomas T. Tidwell

Abstract: Some of the history of the development of physical organic chemistry in Canada from the 1920s is presented, including many of the individuals involved, and their major areas of interest.

Key words: history of physical organic chemistry in Canada, organic reaction mechanisms, free radicals, kinetics.

Résumé : Quelques faits marquants du développement de la chimie organique physique au Canada depuis les années 1920, y compris plusieurs des intervenants et leurs principaux domaines d'intérêt.

Mots clés : histoire de la chimie organique physique au Canada, mécanismes de réactions organiques, radicaux libres, cinétique.

[Traduit par la Rédaction]

The birth on Christmas day in 1900 of E.W.R. (Ned) Steacie was an event that had a far reaching effect for the development of physical organic chemistry in Canada and worldwide. Steacie was a physical chemist, but his research interests led him into the study of free radical reactions of organic molecules during a critical period for the development of this area (1, 2). At that time, about 1930, the appreciation of the role of reactive intermediates such as free radicals and carbocations was rapidly evolving. In a little more than a decade, marked by the appearance of Hammett's text *Physical organic chemistry* in 1940, and Steacie's monograph on free radical chemistry in 1946 (3*a*), there was a major improvement in understanding, and physical organic chemistry changed from a fringe activity to a comprehensive system that promised the power to explain all of organic chemistry, and to enable the rational design of reactions and prediction of chemical properties. Leaders in the field in the period 1945–1965 included E.D. Hughes and C.K. Ingold at University College, London, Paul Bartlett and Frank Westheimer at Harvard, Gardiner Swain at MIT, Saul Winstein and D.J. Cram at UCLA, J.D. Roberts and George Hammond at Caltech, and Cheves Walling and Ron Breslow at Columbia. Many of the physical organic chemists in Canada were to come from these groups.

This period from 1946 coincided with a tremendous growth in the university system in Canada, which included the development of strong research programs in chemistry all across the country, from Newfoundland to British Columbia, as well as at the excellent laboratories at the National Research Council in Ottawa. Physical organic chemistry was a glamorous field at the time, as it had become possible to gain a detailed understanding of what actually took place in organic reactions, including biological processes, and to understand what gave organic molecules their distinctive properties. Synthetic chemists, led by the example of R.B. Woodward at Harvard, also designed new reactions based on mechanistic principles, and so these were halcyon days for physical organic chemistry. Consequently, Canadian universities emphasized the field, and for the last half of the 20th century Canada had a disproportionate influence in this area worldwide. In contrast to the USA, research in physical organic chemistry in industrial laboratories was rather sparse. Exceptions include the spectacular early work on long-lived carbocations carried on by George Olah at the Dow labs in Sarnia around 1960, which was recognized by the award of the Nobel prize in Chemistry some 35 years later, and research in living free radical polymerization by Michael Georges at the Xerox laboratory in Missisauga.

Physical organic chemistry comes in many flavors, and rather than defining the purview of this area it will instead be illustrated by examples of the areas covered in Canada, and the people involved, some of whom may be surprised or even indignant at being placed in this group. Many of the practitioners of the subject, particularly in gas-phase chemistry, considered themselves as physical chemists, but nevertheless made major contributions to the understanding of organic reactions. The choice of topics and people to include is a personal choice, and while 123 individuals are named, others could have been included as well, and apologies are due to those who were left out. The individuals included were generally born before 1963, and many are now past the normal retirement age of 65. As a sign of the times women are scarce in this group, and it is encouraging that so many younger women are now discovering the satisfaction and excitement of the field. There is a younger generation born after 1962, with many new ideas, and augmented with many women, and the story they will write will partly derive from what has gone on before, but will include many things unimagined by the older generations. Perhaps they too, as they get older, will have some interest in their predecessors.

Received 29 June 2005. Published on the NRC Research Press Web site at http://canjchem.nrc.ca on 21 October 2005.

T.T. Tidwell. Department of Chemistry, University of Toronto, Toronto, ON M5S 3H6, Canada. (e-mail: ttidwell@chem.utoronto.ca).

[1]This article is part of a Special Issue dedicated to organic reaction mechanisms.

 doi: 10.1139/V05-178 © 2005 NRC Canada

The Supporting information[2] includes a list of individuals named, with some of their vital statistics, including their main position while working. It is impressive how many of these in earlier times received their undergraduate education and often Master's degrees in Canada, and then went elsewhere for the Ph.D., often at nearby universities such as Iowa State, Illinois, Chicago, and Wisconsin. There was a dearth of active Ph.D. granting institutions in Canada at that time, with McGill University in Montreal being the clear leader. A number of the pioneers in physical organic chemistry attended smaller schools in the Maritimes such as Mount Allison and Acadia Universities. The fledgling prairie universities in Saskatchewan, Alberta, and Manitoba also graduated many chemists who received graduate training elsewhere in the first half of the 20th century. In the growth years, many chemists were also hired from abroad, including many trained at the centers of the field in London and elsewhere in the UK, Los Angeles, and Cambridge, Massachusetts. Canada also exported many chemists who gained fame in chemistry in the USA.

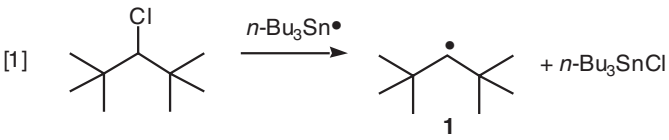
Further information on 21 of the chemists named is available in special issues of the *Canadian Journal of Chemistry* dedicated to particular individuals, as listed in Appendix A. Other sources such as *Canadian Chemical News* and *Proceedings of the Royal Society of Canada* are cited in the Supporting information,[2] and the author would appreciate being informed of other sources that can be added.

Special mention should be made of some of the organic chemists in Canada in the first half of the 20th century who taught and mentored many of those who became physical organic chemists. These include Charles F.H. Allen at McGill, George Wright at Toronto, Robert H. Clark at UBC, and Reuben Sandin at Alberta. These individuals carried on high-quality research, and also inspired future generations of chemists who made Canadian physical organic chemistry rank with the best in the world.

Free radical chemistry

E.W.R. (Ned) Steacie (1900–1962) received his Ph.D. from McGill University in 1926 for research carried out with Frederick Johnson on the solubility of gases in metals, and was also influenced by Otto Maass, an early leader in physical chemistry at McGill. Steacie took a teaching position there, and from about 1929 began the study of gas-phase kinetics of free radical reactions, particularly the pyrolysis of esters, ethers, and alkyl nitrites.

Steacie moved to the National Research Council in Ottawa in 1939 as Director of the Chemistry Division, which was greatly strengthened as a center of chemical research in Canada, particularly in free radical chemistry. Fred Lossing, also a McGill Ph.D. graduate, with Maass, joined the NRC in 1946, and developed a program in gas-phase ion chemstry studied by mass spectrometry. When hired at the NRC to set up a program in mass spectrometry he spent a year at McMaster University in the laboratory of Henry Thode to learn the field. In time his program attracted many co-workers who spread his knowledge and expertise around Canada and elsewhere, and his highly productive career was commemorated in 1990 (3*b*). An early collaborator was Keith Ingold, son of Christopher K. Ingold (1893–1970), who came as a postdoctoral fellow with Lossing in 1951. Keith has had a long career and distinguished career at the NRC, working in free radical chemistry. Included in his accomplishments are studies of hydrocarbon oxidations, "persistent radicals", such as the long-lived di-*tert*-butylmethyl radical (**1**, eq. [1]), the use of "free radical clocks", and free radicals in biological systems (4).



Many of Keith's co-workers at the NRC have also had successful careers in the study of free radicals or other reactive intermediates, including Tony Howard, David Griller, Dan Wayner (now Director General of the Steacie Institute at the NRC), J.C. (Tito) Scaiano, now Professor at the University of Ottawa, and Janusz Lusztyk (now Senior Advisor on Nanotechnology at the NRC). Many other Canadian chemists have been visitors or collaborators with the NRC labs, and the influence on the development of chemistry in Canada has been profound.

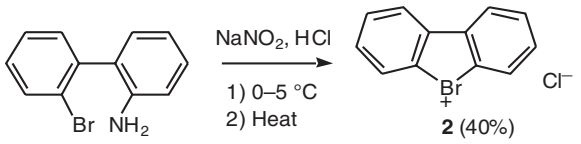
A notable event in physical organic chemistry in Canada was the General Discussion meeting "The reactivity of free radicals" of the Faraday Society of the UK, held in Toronto on 8 and 9 September 1952 (5*a*), with the participation of five future Nobel laureates (R.G.W. Norrish, George Porter, John Polanyi, Linus Pauling, and Gerhard Herzberg). A copy of the program for this meeting is included in the Supporting information,[2] including details of the dinner at the Royal York Hotel in Toronto. This was the first meeting of the Society to be held outside the UK, and it was rumored that initial plans to hold the meeting in the United States were canceled because of fears that certain delegates would not receive visas to the US, a problem that persists 50 years later.

Other prominent individuals involved in research on free radical chemistry in Canada include Ed Janzen (University of Guelph) on the development of spin labels, with a notable citation classic on the subject (5*b*), Jean Lessard (Sherbrooke) using electrochemistry to study radicals, and, Ross Barclay (Mount Allison), who moved from the study of crowded molecules to work on free radicals in biology, Dennis Tanner (Alberta) studied radical halogenation (5*c*), a field rife with controversy, while Nigel Bunce (Guelph) moved from free radical halogenation to prolific studies of organohalogen compounds in the environment. These individuals continued the tradition in organohalogen chemistry begun by Reuben Sandin at Alberta. Among his studies he reported in 1952 (5*d*) the isolation of the first stable bromonium ion, the crys-

[2] Supplementary data for this article are available on the Web site or may be purchased from the Depository of Unpublished Data, Document Delivery, CISTI, National Research Council Canada, Ottawa, ON K1A 0S2, Canada. DUD 4037. For more information on obtaining material refer to http://cisti-icist.nrc-cnrc.gc.ca/irm/unpub_e.shtml.

© 2005 NRC Canada

talline compound **2**, prepared by diazotization of 2-amino-2′-bromobiphenyl (eq. [2]).

[2] 

2 (40%)

Don Arnold, first at UWO and then at Dalhousie, emphasized photochemistry, including free radicals (5*e*), and his former collaborators include Jim Pincock (Dalhousie) and Willie Leigh (McMaster). At the University of Alberta, R.J. Crawford and Karl Kopecky generated free radicals from diazoalkanes (diazenes), as well as other reactive intermediates, while sulfur radicals were studied by Harry Gunning and Otto Strausz, who also studied carbenes and other reactive intermediates. Richard Hiatt at Brock University worked on peroxides, and at the University of British Columbia, Charles McDowell made early applications of electron spin resonance, while Richard Pincock studied radical generation, while Yuan Chow studied radicals at nearby Simon Fraser University.

Carbenes

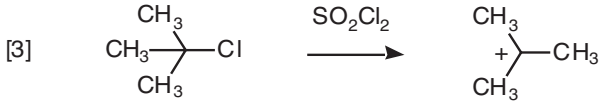
Gerhard Herzberg at the NRC won the Nobel prize in Chemistry in 1971 for studies including carbene generation and structure. John Warkentin (McMaster) has worked in both free radical and carbene chemistry, and, Michael Liu (PEI) has carried on much of his extensive research on carbenes in a largely undergraduate institution.

Ionic reactions in solution

The study of ionic reactions in solution has been a major subject of interest in Canada, with origins that may be traced to several sources, including Keith Laidler at the University of Ottawa, a world renowned figure in the study of reaction kinetics and author of a prominent monograph *Chemical kinetics* (5*f*), as well as many other books. Another school of the study of reaction kinetics in solution was established by Ross Robertson at the NRC, who late in his career went to the University of Calgary. Others included John Scott at Memorial University in Newfoundland, James Hyne (Calgary), Alan Queen (Manitoba), and Ken Leffek (Dalhousie), all of whom came to Canada from the UK and worked with Robertson.

In 1921, Robert H. Clark at the University of British Columbia published a pioneering Canadian physical organic paper on the kinetics of sugar hydrolysis (5*g*), which was in the forefront of the field at the time. Later, he was a mentor of Ross Stewart at UBC, who received his Ph.D. at the University of Washington before returning to UBC. Early in his career Stewart was the Ph.D. supervisor of Keith Yates (5*h*), who became Professor at the University of Toronto, where he studied acid–base reactions, hydrolysis reactions, alkene brominations, computational chemistry, and much else, and whose students included James Pincock, Robert A. McClelland, Robert S. McDonald, Oswald S. Tee, and Robin Cox. Others at Toronto included Jerry Kresge with studies of enols, George Schmid studying additions of sulfenyl and selenyl halides as well as bromination, a topic also pursued by Stan Brown, first at the University of Alberta and later at Queen's University. Tom Tidwell at Toronto specialized in ketenes and electron-deficient carbocations, which were also pursued at York University by Ed Lee-Ruff. Don Lee (University of Regina) has studied the kinetics and mechanisms of oxidation reactions in solution.

Ron Gillespie (McMaster), though nominally an inorganic chemist, studied the protonation of organic compounds, and pioneered the use of highly ionizing solvents. These media were utilized by George Olah (6) in his renowned studies on the direct observation of carbocations in solution. In 1994, Olah was awarded the Nobel Prize for his work on carbocations for which the key first experiments on the *tert*-butyl cation (**3**, eq. [3]).were done in Sarnia. Ted Sorensen at Calgary also studied carbocations in highly acidic solutions by NMR, including important studies of long-lived hydride bridged cations. Jake Stothers (UWO) and Colin Fyfe (Guelph, later UBC) examined other reactive intermediates in solution by NMR, and Laurie Colebrook (Concordia) used NMR in conformational analysis.

[3] 

3

Isotope effects

Arthur Bourns (McMaster) specialized in studies of isotope effects, assisted by the mass spectrometry laboratory of Henry Thode, used to determine isotope ratios (7*a*). Later, he was diverted into an administrative career as President and Chancellor at McMaster, while his students Peter J. Smith (Saskatoon), and Ken Westaway (Laurentian) carried on in this field. Gerald Dunn was one of several Canadian chemists associated with Henry Gilman and others at Iowa State University and his work there included a study of isotope effects (7*b*), which he developed in his career at the University of Manitoba, where his students included John Warkentin (McMaster), Ed Janzen (Guelph), Robert S. McDonald (Mt. St. Vincent), and James Pincock (Dalhousie). Jerry Kresge (Toronto) made fundamental studies on isotope effects and utilized these in the elucidation mechanistic studies involving a variety of reactive intermediates.

Carbocations

Ron Childs (McMaster) who studied with Saul Winstein, continued carbocation studies and was later diverted into administration. Choi Chuk Lee (Saskatchewan) had worked with carbon isotopes at MIT with J.D. Roberts (8) and pursued similar studies of molecular rearrangements using isotopes. Alan Colter (Guelph), another Winstein student, studied solvolysis reactions and ion pairing. Ted Sorensen at the University of Calgary, as previously noted, studied stable ions by NMR. Bob McClelland (Toronto) carried out research on carbocations and later extended this work to nitrenium ions.

© 2005 NRC Canada

Carbanions and elimination reactions

Erwin Buncel began in peroxide chemistry with Alwyn Davies and as a postdoc with Joseph Bunnett became acquainted with azo compounds (9), a field he has pursued, along with work on carbanions. Tony Durst (Ottawa) studied substituent effects on carbanions, and Jake Stothers (UWO) studied these species by NMR. Duncan Hunter (UWO) and Pat Farrell (McGill University) studied elimination reactions, and the latter also examined the properties of solutions.

Bioorganic chemistry

Peter Guthrie (UWO) has made theoretical studies of mechanisms of fundamental reactions such as ester hydrolysis and related processes, while Stan Brown (Alberta, then Queen's) has studied amide hydrolysis, and Ron Kluger (Toronto) has studied enzyme mechanisms. Jik Chin, first at McGill and then at Toronto, has studied biological mechanisms and also organometallic chemistry, while John Bunting at Toronto worked on mechanisms of reactions of heterecocycles, and Bryan Jones (Toronto) studied enzyme models. Normand Voyer (Laval) studied ion channels, and Ossie Tee (Concordia) used cyclodextrins in hydrolysis reactions. Ray Lemieux (Ottawa, the NRC, and Alberta) had a diverse career including studies of conformational analysis and carbohydrate chemistry. Saul Wolfe examined enzyme mechanisms and penicillin chemistry at Queen's and later at Simon Fraser University, with diversions into computational chemistry. Jack Edward (McGill) studied amide hydrolysis, the acid–base properties of amino acids, and explosives. He and Ray Lemieux were responsible for a singularly Canadian invention, the "anomeric effect", widely known as the "Edwards–Lemieux effect". Pierre Deslongschamps (Sherbrooke) also achieved fame in this area, and Jean-Claude Richer (Montreal) studied stereochemistry in heterocyclic rings.

Silicon and germanium chemistry

Adrian Brook (Toronto) was a leader in studies of organosilicon chemistry and his student Kim Baines (UWO) extended these studies to organogermanium compounds. Willie Leigh (McMaster) has investigated silenes and germylenes and Michael Brook (McMaster) studied organosilicon chemistry for materials applications.

Molecular rearrangements, small ring compounds, and thermolysis reactions

Ed Warnhoff (UWO), Robert Fraser (Ottawa), and John Scheffer (UBC) studied rearrangements and molecular structures. At the University of Alberta, Karl Kopecky investigated dioxetanes and diazo compounds, Robert J. Crawford (Alberta) has studied small rings and pyrazolines, and David Darwish pursued the reactions of sulfur compounds. Persephone Cannone (Laval) examined cycloaddition reactions.

Photochemistry

Photochemistry has long been a major interest in Canada, and the Photochemistry Unit at the University of Western Ontario with Paul De Mayo and Don Arnold (who later moved to Dalhousie University) was a major centre for this research. Alan Weedon has continued this tradition, and several physical chemists have also participated. Others active in the area include Peter Yates and Jim Guillet (Toronto), James Pincock (Dalhousie), Denis Gravel (Montreal), Peter Wan (UVic), Ed Lee-Ruff (York U.), and Willie Leigh (McMaster). John Scheffer (UBC) studied photochemistry in the solid state. Tito Scaiano (Ottawa) has been a major contributor in this area, and he and his students, Cornelia Bohne (University of Victoria) and Monica Barra (University of Guelph) have brought a strong South American expertise to Canada.

Computational chemistry

Imre Csizmadia (Toronto) did much to popularize these methods among organic chemists and his students including Paul Mezey (Universty of Saskatchewan), Ray Poirier (Memorial University), and Alan Hopkinson (York University) have also played significant roles. Others active in this area are Russell Boyd (Dalhousie), Arvi Rauk (Calgary), Nick Westiuk (McMaster), Peter Guthrie (UWO) with his unique "no-barrier" theory, Saul Wolfe at Queen's University, later at Simon Fraser University in British Columbia, Dick Bader (McMaster), with his "atoms in molecules" approach, and Errol Lewars (Trent), who evolved from a background in synthetic organic chemistry.

Gas-phase reactions

The study of gas-phase reactions has followed the lead of Fred Lossing at the NRC in Ottawa, and has been carried on by Paul Kebarle (Alberta), Alex Harrison (Toronto), John Holmes (Ottawa), and Diethard Bohme (York). All of these have studied the reactions of organic ions in the gas phase. Carl Coffin at Dalhousie was a student of Maass who made important contributions, but his career was cut short.

Polymers and materials

In addition to individuals studying polymer chemistry there is growing interest in materials chemistry, as exemplified by the work of Bob Lemieux (Queen's University), Tom Fyles (University of Victoria), and Jim Wuest (University of Montreal). This area is expected to assume increasing importance.

Unusual molecules

Reg Mitchell (University of Victoria) for a long time was Canada's main representative in this area, as well as being a great popularizer of chemistry, and has been joined more recently by Graham Bodwell at Memorial University, Newfoundland. Satoru Masamune (Alberta) studied cyclobutadiene and other annulenes, in addition to his major interest in synthesis.

Physical organic minisymposium

Since 1973 physical organic chemistry in Canada has been nourished by the Ontario–Quebec Minisymposium on Physi-

© 2005 NRC Canada

cal Organic Chemistry (POMS), which has served as a forum for this field since its beginning at the instigation of Nick Werstiuk (McMaster), with promotion of the first meeting in Toronto by Keith Yates, Peter Yates, and others. This has included many active participants from the Maritimes, Western Canada, the US, and Europe, and has evolved over the years, reflecting the current state of the field.

Outlook

Physical organic chemistry has played a leading role in Canadian science for more than half a century, and has been a dynamic and developing enterprise. Many of the earlier problems examined by physical organic chemists have been solved and have been replaced by newer and different challenges. This has been an interdisciplinary field from the very beginning, with interests including biological, inorganic, and gas-phase reactions, polymerization, and theoretical chemistry. As the leading areas of chemical research have become increasingly decompartmentalized and the tools of physical organic chemistry have become increasingly pervasive, the boundaries of the field are now often difficult to recognize. Materials chemistry, nanotechnology, biological mechanisms, catalysis, and indeed the search for the origins of life are all physical organic chemistry in new garb. It may be expected that in a further 50 years the field will have evolved in still new directions, but the basic quest for the understanding of how things work will live on.

Acknowledgments

Thanks are due to John Andraos, Bob Crawford, Ossie Tee, John Warkentin, and many others for their assistance with this manuscript, and the Natural Sciences and Engineering Research Council of Canada (NSERC) for financial support.

References

1. T.T. Tidwell. Can. Chem. News, 16–17 May 2000.
2. E.W.R. Steacie. Proc. Roy. Soc. London A, **314**, 1930 (1930).
3. (*a*) E.W.R. Steacie. Atomic and free radical reactions. ACS Monograph 102. Reinhold, New York. 1946; (*b*) E.W.R. Steacie. Int. J. Mass Spectrom. Ion Processes, **101**, 81 (1990).
4 (*a*) J.A. Howard and K.U. Ingold. J. Am. Chem. Soc. **90**, 1056 (1983); (*b*) K.U. Ingold. Acc. Chem. Res. **2**, 1 (1969); (*c*) K.U. Ingold, J. Lustyk, and K.D. Rayner. Acc. Chem. Res. **23**, 219 (1990); (*d*) D. Griller and K.U. Ingold. Acc. Chem. Res. **13**, 317 (1980).
5. (*a*) E. Whittle. Chem. Can. (October), **4**, 56 (1952); (*b*) E.G. Janzen. Acc. Chem. Res. **4**, 31 (1971); (*c*) D.D. Tanner and F.C.P. Law. J. Am. Chem. Soc. **91**, 7535 (1969); (*d*) R.B. Sandin and A.S. Hay. J. Am. Chem. Soc. **74**, 274 (1952); (*e*) J.M. Dust and D.R. Arnold. J. Am. Chem. Soc. **105**, 1221 (1983); (*f*) K.J. Laidler. Chemical kinetics. 1st ed. McGraw Hill, New York. 1950; (*g*) R.H. Clark. J. Am. Chem. Soc. **43**, 1759 (1921); (*h*) R. Stewart and K. Yates. J. Am. Chem. Soc. **80**, 6355 (1958).
6. G.A. Olah. A life of magic chemistry. Wiley, New York. 2000.
7. (*a*) J.G. Lindsay, A.N. Bourns, and H.G. Thode. Carbon 13 isotope effect in the decarboxylation of normal malonic acid. Can. J. Chem. **29**, 192 (1951); (*b*) C. Brynko, G.E. Dunn, H. Gilman, and G.S. Hammond. Isotope effect in the hydrolysis of triphenylsilane-*d*. J. Am. Chem. Soc. **78**, 4909 (1956).
8. R.H. Mazur, W.N. White, D.A. Semenow, C.C. Lee, M.S. Silver, and J.D. Roberts. J. Am. Chem. Soc. **81**, 4390 (1959).
9. J.F. Bunnett, E. Buncel, and K.V. Nahabedian. J. Am. Chem. Soc. **84**, 4136 (1962).

Appendix A. Special issues of the *Canadian Journal of Chemistry*

May 1965	R.B. Sandin	68th Birthday
Dec. 1980	R.U. Lemieux	60th Birthday
June 1981	F.P. Lossing	65th Birthday
May 1983	H.E. Gunning	65th Birthday
Oct. 1984	P. de Mayo	60th Birthday
Nov. 1984	P. Yates	60th Birthday
June 1986	A.N. Bourns	Contributions to Canadian chemistry
Aug. 1987	J.T. Edward	65th Birthday
Aug. 1988	C.A. McDowell	70th Birthday
Nov. 1989	R.J. Gillespie	65th Birthday
Oct. 1990	R. Stewart	65th Birthday
Nov. 1995	J.E. Guillet	Contributions to Canadian chemistry
June 1996	R.F. Bader	65th Birthday
June 1998	E. Buncel	Contributions to Canadian chemistry
June 1999	A.J. Kresge	Contributions to Canadian chemistry
Nov. 2000	A. Brook	Contributions to Canadian chemistry
June 2002	J.B. Jones	65th Birthday
June 2003	D. Arnold	Contributions to Canadian chemistry
June 2004	G. Herzberg	Memorial issue
Nov. 2005	P. Kebarle	Contributions to Canadian chemistry
2006	A. Bader	Contributions to Canadian chemistry

© 2005 NRC Canada

Kinetics and mechanism of acid-catalyzed hydrolysis of the diazo functional groups of 1-diazo-2-indanone and 2-diazo-1-indanone in aqueous solution[1]

Yvonne Chiang, A. Jerry Kresge, Oleg Sadovski, Xiaofeng Zeng, and Yu Zhu

Abstract: Rates of hydrolysis of 1-diazo-2-indanone and 2-diazo-1-indanone were measured in dilute aqueous perchloric acid solutions using both H_2O and D_2O as the solvent, and rates of hydrolysis of the latter substrate were measured in dilute aqueous (H_2O only) formic acid buffer solutions as well. The data for 1-diazo-2-indanone gave the hydronium ion catalytic coefficient $k_H^+ = 5.7 \times 10^{-3}$ (mol/L)$^{-1}$ s^{-1} and the isotope effect $k_H^+/k_D^+ = 2.9$. The normal direction ($k_H/k_D > 1$) of this isotope effect was taken as evidence for a reaction mechanism involving rate-determining hydron transfer from the hydronium ion to the substrate's diazo carbon atom; followed by rapid displacement of diazo nitrogen by a water molecule, giving the observed 1-hydroxy-2-indanone product. The data for 2-diazo-1-indanone, on the other hand, gave a hydronium ion catalytic coefficient two orders of magnitude greater than the value for 1-diazo-2-indanone ($k_H^+ = 5.9 \times 10^{-1}$ (mol/L)$^{-1}$ s^{-1}), and an isotope effect near unity ($k_H^+/k_D^+ = 1.2$). It is argued that this isotope effect represents a situation in which diazo carbon hydronation and displacement of diazo nitrogen are each partly rate determining, a conclusion supported by incipient saturation of buffer catalysis in the formic acid buffer solutions. The 100-fold difference in hydronium ion catalytic coefficients for the two substrates is rationalized in terms of differing electron densities on the diazo carbon atoms.

Key words: diazo compound hydrolysis, solution kinetics, acid catalysis, solvent isotope effects, buffer catalysis saturation.

Résumé : On a mesuré les vitesses d'hydrolyse de la 1-diazoindan-2-one et 2-diazoindan-1-one en solutions aqueuses diluées d'acide perchlorique, en faisant appel tant au H_2O qu'au D_2O comme solvant; les vitesses d'hydrolyse du dernier substrat on aussi été mesurées dans des solutions aqueuses (uniquement avec du H_2O) de tampons à l'acide formique. Les données pour la 1-diazoindan-2-one permettent d'évaluer le coefficient catalytique de l'ion hydronium ($k_H^+ = 5{,}7 \times 10^{-3}$ (mol/L)$^{-1}$ s^{-1}) et l'effet isotopique ($k_H^+/k_D^+ = 2{,}9$). On considère que la direction normale ($k_H/k_D > 1$) de cet effet isotopique est un indice en faveur d'un mécanisme réactionnel impliquant, dans l'étape cinétiquement déterminante, un transfert d'hydron de l'ion hydronium vers l'atome de carbone du diazo du substrat; celui-ci serait suivi d'un déplacement rapide de l'azote du diazo par une molécule d'eau qui conduirait à la formation du 1-hydroxydiazoindan-2-one qui a été observée. Par ailleurs, les données relatives à la 2-diazoindan-1-one indiquent que le coefficient catalytique de l'ion hydronium est de deux ordres de grandeur plus rapide que la valeur pour la 1-diazoindan-2-one ($k_H^+ = 5{,}9 \times 10^{-1}$ (mol/L)$^{-1}$ s^{-1}) et l'effet isotopique près de l'unité ($k_H^+/k_D^+ = 1{,}2$). On suggère que cet effet isotopique représente une situation dans laquelle l'hydronation du carbone du diazo et le déplacement de l'azote du diazo sont tous les deux partiellement cinétiquement importants; cette conclusion est supportée par la saturation induite de la catalyse par le tampon dans les solutions tampons d'acide formique. On rationalise le facteur de cent dans les coefficients catalytiques de l'ion hydronium pour les deux substrats en termes de densités électroniques différentes sur les atomes de carbone du diazo.

Mots clés : hydrolyse de composés diazo, cinétique en solution, catalyse acide, effets isotopiques du solvant, saturation de la catalyse par un tampon.

[Traduit par la Rédaction]

Received 12 September 2004. Published on the NRC Research Press Web site at http://canjchem.nrc.ca on 27 September 2005.

Y. Chiang, A.J. Kresge,[2] O. Sadovski, X. Zeng, and Y. Zhu. Department of Chemistry, University of Toronto, Toronto, ON M5S 3H6, Canada.

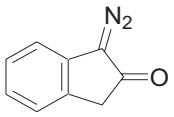
[1]This article is part of a Special Issue dedicated to organic reaction mechanisms.
[2]Corresponding author (e-mail: akresge@chem.utoronto.ca).

 doi: 10.1139/V05-115 © 2005 NRC Canada

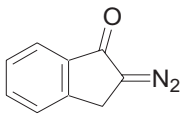
Introduction

The acid-catalyzed hydrolysis of aliphatic diazo compounds is a much-studied reaction that has played an important role in the development of modern ideas on acid–base catalysis (for reviews, see ref. 1). Diazo compounds are also synthetically useful materials: they can, for example, be transformed, via the Wolff rearrangement, into ketenes, which readily undergo a wide variety of useful reactions (2). The synthetic utility of diazo compounds, however, is limited by their facile acid-catalyzed hydrolysis, and information on the nature of this acid-catalyzed reaction, especially on how its rate depends on substrate structure, is consequently of practical value.

In the present paper, we report on an investigation of the acid-catalyzed hydrolysis in aqueous solution of 1-diazo-2-indanone (**1**) and 2-diazo-1-indanone (**2**).



1



2

Although these substances differ only in the relative placement of their diazo and carbonyl functional groups, they differ in reactivity by two orders of magnitude and hydrolyse by different reaction mechanisms.

Experimental section

Materials

1-Diazo-2-indanone

We prepared this substance by diazo group transfer from 4-acetamidobenzenesulfonyl azide (3) to 2-indanone under phase transfer conditions (4). In our hands, however, the yield of product was never greater than ca. 15%. In a typical procedure, 1.00 g (7.6 mmol) of 2-indanone, 2.00 g (8.3 mmol) of 4-acetamidobenzenesulfonyl azide, and 0.050 g of tetrabutylammonium bromide were dissolved in 120 mL of dichloromethane, and 9.0 mL of 1.0 mol/L aqueous sodium hydroxide was added. This mixture was stirred at 0 °C for 3 h and the layers were then separated. The water layer was extracted with two 30 mL portions of dichloromethane, and the combined organic layers were washed with water, dried with sodium sulfate, and the solvent was removed. The residue was purified by column chromatography (silica gel with hexanes–dichloromethane (1:1, *v*:*v*) eluent) and recrystallization from *n*-pentane. The product was a light orange-colored solid. ^{1}H NMR (400 MHz, $CDCl_3$, ppm) δ: 7.24–7.34 (m, 2H), 7.09–7.17 (m, 2H), 3.55 (s, 2H). ^{13}C NMR (100 MHz, $CDCl_3$, ppm) δ: 197.4, 131.2, 129.6, 128.3, 125.5, 125.0, 118.3, 68.4, 42.2. HR-MS calcd. for $C_9H_6N_2O$: 158.0480; found: 158.0483.

2-Diazo-1-indanone

This substance was prepared from the monotosylhydrazone of 1,2-indanedione, as described in the literature (5).

1-Hydroxy-2-indanone

This material was prepared by acid-catalyzed hydrolysis of 1-diazo-2-indanone. A mixture made by combining 50 mL of aqueous 0.04 mol/L perchloric acid with 50 mg of 1-diazo-2-indanone dissolved in 2 mL of acetonitrile was stirred at room temperature overnight and was then extracted with 50 mL of dichloromethane. The aqueous phase was neutralized with sodium hydroxide and then was extracted with dichloromethane three additional times. The combined extracts were dried over magnesium sulfate and the solvent was removed leaving a yellowish oil, which subsequently solidified. Two recrystallizations from dichloromethane–hexane gave a white product. ^{1}H NMR (300 MHz, $CDCl_3$, ppm) δ: 7.6–7.7 (m, 1H), 7.38–7.26 (m, 3H), 5.17 (s, 1H), 3.68 (d, J = 22 Hz, 1H), 3.52 (d, J = 22 Hz, 1H), 3.0 (bs, 1H). ^{13}C NMR (75 MHz, $CDCl_3$, ppm) δ: 214.9, 139.3, 135.7, 129.2, 128.1, 125.2, 125.1, 75.2, 40.8.

2-Hydroxy-1-indanone

This substance was prepared by acid-catalyzed hydrolysis of 2-diazo-1-indanone, as described in the literature (6). The product was a white solid, mp 38 to 39 °C, whose ^{1}H NMR spectrum agreed with a published report (7).

All other materials were best available commercial grades.

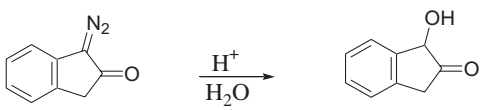
Kinetics

Rates of diazo compound hydrolysis were determined by monitoring the decrease of diazo absorption at λ = 260 nm for 1-diazo-2-indanone and λ = 320 nm for 2-diazo-1-indanone. Measurements were made using a Cary 2200 spectrometer, the temperature of whose cell compartment was controlled at 25.0 ± 0.05 °C. The data so obtained conformed to the first-order rate law well, and observed first-order rate constants were obtained by least-squares fitting of a single exponential function.

Results

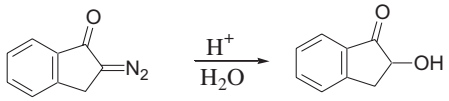
Product analysis

The reaction of diazo carbonyl compounds with the hydronium ion, written here as H^+, in aqueous solution usually gives the corresponding hydroxy compounds as reaction products, as shown in eqs. [1] and [2] for the presently examined substrates. This was shown to be the case here for 1-diazo-2-indanone (**1**) by comparing the ^{1}H NMR spectrum of a spent reaction mixture formed in 0.04 mol/L $HClO_4$ solution with that of an authentic sample of 1-hydroxy-2-indanone (**3**). It was also shown to be the case for 2-diazo-1-indanone (**2**) by comparing the HPLC traces and UV spectra of spent reaction mixtures, formed in 0.001 mol/L $HClO_4$ solution as well as in a 0.2 mol/L formic acid buffer with a buffer ratio of $[HA]/[A^-]$ = 1, with those of authentic samples.

[1] 

1 **3**

© 2005 NRC Canada

[2] 

2 4

Kinetics for 1-diazo-2-indanone

Rates of hydrolysis of 1-diazo-2-indanone were measured in perchloric acid solutions, using both H_2O and D_2O as the solvent, over the concentration range [acid] = 0.04–0.1 mol/L. The ionic strength of these solutions was maintained at 0.10 mol/L by adding sodium perchlorate as required. The data so obtained are listed in Table S1[3] and are displayed in Fig. 1.

It may be seen that observed first-order rate constants increase linearly with increasing acid concentration. The data were therefore subjected to linear least-squares analysis. This produced the H_2O solution second-order rate constant $k_H^+ = (5.70 \pm 0.11) \times 10^{-3}$ (mol/L)$^{-1}$ s^{-1} and a corresponding D_2O solution rate constant, which, in combination with the H_2O result, gave the solvent isotope effect $k_H^+/k_D^+ = 2.87 \pm 0.19$.

Kinetics for 2-diazo-1-indanone

Rates of hydrolysis of 2-diazo-1-indanone were also determined in perchloric acid solutions, again using both H_2O and D_2O as the solvent, over the concentration range [acid] = 0.01–0.1 mol/L at a constant ionic strength of 0.10 mol/L ($NaClO_4$). These data are listed in Table S2[3] and are displayed in Fig. 2. Once again, observed rate constants increased linearly with increasing acid concentration, and linear least-squares analysis gave the H_2O solution rate constant $k_H^+ = (5.88 \pm 0.11) \times 10^{-1}$ (mol/L)$^{-1}$ s^{-1} and the solvent isotope effect $k_H^+/k_D^+ = 1.18 \pm 0.03$.

Rates of hydrolysis of this substrate were also determined in a series of formic acid buffer solutions, all with the same constant stoichiometric buffer ratio ($[HA]_s/[A^-]_s = 1.3$) over the concentration range [buffer] = 0.003–0.3 mol/L, at a constant ionic strength of 0.10 ($NaClO_4$). These data are summarized in Table S3[3] and are displayed in Fig. 3. It may be seen that these observed first-order rate constants also increase with increasing buffer concentration, but not in a linear fashion. Their analysis is detailed in the following section.

Discussion

Perchloric acid solutions

The present results show that the hydrolysis of 1-diazo-2-indanone in perchloric acid solutions is an acid-catalyzed reaction and that it occurs with a substantial hydronium ion isotope effect in the normal direction ($k_H/k_D > 1$): $k_H^+/k_D^+ = 2.87$. This is classic evidence for slow hydron transfer from the hydronium ion to carbon (8), and it suggests that the reaction occurs by rate-determining hydronation of the substrate on its diazo carbon atom followed by more rapid replacement of nitrogen by the hydroxyl group of a water molecule, as shown in eq. [3].

Fig. 1. The relationship between hydronium ion concentration and the rate of hydrolysis of 1-diazo-2-indanone in H_2O (O) and D_2O (Δ) solutions of perchloric acid at 25 °C.

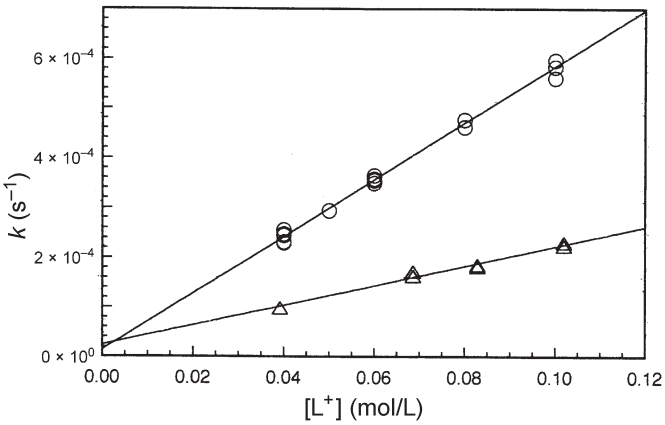


Fig. 2. The relationship between hydronium ion concentration and the rate of hydrolysis of 2-diazo-1-indanone in H_2O (O) and D_2O (Δ) solutions of perchloric acid at 25 °C.

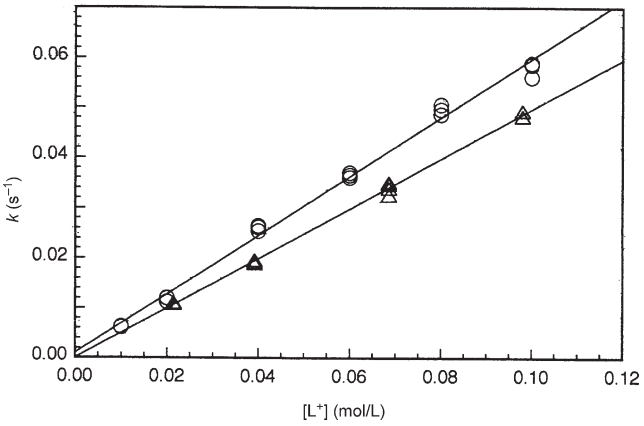
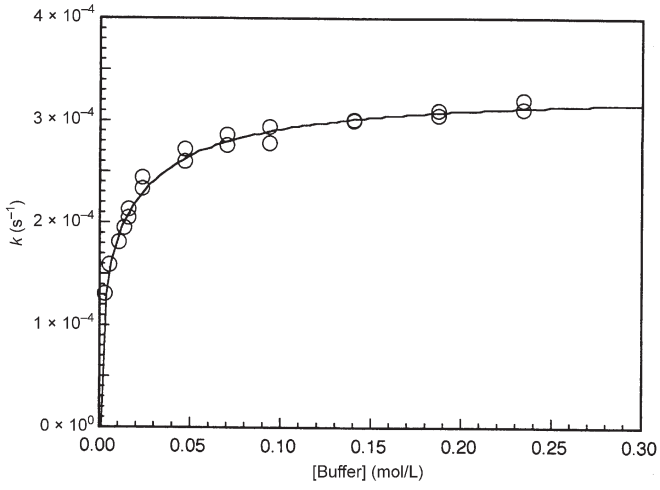
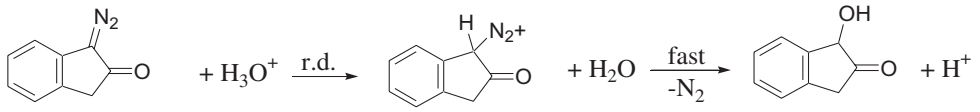


Fig. 3. The relationship between buffer concentration and the rate of hydrolysis of 2-diazo-1-indanone in aqueous (H_2O) formic acid buffer solutions at 25 °C.



[3] Supplementary data for this article (Tables S1–S3) are available on the Web site or may be purchased from the Depository of Unpublished Data, Document Delivery, CISTI, National Research Council Canada, Ottawa, ON K1A 0S2, Canada. DUD 4018. For more information on obtaining material refer to http://cisti-icist.nrc-cnrc.gc.ca/irm/unpub_e.shtml.

© 2005 NRC Canada

[3] 

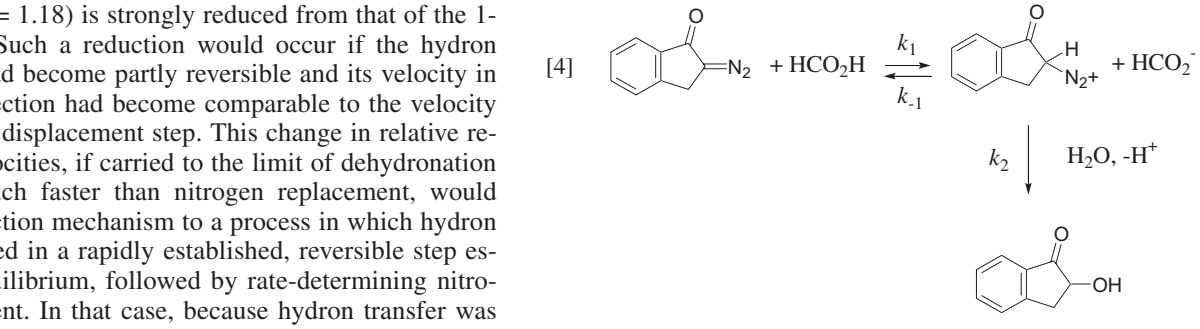
Primary isotope effects on hydron transfer from the hydronium ion are accompanied by an inverse secondary component, contributed by tightening up of bonds to the two nontransferring hydrogen atoms of the hydronium ion unit (9). This reduces the magnitude of the overall effect considerably, and the present isotope effect is in fact a near-maximum value (10). This implies that hydronic motion makes up most of the reaction coordinate and that very little heavy atom participation contributes, as would have been the case if the hydrolysis reaction was a concerted process. The magnitude of the present isotope effect therefore implies that hydron transfer and nitrogen displacement take place in separate steps, as written in eq. [3].

The hydronium ion isotope effect on the hydrolysis of 2-diazo-1-indanone, on the other hand, is quite different: its value ($k_H^+/k_D^+ = 1.18$) is strongly reduced from that of the 1-diazo isomer. Such a reduction would occur if the hydron transfer step had become partly reversible and its velocity in the reverse direction had become comparable to the velocity of the nitrogen displacement step. This change in relative reaction step velocities, if carried to the limit of dehydronation being very much faster than nitrogen replacement, would change the reaction mechanism to a process in which hydron transfer occurred in a rapidly established, reversible step essentially at equilibrium, followed by rate-determining nitrogen displacement. In that case, because hydron transfer was no longer rate-determining, the solvent isotope effect would have no primary component. There would, however, be an equilibrium isotope effect on the hydron transfer step and, since the hydrogen–oxygen bonds of the water molecule product formed in this step are tighter than those of the reactant hydronium ion (9), this isotope effect would be inverse. An example of this kind of reaction is the hydrolysis of diazo acetaldehyde for which the hydronium ion isotope effect is $k_H^+/k_D^+ = 0.55$ (11). A situation intermediate between the limits of a rapidly reversible equilibrium hydron transfer and a rate-determining hydron transfer would be expected to have a hydronium isotope effect intermediate between the limits for these two mechanisms, i.e., a value near unity, as observed.

Hydron transfer could, of course, also take place to the carbonyl oxygen atom of a diazo compound producing an enediol intermediate, whose ketonization would give a hydroxy carbonyl product. Such a reaction, however, with hydronium ion as the hydron donor, would be a strongly uphill oxygen-to-oxygen hydron transfer, whose reverse would be a downhill encounter controlled process, much faster than the subsequent nitrogen displacement step. This would give a strongly inverse hydronium ion isotope effect. An example of such a reaction is the hydrolysis of 1,2-diphenyldiazoethanone for which an isotope effect of $k_H/k_D = 0.57$ has been reported (12), quite different from the isotope effects observed here. Oxygen protonation is also inconsistent with the fact that different hydroxycarbonyl products are formed from the hydrolysis of 1-diazo-2-indanone and 2-diazo-1-indanone (eqs. [1] and [2]), inasmuch as these diazo compounds would both give the same enediol intermediate whose ketonization would produce the same product for both substrates.

Formic acid buffer solutions

Further support for a two-step reaction mechanism with hydron transfer partly rate-determining for the hydrolysis of 2-diazo-1-indanone comes from the curved nature of the buffer dilution plot obtained from rate constants determined in formic acid buffer solutions. The buffer-catalyzed analog of this reaction mechanism is shown in eq. [4], and the rate law that applies to a combination of this route plus the hydronium ion reaction is given as eq. [5]. The concentration variables that appear in this rate law:

[4] 

[5] $$k_{obs} = k_H^+[H^+] + k_1[HCO_2H]/\{1 + (k_{-1}/k_2)[HCO_2^-]\}$$

$[H^+]$, $[HCO_2H]$, and $[HCO_2^-]$ were evaluated for each buffer solution by calculation, using the concentration acidity constant for formic acid applicable at the ionic strength of the rate measurements, $Q_a = 2.80 \times 10^{-4}$ mol/L, based on $pK_a = 3.752$ for formic acid (13) and activity coefficients recommended by Bates (14). The results are listed in Table S3.[3] Least-squares analysis of the rate data using this rate law with $[H^+]$, $[HCO_2H]$, and $[HCO_2^-]$ as independent variables gave $k_H^+ = (4.43 \pm 0.18) \times 10^{-1}$ $(mol/L)^{-1}$ s^{-1}, $k_1 = (1.07 \pm 0.20) \times 10^{-2}$ $(mol/L)^{-1}$ s^{-1}, and $k_{-1}/k_2 = (8.64 \pm 1.53) \times 10^{-1}$ mol/L.

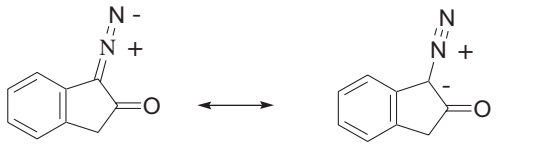
The line shown in Fig. 3 was drawn using these results. It may be seen that the data fit this model well. The value of k_H^+ obtained, moreover, is consistent with $k_H^+ = 5.88 \times 10^{-1}$ $(mol/L)^{-1}$ s^{-1} determined in perchloric acid solutions. The value of k_1, which is the rate constant for carbon protonation of the diazo compound by formic acid, is also a sensible result in that it is nearly two orders of magnitude less than k_H^+, the rate constant for the same hydronation reaction effected by the much more strongly acidic hydronium ion.

Relative reactivities

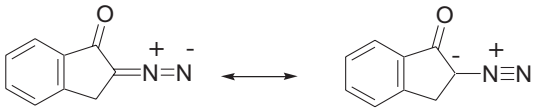
The present results show the hydronium ion catalyzed hydrolysis of 2-diazo-1-indanone to be two orders of magnitude faster than the same reaction of 1-diazo-2-indanone.

© 2005 NRC Canada

Although the mechanisms of these two reactions are not the same, they both involve hydron transfers, either rate-determining or partly rate-determining, to the diazo carbon atom. The rates of both reactions should therefore be influenced by the negative charge density on this carbon atom generated by electron delocalization from the diazo group, as shown by resonance structures **5** and **6**. With both substrates, this charge density is diminished by further delocalization into the adjacent carbonyl groups, and in the case of 1-diazo-2-indanone, it is diminished further by delocalization into the adjacent benzene ring. In the case of 2-diazo-1-indanone, however, the benzene ring is not adjacent to the diazo group, and such further delocalization is not possible. The negative charge density on the diazo carbon atom of 2-diazo-1-indanone is consequently greater than that on the diazo carbon atom of 1-diazo-2-indanone. This makes the diazo carbon atom of the 2-diazo isomer more basic, and more rapidly hydronated, than that of the 1-diazo isomer, as observed.



1 **5**



2 **6**

Acknowledgement

We are grateful to the Natural Sciences and Engineering Research Council of Canada (NSERC) for financial support of this work.

References

1. R.P. Bell. The proton in chemistry. Cornell University Press, Ithaca, New York. 1973. pp. 164–171; M. Regitz and G. Maas. Diazo compounds, properties and synthesis. Academic Press, New York. 1986. pp. 96–165.
2. T.T. Tidwell. Ketenes. Wiley, New York. 1995. Chap. 5.
3. J.S. Baum, D.A. Shook, H.M.L. Davies, and H.D. Smith. Synth. Commun. **17**, 1709 (1987).
4. H. Ledon. Synthesis, 347 (1974); S.M. Kumar. Synth. Commun. **21**, 2121 (1991).
5. M.P. Cava, R.L. Litle, and D.R. Napier. J. Am. Chem. Soc. **80**, 2257 (1958).
6. P.K. Banerjee, D. Mukhopadhyay, and D.N. Chaudhury. J. Indian Chem. Soc. **42**, 115 (1965).
7. S. Dayan, J. Almog, O. Khodzhaev, and S. Rosen. J. Org. Chem. **63**, 2752 (1998).
8. J.R. Keeffe and A.J. Kresge. *In* Techniques of chemistry. Vol. VI. 4th ed. *Edited by* C.F. Bernasconi. Wiley-Interscience, New York. 1986. Part I, Chap. XI.
9. A.J. Kresge, R.A. More O'Ferrall, and M.F. Powell. *In* Isotopes in organic chemistry. Vol. 7. *Edited by* E. Buncel and C.C. Lee. Elsevier, New York. 1987. Chap. 4.
10. A.J. Kresge, D.S. Sagatys, and H.L. Chen. J. Am. Chem. Soc. **99**, 7228 (1977).
11. Y. Chiang, A.J. Kresge, and V.V. Popik. J. Chem. Soc. Perkin Trans. 2, 1107 (1999).
12. J.F. McGarrity, A. Cretton, A.A. Pinberton, D. Swarzenbach, and H.D. Flack. Angew. Chem. Int. Ed. Engl. **22**, 405 (1982); Angew. Chem. Suppl. 551 (1983).
13. H.S. Harned and N.D. Embree. J. Am. Chem. Soc. **56**, 1042 (1934).
14. R.G. Bates. Determination of pH theory and practice. John Wiley and Sons, New York. 1973. p. 49.

© 2005 NRC Canada

The art of discovery in biophysical organic chemistry[1]

Edward M. Kosower

Abstract: Observations made in the course of experiments on pyridinium salts led to important discoveries in physical organic chemistry. The way in which the discoveries were made is likened to art rather than goal-directed "cold logic". We can describe the art of discovery as an effort enhanced by practice and intuition to *recognize novelty* in a finding and *provide productive insight* into its nature. We shall present some examples, and describe what happened after finding an unexpected light absorption band, a surprising solvent effect on spectra, and an unexpectedly stable and beautiful small organic radical.

Key words: art of discovery, solvent polarity parameter, charge-transfer complex, stable free radical, solvent effect on spectra.

Résumé : Des observations faites au cours d' expériences sur des sels pyridiniques ont entraîné d'importantes découvertes dans le domaine de la chimie physique organique. La manière avec laquelle ces découvertes ont été faites semble plus proche de l'art que de la logique pure. On peut décrire l'art de la découverte comme un effort agrémenté par la pratique et par l'intuition à identifier les nouveautés et à donner un éclaircissement productif sur leur nature. Nous présentons ici quelques exemples tels qu'ils se sont manifestés à la suite de l'observation d'une bande d'absorption inattendue, d'un effet surprenant du solvant sur les spectres ainsi que d'un petit radical organique étonnement beau et stable.

Mots clés : art de la découverte, paramètre de polarité d'un solvant, complexe de transfert de charge, radical libre stable, effet de solvant sur un spectre.

One of the most difficult problems facing anyone is that of deciding what to do in life. One picks a direction or a profession on the basis of love for a subject, or out of admiration for an individual, or out of the desire to exploit skills that have been learned (such as playing an instrument, or carpentry, or being a salesperson or businessman). In my case, I was attracted to chemistry at about the age of 12 (in junior high school), and eventually, this was the subject that I studied and in which I made a career. A second difficult question is: What do you actually do within that career? If you are working for a company, problems are assigned to you. If you are a doctor, then problems generally present themselves in the form of patients. If you are a scientist, especially a research scientist, you must choose a problem yourself. It must be original (but still recognizable by others), it must be capable of yielding partial results even when the original question proves to be too difficult to answer, and it must be possible to carry out with means that are reasonably easy to acquire. Success comes as a result of hard work, a good knowledge of the literature, a good understanding of the science that you work in, paying attention to unexpected observations and last, but not least, luck! (remember Louis Pasteur's remark after the discovery of the scientific basis of vaccination that "chance favors the prepared mind"). I will describe in this article how my colleagues and I came to work on certain subjects. It is my hope that these examples will stimulate the reader to ask questions in a different way than that seen in a textbook.

Before we delve into my adventures in discovery, let us consider the meaning of the word, *art*. Of the several definitions that appear in dictionaries, three seem most relevant to our use of the word. These are: 1. Human effort to imitate, supplement, alter, or counteract the work of nature. 2. Skill that is attained by study, practice, or observation. 3. Skill arising from the exercise of intuitive faculties; and what about the word, *discovery*? The most interesting definition is: a productive insight (synonym: breakthrough, find). The art of discovery can be termed an effort enhanced by practice and intuition to *recognize novelty* in a finding and *provide productive insight* into its nature.

The unexpected absorption band

Once upon a time…(*many years ago*) I wanted to study biochemical mechanisms, and chose to spend a year in the laboratory of Frank Westheimer at Harvard University. Frank suggested that I look at the interaction of thiolate anions with pyridinium rings, to see if we could cast some light on the mechanism of action of nicotinamide adenine dinucleotide (NAD). Frank and Birgit Vennesland had just discovered that hydrogen was transferred directly from NADH to acetaldehyde, the first demonstration that a cofac-

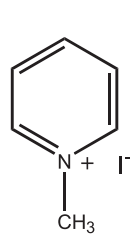
Received 2 February 2005. Published on the NRC Research Press Web site at http://canjchem.nrc.ca on 27 September 2005.

E.M. Kosower. School of Chemistry, Tel-Aviv University, Tel-Aviv 69978, Israel. (e-mail: kosower@post.tau.ac.il).

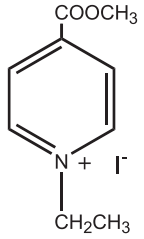
[1]This article is part of a Special Issue dedicated to organic reaction mechanisms.

 doi: 10.1139/V05-120 © 2005 NRC Canada

tor and a substrate made direct contact at an enzyme "active site". In my early experiments with several pyridinium compounds, it appeared that rather basic conditions were required for the formation of thiolate anions, requiring knowledge of the interaction of pyridinium ions with hydroxide ion. I resolved to use the simplest pyridinium ion, the 1-methylpyridinium ion, as a reactant. To alkylate pyridine, there were three possibilities: methyl chloride (a gas), methyl bromide (a low boiling liquid, bp 3.6 °C), and methyl iodide (bp 42 °C). The iodide was the only practical choice, so I began with 1-methylpyridinium iodide as a model for the more complicated molecule, NAD. The reaction with hydroxide ion was expected to be slow, so I measured the spectrum of a reasonably high concentration of 1-methylpyridinium iodide (MP+I-). *The model MP^+I^- had a surprise for us: It absorbed light in an unexpected way, at a wavelength longer than expected. THIS WAS A DISCOVERY, in the recognition of novelty in the behavior of the iodide salt.*



1-Methylpyridinium iodide



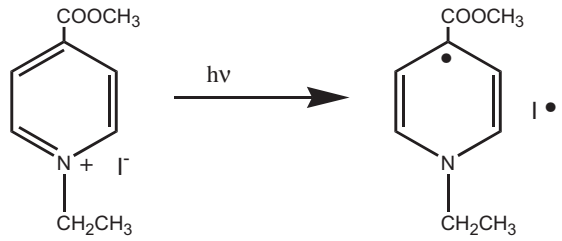
1-Ethyl-4-methoxycarbonyl-pyridinium iodide

Since this discovery was to become the focus of a significant part of my research, it is worth exploring how we came to understand its true nature. At first, I thought that the iodide ion had added to the pyridinium ring (1). Sidney D. Ross, a chemist at Sprague Electric Company refereed the paper and later told me that he thought that charge-transfer complexes might be involved, but recommended its publication anyway. (Referees today would be less kind!). Of course, he was right, and we soon adopted his point of view after reading Mulliken's brilliant papers on charge-transfer complexes and examining the interaction of iodide ion with methyl substituted pyridinium rings. A methyl group should cause the equilibrium for addition at a given position to shift drastically towards dissociation; in fact, there is only a small shift, thus establishing the new absorption as that of a charge-transfer complex of the iodide ion with a pyridinium ring (2, 3). The interpretation of the charge-transfer character of the *novel* light absorption constituted the productive insight in the discovery. This was a significant development in the field of charge-transfer complexes, which are composed of two parts, an electron-rich molecule (a "donor") and an electron-deficient molecule (an "acceptor"). In such complexes, we may describe the light absorption as resulting in an electronic transition in which an electron jumps from an electron-rich molecule (the donor) to its partner in the complex, an electron-poor molecule (the acceptor). In our case, the donor is iodide ion and the acceptor is the 1-methylpyridinium ion. *Charge-transfer transitions* are rather common, and charge-transfer complexes ubiquitous. We shall see another example of such transitions shortly. A further lesson from the study was that dimers can behave differently from monomers, so that concentration dependence of any process or measurement should be carried out whenever possible.

A solvent surprise

Whenever you make a discovery, further questions are raised. What does one do next? We felt that we should learn more about the exciting new charge-transfer transitions, but were hindered by the fact that the absorption maxima were obscured by the pyridinium ion absorption. To move absorptions to longer wavelengths, we reasoned that extending the conjugation of the pyridinium ring would lead to a longer wavelength absorption. More accurately, if we increased the electron affinity of the acceptor we should expect a lower energy charge-transfer transition. To increase solubility, we replaced the 1-methyl group with a 1-ethyl group. The compound, 1-ethyl-4-methoxy-carbonylpyridinium iodide, had a beautiful orange color. To illustrate the power of a little understanding, we were not surprised by the color, thinking that indeed the charge-transfer transition would be more easily observed. A Swiss graduate student had made exactly the same compound some years before and assumed that the color meant that the compound was impure. He recrystallized the salt many times without changing the color. Since he was really trying to prepare the corresponding piperidine, he decided to hydrogenate the "impure" salt. The color disappeared, he obtained a pure piperidine and went on to have a successful career in the Swiss chemical industry. The charge-transfer absorption responsible for the color remained a mystery until we encountered it several years later.

There were hints in our initial work that solvent polarity had an influence on the position of the charge-transfer band. We then took 1-ethyl-4-methoxycarbonylpyridinium iodide and looked at its spectrum in a variety of solvents. We were astounded by the tremendous shifts in the position of the c-t band to longer wavelengths with decreasing solvent polarity. These are illustrated in Fig. 1. *THIS WAS ANOTHER DISCOVERY in the recognition of the novelty of the large solvent sensitivity of the charge-transfer transition.*



1-Ethyl-4-methoxycarbonyl-pyridinium iodide

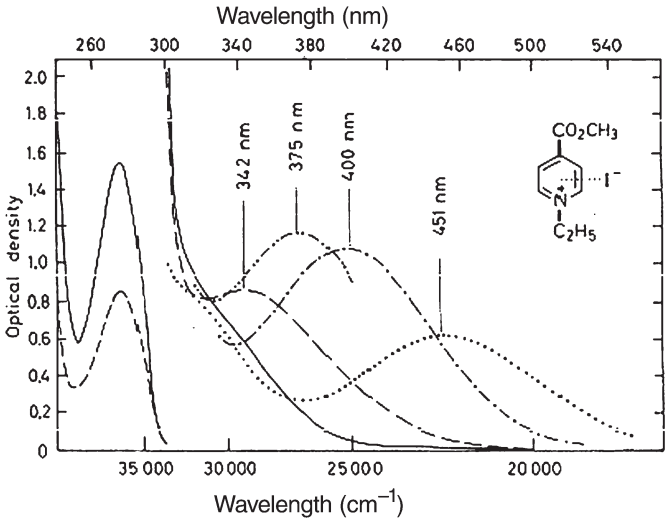
1-Ethyl-4-methoxycarbonyl-pyridinyl radical iodine atom pair

Charge-transfer transition

What was the origin of this large change, essentially the largest ever found for a solvent effect on a spectrum? The basic explanation has to do with the Franck–Condon principle. The solvent molecules are organized around the ground-state donor–acceptor ion pair. The strength of the interaction between the ion pair and the solvent varies with the "polarity" of the solvent, the interaction being stronger for the more polar solvent. Light absorption occurs very rapidly,

© 2005 NRC Canada

Fig. 1. The first charge-transfer band in the absorption spectra of 1-ethyl-4-methoxycarbonylpyridinium iodide in water (——), methanol (- - - -), 2-propanol (-·· –·· -), acetonitrile (–· –· –), and *cis*-1,2-dichloroethene (····) (adapted from refs. 8–10).



within a femtosecond or less. After light absorption, the solvent molecules are still organized as they were for the ground state, but now there is no ion pair. In fact, the organization represents a destabilization of the solvent structure. Roughly speaking, and reflecting an argument by Onsager about the reaction field in a solvent around a molecular dipole, the destabilization is similar to the stabilization of the ion pair by the solvent. We can thus expect a change in the electronic transition energy that is twice the ground-state stabilization, and consequently, a much larger change in the position of light absorption that might be expected for a "usual" solvent-sensitive light absorption such as that for an α,β-unsaturated carbonyl compound. These ideas are summarized in the diagram shown in Fig. 2. The interpretation was the productive insight into the novel solvent effect.

At this point, it became clear to me that such an electronic transition could be useful as a measure of "solvent polarity". I had earned my Ph.D. degree working with Professor Saul Winstein, who, together with Ernie Grunwald, had developed a solvent polarity parameter called *Y*-value, based on the rate of solvolysis of *tert*-butyl chloride in a given solvent. (Today, *Y*-values are based on the rate of solvolysis of adamantyl chloride and are still used to correlate rate constants of reactions). I therefore set out to correlate my solvent polarities with those of Winstein and Grunwald. I used solvent mixtures, methanol–water, ethanol–water, and acetone–water. I made up the mixtures rather randomly and plotted the results (*Y*-value against the transition energy, since these are both energies) as I measured them. I was disappointed at first to find a scatter of points, but as I proceeded, three straight lines emerged on the paper (like Botticelli's Venus arising from the sea). These straight lines converged at the *Y*-value for water, meaning that the spectroscopic parameter was also an effective measure of the polarity of the solvent (4) (Fig. 3)!! After the initial joy had subsided, colleagues in neighboring laboratories urged me to call them *K*-values. I resisted this suggestion, and chose *Z*-

Fig. 2. Energy diagram illustrating the stabilization of the ground state and the destabilization of the excited state for a charge-transfer transition in an ion-pair ground state. The Onsager model is also illustrated (R = reaction field, μ = molecular dipole).

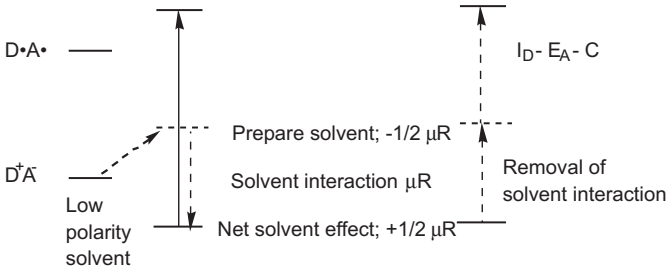
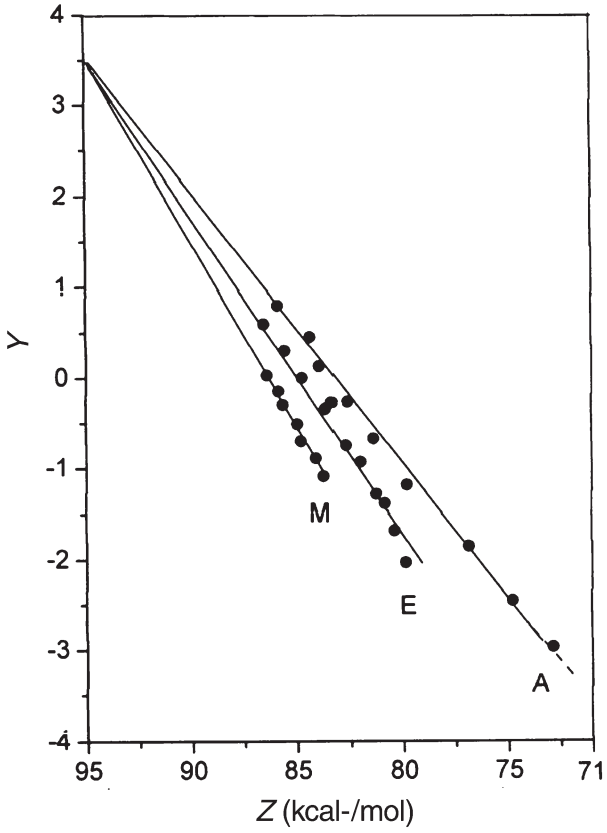


Fig. 3. *Z* vs. *Y* in methanol–water (M), ethanol–water (E), and acetone–water (A). The equations for the lines are Y_M = 0.416 76*Z* – 35.955, Y_E = 0.365 48*Z* – 30.962, and Y_A = 0.287 28*Z* – 23.936.



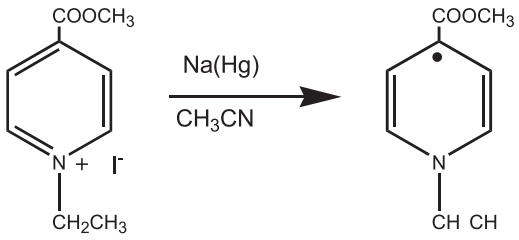
values because they came after *Y*. I then measured a substantial number of *Z*-values (the transition energy for the charge-transfer transition in kcal/mol, 1 cal = 4.184 J) and published the results in the *Journal of the American Chemical Society* (5), along with two other papers on the use of *Z*-values for correlating spectroscopic and kinetic data (6, 7). The paper became a citation classic (No. 47 on the JACS list of most-cited papers) with 1317 citations as of February, 2005).

Trying to gain some insight into the nature of the charge-transfer transition yielded a valuable new chemical resource, a quick and understandable way of measuring solvent polar-

© 2005 NRC Canada

ity. Formulating answers to the many questions raised by the discovery of *Z*-values led to a better understanding of the nature of such parameters. The compounds used to measure the parameter are molecular probes. What is a *probe*? An instrument used to search to the bottom of an object or a problem; also, as a verb, to scrutinize or examine thoroughly. What is a *molecular probe*? A molecular instrument used to scrutinize or examine thoroughly a molecular environment. A molecular probe provides information about the microscopic environment. In contrast, the dielectric constant represents a macroscopic summation or average of all the individual dipolar orientations within the measurement zone. In some cases, like those of *N*-alkylamides, the dielectric constant is high due to dipolar interactions between molecules, while the *Z*-value is relatively low because the microscopic polarity is modest. For a complete discussion of solvents and solvent parameters, the reader is referred to the excellent monograph by Reichardt (8); see also refs. 9 and 10. *Z*-values[2] have recently been used to evaluate the lack of preferential solvation of molecular probes or reactants in solvent mixtures (11).

Small radical is beautiful



1-Ethyl-4-methoxycarbonyl-pyridinium iodide

1-Ethyl-4-methoxycarbonyl-pyridinyl radical

Chemical reduction to radical

According to the theory of charge-transfer transitions, the excited state is formed by electron transfer from the donor to the acceptor. The acceptor pyridinium ring should accept electrons more easily, i.e., at lower excitation energies, as the electron-withdrawing power of the substituent increased. Another way to measure such a behavior is to examine the electrochemical reduction potentials. The potentials indeed fit the idea that the charge-transfer band moved to a longer wavelength with increasing electron affinity of the acceptor. More striking however was the observation that the pyridinyl radicals formed in electrochemical reduction seemed to be stable and colored (12). The prospect of studying small stable radicals was so attractive that E.J. Poziomek (who later went on to a distinguished career in a US Government laboratory) built a vacuum line and carried out the reductions that led to the discovery of the stable 1-ethyl-4-methoxycarbonylpyridinyl radical (13), allowing us to carry out many spectroscopic and kinetic studies (14). The orange 1-ethyl-4-methoxycarbonylpyridinium iodide melted to a scarlet liquid above 112 °C. In a most spectacular and colorful experiment, under high vacuum and in the presence of magnesium, a material distilled from the molten salt and condensed as a royal blue solid on a liquid nitrogen cooled condenser. That solid was shown to be the stable radical. The corresponding 1-methyl-4-cyanopyridinyl radical was shown to dimerize at a rate that could be detected electrochemically, and gave rise eventually to the 1,1′-dimethyl-4,4′-bipyridinium cation radical ("methylviologen") for which we discovered the dimeric complex and measured the ESR spectrum for the first time (15).

Again, asking simple questions about the charge-transfer band we *discovered* a whole new class of stable radicals. Recognizing the *novelty* of the apparent stability of pyridinyl radicals led to the productive insight that such stability might be exploited in a preparative procedure. Using a microsecond flash lamp developed by Lindqvist, we also showed that the pyridinyl radical was formed by the charge-transfer light absorption (16). Further information on pyridinyl radicals is summarized elsewhere (17).

Summary

The art of discovery has been the subject of a few serious studies and is clearly a form of serendipity for which a useful summary may be found on the Web (18). I have tried to give some insight into how one might proceed from an unexpected observation to a new development in science. The examples given are taken from my own early experience, and in most of my subsequent research, I have encountered the same general sequence of events. These would necessitate another article even longer than the present one. Our present research on surface-enhanced IR absorption on silver halide fibers belongs in the same category. If you would ask me what I might be doing a few years from now, I might honestly say that I don't know, but I am sure it will be interesting, exciting, and productive. I can add that enthusiasm and optimism is helpful in smoothing the way to discovery. You have read my story and I look forward to hearing yours!

References

1. E.M. Kosower. J. Am. Chem. Soc. **77**, 3883 (1955).
2. E.M. Kosower. J. Am. Chem. Soc. **78**, 3497 (1956).
3. E.M. Kosower and J.C. Burbach. J. Am. Chem. Soc. **78**, 5838 (1956).
4. E.M. Kosower. J. Am. Chem. Soc. **78**, 5700 (1956).
5. E.M. Kosower. J. Am. Chem. Soc. **80**, 3253 (1958).
6. E.M. Kosower. J. Am. Chem. Soc. **80**, 3261 (1958).
7. E.M. Kosower. J. Am. Chem. Soc. **80**, 3267 (1958).
8. C. Reichardt. Solvents and solvent effects in organic chemistry. 3rd ed. Wiley-VCH, Weinheim. 2003.
9. E.M. Kosower. An introduction to physical organic chemistry. John Wiley and Sons, New York. 1968.
10. E.M. Kosower. Molecular biochemistry. McGraw-Hill, New York. 1962.
11. T.W. Bentley, D.N. Ebdon, E.-J. Kim, and I.S. Koo. J. Org. Chem. **70**, 1647 (2005).
12. W.M. Schwarz, E.M. Kosower, and I. Shain. J. Am. Chem. Soc. **83**, 3164 (1961).

[2] *Z*-value is defined as the position of the maximum of the charge-transfer band of 1-ethyl-4-methoxycarbonylpyridinium iodide expressed in kcal/mol. Z (kcal/mol) = 285 90/λ_{max} (in nm). (The relation is derived from $E = Nhc/4.184\lambda$ in which $N = 6.022\ 14 \times 10^{23}$ mol^{-1}, $h = 6.626\ 08 \times 10^{-34}$ J s, $c = 2.9979 \times 10^{8}$ m/s, and λ is given in nm. Note that 4.1840 J = 1 cal and 10^{-3} kcal = 1 cal).

© 2005 NRC Canada

13. E.M. Kosower and E.J. Poziomek. J. Am. Chem. Soc. **86**, 5515 (1964).
14. E.M. Kosower and I. Schwager. J. Am. Chem. Soc. **86**, 5528 (1964).
15. E.M. Kosower and J.L. Cotter. J. Am. Chem. Soc. **86**, 5524 (1964).
16. E.M. Kosower and L. Lindqvist. Tetrahedron Lett. 4481 (1965).
17. E.M. Kosower. Top. Curr. Chem. **112**, 117 (1983).
18. G. Fine and J. Deegan. Qual. Stud. Educ. **9**, 434 (1996); Three principles of serendip: insight, chance, and discovery in qualitative research [online]. Available from http://www.ul.ie/~philos/vol2/deegan.html.

© 2005 NRC Canada

Kinetics and mechanism of the oxidation of alcohols by tetrapropylammonium perruthenate[1]

W. David Chandler, Zhao Wang, and Donald G. Lee

Abstract: 2-Propanol is oxidized by tetrapropylammonium perruthenate (TPAP) in a reaction that is second order in TPAP and first order in 2-propanol. One of the products, believed to be ruthenium dioxide, is an effective catalyst for the reaction, making it an autocatalytic process. The rate of oxidation is relatively insensitive to the presence of substituents. Primary kinetic deuterium isotope effects are observed when either the hydroxyl or the α hydrogen is replaced by deuterium. The only product obtained from the oxidation of cyclobutanol is cyclobutanone, indicating that the reaction is a two-electron process. Tetrahydrofuran is oxidized at a rate that is several orders of magnitude slower than that observed for 2-propanol, suggesting that the reaction of TPAP with alcohols may be initiated by formation of perruthenate esters. A tentative mechanism consistent with these observations is proposed.

Key words: oxidation, alcohols, tetrapropylammonium perruthenate, reaction mechanism, autocatalysis.

Résumé : La réaction du propan-2-ol par le perruthénate de tétrapropylammonium (PTPA) est du deuxième ordre en PTPA et du premier ordre en propan-2-ol. Un des produits, qu'on suppose être le dioxyde de ruthénium, est un catalyseur efficace de la réaction qui la transforme en processus autocatalytique. La vitesse d'oxydation est pratiquement insensible à la présence de substituants. On observe des effets isotopiques cinétique du deutérium lorsqu'on remplace l'hydrogène de l'hydroxyle ou l'hydrogène en α par du deutérium. Le seul produit obtenu lors de l'oxydation du cyclobutanol est la cyclobutanone, ce qui indique que la réaction se produit par un processus à deux électrons. Le tétrahydrofurane est oxydé à une vitesse qui est de plusieurs ordres de grandeur plus faible que celui observé pour le propan-2-ol, ce qui suggère que la réaction du PTPA avec les alcools est peut-être initiée par la formation d'esters de l'acide perrhuténique. On propose un mécanisme qui est en accord avec les observations.

Mots clés : oxydation, alcools, perrhuténate de tétrapropylammonium, mécanisme de réaction, autocatalyse.

[Traduit par la Rédaction]

Introduction

The historical chemistry of tetrapropylammonium perruthenate (TPAP) has been reviewed (1–3). It is an excellent oxidant for the conversion of primary alcohols to aldehydes and secondary alcohols to ketones in nonaqueous solvents. The reaction is particularly fast, and good yields are usually obtained. Primary alcohols can be oxidized selectively in the presence of secondary alcohols (4) and 1,4- and 1,5-diols are converted to the corresponding five- and six-membered lactones (4, 5).

TPAP has also been used for the oxidation of sulfides to sulfones (6), secondary nitro compounds to ketones (7), and alkylboranes to the corresponding carbonyl compounds (8).

In addition to its use in solvents such as methylene chloride and acetonitrile, TPAP can be used effectively in ionic liquids (9).

Received 20 August 2004. Published on the NRC Research Press Web site at http://canjchem.nrc.ca on 5 October 2005.

W.D. Chandler, Z. Wang, and D.G. Lee.[2] Department of Chemistry, University of Regina, Regina, SK S4S 0A2, Canada.

[1]This article is part of a Special Issue dedicated to organic reaction mechanisms.

[2]Corresponding author (e-mail: dglee@uregina.ca).

Recent applications include the selective oxidation of a secondary alcohol that is part of a molecule that also contains a reactive ether functionality (10), the conversion of a primary alcohol to an aldehyde as a part of the asymmetric total synthesis of pironetin (11), the oxidation of 3-, 11-, 15-, 17-, and 20-hydroxy steroids to the corresponding ketones (12), and the preparation of a pyrrole from the corresponding α-aziridinyl alcohol (13).

TPAP can be used as a stoichiometric oxidant (14–18) or as a catalytic reagent in conjunction with a cooxidant such as *N*-methylmorpholine *N*-oxide (4–14).

Other than our previously published observation that its reactions with alcohols are autocatalytic (19), little is known about the mechanisms of TPAP oxidations. In an attempt to obtain a better understanding of the mechanism, a kinetic study of its reactions with aliphatic alcohols has been undertaken. Although autocatalytic reactions are not easily amenable to kinetic studies, sufficient experimental evidence has been obtained to propose a tentative reaction mechanism.

Experimental

Materials

Methylene chloride, used as the solvent in kinetic experiments, was purified by successive distillations from calcium hydride and tetrabutylammonium permanganate. The purified solvent was stored over molecular sieves.

 doi: 10.1139/V05-114 © 2005 NRC Canada

2-Propanol and the substituted 2-propanols were obtained commercially. They were distilled over calcium oxide and a middle fraction was collected and analyzed using gas chromatography. Purities of 99.9% or greater were obtained by this method. The observed boiling points were in agreement with published values (20). 2-Propanol-2-*d* and 2-propanol-O-*d* were prepared and purified as previously described (21).

Tetrahydrofuran, obtained from Aldrich, was purified by passage through a column of alumina to remove peroxide and fractionally distilled. A freshly purified sample with a boiling point of 64.0–64.2 °C was used in each experiment (22).

Tetrapropylammonium perruthenate, obtained from Aldrich, was dissolved in freshly purified methylene chloride, placed in a 10 mL brown bottle and used immediately in kinetic experiments. The concentration was determined spectrophotometrically from measurement of absorbances at 384 or 270 nm as described in the following.

Spectral studies

The UV–vis spectra of TPAP and its reduction product (RuO_2) have been reproduced in Fig. 1. It is apparent from these spectra that the greatest change in absorbance occurs at about 270 nm when TPAP is reduced by 2-propanol. Therefore, this wavelength is the most logical one to use for kinetic studies. However, before proceeding on that assumption, it was confirmed that the absorbances of both the reactant and the product are proportional to their concentrations at this wavelength. This was done by preparing the corresponding plots of absorbance vs. concentration, as in Figs. 2 and 3. From these plots it is apparent that both TPAP and RuO_2 obey Beer's Law at 270 nm.

Kinetic methods

Determination of reaction rates was achieved by monitoring the increase in absorbance at 270 nm as the reaction progressed. Absorbance measurements were made using a Hewlett Packard 8450A spectrophotometer equipped with a thermostatted cell holder. Each experiment was repeated a minimum of five times and the average reported. The uncertainties noted are standard deviations.

The starting concentrations of the oxidant (TPAP) were between 1.57×10^{-4} and 4.11×10^{-4} mol/L. The concentration of the reductant (2-propanol) was at least 25 times greater in all experiments to ensure that pseudo-order conditions would pertain.

In a typical experiment, 10 mL of a freshly prepared solution of TPAP in methylene chloride was thermostatted at the required temperature in a water bath. An aliquot (2.00 mL) of this solution was then transferred to a cuvette and placed in the cell holder of the HP 8450A spectrophotometer, thermostatted at the same temperature. An excess of alcohol was added using a microliter syringe and the reaction rate was determined by monitoring absorbance changes at 270 nm. Usually, 99 absorbance readings were collected for each kinetic measurement.

A typical plot of absorbance against time is presented in Fig. 4. A sigmoidal plot of this type is typical of autocatalytic reactions. The rate, slow initially, increases dramatically as the product (catalyst) is formed, and then slows down again as the concentrations of reactants are diminished. The autocatalytic nature of the reaction can also be illustrated by plotting the rate (d*A*/d*t*) against time as in Fig. 5. It can be seen that the reaction rate passes through a maximum, giving a "bell-shaped" curve that is diagnostic for autocatalytic reactions (23).

Fig. 1. UV–vis spectrum of tetrapropylammonium perruthenate (TPAP) and its reduction product (RuO_2).

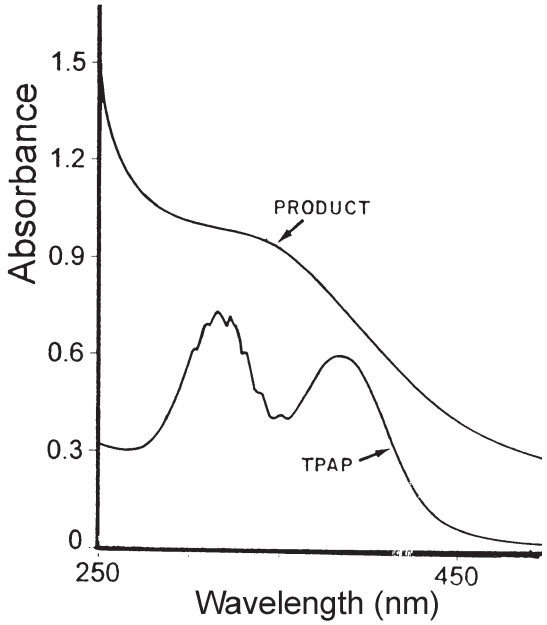
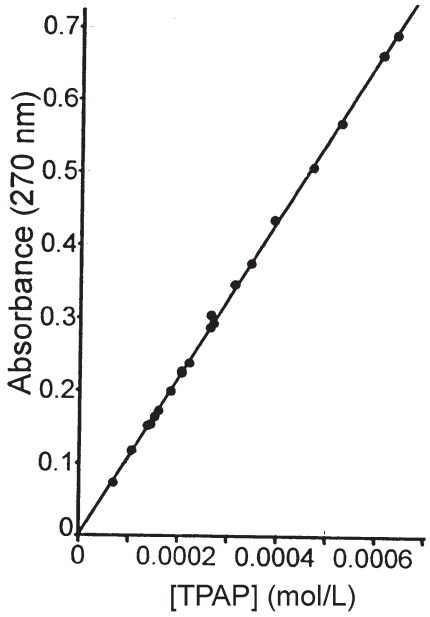


Fig. 2. Beer's Law plot for TPAP at 270 nm. Slope = 1084. Intercept = 0.0013. $r^2 = 0.999$.



Stability of the oxidant

Tetrapropylammonium perruthenate is slowly reduced by the solvent under the experimental conditions used in this study. The pseudo-first-order reaction rate (Fig. 6) is insignificant when compared to the rate at which TPAP is reduced by 2-propanol and shows no evidence of auto-

© 2005 NRC Canada

Fig. 3. Beer's Law plot for the product (RuO_2) formed when TPAP is reduced by 2-propanol. Slope = 3858. Intercept = 0.0071. r^2 = 0.997.

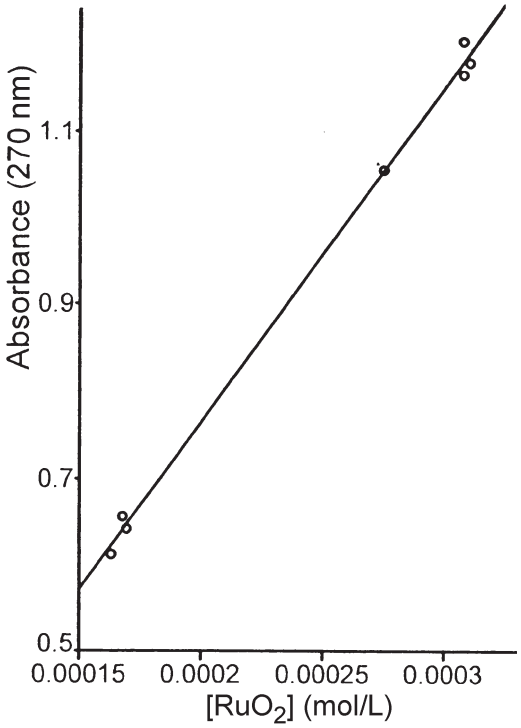
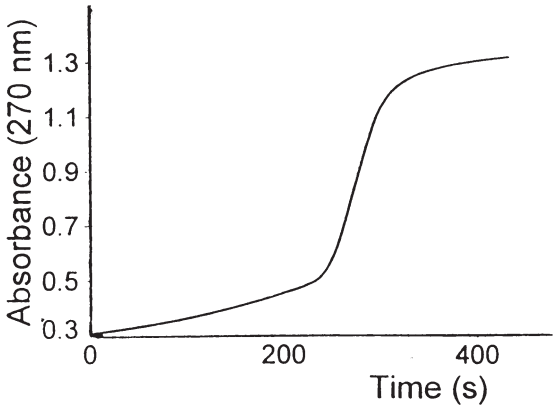


Fig. 4. Plot of the absorbance at 270 nm vs. time for the reduction of TPAP by 2-propanol.



catalysis. Nevertheless, to minimize the potentially large effect of having a small amount of catalyst (RuO_2) present at the beginning of a kinetic experiment, freshly prepared solutions were always used.

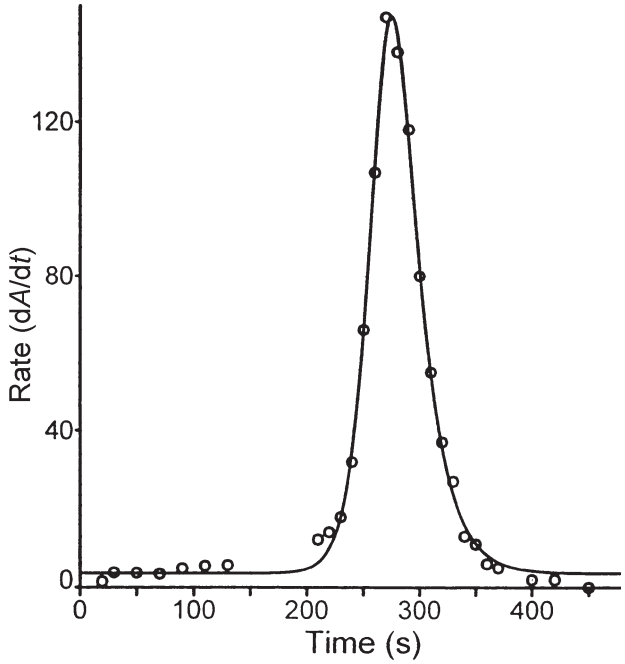
Results

The rate law for the uncatalyzed reaction

The kinetics of an autocatalytic reaction can be analyzed by dividing the rate into two parts — one owing to the uncatalyzed portion of the reaction and one owing to the catalyzed portion, as in eq. [1].

$$[1] \qquad \text{Rate} = \text{Rate}_{\text{uncatalyzed}} + \text{Rate}_{\text{catalyzed}}$$

Fig. 5. Plot of the reaction rate for the reduction of TPAP by 2-propanol vs. time.



The rate of the uncatalyzed reaction was determined from a study of initial reaction rates. Since the catalyzed reaction is much faster than the uncatalyzed reaction, the rate of the autocatalyzed reaction was determined, as described in the following, from a study of the reaction after a significant amount of product had been formed.

At the start of the reaction no product (catalyst) is present and the observed reaction rate is due, therefore, only to the uncatalyzed reaction between tetrapropylammonium perruthenate ($QRuO_4$) and 2-propanol. Consequently, the rate law and rate constant for the uncatalyzed reaction were determined under initial reaction conditions. The general form of the expected rate law, as given in eq. [2], was simplified by using a great excess of 2-propanol. The resulting pseudo-order rate law is expressed in eqs. [3] and [4].

$$[2] \qquad (\mathrm{d}[RuO_2]/\mathrm{d}t)_i = k_u[QRuO_4]_i^m[\text{2-propanol}]^n$$

$$[3] \qquad (\mathrm{d}[RuO_2]/\mathrm{d}t)_i = k_u'[QRuO_4]_i^m$$

$$[4] \qquad k_u' = k_u[\text{2-propanol}]^n$$

Since the absorbance at 270 nm conforms to Beer's Law for both the reactant and the product, the rate law stated in eq. [3] can be expressed in terms of absorbances, as in eqs. [5] and [6].

$$[5] \qquad (\mathrm{d}A/\mathrm{d}t)_i = k_u'A_i^m(\varepsilon_{RuO_2}/\varepsilon_{QRuO_4}{}^m)$$

$$[6] \qquad \ln(\mathrm{d}A/\mathrm{d}t)_i = m\ln A_i + \ln k_u' + \ln(\varepsilon_{RuO_2} - \varepsilon_{QRuO_4}{}^m)$$

The initial reaction rates ($(\mathrm{d}A/\mathrm{d}t)_i$) were easily obtained from tangents to plots of absorbance vs. time at zero time. From a plot of $\ln(\mathrm{d}A/\mathrm{d}t)_i$ vs. $\ln(A_i)$, as in Fig. 7, the reaction was found to be second order with respect to $QRuO_4$. As described in the following, the order with respect to 2-propanol was subsequently found to be unity, resulting in the rate law given in eq. [7] for the uncatalyzed portion of the reaction.

© 2005 NRC Canada

Fig. 6. Plot of the absorbance at 270 nm vs. time for the reduction of TPAP in a methylene chloride solution with no added 2-propanol. Slope = 0.196. Intercept = 6.3×10^{-6}. $r^2 = 0.993$.

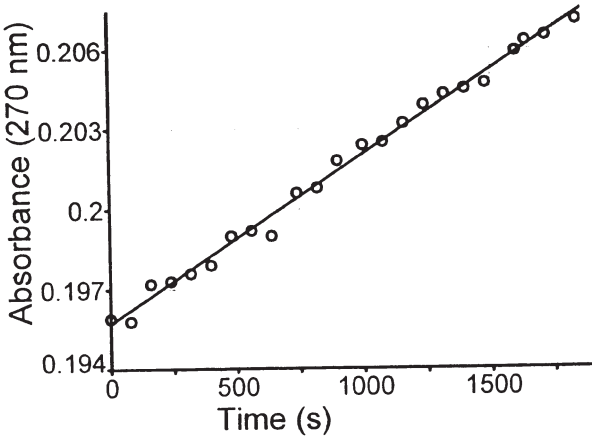
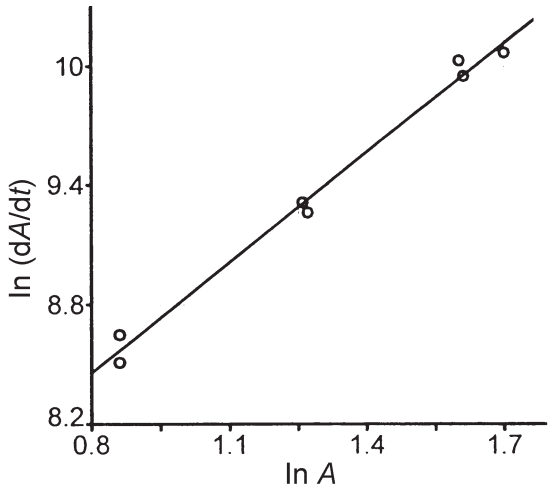


Fig. 7. Plot of the initial rates vs. initial absorbance for the reduction of TPAP by 2-propanol. Slope = 1.8 ± 0.1. Intercept = 6.98. $r^2 = 0.990$.



[7] $(\mathrm{d[RuO_2]}/\mathrm{d}t)_i = -(\mathrm{d[QRuO_4]}/\mathrm{d}t)_i = k_u[\mathrm{QRuO_4}]^2[\text{2-propanol}] = k_u'[\mathrm{QRuO_4}]^2$

The pseudo-second-order rate constants for this reaction (k_u') were then determined from plots of $-\mathrm{d[QRuO_4]}/\mathrm{d}t_i$ vs. $[\mathrm{QRuO_4}]^2$ as in Fig. 8.

Rate law for the catalyzed reaction

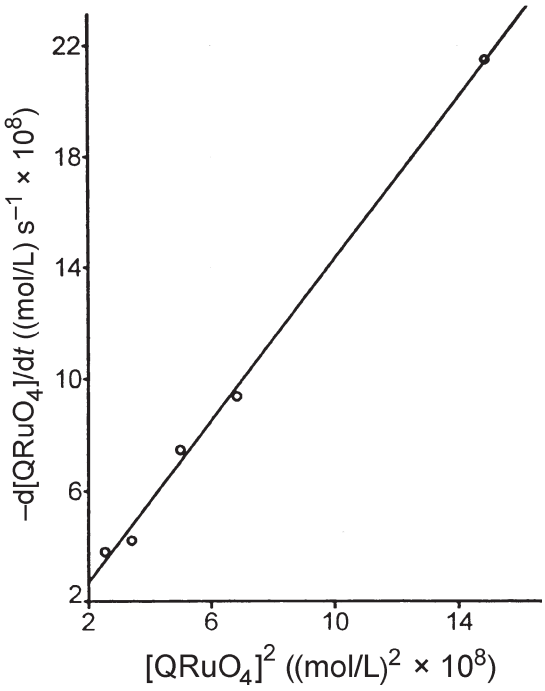
Rates for the catalyzed reaction were determined by taking tangents to the curve obtained from a plot of the absorbances against time after a significant amount of product (RuO_2) had formed. Under these conditions the contribution from the uncatalyzed reaction is negligible, as indicated from the data plotted in Figs. 4 and 5.

The general form of the rate law for the catalyzed portion of the reaction, given in eq. [8], can be simplified to eqs. [9] and [10] by using a large excess of 2-propanol.

[8] $-\mathrm{d[QRuO_4]}/\mathrm{d}t = k_c[\mathrm{QRuO_4}]^p[\mathrm{RuO_2}]^q[\text{2-propanol}]^r$

[9] $-\mathrm{d[QRuO_4]}/\mathrm{d}t = k_c'[\mathrm{QRuO_4}]^p[\mathrm{RuO_2}]^q$

Fig. 8. Plot for the determination of the rate constant (k_u'). Slope (k_u') = 1.45 ± 0.05. Intercept = 0.231. $r^2 = 0.997$.



[10] $k_c' = k_c[\text{2-propanol}]^r$

The concentrations of $QRuO_4$ and RuO_2 can be calculated at any point along a plot of absorbance vs. time (cf. Fig. 4) by use of eqs. [11] and [12] where A_i is the initial absorbance, A_f is the final absorbance, A_t is the absorbance at any time "t", and $\Delta\varepsilon$ is $(\varepsilon_{RuO_2} - \varepsilon_{QRuO_4})$ (24).

[11] $[\mathrm{QRuO_4}] = (A_f - A_t)/\Delta\varepsilon$

[12] $[\mathrm{RuO_2}] = (A_t - A_i)/\Delta\varepsilon$

A combination of eqs. [9] and [11] gives eqs. [13] and [14].

[13] $\mathrm{d}A_t/\mathrm{d}t = k_c'[\mathrm{QRuO_4}]^p[\mathrm{RuO_2}]^q\Delta\varepsilon$

[14] $\ln(\mathrm{d}A_t/\mathrm{d}t) = p\ln[\mathrm{QRuO_4}] + q\ln[\mathrm{RuO_2}] + \ln k_c' + \ln\Delta\varepsilon$

In a series of reactions with differing initial concentrations of $QRuO_4$, rates ($\mathrm{d}A_t/\mathrm{d}t$) were measured by taking tangents to the curves at points where the concentration of RuO_2 was constant. Under conditions of constant $[RuO_2]$, eq. [14] is reduced to eq. [15] where C is a constant. The order with respect to $[QRuO_4]$ obtained from a plot of $\ln(\mathrm{d}A_t/\mathrm{d}t)$ vs. $\ln[QRuO_4]$, as in Fig. 9, was observed to be two. Therefore, the catalyzed portion of the reaction is also second order with respect to the concentration of the oxidant.

[15] $\ln(\mathrm{d}A_t/\mathrm{d}t) = p\ln[\mathrm{QRuO_4}] + C$

Similarly, the apparent order with respect to the concentration of the catalyst (RuO_2) was determined from a series of rate measurements made at constant $QRuO_4$ concentration. Under those conditions, eq. [14] is simplified to eq. [16] where C' is a constant.

© 2005 NRC Canada

Fig. 9. Plot for determining the order of the catalytic reaction with respect to the oxidant. Slope (order) = 2.0 ± 0.1. Intercept = 11.7. r^2 = 0.986.

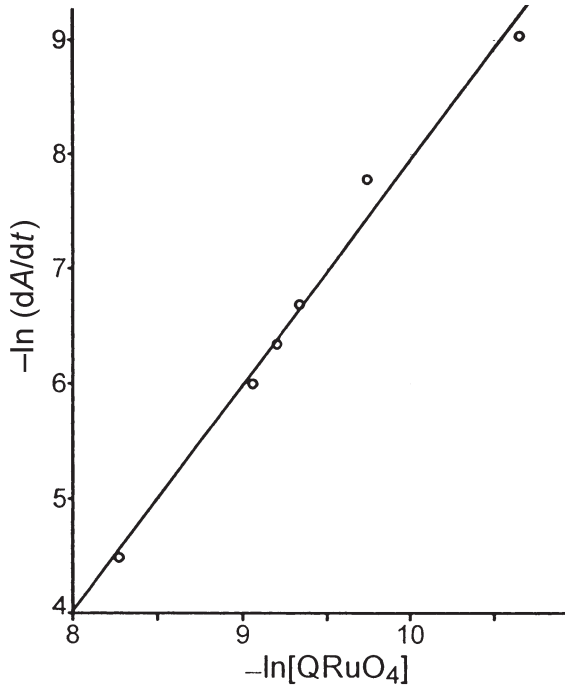
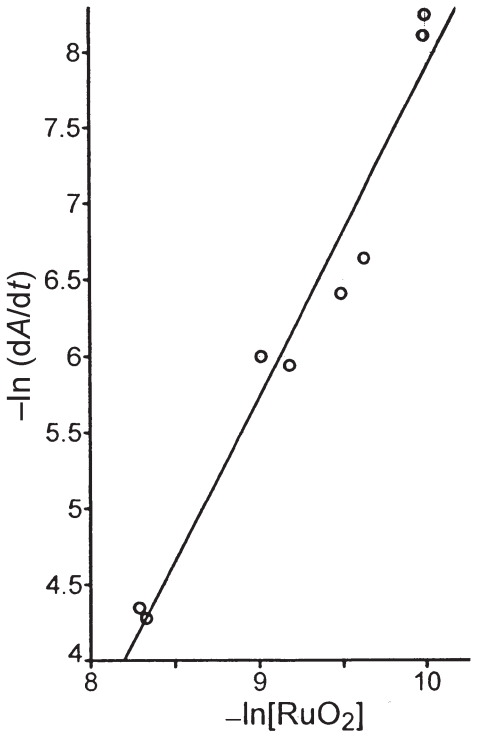


Fig. 10. Plot for determining the apparent order of the catalytic reaction with respect to the catalyst (RuO_2). Slope = 2.1 ± 0.3. Intercept = 13.7. r^2 = 0.957.



[16] $\ln(dA_t/dt) = q \ln[RuO_2] + C'$

The plot of eq. [16], in Fig. 10, indicates that the apparent order with respect to RuO_2 is about two. As described below, the order with respect to 2-propanol was subsequently found to be unity, resulting in the rate law given in eq. [17] for the catalyzed portion of the reaction.

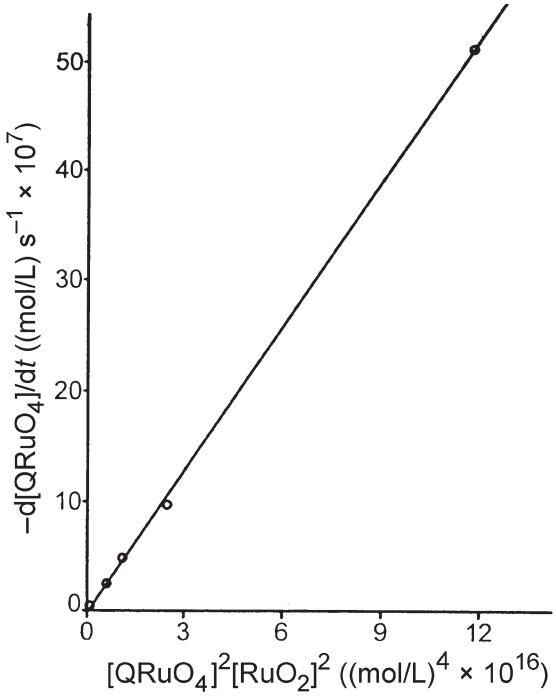
[17] $-d[QRuO_4]/dt = k_c[QRuO_4]^2[RuO_2]^2[\text{2-propanol}]$

The pseudo-fourth-order rate constant (k_c') was then obtained from a plot of $-d[QRuO_4]/dt$ vs. $[QRuO_4]^2[RuO_2]^2$ as in Fig. 11.

The complete rate expression for the reaction determined from this analysis, therefore, is given by eq. [18].

[18] $-d[QRuO_4]/dt = ([QRuO_4]^2[\text{2-propanol}]) \times (k_u + k_c[RuO_2]^2)$

Fig. 11. Plot for the determination of the rate constant (k_c'). Slope = 4.34 ± 0.05. Intercept = 0.245. r^2 = 0.999.



Computer-assisted analysis of reaction rates

Obtaining rate constants for the reaction by use of the classical methods described in the previous section is time consuming and somewhat subject to personal biases. The use of computer-based models for the reaction can eliminate personal biases and greatly reduce the time required for analysis. Accordingly, software written in Turbo Pascal was developed to assist in the analysis of the raw time vs. absorbance data.

The computer program initially estimated pseudo-order rate constants (k_u' and k_c'), and then completed a least-squares regression using an analytic function derived from eq. [19].

[19] $-dA/dt = (k_u' + k_c'[RuO_2]^2)[QRuO_4]^2$

The variable parameters (k_u' and k_c') were then subjected to an iterative regression until the best correlation coefficient was obtained. In this way, it was possible to reproduce the experimental data very closely. The rate constants produced

© 2005 NRC Canada

Table 1. Comparison of rate constants obtained by graphical and computer-assisted analysis.

Rate constant	Graphical analysis[a]	Computer-assisted calculation[b]
k_u' ((mol/L)$^{-1}$ s^{-1})	1.46±0.05	1.57
k_u ((mol/L)$^{-2}$ s^{-1})	123±5	120
k_c'((mol/L)$^{-3}$ s^{-1} × 10^{-9})	4.21±0.05	4.79
k_c ((mol/L)$^{-4}$ s^{-1} × 10^{-9})	354±6	366

Note: Temp. = 25.0 ± 0.1 °C.
[a][2-Propanol] = 0.0119 mol/L.
[b][2-Propanol] = 0.0131 mol/L.

from this computer-assisted analysis compare satisfactorily with the results obtained from the classical analysis described previously. See the data for a typical example given in Table 1.

The data in Table 1 confirm that this approach gives consistent values for the rate constants, with somewhat greater uncertainly in the values for the catalytic rate constants. In an additional test of this approach, an attempt was made to fit the data to a simpler rate law that is first order in oxidant and catalyst, as in eq. [20].

$$[20] \quad -dA/dt = (k_u'' + k_c''[RuO_2])[QRuO_4]$$

The rate constants obtained using eq. [20] were less consistent and the correlation coefficients obtained were much lower than those for eq. [19]. All subsequently reported rate constants are those obtained from computer-assisted analysis of absorbance vs. time data.

From eq. [4], it can be seen that a plot of k_u' vs. [2-propanol] should be linear with a slope equal to k_u, and an intercept near zero, if the initial reaction rate is first order with respect to the concentration of 2-propanol. Similarly, it can be seen from eq. [10] that if the catalytic portion of the reaction is also first order with respect to the concentration of 2-propanol, a plot of k_c' vs. [2-propanol] should be linear with a slope equal to k_c and a zero intercept. The linearity of the two plots, presented in Figs. 12 and 13, confirms that the rate of this reaction is first order in the concentration of 2-propanol throughout.

Isotope effects

Rate constants for the oxidation of 2-propanol-2-*d* and 2-propanol-O-*d* are compared with that of the non-deuterated compound in Table 2. The data indicate that primary kinetic isotope effects are observed for the oxidation of both 2-propanol-2-*d* and 2-propanol-O-*d*.

Substituent effects

Rate constants for the oxidation of 2-propanol and five-substituted 2-propanols were determined to test the sensitivity of the reaction to changes in the nature of the substituents (25). From the data in Table 3 and the corresponding Taft plots in Figs. 14 and 15, it is apparent the rate constants are rather insensitive to substituent effects. The ρ* value for the uncatalyzed reaction is 0.18 and ρ* for the catalytic reaction is –0.43.

Fig. 12. Plot for determining the rate constant (k_u) for the uncatalyzed portion of the reaction. Slope (k_u) = 107 ± 5. Intercept = 0.09. r^2 = 0.976.

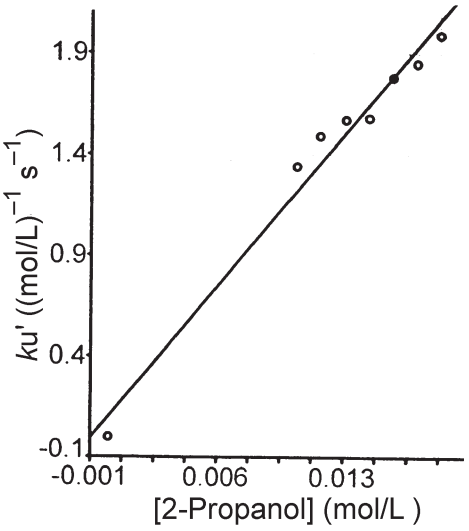
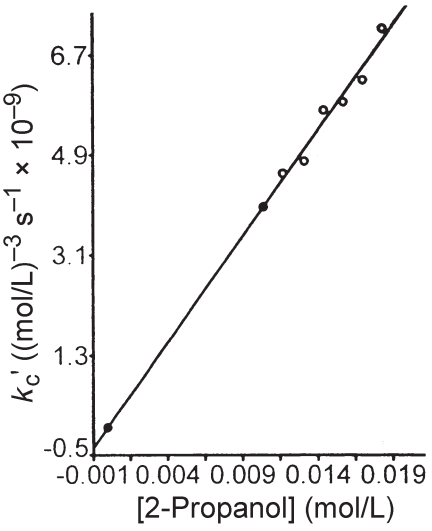


Fig. 13. Plot for determining the rate constant (k_c) for the catalytic portion of the reaction. Slope = (3.81 ± 0.06) × 10^{11}. Intercept = 0.005. r^2 = 0.994.



The oxidation of tetrahydrofuran by $QRuO_4$

When the oxidation of tetrahydrofuran (THF) was studied under similar conditions and with concentrations comparable to those used with 2-propanol in this study, the rates were found to be immeasurably slow. When the concentration of THF was drastically increased (6.14 mol/L), an autocatalytic reaction with a very long induction period was observed, as in Fig. 16.

The effect of moisture

The rate of oxidation of 2-propanol was found to be sensitive to the presence of moisture. When small amounts of water were added under typical reaction conditions, the autocatalytic nature of the absorbance vs. time plots was greatly diminished, as illustrated by the plots in Fig. 17.

© 2005 NRC Canada

Table 2. Isotope effects.

Alcohol	k_u' ((mol/L)$^{-1}$ s^{-1})	k_c' ((mol/L)$^{-3}$ s^{-1} × 10^{-9})	k_{uH}'/k_{uD}'	k_{cH}'/k_{cD}'
2-Propanol	1.57±0.14	4.79±0.76		
2-Propanol-O-*d*	1.17±0.09	1.97±0.76	1.3±0.1	2.4±0.6
2-Propanol-2-*d*	0.47±0.06	1.38±0.76	3.2±0.5	3.5±0.8

Note: Temp. = 25.0 ± 0.1 °C. [ROH] = 1.31 × 10^{-2} mol/L.

Table 3. Substituent effects.

Alcohol	[ROH] (mol/L × 10^2)	k_u ((mol/L)$^{-2}$ s^{-1} × 10^{-9})	k_c ((mol/L)$^{-4}$ s^{-1} × 10^{-9})
2-Butanol	1.09	114±6	282±35
2-Pentanol	0.919	125±10	216±61
2-Hexanol	1.02	104±3	208±3
2-Propanol	1.04	120±13	267±73
1-Methoxy-2-propanol	1.02	135±4	232±9
1,3-Dichloro-2-propanol	1.05	204±15	254±50

Note: Temp. = 25.0 ± 0.1 °C.

Fig. 14. Taft plot for the uncatalyzed reaction. Slope (ρ*) = 0.18. Intercept = 2.08. r^2 = 0.977.

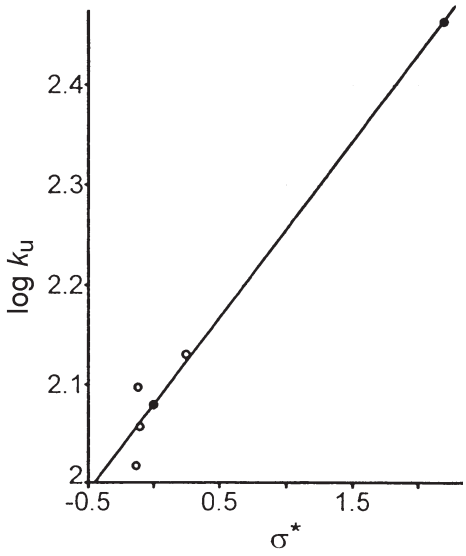
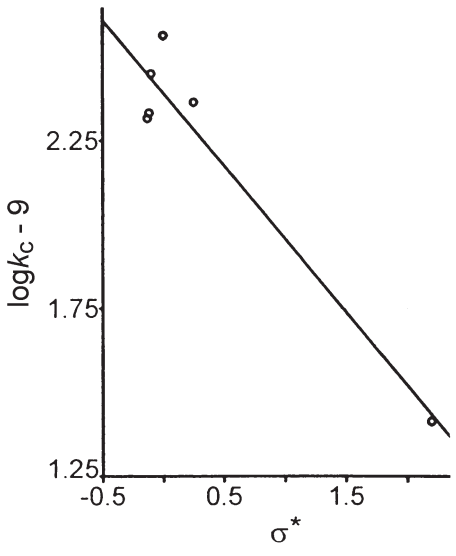


Fig. 15. Taft plot for the catalytic reaction. Slope (ρ*) = –0.43. Intercept = 2.39. r^2 = 0.924.



Consequently, precautions were taken to maintain anhydrous conditions at all times.

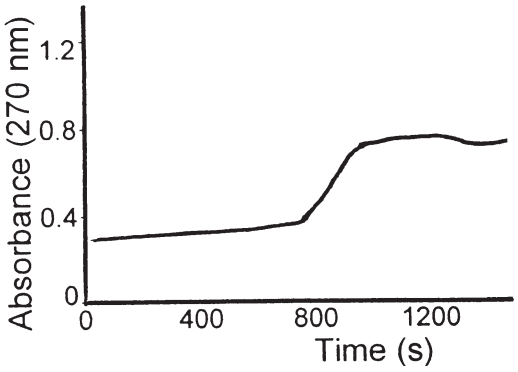
Demonstration of catalysis by the product (RuO_2)

The catalytic nature of the product of the reaction was also demonstrated in an experiment in which additional $QRuO_4$ was added after all of the oxidant initially present had been reduced by an excess of 2-propanol. As indicated by the plot in Fig. 18, the reaction resumed at an accelerated rate without an induction period. After 72 h, however, a fine black solid precipitated and the solution no longer exhibited autocatalysis.

The oxidation of cyclobutanol by $QRuO_4$

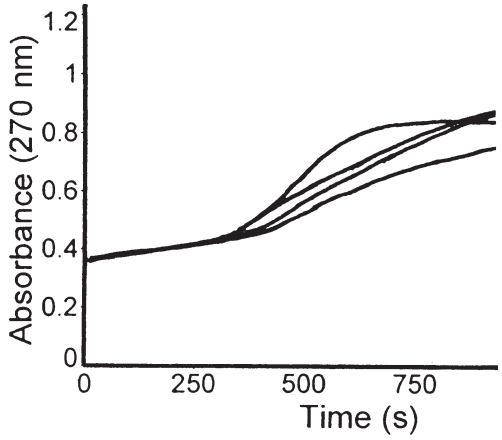
Tetrapropylammonium perruthenate (0.097 g, 0.29 mmol) was added to a 100 mL round-bottomed flask containing cyclobutanol (0.10 g, 1.4 mmol) in 50 mL of methylene

Fig. 16. Plot of the absorbance at 270 nm vs. time for the oxidation of THF (6.14 mol/L) by TPAP.



© 2005 NRC Canada

Fig. 17. Plots illustrating the effect of water on the reaction rates. The top plot was obtained in the absence of added water. The plots below it were obtained for reactions to which 0.5, 1.0, and 1.5 μL of water had been added, respectively.



chloride. The solution was stirred at room temperature until all of the oxidant had been reduced and a brown suspension of RuO_2 remained. After filtering to remove the RuO_2, a clear solution was obtained. Evaporation of the solvent left a product (0.096 g) that was determined by ^1H NMR to contain a nearly quantitative amount of cyclobutanone.

Discussion

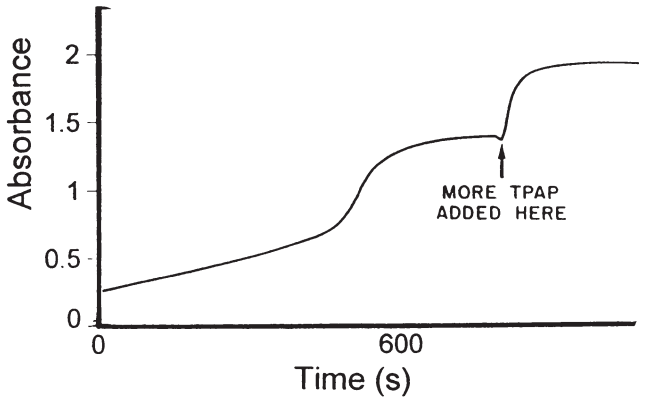
Autocatalysis

The autocatalytic nature of the reaction between tetrapropylammonium perruthenate and 2-propanol is evident from the plots presented in Figs. 4 and 5. The rate of reaction is initially slow because no product (catalyst) is present. However, as the concentration of the product increases, the rate accelerates, with the result that product is produced more and more rapidly. This results in continuous rate increases until the concentration of $QRuO_4$ diminishes, causing the rate to decrease and, finally, to stop.

Although the identity of the product responsible for the autocatalytic nature of the reaction has not been unequivocally established, it is in all likelihood ruthenium dioxide. Evidence in support of this conclusion was obtained by demonstrating that the product from the reduction of ruthenium tetroxide in carbon tetrachloride also catalyzed the reaction between $QRuO_4$ and 2-propanol. When tetrapropylammonium perruthenate was added to a solution prepared by the reduction of RuO_4 with excess 2-propanol, a rapid reduction of $QRuO_4$ occurred without an induction period. Since ruthenium tetroxide is known to be reduced to ruthenium dioxide by alcohols, the observation that this product is also a catalyst for the reaction between $QRuO_4$ and 2-propanol is entirely consistent with the assumption that RuO_2 is responsible for the autocatalysis evident in Figs. 4 and 5 (26).

The catalytic nature of the product was further demonstrated by adding an aliquot of $QRuO_4$ in methylene chloride to a solution in which the reaction of $QRuO_4$ with an excess of 2-propanol had proceeded to completion. As indicated by the plot in Fig. 18, the added $QRuO_4$ was very rapidly reduced without an induction period.

Fig. 18. Plot illustrating the effect of adding additional TPAP after the initial reaction had stopped.



The reaction, therefore, is reminiscent of permanganate reductions in concentrated acid solution that are catalyzed by MnO_2, a product of the reaction (27). In such reactions, the product is a colloid that could act as a surface catalyst.

The observed decrease in catalytic activity in the presence of moisture (Fig. 17) is consistent with the possibility that RuO_2 acts as a surface catalyst whose active sites are blocked by adsorption of water. The observation that the reaction appears to be approximately second order with respect to the concentration of RuO_2 may be an artifact that is related in some way to the average size of the colloidal particles. Other possibilities involving a transition state that includes two molecules of $QRuO_4$, two molecules of RuO_2, and one molecule of 2-propanol are rather speculative (28).

The reaction mechanism

Both the catalytic and noncatalytic portions of the reaction exhibit a similar rate law — first order in 2-propanol and second order in $QRuO_4$. Thus, the transition state must contain two perruthenate ions and a molecule of 2-propanol.

The presence of two perruthenate ions suggests a dimer, similar to those known for other high valent transition metal oxides such as chromate and manganate (29, 30). Two possibilities exist: dimerization of the RuO_4^- ions could take place prior to reaction with the alcohol, as in eqs. [21] and [22], or, an ion of perruthenate and alcohol could react before the second RuO_4^- ion becomes involved, as in eqs. [23] and [24]. Unfortunately, kinetic studies do not help to distinguish between these two possibilities.

[21] $2RuO_4^- \Leftrightarrow Ru_2O_8^{2-}$

[22] $Ru_2O_8^{2-} + ROH \rightarrow$ Products

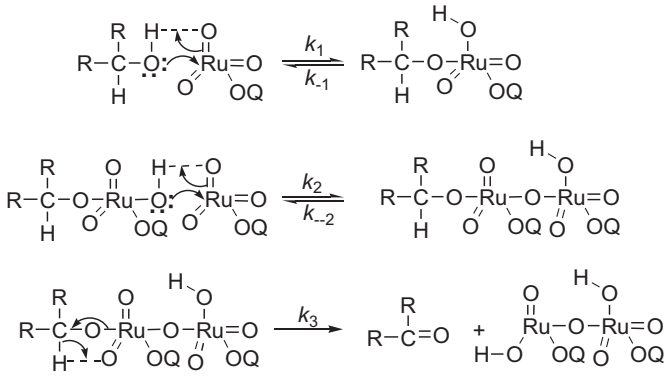
[23] $RuO_4^- + ROH \Leftrightarrow RORuO_4H^-$

[24] $RORuO_4H^- + RuO_4^- \rightarrow$ Products

Regardless of the reaction sequence, it appears that 2-propanol must initially react by formation of an ester. Such a conclusion is consistent with the O-D isotope effect and with the observation that ethers are not readily oxidized by $QRuO_4$. Oxidants such as RuO_4 and MnO_4^- that react with alcohols by an initial cleavage of an α-C—H bond, oxidize alcohols and ethers at comparable rates because the α hydrogens of alcohols and ethers have similar chemical properties

© 2005 NRC Canada

Scheme 1.



(31, 32). However, the reactions of oxidants, such as chromic acid (H_2CrO_4), that are initiated by ester formation, proceed more rapidly when alcohols are the reductants (33).

The observation that cyclobutanol is oxidized to cyclobutanone indicates that the oxidative process is a two-electron transfer. Previous work has established that hydrogen atom transfer from cyclobutanol produces a free radical that opens very rapidly to give acyclic products (34–36). The oxidation of cyclobutanol to cyclobutanone, therefore, indicates that $QRuO_4$ is a two-electron oxidant.

In addition, the low sensitivity of the reaction to substituent changes displayed in the Taft plots (Figs. 14 and 15), suggests a cyclic process in which there is little charge built up on the α carbon in the transition state. A reaction sequence, consistent with these observations, is presented in Scheme 1.

The rate law derived from the reaction sequence in Scheme 1 is consistent with the observed isotope effects since the rate constants for O–D cleavage (k_1) and C–D cleavage (k_3) are both in the numerator of the derived rate law, as indicated in eq. [25].

$$[25] \quad \text{Rate} = (k_1k_2k_3[R_2CHOH][QRuO_4]^2)/(k_{-1}k_{-2} + k_{-1}k_3 + k_2k_3[QRuO_4])$$

Kinetic studies cannot be used to investigate reactions occurring after the transition state; however, the observed 1:1 stoichiometry allows some speculation with respect to the fate of the co-product ($H_2Ru_2O_8Q_2$). If this product (containing two ruthenium atoms, both with an average oxidation state of +6) was reduced to ruthenium(IV) by reaction with the solvent, the stoichiometry would be, $ROH:QRuO_4 = 1:2$. On the other had, if $H_2Ru_2O_8Q_2$ was reduced by 2 mol of 2-propanol, as in eq. [26], the stoichiometry would be, $ROH:QRuO_4 = 3:2$. Both of these possibilities, therefore, appear to be ruled out.

$$[26] \quad 2R_2CHOH + H_2Ru_2O_8Q_2 \rightarrow 2R_2CO + 2QRuO_4H_3$$

One possibility that results in a 1:1 stoichiometry is the suggestion that $H_2Ru_2O_8Q_2$ could dissociate into two different products, one with ruthenium in an oxidation state of +5 (H_2RuO_4Q) and the other, an oxidation state of +7 ($QRuO_4$), as in eq. [27]. Since a ruthenium(V) species would be expected to be very reactive, it would likely be reduced to ruthenium(IV) by reaction with the solvent. The overall result would be a 1:1 stoichiometry.

$$[27] \quad H_2Ru_2O_8Q_2 \rightarrow QRuO_4 + QRuO_4H_2$$

Conclusions

The reaction between alcohols and tetrapropylammonium perruthenate exhibits intense autocatalysis, making it an excellent reagent for synthetic purposes.

The product responsible for the autocatalytic nature of the reaction appears to be ruthenium dioxide.

The presence of moisture decreases the efficiency of the catalyst.

The rate law for the reaction under both noncatalytic and catalytic conditions is first order in the alcohol and second order in the oxidant.

The rate of reaction is much greater for 2-propanol than for THF, suggesting that the reaction involves formation of an intermediate ruthenate ester.

The oxidation of cyclobutanol to cyclobutanone by TPAP indicates that the reaction is a two-electron process.

Primary deuterium kinetic isotope effects are observed for the oxidation of both 2-propanol-2-*d* and 2-propanol-O-*d* by TPAP.

The impact of substituent effects on the reaction rates is not large.

References

1. W.P. Griffith and S.V. Ley. Aldrichimica Acta, **23**, 13 (1990).
2. W.P. Griffith. Chem. Soc. Rev. 179 (1992).
3. S.V. Ley, J. Norman, W.P. Griffith, and S.P. Marsden. Synthesis, 634 (1994).
4. R. Bloch and C. Brillet. Synlett, 829 (1990).
5. S. Kamlage, M. Sefkow, B.L. Paul-Zobel, and M.G. Peter. J. Chem. Soc. Chem. Commun. 331 (2001).
6. K.R. Guertin and A.S. Kende. Tetrahedron Lett. **34**, 5369 (1993).
7. Y. Tokuhaga, M. Ihara, and K. Fukumoto. J. Chem. Soc. Perkin Trans. 1, 207 (1997).
8. M.H. Yates. Tetrahedron Lett. **38**, 2813 (1997).
9. V. Farmer and T. Welton. Green Chem. **4**, 97 (2002).
10. Y.M. Ahn, G.G. Vander Velde, and G.I. Georg. J. Org. Chem. **67**, 7140 (2002).
11. LC. Dias, L.G. de Oliverira, and M.A. de Sousa. Org. Lett. **5**, 265 (2003).
12. C.K. Acosta, P.N. Rao, and H.K. Kim. Steroids, **58**, 205 (1993).
13. I.J. Rosenstein and T.A. Tynan. Synth. Commun. **30**, 1447 (2000).
14. I.E. Marko, A. Gautier, M. Tsukszaki, A. Llobet, E. Plantalech-Mir, C.J. Urch, and S.M. Brown. Angew. Chem. Int. Ed. Engl. **38**, 1960 (1970).
15. S.V. Ley, A. Madin, and N.J.T. Monck. Tetrahedron Lett. **34**, 7479 (1998).
16. D. Diez-Martin, P. Grice, H.C. Kolb, S.V. Ley, and A. Madin. Synlett, 326 (1990).
17. N.J. Anthony, A. Armstron, S.V. Ley, and A. Madin. Tetrahedron Lett. **30**, 3209 (1989).
18. A.C. Dengel, W.P. Griffith, and R.A. Hudson. Transition Met. Chem. (Weinheim, Ger.), **10**, 98 (1985).
19. D.G. Lee, Z. Wang, and W.D. Chandler. J. Org. Chem. **57**, 3276 (1992).
20. D.R. Lide (*Editor*). Handbook of chemistry and physics. 75th ed. CRC Press, Boca Raton, Fla. 1994.

© 2005 NRC Canada

21. D.G. Lee and M. van den Engh. Can. J. Chem. **50**, 2000 (1972).
22. M. Fieser and L.F. Fieser. Reagents for organic synthesis. Vol. 1. J. Wiley, New York. 1972. p. 1140.
23. S.R. Logn. Fundamentals of chemical kinetics. Longman, Essex, UK. 1996. p. 177.
24. K.B. Wiberg. Physical organic chemistry. Wiley, New York. 1964. p. 312.
25. M.B. Smith and J. March. March's advanced organic chemistry. Wiley-Interscience, New York. 2001. p. 431.
26. D.G. Lee and M. van den Engh. *In* Oxidation in organic chemistry. Part B. *Edited by* W.S. Trahanovsky. Academic Press, New York. 1973. p. 177.
27. R. Stewart. *In* Oxidation in organic chemistry, Part A. *Edited by* K.B. Wiberg. Academic Press, New York. 1965. p. 6.
28. Z. Wang. Ph.D. thesis, The University of Regina, Regina, Sask. 1995.
29. P. Atkins and L. Jones. Chemical principles. 3rd ed. Freeman, New York. 2002. p. 614.
30. D.G. Lee and T. Chen. J. Am. Chem. Soc. **115**, 11 231 (1993).
31. M. Hudlicky. Oxidations in organic chemistry. ACS Monograph 186, American Chemical Society, Washington, D.C. 1990. p. 169.
32. D.G. Lee and M. van den Engh. Can. J. Chem. **50**, 3129 (1972).
33. F.H. Westheimer. Chem. Rev. **45**, 419 (1949).
34. K. Meyer and J. Rocek. J. Am. Chem. Soc. **94**, 1209 (1972).
35. J. Rocek and D.E. Aylward. J. Am. Chem. Soc. **97**, 5452 (1975).
36. J. Rocek and A.E. Radkowsky. J. Am. Chem. Soc. **90**, 2986 (1968); **95**, 7123 (1973).

Appendix A

Derivation of eq. [A1] from Scheme A1.

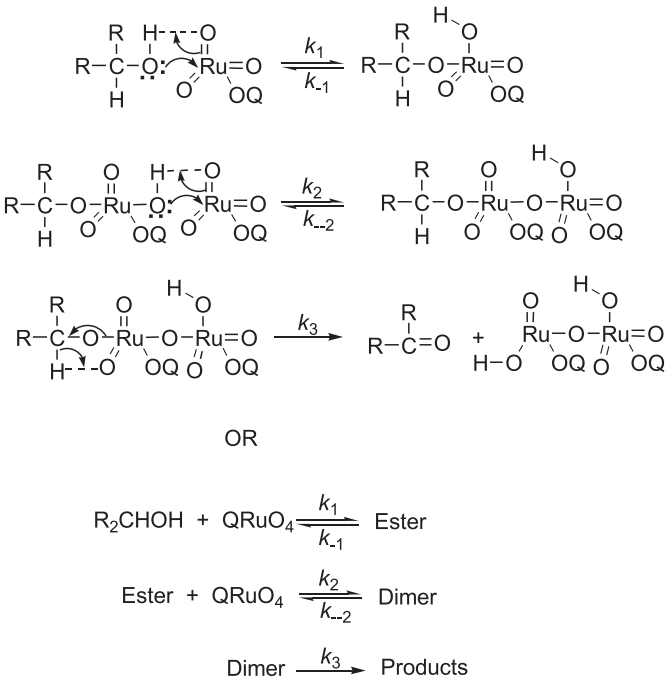
$$[A1]\quad \text{Rate} = (k_1k_2k_3[R_2CHOH][QRuO_4]^2)/(k_{-1}k_{-2} + k_{-1}k_3 + k_2k_3[QRuO_4])$$

Apply the steady state approximation to the intermediates; i.e., to [Ester] and [Dimer].

$$d[\text{Ester}]/dt = k_1[R_2CHOH][QRuO_4] - k_{-1}[\text{Ester}] - k_2[\text{Ester}][QRuO_4] + k_{-2}[\text{Dimer}] = 0$$

$$d[\text{Dimer}]/dt = k_2[\text{Ester}][QRuO_4] - k_{-2}[\text{Dimer}] - k_3[\text{Dimer}] = 0$$

Scheme A1.



$$d[\text{Ester}]/dt + d[\text{Dimer}]/dt = k_1[R_2CHOH][QRuO_4] - k_3[\text{Dimer}] - k_{-1}[\text{Ester}] = 0$$

$$[\text{Ester}] = (k_1[R_2CHOH][QRuO_4] - k_3[\text{Dimer}])/k_{-1}$$

$$[\text{Dimer}] = (k_2[\text{Ester}][QRuO_4])/(k_{-2} + k_3)$$

$$[\text{Dimer}] = (k_1k_2[R_2CHOH][QRuO_4]^2 - k_2k_3[\text{Dimer}][QRuO_4])/(k_{-2} + k_3)(k_{-1})$$

$$[\text{Dimer}] = (k_1k_2[R_2CHOH][QRuO_4]^2)/(k_{-1}k_{-2} + k_{-1}k_3 + k_2k_3[QRuO_4])$$

$$\text{Rate} = k_3[\text{Dimer}] = (k_1k_2k_3[R_2CHOH][QRuO_4]^2)/(k_{-1}k_{-2} + k_{-1}k_3 + k_2k_3[QRuO_4])$$

© 2005 NRC Canada

The remarkable effect of 7-amino substituents on the reactivity of 4-nitrobenzofurazans with nucleophiles[1]

Michael R. Crampton, Chukwuemeka Isanbor, and Thomas C. Willett

Abstract: The reactions of four 4-nitrobenzofurazans (**4a**–**4d**) substituted at the 7 position with (**a**) *N*-ethyl, (**b**) *N*-butyl, (**c**) piperidino, or (**d**) pyrrolidino groups have been examined with sulfite ions and with hydroxide ions in water–DMSO (80:20, *v*/*v*). Addition of sulfite at the 5 position gives σ adducts with equilibrium constants ca. 10^5 lower than that for the formation of the corresponding adduct from 4-nitrobenzofurazan. These reductions are attributed to the stabilization of the parent molecules **4a**–**4d** by conjugative interaction between the 4 and 7 substituents. In alkaline solution, **4a** and **4b** yield the conjugate bases while **4c** and **4d** suffer nucleophilic substitution to give 7-hydroxy-4-nitrobenzofurazan. Reactivity here is relatively high because of the iminium ion character of the substrates.

Key words: benzofurazans, σ adducts, nucleophilic reactivity, substitution.

Résumé : Opérant dans un milieu eau–DMSO (80:20, *v*/*v*), on a étudié les réactions des ions sulfites et des ions hydroxydes avec quatre 4-nitrobenzofurazanes (**4a**–**4d**) substitués en position 7 par (**a**) *N*-éthyle; (**b**) *N*-butyle; (**c**) pipéridino ou (**d**) des groupes pyrrolidino. L'addition de l'ion sulfite en position 5 conduit à des adduits σ dont les constantes d'équilibre sont 10^5 fois plus lentes que celles des formations des adduits correspondants à partir du 4-nitrobenzofurazane. On attribue ces réductions à la stabilisation des molécules parentes **4a**–**4d** par une interaction de conjugaison entre les substituants dans les positions 4 et 7. En solution alcaline, les composés **4a** et **4b** conduisent à la formation des bases conjuguées alors que les composés **4c** et **4d** subissent des réactions de substitution nucléophile qui conduisent à la formation de 7-hydroxy-4-nitrobenzofurazanes. Dans ces cas, la réactivité est relativement grande en raison du caractère d'ion iminium des substrats.

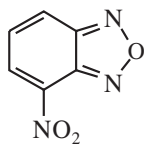
Mots clés : benzofurazanes, adduits σ, réactivité nucléophile, substitution.

[Traduit par la Rédaction]

Introduction

There is current interest in quantitatively measuring reactivity in nucleophile–electrophile combination reactions. Mayr and co-workers (1, 2) have investigated a wide-range of carbon–carbon bond forming reactions. There is also information available on the reactivities of both aromatic and heteroaromatic electron-deficient molecules with neutral and anionic nucleophiles (3, 4). Thus, Terrier, Buncel, and co-workers (5) were recently able to assign electrophilicity values (*E*) of –5.13 for 4,6-dinitrobenzofuroxan (DNBF), an excellent electrophile, and –13.10 for 1,3,5-trinitrobenzene (TNB), a weaker electrophile. These values were obtained in reactions with carbon nucleophiles in acetonitrile. The relative electrophilicities may be expected to show some dependence on the type of nucleophile and the solvent. Thus, the pK_a values (3) corresponding to the covalent reaction with water are 3.75 for DNBF and 13.43 of TNB, showing a rather larger difference than the *E* values.

In thermodynamic terms the stabilities of σ adducts formed by the reaction at the 5 position of 4-nitrobenzofurazan (**1**) are generally comparable with those of the corresponding σ adducts from TNB. However, there are significant differences depending on the nature of the nucleophile and the solvent. Thus, for the reaction with methoxide ions in methanol, values of equilibrium constants are 141 $dm^3\ mol^{-1}$ for **1** (6) and 23 $dm^3\ mol^{-1}$ for TNB (7). For reaction with aliphatic amines in dimethyl sulfoxide (DMSO), values of equilibrium constants are ca. 100 times lower for **1** than for TNB (8, 9). Interestingly, for reactions with sulfite ions (10) or hydroxide ions (11) in water, values are 10^3–10^4 times larger for **1** than for TNB. These differences may be largely due to the effects of solvation. Thus, **2** with a localized negative charge will be well-solvated by water, while **3** with a more delocalized charge will be stabilized by DMSO.



1

Received 15 December 2004. Published on the NRC Research Press Web site at http://canjchem.nrc.ca on 30 September 2005.

M.R. Crampton[2] and T.C. Willett. Chemistry Department, Durham University, Durham, DH1 3LE, UK.
C. Isanbor. Department of Chemistry, University of Lagos, Lagos, Nigeria.

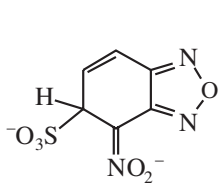
[1]This article is part of a Special Issue dedicated to organic reaction mechanisms.
[2]Corresponding author (e-mail: m.r.crampton@durham.ac.uk).

 doi: 10.1139/V05-116 © 2005 NRC Canada

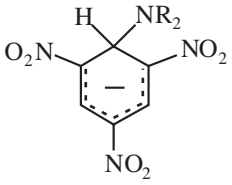
Table 1. Spectroscopic data for parent molecules, σ adducts, and products.

	^{1}H NMR data (δ)[a]				UV absorbance[b]	
Compound	H-5	H-6	J_{56}	Other	λ_{max} (nm)	ε (dm^3 mol^{-1} cm^{-1})
4a	8.53	6.40	8.8	9.54 (NH), 3.51 (2H), 1.28 (3H)	482	2.6×10^4
4b	8.49	6.40	8.8	9.55 (NH), 3.46 (2H), 1.65 (2H), 1.39 (2H), 0.92 (3H)	484	2.8×10^4
4c	8.44	6.64	9.4	4.16 (4H), 1.76 (6H)	510	2.6×10^4
4d	8.46	6.27	9.0	4.19 (2H), 3.69 (2H), 2.10 (4H)	502	3.0×10^4
5a	5.34	5.23	6.2	3.05 (2H), 1.15 (3H)	315	1.2×10^4
5b	5.31	5.19	6.2	2.99, 2.51 (2H), 1.61, 1.55 (2H), 1.29 (2H), 0.83 (3H)	310	1.0×10^4
5c	5.36	5.73	5.8	3.05 (2H), 2.84 (2H), 1.57 (4H), 1.46 (2H)	327	1.1×10^4
6a	7.62[c]	6.42	10.5	3.58 (2H), 1.23 (3H)	393	2.0×10^4
	7.50[c]	6.20	10.5	3.90 (2H), 1.29 (3H)		
6b	7.60[c]	6.44	10.8	3.55 (2H), 1.60 (2H), 1.31 (2H), 0.83 (3H)	392	2.2×10^4
	7.50[c]	6.20	10.8	3.90 (2H), 1.65 (2H), 1.31 (2H), 0.83 (3H)		
8	8.42	6.08	9.7		466	2.7×10^4

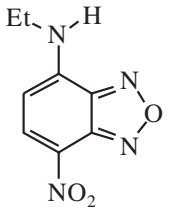
[a]Values for parent molecules **4a**–**4d** are in [^{2}H$_6$]-DMSO. All other values are in D$_2$O–[^{2}H$_6$]-DMSO (80:20, *v*/*v*).
[b]In water–DMSO (80:20, *v*/*v*).
[c]Values for the conformational isomers, see text.



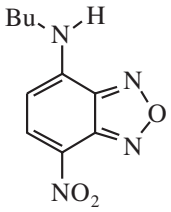
2



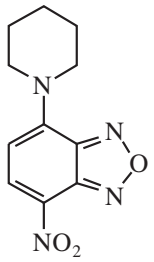
3



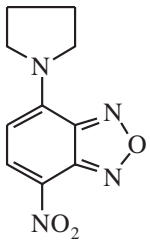
4a



4b



4c



4d

Here, we are concerned with the reactivities of **1** and its 7-substituted derivatives in σ-adduct formation; in particular, the effect of an amino group or substituted amino group at the 7 position.

One source of interest in 4-nitrobenzofurazans is their potential to act as in vitro inhibitors of nucleic acid and protein biosynthesis in animal cells (12–15). Also, the fluorescence characteristics of 7-amino derivatives have been studied (16–18) and their use as fluorescent probes has been investigated (19).

Here, results are reported for the reaction of compounds **4a**–**4d** with sulfite and with hydroxide ions in largely aqueous media. There is evidence for strong conjugation between the groups at the 4 and 7 positions, which stabilizes the parent molecules.

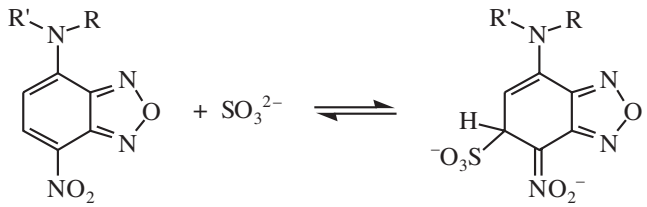
Results and discussion

Most measurements relate to a solvent system of water–DMSO (80:20, *v*/*v*). This system was chosen because of the low solubilities (<5×10^{-5} mol dm^{-3}) of **4b**–**4d** in water. The solubility of **4a** in water was higher, therefore, measurements were made both in water–DMSO (80:20) and in water, allowing a comparison of the solvent systems.

Reaction with sulfite

Spectroscopic results for the parent molecules in DMSO and for the products of the reaction with sulfite in water–DMSO (80:20) are in Table 1. The ^{1}H NMR spectra are consistent with sulfite addition at the 5 position to give **5** as shown in Scheme 1. H-5 shows a large shift to lower frequency (ca. δ 5.3) on adduct formation, while H-6 shows a smaller shift.

Scheme 1.



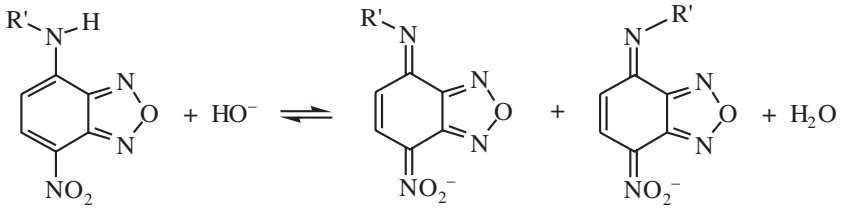
4 **5**

The coupling constant J_{56} is reduced from ca. 9 Hz in the parent to ca. 6 Hz, consistent with the change in hybridization at C-5. Since the shifts of H-5 and H-6 are similar, the assignments may be reversed. Due to the low solubility of **4d** and the low equilibrium constant for adduct formation, useful spectra could not be obtained for **5d**.

The spectra of the adducts were unchanged after several days and there was no evidence for sulfite attack at the 7 position. However, after a week, spectra of **4a** showed small bands at δ 8.42 and 6.08, characteristic of the anion of 7-

© 2005 NRC Canada

Scheme 2.



4a, 4b **6a, 6b**

Table 2. Kinetic and equilibrium results for reaction of **4c**[a] with sulfite in water–DMSO (80:20, *v*/*v*) at 25 °C.

$[SO_3^{2-}]$ (10^{-4} mol dm^{-3})	k_{obs} (s^{-1})	k_{calcd}[b] (s^{-1})	Abs (510 nm)	K_5[c] (dm^3 mol^{-1})
0	—	—	1.27	—
8.0	0.24	0.24	0.90	510
12.0	0.28	0.27	0.79	505
16.0	0.31	0.31	0.71	490
20.0	0.33	0.34	0.64	490
40.0	0.50	0.52	0.41	520
60.0	0.71	0.69	0.32	500
100	0.93	1.04	0.21	508
150	1.42	1.48	0.15	500
200	1.98	1.91	0.11	525

Note: Abs = Absorbance.
[a]Concentration (5×10^{-5} mol dm^{-3}).
[b]Calculated from eq. [1] with k_5 = 87 dm^3 mol^{-1} s^{-1} and k_{-5} = 0.17 s^{-1}.
[c]Calculated as ((1.27 – Abs)/Abs) × (1/$[SO_3^{2-}]$).

Table 3. Summary of kinetic and equilibrium data for reactions with sulfite ions in water–DMSO (80:20, *v*/*v*) at 25 °C.

Compound	k_5 (dm^3 mol^{-1} s^{-1})	k_{-5} (s^{-1})	K_5 (dm^3 mol^{-1})
4a[a]	170	4.5	38
4a	180	1.9	95
4b	154	2.1	73
4c	87	0.17	510
4d	64	19	3.4
1[a,b]	3.3×10^4	0.020	1.65×10^6
TNB[a,c]	3.5×10^4	125	290

[a]Measurements in water.
[b]Data from ref. 10.
[c]Data from ref. 20 for the reaction at unsubstituted ring positions in 1,3,5-trinitrobenzene. Data have not been statistically corrected.

hydroxy-4-nitrobenzofurazan (**8**). Presumably in the sulfite solutions, which are weakly alkaline, hydrolysis occurs very slowly. The failure to observe sulfite attack at the 7 position of **4a**–**4d** is presumably steric in origin. It is known that in **1** itself, attack at the 5 position is followed by a slow isomerization to give the adduct at the 7 position.

Rate and equilibrium measurements for the formation of adducts **4a**–**4d** were made spectrophotometrically in solutions where the sulfite concentration was in large excess of the substrate concentration. In these conditions, a single, first-order process was observed, and rate constants were determined by the stopped-flow method.

Plots of k_{obs} vs. sulfite concentration were linear with a positive intercept on the *y* axis, according to eq. [1], allowing the determination of values of k_5 and k_{-5}. Specific results for the reaction of **4c** are in Table 2. Values of the equilibrium constant K_5 calculated as k_5/k_{-5} were in excellent agreement with those determined using equilibrium absorbance values. Results are collected in Table 3. We will delay the detailed discussion, but note that the adducts formed from **4** have stabilities ca. 10^5 times lower than the corresponding adduct from 1.

$$[1] \qquad k_{obs} = k_5[SO_3^{2-}] + k_{-5}$$

Reaction with hydroxide

There is no spectroscopic evidence for σ-adduct formation from **4a**–**4d** and hydroxide ions in solutions containing up to 1 mol dm^{-3} hydroxide in water–DMSO (80:20, *v*/*v*). Hence, we may estimate that $K_5 < 0.1$ dm^3 mol^{-1}. This contrasts with the behaviour of **1** where the value (11) of the equilibrium constant for reaction with hydroxide at the 5 position is 2700 dm^3 mol^{-1}. However, this behaviour is not unexpected in light of the results with sulfite, which show that values of K_5 are many orders of magnitude lower for **4** than for **1**.

The ^{1}H NMR spectra of **4a** and **4b** in the presence of hydroxide are reported in Table 1 and indicate deprotonation to give the respective conjugate bases **6a** and **6b** as shown in Scheme 2.

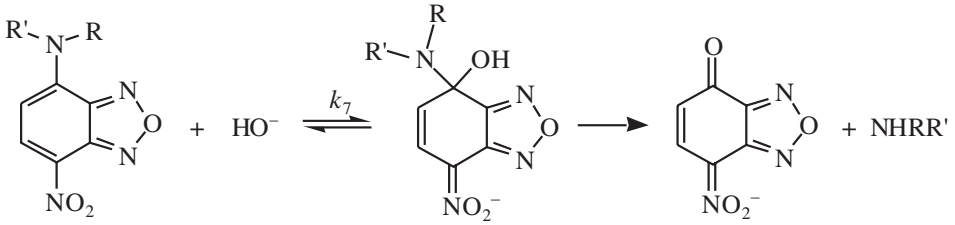
Interestingly, the spectra in each case are compatible with the formation of two conformational isomers as indicated in the scheme. For **6a**, bands for H-5 and H-6 are observed at δ 7.62 and 6.42, J = 10.5 Hz, for the major isomer, and δ 7.50 and 6.20, J = 10.5 Hz, for the minor isomer. For **6a**, the ratio of isomers is 3:1 and for **6b** it is 4:1. Very slow displacement of the 7 substituents is observed so that after 1 week, bands are present due to the anion **8**.

Deprotonation of **4a** and **4b** is accompanied by changes in the UV–vis spectra. In the case of **4b**, λ_{max} is 484 nm in the parent and 392 nm in the anion. These changes were used to measure the pK_a values. An example calculation, in Table 4, yields a pK_a value of 10.15 ± 0.02 for **4b** in water–DMSO (80:20). Values for **4a** were 10.14 ± 0.05 in solvent (80:20) and 10.02 ± 0.02 in water.

In the presence of hydroxide, **4c** and **4d** were irreversibly converted to the anion (**8**) of 7-hydroxy-4-nitrobenzofurazan, which was identified from its ^{1}H NMR and UV–vis spectra (11). Kinetic measurements were made, at λ_{max} for the parent, with hydroxide concentrations in large excess and in the range 0.05–0.20 mol dm^{-3}. First-order kinetics were obtained, and plots of the rate constant vs. hydroxide concentration, which were linear with a zero intercept yielded values of the second-order rate constants. The reaction is likely (3, 4) to proceed by the addition–elimination mecha-

© 2005 NRC Canada

Scheme 3.



4c, 4d **7** **8**

Table 4. Calculation of the pK_a values for **4b**[a] in water–DMSO (80:20, *v*/*v*) at 25 °C.

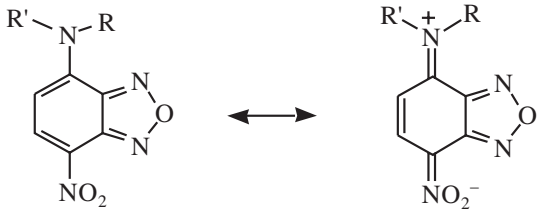
pH[b]	Abs (484 nm)	pK_a[c]
7.0	1.36	—
9.63	1.070	10.14
9.80	0.983	10.16
9.96	0.852	10.17
10.18	0.207	10.13
10.35	0.599	10.14
10.71	0.403	10.17
10.91	0.293	10.11
11.20	0.225	10.15
0.3 NaOH	0.125	—

Note: Abs = Absorbance.
[a]Concentration is 5×10^{-5} mol dm^{-3}.
[b]Borax buffers.
[c]Calculated as pH + log(Abs – 0.125)/(1.36 – Abs).

nism shown in Scheme 3. There was no evidence for the accumulation of the reaction intermediates **7c** and **7d** so that the measured second-order rate constants are likely to represent the values for k_7 for nucleophilic attack at the 7 position. Values obtained were 0.91 ± 0.05 dm^3 mol^{-1} s^{-1} for **4c** and 0.71 ± 0.04 dm^3 mol^{-1} s^{-1} for **4d**. These values may be compared to a value (11) of 0.2 ± 0.1 dm^3 mol^{-1} s^{-1} for hydroxide attack at the 7 position of **1**.

Comparisons

Our results provide evidence for a strong conjugation between the 4-nitro and 7-amino substituents as indicated in **9**. The UV–vis absorbance maxima in **4a**–**4d** are at 482–510 nm, showing a strong bathochromic shift relative to **1** where λ_{max} is 327 nm. A similar, but much weaker, conjugative effect has been noted in 7-methoxy-4-nitrobenzofurazan (**10**) where λ_{max} is 383 nm. It is interesting that in the ^{1}H NMR spectrum of **4d**, the pyrrolidino derivative, the two pairs of α-CH_2 hydrogens show discrete spin-coupled bands at δ 4.19 and 3.69, indicative of the double bond character in the carbon–nitrogen bond.



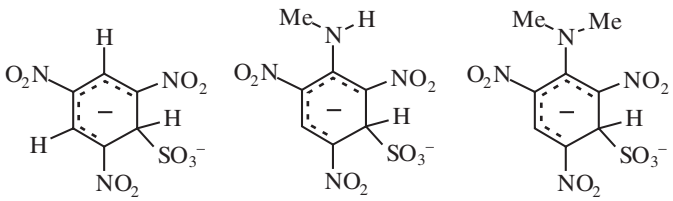
9

When comparing values of rate and equilibrium constants, it must be noted that here values generally refer to water–DMSO (80:20, *v*/*v*), corresponding to a mol fraction of 0.059 in DMSO. The comparisons with other compounds are generally made with results obtained in water. Nevertheless, the proportion of DMSO is small so that effects are likely to be small. Thus, the results in Table 3 for sulfite addition to **4a** indicate an increase in the value of K_5 by a factor of 2.5 on going from water to the mixed solvent. This is in line with other results showing increases in stability for the σ adducts as the proportion of DMSO in the solvent is increased (3, 4, 10).

One effect of the conjugative stabilization shown in **9** is to dramatically decrease values of equilibrium constants for σ-adduct formation at the 5 position. In the case of sulfite addition, the results in Table 3 show that values of K_5 are reduced by factors of ca. 10^5 relative to the value for the reaction of **1**. Values of k_5 are decreased and values of k_{-5} are increased. The overall effect is notably bigger for the pyrrolidino derivative (**4d**) than for the piperidino analogue (**4c**). Related differences between these amines have been reported previously (21–23) and may be attributed to the particular stability of the resonance form **9** in the pyrrolidino derivative.

It is of interest to contrast the effects of an amino substituted in the 4-nitrobenzofurazans with related effects in 1,3,5-trinitrobenzene derivatives. Thus, the values of the equilibrium constants for the formation of the sulfite adducts **10**, **11**, and **12** are (24) 250, 5.4 × 10^4, and 5.4 × 10^4 dm^3 mol^{-1}, respectively. Here, the effect of an *N*-methyl or *N*,*N*-dimethyl substituent is to enhance the stability of the adduct by a factor >100. It is likely that the difference in behaviour in the two systems is largely steric in origin. Hence, in the parent amino-trinitrobenzenes, it is not possible to achieve the degree of planarity required for strong conjugative interaction. The lower aromaticity in the benzofurazans relative to the benzene derivatives (4) may also favour conjugative interaction as shown in **9**.

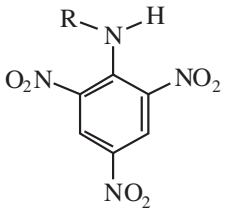
σ-Adduct formation at the 5 position of **4** results in the loss of conjugation between the 4 and 7 substituents, and



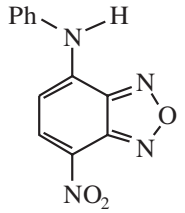
10 **11** **12**

© 2005 NRC Canada

hence, is relatively disfavoured. However, ionization (Scheme 2) is not similarly disadvantaged. Thus, the pK_a values of ca. 10 found for **4a** and **4b** may be compared (3, 4, 25, 26) with corresponding values of ca. 13 for picramide and *N*-alkylpicramides (**13**). In a related fashion, the acidity in water–DMSO (20:80, *v*/*v*) of 7-anilino-4-nitrobenzofurazan (**14**, pK_a 7.68) has been found (27) to be higher than that of 2,4,6-trinitrodiphenylamine (pK_a 8.20).



13



14

The high reactivity of **4c** and **4d** towards hydrolysis (Scheme 3) may be attributed to the contribution of the resonance from **9** to the structure. This gives the carbon–nitrogen bond iminium ion character, hence explaining (28) the reactivity towards the attack of hydroxide. The values obtained for k_7 of ca. 1 dm^3 mol^{-1} s^{-1} may be compared (29) with values of 0.0031 and 0.015 dm^3 mol^{-1} s^{-1} for the corresponding attack of hydroxide on 1-piperidino- and 1-pyrrollidino-2,4,6-trinitrobenzene, respectively. It is interesting that in alkaline solutions, **4a** and **4b**, where anion formation predominates, are very slowly hydrolysed. This is likely to involve hydroxide attack on low concentrations of the parent molecules. As in previous work (10), there is no evidence for an attack of sulfite at the 7 position of 4-nitro-7 substituted benzofurazans, presumably owing to unfavourable steric interactions.

Experimental

Compounds **4a**–**4d** were prepared from 7-chloro-4-nitrobenzofurazan by reaction with 4 equiv. of the appropriate amine in DMSO. Mixtures were stirred for 5 h at room temperature and quenched in ice-cold dilute hydrochloric acid. The precipitates were filtered, washed with water and ethanol, and recrystallized from ethanol. ^{1}H NMR spectra are reported in Table 1, and indicated the absence of impurities. **4a**: mp 164 °C. MS (ES$^+$) *m*/*z* 209 corresponds to $C_8H_9N_4O_3$ (M + H$^+$). **4b**: mp 90 °C. MS (ES$^+$) *m*/*z* 237 corresponds to $C_{10}H_{13}N_4O_3$ (M + H$^+$). **4c**: mp 166 °C. MS (ES$^+$) *m*/*z* 249 corresponds to $C_{11}H_{13}N_4O_3$ (M + H$^+$). **4d**: mp 210 °C. MS (ES$^+$) *m*/*z* 235 corresponds to $C_{10}H_{11}N_4O_3$ (M + H$^+$).

Sulfite solutions were prepared from AnalaR sodium sulfite. To check that no depletion of sulfite concentration occurred because of hydrolysis when making kinetic and equilibrium measurements, measurements were also made in solutions buffered at pH 8.3 using mixtures of sodium sulfite and sodium hydrogen sulfite. The values of rate and equilibrium constants obtained were identical, within experimental error, to those obtained in unbuffered solutions with the same sulfite concentration. Solutions of known hydroxide concentration were made by dilution of AnalaR sodium hydroxide solution. The pH values of buffer solutions, borax or phosphate, were measured using a Jenway 3020 pH meter, calibrated using aqueous buffers. All other materials and solvents were the purest available commercial specimens.

^{1}H NMR spectra were measured using Bruker Ultrashield 400 MHz or Varian Inova 500 MHz spectrometers. Parent molecules were dissolved in [$^2H_6$]-DMSO. Measurements in solutions containing sodium sulfite or sodium deuteroxide were made in water–DMSO (80:20, *v*/*v*) using deuteriated solvents. Parent concentrations were in the range 0.005–0.01 mol dm^{-3} with the nucleophile concentration (ca. 0.1 mol dm^{-3}) in large excess. UV–vis spectra and kinetic measurements were made at 25 °C with a PerkinElmer Lambda 2 spectrophotometer, a Shimadzu UV-2101 PC spectrophotometer, or an Applied Photophysics SX-17 MV stopped-flow instrument. Reported rate constants are the mean of several determinations and are precise to ±5%.

Acknowledgement

We thank the Royal Society, London, for financial assistance to allow C. Isanbor to visit Durham.

References

1. H. Mayr, B. Kempf, and A.R. Ofial. Acc. Chem. Res. **36**, 66 (2003).
2. B. Kempf, N. Hampel, A.R. Ofial, and H. Mayr. Chem. Eur. J. **9**, 1 (2003).
3. E. Buncel, M.R. Crampton, M.J. Strauss, and F. Terrier. Electron deficient aromatic- and heteroaromatic-base interactions. Elsevier, Amsterdam. 1984.
4. F. Terrier. Nucleophilic aromatic displacement. VCH, New York. 1991.
5. F. Terrier, S. Lakhdar, R. Goument, T. Boubaker, and E. Buncel. Chem. Commun. **22**, 2586 (2004).
6. F. Terrier, A.-P. Chatrousse, and F. Millot. J. Org. Chem. **45**, 2666 (1980).
7. C.F. Bernasconi. J. Am. Chem. Soc. **72**, 4682 (1970).
8. M.R. Crampton, J. Delaney, and L.C. Rabbitt. J. Chem. Soc. Perkin Trans. 2, 2473 (1999).
9. L.C. Rabbitt. Ph.D. thesis, University of Durham, Durham, UK. 2000.
10. M.R. Crampton, L.M. Pearce, and L.C. Rabbitt. J. Chem. Soc. Perkin Trans. 2, 257 (2002).
11. M.R. Crampton, R.E.A. Lunn, and D. Lucas. Org. Biomol. Chem. **1**, 3438 (2003).
12. P.B. Ghosh, B. Ternai, and M.W. Whitehouse. J. Med. Chem. **11**, 305 (1968).
13. P.B. Ghosh, B. Ternai, and M.W. Whitehouse. J. Med. Chem. **15**, 255 (1972).
14. M.W. Whitehouse and P.B. Ghosh. Biochem. Pharmacol. **17**, 158 (1968).
15. B.S. Baines, G. Allen, and K. Brocklehurst. Biochem. J. **163**, 189 (1977).
16. T. Hiratsuka and T. Kato. J. Biol. Chem. **262**, 6318 (1987).
17. A. Chattopadhyay. Chem. Phys. Liquids, **53**, 1 (1990).
18. S. Uchiyama, T. Santa, and K. Imai. J. Chem. Soc. Perkin Trans. 2, 2525 (1999).
19. J.M. Boon, R. Shukla, B.D. Smith, G. Licini, and P. Scrimin. Chem. Commun. 260 (2002).
20 C.F. Bernasconi and R.G. Bergstrom. J. Am. Chem. Soc. **95**, 3603 (1973).

© 2005 NRC Canada

21. J.F. Bunnett, S. Sekiguchi, and L.A. Smith. J. Am. Chem. Soc. **103**, 4865 (1981).
22. S. Sekiguchi and J.F. Bunnett. J. Am. Chem. Soc. **103**, 4871 (1981).
23. S. Sekiguchi, T. Suzuki, and M. Hosokawa. J. Chem. Soc. Perkin Trans. 2, 1783 (1989).
24. M.R. Crampton. J. Chem. Soc. B, 1341 (1967).
25. V. Gold and C.H. Rochester. J. Chem. Soc. 1727 (1964).
26. M.R. Crampton and B. Gibson. J. Chem. Soc. Perkin Trans. 2, 752 (1980).
27. J.-C. Halle, M. Mokhtari, P. Soulie, and M.-J. Pouet. Can. J. Chem. **75**, 1246 (1997).
28. E.H. Cordes and W.P. Jencks. J. Am. Chem. Soc. **84**, 832 (1962).
29. E.I. Bujan, V. Remedi, and R.H. de Rossi. J. Chem. Soc. Perkin Trans 2, 969 (2000).

© 2005 NRC Canada

The fragmentation of 7-norbornyloxychlorocarbene — S_Ni-like transition states[1]

Robert A. Moss, Xiaolin Fu, and Ronald R. Sauers

Abstract: 7-Norbornyloxychlorocarbene (**15**) fragments mainly to 7-norbornyl chloride (**16**). A C-2 deuterated analog of **15** (*syn*-**15**-*d*) fragments to labeled chloride **16** with 78% retention and 22% inversion. When the deuterium label is replaced by a *syn*-*exo*-2-methyl group, the resultant carbene **22** fragments to *syn*- and *anti*-7-chloro-*exo*-2-methylnorbornane in a ratio of 1:1.1, corresponding to 48% retention and 52% inversion. Computational studies suggest that the fragmentations proceed via competitive S_Ni-like transition states that lead to either retention or inversion.

Key words: carbenes, carbocations, S_Ni reactions, stereochemistry.

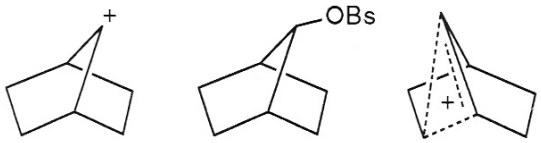
Résumé : La fragmentation du 7-norbornyloxychlorocarbène (**15**) conduit principalement au chlorure de 7-norbornyle (**16**). La fragmentation d'un analogue du composé **15** deutéré en position C-2, le *syn*-**15**-*d*, conduit au chlorure **16** marqué avec 78 % de rétention et 22 % d'inversion. Quand on remplace le deutérium servant de marqueur par un groupe *syn*-*exo*-2-méthyle, le carbène **22** qui en résulte se fragmente en *syn*- et *anti*-7-chloro-*exo*-2-méthylnorbornanes dans un rapport de 1 : 1,1, ce qui correspond à 48 % de rétention et à 52 % d'inversion. Des études par calculs théoriques suggèrent que la fragmentation sur produit par le biais d'états de transition de type S_Ni qui sont en compétition et qui conduisent soit à une rétention soit à une inversion.

Mots clés : carbènes, carbocations, réactions S_Ni, stéréochimie.

[Traduit par la Rédaction]

Introduction

The 7-norbornyl cation **1** has long been a focus of organic reaction mechanism studies (1). Acetolysis of its tosylate precursor proceeded with $k = 8.4 \times 10^{-5}$ s^{-1} at 205 °C, extrapolated to 6.4×10^{-15} s^{-1} at 25 °C, with $\Delta H^* = 35.7$ kcal/mol (1 cal = 4.184 J) and $\Delta S^* = -3.5$ eu (2). This extraordinary lack of reactivity may, in part, be due to angle strain at C-7 (3), although this origin has been downgraded (1) in favor of an electronic origin suggested by Heilbronner, Hoffmann, and co-worker (4) who showed that for reasons of symmetry, the cation at C-7 cannot be stabilized by the ribbon orbitals of the σ skeleton of the underlying six-membered ring.



1 **2** **3**

Received 19 November 2004. Published on the NRC Research Press Web site at http://canjchem.nrc.ca on 5 October 2005.

R.A. Moss,[2] X. Fu, and R.R. Sauers. Department of Chemistry and Chemical Biology, Rutgers, The State University of New Jersey, New Brunswick, NJ 08903, USA.

[1]This article is part of a Special Issue dedicated to organic reaction mechanisms.

[2]Corresponding author (e-mail: moss@rutchem.rutgers.edu).

The solvolysis of 7-norbornyl brosylate (**2**) was depicted as passing through cation **3** by Winstein et al. (5*a*), who studied the stereochemistry and rearrangment attending the acetolysis of **2** at 205 °C. The products included 91% of unrearranged (5*a*) and 90% stereochemically retained (5*b*) acetate **4**, 7% of rearranged *exo*-2-bicyclo[3.2.0]heptyl acetate (**5**), and 2% of the related rearranged olefin **6** (see Scheme 1) (5).

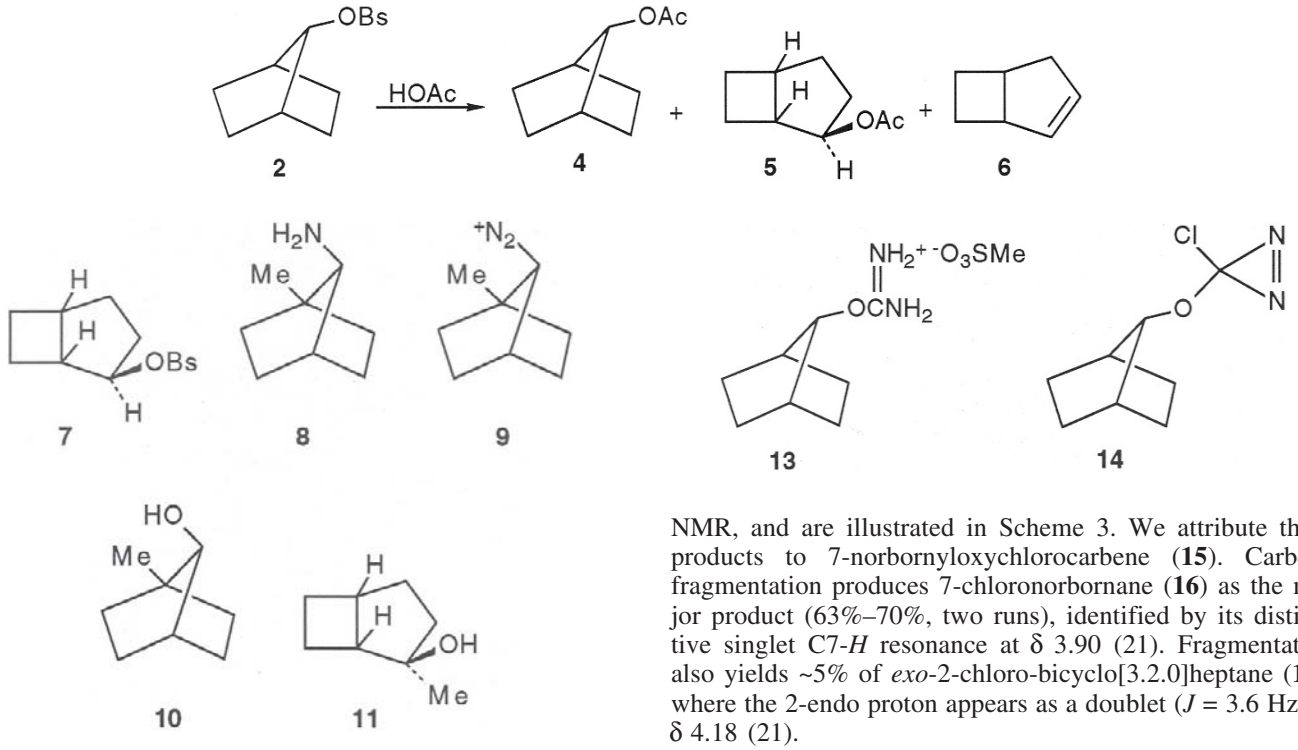
To rationalize the stereoselectivity in the conversion of **2** to **5** (and in accord with the retention in the formation of **4**), cation **3** was suggested as the product-determining intermediate (5).

This postulate was strengthened by the finding that *exo*-2-bicyclo[3.2.0]heptyl brosylate (**7**) underwent acetolysis at 50 °C with anchimeric assistance, extensive rearrangement, and ion pair return to a mixture of 83% of rearranged brosylate **2**, 16% of rearranged acetate **4**, 1% of unrearranged acetate **5**, and a trace of alkene **6** (5*a*). Again, cation **3** was held to account for the course of the reaction.

Furthermore, aqueous nitrous acid deamination of the related (*S*)-1-methyl-7-norbornylamine (**8**), which proceeded via diazonium ion **9**, gave 1-methyl-7-norbornanol (**10**) with high sterochemical retention, as well as the *endo*-2-methyl-*exo*-2-bicyclo[3.2.0]heptanol rearrangement product **11** (6). A cation similar to the solvolysis intermediate was believed to be involved in this deamination reaction (6). More recently, the 7-norbornyl cation has been visualized in a cold SbF_5 matrix by IR spectroscopy, and its structure computed using high level ab initio methods (7, 8). Structures similar to **3** were presented for the 7-norbornyl cation. Our computed structure for this cation will be offered in Fig. 1.

 doi: 10.1139/V05-118 © 2005 NRC Canada

Scheme 1.



We have found the fragmentation of alkoxychlorocarbenes (eq. [1]) to be a valuable, nonsolvolytic entry to several of the most interesting carbocations of organic chemistry (9). These fragmentations, which proceed in both polar (10) and hydrocarbon solvents (11), provide access to (inter alia) the 2-norbornyl cation (12), the 3-nortricyclyl and (or) 5-norbornen-2-yl cations (13), the menthyl and neomenthyl cations (14), and the bicyclo[3.1.0]hexyl cation (15). Here, we describe the application of carbene fragmentation methodology to the 7-norbornyl system. The results provide evidence for the operation of S_Ni-like reaction mechanisms.

[1] $\mathrm{ROCCl} \longrightarrow [\mathrm{R^+\ OC\ Cl^-}] \longrightarrow \mathrm{RCl + CO}$

Results and discussion

7-Norbornyloxychlorocarbene and its products

7-Norbornanol (**12**) was prepared by the sequence of Scheme 2: norbornene was epoxidized with peracetic acid (16); the epoxide was opened to 2-*exo*-bromo-7-*syn*-hydroxynorbornane with HBr (17); and the bromohydrin was debrominated to **12** with a Zn–Cu couple in refluxing 95% ethanol (18). Norboranol **12** was converted to the isouronium mesylate **13** with cyanamide and methanesulfonic acid (19), and the salt was then oxidized to the carbene precursor 3-(7-norbornyloxy)-3-chlorodiazirine (**14**) with NaOCl in aq. DMSO (20). The diazirine was purified by chromatography over silica gel, and characterized by UV (λ_{max} 349 nm in pentane, 355 nm in 1,2-dichloroethane), IR (1541 cm^{-1}, film), and ^1H and ^{13}C NMR spectroscopy (see Experimental).

Diazirine **14** was dissolved in ~2 mL of $CDCl_3$ and irradiated for 1 h at 350 nm. The products were analyzed by NMR, and are illustrated in Scheme 3. We attribute these products to 7-norbornyloxychlorocarbene (**15**). Carbene fragmentation produces 7-chloronorbornane (**16**) as the major product (63%–70%, two runs), identified by its distinctive singlet C7-*H* resonance at δ 3.90 (21). Fragmentation also yields ~5% of *exo*-2-chloro-bicyclo[3.2.0]heptane (**17**), where the 2-endo proton appears as a doublet (J = 3.6 Hz) at δ 4.18 (21).

Trapping of carbene **15** by HCl affords ~14% of dichloride **18** (C7-*H* at δ 4.38, C*H*Cl_2 at δ 7.20), while trapping by adventitious water yields ~1.5% of formate **19** (C7-*H* at δ 4.85, OOC*H* at δ 8.05). There is ample precedent for the formation of these two carbene trapping products (22). As expected (22), generation of carbene **15** in $CDCl_3$ containing (deuterated) pyridine affords a product mixture in which dichloride **18** is suppressed because the pyridine scavenges HCl. Additionally, formate **19** is augmented when carbene **15** is generated in the presence of traces of added water.

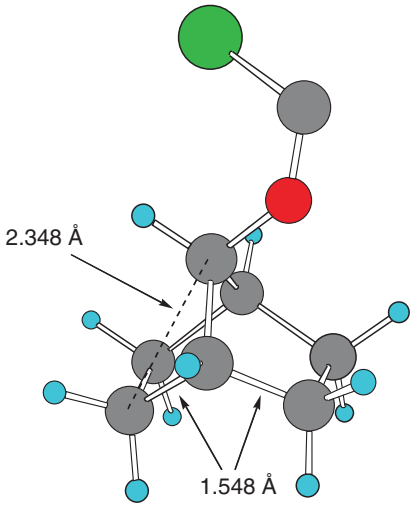
One could formulate the fragmentation of **15** as proceeding via a [**3**$^+$$Cl^-$] ion pair in which return of chloride to C7 produces **16**, whereas chloride attack at C1 generates rearranged chloride **17**. This mechanism agrees with the solvolytic reactions of **2** (Scheme 1) (5) and **7** (5), as well as the deamination of **8** (6). In the following, however, we will suggest that the carbene fragmentation mechanism involves significant S_Ni character. This may also account for the absence of norbornanol, which could have been produced by trapping of the 7-norbornyl cation by traces of water.

Stereochemistry of fragmentation

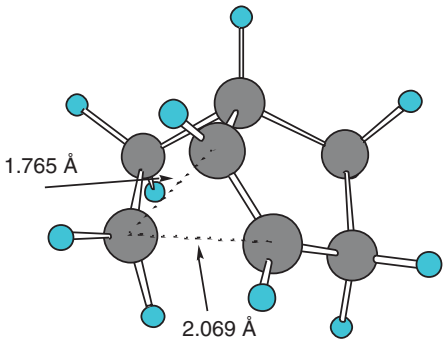
To study the stereochemistry of the **15** → **16** conversion, we prepared deuterium labeled diazirine **14**. Thus, when the Zn–Cu reduction of the bromohydrin of Scheme 2 was carried out in refluxing EtOD, norbornanol **12** was obtained as a mixture of the **12**-*exo*-D and the **12**-*endo*-D isotopomers. Given that the chemical shifts of ^2H are comparable to those of ^1H (23), we can assign signals in the ^2H NMR spectrum by analogy to assignments in the ^1H NMR spectrum. In the latter, the exo and endo C2 and C3 protons of deuterated **12** at δ 1.78 and 1.49 (in $CDCl_3$) appear as multiplets with a total integral value of 3H. In the corresponding ^1H-decoupled

© 2005 NRC Canada

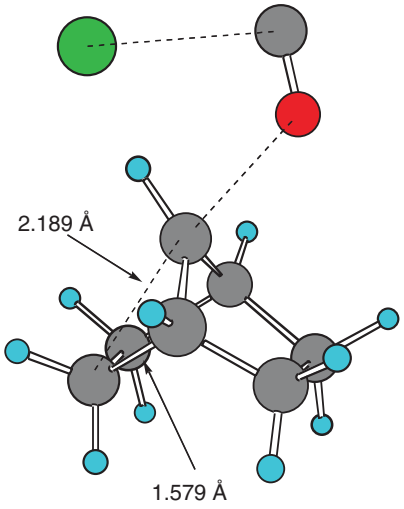
Fig. 1. B3LYP/6-31G(d) computer structures for carbene **15**, 7-norbornyl cation **3**, TS **A**, and TS **B**, showing C1—C2 and C2—C7 distances.



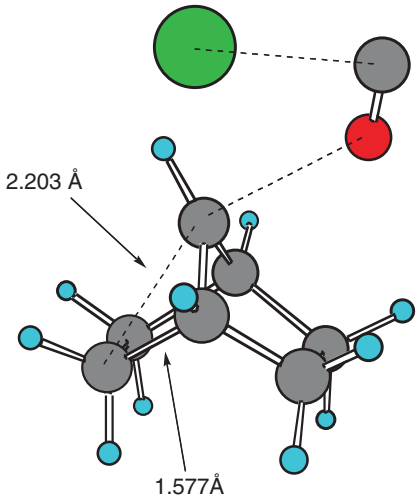
15



3

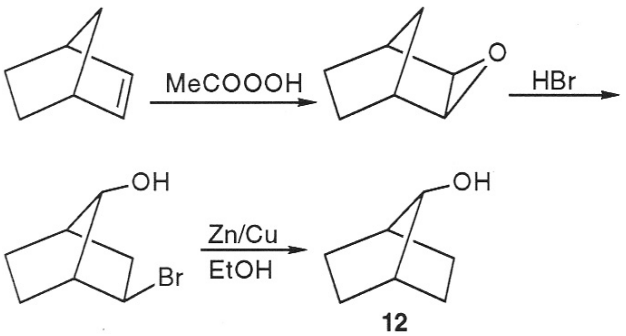


A



B

Scheme 2.

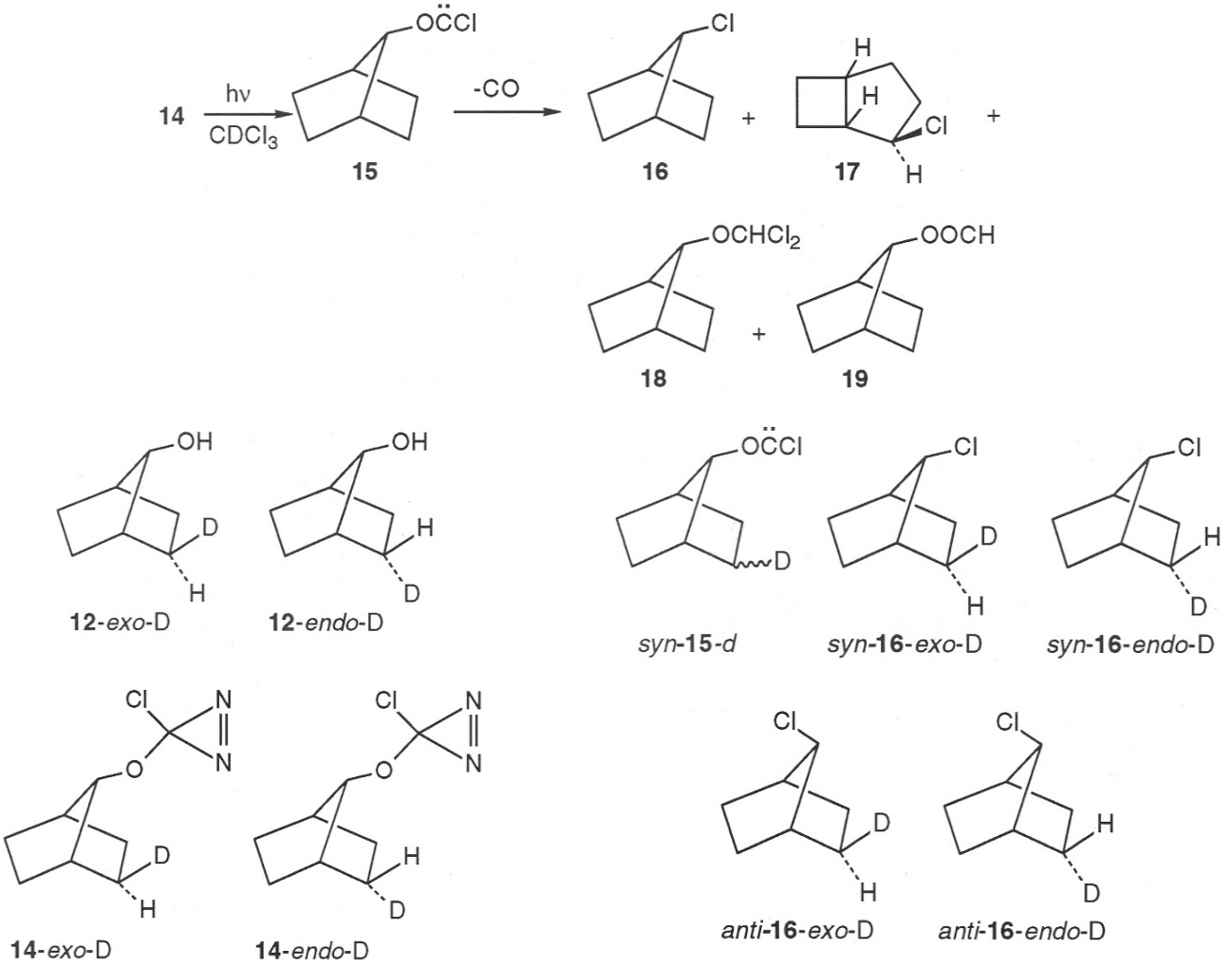


^{2}H NMR spectrum, the deuterons appear as singlets at δ 1.78 (*exo*-2-D) and δ 1.47 (*endo*-2-D) in a ratio of 1.5:1.

Alcohols **12**-*d* were converted to the deuterated diazirines **14**-*exo*-D (δ 1.22 for the ^{2}H in $CDCl_3$) and **14**-*endo*-D (δ 1.45), via the isouronium salts and NaOCl oxidation as above. Photolysis of the **14** isotopomers led, via carbene *syn*-**15**-*d*, to 68% of *syn*-**16**-*exo*-D and *syn*-**16**-*endo*-D (*retention* of configuration), together with *anti*-**16**-*exo*-D and *anti*-**16**-*endo*-D (*inversion*). The proton chemical shifts of **16** have been analyzed by Nash et al. (21*b*), who assign the C2-*exo*-H at δ 1.95, the C2-*endo*-H at δ 1.58, and the four C5 and C6 exo and endo protons at δ 1.29. We can therefore assign (23) the deuterium singlets that we observe in the ^{1}H-decoupled ^{2}H NMR spectrum of the reaction product mix-

© 2005 NRC Canada

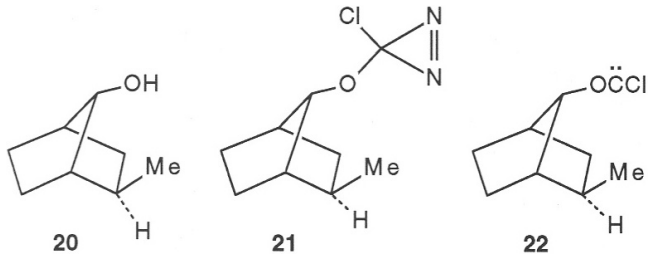
Scheme 3.



ture as *syn*-**16**-*exo*-D (δ 1.94), *syn*-**16**-endo-D (δ 1.59), and *anti*-**16**-*exo*-D plus *anti*-**16**-*endo*-D (both at δ 1.29). The syn/anti product ratio represents retention/inversion for the **15** → **16** conversion. From integration of the appropriate signals in the ^{2}H NMR spectrum, we find retention/inversion = 3.54:1. Therefore, the course of the **15** → **16** fragmentation in $CDCl_3$ is 78% (total) retention, or 56% *net* retention, i.e., there is 22% of inversion.

When D-labeled **15** fragmented in the presence of 3 mol/L *n*-$Bu_4N^+Cl^-$ in $CDCl_3$, ^{2}H NMR analysis gave the retention/inversion ratio of labeled **16** as 2.2 ± 0.3 (two experiments), corresponding to 69% (total) retention or 38% net retention. The small decrease in retention (increase in inversion) of the **15** → **16** conversion in the presence of added chloride may represent a minor incursion of a S_N2 component (chloride attack on carbene **15**) in competition with the normative "unimolecular" fragmentation of the carbene. An inverting attack of azide ion on 1-methyl-7-norbornyl triflate is known (6), as are S_N2 reactions of chloride ion and *primary* alkoxychlorocarbenes (24).

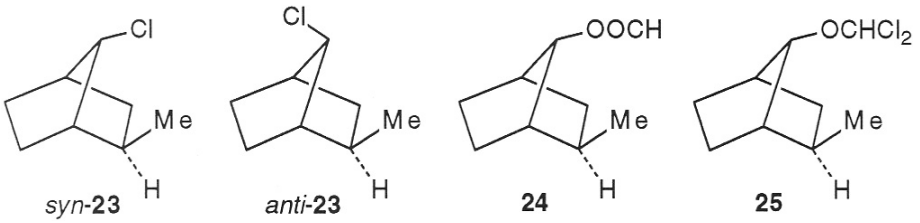
Further stereochemical information on the fragmentation reaction was provided by a methyl labeled analogue of carbene **15**. Thus, *syn*-2-*exo*-methyl-7-norbornanol (**20**) was obtained from the reaction of *exo*-norbornene oxide and methylmagnesium bromide (25). The alcohol was purified by chromatography over silica gel with pentane–ether (4:1), and characterized by ^{1}H and ^{13}C NMR spectroscopy. In the ^{1}H NMR spectrum of **20**, the characteristic C4 bridgehead proton appeared at δ 1.91 (reported at δ 1.97 (25)). Conversion of **20** to the isouronium methanesulfonate (19), followed by oxidation with NaOCl (20) gave diazirine **21** (IR: 1541 cm^{-1}; UV λ_{max}: 349, 366 nm in pentane). The diazirine was also characterized by NMR, as described in the Experimental.

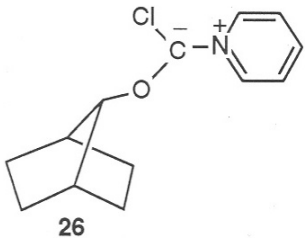


Photolysis (λ > 320 nm) of **21** in $CDCl_3$ gave carbene **22**, which afforded the products shown in Scheme 4. The main products (two runs) were 38% to 39% of *syn*-7-chloro-*exo*-2-methylnorbornane (*syn*-**23**), 38% to 39% of *anti*-7-chloro-

© 2005 NRC Canada

Scheme 4.





exo-2-methylnorborane (*anti*-**23**), 0.8%–1.5% of formate **24**, and 14%–18% of dichloride **25**. There was also 2% to 3% of a product tentatively identified as a methylbicyclo[3.2.0]heptyl chloride, an analogue of **17**.

The identities of **24** and **25** follow from the NMR of their signature protons: for **24**, H7 at δ 4.85 and OOC*H* at δ 8.05; for **25**, H7 at δ 4.30 and C*H*Cl_2 at δ 7.20. Additionally, the yield of dichloride **25** is reduced from 14%–18% to just traces when the fragmentation of **22** occurs in the presence of pyridine.

The identities of key products *syn*-**23** and *anti*-**23** were established by GC–MS (M^+ and $(M + 2)^+$ at *m/e* 144 and 146, respectively), as well as by ^1H and ^{13}C NMR, including various correlation experiments. In particular, the C7 protons of *syn*-**23** and *anti*-**23** appear at δ 3.82 and 4.02, respectively. NMR integration indicates that the two isomers were formed in approximately equal quantities. Capillary GC analysis gave an *anti*/*syn* ratio of 1.1, which increased to 2.4 when the fragmentation of **22** occurred in the presence of 3 mol/L tetrabutylammonium chloride (TBACl).

syn-**23** represents the fragmentation of carbene **22** with retention, while *anti*-**23** indicates inversion. The carbene fragments to chloride **23** with a roughly *equal* balance of retention and inversion. In comparison to the D-labeled carbene **15**, the inversion pathway here has significantly increased: retention/inversion is 3.5:1 for **15**, but 1:1.1 for **22**. The *syn*-*exo*-2-methyl group of **22** appears to hinder chloride return with retention to yield *syn*-**23**, relative to chloride return with inversion to give *anti*-**23**. Computational studies (below) provide a surprising mechanistic rationale.

Kinetics of fragmentation

Absolute rate constants for fragmentations of carbenes **15** and **22** were determined by laser flash photolysis (LFP) (24, 26) using the pyridine ylide method (27). LFP at 351 nm and 25 °C of diazirine **14** in 1,2-dichloroethane (DCE, $A_{351} = 2.1$) in the presence of pyridine produced an absorption assigned to ylide **26** at 424 nm. A correlation of the apparent rate constants for ylide formation (k_{obs}, 1.2–2.8 × 10^6 s^{-1}) vs. pyridine concentration (0.8–7.2 mol/L) was linear (nine points, $r = 0.995$) with a slope of 2.38 × 10^5 $(mol/L)^{-1}$ s^{-1}, equivalent to the rate constant for ylide formation (k_y). The *Y* intercept of 9.91 × 10^5 s^{-1} approximates k_{frag} for the fragmentation of carbene **15** to chlorides **16** and **17**, which constitute ~70% of the reaction products (see Scheme 3). A duplicate kinetics experiment gave similar results, leading to mean values for the rate constants ($k_y = 2.4 \pm 0.3 \times 10^5$ $(mol/L)^{-1}$ s^{-1} and $k_{frag} = 1.02 \pm 0.02 \times 10^6$ s^{-1}).

The latter rate constant is surprisingly high for the fragmentation of ROCCl where R is a *sec*-alkyl group; for example, k_{frag} for cyclopentyl-OCCl is 8.7 × 10^4 s^{-1} (12) and for cyclohexyl-OCCl it is 3.3 × 10^4 s^{-1} (14). Given the substantial kinetic difficulty in the solvolytic formation of the 7-norbornyl cation (2) and the instability of the cation (1, 4), the fast fragmentation of carbene **15** suggests that the transition state is early, and avoids the imposition of much positive charge on C7 of the norbornyl moiety. These ideas will be elaborated in the following.

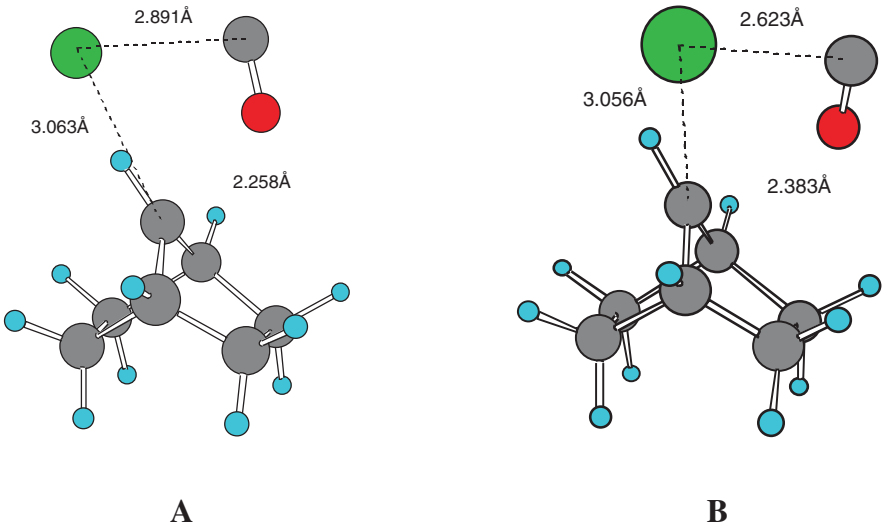
We also studied the LFP of diazirine **14** in the presence of added TBACl. LFP of **14** in DCE with a constant concentration of pyridine and varying quantities (0.008–0.8 mol/L) of TBACl gave a linear correlation (eight points, $r = 0.992$) of k_{obs} for the formation of ylide **26** as a function of chloride concentration. The slope of this correlation can be taken as the second-order rate constant (k_2) for the quenching (or fragmentation) of carbene **15** induced by chloride ion (24, 27), although some of the observed rate enhancement may be due to a "simple" salt effect (also seen with TBA perchlorate). The observed k_2 for carbene **15** (2.4 × 10^6 $(mol/L)^{-1}$ s^{-1}) is very similar to the corresponding rate constant for the reaction of chloride with benzyloxychlorocarbene ($PhCH_2OCCl$), $k_2 = 2.2 \times 10^6$ $(mol/L)^{-1}$ s^{-1} in acetonitrile (24). We conclude that a minor S_N2 decomposition pathway operates for carbene **15** in the presence of an added nucelophile. This agrees with the modest increase in stereochemical inversion for the **15**-*d* → **16**-*d*, conversion with added TBACl (see the previous section).

The fragmentation of **15** was also studied as a function of temperature from –41 to 30 °C. A very good correlation of $\ln k_{frag}$ vs. $1/T$ was obtained (eight points, $r = 0.996$), from which E_a = 3.5 kcal/mol and $A = 4.7 \times 10^8$ s^{-1} ($\Delta S^* = -20$ eu). The low activation energy and strongly negative entropy of activation are fairly typical of ROCCl fragmentations. For example, 1-bicyclo[2.2.2]octyloxychlorocarbene in DCE fragments with E_a = 4.4 kcal/mol and $A = 2.8 \times 10^8$ s^{-1} ($\Delta S^* = -22$ eu) (28).

Finally, we examined the kinetics of fragmentation of carbene **22** using the same methodology applied to carbene **15**. For **22**, $k_{frag} = 7.0 \pm 0.1 \times 10^5$ s^{-1} in DCE, with E_a = 4.2 kcal/mol and $A = 1.8 \times 10^9$ s^{-1} ($\Delta S^* = -18$ eu). The fragmentation of **22** is kinetically comparable to that of carbene

© 2005 NRC Canada

Fig. 2. B3LYP/6-31G(d) transition states for the (in vacuo) fragmentation of carbene **15** to chloride **16**. TS leading to **16** with inversion (**A**), TS leading to **16** with retention **(B**).



15, i.e., the *syn-exo*-2-methyl group of **22** does not induce a major kinetic perturbation.

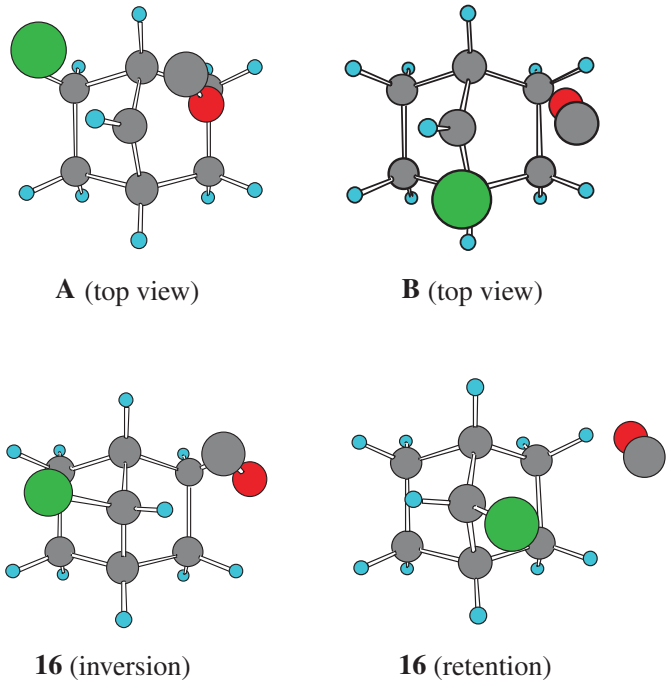
Computational studies

We studied the fragmentation of carbene **15** with DFT methodology. All structures were fully optimized by analytical gradient methods using the GAUSSIAN 98 and GAUSSIAN 03 suites (29*a*), as well as density functional calculations at the 6-31G(d) level, with the exchange potentials of Becke and co-workers (29*a*, 29*b*) and the correlation functional of Lee and co-workers (29*a*, 29*c*).

For the fragmentation of **15** to 7-chloronorbornane (**16**), we located not one, but *two* transition states (cf. Fig. 2, structures **A** and **B**). Transition state **A** (TS **A**) leads to chloride **16** with inversion, whereas TS **B** affords **16** with retention. Each TS was subjected to intrinsic reaction coordinate (IRC) calculations, which verified that they proceeded to chloride **16** in the forward direction and returned to carbene **15** in the reverse direction.

In Fig. 3, we present top views of TS **A** and **B** in which the contrasting skeletal symmetry and geometric relationships of the Cl and C7 atoms are apparent. The inverted and retained IRC end points (chloride **16**) are also illustrated. TS **A** and **B** are energetically comparable: in vacuum, their computed $\Delta H^{\ddagger}$ values (correlated for zero-point energy differences and thermal effects at 298.15 K) are 22.2 (inversion) and 23.3 (retention) kcal/mol. In simulated DCE, using the polarized contiuum model (PCM) (29*a*) and single-point calculations, the $\Delta H^{\ddagger}$ values decrease to 7.3 (inversion) and 7.9 (retention) kcal/mol. The key conclusion is that fragmentation of **15** to **16** should occur with a nearly equal probability of retention and inversion, in agreement with the experimental results for D-labeled **15**, which affords **16**-*d* with a retention/inversion ratio of 3.5:1. A reviewer suggested that the transition state regions for the conversions of **15** to **16** via TS **A** or **B** may be rather broad and flat so that the chloride might explore these regions as dictated by the transition-state geometries, leading to retention or inversion in least motion processes.

Fig. 3. Top views of TS **A** and **B** of Fig. 1 and end points of the IRC calculations on **A** and **B**, which afford chloride **16** with inversion or retention, respectively, relative to carbene **15**.



It is important to note that TS **A** and **B** *do not* evolve to ion pair minima; the lack of complete retention in the **15** → **16** conversion cannot be attributed to stereochemical randomization within an ion pair. When more stable cations can be formed, such as the 1-adamantyl or 3-homoadamantyl cations, IRC calculations indicate that the TS for ROCCl fragmentation gives [R^+Cl^-] ion pairs (10). However, this is not the case for TS **A** or **B**, which approximate those of a S_Ni reaction. A related TS was computationally indicated in the fragmentation of 1-norbornyloxychlorocarbene to 1-norbornyl chloride, where the high-energy 1-norbornyl cation was largely bypassed (10). S_Ni-like TS for the fragmen-

© 2005 NRC Canada

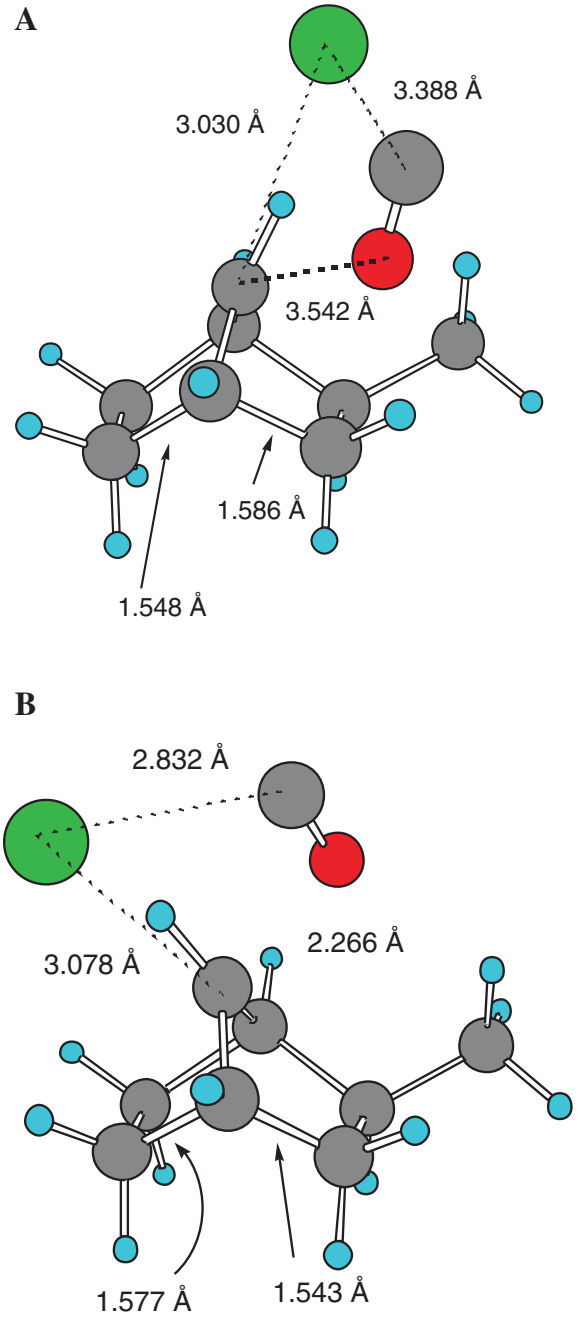
tation of certain secondary ROCCl have been suggested by Jones and co-workers (30), while Schleyer and co-workers have presented experimental and computational evidence for related processes in the fragmentation of alkyl chlorosulfites, a reaction analogous to the fragmentation of alkoxychlorocarbenes (31).

Previously, we suggested that the unexpectedly rapid fragmentation of carbene **15** implies that the TS is "early" and avoids the imposition of significant positive charge on C7. The computational studies support these ideas. Differences between computed ChelpG charges for TS **A** and **B** reveal that there are significant *decreases* in positive charge on C7 in both cases relatve to carbene **15**: –0.30 and –0.27, respectively. These changes are counterbalanced by corresponding increases in negative charge on the chlorine: 0.49 and 0.44, respectively. We interpret these findings to indicate that some positive charge leaks into the carbon framework as the transition states are generated. Related fragmentations that we have studied (e.g., cyclohexyl-OCCl) behave similarly. We conclude that the transition states are relatively early, i.e., between carbene **15** and the 7-norbornyl cation. Structural analyses (see the following) are also consistent with this conclusion.

In Fig. 1, we present the computed Cl—C2 (C3—C4) and C2—C7 (C3—C7) distances for carbene **15**, TS **A**, TS **B**, and the 7-norbornyl cation. Following the C2—C7 distance from carbene **15** (2.348 Å) to TS **A** (2.189 Å) or TS **B** (2.203 Å) and finally to cation **3** (1.765 Å), we observe that the TSs are indeed relatively early; the approach of C7 to C2, which enables the delocalization of positive change, covers only 0.14–0.16 Å in the TS compared to 0.58 Å in the fully developed cation. A similar conclusion emerges from consideration of the Cl—C2 distance, which lengthens as positive charge is delocalized. The expansion is 0.031 or 0.029 Å as carbene **15** goes to TS **A** or TS **B**, respectively, whereas the C1—C2 expansion between carbene **15** and cation **3** is 0.521 Å, about 17 times greater. The computed structure of cation **3** is "between" the 7-norbornyl cation and the (rearranged) 2-bicyclo[3.2.0]heptyl cation. The early TS **A** and **B** are consistent with the low activation energy observed (and computed) for the fragmentation, while the observed negative entropy of activation accords with the cyclic nature of the S_Ni-like TS (see the following).

We turn now to the *syn-exo*-2-methyl substituted carbene **22**. Computational studies at the B3LYP/G-31G(d) level reveal that the methyl group exerts a most subtle effect. For the fragmentation of **22** to chloride **23** we again locate two TSs; these appear in Fig. 4. IRC analysis of TS **B** in the forward direction reveals the formation of *anti*-**23** (i.e., **22** → **23** with inversion), whereas IRC analysis in the reverse direction confirms that TS **B** returns to carbene **22**. The behavior of TS **A**, however, is remarkable: IRC analysis in one direction leads to *anti*-**23** (inversion), while the opposite direction leads not to carbene **22**, but to *syn*-**23** (retention)! Thus, TS **A** bifurcates, leading to *both* products (32). Moreover, the computed activation enthalpy of TS **A** is lower than that of TS **B**, with ΔH^***A** = 18.9 (vacuum) or 3.0 (DCE) vs. ΔH^***B** = 20.8 (vacuum) or 6.0 (DCE), with all values in kcal/mol. Thus, in solution, TS **A** might be expected to dominate and to provide *syn*-**23** and *anti*-**23** in comparable quantities, as is indeed observed. That is, the "racemization"

Fig. 4. B3LYP/6-31G(d) computed transition states for the fragmentations of carbene **22** to *syn*-**23** and *anti*-**23** (see text for discussion).



observed in the fragmentation of carbene **22** to *syn*- and *anti*-**23** is attributable to bifurcation from a S_Ni-like TS (**A**). As in the fragmentation of carbene **15**, ion-pair minima are not detected and presumably cannot account for the inversion component of the reaction.

One caveat: the existence of TS **A** also suggests (32) that there should be a higher, as yet undetected, TS that leads in the forward direction to TS **A** and the reverse direction back to carbene **22**. We do not know the energy of this TS, but given that the experimental activation energies for the fragmentations of carbenes **15** and **22** are comparable at 3.5–

© 2005 NRC Canada

4.2 kcal/mol, ΔH^* for the unknown TS is probably between 4 and 6 kcal/mol (ΔH^* for TS **B** of Fig. 4).

Conclusion

7-Norbornyloxychlorocarbene (**15**) fragments mainly to 7-norbornyl chloride (**16**). An analog of **15** (*syn*-**15**-*d*), labeled with deuterium at C2, fragments to labeled chloride **16** with 78% retention and 22% inversion. When the deuterium label is replaced by a *syn-exo*-2-methyl group, the resulting carbene **22** fragments to *syn*- and *anti*-7-chloro-*exo*-2-methylnorbornane in a ratio of 1:1.1, i.e., with 48% retention and 52% inversion. Computational studies of carbenes **15** and **22** indicate that their fragmentation reactions proceed via S_Ni-like transition states rather than ion pairs. Loss of sterospecificity in the carbene to chloride transformations is due to competition between energetically similar S_Ni-like transition states, which undergo fragmentation with either retention or inversion.

Experimental

General

Pyridine (certified A.C.S. grade) was refluxed over CaH_2, distilled, and stored over 5 Å molecular sieves. Dichloroethane and pentane (HPLC grade) were stored over 5 Å molecular sieves and then used directly.

7-Norbornyloxyuronium methanesulfonate (13)

7-Norbornanol (**12**, Scheme 2), prepared by literature methods (16–18), was converted to the title compound **13** by reaction with cyanamide and methanesulfonic acid according to a literature procedure (19). The desired isouronium salt was obtained as an oil admixed with urea. ^{1}H NMR (400 MHz, DMSO-d_6) δ: 8.55 (s, 4H), 6.65 (br s, urea), 4.70 (s, 1H), 2.47 (s, 3H), 2.23 (s, 2H), 1.07–1.76 (m s, 8H). ^{13}C NMR (100 MHz, DMSO) δ: 161.8 (urea), 161.5, 86.2, 39.8, 38.2, 26.8, 26.5.

3-(7-Norbornyloxy)-3-chlorodiazirine (14)

Isuronium salt **13** was oxidized to diazirine **14** with NaOCl according to Graham's method (20): 1.0 g (4.0 mmol) of **13**, 5.0 g of LiCl in 50 mL of DMSO, and 50 mL of pentane were cooled at 20 °C and treated with 200 mL of 12% aq. NaOCl, saturated with NaCl, added in portions with vigorous shaking. Shaking was continued for 10 min at 15 °C after addition was complete. The reaction mixture was diluted with 100 mL of pentane, the aqueous phase was separated, the pentane phase was washed with 2 × 50 mL of cold brine, and dried over $CaCl_2$ at 0 °C. Diazirine **14** was purified by flash chromatography over silica gel eluted with pentane. The pentane eluate was concentrated by rotary evaporation to give 0.33 g (55%) of diazirine **14**. UV (λ_{max}, pentane, nm): 349, 366. IR (film, cm^{-1}): 1541. ^{1}H NMR (400 MHz, $CDCl_3$) δ: 4.26 (s, 1H), 2.24 (s, 2H), 1.58 (m, 4H), 1.22 (d, J = 7.6 Hz, 4H). ^{13}C NMR (100 MHz, $CDCl_3$) δ: 85.6, 70.9, 38.6, 26.6, 26.0.

7-Norbornanol (*syn*-2-*exo*-D and *syn*-2-*endo*-D mixture)

2-*exo*-Bromo-7-*syn*-hydroxynorbornane (**17**) (24.4 g, 0.13 mol) was refluxed overnight in 200 mL of EtOD with a Zn–Cu couple prepared from 35.0 g (0.55 mol) of Zn dust (33). The cooled reaction mixture was diluted with 100 mL of D_2O and stirred at 25 °C for 2 h. The mixture was concentrated by rotary evaporation, diluted with 200 mL of water, and extracted with 4 × 100 mL of CH_2Cl_2. The combined extracts were dried over $MgSO_4$, and products **12**-*d* were purified by chromatography over silica gel, with elution by pentane–ether (2:1), to give 9.2 g (62%) of solid, mp 125–127 °C. ^{1}H NMR (400 MHz, $CDCl_3$) δ: 3.90 (s, 1H), 2.96 (s, 1H, OH), 1.88 (m, 2H), 1.78, 1.49 (m, 3H), 1.20, 1.10 (m, 4H). ^{2}H NMR (61.4 MHz, $CDCl_3$) δ: 1.78 (*exo*-2-D), 1.47 (*endo*-2-D). ^{13}C NMR (100 MHz, $CDCl_3$) δ: 79.5 (C7), 40.2, 40.1 (Cl, C4), 26.8, 26.6 (C3, C5, C6), 26.5 (t, $J_{D\text{-}C}$ = 13.5 Hz, C2).

3-(7-Norbornyloxy)-3-chlorodiazirine (*syn*-2-*exo*-D and *syn*-2-*endo*-D mixture)

The D-labeled 7-norbornanol was converted to diazirine **14** as described previously for unlabeled 7-norbornanol. ^{1}H NMR (400 MHz, $CDCl_3$) δ: 4.26 (s, 1H), 2.25 (m, 2H), 1.58 (m, 3H), 1.23 (m, 4H). ^{2}H NMR (61.4 MHz, $CDCl_3$) δ: 1.45 (*endo*-2-D), 1.22 (*exo*-2-D). ^{13}C NMR (100 MHz, $CDCl_3$) δ: 85.6 (C7), 70.9 (quat. C), 38.6, 38.5 (C1, C4), 26.6, 26.0 (C3, C5, C6), 26.5 (t, $J_{D\text{-}C}$ = 12.2 Hz, C2).

2-*exo*-Methyl-*syn*-7-hydroxynorbornane (20)

This material was prepared in 21% yield as a colorless oil by the reaction of methylmagnesium bromide and *exo*-norbornene oxide (25). ^{1}H NMR (400 MHz, $CDCl_3$) δ: 3.95 (s, 1H), 2.00 (s, 1H, OH), 1.91 (s, 1H), 1.70 (d, J = 2.4 Hz, 1H), 1.63–1.08 (m, 7H), 1.11 (d, J = 6.8 Hz, 3H). ^{13}C NMR (100 MHz, $CDCl_3$) δ: 80.7, 46.4, 41.5, 37.0, 36.4, 27.8, 25.6, 22.4.

3-(*syn*-2-*exo*-Methyl-7-norbornyloxy)-3-chlorodiazirine (21)

2-Methyl-7-norbornanol (**20**) was converted to the isouronium salt (admixed with urea) by reaction with cyanamide and methansulfonic acid (19), and the oily isouronium salt was oxidized to diazirine **21** by Graham's procedure (20) as described previously for diazirine **14**. UV (λ_{max}, pentane, nm): 349, 366. IR (film, cm^{-1}): 1541. ^{1}H NMR (300 MHz, $CDCl_3$) δ: 4.23 (s, 1H), 2.34 (s, 1H), 1.91, (s, 1H), 1.61–0.85 (m, 7H), 0.87 (d, J = 6.8 Hz, 3H). ^{13}C NMR (75 MHz, $CDCl_3$) δ: 88.1, 66.0, 44.8, 39.5, 36.9, 36.4, 27.0, 25.0, 21.6.

Products

The characteristic resonances in the NMR spectra of products **16**–**19**, the **16**-*d* isotopomers, *syn*-**23**, *anti*-**23**, **24**, and **25** are described in the Results and discussion.

Photolysis

About 200 mg of prepared diazirines **14**, **14**-*d*, or **21** in 2 mL of $CDCl_3$ was placed in a small screw-cap vial or in a NMR tube and irradiated for 1 h with a focused Oriel UV lamp (with a uranium glass filter, λ > 320 nm) or with a Rayonet apparatus housing 350 nm lamps. The resulting NMR analyses are described in the Results and discussion section.

© 2005 NRC Canada

Acknowledgments

We are grateful to Dr. Seho Kim for assistance with various NMR experiments. We are grateful to the National Science Foundation for financial support and to the National Center for Supercomputing Applications for allocation of computer time on the IBM P Series 690 (Grant CHE 030060).

References

1. D.E. Sunko, H. Vancik, Z. Mihalic, V.J. Shiner, Jr., and F.P. Wiglis. J. Org. Chem. **59**, 7051 (1994), and refs. cited therein.
2. S. Winstein, M. Shatavsky, C. Norton, and R.B. Woodward. J. Am. Chem. Soc. **77**, 4183 (1955).
3. D.E. Sunko, H. Vancik, V. Deljac, and M. Milun. J. Am. Chem. Soc. **105**, 5364 (1983).
4. R. Hoffmann, P.D. Mollere, and E. Heilbronner. J. Am. Chem. Soc. **95**, 4860 (1973).
5. (*a*) S. Winstein, F. Gadient, E.T. Stafford, and P.E. Klinedinst, Jr. J. Am. Chem. Soc. **80**, 5895 (1958); (*b*) F.B. Miles. J. Am. Chem. Soc. **90**, 1265 (1968).
6. W. Kirmse and J. Streu. J. Org. Chem. **50**, 4187 (1985).
7. S. Sieber, P.v.R. Schleyer, H. Vancik, M. Mesic, and D.E. Sunko. Angew. Chem. Int. Ed. Engl. **32**, 1604 (1993).
8. M. Mesic, D.E. Sunko, and H. Vancik. J. Chem. Soc. Perkin Trans. 2, 1135 (1994).
9. R.A. Moss. Acc. Chem. Res. **32**, 969 (1999).
10. R.A. Moss, F. Zheng, J.-M. Fedé, L.A. Johnson, and R.R. Sauers. J. Am. Chem. Soc. **126**, 12 421 (2004).
11. R.A. Moss, R.R. Sauers, F. Zheng, X. Fu, T. Bally, and A. Maltsev. J. Am. Chem. Soc. **126**, 8466 (2004).
12. R.A. Moss, F. Zheng, R.R. Sauers, and J.P. Toscano. J. Am. Chem. Soc. **123**, 8109 (2001).
13. R.A. Moss, Y. Ma, R.R. Sauers, and M. Madni. J. Org. Chem. **69**, 3628 (2004).
14. R.A. Moss, L.A. Johnson, M. Kacprzynski, and R.R. Sauers. J. Org. Chem. **68**, 5114 (2003).
15. R.A. Moss and X. Fu. Org. Lett. **6**, 981 (2004).
16. H.M. Walborsky and D.F. Loncrini. J. Am. Chem. Soc. **76**, 5396 (1954).
17. H.M. Walborsky and D.F. Loncrini. J. Org. Chem. **22**, 1117 (1957).
18. S. Winstein and M. Shatavsky. J. Am. Chem. Soc. **78**, 592 (1956).
19. R.A. Moss, G.M. Kaczmarczyk, and L.A. Johnson. Synth. Commun. **30**, 3233 (2000).
20. W.H. Graham. J. Am. Chem. Soc. **87**, 4396 (1965).
21. (*a*) E.A. Hill, R.J. Theissen, C.E. Cannon, R. Miller, R.B. Guthrie, and A.T. Chen. J. Org. Chem. **41**, 1191 (1976); (*b*) J.J. Nash, D.V. Carlson, A.M. Kasper, D.E. Love, K.D. Jordan, and H. Morrison. J. Am. Chem. Soc. **115**, 8969 (1993).
22. R.A. Moss, C.-S. Ge, and L. Maksimovic. J. Am. Chem. Soc. **118**, 9792 (1996).
23. I.C.P. Smith. *In* NMR of newly accessible nuclei. Vol. 2. *Edited by* P. Laszlo. Academic Press, New York. 1983. p. 2.
24. R.A. Moss, L.A. Johnson, D.C. Merrer, and G.E. Lee, Jr. J. Am. Chem. Soc. **121**, 5940 (1999).
25. T.J. Gerteisen and D.C. Kleinfelter. J. Org. Chem. **36**, 3255 (1971).
26. R.A. Moss, L.A. Johnson, S. Yan, J.P. Toscano, and B.M. Showalter. J. Am. Chem. Soc. **122**, 11 256 (2000).
27. J.E. Jackson, N. Soundararajan, M.S. Platz, and M.T.H. Liu. J. Am. Chem. Soc. **110**, 5595 (1988).
28. R.A. Moss, F. Zheng, J.-M. Fedé, Y. Ma, R.R. Sauers, J.P. Toscano, and B.M. Showalter. J. Am. Chem. Soc. **124**, 5258 (2002).
29. (*a*) M.J. Frisch, G.W. Trucks, H.B. Schlegel, G.E. Scuseria, M.A. Robb, J.R. Cheeseman, V.G. Zakrzewski, J.A. Montgomery, Jr., R.E. Stratmann, J.C. Burant, S. Dapprich, J.M. Millam, A.D. Daniels, K.N. Kudin, M.C. Strain, O. Farkas, J. Tomasi, V. Barone, M. Cossi, R. Cammi, B. Mennucci, C. Pommelli, C. Adamo, S. Clifford, J. Ochterski, G.A. Petersson, P.Y. Ayala, Q. Cui, K. Morokuma, D.K. Malick, A.D. Rabuck, K. Raghavachari, J.B. Foresman, J. Cioslowski, J.V. Ortiz, A.G. Baboul, B.B. Stefanov, G. Liu, A. Liashenko, P. Piskorz, I. Komaromi, R. Gomperts, R.L. Martin, D.J. Fox, T. Keith, M.A. Al-Laham, C.Y. Peng, A. Nanayakkara, M. Challacombe, P.M.W. Gill, B.G. Johnson, W. Chen, M.W. Wong, J.L. Andres, C. Gonzales, M. Head-Gordon, E.S. Repogle, and J.A. Pople. GAUSSIAN98. Revision A9 [computer program]. Gaussian, Inc., Pittsburgh, Penn. 1998; M.J. Frisch, G.W. Trucks, H.B. Schlegel, G.E. Scuseria, M.A. Robb, J.R. Cheeseman, J.A. Montgomery, Jr., T. Vreven, K.N. Kudin, J.C. Burant, J.M. Millam, S.S. Iyengar, J. Tomasi, V. Barone, B. Mennucci, M. Cossi, G. Scalmani, N. Rega, G.A. Petersson, H. Nakatsuji, M. Hada, M. Ehara, K. Toyota, R. Fukuda, J. Hasegawa, M. Ishida, T. Nakajima, Y. Honda, O. Kitao, H. Nakai, M. Klene, X. Li, J.E. Knox, H.P. Hratchian, J.B. Cross, C. Adamo, J. Jaramillo, R. Gomperts, R.E. Stratmann, O. Yazyev, A.J. Austin, R. Cammi, C. Pomelli, J.W. Ochterski, P.Y. Ayala, K. Morokuma, G.A. Voth, P. Salvador, J.J. Dannenberg, V.G. Zakrzewski, S. Dapprich, A.D. Daniels, M.C. Strain, O. Farkas, D.K. Malick, A.D. Rabuck, K. Raghavachari, J.B. Foresman, J.V. Ortiz, Q. Cui, A.G. Baboul, S. Clifford, J. Cioslowski, B.B. Stefanov, G. Liu, A. Liashenko, P. Piskorz, I. Komaromi, R.L. Martin, D.J. Fox, T. Keith, M.A. Al-Laham, C.Y. Peng, A. Nanayakkara, M. Challacombe, P.M.W. Gill, B. Johnson, W. Chen, M.W. Wong, C. Gonzalez, and J.A. Pople. GAUSSIAN03. Revision B.02 [computer program]. Gaussian, Inc., Pittsburgh, Penn. 2003. (*b*) A.D. Becke. J. Chem. Phys. **98**, 5648 (1993); (*c*) C. Lee, W. Yang, and R.G. Paar. Phys. Rev. B. **37**, 785 (1988).
30. I.R. Likhotvorik, M. Jones, Jr., A.G. Yurchenko, and P. Krasutsky. Teterahedron Lett. **30**, 5089 (1989).
31. (*a*) P.R. Schreiner, P.v.R. Schleyer, and R.K. Hill. J. Org. Chem. **58**, 2822 (1993); (*b*) P.R. Schreiner, P.v.R. Schleyer, and R.K. Hill. J. Org. Chem. **59**, 1849 (1994).
32. B.K. Carpenter. *In* Reactive intermediate chemistry. *Edited by* R.A. Moss, M.S. Platz, and M. Jones, Jr. Wiley, New York. 2004. p. 925*f*.
33. J.P. Schaefer and E.J. Corey. J. Org. Chem. **24**, 1825 (1959).

© 2005 NRC Canada

The structure, photochemical reactivity, and photophysical properties of adamantyl X-substituted aryl ethers and a comparison with the alkyl groups, methyl, *tert*-butyl, and allyl[1]

A.L. Pincock and J.A. Pincock

Abstract: The structure, photophysical properties, and photochemistry of the adamantyl aryl ethers **1** in both methanol and cyclohexane have been examined. UV absorption spectra, ^{13}C NMR chemical shifts, X-ray structures, and Gaussian calculations (B3LYP/6-31G(d)) indicate that these ethers adopt a 90° conformer in the ground state. In contrast, fluorescence spectra, excited singlet state lifetimes, and calculations (TDDFT) indicated a 0° conformer is preferred in the first excited singlet state S_1. Irradiation in either solvent results in the formation of adamantane and the corresponding phenol as the major products, both derived from radical intermediates generated by homolytic cleavage of the ether bond. The 4-cyano substituted ether **1j** was the only one to form the ion-derived product, 1-methoxyadamantane (16% yield), on irradiation in methanol. Rate constants of bond cleavage for these ethers from S_1 were estimated by two different methods by comparison with the unreactive anisoles **2**, but the effect of substituents was too small to determine structure–reactivity correlations. The temperature dependence of the quantum yields of the fluorescence of the unsubstituted, 4-methoxy and 4-cyano derivatives of **1** and **2** were also determined. These results indicated that the activated process for **1** was mainly bond cleavage for the 4-cyano substrate whereas for **2**, it was internal conversion and intersystem crossing.

Key words: aryl ether photochemistry, fluorescence, excited-state rate constants, excited-state temperature effects.

Résumé : On a étudié la structure, les propriétés photophysiques et la photochimie des oxydes d'adamantyle et d'aryles **1**, tant dans le méthanol que dans le cyclohexane. Les spectres d'absorption UV, les déplacements chimiques en RMN du ^{13}C, les structures obtenues par diffraction des rayons X et les calculs gaussiens (B3LPYP/6-31G(d)) indiquent que dans leur état fondement ces éthers adoptent un conformère à 90°. Par opposition, les spectres de fluorescence, les temps de vie de l'état singulet excité et les calculs (TDDFT) indiquent qu'un conformère à 0° est privilégié dans le premier état singulet excité, S_1. Les produits principaux d'une irradiation dans l'un ou l'autre des solvants sont l'adamantane et le phénol correspondant qui dérivent tous les deux d'intermédiaires radicalaires générés par un clivage homolytique de la liaison éther. L'irradiation dans le méthanol du dérivé **1j** portant un substituant 4-cyano est le seul à conduire à la formation du 1-méthoxyadamantane (rendement de 16 %), le produit dérivé de l'ion. On a utilisé deux méthodes différentes pour évaluer les constantes de vitesse de clivage de la liaison de ces éthers à partir de S_1 par comparaison avec des anisoles non réactifs (**2**); l'effet des substituants est toutefois trop faible pour déterminer des corrélations structure–activité. On a aussi établi la relation entre la température et le rendement quantique de fluorescence des dérivés des composés **1** et **2**, non substitués ou portant des substituants 4-méthoxy ou 4-cyano. Ces résultats indiquent que le processus activé pour le composé **1** est le clivage de la liaison pour le substrat 4-cyano alors que pour le composé **2** il s'agit de la conversion interne et d'un passage intersystème.

Mots clés : photochimie d'éthers aromatiques, fluorescence, constantes de vitesse d'états excités, effets de température sur l'état excité.

[Traduit par la Rédaction]

Introduction

The effect that substituents (X) on aromatic rings (Ar) have on the quantum yields and rate constants of bond cleavage reactions from photochemically generated excited singlet states of substrates of the general class ArY–Z, where the Y—Z bond is the reactive one, continue to attract interest. The objective is to develop excited state structure–reactivity relationships, like the Hammett equation, that are well-established for ground-state reactions. Related to this

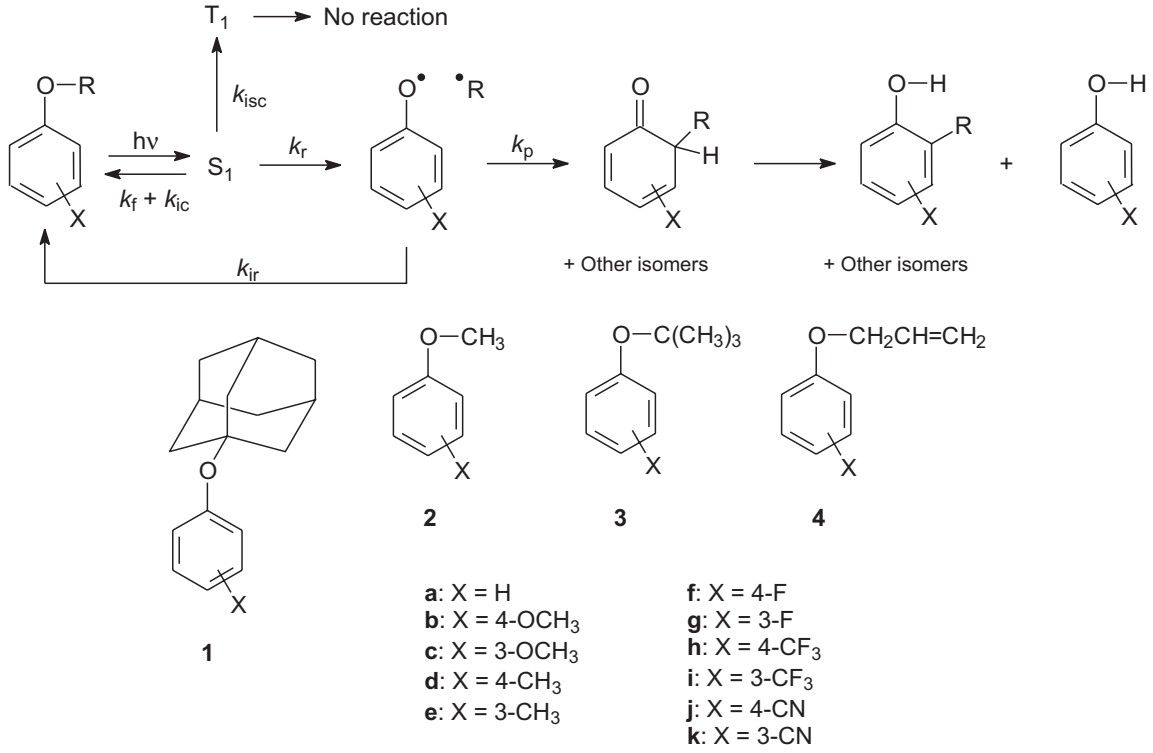
Received 9 December 2004. Published on the NRC Research Press Web site at http://canjchem.nrc.ca on 12 October 2005.

A.L. Pincock and J.A. Pincock.[2] Department of Chemistry, Dalhousie University, Halifax, NS B3H 4J3, Canada.

[1]This article is part of a Special Issue dedicated to organic reaction mechanisms.
[2]Corresponding author (e-mail: james.pincock@dal.ca).

 doi: 10.1139/V05-117 © 2005 NRC Canada

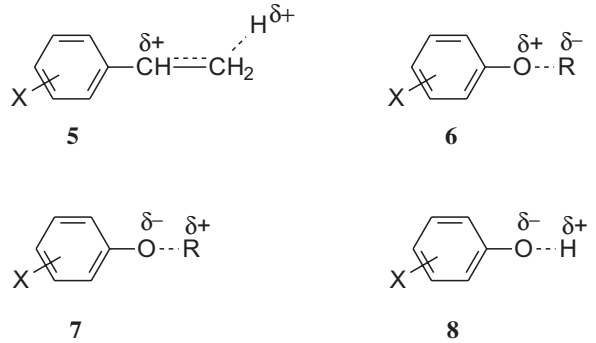
Scheme 1. Mechanism and products formed from the homolytic cleavage of alkyl aryl ethers and rate constants of reaction for S_1.



goal has been one of understanding, in the excited-state cases, the competition between the formation of the products derived from radical pairs (from homolytic cleavage of the Y—Z bond) and ion pairs (from heterolytic cleavage of the Y—Z or from rapid, exergonic redox electron transfer in the first formed radical pair). A general review of the mechanistic principles involved and a survey of the observed reactivity of the Z groups for arylmethyl cases (Y = CH_2) have been published (1).

We now summarize results for four series of the class of compounds ArO-C (**1**–**4**), i.e., phenolic ethers where Y = O and Z = C. New results will be given for the adamantyl aryl ethers **1**, in comparison with the anisoles **2**. Previously, we have reported on the photochemistry and photophysics of the *tert*-butyl (**3**) (2) and allyl ethers (**4**) (3). For these latter two cases, the products of photolysis in either methanol or cyclohexane were, in general, those expected from homolytic cleavage of the carbon–oxygen bond to form a radical pair followed by in-cage coupling (photo-Fries for **3**, photo-Claisen for **4**) or disproportionation (Scheme 1). For both, the reactions were shown to occur from the excited singlet state (S_1) by selective triplet quenching studies.

Rate constants k_r for the reaction from the excited singlet state for the *tert*-butyl compounds **3** were determined by the classic quantum yield (Φ_r) of the reaction method (eq. [1]) (2). The rate constants for S_1 of the reaction (k_r), fluorescence (k_f), internal conversion (k_{ic}), and intersystem crossing (k_{isc}) are shown in Scheme 1. The sum of these is k_t, the reciprocal of τ_s, the excited singlet state lifetime. Measurement of Φ_r by the disappearance of starting material and τ_s by fluorescence decay gives k_r. The rate constants obtained in this way gave a reasonable correlation with $\sigma^{h\nu}$ (4) and $\rho = -0.77$ ($r = 0.975$) for seven of the 10 compounds of set **3** studied where $\sigma^{h\nu}$ values were available. This correlation was surprising because the $\sigma^{h\nu}$ scale was developed from results for the photoprotonation of styrenes and phenylacetylenes, reactions that result in positive charge increases at the benzylic carbon in the rate-determining transition state, **5** for styrenes. A similar transition state (**6**) for the photo-Fries reaction of the *tert*-butyl ethers **3** seems less likely than one of opposite polarity (**7**). However, a very poor (nonexistent) correlation of the rate constants for **3** with the values of σ^{ex} (5–7), which are derived from the excited state pK_as of phenols **8**, was obtained.

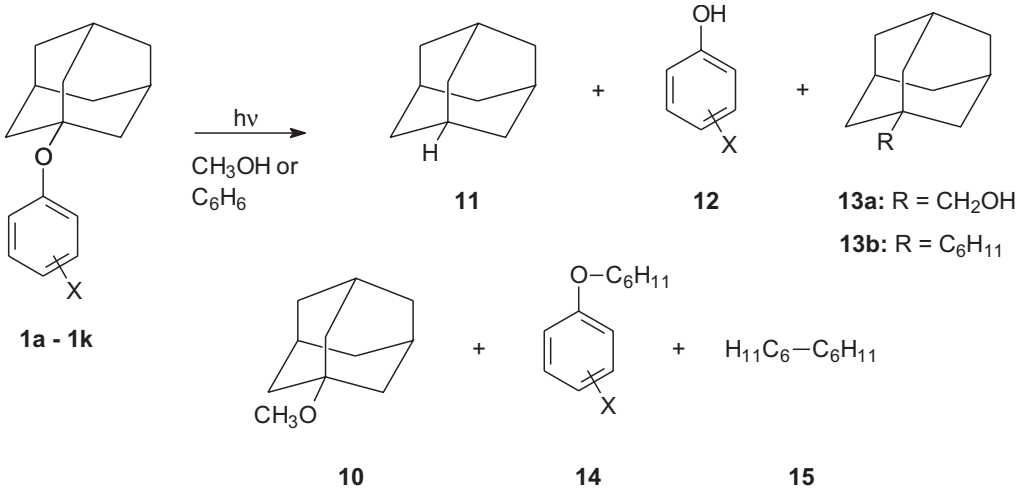


$$[1] \qquad \Phi_r = \frac{k_r}{k_f + k_{ic} + k_{isc} + k_r} = \frac{k_r}{k_t} = k_r \tau_s$$

While studying the *tert*-butyl ethers **3** (2), we also examined the 4-cyano compound **1j** from the adamantyl derivatives. An interesting result was that on photolysis of **1j** in methanol, the ion-derived product 1-methoxyadamantane was obtained in 16% yield. This compound was synthesized

© 2005 NRC Canada

Scheme 2. Products of the photolysis of adamantyl ethers **1** in methanol and cyclohexane.



by reaction of the lithium salt of 1-adamantanol with 4-fluorobenzonitrile (8), a nucleophilic aromatic substitution reaction that relies on the electron-withdrawing nitrile group in the para position. This procedure was unsuccessful for 3-fluorobenzonitrile. Therefore, the other substituted derivatives of **1** were not previously studied.

We now report on the synthesis, photochemistry, photophysical properties, and excited-state rate constants for the complete set of the adamantyl ethers **1**. These compounds have an advantage that the fate of the non-aryl fragment of the ether cleavage reaction can be easily observed. This was not so for the very volatile fragments ($CH_3OC(CH_3)_3$, $CH_3OCH_2CH{=}CH_2$, etc.) expected from sets **3** and **4**.

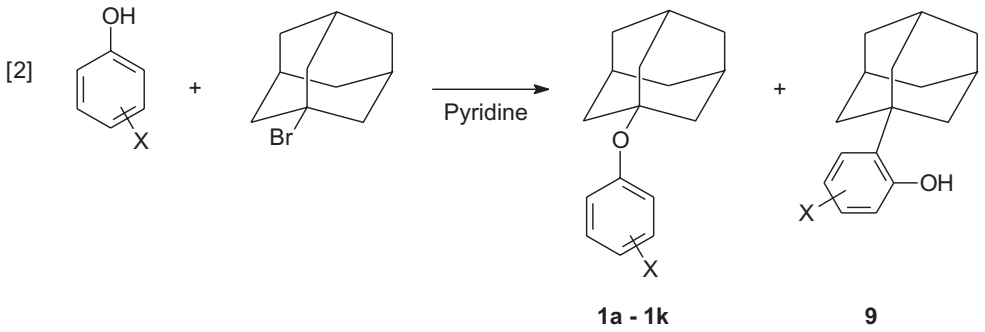
Results and discussion

Synthesis of 1-adamantyl aryl ethers (1a–1k)

The ethers were synthesized by reaction of 1-bromoadamantane (by heating in pyridine) with the corresponding substituted phenols according to a method described previously (9) (eq. [2]). The reaction mixtures were not homogeneous. The reactions were usually monitored by GC-FID until the 1-bromoadamantane (the limiting reagent) had disappeared. The crude product always contained varying amounts of the isomeric (GC–MS) 1-adamantylphenol derivatives **9**, which were not characterized. However, because these isomers were possible products in the photochemistry of the ethers **1**, their GC retention times were useful. They could easily be removed by flash chromatography on silica gel and the ethers purified by crystallization. The yields after purification ranged from 20% to 35%. Characterization data are given in the Experimental section; ^{13}C NMR data, along with those of sets **2**, **3**, and **4**, which will be discussed in the following, are given in Table S1 (Supporting information).[3]

Photochemistry of 1-adamantyl aryl ethers 4a–4k in methanol and cyclohexane

The ethers **1** were photolyzed in either methanol or cyclohexane with 254 nm lamps in a Rayonet reactor at 25 °C. The reactions were reasonably efficient with little dependence on the substituent. For instance, for approximately 100 mg samples, 83% of the unsubstituted compound **1a** and 80% of the 4-methoxy compound **1b** in 100 mL of methanol had reacted after 30 min. The reactions were a factor of two to three times slower in cyclohexane. In both solvents in all cases, except for the 4-cyano compound **1j** in methanol, the products were those expected from the formation of radicals by homolytic cleavage of the C—O bond (Scheme 2). As reported previously (2), 16% of the methyl ether **10** was formed from **1j** in methanol indicating a minor intervention of a pathway involving ion pairs. In agreement with this observation, 4-cyanophenoxide has been used as a leaving group for the generation of diphenylmethyl cations (observable by nanosecond LFP) from diphenylmethyl ethers (10),



[3] Supplementary data for this article are available on the Web site or may be purchased from the Depository of Unpublished Data, Document Delivery, CISTI, National Research Council Canada, Ottawa, ON K1A 0S2, Canada. DUD 4020.

© 2005 NRC Canada

and in the pioneering study by Zimmerman and Somasekhara (11) on photochemically generated triphenylmethyl cations.

The major product from the adamantyl fragment of the ethers **1** for all substrates in both solvents was adamantane **11**, derived from the 1-adamantyl radical and accounting for 70%–90% of the mass balance. This is reasonable on the basis of the fact that hydrogen atom abstraction by the 1-adamantyl radical from both methanol and cyclohexane is somewhat more favourable than by the *tert*-butyl radical (C–H BDE = 99, 96, 99, and 96 kcal/mol for 1-adamantane, methanol, cyclohexane, and 2-methylpropane, respectively) (1 cal = 4.184 J) (12). The major product from the aryl fragment was the corresponding phenol **12**, but these gave very broad and tailing peaks in the GC traces that could not be reliably quantified. Photo-Fries products (GC–MS, 15% yield overall, presumably 2- and 4-(1-adamantyl)phenol) were only observed for **1a** in methanol. Low yields of products **13a**, **13b**, **14**, and **15** (Scheme 2) were also formed from the solvent-derived radicals.

Geometry of aryl ethers 1–4 in the ground state

The geometry and rotational barriers for the methoxy group of anisole have been extensively studied by both experimental and computational methods. Two limiting structures have been considered: **16** with a C(H_3)-O-C1-C2 dihedral angle of $\Phi = 0°$ and **17** with the same angle equal to 90°. For **16**, an sp^2 hybridization model predicts conjugative overlap between the oxygen centered lone pair in a π orbital and the π system of the aromatic ring as indicated by the resonance structures **16a** and **16b**. For **17**, either an sp^2 or sp^3 hybridization model predicts a weaker interaction. Clearly, a vast body of experimental evidence demonstrates that the methoxy group in anisole is a π donor and therefore **16** must be the minimum energy structure on the rotational surface. A more difficult question to answer is the position of **17** on this surface.

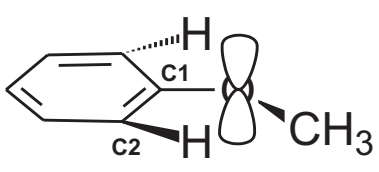
Most experimental studies have indicated a twofold rotational surface with **17** as a maximum at ~4 kcal/mol above **16** (13). Therefore, rotation between the two minima ($\Phi = 0°$ and 180°) would be rapid on the NMR timescale at room temperature. However, long-range C–H NMR coupling constants demonstrate that **17** is in a shallow minimum and therefore the rotational surface is fourfold (14). Calculations by ab initio methods have located this minimum with some basis sets but not with others (13). For instance, at the RHF/6-31G* level, **17** is 1.39 kcal/mol above **16**, and the transition state between the two (Φ = ~65°) is 1.59 kcal/mol above **16**. These same calculations give C-O-C1 bond angles of 119.8° and 115.5° for **16** and **17**, respectively. A conformational minimum similar to **16** has been found for allyl phenyl ether (**4a**: X–H) (15).

In terms of the photochemical reactivity of ethers **1**, **3**, and **4** (as discussed later, the anisoles are photochemically unreactive), **16** has the reactive C—O bond perpendicular to the π system of the aromatic chromophore whereas **17** has the same C—O bond parallel to it. Therefore, **17** should be more reactive. As discussed now, we have used a variety of probes to assess the conformational geometry of aryl ethers in the ground state and conclude that the tertiary alkyl derivatives **1** and **3**, in contrast to the anisoles **2** and the allyl ethers **4**, have preferred geometries analogous to **17**.

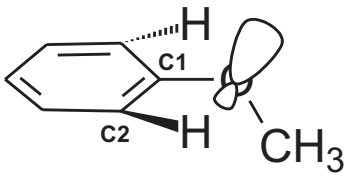
UV absorption spectra of ethers 1–4 in methanol and cyclohexane

The long wavelength absorption band λ_{max} (L_b transition) and molar absorptivity (ϵ) for the 1-adamantyl ethers **1a**–**1k**, and for comparison, the corresponding anisoles **2a**–**2k** in both methanol and cyclohexane as the solvent are reported in Table 1. Values for the *tert*-butyl ethers **3a**–**3i** in methanol and **3a**–**3c** in cyclohexane are also included. The L_b band for the anisoles has a significantly higher ϵ, and the λ_{max} tends to occur at longer wavelengths than the tertiary alkyl cases **1** and **3**. These trends are shown graphically in Fig. 1 for X = H, 4-OCH_3, and CN[4] in both methanol (left in each case) and cyclohexane (right in each case). The spectra for the corresponding allyl derivatives, which have been reported previously (3), are also included in these figures. The spectra for X = 4-CN and 4-CF_3 are not typical of those for the other substitutents because these electron-withdrawing groups interact strongly with the ether oxygen and shift the L_a band to longer wavelengths, partially obscuring the L_b band. The primary ethers (allyl (**4**) and methyl (**2**)) have very similar spectra that differ significantly (higher ϵ values, longer wavelengths) from those of the tertiary alkyl ethers **1** and **3**.

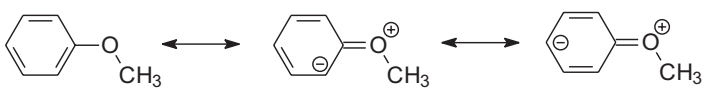
Similar observations have been made previously for anisoles that are sterically crowded by ortho substitution at C-2 and C-6 (16). For instance, the λ_{max} of the L_b band in



16 ($\Phi = 0^o$)



17 ($\Phi = 90^o$)



16a **16b**

[4] These three were chosen to span the complete range of electron-donating and electron-withdrawing abilities of all the substitutents studied.

© 2005 NRC Canada

Table 1. Absorbance and fluorescence data and excited-state rate constants for ethers **1–3** in methanol and cyclohexane.

	X	Solvent[a]	λ_{max}[b] (nm)	ϵ[b] ((mol/L)$^{-1}$ cm^{-1})	$\lambda_{0,0}$[c] (nm)	$E(S_1)$ (kJ/mol)	Φ_f[e]	τ^{sf}[f] (ns)	k_t ($10^7 s^{-1}$)	k_f(exp) ($10^7 s^{-1}$)	k_f (calcd) ($10^7 s^{-1}$)	k_f(exp)/k_f (calcd)[g]	$k_t^M - k_t$ ($10^7 s^{-1}$)
1a	H	M	256	328	280	427	0.23	6.21	16.1	3.7	0.9	3.97	2.9
2a	H	M	271	1680	281	427	0.24[h]	7.58	13.2	3.2	2.4	1.33	
3a	H	M	269	519									
1a	H	C	270	505	279	431	0.21	7.00	14.3	3.0	1.1	2.63	1.5
2a	H	C	271	1930	281	427	0.29[i]	7.80	12.8	3.7	3.6	1.03	
3a	H	C	269	574									
1b	4-OCH_3	M	280	1894	299	402	0.085	2.50	40.0	3.4	2.7	1.24	2.7
2b	4-OCH_3	M	290	2820	305	393	0.11	2.68	37.3	4.1	4.3	0.93	
3b	4-OCH_3	M	280	2000									
1b	4-OCH_3	C	282	2190	298	402	0.090	3.12	32.0	2.6	3.6	0.72	–1.1
2b	4-OCH_3	C	289	3200	304	383	0.12	3.02	33.1	4.0	5.5	0.71	
3b	4-OCH_3	C	280	2140									
1c	3-OCH_3	M	272	1930	281	427	0.084	2.54	39.3	3.8	2.9	1.32	–2.0
2c	3-OCH_3	M	274	2200	285	419	0.076	2.42	41.3	3.1	3.1	1.00	
3c	3-OCH_3	M	272	1723									
1c	3-OCH_3	C	272	1910	283	423	0.106	2.63	38.0	4.0	3.0	1.32	–2.3
2c	3-OCH_3	C	274	2220	284	423	0.093	2.48	40.3	3.7	3.5	1.09	
3c	3-OCH_3	C	272	1777									
1d	4-CH_3	M	269	649	288	414	0.162	5.91	16.9	4.4	1.0	4.36	1.2
2d	4-CH_3	M	279	1880	289	414	0.22	6.37	15.7	3.5	3.1	1.12	
1d	4-CH_3	C	270	759	288	414	0.226	6.62	15.1	3.4	1.3	2.58	1.8
2d	4-CH_3	C	279	2170	290	414	0.33	7.48	13.3	4.4	3.9	1.13	
1e	3-CH_3	M	266	452	283	423	0.17	6.90	14.4	2.4	0.8	3.08	2.0
2e	3-CH_3	M	273	1660	283	423	0.27	8.0	12.4	3.4	2.8	1.21	
1e	3-CH_3	C	266	486	283	423	0.23	7.69	13.0	3.0	0.9	3.26	1.7
2e	3-CH_3	C	273	1810	282	423	0.37	8.79	11.3	4.2	3.4	1.24	
1f	4-F	M	264	1240	284	423	0.14	3.44	29.1	4.0	1.9	2.13	2.2
2f	4-F	M	280	2670	291	410	0.15	3.72	26.9	4.0	4.1	0.98	
3f	4-F	M	269	1200									
1f	4-F	C	271	1550	289	414	0.14	3.54	29.2	4.0	2.6	1.56	3.3
2f	4-F	C	281	2900	290	414	0.18	3.86	25.9	4.0	4.9	0.94	
1g	3-F	M	263	1344	277	431	0.0047	—	—	—	1.9	—	
2g	3-F	M	269	1590	279	431	0.0055	—	—	—	2.3	—	
3g	3-F	M	263	947									
1g	3-F	C	263	905	276	435	0.014	—	—	—	1.7	—	
2g	3-F	C	269	1650	278	431	0.022	0.8	125.0	—	2.9	1.0	
1h	4-CF_3	M	260	434	282	423	0.073	3.76	26.5	1.9	—	—	4.1
2h	4-CF_3	M	270	1060	279	431	0.093	4.47	22.4	2.1	—	—	
3h	4-CF_3	M	260	551									
1h	4-CF_3	C	262	433	281	427	0.10	4.35	22.9	2.3	—	—	3.1
2h	4-CF_3	C	270	1100	280	427	0.13	5.05	19.8	2.6	—	—	
1i	3-CF_3	M	267	1180	289	414	0.037	2.90	34.4	1.3	2.0	0.65	2.8
2i	3-CF_3	M	277	2310	288	414	0.11	3.16	31.6	3.5	3.7	0.95	
3i	3-CF_3	M	273	1163									
1i	3-CF_3	C	268	1290	288	414	0.056	3.17	31.5	1.8	2.5	0.72	2.2
2i	3-CF_3	C	267	2440	289	414	0.16	3.41	29.3	3.2	4.4	0.73	
1j	4-CN	M	274 (sh)	1230	286	419	0.051	2.30	43.5	2.2	—	—	13.9
2j	4-CN	M	271 (sh)	2030	286	419	0.075	3.37	29.6	2.2	—	—	
1j	4-CN	C	267 (sh)	1150	287	419	0.083	4.41	22.6	1.9	—	—	5.6
2j	4-CN	C	274	1310	286	419	0.11	5.88	17.0	1.9	—	—	
1k	3-CN	M	286	1440	305	393	0.094	2.97	33.6	3.1	2.2	1.41	7.5

© 2005 NRC Canada

Table 1 (*concluded*).

	X	Solvent[a]	λ_{max}[b] (nm)	ϵ[b] ((mol/L)$^{-1}$ cm^{-1})	$\lambda_{0,0}$[c] (nm)	$E(S_1)$ (kJ/mol)	Φ_f[e]	τ[sf] (ns)	k_t ($10^7 s^{-1}$)	k_f(exp) ($10^7 s^{-1}$)	k_f (calcd) ($10^7 s^{-1}$)	k_f(exp)/k_f (calcd)[g]	$k_t^M - k_t$ ($10^7 s^{-1}$)
2k	3-CN	M	290	2960	305	393	0.14	3.60	27.7	3.9	4.5	0.87	
1k	3-CN	C	286	1400	300	398	0.14	4.09	24.4	3.5	2.4	1.46	3.7
2k	3-CN	C	288	2980	300	398	0.20	4.83	20.7	4.1	5.1	0.80	

[a]M is methanol, C is cyclohexane.
[b]Obtained from absorption spectra.
[c]Obtained from the overlap of the absorption and fluorescence spectra.
[d]Calculated from $E_{S_1} = 12.0 \times 10^4/\lambda_{0,0}$.
[e]Quantum yield of fluorescence relative to anisole in methanol (0.24) and cyclohexane (0.29), estimated error ±10%.
[f]Singlet lifetime by nanosecond single photon counting. The standard deviations of the fits to the experimental counts are <2%. No value indicates that the lifetime was less than 0.5 ns.
[g]The values of k_f(calcd) could not be obtained for X = 4-CF_3 and 4-CN because the L_a band was at a long enough wavelength so as to obscure the short wavelength portion of the L_b band, preventing the use of eq. [5].
[h]G. Kohler, G. Kittel, and N. Getoff. J. Photochem. **18**, 19 (1985).
[i]I.B. Berlman. Handbook of fluorescence spectra of aromatic molecules. Academic Press, New York. 1971. p. 139.

2,6-dimethylanisole shifts to shorter wavelengths (266 nm) and lower molar absorptivity (620 (mol/L)$^{-1}$ cm^{-1}) compared to anisole itself (269 nm, 2100 (mol/L)$^{-1}$ cm^{-1} (16); 271 nm, 1980 (mol/L)$^{-1}$ cm^{-1} (Table 1),[3] both in cyclohexane). The proposed explanation is that ortho substitution forces the methoxy group into the 90° geometry of **17**, reducing the importance of structures **16a** and **16b** that allow conjugation of the oxygen lone pair with the aryl ring.

^{13}C NMR spectra of ethers 1–4 in $CDCl_3$

Complete ^{13}C NMR spectral data for the adamantyl ethers **1** along with those for the anisoles **2**, *tert*-butyl ethers **3**, and the allyl ethers **4**, are given in Table S1 (Supporting information).[3] The anisole data were taken from the Aldrich compilation (17) and these values were confirmed for the para-substituted compounds by another literature source (18). The allyl ether data, which differ insignificantly from the anisole data, have been reported previously (3). Relative to the anisole derivatives, the ^{13}C chemical shifts at C-4 for both the adamantyl and *tert*-butyl derivatives have higher δ values (deshielded) by an average of 2.57 ± 0.52 ppm (11 compounds) and 2.97 ± 0.38 (nine compounds), respectively. Moreover, these changes vary around these averages in a random way over the range of X groups from electron-donating ones (CH_3O, CH_3) to electron-withdrawing ones (CF_3, CN) in either the meta or para position. Therefore, the contribution that resonance structure **16b** makes is not more important for a resonance electron-withdrawing group like CN.

For ortho-substituted anisoles, the same effect has been observed previously (19) with changes in ^{13}C δ values at C-4 relative to anisole of –0.3 ppm (2-methyl), +3.9 ppm (2,6-dimethyl), +7.2 ppm (2,6-diisopropyl), and +9.7 ppm (2,6-di-*tert*-butyl). These deshielding effects are a consequence of the lowering of the π-electron density at C-4 and reflect the decreasing importance of the resonance contributor **16b** as conformation **17** becomes more dominant. Therefore, the bulky *tert*-butyl and 1-adamantyl alkyl groups are providing a similar steric inhibition to a resonance interaction of the ether oxygen with the benzene ring as the case for two ortho methyl groups on the benzene ring. The effect that these bulky groups have at C-2 and C-6 is even larger (changes in δ values ranging from –10.5 to –11.5 ppm for the adamantyl ethers relative to the anisoles), but these changes probably reflect to some extent a direct steric interaction rather than only the importance of resonance effects.

Molecular orbital calculations

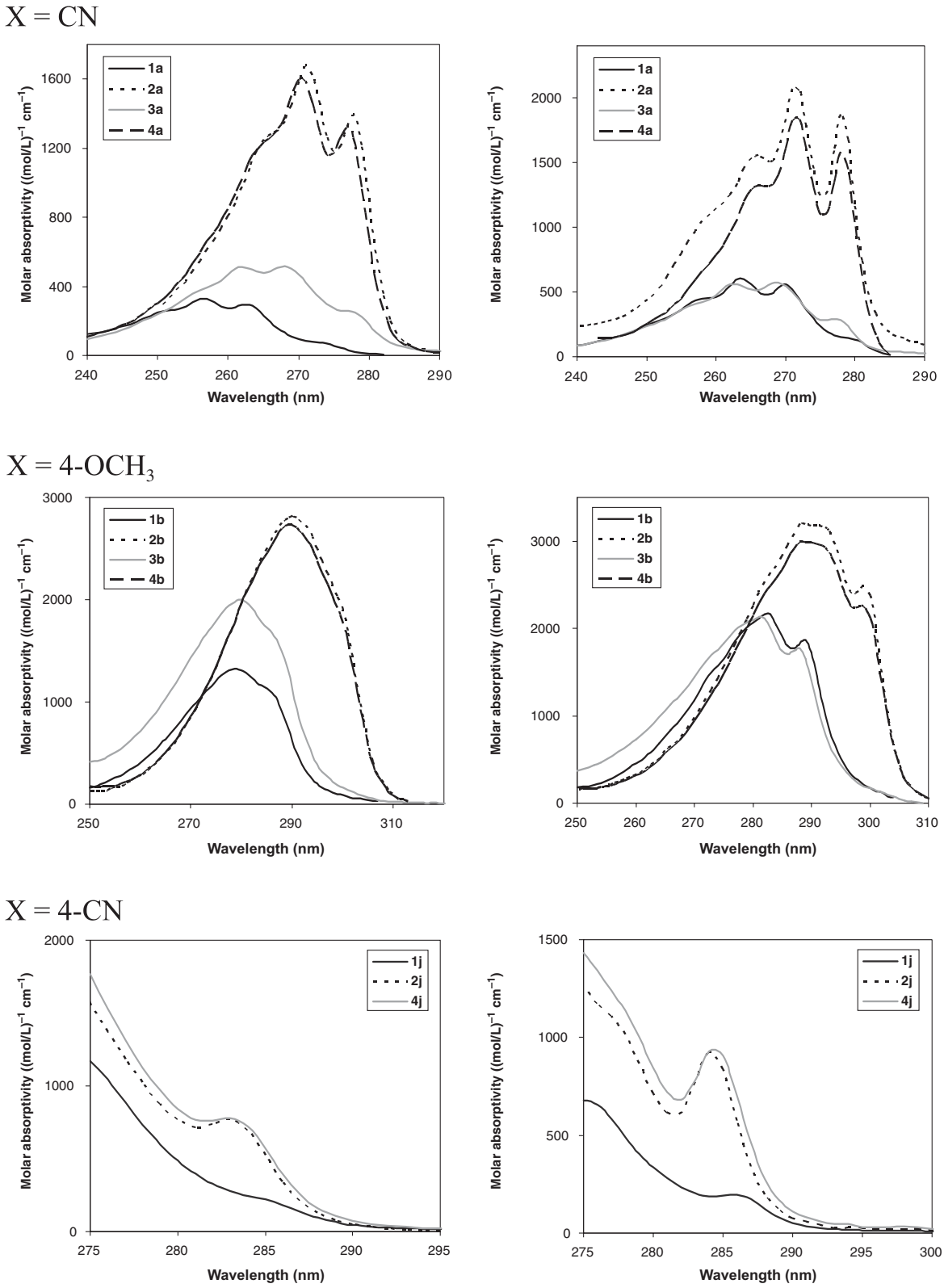
Two views of each of the two stable conformers for 1-adamantyl phenyl ether (**1a**: X = H) are shown in Figs. 2 and 3, the former corresponding to the 0° structure **16** and the latter to the 90° structure **17**. These were obtained as geometry optimized minima by GAUSSIAN 98 (20) at the B3LYP/6-31G(d) level of theory.[5] Similar calculations were performed for the para-substituted cases shown in Table 2 with OH replacing OCH_3 for computational convenience. Frequency analyses indicated that all were minima with all frequencies positive except for small negative values corresponding to methyl rotations for X = CH_3. The lowest energy positive frequencies (~35 cm^{-1} for **16** and ~15 cm^{-1} for **17**) correspond, by visualization in GaussView, to the rotation interconverting **16** and **17**.

After correction for zero point energy, the 90° conformer is calculated to be the more stable for all cases although the difference in energy between the two decreases systematically as the substituent changes from the resonance electron-donating 4-hydroxy group to the electron-withdrawing 4-cyano group. Clearly, this difference is dominated by the steric preference for the 90° geometry, which moves the ortho hydrogens on the benzene ring away from the adamantyl hydrogens. This steric crowding in the 0° structure is indicated by the large calculated O-C1(aryl)-C2(aryl) and C1(adamantyl)-O-C1(aryl) bond angles of 127.5° and 126.8°, respectively, at the ether functional group in contrast to 120.1° and 102.7° for the corresponding angles in the 90° structure. The energetic preference for the 90° conformer is decreased by conjugation of the oxygen lone pair of the ether with the substituent so that the 0° and 90° conformers are calculated to have almost identical stabilities for X = 4-CN. A related observation has been made previously for diphenyl ethers, monosubstituted on one of the two rings (21). The more stable conformer changes from that ring hav-

[5]The optimized geometries in C_1 symmetry have actual dihedral angles of 0.1° for the "0°" structure and 92.7° for the "90°" structure.

© 2005 NRC Canada

Fig. 1. UV absorption spectra of the ethers **1–4** for X = H, 4-OCH_3, and 4-CN in methanol (right) and cyclohexane (left).



ing conjugation to the ether oxygen for 4-CN (0°) to that conjugation being reduced for 4-OH (90°).

A scan of the dihedral angle from –105° to 105° (optimizing all other variables) for the unsubstituted case **1a** gives the energy surface shown in Fig. 4. A very shallow minimum is observed at the 0° geometry with a barrier of approximately 0.2 kJ/mol that separates it from the two identical minima at ±92°. This plot is quite similar to that

© 2005 NRC Canada

Table 2. Calculated (GAUSSIAN 98) values for aryl adamantyl ethers **1** at the two minimum energy conformers.

4-X	Dihedral angle (°)	E(SCF)[a] (Hartree)	ΔE[b] (kJ/mol)	E(SCF + ZPE)[c] (Hartree)	ΔE(ZPE)[b] (kJ/mol)	E(Ex)[d] (kJ/mol)	Osc. strength	$\Delta E(S_1)$[b] (kJ/mol)
OH	0	–772.19879		–771.86533		535.8	0.083	–8.0
OH	90	–772.20166	–7.5	–771.86863	–8.7	552.5	0.059	
F	0	–796.21732		–795.89594		552.5	0.069	–10.8
F	90	–796.21948	–5.7	–795.89863	–7.1	570.1	0.039	
CH_3	0	–736.30263		–735.94560		552.5	0.053	–8.4
CH_3	90	–736.30448	–4.8	–735.94797	–6.2	567.0	0.016	
H	0	–696.98521		–696.65781		565.4	0.035	–6.3
H	90	–696.98691	–4.5	–696.65781	–6.1	577.4	0.009	
CN	0	–789.23183	–1.1	–788.90365		536.3	0.287	–2.1
CN	90	–789.23141		–788.90378	–0.4	539.4	0.234	

[a]Calculated at optimized geometries by B3LYP/6-31G(d).
[b]The negative values indicate the more stable structure of the pair for each X substituent.
[c]After zero point energy correction at optimized geometry.
[d]Calculated by TDDFT/6-31G(d) at the optimized ground-state geometry.

Fig. 2. Two views of the B3LYP/6-31G(d) optimized geometry with a C1(adamantyl)-O-C1(aryl)-C2(aryl) dihedral angle of 0.1°. The O-C1(aryl)-C2(aryl) and the C1(adamantyl)-O-C1(aryl) bond angles are 127.5° and 126.6°, respectively.

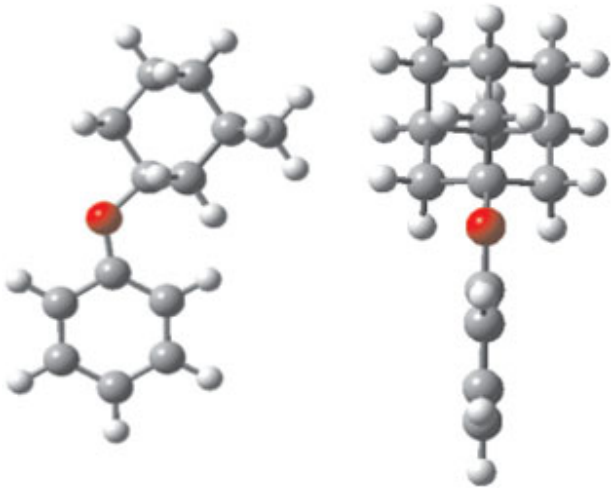
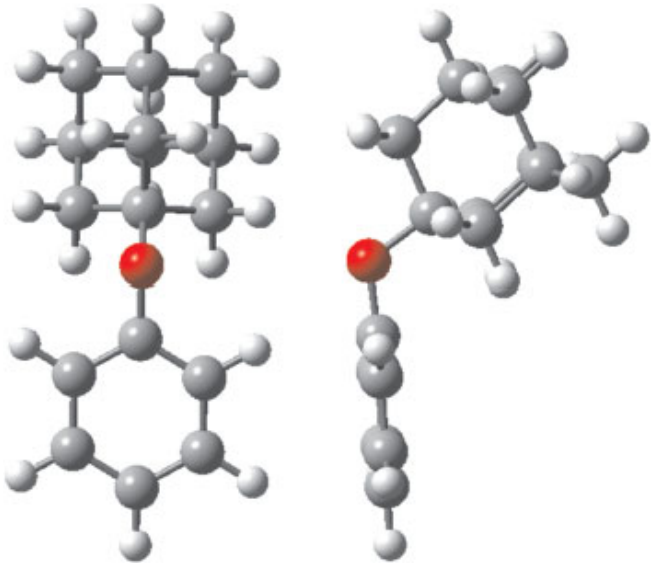


Fig. 3. Two views of the B3LYP/6-31G(d) optimized geometry with a C1(adamantyl)-O-C1(aryl)-C2(aryl) dihedral angle of 92.7°. The O-C1(aryl)-C2(aryl) and the C1(adamantyl)-O-C1(aryl) bond angles are 120.1° and 102.7°, respectively.



calculated for anisole with the contrast that the minimum energy conformation (90° for **1** and 0° for anisole) is complimentary for the two cases.

X-ray structures of adamantyl ethers 1b (X = 4-OCH$_3$) and 1h (X = 4-CF$_3$)

Suitable crystals were obtained for X-ray crystallograph structures[6] for these two compounds and that for **1b** is shown in Fig. 5. In both cases, a geometry similar to the 90° structure is preferred; the observed dihedral angles are 99° for **1b** and 107° for **1h**. These derivations from the symmetrical 90° structures are likely due to intermolecular crystal packing forces.

Geometry of the aryl ethers 1–4 in the excited singlet state

Information about the geometry of aryl ethers in the excited state can be obtained from fluorescence measurements using both excited singlet state lifetimes and steady-state spectra, and MO calculations. The conclusion is that the 0° structure is energetically preferred for S_1.

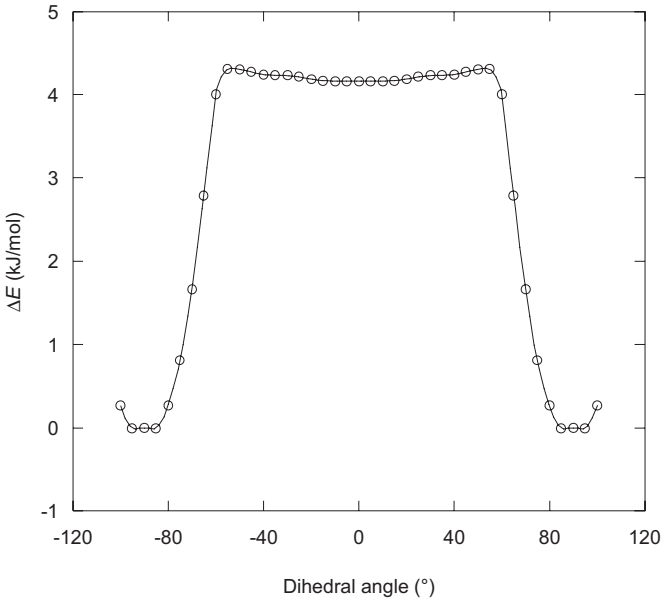
Excited singlet state lifetimes of ethers 1 and 2

The total rate of decay ($k_t = 1/\tau_s$) of the excited singlet state (τ_s from nanosecond single photon counting) along with the fluorescence quantum yields are reported in Table 1 in both methanol and cyclohexane solvents for the adamantyl **1** and methyl ethers **2**. The rate constants of fluorescence ($k_f = \Phi_f k_t$) are also given. Averaged over all substituted compounds, the ratios of $k_f(\mathbf{2})/k_f(\mathbf{1}) = 1.19 \pm 0.35$ and 1.26 ± 0.24 (10 compounds) in methanol and cyclohexane, respectively, are equal to unity, within experimental error. In fact, these ratios are improved to 1.02 ± 0.15 and $1.20 \pm$

[6]T.S. Cameron. Department of Chemistry, Dalhousie University. Unpublished results. 2004.

© 2005 NRC Canada

Fig. 4. Relative energy vs. the C1(adamantyl)-O-C1(aryl)-C2(aryl) dihedral angle for adamantyl phenyl ether by B3LYP/6-31G(d).



0.23, respectively, if the values for X = 3-CF_3, which seem unusually large, are not included in the two averages.

The general theoretical relationship (22, 23) between the radiative lifetime ($\tau_f = 1/k_f$) and the absorbance spectrum is given in eq. [3] where n is the refractive index of the solvent, υ_f is the expectation value for the frequency of the fluorescence spectrum, and the final term is the integrated absorbance spectrum. The constant gives k_f in units of s^{-1} if the frequency values are expressed in wavenumber (cm^{-1}), and molar absorptivity ϵ in the usual units ($(mol/L)^{-1}$ cm^{-1}). This equation is derived on the basis of the oscillator strength model and the important assumption that the excited singlet state and the ground state have similar geometries. It has been used successfully in the past for simple aromatic compounds like benzene, toluene, and *ortho*-xylene (24), and by us for the anisoles **2** and the allyl ethers **4** (3).

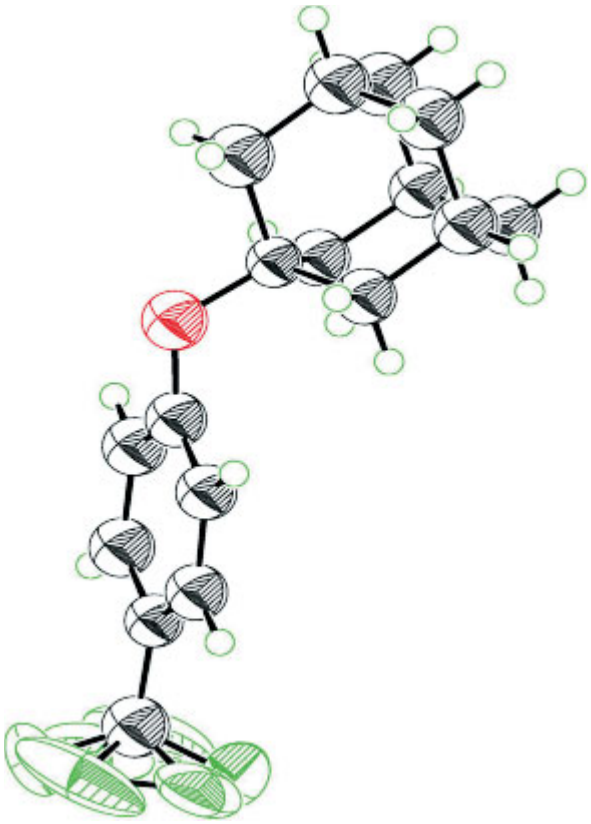
$$[3] \qquad k_f = 2.88 \times 10^{-9} n^2 < \overline{\nu}_f > \int \epsilon \ln \overline{\nu}$$

Equation [3] works very well for the anisoles **2** in both methanol and cyclohexane, $k_f(\text{exp})/k_f(\text{calcd}) = 1.05 \pm 0.10$ (seven compounds) and $k_f(\text{exp})/k_f(\text{calcd}) = 0.96 \pm 0.13$ (10 compounds), respectively. These values are in Table 1.

In contrast, as shown in Table 1, eq. [3] does not work as well for the adamantyl ethers **1**, with $k_f(\text{exp})/k_f(\text{calcd}) = 2.27 \pm 1.14$ (eight compounds) and $k_f(\text{exp})/k_f(\text{calcd}) = 1.98 \pm 0.83$ (eight compounds) in methanol and cyclohexane, respectively. The larger scatter and the average significantly greater than unity is a consequence of the decreases in ϵ for the adamantyl ethers. In general, the lower ϵ values decrease k_f(calcd) values and consequently increase ratios of $k_f(\text{exp})/k_f(\text{calcd})$. As discussed above, these lower values of ϵ for the adamantyl ethers **1** were ascribed to these ethers preferring the 90° geometry rather than the 0° geometry.

The similarity in the experimental k_f values for the anisoles **2** and the adamantyl ethers **1** suggest similar excited-state geometries for both. The good agreement among the k_f values obtained experimentally and from eq. [3] for the anisoles indicates that the ground-state and excited-state geometries are similar, presumably the 0° structure **16**. In contrast, for the adamantyl ethers, the experimental k_f values compare well with the anisoles, whereas those calculated from eq. [3] do not. This implies that the geometry of the adamantyl ethers changes on excitation from the 90° geometry in S_0 to the 0° geometry in S_1.

Fig. 5. X-ray crystal structure of **1h** (X = CF_3).



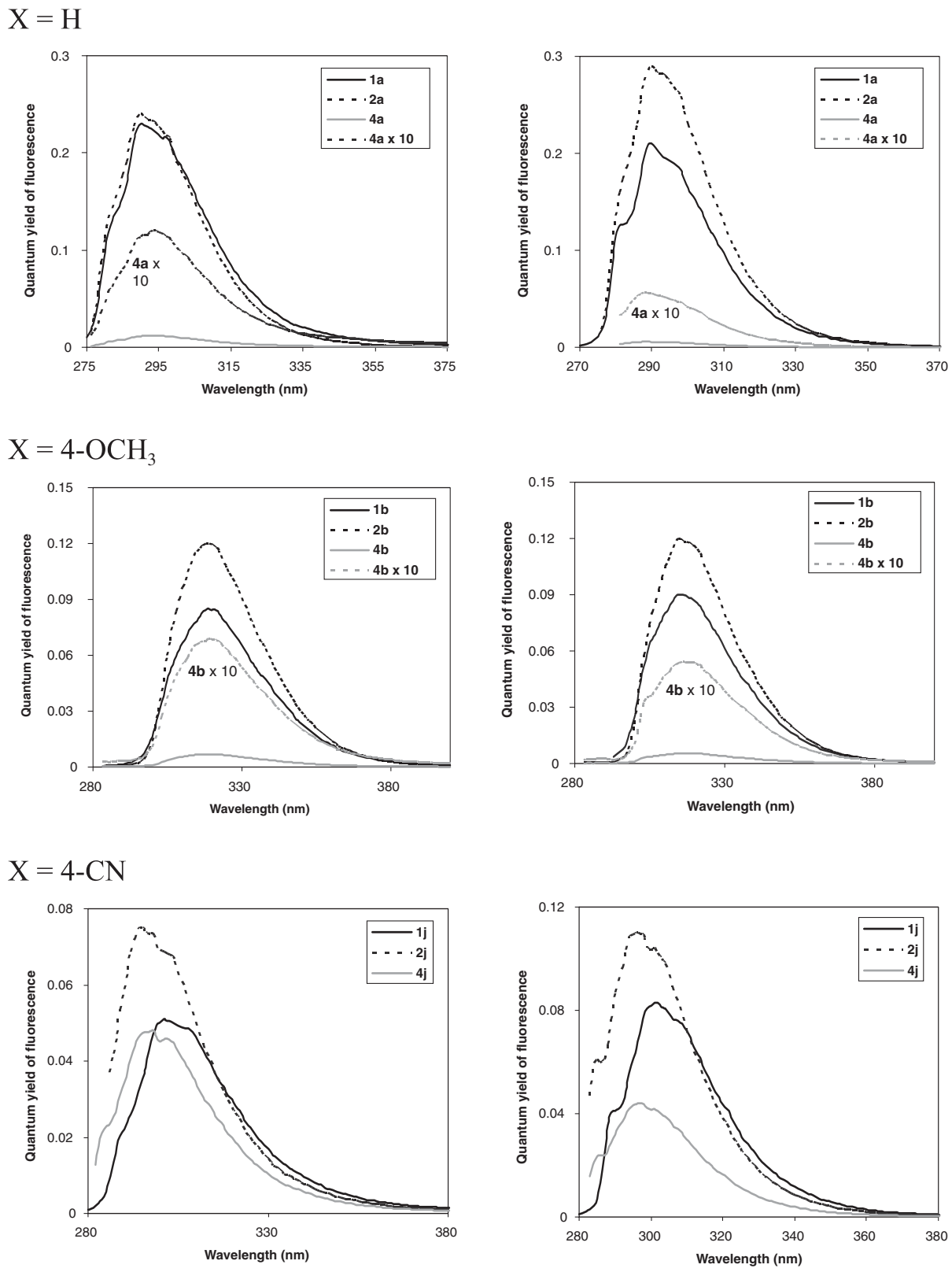
Fluorescence spectra of ethers 1 and 2

Values for the $\lambda_{0,0}$ (from the overlap of emission and excitation spectra), derived singlet state energies (E_{S1} (kJ/mol) = $[1.197 \times 10^5]/\lambda_{0,0}$ (nm)), and fluorescence quantum yields for the anisoles **2** and adamantyl ethers **1** are reported in Table 1. Sample fluorescence spectra for the ethers **1** and **2** with X = H, 4-OCH_3, and 4-CN[4] are shown in Fig. 6, for both methanol (left in each case) and cyclohexane (right in each case). The spectra for the corresponding allyl ethers **4** are also included.

Two features are obvious from the spectra. The first is the very similar wavelength dependence unrelated to the structural change in the alkyl group (from adamantyl to methyl to allyl) in the ether. The only significant exception, a shift to a longer wavelength of about 5 nm for the adamantyl ether, occurs when X = 4-CN in Fig. 6, a case where intramolecular charge transfer in the excited state may be important. Other than this case, the spectra imply that the excited-state geometries of the ethers **1**, **2**, and **4** are similar. This suggestion is reinforced by the similar values of E_{S1} obtained for the anisoles and the adamantyl ethers.

© 2005 NRC Canada

Fig. 6. Fluorescence spectra of the ethers **1**, **2**, and **4** for X = H, 4-OCH_3, and 4-CN in methanol (left) and cyclohexane (right).



The second feature of these spectra is the difference in quantum yields of fluorescence. In general, the adamantyl ethers **1** and the anisoles **2** have similar Φ_fs in either solvent, the adamantyl ether values being somewhat lower. In contrast, the allyl ethers **4** have significantly lower Φ_f values than both **1** and **2**. These decreases for compounds **4** reflect the very large increases in reactivity of the excited singlet state relative to the anisoles **2**. As will be described in the

© 2005 NRC Canada

following, according to eq. [4], the higher values of k_r for the allyl ethers result in higher values of k_t, and, consequently, lower values for $\Phi_f = k_f/k_t$, k_f being essentially constant for any given substituent X but independent of the alkyl group of the ether. The similar values of Φ_f for the adamantyl ethers and the anisoles indicate that the k_r values for the adamantyl compounds do not make a large contribution to the k_t of S_1.

[4] $$k_t = k_f + k_{ic} + k_{isc} + k_r$$

Molecular orbital calculations

Excitation energies to S_1 were calculated by TDDFT/6-31G1(d) (20) using vertical excitations from the optimized ground-state geometries calculated previously for both the $\Phi = 0°$ and 90° conformer, again for the substituents shown in Table 2. In all cases, as expected, the calculated oscillator strength was lower for the 90° than the 0° conformer. Moreover, also in agreement with the UV absorption spectra, the excitation energy was higher for the $\Phi = 90°$ geometry than for the 0° geometry. Combined with the ground-state energies, the relative energies for the excited singlet state ($\Delta E(S_1)$) in Table 1 can be calculated indicating that, for all substitutents, S_1 for the 0° conformer is more stable than S_1 for the 90° conformer. This observation supports the suggestion that excitation of compounds **1** from S_0 at $\Phi = 90°$ gives S_1 at 90°, which then relaxes by rapid rotation to give the more stable conformer S_1 at 0°. Fluorescence emission and reaction should then occur from the 0° conformer.

Rate constants of reaction (k_r) from the excited singlet state of the adamantyl ethers 1

The quantum yield method, as described by eq. [1], for obtaining rate constants for excited-state bond cleavage reactions has a major defect. In all cases where experiments have been designed to detect it, internal return of radical pair intermediates (k_{ir} in Scheme 1) has been observed (1). Therefore, the efficiency of product formation that a quantum yield measures does not give a reliable measure of k_r. In effect, k_{ir} is a form of internal conversion, although not occurring directly from S_1. A knowledge of the fraction of this internal return $[k_{ir}/(k_p + k_{ir})]$, which is undoubtably dependent on the substituent X, could be used to obtain correct values of k_r, but this fraction is a difficult number to obtain experimentally without a suitable probe. For instance, in the cases examined for the allyl ethers (**4a**–**4d**) in both methanol and cyclohexane, the importance of k_{ir} was demonstrated by the fact that the quantum yield method (eq. [1]) gave significantly lower values of k_r than the unreactive model method (eqs. [4] and [5]) (3), described in the following. With no suitable probe for the adamantyl ethers **1**, we decided not to measure quantum yields of reaction.

[5] $$k_t^M = k_f + k_{ic} + k_{isc}$$

The unreactive model method

For the allyl ethers **4**, we recently described an alternate method of measuring k_r for reactions of S_1 that relies on comparing a photochemically reactive compound with an unreactive one that has identical excited-state properties (3). We chose to compare compounds **4** with the anisoles **2**, which are, in comparison, photochemically inert. Either static (Φ_f) or dynamic (τ_s) measurements of fluorescence can be used although the latter is preferred because more reliable experimental values can be obtained. The assumption used is given in eqs. [4] and [5], where the changes in k_t of the reactive series only differ from those (k_t^M) of the model series **2** by k_r. Therefore, subtraction of experimentally determinable values ($k_t - k_t^M = k_r$) should reliably give k_r. Because these are exclusively properties of the excited singlet state, the k_r values obtained are independent of k_{ir}, the internal return process.

This method was applied quite successfully to obtain k_r values for the allyl ethers **4** in both cyclohexane and methanol (3). From absorbance spectra (λ_{max}, ϵ), fluorescence spectra ($\lambda_{0,0}$, E_{S1}), and calculated k_f values, good evidence was provided that the sets **2** and **4** have very similar excited-state properties for any given equivalently substituted pair in either methanol or cyclohexane. The resulting k_r values as a function of substituents spanned almost two orders of magnitude (10^8–10^{10} s^{-1}), and for some cases (3- and 4-methoxy and 3- and 4-methyl), were the dominant mode of decay of S_1. A plot of k_r in methanol vs. k_r in cyclohexane was linear and the slope (0.96) indicated a parallel substituent effect in the two solvents. This observation demonstrates that only radical pair intermediates are being generated, ion pairs not being possible in cyclohexane.

An examination of the k_t (adamantyl ethers **1**) and k_t^M (anisoles **2**) values in Table 1 indicates that the difference required to usefully apply eqs. [4] and [5] is hardly outside experimental error for most substitutents. Small positive values are obtained in most cases, although a few are actually negative. This observation quantitatively demonstrates that the adamantyl ethers have very small values of k_r, the rate constant of reaction, relative to the other modes of decay of the excited singlet state (k_{ic}, k_f, and k_{isc}). The only noticeable trend in the k_r values is towards higher values for those compounds **1j** and **1k** with cyano substitutents at C-3 and C-4, respectively, more so in methanol than in cyclohexane, but particularly for the 4-CN compound in methanol. This correctly accounts for the observation that the 4-cyano compound gives a significant yield of the ion-derived product **10** in methanol. Unfortunately, overall, the changes in k_r are too small to attempt a quantitative substituent effect correlation.

The temperature dependence of the fluorescence method

The effect of temperature on photochemical reactions has received far less attention than it deserves. However, recent studies from the laboratories of Lewis (activation barriers to E to Z isomerization in phenyl substituted alkenes) (25) and Zachariasse (thermally activated internal conversion in amino substitued aromatics) (26) have shown that the measurement of fluorescence quantum yields and lifetimes and intersystem crossing quantum yields over a wide temperature range provides a valuable tool to obtain rate constants for excited singlet state processes. Again, because the properties measured are exclusively those of S_1, the rate constants k_r obtained are independent of processes like k_{ir} or reaction from T_1. We have recently applied this approach to the phototransposition reactions of substituted benzenes (27).

The simplest assumption used is presented in eq. [6], which is the same as eq. [4] except that the reaction process k_r is considered to follow the Arrhenius expression. For

© 2005 NRC Canada

substituted benzenes, the S_0 to S_1 energy gap is large so that $k_{ic} \backsimeq 0$ ($k_{ic} \backsimeq 10^3$ s^{-1} for benzene with $E(S_1) = 444$ kJ/mol).[7] Because $S_1 \rightarrow T_1$ is an exergonic process and considered to be unactivated, the rate of intersystem crossing should be temperature independent. However, Zachariasse and coworkers (26) have clearly shown that for amino substituted aromatics, $S_1 \rightarrow T_n$ intersystem crossing can be an important process that will be activated. Therefore, the total rate of intersystem crossing should be expressed by eq. [7], where k^0_{isc} is the intersystem crossing rate constant at 0 K (temperature independent), and the Arrhenius activation term is for the activated k_{isc}. The activation parameters for this process are characterized by low values of $A_{isc} \backsimeq 10^8$ to 10^9 s^{-1} and $E_{a/isc} \backsimeq$ 4–6 kJ/mol.

$$[6] \qquad k_t = k_f + k_{ic} + k_{isc} + A \exp(-E_a/RT)$$

$$[7] \qquad k_{isc} = k^0_{isc} + A_{isc} \exp(-E_{a/isc}/RT)$$

Values for k_t as a function of temperature have normally been obtained by measuring S_1 lifetimes (τ_s), but this is a very time-consuming process. We have chosen a more rapid method using τ_s and Φ_f at 25 °C (Table 1) to obtain $k_f = \Phi_f/\tau_s$. Then measurement of relative fluorescence quantum yields over a wide temperature range (–25 to 65 °C in methanol and –25 to 95 °C in methylcyclohexane)[8] were done (see Experimental section), and $k_t(T) = \Phi_f(T)/\Phi_f(25\ °C)$ values obtained assuming k_f is constant, independent of temperature. In fact, although k^0_f (the superscript refers to the refractive index (n) of vacuum) is temperature independent, the usual experimental observation for solution measurements is given in eq. [8] where the refractive index of the solvent is temperature dependent. However, over the temperature range studied here, the change in n^2 for the two solvents used is insignificant. From literature values[9] of the variation in refractive index with temperature (28), the k_f values for anisole would only change from 3.1×10^{-7} to 3.3×10^{-7} s^{-1} from –25 to +65 °C in methanol, and from 3.5×10^{-7} to 3.9×10^{-7} s^{-1} from –25 to 95 °C in methylcyclohexane. These ranges do not exceed the estimated error of 10% in k_f (assuming an error of 10% in Φ_f), and consequently, were ignored.

$$[8] \qquad k_f = k^0_f n^2$$

Plots of k_t vs. T are nonlinear and examples are shown in Fig. 7 for anisole, 4-cyanoanisole, and 4-cyanophenyl adamantyl ether (**1j**) in methanol. Other results are compiled in Table 3 for the adamantyl ethers **1** and the corresponding anisoles **2** for X = H, 4-OCH_3, and 4-CN.[4] Excellent fits of this data to eq. [6] were obtained ($r > 0.997$ in all cases) giving an intercept equal to $k_f + k_{isc}$ (assuming $k_{ic} = 0$) and Arrhenius A and E_a values. Using the independently determined experimental values of k_f gives k_{isc}. The consistency of the results is indicated by the similar values of k_{isc} obtained for any given pair of **1** and **2** with the same substituent and in either solvent.

Many of the compounds studied behave in a similar way to anisole in Fig. 7, with very little change in k_t as a function of temperature. As shown in Table 3, this results in low A values ($2.6–8.6 \times 10^9$ s^{-1}) that are characteristic of an activated intersystem crossing process and indicate that the dominant temperature-dependent process for these substrates even at room temperature is $k_{isc,}$ according to eq. [7]. This conclusion was also reached by a previous study on the temperature dependence of k_t (29), in 3-methylpentane and ethanol–methanol (1:1), although the A values ($\sim 2.5 \times 10^8$) reported are even lower than ours. The values of k_{isc} obtained by us for anisole at 25 °C of $(10.0 \pm 1.2) \times 10^{-7}$ s^{-1} (methanol) and $(9.1 \pm 0.9) \times 10^{-7}$ s^{-1} (methylcyclohexane) are in good agreement with literature values of 8.0×10^{-7} s^{-1} (cyclohexane) (30) and 9.4×10^{-7} s^{-1} (isooctane) (31), both obtained from directly measured Φ_{isc}/τ_s values. Moreover, the contribution that k_r makes to the total rate of decay of S_1 for anisole is small because $\Phi_f + \Phi_{isc} = 0.24 + 0.74$ (29) (Ermolaev's rule) in agreement with the observation that irradiation of anisoles does not result in product formation. Very likely, the dialkoxy compounds **2**, with low A and E_a values, also have $\Phi_f + \Phi_{isc} \backsimeq 1$, and therefore they have $\Phi_{isc} \backsimeq 0.9$ in both solvents, on the basis of $\Phi_f \backsimeq 0.1$ (Table 1).

As shown in Fig. 7, 4-cyanoanisole has a larger change in k_t as a function of temperature than does anisole even though both are photochemically unreactive in methanol. This suggests that both k_{isc} and k_r are contributing to the temperature dependence, but that the k_r process does not lead to products. As has been shown previously (26), to separate the activated k_{isc} and k_r rate constants reliably would require a combination of eqs. [6] and [7] and measurements over a much wider range of temperatures so that the process with lower A and E_a values (k_{isc}) would be dominant at low temperatures and k_r (higher A and E_a values) would be dominant at higher temperatures. Quantum yields of intersystem crossing as a function of temperature would also be required.

However, we have recently shown (27) that substituted aromatics undergo an activated process to form prefulvene biradicals. These intermediates (**18**–**20**), as in Scheme 3 for 4-methylbenzontrile (32), provide a pathway for both phototransposition reactions (ortho, meta, para) and also a pathway for k_{ir}, i.e., a chemical rather than photophysical route for internal conversion. We have also estimated (27) a quantum yield of $\Phi_r = 0.29$ for the formation of **18**, and measured a quantum yield of formation of the meta isomer of $\Phi_p = 0.025$ from the para one. Therefore, less than 10% of the intermediate **18** formed undergoes rearrangement to **19**. We suggest that formation of a prefulvene biradical is also the activated k_r process for 4-cyanoanisole. A similar activated internal conversion has been observed (26) for 4-cyanoaniline (and other aromatic amines in hydrocarbon solvents) with $E_a = 35$ kJ/mol and $A \backsimeq 5 \times 10^{12}$ s^{-1}. The authors noted that an activated, but undefined, geometric deformation in S_1 must be providing a pathway for S_1 to S_0 decay.

If this proposal is correct, then the difference in k_r between the anisoles and the adamantyl ethers obtained from the variable temperature studies reflects the increased reactivity of the adamantyl ethers because of C—O bond cleavage. This suggestion assumes that the activated k_{isc} and the

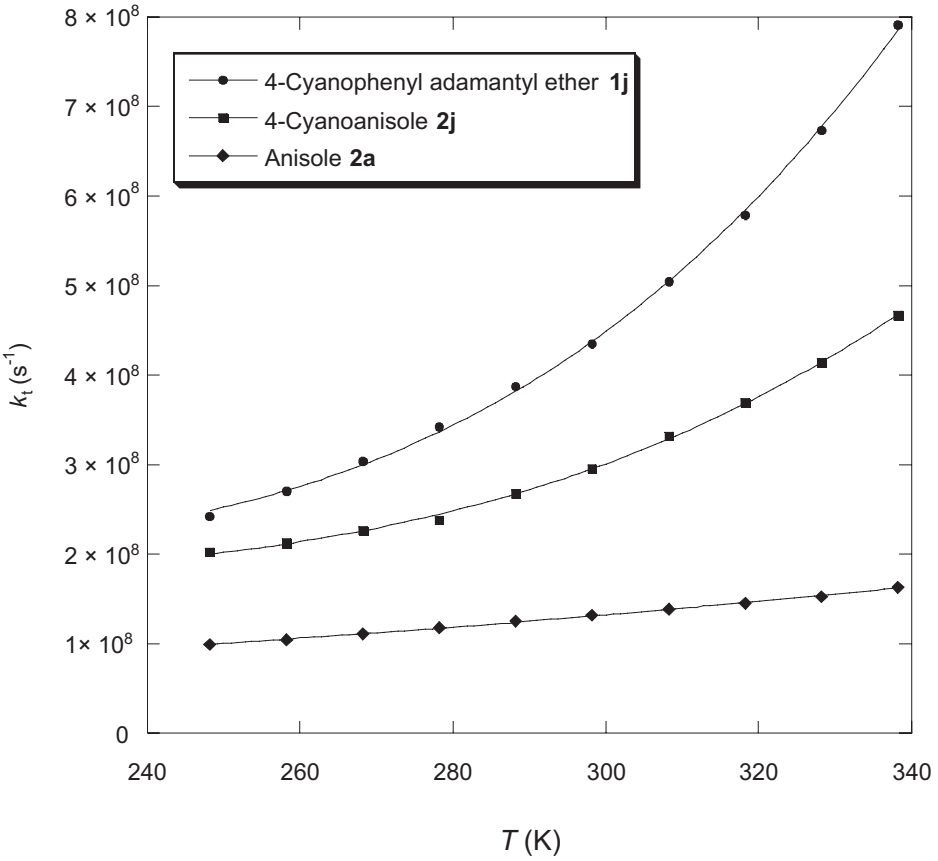
[7] See, in particular, the Introduction section of ref. 26.

[8] For the variable temperature studies, methylcyclohexane, rather than cyclohexane, was used as the solvent to expand the range of experimentally accessible temperatures.

[9] This reference gives values of $dn/dt = -0.000\ 39$/°C for methanol and $-0.000\ 55$/°C for cyclohexane.

© 2005 NRC Canada

Fig. 7. Temperature dependence of k_t and the fits to eq. [6] for the compounds **1j** (X = 4-N), **2j** (X = 4-CN), and **2a** (X = H) in methanol.



4-Cyanophenyl adamantyl ether

y = m1+m2*exp(-m3/(8.314e-3*T))		
	Value	Error
m1	1.9576e+08	8.318e+06
m2	4.4908e+11	1.0285e+11
m3	18.657	0.66811
Chisq	2.107e+14	NA
R	0.99965	NA

4-Cyanoanisole

y = m1+m2*exp(-m3/(8.314e-3*T))		
	Value	Error
m1	1.7267e+08	4.6846e+06
m2	2.0355e+11	5.105e+10
m3	18.377	0.73277
Chisq	6.3681e+13	NA
R	0.99957	NA

Anisole

y = m1+m2*exp(-m3/(8.314e-3*T))		
	Value	Error
m1	6.8121e+07	6.2294e+06
m2	1.8841e+09	4.9421e+08
m3	8.4225	0.90553
Chisq	6.8794e+12	NA
R	0.99914	NA

other k_r processes (for instance, formation of the prefulvene biradical) are similar in rate for the equivalently substituted adamantyl ether and anisole. The difference in the temperature dependence between 4-cyanoanisole (**2j**) and adamantyl 4-cyanophenyl ether (**1j**) is clearly shown in Fig. 7, and the values of Δk_r (25 °C) in the last column of Table 2 support this suggestion. The values are larger in methanol than methylcyclohexane for all substrates studied, in agreement with the observation that the efficiency of photochemical conversion of the adamantyl ethers is greater in methanol. Moreover, both the substituted adamantyl ethers (4-OCH_3, 4-CN) react faster than the unsubstituted one. Most notable is the high k_r value for the 4-CN substrate in methanol, presumably as a result of the k_r process leading to ion pairs from S_1 and the resulting product 1-methoxyadamantane.

Conclusions

A variety of techniques have demonstrated that the adamantyl ethers **1** have a ground-state geometry with a dihedral angle of 90° that reduces conjugation of the ether oxygen with the aryl ring. Upon excitation to S_1, the geometry relaxes to a 0° conformer that increases the conjugation but decreases the overlap between the aromatic π system and the bond that breaks in the excited state. This observation provides an explanation for the low photochemical reactivity of these ethers and the lack of any large substituent effect on the rate constant of bond cleavage from S_1. For substrates that do not react, this technique provides a simple method of determining k_{isc} and Φ_{isc}. The method also allows a comparison between unreactive model compounds (the anisoles) and reactive substrates (the adamantyl ethers) so that the k_r process that leads to products or reactive intermediates can be separated from that which leads back to starting material (k_{ir}), a form of internal conversion.

Experimental

General procedures

Routine ^1H and ^{13}C NMR spectra were obtained in $CDCl_3$ on a Bruker AC 250 F NMR spectrometer in automation mode. The ^{13}C NMR spectra for **1a**–**1j** in Table S1 (Sup-

© 2005 NRC Canada

Table 3. Fits to eq. [6] and derived rate constants for S_1 of adamantyl ethers **1** and anisoles **2**.

	X	Solvent[a]	A^b ($10^9 s^{-1}$)	$E_a{}^b$ (kJ/mol)	$k_f + k_{isc}{}^c$ ($10^7 s^{-1}$)	$k_f{}^d$ ($10^7 s^{-1}$)	$k_{isc}{}^e$ ($10^7 s^{-1}$)	$k_f{}^f$ ($10^7 s^{-1}$)	$k_r{}^g$ ($10^7 s^{-1}$)	$\Delta k_r{}^h$ ($10^7 s^{-1}$)
1a	H	M	3.0 (1.3)	9.2 (1.4)	8.7 (1.0)	3.7 (0.4)	5.0 (1.4)	16.1 (0.2)	7.4 (1.2)	1.0 (1.5)
2a	H	M	1.8 (0.4)	8.4 (0.9)	6.8 (0.2)	3.2 (0.3)	3.6 (0.9)	13.2 (0.1)	6.4 (0.3)	
1a	H	MC	24 (1.0)	16.0 (1.0)	10.6 (0.4)	3.0 (0.3)	7.6 (0.7)	14.3 (0.1)	3.7 (0.5)	0.2 (0.8)
2a	H	MC	3.8 (0.6)	11.6 (0.6)	9.3 (0.2)	3.7 (0.4)	5.6 (0.6)	12.8 (0.1)	3.5 (0.3)	
1b	4-OCH_3	M	4.9 (0.3)	7.7 (0.2)	17.7 (0.1)	3.4 (0.3)	14.3 (0.4)	40.0 (0.4)	25.7 (0.8)	8.9 (1.3)
2b	4-OCH_3	M	3.6 (0.5)	7.6 (0.6)	20.5 (0.1)	4.1 (0.4)	16.4 (0.5)	37.3 (0.4)	16.8 (0.5)	
1b	4-OCH_3	MC	4.4 (0.4)	8.5 (0.4)	17.4 (0.1)	2.6 (0.3)	14.8 (0.4)	32.0 (0.3)	14.6 (0.4)	4.9 (0.9)
2b	4-OCH_3	MC	8.6 (0.6)	10.7 (0.2)	21.6 (0.3)	4.0 (0.4)	17.6 (0.6)	31.3 (0.3)	9.7 (0.5)	
1j	4-CN	M	450 (10)	18.7 (0.7)	19.6 (0.1)	2.2 (0.2)	17.4 (0.3)	43.5 (0.4)	23.9 (0.5)	11.6 (1.3)
2j	4-CN	M	200 (50)	18.4 (0.7)	17.3 (0.5)	2.2 (0.2)	15.1 (0.7)	29.6 (0.3)	12.3 (0.8)	
1j	4-CN	MC	240 (7)	21.0 (1.0)	17.3 (0.4)	1.9 (0.2)	15.4 (0.6)	22.6 (0.2)	4.3 (0.6)	0.3 (1.1)
2j	4-CN	MC	12.3 (6)	14.1 (0.9)	13.0 (0.3)	1.9 (0.2)	11.1 (0.5)	17.0 (0.2)	4.0 (0.5)	

Note: Values in brackets are estimated errors: from fits to eq. [6] for A, E_a, and $(k_f + k_{isc})$; from ±10% for ϕ_f; from ±1% for τ_s; from accumulated errors for calculated quantities.

[a]Solvent: M (methanol), MC (methylcyclohexane).

[b]Arrhenius parameters from eq. [6].

[c]Intercept from eq. [6].

[d]$k_f = \phi_f k_t$.

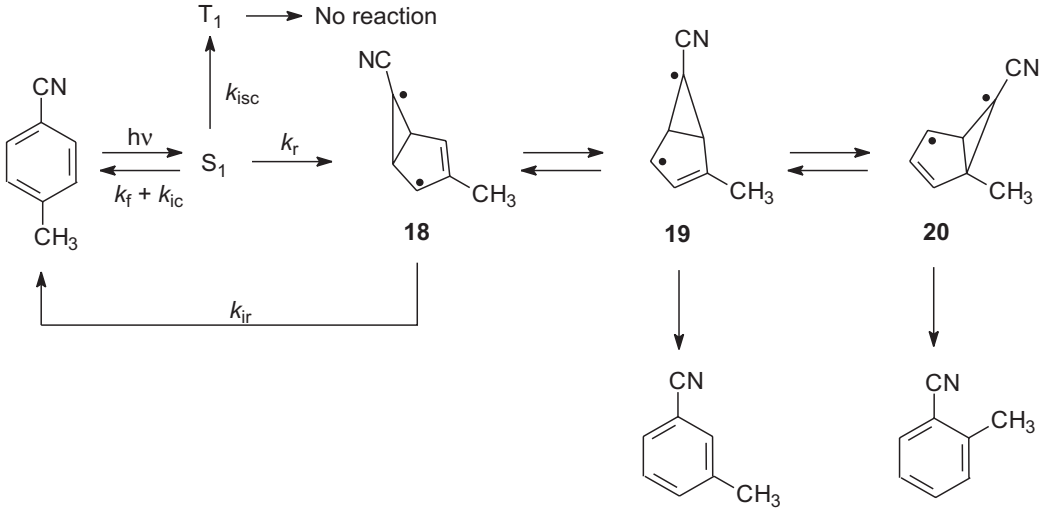
[e]$(k_f + k_{isc}) - k_f$.

[f]$k_t = 1/\tau_s$ from nanosecond single photon counting at 25 °C.

[g]$k_r(25\ °C) = k_t(25\ °C) - (k_f + k_{isc})$.

[h]$k_r(\mathbf{1}) - k_r(\mathbf{2})$ at 25 °C.

Scheme 3. Mechanism for the phototransposition of *para*-methylbenzonitrile to the meta and ortho isomers and associated rate constants of reaction.



porting information)[3] were obtained on a Bruker AVANCE 500 MHz spectrometer with chemical shifts (δ) reported relative to the central line of $CDCl_3$ at 77.16 ppm. GC–MS analyses were performed on a PerkinElmer Autosystem XL instrument with a mass selective detector. The column used was a Supelco 30 m × 0.25 mm MDN-5S 5% phenyl methylsiloxane, film thickness 0.50 μm; temperature program: 60 °C for 1 min; 20 °C/min to 240 °C; 240 °C for 10 min. GC-FID analyses were done in a similar way except on a Supelco DB200 column. Mass spectral data are reported in units of mass over charge (m/z) for all values between 50 and the molecular ion if greater than 10% of the base peak. Intensities are reported as a percent of the base peak. HR-MS were obtained on a CEC 21-110 instrument with a resolution of 5–10 × 10^3. The solvents used for photochemical reactions and fluorescence measurements were used as received: methanol (EM, HPLC), cyclohexane (Aldrich, HPLC), and methylcyclohexane (Aldrich, spectrophotometric grade).

Preparation of the adamantyl aryl ethers 1a–1k

The ethers were synthesized by a modified literature method (9) from 1-bromoadamantane and the substituted phenol (Aldrich). In a typical procedure, a mixture of 8.40 g (75 mmol) of 4-fluorophenol and 3.24 g (15 mmol) of 1-bromoadamantane and 4.5 mL of pyridine was refluxed for 5 h. The reaction mixture was cooled, diluted with 50 mL of water – ethylene glycol (8:1), and extracted with 2 × 15 mL

© 2005 NRC Canada

of hexanes. The extract was washed with 5% NaOH (25 mL), water (2 × 25 mL), dried ($MgSO_4$), and the hexanes evaporated. The crude solid (2.26 g) was purified by flash chromatography using 2.5% ethyl acetate in hexanes to give 1.14 g (31%) of a colourless solid that was recrystallized from methanol.

Characterization of the adamantyl aryl ethers 1a–1k

^{1}H NMR spectra were not particularly diagnostic: the signals expected for the substituted benzene ring, the substituent for X = OCH_3 and CH_3, and the 1-adamantyl ring system (δ 2.17, 1.89, and 1.61, all broad singlets) were all present. ^{13}C NMR spectral data for the ethers **1**, along with those for **2**–**4** are reported in Table S1 (Supporting information).[3] Mass spectral data (GC–MS) were also not particularly diagnostic: a molecular ion (but not for X = 3-CF_3, 4-CF_3, 3-CN, and 4-CN) and $C_{10}H_{15}$, the adamantyl cation as the base peak (100) and its fragment ions at 107 (12), 93 (22), 79 (25), and 77 (13) were observed. Other characterization results: **1a** (X = H): mp 112 to 113 °C (lit. value (33) mp 99 to 100 °C). **1b** (X = 4-OCH_3): mp 48 to 49 °C (lit. value (33) mp 49–51 °C). **1c** (X = 3-OCH_3): mp 44–46 °C. HR-MS calcd. for $C_{17}H_{22}O_2$: 258.1620; found: 258.1628. **1d** (X = 4-CH_3): mp 53.5–54.0 °C (lit. value (33) mp 41–43 °C). **1e** (X = 3-CH_3): mp 69.0–70.0 °C. HR-MS calcd. for $C_{17}H_{22}O$: 246.1671; found: 246.1668. **1f** (X = 4-F): mp 110 to 111 °C. HR-MS calcd. for $C_{16}H_{19}OF$: 246.1420; found: 246.1423. **1g** (X = 3-F): mp 38 to 39 °C. HR-MS calcd. for $C_{16}H_{19}OF$: 246.1420; found: 246.1419. **1h** (X = 4-CF_3): mp 57.5–58.5 °C. **1j** (X = 4-CN): characterized previously (2). **1k** (X = 3-CN): mp 86 to 87 °C.

Irradiation of ethers

A solution of ~100 mg of the appropriate ether in 100 mL of methanol or cyclohexane was purged with nitrogen and then irradiated in a Rayonet photochemical reactor using 16 lamps (75 W, 254 nm). The temperature was kept at 25 °C by circulating water in an immersion tube. Reaction progress was monitored by GC.

Absorbance measurements

Absorbance spectra were recorded at 1 nm resolution using a Cary 100 UV–vis spectrometer thermostatted at 25 °C. Selected examples are shown in Fig. 1. The integrated spectra needed to obtain k_f values from eq. [3] were obtained by summing the 1 nm incremental areas (the absorbance values converted to ε by dividing by the molar concentration) over the complete absorption band. These areas are somewhat uncertain at the short wavelength end because of overlap with the long wavelength tail of the S_2 band so that the absorbance does not reach zero. The wavelength for the minimum in absorbance was used as the cut-off point for the S_1 band. For the 4-cyano and 4-trifluoromethyl derivatives of **1** and **2**, this overlap was too extensive to allow integration of the S_1 band and k_f values were not calculated.

Fluorescence measurements

All samples were degassed by three freeze–pump–thaw cycles and then thermostatted at 25 °C. The substituted anisoles used for comparison were all commercial samples (Aldrich) and were distilled before use. Fluorescence intensity measurements were done using a PTI-210M fluorescence spectrometer with dual model 101 monochromators, a 75 W Xenon lamp, and a model 814 photomultiplier detector. Corrected spectra were obtained. Selected examples are shown in Fig. 6. Fluorescence quantum yields were determined using solutions of matched absorbance by comparison with the known fluorescence quantum yield of 0.24 (30) for anisole in methanol and 0.29 (34) in cyclohexane. The expectation values necessary for calculating the k_f values from eq. [3] were obtained by summing the 1 nm incremental areas over the complete emission band. For temperature-dependent quantum yield measurements, a 1 cm cuvette was thermostatted with stirring in a cuvette holder equipped with a Quantum Northwest TLC 50 temperature controller, which allows relative fluorescence measurements at 10 °C intervals from –25 to 95 °C in methylcyclohexane and –25 to 60 °C in methanol over a 2 h time span. The stability of the lamp over this time period was normally confirmed by rerunning the fluorescence spectrum at 25 °C at the end.

Singlet lifetimes were measured at 25 °C by monitoring fluorescence decay using a PRA time-correlated, single-photon-counting apparatus with a hydrogen flash lamp of with a pulse width of about 1.8 ns.

Acknowledgments

We thank the Natural Sciences and Engineering Research Council of Canada (NSERC) for financial support, Sepracor Canada Ltd., Windsor, Nova Scotia for the donation of chemicals, and Lei Zhang, Department of Chemistry and Biochemistry, Concordia University, Montreal, for assistance with the Gaussian calculations.

References

1. S.A. Fleming and J.A. Pincock. Organic molecular photochemistry. Vol. 3. Marcel Dekker, New York. 1999. p. 211.
2. D.P. DeCosta, A. Bennett, A.L. Pincock, J.A. Pincock, and R. Stefanova. J. Org. Chem. **65**, 4162 (2000).
3. A.L. Pincock, J.A. Pincock, and R. Stefanova. J. Am. Chem. Soc. **124**, 9768 (2002).
4. J. McEwen and K. Yates. J. Phys. Org. Chem. **4**, 193 (1991).
5. E.L. Wehry and L.B. Rogers. J. Am. Chem. Soc. **87**, 4234 (1965).
6. P.J. Baldry. J. Chem. Soc. 951 (1979).
7. (*a*) S.C. Shim, J.W. Park, and H.-S. Ham. Bull. Korean Chem. Soc. **3**, 13 (1982); (*b*) S.C. Shim, J.W. Park, H.-S. Ham, and J.-S. Chung. Bull. Korean Chem. Soc. **4**, 45 (1983).
8. T.F. Wolwode, C. Rose, and T.J. Wandless. J. Org. Chem. **63**, 9594 (1998).
9. H. Masada and Y. Oishi. Chem. Lett. 57 (1978).
10. J. Bartl, H. Mayr, and R.A. McClelland. J. Am. Chem. Soc. **112**, 6918 (1990).
11. H.E. Zimmerman and S. Somasekhara. J. Am. Chem. Soc. **85**, 922 (1963).
12. Y.-R. Luo. Handbook of bond dissociation energies in organic compounds. CRC Press, Boca Raton, Fla. 2003.
13. D.C. Spellmeyer, P.D.J. Grootenhuis, M.D. Miller, L.F. Kuyper, and P.A. Kollman. J. Phys. Chem. **94**, 4491 (1990).
14. (*a*) T. Schaefer and G.H. Penner. Can. J. Chem. **66**, 1635 (1988); (*b*) T. Schaefer and G.H. Penner. Can. J. Chem. **66**,

© 2005 NRC Canada

1641 (1988); (*c*) T. Schaefer and R. Sebastian. Can. J. Chem. **67**, 1148 (1989).
15. E. Taskinen. J. Chem. Soc. Perkin Trans. 2, 1824 (2001).
16. J.C. Dearden and W.F. Forbes. Can. J. Chem. **37**, 1305 (1959).
17. C.J. Pouchert and J. Behnke. The Aldrich library of ^{13}C and ^{1}H NMR spectra. Vol. 2. Aldrich Chemical Company, Milwaukee, Wis. 1993. pp. 175–241.
18. J. Bromilow, R.T.C. Brownlee, D.J. Craik, M. Sadek and R.W. Taft. J. Org. Chem. **45**, 2429 (1980).
19. K.S. Dhami and J.B. Stothers. Can. J. Chem. **44**, 2855 (1966).
20. M.J. Frisch, G.W. Trucks, H.B. Schlegel, G.E. Scuseria, M.A. Robb, J.R. Cheeseman, V.G. Zakrzewski, J.A. Montgomery, Jr., R.E. Stratmann, J.C. Burant, S. Dapprich, J.M. Millam, A.D. Daniels, K.N. Kudin, M.C. Strain, O. Farkas, J. Tomasi, V. Barone, M. Cossi, R. Cammi, B. Mennucci, C. Pomelli, C. Adamo, S. Clifford, J. Ochterski, G.A. Petersson, P.Y. Ayala, Q. Cui, K. Morokuma, N. Rega, P. Salvador, J.J. Dannenberg, D.K. Malick, A.D. Rabuck, K. Raghavachari, J.B. Foresman, J. Cioslowski, J.V. Ortiz, A.G. Baboul, B.B. Stefanov, G. Liu, A. Liashenko, P. Piskorz, I. Komaromi, R. Gomperts, R.L. Martin, D.J. Fox, T. Keith, M.A. Al-Laham, C.Y. Peng, A. Nanayakkara, M. Challacombe, P.M.W. Gill, B. Johnson, W. Chen, M.W. Wong, J.L. Andres, C. Gonzalez, M. Head-Gordon, E.S. Replogle, and J.A. Pople. GAUSSIAN 98. Revision A.11.2 [computer program]. Gaussian Inc., Pittsburgh, Penn. 2001.
21. B. Uno, T. Iwamoto, and N. Okumura. J. Org. Chem. **63**, 9794 (1998).
22. S.J. Strickler and R.A. Berg. J. Chem. Phys. **37**, 814 (1962).
23. J.B. Birks and D.J. Dyson. Proc. R. Soc. London Ser. A, **275**, 135 (1963).
24. R.B. Cundall and L.C. Pereira. J. Chem. Soc. Faraday Trans. **68**, 1152 (1972).
25. F.D. Lewis and X. Zuo. Spectrum (Bowling Green, OH, U.S.), **16**, 8 (2003). Available from www.bgsu.edu/departments/photochem/research/summer2003/spectrum.html.
26. S.I. Druzhinin, A. Demeter, V.A. Galievsky, T. Yoshihara, and K.A. Zachariasse. J. Phys. Chem. **107**, 8075 (2003), and refs. cited therein.
27. C.M. Gonzalez and J.A. Pincock. J. Am. Chem. Soc. **126**, 8870 (2004).
28. J. Timmermans. Physico-chemical constants of pure organic liquids. Vol. 1. Elsevier, New York. 1950.
29. S. Dellonte and G. Marconi. J. Photochem. **30**, 37 (1985).
30. G. Kohler, G. Kittel, and N. Getoff. J. Photochem. **18**, 19 (1982).
31. F.A. Carroll and F.H. Quina. J. Am. Chem. Soc. **94**, 6246 (1972).
32. (*a*) J.A. Pincock. *In* CRC handbook of organic photochemistry and photobiology. 2nd ed. *Edited by* W. Horspool and F. Lenci. CRC Press, Boca Raton, Fla. 2003. pp. 46–1 to 46–19; (*b*) P.J. MacLeod, A.L. Pincock, J.A. Pincock, and K.A. Thompson. J. Am. Chem. Soc. **120**, 13 354 (1998).
33. U. Kraatz. Chem. Ber. **106**, 3095 (1973).
34. I.B. Berlman. Handbook of fluorescence spectra of aromatic molecules. Academic Press, New York. 1971. p. 139.

© 2005 NRC Canada

Kinetics of glycoluril template-directed Claisen condensations — Effect of thionation of the glycoluril[1]

Karen Kam, Mohammad Rahimizadeh, Robert S. McDonald, Paul H.M. Harrison, Hao Chen, Stephen I. Jenkins, and Adrienne Pedrech

Abstract: Apparent rate constants for the *tert*-butoxide promoted Claisen-like condensation of a series of N^1-acetyl-N^6-aroyl-2,5-dithio-3,4,7,8-tetramethylglycolurils (**9a**–**9f**) to give N^1-(3′-aroyl-3′-oxopropionyl)-2,5-dithio-3,4,7,8-tetramethylglycolurils (**10a**–**10f**) were determined by UV spectroscopy. Overall rate accelerations of 3.5- to 18-fold were found relative to the corresponding reactions of the 2,5-dioxo compounds (**7a**–**7f**). Analysis of the Hammett plot for **9** and comparison with that for **7** shows that the key C—C bond-forming step, where the enolate of the acetyl group of the substrate attacks the aroyl carbonyl group, is accelerated by the thio substitution. For electron-withdrawing substituents in the aroyl group, the acceleration is sufficient to make this step nonrate limiting: the Hammett ρ value drops from approx. 1.5 for electron-donating groups to 0.27 for electron-withdrawing groups. Deuterium substitution in the acetyl group reduces the rate slightly, a result consistent with a slow but partially reversible first step in which substrate is deprotonated. A similar acceleration and isotope effect are found when diacetyl glycoluril (**2**) and diacetyl dithio glycoluril (**5**) are compared. The implications of these results are discussed.

Key words: glycoluril, Claisen condensation, kinetics, mechanism.

Résumé : Faisant appel à la spectroscopie UV, on a déterminé les constantes de vitesse apparente des condensations de type Claisen, catalysées par l'ion *tert*-butylate, d'une série de N^1-acétyl-N^6-aroyl-2,5-dithio-3,4,7,8-tétraméthylglycolurils (**9a**–**9f**) conduisant à la formation de N^1-(3′-aroyl-3′-oxopropionyl)-2,5-dithio-3,4,7,8-tétraméthylglycolurils (**10a**–**10f**). On a observé des vitesses globales qui étaient de 3,5 à 18 fois plus rapides que celles des réactions correspondantes avec les composés 2,5-dioxo (**7a**–**7f**). Une analyse de la courbe de Hammett pour les composés **9** et une comparaison avec celle des composés **7** montrent que l'étape clé de formation de la liaison C—C, dans laquelle l'énolate du groupe acétyle du substrat attaque le groupe carbonyle de l'aroyle est accélérée par la substitution thio. Pour les substituants électroaffinitaires du groupe aroyle, l'accélération est suffisante pour que cette étape ne soit plus l'étape cinétiquement déterminante: la valeur ρ de Hammett tombe d'une égale à environ 1,5 pour les groupes électrodonneurs à une valeur de 0,27 pour les groupes électroattracteurs. Une substitution du groupe acétyle par du deutérium réduit légèrement la vitesse, un résultat qui est en accord avec une première étape lente, mais partiellement réversible, dans laquelle le substrat est déprotoné. Une accélération et un effet isotopique semblable ont aussi été observés lorsqu'on a comparé le diacétylglycoluril (**2**) et diacétyldithioglycoluril (**5**). On discute des implications de ces résultats.

Mots clés : glycoluril, condensation de Claisen, cinétique, mécanisme.

[Traduit par la Rédaction]

Introduction

Auxiliaries are frequently pivotal in the design and execution of stereoselective syntheses (1). For example, the oxazolidinones developed by Evans allow highly diastereo- and enantioselective carbon–carbon bond forming reactions, as exemplified by their use in aldol condensations (1, 2). The sulfur congeners of these auxiliaries, the oxazolidinethiones and thiazolidinethiones (3), have also been studied, and have been found to exhibit altered properties compared with the oxygenated compounds; these include enhancement of the acidity of the protons of the *N*-acyl group, altered stereoselectivity, e.g., in aldol reactions (4), and enhanced ease of removal of the auxiliary after the desired aldol reac-

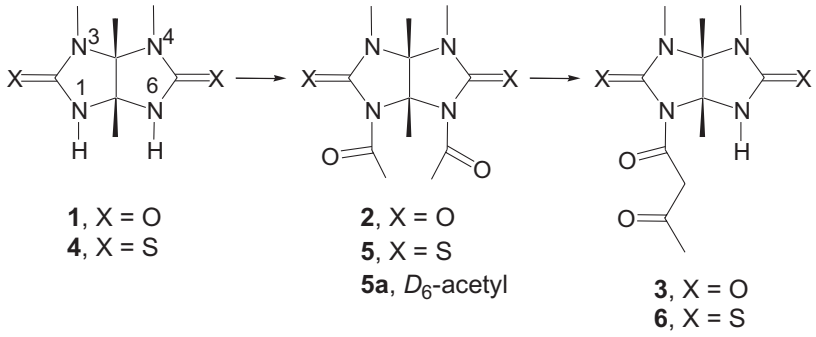
Received 6 December 2004. Published on the NRC Research Press Web site at http://canjchem.nrc.ca on 12 October 2005.

K. Kam, M. Rahimizadeh,[2] P.H.M. Harrison,[3,4] H. Chen, S.I. Jenkins, and A. Pedrech. Department of Chemistry, McMaster University, 1280 Main Street West, Hamilton, ON L8S 4M1, Canada.
R.S. McDonald.[3] Department of Chemistry, Mount St. Vincent University, 166 Bedford Highway, Halifax, NS B3M 2J6, Canada.

[1]This article is part of a Special Issue dedicated to organic reaction mechanisms.
[2]On sabbatical leave from Ferdowski University of Mashad, Iran.
[3]Joint principal authors.
[4]Corresponding author (e-mail: pharriso@mcmaster.ca).

 doi: 10.1139/V05-119 © 2005 NRC Canada

Scheme 1.



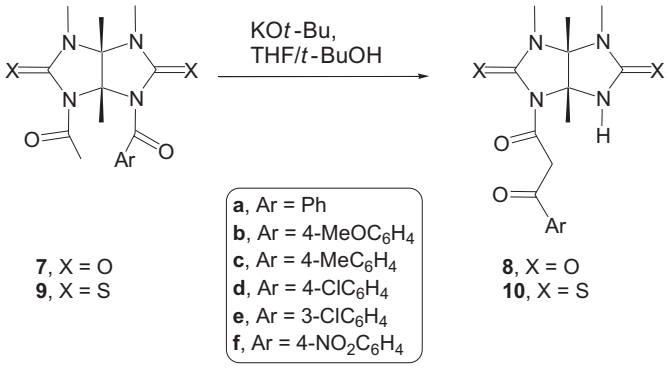
tion is complete (5). Although the effect of substitution of thiocarbonyl for carbonyl groups on nucleophilic substitution by non-carbon nucleophiles has been studied (6), there is little quantitative kinetic data on the extent to which sulfur substitution in auxiliaries influences the key C—C bond-forming chemistry, as results are generally determined as the overall outcome in preparative experiments.

As part of our on-going interest in biomimetic polyketide synthesis, we have developed glycolurils as auxiliaries to promote efficient intramolecular Claisen-like condensations (7). Thus, two sequential or concomitant acylations of 3,4,7,8-tetramethylglycoluril (**1**, Scheme 1) (8) at the N-1 and N-6 sites readily provide diacylglycolurils (e.g., **2**) in which the two acyl entities are held and oriented in proximity to each other. Deprotonation of one acyl moiety with an alkoxide base generates an enolate that is efficiently trapped by the other, electrophilic carbonyl group (9). After collapse of the resulting tetrahedral intermediate and workup, a β-ketoacylglycoluril (e.g., **3**) is generated in high yield (7, 9, 10). The glycoluril thus acts as a bifunctional analog of an Evans oxazolidinone, and the key condensation reaction is the intramolecular equivalent of the known intermolecular acylation of an Evans enolate by an acyl halide (11). In subsequent steps, a sequence of chemical reactions to modify the β-keto group can be effected; this process thus follows the order of events in fatty acid and polyketide biosynthesis (12). Finally, the resulting substituted acylglycoluril can undergo further rounds of acylations and intramolecular condensations (7), thus providing an iterative biomimetic approach to the synthesis of this class of natural products.

We have also described the preparation of thio substituted glycolurils in which one or both of the ureido oxygens has been substituted by sulfur (e.g., **4**) (13), and shown that the thioureido sites are more readily acylated than their ureido counterparts (e.g., conversion of **4** to **5**) (13, 14). The diacylthioglycolurils also rearranged in high yield to β-ketoacyl derivatives, e.g., **5** gives **6**. Although sulfur substitution qualitatively appeared to promote this condensation reaction, we sought a more quantitative way to determine the role of sulfur, and its impact on the various steps of this process.

Recently, we reported a detailed analysis of the condensation reaction using UV spectroscopy to monitor the kinetics of conversion of a series of acetyl aroyl glycolurils (e.g., **7a**–**7f**) into condensation products (e.g., **8a**–**8f**) (Scheme 2) (9). The results show that these reactions proceed cleanly, are first order in both substrate and base, are sensitive to aroyl substituents ($\rho = 1.5$ in a Hammett plot), and exhibit substantial primary kinetic isotope effects when the acetyl group is replaced by CD_3CO. The data were fully consistent with initial deprotonation of starting material at the acetyl group, followed by the proposed Claisen-like carbon–carbon bond formation step; both of these steps are partially rate-limiting, and later steps, including collapse of the ensuing tetrahedral intermediate, are fast. The enolate intermediate formed in the first step partitions between reprotonation by solvent (*t*-BuOH) and attack on the aroyl group; the extent of partitioning depends on the aroyl substituent.

Scheme 2.



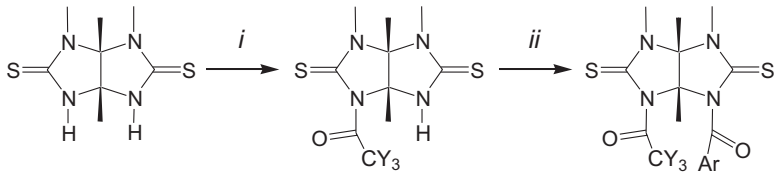
The availability of a rapid kinetic assay to monitor and quantitate the condensation reaction opens up further explorations of this intriguing system. In the present work, we describe the use of this methodology to examine the role of thio substitution in the glycoluril, and present kinetic data for conversion of **9a**–**9f** into **10a**–**10f**, respectively, as well as for the analogous deuterated substrates. Rates for diacetyl glycoluril **2** and its sulfur analog **5** are also compared. The implications of these results for the mechanism of the intramolecular Claisen-like condensation, for the design of more efficient biomimetic systems, and for thionation in chiral auxiliaries in general, are discussed.

Results

Dithioglycoluril **4** was efficiently acetylated to give the monoacetyl compound **11a** as previously reported; **11b** was prepared similarly from [D_6]-acetic anhydride (Scheme 3) (13). The NH site in **11a** reacted readily with benzoyl chloride to give **9a**. Likewise, 4-methoxy-, 4-methyl-, 4-chloro-, 3-chloro-, and 4-nitrobenzoyl chlorides were reacted with

© 2005 NRC Canada

Scheme 3. Reagents: (*i*) *n*-BuLi, THF then $(CY_3CO)_2O$ (1 equiv.); (*ii*) Et_3N, CH_2Cl_2 then ArCOCl, RT, 2.5 h.



4 **11a**, Y = H; **11b**, Y = D

9a, Ar = Ph, Y = H
9b, Ar = 4-$MeOC_6H_4$, Y = H
9c, Ar = 4-MeC_6H_4, Y = H
9d, Ar = 4-ClC_6H_4, Y = H
9e, Ar = 3-ClC_6H_4, Y = H
9f, Ar = 4-$NO_2C_6H_4$, Y = H
12a, Ar = Ph, Y = D
12e, Ar = 3-ClC_6H_4, Y = D
12f, Ar = 4-$NO_2C_6H_4$, Y =D

11a to afford **9b**–**9f**, respectively. The deuterated analogs, **12a**, **12e**, and **12f** were analogously prepared from **11b**.

Rates for rearrangement of **7a**, **9a**–**9f**, and deuterated analogues **12a**, **12e**, and **12f** were obtained as previously described (9). Briefly, each substrate was dissolved in anhydr. THF–*t*-BuOH (50:50), and placed in a sealed UV cuvette. After initiation of reaction with a fivefold or greater molar excess of a solution of base (KO-*t*-Bu) in the same solvent, absorbance at the λ_{max} of the enolate of the condensation product was monitored with time. Pseudo-first-order rate constants (k_{obs}) were determined by best fit, and converted to second-order rate constants (k_{app}) by dividing by base concentration. Slight variations in procedure were required when the rates were large: a lower substrate concentration and the minimal fivefold excess of base were used. In most of the experiments reported herein, and especially in these rapid cases, the reactions had progressed substantially by the time data collection started. Thus, only the last 20%–50% of the reaction progress could be monitored, and the absorbance changes were small, especially when the substrate concentration had been lowered. As a consequence of these effects, the individual kinetic runs had greater errors than those previously reported for the oxygen congeners. These problems were compensated for by performing three to five replicate analyses, and by repeating each measurement with new stock solutions at least once. It was found that the errors associated with curve fitting were small, and thus errors were determined by comparing results from different runs. The resulting average rate constants and errors are presented in Table 1.

Several controls were run during this study, as described previously. Thus, kinetic runs with **9a** and **9b** exhibited isosbestic points when the reaction was monitored in a sequence of rapid UV scans, as had been observed for **7a** (9). Compound **9d** was converted synthetically to condensation product **10d**. When treated with KO-*t*-Bu under similar conditions to those of the kinetics experiments, **10d** gave an essentially identical UV spectrum to that of the final solution at the end of a kinetics experiment with **9d**. This observation confirms that the process being monitored was indeed the expected condensation reaction, as discussed previously for **7a** (9). A plot of k_{obs} for **9a** vs. [Base] was linear, confirming that the reaction is first order in base concentration, as for **7a**. Regression of this plot gave k_{app} for **9a** of 180 ± 12 L mol^{-1} s^{-1}, in good agreement with the value obtained from curve fitting (161 ± 11 L mol^{-1} s^{-1}).

The values for k_{app} for compounds **9a**–**9f** and deuterated congeners thereof are shown in a Hammett plot (15) in Fig. 1, along with the previously reported data for **7a**–**7f** and their deuterated analogues. The results for **9a**–**9f** clearly show a substantial substituent effect, with an increase in rate from the electron-donating 4-methoxy to the withdrawing 4-nitro substituent of eightfold. However, unlike the plot for **7a**–**7f**, the Hammett plot for **9a**–**9f** is clearly nonlinear (r^2 = 0.744 for all data). A more satisfactory fit is obtained when the three data points at high σ are fit to a linear relationship, giving ρ = 0.27 ± 0.05 (r^2 = 0.967). Corresponding regression of the three points at low σ gives a positive value for ρ of 1.4 ± 0.5 (r^2 = 0.821), comparable to the previously reported values for **7a**–**7f** of 1.2–1.5 (9). However, the data may also be accomodated by a curved plot.

The isotope effect for substitution of three deuterons into the acetyl group(s) on the reaction rate constant k_{app} was next examined. Comparison of the rate constants for **9a** vs. **12a**, **9e** vs. **12e**, and **9f** vs. **12f** was made by performing a series of analyses, each of which was composed of five replicate runs; the k^H_{app}/k^D_{app} value obtained for the isotope effect on each of these overall reactions was 1.3 at 25 °C; these values compare with those obtained for **7a**, **7e**, and **7f** vs. their deuterated isotopomers of 1.6–2.6 (9). Overall, the results show a small, but consistent isotope effect in the dithioglycoluril condensations, which was reproduced in each independent analysis. It should be noted that in these experiments, at best only the latter 50% of the reaction progress could be monitored, owing to the high rates for reaction of the dithio analogues. Thus, potentially rapid exchange of deuterium with hydrogen from the *t*-BuOH solvent may mask any inherent isotope effect (see Discussion).

To further investigate the effect of thionation in the glycoluril, we also examined the kinetics for conversion of diacetyl glycolurils **2** and **5** to **3** and **6**, respectively (Scheme 1). In our previous work, we had used acetyl aroyl glycolurils (**7**) exclusively, reasoning that conjugation of the aroyl moiety in the enolate of products **8** would shift the UV absorption

© 2005 NRC Canada

Table 1. Apparent second-order rate constants for the Claisen-like base-induced condensations of diacylglycolurils into enolates of β-ketoacylglycolurils (k_{app}), and relative rate constants (k_{rel}).

Entry	Cmpd	X[a]	R^{1a}	R^{2a}	$k_{app}\pm\sigma$[b] ($L\ mol^{-1}\ s^{-1}$)	$k_{rel}\pm\sigma$[c]	Rel. to[d]	λ_{obs}[e]
1	**7a**	O	Me	Ph	17.2±0.3	1	def[f]	335
2	**9a**	S	Me	Ph	180±40	9.3±0.6	**7a**	345
3	**9b**	S	Me	$4MeOC_6H_4$	50±5	0.41±0.07	**9a**	349
4	**9c**	S	Me	$4MeC_6H_4$	140±9	0.70±0.08	**9a**	345
5	**9d**	S	Me	$4ClC_6H_4$	310±10	1.5±0.1	**9a**	354
6	**9e**	S	Me	$3ClC_6H_4$	330±50	1.5±0.1	**9a**	355
7	**9f**	S	Me	$4NO_2C_6H_4$	400±80	1.9±0.3	**9a**	420
8	**12a**	S	CD_3	Ph	120±10	0.75±0.07	**9a**	341
9	**12e**	S	CD_3	$3ClC_6H_4$	240±30	0.75±0.10	**9e**	355
10	**12f**	S	CD_3	$4NO_2C_6H_4$	330±60	0.75±0.19	**9f**	420
11	**2**	O	Me	Me	8.6±0.3	0.5±0.03	**7a**	300
12	**5**	S	Me	Me	150±20	17±2	**2**	297
13	**5a**	S	CD_3	CD_3	120±20	0.8±0.2	**5**	297

[a]For substrate structures, see the following.
[b]Second-order rate constant at 25 °C, calculated from observed rate constant (k_{obs}) and base concentration (see text), not adjusted relative to a standard (no control). σ is the standard deviation.
[c]Relative rate constant determined from ratio of k_{app} values obtained during the same kinetic run set (controlled). σ is the standard deviation.
[d]Compound used for comparison to calculate k_{rel}.
[e]Observation wavelength for kinetics experiments.
[f]Value defined for comparisons.

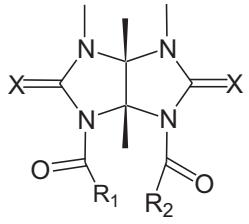
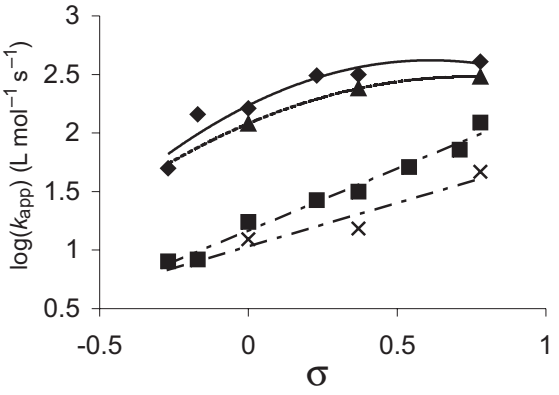


Fig. 1. Hammett plot showing the logarithm of the observed bimolecular rate constant ($\log k_{app}$) plotted against the substituent constant σ for the acetyl aroyl dithioglycoluril substrates **9a**–**9f** (◆) that were studied. Also presented are data for deuterated analogues **12a**, **12e**, and **12f** (▲). The corresponding data for the oxygenated analogues **7** from our previous study (9) are shown for comparison (■, and X for deuterated substrates). Trend lines are shown as an aid to interpretation.



maxima of the product enolates to significantly higher wavelengths than those of the substrates. Indeed, we found that the aroyl groups permitted observation of the reactions in a region of the UV spectrum that was free from absorption owing to other species. However, we were intrigued by the possibility of extending the kinetics measurements to glycolurils bearing only aliphatic acyl groups, since these had been more widely used in our synthetic investigations.

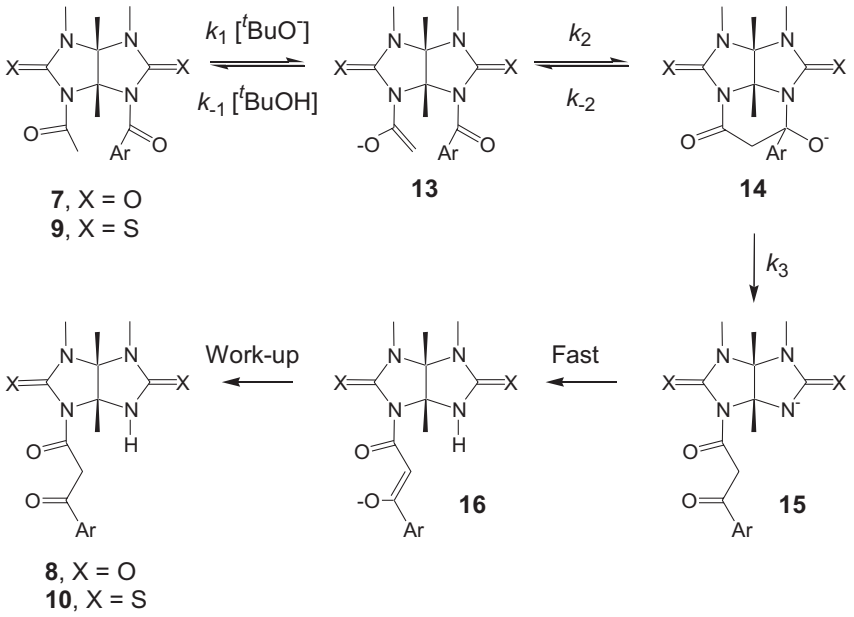
In practice, we found that conversion of both **2** to **3** and **5** to **6** could be readily observed in kinetic runs under conditions otherwise identical to those for **7** and **9**, although λ_{max} for the product enolates was indeed shifted to a lower wavelength (300 nm), where some residual tail-end absorption from starting material was observed. Nonetheless, excellent reproducibility and good fits for the kinetic data were obtained. The rate constants for these reactions are given in Table 1 (entries 11 and 12). Although, as expected for the dramatic change from benzoyl to acetyl, the rate constants are quantitatively different between **2** and **7a** as well as between **5** and **9a**, the differences are remarkably small, suggesting no dramatic change in mechanism. Again, comparing **2** and **5**, thionation accelerates the reaction (17-fold), a result comparable with the effect on acetyl aroyl glycolurils. Further, substitution of CD_3 for CH_3 in both the acetyl groups of **5** slowed the reaction slightly ($k_{app}{}^{H}/k_{app}{}^{D} = 1.25$), a result similar to that observed in **9a** vs. **12a** (Table 1, entry 13).

Discussion

At the outset of this study, we had established that glycoluril **1** can be converted to a range of acetyl aroyl derivatives, and that these undergo efficient intramolecular

© 2005 NRC Canada

Scheme 4. Mechanism proposed for the intramolecular Claisen-like condensation of diacylglycolurils to give β-ketoacylglycolurils.



Claisen-like condensations induced by base, in almost quantitative yield. It had also been shown that the corresponding thio analogue **3** could be more efficiently acylated than **1**, and that a range of nonaromatic diacyldithioglycolurils can undergo the corresponding Claisen-like condensations. The present study shows that acetyl aroyl dithioglycolurils **9a**–**9f** are also readily prepared. That compound **9d** underwent preparative condensation to afford **10d** in reasonable yield (62%, unoptimized), along with the observation that each of **9a**–**9f** gave the enolate of products **10a**–**10f** in the kinetics experiments, shows that this reaction is applicable to the preparation of a range of 3-keto-3-aroylpropanoyl units; these in turn should be of use in synthesis, based on our application of the general methodology described earlier.

Although we had studied the influence of sulfur substitution for oxygen in the glycoluril on the regiochemistry of the condensation reaction, there was no quantitative data to indicate whether this substitution made the key condensation reaction more efficient. Since we had established a rapid method for measuring the reaction rates for conversion of **7** to **8**, and shown that the system obeys straightforward second-order kinetics, we thus set out to evaluate the influence of sulfur substitution on overall reaction rate, and to examine which individual step(s) of the mechanism is (are) influenced by this replacement.

The significantly enhanced overall rate of formation of each of the products **10a**–**10f** from **9a**–**9f** as compared with conversion of **7a**–**7f** to **8a**–**8f** clearly demonstrates that thionation in the glycoluril substantially accelerates the overall reaction (3.5- to 18-fold). A similar effect was found in comparing diacylglycolurils **2** and **5**, demonstrating that the magnitude of the effect appears to be general, and showing for the first time that an aroyl group was not required to observe the kinetics of the condensation reaction. Thus, sulfur substitution improves the overall efficiency of the condensation reaction, a result that was not apparent from the preparative work we had undertaken before. In conjunction with the benefits of thionation that had been shown previously, most notably the ease of acylation as shown here and elsewhere, these results indicate that thioglycolurils may be the auxiliary of choice when using this approach in synthesis.

While these results give the first quantitative measure of the influence of sulfur on the overall reaction rate, comparison of **7** and **9** alone reveals little about the mechanism by which the rate acceleration occurs, since the rates of several steps were comparable in **7a**–**7f**. In the previously proposed mechanism, the first step involved a partially rate-determining deprotonation (step 1, rate constant k_1, Scheme 4) of the diacylglycoluril. Subsequent intramolecular nucleophilic attack (step 2, rate constant k_2) of the ensuing enolate **13** onto the aroyl carbonyl carbon provides tetrahedral intermediate **14**. We previously reasoned that this step was also partly rate-determining, based on the observed positive ρ value in Hammett plots of **7a**–**7f**. However, step 3, the collapse of the tetrahedral intermediate to give **15**, could not be ruled out as a competing slow step. It was reasoned that proton transfer in **15** to give **16**, the species observed in every kinetic experiment, would be rapid.

The faster overall rate upon thionation potentially reflects an acceleration in any or all of the steps involved in the process because k_{app} may be a composite rate constant, depending on which step is influenced. Sulfur substitution might reasonably influence: (*i*) deprotonation, through enhanced kinetic or thermodynamic acidity of the acetyl group via accessibility of the base, enolate stability, or chelate effects, reflected in k_1; (*ii*) condensation, through either enhanced enolate nucleophilicity and (or) activation of the acyl acceptor moiety, either of which would impact k_2; (*iii*) enolate reprotonation, thus altering k_{-1}; or (*iv*) collapse of the tetrahedral intermediate through the enhanced leaving group ability of the thioureido nitrogen in **9** compared to the ureido group in **7**, as would be seen in alteration of k_3. To address the impact of thionation on these individual steps, we determined the rate as a function of aroyl substituent and of deuterium substitution in the acetyl moiety.

The results described here remain fully consistent with

© 2005 NRC Canada

this overall mechanistic scheme (Scheme 4). First-order kinetics in the reactant was observed for all compounds, and it was shown that the reaction of the typical representative **9a** was first order in base, as for **7a**. The rates are somewhat faster than for analogues **7**, but not dramatically altered, again suggesting no overwhelming mechanistic change.

However, the nonlinear Hammett plot for **9a**–**9f** clearly indicates a change in rate-determining step(s). Electron donation in the aroyl entity relative to phenyl decelerates the overall reaction, similar to the effect in **7**. This result is consistent with step 2 remaining at least partially rate-determining. However, with electron-withdrawing groups, there is little influence of substituent on the overall rate ($\sigma = 0.27$), a result consistent with step 2 becoming sufficiently fast with increasing electron withdrawal that it no longer influences the overall rate. Thus, thionation of the glycoluril accelerates step 2 in this regime, and does so to an extent greater than its effect on step 1. Mechanistically, this effect may be the result of either enhanced nucleophilicity of enolate **13** and (or) the enhanced carbonyl group electrophilicity at the aroyl moiety. Further experiments to distinguish these possibilities are now planned.

The observation of a small, but persistent isotope effect upon substitution of CD_3 for Me in the acetyl group in all three thio compounds examined, as well as in diacetyl glycoluril (**5a** vs. **5**) is consistent with step 1 being at least partially rate-determining, as previously proposed for **7**. For the compounds tested, it was not possible to determine from these results whether step 1 was solely the rate-limiting step, since this step may be partially reversible because of exchange with protonated solvent. The resulting gradual dilution of deuterium in the substrate may mask the true isotope effect, as noted previously for **7**. Nonetheless, if reprotonation were extremely fast compared to condensation, then no isotope effect would be expected, since **12** or **5a** would have exchanged completely in the period prior to commencement of measurement. That reprotonation can still compete with condensation in the thio analogues requires that both k_{-1} and k_2 are accelerated relative to the oxygen containing glycolurils.

Finally, it should be noted that the present results are not inconsistent with fast and reversible first and second steps, and a slow collapse of the tetrahedral intermediate in step 3. Although it seems unlikely that sulfur substitution *slows* step 3, further experiments are required to resolve this point.

Conclusions

From a practical standpoint, the results presented provide a rare quantitative measure of the influence of thionation in an auxiliary. Thus, the overall rate acceleration of approx. one order of magnitude, and the demonstration that this effect derives at least partially from acceleration of the key enolate–carbonyl condensation step have implications for the extent to which thionation in other systems such as oxazolidinones may influence the reactions of enolates. Clearly, thioglycoluril **4** is superior to **1** as an auxiliary from the perspective of rate acceleration of the key step of the reaction.

Taken together, the results are consistent with a mechanism for the Claisen-like condensation of acetyl aroyl dithio glycolurils **9a**–**9f** in which a slow (or competitively slow) first step gives enolate **13**. Reprotonation of **13** by *tert*-butanol solvent then competes with intramolecular carbon–carbon bond formation to give tetrahedral intermediate **14**. This quenching of the enolate results in gradual dilution of isotope in analogs **12** containing a trideuteroacetyl group, and masks the true isotope effect on step 1. The C—C bond-forming step is partially rate-determining when the aroyl moiety bears an electron-donating group, but is accelerated by electron-withdrawing groups to the point where it is no longer rate-determining. This effect is in contrast to oxygenated compounds **7**, where step 2 influences the rate even when a 4-nitro substituent is present. Thus, thionation of the glycoluril accelerates the overall condensation rate by accelerating the key condensation step, although it remains to be determined whether other steps are also influenced.

The present results provide a framework for further studies of this intriguing reaction through kinetics experiments. Thus, experiments with monothioglycolurils are underway, to examine the influence of sulfur on one or the other side of the glycoluril, while further experiments with diacyl glycolurils should allow competition experiments between acyl units, so that the mechanistic origins of the previously observed regioselectivities in these reactions can be established.

Experimental section

General

General conditions for preparation and characterization of the glycoluril derivatives were as previously described (9). UV spectroscopy was performed in quartz UV cells bearing a screw cap and septum on a Cary 500 spectrophotometer, with the temperature maintained at 25 °C as previously reported (9). The observation wavelengths used are given in Table 1. The procedures for data manipulation and determination of rate constants were unchanged from our prior work (9). Compound **11a** was prepared as described previously (13).

General procedure for preparation of acetyl aroyl dithioglycolurils 9a–9f

To a solution of **11a** in dichloromethane (15 mL/mmol) at 0 °C was added 2.5–3 equiv. Et_3N. The mixture was stirred for 5 min, then the aroyl chloride (2 to 3 equiv.) was added and stirring was continued for 2.5 h while warming to room temperature. The mixture was extracted three times with 5% HCl. The organic layer was dried over Na_2SO_4, filtered, and concentrated. The product was purified by recrystallization from CH_2Cl_2–hexanes, or by flash chromatography (EtOAc–hexanes, 30:70).

Acetyl benzoyl 2,5-dithioglycoluril (9a)

Compound **11a** (50 mg, 0.18 mmol) and benzoyl chloride (43 μL) gave 62 mg (92%) of **9a**, mp 242–244 °C. UV (THF–*t*-BuOH (50:50), λ_{max}, nm): 244 (ε = 27 000 (mol/L)$^{-1}$ cm^{-1}). IR ($CHCl_3$ cast, cm^{-1}): 2985, 2938 (C-H), 1712 (C=O), 1689 (C=O), 1485, 1402, 1368, 1350, 1333, 1306, 1270, 1240, 1111, 1101. ^{1}H NMR (200 MHz, $CDCl_3$) δ: 7.26–7.55 (5H, m, Ar*H*), 3.38 (3H, s, N-CH_3), 3.25 (3H, s, N-CH_3), 2.70 (3H, s, O=C-CH_3), 2.05 (3H, s, CH_3), 1.71 (3H, s, CH_3). ^{13}C NMR (50 MHz, $CDCl_3$) δ: 179.9, 172.5, 170.3, 134.6, 133.3, 130.4 (2C), 128.3 (2C),

© 2005 NRC Canada

86.8, 86.2, 31.7, 30.8, 28.2, 23.4, 19.0, 16.5. EI-MS *m/z*: 376 [M^+], 246, 193, 142 (base). HR-MS calcd. for $C_{17}H_{20}N_4O_2S_2$: 376.1028; found: 376.1031.

Acetyl 4-methoxybenzoyl 2,5-dithioglycoluril (9b)

Compound **11a** (20 mg, 0.074 mmol) and 4-methoxybenzoyl chloride (38 mg) gave 12 mg (40%) of **9b**. ^{1}H NMR (500 MHz, $CDCl_3$) δ: 7.72 (2H, d, *J* = 8 Hz, Ar*H*), 6.87 (2H, d, *J* = 8 Hz, Ar*H*), 3.83 (3H, s, O-CH_3), 3.35 (3H, s, N-CH_3), 3.24 (3H, s, N-CH_3), 2.67 (3H, s, O=C-CH_3), 2.01 (3H, s, CH_3), 1.68 (3H, s, CH_3). ^{13}C NMR (125 MHz, $CDCl_3$) δ: 180.1, 177.3, 172.4, 169.3, 163.9, 132.8, 127.1, 113.8, 86.7, 86.2, 55.4, 31.6, 30.8, 28.1, 18.9, 16.5.

Acetyl 4-methylbenzoyl 2,5-dithioglycoluril (9c)

Compound **11a** (175 mg, 0.65 mmol) and 4-methylbenzoyl chloride (200 mg) gave 231 mg (91%) of **9c**, mp 230–232 °C. UV (THF–*t*-BuOH (50:50), λ_{max}, nm): 250, 259 (ε = 4650, 4650 (mol/L)$^{-1}$ cm^{-1}). IR ($CHCl_3$ cast, cm^{-1}): 3021 (C-H), 1711 (C=O), 1217, 758. ^{1}H NMR (200 MHz, $CDCl_3$) δ: 7.63 (2H, d, *J* = 8 Hz, Ar*H*), 7.18 (2H, d, *J* = 8 Hz, Ar*H*), 3.36 (3H, s, N-CH_3), 3.23 (3H, s, N-CH_3), 2.68 (3H, s, O=C-CH_3), 2.37 (3H, s, ArCH_3), 2.02 (3H, s, CH_3), 1.69 (3H, s, CH_3). EI-MS *m/z*: 390 [M^+], 260, 142, 119 (base), 91, 56, 43. HR-MS calcd. for $C_{18}H_{22}N_4O_2S_2$: 390.1184; found: 390.1176.

Acetyl 4-chlorobenzoyl 2,5-dithioglycoluril (9d)

Compound **11a** (175 mg, 0.65 mmol) and 4-chlorobenzoyl chloride (228 mg) gave 112 mg (42%) of **9d**, mp 170 to 171 °C. UV (THF–*t*-BuOH (50:50), λ_{max}, nm): 250, 261 (ε = 4100, 4100 (mol/L)$^{-1}$ cm^{-1}). IR ($CHCl_3$ cast, cm^{-1}): 3021 (C-H), 1716 (C=O), 1217, 759. ^{1}H NMR (200 MHz, $CDCl_3$) δ: 7.66 (2H, d, *J* = 8 Hz, Ar*H*), 7.36 (2H, d, *J* = 8 Hz, Ar*H*), 3.38 (3H, s, N-CH_3), 3.24 (3H, s, N-CH_3), 2.73 (3H, s, O=C-CH_3), 2.04 (3H, s, CH_3), 1.72 (3H, s, CH_3). ^{13}C NMR (50 MHz, $CDCl_3$) δ: 179.7, 177.2, 172.5, 169.4, 139.7, 133.1, 131.7 (2C), 128.7 (2C), 86.7, 86.2, 31.8, 30.8, 28.2, 19.0, 16.6. EI-MS *m/z*: 410 [M^+], 280, 142, 43 (base). HR-MS calcd. for $C_{17}H_{19}{}^{35}ClN_4O_2S_2$: 410.0638; found: 410.0640.

Acetyl 3-chlorobenzoyl 2,5-dithioglycoluril (9e)

Compound **11a** (20 mg, 0.074 mmol) and 3-chlorobenzoyl chloride (39 mg) gave 27 mg (90%) of **9e**. ^{1}H NMR (500 MHz, $CDCl_3$) δ: 7.70 (1H, m, Ar*H*), 7.55 (1H, m, Ar*H*), 7.48 (1H, m, Ar*H*), 7.31 (1H, t, *J* = 8 Hz, Ar*H*), 3.38 (3H, s, N-CH_3), 3.23 (3H, s, N-CH_3), 2.73 (3H, s, O=C-CH_3), 2.03 (3H, s, CH_3), 1.70 (3H, s, CH_3). ^{13}C NMR (125 MHz, $CDCl_3$) δ: 179.7, 177.4, 172.6, 169.2, 136.5, 134.4, 133.1, 130.3, 129.4, 128.4, 86.8, 86.2, 31.8, 30.8, 28.1, 19.1, 16.5. EI-S *m/z*: 410 [M^+], 267, 265, 224, 222, 156, 139 (base). HR-MS calcd. for $C_{17}H_{19}{}^{35}ClN_4O_2S_2$: 410.0638; found: 410.0645.

Acetyl 4-nitrobenzoyl 2,5-dithioglycoluril (9f)

Compound **11a** (20 mg, 0.074 mmol) and 4-nitrobenzoyl chloride (21 mg) gave 25 mg (80%) of **9f**. ^{1}H NMR (500 MHz, $CDCl_3$) δ: 8.21 (2H, d, *J* = 9 Hz, Ar*H*), 7.81 (2H, d, *J* = 9 Hz, Ar*H*), 3.40 (3H, s, N-CH_3), 3.21 (3H, s, N-CH_3), 2.77 (3H, s, O=C-CH_3), 2.05 (3H, s, CH_3), 1.72 (3H, s, CH_3). ^{13}C NMR (125 MHz, $CDCl_3$) δ: 179.3, 177.4, 172.7, 168.8, 150.0, 140.2, 131.0, 123.3, 86.7, 86.3, 31.9, 30.8, 28.1, 19.1, 16.4. EI-MS *m/z*: 421 [M^+], 391, 314, 272, 142 (base). HR-MS calcd. for $C_{17}H_{19}N_5O_4S_2$: 421.0878; found: 421.0861.

[2-$^2H_3$]Acetyl-2,5-dithioglycoluril (11b)

To dithioglycoluril **4** (50 mg, 0.22 mmol) in THF (8 mL) was added *n*-BuLi (160 µL of 1.5 mol/L solution in hexanes), and the mixture was stirred for 15 min at room temperature before the addition of acetic anhydride-d_6 (42 µL, 0.44 mmol). After stirring for 1 h, the mixture was quenched with 1 mol/L $NaHSO_4$ (5 mL) and the THF removed on the rotary evaporator. The aqueous residue was extracted with CH_2Cl_2 (2 × 10 mL) and the organic extracts dried over Na_2SO_4. Purification by flash column chromatography (EtOAc–hexanes, 1:1) gave **11b** (28.6 mg, 47%) as a fine white powder. ^{1}H NMR (200 MHz, $CDCl_3$) δ: 3.31 (3H, s, N-CH_3), 3.14 (3H, s, N-CH_3), 1.71 (3H, s, CH_3), 1.59 (3H, s, CH_3). EI-MS *m/z*: 275 [M^+], 143, 84 (base).

[2-$^2H_3$]Acetyl benzoyl 2,5-dithioglycoluril (12a)

Compound **11b** (25 mg, 0.091 mmol) and benzoyl chloride (24 µL) gave 26.3 mg (76%) of **12a**, as for **9a**. ^{1}H NMR (200 MHz, $CDCl_3$) δ: 7.24–7.73 (5H, m, Ar*H*), 3.35 (3H, s, N-CH_3), 3.22 (3H, s, N-CH_3), 2.70 (missing, O=C-CH_3), 2.03 (3H, s, CH_3), 1.69 (3H, s, CH_3). EI-MS *m/z*: 379 [M^+], 246, 143, 105 (base).

[2-$^2H_3$]Acetyl 3-chlorobenzoyl 2,5-dithioglycoluril (12e)

Compound **11b** (20 mg, 0.073 mmol) and 3-chlorobenzoyl chloride (3 equiv.) gave 23 mg (76%) of **12e**, as for **9e**.

[2-$^2H_3$]Acetyl 4-nitrobenzoyl 2,5-dithioglycoluril (12f)

Compound **11b** (20 mg, 0.073 mmol) and 4-nitrobenzoyl chloride (3 equiv.) gave 27 mg (87%) of **12f**, as for **9f**.

4-Chlorobenzoylacetyl dithioglycoluril 10d from 9d

Compound **9d** (60.6 mg, 0.148 mmol) in THF (1.5 mL) was treated with potassium *tert*-butoxide (31.5 mg, 0.28 mmol). The mixture was stirred for 45 min, then quenched with 10% $NaHSO_4$ (3 mL), and extracted with CH_2Cl_2 (2 × 10 mL). The combined organic layers were washed (brine (2 × 10 mL) then water (10 mL)), dried (Na_2SO_4), filtered, and concentrated. Flash column chromatography (60% EtOAc–hexanes) gave 37.1 mg (62%) of **10d**, mp 70 °C dec. UV (THF–*t*-BuOH (50:50), λ_{max}, nm): 250, 330, 370 (sh) (ε = 37 000, 7530 (mol/L)$^{-1}$ cm^{-1}); when treated with excess KO-*t*-Bu: 353 nm (ε = 12 500 (mol/L)$^{-1}$ cm^{-1}). IR ($CHCl_3$ cast, cm^{-1}): 3439 (N-H), 3021 (C-H), 1745, 1672 (C=O), 1329, 1292, 1217, 762. ^{1}H NMR (200 MHz, $CDCl_3$) δ: 8.17 (s, enol C=C*H*), 7.85 (2H, d, *J* = 9 Hz, keto Ar*H*), 7.78 (2H, d, *J* = 9 Hz, enol Ar*H*), 7.46 (2H, d, *J* = 9 Hz, keto Ar*H*), 7.40 (2H, d, *J* = 9 Hz, enol Ar*H*), 7.32 (1H, br s, keto and enol N*H*), 5.73 (1H, d, *J* = 16 Hz, keto COCH_2CO), 4.32 (1H, d, *J* = 16 Hz, keto COCH_2CO), 3.36 (3H, s, enol N-CH_3), 3.27 (3H, s, keto N-CH_3), 3.19 (3H, s, enol N-CH_3), 3.18 (3H, s, keto N-CH_3), 1.85 (3H, s, keto CH_3), 1.83 (3H, s, enol CH_3), 1.65 (3H, s keto and enol CH_3). EI-MS *m/z*: 412, 410 [M^+], 368, 361, 359, 230, 180, 142 (base).

© 2005 NRC Canada

HR-MS calcd. for $C_{17}H_{19}{}^{35}ClN_4O_2S_2$: 410.0638; found: 410.0641.

Acknowledgments

We thank the Natural Sciences and Engineering Research Council of Canada (NSERC) for financial support of this work.

References

1. For examples, see: G. Procter. *In* Asymmetric synthesis. Oxford University Press, Oxford. 1996; K.J. Hale and S. Manaviazar. *In* Advanced asymmetric synthesis. *Edited by* G.R. Stephenson. Chapman and Hall, London. 1996.
2. D.A. Evans, J. Bartroli, and T.L. Shih. J. Am. Chem. Soc. **103**, 2127 (1981). For reviews, see: D.J. Ager, I. Prakash, and D.R. Schaad. Aldrichimica Acta, **30**, 3 (1997); D.J. Ager, I. Prakash, and D.R. Schaad. Chem. Rev. **96**, 835 (1996); D.A. Evans. Aldrichimica Acta, **15**, 23 (1982).
3. For a recent review, see: F. Velazquez and H.F. Olivo. Curr. Org. Chem. **6**, 303 (2004).
4. For selected examples, see: Y. Nagao, S. Yamada, T. Kumagai, M. Ochiai, and E. Fujita. J. Chem. Soc. Chem. Commun. 1418 (1985); M.T. Crimmins, B.W. King, E.A. Tabet, and K. Chaudhary. J. Org. Chem. **66**, 894 (2001).
5. For an example of enhanced cleavage of an acylthiazolidinethione, see: S. Yamada. Angew. Chem. Int. Ed. Engl. **32**, 1083 (1993).
6. For a review, see: E.A. Castro. Chem. Rev. **99**, 3505 (1999); for recent examples, see: I.-H. Um, H.-J. Han, M.-H. Baek, and S.-Y. Bae. J. Org. Chem. **69**, 6365 (2004).
7. S. Sun and P.H.M. Harrison. Tetrahedron Lett. **33**, 7715 (1992); S. Sun and P.H.M. Harrison. J. Chem. Soc. Chem. Commun. 2235 (1994); S. Sun, L. Edwards, and P.H.M. Harrison. J. Chem. Soc. Perkin Trans. 1, 437 (1998); C. Cow, D. Valentini, and P. Harrison. Can. J. Chem. **75**, 884 (1997).
8. H. Biltz. Chem. Ber. **40**, 4806 (1907).
9. M. Rahimizadeh, K. Kam, S.I. Jenkins, R.S. McDonald, and P.H.M. Harrison. Can. J. Chem. **80**, 517 (2002).
10. For crystal structures of **7a** and **8a**, see: C.F. Matta, C.N. Cow, and P.H.M. Harrison. J. Mol. Struct. **660**, 81 (2003).
11. D.A. Evans, M.O. Ennis, T. Le, N. Mandel, and G. Mandel. J. Am. Chem. Soc. **106**, 1154 (1984); D.A. Evans, J.S. Clark, R. Metternich, V.J. Novack, and G.S. Sheppard. J. Am. Chem. Soc. **112**, 866 (1990).
12. T.J. Simpson. *In* Biosynthesis: polyketides and vitamins. *Edited by* F.J. Leeper and J.C. Vederas. Springer, Berlin. 2000. pp. 1–48; J. Staunton and B. Wilkinson. *In* Biosynthesis: Polyketides and vitamins. *Edited by* F.J. Leeper and J.C. Vederas. Springer, Berlin. 2000. pp. 49–92. For recent reviews, see: B.J. Rawlings. Nat. Prod. Rep. **14**, 335 (1997); **15**, 275 (2001); **18**, 190 (2001); **18**, 231 (2001); R. Bentley and J.W. Bennett. Annu. Rev. Microbiol. **53**, 411 (1999); C.W. Carreras, R. Pieper, and C. Khosla. Top. Curr. Chem. **188**, 85 (1997); also see the thematic issue: Polyketide and nonribosomal polypeptide biosynthesis. Chem. Rev. **7** (1997), and refs. cited therein.
13. C. Cow and P. Harrison. J. Org. Chem. **62**, 8834 (1997).
14. P.A. Duspara, C.F. Matta, S.I. Jenkins, and P.H.M. Harrison. Org. Lett. **3**, 495 (2001).
15. L.P. Hammett. J. Am. Chem. Soc. **59**, 96 (1937).

© 2005 NRC Canada

Ambident reactivity of phenoxyl radicals in DNA adduction

Richard A. Manderville

Abstract: Phenols are a class of compounds that can create beneficial effects in vivo owing to their antioxidant properties (through radical scavenging), or they can display hazardous effects owing to their pro-oxidant properties. The mechanism by which phenols act as pro-oxidants stems from their one-electron oxidation into reactive phenoxyl radicals by peroxidase enzymes or redox-active transition metals. In the presence of thiols and molecular oxygen, these reactive phenoxyl radicals stimulate an oxidative stress and cause oxidative damage to biomolecules, which is proposed to contribute to the occurrence of cancer in peroxidase rich tissues. Recent results from our laboratory show that certain phenoxyl radicals can also react directly with the C-8 site of deoxyguanosine to afford oxygen and carbon bonded adducts. This reactivity is consistent with the ambident (oxygen vs. C attachment) electrophilicity of phenoxyl radicals coupled with the susceptibility of the C-8 site of deoxyguanosine to radical attachment. Given that formation of covalent DNA adducts is regarded as the initiation event in the carcinogenic process, C-8 deoxyguanosine adducts of phenolic toxins are expected to contribute greatly to peroxidase driven toxic effects of phenolic xenobiotics. The focus of this review is the role of phenoxyl radicals in direct reactions with DNA and the use of Brown σ^+ values to predict their reactivity.

Key words: DNA adduction, phenoxyl radicals, chlorophenols, ochratoxin A, deoxyguanosine.

Résumé : Les phénols forment une classe de composés qui peuvent avoir des effets bénéfiques in vivo en raison de leurs propriétés antioxydantes (par le biais de leur capacité à piéger les radicaux) ou qui peuvent présenter des effets délétères en raison de leurs propriétés prooxydantes. Le mécanisme par lequel les phénols agissent comme prooxydants découle de leur oxydation, par un mécanisme impliquant un électron qui conduit aux radicaux réactifs phénoxyles, sous l'action des enzymes peroxydases ou des métaux de transition actifs en oxydoréduction. En présence de thiols ou d'oxygène moléculaire, ces radicaux phénoxyles stimulent un stress oxydant et provoquent des dommages oxydants aux biomolécules qui contribueraient, selon les théories actuelles, à l'apparition de cancers dans les tissus riches en peroxydases. Des résultats récents obtenus dans nos laboratoires montrent que certains radicaux phénoxyles peuvent aussi réagir directement avec le site C-8 de la désoxyguanosine pour conduire à la formation d'adduits liés par l'oxygène ou le carbone. Cette réactivité est en accord avec le caractère électrophile ambident (attachement à l'oxygène ou au carbone) des radicaux phénoxyles couplé à la susceptibilité du site C-8 de la désoxyguanosine à des attaques radicalaires. Se basant sur la théorie que la formation d'adduits covalents de l'ADN est considérée comme l'étape qui initie le processus cancérigène, on peut s'attendre à ce que les adduits de toxines phénoliques en C-8 de la désoxyguanosine contribueront fortement aux effets toxiques des xénobiotiques phénoliques activés par les peroxydases. L'objet principal de cette revue est le rôle des radicaux phénoxyles dans les réactions directes avec l'ADN et l'utilisation des valeurs σ^+ de Brown pour prédire leur réactivité.

Mots clés : adduits avec l'ADN, radicaux phénoxyles, chlorophénols, ochratoxine A, désoxyguanosine.

[Traduit par la Rédaction]

Introduction

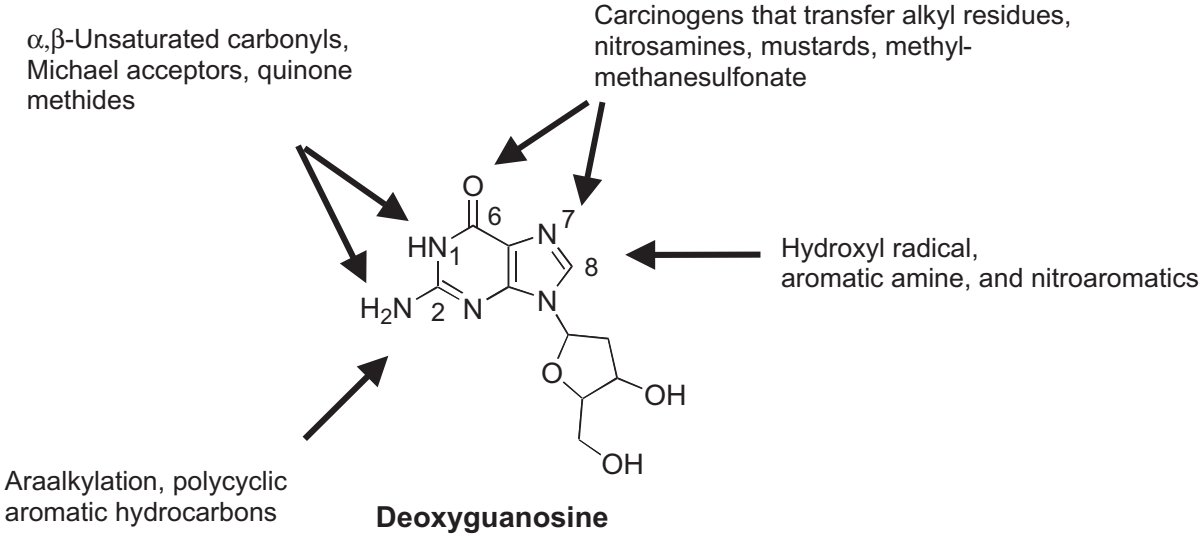
Phenols are ubiquitous substances that possess a wide range of biological activities. Vitamin E and related phenols containing electron-releasing alkyl and methoxy groups possess antioxidant properties through radical scavenging that are beneficial to human health (1). However, certain phenols may also display deleterious pro-oxidant properties that are thought to contribute to aging and disease (2). This pro-oxidant activity is initiated through the one-electron (e) oxidation of phenols into reactive phenoxyl radical intermediates by enzymes with peroxidase activity and redox-active transition metals. These reactive intermediates then undergo a redox-cycling mechanism by hydrogen (H) atom abstraction of essential thiols, such as glutathione (GSH) and protein sulfhydryls, to yield thiyl radicals; this repeatedly generates the parent phenol as a substrate for peroxidase (3). The thiyl radicals react with GSH to generate a GSH disulfide anion radical that can reductively activate molecular oxygen (O_2), which in the presence of transition-metal complexes, can yield the hydroxyl radical that may damage lipids (4), proteins (5), and DNA (6). In addition to an oxidative stress mediated through the phenoxyl radical in vivo, direct covalent reactions of phenoxyl radicals with DNA to

Received 20 February 2005. Published on the NRC Research Press Web site at http://canjchem.nrc.ca on 12 October 2005.

R.A. Manderville. Department of Chemistry, University of Guelph, Guelph, ON N1G 2W1, Canada. (e-mail: rmanderv@uoguelph.ca).

 doi: 10.1139/V05-121 © 2005 NRC Canada

Fig. 1. Summary of the sites on deoxyguanosine that are modified by chemical carcinogens.



yield DNA adducts would contribute to peroxidase driven toxic effects of phenolic xenobiotics (3).

The formation of covalent DNA adducts in vivo is recognized as a common property of most potent carcinogens (7). Shown in Fig. 1 are the sites on deoxyguanosine (dG) that are modified by chemical carcinogens. Those that transfer alkyl residues (nitrosamines, mustards, and methyl-methanesulfonate) target the endocyclic N-7 atom and the exocyclic O-6 atom (7). Polycyclic aromatic hydrocarbons that undergo bioactivation to generate dihydrodiol epoxides and other agents that transfer an araalkyl group tend to target the exocyclic N-2 atom. This site is also modified by α,β-unsaturated carbonyls, Michael acceptors, and quinone methides (8, 9). While it is to be expected that these nucleophilic sites would be targeted by electrophiles, the C-8 site of dG is also a target site of many established carcinogens. For example, those that transfer an arylamine residue and include, aromatic amines, aminoazo dyes, nitroaromatics, and heterocyclic amines found in cooked fish and meats, are known to form nitrogen (N) bonded C-8–dG adducts as the major products (10). The hydroxyl radical also reacts at the C-8 site of dG to form 8-oxo-dG, which is the major oxidative lesion found in DNA, suggesting that the C-8 site of dG is susceptible to radical attack (6).

Recent findings from our work on DNA adduction by phenolic xenobiotics highlights their ability to react covalently with C-8–dG following activation by peroxidase enzymes or redox-active transition metals (11–13). Given that phenols are known to undergo peroxidase mediated oxidation into phenoxyl radicals (14), and C-8–dG adduct formation is in keeping with the susceptibility of C-8–dG to radical attachment, our studies suggest the intermediacy of the phenoxyl radical in covalent bond forming reactions with DNA. Due to their ambident (oxygen (O) vs. carbon (C) attachment) electrophilicity, O adducts and para and ortho C adducts can be formed. Correlation of phenoxyl radical reactivity is also possible due to the fact that remote substituent effects of phenoxyl radicals exhibit a linear correlation with Brown σ^+ constants because of the through-resonance between the electron-deficient phenoxyl radical and the ring substituent (15). The focus of this review is the role of phenoxyl radicals in direct reactions with DNA and the use of σ^+ values to predict reactivity, which is expected to dictate pro-oxidant vs. antioxidant behavior in biological systems.

Chlorophenol (CP) — O adduct formation

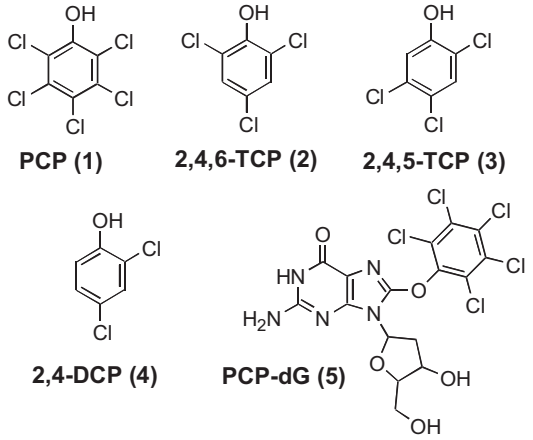
Chlorophenols (CPs) are toxic chemicals that are persistent in the environment. The Environmental Protection Agency (EPA) lists pentachlorophenol (PCP, **1**), 2,4,6-trichlorophenol (TCP, **2**), 2,4,5-TCP (**3**), and 2,4-dichlorophenol (DCP, **4**) as priority pollutants, and of these, **1** and **2** are classified as Group B2 (probable) carcinogens (16). CPs have found use in pesticides, disinfectants, wood preservatives, personal care formulations, and are substantial by-products of wood pulp bleaching with chlorine (17). Human exposure to CPs may occur through drinking water and food and they can be detected in the blood of a high percentage of the population (18). Case reports suggest an association between PCP (**1**) and Hodgkin's disease, soft tissue sarcoma, and acute leukemia (19). Oral animal studies have demonstrated that **1** is a liver carcinogen in mice (20); exposure of rats and mice to **2** resulted in increased incidences of leukemias and hepatocellular carcinomas (16).

It is believed that oxidative metabolism is necessary for CPs to exert their toxic effects. The metabolism of PCP in mammals has been studied extensively and, in general, it has been demonstrated that PCP undergoes cytochrome P450-mediated dechlorination to yield tetrachlorobenzoquinone (TCBQ) and (or) tetrachlorohydroquinone (TCHQ) metabolites (21). The formation of direct DNA adducts by the TCBQ metabolite of PCP has been reported in the liver of mice and rats following mulitiple doses of PCP (22). However, recent in vitro studies show that adduct levels ($36 \pm 9/10^5$ nucleotides) by 100 μmol/L PCP following activation by horseradish peroxidase (HRP) – H_2O_2 are 30-fold higher than levels induced by microsomes that contain cytochrome P450 and 10-fold higher than levels induced by 5 mmol/L TCBQ itself (23).

To gain insight into PCP-mediated DNA adduction, we examined the reaction of PCP (100 μmol/L) with DNA nu-

© 2005 NRC Canada

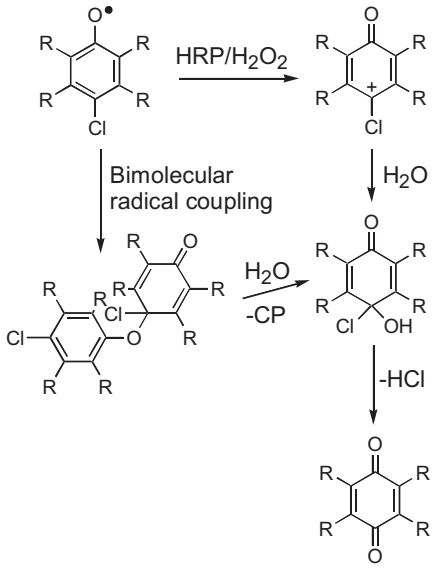
cleosides (2 mmol/L) using HRP–H_2O_2 as the oxidation catalyst and LC–MS (12). Interestingly, these conditions yielded a single DNA adduct that had the five chlorine isotope pattern of PCP and had a molecular ion at $[M - H]^-$ = 528, suggesting attachment of dG with loss of two protons (i.e., PCP(264) + dG(267) – 2H = 529). Isolation and NMR (^1H and ^{13}C) analysis confirmed C-8 attachment by the O site of PCP to yield the adduct PCP–dG (**5**).



Additional experiments were carried out to determine whether **5** could be formed by additional enzyme systems, and whether other DNA bases could react with **1** following HRP–H_2O_2 activation. These experiments showed the reaction to be absolutely specific for dG; no detectable adduct(s) was observed from HRP–H_2O_2 and **1** in the presence of dA, dC, or T. It was also found that the adduct **5** could be generated by treatment of PCP–dG with human myeloperoxidase. However, treatment of PCP–dG with rat liver microsomes that contain cytochrome P450 failed to yield **5** and instead an adduct with $[M - H]^-$ = 440 was detected that was found to co-elute with an adduct induced by reaction of dG with authentic TCBQ. That PCP is a substrate for myeloperoxidase is highly significant given that exposure to PCP has been linked to incidences of leukemia (19). As an analogy, it has been proposed that benzene, via its phenol metabolite, is a leukemogen owing to myeloperoxidase catalyzed oxidation of phenol into the phenolic radical that exhibits pro-oxidant properties (24).

An extension of our studies on HRP-mediated dG adduction by PCP (12) was conducted to include dG adduction by a greater range of CP toxins (**2**–**4**) and to determine whether the pentachlorophenoxyl radical reacts with an actual duplex DNA substrate to form **5** (25). In terms of HRP–H_2O_2 activation, the results with **1** suggested that other CPs (**2**–**4**) would similarly react with dG to yield C-8 O adducts. To test this hypothesis, CP–dG reactions were carried out using conditions analogous to the PCP–dG reaction and were analyzed by LC–MS. Here, it was expected that **2** and **3** would yield an O adduct with a molecular ion at $[M - H]^-$ = 460, while the O adduct from **4** would have a molecular ion at $[M - H]^-$ = 426. However, under conditions favourable for O adduct formation by **1**, the only other CP to yield detectable levels of O adduct was **3**. The major adduct detected for **2**–**4** had UV absorbances at ~275 and 334 nm with a molecular ion at $[M - H]^-$ = 390/392 with a single chlorine isotope. The UV spectrum of the major adduct was similar to

Scheme 1.



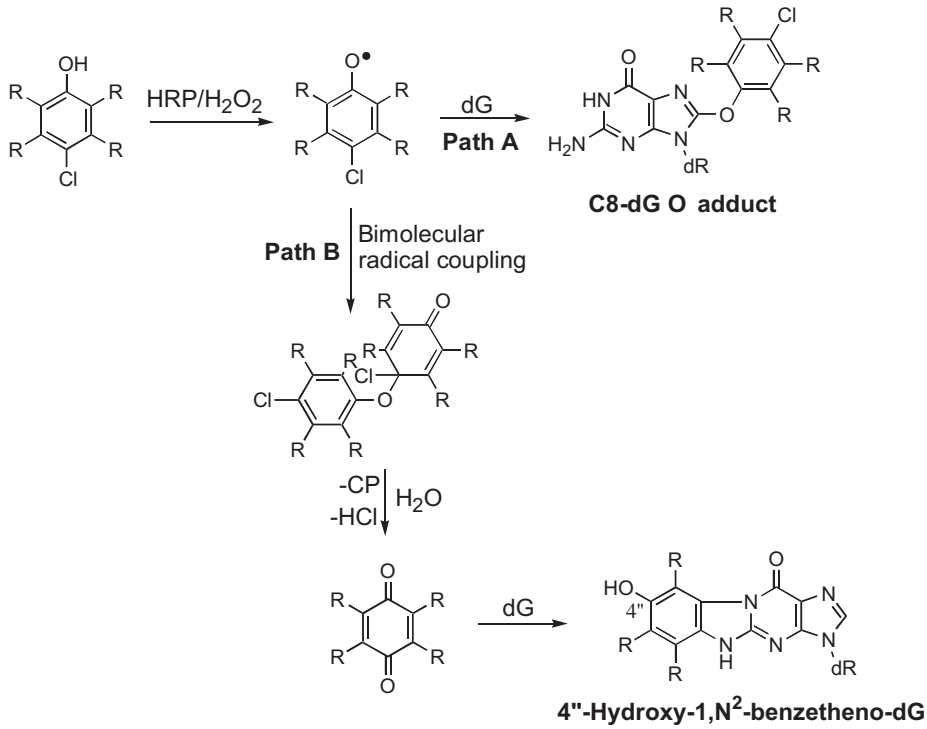
the spectrum reported for the dG adduct generated from 1,4-benzoquinone (BQ) – dG (26), suggesting that bioactivation by HRP–H_2O_2 for these CP substrates (100 µmol/L) yielded a BQ electrophile.

Insight into the intermediacy of a BQ electrophile in dG adduction by CP toxins was gleaned from the literature where the oxidation of halogenated phenols by peroxidase enzymes has been a subject of considerable interest and, in general, the predominant reaction product is a 1,4-BQ (27–31). Thus, as outlined in Scheme 1, the 1,4-BQ may arise by the elimination of HCl from a *gem*-chlorohydrin intermediate derived through HRP-catalyzed 1 e oxidation of a chlorophenoxyl radical to yield a carbocation intermediate that reacts with water. Alternatively, the *gem*-chlorohydrin could arise by hydrolysis of the ether formed by C-O coupling of two chlorophenoxyl radicals. In the case of peroxidase mediated oxidation of **1**, Kazunga et al. (31) presented evidence that the final quinone product (TCBQ) is an artifact of extraction and analytical methods and that the principal product is the ether 2,3,4,5,6-pentachloro-4-pentachlorophenoxy-2,5-cyclohexadienone formed by pentachlorophenoxyl radical coupling. This suggested a common mechanism for HRP–H_2O_2 mediated oxidation of a CP involving bimolecular radical coupling for 1,4-BQ formation. It also suggested the possibility that lowering the concentration of the CP to retard radical coupling would favour C-8-dG O adduct formation for **2**–**4**. Thus, the CP–dG reactions were repeated at 10 µmol/L CP and now all three CPs (**2**–**4**) generated the anticipated C-8–dG O adduct as the major lesion; for **3** the O adduct was the only observable adduct, while **2** and **4** still formed detectable levels of BQ adduct (25).

To determine whether a C-8–dG O adduct forms with a duplex DNA substrate, calf thymus DNA (1 mg/mL) was treated with PCP (100 µmol/L) in phosphate buffer (100 mmol/L, pH 7.4) at 37 °C for 24 h in the presence of HRP (Type VI, 25 units/mL) – H_2O_2 (1 mmol/L) (25). The reacted DNA was precipitated, enzymatically digested, and analyzed by LC–MS using an authentic sample of **5** for comparison. These studies showed that the major DNA le-

© 2005 NRC Canada

Scheme 2.



sion formed from PCP activation by HRP–H_2O_2 had an HPLC retention time, MS–MS fragmentation, and a parent ion identical to those of the authentic adduct standard **5**. This implied that the pentachlorophenoxyl radical reacted with the duplex DNA substrate to form the O bonded C-8 adduct **5** highlighting the in vitro relevance of C-8–dG adducts of phenolic toxins.

The results from these studies on CP-mediated DNA adduction by peroxidase activation allowed us to propose the mechanism summarized in Scheme 2. The reaction is initiated by the production of the chlorophenoxyl radical that may either react directly with dG to furnish the C-8–dG O adduct in an irreversible process (Path A) or self-couple to yield the 1,4-BQ electrophile that reacts with dG to give 4″-hydroxy-1,N^2-benzetheno-dG (Path B). Formation of the benzetheno–dG adduct in Path B may involve initial Schiff base formation from the exocyclic N-2 atom of dG and the carbonyl carbon of the BQ and subsequent nucleophilic attack of the endocyclic N-1 on the vinyl carbon. An alternative pathway, as originally proposed by Jowa et al. (32), would involve initial reaction of N-2 at the vinyl carbon of BQ followed by N-1 attachment to the carbonyl carbon atom to yield 3″-hydroxy-1,N^2-benzetheno-dG. However, the ^{1}H NMR chemical shifts and reaction chemistry for this family of cyclic adducts favour 4″-hydroxy-1,N^2-benzetheno-dG adduct assignment (25).

Differences in CP reactivity may be ascribed to differences in rate constant for the phenoxyl radical bimolecular self-reaction (Path B in Scheme 2). If the bimolecular self-reaction is favourable, then Path B competes effectively with Path A at 100 μmol/L CP substrate, while if the self-reaction is not favourable, then Path A dominates. Increased Cl substitution would be expected to inhibit the bimolecular self-reaction because of steric and (or) electronic repulsion. In this regard, the bimolecular self-reaction rate constant for the phenoxyl radical in H_2O is 2.6×10^9 $(mol/L)^{-1}$ s^{-1} (33) and it has a half-life of ~60 μs in CCl_4 (34). In contrast, the pentachlorophenoxyl radical has a half-life of 30–45 min in aqueous buffer, as determined from direct detection by EPR spectroscopy (28). Clearly Cl substitution increases phenoxyl radical lifetime and this factor would be expected to contribute to phenoxyl radical reactivity in a biological system by enabling the radical time to diffuse away from its site of formation and react with biopolymers.

Ochratoxin A (OTA) — C adduct formation

Ochratoxin A (OTA, **6**) is a mycotoxin produced by several species of *Aspergillus* and *Penicillium* fungi that structurally consists of a *para*-chlorophenolic group containing a dihydroisocoumarin moiety that is amide linked to L-phenylalanine (35). The growth of OTA-producing molds is not readily controlled in stored animal and human foods (36). The toxic effects of OTA include carcinogenicity, mutagenicity, and nephrotoxicity (35). Dietary feeding of OTA induces renal adenomas and carcinomas in male mice and rats (37), and for this reason, it has been classified as group 2B (possible carcinogenic to humans) by the International Agency for Research on Cancer (IARC) (38). The toxin is widespread in temperate areas such as Canada, Denmark, Norway, Germany, Sweden, and the United Kingdom (39). In North America, blood plasma samples collected from volunteers in 16 locations across Canada showed a range of 0.29–2.37 ng/mL with the highest mean concentration in Winnipeg, Manitoba (40). Canadian cancer statistics (2004) estimate 4300 new cases of kidney cancer in Canadians with prevalence in the male population (61%). The highest incidence rate of kidney cancer in males occurs in Manitoba, which correlates with individuals from Manitoba having the highest blood plasma levels of OTA (40). Given

© 2005 NRC Canada

that OTA is an established kidney carcinogen in male rodents (37), OTA may be a cause of kidney cancer in Canadian men.

In Europe, OTA is implicated in a fatal kidney disease called Balkan endemic nephropathy (BEN) (41). BEN is a chronic tubulointerstitial nephropathy described in several rural regions of Bulgaria, Romania, and the former Yugoslavia. Of particular interest are the upper urinary tract tumors (UTT) seen in BEN patients at frequencies much higher than in individuals not suffering from the disease (41). A study of UTT in areas with BEN has demonstrated a direct correlation with OTA exposure (42). The UTT DNAs were studied by the ^{32}P postlabeling method for the presence of OTA-DNA adducts and identified for the first time were OTA-DNA adducts for UTT in patients with BEN that were absent in control tissues. This study provided impetus for the view that OTA-DNA adducts lead to UTT in patients suffering from BEN (42).

One hypothesis for the carcinogenicity of OTA is based on the toxin's genotoxic properties that follow from its biotransformation via an oxidative pathway (43). Because ^{32}P postlabeling studies have suggested a preference for OTA to specifically react with dG (44), we sought to characterize the OTA–dG covalent interaction (11). Initial efforts utilized the photochemistry of OTA to activate the toxin for reaction of dG. Photoirradiation of an OTA (100 μmol/L) – dG (50 mol equiv.) mixture for 2 min in 100 mmol/L phosphate buffer (pH 7.4) generated three major products, as evidenced by electrospray mass spectrometry (ES^-). Two of the products were assigned to the hydroquinone of OTA (OTHQ (**7**), $[M - H]^- = 384$) and the nonchlorinated analogue OTB (**8**) ($[M - H]^- = 368$). The third product also lacked the chlorine isotope pattern of OTA and had a parent ion at $[M - H]^- = 633$. Its MS–MS spectrum exhibited a prominent ion at *m/z* 517 (-deoxyribose (dR)) that was accompanied by ions at *m/z* 473 ($[M - dR - CO_2 - H]^-$) and 429 ($[M - dR - 2CO_2 - H]^-$), suggesting covalent attachment of dG to OTA with loss of HCl (i.e., OTA(403) – Cl(35) + dG(267) – H = 634) (11).

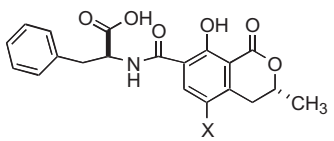
Isolation of the adduct with $[M - H]^- = 633$ and identification by two-dimensional NMR spectroscopy established the adduct structure as the C bonded C-8–dG adduct, OTA–dG (**9**). With the authentic sample of **9** in hand, it was then demonstrated that the same adduct could be formed by treatment of OTA–dG with redox-active transition metals (Fe and Cu) or HRP–H_2O_2 (11).

In collaboration with Dr. Annie Pfohl-Leszkowicz (Toulouse, France) we employed OTA–dG–3′-monophosphate (MP) as a cochromatographic standard for ^{32}P postlabeling studies and demonstrated that OTA–dG co-migrates with the major DNA lesion detected in diseased kidney tissue of rat and with one of four adducts detected in the kidney of the pig (13). The co-migration of OTA–dG with a spot observed by ^{32}P postlabeling emphasizes the biological significance of this compound.

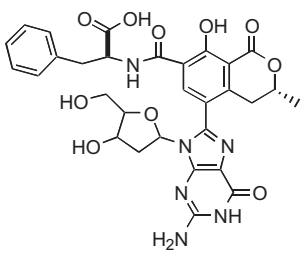
Ambident reactivity of phenols in C-8–dG adduct formation

The isolation and identification of OTA–dG suggested involvement of the OTA phenoxyl radical in covalent bond formation. The toxin undergoes a 1 e oxidative process at ~0.8 V vs. the saturated calomel electrode (SCE) to form the phenoxyl radical (45), and structure–activity relationships implicate the OTA phenoxyl radical in OTA-mediated DNA damage (46). However, unlike CP toxins that favour O adduct formation at C-8–dG (12, 25), OTA favours C adduct formation (11). For OTA, O attachment must be disfavored due to steric (flanking carbonyl moieties) or electronic (delocalization of the OTA phenoxyl radical) factors. Binding of the phenolic O site to a transition metal would also be expected to preclude O attachment. In this regard, Ni(salens) that form phenoxyl radicals upon oxidation are reported to act like OTA and favour C adduct formation at the C-8 site of dG (47). For the amino acid tyrosine, theoretical calculations on DNA adduction by the tyrosyl radical predict ortho C adduct formation because delocalization of the radical favours C attachment and the para position is blocked (48).

In Scheme 3, pathways for ambident reactivity of *para*-chlorophenolic radicals at C-8 of dG are depicted. The O site of the phenolic radical (generated by peroxidase–H_2O_2) is shown reacting at C-8 to yield the N radical intermediate with the sp^3-bound C-8 atom; H atom abstraction (by a phenolic radical) would furnish the O adduct, i.e., **5**. In contrast, C attack would generate the corresponding quinoidal intermediate; homolytic loss of HCl would furnish the O radical that would require an H atom to give the C adduct, i.e., **9**. In the absence of steric factors, the electronic properties of the phenolic radical would be expected to dictate O vs. C adduct formation. Extensive radical delocalization would favour C adduct formation, while O attachment would be favoured for phenoxyl radicals with the unpaired electron localized on the oxygen atom. In this regard, it has been observed that remote substituent effects of phenoxyl radicals exhibit a linear correlation with Brown σ^+ constants because of the through-resonance between the electron-deficient phenoxyl radical and the ring substituent (15, 33). Table 1 gives pK_a values, standard reduction potentials (E°_{red}) for the phenoxyl radical / phenolate ion couples at pH 12, and σ^+ values that are available in the literature for CP substrates, phenol (PhOH), 4-MePhOH, and 4-MeOPhOH (33). A high value of σ^+ suggests that the radical is localized on the oxygen atom, while the negative value for 4-MeOPhOH (–0.78) suggests extensive radical stabilization by the 4-MeO substituent. Not surprisingly, the fully substituted analog PCP has the highest σ^+ value (1.1) and is predicted to be the most reactive O centered radical followed by **3** ($\sigma^+ = 0.61$), **2** ($\sigma^+ = 0.3$), and **4** ($\sigma^+ = 0.21$). Our data shows that the larger value of σ^+ for a CP gives a greater proportion of C-8–dG O adduct. In contrast, tyrosine would have a σ^+ value similar to 4-MePhOH (–0.31), which suggests extensive radical delocalization and is thus predicted to favour C adduct formation.



OTA: X = Cl (6)
OTHQ: X = OH (7)
OTB: X = H (8)



OTA-dG (9)

© 2005 NRC Canada

Scheme 3.

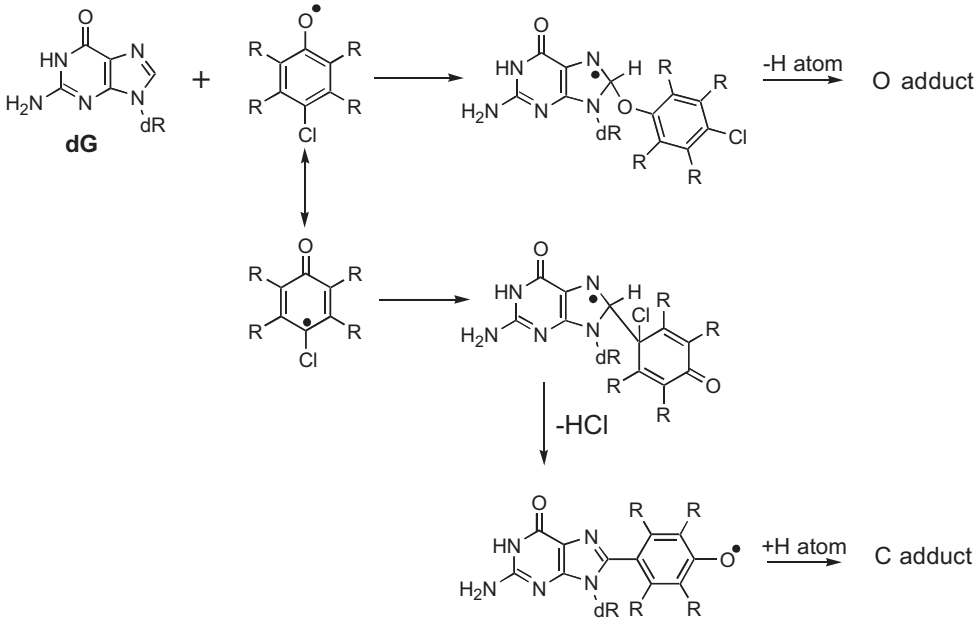


Table 1. Parameters for phenols in aqueous solution.

Phenol	pK_a	E_{red}° (pH 12.0)[a]	σ^+
PhOH	9.98	0.86	0.00
PCP (**1**)	4.74	0.99	1.1
2,4,6-TCP (**2**)	5.99	0.90	0.30
2,4,5-TCP (**3**)	6.72	0.90	0.61
2,4-DCP (**4**)	7.90	0.88	0.21
4-MePhOH	10.28	0.71	–0.31
4-MeOPhOH	10.20	0.58	–0.78

Note: Data taken from ref. 33.
[a]Estimated reduction potential of the phenoxyl radical in volts vs. NHE.

Conclusions

The studies previously discussed demonstrate the ability of phenoxyl radicals to react directly with DNA to yield C-8–dG O or C adducts, as a consequence of the ambident electrophilicity of phenoxyl radicals. Our work provides the first in vitro evidence for C-8–dG O adducts of phenolic toxins by demonstrating that PCP reacts directly with calf thymus DNA to give the O adduct **5** following activation by HRP–H_2O_2. For the natural product OTA, we have isolated and identified the C adduct **9** as the primary OTA–DNA adduct and ^{32}P postlabeling studies support its formation in kidney DNA isolated from pig and rat. Overall, these studies strengthen the hypothesis that direct reactions of phenoxyl radicals with DNA contribute to peroxidase driven toxic effects of phenolic xenobiotics. That physical organic studies have provided σ^+ constants for a wide range of phenols suggests the ability to develop quantitative structure–activity relations (QSAR) for DNA adduction by phenolic xenobiotics. It will be interesting to extend our current work and include a greater range of phenols to determine whether σ^+ values can predict C vs. O adduct formation and pro-oxidant vs. antioxidant behaviour. Current efforts are also focused on the chemical syntheses of C-8–dG adducts (O and C adducts) for site-specific incorporation into duplex DNA for biophysical measurements, NMR structural analysis, and biological testing.

Acknowledgments

Financial support from the National Institutes of Health (R01-CA080787), the Lance Armstrong Foundation, the Environmental Protection Agency (EPA), and the Department of Chemistry at the University of Guelph is acknowledged. I also acknowledge with gratitude the contributions of my coworkers to these studies. Their names appear in the references; special thanks are due to Drs. Jian Dai, Gyungse Park, Dean Lantero, Marcus W. Wright, M. Wade Calcutt, Ronald E. Noftle (Wake Forest University), John D. Simon (Duke University), and Annie Pfohl-Leszkowicz (National High School of Agriculture, Toulouse, France).

References

1. G.W. Burton and K.U. Ingold. Acc. Chem. Res. **19**, 194 (1986).
2. J.L. Bolton. Toxicology, **177**, 55 (2002).
3. R. Goldman, G.H. Claycamp, M.A. Sweetland, A.V. Sedlov, V.A. Tyurin, E.R. Kisin, Y.Y. Tyurina, V.B. Ritov, S.L. Wenger, S.G. Grant, and V. Kagan. Free Radical Biol. Med. **27**, 1050 (1999).
4. T.A. Dix and J. Aikens. Chem. Res. Toxicol. **6**, 2 (1993).
5. E.R. Stadtman. Science (Washington, D.C.), **257**, 1220 (1992).
6. C.J. Burrows and J.G. Muller. Chem. Rev. **98**, 1109 (1998).
7. A. Dipple. Carcinogenesis, **16**, 437 (1995).
8. J.L. Bolton, M.A. Trush, T.M. Penning, G. Dryhurst, and T.J. Monks. Chem. Res. Toxicol. **13**, 135 (2000).
9. W.F. Veldhuyzen, Y.-F. Lam, and S.E. Rokita. Chem. Res. Toxicol. **14**, 1345 (2001).
10. C.E. Elmquist, J.S. Stover, Z. Wang, and C.J. Rizzo. J. Am. Chem. Soc. **126**, 11 189 (2004).

© 2005 NRC Canada

11. J. Dai, M.W. Wright, and R.A. Manderville. J. Am. Chem. Soc. **125**, 3716 (2003).
12. J. Dai, M.W. Wright, and R.A. Manderville. Chem. Res. Toxicol. **16**, 817 (2003).
13. V. Faucet, A. Pfohl-Leszkowicz, J. Dai, M. Castegnaro, and R.A. Manderville. Chem. Res. Toxicol. **17**, 1289 (2004).
14. C. Walsh. Enzymatic reaction mechanisms. W.H. Freeman and Company, New York. 1979. p. 488.
15. J. Lind, X. Shen, T.E. Eriksen, and G. Merényl. J. Am. Chem. Soc. **112**, 479 (1990).
16. IARC. IARC monographs on the evaluation of carcinogenic risks to humans: Occupational exposures in insecticide applications, and some pesticides. Pentachlorophenol. Vol. 53. IARC Press, Lyon, France. 1991. p. 371.
17. S. Ramamoorthy and S. Ramamoorthy. Chlorinated organic compounds in the environment. CRC Press, Boca Raton, Florida. 1997.
18. L. Hovander, T. Malmberg, M. Athanasiadou, I. Athanassiadis, S. Rahm, A. Bergman, and E. Klasson Wehler. Arch. Environ. Contam. Toxicol. **42**, 105 (2002).
19. H.J. Roberts. J. Fla. Med. Assoc. **77**, 86 (1990).
20. E.E. McConnell. Toxicology and carcinogenesis studies of two pentachlorophenol technical-grade mixtures (CAS. No. 87-86-5) in B6C3F1 mice (feed studies). NTP TR349. NIH Publication No. 89-2804. US Department of Health and Human Services, National Institutes of Health, Research Triangle Park, North Carolina. 1988.
21. (*a*) U.G. Ahlborg, K. Larsson, and T. Thunberg. Arch. Toxicol. **40**, 45 (1978); (*b*) B. Van Ommen, A. Adang, F. Muller, and P.J. Van Bladeren. Chem. Biol. Interact. **65**, 247 (1988); (*c*) G. Renner and C. Hopfer. Xenobiotica, **20**, 573 (1990); (*d*) C.-H. Tsai, P.-H. Lin, S. Waidyanathaand, and S.M. Rappaport. Chem. Biol. Interact. **134**, 55 (2001).
22. P.-H. Lin, D.K. La, P.B. Upton, and J.A. Swenberg. Carcinogenesis, **23**, 365 (2002).
23. J.-C. Gautier, J. Richoz, D.H. Welti, J. Markovik, E. Gremaud, F.P. Guengerich, and R.J. Turesky. Chem. Res. Toxicol. **14**, 34 (2001).
24. B.W. Day, V.A. Tyurin, Y.Y Tyurina, M. Liu, J.A. Facey, G. Carta, E.R. Kisin, R.K. Dubey, and V.E. Kagan. Chem. Res. Toxicol. **12**, 28 (1999).
25. J. Dai, A.L. Sloat, M.W. Wright, and R.A. Manderville. Chem. Res. Toxicol. **18**, 771 (2005).
26. A. Chenna and B. Singer. Chem. Res. Toxicol. **10**, 165 (1997).
27. F.P. Guengerich. J. Biol. Chem. **264**, 17 198 (1989).
28. V.M. Samokyszyn, J.P. Freeman, K.R. Maddipati, and R.V. Lloyd. Chem. Res. Toxicol. **8**, 349 (1995).
29. F.W. Wiese, H.C. Chang, R.V. Lloyd, J.P. Freeman, and V.M. Samokyszyn. Arch. Environ. Contam. Toxicol. **34**, 217 (1998).
30. R.P. Ferrari, E. Laurenti, and F. Trotta. JBIC, J. Biol. Inorg. Chem. **4**, 232 (1999).
31. C. Kazunga, M.D. Aitken, and A. Gold. Environ. Sci. Technol. **33**, 1408 (1999).
32. L. Jowa, G. Witz, R. Snyder, S. Winkle, and G.F. Kalf. J. Appl. Toxicol. **10**, 47 (1990).
33. C. Li and M.Z. Hoffman. J. Phys. Chem. B, **103**, 6653 (1999).
34. J. Grodkowski and P. Neta. J. Phys. Chem. **88**, 1205 (1984).
35. J. Dai, G. Park, J.L. Perry, Y.V. Il'ichev, D.A.J. Bow, J.B. Pritchard, V. Faucet, A. Pfohl-Leszkowicz, R.A. Manderville, and J.D. Simon. Acc. Chem. Res. **37**, 874 (2004).
36. F. Galvano, A. Piva, A. Ritieni, and G. Galvano. J. Food Prot. **64**, 120 (2001).
37. G. Boorman. NTP technical report on the toxicology and carcinogenesis studies of ochratoxin A (CAS No 303-47-9) in F344/N rats (gavage studies). NIH Publication No. 89-2813. US Department of Health and Human Services, National Institutes of Health, Research Triangle Park, North Carolina. 1989.
38. J.E. Huff. IARC Sci. Publ. 115, 229 (1991).
39. D. Benford, C. Boyle, W. Dekant, R. Fuchs, D.W. Gaylor, G. Hard, D.B. McGregor, J.I. Pitt, R. Plestina, G. Shephard, M. Solfrizzo, P.J.P. Verger, and R. Walker. Ochratoxin A. Joint Expert Committee Monograph. Vol. 47. FAO/WHO Joint Expert Committee on Food Additives. 2001.
40. P.M. Scott, S.R. Kanhere, B.P. Lau, D.A. Lewis, S. Hayward, J.J. Ryan, and T. Kuiper-Goodman. Food Addit. Contam. **15**, 555 (1998).
41. T. Vrabcheva, T. Petkova-Bocharova, F. Grosso, I. Nikolov, I.N. Chernozemsky, M. Castegnaro, and S. Dragacci. J. Agric. Food Chem. **52**, 2404 (2004).
42. A. Pfohl-Leszkowicz, T. Petkova-Bocharova, I.N. Chernozemsky, and M. Castegnaro. Food Addit. Contam. **19**, 282 (2002).
43. A. Pfohl-Leszkowicz, Y. Grosse, A. Kane, A. Gharbi, I. Baudrimont, S. Obrecht, E.E. Creppy, and G. Dirheimer. *In* Human ochratoxicosis and its pathologies. Vol. 231. John Libbey Eurotext Ltd., London, UK. 1993. p. 129.
44. S. Obrecht-Pflumio and G. Dirheimer. Chem. Biol. Interact. **127**, 29 (2000).
45. M.W. Calcutt, I.G. Gillman, R.E. Noftle, and R.A. Manderville. Chem. Res. Toxicol. **14**, 1266 (2001).
46. C. Malaveille, G. Brun, and H. Bartsch. Mutat. Res. **307**, 141 (1994).
47. J.G. Muller, L.A. Kayser, S.J. Paikoff, V. Duarte, N. Tang, S.E. Rokita, and C.J. Burrows. Coord. Chem. Rev. **185–186**, 761 (1999).
48. F. Ban, M.J. Lundqvist, R.J. Boyd, and L.A. Eriksson. J. Am. Chem. Soc. **124**, 2753 (2002).

© 2005 NRC Canada

Acceleration of the methanolysis of phosphate diesters promoted by $La(OTf)_3$ — The analysis of non-integer $^{s}_{s}$pH/rate profiles resulting from changes in metal ion speciation[1]

Graham T.T. Gibson, Alexei A. Neverov, Allen Chun-Tien Teng, and R.S. Brown

Abstract: In a previous publication (A.A. Neverov and R.S. Brown. Inorg. Chem. **40**, 3588 (2001)) we reported very effective catalysis of the methanolysis of some phosphate diesters (methyl *p*-nitrophenyl phosphate (**1**), bis(*p*-nitrophenyl) phosphate (**2**), and diphenyl phosphate (**3**)) promoted by La^{3+}, and noted a general observation that the plots of $\log k_{cat}$ vs. $^{s}_{s}$pH had non-integer gradients. In this report the origins of that behaviour are studied and analyzed through determination of the speciation of $La^{3+}(^{-}OCH_3)_n$, $(La^{3+})_2(^{-}OCH_3)_m$, $(La^{3+})_2$:phosphate:$(^{-}OCH_3)_y$ forms in solution as a function of $^{s}_{s}$pH. Potentiometric titrations of solutions of $La(OTf)_3$ in methanol at low ($<1 \times 10^{-4}$ mol/L) and high ($>1 \times 10^{-3}$ mol/L) concentration were analyzed through fits of the data to various models to provide speciation diagrams of the various La^{3+} forms in the absence of phosphate. Titrations of La^{3+} in the presence of diphenyl phosphate were also analyzed to provide speciation diagrams for phosphate bound forms. The kinetic data for the La^{3+} catalyzed methanolysis of **1** were analyzed through fitting the kinetic data at low and high $[La^{3+}]$ as a function of $^{s}_{s}$pH to a linear combination of the individual kinetic contributions of each species. Overall the data are best analyzed in the low $[La^{3+}]$ domain as resulting from methoxide attack on a transient complex of phosphate bound to $La^{3+}(^{-}OCH_3)_{0,1}$. In the high $[La^{3+}]$ domain the data fit two kinetically equivalent processes involving either a spontaneous decomposition of $(La^{3+})_2$:**1**$^{-}$:$(^{-}OCH_3)_{2,3,4,5}$ or external methoxide attack on $(La^{3+})_2$:**1**$^{-}$:$(^{-}OCH_3)_{1,2,3,4}$.

Key words: lanthanides, phosphate diester, methanolysis, kinetics, speciation, metal ion catalysis of methanolysis, DNA model methanolysis.

Résumé : Dans une publication antérieure (A.A. Neverov et R.S. Brown. Inorg. Chem. **40**, 3588 (2001)), nous avons rapporté une catalyse très efficace de la méthanolyse de quelques esters de l'acide phosphorique (phosphate de méthyle et de *p*-nitrophényle (**1**), phosphate de bis(*p*-nitrophényle) (**2**) et phosphate de diphényle (**3**)) sous l'influence du La^{3+} et nous avons noté que les gradients des courbes du $\log k_{cat}$ vs. $^{s}_{s}$pH n'étaient pas des nombres entiers. Dans ce travail, nous avons étudié ce comportement et l'avons analysé par une détermination de la spéciation des formes $La^{3+}(^{-}OCH_3)_n$, $(La^{3+})_2(^{-}OCH_3)_m$ et $(La^{3+})_2$:phosphate:$(^{-}OCH_3)_y$ en solution en fonction du $^{s}_{s}$pH. Afin de pouvoir obtenir des diagrammes de spéciation des diverses formes de La^{3+} en l'absence de phosphate, nous avons analysé les résultats de titrages potentiométriques de solutions de $La(OTf)_3$ dans le méthanol, à des concentrations basses ($<1 \times 10^{-4}$ mol/L) et élevées ($>1 \times 10^{-3}$ mol/L), en procédant à divers ajustements des données à divers modèles. Afin d'obtenir des diagrammes de spéciation des formes liées du phosphate, nous avons aussi analysé les données des titrages du La^{3+} en présence de phosphate de diphényle. Les données cinétiques pour la méthanolyse du **1** catalysée par le La^{3+} ont été analysées par le biais d'un ajustement des données à des concentrations faibles et élevées de La^{3+} en fonction de $^{s}_{s}$pH afin d'obtenir une combinaison linéaire des contributions cinétiques individuelles de chaque espèce. Dans l'ensemble, la meilleure façon d'expliquer les données dans le domaine de faible concentration de La^{3+} implique une attaque du méthanolate sur un phosphate intermédiaire lié à un $La^{3+}(^{-}OCH_3)_{0,1}$. Dans le domaine de concentration élevée de La^{3+}, les données peuvent être expliquées par deux processus cinétiquement équivalents impliquant soit une décomposition spontanée d'un complexe $(La^{3+})_2$:**1**$^{-}$:$(^{-}OCH_3)_{2,3,4,5}$ ou une attaque externe d'un méthanolate sur un complexe $(La^{3+})_2$:**1**$^{-}$:$(^{-}OCH_3)_{1,2,3,4}$.

Mots clés : lanthanides, diester de l'acide phosphorique, méthanolyse, cinétique, spéciation, catalyse par un ion métallique d'une méthanolyse, méthanolyse modèle de l'ADN.

[Traduit par la Rédaction]

Received 12 December 2004. Published on the NRC Research Press Web site at http://canjchem.nrc.ca on 18 October 2005.

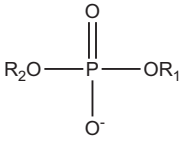
G.T.T. Gibson, A.A. Neverov, A.C.-T. Teng, and R.S. Brown.[2] Department of Chemistry, Queen's University, Kingston, ON K7L 3N6, Canada.

[1]This article is part of a Special Issue dedicated to organic reaction mechanisms.
[2]Corresponding author (e-mail: rsbrown@chem.queensu.ca).

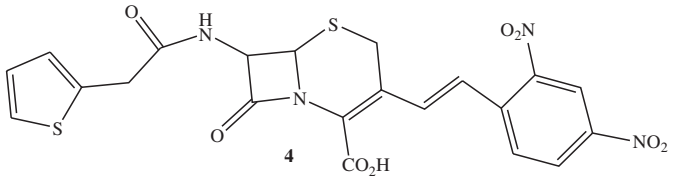
 doi: 10.1139/V05-065 © 2005 NRC Canada

Introduction

Various studies from these labs have shown that La^{3+}, along with 1 equiv. of methoxide in methanol, is an extraordinarily active catalyst for the methanolysis of carboxylate esters (1), β-lactams (2), and a variety of phosphates and thiophosphates including phosphate di- and triesters (3). The phosphate diester linkage is biologically important because it is ideal for preserving genetic information in RNA and DNA because of its kinetic robustness toward hydrolysis. To facilitate what is otherwise a very slow hydrolytic process, Nature provides various metallo-enzymes (4) such as the RNAse from HIV reverse transcriptase (4*a*), 3′–5′ exonuclease from DNA polymerase I (4*b*), and P1 nuclease (4*c*) to cleave phosphate diesters so it is not surprising that a large number of studies have been reported concerning metal-ion-promoted hydrolysis of $(RO)(R'O)PO_2^-$ species (5).



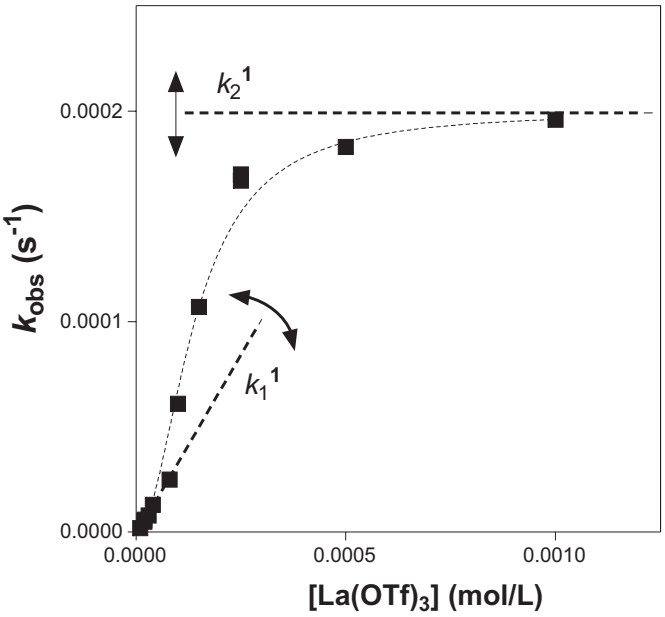
1 $R_2O = OCH_3$, $R_1O = OC_6H_4NO_2$
2 $R_2O = R_1O = OC_6H_4NO_2$
3 $R_2O = R_1O = OC_6H_5$



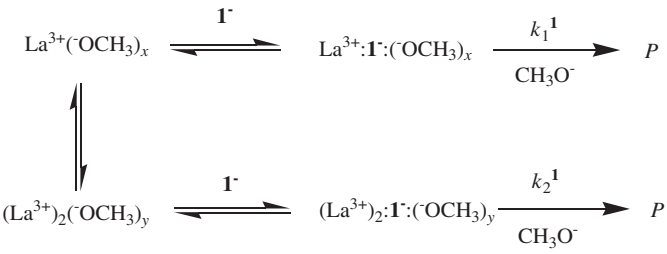
4

Interestingly, metal-catalyzed alcoholysis of phosphate diesters is, to our knowledge, a scarcely investigated area although our own studies (3*a*) showed that the methanolyses of methyl *p*-nitrophenyl phosphate (**1**), bis(*p*-nitrophenyl) phosphate (**2**), and diphenyl phosphate (**3**) were accelerated by as much as 10^{10}-fold in the presence of La^{3+} compared to the background methoxide promoted reaction. Unfortunately, a comprehensive mathematical fit of the kinetic behaviour to a given mechanism that included all the species responsible for catalysis as a function of $^{s}_{s}$pH was not possible due to the complexity of the situation as revealed from kinetic plots of the observed pseudo-first-order rate constant (k_{obs}) for the methanolysis of **1** as a function of $[La^{3+}]$ at various $^{s}_{s}$pH values. Typically, the plots show (3*a*) two $^{s}_{s}$pH-dependent domains of interest, which are illustrated schematically in Fig. 1 (see Figs. 1S and 2S, Supplementary material, for the appearance of these plots at two different $^{s}_{s}$pH values).[3] On the basis of these plots, we rationalized the kinetic behaviour in terms of the simplified process given in Scheme 1, where monomeric and dimeric forms of La^{3+} associated with variable numbers of methoxides in a $^{s}_{s}$pH-dependent way were responsible for the catalysis.

Fig. 1. Plot of pseudo-first-order rate constants for the methanolysis of **1** (2×10^{-5} mol/L) vs. $[La(OTf)_3]$ at 25 °C; $^{s}_{s}$pH = 11.1 (0.02 mol/L triethylamine buffer). Based on data from ref. 3*a*. The values of $k_2^{\mathbf{1}}$ and $k_1^{\mathbf{1}}$ are taken as the limiting plateau value and initial gradient of the plots at given $^{s}_{s}$pH values; double-headed arrows show the direction of change of $k_2^{\mathbf{1}}$ and $k_1^{\mathbf{1}}$ as a function of $^{s}_{s}$pH.



Scheme 1.



At limiting low and high $[La^{3+}]$ we could define the $k_1^{\mathbf{1}}$ and $k_2^{\mathbf{1}}$ as the slope and plateau, respectively, of the k_{obs} vs. $[La^{3+}]$ plots at each $^{s}_{s}$pH, the values being reproduced in Table 1S of the Supplemental material.[3] Curiously, neither $k_1^{\mathbf{1}}$ nor $k_2^{\mathbf{1}}$ shows a unit linear dependence on $[^{-}OCH_3]$, the slopes being 0.35 and 0.5, respectively (3*a*): in the case of the $k_1^{\mathbf{1}}$ plot there is a serious downturn at the highest $^{s}_{s}$pH values.

Typically, log plots of rate constant vs. [lyate], [lyoxide], [catalyst], or $[M^{x+}]$ have integer gradients of 0, 1, or 2, which result from rate-limiting processes having zero-, first-, or second-order dependencies on the concentration of the species of interest. In some common cases such kinetic plots exhibit "saturation" behaviour, with a domain of unit slope evolving into a plateau of zero slope at higher concentration indicative of a substrate associated with the catalytic entity in a kinetically competent 1:1 complex. Non-integer kinetic

[3] Supplementary data for this article are available on the Web site or may be purchased from the Depository of Unpublished Data, Document Delivery, CISTI, National Research Council Canada, Ottawa, ON K1A 0S2, Canada. DUD 4014. For more information on obtaining material refer to http://cisti-icist.nrc-cnrc.gc.ca/irm/unpub_e.shtml.

© 2005 NRC Canada

plots are far less common for ionic reactions[4] (6) although square root dependencies are often observed for reactions catalyzed by metal ions that dimerize to inactive forms such as was found in our recent study of the Zn^{2+} promoted methanolysis of *p*-nitrophenyl acetate and the phosphate triester paraoxon (7), or the Cu^{2+} catalyzed hydrolysis of *p*-nitrophenyl diethyl phosphate (8).

In cases where the speciation of a M^{x+} catalyst changes as a function of its concentration or as a function of pH, one can envision an alteration of the catalytic properties in such a way that the pH / log rate constant profiles can have non-integer gradients or exhibit irregular upward or downward curvature. This phenomenon is probably a general one, the recognition and incorporation of which will prove particularly applicable to studies of mono- and polymetal ion catalysis as a function of pH where the pH / log rate constant profiles do not vary in a regular way (9). Indeed, in a recent analysis of the La^{3+} promoted methanolysis of the β-lactam nitrocefin (**4**) we demonstrated (2) that the nonunit slope for the kinetic data as a function of ${}^{s}_{s}$pH could be accommodated by two kinetically equivalent mechanisms: methoxide attack on $La^{3+}{}_2(\mathbf{4}^-)(^-OCH_3)_n$, n = 0–2, or spontaneous decomposition of the forms $La^{3+}{}_2(\mathbf{4}^-)(^-OCH_3)_n$, n = 1–3.

In this report we analyze the previously obtained rate data for the La^{3+} catalyzed methanolysis of **1** (3*a*) in terms of models involving La^{3+} monomers and dimers with varying numbers of methoxides, the speciation of which depends upon [La^{3+}] concentration and the ${}^{s}_{s}$pH. The speciation of La^{3+} at low (<2 × 10^{-4} mol/L) and high (>1 × 10^{-3} mol/L) metal ion concentrations is computed through analysis of the potentiometric titration data using the program Hyperquad 2000 (10). At high concentrations of metal ion, where the kinetics are suggestive of the formation of $La^{3+}{}_2$ bound phosphate, we have conducted the titrations on solutions of La^{3+} with a fixed 2:1 La^{3+} : diphenyl phosphate ratio, analyzing these to determine the metal ion binding constants and speciation. Finally, we have analyzed the kinetic data in terms of the contributions of the various species present in solution to develop an internally consistent explanation of the shapes of the ${}^{s}_{s}$pH/rate profiles.

Experimental

Materials

Methanol (anhydrous, 99.8%), sodium methoxide (0.5 mol/L in MeOH), lanthanum trifluoromethanesulfonate (99.999%), bis(*p*-nitrophenyl) phosphate (**2**, 99%), and diphenyl phosphate (**3**, 99%) were all purchased from Aldrich and used without any further purification.

${}^{s}_{s}$pH Measurements

The $CH_3OH_2^+$ concentration was determined for kinetic and titration measurements using a Radiometer pHC4000-8 or an Accumet model 13-620-292 combination glass electrode calibrated with Fisher certified standard aqueous buffers (pH = 4.00 and 10.00) as described in our recent papers (11). Values of ${}^{s}_{s}$pH were calculated by subtracting a correction constant of –2.24 from the experimental meter reading (${}^{s}_{w}$pH). This method was described by Bates and co-workers (12*b*, 12*c*) for a molality scale (correction constant –2.34) and later by Bosch and co-workers (13) for a molar correction constant of –2.24 units.

${}^{s}_{s}p\mathit{K}_a$ Determination

The potentiometric titrations of $La(OTf)_3$ and diphenyl phosphate in methanol were performed using a Metrohm model 798 Titrino automatic titrator under anaerobic conditions (Ar) at 25.0 ± 0.1 °C. Methanolic $La(OTf)_3$ and diphenyl phosphate stock solutions (0.02 or 0.002 mol/L) were diluted to the required concentrations by adding anhydrous methanol. The total sample volume in all cases was 20.0 mL. Sodium methoxide titrant, prepared from stock 0.5 mol/L $NaOCH_3$ in a Sure Seal® bottle, was 0.021 or 0.0028 mol/L and was calibrated by titrating Fisher certified standard HCl in water, with the endpoint taken to be ${}^{w}_{w}$pH 7. After each titration the electrode was immersed in pH 4.00 aqueous buffer or a dilute aq. HCl solution for several minutes. The electrode was then rinsed with MeOH, dried with a tissue, and used for the next titration. The electrode was recalibrated often to ensure accurate readings.

The values of the species formation constants in methanol were calculated using the computer program Hyperquad 2000 (version 2.1 NT) (10), with the autoprotolysis constant of pure methanol taken to be $10^{-16.77}$ (13) at 25 °C. The formation constants for the species $La^{3+}{}_2(^-OMe)_n$ (n = 1–5) were determined from the analysis of the potentiometric titration of 1 × 10^{-3} mol/L $La(OTf)_3$. Two such titrations were analyzed separately and their respective species formation constants averaged; the resulting values were used as constants in the subsequent Hyperquad analysis of 2:1 $La(OTf)_3$:phosphate titrations. Similarly, formation constants for the species $La^{3+}(^-OMe)_n$ (n = 1–3) were determined from the analysis of the titration of 1 × 10^{-4} mol/L $La(OTf)_3$. Because the methanolysis of phosphates **1** and **2** in the presence of $La(OTf)_3$ is too fast to perform the titrations of these, **3** was used as a model for all three phosphates studied in the kinetics. The ${}^{s}_{s}p\mathit{K}_a$ of **3** was determined to be 3.47 ± 0.01 from the average result of the Hyperquad analysis of three separate titrations of 1 × 10^{-3} mol/L **3**, and this value was used in subsequent analyses as a constant. The formation constant for the species $La^{3+}{}_2$:$\mathbf{3}^-$, as a model for the species $La^{3+}{}_2$:$\mathbf{1}^-$, was computed from fitting as were other formation constants for species present in a solution of 2:1 La^{3+}:diphenyl phosphate.

Kinetic measurements

The rate of appearance of *p*-nitrophenol accompanying the methanolysis of **2** was followed by monitoring the increase in absorbance of buffered methanol solutions at 311 nm and 25.0 ± 0.1 °C with a Varian Cary 100 Bio UV–vis spectrophotometer. Its extinction coefficient at 311 nm was determined to be 10 878 ± 479 $(mol/L)^{-1}$ cm^{-1} by averaging the slopes of 17 independent plots of Abs. vs. added [*p*-nitrophenol] over 5 × 10^{-5} mol/L < [La^{3+}] < 1 × 10^{-3} mol/L and 2.5 × 10^{-5} mol/L < [*p*-nitrophenol] < 2.25 × 10^{-4} mol/L. Due to the slow rate of reaction at low [La^{3+}], all reactions

[4] Of course, the kinetics of free-radical-initiated chain reactions such as $H_2 + Br_2 \rightarrow 2HBr$, where the first step requires a dissociation of the Br_2 into 2Br radicals, are well-known to follow a square root dependence in [Br_2] (for a discussion of this mechanism see ref. 6).

© 2005 NRC Canada

in this study were followed to 10% completion and k_{obs} was determined in triplicate using the initial rates method. All reactions were performed at $^{s}_{s}$pH 9.21 ± 0.10 (measured after the kinetic run) using a methanol buffer solution of 1.75 × 10^{-2} mol/L *N*-ethylmorpholine ($^{s}_{s}pK_a$ = 8.60 (measured by half neutralization (3*a*)) partially neutralized with 70% $HClO_4$ (BDH). The solutions prepared in this way contain a small, but kinetically insignificant quantity (<0.1%) of water stemming from that present in the MeOH and what is derived from buffer neutralization. To avoid any chloride ion contamination from the glass electrode that might affect the metal ion reactions, the $^{s}_{s}$pH of the reaction solutions was always determined after kinetic measurements.

To investigate whether the kinetics in the low [La^{3+}] domain result from a 1:1 or a 2:2 La^{3+}:**2**$^{-}$ complex at a given $^{s}_{s}$pH (9.21), it was first necessary to establish the point of transition between the ascending and descending wings of the k_{obs} vs. [La^{3+}] plot (see Fig. 1S, Supplemental information).[3] This kinetic experiment was done using [**2**] = 5 × 10^{-5} mol/L and varying [La^{3+}] between 2.5 × 10^{-5} and 4 × 10^{-3} mol/L; the point of transition was determined to occur at 2 × 10^{-4} mol/L [La^{3+}]. To determine if the kinetically active species was a monomeric 1:1 La^{3+}:phosphate complex or a dimeric 2:2 La^{3+}:phosphate complex, [La^{3+}] and [total phosphate] were varied together such that [total phosphate] = [La^{3+}] = 2 × 10^{-4} to 1.2 × 10^{-3} mol/L. Phosphate **2** had poor solubility in the presence of La^{3+} at concentrations higher than 3 × 10^{-4} mol/L, and so its concentration was held constant at 2 × 10^{-4} mol/L in each case, and the far more soluble phosphate **3** was used make up the [total phosphate] throughout the rest of the concentration range.[5]

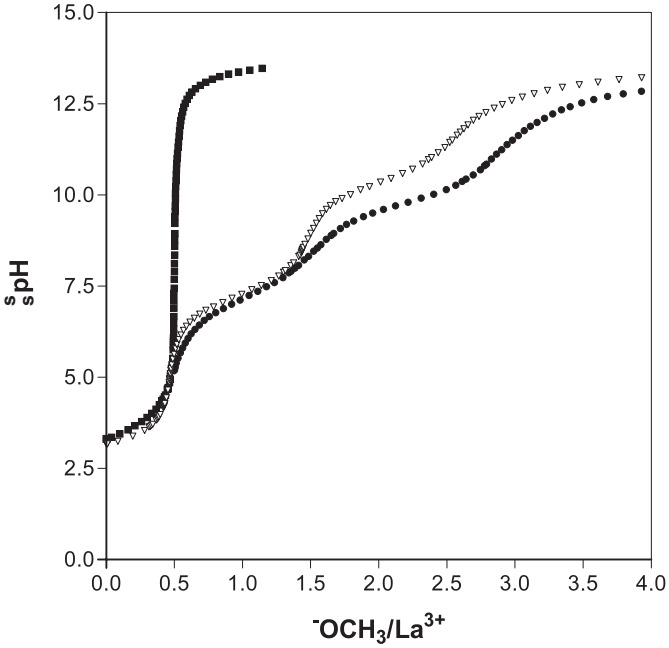
Electrospray MS

Mass spectra were determined in methanol using a Waters/Micromass ZQ (Manchester, UK) single quadrupole mass spectrometer equipped with an electospray source operating at cone voltages between 30 and 70 V. The solutions contained [**3**] = 2 × 10^{-4} mol/L, along with equimolar $La(OTf)_3$ and 4 × 10^{-4} mol/L Bu_4NOCH_3, the latter to create **3**$^{-}$ and add 1 equiv. of methoxide to the metal ion. Samples were infused at a flow rate of 10 μL/min; the spectrometer was externally calibrated and run in positive mode.

Results and discussion

The methodology for fitting the kinetic data as a function of varying [La^{3+}] and $^{s}_{s}$pH involves analyzing the speciation of the metal ion alone at low and high concentrations as a function of $^{s}_{s}$pH and then determining the speciation of the phosphate bound forms of the metal ion. All these data can be gleaned from potentiometric titrations under the appropriate conditions. Following analysis of the speciation, one can then fit the kinetic data (Table 1S, Supplemental material)[3] pertaining to k_1**[1]** (the second-order rate constant for La^{3+} promoted methanolysis of **1** at low [La^{3+}] as a function of $^{s}_{s}$pH) and k_2**[1]** (the plateaued pseudo-first-order rate constant for (La^{3+})$_2$:**1**$^{-}$ methanolysis as a function of $^{s}_{s}$pH) as a linear combination of the contribution of various kinetically active species.

Fig. 2. Potentiometric titration data for 0.001 mol/L $La(OTf)_3$ (●), 0.001 mol/L diphenyl phosphate (■), and a mixture of 0.001 mol/L $La(OTf)_3$ and 0.0005 mol/L diphenyl phosphate (▽) determined in methanol at 25 °C.



Titration analysis

High [La^{3+}] domain (>10^{-3} mol/L)

In the high [La^{3+}] domain of the k_{obs} vs. [La^{3+}] plots for methanolysis of **1** at each $^{s}_{s}$pH the saturation signifies that the active species comprise two metal ions and one phosphate substrate, the latter most likely bridging the two La^{3+} ions to employ double activation (3*a*, 3*b*). Depending on the $^{s}_{s}$pH, the active (La^{3+})$_2$:**1**$^{-}$ species are also proposed to contain a variable number of methoxides from zero to five (3*a*). The six (La^{3+})$_2$:**1**$^{-}$:($^{-}OCH_3$)$_{0-5}$ forms serve as a starting model to fit the potentiometric titration data for 2:1 La^{2+}:phosphate in methanol at 1 × 10^{-3} mol/L La^{3+}, a concentration within the k_2**[1]** domain. Since **1** is too reactive to survive titration in the presence of La^{3+}, the less reactive phosphate **3** was used in the present study as a structural model. While we recognize that the substitution of **3** for **1** might alter the phosphate binding constants and all formation constants for the associated methoxide containing species, the structural variations should not seriously alter the overall conclusions concerning stoichiometry and formation constants. The titration data for representative titrations of (La^{3+})$_2$:**3**$^{-}$, as well as La^{3+} alone and **3** alone for comparison are illustrated in Fig. 2. The formation constants for the background unbound (La^{3+})$_2$ with one to five methoxides were established first by Hyperquad fitting of a (La^{3+})$_2$($^{-}OCH_3$)$_{1-5}$ model to the titration data for 1 × 10^{-3} mol/L $La(OTf)_3$ in

[5] In previous work (ref. 3*b*) we showed that the effect of a second phosphate diester was to act as a bridge between the two La^{3+} ions to facilitate formation of catalytically active dimers, and that a nonreactive or less-reactive phosphate diester can be used to structurally maximize the formation of active (La^{3+})(reactive phosphate)(surrogate phosphate) dimers.

© 2005 NRC Canada

Table 1. Formation constants for $La^{3+}_2(^-OCH_3)_n$ and La^{3+}_2:**3**$^-$:$(^-OCH_3)_n$ species in methanol at [La^{3+}] = 1×10^{-3} mol/L (25.0 °C).

Equilibrium	$\log {}^{s}_{s}K^{a}$	Microscopic ${}^{s}_{s}pK_a{}^{b}$
$[La_2(^-OCH_3)_1]/[La]^2[^-OCH_3]$	12.79±0.01[c]	
$[La_2(^-OCH_3)_2]/[La]^2[^-OCH_3]^2$	22.33±0.22[c]	${}^{s}_{s}pK_a{}^{2}$ = 7.23±0.21[c]
$[La_2(^-OCH_3)_3]/[La]^2[^-OCH_3]^3$	29.64±0.60[c]	${}^{s}_{s}pK_a{}^{3}$ = 9.46±0.38[c]
$[La_2(^-OCH_3)_4]/[La]^2[^-OCH_3]^4$	36.71±0.39[c]	${}^{s}_{s}pK_a{}^{4}$ = 9.70±0.22[c]
$[La_2(^-OCH_3)_5]/[La]^2[^-OCH_3]^5$	42.68±1.08[c]	${}^{s}_{s}pK_a{}^{5}$ = 10.80±0.69[c]
$[La_2(\mathbf{3}^-)]/[La]^2[\mathbf{3}^-]$	10.47±0.47[d]	
$[La_2(\mathbf{3}^-)(^-OCH_3)_1]/[La]^2[\mathbf{3}^-][^-OCH_3]$	20.15±0.51[d]	${}^{s}_{s}pK_a{}^{1}$ = 7.09±0.04[d]
$[La_2(\mathbf{3}^-)(^-OCH_3)_2]/[La]^2[\mathbf{3}^-][^-OCH_3]^2$	29.48±0.51[d]	${}^{s}_{s}pK_a{}^{2}$ = 7.44±0.01[d]
$[La_2(\mathbf{3}^-)(^-OCH_3)_3]/[La]^2[\mathbf{3}^-][^-OCH_3]^3$	36.12±0.42[d]	${}^{s}_{s}pK_a{}^{3}$ = 10.13±0.10[d]
$[La_2(\mathbf{3}^-)(^-OCH_3)_4]/[La]^2[\mathbf{3}^-][^-OCH_3]^4$	42.32±0.52[d]	${}^{s}_{s}pK_a{}^{4}$ = 10.57±0.11[d]
$[La_2(\mathbf{3}^-)(^-OCH_3)_5]/[La]^2[\mathbf{3}^-][^-OCH_3]^5$	47.07±0.03[d]	${}^{s}_{s}pK_a{}^{5}$ = 12.02±0.50[d]

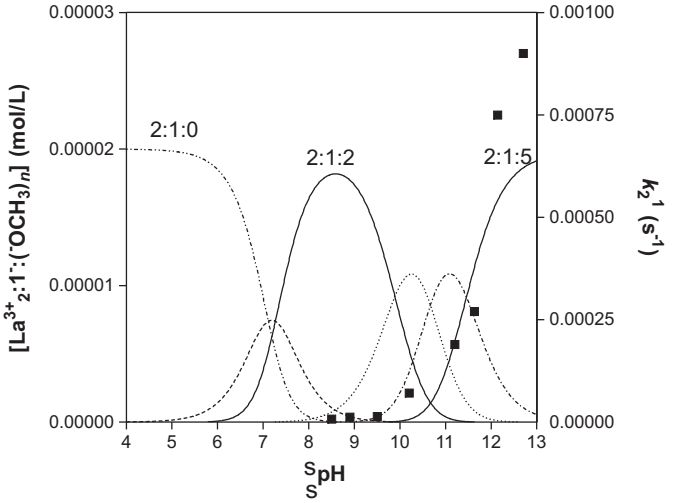
[a]Derived from fits of the potentiometric titration data using the program Hyperquad (10).
[b]Defined as $-\log {}^{s}_{s}K_a$ for La^{3+}_2:**3**$^-$:$(^-OCH_3)_n(HOCH_3)_x \rightleftharpoons La^{3+}_2$:**3**$^-$:$(^-OCH_3)_{n+1}(HOCH_3)_y + H^+$, calculated from data in column 2 as 16.77 – (${}^{s}_{s}pK_a{}^{n} - {}^{s}_{s}pK_a{}^{n-1}$) where 16.77 is the –log of the autoprotolysis constant for pure methanol.
[c]Averages of duplicate titrations of La(OTf)$_3$ (1×10^{-3} mol/L). Errors are calculated as the standard deviation of the mean.
[d]Averages of duplicate titrations of La(OTf)$_3$ (1×10^{-3} mol/L) in the presence of **3** (5×10^{-4} mol/L). Errors calculated as the standard deviation of the mean.

methanol. In Table 1 are presented the average of the log formation constants (log β or $\log {}^{s}_{s}K$) for three separate determinations that were used as constants for all subsequent analyses of the titrations in the presence of **3**. The ${}^{s}_{s}pK_a$ of **3** (3.47 ± 0.01) was also used as an experimentally determined constant, and the autoprotolysis constant for pure methanol ($10^{-16.77}$) (13) was included as the last constant for the fits. Table 1 shows the results for the formation constants of all the species used as the model in the Hyperquad fitting. The concentrations of the various $(La^{3+})_2$:**1**$^-$:$(^-OCH_3)_{0-5}$ species were subsequently computed as a function of ${}^{s}_{s}pH$ from these formation constants using HySS, another program in the Hyperquad 2000 suite. The speciation diagram shown in Fig. 3 was constructed using conditions relevant to the kinetics where [La^{3+}] = 2×10^{-3} mol/L and [**3**] = 2×10^{-5} mol/L. Also superimposed on Fig. 3 are the kinetic data for k_2**1** in units of s^{-1} from Table 1S[3] (3*a*) as a function of ${}^{s}_{s}pH$ to indicate possible species that may contribute to the rate constant. From the appearance of the latter plot, it is clear that no single species is responsible for the kinetic behaviour, and thus a more detailed analysis is required.

Low [La^{3+}] domain (<2 × 10^{-4} mol/L)

Due to the fact that the overall behaviour is a composite of two independent pathways, we analyze the k_{obs} vs. [La^{3+}] data at the limits of two concentration domains. In the low [La^{3+}] domain, the k_{obs} vs. [La^{3+}] plots for the La^{3+} catalyzed methanolysis of **1** show a linear increase corresponding to an apparent second-order process, with the gradient taken to be k_1**1** in units of $(mol/L)^{-1}\ s^{-1}$. The active form is believed to be a transiently formed La^{3+} bound phosphate, formulated preliminarily as La^{3+}:**1**$^-$:$(^-OCH_3)_n$, where the number of methoxides is zero to two depending on the ${}^{s}_{s}pH$. Since not all the substrate is bound in this region, the apparent second-order kinetics could also be accommodated by the process depicted in eq. [1], where k_1**1** = k_{cat}/K_B ($(mol/L)^{-1}\ s^{-1}$), where k_{cat} refers either to the spontaneous decomposition of La^{3+}:**1**$^-$:$(^-OCH_3)_n$ or to the second-order rate constant for the attack of external methoxide on La^{3+}:**1**$^-$:$(^-OCH_3)_{n-1}$.

Fig. 3. Speciation diagram for La^{3+}_2:**1**$^-$:$(^-OCH_3)_n$ forms as a function of ${}^{s}_{s}pH$ computed from the formation constants given in Table 1 for the titration of diphenyl phosphate (2×10^{-5} mol/L) and 2×10^{-3} mol/L La^{3+}. Captions of 2:1:*n* refer to La^{3+}_2:**1**$^-$:$(^-OCH_3)_n$ forms with a variable number of methoxides, (— — —) La^{3+}_2:**1**$^-$:$(^-OCH_3)_1$, (- - - - -) La^{3+}_2:**1**$^-$:$(^-OCH_3)_3$, (—·—·) La^{3+}_2:**1**$^-$:$(^-OCH_3)_4$. Data superimposed on the figure as (■) are first-order rate constants (k_2) for the La^{3+} catalyzed methanolysis of methyl (4-nitrophenyl) phosphate (**1**) from ref. 3*a*.



[1] $La^{3+}(^-OCH_3)_n + \mathbf{1}^- \underset{K_B}{\rightleftharpoons} La^{3+}:\mathbf{1}^-:(^-OCH_3)_n \xrightarrow{k_{cat}} P$

There is some ambiguity as to whether the reaction proceeds through the above monomeric form, or through a double

© 2005 NRC Canada

Table 2. Formation constants for various La^{3+} containing species in methanol at $[La^{3+}] = 1 \times 10^{-4}$ mol/L (25.0 °C).

Equilibrium	$\log {}^{s}_{s}K^{a}$	Microscopic ${}^{s}_{s}pK_a{}^{b}$
$[La(^{-}OCH_3)_1]/[La][^{-}OCH_3]$	9.09±0.08[c]	
$[La_2(^{-}OCH_3)_3]/[La]^2[^{-}OCH_3]^3$	28.35±0.38[c]	
$[La_2(^{-}OCH_3)_4]/[La]^2[^{-}OCH_3]^4$	34.66±0.23[c]	${}^{s}_{s}pK_a{}^{3} = 10.45\pm0.61$[c]
$[La_2(^{-}OCH_3)_5]/[La]^2[^{-}OCH_3]^5$	41.55±0.09[c]	${}^{s}_{s}pK_a{}^{4} = 9.88\pm0.32$[c]

[a]Derived from fits of the potentiometric titration data using the program Hyperquad (10).
[b]Defined as $-\log {}^{s}_{s}K_a$ for $La^{3+}(^{-}OCH_3)_n(HOCH_3)_x \rightleftharpoons La^{3+}(^{-}OCH_3)_{n+1}(HOCH_3)_y + H^+$, calculated from data in column 2 as $16.77 - ({}^{s}_{s}pK^{n} - {}^{s}_{s}pK^{n-1})$ where 16.77 is the –log of the autoprotolysis constant for pure methanol.
[c]Averages of duplicate titrations of $La(OTf)_3$ (1×10^{-4} mol/L). Errors are calculated as the standard deviation of the mean.

phosphate bridged dimer formulated as $(La^{3+})_2$:(phosphate^{-})$_2$:$(^{-}OCH_3)_m$ as was determined to be the case in the La^{3+} promoted methanolysis of 2-hydroxypropyl *p*-nitrophenyl phosphate (3*b*). To cast light on this question, two independent sets of experiments were performed. In the first, the electrospray mass spectrum of a methanol solution containing 2×10^{-4} mol/L of both $La^{3+}(^{-}OTf)_3$ and phosphate diester **3** (chosen because it is kinetically stable during the experimental measurement while **1** is not) displayed masses at *m*/*z* 419.12 and 451.15 indicative of La^{3+}:**3**$^{-}$:$(^{-}OCH_3)(HOCH_3)_{0,1}$, but no masses indicative of any dimeric forms. In the second set of experiments, the kinetics for methanolysis of **2** in the presence of equimolar La^{3+} were determined at an initial concentration corresponding to the point of transition (2×10^{-4} mol/L) between the low and high $[La^{3+}]$ domains observed in the k_{obs} vs. $[La^{3+}]$ plot for the methanolysis of **2**. This same trend and point of transition was previously observed in the methanolysis of **1** ((3*a*), see Fig. 1S, Supplemental material).[3] The kinetics of the methanolysis of **2** were then determined as a function of varying $[La^{3+}]$ concentration, but maintaining the $[La^{3+}]$:$[phosphate]_{total}$ ratio at 1.0. Under these conditions, one anticipates shifting a putative 2(La^{3+}:phosphate) $\rightleftharpoons$ (La^{3+}:phosphate)$_2$ equilibrium to the right so that if the dimeric species is active, an increase in observed rate constant, with possible saturation, will accompany the increase in [La^{3+}:phosphate]. This phenomenon was previously observed with the La^{3+} : 2-hydroxypropyl *p*-nitrophenyl phosphate system (3*b*). Above a concentration of 2×10^{-4} mol/L, the complex of phosphate **2** is poorly soluble in this medium so the additional phosphate concentration was made up with the more soluble **3**, but this change will not alter significantly the kinetic result since the observed reaction concerns the decomposition of **2** (2). The k_{obs} for methanolysis of **2** determined under these conditions is invariant to increasing $[La^{3+}]$ within experimental error ($k_{obs} = (2.43 \pm 0.12) \times 10^{-4}$ s^{-1}, Table 2S, Supplemental material)[3] as expected if the reactive species is the monomeric form La^{3+}:**2**: $(^{-}OCH_3)_n$.

Having established that La^{3+} monomers are active in the low $[La^{3+}]$ domain, we turned our attention to the analysis of the titration data in this concentration range. Shown in Fig. 3S, Supplementary material[3] is the titration curve for a 1×10^{-4} mol/L solution of $La(OTf)_3$ in methanol. The general appearance of this curve is quite different from the profile obtained at 1×10^{-3} mol/L (see Fig. 2) in that the first consumption of methoxide follows a regular titration profile consuming 1 equiv. of methoxide per La^{3+} followed by a much steeper profile for the consumption of additional methoxides. The steeper profile corresponding to the addition of more than 1 equiv. of $^{-}OCH_3$ per La^{3+} suggests that dimers or higher order aggregates are formed in that region. Therefore, for the low $[La^{3+}]$ titrations we analyzed the data in terms of a model comprising La^{3+}, $La^{3+}(^{-}OCH_3)_{0,1}$, and $(La^{3+})_2(^{-}OCH_3)_{3,4,5}$. The goodness-of-fit of this model to the titration profile up to ${}^{s}_{s}$pH 11 is shown in Fig. 3S,[3] and in Table 2 are presented the computed formation constants for all the species in this model. These were then used to compute the speciation diagram using HySS for the kinetically relevant conditions where $[La^{3+}] = 1 \times 10^{-4}$ mol/L. This speciation diagram is represented in Fig. 4 along with the overlaid kinetic data that refer to $k_1^{\mathbf{1}}$ in (mol/L)$^{-1}$ s^{-1} for the La^{3+} catalyzed methanolysis of **1** as a function of ${}^{s}_{s}$pH.

Kinetic analysis

High [La^{3+}] domain (>10^{-3} mol/L)

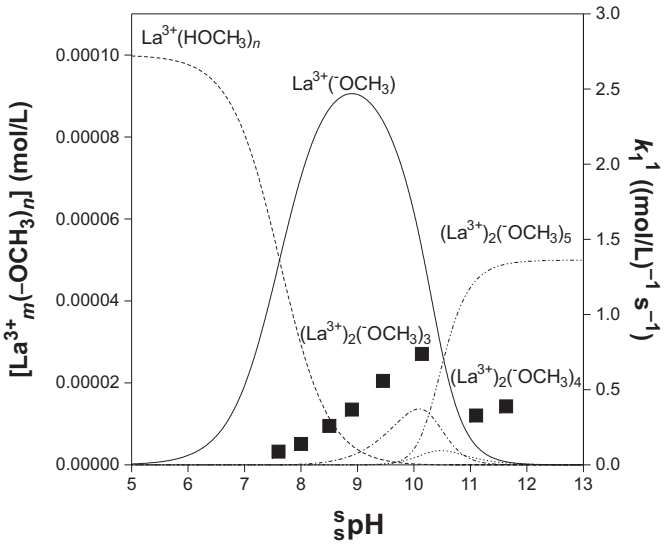
The fits of the titration data to the models previously described provide the concentration of all the participating species as a function of ${}^{s}_{s}$pH in the low and high $[La^{3+}]$ domains. In each domain we can fit the observed rate constants ($k_1^{\mathbf{1}}$ or $k_2^{\mathbf{1}}$) at the various ${}^{s}_{s}$pH values for the La^{3+} catalyzed methanolysis of **1** (3*a*) as linear combinations of the contributions of the individual species. For $k_2^{\mathbf{1}}$ vs. ${}^{s}_{s}$pH in the high $[La^{3+}]$ domain, the appropriate linear combination is given as eq. [2], where each of the $(La^{3+})_2$:**1**$^{-}$:$(^{-}OCH_3)_n$ species contributes its own first-order rate constant ($k_2^{2:\mathbf{1}:n}$) for reaction.

$$[2] \qquad k_2^{\mathbf{1}} = \sum_{n=1}^{5} k_2^{2:\mathbf{1}:n}[(La^{3+})_2:\mathbf{1}^{-}:(^{-}OCH_3)_n]/[\mathbf{1}]_{total}$$

This equation is appropriate for spontaneous breakdown of the substrate-bound species to methanolyzed product via an internal La^{3+} coordinated methoxide mechanism, the transition structure of which is not implied other than it probably contains a dual role for the metal ion as a Lewis acid and deliverer of nucleophilic methoxide. An alternative, and kinetically equivalent, mechanism requires external methoxide attack on the $(La^{3+})_2$:**1**$^{-}$ bound species having one less methoxide than in the internal methoxide model, the appropriate kinetic equation being shown as eq. [3] where

© 2005 NRC Canada

Fig. 4. Speciation diagram for La^{3+} species as a function of $^{s}_{s}$pH computed from the formation constants given in Table 2 for the titration of 1×10^{-4} mol/L La^{3+}. Data superimposed on the figure as (■) are second-order rate constants ($k_1^{\mathbf{1}}$) for the La^{3+} catalyzed methanolysis of methyl (4-nitrophenyl) phosphate (**1**) from ref. 3*a*.



$k'_2{}^{2:\mathbf{1}:n}$ is a second-order rate constant for methoxide attack on each species.

$$[3] \qquad k_2^{\mathbf{1}} = \sum_{n=0}^{4} k'_2{}^{2:\mathbf{1}:n}[(La^{3+})_2:\mathbf{1}^{-}:(^{-}OCH_3)_n][^{-}OCH_3]/[\mathbf{1}]_{total}$$

Given in Table 3 are the rate constants derived from fitting the $k_2^{\mathbf{1}}$ data to eqs. [2] and [3] with the results being displayed in Fig. 5, which includes the individual contributions for all species found to have activity. Their sum generates the overall best fit curve, which is remarkably good given the inherent assumptions of approximating the La^{3+}:**1**$^{-}$ stability constants through the use of **3**. Although the caption for Fig. 5 is specific for the internal methoxide model, the fit is obviously identical for the kinetically equivalent external methoxide model where the $(La^{3+})_2$:**1**$^{-}$:$(^{-}OCH_3)_n$ species responsible for catalysis have one less associated methoxide than in the internal model. The kinetically active forms for the internal methoxide process are $(La^{3+})_2$:**1**$^{-}$:$(^{-}OCH_3)_{2,3,4,5}$, while for the external methoxide process, the reaction is computed to proceed via methoxide attack on $(La^{3+})_2$:**1**$^{-}$:$(^{-}OCH_3)_{1,2,3,4}$.

There is nothing by way of argument that might allow one to prefer one or the other of the described two mechanisms. The computed rate constants for internal methoxide spontaneous decomposition of $(La^{3+})_2$:**1**$^{-}$:$(^{-}OCH_3)_{2,3,4,5}$ are 6.3×10^{-6}, 9.8×10^{-5}, 1.4×10^{-4}, and 1.3×10^{-3} s^{-1}, respectively, consistent with the expectation that the species having the highest basicity for its associated methoxide will react the fastest. For the external methoxide process, the computed second-order rate constants for methoxide on the bound forms with one to four associated methoxides are 1.5×10^4, 3.7×10^2, 2.5×10^2, and 3.3×10^1 $(mol/L)^{-1}$ s^{-1}, respectively, but are well below the limit of ~10^{10} $(mol/L)^{-1}$ s^{-1}, which would be appropriate for a diffusion-limited process involving reaction of an anion and a positively charged species (14). Nevertheless, the rate constants for the external methoxide model are considerably larger than the experimental second-order rate constant for methoxide attack on **1** alone of $(7.9 \pm 0.6) \times 10^{-7}$ $(mol/L)^{-1}$ s^{-1} at 25 °C (3*a*), indicating that complexation of **1** to the $(La^{3+})_2(^{-}OCH_3)_{1,2,3,4}$

Table 3. Computed $k'_2{}^{2:\mathbf{1}:n}$ or $k_2^{2:\mathbf{1}:n}$ rate constants for various species for the La^{3+} catalyzed methanolysis of **1** computed from fits of k_2 vs. $^{s}_{s}$pH data to eq. [2] and [1].

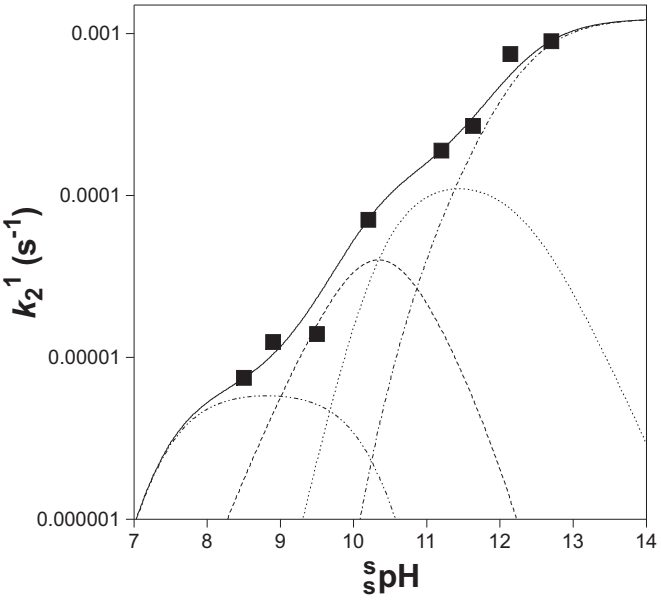
$[La^{3+}{}_2$:**1**$^{-}$:$(^{-}OCH_3)_n]$	$k'_2{}^{2:\mathbf{1}:n}$ or $k_2^{2:\mathbf{1}:n}$
External methoxide model (eq. [3])	
$La^{3+}{}_2$:**1**$^{-}$:$(^{-}OCH_3)_1$	$k'_2{}^{2:\mathbf{1}:1} = (1.5\pm0.2)\times10^{4}$[a]
$La^{3+}{}_2$:**1**$^{-}$:$(^{-}OCH_3)_2$	$k'_2{}^{2:\mathbf{1}:2} = (3.7\pm0.6)\times10^{2}$[a]
$La^{3+}{}_2$:**1**$^{-}$:$(^{-}OCH_3)_3$	$k'_2{}^{2:\mathbf{1}:3} = (2.5\pm0.4)\times10^{2}$[a]
$La^{3+}{}_2$:**1**$^{-}$:$(^{-}OCH_3)_4$	$k'_2{}^{2:\mathbf{1}:4} = (3.3\pm0.5)\times10^{1}$[a]
Internal methoxide model (eq. [2])	
$La^{3+}{}_2$:**1**$^{-}$:$(^{-}OCH_3)_2$	$k_2^{2:\mathbf{1}:2} = (6.3\pm0.9)\times10^{-6}$[b]
$La^{3+}{}_2$:**1**$^{-}$:$(^{-}OCH_3)_3$	$k_2^{2:\mathbf{1}:3} = (9.8\pm1.5)\times10^{-5}$[b]
$La^{3+}{}_2$:**1**$^{-}$:$(^{-}OCH_3)_4$	$k_2^{2:\mathbf{1}:4} = (1.4\pm0.2)\times10^{-4}$[b]
$La^{3+}{}_2$:**1**$^{-}$:$(^{-}OCH_3)_5$	$k_2^{2:\mathbf{1}:5} = (1.3\pm0.2)\times10^{-3}$[b]

Note: Errors computed from the avg. % deviation in the fitted numbers calculated by eq. [2] or [3] from the actual kinetic data. Data fit under the assumption that the various La^{3+}:**3**$^{-}$:$(^{-}OCH_3)_n$ formation constants from Table 1 are realistic approximations for those for the La^{3+}:**1**$^{-}$:$(^{-}OCH_3)$ system.

[a]Values of $k'_2{}^{2:\mathbf{1}:n}$ are actually second-order rate constants in units of $(mol/L)^{-1}$ s^{-1} after accounting for the $^{-}OCH_3$ concentration.

[b]Values of $k_2^{2:\mathbf{1}:n}$ in units of s^{-1}.

Fig. 5. Plot of $k_2^{\mathbf{1}}$ vs. $^{s}_{s}$pH for the $La^{3+}{}_2$ catalyzed methanolysis of **1** and the contributionsof each active species. Lines come from the fit of the kinetic data to eq. [2]. Solid line, composite of all contributions; (—••—••), contribution of $La^{3+}{}_2$(**1**$^{-}$)$(^{-}OCH_3)_2$; (— — —), contribution of $La^{3+}{}_2$(**1**$^{-}$)$(^{-}OCH_3)_3$; (•••), contribution of $La^{3+}{}_2$(**1**$^{-}$)$(^{-}OCH_3)_4$; (—•—•), contribution of $La^{3+}{}_2$(**1**$^{-}$)$(^{-}OCH_3)_5$.



© 2005 NRC Canada

system provides a catalytic enhancement varying from 1.9×10^{10}-fold to 4×10^7-fold, with the least catalysis being observed for methoxide attack on the least positively charged complex.

Low [La^{3+}] domain

As stated previously, in the low [La^{3+}] domain the kinetics are linearly dependent on the metal ion. Thus, the preferred fitting procedure considers that the $k_1^{\mathbf{1}}$ rate constants at each $^{s}_{s}$pH can be described as a linear combination of second-order rate constants (equivalent to k_{cat}/K_B at each $^{s}_{s}$pH) for each of the contributing $(La^{3+})(^{-}OCH_3)_n$ species for the internal methoxide model. For the external methoxide model (eq. [4]), the rate constants are now third-order to accommodate the methoxide concentration that has been factored out.

At low [La^{3+}] the only monomeric species available in solution, as revealed by fits of the potentiometric curve, are $La^{3+}(^{-}OCH_3)_{0,1}$ and it immediately becomes clear that: (1) each species is required to provide a satisfactory fit to the kinetic $k_1^{\mathbf{1}}$ data; and (2) that an additional methoxide is required to explain the activity seen where $La^{3+}(^{-}OCH_3)_1$ is the dominant species to accommodate the increase in rate with $^{s}_{s}$pH. Thus, the internal methoxide mechanism is rendered unlikely because, if operative, the kinetic data would have to track the concentration behaviour of $La^{3+}(^{-}OCH_3)_1$ as a function of $^{s}_{s}$pH, which it does not: correspondingly, the external methoxide mechanism is favoured. Given in Table 4 are the best-fit rate constants from the application of eq. [4], which generate the species contributions to the overall fitted curve presented in Fig. 6 for $k_1^{\mathbf{1}}$ as a function of $^{s}_{s}$pH. The overall fit displayed in Fig. 6, while not as good as obtained for the $k_2^{\mathbf{1}}$ data vs. the $(La^{3+})_2$:$\mathbf{1}^{-}$:$(^{-}OCH_3)_n$ species, is still considered satisfactory in view of the inherent errors in determining the linear region of the k_{obs} vs. $^{s}_{s}$pH profile and the assumed speciation to fit the titration data. The computed constants of 3×10^8 and 5.1×10^6 $(mol/L)^{-2}$ s^{-1} refer to the apparent termolecular processes corresponding to CH_3O^{-} + $\mathbf{1}^{-}$ + $La^{3+}(^{-}OCH_3)_{0,1}$ respectively, the reduction by a factor of ~60-fold in rate constant between the two resulting from Lewis acidity differences attributable to the methoxide content of the respective complexes.

$$[4] \qquad k_1^{\mathbf{1}} = \sum_{n=0}^{1} k_1'^{1:n}[La^{3+}(^{-}OCH_3)_n][^{-}OCH_3]/[La^{3+}]_{total}$$

While the fitting provides the apparent third-order rate constant for the process involving CH_3O^{-} + $\mathbf{1}^{-}$ + $La^{3+}(^{-}OCH_3)_{0,1}$, it is difficult to envision any mechanism where there is not a preequilibrium binding of the substrate to the metal ion followed by attack of methoxide on that complex as in eq. [1]. On the basis of the experimental kinetic saturation plots of k_{obs} vs. [La^{3+}] (3*a*), we estimate the complex between an oppositely charged phosphate and metal ion to have a dissociation constant (K_{dis}) between 2×10^{-4} and 10^{-3} mol/L depending on the metal ion charge as controlled by the number of metal bound methoxides (n = 0, 1). Accordingly, one can calculate the second-order rate constant for methoxide attack on the transiently bound substrate as being between 6×10^4 and 3×10^5 $(mol/L)^{-1}$ s^{-1} in the case of the complex with n = 0, and 10^3 to 5×10^3 $(mol/L)^{-1}$ s^{-1} for the attack of methoxide on the complex with n = 1. Relative to the experimental second-order rate constant for methoxide attack on $\mathbf{1}^{-}$ alone of $(7.9 \pm 0.6) \times 10^{-7}$ $(mol/L)^{-1}$ s^{-1} at 25 °C (3*a*), coordination to $La^{3+}(^{-}OCH_3)_{0,1}$ provides a rate enhancement of at least 10^{11}- to 10^9-fold depending on the overall charge of the metal:substrate complex.

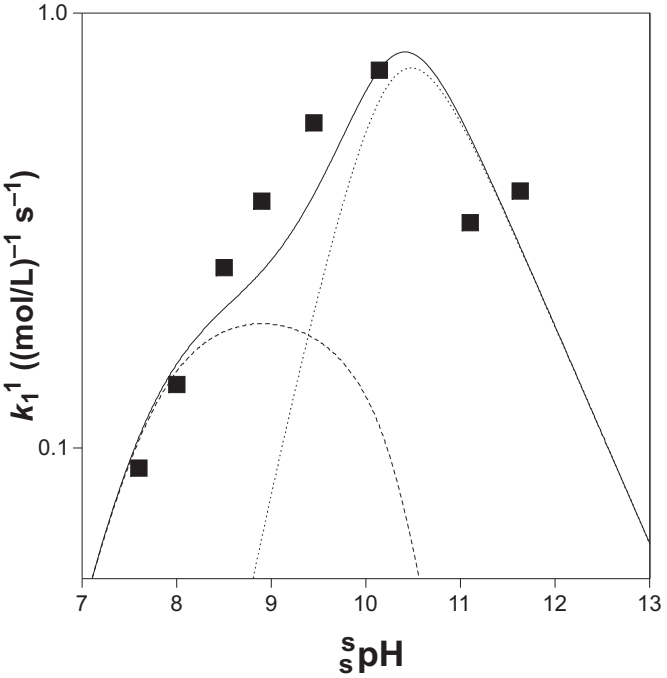
Table 4. Computed $k'^{1:n}_1$ or $k_1^{1:n}$ rate constants for various species for the La^{3+} catalyzed methanolysis of **1** computed from fits of $k_1^{\mathbf{1}}$ vs. $^{s}_{s}$pH data to eq. [4].

$[La^{3+}(^{-}OCH_3)_n]$	$k'^{1:n}_1$
External methoxide model (eq. [4])	
$La^{3+}(^{-}OCH_3)_0$	$k'^{1:0}_1 = (3.0\pm0.6)\times10^{8a}$
$La^{3+}(^{-}OCH_3)_1$	$k'^{1:1}_1 = (5.1\pm0.9)\times10^{6a}$

Note: Errors computed from the avg. % deviation in the fitted numbers calculated by eq. [4] from the actual kinetic data.

[a]Values of $k'^{1:n}_1$ are third-order rate constants in units of $(mol/L)^{-2}$ s^{-1} after accounting for the $^{-}OCH_3$ concentration.

Fig. 6. Plot of $k_1^{\mathbf{1}}$ vs. $^{s}_{s}$pH for the La^{3+} catalyzed methanolysis of **1** and the contributions of each active species. Lines come from the fit of the kinetic data to the external methoxide model given in eq. [4]. Solid line, composite of all contributions; (— — —), contribution of $La^{3+}(^{-}OCH_3)_0$; (···), contribution of $La^{3+}(^{-}OCH_3)_1$.



Conclusions

In this paper we have presented a detailed analysis of the kinetic contributions of various La^{3+} species catalyzing the methanolysis of the phosphate diester **1** for which kinetic data were presented previously (3*a*), but only qualitatively analyzed within the framework of Scheme 1. By coupling the rate data to an analysis of the speciation of the La^{3+} containing complexes present in solution as a function of $^{s}_{s}$pH one can provide a simplified, but satisfactory, model to explain the kinetic behaviour in the high and low [La^{3+}] domains. We anticipate that such an approach will prove

© 2005 NRC Canada

beneficial to explain the origins of nonunit, or irregular dependencies of kinetic profiles of many other metal-ion-catalyzed reactions where the metal ion undergoes changes in speciation as a function of $^{s}_{s}$pH.

There is an interesting observation revealed by comparing these analyses with those previously reported for the La^{3+} promoted catalysis of the methanolysis of neutral substrates such as phosphate triesters (3*c*, 3*d*) and carboxylate esters (1). In those cases, the pH/rate profiles are bell-shaped or distorted bell-shaped and best accommodated by mechanisms involving a dual role for the metal ion as a Lewis acid and deliverer of a metal-coordinated methoxide on a transiently bound neutral substrate. However, in the present cases where there is stronger binding of the anionic phosphate to the metal ion to produce a thermodynamically more stable complex, the pH/rate profiles for both the La^{3+} monomer and dimer cases show gradual increases with non-integral slopes. The preferred analysis involves attack of external methoxide on the relatively stable complex where the main apparent role of the metal ion is to act as a Lewis acid or electrostatic stabilizer of the developing negative charge in the TS. While we offer no detailed explanation of the difference in behaviour between neutral and anionic substrates at this time, it must be related to a counterbalancing of the effects of coordination geometry, Lewis acid activation, relative nucleophilicity of metal-bound and external nucleophiles, and geometry of the activated complexes for each mode of catalysis.

Acknowledgements

The authors gratefully acknowledge the financial assistance of Queen's University and the Natural Sciences and Engineering Research Council of Canada (NSERC) to which G.T.T. Gibson is particularly thankful for the award of a Canada Graduate Scholarship–D. A.C.T. Teng is also indebted to NSERC for the award of an Undergraduate Summer Research Award.

References

1. (*a*) A.A. Neverov, T. McDonald, G. Gibson, and R.S. Brown. Can. J. Chem. **79**, 1704 (2001); (*b*) A.A. Neverov, N.E. Sunderland, and R.S. Brown. Org. Biomol. Chem. **3**, 65 (2005).
2. P.J. Montoya-Pelaez, G.T.T. Gibson, A.A. Neverov, and R.S. Brown. Inorg. Chem. **42**, 8624 (2003).
3. (*a*) A.A. Neverov and R.S. Brown. Inorg. Chem. **40**, 3588 (2001); (*b*) J.S.W. Tsang, A.A. Neverov, and R.S. Brown. J. Am. Chem. Soc. **125**, 1559 (2003); (*c*) J.S.W. Tsang, A.A. Neverov, and R.S. Brown. Org. Biomol. Chem. **2**, 3457 (2004); (*d*) J.S. Tsang, A.A. Neverov, and R.S. Brown. J. Am. Chem. Soc. **125**, 7602 (2003).
4. (*a*) J.F. Davies, Z. Hostomska, Z. Hostomsky, S.R. Jordan, and D.A. Mathews. Science (Washington, D.C.), **252**, 88 (1991); (*b*) L.S. Beese and T.A. Steitz. EMBO J. **10**, 25 (1991); (*c*) A. Lahm, S. Volbeda, and D. Suck. J. Mol. Biol. **215**, 207 (1990).
5. R.S. Brown and A.A. Neverov. J. Chem. Soc. Perkin Trans. 2, 1039 (2002), and refs. 2 and 31 therein.
6. A.A. Frost and R.G. Pearson. Kinetics and mechanism: A study of homogeneous chemical reactions. 2nd ed. John Wiley and Sons, New York. 1965. pp. 236–261.
7. W. Desloges, A.A. Neverov, and R.S. Brown. Inorg. Chem. **43**, 6752 (2004).
8. (*a*) J.R. Morrow and W.C. Trogler. Inorg. Chem. **28**, 2330 (1988); (*b*) (erratum to ref. 8*a*): J.R. Morrow and W.C. Trogler. Inorg. Chem. **31**, 1544 (1992).
9. J. Suh and S.H. Hong. J. Am. Chem. Soc. **120**, 12 545 (1998).
10. Hyperquad 2000 is a computer program that applies nonlinear curve fitting to a titration by adjusting a series of formation constants (log β) for species input to a model, published in: P. Gans, A. Sabatini, and A. Vacca. Talanta, **43**, 1739 (1996).
11. G. Gibson, A.A. Neverov, and R.S. Brown. Can. J. Chem. **81**, 495 (2003).
12. (*a*) C.L. deLigny and M. Rehbach. Recl. Trav. Chim. **79**, 727 (1960); (*b*) R.G. Bates, M. Paabo, and R.A. Robinson. J. Phys. Chem. **67**, 1833 (1963); (*c*) R.G. Bates. Determination of pH: Theory and practice. 2nd ed. John Wiley and Sons, New York. 1964. p. 245.
13. (*a*) I. Canals, J.A. Portal, E. Bosch, and M. Rosés. Anal. Chem. **72**, 1802 (2000); (*b*) E. Bosch, F. Rived, M. Roses, and J. Sales. J. Chem. Soc. Perkin Trans. 2, 1953 (1999); (*c*) F. Rived, M. Rosés, and E. Bosch. Anal. Chim. Acta, **374**, 309 (1998); (*d*) E. Bosch, P. Bou, H. Allemann, and M. Roses. Anal. Chem. **68**, 3651 (1996).
14. (*a*) A. Fersht. Enzyme structure and mechanism. W.H. Freeman and Co., New York. 1985. pp. 147 to 148; (*b*) M. Eigen and L.Z. De Maeyer. Electrochemistry, **59**, 986 (1955).

© 2005 NRC Canada

Deuterium labeling as a test of intramolecular hydride mechanisms in the fragmentation of 2-(1-hydroxybenzyl)-N1′-methylthiamin[1]

Glenn Ikeda and Ronald Kluger

Abstract: 2-(1-Hydroxybenzyl)-N1′-methylthiamin (**1b**) is a model for the addition intermediate in the thiamin catalyzed benzoin condensation. However, N-alkylation alters the reactivity of the compound: instead of undergoing base-catalyzed formation of benzaldehyde and N1′-methylthiamin, it rapidly forms trimethyl amino pyrimidine (**2b**) and phenylthiazole ketone (**3**). The base-catalyzed fragmentation process is faster than the analogous enzymic reaction (in benzoylformate decarboxylase) under the same conditions. One possible mechanism for the rapid fragmentation is an internal hydride transfer from α-C2 to the methylene bridge between the heterocycles. To test the hydride mechanism we prepared α-C2-deuterated **1b** and conducted the fragmentation reaction in normal water. Spectroscopic analysis revealed that the trimethyl aminopyrimidine product does not contain any deuterium, ruling out a hydride transfer mechanism. This supports a mechanism for fragmentation that proceeds instead via a proton transfer from α-C2. Since protonation (and hence, deprotonation) of that site is part of the normal catalytic cycle of benzoylformate decarboxylase, the enzyme must divert the reaction from the lowest energy pathway since it would share a common intermediate with the fragmentation process.

Key words: thiamin, fragmentation, benzoylformate decarboxylase, proton transfer, hydride shift.

Résumé : La 2-(1-hydroxybenzyl)-N1′-méthylthiamine (**1b**) est un modèle pour l'intermédiaire d'addition dans la condensation de la benzoïne catalysée par la thiamine. Toutefois, la N-alkylation altère la réactivité du composé qui, au lieu de subir une réaction catalysée par les bases conduisant à la formation de benzaldéhyde et de N1′-méthylthiamine conduit à la formation rapide de triméthylaminopyrimidine (**2b**) et phénylthiazole cétone (**3**). Le processus de fragmentation catalysé par les bases est plus rapide que la réaction enzymatique analogue (en présence de décarboxylase de benzoylformate) dans les mêmes conditions. Un mécanisme possible pour la fragmentation rapide implique un transfert interne d'hydrure de la position α-C2 vers le pont méthylène entre les hétérocycles. Afin de tenter de confirmer ce mécanisme impliquant un hydrure, le composé **1b** deutéré en α-C2 a été préparé et soumis à une fragmentation dans de l'eau normale. Une analyse spectroscopique a révélé que le produit triméthyl aminopyrimidine ne contient pas de deutérium, ce qui élimine le mécanisme par transfert d'hydrure, mais qui supporte un mécanisme de fragmentation qui se produirait plutôt par le biais d'un transfert de proton à partir de α-C2. Puisque la protonation (et, par voie de conséquence, la déprotonation) de ce site fait partie du cycle catalytique normal de la décarboxylase du benzoylformate, l'enzyme doit faire dévier la réaction de la voie impliquant l'énergie minimale puisqu'il doit partager un intermédiaire commun avec le processus de fragmentation.

Mots clés : thiamine, fragmentation, décarboxylase de benzoylformate, transfert de proton, déplacement d'hydrure.

[Traduit par la Rédaction]

Introduction

The base-catalyzed addition of thiamin to benzaldehyde produces 2-(1-hydroxybenzyl)thiamin (HBnT, **1a**), following the mechanism deduced by Breslow (1, 2).

HBnT also resembles HBnT diphosphate, an intermediate on the pathway of benzoylformate decarboxylase (BFD) (3–5). In the enzymic system, ionization of the hydroxyl group facilitates the elimination of benzaldehyde. However, the major products from decomposition of HBnT in solution are an aminopyrimidine (AP, **2a**) and a phenylthiazole ketone (PTK, **3**) (6). These products were originally reported by Oka et al. for different conditions (7). Base-catalyzed fragmentation overwhelms elimination, being over 10^3 times faster at pH 7 (8). To observe fragmentation without competition from elimination, the N1′-methylated derivative of HBnT (MHBT, **1b**) was prepared, an analogue of the BFD intermediate with N1′ protonated on the enzyme (5).

The fragmentation pathway of HBnT is consistent with the first step being the loss of a proton from α-C2 to generate the delocalized conjugate base, which undergoes the fragmentation reaction as shown (Fig. 1, mechanism 1). The carbanion can also be accessed by decarboxylation (9, 10).

Received 30 March 2005. Published on the NRC Research Press Web site at http://canjchem.nrc.ca on 21 October 2005.

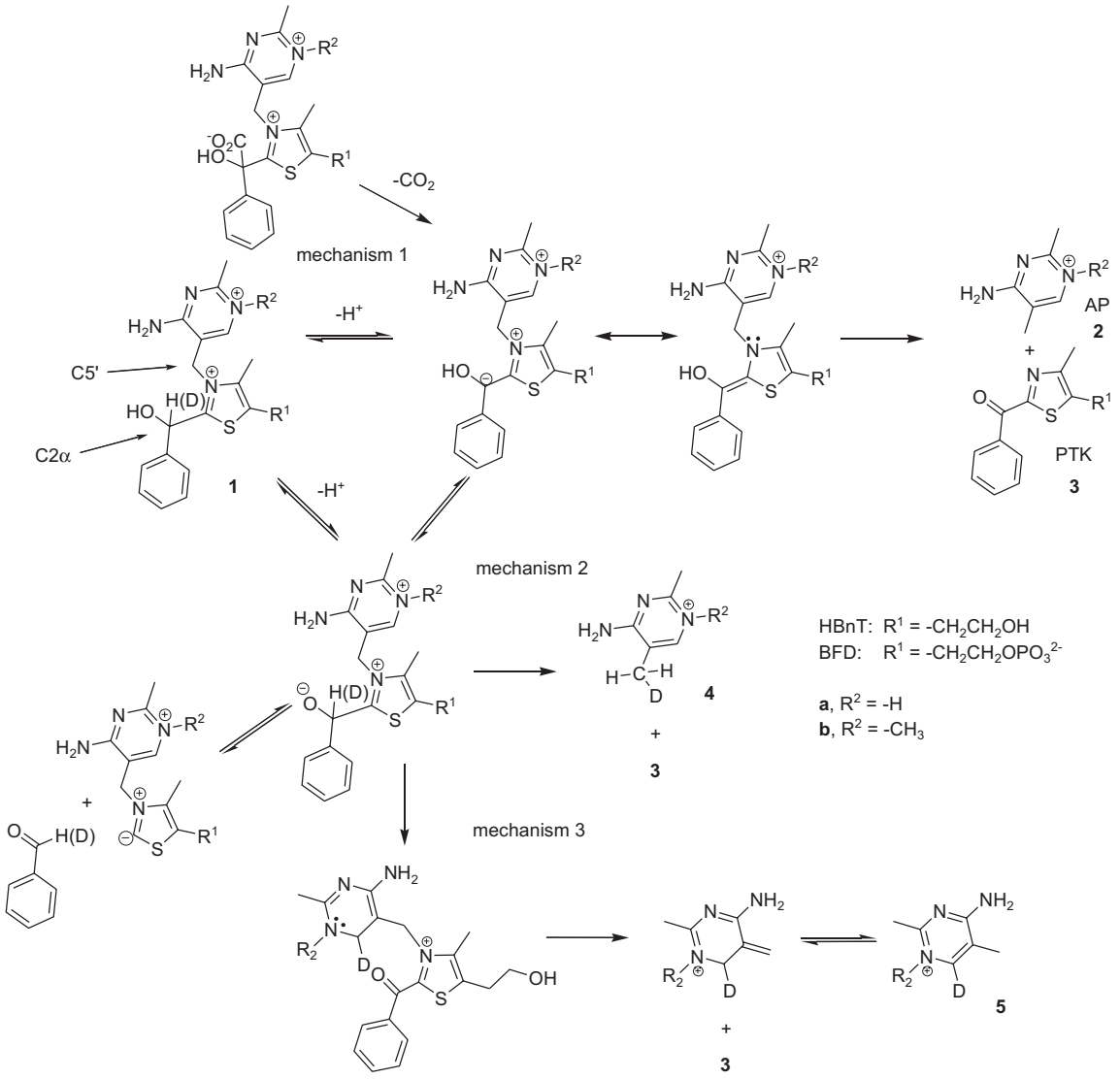
G. Ikeda and R. Kluger.[2] Davenport Chemical Laboratories, Department of Chemistry, University of Toronto, Toronto, ON M5S 3H6, Canada.

[1]This article is part of a Special Issue dedicated to organic reaction mechanisms.

[2]Corresponding author (e-mail: rkluger@chem.utoronto.ca).

 doi: 10.1139/V05-146 © 2005 NRC Canada

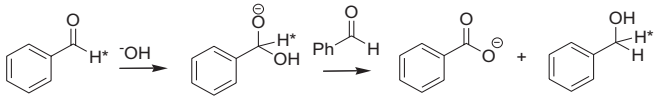
Fig. 1. Mechanisms and deuterium tracing in the fragmentation of HBnT.



An alternative pathway involves the kinetically equivalent oxyanion, obtained from rapid proton transfer from oxygen to carbon that may derive additional stabilization from the positively charged pyrimidine. Fragmentation then would result from an internal Cannizzaro-type reaction (11) involving a hydride shift from α-C2 (Fig. 1, mechanisms 2 and 3). If the hydride mechanism was responsible for the fragmentation, it might involve a manifold of intermediates that are clearly distinct from those formed in the enzymic process. In these mechanisms, the conjugate base of MHBT would react in analogy to the conjugate base of the hydrate of benzaldehyde (Fig. 2). The distinction of hydride and proton transfer mechanisms is reminiscent of the alternatives that were considered as possibilities in the normal catalytic process of glyoxylase I (12–14), which were resolved by the work of Jordan, Kozarich, and their co-workers (13, 14).

The hydride transfer mechanism must give a direct transfer to the acceptor site while a proton transfer mechanism leads to equilibration with the solvent. Thus, we produced the α-C2 deuterated analogue of MHBT (MHBT-*d*) by addition of thiamin addition to deuterobenzaldehyde, and then

Fig. 2. The hydroxide induced Cannizzaro reaction as a model for hydride transfer in MHBT.



conducted the reaction in normal water. The α-C2 carbon acid exchanges very slowly under the conditions of our studies of the fragmentation reaction, so loss of the deuteron will not occur prior to the fragmentation process. The hydride mechanisms require incorporation of the deuterium into the methyl or aryl groups of the pyrimidine product, and the relative rates assure us that this would be detected. Furthermore, proton–deuterium exchange does not occur into the products, so that any loss of deuterium comes from the initial reaction.

The proposed mechanism could potentially give C5′-deuterated AP from the fragmentation of MHBT-*d* in water if the aromatization step occurred with internal deuterium transfer. However, tautomerization would be subject to an

© 2005 NRC Canada

isotope effect and could be solvent-mediated. Therefore, only partial incorporation of deuterium into the C5′ hydrogen is possible in this mechanism.

In the case of BFD, a carbanion must be generated from loss of carbon dioxide from the intermediate generated by addition of thiamin diphosphate to benzoylformate. The same carbanion would be generated from the loss of a proton from the conjugate of thiamin diphosphate and benzaldehyde (HBnT diphosphate). If the fragmentation reaction occurs by a hydride shift mechanism, then this would compete with elimination of the TDP ylide in the enzyme reaction. The enzyme could promote formation of benzaldehyde by controlling the direction of elimination in formation of the carbonyl group, forming the aldehyde rather than the ketone.

Experimental section

The syntheses of MHBT and MHBT-*d* have been previously reported (8, 15). The bisperchlorate of MHBT-*d* (0.3 mmol) was dissolved in 10 mL of water at 25 °C. The solution acidity was maintained at pH 8.0 by addition of 0.1 mol/L potassium hydroxide by an automated burette. After 2 h, the reaction was stopped by addition of hydrochloric acid (1 mol/L) to give an acid concentration in the sample of 0.01 mol/L. The product was purified by extraction with two portions of dichloromethane. Lyophilization of the aqueous layer yielded a mixture of AP and potassium chloride (6–8).

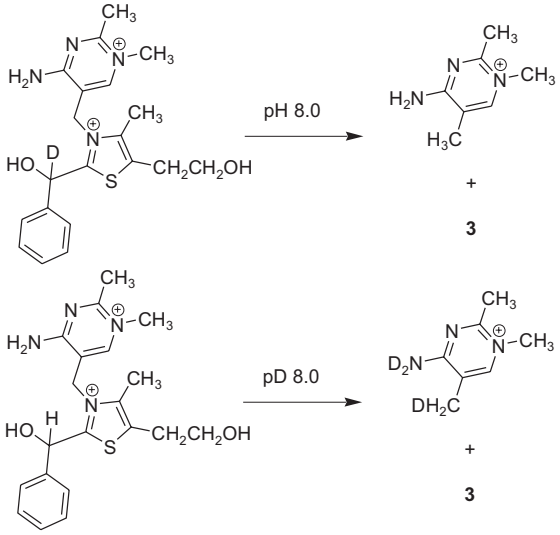
A similar procedure was used for the reaction of MHBT in deuterium oxide. We converted pH meter readings to those for pD by adding 0.4 to the displayed results (16). Fully deuterated acid–base reagents were used. This produced the C5′-monodeuterated analog of AP. ^{1}H NMR (500 MHz, CD_3OD) δ: 8.0 (s, 1H), 3.8 (s, 3H), 2.6 (s, 3H), 2.1 (dt, 3H). EI-MS (high resolution) calcd. for $[N_7H_{10}DN_3]^+$: 138.1016; found: 138.1018.

Results and discussion

No deuterium incorporation occurs into AP from the fragmentation of MHBT-*d* in water (^{1}H NMR and EI-MS (high resolution) calcd. for $[N_7H_{11}N_3]^+$: 137.0953; found: 137.0953). As a control, AP was characterized from the fragmentation of MHBT in deuterium oxide. EI-MS indicates the incorporation of a single deuterium. The location of the deuteron was determined by ^{1}H NMR to be at the C5′ position, which is derived from the methylene bridge between the two heterocycles. The signal for the C5′-methyl group initially consisted of a doublet of triplets ($^2J_{H\text{-}D}$ = 2.1 Hz, $^4J_{H\text{-}H}$ = 0.9 Hz, CD_3OD) from coupling to the geminal deuteron and neighbouring C6′ proton. After confirming the latter assignment by ^{1}H–^{1}H COSY, signal decoupling produced the characteristic 1:1:1 triplet of the monodeuterated methyl group. As the protons of AP do not exchange in deuterium oxide, deuterium incorporation in water would have been detectable under these conditions.

Owing to the absence of deuterated AP products **4** and **5** from the fragmentation of MHBT-*d* in water, we can rule out hydride transfer mechanisms (Fig. 3). Deuterium would be scrambled into solvent from deprotonation of the weak carbon acid to generate the carbanion that is consistent with

Fig. 3. Summary of the results from the deuterium labeling experiments in water and deuterium oxide.



mechanism 1. Monodeuteration of AP from the fragmentation in deuterium oxide is also consistent with mechanism 1 in which C—N bond cleavage occurs with the ionization of C5′ followed by solvent-mediated protonation. Regiospecific deuterium incorporation demonstrates that the isotope comes from solvent and is not transferred internally. The fact that proton–deuterium exchange is not observed in AP indicates that the C5′ methyl group is only weakly acidic, which is consistent with the fragmentation being highly exothermic.

The evidence against an internal hydride transfer supports a mechanism involving the conjugate base at carbon (α-C2). If fragmentation involves the delocalized conjugate base of MHBT, C—N bond cleavage, oxidation of the hydroxyl, and protonation of the C5′ carbon must occur, in steps or in concert. The surprisingly low barrier associated with fragmentation (10^4 s^{-1}) (15) suggests that the transition state of the C—N cleavage process has special stabilization. We note that BFD avoids fragmentation of a similar carbanionic intermediate that is generated by decarboxylation of the addition intermediate from benzoylformate and thiamin diphosphate. The enzyme's normal catalytic route has a higher barrier (k_{cat} = 10^2 s^{-1}) than the fragmentation reaction (17). Since the enzyme-catalyzed reaction necessarily involves a carbanionic structure upon loss of carbon dioxide, the mechanism of fragmentation avoidance is clearly a result of the effects of the enzyme environment (10). The protein manifold of the active site must increase the barrier to fragmentation while lowering that for protonation since the analogous substrates readily undergo fragmentation in solution.

Acknowledgements

We thank the Natural Sciences and Engineering Research Council of Canada (NSERC) for support through an operating grant and for a postgraduate scholarship to GI.

References

1. R. Breslow. Chem. Ind. (London), 893 (1957).
2. R. Breslow. J. Am. Chem. Soc. **79**, 1762 (1957).

© 2005 NRC Canada

3. P.M. Weiss, G.A. Garcia, G.L. Kenyon, W.W. Cleland, and P.F. Cook. Biochemistry, **27**, 2197 (1988).
4. L.J. Dirmaier, G.A. Garcia, J.W. Kozarich, and G.L. Kenyon. J. Am. Chem. Soc. **108**, 3149 (1986).
5. M.S. Hasson, A. Muscate, M.J. McLeish, L.S. Polovnikova, J.A. Gerlt, G.L. Kenyon, G.A. Petsko, and D. Ringe. Biochemistry, **37**, 9918 (1998).
6. R. Kluger, J.F. Lam, and C.-S. Kim. Bioorg. Chem. **21**, 275 (1993).
7. Y. Oka, S. Kishimoto, and H. Hirano. Chem. Pharm. Bull. **18**, 527 (1970).
8. R. Kluger, J.F. Lam, J.P. Pezacki, and C.-M. Yang. J. Am. Chem. Soc. **117**, 11383 (1995).
9. Q. Hu and R. Kluger. J. Am. Chem. Soc. **124**, 14858 (2002).
10. Q. Hu and R. Kluger. J. Am. Chem. Soc. **126**, 68 (2004).
11. C.G. Swain, A.L. Powell, W.A. Sheppard, and C.R. Morgan. J. Am. Chem. Soc. **101**, 3576 (1979).
12. I.A. Rose. Biochim. Biophys. Acta, **25**, 214 (1957).
13. S.S. Hall, A.M. Doweyko, and F. Jordan. J. Am. Chem. Soc. **100**, 5934 (1978).
14. R.V.J. Chari and J.W. Kozarich. J. Biol. Chem. **256**, 9785 (1981).
15. G. Ikeda and R. Kluger. J. Phys. Org. Chem. **17**, 507 (2004).
16. P.K. Glasoe and F.A. Long. J. Phys. Chem. **64**, 188 (1960).
17. E.S. Polovnikova, M.J. McLeish, E.A. Sergienko, J.T. Burgner, N.L. Anderson, A.K. Bera, F. Jordan, G.L. Kenyon, and M.S. Hasson. Biochemistry, **42**, 1820 (2003).

© 2005 NRC Canada

Hydrolysis of aryl hydrogen maleate esters mediated by cyclodextrins — Effect on the intramolecular catalysis[1]

Gabriel O. Andrés, O. Fernando Silva, and Rita H. de Rossi

Abstract: Kinetic studies of the hydrolysis of Z-aryl hydrogen maleates (Z = H, *p*-CH_3, *m*-CH_3, *p*-Cl, *m*-Cl) were carried out in the presence and absence of hydroxypropyl-β-cyclodextrin (HPCD) at variable pH from 1.00 to 3.00. The reaction involves the formation of maleic anhydride as an intermediate and the rate of its formation is strongly dependent on the pH. This is because the neighboring carboxylate group is a better catalyst than the carboxylic group. The rate constant for the formation of maleic anhydride decreases as the HPCD concentration increases in a nonlinear fashion. The results were interpreted in terms of the formation of a 1:1 inclusion complex of the esters with HPCD. The neutral (HA) and anionic (A) species of the substrate have different association constants (K_{CD}^{HA} and K_{CD}^{A}). In all cases studied, K_{CD}^{HA} is higher than K_{CD}^{A} for the same substrate. This difference is responsible for a decrease in the amount of the anionic substrate (reactive species) in the presence of HPCD, which results in a diminution of the observed rate constant. Besides, the rate constant for the reaction of the complexed substrate is smaller than that in the bulk solution indicating that the transition state of the cyclodextrin mediated reaction is less stabilized than the anionic substrate. The values of $\Delta\Delta G^{\ddagger}$ are almost independent of the substituent on the aryl ring and range within 0.48 and 1.05 kcal mol^{-1} (1 cal = 4.184 J). There is no correlation between K_{TS} and the association constant of the substrate indicating that the factors stabilizing the transition state are different from those that stabilize the substrate.

Key words: cyclodextrins, intramolecular catalysis, hydrolysis, inhibition.

Résumé : Opérant à des pH divers allant de 1,00 à 3,00, en présence et en absence de la hydroxypropyl-β-cyclodextrine (HPCD), on a réalisé une étude cinétique de l'hydrolyse de maléates acides de Z-aryle (Z = H, *p*-CH_3, *m*-CH_3, *p*-Cl et *m*-Cl). La réaction implique la formation d'anhydride comme intermédiaire et sa vitesse de formation dépend fortement du pH parce que le groupe carboxylate voisin est un meilleur catalyseur que le groupe carboxylique. La constante de vitesse pour la formation de l'anhydride maléique diminue d'une façon non-linéaire avec une augmentation de la concentration de HPCD. On interprète les résultats en fonction de la formation d'un complexe d'inclusion 1:1 des esters avec le HPCD. Les espèces neutre (HA) et anionique (A) du substrat ont des constantes d'association différentes, K_{CD}^{HA} et K_{CD}^{A}. Dans les cas étudiés, pour un même substrat, les valeurs de K_{CD}^{HA} sont supérieures à K_{CD}^{A}. En présence de HPCD, cette différence est responsable d'une diminution dans la quantité de substrat anionique (espèce réactive), ce qui conduit à la diminution observée de la constante de vitesse. De plus, la constante de vitesse pour la réaction du substrat complexé est plus faible que celle du substrat en solution ce qui indique que l'état de transition de la réaction catalysée par la cyclodextrine est moins stabilisé que celui du substrat anionique. Les valeurs de $\Delta\Delta G^{\ddagger}$ sont pratiquement indépendantes de la nature du substituant sur le noyau aromatique et elles se situent entre 0,48 et 1,05 kcal mol^{-1} (1 cal = 4,184 J). Il n'existe pas de corrélation entre K_{TS} et la constante d'association du substrat ce qui indique que les facteurs stabilisants l'état de transition sont différents de ceux qui stabilisent le substrat.

Mots clés : cyclodextrines, catalyse intramoléculaire, hydrolyse, inhibition.

[Traduit par la Rédaction]

Introduction

Intramolecular catalysis has been used as a model system because it gives important information about enzyme mechanisms (1–3). These reactions are very much dependent on the relative position of the reacting groups and the time that they remain at the proper distance for reaction (4).

Cyclodextrins (CD), which are cyclic oligomers of α-D-glucopyranose, have a well-defined cavity (5). They form inclusion complexes with a wide variety of species in aqueous

Received 26 February 2005. Published on the NRC Research Press Web site at http://canjchem.nrc.ca on 19 October 2005.

G.O. Andrés, O.F. Silva, and R.H. de Rossi.[2] Instituto de Investigaciones en Físico Química de Córdoba (INFIQC), Facultad de Ciencias Químicas, Departamento de Química Orgánica, Universidad Nacional de Córdoba, Ciudad Universitaria, 5000 Córdoba, Argentina.

[1]This article is part of a Special Issue dedicated to organic reaction mechanisms.
[2]Corresponding author (e-mail: ritah@dqo.fcq.unc.edu.ar).

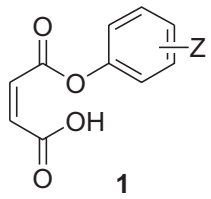
 doi: 10.1139/V05-144 © 2005 NRC Canada

solution (6, 7), and this effect has resulted in multiple industrial applications (8, 9). As a result of the host–guest interaction between the organic substrate and the cyclodextrin, the rate of the reactions usually change and it can also be responsible for interesting changes in reaction mechanisms that are well-documented in the literature (10–12). CDs have been frequently used as microreactors that can catalyze or inhibit organic reactions by including the substrate in their cavity (13, 14).

CDs have also been derivatized to improve some desired property (7, 15), such as hydrophilicity or hydrophobicity (16, 17).

We are interested in the cyclodextrin effect on the intramolecular catalysis because inclusion in the cyclodextrin cavity may change the geometry of the substrate and therefore make intramolecular reaction more favorable (18) or more unfavorable (19) than the reaction of the free substrate.

In previous work, we studied the effect of CD on the hydrolysis of aryl hydrogen phthalate esters (20, 21). We suggested that the Z-aryl ring is included in the CD cavity, and the structure of the substrate is distorted making the intramolecular attack of the carboxylate on the carbonyl of the ester more difficult, and consequently, the rate of the intramolecular reaction decreases. In this paper we report the effect of cyclodextrins on the hydrolysis reaction of Z-aryl hydrogen maleate (**1**) where hydroxypropyl-β-cyclodextrin (HPCD) produces an important decrease in the rate of the anhydride formation, but the behavior is somewhat different from that found for aryl hydrogen phthalate esters indicating differences in the mechanism of the cyclodextrin mediated reaction.



1

Z = H, *p*-CH_3, *m*-CH_3, *p*-Cl, *m*-Cl

Results and discussion

Rate constants for the hydrolysis of Z-aryl hydrogen maleates (Z = *p*-CH_3, *m*-CH_3, H, *p*-Cl, *m*-Cl) and maleic anhydride were obtained by measuring the change in the absorbance at an appropriate wavelength with time. All the kinetics studies were carried out in water containing 3.85% *v*/*v* of acetonitrile (ACN) as the co-solvent and at 25 °C.

Maleic anhydride is an intermediate in the hydrolysis of monoaryl maleate esters (22, 23), therefore it is important to determine the effect of CD on its rate of hydrolysis to understand the effect of cyclodextrin on the hydrolysis of the esters. The reactions of maleic anhydride were studied at pH 2.00 and 3.00 at seven different concentrations of hydroxypropyl-β-cyclodextrin (HPCD) between 2.5 and 30 mmol/L. Only one kinetic process was observed in all cases and the rate constants were the same, within the experimental error, at both pH. The ratio between the rate constant at the highest HPCD concentration (30 mmol/L) and the rate constants without HPCD were 0.93 and 1.01 at pH 2.00 and 3.00, respectively (Supplementary material, Table D1).[3] We also studied the hydrolysis of maleic anhydride at the highest HPCD concentration with different concentrations of a potential competitor for the cyclodextrin cavity (11). The rate constants were not affected by compounds that are known to form inclusion complexes and the observed rate constants were always the same within experimental error (Table D2).[3]

Table 1. Rate constants for the formation of maleic anhydride in the hydrolysis of Z-aryl hydrogen maleates in the presence of different competitors and at constant HPCD concentration.

	p-CH_3[a]	H[b]
Competitor concentration	k_i^{obs} ($\times 10^{-3}$ s^{-1})	k_i^{obs} ($\times 10^{-3}$ s^{-1})
Cyclohexanol ($\times 10^{-3}$ mol/L)		
0	1.37±0.04	4.12±0.03
25	2.21±0.02	5.93±0.4
50	4.24±0.01	10.1±0.1
100	5.3±0.3	11.7±0.6
***tert*-Butyl alcohol ($\times 10^{-3}$ mol/L)**		
100	2.06±0.02	5.6±0.1

Note: Rate constants were obtained in a conventional spectrophotometer at pH 2.00, HPCD concentration 0.03 mol/L, ionic strength 0.5 mol/L, temperature 25 °C, acetonitrile 3.85%. The standard errors were obtained from at least two determinations.

[a]λ = 281 nm.

[b]λ = 271 nm.

The hydrolysis reaction of phenyl-, *p*-methylphenyl-, *m*-methylphenyl-, *p*-chlorophenyl-, and *m*-chlorophenyl hydrogen maleate was studied at pH 1.00, 2.00, 2.50, and 3.00 in the presence of a variable concentration of HPCD (Tables D3–D7).[3] Two kinetic processes were observed at some wavelengths, and they are associated with the formation and hydrolysis of maleic anhydride. To calculate the rate constants for the system we choose a wavelength where the anhydride did not absorb and the formation of Z-phenol is the only process measured. Under these conditions the data can be fitted by a single exponential equation and the rate constants calculated correspond to the formation of the maleic anhydride.

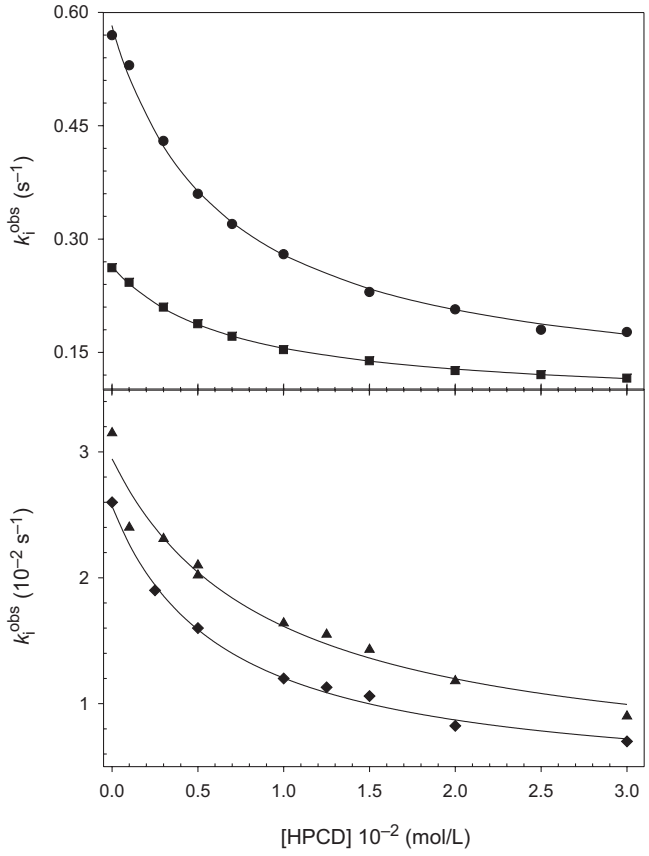
The addition of HPCD decreases the rate of formation of the anhydride, whereas γ-cyclodextrin did not show any effect and α-cyclodextrin showed a minor decrease in rate (Table D8),[3] therefore, the size of the cavity plays an important role on the inhibition observed.

We studied the effect of guests that may be included in the cyclodextrin cavity on the cyclodextrin retarded hydrolysis. At constant HPCD concentration (30 mmol/L) in the presence of cyclohexanol (25–100 mmol/L) and *tert*-butyl alcohol (100 mmol/L), the observed rate constants are higher than in the absence of the competitor (Table 1). The ratios between the rate constants for the hydrolysis in the presence of cyclohexanol at the higher concentration used

[3] Supplementary data for this article are available on the Web site or may be purchased from the Depository of Unpublished Data, Document Delivery, CISTI, National Research Council Canada, Ottawa, ON K1A 0S2, Canada. DUD 4026. For more information on obtaining material refer to http://cisti-icist.nrc-cnrc.gc.ca/irm/unpub_e.shtml.

© 2005 NRC Canada

Fig. 1. Effect of HPCD concentration on the hydrolysis of aryl hydrogen maleates at pH 3. Solvent: water and 3.85% acetonitrile, temperature: 25.0 °C, ionic strength: 0.5 mol/L (NaCl as compensating electrolyte). The symbols for different plots of k_i^{obs} vs. HPCD concentration are: *m*-chlorophenyl hydrogen maleate (●), *p*-chlorophenyl hydrogen maleate (■), *m*-methylphenyl hydrogen maleate (▲), *p*-methylphenyl hydrogen maleate (◆).



(100 mmol/L) and the rate constant for the hydrolysis without the competitor are 3.86 and 2.84 by *p*-methyl- and phenyl hydrogen maleate, respectively. The ratios for the same substrates were 1.50 and 1.36 when the competitor was *tert*-butyl alcohol. The addition of a competitor that binds to the HPCD lowers the free host concentration, resulting in an increase in k_i^{obs} as result of a higher free substrate concentration. Cyclohexanol shows a greater effect than *tert*-butyl alcohol, consistent with the values of the corresponding association constants with β-cyclodextrin, which are 676 and 46 $(mol/L)^{-1}$, respectively (11). These results confirm that there is an effective inclusion complex between the substrate and HPCD because the size of the competitor should not affect any other kind of interaction responsible for the inhibition observed. On the other hand, the smaller effect observed for the phenyl hydrogen maleate is attributed to the smaller association constant in relation to *p*-methyl hydrogen maleate (see the following).

The plot of k_i^{obs} vs. HPCD concentration is nonlinear in all cases (Fig. 1 is representative), and the data were very well fitted by eq. [1]. All the parameters are pH dependent and the value of *c* decreases as the pH increases.

$$[1] \qquad k_i^{obs} = \frac{a + b[\text{HPCD}]}{1 + c[\text{HPCD}]}$$

Based of the results described in the previous section, we suggest the mechanism shown in Scheme 1. The neutral substrate and its anion associates with cyclodextrin with a different association constant. The observed rate constant for Scheme 1 is given by eq. [2].

$$[2] \qquad k_i^{obs} = \frac{k_i + k_{CD}K_{CD}^{A}[\text{HPCD}]}{1 + K_{app}[\text{HPCD}]} f_A$$

where k_i and k_{CD} are the rate constants of the free and complexed anionic substrate, respectively, K_{CD}^{A} is the association constant of the anion of the substrate with HPCD, and K_{app} is given by eq. [3]. It is the product of the association equilibrium constant of the anionic substrate and the fraction of the anion (f_A, eq. [4]) plus the product of the association equilibrium constant of the neutral substrate and the corresponding fraction ($f_{HA} = (1 - f_A)$).

$$[3] \qquad K_{app} = f_A K_{CD}^{A} + (1 - f_A)K_{CD}^{HA}$$

$$[4] \qquad f_A = \frac{K_a}{K_a + H^+}$$

Equation [2] is mathematically equivalent to eq. [1] with $a = k_i f_A$, $b = k_{CD}K_{CD}^{A}f_A$, and $c = K_{app}$. The rate and equilibrium constants obtained are shown in Table 2, which were calculated using eq. [2] to fit all the data obtained at various pH values. In Scheme 1, only the intramolecular reaction of the carboxylate group is considered because it is known that the reaction of the carboxylic acid does not compete with this (22, 23).

We had previously reported for monoaryl esters of phthalic acid that the ratio of association constants for the neutral (K_{CD}^{HA}) and anionic (K_{CD}^{A}) species (20) for the different substrates give values in a range of 6–10. In the case of the monoaryl hydrogen maleates, the difference between the two equilibrium constants is smaller; it amounts only to a factor of two to four (Table 2). Besides there is very small variation of K_{CD}^{HA} and K_{CD}^{A} among the various substrates, which contrasts with the results for monoaryl phthalate esters where there is a significant change in equilibrium constants with the substituents in the aryl ring (20).

The difference in equilibrium constant for the neutral and anionic substrates is important for the observed effect of HPCD because this difference drives the equilibrium toward the neutral species, which is much less reactive than the anionic species (23). Therefore, the absolute inhibition of the observed rate constant is stronger at low pH. For example, in the case of phenyl hydrogen maleate, the relative rates measured at 0 and 30 mmol/L concentrations were 5.1 and 2.7 at pH 1.00 and 3.00, respectively.

Included in Table 2 are the values of K_{TS}. These values have been calculated following the Kurz treatment (24), which was first applied for cyclodextrin mediated reactions by Tee and co-workers (25–27). It represents the hypothetical association equilibrium constant for the transition state for the reaction mediated by cyclodextrin and is defined as the ratio $k_{CD}K_{CD}^{A}/k_i$. The values of K_{TS} are in all cases smaller than the K_{CD}^{A} for the substrates, indicating that inclusion in the cyclodextrin cavity stabilizes the substrate more

© 2005 NRC Canada

Scheme 1.

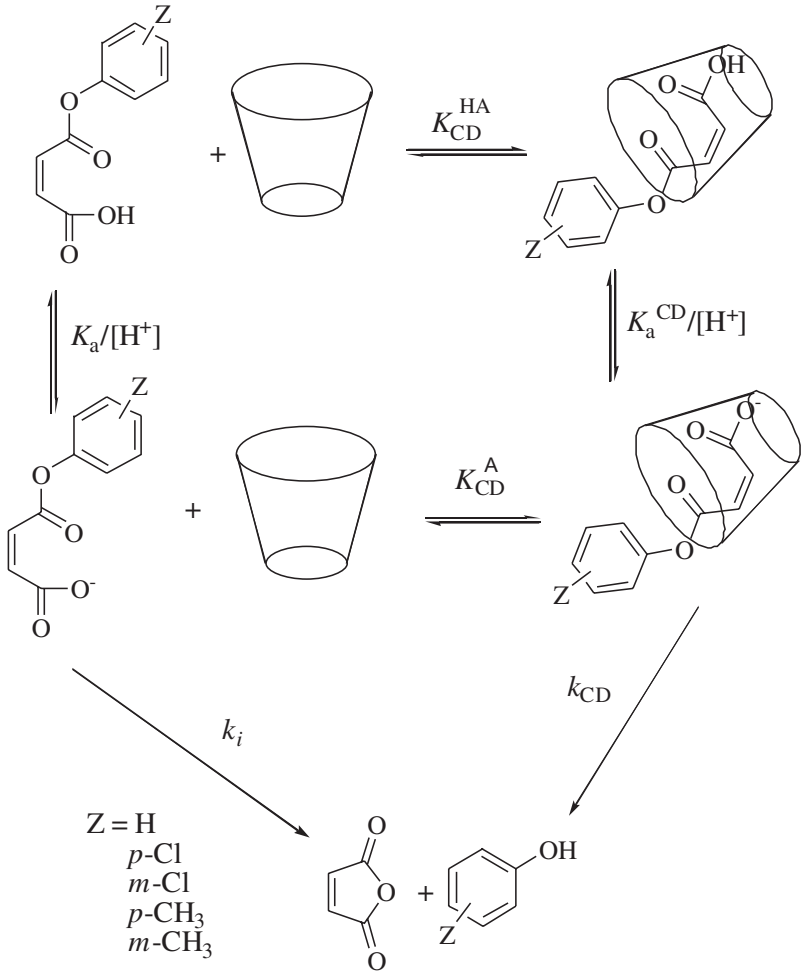


Table 2. Rate and equilibrium constants for the anhydride formation in the hydrolysis of Z-aryl hydrogen maleates mediated by HPCD.

Z	pK_a	k_i ($\times 10^{-2}$ s^{-1})	k_{CD} ($\times 10^{-2}$ s^{-1})	K_{CD}^{A} (mol/L)$^{-1}$	K_{CD}^{HA} (mol/L)$^{-1}$	K_{TS} (mol/L)$^{-1}$[a]	$\Delta\Delta G$ (kcal mol^{-1})[b]
p-Cl	2.64	37.9±0.6	17.0±0.9	101±8	255±18	45	0.48
H	2.43	5.0±0.3	1.5±0.3	104±30	208±57	31	0.72
p-CH_3	2.66	3.7±0.1	0.9±0.1	82±14	313±26	20	0.84
m-CH_3	2.36	3.6±0.1	0.8±0.3	66±22	303±75	15	0.88
m-Cl	2.56	79±2	14±2	141±16	211±31	24	1.05

Note: Obtained from all of the data for each compound and using eq. [2] to fit the data.
[a]The values were determined according to ref. 25.
[b]The difference in free energy for the association of the transition state and the substrate.

than the transition state. In the last column of Table 2, the values of $\Delta\Delta G^{\ddagger}$ that are a measure of the differences in stabilization between substrate and transition state are collected. It is remarkable that the values are about the same for all the substrates, which again contrasts with the results of the aryl phthalate esters where there is a significant variation among the different esters; for instance, $\Delta\Delta G^{\ddagger}$ is 0.20 and 1.59 kcal/mol for the *p*-chloro and *m*-methyl derivative, respectively (20).

We conclude that in this case the orientation of the main complexes is as shown in Scheme 1, namely, with the maleic moiety pointing towards the primary hydroxyl side of the cavity. There are several examples in the literature where anionic compounds are oriented in that way. For instance, benzoate anion and 4-biphenyl carboxylate anion are axially included in the cavity of β-cyclodextrin with an orientation that locates the carboxylate group at the primary hydroxyl side (28) and the same type of orientation was demonstrated for the complex between β-cyclodextrin and β-naphthyloxyacetatate in the solid as well as in solution (29).

The transition state for the attack of the neighboring carboxylate group on the carbonyl carbon of the ester re-

© 2005 NRC Canada

Table 3. IR, ^{13}C NMR, ^{1}H NMR, and melting points for the Z-aryl hydrogen maleates.

Z	IR (cm^{-1})[a]	^{13}C NMR (ppm)[b]		^{1}H NMR (ppm)[b]	mp (°C)
		174.8	129.6	7.21 (m, 5H)	
H	1748.7 (COOH)	167.3	126.6	6.52 (m, J = 12 Hz, 2H)	89.5–92.7
	1708.0 (COOR)	150.5	122.7		
		130.7	121.2		
		175.1	129.6		
		167.7	127.9		
p-Cl	1748.9 (COOH)	148.8	122.7	7.34 (m, 4H)	100.9–102.5
	1705.4 (COOR)	134.7	121.4	6.54 (m, J = 12 Hz, 2H)	
		131.8			
		174.0	129.9		
		167.3	127.0		
m-Cl	1748.8 (COOH)	146.1	122.7	7.27 (m, 4H)	123.6–124.7
	1708.5 (COOR)	133.3	121.9	6.54 (m, J = 12 Hz, 2H)	
		130.4	119.6		
		166.9	132.2		
		165.2	130.1	7.07 (m, 4H)	
p-CH_3	1748.7 (COOH)	147.7	121.0	6.53 (m, J = 12 Hz, 2H)	97.8–100.1
	1708.0 (COOR)	136.4	20.9	2.34 (s, 3H)	
		133.0			
		167.0	129.3		
		165.0	127.4	7.12 (m, 4H)	
m-CH_3	1763.1 (COOH)	149.8	121.6	6.52 (m, J = 12 Hz, 2H)	76.4–79.2
	1702.6 (COOR)	140.0	118.0	2.33 (s, 3H)	
		132.8	21.2		
		130.5			

[a]KBr pellets.
[b]In *d*-chloroform as the solvent.

quires the carboxylate to be in the plane of the ring with the ester group approximately perpendicular. It is well-known that an appropriate geometry in the initial state is a critical factor for a reaction (30, 31). The inclusion of the substrate with the geometry shown in Scheme 1 probably decreases the degree of freedom of the carboxylate group to reach the appropriate geometry for reaction, and therefore, the transition state is destabilized compared to the reaction of the free substrate. It is also possible that the cyclodextrin makes some changes in the most stable conformation of the substrate, making it more difficult to reach the adequate position for intramolecular attack (32).

Conclusions

The intramolecular catalysis of hydrolysis of Z-aryl hydrogen maleate is affected by the presence of HPCD, where the size of the cavity plays an important role. The results presented here indicate that the inhibition of the intramolecular reaction as a result of inclusion in the cavity of the cyclodextrin is due to two main factors. One is the difference between the association constants for the neutral and anionic substrate that drive the equilibrium toward neutral species that is much less reactive than the anion. The second fact is steric restriction imposed for the inclusion in the substrate to reach the transition state, which is evident from a decrease in the stabilization of the transition state compared to the substrate.

From the similarities of the equilibrium constants for the substrates and also the similarities in the destabilization energy of the corresponding transition state we infer that the reactive complexes have the maleic moiety inside the cavity contrary to what was observed for aryl phthalate where inclusion of the aryl ring in the cavity was suggested.

Experimental

Materials

Maleic anhydride (Aldrich) and substituted phenols (Aldrich) were sublimed before use (33). HPCD (average degree of substitution 5.9, PM 1454) (Roquette) was a gift from Ferromet S.A. Argentina and was used without further purification.

The monoaryl esters were prepared from the maleic anhydride and the appropriate phenol by adapting the method described in the literature (34). The esters were characterized by ^{13}C and ^{1}H NMR and IR spectra; all this information along with melting points are summarized in Table 3. IR and NMR spectra were done on Nicolet 5SXC FT-IR (KBr pellets) and Bruker AC 200 (200 MHz) spectrometers, respectively. The purity of the products was also checked by comparing the UV–vis absorption spectrum of a solution containing the fully hydrolyzed esters with one at the same concentration prepared with maleic acid and the corresponding alcohol.

Aqueous solutions were made up from water purified in a Millipore apparatus. Acetonitrile Merck HPLC was dried on silica gel 10% *p*/*v* as described in the literature (33).

© 2005 NRC Canada

Kinetic procedures

The reactions were carried out in a stopped-flow Applied Photophysics SF 17MV apparatus (SF) with unequal mixing. The correspondent Z-aryl hydrogen maleate or the anhydride dissolved in dry acetonitrile was placed in the smaller syringe (0.1 mL). The large syringe (2.5 mL) was filled with a water solution containing all the other ingredients; the cyclodextrin concentration was varied between 0 and 30 mmol/L. The solutions of the substrate for the kinetic determinations were freshly prepared in dry acetonitrile in the appropriate concentration to get a final concentration of 2×10^{-4} mol/L. The total acetonitrile concentration was 3.85% *v*/*v*. When the rate was too slow for the stopped-flow apparatus the kinetic determinations were carried out in a thermostatted cell of a conventional spectrophotometer (Shimadzu UV2101) as described in previous work (21).

All reactions were run at 25.0 ± 0.1 °C and at constant ionic strength (0.5 mol/L) using NaCl as the compensating electrolyte. The pH measurements were carried out using a pH meter at controlled temperature and calibrated with buffers prepared according to the literature (35).

The observed rate constants were determined by measuring the change in absorbance at 250, 268, 271, 273.5, or 281 nm, depending on the substrate. In some of the experiments, the pH of the solution was checked after the reaction by measuring it in the discarded solution, and the change observed were always less than 0.03 pH units. The kinetic traces were fitted with one exponential equation using the software of the SF apparatus.

Acknowledgements

This research was supported in part by the Consejo Nacional de Investigaciones Científicas y Técnicas (CONICET), the Agencia Córdoba Ciencia, Agencia Nacional de Ciencia y Tecnología (FONCYT), Fundacion Antorchas, and the Universidad Nacional de Córdoba, Argentina. G.O.A. and O.F.S. are grateful recipients of CONICET fellowships.

References

1. A.J. Kirby and P.W. Lancaster. J. Chem. Soc. Perkin Trans. 2, 1206 (1972).
2. J. Suh and K.H. Chun. J. Am. Chem. Soc. **108**, 305 (1986).
3. F.M. Menger and M. Ladika. J. Am. Chem. Soc. **110**, 6794 (1988).
4. A.D. Bond, A.J. Kirby, and E. Rodriguez. Chem. Commun. 2266 (2001).
5. M.L. Bender and M. Komiyama. Cyclodextrin chemistry. Springer-Verlag, New York. 1978.
6. K. Takashi. Chem. Rev. **98**, 2013 (1998).
7. R. Breslow and S.D. Dong. Chem. Rev. **98**, 1997 (1998).
8. E.M.M. Del Valle. Proc. Biochem. **39**, 1033 (2004).
9. A.R. Hedges. Chem. Rev. **98**, 2035 (1998).
10. O.S. Tee and B.K. Takasaki. Can. J. Chem. **63**, 3540 (1985).
11. O.S. Tee, M. Bozzi, J.J. Hoeven, and T.A. Gadosy. J. Am. Chem. Soc. **115**, 8990 (1993).
12. M.A. Fernandez and R.H. de Rossi. J. Org. Chem. **62**, 7554 (1997).
13. L. Viola and R.H. de Rossi. Can. J. Chem. **77**, 860 (1999).
14. T.A. Gadosy, M.J. Boyd, and O.S. Tee. J. Org. Chem. **65**, 6879 (2000).
15. V.T. D'Souza and M.L. Bender. Acc. Chem. Res. **20**, 146 (1987).
16. A. Craft and R.A. Bartsch. Tetrahedron, **39**, 1407 (1983).
17. A.R. Khan, P. Forga, K.J. Stine, and V.T. D'Souza. Chem. Rev. **98**, 1977 (1998).
18. D.D. Sternbach and D.M. Bossana. J. Am. Chem. Soc. **104**, 5853 (1982).
19. A.M. Granados and R.H. de Rossi. J. Org. Chem. **66**, 1548 (2001).
20. G.O. Andrés, A.M. Granados, and R.H. de Rossi. J. Chem. Soc. Perkin Trans. 2, 1502 (2002).
21. G.O. Andrés and R.H. de Rossi. ARKIVOC, **10**, 127 (2003).
22. A.J. Kirby. Adv. Org. Chem. **17**, 183 (1980).
23. G.O. Andres and R.H. de Rossi. J. Org. Chem. **70**, 1445 (2005).
24. J. Kurz. J. Am. Chem. Soc. **65**, 987 (1963).
25. O.S. Tee. Carbohydr. Res. **192**, 181 (1989).
26. O.S. Tee, C. Mazza, and X.-X. Du. J. Org. Chem. **55**, 3603 (1990).
27. O.S. Tee and X.-X. Du. J. Am. Chem. Soc. **114**, 620 (1992).
28. H. Hirai, Y. Shiraishi, H. Mihori, K. Saito, and T. Kawamura. Polym. J. **28**, 91 (1996).
29. A. Kokkinou, K. Yannakopoulou, I.M. Mavridis, and D. Mentzafos. Carbohydr. Res. **332**, 85 (2001).
30. E. Hartwell, D.R.W. Hodgson, and A.J. Kirby. J. Am. Chem. Soc. **122**, 9326 (2001).
31. F.M. Menger. Acc. Chem. Res. **18**, 128 (1985).
32. D.W. Griffiths and M.L. Bender. J. Am. Chem. Soc. **95**, 1679 (1973).
33. D.D. Perrin and W.L.G. Armarego. Purification of laboratory chemicals. 3rd ed. Butterworths-Heinemann Ltd, Oxford, UK. 1994.
34. I. Bojanowska and T. Jasinski. Pol. J. Chem. **63**, 455 (1989).
35. D.R. Lide (*Editor*). Handbook of chemistry and physics. 72nd ed. CRC Press, Boca Raton, Fla. pp. 8-30–8-35. 1991 to 1992.

© 2005 NRC Canada

The aromatic character and resonance stabilization energies of substituted cyclopentadienyl and indenyl cations[1]

J.A. Pincock and A.W.H. Speed

Abstract: Calculations (B3LYP/6-31G(d)) have been used to assess the aromaticity of 5-X substituted indenyl (**4**) and cyclopentadienyl (**5**) cations with X = O^-, NH_2, OCH_3, CH_3, F, H, CN, and N_2^+. Two criteria were used, the aromatic stabilization energy (ASE), as determined by isodesmic reactions, and bond alternation, as determined from the Julg index (*A*) on the basis of carbon–carbon bond lengths. Substituent effects on the singlet state of the cyclopentadienyl cations resulted in significant decreases in antiaromatic character for electron-donating groups as indicated by larger *A* values (*A* = –0.25 for X = H and +0.26 for X = NH_2). These decreases paralleled increases in the C-2—C-3 bond length and good linear correlations were obtained between *A* vs. the C-2—C-3 bond length and *A* vs. the ASE. These effects were rationalized by the stabilization by the electron-donating groups of the positive charge at C-5 generated as a consequence of a Jahn–Teller distortion leading to a lowest energy singlet state with a HOMO of a_2 symmetry. In contrast, the lowest energy triplet state for each of the substituted cyclopentadienyl cations has little bond alternation (*A* > 0.9) and, by this criterion, is not significantly antiaromatic. The triplet state is more stable than the singlet state for the unsubstituted case and those with electron-withdrawing groups (ΔE_{ST} = –11.3 and –9.3 kcal/mol for X = H and CN, respectively) (1 cal = 4.184 J), but less stable for electron-donating groups (ΔE_{ST} = +15.0 kcal/mol for X = NH_2). For the indenyl cations **4**, the ASE values were almost independent of the substituent and the *A* values only decreased slightly for electron-donating groups. The *A* values also indicated that the indenyl cations could be divided into two moieties, an X-substituted pentadienyl cation with considerable delocalization and little bond alternation, and a 2,3-butadiene one with considerable bond alternation. This separation also placed the major portion of the positive charge on the pentadienyl part. The lack of symmetry in the substituted indenyl cations rationalizes the selective reactivity of the 5-methoxy-substituted cation at C-1. Finally, the resonance stabilization energies (RSE) of the substituted cations gave a linear correlation with the RSEs of 4-substituted benzylic cations.

Key words: indenyl cations, cyclopentadienyl cations, substituent effects, stabilization energies.

Résumé : On a fait appel à des calculs (B3LUP/6-31G(d)) pour évaluer l'aromaticité de cations indényles (**4**) et cyclopentadiényles (**5**) portant un substituant 5-X dans lesquels X = O^-, NH_2, OCH_3, CH_3, F, H, CN et N_2^+. On a utilisé deux critères, l'énergie de stabilisation aromatique (ESA) telle que déterminée par des réactions isodesmiques et l'alternance des liaisons telle que déterminée par l'indice de Julg (*A*) sur la base des longueurs des liaisons carbone–carbone. Les effets de substituants sur l'état singulet des cations cyclopentadiényles conduit à une diminution significative du caractère antiaromatique avec les groupes électrodonneurs, telle qu'indiquée par des valeurs plus élevées de *A* (*A* = –0,25 pour X = H et +0,26 pour X = NH_2). Ces diminutions sont accompagnées d'une augmentation parallèle de la longueur de la liaison C-2—C-3 et on a obtenu des bonnes corrélations linéaires entre la valeur de *A* en fonction de la longueur de la liaison C-2—C-3 et entre la valeur de *A* en fonction de ESA. On a rationalisé ces effets par la stabilisation par les groupes électrodonneurs de la charge positive en C-5 générée en conséquence d'une distorsion Jahn–Teller conduisant à un état singulet d'énergie le plus faible avec une orbitale moléculaire haute occupée de symétrie a_2. Par opposition, l'état triplet des cations cyclopentadiényles substitués ne présentent pas beaucoup d'alternance des liaisons et, par ce critère, ils ne sont pas très antiaromatiques. L'état triplet est plus stable que l'état singulet dans le cas du produit non substitué ou de ceux portant des groupes électroattracteurs (ΔE_{ST} = –11,3 et –9,3 kcal/mol respectivement pour X = H et CN) (1 cal = 4,184 J), mais plus stable pour les dérivés portant des groupes électrodonneurs (ΔE_{ST} = +15 kcal/mol pour X = NH_2). Pour les cations indényles **4**, les valeurs d'ESA sont presque indépendantes de la nature des substituants et les valeurs de *A* ne diminuent que légèrement avec les groupes électrodonneurs. Les valeurs de *A* indiquent aussi que les cations indényles peuvent être divisés en deux groupes, un cation pentadiényle substitué par un groupe X qui comporte beaucoup de délocalisation et peut d'alternance des liaisons et un buta-2,3-diène qui comporte beaucoup d'alternance de liaison. Ces divisions place aussi une portion importante de la charge positive

Received 23 February 2005. Published on the NRC Research Press Web site at http://canjchem.nrc.ca on 21 October 2005.

J.A. Pincock[2] and A.W.H. Speed. Department of Chemistry, Dalhousie University, Halifax, NS B3H 4J3, Canada.

[1]This article is part of a Special Issue dedicated to organic reaction mechanisms.
[2]Corresponding author (e-mail: james.pincock@dal.ca).

 doi: 10.1139/V05-137 © 2005 NRC Canada

sur la partie pentadiényle. Le manque de symétrie dans les cations indényles substitués permet de rationaliser la réactivité sélective pour la position C-1 du cation substitué par un 5-méthoxy. Enfin les énergies de stabilisation de résonance (ESR) des cations substitués donnent une corrélation linéaire avec les valeurs de ESR des cations benzyliques substitués en position 4.

Mots clés : cations indényles, cations cyclopentadiényles, effets de substituant, énergies de stabilisation.

[Traduit par la Rédaction]

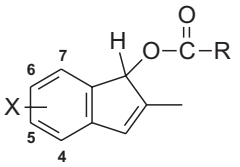
Introduction

We recently reported on the photochemistry of the indenyl esters, acetates (**1a**–**1c**) and pivalates (**2a**–**2c**), in both methanol and cyclohexane solvents (1). In cyclohexane, the products obtained were derived entirely from the radical pair intermediates expected from homolytic cleavage of the carbon–oxygen bond. In methanol, the methyl ethers **3a** and **3b** were obtained in significant yield (from 0% for **2a** to 100% for **1c**) as a consequence of the formation of ion-pair intermediates.

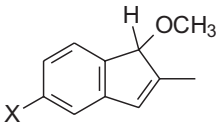
The mechanism of formation of ion-pair intermediates in photosolvolysis reactions has attracted considerable interest recently with two quite different pathways proposed. This topic has recently been reviewed (2). For arylmethyl esters, the first involves direct heterolytic cleavage of the carbon–oxygen bond from the excited singlet state (3). The second proposal is homolytic cleavage from the same excited state followed by rapid redox electron transfer converting the first-formed radical pair to the ion pair (4). For compound **1c**, we tentatively concluded that the former mechanism was the preferred one in contrast to most esters that seem to follow the latter pathway. Independent of the mechanism, the fact that products derived from indenyl cations are formed is certain, perhaps a consequence of the antiaromatic character of these $4n$ π cations, in agreement with Wan and co-workers' (5) proposal for 9-fluorenyl derivatives.

The observation that the 5-methoxy ether **3b** was obtained from either of the starting esters (5-methoxy **1b** or 6-methoxy **1c**) indicates that, as expected, a common indenyl cation **4** is obtained from both, as shown by the two resonance contributors **I-4c** and **II-4c** in Scheme 1. The fact that the methoxy substituted cation **4** reacts with methanol only at C-1 (as in **I**) and not C-1 (as in **II**) is a consequence of the change from C_{2v} symmetry for the unsubstituted indenyl cation **4f** to C_s symmetry by the addition of the methoxy group to C-5. Effectively, C-1 is para to the methoxy group and C-3 is meta in structure **1**–**4c**.

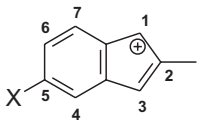
As the benzo analogue of the cyclopentadienyl cation, the indenyl cation has attracted considerable experimental and theoretical interest as a $4n$ antiaromatic ring system (6, 7). Unfortunately, experimental results for substituted cases are scarce. Recently, however, an alkyl (8) and a trifluoromethyl substituted cyclopentadienyl cation (9) and a trifluoromethyl substituted indenyl cation (10) have been the proposed intermediates generated in solvolysis reactions. Nevertheless, the effect that substitutents have on the charge distribution and aromaticity of these cations has not been explored in a systematic way. The limited number of literature results will be summarized in the appropriate context in the following.

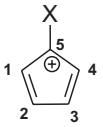


1a: X = H, R = CH_3
1b: X = 5-CH_3O, R = CH_3
1c: X = 6-CH_3O, R = CH_3
2a: X = H, R = *t*-Bu
2b: X = 5-CH_3O, R = *t*-Bu
2c: X = 6-CH_3O, R = *t*-Bu



3a: X = H
3b: X = 5-CH_3O





4a: X = O^-
4b: X = NH_2
4c: X = OCH_3
4d: X = CH_3
4e: X = F
4f: X = H
4g: X = CN
4h: X = N_2^+

5a: X = O^-
5b: X = NH_2
5c: X = OCH_3
5d: X = CH_3
5e: X = F
5f: X = H
5g: X = CN
5h: X = N_2^+

We now report an ab initio molecular orbital study using GAUSSIAN 98 (11) for optimized geometries at the B3LYP/6-31G(d) computational level that probe these issues. This level was chosen so that the results could be conveniently compared with two other recent studies, one on the aromatic character of the unsubstituted cyclopentadienyl and indenyl cations by Jiao, Schleyer, Tidwell, and co-workers (12), and the other on the aromaticity of substituted benzyl cations by Morao and Hillier (13). Moreover, an isodesmic reaction analogous to eq. [1][3] gave calculated reaction energies, which, for our purposes, are independent of the level of theory: +36.28 kcal/mol (MP2(full)/6-31G(d)); +33.14 kcal/mol (MP4SDTQ/6-31G(d)//MP2(full)/6-31G(d)); +33.47 kcal/mol (B3LYP/6-31G(d)); +34.67 kcal/mol (B3LYP/6-31+G(d,p) (14) (1 cal = 4.184 J).

Although our interest in this topic was stimulated by our experimental observations on the photochemistry of the substituted indenyl esters **1** and **2**, we will first present results

[3] The structure used for **8** (X = H) in ref. 14 was 1,3- rather than 1,4-pentadiene.

© 2005 NRC Canada

Scheme 1. The common indenyl cation **4c** from 5-methoxy- (**1b**) and 6-methoxy-2-methyl-indenyl acetate (**1c**).

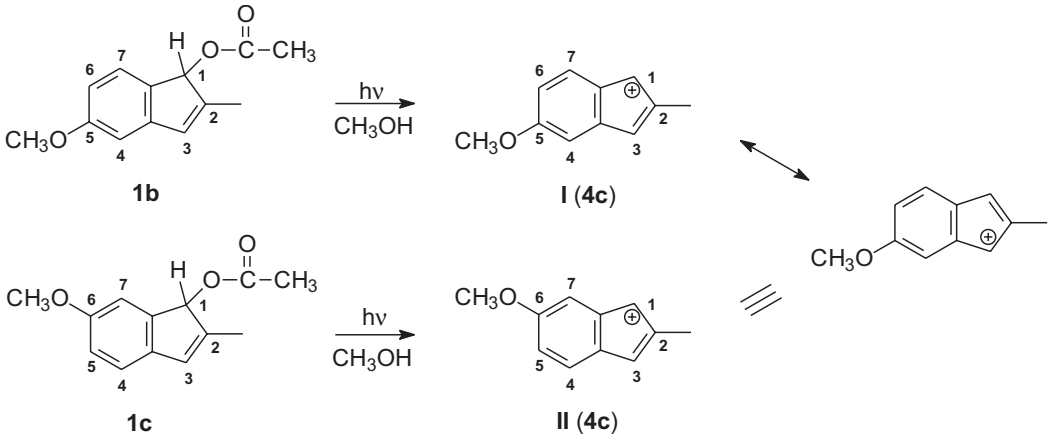


Table 1. Calculated bond lengths and Julg indices (*A*) for the singlet state of the cyclopentadienyl cations **5** with X at C-5 unless otherwise noted.

Cmpd.	X	σ^+	C-2—C-3 (Å)	C-1—C-2 = C-3—C-4 (Å)	C-4—C-5 = C-5—C-1 (Å)	A^a
5a	O^-	–4.27	1.503	1.340	1.511	0.32
5b	NH_2	–1.30	1.516	1.344	1.475	0.26
5c	OCH_3[b]	–0.78	1.526	1.347[c]	1.468[c]	0.15
				1.340	1.481	
5d	CH_3[b]	–0.31	1.547	1.351[d]	1.454[d]	–0.02
				1.341	1.479	
5e	F	–0.07	1.557	1.345	1.454	–0.12
5f	H	0.0	1.575	1.350	1.451	–0.25
5g	CN	0.66	1.556	1.350	1.460	–0.06
5g	2-CN[b]	0.66	1.572	1.374[e]	1.423[e]	–0.15
				1.341	1.468	
5h	N_2^+	1.88	1.615	1.366	1.433	–0.48
5h	2-N_2^+[f]	1.88	1.348	1.517[e]	1.403[e]	0.34
				1.556	1.382	

[a] A = 0.62 for 1,3-cyclopentadiene with C-2—C-3 = 1.470, C-1—C-2 = C-3—C-4 = 1.349, C-4—C-5 = C-5—C-1 = 1.507 Å.
[b] These structures have C_s symmetry, but the HOMO has pseudo a_2 symmetry as in structure **5-I**.
[c] The first bond length of each pair is syn to the methoxy group, the second anti.
[d] The first bond length of each pair is syn to the in-plane hydrogen atom of the methyl group, the second anti.
[e] The first bond length of each pair is C-1—C-2 or C-5—C-1.
[f] This structure has C_s symmetry, but the HOMO has pseudo b_2 symmetry as in structure **5-II**.

for the substituted cyclopentadienyl cations **5** that serve as a useful foundation for the more delocalized indenyl cations **4**.

Results and discussion

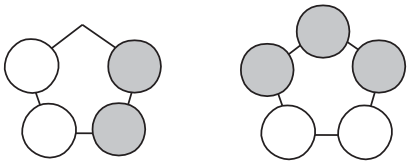
The cations examined (**4a**–**4h** and **5a**–**5h**) were chosen with a range of electron-donating and electron-withdrawing substitutents, as indicated by their Hammett σ^+ values shown in Table 1. Values of σ^+, rather than σ, were chosen on the basis of the direct resonance interaction of the substituent with the positive charge of the cation. The σ^+ values chosen are the same as those used by Morao and Hillier (13), taken from a recent review of Hammett substituent constants (15). The two charged substituents at the extremes, the oxy anion (**a**, X = O^-) and the diazonium cation (**h**, X = N_2^+), without a counter balancing cation for O^- or anion for N_2^+, are not accessible for experimentation, but serve as useful calculated values that reinforce the observed trends for the other, more usual, substitutents.

Aromatic stabilization energy (ASE) of the singlet state of the cyclopentadienyl cations 5

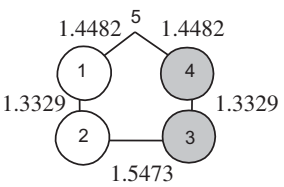
The cyclopentadienyl cation ($C_5H_5^+$) is often used as an introduction to the concept of antiaromaticity. However, as has been known for some time (14) and has been clearly explained in a recent high-level computational study (16), this species is not a single entity. In D_{5h} symmetry, two degenerate π HOMOs are predicted (nodal properties are sketched in **5-D_{5h}**, Fig. 1) and therefore the ground state should be a triplet, in agreement with experimental and computational studies (16). Two Jahn–Teller distortions give the singlet species **5-I** and **5-II** (bond lengths from RHF/6-31G(dp) calculations) C_{2v} geometries, both of which remove the degeneracy of these two orbitals (Fig. 1). In the first, **5-I**, the

© 2005 NRC Canada

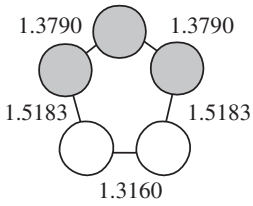
Fig. 1. Structures related to eqs. [1] and [3].



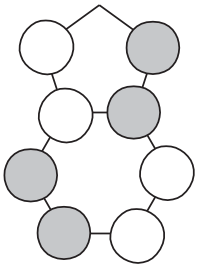
5-D_{5h}



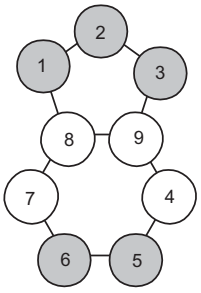
5-I
C_{2v} (a_2)



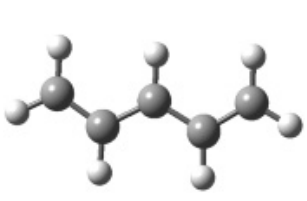
5-II
C_{2v} (b_2)



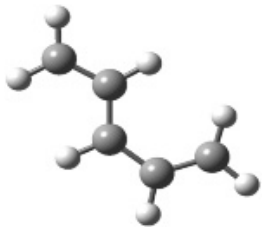
4-I
C_{2v} (a_2)



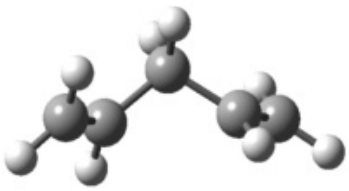
4-II
C_{2v} (b_2)



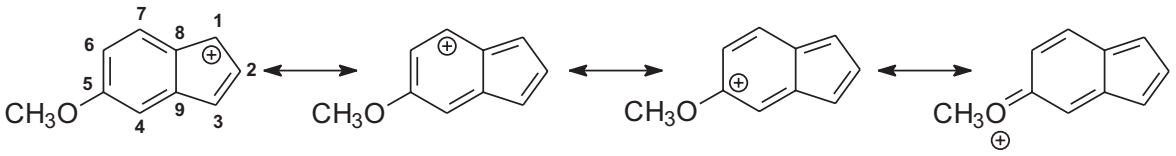
6a



6b



8a



11a **11b** **11c** **11d**

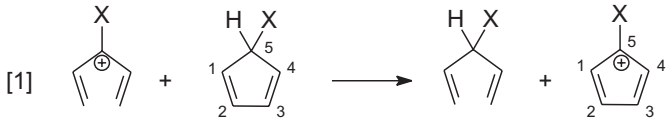
orbital of lower energy, now the HOMO, has a_2 symmetry, the stabilization resulting from lengthening the C-2—C-3[4] bond and decreasing the antibonding interaction. In the second, **5-II**, of b_2 symmetry, the stabilization results from equally increasing both the C-1—C-2 and C-3—C-4 bond lengths. These qualitative arguments have been developed some time ago and reinforced by HMO, MINDO, and ab initio STO-2G methods (17). These two singlet states have been described as a "… *cis*-butadiene moiety …and the other, a combination of an allyl cation and an ethylene…", respectively (12). Therefore, two closed-shell singlet states are possible. These two states are calculated to differ in energy by less than 1 kcal/mol and are higher in energy than the ground-state triplet by 3.4–11.6 kcal/mol, depending on the level of theory (16). At the RHF/6-31G** and CASSCF(4,5)/6-31G** levels of computation, the b_2 state has no imaginary frequencies, but the a_2 does have one of b_2 symmetry. In contrast, at the MP2/6-311G(2d,p) level, the a_2

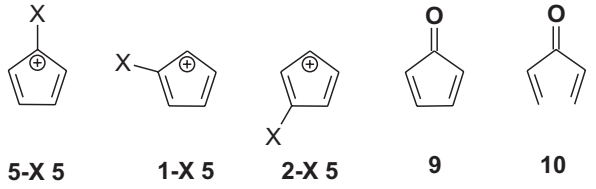
[4] The cyclopentadienyl cations are numbered so that C-5 is on the C_2 axis and across the ring from the unique carbon–carbon bond (C-2—C-3) for each case. This numbering system then agrees with the IUPAC name for 1,3-cyclopentadiene.

© 2005 NRC Canada

state has no imaginary frequencies, but the b_2 one has one, again of b_2 symmetry. An open-shell singlet state is the least stable of all of the states, 11–17 kcal/mol above the triplet ground state (16).

The ASE of the singlet cyclopentadienyl cation **5f** has been previously assessed (12) by the isodesmic reaction in eq. [1] and we have reproduced their reported value of the reaction energy of +42.5 kcal/mol. The energy of **5f** obtained by us, using an input geometry with equal carbon–carbon bond lengths of 1.40 Å, resulted in a minimum energy structure (no imaginary frequencies) with symmetry analagous to **5-I** (bond lengths are in Table 1). Using the values reported in the Supporting information of the previous report (12) for each structure of eq. [1], gives a somewhat different value of +46.8 kcal/mol. The difference between the two values results from the reported value for **8** with X = H. In eq. [1], compounds **6** and **8** are shown so as to indicate the relationship of their bond connectivities to structures **5** and **7**. However, both structures **6** and **8** have conformational possibilities that must be considered. The Supporting information from that publication (12) states that the geometry used for **6** was "all-trans 1,4-pentadienyl ($C_5H_7^+$, C_{2v})", **6a** (Fig. 1) the energy of which we have reproduced. This W conformer is more stable by 3.60 kcal/mol than the sickle conformer **6b** (Fig. 1), and was used by us as the starting geometry for all of the 3-X substituted compounds **6**. We have also reproduced the energies reported for the unsubstituted structures **5** and **7** in eq. [1]. Compound **8** was described, again in the Supporting information of ref. 12, as "trans-1,4-pentadiene (C_5H_8, C_2)". We have found the minimum energy (–195.29777 au) conformer shown in **8a** (Fig. 1) that is more stable than that reported (–195.29087 au). We are not sure what the geometry of that higher energy structure corresponds to, but it was not the value that the authors used to calculate the reported reaction energy of eq. [1].





The situation for the substituted cyclopentadienyl cations **5** is complicated by the three possible positions (C-5, C-1, and C-2) for placing a substituent X on the cyclopentadienyl cation (**5-X 5**, **1-X 5**, and **2-X 5**). Naively, one might consider these three to be resonance contributors because the charge can be moved from one carbon to another using the usual curved-arrow notation. However, because of the unequal bond lengths in the ring this would create structures of differing geometry that cannot be resonance contributors. Therefore, each of these structures is a different species.

For the electron-donating groups, a geometry optimization with no constraints, puts the substituent at C-5 of the structure **5-I** (HOMO, a_2), independent of which carbon is substituted in the initial geometry. A similar minimum energy geometry has been found previously (MP2(full)/6-31G(d)) for the methyl **5d** and other monoalkyl derivatives (14). Therefore, only one minimum energy structure exists with the substituent placed so as to stabilize the high positive charge at C-5 (equal to +0.284)[5] in the parent cyclopentadienyl cation. This charge is largely a consequence of the fact that the HOMO of this ion has a node through this carbon. Significantly, lower charges are at C-1 = +0.147 and C-2 = +0.211.[5]

For the electron-withdrawing groups, structures of differing energy were obtained depending on the input geometry. For X = CN, two minima resulted, a 2-CN and a 5-CN structure. Both of these had C_s symmetry, but with bond lengths and HOMOs corresponding to, but slightly distorted from, the structure of a_2 symmetry, **5-I**. The 2-CN structure was more stable than the 5-CN one by 0.32 kcal/mol. For X = N_2^+, two C_s minima were also obtained: 5-N_2^+ with a HOMO of pseudo a_2 symmetry and 2-N_2^+ with bond lengths and a HOMO corresponding to the b_2 structure **5-II**. The latter structure is the more stable by 20.6 kcal/mol. For both of these electron-withdrawing substituents (CN and N_2^+), the more stable structure results when the substituent is not at the carbon atom of highest positive charge for the cyclopentadienyl cation itself, namely C-5. Computed values for bond lengths of all of the X-substituted cyclopentadienyl cations are in Table 1 and calculated values of the reaction energies, using the 5-substituted structures for **5** are in Table 2. Computed values for all compounds of eq. [1] are in Table S1[6] of the Supporting information.[7]

This isodesmic reaction predicts the effect of transferring a positive charge from the delocalized pentadienyl cation **6** to the delocalized, but antiaromatic, cyclopentadienyl cation **5**. The negatively charged O^- electron-donating group makes structures **5** and **6** the neutral molecules **9** and **10**, respectively, and the positively charged N_2^+ makes them dications. The process of eq. [1] is endergonic, as expected, but is clearly significantly dependent on the substituent X, becoming less disfavoured for electron-donating substituents. For comparison, a very recent computational study of cyclopentadienyl derivatives, including **5a = 9**, indicates that it is slightly antiaromatic on the basis of a negative value (–11.16) for the magnetic susceptibility enhancement and positive values of 8.83 and 5.64 kcal/mol from the energies

[5] All charges given are from Mulliken population analysis with hydrogens summed into the heavy atoms.
[6] As described in the footnote of this Table, structures **7** and **8** (X = O^-), and **8** (X = N_2^+) are not bound, and therefore the reaction energy for these substituents could not be calculated.
[7] Supplementary data for this article are available on the Web site or may be purchased from the Depository of Unpublished Data, Document Delivery, CISTI, National Research Council Canada, Ottawa, ON K1A 0S2, Canada. DUD 4024. For more information on obtaining material refer to http://cisti-icist.nrc-cnrc.gc.ca/irm/unpub_e.shtml.

© 2005 NRC Canada

Table 2. Calculated total reaction energies (kcal/mol) for eqs. [1] and [3]–[7].

X	eq. [1][a]	eq. [3]	eq. [4]	eq. [5][b]	eq. [6]	eq. [7]
O^-	—[c]	–35.5	–1.7	–151.3	–148.4	–145.6
NH_2	7.2	3.3	11.2	–27.0	–26.3	–26.4
OCH_3	14.9	4.2	14.1	–17.2	–11.6	–11.8
CH_3	28.0	11.0	13.5	–7.2	–4.7	–4.7
F	28.6	10.8	15.4	–1.1	2.1	1.9
H	42.5	13.3	13.3	0	0	0
CN	36.0	13.5	14.4	12.6	12.0	12.5
N_2^+	—[c]	21.6	21.2	121.3	109.4	112.9

[a]As described in the text, these values are for the 5-X structure of the cyclopentadienyl cation **5**.
[b]Values from ref. 13.
[c]Structures **7** (X = O^-), **8** (X = O^-), and **8** (X = N_2^+) are not bound. See Table S1 in the Supporting information.[7]

Table 3. Calculated bond lengths, Julg indices (*A*) and singlet–triplet splitting (ΔE_{ST}) for the triplet state (**5T**) of the cyclopentadienyl cations with X at C-5.

Cmpd.	X	C-2—C-3 (Å)	C-1—C-2 = C-3—C-4 (Å)	C-4—C-5 = C-5—C-1 (Å)	*A*	ΔE_{ST} (kcal/mol)
5a	O^-	1.378	1.445	1.462	0.79	28.3
5b	NH_2	1.390	1.436	1.437	0.90	15.0
5c	OCH_3	1.400	1.431[a]	1.439[a]	0.95	11.1
			1.434	1.434		
5d	CH_3[b]	1.415	1.426[b]	1.435[b]	1.00	–2.9
			1.426	1.437		
5e	F	1.416	1.429	1.426	0.99	1.5
5f	H	1.426	1.426	1.426	1.00	–11.3
5g	CN	1.418	1.422	1.439	1.00	–9.3
5h	N_2^+	1.455	1.426	1.431	0.96	–24.2

[a]The first bond length of each pair is syn to the methoxy group, the second anti.
[b]The first bond length of each pair is syn to the in-plane hydrogen atom of the methyl group, the second anti.

of two different reactions (18). Therefore, electron-donating substituents considerably decrease the antiaromatic character of the cyclopentadienyl cation. As will be described in the following, this effect parallels bond alternation effects.

Singlet–triplet splitting (ΔE_{ST}) for the cyclopentadienyl cations 5

The fact that the singlet state of the cyclopentadienyl cations is becoming less antiaromatic (more aromatic) as the electron-donating ability of the substituent increases parallels the ordering of the singlet–triplet splitting. As shown by the ΔE_{ST} values in Table 3, the triplet state (**5T**) is more stable than the singlet by 11.3 kcal/mol for the unsubstituted compound **5f**. In contrast, for the amino substituted case **5b**, the singlet is more stable by 15.0 kcal/mol. A ΔE_{ST} value of 17.9 kcal/mol (CISD at SCF geometries, 3-21G basis set) with very similar bond lengths (C-1—C-2 = C-3—C-4 = 1.447 Å, C-2—C-3 = 1.381 Å, C-4—C-5 = C-5—C-2 = 1.442 Å, see Table 3 for our values for **5T**) has been obtained previously for **5b** (19). As expected, the ΔE_{ST} splitting is very much the largest (23.3 kcal/mol) for the neutral molecule **5a** = **9**.

This substituent effect on the ΔE_{ST} for the cyclopentadienyl cations is analogous to that for carbenes. At the descriptive MO level, a linear carbene has two degenerate nonbonding p orbitals and is a ground-state triplet. Decreasing the bond angle splits the degeneracy and stabilizes the in-plane p orbital as it gains s character. The ground state can then be a closed-shell singlet and the empty π orbital stabilized by electron-donating groups like amino. Suitably substituted carbenes become stable, isolable molecules. These concepts for carbenes have attracted considerable experimental and theoretical interest (20, 21).

Bond alternation in the cyclopentadienyl cations 5 — The Julg index

A number of properties have been used to assess the aromatic character of cyclic conjugated π systems, one of them being geometry (bond length equalization for aromatic systems and bond length alternation for antiaromatic ones). Lee and Wright (16) have argued that "…whether a cyclic compound exhibits aromatic character or not maybe seen most simply by looking at geometry" and "…bearing in mind that the concept of aromaticity has limited chemical use, a definition based on geometry, which is very quick to use, seems most practicable." Although most chemists, including us, would disagree with the first point of the second quote, the second point of that quote is certainly valid. The Julg parameter (*A*), a commonly used index, is given by eq. [2] where *n* is the number of bonds, r_i is any individual bond length, and r_{avg} is the average of all the bond lengths (22). For benzene, with all C—C bonds of equal length, all values of $r = r_{avg}$,

© 2005 NRC Canada

Fig. 2. Plot of *A* (Julg index) vs. the C-2—C-3 bond length (Å) for the cyclopentadienyl cations **5**. The substituent is at C-5 in all cases.

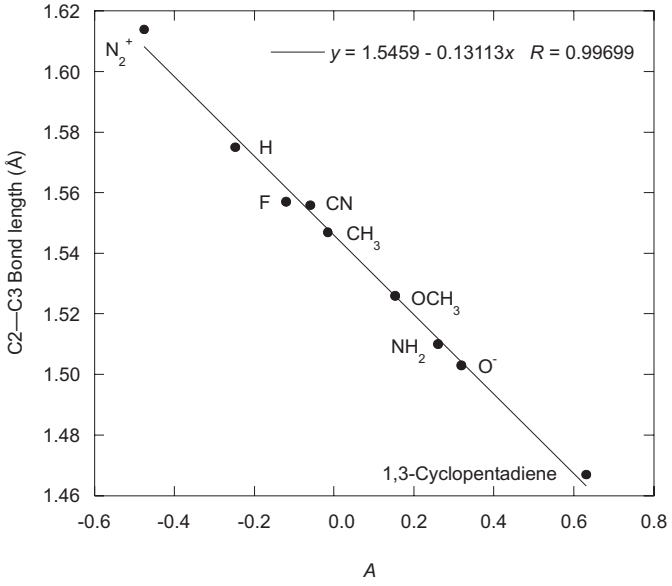
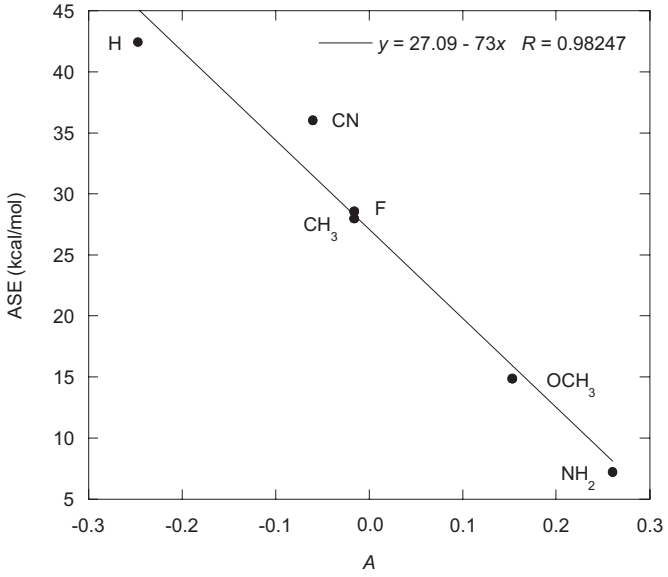


Fig. 3. Plot of *A* (Julg index) vs. the reaction energy (kcal/mol) for eq. [1], the ASE for the cyclopentadienyl cations **5**. The substituent is at C-5 in all cases.



and therefore the second term in eq. [2] equals zero leading to $A = 1$. The scaling factor of 225 is used to force $A = 0$ for Kekulé benzene (1,3,5-cyclohexatriene), a model chosen with alternating C—C bond lengths of 1.33 and 1.52 Å. Therefore, the aromatic cyclopentadienyl anion (12), with all bonds of equal length (1.413 Å, B3LYP/6-31G(d)), also has $A = 1.0$. The butadiene fragment in 1,3-cyclopentadiene (**7**) has $A = 0.618$ (C-1—C-2 = C-3—C-4 = 1.349 Å and C-2—C-3 = 1.470 Å, B3LYP/6-31G(d)) indicative of a greater bond alternation than for the cyclopentadienyl anion.

$$[2] \qquad A = 1 - (225/n)\Sigma[(r_{avg} - r_i)/r_{avg}]^2$$

As a consequence of its antiaromatic character, the singlet state of the cyclopentadienyl cation has considerable bond alteration. The Julg index for this cation has been calculated previously ($A = -0.084$, C-1–C-2 = C-3—C-4 = 1.255 Å, C-2—C-3 = 1.565 Å, MP2(FC)/6-31G(d)) using the carbon string from C-1 to C-4, but omitting the C-4—C-5 and C-5—C-1 bonds (23). In essence, this value reveals the effect that creating a cyclic π system has on the *A* value for a "normal" 1,3-butadiene unit by adding C-5. An even lower value of $A = -0.25$ (C-1—C-2 = C-3—C-4 = 1.350 Å, C-2—C-3 = 1.575 Å, and C-4—C-5 = C-5—C-1 = 1.450 Å in C_{2v} symmetry) is obtained by us using B3LYP/6-31G(d). The major contributor to this low (and negative) value is the long bond length for C-2—C-3.

The *A* values (omitting the C-5—C-1 and C-4—C-5 bonds as in the literature examples), along with the bond lengths, for the singlet state of the 5-X substituted cyclopentadienyl cations are given in Table 1. Similar bond lengths (C-1—C-2 = C-3—C-4 = 1.348 Å, C-2—C-3 = 1.515 Å, C-4—C-5 = C-5—C-1 = 1.489 Å (STO/3-21G) (19) and 1.36, 1.51, and 1.52 Å, respectively, (STO/2G) (17)) for the amino compound **5b** have been reported previously. The *A* values increase from a low of –0.48 for X = N_2^+ to a high of 0.32 for X = O^-, indicating an increase in bond equalization and a decrease in antiaromatic character for electron-donating groups. This increase in *A* is largely determined by the decrease in the C-2—C-3 bond length from a maximum of 1.614 Å for N_2^+ to a minimum of 1.503 Å for O^- compared to the C-1—C-2 and C-3—C-4 bond lengths that average 1.348 ± 0.006 Å over the whole set of X groups. In fact, a very good linear correlation exists between *A* and the C-2—C-3 bond length, including 1,3-cyclopentadiene (Fig. 2). Moreover, a similar linear correlation exists between *A* and the reaction energy for the isodesmic reaction (eq. [1], Fig. 3). The structural conclusion is that electron-donating substituents at C-5 reduce the antiaromatic character of the cyclopentadienyl cation by selectively interacting with the positive charge at C-5. The remaining four carbons become more like a normal butadiene fragment with considerably less bond alteration.

In contrast, the triplet states of the cyclopentadienyl cations have *A* values that are above 0.9[8] (Table 3) indicating that their geometries do not deviate significantly from the D_{5h} symmetry of the unsubstituted case. Therefore, by the bond length criterion, they are not significantly antiaromatic. This makes qualitative sense because the orbitals of **5-I** and **5-II** (Fig. 1) are now both singly occupied in contrast to the singlet state with **5-I** doubly occupied. The opposing symmetry (a_2 vs. b_2) of these two orbitals means that each is bonding where the other is antibonding. The overall result is little bond alternation.

Bond alternation for the singlet states of the indenyl cations 4

The unsubstituted indenyl cation **4f** has a singlet ground state with C_{2v} symmetry, which, unlike the cyclopentadienyl cation, is a consequence of the fusion of the benzene ring to

[8] The exception ($A = 0.79$) is for X = O^-, the neutral cyclopentadienone **9**.

© 2005 NRC Canada

Table 4. Calculated Julg indices (A) and charges (Q) for the singlet state of the indenyl cations **4**.

Cmpd.	X	σ+	A_{cp}[a]	A(Total)	A_1(C-1—C-5)	A_2(C-2—C-4)	r_{av}	Q1	Q3	Q(1–5)/Q(2–4)
4a	O^-	–4.27	0.73	0.62	0.68	0.51	1.426	–0.059	0.000	1.97
4b	NH_2	–1.30	0.77	0.74	0.87	0.49	1.419	0.079	0.095	2.95
4c	OCH_3	–0.78	0.77	0.76	0.94	0.46	1.415	0.102	0.112	2.92
4d	CH_3	–0.31	0.93	0.86	0.96	0.68	1.415	0.152	0.154	1.61
4e	F	–0.07	0.89	0.84	0.96	0.59	1.414	0.157	0.162	2.32
4f	H	0.0	0.97	0.89	0.85	0.87	1.414	0.171	0.171	1.28
4g	CN	0.66	0.97	0.88	0.91	0.77	1.416	0.178	0.183	1.37
4h	N_2^+	1.88	0.99	0.84	0.78	0.81	1.418	0.269	0.272	2.20

[a] A_{cp} is for the cyclopentadienyl part of the indenyl cations using the C-1—C-8, C-8—C-9, and C-9—C-3 bond lengths.

the cyclopentadienyl one rather than the Jahn–Teller distortion of the cyclopentadienyl cation. The π HOMO **4-II** has b_2 symmetry resembling **5-II** for the cyclopentadienyl part and the π LUMO **4-I** has a_2 symmetry resembling **5-I** (nodal properties are sketched in Fig. 1). Therefore, the bond lengths in this state are longest between C-1—C-8 = C-3—C-9 = 1.457 Å[9] (antibonding interaction) and shorter between C-1—C-2 = C-2—C-3 = 1.400 Å and C-8—C-9 = 1.424 Å. However, the bond alternation in the cyclopentadienyl fragment (A_{cp} = 0.97 (Table 4), for the C-1–C-8–C-9–C-3 string, again omitting C-2, the carbon on the C_2 axis), is very small. The b_2 symmetry also results in a very low charge[5] at C-2 = 0.090 and higher ones at C-1 = C-3 = 0.171, in contrast to the cyclopentadienyl cation, which has the highest charge at C-5, the atom on the C-2 axis. Breaking the C_{2v} symmetry by adding an X group at C-5 is therefore expected to have a significant effect on the geometry and charge distribution in the substituted indenyl cations because, for instance, an electron-donating X group is now directly conjugated to the carbon C-1 with the highest positive charge. The electron-donating groups shorten the C-1—C-8 bond and lengthen the C-9—C-3 one giving more bond alternation as in resonance structure **11d** (Fig. 1), the extreme being the neutral molecule **12**. As a consequence, the A_{cp} values (Table 4) are significantly smaller (0.77 for X = NH_2) for the cations with electron-donating groups than for the unsubstituted cation itself.

The total Julg indices for cations **4**, given in Table 4 as A(Total), were calculated in the usual way using the bond lengths around the periphery and do not include the C-8—C-9 bond. The bond lengths used for the unsubstituted compound **4f** were identical to those previously obtained at the same level of theory (12). Worth noting is the fact that the average calculated bond length in compounds **4** is essentially independent of X with an r_{av} = 1.417 ± 0.003 Å, not significantly different from the value of 1.407 ± 0.007 Å for the aromatic indenyl anion (12).

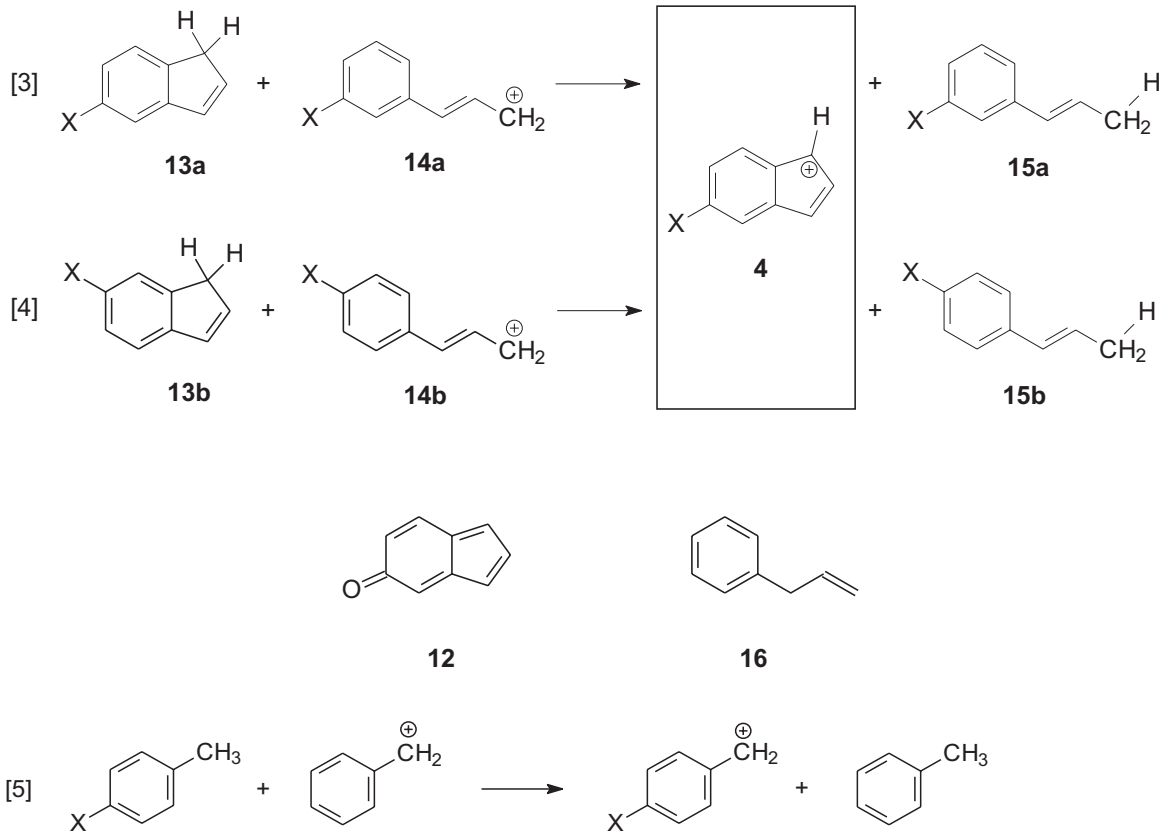
The alternation in the bond lengths for the indenyl cation itself **4f** gives A(Total) = 0.89, less than 1, as expected for an antiaromatic cation but not nearly as low a value as that calculated for the cyclopentadienyl cation (A = –0.25). For the substituted indenyl cations **4**, a trend towards lower values is observed for electron-donating substituents, reaching A = 0.62 for **4a** for X = O^-. A more revealing aspect of the bond alternation is obtained by dividing A(Total) into the two strings, that is A_1 = (C-1–C-8–C-7–C-6–C-5) and A_2 = (C-2–C-3–C-9–C-4). As shown in **11d** for X = methoxy, this separates the indenyl cation into two fragments, an X-terminally substituted pentadienyl cation and a neutral 1,3-butadiene. These A_1 and A_2 values are in Table 4. For the indenyl cation itself, this division makes little difference (A(Total) = 0.89, A_1 = 0.85, and A_2 = 0.87) as expected by its symmetry. However, for the cases substituted with electron-donating groups, $A_1 > A_2$. Most noticeably, for the strong electron-donating groups, the A_2 values are quite low (0.49 for X = NH_2 and 0.46 for X = OCH_3). This four carbon string is analogous to butadiene, but has, for these cases, even stronger bond alternation than butadiene itself (A = 0.63 using the experimental bond lengths of 1.349 Å (C-1—C-2) and 1.467 Å (C-2—C-3)). In contrast, the A_1 values are high (approaching 1.0 for X = NH_2, CH_3, and F) indicating extensive delocalization and bond equalization through this string of atoms. This observation reinforces the high asymmetry induced in indenyl cations by the electron-donating substituents and provides an explanation for their selective reaction at C-1 with nucleophiles.

Aromatic stabilization energy (ASE) of the singlet state of the indenyl cations 4

As for the cyclopentadienyl cations **5**, the ASE of **4** can be defined by an isodesmic reaction model. We have used two isodesmic reactions (eqs. [3] and [4]), again calculating ASE from reaction energies at optimized geometries for each molecule. This model reaction has been used previously (12) for calculations of the ASE of the indenyl cation itself where eqs. [3] and [4] are identical, and a value of ΔE = +20.3 kcal/mol, using B3LYP/6-31G(d), is reported. The concept of this isodesmic reaction is that the positive charge is transferred from a conjugated allyl-aromatic system **14** to an antiaromatic cation **4**. Table 1 of the Supporting information of ref. 12 states that **14** is the "1-phenylallyl cation, ($C_9H_9^+$, C_s)" whose calculated energy we have reproduced, as well as the energies for **4** and **13**, both with X = H. However, the last structure in eqs. [3] and [4] is named as "3-phenylpropene (C_9H_{10}, C_s)" (**16**), which is isomeric with our 1-phenylpropene (**15**, X = H). As expected, using **15**, which is stabilized by conjugation of the alkene with the aryl ring, a lower value of the calculated reaction energy (ΔE = +13.3 kcal/mol) is obtained. The conjugated connection of the alkene with the aryl ring between **13** and

[9] The numbering of atoms, shown in **4-II**, is that same as that in indene.

© 2005 NRC Canada



15 seems to be a more chemically reasonable isodesmic reaction than that between **13** and **16**, and was therefore used by us.

However, a complication arises using eqs. [3] and [4], which are identical only for X = H, the unsubstituted case. For the others, the substituent can be at two possible positions. As discussed previously (see Scheme 1), this change has no effect on the stability of **4**, but will change the energy of each of the other species as they are isomeric in the two equations. These changes are small for the uncharged species (**13a** vs. **13b** and **15a** vs. **15b**), but significant for the charged ones (**14a** vs. **14b**). For instance, the differences in energy between **13a** and **13b** and **15a** and **15b** for X = OCH_3 are only 0.2 and 0.1 kcal/mol, respectively, whereas the difference between **14a** and **14b** for X = OCH_3 is 10.1 kcal/mol, and, as expected, leading to stabilization of the isomer with the electron-donating substituent conjugated (para) to the positive charge in **14b**. The conclusion is that the X group has an effect on the relative stability of **14a** and **14b** that is positionally dependent and therefore different from that on **4** where it is always strongly conjugated. This clearly demonstrates that this isodesmic reaction, used for X = H, is only a suitable choice for assessing substituent effects on the ASE of **4** if the X group is conjugated with the positive charge on both sides of the isodesmic reaction, as in eq. [4].

Calculated values for both isodesmic reactions (eqs. [3] and [4]) as a function of X are given in Table 2. Electronic energies (optimized geometries) for each molecule in both equations are given in the Supporting information[7] (Table S2). For the para cases (**14b**, eq. [4]), the substituent effect is small, essentially negligible for the uncharged cases, indicating that the ASE of the indenyl cation is substituent independent, paralleling its effect on the stability of the propenyl cations **14b**.

Resonance stabilizing energy (RSE) of the singlet state of the indenyl cations 4

Recently, a computational study at a similar level of theory as used here has been published on the effect that substituents have on the relative stability of para-substituted benzyl cations (13). The isodesmic reaction (eq. [5]) was used. The concept here is that RSEs can be calculated for the effect of the substituent relative to the unsubstituted case. The reported values for the calculated reaction energies of eq. [5] are in Table 2. We have applied the analogous eqs. [6] and [7] for the RSEs of the indenyl cations **4**. The advantages that this pair of equations have over the pair from eqs. [3] and [4] are twofold. First, the charged species **4f** on the left-hand side has no substituent and, second, the substituent effect is constant for both the charged species **4** and the uncharged indene **17** on the right-hand side. The only differences in energy are between **17a** and **17b**, which, because they are neutral species, are small. Calculated electronic energies for all structures of eqs. [6] and [7] are in Table S3 of the Supporting information[7] and calculated reaction energies are given in Table 2. As expected, the values obtained are very similar for both substituent positions, and therefore should give a reliable estimate of the RSEs of the indenyl cations **4**.

© 2005 NRC Canada

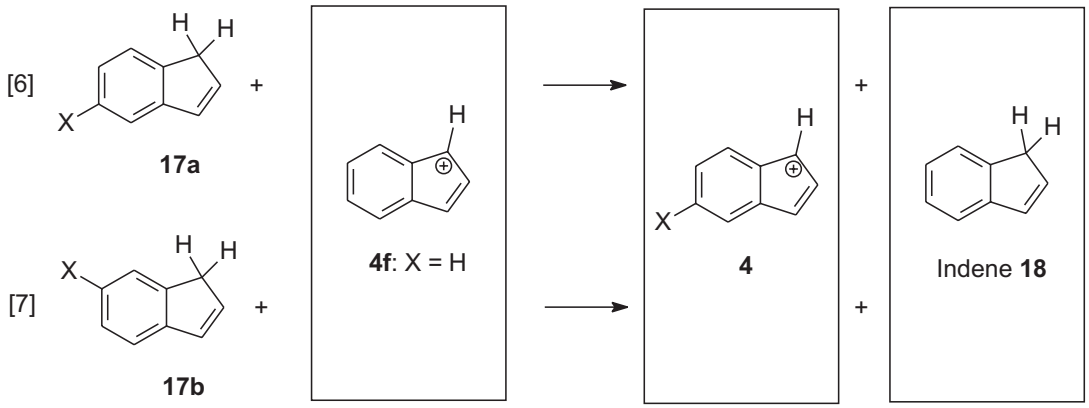
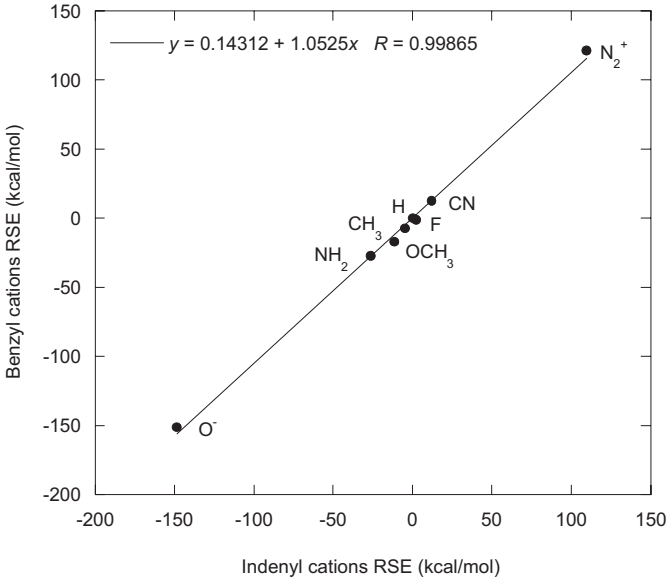


Fig. 4. Plot of the resonance stabilization energy (RSE) of the indenyl cations **4** from eq. [6] vs. the RSE of the benzyl cations from eq. [5].



A plot of the calculated RSEs of the indenyl catons **4** from the reaction energies of eq. [6] vs. those for the benzyl cations of eq. [5] is linear (Fig. 4) with a slope of 1.05. Therefore, substituent effects in reactions that generate indenyl cations should parallel those that generate benzyl or indanyl cations. To our knowledge, only one experimental report on the substituent effects for the generation of indenyl cations is available (24). The rate constants for solvolysis of the 3,5-dinitrobenzoate esters of 1-indenol, 5-methyl-1-indenol, and 5-methoxy-1-indenol gave linear Hammett plots vs. σ^+ with $\rho^+ = -6.0$ (80% aqueous acetone, 80 °C) and $\rho^+ = -5.4$ (2,2,2-trifluoroethanol, 21 °C). These values are very similar to those obtained for the corresponding indanol derivatives: $\rho^+ = -5.3$ (80% aqueous acetone, 21 °C) and $\rho^+ = -5.6$ (2,2,2-trifluoroethanol, 21 °C). Therefore, delocalization of charge in the indenyl cation seems to be unchanged by any antiaromatic effects.

Charge distribution in the indenyl cations 4

Our initial expectation was that the lack of symmetry in the substituted indenyl cations **4** and the resulting lack of symmetry in the charge distribution would rationalize the increased electrophilicity at C-1 relative to C-3 in **4c** with X = OCH_3. In fact, preliminary PM3 calculations indicated this was the case with charges $Q1$ at C-1 = +0.44 and $Q3$ at C-3 = +0.25.[4] However, the higher level Gaussian calculations were not in agreement with this suggestion: the charges at C-1 and C-3 in **4c** equal to +0.102 and +0.112, respectively. These values, along with those calculated for the other substitutents, are given in Table 4. In fact, independent of the substituent, the positive charge is slightly higher at C-3 than at C-1.

However, as the Julg indices indicated and on the basis of the negative σ^+ values, the substituents at the top of Table 4 are expected to strongly delocalize the charge by direct resonance interaction as in contributors **11** (X = OCH_3). Therefore, a more reasonable estimate of the charge distribution in cations **4** should be provided by examining the sum of the charges in the two carbon strings that were used above for the Julg indices: Q(1–5) for C-1–C-8–C-7–C-6–C-5 as shown in **11a** compared to Q(2–4) for the string C-2–C-3–C-9–C-4. The ratios of charges (Q(1–5)/Q(2–4)) in these two strings as a function of substituent are shown in Table 4. These ratios approach a value of three for the strong electron-donating groups indicating that a much larger portion of the positive charge is on the C-1 to C-5 string.[10] This observation correctly rationalizes the observed reactivity of **4c** at C-1 with the nucleophile methanol in the photosolvolysis reactions.

Singlet–triplet splitting (ΔE_{ST}) and bond alternation in the triplet state of the indenyl cations 4

The triplet states of the indenyl cations **5** were all less stable than the corresponding singlet states, as expected for a system without degenerate HOMOs. The ΔE_{ST} values (Table 5) are essentially independent of the substituent with an average of 9.3 ± 0.6 kcal/mol (omitting the values for the charged substituents, which are somewhat higher), 15.3 kcal/mol for O^-, and 14.7 kcal/mol for N_2^+. Moreover, all the A values are high, above 0.9 and approaching 1.0. Therefore, by the bond alternation criterion, the triplet state

[10]Values for **4a** (X = O^-) and **4h** (X = N_2^+) do not follow the trends for the other substituents because the net charge is zero and +2, respectively, for these structures in contrast to +1 for the other cases.

© 2005 NRC Canada

Table 5. Calculated Julg indices (A) and singlet–triplet splittings (ΔE_{ST}) values for the triplet state (**4T**) of the indenyl cations.

Cmpd.	X	A_{cp}	A(Total)	A_1(C-1—C-5)	A_2(C-2—C-4)	r_{av}	ΔE_{ST} (kcal/mol)
4a	O^-	0.97	0.89	0.87	0.93	1.420	15.3
4b	NH_2	0.99	0.93	0.92	0.94	1.413	10.4
4c	OCH_3	0.97	0.95	0.92	0.96	1.413	7.7
4d	CH_3	0.94	0.96	0.94	0.96	1.412	9.1
4e	F	0.94	0.97	0.96	0.98	1.410	9.3
4f	H	0.93	1.00	0.97	0.99	1.411	10.0
4g	CN	0.94	0.96	0.94	0.98	1.413	9.5
4h	N_2^+	0.95	0.95	0.96	0.99	1.416	14.7

of the indenyl cations, as is the case for the cyclopentadienyl cations, are not antiaromatic.

Conclusions

The initial question that led to these computations has been answered. The regiochemistry of the reaction of the 5-methoxyindenyl cation **4c** at C-1, as opposed to C-3, with nucleophiles is a consequence of its lack of symmetry. This cation, along with those others that are substituted with electron-donating groups, can be divided into two parts: a highly delocalized pentadienyl cation and a more localized neutral 1,3-butadiene unit. Bond alternation determinations (Julg index values, A) and substituent effects on resonance stabilization energies that parallel those for benzyl cations support this explanation. This observation emphasizes that substituent effects on resonance stabilization energies and aromatic stabilization energies are not necessarily related.

In addition, substituent effects for cyclopentadienyl cations demonstrated that the antiaromatic character, as determined by an isodesmic reaction, decreased significantly with electron-donating groups. This decrease coincided with a decrease in the bond alternation (again from Julg A values), particularly by the decrease in the C-2—C-3 bond length, as indicated by the correlations in Figs. 2 and 3.

Finally, the singlet–triplet splitting (ΔE_{ST}) for the cyclopentadienyl and indenyl cations were quite different. For the cyclopentadienyl cations, the more stable state changed from the triplet to the singlet for electron-donating groups, whereas the splitting favoured the singlet state independent of the substituent for the indenyl cations. In addition, by the bond alternation criterion, neither the cyclopentadienyl nor the indenyl cations are significantly antiaromatic in the triplet state.

All of these effects agreed qualitatively with the energies and symmetries of the HOMOs and LUMOs (shown in Fig. 1) for the two cations.

Acknowledgements

We thank the Natural Sciences and Engineering Research Council of Canada (NSERC) for financial support and the award of a SRA to AWHS. We also thank Dr. F. Ban for advice on using the GAUSSIAN program.

References

1. J.A. Pincock and I.S. Young. Can. J. Chem. **81**, 1083 (2003).
2. S.A. Fleming and J.A. Pincock. Organic molecular photochemistry. Vol. 3. Marcel Dekker, New York. 1999. p. 211.
3. J.A. Pincock. Acc. Chem. Res. **30**, 43 (1997).
4. (*a*) H.E. Zimmerman. J. Am. Chem. Soc. **117**, 8988 (1995); (*b*) H.E. Zimmerman. J. Phys. Chem. A, **102**, 5616 (1998).
5 (*a*) P. Wan and B. Hall. J. Photochem and Photobiol. A, **56**, 35 (1991); (*b*) P. Wan, B. Chak, and E. Krough. J. Photochem and Photobiol. A, **46**, 49 (1989); (*c*) P. Wan and B. Chank. J. Chem. Soc. Perkin Trans. 2, 1751 (1986); (*d*) P. Wan. J. Org. Chem. **50**, 2583 (1985).
6. K.B. Wiberg. Chem. Rev. **101**, 1317 (2001).
7. A.D. Allen and T.T. Tidwell. Chem. Rev. **101**, 1333 (2001).
8. A.D Allen, M. Sumonja, and T.T. Tidwell. J. Am. Chem. Soc. **119**, 2371 (1997).
9. A.D. Allen and T.T. Tidwell. J. Org. Chem. **66**, 7696 (2001).
10. A.D. Allen, M. Fujio, M. Mohammed, T.T. Tidwell, and Y. Tsui. J. Org. Chem. **62**, 246 (1997).
11. M.J. Frisch, G.W. Trucks, H.B. Schlegel, G.E. Scuseria, M.A. Robb, J.R. Cheeseman, V.G. Zakrzewski, J.A. Montgomery, Jr., R.E. Stratmann, J.C. Burant, S. Dapprich, J.M. Millam, A.D. Daniels, K.N. Kudin, M.C. Strain, O. Farkas, J. Tomasi, V. Barone, M. Cossi, R. Cammi, B. Mennucci, C. Pomelli, C. Adamo, S. Clifford, J. Ochterski, G.A. Pertersson, P.Y. Ayala, Q. Cui, K. Morokuma, N. Rega, P. Salvador, J.J. Dannenberg, D.K. Malick, A.D. Rabuck, K. Raghavachari, J.B. Foresman, J. Cioslowski, J.V. Ortiz, A.G. Baboul, B.B. Stefanov, G. Liu, A Liashenko, P. Piskorz, I. Komaromi, R. Gomperts, R.L. Martin, D.J. Fox, T. Keith, M.A. Al-Laham, C.Y. Peng, A. Nanayakkara, M. Challacombe, P.M.W. Gill, B. Johnson, W. Chen, M.W. Wong, J.L. Andres, C. Conzalez, M. Head-Gordon, E.S. Replogle, and J.A. Pople. GAUSSIAN 98. Revision A. 11.2 [computer program]. Gaussian, Inc., Pittsburgh, Penn. 2001.
12. H. Jiao, P.v.R. Schleyer, Y. Mo, M.A. McAllister, and T.T. Tidwell. J. Am. Chem. Soc. **119**, 7075 (1997).
13. I. Morao and I.H. Hillier. Tetrahedron Lett. **42**, 4429 (2001).
14. B. Reindl and P.v.R. Schleyer. J. Comp. Chem. **19**, 1402 (1998), and refs. therein.
15. C. Hansch, A. Leo, and R.W. Taft. Chem. Rev. **91**, 185 (1991).
16. E.P.F. Lee and T.G. Wright. Phys. Chem. Chem. Phys. **1**, 219 (1999).
17. J. Fabian, A. Melhorn, and N. Tyutyulkov. J. Mol. Struct: THEOCHEM, **151**, 355 (1987).
18. K. Najafian, P.v.R. Schleyer, and T.T. Tidwell. Org. Biomol. Chem. **1**, 3410 (2003).

© 2005 NRC Canada

19. R. Buest, A. Schleitzer, H. Vogel, N. Tyutyulkov, and F. Dietz. Croatia Chem. Acta, **70**, 787 (1997).
20. M. Jones, Jr. and R.A. Moss. *In* Reactive intermediate chemistry. *Edited by* R.A Moss, M.S. Platz, and M. Jones, Jr. John Wiley and Sons, Hoboken, New Jersey. 2004. p. 273.
21. C. Bertrand. *In* Reactive intermediate chemistry. *Edited by* R.A Moss, M.S. Platz, and M. Jones, Jr. John Wiley and Sons, Hoboken, New Jersey. 2004. p. 329.
22. A. Julg and P. François. Theor. Chim. Acta, **8**, 249 (1967).
23. P.v.R. Schleyer, P.K. Freeman, H. Jiao, and B. Goldfuss. Angew. Chem. Int. Ed. Engl. **34**, 337 (1995).
24. E.C. Friedrich and T.M. Tam. J. Org. Chem. **47**, 315 (1982).

© 2005 NRC Canada

An ab initio study of 1,5-suprafacial shifts in 5-substituted 1,3-cyclopentadienes[1,2]

Cory C. Pye and Raymond A. Poirier

Abstract: A computational study of the degenerate 1,5-suprafacial migration of the 5-substituted cyclopentadienes is presented. The substituents considered are the Group 14–17 elements of the second through fifth periods, saturated by hydrogens as needed to fulfill normal valence requirements. The geometry of most transition states are remarkably similar in the carbon framework. The activation barrier to migration was shown to correlate well with a dimensionless "stretching" parameter, especially at the MP2 level.

Key words: 5-substituted 1,3-cyclopentadiene, 1,2-haptotropic shift, 1,5-suprafacial shift, ab initio, transition states.

Résumé : On présente une étude théorique de la migration-1,5 suprafaciale de cyclopentadiènes substitués en position 5. Les substituants considérés les éléments 14 à 17 des périodes deux à cinq, saturés par la quantité appropriée d'atomes d'hydrogène pour satisfaire leurs valences normales. Il est remarquable que la géométrie de la plupart des états de transition est très semblable à celle du squelette carboné. On a montré qu'il existe une bonne corrélation entre la barrière d'activation à la migration et un paramètre d'élongation sans dimension, particulièrement au niveau MP2.

Mots clés : cyclopenta-1,3-diène substitué en position 5, migration-1,2 haptotropique, migration-1,5 suprafaciale, ab initio, états de transition.

[Traduit par la Rédaction]

Introduction

5-Substituted cyclopentadienes are of interest as prototypical rigid systems for the investigation of facial selectivity in the Diels–Alder reaction, as previously discussed (1). In some cases, 5-substituted cyclopentadienes can undergo a degenerate 1,5-suprafacial shift as shown in Fig. 1. This process has been described in many ways, for example, as a hydrogen, metal, or carousel migration; as a prototropic, metallotropic, walk, intramolecular, (1,5)-sigmatropic, circumambulatory rearrangement; as fluxional behavior; and as stereochemical nonrigidity, to name a few. The process has been demonstrated and the activation barrier measured for many substituents, as shown in Table 1. The following quotation from Larrabee's 1974 review (8) provides a snapshot of both the situation 30 years ago, and also an accurate forecast of the situation today: "…it is not yet possible to predict the type of bonding a new structure will exhibit. It may ultimately be possible to make such predictions from large-scale numerical computations. Such bonding descriptions are to be considered incomplete if they do not include a description of the remarkable property found in many σ-bonded organometallic compounds: their fluxional behavior." Even today, the topic remains of much interest, as shown in two recent reviews (9, 10).

Method

Calculations were performed using MUNGAUSS (11), GAUSSIAN 92 (12), or GAUSSIAN 98 (13), utilizing the STO-3G (14), 3-21G (15), 6-31G(d) (16), and 6-31+G(d) (17) basis sets. Huzinaga's basis sets for Ge-Br (4333/433/4) and Sn-I (43333/4333/44), decontracted to {21} in the sp-valence region and polarization functions added, were used in conjunction with the 6-31G(d) basis set (18). Cartesian (6) d functions were used throughout except for STO-3G. Diffuse function exponents were previously presented (1). For brevity, the results and discussion using the STO-3G and 3-21G basis sets are presented in the supplementary material (19).[4]

The MP2 and higher level calculations (20) utilize the frozen core approximation. Default optimization specifications were normally used. For 6-31G(d) and higher, a frequency calculation was performed at the same level and the resulting Hessian used in the following optimization. Z-matrix coordinates constrained to the appropriate symmetry

Received 15 April 2005. Published on the NRC Research Press Web site at http://canjchem.nrc.ca on 19 October 2005.

C.C. Pye.[3] Department of Chemistry, Saint Mary's University, Halifax, NS B3H 3C3, Canada.
R.A. Poirier. Department of Chemistry, Memorial University, St. John's, NL A1B 3X7, Canada.

[1]This article is part of a Special Issue dedicated to organic reaction mechanisms.
[2]Part I in this series is ref. 1.
[3]Corresponding author (e-mail: cory.pye@stmarys.ca).
[4]Supplementary data for this article are available on the Web site or may be purchased from the Depository of Unpublished Data, Document Delivery, CISTI, National Research Council Canada, Ottawa, ON K1A 0S2, Canada. DUD 4029. For more information on obtaining material refer to http://cisti-icist.nrc-cnrc.gc.ca/irm/unpub_e.shtml.

 doi: 10.1139/V05-141 © 2005 NRC Canada

Fig. 1. Degenerate 1,5-suprafacial shift of 5-substituted cyclopentadiene.

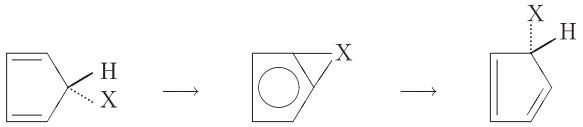


Table 1. Experimental activation barriers for the 1,5-suprafacial shift of 5-substituted cyclopentadienes.

Substituent	Activation barrier (kJ/mol)	Method	System
H	101.7±2.1	^{1}H-VT NMR	-C_5D_5 (2)
CH_3	168.6–185.8	Microflow/GLC	-$CpMe_2$ (3)
SiH_3	59.4±1.0	^{1}H-VT NMR	-Cp (4)
	57.7±0.1	^{13}C lineshape	-Cp (4)
$SiMe_3$	54.4±4.2	^{1}H-VT NMR	-Cp (5)
$GeMe_3$	38.5±4.2	^{1}H-VT NMR	-Cp (6)
$SnMe_3$	32.6±4.2	^{1}H-VT NMR	-Cp (6)
PH_2	131.0±7.5	^{1}H-VT NMR	-$CpMe_5$ (7)
PMe_2	96.2±2.1	^{1}H-VT NMR	-$CpMe_5$ (7)

were used as required to speed up the optimizations. If symmetry constraints led to a transition state instead of a minimum, this would show up as the presence of one or more imaginary frequencies not belonging to the totally symmetric irreducible representation. The Hessian was evaluated at the first geometry for the first level in a series to aid geometry convergence. Molden was used to render the molecular structures (21).

In all tables, bond lengths are given in Å and angles in °. A general trend noticed is that d-polarization functions added to heteroatoms of the second row tend to shorten bonds to adjacent atoms, whereas, when added to heteroatoms of the third and fourth row, they tend to increase bond lengths to adjacent atoms. This was already noted and rationalized (1).

Results and discussion

Geometries

We discuss the geometry of only the transition states (hereafter abbreviated TS). As the cyclopentadienes themselves have been already discussed (1), we refer readers to the figures, tables, and discussion therein. For purposes of naming, the substituent is assumed to be migrating from C5 to C4.

Cyclopentadiene

The structure of the cyclopentadiene TS is shown in Fig. 2. Like the corresponding cyclopentadiene, the structure of the TS for the 1,5-suprafacial hydrogen shift changes little with basis set, with the angular range being about the same, but the bond range being larger (0.03 Å), predominantly about the reaction centers. The 6-31G(d,p) structure differed from the 6-31G(d) one only in the last reported figure, except for the parameters about the reaction centers, which varied in the next to last figure. The structures shown

Fig. 2. Structures of transition states for the 1,5-suprafacial substituent shift.

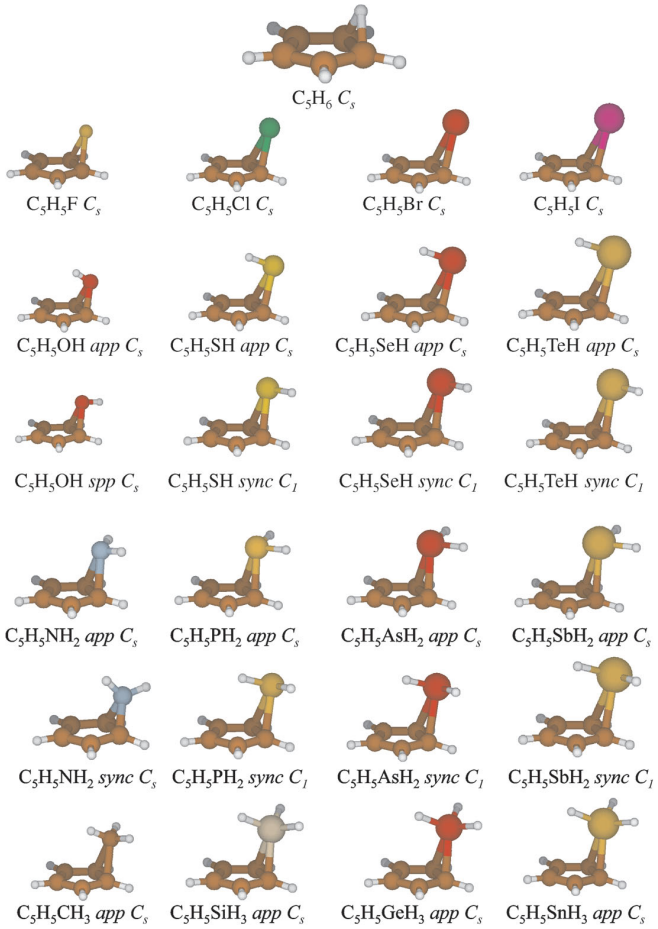


Table 2. Geometry of the 1,5-suprafacial hydrogen shift transition state.

Parameter	HF		MP2	
	6-31G(d)	6-31+G(d)	6-31G(d)	6-31+G(d)
C2—C3	1.3903	1.3925	1.4018	1.4047
C3—C4	1.4001	1.4030	1.4077	1.4108
C4—C5	1.4703	1.4683	1.4894	1.4887
C2—H2	1.0743	1.0742	1.0854	1.0860
C3—H3	1.0719	1.0720	1.0834	1.0843
C4—H4	1.0724	1.0725	1.0839	1.0846
C5—H4′	1.3039	1.3059	1.3009	1.3041
C1-C2-C3	110.23	110.13	110.03	109.93
C2-C3-C4	108.06	108.06	108.32	108.32
C3-C4-C5	106.83	106.88	106.67	106.72
H3-C3-C2	126.67	126.69	126.41	126.41
H4-C4-C3	128.33	128.17	128.55	128.35
H4′-C4-C5	55.68	55.79	55.08	55.20
H4′-C4-C3	107.89	107.90	108.66	108.92

in Tables 2 and S5[4] are in excellent agreement with calculations at the same level previously reported (HF/3-21G (22), 6-31G(d) (23), and MP2/6-31G(d) (23, 24)) and are close to others (B3LYP/6-31G(d) (25, 26)). The C—C bond lengths

© 2005 NRC Canada

Table 3. Geometry of the 1,5-suprafacial halogen shift transition state.

	HF		MP2	
Parameter	6-31G(d)	6-31+G(d)	6-31G(d)	6-31+G(d)
F—C	1.7768	1.8246	1.7885	1.8410
C2—C3	1.4002	1.4043	1.4080	1.4126
C3—C4	1.3853	1.3821	1.3887	1.3873
C4—C5	1.4952	1.5002	1.5138	1.5167
H—C4	1.0684	1.0682	1.0825	1.0826
F-C4-C5	65.12	65.73	64.96	65.67
F-C4-C3	114.26	113.97	113.62	112.88
H-C4-C3	127.38	127.63	127.29	127.59
C1—C	2.3054	2.3035	2.1895	2.1904
C2—C3	1.4028	1.4044	1.4074	1.4100
C3—C4	1.3754	1.3778	1.3895	1.3925
C4—C5	1.5090	1.5080	1.5154	1.5147
H—C4	1.0688	1.0689	1.0832	1.0837
Cl-C4-C5	70.90	70.89	69.75	69.77
Cl-C4-C3	115.00	114.91	114.93	115.16
H-C4-C3	127.70	127.61	126.98	126.80
Br—C	2.4325	2.4200	2.3406	2.3325
C2—C3	1.4021	1.4032	1.4081	1.4103
C3—C4	1.3767	1.3802	1.3894	1.3933
C4—C5	1.5078	1.5054	1.5181	1.5163
H—C4	1.0691	1.0694	1.0839	1.0845
Br-C4-C5	71.95	71.88	71.08	71.03
Br-C4-C3	115.07	115.07	114.73	114.95
H-C4-C3	127.57	127.40	126.99	126.70
I—C	2.6078	2.5976	2.5200	2.5128
C2—C3	1.4003	1.4014	1.4076	1.4096
C3—C4	1.3800	1.3834	1.3927	1.3966
C4—C5	1.5049	1.5025	1.5173	1.5153
H—C4	1.0699	1.0702	1.0848	1.0855
I-C4-C5	73.23	73.19	72.48	72.45
I-C4-C3	115.08	115.05	115.26	115.42
H-C4-C3	127.30	127.13	126.58	126.30

are between the single and double bond lengths of cyclopentadiene, as expected. One surprising feature is the shortening of the C—C bond bisected by the migrating carbon (by over 0.03 Å at the Hartree–Fock level), but this may be related to the lengthening of the migrating C—H bond by over 0.21 Å, making the reactant carbons more sp^2-like. The bond lengths of the hydrogens attached to the reacting carbons decrease by about 0.015 Å to be very close to the usual sp^2 values. The C-C-C angles are within 2° of the idealized 108° of the cyclopentadienyl anion, and the nonmigrating hydrogens are very nearly planar. The migrating H-C-C angle becomes smaller in the TS by a few degrees.

Halocyclopentadienes

The geometries of the 1,5-suprafacial halogen shift TSs are given in Tables 3 and S6.[4] The addition of diffuse function and of correlation has very little effect on the bond angles, except when the associated bonds change significantly.

Table 4. ξ as a function of level and substituent.

	HF		MP2	
Substituent	6-31G(d)	6-31+G(d)	6-31G(d)	6-31+G(d)
H	0.197	0.200	0.183	0.186
F	0.298	0.329	0.279	0.308
Cl	0.279	0.280	0.220	0.221
Br	0.231	0.229	0.186	0.185
I	0.185	0.183	0.147	0.146
OH app	0.221	0.226	0.251	0.265
OH spp	0.250	0.254	0.278	0.289
SH app	0.215	0.212	0.181	0.179
SH sc	0.220	0.220	0.183	0.182
SeH app	0.193	0.191	0.170	0.167
SeH sc	0.185	0.186	0.158	0.158
TeH app	0.160	0.160	0.138	0.136
TeH sc	0.138	0.139	0.120	0.117
NH_2 app	0.095	0.090	0.099	0.094
NH_2 sc	0.097	0.091	0.100	0.093
PH_2 app	0.166	0.170	0.143	0.146
PH_2 sc	0.192	0.194	0.161	0.163
AsH_2 app	0.150	0.153	0.129	0.132
AsH_2 sc	0.173	0.176	0.150	0.151
SbH_2 app	0.109	0.111	0.094	0.095
SbH_2 sc	0.129	0.132	0.112	0.113
CH_3	0.270	0.274	0.246	0.252
SiH_3	0.132	0.135	0.114	0.117
GeH_3	0.135	0.139	0.118	0.120
SnH_3	0.098	0.101	0.085	0.088

Adding diffuse functions tends to shorten the carbon–halogen distance slightly, except for the fluoride, where it lengthens it by about 0.05 Å. Adding correlation significantly shortens the carbon–halogen distance by around 0.10 Å, except for the fluoride, where it increases by 0.01 Å. This demonstrates the extreme importance of diffuse functions for fluorine, and of correlation in these TSs.

The TSs are all remarkably similar in the carbon framework for all halogens, with the only major difference being in the X—C length. We can define a dimensionless measure of the stretching in the TS as

$$[1] \qquad \xi = \frac{r_{\text{transition state}} - r_{\text{reactant}}}{r_{\text{reactant}}}$$

where r is the X—C length at a particular point on the PES. The closer this value is to zero, the less "stretched" the TS is. There is no trend seen in $r_{\text{transition state}} - r_{\text{reactant}}$. As one proceeds from fluorine to iodine, ξ decreases (Table 4), demonstrating that the molecule, on a relative scale, does not need to stretch as much to reach the TS.

Chalcocyclopentadienes

For the 1,5-suprafacial chalcogen shift, one must consider which reactant and product molecules the TS is meant to connect. For the antiperiplanar case, it is clear that the "antiperiplanar" TS should connect them as this involves the least torsional motion of the OH. For the synclinal reactants and products, the situation is not as clearcut. For the alcohol,

© 2005 NRC Canada

Table 5. Activation energies of 1,5-suprafacial group shifts in cyclopentadienes (kJ/mol).

	HF		MP2	
Substituent	6-31G(d)	6-31+G(d)	6-31G(d)	6-31+G(d)
H	162.26	159.24	120.32	116.90
F	270.33	262.53	220.31	208.21
C1	174.03	173.91	148.99	147.21
Br	141.89	143.16	112.34	112.52
I	113.15	113.38	81.68	81.02
OH app	258.92	260.16	195.29	195.79
OH sc	278.36	278.19	212.99	210.40
SH app	180.56	179.97	134.90	132.29
SH sc	179.73	179.03	131.32	129.32
SeH app	148.93	147.76	106.38	104.28
SeH sc	140.79	141.20	95.56	95.58
TeH app	116.73	115.36	78.04	76.32
TeH sc	100.62	100.19	60.89	60.49
NH_2 app	232.48	230.80	191.86	190.11
NH_2 sc	243.27	240.65	202.41	199.28
PH_2 app	136.80	136.35	88.54	86.81
PH_2 sc	153.79	152.39	104.12	102.51
AsH_2 app	105.76	106.37	65.63	66.11
AsH_2 sc	123.09	122.47	80.22	79.87
SbH_2 app	64.67	65.35	34.62	35.42
SbH_2 sc	83.95	83.40	49.34	49.33
CH_3	237.84	235.20	186.16	182.79
SiH_3	93.77	95.00	54.89	55.01
GeH_3	86.80	88.27	50.72	52.27
SnH_3	48.07	50.03	22.68	24.58

Table 6. Activation energies of 1,5-suprafacial group shifts in cyclopentadienes (kJ/mol, single point X/6-31+G(d) at MP2/6-31+G(d) geometry).

Substituent	MP3	MP4SDQ	MP4	QCISD(T)	CCSD(T)
H	137.61	140.23	129.98	135.98	135.97
F	245.07	221.82	192.51	210.58	213.00
Cl	166.52	164.66	144.93	149.20	149.95
Br	130.95	130.66	112.75	117.55	117.99
I	99.30	100.59	84.39	89.31	89.46
OH app	235.59	221.90	195.52	208.46	210.18
OH sc	250.40	235.72	207.43	220.27	222.06
SH app	156.82	157.40	138.72	145.39	145.79
SH sc	153.37	155.08	136.61	142.66	142.86
SeH app	126.16	127.29	110.31	116.28	116.51
SeH sc	116.89	119.12	102.92	108.29	108.34
TeH app	96.19	98.03	83.27	88.78	88.85
TeH sc	79.15	81.74	68.45	73.31	73.28
NH_2 app	214.93	213.12	201.18	208.34	208.98
NH_2 sc	224.14	222.27	210.53	217.44	218.05
PH_2 app	109.93	112.46	98.37	104.70	104.70
PH_2 sc	126.39	128.65	113.43	119.95	120.00
AsH_2 app	85.29	87.61	75.71	80.81	80.78
AsH_2 sc	99.99	102.27	88.99	94.34	94.33
SbH_2 app	49.61	51.60	43.17	47.19	47.15
SbH_2 sc	65.41	67.60	57.36	61.82	61.78
CH_3	210.53	211.07	194.14	201.17	201.37
SiH_3	73.36	75.60	65.74	71.09	71.07
GeH_3	68.96	71.13	61.78	66.73	66.70
SnH_3	35.94	37.65	31.35	34.85	34.81

and for all HF/STO-3G calculations, the C_s symmetric app conformation is a TS, whereas it is a second-order saddle point for other cases. Here, the TS between the synclinal structures is also synclinal. The geometries of the 1,5-suprafacial chalcogen shift TS are given in Table S7 and S8.[4] The basis set trends are similar to those of the halogens, and the TS are similar in the carbon framework. The main difference between the app and spp/sc TSs are the bond lengths and angles involving the migrating group. A pronounced asymmetry develops for the synclinal TSs. The asymmetric TS is lower in energy for the selenium and tellurium cases, and it is also less stretched. For the asymmetrical transition states, the average of the two X—C distances was used to define ξ. Similar trends with ξ were also noticed as a function of period number.

Pnictocyclopentadienes

The geometries of the 1,5-suprafacial pnictogen shift transition states are given in Tables S9 and S10.[4] It appears that the app TSs are reasonable except for the amine, which is, along with all of the spp structures, a second-order saddle point. The app TSs connect the app conformers in the reactant and product. The sc TSs are higher in energy than the app TS where they exist, and are more stretched. For the amine, only one transition state exists that is C_s symmetric and the amine hydrogens are in the symmetry plane (i.e., the nitrogen undergoes an inversion). The C—N distance is much shorter here than in the app conformer. Basis set trends are similar to those of the halogens, with the amine being atypical, like fluorine. The carbon framework of the transition states are remarkably similar, except for the amine. If using the app conformer to define ξ, a similar downward trend is noted. The sc transition states have larger H-X-H and X-C4-C3 angles.

Group 14 cyclopentadienes

The geometries of the 1,2-suprafacial Group 14 shift transition states are given in Table S11.[4] The carbon skeleton is remarkably similar in all four TSs. ξ decreases with increasing atomic number.

Activation energies

The activation barriers for group migration are shown in Tables S12,[4] 5, and 6. Taking the CCSD(T) values as the most accurate, the Hartree–Fock barriers are seen to be too high, whereas the MP2 barriers are too low. Generally, there is little difference between the MP3 and MP4SDQ barriers (3 kJ/mol), and between the QCISD(T) and CCSD(T) barriers (1 kJ/mol), except for first-row substituents. The energy ordering from highest to lowest is HF >> MP4SDQ > MP3 > QCISD(T), CCSD(T) > MP4 > MP2, with the MP3,MP4SDQ and MP2,MP4 pairs occasionally interchanging.

The activation barrier always decreases upon going down a group, but the trend across a row is not always clear. Plots of the activation barrier vs. the stretching parameter are shown in Figs. 3 and 4. Although there is some scatter in the

© 2005 NRC Canada

Fig. 3. Electronic activation barrier vs. stretching parameter (HF/6-31G(d)).

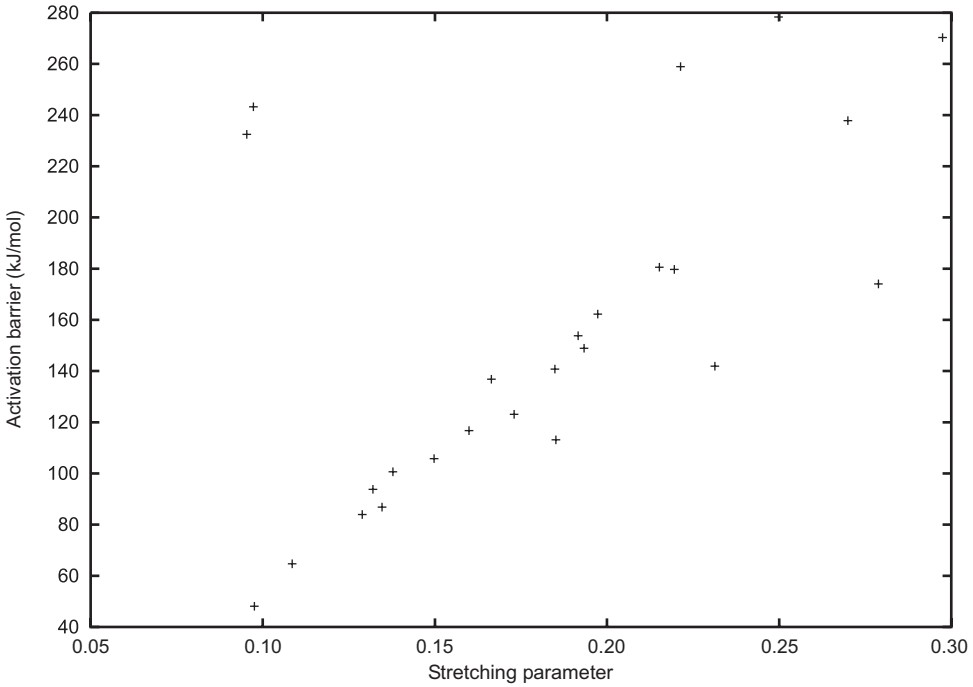
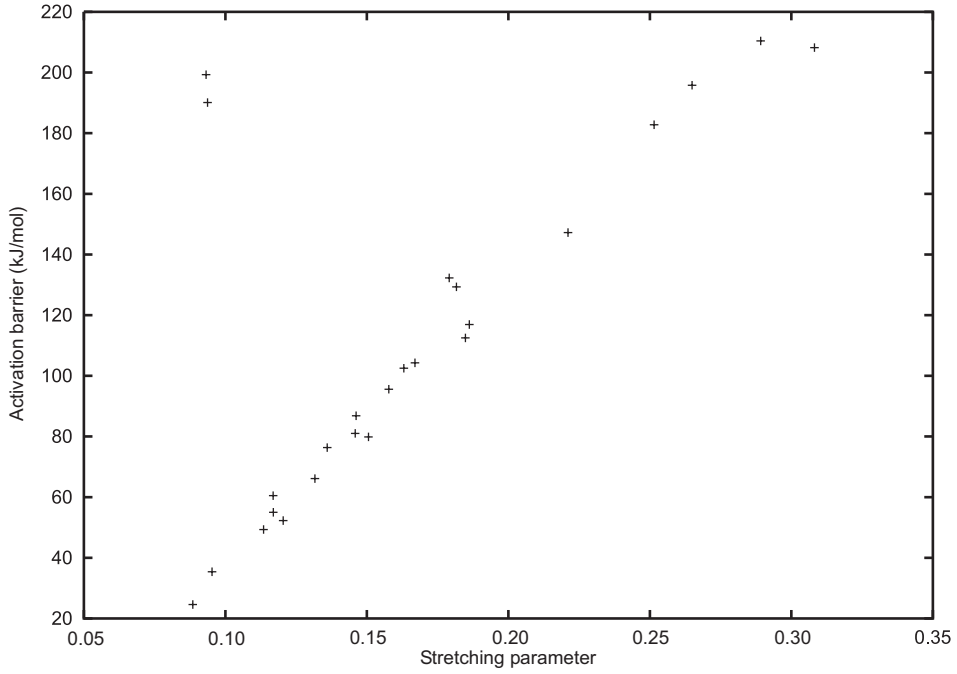


Fig. 4. Electronic activation barrier vs. stretching parameter (MP2/6-31+G(d)).



Hartree–Fock plots, the MP2 activation energies correlate very well with the stretching parameter. The amine is an outlier, as might be expected because of the inversion.

For cyclopentadiene itself, our barriers (kJ/mol) compare well with previous literature, for example, 162.3 (HF/6-31G(d)), 119.7 (MP2/6-31G(d)), and 110.2 (MP2/6-31G(d) + HF/ZPE+therm) (23). Bachrach (23) did not use the frozen core approximation, which accounts for the slight difference in his MP2 result. Our HF/6-31G(d,p) result is 156.63, which shows that polarization functions on hydrogen make a modest contribution (–5.7 kJ/mol) to lowering the activation barrier at the Hartree–Fock level. It is not anticipated that this would lower the barriers when other groups are migrating. Jiao and Schleyer (24) obtained the electronic barriers of 119.7 (MP2/6-31G(d)), 107.5 (MP2/6-311G(d,p)//MP2/6-31G(d)), 124.3 (QCISD(T)/6-311G(d,p)//MP2/6-31G(d)), and 122.2 (MP4/6-311G(d,p)//MP2/6-31G(d)), with MP2/6-31G(d) thermal correction of –5.9. The ZPE and thermal correction tends to cancel the RT correction term needed to obtain the activation energy. The larger 6-311G(d,p) basis

© 2005 NRC Canada

set seems to reduce the barrier by about 10 kJ/mol. B3LYP/6-31G(d) + ZPE calculations place the barrier at 113 kJ/mol (25). To facilitate comparison with our previous paper, and because it is not uniformly defined for the heavier elements, we do not use this larger 6-311G(d,p) basis set. Even at these sophisticated levels, the barrier still has not converged on a reasonable value, although tunnelling effects can account for part of the discrepancy.

The effect of zero-point energy (ZPE) corrections (MP2/6-31+G(d)) is largest for the smaller atoms, whereas the non-ZPE thermal corrections are largest for the largest atoms. In any account, the effects decrease the barrier by less than 10 kJ/mol for hydrogen. For the first-row elements, the barriers are decreased by 5–8 kJ/mol, and for the other elements, typically less than 5 kJ/mol.

From the experimental data presented in Table 1, it seems that methyl substitution has a small effect (5 kJ/mol) on the activation barrier of the migrating group IV atoms. We can thus compare our calculated values with the methyl substituted experimental values. Our best values (electronic) are, for the most part, slightly too high, and the thermal corrections partially correct for this.

The majority of previous work on the (non-hydrogen) shift concerned the application of semiempirical techniques. Dewar (27) found that the barrier of methyl migration in 5-methylcyclopentadiene using MINDO/3 was 194.3 kJ/mol. Cuthbertson and Glidewell (28) examined 5-silylcyclopentadiene using MNDO and found the barrier to be 99.1 kJ/mol. Schoeller (29, 30) predicted the MNDO barrier for the cyclopentadienylphosphane to be 170.3 kJ/mol and stated that the amine prefers inversion over retention of configuration, as we have already noted. MNDO clearly overestimates the barrier, whereas MINDO/3 gives very good results. Most recently, density functional calculations give the barrier (B3LYP/6-311+G(d,p)) as 85.8 and 98.7 kJ/mol for the app and sc isomers of the phosphine, and 63.6 and 75.7 kJ/mol for the app and sc isomers of the arsine. The inversion transition state for the phosphine and arsine was shown to be a higher order saddle point (31). These barriers are lower than ours and are probably more reliable because of the higher quality basis set used.

Conclusions

The structures of the transition states of the 1,5-suprafacial shift of the substituent in 5-substituted cyclopentadienes are, with the exception of the migrating group, very similar. A dimensionless stretching parameter is defined and is shown to correlate well with the activation barrier to this migration, especially at the MP2 level. Our best barriers are estimated to be about 10 kJ/mol too high.

Acknowledgments

We would like to thank the Memorial University of Newfoundland Computing and Communications Department (MUN-CC) and the Saint Mary's University Astronomy and Physics Department (SMU-AP) for computer time. In particular, we would like to thank Digital Equipment Corporation for providing an Alpha server 4100 (MUN-*tempus*), and Sun Microsystems, the Canada Foundation for Innovation, the Atlantic Canada Opportunities Agency, and SMU for providing a 10-processor Sun Enterprise 450 (SMU-*cygnus*). The continuing support of the Natural Sciences and Engineering Research Council of Canada (NSERC) is acknowledged by CP and RP.

References

1. C.C. Pye, J.D. Xidos, D.J. Burnell, and R.A. Poirier. Can. J. Chem. **81**, 14 (2003).
2. W.R. Roth. Tetrahedron Lett. 1009 (1964).
3. J.W. De Haan and H. Kloosterziel. Recl. Trav. Chim. Pays–Bas, **87**, 298 (1968).
4. A. Bonny and S.R. Stobart. J. Chem. Soc. Dalton Trans. 224 (1980).
5. N.M. Sergeyev, G.I. Avramenko, A.V. Kisin, V.A. Korenevsky, and Yu.A. Ustynyuk. J. Organomet. Chem. **32**, 55 (1971).
6. A.V. Kisin, V.A. Korenevsky, N.M. Sergeyev, and Yu.A. Ustynyuk. J. Organomet. Chem. **34**, 93 (1972).
7. P. Jutzi and H. Saleske. Chem. Ber. **117**, 222 (1984).
8. R.B. Larrabee. J. Organomet. Chem. **74**, 313 (1974).
9. P. Jutzi and G. Reumann. J. Chem. Soc. Dalton Trans. 2237 (2000).
10. P.H. Budzelaar, J.J. Engelberts, and J.H. van Lenthe. Organometallics, **22**, 1662 (2003).
11. R.A. Poirier, M.R. Peterson, and A. Yadav. MUNGAUSS [computer program]. Chemistry Department, Memorial University of Newfoundland, St. John's, Newfoundland. 1990.
12. M.J. Frisch, G.W. Trucks, H.B. Schlegel, P.M.W. Gill, B.G. Johnson, M.W. Wong, J.B. Foresman, M.A. Robb, M. Head-Gordon, E.S. Replogle, R. Gomperts, J.L. Andres, K. Raghavachari, J.S. Binkley, C. Gonzalez, R.L. Martin, D.J. Fox, D.J. Defrees, J. Baker, J.J.P. Stewart, and J.A. Pople. 1993. GAUSSIAN 92/DFT. Revision F.4 [computer program]. Gaussian, Inc., Pittsburgh, Penn. 1993.
13. M.J. Frisch, G.W. Trucks, H.B. Schlegel, G.E. Scuseria, M.A. Robb, J.R. Cheeseman, V.G. Zakrzewski, J.A. Montgomery, Jr., R.E. Stratmann, J.C. Burant, S. Dapprich, J.M. Millam, A.D. Daniels, K.N. Kudin, M.C. Strain, O. Farkas, J. Tomasi, V. Barone, M. Cossi, R. Cammi, B. Mennucci, C. Pomelli, C. Adamo, S. Clifford, J. Ochterski, G.A. Peterson, P.Y. Ayala, Q. Cui, K. Morokuma, D.K. Malick, A.D. Rabuck, K. Raghavachari, J.B. Foresman, J. Ciolowski, J.V. Ortiz, A.G. Baboul, B.B. Stefanov, G. Liu, A. Liashenko, P. Piskorz, I. Komaromi, R. Gomperts, R.L. Martin, D.J. Fox, T. Keith, M.A. Al-Laham, C.Y. Peng, A. Nanayakkara, M. Challacombe, P.M.W. Gill, B. Johnson, W. Chen, M.W. Wong, J.L. Andres, C. Gonzalez, M. Head-Gordon, E.S. Replogle, and J.A. Pople. GAUSSIAN 98. Revision A.9 [computer program]. Gaussian, Inc., Pittsburgh, Penn. 1998.
14. H, Li–F.: W.J. Hehre, R.F. Stewart, and J.A. Pople. J. Chem. Phys. **51**, 2657 (1969). He, Ne, Na–Ar: W.J. Hehre, R. Ditchfield, R.F. Stewart, and J.A. Pople. J. Chem. Phys. **52**, 2769 (1980). K, Ca, Ga–Kr: W.J. Pietro, B.A. Levi, W.J. Hehre, and R.F. Stewart. Inorg. Chem. **19**, 2225 (1980). Rb, Se, In–Xe: W.J. Pietro, E.S. Blurock, R.F. Hout, W.J. Hehre, D.J. Defrees, and R.F. Stewart. Inorg. Chem. **20**, 3650 (1981).
15. H–Ne: J.S. Binkley, J.A. Pople, and W.J. Hehre. J. Am. Chem. Soc. **102**, 939 (1980). Na–Ar: M.S. Gordon, J.S. Binkley, J.A. Pople, W.J. Pietro, and W.J. Hehre. J. Am. Chem. Soc. **104**, 2797 (1982). K, Ca, Ga–Kr, Rb, Sr, In–Xe: K.D. Dobbs and W.J. Hehre. J. Comput. Chem. **7**, 359 (1986).
16. C–F 6-31G: W.J. Hehre, R. Ditchfield, and J.A. Pople. J. Chem. Phys. **56**, 2257 (1972). H, C–F polarization functions:

© 2005 NRC Canada

P.C. Hariharan and J.A. Pople. Theor. Chim. Acta, **28**, 213 (1973). Na–Ar: M.M. Francl, W.J. Pietro, W.J. Hehre, J.S. Binkley, M.S. Gordon, D.J. Defrees, and J.A. Pople. J. Chem. Phys. **77**, 3654 (1982).
17. H, Li–F diffuse: T. Clark, J. Chandrasekhar, G.W. Spitznagel, and P.v.R. Schleyer. J. Comput. Chem. **4**, 294 (1983).
18. S. Huzinaga, J. Andzelm, M. Klobutowski, E. Radio-Andzelm, Y. Sakei, and H. Tatewaki. Gaussian basis sets for molecular calculations. Elsevier Science Publishers, Amsterdam. 1984.
19. C.C. Pye. Ph.D. thesis, Memorial University, St. John's, Newfoundland. 1997. Chapter 3, section 2 (pp. 78–91) of this thesis contains a discussion of the STO-3G, 3-21G, and 6-31G(d) Hartree–Fock calculations.
20. A. Szabo and N.S. Ostlund. Modern quantum chemistry: Introduction to advanced electronic structure theory. 1st ed. (revised). McGraw-Hill, New York. 1989, and refs. therein.
21. G. Schaftenaar and J.H. Noordik. J. Comput.–Aided Mol. Des. **14**, 123 (2000).
22. N.G. Rondan and K.N. Houk. Tetrahedron Lett. **25**, 2519 (1984).
23. S.M. Bachrach. J. Org. Chem. **58**, 5414 (1993).
24. H. Jiao and P.v.R. Schleyer. J. Chem. Soc. Faraday Trans. **90**, 1559 (1994).
25. I. Alkorta and J. Elguero. J. Chem. Soc. Perkin Trans. 2, 2497 (1998).
26. B.A. Hess, Jr. and J.E. Baldwin. J. Org. Chem. **67**, 6025 (2002).
27. M.J.S. Dewar. Chem. Br. **11**, 97 (1975).
28. A.F. Cuthbertson and C. Glidewell. J. Organomet. Chem. **221**, 19 (1981).
29. W.W. Schoeller. Z. Naturforsch. B, **38**, 1635 (1983).
30. W.W. Schoeller. Z. Naturforsch. B, **39**, 1767 (1984).
31. S. El Chaouch, J.-C. Guillemin, T. Karpati, and T. Veszpremi. Organometallics, **20**, 5405 (2001).

© 2005 NRC Canada

Solvolysis and ring closure of quinone methides photogenerated from biaryl systems[1]

Yijian Shi and Peter Wan

Abstract: A variety of biaryl quinone methides have been photogenerated with a range of efficiencies from biaryl precursors **4**–**6** and **8**, **10**, and **11**, all having hydroxyl and hydroxymethyl substituents on alternate rings. These novel biaryl quinone methides, which cannot be readily generated via thermal chemistry, are trapped by added nucleophiles such as MeOH and ethanolamine; two that cannot undergo electrocyclic ring closure (from **8** and **11**) are readily observable by nanosecond laser photolysis, with long wavelength maxima (λ_{max}) of 600 and 520 nm, respectively. Photogenerated *o*,*o*′-biaryl quinone methides undergo electrocyclic ring closure to give the corresponding chromene (pyran) products in high yield. Since the precursor biaryl alcohols have highly twisted structures in the ground state (dihedral angle of up to 90° by molecular mechanics calculations), a significant twisting motion to planarity is required to achieve reaction. Using steady-state fluorescence studies, we present evidence to suggest that the mechanism of quinone methide formation may occur via one of the following mechanisms: (*i*) dissociation of the proton from ArOH that precedes twisting; or (*ii*) ArOH dissociation and twisting taking place either simultaneously or in quick succession.

Key words: biaryl quinone methide, photosolvolysis, photodeprotonation, photocyclization.

Résumé : Un certain nombre de biaryl quinone méthides diverses a été photogénéré avec des efficacités variables à partir des précurseurs biarylés **4**–**6**, **8**, **10** et **11** qui portent tous des substituants hydroxyle et hydroxyméthyle sur les autres cycles. Ces nouveaux biaryl quinone méthides, qui ne peuvent pas être générés facilement par le biais de la chimie thermique, peuvent être piégés par l'addition de nucléophiles tel que le méthanol et l'éthanolamine; deux d'entre eux qui ne peuvent pas subir des fermetures électrocycliques de cycles (obtenus à partir de **8** et **11**) peuvent facilement être observés par photolyse laser nanoseconde avec des longueurs d'onde maximales (λ_{max}) de 600 et 520 nm respectivement. Les *o*,*o*′-biaryl quinone méthides photogénérées subissent des fermetures électrocycliques de cycle conduisant à la formation des chromènes (pyran) correspondants, avec des rendements élevés. Puisque les structures de chaque alcool précurseur biarylé sont de nature fortement déformée à l'état fondamental (angle dièdre allant jusqu'à 90° sur la base de calculs de mécanique moléculaire), la réaction ne peut se faire qu'à la suite d'un mouvement de déformation important pour atteindre un état planaire. Faisant appel à des études de fluorescence en état stationnaire, on a obtenu des données qui permettent de suggérer que le mécanisme de formation de la quinoneméthide peut impliquer l'une des voies suivantes: (*i*) une dissociation de proton à partir du ArOH qui précède la déformation ou (*ii*) une dissociation du ArOH et une déformation qui se produisent soit de façon simultanée soit en succession rapide.

Mots clés : biaryl quinone méthide, photosolvolyse, photodéprotonation, photocyclisation.

[Traduit par la Rédaction]

Introduction

The moderate to highly twisted ground-state structures of biaryls (as measured by the dihedral angle between the two phenyl rings) are known, in general, to become more planar when electronically excited. This twisting motion towards planarity inherent in many biaryls on the excited-state surface has been generally rationalized by Zimmerman and Crumrine (1) and Imamura and Hoffmann (2), by noting that the coefficients of the two carbons joining the two aryl rings in the LUMO have the same sign, whereas they have opposite signs in the HOMO. Thus, population of the LUMO on electronic excitation causes an increase in the π-bond strength joining the two aryl groups, hence, a twisting motion to a more planar structure. This phenomenon has been utilized only on a limited basis to design or induce new photochemistry: most of the photochemical reactions reported for biphenyls do not appear to explicitly require a twisting motion to planarity (3). Interest in the photocontrol of supramolecular assemblies (4) and our wish to explore the mechanistic details and scope of quinone methide photogeneration from biaryl systems prompted us to investigate in detail the generality of photocyclization reactions reported by us over several years (5). For example, twisted 2-(2′-hydroxyphenyl)benzyl alcohol (**1**) (dihedral angle of 68°) is efficiently converted (in aq. CH_3CN) to the essentially planar

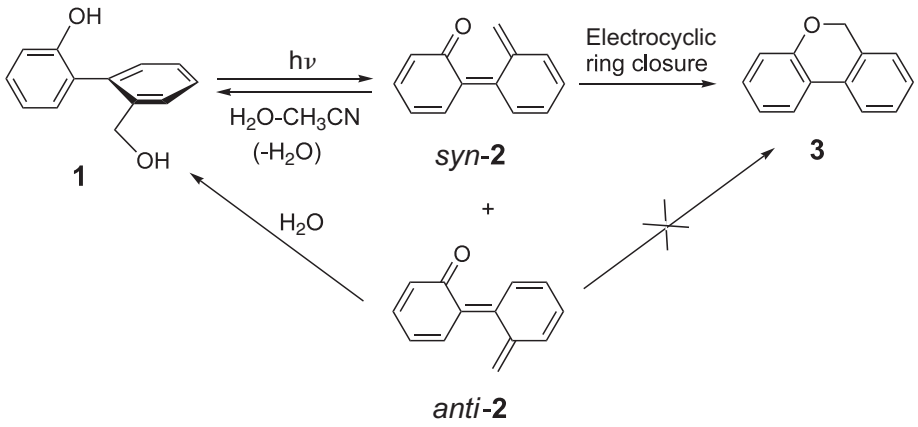
Received 25 January 2005. Published on the NRC Research Press Web site at http://canjchem.nrc.ca on 19 October 2005.

Y. Shi and P. Wan.[2] Department of Chemistry, Box 3065, University of Victoria, Victoria, BC V8W 3V6, Canada.

[1]This article is part of a Special Issue dedicated to organic reaction mechanisms.
[2]Corresponding author (e-mail: pwan@uvic.ca).

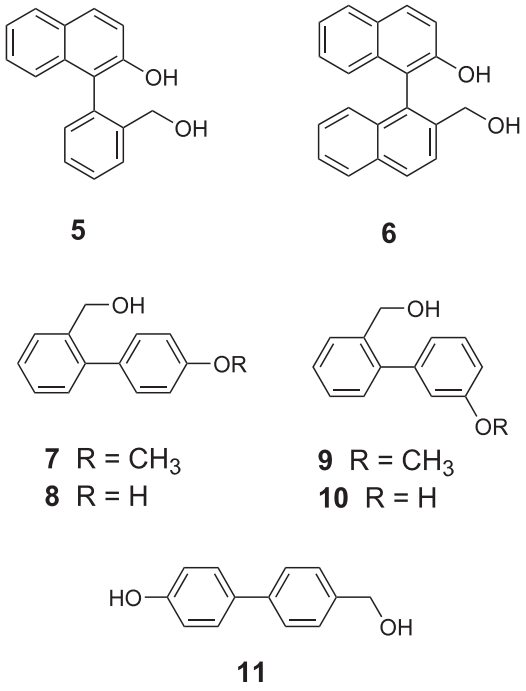
 doi: 10.1139/V05-138 © 2005 NRC Canada

Scheme 1.



5*H*-dibenzo[*b*,*d*]pyran (**3**) (dihedral angle of 24°) via the proposed *o*,*o*′-biphenyl quinone methide *syn*-**2** with high quantum efficiency (Φ up to 0.5 at pH > 11) (Scheme 1) (5). The anti conformer (*anti*-**2**) is presumably also formed but is converted back to substrate **1** by nucleophilic attack by H_2O.

The incorporation of a naphthalene ring will, in general, make such biaryls more twisted than biphenyls owing to higher steric congestion induced by the naphthalene ring. For this reason, we decided to examine the photochemistry of naphthalene incorporated biaryls **4**–**6**, to test whether the photocyclization can occur for these more sterically congested systems. Biphenyl derivatives **7**–**11** were also studied to examine the photochemistry of those systems that cannot undergo photocyclization, but that contain the appropriate hydroxy and hydroxymethyl substituents to enable it to potentially generate the appropriate biphenyl quinone methide intermediate. We show that photocyclization takes place even for the highly sterically congested binaphthyl **6** and that biphenyl quinone methide intermediates are detectable by nanosecond laser flash photolysis only when the cyclization pathway is not available. In addition, photolysis of *m*-hydroxy substituted biphenyl **10** gave rise to a formally non-Kekulé biphenyl quinone methide.



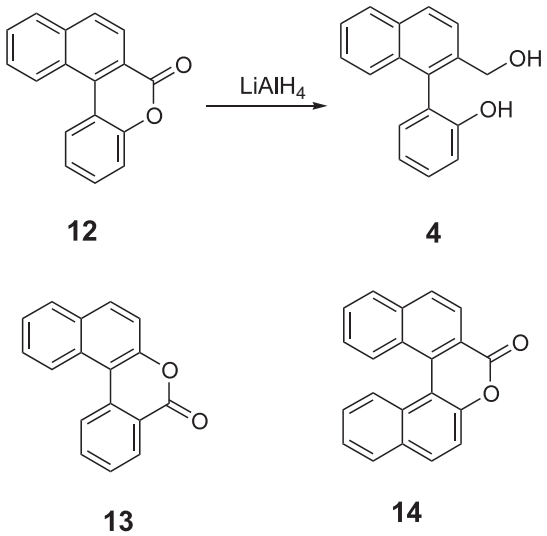
Results and discussion

Materials

Biaryl alcohols **4**–**6** were readily made via $LiAlH_4$ reduction of the corresponding lactones **12**–**14** (e.g., eq. [1]), all known except for lactone **13**, which was made by adapting the procedure reported for **12** and **14** involving use of palladium(II) acetate mediated intramolecular coupling of aryl bromides (6). Biphenyl alcohols **8** and **10** were made by BBr_3 demethylation of methoxybiphenyls **7** and **9**, respectively, which in turn were readily made using palladium(0) mediated Suzuki coupling (7, 8) of the appropriate aryl bromide and arylboronic acid, followed by functional group modification, as shown in Scheme 2 for the synthesis of **7**, which starts from 2-bromotoluene (**15**). Biphenyl alcohol **11** was made by $LiAlH_4$ reduction of commercially available 4-hydroxy-4′-biphenylcarboxylic acid.

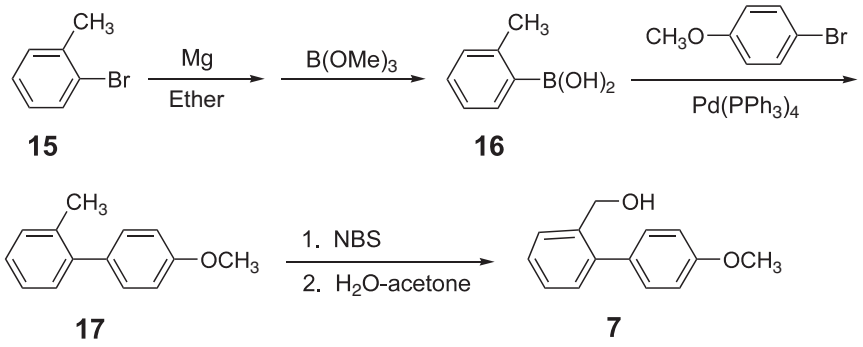
Many *o*,*o*′-disubstituted biphenyls are found in the syn geometry (as shown by *syn*-**18**) as opposed to the *anti* geometry (as shown by *anti*-**18**) with respect to the two *o*-substituents in the solid state (even in the absence of any

[1]



© 2005 NRC Canada

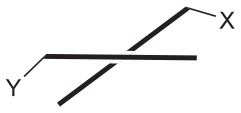
Scheme 2.



intramolecular hydrogen bonding), although the general reason for this remains unclear (9). We have shown that the crystal structure of **1** and its α,α-dimethyl derivative also take on the syn conformation, although for these alcohols intramolecular H bonding may play a role in favouring such a geometry (5*a*). With respect to the other biaryls studied in this work, we anticipate that their diaryl dihedral angles to be quite large, with also a preference for syn geometry. Molecular mechanics calculations (Chem 3D) of **4**–**11** confirm this; indeed the dihedral angles found for **4**–**6** were close to 90°.[2] Although these biaryls are expected to have highly twisted geometries, their solution structures may be different. Roberts (9) has shown there is close agreement between the dihedral angles of biphenyls observed in X-ray crystallography and those deduced from ^{13}C NMR studies. Thus, there is strong reason to believe that all biaryls **4**–**11** have highly twisted structures in solution. Moreover, if the preference for syn geometry observed and (or) predicted in the crystal for *o*,*o*′-disubstituted biaryls is also applicable in solution, then these molecules are also structurally optimized (in solution) to produce *syn* QMs (e.g., *syn*-**2**), which have the correct geometry for electrocyclic ring closure.



syn-**18** (X,Y ortho substituents)



anti-**18** (X,Y ortho substituents)

Product studies

Photolysis (254 or 300 nm) of **4**–**6** in 100% CH_3CN cleanly gave the corresponding ring closure chromene (pyran) products, as shown in Scheme 3 for **4** (correspondingly, **5** gave **20** and **6** gave **21**, Table 1), although with different quantum yields. These ring closure reactions can be conveniently followed by UV–vis spectrophotometry as all the chromene products show a red-shifted strong absorption band. Figure 1 shows the UV–vis spectral changes observed on photolysis of **4** in 100% CH_3CN, which gave chromene **19** quantitatively after sufficient photolysis. Note the presence of vibrational fine structure in the absorption of the photoproduct **19**, which is consistent with its more rigid structure (less torsional flexibility). The presence of isosbestic points throughout the conversion indicates a very clean reaction. The spectral traces for the analogous photochemical conversion of **6** to **21** have been published previously (5*c*) and show the same qualitative features.

The dihedral angle for chromene **21** is a point of interest since this would be the most sterically hindered of all the chromene products. A dihedral angle of 30° was calculated using molecular mechanics (Chem 3D). Thus, the photochemical conversion of **6** to **21** requires a substantial twisting motion, from about 90° to about 30°. Similar twisting motions are required for the conversions of **4** and **5** to the corresponding chromenes.

Photolysis (λ_{ex} = 254 nm) of **4** in H_2O–CH_3CN (1:1, *v*/*v*) results in a photostationary state containing 56% of the chromene product **19** and 44% of alcohol **4** (Fig. 2). Prolonged photolysis does not change this product to starting material ratio. The photostationary state composition was confirmed by exhaustive photolysis of a solution of **19** under the same conditions, which regenerated **4** and gave a photostationary state containing 60% of chromene **19** and 40% of alcohol **4**. Photolysis of **5** (or **6**) under identical conditions resulted in a photostationary state containing >95% chromene product **20** (or **21**) and <5% alcohol starting material.

Photolysis of **4** in neat CH_3OH gave a photostationary state containing approximately 24% of chromene **19** and 76% of the methyl ether product **22**. Prolonged photolysis, however, gave rise to a small amount (~10%) of unidentified side products, owing to the secondary photodecomposition of methyl ether **22**. The reversibility of this reaction was demonstrated by photolysis of chromene **19** in neat CH_3OH, which gave a photostationary state containing 21% of **19** and 79% of **22**. In H_2O–CH_3OH (1:1), photolysis of **19** resulted in a photostationary state containing **19**, **22**, and **4** in a ratio of 8:69:23. When the concentrations of CH_3OH and H_2O are taken into account, the relative rates of CH_3OH and H_2O ad-

[2] Unpublished X-ray analyses (A. MacKinnon, J.A.K. Howard, Y. Shi, and P. Wan) of some single crystals of these compounds confirm the expected large dihedral angles in the solid state. In addition, syn geometry was observed in all of **4**–**6**.

© 2005 NRC Canada

Scheme 3.

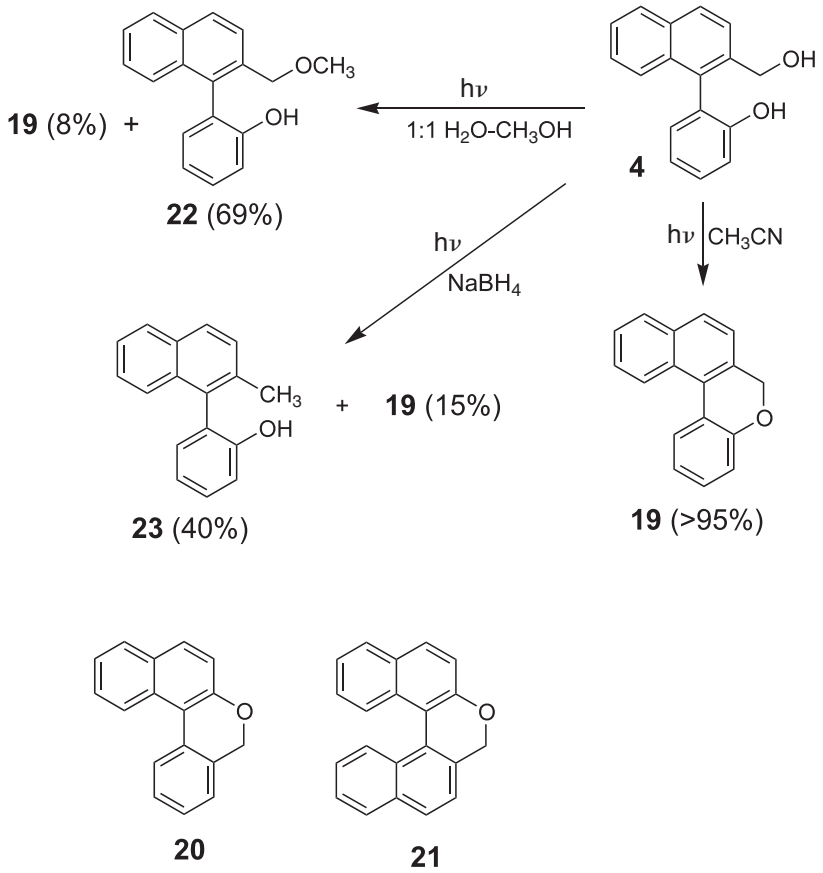


Table 1. Quantum yields for photocyclization of biaryl alcohols **1** and **4**–**6**.

Biaryl alcohol	Product	λ_{max} (nm) (ϵ)[a]	PS ratio[b] in H_2O–CH_3CN (1:1)	Φ[c] (H_2O–CH_3CN) 0% H_2O	1% H_2O	10% H_2O	50% H_2O	Φ[c] (CH_3OH)	Φ[c] (THF)
4	**19**	337 (10 600)	60:40	0.29	0.30	0.25	0.12	0.081	0.39
5	**20**	350 (7 950)	>95:5	0.079	0.090	0.080	0.047	0.039	0.11
6	**21**	350 (11 500)	>95:5	0.11	0.21	0.34	0.18	0.16	0.15
1[d]	**3**	308 (6 775)	≈98:2	0.12	0.10	0.21	0.21		0.11

[a]Absorption max and extinction coefficient (number in brackets) of the product.
[b]Product to biaryl alcohol ratio at the photostationary (PS) state (λ_{ex} = 254 nm).
[c]Product quantum yield (for photocyclization) measured using potassium ferrioxalate actinometry (error: ±10%) (10). Water content quoted is by volume in CH_3CN.
[d]Used for comparison. Some data taken from ref. 5*a*.

dition is approximately 7:1 in favor of CH_3OH. Photolysis of **5** and **6** in the presence of CH_3OH also resulted in the formation of the corresponding methyl ether products accompanied with a reduced yield for the corresponding chromene product. In the presence of $NaBH_4$ (~0.5 mol/L), photolysis of **4** (in 2-propanol or aq. CH_3CN) gave the reduction product **23** and **19** (Scheme 3). Photolysis of **1** and **6** also gave similar reduction products.

Photolysis of the biphenyl alcohols **7** and **8** in H_2O–CH_3OH (1:1) gave the corresponding methyl ether substitution products **24** and **25** (Scheme 4). In the presence of ethyl vinyl ether (~0.4 mol/L), photolysis (254 nm, 15 min) of **8** in aq. CH_3CN (H_2O–CH_3CN, 1:2) gave aldehyde **26** in high yield (>60%). In this reaction, ethyl vinyl ether simply functions as a nucleophile (β-vinyl carbon of ethyl vinyl ether) followed by hydrolysis. No evidence for [4+2] cycloaddition products was observed. Although less efficient, photolysis of **11** under similar conditions also resulted in the formation of the corresponding methyl ether product from CH_3OH, but no aldehyde product was observable in the presence of ethyl vinyl ether.

It was previously observed (5*a*) that when the phenolic OH group of the parent compound **1** was replaced with a methoxy group, photolysis of the substrate in aqueous methanol does not result in the corresponding methyl ether substitution product. This is also true for 3-[2′-

© 2005 NRC Canada

Fig. 1. UV–vis spectral traces showing the smooth conversion of **4** to chromene **19** in 100% CH_3CN (λ_{ex} = 254 nm; each trace represents about 10–20 s photolysis, except for the last trace, which was obtained after extended photolysis, >10 min). The final spectrum obtained is essentially identical to that of pure chromene **19**.

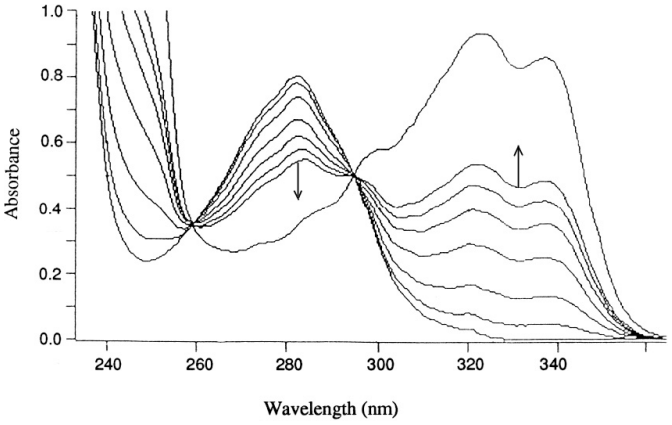
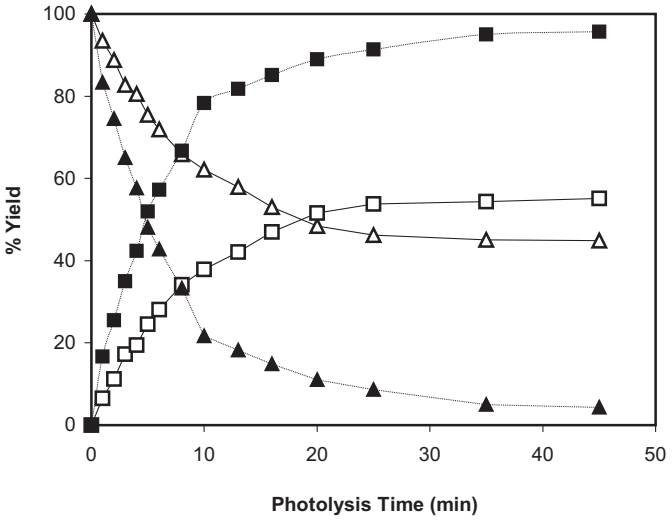
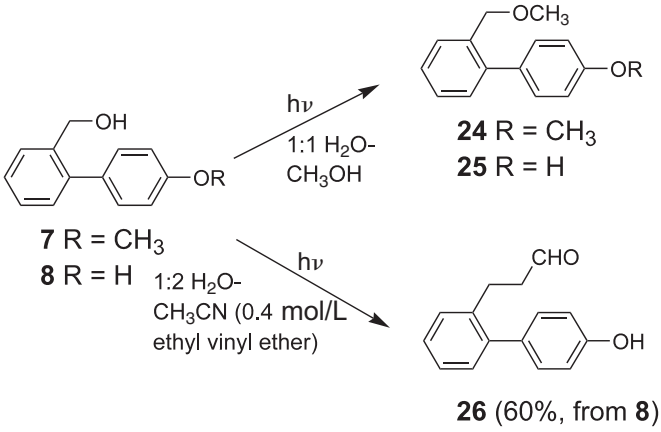


Fig. 2. Plot of % **4** (triangles) and % **19** (squares) vs. photolysis time in 100% CH_3CN (filled) and in CH_3CN–H_2O (1:1) (unfilled).



(hydroxymethyl)phenyl]anisole (**9**), where prolonged irradiation of **9** in CH_3OH–H_2O (1:1) did not give any product, and the starting material was completely recovered.

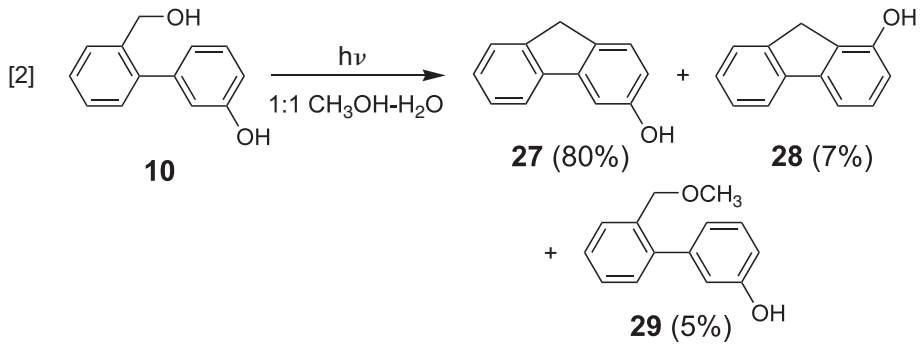
Scheme 4.



Interestingly, irradiation of **10** in CH_3CN–H_2O (1:1) resulted in a major product 3-hydroxyfluorene (**27**) and a minor product in approximately a 10:1 ratio. The minor product had the same molecular weight as **27** and its ^1H NMR spectrum showed only absorption at the aromatic region and a singlet at δ 3.82 ppm, corresponding to Ar-CH_2-Ar. This minor product is consistent with 1-hydroxyfluorene (**28**) (eq. [2]). In CH_3OH–H_2O (1:1), photolysis of **10** gave an additional minor product. The ^1H NMR spectrum of the product mixture is consistent with the formation of the substitution product methyl ether **29** (eq. [2]). The ring closure reaction (to give **27** and **28**) can also be monitored by UV spectrophotometry. Since the absorption spectrum of **27** is red shifted by about 20 nm relative to the starting material (**10**), as the reaction proceeds, a structured new band corresponding to **27** in the 300–320 nm region grows in with photolysis.

Product quantum yields

Product quantum yields for the photocyclization of biaryl alcohols **4–6** and for the photosovolysis/photocyclization of **7–11** were measured using potassium ferrioxalate actinometry (10) (λ_{ex} = 280 nm) as the standard, and UV–vis and (or) ^1H NMR to monitor for reaction progress. Photocyclization product quantum yields for **4–6** are summarized in Table 1. Large solvent dependence was observed in the photocyclization quantum yields. Although H_2O was previously observed to enhance the photocyclization of the parent compound **1** (5*a*), the water effect on the photocyclization of **4** was the opposite. Added H_2O (when the H_2O content ≥10%) noticeably decreased the quantum yield. In contrast



© 2005 NRC Canada

Table 2. Fluorescence data of biaryl alcohols and model compounds.

Compound	τ_f[a] (ns)	Φ_f[b]	k_f^0 (s^{-1})[c] (CH_3CN)	$\Delta\nu$ (w) (cm^{-1})[d] CH_3CN	0.01 mol/L NaOH
Biphenyls					
27				1705(1411)	4235(2063)
11		0.24(0.30)		2979(1574)	4968(2096)
33		0.16(0.19)		3216(1754)	5838(2506)
7		0.15(0.16)			
8		0.13(.026)		3239(1921)	
34		0.12(.087)[e]		3368(2040)	6238(2402)
9		0.12(0.12)			
10		0.14(0.04)		3623(2017)	
30				3003(1801)	5590(2138)
1				3276(1913)	
Naphthols and naphthylphenols					
35				1676(1319)	3034(1583)
5	5.8(10.8)	0.23	4.0×10^7	1834(1525)	2958(1528)
4		0.0059		1689(1899)	
6	6.7	0.15	2.2×10^7	1786(1430)	
31	6.8(15.0)	0.26	3.8×10^7	1737(1361)	2975(1561)
23	3.6	0.050	1.4×10^7	1715(1450)	~7800
32	6.9(3.0)	0.18	2.6×10^7	1680(1354)	6865(2264)

[a]Measured in neat CH_3CN. The lifetime of the corresponding phenolate or naphtholate (in 0.01 mol/L NaOH) quoted in brackets.

[b]Determined in neat CH_3CN using naphthalene and 2-aminopyridine as the standard. The number in brackets was determined in H_2O–CH_3CN (1:1).

[c]Natural fluorescence rate constant as defined by $k_f^0 = \Phi_f/\tau_f$.

[d]$\Delta\nu$ is the Stokes shift and w is the spectral width (at half height), as defined by Berlman (11, 13).

[e]Due to stronger emission from the phenolate ion, Φ_f in aqueous solution was calculated from the Φ_f of **34** in neat CH_3CN and the relative fluorescence intensity in the two solvents.

to **4**, the quantum yield for **6** and **5** showed an initial increase with added water and a decrease at higher water contents. The quantum yield for **5** was also much smaller than those of **4** and **6**. Biaryl alcohol **6** is expected to be most sterically congested system, whereas **4** and **5** are expected to be similar in this respect; therefore, the explanation for the observed quantum yield difference probably lies in an electronic factor that we do not currently understand.

The quantum yield for the photocyclization (to the fluorene ring system) of **10** in CH_3CN–H_2O (1:1) (eq. [2]) was 0.17 (for the formation of both **27** and **28**). There was significant variations in measured quantum yields for the photosolvolysis of the remaining biphenyl alcohols **7**, **8**, and **11**. Photolysis of **8** in H_2O–CH_3OH (1:1) gave **25** with Φ = 0.23, while photolysis of **11** under identical conditions gave the corresponding methyl ether in much lower quantum yield (Φ = 0.026). Substitution of the phenol OH with an OCH_3 group significantly lowers the reactivity of these substrates. For example, the quantum yield (Φ = 0.075) for photolysis of **7** to give **24** is only one-third of that for photolysis of **8** to give **25**. Indeed, there was no methyl ether product (or ring closure product) observable in the photolysis of **9**. In general, the product quantum yields measured previously were unaffected in the pH 1–7 region (slight increases of up to about 10% was observed on lower acidity beyond pH 1). In the pH > 9 region, the compounds were more reactive as indicated by enhanced loss of the substrate, but quantification was problematic because of the formation of more side products as a result of direct excitation of the phenolate.

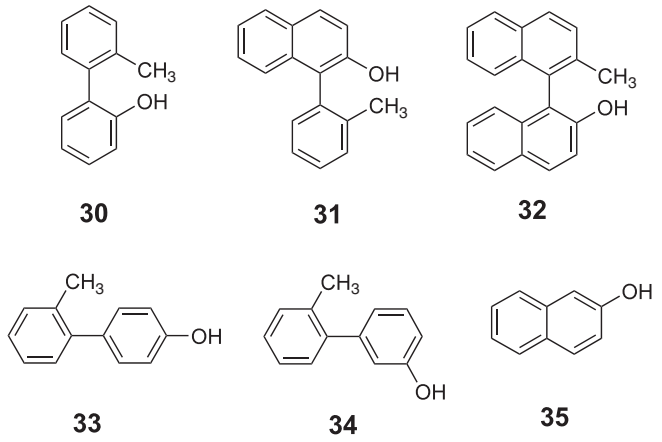
Fluorescence measurements

It is well-known that biphenyl and many of its derivatives have large geometry changes upon electronic excitation (11). When compared with more rigidly planar (in both ground and electronically excited states) molecules such as fluorene and anthracene, these molecules have larger energy differences (thus, a larger Stokes shift) between the Frank–Condon and the fluorescent state. For example, biphenyl and phenyl naphthalenes have significantly larger Stokes shifts (3000–3200 cm^{-1}) than fluorene (1430 cm^{-1}) and 1,2-benzofluorene (1400 cm^{-1}) (in cyclohexane) (11). Thus, excited-state twisting of biaryls can be qualitatively related to the Stokes shift values determined from fluorescence emission spectra (11, 12). In addition, transitions from a more planar initial state (S_0 or S_1) tend to give narrower as opposed to broad spectra (12). Thus, both Stokes shift ($\Delta\nu$) and spectral width (w) of the fluorescence emission band provide useful information with respect to geometry changes associated with the excited state.

Due to highly efficient photocyclization via S_1, some of the biaryl alcohols studied were only weakly fluorescent. Therefore, the fluorescence behavior of a series of model compounds (**7**, **9**, **23**, **27**, and **30**–**35**) that are either nonreactive or reacted only with low quantum efficiency were also studied. The fluorescence spectral properties ($\Delta\nu$, w), fluorescence quantum yields, and the fluorescence lifetimes for some of these compounds are also tabulated in Table 2.

As shown in Table 2, the Stokes shifts ($\Delta\nu$) for all the "loose" biphenyl systems in neat CH_3CN are approximately 3300 ± 300 cm^{-1}, which is significantly larger than that of the

© 2005 NRC Canada

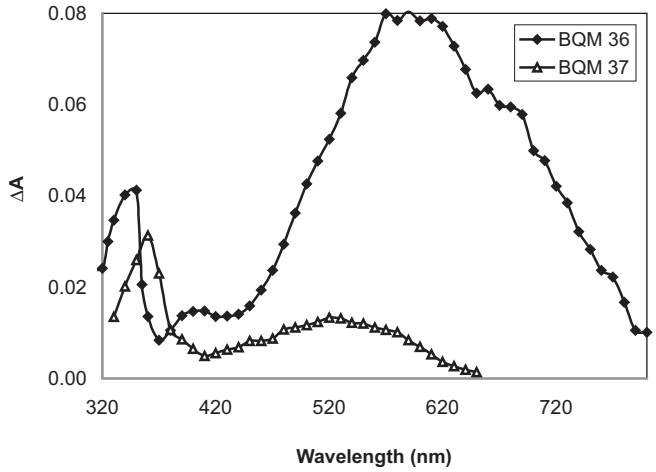


"rigid" biphenyl molecule **27** (1705 cm^{-1}). The spectral width (w) of all the *o*-substituted biphenyl derivatives ($w \approx 1750$–2000 cm^{-1}) is significantly larger than analogs not bearing a substituent at the *o*-position (**11**, $w = 1574$ cm^{-1}) and the rigid compound **27** ($w = 1411$ cm^{-1}). The spectral width of **11** is only slightly larger than that of **27**. This phenomenon is a result of the increased steric repulsion owing to *o*-substitution that results in a less rigid and less planar S_1 in these molecules. A similar trend was also observed in 0.01 N NaOH(aq) solutions, where the emitting species are the corresponding phenolate ions. For example, the Stokes shift and spectral width of **34** ($\Delta\nu = 6238$ cm^{-1}, $w = 2402$ cm^{-1}, model of **10**) and **30** ($\Delta\nu = 5590$ cm^{-1}, $w = 2138$ cm^{-1}, model of **1**) are larger than those of the rigid molecule **27** ($\Delta\nu = 4235$ cm^{-1}, $w = 2063$ cm^{-1}). Thus, it can be concluded that both the neutral and the phenolate ion forms of these biphenyl systems can twist to the more planar geometry upon electronic excitation.

In contrast to the biphenyl systems, biaryls with one or two naphthalene rings (**4**–**6** and their model compounds, bottom half of Table 2) *do not* show large Stokes shifts in neat CH_3CN. The fluorescence spectra of these molecules in neat CH_3CN resemble that of 2-naphthol (**35**) or 2-(hydroxymethyl)naphthalene. The Stokes shifts (~1750 ± 80 cm^{-1}, Table 2) of these compounds are also similar to (or only slightly greater than) that of **35**, but significantly smaller than that of 1-phenylnaphthalene (3200 cm^{-1}) (11), which suggests that these molecules are just as twisted in the S_1 state as in the ground state. The spectral width for these molecules, except for **4**, is also small (~1400–1500 cm^{-1}) indicating rigid S_1 states.

In aqueous solution, neither **4** nor **6** showed any detectable fluorescence emission owing to the very efficient photochemical cyclization from S_1. Thus, model compounds **23** and **32** provided valuable information. In CH_3CN–H_2O (1:1), both of these compounds only gave *one markedly red-shifted* emission band centered at ~560 nm. These emission bands are *identical* to the emission spectra of the corresponding phenolate and (or) naphtholate ions obtained by using 0.01 mol/L NaOH–CH_3CN (1:1) as the solvent. The absence of the emission from the neutral species of **23** and **32** at pH 7 suggests rapid excited-state proton transfer (ESPT) to the solvent. In 0.01 mol/L NaOH–CH_3CN (1:1), the Stokes shift and spectral width ($\Delta\nu = 6865$ cm^{-1}, $w = 2264$ cm^{-1}) of **32** and that of **23** ($\Delta\nu \approx 7800$ cm^{-1}, this emission is too weak for w to be measured accurately) are much larger than the naphtholate ion of **35** ($\Delta\nu = 3034$ cm^{-1}, $w = 1583$ cm^{-1}, Table 2). These extraordinary large Stokes shifts are consistent with large geometry changes in S_1 for the *deprotonated* forms of **32** and **23**. Thus, it seems reasonable that the deprotonated forms of **4** and **6** also twist to the planar (or more planar) geometry in the excited state. The lack of any observable emission from these compounds is due to an inherently efficient cyclization reaction that takes places from this more planar state.

Fig. 3. Transient spectra of biaryl quinone methides **36** and **37** obtained from nanosecond LFP of **8** and **11**, respectively, in 100% H_2O.



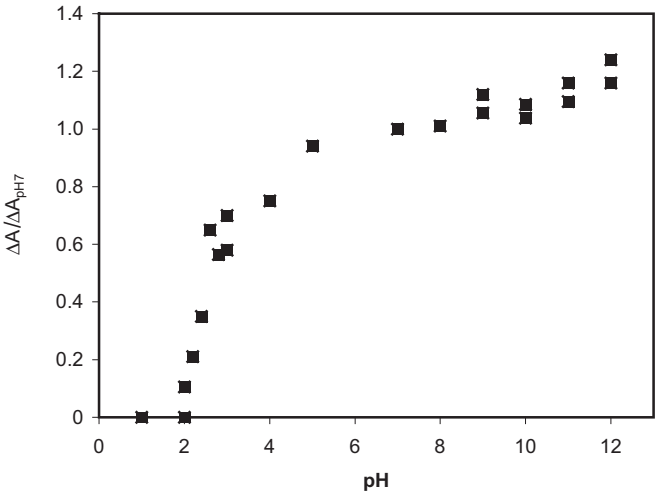
In contrast, **5** and its model compound **31** show strong emissions (at nearly equal intensity) from both the neutral 2-naphthol moiety ($\lambda_{max} \approx 360$ nm) and the naphtholate ion ($\lambda_{max} \approx 425$ nm) in H_2O. In 0.01 mol/L NaOH–CH_3CN (1:1), only the emission of the naphtholate ion was observable, but the spectral properties (Stokes shift, spectral width, and λ_{max}) of this emission closely resemble those of 2-naphthol **35** (the 2-naphtholate ion). It is concluded that **5**, even in its deprotonated form, can not twist to the planar geometry efficiently in S_1, which is required for the ring closure reaction. This is consistent with its low quantum efficiency observed for the ring closure reaction (Table 1).

Laser flash photolysis

Nanosecond laser flash photolysis (LFP) (266 nm, Nd:YAG laser, ≤20 mJ) of **8** in aq. CH_3CN gave a strong and very broad transient absorption spectrum with the major band at ~600 nm (Fig. 3). Although the transient spectrum was broad (450–800 nm), the decay at all wavelengths (including the weak band at 350 nm) was single exponential and had identical rates. It was also observed that the water content of the solvent affected the intensity as well as the decay rate of this transient. In neat CH_3CN, this transient was not observed; in neat H_2O, the intensity of the spectrum was ca. threefold larger than that in CH_3CN–H_2O (1:1). This indicated that H_2O was necessary for the formation of this transient. The λ_{max} of the transient was red shifted with increasing solvent polarity (575 nm in CH_3CN–H_2O (1:1) to 600 nm in neat H_2O). The shape of the spectrum was independent of pH; photolysis of **8** in pH 2.5, 7, and 12 gave essentially the same spectrum, although the intensity varied. The decay rate was not affected by O_2 but showed strong

© 2005 NRC Canada

Fig. 4. pH Dependence for photogeneration of biaryl quinone methide **36** as observed by LFP of **8** (errors are ±10% of quoted value).



solvent and pH dependence. In the CH_3CN–H_2O mixed solvent system, the decay rate increased by ca. three orders of magnitude when the water content changed from 10%–100% H_2O. A plot of the logarithm of the decay rate vs. the molarity of H_2O was essentially linear. The transient could be efficiently quenched by H^+. In pH 4–12, there was essentially no pH effect on the decay rate constant (k_{obs}), although it was slightly affected by added electrolytes (in neat H_2O and 0.01 mol/L NaOH, $k_{obs} = 2.0 \times 10^6$ s^{-1}; in pH 4 and 7 buffered solutions, $k_{obs} = 2.5 \times 10^6$ s^{-1}). However, the decay rate increased dramatically at lower pH (pH 2 to 3), suggesting quenching by H^+. In this pH region, the observable transient intensity also decreased significantly with pH while the fluorescence intensity increased considerably. Due to interference from fluorescence emission and weaker transient absorption, it was not possible to measure the decay rate accurately at low pH. It was estimated that k_{obs} ~10^7 s^{-1} at pH 3 and ~10^8 s^{-1} at pH 2, corresponding to a quenching rate constant (by H^+) of $k_q \approx 10^{10}$ s^{-1} (mol/L)$^{-1}$. The transient was also quenchable by added nucleophiles such as ethanolamine ($k_q = 3.6 \times 10^6$ s^{-1} (mol/L)$^{-1}$).

We thus assigned this transient spectrum to biaryl quinone methide (BQM) **36**. The broad and structureless absorption spectrum is consistent with a ground state that is not rigidly planar. The fact that irradiation of **8** in 0.01 mol/L NaOH gave exactly the same transient spectrum as in pH 7, indicates that this same transient can be generated by irradiation of the corresponding phenolate ion of **8**. The relative quantum efficiency for generating this transient from the neutral form of **8** vs. its deprotonated form (the phenolate ion) is shown in Fig. 4 in which the ΔA at 600 nm at different pH values was measured immediately after each laser pulse, and the ratio $\Delta A/\Delta A_{pH7}$ was plotted against the pH of the solvent. When the energy of the laser pulse and the absorbance of the solution at the excitation wavelength were kept constant, the ratio $\Delta A/\Delta A_{pH7}$ is a direct measure of the relative quantum yield for formation of BQM **36** at this pH (relative to pH 7). It is expected that such a plot would show two transitions, one at pH ≈ 2–4 (corresponding to the pK_a* of the excited-state phenol) and the other at pH ≈ 10 (corresponding to the pK_a of the ground state). This is in fact revealed in Fig. 4. The first titration between pH 2–4 is clearly evident while the second at pH 10–12 is less marked. The modest increase in efficiency upon excitation of the phenolate might be due to the already high yield of the phenolate ion on adiabatic deprotonation from the phenol.

Although product studies showed that the photolysis of **7** in H_2O–CH_3OH (1:1) also gave the corresponding methyl ether product in reasonable yield, LFP of **7** did not produce any observable transient species assignable to quinone methides or carbocations. This seems reasonable since there is no simple mechanism for photogenerating quinone methides from the methoxy compound. Moreover, the anticipated carbocation intermediate responsible for the observed photosolvolysis would be of the benzylic kind and would be too short-lived in aqueous solution to be detectable by nanosecond LFP.

Laser flash photolysis of **11** in aq. CH_3CN also gave a transient absorption spectrum with two major bands at 360 and 525 nm (Fig. 3). Its decay rate in 100% (pH 7) H_2O ($k_{obs} = 1.50 \times 10^4$ s^{-1}) is less than that observed for **36**. The transient is quenched by H^+ and added nucleophiles and thus can be assigned to BQM **37**. A Stern–Volmer plot using $H_2NCH_2CH_2OH$ as a quencher gave $k_q = 2.61 \times 10^5$ s^{-1} (mol/L)$^{-1}$, which is significantly smaller than that observed for **36**. The fact that the spectral width of **37** is narrower than that of **36** is consistent with its more rigid ground state (less steric repulsion at the *o*-position). Unlike **36**, the phenolate ion of **11** gives rise to BQM **37** much more efficiently than the neutral molecule; the relative quantum yield for the photogeneration of **37** is 3.5 times higher at pH 12 than at pH 7.

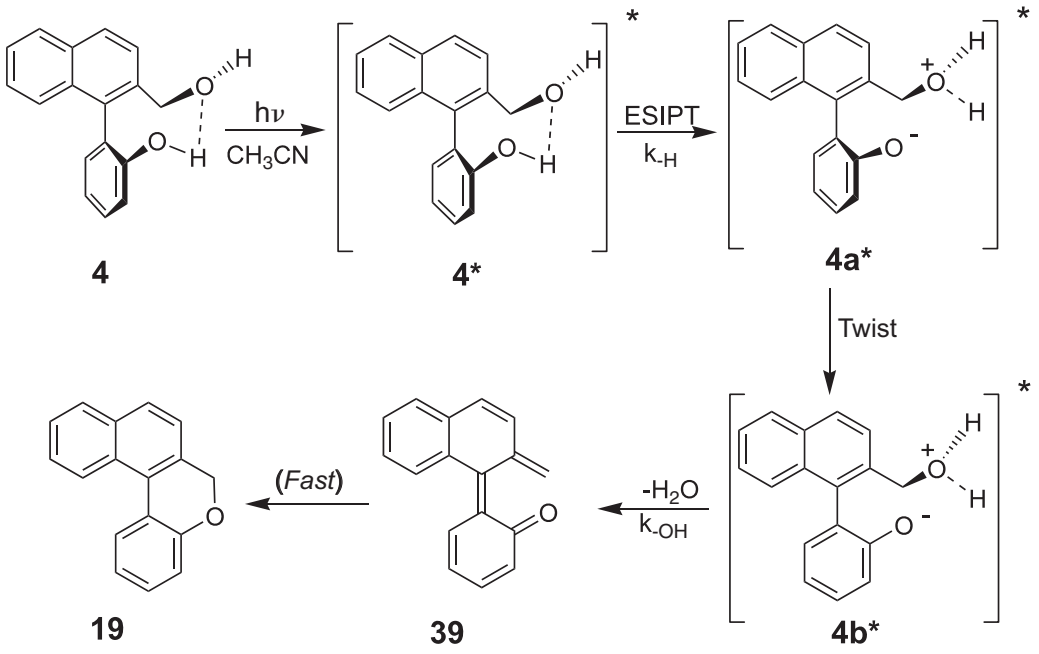
Burnham and Schuster (14) have studied the photochemistry of **6** and **21**. They suggested that the photocyclization of **6** to **21** proceeded via a BQM intermediate (viz., **38**). They also suggested that BQM **38** was observable by nanosecond laser flash photolysis in cyclohexane with a lifetime of 5 μs. However, using nanosecond LFP, we have not been able to detect any transient species in the 450–700 nm region assignable to the BQM for any of **1**, **4**–**6**, and **10** in aq. CH_3CN. We conclude that in aq. CH_3CN any BQM intermediate from these substrates is too short-lived to be detectable on the nanosecond timescale, i.e., electrocyclic ring closure from intermediates such as **39**, to give two new aromatic rings in **19** (Scheme 5) would be expected to be very fast ($k >> 10^9$ s^{-1}).

Reaction mechanisms

We begin our mechanistic discussion for the most reactive compound that undergoes photocyclization, viz., **4** (Scheme 5). The quantum yield for the photocyclization of **4** is high in aprotic solvents such as CH_3CN ($\Phi = 0.3$) and THF ($\Phi = 0.4$). Since a small amount of added H_2O does not change the quantum yield dramatically (Table 1), the reaction cannot be ascribed by a mechanism mediated by traces of residual water or other protic solvent impurities. Although the molecules may be intermolecularly H bonded in the crystalline state, such intermolecular H bonding is not likely in dilute solution in a polar solvent such as CH_3CN. Thus, the reaction in aprotic solvent is most likely via an excited-state intramolecular proton transfer (ESIPT) mechanism, as

© 2005 NRC Canada

Scheme 5.



shown in Scheme 5, in which the ArOH proton is first transferred to the $ArCH_2OH$ oxygen atom of the same molecule via an intramolecular H bond to give **4a***. This is followed by twisting to the planar geometry to give **4b***, followed by the loss of a molecule of H_2O to give the BQM intermediate **39**, which subsequently undergoes electrocyclization in a fast reaction ($k >> 10^9$ s^{-1}) to give the chromene product **19**. This mechanism is supported by the Stokes shift data observed in the fluorescence measurements, which indicated that the neutral forms of **4** and **6** do not twist to the planar geometry, but their deprotonated forms do.

Since the product quantum yield for **4** is also much higher than its analogs (**1**, **5**, and **6**) in aprotic solvents, a faster ESIPT rate could be responsible for this. More insights on this aspect are obtained from the fluorescence quantum yield and fluorescence lifetime studies (Table 2). The kinetic expression for fluorescence quantum yield (Φ_f) is the ratio of the natural fluorescence rate constant (k_f^0) to the sum of the rates for all possible deactivation pathways, given by eq. [3],

$$[3] \qquad \Phi_f = k_f^0/(k_f^0 + \Sigma k_d + \Sigma k_r)$$

where Σk_d represents the sum of nonradiative deactivation rates such as the rate of internal conversion (k_{ic}) and the rate of intersystem crossing (k_{isc}); Σk_r represents the sum of all possible chemical reactions of S_1. According to the proposed mechanism (Scheme 5), Σk_r in this case is the ESIPT rate k_{-H}. For the model compound **23**, Σk_r is zero in neat CH_3CN. If we assume that **4** and **23** have similar k_f^0 and Σk_d values, then k_{-H} can be estimated by eq. [4]:

$$[4] \qquad k_{-H} = (k_f^{\,0} + \Sigma k_d)\left[\frac{(\Phi_f)_{mdl}}{(\Phi_f)_{rec}} - 1\right]$$

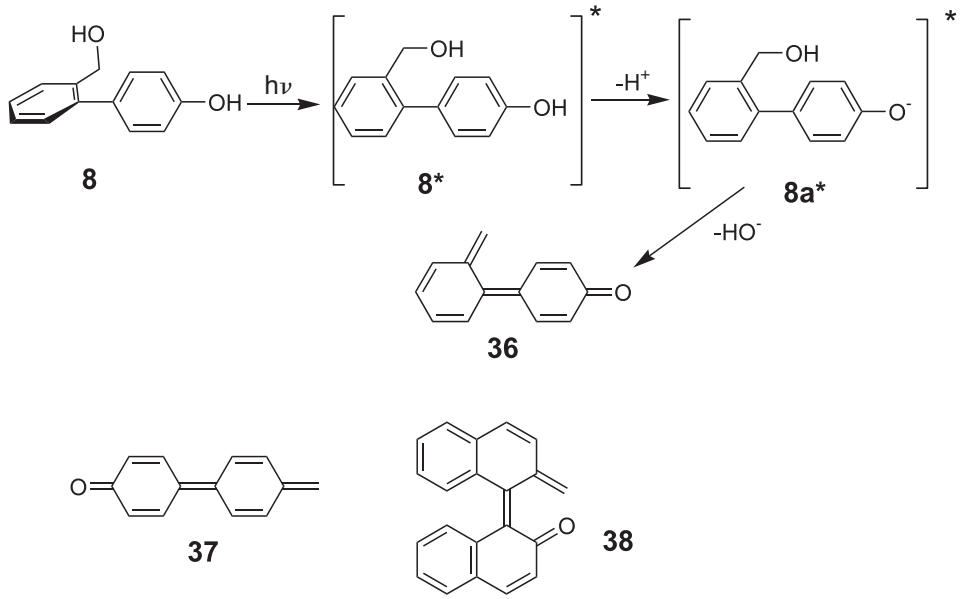
where the rec subscript refers to the reactive compound (i.e., **4**–**6**) and mdl to the corresponding model compound (i.e., **23**, **31**, and **32**); ($k_f^0 + \Sigma k_d$) is the reciprocal of the fluorescence lifetime (τ_f, Table 2) of the model compound. The ESIPT rate k_{-H} estimated for **4** using this method is 2×10^9 s^{-1}, which is nearly two orders of magnitude larger than those for **5** (2×10^7 s^{-1}) and **6** (3×10^7 s^{-1}).

Addition of H_2O to CH_3CN can change the mechanism for photocyclization. It was observed that upon the addition of water (0–2.5 mol/L), the fluorescence intensity of **31** (model of **5**) increased by 11% while both **32** and **23** showed significant fluorescence quenching (fluorescence intensity decreased by 41% and 53%, respectively), suggesting that **23** (or **4**) and **32** (or **6**) undergo efficient ESPT to water. Thus, the increase in cyclization quantum yield with added water (Table 2) can be rationalized as being due to the operation of a more efficient cyclization pathway in water, viz., ESPT to water to generate the phenolate or napththolate ion, followed by twisting to a more planar state and the loss of hydroxide ion. However, when the water content is sufficiently high, the quantum yield for cyclization decreases owing to the competition of nucleophilic attack on the quinone methide by water itself, which leads back to the starting material (i.e., **39** to **4**). In the case of **5**, where the cyclization quantum yield is intrinsically lower, other effects appear to dominate when water is added, making the fluorescence emission stronger at low water content than in pure CH_3CN.

In 0.01 mol/L NaOH, if we also assume that the reactive species has similar k_f^0 and Σk_d values as its model compound, k_{-OH} for **5** (its naphtholate ion) can be estimated from the fluorescence lifetime of **5** (τ_f = 10.8 ns) and that of its model compound **31** (τ_f = 15.0 ns), i.e., $k_{-OH} = (1/10.8 - 1/15) \times 10^9 = 2.6 \times 10^7$ s^{-1}, which is in the same order of magnitude as the natural fluorescence rate constant (k_f^0) for these types of molecules. This also explains the fact that **5** has a strong fluorescence emission in aq. 0.01 mol/L NaOH solution and a lower reaction quantum yield. In contrast, **6** showed complete fluorescence quenching in this medium,

© 2005 NRC Canada

Scheme 6.

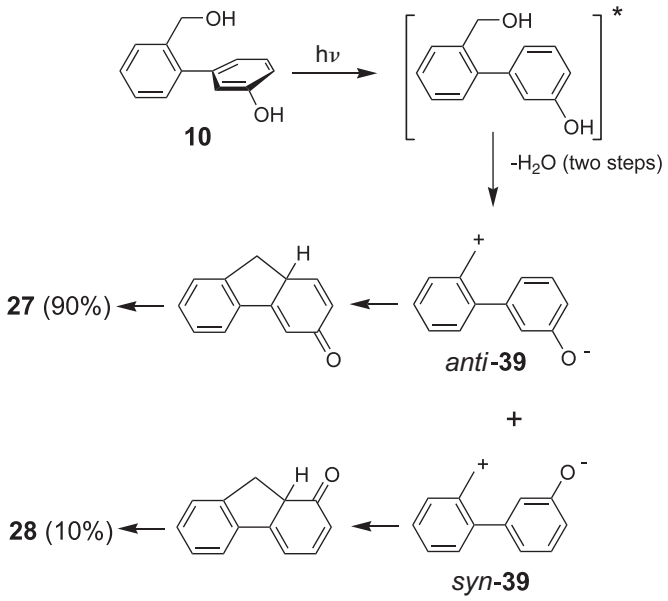


although its model compound **32** does show reasonably strong fluorescence emission. This suggests that k_{-OH} for **6** is much larger than k_f^0, i.e., $k_{-OH} >> 10^7 s^{-1}$. It is therefore clear that the low quantum efficiency observed for the photocyclization of **5** is due to *both* a smaller k_{-H} and a smaller k_{-OH}.

LFP and product studies indicate that the efficiencies for the photogeneration of BQMs **36** and **37** are significantly different, which suggests that **8** and **11** have significantly different reactivities (different deprotonation rate k_{-H} and (or) dehydroxylation rate k_{-OH}). Fluorescence quenching experiments on these systems reveal some interesting insights on these processes. It can be easily seen from Table 2 that significant fluorescence quenching effect is only observable for the biphenyl system bearing both the phenolic and the benzylic OH (and also at the right positions), i.e., **8** and **10**. Φ_f of **8** decreased by a factor of five and that of **10** decreased by a factor of 3.5 when the solvent was changed from neat CH_3CN to H_2O–CH_3CN (1:1), suggesting very large k_{-H} and (or) k_{-OH} for these molecules. When either the CH_2OH moiety (of $ArCH_2OH$) is replaced by CH_3 or the phenolic OH is replaced by an OCH_3, there is either no fluorescence quenching or only a minor quenching effect. In addition, no fluorescence emission from the phenolate ions of **8** and **10** could be detected, although model compounds **33** and **34** did show strong fluorescence emission from their respective phenolate ions. These observations suggest that the deprotonation and dehydroxylation processes in **8** and **10** are unusually fast and may actually be concerted, although it is shown as a step-wise process in Scheme 6. Note that in this mechanism, the twisting about the biphenyl ring system takes place without the need for deprotonation of the phenol, consistent with the fluorescence results.

Although results from product studies indicate that the photolysis of **10** (Scheme 7) should proceed via BQM **39**, LFP studies showed no detectable transients longer than a few ca. 10 ns. This is consistent with the expectation since benzylic-type carbocations **39** should be shorter lived than a few nanoseconds (15). Assuming the presence of BQM **39**

Scheme 7.



intermediates, the working mechanism for the reaction is shown in Scheme 7. The isolation of fluorene products **27** and **28** is consistent with the formation of the zwitterionic BQMs *anti*-**39** and *syn*-**39**. The quantum yield for formation of these intermediates is quite high (Φ = 0.17, vide supra) and indicates that there is substantial charge transfer (electronic communication) between the *o* and *m* positions on *different* rings in the biphenyl system. Note that there is little to no electronic communication between such positions in the ground-state molecule, so the previous finding could be used to design systems where electronic communication can be switched on by photoactivation.

Summary

The main conclusion from this work is that a variety of

© 2005 NRC Canada

biaryl quinone methides (extended analogs of simple benzenoid quinone methides) are readily photogenerable from the corresponding hydroxymethyl substituted phenols (or equivalent compounds) in aqueous solution. Indeed, it would appear that at least for the biphenyl quinone methide series, all isomeric biphenyl quinone methides are photogenerable in aqueous solution, albeit with differing quantum efficiencies. The lifetimes of these quinone methides will range from subnanoseconds to as long as a few milliseconds. Two driving forces have been identified as being responsible for this kind of chemistry: (*i*) the tendency for twisted ground-state biaryls to twist to a more planar geometry in the excited state; and (*ii*) a large degree of charge transfer (to the other ring) inherent in the excited-state phenolate ion.

Experimental section

Instrumentation

^{1}H NMR spectra were recorded on a Bruker WM-250 (250 MHz), AMX (360 MHz), or AC-300 (300 MHz) instrument in $CDCl_3$ or $(CD_3)_2CO$, unless otherwise noted. IR spectra were recorded on a PerkinElmer 283 instrument. UV–vis spectra were measured on a Cary 5 instrument. Mass spectra were obtained on a Finnigan 3300 instrument (CI). High-resolution mass spectra (HR-MS) were obtained on a Kratos Concept H (EI) instrument. Melting points were determined on a Koefler hot stage microscope (uncorrected). Fluorescence spectra were obtained on a Photon Technology International (PTI) A-1010 fluorimeter. Fluorescence lifetimes were determined on a PTI LS-1 instrument in lifetime mode. Gas chromatography was performed on a Varian 3700 instrument with a Hewlett Packard 3390A integrator, with a column temperature of 100–250 °C (initial 100 °C, rate 10 °C/min, final 250 °C). Measurements of pH was carried out on a Corning pH meter 140. Preparative photolyses were carried out using a Rayonet RPR 100 photochemical reactor using 254 or 300 nm lamps. An Oriel 200 W Hg light source and an Applied Photophysis monochromator on an optical bench were employed in small scale photolysis and in product quantum yield determinations.

Common laboratory reagents

Dichloromethane (ACS reagent grade) was distilled before use. Anhydrous THF was obtained by distillation from potassium metal. Anhydrous diethyl ether and dimethyl acetamide were purchased from the Aldrich Chemical Co. and used as received. Other solvents (ACS reagent grade) used for synthetic purposes were used without further purification. Deuterated solvents, D_2O, $CDCl_3$, $(CD_3)_2CO$, CD_3CN, and DMSO-d_6, were purchased from the Cambridge Isotope Laboratory containing 99.9% D. Standard buffer solutions used for fluorescence and LFP studies were purchased from the Fisher Scientific Co. Solvents used for fluorescence studies, CH_3CN (HPLC grade), 95% CH_3CH_2OH, and C_6H_{12} (spectral grade), were checked for spurious emission before use. Anhydrous CH_3CN used for fluorescence studies was distilled over CaH_2 and used immediately. Preparative TLC was carried out on 20 cm × 20 cm silica gel GF Uniplates (Analtech).

Materials

The following compounds were purchased from Aldrich: naphthalene (recrystallized from 95% CH_3CH_2OH), 2-aminopyridine (99.9%, used as secondary standards for fluorescence quantum yield experiments), 2-naphthol (**35**) (recrystallized from 95% EtOH), BBr_3 (1 mol/L in CH_2Cl_2), 2-bromobenzoic acid, 3-bromoanisole, 4-bromoanisole, 2-bromotoluene (**15**), and 4-(4′-hydroxyphenyl)benzoic acid. Biphenyl **1** was synthesized according to a previous method (5*a*). Lactones **12** and **14** were synthesized from known procedures (6).

2′-Naphthyl-2-bromobenzoate

2-Bromobenzoic acid (20 g, 0.1 mol) was dissolved in a mixture of $SOCl_2$ (300 mL) and toluene (500 mL) and refluxed under N_2 for 3 h. The solvent and extra $SOCl_2$ were then removed under reduced pressure distillation to give the acid chloride. The residue was then redissolved in CH_2Cl_2 (500 mL). To this solution, a solution of 2-naphthol (14.4 g) and triethylamine (15 g) in 250 mL CH_2Cl_2 was added dropwise and stirred at room temperature (rt) for several hours. After reaction, the mixture was first washed with water, then dried over $MgSO_4$. The solvent was evaporated to give a brown solid. Pure 2′-naphthyl-2-bromobenzoate was obtained upon recrystallization from toluene (~80%); mp 79 to 80 °C. ^{1}H NMR (250 MHz, $(CD_3)_2CO$) δ: 7.45–7.66 (m, 5H), 7.78–7.88 (m, 2H), 7.90–8.00 (m, 2H), 8.02 (d, 1H, J = 8.8 Hz), 8.06–8.16 (m, 1H). MS (CI) *m*/*z* (relative intensity): 327/329 (M + 1) (14/13), 183/185 (M – $C_{10}H_8O$) (100/99).

5*H*-Dibenzo[*c*,*f*]chromen-5-one (13)

2′-Naphthyl-2-bromobenzoate (5.0 g, 15 mmol), sodium acetate (2.5 g, 30 mmol), triphenylphosphane (2.4 g, 9 mmol), and palladium(II) acetate (0.10 g, 0.45 mmol) were dissolved in dry *N*,*N*′-dimethyl acetamide (180 mL) and heated to 120–130 °C for 24 h. After cooling to rt, CH_2Cl_2 (720 mL) was added. This solution was washed with 10% HCl three times. The organic layer was dried over $MgSO_4$ then the solvent was removed using a rotary evaporator. A mixture of **13** and its β-isomer (3:1 mixture, total 1.5 g, 6 mmol, 40%) was obtained after chromatography (silica gel, CH_2Cl_2). This mixture was separated by slow recrystallization from hexanes (the two isomers separated from the mother liquor at different times). Pure **13** was obtained after an additional recrystallization procedure (final yield 25%); mp 160–162 °C. IR (KBr, cm^{-1}) ν: 3040 (w, C-H aromatic), 1710 (s, C=O), 1605, 1590 (m, C=C), 1500 (m), 1458 (m), 1300 (s), 1270 (s), 1210 (s), 1110 (s), 1065 (s), 805 (s), 780 (m), 740 (s). ^{1}H NMR (250 MHz, $(CD_3)_2CO$) δ: 7.50 (d, 1H, J = 7.9 Hz), 7.60 (ddd, 1H, J = 8, 8, 1 Hz), 7.73 (ddd, 2H, J = 8, 8, 1 Hz), 7.98–8.14 (m, 3H), 8.41 (dd, 1H, J = 8, 1 Hz), 8.75 (d, 1H, J = 8 Hz), 8.85 (d, 1H, J = 8 Hz). HR-MS (EI) calcd. for $C_{17}H_{10}O_2$: 246.0681; found: 246.0688. Chemical anal. calcd. for $C_{17}H_{10}O_2$ (%): C 82.91, H 4.09; found: C 82.80, H 4.08.

General procedure for $LiAlH_4$ reduction

A solution of the substrate in dry THF was added (under stirring, rt) dropwise into a round-bottomed flask charged with $LiAlH_4$ (excess) and a small amount of dry THF. After the addition was completed, the mixture was refluxed for

© 2005 NRC Canada

1 h. Then the mixture was cooled to rt and poured into a mixture of ice and 10% HCl. The corresponding biaryl methanol was obtained after standard extraction (Et_2O–CH_2Cl_2, 1:2), drying ($MgSO_4$), and evaporation (rotary evaporator) of the solvent. Pure product (**4**–**6**) was obtained after recrystallization from toluene (yield ≥90%).

2-[2′-(Hydroxymethyl)-1′-naphthyl]phenol (4)

According to the general procedure for $LiAlH_4$ reduction, 2.5 g of **12** gave 2.4 g of **4** (95%); mp 167 to 168 °C. ^{1}H NMR (360 MHz, CD_3CN) δ: 4.42 (s, 2H, CH_2), 6.99–7.11 (m, 3H), 7.30–7.42 (m, 3H), 7.47 (ddd, 1H, *J* = 7.4, 7.4, 1.5 Hz), 7.74 (d, 1H, *J* = 8.5 Hz), 7.91 (d, 1H, *J* = 8.1 Hz), 7.95 (d, 1H, *J* = 8.6 Hz); additional ^{1}H NMR peaks in $(CD_3)_2CO$: 4.20 (s, broad, 1H, exchangeable with D_2O, OH), 8.03 (s, broad, 1H, exchangeable with D_2O, ArOH). MS (CI) *m*/*z* (relative intensity): 233 (M – OH^-) (100). Chemical anal. calcd. for $C_{17}H_{14}O_2$ (%): C 81.58, H 5.64; found: C 81.54, H 5.54.

1-[2′-(Hydroxymethyl)phenyl]-2-naphthol (5)

According to the general procedure for $LiAlH_4$ reduction, 2.0 g of **13** gave 1.9 g of **5** (95%); mp 167 to 168 °C. ^{1}H NMR (360 MHz, CD_3CN) δ: 4.21 (AB quartet, 2H, *J* = 13.5 Hz, CH_2), 7.06–7.12 (m, 1H), 7.13–7.17 (dd, 1H, *J* = 9, 2 Hz), 7.22 (d, 1H, *J* = 8.8 Hz), 7.27–7.33 (m, 2H), 7.41 (ddd, 1H, *J* = 7.4, 7.4, 1.5 Hz), 7.49 (ddd, 1H, *J* = 7.4, 7.4, 1.5 Hz), 7.67 (d, 1H, *J* = 7.4 Hz), 7.80–7.86 (m, 2H); additional ^{1}H NMR peaks in $(CD_3)_2CO$: 4.10 (s, broad, 1H, exchangeable with D_2O, OH), 8.05 (s, broad, 1H, exchangeable with D_2O, ArOH). MS (CI) *m*/*z* (relative intensity): 233 (M – OH^-) (100). Chemical anal. calcd. for $C_{17}H_{14}O_2$ (%): C 81.58, H 5.64; found: C 81.50, H 5.56.

2-Hydroxy-2′-hydroxymethyl-1,1′-binaphthyl (6)

According to the general procedure for $LiAlH_4$ reduction, 3.0 g of **14** gave 2.8 g of **6** (95%); mp 172 to 173 °C. ^{1}H NMR (360 MHz, CD_3CN) δ: 4.30 (AB quartet, 2H, *J* = 13.3 Hz, CH_2), 6.82 (d, 1H, *J* = 8 Hz), 7.50 (d, 1H, *J* = 8 Hz), 7.19 (ddd, 1H, *J* = 7.6, 7.6, 1.4 Hz), 7.26 (ddd, 1H, *J* = 7.6, 7.6, 1.3 Hz), 7.30 (ddd, 1H, *J* = 7.6, 7.6, 1.3 Hz), 7.31 (d, 1H, *J* = 8.9 Hz), 7.46 (ddd, 1H, *J* = 7.6, 7.6, 1.3 Hz), 7.86 (d, 1H, *J* = 8.6 Hz), 7.90 (d, 1H, *J* ≈ 9 Hz), 7.94 (d, 1H, *J* = 9.0 Hz), 7.98 (d, 1H, *J* ≈ 9 Hz), 8.06 (d, 1H, *J* = 8.4 Hz); additional ^{1}H NMR peaks in $(CD_3)_2CO$: 4.10 (s, broad, 1H, exchangeable with D_2O, OH), 8.20 (s, broad, 1H, exchangeable with D_2O, ArOH). MS (CI) *m*/*z* (relative intensity): 283 (M – OH^-) (100). Chemical anal. calcd. for $C_{21}H_{16}O_2$ (%): C 83.98, H 5.37; found: C 83.54, H 5.24.

4-[4′-(Hydroxymethyl)phenyl]phenol (11)

According to the general procedure for $LiAlH_4$ reduction, 2.0 g of 4-(4′-hydroxyphenyl)benzoic acid (in 200 mL dry THF) gave 1.75 g (93%) of pure **11** after recrystallization from a mixture of toluene and hexanes; mp 205–208 °C. ^{1}H NMR (300 MHz, $(CD_3)_2CO$) δ: 4.18 (t, 1H, *J* = 5.5 Hz, exchangeable with D_2O, OH), 4.64 (d, 2H, *J* = 5.5 Hz, CH_2), 6.90–6.99 (m, 2H), 7.35–7.45 (m, 2H), 7.45–7.60 (m, 4H), 8.43 (s, 1H, exchangeable with D_2O, ArOH). MS (CI) *m*/*z* (relative intensity): 201 (M + 1) (61), 183 (M – OH) (100). Chemical anal. calcd. for $C_{13}H_{12}O_2$ (%): C 77.98, H 6.04; found: C 78.06, H 6.03.

2-Hydroxy-2′-methyl-1,1′-binaphthyl (32)

A sample of 10 mg chromene **21** (photocyclization product of **6**) was refluxed with $LiAlH_4$ in dry THF (ca. 10 mL) for 6 h. After reaction, the solution was then quenched with 5% HCl–ice and extracted with Et_2O (4 × 50 mL). The solvent was evaporated and the residue was purified on preparatory TLC (CH_2Cl_2). Recrystallization from toluene gave a white crystal, mp 163 to 164 °C. ^{1}H NMR (360 MHz, $(CD_3)_2CO$) δ: 2.14 (s, 3H, CH3), 6.85 (d, 1H, *J* ≈ 8 Hz), 7.13 (d, 1H, *J* ≈ 8 Hz), 7.16–7.31 (m, 3H), 7.35–7.43 (m, 2H), 7.55 (d, 1H, *J* = 8.5 Hz), 7.88–7.97 (m, 4H), 7.98 (s, 1H, exchangeable with D_2O, ArOH). ^{13}C NMR δ: 20.3 (CH_3), 119.2, 119.3, 123.7, 125.0, 125.7, 126.4, 126.7, 127.2, 128.6, 128.8, 129.0, 129.6, 129.8, 130.2, 132.4, 133.4, 134.3, 134.8, 136.6, 153.2. HR-MS (EI) calcd. for $C_{21}H_{16}O$: 284.1201; found: 284.1214.

4-(2′-Methylphenyl)anisole (17) and 3-(2′-methylphenyl)anisole

3-Bromoanisole (80 mmol) was dissolved in 100 mL of toluene followed by the addition of $Pd(PPh_3)_4$ (0.70 g). After all the catalyst was dissolved, a solution of boronic acid **16** (100 mmol in 200 mL of 95% ethanol) and a solution of K_2CO_3 (20 g in 100 mL of water) were subsequently added. The mixture was refluxed for 24 h, then worked up by addition of NaOH (10%, ca. 400 mL) followed by extraction into CH_2Cl_2 (3 × 400 mL). The organic layer was dried over $MgSO_4$ and the solvent evaporated to give the crude product as a colourless oil (~90%). This crude product was used directly in the next step without further purification. 3-(2′-Methylphenyl)anisole: ^{1}H NMR (90 MHz, $CDCl_3$) δ: 2.20 (s, 3H, CH_3), 3.79 (s, 3H, OCH_3), 6.85–7.05 (m, 3H), 7.05–7.30 (m, 5H). MS (CI) *m*/*z* (relative intensity): 199 (M + 1) (100). In a similar manner, use of 4-bromoanisole gave 4-(2′-methylphenyl)anisole (**17**): ^{1}H NMR (90 MHz, $CDCl_3$) δ: 2.20 (s, 3H, CH_3), 3.79 (s, 3H, OCH_3), 6.80–7.00 (m, 2H), 7.05–7.35 (m, 6H). MS (CI) *m*/*z* (relative intensity): 199 (M + 1) (100).

4-[2′-(Bromomethyl)phenyl]anisole

To a solution of 16 g of 4-(2′-methylphenyl) anisole **17** (80 mmol) in 250 mL CCl_4, a slurry of 14.2 g of NBS (80 mmol) in 100 mL CCl_4 was added. Then 0.3 g of benzoperoxide was added. The mixture was refluxed for 10 h then allowed to cool to rt and filtered. Upon washing with H_2O (3 × 100 mL), drying over $MgSO_4$, and evaporation of the solvent (rotary evaporator), 20 g (~90%) of crude product was obtained. ^{1}H NMR (90 MHz, $CDCl_3$) δ: 3.79 (s, 3H, OCH_3), 4.35 (s, 2H, CH_2), 6.75–7.05 (m, 2H), 7.05–7.65 (m, 6H). The crude product was used in the next step without further purification.

3-[2′-(Bromomethyl)phenyl]anisole

To a solution of 9.7 g of 3-(2′-methylphenyl) anisole (49 mmol) in 800 mL CCl_4, a slurry of 9.0 g of NBS (50 mmol) in 200 mL CCl_4 was added. Then 0.5 g of benzoperoxide was added. The mixture was refluxed for 30 h and allowed to cool to rt and filtered. Upon washing

© 2005 NRC Canada

with H_2O (3 × 100 mL), drying over $MgSO_4$, and evaporation of the solvent (rotary evaporator), 20 g (~90%) of crude product was obtained. ^{1}H NMR (300 MHz, $CDCl_3$) δ: 3.87 (s, 3H, OCH_3), 4.49 (s, 2H, CH_2), 6.85–7.10 (m, 3H), 7.20–7.45 (m, 4H), 7.50–7.59 (m, 1H). MS (CI) *m/z* (relative intensity): 277/279 (M + 1) (7/6), 197 (M – Br) (100). The crude product was used in the next step without further purification.

4-[2′-(Hydroxymethyl)phenyl]anisole (7) and 3-[2′-(hydroxymethyl)phenyl]anisole (9)

4-[2′-(Bromomethyl)phenyl]anisole (15 g) or 3-[2′-(bromomethyl)phenyl] anisole (15 g) was dissolved in 750 mL of acetone–H_2O (1:1, *v*/*v*) with 5.0 g of added $NaHCO_3$. The mixture was refluxed overnight. The solution was cooled to rt and extracted with CH_2Cl_2 (twice) then with diethyl ether (once). The extract was combined and dried over $MgSO_4$. Upon evaporation of the solvent, 11 g (90%) of crude product was obtained. Pure product was obtained after recrystallization from toluene–hexanes. 4-[2′-(Hydroxymethyl)phenyl]anisole (**7**): mp 77 to 78 °C. ^{1}H NMR (360 MHz, $(CD_3)_2CO$) δ: 4.17 (t, 1H, *J* = 5.5 Hz, exchangeable with D_2O, OH), 4.55 (d, 2H, *J* = 5.5 Hz, CH_2), 6.96–7.01 (m, 2H), 7.18–7.23 (m, 1H), 7.26–7.37 (m, 4H), 7.58–7.63 (m, 1H). MS (CI) *m/z* (relative intensity): 215 (M + 1) (23), 197 (M – OH) (100). Chemical anal. calcd. for $C_{14}H_{14}O_2$ (%): C 78.48, H 6.59; found: C 78.56, H 6.59. 3-[2′-(Hydroxymethyl)phenyl]anisole (**9**): mp 63 to 64 °C. ^{1}H NMR (300 MHz, $(CD_3)_2CO$) δ: 3.80 (s, 1H, OCH_3), 4.25 (t, 1H, *J* = 5.5 Hz, exchangeable with D_2O, OH), 4.65 (d, 2H, *J* = 5.5 Hz, CH_2), 6.85–7.00 (m, 3H), 7.15–7.45 (m, 4H), 7.55–7.66 (d, 1H, *J* = 8Hz). MS (CI) *m/z* (relative intensity): 197 (M – OH) (100). Chemical anal. calcd. for $C_{14}H_{14}O_2$ (%): C 78.48, H 6.59; found: C 78.31, H 6.46.

4-[2′-(Hydroxymethyl)phenyl]phenol (8) and 3-[2′-(hydroxymethyl)phenyl] phenol (10)

A solution of 10 g (36 mmol) 4-[2′-(hydroxymethyl)phenyl]anisole (**7**) or 3-[2′-(hydroxymethyl)phenyl]anisole (**9**) in 750 mL CH_2Cl_2 was added dropwise into a solution of BBr_3 (0.1 mol/L in CH_2Cl_2, 180 mL) at rt over 1 h. The solution was stirred for an additional 4 h. The reaction was quenched by addition of ca. 200 mL of water. The water layer was extracted with diethyl ether (3 × 150 mL). The combined organic extract was dried over $MgSO_4$ and the solvent evaporated to give an oily residue. This residue was dissolved in ca. 500 mL of acetone–H_2O (1:1, *v*/*v*) and refluxed overnight. The solution was cooled to rt and extracted with CH_2Cl_2 (twice) then with diethyl ether (once). The extract was combined and dried over $MgSO_4$. The crude product was obtained upon evaporation of the solvent. Pure product (6.0 g, 80%) was obtained after recrystallization from toluene. 4-[2′-(Hydroxymethyl)phenyl]phenol (**8**): mp 121 to 122 °C. ^{1}H NMR (300 MHz, $(CD_3)_2CO$) δ: 4.10 (t, 1H, *J* = 5.5 Hz, exchangeable with D_2O, OH), 4.55 (d, 2H, *J* = 5.5 Hz, CH_2), 6.83–6.93 (m, 2H), 7.12–7.35 (m, 5H), 7.53–7.62 (m, 1H), 8.45 (s, 1H, exchangeable with D_2O, ArOH). MS (CI) *m/z* (relative intensity): 183 (M – OH) (100). Chemical anal. calcd. for $C_{13}H_{12}O_2$ (%): C 77.98, H 6.04; found: C 78.03, H 6.15. 3-[2′-(Hydroxymethyl)phenyl]phenol (**10**): mp 96 to 97 °C. ^{1}H NMR (300 MHz, $(CD_3)_2CO$) δ: 4.10 (t, 1H, *J* = 5.5 Hz, exchangeable with D_2O, OH), 4.55 (d, 2H, *J* = 5.5 Hz, CH_2), 6.80–6.90 (m, 3H), 7.10–7.40 (m, 4H), 7.60 (d, 1H, *J* = 8 Hz), 8.40 (s, 1H, exchangeable with D_2O, ArOH). MS (CI) *m/z* (relative intensity): 183 (M – OH) (100). Chemical anal. calcd. for $C_{13}H_{12}O_2$ (%): C 77.98, H 6.04; found: C 78.19, H 6.02.

2-(2′-Methyl-1′-naphthyl)phenol (23) and 2-(2′-methylphenyl)phenol (30)

The corresponding biaryl alcohol (**4** or **1**, 50–100 mg) was photolyzed (254 nm) in 100 mL of 2-propanol in the presence of excess (~0.5 g) $NaBH_4$ for 2 h. Then 10% HCl (50–100 mL) was added, and the mixture was extracted with Et_2O–CH_2Cl_2 (1:2, 3 × 80 mL). Pure **23** or **30** were isolated by preparative TLC (CH_2Cl_2–hexanes, second component) as a colourless oil. 2-(2′-Methyl-1′-naphthyl)phenol (**23**): ^{1}H NMR (300 MHz, CD_3CN) δ: 2.18 (s, 3H, CH_3), 6.6 (s, 1H, exchangeable with D_2O, ArOH), 6.95–7.09 (m, 3H), 7.25–7.52 (m, 5H), 7.77–7.90 (m, 2H). MS (CI) *m/z* (relative intensity): 235 (M + 1) (100). 2-(2′-Methylphenyl)phenol (**30**): ^{1}H NMR (360 MHz, $(CD_3)_2CO$) δ: 2.16 (s, 3H, CH_3), 6.89 (ddd, 1H, *J* = 7.4, 7.4, 1.2 Hz), 6.95 (dd, 1H, *J* = 8.0, 1.2 Hz), 7.05 (dd, 1H, *J* = 7.4, 1.7 Hz), 7.11–7.25 (m, 5H), 8.15 (s, 1H, exchangeable with D_2O, ArOH). ^{13}C NMR δ: 20.1, 116.4, 120.3, 126.3, 128.0, 129.3, 129.8, 130.4, 130.9, 131.6, 137.6, 139.6, 155.1. HR-MS (EI) calcd. for $C_{13}H_{12}O$: 184.0888; found: 184.0893.

General procedure for the synthesis of 31, 33, and 34

A solution of the biaryl alcohol **5**, **7**, or **10** (1 equiv.) in CH_2Cl_2 (70 mL per 10 mmol) was added dropwise into a solution of BBr_3 (1.5 equiv., 0.15 mol/L in CH_2Cl_2) at rt over 1 h. The solution was stirred at rt for another 4 h. The reaction was then quenched by the addition of water. The water layer was extracted with diethyl ether (3 × 150 mL). The combined organic extract was dried over $MgSO_4$ and the solvent evaporated on the rotary evaporator to give an oily residue. This residue was dissolved in dry THF and the solution was added (under stirring, rt) dropwise into a round-bottomed flask charged with $LiAlH_4$ (excess) and a small amount of dry THF. After the addition was completed, the mixture was refluxed for 1 h. Then the mixture was cooled to rt and poured into a mixture of ice and 10% HCl. The corresponding biaryl methanol (crude product) was obtained after extraction (Et_2O–CH_2Cl_2, 1:2), drying ($MgSO_4$), and evaporation (rotary evaporator) of the solvent.

1-(2′-Methylphenyl)-2-naphthol (31)

5 (10 mg) was converted to **31** using the preceding general procedure. Pure **31** (8 mg) was obtained as a white solid after purification by preparatory TLC (CH_2Cl_2–hexanes, 1:1), mp 91 to 92 °C. ^{1}H NMR (300 MHz, $(CD_3)_2CO$) δ: 1.99 (s, 3H, CH_3), 7.10–7.20 (m, 2H), 7.25–7.40 (m, 6H), 7.80–7.87 (m, 2H), 7.95 (s, 1H, exchangeable with D_2O, ArOH). MS (CI) *m/z* (relative intensity): 235 (M + 1) (100).

4-(2′-Methylphenyl)phenol (33)

According to the preceding general procedure, 1.07 g of **7** gave 0.85 g (90%) of pure **33** as a white solid after recrystallization from toluene, mp 76 to 77 °C. ^{1}H NMR (360 MHz, DMSO-D_6) δ: 2.21 (s, 3H, CH_3), 6.78–6.84 (m,

© 2005 NRC Canada

2H), 7.09–7.15 (m, 2H), 7.11–7.16 (m, 1H), 7.16–7.22 (m, 2H), 7.22–7.26 (m, 1H), 9.55 (s, 1H, exchangeable with D_2O, ArOH). MS (CI) *m*/*z* (relative intensity): 185 (M + 1) (100).

3-(2′-Methylphenyl)phenol (34)

According to the preceding general procedure, 0.20 g of **10** gave 0.17 g (90%) of pure **34** as a colourless oil. ^{1}H NMR (360 MHz, $(CD_3)_2CO$) δ: 2.24 (s, 3H, CH_3), 6.74–6.87 (m, 3H), 7.14–7.30 (m, 5H), 8.20 (s, 1H, exchangeable with D_2O, ArOH). MS (CI) *m*/*z* (relative intensity): 185 (M + 1) (100).

General photolysis procedure

Preparative scale photolysis was carried out in a Rayonet RPR 100 photochemical reactor using 254 or 300 nm lamps. The reaction mixture was contained in a 100 or 200 mL quartz tube, which was cooled to ≈15 °C using a cold finger (tap water) and purged continuously during photolysis with a stream of argon via a stainless steel syringe needle. Microscale photolysis was carried out in a 3 mL quartz cuvette or in an NMR tube, and irradiated either in a Rayonet RPR 100 photochemical reactor (254 or 300 nm) or on an optical bench (280 nm) equipped with an Oriel 200 W Hg lamp and an Applied Photophysics monochromator. Solutions were purged with a stream of argon via a stainless steel syringe needle for 5 min and sealed before photolysis.

General workup procedure for photolysis in aqueous solution

After photolysis, satd. NaCl solution was added and the mixture was extracted three to five times with either CH_2Cl_2 or Et_2O. The combined organic extract was then dried over $MgSO_4$ and the solvent evaporated on the rotary evaporator.

Photolysis of 2-[2′-(hydroxymethyl)phenyl]phenol (1) in CH_3CN

A solution of **1** (50 mg) in CH_3CN (80 mL) was photolyzed (254 nm) in a quartz tube for 30 min using the general procedure. The solvent was then removed by rotary evaporation. The residue (80% conversion to chromene **3** by ^{1}H NMR) was chromatographed on preparative TLC (silica, hexanes–CH_2Cl_2, 2:1). The first band was collected to give pure 6*H*-benzo[*c*]chromene (**3**) as a colourless oil. ^{1}H NMR (300 MHz, CD_3CN) δ: 5.12 (s, 2H, CH_2), 6.96 (dd, 1H, *J* = 8, 1 Hz), 7.06 (ddd, 1H, *J* = 8, 8, 1 Hz), 7.18–7.44 (m, 4H), 7.76 (d, 1H, *J* = 8 Hz), 7.80 (dd, 1H, *J* = 8, 1 Hz). MS (CI) *m*/*z* (relative intensity): 183 (M + 1) (100).

Photolysis of 2-[2′-(hydroxymethyl)-1′-naphthyl]phenol (4) in aprotic solvent (100% CH_3CN or THF)

A solution of **4** (50 mg) in 100 mL of solvent was photolyzed (254 nm) in a quartz tube for 45 min using the general procedure. The solvent was then removed by rotary evaporation. The residue (>95% conversion to chromene **19** by ^{1}H NMR) was chromatographed on preparative TLC (silica, hexanes–CH_2Cl_2, 2:1). The first band was collected to give pure 6*H*-naphtho[2,1-*c*]chromene (**19**) as a colourless crystal after recrfystallization from CH_3CN; mp 96 to 97 °C (lit. value (16) mp 101 °C). ^{1}H NMR (360 MHz, $(CD_3)_2CO$) δ: 5.13 (s, 2H, CH_2), 7.12–7.23 (m, 2H), 7.33 (ddd, 1H, *J* = 7.9, 7.9, 1.5 Hz), 7.42 (d, 1H, *J* = 8.3 Hz), 7.52 (ddd, 1H, *J* = 7.4, 7.4, 1.4 Hz), 7.58 (ddd, 1H, *J* = 7.6, 7.6, 1.6 Hz), 7.87 (d, 1H, *J* = 8.2 Hz), 7.94–7.98 (m, 1H), 8.05–8.09 (m, 1H), 8.56–8.61 (m, 1H). HR-MS (EI) calcd. for $C_{17}H_{12}O$: 232.0888; found: 232.0892.

For analytical runs (in CH_3CN), the preceding solution was sampled at set irradiation times and injected into the GC to determine the conversion. The GC retention times (t_r) were 12.8 min for **19** and 13.1 min for **4**.

Photolysis of 2-[2′-(hydroxymethyl)-1′-naphthyl]phenol (4) in H_2O–H_3CN (1:1)

A solutionof **4** (50 mg) in 100 mL of solvent was photolyzed (254 nm) in a quartz tube for 45 min using the general procedure. After photolysis, the solution was worked using the general procedure (CH_2Cl_2–Et_2O (2:1), 3 × 150 mL). GC and ^{1}H NMR showed that this sample contained ca. 60% of **19** and ca. 40% of **4**. No side products were detectable. Analytical runs were carried out as described previously, using GC analysis.

Photolysis of 2-[2′-(hydroxymethyl)-1′-naphthyl]phenol (4) in 100% CH_3OH

A solution of **4** (50 mg) in CH_3OH (100 mL) was photolyzed (254 nm) in a quartz tube for 5–45 min using the general procedure. The solvent was then removed by rotary evaporation. The residue (maximum yield, 75% of methyl ether **22** and 25% chromene **19** by ^{1}H NMR) was chromatographed on preparative TLC (silica, CH_2Cl_2). The second band was collected to give pure **22** as a colourless oil. ^{1}H NMR (300 MHz, $(CD_3)_2CO$) δ: 3.24 (s, 3H, OCH_3), 4.35 (AB quartet, 2H, *J* = 12.5 Hz, CH_2), 6.95–7.15 (m, 3H), 7.30–7.55 (m, 4H), 6.69 (d, 1H, *J* = 8.4 Hz), 7.87–7.96 (m, 2H), 8.20 (s, 1H, exchangeable with D_2O, ArOH).

Photolysis of 6H-naphtho[2,1-c]chromene (19) in 100% CH_3CN or THF

A solution of 20 mg of **19** in 60 mL of CH_3CN (or THF) was photolyzed (254 nm) in a quartz tube for 30 min using the general procedure. The solvent was then removed by rotary evaporation. ^{1}H NMR of the residue was identical to that of the starting material **19**.

Photolysis of 6H-naphtho[2,1-c]chromene (19) in H_2O–CH_3CN (1:1)

A solution of 20 mg of **19** in 60 mL of H_2O–CH_3CN (1:1) was photolyzed (254 nm) in a quartz tube for 30 min using the general procedure then worked up using the general procedure (CH_2Cl_2, 3 × 100 mL). The residue contained 60% of **19** and 40% of **4** as determined by ^{1}H NMR.

Photolysis of 6H-naphtho[2,1-c]chromene (19) in H_2O–CH_3OH (1:1)

According to the general procedure for microscale photolysis, a solution (3.0 mL, 2.14×10^{-4} mol/L) of **19** in H_2O–CH_3OH (1:1) was photolyzed in the Rayonet (254 nm) in 30 s intervals. Between each irradiation period, the UV spectrum of the solution was taken. When the UV spectrum of the solution remained unchanged (after a total of five irradiations), the composition of this solution was determined by UV photospectrophotometry by the absorbance of the so-

© 2005 NRC Canada

lution at 337 nm (for **19**, $\varepsilon_{337} = 1.04 \times 10^4$, $\varepsilon_{283} = 3.57 \times 10^3$) and the absorbance increases at 283 nm (for **22** and **4**, $\varepsilon_{283} = 9.23 \times 10^3$), as 8% of **19** and 92% of the ring-opening product **22** + **4**. The solutions for several runs were collected and extracted with CH_2Cl_2 (5 × 5 mL). The combined extracts were dried over $MgSO_4$ and evaporated. ^{1}H NMR of the residue showed that alcohol **4** and methyl ether **22** were formed in a 1:3 ratio, corresponding to a photostationary ratio of 8:23:69 of **19**:**4**:**22**.

Photolysis of 6H-naphtho[2,1-c]chromene (19) in 100% CH_3OH

According to the general procedure for microscale photolysis, a solution (3.0 mL, 1.25×10^{-4} mol/L) of **19** in CH_3OH was photolyzed in the Rayonet (254 nm) in 15 s intervals. Between each irradiation, the UV spectrum of the solution was taken. After 10 irradiations, the UV spectrum remained unchanged. The composition of this solution contained 24% of **19** and 76% of the ring-opening product **22** as determined by the method described previously using UV spectrophotometry. In another attempt, ca. 3 mg of **19** was dissolved in 3 mL of CH_3OH and photolyzed for 5 min. After the photolysis, the solvent was evaporated. ^{1}H NMR of the residue indicated that methyl ether **22** (50%) was the only product.

Photolysis of 1-[2′-(hydroxymethyl)phenyl]-2-naphthol (5) in H_2O–CH_3CN (1:1)

A solution of **5** (50 mg) in 100 mL H_2O–CH_3CN (1:1) was photolyzed (254 nm) in a quartz tube for 90 min and then worked up (CH_2Cl_2–Et_2O (2:1), 3 × 150 mL) using the general procedure. The ^{1}H NMR of the residue showed that 5*H*-dibenzo[*c*, *f*]chromene (**20**) was obtained in 60% yield (with 40% starting material left). Prolonged photolysis (>10 h) could raise the conversion to ca. 90% with decomposition of the product (ca. 10%). Pure **20** was isolated as a white solid by preparative TLC (silica gel, CH_2Cl_2–hexanes (1:1), first band collected). This solid was recrystallized from CH_3CN, mp 55 to 56 °C. ^{1}H NMR (300 MHz, $(CD_3)_2CO$) δ: 5.09 (s, 2H, CH_2), 7.25 (d, 1H, *J* = 8 Hz), 7.35–7.54 (m, 4H), 7.59 (dd, 1H, *J* = 8, 8 Hz), 7.85 (d, 1H, *J* = 9 Hz), 7.93 (d, 1H, *J* = 8 Hz), 8.03 (d, 1H, *J* = 8 Hz), 8.55 (d, 1H, *J* = 9 Hz). HR-MS (EI) calcd. for $C_{17}H_{12}O$: 232.0888; found: 232.0893. Chemical anal. calcd. for $C_{17}H_{12}O$ (%): C 87.91, H 5.21; found: C 87.58, H 5.16.

Analytical runs were carried out in a 3 mL quartz cuvette using the general procedure for microscale photolysis, and the yield of **20** was determined by the absorbance increases of the solution at 350 nm ($\varepsilon_{350} = 7.952$).

Photolysis of 1-[2′-(hydroxymethyl)phenyl]-2-naphthol (5) in 100% CH_3CN or THF

Using the general procedure for microscale photolysis, 3 to approximately 4 mg of **5** was dissolved in 3 mL of solvent and photolyzed in the Rayonet reactor for 10–15 min. After photolysis, the solvent was evaporated. ^{1}H NMR of the residue indicated that **20** was obtained in 10%–20% yield. Due to the low efficiency of this reaction, the conversion was kept low in these experiments to avoid significant decomposition of the reactants.

Photolysis of 1-[2′-(hydroxymethyl)phenyl]-2-naphthol (5) in 100% CH_3OH

Using the general procedure, a sample of ca. 3 mg of **5** in 3 mL of CH_3OH was irradiated in the Rayonet reactor for 15 min then solvent was evaporated. The ^{1}H NMR (300 MHz, $CDCl_3$) of the residue showed a singlet at δ 5.07 corresponding to the formation of **20** (10%). In addition, there was a weak, but sharp, singlet at δ 3.23 (OCH_3) and an AB quartet centred at 4.12 ppm ($J \approx -11$ Hz, CH_2), suggesting the formation of traces of the corresponding methyl ether product (<1%).

Photolysis of 5H-dibenzo[c,f]chromene (20) in H_2O–CH_3OH (1:1)

Using the general procedure for microscale photolysis, a sample of ~2 mg of **20** was dissolved in 3 mL of H_2O–CH_3OH (1:1) and photolyzed in the Rayonet reactor for 30 min and then worked up according to the general procedure. The ^{1}H NMR (300 MHz, $CDCl_3$) of the residue showed that the methyl ether product was obtained in ≈1% yield.

Photolysis of 2-hydroxy-2′-hydroxymethyl-1,1′-binaphthyl (6) in H_2O–CH_3CN (1:1), 100% CH_3CN, or 100% THF

A solution of **6** (50 mg) in 100 mL of solvent was photolyzed (254 nm) in a quartz tube for 30 min, then worked up (CH_2Cl_2–Et_2O (2:1), 3 × 150 mL) using the general procedure (aqueous) or solvent evaporated rotary (nonaqueous). The residue (contained ~90% of **21** by ^{1}H NMR) was chromatographed on preparative TLC (silica, hexanes–CH_2Cl_2, 2:1). The first band was collected to give a white solid, which was recrystallized from CH_3CN to give pure 4*H*-benzo[*f*]naphtho[2,1-*c*]chromene (**21**), mp 176–178 °C. ^{1}H NMR (360 MHz, $(CD_3)_2CO$) δ: 4.99 (d, 1H, *J* = –12.9 Hz, CH_2), 5.36 (d, 1H, *J* = –12.9 Hz, CH_2), 7.30–7.46 (m, 4H), 7.51 (ddd, 1H, *J* = 7.5, 7.5, 1.2 Hz), 7.60–7.67 (m, 3H), 7.93–8.03 (m, 4H). HR-MS (EI) calcd. for $C_{21}H_{14}O$: 282.1045; found: 282.1032. Chemical anal. calcd. for $C_{21}H_{14}O$ (%): C 89.34, H 5.00; found: C 88.97, H 4.84. When photolyzed in neat THF or CH_3CN using the preceding procedure, the reaction also gave the same product, but the efficiency is significantly lower (by ca. 30%–50%).

For analytical runs, two methods were used: (*i*) a solution of **6** was photolyzed in a quartz cuvette, and the formation of **21** was followed by UV spectrophotometry (absorbance at 360 nm, $\varepsilon = 1.04 \times 10^4$ $(mol/L)^{-1}$ cm^{-1}); (*ii*) ~5 mg of **6** was dissolved in 0.4 mL of CD_3CN and purged with Ar for 10 min then sealed in an NMR tube. This sample was irradiated in the Rayonet reactor (in the NMR tube, $\lambda_{ex} = 300$ nm) for a series of set times and the conversions were determined by ^{1}H NMR.

Photolysis of 2-hydroxy-2′-hydroxymethyl-1,1′-binaphthyl (6) in H_2O–CH_3OH (1:1) and 100% CH_3OH

A sample of **6** (20 mg) in 100 mL solvent was photolyzed in the Rayonet reactor for 20 min, then worked up using the method previously described. ^{1}H NMR of the residue showed ca. 15% yield of the methyl ether product and ca. 85% of **21**. The formation of the corresponding methyl ether product was inferred from the observation of the following three sets of characteristic ^{1}H NMR (300 MHz, $(CD_3)_2CO$) peaks δ: 3.19 (s, 3H, OCH_3), 4.23 (AB quartet, 2H, *J* = –13 Hz,

© 2005 NRC Canada

CH_2), and 6.88 (d, 1H, J = 8 Hz). No attempt was made to isolate this product.

Photolysis of 4H-benzo[f]naphtho[2,1-c]chromene (21) in CH_3CN–H_2O (1:1)

A solution of **21** (1.0×10^{-4} mol/L, in H_2O–CH_3CN (1:1)) was placed in a cuvette (3.0 mL) and irradiated at 254 or 300 nm. No changes were detectable by UV–vis spectrophotometry even on prolonged irradiation, indicating the lack of any conversion to the ring-opened product **6**. When this solution was photolyzed on the optical bench using 370 nm, the 360 nm band decreased and a new band at 280 nm grew in, suggesting the formation of **6**.

Photolysis of 4H-benzo[f]naphtho[2,1-c]chromene (21) in CH_3OH–H_2O (1:1)

A solution of **21** (1.0×10^{-4} mol/L in H_2O–CH_3OH (1:1), saturated) was placed in a cuvette (3.0 mL) and irradiated at 254 nm. As the photolysis proceeded, the 360 nm band decreased and a band at 280 nm grew in, suggesting the formation of **6** and (or) the methyl ether substitution product. The spectrum stopped changing at a state corresponding to 20% of chromene **21** and 80% ring-opened products (**6** + the methyl ether product).

Photolysis of 4H-benzo[f]naphtho[2,1-c]chromene (21) in 100% CH_3OH

A solution of **21** (ca. 5 mg in 3 mL CH_3OH) was photolyzed (254 nm) in a quartz cuvette for 5 min, then the solvent was removed by bubbling through the solution with a stream of air. The cuvette was then placed in a round-bottomed flask and left under vacuum for 1 h. ^{1}H NMR of the residue showed that the methyl ether substitution product was obtained in about 30% yield.

Photolysis of 4-[2′-(hydroxymethyl)phenyl]anisole (7) in CH_3OH–H_2O (1:1)

A solution of **7** (90 mg) in CH_3OH–H_2O (1:1, 100 mL) was photolyzed (254 nm) in a quartz tube for 10 min, then worked up (CH_2Cl_2, 3 × 150 mL) using the general procedure. The ^{1}H NMR of the residue showed two products, 4-[2′-(methoxymethyl)phenyl]anisole (**24**) (23%) and 4-(2′-methylphenyl)anisole (~3%). The residue was chromatographed on preparative TLC (silica, hexanes–CH_2Cl_2, 1:1) to give pure **24** as a colourless oil (second band collected). ^{1}H NMR (250 MHz, $(CD_3)_2CO$) δ: 3.28 (s, 3H, $ROCH_3$), 3.82 (s, 3H, $ArOCH_3$), 4.31 (s, 2H, CH_2), 6.95–7.03 (m, 2H), 7.18–7.39 (m, 5H), 7.47–7.53 (m, 1H).

Photolysis of 4-[2′-(hydroxymethyl)phenyl]anisole (7) in different pH

A solution of **7** (1.50 mL, 10 mg in 4.6 mL of CH_3OH) was added to each of the cuvettes charged with either 1.50 mL of H_2O or 0.05 mol/L H_2SO_4, respectively. These samples were irradiated in the Rayonet (254 nm) for 12 min and worked up according to the general procedure. The yields of methyl ether **24** at different pH is in the ratio of 1:1.1:1.2 (pH 7 : pH 1 : H_o = +0.04) as determined by ^{1}H NMR, indicating that the quantum yield increased slightly at low pH.

Photolysis of 4-[2′-(hydroxymethyl)phenyl]phenol (8) in H_2O–CH_3OH (1:1)

A solution of **8** (30 mg) in CH_3OH–H_2O (1:1, 60 mL) was irradiated in a quartz tube for 10 min, then worked up (CH_2Cl_2, 3 × 150 mL) using the general procedure. The ^{1}H NMR of the residue showed 60% yield of 4-[2′-(methoxymethyl)phenyl]phenol (**25**), which was isolated on preparative TLC (silica, CH_2Cl_2) as a colourless oil. ^{1}H NMR (250 MHz, $(CD_3)_2CO$) δ: 3.28 (s, 3H, OCH_3), 4.31 (s, 2H, CH_2), 6.87–6.95 (m, 2H), 7.15–7.35 (m, 5H), 7.45–7.51 (m, 1H), 8.60 (s, broad, exchangeable with D_2O, 1H, ArOH).

Photolysis of 4-[2′-(hydroxymethyl)phenyl]phenol (8) in the presence of ethyl vinyl ether

A solution of **8** (30 mg) in CH_3CN–H_2O (2:1, 100 mL) with 3.5 mL of ethyl vinyl ether added was irradiated in a quartz tube for 15 min according to the general procedure. After photolysis, the solution was worked up (CH_2Cl_2, 3 × 150 mL) using the preceding procedure. ^{1}H NMR showed that there was one major product, 3-[2′-(4″-hydroxyphenyl)phenyl]propanal (**26**), which was purified on preparative TLC (silica, CH_2Cl_2). ^{1}H NMR (300 MHz, $(CD_3)_2CO$) δ: 2.55–2.61 (m, 2H, CH_2), 2.88–2.94 (m, 2H, CH_2), 6.87–6.93 (m, 2H), 7.11–7.17 (m, 3H), 7.18–7.28 (m, 2H), 7.28–7.33 (m, 1H), 8.50 (s, 1H, exchangeable with D_2O, ArOH), 9.64 (t, 1H, J = 1.4 Hz, RCHO).

Photolysis of 4-[2′-(hydroxymethyl)phenyl]phenol (8) at different pH

A solution of **8** (1.50 mL, 9 mg in 4.6 mL of CH_3OH) was added to each of the cuvettes charged with either 1.50 mL of H_2O or 0.05 mol/L H_2SO_4, respectively. These samples were irradiated on the optical bench (280 nm) for 4.0 min, then worked up using the general procedure. The residues of all three samples contained (15 ± 1)% of **25** as determined by ^{1}H NMR, suggesting no pH dependence in this region.

Photolysis of 3-[2′-(hydroxymethyl)phenyl]phenol (10) in CH_3CN–H_2O (1:1)

A solution of **10** (50 mg) in CH_3CN–H_2O (1:1, 100 mL) was photolyzed (254 nm) in a quartz tube for 15 min, then worked up (CH_2Cl_2, 3 × 150 mL) using the general procedure. The ^{1}H NMR of the residue showed ~100% conversion to 3-hydroxyfluorene (**27**) and 1-hydroxyfluorene (**28**) in a ca. 10:1 ratio. The residue was chromatographed on preparative TLC to give a white solid (mixture of **27** and **28**). Recrystallization from toluene–hexanes gave pure **27**, mp 138 to 139 °C. ^{1}H NMR (360 MHz, $(CD_3)_2CO$) δ: 3.78 (s, 2H, CH_2), 6.80 (dd, 1H, J = 8.1, 2.4 Hz), 7.27 (ddd, 1H, J = 7.4, 7.4, 1.3 Hz), 7.30 (d, 1H, J = 2.4 Hz), 7.31–7.39 (m, 2H), 7.50–7.55 (m, 1H), 7.74–7.78 (m, 1H), 8.34 (s, 1H, exchangeable with D_2O, ArOH). MS (CI) m/z (relative intensity): 183 (M + 1) (100). Pure **28** was not isolated. ^{1}H NMR of **28** has CH_2 at δ 3.82 (s).

Photolysis of 3-[2′-(hydroxymethyl)phenyl]phenol (10) in CH_3OH–H_2O (1:1)

A solution of **10** (50 mg) in CH_3OH–H_2O (1:1, 100 mL) was photolyzed (254 nm) in a quartz tube for 15 min, then worked up (CH_2Cl_2, 3 × 150 mL) using the general procedure. The ^{1}H NMR of the residue showed two peaks at

© 2005 NRC Canada

δ 3.27 (OCH_3) and 4.32 ($ArCH_2OR$) with integrations in a 3:2 ratio, in addition to those corresponding to **27** and **28** (≥90%), suggesting the formation (5%–10%) of methyl ether **29**.

Photolysis of 4-[4′-(hydroxymethyl)phenyl]phenol (11) in CH_3OH–H_2O (1:1)

A solution of **11** (40 mg) in CH_3OH–H_2O (1:1, 100 mL) was photolyzed (254 nm) in a quartz tube for 8 min using the general procedure. The solution was then worked up (CH_2Cl_2, 3 × 150 mL) using the general procedure. The residue contained 16% of 4-[4′-(methoxymethyl)phenyl]phenol). Pure 4-[4′-(methoxymethyl)phenyl]phenol was isolated by preparative TLC (silica, hexanes–CH_2Cl_2 (1:1), first band collected) as a colourless oil. ^{1}H NMR (250 MHz, $(CD_3)_2CO$) δ: 3.33 (s, 3H, OCH_3), 4.43 (s, 2H, CH_2), 6.87–6.95 (m, 2H), 7.31–7.40 (m, 2H), 7.40–7.58 (m, 4H), 8.45 (s, 1H, exchangeable with D_2O, ArOH).

Laser flash photolysis

Experiments were carried out at the University of Victoria LFP Facility at 20 ± 2 °C. A Spectra-Physics GCR 12 YAG laser at 266 nm (<30 mJ) was used for excitation and signals were digitized with a Tektronix TDS 520 recorder. Samples of OD ≈ 0.3 at 266 nm were prepared and irradiated in quartz cells. Generally, flow solutions were used to avoid the accumulation of any photoproduct. Samples were continuously purged with a stream of N_2 or O_2.

Fluorescence lifetime measurements

All fluorescence lifetimes were measured on a PTI LS-1 instrument using the time-correlated single photon counting (SPC) technique (typically, using 10 000 counts). Samples were saturated with Ar and the absorbance at the excitation wavelength was adjusted to ~0.1. The lifetime was extracted from the SPC decay trace using the iterative reconvolution program that came with the instrument.

Steady-state fluorescence and fluorescence quantum yield measurements

All fluorescence spectra were recorded on a PTI A-1010 fluorimeter at rt. Samples were degassed by purging with argon gas prior to measurement. The concentrations of all samples were kept at $\leq 10^{-4}$ mol/L (OD ≈ 0.05). In determining the absolute fluorescence quantum yields, two secondary standards, naphthalene (in C_6H_{12}) and 2-aminopyridine (in 0.1 N H_2SO_4), were used.

Photocyclization quantum yields for 1, 4–6, and 10 in CH_3CN–H_2O (1:1)

The quantum yield for the chromene (or hydroxyfluorene) product formation was determined using UV spectrophotometry. Generally, a quartz cuvette containing 3.00 mL solution of the biaryl alcohol substrate was purged with Ar for ~5 min. and then irradiated for a set time (1~10 min) on the optical bench (λ_{ex} = 280 nm, slit 10 nm). The change of absorbance of the solution before and after irradiation (ΔA_λ) at the monitoring wavelength ($\lambda_{mon.}$) was measured. The quantum yield (Φ) was then calculated using the following equation:

$$\Phi = 3.00 \times 10^{-3} \times \Delta A/(\varepsilon_\lambda \times I \times \Delta t)$$

where ε_λ is the extinction coefficient of the product at $\lambda_{mon.}$, I is the light intensity determined using potassium ferrioxalate actinometry (10), and t is the time of irradiation. The initial concentration of the substrate was adjusted such that at 1% conversion, $\Delta A > 0.3$ and the absorbance of the solution at 280 nm >> 2 (typically, $>10^{-4}$ mol/L). The conversion was kept at ca. 1% for all runs. Finally, the sample was irradiated for a longer time to enhance the conversion to ~15% and the conversion rechecked by ^{1}H NMR. The results from ^{1}H NMR were consistent with that measured by UV spectrophotometry. The quantum yields of other solvents were measured relative to that obtained in CH_3CN–H_2O (1:1) using this method. The ε_λ at $\lambda_{mon.}$ are essentially independent of the solvents being studied. The λ_{max} and ε_λ data for all chromene products are summarized in Table 2.

General procedure for determination of photosolvolysis quantum yields for 7–8 and 11

A solution of the substrate (100 mL, typically 4.00 mmol/L in CH_3OH–H_2O (1:1)) and a sample of a reference compound were irradiated in the Rayonet reactor for a set time and worked up using the general procedure. The formation of the methyl ether products (15%–20% conversion) were determined by ^{1}H NMR and GC. The photomethanolysis of two reference compounds, 2,6-dimethoxybenzyl alcohol (Φ = 0.31) and 2-hydroxybenxyl alcohol (Φ = 0.24), were employed (17).

Acknowledgments

This research was supported by the Natural Sciences and Engineering Research Council of Canada (NSERC). We thank Dr. C.-G. Huang for initial studies of some of the biaryl systems.

References

1. H.E. Zimmerman and D.S. Crumrine. J. Am. Chem. Soc. **94**, 498 (1972).
2. A. Imamura and R. Hoffmann. J. Am. Chem. Soc. **90**, 5379 (1968).
3. (*a*) A. Padwa, C. Doubleday, and A. Mazzu. J. Org. Chem. **42**, 3271 (1977); (*b*) S. Lazare, R. Lapouyade, and R. Bonneau. J. Am. Chem. Soc. **107**, 6604 (1985); (*c*) E.C. Taylor, B. Furth, and M. Pfau. J. Am. Chem. Soc. **87**, 1400 (1965); (*d*) K. Mislow and A.J. Gordon. J. Am. Chem. Soc. **85**, 3521 (1963); (*e*) B.S. Udayakumar and G.B. Schuster. J. Org. Chem. **57**, 348 (1992); (*f*) J.S. Swenton, T.J. Ikeler, and G.L. Smyser. J. Org. Chem. **38**, 1157 (1973).
4. V. Balzani and F. Scandola. Supramolecular photochemistry. Ellis Horwood, New York. 1991. Chap. 7.
5. (*a*) C.-G. Huang, K.A. Beveridge, and P. Wan. J. Am. Chem. Soc. **113**, 7676 (1991); (*b*) Y. Shi and P. Wan. J. Chem. Soc. Chem. Commun. 1217 (1995); (*c*) Y. Shi and P. Wan. J. Chem. Soc. Chem. Commun. 273 (1997).
6. (*a*) G. Bringmann, T. Hartung, L. Göbel, O. Schupp, C.L.J. Ewers, B. Schöner, R. Zagst, K. Peters, H.G. von Schnering, and C. Burschka. Liebigs Ann. Chem. 225 (1992); (*b*) G. Bringmann, B. Schöner, O. Schupp, K. Peters, E.-M. Peters, and H.G. von Schnering. Liebigs Ann. Chem. 91 (1994).

© 2005 NRC Canada

7. (*a*) A. Suzuki. Pure Appl. Chem. **63**, 419 (1991); (*b*) A.R. Martin and Y.H. Yang. Acta Chem. Scand. **47**, 221 (1993).
8. C.M. Unrau, M.G. Campbell, and V. Snieckus. Tetrahedron Lett. 2773 (1992).
9. R.M.G. Roberts. Magn. Reson. Chem. **23**, 52 (1985).
10. C. Hatchard and C. Parker. Proc. R. Soc. London Ser. A, **235**, 518 (1956).
11. I. Berlman. Handbook of fluorescence spectra of aromatic molecules. Academic Press, New York. 1971.
12. T.C. Werner. Modern fluorescence spectroscopy. Vol. 2. *Edited by* E.L. Wehry. Plenum Press, New York. Chap. 7.
13. I. Berlman. J. Chem. Phys. **52**, 5616 (1970).
14. K.S. Burnham and G.B. Schuster. J. Am. Chem. Soc. **120**, 12619 (1998).
15. R.A. McClelland. Tetrahedron, **52**, 6823 (1996).
16. G. Bringmann, T. Hartung, L. Göbel, O. Schupp, K. Peters, and H. Schering. Liebigs Ann. Chem. 769 (1992).
17. P. Wan and B. Chak. J. Chem. Soc. Perkin Trans. 2, 1751 (1986).

© 2005 NRC Canada

Time-resolved spectroscopic studies of the photochemistry of some diphenylgermylene (Ph_2Ge:) precursors[1]

Cameron R. Harrington, William J. Leigh, Bryan K. Chan, Peter P. Gaspar, and Dong Zhou

Abstract: The photochemistry of diphenylbis(trimethylsilyl)germane (**2a**) and 1,4-dihydro-5-methyl-1,2,3,4,9,9-hexaphenyl-1,4-germanonaphthalene (**11**) has been studied in solution by steady-state and laser flash photolysis methods with a view to detecting the transient germylene derivative diphenylgermylene (Ph_2Ge), which has previously been shown to be the major product of photolysis of **2a** and a closely related derivative of **11**. Steady-state trapping experiments confirm the formation of Ph_2Ge as the major germanium containing primary product in both cases; with **2a**, the results indicate that other transient species are also formed in minor yields, including phenyl(trimethylsilyl)germylene (Ph(TMS)Ge, ca. 6%) and diphenyl(trimethylsilyl)germyl radicals (Ph_2(TMS)Ge, ≥15%). Laser flash photolysis of **2a** in deoxygenated hexane solution yields a complex mixture of overlapping transient absorptions, which is shown to be comprised of Ph_2Ge, tetraphenyldigermene (**15**) and its oligomerization products, and another species with spectral characteristics similar to the Ph_2(TMS)Ge radical. The latter has been independently generated by hydrogen abstraction from diphenyl(trimethylsilyl)germane by *tert*-butoxyl radicals. Compound **11** extrudes Ph_2Ge more cleanly and efficiently upon photolysis in solution, yet laser flash photolysis affords excited triplet and triplet-derived species as the only detectable transient products; interpretation of the results for this compound is made difficult by its slow thermal decomposition to 5-methyl-1,2,3,4-tetraphenylnaphthalene. It is concluded that in spite of the fact that both **2a** and **11** afford Ph_2Ge in high yield upon photolysis, they are poor precursors for study of the species in solution by time-resolved UV–vis methods, owing to the formation of other, more strongly absorbing transient products than Ph_2Ge, whose lowest energy absorption is characteristically weak.

Key words: germylene, germyl radical, flash photolysis, disilylgermane, photochemistry.

Résumé : Afin d'essayer de détecter le dérivé germylène transitoire, diméthylgermylène (Ph_2Ge), qui avait été reconnu antérieurement comme le produit principal de la photolyse du produit **2a** et de son dérivé apparenté **11**, on a étudié la photochimie du diphénylbis(triméthylsilyl)germane (**2a**) et du 1,4-dihydro-5-méthyl-1,2,3,4,9,9-hexaphényl-1,4-germanonaphtalène (**11**) en solution, par les méthodes de l'état stationnaire et de la photolyse éclair au laser. Les expériences de piégeage de l'état stationnaire confirment dans les deux cas la formation du Ph_2Ge comme produit primaire principal contenant du germanium; avec le produit **2a**, les résultats indiquent que d'autres espèces transitoires se forment aussi, avec des rendements mineurs, dont les radicaux phényl(triméthylsilyl)germylène (Ph(TMS)Ge; rendement d'environ 6 %) et diphényl(triméthylsilyl)germyle (Ph_2(TMS)Ge; rendement supérieur à 15 %). La photolyse éclair au laser du composé **2a** en solution d'hexane désoxygéné mène à la formation d'un mélange complexe d'absorptions transitoires qui se superposent; il a été démontré qu'elles comprennent le Ph_2Ge, le tétraphényldigermène (**15**) et ses produits d'oligomérisation ainsi qu'une autre espèce de caractéristiques spectrales similaires au radical Ph_2(TMS)Ge. Ce dernier a été généré de manière indépendante par abstraction d'hydrogène par des radicaux *tert*-butoxyles à partir du diphényl(triméthylsilyl)germane. Par photolyse en solution, le composé **11** expulse le Ph_2Ge d'une façon beaucoup plus propre et plus efficace, toutefois la photolyse éclair au laser ne fournit comme produits transitoires détectables que le triplet excité et diverses espèces qui en dérivent; l'interprétation des résultats relatifs à ce composé est rendue difficile par sa décomposition thermique lente en 5-méthyl-1,2,3,4-tétraphénylnaphtalène. On en conclut que, même si la photolyse des composés **2a** et **11** mène dans les deux cas à la formation de Ph_2Ge avec un rendement élevé, ils sont de pauvres précurseurs pour l'étude de ces espèces en solution par des méthodes UV–vis résolues dans le temps en raison de la formation d'autres produits transitoires qui absorbent plus fortement que le Ph_2Ge dont la plus faible énergie d'absorption est normalement faible.

Received 9 March 2005. Published on the NRC Research Press Web site at http://canjchem.nrc.ca on 22 October 2005.

C.R. Harrington, W.J. Leigh,[2] B.K. Chan, P.P. Gaspar, and D. Zhou. Department of Chemistry, McMaster University, 1280 Main Street West, Hamilton, ON L8S 4M1, Canada and Department of Chemistry, Washington University, St. Louis, MO 63130, USA.

[1]This article is part of a Special Issue dedicated to organic reaction mechanisms.

[2]Corresponding author: (e-mail: leigh@mcmaster.ca).

 doi: 10.1139/V05-148 © 2005 NRC Canada

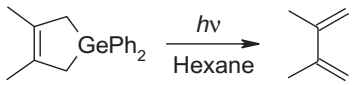
Mots clés : germylène, radical germyle, photolyse éclair, disilylgermane, photochimie.

[Traduit par la Rédaction]

Introduction

Since the report nearly 20 years ago by Ando et al. (1) of the UV spectra of several simple, photochemically generated germylene derivatives in hydrocarbon matrixes at low temperature, there have been a number of studies published on the direct detection and study of reactive diarylgermylenes (2–10) and dialkylgermylenes (6, 11–15) in solution by laser flash photolysis techniques. Most of these studies employed Group 14 catenates as photochemical precursors to these "heavy carbene" analogues, such as **1**–**3** in the case of diphenylgermylene (Ph_2Ge). While steady-state trapping experiments showed that the germylene is the major transient photoproduct in each case, the results of laser photolysis experiments have been highly variable. For example, the UV–vis absorption max of Ph_2Ge has been reported to occur at various positions ranging from 445 to 630 nm, bracketing the value of λ_{max} = 466 nm originally reported by Ando et al. (1) in a 3-methylpentane matrix at 77 K using benzogermanorbornadiene derivative **4** and disilylgermane **2a** as germylene precursors. Thanks to the recent identification of a precursor that yields this reactive species *quantitatively* and in remarkably high quantum efficiency (**5**, eq. [1]), the UV spectrum of Ph_2Ge in hydrocarbon solvents at room temperature has now been conclusively established (9), as have quantitative details of its reactivity toward dimerization (9) and a number of representative metallylene scavengers such as amines, carboxylic acids, halocarbons, Group 14 hydrides, dienes, alkenes, and alkynes (10). In hexane solution at room temperature, diphenylgermylene exhibits λ_{max} = 500 nm (ϵ = 1650 ± 390 $(mol/L)^{-1}$ cm^{-1}) and dimerizes at close to the diffusion-controlled rate to yield the transient 1,1,2,2-tetraphenyldigermene ($Ph_2Ge{=}GePh_2$, λ_{max} = 440 nm, τ ~ 40 μs) (9). None of the UV spectra previously assigned to Ph_2Ge — including that reported by Ando et al. in 3-MP matrices at 77 K (1, 16, 17) — match the one reported more recently in solution using **5** as the precursor.

One of the compounds employed by Ando et al. for the photogeneration of Ph_2Ge — diphenylbis(trimethylsilyl)germane (**2a**) — has also been studied in fluid solution at room temperature by flash photolysis methods (2, 6). Photolysis of the compound in cyclohexane solution in the presence of 2,3-dimethyl-1,3-butadiene (DMB) was found to afford hexamethyldisilane (Si_2Me_6), trimethylphenylsilane ($PhSiMe_3$), and the diene trapping product **5** as the only detectable products (eq. [2]) (6), while laser flash photolysis of the compound afforded a transient that decayed over several hundred microseconds and exhibited λ_{max} = 445 nm (2), blue-shifted somewhat relative to the spectrum recorded for this compound in the earlier matrix experiments (1, 16). Absolute rate constants were determined for reaction of the species with various germylene scavengers, among them oxygen (1.02×10^8 $(mol/L)^{-1}$ s^{-1}), ethyldimethylsilane (k = 1.01×10^4 $(mol/L)^{-1}$ s^{-1}), 1-bromo-2-methylpropane (k = 6.36×10^5 $(mol/L)^{-1}$ s^{-1}), and 2,3-dimethyl-1,3-butadiene (2.75×10^4 $(mol/L)^{-1}$ s^{-1}) (2). Like the UV–vis spectrum, the reactivity of the transient toward the various germylene scavengers examined is in poor agreement with that reported much later for Ph_2Ge using **5** as the precursor (9). It is noteworthy that photolysis of the dimesityl analogue of **2a** (**6**) also affords the corresponding germylene (in this case dimesitylgermylene, Mes_2Ge) quite cleanly, as shown by the results of steady-state trapping experiments, matrix photolysis experiments (1, 16), and laser flash photolysis experiments in solution (7). In this case, the transient spectrum observed (and assigned to Mes_2Ge, λ_{max} ~ 550 nm) in solution (7) matches that obtained in matrix experiments (1, 16) or in solution from other precursors (7, 9) quite closely.

[1] 

5

λ_{max} = 500 nm
τ ~ 2 μs

$Ph_3Ge{-}GePh_3$

1

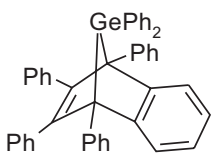
$Ph_2Ge{-}MMe_3$
MMe_3

2

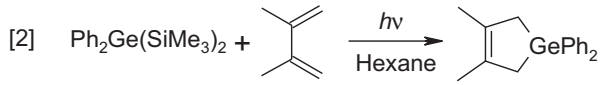
a. M = Si
b. M = Ge

$Ph_2Ge{-}GePh_2$
$Ph_2Ge{\cdot}(GePh_2)n$

3
(n = 1-3)



4

[2] 

2a 0.043 mol/L **5** (61%)

+ Si_2Me_6 (68%)
+ $PhSiMe_3$ (27%)

$Mes_2Ge(SiMe_3)_2$

6
(Mes = 2,4,6-trimethylphenyl)

Recently, we reported a study of the photochemistry of 1,1,1-trimethyl-2,2,2-triphenylsilagermane (**7**) in solution by steady-state and laser flash photolysis methods (18). This compound also yields Ph_2Ge as the major germanium containing photoproduct in solution, but it also affords significant yields of the conjugated germene derived from 1,3-trimethylsilyl migration (**8**) and free radicals owing to triplet-derived Ge—Si bond homolysis (eq. [3]), as revealed by the results of steady-state trapping experiments. Only **8**

© 2005 NRC Canada

and triphenylgermyl radicals could be detected in laser flash photolysis experiments with the molecule, presumably because the absorption spectra of these transients are significantly more intense than that of Ph_2Ge, whose lowest energy (n,p) electronic transition is characteristically weak. Furthermore, the lowest energy absorption band in the UV–vis spectrum of **8** (λ_{max} ~ 475 nm) occurs at a similar position to the much weaker absorption band in the spectrum of the germylene (λ_{max} = 500 nm) under similar conditions. We speculated that an analogous mixture of products might well be expected from photolysis of **2a** under similar conditions, and that the transient spectroscopic behavior reported earlier for this compound might thus be better explained in terms of the corresponding germene (**9**) and (or) the diphenyl(trimethylsilyl)germyl radical (**10**) (18).

[3] $Ph_3GeSiMe_3$ (**7**) $\xrightarrow[\text{Hexane}]{h\nu}$ $Ph_2Ge:$ + $PhSiMe_3$ + $Ph_3Ge\bullet$ + $Me_3Si\bullet$

+ **8** ($GePh_2$, H, $SiMe_3$)

9 ($Ge(Ph)SiMe_3$, H, $SiMe_3$) **10** ($Ph_2GeSiMe_3\bullet$)

In the present paper, we report the results of a reinvestigation of the photochemistry of **2a** in solution by steady-state and laser flash photolysis methods, with a view to providing a secure identification of the transient species observed in the earlier work with this compound, and to see whether discrete evidence for the formation of free Ph_2Ge might be obtained. To aid in the interpretation of the results, germyl radical **10** has been generated by an independent route and its UV–vis spectrum and lifetime recorded under similar conditions to those employed for laser photolysis experiments with **2a**. We have also synthesized an analogue (**11**) of the benzogermanonorbornadiene derivative originally studied by Ando et al. (**4**), and have studied its photochemistry using similar methods. This compound differs from **4** only in the presence of a methyl group situated on the benzannelated ring, which was included so as to facilitate the determination of its purity and the identification of products from photochemical and (or) thermal decomposition, as compounds of this type are known to exhibit pronounced thermal lability under quite mild conditions (19–22).

11 ($GePh_2$, Ph, Ph, Ph, Ph, CH_3)

Results and discussion

The photochemistry of $Ph_2Ge(SiMe_3)_2$ (2a)

The products of photolysis of **2a** in the presence of DMB (see eq. [2]) were originally identified, and their yields established, from a preparative-scale photolysis experiment carried to 64% conversion (6). Because secondary photolysis of **5** can be expected to lead to its preferential loss from the reaction mixture over such extended photolysis times, we began the present study with an examination of the product mixture at much lower conversions. Thus, a deoxygenated 0.05 mol/L solution of **2a** in cyclohexane-d_{12} containing 0.1 mol/L of the diene was irradiated with 254 nm light, monitoring the reaction periodically by (600 MHz) ^{1}H NMR spectroscopy over the 0%–16% conversion range. The NMR spectra of the photolysate showed discrete evidence for the formation of **5** and hexamethyldisilane (Si_2Me_6) in a ca. 1:1 ratio as the only detectable products. GC analysis of a similar photolysis in deoxygenated hexane solution (0.01 mol/L **2a**, 0.03 mol/L DMB) also showed **5** to be the major product of the reaction, but allowed the additional detection of $PhSiMe_3$ in minor amounts (≤6%), along with another minor product that eluted shortly before **2a**. The latter compound, which is formed in similar yield to $PhSiMe_3$, was tentatively identified as 3,4-dimethyl-1-phenyl-1-trimethylsilylgermacyclopent-3-ene (**12**) on the basis of GC–MS evidence. The results of these experiments are summarized in eq. [4].

[4] $Ph_2Ge(SiMe_3)_2$ (**2a**) + 0.03 mol/L $\xrightarrow[\text{Hexane}]{h\nu}$ **5** (89%) + Si_2Me_6 (0.94:1 relative to **5**)

+ **12** (6%) (Ph, Ge, $SiMe_3$) + $PhSiMe_3$ (1:1 relative to **12**)

Interestingly, photolysis of a 0.05 mol/L solution of **2a** in cyclohexane-d_{12} containing methanol (MeOH, 0.5 mol/L) afforded Si_2Me_6 and the Ph_2Ge insertion product **13** as the major products, but the latter was formed in only ca. 60% yield relative to consumed **2a** and in significantly lower yield than the coproduct of Ph_2Ge extrusion, Si_2Me_6. The 0–0.5 ppm region of the spectra also contained singlets attributable to three additional minor products, whose resonances integrated to 10:13:7; the total intensity of the three singlets owing to these products was ca. 30% relative to that of the singlet owing to Si_2Me_6. The most minor of these products was identified by ^{1}H NMR spectroscopy and GC as disilyldigermane **14**, by spiking the mixture with an authentic sample of the compound; the other two were not identified. The results of these experiments are summarized in eq. [5].

Taken together, these results indicate that while extrusion of Ph_2Ge is the dominant photoreaction of **2a**, accounting for ca. 60% of the photochemistry, other minor processes occur as well. One of these is assigned to the alternate germylene extrusion pathway, yielding Ph(TMS)Ge and

© 2005 NRC Canada

[5] $Ph_2Ge(SiMe_3)_2$ + MeOH $\xrightarrow[C_6D_{12}]{h\nu}$ $Ph_2GeH(OMe)$ + $Me_3SiPh_2Ge\text{-}GePh_2SiMe_3$ + other products + Si_2Me_6 (1.17:1 relative to **13**)

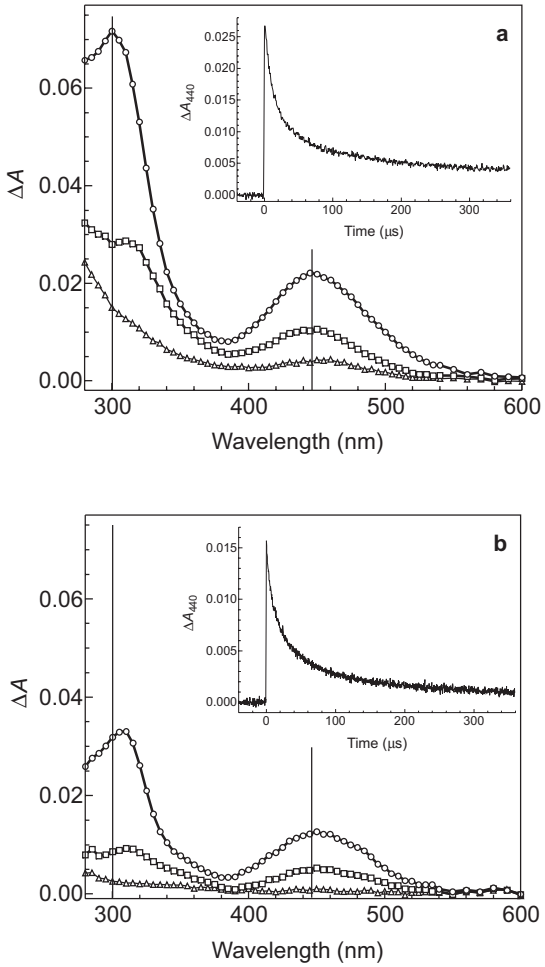
2a — 0.5 mol/L — **13** (60%) — **14** (8%) — 31%

$PhSiMe_3$ in about 6% chemical yield. Another is Si—Ge bond homolysis to yield the trimethylsilyl and diphenyl(trimethylsilyl)germyl radicals, as evidenced by the formation of minor amounts of digermane **14** in the photolysis in the presence of MeOH. This process constitutes at least 15% of the reactive excited-state decay processes of the molecule, based on the observed yield of **14** and the assumption that 50% of the Ph_2(TMS)Ge radicals produced will decay by recombination with trimethylsilyl radical, regenerating **2a**. Interestingly, **14** is not formed in the diene scavenging experiment, and the complete absence of additional $SiMe_3$ resonances in the NMR spectrum of this photolysis mixture indicates that the reason is *not* that the Ph_2(TMS)Ge radical is efficiently scavenged by the diene. A more likely mechanism by which the diene suppresses the formation of free radicals is triplet quenching, since it is known that the formation of radicals in the photolysis of aryldisilanes, arylgermasilanes, and aryldigermanes derives largely from the triplet state, and their formation can be quenched to at least some extent by added diene (18, 23, 24).

Laser flash photolysis experiments with **2a** employed flowed, deoxygenated 1.3×10^{-4} mol/L solutions of the compound in anhydrous hexane, and used the pulses from a KrF excimer laser (248 nm, ~25 ns, ~100 mJ) for excitation. As reported previously (2), laser photolysis of the compound affords strong transient absorptions throughout the 300–600 nm region of the spectrum, which decay over several hundred microseconds with complex kinetics. Figure 1 shows transient spectra recorded at selected time intervals over a ca. 350 μs time window after excitation in the absence and presence of 3 mmol/L acetic acid (AcOH). The spectra in the absence of acid were collected with a view to reproducing the originally reported conditions as closely as possible, while those in the presence of acid were intended to reveal those transient absorptions that remain behind when Ph_2Ge and its oligomerization products are removed from the mixture by trapping with AcOH, a potent germylene scavenger (9, 10). The main (gross) effects of the carboxylic acid are a marked reduction in the intensities of the signals observed throughout the spectrum, and simplification of the complex transient absorptions that arise below ca. 340 nm. In the absence of AcOH (Fig. 1*a*), the spectrum exhibits a band at λ_{max} = 300 nm during the earliest time window monitored, which evolves into a band with λ_{max} ~ 310 nm after ca. 25 μs; only the latter is evident in the region below 340 nm in the presence of the carboxylic acid (Fig. 1*b*). Addition of the acid also reduces the intensity of the long wavelength absorption band centered at λ_{max} ~ 445 nm, and markedly reduces the complexity of the transient decay profile at this wavelength, which decays with multiexponential kinetics in the absence of acid (see inset, Fig. 1*a*). In the presence of 3 mmol/L AcOH the long wavelength absorption decays with clean second-order kinetics (see inset, Fig. 1*b*) and a rate coefficient of $k_{decay}/\varepsilon = (7.4 \pm 0.2) \times 10^5$ cm^{-1} s^{-1} (r^2 = 0.987). The decay kinetics at 310 nm (not shown) are similar to those at 440 nm, suggesting that the two absorption bands in the spectrum of Fig. 1*b* belong to the same (as yet unidentified) transient species. It can thus be concluded that the early (0.64–2.56 μs) spectrum of Fig. 1*a* is the sum of the spectra of at least two transient species of which all but one is eliminated in the presence of 3 mmol/L AcOH.

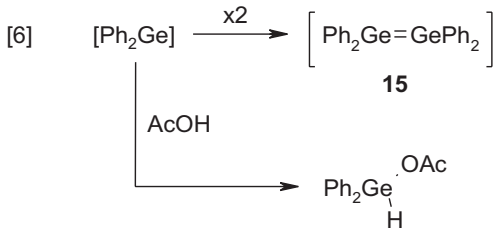
AcOH is known to react with Ph_2Ge irreversibly, with a rate constant of 3.9×10^9 (mol/L)$^{-1}$ s^{-1} (9). Thus, a concentration of 3 mmol/L is sufficient to reduce the lifetime of Ph_2Ge to <100 ns and more or less completely suppress its dimerization to tetraphenyldigermene (**15**), the main mode of decay of the germylene in the absence of scavengers (see eq. [6]) (9). In the absence of scavengers, the concentration

Fig. 1. Transient absorption spectra from laser flash photolysis of a flowed, deoxygenated solution of **2a** (1.3×10^{-4} mol/L) in anhydrous hexane containing (*a*) 0 mmol/L of AcOH and (*b*) 3 mmol/L AcOH, recorded under identical conditions, 0.64–2.56 μs (○), 24–39 μs (□), and 324–325 μs (△) after the pulse. Transient decay traces recorded at a monitoring wavelength of 440 nm are shown as inserts.



© 2005 NRC Canada

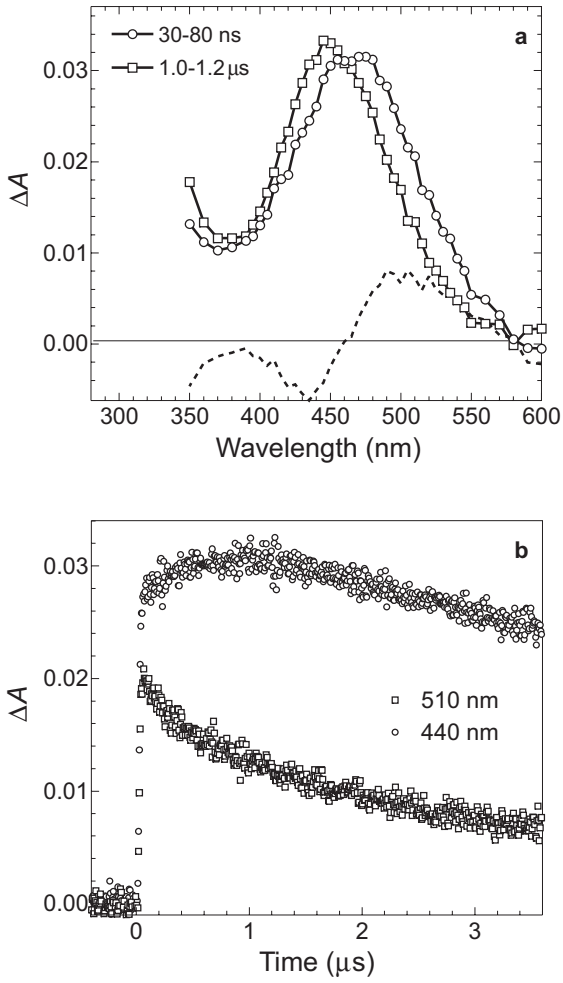
of **15** reaches a maximum in the first ca. 1 μs after the excitation pulse, and then decays over several tens of microseconds (9). We thus attribute that portion of the transient spectrum of Fig. 1*a* that is eliminated in the presence of AcOH to **15** (λ_{max} = 300, 440 nm (9)), formed by dimerization of Ph_2Ge, and its oligomerization product(s). The long wavelength absorption band in the spectrum of **15** is almost exactly coincident with that of the longer lived (nonquenchable) species that was erroneously identified as owing to Ph_2Ge in the original work (2).



Direct evidence for the formation of Ph_2Ge from **2a** was obtained by examination of the transient spectroscopic behavior over shorter timescales. Figure 2 shows transient spectra recorded at selected time intervals within ca. 1 μs after excitation, along with representative transient absorption profiles recorded at 510 and 440 nm. As can be seen from the data, the long wavelength absorption band in the transient spectrum from **2a** is centered at λ_{max} ~ 465 nm during the first ca. 100 ns after excitation, and appears to shift to λ_{max} ~ 445 nm (its position in the spectra of Fig. 1) during the next ~900 ns. Inspection of the transient absorption profile at 440 nm reveals a slight increase in signal strength at this wavelength over this early time period, indicative of the delayed formation of a species that is not present (or at least present in lower concentration) immediately after the ca. 25 ns laser pulse. Thus, the apparent shift in the position of the long wavelength transient absorption during the first microsecond after excitation can be understood as owing to the superposition of three distinct transient absorptions that each evolve differently over this timescale: one that decays almost completely (465 nm < λ_{max} < 550 nm), one that grows in (400 nm < λ_{max} < 460 nm), and one that is essentially nondecaying (λ_{max} ~ 445 nm, see Fig. 1*b*). This behavior is consistent with the initial formation of Ph_2Ge (λ_{max} = 500 nm (9)), which decays over 1 to 2 μs by dimerization to yield **15** (λ_{max} = 440 nm (9)). The timescale over which these changes occur correlates almost precisely with that found in our previous study of these species, generated by laser photolysis of **5** (9). The transient decay profiles shown in Fig. 2 bear only qualitative similarities to those previously obtained from **5** (9), however, owing to the presence of the third transient species, which absorbs relative strongly over the same range of the spectrum, and whose decay proceeds over a much longer timescale.

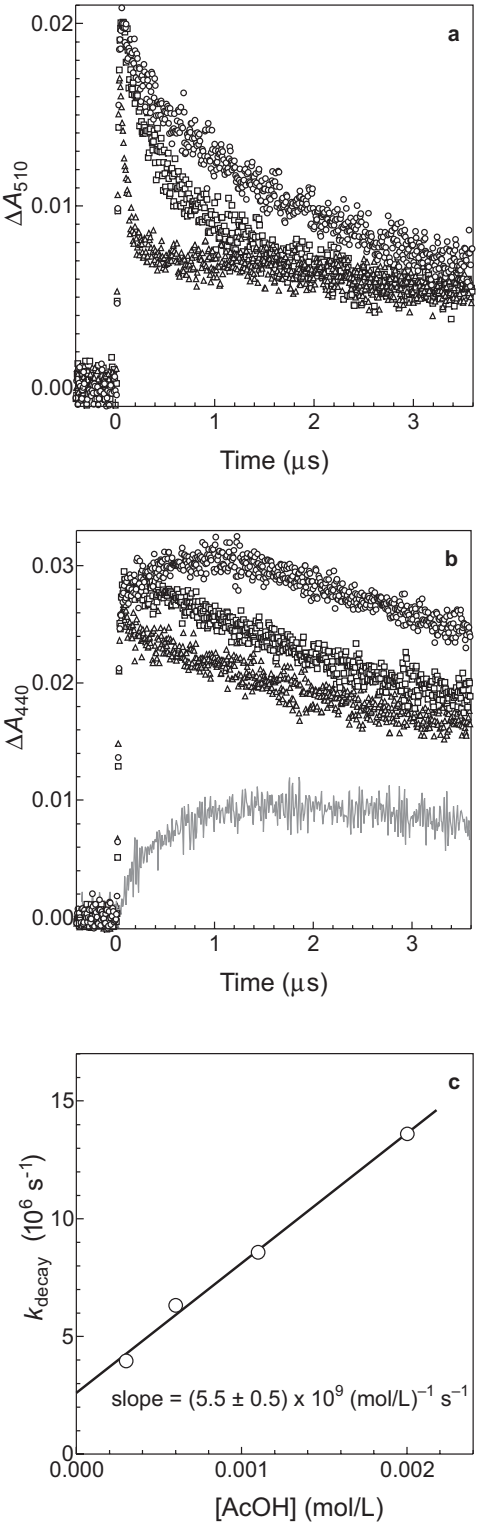
Inspection of the transient absorption profiles over the short timescale as AcOH is added to the solution provides somewhat clearer evidence for the presence of Ph_2Ge and its dimerization product in the transient mixture. Figures 3*a* and 3*b* show a series of decay profiles recorded at the two wavelengths in the presence of 0, 0.1, and 2.0 mmol/L of added carboxylic acid, demonstrating quite clearly that a significant portion of the signal at 510 nm is quenched by the reagent, concomitant with a reduction in the yield of a transient absorbing at 440 nm. Nonlinear least-squares analysis of the initial rapidly decaying portion of the 510 nm decay profiles at several AcOH concentrations as a single exponential decay (with the more slowly decaying residual absorption treated as nondecaying) afforded quite reasonable fits; the resulting pseudo-first-order decay rate constants (k_{decay}) are plotted in Fig. 3*c* vs. AcOH concentration. Linear least-squares analysis of these data according to eq. [7], where k_0 is the effective pseudo-first-order decay rate constant at [AcOH] = 0 and k_{AcOH} is the bimolecular rate constant for scavenging by the carboxylic acid, affords a slope of k_{AcOH} = (5.5 ± 0.5) × 10^9 $(mol/L)^{-1}$ s^{-1}, in excellent agreement with the value reported by us earlier for the O-H insertion reaction of Ph_2Ge with AcOH (k_{AcOH} = 3.9 × 10^9 $(mol/L)^{-1}$ s^{-1} (9)). Figure 3*b* also shows the result of subtracting the decay trace at 440 nm in the presence of 2.0 mmol/L AcOH (where formation of **15** should be more or less completely suppressed) from that recorded in the ab-

Fig. 2. (*a*) Transient absorption spectra from laser flash photolysis of a flowed, deoxygenated solution of **2a** (1.3 × 10^{-4} mol/L) in anhydrous hexane, 30–80 ns (○) and 1.0–1.2 μs (□) after the pulse. The dashed line is the difference between the early and late spectrum. (*b*) Transient absorption profiles recorded at 440 nm (○) and 510 nm (□).



© 2005 NRC Canada

Fig. 3. Transient decay traces recorded with a deoxygenated anhydrous hexane solution of **2a** at (*a*) 510 nm and (*b*) 440 nm in the presence of 0 mmol/L AcOH (○), 0.1 mmol/L AcOH (□), and 2.0 mmol/L AcOH (△). The grey trace in (*b*) is the difference between the 0 and 2.0 mmol/L traces. (*c*) Plot of the rate constant for the initial rapid decay at 510 nm (k_{decay}) vs. [AcOH] over the 0.3–2.0 mmol/L concentration range.



sence of scavenger. This is also in good agreement with the growth–decay profile for **15** that is observed using **5** as the germylene precursor (9).

$$[7] \qquad k_{decay} = k_0 + k_Q[Q]$$

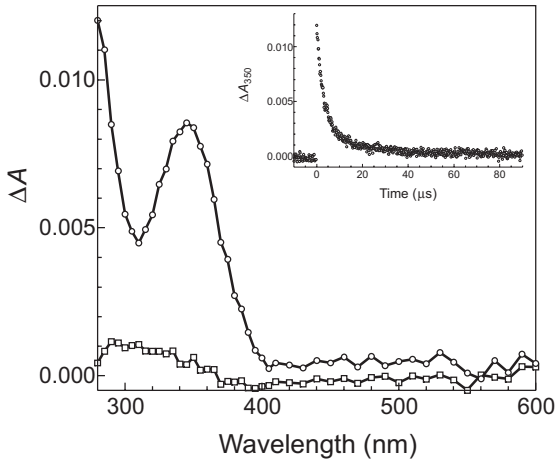
Addition of *n*-butyl amine ($BuNH_2$, 5.0 mmol/L) or MeOH (50 mmol/L) to the hexane solutions of **2a** had similar effects as AcOH on the overall transient behavior (Fig. 1), eliminating the absorptions owing to Ph_2Ge and its products and leaving behind the same long-lived transient species that is observed in the presence of AcOH. Like the carboxylic acid, both of these reagents are potent germylene scavengers, reacting with Ph_2Ge at close to the diffusion-controlled rate in both cases (9).[3] Addition of carbon tetrachloride (CCl_4), chloroform ($CHCl_3$), or oxygen (O_2) to hexane solutions of **2a** in hexane containing 50 mmol/L MeOH caused an increase in the decay rate of the surviving long-lived transient (monitored at 440 nm) in proportion to the concentration of added reagent, and plots of k_{decay} vs. [Q] according to eq. [7] were linear, with slopes of k_{CCl_4} = (7.3 ± 0.7) × 10^6 mol/L^{-1} s^{-1}, k_{CHCl_3} = (1.2 ± 0.1) × 10^4 mol/L^{-1} s^{-1} and k_{O_2} = (6.6 ± 0.8) × 10^7 mol/L^{-1} s^{-1} for CCl_4, $CHCl_3$, and O_2, respectively. The k_{O_2} value is in good agreement with that reported for this species in the original study (k_{O_2} = 1.02 × 10^8 mol/L^{-1} s^{-1}) (2). It is interesting to note that the transient exhibits similar (but two to three times greater) reactivity towards O_2 and CCl_4 as Ph_2Ge does under similar conditions (10), but exhibits ca. 20 times lower reactivity toward $CHCl_3$ (10).

Finally, we examined the flash photolysis behavior of **2a** in deoxygenated tetrahydrofuran (THF) solution, as Ph_2Ge and other reactive germylenes are known to form Lewis acid–base complexes with ethers, with substantially blue-shifted absorption maxima compared to those of the free species (16, 17); for example, generation of Ph_2Ge in a 2-methyltetrahydrofuran glass at 77 K leads to a species absorbing at λ_{max} = 325 nm, which was assigned to the germylene–ether complex (17). The transient spectra obtained by flash photolysis of **2a** in THF solution are similar to those of Fig. 1*b*, but exhibit a weak shoulder on the long wavelength edge of the rising 310 nm absorption, consistent with the presence of the Ph_2Ge-complex. The spectrum of the complex could be isolated by addition of 0.2 mol/L CCl_4 to the solution, which shortened the lifetime of the 310/445 nm transient absorptions to ca. 500 ns and left behind longer lived absorptions ($\tau \sim 2$ μs), centered at λ_{max} = 345 nm that decayed with second-order kinetics (see Fig. 4). The spectrum is in reasonably good agreement with that assigned to the Ph_2Ge–THF Lewis acid–base complex (eq. [8]) in the earlier matrix experiments (17). From the lifetime of the 310/445 nm species under these conditions, a rate constant of ca. 1 × 10^7 mol/L^{-1} s^{-1} can be estimated for its reaction with CCl_4, in good agreement with the value measured in hexane solution (vide supra). The extended lifetime of the Ph_2Ge–THF complex under these conditions presumably results from the fact that it is much less reactive toward CCl_4 than the free germylene, whose concentration is reduced by orders of magnitude relative to that in hexane solution owing to the solvent complexation equilibrium. The "stabilizing"

[3] W.J. Leigh, C.R. Harrington, F. Lollmahomed, and J.J. McDonald. To be published.

© 2005 NRC Canada

Fig. 4. Transient absorption spectra recorded by laser flash photolysis of a deoxygenated 1.3×10^{-4} mol/L solution of **2a** in THF containing 0.2 mol/L CCl_4, 0.6–2.1 μs (○) and 81–85 μs (□) after the (248 nm) laser pulse. The inset shows a transient decay profile recorded at 350 nm.

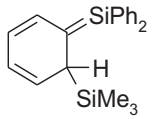


effect of ethers and other Lewis bases on reactive germylenes is well-recognized (25–28).

[8] $Ph_2Ge + O \rightleftharpoons Ph_2Ge^{-}-O^{+}$

The two most reasonable candidates for the 310/445 nm species of Fig. 1*b* are the diphenyl(trimethylsilyl)germyl radical (**10**), which our steady-state results indicate *is* formed upon photolysis of **2a** in significant yield, and the 1-germahexatriene derivative **9**, which would be derived from formal 1,3-trimethylsilyl migration into the ortho position of one of the phenyl groups in the excited singlet state of **2a**. While we have *no* evidence for the formation of **9** from steady-state photolysis experiments, we can nevertheless not easily discount the possibility that it is formed in minor yields and escaped detection in the product studies; trapping of germenes (and silenes) of this general structure by dienes and alcohols is known to afford more than a single product (18, 23, 29). Furthermore, photorearrangements of this type are common in arylgermasilanes (6, 18, 30) and aryldisilanes (31–33) in which the reaction was initially discovered (34). Germene **9** can be expected to be a much stronger absorber than Ph_2Ge, and exhibit similar reactivity to that actually observed for the 310/445 nm transient (18).

The rationale behind the latter statement is as follows. The rate constants for reaction of AcOH and MeOH with germene **8** (one of only two germenes of this type that have been studied (18)) are on the order of 4×10^5 mol/L^{-1} s^{-1} or less, three orders of magnitude lower than the homologous silene derivative (**16**) (18). The reactivity of **9** with nucleophiles can be expected to be significantly lower than that of **8** because of the presence of the trimethylsilyl substituent at Ge, based on analogies in transient silene chemistry; trimethylsilyl substitution at silicon in silenes reduces the reactivity of the Si=C bond by roughly a factor of 10 relative to a methyl substituent (35), which is similar to a phenyl group in its effects on Si=C reactivity (36, 37). Finally, like its silicon counterpart (**16**), germene **8** exhibits significantly higher reactivity toward O_2 and chlorocarbons than it does toward alcohols or other nucleophiles, owing to the radical-like nature of these reactions and the radical-stabilizing effect of the cyclohexadienyl substituent attached to the germenic carbon atom (18). These considerations suggest that the reactivity of the 310/445 nm transient species of Fig. 1*b* is not inconsistent with what might be expected for germene **9**. The only piece of data that argues *against* this assignment is the UV absorption maximum, which lies ca. 35 nm (1800 cm^{-1}) to the *blue* of that exhibited by germene **8** (18). In silenes, replacement of a methyl substituent at silicon with a trimethylsilyl group produces a ca. 4000 cm^{-1} red shift in the UV absorption maximum (35); this fact, coupled with the facts that replacement of one of the phenyl groups in **16** with a methyl group causes a ca. 2000 cm^{-1} blue shift in the absorption maximum (23) and silenes and germenes with the same substituents exhibit essentially identical UV–vis absorption maxima (18, 38), leads to the expectation that the absorption maximum of **9** should be quite similar to that of **8** (λ_{max} ~ 475 nm).



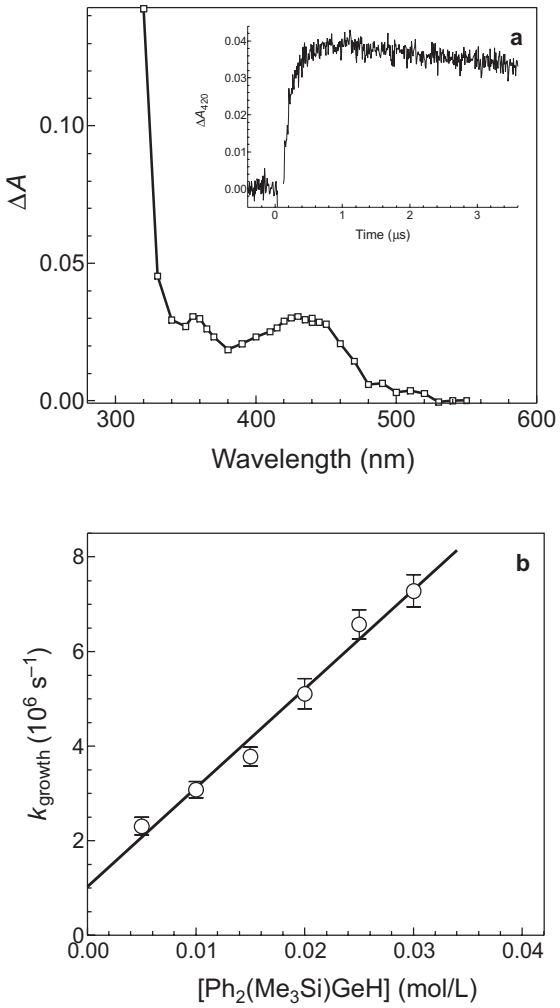
16

To address the other possible transient assignment, germyl radical **10**, we have independently generated the radical by hydrogen abstraction from the corresponding germyl hydride (**17**) by *tert*-butoxyl radicals (eq. [9]), generated by 308 nm laser flash photolysis of 5–30 mmol/L solutions of **17** in di-*tert*-butylperoxide (BOOB) – isooctane (1:4) solution, using a similar procedure to that used previously for the generation of triphenylgermyl and other Group 14 radicals (39, 40). Figure 5 shows the resulting transient absorption spectrum of the radical, a representative transient absorption profile illustrating its growth kinetics, and a plot of the pseudo-first-order rate constant for growth of the radical absorption vs. concentration of **17**, the slope of which is the absolute rate constant for hydrogen abstraction from **17** by *tert*-butoxyl radical. The value obtained, $k = (2.4 \pm 0.4) \times 10^8$ (mol/L)$^{-1}$ s^{-1}, is roughly twice higher than that for the analogous reaction of triphenylgermane (Ph_3GeH) (39),[4] which is the expected result on the basis of comparisons of the corresponding rate constants for hydrogen abstraction from tris(trimethylsilyl)germane and triethylgermane (41), and analogies taken from silicon radical chemistry (42). A possible alternate assignment of the transient product to the diphenylgermyl radical, which might be formed by trimethylsilyl transfer from **17** rather than the expected hydrogen abstraction to form **10**, can be ruled out on the basis of comparisons of the spectrum to that reported for the diphenylgermyl radical (λ_{max} = 325, 405 nm (39*b*)).[5] The authentic spectrum of radical **10**

[4] We also remeasured the rate constant for H abstraction from Ph_3GeH in the course of this work and obtained a value of $k = (1.2 \pm 0.1) \times 10^8$ (mol/L)$^{-1}$ s^{-1}, in excellent agreement with the previously reported value of 9×10^7 (mol/L)$^{-1}$ s^{-1} (39).
[5] We thank a referee for alerting us to this possible alternate assignment.

© 2005 NRC Canada

Fig. 5. (*a*) Transient absorption spectrum of the diphenyl(trimethylsilyl)germyl radical, recorded 3.7–3.9 μs after 308 nm laser photolysis of a 0.040 mol/L solution of $Ph_2Ge(H)SiMe_3$ (**17**) in BOOB–isooctane (1:4, *v*/*v*); the inset shows a typical growth profile of the radical, recorded at a monitoring wavelength of 420 nm. (*b*) Plot of k_{growth} at 420 nm vs. the concentration of added **17**. The solid line represents the linear least-squares fit of the data to eq. [6].



(Fig. 5*a*) agrees reasonably well with the spectrum of the 310/445 nm transient from photolysis of **2a** (Fig. 1*b*), although the match is not precise. We did not attempt to measure rate constants for reaction of authentic **10** with O_2 or with CCl_4 for comparison to those for the 310/445 nm transient, the latter because the germane precursor is unstable in the presence of the halocarbon and light.

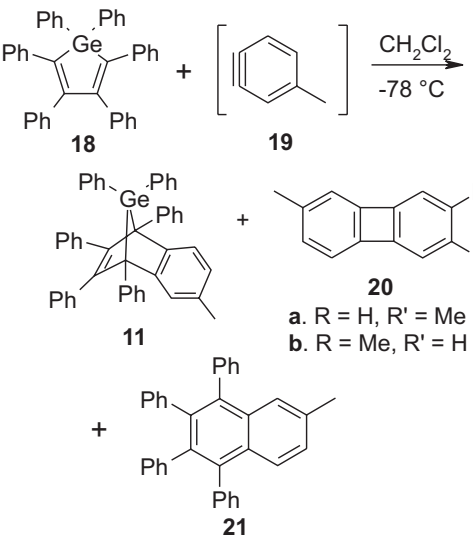
[9] $Me_3Si(Ph)_2Ge{-}H + t\text{-}Bu{-}O\bullet \longrightarrow Me_3Si{-}(Ph)_2Ge\bullet + t\text{-}BuOH$

17 **10**

Table 1 lists the UV absorption maxima and absolute rate constants for reaction of triphenylgermyl radicals (germene **8**) and the 310/445 nm transient from flash photolysis of **2a**. As mentioned previously, the reactivity of the species is similar to that of **8** with the same reagents, significantly more so than it is to the reactivity of the triphenylgermyl radical. In fact, a significantly lower reactivity toward halocarbons and oxygen compared to triphenylgermyl is what one would expect of radical **10**, as the stabilizing effect of trimethylsilyl substitution on both germanium and (in particular) silicon centered radicals is well-known (41–43).

The photochemistry of 1,4-dihydro-5-methyl-1,2,3,4,9,9-hexaphenyl-1,4-germanonaphthalene (11)

Compound **11** was synthesized in ca. 80% yield by cycloaddition of 4-methylbenzyne (**19**) to hexaphenylgermole (**18**; see eq. [10]) in dichloromethane at –78 °C, by an analogous procedure to that reported for the synthesis of **4** (16). The reaction mixture also contained small amounts of the 4-methylbenzyne dimerization products **20** and 6-methyl-1,2,3,4-tetraphenylnaphthalene (**21**); small amounts of **18** are very likely present as well, although the compound could not be specifically detected in the NMR spectrum of the mixture. The amount of **21** in the sample increased slowly relative to **11** over a few hours, thus, the latter was isolated from the reaction mixture by cold (ca. –15 °C) radial chromatography, characterized on the basis of its ^1H and ^{13}C NMR and mass spectra (see the Experimental section), and stored in the dark at –78 °C. However, in spite of reasonable efforts, a sample of **11** containing less than ca. 5% **21** could not be obtained.

[10] 

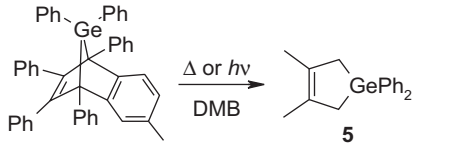
To quantify the thermal lability of **11**, a 0.055 mol/L solution of the compound was prepared in deoxygenated cyclohexane-d_{12} containing 0.5 mol/L DMB and monitored over time at 23 °C by NMR spectroscopy. The mixture contained ca. 10% **21** at the beginning of the experiment, evidently formed by thermal decomposition of **11** subsequent to its initial purification. The NMR spectrum was measured at selected time intervals over the following 20 h, which revealed slow conversion of **11** to **21** and **5** (eq. [11]). A plot of log([**11**]/(mol/L)) vs. time was reasonably linear (r^2 = 0.9886; see Fig. 6) and linear least-squares analysis afforded a first-order rate constant of $(1.6 \pm 0.1) \times 10^{-5}$ s^{-1} for the decomposition of **11**, which yields **21** and Ph_2Ge, trapped as DMB adduct **5** at 23 °C. This corresponds to a half-life of

© 2005 NRC Canada

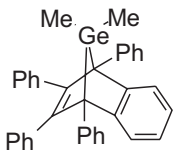
Table 1. Comparison of UV–vis absorption spectra and absolute rate constants for the reaction of the 310/445 nm transient from **2a**, triphenylgermyl radicals (Ph_3Ge), and germene **8** with halocarbons and O_2.

	310/445 nm Transient	Ph_3Ge	**8**
λ_{max} (hexane solution, nm)	310, 445	328, 405 (50)	475 (18)
k_{CCl_4} ((mol/L)$^{-1}$ s^{-1})	7.3×10^6	5.8×10^8 (3)	2.9×10^7 (18)
k_{CHCl_3} ((mol/L)$^{-1}$ s^{-1})	1.2×10^4	5.5×10^7 [6]	$<3\times10^6$ (18)
k_{O_2} ((mol/L)$^{-1}$ s^{-1})	6.6×10^7	3.8×10^9 (3)	9.6×10^7 (18)

ca. 12 h, or (put another way) a decomposition rate of ca. 6% per hour at 23 °C.

[11] 

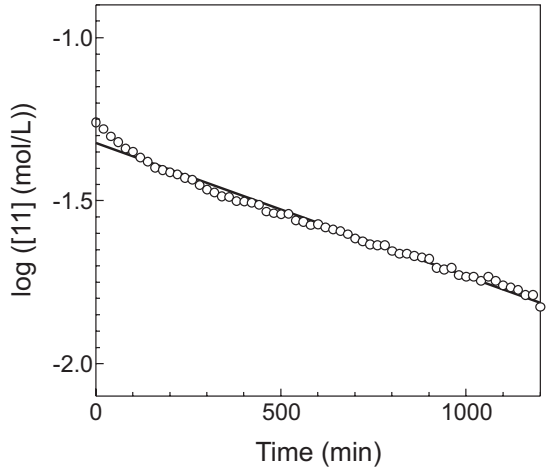
Steady-state photolysis of **11** was carried out on argon outgassed 0.05 mol/L solutions in cyclohexane-d_{12} containing 0.5 mol/L MeOH or DMB with 254 nm light, with the course of the photolyses periodically monitored by ^{1}H NMR spectroscopy; the samples of **11** each contained ca. 10% **21** at the beginning of the experiment. While irradiations and NMR analyses were all carried out at room temperature, the samples were otherwise stored at –78 °C to minimize thermal decomposition. Irradiation to ca. 50% conversion of **11** showed **21** and the corresponding Ph_2Ge trapping products (methoxygermane **13** or germacyclopentene **5**) to be the only detectable photolysis products. While no attempts were made to determine the quantum yield for Ph_2Ge extrusion from the compound, it was estimated to be of similar magnitude to that from **5** for which a value of $\Phi = 0.62$ has been reported (9). Görner et al. (44) reported a quantum yield of $\Phi = 0.4$ for the extrusion of Me_2Ge from the related compound **22** in deoxygenated methylcyclohexane solution.



22

Laser flash photolysis experiments were carried out with flowing, argon outgassed solutions of freshly chromatographed **11** (ca. 5×10^{-5} mol/L, containing ca. 5% **21**) in anhydrous hexane, again using the KrF excimer laser as excitation source. Figure 7 shows a series of transient absorption spectra recorded at various time intervals over the first

Fig. 6. The thermal decomposition of germanorbornadiene **11** in cyclohexane-d_{12} at 23 °C. The solid line represents the linear least-squares fit of the data, affording a first-order rate constant $k = (1.6 \pm 0.1) \times 10^{-5}$ s^{-1}, $r^2 = 0.9886$).

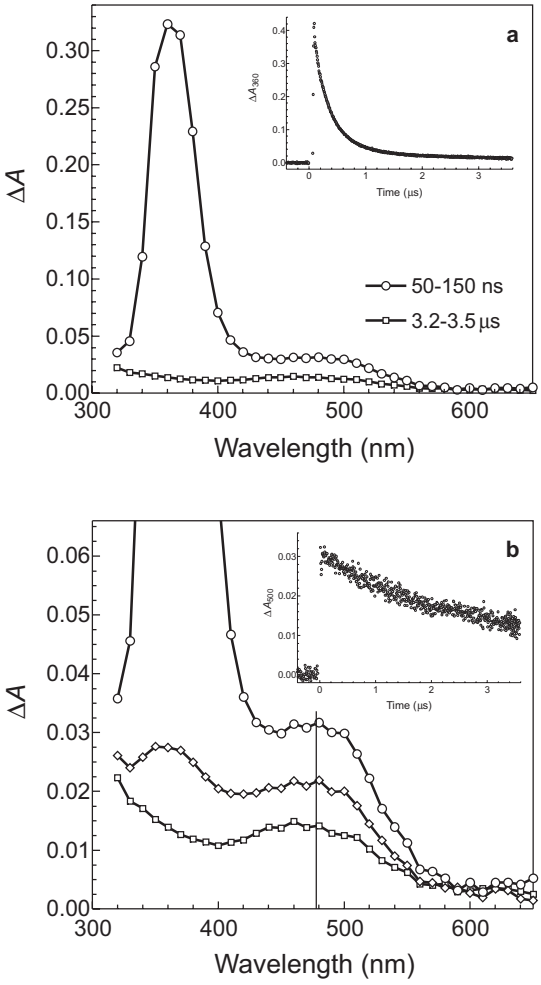


3.6 μs after the laser pulse. The results are consistent with the formation of at least three transient species. The shortest lived transient exhibits very strong absorptions centered at λ_{max} = 360 nm, is formed with the laser pulse, and decays with a lifetime of $\tau \sim 300$ ns. The second species is assigned to the weak shoulder on the 360 nm band in the 50–150 ns spectrum. Its apparent absorption maximum is ca. 480 nm (see the expanded spectra in Fig. 7*b*), which is clearly an underestimate caused by the substantial overlap with the 360 nm band. Nevertheless, the absorptions in the 460–540 nm region of the spectrum are at least five times more intense than would be expected if Ph_2Ge was the only contributor to the absorptions in this range, assuming the germylene is produced at an initial concentration of ca. 10 μmol/L, which is the maximum value we would expect under the conditions of our experiments. The third species is significantly longer lived than the other two and exhibits an apparent $\lambda_{max} \sim 460$ nm, too far to the red to be assigned to the expected germylene dimerization product (digermene **15**). While it is perhaps relevant to point out that the spectrum of this species is similar to that reported in the previous matrix photolysis of **4** (1), we have insufficient information to make a reliable assignment of the species. At no monitoring wavelength in the range studied was a growth in the transient signal discernible, although this is to be expected

[6] W.J. Leigh and N.P. Toltl. Unpublished results.

© 2005 NRC Canada

Fig. 7. (*a*) Transient absorption spectra recorded by laser flash photolysis of a deoxygenated 5×10^{-5} mol/L solution of **11** in anhydrous hexane at 23 °C, 50–150 ns (○) and 3.2–3.5 μs (□) after the (248 nm) laser pulse; the inset shows a transient decay profile recorded at 360 nm. (*b*) An expanded plot of the spectra of (*a*) with a spectrum recorded 1.4–1.6 μs after the pulse included; the vertical line marks the apparent maximum of the long wavelength absorption band in the 50–150 ns spectrum.



considering the substantial overlap with the strongly absorbing species at 360 nm.

Similar experiments carried out on an O_2 saturated solution of **11** verified that Ph_2Ge and its oligomerization products contribute in only a very minor way, if at all, to the transient absorptions observed from flash photolysis of this compound. Under these conditions the transient at 500 nm exhibited a lifetime of ca. 75 ns, and decayed to a residual absorption level roughly 4% of that immediately present after the pulse. A quenching rate constant of $k_{O_2} \sim 9 \times 10^8$ $(mol/L)^{-1}$ s^{-1} can be estimated from the lifetime (using a value of $[O_2] = 0.015$ mol/L for the concentration of O_2 in O_2 saturated hexane), which is ca. 30 times higher than the rate constant reported by us recently for the reaction of Ph_2Ge with O_2 ($k_{O_2} \sim 2.7 \times 10^7$ $(mol/L)^{-1}$ s^{-1} (10)). The other major change noted upon saturation of the solution with O_2 was a change in the form of the decay of the 360 nm transient to biexponential kinetics, with roughly 65% of the absorptions decaying on a very fast timescale and the remaining ~35% exhibiting a lifetime similar to that observed in the absence of O_2. This behaviour suggests that the transient absorptions produced upon flash photolysis of **11** are dominated by triplet or triplet-derived species.

Our results for **11** are similar to those reported for the related compound **22** by Görner and co-workers (44), who assigned the transients observed upon 248 nm laser flash photolysis of the compound to the triplet state of 1,2,3,4-tetraphenylnaphthalene, the coproduct of Me_2Ge photoextrusion from this compound. They were similarly unable to obtain discrete evidence for the formation of a transient assignable to the germylene (44).

As was also reported in the earlier study of **22** (44), virtually identical transient spectroscopic behaviour was observed upon laser flash photolysis of (static) 1×10^{-5} mol/L solutions of the tetraphenylnaphthalene coproduct (**21**, in the present case) in both deoxygenated and oxygen saturated hexane solution, with the transient spectra and lifetimes at various wavelengths coinciding quite closely to those obtained using **11** under corresponding conditions. In this case, saturation of the solution with O_2 decreased the lifetime of the 500 nm transient absorptions to ca. 50 ns from which can be estimated a quenching rate constant of $k_{O_2} \sim 1.3 \times 10^9$ $(mol/L)^{-1}$ s^{-1}, in good agreement with that obtained in experiments using **11** as the precursor.

Görner and co-workers (44) explained their results for **22**, which were much more extensive than the present ones for **11** and involved purer samples (**22** is evidently significantly more stable thermally than **11** (19)), in terms of a mechanism in which the (1,2,3,4-tetraphenylnaphthalene) coproduct of Me_2Ge extrusion is formed in the excited singlet state, which then yields the triplet after intersystem crossing. The alternative possibility that the naphthalene triplet is directly produced along with (singlet) Me_2Ge from the triplet state of the precursor was ruled out on the basis of CIDNP experiments. Because our samples of **11** contained small amounts of the corresponding naphthalene derivative (**21**), we cannot ascertain to what extent the transient mixture produced in our experiments with the Ph_2Ge precursor is contaminated by cophotolysis of the impurity. Nevertheless, our results verify that the transient spectroscopic behaviour observed in flash photolysis experiments with compounds of this type is dominated by triplet and (or) triplet-derived species (for one reason or another), and that simple germylenes such as Ph_2Ge or Me_2Ge are impossible to detect reliably (if at all) in fluid solution from such precursors by time-resolved UV spectroscopic methods.

Summary and conclusions

In spite of the indication from product studies that the direct photolyses of disilylgermane **2a** and benzogermanorbornadiene **11** afford Ph_2Ge in very high yields, they are clearly unsuitable as precursors of the germylene for study by time-resolved UV–vis spectroscopic methods in solution. In the case of **2a**, this is due to the competing formation of a second transient product, which, although it is formed in relatively low yield, absorbs strongly over the same spectral range as Ph_2Ge and its dimerization product (digermene **15**), and is much longer lived than the relatively weakly absorb-

© 2005 NRC Canada

ing germylene. The germylene and its dimer *can* be successfully detected in laser flash photolysis experiments with this compound, but their relatively weak absorptions are superimposed on a background of intense, relatively long-lived absorptions owing to the minor product. This makes them very easy to miss altogether, particularly when little or no independent information on their spectra and reactivities exists, as was the case in the original study. The UV–vis absorption spectrum of the species and its reactivity toward halocarbons and oxygen is broadly consistent with its assignment to the diphenyl(trimethylsilyl)germyl radical, which product studies show is formed in minor, but significant, yields upon photolysis of **2a**. Radical formation is suppressed in the presence of high concentrations of diene, suggesting that the Si—Ge bond homolysis process that is responsible for its formation is derived from the triplet state of the disilylgermane. The alternate assignment of the species to germene **9** cannot be ruled out.

Other factors frustrate attempts to detect the germylene and its dimer in laser flash photolysis experiments with the benzogermanorbornadiene derivative **11**, in spite of the fact that product studies indicate its photodecomposition to proceed cleanly and in relatively high quantum yield. One of these is the compound's rather low thermal stability, which makes it exceedingly difficult to purify to the level necessary for studies of this type; the major product of thermal decomposition (tetraphenylnaphthalene derivative **21**) absorbs strongly at the wavelength necessary to excite the germylene precursor, and its relatively efficiently populated triplet state absorbs very strongly over the same range as the germylene does. Earlier studies with a related compound (44) indicate that even when highly pure samples of the precursor can be obtained, the only transients detectable by time-resolved UV spectroscopic methods are derived from the excited triplet state of the aromatic coproduct. This is thought to be due to the fact that the photodecomposition reaction proceeds adiabatically, ultimately yielding the coproduct in its excited triplet state. In the present experiments with **11**, these two complicating factors combine to make the triplet state of tetraphenylnaphthalene **21** the dominant transient detectable upon laser flash photolysis of the compound in solution at ambient temperatures.

Experimental

^{1}H, ^{13}C, and ^{29}Si NMR spectra were recorded on Bruker AV 200 or AV 600 spectrometers in deuteriochloroform solution unless otherwise noted; ^{1}H and ^{13}C NMR spectra were referenced to the residual solvent proton and ^{13}C signals, respectively. High-resolution electron impact and atmospheric pressure chemical ionization (APCI) mass spectra and exact masses were determined on a Micromass TofSpec 2E (MALDI-TOF mass spectrometer) performed on a Micromass Ultima ESI/APCI triple quadrupole mass spectrometer. IR spectra were recorded on a BioRad FTS-40 FT IR spectrometer and are reported in wavenumbers (cm^{-1}). Gas chromatographic analyses were carried out using a Hewlett-Packard 5890 gas chromatograph equipped with a conventional heated injector, a flame ionization detector, a Hewlett-Packard 3396A integrator, and a SPB-5 capillary column (25 m, 0.25 μm, Supelco, Inc., Bellefonte, Pennsylvania), while GC–MS analyses were carried out using a Micromass GCT instrument interfaced to an Agilent 6890 Series GC system with a J & W DB-XLB 30 m column. Melting points were determined using a Mettler FP82 hot stage mounted on a polarizing microscope and are uncorrected. Radial chromatographic separations were carried out using a Chromatotron® (Harrison Research, Inc., Palo Alto, California) with silica gel 60 plates (4 mm thick) and with hexane as the eluant. Column chromatography was performed on a 30 mm × 600 mm column using silica gel (~100 g, acid washed, 230–400 mesh) (Silicycle). Steady-state photolyses were carried out in a Rayonet® photochemical reactor (Southern New England Ultraviolet Co., Branford, Connecticut) equipped with a merry-go-round apparatus and six RPR-2537 lamps (254 nm).

4-Methyl-2-nitroaniline (Sigma-Aldrich, St. Louis, Missouri), chlorotrimethylsilane (Gelest, Morrisville, Pennsylvania), *tert*-butyllithium (1.7 mol/L in pentane, Sigma-Aldrich), dimethylmalonate (Sigma-Aldrich), and lead tetraacetate (Sigma-Aldrich) were used as received from the suppliers. 2,3-Dimethyl-1,3-butadiene (Sigma-Aldrich) was purified before use by bulb-to-bulb distillation under vacuum. Tetrahydrofuran and hexanes (Caledon reagent grade, Georgetown, Ontario) were dried by passage through activated alumina under nitrogen using a Solv-Tek solvent purification system (Solv-Tek, Inc., Berryville, Virginia). Dichloromethane, methanol, acetone and pentane (all Caledon reagent grade) were used as received. Triethylamine (Sigma-Aldrich) was refluxed over solid KOH and distilled before use. 1,1,2,3,4,5-Hexaphenylgermole was prepared by the procedure of Ferman et al. (45).

Bis(trimethylsilyl)diphenylgermane (2a)

To a flame-dried 150 mL two-neck round-bottom flask equipped with a rubber septum, magnetic stirring bar, and nitrogen inlet was added anhydr. THF (30 mL) via a syringe. The solution was cooled to –40 °C ($MeCN–CO_2$ bath) and 5.2 g (22.8 mmol) of diphenylgermane was added by syringe dropwise through the septum. A solution of *tert*-butyllithium (1.7 mol/L in pentane, 32 mL, 54.4 mmol) was then added dropwise using a syringe in several portions over 10 min. The initial brilliant yellow reaction mixture because of the diphenylgermyl anion transformed to a dark red solution after the half-way point of the addition, signifying the presence of the diphenylgermyl dianion (Ph_2GeLi_2) (46). The solution was stirred at –40 °C for 25 min and then neat chlorotrimethylsilane (9 mL, 7.7 g, 71.3 mmol) was added dropwise via a syringe, causing a slight increase in temperature and the mixture to turn yellow and cloudy. The cooling bath was removed and the reaction mixture was stirred for 24 h, during which time a white precipitate formed. Saturated aqueous ammonium chloride was added slowly until the precipitate dissolved, diethyl ether (25 mL) was added, the layers were separated, and the aqueous portion was extracted with additional ether (3 × 25 mL). The combined ether extracts were washed with saturated brine (25 mL) and water (25 mL), dried over anhydrous magnesium sulphate, filtered, and the solvent was removed on the rotary evaporator. The resulting yellow oil was purified by vacuum distillation (6.7 g, 18.1 mmol, 79%, 110 °C (0.02 mmHg, 1 mmHg = 133.322 4 Pa)) and recrystallized at –40 °C sev-

© 2005 NRC Canada

eral times from acetone–methanol (1:1, *v*/*v*) to yield colourless needles with a melting point of approximately –20 °C. The compound was identified as **2a** by comparison of its ^{1}H and ^{13}C NMR and mass spectra to the previously reported data (6). The purity was estimated to be >99.5% by GC. ^{1}H NMR ($CDCl_3$) δ: 0.20 (s, 18H), 7.21–7.24 (m, 6H), 7.34–7.39 (m, 4H). ^{13}C NMR ($CDCl_3$) δ: 0.33, 127.5, 128.1, 135.8, 139.4. MS (EI) *m*/*z*: 376 (1, ^{76}Ge), 374 (5, ^{74}Ge), 372 (3, ^{72}Ge), 370 (2, ^{70}Ge), 359 (20), 357 (15), 355 (10), 301 (10), 299 (7), 297 (5), 226 (36), 224 (75), 222 (68), 220 (65), 197 (67), 151 (40), 149 (32), 147 (27), 136 (33), 135 (100), 107 (23), 73 (65), 45 (25). Exact mass calcd. for $C_{18}H_{28}GeSi_2$: 374.0941; found: 374.0950.

1,1,2,2-Tetraphenyl-1,2-bis(trimethylsilyl)digermane (14)

To a flame-dried 25 mL one-neck round-bottom flask equipped with a septum and magnetic stirring bar, under nitrogen, was added 1,1,2,2-tetraphenyldigermane (0.51 g, 1.12 mmol) (47) in anhydr. THF (4 mL) via a syringe. The solution was cooled to –40 °C (MeCN–CO_2 bath) and *tert*-butyllithium (1.4 mL, 2.38 mmol) was added dropwise via a syringe in several portions over 10 min. The dark yellow reaction mixture was stirred for 40 min at –40 °C and chlorotrimethylsilane (0.4 mL, 3 mmol) was added dropwise via a syringe over 2 min, causing the mixture to turn colourless. The reaction mixture was warmed to ambient temperature and stirred for 1 h after which saturated aqueous ammonium chloride (2 mL) and distilled water (4 mL) were added slowly until the solution clarified. The work up consisted of dilution with diethyl ether (20 mL) and extraction of the aqueous layer with more ether (2 × 20 mL). The combined organic layers were washed with saturated brine (20 mL) and distilled water (20 mL), dried over magnesium sulphate, filtered, and the solvent was removed on the rotary evaporator. The resulting colourless solid (>95% pure by NMR) was identified as **14** (mp 212–214 °C) on the basis of the following spectroscopic data: IR (solid): 3066 (s), 2956 (m), 1580 (w), 1481 (m), 1429 (m), 1245 (s), 1046 (s), 833 (s). ^{1}H NMR (C_6D_6) δ: 0.14 (s, 18H), 7.11 (t, *J* = 7.2 Hz, 4H), 7.15 (t, *J* = 7.2 Hz, 8H) 7.64 (d, *J* = 7.8 Hz, 8H). ^{13}C NMR (C_6D_6) δ: 0.24, 128.3, 128.4, 136.5, 139.8. ^{29}Si NMR (C_6D_6) δ: –6.1. MS (EI) *m*/*z*: 602 (1), 601 (1), 600 (2), 599 (1), 598 (1.5), 587 (4), 585 (5), 583 (4), 529 (4), 527 (5), 525 (4), 451 (60), 450 (98), 448 (100), 446 (50), 301 (69), 299 (55), 297 (43), 151 (56), 149 (45), 147 (34). Exact mass calcd. for $C_{30}H_{38}Ge_2Si_2$: 602.0936; found: 602.0947.

Diphenyltrimethylsilylgermane (17)

To a 50 mL Schlenk tube connected to a vacuum line and equipped with a magnetic stirring bar was added diphenylgermane (1.18 g, 5.16 mmol) and freshly distilled THF (5 mL). The tube was cooled to –40 °C and *tert*-butyllithium in hexane (1.58 mol/L, 3.26 mL, 5.16 mmol)) was added over 5 min. The resulting yellow mixture was allowed to warm to –20 °C and then stirred for 20 min after which chlorotrimethylsilane (1 mL, freshly distilled from calcium hydride) was added via a syringe, causing the immediate formation of a colourless precipitate. The mixture was warmed to room temperature and stirred for 1 h after which the solvent and excess chlorosilane were removed under high vacuum. The residue was extracted with dry pentane; removal of the pentane under vacuum afforded a colourless liquid. The product was further purified by bulb-to-bulb distillation (twice) to yield a colourless solid (0.55 g, 1.83 mmol, 35%, mp 36.0–37.2 °C), which was identified as **17** on the basis of the following spectral data: IR (solid): 3068 (m), 2955 (s), 2915 (s), 1998 (s, Ge-H), 1483 (m), 1430 (m), 1246 (s), 1088 (m), 976 (w), 836 (s). ^{1}H NMR (C_6D_6) δ: 0.18 (s, 9H), 5.08 (s, 1H), 7.12–7.18 (m, 6H), 7.55–7.57 (m, 4H). ^{13}C NMR (C_6D_6) δ: –0.63, 128.5, 128.6, 135.8, 137.4. ^{29}Si NMR (C_6D_6) δ: –10.1. MS (EI) *m*/*z*: 299.7 (2), 229.9 (13), 228.9 (31), 227.9 (86), 227.0 (100), 226.0 (86), 225.0 (70), 224.1 (56), 223.1 (44), 198.1 (6), 197.1 (25), 195.2 (6), 154.1 (5) 153.1 (15), 152.1 (14), 151.1 (58), 150.1 (15), 149.1 (45), 148.1 (4), 147.1 (32), 136.2 (8), 135.2 (50).

1-Amino-5-methylbenzotriazole was prepared by a modification of the procedure of Campbell and Rees (48), starting from 4-methyl-2-nitronaniline and dimethyl malonate. The original synthetic work did not include NMR or MS data for the compound or its synthetic precursors, so these are listed in the following.

Dimethyl mesoxalate 4-methyl-2-nitrophenylhydrazone

Bronze-coloured crystals, mp 158–160 °C. IR (neat): 2991 (m), 1745 (s), 1725 (s), 1450 (w), 1368 (m), 1174 (m), 944 (w). ^{1}H NMR ($CDCl_3$) δ: 2.35 (s, 3H), 3.87 (s, 3H), 3.93 (s, 3H), 7.24 (d, *J* = 8.5 Hz, 1H), 7.91 (d, *J* = 8.5 Hz, 1H), 7.97 (s, 1H), 14.08 (s, 1H). ^{13}C NMR ($CDCl_3$) δ: 20.3, 52.5, 52.6, 117.1, 124.1, 127.2, 133.4, 134.4, 136.2, 136.9, 161.8, 163.2. MS (EI) *m*/*z*: 295 (2), 141 (5), 89 (6), 87 (20), 72 (100), 71 (99), 57 (85). Exact mass calcd. for $C_{12}H_{13}N_3O_6$: 295.0804; found: 295.0802.

Dimethyl mesoxalate 2-amino-4-methylphenylhydrazone

Orange granules, mp 128 to 129 °C. IR (neat): 3464 (m), 3311 (w), 2990 (w), 1745 (s), 1725 (s), 1680 (m), 1651 (m), 1530 (s), 1440 (m), 1360 (s), 1240 (s), 1200 (m), 800 (m). ^{1}H NMR ($CDCl_3$) δ: 2.22 (s, 3H), 3.80 (s, 3H), 3.86 (s, 3H), 5.0 (bs, 2H), 6.52 (d, *J* = 8.4 Hz, 1H), 6.54 (s, 1H), 6.90 (d, *J* = 8.4 Hz, 1H), 13.29 (s, 1H). ^{13}C NMR ($CDCl_3$) δ: 20.9, 51.8, 51.9, 112.8, 118.5, 119.0, 119.2, 124.4, 136.1, 137.0, 163.4, 164.4. MS (EI) *m*/*z* 265 (2), 263 (3), 205 (8), 177 (5), 159 (5), 146 (5), 133 (5), 120 (10), 119 (12), 91 (50), 85 (80), 84 (100), 71 (60), 49 (85). Exact mass calcd. for $C_{12}H_{15}N_3O_4$: 265.1063; found: 265.1067.

Dimethyl (5-methylbenzotriazol-1-yl)iminomalonate

Yellow powder, mp 115 to 116 °C. IR (neat): 2990 (w), 1745 (s), 1625 (m), 1430 (w), 1300 (m), 1240 (s), 1160 (m), 1030 (s), 812 (s). ^{1}H NMR ($CDCl_3$) δ: 2.51 (s, 3H), 3.99 (s, 3H), 4.02 (s, 3H), 5.1 (bs, 2H), 7.44 (d, *J* = 8.4 Hz, 1H), 7.73 (d, *J* = 8.4 Hz, 1H), 7.79 (s, 1H). ^{13}C NMR ($CDCl_3$) δ: 21.4, 53.5, 53.8, 110.2, 119.4, 130.2, 132.0, 136.2, 140.0, 145.3, 160.8, 162.5. MS (EI) *m*/*z*: 276 (2), 205 (4), 177 (6), 120 (5), 119 (7), 91 (15), 88 (28), 86 (95), 84 (100), 51 (70), 49 (99), 47 (55). Exact mass calcd. for $C_{12}H_{12}N_4O_4$: 276.0859; found: 276.0864.

1-Amino-5-methylbenzotriazole

Colourless needles, mp 91 to 92 °C (lit. value (48) mp 87 to 88 °C). IR (neat): 3295 (m), 3180 (m), 2990 (w), 1745

© 2005 NRC Canada

(m), 1725 (m), 1235 (m), 1150 (m), 1110 (m), 958 (s), 810 (s). ^{1}H NMR ($CDCl_3$) δ: 2.46 (s, 3H), 5.73 (s, 2H), 7.28 (d, J = 8.4 Hz, 1H), 7.47 (d, J = 8.4 Hz, 1H), 7.66 (s, 1H). ^{13}C NMR ($CDCl_3$) δ: 21.4, 109.3, 118.4, 129.9, 130.9, 134.1, 145.0. MS (EI) *m/z*: 148 (4), 133 (4), 120 (25), 119 (35), 92 (20), 91 (90), 86 (75), 84 (100), 77 (15), 65 (22), 51 (17), 50 (75). Exact mass calcd. for $C_7H_8N_4$: 148.0749; found: 148.0750.

1,4-Dihydro-5-methyl-1,2,3,4,9,9-hexaphenyl-1,4-germanonaphthalene (11)

1,4-Dihydro-5-methyl-1,2,3,4,9,9-hexaphenyl-1,4-germanonaphthalene (**11**) was prepared using the method of Ando et al. (17) for the synthesis of **4**. To a flame-dried 100 mL two-neck round-bottom flask equipped with an addition funnel and magnetic stir bar under N_2 was added anhydrous dichloromethane (30 mL) containing 1,1,2,3,4,5-hexaphenylgermole (2.00 g, 3.42 mmol) and 1-amino-5-methylbenzotriazole (0.53 g, 3.59 mmol). The resulting yellowish solution was cooled to –78 °C (*i*-PrOH–CO_2 bath) and a solution of lead tetraacetate (1.67 g, 3.77 mmol) in anhydrous dichloromethane (15 mL) added dropwise with stirring over 50 min. The resulting brown-tinged solution was allowed to warm gradually to room temperature over 1.5 h and then quenched with saturated aqueous sodium carbonate (20 mL). The organic layer was separated, dried with magnesium sulfate, filtered, and the solvent was removed on the rotary evaporator to yield a yellow oil. The oil was purified by radial chromatography in the freezer at –15 °C using precooled dichloromethane–pentane (1:3, *v/v*) as the eluant, which yielded three easily separable fractions. The first two fractions were identified as a 1:1 mixture of 3(3′)-dimethylbiphenylene and 3(4′)-dimethylbiphenylene (**20a** and **20b**, respectively, 0.05 g, 0.28 mmol) (49) and 6-methyl-1,2,3,4-tetraphenylnaphthalene (**21**) (0.35 g, 0.78 mmol) by comparison of their ^{1}H NMR spectra to the literature data. The third fraction (1.8 g, 2.67 mmol, 78%) consisted of a pale yellow powder that was identified as **11** on the basis of the following spectroscopic data: ^{1}H NMR ($CDCl_3$) δ: 2.34 (s, 3H), 6.62 (bs, 4H), 6.80 (d, J = 7.2 Hz, 2H), 6.90–6.96 (m, 7H), 7.07–7.13 (m, 12H), 7.19 (d, J = 7.2 Hz, 1H), 7.39 (d, J = 7.2 Hz, 2H), 7.39 (t, J = 7.2 Hz, 2H), 7.44 (t, J = 7.2 Hz, 1H), 7.75 (d, J = 7.2 Hz, 2H). ^{13}C NMR ($CDCl_3$) δ: 21.5, 61.1, 64.4, 121.8, 122.9, 124.9, 125.5, 125.7, 127.1, 127.6, 128.0, 128.3, 129.7, 129.9, 130.0, 130.1, 131.5, 133.7, 135.0, 135.8, 136.1, 137.1, 138.0, 138.1, 138.3, 138.4, 145.1, 145.8, 146.2, 147.9. MS (APCI) *m/z*: 677.2 (20, ^{76}Ge, M + 1), 675.2 (100, ^{74}Ge, M + 1), 673.1 (60, ^{72}Ge, M + 1), 671.2 (45, ^{70}Ge, M + 1).

Steady-state photolysis experiments

Steady-state photolysis of a deoxygenated solution (ca. 0.75 mL) of **2a** (0.05 mol/L) in cyclohexane-d_{12} containing DMB (0.1 mol/L) was carried out in a quartz NMR tube, monitoring the reaction periodically by ^{1}H NMR spectroscopy over the 0%–16% conversion range. The NMR spectra of the photolysate showed the growth of peaks assignable to hexamethyldisilane (Si_2Me_6, δ 0.049) and **5** (δ: 1.78 (s, 6H) 1.97 (s, 4H), 7.20–7.24 (m, 6H), 7.40–7.43 (m, 4H)) on the basis of comparisons with the spectra of authentic samples; the relative intensities of the Si_2Me_6 singlet and the δ 1.78 ppm singlet owing to **5** averaged to 1.0:3.24, indicating a relative yield of 1:1.08. No other peaks were evident in the 0–0.3 ppm region of the spectrum, although it should be noted that the signal owing to $PhSiMe_3$ (δ 0.233) is almost coincident with that owing to **2a** (δ 0.228). In a second experiment, a deoxygenated hexane solution containing **2a** (0.01 mol/L) and DMB (0.03 mol/L) was photolyzed to ca. 60% conversion with periodic monitoring by GC. The product mixture contained (in order of increasing elution time) $PhSiMe_3$ (2.3%), **12** (2.5%), **5** (41%), and **2a** (50%); Si_2Me_6 elutes with the solvent under these conditions. The products were identified by GC–MS analysis; the product assigned to **12** exhibited the following mass spectrum: MS (EI) *m/z*: 308 (2, ^{76}Ge), 306 (8, ^{74}Ge), 304 (5, ^{72}Ge), 302 (3, ^{70}Ge), 291 (2), 289 (1), 287 (1), 226 (6), 224 (42), 222 (28), 220 (19), 156 (39), 154 (25), 152 (17), 151 (17), 149 (12), 147 (10), 136 (19), 135 (100), 73 (40), 45 (5).

Steady-state photolysis of a deoxygenated solution (ca. 0.75 mL) of **2a** (0.05 mol/L) in cyclohexane-d_{12} containing MeOH (0.5 mol/L) was carried out in a similar manner to that previously described for the DMB trapping experiment. The NMR spectra of the photolysate showed the growth of peaks assignable to Si_2Me_6 (δ 0.049), **13** (δ: 3.54 (s, 3H), 6.12 (s, 1H), 7.2–7.32 (m, 6H), 7.51–7.53 (m, 4H)), and **14** (δ: 0.027 (s, 18H), 7.15–7.19 (m, 12H), 7.36–7.40 (m, 8H)) on the basis of comparisons with the spectra of authentic samples, together with two additional Me_3Si containing species (δ 0.057 and 0.063), which were not identified; the relative intensities of the Si_2Me_6 singlet, the MeO singlet owing to **13** (δ 3.54), and the –$SiMe_3$ singlets owing to **14** (δ 0.027) and the two unidentified components were 1.00 : 0.139 ± 0.013 : 0.114 ± 0.020 : 0.103 ± 0.027 : 0.121 ± 0.006. This gives average relative yields of 1.0 : 0.84 ± 0.07 : 0.11 ± 0.02 : 0.20 ± 0.05 : 0.24 ± 0.02 for the five products, assuming that the singlets for the two unidentified components represent a single trimethylsilyl group each.

Steady-state photolyses (254 nm) of **11** were carried out in similar fashion, on argon outgassed 0.046 mol/L solutions of the compound in cyclohexane-d_{12} containing methanol (0.5 mol/L) and DMB (0.5 mol/L). The photolyses were taken to ca. 60% conversion and were monitored periodically by ^{1}H NMR spectroscopy. In both cases, the formation of the diphenylgermylene adduct (**5** and **13**, respectively) was accompanied by an equal yield of **21**; no other products could be detected in yields greater than ca. 3%. The identities of the products were verified by comparison of the spectra of the crude photolysis mixtures with those of authentic samples.

Thermolysis of benzogermanorbornadiene 11

The thermolysis of **11** was carried out with argon outgassed 0.046 mol/L solutions of the compound in cyclohexane-d_{12} containing DMB (0.5 mol/L). Thermal decomposition of **11** was monitored by 200 MHz ^{1}H NMR spectroscopy, measuring the relative intensities of the δ 2.28 singlet owing to **11** and the residual proton peak owing to the solvent, every 20 min over a 24 h period. The loss of **11** was accompanied by the formation of **21** (δ_{CH_3} 2.31) and **5**.

Laser flash photolysis experiments

Laser flash photolysis experiments with **2a**, **11**, and **21** employed the pulses from a Lambda Physik Compex 120

© 2005 NRC Canada

excimer laser filled with F_2–Kr–Ne mixtures (248 nm, ~25 ns, 100 ± 5 mJ) and a Luzchem Research mLFP-111 laser flash photolysis system, modified as previously described (9). Solutions were prepared at concentrations such that the absorbance at the excitation wavelength was between ca. 0.7 and 0.9, and were continuously flowed through a vacuum oven-dried, thermostatted 7 mm × 7 mm Suprasil flow cell connected to a calibrated 100 mL reservoir, fitted with a glass frit to allow bubbling of argon gas through the solution for at least 30 min prior to and then throughout the duration of each experiment; the entire apparatus was dried in a vacuum oven at 65–85 °C before use. Solution temperatures were measured with a Teflon-coated copper/constantan thermocouple directly inserted into the flow cell. Reagents were added directly to the reservoir by microliter syringe as aliquots of standard solutions. In experiments with those scavengers that absorb at the laser wavelength, the concentrations employed were kept low enough to ensure that the fraction of the excitation light absorbed by the scavenger never exceeded ca. 10%, to avoid complications in the kinetics owing to screening effects or the formation of potentially reactive species from cophotolysis of the scavenger. For experiments using oxygen as a scavenger, solutions of selected O_2–N_2 ratios were prepared by adding the appropriate volume of a nitrogen saturated solution of **1a** in hexane to an oxygen saturated hexane solution of the same concentration in **1a**.

Flash photolysis experiments with compound **17** and triphenylgermane were carried out using Professor J.C. Scaiano's system at the University of Ottawa and a Lumonics EX-530 excimer laser filled with Xe–HCl–Ne mixtures (308 nm, ~6 ns, 70 ± 5 mJ) for excitation. Signals from the monochromator/photomultiplier were captured by a Tektronix 2440 digitizer and transferred to a PowerMacintosh computer programmed in the LabVIEW 4.1 environment from National Instruments (Austin, Texas). Detailed descriptions of similar laser systems have been provided elsewhere (51). Argon outgassed solutions of **18** (5–30 mmol/L) in BOOB–isooctane (1:4, *v*/*v*) were contained in 7 mm × 7 mm (static) quartz cells. Experiments were carried out at room temperature (22 °C). Growth rate constants for radical absorptions were determined by biexponential nonlinear least-squares analysis of the growth–decay profiles, recorded at 420 nm in the case of **17** and 340 nm in the case of triphenylgermane.

Transient decay and growth rate constants were calculated by nonlinear least-squares analysis of the absorbance–time profiles using the PRISM 3.0 software package (GraphPad Software, Inc., San Diego, California) and the appropriate user-defined fitting equations, after importing the raw data from the Luzchem mLFP software. Rate constants were calculated by linear least-squares analysis of decay rate – concentration data (generally four to seven points) that spanned as large a range in transient decay rate as possible. Errors are quoted as twice the standard deviation obtained from the least-squares analyses.

Acknowledgements

We thank the Natural Sciences and Engineering Research Council of Canada (NSERC) for financial support, Teck Cominco Metals Ltd. for a generous gift of germanium tetrachloride, the McMaster Regional Centre for Mass Spectrometry for mass spectra, J.C. Scaiano for the use of his laser photolysis system, and M. Chretien for technical assistance. PPG and DZ are grateful for financial support from the United States National Science Foundation under grants CHE-9981715 and CHE-0316124. BKC thanks the Reactive Intermediate Student Exchange (RISE) and NSERC for summer scholarships.

References

1. W. Ando, T. Tsumuraya, and A. Sekiguchi. Chem. Lett. 317 (1987).
2. S. Konieczny, S.J. Jacobs, J.K. Braddock Wilking, and P.P. Gaspar. J. Organomet. Chem. **341**, C17 (1988).
3. K. Mochida, M. Wakasa, Y. Nakadaira, Y. Sakaguchi, and H. Hayashi. Organometallics, **7**, 1869 (1988).
4. M. Wakasa, I. Yoneda, and K. Mochida. J. Organomet. Chem. **366**, C1 (1989).
5. K. Mochida, I. Yoneda, and M. Wakasa. J. Organomet. Chem. **399**, 53 (1990).
6. K.L. Bobbitt, V.M. Maloney, and P.P. Gaspar. Organometallics, **10**, 2772 (1991).
7. N.P. Toltl, W.J. Leigh, G.M. Kollegger, W.G. Stibbs, and K.M. Baines. Organometallics, **15,** 3732 (1996).
8. K. Mochida, M. Wakasa, and H. Hayashi. Phosphorus Sulfur Silicon Relat. Elem. **150–151**, 237 (1999).
9. W.J. Leigh, C.R. Harrington, and I. Vargas-Baca. J. Am. Chem. Soc. **126**, 16105 (2004).
10. W.J. Leigh and C.R. Harrington. J. Am. Chem. Soc. **127**, 5084 (2005).
11. K. Mochida, N. Kanno, R. Kato, M. Kotani, S. Yamauchi, M. Wakasa, and H. Hayashi. J. Organomet. Chem. **415**, 191 (1991).
12. K. Mochida and S. Tokura. Organometallics, **11**, 2752 (1992).
13. K. Mochida and S. Tokura. Bull. Chem. Soc. Jpn. **65**, 1642 (1992).
14. K. Mochida, K. Kimijima, and H. Chiba. Organometallics, **13**, 404 (1994).
15. M.B. Taraban, O.S. Volkova, V.F. Plyusnin, Y.V. Ivanov, T.V. Leshina, M.P. Egorov, O.M. Nefedov, T. Kayamori, and K. Mochida. J. Organomet. Chem. **601**, 324 (2000).
16. W. Ando, H. Itoh, T. Tsumuraya, and H. Yoshida. Organometallics, **7**, 1880 (1988).
17. W. Ando, H. Itoh, and T. Tsumuraya. Organometallics, **8**, 2759 (1989).
18. W.J. Leigh, N.P. Toltl, P. Apodeca, M. Castruita, and K.H. Pannell. Organometallics, **19**, 3232 (2000).
19. W.P. Neumann and M. Schriewer. Tetrahedron Lett. **21**, 3273 (1980).
20. J. Kocher, M. Lehnig, and W.P. Neumann. Organometallics, **7**, 1201 (1988).
21. W.P. Neumann, E. Michels, and J. Kocher. Tetrahedron Lett. **28**, 3783 (1987).
22. W. Ando and T. Tsumuraya. Organometallics, **8**, 1467 (1989).
23. W.J. Leigh and G.W. Sluggett. J. Am. Chem. Soc. **115**, 7531 (1993).
24. W.J. Leigh and G.W. Sluggett. Organometallics, **13**, 269 (1994).
25. P. Riviere, J. Satge, and A. Castel. C.R. Acad. Sci. Paris, **281**, 835 (1975).
26. J. Barrau, M. Bouchaut, H. Lavayssiere, G. Dousse, and J. Satge. J. Organomet. Chem. **243**, 281 (1983).
27. S. Mazieres, H. Gornitzka, and C. Couret. Polyhedron, **21**, 2827 (2002).

© 2005 NRC Canada

28. N.N. Zemlyansky, I.V. Borisova, M.G. Kuznetsova, V.N. Khrustalev, Y.A. Ustynyuk, M.S. Nechaev, V.V. Lunin, J. Barrau, and G. Rima. Organometallics, **22**, 1675 (2003).
29. W.J. Leigh and G.W. Sluggett. J. Am. Chem. Soc. **116**, 10468 (1994).
30. K. Mochida, H. Kikkawa, and Y. Nakadaira. J. Organomet. Chem. **412**, 9 (1991).
31. M. Ishikawa and M. Kumada. Adv. Organomet. Chem. **19**, 51 (1981).
32. M. Kira and T. Miyazawa. *In* The chemistry of organic silicon compounds. *Edited by* Z. Rappoport and Y. Apeloig. John Wiley and Sons, New York. 1998. p. 1311.
33. M.G. Steinmetz. Chem. Rev. **95**, 1527 (1995).
34. M. Ishikawa, T. Fuchikami, T. Sugaya, and M. Kumada. J. Am. Chem. Soc. **97**, 5923 (1975).
35. W.J. Leigh, R. Boukherroub, and C. Kerst. J. Am. Chem. Soc. **120**, 9504 (1998).
36. T.L. Morkin, T.R. Owens, and W.J. Leigh. *In* The chemistry of organic silicon compounds. Vol. 3. *Edited by* Z. Rappoport and Y. Apeloig. John Wiley and Sons, New York. 2001. p. 949.
37. T.L. Morkin and W.J. Leigh. Acc. Chem. Res. **34**, 129 (2001).
38. N.P. Toltl and W.J. Leigh. J. Am. Chem. Soc. **120**, 1172 (1998).
39. (*a*) C. Chatgilialoglu, K.U. Ingold, J. Lusztyk, A.S. Nazran, and J.C. Scaiano. Organometallics **2**, 1332 (1983); (*b*) K.B. Clark and D. Griller. Organometallics, **10**, 746 (1991).
40. K.U. Ingold, J. Lusztyk, and J.C. Scaiano. J. Am. Chem. Soc. **106**, 343 (1984).
41. C. Chatgilialoglu and M. Ballestri. Organometallics, **14**, 5017 (1995).
42. C. Chatgilialoglu. Chem. Rev. **95**, 1229 (1995).
43. S. Bernadoni, M. Lucarini, G.F. Pedulli, L. Valgimigli, V. Gevorgyan, and C. Chatgilialoglu. J. Org. Chem. **62**, 8009 (1997).
44. H. Görner, M. Lehnig, and M. Weisbeck. J. Photochem. Photobiol. A, **94**, 157 (1996).
45. J. Ferman, J.P. Kakareka, W.T. Klooster, J.L. Mullin, J. Quattrucci, J.S. Ricci, H.J. Tracy, W.J. Vining, and S. Wallace. Inorg. Chem. **38**, 2464 (1999).
46. A. Castel, P. Riviere, J. Satge, and H.Y. Ko. Organometallics, **9**, 205 (1990).
47. A. Castel, P. Riviere, J. Satge, D. Desor, M. Ahbala, and C. Abdenadher. Inorg. Chim. Acta, **212**, 51 (1993).
48. C.D. Campbell and C.W. Rees. J. Chem. Soc. (C), 742 (1969).
49 T. Kitamura, M. Yamane, K. Inoue, M. Todaka, N. Fukatsu, Z. Meng, and Y. Fujiwara. J. Am. Chem. Soc. **121**, 11674 (1999).
50. C. Chatgilialoglu. *In* CRC handbook of photochemistry. Vol II. *Edited by* J.C. Scaiano. CRC Press, Boca Raton, Florida. 1989. p. 3.
51. J.C. Scaiano, M. Tanner, and D. Weir. J. Am. Chem. Soc. **107**, 4396 (1985).

© 2005 NRC Canada

Kinetic isotope effect evidence for the concerted transfer of hydride and proton from hydroxycyclopentadienyl ruthenium hydride in solvents of different polarities and hydrogen bonding ability[1]

Charles P. Casey and Jeffrey B. Johnson

Abstract: The tolyl analogue of Shvo's hydroxycyclopentadienyl ruthenium hydride (**4**) efficiently transfers a hydride and proton to benzaldehyde or acetophenone to produce an alcohol. This reduction can be performed in toluene, methylene chloride, and THF. Reduction of benzaldehyde in toluene and methylene chloride occurs approximately 300 times faster than in THF at 0 °C. Reduction of acetophenone occurs between 75 and 150 times slower than benzaldehyde at 0 °C in each respective solvent. Despite the differences in rate, mechanistic studies have provided evidence for a similar concerted transfer of acidic and hydridic hydrogens in each solvent. Addition of water to THF led to further rate decrease coupled with an increase in the OH/D kinetic isotope effect and a decrease in the RuH/D kinetic isotope effect. Addition of excess alcohol to toluene or methylene chloride results in the significant retardation of the rate of reduction. The slower rate in THF and in the presence of alcohol is attributed to the stabilization of the ground state of ruthenium hydride **4** by hydrogen bonding and the additional energy required to break these bonds prior to carbonyl reduction.

Key words: ruthenium hydrogenation catalysis, hydrogenation mechanism, kinetic isotope effects, ligand–metal bifunctional catalysis.

Résumé : L'analogue tolyle du composé de Shvo, l'hydrure d'hydroxocyclopentadiényle ruthénium (**4**) permet d'effectuer un transfert efficace d'un hydrure et d'un proton vers le benzaldéhyde ou l'acétophénone pour conduire à la production d'un alcool. Cette réduction peut être effectuée dans le toluène, le chlorure de méthylène et le THF. À 0 °C, a réduction du benzaldéhyde dans le toluène et le chlorure de méthylène se produit environ 300 fois plus rapidement que dans le THF. À 0 °C, dans chacun des solvants respectifs, la réduction de l'acétophénone se produit entre 75 et 150 fois plus lentement que celle du benzaldéhyde. Malgré les différences dans les vitesses de réaction, les études de mécanismes ont fourni des données qui militent en faveur d'un transfert similaire d'atomes d'hydrogènes sous les formes de proton et d'hydrure dans chaque solvant. L'addition d'eau au THF conduit à une diminution encore plus grande de la vitesse de réaction couplée à une augmentation de l'effet isotopique cinétique OH/D et à une diminution de l'effet isotopique cinétique RuH/D. L'addition d'un excès d'alcool au toluène ou au chlorure de méthylène conduit à une diminution significative de la vitesse de réduction. La vitesse de réaction sensiblement plus faible dans le THF et en présence d'alcool est attribuée à la stabilisation de l'état fondamental de l'hydrure de ruthénium **4** par une liaison hydrogène et à l'énergie additionnelle requise pour briser ces liens avant la réduction du carbonyle.

Mots clés : catalyse d'hydrogénation par le ruthénium, mécanisme d'hydrogénation, effets isotopiques cinétiques, catalyse bifonctionnelle ligand–métal.

[Traduit par la Rédaction]

Introduction

The development of new catalysts over the past two decades has revolutionized hydrogenation chemistry. The emergence of ligand–metal bifunctional catalysts was initiated by Shvo's report of the hydroxycyclopentadienyl ruthenium hydride catalyst (**1**) (1) and followed by Noyori's development of the (BINAP)Ru(II)(diamine) (**2**) (2) and (arene)Ru(II)(diamine) (**3**) (3) catalysts (Fig. 1). These new species utilize electronically coupled acidic and hydridic hydrogens to catalyze the selective asymmetric reduction of ketones under mild conditions, using hydrogen or 2-

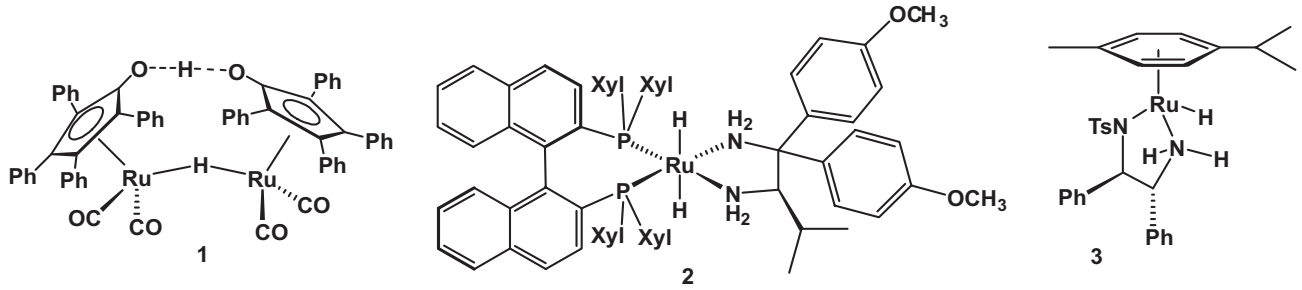
Received 20 January 2005. Published on the NRC Research Press Web site at http://canjchem.nrc.ca on 29 October 2005.

C.P. Casey[2] and J.B. Johnson. Department of Chemistry, University of Wisconsin-Madison, Madison, WI 53706, USA.

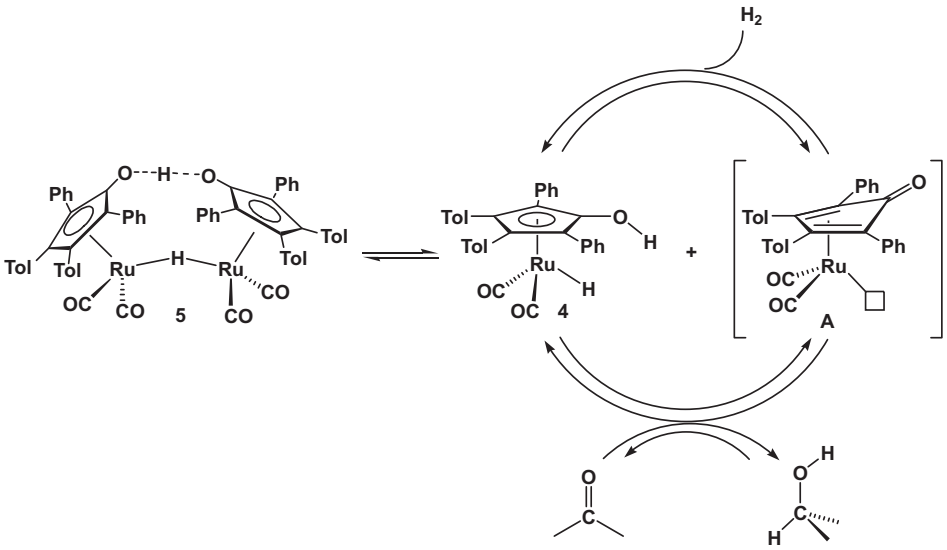
[1]This article is part of a Special Issue dedicated to organic reaction mechanisms.
[2]Corresponding author (e-mail: casey@chem.wisc.edu).

 doi: 10.1139/V05-140 © 2005 NRC Canada

Fig. 1. Ligand–metal bifunctional catalysts.



Scheme 1.



propanol as terminal reductants. These catalysts provide attractive alternatives to stoichiometric reducing agents such as $LiAlH_4$ and $NaBH_4$, and reduce ketones and aldehydes without the need for strongly acidic or basic conditions.

Several studies have been reported that provide mechanistic information about processes catalyzed by Shvo's ruthenium hydride complex. Utilizing the tolyl substituted analogue of Shvo's catalyst, our group has reported evidence consistent with a concerted transfer of the acidic and hydridic hydrogens from **4** to aldehydes (4). In this previous study, however, we could not conclusively exclude a two-step mechanism in which the activation barrier for proton transfer was of similar energy to that for hydride transfer. Here we report studies of ketone reduction performed in an effort to differentiate between these two mechanisms.

Our group has also reported studies of the reduction mechanisms of imines by the monomeric ruthenium hydride **4** (5), the method of hydrogen activation during catalysis (6), as well as a detailed report of the rates of each step within the overall catalytic cycle (Scheme 1).[3] Studies utilizing the Shvo catalyst have been reported in toluene, the solvent primarily used for catalytic reductions, as well as in THF and methylene chloride, solvents used for coupled oxidations, dynamic kinetic resolution, and other isomerization processes (7–9). To assess the validity of the assumption that these mechanisms remain similar in solvents of different natures, we initiated this study to establish the mechanism of aldehyde and ketone reduction by ruthenium hydride **4** in each of these solvents.

Results

Studies of the mechanism of aldehyde reduction in THF-d_8 by the active reducing agent in Shvo's system (ruthenium hydride **4**), have been previously reported by our group (4). These studies, however, were performed in the presence of a small amount of water. Although the role of water was once assumed to be of little consequence to the reaction mechanism, herein we present data that suggests that water slows reduction by stabilization of **4** by hydrogen bonding. The magnitude of each kinetic isotope effect is also dependent upon the concentration of water in solution. Additional data indicates that solvent polarity has little effect on the mechanism of hydrogen transfer, but hydrogen bonding solvents or additives retard reduction.

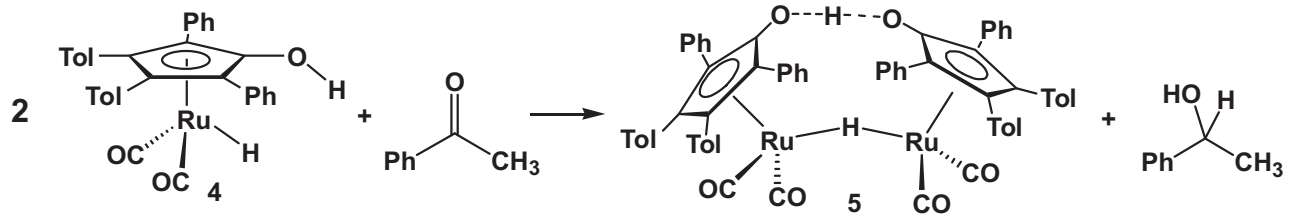
Reduction of acetophenone by 4 in dry toluene-d_8

Reduction of acetophenone by **4** in dry toluene-d_8 resulted in the clean formation of 1-phenylethanol and bridging ruthenium hydride **5** (Scheme 2). The rate of reduction was

[3] C.P. Casey and J.B. Johnson. Unpublished results.

© 2005 NRC Canada

Scheme 2.



monitored by ^{1}H NMR spectroscopy at 6 °C under pseudo-first-order conditions, with a large excess of acetophenone (0.252 mol/L) over **4** (0.0134 mol/L). The first-order disappearance of resonances of **4** (δ 1.85 ($CpTolCH_3$) and –9.26 (RuH)) and the concurrent appearance of resonances consistent with diruthenium hydride **5** (δ 1.80 ($CpTolCH_3$)) and 1-phenylethanol (δ 0.70 (CH_3)) were monitored for at least three half-lives. A plot of concentration vs time was constructed, and the excellent fit to a first-order, nonlinear least-squares equation indicated that the reaction was first-order in ruthenium hydride. Linear dependence upon the concentration of acetophenone (0.185–0.252 mol/L) was observed. These experiments established a second-order rate law for the reduction of acetophenone by **4** (eq. [1]). The rate of ruthenium hydride disappearance is twice that of ketone reduction, as 1 equiv. reduces the ketone while a second traps the proposed unsaturated intermediate to form bridging diruthenium hydride **5**.

$$[1] \qquad -\mathrm{d[ket]}/\mathrm{d}t = -1/2\mathrm{d[\mathbf{4}]}/\mathrm{d}t = k[\mathbf{4}][\mathrm{ket}]$$

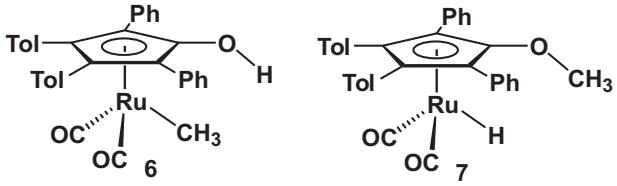
Nature of 4 in toluene

During reduction of acetophenone, the rate displays first-order dependence upon the concentration of **4**. Based upon pulsed gradient spin echo (PGSE) NMR spectroscopy studies (10), however, our group has previously determined that in the absence of hydrogen bonding species, **4** exists as a hydrogen bonded dimer in toluene (6). To test the state of aggregation of **4** in the presence of acetophenone in toluene, we utilized ruthenium methyl complex **6** as a model for **4**, as it has similar hydrogen bonding ability, but displays no reactivity with acetophenone at room temperature (Fig. 2).

In the absence of hydrogen bonding species, PGSE studies indicate that ruthenium methyl complex **6** (9.2 mg, 0.0157 mol/L)[4] has a diffusion constant ($D = 2.09 \times 10^{-11}$ m^2 s^{-1}) similar to that of **5** ($D = 1.98 \times 10^{-11}$ m^2 s^{-1}). This is consistent with **6** being a dimer in toluene, as is **4**. Upon addition of a 15-fold excess of acetophenone (0.229 mol/L), PGSE studies of **6** indicate a larger diffusion constant ($D = 3.40 \times 10^{-11}$ m^2 s^{-1}), similar to that observed for methoxy ruthenium complex **7** (6) ($D = 3.65 \times 10^{-11}$ m^2 s^{-1}). This indicates that in the presence of excess acetophenone, **6** is monomeric, most likely hydrogen bound to acetophenone. Further information is provided in the Supporting information.[5]

The rate of reduction of acetophenone by **4** was monitored at temperatures between –6 and 17 °C. The second-order rate constants $k = 6.67 \times 10^{-3}$ (mol/L)$^{-1}$ s^{-1} at –6 °C, $k = 12.2 \times 10^{-3}$ (mol/L)$^{-1}$ s^{-1} at 0 °C, $k = 16.2 \times 10^{-3}$ (mol/L)$^{-1}$ s^{-1} at 6 °C, $k = 30.5 \times 10^{-3}$ (mol/L)$^{-1}$ s^{-1} at 12 °C, and $k = 43.4 \times 10^{-3}$ (mol/L)$^{-1}$ s^{-1} at 17 °C allowed the determination of the activation parameters $\Delta H^{\ddagger} = 12.5 \pm 1.1$ kcal mol^{-1} (1 cal = 4.184 J) and $\Delta S^{\ddagger} = -21.4 \pm 3.5$ eu.

Fig. 2. Ruthenium models used in PGSE studies.



The kinetic deuterium isotope effects for this reaction in toluene were determined by measuring the rate of reduction of acetophenone with **4** and its isotopomers (**4-RuHOD**, **4-RuDOH**, and **4-RuDOD**) at 6 °C. These rate constants, $k_{RuHOH} = (15.5 \pm 0.6) \times 10^{-3}$ (mol/L)$^{-1}$ s^{-1}, $k_{RuHOD} = (13.5 \pm 0.1) \times 10^{-3}$ (mol/L)$^{-1}$ s^{-1}, $k_{RuDOH} = (4.74 \pm 0.12) \times 10^{-3}$ (mol/L)$^{-1}$ s^{-1}, and $k_{RuDOD} = (4.16 \pm 0.16) \times 10^{-3}$ (mol/L)$^{-1}$ s^{-1}, yielded the kinetic isotope effects provided in Table 1.

Kinetic study of the reduction of benzaldehyde by 4 in toluene-d_8

Kinetic study of the reduction of benzaldehyde by **4** in toluene-d_8 was performed in a similar manner to that described for the reduction of acetophenone. The reduction of benzaldehyde followed second-order kinetics and cleanly yielded benzyl alcohol and **5**. While reduction of acetophenone by **4** was monitored at 6 °C, the reduction of benzaldehyde by **4** was much faster and required lower temperatures (–26 to –49 °C) to obtain convenient rates. Activation parameters for benzaldehyde reduction were $\Delta H^{\ddagger} = 13.0 \pm 1.8$ kcal mol^{-1} and $\Delta S^{\ddagger} = -11.0 \pm 5.1$ eu. Kinetic isotope effects were determined at –37 °C and are reported in Table 1.

Reduction of benzaldehyde by 4 in toluene-d_8 in the presence of ethanol

To assess the effect of the presence of excess ethanol on the rate of reduction, the reduction of benzaldehyde by **4** was performed in toluene containing excess EtOH at –37 °C and monitored by ^{1}H NMR spectroscopy. In the presence of between 0.05 and 0.10 mol/L of EtOH, the rate was independent of ethanol concentration, and displayed first-order

[4] Concentration reported assuming a monomeric nature of each species tested.

[5] Supplementary data for this article are available on the Web site or may be purchased from the Depository of Unpublished Data, Document Delivery, CISTI, National Research Council Canada, Ottawa, ON K1A 0S2, Canada. DUD 4025. For more information on obtaining material refer to http://cisti-icist.nrc-cnrc.gc.ca/irm/unpub_e.shtml.

© 2005 NRC Canada

Table 1. Kinetic isotope effects for the reduction of acetophenone and benzaldehyde by **4** in toluene-d_8, CD_2Cl_2, and THF-d_8.

	Toluene-d_8		CD_2Cl_2		THF-d_8	
Type	PhCHO	$PhCOCH_3$	PhCHO	$PhCOCH_3$	PhCHO	$PhCOCH_3$
k_{RuHOH}/k_{RuHOD}	1.38±0.08	1.15±0.06	1.33±0.13	1.20±0.05	1.30±0.02	1.12±0.05
k_{RuDOH}/k_{RuDOD}	1.37±0.10	1.14±0.05	1.34±0.14	1.17±0.09	1.30±0.08	1.14±0.11
k_{RuHOH}/k_{RuDOH}	2.65±0.18	3.27±0.15	2.51±0.28	2.17±0.15	2.60±0.09	2.50±0.13
k_{RuHOD}/k_{RuDOD}	2.63±0.14	3.24±0.13	2.53±0.24	2.11±0.20	2.60±0.14	2.55±0.24
k_{RuHOH}/k_{RuDOD}	3.63±0.25	3.72±0.20	3.36±0.36	2.54±0.21	3.38±0.19	2.85±0.29

Table 2. Activation parameters and calculated $\Delta G^{\ddagger}$ at 0 °C for reduction of benzaldehyde and acetophenone by **4** in toluene-d_8, CD_2Cl_2, and THF-d_8.

Solvent	Compound	$\Delta H^{\ddagger}$ (kcal mol^{-1})	$\Delta S^{\ddagger}$ (kcal mol^{-1} K^{-1})	$\Delta G^{\ddagger}$ (kcal mol^{-1})
Toluene-d_8	Benzaldehyde	13.0±1.8	–11.0±5.1	16.0
	Acetophenone	12.5±1.1	–21.4±3.5	18.3
CD_2Cl_2	Benzaldehyde	11.9±1.0	–15.6±3.2	16.1
	Acetophenone	10.8±1.2	–28.8±3.8	18.6
THF-d_8	Benzaldehyde	11.2±0.9	–28.9±2.6	19.1
	Acetophenone	17.5±1.2	–15.8±4.0	21.8

Table 3. Isotope effects from reduction of benzaldehyde by the isotopomers of **4** in THF-d_8 in the presence of water (H_2O or D_2O) at 22 °C.[7]

Type	Benzaldehyde (no water)	Benzaldehyde (0.079 mol/L water)	Benzaldehyde (0.120 mol/L water)
k_{RuHOH}/k_{RuHOD}	1.30±0.02	2.30±0.16	2.99±0.35
k_{RuDOH}/k_{RuDOD}	1.30±0.08	2.15±0.34	3.19±0.42
k_{RuHOH}/k_{RuDOH}	2.60±0.09	1.63±0.23	1.32±0.11
k_{RuHOD}/k_{RuDOD}	2.60±0.14	1.52±0.15	1.42±0.24
k_{RuHOH}/k_{RuDOD}	3.38±0.19	3.50±0.25	4.25±0.62

dependence upon **4** and benzaldehyde. The rate constant at –37 °C ($k = 5.6 \times 10^{-3}$ (mol/L)$^{-1}$ s^{-1}) is approximately 3 times slower than the rate constant under completely water and alcohol free conditions ($k = 17.7 \times 10^{-3}$ (mol/L)$^{-1}$ s^{-1}).

The reduction of benzaldehyde by 4 in CD_2Cl_2

The reduction of benzaldehyde by **4** in CD_2Cl_2 also followed second-order kinetics in cleanly forming benzyl alcohol and **5**. Reduction of benzaldehyde between –30 and –47 °C resulted in activation parameters of $\Delta H^{\ddagger} = 11.9 \pm 1.0$ kcal mol^{-1} and $\Delta S^{\ddagger} = -15.6 \pm 3.2$ eu. Use of the isotopomers of **4** at –36 °C provided kinetic deuterium isotope effects (Table 1).

Kinetic study of acetophenone reduction by 4 in CD_2Cl_2

Kinetic study of acetophenone reduction by **4** in CD_2Cl_2 was performed between –6 and 17 °C. The reduction occurs with a second-order rate law. Activation parameters were $\Delta H^{\ddagger} = 10.8 \pm 1.2$ kcal mol^{-1} and $\Delta S^{\ddagger} = -28.8 \pm 3.8$ eu. Reduction by the isotopomers of **4** at 3 °C provided deuterium kinetic isotope effects (Table 1).

The reduction of benzaldehyde by 4 in dry THF-d_8

The reduction of benzaldehyde by **4** in dry THF-d_8 resulted in the clean formation of benzyl alcohol and **5** in a second-order process. Significantly slower benzaldehyde reduction required temperatures approximately 50 °C higher than those used for reduction in toluene-d_8 and CD_2Cl_2. Activation parameters were determined between 10 and 34 °C: $\Delta H^{\ddagger} = 11.2 \pm 0.9$ kcal mol^{-1} and $\Delta S^{\ddagger} = -28.9 \pm 2.6$ eu (Table 2).[6]

Reduction of benzaldehyde by the isotopomers of 4 under completely dry conditions

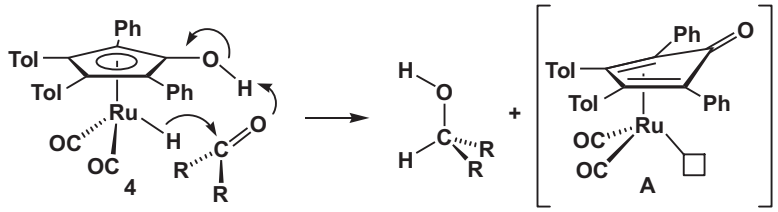
Reduction of benzaldehyde by the isotopomers of **4** under completely dry conditions in THF-d_8 at 22 °C was followed by ^{1}H NMR spectroscopy. The resulting second-order rate constants, $k_{RuHOH} = (15.02 \pm 0.29) \times 10^{-3}$ (mol/L)$^{-1}$ s^{-1}, $k_{RuHOD} = (11.56 \pm 0.13) \times 10^{-3}$ (mol/L)$^{-1}$ s^{-1}, $k_{RuDOH} =$

[6] Activation parameters for this process in the presence of 0.1 mol/L of H_2O or D_2O ($\Delta H^{\ddagger} = 12.0 \pm 1.5$ kcal mol^{-1} and $\Delta S^{\ddagger} = -28 \pm 5$ eu) were previously reported in ref. 4.

[7] Similar kinetic isotope effects were obtained in the presence of 0.1 mol/L of water. See ref. 4.

© 2005 NRC Canada

Scheme 3.



Scheme 4.

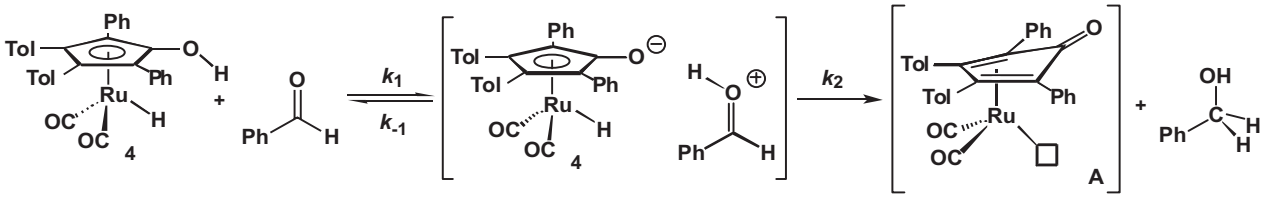
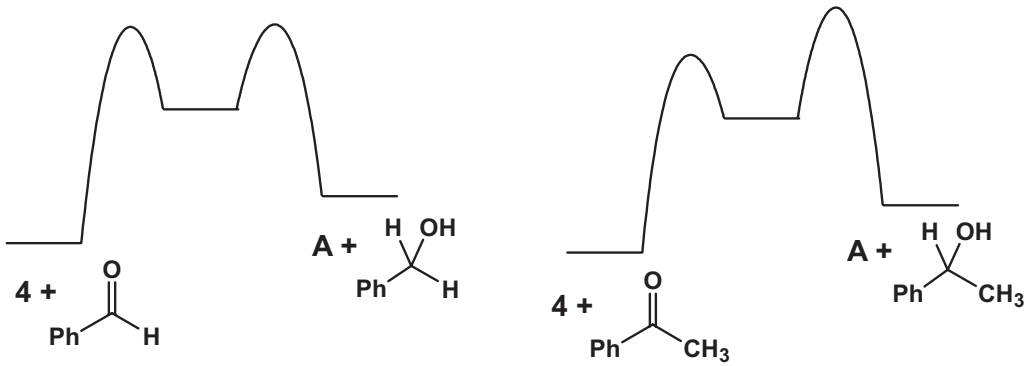


Fig. 3. Relative activation barriers expected for a stepwise hydrogen transfer mechanism to benzaldehyde and acetophenone with proton transfer preceding hydride transfer.



(5.78 ± 0.17) × 10^{-3} (mol/L)$^{-1}$ s^{-1}, and k_{RuDOD} = (4.45 ± 0.28) × 10^{-3} (mol/L)$^{-1}$ s^{-1} were obtained and used to determine the kinetic isotope effects given in Table 3.

Reduction of benzaldehyde by 4 in the presence of 0.079 mol/L of H_2O or D_2O

Reduction of benzaldehyde by **4** in the presence of 0.079 mol/L of H_2O or D_2O in THF-d_8 was followed by ^1H NMR spectroscopy at 22 °C. H_2O was added to the solutions of isotopomers **4-RuHOH** and **4-RuDOH**, while D_2O was added to **4-RuHOD** and **4-RuDOD** providing samples containing 0.079 mol/L of water. The second-order rate constants obtained from these reactions, k_{RuHOH} = (10.62 ± 0.21) × 10^{-3} (mol/L)$^{-1}$ s^{-1}, k_{RuHOD} = (4.60 ± 0.31) × 10^{-3} (mol/L)$^{-1}$ s^{-1}, k_{RuDOH} = (6.52 ± 0.92) × 10^{-3} (mol/L)$^{-1}$ s^{-1}, and k_{RuDOD} = (3.03 ± 0.21) × 10^{-3} (mol/L^{-1} s^{-1}, provided kinetic isotope effects (Table 3)).

Reduction of benzaldehyde by 4 in the presence of 0.120 mol/L of H_2O or D_2O

Reduction of benzaldehyde by **4** in the presence of 0.120 mol/L of H_2O or D_2O in THF-d_8 was performed at 22 °C and monitored by ^1H NMR spectroscopy. Solutions of **4-RuHOH** and **4-RuDOH** contained H_2O, while solutions of **4-RuHOD** and **4-RuDOD** contained D_2O. Second-order rate constants were independently obtained for the reduction of benzaldehyde with each of these isotopomers, k_{RuHOH} = (10.03 ± 0.72) × 10^{-3} (mol/L)$^{-1}$ s^{-1}, k_{RuHOD} = (3.35 ± 0.32) × 10^{-3} (mol/L)$^{-1}$ s^{-1}, k_{RuDOH} = (7.55 ± 0.30) × 10^{-3} (mol/L)$^{-1}$ s^{-1}, and k_{RuDOD} = (2.36 ± 0.52) × 10^{-3} (mol/L)$^{-1}$ s^{-1}. The rate constants for each isotopomer were compared to determine the isotope effects (Table 3).

Reduction of acetophenone by 4 under dry conditions

Reduction of acetophenone by **4** under dry conditions in THF was approximately 80 times slower than reduction of benzaldehyde at comparable temperatures. The formation of 1-phenylethanol and **5** occurred with second-order kinetics. Reduction of acetophenone between 51 and 73 °C yielded activation parameters $\Delta H^{\ddagger}$ = 17.5 ± 1.2 kcal mol^{-1} and $\Delta S^{\ddagger}$ = –15.8 ± 4.0 eu and reduction with the isotopomers of **4** at 67 °C provided kinetic deuterium isotope effects (Table 1).

Discussion

In our initial study of the mechanism of hydrogen transfer from **4** to benzaldehyde, we could not conclusively differentiate between a concerted transfer of hydride and proton (Scheme 3) and a stepwise mechanism in which the two steps have similar barriers ($k_{-1} \approx k_2$, Scheme 4). In a concerted mechanism, isotope effects are observed upon labeling either the acidic or the hydridic hydrogen, and the

© 2005 NRC Canada

Table 4. Predicted kinetic isotope effects for the reduction of benzaldehyde and acetophenone with the doubly labeled isotopomer **4-RuDOD** for concerted and two-step hydrogen transfer mechanisms.

	Toluene-d_8		CD_2Cl_2		THF-d_8	
	PhCHO	$PhCOCH_3$	PhCHO	$PhCOCH_3$	PhCHO	$PhCOCH_3$
Observed k_{RuHOH}/k_{RuDOD}	3.63±0.25	3.72±0.20	3.36±0.36	2.54±0.21	3.38±0.19	2.85±0.29
Predicted concerted	3.64	3.70	3.34	2.53	3.38	2.85
Predicted two-step	3.02	3.41	2.85	2.32	2.90	2.65

doubly labeled isotope effect is the product of the individual isotope effects. In a stepwise mechanism with two similar barriers, isotope effects would also be observed upon labeling of either the acidic or hydridic proton. The doubly labeled isotope effect, however, is predicted to be smaller in magnitude than the product of the individual isotope effects.

In our initial study of the reduction of benzaldehyde, the doubly labeled isotope effect was within error of both the product of the individual isotope effects and the isotope effect predicted for a stepwise mechanism with similar barriers. In an effort to differentiate between these mechanisms, we determined the isotope effects on the reduction of acetophenone. For a two-step mechanism, the more basic nature of the acetophenone oxygen would be expected to lower the barrier for protonation of the carbonyl oxygen; the less electrophilic nature of the carbonyl carbon of acetophenone would be expected to raise the barrier for hydride addition to the carbonyl carbon (Fig. 3).[8] If hydrogen transfer occurs through a stepwise mechanism, elimination (or a decrease) in the OH/OD isotope effect and an increase in the RuH/RuD isotope effect would be expected. In addition, the doubly labeled isotope effect is expected to be substantially less than the product of the individual isotope effects. For a concerted mechanism, isotope effects similar to those seen for benzaldehyde are expected and the doubly labeled isotope effect would be equal to the product of the individual isotope effects.

The observation of similar kinetic isotope effects for both benzaldehyde and acetophenone reduction in the same solvents (Table 1) is consistent with a one-step simultaneous transfer of proton and hydride to the carbonyl group. If a two-step mechanism were operative, then significantly smaller OH/OD isotope effects would be expected for acetophenone reduction compared to benzaldehyde reduction. The product of the individual isotope effects for both acetophenone and benzaldehyde reduction in all three solvents is within error of the doubly labeled isotope effects (Table 4). Furthermore, the isotope effects observed upon labeling RuH or OH are independent of the isotopic identity of the other site. Each of these observations is consistent with the concerted rate-limiting transfer of a proton and hydride to the carbonyl.

For a two-step process, the doubly labeled isotope effect can also be predicted from the individually observed isotope effects. Although the exact magnitude of the isotope effects on the first and second steps varies significantly with the relative rates of the two steps, the isotope effects predicted upon labeling of the hydride, the proton, or both sites are independent of this rate difference. In all cases, the isotope effect predicted for the doubly labeled material is less than the product of the isotope effects observed upon individual labeling.[9] Overall, the observed doubly labeled isotope effect studies are consistent with a concerted transfer mechanism and provide additional support for the simultaneous transfer of proton and hydride to aldehydes and ketones.

Relative reactivity of benzaldehyde and acetophenone

Benzaldehyde was reduced much more rapidly than acetophenone in all the solvents studied. To conveniently measure rates, reactions of acetophenone were run at temperatures ~40 °C higher than benzaldehyde. The rate differences extrapolated to 0 °C were 150 in THF, 101 in CH_2Cl_2, and 75 in toluene.

Hydrogen bonding to 4 decreases reduction rate

The rate of reduction of benzaldehyde showed little dependence on solvent polarity. In going from toluene ($\varepsilon = 2.4$) to CH_2Cl_2 ($\varepsilon = 9.1$) at –45 °C, the rate decreased by 25%. Similarly, the rate of reduction of acetophenone decreased by 45% in going from toluene to CH_2Cl_2. However, the rate of reduction was dramatically slower in the hydrogen bonding solvent THF ($\varepsilon = 7.8$). For benzaldehyde, extrapolation of rate constants to 0 °C indicates that reduction occurs 300 times slower in THF than toluene. Similarly, acetophenone is reduced 600 times slower in THF than toluene.

The rate of reduction decreased greatly upon the addition of alcohol to toluene and decreased slightly upon the addition of water to THF. Addition of 0.05 mol/L of EtOH to toluene resulted in a threefold decrease in the rate of benzaldehyde reduction. Addition of 0.079 mol/L of H_2O to THF resulted in a 30% decrease in the rate of benzaldehyde reduction.

The slower reductions in THF are attributed to hydrogen bonding of THF to the acidic hydrogen of the hydroxycyclopentadienyl ligand of **4**. These hydrogen bonds provide additional stability to the complex, and must be broken, or at least altered, prior to reaction with benzaldehyde. The result is a slightly higher barrier to reaction, and slower benzaldehyde reduction. In contrast, **4** is already hydrogen bonded to a carbonyl oxygen of the substrate in toluene. Similarly, addition of alcohol to toluene results in hydrogen bonding to **4** that must be replaced by hydrogen bonding to the carbonyl group in the transition state. In THF, addition of water leads

[8] The products are placed at a higher energy level than the starting materials because of the instability of proposed unsaturated species **A**. DFT calculations are consistent with these results. See ref. 6.

[9] For a more thorough discussion on the prediction of kinetic isotope effects and determination of kinetic isotope effects on each step in a two-step mechanism, see the Supplementary material.[5]

© 2005 NRC Canada

to somewhat stronger hydrogen bonding of water to **4** than of THF to **4** that must be replaced in the transition state.

Despite the retardation of the reaction rate observed upon addition of ethanol to toluene in the catalytic reactions described in the previous section, no retardation was observed during the course of stoichiometric reduction. This may result from the relatively low ultimate concentration of alcohol, or from competition for hydrogen bonding with the carbonyl species.

Addition of water to THF alters isotope effects

The presence of water also results in significant alteration of the magnitude of the individual isotope effects for the reduction of benzaldehyde in THF. As the concentration of water increases, both individual isotope effects change: the OH/OD isotope effect increases with water concentration, while the RuH/RuD isotope effect decreases. The doubly labeled isotope effect also increases with higher concentrations of water (Table 3).

Deuterium labeling of the hydroxyl proton displayed an isotope effect of 1.30 in THF in the absence of water. Addition of 0.079 mol/L of water (H_2O and D_2O, respectively) led to an increase in the isotope effect to 2.22, and addition of 0.120 mol/L of water led to a further increase to 3.10. Deuterium substitution of ruthenium hydride results in an isotope effect of 2.60 in the absence of water. Addition of water (0.079 mol/L) led to the decrease of this isotope effect to 1.57, and addition of more water (0.120 mol/L) resulted in a further decrease to 1.36.

DFT calculations of the transition state for reduction of $H_2C{=}O$ by (η^5-C_5H_4OH)$Ru(CO)_2H$ indicate an early transition state with only moderate proton transfer from the CpOH to the carbonyl oxygen and moderate hydride transfer from Ru to the carbonyl carbon (5*b*). The increase in OH/OD isotope effect upon addition of water suggests more extensive proton transfer to the carbonyl oxygen at the transition state. Similarly, the decrease in the RuH/RuD isotope effect upon addition of water suggests less extensive transfer of hydride to the carbonyl carbon at the transition state. This is consistent with water stabilizing proton transfer in the transition state.

Conclusion

These studies provide detailed mechanistic evidence that the reduction of ketones and aldehydes occurs through a concerted transfer of the acidic and hydridic hydrogens from the tolyl analogue of Shvo's hydroxycyclopentadienyl ruthenium hydride **4** in toluene, methylene chloride, and THF. In each case, hydrogen transfer is the rate-limiting step of the reaction. The rate of carbonyl compound reduction is much faster in non-hydrogen bonding solvents. Use of the hydrogen bonding solvent THF results in slower reduction rates, in addition to a larger isotope effect on labeling of the acidic proton. These changes are presumably due to stabilization of **4** via hydrogen bonding to the acidic hydrogen.

Experimental

General

All syntheses and sample preparations were prepared following Schlenk techniques or in a nitrogen atmosphere glovebox. Toluene-d_8 and THF-d_8 were distilled from a sodium benzophenone solution immediately prior to use. CD_2Cl_2 was dried over CaH_2 and distilled prior to use. Other solvents were dried and deoxygenated with activated alumina and Q5 purification columns (11). Benzaldehyde and acetophenone were distilled prior to use. NMR spectra were recorded on a 360 MHz spectrometer, and are referenced to residual protons in the deuterated solvent. The temperature of the NMR probe was determined before and after each run with a calibrated internal thermocouple. Ruthenium hydride **4** and isotopomers were prepared according to literature procedure (5).

General kinetic procedure

The general kinetic procedure will be illustrated with a specific example. A standard THF solution of **5** (0.30 mL, 0.007 09 mol/L, prepared in a nitrogen glovebox from 20.2 mg of **5** and 2.5 mL of THF) was prepared in a resealable NMR tube. The sample was degassed by three freeze–pump–thaw cycles. Upon cooling the sample to –196 °C, 1 atm of H_2 was added (1 atm = 101.325 kPa). The sample was then heated at 80 °C to ensure complete conversion to **4-RuHOH**. The solvent was evaporated under low pressure, and the remaining solid was dissolved in 0.25 mL of toluene-d_8 in a nitrogen atmosphere glove box. The sample was cooled to –78 °C and benzaldehyde (100 µL, 0.0492 mmol, 20 equiv.) was added from a 100 µL gas-tight syringe. The NMR tube was resealed, inserted into an NMR spin collar, shaken for ~3 s, and inserted into an NMR spectrometer precooled to –37 °C. The disappearance of **4** and the appearance of benzyl alcohol and ruthenium dimer **5** were followed by ^{1}H NMR spectroscopy for over three half-lives.

[2,5-Ph_2-3,4-Tol_2(η^5-C_4COH)]$Ru(CO)_2CH_3$ (6)

A THF solution of [2,5-Ph_2-3,4-Tol_2(η^5-C_4COH)]Ru-$(CO)_2$Cl (106 mg, 0.175 mmol) and excess CH_3MgBr was refluxed under nitrogen for 4 h and then neutralized with 1.5 mL of 5% HCl (aq). This mixture was extracted with toluene. Evaporation of the toluene extract under vacuum gave **6** as a deep maroon solid (88 mg, 0.150 mmol, 86% yield). IR (CH_2Cl_2, cm^{-1}): 1946, 2008. ^{1}H NMR (toluene-d_8, 360 MHz) δ: 0.82 (s, $RuCH_3$), 1.89 (s, 6H, CpTolCH_3), 4.29 (s, OH), 6.63 (d, ^3J = 8.2 Hz, 4H, aromatics), 6.9–7.2 (m, 10H, aromatics), 7.43 (d, ^3J = 8.2 Hz, 4H, aromatics). ^{13}C{^{1}H} NMR (toluene-d_8, 90 MHz) δ: –15.6 ($RuCH_3$), 21.3 (CpTolCH_3), 88.6 (C3,4 of Cp), 104.2 (C2,5 of Cp), 137.8 (C1 of Cp), 125–137 (eight resonances, aromatics), 203.8 (CO).

Acknowledgements

Financial support from the United States Department of Energy, Office of Basic Energy Sciences, is gratefully acknowledged. Jeffrey Johnson thanks the ACS Organic Division Emmanuil Troyansky Graduate Fellowship for support. Grants from the National Science Foundation (NSF) (CHE-962-9688) and the National Institutes of Health (NIH) (I S10 RR04981-01) for the purchase of NMR spectrometers are acknowledged.

© 2005 NRC Canada

References

1. (*a*) Y. Blum, D. Czarkie, Y. Rahamin, and Y. Shvo. Organometallics, **4**, 1459 (1985); (*b*) Y. Shvo, D. Czarkie, Y. Rahamim, and D.F. Chodosh. J. Am. Chem. Soc. **108**, 7400 (1986); (*c*) N. Menashe and Y. Shvo. Organometallics, **10**, 3885 (1991); (*d*) N. Menashe, E. Salant, and Y. Shvo. J. Organomet. Chem. **514**, 97 (1996).
2. R. Noyori and T. Ohkuma. Angew. Chem. Int. Ed. **40**, 40 (2001).
3. (*a*) K.-J. Haack, S. Hashiguchi, A. Fujii, T. Ikariya, and R. Noyori. Angew. Chem. Int. Ed. Engl. **36**, 285 (1997); (*b*) R. Noyori and S. Hashiguchi. Acc. Chem. Res. **30**, 97 (1997); (*c*) K. Matsumura, S. Hashiguchi, T. Ikariya, and R. Noyori. J. Am. Chem. Soc. **119**, 8738 (1997). The active species of this system has been identified as *trans*-dihydride complex **2**: (*d*) K. Abdur-Rashid, M. Faatz, A.J. Lough, and R.H. Morris. J. Am. Chem. Soc. **123**, 7473 (2001); (*e*) K. Abdur-Rashid, S.E. Clapham, A. Hadzovic, J.N. Harvey, A.J. Lough, and R.H. Morris. J. Am. Chem. Soc. **124**, 15104 (2002).
4. C.P. Casey, S.W. Singer, D.R. Powell, R.K. Hayashi, and M. Kavana. J. Am. Chem. Soc. **123**, 1090 (2001).
5. (*a*) C.P. Casey and J.B. Johnson. J. Am. Chem. Soc. **127**, 1883 (2005); (*b*) C.P. Casey, G.A. Bikzhanova, Q. Cui, and I.A. Guzei. J. Am. Chem. Soc. **127**, 14062 (2005).
6. C.P. Casey, J.B. Johnson, S.W. Singer, and Q. Cui. J. Am. Chem. Soc. **127**, 3100 (2005).
7. (*a*) A.H. Éll, J.S.M. Samec, C. Brasse, and J.-E. Bäckvall. Chem. Commun. 1144 (2002); (*b*) G. Csjernyik, A.H. Éll, L. Fadini, B. Pugin, and J.-E. Bäckvall. J. Org. Chem. **67**, 1657 (2002).
8. (*a*) O. Pàmies and J.-E. Bäckvall. J. Org. Chem. **67**, 1261 (2002); (*b*) F.F. Huerta, A.B.E. Minidis, and J.-E. Bäckvall. Chem. Soc. Rev. **30**, 321 (2001); (*c*) M.-J. Kim, Y.K. Choi, M.Y. Choi, M.J. Kim, and J. Park. J. Org. Chem. **66**, 4736 (2001); (*d*) H.M. Jung, J.H. Koh, M.-J. Kim, and J. Park. Org. Lett. **2**, 2487 (2000).
9. (*a*) H.M. Jung, J.H. Koh, M.-J. Kim, and J. Park. Org. Lett. **2**, 409 (2000); (*b*) J.-E. Bäckvall, and U. Andreasson. Tetrahedron Lett. **34**, 5459 (1993).
10. W.S. Price. Concepts Magn. Reson. **9**, 299 (1997).
11. A.B. Pangborn, M.A. Giardello, R.H. Grubbs, R.K. Rosen, and F.J. Timmers. Organometallics, **15**, 1518 (1996).

© 2005 NRC Canada

Photochemical generation and ^{1}H NMR detection of alkyl allene oxides in solution[1]

Leah E. Breen, Norman P. Schepp, and C.-H. Edmund Tan

Abstract: Irradiation of substituted 5-alkyl-4,5-epoxyvalerophenones leads to the formation of alkyl allene oxides that, in some cases, are sufficiently long-lived to be detected at room temperature by ^{1}H NMR spectroscopy. Absolute lifetime measurements show that the size of the alkyl group has a significant influence on the reactivity of the allene oxide, with *tert*-butyl allene oxide having a lifetime of 24 h in CD_3CN at room temperature that is considerably longer than the 1.5 h lifetime of the ethyl allene oxide. The allene oxides react rapidly with water to give α-hydroxyketones. The mechanism involves nucleophilic attack to the epoxide carbon to give an enol, which can also be detected as an intermediate by ^{1}H NMR spectroscopy.

Key words: allene oxides, mechanisms, absolute reactivity, kinetics, photochemistry.

Résumé : L'irradiation de 5-alkyl-4,5-époxyvalérophénones substituées conduit à la formation d'oxydes d'alkyle et d'allène qui, dans certains cas, ont des temps de vie suffisamment longs pour qu'on puisse les détecter, à la température ambiante, par spectroscopie RMN du ^{1}H. Des mesures de temps de vie absolus montrent que la taille du groupe alkyle joue un rôle important sur la réactivité de l'oxyde d'allène; le temps de vie de l'oxyde de *tert*-butyle et d'allène, dans le CD_3CN et à la température ambiante, est de 24 h ce qui est beaucoup plus long que celui de l'oxyde d'éthyle et d'allène qui n'est que d'une heure et demie. Les oxydes d'allène réagissent rapidement avec l'eau pour conduire à la formation d'α-hydroxycétones. Le mécanisme implique une attaque nucléophile du carbone de d'époxyde pour conduire à un énol qu'on peut aussi détecter comme intermédiaire par spectroscopie RMN du ^{1}H.

Mots clés : oxydes d'allène, mécanismes, réactivité absolue, cinétique, photochimie.

[Traduit par la Rédaction]

Introduction

Allene oxides (1–3) have been studied by theoretical and experimental chemists for several decades. Much of the original interest in these compounds came from their close relationship with cyclopropanones, which are structural isomers of allene oxides (4–9). More recently, they have been implicated as intermediates in the conversion of fatty acids to cyclopentenones and α-ketols in some plants and marine organisms (10, 11), and have also been used as intermediates in synthetic organic chemistry (11–20).

While allene oxides are generally considered to be reactive species, some are sufficiently stable to be isolated (21–24). This has allowed for the spectroscopic analysis of some allene oxides, and has also led to qualitative conclusions concerning the effect of structure on allene oxide stability (1). The chemistry of allene oxides that are too unstable to be isolated has also been examined through the analysis of products from reactions in which the allene oxides are present as undetected, transient intermediates (1, 2). These studies have shown that the reactions of allene oxides are dominated by rearrangement to cyclopropanones and addition of nucleophiles to give α substituted ketones.

Some absolute rate constants for the reactions of allene oxides in solution have been measured (25–27), but this remains one area of allene oxide chemistry that has not yet been extensively examined. Quantitative data concerning the effect of structure, solvent, and other parameters on the reactivity of allene oxides can be readily obtained from absolute reactivity measurements, and this information can lead to mechanistic details that are often difficult to determine from product-based studies. In the present work, we describe results concerning the absolute reactivity of some monoalkyl substituted allene oxides. A key feature of this work is the use of a photochemical method to rapidly generate these allene oxides. As a result, more reactive and previously undetected allene oxides could be examined directly by ^{1}H NMR spectroscopy.

Received 12 October 2004. Published on the NRC Research Press Web site at http://canjchem.nrc.ca on 22 October 2005.

L.E. Breen, N.P. Schepp,[2] and C.-H. Edmund Tan. Department of Chemistry, Dalhousie University, Halifax, NS B3H 4J3, Canada.

[1]This article is part of a Special Issue dedicated to organic reaction mechanisms.

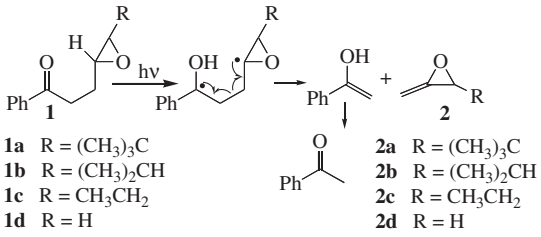
[2]Corresponding author (email: nschepp@dal.ca).

Results and discussion

The photochemical method used to generate the allene oxides in this work is based on the Norrish type II reaction of substituted 4,5-epoxyvalerophenones **1** (eq. [1]). With these substrates, excitation was expected to lead to efficient triplet formation followed by rapid intramolecular hydrogen transfer to generate a 1,4-biradical that fragments to give the desired allene oxide **2**, together with acetophenone.

 doi: 10.1139/V05-139 © 2005 NRC Canada

[1]



1a R = $(CH_3)_3C$
1b R = $(CH_3)_2CH$
1c R = CH_3CH_2
1d R = H

2a R = $(CH_3)_3C$
2b R = $(CH_3)_2CH$
2c R = CH_3CH_2
2d R = H

Initial experiments were carried out using the precursor **1a** (R = $(CH_3)_3C$), which would give the *tert*-butyl allene oxide **2a** that has been isolated by other methods and fully characterized by NMR spectroscopy (23, 28). ^{1}H NMR analysis showed that irradiation of **1a** (ca. 20% depletion) in CD_3CN at room temperature led to the formation of prominent new signals[3] including doublets at 4.34 ppm (J = 3.2 Hz) and 4.28 ppm (J = 3.2 Hz) and a singlet at 3.53 ppm (Fig. 1A), as well as a singlet at 2.60 ppm. The signals at 4.34, 4.28, and 3.53 ppm are the same as those previously assigned to the *tert*-butyl allene oxide (23, 28), with the doublets being assigned to the vinyl protons, and the singlet at 3.50 ppm to the epoxide proton; the signal at 2.60 ppm corresponds to the methyl protons of acetophenone. Thus, the NMR spectra obtained after irradiation clearly showed that fragmentation leading to allene oxide formation as shown in eq. [1] is occurring.

The same method was applied to the generation of other allene oxides with less bulky groups at the epoxide carbon that have until now eluded direct detection. For precursor **1b** (R = $(CH_3)_2CH$), the NMR spectrum after irradiation in CD_3CN showed the formation of overlapping doublets at 4.30 ppm and a doublet at 3.57 ppm (Fig. 1B). The signals at 4.30 and 3.57 ppm are similar to those observed for the *tert*-butyl allene oxide, which is consistent with the assignment of these signals to the isopropyl allene oxide **2b**. Furthermore, the signal at 3.57 ppm is now a doublet, rather then the singlet that appears for the *tert*-butyl allene oxide, as expected for the isopropyl **2b** allene oxide in which the epoxide proton is located adjacent to the CH of the isopropyl moiety. For precursor **1c** (R = CH_3CH_2), irradiation led to the formation of new peaks at 4.29 and 3.71 ppm (Fig. 1C). Again, these chemical shifts and the nature of the splitting are consistent with the assignment of these new peaks to the ethyl allene oxide **2c**.

Irradiation of precursor **1d** in CD_3CN led to no detectable amounts of the parent allene oxide **2d**. A signal at 2.60 ppm owing to the formation of acetophenone was observed, which suggests that allene oxide formation as outlined in eq. [1] had occurred. Thus, our inability to detect allene oxide **2d** is likely due to its high reactivity. To further establish that **2d** was indeed generated, irradiation of **1d** was carried out with 5% D_2O in acetonitrile. Under these conditions, a prominent singlet at 4.01 ppm and triplet at 2.09 ppm were observed. These signals correspond to 1-*d*-3-deuteroxy-2-propanone (29), which is the expected product upon addition of D_2O to allene oxide **2d**. Thus, the parent allene oxide is generated upon irradiation of **1d**, but even in dry acetonitrile it is too short-lived to be detected under our reaction conditions. Since our experimental conditions involved 5 min of irradiation followed by ca. 3 min to acquire the initial ^{1}H NMR spectrum, the lifetime of the parent allene oxide must be less 8 min in neat CD_3CN at room temperature.

Fig. 1. ^{1}H NMR spectra obtained 4 min after irradiation of precursors (A) **1a**, (B) **1b**, and (C) **1c** in CD_3CN at room temperature.

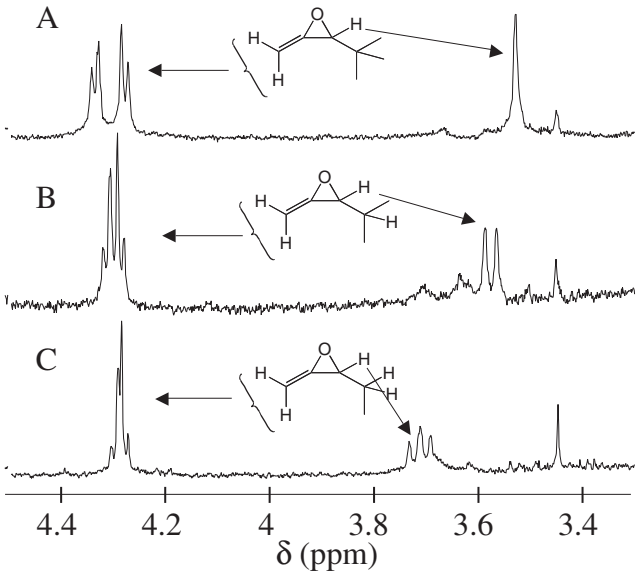
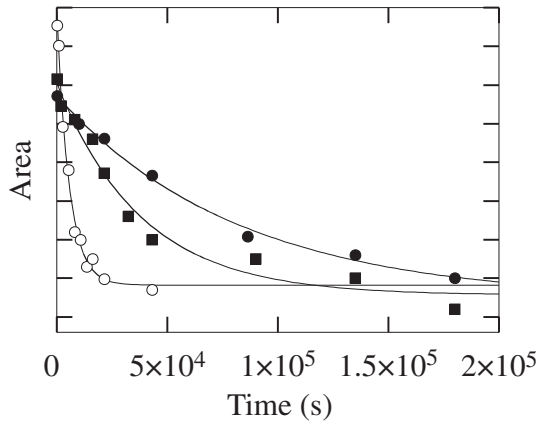


Fig. 2. Integrated area of the vinyl protons of the *tert*-butyl (●), isopropyl (■), and ethyl (○) allene oxides in CD_3CN at 25 °C measured as a function of time after irradiation of the corresponding precursors. The solid lines represent the line-of-best-fit calculated using a first-order rate expression.



Not surprisingly, the allene oxides **2a**–**2c** in neat CD_3CN at room temperature also were not stable, as illustrated by the decrease in the integrated areas of the ^{1}H NMR signals of the vinyl protons as a function of time in Fig. 2. These data can in principle be used to determine the absolute reactivity of the allene oxides; however, given the difficulties in measuring accurate values for the integrated areas, the data were not sufficiently good to distinguish between a first-order decay or a second-order decay of the allene oxides. Nonetheless, the data clearly show a substantial difference in the reactivity of the allene oxides as a function of the size of

[3] Other weak resonances owing to unidentified by-products were also evident in the ^{1}H NMR spectrum.

© 2005 NRC Canada

Table 1. First-order rate constants for the decay of allene oxides **2a**–**2d** in CD_3CN (25 °C).

R	k_{decay} (s^{-1})
tert-Butyl (**2a**)	$(1.2\pm0.2) \times 10^{-5}$
Isopropyl (**2b**)	$(2.4\pm0.4) \times 10^{-5}$
Ethyl (**2c**)	$(1.9\pm0.2) \times 10^{-4}$
H (**2d**)	$>10^{-3}$

the alkyl group, with the isopropyl allene oxide **2b** being considerably more reactive than the *tert*-butyl allene oxide **2a**, and the ethyl allene oxide **2c** showing even greater reactivity. This order of reactivity as a function of the size of the alkyl group is nicely consistent with conclusions made previously (2, 24) that bulky groups directly attached to the epoxide ring serve to enhance the kinetic stability of allene oxides.

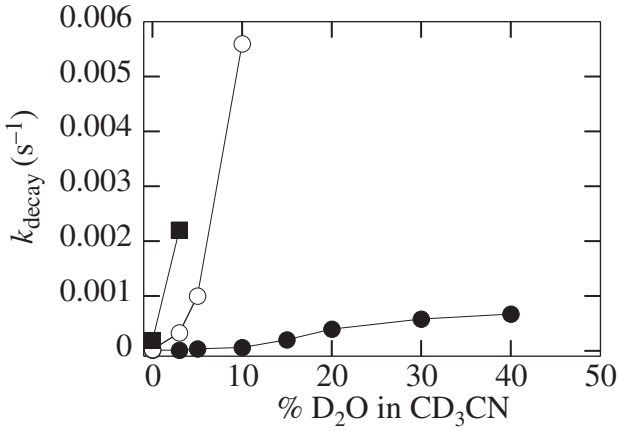
While the decay traces in Fig. 2 fit equally well to first- and second-order rate expressions, a measure of the differences in reactivity can be estimated by comparing rate constants obtained using a first-order fit (Table 1). These results show that the *tert*-butyl allene oxide **2a** and the isopropyl allene oxide decay slowly with rate constants of 1.2×10^{-5} and 2.4×10^{-5} s^{-1}, respectively, which differ only by a factor of two. On the other hand, the ethyl allene oxide **2c** decays about an order of magnitude more quickly with a rate constant of 1.9×10^{-4} s^{-1}. In addition, based on our inability to detect the parent allene oxide, we can estimate that it decays with a rate constant $>10^{-3}$ s^{-1}. The parent allene oxide therefore decays at least 10 times more rapidly than the ethyl derivative, and at least 100 times more rapidly than the bulky *tert*-butyl and isopropyl allene oxides.

The actual reaction of the allene oxides in neat CD_3CN remains unclear. One possibility is that the allene oxides rearrange to the substituted cyclopropanones. However, no ^1H NMR signals corresponding to cyclopropanones could be observed after complete decay of the allene oxides, nor could signals owing to the alkene that would be generated by rapid loss of CO from the cyclopropanone. In fact, no distinct signals were observed to grow as the allene oxides decayed, suggesting that the allene oxides may polymerize or react with solvent to give material difficult to characterize.

Allene oxides are well-known to react with nucleophiles to give α substituted ketones (2), but little is known about the absolute rate constants associated with this nucleophilic addition process. In the present work, the effect of adding D_2O was examined by monitoring the decay of the allene oxides signals in various D_2O–CD_3CN mixtures. Since D_2O was expected to add rapidly to the allene oxides, irradiation of the precursors was carried out in neat CD_3CN, and an ^1H NMR spectrum obtained to ensure that allene oxide formation had occurred. An appropriate amount of D_2O was then added, followed rapidly by the acquisition of a series of spectra. In this way, allene oxide decaying with rate constants less than 0.01 s^{-1} could readily be monitored.

In these experiments, the reduction in the intensity of the vinyl protons of the allene oxides as a function of time fit well to a first-order rate expression giving the pseudo-first-order rate constants that are plotted as a function of D_2O content in Fig. 3. These data clearly show that all three allene oxides decayed considerably more quickly upon the addition of water; however, the reactivity of the allene oxides toward D_2O was strongly dependent on the nature of the alkyl substituent. Thus, in the presence of the *tert*-butyl group, the rate constants for allene oxide decay hardly changed at low D_2O contents, and the *tert*-butyl allene oxide could still be easily observed in 40% D_2O where it decayed with a rate constant of 6.7×10^{-4} s^{-1}. This is in contrast to the results obtained with the isopropyl allene oxide whose decay increased dramatically even in the presence of small amounts of D_2O, and could no longer be observed at D_2O contents >10%. The ethyl allene oxide was even more reactive, with the rate constant for decay increasing 10-fold upon going from neat CD_3CN to 3% D_2O in CD_3CN. At higher D_2O contents, the ethyl allene oxide could no longer be observed.

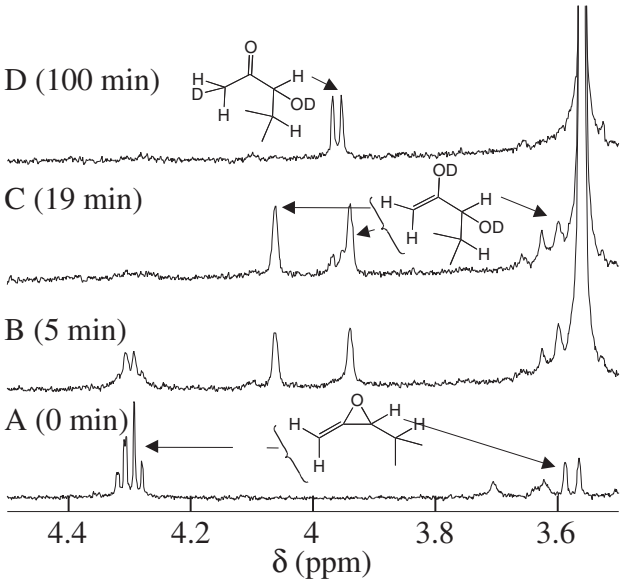
Fig. 3. Rate constants for the decay of the *tert*-butyl (●), isopropyl (○), and ethyl (■) allene oxides in CD_3CN as a function of D_2O content (25 °C).



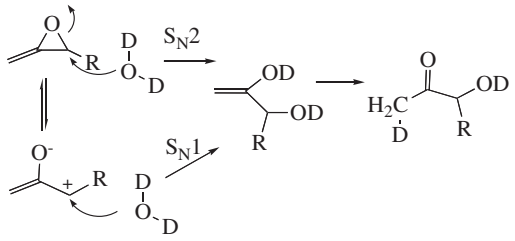
Nucleophilic addition of D_2O to the allene oxides was expected to lead to the formation of the corresponding α-hydroxyketone, and this material was indeed observed by ^1H NMR as the final stable product in the reaction of the allene oxides with D_2O. Two mechanisms for this nucleophilic addition can be envisioned: addition can occur via an S_N1-like mechanism characterized by initial breaking of the epoxide C—O bond followed by addition of the nucleophile, or via an S_N2-like mechanism where the nucleophile directly adds to the intact epoxide ring (eq. [2]). In both cases, the initial product is an enol that then tautomerizes to the more stable ketone form. The formation of the enol intermediate is supported by the sequence of ^1H NMR spectra in Fig. 4. Figure 4A shows the isopropyl allene oxide after irradiation in CD_3CN, but before the addition of D_2O. Five minutes after the addition of 10% D_2O, the allene oxide signals were reduced (Figs. 4B and 4C) and eventually replaced by resonances at 3.9 and 4.1 ppm that correspond to the expected (30) chemical shifts of the vinyl protons of the enol intermediate. A doublet at 3.65 ppm was also observed that can be assigned to the proton on the carbon bearing the hydroxy group of the enol. The enol signals were then replaced by a

© 2005 NRC Canada

Fig. 4. ^{1}H NMR spectra obtained after irradiation of **1b** in CD_3CN, and 5, 19, and 100 min after the addition of 10% D_2O.



[2]



doublet at 3.9 ppm (Fig. 4D), attributed to the proton at the α position of the expected α-hydroxyketone product[4] (29).

While formation of the enol intermediate is consistent with the mechanism shown in eq. [2], its observation was surprising given the high reactivity of most simple enols (31). Two factors may contribute to the unusually long lifetime. First, most absolute rate constant measures for the ketonization of enols have been measured in wholly aqueous solutions; in the 10% aqueous conditions used to observe the enol in Fig. 2B, the enol ketonization process may be somewhat slowed. In fact, in experiments carried out at higher water contents of 30%, the enol could no longer be observed, despite the more rapid disappearance of the allene oxide. Second, the α-hydroxy group may play a role in reducing the reactivity of the enol form by hydrogen bonding. Such hydrogen bonding may reduce the electron density at the enolic OH, thus reducing the overall electrophilicity and the rate constant for addition of a proton to the enolic carbon–carbon double bond.

The effect of structure on the absolute reactivity of the allene oxides with water can also provide some insight into the mechanism of the nucleophilic addition reaction. In particular, rate constants for addition of the nucleophile in the S_N2 mechanism should show a dependence on structure, while in the S_N1-like mechanism, little difference in reactivity upon going from *tert*-butyl to ethyl should be observed. As shown in Fig. 3, a fairly dramatic structural effect is observed, which leads to the conclusion that nucleophilic addition occurs via the S_N2 mechanism.

Conclusions

Our results clearly show that photogeneration of allene oxides by the Norrish type II fragmentation of 4-alkyl-4,5-epoxyvalerophenones leads to formation of simple alkyl substituted allene oxides. Since the allene oxides are generated rapidly, this method allows for the detection of allene oxides that had not previously been observed, and for absolute rate constants to be measured. The use of this photoreaction should be compatible with the generation of broader series of simple alkyl allene oxides, and also with the use of a fast reaction technique like flash photolysis to examine the reactivity of very short-lived allene oxides. Experiments to address those issues are currently under way.

Experimental

Preparation of precursors

Precursors **1a**–**1d** were prepared by addition of the enolate of acetophenone to the appropriate 1-bromo-2-alkene derivative to give the corresponding 1-phenyl-pent-4-en-1-one, followed by epoxidation using *m*-chloroperbenzoic acid. In general, the procedure involved the addition of 1 equiv. of lithium diisopropylamine to acetophenone (1.5 g) in dry THF (15 mL) under an argon atmosphere at –78 °C and stirring for 20 min. One equivalent of 1-bromo-4,4-dimethyl-2-pentene (32) (for **1a**), 1-bromo-4-methyl-2-pentene (33) (for **1b**), 1-bromo-2-pentene (33) (for **1c**), or 1-bromo-2-propene (Aldrich) (for **1d**) was then added, and the mixture allowed to warm up to room temperature over a period of 20 h. The solution was diluted with ether and washed with saturated aqueous ammonium chloride and sodium chloride. The organic layer was dried and the solvent removed under reduced pressure. The crude enone was purified by silica gel column chromatography using 50% dichloromethane in hexanes as the eluant.

Epoxidation was carried out by adding 1.5 equiv. of purified *m*-chloroperbenzoic acid to the enone in CH_2Cl_2. The mixture was stirred for 1.5 h at room temperature. After washing with 5% sodium hydroxide and evaporation of the solvent, the crude product was purified by silica gel column chromatography (20% ethyl acetate in hexanes).

1-Phenyl-6,6-dimethyl-4,5-epoxyheptan-1-one (1a)

^{1}H NMR (ppm) δ: 7.45–8.05 (multiplet, 5H), 3.14 (t, 2H), 2.92–2.97 (m, 1H), 2.56 (d, 1H), 2.08–2.22 (m, 1H), 1.77–1.91 (m, 1H), 0.92 (s, 9H). ^{13}C NMR (ppm) δ: 25.7, 26.5, 30.6, 54.5, 67.1, 127.9, 128.5, 133.0, 136.6, 199.0. HR-MS calcd.: 232.1463; found: 232.1459.

1-Phenyl-6-methyl-4,5-epoxyheptan-1-one (1b)

^{1}H NMR (ppm) δ: 7.45–8.05 (multiplet, 5H), 3.15 (t, 2H), 2.85–2.91 (m, 1H), 2.53–2.57 (d of d, 1H), 2.10–2.23 (m, 1H), 1.78–1.92 (m, 1H), 1.45–1.62 (m, 1H), 1.01 (d, 3H),

[4] The final product also shows the CH_2D protons as a triplet at 2.1 ppm and the methyl groups as doublets at 1.0 and 0.7 ppm.

© 2005 NRC Canada

0.96 (d, 3H). ^{13}C NMR (ppm) δ: 18.3, 18.9, 26.4, 30.3, 34.5, 56.8, 64.5, 127.9, 128.5, 133.0, 136.6, 199.0. HR-MS calcd.: 218.1307; found: 218.1299.

1-Phenyl-4,5-epoxyheptan-1-one (1c)

^{1}H NMR (ppm) δ: 7.45–8.05 (multiplet, 5H), 3.15 (t, 2H), 2.82–2.87 (m, 1H), 2.71–2.77 (m, 1H), 2.12–2.25 (m, 1H), 1.78–1.91 (m, 1H), 1.53–1.64 (m, 2H), 1.00 (t, 3H). ^{13}C NMR (ppm) δ: 9.7, 24.9, 26.3, 34.5, 57.5, 60.2, 127.9, 128.5, 133.0, 136.6, 199.1. HR-MS calcd.: 204.1150; found: 204.1146.

1-Phenyl-4,5-epoxypentan-1-one (1d) (34)

^{1}H NMR (ppm) δ: 7.45–8.05 (multiplet, 5H), 3.20 (t, 2H), 3.10–3.17 (m, 1H), 2.81 (t, 1H), 2.55–2.58 (m, 1H), 2.16–2.24 (m, 1H), 1.80–1.89 (m, 1H). ^{13}C NMR (ppm) δ: 26.8, 34.4, 47.3, 51.5, 127.9, 128.5, 133.1, 136.6.

Irradiation of precursors and determination of rate constants

About 10 mg of **1a**–**1d** were dissolved in 0.750 mL of CD_3CN (Aldrich) in a quartz cuvette (3 mm × 1 cm × 3 cm). The solution was bubbled with nitrogen for 10 min and then irradiated with 308 nm light (60 mJ/pulse, 8 ns pulse) from a Lambda-Physik excimer laser operating at 5 Hz for 5–10 min or with a high-pressure mercury lamp for 15–30 min. Immediately after irradiation, the solution was transferred to an NMR tube and the spectrum obtained using a Bruker AC-250 MHz spectrometer (probe temperature 25 °C). To obtain kinetic data, NMR spectra were obtained at specific time intervals after irradiation. The time intervals varied depending on the lifetime of the allene oxides, but generally six to ten spectra were obtained. The peak area or intensity corresponding to the vinyl protons of the allene oxides was measured in each spectrum (relative to a small amount of CH_2Cl_2 added as an internal standard). These areas or intensities were plotted as a function of time, and rate constants extracted by nonlinear least-squares fitting of the data to a first-order exponential equation.

For studies involving the addition of water, irradiation of the precursor was carried out in the same way in neat CD_3CN. The ^{1}H NMR spectrum was then obtained to ensure allene oxide formation had taken place. A desired amount of D_2O was then added, followed by the acquisition of further NMR spectra at appropriate time intervals. Rate constants were determined in the same way as described in the previous section for reaction in neat CD_3CN. In all cases, the ^{1}H NMR spectra of the final stable product matched closely the published spectra of the corresponding α-hydroxy ketones (29).

Acknowledgements

The authors thank the Natural Sciences and Engineering Research Council of Canada (NSERC) and PetroCanada (Young Innovators Award) for financial support.

References

1. T.H. Chan and B.S. Ong. Tetrahedron, **36**, 2269 (1980).
2. T.H. Chan and B.S. Ong. J. Org. Chem. **43**, 2994 (1978).
3. P.J. Stang. *In* The chemistry of ethers, crown ethers, hydroxyl groups and their sulphur analogues. Vol. 2. *Edited by* S. Patai. Wiley, Chichester, UK. 1980. p. 859.
4. A. Liberles, A. Greenberg, and A. Lesk. J. Am. Chem. Soc. **94**, 8685 (1972).
5. M.E. Zandler, C.E. Choc, and C.K. Johnson. J. Am. Chem. Soc. **96**, 3317 (1974).
6. J.V. Ortiz. J. Org. Chem. **48**, 4744 (1983).
7. B.A. Hess and J.K. Cha. THEOCHEM, **100**, 11 (1993).
8. B.A. Hess, U. Eckart, and J. Fabian. J. Am. Chem. Soc. **120**, 12310 (1998).
9. B.A. Hess, Jr., L. Smentek, A.R. Brash, and J.K. Cha. J. Am. Chem. Soc. **121**, 5603 (1999).
10. N. Tijet and A.R. Brash. Prostaglandins Other Lipid Mediators, **68**–**69**, 423 (2002).
11. E.J. Corey, K. Ritter, M. Yus, and C. Najera. Tetrahedron Lett. **28**, 3547 (1987).
12. J. Grimaldi, M. Malacria, and M. Bertrand. Bull. Soc. Chim. Fr. **7**–**8**, 1731 (1975).
13. M. Bertrand, J.P. Dulcere, G. Gil, J. Grimaldi, and P. Sylvestre-Panthet. Tetrahedron Lett. 3305 (1976).
14. M. Bertrand, J.P. Dulcere, and G. Gil. Tetrahedron Lett. **21**, 4271 (1980).
15. S.J. Kim and J.K. Cha. Tetrahedron Lett. **29**, 5613 (1988).
16. I. Erden, F.P. Xu, J. Drummond, and R. Alstad. J. Org. Chem. **58**, 3611 (1993).
17. I. Erden, F.P. Xu, and W.G. Cao. Angew. Chem. Int. Ed. Engl. **36**, 1516 (1997).
18. M.M. Kabat. J. Org. Chem. **60**, 1823 (1995).
19. M. Shipman, H.R. Thorpe, and I.R. Clemens. Tetrahedron, **55**, 10845 (1999).
20. H. Xiong, R.P. Hsung, C.R. Berry, and C. Rameshkumar. J. Am. Chem. Soc. **123**, 7174 (2001).
21. J.K. Crandall, W.W. Conover, J.B. Komin, and W.H. Machleder. J. Org. Chem. **39**, 1723 (1974).
22. I. Erden and J. Drummond. Tetrahedron Lett. **34**, 1255 (1993).
23. T.H. Chan and B.S. Ong. Tetrahedron Lett. **17**, 3253 (1976).
24. R.O. Camp and F.D. Greene. J. Am. Chem. Soc. **90**, 7349 (1968).
25. A.R. Brash. J. Am. Chem. Soc. **111**, 1891 (1989).
26. A.R. Brash, S.W. Baertschi, C.D. Ingram, and T.M. Harris. Proc. Natl. Acad. Sci. U.S.A. **85**, 3382 (1988).
27. M.D. Clay, J. Durber, and N.P. Schepp. Org. Lett. **3**, 3883 (2001).
28. T. Konoike, T. Hayashi, and Y. Araki. Tetrahedron: Asymmetry, **5**, 1559 (1994).
29. J.A. Katzenellenbogen and S.B. Bowlus. J. Org. Chem. **38**, 627 (1973).
30. B. Capon, D.S. Rycroft, T.W. Watson, and C. Zucco. J. Am. Chem. Soc. **103**, 1761 (1981).
31. Y. Chiang, A.J. Kresge, and N.P. Schepp. J. Am. Chem. Soc. **111**, 3977 (1989).
32. R.W. Hoffmann, H. Brinkman, and G. Frenking. Chem. Ber. **123**, 2387 (1990).
33. D. Seebach and L. Widler. Helv. Chim. Acta, **65**, 1972 (1982).
34. P. Crotti, V. Di Bussolo, L. Favero, F. Macchia, M. Pineschl, and E. Napolitano. Tetrahedron, **55**, 5853 (1999).

© 2005 NRC Canada

Bicyclo[3.2.0]hepta-1,3,6-triene — UV photoelectron spectroscopic and computational studies[1]

T. Bajorek and N.H. Werstiuk

Abstract: Pyrolysis of *N*,*N*-dimethylbicyclo[3.2.0]hepta-3,6-dien-1-amine oxide (**5**) at 120 °C in the source chamber of the UV photoelectron (PE) spectrometer yielded bicyclo[3.2.0]hepta-1,3,6-triene (**6**). The triene dimerizes to yield a mixture of two dimers in equal amounts. A PE spectrum of an authentic mixture of dimers was also recorded for the purpose of spectral subtraction. Pyrolysis of **5** also generates dimethylhydroxylamine (**7**), a spectrum of which was also recorded from an authentic sample. Spectral subtraction allowed the first two ionization potentials of triene **6** at 7.2 and 9.8 eV to be identified. The resultant PE spectrum was compared very favorably with a simulated spectrum obtained from DFT calculations. A QTAIM analysis and calculation of delocalization indexes showed that while homoconjugation between C4 and C6 is negligible there is a weak through-space interaction between the bridgehead carbon atom C1 and C6 of the four-membered ring.

Key words: bicyclo[3.2.0]hepta-1,3,6-triene, UV photoelectron spectroscopy, DFT calculations, QTAIM, delocalization indexes.

Résumé : La pyrolyse de l'oxyde de *N*,*N*-diméthylbicyclo[3.2.0]hepta-3,6-dién-1-amine (**5**) à 120 °C, dans la chambre source d'une spectromètre photoélectronique (PE) UV conduit à la formation de bicyclo[3.2.0]hepta-1,3,6-triène (**6**). Le trimère se dimérise pour conduire à un mélange de deux dimères qui se forment en quantités égales. On a aussi enregistré un spectre PE d'un mélange authentique des dimères afin de pouvoir procéder à une soustraction spectrale. La pyrolyse du composé **5** conduit aussi à la formation de diméthylhydroxylamine (**7**), dont on a aussi enregistré le spectre d'un échantillon authentique. La soustraction spectrale a permis d'identifier les deux premiers potentiels d'ionisation du triène **6** à 7,2 et 9,8 eV. Le spectre PE qui en résulte se compare favorablement avec le spectre simulé obtenu par des calculs basés sur la théorie de la densité fonctionnelle (TDF). Une analyse QTAIM et des calculs d'indices de délocalisation montrent qu'il existe une faible interaction à travers l'espace entre l'atome de carbone de pont C1 et le C6 du cycle à quatre chaînons, même si l'homoconjugaison entre les atomes C4 et C6 est négligeable.

Mots clés : bicyclo[3.2.0]hepta-1,3,6-triène, spectroscopie photoélectronique UV, théorie de la densité fonctionnelle (TDF), QTAIM, indices de délocalisation.

[Traduit par la Rédaction]

Introduction

Bicyclo[3.2.0]hepta-1,3,6-triene (**6**) has been implicated as a reactive intermediate on the C_7H_6 potential energy surface in a number of investigations both experimental (1–3) and computational (4, 5). Although it has not yet been explicitly identified and characterized, its existence was implicated by the isolation and characterization of its dimers (6–10) in solution. Recently, a highly substituted, stable silicon analogue of **6** has been reported with a silicon atom replacing C5 at the bridgehead position (11). Interest in the strained bicyclo[3.2.0]hepta-1,3,6-trienyl ring system remains high.

Received 14 February 2005. Published on the NRC Research Press Web site at http://canjchem.nrc.ca on 22 October 2005.

T. Bajorek and N.H. Werstiuk.[2] Department of Chemistry, McMaster University, 1280 Main St. West, Hamilton, ON L8S 4L8, Canada.

[1]This article is part of a Special Issue dedicated to organic reaction mechanisms.

[2]Corresponding author (e-mail: werstiuk@mcmaster.ca).

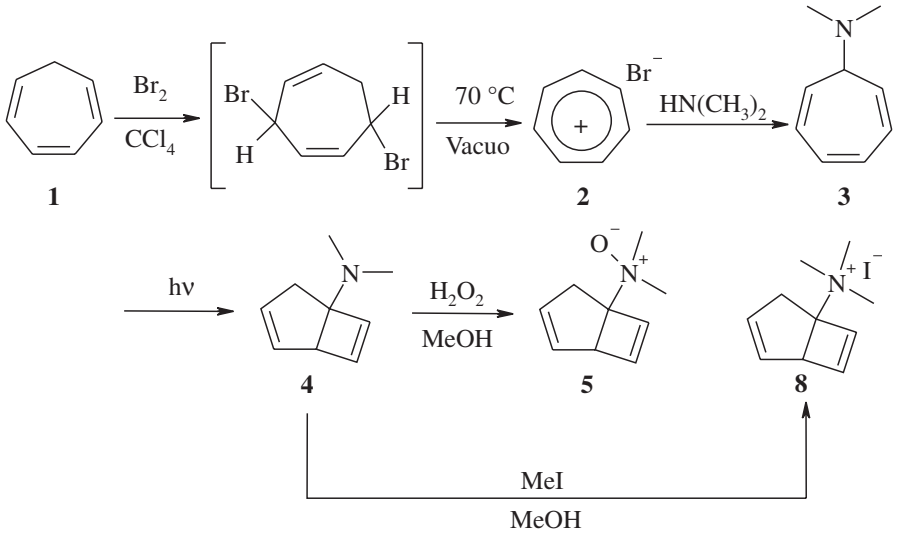
In this paper, we report the first direct experimental evidence for the existence of transient **6** and its ultraviolet (UV) photoelectron spectrum. When combined with MO calculations, UV photoelectron spectroscopy yields information about the electronic structure and bonding of stable as well as transient species that is provided by no other experimental technique. We also undertook a computational study at B3LYP, B3PW91, MP2, and CCSD levels of theory, carried out a QTAIM analysis (12), and evaluated delocalization indexes with LI-DICALC (13, 14) to gain additional information on the bonding of **6** and document the results.

Photoelectron spectroscopic studies

Photoelectron (PE) spectra were recorded with our locally built UV PE spectrometer and calibrated with the 15.6 eV IP band of N_2 that is visible in all spectra (15). Linearity of the spectral scale was checked with the lowest IP bands of methyl iodide at 9.54 and 10.16 eV prior to the experiments. Our unique UV PE spectrometer – CW CO_2 laser apparatus (16) fitted with a heated probe allows us to use the laser as a

 doi: 10.1139/V05-145 © 2005 NRC Canada

Scheme 1.



directed heat source to produce a hot zone as short as 1 mm in length at the tip of a quartz tube positioned about 1 cm from the point of intersection with the ionization beam. We used this setup successfully to obtain PE spectra of short-lived, reactive species such as benzazete and *o*-benzyne (16), l-(2-thiaindane)ketene and benzocyclobutene-thione (17, 18), 1,2-cyclohexadiene (19), (dimethoxy)carbene (20), and *p*-substituted phenylketenes (21) through pyrolysis of suitable precursors. In this case, we used the heated probe to pyrolyze *N*,*N*-dimethylbicyclo[3.2.0]hepta-3,6-dien-1-amine oxide (**5**) contained in a small bottle-shaped quartz vessel located 1 cm from the ionizing beam.

Computational methods

Interpretation of the PE spectrum of the transient was accomplished according to our recently developed (22) and successfully applied (23, 24) routine based on B3LYP (25) calculations. The structure of **6** was optimized at the B3LYP/6-31+G(d) level and used in a single-point calculation on its radical cation performed at the same level of theory. The PE spectrum of **6** was simulated with PESPEC (26). A Gaussian line broadening of 0.4 and a temperature of 300 K were used to simulate the partial PE spectrum with 10 MO energies (HOMO to HOMO-9). Equilbrium optimized geometries of **6** were obtained at the DFT and MP2 levels with GAUSSIAN 98 or GAUSSIAN 03 (27, 28), and frequency calculations were carried out to confirm that the geometries corresponded to minima. The uncorrected energies (E_{elec}) are included in a table as Supplementary information.[3] Wave functions were obtained at the B3LYP, B3PW91, MP2(FC), and CCSD levels. Displays of molecular geometries and molecular orbitals were generated using MOLEKEL (29, 30). QTAIM analyses were carried out with AIMALL (31) and the delocalization indexes were obtained with LI-DICALC (13, 14). The molecular graph of **6** and plots of the C1, C4, and C6 atomic basins were obtained with AIM 2000 (32).

Results and discussion

Synthesis of *N*-oxide 5

The precursor used to generate the transient bicyclo-[3.2.0]hepta-1,3,6-triene (**6**) was *N*,*N*-dimethylbicyclo-[3.2.0]hepta-3,6-dien-1-amine oxide (**5**), synthesized by the oxidation of *N*,*N*-dimethylbicyclo[3.2.0]hepta-3,6-dien-1-amine (**4**) with hydrogen peroxide in methanol. Amine **4** was synthesized according to Scheme 1.

Tropylium bromide (**2**) was synthesized using the procedure of Doering and Knox (33, 34). The bromination of cycloheptatriene (**1**) and subsequent pyrolysis under vacuum at 70 °C yielded tropylium bromide (**2**). Reaction of **2** with dimethylamine gave *N*,*N*-dimethylcyclohepta-1,3,5-trien-7-amine (**3**) (33). Photolysis of amine **3** with a medium pressure mercury arc lamp yielded *N*,*N*-dimethylbicyclo[3.2.0]-hepta-3,6-dien-1-amine (**4**) (35). Treatment of **4** with hydrogen peroxide in methanol gave *N*-oxide (**5**) (36). Alternatively, if amine **4** is treated with excess methyl iodide in ethanol the methiodide salt **8** is obtained (6). This salt was used to generate an authentic sample of a mixture of dimers of **6**.

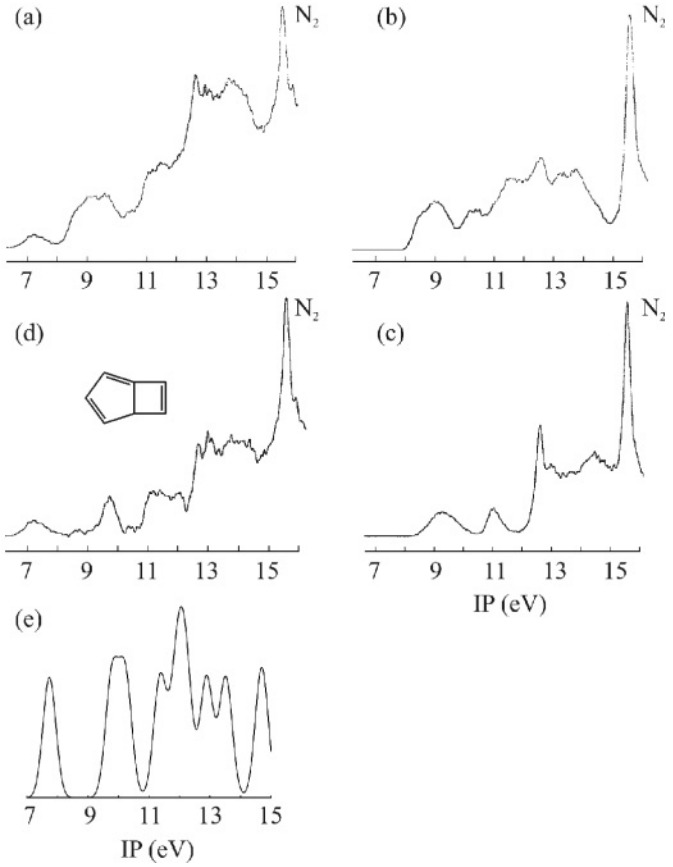
Pyrolysis and PE spectroscopy

The *N*-oxide **5**, placed in a sample vessel and inserted into the tip of an electrically heated probe, was directly pyrolyzed at 120 °C in the source chamber of the spectrometer. The pyrolysis spectrum consists of two main IP bands as illustrated in Fig. 1*a*. The first IP band was observed at 7.2 eV, while the second, very broad IP band spanned the region between 8.5 and 10 eV. In the pyrolysis of **5**, two other products were generated in addition to triene **6**, namely dimethylhydroxylamine (**7**) and two isomers **9** formed by

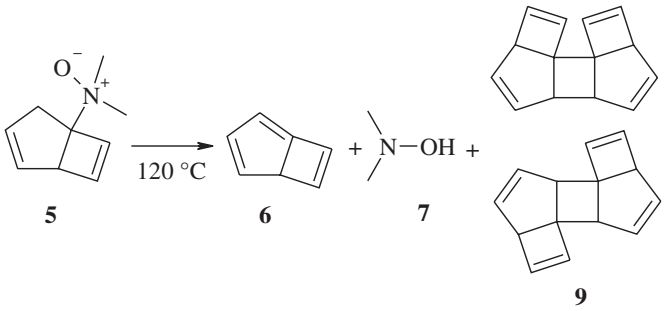
[3] Supplementary data for this article are available on the Web site or may be purchased from the Depository of Unpublished Data, Document Delivery, CISTI, National Research Council Canada, Ottawa, ON K1A 0S2, Canada. DUD 4030. For more information on obtaining material refer to http://cisti-icist.nrc-cnrc.gc.ca/irm/unpub_e.shtml.

© 2005 NRC Canada

Fig. 1. Experimental PE spectra of: (*a*) the pyrolysis of **5**; (*b*) the dimers **9**; (*c*) **7**; (*d*) after subtraction of PE spectra of **9** and **7** from the pyrolysis spectrum; and (*e*) simulated partial PE spectrum of **6**.



Scheme 2.



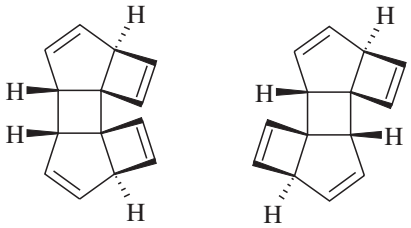
dimerization of triene **6** (Scheme 2) (6). Selected experimental and calculated IPs of **6**, **7**, and **9** are listed in Table 1.

An authentic sample of the dimers was generated from the reaction of potassium *tert*-butoxide with methiodide salt **8** that yielded a 50:50 dimer mixture as reported by Bauld et al. (6). The composition of the dimer mixture was confirmed by GC–MS and showed two signals with identical intensities and areas. Both peaks showed a $M^{+\bullet}$ ion with *m/z* 180. The dimers were not separated because a mixture of the two dimers was needed for the PE spectroscopic experiments. Recently, Billups et al. (9) reported NMR assignments of the two dimers and concluded that the dimers can be represented by the two structures shown in Fig. 2.

Table 1. Selected experimental and calculated IPs of **6**, **7**, and **9** at the B3LYP/6-31+G(d) level.

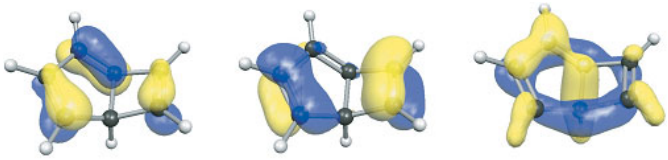
Compound		Ionization potential (eV)		
6	Exp.	7.23	9.76	
	B3LYP	7.73	9.78	10.22
7	Exp.		9.32	11.06
	Lit. (39, 40)		9.18	11.01
	B3LYP		9.10	10.66
9	Exp.		9.04	10.39

Fig. 2. Structure of dimers **9**.



9

Fig. 3. Selected molecular orbitals of triene **6** (contour value 0.08) at the B3LYP/6-31+G(d) level.



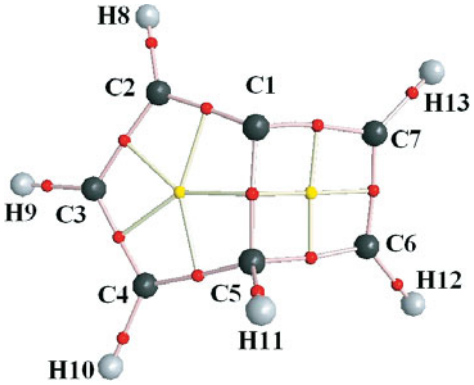
π^- (HOMO) π (HOMO-1) π/σ (HOMO-2)

The photoelectron spectrum of the mixture of dimers shows a very broad IP band in the regions from 8 to 9.5 eV and 10 to 11 eV. That there is no IP band observed below 8 eV (Fig. 1*b*) in the spectrum of the mixture of dimers indicates that the PE spectrum obtained upon the pyrolysis of **5** contains IPs belonging to transient **6**. The photoelectron spectrum of dimethylhydroxylamine **7** was also recorded and revealed that there were no IP bands below 8 eV in its spectrum (Fig. 1*c*). The first broad IP band of **7** was observed in the region between 8 and 10 eV with a vertical ionization potential at 9.3 eV. The second band is narrower than the first and its vertical IP occurs at 11.06 eV. The PE spectra of **7** and the dimers were subtracted from the PE spectrum obtained upon the pyrolysis of **5**, to yield a spectrum showing IP bands at 7.2 and 9.7 eV (Fig. 1*d*). This spectrum is in excellent agreement with the simulated spectrum of bicyclo[3.2.0]hepta-1,3,6-triene (**6**) (Fig. 1*e*), which shows the first IP at 7.7 eV, the second and the third IP at 9.8 and 10.2 eV as a broad IP band that results from the overlap of the two IPs. The molecular orbitals associated with these ionizations are shown in Fig. 3.

The highest occupied molecular orbital (HOMO) is assigned as π^- because it is a π orbital with nodes between C2—C3 and C7—C1. The assignment of π^+ is less obvious; HOMO-1 also has π character, but perhaps HOMO-2, which is a mixed π/σ orbital, best fits the label. Given the nature of HOMO-2, the question arises as to whether or not C4 and

© 2005 NRC Canada

Fig. 4. Molecular graph of triene **6** at the CCSD/6-31+G(d)//MP2(FC)/6-31+G(d) level.



C6 of **6** are homoconjugated. To gain information on this point, we carried out a QTAIM analyses (12) and calculated delocalization indexes with LI-DICALC (13, 14).

QTAIM analysis

The molecular graph of **6** — along with the trajectories linking the (3,+1) ring critical points (yellow) to the (3,–1) bond critical points (red) — generated with AIM 2000 (32) from the wave function obtained at the CCSD/6-31+G(d)//MP2(FC)/6-31+G(d) level is displayed as Fig. 4. The atomic populations, obtained with AIMALL (31), and selected properties of bond and ring critical points, obtained with AIMALL or AIM 2000, are collected in Tables 2 and 3, respectively. It is seen that the carbon atoms bear a marginal negative charge and the hydrogens are slightly positive. The populations obtained at the B3PW91 and CCSD//MP2 levels are very similar. Tetracoordinate carbon C5 is the least negatively charged. As far as the values of ρ at the bond critical points are concerned, the values for the nominal double bonds C1—C2, C3—C4, and C6—C7 are 0.3219, 0.3224, and 0.3309, respectively, somewhat smaller than the value for ethene (0.3404) at the same level of theory. Based on a $\rho(\mathbf{r})_{bcp}$ value of 0.2312 and a laplacian of –0.4864, the C5—C6 bond surprisingly is the weakest of the single C—C bonds. Its distorted bond path is qualitatively in accord with this conclusion. The ellipticity ε ($\lambda_1/\lambda_2 - 1$) of the C1—C2 double bond (0.2786) is significantly smaller than the ellipticities of the other double bonds C3—C4 (0.3287) and C6—C7 (0.3624). Ethene exhibits a value of 0.3640 at the same level of theory with the negative curvatures λ_1 and λ_2 being –0.7295 and –0.5348, respectively. The values are –0.6702 and –0.5241 for the C1—C2 bond of **6** so the decrease in ellipticity is due to a decrease in λ_1 relative to ethene. The curvatures for the C6—C7 double bond are –0.7030 and –0.5140 so ε is 0.3674. The ring critical point of the four-membered ring exhibits a substantially larger value for ρ (0.0986) than the five-membered ring (0.0452).

Delocalization indexes

Using equations developed at the HF level to calculate localization indexes (LIs) and delocalization indexes (DIs) (13, 14), we recently extended the idea of Fermi correlation by expressing LIs and DIs in terms of natural molecular orbitals η_l with occupation numbers n_l, and obtained eqs. [1] (the Fermi hole density), [2], and [3] that allowed us to determine LIs and DIs for correlated wave functions (13, 14).

Table 2. QTAIM atom electron populations and charges of triene **6** at various levels of theory.

Atom	B3PW91/6-31+G(d)	CCSD//6-31+G(d)//MP2(FC)/6-31+G(d)
C1	6.04313[a] (–0.04313)[b]	6.04753 (–0.04753)
C2	6.06622 (–0.06622)	6.07038 (–0.07038)
C3	6.05285 (–0.05285)	6.05689 (–0.05689)
C4	6.08706 (–0.08706)	6.09164 (–0.09164)
C5	6.01141 (–0.01141)	6.00559 (–0.00559)
C6	6.07181 (–0.07181)	6.07711 (–0.07711)
C7	6.06389 (–0.06389)	6.06792 (–0.06792)
H8	0.93842 (0.06158)	0.93391 (+0.06619)
H9	0.94532 (0.05468)	0.94054 (+0.05946)
H10	0.94213 (0.05787)	0.93775 (+0.06225)
H11	0.94261 (0.05739)	0.94331 (+0.05686)
H12	0.91779 (0.08221)	0.91563 (+0.08437)
H13	0.91883 (0.08117)	0.91252 (+0.08748)
Total electrons (Charge)	48.0016 (–0.0016)	48.0004 (–0.0004)

[a]The atom electron population.
[b]The atomic charge in parentheses.

[1] $$h(\mathbf{r_1},\mathbf{r_2}) = \sum_l \sum_m n_l^{1/2} n_m^{1/2} [\eta_l^*(\mathbf{r_1})\eta_l(\mathbf{r_2})\eta_m^*(\mathbf{r_2})\eta_m(\mathbf{r_1})]/\rho(\mathbf{r_1})$$

[2] $$F(\Omega,\Omega) = \int_\Omega d\mathbf{r_1} \int_\Omega d\mathbf{r_2} \rho(\mathbf{r_1}) h(\mathbf{r_1},\mathbf{r_2}) = -\sum_{l,m} n_l^{1/2} n_m^{1/2} S_{l,m}^2(\Omega)$$

[3] $$F(\Omega,\Omega') = -\sum_{l,m} n_l^{1/2} n_m^{1/2} S_{l,m}(\Omega) S_{l,m}(\Omega')$$

The LI λ(A) and DI δ(A,B) are calculated from eqs. [4] and [5], respectively. We used νPΩ and Ω′ rather than A and B in the eqs. [4] and [5] to emphasize the fact that we are dealing with the physical spaces (the basins) of atoms A and B. The $S_{l,m}$ is obtained directly from the atomic overlap matrix for each Ω obtained from integration of the atomic basins with PROAIMV or PROMEGA of AIMALL (31).

[4] $$\lambda(A) = |F(\Omega,\Omega)|$$

[5] $$\delta(A,B) = 2|F(\Omega,\Omega')|$$

The occupation numbers n_l and n_m are available from the wave function file obtained with GAUSSIAN 98 or GAUSSIAN 03 calculations. The DIs are defined by eq. [5] from the integration of the density of the Fermi hole on two atomic basins Ω and Ω′, so Ω,Ω′ represents the extent to which the electrons in Ω basin are delocalized over the Ω′ basin and vice versa. Consequently, the sum of the LIs and the DIs/2 should equal the total number of electrons in the molecule. Though in strict sense, the density of the Fermi hole cannot be defined within the framework of the DFT theory, recent calculations have demonstrated that the DIs and LIs obtained from Kohn–Sham spin orbitals are similar to those computed with HF wave functions (37). As a result, any atomic population ($N(\Omega)$) can be partitioned into two

© 2005 NRC Canada

Table 3. Selected properties (density, laplacian, and ellipiticty) of selected bond and ring critical points of triene **6** at the CCSD//6-31+G(d)//MP2(FC)/6-31+G(d) level.

Critical point	C1—C2[a]	C2—C3[a]	C3—C4[a]	C4—C5[a]	C5—C6[a]	C6—C7[a]	C1—C7[a]	C1—C5[a]	RCP1[b]	RCP2[c]
$\rho(\mathbf{r})$[d]	0.3219	0.2808	0.3224	0.2647	0.2312	0.3309	0.262	0.2544	0.0452	0.0986
$\nabla^2\rho$[d]	–0.8824	–0.7215	–0.8845	–0.6499	–0.4864	–0.9153	–0.6192	–0.5953	0.3205	0.4369
ε (Ellipticity)	0.2786	0.1295	0.3287	0.0418	0.0345	0.3674	0.0976	0.0501	—	—

[a]The (3,–1) bond critical points between pairs of atoms.
[b]The (3,+1) ring critical point of the five-membered ring.
[c]The (3,+1) ring critical point of the four-membered ring.
[d]In atomic units.

Table 4. Selected delocalization indexes and % pair delocalization between pairs of atoms of triene **6** at the CCSD//6-31+G(d)//MP2(FC)/6-31+G(d) and B3PW91/6-31+G(d) levels.

Atom pairs Ω and Ω′	C1—C2	C2—C3	C3—C4	C4—C5	C5—C6	C6—C7	C1—C7	C1—C5	C4—C6[a]
Delocalization index	1.292 (*1.586*)[b]	0.989 (*1.165*)	1.336 (*1.650*)	0.894 (*1.042*)	0.811 (*0.954*)	1.375 (*1.715*)	0.917 (*1.094*)	0.798 (*0.950*)	0.051 (*0.081*)[c]
% of pairs delocalized from basin Ω to basin Ω′[d]	38.08 (*38.74*)	29.40 (*28.46*)	39.50 (*40.25*)	26.60 (*25.42*)	22.80 (*22.60*)	41.53 (*42.13*)	27.54 (*26.87*)	23.53 (*22.49*)	1.51 (*1.99*)

[a]This is the homoconjugative interaction.
[b]The values in italics were obtained at the B3PW91/6-31+G(d) level.
[c]All the DIs for C4 are: 0.0911 (C1), 0.0575 (C2), 1.3364 (C3), 0.8936 (C5), 0.0508 (C6), 0.0184 (C7), 0.0064 (H8), 0.0030 (H9), 0.8314 (H10), 0.0319 (H11), 0.0030 (H12), 0.0024 (H13); for C6: 0.1107 (C1) (at the B3LYP level 0.1448), 0.0505 (C2), 0.0187 (C3), 0.0508 (C4), 0.8112 (C5), 1.3755 (C7), 0.00234 (H8), 0.0017 (H9), 0.0015 (H10), 0.0308 (H11), 0.8243 (H12), 0338 (H13). The LIs for C4 and C6 are 4.4116 and 4.4212, respectively.
[d]% of pairs delocalized between a given basin Ω and another basin Ω′ is given by $[DI(\Omega,\Omega') \times 100]/\Sigma DI$.

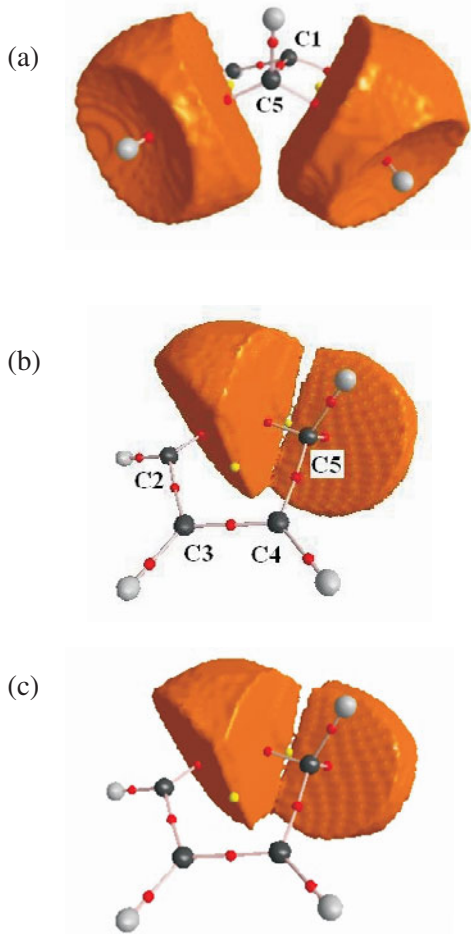
components, one containing the delocalized electron population ($N_{DI}(\Omega)$), and another corresponding to the localized electronic charge at the HF (DFT), and correlated levels of theory and the % pair delocalization can be calculated. We have published a comparison of LIs and DIs obtained at the HF, DFT, and various correlated levels of theory and on the whole, inclusion of correlation tends to reduce the DIs relative to the HF and DFT levels. DIs obtained at the DFT level can be significantly overestimated. In this paper, we include the DIs between pairs of atoms of **6** along with % pair delocalization in each case. The data are collected in Table 4. For homonuclear molecules like ethane and ethene, the archetypal examples of molecules with single and double covalent bonds, the DIs should approach 1 and 2, an indication that one and two pairs of electrons are shared between two carbon atoms, respectively. The DIs for the C—C and C=C bonds of ethane and ethene at the CCSD/6-31+G(d)//MP2(FC)/6-31+G(d) level are 0.877 (Σ(LIs + DIs/2) = 18.0006) and 1.515 (Σ(LIs + DIs/2) = 18.0002), respectively. That DFT methods overestimate DIs is seen in the fact that at the B3PW91/6-31+G(d) level, the DIs are 1.029 and 1.931 for ethane and ethene, respectively. The same trend is seen in the data for **6** in Table 4. At the CCSD/6-31+G(d)//MP2(FC)/6-31+G(d) level, the DIs for the nominal double bonds of **6** are smaller than the DI of ethene. For the single bonds, the DIs are smaller than the DI of ethane except for C2—C3 where the value is 0.989 in keeping with the fact some double character is expected between C2 and C3. While Austen (38) has shown that DIs decrease when charge transfer occurs between atoms of diatomics, based on the electron populations (Table 2), there appears to no significant differential charge transfer between the carbon atoms of **6**. There is a significant difference between the populations of the hydrogens connected to C6 and C7 and the other hydrogens of **6** indicating that there is more charge transfer in these cases and the DIs for C6—H12 and C7—H3 are 0.8243 and 0.8256, respectively, somewhat smaller than the DIs for the other vinylic C—Hs: 0.8283 (C2—H8), 0.8285 (C3—H9), 0.8314 (C4—H10). Of particular importance in the case of **6** is the fact that the DI and the % pair delocalized between the C4—C6 basins — the potential homoconjugative interaction — are negligibly small at 0.051 and 1.52, respectively. That the homoconjgative interaction between C4 and C6 is negligible is also seen in the display of the C4 and C6 basins in Fig. 5*a* obtained with AIM 2000 with the B3LYP/6-31+G(d) wave function so a direct comparison can be made with the MOs displayed in Fig. 3. Even at the B3LYP/6-31+G(d) level in which DIs are overestimated, the basins are not close to each other at an isosurface contour value of 0.005. Moreover, even at a contour value of 0.001 (not shown) that is normally used to define van der Waals surfaces, the C4 and C6 basins are not close to each other. The zero-flux surfaces between the hydrogen and carbon basins are clearly see in Fig. 5*a*. The atomic basins obtained at the B3PW91/6-31+G(d) level (not shown) were not discernibly different from the B3LYP basins. Most interesting is the fact that there is a significant DI (0.1448 at B3LYP/6-31+G(d) and 0.1107 at CCSD/6-31+G(d)//MP2(FC)/6-31+G(d); see footnote *c* of Table 4) between C1 and C6. As seen in Figs. 5*b* and 5*c*, while it is not possible to visually discern differences in the displays, the wedge-shaped basins are in very close proximity in accord with the DIs being >0.1.

Conclusions

The pyrolysis of *N*,*N*-dimethylbicyclo[3.2.0]hepta-3,6-dien-1-amine oxide (**5**) in the source of the PE spectrometer made it possible to record a PE spectrum that consists of IP bands corresponding to the transient bicyclo[3.2.0]hepta-

© 2005 NRC Canada

Fig. 5. Atomic basins of: (*a*) C4 and C6 (B3LYP/6-31+G(d)); (*b*) C1 and C6 (B3LYP/6-31+G(d)); and (*c*) (CCSD/6-31+G(d)//MP2(FC)/6-31+G(d)) at an isosurface contour value of 0.005.



1,3,6-triene (**6**). The initial pyrolysis spectrum was obscured by IPs corresponding to the dimers **9** of the triene and dimethylhydroxylamine **7**. Upon subtraction of the PE spectra of **9** and **7**, the IPs of the transient **6** were clearly exposed. The experimental and simulated PE spectra of **6** are in excellent agreement and illustrate the first direct experimental observation of the elusive bicyclo[3.2.0]hepta-1,3,6-triene (**6**). The molecular structure of **6** was studied with QTAIM and a comparison of delocalization indexes showed that there is no homoconjugation between C4 and C6. Nevertheless, a delocalization index >0.1 between C1 and C6 indicated the presence of a minor homoconjugative interaction between these atoms and this was corroborated by the fact that there is slight contact between the basins of these atoms. We expect that a combination of delocalization indexes and plots of atomic basins will be the method of choice for evaluating homoconjugation and delocalization, especially in reactive intermediates. We are currently studying delocalization in a variety of so-called nonclassical carbocations and carbenes and a range of carbanions using this approach.

Experimental

The PE spectra were recorded at pressures between 2 to 6×10^{-3} torr (1 torr = 133.322 4 Pa) on a locally built UV PE spectrometer and were calibrated with the IP band of N_2 that is visible at 15.6 eV in all spectra (15). Linearity of the spectral scale was checked with the lowest IP bands of methyl iodide at 9.54 and 10.16 eV prior to the experiments. *N*-oxide **5** was placed in a small bottle-shaped quartz sample tube that was inserted into the tip of the heated probe and pyrolyzed in the source of the spectrometer. The tip of the sample tube was located 1 cm from the ionizing beam. The sample was dried under source vacuum for at least 12 h and the temperature was raised until pyrolysis occurred (120 °C) and a suitable sample pressure was achieved. Spectra were obtained by collecting and averaging 20–30 scans. Spectra of the dimers and dimethylhydroxylamine were obtained using our external sample introduction system.

Interpretation of the PE spectrum of the transient was aided by the application of a recently developed (22) and successfully applied (23, 24) routine based on B3LYP calculations. The equilibrium optimized geometry of **6** was obtained at the B3LYP/6-31+G(d) level of theory and used in single-point calculations on the radical cation at the same level of theory. The simulated PE spectrum of **6** was obtained from the MO results using a Fortran program PESPEC (26). A Gaussian line broadening of 0.4 and a temperature of 300 K were used to simulate the partial PE spectrum with 10 MO energies (HOMO to HOMO-9). DFT, MP2, and CCSD calculations were carried out with GAUSSIAN 98 or GAUSSIAN 03 (27, 28). Displays of molecular geometries and molecular orbitals were generated using MOLEKEL (29, 30). QTAIM analyses were carried out with AIMALL (31) and the delocalization indexes were obtained with LI-DICALC (13, 14). The molecular graph of **6** and plots of the C1, C4, and C6 atomic basins were obtained with AIM 2000 (32). The grid-point file for **6** contained over 900 000 points calculated at a mesh size of 0.125, and the surfaces displayed in Fig. 5 were obtained by triangularization using the grid points of the 0.005 isosurface. This accounts for the relatively uneven appearance of the isosurfaces. To obtain smoother surfaces would have required long calculations and the generation larger than 100 MB in size.

Tropylium bromide (2) (33, 34)

A solution of 1,3,5-cycloheptatriene (24.2 g, 0.263 mol) in dichloromethane (200 mL) was placed in a round-bottomed flask cooled in a dry ice – acetone bath. A solution of bromine (15 mL) in dichloromethane (120 mL) was added dropwise. After the addition, the reaction was allowed to come to room temperature. Removal of solvent resulted in a dark brown oil, which was heated with stirring under vacuum in a round-bottomed flask fitted with a downward distillation apparatus at a temperature of 70 °C overnight. The dark solid residue was ground with mortar and pestle under dichloromethane and was filtered. Tropylium bromide was collected as a pale green solid.

N,*N*-Dimethylcyclohepta-1,3,5-trien-7-amine (3)

N,*N*-Dimethylcyclohepta-1,3,5-trien-7-amine was synthesized according to a procedure by Doering and Knox (33).

A solution of tropylium bromide (5.8 g) in 35 mL of distilled water was treated with 20% dimethylamine in water (40 mL). Immediately upon this addition a light brown oil separated. The solution was extracted with pentane (2 ×

© 2005 NRC Canada

20 mL). The combined organic extracts were dried with anhydr. $MgSO_4$. Filtration and removal of solvent resulted in 3.5 g of a yellow oil. Purity of the product was confirmed by NMR. ^{1}H NMR ($CDCl_3$) δ: 1.86 (t, 1H), 2.37 (s, 6H), 5.45 (m, 2H), 6.17 (m, 2H), 6.71 (m, 2H). ^{13}C ($CDCl_3$) δ: 43.2, 65.6, 122.8, 123.5, 130.6.

***N*,*N*-Dimethylbicyclo[3.2.0]hepta-3,6-dien-1-amine (4) (35)**

A solution of *N*,*N*-dimethylcyclohepta-1,3,5-trien-7-amine (2 g) in 1 L of hexanes (Omnisolve) was degassed for 1 h with nitrogen and photolyzed with a medium pressure mercury arc lamp for 6.5 h. The solution was then filtered to remove precipitated polymeric material and the solvent was removed using a rotary evaporator affording 1.6 g of the bicyclic amine. The product was checked by NMR and was used in PE spectroscopic experiments without further purification. ^{1}H NMR ($CDCl_3$) δ: 2.23–2.28 (m, 2H), 2.25 (s, 6H), 3.48 (m, 1H), 5.74 (m, 2H), 6.31 (br s, 2H).

***N*,*N*-Dimethylbicyclo[3.2.0]hepta-3,6-dien-1-amine oxide (5) (36)**

A solution of tertiary amine **4** (1 g) in 30 mL of methanol was treated with 30% hydrogen peroxide (2 g). The solution was stirred overnight at room temperature under nitrogen. Excess hydrogen peroxide was quenched with palladium on charcoal. The solution was filtered and the solvent was removed on a rotary evaporator. The sample was dried under vacuum to yield a tan solid. *N*-oxide **5** was identified by NMR in deuterated methanol. ^{1}H NMR (CD_3OD) δ: 3.33 (s, 3H), 3.36 (s, 3H), 3.95 (br s, 1H), 5.83 (br s, 2H), 6.26 (d, 2H), 6.55 (d, 2H).

Acknowledgements

We gratefully acknowledge financial support by the Natural Sciences and Engineering Research Council of Canada (NSERC).

References

1. C. Wentrup, E. Wentrup-Byrne, and P. Müller. Chem. Commun. 210 (1977).
2. O.L. Chapman and C.J. Abelt. J. Org. Chem. **52**, 1218 (1987).
3. R.J. McMahon, C.J. Abelt, O.L. Chapman, J.W. Johnson, C.L. Kreil, J.-P. LeRoux, A.M. Mooring, and P.R. West. J. Am. Chem. Soc. **109**, 2456 (1987).
4. M.W. Wong and C. Wentrup. J. Org. Chem. **61**, 7022 (1996).
5. E.V. Patterson and R.J. McMahon. J. Org. Chem. **62**, 4398 (1997).
6. N.L. Bauld, C.E. Dahl, and Y.S. Rim. J. Am. Chem. Soc. **91**, 2787 (1969).
7. R. Breslow, W. Washburn, and R.G. Bergman. J. Am. Chem. Soc. **91**, 196 (1969).
8. R. Breslow and W. Washburn. J. Am. Chem. Soc. **92**, 428 (1970).
9. W.E. Billups, R.K. Saini, V.A. Litosh, L.B. Alemany, W.K. Wilson, and K.B. Wiberg. J. Org. Chem. **67**, 4436 (2002).
10. W.T. Brown and W.M. Jones. J. Org. Chem. **44**, 3090 (1979).
11. Y. Kon, J. Ogasawara, K. Sakamoto, C. Kabuto, and M. Kira. J. Am. Chem. Soc. **125**, 9310 (2003).
12. R.F.W. Bader. Atoms in molecules. Oxford Science Publications, Oxford, UK. 1990.
13. Y.-G. Wang and N.H. Werstiuk. J. Comput. Chem. **24**, 379 (2003).
14. Y.-G. Wang, C. Matta, and N.H. Werstiuk. J. Comput. Chem. **24**, 1720 (2003).
15. N.H. Werstiuk, D.N. Butler, and E. Shahid. Can. J. Chem. **65**, 760 (1986).
16. N.H. Werstiuk, J. Ma, and C.D. Roy. Can. J. Chem. **73**, 146 (1995).
17. N.H. Werstiuk, J. Ma, C.D. Roy, A.J. Kresge, and E.A. Jefferson. Can. J. Chem. **73**, 1738 (1995).
18. N.H. Werstiuk, J. Ma, C.D. Roy, A.J. Kresge, and E.A. Jefferson. Can. J. Chem. **73**, 2536 (1995).
19. N.H. Werstiuk, J. Ma, and C.D. Roy. Can. J. Chem. **74**, 1903 (1996).
20. H.M. Muchall, N.H. Werstiuk, B. Choudhury, J. Warkentin, and J. Pezacki. Can. J. Chem. **76**, 238 (1998)
21. N.H. Werstiuk, H.M. Muchall, J. Ma, and M.T.H. Liu. Can. J. Chem. **76**, 1162 (1996).
22. H.M. Muchall, N.H. Werstiuk, and B. Choudhury. Can. J. Chem. **76**, 221 (1998).
23. T. Bajorek and N.H. Werstiuk. Can. J. Chem. **82**, 80 (2004).
24. T. Bajorek and N.H. Werstiuk. Chem. Commun. (Cambridge), 648 (2002).
25. A.D. Becke. J. Chem. Phys. **98**, 5648 (1993).
26. N.H. Werstiuk, G. Timmins, J. Ma, and T.A. Wildman. Can. J. Chem. **70**, 1971 (1992).
27. M.J. Frisch, G.W. Trucks, H.B. Schlegel, G.E. Scuseria, M.A. Robb, J.R. Cheeseman, V.G. Zakrzewski, J.A. Montgomery, R.E. Stratmann, J.C. Burant, S. Dapprich, J.M. Millam, A.D. Daniels, K.N. Kudin, M.C. Strain, O. Farkas, J. Tomasi, V. Barone, M. Cossi, R. Cammi, B. Mennucci, C. Pomelli, C. Adamo, S. Clifford, J. Ochterski, G.A. Petersson, P.Y. Ayala, Q. Cui, K. Morokuma, D.K. Malick, A.D. Rabuck, K. Raghavachari, J.B. Foresman, J. Cioslowski, J.V. Ortiz, B.B. Stefanov, G. Liu, A. Liashenko, P. Piskorz, I. Komaromi, R. Gomperts, R.L. Martin, D.J. Fox, T. Keith, M.A. Al-Laham, C.Y. Peng, A. Nanayakkara, C. Gonzalez, M. Challacombe, P.M.W. Gill, B.G. Johnson, W. Chen, M.W. Wong, J.L. Andres, M. Head-Gordon, E.S. Replogle, and J.A. Pople. GAUSSIAN 98. Revision A.9 [computer program]. Gaussian, Inc., Pittsburgh, Penn. 1998.
28. M.J. Frisch, G.W. Trucks, H.B. Schlegel, G.E. Scuseria, M.A. Robb, J.R. Cheeseman, J.A. Montgomery, Jr., T. Vreven, K.N. Kudin, J.C. Burant, J.M. Millam, S.S. Iyengar, J. Tomasi, V. Barone, B. Mennucci, M. Cossi, G. Scalmani, N. Rega, G.A. Petersson, H. Nakatsuji, M. Hada, M. Ehara, K. Toyota, R. Fukuda, J. Hasegawa, M. Ishida, T. Nakajima, Y. Honda, O. Kitao, H. Nakai, M. Klene, X. Li, J.E. Knox, H.P. Hratchian, J.B. Cross, C. Adamo, J. Jaramillo, R. Gomperts, R.E. Stratmann, O. Yazyev, A.J. Austin, R. Cammi, C. Pomelli, J.W. Ochterski, P.Y. Ayala, K. Morokuma, G.A. Voth, P. Salvador, J.J. Dannenberg, V.G. Zakrzewski, S. Dapprich, A.D. Daniels, M.C. Strain, O. Farkas, D.K. Malick, A.D. Rabuck, K. Raghavachari, J.B. Foresman, J.V. Ortiz, Q. Cui, A.G. Baboul, S. Clifford, J. Cioslowski, B.B. Stefanov, G. Liu, A. Liashenko, P. Piskorz, I. Komaromi, R.L. Martin, D.J. Fox, T. Keith, M.A. Al-Laham, C.Y. Peng, A. Nanayakkara, M. Challacombe, P.M.W. Gill, B. Johnson, W. Chen, M.W. Wong, C. Gonzalez, and J.A. Pople. GAUSSIAN 03. Revision B.02 [computer program]. Gaussian, Inc., Pittsburgh, Penn. 2003.
29. P. Flükiger, H.P. Lüthi, S. Portman, and J. Weber. MOLEKEL 4.3 [computer program]. Swiss Center for Scientific Computing, Manno, Switzerland. 2000–2002.
30. S. Portman and H.P. Lüthi. Chimia, **54**, 766 (2000).

© 2005 NRC Canada

31. T.A. Keith and R.F.W. Bader. AIMALL [computer program]. McMaster University, Hamilton, Ontario. 1997.
32. F. Biegler-Konig. AIM 2000 [computer program]. University of Applied Science, Bielefeld, Germany.
33. W.E. von Doering and L.H. Knox. J. Am. Chem. Soc. **79**, 352 (1957).
34. W.E. von Doering and L.H. Knox. J. Am. Chem. Soc. **76**, 3203 (1954).
35. A.P. Ter Borg, E. Razenberg, and H. Kloosterziel. Recl. Trav. Chim. **84**, 1230 (1965).
36. A.C. Cope and E. Ciganek. *In* Organic synthesis. Collect. Vol. IV. *Edited by* N. Rabjohn. Wiley, New York. 1963. p. 612.
37. J. Poater, M. Solà, M. Duran, and X. Fradera. Theor. Chem. Acc. **107**, 362 (2002).
38. M.A. Austen. Ph.D. thesis, McMaster University, Hamilton, Ontario. 2003.
39. P. Rademacher and B. Freckmann. J. Electron Spectrosc. Relat. Phenom. **19**, 251 (1980).
40. W. Schafer and A. Schweig. Angew. Chem. Int. Ed. Engl. **11**, 836 (1972).

© 2005 NRC Canada

Reactions of acetoxy(methylthio)carbene and *S*-methyl thiopyruvate[1]

Arkadiusz Klys, Wojciech Czardybon, John Warkentin, and Nick Henry Werstiuk

Abstract: Thermolysis of 2-acetoxy-5,5-dimethyl-2-methylthio-Δ^3-1,3,4-oxadiazoline in benzene at 110 °C afforded *S*-methyl 2-oxopropanethioate (*S*-methyl thiopyruvate) from 1,2-acyl migration in acetoxy(methylthio)carbene, as well as *S*,*S*-dimethyl 2-acetoxy-2-methylpropanebis(thioate) and *S*-methyl 2-acetoxy-2-(methylthio)butanethioate. The latter two, both composed of two carbene units, are derived from reaction of the first product with the carbene.

Key words: acetoxy(methylthio)carbene, carbene, *S*-methyl thiopyruvate, rearrangement.

Résumé : La thermolyse de la 2-acétoxy-5,5-diméthyl-2-méthylthio-Δ^3-1,3,4-oxadiazoline, dans le benzène à 110 °C, conduit à la formation du 2-oxopropanethioate de *S*-méthyle (thiopyruvate de *S*-méthyle) qui provient d'une migration 1,2 d'un groupe acyle dans l'acétoxy(méthylthio)carbène, ainsi que du 2-acétoxy-2-méthylpropanebis(thioate) de *S*,*S*-diméthyle et du 2-acétoxy-2-(méthylthio)butanethioate de *S*-méthyle. Ces deux derniers produits, qui sont formés de deux unités de carbène, dérivent de la réaction du premier produit avec le carbène.

Mots clés : acétoxy(méthylthio)carbène, carbène, thiopyruvate de *S*-méthyle, réarrangement.

Introduction

Recently, we reported the generation of acetoxy(methoxy)carbene (**2**) by thermolysis of 2-acetoxy-5,5-dimethyl-2-methoxy-Δ^3-1,3,4-oxadiazoline (**1**, Scheme 1) (1). Thermolysis of **1** is relatively complex, affording the carbene as well as 2-diazopropane as shown in the abbreviated Scheme 1. The carbene did not fragment to radicals, but it rearranged to methyl pyruvate (**3**) by acetyl migration from oxygen to the carbene carbon, a known process for other acetoxycarbenes (2–7).

We now report that thermolysis of **4** does not afford 2-diazopropane, but gives acetoxy(methylthio)carbene (**5**) under the same conditions. The latter also undergoes a 1,2-acyl shift, but the final products contained not only the rearrangement product (**6**), analogous to **3**, but also two additional compounds. In particular, **4** afforded **6** (the known propanethioic acid, 2-oxo-, *S*-methyl ester, also known as *S*-methyl thiopyruvate) and two additional compounds (**8** and **10**), each made up of two carbene units (Scheme 2).

The precursor of **5** was 2-acetoxy-5,5-dimethyl-2-methylthio-Δ^3-1,3,4-oxadiazoline (**4**) prepared from **9** according to Scheme 3.

Thermolysis of **4** in benzene gave **6**, **8**, and **10**. Formation of **6** probably occurs by concerted acetyl transfer from oxygen to the carbene carbon, as was found for other acyloxy carbenes (2–8). Formation of compounds **6** and **8** is most easily formulated in terms of zwitterionic intermediates (9) formed by reaction of **6** with **5** (Scheme 4).

The first formed *S*-methyl thiopyruvate (**6**) reacts with the carbene preferentially at the ketonic carbon, which must be more electrophilic than the thioester carbonyl carbon. Most likely, transfer of an acyl group occurs through a five-membered transition state to afford the solid **8**. Attack at the thioester carbonyl group, followed by an analogous transfer affords the liquid **10**.

The structure of **8** was confirmed by means of single crystal X-ray diffraction[4] and that of **10** was determined by NMR and mass spectrometry, with reference to the spectra of **8**, chemical shift tables, (10) and chemical shift predictions from the ChemDraw program. Good models for **8** were not found. Attack of dialkoxycarbenes on carbonyl groups has been observed (11), but we are not aware of analogous reactions of acetoxy(methylthio)carbene. Transfer of an acetyl group in zwitterionic intermediates such as **7** and **9** also appears to be unprecedented.

Received 27 April 2005. Published on the NRC Research Press Web site at http://canjchem.nrc.ca on 22 October 2005.

A. Klys, W. Czardybon, J. Warkentin,[2] and N.H. Werstiuk.[3] Department of Chemistry, McMaster University, 1280 Main St. W., Hamilton, ON L8S 4M1, Canada.

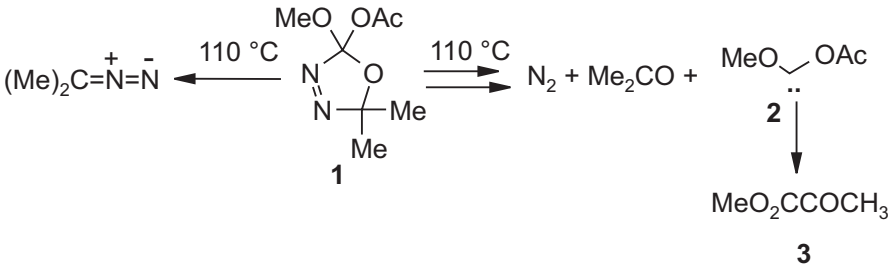
[1]This article is part of a Special Issue dedicated to organic reaction mechanisms.

[2]Corresponding author (e-mail: warkent@mcmaster.ca).
[3]Corresponding author (e-mail: werstiuk@mcmaster.ca).

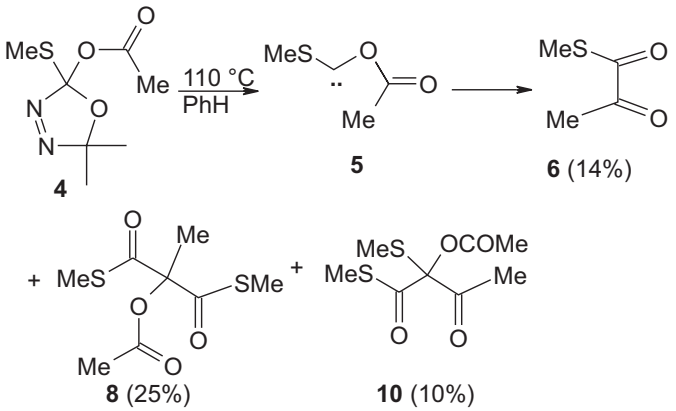
[4]Supplementary data for this article are available on the Web site or may be purchased from the Depository of Unpublished Data, Document Delivery, CISTI, National Research Council Canada, Ottawa, ON K1A 0S2, Canada. DUD 4036. For more information on obtaining material refer to http://cisti-icist.nrc-cnrc.gc.ca/irm/unpub_e.shtml. CCDC 274864 contains the crystallographic data for this manuscript. These data can be obtained, free of charge, via www.ccdc.cam.ac.uk/conts/retrieving.html (Or from the Cambridge Crystallographic Data Centre, 12 Union Road, Cambridge CB2 1EZ, UK; fax +44 1223 336033; or deposit@ccdc.cam.ac.uk).

 doi: 10.1139/V05-151 © 2005 NRC Canada

Scheme 1.



Scheme 2.



Although the zwitterions **7** and **9** are conjectural intermediates, there is some precedent for formation of persistent charge-separated structures from reactions of a nucleophilic carbene. Imidazol-2-ylidenes react with tetracoordinate silicon compounds (12), with stannylenes (13), and with a plumbylene (14), for example, to produce species that are zwitterions or resonance hybrids that have zwitterionic contributors. An imidazol-2-ylidene also attacks CS_2 to form an isolable zwitterion (15) (Scheme 5).

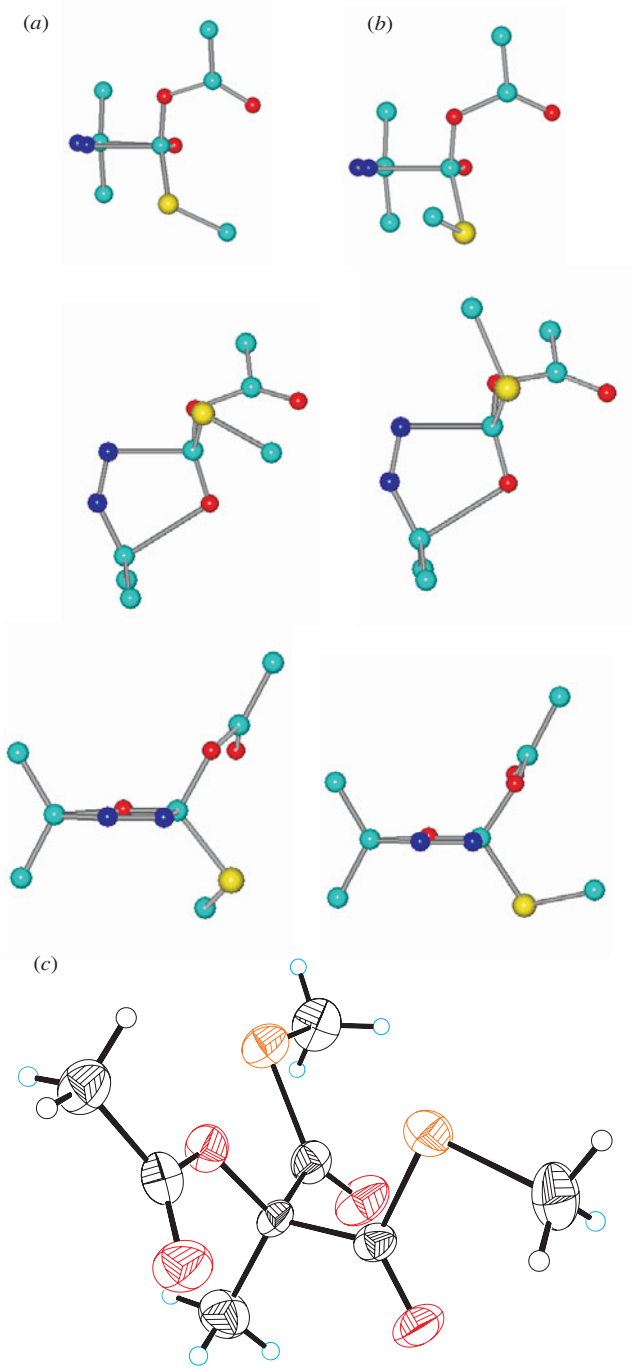
The reasons for the different thermolysis behaviours of **1** and **4** are not well understood but some potential causes of the differences were examined by means of computation. First, the free energy barriers to fragmentation of the two oxadiazolines might be different, either favouring fragmentation of **1** in the sense that affords 2-diazopropane (7) or favouring fragmentation of **4** in the sense that affords **5**. Either could account for the fact that **1** affords 2-diazopropane while **4** does not. To account for the fact that **4** affords **8** and **10** whereas **1** does not produce analogous 2:1 products, one could imagine that the reactivity of **5** toward **6** could be higher than that of **2** toward **3**.

Optimized equilibrium geometries and transition states were obtained at the Becke3PW91/6-31+G** (16*a*) level, which includes the three-parameter Becke–Perdew–Wang (Becke3PW91) exchange-correlation potential (16*b*) using either GAUSSIAN 98 (16*a*) or GAUSSIAN 03 (16*c*).

Computation of the free energy barriers for fragmentation of the oxadiazolines at 110 °C was carried out for both the gauche and antigauche conformations, where gauche and antigauche are defined in Fig. 1.

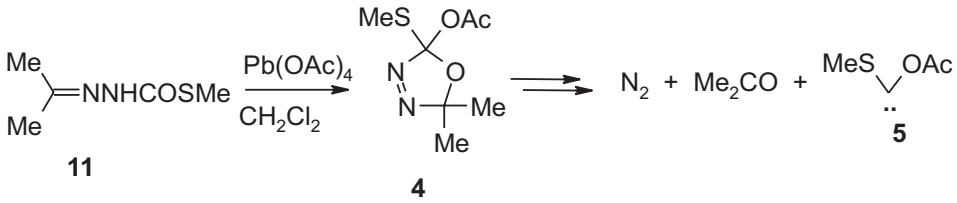
For **1**, the antigauche conformation is more favourable for diazopropane formation ($G^{\ddagger}$ = 24.6 kcal mol^{-1}, 1 cal = 4.184 J), while the gauche conformation is favoured for ylide formation ($G^{\ddagger}$ = 26.9 kcal mol^{-1}) (7). For **4**, the

Fig 1. Different views of the gauche and antigauche conformations of the transition state for formation of diazopropane from **4**, with hydrogen atoms omitted for clarity: (*a*) antigauche conformation; (*b*) gauche conformation. (*c*) ORTEP rendition of **8**.

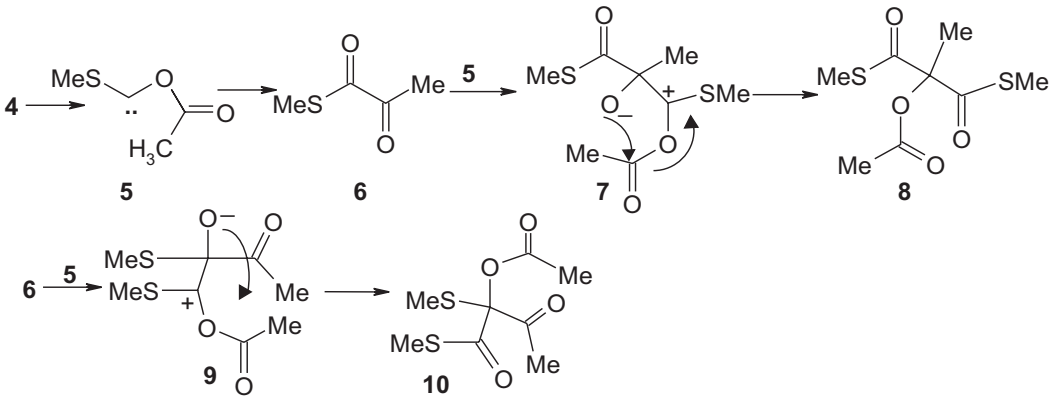


© 2005 NRC Canada

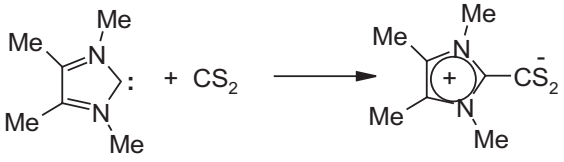
Scheme 3.



Scheme 4.



Scheme 5.



antigauche conformation is again favoured for diazopropane formation ($G^{\ddagger}_{\text{diazopropane}}$ = 20.2 kcal mol^{-1}), while the gauche conformation is slightly favoured for ylide formation (22.5 kcal mol^{-1}).

It is clear that the computations do not predict all of the experimental results, which indicate that **1** should fragment to 2-diazopropane at 110 °C (which it does) and that **4** should also do so (which it does not). However, the free energy differences for the two possible thermolysis paths open to **1** and **4** are only about 2 kcal mol^{-1}, which could easily be within the combined errors in the computations (Table 1).

Calculated free energies of activation for rearrangement (1,2-acyl migration) of the carbenes gave 16.6 and 13.1 kcal mol^{-1} for **2** and **5**, respectively. This result suggests that **5** probably rearranges more rapidly than **2**. As a reasonable explanation for the fact that **5** affords not only **6**, but also **8** and **10**, we suggest that **5** is significantly more reactive toward **6** than **2** is toward **3**. The methylthio group is poorer (compared to the methoxy group) at conjugative stabilization of both a carbene and a carbonyl group and that feature could make both **5** and **6** more reactive than their oxy counterparts (**2** and **3**). Ketoester **6** can be regarded as somewhat like an α-diketone rather than a simple α-ketoester, with a consequent increase in reactivity of both carbonyl groups toward nucleophiles.

Summary

Acetoxy(methylthio)carbene rearranges in benzene at 110 °C by 1,2-acyl migration to *S*-methyl thiopyruvate. The latter reacts with the carbene at both carbonyl groups to afford *S*,*S*-dimethyl 2-acetoxy-2-methylpropanebis(thioate) and *S*-methyl 2-acetoxy-2-(methylthio)butanethioate. Those products probably arise by acetyl group transfer, through five-membered transition states, in zwitterionic intermediates. Support for the formation of the carbene via cycloreversion of an oxadiazoline precursor to a carbonyl ylide, and rearrangement of the carbene by concerted acyl group transfer, was sought by means of computation.

Experimental

General

^{1}H NMR spectra were obtained from solutions in C_6D_6 or $CDCl_3$, with Bruker spectrometers operating at 200 or 600 MHz, unless otherwise indicated, and are referenced to the signal at 7.16 attributed to C_6HD_5 or to $CHCl_3$ at 7.26 ppm. ^{13}C NMR spectra, run at 50.9 or 150.9 MHz, in C_6D_6 or $CDCl_3$, are referenced to the center line of the solvent triplet at 128.1 or 77.2 ppm, respectively. Mass spectra were run with a Micromass/Waters GCT time-of-flight instrument. GC separations were performed with a 6 ft × 4.0 mm (1 ft = 0.0348 m) (internal) column containing 10% OV 101. The helium flow rate was 40 mL min^{-1} and the temperature program was 60 °C for 3 min, then 5 °C / min to 200 °C. IR spectra were taken with neat samples on a Bruker Tensor 27 FT IR instrument equipped with a Harrick ATR accessory and a ZnSe crystal.

Yields are calculated in the usual way, as 100 (mol product)/mol **4**, with the different stoichiometries involved in the formation of **6**, **8**, and **10** being taken into account. For example, 2 mol of **4** are required to make 1 mol of **8**. About 80% of the potential carbene units from **4** were accounted for by products **6**, **8**, and **10**.

© 2005 NRC Canada

Table 1. Energies expressed as total energies, zero point corrected total energies, free energies, and enthalpies calculated at the B3PW91/6-31+G** level.

(*a*) MeSOAc system					
	gauche		antigauche		
Thermochemical parameter[a]	TS to ylide	TS to diazopropane	TS to ylide	TS to diazopropane	TS carbene (W) to pyruvate
ΔE_{elec}[b]	27.10	25.91	27.63	24.88	13.15
ΔE_o[c]	24.31	23.43	24.75	22.41	12.41
$\Delta E_{110\ °C}$[d]	25.19	24.28	25.65	23.28	12.05
$\Delta H_{25\ °C}$[e]	25.06	24.19	25.51	23.19	12.14
$\Delta H_{110\ °C}$	25.19	24.28	25.65	23.28	12.05
$\Delta G_{25\ °C}$[f]	23.10	21.85	23.64	20.86	12.86
$\Delta G_{110\ °C}$	22.52	21.16	23.09	20.18	13.08
(*b*) MeOOAc system					
	gauche		antigauche		
Thermochemical parameter[a]	TS to ylide	TS to diazopropane	TS to ylide	TS to diazopropane	TS carbene (W) to pyruvate
ΔE_{elec}[b]	34.53	31.43	37.22	29.84	16.71
ΔE_o[c]	30.64	28.78	32.17	27.18	15.96
$\Delta E_{110\ °C}$[d]	32.24	28.06	32.78	28.07	15.57
$\Delta H_{25\ °C}$[e]	31.98	29.53	34.05	27.97	15.70
$\Delta H_{110\ °C}$	32.24	28.01	32.74	28.07	15.57
$\Delta G_{25\ °C}$[f]	28.33	27.45	28.24	25.51	16.34
$\Delta G_{110\ °C}$	26.93	30.16	29.86	24.58	16.60

[a]At the B3PW91/6-31+G** level in kcal mol^{-1}.
[b]E_{elec} is the uncorrected total energy.
[c]$E_o = E_{elec}$ + ZPE.
[d]$E = E_o + E_{vib} + E_{rot} + E_{trans}$.
[e]$H = E + RT$.
[f]$G = H - TS$.

2-Acetoxy-5,5 dimethyl-2-methylthio-Δ^3-1,3,4-oxadiazoline (4)

To a stirred solution of $Pb(OAc)_4$ (8.4 g) in CH_2Cl_2 at 0 °C was added hydrazone **11** (17) (2 g, 13.7 mmol). After 3 h the solution was filtered through Celite to remove $Pb(OAc)_2$ and the organic filtrate was washed with 100 mL of aq. (5%) $NaHCO_3$ before it was dried. Evaporation of the solvent left a yellow oil (1.9 g, 68%) that was a mixture of **4** and an acyclic isomer. Very fast chomatography on "old" neutral alumina (hydrated in an open beaker for 3 days) in a 15 cm × 3 cm column with hexane–EtOAc (95:5), collection of the first fraction, evaporation of the solvent immediately, and recrystallization from pentane at –20 °C gave 1.3 g (46%) of colorless crystalline **4**. ^{1}H NMR (200 MHz, $CDCl_3$) δ: 1.56 (s, 3H), 1.65 (s, 3H), 2.13 (s, 3H), 2.41 (s, 3H). ^{13}C NMR (50.3 MHz, $CDCl_3$) δ: 13.55, 21.62, 23.35, 23.61, 125.72, 133.16, 166.98. MS (CI, NH_3) *m/z* calcd. for $C_7H_{13}N_2O_3S$: 205.0642 $(M + H)^+$; found: 205.0647.

Thermolysis of 4

Oxadiazoline **4** (204 mg, 1 mmol) in dry benzene (5 mL) was heated for 24 h at 110 °C. The solvent was then evaporated in vacuo and products **7** and **8** were separated by radial chromatography on a 2 mm silica plate with hexane–EtOAc (95:5). Product **6** was separated by GC with a 6 ft × 4.0 mm (internal) column containing 10% OV 101, which also separated **8** from **10**. The helium flow rate was 40 mL min^{-1} and the temperature program was 60 °C for 3 min, then 5 °C / min to 200 °C. The total yield of products was determined by analysis of the ^{1}H NMR spectrum of the crude product containing an internal standard. The same yields were calculated from GC data.

Propanethioic acid, 2-oxo-, *S*-methyl ester (6) (18)

Pale yellow oil. Yield: 14%. IR (cm^{-1}): 1722, 1670. ^{1}H NMR (200 MHz, $CDCl_3$) δ: 2.35 (s, 3H), 2.43 (s, 3H). ^{13}C NMR (50.3 MHz, $CDCl_3$) δ: 11.42, 24.06, 191.86, 193.20.

S,*S*-Dimethyl 2-acetoxy-2-methylpropanebis(thioate) (8)

White solid. Yield: 25%. IR (cm^{-1}): 1753, 1697, 1663. The C=O stretching frequencies of esters, in nonpolar solvents, are in the range 1735–1750 cm^{-1} (19). ^{1}H NMR (200 MHz, $CDCl_3$) δ: 1.88 (s, 3H), 2.22 (s, 3H), 2.32 (s, 6H). ^{1}H NMR (200 MHz, C_6D_6) δ: 1.72 (s, 3H), 1.84 (s, 6H), 1.96 (s, 3H). ^{1}H NMR chemical shifts ($CDCl_3$) predicted with the use of ChemDraw: 1.86, 2.01, 2.27. ^{13}C NMR (50.3 MHz, $CDCl_3$) δ: 11.4 (SCH_3), 21.2 (CH_3 or CH_3CO_2), 21.4 (CH_3 or CH_3CO_2), 91.5 (quat. carbon), 168.6 (O_2CCH_3), 195.4 (O_2CSCH_3) (assignments based on ref. 10). ^{13}C NMR chemical shifts ($CDCl_3$) predicted with the use of ChemDraw: 15.5, 17.2, 17.3, 117.1, 171.0, 197.6. HR-MS (CI, NH_3) *m/z* calcd. for $C_8H_{13}O_4S_2$: 237.0255 (M +

© 2005 NRC Canada

H)$^+$; found: 237.0255. The structure of **8** was confirmed by means of single crystal X-ray diffraction.

S-Methyl 2-acetoxy-2-(methylthio)butanethioate (10)

Pale yellow oil. Yield: 10%. IR (cm^{-1}): 1754. ^1H NMR (200 MHz, $CDCl_3$) δ: 2.12 (s, 3H), 2.24 (s, 3H), 2.36 (s, 3H), 2.42 (s, 3H). ^1H NMR chemical shifts ($CDCl_3$) predicted with the use of ChemDraw: 2.01, 2.09, 2.09, 2.27. ^{13}C NMR (50.3 MHz, $CDCl_3$) δ: 12.4 (CH_3S or CH_3SC=O), 12.6 (CH_3S or CH_3SC=O), 21.0 (CH_3CO_2), 26.3 (CH_3C=O), 98.6 (quat. carbon), 169.1 (O_2CCH_3), 193.9 (O=$CSCH_3$ or O=CCH_3), 194.7 (O=$CSCH_3$ or O=CCH_3) (assignments based on ref. 10). ^{13}C NMR chemical shifts ($CDCl_3$) predicted with the use of ChemDraw: 7.6, 14.8, 15.0, 16.6, 130.4, 171.0, 196.5, 206.0. MS (CI, NH_3) *m/z*: 254 (M + NH_4)$^+$, 100%, 237 (M + H)$^+$, 12%. HR-MS (CI, NH_3) *m/z* calcd. for $C_8H_{16}NO_4S_2$: 254.0521 (M + NH_4)$^+$; found: 254.0524.

Search for 2-diazopropane

Phenol generates the stable isopropyl phenyl ether (1) from 2-diazopropane. Thermolysis of oxadiazoline **4** (0.20 g, 0.98 mmol) in benzene (1 mL) in the presence of phenol (0.184 g, 1.96 mmol) and analysis of the crude reaction mixture by gas chromatography, with authentic ether as the reference in hand, showed at most a trace of the ether. Mass spectrometry of the same crude product and a careful search for *m/z* = 136.19 ($C_9H_{12}O$) failed to show any signal above noise. The detection limit by this method was estimated to be well below 1%.

Acknowledgements

The authors are grateful to Professor Jim Britten, who carried out the crystallography, and to the Natural Sciences and Engineering Research Council of Canada (NSERC) for financial support.

References

1. W. Czardybon, A. Klys, J. Warkentin, and N.H. Werstiuk. Can. J. Chem. **81**, 1438 (2003).
2. M. Békhazi and J. Warkentin. J. Org. Chem. **47**, 4870 (1982).
3. R.A. Moss, S. Xue, and W. Liu. J. Am. Chem. Soc. **116**, 1583 (1994).
4. R.A Moss, S. Xue, W. Liu, and K. Krogh-Jesperson. J. Am. Chem. Soc. **118**, 12588 (1996).
5. R.A. Moss, S. Xue, W. Ma, and H. Ma. Tetrahedron Lett. **38**, 4379 (1997).
6. R.A. Moss and D.C. Merrer. Tetrahedron Lett. **39**, 8067 (1998).
7. W. Czardybon, J. Warkentin, and N.H. Werstiuk J. Phys. Org. Chem. **18**, 486 (2005).
8. R.F.C. Brown, F.W. Eastwood, S.T. Lim, and G.L. McMullen. Aust. J. Chem. **29**, 1705 (1976).
9. H. Zhou, G. Mloston, and J. Warkentin. Org. Lett. **7**, 487 (2005).
10. H.-D. Kalinowski, S. Berger, and S. Braun. Carbon-13 NMR spectroscopy. Wiley, New York. 1988. pp. 193–198.
11. (*a*) M. Dawid and J. Warkentin. Can. J. Chem. **81**, 598 (2003); (*b*) M. Dawid, G. Mloston, and J. Warkentin. Chem. Eur. J. **8**, 2184 (2002); (*c*) P.C. Venneri and J. Warkentin. Can. J. Chem. **78**, 1194 (2000).
12. N. Kuhn, T. Kratz, D. Bläser, and R. Boese. Chem. Ber. **128**, 245 (1995).
13. A. Schäfer, M. Weidenbruch, W. Saak, and S. Pohl. J. Chem. Soc. Chem. Commun. 1157 (1995).
14. F. Stabenow, W. Saak, and M. Weidenbruch. Chem. Commun. (Cambridge), 1131 (1999).
15. N. Kuhn, H. Bohnen, and G. Henkel. Z. Naturforsch. B, **49b**, 1473 (1994).
16. (*a*) M.J. Frisch, G.W. Trucks, H.B. Schlegel, G.E. Scuseria, M.A. Robb, J.R. Cheeseman, V.G. Zakrzewski, J.A. Montgomery, Jr., R.E. Stratmann, J.C. Burant, S. Dapprich, J.M. Millam, A.D. Daniels, K.N. Kudin, M.C. Strain, O. Farkas, J. Tomasi, V. Barone, M. Cossi, R. Cammi, B. Mennucci, C. Pomelli, C. Adamo, S. Clifford, J. Ochterski, G.A. Petersson, P.Y. Ayala, Q. Cui, K. Morokuma, D.K. Malick, A.D. Rabuck, K. Raghavachari, J.B. Foresman, J. Cioslowski, J.V. Ortiz, A.G. Baboul, B.B. Stefanov, G. Liu, A. Liashenko, P. Piskorz, I. Komaromi, R. Gomperts, R.L. Martin, D.J. Fox, T. Keith, M.A. Al-Laham, C.Y. Peng, A. Nanayakkara, M. Challacombe, P.M.W. Gill, B. Johnson, W. Chen, M.W. Wong, J.L. Andres, C. Gonzalez, M. Head-Gordon, E.S. Replogle, and J.A. Pople. GAUSSIAN 98 [computer program]. Gaussian, Inc., Pittsburgh, Penn. 1998; (*b*) J.P. Perdew and Y. Wang. Phys. Rev. B, **45**, 13244 (1992); (*c*) M.J. Frisch, G.W. Trucks, H.B. Schlegel, G.E. Scuseria, M.A. Robb, J.R. Cheeseman, J.A. Montgomery, Jr., T. Vreven, K.N. Kudin, J.C. Burant, J.M. Millam, S.S. Iyengar, J. Tomasi, V. Barone, B. Mennucci, M. Cossi, G. Scalmani, N. Rega, G.A. Petersson, H. Nakatsuji, M. Hada, M. Ehara, K. Toyota, R. Fukuda, J. Hasegawa, M. Ishida, T. Nakajima, Y. Honda, O. Kitao, H. Nakai, M. Klene, X. Li, J.E. Knox, H.P. Hratchian, J.B. Cross, C. Adamo, J. Jaramillo, R. Gomperts, R.E. Stratmann, O. Yazyev, A.J. Austin, R. Cammi, C. Pomelli, J.W. Ochterski, P.Y. Ayala, K. Morokuma, G.A. Voth, P. Salvador, J.J. Dannenberg, V.G. Zakrzewski, S. Dapprich, A.D. Daniels, M.C. Strain, O. Farkas, D.K. Malick, A.D. Rabuck, K. Raghavachari, J.B. Foresman, J.V. Ortiz, Q. Cui, A.G. Baboul, S. Clifford, J. Cioslowski, B.B. Stefanov, G. Liu, A. Liashenko, P. Piskorz, I. Komaromi, R.L. Martin, D.J. Fox, T. Keith, M.A. Al-Laham, C.Y. Peng, A. Nanayakkara, M. Challacombe, P.M.W. Gill, B. Johnson, W. Chen, M.W. Wong, C. Gonzalez, and J.A. Pople. GAUSSIAN 03 [computer program]. Gaussian, Inc., Pittsburgh, Penn. 2003.
17. E. Nachbaur and W. Gottardi. Monatsh. Chem. **95**, 779 (1964).
18. K. Ogura, N. Katoh, I. Yoshimura, and G. Tsuchihashi. Tetrahedron Lett. 375 (1978).
19. I. Fleming and D.H. Williams. Spectroscopic methods in organic chemistry. McGraw-Hill, London. 1966. p. 61.

© 2005 NRC Canada

Effect of modification of the electrophilic center on the α effect[1]

Ik-Hwan Um, Ji-Youn Lee, Sun-Young Bae, and Erwin Buncel

Abstract: We report on a nucleophilic study of esters R-C(=X)-Y-Ar in which the electrophilic center has been modified by replacing O by S in the leaving group or carbonyl center: 4-nitrophenyl acetate (**1**), *S*-4-nitrophenyl thioacetate (**2**), 4-nitrophenyl benzoate (**3**), and *O*-4-nitrophenyl thionobenzoate (**4**). The studies include O^- and S^- nucleophiles as well as α nucleophiles in H_2O at 25.0 ± 0.1 °C. The sulfur nucleophile (4-chlorothiophenoxide, 4-$ClPhS^-$) exhibits significant enhanced reactivity for the reactions with thiol and thione esters **2** and **4** compared with their oxygen analogues **1** and **3**. On the contrary, the common nucleophile OH^- is much less reactive towards **2** and **4** compared with **1** and **3**. The effect of changing both the electrophilic center and the nucleofugic center on the reactivity of the other oxygen nucleophiles is not so significant: 4-chlorophenoxide (4-$ClPhO^-$) is four to six times more reactive in the reactions with thiol and thione esters **2** and **4** compared with their oxygen analogues **1** and **3**. The α effects exhibited by butan-2,3-dione monoximate (Ox^-) and HOO^- are strongly dependent on the nature of the electrophilic center of the substrates, indicating that the difference in the ground-state solvation energy cannot be fully responsible for the α effect. Our results clearly emphasize the strong dependence of the α effect on the substrate structure, notably, the nature of the electrophilic center. The impact of change in the nucleofuge (**1**→**2**) and the electrophilic center (**3**→**4**) on reactivity indicates that α nucleophiles will need to be "purpose built" for decontamination and nucleophilic degradation of specific biocides.

Key words: α effect, nucleophilicity, nucleofuge effect, electrophilicity, polarizability.

Résumé : On a effectué une étude nucléophile des esters suivants, de formule générale R-C(=X)-Y-Ar, dans lesquels le centre électrophile a été modifié en remplaçant l'oxygène par un soufre dans le groupe partant ou dans le centre carbonyle: acétate de 4-nitrophényle (**1**), thioacétate de *S*-4-nitrophényle (**2**), benzoate de 4-nitrophényle (**3**) et thionobenzoate de *O*-4-nitrophényle (**4**). L'étude réalisée dans l'eau, à 25,0 ± 0,1 °C, inclut des nucléophiles O^- et S^- ainsi que des nucléophiles en α. Le nucléophile sulfuré (4-chlorothiophénolate, 4-$ClPhS^-$) présente une réactivité fortement accrue pour les réactions avec les esters thiolique et thionique **2** et **4** par comparaison avec leurs analogues oxygénés **1** et **3**. L'effet qui résulte d'un changement à la fois du centre électrophile et du centre nucléofuge sur la réactivité des autres d'oxygènes nucléophiles n'est pas aussi significatif: le 4-chlorophénolate (4-$ClPhO^-$) est de quatre à six fois plus réactif dans les réactions avec les esters thiolique et thionique **2** et **4** par comparaison avec leurs analogues oxygénés **1** et **3**. Les effets α présentés par le monoxoimate de la butane-2,3-dione (Ox^-) ou le HOO^- dépendent fortement de la nature du centre électrophile des substrats, ce qui indique que la différence dans l'énergie de solvatation de l'état fondamental n'est pas complètement responsable de l'effet α. Ces résultats mettent clairement en évidence la forte dépendance de l'effet α sur la structure du substrat, particulièrement, la nature du centre électrophile. L'impact d'un changement dans le centre nucléofuge (**1**→**2**) et le centre électrophile (**3**→**4**) sur la réactivité indique que les nucléophiles en α devront être synthétisés sur mesure pour la décontamination et la dégradation nucléophile de biocides spécifiques.

Mots clés : effet α, caractère nucléophile, effet nucléofuge, caractère électrophile, polarisabilité.

[Traduit par la Rédaction]

Introduction

Since α-effect nucleophiles exhibit abnormally enhanced nucleophilicity toward a variety of electrophilic centers (1), they can be used effectively for nucleophilic breakdown of neurotoxins, antidotes for nerve gases, cleanup of contaminated sites, etc. (2–5). A great deal of effort has been made to investigate the importance of determining factors that govern α nucleophilicity so as to design better decontaminants (1, 6–10).

Many factors have been suggested to influence the magnitude of the α effect. Dixon and Bruice (11) demonstrated

Received 8 March 2005. Published on the NRC Research Press Web site at http://canjchem.nrc.ca on 22 October 2005.

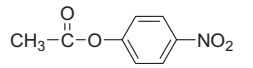
I.-H. Um,[2] J.-Y. Lee, and S.-Y. Bae. Department of Chemistry, Ewha Womans University, Seoul 120-750, Korea.
E. Buncel.[3] Department of Chemistry, Queen's University, Kingston, ON K7L 3N6, Canada.

[1]This article is part of a Special Issue dedicated to organic reaction mechanisms.
[2]Corresponding author (e-mail: ihum@mm.ewha.ac.kr).
[3]Corresponding author (e-mail: buncele@chem.queensu.ca).

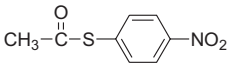
 doi: 10.1139/V05-157 © 2005 NRC Canada

that the α effect increases as β_{nuc} increases, and it is also known that the α effect increases with increasing s character of the electrophilic center (i.e., $sp^3 < sp^2 < sp$) (12, 13), though some exceptions exist (14, 15).

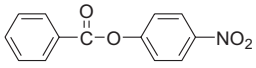
We have recently shown that the α effect is significantly dependent on the nature of the solvent medium for reactions of 4-nitrophenyl acetate (**1**) with butan-2,3-dione monoximate (Ox^-) and 4-chlorophenoxide (4-ClPhO^-) as an α and its reference normal nucleophile, respectively, in DMSO–H_2O (8) and in MeCN–H_2O mixtures of varying compositions (9, 10). A bell-shaped profile has been obtained for the reactions performed in aq. DMSO (8) while in aq. MeCN, an increasing α effect was observed in the plot of the α effect vs. mol% of the organic solvent (9, 10). Interestingly, as well, the α effect has been found to be strongly dependent on the nature of the electrophilic center atom for the reactions of **1**, 4-nitrophenyl benzensulfonate, and diphenylphophinate with Ox^- and $ClPhO^-$ in DMSO–H_2O mixtures, i.e., the α effect decreases in the order C=O > SO_2 > P = O over the range of solvent composition (8*c*, 8*d*).



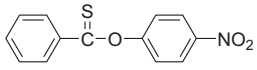
1: PNPA



2: PNPTA



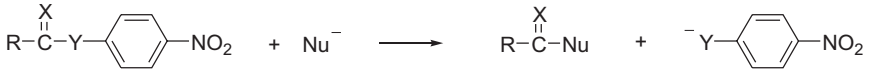
3: PNPB



4: PNPTB

In a more systematic study, we have extended our study to the reactions of **1**–**4** in which both the electrophilic center and the nucleofugic center are modulated from oxygen to sulfur. Replacement of O by a polarizable S atom in the leaving group of **1**, or in the carbonyl bond of **3**, would increase the electrophilicity of the electrophilic center by increasing the polarizability without changing the structure (16–18). Besides, replacement of O by a polarizable S atom in the leaving group of **1** would increase its nucleofugality since thiol is more acidic than the corresponding alcohol by 2–4 pK_a units (16).

Equation [1] shows the overview of the reactions studied. Here, nucleophilic attack occurs at the electrophilic center (C=X). This center is modified by the attached group, R (CH_3 or C_6H_5), the nucleofuge, YAr (where Y = O or S), and the heteroatom, X (X = O or S). The kinetics of the nucleophilic substitution reactions of **1**–**4** have been examined using five different anionic nucleophiles, a sulfur centered nucleophile and four oxygen nucleophiles including two α-effect nucleophiles.

[1] 

R = CH_3 or C_6H_5

X = O or S, Y = O or S

Nu^- = 4-ClPhS^-, 4-ClPhO^-, Ox^-, HOO^-, HO^-

Table 1. Summary of second-order rate constants (k, $(mol/L)^{-1}$ s^{-1}) for the reactions of **1**–**4** with various anionic nucleophiles in H_2O at 25 °C.

Nu^-	pK_a (NuH)	**1**	**2**	**3**	**4**
4-ClPhS^-	7.50	0.143	42.7	0.025	342
4-ClPhO^-	9.38	0.685	2.53	0.260	1.53
Ox^-	9.42	65.8	61.0	23.0	48.9
HOO^-	11.7	3450	3460	1480	1570
HO^-	15.7	11.8	5.90	4.20	0.470

The systematic change in the environment of the electrophilic center has resulted in a significant effect on the reactivity of the anionic nucleophiles studied. We report the remarkable differential effects of changing the nucleofuge (**1**→**2**), the acyl group (**1**→**3**), and the electrophilic center (**3**→**4**) on reactivity of these nucleophiles.

Results

Kinetic studies were performed spectrophotometrically under pseudo-first-order conditions with the nucleophile in excess. Pseudo-first-order rate constants (k_{obs}) were obtained from the equation, $\ln(A_\infty - A_t) = -k_{obs}t + c$. The correlation coefficients of the plots were usually higher than 0.9995. Generally, five different concentrations of nucleophile solutions were used to determine the second-order rate constant from the slope of the linear plot of k_{obs} vs. nucleophile concentration. It is estimated from replicate runs that the uncertainty in the rate constants is less than ±3%, except for the reactions with 4-ClPhS^- where rate constants have a larger uncertainty owing to oxidation to the disulfide. The second-order rate constants determined in this way are summarized in Table 1 and the kinetic conditions and results are given in the Supporting information.[4]

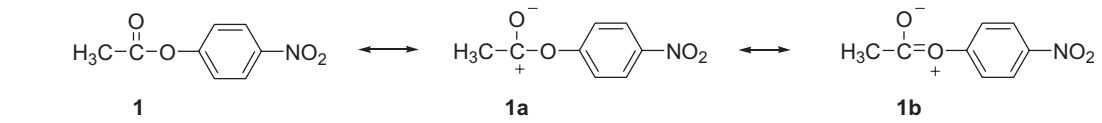
Discussion

Replacing O by S in the leaving group (1→2) — Nucleofuge effect

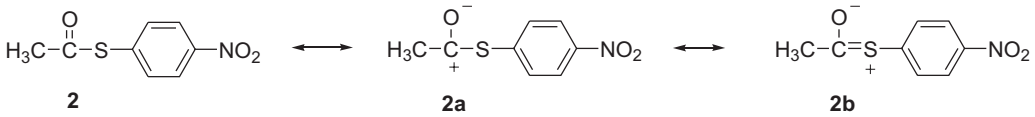
Replacement of the oxygen by a polarizable sulfur in the leaving group of **1** would result in an increase in nucleofugality of the leaving group as well as in the electrophilicity of the electrophilic center without changing its structure. This argument can be supported by the ^{13}C NMR chemical shifts of the carbonyl carbon and the C=O

[4] Supplementary data for this article are available on the Web site or may be purchased from the Depository of Unpublished Data, Document Delivery, CISTI, National Research Council Canada, Ottawa, ON K1A 0S2, Canada. DUD 4033. For more information on obtaining material refer to http://cisti-icist.nrc-cnrc.gc.ca/irm/unpub_e.shtml.

© 2005 NRC Canada



1 **1a** **1b**



2 **2a** **2b**

stretching vibrations of thiol relative to the oxygen esters. Thiol esters exhibit 20–30 ppm downfield shifts relative to their oxygen analogues in the ^{13}C NMR spectra (17), while the C=O stretching vibration for thiol esters shifts to ca. 40–60 cm^{-1} lower frequencies than for the corresponding oxygen esters (18), indicating that the carbonyl carbon of thiol esters has greater partial positive charge and weaker double bond character than that of the corresponding oxygen esters (17, 18).

Thus, one can suggest that the contribution of resonance structures **1b** and **2a** is more important than **2b** and **1a**, respectively. This is also in accord with the fact that overlap between 2p and 3p orbitals is weaker than between 2p orbitals. Accordingly, the thiol ester **2** would exhibit enhanced electrophilicity compared to its oxygen analogue **1**. Furthermore, the fact that 4-nitrothiophenoxide (pK_a = 4.54) is less basic than 4-nitrophenoxide (pK_a = 7.14) (16) by 2.6 pK_a units in H_2O is in accord with the proposal that the former is a better nucleofuge. Thus, one might expect **2** should be more reactive than **1**. The following results interestingly reflect on these expectations.

Sulfur vs. oxygen nucleophiles

Our results show that the thiol ester **2** is ca. 300 times more reactive than its oxygen analogue **1** toward the sulfur nucleophile 4-ClPhS$^-$. As shown in Table 1, the rate constant for the reaction of 4-ClPhS$^-$ increases from 0.143 to 42.7 $(mol/L)^{-1}$ s^{-1} as the substrate is changed from **1** to **2**. On the contrary, **2** is less reactive than **1** in reaction with OH$^-$ by a factor of 2: the rate constant for the reaction of OH$^-$ decreases from 11.8 to 5.90 $(mol/L)^{-1}$ s^{-1} as the substrate changes from **1** to **2**. The decrease in the reactivity of OH$^-$ on changing the substrate from **1** to **2** is unexpected on the basis of the argument given in the previous section.

One might suggest that the nature of the rate-determining step (RDS) is responsible for the absence of the predicted nucleofuge effect for the reactions with OH$^-$, since an enhanced nucleofugality would be ineffective for reactions in which the leaving-group departure occurs after the RDS. Now, previous work suggests that alkaline hydrolysis of aryl acetates proceeds through an addition intermediate in which its formation is the RDS (19). Accordingly, one can expect that the nucleofuge effect would be absent for reactions of OH$^-$ with **1** and **2**. Contrastingly, the reactions of **1** and **2** with 4-ClPhS$^-$ have been reported to proceed through an addition intermediate but with a different RDS, i.e., breakdown of the intermediate for the reaction with **1** and its formation for the reaction with **2** (16). Thus, one might attribute the differential nucleofuge effect shown by 4-ClPhS$^-$ and OH$^-$ to the difference in their RDS. However, this argument cannot explain why in the reaction with OH$^-$ **2** is less reactive than **1**.

The differential nucleofuge effect shown by 4-ClPhS$^-$ and OH$^-$ in their reactions with **1** and **2** is in accord with the hard and soft acids and bases principle (HASB) (20): 4-ClPhS$^-$ is known to be highly soft while OH$^-$ is a hard base. Accordingly, basicity of the two nucleophiles does not govern their nucleophilicity, since the polarizable 4-ClPhS$^-$ is seven times more reactive than the charge localized OH$^-$ toward the polarizable thiol ester **2**, although 4-ClPhS$^-$ is less basic than OH$^-$ by 8.2 pK_a units (21).

Hydroxide vs. aryloxide nucleophiles

Table 1 demonstrates that the thiol ester **2** is more reactive than its oxygen analogue **1** toward 4-ClPhO$^-$ by a factor of 4: the rate constant for the reaction with 4-ClPhO$^-$ increases from 0.685 to 2.53 $(mol/L)^{-1}$ s^{-1} as the substrate is changed from **1** to **2**. Thus, 4-ClPhO$^-$, though an oxygen nucleophile, exerts higher reactivity toward the polarizable thiol ester **2** than toward its oxygen analogue **1**. This contrasts to the result obtained for the reaction with OH$^-$. Previous work suggests that the reactions of **1** and **2** with 4-ClPhO$^-$ proceed through an addition intermediate in which leaving-group departure occurs after the RDS (16, 22). It follows that the rate enhancement shown by 4-ClPhO$^-$ on changing the substrate from **1** to **2** is not due to a nucleofuge effect.

The negative charge on the oxygen atom of 4-ClPhO$^-$ can be delocalized on the phenyl ring by resonance as shown in the following. In agreement with this, the charge density of the oxygen atom of 4-ClPhO$^-$ has been calculated to be –0.777 at the MP2/6-31+G* level. It would seem reasonable to suggest that the difference in charge density between the oxygen atoms of OH$^-$ and 4-ClPhO$^-$ is responsible for the differential nucleofuge effect shown by OH$^-$ and 4-ClPhO$^-$ for the reactions with **1** and **2**. However, one can find from Table 1 that OH$^-$ is 17 times more reactive than 4-ClPhO$^-$ for the reaction with **1**, but only 2.3 times more reactive for the reaction with **2**, although the former is more basic than the latter by 6.3 pK_a units. Clearly, the rate constant ratio (k^{OH^-}/k^{ClPhO^-} = 2.3) for the reaction of **2** with OH$^-$ and 4-ClPhO$^-$ is unexpectedly small if one considers the large difference in the basicity of the two nucleophiles.



The α effect — Oximate vs. chlorophenoxide nucleophiles

Ox$^-$ exhibits only a slight decrease in its reactivity for the reaction with the thiol ester **2** compared to its oxygen ester **1**,

© 2005 NRC Canada

the rate constant decreasing from 65.8 to 61.0 $(mol/L)^{-1}$ s^{-1}. This small decrease in reactivity for Ox^- on changing the substrate contrasts to the result obtained for the reactions of 4-$ClPhO^-$.

The negative charge of the nucleophilic oxygen atom of Ox^- can be delocalized by resonance as shown in the folllowing, but it resides on the two electronegative oxygen atoms. In fact, the charge density on the nucleophilic oxygen and the carbonyl oxygen atoms has been calculated to be –0.565 and –0.670, respectively on the MP2/6-31+G* level. This could be one possible reason why Ox^- and 4-$ClPhO^-$ exhibit a contrasting nucleofuge effect.



As an α-effect nucleophile, Ox^- exhibits higher reactivity for the reactions with **1** and **2** than its reference normal nucleophile (4-$ClPhO^-$) of equal pK_a (8). As shown in Table 2, the α effect ($k^{Ox^-}/k^{4\text{-}ClPO^-}$) decreases from 96 to 24 as the substrate changes from **1** to **2**, indicating that the magnitude of the α effect is highly dependent on the nature of the substrates.

The α effect — HOO^- vs. OH^-

HOO^- exhibits nearly the same reactivity for the reactions with **1** and **2**: the rate constants shown in Table 1 are 3450 and 3460 $(mol/L)^{-1}$ s^{-1} for the reactions with **1** and **2**, respectively. This is an interesting result, since 4-$ClPhS^-$ exhibits a rate increase of 300, while OH^- results in a rate decrease of 2 on changing the substrate from **1** to **2**.

Although HOO^- is less basic than OH^- by 4 pK_a units, these two nucleophiles have often been employed as an α and the reference normal nucleophiles owing to the similarity of their structures (1). The magnitude of the α effect is larger for the reaction with the thiol ester **2** than for that with the oxygen analogue **1**. As shown in Table 2, the α effect shown by HOO^- (k^{HOO^-}/k^{HO^-}) increases from 290 to 590 as the substrate changes from **1** to **2**. The substrate-dependent α effect is also seen for the Ox^- system, but the α effect exhibited by Ox^- is smaller for the reaction with the thiol ester **2** ($k^{Ox^-}/k^{4\text{-}ClPO^-}$ = 24) than with the oxygen analogue **1** ($k^{Ox^-}/k^{4\text{-}ClPO^-}$ = 96), which is in agreement with the HASB principle.

Replacing O by S at the electrophilic center (3→4) — The heteroatom effect

It is generally considered that a C=S bond is more polarizable than a C=O bond, on the grounds that the overlap between the 2p and 3p orbitals in a C=S bond is not as strong as that between the 2p orbitals in a C=O bond, indicating that the contribution of **4a** is more significant than that of **3a**. ^{13}C NMR spectra for substrates **3** and **4** are in agreement with this argument. The chemical shifts for the carbon atoms of the C=O and C=S bonds in **3** and **4** are 163.8 and 209.8 ppm, respectively. Such a large downfield shift (46 ppm) suggests that the carbon atom of the C=S bond in **4** has greater positive charge than that of the C=O bond in **3**, consistent with the previous proposal that the contribution of **4a** outweighs that of **3a**. In turn, **4** is expected to be more electrophilic and more reactive than **3**.

Table 2. Summary of the α-effect shown by HOO^- and Ox^- for the reactions of **1**–**4** in H_2O at 25 °C.

Substrate	k^{HOO^-}/k^{HO^-}	$k^{Ox^-}/k^{4\text{-}ClPhO^-}$
PNPA (**1**)	290	96
PNPTA (**2**)	590	24
PNPB (**3**)	350	88
PNPTB (**4**)	3300	32

Sulfur vs. oxygen nucleophiles

Our results show a striking major effect of changing the heteroatom X from O to S for the reactions of **3** and **4** with the sulfur nucleophile, 4-$ClPhS^-$. The rate constant (Table 1) for the reactions of 4-$ClPhS^-$ increases from 0.025 to 342 $(mol/L)^{-1}$ s^{-1} as the heteroatom X changes from O to S (**3**→**4**). Thus, the rate enhancement on changing the substrate from **3** to **4** for the reaction with 4-$ClPhS^-$ is 14 000, which is greater than for the reactions of **1** and **2** with 4-$ClPhS^-$ ($k^{4\text{-}ClPhS^-}$(**2**)/$k^{4\text{-}ClPhS^-}$(**1**) = 300).

On the contrary, the rate constant for the reaction of OH^- decreases from 4.20 to 0.470 $(mol/L)^{-1}$ s^{-1} on changing the heteroatom X from O to S. Thus, the thione ester **4** is nine times less reactive than its oxygen analogue **3** for the reaction with OH^-.

Such a rate retardation is quite unexpected, since **4** would be expected to be more reactive than **3**. This indicates that the reactivity of OH^- is exceedingly low toward the polarizable thione ester **4**.

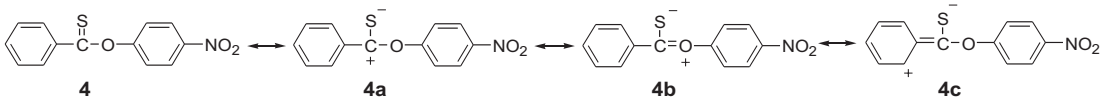
It is also noted that 4-$ClPhS^-$ is 180 times less reactive than OH^- in the reaction with **3**, but 730 times more reactive than OH^- in the reactions with **4**, although the former nucleophile is 8.2 pK_a units less basic than the latter. Thus, basicity alone cannot determine the nucleophilicity for the reaction with polarizable electrophiles.

Hydroxide vs. aryloxide nucleophiles

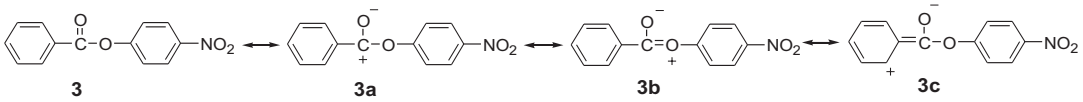
4-$ClPhO^-$ exhibits a rate enhancement of 6 on changing the heteroatom X from O to S (Table 1). Unexpectedly, while an oxygen nucleophile, 4-$ClPhO^-$ is more reactive in the reaction with the thione ester **4** than with the oxygen analogue **3**. The rate constant ratio ($k^{OH^-}/k^{4\text{-}ClPhO^-}$) decreases as the substrate changes from **3** to **4**, i.e., $k^{OH^-}/k^{4\text{-}ClPhO^-}$ = 16 and 0.3, for the reactions with **3** and **4**, respectively. Interestingly, although it is much more basic, OH^- is three times less reactive than 4-$ClPhO^-$ in the reaction with **4**.

The α effect — The oximate α nucleophile

Table 1 shows that Ox^- exhibits a rate enhancement by a factor of 2 on changing the substrate from **3** to **4**. The rate enhancement shown by Ox^- is smaller than that by 4-$ClPhO^-$ on changing substrates from **3** to **4**. Accordingly, the α effect decreases from 88 to 32 as the substrate changes



© 2005 NRC Canada



from the oxygen ester **3** to its sulfur analogue **4**. A similar result is obtained for the reactions with **1** and **2** as mentioned in the preceding section, i.e., the α effect exhibited by Ox^- is larger for the oxygen ester **1** than for its sulfur analogue **2**.

We have recently shown that the magnitude of the α effect is dependent on the nature of the electrophilic center for the series **1**, 4-nitrophenyl diphenylphosphinate and benzensulfonate, with Ox^- and 4-$ClPhO^-$ (8). The α effect ($k^{Ox^-}/k^{4\text{-}ClPhO^-}$) was found to decrease as the electrophilic center is changed from C=O to SO_2 and P=O (8*d*).

Calorimetric measurements have shown that Ox^- is ca. 4 kcal/mol (1 cal = 4.184 J) less solvated than 4-$ClPhO^-$ in H_2O (8*b*), indicating that a solvation effect could be responsible for the α effect shown by Ox^-, at least in part. In fact, we have recently shown that the magnitude of the α effect for the reaction of **2** with Ox^- and 4-$ClPhO^-$ is linearly proportional to the solvation energy difference between the α-effect nucleophile Ox^- and the normal nucleophile 4-$ClPhO^-$ in DMSO–H_2O mixtures of varying compositions (22). However, the substrate-dependent α effect found in the present and previous systems suggests that a solvation effect cannot be solely responsible for the origin of the α effect (8–10, 22).

The α effect — HOO^- vs. OH^-

The reactivity of HOO^- has been found to be independent of the nature of the electrophilc center in the present study. As shown in Table 1, HOO^- exhibits nearly the same second-order rate constant on changing the substrate from **3** to **4** or from **1** to **2**. This is interesting since the structurally similar OH^- exhibits significant rate retardation on changing the nature of the electrophilic center, from **3** to **4** or from **1** to **2**. Accordingly, HOO^- exhibits substrate-dependent α effects, i.e., k^{HOO^-}/k^{HO^-} increases from 290 to 590 and from 350 to 3300 as the substrate is changed from **1** to **2** and **3** to **4**, respectively. The α effect shown by HOO^- is larger for the reactions with thiol and thione esters **2** and **4** than for the corresponding oxygen esters **1** and **3**. Interestingly, this contrasts with the result obtained for Ox^-, which exhibits smaller α effects for the reactions with thiol and thione esters **2** and **4**.

OH^- has often been found to exhibit a negative deviation from Brønsted-type plots for various nuclephilic substitution reactions, which Jencks et al. (23) attributed to abnormal solvation. In fact, OH^- has been shown to be 12, 32, and 38 kcal/mol more solvated than HOO^-, PhO^-, and PhS^-, respectively, in H_2O (24). Thus, one might similarly attribute the unusually low reactivity of OH^- in this system to a solvation effect, at least in part. This would be consistent with the finding that OH^- exhibits nearly the same reactivity as HOO^- in gas-phase reactions with methyl formate (25). However, if the GS solvation effect were mainly responsible for the α effect shown by HOO^- in this study, then the α effect should have remained nearly constant irrespective of the nature of the substrate. In fact, the α effect has been shown to be significantly dependent on the nature of the electrophilic center. Thus, the ground-state (GS) solvation effect cannot be solely responsible for the α effect shown by HOO^-. This is consistent with our recent conclusion that TS stabilization is also a contributing factor responsible for the α effect (1, 8, 9).

Acyl group effect — Acetate vs. benzoate (1→3)

We have recently shown that the contribution of the resonance structure **3c**, which is not possible for **1**, is likely responsible for the decrease in reactivity of aryl benzoates in nucleophilic substitution reactions with various amines and anionic nucleophiles such as OH^-, N_3^-, and CN^- (26–28). Thus, replacement of the methyl group in **1** by a phenyl group would cause a rate retardation owing to stabilization of the GS in **3** by resonance (**3c**) and (or) enhanced steric hindrance.

As shown in Table 1, the acetate ester **1** is two to seven times more reactive than the benzoate ester **3** toward all the nucleophiles investigated in this study. Steric hindrance appears to be more significant for the reaction with the large 4-$ClPhS^-$ since the rate constant ratio for the reactions of **1** and **3** is much larger for the reactions with 4-$ClPhS^-$ than for those with the other oxygen nucleophiles, e.g., $k(\mathbf{1})/k(\mathbf{3})$ = 2 to 3 for the reactions with HOO^-, Ox^-, and 4-$ClPhO^-$, but $k(\mathbf{1})/k(\mathbf{3})$ = 7 for the reactions with the large sulfur nucleophile (4-$ClPhS^-$).

Conclusions

The present study has allowed us to conclude the following: (1) the sulfur nucleophile (4-$ClPhS^-$) exhibits significantly enhanced reactivity for the reactions with the thiol and thione esters **2** and **4** compared to their oxygen analogues **1** and **3**, respectively; (2) on the contrary, the common oxygen nucleophile OH^- is much less reactive in the reactions with the sulfur containing substrates **2** and **4**; (3) the strong solvation of OH^- in H_2O cannot be solely responsible for the unusually low reactivity shown by OH^- in the reactions with thiol and thione esters **2** and **4**; (4) the α effects shown by Ox^- and HOO^- are strongly dependent on the nature of the electrophilic center of the substrates, indicating that the difference in the GS solvation energy cannot be fully responsible for the α effect; (5) our results clearly emphasize the strong dependence of the α effect on the substrate structure, notably, the nature of the electrophilic center. The impact of change in the nucleofuge (**1**→**2**) and heteroatom X (**3**→**4**) on reactivity indicates that α nucleophiles will need to be "purpose built" for decontamination and nucleophilic degradation of specific biocides.

Experimental section

Materials

Substrates **1**–**4** have been readily prepared by reaction of the corresponding acid chloride with 4-nitrophenol or 4-nitrothiophenol in the presence of triethylamine in anhydrous ether. Their purity was checked by melting points and

© 2005 NRC Canada

spectroscopic data such as IR and NMR spectra. Other materials were of the highest quality available and were generally recrystallized before use. Glass-distilled water was further boiled and cooled under nitrogen just before use.

Kinetics

Kinetic studies were performed using a Scinco S-3100 PDA UV–vis spectrophotometer for slow reactions ($t_{1/2} \geq 10$ s) or an Applied Photophysics SX-17MV stopped-flow spectrophotometer for fast reactions ($t_{1/2} < 10$ s) equipped with a constant-temperature circulating bath. The reactions were followed by monitoring the appearance of 4-nitrophenoxide (or 4-nitrothiophenoxide for the reaction of **2**). Each reaction was monitored up to 10 half-lives.

Typically, a reaction was initiated by adding 5 μL of a ca. 0.01 mol/L solution of substrates in MeCN by a gas-tight syringe to a 10 mm quartz UV cell containing 2.50 mL of a thermostatted reaction mixture made of an aliquot of nucleophile solution. The stock solutions (ca. 0.2 mol/L) of 4-ClPhO$^-$, Ox$^-$, and HOO$^-$ were prepared by dissolving 2 equiv. of 4-ClPhOH, OxH, and HOOH and 1 equiv. of standardized NaOH solution to keep the pH constant by making self-buffered solutions. However, owing to the low solubility of 4-ClPhSH in water, the concentration of 4-ClPhS$^-$ stock solution was prepared by mixing ca. 0.011 mol/L of 4-ClPhSH and 0.010 mol/L of NaOH. The kinetic conditions and results are summarized in the Supporting information.[4] Other detailed kinetic methods were reported previously (8*b*, 8*c*).

Product analysis

One of the reaction products, 4-nitrophenoxide (or 4-nitrothiophenoxide for the reactions of substrate **2**), was determined quantitatively by measuring the optical density using a UV–vis spectrophotometer in all cases. Other products (e.g., *S*-4-chlorophenyl thioacetate, *S*-4-chlorophenyl thiobenzoate, and 4-chlorophenyl dithiobenzoate for the reactions of substrates **1**–**4** with 4-chlorothiophenoxide, respectively) were analyzed by a GC technique. The quantitative analysis was performed using the authentic samples by a Varian 3800 Model GC with a DB 624 column (30 m × 0.32 mm × 1.8 μm) for *S*-4-chlorophenyl acetate (retention time 13.50 min at the injector temperature of 250 °C, the column temperature starting at 50 °C and increased by 15 °C/min) and with a DB 5 column (30 m × 0.32 mm × 0.25 μm) for *S*-4-chlorophenyl thiobenzoate and 4-chlorophenyl dithiobenzoate (retention time 11.23 and 10.43 min, respectively, at the injector temperature of 250 °C, the column temperature starting at 50 °C and increased by 20 °C/min).

Acknowledgments

I.H.U. is grateful for the financial support from the Korea Research Foundation (KRF-2002-070-C00061) and to Sang-Eun Jeon for analysis of the reaction products by GC. E.B. thanks the Natural Sciences and Engineering Research Council of Canada (NSERC) for a research grant. The authors also acknowledge helpful discussions with Professors J.M. Dust, S. Hoz, and J.F. King (29).

References

1. Reviews: (*a*) E. Buncel and I.H. Um. Tetrahedron, **60**, 7801 (2004); (*b*) E. Buncel and S. Hoz. Isr. J. Chem. **26**, 313 (1985); (*c*) A.P. Grekov and V.Y. Veselov. Usp. Khim. **47**, 1200 (1978); (*d*) N.J. Fina and J.O. Edwards. Int. J. Chem. Kinet. **5**, 1 (1973).
2. H. Morales-Rojas and R.A. Moss. Chem. Rev. **102**, 2497 (2002).
3. (*a*) J.S. Tsang, A.A. Neverov, and R.S. Brown. J. Am. Chem. Soc. **125**, 7602 (2003); (*b*) J.S. Tsang, A.A. Neverov, and R.S. Brown. J. Am. Chem. Soc. **125**, 1559 (2003); (*c*) A.A. Neverov and R.S. Brown. Inorg. Chem. **40**, 3588 (2001); (*d*) A.A. Neverov, G. Gibson, and R.S. Brown. Inorg. Chem. **42**, 228 (2003); (*e*) S.G. Srivatsan and S. Verma. Chem. Commun. 515 (2000); (*f*) J. Toullec and M. Mohamed. Chem. Commun. 221 (1996).
4. (*a*) V. Balakrishnan, X. Han, G.W. VanLoon, J.M. Dust, J. Tollec, and E. Buncel. Langmuir. **20**, 6586 (2004); (*b*) R. Nagelkerke, G.R.J. Thatcher, and E. Buncel. Org. Biomol. Chem. **1**, 163 (2003); (*c*) E. Buncel, R. Nagelkerke, and G.R.J. Thatcher. Can. J. Chem. **81**, 53 (2003).
5. I.H. Um, S.E. Jeon, M.H. Baek, and H.R. Park. Chem. Commun. 3016 (2003).
6. (*a*) F. Terrier, E. Le Guevel, A.P. Chatrouse, G. Moutiers, and E. Buncel. Chem. Commun. 600 (2003); (*b*) E. Buncel, C. Cannes, A.P. Chatrousse, and F. Terrier. J. Am. Chem. Soc. **124**, 8766 (2002); (*c*) A.P. Moutiers, E. Le Guevel, L. Villien, and F. Terrier. J. Chem. Soc. Perkin Trans. 2, 7 (1997); (*d*) F. Terrier, G. Moutiers, L. Xiao, E. Le Guvel, and F. Guir. J. Org. Chem. **60**, 1748 (1995); (*e*) F. Terrier, P. McCormack, E. Kizilian, J.C. Halle, P. Demerseman, F. Guir, and C. Lion. J. Chem. Soc. Perkin Trans. 2, 153 (1991); (*f*) G. Moutiers, E. Le Guevel, C. Cannes, F. Terrier, and E. Buncel. Eur. J. Org. Chem. **17**, 3279 (2001).
7. (*a*) C.F. Bernasconi and C. Murray. J. Am. Chem. Soc. **108**, 5251 (1986); (*b*) D.J. Palling and W.P. Jencks. J. Am. Chem. Soc. **106**, 4869 (1984).
8. (*a*) E. Buncel and I.H. Um. J. Chem. Soc. Chem. Commun. 595 (1986); (*b*) I.H. Um and E. Buncel. J. Org. Chem. **65**, 577 (2000); (*c*) R.M. Tarkka and E. Buncel. J. Am. Chem. Soc. **117**, 1503 (1995); (*d*) I.H. Um, J.Y. Hong, and E. Buncel. Chem. Commun. 27 (2001).
9. (*a*) I.H. Um, Y.M. Park, and E. Buncel. Chem. Commun. 1917 (2000); (*b*) I.H. Um, E.J. Lee, and E. Buncel. J. Org. Chem. **66**, 4859 (2001).
10. I.H. Um, H.W. Lee, J.S. Lee, H.J. Moon, and D.S. Kwon. J. Org. Chem. **62**, 5939 (1997).
11. H.J. Dixon and T.C. Bruice. J. Am. Chem. Soc. **94**, 2052 (1972).
12. E. Buncel, C. Chuaqui, and H. Wilson. J. Am. Chem. Soc. **104**, 4896 (1982).
13. (*a*) K.R. Fountain, C.J. Felkerson, J.D. Driskell, and B.D. Lamp. J. Org. Chem. **68**, 1810 (2003); (*b*) K.R. Fountain, D.B. Tad-y, T.W. Paul, and M.V. Golynskiy. J. Org. Chem. **64**, 6547 (1999); (*c*) K.R. Fountain and K.D. Patel. J. Org. Chem. **62**, 4795 (1997).
14. I.H. Um, J.S. Lee, and S.M. Yuk. J. Org. Chem. **63**, 9152 (1998).
15. I.H. Um, E.J. Lee, J.A. Seok, and K.H. Kim. J. Org. Chem. **70**, 7530 (2005).
16. D.J. Hupe and W.P. Jencks. J. Am. Chem. Soc. **99**, 451 (1977).
17. W.J. Middleton, E.G. Howard, and W.H. Sharkey. J. Org. Chem. **30**, 1375 (1965).

© 2005 NRC Canada

18. J. Jenssen. *In* The chemistry of carboxylic acids and esters. *Edited by* S. Patai. Wiley-Interscience Publishers, London. 1965. Chap. 15.
19. E. Buncel, I.H. Um, and S. Hoz. J. Am. Chem. Soc. **111**, 971 (1989).
20. (*a*) R.G. Pearson. J. Am. Chem. Soc. **85**, 3533 (1963); (*b*) T.L. Ho. *In* Hard and soft acids and bases. *Edited by* R.G. Pearson. Academic Press, New York. 1977.
21. W.P. Jencks and F. Regenstein. *In* Handbook of biochemistry. Selected data for molecular biology. *Edited by* H.A. Sober. The Chemical Rubber Co., Cleveland, Ohio. 1968.
22. I.H. Um and E. Buncel. J. Am. Chem. Soc. **123**, 11 111 (2001).
23. W.P. Jencks, S.R. Brant, J.R. Gandler, G. Fendrich, and C. Nakamura. J. Am. Chem. Soc. **104**, 7046 (1982).
24. J.F. Ritchie. J. Am. Chem. Soc. **105**, 7313 (1983).
25. C.H. DePuy, E.W. Della, J. Filley, J.J. Grabowski, and V.M. Bierbaum. J. Am. Chem. Soc. **105**, 2481 (1983).
26. (*a*) I.H. Um, K.H. Kim, H.R. Park, M. Fujio, and Y. Tsuno. J. Org. Chem. **69**, 3937 (2004); (*b*) I.H. Um, S.E. Lee, and H.J. Kwon. J. Org. Chem. **67**, 8999 (2002); (*c*) I.H. Um, J.S. Min, J.A. Ahn, and H.J. Hahn. J. Org. Chem. **65**, 5659 (2000).
27. (*a*) I.H. Um, J.Y. Hong, J.J. Kim, O.M. Chae, and S.K. Bae. J. Org. Chem. **68**, 5180 (2003); (*b*) I.H. Um, S.M. Chun, M. Fujio, and Y. Tsuno. J. Org. Chem. **69**, 3166 (2004).
28. I.H. Um, H.J. Han, J.A. Ahn, S. Kang, and E. Buncel. J. Org. Chem. **67**, 8475 (2002).
29. J.F. King, Z.R. Guo, and D.F. Klassen. J. Org. Chem. **59**, 1095 (1994).

© 2005 NRC Canada

Computational studies of the properties of phenyloxenium ions — A comparison with phenylnitrenium and phenylcarbenium ions[1]

Stephen A. Glover and Michael Novak

Abstract: Properties of phenyloxenium ion **13a**, phenylnitrenium ion **14a**, and their 4-methyl and 4-phenyl analogues have been studied at the HF/6-31G* and pBP/DN*//HF/6-31G* levels to explain differences in their relative ease of formation and their stabilities. The phenyloxenium ions **13** are ground-state singlets but S_0–T_1 gaps are smaller than those of the corresponding nitrenium ions. The S_0 states are stabilized by donor methyl and phenyl substituents in both classes of ions, but phenyloxenium ion has much greater charge localization on the ring, primarily at the 4 position. Evidence for this difference stems from ground-state HF/6-31G*geometries, dipole moments, and vibrational frequencies. Nitrenium ions exhibit some quinoidal character, but the calculated C—N bond lengths are longer than those of their 4-hydroxy-2,5-cyclohexadienone imine hydration products **17** and the symmetric C-N stretching frequencies are ca. 60–100 cm^{-1} less than those of **17**. However, the C—O bond lengths and stretching frequencies of the phenyloxenium ions are slightly shorter and greater, respectively, than those of their 4-hydroxy-2,5-cyclohexadienone hydration products (**16**). The oxenium ions are best described by their 4-oxo-2,5-cyclohexadienyl carbenium resonance structures. Accordingly, a 4-phenyl group stabilizes the phenyloxenium ion more than the phenylnitrenium ion leading to a planar geometry and considerably more charge in the distal ring, thus accounting for regioselectivities of azide reactions. Isodesmic comparisons of the energy difference between phenyloxenium and phenylnitrenium ions and their neutral hydration products explains their relative stabilities under aqueous conditions; whereas 4-biphenylyloxenium ion **13c** has a lifetime in water of 12 ns as opposed to the corresponding nitrenium ion **14c** (300 ns), the 4-methylphenyloxenium ion **13b** is less stable to hydration by 18.7 kcal mol^{-1} (1 cal = 4.184 J) and cannot be observed under the conditions used to generate **13c**.

Key words: oxenium ions, nitrenium ions, computational chemistry, nucleophilic addition, singlet state properties.

Résumé : Les propriétés de l'ion phényloxénium **13a**, de l'ion phénylnitrénium **14a** et de leurs analogues 4-méthyl- et 4-phényl- ont été étudiées aux niveaux HF/6-31G* et pBP/DN*//HF/6-31G* pour tenter d'expliquer les différences dans leurs facilités relatives de formation dans leurs stabilités. Les ions phényloxénium **13** sont des singulets à l'état fondamental, toutefois les écarts S_0–T_1 sont plus faibles que ceux des ions nitrénium correspondants. Dans les deux classes d'ions, les états S_0 sont stabilités par les substituants donneurs méthyle et phényle; toutefois, la délocalisation de la charge sur le cycle est beaucoup plus grande avec l'ion phényloxénium, particulièrement vers la position 4. Les bases pour ces différences sont tirées des géométries HF/6-31G* de l'état fondamental, des moments dipolaires et des fréquences de vibration. Les ions nitrénium exhibent un caractère quinoïdal, mais les longueurs calculées des liaisons C—N sont supérieures à celle de leur produit d'hydratation, l'imine de la 4-hydroxycyclohexa-2,5-diénone (**17**) et les fréquences d'élongation symétrique du C-N sont de 60 à 100 cm^{-1} inférieures à celle du composé **17**. Toutefois, les longueurs des liaisons C—O et les fréquences d'élongation des ions phényloxénium ne sont respectivement que faiblement plus courtes et plus longues que celles de leur produit d'hydratation, la 4-hydroxycyclohexa-2,5-diénone (**16**). La meilleure façon de décrire les ions oxénium correspond aux structures de résonance du carbénium 4-oxocyclohexa-2,5-diényle. En conséquence, un groupe 4-phényle stabilise plus un ion phényloxénium que l'ion phénylnitrénium conduisant à une géométrie planaire et beaucoup plus de charge dans le noyau distal, ce qui expliquerait les régiosélectivités des réactions avec l'ion azoture. Des comparaisons isodesmiques des différences d'énergie entre les ions phényloxénium et phénylnitrénium et leurs produits neutres d'hydratation explique leurs stabilités relatives dans des conditions aqueuses; alors que le temps de vie de l'ion 4-biphényloxénium **13c** dans l'eau est de 12 ns par rapport à 300 ns pour celui de l'ion nitrénium correspondant **14c**, l'ion 4-méthylphényloxénium **13b** est moins stable à l'hydratation par 18,7 kcal mol^{-1} (1 cal = 4,184 J) et il ne peut pas être observé dans les conditions utilisées pour générer le composé **13c**.

Received 28 March 2005. Published on the NRC Research Press Web site at http://canjchem.nrc.ca on 25 October 2005.

S.A. Glover.[2] School of Biological, Biomedical and Molecular Sciences, University of New England, Armidale, New South Wales 2350, Australia.
M. Novak. Department of Chemistry and Biochemistry, Miami University, Oxford, OH 45056, USA.

[1]This article is part of a Special Issue dedicated to organic reaction mechanisms.
[2]Corresponding author (e-mail: sglover@une.edu.au).

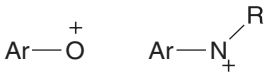
 doi: 10.1139/V05-149 © 2005 NRC Canada

Mots clés : ions oxénium, ions nitrénium, chimie théorique, addition nucléophile, propriétés de l'état singulet.

[Traduit par la Rédaction]

Introduction

Arylnitrenium ions **2**, which are widely accepted to be the intermediates derived from metabolites of carcinogenic aromatic amines, have been studied extensively. As a result, factors affecting their stability, their lifetimes under aqueous conditions and their reactivity with a range of inorganic and biological nucleophiles have been the subject of many investigations (1–15). Undoubtedly, these ions are strongly delocalized and they can best be regarded as 4-imino-2,5-cyclohexadienyl carbocations, although they do retain some electrophilic reactivity at nitrogen (4–7, 11, 15–25). Delocalization leads to predominant reaction on the aryl ring with attendant disruption of aromaticity. The intrinsic barrier resulting from this loss of aromaticity leads to long lifetimes in aqueous solution, which in certain instances accounts for elevated carcinogenic behaviour. The lifetimes of 4-biphenylylnitrenium ion (300 ns at 30 °C) and its bridged counterpart, 2-fluorenylnitrenium ion (30 μs at 20 °C) derived from mutagenic and carcinogenic arylamines, are longer in aqueous solution than those of nitrenium ions derived from noncarcinogenic arylamines (4, 13, 16, 18, 26).

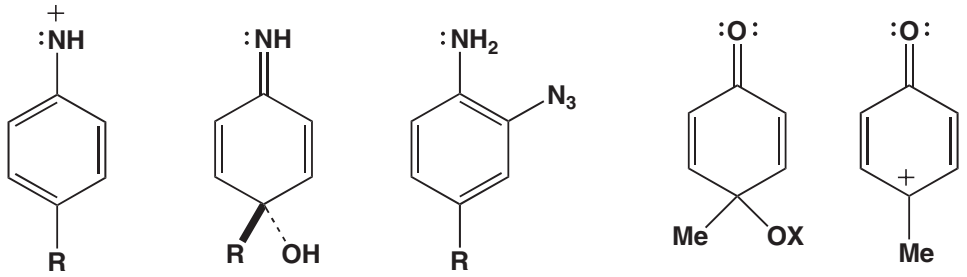


1 **2**

The oxygen counterparts of arylnitrenium ions (aryloxenium ions **1**), have, on the other hand, received relatively little attention. They have been proposed to explain the products of the synthetically useful electrochemical and chemical oxidations of phenols (27–33), and the copper-catalysed generation of commercially useful polymers such as poly(2,6-dimethyl-1,4-phenylene oxide) (34, 35). Reactions on both the aryl substituent (28, 29, 31, 32) as well as upon oxygen (30, 33) have been ascribed to the electrophilic behaviour of these species, but the regiochemistry of reactions of purported examples of **1** generated from different sources is confusing; surprisingly, little is known of the reactivity and selectivity of these species, or even whether they have actually been generated in the cases in which they have been invoked. The possible formation of **1** with electron-deficient aryl groups is particularly intriguing (29). Compounding this, there is the possible involvement of triplet ions. A recent report has described a relatively unreactive, hindered form of **1** but this long-lived (0.55 μs) species provides little insight into the reactions of more transient members of this class of ions (36).

We recently described the solvolysis of the 4-acetoxy-4-phenyl-2,5-cyclohexadienone (**3**) and showed that, in neutral, acidic, and basic aqueous media, it solvolyses to 4-biphenylyloxenium ion **4** (37, 38). This ion has a lifetime in water at 30 °C of 12 ns, considerably longer than the analogous 1-(4-biphenylyl)ethyl and 4-phenylcumyl carbenium ions (0.1 and 0.5 ns, respectively) (39, 40), but more than an order of magnitude shorter than that of 4-biphenylylnitrenium ion **8a** (13). Water reacts at the 4 position giving the 4-phenylquinol **5**, but in the competition reactions with azide, from which its lifetime was determined, both the 2- and the 4′-azidobiphenols (**6** and **7**) were formed in a 4.7:1 ratio (Scheme 1) (37).

In similar competition reactions, 4-biphenylylnitrenium ion **8a** afforded the 4-hydroxy-4-phenyl-2,5-cyclohexadienone imine (**9a**) and only the 2-azidobiphenylamine (**10a**) (4). Thus, apart from their differences in lifetimes, 4-biphenylyloxenium and 4-biphenylylnitrenium ions differ in the regiochemistry of azide addition. The isolation of appreciable quantities of the 4′-regioisomer signals significantly greater delocalization of positive charge in the oxenium ion (37). In addition, substituents influence the stabilities of nitrenium ions and oxenium ions to a different extent. While 4-methylnitrenium ion **8b** has been detected from solvolysis of *N*-(4-methylphenyl)-*O*-pivaloyl hydroxylamine (lifetime of 0.8 ns in aqueous acetonitrile at 20 °C) and reacts with water and azide giving **9b** and **10b** (16, 17), we were not able to observe 4-methylphenyloxenium ion **12** from solvolysis of **11a** under any conditions. While the 4-methylquinol **11b** is formed, it does so through normal ester hydrolysis; in aqueous conditions and with 10 atom% ^{18}O water there is little or no incorporation of ^{18}O into the 4-hydroxyl of the product **11b** that is formed upon solvolysis of **11a**. However, there is full incorporation into **5** upon solvolysis of **3** (38). Relative to the phenylnitrenium ion, either the phenyloxenium ion is



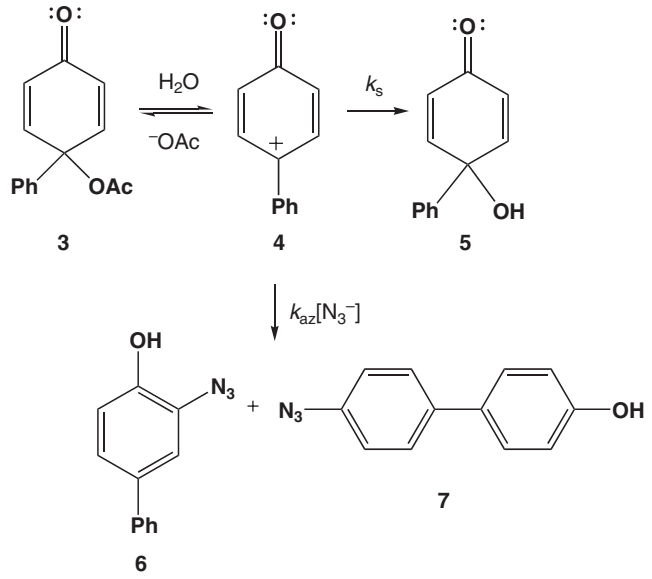
8 **9** **10** **11** **12**

a; R = Ph
b; R = Me

a; X = Ac
b; X = H

© 2005 NRC Canada

Scheme 1.



stabilized far more weakly by a 4-methyl substituent or, alternatively, a 4-phenyl group can provide extra stabilization.

4-Biphenylyloxenium ion generated in this manner appears to react as a singlet species, but, as with nitrenium ions, oxenium ions can be both singlet and triplets. For the simplest form (HO^+), the triplet is lower in energy by 54 kcal mol^{-1} (1 cal = 4.184 J) (41), but electron-donating substituents are expected to stabilize the singlet state more than the triplet state. An earlier MNDO study indicated that singlet states of phenylnitrenium ion and *N*-formylphenylnitrenium ion were lower than the triplet states by about 20 kcal mol^{-1} (42). At the UHF/6-31G* level, singlet phenyloxenium ion is computed to be more stable than its triplet form by only 4 kcal mol^{-1} (34), but Li et al. (43) demonstrated that for both phenylnitrenium ion and phenyloxenium ion the computed energy difference was strongly dependent upon the size of the basis set and, particularly, on the inclusion of correlation energy. However, their calculations utilized HF/STO-3G optimized geometries. Using density functional theory, Cramer and co-workers (25, 44) have calculated singlet states of arylnitrenium ions to be significantly more stable than the triplets (by between 13 and 28 kcal mol^{-1}), and the gap is greatest with electron-donor groups at the 4 position.

In this study, we have compared the influence of 4-methyl and 4-phenyl substituents upon S_0–T_1 energies of phenyloxenium and phenylnitrenium ions and singlet ground-state properties of these, and their carbenium analogues, with a view to understanding the differences in their lifetimes and reactivities.

Methods

Geometries were optimized up to the HF/6-31G* (closed shell) and UHF/6-31G* (triplets) levels and these were used to compute energies, including correlation energies, at the density functional level (pBP/DN*//HF/6-31G*) using the Spartan suite of programs (45, 46). Energies at the pBP/DN*//HF/6-31G* level were on average 1 to 2 kcal mol^{-1} higher than those obtained from full optimization at the pBP/DN* level. Energies of orthogonal conformations of biphenylyl ions were obtained by constraining the inter-ring dihedral angles at 90° and fully optimizing the remaining structural parameters. HF/6-31G* geometries differed only marginally and systematically from those obtained by full DFT analysis and hence were used for comparative purposes. Gas-phase vibrational frequencies were determined using HF/6-31G* optimized geometries and corrected according to the HF/6-31G* scaling factor (0.8953) published by Scott and Radom (47). Trends in these were mirrored in vibrational frequencies of the pBP/DN* fully optimized structures where calculated. The pBP/DN* DFT method was benchmarked against higher level DFT methods by comparing singlet–triplet energies for unsubstituted, 4-chlorophenyl and 4-methylphenyl ions with previously published data. Singlet–triplet splittings were obtained at the pBP/DN*//HF/6-31G* level and, where practical, at the pBP/DN* level.

Isodesmic rxns. [1]–[3] were used to evaluate the relative hydration energies of 4-methylphenyloxenium ion **13b** and 4-biphenylyloxenium ion **13c** relative to the parent phenyloxenium ion **13a** as well as the relative stabilities of 4-methylphenylnitrenium ion **14b** and 4-biphenylylnitrenium ion **14c** relative to the parent phenylnitrenium ions **14a**. Relative hydration energies of phenyloxenium ion **13a** and phenylnitrenium ion **14a**, 4-methylphenyloxenium ion **13b** and 4-methylphenylnitrenium ion **14b**, and 4-biphenylyloxenium ion **13c** and 4-biphenylylnitrenium ion **14c** were determined likewise.

Isodesmic reactions were carried out using: (*i*) HF/6-31G* energies without electron correlation; (*ii*) pBP/DN*//HF/6-31G* with electron correlation and including ZPEs; (*iii*) pBP/DN*//HF/6-31G* with electron correlation, including ZPEs and free energies at 298.15 °C. A comparison of isodesmic reaction energies confirms that, for the most part, the inclusion of electron correlation or thermodynamic quantities makes little difference to the results. Where all relevant species could be fully optimized at the pBP/DN* level, isodesmic energies were almost identical to those obtained by the pBP/DN*//HF/6-31G* method.

Energies are given in atomic units (au) or kcal mol^{-1}. Bond lengths are given in Å and vibrational frequencies are reported in cm^{-1}. Dipole moments are given in Debye (D). Energies for all ions and molecules in this study are presented in Tables 1 and 2.

Results and discussion

Singlet–triplet splittings

Energies of singlet and triplet states of **13a**–**13c** and **14a**–**14d** as well as S_0–T_1 splittings at the HF/6-31G*, pBP/DN*//HF/6-31G*, and pBP/DN* levels are presented in Table 1.

S_0–T_1 splittings for unsubstituted-, **14a**, 4-methyl-, **14b,** and 4-chlorophenylnitreniumions, **14d**, have been determined previously at the BPW91/cc-pVDZ level and indicate that methyl and chloro (S_0–T_1 = –21.9 and –21.3 kcal mol^{-1}, respectively) lower the singlet state marginally relative to the triplet state when compared to phenylnitrenium ion (S_0–T_1 = –18.8 kcal mol^{-1}) (44). The pBP/DN* level performed

© 2005 NRC Canada

Table 1. HF/6-31G*, pBP/DN*//HF/6-31G*, and pBP/DN* total energies (au) and zero-point energies, free energies, and S_0–T_1 splittings (kcal mol^{-1}) for **13a–13c** and **14a–14d**.

Method	Type	**13a**	**13b**	**13c**	**14a**	**14b**	**14c**	**14d**
HF/6-31G*	T_1	–304.67688	–3443.72152	–534.25228	–284.85064	–323.89344	–514.42163	
	T_1^{90} $(\Delta E)_T$[a]			–534.23654 (9.8)				
	S_0	–304.66543	–343.72070	–534.25212	–284.85012	–323.90167	–514.42703	
	S_0^{90} $(\Delta E)_S$[a]			–534.22898 (14.5)			–514.41016 (10.5)	
	S_0–T_1	7.2	0.5	0.1	0.3	–5.2	–3.4	
pBP/DN*//HF/6-31G	T_1	–306.58635	–345.92174	–537.73050	–286.70995	–326.04468	–517.85319	
	T_1^{90} $(\Delta E)_T$[a]			–537.72669 (2.4)				
	S_0	–306.60706	–345.94925	–537.76495	–286.74054	–326.07909	–517.88898	
	(ZPE, *G*)[b]	(55.72, 36.5)	(72.54, 51.7)	(105.86, 83.1)	(63.83, 44.83)	(80.35, 60.21)	(113.45, 91.89)	
	S_0^{90} $(\Delta E)_S$[a]			–537.73537 (18.6)			–517.86702 (13.8)	
	S_0–T_1	–13.0	–17.3	–21.6	–19.2	–21.6	–22.5	
pBP/DN*[c]	T_1	–306.58830	–345.92421	—[d]	–286.70749	–326.04147		–746.37877
	(ZPE)	(52.95)	(69.36)		(59.87)	(76.72)		(54.38)
	S_0	–306.61024	–345.95367	–537.77092	–286.74344	–326.08333		–746.42314
	(ZPE)	(55.43)	(71.48)		(63.34)	(79.47)		(57.59)
	$(S_0–T_1)_{ZPE}$	–11.4	–16.4	—	–19.0	–22.6		–24.6
	$(S_0–T_1)_{ZPE}$[e]				–18.8	–21.9		–21.3

[a]Difference in energy between the orthogonal and geometry-optimized biphenyl geometries in kcal mol^{-1}.
[b]Zero-point energies and free energies (kcal mol^{-1}) from frequency calculations at the pBP/DN*//HF/6-31G* level.
[c]Geometry optimized at the pBP/DN* level.
[d]Calculation failed because of SCF convergence difficulties.
[e]BPW91/cc-pVDZ value from ref. 44.

© 2005 NRC Canada

Table 2. HF/6-31G*, pBP/DN*//HF/6-31G*, and pBP/DN* energies (au) and zero-point energies and free energies (kcal mol^{-1}) for **15a–15c**, **16a–16c**, and **17a–17c**.

Method	Type	15a	15b	15c	16a	16b	16c	17a	17b	17c
HF/6-31G*	S_0	–268.886732	–307.93433	–498.45358	–380.38881	–419.42716	–609.93427	–360.53951	–399.57797	–590.08976
	S^{90}			–498.44300						
	$(\Delta E)_S$[a]			(6.6)						
pBP/DN*// HF/6-31G	S_0	–270.71771	–310.05274	–501.85666	–382.78554	–422.11152	–613.89610	–362.88591	–402.21018	–594.00042
	(ZPE, *G*)	(71.27, 52.61)	(87.90, 67.86)	(119.61, 116.37)	(65.83, 46.47)	(81.97, 61.77)	(114.47, 92.32)	(72.9, 53.3)	(89.5, 69.1)	(122.0, 99.7)
	S^{90}			–501.84012						
	$(\Delta E)_S$[a]			(10.4)						
pBP/DN*[b]	S_0				–382.79152	–422.11753		–362.89190	–402.21669	
	(ZPE)				(65.1)	(81.3)		(72.2)	(88.7)	

[a]Difference in energy between the orthogonal and geometry-optimized biphenyl geometry in kcal mol^{-1}.
[b]Geometry optimized at the pBP/DN* level.

similarly for the unsubstituted and 4-methylphenylnitrenium ion (S_0–T_1 = –19.0 and –22.6 kcal mol^{-1}) and the splitting for the 4-chlorinated analogue was marginally higher (–24.5 kcal mol^{-1}). While there are no experimental values with which to compare these computed splittings, the pBP/DN* method works at least as well as Cramer's density functional approach using the correlation consistent polarized Valence double zeta basis set (44).

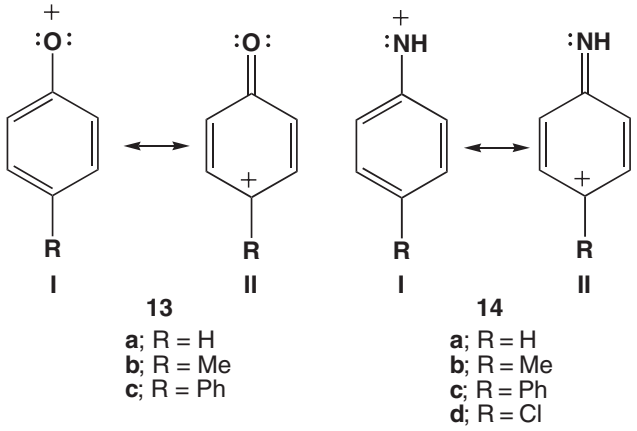
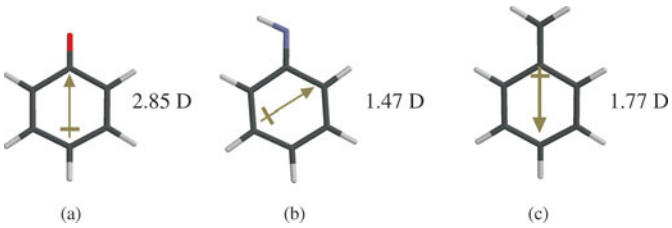


Table 1 gives the S_0–T_1 energy differences for phenyloxenium **13a** and its 4-methyl and 4-phenyl counterparts (**13b** and **13c**). HF/6-31G* predicts triplet states to be marginally lower than the singlet states. However, as expected, the inclusion of electron correlation at the pBP/DN* level radically alters the singlet state energy relative to the triplet state, at least in the cases studied. SCF convergence difficulties prevented calculation of the triplet state of **13c**, but the S_0–T_1 energies for **13a** and **13b** (–11.4 and –16.4 kcal mol^{-1}, respectively) indicate that, like phenylnitrenium ions, the donor methyl substituent stabilized the singlet state relative to hydrogen. While the S_0–T_1 differences are negative, the magnitude of the splitting is smaller than that found for the corresponding phenylnitrenium ions (–19.0 and –22.6 kcal mol^{-1}) although the impact of the donor methyl group appears greater in the oxenium ion case. The single point pBP/DN*//HF/6-31G* method, for which a value could also be obtained for **13c**, shows a similar trend for **13a** and **13b**, with comparable singlet–triplet splittings. However, the results indicate that a 4-phenyl group more strongly stabilizes the singlet state relative to the triplet state. This stabilization (–8.6 kcal mol^{-1} relative to **13a**) is significantly greater than that computed for the corresponding nitrenium ion (–3.2 kcal mol^{-1}).

In these reduced valence cations, it is expected that electron-donating groups will stabilize singlet states more than the triplets in line with conventional molecular orbital arguments; cationic resonance stabilization results in lowering in energies of valence electrons (in the HOMO), but the triplet states are radical-like, having one electron localized in a p_y orbital on the heteroatom and one more electron in the π system than the S_0 state. However, when compared to phenylnitrenium ions **14**, the greater stabilization by methyl and phenyl relative to hydrogen in the phenyloxenium ion case suggests that there is greater localization of positive charge on the 4 position. In valence bond terminology, there

© 2005 NRC Canada

Fig. 1. Dipole moments in S_0 states of: (*a*) phenyloxenium **13a**, (*b*) phenylnitrenium **14a**, and (*c*) phenylcarbenium **15a** ions.



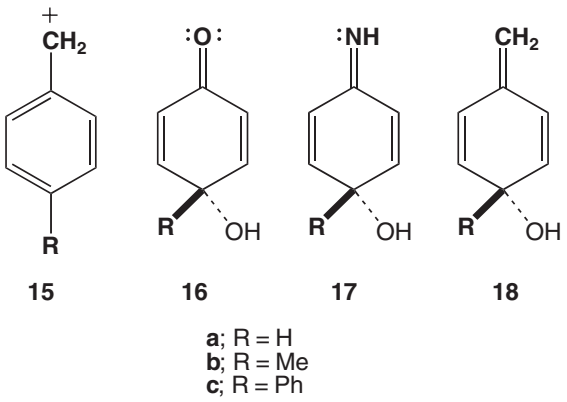
is a greater preponderance of (II) in the resonance hybrid of **13** than is the case in **14**. The HF/6-31G* S_0 and T_1 ground-state geometries of **13c** are planar, signifying extensive π delocalization into the distal ring in both species. However, this would be expected to be more important in the singlet state than in the triplet state; while localization of charge on the 4 position in phenyloxenium ion is a consequence of the electronegativity of oxygen, in the triplet state there is no similar driving force for spin localization onto that position. The barriers to rotation about the connecting bond for the S_0 and T_1 states, computed at the pBP/DN*//HF/6-31G* level from the orthogonal conformations, are 18.6 and 2.4 kcal mol^{-1}, respectively. In addition, the interconnecting bond in the singlet state (1.421 Å) is considerably shorter than that in the triplet state (1.431 Å).

Properties of S_0 state phenyloxenium, phenylnitrenium, and phenylcarbenium ions

Evidence for a higher degree of localization of positive charge at the 4 position in **13** relative to **14** and **15** can be found in the properties of their respective S_0 states. Figure 1 illustrates the orientations and magnitudes of HF/6-31G* computed dipole moments in phenyloxenium **13a**, phenylnitrenium **14a**, and phenylcarbenium **15a** ions.

The electron deficiency in **15a** is clearly on the exocyclic carbon (Fig. 1*c*). In contrast, the magnitude and orientation of the dipole moment predicted for S_0 phenyloxenium ion **13a** clearly indicates a strong localization of positive charge at the 4 position in the ring. From the magnitude and orientation of the dipole moment in **14a**, appreciably less charge must reside on the ring. The contribution to the dipole in the direction of nitrogen and along the axis of the ring-to-nitrogen bond is estimated at 1.41 D, considerably less than for **13a**.[3] While computed charges should be treated with caution, in support of this, HF/6-31G* electrostatic charges at *O* in **13a** and *NH* in **14a** are –0.36 and –0.16, respectively, and for each species, total electrostatic charges at the ortho carbons are respectively +0.06 and –0.09 while at the para carbon they are calculated to be +0.4 and +0.24.

Greater localization of charge at the 4 position in **13** is evident from the optimized ground-state geometries. HF/6-31G* optimized geometries for **13a**, **14a**, and **15a** are presented together with those of the respective 4-hydroxylated products **16a**, **17a**, and **18a** in Fig. 2. A comparison of the bond lengths of **13a** (Fig. 2*a*) with those for **16a** (Fig. 2*d*) clearly indicates that the phenyloxenium ion has a stronger carbonyl bond than the hydration product as evidenced by the shorter C—O bond length. In addition, the degree of bond alternation around the ring in **13a** and **16a** is relatively similar. In contrast, the C—N bond in **14a** (Fig. 2*b*) is longer than that in the neutral imine (Fig. 2*e*). Although there is bond alternation around the ring, a comparison with that in **13a** (Fig. 2*a*) indicates a smaller degree of alternation in the nitrenium ion. In the carbenium ion case (Fig. 2*c*), the geometry accords with the exocyclic cationic form; the CH_2—C bond, in this case, is much longer than the cross-conjugated double bond in the hypothetical hydration product **18a** (Fig. 2*f*).



The short C=O bonds and high degree of alternation in the phenyl rings was reproduced in the 4-methyl (**13b**) and 4-biphenylyl (**13c**) cases and this was better reflected in both the C=O and the symmetric and antisymmetric $C_2{=}C_3$ ($C_5{=}C_6$) vibrational frequencies determined from full frequency analyses on the S_0 states of **13a**–**13c** and **14a**–**14c**. These, together with the vibrational frequencies for the hydrated adducts **16a**–**16c** and **17a**–**17c**, are presented in Table 3.

Introduction of a 4-methyl and 4-phenyl substituent stabilizes positive charge at the 4 position or, in valence bond terms, the resonance hybrid II of **13**. This is evidenced by greater differences between the C=O vibrational frequencies in **13b** and **13c** relative to the corresponding hydrated adducts **16b** and **16c**. While the $C_1{=}C_2/C_5{=}C_6$ symmetric and asymmetric stretch frequencies are lower than those in the neutral hydrated adducts, these too increase with electron donor substitution reflecting strengthening of the C=C bonds (Table 3). The effect of the 4 substituents upon the corresponding nitrenium ions is, however, much more marked. While the C=N stretch frequencies in **14a**–**14c** are significantly lower than those in the hydrated adducts **17a**–**17c**, the difference reduces by 20 and 47 cm^{-1}, respectively, upon introduction of a 4-methyl and 4-phenyl substituent. This indicates that while the oxenium ion **13** is essentially in resonance form II, the nitrenium ion **14** has an appreciable contribution from I; upon substitution by an electron donor methyl or phenyl group, the proportion of II is increased more markedly leading to larger changes in C=NH vibrational frequencies. In other words, unlike **13a**, **14a**, on account of the reduced electronegativity of nitrogen, can still sustain some positive charge on the nitrogen. This picture

[3] Dipole moment = 1.468 D, x = 1.16, y = 0.000, z = 0.890, CNH angle = 114°; the component from the N—H bond in the z direction, which is along the C—N bond, is –(1.16 tan 24°) = –0.516 D.

© 2005 NRC Canada

Fig. 2. Optimized bond lengths for: (*a*) phenyloxenium ion **13a**, (*b*) phenylnitrenium ion **14a**, and (*c*) phenylcarbenium ion **15a** and their hydrated adducts (*d*) **16a**, (*e*) **17a**, and (*f*) **18a**.

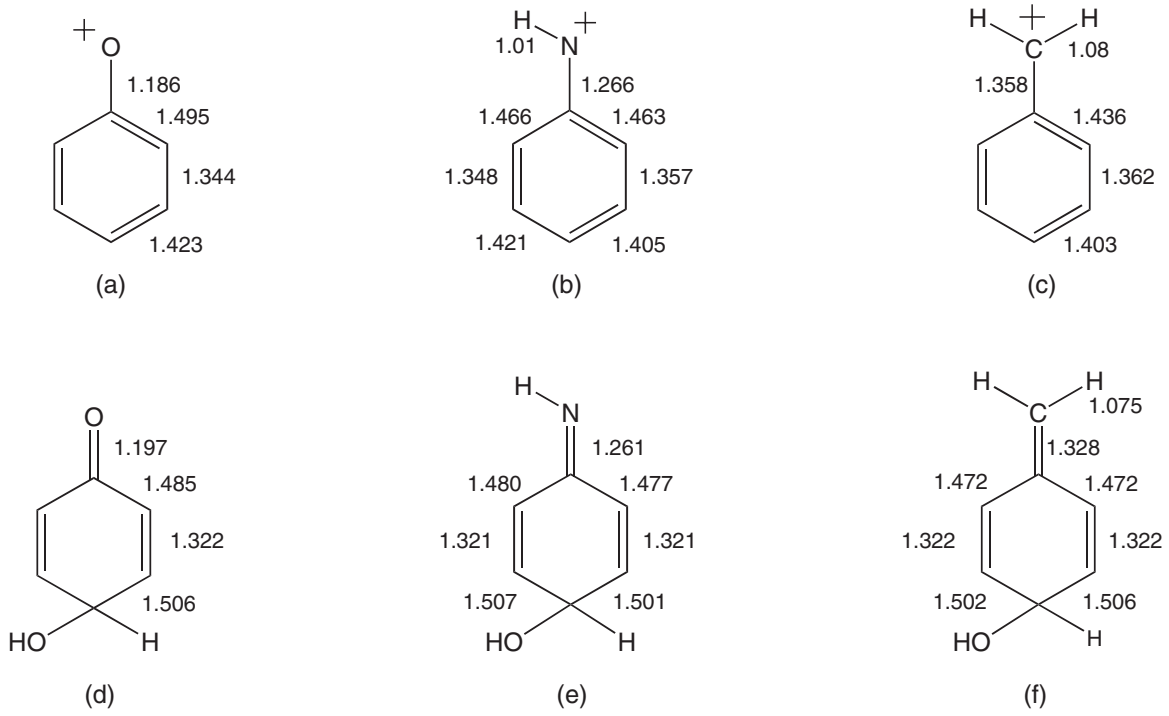


Table 3. HF/6-31G* vibrational frequencies (cm^{-1}) for phenyloxenium ions **13a**–**13c**, phenylnitrenium ions **14a**–**14c**, and their hydrated adducts **16a**–**16c** and **17a**–**17c**.

Bond	**13a**	**16a**	Δν	**13b**	**16b**	Δν	**13c**	**16c**	Δν
C=O	1799.6	1790.6	9.0	1807.6	1789.7	17.9	1812.1	1788.8	23.3
C=C(s)	1604.4	1681.4	–77.0	1623.2	1682.3	–59.1	1643.8	1678.7	–34.9
C=C(as)	1541.7	1649.1	–107.4	1541.7	1647.4	–105.6	1586.5	1643.8	–57.3
Bond	**14a**	**17a**	Δν	**14b**	**17b**	Δν	**14c**	**17c**	Δν
C=NH	1627.7	1735.1	–107.4	1648.2	1736.0	–87.7	1671.5	1731.5	–60.0
C=C(s)	1584.7	1660.8	–76.1	1598.1	1660.8	–62.7	1614.2	1652.7	–38.5
C=C(as)	1535.4	1654.5	–119.1	1518.4	1654.5	–136.1	1542.6	1648.2	–105.6

accords with reactivity patterns of arylnitrenium ions in that nucleophiles react on both the ring and at nitrogen (4–7, 12, 14, 48, 49).

Relative stabilities

Isodesmic rxn. [1] was used to estimate the hydration energies of phenyloxenium ions **13a**–**13c** relative to their corresponding nitrenium ions **14a**–**14c** and reflect relative stabilities of the correspondingly substituted ions.

From energies in Tables 1 and 2, the isodesmic energies from eq. [1] were calculated at the three levels indicated in

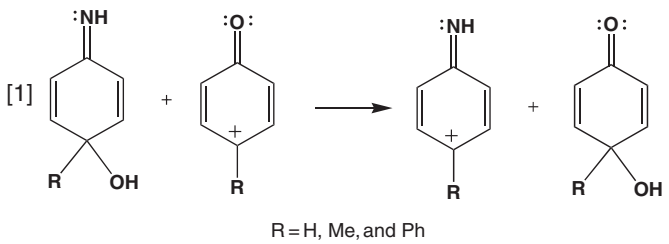


Table 4. The data show these energies to be largely independent of electron correlation as well as ZPEs and free energies in line with previous findings (50). The negative values indicate that, relative to their hydrated adducts **17** and **16**, phenylnitrenium ions are, in all three instances, more stable than the corresponding phenyloxenium ions, in line with their more delocalized positive charge. The difference between stabilities of **14c** and **13c** is in accord with the relative lifetimes of these ions in aqueous solution as determined from our competition reactions with azide (300 ns in the case of **14c** as opposed to 12 ns in the case of **13c** at 30 °C (37)). However, while a 4-methyl group exerts only a small influence upon the energies, the 4-phenyl group clearly provides greater relative stabilization to **13c** than to **14c** (the energy difference reduces in magnitude from 18 to 19 kcal mol^{-1} in the case of unsubstituted and methylated ions to 11 kcal mol^{-1} in the case of biphenylyl ions).

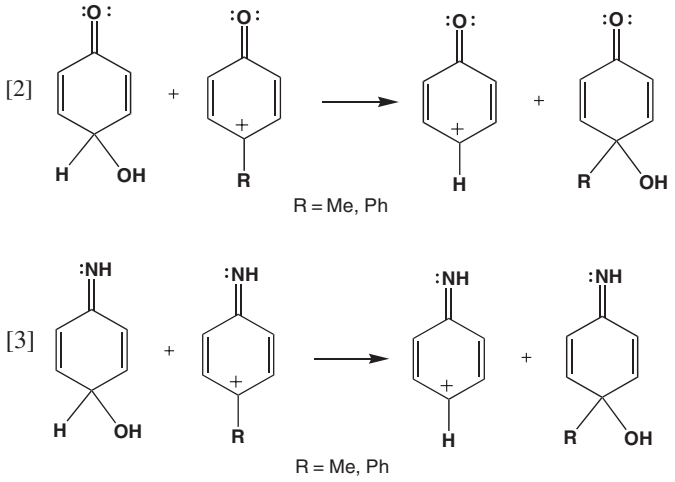
A similar conclusion can be reached from isodesmic reactions comparing the relative hydration energies of 4-methyl- **13b** and 4-biphenylyloxenium ions **13c** with the

© 2005 NRC Canada

Table 4. Isodesmic reaction energies from rxns. [1]–[3].

Isodesmic reaction	R	ΔE_{react} HF/6-31G*	ΔE_{react} pBP/DN*//HF/6-31G*+ZPE	ΔE_{react} pBP/DN*//HF/6-31G*+ZPE+G
[1][a]	H	–21.3	–19.8	–19.3
[1][a]	Me	–18.9	–19.2	–18.4
[1][a]	Ph	–12.2	–12.3	–11.0
[2][b]	Me	10.6	9.5	10.3
[2][b]	Ph	25.9	28.2	29.0
[3][c]	Me	8.2	9.0	9.4
[3][c]	Ph	16.7	20.8	20.6

[a]Stability of phenyloxenium ions **13a**–**13c** relative to the nitrenium ions **14a**–**14c**.
[b]Stability of **13b** and **13c** relative to **13a**.
[c]Stability of **14b** and **14c** relative to **14a**.



unsubstituted ion **13a** (rxn. [2]) and rxn. [3] that gives corresponding estimates for the nitrenium ions **14b** and **14c** relative to **14a**.

Data for rxns. [2] and [3] in Table 4 clearly indicate that both methyl and phenyl stabilize both ions (positive values). However, whereas a 4-methyl group results in similar stabilization of the ions **13a** and **14a**, a 4-phenyl substituent stabilizes phenyloxenium ion by between 8 and 9 kcal mol^{-1} relative to the phenylnitrenium ion. This is a critical difference. This stabilization accounts for the fact that it is possible to generate and trap **13c** in aqueous media in a similar manner to the generation and trapping of **14b** and **14c** (4, 13, 16, 17, 37, 50). However, **13b** could not be observed under any of the conditions used for the trapping of **13c** (37, 38). We estimate, using the differences in hydration energies from isodesmic rxn. [2] (Table 4), and previously published correlations of nitrenium ion lifetimes and hydration energies of rxn. [3] that the lifetime of the 4-methylphenyloxenium would be of the order of 3–5 ps, approaching that of a transition state rather than an intermediate (38, 50).

The increased stabilization of phenyloxenium ion by a 4-phenyl group relative to phenylnitrenium ion also manifests itself in the ground-state geometries of the two ions (Fig. 3). Whereas **15c** and **14c** are nonplanar with inter-ring dihedrals of 22° and 28°, respectively, **13c** is computed to be planar at the HF/6-31G* level. The extent to which there is overlap between the two rings is also evident from the length of the connecting bonds as well as the barriers to rotation around the rings. The twist angles in biphenyls are determined by a balance between electronic and steric influences. In the case of **13c**, the resonance interaction is strong enough to overcome the strain imposed by the repulsion between *m* and *o′* hydrogens and the barrier to rotation about the C4—C4′ bond is clearly significantly higher than that for **14c** and **15c**.

The degree of delocalization in **13c**, **14c**, and **15c** clearly manifests itself in the nature of the LUMOs of all three. Relative contributions to the LUMO at the exocyclic atom and the 4 positions vary inversely (Fig. 4) and similar variations in LUMO contributions were found for the corresponding phenyl- and 4-methylphenylenium ions. Accordingly, in aqueous conditions, attack of water at the 4 position is the major process with biphenylyloxenium ion (37, 38), while biphenylylcarbenium ion reacts at the benzylic position. As alluded to previously, biphenylylnitrenium reacts with water at the 4 position, but is also known to react at nitrogen (4–7, 12, 14, 48, 49). In this series, there is also a progressively greater contribution to the LUMO from the distal ring from twisted **15c** to planar **13c** (Fig. 4). Solvolysis studies on biphenylyloxenium ion indicate that water ($k_s = 8.4 \times 10^7$ s^{-1}) and, to a degree, acetate ($k_{OAc} = 2.8 \times 10^8$ $(mol/L)^{-1}$ s^{-1}) are more selective nucleophiles than Br^- ($k_{Br^-} = 3.9 \times 10^9$ $(mol/L)^{-1}$ s^{-1}) and azide ($k_{Az} = 6.5 \times 10^9$ $(mol/L)^{-1}$ s^{-1}) (38). Our experimental studies have detected addition of water and acetate to the 4 position in 4-biphenylyloxenium ion (37). With the more reactive azide, the major products were **6** and **7**. While reversible attack of azide at the 4 position cannot be discounted, the formation of these products reflects the lower selectivity of azide when compared to water. In addition, the formation of the 4′-azidobiphenol (**7**) from azide–water competition reactions with **3** (Scheme 1) and the failure to detect the attack of azide at the 4′ position on the corresponding nitrenium ion, reflects the attendant planarity in this ion and the increased delocalization of the positive charge in **13c**. Bromide appeared to react on **13c** giving only 2-bromo-4-biphenol (37).

Conclusion

Phenyloxenium ions **13** are predicted to have a S_0 ground state that is lowered, relative to the T_1 state, by electron donor substituents. Analysis of computed ground-state geometries and IR vibrational frequencies shows that phenyloxenium ion is best described as a 4-oxo-2,5-cyclohexadienyl cation. Accordingly, it is stabilized effectively by a 4-phenyl substituent, which is coplanar to maximize charge delocalization. This results in products from attack of

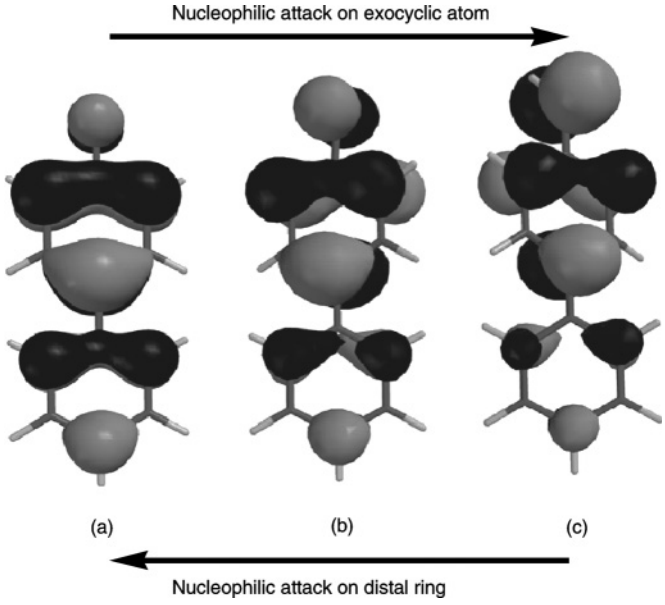
© 2005 NRC Canada

Fig. 3. Ground-state HF/6-31G* geometries, twist angles, inter-ring bond lengths, and rotational barriers (pBP/DN*//HF/6-31G*) for: (*a*) 4-biphenylyloxenium ion **13c**, (*b*) 4-biphenylylnitrenium ion **14c**, and (*c*) 4-biphenylylcarbenium ion **15c**.



	(a)	(b)	(c)
Dihedral (°)	0.0	21.9	28.3
C—C (Å)	1.421	1.437	1.457
Barrier (kcalmol^{-1})	18.6	13.8	10.4

Fig. 4. LUMO contributions to: (*a*) 4-biphenylyloxenium ion **13c**, (*b*) 4-biphenylylnitrenium ion **14c**, and (*c*) 4-biphenylylcarbenium ion **15c**.



nonselective nucleophiles like azide on both rings. The 4-methyl analogue **13b** is predicted to be considerably less stable in support of the experimental finding that it cannot be observed under conditions in which **13c** is readily detected. Relative to their hydrated products, 4-biphenylyloxenium ion is predicted to be less stable than 4-biphenylylnitrenium ion in support of their respective lifetimes in aqueous conditions. The difference in properties between nitrenium and oxenium ions can be ascribed to differences in the electronegativity of oxygen and nitrogen. Whereas nitrogen can sustain partial positive charge, the more electronegative oxygen atom in the phenyloxenium ion causes a high degree of charge localization on the ring. The attendant destabilization of oxenium ions relative to nitrenium ions is reflected in the aqueous solution lifetimes of **13c** and **14c** and in the difference in the ability to detect **14b** and **13b**.

Acknowledgments

The authors are grateful to Miami University for sabbatical leave to MN and the University of New England for a University Research Grant to SAG. Ackowledgement is also made to the Donors of the American Chemical Society Petroleum Research Fund for partial support of this research (Grant No. 43176-AC4).

References

1. M. Novak, K.A. Martin, and J.L. Heinrich. J. Org. Chem. **54**, 5430 (1989).
2. J.S. Helmick, K.A. Martin, J.L. Heinrich, and M. Novak. J. Am. Chem. Soc. **113**, 3459 (1991).
3. M. Novak and K.S. Rangappa. J. Org. Chem. **57**, 1285 (1992).
4. M. Novak, M.J. Kahley, E. Eiger, J.S. Helmick, and H.E. Peters. J. Am. Chem. Soc. **115**, 9453 (1993).
5. M. Novak and S.A. Kennedy. J. Am. Chem. Soc. **117**, 574 (1995).
6. M. Novak and J. Lin. J. Am. Chem. Soc. **118**, 1302 (1996).
7. S.A. Kennedy, M. Novak, and B.A. Kolb. J. Am. Chem. Soc. **119**, 7654 (1997).
8. M. Novak, L.L. Xu, and R.A. Wolf. J. Am. Chem. Soc. **120**, 1643 (1998).
9. M. Novak and S.A. Kennedy. J. Phys. Org. Chem. **11**, 71 (1998).
10. M. Novak, J.K. Kayser, and M.E. Brooks. J. Org. Chem. **63**, 5489 (1998).
11. M. Novak and S. Rajagopal. *In* Advances in physical organic chemistry. *Edited by* T.T. Tidwell and J.P. Richard. Academic Press, London. 2001. p. 167.
12. J.C. Fishbein and R.A. McClelland. J. Am. Chem. Soc. **109**, 2824 (1987).
13. R.A. McClelland, P.A. Davidse, and G. Hadzialic. J. Am. Chem. Soc. **117**, 4173 (1995).
14. R.A. McClelland, A. Ahmad, A.P. Dicks, and V.E. Licence. J. Am. Chem. Soc. **121**, 3303 (1999).
15. R. Bose, A.R. Ahmed, A.P. Dicks, M. Novak, K.J. Kayser, and R.A. McClelland. J. Chem. Soc. Perkin Trans. 2, 1591 (1999).
16. M. Novak, M.J. Kahley, J. Lin, S.A. Kennedy, and L.A. Swanegan. J. Am. Chem. Soc. **116**, 11626 (1994).

© 2005 NRC Canada

17. M. Novak, M.J. Kahley, J. Lin, S.A. Kennedy, and T.G. James. J. Org. Chem. **60**, 8294 (1995).
18. R.A. Davidse, M.J. Kahley, R.A. McClelland, and M. Novak. J. Am. Chem. Soc. **116**, 4513 (1994).
19. R.A. McClelland. Tetrahedron, **52**, 6823 (1996).
20. R.A. McClelland, M.J. Kahley, P.A. Davidse, and G. Hadzialic. J. Am. Chem. Soc. **118**, 4794 (1996).
21. P. Sukhai and R.A. McClelland. J. Chem. Soc. Perkin Trans. 2, 1529 (1996).
22. D. Ren and R.A. McClelland. Can. J. Chem. **76**, 78 (1998).
23. A.P. Dicks, A.R. Ahmed, R. D'Sa, and R.A. McClelland. J. Chem. Soc. Perkin Trans. 2, 1 (1999).
24. P. Ramlall and R.A. McClelland. J. Chem. Soc. Perkin Trans. 2, 225 (1999).
25. S. Srivastava, P.H. Ruane, J.P. Toscano, M.B. Sullivan, C.J. Cramer, D. Chiapperino, E.C. Reed, and D.E. Falvey. J. Am. Chem. Soc. **122**, 8271 (2000).
26. M. Novak and S. Rajagopal. Chem. Res. Toxicol. **15**, 1495 (2002).
27. J.S. Swenton, K. Carpenter, Y. Chen, M.L. Kerns, and G.W. Morrow. J. Org. Chem. **58**, 3308 (1993).
28. R.A. Abramovitch, M. Inbasekaran, and S. Kato. J. Am. Chem. Soc. **95**, 5428 (1973).
29. R.A. Abramovitch, G. Alvernhe, R. Bartnik, N.L. Dassanayake, M. Inbasekaran, and S. Kato. J. Am. Chem. Soc. **103**, 4558 (1981).
30. J.A.R. Rodrigues, R.A. Abramovitch, J.D.F. de Sousa, and G.C. Leiva. J. Org. Chem. **69**, 2920 (2004).
31. Y. Endo, K. Shudo, and T. Okamato. J. Am. Chem. Soc. **99**, 7721 (1977).
32. Y. Endo, K. Shudo, and T. Okamato. J. Am. Chem. Soc. **104**, 6393 (1982).
33. K. Shudo, Y. Orihara, T. Ohta, and T. Okamato. J. Am. Chem. Soc. **103**, 943 (1981).
34. P.J. Baesjou, W.L. Driessen, G. Challa, and J. Reedijk. J. Am. Chem. Soc. **119**, 12 590 (1997).
35. S. Kobayashi and H. Higashimura. Prog. Polym. Sci. **28**, 1015 (2003).
36. A.F. Hegarty and J.P. Keogh. J. Chem. Soc. Perkin Trans. 2, 758 (2001).
37. M. Novak and S.A. Glover. J. Am. Chem. Soc. **126**, 7748 (2004).
38. M. Novak and S.A. Glover. J. Am. Chem. Soc. **127**, 8090 (2005).
39. J.P. Richard, M.E. Rothenberg, and W.P. Jencks. J. Am. Chem. Soc. **106**, 1361 (1984).
40. J.P. Richard and W.P. Jencks. J. Am. Chem. Soc. **104**, 4689 (1982).
41. S. Katsumata and D.R. Lloyd. Chem. Phys. Lett. **45**, 519 (1977).
42. S.A. Glover and A.P. Scott. Tetrahedron, **45**, 1763 (1989).
43. Y. Li, R.A. Abramovitch, and K.N. Houk. J. Org. Chem. **54**, 2911 (1989).
44. M.B. Sullivan, K. Brown, C.J. Cramer, and D.G. Truhlar. J. Am. Chem. Soc. **120**, 11 778 (1998).
45. SPARTAN. Version 5.0 [computer program]. Wavefunction Inc., Irvine, Calif. 1993–1997.
46. MacSpartan Pro. Version 1 [computer program]. Wavefunction, Inc., 18401 Van Karman Avenue, Suite 370, Irvine, Calif. 2000.
47. A.P. Scott and L. Radom. J. Phys. Chem. **100**, 16502 (1996).
48. F.F. Kadlubar. Environ. Health Perspect. **62**, 19 (1985).
49. F.A. Beland and F.F. Kadlubar. *In* Chemical carcinogenesis and mutagenesis. 8th ed. *Edited by* C.S. Cooper and P.L. Grover. Springer-Verlag, Berlin. 1990. p. 267.
50. M. Novak and J. Lin. J. Org. Chem. **64**, 6032 (1999).

© 2005 NRC Canada

The role of molecular geometry in the Wolff rearrangement of α-diazocarbonyl compounds — Conformational control or structural constraints?[1]

Vladimir V. Popik

Abstract: Relaxed scans of potential energy surfaces for the loss of nitrogen from four different diazocarbonyl compounds: 3-diazo-2-butanone (**1**), 2-diazocyclohexanone (**2**), methyl diazomalonate (**3**), and diazo Meldrum's acid (**4**), were conducted at the B3LYP/6-31+G(d,p) level. The geometries of species and transition states involved in the process were optimized at the B3LYP/6-311+G(3df,2p) level, while electronic energies were computed using the MP2(full)/aug-cc-pVTZ method. These calculations suggest that the rigidity of cyclic molecules, rather than the conformational structure of the starting diazocarbonyl compounds, defines the pathway of the dediazotization reaction. In acyclic diazocarbonyl compounds, loss of nitrogen results in the formation of a carbene, which is stabilized by the overlap of the system of carbonyl group and the unshared electron pair of a singlet carbene. On the contrary, in small- to medium-sized cyclic systems, carbonyl carbenes are unable to attain a stabilizing orthogonal conformation. Consequently, cyclic carbonyl carbenes are less stable, and the concerted Wolff rearrangement becomes the predominant process. Transition states for the concerted Wolff rearrangement and for the formation of carbonyl carbenes have a very similar geometry.

Key words: diazocarbonyl compounds, Wolff rearrangement, conformation, carbene, ketene.

Résumé : Opérant au niveau B3LYP/6-31+G(d,p) de la théorie, on a effectué un balayage des surfaces d'énergie potentielle pour la perte de l'azote à partir de quatre composés diazocarbonyles différents: 3-diazobutan-2-one (**1**), 2-diazocyclohexanone (**2**), diazomalonate de méthyle (**3**) et l'acide diazo de Meldrum (**4**). Les géométries des espèces et des états de transition impliqués dans le processus ont été optimisées au niveau B3LYP/6-311+G(3df,2p) alors que les énergies électroniques ont été calculées à l'aide de la méthode MP2(full)/aug-cc-pVTZ. Ces calculs suggèrent que la rigidité des molécules cycliques, plutôt que la structure conformationnelle des composés diazocarbonyles de départ, définit la voie réactionnelle de la réaction de dédiazotation. Dans les composés diazocarbonyles acycliques, la perte d'azote conduit à la formation d'un carbène qui est stabilisé par un recouvrement du système de groupe carbonyle et de la paire d'électrons non partagée du carbène singulet. Au contraire, dans les composés comportant des cycles petits ou moyens les carbonyl carbènes ne sont pas en mesure d'atteindre une conformation orthogonale stabilisante. En conséquence, avec les composés cycliques, les carbonyl carbènes sont moins stables et le réarrangement de Wolff concerté devient le processus prédominant. Les états de transition pour le réarrangement de Wolff concerté et la formation d'un carbonyl carbène ont des géométries très semblables.

Mots clés : composés diazocarbonyles, réarrangement de Wolff, conformation, carbène, cétène.

[Traduit par la Rédaction]

Introduction

Thermolysis or light-induced decomposition of α-diazocarbonyl compounds usually leads to products formed by the trapping of two different reactive intermediates, i.e., ketenes and α-carbonyl carbenes (1, 2). The generally accepted explanation of this dual reactivity is presented in Scheme 1. The loss of nitrogen from α-diazocarbonyl compounds results in the formation of α-carbonyl carbenes, which can exist in two different electronic states, i.e., singlet or triplet (3–5). Thermal decomposition or direct photolysis of α-diazocarbonyl compounds is usually dominated by the chemistry of singlet carbenes. Carbenes are very reactive species and readily undergo an O-H or C-H insertion, add to π bonds, or form ylides (6). Alternatively, an α-carbonyl carbene can rearrange to form a ketene. The latter can also be formed directly from the diazo compound, bypassing the α-carbonyl carbene step by the migration of the substituent X concerted with the loss of nitrogen (1, 7). Ketenes react with nucleophiles to produce corresponding enols, which then rapidly ketonize to yield the final product — carboxylic acid derivatives (8). The overall process is known as the Wolff rearrangement.

The ratio of ketene derived to carbenic products depends on the relative rates of bimolecular reactions of the α-carbonyl

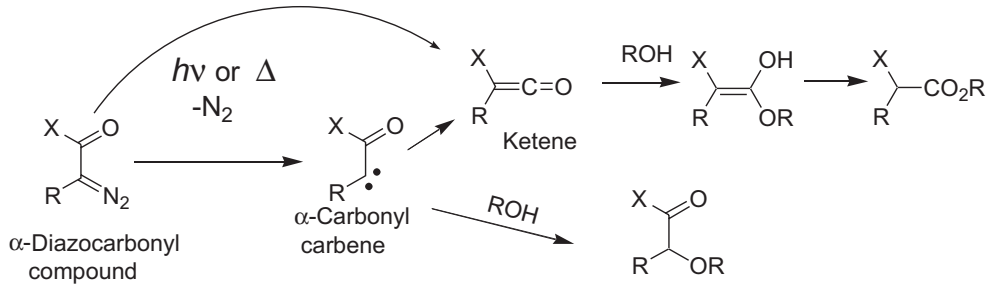
Received 11 April 2005. Published on the NRC Research Press Web site at http://canjchem.nrc.ca on 3 November 2005.

V.V. Popik. Center for Photochemical Sciences, Bowling Green State University, Bowling Green, OH 43403, USA. (e-mail: vpopik@bgnet.bgsu.edu).

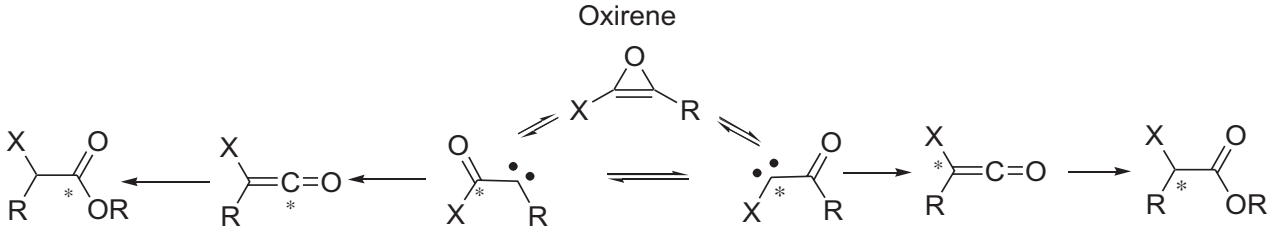
[1]This article is part of a Special Issue dedicated to organic reaction mechanisms.

 doi: 10.1139/V05-152 © 2005 NRC Canada

Scheme 1.



Scheme 2.



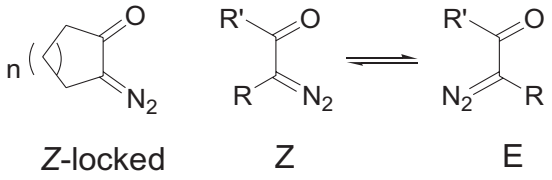
carbene and its rearrangement to ketene. The concentration and the reactivity of carbene trapping reagents also affect the outcome of the reaction.

Another important feature of an α-carbonyl carbene intermediate, which allows for the detection of even very short-lived carbenes, is α-carbonyl carbene – α-carbonyl carbene isomerization, which is believed to proceed via an antiaromatic oxirene (Scheme 2) (9). Isotopic labeling of the diazo or carbonyl group carbon atom is commonly used to detect carbonyl carbene isomerization (10, 11).

The factors that direct the decomposition of α-diazocarbonyl compounds into a concerted Wolff rearrangement or carbene pathway are still not well-understood. It has been observed that cyclic diazo ketones usually produce high or quantitative yields of ketenes; while in the case of their acyclic analogs, the Wolff rearrangement is often accompanied or even completely suppressed by carbene reactions (12, 13). The low-temperature NMR experiments unequivocally proved that α-diazocarbonyl compounds exist as an equilibrium of two conformations with *s*-Z and *s*-E arrangements of diazo and carbonyl groups (Scheme 3) (14, 15). The *s*-Z isomer usually predominates in the equilibrium, unless steric repulsions of substituents R and R′ destabilize it in favor of the *s*-E form (3, 16).

Based on the differences in the reactivity of 3,3,6,6-tetramethyl-2-diazocyclohexanone, which is locked in the *s*-Z configuration, and 2,2,5,5-tetramethyl-4-diazo-3-hexanone,[2] which is forced to adopt the *s*-E conformation by bulky *tert*-butyl substituents, Kaplan and co-workers (13, 14*a*, 14*b*) postulated that *s*-Z conformers of α-diazocarbonyl compounds undergo a concerted Wolff rearrangement to ketenes, whereas the *s*-E form loses nitrogen to produce α-carbonyl carbene. The latter can undergo isomerization into ketenes or be trapped by external reagents. While this hypothesis has been adopted by other authors (6*a*, 17), some established *s*-E diazo ketones produce ketenes with ease (18). In addition,

Scheme 3.



the Wolff rearrangement of acyclic *Z*-diazo ketones is often accompanied by isotope scrambling, indicating participation of the α-carbonyl carbene (10).

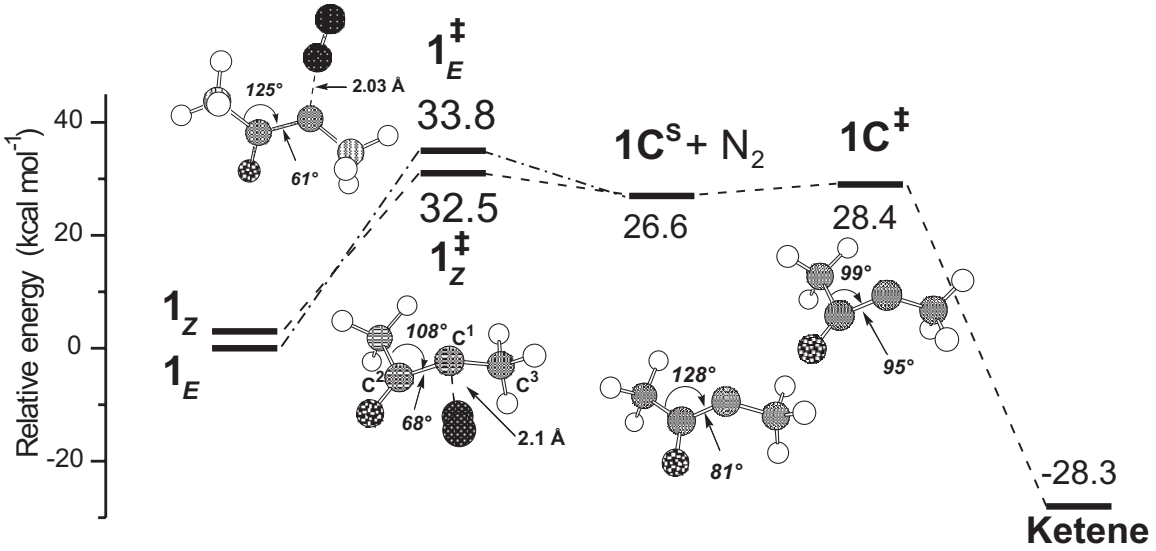
To get a better understanding of the influence of structural factors on the reactivity of α-diazocarbonyl compounds, we undertook a detailed quantum mechanical study of four α-diazocarbonyl compounds: 3-diazo-2-butanone (**1**), 2-diazocyclohexanone (**2**), methyl diazomalonate (**3**), and diazo Meldrum's acid (**4**).

Diazo ketone **1** exists in solutions as a mixture of E and Z isomers (14*d*, 19) and produces a high yield of the Wolff rearrangement product upon irradiation (20). This reaction is accompanied by a complete scrambling of the ^{13}C label, indicating that it proceeds via the formation acetylmethyl carbene (10). Diazocyclohexanone **2** also undergoes the Wolff rearrangement upon irradiation or thermolysis (12*a*); however, isotope labeling experiments suggested a concerted mechanism (11). One of the most impressive examples of the structural control of the Wolff rearrangement is found in the family of diazomalonic acid esters. Cyclic isopropylidene diazomalonate (**4**) undergoes an efficient Wolff rearrangement both thermally (21) and photochemically (21, 22), while acyclic diazomalonates, such as **3**, produce only carbenic products in solution (23, 24). The reasons for such different reactivity are not clear, since **3** has the same Z,Z conformation of the 2-diazo-1,3-dicarbonyl fragment as the cyclic diazodiester **4** (23*c*).

[2] Geometrial optimization of this diazo compound that we conducted at the B3LYP/6-311+G(3df,2p) level of theory produced a planar *s*-E conformation.

© 2005 NRC Canada

Fig. 1. Schematic potential energy profiles for the decomposition of Z and E conformers of 3-diazo butanone (**1**). Structures represent B3LYP/6-311+G(3df,2p) optimized geometries of α-carbonyl carbene $\mathbf{1C^S}$ and transition states for the loss of nitrogen from *Z*-($\mathbf{1}_Z^{\ddagger}$) and *E*-($\mathbf{1}_E^{\ddagger}$) forms of the substrate and the Wolff rearrangement of the carbene ($\mathbf{1C}^{\ddagger}$). The bond distances are shown in Å, while bond angles and dihedral angles (highlighted in *italics*) are in degrees.



Results and discussion

Computational methods

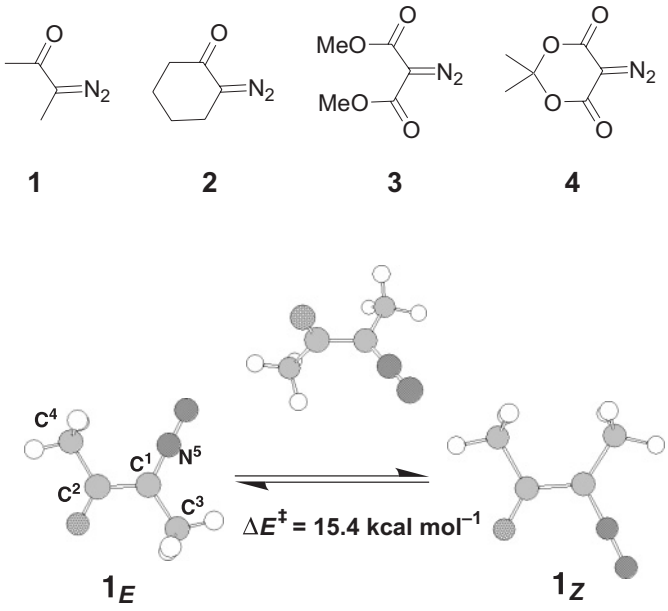
Geometries of the diazocarbonyl compounds **1**–**4** and the species involved in their decomposition were preoptimized at the B3LYP/6-31+G(d,p) level and then reoptimized using the extended triple-ζ 6-311+G(3df,2p) basis set. Some structures were also optimized at the MP2/6-31+G(d,p) level, while single-point energy calculations were conducted using the MP2(full)/aug-cc-pVTZ method.

3-Diazo-2-butanone (**1**) can exist in *E*-($\mathbf{1}_E$) and *Z*-($\mathbf{1}_Z$) conformations. According to the DFT calculation, both conformations are planar and the E conformation is 1.6 kcal mol^{-1} lower in energy (Scheme 4). In the transition state for the E to Z isomerization, the diazo group is orthogonal to the carbonyl group, and the process has an activation barrier of 15.4 kcal mol^{-1}. These numbers agree well with experimental values ($\Delta H°$= 1.45 kcal mol^{-1} and $\Delta H^{\ddagger}$ = 15.6 kcal mol^{-1} in $CDCl_3$) (1 cal = 4.184 J) (14*d*).

The loss of nitrogen from both conformers of diazobutanone **1** results in the formation of a singlet carbonyl carbene $\mathbf{1C^S}$ (Fig. 1). The electronic energies and representative structural parameters for the singlet carbenes $\mathbf{1C^S}$, transition states for deazotization of *E*-($\mathbf{1}_E^{\ddagger}$) and *Z*-($\mathbf{1}_Z^{\ddagger}$) conformers of diazobutanone, as well as for the Wolff rearrangement of the α-carbonyl carbene ($\mathbf{1C}^{\ddagger}$) are shown in Fig. 1.

The carbonyl group in singlet carbene $\mathbf{1C^S}$ is almost orthogonal to the plane of the carbene (C2-C1-C3, Fig. 1). Such geometry provides a better overlap of the orbital containing an unshared pair of electrons localized on the carbene carbon with the π system of the carbonyl groups. The triplet acetylmethyl carbene ($\mathbf{1C^T}$), on the other hand, was found to be planar. Similar differences in geometry were reported for several other α-carbonyl carbenes (21, 23*c*, 25). It is interesting to note that the B3LYP/6-311+G(3df,2p) calculations predict that triplet $\mathbf{1C^T}$ is slightly higher in energy

Scheme 4.

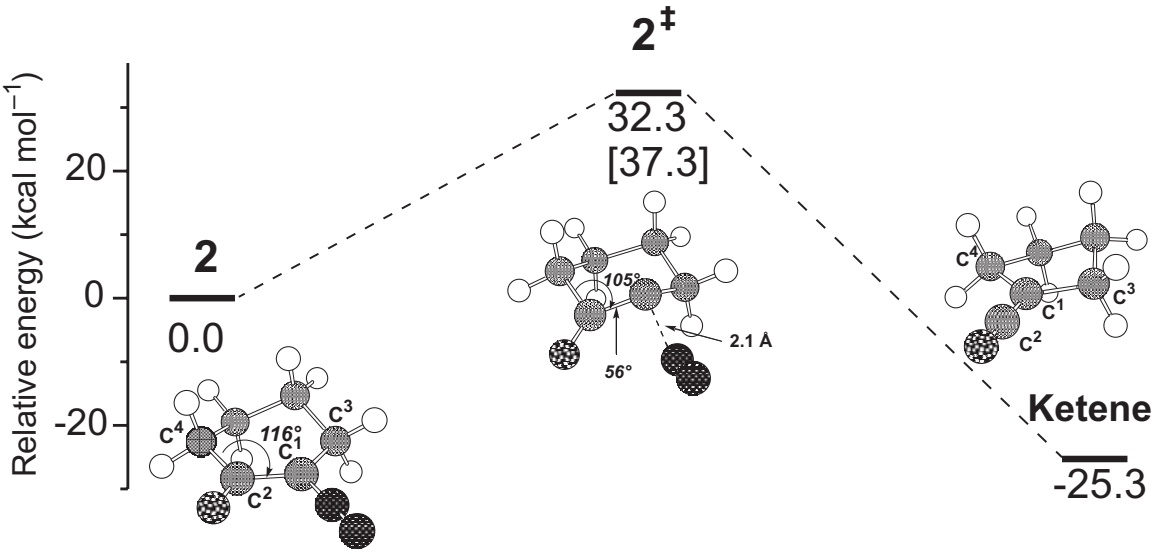


($\Delta E°$ = 0.8 kcal mol^{-1}) than its singlet counterpart, indicating that this α-carbonyl carbene has the singlet ground state. This conclusion is supported by the results of MP2 calculations. Optimization of $\mathbf{1C^T}$ and $\mathbf{1C^S}$ geometries at the UMP2/6-311+G(d,p) level produces exactly the same relative stability. Single-point UMP2(full)/aug-cc-pVTZ calculations predict an even larger singlet–triplet gap of –6.0 kcal mol^{-1}.

Another interesting feature of the thermal decomposition of diazo ketone **1** is the difference in the thermal stability of E and Z conformers. While the E conformation is more stable and is predominant in the equilibrium, the transition state for the decomposition of the Z conformer ($\mathbf{1}_Z^{\ddagger}$) is lower in energy by 1.3 kcal mol^{-1} (or 2.2 kcal mol^{-1} at the

© 2005 NRC Canada

Fig. 2. Schematic potential energy profile for the decomposition of 2-diazohexanone (**2**). Energy are calculated at the B3LYP/6-311+G(3df,2p) and MP2(full)/aug-cc-pVTZ (in brackets) levels. Structures represent B3LYP/6-311+G(3df,2p) optimized geometries of **2**, transition states for the loss of nitrogen $\mathbf{2}^{\ddagger}$, and the cyclopentanylidene. The bond distances are shown in Å, while bond angles and dihedral angles (highlighted in *italics*) are in degrees.



MP2(full)/aug-cc-pVTZ level). A similar difference was observed for diazoacetone (1.5 kcal mol^{-1}).[3] These results suggest that the thermal decomposition of diazobutanone **1** proceeds mostly through the Z conformer, while photochemical reactions are dominated by the excitation of the E form of the substrate. The geometries of the transition states $\mathbf{1}_Z^{\ddagger}$ and $\mathbf{1}_E^{\ddagger}$ are also quite different. The carbonyl group valence angle in $\mathbf{1}_E^{\ddagger}$ is 125°, which is higher than in the starting material (116°) and is very close to the resulting carbene ($\mathbf{1C}^S$, 128°). The carbonyl angle in $\mathbf{1}_Z^{\ddagger}$, on the other hand, is even smaller than in the starting diazobutanone **1**. At first we interpreted this observation as an indication of a concerted mechanism for the *Z*-diazobutanone. However, IRC calculations, as well as optimization of the $\mathbf{1}_Z^{\ddagger}$ structure after ca. 10% displacement along the reaction path for the normal coordinate of the imaginary vibrational frequency, connect this transition state only to carbene $\mathbf{1C}^S$ and not to dimethylketene. This observation is in sharp contrast with a recent DFT study of diazoacetone decomposition.[3] The E conformer of the latter loses nitrogen to produce a carbene, while the Z conformer undergoes a concerted Wolff rearrangement. We thoroughly explored the corresponding area of PES, but were unable to locate the transition state for the concerted Wolff rearrangement of $\mathbf{1}_Z$. A similar fluctuation of the carbonyl valence angle was previously reported in the carbene-producing decomposition of the Z,Z conformer of methyl diazomalonate (25*b*).

2-Diazocyclohexanone (**2**) has a planar Z arrangement of the diazo and carbonyl groups locked by the cyclic structure (Fig. 2). DFT calculations predict that the thermal decomposition of **2** results in a concerted Wolff rearrangement, i.e., ketene is formed directly from the diazoketone precursors without a carbene intermediate. The corresponding cyclic carbonyl carbene (**2C**) is not even a real species. Every attempt at optimization of the geometry of **2C** using the DFT, HF, or MP2 method collapsed to a ketene structure. This observation allows us to conclude that the thermal Wolff rearrangement of **2** is a truly concerted process. However, it is interesting to note that the geometry of the diazocarbonyl fragment in the transition state $\mathbf{2}^{\ddagger}$ is surprisingly similar to that of $\mathbf{1}_Z^{\ddagger}$ (Fig. 2). The carbonyl group valence angle is 105°, while the dihedral angle between the carbonyl group and carbene planes is 56°. In other words, the geometry of the transition state for the concerted Wolff rearrangement of **2** is very close to that of a free α-carbonyl carbene. The electronic energies and representative structural parameters for **2** and the transition state for the concerted Wolff rearrangement $\mathbf{2}^{\ddagger}$ are shown in Fig. 2.

The potential energy diagrams for the decomposition of **3** and **4** were reported previously (25*b*). The loss of nitrogen from any of the three conformers of **3** results in the formation of biscarbomethoxycarbene. As in the case of **1** (vide supra), we were unable to locate a transition state for the concerted Wolff rearrangement of **3**. For the cyclic isopropylidene diazomalonate **4**, on the other hand, the concerted Wolff rearrangement is the preferred decomposition pathway. The results of quantum mechanical calculations agree well with experimental data on photolysis and thermolysis of **3** and **4** mentioned in the Introduction (22–25).

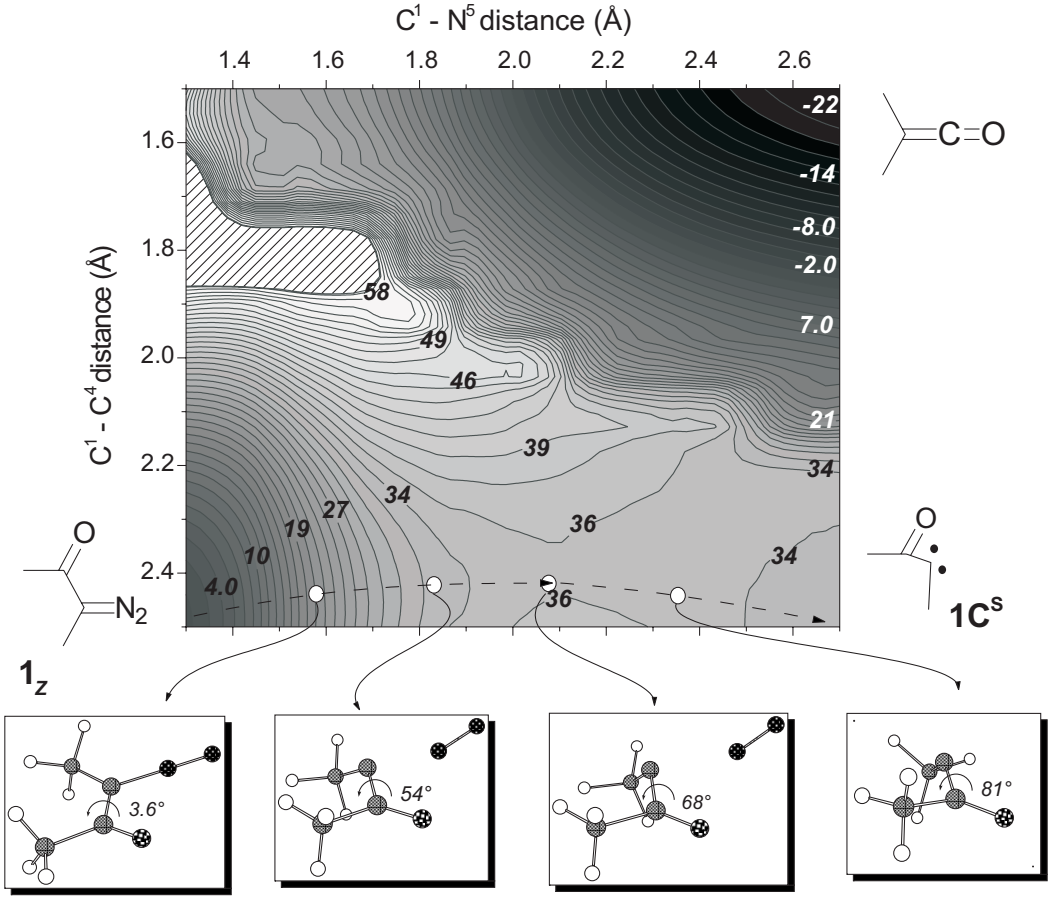
Potential energy surface (PES) scans

To analyze the effect of structural factors on the thermal decomposition of diazoketones, 3-D relaxed PES scans for the decomposition of diazo compounds **1**–**4** were conducted at the B3LYP/6-31+G(d,p) level of theory. The distances between nitrogen and carbon (C1) atoms of the diazo group, as well as between C1 and the atom migrating in the Wolff rearrangement (C4 or O4), were fixed in steps, while other de-

[3] J. Liu, V. Popik, C.M. Hadad, and M.S. Platz. Submitted for publication.

© 2005 NRC Canada

Fig. 3. Contour plot of the potential energy surface (PES) for the extrusion of nitrogen from *Z*-3-diazobutanone ($\mathbf{1}_Z$). Values shown on the isoergic lines represent the relative energy in kcal mol^{-1} (referenced to the starting diazo compound $\mathbf{1}_Z$). Structures shown under the PES plot represent optimized geometries of the system corresponding to the PES coordinates marked with empty circles.



grees of freedom were fully optimized. The bottom left corner of the contour plots correspond to the energy of the initial diazocarbonyl compound (**1**, **2**, **3**, or **4**). The extension of the C1—N bond without explicitly changing the C1—C4 (C1—O4 for **3** and **4**) distance leads to the formation of an α-carbonyl carbene (bottom right corner), while the elongation of the C1—N bond accompanied by the shortening of the C1—C4 distance leads to a ketene (upper right corner, Figs. 3–6).

The analysis of the PES plots for decomposition of the α-diazocarbonyl compounds **1**–**4**, shown in Figs. 3–6, allows us to conclude that the synchronous Wolff rearrangement is an unfavorable process for all of these substrates. Simultaneous cleavage of the C1—N bond and the migration of the substituent (C4 or O4) result in a steep rise in energy. The extrusion of nitrogen from diazo compounds **1**–**4** initially proceeds by the elongation of the C1—N bond only, while the C1—C4 (C1—O4) distance remains virtually unchanged. During this initial stage of decomposition, the carbon atom of the diazo group (C1) moves out of the plane of the carbonyl group (or groups). The changes in geometry of α-diazocarbonyl compounds **1**–**4** along the reaction path are illustrated by structures shown in Figs. 3–6.

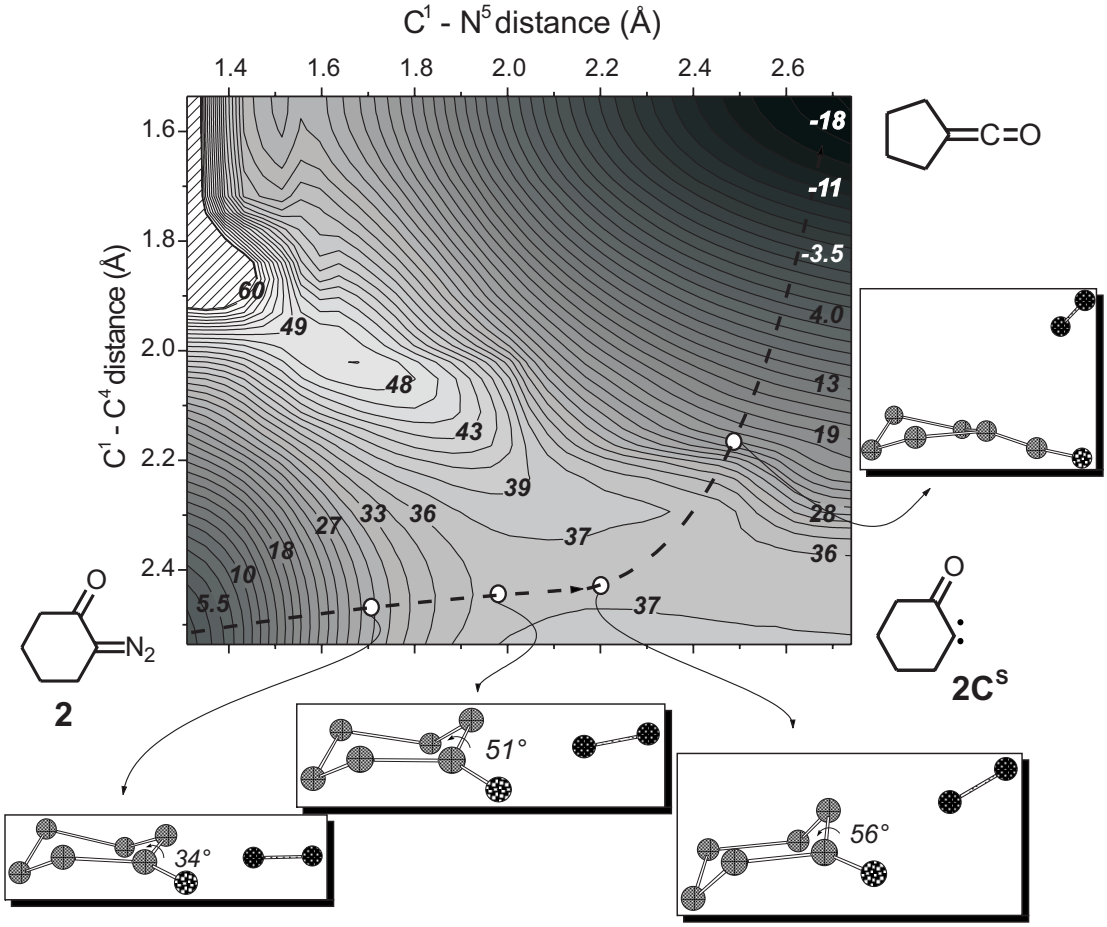
The valley on the PES follows the elongation of the C1—N bond, eventually reaching the energy plateau at ca. 2.1–2.3 Å. In the plateau region of the PES, even significant changes in C1—N and C1—C4 (C1—O4) distances cause very little variation in energy. Transition states for both the concerted and stepwise Wolff rearrangement are located on this plateau and possess very similar geometries, which resemble that of an α-carbonyl carbene. Gradients felt by the system on the energy plateau define the outcome of the reaction, i.e., formation of the carbene or rearrangement to the ketene.

The PES plot for the decomposition of the Z conformer of 3-diazobutanone **1** shows that the energy plateau is reached comparatively early, at a C1—N distance of ca. 2.1 Å (Fig. 3). The dihedral angle between the carbonyl group and the C2-C1-C3 plane in this region is ca. 70°, which is very close to the geometry of the singlet acetylmethyl carbene ($\mathbf{1C}^{\mathbf{S}}$). There are downhill gradients leading from the plateau on the PES in the direction of the carbene $\mathbf{1C}^{\mathbf{S}}$ formation and the migration of C4. In other words, the landscape of the PES suggests the possibility of both a concerted Wolff rearrangement and an α-carbonyl carbene formation. However, the full saddle point optimization (opt = ts) of several geometries on this plateau converged to the same structure, i.e., the transition state for the carbene formation $\mathbf{1}_Z^{\ddagger}$ (vide supra).

The energy plateau on the PES for the dediazotization of **2** is also reached at a C1—N distance of ca. 2.1 Å (Fig. 4).

© 2005 NRC Canada

Fig. 4. Contour plot of the potential energy surface (PES) for the extrusion of nitrogen from 2-diazocyclohexanone (**2**). Values shown on the isoergic lines represent the relative energy in kcal mol^{-1} (referenced to **2**). Structures shown under the PES plot represent optimized geometries of the system corresponding to the PES coordinates marked with empty circles.



However, the deviation of C1 from planarity is substantially smaller, i.e., 51°–56°, apparently because of structural constraints. The only downhill gradient evident from the PES plot leads to the migration of the substituent C4 and the formation of the ketene. Therefore, the thermal Wolff rearrangement of **2** is predicted to be a concerted reaction. In fact, there is no energy minimum corresponding to the singlet carbonyl carbene **2C^S** (vide supra). In our opinion, this phenomenon stems from the inability of cyclic carbene **2C^S** to adopt a stable orthogonal conformation.

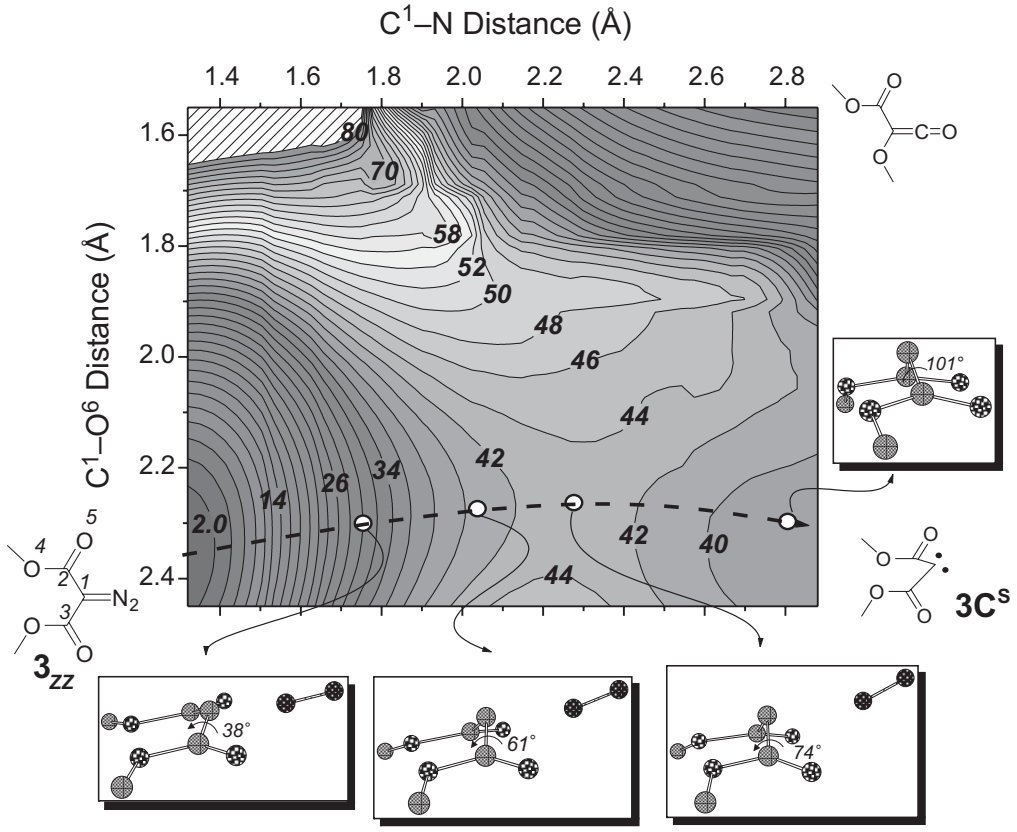
The landscape of PES surrounding methyl diazomalonate **3** (Fig. 5) is very similar to that of diazo ketone **1**. The extrusion of nitrogen from **3** initially proceeds by the elongation of the C1—N bond, while the C1—O4 distance remains virtually unchanged. This process is also accompanied by the shift of the carbon atom of the diazo group (C1) up from the plane of carbonyl groups reaching a dihedral angle of 74°. The energy plateau, however, is reached somewhat later, at a C1—N distance of ca. 2.25 Å, and lies higher in energy by ca. 8 kcal mol^{-1} more than in the case of **1**. This observation can be explained by the reduced ability of the ester carbonyl groups to participate in the resonance stabilization of the emerging carbene. There is a substantial downhill gradient leading the system from the high energy plateau towards the formation of biscarbomethoxycarbene **3C^S**, while the migration of the substituent (O4) is still an uphill process. The elongation of the C1—N bond beyond 2.3 Å in methyl diazomalonate **3** is, therefore, accompanied by an increase in the dihedral angle between the C3-C1-C2 plane and planes of carbonyl groups and results in an energy reduction, leading the system to the formation of a carbene (Fig. 5).

The energy plateau on the PES for the dediazotization of **4** is reached even later, at a C1—N distance of 2.45 Å and is ca. 16 kcal mol^{-1} higher than in the case of diazocyclohexanone **2** (Fig. 6). This increased energy barrier agrees well with the high thermal stability of this compound. The high activation energy of the thermal decomposition reaction is apparently due to both a reduced resonance stabilization of the emerging occupied orbital of carbene and structural rigidity, which does not allow **4** to achieve orthogonal conformation. In fact, the dihedral angle between the C2-C1-C3 plane and the carbonyl groups never extends above 60° at any point on this PES.

As a result, the elongation of the C1—N bond beyond 2.45 Å requires additional energy, while the migration of a substituent from that point on the PES is an exoergic process. In other words, **4** is predicted to undergo a concerted Wolff Rearrangement.

© 2005 NRC Canada

Fig. 5. Contour plot of the potential energy surface (PES) for the extrusion of nitrogen from the Z,Z conformer of methyl diazomalonate (**3**). Values shown on the isoergic lines represent the relative energy in kcal mol^{-1} (referenced to $\mathbf{3}_{ZZ}$). Structures shown under the PES plot represent optimized geometries of the system corresponding to the PES coordinates marked with empty circles.



In contrast with diazocyclohexanone **2**, the carbene **4C^S**, which can be produced from the cyclic diazomalonate **4**, is predicted to be a real intermediate by DFT calculations (21). There is an energy minimum on the PES corresponding to **4C^S**, and this structure has no imaginary frequencies. The energy well for this cyclic singlet dicarbonyl carbene is very shallow, and there's virtually no barrier ($\Delta E^{\ddagger} < 1$ kcal mol^{-1}) for the rearrangement to ketene (21). In addition, the energy of **4C^S** is higher than the energy of the transition state for the concerted Wolff rearrangement of **4**.

Conclusions

Analysis of the PES for the decomposition of four diazocarbonyl compounds — two cyclic structures with locked Z (**2**) and Z,Z (**4**), and Z (**1**) and Z,Z (**3**) conformers of their acyclic analogs — allows us to conclude that the outcome of the dediazotization reaction, i.e., the concerted Wolff rearrangement or formation of an α-carbonyl carbene, is defined by the structural constraints of the molecule. Both processes start by the extension of the C1—N bond accompanied by the out-of-plane shift of C1 until the system reaches the energy plateau at a C1—N distance in the 2.1–2.45 Å range. The direction of further transformation depends on the relative stability of the corresponding carbonyl carbene. Relatively deep energy wells correspond to carbenes produced from acyclic diazocarbonyl compounds (**1** and **3**), since they adopt an orthogonal conformation, which allows for a stabilizing conjugation of the π system of the carbonyl group with the lone pair of a singlet carbene. In cyclic diazocarbonyl compounds, such as **2** and **4**, carbenes are much higher in energy because they are unable to attain a stabilizing orthogonal conformation. Migration of the substituent, i.e., concerted Wolff rearrangement, becomes the only downhill process.

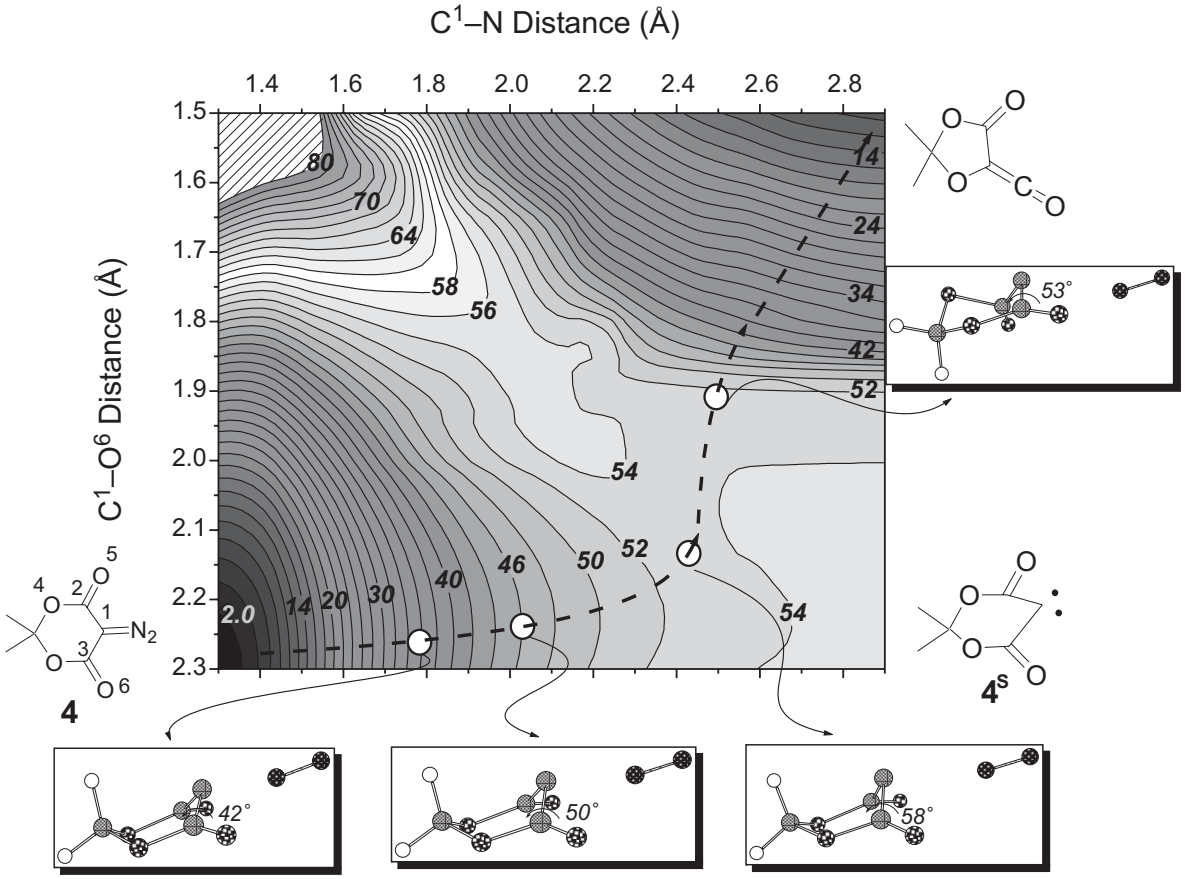
Experimental section

Theoretical procedures

Quantum mechanical calculations were carried out using the GAUSSIAN 98 suit of programs (26). Levels of theory examined ranged from the hybrid B3LYP (27) DFT calculations with the 6-31+G(d,p) (28) basis sets to the high-level composition procedure MP2(full)/aug-cc-pVTZ//B3LYP/6-311+G(3df,2p). For all the DFT calculations, zero-point vibrational energy (ZPVE) corrections, required to correct the raw relative energies to 0 K, were obtained from the B3LYP/6-31+G(d,p) method. Analytical second derivatives were computed to confirm each stationary point to be a minimum by yielding zero imaginary vibrational frequencies for the intermediates and one imaginary vibrational frequency for each transition state. The vibrational frequencies were scaled by 0.9772 (29). Initial geometry optimization, IRC calculations for transition states, and relaxed scans of poten-

© 2005 NRC Canada

Fig. 6. Contour plot of the potential energy surface (PES) for the extrusion of nitrogen from diazo Meldrum's acid (**4**). Values shown on the isoergic lines represent the relative energy in kcal mol^{-1} (referenced to **4**). Structures shown under the PES plot represent optimized geometries of the system corresponding to the PES coordinates marked with empty circles.



tial energy surfaces were conducted at the B3LYP/6-31+G(d,p) level. In the PES scans, the C1—C4 (or O4) and C1—N coordinates were fixed in steps, while the other degrees of freedom were fully optimized. Each of the four potential energy surfaces consisted of about 160 points corresponding to different values of C1—C4 (or O4) and C1—N distances.

Acknowledgment

We are grateful to the National Institutes of Health for partial support of this project (NIH R15 CA91856-01A1).

References

1. W. Kirmse. Eur. J. Org. Chem. 2193 (2002).
2. (*a*) H. Meier and K.-P. Zeller. Angew. Chem. Int. Ed. Engl. **14**, 32 (1974); (*b*) M. Regitz and G. Maas. Diazo compounds. Academic Press, Orlando, Fla. 1986; (*c*) T. Ye and A.M. McKervey. Chem. Rev. **94**, 1091 (1994); (*d*) M.P. Doyle, M.A. McKervey, and T. Ye. Modern catalytic methods for organic synthesis with diazo compounds. Wiley-Interscience, New York. 1998. pp. 487–534; (*e*) K.-P. Zeller, H. Meier, and E. Muller. Tetrahedron, **28**, 5831 (1972).
3. (*a*) J.L. Wang, I.R. Likhtvorik, and M.S. Platz. J. Am. Chem. Soc. **121**, 2883 (1999); (*b*) I.R. Likhtvorik, Z. Zhu, E.L. Tae, E. Tippmann, B.T. Hill, and M.S. Platz. J. Am. Chem. Soc. **123**, 6061 (2001).
4. A.P. Scott, M.S. Platz, and L. Radom. J. Am. Chem. Soc. **123**, 6069 (2001), and refs. cited therein.
5. (*a*) R.J. McMahon, O.L. Chapman, R.A. Hayes, T.C. Hess, and H.-P. Krimmer. J. Am. Chem. Soc. **107**, 7597 (1985); (*b*) J.J. Novoa, J.J.W. McDouall, and M.A. Robb. J. Chem. Soc. Faraday Trans. 2, **83**, 1629 (1987).
6. (*a*) J.P. Toscano. *In* Advances in carbene chemistry. Vol. 2. *Edited by* U.H. Brinker. JAI Press, Greenwich, Conn. 1998. pp. 216–245; (*b*) M. Jones and R.A. Moss. Carbenes. Wiley, New York. 1973; (*c*) H. Zollinger. Diazo chemistry II. VCH Publishers, New York. 1995. pp. 305–357; (*d*) W. Kirmse. *In* Advances in carbene chemistry. *Edited by* U.H. Brinker. JAI Press Inc., Greenwich, Conn. 1994. pp. 1–57; (*e*) D.J. Miller and C.J. Moody. Tetrahedron, **40**, 10811 (1995).
7. T.T. Tidwell. Ketenes. Wiley, New York. 1976. pp. 84–100.
8. A.J. Kresge. Chem. Soc. Rev. **25**, 275 (1996).
9. (*a*) E. Lewars. Can. J. Chem. **78**, 297 (2000), and refs. cited therein; (*b*) K.S. Sung. Can. J. Chem. **78**, 562 (2000); (*c*) G. Vacek, J.M. Galbraith, Y. Yamaguchi, H.F. Schaefer, R.H. Nobes, A.P. Scott, and L. Radom. J. Phys. Chem. **98**, 8660 (1994); (*d*) R.H. Nobes, H.F. Schaefer III, and L. Radom. J. Am. Chem. Soc. **116**, 10159 (1994); (*e*) E.G. Lewars. Chem.

© 2005 NRC Canada

Rev. **83**, 519 (1983); (*f*) M. Torres, E.M. Lown, H.E. Gunning, and O.P. Strausz. Pure Appl. Chem. **52**, 1623 (1980); (*g*) H. Tomioka, H. Okuno, S. Kondo, and Y. Izawa. J. Am. Chem. Soc. **102**, 7123 (1980); (*h*) K.-P. Zeller. Angew. Chem. Int. Ed. Engl. **16**, 781 (1977).

10. (*a*) I.G. Csizmadia, J. Font, and O.P. Strausz. J. Am. Chem. Soc. **90**, 7360 (1968); (*b*) J. Fenwick, G. Frater, K. Ogi, and O.P. Strausz. J. Am. Chem. Soc. **95**, 124 (1973); (*c*) K.-P. Zeller. Angew. Chem. Int. Ed. Engl. **16**, 781 (1977); (*d*) K.-P. Zeller. Liebigs. Ann. Chem. 2036 (1979); (*e*) H. Schwarz. Angew. Chem. **99**, 153 (1987).
11. U. Timm, K.-P. Zeller, and H. Meier. Tetrahedron, **33**, 453 (1977).
12. (*a*) L. Horner, I.K. Korobitsyna, L.L. Rodina, and T.P. Sushko. Zh. Org. Khim. **4**, 175 (1968); (*b*) U. Timm, K.-P. Zeller, and H. Meier. Tetrahedron, **33**, 453 (1977); (*c*) H. Tomioka, H. Okuno, and Y. Izawa. J. Org. Chem. **45**, 5278 (1980); (*d*) H. Rau and M. Bokel. J. Photochem. Photobiol. A, **53**, 311 (1990); (*e*) L.M. Hadel, V.M. Maloney, M.S. Platz, W.G. McGimpsey, and J.C. Scaiano. J. Phys. Chem. **90**, 2488 (1986); (*f*) H. Tomioka, K. Hirai, K. Tabayashi, and S. Murata. J. Am. Chem. Soc. **112**, 7692 (1990); (*g*) Y. Chiang, A.J. Kresge, P. Pruszynski, N.P. Schepp, and J. Wirz. Angew. Chem. Int. Ed. Engl. **30**, 1366 (1990); (*h*) A.B. Charette, R.P. Wurz, and T. Ollevier. Helv. Chim. Acta, **85**, 4468 (2002); (*i*) E. Tippmann, G. Holinga, and M.S. Platz. Org. Lett. **5**, 4919 (2003).
13. F. Kaplan and M.L. Mitchell. Tetrahedron Lett. **9**, 759 (1979).
14. (*a*) F. Kaplan and G.K. Meloy. Tetrahedron Lett. 2427 (1964); (*b*) F. Kaplan and G.K. Meloy. J. Am. Chem. Soc. **88**, 950 (1966); (*c*) H. Kessler and D. Rosenthal. Tetrahedron Lett. 393 (1973); (*d*) R. Curci, F. DiFuria, and V. Lucchini. Spectrosc. Lett. **7**, 211 (1974); (*e*) R.L. Lichter, P.R. Srinivasan, A.B. Smith III, R.K. Dieter, and C.T. Denny. Chem. Commun. 366 (1977); (*f*) F.L. Dickert, F.M. Soliman, and H.J. Bestmann. Tetrahedron Lett. **23**, 2639 (1982).
15. (*a*) V.A. Nikolaev, L.L. Rodina, and I.K. Korobitsyna. Zh. Org. Khim. **10**, 1555 (1974); (*b*) W. Lauer, V. Krause, H. Wengenroth, and H. Meier. Chem. Ber. **121**, 465 (1988); (*c*) V.A. Nikolaev and V.V. Popik. Zh. Org. Khim. **25**, 1014 (1989).
16. (*a*) S. Sorriso. *In* The chemistry of diazonium and diazo groups. *Edited by* S. Patai. Wiley, Chichester. 1978. pp. 95–136; (*b*) J.M. Goodman, J.J. James, and A. Whiting. J. Chem. Soc. Perkin Trans. 2, 109 (1994).
17. (*a*) H. Tomioka, H. Okuno, and Y. Izawa. J. Org. Chem. **45**, 5278 (1980); (*b*) H. Tomioka, M. Kondo, and Y. Izawa. J. Org. Chem. **46**, 1090 (1981); (*c*) C. Marfisi, P. Verlaque, G. Davidovics, J. Pourcin, L. Pizzala, J.-P. Aycard, and H. Bodot. J. Org. Chem. **48**, 533 (1983); (*d*) M. Tsuda, S. Oikawa, and K. Nagayama. Chem. Pharm. Bull. **35**, 1 (1987); (*e*) M. Tsuda and S. Oikawa. Chem. Pharm. Bull. **37**, 573 (1989); (*f*) M. Torres, R.K. Gosavi, E.M. Lown, E.J. Piotrkowski, B. Kim, J.L. Bourdelande, J. Font, and O.P. Strausz. Stud. Phys. Theor. Chem. **77**, 184 (1992); (*g*) J.P. Toscano, M.S. Platz, V. Nikolaev, and V. Popik. J. Am. Chem. Soc. **116**, 8146 (1994).
18. K.-P. Zeller. Chem. Ber. **112**, 678 (1979); J. Fenwick, G. Frater, K. Ogi, and O.P. Strausz. J. Am. Chem. Soc. **95**, 124 (1973); M. Torres, J. Ribo, A. Clement, and O.P. Strausz. Can. J. Chem. **61**, 996 (1983).
19. (*a*) C. Wentrup and H. Dahn. Helv. Chim. Acta, **53**, 1637 (1970); (*b*) S. Sorriso and A. Foffani. J. Chem. Soc. Perkin Trans. 2, 2142 (1973).
20. C. Bachmann, T.Y. N'Guessan, F. Debu, M. Monnier, J. Pourcin, J.-P. Aycard, and H. Bodo. J. Am. Chem. Soc. **112**, 7488 (1990), and refs. cited therein.
21. A. Bogdanova and V.V. Popik. J. Am. Chem. Soc. **125**, 14153 (2003).
22. (*a*) V.A. Nikolaev, N.N. Khimich, and I.K. Korobitsyna. Khim. Geterotsikl. Soedin. 321 (1985); (*b*) T. Lippert, A. Koskelo, and P.O. Stoutland. J. Am. Chem. Soc. **118**, 1551 (1996); (*c*) M.A. Winnik, F. Wang, T. Nivaggioli, Z. Hruska, H. Fukumura, and H. Masuhara. J. Am. Chem. Soc. **113**, 9702 (1991); (*d*) R.V. Stevens, G.S. Bisacchi, L. Goldsmith, and C.E. Strouse. J. Org. Chem. **45**, 2708 (1980); (*e*) S.L. Kammula, H.L. Tracer, P.B. Shelvin, and M. Jones, Jr. J. Org. Chem. **42**, 2931 (1977).
23. (*a*) J.-L. Wang, J.P. Toscano, M.S. Platz, V. Nikolaev, and V.V. Popik. J. Am. Chem. Soc. **117**, 5477 (1995); (*b*) M. Jones, Jr., W. Ando, M.E. Hendrick, A. Kulczucki, P.M. Howley, K.F. Hummel, and D.S. Malament. J. Am. Chem. Soc. **94**, 7469 (1972); (*c*) A. Bogdanova and V.V. Popik. J. Am. Chem. Soc. **126**, 11293 (2004).
24. In the absence of trapping reagent, e.g., in cryogenic matrix or in the gas phase, dicarbalkoxycarbene can undergo Wolff rearrangement: P. Visser, R. Zuhse, M.W. Wong, and C. Wentrup. J. Am. Chem. Soc. **118**, 12598 (1996).
25. A.P. Scott, M.S. Platz, and L. Radom. J. Am. Chem. Soc. **123**, 6069 (2001), and refs. cited therein.
26. GAUSSIAN 98 [computer program]. M.J. Frisch, G.W. Trucks, H.B. Schlegel, G.E. Scuseria, M.A. Robb, J.R. Cheeseman, V.G. Zakrzewski, J.A. Montgomery, Jr., R.E. Stratmann, J.C. Burant, S. Dapprich, J.M. Millam, A.D. Daniels, K.N. Kudin, M.C. Strain, O. Farkas, J. Tomasi, V. Barone, M. Cossi, R. Cammi, B. Mennucci, C. Pomelli, C. Adamo, S. Clifford, J. Ochterski, G.A. Petersson, P.Y. Ayala, Q. Cui, K. Morokuma, P. Salvador, J.J. Dannenberg, D.K. Malick, A.D. Rabuck, K. Raghavachari, J.B. Foresman, J. Cioslowski, J.V. Ortiz, A.G. Baboul, B.B. Stefanov, G. Liu, A. Liashenko, P. Piskorz, I. Komaromi, R. Gomperts, R.L. Martin, D.J. Fox, T. Keith, M.A. Al-Laham, C.Y. Peng, A. Nanayakkara, M. Challacombe, P.M.W. Gill, B. Johnson, W. Chen, M.W. Wong, J.L. Andres, C. Gonzalez, M. Head-Gordon, E.S. Replogle, and J.A. Pople. Gaussian, Inc., Pittsburgh, Penn. 2001.
27. A.D. Becke. J. Chem. Phys. **98**, 5648 (1993).
28. W.J. Hehre, L. Radom, P.v.R. Schleyer, and J.A. Pople. Ab initio molecular orbital theory. Wiley, New York. 1986.
29. A.P. Scott and L. Radom. J. Phys. Chem. **100**, 16 502 (1996).

© 2005 NRC Canada

REVIEW / SYNTHÈSE

A comparison of the mechanisms of hydrolysis of benzimidates, esters, and amides in sulfuric acid media[1,2]

Robin A. Cox

Abstract: The mechanisms given in textbooks for both ester and amide hydrolysis in acid media are in need of revision. To illustrate this, benzimidates were chosen as model compounds for oxygen protonated benzamides. In aqueous sulfuric acid media they hydrolyze either by a mechanism involving attack of two water molecules at the carbonyl carbon to give a neutral tetrahedral intermediate directly, as in ester hydrolysis, or by an S_N2 attack of two water molecules at the alkyl group of the alkoxy oxygen to form the corresponding amide, or by both mechanisms, depending on the structure of the benzimidate. The major line of evidence leading to these conclusions is the behavior of the excess acidity plots resulting from the rate constants obtained for the hydrolyses as functions of acid concentration and temperature. The first of these mechanisms is in fact very similar to one found for the hydrolysis of benzamides, as inferred from: (1) similar excess acidity plot behaviour; and (2) the observed solvent isotope effects for amide hydrolysis, which are fully consistent with the involvement of two water molecules, but not with one or with three (or more). This mechanism starts out as essentially the same one as that found for ester hydrolysis under the same conditions. Differences arise because the neutral tetrahedral intermediate, formed directly as a result of the protonated substrate being attacked by two water molecules (not one), possesses an easily protonated nitrogen in the amide and benzimidate cases, explaining both the lack of ^{18}O exchange observed for amide hydrolysis and the irreversibility of the reaction. Protonated tetrahedral intermediates are too unstable to exist in the reaction media; in fact, protonation of an sp^3 hybridized oxygen to put a full positive charge on it is extremely difficult. (This means that individual protonated alcohol or ether species are unlikely to exist in these media either.) Thus, the reaction of the intermediate going to product or exchanged reactant is a general-acid-catalyzed process for esters. For amide hydrolysis, the situation is complicated by the fact that another, different, mechanism takes over in more strongly acidic media, according to the excess acidity plots. Some possibilities for this are given.

Key words: esters, amides, benzimidates, hydrolysis, excess acidity, mechanism, acid media.

Résumé : Les mécanismes donnés dans les manuels de chimie pour les hydrolyses tant des esters que des amides en milieu acide demandent à être révisés. Pour illustrer ce point, on a choisi les benzimidates comme composés modèles de benzamides protonés à l'oxygène. Dans des milieux contenant de l'acide sulfurique aqueux, suivant la nature du benzimidate, ils s'hydrolysent soit par un mécanisme impliquant une attaque de deux molécules d'eau au niveau du carbone portant le groupe carbonyle et ils conduisent directement à la formation d'un intermédiaire tétraédrique neutre, tel que dans le cas des hydrolyses d'esters, soit par une attaque S_N2 de deux molécules d'eau au niveau du groupe alkyle de l'oxygène alkoxy pour former l'amide correspondant ou par une combinaison des deux mécanismes. La principale ligne de signes conduisant à ces conclusions est le comportement des courbes d'excès d'acidité qui résultent des constantes de vitesse obtenues pour les hydrolyses en fonctions de la concentration de l'acide et de la température. Le premier de ces mécanismes est en fait très semblable à celui qu'on retrouve pour les benzamides, tel qu'on peut en déduire sur la base (1) de comportement semblable de la courbe d'excès d'acidité et (2) les effets isotopiques de solvant observés pour l'hydrolyse de l'amide qui est pleinement en accord avec une implication de deux molécules d'eau, mais pas avec une ou avec trois ou plus. Ce mécanisme débute essentiellement de la même manière que celui observé pour l'hydrolyse des esters dans les mêmes conditions. Les différences apparaissent parce que l'intermédiaire tétraédrique

Received 18 March 2005. Published on the NRC Research Press Web site at http://canjchem.nrc.ca on 1 November 2005.

Dedicated to the future progress of physical organic chemistry in Canada.

R.A. Cox. 16 Guild Hall Drive, Scarborough, ON M1R 3Z8, Canada. (e-mail: robin.a.cox@sympatico.ca).

[1]This article is part of a Special Issue dedicated to organic reaction mechanisms.
[2]Part 27 of the series "Mechanistic studies in strong acids" of which part 26 is ref. 28.

 doi: 10.1139/V05-142 © 2005 NRC Canada

neutre, qui se forme directement par une attaque du substrat protoné par deux (pas une) molécules d'eau, comporte dans les cas de l'amide et du benzimidate, un azote qui peut facilement être protoné et ceci explique le fait que, lors de l'hydrolyse de l'amide, il n'y a pas d'échange de ^{18}O et que la réaction est irréversible. Les intermédiaires tétraédriques protonés sont trop instables pour exister dans le milieu réactionnel; en fait, la protonation d'un atome d'oxygène à hybridation sp^3 pour y placer une charge positive complète est extrêmement difficile. (Ceci signifie qu'il est peu probable que les espèces alcool ou éther protonées individuelles puissent exister dans ces milieux). Pour les esters, la réaction de l'intermédiaire conduisant au produit ou au réactif ayant subi un échange est donc un processus soumis à une catalyse acide générale. Pour l'hydrolyse des amides, la situation est compliquée par le fait que, en milieux fortement acides, selon les courbes d'excès d'acidité, un autre mécanisme, différent, prendrait le pas. On donne quelques possibilités pour ceci.

Mots clés : esters, amides, benzimidates, hydrolyse, acidité en excès, mécanisme, milieu acide.

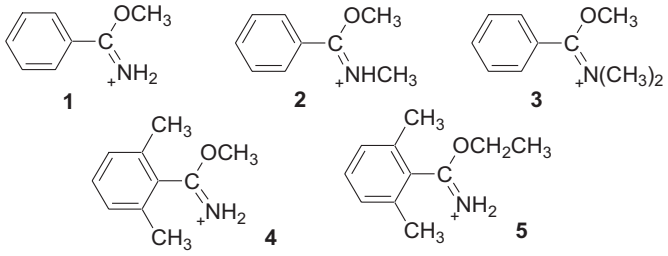
[Traduit par la Rédaction]

Introduction

The excess acidity method for dealing with experimental data obtained as a function of acid concentration in acid media (1, 2) has shown itself to be a very useful way of obtaining information regarding the mechanisms of reactions that take place in these solutions, as well as providing standard-state pK_{BH+} and $\log k_0$ values, and $\Delta H^{\ddagger}$ and $\Delta S^{\ddagger}$ values if data at different temperatures are available, which can be directly compared with one another and with values obtained for other reactions in aqueous and buffer media (2). Particularly for A2 reactions, the water activities in these media are often also needed (2), and it has recently been found that the values used historically for delineating reaction mechanisms in these media are the wrong ones, being mol-fraction-based values and thus having a different standard state from the molarities used for C_{H+} and the other concentrations (2). (This means that Bunnett *w* values (3) and Yates *r* values (4) listed in the literature are wrong, but these treatments are superceded by the excess acidity treatment anyway.) It has recently been found (2) that using the correct water activities makes no difference to the mechanism long since (5) deduced for ester hydrolysis in relatively dilute acids (up to a water:acid ratio of 1:1, which is 84.48 wt% for sulfuric acid) (5, 6). This is given in Scheme 1, and involves the participation of two water molecules with the protonated substrate in the rate-determining step to give a neutral tetrahedral intermediate directly (despite what is said in almost every introductory organic chemistry text (7), shown at the upper right in Scheme 1).

The Scheme 1 mechanism for esters is now widely accepted; in fact, a recent isotope effect study of the hydrolysis of methyl formate in dil. aq. HCl media has allowed delineation of the bond-making and bond-breaking processes in some detail (8). Recent theoretical calculations are also in agreement (9).

For amides, it had been thought that three (4, 10), or three and then one (11) water molecules were involved in the hydrolysis; but in contrast to the ester case, use of the correct water activity values does make a difference to the analysis (2), the correct number more likely being two (2). To clarify this situation, and because a previous analysis of lactam hydrolysis also used incorrect water activities and was inconclusive anyway (12), it was decided to reanalyze some rate constant results obtained for the hydrolysis of benzimidates in aqueous sulfuric acid media (13–15). Benzimidates are model compounds for oxygen protonated amides, the most likely protonated intermediates involved in amide hydrolysis (11). The compounds studied were **1**–**3**, in the case of **2** and **3** as their BF_4^- salts (13, 14), and **4** and **5** (15), for which rate constant data as functions of both acid concentration and temperature were available.



Results

Hydrolysis rate constants (k_ψ) as a function of acid concentration and temperature for **1**–**3** are taken from Smith and Yates (13, 14) and for **4** and **5** from McClelland (15). Values of the excess acidity *X* and correct water activities (a_{Nu}) were those used before (2). Recently, a new set of measurements of bisulfate ion concentration as a function of acid concentration and temperature in the sulfuric acid medium has become available (16); this was added to the computer program used to calculate concentrations and activities (2), but was not needed for this work.

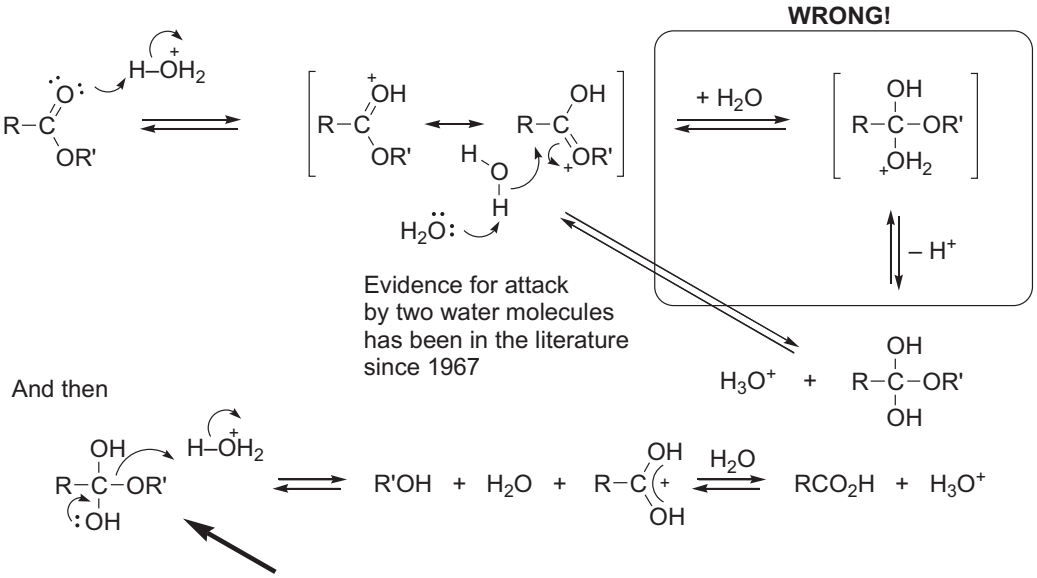
$$[1] \qquad \log k_\psi = \log k_0 + (m^{\ddagger} - 1)m^*X + \log a_{Nu}$$

$$[2] \qquad \log k_0 = 10.31883 + \log T - (\Delta G^{\ddagger}/RT \ln 10) + (\Delta H^{\ddagger}/RT \ln 10)((T - \theta)/T)$$

The excess acidity rate equation that applies here, since the substrates already contain a full positive charge, is eq. [1] (2), with the nucleophile (Nu) being water; k_0 is the rate constant for the reaction in the standard state, infinite dilution in a hypothetical ideal 1 mol/L acid solution. The parameters m^* and $m^{\ddagger}$ are slope parameters applying to the transition state ($m^{\ddagger}$) (and the protonated substrate (m^*), irrelevant here). Since rate constants at several temperatures were available, $\log k_0$ was expanded according to the Clarke and Glew (17) formulation of eq. [2] (which I find preferable to the usual Eyring expansion (18), giving better numbers with the correct errors). The numerical term contains

© 2005 NRC Canada

Scheme 1.

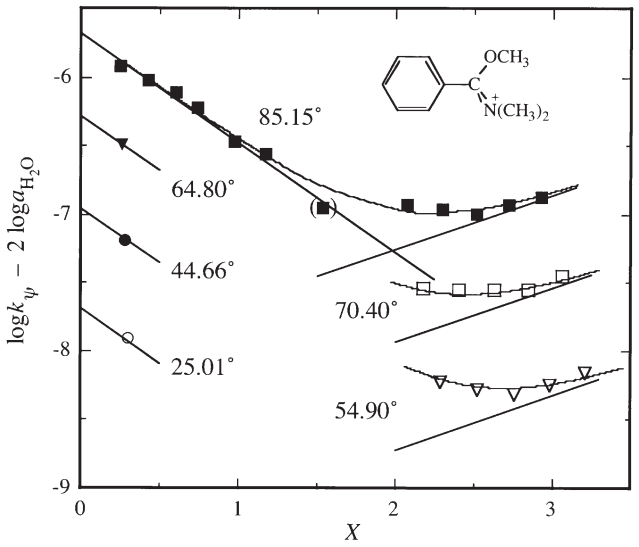


the Planck and Boltzmann constants (18), R is the gas constant (1.985 89 here), T the absolute temperature, and θ is the reference temperature of 298.15 K, 25 °C, at which the activation parameters are valid (17). The entropies of activation ($\Delta S^{\ddagger}$) are easily obtained from the free energies and enthalpies of activation, $\Delta G^{\ddagger}$ and $\Delta H^{\ddagger}$.

Using all of the experimental data simultaneously results in a triple linear regression with the variables being X, $\log a_{H_2O}$, and $((T - \theta)/T)$. When this is carried out for **1**, the slope against the water activity, the number of water molecules kinetically involved in the reaction (which I will continue to call r) calculates to 1.92 ± 0.16. For **4**, for which fewer, more error-prone, experimental data are available, r calculates to 2.55 ± 0.26. The slopes against X are quite different, being negative for **1** and positive for **4**, indicating different mechanisms. The situation is more complex for **2** and **3**, which react by both mechanisms, and the data require curve-fitting. There are too few data points available for **5** to give a reliable r value. Consequently, r was given the fixed value of 2.00 to simplify the computations, particularly for **2** and **3**.

The resulting excess acidity plot for **1** has already been published (Fig. 16 in ref. 2), and the plots for **3** and **4** are given here as Figs. 1 and 2. All these plots have 2 $\log a_{H_2O}$ subtracted from the y axis to be displayed as more easily understood lines. The parameters for all of the substrates reacting by the two mechanisms, $\log k_0$ values at 25 °C, excess acidity slopes, and the calculated activation parameters, are given in Table 1. The Table 1 information must be regarded as replacing similar information for some of these compounds previously given (11).

Fig. 1. Excess acidity plot against X according to eq. [1] for the hydrolysis of **3** at several temperatures, showing the two mechanisms.



Discussion

Ester hydrolysis

As shown in Scheme 1, ester hydrolysis in acidic media requires two water molecules. The reason for this is that protonated tetrahedral intermediates do not exist in these primarily aqueous media (19). They are too unstable to have finite lifetimes, and as Jencks points out, in order for a species to be a reaction intermediate, it must be capable of existing (have a finite lifetime, however short) in the reaction solution (19). In these Grötthus chain-transfer aqueous media, proton transfer takes place along hydrogen bonds, and the lifetime of any individual species with a full positive charge on an sp^3-hybridized oxygen is *really* short. As recent theoretical calculations (20) have shown, one cannot speak of individual H_3O^+ molecules as existing in these solutions at all, at least at room temperature, and the positive charge is effectively borne by the entire solvent, not by any

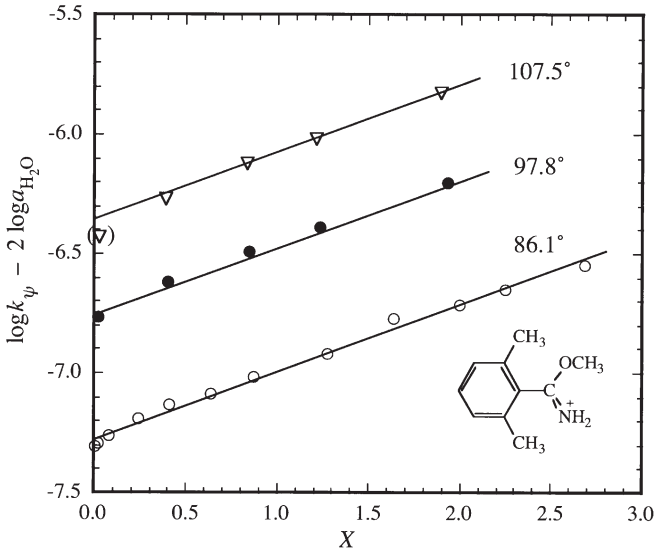
© 2005 NRC Canada

Table 1. Standard-state values at 25 °C for $\log k_0$, activation enthalpies and entropies, and excess acidity slopes, for benzimidates **1**–**5** reacting via the two mechanisms.

Compound	$\log k_0$	$\Delta H^{\ddagger}$ (kcal mol^{-1})	$\Delta S^{\ddagger}$ (cal K^{-1} mol^{-1})	$m^*(m^{\ddagger} - 1)$
A2 mechanism				
1	–7.484±0.012	19.786±0.095	–26.42±0.32	–0.3299±0.0048
2	–7.372±0.033	17.07±0.30	–35.0±1.0	–0.470±0.033
3	–7.694±0.028	15.71±0.26	–41.06±0.90	–0.797±0.039
S_N2 mechanism				
2	–10.9±1.0	28.1±3.4	–14±12	0.36±0.22
3	–11.25±0.31	25.33±0.83	–25.1±3.1	0.397±0.078
4	–10.632±0.046	26.26±0.33	–19.1±1.1	0.2823±0.0057
5	–10.857±0.075	25.88±0.57	–21.4±1.9	0.3667±0.0073

Note: The errors given are standard deviations.

Fig. 2. Excess acidity plot against X according to eq. [1] for the hydrolysis of **4** at several temperatures, showing the involvement of two water molecules.



one specific oxygen atom (20). Referring to H_3O^+ is simply a convenience.

As a consequence, the reverse reaction back to starting material, often exchanged if the reaction is performed in ^{18}O-enriched media, must be general-acid-catalyzed as shown in Scheme 1. In practice, this would be very difficult to detect, and has not been looked for.

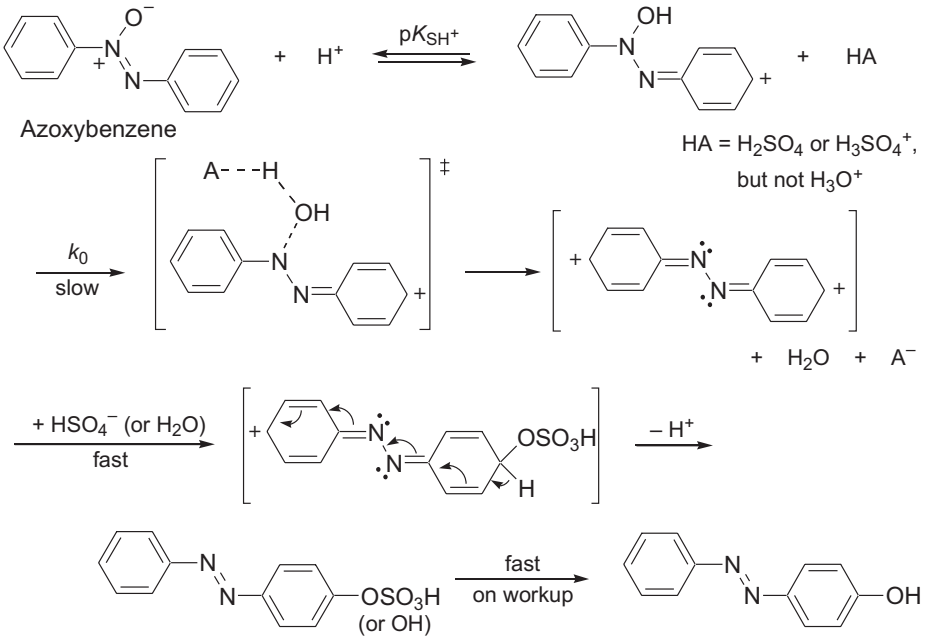
As another consequence, specific protonated alcohol molecules cannot exist in these media either. There are several reported measurements of pK_{BH}^+ values for alcohols in the literature, with reported values around –2 (21, 22). Not surprisingly, these are close to the value –1.743 taken for water, but this is a wholly artificial number, defined so as to be consistent with the definition used for weak acids in solution (23). As discussed, in aqueous acids the positive charge on what is referred to as H_3O^+ is in fact distributed into the solution as a whole (there is nothing equivalent to the "HA" of the definition as a definite species), and the same must be true of acidic alcohol solutions as well, with alcohol molecules taking the place of a quantity, up to maybe 10% for NMR studies, of the water molecules. The reported pK_{BH}^+ values are obtained from the variation of NMR chemical shifts or chemical shift differences of alcohols (proton or ^{13}C) in media of increasing acidity (21, 22), but, since the time base for NMR chemical shift measurements is in the millisecond range, the reported values cannot possibly refer to the increasing concentration of specific ROH_2^+ species but rather to the gradually increasing average positive charge on the alcohol oxygen with increasing acidity — a medium effect. This is different from the protonation of (say) esters or amides, also studied by ^{1}H NMR spectroscopy (24), where the positive charge can be delocalized internally by resonance, and one can speak of specific protonated species with finite lifetimes. It has always been a puzzle to me that I could not use the excess acidity treatment (2) to give accurate alcohol pK_{BH}^+ values, despite the existence of a great deal of very good, accurate chemical shifts as a function of acidity information, particularly for ethanol (21). I now know the reason — I should have been analyzing the spectra as a medium effect (25) and not as a protonation equilibrium. I will report further on this in the future.[3] Perhaps we will have to come up with different terminology, and not call the numbers measured for alcohols and related molecules in which the positive charge has perforce to be concentrated on a specific sp^3-hybridized oxygen with no delocalization possibilities, pK_{BH}^+ values at all.

Thus, it is highly likely that protonation of an sp^3-hybridized oxygen with no delocalization possibilities is in fact very difficult. There are hints of this in the literature. Azoxybenzene (see Scheme 2) has an entire formal negative charge on the oxygen, and the balancing positive charge on the azoxy nitrogen is delocalized into at least one and maybe both of the aromatic rings (26). One might think that protonation of this oxygen should be easy, but such is not the case, the molecule having a pK_{BH}^+ of –5.15 (half-protonated in 70% H_2SO_4) (26). The second protonation of this oxygen, required for the Wallach rearrangement of azoxybenzene (27, 28) (Scheme 2), is not an equilibrium process but rather requires general acid catalysis by H_2SO_4 or $H_3SO_4^+$, H_3O^+ not being a strong enough acid to catalyze the reaction at all (29). The formal O^- of nitro groups does not protonate before the superacid acidity region (30). The reported "pK_{BH}^+" values of ethers in the –1 to –2 range (31) could be taken to

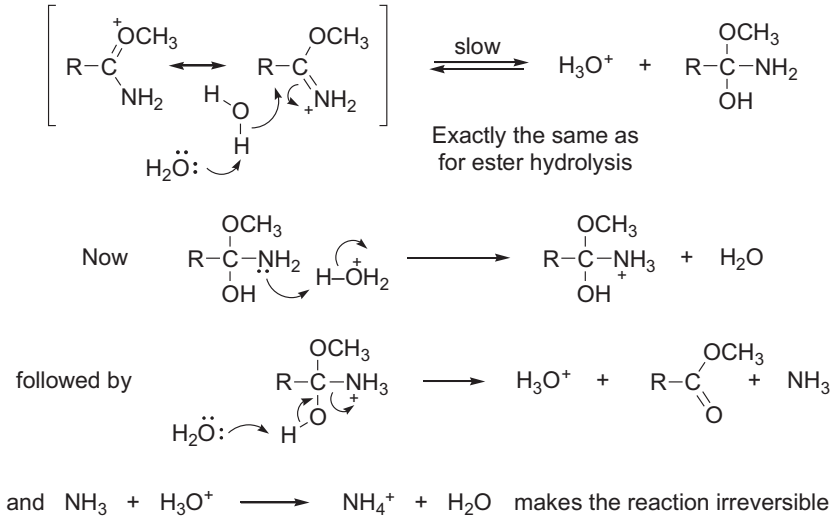
[3] R.A. Cox. Work in progress.

© 2005 NRC Canada

Scheme 2.



Scheme 3.



indicate that ethers should hydrolyze easily in dilute acid, but in fact, as is well-known, this process is very difficult, requiring boiling in strong acids having a strongly nucleophilic anion (HBr or HCl). Aromatic ethers, anisole, and related molecules with more alkoxy groups have reported pK_{BH}^+ values in the –3 to –11 range (32) and are as likely to protonate on one of the ring carbons as on one of the oxygens (33). Alcohols do undergo ^{18}O exchange in acid media, but this is not exactly a facile reaction either (34).

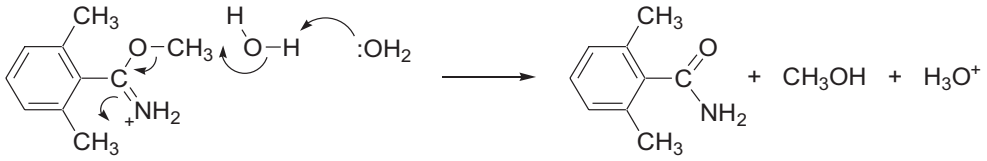
Benzimidate hydrolysis

Returning to the subject of this paper, the excess acidity plots, particularly Fig. 16 in ref. 2 and Fig. 2 here, are only linear on the assumption of two water molecules being involved in both of the benzimidate hydrolysis reaction mechanisms. The hydrolysis mechanism undergone by **1**, and by **2** and **3** at the lower acidities, is shown in Scheme 3. The *o*-methyl groups suppress this mechanism for **4** and **5** (15), and these are instead attacked at the O-methyl group by two water molecules as shown in Scheme 4. This mechanism also becomes important for **2** and **3** at the higher acidities. Product analysis supports both of these schemes (13–15); the amide products of Scheme 4 are less reactive than the imidates and their hydrolysis does not cause complications (13–15).

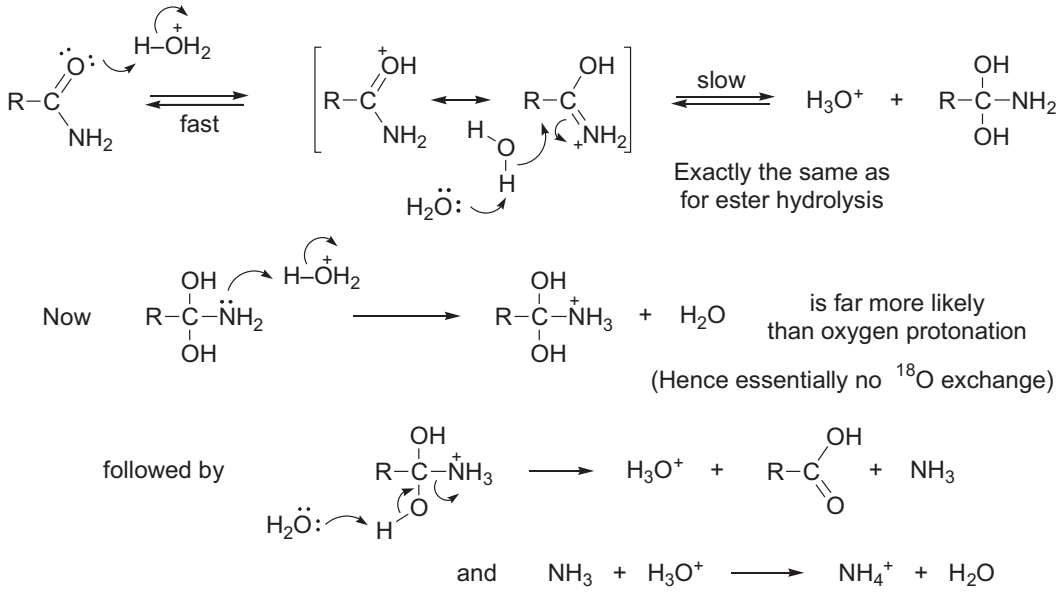
The rate-determining step in Scheme 3 is essentially the same as it is for the ester hydrolysis in Scheme 1, but the tetrahedral intermediate now possesses a basic nitrogen atom (pK_{BH}^+ probably not far from that of ammonia) and loss of ammonia and its protonation to NH_4^+ makes the reaction essentially irreversible. The Scheme 4 mechanism is a straightforward S_N2 process.

© 2005 NRC Canada

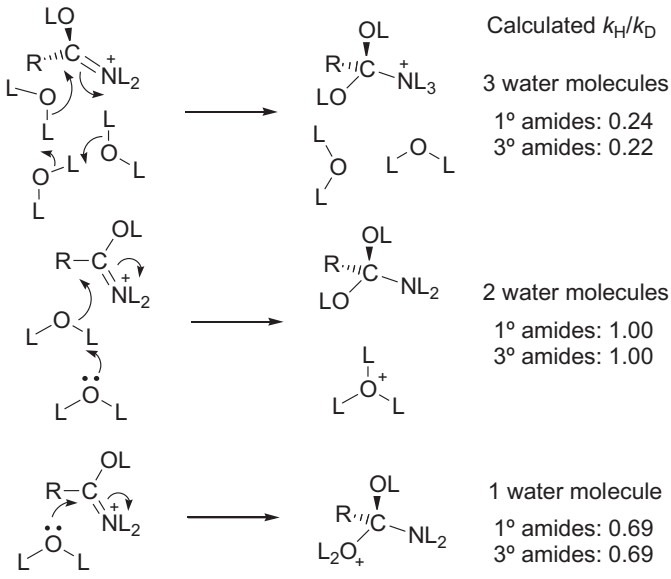
Scheme 4.



Scheme 5.



The information in Table 1 shows that, at least in the standard state, the Scheme 4 S_N2 reaction is a much more difficult process than is the Scheme 3 one, with rate constants essentially a thousand times smaller. Also the activation enthalpies are some 8 kcal mol^{-1} higher, but these are compensated to some extent by the less negative entropies of activation, as is often the case. This is probably simply because the attacking water molecules "see" more positive charge in the Scheme 3 case. However, the excess acidity slopes (probably related to the transition-state activity coefficient behaviour (35)) are quite different, negative for the Scheme 3 process but positive for the Scheme 4 one, which is why it takes over from the Scheme 3 mechanism in the more strongly acidic solutions for **2** and **3**.



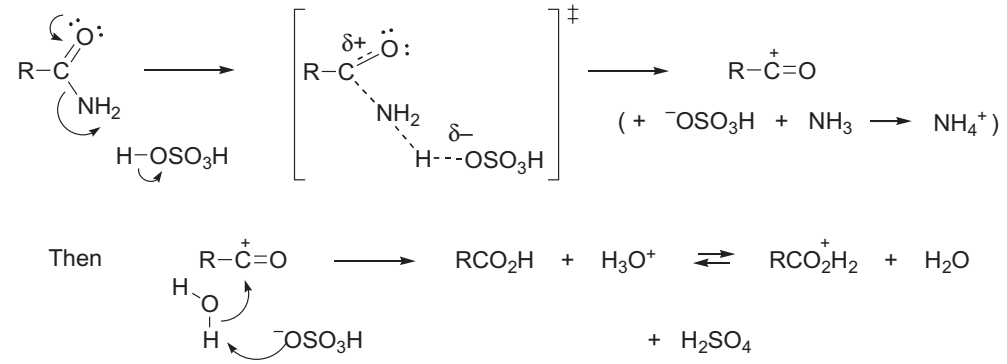
Amide hydrolysis

By straightforward analogy, the hydrolysis mechanism for amides must therefore be that of Scheme 5, at least in the more dilute acid region. A great deal of high-quality experimental data is available for the hydrolysis of the benzamide equivalents of **1**–**3**; hydrolysis rate constants as functions of acid concentration and temperature (10, 14, 36), in aqueous sulfuric, perchloric, and hydrochloric acid media. Several years' work on this[3] unequivocally shows that, at least in the more dilute acidity region, two water molecules react with an oxygen protonated amide in the rate-determining step, according to the excess acidity plots for these compounds, exactly as found for the benzimidates in this study. This is in accord with an accumulating amount of other evidence. For instance, standard fractionation factors (37) can be used to calculate solvent isotope effects for amides reacting in regular and deuterated media with one, two, and three water molecules (shown in the following) (38).

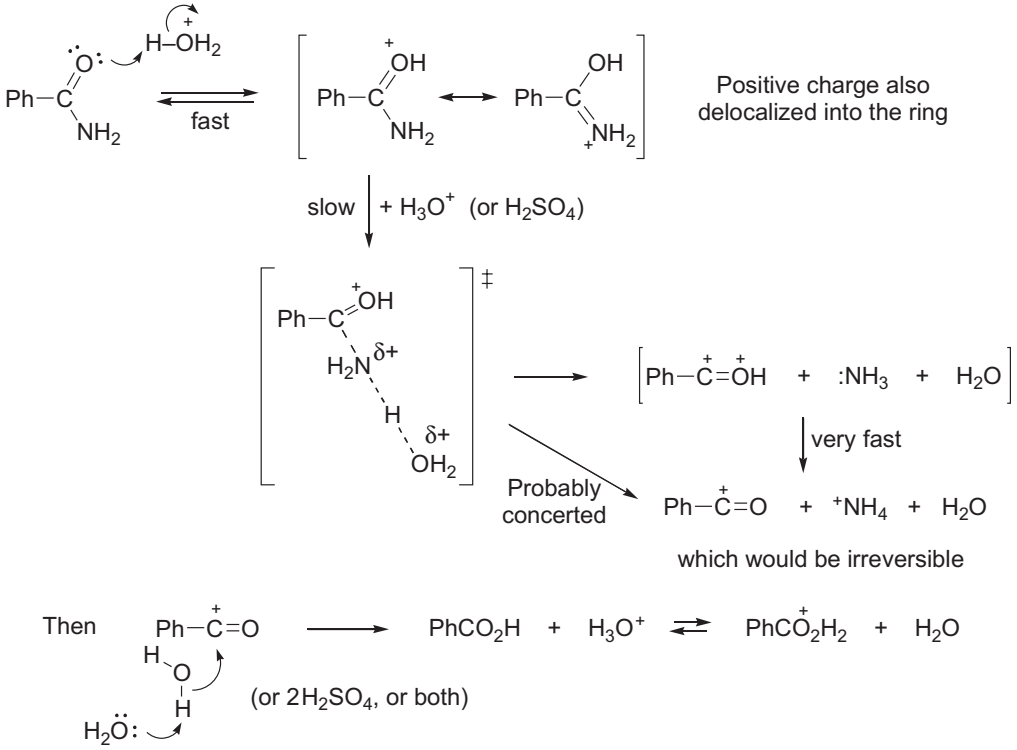
The experimentally measured number (38) is 1.00, exactly in accord with the two-water-molecule mechanism, but certainly not for one involving one or three water molecules. Ironically, we have favoured both of the latter in the past (11). Originally, we liked the three-water-molecule mechanism because it enabled an *N*-protonated tetrahedral interme-

© 2005 NRC Canada

Scheme 6.



Scheme 7.



diate to be formed directly (see the previous section), but the solvent isotope effect work rules this out. Also Guthrie's multidimensional analysis is inconsistent with the involvement of three water molecules (39).[4] Scheme 5 is the correct mechanism.

Many years ago it was found that amide hydrolysis in acid involves very little ^{18}O exchange when the reaction is carried out in ^{18}O-enriched media (40), which is what would be expected according to Scheme 5 with its tetrahedral intermediate containing a highly basic nitrogen. Some exchange does take place, however; the early and the more recent work has been summarized in some detail (41), the Scheme 5 hydrolysis mechanism still being favoured (41).

However, this is not the whole story. My own work on the hydrolysis of the benzamide equivalents of **1**–**3**[3] is not yet ready for publication because another mechanism takes over from the Scheme 5 one in media in which there is still plenty of water present; the excess acidity plots begin to deviate upwards from the behavior predicted according to Scheme 5. At the time of writing, I do not know what this second mechanism is. Originally, we thought that bisulfate ion was taking over from water as a nucleophile in sulfuric acid (11), but this seems less likely now because the same behaviour is observed in perchloric acid media, where there is no alternate nucleophile present.[3]

One possibility is given as Scheme 6, where proton transfer is to nitrogen rather than to oxygen, possibly general-acid-catalyzed as shown (undissociated H_2SO_4 being the

[4] J.P. Guthrie. Personal communication (2002).

© 2005 NRC Canada

general acid in Scheme 6), forming an acylium ion that would rapidly collapse with water or bisulfate. General acid catalysis in strong acid media, first investigated by the Kresge group (42) and subsequently by us in connection with the Wallach rearrangement (29) (Scheme 2) actually appears to be much more common than is generally supposed. However, Scheme 6 starts from the unprotonated amide, which is decreasing in concentration with increasing acidity, and thus the reaction should rapidly slow down with increasing acidity, which it does not. Of course there could be a tautomerization from oxygen protonated amide to nitrogen protonated amide first, and this could then break up to acylium ion and ammonia in a simple A1 process, constituting another possible mechanism. The excess acidity behaviour does not really fit either of these very well, but an A1 process does seem possible.[3]

An intriguing possibility is shown in Scheme 7, which has the advantage of starting from the oxygen protonated amide, meaning that the rate would not decrease with increasing acidity as the Scheme 6 mechanism would predict. This is also visualized as being a general-acid-catalyzed process as shown. It is, of course, not likely that the protonated acylium species of Scheme 7 would actually form; the departing ammonia molecule would most likely take the OH^+ proton with it as NH_4^+ in a concerted process, but this is rather difficult to draw, so I have shown it as a separate process in Scheme 7. There is, in fact, precedent for a mechanism like this in the Wallach rearrangement of azoxybenzene (27, 29), given here for comparison as Scheme 2 (28), so it is not as unlikely as it appears at first glance. The Scheme 7 mechanism would also show no ^{18}O exchange (this experiment has only been carried out at relatively low acidities for amides) and would presumably only apply to amides in which the charge on the protonated species can be dispersed in some way, into the ring for the benzamides. Thus, ordinary alkyl amides may not show this behavior.

Acknowledgements

It is a pleasure to acknowledge many discussions of the material in this commentary with my friends and colleagues over the years, among them Stan Brown, Erwin Buncel, Peter Guthrie, John Marlier, Charles Perrin, Tom Tidwell, and particularly Jerry Kresge, who helped with the solvent isotope effect calculations. I think we are all pretty much in agreement now, at least on the basics.

References

1. R.A. Cox and K. Yates. Can. J. Chem. **57**, 2944 (1979); R.A. Cox. Acc. Chem. Res. **20**, 27 (1987).
2. R.A. Cox. Adv. Phys. Org. Chem. **35**, 1 (2000).
3. J.F. Bunnett. J. Am. Chem. Soc. **83**, 4956 (1961); and subsequent papers.
4. K. Yates and J.B. Stevens. Can. J. Chem. **43**, 529 (1965); K. Yates and J.C. Riordan. Can. J. Chem. **43**, 2328 (1965); and subsequent papers.
5. K. Yates and R.A. McClelland. J. Am. Chem. Soc. **89**, 2686 (1967).
6. K. Yates. Acc. Chem. Res. **4**, 136 (1971).
7. For instance: P.Y. Bruice. Organic chemistry. 3rd. ed. Prentice Hall, Inc., Upper Saddle River, New Jersey. 2001. p. 960; T.W.G. Solomons and C.B. Fryhle. Organic chemistry. 7th. ed. John Wiley and Sons, Inc., New York. 2000. p. 829.
8. J.F. Marlier, T.G. Frey, J.A. Mallory, and W.W. Cleland. J. Org. Chem. **70**, 1737 (2005).
9. C.-K. Kim, I.Y. Lee, D.S. Chung, B.-S. Lee, and I. Lee. Bull. Korean Chem. Soc. **19**, 993 (1998); F. Haeffner, C.-H. Hu, T. Brinck, and T. Norin. THEOCHEM, **459**, 85 (1999); K. Hori, Y. Hashitani, Y. Kaku, and K. Ohkubo. THEOCHEM, **461–462**, 589 (1999).
10. C.R. Smith and K. Yates. J. Am. Chem. Soc. **93**, 6578 (1971).
11. R.A. Cox and K. Yates. Can. J. Chem. **59**, 2853 (1981).
12. R.A. Cox. Can. J. Chem. **76**, 649 (1998).
13. C.R. Smith and K. Yates. J. Am. Chem. Soc. **94**, 8811 (1972).
14. C.R. Smith. Ph.D. thesis, University of Toronto, Toronto, Ontario. 1971.
15. R.A. McClelland. J. Am. Chem. Soc. **97**, 3177 (1975).
16. C.E.L. Myhre, D.H. Christensen, F.M. Nicolaisen, and C.J. Nielsen. J. Phys. Chem. A, **107**, 1979 (2003).
17. E.C.W. Clarke and D.N. Glew. Trans. Faraday Soc. **62**, 539 (1966).
18. K.J. Laidler. Theories of chemical reaction rates. McGraw-Hill, Inc., New York. 1969. Chap. 3.
19. W.P. Jencks. Acc. Chem. Res. **13**, 161 (1980).
20. S.V. Shevkunov. Russ. J. Gen. Chem. **74**, 1471 (2005).
21. D.G. Lee and R. Cameron. J. Am. Chem. Soc. **93**, 4724 (1971).
22. D.G. Lee and K.J. Demchuk. Can. J. Chem. **65**, 1769 (1987); W.D. Chandler and D.G. Lee. Can. J. Chem. **68**, 1757 (1990).
23. F. Ruff and I.G. Csizmadia. Organic reactions: equilibria, kinetics and mechanisms. Elsevier Science B.V., Amsterdam. 1994. p. 320.
24. D.G. Lee and M.H. Sadar. J. Am. Chem. Soc. **96**, 2862 (1974); R.A. Cox, L.M. Druet, A.E. Klausner, T.A. Modro, P. Wan, and K. Yates. Can. J. Chem. **59**, 1568 (1981).
25. R.A. Cox and K. Yates. Can. J. Chem. **59**, 1560 (1981).
26. E. Buncel and B.T. Lawton. Can. J. Chem. **43**, 862 (1965).
27. R.A. Cox and E. Buncel. *In* The chemistry of the hydrazo, azo and azoxy groups. Vol. 1. *Edited by* S. Patai. John Wiley and Sons, London. 1975. p. 775; R.A. Cox and E. Buncel. *In* The chemistry of the hydrazo, azo and azoxy groups. Vol. 2. *Edited by* S. Patai. John Wiley and Sons, London. 1997. p. 569.
28. R.A. Cox, D.Y.K. Fung, I.G. Csizmadia, and E. Buncel. Can. J. Chem. **81**, 535 (2003).
29. R.A. Cox. J. Am. Chem. Soc. **96**, 1059 (1974).
30. J.C.D. Brand. J. Chem. Soc. 997 (1950); R.J. Gillespie, T.E. Peel, and E.A. Robinson. J. Am. Chem. Soc. **93**, 5083 (1971).
31. P. Bonvicini, A. Levi, V. Lucchini, G, Modena, and G. Scorrano. J. Am. Chem. Soc. **95**, 5960 (1973).
32. A.J. Kresge, H.J. Chen, L.E. Hakka, and J.E. Kouba. J. Am. Chem. Soc. **93**, 6174 (1971).
33. A.J. Kresge, Y. Chiang, and L.E. Hakka. J. Am. Chem. Soc. **93**, 6167 (1971).
34. C.A. Bunton, A. Konasiewicz, and D.R. Llewellyn. J. Chem. Soc. 604 (1955); C.A. Bunton and D.R. Llewellyn. J. Chem. Soc. 3402 (1957).
35. A. Bagno, G. Scorrano, and R.A. More O'Ferrall. Rev. Chem. Intermed. **7**, 313 (1987).
36. J.A. Leisten. J. Chem. Soc. 765 (1959); S. Rysman de Lockerente, P. van Brandt, A. Bruylants, M. de Buyl-Gaudissart, and D. Hubert. Bull. Cl. Sci. Acad. Roy. Belg. **58**, 180 (1972); T. Yamana, Y. Mizukami, A. Tsuji, and M. Ikuta. Chem. Pharm. Bull. **20**, 1778 (1972); C.A. Bunton,

© 2005 NRC Canada

S.J. Farber, A.J.G. Milbank, C.J. O'Connor, and T.A. Turney. J. Chem. Soc. Perkin Trans. 2, 1869 (1972); M.S. Shingare, D.B. Ingle, and D.D. Khanolkar. J. Indian Chem. Soc. **52**, 599 (1975).
37. F. Ruff and I.G. Csizmadia. Organic reactions: equilibria, kinetics and mechanisms. Elsevier Science B.V., Amsterdam. 1994. p. 241.
38. A.J. Bennet, H. Slebocka-Tilk, R.S. Brown, J.P. Guthrie, and A. Jodhan. J. Am. Chem. Soc. **112**, 8497 (1990).
39. J.P. Guthrie. Can. J. Chem. **83**, 1 (2005).
40. R.A. McClelland. J. Am. Chem. Soc. **97**, 5281 (1975).
41. R.S. Brown, A.J. Bennet, and H. Slebocka-Tilk. Acc. Chem. Res. **25**, 481 (1992).
42. A.J. Kresge, L.E. Hakka, S.G. Mylonakis, and Y. Sato. Discuss. Faraday Soc. 75 (1965)

© 2005 NRC Canada

Scientific genealogies of physical and mechanistic organic chemists[1]

John Andraos

Abstract: Scientific genealogy trees of scientists who contributed to the study of organic reaction mechanisms over the last century are presented. The trees show doctoral and post-doctoral connections among scientists as well as connections between scientific ideas. Contributions made by scientists working in laboratories at Canadian universities and at the National Research Council of Canada are noted throughout. These trees, covering more than two centuries, are of interest to senior scientists and young students of science alike in understanding the evolution of scientific ideas and in career development for aspiring scientists. Key patterns revealed by these trees pertaining to ideas and discoveries made, how they were made, connections between them, and who made them are also discussed.

Key words: reaction mechanisms, physical organic chemistry, scientific genealogies.

Résumé : On présente les arbres généalogiques des scientifiques qui ont contribué à l'étude des mécanismes des réactions organiques au cours du dernier siècle. Les arbres mettent aussi en évidence les relations doctorales et postdoctorales ainsi que les corrélations entre idées scientifiques. Dans toute cette présentation, on met en relief toutes les contributions des scientifiques qui ont travaillé dans les laboratoires des universités canadiennes et ceux du Conseil national de recherches du Canada. Ces arbres, qui couvrent plus de deux siècles, présentent de l'intérêt autant pour les scientifiques bien établis que pour les jeunes étudiants des sciences en leur permettant de comprendre l'évolution des idées scientifiques et le développement des carrières des scientifiques ambitieux. On discute aussi des patrons clés révélés par ces arbres en relation avec les idées et les découvertes qui ont été faites, qui les a faites, comment elles ont été faites et des relations entre elles.

Mots clés : mécanismes réactionnels, chimie organique physique, généalogies de scientifiques.

[Traduit par la Rédaction]

Introduction

In keeping with the theme of this special issue to emphasize the historical and current importance of mechanistic chemistry and the international impact that Canadian scientists have made to it, this paper presents scientific genealogy trees of prominent scientists who have made significant contributions to physical organic chemistry and reaction intermediate studies. Figure 1 shows a "super" tree with a timeline covering more than a century of scientific work that depicts key players as lynch pin nodes in the overall grand scheme of things. Detailed specific trees emanating from these people are available in the Supplementary material.[2] All of these trees were constructed using biographical information obtained from various sources: Poggendorff's Biographisches-literarisches Handwortenbuch zur Geschichte der exacten Naturwissenschaften (2nd ed., Wiley-VCH, Berlin), Biographical Memoirs of Fellows of the Royal Society (Vols. 1–50, The Royal Society, London), Obituary Notices of Fellows of the Royal Society (Vols. 1–9, The Royal Society, London), Biographical Memoirs of Fellows of the National Academy of Sciences of the United States of America (Vols. 1–84, National academy of Sciences, Washington, D.C.), Dictionary of Scientific Biography *Edited by* Charles C. Gillispie (Charles Scribner's Sons, New York), and various biographical references compiled in ref. 1. The following code applies to the trees: solid lines indicate doctoral advisor links, dashed lines indicate post-doctoral advisor links, boxes indicate people who brought knowledge from one country to another, and maple leaf icons indicate scientists who made contributions at Canadian universities and at the National Research Council of Canada. For each entry the name of the scientist is given along with the university where they did their doctoral work, the year of their Ph.D., and a chronological list of their notable contributions to the fields of physical organic chemistry and reaction intermediates. References to these contributions may be found in Tables S1, S2, S5, and S6 (Supplementary material) of

Received 10 May 2005. Published on the NRC Research Press Web site at http://canjchem.nrc.ca on 2 November 2005.

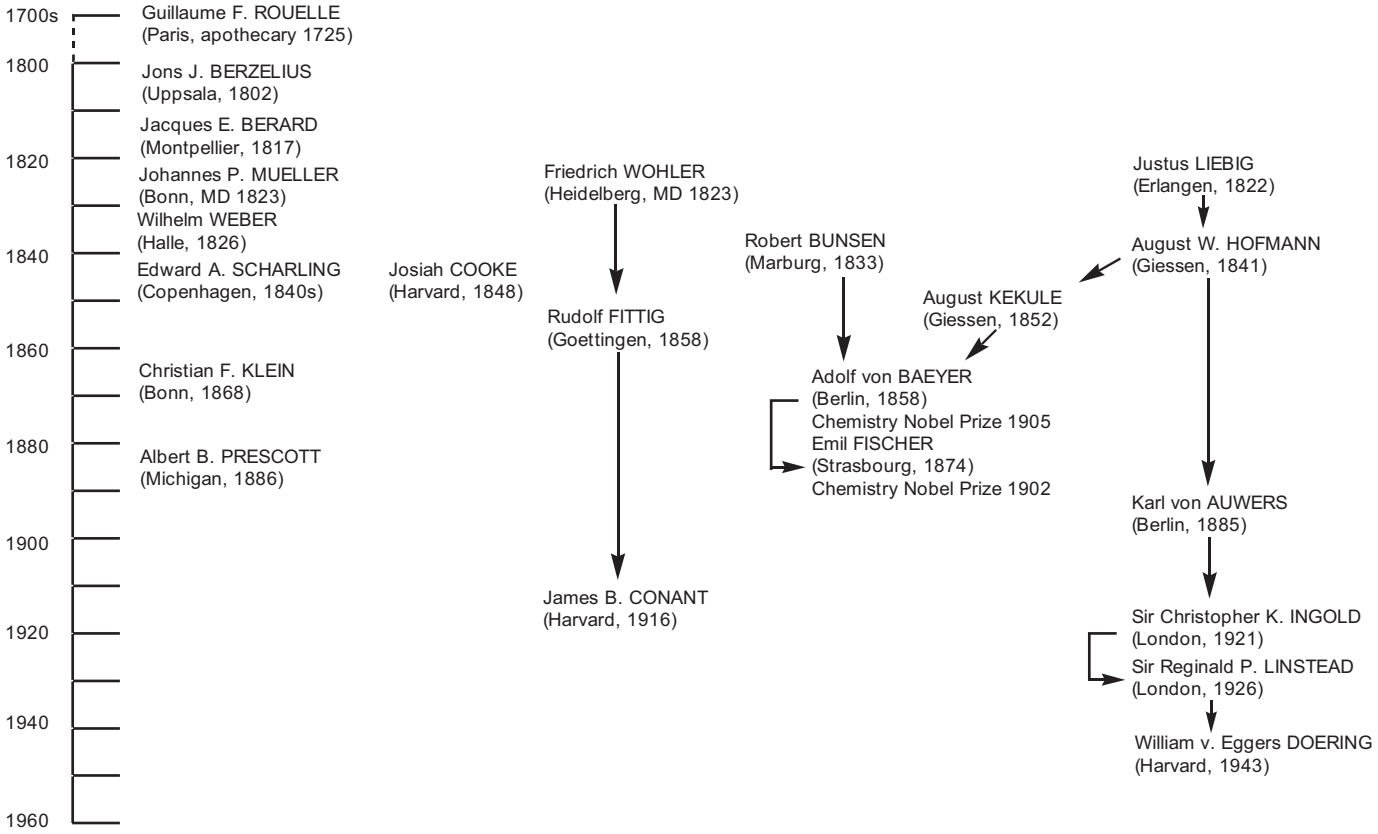
J. Andraos. Department of Chemistry, York University, Toronto, ON M3J 1P3, Canada. (e-mail: jandraos@yorku.ca).

[1]This article is part of a Special Issue dedicated to organic reaction mechanisms.

[2]Figures S1–S37 showing scientific genealogies of scientists contributing to organic reaction mechanisms and reaction intermediates. Canadian scientists are designated with a maple leaf icon. Supplementary data for this article are available on the Web site or may be purchased from the Depository of Unpublished Data, Document Delivery, CISTI, National Research Council Canada, Ottawa, ON K1A 0S2, Canada. DUD 4038. For more information on obtaining material refer to http://cisti-icist.nrc-cnrc.gc.ca/irm/unpub_e.shtml.

 doi: 10.1139/V05-158 © 2005 NRC Canada

Fig. 1. Summary "super" scientific genealogy tree of key scientists whose scientific offspring contributed significantly to the development of mechanistic chemistry and to the discovery of reaction intermediates along with the timeline of the doctoral degree.



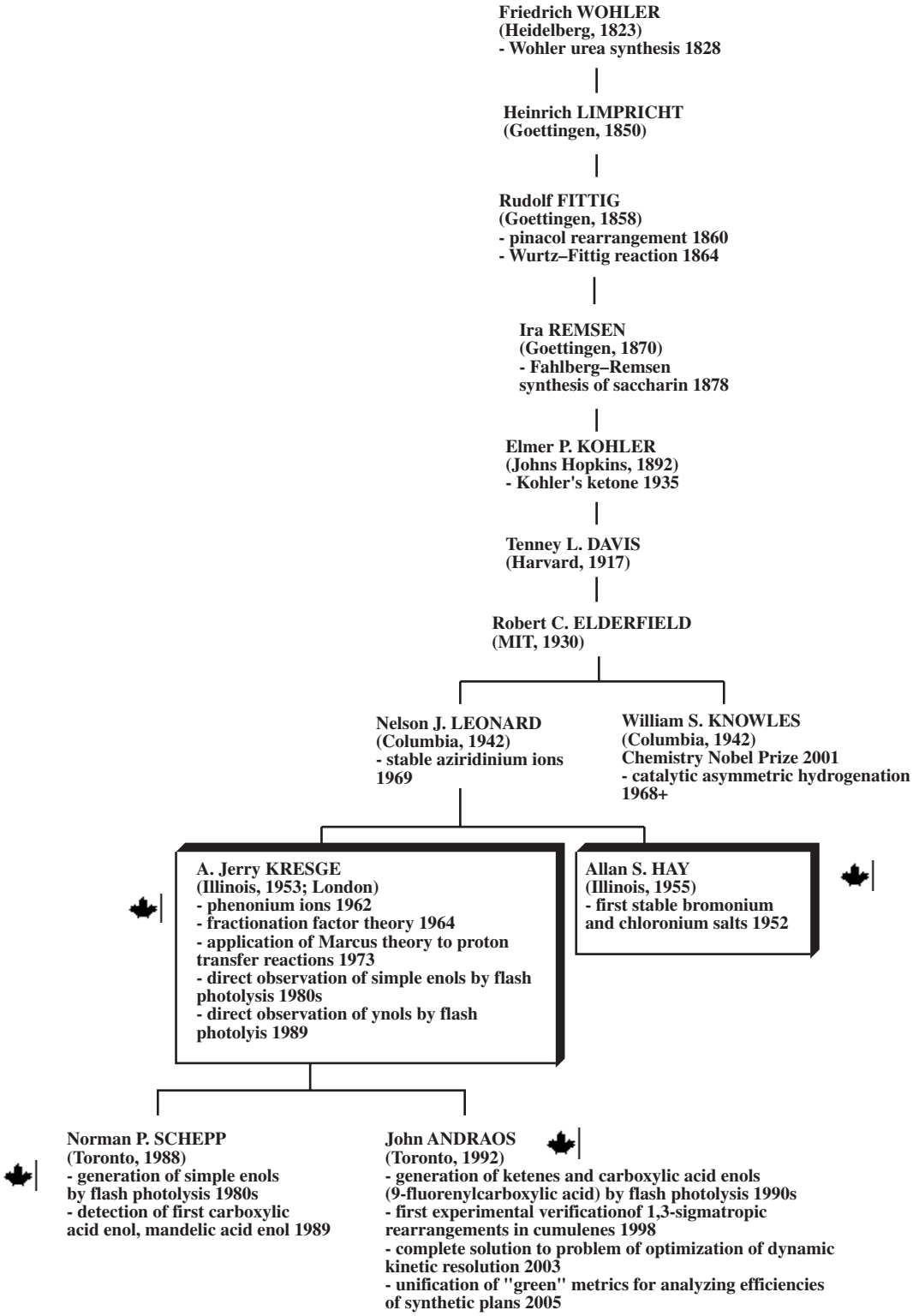
the following paper (2). These trees effectively trace how knowledge in physical organic chemistry emerged as a whole and how it came to Canada from the earliest times up to the year 2004. All professors of chemistry in Canada who made contributions to physical organic chemistry are included. In addition, particular attention was made to include in the compilation all Canadian contributors to this special issue. As an example, my personal scientific genealogy tree is shown in Fig. 2.

Though at first sight this compilation has obvious appeal to readers who may be interested only in the history of science, it is of far more fundamental and practical value with respect to conducting original research. From readings of biographical memoirs of famous scientists, one recognizes that nearly all of them can attribute their success in science in significant measure to their knowledge of how ideas progressed down the line from their forebears rather early in their careers in addition to the obvious traits of possessing intelligence, command of, and enthusiasm for their subject. Stamina, perseverance, and maintaining focus on key questions to be answered are particularly important virtues that academics require in the course of their work throughout their careers, especially when they are faced with convincing their peers of novel ideas that challenge established paradigms brought forward by scientists in positions of power and authority (3). One often can correctly guess that one must really have a good idea when one encounters stiff resistance to that idea. One is reminded of the following relevant statements made by a philosopher and physicist, respectively. "All truth passes through three stages before it is recognized. First, it is ridiculed. Second, it is violently opposed. Third, it is regarded as self-evident." (Arthur Schopenhauer, 1788–1860) (4). "A new scientific truth does not triumph by convincing its opponents and making them see the light, but rather because its opponents eventually die, and a new generation grows up that is familiar with it." (Max Planck, 1858–1947) (5).

Probably the most celebrated illustrations of these insights are the comments of Hermann Kolbe (1818–1884) on the imaginative ideas of Jacobus van't Hoff (1852–1911, first recipient of the Nobel Prize in Chemistry in 1901) concerning the connection between the observation of optical activity in compounds and the presence of asymmetric carbon atoms in their molecular structures as exemplified by the following quotations. "…the weeds of a seemingly learned and brilliant but actually trivial and empty Philosophy of Nature, which, after having been replaced some fifty years ago by the exact sciences, is now once more dug up by pseudo-scientists from the lumber room of human fallacies, and like a trollop, newly attired in elegant dress and make-up, is smuggled into respectable company, to which she does not belong." (6*a*). "Not long ago, I expressed the view that the lack of general education and of thorough training in chemistry was one of the causes of the deterioration of chemical research in Germany. Will anyone to whom my worries seem exaggerated please read, if he can, a recent memoir by a Herr van't Hoff on *La Chimie dans l'Espace*, a document crammed to the hilt with outpourings of childish fantasy…This Dr. J.H. van't Hoff, employed by the Veterinary Academy of Utrecht, has, so it seems, no taste for accurate

© 2005 NRC Canada

Fig. 2. Sample scientific genealogy tree showing doctoral advisor – student connections and flow of scientific ideas.



chemical research. He finds it more convenient to mount his Pegasus (evidently taken from the stables of the Veterinary Academy) and to announce how, on his bold flight to Mount Parnassus, he saw atoms arranged in space." (6*b*).

A modern example documented in recent celebrations of the most cited papers in the *Journal of the American Chemical Society* in the last 125 years is that of Lineweaver and Burk whose classic paper (7) is the most cited in that journal and yet at the time of review it was rejected several times by six reviewers, but the editor of the day took the risk and allowed publication (8). Now, of course, Lineweaver–Burk plots are routinely used in pharmacokinetic studies and are mentioned in virtually every undergraduate biochemistry textbook. Interestingly, the idea of plotting enzyme data in

© 2005 NRC Canada

this way came to them in their discussions when viewing data plots upsidedown as they were seated opposite each other at a desk! Another case is the postulation and discovery of the Koelsch radical in 1937 (9*a*), which was confirmed by ESR spectroscopy two decades later in 1957 (9*b*). This is actually an excellent example of how a new powerful technique helped to solve an old problem and thereby confirm prior indirect evidence of the existence of a chemical species.

Close examination of these genealogy trees reveals several important and revealing patterns that are relevant to the progression of the science itself and the career developments of the practitioners themselves. The following discussion is thus focused on two specific areas: the development of scientific discoveries in physical organic chemistry and reaction intermediates over time, and career development patterns among successful practitioners in the field. In the scientific development category we have: (1) leading chemists claiming discovery of the most number of reaction intermediates; (2) leading chemists claiming discovery of the most number of concepts in physical organic chemistry; (3) synthetic chemists who used principles and concepts in physical organic chemistry to advantage in organic synthesis; (4) physical and theoretical chemists who contributed to the development of physical organic chemistry concepts; and (5) highlights of achievements by Canadian chemists. In the career development category we have: (1) idea generation and connections, and distinguishing innovators from followers; and (2) leading academics in Canada who spawned the next generation of physical organic chemists in Canada. In the following compilation, leading scientists are listed in alphabetical order with their contributions. No ranking with respect to most important vs. least important discoveries is implied since all contributions are noteworthy and meritous. Other scientists not given here who made contributions are noted in the genealogy trees (see Supplementary material).[2]

Leading chemists claiming discovery of the most reaction intermediates include:

- Paul D. Bartlett (bridged halonium ions (1936–1937), aziridinium ions (1947), and episulfonium ions (1949))
- Keith U. Ingold (detection of phenyl radical (1953), benzyl radicals (1966), cumyloxy radicals (1969), peroxy radicals (1969), β-scission mechanism (1969), phosphinoyl radicals (1973), phosphinyl radicals (1973), and phosphinothionyl radicals (1973) by laser flash photolysis and electron spin resonance techniques)
- George A. Olah (bridged halonium ions (1951), arenium ions (1956), dications (1966), phenonium ions (1969), and benzidine rearrangement dication (1972), all by generation in magic acid and detected by NMR spectroscopy)
- Wilhelm Schlenk (stable carbanions (1910), ketyl radicals and radical anions (1911), metal radical anions (1914), the Schlenck–Brauns biradical or hydrocarbon (1915), and *p*-quinodimethanes (1919))
- Julius Stieglitz (nitrenes (1896), carbocations (1899), tetrahedral intermediates (1899), and nitrenium ions (1913), all conjectured from comparative analysis of product structures with substrate structures)
- Hermann Staudinger (ketenes (1905), *o*-quinonemethide (1911), and nitrenes (1917))
- Saul Winstein (bridged halonium ions (1939), acetoxonium ions (1942), nonclassical norbornyl cation (1949), methoxonium ions (1952), phenonium ions (1952), and stable *p*-quinonemethides (1960))

Leading physical organic chemists claiming introduction of the most number of named concepts in the field include:

- Louis P. Hammett (linear free energy relationships (1924), solvolysis reactions (1927), Hammett acidity function (1932), Hammett equation (1935), substitutent effects and constants (1935), general acidity functions (1937), Zucker–Hammett hypothesis (1939), and Acree–Curtin–Hammett principle (1954))
- Sir Christopher K. Ingold (concept of inductive effect (1923), concept of mesomeric or resonance effect (1924), concept of partial charges in chemical structures (1926), E1cb (1933), SN1 and SN2 (1934), E1 and E2 (1937–1948), and A1 and A2 (1941) mechanism categorizations, isotopic labelling experiment (1935), common ion effect (1940), normal salt effect (1940), principle of microscopic reversibility (1953–1969))
- William P. Jencks (tetrahedral intermediates and catalysis in esterification reactions (1964), More O'Ferrall – Jencks diagram (1970), Jencks azide clock (1977), and Keeffe–Jencks equations (1981)
- C. Garner Swain ("push–pull" mechanism (1948), Swain–Scott equation (1953), Swain–Schaad equation (1958), and Swain–Lupton equation (1968))
- Saul Winstein (anchimeric assistance or neighbouring group participation in solvolysis reactions (1939), normal salt effect (1940), Grunwald–Winstein equation (1948), intimate and solvent separated ion pairs (1952), special salt effects (1954), Winstein–Holness equation (1955), and concept of homoaromaticity and homoconjugation (1959))

Leading synthetic chemists who have used mechanistic ideas to advantage in organic synthesis strategies include:

- Adolf von Baeyer (concept of angle strain (1885) and carbonium ion theory (1901))
- Sir Derek H.R. Barton (the role of conformation in organic synthesis (1952))
- Emil Fischer (lock and key model of enzyme catalysis (1894), experimental verification of tetrahedral asymmetry at carbon (1914))
- Ernst O. Fischer (synthesis of transition-metal complexes of carbenes (1964), carbynes (1973), and ketenes (1983))
- Moses Gomberg and Werner Bachmann (synthesis of *o*- and *p*-quinonemethides (1913) and synthesis of stable metal ketyl radicals and ketyl radical anions (1927))
- Raymond U. Lemieux (Edward–Lemieux anomeric effect (1955–1969))
- Hans Meerwein (Wagner–Meerwein rearrangement reaction (1922), synthesis of Meerwein oxonium salts (1937), and discovery of insertion of carbenes into C—H bonds (1942))
- Sir Robert Robinson (curly arrow notation for reaction mechanisms depicting electron flow from electron donor sites to electron acceptor sites (1922–1932) and electronic theory of organic chemistry (1926))
- Georg Wittig (Diels–Alder trapping of generated benzyne intermediate (1942), synthesis of *o*-quinodimethanes (1948), launched ylide chemistry (1948), and developed

© 2005 NRC Canada

the Wittig reaction and Wittig reagents to effect ketone–olefin transformations (1954))
- Robert B. Woodward (elucidation of structure of metallocene "sandwich" complexes (1952), concept of Woodward–Hoffmann rules to explain stereochemical product outcomes in thermal and photochemical electrocyclic reactions (1965))

Leading physical and theoretical chemists who made important contributions to mechanistic chemistry include:
- Henry Eyring (development of the absolute rate and transition state theory and Eyring equation (1935), electrode kinetics (1939), heterogeneous catalysis (1940), and solvent effects in kinetics (1940))
- Gerhard Herzberg (detection and spectroscopic identification of methyl radicals and singlet and triplet methylene (1956–1959))
- Gilbert N. Lewis (development of concepts of covalent bonding (1916), octet rule (1916), electrophilicity and nucleophilicity (1921), Lewis acidity and basicity (1923), and inductive effect (1923), advanced the idea that radicals and other paramagnetic species could be studied by magnetic methods (1923), investigated the effect of resonance on electronic transitions (1939), and discovery of the triplet state of ketones (1944))
- Rudolph A. Marcus (development of the Rice–Ramsperger–Kassel–Marcus theory (1951) and development of concepts in electron transfer theory including the Marcus equation and prediction of the inverted region (1956))
- Ronald G.W. Norrish and Lord George Porter (discovery of the Norrish type I and type II reactions (1935), development of the flash photolysis technique (1949), detection of acetoxy radicals (1952), benzyl radicals (1957), and phenyl radicals (1968))
- Linus Pauling (concept of electronegativity and development of the Pauling scale (1932), investigation of aromatic sigma complexes (1935), concept of hybridization in bonding (1948), and development of the Corey–Pauling–Koltun (CPK) space-filling models (1959))
- Michael Polanyi (development of the Bell–Evans–Marcus–Hammond–Polanyi–Thornton–Leffler principle (1936))
- Edward Teller (Renner–Teller effect (1934), Teller–Redlich product rule (1935), Jahn–Teller effect (1936), and the concept of principle of least motion (1938))

Great Canadian contributors to mechanistic and reaction intermediates chemistry include:
- Ronald J. Gillespie (valence shell electron repulsion theory (1963) and use of magic or superacid media to detect carbocation intermediates (1968))
- Keith U. Ingold (detection of phenyl radical (1953), peroxy radicals (1969), β-scission mechanism (1969), phosphinoyl radicals (1973), phosphinyl radicals (1973), and phosphinothionyl radicals (1973) by laser flash photolysis and electron spin resonance techniques)
- A. Jerry Kresge (fractionation factor theory applied to solvent isotope effects (1964), application of Marcus electron transfer theory to proton transfer reactions (1973), and direct observations of enol (1980s), ynol (1989), ketene (1990s), and quinomethide intermediates by flash photolysis (2000s))
- Keith J. Laidler (application of theory of absolute reaction rates to problems in heterogenous catalysis (1940), electrode kinetics (1939), and solvent effects in kinetics (1940), investigation of kinetics of the urea–urease system (1949), thermal free-radical reactions (1951), investigation of pH effects on enzyme kinetics (1955), and investigation of temperature effects on enzyme kinetics (1979))
- Frederick P. Lossing (detection of phenyl radical (1953), *p*-quinodimethanes (1955), and acetoxyl radical (1955) by mass spectrometry, and investigation of free radicals in the gas phase by mass spectrometry (1957)
- Rudolph A. Marcus[3] (development of the Rice–Ramsperger–Kassel–Marcus theory (1951) and development of concepts in electron transfer theory including the Marcus equation and prediction of the inverted region (1956))
- E.W.R. Steacie (detection of benzyl radical (1954) and acetoxyl radical (1955))
- Thomas T. Tidwell (synthesis of persistent bis(trimethylsilyl)ketenes (1992), synthesis of persistent allenylketenes (1997), synthesis of persistent silylketenes (1999))
- J.C. Tito Scaiano (development of the probe technique for detecting spectroscopically "invisible" transients (1977), development of time-resolved microwave dielectric absorption spectroscopy (1982, with Professor Richard Fessenden), development of the two-laser two-colour laser flash photolysis experiment for detecting excited state species tandemly generated from short-lived ground state transients (1984), trapping of carbenes to yield ylides such as pyridine ylide and thiocarbonyl ylides (1986), detection of ketene zwitterions by flash photolysis (1992), and development of the laser drop experiment for studying multiphoton excitation of photoprecursors (1993)

Successful academics invariably obtained their doctoral degrees and post-doctoral apprenticeships with scientists who were contemporary leaders in their fields. Horizontal comparisons across a contemporary generation in any tree reveal which ideas and discoveries were brought forward at nearly the same time. These also reveal people who may have been fellow colleagues, graduate students, or post-doctoral fellows at the bench in the same laboratory. A common trend is for people to do their post-doctoral training with the doctoral advisor of their own doctoral advisor, in effect their scientific "grandfather". This pattern is particularly effective in securing consistent and credible recommendation letters from people who know one another professionally as well as personally. The German term *doktorvater* (doctor father) best describes a successful intellectual relationship between student and advisor. The following quotation from the Acknowledgements page of the 1933 M.Sc. thesis of Carl A. Winkler describing his relationship with his advisor Otto Maass is particularly pertinent. "In the brief space of two years since this work was begun, under

[3] Rudolph A. Marcus is included among the Canadians since he was born and raised in Montreal, Quebec and did his graduate work under Professor Carl Winkler at McGill University in 1946 and then became a post-doctoral fellow at NRC in Ottawa under E.W.R. Steacie. His theoretical training and later accomplishments in the study of electron transfer reactions came about from his association with Professor Oscar K. Rice at the University of North Carolina, who allowed him the freedom to pursue his ideas and publish on his own.

© 2005 NRC Canada

the direction of Dr. O. Maass, the writer has become aware of having worked not under, but with him. His generous assistance, invaluable and kindly criticisms, and unbound optimism, are emphasized by all those who have privileged to work with him. The interest which Dr. Maass evinces in the individual as a chemist is paralleled by his interest in the chemist as an individual. The author feels that to have worked with Dr. Maass is to have experienced the utmost in satisfactory relationships between student and director." (10).

From the trees presented here one can readily deduce how personal relationships among scientists through advisor–student connections explain alliances with respect to collaborations or even rivalries and personal conflicts. In practical terms, it readily explains success in obtaining academic positions and academic job placement in particular institutions. Not surprisingly from the above quote, nearly 50 professors of chemistry across Canada, including Rudolf Marcus (1992 Nobel Chemistry Laureate), can trace their scientific genealogies directly to the Maass–Winkler combination, a statistical legacy that will likely remain unbroken. All of this information is hidden in the scientific literature and may not be so readily revealed, whether intentionally or unintentionally, particularly to new entering students in the field who may have the drive and intelligence to make the committment to research, but require career guidance to channel their efforts in the right direction. The demands of fulfilling degree requirements and maintaining focus on the research problems at hand pose additional challenges to maintain the "big picture" outlook. Networking at conferences and talking with people at colloquia and other gatherings is the best way to penetrate this important area of knowledge as it is essential for successful career development.

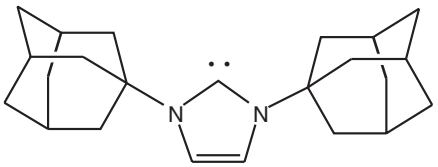
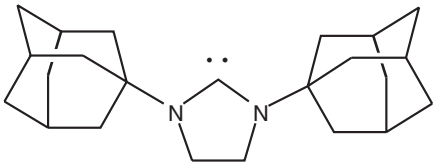
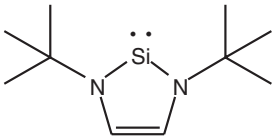
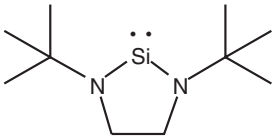
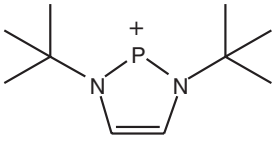
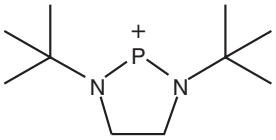
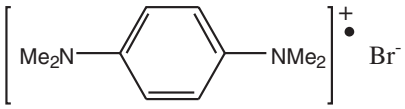
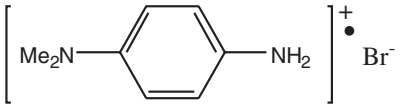
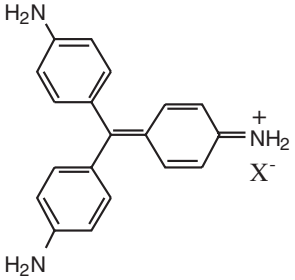
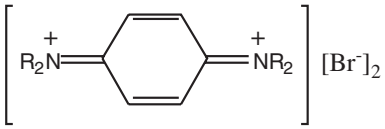
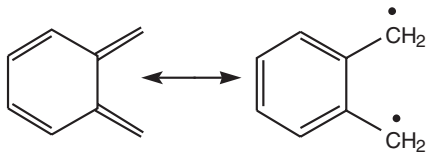
Another important spin-off of such genealogy trees is that predictability of what is important and worth looking into as a viable research question or area markedly improves when one knows the chronology of ideas and associates themselves with the key players in shaping those ideas or at least their direct scientific descendants. Naturally, as one would expect, the likelihood of making the "right connections" between various research areas increases as the size of the entire knowledge database grows. However, serendipity in the form of unexpected occurrences and chance "mistakes" always plays a strong hand and one must be prepared to recognize opportunities and act on them where possible. The most profound and dramatic connections often turn out to be those made between, at first sight, seemingly disparate fields. Nevertheless, despite the complexity of the maze, one is able to discern a certain logic in the ideas discovered over time, so that rather than them being presented or learned as a loose collection of dry facts, the trees serve to organize them into a meaningful whole. The big payoff is that student interest in the subject is enhanced and memory retention of information increases. A great motivation is the tantalizing prospect that if successful in significantly advancing the field, an aspiring student may one day join this growing "tree of knowledge". What is important is knowing the connections between ideas and the context and circumstances in which those discoveries were made, ascertaining the limitations and levels of approximation employed, performing full graphical critical point and dimensional analyses of key equations, and representing ideas using visualization techniques if possible. All of these can be best achieved by reading the published works of the originators of the discoveries themselves rather than relying solely on a textbook author's "hand-me-down" interpretation of them. Peter Dervan's following quote exemplifies the value of doing just that and how teaching can influence research. "During my first years at Cal Tech, I experienced how profoundly classroom teaching would influence my research. I taught Advanced Organic Chemistry, a reaction mechanisms course for graduate students. I never had the time to read in detail the original seminal papers of Winstein, Doering, Roberts, Olah and other pioneers of the field. Upon reading those key papers published mostly in the 1950s, I realized that these researchers set the stage for several decades of new inquiry in the field of reactive intermediates. My research should not be closing problems but rather opening new areas. I decided to choose a research problem that seemed hopeless in terms of current understanding, but would be suitable for thirty years of scientific inquiry." (11).

Those researchers who follow this track early in their career paths are able to ask more penetrating questions and to chart new directions with greater confidence and thereby do worthwhile research of high quality. Knowing what is important and what is not is one of the key skills in charting a research agenda. In short, being able to see the big picture is imperative for success. Hence, the impact on one's research plans is tremendous. In this vain, distinguishing innovators from followers becomes important. The reader may peruse these trees at leisure and consult them over several times and new ideas and revelations will surface. The reader is invited to explore these trees in a self-discovery approach and verify for themselves the previous points through their own personal experiences.

Table 1 lists some examples in the field of reaction intermediates of important idea and discovery connections between innovators and followers who themselves, in many cases, became innovators in their own right. Perusal of this list, particularly the structural similarities between juxtaposed reaction intermediates, illustrates and emphasizes points made in the preceding paragraph. Not surprisingly, therefore, students who have trained with any of the key scientific contributors or their immediate descendants are highly sought after as the next generation of academics. The thinking here is that their mentors' successes will likely rub off on them as they chart their own research agendas, particularly if their doktorvater relationship had been positive. In fact, the most effective way for a scientist's work to live beyond their time is for them to populate the next generation of academics with people that they have mentored, otherwise their names and work will inevitably be driven to extinction. This virtually guarantees that their ideas, contributions, and views will continue to influence scientific thought. Moreover, this strategy has a pay off for the advisor in the form of a "boomerang effect" with respect to fame, personal ego, the acquisition of prizes and research funds to continue their scientific work, and a growing publication list. However, this boomerang effect works in one direction; that is, if an advisor's students are sought after it implies that the above benefits follow, but the converse may not always be true

© 2005 NRC Canada

Table 1. Idea and discovery connections between key players in physical organic and reaction intermediate chemistry through doctoral and post-doctoral scientific lineages.

Innovating idea or discovery	Following idea or discovery
A.J. Arduengo, III: synthesis of stable imidazolylidenes and imidazolinylidenes (Arduengo carbenes) (1991)	M.K. Denk: synthesis of stable silylene analogues of Arduengo and Wanzlich carbenes (1994), phosphenium ions (1999)
 	   
A. von Baeyer: radical cations in the study of Wurster salts (1875) and synthesis of triphenylmethane dyes (1901 - 1905)	R. Willstätter: radical cations in the study of extended p-quinoid structures of p-phenylenediamine (1908) and study of o-quinodimethanes (1907)
 Wurster's blue  Wurster's red 	 

© 2005 NRC Canada

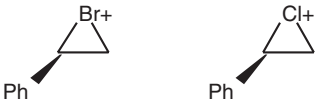
Table 1 (*continued*).

A. von Baeyer: concept of angle strain in ring systems (1885)

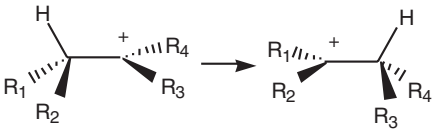
H. Sachse: Mohr-Sachse boat and chair conformations of cyclohexane (1890)

P.D. Bartlett: bridged bromonium and chloronium ions in the bromination and chlorination of styrene (1936 - 1937); aziridinium ions (1947); episulfonium ions (1949)

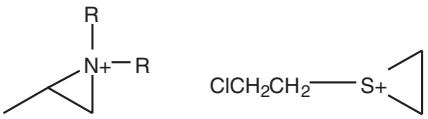
D.S. Tarbell: bridged bromonium and chloronium ions in the bromination and chlorination of styrene (1936 - 1937)



F.E. Condon and A. Schneider: Bartlett-Condon-Schneider reaction involving 1,2-proton shifts in carbocation intermediates (1944)



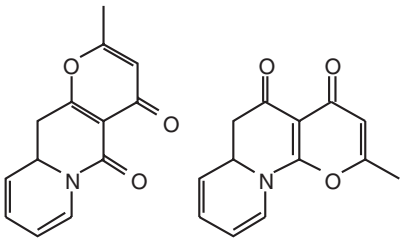
C.G. Swain: aziridinium ions (1947) and episulfonium ions in the solvolysis of mustards (1949)



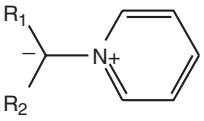
D.H.R. Barton: role of conformation in predicting product outcomes in organic synthesis (1952)

N. Holness: Winstein-Holness equation relating overall rate constant for appearance of product to relative populations of starting conformers (1955)

J. Berson: elucidation of the structure of pyridine adducts of ketene (1956)[a]



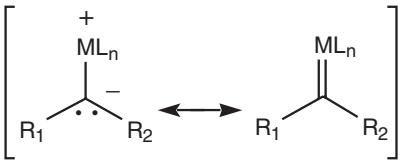
M.S. Platz: trapping of spectroscopically invisible carbenes with pyridine to yield coloured pyridine ylides in LFP experiments (1986)



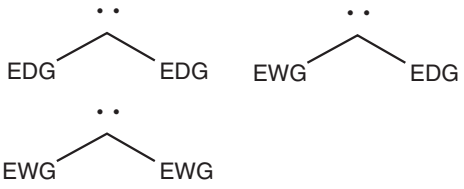
© 2005 NRC Canada

Table 1 (*continued*).

G.L. Closs: discovery of carbenoids in cyclopropanation of olefins (1964); first absolute rate constant measurement of carbene reaction by LFP (1976)



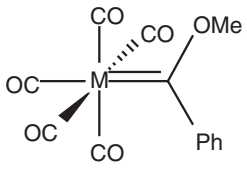
R.A. Moss: Hammett analysis of carbene and olefin reaction (1975); concept of philicity in singlet carbenes (1977)



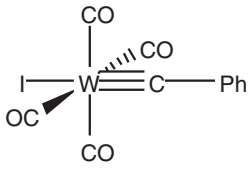
H. Eyring: development of the absolute rate and transition state theory and Eyring equation (1935), application of the absolute rate theory to electrode kinetics (1939), heterogeneous catalysis (1940)

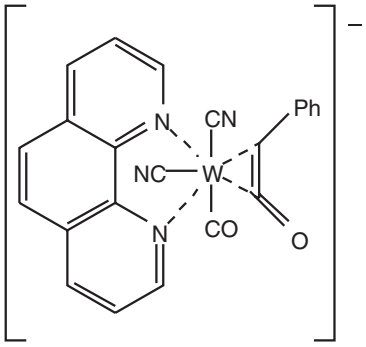
K.J. Laidler: application of the absolute rate theory to electrode kinetics (1939), heterogeneous catalysis (1940), solvent effects in kinetics (1940), investigation of kinetics of the urea-urease system (1949), thermal free radical reactions (1951), investigation of pH effects on enzyme kinetics (1955), temperature effects on enzyme kinetics (1979)

Ernst O. Fischer: synthesis of transition metal complexes of carbenes (1964), carbynes (1973), and ketenes (1983)



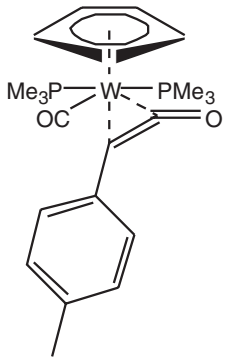
M = W, Cr, Mo





$[Ph_3P\text{-}N{=}PPh_3]^+$

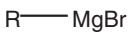
F. Kreissl: synthesis of transition metal complexes of ketenes (1976)



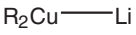
© 2005 NRC Canada

Table 1 (*continued*).

V. Grignard: organometallic compounds and Grignard organomagnesium reagents for carbon-carbon bond forming reactions (1900)



H. Gilman: Gilman organocuprate reagents for carbon-carbon bond forming reactions (1936)



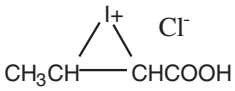
L.P. Hammett: concept of linear free energy relationships (1924) and Hammett equation (1935)

$\log\left(\frac{K_X}{K_H}\right) = \rho\sigma$ (for equilibrium reactions) $\log\left(\frac{k_X}{k_H}\right) = \rho\sigma$ (for irreversible reactions)
where σ is the substituent constant and ρ is the reaction constant

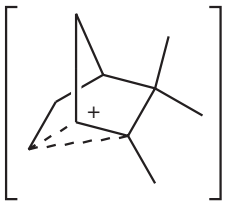
R.W. Taft Jr.: Taft equation (1952)

$\log\left(\frac{k_X}{k_H}\right) = \rho^*\sigma^* - SE_S$
where σ^* is the substitutent polar effect constant, E_S is the substituent steric effect constant, and ρ^* and S are the corresponding reaction constants

C.K. Ingold: bridged halonium ions in the reaction of 2-butenoic acid with ICl (1931)



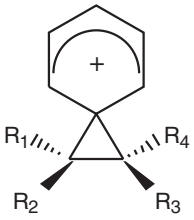
C.L. Wilson: suggestion of bridged carbocations as intermediates in the Wagner–Meerwein rearrangement of camphoryl chloride (1939)



A.G. Brook: bridged mercurinium ions in the oxymercuration of olefins (1950)



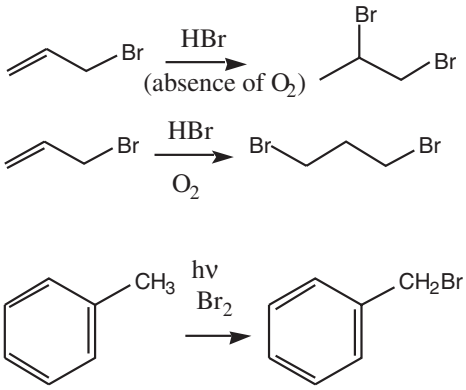
D.J. Cram (1949), S. Winstein (1952), A.J. Kresge (1962): study of phenonium ions



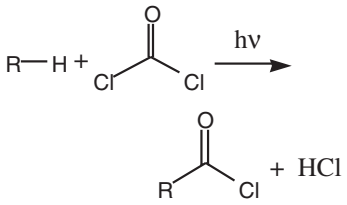
© 2005 NRC Canada

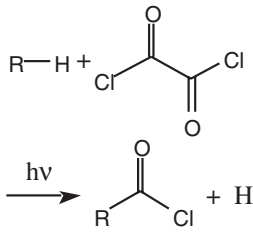
Table 1 (*continued*).

M.S. Kharash: study of radicals in solution phase reactions (1930s)

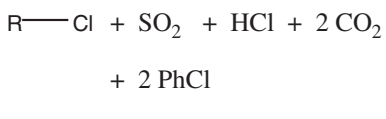


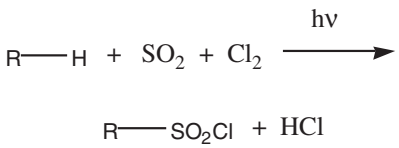
H.C. Brown: study of radicals in chloroformylation and chlorosulfonation reactions (1940)



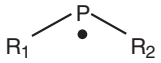




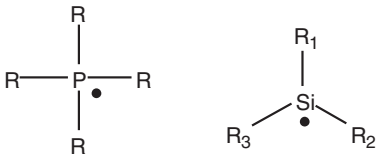




W.H. Urry: phosphinyl radicals (1945)



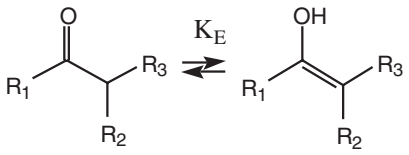
C. Walling: phosphoranyl radicals (1959) and silyl radicals (1966)



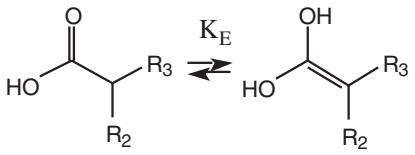
© 2005 NRC Canada

Table 1 (*continued*).

A.J. Kresge: detection and measurement of keto-enol equilibrium constants for simple ketones in aqueous solution (e.g., acetone) (1984)



N.P. Schepp: detection and measurement of keto-enol equilibrium constants for enols of carboxylic acids in aqueous solution (mandelic acid) (1989)



G.N. Lewis: concept of covalent bonding (1916)

W.M. Latimer and W.H. Rodebush: concept of hydrogen bonding (1920)

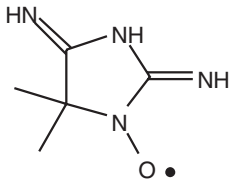
J.U. Nef: concept of tautomerism (1877)

S.F. Acree: proposed Acree -Curtin-Hammett principle based on product studies of diazomethanation of various tautomeric forms of phenylurazoles (1907)

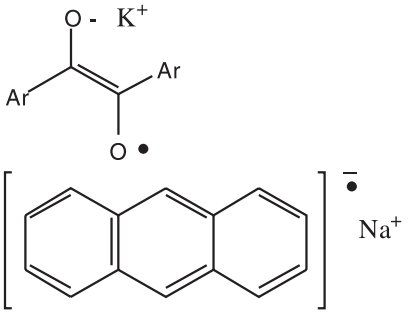
R.G.W. Norrish: discovery of the Norrish Type I and Type II photoreactions (1935); development of flash photolysis technique (1949)

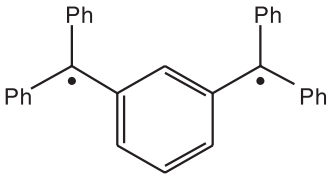
G. Porter: development of flash photolysis technique (1949)
J. Wirz: detection of ynol intermediate by laser flash photolysis (1989)

O. Piloty: synthesis of the first organic nitroxide, porphyrexide (1901)



W. Schlenk: synthesis of stable ketyl radicals (1911), metal radical anions (1914), and the Schlenk-Brauns hydrocarbon (biradical) (1915)

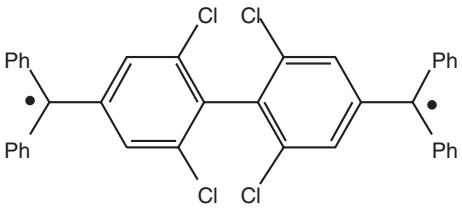




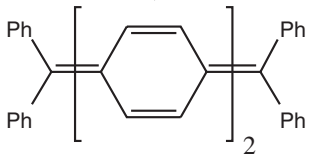
E.F.W. Müller: synthesis of Müller's hydrocarbon (biradical) (1935), Müller-Müller-Rodloff biradical rule (1935); magnetic susceptibility measurements on ketyl radicals and ketyl radical anions (1936); discovery of 2,4,6-tri-*t*-butylphenoxy radical (1955)

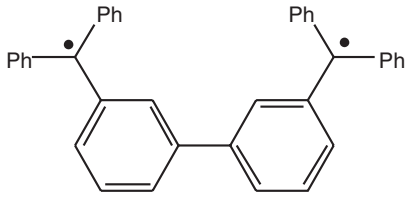
© 2005 NRC Canada

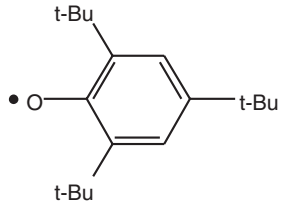
Table 1 (*continued*).









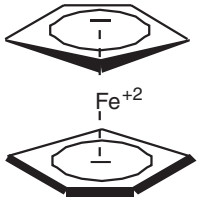


S.P.L. Sorensen: development of pH scale (1909)	J.N. BrØnsted: development of acidity concept (1923), catalysis law (1924 - 1928)
J.K.W.F. Tiemann: first proposal of nitrenes as intermediates in the Lossen rearrangement (1891)	J. Stieglitz: suggestion of nitrenes as intermediates (1896) H. Staudinger: nitrenes (1917)

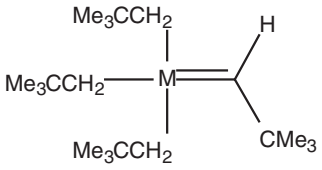
© 2005 NRC Canada

Table 1 (*concluded*).

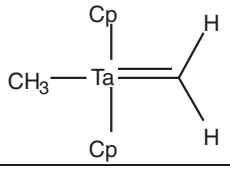
G. Wilkinson: elucidation of the structure of ferrocene (1952)



R.R. Schrock: synthesis of tantalum and niobium carbene complexes (Schrock carbenes) (1974)



M = Ta, Nb



Note: See Tables S1, S5, and S6 in the Supplementary material in the following paper (2) for the original references.
[a]J.A. Berson and W.M. Jones. J. Am. Chem. Soc. **78**, 1625 (1956).

depending on how generous or selfish an advisor is in letting their students pursue their own ideas and allow them to shine. This leads to the key question a research student should ask of their prospective advisor before ranking them according to their area of research, prizes, their publication list, and other recognition measures: "What were the career fates of past students and research fellows who passed through that research group?". Sydney Brenner (2002 Physiology and Medicine Nobel Laureate) offers the following succinct insight in his autobiographical sketch on the point of reprioritization of selection criteria of advisors for students when choosing their potential research mentors (12): "I believe that a scientist should be judged by the quality of the people he has helped to produce and not by prizes or other honours bestowed on him."

These positive influences are tempered by the fact that the achievements of a research advisor are linked directly to the successes of their students. Simply put, an advisor is only as good as his or her students. Also, another tempering point is that there is an expectation and promise that these budding scientists make notable future discoveries and expand fundamental knowledge over their own careers. In this vein, faculty members in Canada who have been most successful in placing their students and post-doctoral fellows in academic positions in departments of chemistry in Canada in the fields of pure and applied physical organic chemistry and related areas are given in the following. University names in parentheses denote where these people have worked or are currently charting their careers.

Ronald J. Gillespie:
Felix Aubke (University of British Columbia)
Thomas Birchall (McMaster University)
Howard J. Clase (Memorial University)
Philip A.W. Dean (University of Western Ontario)
John S. Hartman (Brock University)
John B. Milne (University of Ottawa)
Jack Passmore (University of New Brunswick)
J. Wilson Quail (University of Saskatchewan)
Edward A. Robinson (University of Toronto)
Gary J. Schrobilgen (McMaster University)
John B. Senior (University of Saskatchewan)
Robert C. Thompson (University of British Columbia)
William A. Whitla (Mount Allison University)
J.C. Tito Scaiano:
Pamela A. Arnold (University of Ottawa)
Jeffrey T. Banks (Acadia University, University of New Brunswick)
Monica Barra (University of Waterloo)
Cornelia Bohne (University of Victoria)
Gonzalo Cosa (McGill University)
Frances L. Cozens (Dalhousie University)
Christopher Evans (Ryerson University)
William J. Leigh (McMaster University)
Matthew J. Lukeman (Acadia University)
William Skene (Université de Montréal)
Keith Yates:
Robin A. Cox (University of Toronto)
Alan C. Hopkinson (York University)
Robert A. McClelland (University of Toronto)
Robert S.B. McDonald (Mt. Saint Vincent University)
Paul G. Mezey (University of Saskatchewan, Memorial University)
James A. Pincock (Dalhousie University)
Oswald S. Tee (Concordia University)
Peter Wan (University of Victoria)
Keith U. Ingold:
Jeffrey T. Banks (Acadia University, University of New Brunswick)
Philip J. Dutton (University of Windsor)
Linda J. Johnston (NRC, Ottawa)
Janusz Lusztyk (NRC, Ottawa)
J.C. Tito Scaiano (NRC, University of Ottawa)
Danial D.M. Wayner (NRC, Ottawa)
Russell J. Boyd:

© 2005 NRC Canada

Axel D. Becke (McMaster University)
Natalie M. Cann (Queen's University)
Katherine V. Darvesh (Mt. Saint Vincent University)
James W. Gauld (University of Windsor)
Brian A. Pettitt (University of Winnipeg)
Stacey D. Wetmore (Mount Allison University)
Ross E. Robertson:
James B. Hyne (University of Calgary)
Kenneth T. Leffek (Dalhousie University)
Alan Queen (University of Manitoba)
John Marshall William Scott (Memorial University)
Allan R. Stein (Memorial University)
John Steve Hartman (Brock University)
E.W.R. Steacie:
James B. Farmer (University of British Columbia)
Hyman D. Gesser (University of Manitoba)
Harry E. Gunning (University of Alberta)
Douglas G. James (University of British Columbia)
John C. Polanyi (University of Toronto)
David C. Walker (University of British Columbia)
Imre G. Csizmadia:
John D. Goddard (University of Guelph)
Alan C. Hopkinson (York University)
Roy E. Kari (Laurentian University)
Paul G. Mezey (University of Saskatchewan, Memorial University)
Raymond A. Poirier (Memorial University)
Keith J. Laidler:
Harvey Kaplan (University of Ottawa)
Michael T.H. Liu (University of Prince Edward Island)
Leon F. Loucks (University of Prince Edward Island)
Keith G. McCurdy (University of Lethbridge)
Donald J. McKenney (University of Windsor)
Ronald H. Kluger:
B. Jik Chin (University of Toronto)
Andew S. Grant (Mount Allison University)
Scott D. Taylor (University of Toronto)
Gregory R.J. Thatcher (was at Queen's University)
John Paul Pezacki (NRC, Ottawa)
John Warkentin:
Robin A. Cox (University of Toronto)
Adrian L. Schwan (University of Guelph)
John Paul Pezacki (NRC, Ottawa)
Paul R. West (University of Victoria)
Saul Wolfe:
Howard Alper (University of Ottawa)
Glenn E. Palmer (University of Prince Edward Island)
Arvi Rauk (University of Calgary)
Donald F. Weaver (Dalhousie University)
Donald R. Arnold:
James A. Pincock (Dalhousie University)
William J. Leigh (McMaster University)
Danial D.M. Wayner (NRC, Ottawa)
Richard F.W. Bader:
Andre D. Bandrauk (Université de Sherbrooke)
Thanh T. Nguyen Dang (Laval University)
Kathleen M. Gough (University of Manitoba)
Adrian G. Brook:
Kim M. Baines (Univesity of Western Ontario)
Gary J.D. Peddle (University of Alberta)
Cecil M. Warner (University of Guelph)
Erwin Buncel:
Helen A. Joly (Laurentian University)
Richard A. Manderville (University of Guelph)
David R.J. Palmer (University of Saskatchewan)
James T.C. Wojtyk (University of Prince Edward Island)
A. Jerry Kresge:
Andrew S. Grant (University of Winnipeg, Mount Allison University)
Norman P. Schepp (Dalhousie University)
Robert A. McClelland:
Judy L. Bolton (was at Queen's University, now at University of Illinois at Chicago)
R. Bruce Lennox (McGill University)
Frances L. Cozens (Dalhousie University)
Thomas T. Tidwell:
Richard F. Langler (Mount Allison University)
Daryoush Tahmessebi (St. Francis Xavier University, Brandon University)

Acknowledgements

Parts of this work were presented at the 29th Ontario–Quebec Physical Organic Chemistry Mini-Symposium, 2–4 November, 2001, York University, Toronto, Ontario.

Though best efforts were made in this work to recognize as many key contributors to the study of reaction intermediates as far as possible, any remaining errors and (or) omissions in any of the compilations is unintentional.

References

1. J. Andraos. Named things in chemistry and physics [online]. Available from http://www.careerchem.com/NAMED/Homepage.html [accessed July 2004]. 2001.
2. J. Andraos. Can. J. Chem. **83**, 1415 (2005).
3. H.C. Brown and P.v.R. Schleyer. The nonclassical ion problem. Plenum Press, New York. 1977. pp. 8 to 9.
4. A. Schopenhauer. On the wisdom of life: essays and aphorisms. Translated by R.J. Hollingdale. Penguin, Middlesex. 1970.
5. M. Planck. Scientific autobiography and other papers. Translated by F. Gaynor. Philosophical Library, New York. 1949. pp. 33 to 34. See also: C.C. Gaither and A.E. Cavazos-Gaither. Scientifically speaking: a dictionary of quotations. Institute of Physics Publishing, Bristol. 2000. p. 348.
6. (*a*) A.W.H. Kolbe. J. Prakt. Chem. **14**[n.f.], 268 (1876); (*b*) A.W.H. Kolbe. J. Prakt. Chem. **15**[n.f.], 473 (1877). See also: M. Polanyi. Personal knowledge: towards a post-critical philosophy. The University of Chicago Press, Chicago. 1962. pp. 155 to 156.
7. H. Lineweaver and D. Burk. J. Am. Chem. Soc. **56**, 658 (1934).
8. R. Dagani. Chem. Eng. News, **81**, 26 (2003).
9. (*a*) C.F. Koelsch. J. Am. Chem. Soc. **54**, 4744 (1932); (*b*) C.F. Koelsch. J. Am. Chem. Soc. **79**, 4439 (1957).
10. C.A. Winkler. M.Sc. thesis, McGill University, Montreal, Quebec. 1933.
11. P. Dervan. Bioorg. Med. Chem. **9**, 2215 (2001).
12. T. Frängsmyr (*Editor*). Les Prix Nobel. The Nobel Prizes 2002 [online]. Available from http://www.nobelprize.org/medicine/laureates/2002/brenner-autobio.html [accessed May 2005]. 2003.

© 2005 NRC Canada

Reaction intermediates in organic chemistry — The "big picture"[1]

John Andraos

Abstract: An overview of the discovery of reaction intermediates and associated concepts in physical organic chemistry is presented. Particular attention is paid to chronology of ideas, frequency of occurrence of reaction intermediates in the library of organic reactions used in organic synthesis, and the lexicon of scientific terms used in the language of physical organic chemistry. General logic decision trees are presented for the unique or near unique identification of reaction intermediates based on experimental techniques and common patterns of reactivity documented in the literature over the last century. Contributions made by scientists working in laboratories at Canadian universities and at the National Research Council of Canada are noted throughout.

Key words: physical organic chemistry, mechanistic chemistry, reaction intermediates.

Résumé : On présente une revue de la découverte d'intermédiaires réactionnels et de concepts apparentés en chimie organique physique. On porte une attention particulière à la chronologie des idées, la fréquence de la mention des intermédiaires réactionnels dans les relevés de réactions organiques utilisées en synthèse organique et le lexique des termes scientifiques utilisés dans le langage de la chimie organique physique. On présente des arbres décisionnels logiques et généraux pour l'identification unique ou pratiquement unique d'intermédiaires réactionnels basés sur des techniques expérimentales et sur des patrons communs de réactivité documentés dans la littérature pendant plus d'un siècle. On note partout les contributions faites par les scientifiques travaillant dans les laboratoires des universités canadiennes et dans ceux du Conseil national de recherches du Canada.

Mots clés : chimie organique physique, chimie mécanistique, intermédiaires réactionnels.

[Traduit par la Rédaction]

Introduction

The development of physical organic chemistry concepts is inextricably linked to the discovery and identification of reaction intermediates (1). Once chemists began amassing a library of chemical reactions that made it possible for one chemical structure to be transformed into another, thereby ushering in the vast and unlimited field of organic synthesis, it soon became apparent that patterns of reactivity among common structures emerged as a consequence of such transformations. The central questions of how and why particular products resulted in a given reaction from known substrate structures launched the field of mechanistic chemistry. These questions in turn evolved into others such as "how fast a particular reaction proceeds" and "how can one control the product outcome". The former launched an era of instrumentation development where various time-resolved techniques were invented to probe the temporal gap between substrate and product(s) of a given reaction. The latter question launched investigations into what parameters were important and to what degree in determining product outcomes. All of these questions were greatly influenced by ongoing parallel theoretical and experimental developments in the understanding, determination, and verification of chemical structure. Much of the success in structure elucidation and prediction and in time-resolved studies of reaction intermediates may be attributed to the birth of quantum mechanics and spectroscopy, which were the children of the happy marriage between physics and chemistry. Over time a certain "logic" to the understanding of organic reaction transformations emerged. Essentially the whole field of physical organic chemistry can be reduced to an algorithm that attempts to solve the inverse problem of determining the minimum possible set of elementary steps constituting a reaction mechanism that is consistent with experimental observations. It must also satisfy the fundamental condition that the sum of the elementary steps is the overall chemically balanced stoichiometric equation as prescribed by Lavoisier's conservation of mass law. This set of elementary steps may or may not involve transient structures or reaction intermediates between the known substrate structures and identified product structures. Transient structures may be observed directly or inferred indirectly. This inverse problem is akin to the one in algebra of factoring a complex polynomial into its constituent factors, or in number theory of factoring a natural number into its prime factors. However, an important difference between the two related inverse problems is that in mechanistic chemistry the set of "factors" may not be unique and that an iron-clad deductive proof of mechanism

Received 15 April 2005. Published on the NRC Research Press Web site at http://canjchem.nrc.ca on 8 November 2005.

J. Andraos. Department of Chemistry, York University, Toronto, ON M3J 1P3, Canada. (e-mail: jandraos@yorku.ca).

[1]This article is part of a Special Issue dedicated to organic reaction mechanisms.

 doi: 10.1139/V05-175 © 2005 NRC Canada

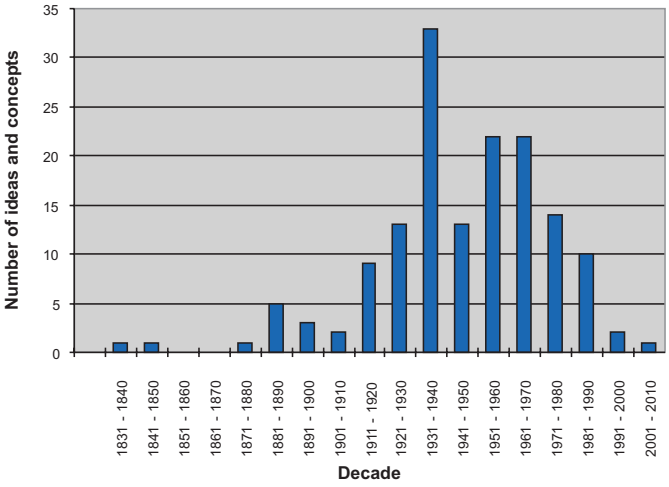
cannot be done. The best one can hope for is consistency among various observations and techniques used. This effectively means that every postulated mechanism, or "set of factors", is only confirmed by experimental evidence and techniques that are available at the time of discovery, and hence is always open to later revision pending reexamination by new techniques. Laidler in a commentary on the use and misuse of the concept of rate-controlling step states that "reaction mechanism can never be established with a high degree of confidence" (2). In mathematics the analogous proof once confirmed is always true for all time.

This paper outlines key developments in physical organic chemistry and shows how they have impacted studies of reaction intermediates. The approach is to present the "big picture", tracing both ideas and people in the field so that the reader can get a sense of scale of what has been accomplished as well as take stock of where we are at today in the field and identify new fruitful areas of future research. Particular attention is paid to chronology of ideas, frequency of occurrence of reaction intermediates in the library of organic reactions used in organic synthesis, and the lexicon of scientific terms used in the language of physical organic chemistry. General logic decision trees are presented for the unique or near unique identification of reaction intermediates based on experimental techniques and common patterns of reactivity documented in the literature over the last century. In keeping with the theme of this special issue, contributions made by scientists working in laboratories at Canadian universities and at the National Research Council of Canada are noted throughout.

Chronology of concepts in physical organic chemistry

Figure 1 shows a histogram of the timeline of discovery of key concepts in the field of physical organic chemistry and Table S1 (Supplementary material)[2] specifies them in a list along with the respective names of scientists who made these contributions. The celebrated ideas are named after particular scientists and the remainder are given special names. It is instructive to point out that when one begins learning about a field of science for the first time one can fast track their study by focusing on the "named things" in that field, since these represent the sign posts of what is important in the subject in question, especially ones that have stood the test of time, usage, and further experimentation by scientists at large. In a number of instances, ideas have been attributed to scientists with established reputations despite them not being the original discoverers. Recent works (3) have documented this phenomenon of incorrect attributions of discovery, priority, and credit of chemical names and eponyms in organic and physical chemistry. Examples relevant to the present compilation (4) include: (*i*) the Le Châtelier's principle of equilibria (1884) (5), which was discovered a few months earlier by Jacobus H. van't Hoff (1884) (6); (*ii*) the Arrhenius equation (1889) (7) also discovered earlier by van't Hoff (1884) (6); (*iii*) the steady-state

Fig. 1. Histogram showing timeline of discovery of key concepts in physical organic chemistry (growth of ideas and concepts).

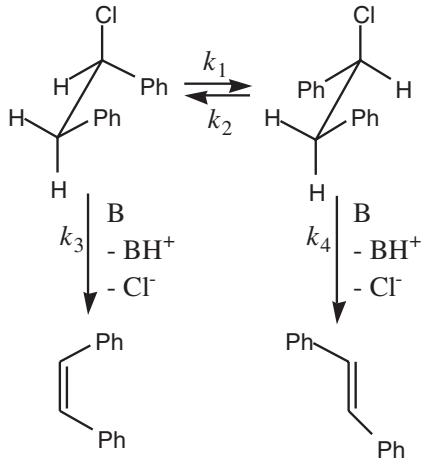


approximation in chemical kinetics credited to Max Bodenstein in 1913, which was described earlier in that year by David Leonard Chapman and his student L.K. Underhill (8); (*iv*) the Michaelis–Menten mechanism of enzyme kinetics (9) (1913), which was first described earlier in 1892–1902 by Adrian J. Brown (10) and by Victor Henri (11) in 1901–1903 following work done in the laboratories of Wilhelm Ostwald in Leipzig and culminating in a doctoral thesis on the enzyme kinetics of diastase; (*v*) the Orton rearrangement (12) (1902) discovered earlier by Georg Bender (13) in 1866; and (*vi*) the Curtin–Hammett principle (14) (1954), which was originally formulated in 1907 by Solomon F. Acree (15). The last case has not been discussed before in the literature and deserves further comment here. No references to Acree's early work are mentioned in any of the well-known papers by Curtin, Hammett, and others including an extensive review of the topic by Seeman (16). Only two citations in the literature appear to mention Acree's contribution (17, 18). Hammett, in his book, refers to the principle as the "Curtin principle", but makes the following footnote: "Because Curtin is very generous in attributing credit, this is sometimes referred to as the Curtin–Hammett principle". Curtin, in turn, in his 1954 paper, published in an obscure journal and likely read by few chemists, refers to a private communication from Hammett in 1950 attributing that the idea originated from Hammett in his comment: "It was pointed out by Professor L.P. Hammett in 1950 that if the transition state theory is accepted and if rotation between the various possible conformations of the starting material is very rapid compared to the rate of the reaction, the relative amounts of products formed from the two critical conformations are completely independent of the relative populations of the conformations and depend only upon the difference in free energy of the transition states." The chemical reaction referred to in Curtin's work is the E2-base-catalyzed elimination of halide from 1,2-diphenyl-1-chloroethane to yield *cis*- and *trans*-stilbene (Scheme 1). Curiously, Curtin's paper

[2] Supplementary data for this article are available on the Web site or may be purchased from the Depository of Unpublished Data, Document Delivery, CISTI, National Research Council Canada, Ottawa, ON K1A 0S2, Canada. DUD 4039. For more information on obtaining material refer to http://cisti-icist.nrc-cnrc.gc.ca/irm/unpub_e.shtml.

© 2005 NRC Canada

Scheme 1.



cis-stilbene *trans*-stilbene

does not present a precise mathematical relationship describing the phenomenon, but Hammett does in his book with the following equation given in eq. [1].

$$[1] \qquad \frac{\mathrm{d[trans-stilbene]}/\mathrm{d}t}{\mathrm{d[cis-stilbene]}/\mathrm{d}t} = \frac{q^{\#}_{\mathrm{trans}}}{q^{\#}_{\mathrm{cis}}}$$

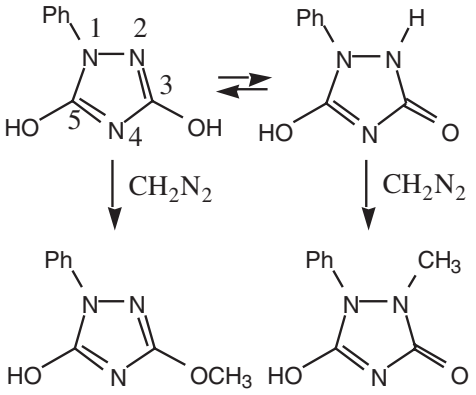
where the qs refer to transition-state partition functions for the elimination steps, which in turn are related to the corresponding rate constants. However, Acree in 1907 studied the oxygen and nitrogen alkylations of tautomeric mixtures of 1-phenyl urazoles with diazomethane in ether solution (Scheme 2). He correctly concluded that "it is perfectly obvious that such reactions … do not give us decisive evidence in regard to the relative amounts of the enol and keto forms in any given amide group in which the change from one tautomeric form to the other is very rapid in comparison with the reactions between the two forms and the alkylating reagents." Furthermore, Acree derived an expression, identical in form to the Winstein–Holness equation, for the observed second-order rate constant for the appearance of total product as a function of the relative populations of the urazole enol and keto forms nearly a half-century before Winstein and Holness's celebrated paper of 1955 (19). The thread of this principle was taken up again nearly 50 years later in 2003 (18) when an experimentally accessible efficiency parameter, defined only in terms of the four relevant rate constants (see eq. [2]), was introduced as a means to gauge the true efficiency of resolution of a chemical system obeying kinetic schemes as shown in Schemes 1 and 2 and having starting materials that are stereochemically related. This parameter was able to account for all experimentally observed cases between and including the limits of complete dynamic kinetic resolution (Acree–Curtin–Hammett conditions) and complete kinetic resolution (anti-Acree–Curtin–Hammett conditions).

$$[2] \qquad \varepsilon_{\mathrm{DKR}} = \frac{rv+u}{rv+u+1}$$

where $r = k_3/k_4$, $u = k_1/k_3$, and $v = k_2/k_3$.

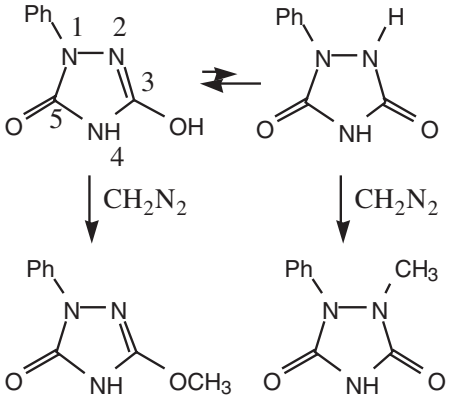
Scheme 2.

2,3-amide group tautomerism



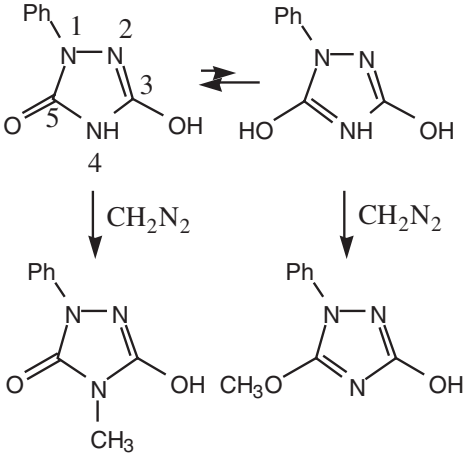
major minor

2,3-amide group tautomerism



major minor

4,5-amide group tautomerism

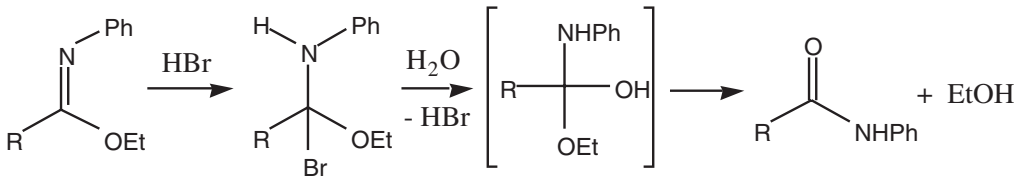


major minor

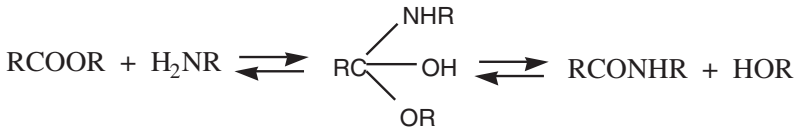
Before the notion of reaction intermediates was even conceived, mathematical laws of chemical kinetics (20) and the concept of catalysis (21) were already established by Jons J.

© 2005 NRC Canada

Scheme 3.



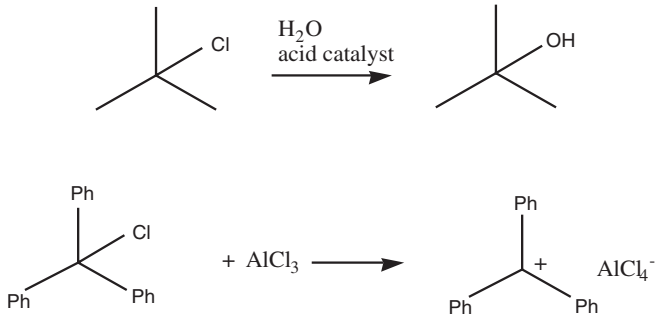
As written by Julius Stieglitz (1899):



Berzelius, Wilhelm Ostwald, and Jacobus H. van't Hoff. Ludwig Wilhelmy carried out the first reported kinetics experiment in 1850 when he examined the acid-catalyzed hydrolysis of cane sugar to invert sugar by polarimetry (22). The concept of the existence of reaction intermediates as chemical species of fleeting lifetimes originated in 1899 when Julius Stieglitz suggested the first mechanism of a chemical reaction when he examined the acid-catalyzed hydration of imidoethers via tetrahedral intermediates (Scheme 3) (23). James Norris in 1901 postulated the existence of carbocations, as it turns out the most extensively studied reaction intermediate class of all, when he examined the solvolysis of tertiary alkyl halides in acidic media (Scheme 4) (24). Almost simultaneously Adolf von Baeyer formulated the carbonium ion theory to account for the chemical behaviour and colour of triphenylmethane dyes such as fuchsine and crystal violet (Scheme 5) (25). A prominent American scientist, Gilbert N. Lewis, in the early part of the last century laid the foundation for a number of concepts that contributed greatly to the study of reaction mechanisms and reaction intermediates: octet rule in bonding (26), electrophilicity and nucleophilicity (27), inductive effect,[3] the prediction that radicals could be studied by magnetic methods,[4] Lewis acids and bases as electron acceptors and donors (27*b*), and the effect of resonance on electronic transitions (28).

Examination of the histogram in Fig. 1 shows the first "golden age" of physical organic chemistry in the 1930s and 1940s when simple reaction mechanisms were systematically categorized by type for the first time and new nomenclatures were introduced by Sir Christopher K. Ingold and his school such as Elcb (29), S_N1 and S_N2 (30), E1 and E2 (31), A1 and A2 (32), and B1 and B2 (32). Up to that time about 200 named organic reactions were already known since Wöhler's urea synthesis (33). The earliest attempts to understand reactivity in a systematic way were made by Sir Robert Robinson who formulated the familiar curly arrow notation to symbolize electron flow from electron donor groups to electron acceptor groups in an effort to determine patterns of reactivity in aromatic substitution reactions and to understand electronic effects of substituents on aromatic

Scheme 4.



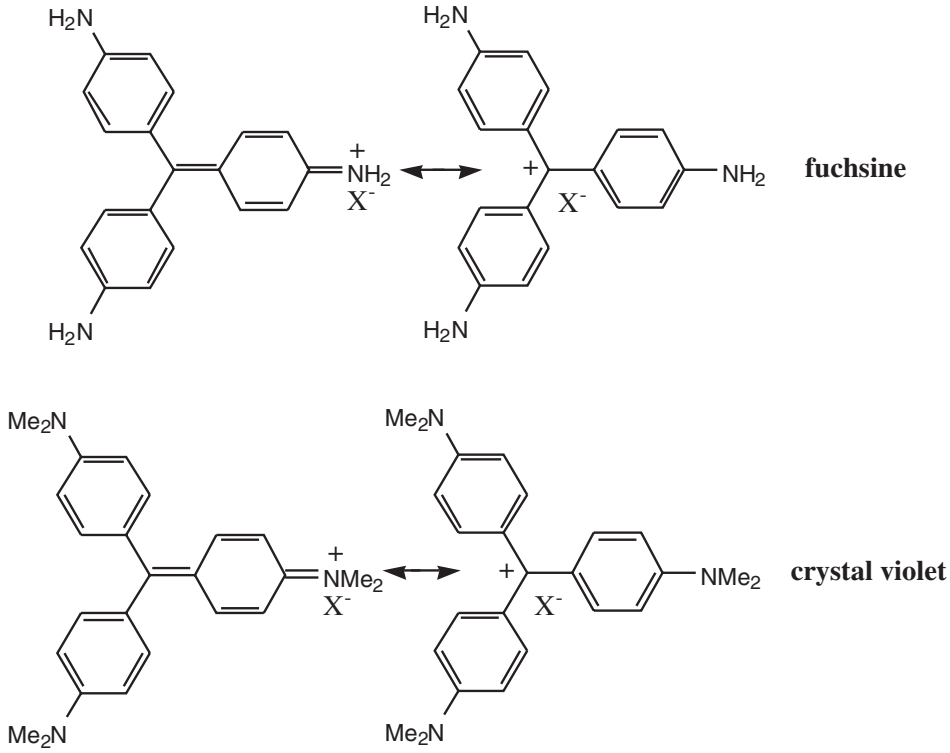
rings (34), and by Arnold F. Holleman who introduced the concept of directing groups in such reactions (35). Both Robinson and Ingold formulated the electronic theory of organic chemistry (36) though a bitter controversy over priority developed between them (37). The next major advances to be put forward during this period were by Johannes Brönsted (38), who introduced a linear double logarithmic correlation between rate constants and acid strength for acid- and base-catalyzed proton transfer reactions, by Louis Hammett (39), who introduced the general concept of linear free energy relationships and the quantitative partitioning of substituent effects via substituent constants, and by Henry Eyring (40), who introduced transition-state theory that linked measurable kinetic and thermodynamic parameters to explain the dynamics of bond-making and bond-making processes in elementary steps of a reaction mechanism. In a short time after the discovery of deuterium by Harold Urey in 1932 (41) powerful techniques for probing the nature of such transition states, particularly those pertaining to the rate-determining step, emerged; namely the determination of isotope effects on rate constants and equilibrium constants (42), isotopic labelling experiments (43), and isotopic exchange experiments (44). All of these advances helped to rationalize chemical reactions and gave chemists the confidence to predict product outcomes for new reactions that had yet to be carried out.

In the second golden age of physical organic chemistry in the 1950s and 1960s, attention shifted to the United States

[3] See ref. 20*a*, p. 139.
[4] See ref. 20*a*, p. 80, 148.

© 2005 NRC Canada

Scheme 5.



where the following people figured prominently in further developing ideas in the field: Paul D. Bartlett (Harvard), Ronald Breslow (Columbia), William von Eggers Doering (Columbia), George S. Hammond (Iowa State, Cal Tech), William P. Jencks (Brandeis), George A. Olah (USC), C. Garner Swain (MIT), Robert W. Taft, Jr. (Pennsylvania State, UC Irvine), Frank H. Westheimer (Harvard), and Saul Winstein (UCLA). Though Canadian university students of chemistry have heard of Winstein's name in connection with several concepts in physical organic chemistry as attested by the many things named after him, very few, if any, know that he was born and raised in Montreal, Quebec before embarking on a doctoral degree at Cal Tech under Howard J. Lucas and launching his legendary career at UCLA (45).

In this time period the invention of time-resolved techniques (46) for probing fast reactions resulted in an explosion of research on monitoring the temporal behaviours of a wide variety of transients in various media whose lifetimes are in the submillisecond to picosecond time domains. This second golden age was characterized by technological advances in instrumentation, which made it possible to probe the earliest stages of chemical processes in a reaction mechanism. The strength of these methods led mainly by flash photolysis provided direct observation of reaction intermediates by various kinetic and spectroscopic means. Both kinetic decay (or growth) curves and spectra of transients could thus be obtained. The invention of lasers by physicists and other electronic equipment by engineers and skilled technicians to rapidly convert optical signals into electrical signals and to capture, digitize, and store kinetic waveforms for subsequent analysis helped to propel this technique to the forefront of research. Modern day physical organic chemists ought to therefore give these scientists the credit and respect that they so rightly deserve. The main condition for making the chemistry work by this method was the fact that targeted transients had to be generated by some photochemical reaction. Other techniques based on rapid mixing of solutions such as stopped-flow (46) or on applying sudden perturbations of temperature on solutions, commonly called the T-jump technique (46), also contributed to the study of reaction intermediates, but to a lesser extent. Virtually every kind of spectroscopy has been modified to become time-resolved in one way or another. Another useful technique pioneered by George C. Pimentel (47) to probe reaction intermediates is that of generating them in noble gas matrices at low temperatures and inferring their structure by IR, microwave, or UV spectroscopy in conjunction with theoretical calculations of their geometries at various levels of theory. IR spectroscopy is particularly useful since observed spectra can be directly compared with vibrational frequencies calculated from analyses of corresponding geometry optimized structures.

In recent years emphasis has shifted to the syntheses of thermodynamically and (or) kinetically stable analogs of reaction intermediates, essentially putting them in a bottle. This has lead to a number of chemical curiosities (see Table S6 in the Supplementary materials).[2] Success can be achieved by judicious choice of substituents so as to impart stabilization by electronic and (or) steric effects or by generating them in exotic media that stabilize their structures such as "magic acid" (48), or by caging the intermediates in highly restricting media such as zeolite supercages (49). Another new frontier that is being examined is the probing of organometallic intermediate structures in important carbon–

© 2005 NRC Canada

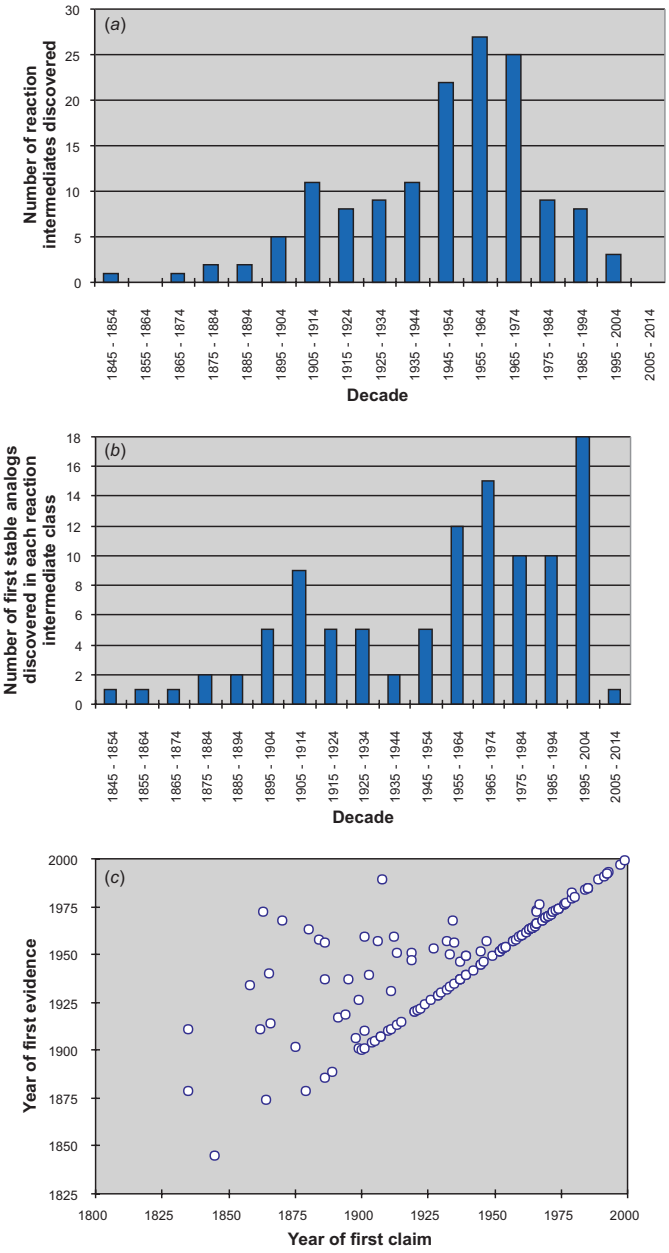
carbon bond-forming reactions that utilize organometallic catalysts, particularly those containing palladium and other transition metals (50).

Table S2 (Supplementary material)[2] summarizes important coined terms used in physical organic chemistry and reaction intermediate studies. It is instructive to point out here that a very effective way for a scientist to carve out their scientific niche and get attention for their work is to coin a particular word or phrase that over time will end up being synonymous with the discovery that they have made or the concept that they initiated and their persona. Perusal of this list shows some well-known coined name – scientist associations as well as some surprises, which even the seasoned practitioner in the field may learn about for the first time. The true measure of worth and recognition of an idea or concept is when other scientists use that idea or concept in their own work and even go further by building on top of it.

Chronology of discovery of reaction intermediates

Figures 2*a* and 2*b* show timelines of discovery of reaction intermediates and of stable analogs. Original references, including reviews, and schemes depicting reactions for all of these intermediates are compiled in the extensive database of Tables S5 and S6 (Supplementary material).[2] The histogram in Fig. 2*a* shows that the greatest number of intermediates were discovered during the second golden age of physical organic chemistry (mid-1940s to mid-1970s) that coincided with the advent of time-resolved techniques. Table 1 gives a detailed list of this chronology from Fremy's nitroxide radical salt (1845) to Thomas Tidwell's bisketenes (2000). Figure 2*b* shows the timeline of discovery of stable analogs of reaction intermediates, where it is observed that most of the advances have been made in the last 40 years particularly between 1995 and 2004. Figure 2*c* shows the correlation between first claim and first evidence of intermediate identification by experimental means. Not surprisingly the correlation is worse from the mid-19th century to the mid-20th century and improves markedly from about 1950 to the present day. During the early years, many intermediates were conjectured with little experimental evidence. Several years had to pass before their identities were finally confirmed, again largely thanks to technological advances that had to be developed in order for this to happen. Notable intermediates with extended time gaps between claim and discovery include: (*i*) the dication intermediate in the benzidine rearrangement confirmed by George Olah in 1972, 109 years after A.W. Hofmann's discovery of the rearrangement reaction in 1863; (*ii*) oxirene in Wolff rearrangement confirmed by Imre G. Csizmadia and Otto P. Strausz in 1968, 98 years after Marcellin Berthelot's first claim in 1870, which was later proven false, for the oxidation of propyne in the presence of chromic acid; (*iii*) Wallach intermediate confirmed by George Olah in 1963 in magic acid, 83 years after Otto Wallach's discovery of the rearrangement of aromatic azo-*N*-oxides; (*iv*) ynols confirmed by Robin Hochstrasser, Jakob Wirz, and A. Jerry Kresge in 1989, 81 years after Hermann Staudinger's confirmation that the ketene structure is not that of a hydroxyacetylene and 69 years after Charles D. Hurd's conjecture of the keteno–ynol tautomerism; (*v*) ketyl radicals

Fig. 2. (*a*) Histogram showing the timeline of discovery of reaction intermediates. See Table S5[2] for specific structures and references. (*b*) Histogram showing the timeline of discovery of the first stable analogs of reaction intermediates in each class by direct synthesis. See Table S6 in the Supplementary material[2] for specific structures and references. (*c*) Graph showing the correlation between first claim and first evidence of intermediate identification by experimental means.



confirmed by Wilhelm Schlenk in 1911, 76 years after A. Laurent's observation of coloured solutions of aromatic ketones upon exposure to sodium metal in 1835; (*vi*) acetoxyl radicals confirmed in 1934, 76 years after B.C. Brodie's discovery of benzoyl peroxide in 1858; (*vii*) episulfonium ions confirmed by Reynold C. Fuson in 1940, 75 years after A. Cahours's synthesis of thiirane from dimethylsulfide and 1,2-dibromoethane in 1865; (*viii*) phenyl cation confirmed by Edward S. Lewis in 1954, 74 years after the discovery of

© 2005 NRC Canada

Table 1. Chronology of discovery of reaction intermediates.

Year	Reaction intermediate discovered (scientists)[a]
1845	Fremy's nitroxide radical
1874	Sulfonium ions (A. von Oefele, C. Schoeller, A. Cahours)
1879	Radical cations (A. Laurent, C. Wurster, H. Wieland)
1879	Wurster salts
1886	Janovsky complex
1889	Meisenheimer–Jackson complexes
1900	Gomberg radical
1901	Carbocations (J. Stieglitz, J.F. Norris, A. Baeyer)
1901	Piloty's nitroxide radical
1902	Enols (E. Erlenmeyer, A. Lapworth)
1904	Thiele biradical
1905	Ketenes (H. Staudinger)
1906	Phosphonium ions (A. Michaelis, A.E. Arbuzov)
1907	Chichibabin biradical
1907	*o*-Quinodimethanes (R. Willstaetter)
1910	Carbanions (V. Grignard, W. Schlenk)
1910	Niementowski's nitroxide radical
1911	Ketyl radicals (A. Laurent, W. Schlenk)
1911	Carbenes (A. Geuther, H. Staudinger, J. Hine)
1911	*o*- and *p*-Quinonemethides (H. Staudinger)
1913	2,4- and 2,5-Cyclohexadienones (H. McCombie)
1914	Radical anions (M. Berthelot, W. Schlenk)
1915	Schlenk–Brauns biradical
1917	Nitrenes (F. Tiemann, H. Staudinger)
1919	Phosphonium ylides (A. Michaelis, H. Staudinger)
1920	Hydronium ions (L.S. Bagster, G. Cooling, M. Volmer)
1920	Hydrazyl radicals
1921	Pyridine ylides (W. Scheider)
1922	Sulfimine ylides (F. Mann, W.J. Pope)
1924	Flavylium salts (R. Robinson)
1926	Tetrahedral intermediates (J. Stieglitz, F. Swarts)
1926	Kenyon–Banfield radical
1929	Gas-phase alkyl radicals (F. Paneth)
1929	Ammonium ylides (C.K. Ingold)
1930	Sulfonium ylides (C.K. Ingold)
1931	Halonium ions (A. McKenzie, R. Kuhn, C.K. Ingold)
1932	Iminium ions (T.D. Stewart, W.E. Bradley)
1933	Solution-phase alkyl radicals (M.S. Kharasch)
1934	Acetoxy radicals (B.C. Brodie, D.H. Hey, W.A. Waters)
1935	Norrish type I and II biradcials
1937	Benzyl radicals (A. Michaelis, M.S. Kharasch)
1937	Aryl radicals (E. Bamberger, O. Kuehling, W.A. Waters)
1937	Acylium ions (L.P. Hammett, M. Bender)
1937	Acylammonium ions
1937	Meerwein salts
1939	Benzoyl radicals (J.F. Norris, H.H. Glazebrook, T.G. Pearson)
1939	Müller–Neuhoff biradical
1939	Mercurinium ions (H.J. Lucas)
1940	Episulfonium ions (A. Cahours, R.C. Fuson)
1942	Acetoxonium ions (S. Winstein)
1945	Phosphinyl radicals (M.S. Kharasch)
1945	Excited-state triplet ketones (G.N. Lewis, M. Kasha)
1946	Nitronium ions (C.K. Ingold, R.J. Gillespie)
1946	Aziridinium ions (J.S. Fruton, M. Bergmann)
1947	*p*-Quinodimethanes (W. Schlenk, M. Szwarc)
1949	Bridged carbocations (C.L. Wilson, S. Winstein)
1949	Nonclassical ions (C.L. Wilson, S. Winstein)
1949	Phenonium ions (D.J. Cram, S. Winstein)
1950	Germylenes (P. Royen, R. Schwarz, S.N. Glarum, C.A. Kraus)
1951	Nitrenium ions (J. Stieglitz, C.K. Ingold)
1951	Metallocenes (F. Hein, P.L. Pauson, G. Wilkinson, R.B. Woodward)
1952	Aromatic π complexes (M.J.S. Dewar, H.C. Brown)
1952	Metal carbenoids (P. Yates)
1952	Nitrosonium ions (C.K. Ingold)
1952	Methoxonium ions (S. Winstein)
1953	Benzynes (W.E. Bachmann, H.T. Clarke, J.D. Roberts)
1953	Aromatic σ complexes (M. Kilpatrick, G.A. Olah, H.C. Brown)
1953	Doering–Zeiss intermediate
1953	Peroxy radicals
1953	Phenoxyl radicals (E. Muller, C.D. Cook)
1954	Phosphonium betaines (G. Wittig)
1954	Tropylium ions (W.v.E. Doering)
1956	Nitrilium ions (E. Beckmann, F. Klages, W. Grill, I. Ugi)
1956	Wheland intermediate (H.C. Brown, G.A. Olah)
1957	Aminyl radicals (H. Wieland)
1957	Koelsch radical
1957	Silyl radicals (F.C. Whitmore, R.N. Haszeldine)
1957	Cyclopropenyl cations (R. Breslow)
1957	Flavinium salts (A. Robertson, W.B. Whalley)
1958	Phenyl cation (T. Sandmeyer, E.S. Lewis)
1958	1,3-Dioxolenium ions (H. Meerwein)
1959	Pyrylium salts (A. Werner, A.T. Balaban)
1959	Nitroxyl radicals (H. Wieland, K.H. Meyer, O.L. Lebedev)
1959	Phosphoranyl radicals (C. Walling)
1960	Thicarbonyl ylide (G. Wittig)
1960	Vinyl cations (C.A. Grob, P.E. Peterson)
1960	Wanzlich carbenes
1962	Nitrile ylide (R. Huisgen)
1962	Carbonyl oxide (Criegee zwitterion) (R. Criegee, P.D. Bartlett)
1963	Wallach intermediate (O. Wallach, **E. Buncel**, G.A. Olah)
1963	1,3-Dipole traps (R. Huisgen)
1963	Dinitrenes (A.M. Trozzolo, E. Wasserman)
1963	Verdazyl radicals (R. Kuhn)
1964	Violenes (S. Hünig)
1964	Thiophenoxyl radicals (U. Schmidt)
1964	Phenylselanyl radicals (U. Schmidt)
1964	Fischer carbene
1964	Vinylidene carbenes (H.D. Hartzler, W.J. le Noble)
1964	Iminoxyl radicals (J.R. Thomas)
1965	Phosphinoyl radicals
1966	Dications in magic acid (G.A. Olah)
1966	Acyl radicals (H.G. Kuivila, E.J. Walsh, Jr.)
1966	Stannyl radicals
1966	Silylenes (P.P. Gaspar)
1968	Oxirene (M. Berthelot, W. Madelung, **I.G. Csizmadia**, **O. Strausz**)
1968	Vinylidenes (G.H. Coleman, R.D. Maxwell, M.S. Newman, P.J. Stang)
1968	Allene oxides (J.K. Crandall)

© 2005 NRC Canada

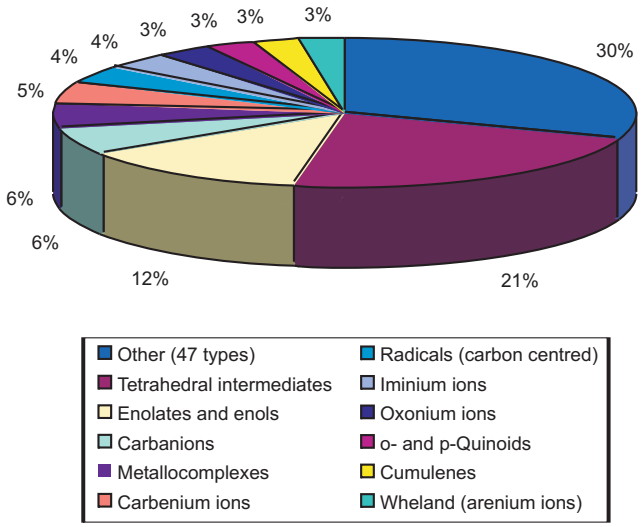
Table 1 (*concluded*).

Year	Reaction intermediate discovered (scientists)[a]
1968	Trinitrenes (E. Wasserman)
1969	Azomethines
1969	*N*-Alkoxy-*N*-alkylamino radicals
1969	Thiirenium ions (G. Modena)
1970	Carbonyl ylide (**D.R. Arnold**)
1970	Phosphinothioyl radicals
1970	Transition-metal vinyl cation complexes (H.C. Clark, R.J. Puddephatt)
1971	Nicholas cation
1972	Dication in benzidine rearrangement (A. Hofmann, G.A. Olah)
1972	Transition metal vinylidene complexes (O.S. Mills, A.D. Redhouse, R.B. King)
1972	Amido radicals
1972	Transition-metal keteniminium complexes
1973	Oxenium ions (R.A. Abramovitch)
1973	Transition-metal carbyne complexes (E.O. Fischer)
1974	Carbynes (**O.P. Strausz**)
1974	Propadienones (R.F.C. Brown)
1974	Schrock carbene
1976	Thionitroxide radicals (J.E. Bennett, W.C. Danen)
1976	Thioaminyl radicals (W.C. Danen)
1976	Transition-metal ketenyl complexes (F.R. Kreissl)
1976	Transition-metal vinylidenecarbene (allenylidene) complexes (E.O. Fischer)
1977	Transition-metal silene complexes
1979	Butatrienones (R.F.C. Brown)
1980	2,4- and 2,5-Cyclohexadienimines
1982	Ketene zwitterions (R. Gompper, U. Wolf, J. Pacansky, **J.C. Scaiano**)
1984	Trapping of carbenes via ylide formation (**J.C. Scaiano**, M.S. Platz)
1985	Bertrand carbene
1985	*N*-Thiosulfonamidyl radicals (Y. Miura)
1985	Distonic radical cation (L. Radom)
1989	Ynols (H. Staudinger, C.D. Hurd, R. Hochstrasser, J. Wirz, **A.J. Kresge**)
1989	Oxonium ylides (W. Kirmse)
1991	Arduengo carbene
1992	Iminopropadienones (C. Wentrup)
1992	Trimethylsilyl substituted bisketenes (**T.T. Tidwell**)
1993	Silylium ions (C.A. Reed)
1997	Allenylketenes (**T.T. Tidwell**)
1999	Phosphenium ions (**M.K. Denk**)

Note: See Table S5 in the Supplementary material[2] for references.
[a]Bolded entries represent contributions by scientists working in Canadian universities or at the National Research Council of Canada.

the Sandmeyer reaction in 1884; (*ix*) nitrilium ions confirmed by F. Klages, Ivar Ugi, and A. Hassner between 1956 and 1966, 70–80 years after the discovery of the Beckmann rearrangement of 1886; (*x*) pyrylium ions confirmed by A. Balaban's synthesis of pyrylium salts in 1959, 58 years after Alfred Werner's initial observations in 1901; (*xi*) benzyl radicals confirmed by Morris S. Kharasch in 1937, 51 years after August Michaelis's synthesis of tribenzylarsine from benzyl chloride and arsenic trichloride in 1886; and (*xii*) carbenes confirmed by Hermann Staudinger in 1911 in the thermal and photochemical Wolff rearrangement of diazoketones and by Jack Hine in 1950 in the haloform hydrolysis reaction under basic conditions 49 and 88 years, respectively, after A. Geuther's conjecture of their existence in the hydrolysis of chloroform in base in 1862.

Fig. 3. Pie chart showing the frequency of occurrence of reaction intermediate types in named organic reactions that constitute the library of reactions used in organic synthesis.



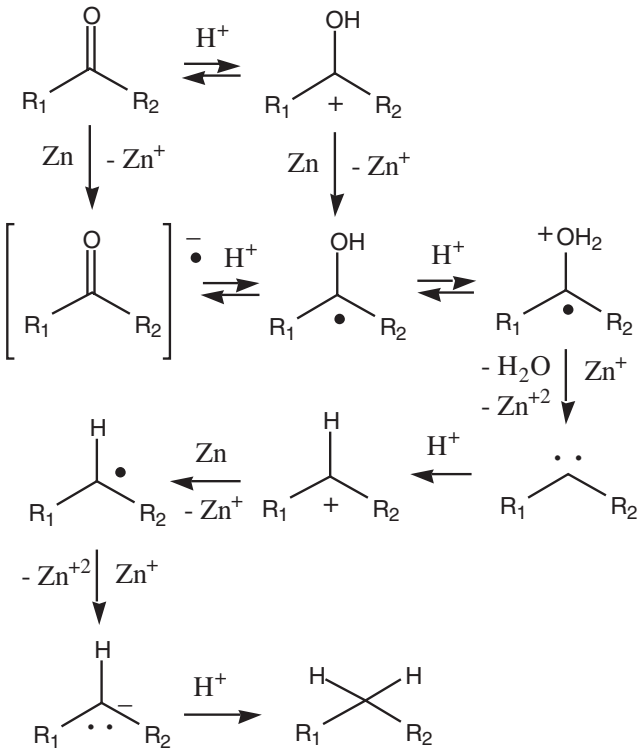
Reaction intermediates in organic synthesis

Figure 3 illustrates the frequencies of occurrence of each of the major classes of intermediates in the library of organic reactions used in synthesis and Table S3 (Supplementary material)[2] lists the specific reactions corresponding to each intermediate type. Organic reactions may be classified succinctly according to the following types: carbon–carbon and non-carbon–carbon bond-forming reactions (includes additions, cyclizations, and couplings), condensations, multicomponent reactions, oxidations and reductions with respect to the substrate of interest, rearrangements, substitutions, and fragmentations or eliminations. The first four reaction types figure prominently in skeletal building, or *aufbau* type, reactions, which are the most important class of organic reaction in synthesis. The documentation of carbon–carbon bond-forming reactions dates back to the early part of the 19th century with Faraday's electrochemical synthesis of hydrocarbons from carbon monoxide, carbonic acid, and hydrogen in 1834 (51), Robert Kane's aldol condensation in 1838 (52), and Strecker's synthesis of α-cyanoamines from aldehydes, hydrocyanic acid, and ammonia in 1850 (53). The top five most frequently appearing intermediates in organic reactions based on a library of 435 reactions (4, 54) are: tetrahedral intermediates (21%), enols and enolates (12%), carbanions (6%), metallocomplexes (6%), and carbenium ions (5%).

The ease or difficulty in elucidating reaction mechanisms depends on the reaction type. Tetrahedral intermediates, enols, enolates, and carbanions figure heavily in skeletal building reactions. It is fairly straightforward to write out reasonable reaction mechanisms for organic reactions involving these

© 2005 NRC Canada

Scheme 6.



species in carbon–carbon and non-carbon–carbon bond-forming reactions, condensations, and multicomponent reactions. Historically, substitution reactions and their associated mechanistic types (SN1, SN2, E1, E1cb, E2, and electrophilic and nucleophilic aromatic), as noted previously, are the best characterized. The elucidation of rearrangement reactions, on the other hand, is less straightforward and is strongly connected to the identification of specific reaction intermediates. Studies of carbenium ions and other cationic intermediates in acid-catalyzed reactions are particularly noteworthy in this regard such as the Wagner–Meerwein rearrangement. Generally, this class of reactions is the most challenging to elucidate and are often the subject of mechanistic puzzles. Labelling experiments are particularly helpful in decoding molecular reorganization processes. Oxidation and reduction reactions with respect to the substrate of interest are the least well-characterized mechanistically in terms of acquiring spectroscopic and kinetic data. This may be due to the fact that many of them occur in heterogeneous media, involve metals or organometallic species, or are surface reactions where traditional methods employed successfully in homogeneous phases may not be adequate to handle the complexities of kinetic treatments, in particular. It is probably in this class of reactions where mechanistic chemists may find it fruitful to explore uncharted territory, particularly with respect to inventing improved redox catalysts for industrial processes and understanding redox cascades in biological processes such as photosynthesis and nitrogen fixation that involve metal-containing enzymes. However, organometallic esters have been reasonably characterized for simple oxidation reactions such as the Criegee glycol cleavage (cyclic lead ester), Hooker oxidation (cyclic manganate ester), Jones oxidation (chromate ester), Lemieux–Johnson oxidation of olefins to 1,2-diols (cyclic osmate ester), Lemieux–Johnson oxidative cleavage of olefins to aldehydes (cyclic osmate ester), permanganate oxidation of olefins to 1,2-diols (cyclic manganate ester), Sarett procedure (chromate ester), Sharpless oxyamination (cyclic osmate ester and cyclic osmate amide), and Sharpless–Jacobsen dihydroxylation (cyclic osmate esters). Ozonides are also well-documented as intermediates in the Harries ozonolysis reaction. Browsing through Table S3[2] shows that reduction reactions may involve carbanion, carbene, radical, radical anions, or ylide intermediates. It is interesting to note that the Clemmensen reduction of ketone groups to methylene groups in acidic media potentially proceeds by the greatest number of intermediate types of any reaction. As shown in Scheme 6, the four-electron redox reaction can be postulated to proceed successively via radical anion, ketyl radical, carbene, carbenium ion, carbon centered radical, and finally carbanion intermediates. Table S4 (Supplementary material)[2] lists those named organic reactions that do not proceed via reaction intermediates and thus occur by concerted processes involving either asynchronous or synchronous bond-forming and bond-breaking processes in the transition states.

Identification of reaction intermediates — The underlying logic of it all

In determining the identity of a reaction intermediate in a thermal or photochemical transformation there are a number of steps that need to be followed. The first thing is to precisely determine the structures of the starting substrate structures as well as the final product structures, including their distribution. At this stage, comparison of product and reactant structures can lead to educated guesses as to the possible structures of transient species. This kind of analysis was the basis of understanding rearrangement reactions such as the Wagner–Meerwein rearrangement where carbocationic intermediates were postulated, or the Wolff and Curtius rearrangements where carbene and nitrene intermediates were conjectured. Julius Stieglitz, James F. Norris, and Frank C. Whitmore were the first to successfully use this technique in predicting likely transient species in such reactions (23, 24, 55). Astute chemists know that often it is the minor products of a reaction that give the most important clues as to the kind of mechanism that may be operative and the speciation of the suspect transient. Examples include liberated gases such as nitrogen (eliminated in Bamford–Stevens oxidation of hydrazones via carbenes, Curtius rearrangement via nitrenes, cyclopropanation with diazomethane via carbenes, diimide reduction via radicals, 1,3-dipolar additions of 1,2-diazoles to olefins, Gatterman reaction via arylium ions or aryl radicals, Gomberg–Bachmann and Meerwein arylation reactions via aryl cations, McFadyen–Stevens reaction via nitrenes, radical dehalogenation via radicals, Sandmeyer reaction via arylium ions or aryl radicals, Schiemann reaction via arylium ions or aryl radicals, Schmidt rearrangement via nitrenes, Staudinger reaction via nitrenes, Tiffeneau–Demjanov reaction via ring expansion, von Richter reaction via carbanions, Wharton reaction via tetrahedral intermediates, Wolff rearrangement reaction via carbenes, and Wolff–Kishner re-

© 2005 NRC Canada

duction via carbanions, iminium ions, and tetrahedral intermediates), hydrogen (eliminated in Chichibabin reaction via carbanions, Corey–Bakshi–Shibata reduction via ylides, Corey–Chaykovsky epoxidation reaction via carbanions, Gribble reduction of diarylketones via tetrahedral intermediates, Wadsworth–Horner–Emmons reaction via carbanions, and Williamson ether synthesis via alkoxides), carbon dioxide (decarboxylations in Borodin–Hunsdiecker reaction via acetoxy radicals, Corey–Winter reaction via carbenes and ylides, Dakin–West reaction via tetrahedral intermediates, diimide reduction via radicals, Eschweiler–Clarke reaction via iminium ions, Hofmann–Martius rearrangement via nitrenes, Hooker oxidation via enols, Kochi reaction via carbenium ions, Leuckart reaction via tetrahedral intermediates, Lossen rearrangement via nitrenes, malonates, and acetoacetates via tetrahedral intermediates, Perkin rearrangement via tetrahedral intermediates, and Schmidt rearrangement via nitrenes), ethylene (eliminated in ring-closing metathesis reactions via organometallic intermediates), hydrogen sulfide (eliminated in Willgerodt–Kindler reaction via tetrahedral intermediates and thiirenium ions), and sulfur dioxide (Ramberg–Bäckland rearrangement via carbanions). Products arising from recombination of fragments generated in a reaction are a signature of radicaloid processes such as 1,2-diphenylethane (dibenzyl), which arises by recombination of benzyl radicals.

There are a number of techniques that can be used to probe or interrogate a reaction between reactants and products. These fall into two main categories: indirect or direct methods. Under indirect methods we have: trapping or quenching kinetic and spectroscopic experiments, which introduce one or more chemical species that react noncompetitively or competitively with the generated intermediate, isolation of the trapped products from the quenching method, isotopic labelling studies, and pH – rate profile behaviour. Under direct methods we have: kinetic and spectroscopic time-resolved techniques that estimate the lifetimes and spectral properties of transient species, direct isolation or "freezing out" of intermediates in restricting media, and direct synthesis of thermodynamically and (or) kinetically stable analogs.

In the quenching technique one aims to use probe molecules that are unique or near-unique traps for the particular transient investigated, rather than promiscuous ones. One key assumption that needs to be experimentally verified is that the trapping agents should not undergo secondary reactions under the prescribed experimental conditions. Examples of specific traps are azide ion for carbenium ions; whereas, examples of promiscuous traps are oxygen that can quench excited state triplet species by triplet–triplet annhilation and carbon centred radicals to give peroxy radicals, and pyridine that can quench ketenes to ketene zwitterions and carbenes to pyridine–carbene ylides. However, specific quenching may not be so simple and often the strategy is to use a combination of trapping agents and then to look for consistency in their kinetic and spectroscopic behaviour. If an intermediate is suspected to be electrophilic then nucleophilic traps are selected, as in the case of cationic transients that are quenched by nucleophilic species with electron-donating groups, lone pairs of electrons, or negatively charged atoms. If an intermediate is suspected to be nucleophilic then electrophilic traps are chosen, as in the case of anionic transients that are quenched by electrophilic species with electron-withdrawing groups, electron-accepting centres, or positively charged atoms. Table 2 summarizes sets of quenchers that have been used to identify various reaction intermediate families. Sometimes trapping agents lead to secondary transients that themselves degrade. The probe technique to "see" spectroscopically invisible transients is particularly important here (56). For example, carbenes absorbing in the UV may be quenched by pyridine to yield coloured carbene ylides absorbing in the visible range, which in turn may be trapped with dimethoxycarbonylacetylene (Scheme 7). Transient ketenes may be first quenched by pyridine to produce ketene zwitterions. These adducts can conceivably undergo further trapping reactions with 1,4-dipolarophiles by analogy with pyridine carbene ylides that can be trapped with 1,3-dipolarophiles (Scheme 8) (57).

Isolation of the final products from quenching experiments can further corroborate structural assignments of the investigated transient species. Stereochemical aspects are often very helpful in this regard. Notable examples are the establishment of the connection between the Walden inversion rule and the S_N2 mechanism (58) and the trapping of singlet vs. triplet carbenes by olefins to give cyclopropane derivatives (59). The trapping of transients to yield stable isolable compounds such as transition-metal complexes has also been of great value. Ernst O. Fischer's pioneering work in trapping carbenes, carbynes, and ketenes using tungsten, molybdenum, and chromium carbonyls are good examples of this technique (60).

Deuterium and C13 labelling studies, including the measurement of kinetic primary and secondary isotope effects, can inform which bonds are being made and broken in particular steps in the proposed mechanism, particularly the rate-determining step. Scrambling of isotopic labels usually infers the presence of a symmetrical intermediate. For example, oxirenes have been inferred as possible intermediates in the Wolff rearrangement of diazoketones to carbenes and then ketenes (61), and thiirenium ions have been inferred in the cyclization–elimination reaction of thioalkoxy substituted vinyl sulfonates (62). If it is suspected that the transient structure has ionizable groups then the acquisition of pH – rate profiles are particularly useful, since their shapes reveal important kinetic and thermodynamic parameters. Enols are particularly noteworthy. Also, the form of buffer catalysis gives insights about whether general or specific acid- or base-catalysis mechanisms are operative. An important point to keep in mind is that such experiments need to be conducted in aqueous media so that meaningful kinetic and thermodynamic parameters can be determined, as well as their dependencies on acid or base concentration. Also, for meaningful comparisons to be made between related chemical structures of any reaction intermediate class, it is best to conduct experiments in a uniform medium under a standard set of conditions. For example, aqueous solution at an ionic strength of 0.1 mol/L NaCl or $NaClO_4$ at 25 °C and 1 atm (1 atm = 101.325 kPa).

The determination of rate laws for the dependence of observed rate constants on concentrations of various species gives important information about the molecularity and

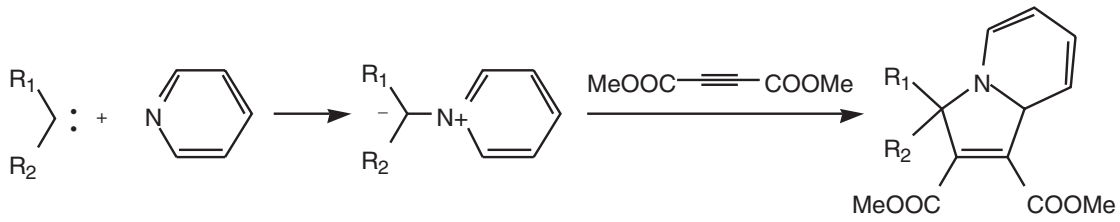
© 2005 NRC Canada

Table 2. List of quenchers used for each reaction intermediate group.

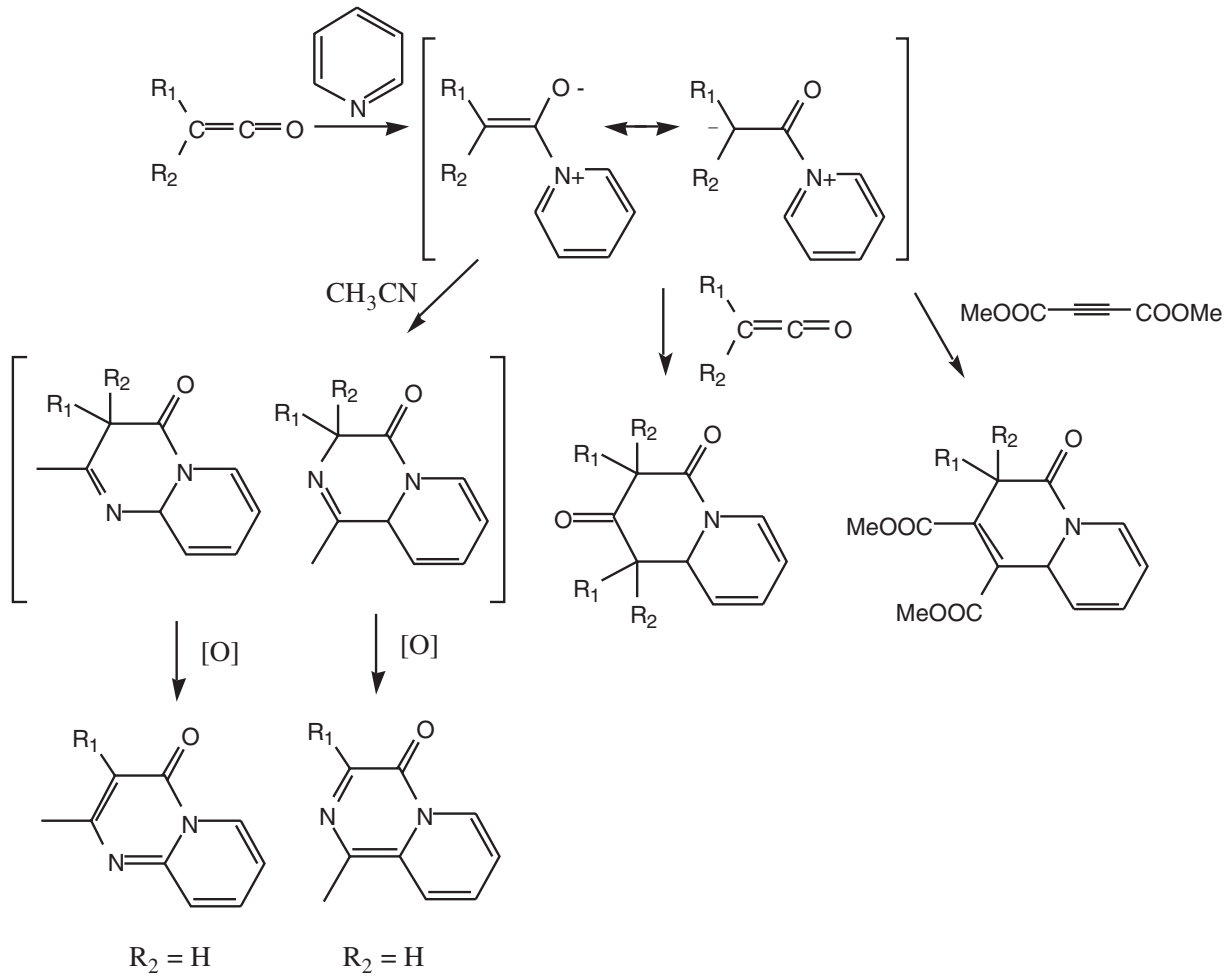
Reaction intermediate group	Quenchers used
Carbenes	Alcohols
	Diazocompounds
	Halogen donors (e.g., carbon tetrachloride, chloroform)
	Hydrogen donors (e.g., *n*-hexane, methanol, isopropanol, isooctane, trialkyltin hydride)
	Imines
	Ketones (e.g., Michler's ketone, acetone)
	Maleic acid, dimethyl ester
	Nitriles (e.g., acetonitrile)
	Olefins
	Oxygen
	Pyridine
	2,2,6,6-Tetramethylpiperidine-*N*-oxide (TEMPO)
	Thioketones (e.g., adamantanethione)
	Thiols
	Triethylamine
Carbocations	Alcohols (e.g., methanol, ethanol, hexafluoroisopropanol, trifluoroethanol)
	Azide ion
	1,3,5-Trimethoxybenzene
1,3-Dipoles	Hydrogen donors (e.g., *n*-hexane, methanol, isopropanol, isooctane, trialkyltin hydride)
	Olefins
Excited state triplets	Aromatics (e.g., azulene, xylenes, 1,4-dimethoxybenzene, 9,10-dibromoanthracene)
	Diethylsulfide
	Iodine
	Methyl viologen
	Olefins (e.g., acrylonitrile, styrene, methylmethacrylate, vinylacetate, 1,1-diphenylethene)
	Oxgyen
	Peroxy compounds (e.g., di-*tert*-butylperoxide, benzoyl peroxide)
	Phenols
	2,2,6,6-Tetramethylpiperidine-*N*-oxide (TEMPO)
	Triethylamine
	Nitrous oxide
	Di-*tert*-butylnitroxide
Ketenes	Alcohols
	Primary and secondary amines
	Pyridine
	2,2,6,6-Tetramethylpiperidine-*N*-oxide (TEMPO)
	Water
Nitrenes	Nitriles (e.g., acetonitrile)
Radicals	Alcohols
	Chloranil
	1,4-Cyclohexadiene
	2,3-Dichloro-5,6-dicyanobenzoquinone (DDQ)
	Halogen donors (e.g., carbon tetrachloride, chloroform)
	Hydrogen donors (e.g., *n*-hexane, methanol, isopropanol, isooctane, trialkyltin hydride)
	$Ni(acac)_2$, $Fe(acac)_3$
	Nitrones
	Nitroso compounds
	Olefins
	Oxygen
	2,2,6,6-Tetramethylpiperidine-*N*-oxide (TEMPO)
	Tetracyanoethylene (TCNE)
	Tetracyano-*p*-quinodimethane (TCNQ)
	Thiols

© 2005 NRC Canada

Scheme 7.



Scheme 8.



structure of the rate-limiting transition state. Limiting or asymptotic approximations with respect to relative rate constant magnitudes and (or) concentrations of catalyst, quencher, or reactant such as preequilibrium and steady-state approximations are especially useful in verifying rate law behaviours under simplified experimental conditions.

Direct methods are the most convincing in identifying transients, but comparisons of results with known reactions and with other indirect methods previously described are still necessary to obtain a complete story. Time-resolved techniques such as flash photolysis, pulse radiolysis, stopped-flow, and temperature jump allow both detailed kinetic and spectroscopic measurements to be made. In flash photolysis, pulse radiolysis, and temperature-jump techniques, chemical systems are suddenly perturbed by excitation pulses of light, electron beams, or heat, which results in the generation of the transient in solution. The stopped-flow technique involves rapid mixing of two solutions containing substrates. A thermal reaction proceeds giving rise to corresponding transient species once these solutions come into contact with one another. In all cases, once a transient is generated the optical density of the reaction solution is altered and the temporal dependence of this optical density change is monitored. The reaction solution is said to be "probed" by some spectroscopic means such as by UV–vis, IR, EPR, or NMR. Characteristic kinetic behaviours with respect to quenching experiments, such as magnitude of quenching rate constants, order of reaction, dependence of observed rate constants on catalyst concentration, and mathematical forms of the disappearance of substrate and appear-

© 2005 NRC Canada

ance of product as functions of time, and characteristic spectroscopic absorption markers, such as unique absorption bands, help to eliminate false candidates and narrow down the possibilities. The key condition to "catch" or view a transient is that the time resolution of the apparatus used must be smaller than the expected lifetime of the transient. Time resolutions range from several seconds in standard UV spectrophotometric devices to picoseconds in laser flash photolysis apparatuses. Obvious chemical constraints in using these techniques are the kinds of chemical reactions and precursors that are available to generate the appropriate intermediates. Photoreactions are necessary if flash photolysis is to be used and thermal reactions are necessary if T-jump or stopped flow is to be used. Often the choice of precursor is dictated by the suspected identity of the transient. Again, the library of known reactions is of great value in this selection.

Generation of intermediates in highly restricting media such as low-temperature noble gas matrices or organic glasses, or at room temperature in zeolites where the possibility of further reaction is severely impeded is also a powerful way of directly viewing transient species. Transients may be generated photochemically from appropriate precursors that are themselves trapped in a restricting matrix, or by flash vacuum pyrolysis of a substrate in the gas phase where the target intermediate is first generated and then subsequently trapped at 10 K in an argon matrix deposited on a KBr window using a cryostat apparatus. Once trapped, the spectrum of a transient may be obtained and its structure inferred from difference spectra in which the background spectrum of the matrix medium is subtracted out. Often such studies are done in conjunction with computational studies to determine their theoretically predicted IR, UV, or microwave spectra and to compare these with the experimental ones. Matching of spectra constitutes corroborative evidence for transient identification.

The most direct method is the synthesis of a thermodynamically stable analog, effectively bottling the intermediate as a *bona fide* isolable compound. This allows the complete characterization of the structure by conventional means such as boiling point, melting point, ^{1}H and ^{13}C NMR, IR, and UV spectroscopy, mass spectrometry, and X-ray crystallography. To make this strategy work, all available knowledge gained from previous methodologies is used. Thermodynamic stability is influenced by such factors as increased steric crowding, counterbalancing electronic effects by judicious choice of substituents, and topology. Highly stable analogs of reaction intermediates as summarized in Table S6 (Supplementary material)[2] have been found by using one or more of these strategies. Often such chemical curiosities have been discovered by accident rather than by design.

Like most of the thinking done in an empirical science, chemistry relies heavily on comparing new results with the growing empirically derived database or library of past results. The common paradigm is to select special reactions or conditions as "standards", which can be used as yardsticks or comparators for other reactions or conditions.[5] This, for example, is the basis of the linear free energy relationship analysis and compilation of various substituent constants advanced by Hammett, Taft, and others. Substituent effect experiments fine-tune our understanding of the nature of the rate-determining step, which involves a key intermediate. Such questions as charge distribution in the rate-determining transition state, its position along the reaction coordinate relative to reactants and immediate products, and degree of proton transfer, if applicable, may be answered. Also, changes in curvature of Brønsted and Hammett plots and pH – rate profiles may be interpreted as changes in rate-determining step occurring if downward bends (concave down curvature) are observed or as changes in reaction mechanism occurring if upward bends (concave up curvature) are observed.

Naturally, as the database of knowledge increases, comparisons between new and known reactions become more reliable and hence one's guesses as to the identity of reaction intermediates improve markedly. In terms of the decision trees shown in Figs. 4*a*–4*d*, one need not start at the top and work their way down, but begin somewhere in the middle and quickly gravitate to the likely transient structure in a few iterations of experimentation.

If one knew nothing about a suspected transient at all or had no precedent of analogous reactions to go by in the identification process, then the multiplicity assignment of the transient becomes the uppermost question in the decision tree. Overall, the key concept is to corroborate evidence from various methods so that a consistent picture is built for transient identification, keeping in mind the caveat given in the introduction that *definitive* proof is not possible, but *corroborative* proof is. It may be argued that corroborative proof may evolve into definitive proof the longer the evidence stands the test of time and further experimentation by ever more techniques. Corroboration of experimental results with theoretical computational studies of possible stable geometries and energetics of chemical species from reactants to products, including intervening intermediate structures with associated transition states in each step, is also a very useful strategy. The aim is to map out a complete energy reaction coordinate profile or surface showing the number of sequential elementary steps, the number of relevant transition states, the number of possible intermediates, the structures of all chemical species, and the energy differences between one structure and the next. Relationships such as the ones shown in eq. [3] become useful. The determination of reaction energy barriers and relative thermodynamic stabilities of reactants and products is important in identifying kinetic and thermodynamic control processes, particularly when they operate synergistically or antagonistically

[5] Unfortunately, nucleophilicity, which is a ubiquitous chemical phenomenon, continues to be poorly described in pure quantitative terms from a theoretical point of view. No one universal standard reaction or set of standard reactions have been found to describe nucleophilicity adequately for all chemical structures or reaction types. Practically all existing scales break down at some point. The best that has been accomplished is to use entirely empirical approaches such as the ones advanced by Mayr and co-workers (63) based on extensive families of correlations. On the other hand, proton and electron transfer reactions are both rigorously described in theoretical and quantitative terms. In such reactions protons or electrons are either consumed or produced regardless of the chemical structures of reactants and products involved. This commonality greatly simplifies comparisons between reactions.

© 2005 NRC Canada

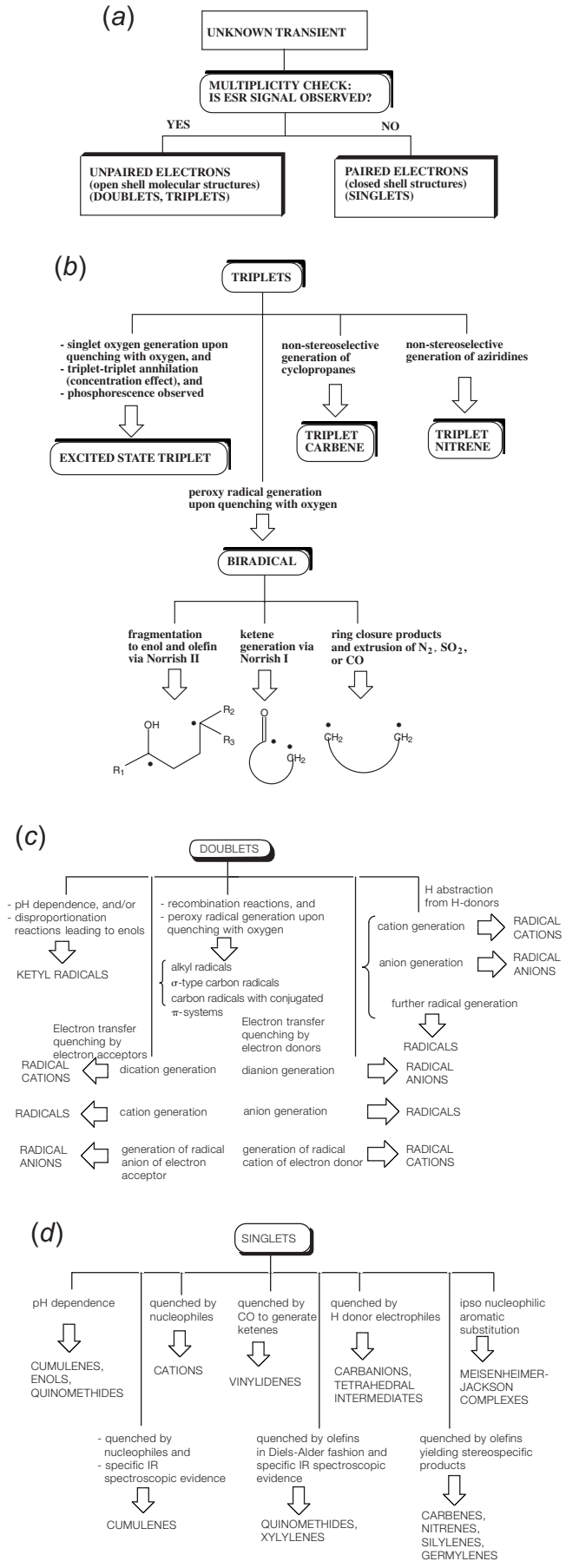
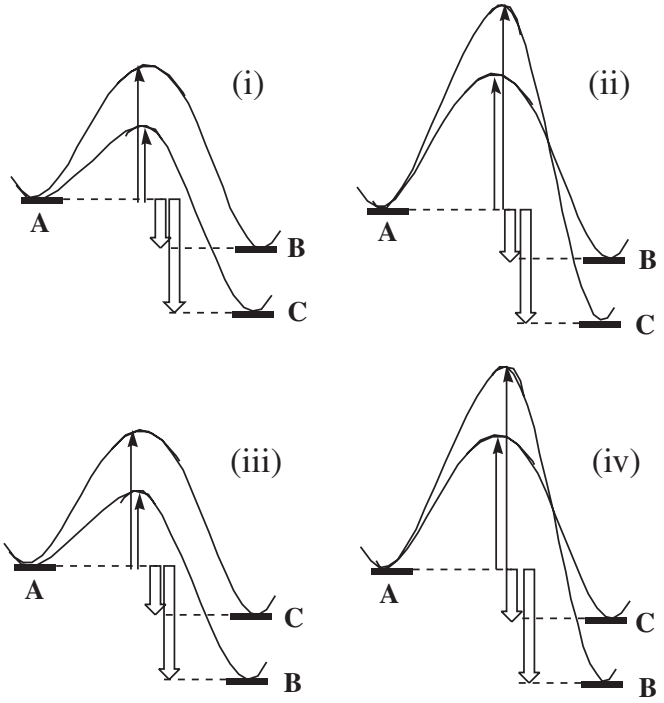


Fig. 4. (*a*) Decision tree showing the main separation of reaction intermediates according to multiplicity. (*b*) Decision tree for the identification reaction intermediates that have a triplet multiplicity. (*c*) Decision tree for the identification reaction intermediates that have a doublet multiplicity. (*d*) Decision tree for the identification reaction intermediates that have a singlet multiplicity.

Fig. 5. Kinetic and thermodynamic control processes for reaction scheme A → B + C. (*i*) Product C is both a thermodynamically and kinetically controlled product (synergistic); (*ii*) product C is a thermodynamically controlled product and product B is a kinetically controlled product (antagonistic); (*iii*) product B is both a thermodynamically and kinetically controlled product (synergistic); (*iv*) product B is a thermodynamically controlled product and product C is a kinetically controlled product (antagonistic).



(see Fig. 5). Complimentary agreement between experiment and theory is particularly satisfying in such analyses.

[3] Number of elementary steps in mechanism =

Number of transition states in mechanism

Number of reaction intermediates in mechanism =

Number of elementary steps in mechanism – 1

Within the realm of experimentation, probably the strongest evidence that can be obtained for the identity of a particular transient is if it can be generated from different precursors and by different techniques and if it can be shown that its spectroscopic and kinetic behaviours are the same irrespective of its origin or method of generation.

© 2005 NRC Canada

Acknowledgements

Parts of this work were presented at the 29th Ontario–Quebec Physical Organic Chemistry Mini-Symposium, 2–4 November 2001, York University, Toronto, Ontario.

The author thanks Wahab Farooq (University of Karachi, Pakistan) for contributions to the list of coined terms in physical organic chemistry. Though best efforts were made in this work to recognize as many key contributors to the study of reaction intermediates as far as possible, any remaining errors and (or) omissions in any of the compilations is unintentional.

References

1. (*a*) A.A. Frost and R.G. Pearson. Kinetics and mechanism: a study of homogeneous chemical reactions. 2nd ed. Wiley, New York. 1961; (*b*) J. Hine. Physical organic chemistry. McGraw-Hill Book Co., Inc., New York. 1962; (*c*) J.E. Leffler and E. Grunwald. Rates and equilibria of organic reactions. Wiley, New York. 1963; (*d*) W.P. Jencks. Catalysis in chemistry and enzymology. McGraw-Hill Book Co., Inc., New York. 1969; (*e*) C.K. Ingold. Structure and mechanism in organic chemistry. 2nd ed. Cornell University Press, Ithaca, New York. 1969; (*f*) L.P. Hammett. Physical organic chemistry: reaction rates, equilibria, and mechanisms. McGraw-Hill Book Co., Inc., New York. 1970; (*g*) S.P. McManus (*Editor*). Organic reactive intermediates. Academic Press, New York. 1973; (*h*) R.P. Bell. The proton in chemistry. 2nd ed. Chapman & Hall, London. 1973; (*i*) C.D. Ritchie. Physical organic chemistry: the fundamental concepts. Marcel Dekker, New York. 1975; (*j*) C. Wentrup. Reactive molecules: the neutral reactive intermediates in organic chemistry. Wiley, New York. 1984; (*k*) R.A.Y. Jones. Physical and mechanistic organic chemistry. 2nd ed. Cambridge University Press, Cambridge. 1984; (*l*) N.S. Isaacs. Physical organic chemistry. Wiley, New York. 1987; (*m*) T.H. Lowry and K.S. Richardson. Mechanisms and theory in organic chemistry. Harper and Row Publishers, New York. 1987; (*n*) K.J. Laidler. Chemical kinetics. Harper and Row Publishers, New York. 1987; (*o*) J.C. Scaiano (*Editor*). CRC handbook of organic photochemistry. Vols. I and II. CRC Press, Boca Raton, Fla. 1989; (*p*) J.H. Espenson. Chemical kinetics and reaction mechanisms. 2nd ed. McGraw-Hill, Inc., New York. 1995; (*q*) T.T. Tidwell, Z. Rappoport, and C.L. Perrin (*Editors*). Pure Appl. Chem. **69**, 211 (1997), and refs. therein; (*r*) F.A. Carroll. Perspectives in structure and mechanism in organic chemistry. Brooks/Cole Publishing Co., Pacific Grove, Calif. 1998; (*s*) R.A. Moss, M.S. Platz, and M. Jones, Jr. Reactive intermediate chemistry. Wiley, New York. 2004.
2. K.J. Laidler. J. Chem. Ed. **65**, 250 (1988).
3. (*a*) P. Cintas. Angew. Chem. Int. Ed. **43**, 5888 (2004); (*b*) R.J. de Levie. J. Chem. Ed. **77**, 610 (2000); (*c*) R. Hinch and S. Schnell. J. Math. Chem. **35**, 253 (2004); (*d*) K.J. Laidler. Acc. Chem. Res. **28**, 187 (1995).
4. J. Andraos. Named things in chemistry and physics {online]. Available from http://www.careerchem.com/NAMED/Homepage.html [accessed July 2004]. 2000.
5. H.L. Le Châtelier. Compt. Rend. **99**, 786 (1884).
6. J.H. van't Hoff. Études de dynamique chimique. F. Muller, Amsterdam. 1884.
7. S. Arrhenius. Z. Phys. Chem. **4**, 226 (1889).
8. (*a*) M. Bodenstein and W. Dux. Z. Phys. Chem. **85**, 297 (1913); (*b*) M. Bodenstein. Z. Phys. Chem. **85**, 329 (1913); (*c*) D.L. Chapman and L.K. Underhill. J. Chem. Soc. **103**, 496 (1913).
9. L. Michaelis and M.L. Menten. Biochem. Z. **49**, 333 (1913).
10. (*a*) A.J. Brown. J. Chem. Soc. Trans. **61**, 369 (1892); (*b*) A.J. Brown. J. Chem. Soc. Trans. **81**, 373 (1902).
11. (*a*) V. Henri. Lois générales de l'action des diastases. Hermann, Paris. 1903; (*b*) V. Henri. Compt. Rend. **133**, 891 (1901); (*c*) V. Henri. Z. Phys. Chem. **39**, 194 (1901); (*d*) V. Henri. Compt. Rend. **135**, 916 (1902).
12. K.P.C. Orton. Proc. R. Soc. London, **71**, 156 (1902).
13. (*a*) G. Bender. Chem. Ber. **19**, 2272 (1886); (*b*) J. Shorter. Chem. Soc. Rev. **27**, 355 (1998); (*c*) J. Shorter. Chem. Br. **31**, 310 (1995).
14. (*a*) D.Y. Curtin. Rec. Chem. Prog. **15**, 111 (1954); (*b*) L.P. Hammett. Physical organic chemistry: reaction rates, equilibria, and mechanisms. 2nd ed. McGraw-Hill, New York. 1970. p. 119 to 120.
15. S.F. Acree. Am. Chem. J. **38**, 1 (1907).
16. J.I. Seeman. Chem. Rev. **83**, 83 (1983).
17. D.S. Tarbell and A.T. Tarbell. Essays on the history of organic chemistry in the United States, 1875–1955. Folio Publishers, Nashville, Tenn. 1986. Chap. 4.
18. J. Andraos. J. Phys. Chem. A, **107**, 2374 (2003).
19. S. Winstein and N.J. Holness. J. Am. Chem. Soc. **77**, 5562 (1955).
20. (*a*) J.H. van't Hoff. Vorlesungen über Theoretische und Physikalische Chemie. Friedrich Viewig und Sohn, Braunschweig. 1898; (*b*) J.H. van't Hoff. Etudes de dynamique chimique. Frederik Muller & Co., Amsterdam. 1884; (*c*) J.H. van't Hoff. Leçons de chimie physique. 1re Partie. Hachette, Paris. 1860–1869.
21. (*a*) J.J. Berzelius. Jahresberichte, **15**, 237 (1835); (*b*) W. Ostwald. J. Prakt. Chem. **27**, 1 (1883).
22. (*a*) L.F. Wilhelmy. Ann. Phys. **81**, 413 (1850); (*b*) L.F. Wilhelmy. Ann. Phys. **81**, 499 (1850).
23. J. Stieglitz. Am. Chem. J. **21**, 101 (1899).
24. (*a*) J.F. Norris and W.W. Sanders. Am. Chem. J. **25**, 54 (1901); (*b*) J.F. Norris. Am. Chem. J. **25**, 117 (1901); (*c*) J.F. Norris. Am. Chem. J. **38**, 627 (1907).
25. (*a*) A. von Baeyer and V. Villiger. Chem. Ber. **34**, 1189 (1901); (*b*) A. von Baeyer and V. Villiger. Chem. Ber. **34**, 3013; (*c*) F. Kehrmann and F. Wentzel. Chem. Ber. **34**, 3815 (1901); (*d*) A. von Baeyer. Chem. Ber. **38**, 3815 (1905).
26. G.N. Lewis. J. Am. Chem. Soc. **38**, 762 (1916).
27. (*a*) G.N. Lewis. Valence and the structure of atoms and molecules. Chemical Catalog Co., New York. 1923. p. 141; (*b*) G.N. Lewis. J. Franklin Inst. **226**, 293 (1938).
28. G.N. Lewis and M. Calvin. Chem. Rev. **25**, 273 (1939).
29. (*a*) E.D. Hughes and C.K. Ingold. J. Chem. Soc. 523 (1933); (*b*) E.D. Hughes, C.K. Ingold, and C.S. Patel. J. Chem. Soc. 526 (1933).
30. (*a*) C.K. Ingold. Chem. Rev. **15**, 225 (1934); (*b*) J.L. Gleave, E.D. Hughes, and C.K. Ingold. J. Chem. Soc. 236 (1935); (*c*) E.D. Hughes. J. Am. Chem. Soc. **57**, 708 (1935).
31. (*a*) E.D. Hughes, C.K. Ingold, and A.D. Scott. J. Chem. Soc. 1271 (1937); (*b*) E.D. Hughes and B.J. MacNulty. J. Chem. Soc. 1283 (1937); (*c*) M.L. Dhar, E.D. Hughes, C.K. Ingold, A.M.M. Mandour, G.A. Maw, and L.I. Woolf. J. Chem. Soc. 2093 (1948).
32. J.N.E. Day and C.K. Ingold. Trans. Faraday Soc. **37**, 686 (1941).
33. F. Wöhler. Ann. Chim. **37**, 330 (1828).
34. (*a*) W.O. Kermack and R. Robinson. J. Chem. Soc. **121**, 427 (1922); (*b*) R. Robinson. Two lectures on an outline of an electrochemical (electronic) theory of the course of organic reac-

© 2005 NRC Canada

tions. Institute of Chemistry of Great Britain and Ireland, London. 1932.
35. (*a*) A.F. Holleman. Die Direkte Einfuhrung von Substituenten in den Benzolkern. Verlag von Veit & Co., Leipzig. 1910; (*b*) A.F. Holleman. Chem. Rev. **1**, 137 (1924).
36. (*a*) J. Allan and R. Robinson. J. Chem. Soc. 376 (1926); (*b*) A.E. Oxford and R. Robinson. J. Chem. Soc. 383 (1926); (*c*) R. Robinson and J.C. Smith. J. Chem. Soc. 392 (1926); (*d*) J. Allan, A.E. Oxford, and R. Robinson. J. Chem. Soc. 411 (1926); (*e*) T.R. Lea and R. Robinson. J. Chem. Soc. 903 (1926); (*f*) C.K. Ingold and E.H. Ingold. J. Chem. Soc. 310 (1926).
37. (*a*) R. Robinson. Memoirs of a minor prophet: 70 years of organic chemistry. Vol. 1. Elsevier, Amsterdam. 1976; (*b*) T. Williams. Robert Robinson: chemist extraordinary. Clarendon Press, Oxford. 1990; (*c*) K.T. Leffek. Sir Christopher Ingold: a major prophet of organic chemistry. Nova Lion Press, Victoria, B.C. 1996; (*d*) P. Laszlo. Ambix, **50**, 261 (2003); (*e*) T.M. Brown, A.T. Dronsfield, and P.J.T. Morris. Educ. Chem. **40**, 129 (2003); (*f*) M.D. Saltzmann. J. Chem. Ed. **57**, 484 (1980); (*g*) J. Shorter. Nat. Prod. Rep. **4**, 61 (1987).
38. (*a*) J.N. Brönsted and K. Pedersen. Z. Phys. Chem. **108**, 185 (1924); (*b*) J.N. Brönsted. Z. Phys. Chem. **115**, 337 (1925); (*c*) J.N. Brönsted and E.A. Guggenheim. J. Am. Chem. Soc. **49**, 2554 (1927); (*d*) J.N. Brönsted. Chem. Rev. **5**, 231 (1928).
39. (*a*) L.P. Hammett. Chem. Rev. **17**, 125 (1935); (*b*) L.P. Hammett. J. Am. Chem. Soc. **59**, 96 (1937).
40. (*a*) H. Eyring. Z. Phys. Chem. B, **12**, 279 (1931); (*b*) H. Eyring. J. Chem. Phys. **3**, 107 (1935); (*c*) H. Eyring. Chem. Rev. **17**, 65 (1935); (*d*) H. Eyring. Trans. Faraday Soc. **34**, 41 (1938).
41. (*a*) H.C. Urey, F.G. Brickwedde, and G.M. Murphy. Phys. Rev. **39**, 164 (1932); (*b*) H.C. Urey, F.G. Brickwedde, and G.M. Murphy. Phys. Rev. **40**, 1 (1932).
42. (*a*) O. Reitz. Z. Phys. Chem. **A177**, 85 (1936); (*b*) O. Reitz. Naturwissenshaften, **24**, 814 (1936); (*c*) O. Reitz. Z. Elektrochem. **43**, 659 (1937); (*d*) O. Reitz. Z. Phys. Chem. **A179**, 119 (1937); (*e*) O. Reitz. Z. Elektrochem. **44**, 72 (1938); (*f*) O. Reitz. Z. Elektrochem. **44**, 693 (1938); (*g*) O. Reitz. Z. Elektrochem. **45**, 100 (1939); (*h*) O. Reitz. Z. Phys. Chem. **A183**, 371 (1939); (*i*) O. Reitz and J. Kopp. Z. Phys. Chem. **A184**, 429 (1939).
43. (*a*) D. Rittenberg, W. Bleakney, and H.C. Urey. J. Chem. Phys. **2**, 48 (1934); (*b*) R. Schoenheimer and D. Rittenberg. J. Biol. Chem. **111**, 163 (1935); (*c*) R. Schoenheimer, D. Rittenberg, and M. Graff. J. Biol. Chem. **111**, 183 (1935); (*d*) D.J.G. Ives and H.N. Rydon. J. Chem. Soc. 1735 (1935); (*e*) E.D. Hughes, F. Juliusburger, S. Masterman, B. Topley, and J. Weiss. J. Chem. Soc. 1525 (1935); (*f*) C.K. Ingold, E. de Salas, and C.L. Wilson. J. Chem. Soc. 1328 (1936); (*g*) D.J.G. Ives. J. Chem. Soc. 81 (1938); (*h*) D.J.G. Ives and G.C. Wilks. J. Chem. Soc. 1455 (1938); (*i*) R. Schoenheimer and D. Rittenberg. Science (Washington, D.C.), **87**, 221 (1938); (*j*) D.J.G. Ives and R.H. Kerlogue. J. Chem. Soc. 1362 (1940); (*k*) R. Schoenheimer and D. Rittenberg. Physiol. Rev. **20**, 218 (1940); (*l*) R.E. Kohler, Jr. Hist. Stud. Phys. Sci. **8**, 257 (1977).
44. (*a*) H.C. Urey and L.J. Grieff. J. Am. Chem. Soc. **57**, 321 (1935); (*b*) L.A. Webster, M.H. Wahl, and H.C. Urey. J. Chem. Phys. **3**, 129 (1935).
45. W.G. Young and D.J. Cram. Biog. Memoirs Natl. Acad. Sci. **43**, 321 (1973).
46. G.G. Hammes (*Editor*). Investigation of rates and mechanisms of reactions. Parts I and II. Wiley, New York. 1974.
47. (*a*) E. Whittle, D.A. Dows, and G.C. Pimentel. J. Chem. Phys. **22**, 1943 (1954); (*b*) E.D. Becker and G.C. Pimentel. J. Chem. Phys. **25**, 224 (1954).
48. (*a*) R.J. Gillespie. Acc. Chem. Res. **1**, 202 (1968); (*b*) R.J. Gillespie. Can. Chem. Ed. **4**, 9 (1969); (*c*) R.J. Gillespie and T.E. Peel. Adv. Phys. Org. Chem. **9**, 1 (1971); (*d*) R.J. Gillespie. Endeavour, **32**, 3 (1973); (*e*) R.J. Gillespie. Proton Transfer React. 1 (1975); (*f*) G.A. Olah and A. Commeyras. J. Am. Chem. Soc. **91**, 2929 (1969); (*g*) G.A. Olah, A.T. Ku, and J.A. Olah. J. Org. Chem. **35**, 3925 (1970); (*h*) G.A. Olah, G.K.S. Prakash, and J. Sommer. Superacids. Wiley, New York. 1984; (*i*) G.A. Olah. J. Org. Chem. **65**, 5943 (2001).
49. J.C. Scaiano and H. Garcia. Acc. Chem. Res. **32**, 783 (1999).
50. S.A. Blum, K.L. Tan, and R.G. Bergman. J. Org. Chem. **68**, 4127 (2003).
51. M. Faraday. Pogg. Ann. Phys. Chem. **33**, 433 (1834). Michael Faraday's contributions to chemistry also include the discovery of benzene (Phil. Trans. Roy. Soc. London **115**, 440 (1825) and gas hydrates (Phil. Trans. Roy. Soc. London **133**, 160 (1823)), and the synthesis of perchloro organic compounds such as hexachloroethane, tetrachloroethylene, and hexachlorobenzene (Ann. Chim. Phys. **18**, 48 (1821)).
52. (*a*) R. Kane. Pogg. Ann. Phys. Chem. **44**, 475 (1838); (*b*) R. Kane. J. Prakt. Chem. **15**, 129 (1838).
53. A. Strecker. Justus Liebigs Ann. Chem. **75**, 27 (1850).
54. (*a*) J.J. Li. Name reactions: a collection of detailed reaction mechanisms. Springer-Verlag, Berlin. 2002; (*b*) H. Krauch and W. Kunz. Organic name reactions: a contribution to the terminology of organic chemistry, biochemistry, and theoretical organic chemistry (translated by J.M. Harkin). Wiley, New York. 1964; (*c*) J.F. Bunnett. Pure Appl. Chem. **53**, 305 (1981); (*d*) R.A.Y. Jones and J.F. Bunnett. Pure Appl. Chem. **61**, 725 (1989); (*e*) W.H. Powell. Pure Appl. Chem. **65**, 1357 (1993); (*f*) G.P. Moss, P.A.S. Smith, and D. Tavernier. Pure Appl. Chem. **67**, 1307 (1995).
55. (*a*) F.C. Whitmore. Ann. Rep. Prog. Chem. (Chem. Soc. London), **30**, 177 (1933); (*b*) F.C. Whitmore. J. Am. Chem. Soc. **54**, 3274 (1932); (*c*) F.C. Whitmore. Chem. Eng. News, **26**, 688 (1948).
56. (*a*) R.L. Barcus, L.M. Hadel, L.J. Johnston, M.S. Platz, T.G. Savino, and J.C. Scaiano. J. Am. Chem. Soc. **108**, 3928 (1986); (*b*) D. Griller, L.M. Hadel, A.S. Nazran, M.S. Platz, P.C. Wong, T.G. Savino, and J.C. Scaiano. J. Am. Chem. Soc. **106**, 2227 (1984).
57. Precedence for this suggestion comes from the confirmation of the pyranodihydroquinolizone structure of the stable Wollenberg's yellow (O. Wollenberg. Chem. Ber. **67**, 1675 (1934)) formed by passing excess ketene gas in pyridine (J.A. Berson and W.M. Jones. J. Am. Chem. Soc. **78**, 1625 (1956)), and by the analogous structure of the unstable adduct formed when excess diphenylketene reacts with pyridine: H. Staudinger, H.W. Klever, and P. Kober. Justus Liebigs Ann. Chem. **374**, 1 (1910).
58. (*a*) H. Phillips. J. Chem. Soc. **123**, 44 (1923); (*b*) J. Kenyon and H. Phillips. Trans. Faraday Soc. **26**, 451 (1930); (*c*) H. Phillips and J. Kenyon. J. Chem. Soc. 108 (1932); (*d*) H. Phillips and J. Kenyon. J. Chem. Soc. 1232 (1932); (*e*) H. Phillips and J. Kenyon. J. Chem. Soc. 179 (1933).
59. P.S. Skell and A.Y. Garner. J. Am. Chem. Soc. **78**, 5430 (1956).
60. (*a*) E.O. Fischer and A. Maasbol. Angew. Chem. Int. Ed. Engl. **3**, 580 (1964); (*b*) E.O. Fischer, C.G. Kreiter, J. Müller, G. Huttner, and H. Lorenz. Angew. Chem. Int. Ed. Engl. **12**, 564 (1973); (*c*) F.R. Kreissl, A. Frank, U. Schubert, T.L. Lindner, and G. Hutner. Angew. Chem. **88**, 649 (1976); (*d*) E.O. Fischer, A.C. Filippou, H.G. Alt, and K. Ackermann. J. Organomet. Chem. **254**, C21 (1983).

© 2005 NRC Canada

61. (*a*) I.G. Csizmadia, J. Font, and O. Strausz. J. Am. Chem. Soc. **90**, 7360 (1968); (*b*) K.P. Zeller, H. Meier, H. Kolshorn, and E. Mueller. Chem. Ber. **105**, 1875 (1972).
62. G. Capozzi, G. Melloni, G. Modena, and U. Tonellato. Chem. Commun. 1520 (1969).
64. (*a*) M. Hofmann, N. Hampel, T. Kanzian, and H. Mayr. Angew. Chem. Int. Ed. **43**, 5402 (2004); (*b*) A.R. Ofial and H. Mayr. Macromolecular Symposia, **215**, 353 (2004); (*c*) H. Mayr, B. Kempf, and A.R. Ofial. Acc. Chem. Res. **36**, 66 (2003); (*d*) H. Mayr and M. Patz. Angew. Chem. Int. Ed. Engl. **33**, 938 (1994).

© 2005 NRC Canada

Competitive endo- and exo-cyclic C–N fission in the hydrolysis of *N*-aroyl β-lactams[1]

Wing Y. Tsang, Naveed Ahmed, Karl Hemming, and Michael I. Page

Abstract: The balance between endo- and exo-cyclic C–N fission in the hydrolysis of *N*-aroyl β-lactams shows that the difference in reactivity between strained β-lactams and their acyclic analogues is minimal. Attack of hydroxide ion occurs preferentially at the exocyclic acyl centre rather than that of the β-lactam during the hydrolysis of *N*-*p*-nitrobenzoyl β-lactam. In general, both endo- and exo-cyclic C–N bond fission occurs in the alkaline hydrolysis of *N*-aroyl β-lactams, the ratio of which varies with the aryl substituent. Hence, the Brønsted β-values differ for the two processes: –0.55 for the ring-opening reaction and –1.54 for the exocyclic C–N bond fission reaction. For the pH-independent and acid-catalysed hydrolysis of *N*-benzoyl β-lactam, less than 3% of products are derived from exocyclic C–N bond fission.

Key words: β-lactams, hydrolysis, linear free energy relationships, strain.

Résumé : La balance entre la fission C–N endo- et exocyclique lors de l'hydrolyse de *N*-aroyl β-lactames montre que la différence de réactivité entre des lactames tendus et leurs analogues acyles est minimale. L'attaque par l'ion hydroxyde se fait préférentiellement au niveau du centre acyle exocyclique plutôt que sur celui du β-lactame lors de l'hydrolyse du *N*-*p*-nitrobenzoyl β-lactame. En général, il se produit des fissions des liaisons C–N tant endo- que exocycliques lors de l'hydrolyse alcaline des *N*-aroyl β-lactames et le rapport des deux varie en fonction de la nature du substituant. En conséquence, les valeurs β de Brønsted diffèrent pour les deux processus étant égales à –0,55 pour la réaction d'ouverture de cycle et de –1,54 pour la réaction de fission de la liaison C–N exocyclique. Les hydrolyses indépendantes du pH et catalysées par les acides du *N*-benzoyl β-lactame fournissent moins que 3 % de produits dérivés de la fission de la liaison C–N exocyclique.

Mots clés : β-lactames, hydrolyse, relations linéaires d'énergie libre, tension.

[Traduit par la Rédaction]

Introduction

β-Lactam antibiotics such as penicillins (**1**) and cephalosporins are often considered unusually reactive when compared with normal amides because most of their biologically important reactions involve the opening of the highly strained four-membered ring (1, 2). The effect of ring strain on the reactivity of β-lactams may be demonstrated by comparing the rates of the reactions of monocyclic β-lactams with their acyclic analogues. For example, and perhaps contrary to expectation, the rate of alkaline hydrolysis of β-lactams is, at most, 100-fold greater than that of an analogous acyclic amide. The second-order rate constant for the hydroxide ion catalysed hydrolysis of *N*-methyl β-lactam is only threefold greater than that for *N*,*N*-dimethyl acetamide (3).

Incorporating a benzamide as a potential leaving group into a simple azetidin-2-one gives the imide *N*-benzoyl β-lactam (**2**), which contains an endocyclic and an exocyclic acyl centre both of which are potential sites for nucleophilic attack. The hydrolysis of **2** could occur by two routes. For example, the hydroxide ion could attack the exocyclic carbonyl to generate benzoic acid and the intact β-lactam (Scheme 1, route a). The β-lactam could then undergo further reaction with the hydroxide ion to give a ring-opened β-amino acid. Alternatively, the hydroxide ion could attack the endocyclic β-lactam carbonyl to give a ring-opened product **3** (Scheme 1, route b). Many would expect this to be the dominant reaction pathway based on the belief that ring strain increases the reactivity of β-lactams. We were interested in exploring the balance between endo- and exo-cyclic C–N fission as a function of substituents in the aroyl group, and herein report further evidence that the difference in reactivity between strained β-lactams and their acyclic analogues is minimal.

Received 3 March 2005. Published on the NRC Research Press Web site at http://canjchem.nrc.ca on 11 November 2005.

W.Y. Tsang, N. Ahmed, K. Hemming, and M.I. Page.[2] Department of Chemical and Biological Sciences, The University of Huddersfield, Queensgate, Huddersfield, HD1 3DH, UK.

[1]This article is part of a Special Issue dedicated to organic reaction mechanisms.

[2]Corresponding author (e-mail: m.i.page@hud.ac.uk).

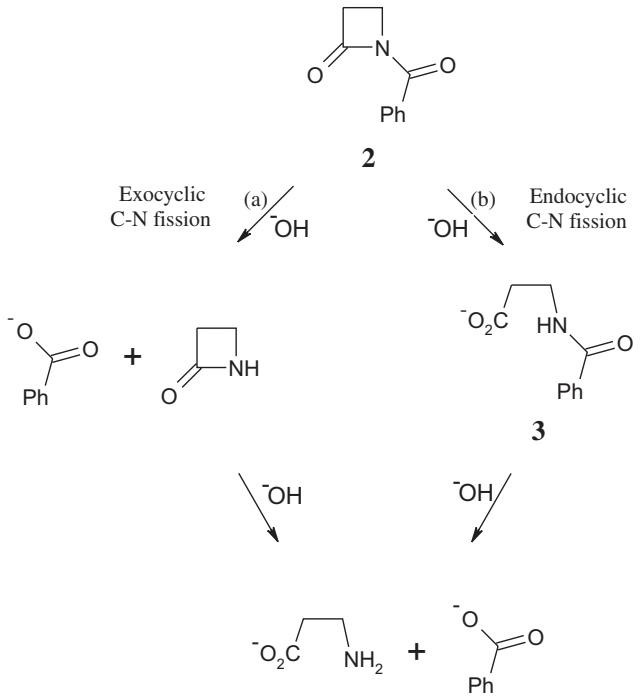
Experimental section

Synthesis

N-Aroyl β-lactams were prepared according to the following general procedure: To a stirred solution of azetidin-2-one (0.5 g, 7.03 mmol) in dry dichloromethane (DCM, 20 mL) was added 4,4-dimethylaminopyridine (0.1 g, 0.82 mmol) at –78 °C, and a solution of aroyl chloride (1.57 g, 8.46 mmol) in dichloromethane (10 mL) dropwise over 5 min. Triethylamine (0.98 mL, 7.02 mmol) was added dropwise

 doi: 10.1139/V05-153 © 2005 NRC Canada

Scheme 1.



over 10 min forming a white precipitate. The reaction mixture was stirred at –78 °C for 1 h and for a further 24 h at ambient temperature. DCM (10 mL) was added to the reaction mixture, and the solution was washed with water (15 mL) and saturated brine (2 × 15 mL). The organic layer was dried over anhydr. Na_2SO_4, and the solvent was removed under reduced pressure by rotary evaporation at 30 °C to yield a pale yellow oil, which was purified by column chromatography.

1-(4′-Methoxybenzoyl)-1-azetidin-2-one

Yield: 0.6 g (42%); mp 125–127 °C. IR υ_{max} (cm^{-1}, $CHCl_3$): 3020, 3009, 2975, 2912, 2842, 1784, 1668, 1606, 1325, 1259, 1195, 1108, 1028. ^1H NMR ($CDCl_3$) δ: 7.99 (2H, d, J = 8.88 Hz), 6.92 (2H, d, J = 8.97 Hz), 3.85 (3H, s, CH_3), 3.77 (2H, t, J = 5.44 Hz, CH_2N), 3.02 (2H, t, J = 5.45 Hz, CH_2CO). ^{13}C NMR ($CDCl_3$) δ: 165.23 (C=O), 163.92 (C=O), 132.57 (quaternary carbon), 131.92 (ArCH), 123.76 (quaternary carbon), 113.948 (ArCH), 55.21 (CH_3), 36.45 (CH_2N), 34.44 (CH_2CO). HR-EI-MS calcd. for $C_{11}H_{11}NO_3$: 206.0812 $[M + H]^+$; found: 206.0812.

1-Benzoyl-1-azetidin-2-one

Yield: 0.91 g (65%). IR υ_{max} (cm^{-1}, $CHCl_3$): 3020, 1786, 1673, 1327, 1298, 1216, 1192. ^1H NMR ($CDCl_3$) δ: 8.00 (2H, d, J = 7.43 Hz), 7.61 (1H, t, J = 7.29 Hz), 7.49 (2H, t, J = 7.83 Hz), 3.81 (2H, t, J = 5.49 Hz), 3.14 (2H, t, J = 5.49 Hz). ^{13}C NMR ($CDCl_3$) δ: 166.26 (C=O), 163.95 (C=O), 133.19 (PhCH), 131.83 (quaternary carbon), 129.69 (PhCH), 128.12 (PhCH), 36.77 (CH_2), 35.05 (CH_2).

1-(4′-Chlorobenzoyl)-1-azetidin-2-one

Yield: 0.85 g (58%). IR υ_{max} (cm^{-1}, $CHCl_3$): 3020, 1788, 1673, 1593, 1404, 1324, 1284, 1217, 1093. ^1H NMR ($CDCl_3$) δ: 7.95 (2H, d, J = 6.68 Hz), 7.44 (2H, d, J = 8.66 Hz), 3.77 (2H, t, J = 5.5 Hz, CH_2N), 3.12 (2H, t, J = 5.61 Hz, CH_2CO). ^{13}C NMR ($CDCl_3$) δ: 165.01 (C=O), 163.84 (C=O), 139.51 (quaternary carbon), 131.14 (CH), 130.1 (quaternary carbon), 128.44 (ArCH), 36.73 (CH_2N), 34.99 (CH_2CO). HR-EI-MS calcd. for $C_{10}H_8NO_2Cl$: 210.0316 $[M + H]^+$; found: 210.0316.

1-(4′-Nitrobenzoyl)-1-azetidin-2-one

Yield: 1.23 g (80%); mp 130 to 131 °C. IR υ_{max} (cm^{-1}, $CHCl_3$): 3020, 1787, 1686, 1599, 1523, 1397, 1309, 1252, 1204, 992. ^1H NMR ($CDCl_3$) δ: 8.33 (2H, d, J = 8.75 Hz), 8.14 (2H, d, J = 8.74 Hz), 3.85 (2H, t, J = 5.58 Hz, CH_2N), 3.2 (2H, t, J = 5.57 Hz, CH_2CO). ^{13}C NMR ($CDCl_3$) δ: 164.16 (C=O), 163.79 (C=O), 150.29 (quaternary carbon), 137.32 (quaternary carbon), 130.76 (CH), 123.28 (CH), 37.0 (CH_2N), 35.5 (CH_2CO).

Kinetic procedures

Standard UV spectroscopy was carried out on a Cary 1E UV–vis spectrophotometer (Varian, Australia) equipped with a 12-compartment cell block. The instrument was used in a double beam mode, allowing six reaction cells to be followed in a single run. The cell block was thermostatted using a Peltier system.

The pH measurements were made with a ϕ40 pH meter (Beckman, Fullerton, California) using a semi-micro calomel electrode (Beckman). A calibration of the pH meter was carried out at 30 °C using pH 6.99 ± 0.01, 4.01 ± 0.02, or 9.95 ± 0.02 calibration buffers. For solution pH ≥ 3 and ≤ 11, the pH was controlled by the use of ≤0.2 mol/L buffer solutions of formate (pK_a 3.75), ethanoate (pK_a 4.72), MES (pK_a 6.1), MOPS (pK_a 7.2), TAPS (pK_a 8.4), CAPSO (pK_a 9.6), and CAPS (pK_a 10.4). Buffer solutions were prepared by partial neutralization of their sodium salts to the required pH. Hydroxide ion concentrations were calculated using pK_w (H_2O) = 13.83 at 30 °C (4).

In all experiments, temperatures were maintained at 30 °C and ionic strength at 1.0 mol/L with AnalaR grade KCl unless otherwise stated. AnalaR grade reagents and deionized water were used throughout. Organic solvents were glass-distilled prior to use and stored under nitrogen.

Reactions studied by UV spectrophotometry were commenced by injections (20 μL) of acetonitrile stock solutions 2×10^{-2} mol/L of the substrate into the cells containing preincubated buffer (2.0 mL). Final reaction cells contained ≤1% acetonitrile (*v*/*v*). The pH of the reaction cells was measured before and after each kinetic run at 30 °C; kinetic runs experiencing a change >0.05 units were rejected. Reactant disappearance or product appearance were followed at absorbance change maxima for individual compounds. The solubility of compounds was ensured by working within the linear range of absorbance in corresponding Beer–Lambert plots. Reaction concentrations were generally within the range of 2×10^{-5} to 2×10^{-4} mol/L. Pseudo-first-order rate constants from exponential plots of absorbance against time or gradients of initial slopes were obtained using the Cary Win UV kinetics application (Version 02.00(26)). The pH–rate profiles were modelled to theoretical equations using the Scientist program (V2.02, Micromath Software Ltd, Saint Louis, Missouri).

© 2005 NRC Canada

HPLC analysis

HPLC analysis was carried out on the Beckman System Gold HPLC with the 127 solvent module running a linear gradient program from solvent A (94% water, 5% acetonitrile, and 1% formic acid) to solvent B (20% water, 79% acetonitrile, and 1% formic acid) over a period of 30 min, using a RP-18 (5 μm) LiChrospher® 100 column, and monitored by the 168 diode array detector at 228 nm.

Results and discussion

The hydrolysis of *N*-benzoyl β-lactam

The rate of hydrolysis of **2** was studied by UV spectrophotometry in buffered solutions of various pH with 1% acetonitrile – water (*v*/*v*) and 1.0 mol/L ionic strength (KCl) at 30 °C. The hydrolysis of **2** shows simple first-order kinetics to give an observed rate constant (k_{obs}). The pseudo-first-order rate constant (k_{int}) for hydrolysis, obtained by extrapolating k_{obs} to zero-buffer concentration, shows acid-catalysed, pH-independent, and alkaline hydrolysis terms, the relative importance of which vary with pH (Fig. 1). The pseudo-first-order rate constant (k_{int}) has a first-order dependence on acid and hydroxide ion concentration, as indicated by the slope of unity on the acid and basic limb, respectively, of the plot of the logarithm of the rate constant (k_{int}) against pH. The pseudo-first-order rate constant can be fitted to eq. [1] using the Scientist program:

$$[1] \qquad \frac{\text{Rate}}{[\beta\text{-lactam}]} = k_{int} = k_o + k_H[H^+] + k_{OH}[OH^-]$$

The rate constants for acid-catalysed hydrolysis (k_H), pH-independent hydrolysis (k_o), and alkaline hydrolysis (k_{OH}) of **2** are $k_H = 3.19 \times 10^{-5}$ (mol/L)$^{-1}$ s^{-1}, $k_o = 8.92 \times 10^{-7}$ s^{-1}, and $k_{OH} = 11.2$ (mol/L)$^{-1}$ s^{-1}. The latter is in the range commonly observed for the alkaline hydrolysis of imides (5).

Alkaline hydrolysis of *N*-benzoyl β-lactam

The site of nucleophilic attack by the hydroxide ion on **2** is not obvious because the rates of alkaline hydrolysis of β-lactams with weakly basic leaving groups are similar to those for analogous acyclic amides (2, 6). The rate of alkaline hydrolysis was also studied by pH-stat to monitor the progress of the reaction by titrating against a NaOH solution. One equivalent of NaOH to the β-lactam concentration was consumed for the overall reaction, and the calculated second-order rate constant (k_{OH}) for the alkaline hydrolysis of **2** from a single pH-stat experiment, carried out at pH 10.50, was very similar to that determined by UV spectrophotometry. At the end of the reaction, the solution was analysed by HPLC with a UV detector. The presence of benzoic acid is clearly demonstrated as a new signal. No benzoic acid would be formed from the hydrolysis of the β-amido acid **3** under these conditions (Scheme 1, route b). Any hydrolysis to give benzoic acid via route b would also consume more than 1 equiv. of hydroxide ion to the β-lactam concentration in contrast to 1 equiv. as seen in the pH-stat experiment. The benzoic acid must then be formed from the alkaline hydrolysis of the exocyclic amide (Scheme 1, route a). Competing exo- and endo-cyclic C–N bond fission was also confirmed by studying the hydrolysis reaction in 1.0 mol/L NaOD–D_2O by ^{1}H NMR. The spectrum, taken immediately after mixing, shows no starting material but two pairs of distinctive triplets in the methylene region. One pair of the triplets belongs to the simple unsubstituted azetidin-2-one, identified by spiking the reaction mixture with the compound. For the other pair of triplets, two-dimensional ^{1}H, ^{13}C HMBC NMR shows a cross peak between the exocyclic carbonyl carbon and one of the triplets, which indicates that the exocyclic carbonyl was still attached to the ring skeleton, i.e., the β-amido acid hydrolysis product **3**.

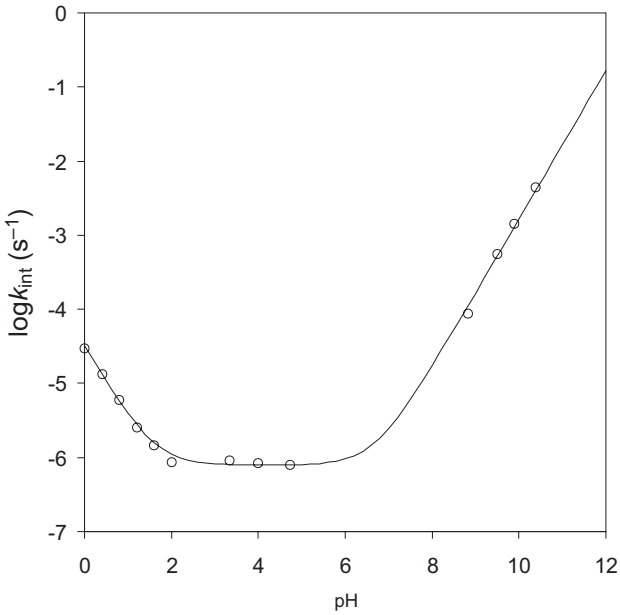


Fig. 1. The pH–rate profile for the hydrolysis of *N*-benzoyl β-lactam (**2**) in 1% acetonitrile – water (*v*/*v*) at 30 °C with 1.0 mol/L ionic strength.

The fractions of the unsubstituted azetidin-2-one and the β-amido acid **3** in H_2O, calculated using the ratio of their NMR signal integrals, are 0.19 and 0.81, respectively. The product ratio was the same when the reaction was carried out at pH 10.50, maintained by pH-stat. This indicates that the rates of hydrolysis of the β-lactam and the exocyclic amide have the same dependence on the hydroxide ion concentration. As the relative rates between two competing pathways in a parallel reaction are proportional to their product distribution (7), the second-order rate constant for the alkaline hydrolysis of the β-lactam of **2** (k_{OH}^{endo}) is 9.07 (mol/L)$^{-1}$ s^{-1} and that for the alkaline hydrolysis of the exocyclic amide (k_{OH}^{exo}) is 2.13 (mol/L)$^{-1}$ s^{-1} (Table 1).

The hydrolysis of *N*-benzoyl β-lactam shows no deuterium incorporation in the hydrolysis product β-amido acid, indicative of a direct addition–elimination mechanism of acyl transfer. The hydrolysis of *N*-acyl β-lactams thus occurs by competitive attack at the endo- and exo-cyclic carbonyl centres. The fact that exocyclic attack is competitive with endocyclic is yet another example of the surprisingly small difference in reactivity between β-lactams and acyclic amides (2, 6). If the rate-limiting step is attack of hydroxide ion on the β-lactam carbonyl carbon to form a tetrahedral intermediate, then the release of strain in the four-membered ring would not be realized in the transition state, although one may have anticipated a preferential conversion of a three-coordinate to a four-coordinate carbon in the four-

© 2005 NRC Canada

Table 1. The second-order rate constants for the hydrolysis at the endo- and exo-cyclic carbonyl centres of *N*-benzoyl β-lactam (**2**) in water and deuterium oxide with 1% acetonitrile (*v*/*v*) and 1.0 mol/L ionic strength (KCl) at 30 °C.

	Observed rate constants	Rate constants for endocyclic C–N fission	Rate constants for exocyclic C–N fission
k_{OH} ((mol/L)$^{-1}$ s^{-1})	11.2	9.07	2.13
k_{OD} ((mol/L)$^{-1}$ s^{-1})	15.1	12.2	2.87
SKIE[a]		0.74	0.74

[a]SKIE (solvent kinetic isotope effect).

membered ring. If the rate-limiting step is the breakdown of the tetrahedral intermediate or if the reaction is concerted, then this appears to be another example of the reluctance of four-membered rings to undergo facile opening (2, 8).

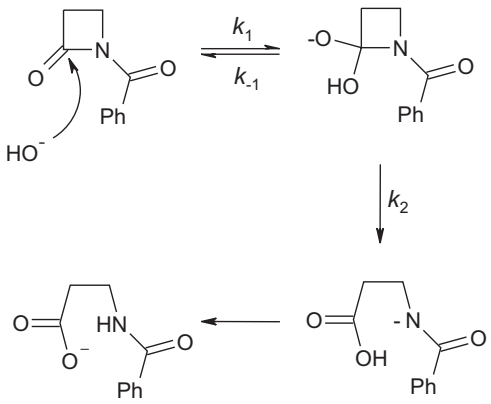
The apparent second-order rate constant (k_{OD}^{app}) for the alkaline hydrolysis of **2** in D_2O, using pK_w^{D2O} = 14.699 (4) and pD = pH meter reading + 0.40 (9), is 15.1 (mol/L)$^{-1}$ s^{-1}. The fraction of the unsubstituted azetidin-2-one and the β-amido acid **3** obtained from the ^{1}H NMR signal integrals of the products of the reaction in 1.0 mol/L NaOD–D_2O is identical to that obtained in 1.0 mol/L NaOH–H_2O. Therefore, the second-order rate constant for the alkaline hydrolysis of the exocyclic amide (k_{OD}^{exo}) is 2.87 (mol/L)$^{-1}$ s^{-1} and that for the alkaline hydrolysis of the β-lactam (k_{OD}^{endo}) is 12.2 (mol/L)$^{-1}$ s^{-1} (Table 1). As the ratio between the alkaline hydrolysis of the exocyclic amide and the β-lactam is the same in water and in deuterium oxide, the two reactions have, within experimental error, the same solvent kinetic isotope effect (k_{OH}/k_{OD}) of 0.74 (Table 1). The inverse solvent isotope effect is compatible with a rate-limiting formation of the tetrahedral intermediate or its breakdown by anion expulsion (Scheme 2).

The rate-limiting step for the alkaline hydrolysis of acyclic amides is normally the breakdown of the tetrahedral intermediate with partial protonation on the leaving group amine nitrogen (6, 10). However, with **2**, protonation on the amide nitrogen is thermodynamically unfavourable. The leaving group may be expelled in the rate-limiting step as an amide anion without N protonation **4** and is compatible with the observed inverse solvent kinetic isotope effect. C–N bond fission expelling an amide anion from the tetrahedral intermediate would be rate limiting if the expulsion of the amide anion is slower than the expulsion of an incoming hydroxide ion in the intermediate, i.e., $k_2 < k_{-1}$ (Scheme 2). The pK_a of amides like benzamide is about 15, so the pK_a of the conjugate acids of the groups expelled, water and amide, are very similar. The relative rate of C–O fission expelling alkoxide anions compared with C–N fission expelling amines of the same basicity is not easy to predict. Some reactions appear to favour amine expulsion (11), whereas others have faster rates for oxygen (2). A large negative charge development on the leaving group nitrogen is expected for expulsion of an amide anion. The hydrolysis was further studied by using linear free energy relationships to elucidate changes in effective charge in the transition state by monitoring the effect of changing the aryl substituents on reactivity.

Structure–activity relationships for the alkaline hydrolysis of *N*-aroyl β-lactams

The rates of alkaline hydrolysis of some aryl substituted

Scheme 2.



N-aroyl β-lactams were studied as a function of pH in 1% acetonitrile – water (*v*/*v*) with 1.0 mol/L ionic strength (KCl) at 30 °C by UV spectrophotometry. The pseudo-first-order rate constants (k_{int}) for the buffer-independent hydrolysis were obtained by extrapolating the observed rate constant to zero-buffer concentration. The apparent second-order rate constant (k_{OH}^{app}) for alkaline hydrolysis was obtained from the slope of the plot of the pseudo-first-order rate constant (k_{int}) against the hydroxide ion concentration. Using the fraction of products obtained, as previously described using ^{1}H NMR, the apparent second-order rate constants (k_{OH}^{app}) are then separated into the second-order rate constants for the alkaline hydrolysis of the exocyclic amide (k_{OH}^{exo}) and for the alkaline hydrolysis of the β-lactam (k_{OH}^{endo}) (Table 2). The product ratios between the unsubstituted azetidin-2-one and the β-amido acid hydrolysis product, and hence the relative rates of endo- and exo-cyclic C–N bond fission, depend on the nature of the para-substituents in the benzamide residue. Electron-withdrawing substituents favour attack at the exocyclic amide, presumably reflecting the relative importance of the electrophilicity of the carbonyl centre compared with the nucleofugality of the leaving group. The more electron-withdrawing is the substituent, the higher the ratio of exocyclic to endocyclic C–N bond fission and the greater the formation of the simple azetidin-2-one relative to the β-amido acid **3** as products. Exocyclic C–N bond fission is the dominant reaction in the alkaline hydrolysis of *N*-*p*-nitrobenzoyl β-lactam in preference to β-lactam hydrolysis (Table 2).

The observation that electron-withdrawing substituents enhance the rate of reaction is compatible with either rate-limiting formation of the tetrahedral intermediate or its breakdown with amide anion expulsion occurring in the

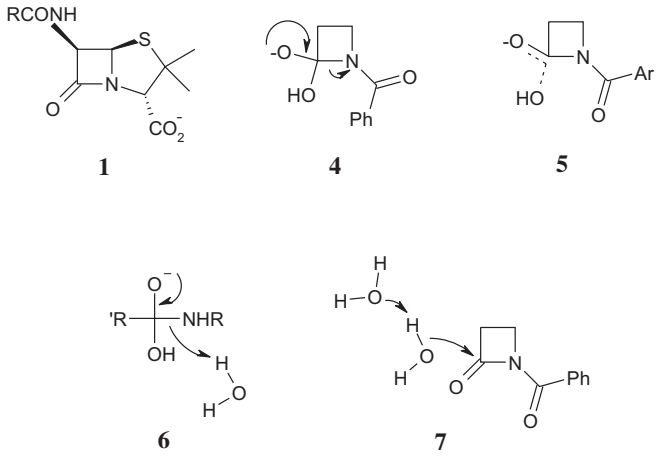
© 2005 NRC Canada

Table 2. The second-order rate constants (SD ± 5%) for the alkaline hydrolysis of *N*-aroyl β-lactams in 1% acetonitrile – water (*v*/*v*) with 1.0 mol/L ionic strength (KCl) at 30 °C.

	pK_a	k_{OH}^{app} ((mol/L)$^{-1}$ s^{-1})	Fraction of endocyclic C–N fission	k_{OH}^{endo} ((mol/L)$^{-1}$ s^{-1})	Fraction of exocyclic C–N fission	k_{OH}^{exo} ((mol/L)$^{-1}$ s^{-1})
p-NO_2	3.44	57.7	0.46	26.5	0.54	31.2
p-Cl	3.99	18.2	0.76	13.8	0.24	4.37
p-H	4.20	11.2	0.81	9.07	0.19	2.13
p-OMe	4.47	8.08	0.90	7.27	0.10	0.81
o-COOH	5.28	2.60	1.00	2.60	0.0	—

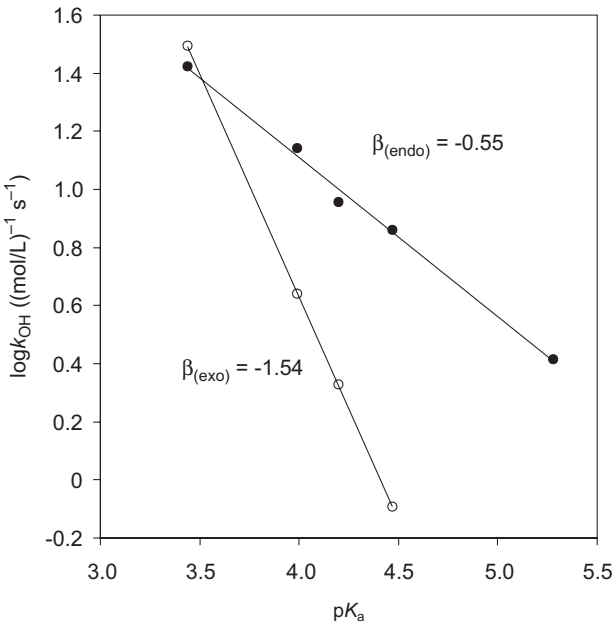
Note: The pK_a of the carboxylic acid corresponding to exocyclic aryl carboxamide is given as an indicator of the inductive effect of the substituent in the aromatic ring. pK_a values are taken from ref. 12.

transition state. The difficulty with correlating the reaction rate to the ionization of the leaving group is the lack of available ionization constants of substituted benzamides. The ionization constants of substituted benzoic acids, as analogues of benzamides, were therefore used for the correlation.



The Brønsted-type plot of the rate constants for the alkaline hydrolysis of the β-lactam ring of *N*-aroyl β-lactams against the pK_a of the corresponding benzoic acids is shown in Fig. 2. This shows a good linear correlation, the slope of which gives the Brønsted β_{lg} value for the alkaline hydrolysis of *N*-aroyl β-lactams as –0.55. This indicates that in the transition state of the rate-limiting step of hydrolysis, the effective charge on the nitrogen atom in the amine leaving group becomes more negative relative to the reactant state by 0.55. The effective charge on the nitrogen of β-lactams is expected to be very similar to that of acyclic amides of +0.7 (13). There is no data on the effective charge on the nitrogen in imides. If there is no levelling of the resonance effect, then presumably the charge could be as high as 1.4. If amide resonance is reduced, then, effectively, imides could be treated as amides to which is attached an electron-withdrawing acyl group not involved in further resonance stabilization. This would make the effective charge on the imide nitrogen greater than 0.7 but less than 1.4. A crude estimation may be obtained from the difference in σ and σ$^-$ values for a *para*-acyl substituent, i.e., 0.50 and 0.84, respectively (13). The additional positive charge on the imide nitrogen due to a second electron-withdrawing but non-resonating acyl substitutent would be (0.5/0.84) × 0.7 = 0.42. This would make the effective charge on the imide nitrogen +1.1. This will be used in subsequent discussions, but a slightly smaller or larger value makes little difference to the conclusions.

Fig. 2. Brønsted plot for the second-order rate constant (k_{OH}), for the alkaline hydrolysis at the endocyclic (●) and exocyclic (○) carbonyl centre of *N*-aroyl β-lactams against the pK_a of the corresponding benzoic acid in 1% acetonitrile – water (*v*/*v*) at 30 °C. I = 1.0 mol/L (KCl).



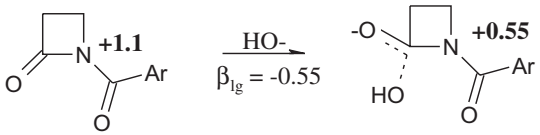
The observed Brønsted value of –0.55 for the alkaline hydrolysis of the β-lactam ring of *N*-aroyl β-lactams is compatible with a late transition state for the formation of the tetrahedral intermediate **5**. The effective charge of +0.55 on N in the transition state structure indicates little or no C–N bond fission and that the nitrogen atom is still involved in normal amide resonance with the aroyl residue (Scheme 3). For comparison, the Brønsted β_{lg} value for the alkaline hydrolysis of N-substituted amides is –0.07 (6), which was interpreted in terms of general-acid-catalysed breakdown of the tetrahedral intermediate owing to partial proton transfer from water **6**. The rates of alkaline hydrolysis of *N*-aryl β-lactams generate a Brønsted β_{lg} of –0.44, which was taken as evidence of rate-limiting formation of the tetrahedral intermediate (2, 14).

© 2005 NRC Canada

Table 3. The apparent rate constants (SD ± 5%) and kinetic parameters for the acid-catalysed hydrolysis, pH-independent hydrolysis, and alkaline hydrolysis of *N*-benzoyl β-lactam (**2**) in 1% acetonitrile – water (*v*/*v*) with 1.0 mol/L ionic strength (KCl) at different temperatures.

	k ((mol/L)$^{-1}$ s^{-1})						
	20.0 °C	30.0 °C	40.0 °C	50.0 °C	60.0 °C	$\Delta S^{\ddagger}$ (J K^{-1} mol^{-1})	$\Delta H^{\ddagger}$ (kJ mol^{-1})
H_2O	3.77×10^{-7}	8.92×10^{-7}	1.34×10^{-6}	2.01×10^{-6}	3.53×10^{-6}	–228 ± 9	40.9 ± 2.8
HO^-	6.72	11.2	22.2	37.7	69.7	–77.3 ± 4.2	44.8 ± 1.3
H^+	9.66×10^{-6}	3.19×10^{-5}		3.78×10^{-4}	1.12×10^{-3}	–19.1 ± 6.7	94.5 ± 0.4

Scheme 3.



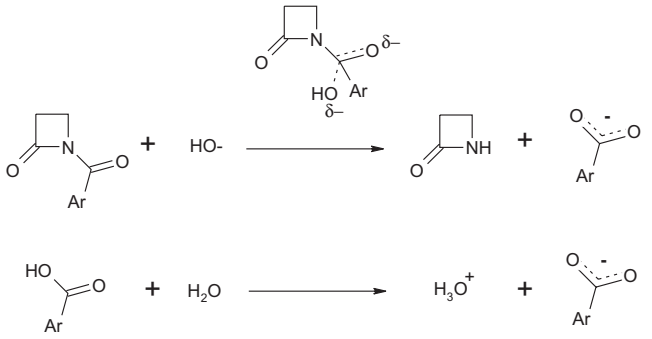
Extrapolating the data for the Brønsted plot for the alkaline hydrolysis of *N*-aryl β-lactams to the rate constant for the alkaline hydrolysis of *N*-benzoyl β-lactam gives an apparent pK_a of –7.5 for the leaving group amine. Formally this corresponds to the N protonation of benzamide, but as protonation of amides corresponds to O rather than N protonation, the predicted pK_a for N protonation of an amide is not unreasonable.

The Brønsted-type plot for the alkaline hydrolysis of the exocyclic amide of *N*-aroyl β-lactams against the pK_a of the corresponding benzoic acids is shown in Fig. 2. The plot is again reasonably linear, but the dependence of the rate on the pK_a is much greater with an apparent Brønsted β of –1.54. The correlation is intriguing, as the product of the exocyclic amide hydrolysis and that of ionization of the carboxylic acid are the same (Scheme 4). The Brønsted value of –1.54 indicates that the effective charge at the reaction centre in the transition state for the amide hydrolysis is more negative than that in the reactant imide compared with the charge in the carboxylate ion relative to that in the undissociated acid. This indicates that there is a relatively greater negative charge density in the transition state for the hydrolysis reaction than that in the carboxylate anion. This may indicate a rate-limiting formation of the tetrahedral intermediate with a late transition state or an early one in a rate-limiting breakdown because in the tetrahedral intermediate the negative charge is more localized. A similar linear free energy relationship was observed for the rates of alkaline hydrolysis of esters against the pK_a of the product carboxylic acid, which gave a Brønsted value of –1.3 (15). The localized negative charge on the oxygen anion in the tetrahedral intermediate is more dependent on the stabilizing effect of electron-withdrawing groups than the more stable delocalized negative charge in the carboxylate anion.

pH-Independent hydrolysis

The rate of hydrolysis of **2** is pH independent from pH 2–6 (Fig. 1). A product analysis using HPLC of the reaction at pH 3.99 (0.1 mol/L acetate buffer), ionic strength 1.0 mol/L (KCl), and at 60 °C was undertaken. The signal for **2** disappeared with time in an exponential manner, but that for benzoic acid, identified by spiking with the compound, was

Scheme 4.



formed in the hydrolysis in barely detectable amounts. Less than 3% of the hydrolysis pathway now occurs by exocyclic C–N fission. Furthermore, the acetate buffer probably affects the relative rates of hydrolysis of the β-lactam and the exocyclic amide. Buffer catalysis accounts for 17% of the observed rate of hydrolysis under the same experimental conditions as determined from kinetic measurements at different acetate concentrations. If, in an extreme case, the buffer-catalysed hydrolysis of **2** occurs exclusively at the exocyclic amide, a minimum of 17% of the product would be benzoic acid. However, as only a maximum of 3% is attributed to the hydrolysis of the exocyclic amide in the acetate buffer at pH 4, the pH-independent hydrolysis of **2** probably occurs exclusively with endocyclic C–N bond fission. This is in contrast to the 4:1 ratio of β-lactam and exocyclic amide hydrolysis seen for the alkaline hydrolysis of **2**. The exocyclic acyl centre must show a greater selectivity (β_{nuc}) towards nucleophilic attack by water and hydroxide ion, than that of the β-lactam.

The rate of hydrolysis of **2** was studied at different temperatures by UV spectrophotometry (Table 3). The entropy of activation ($\Delta S^{\ddagger}$) for the pH-independent hydrolysis is –228 J K^{-1} mol^{-1}, which is threefold more negative compared with –77.3 J K^{-1} mol^{-1} for the alkaline hydrolysis. The more negative entropy of activation for the pH-independent hydrolysis compared to that for the alkaline hydrolysis suggests a more ordered system for the pH-independent hydrolysis. The solvent kinetic isotope effect (k_{H_2O}/k_{D_2O}) for the pH-independent hydrolysis of **2** is 1.25, which indicates the transition state in the rate-limiting step involves a degree of proton transfer (Table 4). The entropy of activation ($\Delta S^{\ddagger}$) and the solvent kinetic isotope effect (k_{H_2O}/k_{D_2O}) is compatible with a hydrolysis mechanism involving nucleophilic attack by water that is general-base-catalysed by another water molecule such as that shown in **7**.

© 2005 NRC Canada

Table 4. The rate constants for the acid-catalysed hydrolysis (k_H), pH-independent hydrolysis (k_o), and alkaline hydrolysis (k_{OH}) of the β-lactam of *N*-aroyl β-lactams in 1% acetonitrile – water (*v*/*v*) with 1.0 mol/L ionic strength (KCl) at 30 °C.

	pK_a	k_o (s^{-1})	k_H ($(mol/L)^{-1}$ s^{-1})	k_{OH}^{endo} ($(mol/L)^{-1}$ s^{-1})
p-NO_2	3.44	3.51×10^{-6}	1.38×10^{-5}	26.5
p-Cl	3.99	1.23×10^{-6}	2.68×10^{-5}	13.8
p-H	4.20	8.92×10^{-7} (H_2O) 7.16×10^{-7} (D_2O)	3.19×10^{-5}	9.07
p-OMe	4.47	6.04×10^{-7}	7.75×10^{-5}	7.27
o-COOH	5.28			2.60

Note: The pK_a of the carboxylic acid corresponding to exocyclic aryl carboxamide is given as an indicator of the inductive effect of the substituent in the aromatic ring. pK_a values are taken from ref. 12.

The first-order rate constants (k_o) for the pH-independent hydrolysis of aryl substituted *N*-aroyl β-lactams were determined (Table 4) and generated a Brønsted β_{lg} value of –0.77. The Brønsted β_{lg} value for the pH-independent hydrolysis is slightly more negative than that for the alkaline hydrolysis (β_{lg} = –0.55) indicating a later transition state probably owing to water being a much weaker nucleophile than hydroxide ion.

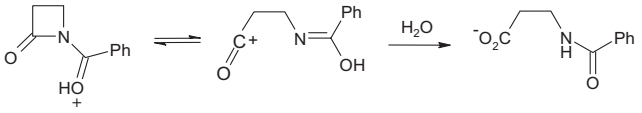
Acid-catalysed hydrolysis

The acid-catalysed hydrolysis of **2** in 1.0 mol/L hydrochloric acid was also followed by HPLC at 30 °C. The signal for **2** disappeared with time in an exponential manner, but that for benzoic acid, identified by spiking with the compound, did not show any significant increase. It is estimated that benzoic acid formation accounted for less than 3% of the hydrolysis pathway.

The second-order rate constants (k_H) for the acid-catalysed hydrolysis of the β-lactam of *N*-aroyl β-lactams increase with electron-donating substituents in the aryl ring of the amide leaving group (Table 4). The rate constants are reasonably well-correlated with the pK_a of the corresponding benzoic acid to give a Brønsted β_{lg} value of 0.68. The change in effective charge of +0.68 indicates a transition state with significant protonation on the amide leaving group. There are three possible sites for protonation of **2**: the β-lactam nitrogen is the least basic compared with the β-lactam and the exocyclic carbonyl oxygens. Protonation on the exocyclic carbonyl oxygen is probably more favourable than protonation on the β-lactam carbonyl oxygen, as the carbonyl oxygen becomes less basic when it is attached to a four-membered ring system (16). Also, protonation on the exocyclic carbonyl oxygen may increase the nucleofugality of the leaving group in β-lactam ring opening.

The second-order rate constants for the acid-catalysed hydrolysis of **2** shows a greater dependence on temperature than that for alkaline hydrolysis (Table 3). The entropy of activation ($\Delta S^{\ddagger}$) for the acid-catalysed hydrolysis is –19.1 J K^{-1} mol^{-1}, which is threefold less negative compared with –77.3 J K^{-1} mol^{-1} for alkaline hydrolysis. The smaller entropy of activation for the acid-catalysed hydrolysis may be indicative of an A1 pathway and a unimolecular breakdown of the conjugate acid of the *N*-aroyl β-lactam. The acid-catalysed hydrolysis of the β-lactam in penicillins **1** and other β-lactams has been suggested to involve an A1 mechanism with protonation on the β-lactam nitrogen leading to intermediate formation of an acylium ion (6, 16). If the acid-catalysed hydrolysis of *N*-benzoyl β-lactam occurs by an A1 mechanism with O protonation on the exocyclic carbonyl, C–N bond fission would form a highly unstable acylium ion and an enol amide (Scheme 5).

Scheme 5.



In conclusion, it has been shown that the alkaline hydrolysis of *N*-aroyl β-lactams occurs at similar rates at the β-lactam and the exocyclic amide centres. Despite the strain energy of the four-membered ring, it is not released in the transition state to lower the activation energy and favour exclusive endocyclic C–N ring fission. The reluctance of four-membered rings to open rapidly has been noted previously (2). The competitive rates of hydrolysis at the endocyclic and exocyclic carbonyl centres provide an opportunity to investigate the relationship between the specificity and reactivity of the acyl centres towards enzymes.

Acknowledgment

We thank the University of Huddersfield for financial support and Andrew Williams for discussion.

References

1. M.I. Page. *In* The chemistry of β-lactams. *Edited by* M.I. Page. Blackie, Glasgow. 1992.
2. M.I. Page. Adv. Phys. Org. Chem. **23**, 165 (1987).
3. N.J. Baxter, L.J.M. Rigoreau, A.P. Laws, and M.I. Page. J. Am. Chem. Soc. **122**, 3375 (2000); K. Bowden and K. Bromley. J. Chem. Soc. Perkin Trans. 2, 2111 (1990).
4. A.K. Covington, R.A. Robinson, and R.G. Bates. J. Phys. Chem. **70**, 3820 (1966).
5. J.T. Edward and K.A. Terry. J. Chem. Soc. 3527 (1957).
6. M.I. Page. Acc. Chem. Res. **17**, 144 (1984); P. Proctor, N.P. Gensmantel, and M.I. Page. J. Chem. Soc. Perkin Trans. 2, 1185 (1982).
7. A.A. Frost and R.G. Pearson. Kinetics and mechanism: a study of homogeneous chemical reactions. Wiley, New York. 1953.
8. M.I. Page, P. Webster, and L. Ghosez. J. Chem. Soc. Perkin Trans. 2, 805 (1990).
9. P.K. Glascoe and F.A. Long. J. Phys. Chem. **64**, 188 (1960).

© 2005 NRC Canada

10. J.J. Morris and M.I. Page. J. Chem. Soc. Perkin Trans. 2, 679 (1980); 685 (1980); R.S. Brown, A.J. Bennet, and H. Slebocka-Tilk. Acc. Chem. Res. **25**, 481 (1992).
11. N. Gravitz and W.P. Jencks. J. Am. Chem. Soc. **96**, 499 (1974).
12. E.A. Braude and F.C. Nachod. Determination of organic structures by physical methods. Academic Press, New York. 1955.
13. M.I. Page and A. Williams. Organic and bio-organic mechanisms. Addison-Wesley Longman, Harlow, UK. 1997.
14. G.M. Blackburn and J.D. Plackett. J. Chem. Soc. Perkin Trans. 2, 1366 (1972).
15. P. Barton, A.P. Laws, and M.I. Page. J. Chem. Soc. Perkin Trans. 2, 2021 (1994).
16. P. Wan, T.A. Modro, and K. Yates. Can. J. Chem. **58**, 2423 (1980).

© 2005 NRC Canada

A temperature-annealing effect on the host–guest complexation with γ-cyclodextrin[1]

P. John Wright and Cornelia Bohne

Abstract: Pyrene binds to γ-cyclodextrin and forms host–guest complexes with different stoichiometries. The fluorescence of pyrene was employed as a qualitative signature for these different complexes. Solutions prepared at room temperature were shown not to be in thermodynamic equilibrium, since a heating cycle of 20 min at 80 °C followed by cooling led to changes in the relative concentrations of the pyrene–γ-cyclodextrin complexes. This temperature-annealing effect has consequences when determining thermodynamic parameters such as equilibrium constants and host–guest stoichiometries.

Key words: cyclodextrin, pyrene, aggregates, fluorescence.

Résumé : Le pyrène se lie à la γ-cyclodextrine pour former des complexes hôte–invité de stoechiométries diverses. On a utilisé la fluorescence du pyrène comme signature qualitative de ces différents complexes. On a démontré que des solutions préparées à la température ambiante ne présentent pas d'équilibre thermodynamique puisqu'un cycle de chauffage de 20 min à 80 °C, suivi par un refroidissement, conduit à des changements dans les concentrations relatives des complexes pyrène–γ-cyclodextrine. Cet effet d'annellation lié à la température a des conséquences lorsqu'on veut déterminer des paramètres thermodynamiques, tels les constantes d'équilibre et les stoechiométries hôte–invité.

Mots clés : cyclodextrine, pyrène, agrégats, fluorescence.

[Traduit par la Rédaction]

Introduction

Cyclodextrins (CDs) are cyclic oligosaccharides that serve as hosts for guest complexation owing to their relatively hydrophobic cavity. CDs have been extensively employed to study host–guest complexation (1–5) and biomimetic systems (6–9). From a technological point of view, applications of CDs can be found in separation methods (10) and in food and drug formulations (11, 12). Most CDs complex guests with a 1:1 (guest:CD) stoichiometry (3), but CDs can also be involved in higher order complexes where more than one CD molecule is present in the complex.

In the thermodynamic characterization of CD host–guest complexes, it is normally assumed that aqueous CD solutions follow an ideal behavior, i.e., for a given weight of CD solubilized in water, the CD molecules are present as monomers. However, there is evidence that this assumption is not always applicable, especially at high CD concentrations. The osmotic pressures and activity coefficients for α- and γ-CD decrease with an increase in the CD concentration (≤120 mmol/L) (13), and the formation of CD dimers are suggested to be responsible for this effect. Light scattering experiments showed that solutions of CDs (≤50 mmol/L) contained aggregates (14, 15) larger than 100 nm, suggesting that the aggregate contains several CD molecules. The aggregation was more prominent for β-CD than for α- and γ-CD, and in the latter two cases it was suggested that the contribution of the aggregates to the total amount of the CD dissolved in aqueous solutions was small (15, 16). Aggregation can be minimized by increasing the temperature or the ionic strength of the solution (15). Indeed, the formation of aggregates, leading to hazy solutions and the formation of precipitates, is a problem in drug formulation (17).

The objective of this work was to determine if CD–guest solutions prepared at room temperature by dissolving the guest and CD in water constitutes a system in thermodynamic equilibrium. An annealing process was employed in which the solution was heated to a high temperature (80 °C) followed by cooling. The solubility of CDs is known to increase when the temperature is raised (4, 18), and the formation of aggregates is diminished at high temperatures (15). In addition, for a guest-appended CD, initial heating of the sample to 85 °C was shown to influence the types of complexes formed (19).

The addition of salts can affect the magnitude of the equilibrium constants between guests and CDs for 1:1, 1:2, and 2:2 (guest:CD) complexes (20–23). The effect depends on the nature and the concentration of the salts. It can be ascribed either to competitive complexation of anions to the CD cavity, since some anions were shown to bind weakly to CDs (24, 25), or to the water structure breaking–making effect of the salts, which is related to the Hoffmeister's series for protein solubility. The effect of salts on solute solubility is an empirical observation for which the mechanistic interpretation is not completely elucidated (26–30). Anions such as $^{-}$SCN and I^{-} are structure-breaking agents, and the

Received 2 May 2005. Published on the NRC Research Press Web site at http://canjchem.nrc.ca on 10 November 2005.

P.J. Wright and C. Bohne.[2] Department of Chemistry, University of Victoria, PO Box 3065, Victoria, BC V8W 3V6, Canada.

[1]This article is part of a Special Issue dedicated to organic reaction mechanisms.

[2]Corresponding author (e-mail: bohne@uvic.ca).

 doi: 10.1139/V05-159 © 2005 NRC Canada

hydration energy of these ions is low, leaving more water molecules available to interact with other solutes. NaCl is neutral with respect to its solvation ability and does not significantly affect the solvation ability of water; whereas the sulfate anion is a structure-making agent. Since the addition of salts was shown to inhibit aggregation of CDs (15), we studied the effect of salt addition on the annealing effect for host–guest complexation.

We chose the pyrene–γ-CD system to investigate the effect of temperature annealing because three γ-CD complexes with different stoichiometries are formed (1:1, 1:2, and 2:2; Scheme 1) (31, 32). This system is expected to be more sensitive to the presence of CD aggregates than a system containing only a 1:1 host–guest complex. In addition, the investigation on the binding dynamics of pyrene to γ-CD showed that slow processes were present that occurred over tenths of seconds, which were likely to be related to the rearrangement of pyrene within CD complexes (31). A further rationale for using pyrene as the guest is that its photophysics are sensitive to the polarity of the environment and to the formation of pyrene dimers. The latter leads to the emission characteristically observed for excimers, which in an unconstrained solution are due to the interaction of a singlet excited state of pyrene with a ground-state molecule of pyrene. In the presence of γ-CD, the "excimer-like" broad emission centered around 473 nm is due to the inclusion of two pyrene molecules in the γ-CD complex (2:2) (31, 32). The intensities of the vibronic bands for the pyrene monomer emission respond differently to the solvent polarity. For this reason, the intensity ratio for the emission peak at 373 nm with respect to the intensity at 383 nm (I:III ratio) is high in water and low in nonpolar solvents (33, 34).

[1] Pyrene + γ-CD → Pyrene–γ-CD (1:1)

[2] Pyrene–γ-CD + γ-CD → Pyrene–$(\gamma\text{-CD})_2$ (1:2)

[3] 2Pyrene–γ-CD → $(\text{Pyrene})_2$–$(\gamma\text{-CD})_2$ (2:2)

Experimental

Materials

Pyrene (Aldrich, 99%) was recrystalized once from 95% ethanol, and its purity was checked in single photon counting experiments in which a mono-exponential decay was observed. γ-CD was either a gift from Cargill (lot No. F8025-12) or purchased from Cyclodextrin Technologies Development Inc. (lot 110080P008), and it was used without purification.

NaI (Aldrich, 99%), NaCl (Anachemia, 99%), Na_2SO_4 (BDH, 99%), NaSCN (Aldrich, 99%), and methanol (ACP, spectrograde) were used without purification. The water employed was deionized using a Sybron Barnstead system (≥17.8 MΩ).

Equipment

UV–vis absorption spectra were recorded on a Cary 1 spectrometer. Steady-state fluorescence spectra were measured with a PTI QM-2 fluorimeter and the temperature of the sample was kept constant using a Haake F3 bath. The excitation wavelength was 331 nm, and the emission spectra were measured between 350 and 600 nm. The bandwidths for the excitation and emission monochromator slits were 1.5 nm. The spectra were corrected for a baseline run containing all components with the exception of pyrene, which was subtracted from the fluorescence spectrum of pyrene. This procedure corrected for the Raman emission of the solvent and the small impurity emission present in the γ-CD sample. For quantitative measurements of the emission intensity, a standard deoxygenated and sealed sample containing pyrene in cyclohexane was employed for normalization purposes.

Time-resolved fluorescence measurements were performed with an Edinburgh OB 920 single photon counting system. The excitation source was a hydrogen-filled lamp. The instrument response function was collected with a Ludox (Aldrich) solution by scattering light at the excitation wavelength. A Lauda RM6 bath was used to keep the sample at a constant temperature. The excitation and emission wavelengths were set to 331 and 383 nm, respectively, and the bandpass for the excitation and emission monochromators was ca. 16 nm (2 mm slits). An iris was employed to ensure that the frequency for the stop pulses was less than 2.5% of the frequency for the excitation pulses. Data were analyzed using the Edinburgh software based on nonlinear least-squares fitting of the experimental data to a sum of exponentials. The instrument response function was very narrow for the time window measured (1 μs), and for this reason reconvolution of the decay with the instrument response function was not necessary. The fluorescence decays were fit to the sum of exponentials, and the goodness of the fit was judged by the χ^2 values (<1.2), the inspection of the randomness of the residuals, and the autocorrelation (35).

Methods

Sample preparation

Aqueous pyrene solutions (0.5 μmol/L) were prepared by injecting small amounts of a pyrene methanolic solution (0.5–1.5 mmol/L) into water in which the desired concentration of γ-CD had been dissolved. The samples were shaken for at least 12 h. Solutions containing NaCl, Na_2SO_4, or NaSCN were prepared as above by first preparing aqueous solutions of the salts. All measurements were performed in aerated solutions.

Temperature variation

Fluorescence spectra at the various temperatures were obtained by starting the collection of spectra at the lowest temperature (ca. 7 °C). Samples were kept at each temperature for at least 20 min. In some instances longer equilibration times were required to achieve constant emission intensities. After the spectra were collected at 59 °C, the sample was heated to 80 °C for 20 min and subsequent spectra were collected at decreasing temperatures. Experiments were also performed for which the annealing times were varied (20, 40, and 60 min). Spectra were recorded at 20 °C, and the samples were then heated to 80 °C and kept for the required time at the higher temperature before being cooled to 20 °C.

Determination of the I:III ratio and excimer emission intensity

The fluorescence intensities for the I and III bands of the monomer emission were measured at the emission maxima of 373 and 383 nm, respectively. The pyrene excimer emis-

© 2005 NRC Canada

sion intensity was measured at 473 nm, and was corrected for the residual monomer emission at 473 nm by

$$[4] \qquad E_{cor} = I_{473} - I_{383}\left(\frac{I_{473}(aq)}{I_{383}(aq)}\right)$$

where I_{473} is the uncorrected intensity measured, and the intensity at 383 nm (I_{383}) is multiplied by the ratio of intensities at 473 and 383 nm determined for the pyrene monomer emission in water (0.015).

Fluorescence quenching

Iodide was used as a quencher, and aqueous stock solutions (ca. 2.0 mol/L) were prepared daily and kept in the dark for the duration of the experiment. All experiments were acquired at 20.4 °C. Annealed samples were heated to 80 °C for 20 min and then recooled to 20.4 °C before the addition of quencher. The maximum quencher concentration employed was 50 mmol/L. The intensity in the absence of quencher (I_0) was corrected for the dilution of the fluorophore with the addition of quencher. The emission intensity for the monomer was recorded at 383 nm, which corresponds to the emission band that is insensitive to solvent polarity.

Results

Pyrene in the presence of γ-CD forms three types of complexes with 1:1, 1:2, and 2:2 (pyrene:γ-CD) stoichiometries (31, 32). The excimer-like emission of pyrene is a signature for the 2:2 complex. Therefore, the ratio of the excimer to the monomer emission intensities (E:M) is a measure of the fraction of pyrene in the 2:2 complex compared with the fraction of monomeric pyrene. The monomer emission of pyrene is a combination of the emission of free pyrene in solution and pyrene in the 1:1 and 1:2 complexes. The I:III ratio corresponds to the sum of the I:III ratios for each pyrene monomeric species taking into account the relative contribution of each species. For the experimental conditions employed in this work, the I:III ratio of pyrene was 1.75 ± 0.02 in water and was 0.58 ± 0.01 in cyclohexane. The I:III ratio for pyrene in the 1:2 complex was previously determined to be close to the ratio in cyclohexane (31). Pyrene in the 1:1 complex has an I:III ratio that is lower than in water, but not as low as in the 1:2 complex. It is important to note that the previous interpretation of the formation of the 1:2 complex (31, 32) was based on the implicit assumption that γ-CD is monomeric in aqueous solution. These experiments would be equally consistent with the incorporation of one pyrene molecule in an aggregate containing two or more γ-CDs. For this reason, we will identify the pyrene–γ-CD complex where the guest is in a very nonpolar environment as a 1:*n* complex.

The temperature annealing experiments in which the pyrene emission in the presence of γ-CD was measured at several temperatures, took approximately 12 h to complete. We also observed that nonannealed samples of pyrene–γ-CD that were kept for a period of months in the dark formed hazy solutions. For this reason, it was important to establish that the changes in the emission spectra observed in the annealing experiment were not due to slow changes to the solution that would occur regardless of a temperature change. A control experiment was run in which a sample was divided in half. One half was kept at room temperature and the other half was used for the temperature-annealing experiment. The fluorescence spectra for both samples were measured after 12 and 24 h of sample preparation and completion of the experiment. The pyrene emission intensities, I:III ratios, and E:M ratios did not change over this period of time in either case. This result showed that no loss of pyrene owing to its adsorption onto the glass surface of the vials occurred and that the sample composition did not change over a 24 h period.

NaCl, Na_2SO_4, and NaSCN were used as electrolytes to study the effect of salt addition on pyrene complexation to γ-CD. None of these salts (0.2 mol/L) had an effect on the I:III ratio for pyrene (0.5 μmol/L) in an aqueous solution (1.75 ± 0.02). The I:III ratio in water is known to decrease with increasing temperature, whereas the value for this ratio is constant in cyclohexane (36). A temperature-annealing experiment for pyrene in water showed that upon cooling, the same I:III ratios were obtained at each temperature as those measured prior to heating the sample. The fluorescence decays for pyrene in water in the absence and presence of NaCl or Na_2SO_4 were mono-exponential, and the singlet excited state lifetime was 135 ± 2 ns. This value was the same as previously reported for pyrene in aerated aqueous solutions (36, 37). In the presence of thiocyanide, a shorter lifetime of 85 ns was measured indicating that $^{-}$SCN quenches the singlet excited state of pyrene with a moderate efficiency (2.2×10^7 $(mol/L)^{-1}$ s^{-1}).

The temperature-annealing experiments were performed by measuring the steady-state pyrene emission spectra starting at a low temperature (ca. 7 °C) and progressively increasing the temperature to ca. 60 °C. At this point the sample cell was removed from the fluorimeter and was heated in an external bath at 80 °C for 20 min. After the heating period, the emission spectra were measured at decreasing temperatures. The amount of 2:2 complex in the presence of 20 mmol/L γ-CD compared with pyrene in the monomeric form was higher at the lower temperatures (Figs. 1 and 2). In addition, the I:III ratio was lower when the temperature was low (Fig. 2). Annealing of the solution at 80 °C led to a decrease in the excimer intensity and an increase in the I:III ratio for the spectra measured at 59.3 °C (compare points **b** and **c** in Fig. 2). These results indicate that annealing at high temperatures decreases the amount of 2:2 complex and that the monomeric pyrene species were on average located in a more polar environment. Further cooling of the solution after the annealing procedure led to an increase in the excimer intensity at the expense of the monomer intensity, but only a moderate decrease was observed for the I:III ratio (Fig. 2). The same behavior was observed for solutions in the presence of NaCl or Na_2SO_4. In contrast, the behavior in the presence of NaSCN was different (Fig. 3). The annealing process led to a marked increase of the E:M ratio (inset Fig. 3).

In the presence of 50 mmol/L γ-CD at temperatures equal to or below 20 °C, the fraction of monomeric pyrene in solution is negligible based on calculations using the equilibrium constants previously determined at 20 °C (31). At this high γ-CD concentration, the I:III ratio at temperatures equal to

© 2005 NRC Canada

Fig. 1. Pyrene fluorescence spectra in the presence of 20 mmol/L γ-CD and 0.2 mol/L NaCl at 7.0 °C (black, **a**), 20.4 °C (red, **b**), and 59.3 °C (blue, **c**). (A) The first spectrum was taken at 7 °C and the temperature was raised to 59.3 °C. (B) The sample was annealed for 20 min at 80 °C and the first spectrum after the annealing process was taken at 59.3 °C, and the sample was then cooled.

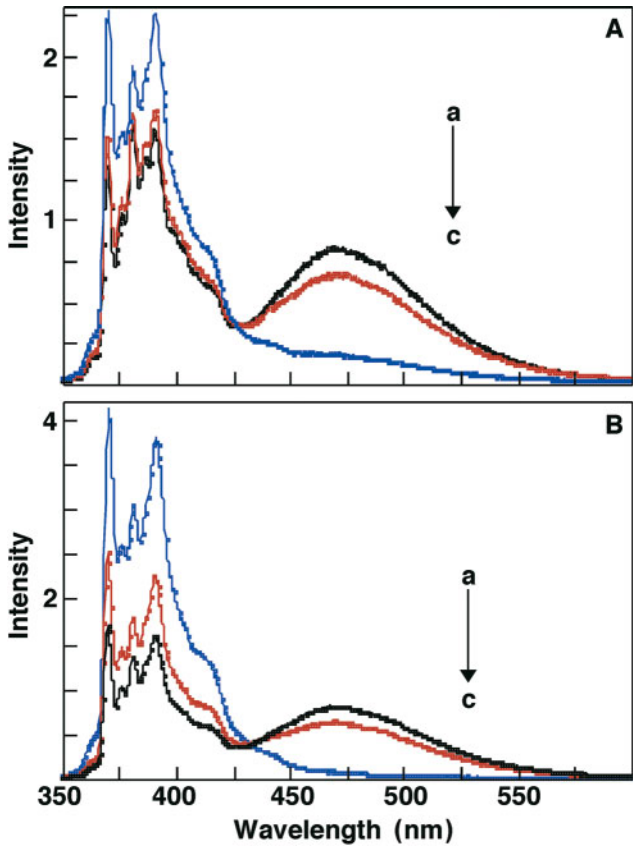
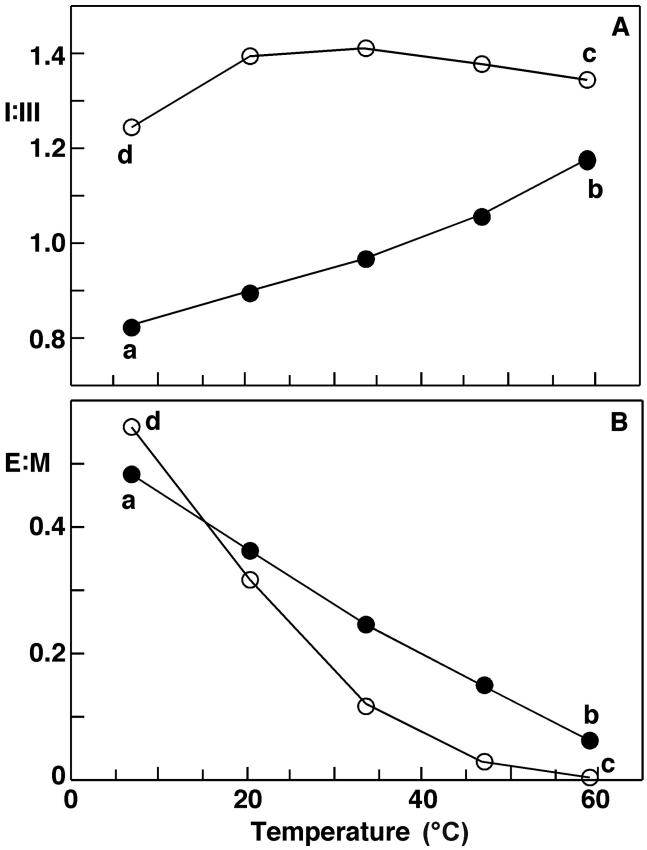


Fig. 2. Change of the I:III (A) and the E:M ratios (B) of the pyrene fluorescence in the presence of 20 mmol/L γ-CD and 0.2 mol/L NaCl as the temperature was raised (solid symbols, from **a** to **b**). The sample was annealed for 20 min at 80 °C (from **b** to **c**) followed by cooling of the sample (open symbols from **c** to **d**). The solid lines were added to connect the data points for the heating and cooling cycles and do not have any physical meaning.



or below 20 °C was a measure of the fraction of pyrene in a 1:1 and 1:*n* complex. For all salts employed, the I:III ratio at 20 °C was higher after the annealing process (Fig. 4).

A control experiment was performed in which samples were heated from 20 to 80 °C and kept at the higher temperature for 20, 40, or 60 min. The purpose of this experiment was to determine if heating of the samples containing the pyrene–γ-CD complexes for longer periods of time would enhance the changes observed for the shorter heating period. This experiment was performed for pyrene in 20 mmol/L γ-CD in the absence of salt and in the presence of NaCl or NaSCN. Some loss of pyrene was observed after the longer heating periods, probably owing to evaporation. For this reason, the only possible comparison was for the I:III ratios. The I:III ratios measured at 20 °C increased from 0.70 to 1.37 ± 0.03 for the three heating periods in the case of the pyrene–γ-CD system in the absence of added salt. The increase observed in the presence of NaSCN was from 0.60 to 1.11 ± 0.06; whereas in the presence of NaCl the change was from 0.73 to 1.4 ± 0.1. These results show that heating for 20 min was sufficient to achieve the annealing process.

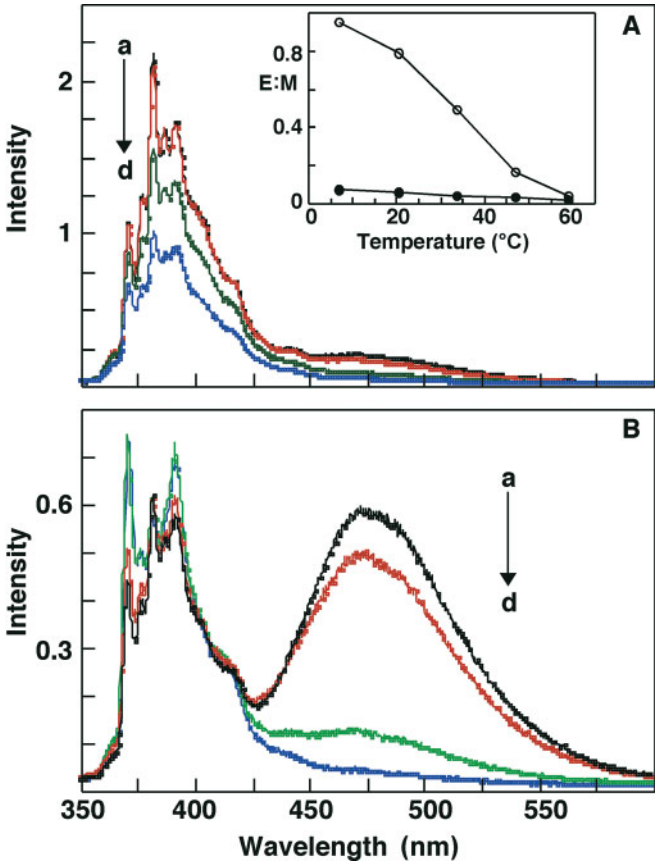
The lifetimes of the pyrene monomer emission in the presence of 20 mmol/L γ-CD were determined using the single photon counting technique. The emission decays were measured at 20 °C before and after annealing the samples at 80 °C for 20 min. The decays were fitted to the sum of two exponentials, where the shorter lifetime around 120–140 ns corresponds to the pyrene in the 1:1 complex, and the component with a long lifetime (330–350 ns) corresponds to the pyrene in the 1:*n* complex. The objective of the lifetime studies was to determine if a change occurred for the pre-exponential factors, which are related to the concentration of the 1:1 and 1:*n* species. In the presence and absence of all salts, the pre-exponential factor corresponding to the short lifetime increased after the annealing process at the expense of the pre-exponential factor for the longer lifetime.

Iodide anions are efficient quenchers of the emission of pyrene, where the quenching rate constant (k_q) is 1.1×10^9 $(mol/L)^{-1}$ s^{-1} (38). For steady-state emission spectra, quenching is observed as a decrease of the intensity (I) compared with the intensity (I_0) in the absence of quencher (Q), where the Stern–Volmer constant (K_{SV}) is equal to the product of the quenching rate constant and the lifetime in the absence of quencher. In the case of pyrene in water, the value for K_{SV} is 162 $(mol/L)^{-1}$.

$$[5] \qquad I_0/I = 1 + K_{SV}[Q]$$

© 2005 NRC Canada

Fig. 3. Pyrene fluorescence spectra in the presence of 50 mmol/L γ-CD and 0.2 mol/L NaSCN at 7.0 °C (black, **a**), 20.4 °C (red, **b**), 46.9 °C (green, **c**), and 59.3 °C (blue, **d**). (A) The first spectrum was taken at 7 °C and the temperature was raised to 59.3 °C. (B) The sample was annealed for 20 min at 80 °C and the first spectrum after the annealing process was taken at 59.3 °C and the sample was then cooled. The inset shows the E:M ratio for the heating (solid symbols) and cooling process (open symbols).



Complexation of pyrene to γ-CD led to a marked decrease in the quenching efficiency by iodide anions (31). Quenching experiments by iodide for the monomer emission were performed to determine if the annealing process significantly altered the protection efficiency provided by γ-CD. The I:III ratios of pyrene are known to decrease with the addition of iodide anions because the pyrene species with high I:III ratios (i.e., free pyrene and 1:1 complex) are quenched more efficiently than the pyrene in the 1:*n* complex (31). The decrease of the I:III ratio was observed for the sample before and after the annealing process at 80 °C (Fig. 5). In the absence of salt, the quenching efficiency for samples containing 20 mmol/L γ-CD was similar before and after the annealing process (K_{SV} = 12 ± 1 (mol/L)$^{-1}$). When NaCl or Na_2SO_4 was added to these samples, the quenching efficiency after the annealing process was higher than before the temperature was raised (Fig. 6). However, when the γ-CD concentration was 50 mmol/L, the quenching efficiency after the annealing process was always smaller in the absence of salt and in the presence of NaCl or Na_2SO_4 (Fig. 6). Quenching experiments in the presence of NaSCN were

Fig. 4. Change of the I:III ratio of the pyrene fluorescence in the presence of 50 mmol/L γ-CD as the temperature was raised (solid symbols, from **a** to **b**). The sample was annealed for 20 min at 80 °C (from **b** to **c**) followed by cooling of the sample (open symbols from **c** to **d**). ○, absence of salt; □, presence of 0.2 mol/L NaCl; △, presence of 0.2 mol/L Na_2SO_4, and ▽, presence of 0.2 mol/L NaSCN. The solid lines were added to connect the data points for the heating and cooling cycles and do not have any physical meaning.

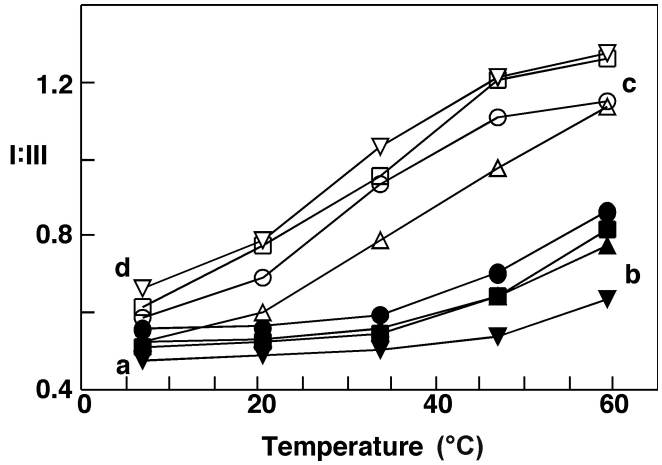
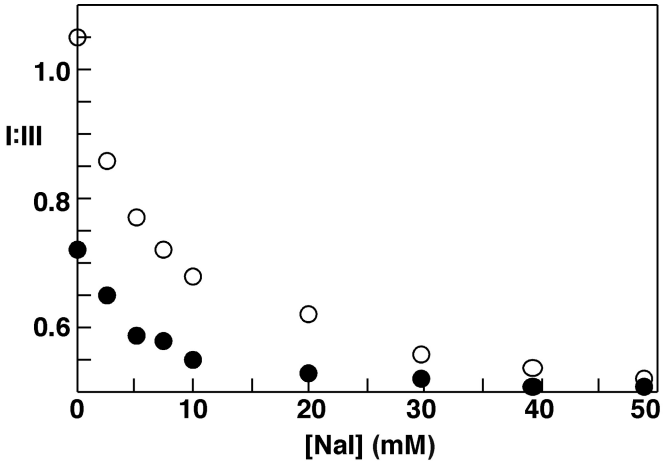


Fig. 5. Dependence of the I:III ratio for pyrene in the presence of 20 mmol/L γ-CD with the iodide anion concentration at 20.4 °C. The closed symbols are for a sample prepared at room temperature and the open symbols are for the same sample after temperature annealing at 80 °C for 20 min.



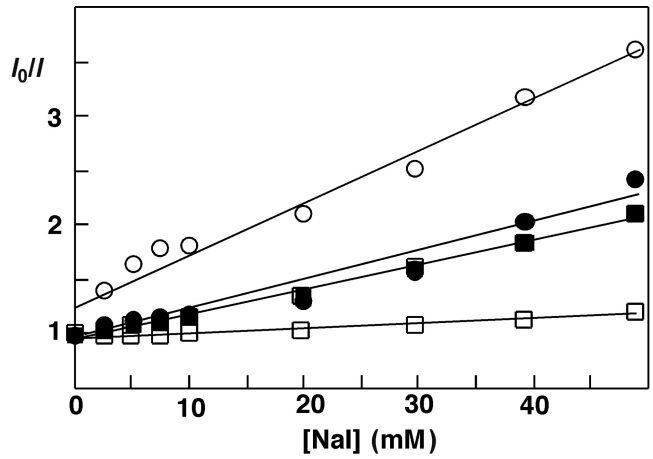
complex because both iodide and thiocyanide anions are quenchers of the pyrene emission, and a detailed analysis was not pursued.

Discussion

The very slow change of the pyrene–γ-CD solution over periods of months is evident from the formation of hazy solutions. This phenomenon seems to be common and is known to be a problem in drug formulation (17). The presence of aggregates when CDs are dissolved in water has been previously reported (14–16), and it could lead to

© 2005 NRC Canada

Fig. 6. Quenching plot at 20.4 °C for the pyrene monomer fluorescence measured at 383 nm in the presence of 0.2 mol/L Na_2SO_4 for γ-CD concentrations of 20 mmol/L (○) and 50 mmol/L (□). The solid symbols correspond to samples prepared at room temperature and the open symbols are for samples after temperature annealing at 80 °C for 20 min. The solid lines correspond to the fit of the experimental data to eq. [5].



changes in the host–guest composition for CD solutions. The objective of this work was to determine whether the presence of aggregates for aqueous γ-CD solutions was an important factor when determining the types of host–guest complexes formed. The temperature-annealing experiments performed determined that dissolving CD in water and letting the samples equilibrate for 12 h does not yield solutions at a thermodynamic equilibrium.

A consequence of CD aggregation would be the decrease of the effective monomer concentration, and in the case of the formation of only 1:1 complexes, the aggregate presence would yield apparent equilibrium constants that are too high. The investigation of the aggregation effect for systems where only 1:1 complexes are formed would require the determination of equilibrium constants for different annealing procedures. The pyrene–γ-CD system can be more conveniently used as a diagnostic system for the temperature-annealing effect because more than one CD complex is present and the change in the fraction of each CD species can be identified from changes in the I:III and E:M ratios. Changes in the I:III ratio can be qualitatively related to the changes in the ratio of the 1:1 complex to the sum of the 1:1 and 1:*n* complexes; whereas changes in the E:M ratio indicate how prevalent the formation of the 2:2 complex is compared with the CD complexes containing one pyrene. The objective of this work was to qualitatively determine the extent to which the formation of aggregates affects the distribution of host–guest complexes involving γ-CDs. The intent was not to determine the thermodynamics (equilibrium constants and host–guest stoichiometries) for each experimental condition (different temperatures and presence of different salts) investigated.

The increase in temperature led to a decrease in the E:M ratio and an increase in the I:III ratio, suggesting a decrease in the concentrations of the 1:*n* and 2:2 complexes. This trend was observed for γ-CD concentrations of 20 and 50 mmol/L. A temperature dependence on the equilibrium constants is an expected result. The result that is not consistent with a solution in thermodynamic equilibrium is the fact that upon cooling the samples, the distribution of the CD complexes was not the same as observed before the heating cycle. The different values for the I:III and E:M ratios during the cooling procedure are indicative of changes in the sample composition.

The solubility of CDs increases as the temperature is raised (18), and an increase in temperature was shown to decrease the amount of CD aggregates in solution (15). For this reason, we infer that the annealing process breaks up CD aggregates containing two or more CD molecules. No further changes to the pyrene spectroscopy were observed when the annealing time at 80 °C was increased from 20 to 60 min, suggesting that the annealing process was complete within 20 min.

The I:III ratio increases and the E:M decreases for a solution of pyrene–γ-CD (20 mmol/L) at 59.3 °C after the annealing process. The breakup of the CD aggregates leads to an increase in the monomeric pyrene in the form of free pyrene or pyrene in the 1:1 complex, which is responsible for the increase in the I:III ratio. Two different processes could explain the decrease in the 2:2 concentration after the annealing procedure: (*i*) the concentration of the 1:1 complex decreases, and since the 2:2 complex is formed from two 1:1 complexes, the concentration of the 2:2 complex also decreases; or (*ii*) some of the pyrene dimers are formed within aggregates, which upon dissociation liberate pyrene, leading to a decrease in the excimer intensity. When the solutions are cooled, the E:M ratios for temperatures of 20 and 7 °C are either similar or somewhat higher than those observed for the samples that were not annealed. If dimers were formed in CD aggregates containing more than two γ-CDs, these aggregates should also have been present at the low temperatures before the annealing procedure and the E:M ratio should have decreased during the cooling cycle. Therefore, the significant decrease of the E:M ratio at 59.3 °C is due to a decrease in the concentration of the 1:1 complex. The increase of the pre-exponential factors in the fluorescence decay kinetics for the species with the shorter lifetime supports the assignment that the fraction of 1:*n* complexes decreases after the annealing process at 80 °C.

At 50 mmol/L γ-CD, the concentration of the 2:2 complex is ca. 5 to 10 times lower than at a CD concentration of 20 mmol/L. In addition, at the higher γ-CD concentration the concentration of free pyrene at 20 °C is negligible. This situation is not altered after the annealing period at 80 °C for temperatures below 25 °C. At higher temperatures the I:III ratio is close to one, suggesting that some free pyrene could be present in solution. At 59.3 °C, the annealing process clearly led to a change in the composition of the monomeric pyrene species, suggesting that there was a substantial breakup of the γ-CD aggregates.

The quenching experiments by iodide in the presence of 50 mmol/L γ-CD at 20 °C showed that after the annealing process at 80 °C the quenching efficiency decreased. Under these conditions the I:III ratio is lower than 0.7. These results indicate that even after the annealing process pyrene was located in 1:*n* complexes and that the singlet excited state of pyrene was more protected than before the annealing process. Relocation of the pyrene closer to the oxygens that

© 2005 NRC Canada

line the interior of the CD cavities could explain the increase in the I:III ratio despite the higher protection of the excited pyrene from quenching by iodide anions in the aqueous phase.

The annealing process of the pyrene–γ-CD system was studied in the presence of various salts. The three factors that motivated these studies were the fact that the addition of salts was previously shown to change the equilibrium constants between guests and CDs (20–22); the fact that it was suggested that an increase in the ionic strength could break up the CD aggregates (15); and the fact that we used an ionic quencher to investigate the protection provided by the CD for the interaction of the included guest with the quencher. The salts employed were chosen to represent an anion that is strongly hydrated and is therefore called a structure-making salt (Na_2SO_4), a salt with low hydration energy (NaSCN, structure breaking), and a salt which is relatively neutral with respect to its solvation ability (NaCl). The addition of NaCl was used to test how the ionic strength affects the system without affecting the hydration ability of the solvent. Iodide was used as the quencher and according to the classification above, it is a structure-breaking salt.

The changes in the I:III and E:M ratios in the heating and cooling cycles were similar for pyrene–γ-CD solutions in the absence of salt and in the presence of NaCl and Na_2SO_4 at both γ-CD concentrations studied (20 and 50 mmol/L). Therefore, the increase in ionic strength or the addition of structure-making salts at moderate concentrations (0.2 mol/L) did not significantly alter the redistribution of species during the temperature-annealing process. A more subtle effect was observed when analyzing the quenching results, where in the absence of salts the quenching efficiency did not change for a concentration of 20 mmol/L γ-CD, but it increased in the presence of NaCl and Na_2SO_4. The reasons for this difference are not immediately obvious and are not observed at the higher γ-CD concentration (50 mmol/L), where the quenching efficiency decreased in the absence of salt and in the presence of NaCl and Na_2SO_4. The fact that the same trends were observed in the presence of NaCl and Na_2SO_4 is a good indication that the addition of up to 50 mmol/L iodide does not alter the distribution of the pyrene–γ-CD complexes. The iodide anion is a structure-breaking salt, and if its addition was substantially changing the distribution of the pyrene–γ-CD complexes, one would expect this effect to be attenuated in the presence of a structure-making salt such as Na_2SO_4.

The addition of NaSCN led to a much larger change in the E:M ratio during the annealing process when compared with the changes observed in the absence of salt and in the presence of NaCl and Na_2SO_4. One important difference is that the thiocyanide anion was shown to bind to α- and β-CD, whereas the chloride and sulfate anions seem to bind only weakly to CDs (23–25). It is possible that the changes observed in the presence of NaSCN were due to competitive binding in addition to a change in the hydration ability of water. A further increase in complexity is the fact that the thiocyanide anion was shown to quench the singlet excited state of pyrene. This effect would lead to a larger decrease of the emission intensity when pyrene relocates from the 1:*n* complexes to the 1:1 complex and to water. The only conclusion we can reach for the addition of NaSCN in this qualitative study is that its effect is very different from that for NaCl and Na_2SO_4. Any mechanistic determination to see if this observation is due to the presence of a water-structure-breaking salt or due to competitive binding would require detailed studies where equilibrium constants are determined, which are beyond the scope of this study.

Conclusions

The temperature-annealing experiments showed that samples of γ-CD prepared at room temperature and left to equilibrate for 12 h do not achieve a thermodynamic equilibrium. The formation of aggregates affects the concentration of guest–CD complexes present in solution. A consequence of this observation is that equilibrium constants determined under conditions where CD aggregates are present in solution are incorrect. This problem may be more pronounced in the case of β-CD, where the formation of aggregates was reported to be more prevalent than for α- and γ-CD (15). An additional uncertainty is that the degree of hydration may have an effect on the formation of aggregates, since it was shown that the dissolution rate of hydrated and anhydrous β-CD are very different (18). The presence of aggregates and the different methods of sample preparation are probably the reason why for some systems the equilibrium constants and guest–CD stoichiometries reported show significant discrepancies. Indeed, this may be the reason for the large differences observed for the pyrene–γ-CD system used in this study (31, 32, 39, 40). To ensure that a thermodynamic equilibrium is achieved, we advise that solutions containing CDs should be heated at high temperature for a period of time before the guest–CD solutions are prepared.

Acknowledgements

The authors thank the Natural Sciences and Engineering Research Council of Canada (NSERC) for the financial support for this research, Cargill for the generous gift of γ-CD, and L. Netter for support with software development.

References

1. P. Bortolus and S. Monti. Adv. Photochem. **21**, 1 (1996).
2. K.A. Connors. Chem. Rev. **97**, 1325 (1997).
3. M.V. Rekharsky and Y. Inoue. Chem. Rev. **98**, 1875 (1998).
4. J. Szejtli. *In* Comprehensive supramolecular chemistry. Vol. 3, Cyclodextrins. *Edited by* J. Szejtli and T. Osa. *Series edited by* J.L. Atwood, J.E.D. Davies, D.D. MacNicol, F. Vögtle, and J.-M. Lehn. Elsevier Science Ltd., New York. 1996. pp. 5–40.
5. J. Szejtli. Chem. Rev. **98**, 1743 (1998).
6. R. Breslow. Science (Washington, D.C.), **218**, 532 (1982).
7. M. Komiyama. *In* Comprehensive supramolecular chemistry. Vol. 3, Cyclodextrins. *Edited by* J. Szejtli and T. Osa. *Series edited by* J.L. Atwood, J.E.D. Davies, D.D. MacNicol, F. Vögtle, and J.-M. Lehn. Elsevier Science Ltd., New York. 1996. pp. 401–422.
8. I. Tabushi. Acc. Chem. Res. **15**, 66 (1982).
9. I. Tabushi and Y. Kuroda. Adv. Cat. **32**, 417 (1982).
10. J. Snopek, E. Smolková-Keulemansová, T. Cserháti, K.H. Gahm, and A. Stalcup. *In* Comprehensive supramolecular chemistry. Vol. 3, Cyclodextrins. *Edited by* J. Szejtli and T. Osa. *Series edited by* J.L. Atwood, J.E.D. Davies, D.D.

© 2005 NRC Canada

MacNicol, F. Vögtle, and J.-M. Lehn. Elsevier Science Ltd., New York. 1996. pp. 515–572.
11. T. Nagai and H. Ueda. *In* Comprehensive supramolecular chemistry. Vol. 3, Cyclodextrins. *Edited by* J. Szejtli and T. Osa. *Series edited by* J.L. Atwood, J.E.D. Davies, D.D. MacNicol, F. Vögtle, and J.-M. Lehn. Elsevier Science Ltd., New York. 1996. pp. 441–450.
12. T.A. Reineccius, G.A. Reineccius, and T.L. Peppard. J. Food Sci. **67**, 3271 (2002).
13. K. Miyajima, M. Sawada and M. Nakagani. Bull. Chem. Soc. Jpn. **56**, 3556 (1983).
14. A.W. Coleman, I. Nicolis, N. Keller and J.P. Dalbiez. J. Inclusion Phenom. Mol. Recognit. Chem. **13**, 139 (1992).
15. G. González-Gaitano, P. Rodríguez, J.R. Isasi, M. Fuentes, G. Tardajos and M. Sánchez. J. Inclusion Phenom. Macrocyclic Chem. **44**, 101 (2002).
16. G.G. Gaitano, W. Brown, and G. Tardajos. J. Phys. Chem. B, **101**, 710 (1997).
17. L. Szente, J. Szejtli, and G.L. Kis. J. Pharm. Sci. **87**, 778 (1998).
18. M.J. Jozwiakowski and K.A. Connors. Carbohyd. Res. **143**, 51 (1985).
19. S.R. McAlpine and M.A. Garcia-Garibay. J. Am. Chem. Soc. **120**, 4269 (1998).
20. T.C. Barros, K. Stefaniak, J.F. Holzwarth, and C. Bohne. J. Phys. Chem. A, **102**, 5639 (1998).
21. J. Dey, E.L. Roberts, and I.M. Warner. J. Phys. Chem. A, **102**, 301 (1998).
22. S. Sau, B. Solanki, R. Orprecio, J. van Stam, and C.H. Evans. J. Inclusion Phenom. Macrocyclic Chem. **48**, 173 (2004).
23. Z. Yi, C. Zhao, Z. Huang, H. Chen, and J. Yu. Phys. Chem. Chem. Phys. **1**, 441 (1999).
24. R.P. Rohrbach, L.J. Rodriguez, E.M. Eyring, and J.F. Wojcik. J. Phys. Chem. **81**, 944 (1977).
25. J.F. Wojcik and R.P. Rohrbach. J. Phys. Chem. **79**, 2251 (1975).
26. K.D. Collins and M.W. Washabaugh. Q. Rev. Biophys. **18**, 323 (1985).
27. M.C. Gurau, S.-M. Lim, E.T. Castellana, F. Albertorio, S. Kataoka, and P.S. Cremer. J. Am. Chem. Soc. **126**, 10522 (2004).
28. G. Karlström. Phys. Chem. Chem. Phys. **5**, 3238 (2003).
29. A.W. Omta, M.F. Kropman, S. Woutersen, and H.J. Bakker. Science (Washington, D.C.), **301**, 347 (2003).
30. J.N. Sachs and T.B. Woolf. J. Am. Chem. Soc. **125**, 8742 (2003).
31. A.S.M. Dyck, U. Kisiel, and C. Bohne. J. Phys. Chem. B, **107**, 11652 (2003).
32. S. Hamai. J. Phys. Chem. **93**, 6527 (1989).
33. D.C. Dong and M.A. Winnik. Photochem. Photobiol. **35**, 17 (1982).
34. K. Kalyanasundaram and J.K. Thomas. J. Am. Chem. Soc. **99**, 2039 (1977).
35. C. Bohne, R.W. Redmond, and J.C. Scaiano. *In* Photochemistry in organized and constrained media. *Edited by* V. Ramamurthy. VCH Publishers, New York. 1991. pp. 79–132.
36. H. Yang and C. Bohne. J. Phys. Chem. **100**, 14533 (1996).
37. W. Xu, J.N. Demas, B.A. DeGraff, and M. Whaley. J. Phys. Chem. **97**, 6546 (1993).
38. C. Ju and C. Bohne. Photochem. Photobiol. **63**, 60 (1996).
39. K. Kano, I. Takenoshita, and T. Ogawa. Chem. Lett. 321 (1982).
40. N. Kobayashi, R. Saito, H. Hino, Y. Hino, A. Ueno, and T. Osa. J. Chem. Soc. Perkin Trans. 2, 1031 (1983).

© 2005 NRC Canada

Dissociation of the phenanthroimidazole dimer — A highly delocalized radical — Gomberg revisited[1]

Eric Kiepek, Yuhui Zhou, Shmaryahu Hoz, Ester Rozental, Peter M. Kazmaier, and Erwin Buncel

Abstract: Results of a calculational study at the B3LYP/6-3/G* level concerning the dimerization of the phenanthroimidazole radical are reported herein. The optimized minimum energies of six dimer structures corresponding to C—C, C—N, and N—N bonding have been obtained. The lowest energy dimer is found to be that resulting from N—N bonding (**12**). However, this does not correspond to an X-ray structure study of the experimentally isolated dimer (**13**), which reveals C—N bonding, as is also deduced from an NMR investigation. The variance between the experimental structure and the calculational lowest energy one is examined on the basis of steric interactions: virtually retained planarity, and hence, full conjugation in the two phenanthroimidazole halves in **12**, vs. twisting and lack of coplanarity in the other dimer structures. Importantly, spin density calculations reveal a negligible spin density on the nitrogens, rendering dimer **12** formation through N—N bonding highly improbable. A bond dissociation energy of 16.5 kcal/mol (1 cal = 4.184 J) is calculated for the experimental dimer **13**, which is by far the lowest C—N bond energy recorded so far in the literature. As well, this value is of the same order of magnitude as the calculated C—C BDE in hexaphenylethane, which had been postulated by Gomberg in 1900 as the molecule formed on dimerization of the triphenymethyl radical, but so far not observed experimentally.

Key words: delocalized radical dimerization, phenanthroimidazole dimer, Gomberg's dimer, X-ray structure, C—N bond dissociation energy.

Résumé : On a effectué des calculs au niveau B3LYP/6-3/G* sur la dimérisation du radical phénanthroimidazole. On a obtenu les énergies minimales optimisées de six structures dimères correspondant aux liaisons C—C, C—N et N—N. On a trouvé que le dimère de plus faible énergie résulte de la liaison N—N (**12**). Toutefois, ce résultat de calcul ne correspond pas à l'étude de structure par diffraction des rayons X qui a été faite sur le dimère **13** isolé expérimentalement et dans laquelle on observe une liaison C—N, tel qu'on peut aussi le déduire d'une étude par spectroscopie RMN. Pour essayer d'expliquer les causes de la variance entre l'énergie minimale déduite sur la base de calculs théoriques et la structure observée expérimentalement, on a fait appel aux interactions stériques ainsi qu'au caractère planaire maintenu et, en conséquence, à la conjugaison complète des deux moitiés de phénanthroimidazole dans **12** par opposition à la déformation et au manque de caractère coplanaire dans les autres structures dimères. Il est aussi important de noter que les calculs de densité de spin révèlent la présence d'une densité de spin négligeable sur les azotes qui rend la formation du dimère **12** par une liaison N—N très improbable. On a évalué à 16,5 kcal/mol (1 cal = 4,184 J) l'énergie de dissociation de liaison pour le dimère expérimental **13** et cette valeur est de loin l'énergie de liaison C—N enregistrée à ce jour dans la littérature. De plus, cette valeur est du même ordre de grandeur que celle calculée pour la liaison BDE C—C de l'hexaphénylméthane qui, selon Gomberg en 1900, serait la molécule qui se formerait lors de la dimérisation du radical triphénylméthyle mais qui n'a jamais été observée expérimentalement.

Mots clés : dimérisation d'un radical délocalisé, dimère phénanthroimidazole, dimère de Gomberg, structure déterminée par rayons X, énergie de dissociation d'une liaison C—N.

[Traduit par la Rédaction]

Received 27 April 2005. Published on the NRC Research Press Web site at http://canjchem.nrc.ca on 11 November 2005.

This paper is dedicated to Professor Alwyn G. Davies.

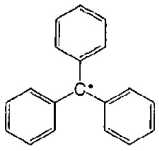
E. Kiepek, Y. Zhou, and E. Buncel.[2] Department of Chemistry, Queen's University, Kingston, ON K7L 3N6, Canada.
S. Hoz[3] **and E. Rozental.** Bar Ilan University, Ramat-Gan 52100, Israel.
P.M. Kazmaier. Xerox Research Centre of Canada, Mississauga, ON L5K 2L1, Canada.

[1]This article is part of a Special Issue dedicated to organic reaction mechanisms.
[2]Corresponding author (e-mail: buncele@chem.queensu.ca).
[3]Corresponding author (e-mail: shoz@mail.biu.ac.il).

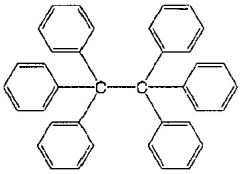
 doi: 10.1139/V05-177 © 2005 NRC Canada

Introduction

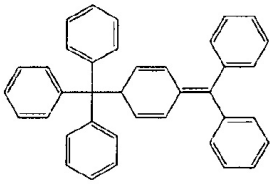
The dimerization of delocalized radicals has been of interest since 1900 when Gomberg concluded that dimerization of the triphenylmethyl radical **1** produced, in a straightforward manner, the anticipated hexaphenylethane **2** (1). However, it was much later, in 1968, that the correct structure of the dimer was shown to be the unsymmetrical molcule **3** (2). This brought forth new interest, including attempts to synthesize the authentic molecule **2** (3), so far without success.



1



2



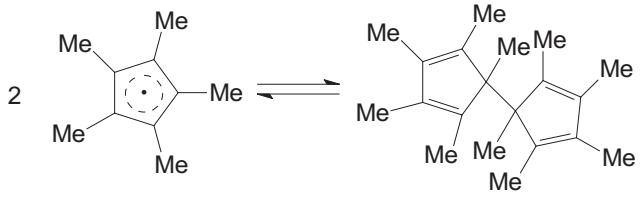
3

Discussions concerning the possible synthesis of **2** are of course tied to its bond dissociation energy (BDE) and various calculational methods have been directed toward this end. Very recently, applying a three-level hybrid quantum mechanical (ONIOM) method, Vreven and Morokuma (4) derived a BDE of 16.6 kcal/mol (1 cal = 4.184 J) for **2**, and hence concluded that its synthesis could in fact be feasible.

Davies and Lusztyk (5) experimentally investigated a somewhat related dimerization (Scheme 1), namely that of the delocalized pentamethylcyclopentadienyl radical **4**, which produced the dimer **5** in a diffusion-controlled process ($2k_t = 2 \times 10^9$ (mol/L)$^{-1}$ s^{-1} at 25 °C in hexane). The dimer, in turn, on heating to 70–120 °C dissociates to the radical, identified by its ESR spectrum. In a subsequent study, Ingold and co-workers (6) studied the equilibrium as a function of temperature (92–120 °C) and thereby obtained ΔH = 18.8 kcal/mol as the enthalpy of dissociation, i.e., comparable to the calculated BDE of hexaphenylethane referred to previously (4). Factors contributing to the ease of dissociation of dimer **5** are the strain energy, calculated by MM2 as 33.4 kcal/mol (6), and the inherent resonance stabilization of the Me_5C_5 radical **4** (5).

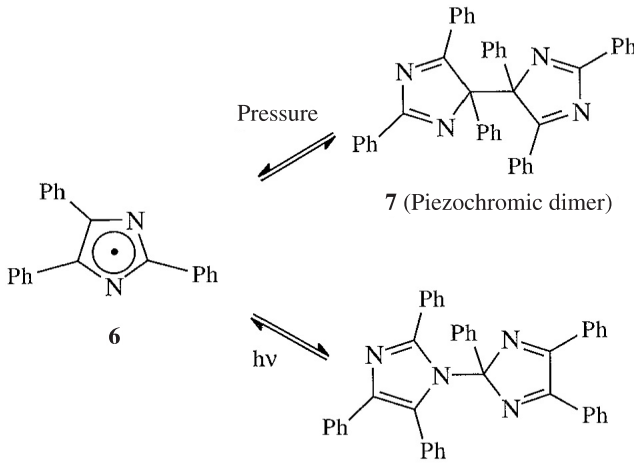
Our interest in these and related systems arose from the reports that the radical **6**, formed on oxidation of triphenylimidazole (7), gives rise to piezochromic dimer **7** under pressure and photochromic dimer **8** on irradiation (Scheme 2). As part of a wider study on thermochromic and photochromic molecules (8), it was our aim to devise pressure- and sheer-sensitive dye molcules that could be used as sensors in polymer processing (9). We thus extended

Scheme 1.



4 **5**

Scheme 2.



7 (Piezochromic dimer)

8 (Photochromic dimer)

the conjugation system shown in Scheme 1 to the radical derived from 2-(*p*-bromophenyl)phenanthroimidazole **9** (X = Br) and its dimerization, shown in Scheme 3 (10).

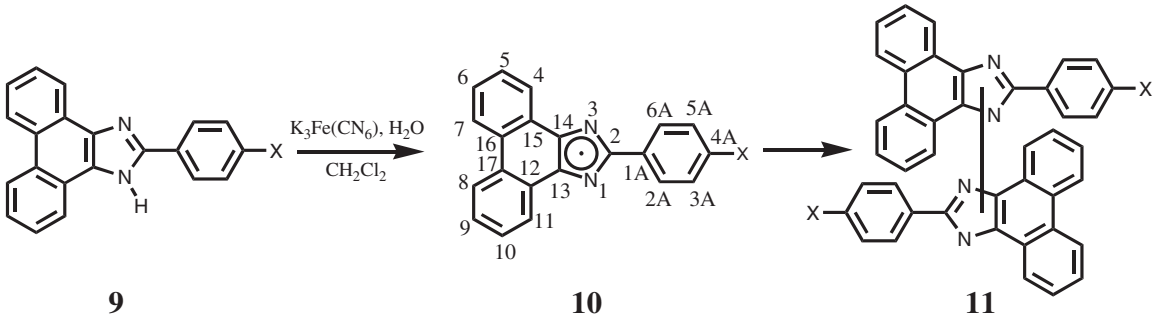
As in the case of the triphenylmethyl radical, where dimerization can occur in more than one sense, there are actually six modes available for recombination of radical **10**: via N—N bonding (**12**), C—N bonding (**13**, **14**), and C—C bonding (**15**–**17**) (Fig. 1). We have presented NMR evidence (10) that the dimer produced has the structure **13** (X = Br), i.e., C—N bonding.

In the current work we have undertaken a computational study of the unsubstituted molecule **11** (X = H) aimed to determine the relative energies of the six possible dimers as well as their bond dissociation energies. Unexpectedly, we have found that the computationally lowest energy dimer is not **13** with C—N bonding, but **12** with N—N bonding. To resolve this contradiction, an X-ray structure analysis was undertaken (**11**, X = Br) and has confirmed the earlier NMR structure of **13** (X = Br) for the isolated dimer. We conclude that the fact that **12**, the computationally most stable isomer, is not the one experimentally obtained, stems from a kinetic barrier owing to low spin densities on the nitrogen atoms.

Another finding of interest is of a very low C—N BDE in **13** (X = H, 16.5 kcal/mol), apparently the lowest C—N BDE recorded so far.

© 2005 NRC Canada

Scheme 3.



9 **10** **11**

Table 1. B3LYP/6-31G* energy calculations of the six dimers and the free radical.

Dimer	*E* (au)	ZPE (au)	E_o' (au)	Counterpoise correction (au)	E_o (au)
12	–1835.1965	0.5662	–1834.6413	–0.0262	–1834.6675
13	–1835.1752	0.5654	–1834.6209	–0.0272	–1834.6481
14	–1835.1552	0.5649	–1834.6014	–0.0271	–1834.6285
15	–1835.1611	0.5648	–1834.6073	–0.0296	–1834.6369
16	–1835.1554	0.5648	–1834.6016	–0.0291	–1834.6308
17	–1835.1523	0.5645	–1834.5989	–0.0281	–1834.6270
Radical	–917.5861	0.2806	–917.3109		–917.3109

Results

Calculational studies — Dimer energies, bond dissociation energies, radical spin densities, and CH_3· addition energies

1. Dimer energies

*(a) Geometry optimized minimum energies (*E*)*

Optimized minimum energies of the six dimer structures using the B3LYP/6-31G*//B3LYP/6-31G* methodology are given in Table 1 while the corresponding optimized geometries are shown in Fig. 2.

(b) Zero point corrected energy (E_o'*)*

A frequency calculation was performed to obtain the zero point vibrational energy (E_{ZPE}). This value was added to E to give the zero point corrected energy (E_o').

[1] $$E_o' = E + E_{ZPE}$$

The resulting E_o' values are included in Table 1.

(c) Counterpoise and zero point corrected energies (E_o*)*

The counterpoise energy correction (E_{corr}) (11) was performed next for all six dimers and the values are given in Table 1. The counterpoise and zero point corrected energies (E_o) are then given by:

[2] $$E_o = E + E_{ZPE} + E_{corr}$$

(d) Relative dimer energies

According to Table 1, the lowest E_o value corresponds to dimer **12** and this was arbitrarily selected as the reference level with E_o = O. The relative energies (ΔE_o) of the other dimers are then given in Table 2. They range from ΔE_o = 12.2 kcal/mol for dimer **13** to ΔE_o = 25.4 kcal/mol for **17**.

2. Bond dissociation energies

To calculate BDEs, calculations for the radical were first performed using the methodology in sections 1(*a*) and 1(*b*). Data are included in Table 1. The radical structure is shown in Scheme 3.

Bond dissociation energies are calculated via the equation:

[3] $$BDE = 2E_o^{Rad} - E_o$$

where the E_o values (eq. [2]) are taken from Table 1, while E_o^{Rad} is the geometry optimized minimum energy of the free radical species and is also found in Table 1.

3. Radical spin densities

Spin densities of the optimized minimum energy structure **10** (X = H) were obtained using the B3LYP/6-31G* methodology. Spin density values at the various atomic centres of the radical are tabulated in Table 3.

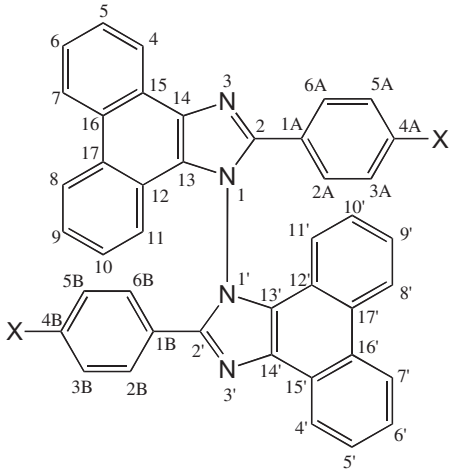
4. CH_3· addition to radical

The change in energy on going from an sp^2 hybridized state of the radical to the sp^3 state on methylation was evaluated for the C2, C13, and N1 atomic centres. Geometry optimization was performed as in sections 1(*a*) and 1(*b*). Table 4 presents the relevant energy terms.

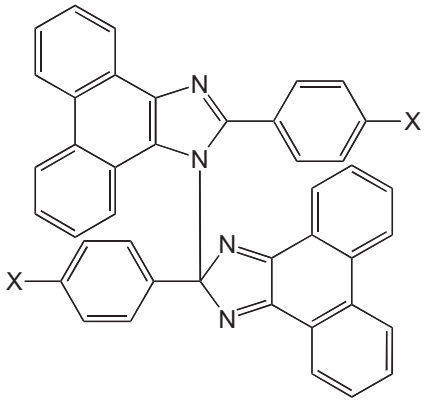
According to Table 4, the lowest E_o value is found for the N1-Me structure and this is taken as the zero level for comparison with the other two structures. One hence obtains for the C2-Me and C13-Me structures ΔE_o^{Me} values of 12.3 and 18.5 kcal/mol, respectively.

© 2005 NRC Canada

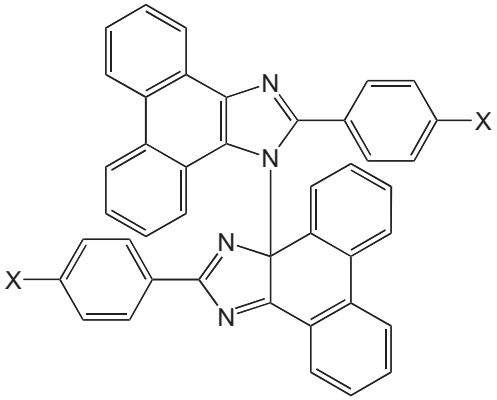
Fig. 1. Possible structures arising from the dimerization of radical **10**.



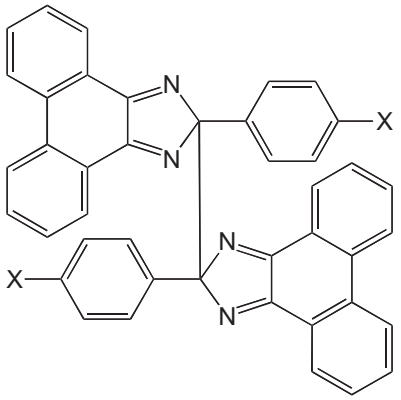
12



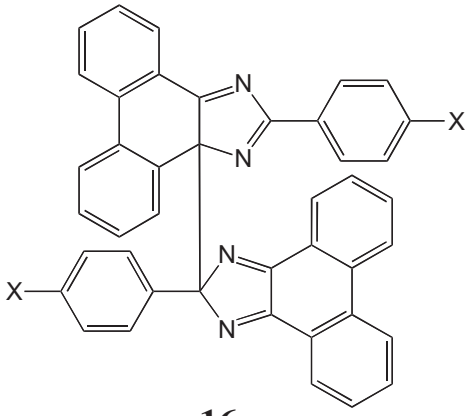
13



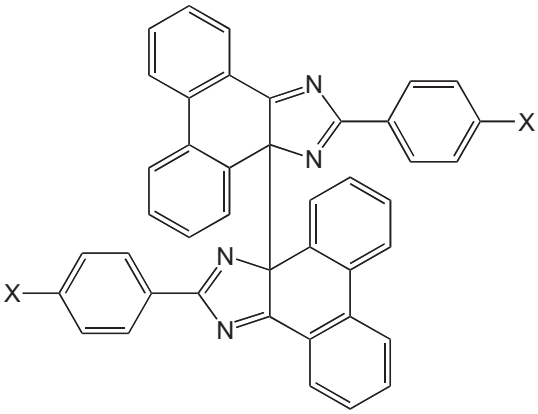
14



15



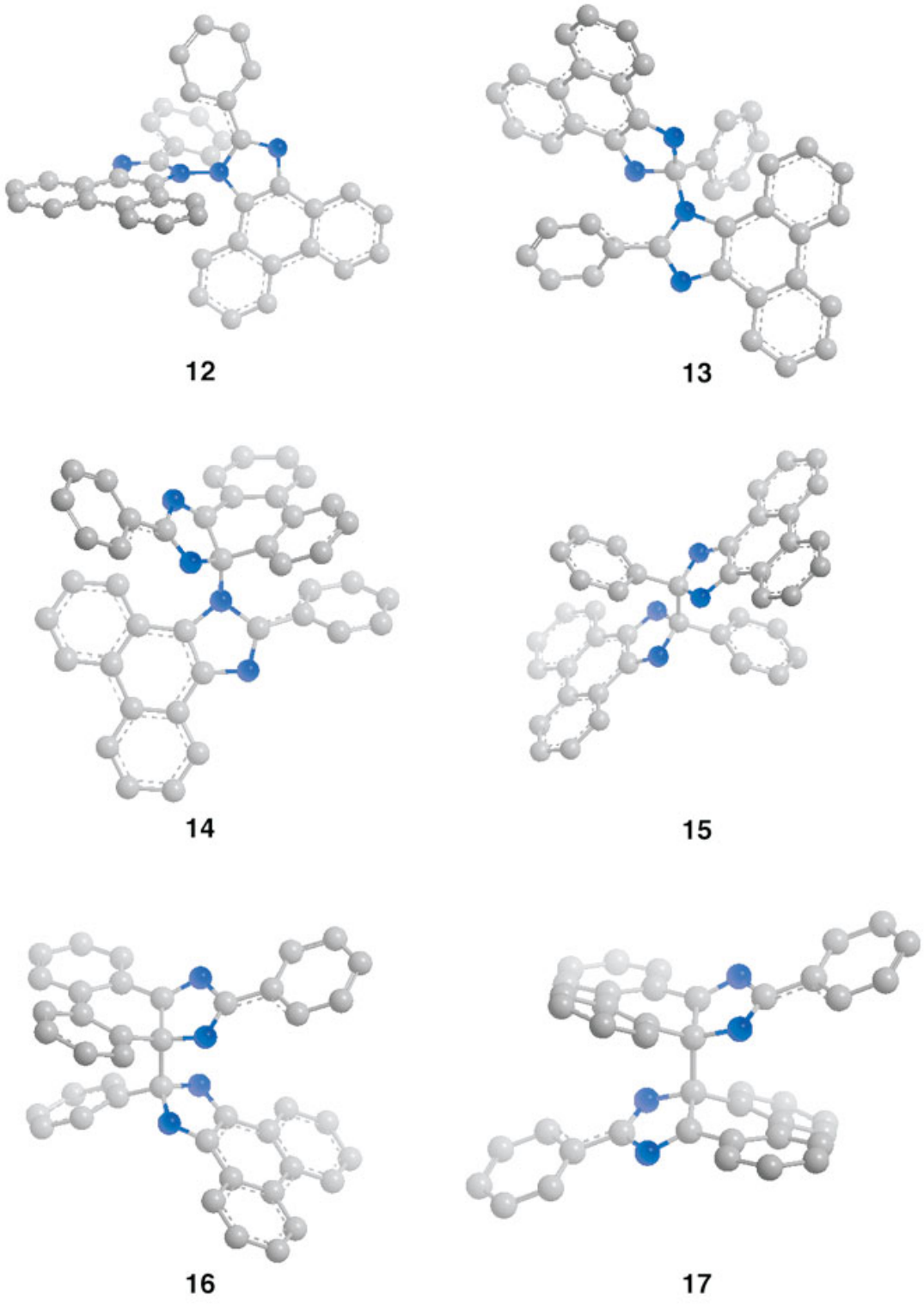
16



17

© 2005 NRC Canada

Fig. 2. Three-dimensional structures of the six possible molecules formed in the dimerization of **10**. Note the loss of planarity and aromaticity of one or more phenanthrene groups in **14**, **16**, and **17**, the three least stable dimers.



© 2005 NRC Canada

Table 2. Dimer energies relative to dimer **12**, taken as zero, and bond dissociation energies for cleavage of the bond to generate two phenanthroimidazole radicals.

Dimer	ΔE_o (kcal/mol)	BDE (kcal/mol)
12	0.0	28.7
13	12.2	16.5
14	24.5	4.2
15	19.2	9.4
16	23.1	5.6
17	25.4	3.2

Table 3. Spin density distribution in radical **10**.

Atom[a]	Electron spin density
N1	–0.0525
C2	0.326
N3	–0.0523
C4	0.101
C5	–0.0421
C6	0.0983
C7	–0.0307
C8	–0.0307
C9	0.0984
C10	–0.0422
C11	0.101
C12	–0.0761
C13	0.257
C14	0.257
C15	–0.076
C16	0.0679
C17	0.068
C1A	–0.0724
C2A	0.114
C3A	–0.06218
C4A	0.14
C5A	–0.0618
C6A	0.114

[a]See Scheme 3 for numbering.

X-ray structure

Figure 3 shows the structure of dimer **13** (X = Br) together with the atom numbering scheme. The cell packing is shown in Fig. 4.[3]

Discussion

As noted in the Introduction, the dimerization of delocalized radicals has been of interest since Gomberg's studies with the triphenylmethyl radical in 1900 (1). That and the follow-up studies demonstrated that delocalized radicals can recombine in more than one sense giving rise to two or more structurally different dimer isomers. Dimerization of the phenanthroimidazole radical system can in principle give rise to six likely dimers that would be produced via N—N, C—N, and C—C bonding. We have previously reported a NMR study of the isolated dimer, which indicated a structure involving C—N bonding (10).

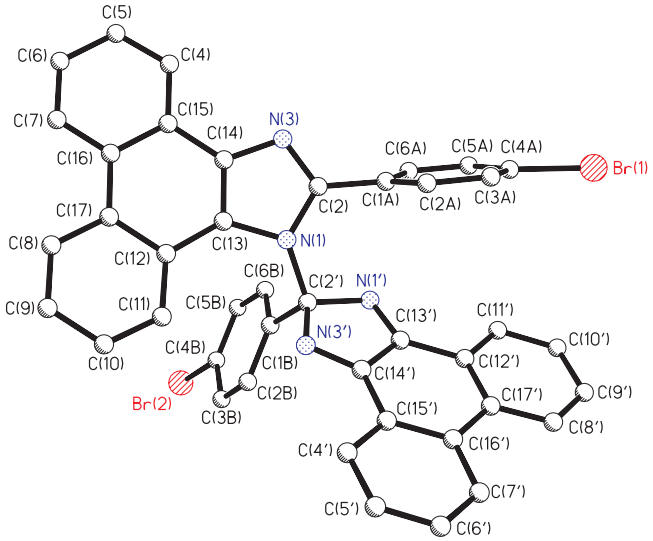
In light of the continuing theoretical and experimental studies pertaining to the dimerization of delocalized radicals (4–6) and the unusual nature of the phenanthroimidazole system, it was desirable to follow up the NMR study with calculation of the relative energies of the six dimers and the corresponding N—N, C—N, and C—C bond dissociation energies in juxtaposition. In the following, we discuss the divergence revealed between the results of the calculational studies on relative dimer energies vis-à-vis the actual structure obtained earlier by NMR and currently confirmed by X-ray work.

Next, we discuss the origin of the variance between the X-ray data and the computed structure. Finally, we return to the conundrum posed by Gomberg's original conclusions.

Table 4. B3LYP/6-31G* energy calculations for the radical methylated at three atomic centres.

Methylated radical	E (au)	ZPE (au)	E_o (au)	ΔE_o (au)
N1-Me	–957.5279	0.3224	–957.2118	0.0000
C2-Me	–957.5006	0.3145	–957.1923	0.0196
C13-Me	–957.4969	0.3209	–957.1823	0.0295

Fig. 3. Structure of dimer **13** as determined using X-ray crystallography.



[3] Supplementary data for this article are available on the Web site or may be purchased from the Depository of Unpublished Data, Document Delivery, CISTI, National Research Council Canada, Ottawa, ON K1A 0S2, Canada. DUD 4032. For more information on obtaining material refer to http://cisti-icist.nrc-cnrc.gc.ca/irm/unpub_e.shtml. CCDC 279725 contains the crystallographic data for this manuscript. These data can be obtained, free of charge, via www.ccdc.cam.ac.uk/conts/retrieving.html (Or from the Cambridge Crystallographic Data Centre, 12 Union Road, Cambridge CB2 1EZ, UK; fax +44 1223 336033; or deposit@ccdc.cam.ac.uk).

© 2005 NRC Canada

Fig. 4. Cell packing of dimer **13** as determined by X-ray crystallography.

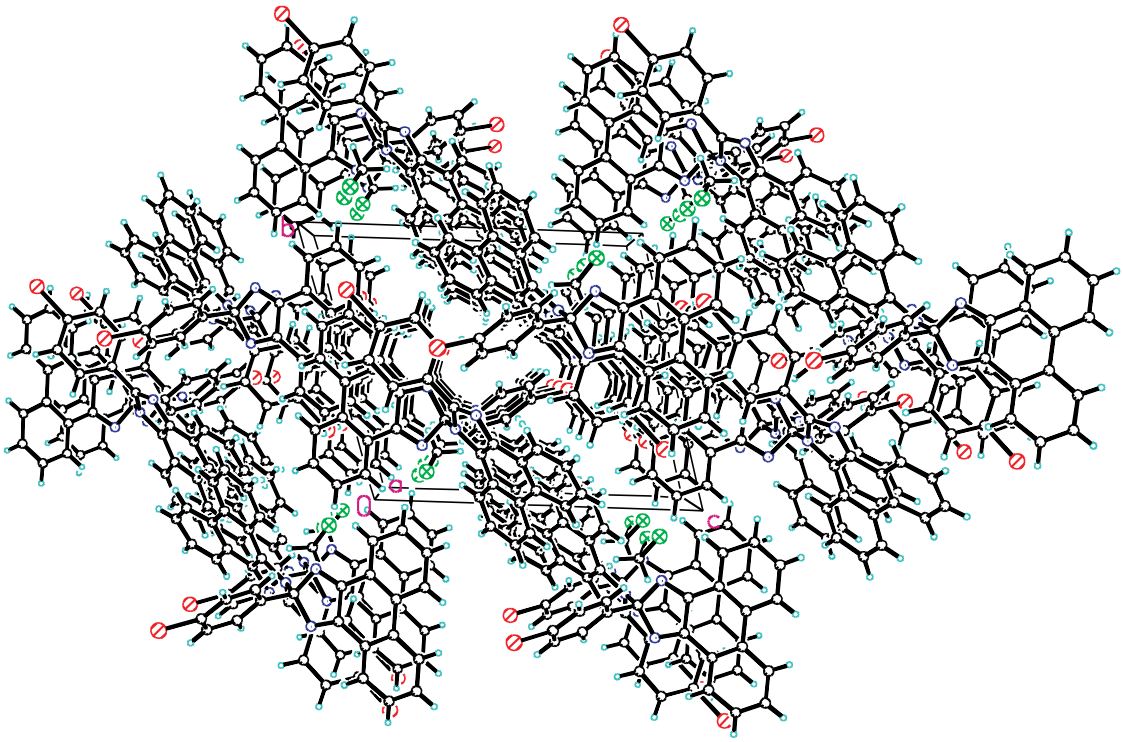
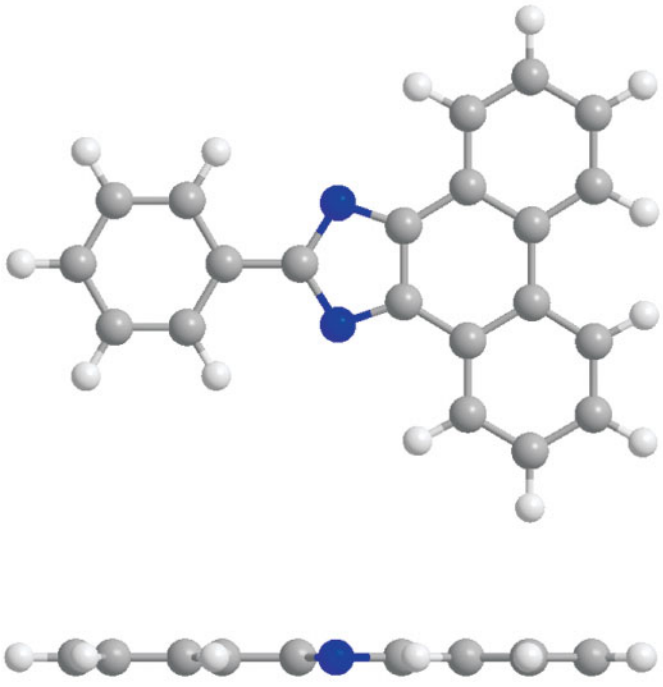


Fig. 5. Three-dimensional structure of radical **10**. Note the planarity of the molecule.



Theoretical study of dimerization of free radical 10

Optimization of the free radical species using B3LYP/6-31G* calculations of the optimized geometry yields a planar structure (**10**, Fig. 5) with C_{2v} symmetry. This allows maximum conjugation among the π systems comprising the imidazole, the phenanthro, and phenyl rings.

As mentioned previously, combination of the two radicals (**10**) can occur in six different ways: N—N bonding results in only one unique product because of symmetry (**12**); N—C bonding can occur in two ways, N1 to C2 (**13**) and N1 to C13 (**14**) of the second radical; C—C bonding occurs as C2 to C2 (**15**), C2 to C13 (**16**), or C13 to C13 (**17**) of the second radical (Fig. 1). The relative stabilization and bond dissociation energies of the various dimers are presented in Table 4 and in Fig. 6 in graphical form.

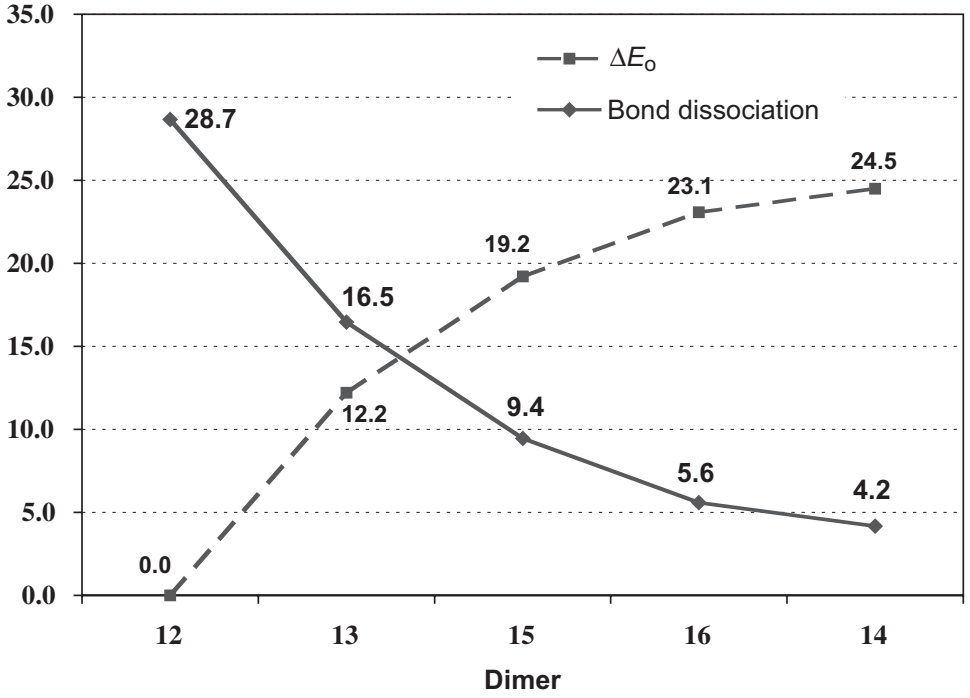
Interestingly, the computationally most stable structure is **12** (N—N bonding), whereas **13** (C—N bonding) is the isomer obtained experimentally. Before dealing with this conundrum, we will first discuss the order of stability of the various isomers.

Stability order of the dimers

Since the energetics of bond formation between two radicals is the outcome of the structural changes made in each of these radicals, we have separately studied the effect of bonding at the three different sites: N1, C2, and C13 on the monomeric unit. This was achieved by the addition of a methyl radical to the monomer radical at these positions. The results are given in Table 4. As can be seen from this table, the most stable bond is formed with the nitrogen, probably because this does not impact on the aromaticity of any of the rings, and planarity is maintained. On the other hand, methylation at C2 disrupts the aromaticity of the imidazole ring while methylation at C13 disrupts the aromaticity of both the imidazole and the phenanthro systems. This is reflected in the stability order. Thus, except for a slight change of pattern, the stability order of the dimers reflect the num-

© 2005 NRC Canada

Fig. 6. The relative stabilities (dashed line) and bond dissociation energies (solid line) of the six dimers.



ber of rings in which aromaticity is disrupted. The computationally most stable dimer (**12**) is the one in which aromaticity is retained for all rings. The least stable isomer is **17** in which four ring systems have lost aromaticity. In between, the only deviation from this order is in the two isomers **14** and **16** where the difference between them amounts to only 1.4 kcal/mol. The loss of planarity of the phenanthro systems of dimers **14**, **16**, and **17** can be seen readily in the three-dimensional structures shown in Fig. 2.

It is significant that the experimentally obtained isomer (**13**), having disrupted aromaticity in one ring, comes second to the most stable computed isomer (**12**). To resolve this contradiction between computational and experimental structural assignments, we opted for the unambiguous X-ray structure determination. In fact, X-ray analysis has shown that, indeed, the structure of the experimentally isolated dimer corresponds to **13**.

Shown in Fig. 7 are two perspective structures of each of these two isomers. The important structural characteristics of **12** and **13** previously discussed are readily seen in these perspectives. The perspectives of the other dimers are given in the Supplementary material.[3]

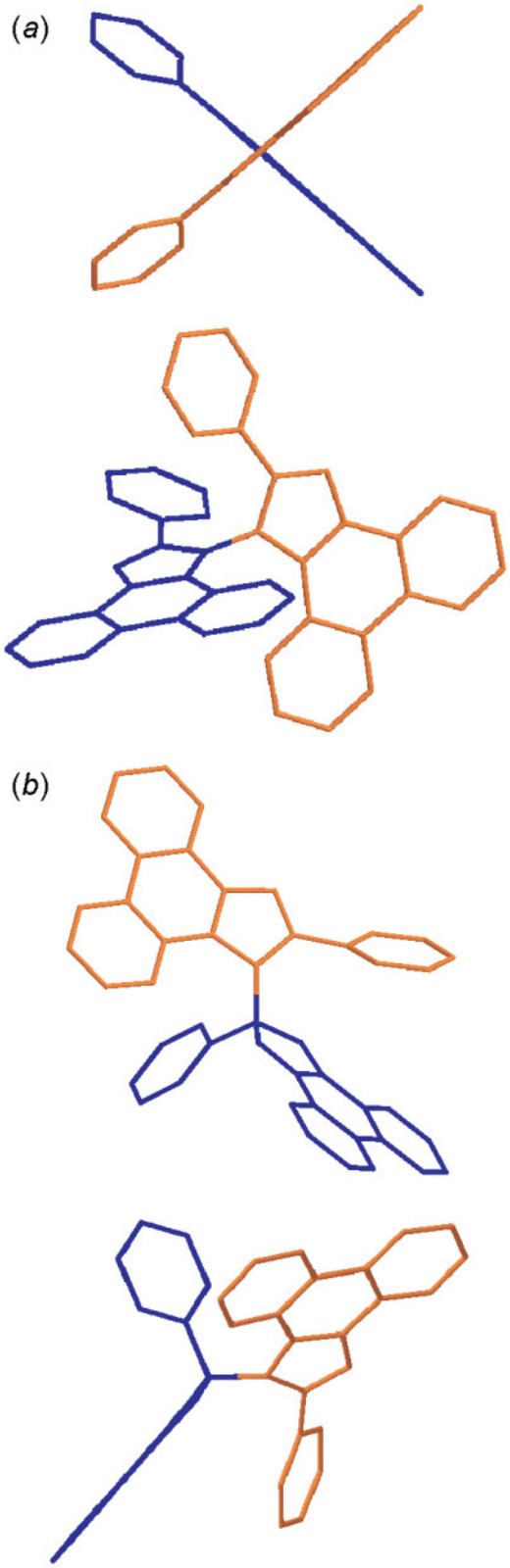
The origin of the conundrum implicit in the results presented hitherto remains to be considered. In fact, it is appropriate to address two questions: (*a*) it is common knowledge that N—N bonds are rather weak. Then what is the reason that in the present system the N—N bonding is the strongest one (28.7 kcal/mol) as opposed to C—N bonding (16.5 kcal/mol) of the isolated dimer (Table 2)? (*b*) On the assumption that the computations indeed reflect the actual stabilities, then why is the computationally most stable isomer not the one isolated?

In fact, the first question casts doubt on the validity of these calculations. We believe that in general, the reason for the low binding energy between nitrogen atoms results from the interelectronic pair–pair repulsion. Where this interaction does not exist, for example, in the triple bond of the N_2 molecule, the bond energy of this molecule (225 kcal/mol) is larger by 25 kcal/mol than that of the triple bond in acetylene (200 kcal/mol). In the present system, the two planar units in **12** are orthogonal to each other (see Figs. 2 and 7*a*) in this way avoiding a destabilizing interaction between the two p–π systems on the nitrogens. In addition, this isomer is the only system among the six where aromaticity is retained in all rings and planarity is not hampered. Therefore, general considerations indeed point to this isomer as being the most stable one.

We now turn to the second question — why isomer **12** is not obtained. We assume that this is a result of a kinetic selectivity; namely, this (N—N) isomer is slow to be formed. A possible origin for sluggishness in radical combination reactions could be because of low spin densities on the relevant atoms. To explore this possibility, we have calculated the spin density distribution in the radical monomer. The results are given in Table 3. The data in this table show that the spin density on the nitrogen is indeed very small (~5%). While this does not rule out the possibility of the N—N bond formation or reflect on its strength, it reflects on the probability of its formation upon encountering two radicals in the appropriate orientation (~0.25%). The fact that the spin density on C2 is 32% significantly increases the probability for the formation of **13**. Using this logic, it might be assumed that dimer **15** (C2—C2) would be the dominant dimer formed; however, the bond dissociation energy of **15** is calculated at 9 kcal/mol, making the formation of the stable dimer highly unlikely. Thus, working under thermodynamic control conditions, **12** would probably have been the experimentally obtained isomer. However, under the experi-

© 2005 NRC Canada

Fig. 7. (*a*) Perspective presentation of dimer **12**. (*b*) Perspective presentation of dimer **13**.



mental conditions used, the equilibrium is shifted to one side by the precipitation of **13**, giving rise in this way to the formation of the thermodynamically less stable isomer.

Comparison of the X-ray data with the calculated structure

The overall structure of dimer **13** as determined by X-ray analysis and the computed optimized geometry using B3LYP is shown in Fig. 8. Clearly, there is a close correspondence.

For all atoms, the bond lengths and angles of dimer **13** calculated by the B3LYP/6-31G* geometry optimization were within 1% of the bond lengths and angles measured by X-ray. The maximum difference in bond lengths between the theoretical geometry and the measured geometry was 3.3% (C1B—C2B). However, the dihedral angle is not the same for all atoms in the computed and X-ray geometries. These differences arise from different degrees of rotation along both the N1—C2 bond axis and the C2—C1A bond axis in the two different geometries. The differing amounts of rotation along these axes result in: (1) the two halves of the dimers being slightly more rotated in the measured X-ray geometry than in the calculated geometry; and (2) the phenyl group being more rotated (i.e., less in plane with the imidazole group) in the X-ray model than in the computed model. It is important to note that the X-ray data was collected from a crystal structure in which many dimers were stacked in a crystalline form (see Fig. 4), while the computed model was based on a single molecule, isolated in space. Despite these differences, there is quite good agreement between the two structures. Bond lengths, bond angles, and dihedral angles for the X-ray geometry and the calculated geometry are reported as Supplementary material (Tables S6–S8).[3]

Gomberg's premature assignment, Morukama's predictions, and dimer bond energies

Gomberg's mistaken assignment of structure on recombination of two triphenylmethyl radicals and the subsequent correction some 60 years later (vide supra) have become classics of modern chemistry. Though hexaphenylethane, Gomberg's predicted dimer, has not yet been synthesized, Morukama's recent calculations, which have assigned a BDE of 16.6 kcal/mol to the central C—C bond, have led these authors to suggest that synthesis of hexaphenylethane should, in fact, be possible.

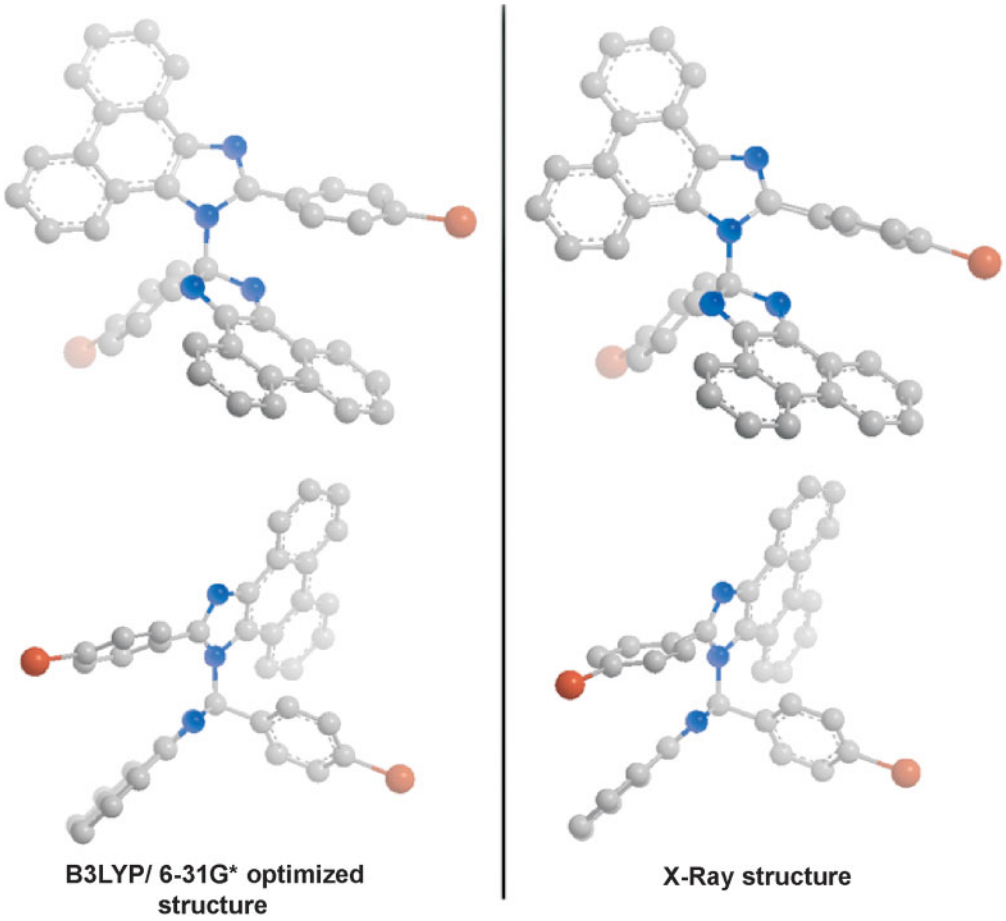
Our study poses an interesting juxtaposition to the previous section. On one hand, the calculations have shown that the actual dimer isomer (**13**) produced from the dimerization of radical **10** is not the most thermodynamically stable one. On the other hand, however, the BDE of the C—N in dimer formation is calculated as 16.5 kcal/mol, i.e., only a shade below Morukama's calculated BDE. Note also that a normal C—N bond is quoted as having a BDE of ca. 70 kcal/mol, easily making our C—N bond as having the lowest recorded BDE. (According to a recent compilation, the lowest C—N BDE reported so far is 26.3 kcal/mol) (12).

Conclusions

An X-ray structure study on the molecule formed by dimerization of the phenanthroimidazole radical **10** has been shown to be **13** resulting from C—N bond formation between two radicals. This agrees with conclusions based on a NMR study. However, as a contradistinction, the results of a computational study using the B3LYP/6-31G* methodology

© 2005 NRC Canada

Fig. 8. A comparison of the B3LYP/6-31G* optimized geometry of dimer **13** with X = Br with the experimentally measured geometry of the same molecule. Note that the phenyl group (in the upper half of the dimer) is slightly less in plane with the imidazole group in the X-ray structure than in the B3LYP/6-31G* structure. (See Supplementary Tables S6–S8 for detailed comparison of the X-ray and computed geometries: bond angles, bond lengths, and dihedral angles).[3]



has revealed that the lowest energy dimer results not from C—N (or C—C) bond formation, but rather from N—N bond formation. We concluded that although **12** is the computationally most stable isomer, the low spin density on the nitrogen kinetically discourages N—N bond formation. An interesting juxtaposition in the present results vis-à-vis Gomberg's dimer and Morukama's calculations is revealed by the present work.

Experimental section

X-ray structure determination

A crystal of the compound (yellowish, plate-shaped, size 0.4 mm × 0.2 mm × 0.1 mm) was mounted and sealed on a glass fiber with epoxy glue. Data collection was performed on a Bruker SMART CCD 1000 X-ray diffractometer with graphite monochromated Mo K_α radiation (λ = 0.710 73 Å), operating at 50 kV and 35 mA at 27 °C over 2θ ranges of 3.62°~56.76°. No significant decay was observed during the data collection.

Data were processed on a Pentium PC using the Bruker AXS Windows NT SHELXTL software package (version 5.10) (13). Neutral atom scattering factors were taken from Cromer and Waber (14). The raw intensity data were converted (including corrections for scan speed, background, and Lorentz and polarization effects) to structure amplitudes and their esds using the program SAINT, which corrects for *L*p and decay. Absorption corrections were applied using the SADABS program. The crystal is a triclinic space group *P*-1, based on the systematic absences, *E* statistics, and successful refinement of the structure. The structure was solved by direct methods. Full-matrix least-square refinements minimizing the function $\Sigma w(F_o^2 - F_c^2)^2$ were applied to the compound. All non-hydrogen atoms were refined anisotropically. The positions for all hydrogen atoms were calculated, and their contributions were included in the structure factor calculations with isotropic thermal parameters 1.2 times that of the attached carbon atoms (1.5 times for methyl hydrogens).

Convergence to final R_1 = 0.0554 and wR_2 = 0.1469 by using 8249 independent reflections and 460 parameters was achieved (eq. [4]), with the largest residual peak and hole to be 0.848 and –0.275 e/Å^3, respectively. Crystallographic data, experimental details, and refinement summary are given in Table 5. The molecular structure and cell packing are shown in Figs. 3 and 4.

© 2005 NRC Canada

Table 5. Crystal data.

Identification code	aw14
Empirical formula	$C_{42}H_{25}Br_2N_4 \cdot 0.5CH_2Cl_2$
Formula weight	787.94
Temperature (K)	300(2)
Wavelength (Å)	0.710 73
Crystal system	Triclinic
Space group	*P*-1
Unit cell dimensions	
a (Å)	11.681(5)
b (Å)	13.096(6)
c (Å)	13.673(6)
α (°)	103.971(8)
β (°)	90.773(8)
γ (°)	116.353(7)
Volume (Å^3)	1 801.2(14)
Z	2
Density (calcd., Mg/m^3)	1.453
Absorption coefficient (mm^{-1})	2.361
F(000)	792
Crystal size (mm^3)	0.4 × 0.2 × 0.1
θ Range for data collection (°)	1.81–28.38
Index ranges	$-15 \le h \le 15$, $-17 \le k \le 17$, $-16 \le l \le 18$
Reflections collected	12 995
Independent refelctions	8 249 [*R*(int) = 0.018 7]
Completeness to θ = 28.38 (%)	91.4
Absorption correction	Empirical (Bruker SADABS)
Max and min transmission	1.000 0, 0.761 9
Refinement method	Full-matrix least-squares on F^2
Data / restraints / parameters	8 249 / 0 / 460
Goodness-of-fit on F^2	0.843
Final *R* indices ($I > 2\sigma(I)$)	R_1 = 0.055 7, wR_2 = 0.146 5
R indices (all data)	R_1 = 0.114 3, wR_2 = 0.161 7
Largest diff. peak and hole (e Å^{-3})	0.846 and –0.393

[4] $$R_1 = \Sigma||F_o| - |F_c||/\Sigma|F_o|$$

$$wR_2 = \{\Sigma[w(F_o^2 - F_c^2)^2]/\Sigma[w(F_o^2)^2]\}^{1/2}$$

where $w = 1/[\sigma^2(F_o^2) + (0.075P)^2]$ and $P = [\max(F_o^2,0) + 2F_c^2]/3$.

Computations

All computations were preformed using GAUSSIAN 98 and carried out at the High Performance Computing Virtual Laboratory (HPCVL) at Queen's University.

Acknowledgements

We thank the Natural Sciences and Engineering Research Council of Canada (NSERC) and Materials Manufacturing Ontario (MMO) for financial support, Dr. Ruiyaho Wang for the X-ray structure determination, and Professor Bernie Schlegel for discussion.

References

1. M. Gomberg. J. Am. Chem. Soc. **22**, 757 (1900).
2. H. Lankamp, W.Th. Nauta, and C. MacLean. Tetrahedron Lett. 249 (1968).
3. C.R. Arkin, B. Cowans, and B. Kahr. Chem. Mater. **8**, 1500 (1996).
4. T. Vreven and K. Morokuma. J. Phys. Chem. A, **106**, 6167 (2002).
5. A.G. Davies and J. Lusztyk. J. Chem. Soc. Perkin Trans. 2, 692 (1981).
6. P.N. Culshaw, J.C. Walton, L. Hughes, and K.V. Ingold. J. Chem. Soc. Perkin Trans. 2, 879 (1993).
7. T. Hayashi and K. Maeda. Bull. Chem. Soc. Jpn. **33**, 565 (1960).
8. (*a*) E. Buncel. Can. J. Chem. **78**, 1251 (2000); (*b*) S. Swansberg, E. Buncel, and R.P. Lemieux. J. Am. Chem. Soc. **122**, 6594 (2000); (*c*) J.T.C. Wojtyk, P.M. Kazmaier, and E. Buncel. J. Chem. Soc. Chem. Commun. 1703 (1998); (*d*) E. Buncel and K.-s. Cheon. J. Chem. Soc. Perkin Trans. 2, 1241 (1998); (*e*) R.A. Cox, E. Buncel, and S. Patai (*Editors*). The chemistry of hydrazo, azo, and azoxy groups. Vol. 2. Wiley-Interscience, New York. 1997; (*f*) S.-R. Keum, K.-B. Lee, P.M. Kazmaier, and E. Buncel. Tetrahedron Lett. **35**, 1015 (1994); (*g*) R.A. Cox, I. Onyido, and E. Buncel. J. Am. Chem. Soc. **114**, 1358 (1992); (*h*) E. Buncel and S. Rajagopal. Acc. Chem. Res. **23**, 226 (1990); (*i*) D.L.H. Williams and E. Buncel. *In* Isotopes in organic chemistry. Vol. 5. *Edited by* E.

© 2005 NRC Canada

Buncel and C.C. Lee. Elsevier, Amesterdam. 1980. pp. 184–197; (*j*) R.A. Cox and E. Buncel. *In* The chemistry of the hydrazo, azo, and azoxy groups. *Edited by* S. Patai. Wiley, London. 1975. pp. 775–859; (*k*) A.J. Dolenko and E. Buncel. *In* The chemistry of the hydrazo, azo, and azoxy groups. *Edited by* S. Patai. Wiley, London. 1975. pp. 725–773; (*l*) E. Buncel. Acc. Chem. Res. **8**, 132 (1975); (*m*) E. Buncel. *In* Mechanisms of molecular migrations. Vol. 1. *Edited by* B.S. Thyagarajan. Wiley, New York. 1968. pp. 61–119; (*n*) D. Abdallah, M.A.A. Ghani, M.F. Cunningham, P.M. Kazmaier, B. Keoshkerian, and E. Buncel. Can. J. Chem. **82**, 1393 (2004); (*o*) M.A.A. Ghani, D. Abdallah, P.M. Kazmaier, B. Keoshkerian, and E. Buncel. Can. J. Chem. **82**, 1403 (2004).

9. (*a*) D.C. Clark and W.E. Baker. Annu. Conf. Polym. Process. Soc., Secaucus, N.J. Paper 6. June 1997; (*b*) A.C. Cordo and B.M. Kosowki. Int. Annu. Conf. ICT, 25th. 1994. p. 1.
10. Y. Zhou, W.E. Baker, P.M. Kazmaier, and E. Buncel. Can. J. Chem. **76**, 884 (1998).
11. (*a*) A.E. Frisch and M.J. Frisch. GAUSSIAN 98 user's reference. 2nd ed. Gaussian Inc., Pittsburgh, Penn. 1994–1999. p. 245; (*b*) M.J. Frisch, J.E. Del Bene, J.S. Binkley, and H.F. Schaefer III. J. Chem. Phys. **84**, 2279 (1986); (*c*) D.W. Schwenke and D.G. Truhlar. J. Chem. Phys. **82**, 2418 (1985).
12. Y.-R. Luo. Handbook of bond dissociation energies of organic compounds. CRC Press, New York. 2003.
13. SHELXTL NT. Version 5.10 [computer program]. Bruker AXS Inc., Madison, Wis. 1999.
14. D.T. Cromer and J.T. Waber. International tables for X-ray crystallography. Vol. 4. Kynoch Press, Birmingham, UK. 1974. Table 2.2A.

© 2005 NRC Canada

Photochemistry of 9-methylbicyclo[3.3.1]nonyl aryl ketones — A novel 1,5-disproportionation of 1,4-hydroxy biradicals and asymmetric induction using the solid-state ionic chiral auxiliary method[1]

Shuang Chen, Brian O. Patrick, and John R. Scheffer

Abstract: A novel 1,5-disproportionation reaction has been discovered for 1,4-hydroxy biradicals derived from the photolysis of 9-methylbicyclo[3.3.1]nonyl phenyl ketones (**1**), which undergo mainly Yang cyclization both in solution and the solid state. By applying the solid-state ionic chiral auxiliary method of asymmetric synthesis to the Yang cyclization, enantiomeric excesses as high as 95% were achieved at high reaction conversions. The origin of the reaction selectivity is discussed with the help of X-ray crystallography. In addition, the solid-state photoreaction of ketone **1b** was found to occur in a single crystal-to-single crystal fashion.

Key words: photochemistry, 1,4-hydroxy biradical, disproportionation, asymmetric induction, ionic chiral auxiliary, single crystal-to-single crystal reaction.

Résumé : On a découvert une nouvelle réaction de dismutation pour les 1,4-dihydroxy biradicaux obtenus par photolyse des 9-méthylbicyclo[3.3.1]nonyl (phényl) cétones (**1**) qui subissent principalement une cyclisation de Yang tant en solution qu'à l'état solide. En appliquant à la cyclisation de Yang la méthode de l'auxiliaire chiral ionique en phase solide, il a été possible d'obtenir des excès énantiomériques pouvant atteindre 95 % avec des taux de conversion élevés. On discute de l'origine de la sélectivité de la réaction à l'aide de la cristallographie des rayons X. De plus, on a trouvé que, à l'état solide, la réaction de la cétone **1b** s'effectue d'une façon allant d'un cristal unique à un cristal unique.

Mots clés : photochimie, 1,4-dihydroxy biradical, dismutation, induction asymétrique, auxiliaire chiral ionique, réaction d'un cristal unique à un cristal unique.

[Traduit par la Rédaction]

Introduction

Triplet 1,4-hydroxy biradicals formed in the γ-hydrogen abstraction step of the photochemical Norrish–Yang type II reaction have three possible fates: reverse hydrogen transfer to regenerate the starting ketone in its ground state, cleavage of the central carbon–carbon bond to form an alkene and an enol, and Yang cyclization to form a cyclobutanol derivative (Scheme 1) (1). In this paper, we report a fourth reaction pathway, a novel 1,5-disproportionation, observed for the 1,4-hydroxy biradicals derived from hydrogen abstraction of 9-methylbicyclo[3.3.1]nonyl phenyl ketones (**1**). The study of the photochemistry of 9-methylbicyclo[3.3.1]nonyl phenyl ketones (**1**) complements our earlier studies on the solid-state Norrish–Yang type II photochemistry of adamantyl phenyl ketones and norbornyl phenyl ketones (**2** and **3**) (Scheme 1) (2, 3). In these two previous systems, hydrogen abstraction occurred from either a rigid six-membered ring or a rigid five-membered ring, while in the bicyclo[3.3.1]nonyl phenyl ketone system hydrogen abstraction occurs from a relatively flexible six-membered ring, allowing for the effects of small changes in ring geometry on the hydrogen abstraction process and the reaction outcome to be examined. Moreover, 9-methylbicyclo[3.3.1]nonyl phenyl ketones (**1**) are achiral molecules that give mainly chiral Yang photocyclization products upon photolysis. As hydrogen abstraction of either of the two enantiotopic γ-hydrogen atoms could occur, this allows the enantioselectivity of the reaction to be studied using the solid-state ionic chiral auxiliary method (4).

Received 21 January 2005. Published on the NRC Research Press Web site at http://canjchem.nrc.ca on 10 November 2005.

S. Chen, B.O. Patrick, and J.R. Scheffer.[2] Department of Chemistry, University of British Columbia, 2036 Main Mall, Vancouver, BC V6T 1Z1, Canada.

[1]This article is part of a Special Issue dedicated to organic reaction mechanisms.

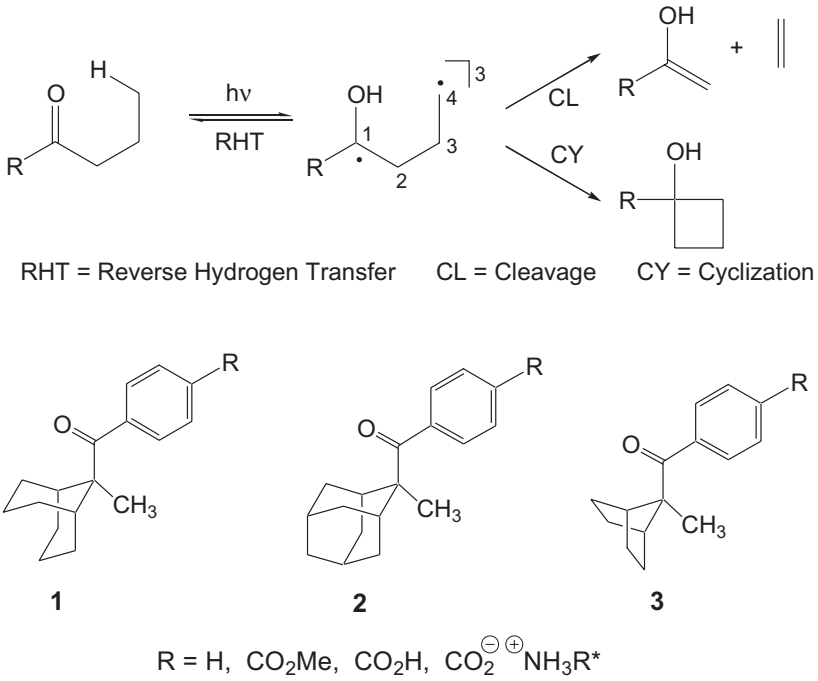
[2]Corresponding author: (e-mail: scheffer@chem.ubc.ca).

Results and discussion

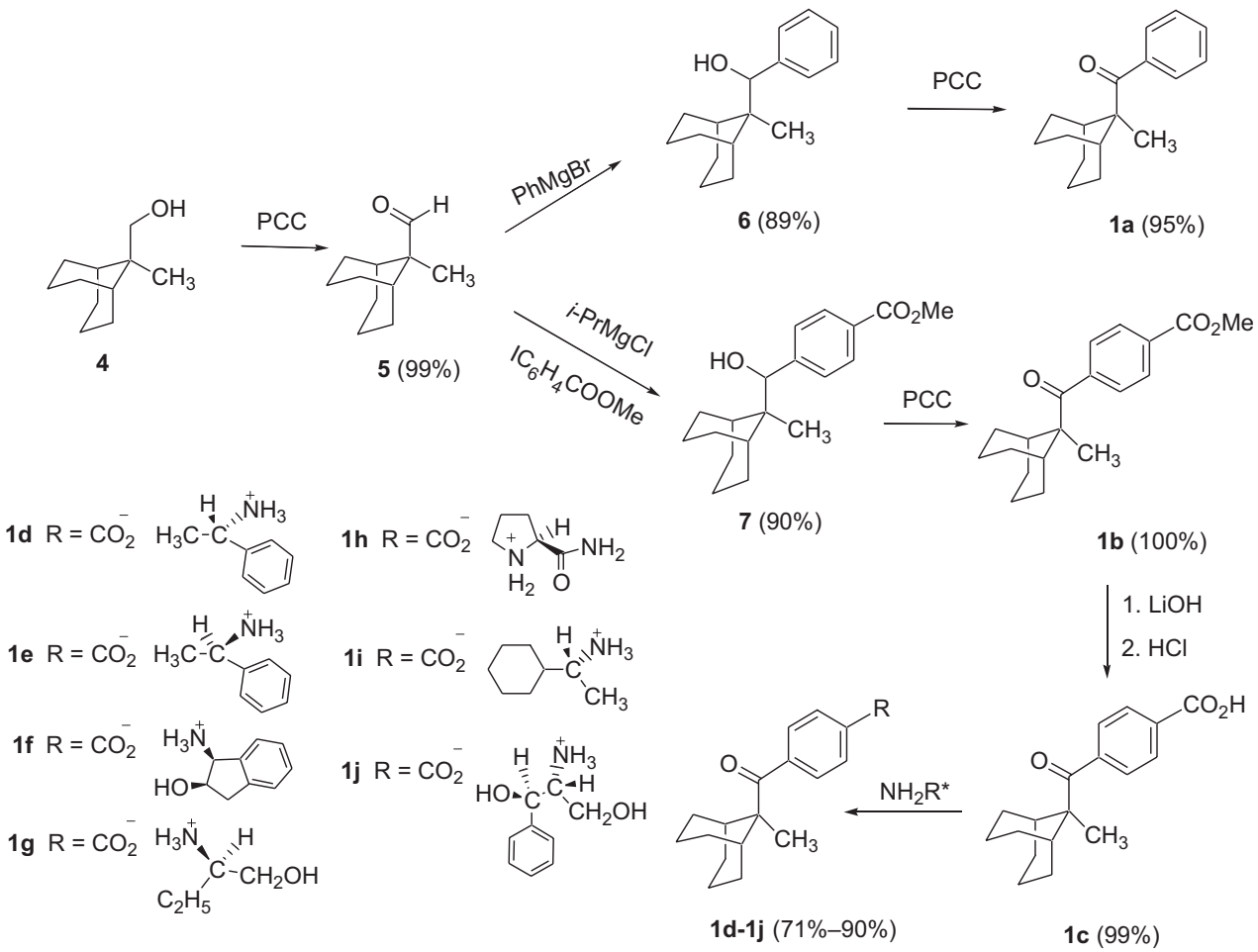
9-Methylbicyclo[3.3.1]nonyl phenyl ketones (**1a** and **1b**) were prepared by standard synthetic methods (Scheme 2) from the known compound 9-methylbicyclo[3.3.1]nonyl methanol (**4**) (5). Hydrolysis of ester **1b** afforded the corresponding keto acid **1c**, which was then reacted with various optically pure amines to form chiral salts **1d**–**1j** through acid–base chemistry. All these compounds were fully characterized by ^{1}H and ^{13}C NMR, FT-IR, HR-MS, UV, and elemental analysis (see details in the Experimental section).

 doi: 10.1139/V05-147 © 2005 NRC Canada

Scheme 1.

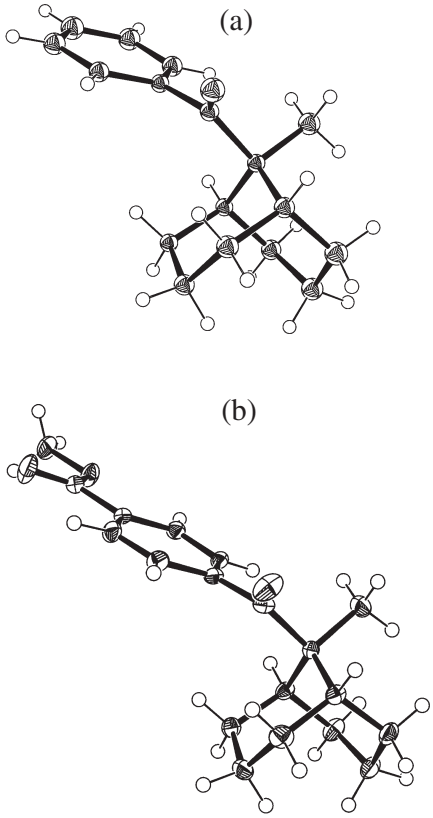


Scheme 2.



© 2005 NRC Canada

Fig. 1. ORTEP representation of (*a*) ketone **1a** and (*b*) ketone **1b**.



Single crystal X-ray crystallographic determinations were also performed for compounds **1a** and **1b** (Fig. 1).

The photochemistry of aryl ketones **1a** and **1b** was explored in both solution and the crystalline state. The reaction products were readily obtained by preparative scale solution photolysis and the solid-state reactions were performed on an analytical scale to determine the mode of reactivity in that medium. The details of the experiments as well as the apparatus used are given in the Experimental section. Table 1 and Scheme 3 summarize the photochemical results in both media. As shown in Scheme 3 and Table 1, like the analogous compounds **2** and **3** (2, 3), solution photolysis of ketones **1a** and **1b** primarily yielded Yang photocyclization products **9a** and **9b**.

Interestingly, photolysis of ketones **1a** and **1b** also afforded small amounts (<5%) of the unusual 1,5-disproportionation products **10a** and **10b** (Scheme 3). These minor products are presumably formed by a novel disproportionation of the intermediate 1,4-hydroxy biradical **8** in which a hydrogen atom on C5 is transferred to the radical center on C1. As far as we are aware, this type of disproportionation reaction is unknown for 1,4-hydroxy biradicals, although the corresponding process has been observed for a 1,5-hydroxy biradical (6). The stereochemistry of the major photoproducts (**9a** and **9b**) was later determined to be that in which the aryl group is in the endo position, although generation of *exo*-aryl products is theoretically possible. It is interesting to note that in the photochemistry of 9-methyl substituted ketones **1a** and **1b**, no Norrish type I or type II photocleavage products could be identified, although traces (<1%) of several unknown photoproducts could be detected by GC. The

Table 1. Photolysis of ketones **1a** and **1b** in solution and the crystalline state.

				Products (%)[b]			
Ketone	Medium	Time (h)	Conversion (%)[a]	**9a**	**10a**	**9b**	**10b**
1a	CH_3CN[c]	1	65	62	2		
		2	89	85	3		
		8	100	92	3		
	Crystal[c]	24	100	92	5		
1b	CH_3CN[c]	1	98			91	4
	Crystal[c]	24	100			90	5

[a]Percentage of total GC integral owing to the disappearance of the corresponding starting material.
[b]Percentage of total GC integral owing to the corresponding product.
[c]The combined percentage of the reported compounds is less than unity because of some unidentified GC peaks.

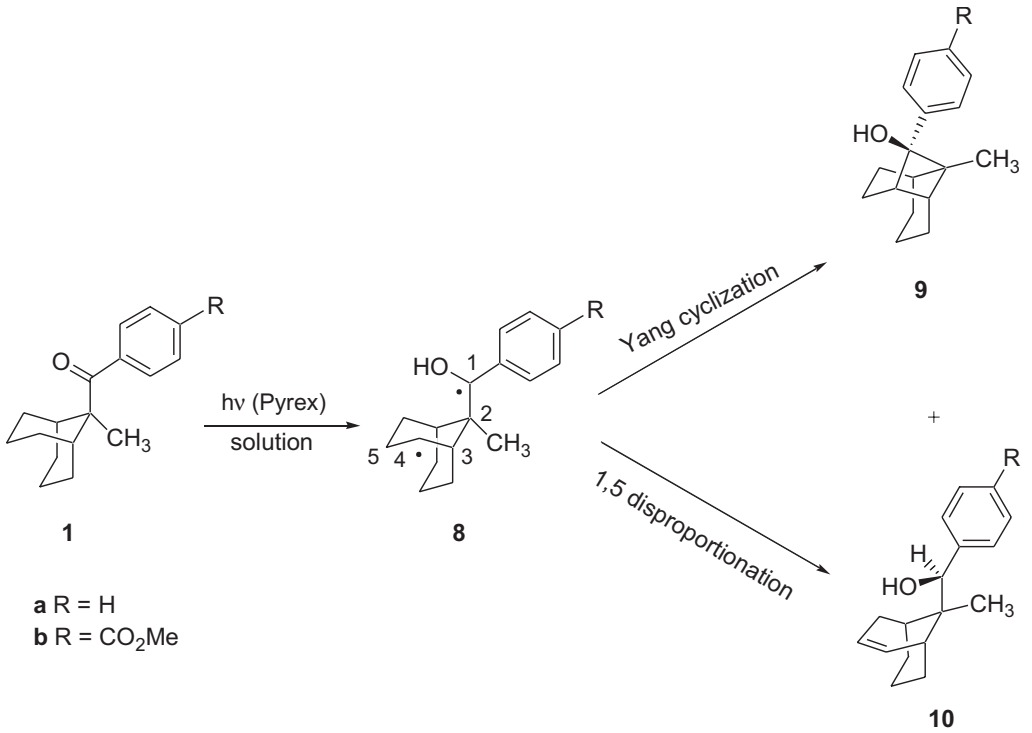
results of solid-state photolysis of ketones **1a** and **1b** were strikingly similar to their solution counterparts, with **1a** and **1b** affording photoproducts **9a** and **9b** (90%–92%) and **10a** and **10b** (5%). All the photoproducts were fully characterized by 1D ^1H and ^{13}C (BB and APT) NMR, 2D ^1H–^1H COSY, ^1H–^{13}C HMQC, HMBC and NOESY, FT-IR, HR-MS, as well as by elemental analysis. The structures of photoproducts **10a**, **9b**, and **10b** were also confirmed by X-ray crystallography (Fig. 2). The details of the separation conditions along with the analytical data for each of the products are given in the Experimental section.

As described above, 9-methylated bicyclo[3.3.1]nonyl phenyl ketones **1a** and **1b** underwent Yang photocyclization and yielded *endo*-aryl cyclobutanols **9a** and **9b** as major photoproducts, both in solution and the solid state. In this case, it is relevant to ask why neither *exo*-aryl cyclobutanols nor photocleavage products were obtained. To answer this question, consider the idealized reaction pathway shown in Scheme 4. X-ray crystallography shows that in the crystalline state ketones **1a** and **1b** adopt chair–chair conformations in which the benzoyl group is in the axial position and the mean plane of the carbonyl group is roughly orthogonal to the plane bisecting the bicyclo[3.3.1]nonane ring between γ-hydrogen atoms H_x and H_y. In this case, H_x is in closer proximity to the carbonyl oxygen than H_y (for H_x: d = 2.50 Å in ketone **1a**, and 2.52 Å in ketone **1b**; for H_y: d = 3.49 Å in ketone **1a**, and 3.69 Å in ketone **1b**). The other γ-hydrogen abstraction parameters (ω, Δ, and θ) in Table 2 also suggest that H_x is in a more favorable position for hydrogen abstraction than H_y (7).

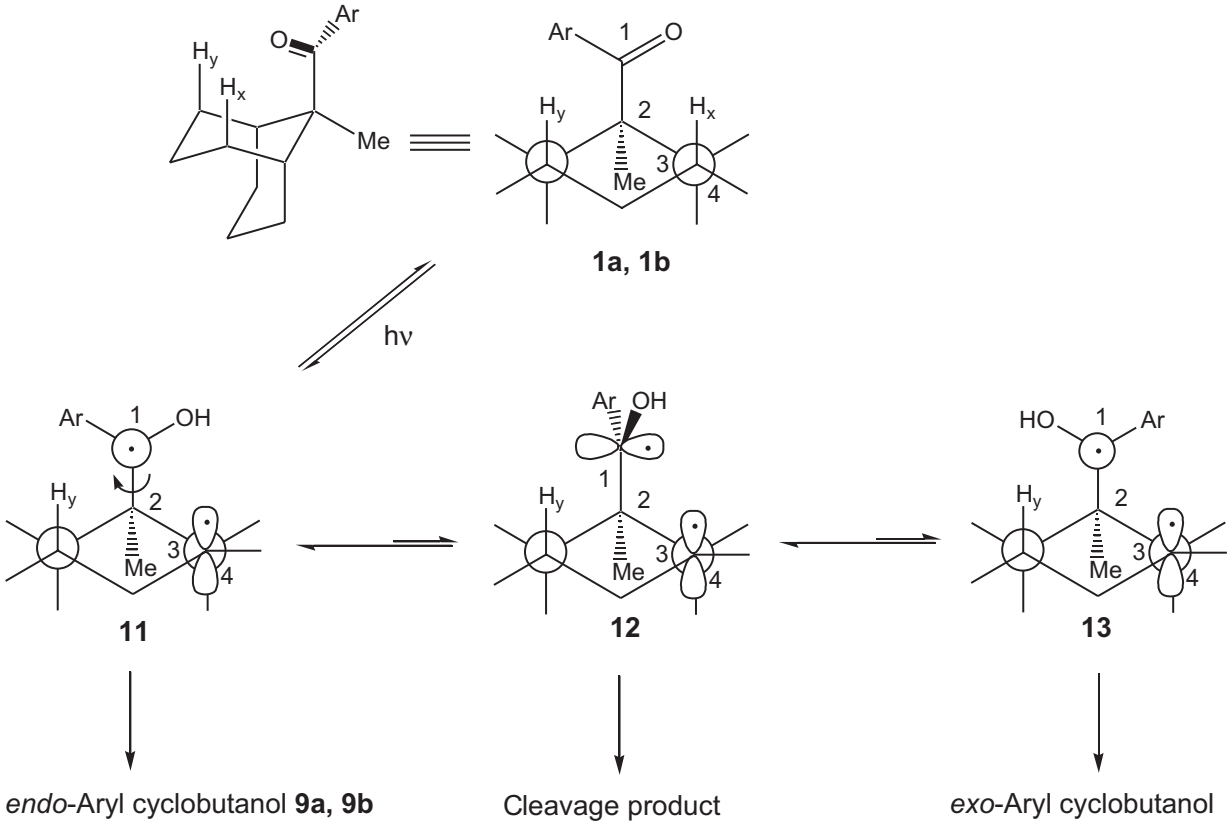
Upon photoexcitation and hydrogen abstraction, 1,4-hydroxy biradical intermediate **11** will be generated. Since hydrogen abstraction in the solid state is considered to occur with minimum movement of the heavy atoms, geometric data derived from the ground-state ketone can be used to analyze the behavior of the corresponding 1,4-hydroxy biradical intermediate (8). For this purpose, we define two torsional angles with reference to Fig. 3*a*, which is a depiction of the 1,4-hydroxy biradicals derived from ketones **1a** and **1b**. Angle φ_1 is defined as the dihedral angle between the C2—C3 bond and the p orbital on C1, and the angle φ_4 is likewise defined as the analogous angle between the C2—C3 bond and the p orbital on C4. The p orbitals at C1 and

© 2005 NRC Canada

Scheme 3.

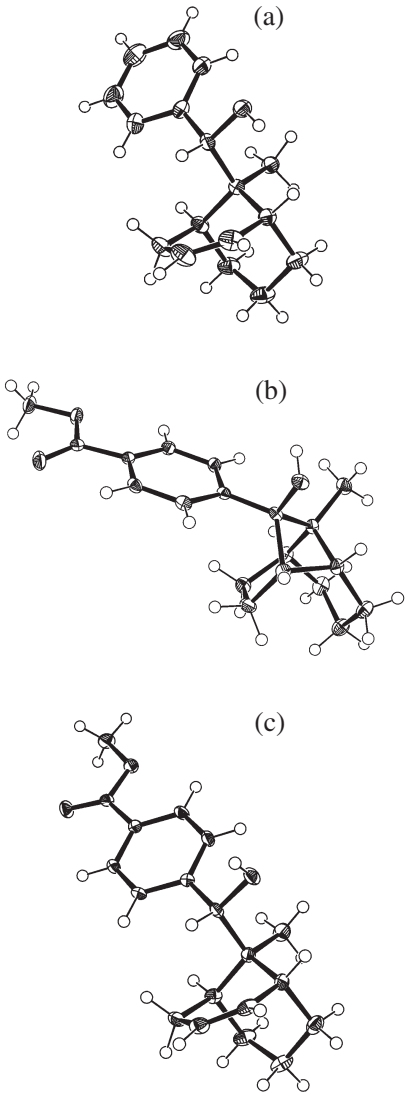


Scheme 4.



© 2005 NRC Canada

Fig. 2. ORTEP representation of photoproducts (*a*) **10a**, (*b*) **9b**, and (*c*) **10b**.



C4 are assumed to be orthogonal to the O-C1-C2 and C3-C4-C5 planes, respectively. It is generally believed that cleavage of 1,4-hydroxy biradicals is favored by good overlap between the p orbitals on C1 and C4 with the C2—C3 bond (9). The overlap between these orbitals is proportional to $\cos\varphi_1$ and $\cos\varphi_4$ (10), and the best geometry for cleavage can be expected when φ_1 and $\varphi_4 = 0°$ and $\cos\varphi_1 = \cos\varphi_4 = 1$. The values of $\cos\varphi_1$ and $\cos\varphi_4$ for the two ketones investigated in the present study are given in Table 3. Also shown in Table 3 are the values of the angle β, defined as the dihedral angle between the p orbital on C1 and the C2–C4 vector (Fig. 3*b*). The most favorable geometry for cyclization exists when $\beta = 0°$, i.e., when the p orbital on C1 is pointing directly at the p orbital on C4. Table 3 also gives the values of the distance (*D*), defined as the distance between C1 and C4. For Yang photocyclization to be successful, the radical-containing carbon atoms C1 and C4 must be close to one another, i.e., $D < 3.4$ Å, which is the sum of the van der Waals radii for two carbon atoms (11).

Table 2. Hydrogen atom abstraction parameters for compounds **1a** and **1b**.

Ketone	H	*d* (Å)[a]	ω (°)[b]	Δ (°)[c]	θ (°)[d]
1a	H_x	2.50	57	86	118
	H_y	3.49	91	41	105
1b	H_x	2.52	63	78	119
	H_y	3.69	94	35	105
Ideal value		2.7±0.2	0	90–120	180

[a]C=O···H_γ distance.
[b]Deviation of H_γ from the mean plane of the carbonyl group.
[c]C=O···H_γ angle.
[d]C-H_γ···O angle.

Fig. 3. (*a*) Idealized 1,4-hydroxybiradical intermediate. (*b*) Depiction of the angle β.

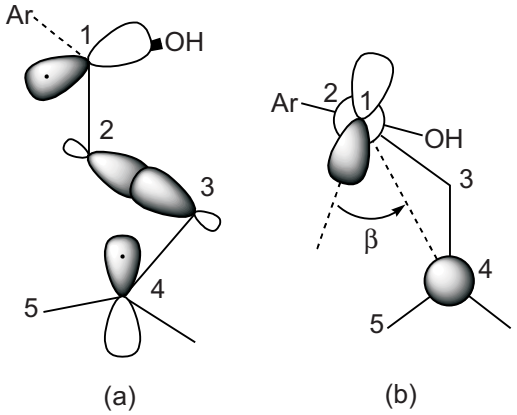


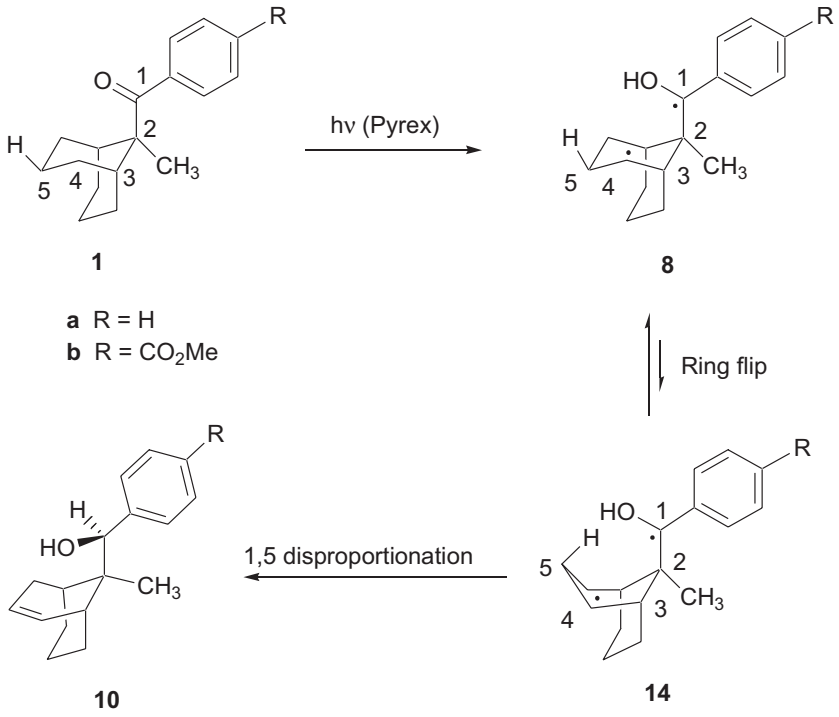
Table 3. Geometric data for ketones **1a** and **1b**.

Ketone	φ_1 (°)	$\cos\varphi_1$	φ_4 (°)	$\cos\varphi_4$	β (°)	*D* (Å)
1a	65	0.42	35	0.82	35	3.01
1b	59	0.52	36	0.81	28	2.90

With $\cos\varphi_4 \approx 80\%$ and $\cos\varphi_1 \approx 50\%$ (only 50% of maximum overlap between the p orbital on C1 and the C2—C3 bond), the geometry of biradical intermediate **11** is poor for cleavage, as cleavage requires good overlap of both p orbitals with the cleaving C2—C3 bond. But this biradical has a good geometry for cyclization, with $\beta \approx 30°$ (indicating there is reasonably good overlap of the two p orbitals at C1 and C4) and $D = 2.90$ Å in ketone **1b**, and 3.01 Å in ketone **1a**. As a result, cyclization of biradical **11** with retention of configuration at C1 and C4 leads to the predominant *endo*-aryl photoproducts **9a** and **9b**. On the other hand, for cleavage to occur, an approximate 90° rotation of the aryl and hydroxyl groups about the C1—C2 bond of biradical **11** is required to align the p orbital on C1 with the C2—C3 σ bond (see Scheme 4, structure **12**). An additional 90° rotation of the aryl and hydroxyl groups about the C1—C2 bond leads to biradical **13**, closure of which would give *exo*-aryl cyclobutanol products. Both processes require rotations about the C1—C2 bond and are unfavorable because of Ar/α-CH_3 eclipsing, a phenomenon known as the "α-alkyl group effect" (12). Therefore, *endo*-aryl cyclobutanols **9a**

© 2005 NRC Canada

Scheme 5.



and **9b** are the major products formed in the photoreaction of ketones **1a** and **1b**.

Formation of minor photoproducts **10a** and **10b** observed in the photolysis of ketones **1a** and **1b** can be seen to be the result of a 1,5-disproportionation of biradical intermediate **14**, which in turn is formed by a ring flip of initially formed biradical **8** (Scheme 5).[3] X-ray crystallographic analysis showed that the distance between C1 and the equatorial hydrogen atom on C5 in ketones **1a** and **1b** is 4.08 and 4.02 Å, respectively. It is unlikely that 1,5-disproportionation could take place directly from the chair–chair biradical **8** without a significant geometry change of the bicyclic ring. On the other hand, a ring flip of biradical **8** at the C5 end leads to the boat–chair biradical **14** in which the flagpole hydrogen atom on C5 is brought close to the radical center on C1 (13), and a 1,5-disproportionation process should easily occur. Because this ring-flipping process is energetically unfavorable, in an established equilibrium, the population of biradical **14** is less than that of biradical **8**. Moreover, because 1,5-disproportionation requires breaking a C—H bond, it is likely to be a slower process than Yang cyclization. Therefore, only small amounts of disproportionation products **10a** and **10b** were observed in the photolysis of ketones **1a** and **1b**.

In comparison with our previous studies on the photochemistry of adamantyl phenyl and norbornyl phenyl ketones (**2** and **3**) in which Yang cyclization was found to be the sole reaction pathway (no 1,5-disproportionation product was obtained owing to the rigidity of adamantyl and norbornyl ring skeletons) (2, 3), the present study not only corroborates this main reaction pattern for bicyclic and tricyclic phenyl ketones, but also shows that small changes in the flexibility of the bicyclic ring system can lead to a new reaction pattern, in this case a novel 1,5-disproportionation reaction.

To apply the solid-state ionic chiral auxiliary method to asymmetric induction in the photochemistry of 9-methylbicyclo[3.3.1]nonyl phenyl ketones, a number of crystalline salts (**1d–1j**, Scheme 2) were prepared by reaction of keto acid **1c** with commercially available optically pure amines. The amines were selected according to two criteria: (*i*) the pK_a of the reacting acid should be lower than that of the protonated amine by about 3 pK_a units (14, 15) because this ensures complete proton transfer from the acid to the amine instead of formation of a neutral hydrogen bonded complex; (*ii*) the amine selected should not possess chromophores that interfere with the aryl ketone absorption at 320–330 nm. The formation of an ammonium carboxylate linkage between the acid and amine was confirmed by the melting point and FT-IR spectrum of each salt. The melting points of all the salts are different from both those of keto acid **1c** and the corresponding amines. In the IR spectrum of keto acid **1c**, the C=O stretches of the ketone and carboxylic acid exist as broadened bands at 1695 and 1680 cm^{-1}, respectively. In the spectra of the salts, these absorptions are replaced by a single sharper band at ~1675 cm^{-1} corresponding to the C=O stretch of the ketone. At the same time, two new intense bands (1300–1600 cm^{-1}) owing to the symmetric and asymmetric stretches of the carboxylate anion are observed (16). The 1:1 acid–base stoichiometry of all the salts was confirmed by ^{1}H NMR spectroscopy, ESI (or LSI-MS) mass spectrometry, and elemental analysis.

[3] An alternative mechanism for the formation of minor photoproducts **10a** and **10b** involving initial δ-hydrogen atom abstraction followed by disproportionation is deemed unlikely on two counts: the general and well-established kinetic preference for γ over δ-hydrogen abstraction (1*a*), and in the specific case of ketones **1a** and **1b**, impossibly long C=O···H_δ distances (4.40 and 4.38 Å, respectively).

© 2005 NRC Canada

To determine whether the ionic chiral auxiliary has any effect on the product distribution or the steric course of the photoreaction in solution, a number of the optically active salts were photolyzed in a mixture of acetonitrile and water. Following irradiation, the reaction mixture was treated with excess ethereal diazomethane solution to form the corresponding methyl esters **9b** and **10b**. All the solution-state reactions essentially afforded the same product ratio of cyclobutanol **9b** and alkene **10b** as that observed in the solution photolysis of keto ester **1b**. Photoproduct **9b** was subsequently determined to be racemic. The enantiomeric excess of photoproduct **10b** was not measured owing to its small quantity in the reaction mixture. These results show that, in solution, the anisotropy of the chiral ammonium ion has no influence on the reaction selectivity.

Each of the salts listed in Scheme 2 was irradiated in the crystalline state. No color change or melting of the crystals was observed during the reaction, and following irradiation, the crystals were dissolved in ethyl acetate or methanol and treated with excess ethereal diazomethane to form the corresponding methyl esters **9b** and **10b**. Following diazomethane treatment, the organic layer containing the esterified photoproducts and starting material was washed with water and filtered through a short-path silica gel column to remove the chiral auxiliary. The mixture was then analyzed by GC for yield and conversion. Owing to the overlap of the product and starting ketone peaks in the chiral HPLC analysis, achiral preparative HPLC was used to isolate photoproduct **9b** (Waters Radialpak™ μPorasil™ silica column, 10% EtOAc in hexanes, 5 mL/min). Following purification, the enantiomeric excess of photoproduct **9b** was measured using chiral HPLC (Chiralcel® OC column, 2% isopropanol in hexanes, 0.5 mL/min). The results of the solid-state photolysis of chiral salts **1d**–**1j** are summarized in Table 4. Irradiation of the salts in the crystalline state leads to asymmetric induction with product ees ranging from 3% to 95%. The highest ee was observed for salt **1i** formed between acid **1c** and (*R*)-(–)-1-cyclohexylethylamine, where an enantiomeric excess of 95% was achieved at 38% reaction conversion.

Photolysis of the (*S*)-(–)-1-phenylethylamine and (*R*)-(+)-1-phenylethylamine salts (**1d** and **1e**) afforded nearly equal optical yields of the enantiomers of cyclobutanol **9b** (after diazomethane workup). This allows direct access to both enantiomers by simple exchange of the ionic chiral auxiliary. Table 4 also shows that the product ee declines with increasing reaction conversion. This is not unexpected, since the salts react to give products that presumably do not "fit" into the original crystal lattice, and defect sites are generated. As the reaction proceeds, the rigidity and regularity of the crystal lattice is gradually lost. As a result, the topochemical control is reduced and enantioselectivity declines. Low-temperature photolysis can be used to partially compensate this effect. As shown in Table 4, for reactions conducted at reduced temperature (–20 °C), enantioselectivities are better than those obtained at room temperature. Specifically, at –20 °C, quantitative conversion to cyclobutanol **9b** from salt **1d** occurred in 81% ee in comparison to 70% ee at room temperature. Further reducing the reaction temperature to –70 °C provided limited improvement in enantioselectivity, while much longer irradiation times were required.

To date, salts **1d**–**1j** have resisted attempts to determine their X-ray crystal structures; thus, we were not able to correlate the observed enantioselectivity with the solid-state structure. Nevertheless, the high ees observed in the solid state can be explained by a conformational effect, a situation that has been seen in other solid-state enantioselective Norrish–Yang type II reactions (17). In the solid state, the role of the ionic chiral auxiliary is to preorganize the photoreactant in a homochiral conformation in which the carbonyl group of the substrate is positioned to abstract only one of the two diastereotopic γ hydrogens in the initial step of the photoreaction. With topochemical control persisting in the solid state, formation of a single enantiomer of the product is achieved following removal of the chiral auxiliary, thereby transforming conformational chirality into configurational chirality.

Among the salts studied, salt **1j** showed a particularly low enantioselectivity (3% ee). The low enantioselectivity observed is likely due to the phenomenon of *conformational enantiomerism* (18) in which equal amounts of both enantiomeric conformers of the photolabile carboxylate exist within the crystal lattice. Each conformer abstracts one of the two diastereotopic γ hydrogens and forms opposite enantiomers of the same photoproduct after workup. In addition,

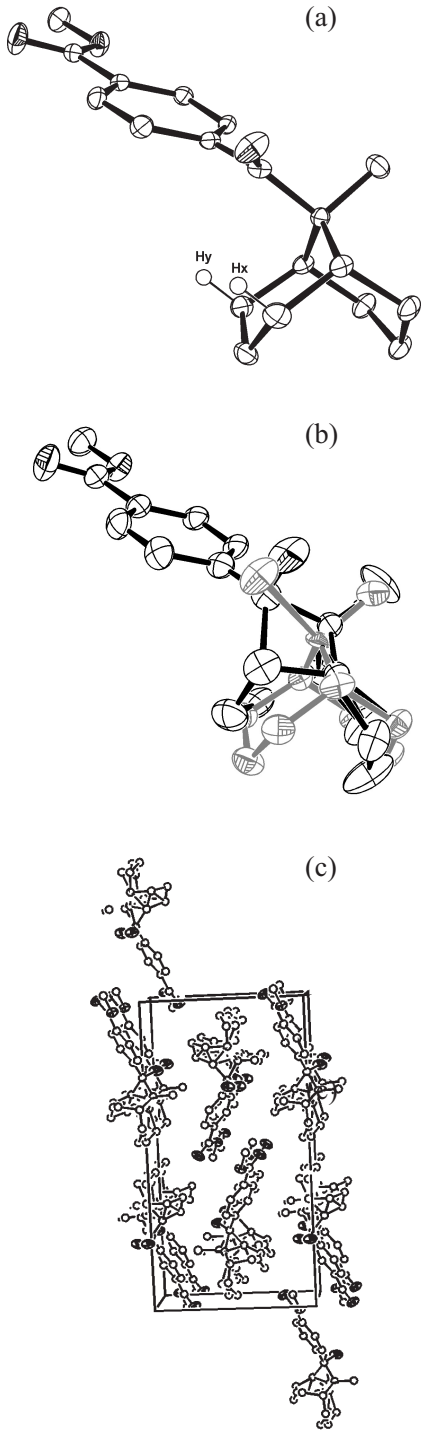
Table 4. Solid-state photolysis of optically pure salts **1d**–**1j**.

Salt	Temp. (°C)	Time (min)	Conv. (%)[a]	ee (%)[b]	[α][c]
1d	r.t.[d]	120	>99	70	+
	–20	15	31	91	+
	–20	30	60	86	+
	–20	240	>99	81	+
	–70	180	44	86	+
1e	r.t.[d]	120	>99	73	–
	–20	15	36	90	–
	–20	30	72	86	–
	–20	60	89	86	–
	–70	120	93	80	–
1f	r.t.[d]	120	83	49	+
	–20	60	55	86	+
	–20	180	73	60	+
	–20	300	95	54	+
1g	r.t.[d]	120	98	25	–
	–20	30	21	38	–
	–20	240	81	29	–
1h	r.t.[d]	120	94	60	+
	–20	30	26	94	+
	–20	180	87	77	+
	–70	180	56	93	+
1i	r.t.[d]	120	>99	36	–
	–20	10	38	95	–
	–20	30	64	84	–
	–20	120	97	70	–
1j	r.t.[d]	120	>99	3	+
	–20	60	35	17	+
	–20	240	84	7	+
	–70	180	68	6	+

[a]Percentage of total GC integral owing to the disappearance of the corresponding starting material.
[b]The enantiomeric excess for photoproduct **9b** was determined using a Chiralcel® OC HPLC column.
[c]Sign of rotation of **9b** at the sodium D-line.
[d]Room temperature.

© 2005 NRC Canada

Fig. 4. ORTEP representation of: (*a*) ketone **1b** showing γ hydrogens H_x and H_y; (*b*) mixed crystal composed of 75% of ketone **1b** (gray) and 25% of photoproduct **9b** (black); (*c*) crystal packing diagram of the mixed crystal.



crystal disorder could also be a cause for the low enantioselectivity observed in the photolysis of salt **1j**. In a disordered crystal, two or more conformations of the reactive ion are distributed randomly throughout the crystal (static disorder) or are thermally interconverting (dynamic disorder). Since attempts to grow crystals of salt **1j** suitable for X-ray analysis were not successful, the exact reason for the low enantioselectivity of salt **1j** remains to be determined.

During our photochemical studies, we noticed that crystals of ketone **1b** did not change in appearance upon irradiation. This suggested the occurrence of a single-crystal-to-single-crystal reaction (19), which allowed the structures of both reactant and product to be obtained at various stages of reaction. Figure 4*a* shows the crystal structure of ketone **1b** prior to photolysis, and Fig. 4*b* depicts the superposition of ketone **1b** and its photoproduct in the mixed crystal following 25% conversion to the corresponding cyclobutanol **9b**. The extent of conversion was determined through refinement of the atom site occupancy factors in the X-ray crystallographic study. Figure 4*a* predicts preferential abstraction of H_x over H_y, and in agreement with this, the molecular structure of the photoproduct shows that the carbon atom to which H_x was attached is in fact part of the newly formed four-membered ring. The crystal structures also reveal that closure of the biradical does occur with "retention of configuration" at the carbonyl carbon. The reactant and product have similar geometries in which the aryl group portion of the molecule remains essentially unchanged during photolysis, while an upward movement of the γ carbon occurs to allow for cyclobutane ring formation. The corresponding alteration of the bicyclic ring skeleton is significant but a close atom-for-atom correspondence between the photoreactant and photoproduct is maintained. Also observed was a change in the orientation of the carbon–oxygen bond during the change in hybridization at the carbonyl carbon from sp^2 to sp^3. Accompanying this was a change in the length of the C—O bond from 1.22 to 1.33 Å. While these motions are significantly greater than those accompanying other unimolecular single crystal-to-single crystal photoreactions,[4] the overall packing arrangement of the crystal (Fig. 4*c*) remains unchanged, and as a result, the process still occurs in a topochemical fashion.

Summary

The photochemistry of several 9-methylbicyclo[3.3.1]-nonyl phenyl ketones was studied in solution and the solid state. In both media, Yang photocyclization was found to be the major process for α-methylated bicyclo[3.3.1]nonyl phenyl ketones (**1a** and **1b**), with *endo*-aryl cyclobutanols (**9a** and **9b**) being the major products. An unusual 1,4-hydroxy biradical disproportionation reaction was also observed during the photolysis of ketones **1a** and **1b**, although it was a minor process (<5%). By utilizing the *ionic chiral auxiliary* method, high enantioselectivities (up to 95%) were achieved for a number of the optically active salts on photolysis in the solid state. In addition, structure–reactivity correlation studies were performed based on the crystal structure data of ketones **1a** and **1b** to rationalize their photochemical behavior. The solid-state photoreaction of ketone **1b** was found to occur in a topochemically controlled, single crystal-to-single crystal fashion.

[4] For examples of unimolecular single-crystal-to-single-crystal photochemical reactions, see refs. 2 and 3.

© 2005 NRC Canada

Experimental section

Commercial spectral grade solvents were used for photochemical experiments unless otherwise stated. For synthetic use tetrahydrofuran and diethyl ether were dried over the sodium ketyl of benzophenone, dichloromethane was dried over calcium hydride, and acetonitrile was distilled from P_2O_5. All reactions were performed under a nitrogen atmosphere unless otherwise noted. Melting points were determined on a Fisher-Johns hot-stage apparatus and were uncorrected. Analytical TLC was performed on 0.20 mm silica gel 60-F plates and visualized under UV light and (or) by staining with I_2 or phosphomolybdic acid. Preparative chromatography was performed using either the flash column method with silica gel (particle size 230–400 mesh) or radial elution chromatography on a Harrison Research Chromatron (model 7924T) with self-coated silica gel plates (1 or 2 mm thickness with EM Science silica gel 60 PF254 containing gypsum 7749-3). IR spectra were recorded on a PerkinElmer 1710 Fourier transform spectrometer. UV spectra were recorded on a PerkinElmer Lambda-4B UV–vis spectrometer at 25 °C. High-resolution mass spectra were obtained from a Kratos MS 50 instrument using electron impact (EI) ionization at 70 eV, a Kratos MS 80 spectrometer using desorption chemical ionization (CI) with the ionizing gas noted, a Kratos Concept IIHQ hybrid spectrometer using liquid secondary ionization (LSI-MS), or a Micromass LCT spectrometer using electrospray ionization (ESI). Elemental analyses were performed by the University of British Columbia (UBC) microanalytical service on a Carlo Erba CHN Model 1106 analyzer. ^{1}H NMR spectra were obtained at either 300 or 400 MHz on Bruker AV-300 or Bruker AV-400 instruments. ^{13}C NMR spectra were recorded at either 75 or 100 MHz. Some spectra are supported by data from the attached proton test (APT). Where these are given, (-ve) denotes a negative APT peak corresponding to a methine (CH) or methyl (CH_3) carbon centre, while no assignment signifies a quaternary or methylene (CH_2) carbon center.

9-Methylbicyclo[3.3.1]nonyl carboxaldehyde (5) and 9-methylbicyclo[3.3.1]nonyl phenyl methanol (6)

A mixture of PCC (1.40 g, 6.48 mmol) and Celite® 545 (2.79 g) was ground with a mortar and pestle until homogeneous. This solid was added to a solution of alcohol **4** (5) (545 mg, 3.24 mmol) in anhydrous dichloromethane (40 mL) and the mixture stirred for 2 h at room temperature. The reaction mixture was filtered through a column of Florisil® and the remaining solids triturated well with anhydr. Et_2O. Removal of solvent in vacuo gave aldehyde **5** (538 mg, 100%) as colorless oil, which was found to be unstable and was used without further purification. To a cold (0 °C) solution of phenyl magnesium bromide in THF (25 mL) was added aldehyde **5** (538 mg, 3.24 mmol in 5 mL of THF). The reaction was stirred in the cold (0 °C) for 2 h and quenched with 5% aq. NH_4Cl solution (15 mL). THF was removed and the resultant aqueous phase was extracted with Et_2O (3 × 20 mL). The combined ethereal extracts were washed with H_2O (20 mL) and brine (20 mL), followed by drying ($MgSO_4$) and removal of the solvent in vacuo. Silica gel chromatography (5% EtOAc in petroleum ether) afforded alcohol **6** (706 mg, 89%) as a white solid, mp 118–118.5 °C (EtOAc – petroleum ether). IR (KBr, cm^{-1}): 3395, 2943, 2912, 2868, 1491, 1461, 1020, 892, 761, 732, 703, 567. ^{1}H NMR ($CDCl_3$, 400 MHz) δ: 0.85 (s, 3H), 1.27 (br, 1H), 1.39 (m, 1H), 1.50–1.62 (m, 4H), 1.66 (s, 1H), 1.68–1.99 (m, 5H), 2.00–2.20 (m, 2H), 2.37 (m, 1H), 5.40 (s, 1H), 7.23 (m, 1H), 7.29 (m, 2H), 7.37 (m, 2H). ^{13}C NMR ($CDCl_3$, 100 MHz) δ: 16.54 (-ve), 20.58, 20.87, 27.20, 27.60, 27.74, 27.85, 32.24 (-ve), 32.92 (-ve), 39.65, 74.13 (-ve), 126.93 (-ve), 127.47 (-ve), 127.55 (-ve), 142.45. HR-MS (CI) calcd. for $C_{17}H_{24}O$: 244.1827; found: 244.1834. Anal. calcd. for $C_{17}H_{24}O$: C 83.55, H 9.90; found: C 83.95, H 10.02.

9-Benzoyl-9-methylbicyclo[3.3.1]nonanes (1a)

A mixture of PCC (1.15 g, 5.33 mmol) and Celite® 545 (2.30 g) was ground with a mortar and pestle until homogeneous. This solid was added to a solution of alcohol **6** (651 mg, 2.66 mmol) in anhydrous dichloromethane (30 mL) and the reaction mixture was stirred for 10 h at room temperature. The reaction mixture was filtered through a column of Florisil® and the remaining solids well triturated with anhydr. Et_2O. Removal of solvent in vacuo and silica gel chromatography (3% Et_2O in petroleum ether) gave ketone **1a** (612 mg, 95%) as a white solid, mp 67 to 68 °C (EtOAc – petroleum ether). UV–vis (2.39×10^{-4} mol/L, MeOH, nm ((mol/L)$^{-1}$ cm^{-1})): 285 (1178), 330 (720). IR (KBr, cm^{-1}): 2960, 2913, 2865, 1672, 1444, 1266, 1232, 1216, 1124, 963, 932, 721, 696, 663. ^{1}H NMR ($CDCl_3$, 300 MHz) δ: 1.30–1.93 (m, 13H), 2.02–2.17 (m, 2H), 2.34 (br, 2H), 7.33–7.46 (m, 3H), 7.70–7.75 (m, 2H). ^{13}C NMR ($CDCl_3$, 75 MHz) δ: 20.20, 20.98, 23.63 (-ve), 26.82, 29.02, 33.90 (-ve), 50.79, 127.84 (-ve), 127.97 (-ve), 130.83 (-ve), 139.34, 209.84. HR-MS (EI) calcd. for $C_{17}H_{22}O$: 242.1671; found: 242.1670. Anal. calcd. for $C_{17}H_{22}O$: C 84.25, H 9.15; found: C 84.45, H 9.13. This structure was confirmed by X-ray crystallographic analysis.

(9-Methyl)bicyclo[3.3.1]non-9-yl (*p*-carbomethoxy)phenyl methanol (7)

A mixture of PCC (3.71 g, 17.2 mmol) and Celite® 545 (5.00 g) was ground with a mortar and pestle until homogeneous. This solid was added to a solution of alcohol **4** (5) (1.81 g, 10.8 mmol) in anhydrous dichloromethane (120 mL) and the mixture was stirred for 2 h at room temperature. The reaction mixture was filtered through a column of Florisil® and the remaining solids well triturated with anhydr. Et_2O. Removal of solvent in vacuo gave aldehyde **5** (1.79 g, 99%) as colorless oil, which was used without further purification. To a cold (–40 °C) solution of methyl 4-iodobenzoate (2.85 g, 10.9 mmol) in THF (60 mL) was added isopropylmagnesium chloride (5.7 mL of a 2.0 mol/L solution in THF, 11.4 mmol) over 10 min. The reaction was stirred in the cold (–40 °C) for 1 h. A solution of aldehyde **5** (1.73 g, 10.4 mmol) previously obtained in THF (20 mL) was added. The reaction was stirred at –40 °C for 3 h and quenched with 5% aq. NH_4Cl (100 mL). THF was removed in vacuo and the resultant aqueous phase was extracted with Et_2O (3 × 70 mL). The combined ethereal extracts were washed with brine (2 × 100 mL), followed by drying ($MgSO_4$) and removal of the solvent in vacuo. Silica gel chromatography (14% EtOAc in petroleum ether) afforded alcohol **7** (2.82 g, 90%) as a white powder, mp 135–137 °C (EtOAc – petro-

© 2005 NRC Canada

leum ether). IR (KBr, cm^{-1}): 3516 (br), 2950, 2913, 2868, 1724, 1610, 1490, 1460, 1436, 1283, 1192, 1111, 1034, 1018, 909, 869, 812, 770, 736, 715, 573. ^1H NMR ($CDCl_3$, 300 MHz) δ: 0.79 (s, 3H), 1.90–2.40 (m, 15H), 3.88 (s, 3H), 5.43 (s, 1H), 7.42 (d, *J* = 8.4 Hz, 2H), 7.93 (d, *J* = 8.4 Hz, 2H). ^{13}C NMR ($CDCl_3$, 75 MHz) δ: 16.56 (-ve), 20.48, 20.78, 27.15, 27.62 (br), 27.76, 32.19 (-ve), 32.90 (-ve), 39.91, 52.00 (-ve), 73.82 (-ve), 127.49 (-ve), 128.68 (-ve), 147.91 (br), 167.07. HR-MS (CI) calcd. for $C_{19}H_{30}NO_3$: 320.2226 $(M + NH_4)^+$; found: 320.2222. Anal. calcd. for $C_{19}H_{26}O_3$: C 75.46, H 8.67; found: C 75.48, H 8.73.

9-(*p*-Carbomethoxybenzoyl)-9-methylbicyclo[3.3.1]nonane (1b)

A mixture of PCC (3.09 g, 14.3 mmol) and Celite® 545 (5.0 g) was ground with a mortar and pestle until homogeneous. This solid was added to a solution of alcohol **7** (2.71 g, 8.96 mmol) in anhydrous dichloromethane (100 mL) and the resulting mixture was stirred for 12 h at room temperature. The reaction mixture was filtered through a column of Florisil® and the remaining solids triturated well with anhydr. Et_2O. Removal of solvent in vacuo gave ketone **1b** (2.69 g, 100%) as a white solid, mp 137 to 138 °C (EtOAc–hexanes). ^1H NMR ($CDCl_3$, 300 MHz) δ: 1.48 (s, 3H), 1.32–1.94 (m, 10H), 2.08 (m, 2H), 2.29 (br, 2H), 3.92 (s, 3H), 7.74 (d, *J* = 8.5 Hz, 2H), 8.03 (d, *J* = 8.5 Hz, 2H). ^{13}C NMR ($CDCl_3$, 75 MHz) δ: 20.10, 20.89, 23.64 (-ve), 26.71, 29.03, 33.74 (-ve), 51.04, 52.32 (-ve), 127.69 (-ve), 129.27 (-ve), 131.89, 143.20, 166.36, 209.71. IR (KBr, cm^{-1}): 2950, 2906, 2857, 1722, 1666, 1497, 1435, 1401, 1279, 1235, 1190, 1108, 1017, 960, 934, 862, 738, 703. UV–vis (1.46×10^{-4} mol/L, MeOH, nm ($(mol/L)^{-1}$ cm^{-1})): 285 (1459), 330 (194). HR-MS (EI) calcd. for $C_{19}H_{24}O_3$: 300.1725; found: 300.1729. Anal. calcd. for $C_{19}H_{24}O_3$: C 75.97, H 8.05; found: C 75.80, H 8.00. This structure was confirmed by X-ray crystallographic analysis.

9-(*p*-Carboxybenzoyl)-9-methylbicyclo[3.3.1]nonane (1c)

To a solution of ester **1b** (2.45 g, 8.16 mmol) in THF (50 mL) was added a solution of lithium hydroxide monohydrate (3.42 g, 81.6 mmol, in 25 mL of water). The reaction was stirred at room temperature for 20 h. The reaction solution was diluted with Et_2O (200 mL) and extracted with water (3 × 100 mL). The combined aqueous extracts were acidified with concd. HCl and extracted with Et_2O (3 × 100 mL). The combined organic extracts were washed with water (100 mL) and brine (100 mL), then dried over $MgSO_4$. Removal of solvent in vacuo yielded acid **1c** (2.31 g, 99%) as a white powder, mp 224–226 °C (EtOH–H_2O). IR (KBr, cm^{-1}): 3080–2720 (br), 2950, 2906, 2863, 1695, 1680, 1568, 1505, 1431, 1401, 1316, 1295, 1214, 1126, 968, 933, 860, 807, 761, 731, 698, 543. ^1H NMR (DMSO, 300 MHz) δ: 1.20–2.16 (m, 15H), 2.22 (br, 2H), 7.82 (d, *J* = 8.2 Hz, 2H), 7.98 (d, *J* = 8.2 Hz, 2H). (No COOH signal was observed owing to proton exchange with a trace amount of water in the solvent). ^{13}C NMR (DMSO, 75 MHz) δ: 19.66, 20.41, 23.05 (-ve), 26.16, 28.47, 33.10 (-ve), 50.22, 127.71 (-ve), 129.12 (-ve), 132.78, 142.24, 166.66, 209.02. UV–vis (1.68×10^{-4} mol/L, MeOH, nm ($(mol/L)^{-1}$ cm^{-1})): 285 (2994), 335 (333). HR-MS (EI) calcd. for $C_{18}H_{22}O_3$: 286.1569; found: 286.1567. Anal. calcd. for $C_{18}H_{22}O_3$: C 75.50, H 7.74; found: C 75.23, H 7.67.

(*S*)-(–)-1-Phenylethylamine salt (1d)

Keto acid **1c** (86 mg, 0.30 mmol) and (*S*)-(–)-1-phenylethylamine (40 μL, 38 mg, 0.31 mmol) were dissolved in a hot mixture of acetonitrile and methanol. Upon cooling to room temperature, filtration gave salt **1d** as colorless needles (98 mg, 80%), mp 211–213 °C (MeOH–CH_3CN). IR (KBr, cm^{-1}): 3447, 2915, 2862, 2767, 1667, 1615, 1518, 1455, 1395, 1232, 1219, 1124, 1092, 965, 932, 844, 825, 764, 745, 695, 539. ^1H NMR (CD_3OD, 300 MHz) δ: 1.30–2.25 (m, 18H), 2.33 (br, 2H), 4.42 (q, *J* = 6.8 Hz, 1H), 7.41 (m, 5H), 7.73 (d, *J* = 8.4 Hz, 2H), 7.95 (d, *J* = 8.4 Hz, 2H). ^{13}C NMR (CD_3OD, 75 MHz) δ: 20.96 (-ve), 21.26, 22.01, 24.16 (-ve), 27.80, 30.11, 35.25 (-ve), 52.05, 52.26 (-ve), 127.60 (-ve), 128.44 (-ve), 129.89 (-ve), 130.05 (-ve), 130.26 (-ve), 140.11, 141.37, 141.99, 173.98, 212.09. HR-MS (LSI-MS) calcd. for $C_{26}H_{34}NO_3$: 408.2539 $(M + H^+)$; found: 408.2538. Anal. calcd. for $C_{26}H_{33}NO_3$: C 76.62, H 8.16, N 3.44; found: C 76.34, H 8.15, N 3.43.

(*R*)-(+)-1-Phenylethylamine salt (1e)

Keto acid **1c** (57 mg, 0.20 mmol) and (*R*)-(+)-1-phenylethylamine (27 μL, 25 mg, 0.21 mmol) were dissolved in a hot mixture of acetonitrile and methanol. Upon cooling to room temperature, filtration gave salt **1e** as colorless needles (64 mg, 79%), mp 211–213 °C (MeOH–CH_3CN). IR (KBr, cm^{-1}): 3446, 2915, 2864, 2766, 1668, 1615, 1519, 1456, 1396, 1232, 1219, 1124, 1092, 966, 933, 844, 825, 764, 744, 695, 539. ^1H NMR (CD_3OD, 300 MHz) δ: 1.30–2.25 (m, 18H), 2.33 (br, 2H), 4.42 (q, *J* = 6.8 Hz, 1H), 7.41 (m, 5H), 7.73 (d, *J* = 8.4 Hz, 2H), 7.95 (d, *J* = 8.4 Hz, 2H). ^{13}C NMR (CD_3OD, 75 MHz) δ: 20.96 (-ve), 21.26, 22.01, 24.16 (-ve), 27.80, 30.11, 35.25 (-ve), 52.05, 52.26 (-ve), 127.60 (-ve), 128.44 (-ve), 129.89 (-ve), 130.05 (-ve), 130.26 (-ve), 140.20, 141.37, 141.99, 173.98, 212.09. HR-MS (ESI) calcd. for $C_{26}H_{34}NO_3$: 408.2539 $(M + H^+)$; found: 408.2544. Anal. calcd. for $C_{26}H_{33}NO_3$: C 76.62, H 8.16, N 3.44; found: C 76.35, H 8.46, N 3.47.

(1*S*,2*R*)-(–)-*cis*-1-Amino-2-indanol salt (1f)

Salt **1f** was prepared by dissolving 57 mg (0.20 mmol) of keto acid **1c** and 31 mg (0.21 mmol) of (1*S*,2*R*)-(–)-*cis*-1-amino-2-indanol in a hot mixture of acetonitrile and methanol. Upon cooling to room temperature, filtration gave salt **1f** as an off-white powder (71 mg, 81%), mp 190 °C (dec) (MeOH–CH_3CN). IR (KBr, cm^{-1}): 3235, 2913, 2862, 2625, 1670, 1619, 1580, 1535, 1452, 1397, 1267, 1216, 1093, 966, 932, 844, 823, 803, 741, 567. ^1H NMR (CD_3OD, 300 MHz) δ: 1.28–2.00 (m, 13H), 2.18 (m, 2H), 2.33 (br, 2H), 3.01 (dd, *J* = 5.9, 16.3 Hz, 1H), 3.22 (dd, *J* = 6.4, 16.3 Hz, 1H), 4.54 (d, *J* = 5.9 Hz, 1H), 4.70 (dd, *J* = 5.9, 11.3 Hz, 1H), 7.31 (m, 3H), 7.46 (d, *J* = 7.3 Hz, 2H), 7.73 (d, *J* = 8.4 Hz, 2H), 7.96 (d, *J* = 8.4 Hz, 2H). ^{13}C NMR (CD_3OD, 75 MHz) δ: 21.24, 22.00, 24.15 (-ve), 27.80, 30.10, 35.24 (-ve), 40.09, 52.05, 58.71 (-ve), 72.08 (-ve), 126.14 (-ve), 126.64 (-ve), 128.40 (-ve), 129.44 (-ve), 129.89 (-ve), 130.77 (-ve), 138.47, 141.28, 141.99, 142.77, 174.11, 212.11. HR-MS (ESI) calcd. for $C_{27}H_{34}NO_4$: 436.2488 $(M + H^+)$; found: 436.2486. Anal.

© 2005 NRC Canada

calcd. for $C_{27}H_{33}NO_4$: C 74.45, H 7.64, N 3.22; found: C 74.38, H 7.68, N 3.23.

(*R*)-(–)-2-Amino-1-butanol salt (1g)

Salt **1g** was prepared by dissolving 57 mg (0.20 mmol) of keto acid **1c** and 19 mg (0.21 mmol) of (*R*)-(–)-2-amino-1-butanol in hot methanol. Upon cooling to room temperature, filtration gave salt **1g** as an off-white powder (53 mg, 71%), mp 159–162 °C (MeOH). IR (KBr, cm^{-1}): 3367, 2960, 2910, 2871, 1681, 1667, 1595, 1524, 1463, 1387, 1263, 1232, 1217, 1124, 1083, 964, 931, 869, 803, 747, 570. ^{1}H NMR (CD_3OD, 300 MHz) δ: 1.01 (t, *J* = 7.6 Hz, 3H), 1.25–2.00 (m, 15H), 2.18 (m, 2H), 2.33 (br, 2H), 3.08 (m, 1H), 3.54 (dd, *J* = 6.7, 11.7 Hz, 1H), 3.75 (dd, *J* = 3.7, 11.7 Hz, 1H), 7.73 (d, *J* = 8.5 Hz, 2H), 7.96 (d, *J* = 8.5 Hz, 2H). ^{13}C NMR (CD_3OD, 75 MHz) δ: 10.16 (-ve), 21.25, 22.00, 23.67, 24.16 (-ve), 27.81, 30.11, 35.25 (-ve), 52.05, 55.98 (-ve), 61.99, 128.44 (-ve), 129.88 (-ve), 141.43, 141.96, 174.17, 212.11. HR-MS (ESI) calcd. for $C_{22}H_{34}NO_4$: 376.2488 (M + H^+); found 376.2488. Anal. calcd. for $C_{22}H_{33}NO_4$: C 70.37, H 8.86, N 3.73; found: C 70.28, H 8.90, N 3.76.

L-Prolinamide salt (1h)

Salt **1h** was prepared by dissolving keto acid **1c** (57 mg, 0.20 mmol) and L-prolinamide (24 mg, 0.21 mmol) in a hot mixture of acetonitrile and methanol. Upon cooling to room temperature, filtration gave salt **1h** (72 mg, 90%) as a white powder, mp 210–211.5 °C (MeOH–CH_3CN). IR (KBr, cm^{-1}): 3365, 3232, 2935, 2909, 2871, 1715, 1680, 1631, 1591, 1544, 1383, 1217, 1015, 963, 931, 827, 804, 744, 668, 641, 567. ^{1}H NMR (CD_3OD, 300 MHz) δ: 1.20–2.00 (m, 16H), 2.17 (m, 2H), 2.33 (br, 2H), 2.39, (m, 1H), 3.31 (m, 2H), 4.19 (dd, *J* = 6.4, 8.4 Hz, 1H), 7.73 (d, *J* = 8.4 Hz, 2H), 7.97 (d, *J* = 8.4 Hz, 2H). ^{13}C NMR (CD_3OD, 75 MHz) δ: 21.23, 21.99, 24.15 (-ve), 25.38, 27.79, 30.10, 31.25, 35.24 (-ve), 47.34, 52.07, 60.99 (-ve), 128.48 (-ve), 129.93 (-ve), 140.68, 142.21, 173.01, 173.71, 212.07. HR-MS (ESI) calcd. for $C_{23}H_{33}N_2O_4$: 401.2440 (M + H^+); found: 401.2451. Anal. calcd. for $C_{23}H_{32}N_2O_4$: C 68.97, H 8.05, N, 6.99; found: C 69.10, H 8.09, N 6.98.

(*R*)-(–)-1-Cyclohexylethylamine salt (1i)

Salt **1i** was prepared by dissolving keto acid **1c** (57 mg, 0.20 mmol) and (*R*)-(–)-1-cyclohexylethylamine (31 μL, 27 mg, 0.21 mmol) in hot methanol. Upon cooling to room temperature, filtration gave salt **1i** as a white powder (71 mg, 86%), mp 192–195 °C (MeOH). IR (KBr, cm^{-1}): 3443, 2929, 2862, 2603, 2551, 2361, 2342, 2203, 1666, 1635, 1578, 1537, 1450, 1382, 1263, 1232, 1216, 1126, 964, 932, 868, 821, 804, 745, 568. ^{1}H NMR (CD_3OD, 300 MHz) δ: 0.98–2.00 (m, 27H), 2.18 (m, 2H), 2.33 (br, 2H), 3.06 (m, 1H), 7.73 (d, *J* = 8.4 Hz, 2H), 7.96 (d, *J* = 8.4 Hz, 2H). ^{13}C NMR (CD_3OD, 75 MHz) δ: 16.07 (-ve), 21.24, 22.00, 24.15 (-ve), 26.92, 27.00, 27.08, 27.81, 28.82, 30.01, 30.11, 35.26 (-ve), 42.75 (-ve), 52.05, 53.39 (-ve), 128.42 (-ve), 129.85 (-ve), 141.61, 141.90, 174.20, 212.09. HR-MS (ESI) calcd. for $C_{26}H_{40}NO_3$: 414.3008 (M + H^+); found: 414.3009. Anal. calcd. for $C_{26}H_{39}NO_3$: C 75.50, H 9.50, N 3.39; found: C 75.31, H 9.55, N 3.46.

(1*R*,2*R*)-(–)-2-Amino-1-phenyl-1,3-propanediol salt (1j)

Salt **1j** was prepared by dissolving keto acid **1c** (57 mg, 0.20 mmol) and (1*R*,2*R*)-(–)-2-amino-1-phenyl-1,3-propanediol (35 mg, 0.21 mmol) in a hot mixture of acetonitrile and methanol. Upon cooling to room temperature, filtration gave salt **1j** as a white powder (76 mg, 84%), mp 142 to 143 °C (MeOH–CH_3CN). IR (KBr, cm^{-1}): 3367, 2914, 2864, 1668, 1582, 1542, 1493, 1453, 1386, 1229, 1124, 1039, 968, 960, 932, 868, 840, 803, 746, 700, 572, 540. ^{1}H NMR (CD_3OD, 300 MHz) δ: 1.25–1.73 (m, 8H), 1.51 (s, 3H), 1.89 (m, 2H), 2.17 (m, 2H), 2.33 (br, 2H), 3.26 (m, 1H), 3.47 (m, 2H), 4.73 (d, *J* = 8.6 Hz, 1H), 7.37 (m, 5H), 7.72 (d, *J* = 8.6 Hz, 2H), 7.96 (d, *J* = 8.6 Hz, 2H). ^{13}C NMR (CD_3OD, 75 MHz) δ: 21.23, 21.98, 24.15 (-ve), 27.81, 30.10, 35.26 (-ve), 52.06, 60.23, 60.29 (-ve), 72.54 (-ve), 127.86 (-ve), 128.42 (-ve), 129.51 (-ve), 129.74 (-ve), 129.89 (-ve), 141.38, 141.97, 142.23, 174.13, 212.15. HR-MS (ESI) calcd. for $C_{27}H_{36}NO_5$: 454.2593 (M + H^+); found: 454.2599. Anal. calcd. for $C_{27}H_{35}NO_5$: C 71.50, H 7.78, N 3.09; found: C 71.34, H 8.05, N 3.41.

Photochemistry

Both solution- and solid-state photolyses were carried out by using a 450 W Hanovia medium-pressure mercury lamp in a water-cooled immersion well. Light from the lamp was filtered through a Pyrex (λ ≥ 290 nm) immersion well. For preparative scale solution-state photolyses, samples were dissolved in HPLC grade or spectral grade solvents and were purged with nitrogen for at least 15 min prior to irradiation. The reactions were performed either in sealed reaction vessels or under a positive pressure of nitrogen. Yields and conversions were calculated based on the mass of the isolated products. For analytical solid-state photolyses, the procedure consisted of crushing ca. 5 mg of the salt to be photolyzed between two Pyrex microscope slides, taping the plates together, sealing the resulting sandwiches in polyethylene bags under a positive nitrogen atmosphere, and irradiating the ensembles with the output from a water-cooled 450 W medium-pressure mercury lamp. Photolyses were generally carried out at room temperature. For some runs that required low temperature during photolysis, a Cryocool CC-100 II immersion cooling system (Neslab Instrument Inc.) was used with ethanol as the coolant. The salts were irradiated for varying lengths of time to determine the dependence of the ee values on the extent of conversion. To achieve high conversions it was usually necessary to rotate the sample 180° midway through the irradiation, exposing the rear side of the slide to the light and allowing as much of the sample as possible to react. For neutral molecules, the sample was directly analyzed by GC. The reaction mixtures containing chiral organic salts were first derivatized to their corresponding methyl esters by treatment with excess ethereal diazomethane solution and then washed with water and subjected to short-path silica gel chromatography to remove the chiral auxiliary. The mixtures were then analyzed by GC for conversion as well as product composition. Yields and conversions of the solid-state reactions were determined based on the average integration of at least two GC analyses. The overall precision of the reported GC results is estimated to be ±1%.

© 2005 NRC Canada

Preparative photolysis of ketone 1a

A solution of ketone **1a** (485 mg, 2.00 mmol) in acetonitrile (40 mL) was purged with nitrogen for 30 min and irradiated for 7 h. Removal of the solvent in vacuo followed by silica gel chromatography (6% EtOAc in petroleum ether) afforded starting material **1a** (17 mg, 4%), cyclobutanol **9a** (442 mg, 91%), and alkene **10a** (19 mg, 4%).

Data for cyclobutanol 9a

Colorless oil. IR (KBr, cm^{-1}): 3441, 3027, 2923, 2874, 1479, 1452, 996, 882, 775, 702. ^{1}H NMR (C_6D_6, 400 MHz) δ: 0.89 (m, 1H), 1.14 (m, 1H), 1.23–1.27 (m, 1H), 1.28 (s, 3H), 1.33–1.39 (m, 2H), 1.52–1.77 (m, 5H), 1.82–1.97 (m, 2H), 2.60 (m, 1H), 2.71 (m, 1H), 7.07–7.18 (m, 5H). ^{13}C NMR ($CDCl_3$, 75 MHz) δ: 17.77 (-ve), 18.29, 20.23, 22.55, 24.53, 27.56, 36.11 (-ve), 37.62 (-ve), 46.26, 46.37 (-ve), 82.64, 125.29 (-ve), 127.17 (-ve), 128.65 (-ve), 144.04. HR-MS (EI) calcd. for $C_{17}H_{22}O$: 242.1671; found: 242.1672. Anal. calcd. for $C_{17}H_{22}O$: C 84.25, H 9.15; found: C 84.00, H 9.13.

Data for alkene 10a

Melting point: 55–56.5 °C (EtOAc – petroleum ether). IR (KBr, cm^{-1}): 3431, 3057, 3015, 2940, 2918, 2864, 1492, 1472, 1453, 1015, 899, 763, 712, 608. ^{1}H NMR (CD_2Cl_2, 300 MHz) δ: 0.90 (s, 3H), 1.18–1.43 (m, 4H), 1.52–2.04 (m, 5H), 2.48 (m, 1H), 2.70 (m, 1H), 4.97 (br, 1H), 5.73 (m, 1H), 6.00 (m, 1H), 7.20–7.40 (m, 5H). ^{13}C NMR (CD_2Cl_2, 75 MHz) δ: 15.77 (-ve), 16.57, 24.75, 29.52, 32.32, 33.22 (-ve), 35.48 (-ve), 40.04, 75.92 (-ve), 127.23 (-ve), 127.77 (-ve), 128.12 (-ve), 128.97 (-ve), 129.16 (-ve), 143.07. HR-MS (EI) calcd. for $C_{17}H_{22}O$: 242.1671 (M^+); found: 242.1672. Anal. calcd. for $C_{17}H_{22}O$: C 84.25, H 9.15; found: C 84.05, H 9.15. This structure was confirmed by X-ray crystallographic analysis.

Preparative photolysis of ketone 1b

A solution of ketone **1b** (501 mg, 1.67 mmol) in acetonitrile (50 mL) was purged with nitrogen for 30 min and irradiated for 6 h. Removal of the solvent in vacuo followed by silica gel chromatography (11% EtOAc in petroleum ether) afforded cyclobutanol **9b** (446 mg, 89%) and alkene **10b** (27 mg, 5%).

Data for cyclobutanol 9b

Melting point: 149 to 150 °C (EtOAc – petroleum ether). IR (KBr, cm^{-1}): 3482, 2958, 2927, 2879, 1723, 1609, 1439, 1279, 1106, 1007, 861, 781, 712. ^{1}H NMR (C_6D_6, 400 MHz) δ: 0.85 (m, 1H), 0.98 (m, 1H), 1.20 (s, 3H), 1.21–1.35 (m, 3H), 1.45–1.65 (m, 5H), 1.83 (m, 2H), 2.52 (m, 1H), 2.66 (m, 1H), 3.53 (s, 3H), 7.09 (d, J = 8.2 Hz, 2H), 8.11 (d, J = 8.2 Hz, 2H). ^{13}C NMR (C_6D_6, 100 MHz) δ: 17.70 (-ve), 18.61, 20.46, 22.87, 24.61, 27.73, 36.19 (-ve), 37.62 (-ve), 46.42, 46.79 (-ve), 51.61 (-ve), 81.87, 125.73 (-ve), 129.45, 130.32 (-ve), 149.34, 166.64. HR-MS (EI) calcd. for $C_{19}H_{24}O_3$: 300.1725; found: 300.1726. Anal. calcd. for $C_{19}H_{24}O_3$: C 75.97, H 8.05; found: C 75.96, H 8.28. This structure was confirmed by X-ray crystallographic analysis.

Data for alkene 10b

Melting point: 148–150 °C ($CHCl_3$–hexanes). IR (KBr, cm^{-1}): 3524, 3017, 2950, 2921, 2862, 1723, 1706, 1610, 1436, 1281, 1111, 1016, 860, 772, 724, 705, 612. ^{1}H NMR (C_6D_6, 400 MHz) δ: 0.85 (s, 3H), 1.03–1.12 (m, 2H), 1.20–1.30 (m, 3H), 1.48–1.80 (m, 4H), 2.35 (br, 1H), 2.53 (br, 1H), 3.53 (s, 3H), 4.30 (s, 1H), 5.62 (m, 1H), 5.83 (m, 1H), 7.29 (d, J = 8.3 Hz, 2H), 8.13 (d, J = 8.3 Hz, 2H). ^{13}C NMR (C_6D_6, 75 MHz) δ: 15.71 (-ve), 16.52, 24.57, 29.36, 32.11, 32.90 (-ve), 36.16 (-ve), 40.09, 51.57 (-ve), 75.22 (-ve), 128.05 (-ve), 128.55 (-ve), 129.04 (-ve), 129.19 (-ve), 129.35, 148.50, 166.82. HR-MS (CI) calcd. for $C_{19}H_{28}NO_3$: 318.2069 ($M + NH_4^+$); found: 318.2069. Anal. calcd. for $C_{19}H_{24}O_3$: C 75.97, H 8.05; found: C 75.89, H 8.36. This structure was confirmed by X-ray crystallographic analysis.

X-ray crystal structure analyses

Crystal data for compounds **1a**, **1b**, **9b**, **10a**, and **10b** were collected using a Rigaku/AFC7 four-circle diffractometer equipped with an ADSC Quantum CCD detector. The X-ray source was graphite-monochromated Mo Kα radiation (λ = 0.710 73 Å). Structures were solved by means of direct methods (SHELXS-97 (20) for **1a**, SIR92 (21) for **1b**, **9b**, **10a**, and **10b**), and all refinements were carried out by full-matrix least-squres procedures (SHELXL-97) (22) using anisotropic displacement parameters for all non-hydrogen atoms. Hydrogen atoms were introduced in calculated positions and only one overall isotropic displacement parameter was refined. The CCDC reference numbers are CCDC 255968–255972 for compounds **1a**, **1b**, **9b**, **10a**, and **10b**, respectively, and 260038 for the mixed crystal resulting from partial solid-state photolysis of ketone **1b**.[5]

Crystal structure determination of ketone 1a

Single crystals of **1a** were recrystallized from EtOAc – petroleum ether, mounted in inert oil, and transferred to the cold nitrogen stream of the diffractometer. Crystal data: $C_{17}H_{22}O$, MW = 242.35, triclinic, a = 6.938 Å, b = 10.104 Å, c = 10.197 Å, α = 101.473°, β = 98.041°, γ = 104.520°, V = 664.48 Å^3, T = 173 K, space group P, Z = 2, μ(Mo Kα) = 0.073 mm^{-1}, reflections measured = 4092, unique = 2552, $R1$ = 0.0402, $wR2$ = 0.1053, GoF = 1.046.

Crystal structure determination of ketone 1b and its single crystal-to-single crystal reaction

Single crystals of **1b** were recrystallized from EtOAc–hexanes, mounted in inert oil and transferred to the cold nitrogen stream of the diffractometer. Crystal data: $C_{19}H_{24}O_3$, MW = 300.38, monoclinic, a = 6.5508(3) Å, b = 11.0233(6) Å, c = 21.4693(13) Å, β = 92.627(2)°, V =

[5] Supplementary data for this article are available on the Web site or may be purchased from the Depository of Unpublished Data, Document Delivery, CISTI, National Research Council Canada, Ottawa, ON K1A 0S2, Canada. DUD 4027. For more information on obtaining material refer to http://cisti-icist.nrc-cnrc.gc.ca/irm/unpub_e.shtml. CCDC 255968–255972 and 260038 contain the crystallographic data for this manuscript. These data can be obtained, free of charge, via www.ccdc.cam.ac.uk/conts/retrieving.html (or from the Cambridge Crystallographic Data Centre, 12 Union Road, Cambridge CB2 1EZ, UK; fax +44 1223 336033; or deposit@ccdc.cam.ac.uk).

© 2005 NRC Canada

1548.70(14) Å^3, T = 173 K, space group $P2_1/c$, Z = 4, μ(Mo Kα) = 0.085 mm^{-1}, reflections measured = 13 627, unique = 3307, $R1$ = 0.0411, $wR2$ = 0.1059, GoF = 1.046. Same crystal photolyzed to 25% conversion: $C_{19}H_{24}O_3$, MW = 300.38, monoclinic, a = 6.5305(2) Å, b = 11.2200(4) Å, c = 21.4348(7) Å, β = 91.892(1)°, V = 1569.72(1) Å^3, T = 173 K, space group $P2_1/c$, Z = 4, μ(Mo Kα) = 0.085 mm^{-1}, reflections measured = 24 848, unique = 2768, $R1$ = 0.0424, $wR2$ = 0.1125, GoF = 1.058.

Crystal structure determination of ketone 9b

Single crystals of **9b** were recrystallized from EtOAc – petroleum ether, mounted in inert oil, and transferred to the cold nitrogen stream of the diffractometer. Crystal data: $C_{19}H_{24}O_3$, MW = 300.38, triclinic, a = 6.2815(4) Å, b = 7.2477(6) Å, c = 18.7120(17) Å, α = 79.329(9)°, β = 82.478(10)°, γ = 69.225(8)°, V = 780.75(11) Å^3, T = 173 K, space group P, Z = 2, μ(Mo Kα) = 0.085 mm^{-1}, reflections measured = 3144, unique = 3144, $R1$ = 0.0367, $wR2$ = 0.1027, GoF = 1.086.

Crystal structure determination of ketone 10a

Single crystals of **10a** were recrystallized from EtOAc – petroleum ether, mounted in inert oil, and transferred to the cold nitrogen stream of the diffractometer. Crystal data: $C_{17}H_{22}O$, MW = 242.35, monoclinic, a = 10.4796(10) Å, b = 19.2773(18) Å, c = 13.6457(13) Å, β = 93.507(3)°, V = 2751.5(5) Å^3, T = 173 K, space group $P2_1/c$, Z = 8, μ(Mo Kα) = 0.070 mm^{-1}, reflections measured = 23 886, unique = 5933, $R1$ = 0.0618, $wR2$ = 0.1553, GoF = 1.128.

Crystal structure determination of ketone 10b

Single crystals of **10b** were recrystallized from $CHCl_3$–hexanes, mounted in inert oil, and transferred to the cold nitrogen stream of the diffractometer. Crystal data: $C_{19}H_{24}O_3$, MW = 300.38, monoclinic, a = 15.1864(11) Å, b = 6.8150(5) Å, c = 14.9981(10) Å, β = 90.383(4)°, V = 1552.20(19) Å^3, T = 173 K, space group $P2_1/n$, Z = 4, μ(Mo-K_α) = 0.085 mm^{-1}, reflections measured = 3331, unique = 3331, $R1$ = 0.0378, $wR2$ = 0.0949, GoF = 0.928.

Acknowledgements

Financial support from the Natural Sciences and Engineering Research Council of Canada (NSERC) is gratefully acknowledged.

References

1. For general reviews of the Norrish–Yang type II reaction, see: (*a*) P.J. Wagner and B.S. Park. *In* Organic photochemistry. Vol. 11. *Edited by* A. Padwa. Marcel Dekker, New York. 1991. Chap. 4; (*b*) A.G. Griesbeck, S. Buhr, M. Fiege, H. Schmickler, and J. Lex. J. Org. Chem. **63**, 3847 (1998). Cyclobutanol products in Norrish type II photochemistry were first reported by: N.C. Yang and D.H. Yang. J. Am. Chem. Soc. **80**, 2913 (1958).
2. M. Leibovitch, G. Olovsson, J.R. Scheffer, and J. Trotter. J. Am. Chem. Soc. **120**, 12755 (1998).
3. B.O. Patrick, J.R. Scheffer, and C. Scott. Angew. Chem. Int. Ed. **42**, 3775 (2003).
4. For general reviews of the solid-state ionic chiral auxiliary method of asymmetric synthesis, see: (*a*) J.N. Gamlin, R. Jones, M. Leibovitch, B.O. Patrick, J.R. Scheffer, and J. Trotter. Acc. Chem. Res. **29**, 203 (1996); (*b*) J.R. Scheffer. Can. J. Chem. **79**, 349 (2001).
5. D. Braga, S. Chen, H. Filson, L. Maini, M.R. Netherton, B.O. Patrick, J.R. Scheffer, C. Scott, and W. Xia. J. Am. Chem. Soc. **126**, 3511 (2004).
6. P.J. Wagner and G. Laidig. Tetrahedron Lett. **32**, 895 (1991).
7. The preference for abstraction of H_x over H_y in the case of ketones **1a** and **1b** is in accord with previous work from our laboratory on the geometric requirements for Norrish–Yang type II hydrogen abstraction. See: H. Ihmels and J.R. Scheffer. Tetrahedron **55**, 885 (1999).
8. E. Cheung, M.R. Netherton, J.R. Scheffer, and J. Trotter. Org. Lett. **2**, 77 (2000).
9. P.J. Wagner, P.A. Kelso, and A.E. Kempainen. J. Am. Chem. Soc. **90**, 5896 (1968).
10. J.K. Burdett. Molecular shapes. Wiley-Interscience, New York. 1980. p. 6.
11. A. Bondi. J. Phys. Chem. **68**, 441 (1964).
12. (*a*) F.D. Lewis and T.A. Hilliard. J. Am. Chem. Soc. **92**, 6672 (1970); (*b*) F.D. Lewis and R.A. Ruden. Tetrahedron Lett. 715 (1971); (*c*) P.J. Wagner, P.A. Kelso, A.E. Kemppainen, J.M. McGrath, H.N. Schott, and R.G. Zepp. J. Am. Chem. Soc. **94**, 7506 (1972).
13. The distance between the flagpole hydrogen atom on C5 and the radical center on C1 in boat–chair biradical **14** is estimated to be 2.3 Å, as the calculated flagpole hydrogen to hydrogen distance in the boat conformation of cyclohexane is 2.36 Å. See: F. Freeman, A. Phornvoranunt, and W.J. Hehre. J. Phys. Org. Chem. **12**, 176 (1999).
14. (*a*) M.C. Etter and D.A. Adsmond. J. Chem. Soc. Chem. Commun. 589 (1990); (*b*) S.L. Johnson and K.A. Rumon. J. Phys. Chem. **69**, 74 (1965).
15. For exceptions to this rule, see: R.-F. Liao, J.W. Lauher, and F.W. Fowler. Tetrahedron, **52**, 3153 (1996).
16. D. Dolphin and A. Wick. Tabulation of infrared spectral data. Wiley, New York. 1977. p. 295.
17. For a similar situation in which the enantioselectivity of a Norrish–Yang photoreaction in the crystalline state is governed by preferential abstraction of the geometrically favored γ-hydrogen atom, see ref. 2 as well as: S. Chen, B.O. Patrick, and J.R. Scheffer. J. Org. Chem. **69**, 2711 (2004).
18. E. Cheung, T. Kang, M.R. Netherton, J.R. Scheffer, and J. Trotter. J. Am. Chem. Soc. **122**, 11 753 (2000).
19. For a discussion of photochemical solid-to-solid reactions (including single crystal-to-single crystal transformations), see: A.E. Keating and M.A. Garcia-Garibay *In* Molecular and supramolecular photochemistry. Vol. 2. *Edited by* V. Ramamurthy and K.S. Schanze. Marcel Dekker, New York. 1998. Chap. 5.
20. (*a*) G.M. Sheldrick. SHELXS-97: A program for automatic solution of crystal structures [computer program]. University of Göttingen, Göttingen, Germany. 1997. Release 97-2; (*b*) G.M. Sheldrick. Acta Crystallogr. Sect. D, **D49**, 18 (1993).
21. A. Altomare, G. Cascarano, C. Giacovazzo, and A. Gualardi. J. Appl. Crystallogr. **26**, 343 (1993).
22. G.M. Sheldrick. SHELXL-97: A program for crystal structure refinement [computer program]. University of Goettingen, Germany. 1997. Release 97-2.

© 2005 NRC Canada

Regioselective S—O vs. C—O bond cleavage in sulfenate ester radical anions[1]

Donald L.B. Stringle and Mark S. Workentin

Abstract: The electron transfer (ET) reduction of benzyl benzenesulfenate ester (**1**) and *tert*-butyl benzenesulfenate ester (**2**) was investigated using electrochemical techniques. Analysis of the cyclic voltammetry of each compound suggests that the ET reduction proceeds via a stepwise dissociative mechanism. The voltammograms of **1** are similar to those of diaryl disulfides and it was found through controlled potential electrolysis (CPE) product studies that ET reduction leads to S—O bond cleavage. The voltammograms of **2** are dramatically different with a sharper dissociative wave occurring at a more negative peak potential. CPE experiments indicate products that result from ET leading to C—O bond cleavage in this case. DFT calculations of the singly occupied molecular orbitals (SOMOs) of **1** and **2** were performed and offer a rationale for the different reactivity of the two radical anions.

Key words: sulfenate esters, dissociative electron transfer, electrochemistry, radical anions.

Résumé : On a étudié la réaction de réduction par transfert d'électron (TE) du benzènesulfénate de benzyle (**1**) et du benzènesulfénate de *tert*-butyle (**2**) en faisant appel à des techniques électrochimiques. L'analyse de la voltampérométrie cyclique de chaque composé suggère que la réduction par TE se produit par un mécanisme par dissociations successives. Le voltampérogramme du composé **1** est semblable à celui des disulfures de diaryles et, sur la base d'études des produits par électrolyse à potentiel contrôlé (EPC), on a trouvé que la réduction par TE conduit à une coupure de la liaison S—O. Le voltampérogramme du composé **2** est dramatiquement différent et il présente une vague dissociative qui se présente à un pic de potentiel beaucoup plus négatif. Les études d'EPC indiquent que, dans ce cas, les produits qui résultent d'un TE proviennent d'une coupure d'une liaison C—O. Des calculs effectués sur la base de la théorie de la densité fonctionnelle des orbitales moléculaires à occupation singulet (SOMO) des composés **1** et **2** et ils permettent de présenter une rationalisation pour les réactivités différentes des deux radicaux anions.

Mots clés : esters de l'acide sulfénique, transfert d'électron avec dissociation, électrochimie, radicaux anions.

[Traduit par la Rédaction]

Introduction

A major focus of our group has been the study of dissociative electron transfer (ET) reactions through electrochemical methods. The work provides an opportunity to investigate many aspects of ET reactions, but also allows for investigation into the reactivity of the intermediate species formed upon ET. Studies of 9,10-diphenylanthracene endoperoxide found that upon ET reduction, O—O bond cleavage occurred generating an alkoxyl radical (1, 2). It was observed that an O-neophyl type rearrangement at the alkoxyl radical could occur in competition with its ET reduction. Similarly, the dissociative ET reduction of 3,3,6,6-tetraaryl-1,2-dioxanes involved formation of a distonic radical anion (where the radical and anionic centres are spatially and electronically distinct), which could be reduced or could fragment (3). The fragmentation pathway led to a homogeneous ET-fragmentation radical anion chain reaction that was responsible for a potential dependence on the product ratios of controlled potential electrolysis (CPE) experiments. Both cases demonstrate the unique reactivity that can be observed upon generation of radical anion species by electrochemical means, and how the reactivity can be controlled by adjusting the potential at which they are formed. In this sense, the electrochemical generation of radical anions makes for ideal circumstances to investigate their reactivity.

The study of sulfenate esters developed as an extension to our work on the ET reduction of peroxides (4–7) and endoperoxides (1–3, 8–10) and the work of others concerning the ET reduction of diaryl disulfides (11–14). The ET reduction of the O—O bonds in peroxides and endoperoxides and the S—S bonds in diaryl disulfides are characterized by unusually large values for the intrinsic barrier for the ET ($\Delta G_0^{\ddagger}$). For the ET reduction of peroxides and endoperoxides the ET is shown to cleave the O—O bond via a concerted dissociative mechanism where electron uptake and bond cleavage are simultaneous. In this case, the large intrinsic barrier is a result of a contribution from the bond dissociation energy of the fragmenting bond. In contrast, the reduction of diaryl disulfides was shown to follow a stepwise dissociative mechanism, with the formation of a radical anion intermediate that leads to fragmentation of the S—S bond in a second

Received 27 April 2005. Published on the NRC Research Press Web site at http://canjchem.nrc.ca on 10 November 2005.

D.L.B. Stringle and M.S. Workentin.[2] Department of Chemistry, The University of Western Ontario, London, ON N6A 5B7, Canada.

[1]This article is part of a Special Issue dedicatted to organic reaction mechanisms.

[2]Corresponding author (e-mail: mworkent@uwo.ca).

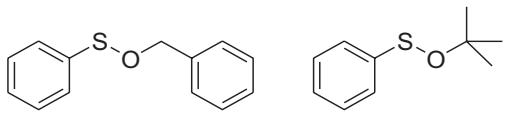
 doi: 10.1139/V05-164 © 2005 NRC Canada

Table 1. Data obtained from the CVs of **1** and **2** (1.0–3.0 mmol/L) in 0.1 mol/L TBAP–DMF solution.

Parameters	Scan rates (V/s)	**1**	**1** + acid/MeOTs[a]	**2**	**2** + acid[b]
E_p (V vs. SCE)	0.1	–1.68	–1.67	–2.28	–2.29
	1.0	–1.76	–1.75	–2.36	–2.35
	10.0	–1.89	–1.89	–2.48	–2.43
$\Delta = (E_{p/2} - E_p)$ (mV)	0.1	117	96	83	86
	1.0	124	91	95	96
	10.0	156	127	129	110
$I_p/v^{1/2}$ (mA $s^{1/2}$ $V^{-1/2}$)[c]		107	164	144	170
$\alpha = 1.85\frac{RT}{F}\Delta$	0.1	0.41	0.50	0.58	0.60
	1.0	0.38	0.52	0.50	0.55
		0.31	0.37	0.37	0.49
$\alpha_{app} = \frac{RT}{nF}\left(\frac{\partial \ln v}{\partial E_p}\right)$		0.35	0.38	0.28	0.41
$\partial E_p/\partial$ log ν (mV)		–83	–78	–103	–72
$n = Q/mF$ (F/mol)[d]		1.1	1.9	1.1	2.0

[a]Average of multiple experiments where either acetanilide or TFE was used in at least two times excess in combination with at least 1 equiv. of MeOTs.
[b]CVs preformed in the presence of at least a two times excess of acetanilide.
[c]Corrected for a 2 mmol/L solution.
[d]Equation determines the stoichiometry of an electroysis based on the charge introduced into the cell (Q), the mol of analyte (m), and Faraday constant.

Scheme 1.



1 **2**

step. For the disulfides, the large intrinsic barrier was shown to be the result of contributions due to a significant S—S bond stretching upon ET forming a loosely bound radical anion intermediate. To further examine the factors that govern the stepwise vs. concerted mechanism in these types of bonded systems, we initiated this study of the ET to sulfenate esters, which contain a single S—O bond.

Although isoelectronic with peroxides (O—O) and disulfides (S—S), the S—O bonded sulfenate esters might reasonably be expected to show some differences in reactivity because the relative size and electronegativity of the two atoms in the bond are different. Because the chemistry of a compound initiated by ET and photochemical excitation often follow similar pathways, then it is constructive to note that in the many investigations of the photochemistry of sulfenate esters it is uniformly demonstrated that S—O bond cleavage occurs upon excitation (15, 16), similar to both peroxides and disulfides that undergo photolytic O—O and S—S cleavage, respectively. This offers reason to suspect that upon ET reduction these compounds would then undergo S—O cleavage as well. However, a computational study by Gregory and Jenks (17) suggests that compared to R-O-O-R′ peroxides, sulfenic esters (R-S-O-R′) can have much weaker R′—O bonds than the stronger central S—O or the corresponding R—S bonds. This suggests that sulfenic esters may indeed exhibit different reactivity compared to peroxides and disulfides. In this study the ET reduction of benzyl benzenesulfenate ester (**1**) and *tert*-butyl benzenesulfenate ester (**2**), shown in Scheme 1, was examined. These substrates vary only in the ester functionality, which is ideal for probing the impact of this group on the reactivity. Both substrates are derivatives of benzenesulfenic acid, which provides a convenient handle for comparison to diaryl disulfides. The work reported here details the analysis of the cyclic voltammetry (CV) and the CPE for each compound to determine the mechanism of the initial ET and investigate the reactivity of any radical anion species formed through ET reduction.

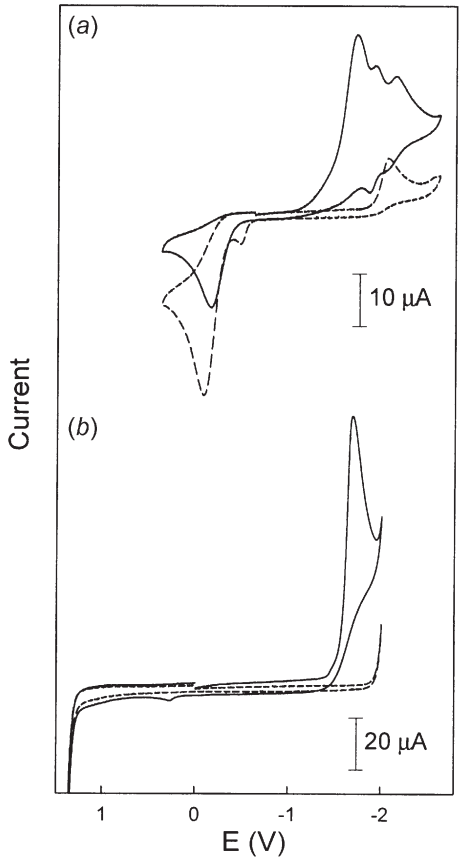
Results and discussion

ET reduction of benzyl benzenesulfenate ester (1)

The cyclic voltammetry of **1** was performed in dimethylformamide (DMF) with 0.1 mol/L tetrabutylammonium perchlorate (TBAP) as supporting electrolyte. The pertinent CV data for both **1** and **2** are listed in Table 1. A representative CV of **1** in the absence of acid is shown in Fig. 1*a*. When scanning cathodically, a broad wave with low peak current is observed at –1.68 V vs. SCE at 0.1 V/s, which is assigned as the dissociative wave of **1**. This wave is irreversible at all scan rates investigated (0.1–50.0 V/s). The peak current corrected for scan rate and concentration is 107 μA for a 2 mmol/L solution. The peak current provides an indication of the number of electrons involved in the reduction step. The E_p shifts negatively with increasing scan rate by 83 mV/decade. The peak breadth also increases, from values of 117 to 124 mV at 0.1 and 1.0 V/s, respectively, which leads to the corresponding decrease in the transfer coefficient (α), with values of 0.41 and 0.38 at the same scan

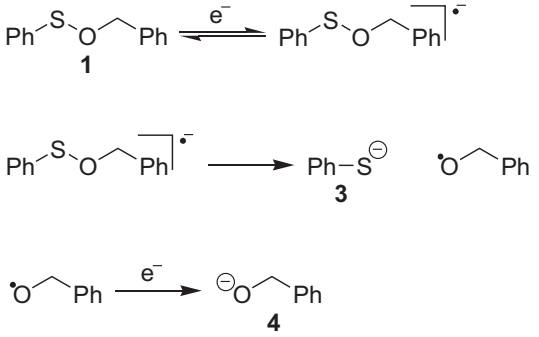
© 2005 NRC Canada

Fig. 1. Representative CVs of **1** in 0.1 mol/L TBAP–DMF at 0.1 V/s: (*a*) **1** (2.3 mmol/L) before (solid line) and after (dashed line) introduction of 6.1 C of charge into the cell; (*b*) **1** (2.2 mmol/L) in the presence of acetanilide (40 mmol/L) and MeOTs (40 mmol/L) before (solid line) and after (dashed line) introduction of 10.3 C of charge into the cell.



rates. A shoulder is present on the tail of this wave and following this is another small wave that appears to be quasi-reversible. Both of the latter two features are present due to the reduction of products formed from parent–child reactions, where **1** (the parent) reacts with a basic or nucleophilic anionic species (the child) generated from the ET reduction of **1**. Reversing to scan anodically, a large oxidation near 0 V vs. SCE is observed and is attributed primarily to the oxidation of phenylthiolate (**3**) to the phenylthiyl radical (18). Because of the similarity in oxidation potentials, this wave may also include the oxidation of phenylmethoxide anion (**4**), and at slower scan rates this wave does appear to be composed of two overlapping oxidation peaks. The presence of **3** is confirmed by reversing the scan direction to scan cathodically following this large oxidation peak. A reduction wave attributable to diphenyl disulfide is observed, though this wave is exceedingly broad because of fouling of the working electrode by the putative phenylthiyl radicals. The analysis of the CVs indicates that the ET reduction occurs by the mechanism shown in Scheme 2. The initial ET occurs to form a radical anion intermediate, which then cleaves at the S—O bond in a separate step. The cleavage of the radical anion generates phenylthiolate (**3**) and the phenylmethoxyl radical. The alternate mode of cleavage (phenylthiyl radical and phenylmethoxide anion) is less favoured as the phenylthiyl radical is estimated to have a more negative reduction potential than the phenylmethoxyl radical (18). Regardless of the mode of cleavage, the reduction potential of the radical formed is far positive of the reduction potential of **1** and undergoes a rapid ET to give the phenylmethoxide anion (**4**).

Scheme 2. Proposed mechanism for the ET reduction of **1**.



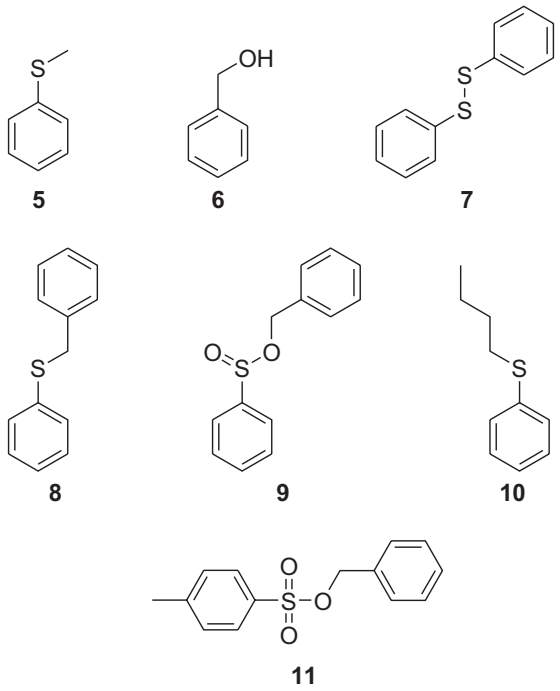
The reduction waves following the dissociative wave of **1** are due to products from the reactions involving the anionic species **3** or **4** reacting with **1** or the medium. The addition of an acid, such as acetanilide or 2,2,2-trifluoroethanol (TFE), will result in the protonation of **4**, eliminating any reactions of this anion with **1**. The pK_as of benzenethiol, acetanilide, and TFE as determined in DMSO are 10.3, 21.45, and 23.45, respectively (19). Given the relative pK_a values for these compounds, it is apparent why acetanilide and TFE have a limited capacity to protonate **3**. Therefore, the addition of these acids does not hinder the ability of **3** to react with **1**, even when present in large excess. In this case, to trap any **3** produced in the reduction of **1** a nucleophile trap such as methyl *p*-toluenesulfonate (MeOTs) or methyl iodide (MeI) is added.

The addition of both an acid and nucleophile trap is necessary to observe the full peak current. For example, the addition of 2 equiv. of TFE results in an increase in the peak current from 107 to 148 μA. The addition of 1 equiv. of MeOTs caused a further increase from 148 to 164 μA. It was also observed that addition of MeOTs alone was not capable of stopping the parent–child reactions, as an increase in the peak current of the dissociative wave is observed with the addition of acetanilide to a cell containing **1** and a large excess of MeOTs. It would seem that both the anions generated from reduction of **1** are participating in some form of parent–child reaction, therefore it is necessary to add both an acid and a nucleophile trapping agent to observe the maximum peak current.

The voltammetry responds differently to the addition of each reagent. Upon initial addition of acid the peak sharpens, especially apparent at higher scan rates, with α values ranging from 0.44 at 0.1 V/s to 0.53 at 1.0 V/s and then down to 0.37 at 10.0 V/s. The E_p continues to shift negatively as in the absence of acid by 74 mV/decade. The dissociative wave sharpens even further with the addition of MeOTs, most noticeably at the foot of the wave. This is carried over to the values of α, ranging from 0.50 to 0.52 to 0.37 at 0.1, 1.0, and 10.0 V/s, respectively. The addition of both reagents to the cell eliminates the shoulder on the tail

© 2005 NRC Canada

Scheme 3. Products obtained from the CPE of **1**.

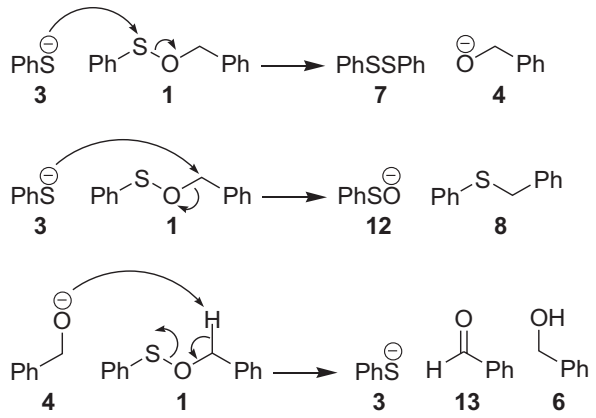


of the dissociative wave and no reduction waves are observed following it prior to the reduction of MeOTs occurring around –2.1 V vs. SCE. This is evidence that it has stopped any parent–child reactions and any products from the reduction that have been trapped are not electroactive in the potential window investigated. The large oxidation near 0 V vs. SCE also disappears, though it remains present in the voltammetry of **1** until MeOTs is added, again confirming its assignment as the oxidation of **3**.

Analysis of the data obtained from voltammograms performed in the presence of both acid and a nucleophile trapping agent allows an important conclusion concerning the mechanism of reduction to be drawn. The values for the peak width, peak current, and the shift in the peak potential are all similar to an electrochemically reversible process (i.e., the reduction of nitrobenzene) suggesting that the bond cleavage, and not the ET, is the rate-determining step. This implies that the ET reduction is occurring by a stepwise dissociative mechanism.

CPE experiments carried out in the absence of both acid and MeOTs required only 1.1 electron equiv., this value being the average obtained over several experiments. CVs taken before and after complete electrolysis are shown in Fig. 1*a*. Following complete reduction, the dissociative wave has completely disappeared while a small irreversible wave at more negative potentials is present. Scanning anodically, it was found that the peak attributed to the oxidation of **3** significantly increased. The cell solution was acidified and MeOTs was added following the electrolysis to aid in product isolation. The majority of the DMF and TFE were removed in vacuo with mild heating (60 °C). The residue was then subjected to column chromatography. Analysis of the fractions obtained by GC and GC–MS indicated the products summarized in Scheme 3. The major products of the reduction, methyl phenyl sulfide (**5**), benzyl alcohol (**6**), and diphenyl disulfide (**7**), could be identified using GC by comparison with authentic samples. Benzyl phenyl sulfide (**8**), a minor product, could also be identified by GC comparison. The identities of these products were further confirmed by mass spectrometry. The identities of the other minor products of reduction, benzylbenzenesulfinate (**9**), *n*-butyl phenyl sulfide (**10**), and benzyl *p*-toluenesulfonate (**11**), are based on their mass spectra. There were some minor products present that could not be conclusively identified by their mass spectra. Compounds **6**–**9** are products derived from parent–child processes. The remaining products are attributed to secondary reactions involving products of the reduction (**3** and **4**) with the solvent, electrolyte, or MeOTs. Because of the significance of these secondary reactions, a similar electrolysis was carried out, only switching to acetonitrile (MeCN) as the solvent, which was then worked up as previously described. GC–MS analysis revealed that switching the electrolysis solvent did not simplify the product mixture, and that products produced from reaction with MeCN were also present.

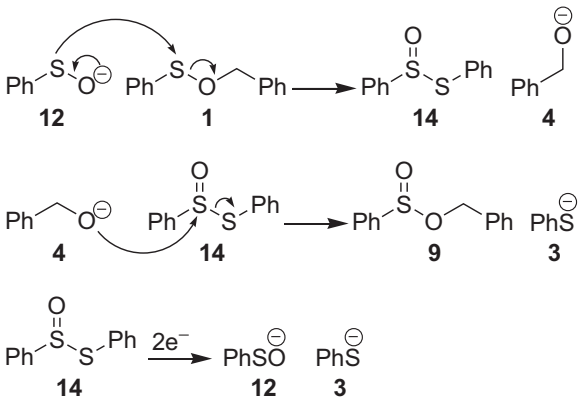
Scheme 4. Parent–child reactions involved in the ET reduction of **1**.



Based on the products observed in the DMF electrolysis, the reactions shown in Scheme 4 have been postulated for the parent–child processes. The first reaction is a nucleophilic attack at the sulfur atom of **1** by **3** to give diphenyl disulfide (**7**) and **4**. The reaction is believed to be occurring, but is in essence inconsequential as **4** is produced by direct ET to **1**. Also, at the potential at which the electrolysis is performed, any **7** formed by this reaction will be reduced to give 2 equiv. of **3**. This reaction will not affect either the products observed or the charge required for complete electrolysis. The second reaction involves attack at the benzyl carbon of **1** by **3** to give the benzenesulfenate anion and benzyl phenyl sulfide (**8**). This reaction accounts for the observance of **8** as a product from electrolysis and accounts for the lower charge consumption, as the reduction potential of **8** is negative of the electrode potential during electrolysis. The final parent–child reaction is the deprotonation of the benzyl carbon of **1** to give benzyl alcohol (**6**), benzaldehyde (**13**), and **3**. Benzaldehyde was observed as a minor product in the CPE experiments carried out in MeCN. The reduction potential of **13** is very close to that of **1** with $E^{\circ}_{\mathbf{13}} = -1.85$ V vs. SCE, and it is suggested that the shoulder on the dissociative wave is due to the reduction of **13** (Fig 1*a*). For

© 2005 NRC Canada

Scheme 5. Reactions accounting for the formation of **9**.

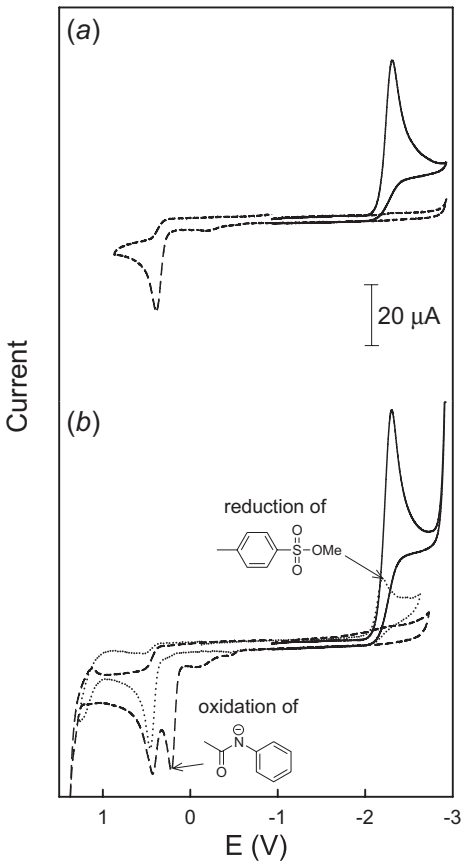


these reasons it is suspected that **13** will be reduced to its radical anion during the electrolysis of **1**. Reduction of **13** in aprotic solvent leads to the formation of 1,2-diphenylethane-1,2-diol (20–25); however, this compound was not observed as a product of our experiments. As the presence of acid is required to observe the full peak current of the dissociative wave of **1**, there must be a parent–child reaction involving **4** and **1**. Also, reaction between **4** and **1** to give **13** will result in a net decrease in the charge required for complete electrolysis, even if **13** is reduced to its radical anion. The products that were not conclusively identified were consistent with products from reactions between **3** and **13** and could account for the lack of products serving as evidence of the presence of **13**. On these grounds, we propose the reaction shown in Scheme 4 as the most likely reaction between **1** and **4**.

The formation of benzyl benzenesulfinate (**9**) cannot be directly accounted for through a parent–child reaction. However, in the reaction leading to **8** the benzenesulfenate anion (**12**) is generated. A possible reaction of this anion with **1** is illustrated in Scheme 5. Attack at the sulfur atom of **1** by **12** generates phenyl benzenethiosulfinate (**14**), while releasing **4**. A subsequent reaction between **4** and **14** could lead to the formation of **9**. Compound **14** could also be generated from attack of **12** on **7** with the release of **3**. The other primary process available to **14** would be ET reduction, which would lead to the generation of **12** and **3**.

When the reduction is performed in the presence of both MeOTs and acetanilide, a smooth conversion to phenyl methyl sulfide and benzyl alcohol by two-electron reduction is observed. It can be seen in Fig. 1*b* that no electroactive reagents remain following complete reduction of **1**. Both HPLC and GC results confirm quantitative formation of phenyl methyl sulfide (**5**). GC was used to determine the concentration of benzyl alcohol produced under these conditions, though it was difficult to achieve consistent results, even for the standards used for calibration. GC calibration indicates that 76% of the maximum amount of benzyl alcohol is recovered when the reduction is carried out with acid and MeOTs. These results were consistent with quantitative formation of benzyl alcohol given the error associated with these measurements. Considering that **5** is formed quantitatively and the two-electron stoichiometry for the complete reduction, it is assumed that a less than quantitative return of benzyl alcohol is primarily due to loss during the work-up.

Fig. 2. Representative CVs of **2** in 0.1 mol/L TBAP–DMF at 0.1 V/s: (*a*) **2** (2.4 mmol/L) before (solid line) and after (dashed line) introduction of 6.0 C of charge into the cell; (*b*) **2** (2.3 mmol/L) in the presence of acetanilide (40 mmol/L) before (solid line) and after (dashed line) introduction of 11.2 C of charge into the cell and following the subsequent addition of 2.7 mmol/L MeOTs (dotted line).



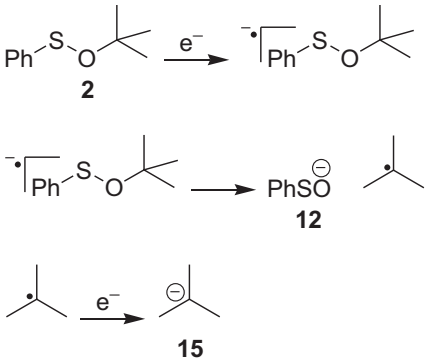
Analysis of the CV and CPE experimental data leads to the conclusion that the ET reduction of **1** occurs via a stepwise dissociative mechanism and the intermediate radical anion cleaves at the S—O bond.

ET reduction of *tert*-butyl benzenesulfenate ester (2)

The CV experiments of **2** were performed in 0.1 mol/L TBAP in DMF and the relevant voltammetric data are listed in Table 1 for comparison to the CV data obtained for compound **1**. A representative CV of **2** in 0.1 mol/L TBAP–DMF solution is shown in Fig. 2. A narrow, irreversible wave is observed at –2.28 V vs. SCE at 0.1 V/s. A negative shifting of the E_p with increasing scan rate is observed at a rate of 103 mV/decade. The peak width increases with increasing scan rate leading to decreasing values of the transfer coefficient. The α values at 0.1, 1.0, and 10.0 V/s are 0.58, 0.50, and 0.37, respectively. These data are in accord with the heterogeneous ET occurring by a stepwise dissociative mechanism, although the shifting of the E_p is higher than generally observed for systems proceeding by a stepwise mechanism. The dissociative wave is the only peak present on the cathodic scan, and reversing to the anodic scan reveals only small oxidation waves, starting at –0.4 V

© 2005 NRC Canada

Scheme 6. Mechanism for the ET reduction of **2**.

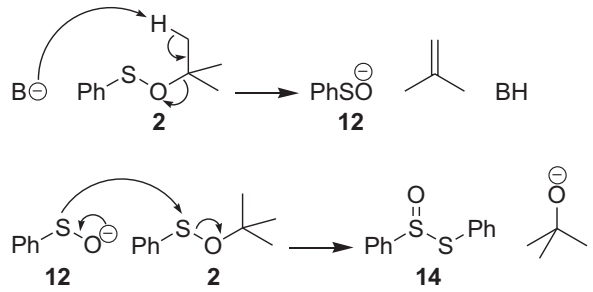


vs. SCE through to the largest oxidation wave occurring at 0.45 V vs. SCE at 0.2 V/s. The origin of these oxidations will be discussed in the context of the electrolysis experiments. It is sufficient at this point to note that unlike the voltammograms for **1**, only a small oxidation is present near 0 V vs. SCE. This is an indication that **3** is being produced only in a limited quantity, and the addition of nucleophile traps is deemed unnecessary when studying the electrochemistry of **2**. In comparison, for the reduction of **1** a large oxidation wave due to **3** is observed indicating a significant amount of **3** is produced, leading to the conclusion that the radical anion dissociates by S—O cleavage. Limited production of **3** is an indication that S—O bond cleavage is not occurring appreciably and that instead the radical anion of **2** dissociates by breaking the C—O bond as illustrated in Scheme 6. In this scheme, compound **2** is initially reduced by an ET to its radical anion, which then fragments in a separate step. The C—O bond is cleaved in the fragmentation step resulting in the formation of benzenesulfenate anion (**12**) and the *tert*-butyl radical. The standard reduction potential of this radical is estimated to be –1.54 V vs. SCE (18), which is positive of the E_p of **2**, therefore a heterogeneous ET can reduce this radical to give the *tert*-butyl anion (**15**).

The addition of a weak, nonnucleophilic acid, such as acetanilide or TFE, causes a significant increase in the peak current. The peak current values, corrected for both concentration and scan rate are 147 μA without acid and 170 μA with acid for a 2 mmol/L solution. Again, some parent–child interaction is responsible for a lower observed peak current in the absence of a reagent to trap the reactive species. The peak not only increased in current, but became narrower, which was especially apparent at higher scan rates. This is demonstrated in the value of the transfer coefficient, ranging from 0.55 to 0.50 and 0.43 at scan rates of 0.1, 1.0, and 10.0 V/s, respectively. Also, the observed shift in the E_p with increasing scan rate decreased from 103 to 72 mV/decade, a value that is more consistent with ET by a stepwise dissociative mechanism. The addition of acid did not dramatically affect the oxidation waves observed in the absence of acid, as it appears that the products responsible for these oxidation peaks are produced in the same quantity in the presence and absence of acid.

To confirm that C—O bond cleavage was occurring in the ET reduction of **2**, CPE experiments were necessary. Performing CPE in the absence of acid required only 1.1 electron equiv. for the complete reduction of **2**. This

Scheme 7. Parent–child reactions involved in the ET reduction of **2**.



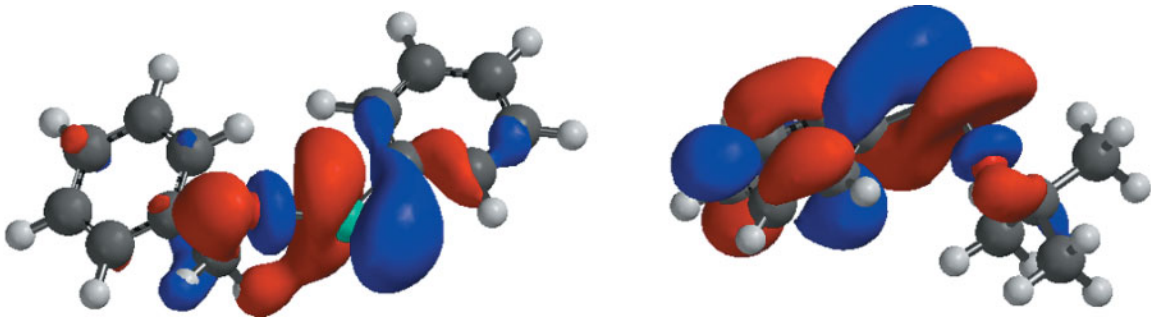
demonstrates that the parent–child process is highly effective when reduction is carried out on the electrolysis scale. Figure 2*a* shows CVs of **2** taken before and after the electrolysis. It can be seen that following electrolysis there are no products that are electroactive at negative potentials. However, anodic scans reveal that a large oxidation peak is present at 0.45 V vs. SCE at 0.2 V/s. Small peaks occurring at slightly more negative potentials are also present. Electrolysis performed with a large excess of acetanilide present require 1.96 F/mol (i.e., 2 electron equiv.) for complete reduction indicating that only acid is necessary to effectively suppress any parent-child reactions. Figure 2*b* shows the before and after CVs from the CPE of **2** with acid and it is seen that again no reducible products are observed and the large oxidation at 0.45 V vs. SCE seen in the voltammetry following CPE without acid is present. There is a large peak just negative of this oxidation, which is due to the oxidation of the acetanilide anion. Figure 2*b* shows that the addition of MeOTs following electrolysis will remove the oxidation peak of the acetanilide anion along with the smaller oxidation waves also present. The large wave at 0.45 V remains unaffected by the addition of MeOTs. Washing of the cell contents with an organic solvent and water proved inadequate in identifying the products of reduction as essentially no products could be detected in the organic residue by GC or ^{1}H NMR spectroscopy. In place of typical product analysis, it was decided to further analyze the large oxidation wave present in the CVs of the products of electrolysis.

Given that little to no **3** was observed in the CVs of **2**, C—O bond cleavage is believed to be occurring as shown in Scheme 6. Based on the anions formed from this reduction, the reactions illustrated in Scheme 7 are the proposed parent–child reactions believed to be occurring. The first reaction involves removal of a proton from the terminal methyl groups of **2**. The base involved in this reaction could be the *tert*-butyl anion or more likely the basic species generated from proton abstraction by the *tert*-butyl anion. Deprotonation of **2** generates isobutylene and benzenesulfenate anion (**12**). Therefore, the same product is observed in the voltammetry whether formed from direct reduction or from deprotonation of **2**. This accounts for the observance of the same oxidation wave following the electrolysis of **2** with or without acid.

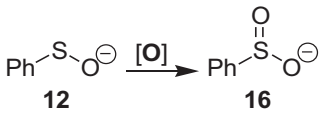
The second possible parent–child reaction involves nucleophilic attack of **2** by **12**. This process is identical to that proposed in the formation of **9** from the ET reduction of **1**, as previously shown. Again, phenyl thiobenzenesulfinate (**14**) is produced only now with the *tert*-butoxide anion as

© 2005 NRC Canada

Fig. 3. Depiction of the SOMOs of the radical anions of **1** (left) and **2** (right) as determined by DFT calculations.



Scheme 8.



the leaving group. The presence of *tert*-butoxide is believed to account for the small oxidation wave at –0.4 V vs. SCE in the CVs of **2**. Any **14** produced will likely be reduced to return to **12** and **3** (Scheme 5) and this reaction accounts for the oxidation wave at 0 V vs. SCE attributed to the oxidation of **3**.

However, the primary product from CPE of **2** in the presence and absence of acid is responsible for the oxidation peak at 0.45 V vs. SCE. We attribute this peak to the oxidation of benzenesulfinate (**16**), which is formed from the oxidation of **12** (Scheme 8). Evidence in favour of this assignment comes from the addition of sodium benzenesulfinate to the cell solution following CPE of **2**. The peak at 0.45 V increased in peak current and no new peaks were observed, while the E_p remained relatively constant indicating that the peak was likely due to the oxidation of benzenesulfinate. Independent CV experiments were performed that confirmed that the E_p of the sodium benzenesulfinate coincided with that of the oxidation wave observed in the electroysis of **2**. By varying the concentration of the sodium benzensulfinate the current response was calibrated and the concentration of **16** formed in the electrolysis was determined. As much as 75% of **2** was converted to **16** in the electrolysis performed without acid, and **16** was present in 96% of the starting concentration of **2** for CPE experiments performed with acid. How the conversion of **12** to **16** occurs is not completely understood. Previous studies of the electrolysis of phenyl benzenethiosulfinate also reported a similar oxidation wave that was attributed to **16** (26). In this study it was hypothesized that a disproportionation reaction between two molecules of **12** was occurring to give **3** and **16**. While it is possible that this process occurs, the relative peak currents of the oxidation peaks due to **3** and **16** indicate that it is not the primary process leading to the generation of **16**. It is difficult to assign a particular pathway for the oxidation of benzenesulfenate. Oxidation by perchlorate is unfavourable and oxidation by the solvent requires a significant amount of residual water to be present. It should be recognized that the E_p of an irreversible wave is not the most reliable means of identifying an unknown present in solution and that the wave could be due to the oxidation of benzenesulfenate and that the oxidation peaks of benzenesulfenate and benzenesulfinate simply coincide. Since benzenesulfenate is a highly unstable species, it was not possible to obtain an authentic sample to check this assertion.

Table 2. Bond lengths (Å) calculated for the equilibrium conformers of **1** and **2** and their respective radical anions.

Bond	**1** (Å)	$\mathbf{1}^{\cdot-}$ (Å)	**2** (Å)	$\mathbf{2}^{\cdot-}$ (Å)
C—S	1.764	1.734	1.765	1.787
S—O	1.702	1.776	1.702	1.668
O—C	1.423	1.384	1.441	1.439

DFT calculations of the SOMOs

It is interesting to compare the differences in the ET reactions of **1** and **2** that result as a difference in the O group. The most intriguing result of changing the ester moiety is the resulting change in the mode of fragmentation of the radical anions. The factors that result in the difference in cleavage reactions are not obvious. The same anionic fragment, either phenyl thiolate (**11**) or benzenesulfinate (**22**), would result from S—O and C—O cleavage of each compound, so it is not related to a thermodynamic advantage imparted by the stability of the anionic product. In both cases the carbon radical formed from C—O cleavage would be relatively stable; estimates of the reduction potentials of the benzyl radical and the *tert*-butyl radical have them near –1.34 and –1.54 V vs. SCE (18), respectively.

The difference seems to be related to differences in the electronic configuration of the radical anion intermediate for each of **1** and **2**. The SOMO for each of these compounds was determined by performing PM3 calculations to determine the equilibrium conformer of the radical anion and then density functional theory calculations at the BLYP-3//6-31** level were performed to arrive at the SOMO for each compound. The results of these computations are depicted in Fig. 3. The SOMO of the radical anion of **1** was largely associated with the S—O bond while the SOMO of the radical anion of **2** was largely delocalized over the phenyl ring and S atom. The respective bond lengths of the starting compound and its radical anion determined by PM3 calculations are given in Table 2. The ET to **1** causes significant lengthening of the S—O bond, while the S—O bond of **2** shortens upon ET. For **1** the majority of the additional charge is associated with the S—O bond and S—O cleavage is the result. For **2** the charge is delocalized onto the phenyl ring with only a limited effect on the S—O and C—O bonds, and

© 2005 NRC Canada

cleavage follows the most thermodynamically favourable pathway. Gregory and Jenks (17) have performed calculations for the homolytic cleavage of disulfides, peroxides, and sulfenate esters. While it was found that S—S and O—O cleavage were the most energetically viable pathways for disulfides and peroxides, the results indicated that fissure at the C—O bond is the most thermodynamically favourable mode of cleavage for a sulfenate ester. Our experimental results indicate that such an advantage is present in the radical anion of **2** as well.

Regioselective bond cleavages were observed by Houmam et al. (27) in their study of the ET reduction of benzyl thiocyanates, where differences in the mode of cleavage were observed for benzylthiocyanate and 4-nitrobenzylthiocyanate. The differences in this case were related to the radical anion intermediate, with benzylthiocyanate forming a σ* type radical anion akin to compound **1** and nitrobenzylthiocyanate forming a π* radical anion intermediate as was observed for **2**. In this case, the difference in the electron distribution of the radical anions of **1** and **2** must be related to the nature of the ester functionality as opposed to the aromatic moiety. The electron-donating capacity of the *tert*-butyl group increases the electron density on the O atom shifting the SOMO onto the aromatic ring. The benzyl group has the opposite effect, decreasing the electron density at the O atom and drawing the SOMO onto the S—O bond.

Conclusions

The ET reduction of benzyl benzenesulfenate ester (**1**) and *tert*-butyl benzenesulfenate ester (**2**) has been investigated. In each case, ET reduction generates a radical anion intermediate that subsequently undergoes bond cleavage. The bond that cleaves upon reduction, however, differs for the two compounds. ET reduction of **1** leads to S—O bond cleavage to give phenylthiolate and phenylmethoxide in an overall two-electron process. Complicating secondary reactions are effectively suppressed by addition of appropriate trapping reagents. The ET reduction of **2** leads to C—O cleavage of the radical anion. In the presence of acid the reduction proceeds to quantitatively generate benzenesulfenate. The difference in the mode of cleavage for these two radical anions is most likely related to the electron distribution in the radical anion. The additional charge on the radical anion of **1** is largely associated with the S—O bond, leading to significant S—O bond stretching upon ET and ultimately, bond fragmentation. The additional electron on the radical anion of **2** is largely associated with the phenyl ring and S atom so the dissociation of the radical anion follows the most thermodynamically favourable pathway, which in this case is C—O cleavage.

Experimental

General

The NMR spectra were obtained using a Varian Mercury 400 MHz spectrometer using the solvent peak ($CDCl_3$, 7.28 ppm) as the reference. ^1H and ^{13}C NMR spectra were recorded at 400.1 and 100.6 MHz, respectively. Mass spectra were performed using a MAT 8200 Finigan high-resolution mass spectrometer. GC was performed using an Agilent technologies GC 6890N gas chromatograph. HPLC was carried out using a Waters 600 controller and Waters Delta 600 pump, a Waters 2487 dual λ absorbance detector all interfaced to a PC using Millenium software, and a Hamilton PRP-1 column.

Calculations were performed on a PC using the SPARTAN program, which performed the PM3 and DFT calculations. The method for the calculations of the SOMOs of the sulfenate ester radical anions involved a geometry optimization of the structure using semiempirical PM3 calculations followed by a single-point energy DFT calculation using the B3LYP//6-31G** basis set.

Electrochemical apparatus and procedures

Cyclic voltammetry was performed using either a PAR 283 or PAR 263 model EG & G potentiostat interfaced to a personal computer using the M270 DOS-based software. A standard three electrode arrangement, with working, counter, and reference electrodes, was employed. The cell was maintained at a constant temperature of 25 °C with continuous purging using high purity Ar gas throughout the experiment. The working electrode was a 3 mm diameter glassy carbon rod (Tokai) sealed in a glass tube with epoxy resin. The working electrode was cleaned prior to use by polishing with 0.25 μm diamond paste, rinsing with 2-propanol, and placed in a sonicator in 2-propanol for 10 min. Electrochemical activation of the electrode was performed by cycling several times between 0 and –2.7 V at 0.2 V/s in the background solution. The counter electrode was a platinum plate, which was symmetrically placed under the working electrode. The reference electrode consisted of a silver wire immersed in a 0.1 mol/L solution of the electrolyte in the appropriate solvent contained in a narrow glass tube with a fine sintered glass tip. The reference potential was calibrated following each experiment using the ferrocene/ferrocenium couple whose standard potential under our conditions was 0.464 V vs. SCE. All reported potentials are referenced to SCE.

The CPE experiments were carried out using the same cell set up protocol and a similar cell arrangement. In controlled potential electrolysis, there is the inclusion of a second working electrode, which is a 2.5 cm (dia.) × 0.8 cm (width) glassy carbon disk, custom fit into a Teflon jacket that attaches to a Radiometer ED-101 rotating disk assembly. A radiometer CTV101 speed control unit was used to regulate the velocity of the rotating disk electrode (RDE), which was maintained at 4500 rpm for these experiments.

Materials

Dry solvents were obtained from an Innovative Technology SPS-400-5 solvent purification system and were stored a maximum of 5 days under an N_2 atmosphere. Tetrabutylammonium perchlorate (Aldrich, Fluka) was purified by multiple recrystallizations from 95% EtOH and the crystals subsequently vacuum-dried at 60 °C overnight. The recrystallized and dried electrolyte was then stored in a dehumidifying cabinet. Benzyl alcohol, benzaldehyde, diphenyl disulfide, thioanisole, benzenethiol, sulfuryl chloride, and *m*-chloroperbenzoic acid were purchased from Aldrich and purified by standard procedures when necessary.

© 2005 NRC Canada

Benzyl benzenesulfenate ester (1)

Compound **1** was prepared by the reaction of lithium phenylmethoxide and benzenesulfenyl chloride as previously reported (28). The crude product was a deep yellow oil, which was purified by vacuum distillation at 100 °C and >0.5 mmHg (1 mmHg = 133.322 4 Pa) using a Kugelrohr apparatus to give a pale yellow oil. ^{1}H NMR ($CDCl_3$) δ: 7.40–7.43 (m, 2H), 7.26–7.32 (m, 4H), 7.17–7.22 (m, 2H), 7.09–7.15 (m, 2H), 4.70 (s, 2H). ^{13}C NMR ($CDCl_3$) δ: 140.13, 136.92, 128.96, 128.39, 127.32, 127.02, 126.69, 124.32, 79.50.

tert-*Butyl benzenesulfenate ester (2)*

Compound **2** was prepared by reaction of *tert*-butyl alcohol and benzenesulfenyl chloride in the presence of pyridine as previously reported (29). Purification was performed by column chromatography using hexanes – ethyl acetate (4:1) as the eluent to give a clear, colourless oil. ^{1}H NMR ($CDCl_3$) δ: 7.66–7.70 (m, 2H), 7.49–7.53 (m, 3H), 1.56 (s, 9H). ^{13}C NMR ($CDCl_3$) δ: 146.46, 131.54, 128.90, 124.86, 82.87, 29.87.

Benzyl phenyl sulfide (8)

Compound **8** was prepared by the addition of a solution of benzylbromide (5.9 mmol) in ~25 mL CH_2Cl_2 to a flask containing benzenethiol (5.8 mmol) and pyridine (6.2 mmol) dissolved in 25 mL of CH_2Cl_2. The reaction mixture was washed with aq. K_2CO_3 solution, which was then washed with CH_2Cl_2. The organic extracts were combined and washed three times with H_2O and dried over anhydr. Na_2SO_4. The crude product was purified by column chromatography with hexanes – ethyl acetate (10:1) as the eluent. ^{1}H NMR ($CDCl_3$) δ: 7.21–7.37 (m, 10H), 4.17 (s, 2H). ^{13}C NMR ($CDCl_3$) δ: 137.33, 136.28, 129.64, 128.73, 128.39, 127.08, 127.02, 126.21, 38.88.

Phenyl benzenethiosulfinate (14)

Compound **14** was prepared by the oxidation of diphenyl disulfide with *m*-chloroperbenzoic acid according to accepted literature methods (30–32). Column chromatography was employed for the purification using hexanes – ethyl acetate (10:1) as the eluent. ^{1}H NMR ($CDCl_3$) δ: 7.64–7.68 (m, 2H), 7.47–7.56 (m, 5H), 7.41–7.46 (m, 1H), 7.34–7.40 (m, 2H). ^{13}C NMR ($CDCl_3$) δ: 143.96, 135.33, 131.50, 130.26, 129.24, 128.89, 127.52, 124.29.

Identification of products from the CPE experiments of 1

Product mixtures and authentic samples were subjected to analysis by GC using a 15 m HP-5 column. The method used to obtain the gas chromatograms is as follows: the initial temperature is 80 °C and upon initiation the temperature is increased to 280 °C at a rate of 15°/min and held at 280 °C for 5 min. Following partial separation of the products into two major fractions by column chromatography, the fractions of the product mixture were analyzed by GC–MS. The method for the GC of these analyses is as follows: the temperature is initially set at 60 °C and held for 3 min. The temperature is then ramped to 300 °C by 15°/min.

Methyl phenyl sulfide (5)

The presence of **5** in the product mixtures could be inferred from the observation of a peak in the GC chromatogram of the product mixture with the same retention time as an authentic sample of **5** purchased from Aldrich. GC–MS of this peak had the following major peaks: 124 (100%) M^+, 109 (47%) $M^+ - CH_3$, 91 (57%) $M^+ - SH$, 78 (65%) $M^+ - SCH_2$.

Benzyl alcohol (6)

The presence of **6** in the product mixtures was determined from the observation of a peak in the GC chromatograms of the products with the same retention time as an authentic sample of **6** purchased from Aldrich. The corresponding peak in the GC–MS had the following mass spectrum characteristics: 108 (100%) M^+, 91 (25%) $M^+ - OH$, 79 (75%) $M^+ - CHO$.

Diphenyl disulfide (7)

The presence of **7** in the product mixtures was determined from the observation of a peak in the GC chromatograms of the products with the same retention time as an authentic sample of **7** purchased from Aldrich. The corresponding peak in the GC–MS had the following mass spectrum characteristics: 218 (100%) M^+, 185 (28%) $M^+ - HS$, 154 (30%) $M^+ - H_2S_2$, 140 (10%) $M^+ - C_6H_6$, 109 (99%) $M^+ - SC_6H_6$, 65 (42%), 109 – CS.

Benzyl phenyl sulfide (8)

The presence of **8** in the product mixtures was determined from the observation of a peak in the GC chromatograms of the products with the same retention time as an authentic sample of **8** prepared as previously described. The corresponding peak in the GC–MS had the following mass spectrum characteristics: 200 (83%) M^+, 109 (19%) $M^+ - C_7H_7$, 91 (100%) $M^+ - C_6H_5S$, 65 (45%), 109 – CS.

Benzyl benzenesulfinate (9)

The presence of **9** in the product mixtures was determined from the analysis of the GC–MS of the product mixture. The peak assigned to this product had the following mass spectrum characteristics: 232 (1%) M^+, 167 (6%) $M^+ - C_5H_5$, 153 (2%) 167 – CH_2, 125 (6%) $M^+ - C_7H_7O$, 91 (100%) $M^+ - C_6H_5O_2S$, 77 (23%) 91 – CH_2, 65 (9%) $M^+ - C_8H_8O_2S$.

n-*Butyl phenyl sulfide (10)*

The presence of **10** in the product mixtures was determined from the analysis of the GC–MS of the product mixture. The peak assigned to this product had the following mass spectrum characteristics: 166 (77%) M^+, 152 (4%) $M^+ - CH_2$, 123 (100%) $M^+ - C_3H_7$, 109 (49%) $M^+ - C_4H_9$, 91 (5%) $M^+ - C_3H_7S$, 77 (11%) $M^+ - SC_4H_9$, 65 (12%), 109 – CS.

Benzyl* p-*toluenesulfonate (11)

The presence of **11** in the product mixtures was determined from the analysis of the GC–MS of the product mixture. The peak assigned to this product had the following mass spectrum characteristics: 262 (12%) M^+, 244 (3%) $M^+ - H_2O$, 186 (3%) $M^+ - C_6H_5$, 107 (100%) $M^+ - C_7H_7O_2S$, 91 (12%) $M^+ - C_7H_7O_3S$, 79 (52%), 107 – CO.

© 2005 NRC Canada

Benzaldehyde (13)

The presence of **13** in the product mixtures from CPE experiments performed in MeCN was determined from the observation of a peak in the GC chromatograms of the products with the same retention time as an authentic sample of **13** purchased from Aldrich. The corresponding peak in the GC–MS had the following mass spectrum characteristics: 108 (100%) M^+, 91 (26%) $M^+ - OH$, 79 (73%) $M^+ - CHO$.

References

1. R.L. Donkers, J. Tse, and M.S. Workentin. Chem. Commun. 135 (1999).
2. R.L. Donkers and M.S. Workentin. J. Am. Chem. Soc. **126**, 1688 (2004).
3. D.L.B. Stringle, R.N. Campbell, and M.S. Workentin. Chem. Commun. 1246 (2003).
4. M.S. Workentin, F. Maran, and D.D.M. Wayner. J. Am. Chem. Soc. **117**, 2120 (1995).
5. S. Antonello, M. Musumeci, D.D.M. Wayner, and F. Maran. J. Am. Chem. Soc. **119**, 9541 (1997).
6. R.L. Donkers, F. Maran, D.D.M. Wayner, and M.S. Workentin. J. Am. Chem. Soc. **121**, 7239 (1999).
7. D.C. Magri and M.S. Workentin. Org. Biomol. Chem. **1**, 3418 (2003).
8. M.S. Workentin and R.L. Donkers. J. Am. Chem. Soc. **120**, 2664 (1998).
9. R.L. Donkers and M.S. Workentin. J. Phys. Chem. B, **102**, 4061 (1998).
10. R.L. Donkers and M.S. Workentin. Chem. Eur. J. **7**, 4012 (2001).
11. T.B. Christensen and K. Daasbjerg. Acta Chem. Scand. **51**, 307 (1997).
12. K. Daasbjerg, H. Jensen, R. Benassi, F. Taddei, S. Antonello, A. Gennaro, and F. Maran. J. Am. Chem. Soc. **121**, 1750 (1999).
13. S. Antonello, R. Benassi, G. Gavioli, F. Taddei, and F. Maran. J. Am. Chem. Soc. **124**, 7529 (2002).
14. S. Antonello, K. Daasbjerg, H. Jensen, F. Taddei, and F. Maran. J. Am. Chem. Soc. **125**, 14905 (2003).
15. W.H. Horspool. The chemistry of sulphenic acids and their derivatives. Edited by S. Patai. John Wiley and Sons, Chichester. 1990.
16. (*a*) D.J. Pasto, F. Cottard, and C. Picconatto. J. Org. Chem. **59**, 7172 (1994); (*b*) D.J. Pasto and G.L. L'Hermine. J. Org. Chem. **55**, 5815 (1990); (*c*) D.J. Pasto and G.L. L'Hermine. Tetrahedron, **49**, 3259 (1993); (*d*) D.J. Pasto and F. Cottard. J. Org. Chem. **59**, 4642 (1994).
17. D.D. Gregory and W.S. Jenks. J. Org. Chem. **63**, 3859 (1998).
18. K. Daasbjerg, S.U. Pedersen, and H. Lund. *In* General aspects of the chemistry of radicals. *Edited by* Z.B. Alfassi. John Wiley and Sons, Chichester. 1999. p. 385.
19. F.G. Bordwell. Acc. Chem. Res. **21**, 456 (1988).
20. S.G. Mairanovskii. Bull. Acad. Sci. USSR, 2003 (1961).
21. E. Laviron. Coll. Czech. Chem. Commun. **30**, 4219 (1965).
22. L. Nadjo and J.-M. Savéant. J. Electroanal. Chem. **33**, 419 (1971).
23. J.W. Hayes, I. Ruzic, D.E. Smith, G.L. Booman, and J.R. Delmastro. J. Electroanal. Chem. **51**, 269 (1974).
24. V.D. Parker and O. Lerflaten. Acta. Chem. Scand. Ser. B, **B37**, 403 (1983).
25. C.P. Andrieux, M. Grzeszczuk, and J.-M. Savéant. J. Am. Chem. Soc. **113**, 8811 (1991).
26. B. Persson. J. Electroanal. Chem. **86**, 313 (1978).
27. A. Houmam, E.M. Hamed, P. Hapiot, J.M. Motto, and A.L. Schwan. J. Am. Chem. Soc. **125**, 12676 (2003).
28. E.G. Miller, D.R. Rayner, H.T. Thomas, and K. Mislow. J. Am. Chem. Soc. **90**, 4861 (1968).
29. L. Goodman and N. Kharasch. J. Am. Chem. Soc. **77**, 6541 (1955).
30. L.D. Small, J.H. Bailey, and C.J. Cavalitto. J. Am. Chem. Soc. **69**, 1710 (1947).
31. S.W. Bass and S.A. Evans. J. Org. Chem. **45**, 710 (1980).
32. D.J. Pasto and F. Cottard. J. Am. Chem. Soc. **116**, 8973 (1994).

© 2005 NRC Canada

The mechanisms of hydrolysis of alkyl *N*-alkylthioncarbamate esters at 100 °C[1]

Eduardo Humeres, Maria de Nazaré M. Sanchez, Conceição M.L. Lobato, Nito A. Debacher, and Eduardo P. de Souza

Abstract: The hydrolysis of ethyl *N*-ethylthioncarbamate (ETE) at 100 °C was studied in the range of 7 mol/L HCl to 4 mol/L NaOH. The pH–rate profile showed that the hydrolysis occurred through specific acid catalysis at pH < 2, spontaneous hydrolysis at pH 2–6.5, and specific basic catalysis at pH > 6.5. The Hammett acidity plot and the excess acidity plot against X were linear. The Bunnett–Olsen plot gave a negative slope indicating that the conjugate acid was less hydrated than the neutral substrate. It was concluded that the acid hydrolysis occurred by an A1 mechanism. The neutral species hydrolyzed with general base catalysis shown by the Brønsted plot with $\beta = 0.48 \pm 0.04$. Water acted as a general base catalyst with (pseudo-)first-order rate constant, $k_N = 3.06 \times 10^{-7}$ s^{-1}. At pH > 6.5 the rate constants increased, reaching a plateau at high basicity. The basic hydrolysis rate constant of ethyl *N*,*N*-diethylthioncarbamate, which must react by a $B_{Ac}2$ mechanism, increased linearly at 1–3 mol/L NaOH with a second-order rate constant, $k_2 = 2.3 \times 10^{-4}$ (mol/L)$^{-1}$ s^{-1}, which was 10 times slower than that expected for ETE. Experiments of ETE in 0.6 mol/L NaOH with an excess of ethylamine led to the formation of diethyl thiourea, presenting strong evidence that the basic hydrolysis occurred by the E1cb mechanism. In the rate-determining step, the E1cb mechanism involved the elimination of ethoxide ion from the thioncarbamate anion, producing an isothiocyanate intermediate that decomposed rapidly to form ethylamine, ethanol, and COS.

Key words: alkylthioncarbamate esters, ethyl *N*-ethylthioncarbamate, ethyl *N*,*N*-diethylthioncarbamate, hydrolysis, mechanism.

Résumé : Opérant à 100 °C, dans des milieux allant du HCl à 7 mol/L au NaOH à 4 mol/L, on a étudié la réaction d'hydrolyse du *N*-éthylthionecarbamate d'éthyle (ETE). Le profile de la vitesse en fonction du pH montre que l'hydrolyse se produit par le biais d'une catalyse acide spécifique à des pH inférieurs à 2, par une hydrolyse spontanée à des pH allant de 2 à 6,5 et par une hydrolyse par catalyse basique à des pH supérieurs à 6,5. La courbe d'acidité de Hammett et la courbe d'excès d'acidité en fonction de X sont linéaires. La courbe de Bunnett–Olsen donne une pente négative qui indique que l'acide conjugué est moins hydraté que le substrat neutre. On en conclut que l'hydrolyse acide se produit par un mécanisme A1. L'espère neutre s'hydrolyse par une catalyse générale basique mise en évidence par la courbe de Brønsted avec une valeur de $\beta = 0{,}48 \pm 0{,}04$. L'eau agit comme catalyseur basique général avec une constante de vitesse de (pseudo-)premier ordre, $k_N = 3{,}06 \times 10^{-7}$ s^{-1}. À des pH supérieurs à 6,5, les constantes de vitesse augmentent pour atteindre un plateau aux pH élevés. Pour l'hydrolyse basique du *N*,*N*-diéthylthionecarbamate d'éthyle, qui doit obligatoirement réagir par un mécanisme $B_{Ac}2$, la constante de vitesse augmente d'une façon linéaire dans le NaOH à des concentrations allant de 1 à 3 mol/L et la constante de vitesse du deuxième ordre, $k_2 = 2{,}3 \times 10^{-4}$ (mol/L)$^{-1}$ s^{-1}, est 10 fois plus lente que celle attendue pour l'ETE. Des expériences avec l'ETE dans du NaOH à 0,6 mol/L, en présence d'un excès d'éthylamine, conduit à la formation de diéthylthiourée, ce qui suggère fortement que l'hydrolyse basique se produit par un mécanisme E1cb. Dans l'étape cinétiquement déterminante, le mécanisme E1cb implique l'élimination de l'ion éthylate à partir de l'anion thionecarbamate avec formation d'un intermédiaire isothiocyanate qui se décompose rapidement pour former de l'éthylamine, de l'éthanol et du COS.

Mots clés : alkylthionecarbamates d'esters, *N*-éthylthionecarbamate d'éthyle, *N*,*N*-diéthylthionecarbamate d'éthyle, hydrolyse, mécanisme.

[Traduit par la Rédaction]

Received 29 April 2005. Published on the NRC Research Press Web site at http://canjchem.nrc.ca on 11 November 2005.

E. Humeres,[2,3] M.N.M. Sanchez, C.M.L. Lobato, N.A. Debacher, and E.P. de Souza. Departamento de Química, Universidade Federal de Santa Catarina, 88040-900 Florianópolis, SC, Brazil.

[1]This article is part of a Special Issue dedicated to organic reaction mechanisms.

[2]Present address: Grupo de Reactividad Química y Fotoreactividad, Departmento de Físico Química e Ingeniería Química, Universidade A Coruña, Rúa Alejandro de la Sota, 1. E-15008 A Coruña, Galicia, España.
[3]Corresponding author (e-mail: humeres@mbox1.ufsc.br).

 doi: 10.1139/V05-165 © 2005 NRC Canada

Introduction

The reaction of carbon dioxide and carbon disulfide with alkoxides, halides, and amines produces derivatives that are important pesticides (eq. [1]) (1). Carbamic acid acid esters (**1**, X = O) are widely used as insecticides because of their ability to inhibit the enzyme acetylcholinesterase. Thioncarbamic esters (**1**, X = S) are used as fungicides and bactericides (2), nematocides (3), collectors in flotation (4), and in a variety of industrial applications (5). The formation of the highly stable thioncarbamate group has been used to immobilize enzymes in a cellulose matrix (eq. [1], R = cellulose, R″ = enzyme) (6).

The biological activity depends on the C=X group (X = O, S) because of the different properties of the oxo and sulfo groups. The carbonyl can stabilize α-carbocations better than sulfur, but this capacity is inverted for carbanions. The thiocarbonyl is a powerful electron-withdrawing group because sulfur can easily accept electrons.

There is a duality of mechanisms for the basic hydrolysis of carbamates and thioncarbamate esters depending on the availability of a proton on the nitrogen atom of the ester. Mechanism $B_{Ac}2$ applies if there is no proton on the nitrogen (*N*,*N*-disubstituted nitrogen), but if the nitrogen contains a proton, mechanism E1cb might apply, although not necessarily. All aryl esters follow this pattern. Alkyl carbamates apparently follow the $B_{Ac}2$ mechanism. However, no information exists about the mechanisms involved in the hydrolysis of alkyl thioncarbamate esters.

In this work, we studied the hydrolysis (at 100 °C) of ethyl *N*-ethylthioncarbamate in the range of 7 mol/L of HCl to 4 mol/L of NaOH, to obtain an insight into the mechanisms involved.

Experimental

Materials

Reagents were all of analytical grade and were used without further purification. Distilled water was deionized and deoxygenated by boiling and cooling under nitrogen. Ethylamine was distilled (bp 18 °C), condensed in a trap cooled with liquid nitrogen, and bubbled into water to obtain a 2 mol/L solution. UV spectra and kinetics were obtained using a Cary 219 spectrophotometer. All compounds were identified by ^{1}H NMR and IR spectra.

Ethyl *O*-ethylxanthate (EXE)

Potassium *O*-ethylxanthate (EXK) was obtained using the classical procedure (7), adding 60 mL of carbon disulfide to a cooled solution of 56 g (1 mol) potassium hydroxide in 200 mL of ethanol. The product was recrystallyzed twice in ethanol; λ_{max} (ethanol) 301 nm. Ethyl *O*-ethylxanthate was obtained after refluxing a solution of EXK (32 g, 0.2 mol) and ethyl bromide (21.8 g, 0.2 mol) for 4 h in 50 mL of ethanol. The product was washed with water, dried over anhydrous sodium sulfate, and distilled under vacuum: bp 35 °C at 1 mmHg (lit. value (8) bp 78 °C at 18 mmHg) (1 mmHg = 133.322 4 Pa); λ_{max} (water) 283 nm.

Ethyl *N*-ethylthioncarbamate (ETE)

Ethyl *O*-ethylxanthate (13.3 g, 0.1 mol) was dissolved in 10 mL of ethanol, and an aqueous solution of ethylamine (0.11 mol) at pH 11 was added with cooling, allowing the solution to react for 24 h at 10 °C under constant stirring. The ethanol was eliminated under vacuum in a rotatory evaporator and the product was washed with water, dried over anhydrous sodium sulfate, and distilled under vacuum: bp 74 °C at 1 mmHg (lit. value (9) bp 78 °C at 3 mmHg); λ_{max} (water) 242 nm.

Ethyl *N*,*N*-diethylthioncarbamate (DETE)

A solution of 10 g (75 mmol) of EXE and 6 g (82 mmol) of diethylamine in 200 mL of ethanol was allowed to react at room temperature. The reaction was followed via UV spectrophotometry by the disappearance of the band at 283 nm because of EXE and the appearance of the band at 245 nm because of DETE. The product was distilled under vacuum: bp 85 °C at 1 mmHg; λ_{max} (water) 245 nm.

1,3-Diethyl thiourea (DETU) (10)

Ethyl isothiocyanate (4.5 g of a 90% aqueous solution) was slowly added to 8.7 g of a 70% aqueous solution of ethylamine. The reaction was exothermic and the mixture was cooled in an ice bath. The water was evaporated at 60 °C, and the crystals were recrystallized twice in dried ethanol; mp 77.1 °C (lit. value (11, 12) mp 72–78 °C); λ_{max} (methanol) 210 and 234 nm.

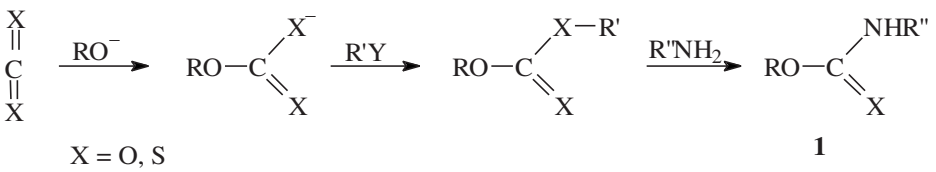
Reverse base dissociation constant of ethyl *N*-ethylthioncarbamate ($-pK_b$)

The dissociation constant was obtained at 25 °C from a series of measurements of the absorbance at 242 nm of a ca. 10^{-5} mol/L solution of the substrate, in the range of H_- = 10–15. The initial solution was 0.01 mol/L NaOH and known volumes of a 8 mol/L NaOH solution were added, correcting the absorbance for the dilution and the absorbance of the base. The UV spectra in the range of pH 7 to 2.7 mol/L NaOH, μ = 5 (NaCl) showed a single isosbestic point at 228 nm. Inversion of the basicity after the titration showed that the dissociation at 25 °C was reversible, with no noticeable reaction. The value of $-pK_b = 13.6 = pK_2$ (see the following) was calculated from the inflection point of the plot of the corrected absorbance vs. H_- for NaOH (Fig. 1) (13).

Correction of pH and pK_a with temperature

The pH of the solutions was measured at 25 °C and corrected to 100 °C as described elsewhere (14). The same

[1]

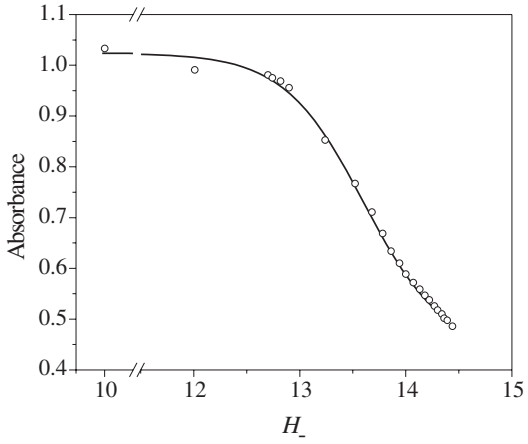


X = O, S

1

© 2005 NRC Canada

Fig. 1. Titration curve of ETE at 25 °C.



method was followed to calculate the pK_as of the buffers at 100 °C.

Kinetics

Kinetics were studied at 100 °C in distilled deoxygenated water in the range of H_o = –2.4 to 4 mol/L NaOH. The kinetic solution (50 mL) had a final concentration of ca. 10^{-4} mol/L; samples of 3 mL were placed in sealed glass ampoules and immersed in a thermostat at 100 °C. The samples were collected at different times and quenched in a Dewar bath with salted ice. The kinetics were followed spectrophotometrically at 25 °C by the disappearance of ETE at 242 nm or at 230 nm for the basic hydrolysis. The disappearance of DETE was followed at 245 nm. All runs were followed for at least three half-lives and the ln ΔA vs. time plots produced straight lines that were considered when $r \geq 0.99$. The pH of unbuffered runs was controlled at the end of the experiment and showed no change.

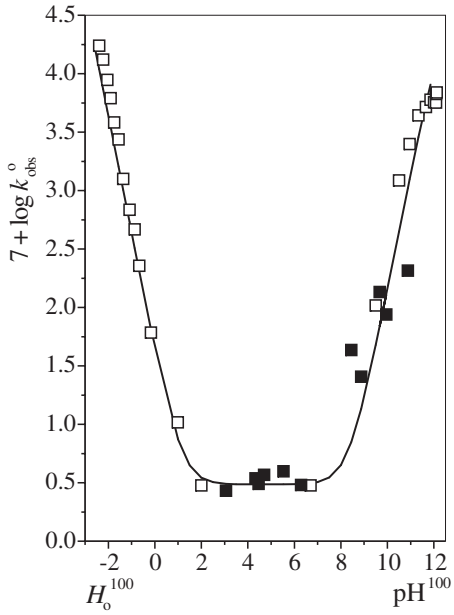
For the kinetics under strong basic conditions, the rate constants were also calculated by the Guggenheim method (15) because of a precipitate of sulfur that interfered with the absorbance readings. The rate constants for the slowest kinetics were obtained from initial rates.

Product analysis

The products of the hydrolysis of ETE were characterized in a preparative run at 2.5 mol/L NaOH and 100 °C, allowing a 50 min reaction. A sample was extracted with chloroform, and ethylamine was identified as a product by GLC. Another sample was extracted with cyclohexane, and ethanol was also identified as a product by GLC.

To trap the isothiocyanate intermediate, a preparative run of the hydrolysis of ETE in the presence of ethylamine was carried out. An aqueous solution of 4.5 mmol/L ETE, 0.6 mol/L NaOH, and 3 mol/L ethylamine was refluxed for 30 min, and after cooling, it was neutralized with HCl. The products were extracted with chloroform, concentrated in a rotatory evaporator, dried over anhydrous sodium sulphate, and then analyzed by TLC (silica gel, MeOH). A single spot was found with R_f 0.75, the same as an authentic sample of 1,3-diethyl thiourea. This result was confirmed by UV spectra.

Fig. 2. pH–rate profile of the hydrolysis of ETE at 100 °C. Unbuffered (□) and values extrapolated to zero buffer concentration (■).



Activation parameters

Activation parameters were calculated from the rate constants in the temperature range of 90–110 °C by least-squares fitting to the Eyring equation.

Results and discussion

pH–rate profile of ETE

The pH–rate profile was obtained at 100 °C in the range of H_o = –2.4 to pH 12 (Fig. 2). The values of k^o_{obs} were obtained in the absence of buffer or extrapolated to zero buffer concentration, and the pH was corrected for the temperature as has been previously described (14).

In the acid range of pH < 2, HCl was used and the H_o values obtained at 25 °C from the excess acidity X, and the HCl acid molarity (C_{H^+}) was corrected at 100 °C for the change of the excess acidity X with temperature (eqs. [2] and [3]) (16).

[2] $$-H_o = X + \log C_{H^+}$$

[3] $$X_T = X_{25^\circ}\left(\frac{298.15}{T}\right)$$

At pH > 10, H_- was calculated from

[4] $$H_- = pK_w^{100} + \log[OH^-]$$

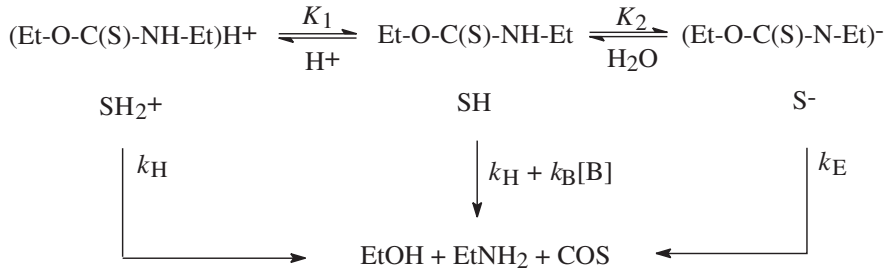
where pK_w^{100} = 12.26 (14*b*, 17).

In the 0.05–1.0 mol/L NaOH range at 25 °C, these values are less than 0.1% different from those obtained from the acidity function using thioacetamide as an indicator (13).

The profile was divided into three regions. At pH < 2, $\log k^o_{obs}$ increases with acid concentration by a specific acid catalysis mechanism. In the range of pH 2–6.5, the rate constants were independent of the pH. A specific basic hydroly-

© 2005 NRC Canada

Scheme 1. Kinetic scheme of the hydrolysis of ETE.



sis occurred at pH > 6.5, and the rate constants reached a plateau in the region of pH > 12. The pH–rate profile can be described according to Scheme 1 by eq. [5].

$$[5] \qquad k^{o}_{obs} = k_H \frac{a_{H^+}}{K_1 K'} + \frac{k_N}{K'} + \frac{k_E K_2 [OH^-]}{K_w K'}$$

where

$$K' = \frac{a_{H^+}}{K_1} + 1 + \frac{K_2}{a_{H^+}} \text{ and } a_{H^+} = h_o \text{ when pH} < 2.$$

In Scheme 1, K_1 and K_2 are the acid and reverse base dissociation constants of species SH_2^+ and SH, respectively, k_H is the specific acid hydrolysis rate constant, and k_N and k_E are the rate constants of spontaneous and basic hydrolysis, respectively. Equation [5] assumes that the basic hydrolysis occurs by the E1cb mechanism as will be discussed in the following.

Acid hydrolysis

At HCl concentrations higher than 1 mol/L, the terms due to spontaneous and basic hydrolysis in eq. [5] are very small compared to those of acid hydrolysis because

$$k_H \frac{a_{H^+}}{K_1 K'} >> \frac{k_N}{K'} + \frac{k_E K_2 [OH^-]}{K_w K'}$$

and eq. [5] becomes

$$[6] \qquad k^{o}_{obs} = \frac{k_H h_o}{h_o + K_1}$$

and, when the ester is predominantly protonated, $k^{o}_{obs} = k_H$ at that acidity range.

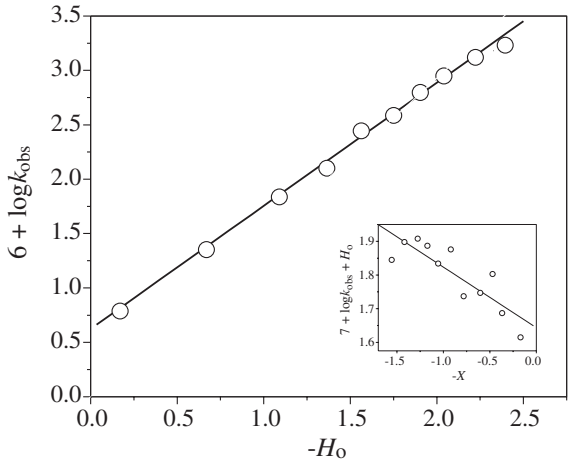
Several plots showed that the acid hydrolysis occurred by the A1 mechanism. The Hammett plot of $\log k_{obs}$ vs. $-H_o$ (Fig. 3) was linear with a slope of 1.14 (r = 0.999), close to the unity value expected by the Zucker–Hammett hypothesis for this mechanism (18).

The pH–rate profile suggests that in the of 1–7 mol/L HCl concentration range, the substrate is unprotonated, and the relevant rate equation is eq. [7] (19)

$$[7] \qquad \log k^{o}_{obs} - \log C_{H^+} = \log \frac{k_o}{k_1} + m^{\ddagger} m^* X$$

where k_o is the medium-independent specific acid catalysis rate constant. The excess acidity assumption is that the term containing the activity coefficient of the transition state $f_{\ddagger}$ is linearly related to the activity coefficient ratio containing the conjugate acid SH_2^+ (20), and that this is linear in X (eq. [8]).

Fig. 3. Hammett plot for the acid hydrolysis of ETE at 100 °C. Insert: Bunnett–Olsen plot.



$$[8] \qquad \log \frac{f_{SH} f_{H^+}}{f_{\ddagger}} = m^{\ddagger} \log \frac{f_{SH} f_{H^+}}{f_{SH_2^+}} = m^{\ddagger} m^* X$$

The excess acidity slope value (m^*) is associated with solvation differences between SH and SH_2^+ (21). For A1 reactions, $m^{\ddagger} > 1$ and the excess acidity plots are linear for A1 mechanisms, while these plots are curved for A2 mechanisms.

The linearity of the excess acidity plot against X of the hydrolysis of ETE in HCl is shown in Fig. 4, where $m^{\ddagger} m^*$ = 1.18, $\log (k_o/K_1)$ = –5.36, and r = 0.996.

We do not know the value of m^* for ETE, but the Bunnett–Olsen plot gave $\phi_{\ddagger}$ = –0.18 (r = 0.854) from eq. [9] for unprotonated substrates (Fig. 3, insert) (22).

$$[9] \qquad \log k^{o}_{obs} + H_o = \left(\log \frac{k_o}{K_1} \right) + \phi_{\ddagger} (H_o + \log C_{H^+})$$

Although the correlation coefficient is lower, the negative slope indicates that SH_2^+, whose structure should be closer to the transition state, is less hydrated than SH as expected for the A1 mechanism. We note that for HCl, $H_o + \log C_{H^+} = -X$, and eq. [9] is equivalent to eq. [7], where $m^{\ddagger} m^* = 1 - \phi_{\ddagger}$, and the value of $\log (k_o/K_1) = -5.36$ is the same as that found in the excess acidity plot.

In Table 1, it can be observed that the activation parameters for the acid hydrolysis at 2.5 mol/L HCl, $\Delta G^{\ddagger} = \Delta H^{\ddagger}$, because $\Delta S^{\ddagger}$ (–1.6 ± 2.2 cal mol^{-1} K^{-1}, 1 cal = 4.184 J) is

© 2005 NRC Canada

Table 1. Activation parameters for the hydrolysis of ETE at 100 °C.

Hydrolysis	Concentration	$\Delta G^{\ddagger}$ (kcal mol^{-1})	$\Delta H^{\ddagger}$ (kcal mol^{-1})	$\Delta S^{\ddagger}$ (cal mol^{-1} K^{-1})
Acid	HCl (2.5 mol/L)	29.5±1.7	28.9±0.9	–1.6±2.2
Water catalysis	pH 5.5	32.8±2.9	22.6±1.4	–27.4±3.8
Basic	NaOH (2.5 mol/L)	26.2±1.6	14.0±0.6	–34.5±1.5
Basic (DETE)	NaOH (2.0 mol/L)	27.7±1.8	21.3±.0.9	–17.2±2.5

Note: Standard state: 1 mol/L, 100 °C.

Fig. 4. Excess acidity plot against X of the hydrolysis of ETE in HCl at 100 °C.

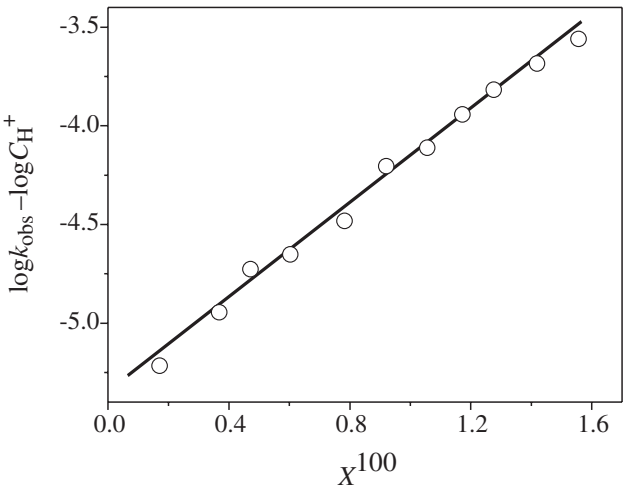
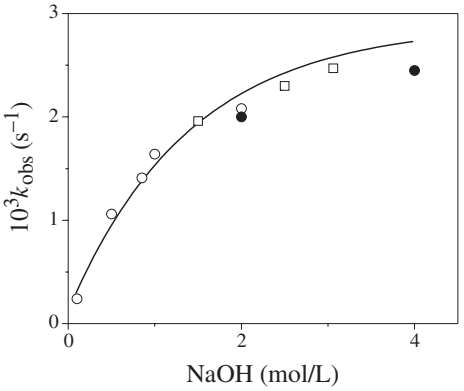


Fig. 5. Basic hydrolysis of ETE at 100 °C. Average from values calculated from the Guggenheim method and assuming absorbance = 0 at t_∞ (○); calculated from the Guggenheim method (□); average calculated from the Guggenheim method at 4 μ (NaCl) (●).



close to zero considering the standard deviation. This value is characteristic of an A1 mechanism (23).

The conjugate acid SH_2^+ should be preferentially N-protonated to produce ethylamine by breaking the N—C bond, and an ethyl thionformyl cation (S=C$^+$-OEt), which hydrolyzes rapidly to produce COS and ethanol.

Basic hydrolysis

At pH > 6.5, the pH–rate profile of ETE presented an increase of the rate constants that reached a plateau at high basicity (Fig. 5).

At high basicity, $K' = 1 + \dfrac{K_2}{a_{H^+}}$

because $1 + \dfrac{K_2}{a_{H^+}} >> \dfrac{a_{H^+}}{K_1}$.

Also $k^{o}_{obs} >> k_N$ and $\dfrac{k_E K_2[OH^-]}{K_w K'} >> k_H \dfrac{a_{H^+}}{K_1 K'} + \dfrac{k_N}{K'}$.

Therefore,

$$[10] \qquad k^{o}_{obs} = \frac{k_E K_2[OH^-]}{K_w + K_2[OH^-]} = \frac{k_E K_2}{a_{H^+} + K_2}$$

The reciprocal plot of $1/k^{o}_{obs}$ vs. $1/[OH^-]$ was linear (r = 0.999) and allowed the calculation of $k_E = 3.79 \times 10^{-3}$ s^{-1} and $pK_2 = -pK_b = 12.43$. At 25 °C the experimental value of pK_2 was 13.6. The difference of 1.2 pK units with temperature is about the same as that found for the *N*-aryl thioncarbamate series (24).

Equation [5] assumed that the specific basic catalysis occurs through the E1cb mechanism, but it is also possible that it occurs by a $B_{Ac}2$ mechanism as shown in Scheme 2. Both have been observed for carbamate esters (25, 26).

The E1cb mechanism eliminates ethoxide ion from the thioncarbamate anion in the rate-determining step, producing an isothiocyanate intermediate that decomposes rapidly to form ethylamine and COS as products. The $B_{Ac}2$ mechanism produces a tetrahedral intermediate in the slow step, which forms the products through several consecutive fast reactions. Neither of these mechanisms can be kinetically distinguished, as shown by eqs. [11] and [12].

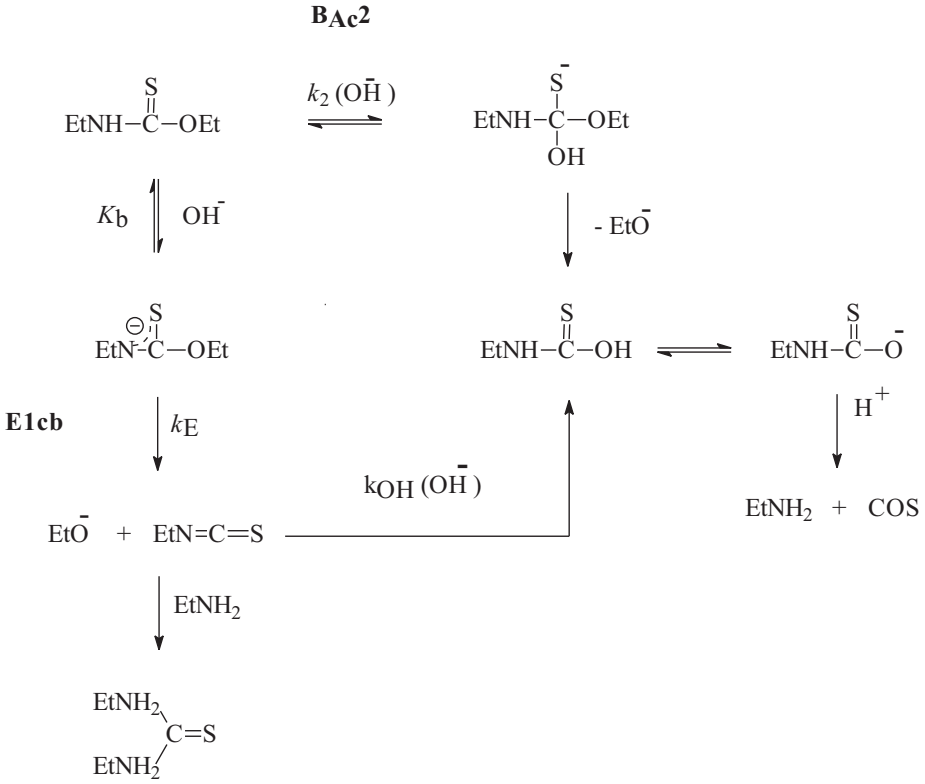
$$[11] \qquad k_{obs} = \frac{k_E K_2}{a_{H^+} + K_2} \text{ (E1cb)}$$

$$[12] \qquad k_{obs} = \frac{k_2 K_w}{a_{H^+} + K_2} \text{ ($B_{Ac}2$)}$$

For ETE, the reciprocal plot from the $B_{Ac}2$ kinetic equation gave $k_2 = 2.58 \times 10^{-3}$ (mol/L)$^{-1}$ s^{-1} and the same pK_2 = 12.43 found from the E1cb equation. To hydrolyze by E1cb mechanism, the substrate must form the conjugate base by ionization of the N—H bond. Therefore, the basic hydrolysis of DETE must occur by the $B_{Ac}2$ mechanism. The hydrolysis rate constant of DETE increased linearly at 1–3 mol/L of NaOH with a second-order rate constant, $k_2 = 2.3 \times 10^{-4}$ (mol/L)$^{-1}$ s^{-1}, i.e., 10 times slower than the value expected for ETE. It has been noted in earlier works that *N*-alkyl carbamate esters hydrolyze more rapidly than *N*,*N*-dialkyl esters (27, 28).

© 2005 NRC Canada

Scheme 2. Mechanisms involved in the basic hydrolysis of ETE at 100 °C.



The alternative of either mechanism depends on the difference of free energy of activation to overpass the kinetic barrier. Comparison of $\Delta G^{\ddagger}$ of DETE and ETE results in a difference of ca. 1 kcal mol^{-1} more favorable to the E1cb path (Table 1). For ETE, the total barrier is divided into two terms: the basic N-H ionization to form the thioncarbamate anion (pK_2 = 13.6, Scheme 1, $\Delta G^{\ddagger}$ = 21.2 kcal mol^{-1}), and the expulsion of the ethoxide anion producing ethyl isothiocyanate ($\Delta G^{\ddagger}$ = 26.2 kcal mol^{-1}). In comparison to the carbamate analogues, the path through the E1cb mechanism of ETE is greatly favored because of the decrease in pK_2 owing to the strong electron-withdrawing effect of the thiocarbonyl group. It corresponds to a pK_a = 24.7 at 100 °C, or 16 pK units higher than ethylamine. This is a reasonable value because, for alkyldithiocarbamates, a decrease in the basicity of the N by 14 pK units with respect to the parent amine was calculated (29).

For the carbamate ester series, it was observed that reactions occurring through the E1cb mechanism were much faster than those ocurring through the $B_{Ac}2$ mechanism (25–27, 30) because of a sharp decrease in $\Delta H^{\ddagger}$ (25–27). The activation parameters of ETE and DETE are also consistent with this observation as shown in Table 1.

One important feature of the E1cb mechanism is the formation of the ethyl isothiocyanate intermediate. Experiments with ETE in 0.6 mol/L of NaOH in the presence of an excess of ethylamine showed the formation of diethyl thiourea (Scheme 2). Diethyl thiourea could only be formed from the isothiocyanate because ethylaminolysis of ethyl *O*-ethylxanthate produced only ethyl *N*-ethylthioncarbamate, and the reaction did not go further (31). Therefore, this result provides strong evidence that the basic hydrolysis occurs by the E1cb mechanism, the same as was found for aryl *N*-arylcarbamates (26), aryl *N*-arylthioncarbamates (32), and ethyl *N*-arylthioncarbamates (24).

The curve of the pH–rate profile in Fig. 2 was drawn using eq. [5], written as eq. [13]

$$[13] \quad k^{o}_{obs} = \frac{k_H}{K_1} a_{H^+} + k_N + \frac{k_E K_2}{a_{H^+} + K_2}$$

where $\log \frac{k_H}{K_1} = -5.36$.

General catalysis

The E1cb mechanism in Scheme 2 involves a fast preequilibrium deprotonation by hydroxide ion followed by a slow elimination of the ethoxide ion. However, for weak bases the deprotonation step is the rate-determining step, followed by a fast elimination reaction. This mechanism leads to general base catalysis.

General base catalysis was observed for ETE in the pH 3–11 range (Table 2) for conjugate bases of oxy acids and ammonium ion. The rate constants increased linearly with increasing concentration of the general base. No catalysis was detected for acetate within the experimental error. For succinate, tetraborate, and carbonate, monoanion and dianion species are present at the experimental pH, and both can act as catalysts. The molar fractions of the monoanions and dianions were considered to calculate the second-order general base catalysis rate constant (k_B).

The Brønsted plot of logk_B vs. pK_a, statistically corrected (Fig. 6), gave a straight line for the conjugate bases of oxy acids (without hydroxide ion) with β = 0.48 ± 0.04 (r = 0.989). Ethylamine was about two orders of magnitude more

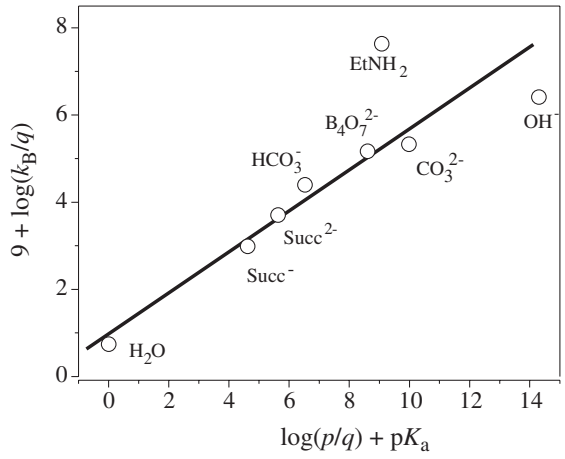
© 2005 NRC Canada

Table 2. General catalysis of the hydrolysis of ethyl *N*-ethylthioncarbamate at 100 °C.

Acid	Conjugate base	pK_a at 25 °C	pK_a at 100 °C	k_B ((mol/L)$^{-1}$ s^{-1})
Hydron				
H_3O^+	H_2O	(–1.75)	0.0	5.5×10^{-9}[a]
Succinic acid				
$HOOC(CH_2)_2COOH$	$HOOC(CH_2)_2COO^-$	4.21[b]	4.32[c,d,e]	9.75×10^{-7}
	$-OOC(CH_2)_2COO^-$	5.64[b]	5.93[c,d,e]	1.02×10^{-5}
Tetraborate monoanion				
$HB_4O_7^-$	$B_4O_7^{2-}$	9.24[c]	8.91[f]	2.94×10^{-4}
Carbonic acid				
H_2CO_3	HCO_3^-	6.35[b]	6.23[d]	2.50×10^{-5}
	CO_3^{2-}	10.33[c]	10.28[g]	4.27×10^{-4}
Ethylammonium ion				
$CH_3CH_2NH_3+$	$CH_3CH_2NH_2$	10.63[b]	8.60[d,h,i]	4.3×10^{-2}
Water				
H_2O	OH^-	15.74[j]	14.0[g]	2.58×10^{-3}[k]

[a] k_N at 1 mol/L concentration.
[b] V.E. Bower and R.G. Bates. *In* Handbook of analytical chemistry. 1st ed. *Edited by* L. Meites. McGraw Hill, New York. 1963.
[c] R.G. Bates and R. Gary. J. Res. Nat. Bur. Stand. **65A**, 495 (1961).
[d] H.S. Harned and N.D. Embree. J. Am. Chem. Soc. **56**, 1050 (1934).
[e] pK_{a1}: t_m = 46.60, pK_m = 4.185; pK_{a2}: t_m = 22.63, pK_m = 5.638.
[f] Reference 14*a*.
[g] Reference 14*b*.
[h] Reference 11.
[i] Calculated for ethylammonium (pK_m = 5.857, t_m = 334).
[j] H.S. Harned and R.A. Robinson. Trans. Faraday Soc. **36**, 973 (1940).
[k] From eq. [12] assuming a $B_{Ac}2$ mechanism.

Fig. 6. Brønsted plot of the general catalysis of the hydrolysis of methyl *N*-methylthioncarbamate at 100 °C. Without considering ethylamine and hydroxide ion, $\beta = 0.48 \pm 0.04$ ($r = 0.989$).



effective as a catalyst than the corresponding oxy acid, which is to be expected, since it is a better nucleophile toward the thiocarbonyl group. The second-order rate constant k_B for OH^- was calculated assuming the $B_{Ac}2$ mechanism (eq. [12]), and its low value is attributed to the high hydration of the ion (13). Nevertheless, the fast and reversible deprotonation of ETE at 25 °C (see Experimental) showed that the specific basic catalysis must form the ester anion in a fast step at 100 °C, which slowly decomposed to produce ethyl isothiocyanate by the E1cb mechanism.

For the series of carbamate and thioncarbamate esters, only a small general base catalysis was observed for *p*-nitrophenyl *N*-methylcarbamate (30), and no general catalysis was observed for alkyl *N*-arylthioncarbamates (24) or aryl *N*-arylthioncarbamates (32). The slow proton transfer step from ETE is a consequence of the high pK_a (24.7) of the N-H dissociation. For *N*-arylthioncarbamates, the dissociation is ca. 3 pK units more favorable.

Water catalysis

The Brønsted plot showed that water acts as a general base in the pH-independent region of the pH–rate profile, and therefore in that region, k_{obs} can be expressed by eq. [14], where k_N is the water-catalyzed (pseudo-)first-order rate constant, and k_B is the catalytic coefficient of the general bases.

$$[14] \quad k_{obs} = k_N + k_B[B]$$

The value of $k_N = 3.06 \times 10^{-7}$ s^{-1} was obtained from the average of k_{obs} extrapolated to zero buffer concentration in the pH 2–6.5 range. The total molecularity of the reaction is at least two, but the exact value cannot be determined from the kinetic data, since the water concentration remained constant. In the absence of other general bases, the water-catalyzed, pH-independent hydrolysis is the only reaction.

The activation parameters for the water catalysis are shown in Table 1. It is known that water can catalyze a reaction as a nucleophile, a general acid, or a general base. The hydrolysis of activated amides and carboxylic esters are water-catalyzed between pH 2.0 and 5.5 via a dipolar activated complex in which two water molecules, one acting as a nucleophile and one acting as a general base, are involved (33). In carboxylic ester hydrolysis, values of the entropy of activation of –30 to –40 cal mol^{-1} K^{-1} are common (34),

© 2005 NRC Canada

while for primary and secondary halides and sulfonates they are ca. –10 cal mol^{-1} K^{-1} (35). For reactions where the nucleophilic attack of water on a thiocarbonyl is catalyzed by a second molecule of water, the entropy of activation is in the –40 to –25 cal mol^{-1} K^{-1} range (36). The value of the entropy of activation (–27.3 cal mol^{-1} K^{-1}) for the water catalysis of ETE is consistent with the postulated mechanism, considering the lack of examples where water catalyzes a reaction exclusively as a general base. The large value of β = 0.48 obtained from the Brønsted plot suggests that the transition state is highly polar resulting in electrostriction of the bulk solvent, inducing a number of water molecules to be tightly constrained, which results in a large negative entropy of activation.

Conclusions

The acid hydrolysis of ETE at 100 °C occurs through an A1 mechanism, most likely with N-protonation and formation of ethylamine by N—C bond breakage, and an ethyl thionformyl cation ($S=C^{+}$-OEt) that hydrolyzes rapidly to produce COS and ethanol.

At pH 2–6.5, where the main species is the neutral substrate, the hydrolysis is pH-independent and is catalyzed by water as a general base. General bases catalyze the slow proton transfer from the neutral species to form an isothiocyanate intermediate.

The ETE anion hydrolyzes with specific basic catalysis by E1cb mechanism, forming ethyl isothiocyanate in the rate-determining step, which decomposes rapidly to products.

Acknowledgements

The scholarship for E.P.de S. and the research fellowship for E.H. of the Brazilian Conselho Nacional de Pesquisa Científica e Tecnológica (CNPq) are gratefully acknowledged.

References

1. (*a*) R. Huxtable. Biochemistry of sulfur. Plenum Press, New York. 1986; (*b*) G.D. Thorn and R.A. Ludwig. The dithiocarbamates and related compounds. Elsevier, Amsterdam. 1962; (*c*) R.J. Cremlyn. *In* Herbicides and fungicides. *Edited by* N.R. McFarlane. The Chemical Society Spec. Publ., London. 1976; (*d*) R.J. Cremlyn. Pesticides. Preparation and mode of action. Wiley, Chichester. 1978; (*e*) J.R. Corbett, K. Wright, and A.C. Baillie. The biochemical mode of action of pesticides. Academic, London. 1984.
2. (*a*) D. Martin. Monatsber. Dtsch. Akad. Wiss. Berlin, **7**, 520 (1964); (*b*) S. Rich and J.G. Horsfall. Conn. Agric. Exp. St. **639**, 1 (1961); (*c*) D. Martin. Sitzungsber. Dtsch. Akad. Wiss. Berlin, **6**, 56 (1962); (*d*) T. Noguchi, Y. Hashimoto, K. Miyazaki, and K. Aritsune. Yakugaku Zasshi, **88**, 335 (1968); (*e*) T. Noguchi, K. Miyazaki, K. Aritsune, Y. Hashimoto, S. Kosaka, M. Kikuchi, and R. Sakimoto. Yakugaku Zasshi, **88**, 344 (1968).
3. T. Noguchi, K. Miyazaki, K. Kikawa, and Y. Hashimoto. Yakugaku Zasshi, **88**, 465 (1968).
4. (*a*) A.V. Glembotskii, L. Shubov, and A.K. Livishits. Tsvetn. Metall. **41**, 8 (1968); (*b*) W.A. Douglas. US Patent 1 674 166, 1928; (*c*) G.H. Harris and A. Fichback. US Patent 2 691 635, 1954.
5. (*a*) G. Wener. US Patent 2 2276 553, 1942; (*b*) C.F.H. Allen and P.W. Vittum. US Patent 2 313 498, 1943; (*c*) G.W.Staton and F.A. Ehlers. US Patent 2 735 833, 1956; (*d*) J. Claudim, J.P. Sisley, and G. Bilger. French Patent 881 458, 1943; (*e*) W.D. Stevenson and S. Smiles. J. Chem. Soc. 1740 (1930); (*f*) C.T. Griensheim. German Patent 859 458, 1952; (*g*) M.F. Torrence. US Patent 2 658 091, 1953; (*h*) R.H. Cooper. US Patent 2 333 468, 1943; (*i*) T.F Wood and J.H. Garder. J. Am. Chem. Soc. **63**, 2741 (1941).
6. E. Humeres, L.F. Sequinel, M. Nunes, C.M.S. Oliveira, and P.J. Barrie. J. Phys. Org. Chem. **7**, 287 (1994).
7. A.I. Vogel. A textbook of practical organic chemistry. Longmans, London. 1971. p. 499.
8. G. Bulmer and F.G. Mann. J. Chem. Soc. 666 (1945).
9. M.C. Rezende. M.Sc. dissertation, Universidade Federal de Santa Catarina, Florianópolis, Brazil. 1976.
10. K. Horiuti and Y. Kurosu. Tokyo Iji Shinshi, 968 (1940).
11. J.A. Dean (*Editor*). Lange's handbook of chemistry. 13th ed. McGraw Hill, New York. 1985.
12. D.R. Lid (*Editor*). Handbook of chemistry and physics. 80th ed. CRC Press, New York. 1999–2000.
13. C.D. Ritchie and J.F. Coetze. Solute–solvent interactions. Marcel Dekker, New York. 1969. Chap. 3.
14. (*a*) E. Humeres, J. Quijano, and M.M.S. de Souza. J. Bras. Chem. Soc. **1**, 99 (1990); (*b*) E. Humeres, J. Quijano, and M.M.S. de Souza. Atual. Fis. Quim. Org. *Edited by* E. Humeres. IOESC, Florianópolis, Brazil. 1987. p. 198.
15. E.A. Guggenheim. Philos. Mag. **2**, 538 (1926).
16. R.A. Cox. Adv. Phys. Org. Chem. **35**, 1 (2000).
17. H.S. Harned and R.A. Robinson. Trans. Faraday Soc. **36**, 973 (1940).
18. L. Zucker and L.P. Hammett. J. Am. Chem. Soc. **61**, 2791 (1939).
19. (*a*) R.A. Cox. Acc. Chem. Res. **20**, 27 (1987); (*b*) R.A. Cox and K. Yates. Can. J. Chem. **57**, 2944 (1979).
20. (*a*) A.J. Kresge, R.A. More O'Ferrall, L.E. Hakka, and V.P. Vitullo. J. Chem. Soc. Chem. Commun. 46 (1965); (*b*) A.J. Kresge, S.G. Mylonakis, Y. Sato, and V.P. Vitullo. J. Am. Chem. Soc. **93**, 6181 (1971).
21. A. Bagno, G. Scorrano, and R.A. More O'Ferrall. Rev. Chem. Intermed. **7**, 313 (1987).
22. V. Luchini, G. Modena, G. Scorrano, and U. Tonellato. J. Am. Chem. Soc. **99**, 3387 (1977).
23. (*a*) L.L. Schaleger and F.A. Long. Adv. Phys. Org. Chem. **1**, 1 (1963); (*b*) J. Koskikallio and E. Whalley. Trans. Faraday Soc. **55**, 809 (1959); (*c*) F. Brescia and V.K. Lamer. J. Am. Chem. Soc. **62**, 612 (1940); (*d*) P. Salomaa. Suom. Kemistil. B, **B33**, 11 (1960); (*e*) L.K. Briche and L.P. Lindsay. J. Am. Chem. Soc. **82**, 3538 (1960).
24. E. Humeres, C. Zucco, M. Nunes, N.A. Debacher, and R.J. Nunes. J. Phys. Org. Chem. **15**, 570 (2002).
25. L.W. Dittert and R. Higuchi. J. Pharm. Sci. **52**, 852 (1963).
26. (*a*) A.F. Hegarty and L.N. Frost. J. Chem. Soc. Chem. Commun. 500 (1972); (*b*) A.F. Hegarty and L.N. Frost. J. Chem. Soc. Perkin Trans. 2, 1719 (1973).
27. L.W. Dittert. Diss. Abstr. **22**, 1837 (1961).
28. I. Christenson. Acta Chem. Scand. **18**, 398 (1964).
29. E. Humeres, M.M.S. de Souza, N.A. Debacher, J.D. Franco, and A. Schutz. J. Org. Chem. **63**, 1598 (1998).
30. M. Bender and R.B. Homer. J. Am. Chem. Soc. **30**, 3975 (1965).
31. E. Humeres, V. Soldi, M. Klug, M. Nunes, C.M.S. Oliveira, and P.J. Barrie. Can. J. Chem. **77**, 1050 (1999).

© 2005 NRC Canada

32 (*a*) G. Sartore, M. Bregon, and J.P. Calmon. Tetrahedron Lett. **36**, 3133 (1974); (*b*) A. Williams, S.V. Hill, and S. Thea. J. Chem. Soc. Perkin. Trans. 2, 437 (1983).
33. (*a*) T.H. Fife and D.M. McMahon. J. Am. Chem. Soc. **91**, 7481 (1969); (*b*) W. Karzijn and J.B.F.N. Engberts. Tetrahedron Lett. 1787 (1978); (*c*) J.F.F. Engbersen and J.B.F.N. Engberts. J. Am. Chem. Soc. **97**, 1563 (1975); (*d*) N.J. Buurma, L. Pastorello, M.J. Blandamer, and J.B.F.N. Engberts. J. Am. Chem. Soc. **123**, 11848 (2001).
34. S.L. Johnson. Adv. Phys. Org. Chem. **5**, 237 (1967).
35. (*a*) R.L. Heppolette and R.E. Robertson. Proc. R. Soc. London Ser. A, **A252**, 273 (1959); (*b*) R.L. Heppolette and R.E. Robertson. Can. J. Chem. **44**, 677 (1966); (*c*) R.E. Robertson. Can. J. Chem. **35**, 613 (1957); (*d*) R.E. Robertson, A. Stein, and S.E. Sugamori. Can. J. Chem. **44**, 685 (1966).
36. E. Humeres, L.F. Sequinel, M. Nunes, C.M.S. Oliveira, and P.J. Barrie. Can. J. Chem. **76**, 960 (1998).

© 2005 NRC Canada

The HERON reaction — Origin, theoretical background, and prevalence[1]

Stephen A. Glover, Arvi Rauk, Jeanne M. Buccigross, John J. Campbell, Gerard P. Hammond, Guoning Mo, Luke E. Andrews, and Ashley-Mae E. Gillson

Abstract: The origin of the HERON reaction is reviewed from a historical perspective and shown to have its foundation in the unusual properties of bisheteroatom-substituted amides, so-called anomeric amides. The reaction involves migration of anomerically destabilized oxo-substituents on an amide nitrogen to the amide carbon and dissociation of the amide bond. Computational work providing a theoretical basis for the reaction is presented, together with physical organic measurements that support results therefrom. The rearrangement has been observed in a number of chemical transformations of *N*-alkoxy-*N*-aminoamides, reactions of 1-acyloxy-1-alkoxydiazenes, *N*-alkoxy-*N*-aminocarbamates, *N*-alkoxyhydroxamic acids, as well as in the gas-phase reactions of *N*-acyloxy-*N*-alkoxyamides.

Key words: HERON reaction, anomeric amides, rearrangements, hindered esters, concerted reactions.

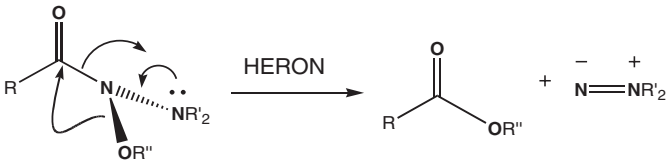
Résumé : On a fait une revue historique de l'origine de la réaction HERON et on montre que sa base réside dans les propriétés inhabituelles des amides portant des substituants bishétéroatomiques, les amides dits anomères. La réaction implique la migration de substituants oxo anomériquement déstabilisée de l'azote d'un amide vers le carbone de l'amide accompagnée d'une dissociation de la liaison amide. On présente un ensemble de calculs théoriques qui sert de base pour expliquer la réaction ainsi que des mesures de chimie organique physique qui supportent les résultats de ces calculs. Le réarrangement a été observé dans un certain nombre de transformations chimiques de *N*-alkoxy-*N*-aminoamides, dans les réactions de 1-acyloxy-1-alkyoxydiazènes, de *N*-alkoxy-*N*-aminocarbamates et d'acides *N*-alkoxyhydroxamiques ainsi que dans les réactions en phase gazeuse de *N*-acyloxy-*N*-alkoxyamides.

Mots clés : réaction HERON, amides anomères, réarrangements, esters stériquement empêchés, réactions concertées.

Introduction

The HERON reaction (Scheme 1) was conceived during our investigations into the reactions of a highly unusual class of mutagenic amides, the *N*-acyloxy-*N*-alkoxyamides (1, 2). It was annointed at the Second Heron Island Conference on Reactive Intermediates and Unusual Molecules, which was held on Heron Island in 1994, and, more recently, confirmed as a named reaction in the 13th edition of *The Merck Index* (3). *N*-Acyloxy-*N*-alkoxyamides are members of the class of anomeric amides that bear two heteroatoms bonded to the amide nitrogen (4). These highly unusual amides are direct-acting mutagens in that they mutate *Salmonella typhimurium* in the Ames test without the need for metabolic activation. Since the initial discovery (5, 6), we have synthesized well over 70 examples and nearly all those that we have tested are mutagenic (7). The direct mutagenicity of this class of amides has led to a quantitative structure–activity relationship (QSAR) from which we can predict the mutagenic activity of virtual congeners, but, equally as interesting, we can identify and quantify unusual molecular interactions of structural elements with DNA (8).

Scheme 1.



Structure of anomeric amides

N-Acyloxy-*N*-alkoxyamides, as with all anomeric amides, possess pyramidalized nitrogen atoms (4). Early computational work at the AM1 level confirmed a tendency to highly developed sp^3 hybridization at nitrogen (2, 4), and, subsequently, so too have more rigorous ab initio calculations at both the HF/6-31G* and the B3LYP/6-31G* density functional theory (DFT) levels of theory (9–11). This conformational

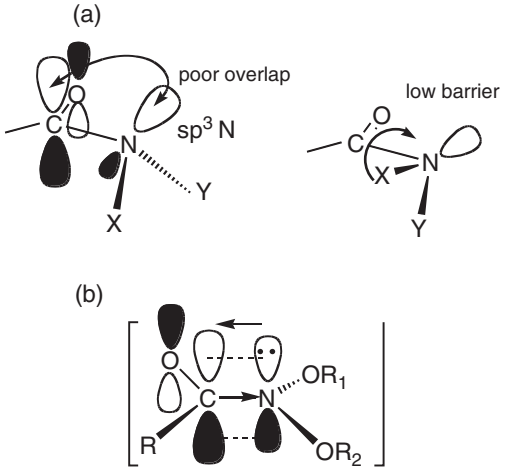
Received 12 May 2005. Published on the NRC Research Press Web site at http://canjchem.nrc.ca on 22 November 2005.

S.A. Glover,[2] J.J. Campbell, G.P. Hammond, G. Mo, L.E. Andrews, and A.-M.E. Gillson. School of Biological, Biomedical and Molecular Sciences, University of New England, Armidale, New South Wales 2350, Australia.
J.M. Buccigross. Department of Chemistry and Physical Sciences, College of Mount St. Joseph, Cincinnatti, OH 45233-1670, USA.
A. Rauk. Department of Chemistry, University of Calgary, Calgary, AB T2N 1N4, Canada.

[1]This article is part of a Special Issue dedicated to organic reaction mechanisms.
[2]Corresponding author (e-mail: sglover@une.edu.au).

 doi: 10.1139/V05-150 © 2005 NRC Canada

Fig. 1. (*a*) Facile amide isomerism in anomeric amides. (*b*) Stabilization that raises isomerization barriers in planar amides.



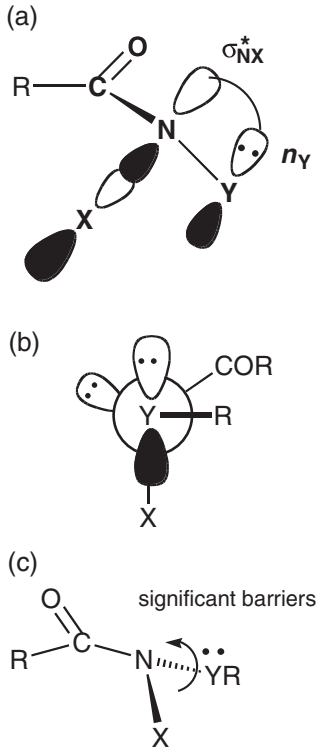
change is readily interpreted in terms of electronegativity of the nitrogen substituents.

It is well-known that atoms geminally substituted with heteroatoms tend towards pyramidality. In qualitative terms, relative to sp^2 hybridization, sp^3 hybridization at the central atom and the consequent increase in p character in the σ bonds enables electron density to be closer to the more electronegative ligands. Thus, anomeric amides possess a nitrogen that substantially deviates from planarity and the increased "s" content of the lone pair drastically reduces lone pair delocalization onto the carbonyl. The intrinsic barrier to rotation about the N—C(O) bonds (Fig. 1*a*), a barrier that is significant in normal amides (12) and hydroxamic esters, (9, 13) and which often leads to dynamic effects in their ^1H NMR spectra at room temperature, is largely lost. Wiberg (14) recently argued that the barrier in "normal" amides is a combination of a π type HOMO–LUMO overlap between the lone pair on nitrogen and the $\pi^*_{C=O}$ molecular orbital combined with a synergistic σ type back donation to the electronegative sp^2 nitrogen (Fig. 1*b*). In anomeric amides both effects disappear on account of the sp^3 hybridization at nitrogen and barriers to isomerization have been found to be drastically reduced or are too low to be measured by dynamic NMR methods (4, 10). Ab initio calculations confirm these properties (4, 9, 10, 15).

N-Acyloxy-*N*-alkoxyamides amides should have longer than normal N—C(O) bonds and shorter carbonyl bonds resulting in higher than expected IR carbonyl stretch frequencies. This has been experimentally determined in that all *N*-acyloxy-*N*-alkoxyamides exhibit amide carbonyl stretch frequencies between 1710 and 1760 cm^{-1} (4). In addition, these amides sustain anomeric effects through the amide nitrogen by which the lone pair on one heteroatom (Y) interacts with the σ* orbital between nitrogen and the other heteroatom X (Fig. 2*a*), thus shortening the Y—N bond and weakening the N—X bond. The ground-state conformations in anomeric amides should facilitate this overlap and, depending upon its strength, barriers to rotation about the N—Y bond can be expected to be greater than predicted by steric effects alone (Figs. 2*b* and 2*c*).

The structural features outlined above have been verified by X-ray crystallography. We recently published the structures of the "most pyramidal" amides, both *N*-acyloxy-*N*-alkoxyamides, which verify the conformational effects previously described (Fig. 3*a*) (16). Not only do they exhibit highly pyramidal nitrogens (avg. angle ~ 108°) and very long N—C bonds, their alkoxy O—N bonds are shortened while the N—O acyl bond is long. Similarly, the related *N*,*N*′-dialkoxy-*N*,*N*′-diacylhydrazine possesses pyramidal nitrogens, long N—C bonds and a short N—N bond (Fig. 3*b*). Both structures exhibit a conformational preference that clearly optimizes either the n_O— σ^*_{NO} or the n_N—σ^*_{NO} overlap (15, 16).

Fig. 2. (*a*) Anomeric overlap, (*b*) conformational preference, and (*c*) rotationally restricted bond in anomeric amides.



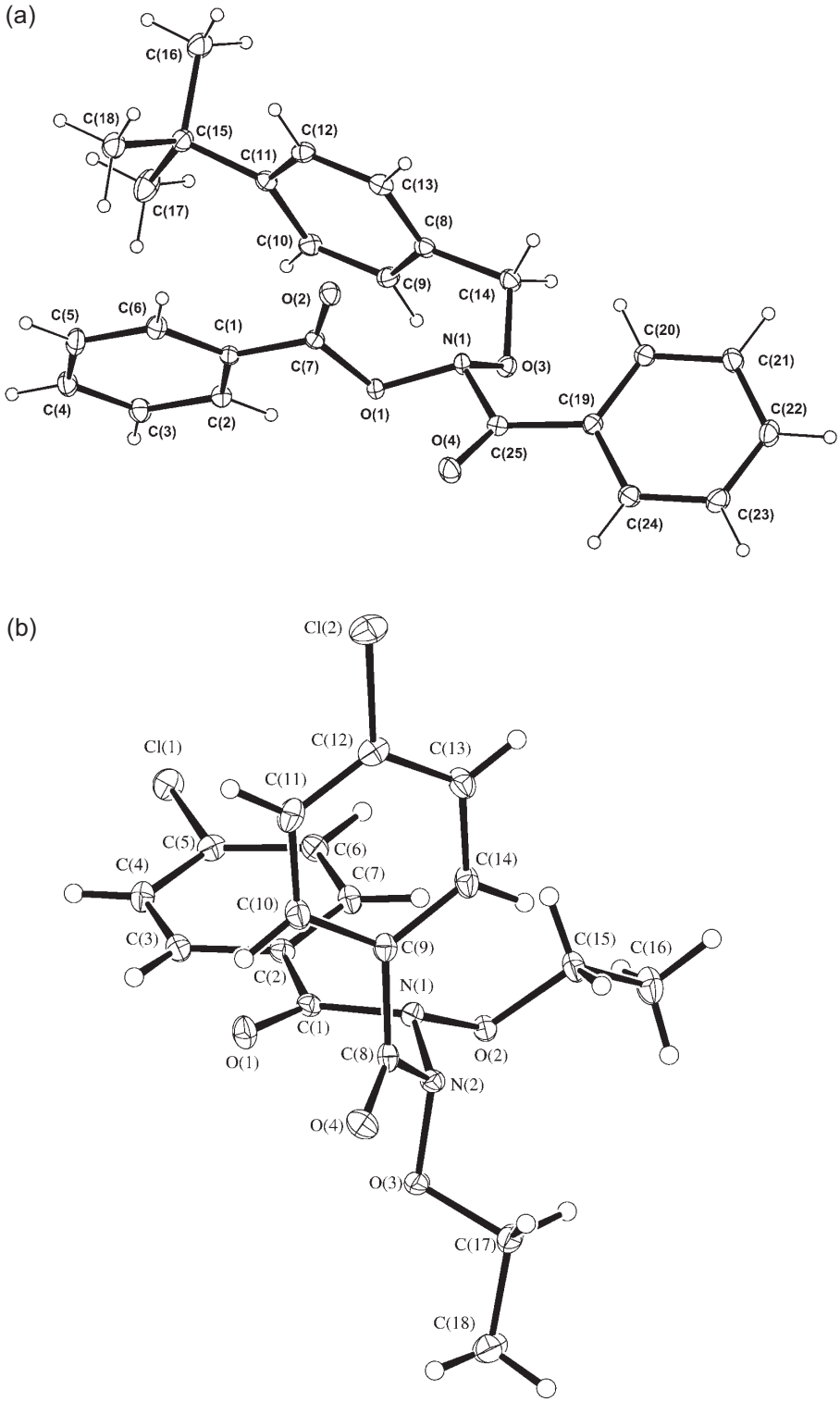
Reactivity of anomeric amides

The XNY system should be polarized as shown in Fig. 4. Where Y is a strong electron pair donor (e.g., nitrogen), and X a strongly electron affinic atom such as halogen or in the case of *N*-acyloxy-*N*-alkoxyamides, the acyloxy oxygen, elimination might be expected yielding in the process a stabilized nitrenium ion (Fig. 4*a*). Work in these laboratories and elsewhere has established that nitrenium ions are strongly stabilized by neighbouring heteroatoms (17–28). Such a process would be promoted by polar solvents as well as acid or Lewis acid complexation with X. Thus, unimolecular decomposition would be expected in strongly anomeric systems.

In S_N2 reactions, substituents at the central atom that can stabilize cationic character will also stabilize the S_N2 transition state leading to longer bonds to both the nucleophile and the leaving group (29–31). Thus, in systems with moderate anomeric overlap, this together with negative hyperconjugation and anchimeric assisted weakening of the N—X bond should promote S_N2 reactions at nitrogen leading to loss of X^- (Fig. 4*b*).

© 2005 NRC Canada

Fig. 3. ORTEP depictions of: (*a*) *N*-benzoyloxy-*N*-(4-*tert*-butylbenzyloxy)benzamide and (*b*) *N*,*N*′-di(*p*-chlorobenzoyl)-*N*,*N*′-diethoxyhydrazine with thermal ellipsoids depicted at the 20% and 25% levels, respectively.



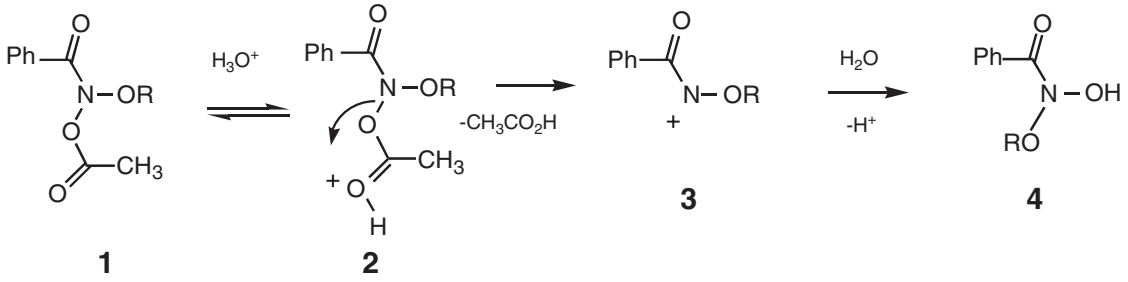
Discussion

The HERON reaction

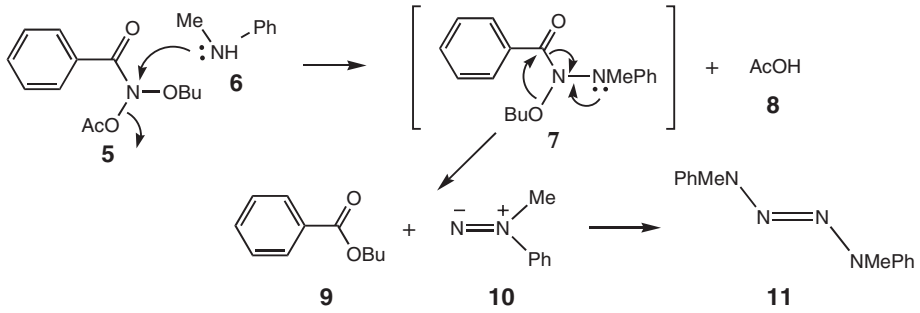
As a part of an investigation into the mechanism of their mutagenic action we subjected *N*-acetoxy-*N*-alkoxybenzamides **1** to a range of solvolytic studies and reactions with potential biological nucleophiles (1, 4, 6, 11, 21, 32–34). They hydrolyse very slowly at neutral pH, but, as predicted, upon protonation on the acetoxy group **2** with acid catalysis in aqueous acetonitrile, they undergo rapid decomposition by the unusual $A_{Al}1$ mechanism leading to *N*-acyl-*N*-alkoxynitrenium ions **3**, which react rapidly with water leading to

© 2005 NRC Canada

Scheme 2.



Scheme 3.



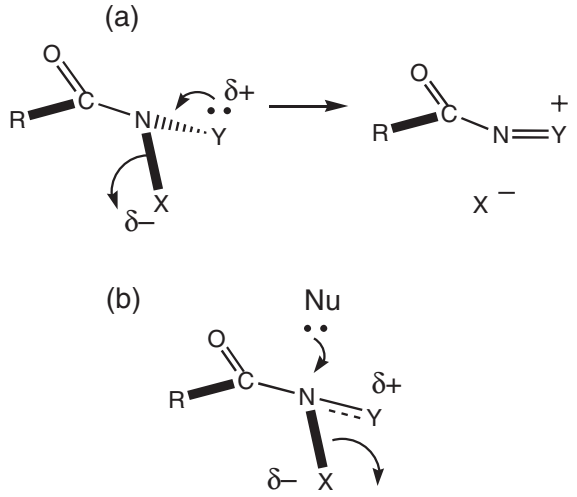
N-alkoxyhydroxamic acids **4** and a variety of secondary products (Scheme 2).

However, a fundamental difference between these and all other conventional amides is that they are susceptible to S_N2 reactions at the amide nitrogen. Treatment of *N*-acyloxy-*N*-alkoxybenzamides with aromatic amines in methanol results in S_N2 displacement of the acyloxy group to give, as intermediates, *N*-alkoxy-*N*-arylaminobenzamides (1, 11, 35). These too are strongly anomeric on account of a high energy lone pair on nitrogen and the electronegative oxygen of the alkoxyl group. With *N*-methyl aniline (**6**) in methanol or aqueous acetonitrile, *N*-acetoxy-*N*-butoxybenzamide (**5**) afforded an excellent yield of butyl benzoate (**9**) and acetic acid (**8**). Close examination of these highly coloured reaction mixtures indicated the presence of crystals of *N*,*N*′-dimethyl-*N*,*N*′-diphenyl tetrazene (**11**) (Scheme 3). A crossover experiment using a mixture of *N*-acetoxy-*N*-butoxy-*p*-toluamide and *N*-acetoxy-*N*-ethoxybenzamide afforded clean yields of butyl *p*-toluate and ethyl benzoate, thus pointing to an intramolecular rearrangement.

In Scheme 3, the S_N2 reaction leads to the intermediate *N*-butoxy-*N*-(*N*′-methylanilino)benzamide (**7**). Anomeric weakening of the N—O bond in **7** results not in heterolysis to alkoxide ion, which would be energetically unfavourable, but rather migration of the butoxyl group from the amide nitrogen to the carbonyl carbon and heterolysis of the N—C bond. This reaction results in the formation of 1-methyl-1-phenyldiazene (**10**), which under the reaction conditions dimerizes to the tetrazene **11**. These rearrangement processes are characterized by a transition state in which the alkoxyl group migrates from the amide nitrogen to the carbonyl carbon (Fig. 5*a*) and therefore involves heteroatom rearrangements on nitrogen, the HERON reaction[3] (2).

Thus, the HERON reaction, as well as the unique properties of *N*-acyloxy-*N*-alkoxyamides, can be ascribed to the configuration at nitrogen, namely bisheteroatom substitution.

Fig. 4. (*a*) Anomerically induced elimination. (*b*) S_N2 reaction at nitrogen.



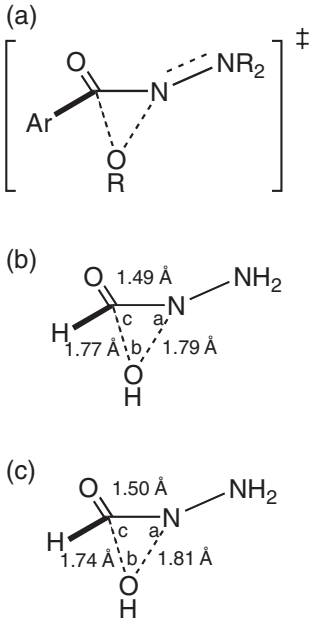
Computational verification of the HERON reaction

This reaction, though published in the early 1990s, was named in the literature in a 1995 paper in which we presented a semiempirical molecular orbital treatment of the HERON reactions of a range of anomeric amides (2). AM1 predicted, adequately, the ground-state properties of various anomeric amides, as well as the relative propensity for HERON migration of a variety of geminal heteroatom substituents on nitrogen. In general, the activation energy was lowered with an amino substituent and more electronegative migrating atoms or electron-deficient groups. In the case of

[3] Presented to the 2nd Heron Island Conference on Reactive Intermediates and Unusual Molecules. The authors are grateful to Professor Richard Wong who suggested that the reaction deserved to be named.

© 2005 NRC Canada

Fig. 5. (*a*) Transition state for a HERON reaction of an *N*-alkoxy-*N*-aminoamide. Computed transition states for the migration of hydroxyl in *N*-amino-*N*-hydroxyformamide at: (*b*) AM1 (a = 65°, b = 45°, and c = 65°) and (*c*) HF/6-31G* (a = 63°, b = 48°, and c = 69°) levels.

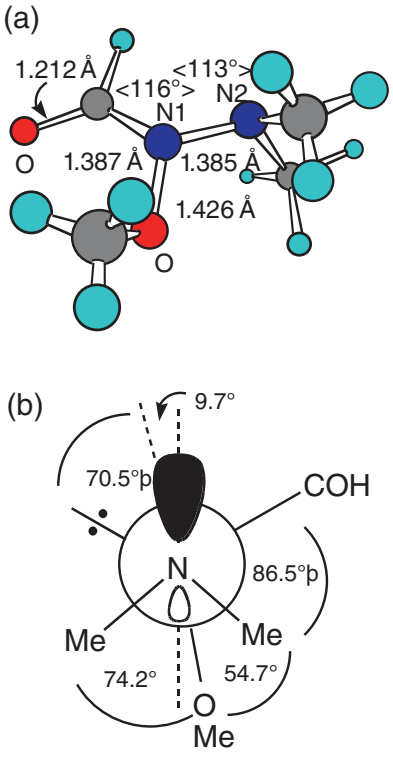


N-alkoxy-*N*-aminoamides, we attributed this to better anomeric weakening of the N—OR bond through a favourable interaction between a high energy nitrogen lone pair and a low energy N—OR σ* orbital. A transition state was predicted that indicated partial bonding between the migrating oxygen and both the amide nitrogen and carbon atoms in a plane perpendicular to that of N-C=O (Fig. 5*b*). The amide bond was largely unaltered. A similar result was obtained from HF/6-31G* calculations (Fig. 5*c*).

In a comprehensive study using DFT, we showed that anomeric substitution can be expected to lead to the conformational changes outlined in Fig. 2 in a wide range of amides (9). At this more reliable computational level, bis-heteroatom substitution leads to pyramidal amide nitrogens, lengthened N—CO bonds, shortened Y—N bonds, conformations about which optimize n_Y— σ^*_{NX} overlap. A subsequent, detailed B3LYP/6-31G* investigation of the congener, *N*-methoxy-*N*-dimethylaminoformamide, a model for the intermediate **7** in the HERON reaction indicated all these features (Fig. 6*a*) (10) and predicted: a strongly pyramidal nitrogen (avg. angles at nitrogen of 116°); a long N—C bond of 1.39 Å (computed to be 1.36 Å in formamide); a short N—N bond of 1.38 Å (1.45 Å in hydrazines); an extraordinarily low barrier of 13 kcal mol^{-1} (1 cal = 4.184 J) to E–Z isomerization about the N—C bond (typically 19–24 kcal mol^{-1} in conventional amides); a remarkably high barrier of 14 kcal mol^{-1} to rotation about the formally single N—N bond; an orientation of the amino substituent that optimized the anomeric overlap with the vicinal N—O bond (Fig. 6*b*).

A DFT evaluation of the HERON reaction of *N*-methoxy-*N*-dimethylaminoformamide to give methyl formate and 1,1-dimethyldiazene confirmed the earlier predictions at the AM1 and HF/6-31G* level (Fig. 7). The activation energy in

Fig. 6. (*a*) Lowest energy conformation of *N*-methoxy-*N*-dimethylaminoformamide (< x > = avg. angle). (*b*) Newman projection along the N—N bond.



the gas phase is modest at 21.4 kcal mol^{-1}, and the rearrangement is predicted to be exothermic by some 5.5 kcal mol^{-1} (36). The transition-state geometry shows that the N—C bond is intact, and the carbonyl bond is virtually unaltered. An intrinsic reaction coordinate study indicated that the N—C bond cleaves in concert with O—C bond formation after the transition state. In essence, this reaction represents an intramolecular S_N2 reaction on the amide carbonyl. Further analysis of the computed transition state indicates the charge redistribution (Fig. 7). Predictably, N2 becomes more positive at the transition state, while N1 and the migrating group develop negative charge. Electron-releasing groups on the donor nitrogen and electron-withdrawing groups on the migrating oxygen should lower the energy of the transition state, which should also proceed better in polar solvents that can stabilize this charge separation. Interestingly, there is no appreciable change in charge at the carbonyl and neither electron-donor groups nor electron-withdrawing groups at this position should exert a major influence upon the energetics of the reaction.

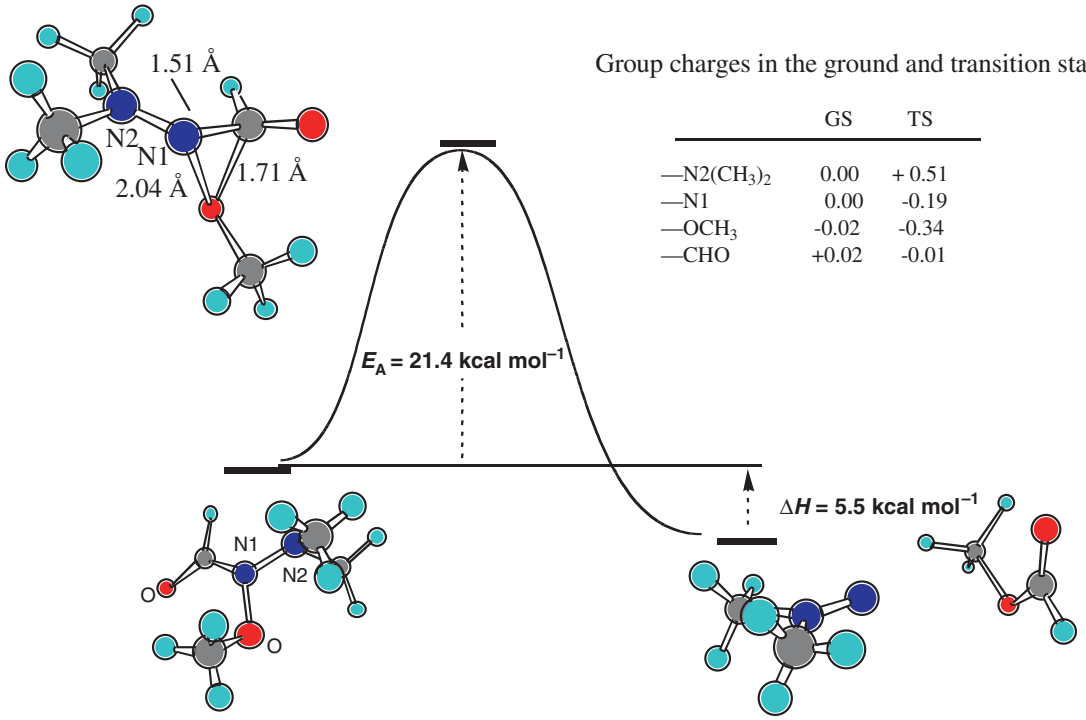
Experimental evidence in support of these computational results has accrued from a number of reactivity studies.

The HERON reaction of *N*-amino-*N*-alkoxyamides

We have routinely used the S_N2 reaction of *N*-acyloxy-*N*-alkoxyamides and *N*-methylaniline as a measure of their susceptibility to nucleophilic attack at nitrogen, and hence, to possible reactions with nucleophilic centres in DNA. The reactions can be followed in d_4-methanol and can be monitored through the disappearance of the mutagen or aniline and the formation of ester and tetrazene. HERON

© 2005 NRC Canada

Fig. 7. Energetics and transition-state properties for the HERON reaction of *N*-methoxy-*N*-dimethylaminoformamide to 1,1-dimethyldiazene and methyl formate.



rearrangement of the intermediate *N*-alkoxy-*N*-(*N*-methylanilino)benzamides proceeds with a low activation energy in methanol as it has never been detected under these reaction conditions, even at temperatures well below ambient (34). This is not surprising as the B3LYP/6-31G* activation energy for the model reaction in the gas phase is an upper limit and it would probably be significantly lower in solution.

A related class of analogues, the *N*,*N*′-diacyl-*N*,*N*′-dialkoxyhydrazines **12**, are readily generated by oxidative dimerization of hydroxamic esters (37–40) and by dimerization of alkoxyamidyl radicals formed upon oxidation of hydroxamic esters or photolysis of *N*-alkoxy-*N*-haloamides (41, 42). In a recent study we have demonstrated that these hydrazines exhibit all the hallmarks of anomeric amides (15). Their carbonyl stretch frequencies in solution are in the range of 1700–1744 cm^{-1}, while those of their precursor hydroxamic esters are in the range 1680–1690 cm^{-1} (4, 15). This accords with pyramidal nitrogen atoms, and in the case of *N*,*N*′-diacetyl-*N*,*N*′-di(*p*-chlorobenzyloxy)hydrazine, dynamic NMR methods afforded a low amide isomerization barrier of just 12.9 kcal mol^{-1}. For a range of such *N*,*N*′-diacyl-*N*,*N*′-dialkoxyhydrazines, we also obtained barriers for isomerization about the N—N bond that were in the range of 15–17 kcal mol^{-1}, which is indicative of a strong NNO anomeric interaction (15). Furthermore, from IR studies, these hydrazines appear to be unsymmetrical in both the solution and the solid phase, displaying two carbonyls;[4] one-half of the hydrazine can be regarded as a donor substituent on the other anomerically substituted nitrogen.

This spectroscopic evidence is supported by the X-ray structure of *N*,*N*′-di(*p*-chlorobenzoyl)-*N*,*N*′-diethoxyhydrazine (Fig. 3*b*). This *N*,*N*′-diacyl-*N*,*N*′-dialkoxyhydrazine is asymmetrical in nature and both nitrogens are strongly pyramidal with avg. angles at N(1) and N(2) of 113.6° and 114.4°, respectively. Furthermore, there is evidence for an anomeric interaction in the direction of N(2). The N(2)—O(3) bond nearly bisects the C(1)-N(1)-O(2) angle with torsion angles of 69.4° and –66.7° to N(1)—C(1) and N(1)—O(2) bonds, respectively, while the N(2)—O(3) bond is nearly 0.01 Å longer then the N(1)—O(2) bond. Both could be accounted for by overlap between the N(1) lone pair and the N(2)—O(3) antibonding orbital.

Upon mild heating, *N*,*N*′-diacyl-*N*,*N*′-dialkoxyhydrazines were known to decompose intramolecularly to 2 equiv. of ester and nitrogen by a reaction mechanism originally purported to involve two, four-centre rearrangements (Scheme 4, path A). Rate-enhancing donor acyl substituents were believed to stabilize intrinsic acylium character in the first, rate-determining step (39, 43).

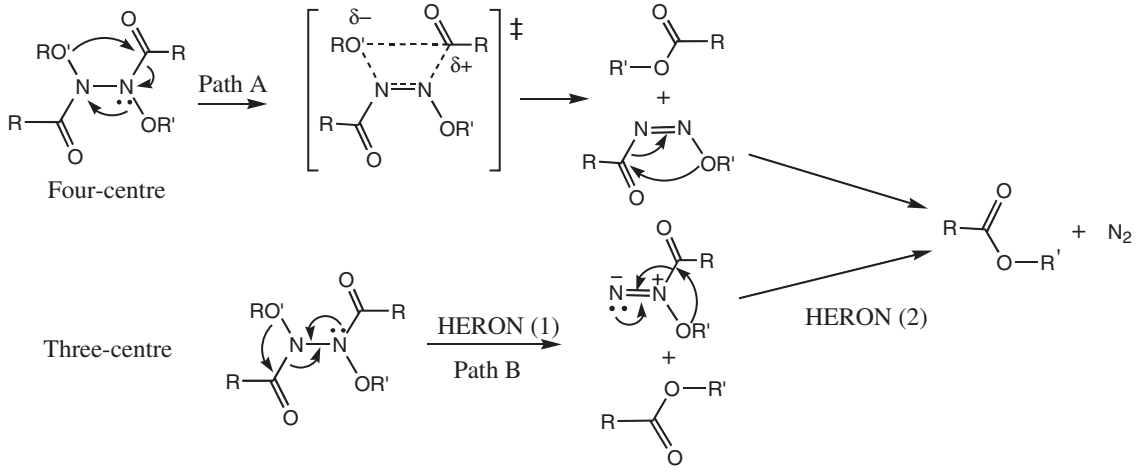
The discovery of the HERON reaction process instigated a reevaluation of the mechanistic details of this reaction by our group (44) and, coincidentally, by Barton and co-workers (40). Both studies involved the synthesis and thermal decomposition of an asymmetrical hydrazine. In our study, *N*-benzoyl-*N*-benzyloxy-*N*′-butoxy-*N*′-(*p*-chlorobenzoyl)hydrazine (**12a**) decomposed at room temperature in $CDCl_3$ affording largely benzyl benzoate (**13a**) and butyl *p*-chlorobenzoate (**13b**) from two, three-centre processes (Scheme 4, path B). Similarly, Barton and co-workers exclusively rearranged **12b** to a 1:1 mixture of **13c** and **13d** (40).

AM1 calculations carried out by both ourselves (44) and Barton's group (40), and subsequent high level calculations

[4] These are due to symmetrical and asymmetrical coupled stretch modes rather than individual frequencies for each carbonyl (15).

© 2005 NRC Canada

Scheme 4.

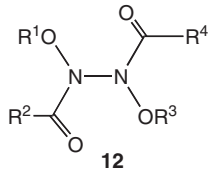


carried out by Thomson and Hall (45) on **12d**–**12f**, supported this mechanism in which the second step, also a HERON-type reaction, has a very low activation barrier. For hydrazine model **12d**, they calculated an activation barrier of 25 kcal mol^{-1} at the CCSD(T)//B3P86 level for HERON (1) in Scheme 4, a step that was exothermic by 13 kcal mol^{-1}. At the B3P86//B3P86 level, activation barriers for **12d**, **12e**, and **12f** were 24, 23, and 35 kcal mol^{-1}, respectively. The second HERON reaction (HERON (2), Scheme 4) of the diazene intermediate is computed to have a low activation barrier of just 2 kcal mol^{-1} and the extrusion of nitrogen is exothermic by 104 kcal mol^{-1}! Similar results were obtained for HERON (2) for the methylated models **12e** and **12f**. They also reported that a concerted pathway to two molecules of ester and nitrogen was not viable.

The transition state for HERON (1), computed for the rearrangement of methoxyl in **12f**, resembled that previously computed for the HERON reaction of *N*-methoxy-*N*-dimethylaminoformamide to give methyl formate and 1,1-dimethyldiazene (36). The transition state for the second step was very early in accordance with the exothermic nature of this step. B3LYP/6-31G*calculations from our group for a similar rearrangement of 1-formyl-1-methoxydiazene confirmed this and will be dealt with later in this review (46).

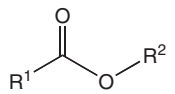
The initial, rate-determining step in the HERON reaction of hydrazines **14a**–**14e** and **15a**–**15e** proceeds with modest activation barriers of between 22 and 30 kcal mol^{-1} and negative entropies of activation (36). Thus, the experimental values are in excellent agreement with our activation energy for the HERON reaction of *N*,*N*-dimethylamino-*N*-methoxyformamide (21 kcal mol^{-1}, Fig. 7) and those computed by Thomson and Hall (45) for models **12d**–**12f**.

The unimolecular rate constants at 298 K for decomposition of a series of *N*,*N*′-di(*p*-substituted benzoyl)-*N*,*N*′-diethoxyhydrazines (**14a**–**14e**) in mesitylene correlated with Hammett σ^+ constants with $\rho = -0.35$, reflecting the stabilization of the transition state by electron-releasing acyl substituents adjacent to the donor nitrogen (Fig. 8*a*). The rates constants at 298 K for a series of *N*,*N*′-diacetyl-*N*,*N*′-di(*p*-substituted benzyloxy)hydrazines (**15a**–**15e**) correlated with Hammett σ constants, but with positive slope ($\rho = 1.02$), thus reflecting the stabilization of the transition state by electron-withdrawing alkoxyl substituents (Fig. 8*b*). Both results con-



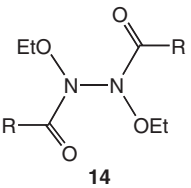
12

a: $R^1 = C_6H_4CH_2$, $R^2 = C_6H_5$ $R^3 = Bu$, $R^4 = p\text{-}ClC_6H_4$
b: $R^1 = CH_3$, $R^2 =$ cyclohexyl $R^3 = C_6H_5(CH_2)_2$, $R^4 = C_6H_5CH_2$
c: $R^1 = R^3 = Bu^t$, $R^2 = R^4 =$ 1-adamantyl
d: $R^1 = R^2 = R^3 = R^4 = H$
e: $R^2 = R^4 = CH_3$, $R^1 = R^3 = H$
f: $R^1 = R^2 = R^3 = R^4 = CH_3$



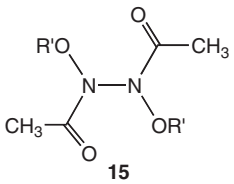
13

a: $R^1 = C_6H_5$, $R^2 = C_6H_5CH_2$
b: $R^1 = p\text{-}ClC_6H_4$, $R^2 = Bu$
c: $R^1 =$ cyclohexyl, $R^2 = CH_3$
d: $R^1 = C_6H_5CH_2$, $R^2 = C_6H_5(CH_2)_2$
e: $R^1 =$ 1-adamantyl, $R^2 = Bu^t$
f: $R^1 = R^2 = H$
g: $R^1 = CH_3$, $R^2 = H$
h: $R^1 = R^2 = CH_3$



14

a: $R = p\text{-}CH_3OC_6H_4$
b: $R = p\text{-}CH_3C_6H_4$
c: $R = C_6H_5$
d: $R = p\text{-}ClC_6H_4$
e: $R = p\text{-}NO_2C_6H_4$



15

a: $R' = p\text{-}CH_3OC_6H_4CH_2$
b: $R' = p\text{-}CH_3C_6H_4CH_2$
c: $R' = C_6H_5CH_2$
d: $R' = p\text{-}ClC_6H_4CH_2$
e: $R' = p\text{-}NO_2C_6H_4CH_2$

firmed the charge distribution at the transition state for the HERON rearrangement (Fig. 7) (36). Furthermore, members of the benzoyl series react about two orders of magnitude faster at 298 K than the benzyloxy series (typically 3×10^{-6} vs. 5×10^{-8} L mol^{-1} s^{-1}). This can be understood since, in the benzoyl series, a donor group facilitates development of positive charge at the donor nitrogen but has little effect upon the acyl carbon in the migration, since this accrues little charge in the transition state (Figs. 7 and 8*a*). However, while an electron-withdrawing group on the alkoxyl group will stabilize negative charge in the migrating group, it will destabilize the developing positive charge on the adjacent donor nitrogen (Figs. 7 and 8*b*).

Thus, the thermal rearrangement of *N*,*N*′-diacyl-*N*,*N*′-dialkoxyhydrazines to esters and nitrogen is a HERON reac-

© 2005 NRC Canada

Scheme 5.

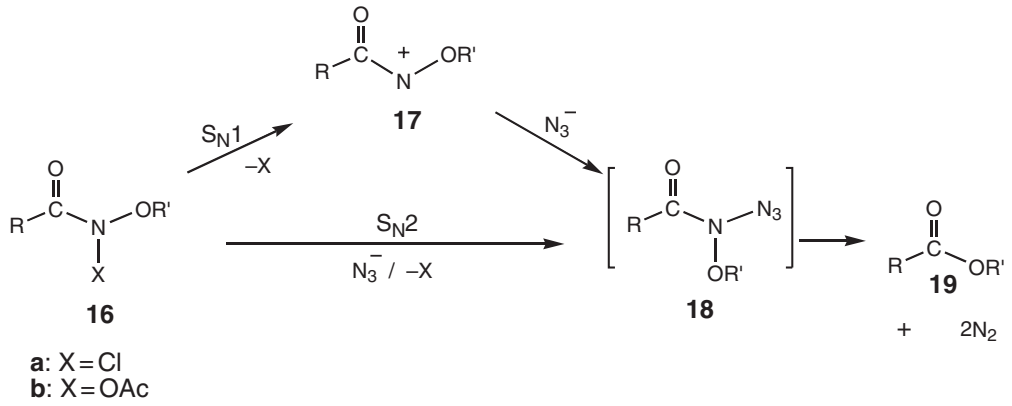
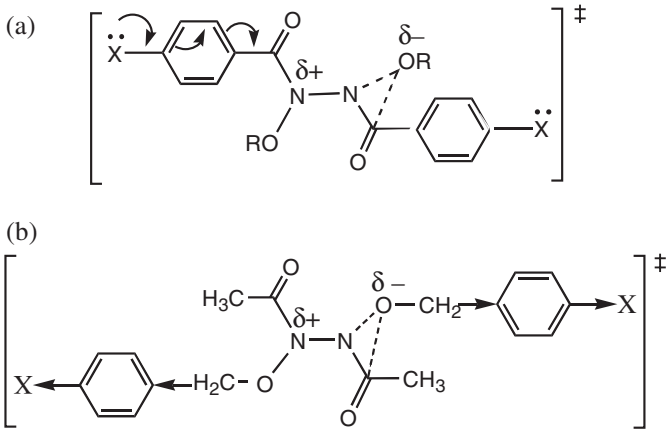


Fig. 8. Influence on the HERON transition states of: (*a*) electron-rich benzoyl groups in **14**; and (*b*) electron-deficient benzyloxy groups in **15**.



tion and their reduced rates of reactivity (probably on account of weaker donor capacity of one nitrogen because of acyl substitution) enabled us to confirm the theoretical transition-state properties.

This concerted reaction was flagged by Barton and coworkers (40) as an excellent synthesis of sterically hindered esters. For example, decomposition of **12c** afforded *tert*-butyl 1-adamantanecarboxylate (**13e**) in 87% yield.

The HERON reaction of 1-acyl-1-alkoxydiazenes

N-Alkoxy-*N*-chloroamides (**16a**) and *N*-acetoxy-*N*-alkoxyamides (**16b**) react with sodium azide at room temperature giving the ester **19**, derived from the alkoxyl and acyl groups of the hydroxamic ester, as well as nitrogen. In the case of both *N*-alkoxy-*N*-chloroamides and *N*-acyloxy-*N*-alkoxyamides, crossover experiments indicated that the reaction exclusively yields the carboxylic ester derived from the corresponding alkoxyl and acyl group (35). Both an S_N1 process involving the nitrenium ion **17** and direct S_N2 mechanism are possible under these conditions (Scheme 5). The reactions are extremely fast in aqueous organic solvents but can be monitored dilatometrically at 295 K and have been found to proceed by the bimolecular process yielding 2 equiv. of nitrogen, with rate constants of around 2 L mol^{-1} s^{-1}. Bimolecular reactions of *N*-acyloxy-*N*-alkoxyamides with *N*-methylanilines (34) and glutathione or L-cysteine methyl ester[5] are slower by two to three orders of magnitude. *N*-Alkoxy-*N*-azidoamides **18** are believed to form as reactive intermediates (35, 46).

Calculations on the lowest energy structure for *N*-azido-*N*-methoxyformamide (**20**) at HF/6-31G* (35) and B3LYP/6-31G* (46) indicate that the azido adduct lies at a potential energy minimum and is typically anomeric with avg. angles at nitrogen of 112° and 113° (Fig. 9*a*), and a conformation that supports one anomeric overlap, that being between the oxygen lone pair and the N1—N2 bond (Figs. 9*b* and 9*c*).

Production of methylformate and two molecules of nitrogen can occur by three routes. The first possibility involves a HERON reaction yielding ester **21** and tetrazene **22**, which is the source of 2 equiv. of nitrogen (Scheme 6, path A). Alternatively, an initial loss of nitrogen could give 1,1-diazene (Scheme 6, path B), which undergoes a HERON reaction producing ester and a second equivalent of nitrogen (Scheme 6, path C). The latter process is identical to the HERON (2) step in the decomposition of *N*,*N*′-diacyl-*N*,*N*′-dialkoxyamides (Scheme 4). A concerted rearrangement with loss of nitrogen (Scheme 6, path D) is also possible. Once again, we have used computational methods to determine the most likely reaction mechanism. All three reactions are highly exothermic (137 kcal mol^{-1}), but neither path A nor path D was found to be a viable competitor to the stepwise dissociation into 1,1-diazene (**23**) and nitrogen (Scheme 6, paths B and C). The azidonitrene in path A decomposes with zero activation energy to two molecules of nitrogen and no transition state for the concerted pathway could be found without prior loss of nitrogen as occurs in path B. Loss of nitrogen from *N*-azido-*N*-methoxyformamide in path B is exothermic by between 42 and 44 kcal mol^{-1} depending upon the ground-state geometry and has very low activation barriers of between 5 and 8 kcal mol^{-1}. The transition states all show stretching of the N4—N5 bonds of about 0.24 Å and sp^2 hybridization at the amide nitrogen. In addition, the N3—N4 bonds shorten by about 0.11–0.13 Å. The connected ground-state, transition-state, and 1,1-diazene ge-

[5] At 308 K, gluthione reacted in d_6-DMSO–D_2O with bimolecular rate constants of around 2.6 × 10^{-2} L mol^{-1} s^{-1}; at 303 K in d_4-methanol, L-cysteine methyl ester reacted with a rate constant of 1.6 × 10^{-2} L mol^{-1} s^{-1}.

© 2005 NRC Canada

Scheme 6.

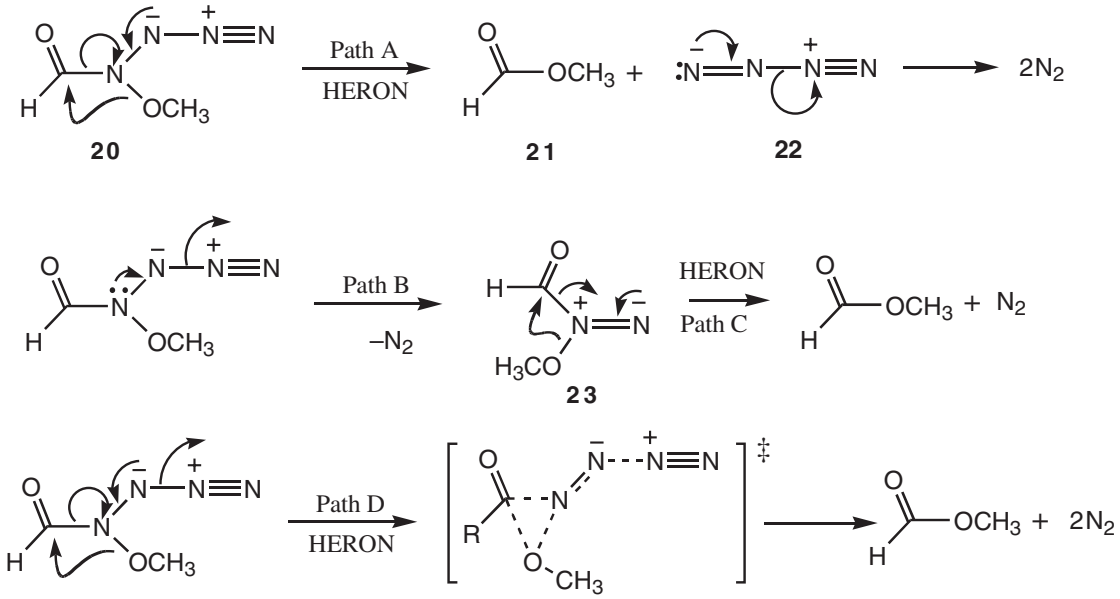
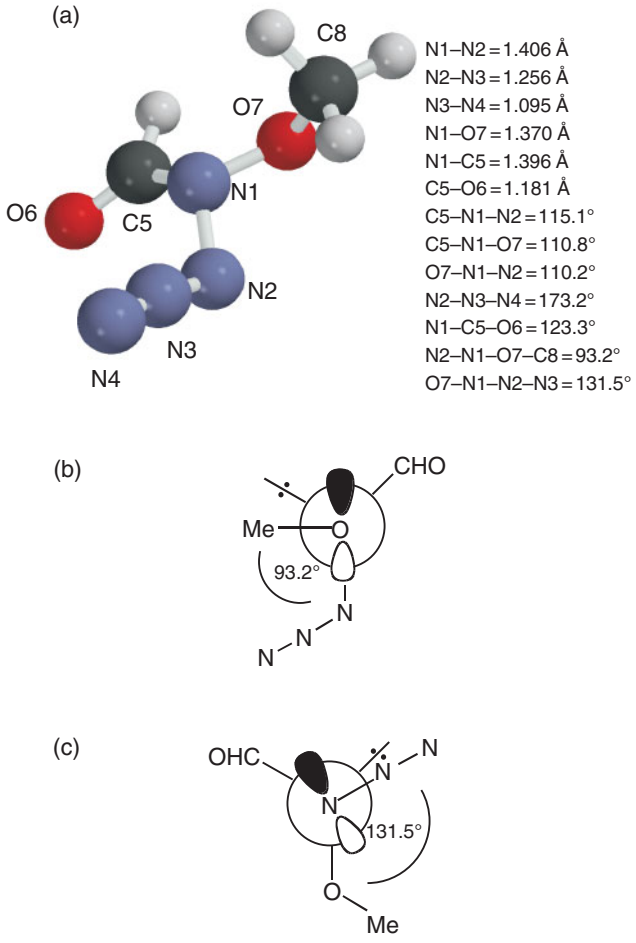


Fig. 9. (*a*) HF/6-31G* geometry of *N*-azido-*N*-methoxyformamide. (*b*) Newman projection along the O7—N1 bond. (*c*) Newman projection along the N2—N1 bond.



ometries from the lowest energy conformer of *N*-azido-*N*-methoxyformamide are given in Fig. 10.

Rearrangement of 1-formyl-1-methoxydiazene to nitrogen and methylformate (Scheme 6, path C) is a HERON reaction and is an identical process to the second step for the thermal decomposition of *N*,*N*′-diacyl-*N*,*N*′-dialkoxyhydrazines. At the B3LYP/6-31G* level, the transition state (Fig. 10*d*) is early with an activation barrier of only 2.8 kcal mol^{-1}, and the second step is overall exothermic by approximately 95 kcal mol^{-1}. Our result is completely in line with that of Hall and Thomson's (45), previously described for the simpler system (E_A = 2 kcal mol^{-1}, ΔE = 104 kcal mol^{-1}).

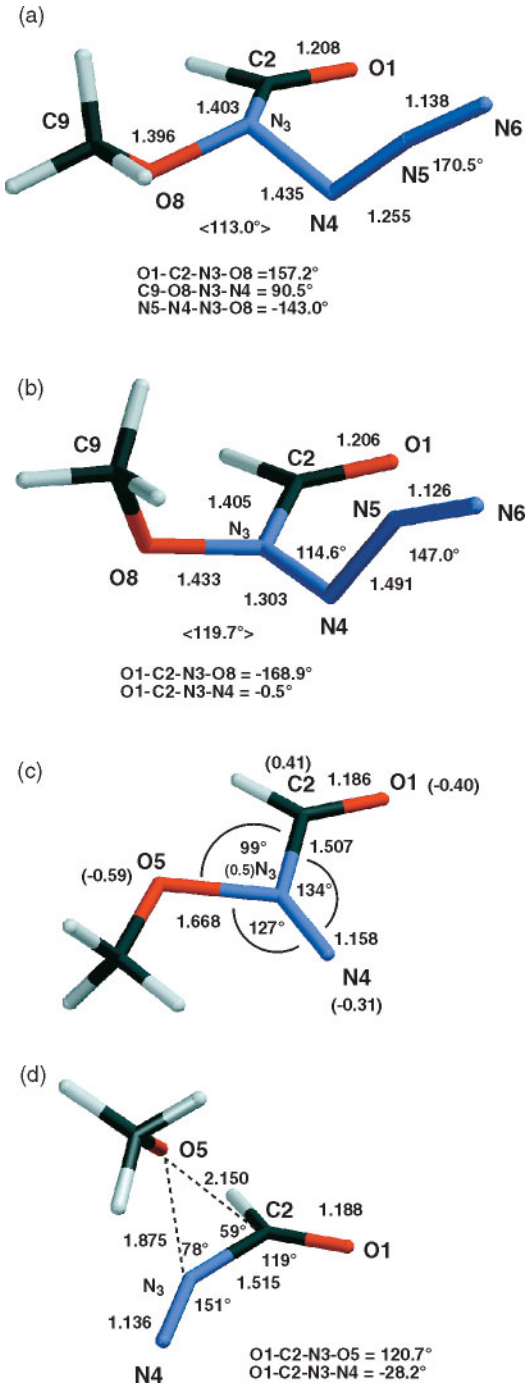
We have utilized the favourable energetics and concerted rearrangement of *N*-alkoxy-*N*-azidoamides to esters and nitrogen in the facile synthesis of highly hindered esters from *N*-chlorohydramic esters (Table 1). Yields rival those of Barton's group (40) from HERON decomposition of the hydrazines. Precursors for both syntheses are the hydroxamic esters, but the hydrazine method involves prior oxidative dimerization, whereas the intermediates in our synthesis are the *N*-chlorohydroxamic esters that are very readily generated from hydroxamic esters in quantitative yield using *tert*-butyl hypochlorite.

The HERON reaction in alcoholysis of dialkyl azodicarboxylates

Azodicarboxylates **24** are a class of nitrogen electrophiles that have been used widely in the Mitsunobu reaction, an effective synthetic protocol for activating alcohols to esterification (largely with inversion of configuration) (47–49). Reactions in alcohols have produced both symmetrical and unsymmetrical dialkylcarbonates as side products or as the major product (50, 51). Direct alcoholysis of azodicarboxylate esters has been described by several groups (38, 52–54). Azodicarboxylates **24** were reported to be stable in ethanol, but vigorously decomposed upon addition of bases such as alkoxides and sodium acetate (52). The hydrazines **25** were believed to be unstable intermediates, although reports are contradictory. Galynker and Still (55) reported that

© 2005 NRC Canada

Fig. 10. (*a*) Ground-state geometry for *N*-azido-*N*-methoxyformamide. (*b*) First transition state for the loss of nitrogen (Scheme 6, path B). (*c*) Ground-state geometry of 1-formyl-1-methoxydiazene. (*d*) Transition state for the HERON reaction of 1-formyl-1-methoxydiazene (Scheme 6, path C).



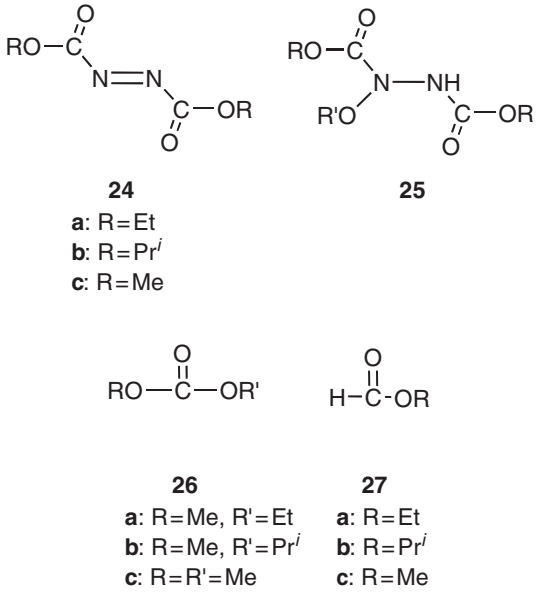
they were major, stable side products from Mitsonobu tosylation reactions. However, based on our observations azodicarboxylates **24** are most likely to undergo a HERON rearrangement upon nucleophilic addition.

In support of this, we found that diethyl azodicarboxylate (**24a**) and diisopropyl azodicarboxylate (**24b**) were completely stable in methanol, but upon addition of sodium methoxide, sodium acetate, or sodium hydroxide, they decomposed with a spontaneous evolution of an equivalent of nitrogen, liberation of heat, and a change of colour from the characteristic yellow of the azodicarboxylates to pink. The products of decomposition in a methanolic solution of sodium methoxide or sodium acetate were identified spectroscopically and by GLC as ethyl methyl carbonate (**26a**) and ethyl formate (**27a**), and in the case of the reaction of **24b**, ^{1}H NMR analysis of the reaction mixture indicated the presence of methyl isopropyl carbonate (**26b**) and isopropyl formate (**27b**) in an approximate ratio of 1:1.

Table 1. Ester (RCOOR′) formation from the reaction of alkyl *N*-alkoxy-*N*-chloroamides (RCONClOR′) with sodium azide in aqueous acetonitrile.

Ester	R	R′	Crude yield (%)
19a	Ph	$(CH_3)_3C$	87
19b	$(CH_3)_3C$	$(CH_3)_3C$	30[a]
19c	1-Adamantyl	$(CH_3)_3C$	82[b]
19d	$(CH_3)_3C$	Cyclohexyl	97
19e	Ph	$(CH_3)_2CH$	92
19f	Ph	$PhCH_2$	93
19g	CH_3	$PhCH_2$	92
19h	*p*-$NO_2C_6H_4$	Et	94
19i	Ph	Et	94

[a]GLC analysis; reaction accompanied by formation of pivalic acid (29%).
[b]Traces of adamantane carboxylic acid were also detected.



24 **25**

a: R=Et
b: R=Pr^i
c: R=Me

26 **27**

26
a: R=Me, R'=Et
b: R=Me, R'=Pr^i
c: R=R'=Me

27
a: R=Et
b: R=Pr^i
c: R=Me

In support of this, we found that diethyl azodicarboxylate (**24a**) and diisopropyl azodicarboxylate (**24b**) were completely stable in methanol, but upon addition of sodium methoxide, sodium acetate, or sodium hydroxide, they decomposed with a spontaneous evolution of an equivalent of nitrogen, liberation of heat, and a change of colour from the characteristic yellow of the azodicarboxylates to pink. The products of decomposition in a methanolic solution of sodium methoxide or sodium acetate were identified spectroscopically and by GLC as ethyl methyl carbonate (**26a**) and ethyl formate (**27a**), and in the case of the reaction of **24b**, ^{1}H NMR analysis of the reaction mixture indicated the presence of methyl isopropyl carbonate (**26b**) and isopropyl formate (**27b**) in an approximate ratio of 1:1.

Formation of mixed carbonates might be rationalized by carbonyl addition followed by acyl cleavage. However, there is ample evidence from Mitsonobu chemistry that azodicarboxylates undergo nucleophilic attack at nitrogen. The HF/6-31G* computed lowest energy conformer of dimethyl azodicarboxylate has the ester groups orthogonal to the nitrogen double bond and the LUMO of **24c** is essentially a pure $\pi^*_{N=N}$ orbital (Fig. 11*a*). The second lowest unoccupied orbital possesses $\pi^*_{C=O}$ character, but is nearly 2.5 eV higher in energy. Nucleophiles, including methoxide, would be pre-

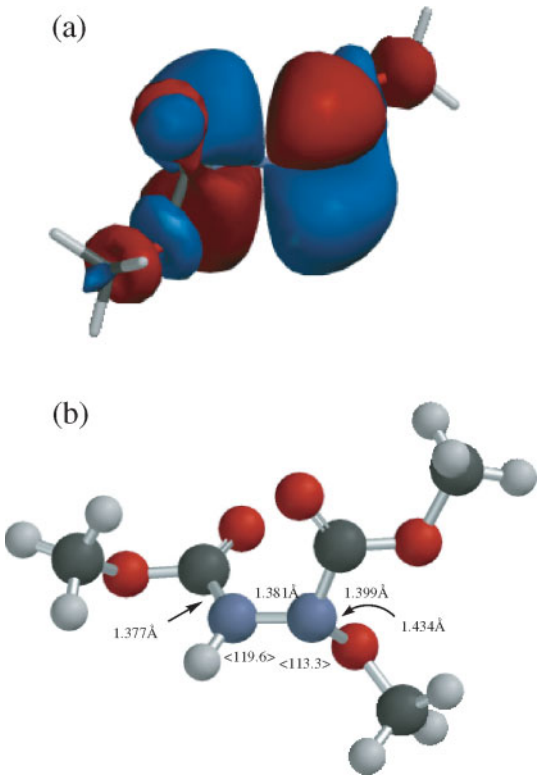
© 2005 NRC Canada

Table 2. Computed B3LYP/6-31G*//HF/6-31G* energies for reactants and products from the reaction of dimethyl azodicarboxylate (**32**) and methoxide ion.

Structure	HF/6-31G* (au)	B3LYP/6-31G*//HF/6-31G* (au)	SM5.4 (kcal mol^{-1}) (ref. 56)
Carbonyl adduct (**28**)	–677.72754	–681.52136	–59.1
Azo adduct (**29**	–677.71817	–681.51338	–65.0
HERON t.s. (**32**, R = Me)	–677.68059	–681.50298	–56.6
Carbonate (**26c**)	–341.70052	–343.60391	–0.9
Acyl anion (**34**, R = Me)	–227.13615	–228.41052	–67.7
Nitrogen	–108.94395	–109.52189	0.6
Reaction energies (kcal mol^{-1})	HF/6-31G*	B3LYP/6-31G*//HF/6-31G*	SM5.4 (ref. 56)
E_A	23.6	6.5	8.4
ΔE_{HERON}[a]	–5.9	–5.0	6.0
ΔE_{React}[b]	–39.2	–14.4	–3.0

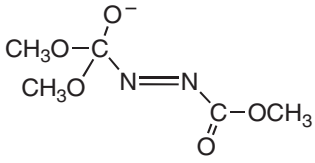
[a]Reaction energy for the transformation of **29** into **28**.
[b]Reaction energy for the transformation of **29** into **26c**, **34** (R = Me), and nitrogen.

Fig. 11. (*a*) HF/6-31G* LUMO orbital of dimethyl azodicarboxylate (**24c**). (*b*) HF/6-31G* geometry of *N,N′*-dicarbomethoxy-*N*-methoxyhydrazine.

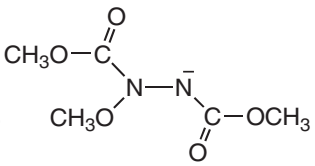


dicted to attack azodicarboxylates exclusively at the nitrogen atoms. In addition, while the anionic carbonyl adduct **28** is slightly more stable than the azo adduct **29** in the gas phase, it is slightly less stable if aqueous solvation is incorporated (Table 2).

Scheme 7 depicts possible mechanisms for the conversion of dialkyl azodicarboxylates into mixed carbonates. Attack at the azo group would result in the intermediate **30** in which the neighbouring nitrogen has anionic character. The anion could be protonated giving **31** (Scheme 7, path A) or, alternatively, could undergo a HERON reaction (Scheme 7, path B) with the formation of the mixed dialkyl carbonate **26** and



28



29

alkyl formate anion **34**, which ultimately leads to alkyl formate **27**.

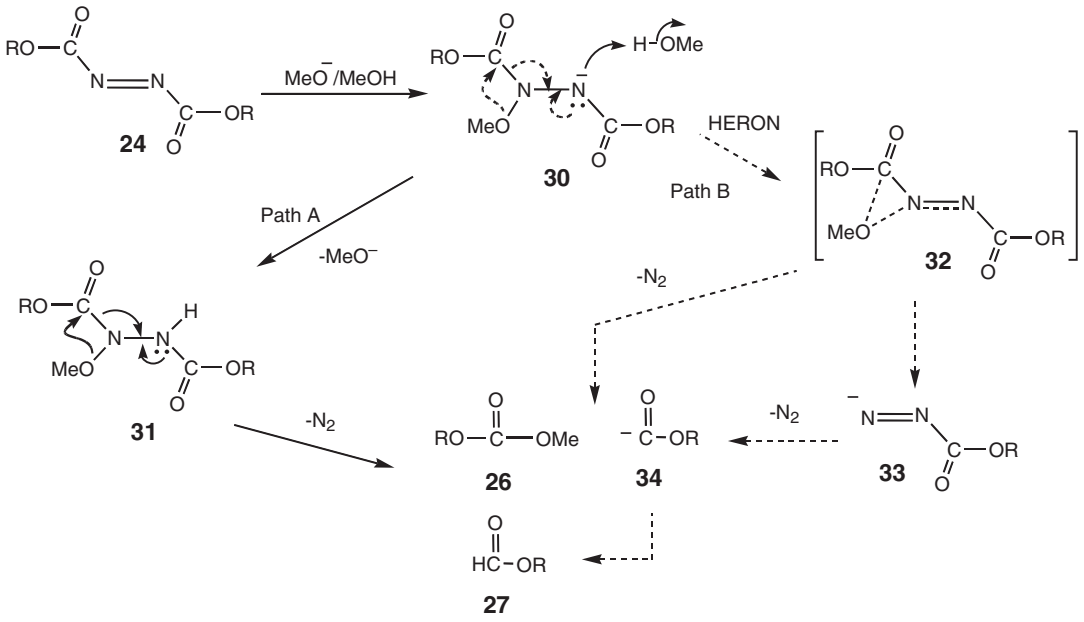
However, path A followed by HERON reaction of **31** is less likely. Firstly, methoxide must be a stronger base than **30**, and secondly, **31** is likely to be much more stable than the *N,N′*-diacyl-*N,N′*-dialkoxyhydrazines; according to HF/6-31G* calculations (Fig. 11*b*), the amide lone pair is strongly conjugated with the carbonyl, since the nitrogen is largely sp^2 at the protonated nitrogen (avg. angle at nitrogen 119.6°). Compared to the *N,N′*-diacyl-*N,N′*-dialkoxyhydrazines, which are computed to have N—N bond lengths of around 1.355 Å (15), this "half-anomeric" hydrazine has a much longer N—N bond (1.381 Å), reflecting poor anomeric overlap. In keeping with this, we could not locate a transition state for a HERON reaction of this structure.

In **30**, the anionic lone pair is very high in energy resulting in a strong anomeric overlap and driving force for the rearrangement. The process has an analogy in the previously reported, facile HERON reaction of the conjugate anion of *N*-alkoxyhydroxamic esters described in the following example (33).

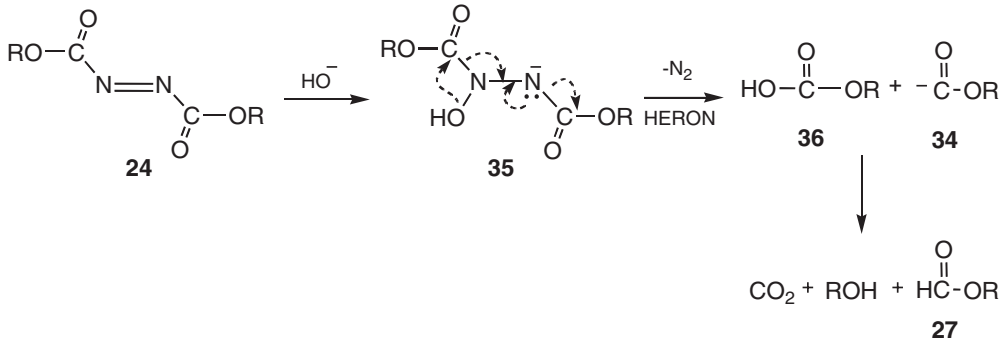
Table 2 gives calculated energies for the reactant, transition state, and products from the HERON reaction of *N,N′*-dicarbomethoxy-*N*-methoxy anion (**29**). In the gas phase, the rearrangement has an extremely low E_A of 6.5 kcal mol^{-1} (14.8 kcal mol^{-1} with solvation), and in this case, leads initially to the carbonyl adduct **28**, which is similar in energy and is a stationary point. It is proposed that **28** directly decomposes to nitrogen and an acyl anion, which scavenges a proton from methanol. The methoxycarbonyldiazene anion (**33**) (R = Me) that would be formed by cleavage of the amide bond is computed to be a metastable point on the energy surface and spontaneously rearranges to an acyl anion and nitrogen. Overall, the reaction is exothermic by 14.4 kcal mol^{-1} (17.4 kcal mol^{-1} with solvation).

© 2005 NRC Canada

Scheme 7.



Scheme 8.



In a methanolic solution of potassium hydroxide, **24a** and **24b** exothermically decomposed with immediate evolution of nitrogen and formation of ethyl and isopropyl formate. In the case of **24b**, isopropanol was isolated as a product. Reaction according to Scheme 7 would result in formation of the alkyl hydrogen carbonate **36**, which under the basic reaction conditions, would probably decompose to alcohol and carbon dioxide (Scheme 8).

The formation of alkyl formate by this reaction represents a more acceptable route than that proposed by Vederas and co-workers (57) for the formation of steroidal formate ester (**39**) from *N*-bromosuccinimide oxidation of chiral diazane (**37**) (Scheme 9). The intermediate azodicarboxylate **38** was thought to react with water giving **40** by attack at carbonyl. Decarboxylation and radical decomposition of **40** via **41** completed the process. Homolytic decomposition of **40** to give **41** is considered by the author to be a highly unlikely process as is the reaction of water at the carbonyl of **38**.

The HERON reaction of *N*-alkoxyhydroxamic acids

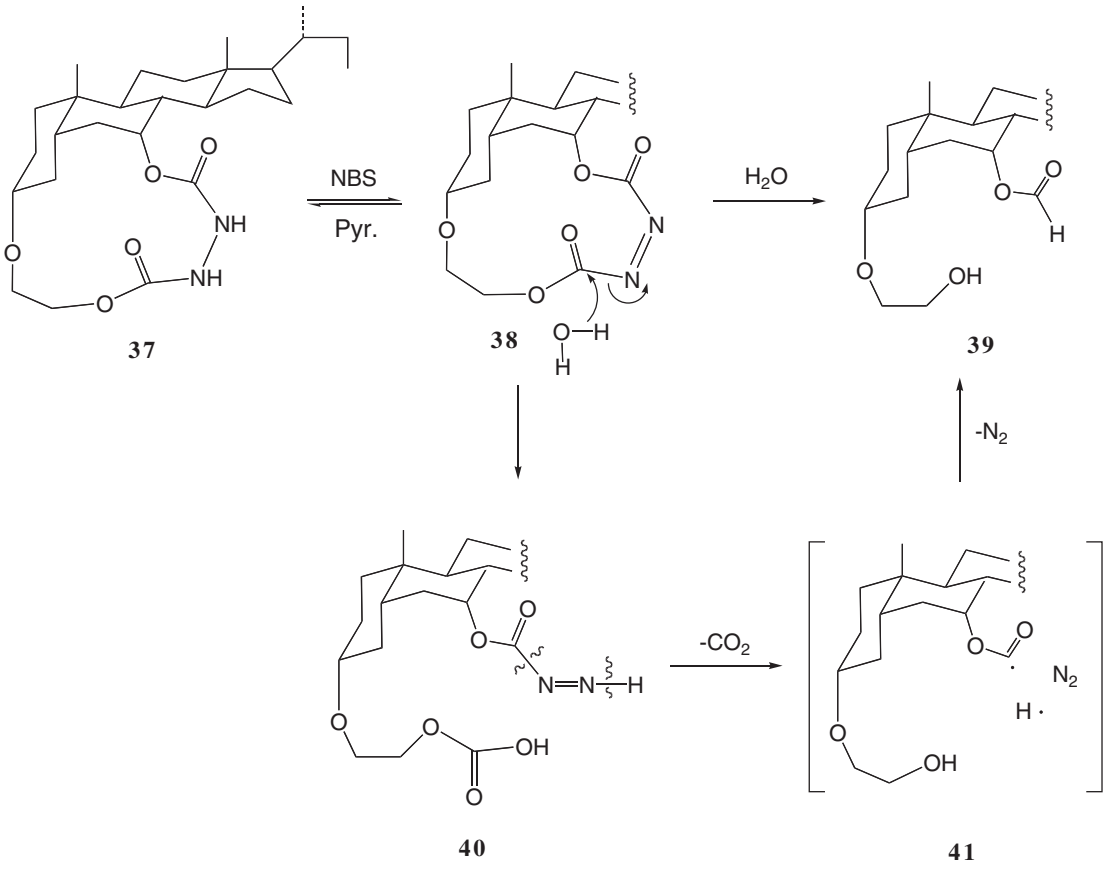
Treatment of *N*-acyloxy-*N*-alkoxybenzamides (**42a**) with dilute aqueous sodium hydroxide, at room temperature, resulted in the rapid formation of alkyl benzoates **19** (33). A crossover experiment using *N*-acetoxy-*N*-butoxy-*p*-chlorobenzamide and *N*-acetoxy-*N*-benzyloxybenzamide resulted in the exclusive formation of butyl *p*-chlorobenzoate (46%) and benzyl benzoate (43.3%) esters along with the hydrolysis products, *p*-chlorobenzoic and benzoic acid. This result indicates that ester formation involves an intramolecular process.

Using a series of *N*-(*p*-substituted benzoyloxy) mutagens, it was shown to occur by S_N2 reaction of hydroxide at nitrogen, which gives hydroxamic acid (**43**) as an intermediate (Scheme 10) (33). The presence of excess base would ensure conversion of the hydroxamic acid intermediate into the conjugate anion **44** resulting in a HERON reaction and formation of ester **19** and presumably NO^-. The formation of noncrossover esters in the acid-catalysed solvolyses of *N*-acetoxy-*N*-alkoxyamides **1** at low acid concentrations, according to Scheme 2, has also been observed. Such reactions produce the *N*-alkoxy-*N*-benzoylnitrenium ion **3** from **2** and, by solvolysis, *N*-alkoxyhydroxamic acid (**4**) directly (32).

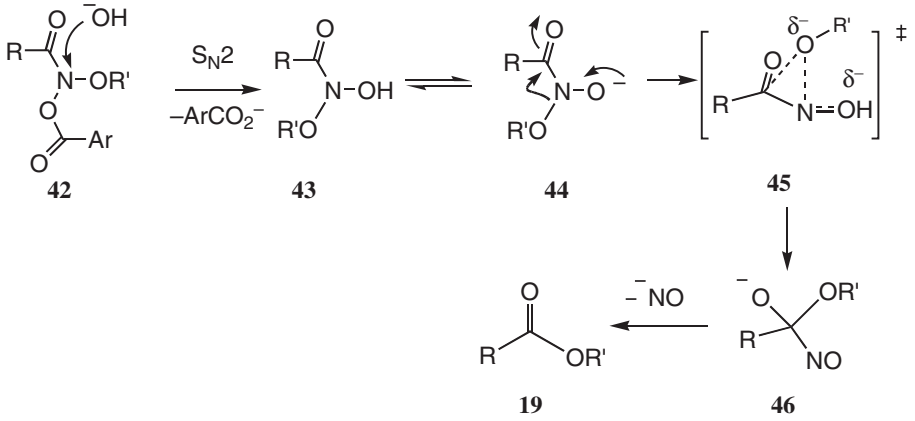
While the lone pair on the hydroxy oxygen of hydroxamic acid (**43**) would be tightly bound, resulting in a weak n_{OH}—σ^*_{N-OR} interaction, the anion **44** would possess a high energy pair of electrons, thus enhancing the anomeric effect

© 2005 NRC Canada

Scheme 9.



Scheme 10.



a: R = Ph, R' = Bn
b: R = R' = Me

in a similar fashion to the amide anion **30** previously described and which drives that HERON reaction. Calculations on the rearrangement of *N*-methoxy-*N*-methanohydroxamate anion (**44b**) (Fig. 12*a*) to methyl formate (**19b**) indicated an early transition state (**45b**) (Fig. 12*b*) that leads to the tetrahedral alkoxide intermediate (**46b**) (Fig. 12*c*), which presumably decomposes by elimination of NO^-. B3LYP/6-31G*//HF/6-31G* results (Table 3) gave an activation energy for the HERON step of only 5.3 kcal mol^{-1} (10.0 kcal mol^{-1} including solvation effects). Formation of the tetrahedral intermediate was exothermic by 10.7 kcal mol^{-1} and the overall reaction was endothermic by 21 kcal mol^{-1} with solvation, which suggests reversibility of the HERON step in this case.

Recently, Shtamburg et al. (58) studied the methanolysis of a variety of *N*-acetoxy-*N*-alkoxy derivatives of carbamate **47a**, urea **47b**, and benzamide **50** and found that, with the exception of the benzamide, acyloxy substitution at nitrogen

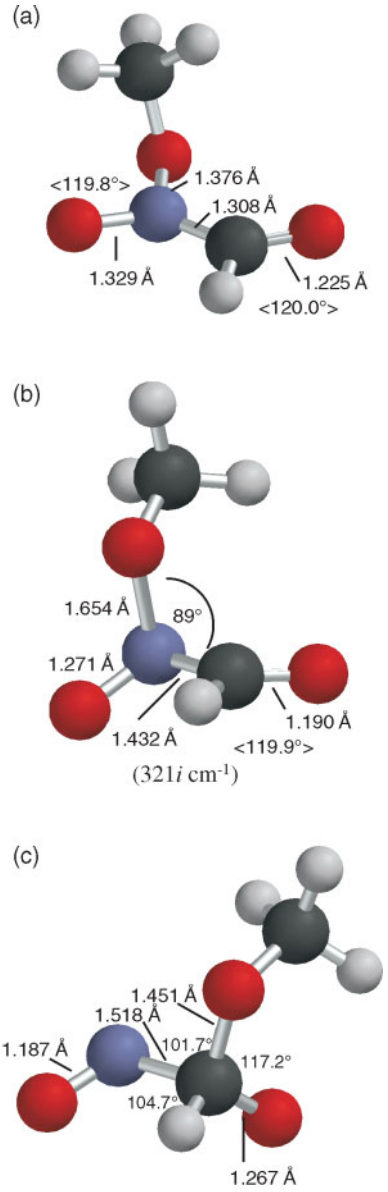
© 2005 NRC Canada

Table 3. Computed B3LYP/6-31G*//HF/6-31G* energies for reactants and products from the rearrangement of *N*-methoxymethanohydroxamate anion (**44b**).

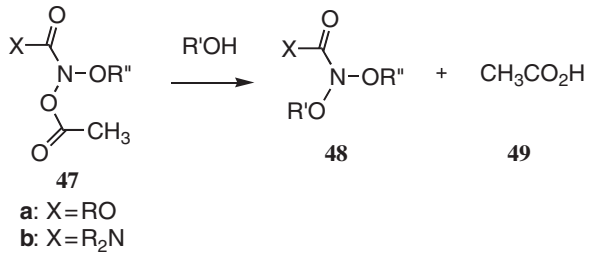
Structure	HF/6-31G* (au)	B3LYP/6-31G*//HF/6-31G* (au)	SM5.4 (kcal mol^{-1}) (ref. 56)
Hydroxamate (**44b**)	–356.95534	–358.93375	–67.4
HERON t.s. (**45b**)	–356.93625	–358.9252	–62.8
Alkoxide (**46b**)	–356.98422	–358.95114	–67.2
Methyl formate (**19b**)	–227.77945	–229.05208	–3.5
NO^-	–129.13602	–129.80825	–88.5
Reaction energies (kcal mol^{-1})	**HF/6-31G***	**B3LYP/6-31G*//HF/6-31G***	**SM5.4 (ref. 56)**
E_A	12.0	5.4	4.6
ΔE_{HERON}[a]	–18.1	–10.9	0.3
ΔE_{React}[b]	25.0	46.1	–24.5

[a]Reaction energy for the transformation of **44b** to **46b**.
[b]Reaction energy for the transformation of **44b** to **19b** and NO^-.

Fig. 12. HF/6-31G* geometries for: (*a*) the ground state of *N*-methoxymethanohydroxamate (**44b**); (*b*) HERON transition state **45b**; and (*c*) tetrahedral intermediate **46b**.



Scheme 11.



and loss of acetic acid was a useful means of obtaining the corresponding symmetrical and asymmetrical *N*,*N*-dialkoxy derivatives **48** (Scheme 11).

The reaction with *N*-acetoxy-*N*-ethoxybenzamide (**50**) did not result in substitution at nitrogen and a reaction in an aprotic medium with sodium methoxide afforded methyl and ethyl benzoates. They attributed the formation of methyl benzoate to methoxide reaction at the amide carbonyl and the formation of ethyl benzoate (**53**) to a HERON reaction. Presumably, in this medium, attack at the carbonyl of the acetoxyl group would directly lead, by fragmentation of **51**, to the conjugate anion of the *N*-ethoxybenzohydroxamic acid (**52**), followed by the HERON migration of the ethoxy substituent from nitrogen to the benzamide carbonyl (Scheme 12).

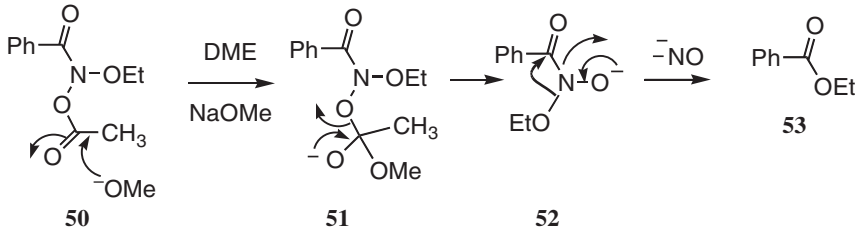
The HERON reaction of *N*-acyloxy-*N*-alkoxyamides in the gas phase

HERON rearrangement of *N*-acyloxy-*N*-alkoxyamides has not been observed. In polar solvents (aqueous acetonitrile) anomeric weakening of the AcO—N bond favours heterolysis over migration of the acyloxy substituent. Migration would yield anhydrides, which have never been observed as side products from the $A_{Al}1$ or S_N2 reactions of *N*-acyloxy-*N*-alkoxyamides of our group (1, 6, 21, 32–34) or Shtamburg's recent studies (58).

ESI-tandem mass spectrometric studies on a number of *N*-acyloxy-*N*-alkoxyamides indicated that under these conditions, free from solvent, the sodiated parent ion can be detected, which fragmented under collision-induced dissociative conditions into three sodiated product ions (Table 4). These products exhibited masses corresponding to the sodiated *N*-alkoxyamidyl radical (**54**), which in most cases was the

© 2005 NRC Canada

Scheme 12.



Scheme 13.

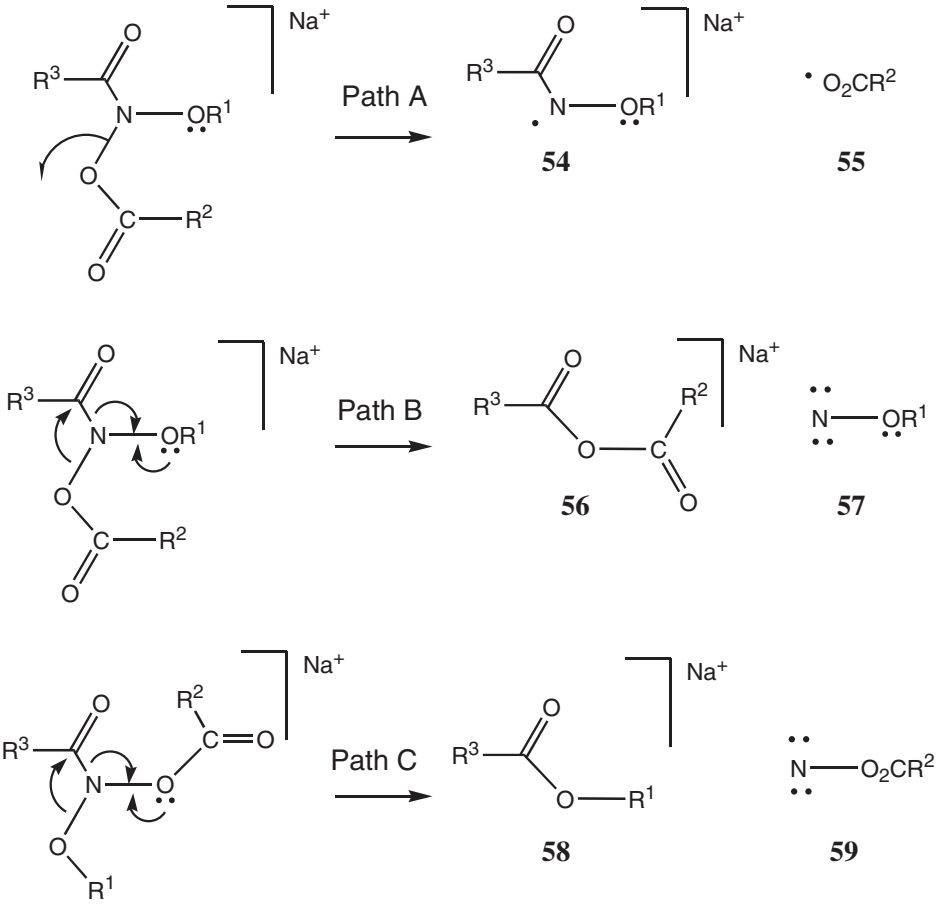


Table 4. Values of *m*/*z* for sodiated ions from the ESI-MS of *N*-acyloxy-*N*-alkoxyamides **60a–60l**.

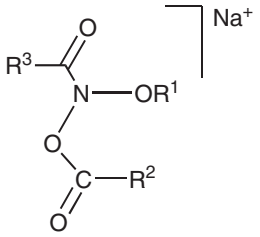
Structure	**60**	**54**	**56**	**58**
a	274	215	187	201
b	302	243	215	229
c	362	303	275	—
d	404	345	317	—
e	370	249	249	235
f	426	305	249	291
g	336	215	249	—
h	288	167	201	Trace
i	302	181	215	—
j	394	273	307	—
k	316	195	229	—
l	330	209	243	—

Note: ESI conditions in positive ion mode: H_2O–MeOH, drying gas 350 °C, capillary = 30 V, CID = –5 to –30 eV.

major pathway (Scheme 13, path A), but the second most intense product ion was the sodiated anhydride **56** formed through HERON rearrangement of the acyl group (Scheme 13, path B). The alternative ester **62** that would be formed through a HERON migration of the alkoxy group (Scheme 13, path C) was a weak product ion in all cases where it was present and absent in the fragmentations of all aliphatic amides (**60h–60l**). The fragments from the reaction processes are presumed to be acyloxyl radical (**55**), alkoxynitrene (**57**), and acyloxynitrene (**59**).

According to B3LYP/6-31G*//HF/6-31G* calculations on **60m** and its HERON rearrangement products in the gas phase, migration of the acyloxyl group is favoured over the alkoxyl group by about 4 kcal mol^{-1} (Table 5). The transition states (Figs. 13*b*–13*d*) are relatively similar with the migrating oxygen perpendicular to the ONC(O) plane, though the HERON transition state for acyl appears looser (Fig. 13*b*), which would be expected because of the polarities involved.

© 2005 NRC Canada



60

a: R^1=Bu, R^2=Me, R^3=Ph
b: R^1=Bu, R^2=Me, R^3=3,5-diMeC_6H_3
c: R^1=Bu, R^2=Me, R^3=fluoren-1-yl
d: R^1=Bu, R^2=Me, R^3=2-anthraquinon-2-yl
e: R^1=R^2=R^3=Ph
f: R^1=4-Bu^t, R^2=R^3=Ph
g: R^1=Bu, R^2=R^3=Ph
h: R^1=Bu, R^2=Ph, R^3=n-Pr
i: R^1=Bu, R^2=Ph, R^3=Bu^i
j: R^1=Bu, R^2=Ph, R^3=1-Ad
k: R^1=Bu, R^2=Ph, R^3=Bu^t
l: R^1=Bu, R^2=Ph, R^3=neopentyl
m: R^1=Me, R^2=R^3=H

Table 5. Computed energies for ground state and migration transition states for **60m**.

Structure	B3LYP/6-31G* (au)	Relative energy (kcal mol^{-1})	Frequency (cm^{-1})
Fig. 13*a*	–472.851865	0.0	
Fig. 13*b*	–472.790221	38.7	271*i*
Fig. 13*c*	–472.782035	43.4	210*i*
Fig. 13*d*	–472.783513	42.9	282*i*

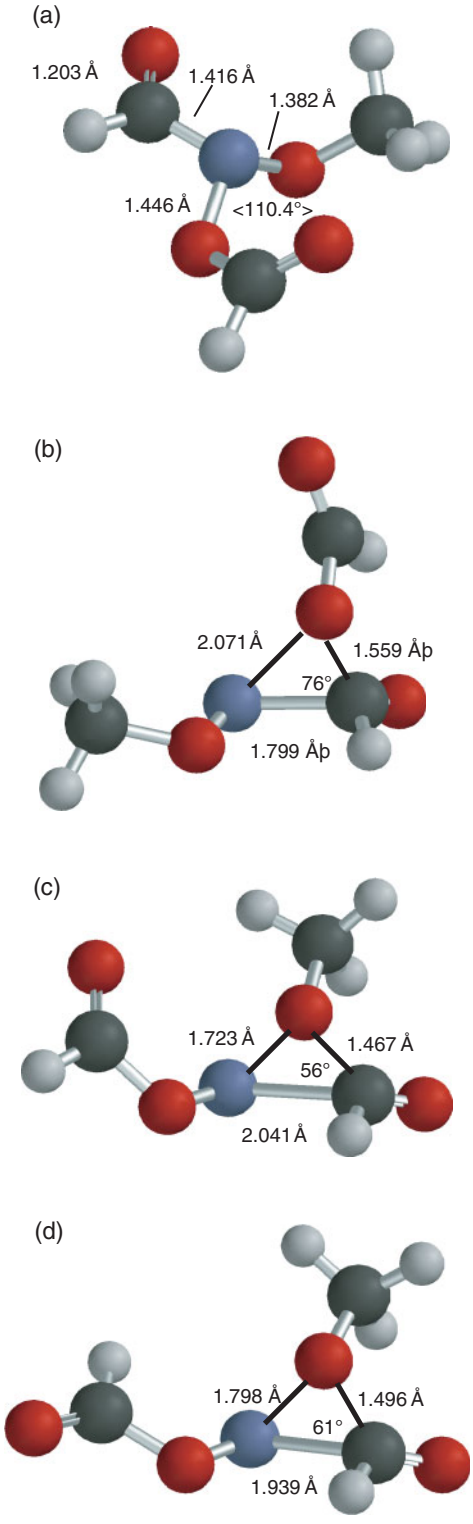
Two conformations of the transition state for methoxyl migration (Figs. 13*c* and 13*d*) were found with very similar energies.

The magnitude of the activation energies indicates that such migrations are unlikely to compete with heterolysis of the N—OAc bond, particularly in polar solvents. While the influence of the spectator sodium ion on these reactions is unknown, clearly, the ESI-MS–MS data reflects the expected migration tendencies of acyl vs. alkoxyl moieties in these substrates. The alkoxyl oxygen, though much more electronegative than nitrogen, is a better donor atom than the acyloxy oxygen, which is bonded to an electron-withdrawing carbonyl carbon, and hence, the acyl group migration would be preferred.

Conclusions

The HERON reaction is one of the newest named reactions (3). In this review we have outlined the discovery of this reaction, theoretical support for the process, as well as instances where there are good grounds to expect its participation. Certainly, it is involved in the reactions of NNO anomeric amides that have tetrahedral amide nitrogens, which is a consequence of the favourable anomeric interaction in those configurations. These reactions, which involve migration of groups from an amide nitrogen to an amide carbonyl carbon, contrast with the known migrations in the reverse direction that are exemplified by the well-documented Hoffman (59), Lossen (60), and Curtius (61) reactions. The reaction is also found in the conversion of 1-acyl-1-alkoxydiazenes, a second step in the thermal decompositions

Fig. 13. B3LYP/6-31G* geometries for: (*a*) the ground state of *N*-formyloxy-*N*-methoxyformamide (**60m**), and transition states for the migration of: (*b*) acyloxyl; and (*c*) and (*d*) alkoxyl groups.



© 2005 NRC Canada

of *N*,*N*′-diacyl-*N*,*N*′-dialkoxyhydrazines and *N*-alkoxy-*N*-azidoamides that are formed by S_N2 reactions of azide with *N*-chloro- and *N*-acyloxy-*N*-alkoxyamides. The mechanism is also implicated in the reactions of some ONO anomeric amides as exemplified by the rearrangements of alkoxyl groups in basic or weakly acidic solutions of *N*-alkoxyhydroxamic acids, and, most recently, in the gas-phase rearrangements of *N*-acyloxy-*N*-alkoxyamides. In the future, other anomeric amides such as *N*-alkoxy-*N*-haloamides or *N*-amino-*N*-haloamides may well be found to undergo HERON processes.

Acknowledgements

SAG is grateful to the Australian Research Council and the University of New England for financial support.

References

1. J.J. Campbell and S.A. Glover. J. Chem. Soc. Perkin Trans. 2, 1661 (1992).
2. J.M. Buccigross and S.A. Glover. J. Chem. Soc. Perkin Trans. 2, 595 (1995).
3. S.A. Glover. *In* The Merck Index. 13th ed. *Edited by* M.J. O'Neil. Merck & Co., Inc., Whitehouse Station, New Jersey. 2001. p. ONR-48.
4. S.A. Glover. Tetrahedron, **54**, 7229 (1998).
5. R.G. Gerdes, S.A. Glover, J.F. Ten Have, and C.A. Rowbottom. Tetrahedron Lett. **30**, 2649 (1989).
6. J.J. Campbell, S.A. Glover, and C.A. Rowbottom. Tetrahedron Lett. **31**, 5377 (1990).
7. T.M. Banks, A.M. Bonin, J.J. Campbell, S.A. Glover, G.P. Hammond, A.S. Prakash, and C.A. Rowbottom. Mutat. Res. **494/1–2**, 115 (2001).
8. L.E. Andrews, T.M. Banks, A.M. Bonin, S.F. Clay, A.-M.E. Gillson, and S.A. Glover. Aust. J. Chem. **57**, 377 (2004).
9. S.A. Glover and A. Rauk. J. Org. Chem. **61**, 2337 (1996).
10. S.A. Glover and A. Rauk. J. Org. Chem. **64**, 2340 (1999).
11. S.A. Glover. ARKIVOC. Issue in Honour of Professor O.S. Tee, ms OT-308C [online]. Available from http://www.arkat-usa.org/ark/journal/2001/I12_Tee/OT-308.htm. 2001.
12. L.M. Jackman and F.A. Cotton. Dynamic nuclear magnetic resonance spectroscopy. Academic Press, New York. 1975. p. 203.
13. L. Bauer and O. Exner. Angew. Chem. Int. Ed. Engl. **13**, 376 (1974).
14. K.B. Wiberg. *In* The amide linkage. Selected structural aspects in chemistry, biochemistry and materials science. *Edited by* A. Greenberg, C.M. Breneman, and J.F. Liebman. John Wiley and Sons, Inc., New York. 2000.
15. S.A. Glover, G. Mo, A. Rauk, D. Tucker, and P. Turner. J. Chem. Soc. Perkin Trans. 2, 2053 (1999).
16. A.-M.E. Gillson, S.A. Glover, D.J. Tucker, and P. Turner. Org. Biomol. Chem. **1**, 3430 (2003).
17. S.A. Glover, A. Goosen, C.W. McCleland, and J.L. Schoonraad. J. Chem. Soc. Perkin Trans. 2, 2255 (1984).
18. S.A. Glover, A. Goosen, C.W. McCleland, and J.L. Schoonraad. Tetrahedron, **43**, 2577 (1987).
19. S.A. Glover and A.P. Scott. Tetrahedron, **45**, 1763 (1989).
20. S.A. Glover, C.A. Rowbottom, A.P. Scott, and J.L. Schoonraad. Tetrahedron, **46**, 7247 (1990).
21. J.J. Campbell, S.A. Glover, G.P. Hammond, and C.A. Rowbottom. J. Chem. Soc. Perkin Trans. 2, 2067 (1991).
22. S.A. Glover, K.M. Jones, I.R. McNee, and C.A. Rowbottom. J. Chem. Soc. Perkin Trans. 2, 1367 (1996).
23. M. Kawase, T. Kitamura, and Y. Kikugawa. J. Org. Chem. **54**, 3394 (1989).
24. Y. Kikugawa and M. Kawase. J. Am. Chem. Soc. **106**, 5728 (1984).
25. Y. Kikugawa and M. Shimada. Chem. Lett. 1771 (1987).
26. E. Miyazawa, T. Sakamoto, and Y. Kikugawa. J. Org. Chem. **68**, 5429 (2003).
27. D.J. Wardrop and A. Basak. Org. Lett. **3**, 1053 (2001).
28. D.J. Wardrop, C.L. Landrie, and J.A. Ortîz. Synlett, **9**, 1352 (2003).
29. E.R. Thornton. J. Am. Chem. Soc. **89**, 2915 (1967).
30. W.P. Jencks. Chem. Rev. **72**, 705 (1972).
31. A. Pross. Theoretical and physical principles of organic chemistry. John Wiley and Sons, Inc., New York. 1995. p. 49.
32. A.M. Bonin, S.A. Glover, and G.P. Hammond. J. Chem. Soc. Perkin Trans. 2, 1173 (1994).
33. A.M. Bonin, S.A. Glover, and G.P. Hammond. J. Org. Chem. **63**, 9684 (1998).
34. J.J. Campbell and S.A. Glover. J. Chem. Res. (S) **8**, 474 (1999); J. Chem. Res. (M), **8**, 2075, (1999).
35. S.A. Glover and G. Mo. J. Chem. Soc. Perkin Trans. 2, 1728 (2002).
36. S.A. Glover, G. Mo, and A. Rauk. Tetrahedron, **55**, 3413 (1999).
37. R.O.C. Norman, R. Purchase, and C.B. Thomas. J. Chem. Soc. Perkin Trans. 1, 1701 (1972).
38. R.J. Crawford and R. Raap. J. Org. Chem. **28**, 2419 (1963).
39. J.H. Cooley, M.W. Mosher, and M.A. Khan. J. Am. Chem. Soc. **90**, 1867 (1968).
40. M.V. De Almeida, D.H.R. Barton, I. Bytheway, J.A. Ferriera, M.B. Hall, W. Liu, D.K. Taylor, and L. Thomson. J. Am. Chem. Soc. **117**, 4870 (1995).
41. A.R. Forrester, E.M. Johansson, and R.H. Thomson. J. Chem. Soc. Perkin Trans. 1, 1112 (1979).
42. S.A. Glover, A. Goosen, C.W. McCleland, and J.L. Schoonraad. J. Chem. Soc. Perkin Trans. 1, 2255 (1984).
43. J.H. Cooley, D.H. Stone, and H. Oguri. J. Am. Chem. Soc. **42**, 3096 (1977).
44. J.M. Buccigross, S.A. Glover, and G.P. Hammond. Aust. J. Chem. **48**, 353 (1995).
45. L.M. Thomson and M.B. Hall. J. Phys. Chem. A, **104**, 6247 (2000).
46. S.A. Glover and A. Rauk. J. Chem. Soc. Perkin Trans. 2, 1740 (2002).
47. O. Mitsonobu. Synthesis, 1 (1981).
48. M. Verasi, K.A.M. Walker, and M.L. Maddox. J. Org. Chem. **52**, 4235 (1987).
49. D.L. Hughes, R.A. Reamer, J.J. Bergan, and E.J.J. Grabowski. J. Am. Chem. Soc. **110**, 6487 (1988).
50. G. Grynkiewicz, J. Jurczak, and A. Zamojski. Tetrahedron, **31**, 1411 (1975).
51. Z. Barneis, Y. Broeir, and S. Bittner. Chem. Ind. (London), 526 (1976).
52. E. Fahr and H. Lind. Angew. Chem. Int. Ed. Engl. **5**, 372 (1966).
53. J.C.J. MacKenzie, A. Rodgman, and G.F. Wright. J. Org. Chem. **17**, 1666 (1952).
54. O. Diels and C. Wulff. Liebigs Ann. Chem. **437**, 309 (1924).
55. I. Galynker and W.C. Still. Tetrahedron Lett. **43**, 4461 (1982).
56. C.C. Chambers, G.D. Hawkins, C.J. Cramer, and D.G. Truhlar. J. Phys. Chem. **100**, 16385 (1996).
57. J.M. Harris, E.A. Bolessa, and J.C. Vederas. J. Chem. Soc. Perkin Trans. 1, 1951 (1995).

© 2005 NRC Canada

58. V.G. Shtamburg, E.A. Klots, A.P. Pleshkova, V.I. Avramenko, S.P. Ivonin, A.V. Tsygankov, and R.G. Kostyanovsky. Russ. Chem. Bull. **52**, 2252 (2003).
59. A.W. Hoffman. *In* The Merck Index. 13th ed. *Edited by* M.J. O'Neil. Merck & Co., Inc., Whitehouse Station, New Jersey. 2001. p. ONR-51.
60. W. Lossen. *In* The Merck Index. 13th ed. *Edited by* M.J. O'Neil. Merck & Co., Inc., Whitehouse Station, New Jersey. 2001. p. ONR-63.
61. T. Curtius. *In* The Merck Index. 13th ed. *Edited by* M.J. O'Neil. Merck & Co., Inc., Whitehouse Station, New Jersey. 2001. p. ONR-23.

© 2005 NRC Canada

Deuterium kinetic isotope effects on the thermal isomerizations of deuteriocyclopropane to deuterium-labeled propenes[1]

John E. Baldwin and Stephanie R. Singer

Abstract: The gas-phase thermal isomerizations of deuteriocyclopropane to the four possible monodeuterium-labeled propenes have been followed at 435 °C. The observed distribution of products provides estimates of two deuterium kinetic isotope effects, the secondary k_H^s/k_D^s for the carbon–carbon bond cleavage leading to trimethylene diradical reactive intermediates and the primary k_H^p/k_D^p ratio for a [1,2] shift of a hydrogen or deuterium leading from the diradical to a labeled propene. The values determined are k_H^s/k_D^s = 1.09 ± 0.03 and k_H^p/k_D^p = 1.55 ± 0.06. The experimental k_H^s/k_D^s value found agrees well with some, but not all, earlier calculated values and conjectures.

Key words: cyclopropane, thermal rearrangement, kinetic isotope effects.

Résumé : Opérant à 435 °C, on a étudié les réactions d'isomérisation thermiques en phase gazeuse du deutérocyclopropane qui conduisent aux quatre propènes monodeutérés possibles. La distribution observée des produits permet d'évaluer deux des effets isotopiques cinétiques, l'effet isotopique secondaire k_H^s/k_D^s pour la rupture de la liaison carbone–carbone conduisant à la formation d'intermédiaires réactifs diradicalaires triméthylènes et le rapport primaire k_H^p/k_D^p pour le déplacement [1,2] d'un atome d'hydrogène ou de deutérium qui conduit du diradical à un propène marqué. Les valeurs déterminées sont k_H^s/k_D^s = 1,09 ± 0,03 et k_H^p/k_D^p = 1,55 ± 0,06. La valeur expérimentale trouvée pour k_H^s/k_D^s est en bon accord avec les quelques-unes des hypothèses et des valeurs calculées antérieurement, mais pas nécessairement toutes.

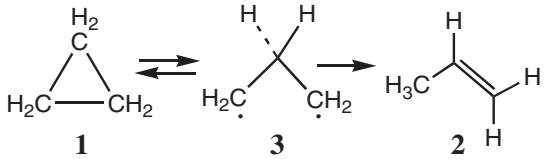
Mots clés : cyclopropane, réarrangement thermique, effets isotopiques cinétiques.

[Traduit par la Rédaction]

Introduction

The thermal chemistry of cyclopropane is marvelously complex relative to the small size and high symmetry of the hydrocarbon. This minimal cycloalkane (**1**) undergoes a thermal structural isomerization to propene (**2**) (1, 2). Deuterium-labeled analogs exhibit thermal stereomutations (3), which have been demonstrated to occur through both one-center and two-center epimerizations (4). The structural isomerization and the two types of stereomutations are generally held to involve transient formation of a trimethylene diradical reactive intermediate (**3**), which may revert to cyclopropane or shift a hydrogen from C2 to C1 to afford propene (5–8). The transition-state structure for the rate-determining step in this formulation leading from **3** to **2** has been characterized in several high-level theoretical calculations (9–12).

Interpretations of experimental data providing information about rate constants for the one-center and two-center thermal epimerizations observed for the 1,2-d_2-labeled cyclopropanes depend on secondary deuterium kinetic isotope effects. The importance of k_H^s/k_D^s is easy to grasp: the C1—C2 and C1—C3 bonds of 1,2-d_2-labeled cyclopropanes might well break at different rates. A net one-center epimerization at C1 could occur through cleavage of the C1—C2 bond (rate constant k_1) or when C1—C3 breaks (rate constant k_1'). Simultaneous two-center epimerizations at C1 and C2 (rate constant k_{12}) or at C1 and C3 (rate constant k_{13}) could occur at different rates. The latter two-center event would contribute to an observable one-center epimerization at C1. All of which gets complicated. With rate constant ratios defined as $f_1 = k_1'/k_1$ and $f_{12} = k_{13}/k_{12}$, the two experimental observables, k_i (for the geometrical isomerization equilibrating *cis*- and *trans*-1,2-d_2-cyclopropane) and k_α (for racemization of nonracemic *trans*-1,2-d_2-cyclopropane), are related to the mechanistic rate constant ratio k_{12}/k_1 as in eqs. [1] and [2] (13).



1 **3** **2**

$$[1] \quad \frac{k_i}{k_\alpha} = \frac{2 + \dfrac{(2f_{12}k_{12})}{(k_1 + f_1k_1)}}{1 + \dfrac{(k_{12} + f_{12}k_{12})}{(k_1 + f_1k_1)}}$$

Received 27 April 2005. Published on the NRC Research Press Web site at http://canjchem.nrc.ca on 18 November 2005.

J.E. Baldwin[2] and S.R. Singer. Department of Chemistry, Syracuse University, Syracuse, NY 13244, USA.

[1]This article is part of a Special Issue dedicated to organic reaction mechanisms.

[2]Corresponding author (e-mail: jbaldwin@syr.edu).

 doi: 10.1139/V05-167 © 2005 NRC Canada

$$[2]\qquad \frac{k_{12}}{k_1} = \frac{2 - \dfrac{k_i}{k_\alpha}}{\dfrac{k_i}{k_\alpha}\dfrac{(1+f_{12})}{(1+f_1)} - \dfrac{2f_{12}}{(1+f_1)}}$$

One way to simplify eq. [2] is to suppose, quite reasonably, that $f_1 \approx f_{12}$, and let $f = f_1 = f_{12}$ (13). One is left with an equation linking two observables with three unknowns (eq. [3]).

$$[3]\qquad \frac{k_{12}}{k_1} = \frac{2 - \dfrac{k_i}{k_\alpha}}{\dfrac{k_i}{k_\alpha} - \dfrac{2f}{(1+f)}}$$

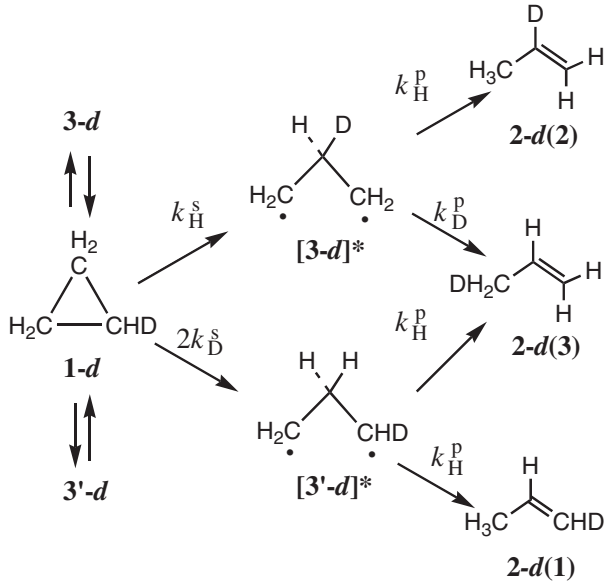
If one could estimate a reliable value of f, then k_{12}/k_1 could be derived from a reliable experimental k_i/k_α ratio. For example, if k_i/k_α were 1.07 as was reported for stereomutations of a nonracemic *trans*-1,2-d_2-cyclopropane at 422.5 °C and f were assumed to be 1.1 (4), then according to eq. [3], k_{12}/k_1 would be 42, a large number leading to the conclusion that the "double methylene rotation mechanism operates to the virtual exclusion of any other pathway" (4). Or one could view the experimental data as leading to the conclusion that double methylene rotation is favored over single methylene rotation by a factor of ≈50 (14).

Later experimental work with a nonracemic 1-^{13}C-1,2,3-d_3-cyclopropane concluded that k_{12}/k_1 is 1 ± 0.2 (15), a finding that has prompted considerable theoretical attention but no consensus on the mechanistic details of the stereomutations or on the dynamics of trimethylene diradicals.

Three groups have provided theory-based estimates of f or k_H/k_D (k_{12}) based on harmonic vibrational frequencies and various kinetic models: 1.13 and 1.12 (at 422.5 °C) (16, 17), and 1.09 (at 400 °C) (18). Other calculations have given rise to theory-based estimates of k_{12}/k_1, an undertaking sensitive to the kinetic model adopted, especially whether or not trimethylene is an intermediate to which transition-state theory may be applied, the potential energy surface used, and whether semiclassical or quantum dynamics calculations are employed. These published theory-based k_{12}/k_1 ratios are 0.94 (17), 1.18 (18), 1.35 (13), 2.2 (19), 2.3 (13), 3.5 (13), and 4.73 (18). The lower ratios are favored when transition-state theory models are applied to the transient trimethylene diradical (20); the higher ratios are calculated using dynamic models in which redistributions of vibrational energy compete poorly with momentum-preserving transits of the diradical over the potential energy surface.

The values of calculated k_H/k_D (k_{12}) ratios depend on the accuracy of theory-derived transition structures and vibrational frequencies, the broad potential energy surface on which the trimethylene diradical lives its brief existence, and whether explicit consideration of torsional potentials may be appropriate; the calculated values may not be correct. Other reasonable values might be more accurate (13). If the ratio f is uncertain within the range 0.8–1.1, and if k_i/k_α were 1.07, then corresponding values of k_{12}/k_1 would be in the range from 5 to 42 (13). Or if f were 0.8 and k_i/k_α were indeed 1.07 then k_{12}/k_1 would be 5, a value close to one theory-based estimate (18). The k_{12}/k_1 ratio is obviously a sensitive function of the value of f. But the k_{12}/k_1 ratio is also a sensitive function of the experimental value of k_i/k_α (eq. [3]).

Fig. 1. Isomerization paths from **1-*d*** to four monodeuteriopropenes.



There have been no *experimentally* estimated values of the secondary deuterium kinetic isotope effect associated with homolytic thermal cleavage of a cyclopropane C—C bond, and no attempts yet published to face the more exacting challenge of measuring the k_H^s/k_D^s ratios for k_1 and k_{12} for the stereomutations of appropriate isotopically labeled cyclopropanes. The present work describes experiments leading to two deuterium kinetic isotope effects of import to thermal cyclopropane-to-propene isomerizations, the secondary k_H^s/k_D^s ratio for C—C bond cleavage and the primary k_H^p/k_D^p effect on [1,2] shifts leading from a deuterium-labeled trimethylene diradical to labeled propenes.

Results and discussion

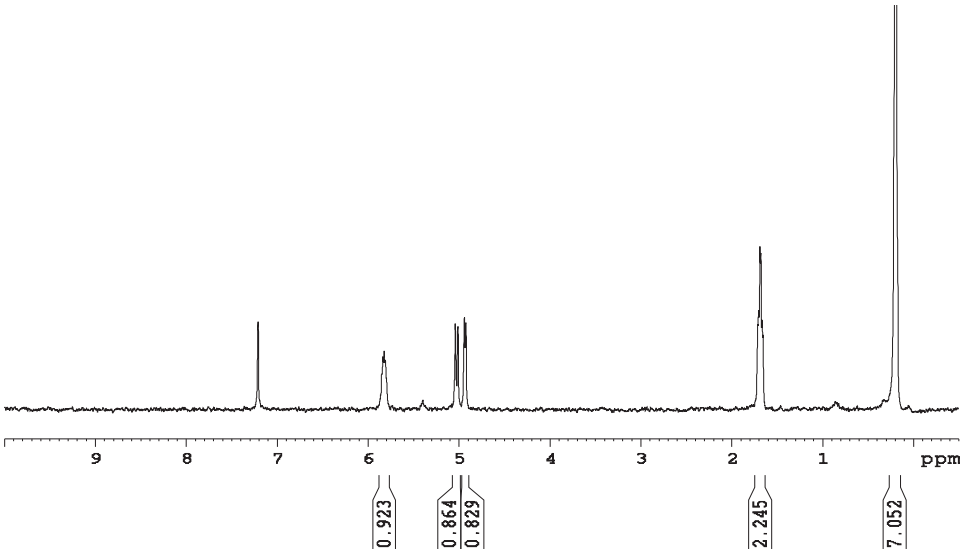
Deuteriocyclopropane (**1-*d***) was identified as a labeled cyclopropane suitable for gaining an experimental value for the secondary k_H^s/k_D^s effect on the C—C cleavage of cyclopropane. It is easily made and presents no complications related to stereomutations: all one-center and two-center epimerizations for this molecule are unobservable. The isomerizations of **1-*d*** could lead to four monodeuterium-labeled propenes, as diagrammed in Fig. 1. The E- and Z-isomers of **2-*d*(1)** are not shown explicitly.

The model depicted in Fig. 1 recognizes that the lifetime of trimethylene diradicals, about 120 fs (20), is too short for significant intramolecular redistributions of vibrational energy under the gas-phase reaction conditions. Trimethylene diradicals **3-*d*** and **3′-*d***, which lack sufficient vibrational energy to give propenes, revert to **1-*d***. Related trimethylene diradicals with additional isotopic labeling could give rise to stereoisomeric cyclopropanes but not related propenes.

The fractions of trimethylene diradicals having sufficient thermal energy to proceed to propene products would be proportional to $k_H^s/(k_H^s + 2k_D^s)$ for [**3-*d***]* and $2k_D^s/(k_H^s + 2k_D^s)$ for [**3′-*d***]*. The second isotopomer [**3′-*d***]* would be favored, for two CHD—CH_2 bonds of **1-*d*** could be broken.

© 2005 NRC Canada

Fig. 2. ^{2}H NMR spectrum at 92.1 MHz of propene-*d* isomers from the thermal rearrangement of **1-*d*** for 12.5 h at 435 °C.



Diradical [**3-*d***]* could react with rate constant k_H^p to yield **2-*d*(2)**, and with rate constant k_D^p to afford **2-*d*(3)**. The second energized trimethylene diradical ([**3′-*d***]*) could react further through $k^p{}_H$ to give **2-*d*(3)** and through k_H^p in the other direction to provide a mixture of both isomers of **2-*d*(1)**.

All four rate constants for hydrogen shifts in Fig. 1 (k_H^s, k_H^p leading to **2-*d*(2)**, k_H^p leading to **2-*d*(3)**, and k_H^p leading to **2-*d*(1)**) might be conditioned by secondary k_H/k_D effects. The possible β-secondary k_H/k_D contribution to the k_H^s/k_D^s ratio will be considered further when comparisons with theory-predicted k_H^s/k_D^s values are made. Possible secondary effects for the [1,2] shifts associated with rate constants k_H^p for reactions of [**3-*d***]* or [**3′-*d***]* were neglected. The k_H^p/k_D^p ratio was assumed to be largely determined by the primary [1,2] shifts of H vs. D.

Given the model of Fig. 1, the relative concentrations of deuterium-labeled propenes in product mixtures would be as expressed in the proportional relationships shown in eqs. [4]–[6].

[4] $$\textbf{2-}\boldsymbol{d}\textbf{(1)} \propto 2k_H^p k_D^s/(k_H^s + 2k_D^s)$$

[5] $$\textbf{2-}\boldsymbol{d}\textbf{(2)} \propto k_H^p k_H^s/(k_H^s + 2k_D^s)$$

[6] $$\textbf{2-}\boldsymbol{d}\textbf{(3)} \propto (k_H^s k_D^p + 2k_D^s k_H^p)/(k_H^s + 2k_D^s)$$

These proportionalities may be expressed more conveniently by dividing the right-hand sides of each of these three expressions by $k_D^s k_D^p/(k_H^s + 2k_D^s)$ (eqs. [7]–[9]).

[7] $$\textbf{2-}\boldsymbol{d}\textbf{(1)} \propto 2k_H^p/k_D^p$$

[8] $$\textbf{2-}\boldsymbol{d}\textbf{(2)} \propto (k_H^s/k_D^s) \times (k_H^p/k_D^p)$$

[9] $$\textbf{2-}\boldsymbol{d}\textbf{(3)} \propto k_H^s/k_D^s + 2k_H^p/k_D^p$$

The product mixtures from a series of five gas-phase thermal rearrangements of **1-*d*** at 435 °C with cyclopentane as the bath gas were analyzed by ^{2}H NMR in nine independent integrations. A representative spectrum of a product mixture is shown in Fig. 2. The ^{2}H NMR resonance signals are as expected (21), with the distinct vicinal $^3J_{H\text{-}D}$ coupling constants for the E- and Z-isomers of **2-*d*(1)** in clear evidence. Unreacted **1-*d*** is evident as a doublet centered at 0.22 ppm, with $^2J_{H\text{-}D}$ = 0.95 Hz.

The intensities of the various ^{2}H NMR absorptions were determined without broadband proton decoupling so as to obviate possible NOE effects. For all but one integration, the pulse delay was 50 s; for the last 20 h run, the delay was 10 s. No significant differences in relative intensities at different reaction times were noted (Table 1), and no appreciable complications from secondary reactions were evident. Two minor absorptions (at 5.4 and 0.9 ppm) were contributed by unidentified side products (Fig. 2).

The relative ^{2}H NMR integral intensities of Z- and E-isomers of **2-*d*(1)** were 17.2 ± 0.46% and 17.3 ± 0.39%, respectively, equal within experimental uncertainties. The relative intensities for **2-*d*** isomers and for unreacted **1-*d*** as a function of reaction time showed a simple exponential decay of starting material corresponding to a rate constant for isomerzations of 1.13×10^{-5} s^{-1}. The high-pressure rate constant for rearrangement of unlabeled cyclopropane at 435 °C may be calculated from the activation parameters reported by Chambers and Kistiakowsky (22), $\log_{10} A$ = 15.17, E_a 65.0 kcal/mol (1 cal = 4.184 J): it is 1.29×10^{-5} s^{-1}, just slightly larger than the rate constant derived here. The difference may be ascribed to a combination of two factors: the pressure in the kinetic bulb during thermal reactions with cyclopentane present as a bath gas (113 to 114 torr, 1 torr = 133.322 4 Pa), is less than would be required to give kinetic behavior at the high-pressure limit, and deuterium kinetic isotope effects could lower the rate of isomerization moderately.

The experimental data summarized in Table 1 and the relationships shown in eqs. [7]–[9] lead easily to values for the two deuterium isotope effects involved, k_H^s/k_D^s for cleaving a cyclopropane C—C bond and k_H^p/k_D^p for shifting a hydrogen or deuterium from C2 to C1 in the trimethylene diradical **3-*d***. The three expressions (eqs. [7]–[9]) are just proportionalities; they can be used to formulate two independent equations with two unknowns. From eqs. [7] and [8], eq. [10] follows, and $k_H^s/k_D^s = 2 \times 18.8/34.6 = 1.09$.

© 2005 NRC Canada

Table 1. Relative intensities of ^{2}H NMR absorptions for propene-*d* products from thermal isomerizations of deuteriocyclopropane at 435 °C.

Time (h)	**2-*d*(2)** (%) (5.87 ppm)	**2-*d*(1)** (Z and E) (%) (5.07 and 4.98 ppm)	**2-*d*(3)** (%) (1.64 ppm)
7.5	18.6	34.7	46.7
10	18.9	35.4	45.7
10	18.8	35.2	46.0
12.5	19.7	34.5	45.8
12.5	19.0	34.8	46.2
5	18.0	33.3	48.7
20	18.9	33.9	47.2
20	18.4	34.4	47.2
20	18.5	35.3	46.2
Average	18.8	34.6	46.6
Standard deviation	0.4	0.6	0.8
Relative error	1.9	1.7	1.7

[10] $$[\mathbf{2\text{-}d(1)}]/[\mathbf{2\text{-}d(2)}] = 2/(k_H^s/k_D^s)$$

An equation may be constructed from eqs. [8] and [9] with but a single unknown, the primary kinetic isotope effect rate-constant ratio, k_H^p/k_D^p (eq. [11]).

[11] $$[\mathbf{2\text{-}d(3)}]/[\mathbf{2\text{-}d(2)}] = (k_H^s/k_D^s + 2k_H^p/k_D^p)/[(k_H^s/k_D^s) \times (k_H^p/k_D^p)]$$

Rearranging eq. [11] to express k_H^p/k_D^p as a function of knowns gives eq. [12], which leads at once to the solution $k_H^p/k_D^p = 1.55$.

[12] $$k_H^p/k_D^p = (k_H^s/k_D^s)/\{(k_H^s/k_D^s) \times [\mathbf{2\text{-}d(3)}]/[\mathbf{2\text{-}d(2)}] - 2\}$$

When the experimental uncertainties in the integrated NMR absorption intensities are taken into account, the two isotope effects and error estimates are $k_H^s/k_D^s = 1.09 \pm 0.03$ and $k_H^p/k_D^p = 1.55 \pm 0.06$.

How significantly would these estimates be altered if a minor contribution to the overall isomerization from a different path, one involving a direct rate-determining isomerization of **1-*d*** to a monodeuterium-labeled singlet 1-propylidene reactive intermediate, followed by a very rapid [1,2]-hydrogen or [1,2]-deuterium shift (12)? Were this hypothetical path a contributor, there would be some bias favoring the formation of **2-*d*(2)** at the expense of the other three propene-*d* isotopomers. Primary kinetic isotope effects could be involved at two stages, during formation of a propylene-*d* intermediate or during a [1,2] shift. But a contribution of as much as 10% by such a path would not lead to significant changes in the estimated values for k_H^s/k_D^s (1.09 ± 0.03) and k_H^p/k_D^p (1.55 ± 0.06). Were the primary k_H/k_D effects on the cyclopropane to 1-propylene to propene route equal to 1.6, and the secondary effect 1.09 once again, the changes in the calculated distributions of **2-*d*** isomers would lead to calculated k_H^s/k_D^s and k_H^p/k_D^p values of 1.11 and 1.63, estimates very close to the values based on taking the trimethylene diradical intermediate mechanistic model to be the only path. A minor contribution from the 1-propylidene route would not influence the two kinetic isotope effect estimations significantly (23).

The kinetic model adopted and the experimental observations of the present work define k_H^s/k_D^s as the ratio of rate constants leading from **1-*d*** to [**3-*d***]* and from **1-*d*** to [**3′-*d***]*. The value obtained for k_H^s/k_D^s (1.09 ± 0.03) is a composite of α and β effects. The α effect influences the cleavage leading to **3′-*d*** and the β effect influences the cleavage leading to **3-*d***, each relative to the rate constant for cleaving one C—C bond in unlabeled cyclopropane. Thus, k_H^s/k_D^s is a ratio of one rate constant modified by a β secondary effect divided by one conditioned by an α effect.

Direct comparisons with the theory-derived values for k_{13} vs. k_{12} rate constants in 1,2-d_2-cyclopropanes previously cited, 1.13 and 1.12 (at 422.5 °C) (16, 17) and 1.09 (at 400 °C) (18), are appropriate, for k_{13} in conditioned by the product of one α and one β effect, while k_{12} is conditioned by the product of two α effects. The k_{13}/k_{12} ratio, the *f* factor, is equivalent to the present k_H^s/k_D^s ratio. Thus, the experimental value 1.09 ± 0.03 is completely consistent with the value assumed in 1975 (4) and with the several subsequent theory-derived values (16–18).

The hypothetical $k_H^s/k_D^s = 0.8$ value may successfully serve as a device for reinterpreting one reported k_i/k_α value for 1,2-d_2-cyclopropanes (1.07) as consistent with $k_{12}/k_1 \approx 5$, a ratio found in one theory-based model for the stereomutations (18). With $k_H^s/k_D^s = 0.8$, the earlier conclusion (4) that $k_{12}/k_1 \approx 42$ could be abandoned, while the experimentally reported (4) rate constant ratio ($k_i/k_\alpha = 1.07$) could remain unquestioned. The present experimental value ($k_H^s/k_D^s = 1.09 \pm 0.03$) makes the hypothetical $k_H^s/k_D^s = 0.8$ value seem unlikely. The discrepancies in the literature as to the k_{12}/k_1 ratio for cyclopropane stereomutations may hinge more plausibly on problems associated with experimental determinations of k_i and k_α values than in different judgments on the k_H^s/k_D^s ratio (15*e*).

Experimental section

Deuteriocyclopropane

To an oven-dried, heavy-walled tube fitted with a stopcock and provided with an argon atmosphere and a tiny stir-

© 2005 NRC Canada

ring bar was added, in turn, AIBN (0.10 g, 0.61 mmol), Bu_3SnD (2.0 g, 1.8 mL, 6.8 mmol), and cyclopropyl bromide (0.39 g, 3.2 mmol). The stopcock was closed and the reaction tube was heated at 85 °C for 5 h. The reaction mixture was then cooled to room temperature; the stopcock was opened to allow the volatile materials in the product mixture to be collected in an evacuated glass coil cooled in liquid nitrogen. The deuterium-labeled cyclopropane product was purified and isolated by preparative gas chromatography (15*c*) using a modified Varian Aerograph A90-P3 instrument and a 0.63 cm × 3.7 m 20% SE-30 60/80 mesh Chromosorb W HMDS column.

Thermal isomerizations

The glass collection vessel containing the preparative GC purified **1-*d*** was connected to a glass adapter containing 3 Å molecular sieves; the adapter led to a vacuum line. The sample was cooled with liquid nitrogen and the helium present was removed from the collection vessel and the vacuum line. The cooling bath was removed to allow the gas to volatilize and fill the vacuum line. The pressure of gas in the line was noted, and the **1-*d*** sample was condensed in a small cold finger in the vacuum line close to the kinetic bulb with liquid nitrogen and a small Dewar. The pressure remaining in the line was noted, and a stopcock was closed to isolate the condensed **1-*d***. The difference in the two pressures recorded and the volume of the line defined the amount of **1-*d*** that had been condensed. The **1-*d*** remaining in the line was removed. Cyclopentane (anhydrous, Aldrich, Milwaukee, Wisconsin) in a glass coil was degassed 3 times using a freeze–thaw routine, allowed to warm, and admitted to the vacuum line. The pressure in the line was noted, the cyclopentane was condensed into the small cold finger containing the **1-*d*** sample, the stopcock was closed to isolate the condensed hydrocarbons, and the pressure in the line from the remaining cyclopentane was noted. The two pressure readings provided a measure of the amount of cyclopentane that had been condensed. The cyclopentane remaining in the line was pumped off.

The condensed mixture of **1-*d*** and cyclopentane was allowed to expand into an evacuated 280 mL kinetic bulb over a 2 min period by appropriate manipulations of stopcocks and warming the cold finger with hot water. The kinetic bulb was closed, the small amount of reactant and cyclopentane remaining between the cold finger and the cut-off stopcock atop the kinetic bulb was determined manometrically and then evacuated from the vacuum line.

When the designated time for a thermal isomerization had elapsed, the reaction mixture was quickly transferred from the kinetic bulb and collected in an evacuated u-tube immersed in liquid nitrogen. Subsequently the product mixture was transferred from the u-tube to a degassed NMR tube containing $CHCl_3$ and immersed in liquid nitrogen; the tube was sealed and the product mixture was analyzed by ^2H NMR spectroscopy at 92.1 MHz.

Thermal runs over 7.5, 10, 12.5, and 20 h used from 8.7 to 9.2 mg of **1-*d*** and 42 to 43 mg of cyclopentane; pressures in the kinetic bulb were 113 to 114 torr. The single run over 15 h employed 8.3 mg of **1-*d*** and no cyclopentane; the pressure was only 24 torr. The isomerization for this run was notably slower, but the distribution of **2-*d*** products was consistent with the distributions observed in other product mixtures (Table 1). The conversion vs. time data used to calculate the rate constant 1.29×10^{-5} s^{-1} for the **1-*d*** to **2-*d*** isomerizations did not include the run in which cyclopentane was not present.

Acknowledgments

We thank the National Science Foundation for support of this work through CHE-0211120 and Mr. David J. Kiemle of the SUNY College of Forestry and Environmental Science for recording the ^2H NMR spectra.

References

1. S. Tanatar. Ber. Dtsch. Chem. Ges. **29**, 1297 (1896).
2. L. Birladeanu. J. Chem. Ed. **75**, 603 (1998).
3. B.S. Rabinovitch, E.W. Schlag, and K.B. Wiberg. J. Chem. Phys. **28**, 504 (1958).
4. (*a*) J.A. Berson and L.D. Pedersen. J. Am. Chem. Soc. **97**, 238 (1975); (*b*) J.A. Berson, L.D. Pedersen, and B.K. Carpenter. J. Am. Chem. Soc. **98**, 122 (1976).
5. S.W. Benson. J. Chem. Phys. **34**, 521 (1961).
6. R. Hoffmann. J. Am. Chem. Soc. **90**, 1475 (1968).
7. J.A. Horsley, Y. Jean, C. Moser, L. Salem, R.M. Stevens, and J.S. Wright. J. Am. Chem. Soc. **94**, 279 (1972).
8. Y. Yamaguchi, H.F. Schaefer, and J.E. Baldwin. Chem. Phys. Lett. **185**, 143 (1991).
9. C. Doubleday, Jr. J. Phys. Chem. **100**, 3520 (1996).
10. K.-N. Fan, Z.-H. Li, W.-N. Wang, H.-H. Huang, and W. Huang. Chem. Phys. Lett. **277**, 257 (1997).
11. F. Dubnikova and A. Lifshitz. J. Phys. Chem. A, **102**, 3299 (1998).
12. H.F. Bettinger, J.C. Rienstra-Kiracofe, B.C. Hoffman, H.F. Schaefer, J.E. Baldwin, and P.v.R. Schleyer. Chem. Commun. (Cambridge), 1515 (1999).
13. (*a*) C. Doubleday, Jr., K. Bolton, and W.L. Hase. J. Phys. Chem. A, **102**, 3648 (1998); See also: (*b*) C. Doubleday, Jr., K. Bolton, G.H. Peslherbe, and W.L. Hase. J. Am. Chem. Soc. **118**, 9922 (1996); (*c*) K. Bolton, W.L. Hase, and C. Doubleday, Jr. Ber. Bunsen-Ges. **101**, 414 (1997); (*d*) K. Bolton, W.L. Hase, and C. Doubleday, Jr. J. Phys. Chem. B, **103**, 3691 (1999).
14. W.T. Borden. *In* Reactive intermediate chemistry. *Edited by* R.A. Moss, M.S. Platz, and M. Jones, Jr. John Wiley and Sons, New York. 2004. pp. 961–1004.
15. (*a*) S.J. Cianciosi, N. Ragunathan, T.B. Freedman, L.A. Nafie, D.K. Lewis, D.A. Glenar, and J.E. Baldwin. J. Am. Chem. Soc. **113**, 1864 (1991); (*b*) T.B. Freedman, S.J. Cianciosi, N. Ragunathan, J.E. Baldwin, and L.A. Nafie. J. Am. Chem. Soc. **113**, 8298 (1991); (*c*) J.E. Baldwin and S.J. Cianciosi. J. Am. Chem. Soc. **114**, 9401 (1992); (*d*) J.E. Baldwin, S.J. Cianciosi, D.A. Glenar, G.J. Hoffman, I.-W. Wu, and D.K. Lewis. J. Am. Chem. Soc. **114**, 9408 (1992); (*e*) J.E. Baldwin. *In* The chemistry of the cyclopropyl group. Vol 2. *Edited by* Z. Rappoport. John Wiley, Chichester. 1995. pp. 469–494; (*f*) T.B. Freedman, D.L. Hausch, S.J. Cianciosi, and J.E. Baldwin. Can. J. Chem. **76**, 806 (1998).
16. S.J. Getty, E.R. Davidson, and W.T. Borden. J. Am. Chem. Soc. **114**, 2085 (1992).
17. J.E. Baldwin, Y. Yamaguchi, and H.F. Schaefer. J. Phys. Chem. **98**, 7513 (1994).

© 2005 NRC Canada

18. D.A. Hrovat, S. Fang, W.T. Borden, and B.K. Carpenter. J. Am. Chem. Soc. **119**, 5253 (1997); **120**, 5603 (1998).
19. E.M. Goldfield. Faraday Discuss. **110**, 185–205 (1998).
20. S. Petersen, J.L. Herek, and A.H. Zewail. Science (Washington, D.C.), **266**, 1359 (1994).
21. R.V. Dubs and W. von Philipsborn. Org. Magn. Reson. **12**, 326 (1979).
22. (*a*) T.S. Chambers and G.B. Kistiakowsky. J. Am. Chem. Soc. **56**, 399 (1934); See also: (*b*) H.O. Prichard, R.G. Sowden, and A.F. Trotman-Dickenson. Proc. R. Soc. London Ser. A, **217**, 563 (1953); (*c*) E.W. Schlag and B.S. Rabinovitch. J. Am. Chem. Soc. **2**, 5996 (1960); (*d*) E.V. Waage and B.S. Rabinovitch. J. Phys. Chem. **76**, 1695 (1972).
23. J.E. Baldwin, L.S. Day, and S.R. Singer. J. Am. Chem. Soc. **127**, 9370 (2005).

© 2005 NRC Canada

The kinetics of the spontaneous, proton- and Al^{III}-catalysed hydrolysis of 1,5-anhydrocellobiitol — Models for cellulose depolymerization in paper aging and alkaline pulping, and a benchmark for cellulase efficiency[1]

John William Baty and Michael L. Sinnott

Abstract: The kinetics of the spontaneous, proton- and Al^{III}-catalysed hydrolyses of the C1—O4′ bond in 1,5-anhydrocellobiitol have been measured at elevated temperatures (125.0–220.0 °C). Data for the first two processes extrapolate to the expression $k = (8.6 \pm 2.1 \times 10^{-16}) + (1.4 \pm 0.2 \times 10^{-9\text{-pH}})$ s^{-1} at 25 °C. These room-temperature figures were used to model cellulose depolymerization by the af Ekenstam equation. The spontaneous process is too slow to contribute to loss of paper strength on aging, and even the acid-catalysed process is significant only below ~pH 4.0. However, the spontaneous hydrolysis readily accounts for the reduction of cellulose degree of polymerization (DP) during alkaline (e.g., kraft) pulping of cellulose fibres. Efficient electrophilic catalysis by Al^{III} was observed at 150.0 °C in 0.1 mol/L succinate buffers of room temperature pH 3.05 and 3.35 ($k_2 = 8.1 \pm 0.4 \times 10^{-3}$ and $4.2 \pm 0.2 \times 10^{-3}$ $(mol/L)^{-1}$ s^{-1}, respectively). The apparent activation energy of the Al^{III}-catalysed process was 31 ± 4 kJ mol^{-1}, lower than that of the proton-catalysed path, suggesting the electrophilic catalysis increases in importance as the temperature approaches ambient. Consequently, it appears that the culprit in the impermanence of "rosin-alum"-sized paper is Al^{III}, directly acting as a Lewis acid, not the Al^{III} hydration sphere as a Brønsted acid. Conservation measures should either address this or be generic (e.g., low-temperature storage).

Key words: cellulose, hydrolysis, kraft pulping, paper conservation, rosin-alum sizing.

Résumé : Opérant à des températures élevées (125,0 à 220,0 °C), on a mesuré les vitesses des réactions d'hydrolyse, spontanée et catalysées par le proton ou l'aluminium(III), de la liaison C1—O4′ du 1,5-anhydrocellobiitol. Les données pour les deux premiers processus conduisent à l'expression $k = (8{,}6 \pm 2{,}1 \times 10^{-16}) + (1{,}4 \pm 0{,}2 \times 10^{-9\text{-pH}})$ s^{-1} extrapolée à 25 °C. On a utilisé ces valeurs à la température ambiante comme modèle pour la dépolymérisation de la cellulose par l'équation de af Ekenstam. Le processus spontané est trop lent pour contribuer à une perte de la force du papier avec l'âge; le processus catalysé par un acide n'est significatif qu'à des pH inférieurs à environ 4,0. Toutefois, l'hydrolyse spontanée permet d'expliquer facilement la réduction du degré de polymérisation (DP) de la cellulose durant le traitement alcalin (kraft) des fibres de cellulose. On a observé une catalyse électrophile efficace par l'aluminium(III) à 150,0 °C, dans des tampons de succinate, à la température ambiante et à des pH de 3,05 et 3,35 ($k_2 = 8{,}1 \pm 0{,}4 \times 10^{-3}$ et $4{,}2 \pm 0{,}2 \times 10^{-3}$ $(mol/L)^{-1}$ s^{-1} respectivement). L'énergie d'activation apparente pour le processus catalysé par l'aluminium(III) est de 31 ± 4 kJ mol^{-1}, inférieure à celle du processus catalysé par le proton, ce qui suggère que la catalyse électrophile augmente en importance lorsque la température tend vers la température ambiante. En conséquence, il semble que le coupable de la non permanence du papier collage à la rosine et à l'alun serait l'aluminium(III) qui agirait directement comme acide de Lewis et non pas la sphère d'hydratation de l'aluminium(III) qui agirait comme un acide de Brønsted. Les mesures de conservation devraient tenir compte de ces conclusions ou être génériques, tel qu'un entreposage à basse température.

Mots clés : cellulose, hydrolyse, pulpage alcalin, conservation du papier, traitement à la rosine et à l'alun.

[Traduit par la Rédaction]

Received 20 April 2005. Published on the NRC Research Press Web site at http://canjchem.nrc.ca on 25 November 2005.

J.W. Baty.[2] School of Materials, University of Manchester, POB 88, Sackville Street, Manchester, M60 1QD, UK.
M.L. Sinnott.[3] School of Applied Sciences, University of Huddersfield, Queensgate, Huddersfield, HD1 3DH, UK.

[1]This article is part of a Special Issue dedicated to organic reaction mechanisms.
[2]Present address: 1201 Lincoln Mall, Apt. 400, Lincoln, NE 68508-2800, USA.
[3]Corresponding author (e-mail: m.l.sinnott@hud.ac.uk).

 doi: 10.1139/V05-168 © 2005 NRC Canada

Introduction

The loss of mechanical strength of cellulose fibres with age is an important limiting factor in the preservation of paper documents and, to a lesser extent, textiles. The degradation of paper in particular threatens much of our written cultural heritage (1). Loss of paper strength is associated with a decrease in the degree of polymerization (DP) of the cellulose in the paper fibres (2*a*). Some depolymerization arises from initial oxidation of the hydroxyls in cellulose to carbonyl groups, which can then promote E1cb-like elimination of O4 and its substituent, leading to cellulose chain cleavage. The oxidation can arise from excess use of oxidative bleaching agents or photooxidation (3).

However, much paper degradation (particularly that occurring under conditions of archival storage) does not occur by these routes, and appears to be a hydrolysis. Hydrolytic degradation is confirmed by the detection of glucose, cellobiose, and cellotriose in naturally aged papers (4). Paper is 4%–9% water by weight (5), and the aqueous hydrolysis of the β(1→4) link in the noncrystalline regions of the cellulose fibre is the depolymerization route.

We here report studies of the kinetics of hydrolysis of 1,5-anhydrocellobiitol by spontaneous and electrophile-catalysed routes. We also report data on the hydrolysis of this compound by the well-known acid-catalysed mechanism, but at high-temperature and (room-temperature) pH 3.1–4.0, to permit comparison with the first two routes without large extrapolation of acid strength. This compound, rather than cellobiose itself, was used as the model for the β(1→4) link in cellulose to avoid the carbonyl group rearrangement and elimination reactions, which had vitiated a previous attempt to measure the rate of spontaneous hydrolysis of a β(1→4) glucan link (6).

The spontaneous hydrolysis of 2,4-dinitrophenyl glycosides has been known for some time (7) and effects of glycone structure have been studied in detail (8). Since the glucopyranosyl cation is "too unstable to exist" in contact with an anionic leaving group (9), such hydrolyses are S_N2 (A_ND_N) reactions with "exploded" transition states with little bonding to either nucleophilic water or the leaving group (10). Multiple kinetic isotope effects with fluoride as a leaving group support such a picture (11). The $\log k_{hyd}$ vs. pH plot for 2,4-dinitrophenyl β-galactopyranoside was horizontal between pH 2 and 8, that for *p*-nitrophenyl β-glucopyranoside between pH 3 and 6 (12). However, the expectation that the horizontal region for such plots would get smaller as the leaving group became worse was confounded by the recent discovery of a spontaneous hydrolysis pathway for methyl glycosides. Wolfenden et al. (13) measured the rates of methyl β- and α-D-glucopyranoside and -ribofuranoside hydrolysis at 180–260 °C and observed rates independent of the buffer room-temperature pH between 7 and 11. Their data for methyl β-D-glucopyranoside extrapolate to a rate of $4.7 \pm 2.1 \times 10^{-15}$ s^{-1} at 25 °C, a figure they noted may be of significance to paper degradation. We considered that departure of the 4-anion of glucose might be faster than that of methoxide for steric and electronic reasons. The anticipated β_{lg} value of the spontaneous hydrolysis of glycosides is expected to be between that for the spontaneous hydrolyses of aryloxytetrahydropyrans (–1.18) and methoxymethyl carboxylates (–0.82) (14). The former generates a solvent-equilibrated tetrahydropyranyl cation; the latter is an unambiguous S_N2 (A_ND_N) reaction. The pK_a of methanol is 15.54 (15); whereas that for the 2-OH of glucose is 14.0 (16), and the 4-OH is likely to be similar. Further, it seems as if the β(1→4) linkage between two hexopyranose units is somewhat crowded: equilibrium constants for the hydrolysis of lactose and allolactose (the β(1→6) isomer) at 37 °C are 152 ± 19 mol/L and ~44 mol/L, respectively (17). It seemed likely that the spontaneous hydrolysis of 1,5-anhydrocellobiitol would be faster than that of methyl β-D-glucopyranoside by over one order of magnitude because of electronic effects, and a factor of ~2 through steric acceleration. Were this to be the case at room temperature, spontaneous hydrolysis would be a major contributor to paper degradation.

Paper from around the middle of the 19th century until about the mid-1970s loses mechanical strength comparatively quickly, so that 19th and early 20th century documents can be in worse condition than books and papers from the 17th and 18th centuries. The culprit is "rosin-alum" sizing (sizing with diterpene acids and aluminium sulfate — not $KAl(SO_4)_2{\cdot}12H_2O$), invented in 1800 and widespread by the 1840s (18). Paper conservators have hitherto assumed that rosin-alum-sized paper principally degrades via the proton-catalysed mechanism, with the aluminium hydration sphere acting as a source of protons (19). Policies of mass deacidification of documents have followed from this assumption (20) despite occasional paper technology studies suggesting the picture was more complicated. For example, differing activation energies from differential thermal analyses led Parks to conclude, "Sulfuric acid has a destabilizing effect qualitatively different from that of [aluminium sulfate]…" (21). Barański et al. (22) measured the macroscopic kinetics of the degradation of $Al_2(SO_4)_3$-impregnated papers and concluded that mixed-control-type kinetic equations, taking into account other processes, were required. In 1993, it was remarked "Considering that rosin sizing is still widely used after 140 years, and that in commercial operations aluminium compounds are invariably involved, it is a matter for some astonishment that we still do not know for certain the exact mechanism by which aluminium compounds affect permanence…" (23).

We hypothesized that Al^{III} species in rosin-alum-sized paper might be directly acting as electrophiles rather than as a source of protons. The hypothesis had a chemical precedent in the electrophilic catalysis of the hydrolysis of 8-quinolinyl β-D-glucopyranosides by first-row transition metal ions (24, 25) and a possible biochemical one in the Mg^{II}-dependence of the hydrolysis of *O*-glycosides by the *lacZ* β-galactosidase of *Escherichia coli* (26). A preliminary report of catalysis of 1,5-anhydrocellobiitol hydrolysis by Al^{III} has been published (27); we now report full details and apply the measured rate data to the depolymerization of cellulose, modelled with the af Ekenstam equation.

The proton-catalysed hydrolysis of cellulose has received much attention over the years. Macroscopic kinetic studies have been prompted by technology, such as the industrial manufacture of microcrystalline cellulose (28), the development of biomass fuels and feeds (29, 30*a*), the acid pulping of biomass for paper (30*b*), and the permanence and conservation of cellulosic textiles and paper (31, 32). The acid-

© 2005 NRC Canada

catalysed hydrolysis of glycosides in general has been extensively studied. Pyranosides hydrolyse by initial protonation of the exocyclic oxygen atom followed by C1-O1 fission. In the case of alkyl glycosides, the protonation step is a pre-equilibrium one (i.e., specific acid catalysis) (33, 34). Any nucleophilic involvement is questionable. The leaving group is electrically neutral (and, with a late transition state, results in $\beta_{lg} \sim 0$). Recent work on 2-deoxy-β-glucopyranosyl pyridinium salts, with likewise an electrically neutral leaving group, suggests that the rate-determining step is formation of a solvent-separated ion-pair-molecule complex (i.e., $X^-//Glu^+Py$) (35). An analogous process would explain the dependence of acid-catalysed hydrolysis reactions on the nature, but not the nucleophilicity, of anions present (33, 36). Limited data for the hydrolysis of 1,5-anhydrocellobiitol in mildly acid media were therefore obtained, largely to establish the "turnround" point on the pH–rate profile, and to compare to the electrophile-catalysed process.

Materials and methods

1,5-Anhydrocellobiitol ((4-*O*-β-D-glucopyranosyl)-1,5-anhydro-D-glucitol) was prepared according to Zhang (37), who adapted Fletcher's route to 1,5-anhydroglucitol (38). Reduction of ethyl (heptacetyl-β-cellobiosyl) xanthate with Raney nickel afforded hepa-*O*-acetyl-1,5-anhydrocellobiitol, mp 194 to 195 °C (lit. value (39) mp 194 to 195 °C). Zemplén deacetylation afforded a material mp of 170 °C (decomp.), lit. value (39) mp 172 °C (decomp.), $[\alpha]_D^{20}$ 29° (lit. value 29.3). Spin-decoupled ^{13}C NMR 10 lines, d 103 (C1), double intensity 76.5 (C6 and C6′), and 79.5 (C5 and C5′).

Reaction solutions containing 1,5-anhydrocellobiitol substrate in buffer (including, where applicable, catalysts or catalytic controls) were sealed inside small ampoules made from melting point capillaries (Fisher Scientific Co.) and submerged into a thermostatted oil bath (Labovisco-PMT Tamson TC 9E). Oil temperatures were verified using a mercury-in-glass thermometer calibrated by the UK National Physical Laboratory, Teddington. After various time intervals the ampoules were removed, opened, and the proportions of 1,5-anhydrocellobiitol and 1,5-anhydroglucitol analyzed by high-performance liquid chromatography – refractive index detection (pH 3.0–4.0, all components by Gilson Medical Instruments, Inc., supplied by Anachem Ltd., Luton, Beds, UK, except the column by YMC (YMC-Polyamine II)) or high-performance anion exchange chromatography – pulsed amperometric detection (pH 4.7–11.0, all components by Dionex (UK) Ltd., Camberley, Surrey, UK, including the CarboPac PA-10 column). Because of the high surface area of the capillaries and the exposure time of hours to days, warm-up and cool-down times were negligible.

The concentration of substrate in the sample solutions was selected for optimal detection. For refractive index detection (HPLC) this was 10 mmol/L and for pulsed amperometric detection (HPAE) it was 3.07×10^{-4} mol/L. One hydrolysis product of 1,5-anhydrocellobiitol, glucose, is expected to degrade rapidly at high temperatures to carboxylic acids and other compounds (13, 40). To accommodate these, a ratio of 10:1 molar ionic strength buffer to molar substrate was selected for all reactions conducted. The pH of all samples was measured at room temperature and rechecked with narrow-range pH paper after exposure. Oxygen – acid buffer systems, with small heats of ionization, were used to minimize dpH/d*T*. Further criteria for buffer suitability were solubility in the chromatographic mobile phase and noninterference with detection. For HPLC–RI, succinic acid – succinate buffers (pH 3.0–4.0) were selected. For HPAE–PAD, acetic acid – acetate (pH 4.7), monobasic phosphate – dibasic phosphate (pH 5.9–7.5), and dibasic phosphate – tribasic phosphate (pH 9.6–10.7) were used.

We considered general acid catalysis of substrate hydrolysis by buffers highly unlikely in these studies. General acid catalysis of glycosides is favoured where acidic leaving groups make the conjugate acid of the substrate too unstable to exist (34). The mode of acid catalysis of the hydrolysis of *p*-nitrophenyl glucopyranoside changes from general at 45 °C to specific at 75 °C (41).

The Al^{III} ion has a complicated aqueous coordination chemistry, with certain insoluble species predominating under certain conditions (42). Therefore, in the electrophilic catalysis study, samples were monitored for any loss of homogeneity. Samples exhibiting a loss of homogeneity were discarded because of the risk of crystal entrainment. The Al^{III} ion was added as $Al_2(SO_4)_3 \cdot nH_2O$, the salt employed in the rosin-alum-sizing method. In the study comparing the rates of proton vs. electrophilic catalysis, concentrations of $Al_2(SO_4)_3$ ranging from 0 to 20 mmol/L were employed.

Results and discussion

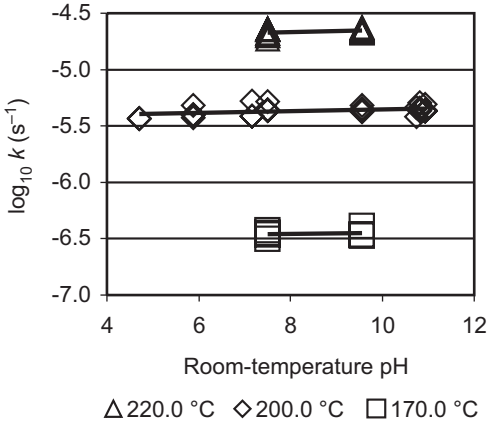
The spontaneous hydrolysis of 1,5-anhydrocellobiitol

Figure 1 shows $\log_{10}k_{obs}$ for hydrolysis of 1,5-anhydrocellobiitol as a function of room-temperature pH at three temperatures; individual constants are listed in the Supplementary material.[4] The gradients of these plots are 0.017 ± 0.005 at 220.0 °C, 0.007 ± 0.004 at 200.0 °C, and 0.005 ± 0.012 at 170.0 °C, effectively zero. The alkaline degradation mechanisms of 1,5-anhydrocellobiitol observed by Brandon occurred in NaOH solution (0.5–2.5 mol/L, H_- 14–15) (43*a*) and are therefore unlikely to be important in our pH range. As expected, a pH-independent reaction similar to methyl β-D-glucopyranoside has been observed. At 220.0 °C, where the two sets of data can be compared without extrapolation, the rate for 1.5-anhydrocellobiitol is about an order of magnitude faster than for methyl β-D-glucopyranoside ($\log_{10}k_{obs}$ = –4.66 ± 0.03 and ~–5.8, respectively), confirming our analysis of electronic and steric effects. The E_a from data at 220.0, 200.0, and 170.0 °C is 149 ± 2 kJ mol^{-1} at (room-temperature) pH 7.5, and 151 ± 2 kJ mol^{-1} at (room-temperature) pH 9.6. An average figure for the entropy change of activation at ambient temperature ($\Delta S^{\ddagger}_{25\,°C}$) is calculated to be –38 ± 3 J mol^{-1} K^{-1}.

[4] Supplementary data for this article are available on the Web site or may be purchased from the Depository of Unpublished Data, Document Delivery, CISTI, National Research Council Canada, Ottawa, ON K1A 0S2, Canada. DUD 4045. For more information on obtaining material refer to http://cisti-icist.nrc-cnrc.gc.ca/irm/unpub_e.shtml.

© 2005 NRC Canada

Fig. 1. k_{obs} vs. room-temperature pH. The pH dependence of the spontaneous hydrolysis of 1,5-anhydrocellobiitol measured at three temperatures.



Our E_a figure is significantly higher than the value from Wolfenden et al. (13) for the spontaneous hydrolysis of methyl β-D-glucopyranoside (124 ± 6 kJ mol^{-1}), but is in line with their unpublished results on the spontaneous hydrolysis of trehalose (155 kJ mol^{-1}, personal communication from R. Wolfenden). The value for the spontaneous hydrolysis of methyl β-D-glucopyranoside is similar to that of several 2,4-dinitrophenyl β-D-glycopyranosides (108–126 kJ mol^{-1}), which, however, react some 10^{10}-fold faster (8). Our value for $\Delta S^{\ddagger}_{25\,°C}$ is lower than has been observed in other spontaneous hydrolysis systems, but not as low as observed by Wolfenden et al. (13) for methyl β-D-glucopyranoside (–99.6 ± 3.1 J mol^{-1} K^{-1}). The difference in our E_a for 1,5-anhydrocellobiitol from the value obtained by Wolfenden et al. (13) for methyl β-D-glucopyranoside is such that while the spontaneous hydrolysis of 1,5-anhydrocellobiitol is faster at the temperatures tested, it extrapolated to lower rates at ambient temperatures (8.6 ± 2.1 × 10^{-16} s^{-1} at 25.0 °C as against 4.7 ± 2.1 × 10^{-15} s^{-1}). It may be that departure of methoxide requires immobilization of a water molecule as proton donor, but that departure of the glucose 1-anion or 4-anion does not.

True endoglucanases have k_{cat} values around 30 s^{-1} when acting on long cellooligosaccharides (44). They therefore achieve a rate enhancement of ~3 × 10^{16} over the uncatalysed mechanism measured with our model.

Depolymerization of cellulose modelled using the af Ekenstam equation

af Ekenstam derived eq. [1] relating the degree of polymerization to the first-order rate constant for the cleavage of a specific linkage. Random chain fission and rates of cleavage independent of position in the chain were assumed (45).

$$[1] \qquad \ln(1 - DP_t^{-1}) - \ln(1 - DP_0^{-1}) = -kt$$

where DP_0 and DP_t are the degrees of polymerization initially and at time t, respectively, and k is the first-order microscopic rate constant for cleavage of an individual linkage, assumed to be invariant across the chain. Whilst this equation is normally used to calculate k from DP data, we reversed the process, inputting k from our model studies. This assumes that the cellulose is in dilute aqueous solution, like the model. The periodic crystalline regions of native cellulose, which are sites of very limited aqueous chemistry, are therefore neglected. Therefore, our results will overestimate the true rate of cellulose depolymerization by a particular mechanism.

Fig. 2. DP vs. t at 25 °C. Calculated from af Ekenstam eq. [1], substituting a DP_0 of 1300 and the extrapolated values for $k_{25\,°C}$ from methyl β-D-glucopyranoside (13) and 1,5-anhydrocellobiitol.

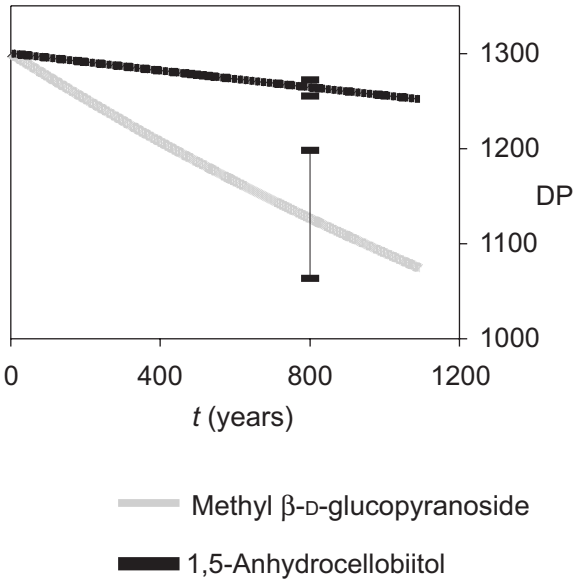


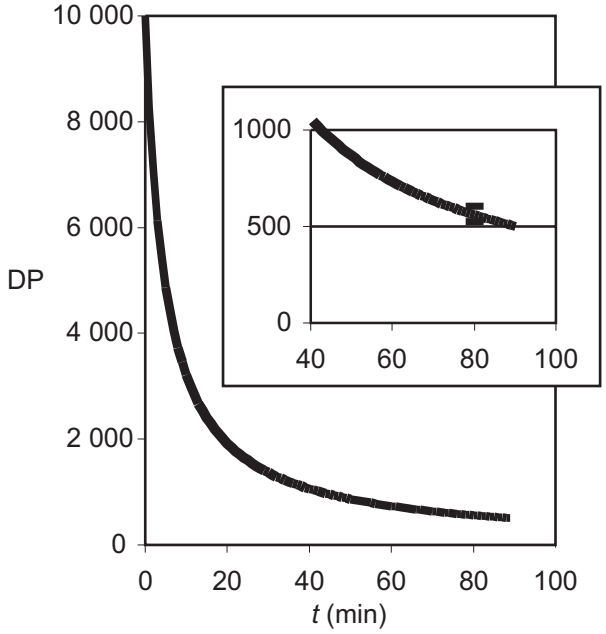
Figure 2 models cellulose depolymerization due to the spontaneous hydrolysis mechanism over time at 25 °C. The DP_0 used (1300) is that commonly taken for the cellulose in softwood kraft pulp (2*b*, 46); the specific rate constants used are that previously given for 1,5-anhydrocellobiitol and that reported by Wolfenden et al. (13) for methyl β-D-glucopyranoside. These models strongly suggest that spontaneous hydrolysis is not likely to be a problem encountered in neutral and alkaline papers in archives. The retained DP of ~1250 after 1000 years is far more than the ~400 at which brittleness becomes a problem in paper (2*a*).

A major element of the kraft process of paper pulping is the "cook phase" in which wood chips are exposed to conditions of pH 12–14 and 170–173 °C for roughly 90 min after warm-up (47). In this process, a DP loss from the biosynthetic ~10 000 (30*c*) to ~1300 occurs (2*b*). This loss in DP has been attributed to alkaline degradation mechanisms including β-alkoxy elimination (also known as the "peeling reaction" because it proceeds endwise) and unimolecular nucleophilic substitution that results from hydroxyl ionization. Previous molecular model studies of this process have not identified a spontaneous hydrolysis mechanism (43*b*, 48–50).

Figure 3 plots DP vs. t, showing the depolymerization of cellulose because of spontaneous hydrolysis modelled with 1,5-anhydrocellobiitol using the af Ekenstam eq. [1] and a DP_0 value of 10 000. The specific rate constant used in this model (3.5 ± 0.3 × 10^{-7} s^{-1}) is the average value of two data series obtained with good precision at 170.0 °C. (See Fig. 1 and Supplementary material).[4] As previously argued, the hydrolysis of 1,5-anhydrocellobiitol observed at these pH values will be exclusively due to the spontaneous hydrolysis

© 2005 NRC Canada

Fig. 3. DP vs. t at 170.0 °C. Depolymerization of cellulose during kraft cooking owing exclusively to spontaneous hydrolysis, modelled with 1,5-anhydrocellobiitol using af Ekenstam eq. [1] and a DP_0 of 10 000. The k_{obs} value used is an average of two data series (pH 7.5 and 9.6) obtained at 170.0 °C. Inset: Detail of depolymerization (40–90 min).



mechanism. As shown in the inset of Fig. 3, this model predicts that spontaneous hydrolysis alone reduces the DP of the cellulose to 502 ± 37 after 90 min under kraft cooking conditions, which is appreciably shorter than the actual DP after kraft cooking. An overestimate of DP loss, however, is expected here for two reasons. First, as previously noted, this model assumes that all of each cellulose chain is soluble. Second, in native wood chips, cellulose is part of a composite in which the matrix is (hydrophobic) lignin. On the introduction of the wood chips into the digester, only the surface of the chips is in contact with the kraft cooking liquor. Nonetheless, the reduction in DP is so large as to point unambiguously to the spontaneous hydrolysis mechanism as a primary mechanism of cellulose depolymerization in the kraft process.

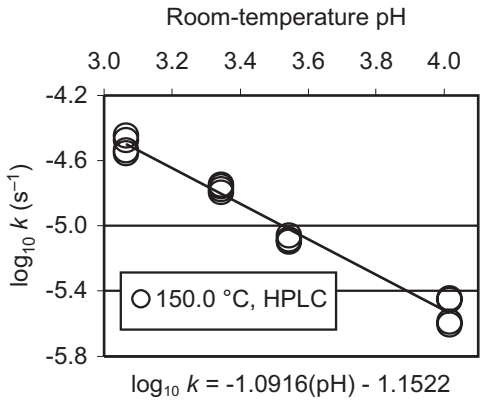
Given the relation between DP and paper strength, spontaneous hydrolysis is the primary mechanism in limiting the strength of papers made from kraft pulp.

The proton-catalysed hydrolysis of 1,5-anhydrocellobiitol

The slope of the plot (Fig. 4) of $\log_{10}k_{obs}$ (150.0 °C) vs. room temperature pH between pH 3.1 and 4.0 has a value of 1.09 ± 0.04, showing the expected 1:1 dependence of the specific rate constant to proton concentration. The pH changes were brought about by changing the buffer ratio in the same buffer system (succinic acid – succinate), which means that changes of pH within the series are temperature-independent, even if the change in absolute pH with temperature is large.

The E_a obtained from k_{obs} (room-temperature pH 3.5) between 140.0 and 175.0 °C, is 140 ± 1 kJ mol^{-1} (27). Extrapolation to 25.0 °C gives a value of 4.5 ± 0.7 × 10^{-13} s^{-1}, 525 times faster than the spontaneous hydrolysis. Equating $-\log_{10}[H^+]$ with measured pH at 25.0 °C gives a second-order rate constant for the proton-catalysed reaction of 1.4 ± 0.2 × 10^{-9} (mol/L)$^{-1}$ s^{-1}. For the hydrolysis at 25.0 °C, we can thus write eq. [2], valid from very acidic conditions to ~pH 12.3.

Fig. 4. $\log_{10}k_{obs}$ vs. pH. The pH dependence of the specific acid catalysis of 1,5-anhydrocellobiitol (150.0 °C).



$$[2] \quad k_{hyd,\ 25\ °C} = (8.6 \pm 2.1 \times 10^{-16}) + (1.4 \pm 0.2 \times 10^{-9\text{-pH}})\ s^{-1}$$

Therefore, the acid-catalysed hydrolysis becomes comparable with the spontaneous one only at pH 6.0.

The activation energy calculated for hydrolysis in succinic acid buffers of room-temperature pH 3.5 will include the heat of ionization of succinic acid. The value (140 ± 1 kJ mol^{-1}) is close to activation energies measured with stoichiometric concentrations of mineral acids (e.g., 141.3 kJ mol^{-1} for methyl β-D-glucopyranoside, 138.8 kJ mol^{-1} for 2-propyl β-D-glucopyranoside, or 134.2 kJ mol^{-1} for the sterically acclerated 1-adamantyl β-D-glucopyranoside (51)), which do not include such a contribution. Therefore, the heat of ionization of succinic acid appears to be low, as is expected for an oxygen acid.

Modelling depolymerization using the af Ekenstam equation

Figure 5 models the depolymerization of cellulose in paper fibres ($DP_0 \cong 1300$) using af Ekenstam eq. [1] inputting the extrapolated value of $k_{25.0\ °C}$ (4.5 ± 0.7 × 10^{-13} s^{-1}) for 1,5-anhydrocellobiitol at pH 3.5. The other pH values were calculated from the pH 3.5 extrapolated value, assuming rates that were first-order in protons. The af Ekenstam equation will overestimate the rate of hydrolysis, since it assumes an aqueous environment throughout all cellulose chains. It is clear that even paper of pH 3.5 — at the lower end of the range of even "acid" papers — will have a usable lifetime of several decades before it reaches the failure criterion of DP = 400, the point at which paper becomes unusably brittle (2*a*). Although of greater significance than spontaneous hydrolysis, it seems unlikely that proton catalysis plays a major role in paper aging.

© 2005 NRC Canada

Fig. 5. Four hundred years of aging: DP vs. *t* at 25 °C. The depolymerization of cellulose in papermaking fibres modelled using af Ekenstam eq. [1], substituting 1300 for DP_0, and specific rate constants obtained from the model compound, 1,5-anhydrocellobiitol. The rate at pH 3.5 (succinic acid – succinate buffer, no Al^{III}) was extrapolated. All other pH values were calculated from the extrapolated rate based on first-order kinetics in H^+.

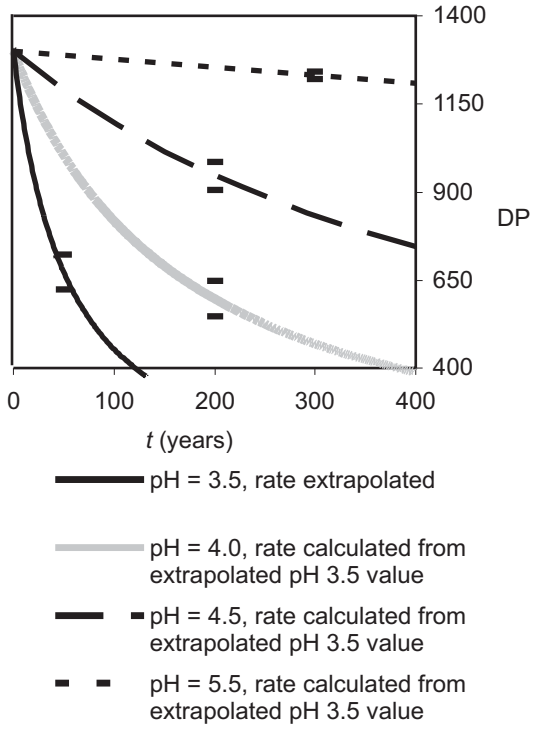
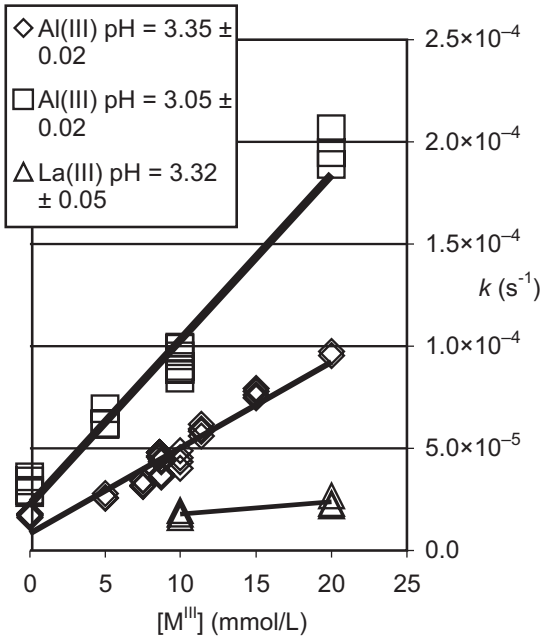


Fig. 6. *k* vs. [M^{III}]. First-order rate constants for hydrolysis of 1,5-anhydrocellobiitol (150.0 °C) as a function of added trivalent metal sulfates (27).



The Al^{III}-catalysed hydrolysis of 1,5-anhydrocellobiitol

Figure 6 shows the effect of added $Al_2(SO_4)_3$ and $La_2(SO_4)_3$ on k_{obs} for hydrolysis (150.0 °C) of 1,5-anhydrocellobiitol (10 mmol/L) in 100 mmol/L succinate buffers with the room-temperature pH values shown. The much greater effect of Al^{III} than La^{III} establishes that the increase in rate is not due to a change in ionic strength. (Although maximum added salt concentration was only 20% that of the buffer, if the concept of ionic strength, defined as $1/2\ \Sigma c_i z_i^2$, is applicable to these concentrated solutions, it is not constant, since we used salts of a divalent anion and trivalent cation (27)).

Competitive chelation of Al^{III} by succinate, substrate hydroxyls, and substrate glycosidic oxygen is expected, with Al^{III} in solution likely to be completely coordinated by the succinate and sulfate (42). Because of this anation, the rate of hydrolysis is expected to be lower than that which would be observed with $AlCl_3$, which possesses a noncoordinating cation (42, 52). Despite anation, unambiguous effects over the control are still observed. A clear pH dependence in the rate of the electrophilic hydrolysis is noted in this pH range. The apparent second-order rate constant at pH 3.05 is 8.1 ± 0.4 × 10^{-3} $(mol/L)^{-1}$ s^{-1}; at pH 3.35 it is 4.2 ± 0.2 × 10^{-3} $(mol/L)^{-1}$ s^{-1}, showing approximate proportionality of the second-order rate constant to the proton concentration.[5]

Presumably, this is due to protonated aluminium species being more electrophilic than unprotonated ones. Aluminium(III) exists in a variety of coordination compounds under papermaking conditions and it is not certain whether this particular pH dependence will extend to other pH ranges. It does suggest, however, that the relative importance of electrophilic catalysis to proton catalysis under ambient conditions will be pH-independent (27).

At 20 mmol/L of Al^{III}, k_{obs} was measured at 150.0 and 125.0 °C in buffers of room-temperature pH 3.33, and gave an E_a value of 109 ± 3 kJ mol^{-1} (27). This is appreciably lower than the value for proton-catalysed hydrolysis, suggesting that the electrophilic pathway will increase in importance as the temperature is lowered. Although the proton-catalysed pathway contributes ~10% to k_{obs} at 20 mmol/L of Al^{III} at 150.0 °C, the lower energy of activation means that this contribution, small anyway, decreases with temperature.

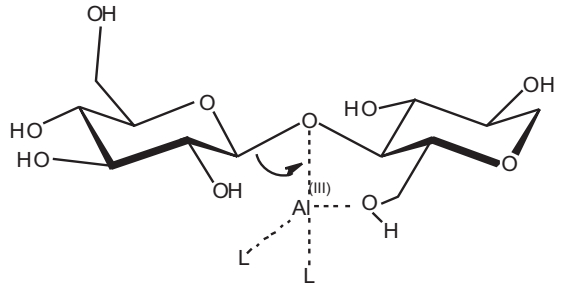
Conceivably, a kinetically equivalent pathway of hydrolysis could proceed, not from the coordination of Al^{III} with cellulose as in Scheme 1, but from the kinetically equivalent nucleophilic attack by an Al^{III}-coordinated oxygen atom on the conjugate acid of the substrate as in Scheme 2. However, as discussed in the Introduction, the sensitivity of such processes to nucleophilicity varies from weak to imperceptible. For example, in 2,4-dinitrophenolate production from 2,4-dinitrophenyl β-D-glucopyranoside, Bennet and Sinnott (53) showed sodium azide (1.0 mol/L) increased the rate by only 40%.

Electrophilic catalysis by Al^{III} was demonstrated with mmol/L concentrations of catalyst and substrate in homogeneous solution. In rosin-alum-sized paper there is more than enough aluminium to catalyse such a process: Priest et al.

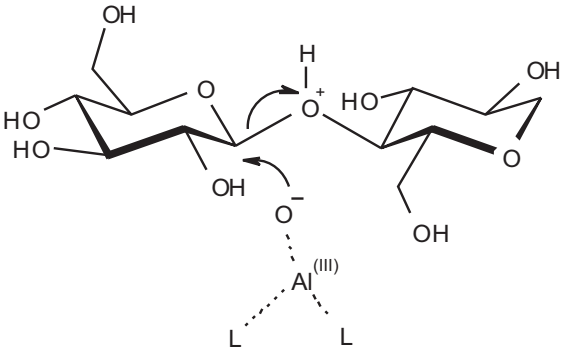
[5] In the preliminary communication, an error of 10^2 in these derived constants, immediately apparent from the displayed graphs, was unfortunately made.

© 2005 NRC Canada

Scheme 1. 1,5-Anhydrocellobiitol, showing a possible coordination pattern for Al^{III} (27). Coordination by O6′ is speculative, but has a possible precedent in the intramolecular conversion of lactose into allolactose by the *lacZ* β-galactosidase of *E. coli* where Mg^{II} may be the electrophile (26).



Scheme 2. A kinetically equivalent pathway to the electrophile-catalysed hydrolysis: hydrolysis proceeding from nucleophilic substitution of an Al^{III}-coordinated oxygen atom. This mechanism is deemed unlikely to cause the observed acceleration because of the minimal effect of even very strong nucleophiles in these systems (52).



(54) found a range of 1.3%–6.7% $Al_2(SO_4)_3$ (average 3.8%) per weight of oven-dried 20th century papers (AAS of acid extracts). Thus, in principle, concentrations of Al^{III} in the molar range are possible in the 5%–7% aqueous phase in such papers, although in practice much of the aluminium will be precipitated or adsorbed.

Mechanism of electrophilic catalysis of 1,5-anhydrocellobiitol hydrolysis by Al^{III}

Given the rate of water exchange in the inner sphere of Al^{III} (55), ligand exchange about Al^{III} is unlikely to be rate-determining. The identities of these ligands in the model system will include aquo, sulfate, and succinate, whilst in the paper sheet they will be many and various. Particularly given that in crystalline cellulose I the conformation about C5-C6 is the usually disfavoured *tg* conformation (56), the possibility exists that Al^{III} is chelated as shown in Scheme 1 in the productive complex. A possible biochemical precedent for 6-OH coordination may be found in the intramolecular conversion of lactose into allolactose by *E. coli* β-galactosidase, which contains an active-site Mg^{II} (26). Aluminium(III), which has a similar Pauling ionic radius (50 pm) to Mg^{II} (65 pm), is expected to coordinate in a similar manner.

Figure 7 models the depolymerization of cellulose using the af Ekenstam eq. [1] inputting 1300 for DP_0 and k_{obs} values from 20 mmol/L $Al_2(SO_4)_3$ catalysed 1,5-anhydrocellobiitol samples (room temperature pH 3.33) extrapolated to 25 °C. This model suggests that paper of this composition would be extremely impermanent, reaching the failure criterion of DP ≅ 400 after 96 days. Such impermanence will be exaggerated, particularly as raising the pH will decrease the electrophilicity of the aluminium in the paper sheet. However, Murray (57), implicating rosin-alum sizing soon after its introduction, commented, "One letter which I had forwarded by post fell to pieces by the way…". Even papers of such pronounced impermanence can be preserved for centuries using the preservation technique of cold storage. The same k_{obs} values used in Fig. 7 (20 mmol/L $Al_2(SO_4)_3$, pH 3.33), but extrapolated to –20 °C, are plotted using af Ekenstam eq. [1] in Fig. 8.

Fig. 7. DP vs. *t* at 25 °C. The depolymerization of cellulose in papermaking fibres modelled using af Ekenstam eq. [1], substituting a DP_0 of 1300 and $k_{25\ °C}$ for 1,5-anhydrocellobiitol hydrolyses as labelled.

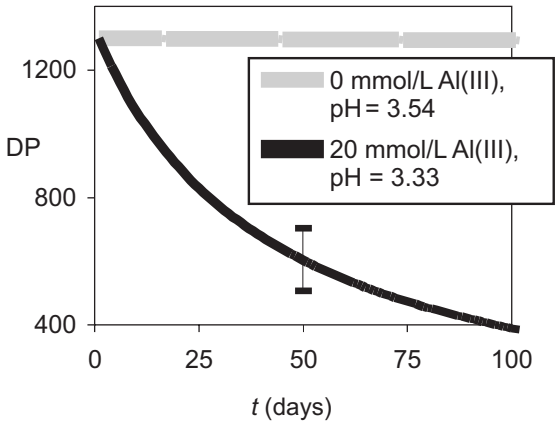
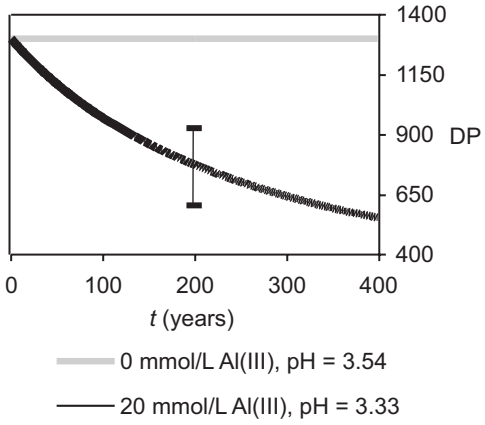


Fig. 8. Four hundred years of aging at –20 °C: DP vs. *t* at 25 °C. The depolymerization of cellulose in papermaking fibres under cold storage conditions. Modelled using the af Ekenstam eq. [1], substituting 1300 for DP_0, and specific rate constants obtained from the model compound, 1,5-anhydrocellobiitol.



Conclusions

The spontaneous hydrolysis of the β(1→4) link in cellulose, modelled in 1,5-anhydrocellobiitol, is too slow to contribute to reduction in degree of polymerization of cellulose

© 2005 NRC Canada

(and hence loss of paper strength) during aging of paper under archival storage conditions, but does completely account for the reduction in cellulose DP during kraft pulping. The proton-catalysed pathway is adequate to account for reduction in cellulose DP during aging only of the most acidic papers. Efficient electrophilic catalysis by Al^{III} has been demonstrated, and is likely to be the origin of the impermanence of all rosin-alum-sized papers.

Whilst more work is needed to determine the details of the Al^{III}-catalysed hydrolysis, it is clear that programs of document deacidification (such as that currently under way in the US Library of Congress (20)) will have, at best, a direct effect only on the most acidic of papers, and only the indirect one of reducing the electrophilicity of metal ions on other acid papers. Deacidification procedures that add metals (especially deacidification by dimethyl cadmium) are likely to be counterproductive.

It would appear that generic document storage techniques should be more widely adopted. The preservation technique of cold storage, widely used to preserve photographic materials, slows the rate of all detrimental reactions and does not entail the chemical alteration of the object. If a chemical alteration is absolutely necessary, it should at least target the real culprit of impermanence, e.g., complex the Al^{III} ion in rosin-alum-sized papers with fluoride.

Acknowledgements

We thank the Textiles and Paper Group, School of Materials, University of Manchester, for two years of postgraduate support for JWB, and Dr. Yazmin Hernandez and Dr. Richard Hughes, University of Huddersfield, for help with operation of the HPAEC-PAD system.

References

1. S.A. Buchanan. *In* Paper preservation: current issues and recent developments. *Edited by* P. Luner. Tappi Press, Atlanta, Georgia. 1989. p. 24.
2. (*a*) R.J. Heywood. Ph.D. thesis, University of Surrey, Guildford, Surrey, UK. 1997. p. 131; (*b*) pp. 102 to 103.
3. P.M. Whitmore and J. Bogaard. Restaurator, **15**, 26 (1994).
4. D. Erhardt, C.S. Tumosa, and M.F. Mecklenburg. *In* Historic textiles, papers and polymers in museums. *Edited by* J.M. Cardamome and M.T. Baker. ACS Symp. Ser. 779. American Chemical Society, Washington, D.C. 2001. p. 23.
5. J.D. Peel. Paper science and paper manufacture. Angus Wilde, Vancouver. 1999. p. 52.
6. G. Legler, M.L. Sinnott, and S.G. Withers. J. Chem. Soc. Perkin Trans. 2, 1376 (1980).
7. D. Cocker and M.L. Sinnott. J. Chem. Soc. Perkin Trans. 2, 1391 (1975).
8. M.N. Namchuk, J.D. McCarter, A. Becalski, T. Andrews, and S.G. Withers. J. Am. Chem. Soc. **122**, 1270 (2000).
9. N.S. Banait and W.P. Jencks. J. Am. Chem. Soc. **113**, 7951 (1991).
10. W.P. Jencks. Chem. Soc. Rev. **10**, 345 (1981).
11. Y. Zhang, J. Bommuswamy, and M.L. Sinnott. J. Am. Chem. Soc. **116**, 7557 (1994).
12. D. Piszkiewicz and T.C. Bruice. J. Am. Chem. Soc. **90**, 2156 (1968).
13. R. Wolfenden, X. Lu, and G. Young. J. Am. Chem. Soc. **120**, 6814 (1998).
14. G.-A. Craze and A.J. Kirby. J. Chem. Soc. Perkin Trans. 2, 354 (1978).
15. P. Ballinger and F.A. Long. J. Am. Chem. Soc. **82**, 795 (1960).
16. H. Nielsen and P.E. Sörensen. Acta Chem. Scand. Ser. A, **37**, 105 (1983).
17. A.C. Elliott, K. Srinvasan, M.L. Sinnott, P.J. Smith, J. Bommuswamy, Z. Guo, B.G. Hall, and Y.L. Zhang. Biochem. J. **282**, 155 (1992).
18. D. Hunter. Papermaking: the history and technique of an ancient craft. Dover, New York. 1943. p. 523.
19. For example, see the introduction in: D.J. Priest and M. Farrar. *In* Proceedings of symposium 88, Ottawa, Ontario, 3–7 October 1988. *Edited by* H.D. Burgess. Canadian Institute of Conservation, Ottawa, Ontario. 1994. p. 255.
20. The Library of Congress. Saving the written word: Library of Congress awards mass deacidification contract. Press release [online]. Available from http://www.loc.gov/today/pr/2001/01-155.html [accessed 25 March 2005]. 2001.
21. E.J. Parks. Tappi J. **54**, 537 (1971).
22. A. Barański, R. Dziembaj, A. Konieczna-Molenda, J.M. Lagan, and S. Walas. Pol. J. Chem. Technol. **6**, 1 (2004).
23. N. Gurnagul, R.C. Howard, X. Zou, T. Uesaka, and D.H. Page. J. Pulp Paper Sci. **19**, J160 (1993).
24. C.R. Clark, R.W. Hay, and I.C.M. Dea. J. Chem. Soc. D, **13**, 794 (1970).
25. C.R. Clark and R.W. Hay. J. Chem. Soc. Perkin Trans. 2, 1943 (1973).
26. M.L. Sinnott. Chem. Rev. **90**, 1171 (1990).
27. J. Baty and M.L. Sinnott. Chem. Commun. (Cambridge), **7**, 866 (2004).
28. For example, see: Enerex Botanicals Ltd. Microcrystalline cellulose I.P.: the excipient of choice [online]. Available from http://www.enerex.ca/articles/microcrystalline_cellulose.htm [accessed 18 April 2005]. 1997–2004.
29. J.S. Kim, Y.Y. Lee, and R.W. Torget. Appl. Biochem. Biotechnol. **91–93**, 331 (2001).
30. (*a*) E. Sjöström. Wood chemistry: fundamentals and applications. 2nd ed. Academic Press, San Diego. 1993. p. 230; (*b*) p. 132; (*c*) p. 59.
31. J.M. Cardamone. *In* Historic textiles, papers, and polymers in museums. *Edited by* J.M. Cardamone and M.T. Baker. ACS Symp. Ser. 799. American Chemical Society, Washington, D.C. 2001. p. 8.
32. J. Stanley. Ph.D. thesis, The Victoria University of Manchester, Manchester, UK. 1992. p. 110.
33. B. Capon. Chem. Rev. **69**, 407 (1969).
34. M.L. Sinnott. *In* The chemistry of enzyme action. New comprehensive biochemistry. Vol. 6. *Edited by* M.I. Page. *Series Edited by* A. Neuberger and L.L.M. van Deenen. Elsevier, Amsterdam. 1984. p. 389.
35. X. Huang, C. Surry, T. Hiebert, and A.J. Bennet. J. Am. Chem. Soc. **117**, 10614 (1995).
36. A.J. Bennet, M.L. Sinnott, and W.S.S. Wijesundera. J. Chem. Soc. Perkin Trans. 2, 1233 (1985).
37. Y. Zhang. Ph.D. thesis, University of Illinois at Chicago, Chicago, Illinois. 1994. p. 87.
38. H.G. Fletcher, Jr. J. Am. Chem. Soc. **69**, 706 (1947).
39. H.G. Fletcher, Jr. and C.S. Hudson. J. Am. Chem. Soc. **70**, 310 (1948).
40. R. Larralde, M.P. Robertson, and S.L. Miller. Proc. Natl. Acad. Sci. U.S.A. **92**, 8158 (1995).

© 2005 NRC Canada

41. A.J. Bennet, A.J. Davis, L. Hosie, and M.L. Sinnott. J. Chem. Soc. Perkin Trans. 2, 581 (1987).
42. L. Neimo. *In* Papermaking chemistry. Papermaking science and technology. Vol. 4. *Edited by* L. Neimo. *Series Edited by* J. Gullichsen and H. Paulapuro. Fapet, Helsinki, Finland. 1999. p. 94.
43. (*a*) R.E. Brandon. Ph.D. thesis, Lawrence University, Appleton, Wisconsin. 1973. p. 54 and 63; (*b*) all chapters.
44. For example, see: M. Schülein, D.F. Tikhomirov, and C. Schou. *In* Trichoderma reesei cellulases and other hydrolases. *Edited by* P. Suominen and T. Reinikainen. Akateminen Kirjakauppa, Helsinki, Finland. 1993. p. 109.
45. A. af Ekenstam. Ber. **69**(B), 553 (1936).
46. D.H. Schroff and A.W. Stannett. I.E.E. Proc. C, **132**, 312 (1985).
47. T.M. Grace, B. Leopold, and E.W. Malcolm (*Editors*). Alkaline pulping. 3rd ed. Pulp and paper manufacturing. Vol. 5. Joint Textbook Committee of the Paper Industry (TAPPI and CPPA), Atlanta, Georgia and Montreal, Quebec. 1989. p. 9.
48. D.A. Blythe and L.R. Schroeder. J. Wood Chem. Technol. **5**, 313 (1985).
49. R.E. Brandon, L.R. Schroeder, and D.C. Johnson. *In* Cellulose technology research symposium (1974). ACS Symp. Ser. 10. American Chemical Society, Washington, D.C. 1975. p. 125.
50. R.M. Kaylor, D.R. Dimmel, A.J. Ragauskas, and C.L. Liotta. J. Wood Chem. Technol. **15**, 431 (1995).
51. D. Cocker, L.E. Jukes, and M.L. Sinnott. J. Chem. Soc. Perkin Trans. 2, 190 (1973).
52. See the macroscopic kinetics studies of both $Al_2(SO_4)_3{\cdot}nH_2O$ and $AlCl_3{\cdot}nH_2O$ in: D.C. Chamberlain. Ph.D. thesis, The Victoria University of Manchester, Manchester, UK. 1991. p. 104, 112, and 140.
53. A.J. Bennet and M.L. Sinnott. J. Am. Chem. Soc. **108**, 7787 (1986).
54. D.J. Priest, J. Stanley, and A. Karademir. *In* IPC conference papers London 1997: Proceedings of the Fourth International Conference of the Institute of Paper Conservation, London, 6–9 April 1997. Institute of Paper Conservation, London. 1998. p. 291.
55. A.E. Martell (*Editor*). Coordination chemistry. ACS Monograph 168. Vol. 2. American Chemical Society, Washington, D.C. 1978; Data reassembled in: S. Kobayashi and K. Manabe. Acc. Chem. Res. **35**, 209 (2002).
56. J. Sugiyama, J. Persson, and H. Chanzy. Macromolecules, **24**, 2461 (1991).
57. J. Murray. Observations and experiments on the bad composition of modern paper with a description of a permanent writing ink which cannot be discharged. G. & B. Whittaker, London. 1824. Quoted in: J. Stanley. Ph.D. thesis, The Victoria University of Manchester, Manchester, UK. 1992. p. 1.

© 2005 NRC Canada

Benzenesulfonyl chloride with primary and secondary amines in aqueous media — Unexpected high conversions to sulfonamides at high pH[1]

James F. King, Manjinder S. Gill, and Petru Ciubotaru

Abstract: We have determined pH–yield profiles under pseudo-first-order conditions of the reactions of benzenesulfonyl chloride with a set of primary and secondary water-soluble alkylamines, and have found with certain amines, such as dibutylamine, a profile taking the form of a sigmoid pH–yield curve with relatively high yields of the sulfonamide persisting with increasing basicity up to and including 1.0 mol/L sodium hydroxide. This behaviour is quantitatively accounted for by invoking, in addition to the usual second-order reaction of the sulfonyl chloride with the amine, two third-order terms (*i*) one first-order in sulfonyl chloride, amine and hydroxide anion, and (*ii*) another first-order in sulfonyl chloride and second-order in the amine. The importance of the third-order terms correlates approximately with the total number of alkyl carbon atoms in the amine, and this in turn is regarded as related to the hydrophobic character of the amine. Experiments to test this picture included: (*i*) observation of a bell-shaped curve with bis(2-methoxyethyl)amine, (*ii*) in the reaction of dibutylamine in THF–H_2O (1:1), and also (*iii*) in the reaction of dibutylamine in 1.0 mol/L tetrabutylammonium bromide, and (*iv*) increase in the contributions of the third-order terms in 1.0 mol/L aqueous sodium chloride. Preparative reactions with dibutylamine, 1-octylamine, and hexamethylenimine in 1.0 mol/L aqueous sodium hydroxide with a 5% excess of benzenesulfonyl chloride gave, respectively, 94%, 98%, and 97% yields of the corresponding sulfonamides.

Key words: sulfonyl chlorides, primary and secondary amines, pH–yield profiles, organic synthesis in water, hydrophobic effects.

Résumé : On a déterminé les profils pH–rendement dans des conditions de pseudo-premier ordre des réactions du chlorure de benzènesulfonyle avec un ensemble d'alkylamines primaires et secondaires solubles dans l'eau et on a trouvé avec certaines amines, telle la dibutylamine, que le profil de la courbe pH–rendement prend une forme sigmoïde, avec des rendements relativement élevés de sulfonamide qui persistent avec une augmentation de la basicité jusqu'à l'hydroxyde de sodium 1,0 mol/L. Ce comportement peut être expliqué quantitativement en invoquant, en plus de la réaction habituelle du deuxième ordre du chlorure de sulfonyle avec l'amine, deux termes de troisième ordre (*i*) une du premier ordre en chlorure de sulfonyle, en amine et en ion hydroxyde et (*ii*) un autre du premier ordre en chlorure de sulfonyle et du deuxième ordre en amine. L'importance des termes du troisième ordre donne une corrélation approximative avec le nombre total d'atomes de carbone de la chaîne alkyle de l'amine et ceci peut alors être considéré comme relié au caractère hydrophobe de l'amine. Les expériences réalisées pour évaluer cette hypothèse incluent (*i*) l'observation d'une courbe en forme de cloche avec la bis(2-méthoxyéthyl)amine et (*ii*) dans la réaction avec la dibutylamine dans un mélange THF–H_2O (1 : 1) et aussi (*iii*) dans la réaction de la butylamine dans le bromure de tétrabutylammonium à 1,0 mol/L et (*iv*) une augmentation dans les contributions des termes du troisième ordre dans le chlorure de sodium aqueux à 1,0 mol/L. Les réactions préparatives avec de la dibutylamine, de la 1-octylamine et de l'hexaméthylèneimine dans de l'hydroxyde de sodium aqueux à 1,0 mol/L, en présence d'un excès de 5 % de chlorure de benzènesulfonyle ont donné respectivement des rendements de 94 %, 98 % et 97 % des sulfonamides correspondants.

Mots clés : chlorures de sulfonyle, amines primaires et secondaires, profils pH–rendement, synthèse organique en milieu aqueux, effets hydrophobes.

[Traduit par la Rédaction]

Received 7 April 2005. Published on the NRC Research Press Web site at http://canjchem.nrc.ca on 25 November 2005.

J.F. King,[2] M.S. Gill, and P. Ciubotaru. Department of Chemistry, The University of Western Ontario, London, ON N6A 5B7, Canada.

[1]This article is part of a Special Issue dedicated to organic reaction mechanisms.
[2]Corresponding author (e-mail: scijfk@uwo.ca).

 doi: 10.1139/V05-154 © 2005 NRC Canada

Introduction

In recent times we have seen an increase of interest in the use of water as a solvent for organic synthesis. Selectivity and simplicity, and perhaps most significantly, cheapness, low toxicity, and general environmental acceptability, are among the benefits ascribed to reactions in water (1). Our role in this revival has included pointing to eqs. [1] and [2] for, respectively, (*i*) finding pH_{max}, the optimal pH for carrying out reactions in water between a nucleophile (Nu) and a hydrolysable electrophile (E), and (*ii*) pointing to the merits of pH–yield profiles for seeing the variation in yield with change in pH in such reactions when carried out under pseudo-first-order conditions (2).

$$[1] \qquad pH_{max} = 1/2\ [\log(k_w/k_{OH}) + pK_w + pK_a]$$

$$[2] \qquad f_p = \frac{k_N[Nu]}{k_w + k_{OH}[OH^-] + k_N[Nu]} = \frac{k_N Nu_T K_a/([H^+] + K_a)}{k_w + k_{OH}K_w/[H^+] + k_N Nu_T K_a/([H^+] + K_a)}$$

We were gratified to find in the reactions tested experimentally, namely, benzenesulfonyl chloride with amines or phenoxide anions, benzoyl chloride or acetic anhydride with amines, and allyl bromide with β-dicarbonyl enolates, that eq. [1] was invariably obeyed and eq. [2] commonly followed. (Rate constants are defined in Scheme 1; [Nu] = concentration of free amine, $Nu_T = [Nu] + [NuH^+]$, i.e., the total concentration of the amine species).

Two forms of deviation from eq. [2] have been encountered, and to see how these may arise, it is appropriate to recall that conformance to eqs. [1] and [2] requires that the rate law for the nucleophile–electrophile reaction in water be given by eq. [3].

$$[3] \qquad k_{obs} = k_w + k_{OH}[OH^-] + k_N[Nu]$$

One form of deviation from eq. [2] was noted in the reactions of benzenesulfonyl chloride with phenoxide anions (3) and also with acetic anhydride and primary or secondary amines (2*b*), and was ascribed to the consumption of a portion (usually <10%) of the electrophile (E) by hydrolysis assisted by the nucleophile (Nu) acting as a general base. Addition of a term, $k_{GB}[Nu]$, to eq. [3], and modifying eq. [2] by including the $k_{GB}[Nu]$ term in the denominator as in eq. [4], led to quantitative agreement of theory and experiment.

$$[4] \qquad f_p = \frac{k_N Nu_T K_a/([H^+] + K_a)}{k_w + k_{OH}K_w/[H^+] + (k_N + k_{GB})Nu_T K_a/([H^+] + K_a)}$$

The second deviation from eq. [2] was initially noted in the reaction of benzenesulfonyl chloride with benzylamine (Fig. 2 of ref. 2*a*); eq. [3] accurately predicts the yields for pH values 6–11, but not for pH 12, where the experimental yield is 65% and the predicted yield only 45%. We decided to look more closely into this system and found, as is described in this paper, an apparently hitherto unobserved third-order reaction in which we have evidence of the intervention of hydrophobic effects. As a corollary to this conclusion, we wish to draw attention to the usefulness of pH–yield experiments in the general problem of elucidating the factors influencing the interaction of water with organic materials. The present paper is largely taken from two theses (4); preliminary descriptions of our initial observations have been given in conference presentations (5).

Scheme 1.

First order reaction

$$PhSO_2Cl + 2\ H_2O \xrightarrow{k_w} PhSO_2OH + Cl^- + H_3O^+$$

Second order reactions

$$PhSO_2Cl + H_2O + OH^- \xrightarrow{k_{OH}} PhSO_2OH + Cl^- + H_2O$$

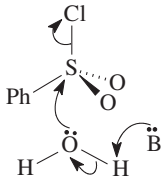
$$PhSO_2Cl + RR'NH + H_2O \xrightarrow{k_N} PhSO_2NRR' + Cl^- + H_3O^+$$

$$PhSO_2Cl + H_2O + RR'NH \xrightarrow{k_{GB}} PhSO_2OH + Cl^- + RR'NH_2^+$$

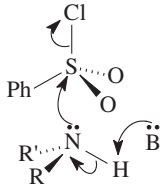
Third order reactions

$$PhSO_2Cl + 2\ RR'NH \xrightarrow{k_{NN}} PhSO_2NRR' + Cl^- + RR'NH_2^+$$

$$PhSO_2Cl + RR'NH + OH^- \xrightarrow{k_{NOH}} PhSO_2NRR' + Cl^- + H_2O$$



1



2

B = H_2O, RR'NH, OH^-

Results and discussion

Methods and materials

The products of the reactions showed acceptable IR and ^1H and ^{13}C NMR spectra, and, where the sulfonamide was previously known, the properties were in accord with earlier reports. Those sulfonamides not previously reported have been characterized by spectra and high-resolution mass spectrum (HR-MS) molecular weight determination as described in the Experimental; further spectroscopic information on the known compounds is given elsewhere (4).

Our procedures for rate measurement by pH-stat (6) and determination of product yields by simple weighing of products (2) have already been described. In our initial experiments, we encountered a difficulty in reproducing results at high pH, and at least some of the problem is believed to arise because of the high rates of the reactions being observed and their sensitivity to mixing procedures. By using very rapid stirring and making sure that the mixing protocols varied as little as possible from one run to another, a fair measure of reproducibility was generally observed; further details are provided in the Experimental section. For reac-

© 2005 NRC Canada

Fig. 1. pH–yield profiles for the reaction of benzenesulfonyl chloride (initial concentration 7.8×10^{-4} mol/L) with primary amines (0.01 mol/L) in water at 25.0 °C. Allylamine (●); benzylamine (□); and butylamine (▲). Points are experimental and lines are drawn using eq. [5] and the appropriate parameters from Table 1.

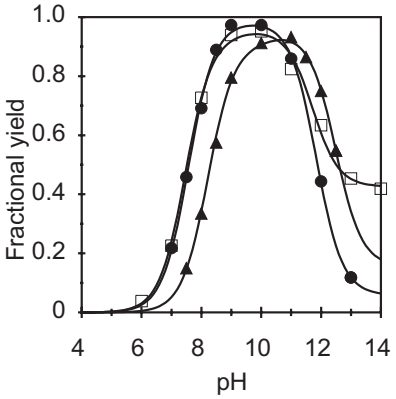


Fig. 2. pH–yield profiles for the reaction of benzenesulfonyl chloride (initial concentration 7.8×10^{-4} mol/L) with primary amines (0.01 mol/L) in water at 25.0 °C: 2-Methoxyethylamine (□); 1-octylamine (●); and *tert*-butylamine (▲). Points are experimental and lines are drawn using eq. [5] and the appropriate parameters from Table 1.

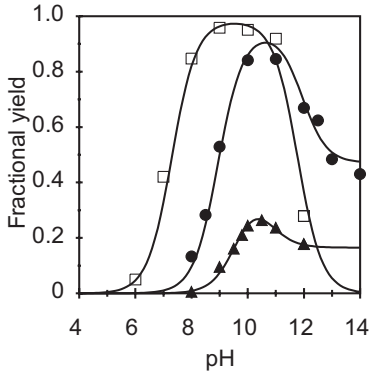


Fig. 3. pH–yield profiles for the reaction of benzenesulfonyl chloride (initial concentration 7.8×10^{-4} mol/L) with secondary amines (0.01 mol/L) in water at 25.0 °C: Dimethylamine (●); dibutylamine (▼); dipropylamine (■); and diethylamine (▲). Points are experimental and lines are drawn using eq. [5] and the appropriate parameters from Table 1.

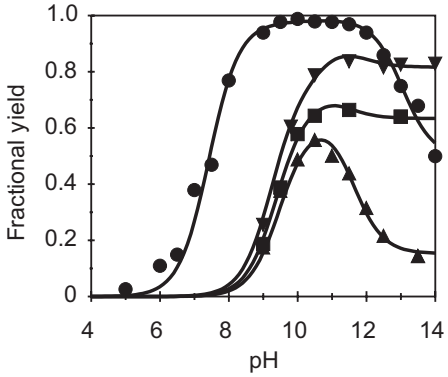
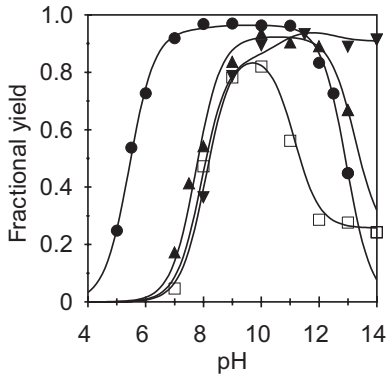


Fig. 4. pH–yield profiles for the reaction of benzenesulfonyl chloride (initial concentration 7.8×10^{-4} mol/L) with secondary amines (0.01 mol/L) in water at 25.0 °C: Morpholine (●); piperidine (▲); diallylamine (□); and hexamethylenimine (▼). Points are experimental and lines are drawn using eq. [5] and the appropriate parameters from Table 1.



tions on a scale too small for the weights to be informative, yields were determined by quantitative UV analysis or by gas chromatography as indicated in the Experimental section.

pH–yield profiles

Initial pH–yield profiles with primary and secondary amines (Figs. 1–4) revealed a consistent pattern. The amines with the smallest or most hydrophilic alkyl groups, e.g., allylamine and butylamine (Fig. 1), 2-methoxyethylamine (Fig. 2), and morpholine and piperidine (Fig. 4) and, to a lesser extent, dimethylamine (Fig. 3) and piperidine (Fig. 4), showed roughly bell-shaped curves as observed earlier. Others, however, notably dibutylamine (Fig. 3) and hexamethylenimine (Fig. 4), showed sigmoid pH–yield curves strongly reminiscent of simple titration curves. Other amines, e.g., diethylamine, dipropylamine, benzylamine, octylamine, and *tert*-butylamine, showed intermediate behaviour, with a clearly visible maximum yield near the expected pH_{max}, but with the yield in the pH 13 to 14 region not near zero but rather roughly half of that at pH_{max}.

This observation that the amines with the largest number of carbons showed the greatest tendency for a high yield of sulfonamide at high pH suggested that the hydrophobic alkyl groups could be leading to some form of association of organic molecules, especially at high pH where two factors, (*i*) maximum concentrations of the (unprotonated) amines and (*ii*) highest ionic strength due to the high concentration of NaOH, combine to provide an environment most likely to yield molecular association. One way of treating such hydrophobic factors would be to postulate two third-order terms involving, respectively, (*i*) sulfonyl chloride and two molecules of the amine (the k_{NN} term) and (*ii*) sulfonyl chloride, amine, and sodium hydroxide (the k_{NOH} term). These are included in the full reaction scheme shown in Scheme 1. The rate constants derived from this treatment of the pH–rate and pH–yield results are given in Table 1.

One should note in Scheme 1 that the simple second-order reaction of the sulfonyl chloride with amine to yield the sulfonamide (the k_N reaction), as well as the simple hydrolysis term (k_W term), are written with a molecule of water not

© 2005 NRC Canada

Table 1. Rate constants for the reaction of benzenesulfonyl chloride with primary and secondary amines in water at 25.0 °C.

Amine	pK_a[a]	k_{Nu}[b] ((mol/L)$^{-1}$ s^{-1})	k_N[c] ((mol/L)$^{-1}$ s^{-1})	k_{GB}[c] ((mol/L)$^{-1}$ s^{-1})	k_{NN}[c] ((mol/L)$^{-2}$ s^{-1})	k_{NOH}[c] ((mol/L)$^{-2}$ s^{-1})
Allylamine	9.49		25	<0.1	4.7×10^2	2.5×10^2
Benzylamine	9.34	22.7	21.5	1.2	1.4×10^3	3.0×10^3
2-Methoxyethylamine	9.2	23.8	23.8	<0.1	<1	<1
Butylamine	10.59	70.2	65.3	4.9	7.5×10^3	7.5×10^2
Octylamine	10.65	73	73	<0.1	1.1×10^5	1.7×10^4
tert-Butylamine	10.55		1	0.09	(3)	8.0×10^2
Dimethylamine	10.64	499	489	10	4.6×10^4	3.8×10^3
Diethylamine	10.98	6.1	6.1	<0.1	6.0×10^2	7.3×10^2
Dipropylamine	11	8.9	8.9	<0.1	5×10^2	7.0×10^3
Dibutylamine	11.25	25.7	25.7	<0.1	4×10^3	1.8×10^4
Diallylamine	9.29		5.4	0.4	<1	1.3×10^3
Piperidine	11.22	899	8.4×10^2	60	(2×10^2)	1.1×10^3
Morpholine	8.36	126	1.2×10^2	6	2.6×10^2	<1
Hexamethylenimine	11.11	440	3.8×10^2	60	9.0×10^4	4.0×10^4
Bis(2-methoxyethyl)amine	8.89	1.94	1.94	<0.01	(1×10^2)	3.4×10^2

[a] pK_a values are from the collection of Jencks and Regenstein (7), except for the value for hexamethylenimine, which is from ref. 8, and that for bis(2-methoxyethyl)amine, which was determined by the method of Albert and Serjeant (9).

[b] The k_{Nu} values were obtained from pH-stat rate measurements of the reaction of benzenesulfonyl chloride (initial concentration 0.001 mol/L) with 0.01 mol/L solutions of the amine in water at 25.0 °C, as previously described (6). This procedure yields k_{Nu} as defined by the following modified form of eq. [3]: $k_{obs} = k_w + k_{OH}[OH^-] + k_{Nu}[Nu]$, where $k_{Nu} = k_N + k_{GB}$; Rogne's values (10) for k_w and k_{OH} (3.06×10^{-3} s^{-1} and 40.4 (mol/L)$^{-1}$ s^{-1}, respectively) were used.

[c] The values of k_N, k_{GB}, k_{NN}, and k_{NOH} were obtained by an iterative manual least-squares procedure involving (*i*) assuming initially that $k_N \approx k_{Nu}$ (i.e., $k_{GB} \approx 0$) and finding (by the least-squares method) values for k_{NN} and k_{NOH} using eq. [5], (*ii*) evaluation of k_{GB} from the three to five f_p points at lowest pH (believed to be only minimally influenced by k_{NN} and k_{NOH}) and finding the best least-squares fit within the constraint $k_N + k_{GB} = k_{Nu}$, and, where appropriate, (*iii*) another round of least-squares calculations using both k_N and k_{GB} values carried out to obtain k_{NN} and k_{NOH} yielding minimal least-squares sums. In the three cases for which k_{Nu} values were not measured, a preliminary value of k_N was obtained by the best least-squares fit of the three to five f_p points at lowest pH, followed then by the procedure previously given for the other amines starting with k_{Nu}. The value preceded by the less than sign (<) has been found to give a poorer least-squares fit than zero, i.e., the parameter is experimentally indistinguishable from zero. Parentheses enclosing a few values indicate low reliability as indicated by a low sensitivity of the least-squares sum to change in that parameter.

required by minimal stoichiometry. This "extra" molecule of water is included to reflect the high likelihood of general base catalysis by water in these reactions in accord with Jenck's "libido rule" (11), which asserts that general base catalysis is observed when the hydrogen being removed in the reaction changes its acidity during the course of the reaction from initially too weak to react with the general base, to finally strong enough to readily protonate the general base. In the present reaction of benzenesulfonyl chloride with an amine, the hydrogen on the amine starts with a pK_a around 35 and ends up in the absence of general base intervention in an *N*-protonated sulfonamide with a pK_a around –5 or lower (12); note that water, the amine, and hydroxide anion (pK_as of conjugate acids are –1.7, ~10, and 15.7, respectively) are all capable of acting as general bases for sulfonamide formation. General base catalysis by a second molecule of water in the simple hydrolysis of sulfonyl chlorides has been discussed elsewhere (13). The merit of looking at the simple sulfonamide formation in this way becomes apparent on inspection of structures **1** and **2** whereby one may see that the third-order terms (k_{NOH} and k_{NN}) are simply the aminolysis analogues of the hydrolyses involving general base catalysis by hydroxide and the amine, respectively.

With the addition of the third-order reactions, we obtain eq. [5], the equation describing the pH–yield profile.

$$[5] \qquad f_p = \frac{k_N[Nu] + k_{NN}[Nu]^2 + k_{NOH}[Nu][OH^-]}{k_w + k_{OH}[OH^-] + k_N[Nu] + k_{GB}[Nu] + k_{NN}[Nu]^2 + k_{NOH}[Nu][OH^-]}$$

Equation [5] may be expanded to be a function of $[H^+]$ (or pH) by substituting $[Nu] = Nu_T K_a/[H^+]$ and $[OH^-] = K_W/[H^+]$.

As is shown in Figs. 5 and 6, by including the k_{NN} and k_{NOH} terms the pH–yield profiles for three different initial concentrations of dibutylamine are satisfactorily reproduced by the same values of two parameters (k_{NN} and k_{NOH}), along with, of course, the previously measured rate constants k_w, k_{OH}, and k_{Nu}. With the other amines the same parameters (including also a k_{GB} term with some amines) in varying degrees of relative importance suffice to provide a satisfactory fit to the observed pH–yield profiles.

By this treatment the only two reactions of any consequence in this pH 13 to 14 region are the hydroxide promoted reactions, the k_{OH} reaction leading to the hydrolysis

© 2005 NRC Canada

Fig. 5. pH–yield profiles for the reaction of benzenesulfonyl chloride with three concentrations of dibutylamine: 0.01 mol/L (□), 0.005 mol/L (▲), and 0.001 mol/L (●). Points are experimental and lines are drawn using eq. [5] and the appropriate parameters from Table 1.

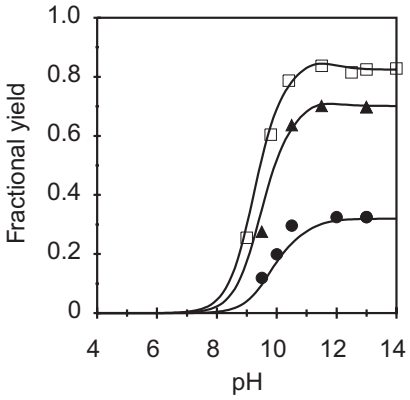
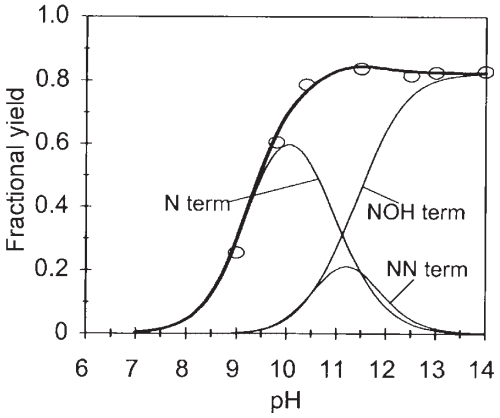


Fig. 6. pH–yield profiles for the reaction of benzenesulfonyl chloride with dibutylamine (0.01 mol/L) showing the estimated contributions of the individual sulfonamide forming reactions. The individual reactions are each shown by a light line with the appropriate subscript for that reaction from Scheme 1; the bold line gives f_p, the sum of the three component contributions.



product and the k_{NOH} process giving the sulfonamide, and hence the product ratio (amide:acid) for the reaction in the pH 13 to 14 region is given simply by the ratio of the rates of these two processes, i.e., $k_{NOH}[Nu][OH^-]/k_{OH}[OH^-]$. At high pH, $Nu_T \approx [Nu]$ and with cancelling of the $[OH^-]$s, the product ratio $\approx k_{NOH}Nu_T/k_{OH}$. Similar reasoning from eq. [5] gives $f_{p14} \approx k_{NOH}Nu_T/(k_{NOH}Nu_T + k_{OH})$, which in turn leads to a serviceable approximation for obtaining a rough value for k_{NOH}, i.e., $k_{NOH} \approx k_{OH}/[(1/f_{p14} - 1)Nu_T]$, where f_{p14} is the (actual or extrapolated) fractional yield at pH 14.

The case for the k_{NN} term is perhaps less obvious than that for k_{NOH} but it appears appropriate to include it at this stage because (*i*) it yields a substantially better fit to most observed pH–yield curves, and (*ii*) it appears to be such an eminently likely process that its possible role would have to be specifically examined anyway. As expected, the contribution of the k_{NN} term diminishes to negligible at very low amine concentrations.

It should be mentioned that the k_{GB} term is of limited importance for most reactions in "straight" water. It was evidently negligible (<1) for six of the amines and was found to be less than 10% of k_N in all cases except hexamethylenimine; as will be discussed later, one of the effects of using 1 mol/L NaCl as solvent is a detectable increase in the k_{GB} term for certain amines.

An essential feature to notice in the rate constants in Table 1 is the variation as the alkyl group increases in number of carbon atoms. We illustrate by noting the pattern in k_N for the sequence dimethylamine, diethylamine, dipropylamine, and dibutylamine (490, 6.1, 8.9, and 25.7 $(mol/L)^{-1}$ s^{-1}, respectively). The drop in rate on changing from methyl to ethyl is common among nucleophilic reactions of alkylamines and is ascribed to increased nonbonding interactions in the transition state with the extra carbon in the alkyl group (14). With most nucleophilic reactions, however, the following pattern is found: ethyl ≥ propyl ≥ butyl, etc. With k_N, however, there appears to be a small increase with size: ethyl ≈ propyl < butyl. This, we suggest, points to a hydrophobic effect (1*a*, 15) even with the second-order terms. The effect on the third-order rate constants is more dramatic, with the k_{NOH} values for diethylamine, dipropylamine, and dibutylamine being 7.3×10^2, 7×10^3, and 1.8×10^4 $(mol/L)^{-2}$ s^{-1}, respectively. In our view, it is fully consistent with the influence of hydrophobic effects, to regard both the second-order (k_N) and third-order (k_{NOH}) reactions as proceeding by way of an initial amine – sulfonyl chloride complex and that the complex reacts in a second step with either water or hydroxide anion, respectively. The formation of this complex is increased as the number of carbons in the alkyl group(s) (and hence the hydrophobic character) of the amine increases. With the second-order process, the second step of the reaction is believed to involve reaction of this complex with water acting as a general base as shown in structure **2** (B = H_2O). This reaction is comparatively slow, and the transition states accordingly reflect well-developed steric effects of the alkyl groups; increase of the "size" of the alkyl group will therefore have two distinct effects: (*i*) acceleration of the reaction by the hydrophobic effect; and (*ii*) slowing of the reaction by the steric effect, with the net result in this instance being a modest increase (approximately fourfold) on going from ethyl to butyl. With the third-order (k_{NOH}) process, the second step, namely reaction of the complex with hydroxide anion (**2**, B = OH^-), is a fast reaction with an early transition state in which the steric effects of the alkyl groups plays a smaller role than the hydrophobic effect; the result is a 25-fold change on going from diethylamine to dibutylamine.

Tests of the proposed mechanisms

The agreement of the observed and calculated pH–yield curves and the consistency of the rate constants with a picture invoking a hydrophobic effect, though gratifying, is not in itself sufficient to establish the mechanism outlined in Scheme 1. Views on the complex field of hydrophobic effects (1*a*, 15) appear to concur in that the effect is (*i*) increased by addition of certain solutes, especially salts such as sodium chloride and sodium hydroxide, labeled as "salting out"or "hydrophobic", and (*ii*) diminished by other solutes such as organic solvents (ethanol, DMSO, THF) or certain other salts labeled as "salting in" or "antihydropho-

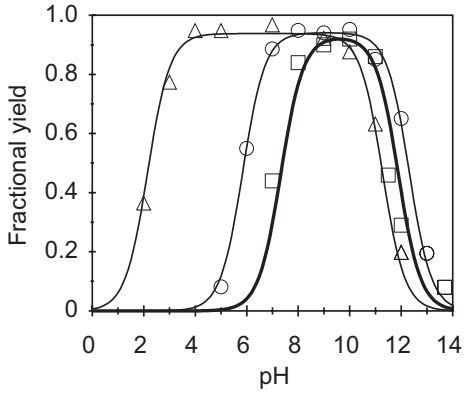
© 2005 NRC Canada

Table 2. Rate constants for the reaction of benzenesulfonyl chloride with primary and secondary amines in mixed aqueous media at 25.0 °C.

Amine	pK_a' [a]	k_{Nu} [b] ((mol/L)$^{-1}$ s^{-1})	k_N [b] ((mol/L)$^{-1}$ s^{-1})	k_{GB} [b] ((mol/L)$^{-2}$ s^{-1})	k_{NN} [b] ((mol/L)$^{-2}$ s^{-1})	k_{NOH} [b] ((mol/L)$^{-2}$ s^{-1})
THF–H_2O (1:1)						
Aniline	3.5		0.32	0.01		
Benzylamine	8.22		3.5	0.2		
Dibutylamine	9.3		1.3	0.08		
NaCl (1 mol/L in H_2O)						
Dimethylamine	10.98	891	820	71	4.9×10^4	3.9×10^3
Diethylamine	11.16	11.1	7.9	3.2	7.8×10^2	1.78×10^3
Dipropylamine	11.21	12.3	11.9	0.4	3.8×10^3	1.1×10^4
Dibutylamine	11.17	16.2	16.2	<0.1	4.0×10^3	2.5×10^4

[a]Apparent pK_a values determined in the specified media by the procedure of Albert and Serjeant (9). pH values were meter readings in the medium in question, after standardization with aqueous buffers.
[b]Rate constants were obtained as described in footnotes *b* and *c* of Table 1.

Fig. 7. pH–yield profiles for the reaction of benzenesulfonyl chloride (initial concentration 7.8×10^{-4} mol/L) with amines (0.01 mol/L) in THF–H_2O (1:1) at 25.0 °C: aniline (Δ), benzylamine (○), and dibutylamine (□). Points are experimental and lines are drawn using eq. [5] and the appropriate parameters from Table 2, plus $k_w = 1.5. \times 10^{-4}$ s^{-1} and $k_{OH} = 1.8$ (mol/L)$^{-1}$ s^{-1} determined from the pH–rate profile for this medium (4*a*).



bic", such as guanidinium bromide or tetrabutylammonium bromide. Accordingly, we have determined the effect of adding examples of hydrophobic and antihydrophobic solutes to the reaction mixtures and seeing the effect on the pH–yield profiles.

Reactions in THF–H_2O (1:1)

Our first venture was to carry out the reaction in aq. THF (1:1). The results for aniline, benzylamine, and dibutylamine are shown in Fig. 7. The curve for aniline is qualitatively similar to that in water alone but with a lowered value for k_N (in water, $k_N = 4.6$, $k_{GB} \approx 0$ (mol/L)$^{-1}$ s^{-1} (2*a*); in THF–H_2O (1:1), $k_N = 0.32$, $k_{GB} \approx 0.006$ (mol/L)$^{-1}$ s^{-1}; see Table 2). The effect on the other two amines was much more striking — and gratifying. With benzylamine there was no sign of any hydrophobic effect and with dibutylamine only a small sign of a possible third-order term was in evidence. Clearly, in THF–H_2O (1:1) the putative hydrophobic effect is very much reduced.

It is of interest that with THF–H_2O (1:4), the pH–yield profile for benzylamine is qualitatively very similar to that in water alone; a third-order term (k_{NOH}), somewhat reduced relative to k_N, is required to fit the curve adequately (4*a*).

It should be noted that the aq. THF experiments were also of interest for the practical purpose of determining the effects of cosolvent on the validity of our pH_{max} equation (eq. [1]) for use with amines with sufficiently low water solubility to make the experiment impracticable without addition of cosolvent. The chief effect of adding the organic solvent appears to be the well-known lowering of the apparent pK_a of the amine; the pK_a' values are shown in Table 2. pH_{max} values calculated from eq. [1] using pK_a' values determined in the solvent in question are in good accord with the experimental ones. pH_{max}, as given in eq. [1], may be regarded as the average of pK_a and pH_i, with $pH_i = k_W/k_{OH} + K_w$, where pH_i is the inflection point in a pH–rate profile (i.e., the pH at which $k_W = k_{OH}[OH^-]$). Values of pH_i for a sizable array of electrophilic reagents were tabulated in our earlier study (2*a*), and it was of interest to see the effect of solvent change on pH_i. We found, in fact, that the pH_i values are very similar: 9.88 in water (2*a*), 9.95 in THF–H_2O (1:4), and 9.92 in THF–H_2O (1:1). This suggests that the effect of the solvent change is similar for both the water and hydroxide promoted reactions.

Bis(2-methoxyethyl)amine

If indeed the effect noted at high pH with dibutylamine is, in fact, due to hydrophobic association of benzenesulfonyl chloride and dibutylamine, it is to be expected that a secondary amine of similar size and shape, but with relatively hydrophilic groups on the nitrogen atom, would show less of this effect. To test this idea we have studied the reaction of bis(2-methoxyethyl)amine ($(CH_3OCH_2CH_2)_2NH$), which is an approximate isostere of dibutylamine in which one methylene group in each chain is replaced by the relatively polar ether oxygen. The pH–yield profile for bis(2-methoxyethyl)amine is shown in Fig. 8. As may be readily seen from inspection of the curve or by inspection of the k_{NN} and k_{NOH} values (Table 1), the results are consistent with a much reduced hydrophobic effect relative to dibutylamine.

Reactions in aq. NaCl solutions

pH yield profiles for dimethylamine, dipropylamine, and dibutylamine in 1 mol/L aqueous sodium chloride solution are shown in Fig. 9, and those for diethylamine in both 1

© 2005 NRC Canada

Fig. 8. pH–yield profile for the reaction of benzenesulfonyl chloride (initial concentration 7.8×10^{-4} mol/L) with bis(2-methoxyethyl)amine (0.01 mol/L). Points are experimental and the line is drawn using eq. [5] and the appropriate parameters from Table 1.

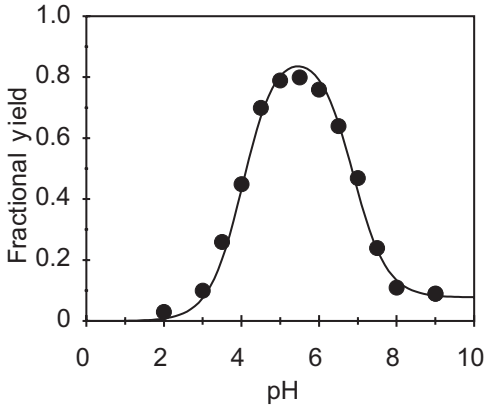
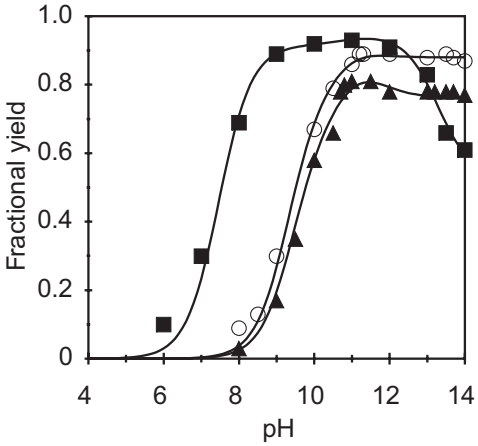


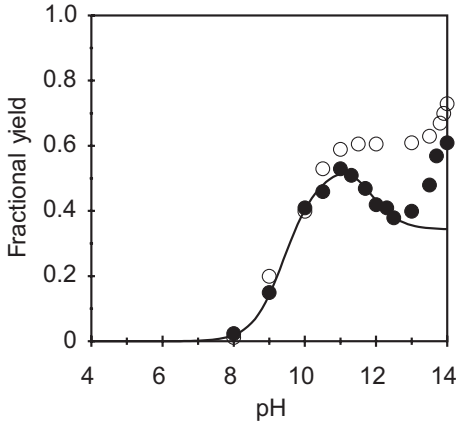
Fig. 9. pH–yield profiles for the reaction of benzenesulfonyl chloride (initial concentration 7.8×10^{-4} mol/L) with amines (0.01 mol/L) in aq. NaCl (1.0 mol/L) at 25.0 °C: dimethylamine (■); dibutylamine (○); and dipropylamine (▲). Points are experimental and lines are drawn using eq. [5] and the appropriate parameters from Table 2, plus $k_w = 2.74. \times 10^{-3}$ s^{-1} and $k_{OH} = 34.1$ (mol/L)$^{-1}$ s^{-1} determined from the pH–rate profile for this medium (4*b*).



and 2 mol/L NaCl solutions in Fig. 10; the derived rate constants for the reactions in 1 mol/L NaCl are listed in Table 2.

In considering these results we must remember that much of the effect of the sodium chloride is due to a change in ionic strength, i.e., it leads to a more polar medium that is more favorable than plain water to the development of charge separation in the transition state. Most of the changes that are observed in the reactions of dimethylamine are consistent with such an ionic strength effect. We note, for example, a modest increase in k_N and, interestingly, a more substantial effect (sevenfold increase) in k_{GB}. This latter result is consistent with greater charge separation in the transition state in the k_{GB} term than in the k_N process. A sizable increase in k_{GB} (relative to k_N) is also noted with diethylamine along with a smaller increase with dipropylamine, again presumably for the same reason.

Fig. 10. pH–yield profiles for the reaction of benzenesulfonyl chloride (initial concentration 7.8×10^{-4} mol/L) with diethylamine (0.01 mol/L) in aq. NaCl at 25.0 °C: 1.0 mol/L (●) and 2.0 mol/L (○). Points are experimental and the line is drawn using eq. [5] as described for Fig. 9.



The hydrophobic effect is expected to be stronger in sodium chloride solution than in water, and consistent with this is the observation in the rise in the "plateau level", i.e., the value of f_p in the pH range 11–14 with both dipropylamine and dibutylamine, reflecting a small increase in k_{NOH} relative to k_N on going from water to 1 mol/L NaCl solution.

The case of diethylamine is particularly interesting, showing not only an increase in the plateau level (around pH 12 to 13), but also a further increase in f_p presumably associated with an increase of k_{NOH} with change in ionic strength as the pH changes from 13 to 14. If this picture is correct, it is interesting — and surprising — that no analogous change in the pH region 13 to 14 is apparent with dipropylamine or dibutylamine. One possibility is that with these amines any changes in k_{NOH} are cancelled by other effects such as association of the amine with concomitant reduction in the concentration of the free amine and hence of the rate of the reaction. It is of interest in this connection to look at the solubilities (at 25 °C) of these amines in water and 1 mol/L NaCl solution: dibutylamine, 0.0348 and 0.0226 mol/L, respectively; dipropylamine, 0.4434 and 0.2483 mol/L, respectively; diethylamine, soluble in all proportions in both media. The hydrophobic effect (salting out) clearly shows with both dibutylamine and dipropylamine. Note that no line is drawn through the points for 2 mol/L NaCl, as we were unable to measure k_w and k_{OH} in this medium; the standard kinetic plots did not yield straight lines pointing, not surprisingly, to nonideal solution behaviour.

It is evident that the full picture is probably very complex and that an extensive study would be required for a more complete understanding of the reactions in NaCl. It is our view, however, that our observations, when taken with other results presented in this study, are in full accord with the presence of a hydrophobic effect on the k_{NOH} terms of the reactions of diethylamine, dipropylamine, and dibutylamine in NaCl solutions.

Reactions in aqueous tetrabutylammonium bromide solution

Solutions of tetrabutylammonium bromide are known to lead to salting in of organic solutes. Accordingly, in the light

© 2005 NRC Canada

Table 3. Observed % yields in the reactions of benzenesulfonyl chloride with primary and secondary amines under preparative conditions.

Amine	% Yield below pH_{max} (pH)	% Yield at pH_{max}[a] (pH)	% Yield in 1.0 mol/L NaOH
Butylamine	86.5 (8.2)	99.0 (10.2)	44.9, 44.0
2-Methoxyethylamine	58.1 (7.0)	99.2 (9.5)	56
1-Octylamine	96.1 (8.5)	96.5 (10.3)	98.3
Dimethylamine			91
Diethylamine	51.7 (9.0)	94.8 (10.4)	87
Dibutylamine	77.7 (9.0)	88.4, 86.5 (10.6)	94
Dipentylamine[b]	94.3 (9.0)	96.6 (10.5)	97.8
Morpholine	44.8 (5.5)	99.0 (9.15)	73.2
Piperidine	75.5 (8.0)	94.9 (10.55)	89
Hexamethylenimine	85.1 (8.0)	99.6 (10.6)	97
Diisobutylamine[c]			69.9
Diallylamine			76.9
Bis(2-methoxyethyl)amine		91.0 (9.39)	59.0, 61.0

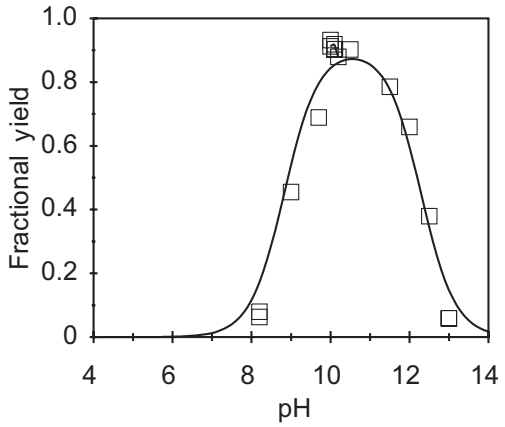
Note: Benzenesulfonyl chloride (0.67 mL, 5.25 mmol) added to a solution (50 mL) of the amine (0.1 mol/L) either (*i*) adjusted to the specified pH or (*ii*) in 1.0 mol/L aq. NaOH at 25 °C.

[a] pH_{max} calculated from eq. [1] using the pK_a values given in footnotes *b* and *c* and in Table 1.

[b] pK_a = 11.18 (17).

[c] pK_a = 10.50 (7).

Fig. 11. pH–yield profile for the reaction of benzenesulfonyl chloride (initial concentration 0.001 mol/L) with dibutylamine (0.01 mol/L) in aqueous tetrabutylammonium bromide (1.0 mol/L) at 25.0 °C. Points are experimental. The line is drawn using eq. [2] with $k_w = 3.06 \times 10^{-3}$ s^{-1}, $k_{OH} = 40.4$ (mol/L)$^{-1}$ s^{-1}, and $k_N = 71$ (mol/L)$^{-1}$ s^{-1} (see text).



of what has already been presented in this paper, it is to be expected that the postulated hydrophobic effect would be reduced by carrying out the reaction in aqueous tetrabutylammonium bromide solution. In accord with this picture we noted that the solubility of dibutylamine increased from 0.0348 mol/L in water to 0.0834 mol/L in 1.0 mol/L aqueous tetrabutylammonium bromide solution.

The pH–yield profile for the reaction of benzenesulfonyl chloride (0.001 mol/L) with dibutylamine (0.01 mol/L) in 1 mol/L $Bu_4N^+Br^-$ at 25 °C is shown in Fig. 11. It is immediately evident that the points form the normal bell shape associated with a system conforming to eq. [2] without any need to invoke third-order terms. The line shown, which is obtained from eq. [2] using the k_w, k_{OH}, and pK_a parameters for water plus $k_N = 71$ (mol/L)$^{-1}$ s^{-1} (a value obtained by a manual least-squares fit to the experimental points), is presented to illustrate that the data for the reaction in tetrabutylammonium bromide can indeed be readily accommodated on the basis of eq. [2] without invoking k_{NOH} or k_{NN}. In other words, the phenomena leading to the sigmoid pH–yield curve with benzenesulfonyl chloride and dibutylamine in water would appear to have disappeared in the tetrabutylammonium bromide solution, as predicted by the hydrophobic effect picture.

Yields at high pH under preparative conditions

The pseudo-first-order conditions used in determining most of the pH–yield profiles in this study involved low concentrations of the sulfonyl chloride with a 10-fold or greater excess of the (total) amine. It is of interest to see to what extent the unusual features of reactions at high pH shown in our pH–yield experiments show up under reaction conditions more typical of organic synthesis.

Reactions were carried out by adding a 5% excess of benzenesulfonyl chloride to a 0.1 mol/L solution of the amine; these concentrations are distinctly higher than those used in constructing the pH–yield profiles. As may be seen from the results in Table 3, the yields at pH_{max} are high (usually close to or above 95%); yields below pH_{max} are invariably lower though the difference is small in some cases. The yields in 1.0 mol/L NaOH ("pH 14") generally follow expectation based on pH–yield profiles. Some of the yields in 1.0 mol/L NaOH are high, e.g., octylamine (98.3%), dipentylamine (97.8%), and hexamethylenimine (97.0%). For these substrates, the high pH procedure is a simple and surprisingly efficient procedure for preparing the benzenesulfonamides; note that the reaction leading to these yields is primarily (99% or more) due to the k_{NOH} term.

These results prompted us to see if any other electrophiles reacted with dibutylamine with any sign of the involvement of third-order terms. Accordingly, we compared preparative runs at pH 11.40 (pH_{max}) and in 1.0 mol/L NaOH between benzoyl chloride and dibutylamine and obtained yields of

© 2005 NRC Canada

97.5% and 84.2% (4*a*), respectively; neither this nor a limited number of points in a (partial) pH–yield profile pointed to any sign of a third-order term. In addition, we had previously examined the pH–yield behaviour of acetic anhydride with primary and secondary amines (2*b*), but had not specifically looked at the reaction with dibutylamine. A pH–yield profile of this reaction over the pH range 8.0–13.0 was found (4*b*) to be well-described by eq. [4] with $k_N = 2.5 \times 10^3$ $(mol/L)^{-1}$ s^{-1} and $k_{GB} = 90$ $(mol/L)^{-1}$ s^{-1} taken with the parameters previously used (2*b*). We conclude that neither benzoyl chloride nor acetic anhydride shows a detectable third-order term in its reaction with dibutylamine under our conditions. It is probably not surprising that acetic anhydride should show no detectable third-order term, since the anhydride must be comparatively hydrophilic. The observation of a third-order term with benzenesulfonyl chloride and the failure to see any sign of a third-order term with its carbonyl analogue, benzoyl chloride, raises the interesting question: Why the difference? We have no firm evidence on the point, but we note that the arrangement shown by **2** could be close to an energy minimum for the electrophile–nucleophile complex prior to any reaction. Movement of the electrons as shown should take place readily and directly lead to the sulfonamide in the favourable conformation in which the free electron pair on the nitrogen is gauche to both oxygens (16). With benzoyl chloride, on the other hand, no such favourable arrangement of the amine – acid chloride complex comes readily to mind.

Concluding comment

In this study we present evidence that the general reaction of benzenesulfonyl chloride with primary and secondary amines in water requires at least one, and probably two, third-order terms (the k_{NOH} and k_{NN} terms, respectively). The principal observation that led to this proposal was obtained from pH–yield profiles, which showed, in all but the simplest or most hydrophilic amines, higher yields of the sulfonamide than predicted by the simplest mechanism. The third-order terms show up especially with simple alkylamines containing six or more alkyl carbon atoms, in accord with the intervention of hydrophobic phenomena. Experiments designed to disclose hydrophobic influences are in accord with this view.

In principle, the existence of the third-order terms should be detectable by conventional pH–rate studies, but as may be seen from the rate constants in Table 1, the half-lives of the reactions in the pH range in which the third-order terms are important, are inconveniently short for at least the simpler rate measurement techniques. The method of pH–yield profiles is a very easy procedure, which readily leads to information on an array of pH-dependent processes. Use of this procedure appears to be limited by variable yields under ostensibly identical conditions; this circumstance appears to arise as a result of either (*i*) extremely fast reactions that lead to difficulties with mixing effects or (*ii*) problems arising from low solubilities. Within the range in which reproducible results are readily obtained, pH–yield profiles can be a convenient source of valuable information, and further exploitation of the method is foreseen.

Experimental

Kinetic determinations were carried out with a pH-stat apparatus consisting of a Radiometer pH meter (PHM 25) equipped with GK2401B combination glass electrode (pH range 0–14, temperature range 0–100 °C), and an Aminco automatic burette with a 3 mL syringe reservoir. The reaction vessel used was a Radiometer V520 vessel equipped with a Radiometer V525 thermostatting jacket. The temperature was maintained with the aid of a Haake FJ constant temperature circulating apparatus. Stirring was accomplished with the use of a magnetic stirrer and the time was measured with a Precision Scientific Co. electric timer. The pH apparatus used for the pH–yield profiles consisted of either a Sargent-Welch 6000 meter with a Fisher all range (pH 1–14) combination electrode or a Radiometer pH meter (PHM 25) as previously described. Evaporation of solvents was carried out with a Büchi Rotovap apparatus connected to a water aspirator, and last traces of solvent were removed under vacuum until constant weight of the product was attained. Melting points were obtained using either a Kofler hot stage or a Gallenkamp apparatus and are uncorrected. ^1H and ^{13}C NMR spectra were obtained using Varian Gemini 300 and Varian Gemini 200 spectrometers. IR spectra were obtained with either a PerkinElmer 2000 FT-IR spectrometer or a Nicolet 205 FT-IR spectrometer. Reagent grade NaCl was used in the experiments carried out in aqueous salt solutions; in a few experiments with secondary amines, recrystallized NaCl was used, but no significant difference from reagent grade NaCl was detected. Benzenesulfonyl chloride and all the amines were fractionally distilled prior to use. Dichloromethane was dried over calcium hydride and distilled prior to use. The hydrochloride salts of amines were prepared by addition of hydrogen chloride to solutions of the amines in ether. The hydrochloride precipitates were collected by filtration, recrystallized, and dried to constant weight; melting points agreed with literature values. Authentic specimens of the sulfonamides for comparison were typically prepared from reaction of benzenesulfonyl chloride with excess amine or with an equivalent amount of amine in the presence of excess triethylamine, in dichloromethane at 0 °C to rt for 1–3 h. The reaction mixture was treated with water; the aqueous layer was made acidic and was extracted with dichloromethane (3 × 50 mL). The organic layer was dried over anhydr. $MgSO_4$ and the solvent evaporated to the give the corresponding sulfonamides in good yields (60%–90%). Melting points (where previously reported) were in accord with literature values; all sulfonamides showed IR, ^1H and ^{13}C NMR spectra, and exact mass values in accord with the assigned structures. Further details on known sulfonamides may be found elsewhere (4); properties of previously unknown sulfonamides are given in the following.

N-(2-Methoxyethyl)benzenesulfonamide

Clear liquid. IR (neat, cm^{-1}) ν_{max}: 3283 (br, s), 2930 (s), 2892 (s), 1448 (s), 1329 (s), 1162 (s), 1126 (s), 1090 (s), 1026 (w), 955 (w). ^1H NMR δ: 3.12 (q, 2H), 3.23 (s, 3H), 3.38 (t, 2H), 5.44 (t, 1H, NH), 7.48–7.61 (m, 3H), 7.85–7.90 (m, 2H). ^{13}C NMR δ: 42.7, 58.5, 70.4, 126.8, 129.0, 132.5, 139.8. HR-MS calcd. for $C_9H_{13}NO_3S$: 215.0616; found: 215.0619.

© 2005 NRC Canada

***N*,*N*-Dipentylbenzenesulfonamide**

Clear liquid. IR (neat, cm^{-1}) ν_{max}: 2958 (s), 2933 (s), 2872 (s), 1467 (w), 1447 (s), 1341 (s), 1157 (vs), 1091 (s), 1044 (w), 950 (w). ^1H NMR δ: 0.87 (t, 6H), 1.19–1.35 (m, 8H), 1.51 (quintet, 4H), 3.11 (t, 4H), 7.46–7.58 (m, 3H), 7.79–7.83 (m, 2H). ^{13}C NMR δ: 13.9, 22.2, 28.2, 28.8, 48.1, 126.9, 128.9, 132.1, 140.1. HR-MS calcd. for $C_{16}H_{27}NO_2S$: 297.1763; found: 297.1766.

***N*-Phenylsulfonylhexamethylenimine**

White solid, mp 34–34.5 °C. IR (cm^{-1}) ν_{max}: 3029 (w), 2936 (w), 1447 (w), 1331 (s), 1158 (vs), 1092 (w), 1045 (w). ^1H NMR δ: 1.54–1.60 (m, 4H), 1.68–1.76 (br m, 4H), 3.27 (t, 4H), 7.47–7.56 (m, 3H), 7.78–7.81 (m, 2H). ^{13}C NMR δ: 26.8, 29.0, 48.1, 126.8, 128.9, 132.1, 139.4. HR-MS calcd. for $C_{12}H_{17}NO_2S$: 239.0980; found: 239.0982.

***N*,*N*-Bis(2-methoxyethyl)benzenesulfonamide**

Pale yellow liquid, bp 160–162 °C (1 torr, 1 torr = 133.322 4 Pa). IR (cm^{-1}) ν_{max}: 2935 (s), 2883 (s), 1445 (s), 1337 (s), 1167 (s), 1120 (s), 941 (s), 735 (s), 685 (s), 590 (s). ^1H NMR δ: 3.22 (s, 6H), 3.34, (t, 4H), 3.46 (t, 4H), 7.44–7.55 (m, 3H), 7.56–7.79 (m, 2H). ^{13}C NMR δ: 48.5, 58.6, 71.3, 126.9, 128.8, 132.3, 139.7. HR-MS calcd. for $C_{12}H_{19}NO_4S$: 273.1034; found: 273.1028.

Reaction of benzenesulfonyl chloride with amines

Construction of pH–yield profiles

Benzenesulfonyl chloride (50 μL, 0.392 mmol) was quickly injected from a 50 μL syringe into a vigorously stirred solution of the amine (0.01 mol/L or 0.02 mol/L) in water (500 mL) in a 800 mL beaker, previously adjusted to the desired pH with dilute HCl or NaOH. The pH was maintained by dropwise addition of NaOH (0.5 mol/L or 0.1 mol/L) until it remained stable. The reaction mixture was acidified to pH 2 with 1 mol/L H_2SO_4 and extracted with dichloromethane; the organic layer was dried over anhydr. $MgSO_4$, filtered, and the solvent was evaporated as previously described. The product was identified by comparison of its ^1H NMR with that of an authentic sample. The yields were calculated from the constant weight of the product, based on the theoretical yield, and shown as experimental points in the figures. For the reactions at pH 14 and 13, 1 mol/L NaOH and 0.1 mol/L NaOH (500 mL), respectively, were used. In the reaction with dimethylamine the beaker was covered with Parafilm owing to the volatility of the amine. Reactions in NaCl solutions were carried out similarly, except for the use of 0.5, 1.0, or 2.0 mol/L NaCl solutions in place of water.

Reactions at lower concentrations required a modified procedure. The reaction was conducted with amine concentrations of 0.002 or 0.001 mol/L and was carried out as previosuly described except that the extracted solution of dichloromethane was dried over anhydr. $MgSO_4$ and filtered into a volumetric flask (100 or 250 mL) and the volume was made up to mark with dichloromethane. The UV spectrum of the solution was obtained and absorption at a particular wavelength was recorded, for example, for *N*,*N*-dibutylbenzenesulfonamide at λ = 275 nm. The yields were calculated from a calibration curve, which was obtained from solutions of the corresponding sulfonamide (product) of known concentrations in dichloromethane vs. the UV absorptions at that particular wavelength.

For reactions in THF–H_2O, the previous procedure was followed except that instead of water (500 mL), THF + H_2O (100 + 400 mL) was used for THF–H_2O (20:80) and THF + H_2O (250 + 250 mL) was used for THF–H_2O (50:50). After the reaction was completed at a particular pH, the pH of the reaction mixture was adjusted to 7 and most of the THF was removed on the rotatory evaporator. The reaction mixture was acidified to pH 2, followed by the workup as described before. The yields are shown in Fig. 7 and the derived rate constants listed in Table 2.

Reactions in tetrabutylammonium bromide (for reasons of economy) were carried out on a relatively small scale: benzenesulfonyl chloride (4.43 mg, 0.0251 mmol) in THF (32 μL) was injected into 25 mL of an aqueous solution of 1.0 mol/L in $Bu_4N^+Br^-$ and 0.01 mol/L in dibutylamine adjusted to the desired pH as previously described. Workup involved acidification to pH 1 with HBr, extraction with ether (3 × 10 mL), drying of the extract with $MgSO_4$, and evaporation of the solvent to 25 mL. A known quantity of nitrobenzene was added as internal standard and the amount of sulfonamide determined by GC. Two larger scale runs using 0.032 mL of benzenesulfonyl chloride in 250 mL of a solution 1 mol/L in tetrabutylammonium bromide and 0.01 mol/L in dibutylamine carried out as previously described with simple weighing of the product, gave yields of 17% and 69% at pH 14.0 and 10.0, respectively, in agreement with the smaller scale results.

Reactions under preparative conditions

Benzenesulfonyl chloride (0.67 mL, 5.25 mmol) was injected into a solution of the amine (0.1 mol/L) in 50 mL of water contained in a 100 mL beaker and previously adjusted to the desired pH, and the mixture stirred until reaction was complete (typically 1 to 2 h). The mixture was then acidified to pH 2 with 1 mol/L H_2SO_4 and worked up by extraction with dichloromethane as described for the pH–yield profiles in water; yields are listed in Table 3.

Acknowledgements

We are grateful to the Natural Sciences and Engineering Research Council of Canada (NSERC) for financial support of this study. We thank Professor Mark Workentin for the use of his GC apparatus and John Villella, Kevin Kulbaba, and Rana Ibrahim for valuable preliminary experiments.

References

1. (*a*) R. Breslow. Acc. Chem. Res. **24**, 159 (1991); (*b*) P.A. Grieco. Aldrichimica Acta, **24**, 59 (1991); (*c*) C.J. Li. Chem. Rev. **93**, 2023 (1993); (*d*) A. Lubineau, J. Augé, and Y. Queneau. Synthesis, 741 (1994); (*e*) P.A. Grieco (*Editor*). Organic synthesis in water. Blackie Academic and Professional, London. 1998; (*f*) C.J. Li and T.H. Chan. Organic reactions in aqueous media. Wiley, New York. 1997; (*g*) R. Breslow. *In* Green chemistry frontiers in benign chemical syntheses and processes. *Edited by* P.T. Anastas and T.C. Williamson. Oxford University Press, Oxford. 1998. Chap. 13; (*h*) C.-J. Li. *In* Green chemistry frontiers in benign chemical syntheses and

© 2005 NRC Canada

processes. *Edited by* P.T. Anastas and T.C. Williamson. Oxford University Press, Oxford. 1998. Chap. 14; (*i*) A. Lubineau and J. Augé. Top. Curr. Chem. **206**, 1 (1999).
2. (*a*) J.F. King, R. Rathore, J.Y.L. Lam, Z.R. Guo, and D.F. Klassen. J. Am. Chem. Soc. **114**, 3028 (1992); (*b*) J.F. King, Z.R. Guo, and D.F. Klassen. J. Org. Chem. **59**, 1095 (1994).
3. J.Y.L. Lam. Ph.D. thesis, The University of Western Ontario, London, Ontario. 1992.
4. (*a*) M.S. Gill. Ph.D. thesis, The University of Western Ontario, London, Ontario. 1996; (*b*) P. Ciubotaru. M.Sc. thesis, The University of Western Ontario, London, Ontario. 1999.
5. (*a*) J.F. King, M.S. Gill, and D.F. Klassen. Pure Appl. Chem. **68**, 825 (1996); (*b*) J.F. King, M.S. Gill, and P. Ciubotaru. Sixth European Symposium on Organic Reactivity (ESOR-VI), Louvain-la-Neuve, Belgium. July 1997. Abstract OC31.
6. J.F. King, S. Skonieczny, and J.Y.L. Lam. J. Am. Chem. Soc. **114**, 1743 (1992).
7. W.P. Jencks and J. Regenstein. Handbook of biochemistry and molecular biology. 3rd ed. Vol. 1. *Edited by* G.D. Fasman. CRC Press, Cleveland. 1976. p. 305.
8. S. Bergström and G. Olofsson. J. Solution Chem. **7**, 497 (1978).
9. A. Albert and E. P. Serjeant. Ionization constants of acids and bases: a laboratory manual. Methuen, London. 1962.
10. O. Rogne. J. Chem. Soc. B, 1294 (1968).
11. W.P. Jencks. J. Am. Chem. Soc. **94**, 4731 (1972).
12. J.F. King. *In* The chemistry of sulphonic acids, esters, and their derivatives. *Edited by* S. Patai and Z. Rappoport. Wiley, Chichester. 1991. Chap. 6. p. 249.
13. J.F. King and K.C. Khemani. Can. J. Chem. **67**, 2162 (1989).
14. (*a*) J.-L.M. Abboud, R. Notario, J. Bertrán, and M. Solà. Prog. Phys. Org. Chem. **19**, 1 (1993); (*b*) W.A. Henderson, Jr. and C.J. Schultz. J. Org. Chem. **27**, 4643 (1962); (*c*) H.K. Hall, Jr. J. Org. Chem. **29**, 3539 (1964); (*d*) K. Okamoto, S. Fukui, I. Nitta, and H. Shingu. Bull. Chem. Soc. Jpn. **40**, 2350; **40**, 2354 (1967).
15. (*a*) W. Blokzijl and J.B.F.N. Engberts. Angew. Chem. Int. Ed. Engl. **32**, 1545 (1993); (*b*) J.B.F.N. Engberts and M.J. Blandamer. Chem. Commun. (Cambridge), 1701 (2001); (*c*) R. Breslow. Acc. Chem. Res. **37**, 471 (2004); (*d*) S. Otto and J.B.F.N. Engberts. J. Org. Biomol. Chem. **1**, 2809 (2003).
16. (*a*) T. Jordan, H.W. Smith, L.L. Lohr, Jr., and W.N. Lipscomb. J. Am. Chem. Soc. **85**, 846 (1963); (*b*) W.B. Jennings and R. Spratt. Chem. Commun. (Cambridge), 1418 (1970); (*c*) J.F. King, K.C. Khemani, S. Skonieczny, and N.C. Payne. Rev. Heteroatom Chem. **1**, 80 (1988).
17. N.F. Hall and M.R. Sprinkle. J. Am. Chem. Soc. **54**, 3469 (1932).

© 2005 NRC Canada

Formation and stability of organic zwitterions — The carbon acid pK_as of the trimethylsulfonium and tetramethylphosphonium cations in water[1]

Ana Rios, AnnMarie C. O'Donoghue, Tina L. Amyes, and John P. Richard

Abstract: We report second-order rate constants of k_{DO} = 7.5 × 10^{-4} and 9.9 × 10^{-5} $(mol/L)^{-1}$ s^{-1} for exchange for deuterium of the first methyl proton of the trimethylsulfonium and tetramethylphosphonium cations, respectively, in D_2O at 25 °C and I = 1.0 (KCl). The data were analyzed to give the following carbon acidities for these cationic carbon acids in water: $(CH_3)_3S^+$, pK_a = 28.5; $(CH_3)_4P^+$, pK_a = 29.4. These acidities are close to those of the neutral carbon acids acetonitrile and dimethylacetamide. This provides evidence that a portion of the stabilization of the cyanomethyl carbanion is due to resonance delocalization of negative charge from carbon to cyano nitrogen.

Key words: carbon acids, carbanions, ylides, proton transfer.

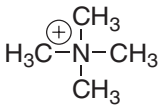
Résumé : Opérant dans le D_2O, à 25 °C et une valeur de I = 1,0 (KCl), on a déterminé que les constantes de vitesse du deuxième ordre pour l'échange du deutérium du premier proton méthyle des cations triméthylsulfonium et tétraméthylphosphonium sont respectivement de k_{DO} = 7,5 × 10^{-4} et 9,9 × 10^{-5} $(mol/L)^{-1}$ s^{-1}. Les données ont été analysées pour en tirer les acidités carboniques suivantes pour ces acides carboniques cationiques dans l'eau: $(CH_3)_3S^+$, pK_a = 28,5 et $(CH_3)_4P^+$, pK_a = 29,4. Ces acidités se rapprochent de celles d'autres acides carboniques, tel l'acétonitrile et le diméthylacétamide. Ces résultats montrent qu'une portion de la stabilization du carbanion cyanométhyle est due à une délocalization de résonance de la charge négative du carbone vers l'azote du groupe cyano.

Mots clés : acides carboniques, carbanions, ylures, transfert de proton.

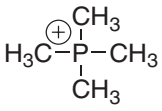
[Traduit par la Rédaction]

Introduction

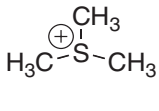
We are interested in characterizing the effects of strongly electron-withdrawing substituents on carbon acidity and have reported the kinetic and thermodynamic acidities of a variety of weak carbon acids in water (1–12). The very low carbon acidity of methane (13) is increased by substituents that provide polar and (or) resonance stabilization of negative charge at the methyl carbanion; and the most powerful purely polar stabilization of a methyl carbanion is provided by a cationic group at a neighboring atom. In 1955 Doering and Hoffmann (14) reported rate constants for deprotonation of the tetramethylammonium, tetramethylphosphonium, and trimethylsulfonium cations by hydroxide ion at several temperatures. Their data showed that the tetramethylammonium cation is a significantly weaker carbon acid than the tetramethylphosphonium and trimethylsulfonium cations. Thus, the ylides of phosphonium and sulfonium cations are stabilized relative to the corresponding ylides of ammonium cations by the greater polarizability of phosphorus and sulfur than of nitrogen, and possibly by hyperconjugation (15, 16) and back-bonding from carbon to the *d*-orbitals of phosphorus and sulfur (17).



Me_4N^+



Me_4P^+



Me_3S^+

In recent years there have been several studies that document the relatively strong carbon acidity of alkyl sulfonium (18–26) and alkyl phosphonium (27, 28) cations. However, the carbon acid pK_as for the parent tetramethylphosphonium and trimethylsulfonium cations in aqueous solution have not been reported. To this end, we have determined the rate constants for deprotonation of the tetramethylphosphonium cation (**Me_4P^+**) and trimethylsulfonium cation (**Me_3S^+**) in D_2O at 25 °C, using modern NMR methods to monitor transfer of deuterium from the solvent to carbon acid. Our results agree well with the results of Doering and Hoffmann (14); they extended earlier work by showing that there is no catalysis of deprotonation of these cationic carbon acids by buffer bases. An analysis of these data by the methods that we have developed to determine equilibrium carbon acidities in water (1–

Received 25 April 2005. Published on the NRC Research Press Web site at http://canjchem.nrc.ca on 25 November 2005.

A. Rios. Departamento de Química Física, Facultad de Química, Universidad de Santiago, 15706 Santiago de Compostela, Spain.
A.C. O'Donoghue. Department of Chemistry, University College Dublin, Belfield, Dublin 4, Ireland.
T.L. Amyes and J.P. Richard.[2] Department of Chemistry, University at Buffalo, SUNY, Buffalo NY 14260 USA.

[1]This article is part of a Special Issue dedicated to organic reaction mechanisms.
[2]Corresponding author (e-mail: jrichard@chem.buffalo.edu).

 doi: 10.1139/V05-155 © 2005 NRC Canada

12) provides the carbon acid pK_as for deprotonation of $\mathbf{Me_4P^+}$ and $\mathbf{Me_3S^+}$ in water.

Experimental

Materials

All organic and inorganic chemicals were reagent grade or better and were used without further purification. Trimethylsulfonium methyl sulfate, tetramethylphosphonium chloride, tetramethylammonium chloride, quinuclidine hydrochloride, 1,1,1,3,3,3-hexafluoro-2-propanol (HFIP), 2,2,2-trifluoroethanol (TFE), and KOD (40% wt, +98% D) were from Aldrich. Deuterium oxide (99.9% D) and deuterium chloride (35% *w*/*w*, 99.5% D) were from Cambridge Isotope Laboratories.

Preparation of solutions

The acidic proton of quinuclidine hydrochloride was exchanged for deuterium before use as described previously (1). TFE and HFIP were dissolved directly in D_2O (99.9% D), but at no time did this introduce >0.5 atom% of protium into the solvent. Quinuclidine, trifluoroethanol, and HFIP buffers were prepared by dissolving their acidic forms and KCl in D_2O followed by the addition of KOD to give the desired acid:base ratio or pD at I = 1.0 (KCl).

Solution pD was determined at 25 °C using an Orion Model 720A pH meter equipped with a Radiometer GK2321C or pHC4006-9 combination electrode. Values of pD were obtained by adding 0.40 to the observed reading of the pH meter (29). The concentration of deuterioxide ion at any pD was calculated from eq. [1], where $K_w = 10^{-14.87}$ (mol/L)^2 is the ion product of D_2O at 25 °C (30) and γ_{OL} = 0.79 or 0.75 is the apparent activity coefficient of lyoxide ion under our experimental conditions determined by the GK2321C or the pHC4006-9 electrode, respectively (2).

$$[1] \qquad [DO^-] = \frac{10^{pD-pK_w}}{\gamma_{OL}}$$

^{1}H NMR spectroscopy

^{1}H NMR spectra at 500 MHz were recorded in D_2O at 25 °C on a Varian Unity Inova 500 spectrometer. The relaxation times for the methyl protons of $\mathbf{Me_3S^+}$ and $\mathbf{Me_4P^+}$, determined for 10 mmol/L solutions of substrate at I = 1.0 (KCl), were found to be in the range of T_1 = 6 to 7 s. The relaxation delay between pulses was at least 10-fold greater than the longest T_1 of the protons of interest. Chemical shifts were reported relative to HOD at 4.67 ppm. Baselines were subjected to a first-order drift correction before the determination of the integrated peak areas.

Kinetic measurements

All reactions were carried out in D_2O at 25 °C and a constant ionic strength of 1.0 maintained with potassium chloride. The deuterium exchange reactions of $\mathbf{Me_3S^+}$ and $\mathbf{Me_4P^+}$ in buffered solutions were initiated by mixing solutions of the substrate and the buffer at the same pD and ionic strength (I = 1.0, KCl) to give a final substrate concentration of 10 mmol/L. The reactions of $\mathbf{Me_4P^+}$ and $\mathbf{Me_4N^+}$ in alkaline solutions of D_2O were initiated by mixing solutions of the substrate and KOD at the same ionic strength (I = 1.0, KCl) to give a final substrate concentration of 10 mmol/L. At timed intervals an aliquot (600 μL) was removed from the reaction mixture and the pD was adjusted to 7 to 8 by the addition of concentrated DCl and 50 μL of 0.4 mol/L phosphate buffer in D_2O. The aliquots were either analyzed immediately by ^{1}H NMR spectroscopy or were frozen for analysis at a later time.

The exchange for deuterium of the first proton of the methyl groups of $\mathbf{Me_3S^+}$ was followed by monitoring the disappearance of the singlet at 2.911 ppm owing to the CH_3 groups and the appearance of the triplet at 2.899 ppm (J_{HD} = 2 Hz) owing to the CH_2D groups, by ^{1}H NMR. The exchange for deuterium of the first proton of the methyl groups of $\mathbf{Me_4P^+}$ was followed by monitoring the disappearance of the doublet at 1.867 ppm (J_{HP} = 16 Hz) owing to the CH_3 groups and the appearance of the doublet of triplets at 1.852 ppm (J_{HP} = 16 Hz, J_{HD} = 2.5 Hz) owing to the CH_2D groups. The reactions were followed during the exchange for deuterium of up to 25% and 5% of the first proton of the methyl groups of $\mathbf{Me_3S^+}$ and $\mathbf{Me_4P^+}$, respectively.

$$[2] \qquad R = \frac{A_{CH_3}}{A_{CH_3} + \frac{A_{CH_2D}}{2}}$$

$$[3] \qquad \ln R = -k_{obsd}t$$

Values of R, which is a measure of the progress of the deuterium exchange reaction (4, 31), were calculated according to eq. [2], where A_{CH_3} and A_{CH_2D} are the integrated areas of the signals owing to the CH_3 and CH_2D groups, respectively. During the early stages of the reaction of $\mathbf{Me_3S^+}$, it was possible to obtain baseline separation of only the most upfield peak of the triplet owing to the CH_2D groups. In these cases, the total integrated area of the triplet due to the CH_2D groups (A_{CH_2D}) was obtained by multiplying the integrated area of the resolved peak by three, and the area of the singlet owing to the CH_3 groups (A_{CH_3}) was obtained as the difference between the total peak area for both the singlet and the triplet and A_{CH_2D} (2). For the reaction of $\mathbf{Me_4P^+}$, only the most upfield peak of the doublet of triplets due to the CH_2D groups was cleanly resolved. The area of the doublet of triplets due to the CH_2D groups (A_{CH_2D}) was obtained by multiplying the integrated area of the resolved peak by six, and the area of the doublet due to the CH_3 groups (A_{CH_3}) was obtained as the difference between the total peak area for all the signals and A_{CH_2D}.

Semilogarithmic plots of reaction progress (R) against time were linear with negative slopes equal to k_{obsd} (s^{-1}, eq. [3]), which is the rate constant for exchange of a *single* proton of the substrate.

A triplet at 3.164 ppm (J = 0.5 Hz) was observed for the four equivalent methyl groups of the tetramethylammonium cation. No signal for a CH_2D group was observed after the incubation of the substrate in the presence of 1.0 mol/L KOD at 25 °C for 16 days. Several spurious signals appeared during this prolonged reaction time, but no attempt was made to assign these signals.

© 2005 NRC Canada

Table 1. First-order rate constants for exchange for deuterium of the first proton of **Me_4P^+** and **Me_3S^+** in D_2O at 25 °C and I = 1.0 (KCl).

Carbon acid	Brønsted base	f_B[a]	$[B]_T$ (mol/L)[b]	pD	$[DO^-]$ (mol/L)[c]	k_{ex} (s^{-1})[d]
$(CH_3)_4P^+$	DO^-				0.29	2.8×10^{-5}
					0.22	2.2×10^{-5}
					0.17	1.6×10^{-5}
					0.13	1.2×10^{-5}
					0.042	3.9×10^{-6}
	$CF_3CH_2O^-$	0.2	0.092	12.22	2.83×10^{-3}	3.1×10^{-7}
			0.18	12.30	3.40×10^{-3}	3.6×10^{-7}
			0.28	12.34	3.73×10^{-3}	3.4×10^{-7}
			0.37	12.37	4.00×10^{-3}	3.7×10^{-7}
$(CH_3)_3S^+$	$(CF_3)_2CHO^-$	0.90	0.05	10.77	1.01×10^{-4}	1.0×10^{-7}
			0.10	10.77	1.01×10^{-4}	9.6×10^{-8}
			0.25	10.83	1.15×10^{-4}	9.8×10^{-8}
			0.50	10.91	1.39×10^{-4}	1.1×10^{-7}
	Quinuclidine	0.20	0.05	11.50	5.40×10^{-4}	3.7×10^{-7}
			0.20	11.47	5.04×10^{-4}	3.3×10^{-7}
		0.40	0.05	11.92	1.42×10^{-3}	9.0×10^{-7}
			0.20	11.89	1.32×10^{-3}	7.6×10^{-7}
	$CF_3CH_2O^-$	0.10	0.05	12.04	1.87×10^{-3}	1.42×10^{-6}
			0.20	12.12	2.25×10^{-3}	1.42×10^{-6}

[a]Fraction of the Brønsted catalyst in the reactive basic form.
[b]Total concentration of the Brønsted catalyst.
[c]Concentration of deuterioxide ion at the pD of the experiment calculated from eq. [1].
[d]Observed first-order rate constant for deuterium exchange determined by ^1H NMR spectroscopy.

Results

The exchange for deuterium of the first proton of the methyl groups of **Me_3S^+** and **Me_4P^+** in D_2O at 25 °C and I = 1.0 (KCl) was followed by ^1H NMR spectroscopy at 500 MHz (Scheme 1). Deuterium exchange at **Me_3S^+** results in disappearance of the singlet at 2.911 ppm owing to the CH_3 groups and appearance of an upfield-shifted triplet at 2.899 ppm owing to the CH_2D groups. Similarly, exchange at **Me_4P^+** results in disappearance of the doublet at 1.867 ppm and the appearance of a doublet of triplets at 1.852 ppm owing to the CH_2D groups. The deuterium isotope effect on the ^1H NMR chemical shift and the H–D coupling constant are similar to those observed in our previous work (1, 2, 4–6, 9, 10, 32, 33).

First-order rate constants (k_{obsd} (s^{-1})) for exchange for deuterium of a *single* proton of the cationic carbon acids were determined as the slopes of semilogarithmic plots of reaction progress R (eq. [2]) against time according to eq. [3] (not shown). The reaction of **Me_3S^+** to give the monodeuteriated product occurs nine times as fast as the exchange of a *single* proton of the reactant, so that $k_{ex} = 9k_{obsd}$ where k_{ex} (s^{-1}) is the first-order rate constant for exchange of the first proton of the reactant to give the monodeuteriated product (Scheme 1A) (4, 31). Similarly, the reaction of **Me_4P^+** to give the monodeuteriated product occurs 12 times as fast as the exchange of a *single* proton of the reactant, so that $k_{ex} = 12k_{obsd}$ (Scheme 1B) (4, 31).

Table 1 gives the values of k_{ex} (s^{-1}) for the deuterium exchange reactions of **Me_3S^+** and **Me_4P^+** in the presence of various concentrations of deuterioxide ion or added buffers in D_2O at 25 °C and I = 1.0 (KCl). There is no significant change in the value of k_{ex} for the deuterium exchange reaction of **Me_4P^+** as the concentration of trifluoroethanol buffer is increased from 0.092 to 0.37 mol/L at pD 12.3. Similarly, the value of k_{ex} for the deuterium exchange reaction of **Me_3S^+** is independent of the concentration of added hexafluoroisopropanol, quinuclidine, or trifluoroethanol buffers (Table 1). The absence of buffer catalysis of deuterium exchange shows that, in basic solution, these cationic carbon acids are deprotonated exclusively by the solvent.

Scheme 1.

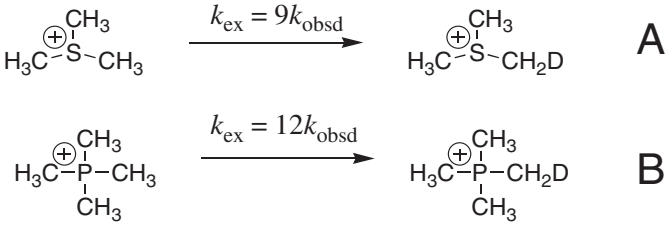


Figure 1 shows the dependence of k_{ex} (s^{-1}) on the concentration of deuterioxide ion in D_2O for the deuterium exchange reaction of **Me_4P^+**. The slope of this correlation gives $k_{DO} = 9.9 \times 10^{-5}$ $(mol/L)^{-1}$ s^{-1} (eq. [4]) where k_{DO} is the second-order rate constant for deuterium exchange catalyzed by the deuterioxide ion.

$$[4] \qquad k_{ex} = k_{DO}[DO^-]$$

© 2005 NRC Canada

Fig. 1. Dependence of k_{ex} (s^{-1}) for exchange for deuterium of the first proton of $\mathbf{Me_4P^+}$ on the concentration of deuterioxide ion in D_2O at 25 °C and I = 1.0 (KCl). The slope gives the second-order rate constant (k_{DO}) for DO^--catalyzed deuterium exchange.

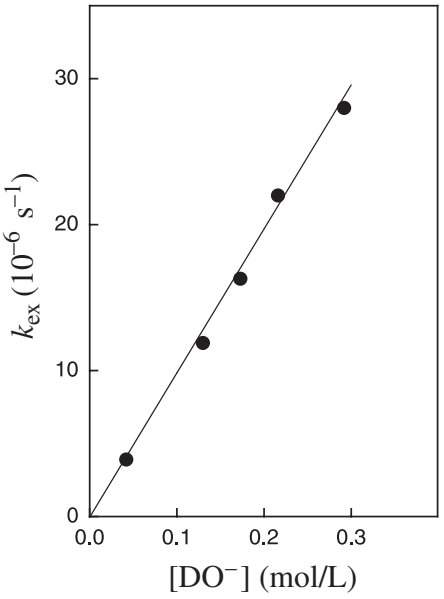


Figure 2 shows the pD–rate profiles for the deuterium exchange reactions of $\mathbf{Me_4P^+}$ (●) and $\mathbf{Me_3S^+}$ (◆). In cases where values of k_{ex} were determined over a range of buffer concentrations (Table 1), the values of pD and k_{ex} for the reaction at the lowest buffer concentration were used for Fig. 2. The solid line through the data for $\mathbf{Me_4P^+}$ was calculated from the value of $k_{DO} = 9.9 \times 10^{-5}$ $(mol/L)^{-1}$ s^{-1} using eq. [5]. A value of $k_{DO} = 7.5 \times 10^{-4}$ $(mol/L)^{-1}$ s^{-1} for $\mathbf{Me_3S^+}$ was determined from the fit of the data to eq. [5] (10). Figure 2 also shows data for the deuterium exchange reactions of acetonitrile (■) (4) and dimethylacetamide (▲) (10) taken from our earlier work.

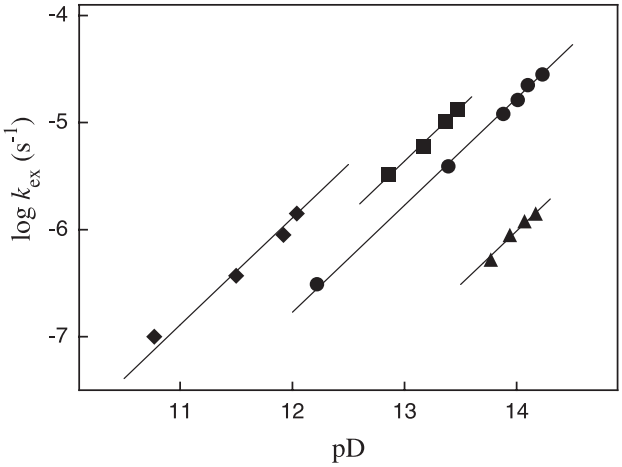
$$[5] \qquad \log k_{ex} = \log\left(\frac{k_{DO}K_w}{\gamma_{OL}}\right) + \text{pD}$$

There was no detectable formation of a CH_2D group after the reaction of $\mathbf{Me_4N^+}$ in 1.0 mol/L KOD in D_2O at 25 °C for 16 days. During this time, the appearance of several unidentified NMR signals showed that there were other reaction(s) of $\mathbf{Me_4N^+}$, but these were not characterized. A peak for a CH_2D group that is 1% of the area of the peak due to the CH_3 groups could have been easily detected in these experiments. This was used to calculate an upper limit of $k_{DO} < 4 \times 10^{-8}$ $(mol/L)^{-1}$ s^{-1} for the deuterium exchange reaction of $\mathbf{Me_4N^+}$ catalyzed by deuterioxide ion.

Discussion

The present work was initiated for the following reasons: (1) We wanted to determine second-order rate constants for the deuterioxide ion catalyzed deuterium exchange reactions of $\mathbf{Me_4P^+}$ and $\mathbf{Me_3S^+}$ using modern analytical methods and under the same conditions used in our other studies of the acidity of weak carbon acids. (2) We wanted to determine if these deuterium exchange reactions are catalyzed by buffer bases. (3) We wanted to obtain pK_as for these cationic carbon acids in water and to draw comparisons with the other data that we have reported over the last decade or so.

Fig. 2. pD–rate profiles of k_{ex} for deuterioxide ion catalyzed exchange for deuterium of the first proton of $\mathbf{Me_3S^+}$ (◆, this work), $\mathbf{Me_4P^+}$ (●, this work), CH_3CN (■, data from ref. 4), and $CH_3C(O)NMe_2$ (▲, data from ref. 10) in D_2O at 25 °C and I = 1.0 (KCl).



In 1955 Doering and Hoffmann (14) monitored the deuterium exchange reactions of several cationic carbon acids in D_2O by combustion of the recovered carbon acid to a mixture of D_2O and H_2O, whose deuterium enrichment was then determined by the "method of the falling drop". Table 2 shows that the second-order rate constants (k_{DO}) for deuterioxide-ion-catalyzed exchange of the first proton of $\mathbf{Me_4P^+}$ and $\mathbf{Me_3S^+}$ determined here agree to within 33% with the earlier values of Doering and Hoffmann (14). The slightly higher values reported in the earlier work were obtained at a temperature of 26.8 °C compared with 25 °C used in this work.

Rate-determining step for hydron exchange

The rate constant (k_{DO}) for exchange of the first proton of these cationic carbon acids in D_2O may be limited either by the chemical step of proton transfer from the substrate to deuterioxide ion (k_p, Scheme 2), or if this step is reversible ($k_{-p} >> k_{reorg}$), by the rate constant for reorganization of solvent to place a molecule of D_2O in a position to deliver a labeled hydron to the ylide, $k_{reorg} \approx 10^{11}$ s^{-1} (Scheme 2) (4, 11, 34). It has been shown in earlier work that reorganization of solvent is largely rate-determining for the lyoxide ion catalyzed deprotonation of cyanoalkanes (4). The following comparisons between proton transfer at cyanoalkanes and at $\mathbf{Me_4P^+}$ and $\mathbf{Me_3S^+}$ provide strong evidence that these reactions proceed with the common rate-determining step of solvent reorganization.

(1) There is a simple correlation between the decreasing importance of buffer catalysis of carbon deprotonation on moving from dihydroxyacetone phosphate (35) to acetamide (10) (Scheme 3) and the increasing reactivity and decreasing lifetime of the carbanion product of carbon deprotonation (10). No buffer catalysis is observed for the limiting case where the reorganization of solvent

© 2005 NRC Canada

Table 2. Kinetic and thermodynamic acidity of simple weak carbon acids in aqueous solution.

Carbon acid	k_{DO} ((mol/L)$^{-1}$ s^{-1})[a]	k_{HO} ((mol/L)$^{-1}$ s^{-1})[b]	k_{HOH} (s^{-1})[c]	pK_a[d]	pK_a (CH_3)[e]
$(CH_3)_4N^+$	$<4\times10^{-8}$[f]	$<1.7\times10^{-8}$[g]	10^{11}	>32.8	>33.4
$(CH_3)_4P^+$	9.9×10^{-5}[h]	4.1×10^{-5}[g]	10^{11}	29.4	30.0
$(CH_3)_3S^+$	(1.2×10^{-4})[i] 7.5×10^{-4}[h] (1.0×10^{-3})[i]	3.1×10^{-4}[g]	10^{11}	28.5	29.0
CH_3CN[j]	2.7×10^{-4}	1.1×10^{-4}	10^{11}	28.9	28.9
$CH_3C(O)NMe_2$[k]	5.7×10^{-6}	2.9×10^{-6}[k]	7.3×10^{9}[k]	29.4	29.4

Note: At 25 °C and I = 1.0 (KCl).

[a]Second-order rate constant for deprotonation of the carbon acid by deuterioxide ion in D_2O.

[b]Second-order rate constant for deprotonation of the carbon acid by hydroxide ion in H_2O.

[c]First-order rate constant for protonation of the carbanion by solvent water, estimated as $k_{HOH} = k_{reorg} = 10^{11}$ s^{-1}, where k_{reorg} is the rate constant for solvent reorganization (see text).

[d]Acidity of the carbon acid in water, calculated according to eq. [6] of the text.

[e]Statistically corrected acidity of a *single methyl* group of the carbon acid.

[f]Upper limit calculated as the rate constant for a reaction that would have given a value of R = 1/1.005 (eq. [2]) after 16 days (see text).

[g]Calculated from the value of k_{DO} using the relationship $k_{HO} = k_{DO}/2.4$, where 2.4 is the maximum secondary solvent deuterium isotope effect on the reactivity of lyoxide ion (see text).

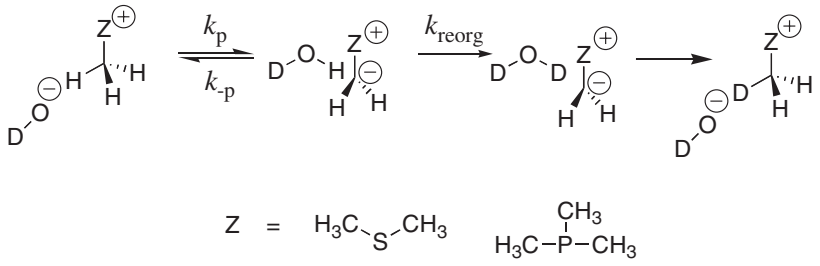
[h]Data from Table 1.

[i]Data from ref. 14.

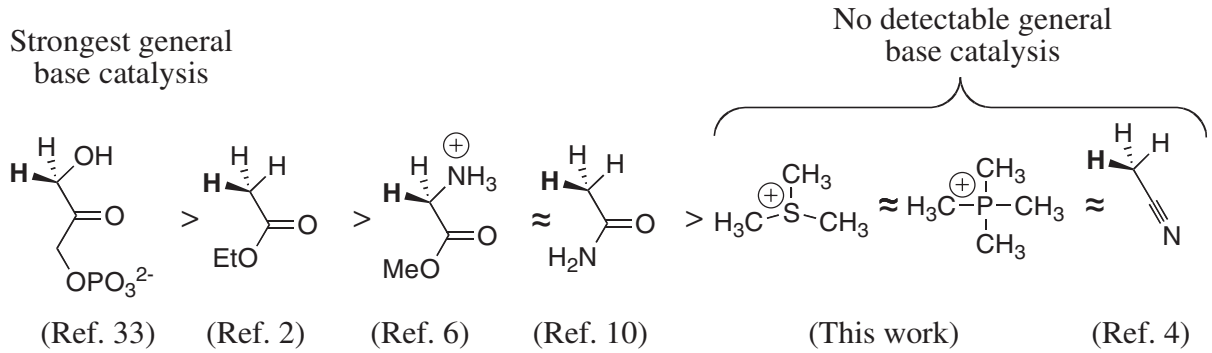
[j]Data for acetonitrile were taken from ref. 4.

[k]Data for dimethylacetamide were taken from ref. 10.

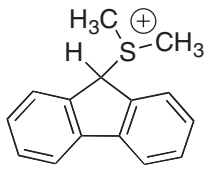
Scheme 2.



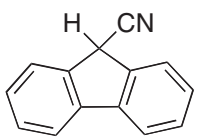
Scheme 3.



to place a molecule of D_2O in a position to deliver a labeled hydron to the carbanion is rate-determining, because it is not possible for the buffer catalyst to increase the rate of solvent reorganization. Therefore, the observation that there is no buffer catalysis of carbon deprotonation either of cyanoalkanes (4) or of **Me_4P^+** and **Me_3S^+** (this work) is consistent with a common rate-determining step of solvent reorganization (k_{reorg}, Scheme 2) for these three proton transfer reactions.



1



2

© 2005 NRC Canada

(2) There are similar intrinsic rate constants at $\Delta pK_a = 0$ of $k_o \approx 10^4$ (mol/L)$^{-1}$ s^{-1} for deprotonation of the dimethyl-9-fluorenylsulfonium ion (**1**) by primary amines in water–DMSO (95:5) (20) and $k_o \approx 10^{3.6}$ (mol/L)$^{-1}$ s^{-1} for deprotonation of 9-cyanofluorene (**2**) in water–DMSO (90:10) (18). This shows that the α-SMe_2^+ and α-CN substituents have similar effects on the Marcus intrinsic barrier for proton transfer at carbon. The rate constants $k_{DO} = 2.7 \times 10^{-4}$ (mol/L)$^{-1}$ s^{-1} for deprotonation of acetonitrile (4) and $k_{DO} = 7.5 \times 10^{-4}$ (mol/L)$^{-1}$ s^{-1} for deprotonation of **Me_3S^+** (this work) are also similar. The reactions, which proceed with similar rate constants and Marcus intrinsic barriers, also have a similar thermodynamic drive force (12, 36, 37). Therefore, if $k_{-p} > k_{reorg} \approx 10^{11}$ s^{-1} for deprotonation of CH_3CN, as proposed in earlier work (4, 34), then the same relationship must hold for deprotonation of **Me_3S^+**. We are not aware of any data that would allow us to estimate the effect of an α-PMe_3^+ substituent on the intrinsic barrier to deprotonation of carbon.

Carbon acid pK_as

Table 2 gives the carbon acid pK_as for deprotonation of **Me_4P^+** and **Me_3S^+** in water obtained in this work. These pK_as were calculated using eq. [6] derived from Scheme 4 where k_{HO} is the second-order rate constant for deprotonation of the carbon acid by hydroxide ion in H_2O (Table 2), $k_{HOH} = k_{reorg} = 10^{11}$ s^{-1} is the first-order rate constant for protonation of the carbanion zwitterion by solvent water (4, 10, 11, 34), and $K_w = 10^{-14}$ (mol/L)^2 is the ion product of water.

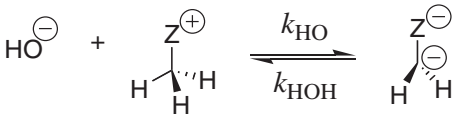
$$[6] \qquad pK_a = pK_w + \log\left(\frac{k_{HOH}}{k_{HO}}\right)$$

The values of k_{HO} (Table 2) were calculated from the corresponding rate constants for deprotonation of the carbon acids by deuterioxide ion (Table 1) using the relationship $k_{HO} = k_{DO}/2.4$ where 2.4 is the maximum secondary solvent deuterium isotope effect on the reactivity of lyoxide ion (38). This is appropriate because almost the entire difference in the basicity of deuterioxide and hydroxide ions will be expressed in the transition state for carbanion formation when solvent reorganization is rate-determining for exchange (4). The principle of microscopic reversibility requires that the reverse protonation of these carbanion zwitterions by solvent water is also limited mainly by solvent reorganization, with a rate constant on the order of that for the dielectric relaxation of water, $k_{HOH} = k_{reorg} = 10^{11}$ s^{-1} (39–41).

The greater carbon acidity of **Me_3S^+** and **Me_4P^+** than of **Me_4N^+** (Table 1) is well-known (14). It represents the greater stabilization of sulfur and phosphorus than of nitrogen ylides from polarization of charge by the larger third-row atoms and, possibly, by hyperconjugation (15, 16) and back-bonding from carbon to the d orbitals of sulfur and phosphorus (17).

We are not able to account for the difference between the reported pK_as of 28.5 (Table 2) and 18.2 (42) for deprotonation of **Me_3S^+** in water and DMSO, respectively. The change from DMSO to water causes a large decrease in pK_a when the conjugate base of the acid is a strong hydrogen bond acceptor (42), and this solvent effect on pK_a becomes less with decreasing stabilization of the conjugate base by hydrogen bonding to water. However, a substantially lower pK_a for **Me_3S^+** in the organic solvent DMSO than in water would require an unprecedented preferential solvation of the products of proton transfer by DMSO. The pK_a of 18.2 for deprotonation of **Me_3S^+** in DMSO is also inconsistent with the pK_a of 17.8 for deprotonation of the benzylic carbon of **$Me_2(PhCH_2)S^+$** in DMSO (24) because the α-phenyl substituent should result in a substantial increase in carbon acidity. We note that the pK_a of 18.2 for **Me_3S^+** in DMSO was reported in a Table in a review article (42), but to the best of our knowledge, it has not been further documented.

Scheme 4.



Substituent effects on carbon acidity

Computational studies provide evidence for formal resonance delocalization of negative charge onto nitrogen at the cyanomethyl carbanion (43). However, it is not clear whether this delocalization of charge results in a large stabilization of this carbanion. For example, delocalization of negative charge at the acetate anion provides a simple explanation for the relatively high acidity of acetic acid. However, it has been proposed that this high acidity is largely due to inductive stabilization of negative charge by the electron-withdrawing carbonyl group (44). The following observations provide evidence that there is significant stabilization of the cyanomethyl carbanion by both polar and resonance interactions between the negative charge and the α-CN group.

(1) The polar effect of a cationic α-substituent on carbanion stability must be larger than the polar effect of the neutral α-cyano group, where the interaction is between the formal negative charge of the carbanion and the *partial* positive charge of the cyano dipole. Therefore, the essentially identical values of pK_a = 28.9 for acetonitrile (4) and pK_a = 29.0 for a *single methyl* group of **Me_3S^+** (Table 2) show that there is sufficient resonance stabilization of the cyanomethyl carbanion to balance the greater stabilization of the sulfur ylide from polarization and back-bonding effects.

(2) The Hammett substituent constants σ = 0.82 for *p*-NMe_3^+ and σ = 0.66 for *p*-CN (45) show that a *p*-NMe_3^+ substituent provides a larger stabilization of negative charge than does a *p*-CN substituent when the interaction occurs across a benzene ring. By comparison, the observation that pK_a = 28.9 for acetonitrile is much lower than pK_a > 33.4 for a *single methyl* group of **Me_4N^+** (Table 2) shows that an α-CN substituent provides a substantially larger stabilization of negative charge at a neighboring carbon than does an α-NMe_3^+ group. This shows that there is sufficient resonance stabilization of the cyanomethyl carbanion to balance the greater polar stabilization of the nitrogen ylide.

© 2005 NRC Canada

It is interesting that no large intrinsic barrier to proton transfer arises from the requirement for the movement of negative charge from nitrogen to carbon on moving to the transition state for protonation of α-cyano carbanions (4, 12, 46, 47). As discussed earlier (4), the proton transfer to α-cyano carbanions resembles proton transfer to acetate anion (48) in that the requirement for localization of negative charge at the reacting basic atom (carbon or oxygen) proceeding to the transition state does not result in a large intrinsic barrier for proton transfer.

The α-fluorenyl group at the dimethyl-9-fluorenylsulfonium ion (**1**, pK_a = 13.7 in water–DMSO (95:5) (20)) causes a 16-unit decrease in the statistically corrected pK_a of 29.5 for a *single proton* of $\mathbf{Me_3S^+}$, while the α-fluorenyl group at 9-cyanofluorene (**2**, pK_a = 10.7 in water–DMSO (90:10) (18)) causes a larger 19-unit decrease in the statistically corrected pK_a of 29.4 for a *single proton* of acetonitrile. This shows that the addition of an α-fluorenyl group results in a larger attenuation of the α-SMe_2^+ than of the α-CN substituent effect on carbon acidity. We suggest that this reflects the particularly sharp falloff ($1/r^4$) in the stabilization of negative charge by polarization onto a atom with increasing radius of separation of the interacting centers (45).

Acknowledgement

We acknowledge the National Institutes of Health (GM 39754) for generous support of this work.

References

1. T.L. Amyes and J.P. Richard. J. Am. Chem. Soc. **114**, 10297 (1992).
2. T.L. Amyes and J.P. Richard. J. Am. Chem. Soc. **118**, 3129 (1996).
3. R.W. Nagorski, T. Mizerski, and J.P. Richard. J. Am. Chem. Soc. **117**, 4718 (1995).
4. J.P. Richard, G. Williams, and J. Gao. J. Am. Chem. Soc. **121**, 715 (1999).
5. A. Rios and J.P. Richard. J. Am. Chem. Soc. **119**, 8375 (1997).
6. A. Rios, T.L. Amyes, and J.P. Richard. J. Am. Chem. Soc. **122**, 9373 (2000).
7. Y. Chiang, A.G. Griesbeck, H. Heckroth, B. Hellrung, A.J. Kresge, Q. Meng, A.C. O'Donoghue, J.P. Richard, and J. Wirz. J. Am. Chem. Soc. **123**, 8979 (2001).
8. A. Rios, J. Crugeiras, T.L. Amyes, and J.P. Richard. J. Am. Chem. Soc. **123**, 7949 (2001).
9. A. Rios, J.P. Richard, and T.L. Amyes. J. Am. Chem. Soc. **124**, 8251 (2002).
10. J.P. Richard, G. Williams, A.C. O'Donoghue, and T.L. Amyes. J. Am. Chem. Soc. **124**, 2957 (2002).
11. T.L. Amyes, S.T. Diver, J.P. Richard, F.M. Rivas, and K. Toth. J. Am. Chem. Soc. **126**, 4366 (2004).
12. J.P. Richard, T.L. Amyes, and M.M. Toteva. Acc. Chem. Res. **34**, 981 (2001).
13. A. Streitwieser, M.R. Granger, F. Mares, and R.A. Wolf. J. Am. Chem. Soc. **95**, 4257 (1973).
14. W.v.E. Doering and A.K. Hoffmann. J. Am. Chem. Soc. **77**, 521 (1955).
15. R.K. Bansal, N. Gupta, S. Singh, K. Karaghiosoff, P. Mayer, and M. Vogt. Tetrahedron Lett. **45**, 7771 (2004).
16. J.F. King, R. Rathore, Z. Guo, M. Li, and N. Payne. J. Am. Chem. Soc. **122**, 10 308 (2000).
17. D.A. Dixon, T.H. Dunning, R.A. Eades, and P.G. Gassman. J. Am. Chem. Soc. **105**, 7011 (1983).
18. C.F. Bernasconi and F. Terrier. J. Am. Chem. Soc. **109**, 7115 (1987).
19. C.J. Murray and W.P. Jencks. J. Am. Chem. Soc. **110**, 7561 (1988).
20. C.J. Murray and W.P. Jencks. J. Am. Chem. Soc. **112**, 1880 (1990).
21. N.H. Werstiuk and S. Banerjee. J. Org. Chem. **46**, 470 (1981).
22. G. Barbarella, A. Garbesi, and A. Fava. Helv. Chim. Acta, **54**, 253 (1971).
23. V. Cere, C. Paolucci, S. Pollicino, E. Sandri, and A. Fava. Tetrahedron Lett. **24**, 839 (1983).
24. J.-P. Cheng, B. Liu, Y. Zhao, Y. Sun, X.-M. Zhang, and Y. Lu. J. Org. Chem. **64**, 604 (1999).
25. O. Hofer and E.L. Eliel. J. Am. Chem. Soc. **95**, 8045 (1973).
26. O.T. Magnusson and P.A. Frey. Bioorg. Chem. **30**, 53 (2002).
27. X.-M. Zhang and F.C. Bordwell. J. Am. Chem. Soc. **116**, 968 (1994).
28. A.-P. Bettencourt, A.M. Freitas, M.I. Montenegro, M.F. Nielsen, and J.H.P. Utley. J. Chem. Soc. Perkin Trans. 2, 515 (1998).
29. P.K. Glasoe and F.A. Long. J. Phys. Chem. **64**, 188 (1960).
30. A.K. Covington, R.A. Robinson, and R.G. Bates. J. Phys. Chem. **70**, 3820 (1966).
31. C.J. Halkides, P.A. Frey, and J.B. Tobin. J. Am. Chem. Soc. **115**, 3332 (1993).
32. R.W. Nagorski and J.P. Richard. J. Am. Chem. Soc. **118**, 7432 (1996).
33. J.P. Richard and R.W. Nagorski. J. Am. Chem. Soc. **121**, 4763 (1999).
34. J.C. Fishbein and W.P. Jencks. J. Am. Chem. Soc. **110**, 5087 (1988).
35. J.P. Richard. J. Am. Chem. Soc. **106**, 4926 (1984).
36. R.A. Marcus. J. Phys. Chem. **72**, 891 (1968).
37. A.J. Kresge. Chem. Soc. Rev. **2**, 475 (1973).
38. A.J. Kresge, R.A. More O'Ferrall, and M.F. Powell. *In* Isotopes in organic chemistry. Vol. 7. *Edited by* E. Buncel and C.C. Lee. Elsevier, New York. 1987.
39. K. Giese, U. Kaatze, and R. Pottel. J. Phys. Chem. **74**, 3718 (1970).
40. U. Kaatze. J. Chem. Eng. Data, **34**, 371 (1989).
41. U. Kaatze, R. Pottel, and A. Schumacher. J. Phys. Chem. **96**, 6017 (1992).
42. F.G. Bordwell. Acc. Chem. Res. **21**, 456 (1988).
43. K.B. Wiberg and H. Castejon. J. Org. Chem. **60**, 6327 (1995).
44. M.R.F. Siggel, A. Streitwieser, and T.D. Thomas. J. Am. Chem. Soc. **110**, 8022 (1988).
45. J. Hine. Structural effects on equilibria in organic chemistry. Wiley, New York. 1975.
46. C.F. Bernasconi. Acc. Chem. Res. **20**, 301 (1987).
47. F. Hibbert, F.A. Long, and E.A. Walters. J. Am. Chem. Soc. **93**, 2829 (1971).
48. M. Eigen. Angew. Chem. Int. Ed. Engl. **3**, 1 (1964).

© 2005 NRC Canada

Synthesis of novel sulfonyl-stabilized phosphorus ylides, and the kinetics and mechanism of their conventional and flash vacuum pyrolysis reactions[1]

Rasha F. Al-Bashir, Nouria A. Al-Awadi, and Osman M.E. El-Dusouqui

Abstract: Nine substituted sulfonyl-stabilized phosphorus ylides were prepared by treating their intermediate ylide analogues with phenylmethanesulfonyl fluoride. The stoichiometric ratio of the reactants for each preparation needed to be adjusted according to the basicity of each ylide intermediate. The nine ylide compounds were then subjected to conventional (sealed-tube) gas-phase pyrolysis at 470–545 K. The pyrolytic reactions were homogeneous and obeyed a first-order rate equation. The values of the Arrhenius log A (s^{-1}) and E_a (kJ mol^{-1}) obtained for these reactions averaged 11.12 ± 2.00 and 131.8 ± 24.4, respectively. Analysis of the pyrolysates from conventional pyrolysis and from flash vacuum pyrolysis at 600 K showed the products to be complex mixtures of triphenylphosphine, triphenylphosphine oxide, triphenylphosphine sulfide, and symmetric and unsymmetric alkenes. Conventional pyrolysis also gave novel mixed sulfones and, for the *p*-methoxyaryl substituent, *p*-anisaldehyde. The products of the reactions under study are explained on the basis of a mechanism involving a sulfonyl carbene intermediate, and the reaction mechanism is used to rationalize the kinetic results and molecular reactivities.

Key words: ylides, synthesis, pyrolysis, kinetics, mechanism.

Résumé : La réaction d'analogues d'ylures intermédiaires avec le fluorure de phénylméthanesulfonyle a permis de préparer neuf ylures de phosphores substitués, stabilisés par un groupe sulfonyle. Le rapport stoechiométrique des réactifs nécessaires pour chacune des préparations a été ajusté en fonction de la basicité de chaque ylure intermédiaire. On a ensuite soumis chacun des neuf ylures à une pyrolyse à phase gazeuse, en tube scellé, à des températures allant de 470 à 545 K. Les réactions pyrolytiques sont homogènes et obéissent à une équation de vitesse du premier ordre. Les valeurs moyennes pour les paramètres d'Arrhenius, log A (s^{-1}) et E_a (kJ mol^{-1}), obtenues pour ces réactions sont respectivement de 11,12 ± 2,00 et de 131,8 ± 24,4. L'analyse des produits de pyrolyse conventionnelle et de pyrolyse éclair sous vide à 600 K montrent que les produits correspondent à des mélanges complexes comprenant de la triphénylphosphine, de l'oxyde de triphénylphosphine, de sulfure de triphénylphosphine ainsi que des alcènes symétriques et non symétriques. La pyrolyse conventionnelle conduit aussi à de nouvelles sulfones mixtes et, dans le cas du substituant *p*-méthoxyaryle, à du *p*-anisaldéhyde. Les produits des réactions obtenus dans cette étude sont expliqués sur la base d'un mécanisme impliquant un intermédiaire sulfonylcarbène et on utilise le mécanisme réactionnel pour rationaliser les résultats cinétiques et les réactivités molaires.

Mots clés : ylures, synthèse, pyrolyse, cinétique, mécanisme.

[Traduit par la Rédaction]

Introduction

Reports on the synthesis of sulfonyl-stabilized phosphorus ylides suggest two formal steps in the preparation: first, a base, butyl lithium (BuLi), reacts with the appropriate quaternary phosphonium halide salt (QS) in a nitrogen atmosphere to give an intermediate ylide, which then proceeds to react with the designated sulfonyl fluoride (RSO_2F) to form the target ylide (1–4). In the present study, this procedure was found, however, not to be uniform and straightforward, as the stoichiometric ratio of the reactants (QS:BuLi:RSO_2F) needed to be adjusted according to the basic strength of the ylide intermediate formed in the first step. Besides, it has been noted that α-sulfonyl ylides cannot be prepared by treatment of the intermediate ylides with sulfonyl chloride derivatives, since this procedure results in the formation of α-chloro ylides instead of the target sulfonyl-stabilized phosphorus ylides (4). Hence, sulfonyl fluorides were used instead.

Aitken et al. (1) have shown that flash vacuum pyrolysis at 600 K of sulfonyl-stabilized phosphorus ylides gave Ph_3P, Ph_3PO, Ph_3PS, and alkenes (either symmetric or unsymmetric). These products are consistent with the formation of

Received 9 May 1005. Published on the NRC Research Press Web site at http://canjchem.nrc.ca on 25 November 2005.

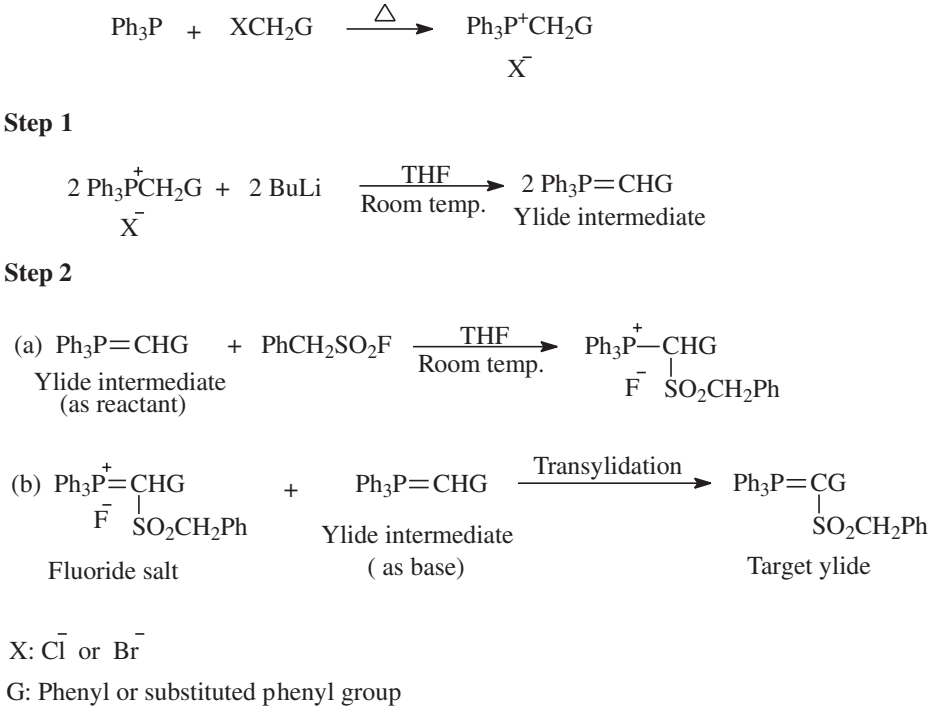
R.F. Al-Bashir, N.A. Al-Awadi,[2] and O.M.E. El-Dusouqui. Department of Chemistry, University of Kuwait, P.O. Box 5969, Safat 13060, Kuwait.

[1]This article is part of a Special Issue dedicated to organic reaction mechanisms.

[2]Corresponding author (e-mail: nouria@kuc01.kuniv.edu.kw).

 doi: 10.1139/V05-210 © 2005 NRC Canada

Scheme 1. Reaction pathway for ylides **3**–**9**.



a sulfonyl carbene intermediate. The phosphorus oxides and sulfides can be accounted for by the separate extrusion of Ph_3P and SO_2, which then partly combine to give Ph_3PO and Ph_3PS, and the validity of this was confirmed by control experiments (1). The sulfonyl-stabilized ylides were obtained as stable, high-melting solids with characteristic spectral data including diagnostic ^{31}P NMR signals at δ 16.9–21.7 ppm. Here, we report the results of a study on the kinetics and reaction product of thermolysis of nine substituted sulfonyl-stabilized phosphorus ylides using conventional (sealed-tube (ST); static) pyrolysis (CP), and compare the products of reaction with those from flash vacuum pyrolysis (FVP). The kinetic investigation also provides a novel insight into molecular reactivities and the effects of substituents on the pyrolysis of stabilized phosphorus ylides.

The nine ylide compounds under study are derivatives of [(benzylsulfonyl)methylene](triphenyl)phosphorane (Ph_3P=C(G)SO_2CH_2Ph) in which the substituent (G) is: *p*-CNC_6H_4 (**1**), *p*-$NO_2C_6H_4$ (**2**), *m*-$NO_2C_6H_4$ (**3**), *p*-ClC_6H_4 (**4**), *m*-ClC_6H_4 (**5**), C_6H_5 (**6**), *p*-$CH_3C_6H_4$ (**7**), *p*-$CH_3OC_6H_4$ (**8**), and CH_3 (**9**), respectively.

Results and discussion

Synthesis

Synthesis of ylides **3**–**9** according to literature procedures (1) required the ratio of the reactants, quaternary phosphonium halide salt ($Ph_3P^+CH_2GX^-$) : BuLi : phenylmethanesulfonyl fluoride ($PhCH_2SO_2F$), to be 2:2:1; as these reactions involve transylidation to regenerate one molecule of quaternary phosphonium fluoride salt (Scheme 1). In these cases, the basicity of the ylide intermediate formed in step 1 is high enough for it to act also as the base needed to abstract the proton from the quaternary phosphonium salt formed in step 2*a* to give the target ylide in transylidation step 2*b*. The electron-withdrawing substituents (CN and *p*-NO_2) of the phenyl group in ylides **1** and **2**, respectively, will decrease the protophilic character of the multiple bond of these ylides relative to that of ylides **3**–**9**, and so the amount of BuLi base had to be doubled to avoid formation of excess ylide intermediate and to provide the base required in step 2*b* (Scheme 2). Accordingly, the reactant ratio of quaternary phosphonium halide salt : BuLi : phenylmethanesulfonyl fluoride was adjusted to 1:2:1.

Attempts to synthesize ylide **1** (G = *p*-CNC_6H_4) using the ratio of 2:2:1 failed to give any ylide product. Besides, it is of interest to note that the reactant ratio of 1:2:1, which gave ylide **2** (G = *p*-$NO_2C_6H_4$) in 72% yield, failed to give ylide **3** (G = *m*-$NO_2C_6H_4$), which, however, was obtained in 65% yield when the reactant ratio of 2:2:1 was used instead; this same ratio was also used for ylides **3**–**9**. The present findings indicate that the basicity of the ylide intermediate obtained in the initial step of the reaction determines whether the intermediate ylide is basic enough to act as the proton scavenger in the transylidation reaction, or that the stronger BuLi base is needed to complete the reaction. The stoichiomeric ratio of the reactants as well as the % yield of the target ylides correlate well with the expected relative basicities of the intermediate ylides as judged by the electron-donating and electron-withdrawing effect of the group in substituent G.

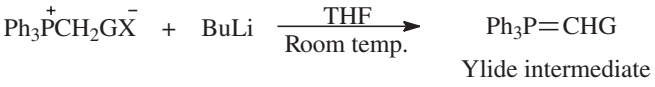
Pyrolysates and reaction mechanism

Reaction products for complete pyrolysis were obtained for all nine substrates (*i*) in a FVP (flow) reactor at 600 K, and (*ii*) in a sealed-tube pyrolyser (static method) at temperatures exceeding those used in the kinetic investigations. The static-method reactions (CP reaction) were allowed ample residence time to ensure maximum pyrolysis. The constituents of the pyrolysates obtained by this method were isolated

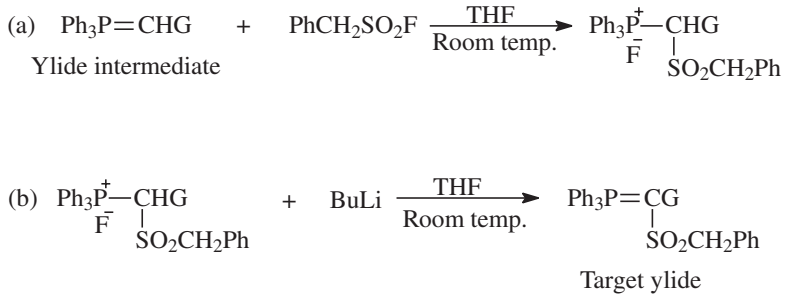
© 2005 NRC Canada

Scheme 2. Reaction pathway for ylides **1** and **2**.

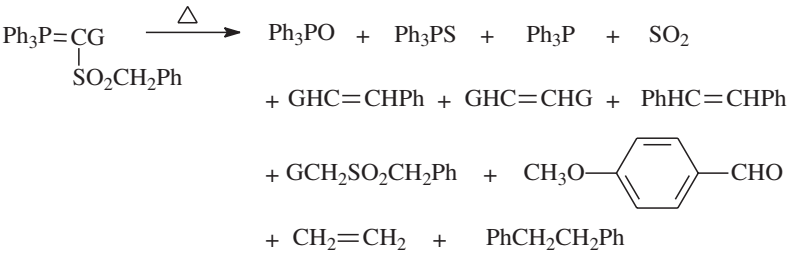
Step I



Step II



Scheme 3. Composition of the products of gas-phase pyrolysis of ylides **1**–**9**.



using preparative liquid chromatography (PLC) and analyzed using GC–MS, FT-IR, and ^{1}H NMR techniques. The pyrolysates from FVP were collected in a cold trap. FVP and CP gave identical products of Ph_3P, Ph_3PO, Ph_3PS, and alkenes (symmetric and unsymmetric) (Scheme 3). However, static pyrolysis of the ylides followed by PLC gave better separation and isolation profiles of alkenes, and allowed the identification of more reaction products, including *p*-anisaldehyde and mixed sulfones, which were not detected in the pyrolysates from FVP. It is noteworthy that the static (sealed-tube) method provides longer residence time for novel pyrolytic reaction pathways. Identification and characterization of the constituents of the pyrolysates are detailed in the Experimental section.

[(Benzylsulfonyl)(4-cyanophenyl)methylene](triphenyl)-phosphorane (ylide 1)

The analysis of the pyrolysates — separated as oils — showed 4-cynostilbene, which was separated in pure form on PLC. *trans*-Stilbene and novel *trans*-4,4′-dicyanostilbene were also isolated in a very pure state as well from a separate fraction. In a third fraction, (4-cyanobenzyl)benzyl sulfone identified for the first time in the present study, was isolated as a novel sulfone only by CP.

[(Benzylsulfonyl)(4-nitrophenyl)methylene](triphenyl)-phosphorane (ylide 2)

Analysis by ^{1}H NMR, IR, and MS showed a mixture of alkenes, namely, *trans*-4-nitrostilbene and *trans*-stilbene, both clearly identified. A major fraction, novel (4-nitrobenzyl)benzylsulfone, isolated by CP only, was properly characterized and identified.

[(Benzylsulfonyl)(3-nitrophenyl)methylene](triphenyl)-phosphorane (ylide 3)

The analysis of the products of reaction of this ylide showed a mixture of two alkenes: *trans*-3-nitrostilbene (major fraction) and *trans*-stilbene; the latter identified only through the static method. Besides, (3-nitrobenzyl)benzyl sulfone was isolated and clearly identified as a novel compound using the static pyrolysis technique.

[(Benzylsulfonyl)(4-chlorophenyl)methylene](triphenyl)-phosphorane (ylide 4)

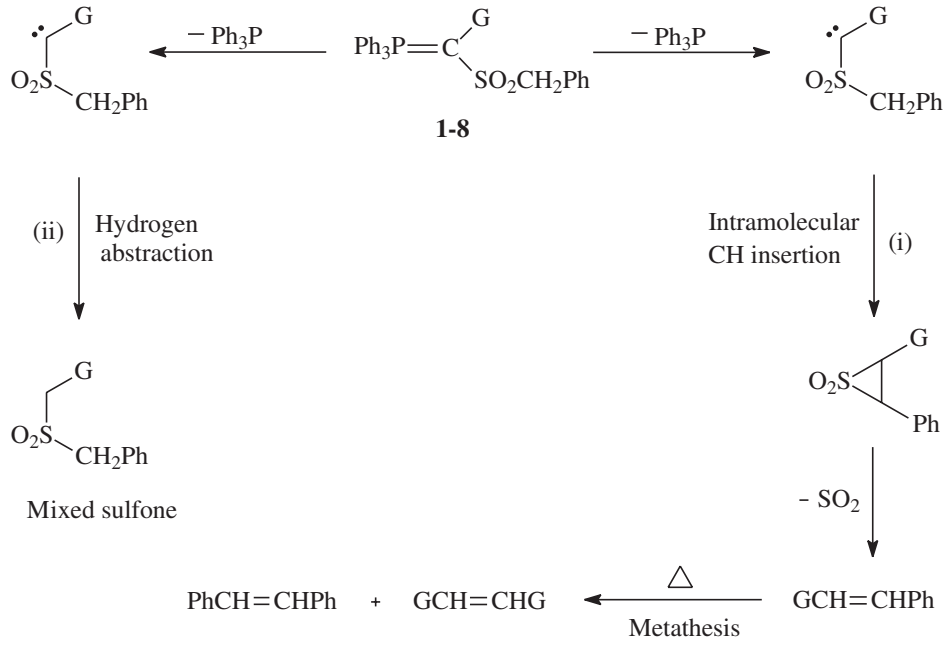
The spectral analysis (^{1}H NMR, IR, and MS) of the products proved the presence of 4,4′-dichlorostilbene, which was separated in a pure form by PLC. Both *trans*-4-chlorostilbene and *trans*-stilbene were present as well in small amounts. The ^{1}H NMR for *trans*-4-chlorostilbene in $CDCl_3$ showed signals (5) at δ 6.83 (1H, d, J = 16.4 Hz), 6.91 (1H, d, J = 16.4 Hz), 7.07–7.42 (9H, m). MS *m/z*: 216 (34% abundance) molecular ion, 215 (17%), 214 (100%) base peak, 179 (45%), 178 (59%). Novel (4-chlorobenzyl)benzyl sulfone obtained by the static technique was separated as a pure fraction on PLC.

[(Benzylsulfonyl)(3-chlorophenyl)methylene](triphenyl)phosphorane (ylide 5)

Reaction product separation on PLC showed 3-chlorostilbene, 3,3′-dichlorostilbene, and *trans*-stilbene. ^{1}H

© 2005 NRC Canada

Scheme 4. Generation and further reaction of the sulfonyl carbene intermediate of ylides **1**–**8**.



NMR for *trans*-3,3′-dichlorostilbene in $CDCl_3$ showed diagnostic signals (6) at δ 7.03 (2H, s), 7.32–7.42 (8H, m), and for *trans*-3-chlorostilbene (7) at δ 6.85 (1H, d, *J* = 16.5 Hz), 6.92 (1H, d, *J* = 16.5 Hz), 7.11–7.42 (9H, m). (3-Chlorobenzyl)benzyl sulfone was also isolated for the first time in this study using CP.

It is to be noted that FVP does not give the sulfone products.

Ylides 6, 7, and 9

The FVP at 600 K of these ylides has been studied before (1). In each case a mixture of Ph_3P, Ph_3PO, and Ph_3PS was produced together with various alkenes, exactly as observed in the present study for ylides **1**–**5**. Static pyrolysis of these ylides gave products identical to those obtained through FVP.

[(Benzylsulfonyl)(4-methoxyphenyl)methylene](triphenyl)-phosphorane (ylide 8)

The spectral analysis of the products by both FVP and the static method showed *trans*-methoxystilbene; δ_H ($CDCl_3$) (6): 4.01 (3H, s), 6.88 (2H, d, *J* = 8.5 Hz), 6.98 (1H, d, *J* = 16.3 Hz), 7.08 (1H, d, *J* = 16.3 Hz), 7.10–7.55 (m, 7H). MS *m*/*z*: 210 ($M^{+\cdot}$, 22% abundance) molecular ion, 209 (100%) base peak, and fragment ions at 194 (12%), 195 (6%), 165 (33%), 166 (10%), 152 (6%), 135 (16%), 121 (33%).

In a separate fraction, *trans*-4,4′-dimethoxystilbene was identified; δ_H ($CDCl_3$) (8): 3.86 (6H, s), 6.91 (4H, d, *J* = 6.85 Hz), 6.95 (2H, s), 7.45 (4H, d, *J* = 6.85 Hz). MS *m*/*z*: 240 ($M^{+\cdot}$, 100%), molecular ion and base peak, fragment ions (9) at 226 (18%), 225 (49%), 165 (45%), 153 (28%), 152 (32%), 120 (12%). Besides, *trans*-stilbene was also isolated in a third fraction, but the sulfone fraction could not be identified even on using CP. Instead, 4-methoxybenzyaldehyde (*p*-anisaldehyde) was isolated in a very pure state.

According to these results, the composition of the products of the gas-phase pyrolysis of the substituted sulfonyl-stabilized ylides (**1**–**9**) was as shown in Scheme 3. Based on the overall pyrolysate composition, a feasible reaction mechanism is proposed to account for the product of the gas-phase pyrolytic reaction of the sulfonyl-stabilized phosphorus ylides (**1**–**9**) under study. The mechanism involves the formation and further reaction of a sulfonyl carbene intermediate (1).

In the case of ylides **1**–**8** (Scheme 4): (*i*) The carbene intermediate obtained reacts by an intramolecular CH insertion process to give thiirane dioxide, followed by loss of SO_2, alkene metathesis, and the partial reaction of Ph_3P with SO_2 to give Ph_3PO and Ph_3PS; (*ii*) the carbene intermediate abstracts hydrogen in a novel reaction, observed only in pyrolysis by the static method of ylides **1**–**5** (all with an electron-withdrawing group in substituent G), to give mixed sulfones (Scheme 4). It is to be noted that for ylide **6** (G = Ph) and ylides **7** and **8** (electron-donating groups in G) no such sulfone products were detected in the pyrolysates. The formation of 4-methoxybenzaldehyde (*p*-anisaldehyde) by ylide **8** involves a novel route in which the carbene centre seems to abstract O and H possibly through a free radical pathway to give the aldehyde. An earlier study on the pyrolysis of arylsulphonyl-stabilized phosphorus ylides reports aldehyde formation for substrates in which the aryl substituent is an *o*-methoxyphenyl group (1).

When G = CH_3 (ylide **9**), literature reports (1, 3) suggest two pathways (Scheme 5) for the reaction of the sulfonyl carbene intermediates.

Kinetic analysis

The kinetic data of the pyrolytic gas-phase elimination reactions of the nine ylides (**1**–**9**) under study are given in Table 1. Each rate constant at any given temperature represents an average from a set of three values obtained in three separate kinetic runs conducted at the same temperature. The agreement among the values of the rate constant in each set is within ±2%. Each kinetic run was monitored until 90%–95% of the reaction was completed, and the range of 44 ±

© 2005 NRC Canada

Scheme 5. Reaction pathway of ylide **9**.

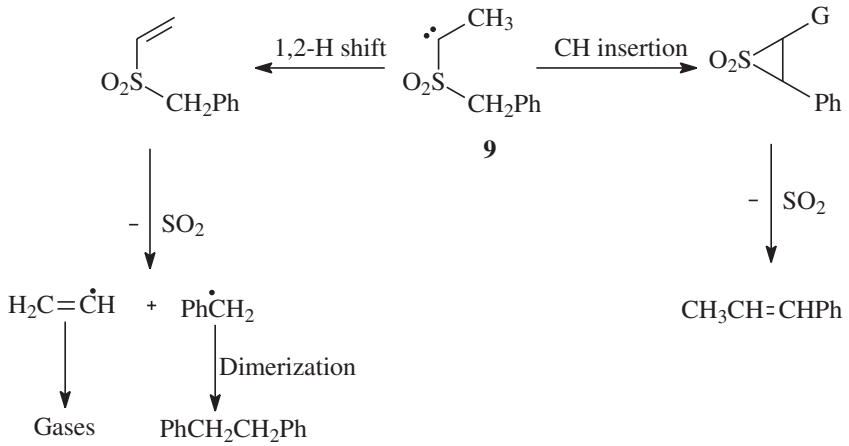


Table 1. Rate constants (k, s^{-1}), Arrhenius log A and E_a, entropies of activation ($\Delta S^{\ddagger}$), and rate constants at 500 K of the gas-phase pyrolysis of sulfonyl-stabilized phosphorus ylides (**1**–**9**).

Ylide	G	T (K)	10^4k (s^{-1})	log A (s^{-1})	E_a (kJ mol^{-1})	$10^4k_{500\ K}$ (s^{-1})	$\Delta S^{\ddagger}_{500\ K}$ (J K^{-1} mol^{-1})
1	*p*-CNC_6H_4	495.4	2.899	10.11±0.26	129.4±2.51	3.93	–55.62
		502.4	4.737				
		515.0	9.194				
		520.4	13.53				
		526.2	18.87				
		533.2	27.08				
2	*p*-$NO_2C_6H_4$	487.0	2.368	13.12±0.25	156.1±2.43	6.41	+1.895
		494.8	4.313				
		502.4	8.705				
		509.4	13.19				
		516.6	20.00				
		529.4	53.36				
3	*m*-$NO_2C_6H_4$	492.4	3.939	8.63±0.08	113.4±0.79	6.11	–84.10
		499.2	5.745				
		507.0	8.680				
		513.8	12.50				
		520.6	17.90				
		527.8	25.72				
		534.8	34.74				
4	*p*-ClC_6H_4	494.8	2.748	8.65±0.18	115.6±1.84	3.78	–83.64
		502.6	4.502				
		509.7	6.269				
		523.4	13.62				
		538.2	26.17				
		544.8	37.59				
5	*m*-ClC_6H_4	494.2	2.122	7.67±0.15	107.4±1.55	2.88	–102.3
		506.2	3.942				
		515.6	6.116				
		522.5	9.016				
		530.0	12.92				
		536.2	15.91				
		543.7	22.88				
6	C_6H_5	500.8	5.527	9.75±0.06	124.7±0.63	5.32	–62.61
		508.4	8.917				
		516.2	13.39				
		524.2	21.17				

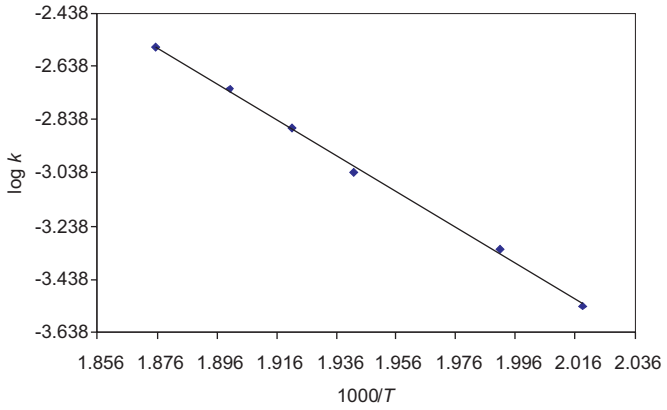
© 2005 NRC Canada

Table 1 (*concluded*).

Ylide	G	T (K)	10^4k (s^{-1})	log A (s^{-1})	E_a (kJ mol^{-1})	$10^4k_{500\ K}$ (s^{-1})	$\Delta S^{\ddagger}_{500\ K}$ (J K^{-1} mol^{-1})
		531.4	31.64				
		539.0	46.49				
		545.2	63.72				
7	*p*-$CH_3C_6H_4$	479.2	3.656	9.13±0.14	115.3±1.34	12.0	–74.54
		493.8	8.356				
		501.6	12.74				
		509.4	20.14				
		524.0	43.28				
8	*p*-$CH_3OC_6H_4$	475.0	2.190	11.53±0.34	134.0±3.26	12.5	–28.53
		483.0	3.882				
		491.6	6.849				
		498.2	10.95				
		505.0	19.03				
		512.2	25.11				
		520.4	47.33				
9	CH_3	470.4	3.194	8.43±0.14	107.4±1.25	16.2×10^{-4}	–87.95
		476.4	4.366				
		483.6	6.871				
		490.4	9.945				
		497.2	14.14				
		504.4	20.54				
		511.8	28.52				

6 K over which the reactions were followed is in accord with the temperature range deemed necessary for reliable kinetic analysis of thermal gas-phase elimination reactions (10, 11). Arrhenius parameters were obtained using the results from Table 1. The Arrhenius plots were linear over the studied temperature and reaction range, with correlation coefficients of the order of 0.990 ± 0.009. A representative plot is given in Fig. 1 for [(benzylsulphonyl)(4-cyanophenyl)methylene](triphenyl)phosphorane (ylide **1**), with a correlation coefficient of 0.999. Arrhenius log A (s^{-1}), $\Delta S^{\ddagger}$ (J K^{-1} mol^{-1}), the energy of activation (E_a, kJ mol^{-1}), and the first-order rate constants (k, s^{-1}) of the pyrolysis reactions at 500 K are recorded in Table 1. The values for $\Delta S^{\ddagger}$ (J K^{-1} mol^{-1}) are negative or small (positive) suggesting higher structural organization and the formation of an ordered transition state.

Fig. 1. Arrhenius plot for the pyrolysis of ylide **1**.



Molecular reactivities and substituent effects

The first-order rate constants at 500 K of the gas-phase pyrolytic reactions of ylides **1**–**9** and the rate constant ratio (relative rate, k_{rel}) of the ylides are summarized in Table 2.

The main features of the kinetic results are as follows:

1. The rate of pyrolysis of ylide **9**, where G = CH_3, is ca. 3 times faster than the rate of pyrolysis of ylide **6**, where G = C_6H_5; this represents the highiest increment in reactivity in the series of ylides under consideration and is attributed to the fact that the reactive carbene intermediate of ylide **9** can react either by 1,3-H insertion or 1,2-H insertion followed by the elimination of SO_2. The pyrolysates 1-phenylpropene and dibenzyl prove the possibility of both modes of insertion, where G is the aromatic phenyl group, the carbene intermediate can react only by 1,3-insertion.
2. Introducing *p*-methyl and *p*-methoxy groups into the aromatic ring ylides **7** and **8** respectively, has increased the rate of pyrolysis by almost 2.3 times for both ylides; this could be explained in terms of the electron-donating nature of these substituents and their influence on the carbene intermediate suggested (Schemes 4 and 5).
3. When electron-withdrawing substituents (*p*-Cl, *m*-Cl, and *p*-CN) were introduced into ylides **4**, **5**, and **7**, respectively, the reactivity was reduced; this indicates that these substituents destabilize the carbene intermediate.
4. Introducing the nitro group at the *para* and *meta* positions of ylides **3** and **4**, respectively, resulted in no change on the reactivity compared to ylide **6** (G = C_6H_5); this unique behaviour of the nitro group in the gas-phase thermal elimination reactions of organic compounds has been reported in other studies (12).

© 2005 NRC Canada

Table 2. Rate constants (k, s^{-1}) at 500 K and the rate constant ratio (relative rate, k_{rel}) of the pyrolysis of sulfonyl-stabilized phosphorus ylides (**1**–**9**).

Ylide	G	10^4 k (s^{-1})	k_{rel}
1	*p*-CNC_6H_4	3.926	0.738
2	*p*-$NO_2C_6H_4$	6.406	1.20
3	*m*-$NO_2C_6H_4$	6.109	1.15
4	*p*-ClC_6H_4	3.782	0.711
5	*m*-ClC_6H_4	2.881	0.542
6	C_6H_5	5.317	1.00
7	*p*-$CH_3C_6H_4$	12.00	2.26
8	*p*-$CH_3OC_6H_4$	12.48	2.35
9	CH_3	16.17	3.04

5. It is important to note that these sulfonyl carbene intermediates are already stabilized by conjugative interaction with the sulfonyl group (Scheme 6), and this might be the reason behind the relatively small substituent effects obtained.

These features of the kinetic results support the reaction pathways suggested and that the formation of the carbene intermediate is the rate-controlling step.

Experimental

Materials, techniques, and instrumentation

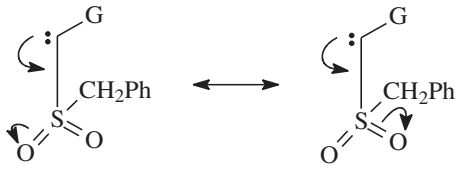
The required quaternary phosphonium salts were prepared by the reaction of the appropriate alkyl halide with triphenylphosphine in boiling toluene. The phenylmethanesulfonyl fluoride, BuLi, and dry THF are commercially available from Aldrich. Further drying of THF was made by distillation from potassium benzophenone ketyl under N_2. The ylides and the constituents of their pyrolysates were characterized using GC–MS, FT-IR, ^{1}H NMR, ^{13}C NMR, and ^{31}P NMR spectroscopy. Instrumentation included a Finnigan Mat INCOSXL for GC–MS studies, a PerkinElmer 2000 spectrometer for FT-IR, and a Bruker DPX 400 spectrometer for the NMR analysis. Kinetic runs and pyrolysates preparation for reaction product analysis using a sealed-tube pyrolyser (conventional static pyrolysis) were conducted in a Chemical Data System (CDS) custom-made pyrolyzer comprising an insulated aluminum block fitted with a platinum-resistance thermometer and thermocouple connected to a Comark microprocessor thermometer. The temperature of the aluminum block was controlled by a digital Eurotherm 093 precision temperature regulator. Aluminum was chosen for its low temperature gradient and resistance to elevated temperatures. HPLC analysis of kinetic runs was carried out on a Waters prope (pump model 515 and UV detector model 2487).

FVP was conducted in a fused-quartz tube, which was housed in a sublimation oven. The latter was connected to a hot zone pyrolyzer under low pressure ending with a U-shaped trap cooled in liquid nitrogen.

Synthesis and characterization of ylides (1–9)

The details of the synthesis of the novel sulfonyl-stabilized ylides **1** and **3**–**5** are given in the following, while ylides **2** and **6**–**9** were prepared following literature procedures (1, 3). The general procedure A for the synthesis of ylides **1** and **2**, and procedure B for the preparation of ylides **3**–**9** are described hereafter.

Scheme 6. Carbene intermediate stabilization by conjugative interaction with sulfonyl groups.



Synthesis

Procedure A

In the synthesis of ylides **1** and **2**, a solution of 1.6 mol/L BuLi in hexane (7.5 mmol) was slowly added from a syringe to a stirred suspension of the corresponding quaternary phosphonium salt (7.5 mmol) in dry THF (50 mL) at room temperature under nitrogen. The mixture was stirred for about 1 h, and then an equivalent amount of phenylmethanesulfonyl fluoride (7.5 mmol) in dry THF (ca. 5 mL) was added all at once. The reaction mixture was stirred further for 5 h, followed by the addition of another portion of BuLi in hexane (7.5 mmol). The crude material was dissolved in dichloromethane (100 mL), washed with water (3 × 75 mL), dried, and concentrated under vacuum. The residual oil was triturated with a suitable solvent to obtain the pure ylide.

Procedure B

For the preparation of ylides **3**–**9**, a suspension of the appropriate quaternary phosphonium salt (15 mmol) in dry THF (100 mL) was stirred at room temperature under nitrogen while a solution of 1.6 mol/L BuLi in hexane (15.6 mmol) was slowly added from a syringe. The mixture was stirred further for about 1 h, and then a solution of phenylmethanesulfonyl fluoride (7.5 mmol) in dry THF (10 mL) was added dropwise to the ylide solution. The mixture was kept stirring overnight, and the reaction mixture was then filtered and the filtrate was evaporated. The residue was dissolved in dichloromethane (150 mL) and washed with water (3 × 75 mL), dried and the solvent evaporated (1, 3).

A problem encountered in the preparation of stabilized ylides in general, and in the synthesis of the present ylides, they were often difficult to crystallize in pure form from the oils obtained following the evaporation step. Since the products hydrolyzed when chromatography was attempted, and decomposed on sublimation, the safer option was their trituration with suitable solvents to obtain the pure ylides (13).

Characterization

Ylides **2** and **6**–**9** were gratefully received from Dr. Alan Aitken, University of St. Andrews, St. Andrews, Fife UK. The ylides were purified, recrystallized from dichloromethane–ether (ylide **2**), ethylacetate (ylides **6**–**9**), and characterized before use.

© 2005 NRC Canada

[(Benzylsulfonyl)(4-cyanophenyl)methylene](triphenyl)-phosphorane (1)

The quaternary phosphonium salt, 4-cyanobenzyltriphenylphosphonium bromide (**$Ph_3P^+CH_2$*p*-$NCC_6H_4Br^-$**), was prepared by refluxing 10.49 g of triphenylphosphine (0.04 mol) and 7.84 g (0.04 mol) of α-bromo-*p*-tolunitrile in 60 mL toluene for 18 h to get 11 g (ca. 60%) of the salt; mp 326–329 °C (14). ^{1}H NMR ($CDCl_3$) (15) δ_H: 5.92 (2H, d, J = 15.6 Hz), 7.32 (2H, d, J = 8 Hz), 7.43 (2H, dd, J = 2.3, 8.2 Hz), 7.57–7.61 (6H, m), 7.73–7.83 (9H, m). ^{13}C NMR (DMSO) ($J_{P\text{-}C}$) δ_C: 29.17 (d, J = 46.6 Hz, P-CH_2), 112.22 (d, J = 3.8 Hz), 118.50 (d, J = 85.3 Hz, C-1 of P-Ph), 119.37 (d, J = 2 Hz), 131.26 (d, J = 12.5 Hz, C-3 of P-Ph), 132.80 (d, J = 5.4 Hz), 133.64 (d, J = 3 Hz, C-4 of P-Ph), 135.09 (d, J = 10 Hz, C-2 of P-Ph), 135.15 (d, J = 8.2 Hz), 136.32 (d, J = 2.7 Hz). ^{31}P NMR ($CDCl_3$) δ_P: 25.12. Anal. calcd. for $C_{26}H_{21}BrNP$ (%): C 68.12, H 4.58, N 3.06; found: C 68.10, H 4.63, N 3.17.

The target ylide **1** was prepared by treating the obtained salt with BuLi followed by phenylmethanesulfonyl fluoride in a 1:2:1 ratio, as shown in procedure B. The yellow material that remained after evaporation of the solvent was triturated with diethyl ether to afford a solid material, which was recrystallized from acetonitrile to give 1.80 g of yellow crystals (ca. 45%); mp 276–278 °C. IR υ_{max} (cm^{-1}): 2216, 1594, 1285, 1263, 1177, 1141, 1101, 994, 695, 544, 514. ^{1}H NMR ($CDCl_3$) δ_H: 3.88 (2H, s), 6.95 (2H, d, J = 8 Hz), 7.09 (2H, d, J = 8 Hz), 7.16 (2H, d, J = 8 Hz), 7.25–7.28 (2H, m), 7.30–7.34 (1H, m), 7.40–7.45 (6H, m), 7.54–7.61 (9H, m). ^{13}C NMR ($CDCl_3$) ($J_{P\text{-}C}$) δ_C: 51.3 (d, J = 126 Hz, P=C), 62.9 (CH_2), 106.5 (C≡N), 120.13, 126.55 (d, J = 92 Hz, C-1 of P-Ph), 128.37, 128.77, 129.10 (d, J = 12 Hz, C-3 of P-Ph), 131.17 (2C), 131.46 (d, J = 9 Hz), 132.37 (d, J = 5.4 Hz), 132.67 (d, J = 3 Hz, C-4 of P-Ph), 132,46 (d, J = 9.7 Hz), 134.48 (d, J = 10 Hz, C-2 of P-Ph), 142.65 (d, J = 9.5 Hz). ^{31}P NMR ($CDCl_3$) δ_P: 19.36. MS *m*/*z*: 531 ($M^{+\cdot}$, 2), 440 (25), 392 (14), 376 (16), 277 (18), 262 (68), 183 (55), 105 (100). Anal. calcd. for $C_{33}H_{26}NO_2PS$ (%): C 74.58, H 4.90, N 2.64, S 6.03; found: C 74.71, H 5.12, N 3.01, S 5.68.

[(Benzylsulfonyl)(4-nitrophenyl)methylene](triphenyl)-phosphorane (2)

Obtained by treating the obtained salt with BuLi followed by phenylmethanesulfonyl fluoride in a 1:2:1 ratio. Yield: 72%, mp 275 to 276 °C (3). IR υ_{max} (cm^{-1}): 1582, 1490, 1334, 1284, 1264, 1142, 1107, 992, 936, 695 (3). ^{1}H NMR ($CDCl_3$) δ_H (3): 3.86 (2H, s), 6.84 (2H, d, J = 8.9 Hz), 7.11 (2H, d, J = 7.1 Hz), 7.29–7.34 (3H, m), 7.43–7.48 (6H, m), 7.56–7.66 (9H, m), 7.71 (2H, d, J = 8.8 Hz). ^{13}C NMR ($CDCl_3$) ($J_{P\text{-}C}$) δ_C: 54.03 (d, J = 124 Hz, P=C), 63.10, 123.10, 126.00 (d, J = 92 Hz, C-1 of P-Ph), 128.55, 128.87, 129.29 (d, J = 12 Hz, C-3 of P-Ph), 130.53 (d, J = 6 Hz), 131.00, 131.52, 132.93 (d, J = 3 Hz, C-4 of P-Ph), 134.63 (d, J = 10 Hz, C-2 of P-Ph), 143.11, 145.81 (d, J = 10 Hz). ^{31}P NMR ($CDCl_3$) δ_P: 19.21. MS *m*/*z*: 551 ($M^{+\cdot}$, 20), 460 (38), 412 (18), 396 (16), 277 (85), 262 (100), 201 (22), 183 (96), 108 (36), 91 (85). Anal. calcd. for $C_{32}H_{26}NO_4PS$ (%): C 69.69, H 4.74, N 2.54, S 5.81; found: C 69.49, H 4.80, N 2.70, S 5.28.

[(Benzylsulfonyl)(3-nitrophenyl)methylene](triphenyl)-phosphorane (3)

The quaternary salt, 3-nitrobenzyltriphenylphosphonium chloride (**$Ph_3P^+CH_2$*m*-NO_2-$C_6H_4Cl^-$**), was prepared by refluxing 10.49 g (0.04 mol) of triphenylphosphine and 6.9 g (0.04 mol) of 3-nitrobenzyl chloride in 30 mL benzene for 28 h. After cooling, the solid was collected and washed with diethyl ether to obtain 11 g (~63%) of the salt; mp 255–258 °C (16). ^{1}H NMR ($CDCl_3$) δ_H: 6.08 (2H, d, J = 15.2 Hz), 7.29 (1H, t, J = 8 Hz), 7.58–7.64 (7H, m), 7.74–7.76 (3H, m), 7.84–7.89 (6H, m), 7.95 (1H, d, J = 8 Hz), 8.04 (1H, d, J = 8 Hz). ^{13}C NMR ($CDCl_3$) ($J_{P\text{-}C}$) δ_C: 30.18 (d, J = 46.8 Hz, P-CH_2), 118.01 (d, J = 85.4 Hz, C-1 of P-Ph), 123.41 (d, J = 3.4 Hz), 126.17 (d, J = 5 Hz), 130.31 (d, J = 3 Hz), 130.81 (d, J = 12.5 Hz, C-3 of P-Ph), 131.17 (d, J = 19.6 Hz), 134.98 (d, J = 10 Hz, C-2 of P-Ph), 135.65 (d, J = 3 Hz, C-4 of P-Ph), 139.41 (d, J = 5.4 Hz), 148.14 (d, J = 3.6 Hz). ^{31}P NMR ($CDCl_3$) δ_P: 25.55. MS *m*/*z*: 398 ($M^{+\cdot} - Cl^-$). Anal. calcd. for $C_{25}H_{21}ClNO_2P$ (%): C 69.20, H 4.84, N 3.23; found: C 69.14, H 4.86, N 3.32.

The target ylide **3** was obtained by treating the salt with BuLi followed by the addition of phenylmethanesulfonyl fluoride in a 2:2:1 ratio, as per procedure A. The residual oil was triturated and recrystallized from ethyl acetate to give 2.68 g of yellow crystals (ca. 65%) of the target ylide: mp 233–235 °C. IR υ_{max} (cm^{-1}): 1518, 1438, 1340, 1276, 1257, 1100, 1012, 997, 745, 693, 551. ^{1}H NMR ($CDCl_3$) δ_H: 3.95 (2H, s), 7.13–7.17 (3H, m), 7.23–7.27 (3H, m), 7.40–7.44 (6H, m), 7.51–7.61 (10H, m), 7.63–7.65 (1H, m), 7.73–7.75 (1H, m). ^{13}C NMR ($CDCl_3$) ($J_{P\text{-}C}$) δ_C: 48.71 (d, J = 128 Hz, P=C), 62.7 (CH_2), 119.40 (d, J = 1 Hz), 126.47 (d, J = 92 Hz, C-1 of P-Ph), 127.87, 128.12, 128.33, 128.39 (d, J = 3.7 Hz), 128.69 (d, J = 12 Hz, C-3 of P-Ph), 130.79, 130.97, 132.16 (d, J = 3 Hz, C-4 of P-Ph), 133.97 (d, J = 10 Hz, C-2 of P-Ph), 137.81 (d, J = 10 Hz), 140.18 (d, J = 4.5 Hz), 147.20. ^{31}P NMR ($CDCl_3$) δ_P: 20.3. MS *m*/*z*: 551 ($M^{+\cdot}$, 2), 461 (12), 412 (8), 396 (10), 277 (60), 262 (100), 201 (15), 183 (84), 108 (38), 91 (96). Anal. calcd. for $C_{32}H_{26}NO_4PS$ (%): C 69.69, H 4.72, N 2.54, S 5.81; found: C 69.80, H 4.82, N 2.50, S 5.46.

[(Benzylsulfonyl)(4-chlorophenyl)methylene](triphenyl)-phosphorane (4)

The quaternary salt, 4-chlorobenzyltriphenylphosphonium chloride (**$Ph_3P^+CH_2$*p*-Cl-$C_6H_4Cl^-$**), was prepared by refluxing 10.49 g triphenylphosphine (0.04 mol) and 6.5 g 4-chlorobenzyl chloride (0.04 mol) in 70 mL toluene for 21 h. After cooling, the solid was filtered and washed with diethyl ether to obtain 13.15 g (ca. 78%) of the salt: mp 290–293 °C (17, 18). ^{1}H NMR ($CDCl_3$) (15) δ_H: 5.71 (2H, d, J = 14.8 Hz), 7.0 (2H, d, J = 8 Hz), 7.11–7.12 (2H, m), 7.55–7.59 (6H m), 7.69–7.80 (9H, m). ^{13}C NMR ($CDCl_3$) ($J_{P\text{-}C}$) δ_C: 30.11 (d, J = 46.2 Hz, P-CH_2), 118.40 (d, J = 85 Hz, C-1 of P-Ph), 126.99 (d, J = 6.9 Hz), 129.26 (d, J = 3.2 Hz, C-4 of P-Ph), 130.61 (d, J = 12.5 Hz, C-3 of P-Ph), 133.69 (d, J = 5.4 Hz), 134.75 (d, J = 4.7 Hz), 135.06 (d, J = 10 Hz, C-2 of P-Ph), 135.38. ^{31}P NMR ($CDCl_3$) δ_P: 24.79. MS *m*/*z*: 389/387 ($M^{+\cdot}$ + 2/$M^{+\cdot} - Cl^-$). Anal. calcd. for $C_{25}H_{21}Cl_2P$ (%): C 70.92, H 4.96; found: C 70.90, H 5.02.

The target ylide **4** was prepared by treating the salt with BuLi followed by phenylmethanesulfonyl fluoride in a 2:2:1

© 2005 NRC Canada

ratio, as shown in procedure A. The obtained colourless material was recrystallized from ethyl acetate to give 2.59 g (ca. 64%) of the ylide: mp 232–234 °C. IR υ_{max} (cm^{-1}): 1584, 1485, 1436, 1269, 1104, 1018, 935, 757, 732, 694, 542. ^1H NMR ($CDCl_3$) δ_H: 3.97 (2H, s), 6.98 (2H, d, J = 8 Hz), 7.05–7.15 (4H, m), 7.27–7.30 (2H, m), 7.35–7.39 (7H, m), 7.48–7.53 (9H, m). ^{13}C NMR ($CDCl_3$) (J_{P-C}) δ_C: 46.6 (d, J = 129 Hz, P=C), 62.06 (CH_2), 127.68 (d, J = 92 Hz, C-1 of P-Ph), 128.05 (2C), 128.17 (d, J = 1.4 Hz), 128.63, 128.68 (d, J = 1.9 Hz), 128.89 (d, J = 12 Hz, C-3 of P-Ph), 131.61, 131.69, 132.18 (d, J = 3 Hz, C-4 of P-Ph), 134.16 (d, J = 3.6 Hz), 134.28 (d, J = 10 Hz, C-2 of P-Ph), 136.63 (d, J = 4 Hz). ^{31}P NMR ($CDCl_3$) δ_P: 19.61. MS *m/z*: 542/540 ($M^{+\cdot}$ + 2/$M^{+\cdot}$, 35/60%), 415 (30), 401 (45), 385 (80), 351 (40), 277 (100), 262 (75), 201 (45), 199 (42), 183 (80), 139 (58), 1 (64). Anal. calcd. for $C_{32}H_{26}ClO_2PS$ (%): C 71.04, H 4.81, S 5.92; found: C 71.21, H 4.92, S 6.03.

[(Benzylsulfonyl)(3-chlorophenyl)methylene](triphenyl)-phosphorane (5)

The quaternary salt, 3-chlorobenzyltriphenylphosphonium chloride (**$Ph_3P^+CH_2$*m*-Cl-$C_6H_4Cl^-$**), was prepared by refluxing 10.49 g of triphenylphosphine (0.04 mol) with 6.44 g of 3-chlorobenzyl chloride (0.04 mol) in benzene for 48 h to obtain 13.90 g (ca. 82%) of the salt: mp 320–323 °C (19). ^1H NMR ($CDCl_3$) δ_H: 5.66 (2H, d, J = 15.2 Hz), 6.87 (1H, d, J = 2 Hz), 7.02 (1H, t, J = 8 Hz), 7.12 (1H, d, J = 7.6 Hz), 7.15 (1H, d, J = 7.6 Hz), 7.57–7.61 (6H, m), 7.71–7.81 (9H, m). ^{13}C NMR ($CDCl_3$) (J_{P-C}) δ_C : 30.62 (d, J = 46.5 Hz, P-CH_2), 118.30 (d, J = 85.40 Hz, C-1 of P-Ph), 128.91 (d, J = 3.8 Hz), 130.35 (d, J = 8.4 Hz), 130.55 (d, J = 3.3 Hz, C-4 of P-Ph), 130.70 (d, J = 12.5 Hz, C-3 of P-Ph), 130.76, 131.73 (d, J = 5.3 Hz), 134.72 (d, J = 3.8 Hz), 134.98 (d, J = 10 Hz, C-2 of P-Ph), 135.51 (d, J = 2.7 Hz). ^{31}P NMR ($CDCl_3$) δ_P: 25.05. MS *m/z*: 389/387 ($M^{+\cdot}$ + 2/$M^{+\cdot}$ – Cl^-). Anal. calcd. for $C_{25}H_{21}Cl_2P$ (%): C 70.92, H 4.96; found: C 70.96, H 4.96.

The target ylide **5** was prepared by treating the obtained salt with BuLi and phenylmethanesulfonyl fluoride according to procedure A, in a 2:2:1 ratio. The obtained colorless material was recrystallized from ethyl acetate to obtain 3.25 g of the pure colorless crystals (ca. 80%) of the target ylide mp 216–218 °C. IR υ_{max}(cm^{-1}): 1584, 1436, 1270, 1103, 811, 760, 542, 503. ^1H NMR ($CDCl_3$) δ_H: 3.99 (2H, s), 6.90–7.00 (2H, m), 7.04 (1H, s), 7.10–7.15 (2H, m), 7.25–7.31 (4H, m), 7.37–7.40 (6H, m), 7.48–7.55 (9H, m). ^{13}C NMR ($CDCl_3$) (J_{P-C}) δ_C: 47.5 (d, J = 129 Hz, P=C), 62.29 (CH_2), 125.6 (d, J = 2 Hz), 127.53 (d, J = 92 Hz, C-1 of P-Ph), 128.13, 128.64, 128.71, 128.89 (d, J = 12 Hz, C-3 of P-Ph), 128.98, 131.59 (d, J = 2.1 Hz), 132.06 (d, J = 2.9 Hz), 132.24 (d, J = 3 Hz, C-4 of P-Ph), 134.17, 134.30 (d, J = 10 Hz, C-2 of P-Ph), 134.89 (d, J = 4.1 Hz), 137.7 (d, J = 9 Hz). ^{31}P NMR ($CDCl_3$) δ_P: 19.84. MS *m/z*: 542/540 ($M^{+\cdot}$ + 2/$M^{+\cdot}$, 8/18%), 451/449 ($^{37/35}Cl$ – M^+ – $PhCH_2$, 35/100), 401 (50), 385 (85), 351 (40), 262 (46), 241 (40), 183 (85), 165 (78), 139 (75). Anal. calcd. for $C_{32}H_{26}ClO_2PS$ (%): C 71.04, H 4.81, S 5.92; found: C 71.17, H 4.96, S 5.66.

[(Benzylsulfonyl)(phenyl)methylene](triphenyl)phosphorane (6)

Obtained by treating the obtained salt with BuLi followed by phenylmethanesulfonyl fluoride in a 2:2:1 ratio. Yield: 78%; mp 210–212 °C (1, 3). IR υ_{max} (cm^{-1}): 1590, 1484, 1435, 1266, 1240, 1094, 1021, 939, 708, 692, 545, 526. ^1H NMR ($CDCl_3$) (1) δ_H: 4.00 (2H, s), 7.03–7.15 (4H, m), 7.26–7.37 (12H, m), 7.47–7.54 (9H, m). ^{13}C NMR ($CDCl_3$) (J_{P-C}) (1) δ_C: 46.80 (d, J = 129 Hz, P=C), 61.83 (CH_2), 125.85 (d, J = 2 Hz), 127.91, 128.09 (d, J = 92 Hz, C-1 of P-Ph), 128.13, 128.50, 128.73 (d, J = 12 Hz, C-3 of P-Ph), 131.70, 131.94 (d, J = 3 Hz, C-4 of P-Ph), 134.27 (d, J = 10 Hz, C-2 of P-Ph), 135.20 (d, J = 9 Hz), 135.29 (d, J = 9 Hz), 135.94 (d, J = 4 Hz). ^{31}P NMR ($CDCl_3$) δ_P: 19.61 (1). MS *m/z*: 506 ($M^{+\cdot}$, 60), 416 (57), 415 (48), 368 (64), 351 (90), 273 (18), 165 (64), 105 (100). Anal. calcd. for $C_{32}H_{27}O_2PS$ (%): C 75.89, H 5.34, S 6.32; found: C 75.85, H 5.44, S 6.21.

[(Benzylsulfonyl)(4-methylphenyl)methylene](triphenyl)-phosphorane (7)

Obtained by treating the obtained salt with BuLi followed by phenylmethanesulfonyl fluoride in a 2:2:1 ratio. Yield: 74%; mp 186–189 °C (1). IR υ_{max} (cm^{-1}): 1625, 1502, 1483, 1435, 1264, 1244, 1144, 1106, 1094, 1043, 1028, 935, 864, 788, 754, 714, 694 (1). ^1H NMR ($CDCl_3$) (1) δ_H: 2.24 (3H, s), 3.99 (2H, s), 6.87 (2H, d, J = 8 Hz), 7.13–7.16 (4H, m), 7.24–7.36 (9H, m), 7.45–7.52 (9H, m). ^{13}C NMR ($CDCl_3$) (J_{P-C}) δ_C: 21.5 (CH_3), 46.6 (d, J = 129 Hz, P=C), 61.6 (CH_2), 128.30 (d, J = 92 Hz, C-1 of P-Ph), 128.58 (d, J = 12 Hz, C-3 of P-Ph), 128.63, 128.75, 128.97 (d, J = 1 Hz), 131.73, 131.86 (d, J = 3 Hz, C-4 of P-Ph), 131.96, 132.01, 134.26 (d, J = 10 Hz, C-2 of P-Ph), 135.63 (d, J = 2 Hz), 136.11 (d, J = 4 Hz). ^{31}P NMR ($CDCl_3$) δ_P: 19.49. MS *m/z*: 520 ($M^{+\cdot}$, 60), 429 (50), 416 (5), 380.7 (40), 365 (100), 277 (5), 262 (30), 165 (65), 119 (90), 91 (75). Anal. calcd. for $C_{33}H_{29}O_2PS$ (%): C 76.15, H 5.58, S 6.15; found: C 76.17, H 5.64, S 5.79.

[(Benzylsulfonyl)(4-methoxyphenyl)methylene](triphenyl)-phosphorane (8)

Obtained by treating the obtained salt with BuLi followed by phenylmethanesulfonyl fluoride in a 2:2:1 ratio. Yield: 86%; mp 193–195 °C (3). IR υ_{max} (cm^{-1}): 2829, 1598, 1503, 1438, 1242, 1095, 1049, 750, 694 (3). ^1H NMR ($CDCl_3$) (3) δ_H: 3.75 (3H, s), 4.13 (2H, s), 6.62 (2H, d, J = 8 Hz), 7.16–7.18 (4H, m), 7.27–7.29 (2H, m), 7.32–7.35 (7H, m), 7.45–7.50 (9H, m). ^{13}C NMR ($CDCl_3$) (J_{P-C}) δ_C: 45.85 (d, J = 129 Hz, P=C), 55.61 (CH_3), 61.55 (CH_2), 113.72, 126.97 (d, J = 8.4 Hz), 127.86, 128.28 (d, J = 92 Hz, C-1 of P-Ph), 128.60, 128.71 (d, J = 12 Hz, C-3 of P-Ph), 131.70, 131.87 (d, J = 3 Hz, C-4 of P-Ph), 132.04, 134.20 (d, J = 10 Hz, C-2 of P-Ph), 137.94 (d, J = 3 Hz), 158.35 (d, J = 2 Hz). ^{31}P NMR ($CDCl_3$) δ_P: 19.80. MS *m/z*: 536 ($M^{+\cdot}$, 40), 397.1 (25), 365 (30), 381 (100), 278 (50), 262 (55), 183 (70), 152 (40), 121 (50), 91 (75). Anal. calcd. for $C_{33}H_{29}O_3PS$ (%): C 73.88, H 5.41, S 5.97; found: C 73.80, H 5.51, S 5.55.

[(Benzylsulfonyl)(methyl)methylene](triphenyl)phosphorane (9)

Obtained by treating the obtained salt with BuLi followed by phenylmethanesulfonyl fluoride in a 2:2:1 ratio. Yield: 62%; mp 170–172 °C (1). ^1H NMR ($CDCl_3$) (1) δ_H: 1.58 (3H, d, J = 14 Hz), 3.97 (2H, s), 7.27 (5H, s), 7.7–7.4

© 2005 NRC Canada

Table 3. Conditions for kinetics and HPLC analysis of sulfonyl-stabilized phosphorus ylides **1–9** (**$Ph_3P{=}CGSO_2CH_2Ph$**).

Ylide	G	Internal standard	UV detector (λ, nm)	*T* range (K)	Eluent (CH_3CN:H_2O)
1	*p*-CNC_6H_4	1,2,4-Trichlorobenzene	256	495–533	60:40+0.1% AcOH
2	*p*-$NO_2C_6H_4$	Chlorobenzene	210	487–529	70:30
3	*m*-$NO_2C_6H_4$	Chlorobenzene	256	492–535	70:30
4	*p*-ClC_6H_4	Chlorobenzene	256	495–545	70:30
5	*m*-ClC_6H_4	Chlorobenzene	256	494–544	70:30
6	C_6H_5	1,3-Dichlorobenzene	210	501–545	62:38
7	*p*-$CH_3C_6H_4$	Chlorobenzene	256	479–524	60:40+0.1% AcOH
8	*p*-$CH_3OC_6H_4$	Chlorobenzene	256	475–520	60:40+0.1% AcOH
9	CH_3	1,2,4-Trichlorobenzene	210	470–512	60:40+0.1% AcOH

(15H, m). ^{31}P NMR ($CDCl_3$) (1) δ_P: 20.8. Anal. calcd. for $C_{27}H_{25}O_2PS$ (%): C 72.97, H 5.63, S 7.21; found: C 72.68, H 5.42, S 6.98.

Characterization of novel products of the pyrolysis of ylides 1–4

Ylide 1

trans-*4,4′-Dicyanostilbene (*p-*$NCC_6H_4CH{=}CHC_6H_4CN$*-*p*)*

IR υ_{max} (cm^{-1}): 2224, 949, 773. ^{1}H NMR ($CDCl_3$) δ_H: 7.21 (2H, s), 7.63 (4H, d, *J* = 8 Hz), 7.69 (4H, d, *J* = 8 Hz). MS *m/z*: 231 (18), 230 ($M^{+\cdot}$, 100), 229 (44), 228 (13), 215 (15), 202 (12).

(4-Cyanobenzyl)benzyl sulfone (4-$NCC_6H_4CH_2SO_2CH_2C_6H_5$*)*

IR υ_{max} (cm^{-1}): 2229, 1731, 1664, 1496, 1313, 1120, 773, 644. ^{1}H NMR ($CDCl_3$) δ_H: 4.15 (2H, s), 4.24 (2H, s), 7.41–7.50 (7H, m), 7.70 (2H, d, *J* = 8 Hz). MS *m/z*: 271 ($M^{+\cdot}$, 13), 207 (40), 206 (34), 130 (11), 116 (49).

Ylide 2

(4-Nitrobenzyl)benzyl sulfone (4-$NO_2C_6H_4CH_2SO_2CH_2C_6H_5$*)*

IR υ_{max} (cm^{-1}): 1525, 1349, 1296, 1116, 907, 730. ^{1}H NMR ($CDCl_3$) δ_H: 4.20 (s, 2H), 4.26 (s, 2H), 7.44–7.48 (m, 5H), 7.55 (d, 2H, *J* = 8.8 Hz), 8.27 (d, 2H, *J* = 8.7 Hz).

Ylide 3

(3-Nitrobenzyl)benzyl sulfone (3-$NO_2C_6H_4CH_2SO_2CH_2C_6H_5$*)*

IR υ_{max} (cm^{-1}): 1528, 1352, 1320, 1256, 1118, 1077, 815, 699, 641. ^{1}H NMR($CDCl_3$) δ_H: 4.2 (2H, s), 4.28 (2H, s), 7.43–7.48 (5H, m), 7.61 (1H, t, *J* = 8 Hz), 7.76 (1H, d, *J* = 7.7 Hz), 8.18 (1H, brs), 8.28 (1H, dd, *J* = 1, 8.2 Hz). ^{13}C NMR ($CDCl_3$) + DEPT135 δ_C: 57.01 (CH_2), 59.81 (CH_2), 124.43, 126.33, 127.62, 129.4, 129.73, 129.89, 130.36, 131.09, 137.43, 145.5. MS *m/z*: 291 ($M^{+\cdot}$, 3), 227 (8), 178 (24), 165 (32), 152 (14), 105 (62).

Ylide 4

(4-Chlorobenzyl)benzyl sulfone (4-$ClC_6H_4CH_2SO_2CH_2C_6H_5$*)*

IR υ_{max} (cm^{-1}): 1492, 1300, 1116, 902, 724. ^{1}H NMR ($CDCl_3$) δ_H: 4.10 (2H, s), 4.18 (2H, s), 7.32 (2H, d, *J* = 8.4 Hz), 7.38–7.45 (7H, m). ^{13}C NMR ($CDCl_3$) + DEPT135 δ_C: 57.4 (CH_2), 58.8 (CH_2), 126.2, 127.8, 129.5, 129.6, 129.6, 131.2, 132.6, 135.8. MS *m/z*: 282 (2), 280 ($M^{+\cdot}$, 6), 279 (2), 219 (2), 218 (18), 217 (10), 216 (32), 127 (50), 126 (18), 125 (100), 91 (100).

Ylide 5

(3-Chlorobenzyl)benzyl sulfone (3-$ClC_6H_4CH_2SO_2CH_2C_6H_5$*)*

IR υ_{max} (cm^{-1}): 1598, 1476, 1318, 1118, 904, 728, 648, 609. ^{1}H NMR ($CDCl_3$) δ_H : 4.09 (2H, s), 4.19 (2H, s), 7.29 (1H, d, *J* = 8 Hz), 7.35 (2H, d, *J* = 8 Hz), 7.37–7.45 (6H, m). MS *m/z*: 283 (6), 281 ($M^{+\cdot}$ + 1, 18), 218 (18), 217 (14), 216 (30), 183 (8), 181 (22), 157 (15), 155 (10), 127 (24), 125 (50).

Kinetic measurements and product analysis

Stock solution (7 mL) was prepared by dissolving 6–10 mg of the ylide in acetonitrile as the solvent to give a concentration of 1000–2000 ppm. Internal standard was then added, the amount of which was adjusted to give the desired peak area ratio of ylide to standard (2.5:1). The solvent and the internal standard were selected because both are stable under the conditions of pyrolysis and they do not react with either ylide or product. The internal standards used in this study were chlorobenzene, 1,3-dichlorobenzene, and 1,2,4-trichlorobenzene. Each mixture was filtered before use to ensure a homogenous solution.

The weight ratio of the ylide with respect to the internal standard was calculated from the ratio of the ylide peak area to the peak area of the internal standard. The kinetic rate was obtained by tracing the rate of disappearance of the ylide with respect to the internal standard as follows:

An aliquot part (0.2 mL) of each solution containing the ylide and the internal standard was pipetted into the reaction tube, and the tube was placed in the pyrolyzer for 6 min under nonthermal conditions. A sample was analyzed using the HPLC probe with the UV detector at a wavelength of 256 or 210 nm, and the standardization value (A_o) was then calculated. Several HPLC measurements were obtained with an accuracy of ≥2%. The temperature of the pyrolysis block was then raised until approximately 10% pyrolysis was deemed to occur over 900 s. This process was repeated after each 10–15 °C rise in the temperature of the pyrolyzer until >90% pyrolysis was achieved. The relative ratios of the integration values of the sample and the internal standard (*A*) at the pyrolysis temperature were then calculated. At least three kinetic runs were carried out at each reaction temperature following each 10–15 °C rise in the pyrolyzer temperature to ensure reproducible values of *A*. Treatment of the

© 2005 NRC Canada

kinetic data and calculation of Arrhenius parameters and reaction rate constants have been detailed elsewhere (10, 20, 21). The conditions for kinetic and HPLC analyses of the ylides **1**–**9** are summarized in Table 3.

Acknowledgements

One of the authors (R.F.A.) wishes to thank the College of Graduate Studies, Kuwait University for a PhD candidacy. Kuwait University Research Grant SC 01/99 and ANALAB and SAF Grant Nos. GS 01/01 and GS 03/01 are gratefully acknowledged.

References

1. R.A. Aitken, M.J. Drysdale, G. Ferguson, and A.J. Loug. J. Chem. Soc. Perkin Trans. 1, 875 (1998).
2. R.A. Aitken and M.J. Drysdale. J. Chem. Soc. Chem. Commun. 512 (1991).
3. B.A. Reith, J. Strating, and A.M. Van Leusen. J. Org. Chem. **39**, 2729 (1974).
4. A.M. Van Leusen, B.A. Reith, A.J.W. Iedema, and J. Strating. Recl. Trav. Chim. Pays–Bas, **91**, 37 (1972).
5. Y. Shen and J. Yao. J. Chem. Res. Synop. 394 (1996).
6. L. Engman. J. Org. Chem. **49**, 3559 (1984).
7. H. Güsten and M. Salzwedel. Tetrahedron, **23**, 187 (1967).
8. H. Ndayikengurukiye, S. Jacobs, and W. Tachelet. Tetrahedron, **53**, 13811 (1997).
9. Mass Spectrometry Data Centre. Eight peak index of mass spectra. 4th ed. Royal Society of Chemistry, Cambridge. 1991.
10. N.A. Al-Awadi, M.H. Elnagdi, K. Kaul, S. Ilingovan, and O.M.E. El-Dusouqui. J. Phys. Org. Chem. **12**, 1 (1999).
11. R. Taylor. *In* The chemistry of functional groups: Supplement B. *Edited by* S. Patai. John Wiley, Chichester. 1979. p. 876.
12. H.H. Dib, N.A. Al-Awadi, Y.A. Ibrahim, and O.M.E. El-Dusouqui. Tetrahedron, **59**, 9455 (2003).
13. R.A. Aitken, J.I.G. Cadogan, and I. Gosney. Phosphorus, sulfur and silicon. Vol. 101. OPA, Amsterdam. 1995. p. 281.
14. A. Mylona, J. Nikokavouras, and I.M. Takakis. J. Chem. Res. Miniprint, **12**, 3514 (1986).
15. C. Imrie, T.A. Modro, E.R. Rohwer, and C.C.P. Wagener. J. Org. Chem. **58**, 5643 (1993).
16. H.H. Mel'nikow, A.E. Kretow, and Z. Mel'zer. Zh. Obshch. Khim. **7**, 461 (1937).
17. H. Higashi. Bull. Chem. Soc. Jpn. **43**, 3236 (1970).
18. A. Shafiee, K.M. Semnani, and A. Foroumadi. J. Heterocycl. Chem. **33**, 671 (1996).
19. B.R. Baker and R.E. Gibson. J. Med. Chem. **14**, 315 (1971).
20. N.A. Al-Awadi, K. Kaul, and O.M.E. El-Dusouqui. J. Phys. Org. Chem. **13**, 499 (2000).
21. N.A. Al-Awadi, O.M.E. El-Dusouqui, K. Kaul, and H.H. Dib. Int. J. Chem. Kinet. **32**, 403 (2000).

© 2005 NRC Canada

Comparison of the nucleophilicities of alcohols and alkoxides[1]

Thanh Binh Phan and Herbert Mayr

Abstract: The kinetics of the reactions of benzhydrylium ions with some alcohols and alkoxides dissolved in the corresponding alcohols were photometrically investigated. Using the correlation equation log k (20 °C) = $s(E + N)$, the N and s parameters of methoxide, ethoxide, *n*-propoxide, and isopropoxide in alcohol–acetonitrile (91:9, *v*/*v*) were determined. The cosolvent acetonitrile has only a little influence on the rate constants of the reactions of alcohols and alkoxides. The order of N values ($OH^- << MeO^- < EtO^- < n\text{-}PrO^- < i\text{-}PrO^-$) shows that alkoxides differ only moderately in reactivity but are considerably more nucleophilic than hydroxide. As a consequence, the nucleophilic reactivity of a 0.5 mmol/L aqueous hydroxide solution increases by a factor of 13 when 10% (*v*/*v*) methanol is added. In 1–10 mmol/L alkoxide solutions in alcohols, weak electrophiles react considerably faster with alkoxides than with the corresponding alcohols. With increasing electrophilicity, the preference for alkoxides decreases, and electrophiles of $-3 < E < 3$ react with alkoxides (1–10 mmol/L) and alcohols with comparable rates. Stronger electrophiles will react with alcohols exclusively when alkoxides are present in concentrations ≤10 mmol/L.

Key words: kinetics, alcohol, alkoxide, linear free energy relationship, nucleophilicity.

Résumé : Faisant appel à la photométrie, on a étudié la cinétique des réactions d'ions benzhydrylium avec quelques alcools et alcoolates dissous dans les alcools correspondants. Utilisant l'équation de corrélation log k (20 °C) = $s(E + N)$ on a déterminé les paramètres N et s du méthylate, de l'éthylate, du propylate et de l'isopropylate dans un mélange 91 : 9 (*v*/*v*) d'alcool et d'acétonitrile. L'acétonitrile utilisé comme cosolvant n'a que peu d'effet sur les constantes de vitesse des réactions des alcools et des alcoolates. L'ordre des valeurs de N ($OH^- << MeO^- < EtO^- < n\text{-}PrO^- < i\text{-}PrO^-$) montre que les réactivités des alcoolates ne diffèrent que légèrement, mais qu'ils sont beaucoup plus nucléophiles que l'hydroxyde. En conséquence, la réactivité nucléophile d'une solution d'hydroxyde aqueux à une concentration de 0,5 mmol/L augmente par un facteur de 13 quand on lui ajoute 10 % (*v*/*v*) de méthanol. Dans des solutions d'alcoolates à des concentrations allant de 1 à 10 mmol/L, les électrophiles faibles réagissent beaucoup plus rapidement avec les alcoolates qu'avec les alcools correspondants. Avec une augmentation du caractère électrophile, la préférence des alcoolates diminue et les électrophiles de $-3 < E < 3$ réagissent avec les alcools et les alcoolates (à des concentrations allant de 1 à 10 mmol/L) avec des vitesses comparables. Les électrophiles plus forts ne réagissent qu'avec les alcools lorsque les alcoolates sont présents à des concentrations inférieures à 10 mmol/L.

Mots clés : cinétique, alcool, alcoolate, relation linéaire d'énergie libre, caractère nucléophile.

[Traduit par la Rédaction]

Introduction

Knowledge of relative nucleophilicities of alcohols and alkoxides is essential for the understanding of the course of numerous nucleophilic additions and substitutions involving these reagents. However, alcohols and alkoxides widely differ in nucleophilicity, and the choice of reaction partners that are suitable for kinetic investigations with both types of reagents has not been trivial (1).

Recently, we have demonstrated that benzhydrylium ions of variable reactivity can be used as reference electrophiles for comparing *n*-, π-, and σ-nucleophiles of widely differing reactivity (2). Equation [1], where E is an electrophilicity parameter and N and s are nucleophile specific parameters, allows one to predict rate constants for the reactions of nucleophiles with benzhydrylium ions with a standard deviation of less than a factor of 2; rate constants for the reactions with other types of carbocations and with Michael acceptors can be calculated with an accuracy better than a factor of 10–100 (2, 3). This precision is remarkable in view of the large structural variety and the more than 30 orders of magnitude presently covered by this correlation.

$$\log k\ (20\ ^\circ\mathrm{C}) = s(N + E) \qquad [1]$$

Recently, we have reported nucleophilicity parameters for typical solvents, which we have termed N_1 to indicate that

Received 27 April 2005. Published on the NRC Research Press Web site at http://canjchem.nrc.ca on 25 November 2005.

T.B. Phan and H. Mayr.[2] Department Chemie und Biochemie der Ludwig-Maximilians-Universität München, Butenandtstrasse 5-13 (Haus F), D-81377 München, Germany.

[1]This article is part of a Special Issue dedicated to organic reaction mechanisms.

[2]Corresponding author (e-mail: Herbert.Mayr@cup.uni-muenchen.de).

 doi: 10.1139/V05-170 © 2005 NRC Canada

their use in eq. [1] gives rise to first-order rate constants (4). Alkoxides, one of the most important classes of nucleophiles, have so far not yet been characterized in this way. Since knowledge of their *N* and *s* parameters is crucial for a systematic analysis of nucleophilic aromatic substitutions as well as of S_N2 reactions, we set out to determine their nucleophilicity parameters as defined by eq. [1].

Results and discussion

Nucleophilic reactivities of alcohols

The rates of the reactions of methanol and ethanol with a series of benzhydrylium ions (Table 1) have been previously reported (4). We have now employed the same method for determining the rates of the reactions of *n*-propanol and isopropanol with benzhydrylium ions (eq. [2]).

[2] $$Ar_2CH^+BF_4^- + ROH \rightarrow Ar_2CHOR + HBF_4$$

Due to the presence of amino substituents in the aryl groups, the addition of extra bases for neutralizing the liberated HBF_4 was not necessary. Most of the reactions were studied with 9% acetonitrile (*v*/*v*) as the cosolvent by mixing 10 volume parts of alcohol with one volume part of a solution of $Ar_2CH^+BF_4^-$ in acetonitrile in a stopped-flow instrument. However, the reactions of $(lil)_2CH^+$ and $(jul)_2CH^+$ with alcohols are sufficiently slow that they can also be studied in pure alcohols. Since the first-order decay rates of $(lil)_2CH^+$ and $(jul)_2CH^+$ in *n*-propanol–acetonitrile (91:9, *v*/*v*) are only 46% and 10% slower than in pure *n*-propanol, respectively (see the footnotes of Table 2), the influence of the cosolvent acetonitrile is only of minor importance for the following structure reactivity discussions.

Plots of $\log k_1$ (Table 2) vs. the electrophilicity parameter (*E*) of the benzhydrylium ions (Table 1) gave straight lines (Fig. 1) from which, according to eq. [1], the nucleophilicity parameter (N_1) and slope parameter (*s*) were derived (Table 3). Division of the first-order rate constants in Table 2 by the molar concentrations of the alcohols gave second-order rate constants. Their plots vs. *E* gave correlation lines, which are parallel to those in Fig. 1, and gave rise to the nucleophilicity parameters (*N*), which are also listed in Table 3.

Nucleophilic reactivities of alkoxides

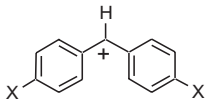
Because of the fast reactions of most benzhydrylium ions with alcohols, it was again necessary to study the reactivities of alkoxides in the corresponding alcohols in the presence of 9% (*v*/*v*) acetonitrile. Such solutions were obtained by mixing 10 parts of a solution of sodium alkoxide in the corresponding alcohol with 1 part of a solution of a benzhydrylium tetrafluoroborate in acetonitrile in a stopped-flow instrument. The reactions of $(lil)_2CH^+$ with alcohols were slow enough, however, that for this carbenium ion the influence of the cosolvent acetonitrile could be studied.

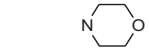
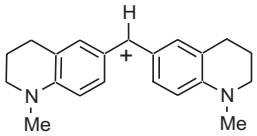
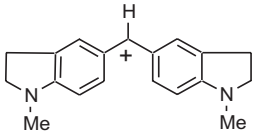
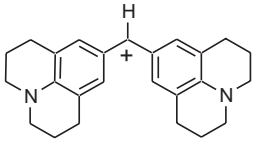
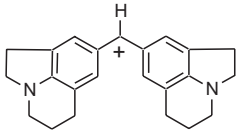
Figure 2 shows that the pseudo-first-order rate constant (k_{obs}) for the decay of $(lil)_2CH^+$ increases linearly with $[MeO^-]$ in both pure methanol and in methanol–acetonitrile (91:9, *v*/*v*). The nucleophilic reactivity of methoxide is approximately 42% larger in pure methanol than in methanol–acetonitrile (91:9, *v*/*v*) (Fig. 2). Analogously, the nucleophilic reactivities of OH^- in H_2O and of other alkoxides in the corresponding alcohols slightly decrease when 9% acetonitrile is added as a cosolvent (Table 4).

The intercepts of almost zero shown in Fig. 2 reflect the observation that the rates of the reactions of the alcohols with the carbocations (4) are negligible compared with the

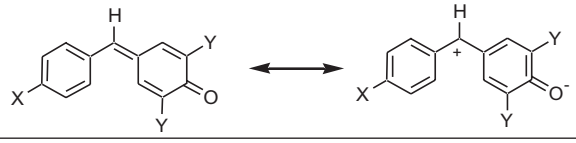
Table 1. (*a*) Benzhydrylium ions and (*b*) quinone methides used as reference electrophiles.

(*a*) Benzhydrylium ions.



Abbr.	X	*E*[a]
Ph_2CH^+	H	+5.90
$(ani)_2CH^+$	OCH_3	0
$(mfa)_2CH^+$	$N(CH_3)CH_2CF_3$	–3.85
$(dpa)_2CH^+$	NPh_2	–4.72
$(mor)_2CH^+$		–5.53
$(mpa)_2CH^+$	$N(Ph)CH_3$	–5.89
$(dma)_2CH^+$	$N(CH_3)_2$	–7.02
$(pyr)_2CH^+$	$N(CH_2)_4$	–7.69
$(thq)_2CH^+$		–8.22
$(ind)_2CH^+$		–8.76
$(jul)_2CH^+$		–9.45
$(lil)_2CH^+$		−10.04

(*b*) Quinone methides.



Abbr.	X	Y	*E*[b]
$ani(Ph)_2QM$	OCH_3	C_6H_5	–12.18
$dma(Ph)_2QM$	$N(CH_3)_2$	C_6H_5	–13.39
$tol(t\text{-}Bu)_2QM$	CH_3	$C(CH_3)_3$	–15.83
$ani(t\text{-}Bu)_2QM$	OCH_3	$C(CH_3)_3$	–16.11
$dma(t\text{-}Bu)_2QM$	$N(CH_3)_2$	$C(CH_3)_3$	–17.29

[a]From ref. 2.
[b]From ref. 5.

© 2005 NRC Canada

Table 2. First-order rate constants (k_1, s^{-1}, at 20 °C) for the reactions of benzhydrylium ions (Ar_2CH^+) with alcohols in alcohol–acetonitrile (91:9, *v*/*v*).

	k_1 (s^{-1})			
Ar_2CH^+	MeOH–MeCN (91:9)[a]	EtOH–MeCN (91:9)[a]	*n*-PrOH–MeCN (91:9)	*i*-PrOH–MeCN (91:9)
$(lil)_2CH^+$	6.14×10^{-3}	3.52×10^{-3}	3.60×10^{-3}[b]	—
$(jul)_2CH^+$	—	—	1.36×10^{-2}[c]	1.58×10^{-3}
$(ind)_2CH^+$	—	3.82×10^{-2}	4.07×10^{-2}	5.05×10^{-3}
$(thq)_2CH^+$	2.17×10^{-1}	—	1.17×10^{-1}	1.93×10^{-2}
$(pyr)_2CH^+$	9.32×10^{-1}	2.72×10^{-1}	3.36×10^{-1}	7.42×10^{-2}
$(dma)_2CH^+$	2.31	9.24×10^{-1}	1.09	5.00×10^{-1}
$(mpa)_2CH^+$	2.79×10^{1}	1.45×10^{1}	—	—
$(mor)_2CH^+$	2.65×10^{1}	1.38×10^{1}	1.53×10^{1}	6.68
$(dpa)_2CH^+$	3.60×10^{2}	2.60×10^{2}	—	—
$(mfa)_2CH^+$	4.02×10^{2}	2.55×10^{2}	—	—
$(ani)_2CH^+$	4.95×10^{6}	4.33×10^{6}	—	—

[a]From ref. 4.
[b]$k_1 = 6.71 \times 10^{-3}$ s^{-1} in 100% *n*-PrOH (this work).
[c]$k_1 = 1.51 \times 10^{-2}$ s^{-1} in 100% *n*-PrOH (this work).

Fig. 1. Correlation of the first-order rate constants ($\log k_1$) for the reactions of ROH–acetonitrile (91:9, *v*/*v*) with benzhydrylium ions at 20 °C vs. their electrophilicity parameters (*E*).

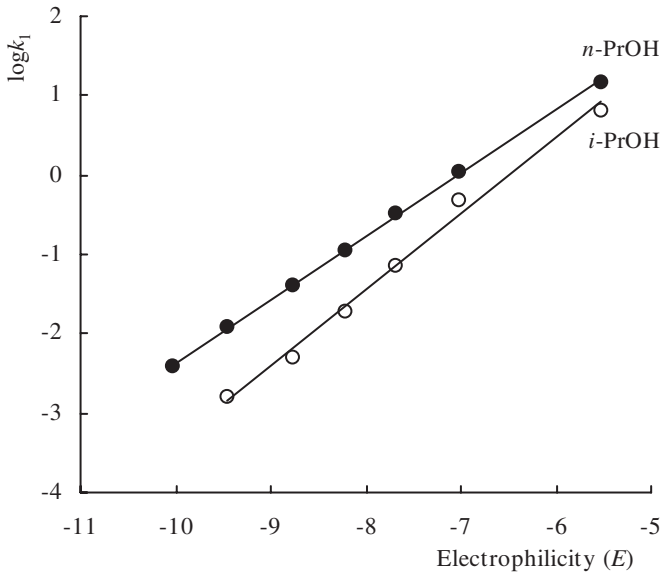


Fig. 2. Plot of the pseudo-first-order rate constants (k_{obs}, s^{-1}, at 20 °C) for the decay of the $(lil)_2CH^+BF_4^-$ concentration in pure methanol and in methanol–acetonitrile (91:9, *v*/*v*) vs. the concentration of sodium methoxide.

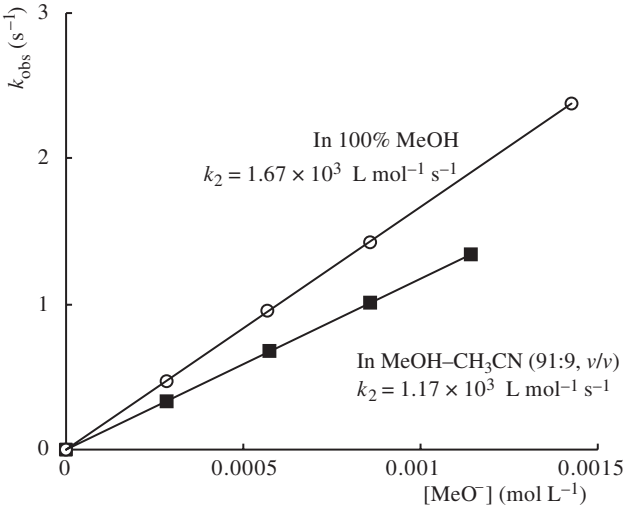


Table 3. Nucleophilicity parameters (N_1, for first-order rate constants), (*N*, for second-order rate constants), and slope parameters (*s*) for mixtures of ROH–acetonitrile (91:9, *v*/*v*).

ROH	N_1	*N*	*s*	Ref.
MeOH	7.45	5.89	0.87	4
EtOH	7.10	5.77	0.90	4
n-PrOH	7.05	5.69	0.80	This work
i-PrOH	6.49	5.37	0.96	This work

corresponding reaction rates of the alkoxides. Therefore, an easy separation of the two processes is possible.

Plots of pseudo-first-order rate constants vs. alkoxide concentrations analogous to those shown in Fig. 2 gave the second-order rate constants for the reactions of alkoxides

Table 4. Second-order rate constants (k_2, L mol^{-1} s^{-1}, at 20 °C) for the reactions of $(lil)_2CH^+BF_4^-$ with hydroxide in water–acetonitrile mixtures and with alkoxides in the corresponding alcohols, and in alcohol–acetonitrile (91:9, *v*/*v*).

	k_2 (L mol^{-1} s^{-1})	
RO^-	In ROH	In ROH–MeCN (91:9, *v*/*v*)
HO^-[a]	2.16[b]	1.65
MeO^-	1.67×10^3	1.17×10^3
EtO^-	7.88×10^3	6.45×10^3
n-PrO^-	2.30×10^4	1.88×10^4
i-PrO^-	4.66×10^4	3.10×10^4

[a]From ref. 6.
[b]In water–acetonitrile (99.6:0.4, *v*/*v*).

© 2005 NRC Canada

Table 5. Second-order rate constants (k_2, L mol^{-1} s^{-1}, at 20 °C) for the reactions of benzhydrylium ions (Ar_2CH^+) with hydroxide and alkoxides in ROH–acetonitrile mixtures.

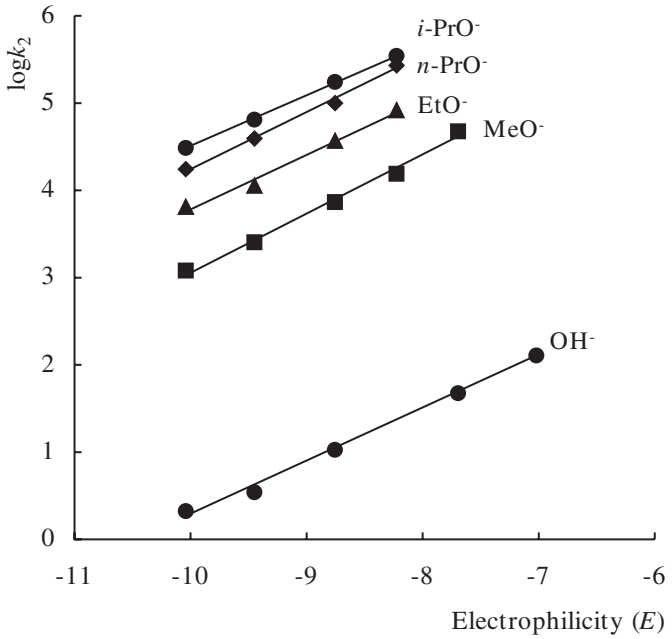
	k_2 (L mol^{-1} s^{-1})				
Ar_2CH^+	HO^-[a]	MeO^-[b]	EtO^-[b]	n-PrO^-[b]	i-PrO^-[b]
$(lil)_2CH^+$	2.16	1.17×10^3	6.45×10^3	1.88×10^4	3.10×10^4
$(jul)_2CH^+$	3.44	2.48×10^3	1.15×10^4	3.69×10^4	6.30×10^4
$(ind)_2CH^+$	1.08×10^1	7.41×10^3	3.58×10^4	1.09×10^5	1.75×10^5
$(thq)_2CH^+$	—	1.56×10^4	8.32×10^4	2.61×10^5	3.47×10^5
$(pyr)_2CH^+$	4.85×10^1	4.80×10^4	—	—	—
$(dma)_2CH^+$	1.31×10^2	—	—	—	—

[a]In water–acetonitrile (99.6:0.4, *v*/*v*), from ref. 6.
[b]In alcohol–acetonitrile (91:9, *v*/*v*), this work.

Table 6. Second-order rate constants (k_2, L mol^{-1} s^{-1}, at 20 °C) for the reactions of alkoxides with quinone methides in the corresponding alcohols.

	k_2 (L mol^{-1} s^{-1})			
Quinone methide	MeO^- in MeOH	EtO^- in EtOH	n-PrO^- in n-PrOH	i-PrO^- in i-PrOH
dma(t-Bu)$_2$QM	1.45×10^{-1}	1.56×10^{-1}	1.81×10^{-1}	9.44×10^{-1}
ani(t-Bu)$_2$QM	4.96×10^{-1}	5.50×10^{-1}	5.96×10^{-1}	2.58
tol(t-Bu)$_2$QM	6.12×10^{-1}	6.32×10^{-1}	—	—
dma(Ph)$_2$QM	5.35×10^1	—	—	—
ani(Ph)$_2$QM	1.68×10^2	—	—	—

Fig. 3. Plot of the second-order rate constants (logk_2) of the reactions of hydroxide in water–acetonitrile (99.6:0.4, *v*/*v*) and alkoxides in ROH–acetonitrile (91:9, *v*/*v*) with benzhydrylium ions at 20 °C (from Table 5) vs. the electrophilicity parameters (*E*) (from Table 1) of the benzhydrylium ions.



with benzhydrylium ions listed in Table 5. The second-order rate constants of the reactions of alkoxides with quinone methides in pure alcohols (Table 6) have been analogously obtained.

Table 7. Nucleophilicity (*N*) and slope parameters (*s*) for alkoxides in the corresponding alcohols.

	ROH–CH_3CN (91:9)		100% ROH	
RO^-	N^a	s^a	N^b	s^b
OH^-	—	—	10.47[c]	0.61[c]
MeO^-	14.51	0.68	15.78	0.56
EtO^-	16.08	0.62	15.78	0.65
n-PrO^-	16.73	0.63	16.03	0.70
i-PrO^-	17.71	0.58	17.03	0.63

[a]From reactions with benzhydrylium ions (Table 5).
[b]From reactions with benzhydrylium ions and quinone methides (Tables 5 and 6).
[c]From ref. 6.

Plots of the rate constants listed in Table 5 vs. the electrophilicity parameter *E* (Fig. 3) show an increase of the nucleophilicities of RO^- in ROH–CH_3CN mixtures in the order $OH^- << MeO^- < EtO^- < n\text{-}PrO^- < i\text{-}PrO^-$.

Intercepts and slopes of the correlations in Fig. 3 give the *N* and *s* parameters listed in the left part of Table 7. Since the cosolvent acetonitrile has only a little influence on the rate constants of the reactions of alkoxides with benzhydrylium ions (Table 4), one can combine the rate constants for the reactions of RO^- with benzhydrylium ions in alcohol–acetonitrile (91:9, *v*/*v*) (Table 5) and the corresponding rate constants for the reactions of RO^- with quinone methides in pure alcohols (Table 6) to give the reactivity parameters *N* and *s* listed on the right of Table 7.

Table 8 compares the relative reactivities of HO^- and RO^- in H_2O and ROH, respectively, toward $(ind)_2CH^+$, 1,3,5-trinitrobenzene (7), *n*-butyl bromide (8), and benzyl chloride (9).

© 2005 NRC Canada

Table 8. Relative reactivities of RO^- in ROH toward different electrophiles.

Electrophile	HO^- in H_2O	MeO^- in MeOH	EtO^- in EtOH	*n*-PrO^- in *n*-PrOH	*i*-PrO^- in *i*-PrOH	Ref.
$(ind)_2CH^+BF_4^-$	0.00030	0.21	1.00	3.04	4.89	[a]
1,3,5-Trinitrobenzene	0.0011	0.21	1.00	—	—	[b]
n-BuBr	0.0800	0.82	1.00	—	0.40	[c]
$PhCH_2Cl$	—	0.91	1.00	0.87	0.44	[d]

[a]At 20 °C (this work).
[b]At 25 °C, from ref. 7.
[c]At 26 °C, from ref. 8.
[d]At 60 °C, from ref. 9.

Table 9. Effect of alcohol additives on the pseudo-first-order rate constants (k_{obs}, s^{-1}, at 20 °C) of the decay of $(jul)_2CH^+BF_4^-$ (0.014 mmol/L) in basic water–acetonitrile (91:9, *v*/*v*) solutions ($[OH^-] + [RO^-]$ = 0.5 mmol/L).

	k_{obs} (s^{-1})		
Alcohol (%)[a]	MeOH (pK_a = 15.5[b])	EtOH (pK_a = 15.9[b])	*n*-PrOH (pK_a = 16.1[b])
0	1.39×10^{-3}	1.39×10^{-3}	1.39×10^{-3}
1	2.66×10^{-3}	1.44×10^{-3}	1.66×10^{-3}
3	5.96×10^{-3}	2.09×10^{-3}	2.02×10^{-3}
5	1.09×10^{-2}	3.03×10^{-3}	2.67×10^{-3}
10	1.86×10^{-2}	6.67×10^{-3}	6.25×10^{-3}

[a]% (*v*/*v*).
[b]In H_2O, from ref. 20.

It is obvious that the relative reactivities of hydroxide and alkoxides (dissolved in their conjugate acids H_2O or ROH) toward carbocations, 1,3,5-trinitrobenzene, and alkyl halides depend on the electrophiles. While methoxide in methanol is 5 times less reactive than ethoxide in ethanol toward carbocations and 1,3,5-trinitrobenzene, their reactivities in S_N2 reactions are almost identical (Table 8). How can one explain these differences?

Previously, good correlations between Ritchie's nucleophilicity parameter (N_+) (derived from reactions with carbocations (1*a*, 10)) and Swain–Scott's parameter (*n*) (derived from reactions with methyl halides (11)), as well as between our nucleophilicity parameter (N_1) (derived from reactions with benzhydrylium ions (4)) and Kevill's solvent nucleophilicity (N_T) (derived from reactions with methylsulfonium ions (12)), have been reported (4, 13, 14).

Since the electrophilicities of the benzhydrylium ions have been demonstrated to be almost independent of the solvent (15), one can assume that the relative reactivities toward $(ind)_2CH^+$ (first line of Table 8) predominantly reflect the relative nucleophilicities of hydroxide and alkoxides in the corresponding solvents, i.e., *i*-PrO^- in *i*-PrOH is 5 times more nucleophilic than EtO^- in EtOH, which is 5 times more nucleophilic than MeO^- in MeOH. In S_N2 reactions, the differences in nucleophilicity will generally be attenuated, and we have reported that approximately half of the differences in nucleophilicities toward carbocations are found in S_N2 reactions with methyl sulfonium ions (4). The S_N2 reactions with alkyl halides will furthermore be affected by the variable electrophilic component of the solvent as expressed by Winstein–Grunwald's solvent ionizing power (*Y*) (16), which decreases in the order H_2O >> MeOH > EtOH > *i*-PrOH (17). A combination of the two effects, as expressed by the extended Winstein–Grunwald equation (12*b*, 18) accounts for the different reactivity order toward *n*-BuBr and $PhCH_2Cl$. Thus, MeO^- in MeOH and EtO^- in EtOH show similar reactivities toward these alkyl halides because the higher nucleophilicity of EtO^- as compared to that of MeO^- (Table 7) is compensated by the higher ionizing power of MeOH as compared to that of ethanol. The reactivity order *i*-PrO^- in *i*-PrOH < EtO^- in EtOH in reactions with *n*-BuBr and $PhCH_2Cl$ can be analogously be attributed to the variable electrophilic contribution of the solvents.

The striking differences in nucleophilicity between basic aqueous and basic alcoholic solutions shown in Fig. 3 suggest that the nucleophilicities of basic aqueous solutions may considerably be enhanced by adding small amounts of alcohols. Table 9 and Fig. 4 indicate that this is indeed the case. However, because of the higher pK_a values of propanol and ethanol, 10% (*v*/*v*) of these alcohols cause an increase of only a factor of 4 to 5. In contrast, 10% (*v*/*v*) methanol increases the nucleophilicity of a 0.5 mmol/L OH^- solution by a factor of 13 (19). This tremendous effect, resulting from the low pK_a value of methanol and the high nucleophilicity of methoxide, may be utilized in synthetic procedures.

Comparison of alcohols and alkoxides

Let us finally turn to the comparison of the nucleophilicities of alcohols and alkoxides, which can be derived from Tables 2 and 5. It was found that the second-order rate constants for alkoxides are generally 5–7 orders of magnitude greater than the first-order rate constants for alcohols. As a consequence, in 10 or 1 mmol/L solutions of alkoxides in alcohols, weak electrophiles will react almost exclusively with alkoxides and not with the solvents (Fig. 5). This ratio decreases with increasing reactivities of the carbocations be-

© 2005 NRC Canada

Fig. 4. Effect of alcohol additives on the pseudo-first-order rate constants (k_{obs}, s^{-1}, at 20 °C) of the decay of $(jul)_2CH^+BF_4^-$ (0.014 mmol/L) in basic water–acetonitrile (91:9, *v*/*v*) solutions ($[OH^-] + [RO^-] = 0.5$ mmol/L).

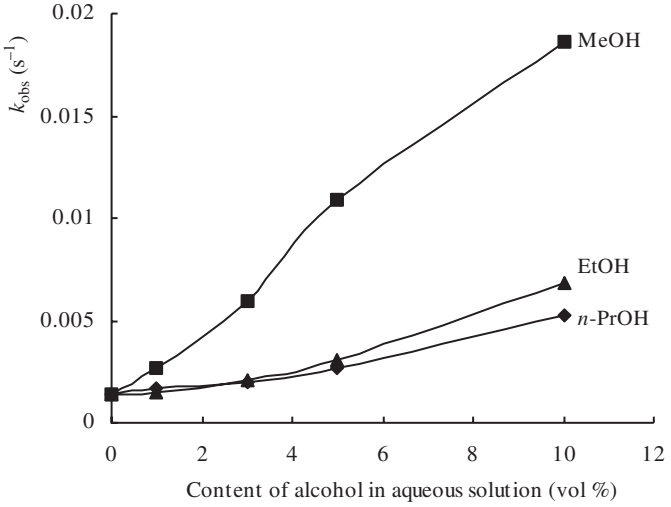
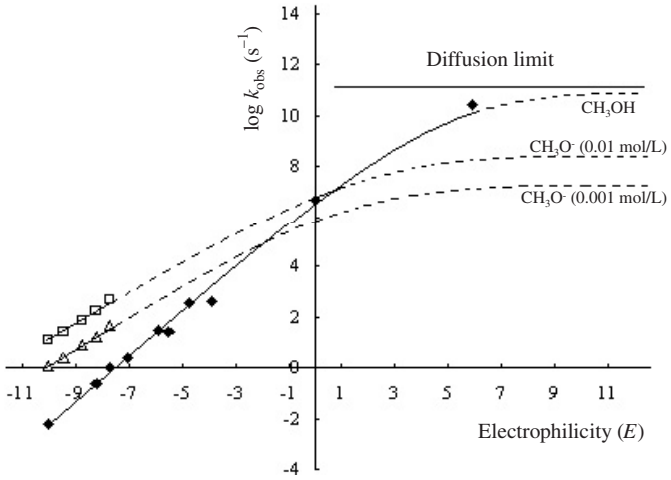


Fig. 5. Pseudo-first-order rate constants (k_{obs}, s^{-1}, at 20 °C) for the reactions of carbocations with methoxide and methanol in 1 and 10 mmol/L solutions of methoxide in methanol–acetonitrile (91:9, *v*/*v*). The rate constant for the reaction of Ph_2CH^+ (E = 5.90) with methanol was taken from ref. 22.



cause of the greater slopes of the alcohol correlations, and in the range $-3 < E < 3$, crossing of the correlation lines takes place. Highly reactive carbocations will almost exclusively react with the solvent that is present in higher concentration and not with the more nucleophilic alkoxides (21).

Though the kinetic investigations in this study were performed with benzhydrylium ions and quinone methides as reference electrophiles, the conclusions are of more general validity. Since eq. [1] has been demonstrated to generally hold for reactions of nucleophiles with various types of π electrophiles (5, 23*a*), e.g., other types of carbocations (3), Michael acceptors (23*b*), and electron-deficient arenes (24, 25), one can use the reactivity parameters determined in this work to predict whether alcohols or alkoxides are the effective nucleophiles in reactions of these electrophiles with alcoholic alkoxide solutions.

Experimental

Materials

Solvents

Reagent grade methanol (99.8%) was purchased from Acros (Nidderau), and absolute ethanol and *n*-propanol were distilled from magnesium and iodine. Anhydrous isopropanol (99.5%) was purchased from Aldrich (Munich). Anhydrous acetonitrile (99.5%) was purchased from Merck (Darmstadt).

Alkoxides

Sodium methoxide and sodium ethoxide were purchased from Acros (Nidderau). Stock solutions of other sodium alkoxides (*n*-propoxide and isopropoxide) were prepared by adding freshly cut sodium metal prewashed in the corresponding solvents to pure solvents maintained in an atmosphere of dry nitrogen. Solutions thus prepared were stored under dry nitrogen and analyzed immediately before use by titration with 0.1 mol/L HCl to the phenolphthalein-endpoint. Stock solutions of the sodium alkoxides were usually 0.1–0.15 mol/L. Solutions of lower concentrations were prepared by dilution.

Kinetic measurements

Because the reactions of the colored reference electrophiles with nucleophiles gave rise to colorless products, the decay of the absorptions of the electrophiles was followed by UV–vis spectroscopy (4, 6, 15*a*, 26).

The temperature of the solutions during all kinetic studies was kept constant (20 ± 0.1 °C) by using a circulating bath thermostat.

The rates of slow reactions ($\tau_{1/2} > 10$ s at 20 °C) were determined by using a J&M Tidas diode array spectrophotometer, which was controlled by Labcontrol Spectacle software and connected to a Hellma 661.502-QX quartz Suprasil immersion probe (5 mm light path) via fiber optic cables and standard SMA connectors. Hi-Tech SF-61DX2 stopped-flow spectrophotometer systems (controlled by Hi-Tech KinetAsyst2 software) were used for the investigation of rapid reactions (10 ms < $\tau_{1/2}$ < 10 s at 20 °C).

The stopped-flow experiments were performed by mixing 10 volume parts of the alcohols or solutions of the alkoxides in the corresponding alcohols with 1 volume part of the solutions of the reference electrophiles in acetonitrile to yield 91:9 (*v*/*v*) mixtures of alcohols and acetonitrile. The first-order or pseudo-first-order rate constants (k_{obs}, s^{-1}) were obtained by least-squares fitting of the absorbance A of the electrophiles to the single-exponential ($A_t = A_0 \exp(-k_{obs}t) + C$).

The first-order rate constants (k_1, s^{-1}) of the reactions of alcohols with the reference electrophiles were calculated as mean values of the k_{obs} obtained from several runs.

Alkoxide concentrations were at least 10 times as high as those of the electrophiles, resulting in pseudo-first-order kinetics with an exponential decay of the electrophile concentrations. As the k_{obs} increase linearly with the concentrations of the alkoxides, the slopes of the correlations correspond to

© 2005 NRC Canada

the second-order rate constants (k_2, L mol^{-1} s^{-1}) of the reactions of the alkoxide ions with the electrophiles.[3]

Acknowledgements

Financial support by the Deutsche Forschungsgemeinschaft and the Fonds der Chemischen Industrie is gratefully acknowledged. We thank Dr. T. Lemek for experimental support and Dr. A.R. Ofial for helpful discussions.

References

1. (*a*) C.D. Ritchie. Acc. Chem. Res. **5**, 348 (1972); (*b*) C.D. Ritchie. Can. J. Chem. **64**, 2239 (1986).
2. H. Mayr, T. Bug, M.F. Gotta, N. Hering, B. Irrgang, B. Janker, B. Kempf, R. Loos, A.R. Ofial, G. Remennikov, and H. Schimmel. J. Am. Chem. Soc. **123**, 9500 (2001).
3. (*a*) H. Mayr and M. Patz. Angew. Chem. **106**, 990 (1994); Angew. Chem. Int. Ed. Engl. **33**, 938 (1994); (*b*) H. Mayr, B. Kempf, and A.R. Ofial. Acc. Chem. Res. **36**, 66 (2003); (*c*) H. Mayr and A.R. Ofial. *In* Carbocation chemistry. *Edited by* G.A. Olah and G.K.S. Prakash. Wiley, Hoboken, New Jersey. 2004. Chap. 13. p. 331; (*d*) H. Mayr and A.R. Ofial. Pure Appl. Chem. In press.
4. S. Minegishi, S. Kobayashi, and H. Mayr. J. Am. Chem. Soc. **126**, 5174 (2004).
5. R. Lucius, R. Loos, and H. Mayr. Angew. Chem. **114**, 97 (2002); Angew. Chem. Int. Ed. **41**, 91 (2002).
6. S. Minegishi and H. Mayr. J. Am. Chem. Soc. **125**, 286 (2003).
7. C.F. Bernasconi. J. Am. Chem. Soc. **92**, 4682 (1970).
8. W. Reeve, C.M. Erikson, and P.F. Aluotto. Can. J. Chem. **57**, 2747 (1979).
9. I.G. Murgulescu, D. Oancea, and G. Mincu. Rev. Roum. Chim. **14**, 3 (1969).
10. C.D. Ritchie. J. Am. Chem. Soc. **97**, 1170 (1975).
11 C.G. Swain and C.B. Scott. J. Am. Chem. Soc. **75**, 141 (1953).
12. (*a*) D.N. Kevill and S.W. Anderson. J. Org. Chem. **56**, 1845 (1991); (*b*) D.N. Kevill. *In* Advances in quantitative structure-property relationships. Vol. 1. *Edited by* M. Charton. JAI Press, Greenwich, Connecticut. 1996. pp. 81.
13. J.W. Bunting, J.M. Mason, and C.K.M. Heo. J. Chem. Soc. Perkin Trans. 2, **11**, 2291 (1994).
14. J.P. Richard, M.M. Toteva, and J. Crugeiras. J. Am. Chem. Soc. **122**, 1664 (2000).
15. Rate constants for the reactions of Ar_2CH^+ with neutral π systems and hydride donors are almost unaffected by solvent polarity: (*a*) H. Mayr, R. Schneider, C. Schade, J. Bartl, and R. Bederke. J. Am. Chem. Soc. **112**, 4446 (1990); (*b*) H. Mayr, N. Basso, and G. Hagen. J. Am. Chem. Soc. **114**, 3060 (1992); (*c*) M.A. Funke and H. Mayr. Chem. Eur. J. **3**, 1214 (1997).
16. E. Grunwald and S. Winstein. J. Am. Chem. Soc. **70**, 846 (1948).
17. T.W. Bentley and G. Llewellyn. *In* Progress in physical organic chemistry. *Edited by* R.W. Taft. John Wiley and Sons, Inc., New York. 1990.
18. S. Winstein, A.H. Fainberg, and E. Grunwald. J. Am. Chem. Soc. **79**, 4146 (1957).
19. (*a*) The influence of alcohols on the nucleophilicity of basic aqueous solutions has previously been studied in reactions with 1,3,5-trinitrobenzene: C.F. Bernasconi and R.G. Bergstrom. J. Org. Chem. **36**, 1325 (1971); (*b*) Relative reactivities of water and alcohol toward carbocations in mixed solvents have extensively been studied: T.W. Bentley, D.N. Ebdon, E.-J. Kim, and I.S. Koo. J. Org. Chem. **70**, 1647 (2005).
20. (*a*) R. Stewart. *In* The proton: Applications to organic chemistry. Organic chemistry – A series of monographs. Vol. 46. *Edited by* H.H. Wasserman. Academic Press, Orlando, Florida. 1985; (*b*) W.N. Olmstead, Z. Margolin, and F.G. Bordwell. J. Org. Chem. **45**, 3295 (1980).
21. An analogous relationship has been reported for the relative reactivities of $CF_3CH_2O^-$ and CF_3CH_2OH: J.P. Richard and W.P. Jencks. J. Am. Chem. Soc. **106**, 1373 (1984).
22. R.A. McClelland. *In* Reactive intermediate chemistry. *Edited by* R.A. Moss, M.S. Platz, and M. Jones, Jr. John Wiley and Sons, Inc., Hoboken, N.Y. 2004. Chap. 1. pp. 3–40.
23. (*a*) R. Lucius and H. Mayr. Angew. Chem. **112**, 2086 (2000); Angew. Chem. Int. Ed. **39**, 1995 (2000); (*b*) T. Lemek and H. Mayr. J. Org. Chem. **68**, 6880 (2003).
24. F. Terrier, S. Lakhdar, R. Goumont, T. Boubaker, and E. Buncel. Chem. Commun. (Cambridge), 2586 (2004).
25. G.Ya. Remennikov, B. Kempf, A.R. Ofial, K. Polborn, and H. Mayr. J. Phys. Org. Chem. **16**, 431 (2003).
26. (*a*) H. Mayr and A.R. Ofial. Einsichten-Forschung an der LMU München, **20**, 30 (2001); (*b*) A.D. Dilman, S.L. Ioffe, and H. Mayr. J. Org. Chem. **66**, 3196 (2001).

[3] Supplementary data for this article are available on the Web site or may be purchased from the Depository of Unpublished Data, Document Delivery, CISTI, National Research Council Canada, Ottawa, ON K1A 0R6, Canada. DUD 4048. For more information on obtaining material refer to http://cisti-icist.nrc-cnrc.gc.ca/irm/unpub_e.shtml.

© 2005 NRC Canada

Acid enol and dihydropyridine intermediates in pyridylketene hydration — A computational study[1]

Andrei V. Fedorov, Katayoun Najafian, Thomas T. Tidwell, and Sinisa Vukovic

Abstract: 3-Pyridylketene (3-**1**) is found experimentally to undergo hydration forming an intermediate acid enol 3-**2**; whereas 2- and 4-pyridylketenes (2-**1** and 4-**1**), instead, form (carboxymethylene)dihydropyridine intermediates 2-**4** and 4-**4**, which live much longer than 3-**2**. Density functional calculations have been carried out to elucidate the hydration reactivity of these ketenes, and reveal that the dihydropyridine intermediates 2-**4** and 4-**4** are more stable than the unobserved acid enols 2-**2** and 4-**2** by 6.23 and 12.2 kcal/mol, respectively. For 3-**1** a pathway was calculated utilizing two H_2O molecules leading to the acid enol intermediate 3-**2**, which then forms 3-pyridylacetic acid (3-**3**). Hydration of 4-pyridylketene involves net 1,6-addition of water, and a pathway involving a bridge of six H_2O molecules connecting the pyridyl nitrogen and the carbonyl carbon was determined.

Key words: mechanisms of pyridylketene hydration, computations, enols, dihydropyridines.

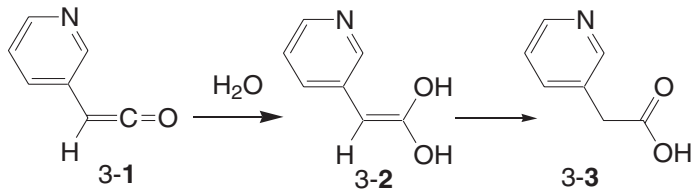
Résumé : On a démontré expérimentalement que le 3-pyridylcétène (3-**1**) subit une hydratation qui conduit à la formation d'un intermédiaire acide énolique 3-**2** alors que les 2- et 4-pyridylcétènes (2-**1** et 4-**1**) conduisent plutôt à la formation d'intermédiaires (carboxyméthylène)dihydropyridines 2-**4** et 4-**4** dont les temps de vie sont beaucoup plus longs que celui du composé 3-**2**. On a effectué des calculs de densité fonctionnelle pour élucider la réactivité de ces cétènes vis-à-vis de l'hydratation et ils ont démontré que les intermédiaires dihydropyridines 2-**4** et 4-**4** sont beaucoup plus stables que les acides énoliques 2-**2** et 4-**2** qui n'ont jamais été isolés et que les différences d'énergie sont respectivement de 6,23 et 12,2 kcal/mol. Pour le composé 3-**1**, on a calculé une voie réactionnelle qui fait appel à deux molécules d'eau et qui conduit à l'intermédiaire acide énolique 3-**2** et finalement à l'acide 3-pyridylacétique (3-**3**). L'hydratation du 4-pyridylcétène implique une addition 1,6 d'eau et on a déterminé une voie réactionnelle impliquant un pont de six molécules d'eau reliant l'azote de la pyridine et le carbone du groupe carbonyle.

Mots clés : mécanisme de l'hydratation de pyridylcétènes, calculs, énols, dihydropyridine.

[Traduit par la Rédaction]

Introduction

In recent experimental studies in our laboratory (1) the 2-, 3-, and 4-pyridylketenes (2-**1**, 3-**1**, and 4-**1**) were generated as transient intermediates by laser flash photolysis of the corresponding diazo ketones in CH_3CN solution, with confirmation of the structures by the observation of the characteristic ketenyl absorptions at 2127, 2125, and 2128 cm^{-1}, respectively, using time-resolved infrared spectroscopy (TRIR) (1*d*). Studies of the hydration reactivity of these species using UV spectroscopy (1*a*) have shown that 3-**1** undergoes hydration to 3-pyridylacetic acid (3-**3**) via a transient acid enol intermediate 3-**2** comparable to that formed from phenylketene (1*b*). Two processes were observed in the reaction of 3-**1** and were assigned to the formation and decay of acid enol intermediate 3-**2** (eq. [1]) (1*a*). However, hydration of 2-**1** and 4-**1** did not form observable enols **2**, but instead, gave transient intermediates identified as (carboxymethylene)dihydropyridines (2-**4** and 4-**4**), resulting from the conjugate addition of H_2O (eqs. [2] and [3]) (1*a*). In the case of 2-**1**, the longer-lived transient decayed with biexponential kinetics, and it was proposed that both *Z*-2-**4a**

[1] 

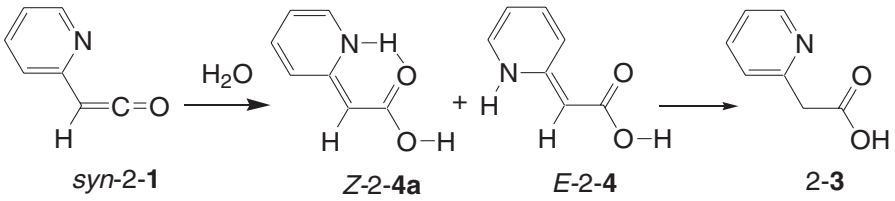
3-**1** 3-**2** 3-**3**

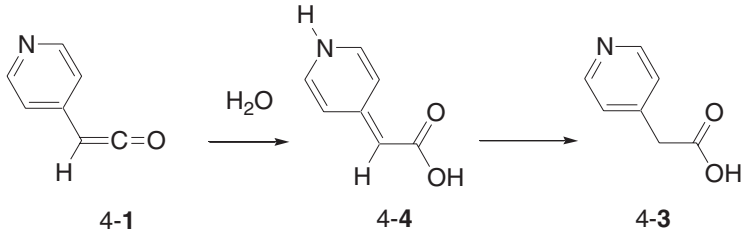
Received 30 March 2005. Published on the NRC Research Press Web site at http://canjchem.nrc.ca on 29 November 2005.

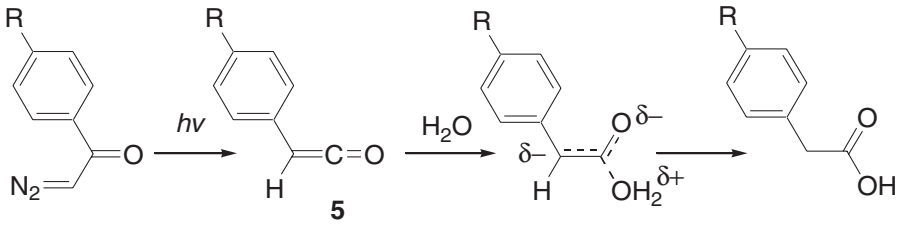
A.V. Fedorov,[2] K. Najafian, T.T. Tidwell,[3] and S. Vukovic. Department of Chemistry, University of Toronto, Toronto, ON M5S 3H6, Canada.

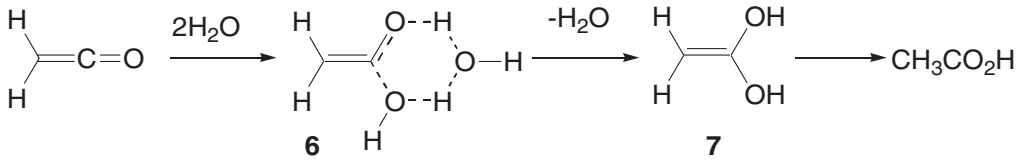
[1]This article is part of a Special Issue dedicated to organic reaction mechanisms.
[2]Current address: Wright Photoscience Laboratory, Department of Chemistry, Bowling Green State University, Bowling Green, OH 43403, USA.
[3]Corresponding author (e-mail: ttidwell@chem.utoronto.ca).

 doi: 10.1139/V05-162 © 2005 NRC Canada

[2] 

[3] 

[4] 

[5] 

and *E*-2-**4** were formed, possibly from the two conformers of 2-**1** (1*a*).

Previous examinations of the mechanisms of ketene hydration (2) include the classic experimental studies of arylketenes (2*a*) and of ketene itself (2*b*), and theoretical studies for ketene (3). The rate constants for the reaction of arylketenes **5** with H_2O were correlated with Hammett σ constants for the substituents with a slope of 1.2 (2*b*), indicative of rate-limiting nucleophilic attack of water on the carbonyl carbon in the ketene plane (2), with stabilization of partial negative charge in the transition state by the aryl group (eq. [4]) (3*a*).

Computational studies of the hydration of ketene favor structures in which multiple water molecules are involved, and for two H_2O molecules a cyclic transition state **6** is preferred, with a much lower barrier than for the addition of a single water molecule (3). This leads to the enol **7** of acetic acid (eq. [5]), and for some ketenes the acid enol intermediates have been detected by UV spectroscopy, including the recent studies of phenylketene (**5**, R = H) itself (1*b*). The acid enol $Ar_2C{=}C(OH)_2$ from ditipylketene ($Ar_2C{=}C{=}O$, Ar = 2,4,6-*i*-$Pr_3C_6H_2$) has been directly observed as a long-lived species in solution by NMR (4).

The N-H···O hydrogen bonding in *Z*-2-**4** (eq. [2]) is of additional interest for its resemblance to that observed in similar systems involving N-H···O hydrogen bonding proposed to be stabilized by resonance-assisted hydrogen bonds (RAHB) (5). The related example of intramolecular hydrogen bonding in the enol of acetylacetone has also been recently reinvestigated (5*d*).

The goal of the present study was a computational examination of the hydration of the pyridylketenes (2-**1**, 3-**1**, and 4-**1**), with an effort to answer such questions as the contrast between the behavior of 4-**1** in hydration and amination, forming a dihydropyridine and an enol, respectively, and to test the validity of the interpretations of the experimental results. It was also intended to see if any evidence for stabilization due to RAHB or pseudopericyclic transition states (6) could be found.

Results

Structures and energies of 2-**1**, 3-**1**, and 4-**1** and their hydration products were calculated at the B3LYP/6-311+G**//B3LYP/6-311+G** level using GAUSSIAN 98 (7), as reported in Table 1. The energies were corrected using calculated zero point vibrational energies (ZPVE). Relative energies (kcal/mol) for the different conformations were *syn*-2-**1** (0.0), *anti*-2-**1** (1.3), *syn*-3-**1** (4.2), *anti*-3-**1** (3.9), and 4-**1** (2.9); and the barriers to rotation about the aryl–ketenyl bond relative to the minimum energy conformation for each isomer were 7.2, 3.7, and 4.8 kcal/mol, respectively (Table 1).

The hydration products for the addition of one and two H_2O molecules examined include complexes **14**, transition structures **15**, acid enols **2**, (carboxymethylene)dihydropyridine

© 2005 NRC Canada

Table 1. Energies (Hartrees) for hydration of pyridylketenes **1** (B3LYP/6-311+G**//B3LYP/6-311+G**).

Structure	E + ZPVE[a]	ΔE (kcal/mol)
syn-2-**1**	–399.706 650	0.0
anti-2-**1**	–399.704 542	1.32
TS-2-**1**	–399.695 155	7.21
H_2O	–76.437 174	
syn-2-**1** + H_2O	–476.143 824	0.0
syn-2-**1** + $2H_2O$	–552.580 998	0.0
syn-2-**1** + $3H_2O$	–628.018 172	0.0
anti-2-**1** + H_2O	–476.141 716	0.0 (1.32)
syn-2-**2a**	–476.143 366	0.29
syn-2-**2a** + H_2O	–552.580 540	0.30 (0.0)
syn-2-**2a**·H_2O	–552.589 642	(–5.43)
anti-2-**2a**	–476.147 963	–3.92 (5.25)
anti-2-**2a**·H_2O	–552.595 391	–10.36
syn-2-**2b**	–476.169 857	–16.34
syn-2-**2b** + H_2O	–552.607 031	–16.34
syn-2-**2b**·H_2O	–552.618 123	–23.30
2-**2b**·H_2O + H_2O	–629.055 297	–23.30
syn-2-**2c**	–476.165 166	–13.39
syn-2-**3a**	–476.182 220	–24.09
syn-2-**3a** + H_2O	–522.619 394	–24.09
syn-2-**3b**	–476.179 328	–22.28
2-**3c**	–476.180 427	–22.97
2-**3c**·H_2O	–552.630 401	–31.00
2-**3c**·H_2O + H_2O	–629.067 574	–31.00
Z-2-**4a**	–476.178 927	–22.03
Z-2-**4a** + H_2O	–522.616 102	–22.03
Z-2-**4a**·H_2O	–552.628 129	–29.57
E-2-**4a**	–476.166 238	–15.39 (–14.07)
Z-2-**4b**	–476.171 023	–17.07
Z-2-**4b** + H_2O	–522.608 197	–17.07
Z-2-**4b**·H_2O	–522.622 124	–25.81
E-2-**4b**	–476.162 663	–11.83 (–13.14)
E-2-**4b** + H_2O	–522.599 837	–11.82
Z-2-**4b**·H_2O	–552.622 124	–25.81
syn-2-**14a**	–476.146 937	–2.0
syn-2-**14b**	–552.593 152	–7.63
syn-2-**15a**	–476.076 895	42.00
syn-2-**15b**	–552.552 608	17.81
syn-2-**16a**	–552.560 211	13.04
syn-2-**16b**	–629.009 094	5.70
syn-3-**1** (*syn*-3-PyCH=C=O)	–399.699 903	4.23 (0.30)
anti-3-**1**	–399.700 391	3.93 (0.0)
TS-3-**1**	–399.694 556	7.59 (3.66)
syn-3-**1** + $2H_2O$	–522.574 251	0.0
syn-3-**2**	–552.590 633	–10.28
syn-3-**3**	–552.627 097	–33.16
syn-3-**14**	–552.586 727	–7.83
syn-3-**15**	–522.553 199	13.21
4-**1** (4-PyCH=C=O)	–399.702 012	2.91 (0.0)
TS-4-**1**	–399.694 275	7.76 (4.85)
4-**1** + H_2O	–476.139 186	0.0
4-**1** + $2H_2O$	–552.576 360	0.0
4-**1** + $3H_2O$	–629.013 535	0.0
4-**1** + $4H_2O$	–705.450 708	0.0
4-**1** + $6H_2O$	–858.325 056	(0.0)
4-**1**·$6H_2O$	–858.384 424	(–37.25)
4-**2**	–476.145 731	–4.11
4-**2**·H_2O	–552.593 497	–10.75
4-**2**·$3H_2O$	–705.488 787	–23.89
4-**2**·$3H_2O$ (in H_2O)	–705.489 485	–24.33
4-**3**	–476.177 170	–23.83
4-**3** + H_2O	–552.614 344	–23.83
4-**3** + $3H_2O$	–705.488 692	–23.83
4-**4**	–476.165 149	–16.29
4-**4**·$3H_2O$	–705.508 591	–36.32
4-**4**·$3H_2O$ (in H_2O)	–705.509 710	–37.02
4-**14a**	–476.143 086	0.0
4-**14b**	–552.588 709	–7.75
4-**15a**	–476.078 625	38.00
4-**15b**	–552.556 270	12.61

Table 1 (*concluded*).

[a]ZPVE = zero point vibrational energy.

intermediates 2-**4** and 4-**4**, and product arylacetic acids **3**. Energies are given in Table 1, and the reaction profile for hydration of *syn*-2-pyridylketene (*syn*-2-**1**) with two H_2O molecules is shown in Fig. 1. This shows the formation of initial complex 2-**14b**, transition structure 2-**15b**, and acid enol *syn*-2-**2a**·H_2O, which is 5.4 kcal/mol more stable than the reactants. The isomeric acid enol *syn*-2-**2b**·H_2O is a further 17.9 kcal/mol more stable, and this provides a measure of the strength of the intramolecular hydrogen bond. The dihydropyridine tautomer *Z*-2-**4a**·H_2O is more stable by an additional 6.3 kcal/mol, with a hydrogen bond length NH···O of 1.812 Å, while the acid *syn*-2-**3c**·H_2O is another 1.4 kcal/mol more stable. Profiles for the other reactions are given in Figs. S1–S3 (Supporting information).[4] For comparison a number of structures were also calculated at the B3LYP/6-31++G**//B3LYP/6-31++G** level, and the energy differences between pairs of intermediates were very similar in all cases at the two levels of theory (Table S2, Supporting information).[4]

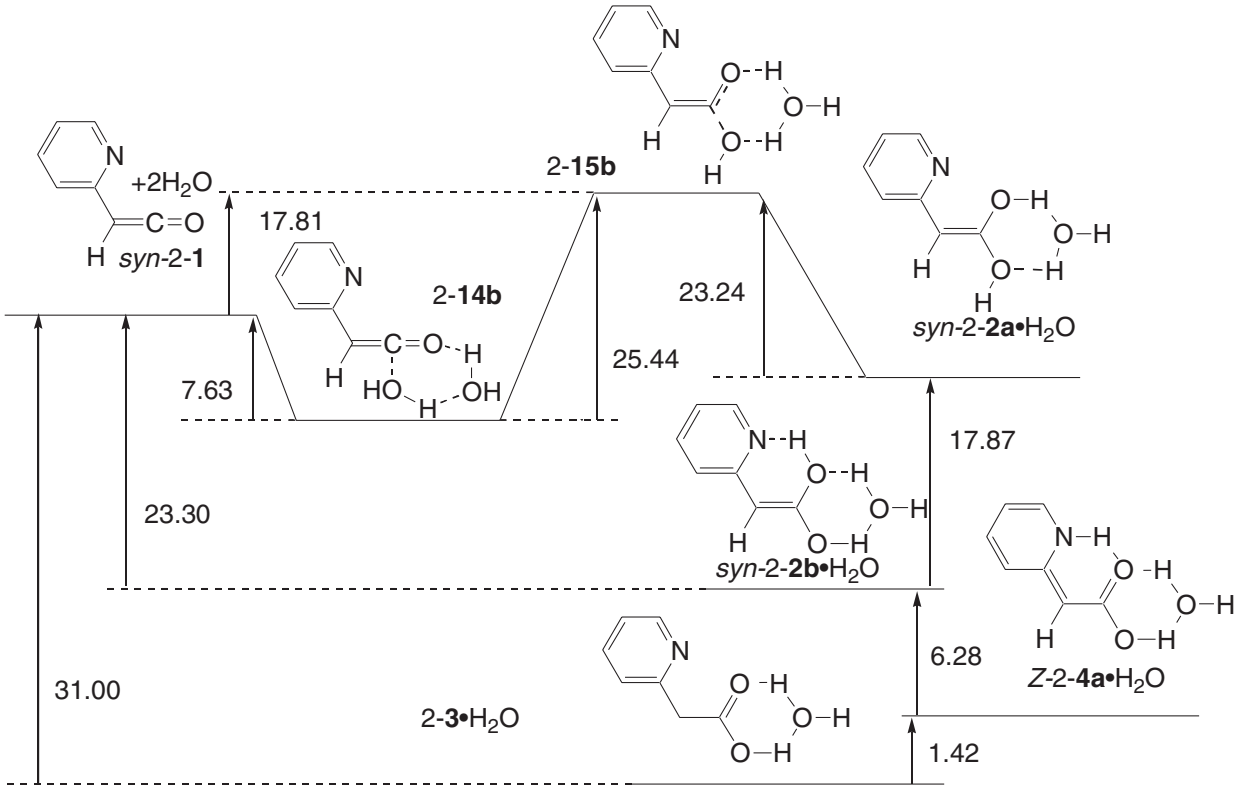
The initially formed acid enols 2-**1**, 3-**1**, and 2-**2a** are calculated to be 5.4, 10.3, and 10.8 kcal/mol, respectively, more stable than the separated reactants. 2-Carboxymethylene-1,4-dihydropyridine (2-**4**) is 12.2 kcal/mol more stable than the acid enol 4-**2** (Scheme 1).

The conversion from 4-pyridylketene to 4-carboxymethylene-1,4-dihydropyridine (4-**4**) in water is expected to involve the participation of a bridge of water molecules to enable proton addition to nitrogen and OH addition to the ketenyl carbon by a relay mechanism in which successive proton transfers occur. To simulate this process, the struc-

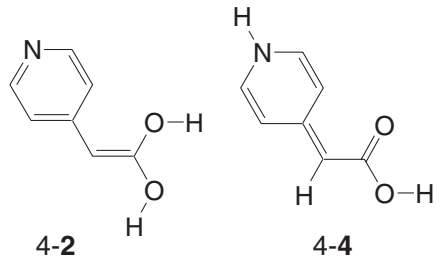
[4] Supplementary data for this article are available on the Web site or may be purchased from the Depository of Unpublished Data, Document Delivery, CISTI, National Research Council Canada, Ottawa, ON K1A 0R6, Canada. DUD 4047. For more information on obtaining material refer to http://cisti-icist.nrc-cnrc.gc.ca/irm/unpub_e.shtml.

© 2005 NRC Canada

Fig. 1. B3LYP/6-311+G**//B3LYP/6-311+G** calculated energy changes (kcal/mol) for hydration of 2-pyridylketene (2-**1**).



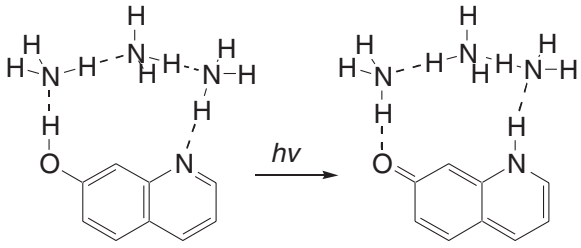
Scheme 1. Relative energies (kcal/mol) of hydrates of 4-pyridylketene (4-**1**).



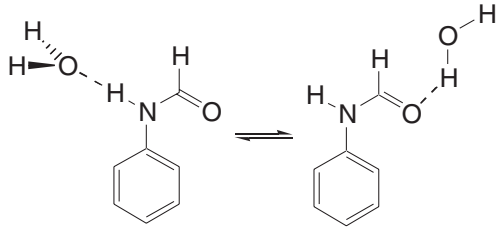
tures of reaction with a chain of six H_2O molecules between the nitrogen and the ketenyl group were calculated. These include an initial ketene complex 4-**1**·6H_2O, the complexed acid enol 4-**2**·5H_2O, and 4-**4**·5H_2O (Fig. 2). The complexed ketene 4-**1**·6H_2O has the water bridge largely in the plane of the pyridylketene and was calculated to be 37.3 kcal/mol more stable than the separated reactants at the B3LYP/6-311+G**//B3LYP/6-311+G** level (Table 1). This stabilization arises from the seven hydrogen bonds present in the complex. The water bridges in 4-**4**·5H_2O and in the acid enol 4-**2**·5H_2O are above the pyridyl plane, and the dihydropyridine 4-**4**·5H_2O is computed to be more stable than the enediol 4-**2**·5H_2O by 7.4 kcal/mol at the B3LYP/6-31G*//B3LYP/6-31G* level (Table S3, Supporting information).[4] This compares to the difference among the intermediates without the 5H_2O of 12.2 kcal/mol (Scheme 1).

Other similar structures with the same or different numbers of water molecules are expected to contribute to the species present in solution, and no single structure, but rather many, would be involved in the transformation in solution. An analogous relay mechanism for hydrogen transfer between oxygen and quinolyl nitrogen utilizing a bridge of three NH_3 molecules has recently been demonstrated by an experimental and computational study (eq. [6]) (8*a*). In another example of this type of process, the barrier to migration of a single water molecule hydrogen bonded to the nitrogen moving to the carbonyl oxygen of *N*-phenyl formamide was measured experimentally and calculated at the B3LYP/6-31+G* level, with a calculated barrier of 3.2 kcal/mol compared with the averaged experimental barrier of 2.6 kcal/mol (eq. [7]) (8*b*). Other reactions involving chains of water molecules to effect proton transfer have also been reported (8*c*–8*e*).

[6]

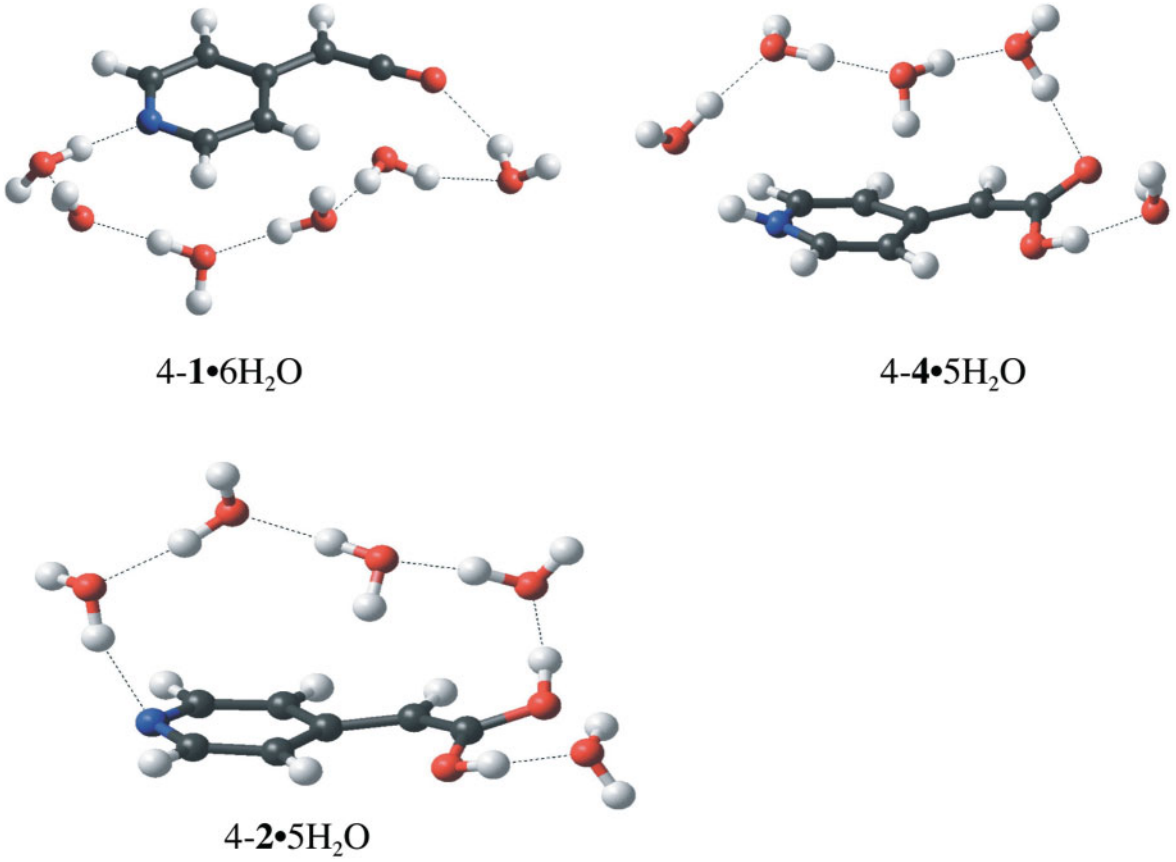


[7]

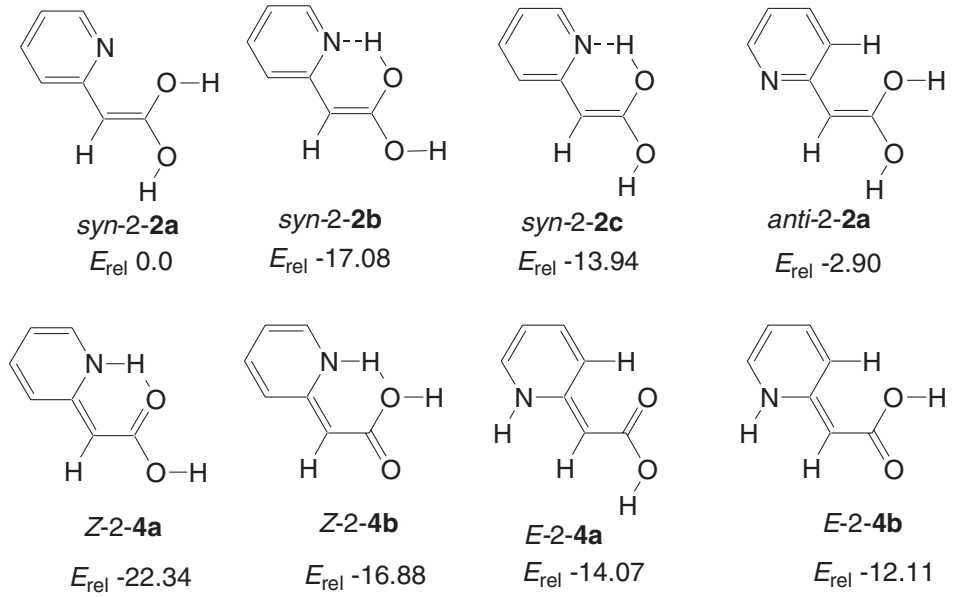


© 2005 NRC Canada

Fig. 2. Calculated structures of 4-pyridylketene complex (4-**1**·6H_2O), dihydropyridine 4-**4**·5H_2O, and acid enol 4-**2**·5H_2O (B3LYP/6-31G*//B3LYP/6-31G*) from hydration of ketene 4-**1** with a bridge of six H_2O molecules.



Scheme 2. Relative energies (kcal/mol) of hydrates of 2-pyridylketene (2-**1**).



Calculated relative energies (Table 1) of various monohydrates of 2-pyridylketene are summarized in Scheme 2, and the 2-carboxymethylene-1,2-dihydropyridine intermediate *Z*-2-**4a** with an intramolecular hydrogen bond from the carbonyl oxygen to the pyridyl nitrogen was calculated to be 5.5 kcal/mol more stable than *Z*-2-**4b** with a hydrogen bond to the hydroxyl oxygen, and 5.3 kcal/mol more stable than the hydrogen bonded acid enol *syn*-2-**2b**. The energy difference between the acid enols *syn*-2-**2a** and *syn*-2-**2b** of 17.1 kcal/mol provides a measure of the strength of

© 2005 NRC Canada

the hydrogen bond in the acid enols. The hydrogen bonded dihydropyridine *Z*-2-**4a** is 8.3 kcal/mol more stable than *E*-2-**4a**.

Discussion

The transition structures **15** for the addition of two H_2O molecules to the ketenyl group with the formation of acid enols are 17.8, 13.2, and 12.6 kcal/mol, respectively, higher in energy than the separated reactants for 2-**1**, 3-**1**, and 4-**1**. These follow the order of the experimental rate constant ratios of the ketenes 4-**1**:3-**1**:2-**1** of 4.5:2.3:1.0 for hydration and 17:4.0:1.0 for amination. Therefore, 4-pyridylketene has the lowest calculated barrier and is the most reactive, while 2-pyridylketene has the highest calculated barrier and the lowest observed reactivity. The computed stability of the isomers at the B3LYP/6-311+G** level is 2-**1** > 4-**1** > 3-**1**, so the orders of reactivity do not strictly follow the ground state stabilities. The rate constant ratio ($k_{(\text{ketene to intermediate})}/k_{(\text{intermediate to product})}$) for amination of 4-**1** is 6.2, but for hydration of 4-**1** this ratio is 2.4×10^3. The difference between the two lies in the fact that hydration of 4-**1** results in the formation of a long-lived intermediate shown to be 4-**4** (eq. [3]); whereas no such intermediate is detected in amination.

The fundamental difference in the reaction pathways is that in hydration 1,6-addition to 4-pyridylketene can occur by a relay mechanism through a network of water molecules to effect nucleophilic addition to the carbonyl carbon together with electrophilic protonation at nitrogen (Fig. 2; see also Scheme S5, Supporting information).[4] This can be readily achieved in solvent H_2O, as illustrated for six H_2O molecules in Fig. 2, but is not feasible for amination, in which the concentration of *n*-butylamine in CH_3CN used was between 10^{-4} and 10^{-3} mol/L (1*d*). This is well-illustrated by the reaction of eq. [6], in which stepwise transfer of the proton through the ammonia "wire" was demonstrated experimentally and computationally (8*a*). 4-Carboxymethylene-1,4-dihydropyridine (4-**4**) is relatively long-lived, as conversion of this species to the product acid also requires the participation of a number of water molecules. It may be seen that one of the water molecules in 4-**4**·5H_2O (Fig. 2) has a water molecule well-positioned for proton donation to C2 of the incipient pyridylacetic acid.

The dihydropyridine intermediates 2-**4** can be assigned as the *E*-2-**4** and *Z*-2-**4** structures, respectively, and their formation in a 28:72 ratio corresponds to the equilibrium ratio of the anti and syn conformations of 2-pyridylketene (2-**1**) predicted by computations and observed experimentally by trapping in an argon matrix at 10 K (9). However, the conformations of 2-**1** may have different reactivities. Dihydropyridine *Z*-2-**4** is stabilized by an intramolecular hydrogen bond and is longer lived than the E stereoisomer. Both of the dihydropyridyl structures (*Z*-2-**4** and *E*-2-**4**) are longer lived than the enol 3-**2** (eq. [6]), and this may reflect the greater stability of *Z*-2-**4** and *E*-2-**4** and the greater degree of bond reorganization needed for conversion to the acid.

Conclusion

In summary, the computations predict that the transient carboxymethylene–dihydropyridines formed in hydration of 2-**1** and 4-**1** are more stable than the acid enols, which is in agreement with experiment. The computed reaction pathway for hydration of 3-**1** leads to an acid enol transient, and no dihydropyridine is possible. Structures of isomeric dihydropyridine transients from hydration of 2-**1** have also been calculated, and these correspond to the two experimentally observed transients in this reaction. A structure with a bridge of six H_2O molecules between the carbonyl carbon of 2-**1** and the pyridyl nitrogen has been calculated, as well as the structure of the dihydropyridine that would result from proton addition to nitrogen and OH addition to ketenyl carbonyl by a relay mechanism involving six H_2O molecules connecting the ring nitrogen and the keteneyl group. No evidence for the conceptually attractive pseudopericyclic mechanism is found for hydration of 2-**1**, and the computational studies provide no evidence for or against the stabilization of the dihydropyrine intermediate *Z*-2-**4a** by resonance-assisted hydrogen bonding.

Acknowledgement

Financial support by the Natural Sciences and Engineering Research Council of Canada (NSERC), the Petroleum Research Fund administered by the American Chemical Society, and a Killam Fellowship from the Canada Council for the Arts to T.T.T. is gratefully acknowledged.

References

1. (*a*) A.D. Allen, A.V. Fedorov, T.T. Tidwell, and S. Vukovic. J. Am. Chem. Soc. **126**, 13790 (2004); (*b*) Y. Chiang, A.V. Fedorov, A.J. Kresge, I. Onyido, and T.T. Tidwell. J. Am. Chem. Soc. **126**, 9382 (2004); (*c*) A.D. Allen, A.V. Fedorov, K. Najafian, T.T. Tidwell, and S. Vukovic. Pure Appl. Chem. **76**, 1953 (2004); (*d*) A.W. Acton, A.D. Allen, L.M. Antunes, A.V. Fedorov, K. Najafian, T.T. Tidwell, and B.D. Wagner. J. Am. Chem. Soc. **124**, 13790 (2002).
2. (*a*) E. Bothe, H. Meier, D. Schulte-Frohlinde, and C. von Sonntag. Angew. Chem. Int. Ed. Engl. **15**, 380 (1976); (*b*) E. Bothe, A.M. Dessouk, and D. Schulte-Frohlinde. J. Phys. Chem. **84**, 3270 (1980); (*c*) A.D. Allen, A.J. Kresge, N.P. Schepp, and T.T. Tidwell. Can. J. Chem. **65**, 1719 (1987); (*d*) J. Andraos and A.J. Kresge. J. Photochem. Photobiol. A, **57**, 165 (1991); (*e*) A.D. Allen, J. Andraos, A.J. Kresge, and M.A. McAllister. J. Am. Chem. Soc. **114**, 1878 (1992); (*f*) J. Andraos and A.J. Kresge. Can. J. Chem. **78**, 508 (2000); (*g*) Y. Chiang, A.J. Kresge, and V.V. Popik. J. Chem. Soc. Perkin Trans. 2, 1107 (1999).
3. (*a*) M.T. Nguyen and A.F. Hegarty. J. Am. Chem. Soc. **106**, 1552 (1984); (*b*) P.N. Skancke. J. Phys. Chem. **96**, 8065 (1992); (*c*) M.T. Nguyen and G. Raspoet. Can. J. Chem. **77**, 817 (1999); (*d*) J.P. Guthrie. Can J. Chem. **77**, 934 (1999); (*e*) X. Duan and M. Page. J. Am. Chem. Soc. **117**, 5114 (1995).
4. (*a*) J. Frey and Z. Rappoport. J. Am. Chem. Soc. **118**, 5169 (1996); (*b*) J. Frey and Z. Rappoport. J. Am. Chem. Soc. **118**, 5182 (1996).
5. (*a*) P. Gilli, V. Bertolasi, V. Ferretti, and G. Gilli. J. Am. Chem. Soc. **122**, 10405 (2000); (*b*) J. Chin, F. Mancin, N.

© 2005 NRC Canada

Thavarajah, D. Lee, A. Lough, and D.S. Chung. J. Am. Chem. Soc. **125** 15276 (2003); (*c*) A. Filarowski, A. Koll, and T. Glowiak. J. Chem. Soc. Perkin Trans. 2, 835 (2002); (*d*) R. Srinivasan, J.S. Feenstra, S.T. Park, S. Xu, and A.H. Zewail. J. Am. Chem. Soc. **126**, 2266 (2004).

6. (*a*) D.M. Birney, X. Xu, S. Ham, and X. Huang. J. Org. Chem. **62**, 7114 (1997); (*b*) C. Zhou and D.M. Birney. J. Am. Chem. Soc. **124**, 5231 (2002); (*c*) S. Ham and D.M. Birney. J. Org. Chem. **61**, 3962 (1996); (*d*) W.W. Shumway, N.K. Dalley, and D.M. Birney. J. Org. Chem. **66**, 5832 (2001); (*e*) for a recent computational examination of pseudopericyclic reactions, see: J. Rodriguez-Otero, E.M. Cabaleiro-Lago, J.M. Hermida-Ramón, and A. Pena-Gallego. J. Org. Chem. **68**, 8823 (2003).
7. M.J. Frisch, G.W. Trucks, H.B. Schlegel, G.E. Scuseria, M.A. Robb, J.R. Cheeseman, V.G. Zakrzewski, J.A. Montgomery, Jr., R.E. Stratmann, J.C. Burant, S. Dapprich, J.M. Millam, A.D. Daniels, K.N. Kudin, M.C. Strain, O. Farkas, J. Tomasi, V. Barone, M. Cossi, R. Cammi, B. Mennucci, C. Pomelli, C. Adamo, S. Clifford, J. Ochterski, G.A. Petersson, P.Y. Ayala, Q. Cui, K. Morokuma, D.K. Malick, A.D. Rabuck, K. Raghavachari, J.B. Foresman, J. Cioslowski, J.V. Ortiz, A.G. Baboul, B.B. Stefanov, G. Liu, A. Liashenko, P. Piskorz, I. Komaromi, R. Gomperts, R.L. Martin, D.J. Fox, T. Keith, M.A. Al-Laham, C.Y. Peng, A. Nanayakkara, M. Challacombe, P.M.W. Gill, B. Johnson, W. Chen, M.W. Wong, J.L. Andres, C. Gonzalez, M. Head-Gordon, E.S. Replogle, and J.A. Pople. GAUSSIAN 98. Revision A.9 [computer program]. Gaussian, Inc., Pittsburgh, Penn. 1998.
8. (*a*) C. Tanner, C. Manca, and S. Leutwyler. Science, **302**, 1736 (2003); (*b*) J.R. Clarkson, E. Baquero, V.A. Shubert, E.M. Myshakin, K.D. Jordan, and T.S. Zwier. Science, **307**, 1443 (2005); (*c*) J.G. Cole and P. Wan. Can. J. Chem. **80**, 46 (2002); (*d*) M. Fischer and P. Wan. J. Am. Chem. Soc. **121**, 4555 (1999); (*e*) M. Flegel, M. Lukeman, L. Huck, and P. Wan. J. Am. Chem. Soc. **126**, 7890 (2004).
9. A. Kuhn, C. Plüg, and C. Wentrup. J. Am. Chem. Soc. **122**, 1945 (2000).

© 2005 NRC Canada

The addition of alkynes to a tetrasilyldisilene — Evidence for a biradical intermediate[1]

Stephen E. Gottschling, Michael C. Jennings, and Kim M. Baines

Abstract: The addition of two newly developed mechanistic probes, (*trans*,*trans*-2-methoxy-3-phenylcyclopropyl)ethyne (**1**) and (*trans*,*trans*-2-methoxy-1-methyl-3-phenylcyclopropyl)ethyne (**2**), to tetrakis(*tert*-butyldimethylsilyl)disilene (**3**) has been investigated. The addition of **1** to **3** gave 1-[2-(*cis*-2-methoxy-3-phenylcyclopropylidene)vinyl]-1,1,2,2-tetrakis-(*tert*-butyldimethylsilyl)disilane (**5**) as the major product; whereas addition of alkyne **2** to the disilene gave three stereoisomers of 1,1,2,2-tetrakis(*tert*-butyldimethylsilyl)-6-methoxy-5-methyl-7-phenyl-1,2-disilacyclohepta-3,4-diene (**7**–**9**) and 1,1,2,2-tetrakis(*tert*-butyldimethylsilyl)-3-(*trans*,*trans*-2-methoxy-1-methyl-3-phenylcyclopropyl)-1,2-disilacyclobut-3-ene (**10**) as the major products. The formation of cycloheptaallenes **7**–**9** provides convincing evidence that the addition of alkynes to tetrasilyldisilenes involves the formation of a biradical intermediate.

Key words: disilene, alkyne, cycloaddition, reaction mechanism, mechanistic probe.

Résumé : On a étudié l'addition de deux sondes mécanistiques développées récemment, le (*trans*,*trans*-2-méthoxy-3-phénylcyclopropyl)éthyne (**1**) et le (*trans*,*trans*-2-méthoxy-1-méthyl-3-phénylcyclopropyl)éthyne (**2**) sur le tétrakis(*tert*-butyldiméthylsilyl)disilène (**3**). L'addition du composé **1** sur **3** conduit à la formation du 1-[2-(*cis*-méthoxy-3-phényl-cyclopropylidène)vinyl]-1,1,2,2-tétrakis(*tert*-butyldiméthylsilyl)disilane (**5**) comme produit principal alors que l'addition de l'alcyne **2** au disilène conduit à trois stéréoisomères du 1,1,2,2-tétrakis(*tert*-butyldiméthylsilyl)-6-méthoxy-5-méthyl-7-phényl-1,2-disilacyclohepta-3,4-diène (**7**–**9**) et au 1,1,2,2-tétrakis(*tert*-butyldiméthylsilyl)-3-(*trans*,*trans*-2-méthoxy-1-méthyl-3-phénylcyclopropyl)-1,2-disilacyclobut-3-ène (**10**) comme produits principaux. La formation des cycloheptaallènes **7**–**9** apporte une preuve évidente que l'addition d'alcynes à des tétrasilyldisilènes implique la formation d'une intermédiaire biradicalaire.

Mots clés : disilène, alcyne, cycloaddition, mécanisme réactionnel, sonde mécanistique.

[Traduit par la Rédaction]

Introduction

The discovery of stable disilenes over 20 years ago was significant not only because it permitted a detailed characterization of these novel compounds, but also because it provided a facile route to derivatives that could easily be elaborated to more complex structures not readily available by any other means (1). Since their discovery, many researchers have explored the synthetic utility of disilenes; however, without a more complete understanding of the mechanisms of their reactions (2), the applications of this chemistry will be limited. With this goal in mind, we have investigated the mechanisms of the addition of both aldehydes (3, 4) and alkynes (5) to tetramesityldisilene.

In our study of the mechanism of the addition of alkynes to tetramesityldisilene, we have utilized the rapid ring-opening rearrangement of α-cyclopropylvinyl radicals or cations as mechanistic probes (5). The judicious placement of appropriate substituents on cyclopropyl alkynes **1** and **2** enables the discrimination between the formation of an α-cyclopropylvinyl radical, cation, or anion based on the regioselective rearrangements of these intermediates, or lack thereof. We have demonstrated that the vinyl radical will open rapidly ($k_R \sim 10^{10}$ s^{-1}) and regioselectively toward the phenyl substituent, whereas a vinyl cation adjacent to the three-membered ring opens rapidly ($k_R \sim 10^{10}$–10^{12} s^{-1}) toward the methoxy substituent (Scheme 1). The vinyl anion (as modeled by the lithium derivative) is stable towards ring opening (6). Furthermore, the large rate constants for the structural rearrangements of the radical and cation ensures that the ring opening will effectively compete with other possible reactions.

The addition of cyclopropyl alkyne **2** to the prototypical tetraaryldisilene (tetramesityldisilene (5)) resulted in the formation of four products: three stereoisomers of 1,1,2,2-tetramesityl-6-methoxy-5-methyl-7-phenyl-1,2-disilacyclohepta-3,4-diene and 1,1,2,2-tetramesityl-3-(2-methoxy-1-methyl-3-phenylcyclopropyl)disilacyclobut-3-ene (Scheme 2). The structure of the seven-membered ring, particularly the placement of the phenyl substituent, provides convincing

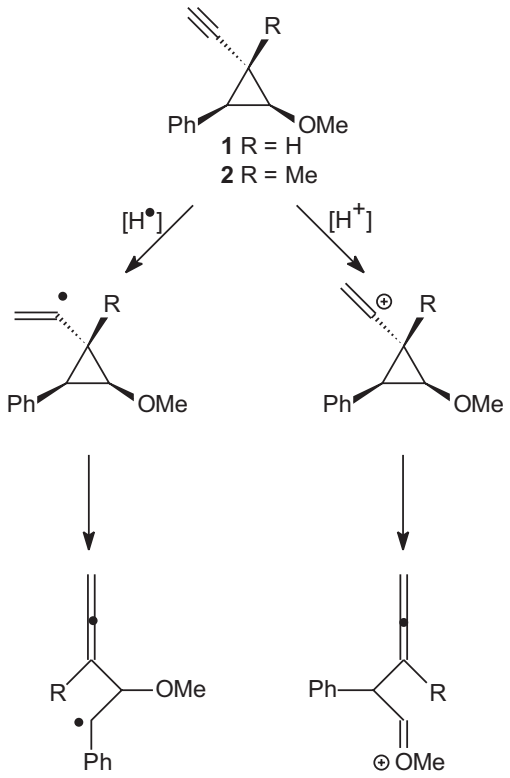
Received 10 May 2005. Published on the NRC Research Press Web site at http://canjchem.nrc.ca on 29 November 2005.

S.E. Gottschling, M.C. Jennings, and K.M. Baines.[2] Department of Chemistry, University of Western Ontario, London, ON N6A 5B7, Canada.

[1]This article is part of a Special Issue dedicated to organic reaction mechanisms.
[2]Corresponding author (e-mail: kbaines2@uwo.ca).

 doi: 10.1139/V05-169 © 2005 NRC Canada

Scheme 1.



evidence that the addition of the alkyne to the disilene involved the formation of a 1,4-biradical intermediate, which opened regioselectively towards the phenyl substituent before ring closure. Closure of the biradical to give the disilacyclobutene appears to compete with ring opening.

We now wish to extend our study and examine the mechanism of the addition of the alkyne probes to other prototypical disilenes. A comparison of the reactivity of tetraaryl- and tetrasilyl-substituted disilenes reveals some notable differences, particularly in reactions with alkenes (1*f*, 7) and alkynes (7*a*, 8). In general, the tetrasilyldisilenes are more prone to ene reactions than are their aryl counterparts. Furthermore, silyl substitution on the double bond also dramatically influences the E/Z isomerization barrier in disilenes: the barrier is much greater in tetraaryldisilenes than in the silyl derivatives (~25 vs. 15 kcal/mol, respectively) (1 cal = 4.184 J) (1*f*, 1*i*). Given these differences, we have now investigated the addition of the alkyne mechanistic probes **1** and **2** to tetrakis(*tert*-butyldimethylsilyl)disilene (**3**), and have compared the results with our previous work on tetramesityldisilene (5).

Results

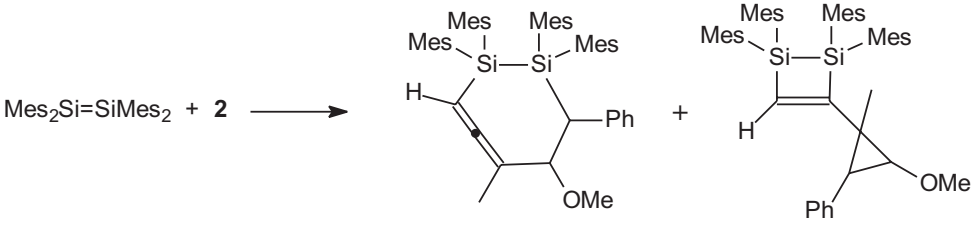
An excess of alkyne **1** was added to a deep orange solution of disilene **3** obtained by photolysis of hexakis(*tert*-butyldimethylsilyl)cyclotrisilane (**4**) (9) in hexanes. The solution was allowed to stir for 16 h. Chromatographic purification of the crude oil obtained after removal of the solvent from the reaction mixture yielded one major product identified as 1-[2-(*cis*-2-methoxy-3-phenyl-cyclopropylidene)vinyl]-1,1,2,2-tetrakis(*tert*-butyldimethylsilyl)disilane (**5**) (see Scheme 3). The structure of **5** was assigned based on the NMR and IR spectroscopic data of the compound. An absorption at 1972 cm^{-1} in the IR spectrum of **5** as well as a signal at 197.73 ppm in the ^{13}C NMR spectrum of **5** are consistent with the presence of an allene moiety. The IR spectrum of **5** also contained an absorption at 2064 cm^{-1}, characteristic of an Si—H bond. The ^{1}H, ^{13}C, and ^{29}Si NMR spectra of **5** revealed a complete lack of symmetry in the molecule. Finally, the chemical shifts, splitting pattern, and coupling constants of a three-spin system, 5.80 ppm (dd, J = 3.3, 5.7 Hz), 3.84 ppm (dd, J = 3.3, 5.7 Hz), and 2.81 ppm (t, J = 5.7 Hz), were consistent with an allenylidene cyclopropane moiety with two vicinal substituents (phenyl and methoxy) on the three-membered ring. The cis stereochemistry of the vicinal cyclopropyl hydrogens was assigned based on the observed coupling constant between these two nuclei (J = 5.7 Hz). Coupling constants for cis vicinal hydrogens on a 1-methoxy-2-phenyl-substituted cyclopropane typically range between 6 and 8 Hz (6, 10); the coupling constants for the trans isomers are 2–4 Hz in magnitude (11). 1,4-Di-*tert*-butyl-2-hydroxy-1,1,4,4-tetramethyl-2,3-bis(*tert*-butyldimethylsilyl)tetrasilane (**6**) (7*a*) was also isolated from the reaction mixture in low yield. Presumably, disilane **6** is formed by reaction of **3** with adventitious water.

An excess of alkyne **2** was added to a deep orange solution of disilene **3**, once again, obtained by photolysis of hexakis(*tert*-butyldimethylsilyl)cyclotrisilane (**4**) (9) in hexanes. The solution was allowed to stir for 20–40 h. Analysis of the crude product by ^{1}H NMR spectroscopy revealed a mixture of **7**, **8**, **9**, **10**, and **6** (~27:14:16:32:11, respectively) in addition to unreacted **2** and **4** (Scheme 4). Compounds **7** (9%–24% isolated yield), **8** (0%–9% isolated yield), **10** (26%–29% isolated yield), **6** (6%–13% isolated yield), **4** (11%–15% recovery), and **2** (1%–6% recovery) were isolated by chromatographic separation of the crude residue. Compound **9** was not isolated after chromatography and was therefore identified and characterized by analysis of the crude product mixture. Compound **11** (7%–15%), although not observed in the ^{1}H NMR spectrum of the crude product, was also isolated from the chromatographic plate.

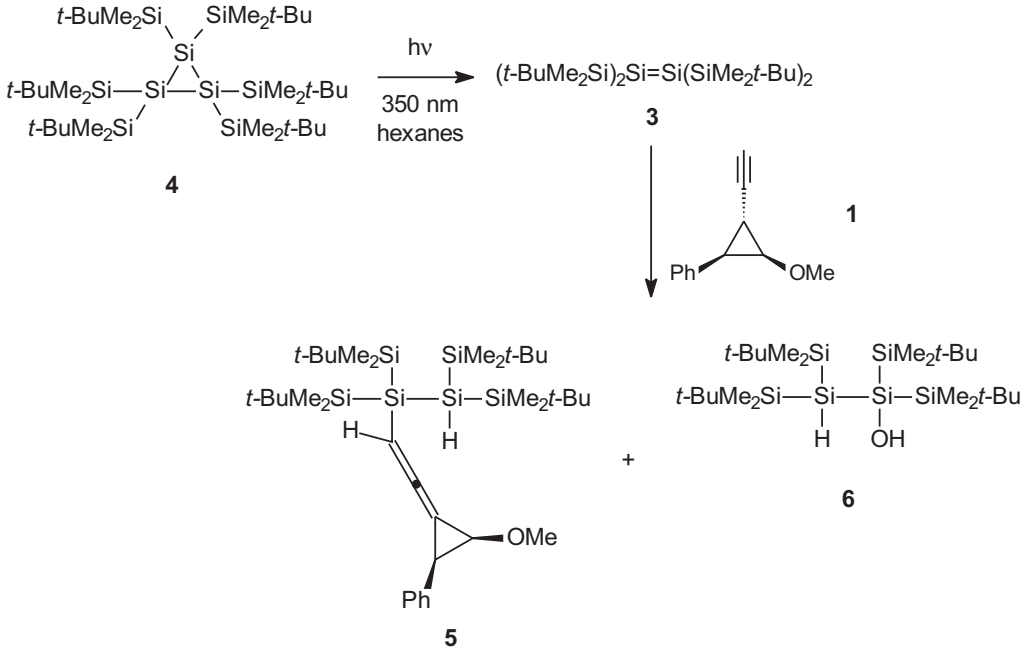
The structures of **7**–**9** were determined by ^{1}H, ^{1}H–^{1}H gCOSY, ^{1}H–^{13}C gHMQC and gHMBC, ^{1}H–^{29}Si gHMBC NMR and IR spectroscopy. The rationale behind the structural assignment is discussed for **7**. Similar logic was used to establish the structures of **8** and **9**. An absorption at 1926 cm^{-1} in the IR spectrum of **7**, as well as a signal at 211.8 ppm in the ^{13}C spectrum, indicated the presence of an allene group in the molecule. The correlations observed in the ^{1}H–^{1}H gCOSY spectrum of **7** and the multiplicities of the signals observed in the ^{1}H NMR spectrum of **7** are consistent with a $CH{=}C{=}C(CH_3)CHCH$ spin system (fragment 1, Scheme 5): 1.81 ppm (d, 3H, J = 3.7 Hz), 3.95 ppm (d, 1H, J = 9.8 Hz), 4.83 (dd, 1H, J = 2.0, 9.8 Hz), 5.64 ppm (dq, 1H, J = 2.0, 3.7 Hz). A correlation was observed in the ^{1}H–^{1}H gCOSY spectrum of **7** between the signal at 4.83 ppm and the one at 5.64 ppm, assigned to the allenic proton. No such correlation is observed for the signal at 3.95 ppm in the ^{1}H NMR spectrum of **7**. Additionally, a correlation was observed in the ^{1}H–^{13}C gHMBC NMR spectrum of **7** between the signal at 4.83 ppm in the ^{1}H dimension and the signal at 211.8 ppm in the ^{13}C dimension

© 2005 NRC Canada

Scheme 2.



Scheme 3.

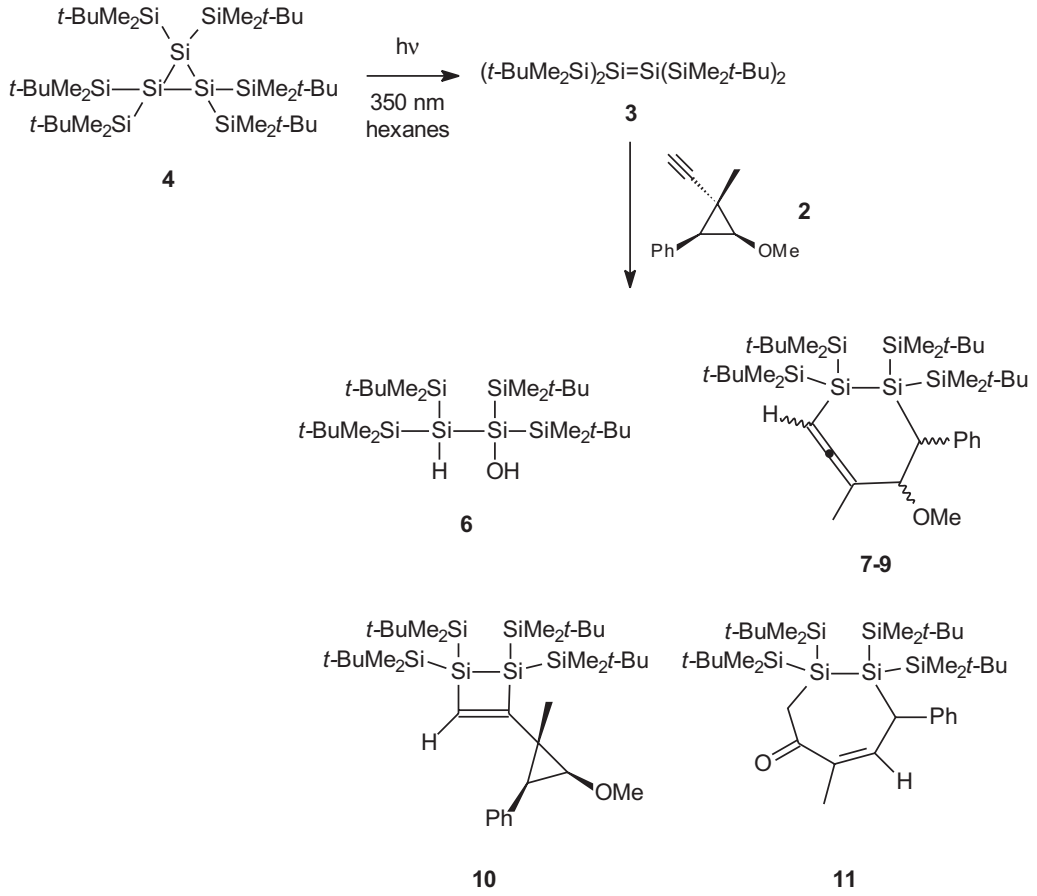


assigned to the sp-hydridized central allenic carbon. No such correlation was observed for the signal at 3.95 ppm in the ^{1}H dimension. All of these data lead to the assignment of the ^{1}H signals as shown fragment 1 (Scheme 5).

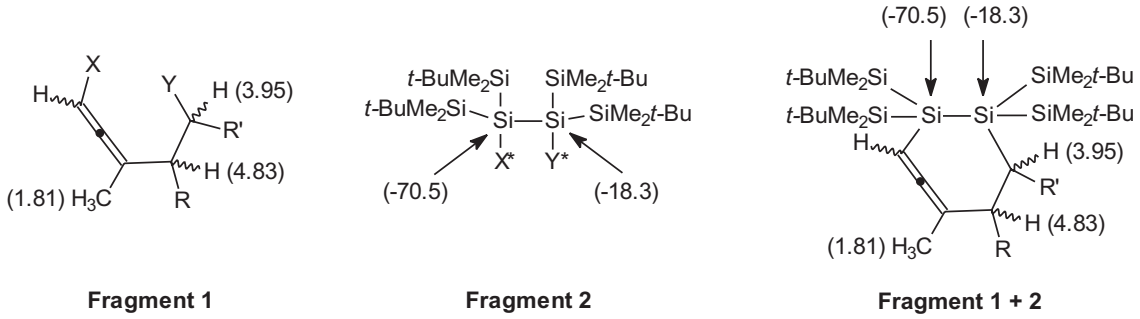
Examination of the ^{1}H NMR spectrum of **7** in the range of 0–1.5 ppm reveals six different signals integrating for 3H each (SiMe), one signal integrating for 6H ($SiMe_2$), and four signals each integrating for 9H (*t*-Bu). In addition, the presence of six different signals in the ^{29}Si dimension of the ^{1}H–^{29}Si gHMBC spectrum of **7**: four signals at 0.5, –1.1, –1.3, and –2.3 ppm, assigned to the four *t*-$BuMe_2Si$ groups based on the chemical shift and the observed correlations, and two signals at –70.5 and –18.3 ppm assigned to the ring silicons. The upfield signals also correlated to four SiMe groups providing evidence that the *t*-$BuMe_2Si$ groups remained attached to silicon. These data are consistent with a tetrakis(*tert*-butyldimethylsilyl)disilane fragment in which no symmetry exists (fragment 2, Scheme 5). Correlations were observed in the ^{1}H–^{29}Si gHMBC spectrum of **7** between the doublet at 1.81 ppm in the ^{1}H dimension, assigned to the vinylic methyl group, and the signal at –70.5 ppm in the ^{29}Si dimension, and thus, the signal at –70.5 ppm was assigned to the ^{29}Si atom attached to the sp^2-hybridized carbon. Additionally, a correlation was observed between the doublet at 3.95 ppm in the ^{1}H dimension and the signals at –18.3 and –70.5 ppm in the ^{29}Si dimension. These correlations suggest that fragments 1 and 2 are linked as shown in Scheme 5 to make a 1,2-disilacyclohepta-3,4-diene ring. The gHMBC and gHMQC spectra were critical in the assignment of the regiochemistry of the phenyl and methoxy groups on the seven-membered ring. A correlation was observed between the doublet of doublets at 4.83 ppm in the ^{1}H dimension of the ^{1}H–^{13}C gHMQC spectrum of compound **7** and the signal at 82.0 ppm in the ^{13}C dimension. A correlation was also observed between the doublet at 3.95 ppm in the ^{1}H dimension and the signal at 46.4 ppm in the ^{13}C dimension. The ^{13}C chemical shifts are consistent with the H assigned to the signal at 4.83 ppm being located on the carbon adjacent to the methoxy group, and the H giving rise to the signal at 3.95 ppm being located on the carbon attached to the phenyl group. Further evidence for the assignment of this regiochemistry was observed in the ^{1}H–^{13}C gHMBC NMR spectrum of **7**. A correlation was observed between the doublet of doublets at 4.83 ppm in the ^{1}H dimension and the signal at 56.80 ppm in the ^{13}C dimension assigned to the methoxy group. A correlation was also observed between the doublet at 3.95 ppm in the ^{1}H dimension and signals at 143.8 and 131.3 ppm in the ^{13}C dimension assigned to the ipso and ortho carbon atoms of the phenyl group, respectively. Finally, in the ^{1}H–^{29}Si gHMBC NMR spectrum of **7**, correlations were observed between the doublet at 3.95 ppm in the ^{1}H dimension and signals at –18.3 and –70.5 ppm (vide

© 2005 NRC Canada

Scheme 4.



Scheme 5.



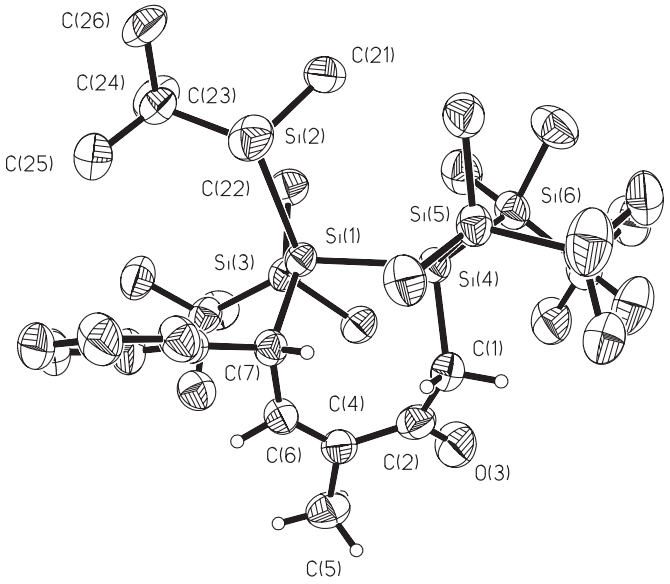
$^{1}H/^{29}Si$ chemical shifts are given in brackets

supra), and at –1.1 and –1.3 ppm in the ^{29}Si dimension, which have been assigned to the endocyclic ring silicon atoms and the silicon atoms in the *tert*-butyldimethylsilyl groups attached to the silicon at –18.3 ppm, respectively. The doublet of doublets at 4.83 ppm in the ^{1}H dimension correlated to only one ^{29}Si signal at –18.3 ppm. These data are completely consistent with the proposed regiochemistry in **7**. Similar correlations were observed in the NMR spectra of disilacyclohepta-1,2-dienes **8** and **9**. The regiochemistry of all three isomers was determined to be the same.

A molecular ion was not observed in the EI-MS of **7** or **8**. A signal was, however, observed at *m*/*z* 688, which is consistent with the molecular weight of the disilacycloheptenone **11**, which was isolated after chromatographic separation of the crude product mixture. It is believed that compounds **7** and **8** are converted to **11** during the course of mass spectrometric analysis. Compound **11** was identified and characterized by ^{1}H, ^{1}H–^{1}H gCOSY, ^{1}H–^{13}C gHMQC and gHMBC, ^{1}H–^{29}Si gHMBC NMR and IR spectroscopy, as well as mass spectrometry. The identity of **11** was unambiguously confirmed by X-ray analysis (Fig. 1). The most notable feature of the structure is the Si(1)—Si(4) bond length of 2.4572(13) Å, which is considerably longer that the average bond length of 2.35 Å. This is likely due to the steric crowd-

© 2005 NRC Canada

Fig. 1. Molecular structure of 1,1,2,2-tetrakis(*tert*-butydimethylsilyl)-5-methyl-3-phenyl-1,2-disilacyclohept-4-en-6-one (**11**). Thermal ellipsoids are drawn at the 50% probability level.



ing of the bulky *tert*-butyldimethylsilyl substituents. Consistent with this, distortions about the silicon atoms were also observed: C(7)-Si(1)-Si(4) (96.99(11)°), C(23)-Si(2)-Si(1) (121.97(12)°), C(33)-Si(3)-Si(1) (122.43(12)°), C(1)-Si(4)-Si(5) (96.89(11)°), C(53)-Si(5)-Si(4) (118.71(12)°), and C(63)-Si(6)-Si(4) (117.30(14)°). All other bond lengths and angles were within normal values.

The highest mass ion cluster in the mass spectrum of **10** was observed at *m/z* 702, consistent with the formation of a 1:1 adduct between disilene **3** and alkyne **2**. Six different ^{29}Si were apparent in the ^{1}H–^{29}Si gHMBC spectrum of **10**: 4.8, 1.3, –0.7, –1.3, –45.7, and –66.0 ppm. The four downfield signals can be assigned to the four *t*-BuMe_2Si groups based on the observed correlations in the ^{1}H–^{29}Si gHMBC NMR spectrum: each signal correlated to both SiMe and *t*-Bu signals in the ^{1}H dimension. Furthermore, correlations were observed between the SiMe groups in the ^{1}H dimension and the signals at –66 and –45.7 ppm in the ^{29}Si dimension, leading to the conclusion that the *t*-BuMe_2Si groups are attached to silicon. Signals at 174.65 and 140.07 ppm were observed in the ^{13}C NMR spectrum of **10** and were assigned to the sp^2-hybridized carbons in a dimetallacyclobutene ring based on observed correlations in the ^{1}H–^{13}C gHMQC and gHMBC NMR spectra of **10,** and by comparison to the chemical shifts of ring carbons in related dimetallacyclobutenes (12). Furthermore, the vinylic hydrogen exhibited a measurable coupling constant to both ring silicons providing additional evidence for the disilacyclobutene structure. All remaining NMR spectroscopic data were consistent with a structure in which the cyclopropane ring was intact. The cis stereochemistry of the phenyl and methoxy substituents on the cyclopropyl ring was assigned based on the coupling constant of the ring hydrogens (J = 6.7 Hz) (6, 10, 11). The stereochemical relation of the methyl substituent to the phenyl and methoxy groups was not determined but has been tentatively assigned as cis to both substituents on the assumption that its stereochemical configuration remained unchanged during the course of the reaction.

Discussion

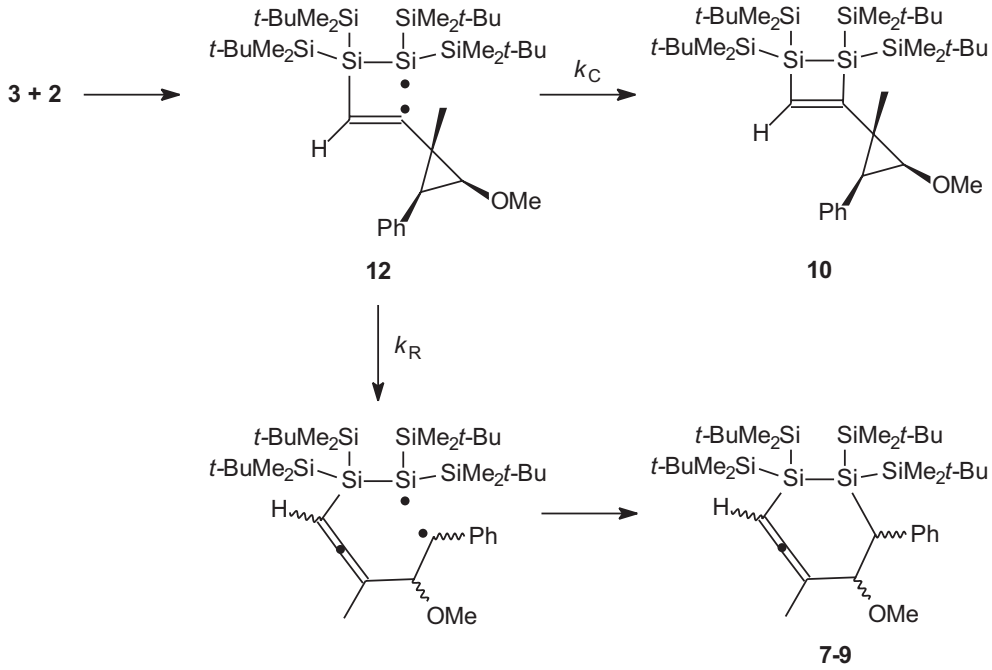
Addition of alkyne **1** to tetrasilyldisilene **3** resulted in the formation of allene **5** as the major product (Scheme 3). Allene **5** appears to be the result of a formal ene reaction between the alkyne and the disilene. Interestingly, Kira and coworkers (7*a*) observed the formation of a 2-allenyltetrasilane upon the addition of 1-hexyne to disilene **3**. Analysis of the structure of allene **5** provides little insight into the mechanism by which the ene reaction has occurred. While no ring opening of the cyclopropane was observed, it is not possible to confidently state that a vinyl radical or cation was *not* formed adjacent to the cyclopropyl ring during the course of the reaction because the relative rates of cyclopropyl ring opening and disproportionation of a biradical (or zwitterion) through a six-membered ring transition state are unknown. Alternatively, it is possible that the reaction proceeds through a concerted pathway or a pathway involving formation of zwitterionic intermediate in which a vinyl anion is adjacent to the cyclopropyl ring. Opening of the cyclopropyl ring is not expected to occur under these conditions.

In an attempt to avoid formation of an allene, alkyne **2** was added to disilene **3**. Alkyne **2** lacks a hydrogen in the appropriate position for an ene reaction. Addition of alkyne **2** to **3** resulted in the formation of compounds **6–10** (Scheme 4). Once again, 2-hydroxytetrasilane (**6**) is most likely formed by the addition of adventitious water to the disilene.

The formation of disilacycloheptadienes **7–9** provides clear evidence that cyclopropyl ring opening has occurred upon addition of alkyne **2** to disilene **3,** consistent with the formation of a reactive intermediate during the course of the reaction. The relative position of the phenyl substituent within disilacycloheptadienes **7–9** has been determined to be adjacent to the ring silicon in all isomers by NMR spectroscopy. This regiochemistry is consistent with cyclopropylvinyl rearrangement occurring towards the phenyl group and provides unambiguous evidence that the addition of alkynes to the tetrasilyldisilene occurs through a stepwise reaction mechanism via the formation of a *biradical* intermediate as shown in Scheme 6. Thus, addition of alkyne **2** to disilene **3** leads to the 1,4-biradical intermediate **12**. Biradical **12** can then either cyclize to form disilacyclobutene **10** or regioselectively rearrange towards the phenyl substituent to form a new 1,7-biradical, which can then close to yield the observed products (**7–9**). The formation of disilacyclobutene **10** indicates that ring closure (k_C) of biradical **12** effectively competes with rearrangement. Analysis of the product ratios (disilacycloheptadienes–disilacyclobutenes) determined by ^{1}H NMR spectroscopy by competition kinetics allows the rate constant for ring closure (k_C) to be estimated. Using the value of 1.6×10^{10} s^{-1} as an approximation for the rate constant for rearrangement (k_R) of biradical **12** (6*b*), k_C was estimated to be 9×10^{9} s^{-1}. This is remarkably similar to the estimate obtained for the rate constant for ring closure of the analogous 1,4-biradical in the addition of alkyne **2** to tetramesityldisilene (4×10^{9} s^{-1}). The formation of **7–9** is

© 2005 NRC Canada

Scheme 6.



not consistent with a mechanism in which a zwitterionic intermediate is formed. If a cation were generated adjacent to the cyclopropyl ring, the evidence indicates that the rearrangement would occur towards the methoxy substituent; if an anion was generated adjacent to the cyclopropyl ring, the evidence indicates that no rearrangement would occur (6*a*).

Compound **11** was not observed in the crude reaction mixture; however, it was isolated after chromatographic separation of the products. The disilacycloheptadienone is likely formed from all three disilacyclohepta-3,4-diene isomers (**7**–**9**) by hydration of the allene moiety followed by loss of methanol to produce the observed enone. The presence of the allene functionality within the seven-membered ring of compounds **7**–**9** imparts a significant amount of ring strain (13). It is, therefore, not surprising that the hydration of the allene would readily occur to relieve some of this strain. The stability of the tetrasilyl-substituted disilacyclohepta-1,2-diene ring system towards hydration can be compared with the analogous mesityl-substituted ring systems, formed by the addition of alkyne **2** to tetramesityldisilene (5). In this case, hydration of the allene moiety did not occur upon chromatography. Evidently, the mesityl group is more effective at shielding the strained allene moiety. Assuming **11** is formed from all three disilacycloheptadiene isomers, the position of the phenyl substituent adjacent to the ring silicon in **11** provides additional evidence for the regiochemical assignments of the phenyl and methoxy substituents in **7**–**9**.

The organic modification of silicon surfaces is currently of much interest (14). In particular, the reactivity of silicon dimers on the reconstructed Si(100) 2 × 1 surface towards alkynes has been extensively studied (15). We believe that tetrasilyldisilenes may act as excellent models for the strained dimers on the reconstructed Si(100) 2 × 1 surface. Indeed, the addition of alkynes to the dimers on the surface has been theoretically examined (16). The cycloaddition of acetylene or butadiyne to the surface was found to follow a pathway involving a biradical intermediate. Our experimental results corroborate these findings.

In summary, the results presented herein, taken with our previous work (5), indicate that the addition of alkynes to both tetraaryl- and tetrasilyl-substituted disilenes involves the formation of a biradical intermediate. Furthermore, our work suggests that the reactivity of molecular disilenes and the silicon dimers of the reconstructed Si(100) 2 × 1 surface are comparable.

Experimental

General details

All experiments were carried out in flame-dried glassware under an inert atmosphere of argon. Hexanes were dried either using a solvent purification system (Innovative Technology Inc., Newburyport, Massachusetts) in which the solvent was passed through an alumina-packed column or by distillation from LAH. Chromatography was carried out on conventional preparative plates or by column chromatography using silica gel. Photolyses were carried out at 350 nm using a Rayonet photochemical reactor. NMR spectra were recorded on a Varian Mercury 400, a Varian Inova 400, or a Varian Inova 600 NMR spectrometer. The standards were as follows: residual C_6D_5H (7.15 ppm) for ^1H; C_6D_6 central transition (128.00 ppm) for ^{13}C; and Me_4Si as an external standard (0.00 ppm) for ^{29}Si. The ^{13}C chemical shifts of compounds **7**–**9** and **11** were extracted from the ^1H–^{13}C gHSQC and gHMBC spectra. IR spectra were obtained as thin films on a PerkinElmer System 2000 FT IR spectrometer. Electron impact (70 eV) mass spectra were obtained using a Finnegan MAT model 8200 mass spectrometer (reported in mass-to-charge units (*m*/*z*) with ion identity and intensities relative to the base peak in parentheses). (*trans*,*trans*-2-Methoxy-3-phenylcyclopropyl)ethyne (**1**) (6*a*), (*trans*,*trans*-2-methoxy-1-methyl-3-phenylcyclopropyl)ethyne (**2**) (6*a*),

© 2005 NRC Canada

and hexakis(*tert*-butyldimethylsilyl)cyclotrisilane (**4**) (9) were prepared according to the previously reported procedures.

Addition of 1 to 3

4 (43.0 mg, 0.06 mmol) was dissolved in degassed hexanes (5 mL) and photolyzed for 24 h at 10 °C to give a deep red-orange solution. A solution of **1** (17.1 mg, 0.1 mmol) dissolved in degassed hexanes (3 mL) was added to the red-orange solution. The mixture was allowed to stir for 16 h. During this time, the deep red-orange colour faded to pale orange. The solvent was removed by rotary evaporation to give a light orange residue. After separation of the residue by preparative TLC (hexanes–CH_2Cl_2, 90:10), **5** (36.3 mg, 81% yield based on 21% recovery of **4**), **6** (7*a*) (2.4 mg, 7%), **4** (9.2 mg, 21% recovery), and **1** (6.0 mg, 35% recovery) were obtained.

*1-[2-(***cis***-2-Methoxy-3-phenylcyclopropylidene)vinyl]-1,1,2,2-tetrakis(***tert***-butyldimethylsilyl)disilane (5)*

IR (thin film, cm^{-1}): 2950 (s), 2889 (m), 2848 (s), 2064 (m), 1972 (s), 1470 (m), 1250 (m), 1112 (m), 1004 (m), 799 (s). ^{1}H NMR (C_6D_6) δ: 7.48 (d, 2H, *o*-PhH, *J* = 7.9 Hz), 7.23 (t, 2H, *m*-PhH, *J* = 7.3 Hz), 7.10 (t, 1H, *p*-PhH, *J* = 7.3 Hz), 5.80 (dd, 1H, C=CH, *J* = 3.3, 5.7 Hz), 3.84 (dd, 1H, CHOMe, *J* = 3.3, 5.7 Hz), 3.49 (s, 1H, SiH), 2.94 (s, 3H, OMe), 2.81 (t, 1H, CHPh, *J* = 5.7 Hz), 1.19 (s, 9H, *t*-Bu), 1.07 (s, 9H, *t*-Bu), 1.05 (s, 18H, 2 *t*-Bu), 0.53 (s, 3H, SiMe), 0.43 (s, 3H, SiMe), 0.38 (s, 3H, SiMe), 0.38 (s, 3H, SiMe), 0.35 (s, 3H, SiMe), 0.33 (s, 3H, SiMe), 0.31 (s, 6H, 2SiMe). ^{13}C NMR (C_6D_6) δ: 197.73 (C=*C*=C), 137.09 (*i*-PhC), 129.31 (*o*-PhC), 127.94 (*m*-PhC), 126.34 (*p*-PhC), 83.50 (SiCH=), 76.95 (*C*=C=CH), 63.35 (*C*HOMe), 57.92 (OMe), 33.27 (PhCH), 28.72, 28.54, 27.89, 27.86 (Me), 19.22, 19.16 (*C*Me), 0.08 (broad), –0.73 (broad), –0.86 (broad), –1.41, –1.50 (broad), –1.75 (SiMe). ^{29}Si NMR (C_6D_6) δ: –117.64 (SiH, *J* = 148 Hz), 1.93, 1.59 (*t*-BuMe_2*Si*SiH), 0.37, –0.03 (s, *t*-BuMe_2*Si*SiCC=C), –79.59 (SiCH=C). EI-MS m/*z* (%): 688 (M^+, 3), 673 (M^+ – Me, 3), 631 (M^+ – *t*-Bu, 7), 573 (M^+ – *t*-BuMe_2Si, 20), 429 (M^+ – (*t*-BuMe_2Si)$_2$SiH, 29), 73 ($SiMe_3$, 100). HR-MS calcd. for $C_{36}H_{72}OSi_6$: 688.4199 (M^+); found: 688.4206.

Addition of 2 to 3

4 (44 mg, 0.06 mmol) was dissolved in degassed hexanes (4 mL). The solution was photolyzed at 350 nm for 30 h at room temperature to give a deep red-orange solution. A solution of **2** (22.0 mg, 0.12 mmol) dissolved in degassed hexanes (2 mL) was added to the red-orange solution. The mixture was allowed to stir for 40 h. During this time, the deep red-orange colour of the solution faded to pale orange. The solvent was then removed by rotary evaporation to give a light yellow residue (67.3 mg). Analysis of the crude product by ^{1}H NMR spectroscopy revealed a mixture of **7**, **8**, **9**, **10**, and **6** (~27:14:16:32:11, respectively). The components of the residue were separated by preparative TLC (hexanes–CH_2Cl_2, 50:50) to yield **10** (11.5 mg, 22%), **7** (12.3 mg, 24%), and **11** (7.3 mg, 15%). A band was also obtained containing a mixture of **4**, **8**, **10**, **6**, and **2** (28:26:18:20:8, 20 mg). Separation of this band (hexanes–CH_2Cl_2, 90:10) yielded **4** (5.7 mg, 13% recovery), **10** (3.1 mg, 6% for a 28% total yield), **2** (0.3 mg, 1% recovery), and a mixture (3.3 mg, 81:19) of **6** (7%) (7*a*) and **4** (1% for a 14% total recovery). It was difficult to obtain **7** and **11** cleanly; they were contaminated with minor amounts of unidentified compounds. When the crude reaction mixture was chromatographically separated using a different eluent (hexanes–CH_2Cl_2, 75:25), **8** (9%) was obtained as a mixture with **6** (**8**:**6** = 40:60) and was characterized as such. Compound **9** was identified in the crude reaction mixture but could not be isolated.

Table 1. Crystal data for **11**.

Empirical formula	$C_{36}H_{72}OSi_6$
Formula mass	689.48
Colour and habit	Colourless plate
Crystal dimensions (mm)	0.35 × 0.25 × 0.10
Crystal system	Triclinic
Space group	*P*-1
Z	2
a (Å)	9.430 7(6)
b (Å)	11.793 0(5)
c (Å)	19.865 6(8)
α (°)	97.676(3)
β (°)	95.360(3)
γ (°)	102.652(3)
Collection ranges	$-11 \le h \le 9$, $-13 \le k \le 14$, $-23 \le l \le 23$
Temperature (K)	296(2)
Volume (Å^3)	2 119.15(18)
D_{calcd} (mg/m^3)	1.081
Radiation	Mo K_α (λ = 0.710 73 Å)
Absorption coeff. (mm^{-1})	0.222
Absorption correction	Multiscan
F(000)	760
θ Range for data collection (°)	2.72–25.00
Reflections collected	23 050
Independent reflections	7 206 (R_{int} = 0.093)
Completeness to θ = 25.00° (%)	96.8
Data, restraints, parameters	7 206, 0, 376
Max and min transmission	0.978 1 and 0.926 4
Goodness-of-fit on F^2	1.036
Final *R* indices [$I > 2\sigma(I)$]	R_1 = 0.065 4, wR_2 = 0.171 6
R indices (all data)	R_1 = 0.093 0, wR_2 = 0.195 1
Refinement method	Full-matrix least-squares on F^2
Largest diff. peak and hole (e Å^{-3})	0.606 and –0.399

Crystals of **11** were grown from a concentrated methylene chloride solution by slow diffusion of acetonitrile. A colourless plate was mounted on a glass fibre. Data were collected at room temperature (23 °C) on a Nonius Kappa CCD diffractometer with COLLECT (Nonius B.V., Delft, The Netherlands, 1998). The unit cell parameters were calculated and refined from the full data set. Crystal cell refinement and data reduction were carried out using DENZO (Nonius B.V., Delft, The Netherlands, 1998). The data were scaled using SCALEPACK (Nonius B.V., Delft, The Netherlands, 1998). The crystal data and refinement parameters for **11** are listed in Table 1. The SHELXTL-NT V6.1 (Bruker AXS,

© 2005 NRC Canada

Madison, Wisconsin) suite of programs was used to solve the structure by direct methods. Subsequent difference Fourier syntheses allowed the remaining atoms to be located. The molecule was very well behaved. All of the non-hydrogen atoms were refined with anisotropic thermal parameters. The hydrogen atom positions were geometrically calculated and were included as riding on their respective carbon atoms. The largest residue electron density peak (0.606 e $Å^{-3}$) was associated with one of the Si—Si bonds. CCDC 270736 (**11**) contains the supplementary crystallographic data for this paper.[3]

1,1,2,2-Tetrakis(*tert*-butyldimethylsilyl)-6-methoxy-5-methyl-7-phenyl-1,2-disilacyclohepta-3,4-diene (7)

IR (thin film, cm^{-1}): 2956 (s), 2928 (s), 2894 (m), 2855 (s), 1926 (w), 1461 (m), 1250 (m), 1090 (m), 835 (s), 799 (s). ^{1}H NMR (C_6D_6) δ: 7.09–7.22 (m, *o,m*-PhH), 7.00 (t, 1H, *p*-PhH, *J* = 7.4 Hz), 5.64 (dq, 1H, C=CHSi, *J* = 3.7, 2.0 Hz), 4.83 (dd, 1H, CHOMe, *J* = 2.0, 9.8 Hz), 3.95 (d, 1H, CHPh, *J* = 9.8 Hz), 2.96 (s, 3H, OMe), 1.81 (d, 3H, Me, *J* = 3.7 Hz), 1.31 (s, 9H, *t*-Bu), 1.21 (s, 9H, *t*-Bu), 1.10 (s, 9H, *t*-Bu), 0.87 (s, 3H, SiMe), 0.74 (s, 9H, *t*-Bu), 0.57 (s, 3H, SiMe), 0.53 (s, 3H, SiMe), 0.45 (s, 3H, SiMe), 0.41 (s, 6H, 2SiMe), 0.10 (s, 3H, SiMe), 0.09 (s, 3H, SiMe). ^{13}C NMR (C_6D_6) δ: 211.8 (C=*C*=C), 143.8 (*i*-PhC), 131.3 (*o*-PhC), 125.7 (*m*-PhC), 96.5 (C=*C*Me), 84.5 (C=*C*HSi), 82.0 (*C*HOMe), 56.8 (OMe), 46.4 (PhCH), 29.9, 29.6, 29.5, 28.8 (SiC*Me*$_3$), 22.5, 22.1, 21.8, 20.1 (Si*C*Me$_3$), 12.8 (Me), 3.4, 2.4, 2.2, 2.0, 1.6, 0.4, –0.2, –0.5 (SiMe). ^{29}Si NMR (C_6D_6) δ: –70.5 (SiCH=C), –18.3 (SiCHPh), 0.5, –1.1, –1.3, –2.3 (*t*-BuMe$_2$Si). EI-MS *m/z* (%): 688 (7), 603 (27), 532 (19), 475 (7), 419 (10), 275 (31), 73 (SiMe$_3$, 100).

1,1,2,2-Tetrakis(*tert*-butyldimethylsilyl)-6-methoxy-5-methyl-7-phenyl-1,2-disilacyclohepta-3,4-diene (8)

IR (thin film, cm^{-1}): 3666 (w), 2954 (s), 2926 (s), 2895 (m), 2855 (s), 2060 (w), 1931 (w), 1462 (m), 1253 (m), 1093 (m), 1004 (m), 800 (s). ^{1}H NMR (C_6D_6) δ: 7.58 (dd, 2H, *o*-PhH, *J* = 8.0, 1.3 Hz), 7.17 (t, 2H, *m*-PhH, *J* = 7.6 Hz), 7.03 (tt, 1H, *p*-PhH, *J* = 7.4, 1.2 Hz), 5.70 (q, 1H, C=CHSi, *J* = 3.9 Hz), 3.84 (s, 1H, CHPh), 3.33 (d, 1H, CHOMe, *J* = 0.6 Hz), 3.06 (s, 3H, OMe), 1.55 (d, 3H, Me, *J* = 3.9 Hz), 1.33 (s, 9H, *t*-Bu), 1.21 (s, 9H, *t*-Bu), 1.14 (s, 9H, *t*-Bu), 0.84 (s, 3H, SiMe), 0.71 (s, 9H, *t*-Bu), 0.66 (s, 3H, SiMe), 0.49 (s, 3H, SiMe), 0.47 (s, 3H, SiMe), 0.430 (s, 3H, SiMe), 0.428 (s, 3H, SiMe), 0.39 (s, 3H, SiMe), 0.05 (s, 3H, SiMe). ^{13}C NMR (C_6D_6) δ: 210.9 (C=*C*=C), 149.5 (*i*-PhC), 129.6 (*o*-PhC), 126.2 (*p*-PhC), 92.0 (C=*C*Me), 88.0 (*C*HOMe), 85.6 (C=*C*HSi), 55.1 (OMe), 44.7 (PhCH), 29.9, 29.8, 29.6, 28.6 (SiC*Me*$_3$), 22.8 (2C), 21.8, 20.0 (Si*C*Me$_3$), 18.1 (Me), 3.4, 2.6, 2.0, 1.9, 1.6, 0.6, 0.4, –0.1 (SiMe). ^{29}Si NMR (C_6D_6) δ: –69.1 (SiCH=C), –35.5 (SiCHPh), 0.7, –0.3, –1.9, –2.1 (*t*-BuMe$_2$Si). EI-MS *m/z* (%): 688 (6), 603 (19), 532 (15), 475 (6), 419 (9), 275 (27), 73 (SiMe$_3$, 100).

1,1,2,2-Tetrakis(*tert*-butyldimethylsilyl)-6-methoxy-5-methyl-7-phenyl-1,2-disilacyclohepta-3,4-diene (9)

^{1}H NMR (C_6D_6) δ: 5.52 (dq, 1H, C=C(H)Si, *J* = 3.7, 1.4 Hz), 4.61 (d, 1H, CHOMe, *J* = 11.1 Hz) 3.46 (d, 1H, CHPh, *J* = 11.1 Hz), 2.97 (s, 3H, OMe), 1.83 (d, 3H, Me, *J* = 3.5 Hz). ^{13}C NMR (C_6D_6) δ: 211.9 (C=*C*=C), 145.3 (*i*-PhC), 130.5 (*o*-PhC), 87.4 (C=*C*Me), 87.7 (*C*HOMe), 82.5 (C=*C*HSi), 51.8 (OMe), 39.2 (PhCH), 17.7 (Me). ^{29}Si NMR (C_6D_6) δ: –48.4 (SiCH=C), –35.5 (SiCHPh).

1,1,2,2-Tetrakis(*tert*-butyldimethylsilyl)-3-(trans,trans-2-methoxy-1-methyl-3-phenylcyclopropyl)-1,2-disilacyclobut-3-ene (10)

IR (thin film, cm^{-1}): 2959 (s), 2927 (s), 2893 (m), 2856 (s), 1600 (w), 1498 (m), 1460 (m), 1385 (m), 1359 (m), 1252 (m), 1112 (m), 1080 (m), 1006 (m), 796 (s), 750 (m), 699 (m). ^{1}H NMR (C_6D_6) δ: 7.56 (d, 2H, *o*-PhH, *J* = 7.6 Hz), 7.23 (t, 2H, *m*-PhH, *J* = 7.3 Hz), 7.08 (t, 1H, *p*-PhH, *J* = 7.3 Hz), 6.50 (s, 1H, C=CH), 3.48 (d, 1H, CHOMe, *J* = 6.7 Hz), 3.24 (s, 3H, OMe), 2.38 (d, 1H, CHPh, *J* = 6.7 Hz), 1.37 (s, 3H, Me), 1.10 (s, 27H, 3 *t*-Bu), 1.08 (s, 9H, *t*-Bu), 0.45 (s, 3H, SiMe), 0.43 (s, 3H, SiMe), 0.42 (s, 3H, SiMe), 0.41 (s, 3H, SiMe), 0.39 (s, 3H, SiMe), 0.37 (s, 3H, SiMe), 0.35 (s, 3H, SiMe), 0.35 (s, 3H, SiMe). ^{13}C NMR (C_6D_6) δ: 174.65 (*C*=CH), 140.07 (C=*C*H), 137.27 (*i*-PhC), 130.55 (*o*-PhC), 127.89, 126.10 (*m,p*-PhC), 71.83 (*C*HOMe), 58.59 (OMe), 35.81 (PhCH), 32.35 (*C*Me), 29.43, 29.30, 29.24 (SiC*Me*$_3$), 20.11, 20.04, 19.86, 19.68 (Si*C*Me$_3$), 13.74 (Me), 1.17, 1.01, 0.66, 0.60, 0.42, 0.33, 0.02, 0.14 (SiMe). ^{29}Si NMR (C_6D_6) δ: –45.7 (*J* = 24 Hz, Si-C=CH), –66.0 (*J* = 8 Hz, Si-CH=), 4.8, 1.3, –0.7, –1.3 (*t*-BuMe$_2$Si). EI-MS *m/z* (%): 702 (M^+, 9), 687 (M^+ – Me, 3), 645 (M^+ – *t*-Bu, 7), 587 (M^+ – *t*-BuMe$_2$Si, 45), 73 (SiMe$_3$, 100). HR-MS calcd. for $C_{37}H_{74}OSi_6$: 702.4355 (M^+); found: 702.4379.

1,1,2,2-Tetrakis(*tert*-butyldimethylsilyl)-5-methyl-3-phenyl-1,2-disilacyclohept-4-en-6-one (11)

IR (cm^{-1}): 2959 (m), 2917 (s), 2847 (s), 1736 (w), 1682 (w), 1650 (w), 1472 (m), 1258 (m), 1087 (m), 1025 (m), 800 (m). ^{1}H NMR (C_6D_6) δ: 7.52 (d, 2H, *o*-PhH, *J* = 8.0 Hz), 7.12 (t, 1H, *m*-PhH, *J* = 6.8 Hz), 6.99 (t, 2H, *p*-PhH, *J* = 7.2 Hz), 6.03 (d, 1H, C=C(H), *J* = 8.6 Hz), 4.36 (d, 1H, CHPh, *J* = 8.6 Hz), 3.21 (d, 1H, SiCH(H), *J* = 10.0 Hz), 2.82 (d, 1H, SiCH(H), *J* = 10.0 Hz), 1.76 (s, 3H, Me), 1.23 (s, 9H, *t*-Bu), 1.18 (s, 9H, *t*-Bu), 1.13 (s, 9H, *t*-Bu), 0.77 (s, 9H, *t*-Bu), 0.71 (s, 3H, SiMe), 0.44 (s, 3H, SiMe), 0.43 (s, 3H, SiMe), 0.41 (s, 3H, SiMe), 0.38 (s, 3H, SiMe), 0.33 (s, 3H, SiMe), 0.16 (s, 3H, SiMe), 0.10 (s, 3H, SiMe). ^{13}C NMR (C_6D_6) δ: 205.4 (C=O), 146.3 (*i*-PhC), 129.2 (*o*-PhC), 126.2, 126.1 (*m,p*-PhC), 138.1 (C=*C*H), 136.2 (C=*C*Me), 36.7 (PhCH), 32.4 (SiCH$_2$), 29.9, 29.4, 29.3, 29.1 (SiC*Me*$_3$), 22.4, 22.0, 21.7, 19.8 (Si*C*Me$_3$), 21.1 (Me), 2.4, 2.2, 2.1, 1.2, 1.0 (2C), 0.6, 0.1 (SiMe). ^{29}Si NMR (C_6D_6) δ: –55.0 (SiCH$_2$), –40.8 (SiCHPh), 1.3, –0.5, –1.1, –1.9 (*t*-BuMe$_2$Si). EI-MS *m/z* (%): 688 (M^+, 25), 631 (M^+ – *t*-Bu, 4), 573

[3] Supplementary data for this article are available on the Web site or may be purchased from the Depository of Unpublished Data, Document Delivery, CISTI, National Research Council Canada, Ottawa, ON K1A 0R6, Canada. DUD 4046. For more information on obtaining material refer to http://cisti-icist.nrc-cnrc.gc.ca/irm/unpub_e.shtml. CCDC 270736 contains the crystallographic data for this manuscript. These data can be obtained, free of charge, via www.ccdc.cam.ac.uk/conts/retrieving.html (or from the Cambridge Crystallographic Data Centre, 12 Union Road, Cambridge CB2 1EZ, UK; fax +44 1223 336033; or deposit@ccdc.cam.ac.uk).

© 2005 NRC Canada

(M^+ – *t*-$BuMe_2Si$, 37), 73 ($SiMe_3$, 100). HR-MS calcd. for $C_{36}H_{72}OSi_6$: 688.4199 (M^+); found: 688.4189.

Acknowledgements

We thank the Natural Sciences and Engineering Research Council of Canada (NSERC), the University of Western Ontario, and the Ontario Photonics Consortium for financial support.

References

1. For reviews on disilene chemistry, see: (*a*) M. Kira. J. Organomet. Chem. **689**, 4475 (2004); (*b*) N. Wiberg. *In* Silicon chemistry: From the atom to extended systems. *Edited by* P. Jutzi and U. Schubert. Wiley-VCH Verlag GmbH and Co., Weinheim, Germany. 2003. pp. 85–99; (*c*) M. Weidenbruch. Organometallics, **22**, 4348 (2003); (*d*) M. Weidenbruch. *In* Chemistry of organic silicon compounds. Vol. 3. *Edited by* Z. Rappoport and Y. Apeloig. John Wiley and Sons Ltd., Chichester, UK. 2001. pp. 391–428; (*e*) M. Kira. Pure Appl. Chem. **72**, 2333 (2000); (*f*) M. Kira and T. Iwamoto. J. Organomet. Chem. **611**, 236 (2000); (*g*) M.A. Chaubon, H. Ranaivonjatovo, J. Escudié, and J. Satgé. Main Group Met. Chem. **19**, 145 (1996); (*h*) M. Driess and H. Gruetzmacher. Angew. Chem. Int. Ed. Engl. **35**, 828 (1996); (*i*) R. Okazaki and R. West. Adv. Organomet. Chem. **39**, 231 (1996); (*j*) M. Weidenbruch. Coord. Chem. Rev. **130**, 275 (1994); (*k*) T. Tsumuraya, S.A. Batcheller, and S. Masamune. Angew. Chem. Int. Ed. Engl. **30**, 902 (1991); (*l*) G. Raabe and J. Michl. *In* The chemistry of organic silicon compounds. *Edited by* S. Patai and Z. Rappoport. Wiley, New York. 1989. pp. 1015–1142; (*m*) R. West. Angew. Chem. Int. Ed. Engl. **26**, 1201 (1987); (*n*) A.H. Cowley and N.C. Norman. Prog. Inorg. Chem. **34**, 1 (1986).
2. (*a*) T.L. Morkin, T.R. Owens, and W.J. Leigh. *In* Chemistry of organic silicon compounds. Vol. 3. *Edited by* Z. Rappoport and Y. Apeloig. John Wiley and Sons Ltd., Chichester, UK. 2001. pp. 949–1026; (*b*) H. Sakurai. *In* Chemistry of organic silicon compounds. Vol. 2. *Edited by* Z. Rappoport and Y. Apeloig. John Wiley and Sons Ltd., Chichester, UK. 1998. pp. 827–855.
3. (*a*) M.S. Samuel, H.A. Jenkins, D.W. Hughes, and K.M. Baines. Organometallics, **22**, 1603 (2003); (*b*) C.E. Dixon, D.W. Hughes, and K.M. Baines. J. Am. Chem. Soc. **120**, 11049 (1998).
4. N.J. Mosey, K.M. Baines, and T.K. Woo. J. Am. Chem. Soc. **124**, 13306 (2002).
5. S.E. Gottschling, K.K. Milnes, M.C. Jennings, and K.M. Baines. Organometallics, **24**, 3811 (2005).
6. (*a*) S.E. Gottschling, T.N. Grant, K.K. Milnes, M.C. Jennings, and K.M. Baines. J. Org. Chem. **70**, 2686 (2005); (*b*) K.K. Milnes, S.E. Gottschling, and K.M. Baines. Org. Biomol. Chem. 2004, **2**, 3530.
7. (*a*) T. Iwamoto, H. Sakurai, and M. Kira. Bull. Chem. Soc. Jpn. **71**, 2741 (1998); (*b*) C.E. Dixon, J.A. Cooke, and K.M. Baines. Organometallics, **16**, 5437 (1997); (*c*) C.E. Dixon, H.W. Liu, C.M. Vander Kant, and K.M. Baines. Organometallics, **15**, 5701 (1996); (*d*) A.D. Fanta, D.J. DeYoung, J. Belzner, and R. West. Organometallics, **10**, 3466 (1991).
8. (*a*) D.J. De Young, M.J. Fink, and R. West. Main Group Met. Chem. **10**, 19 (1987); (*b*) D.J. De Young and R. West. Chem. Lett. **6**, 883 (1986).
9. M. Kira, T. Iwamoto, M. Maruyama, T. Kuzuguchi, D. Yin, C. Kabuto, and H. Sakurai. J. Chem. Soc. Dalton Trans. 1539 (2002).
10. M.S. Samuel and K.M. Baines. J. Am. Chem. Soc. **124**, 13306 (2002).
11. (*a*) M. Sugawara and J. Yoshida. Synlett, 1057 (1998); (*b*) E. Wenkert, M.E. Alonson, B.L. Buckwalter, and E.L. Sanchez. J. Am. Chem. Soc. **105**, 2021 (1983); (*c*) K. Sato, H. Hagiwara, H. Uda, M. Sato, and N. Harada. J. Am. Chem. Soc. **98**, 8281 (1976).
12. (*a*) N. Wiberg, W. Neidermayer, and K. Polborn. Z. Anorg. Allg. Chem. **628**, 1045 (2002); (*b*) V.Y. Lee, M. Ichinohe, and A. Sekiguchi. J. Organomet. Chem. **636**, 41 (2001); (*c*) N. Fukaya, M. Ichinohe, Y. Kabe, and A. Sekiguchi. Organometallics, **20**, 3364 (2001); (*d*) N. Fukaya, M. Ichinohe, and A. Sekiguchi. Angew. Chem. Int. Ed. **39**, 3881 (2000). (*e*) K.M. Baines, C.E. Dixon, J.M. Langridge, H.W. Liu, and F. Zhang. Organometallics, **18**, 2206 (1999); (*f*) J. Belzner, H. Ihmels, B.O. Kneisel, and R. Herbst-Irmer. J. Chem. Soc. Chem. Commun. 1989 (1994).
13. (*a*) I.V. Komarov. Russ. Chem. Rev. **70**, 991 (2001); (*b*) R.P. Johnson. *In* Molecular structure and energetics. Vol. 3. *Edited by* J.F. Liebman and A. Greenberg. VCH, Weinheim, Germany. 1986. pp. 85–140.
14. (*a*) J. Buriak. Chem. Rev. **102**, 1271 (2002); (*b*) R.J. Hamers, S.K. Coulter, M.D. Ellison, J.S. Hovis, M.P. Schwartz, C.M. Greenlief, and J.N. Russell, Jr. Acc. Chem. Res. **33**, 617 (2000).
15. (*a*) M.V. Lee, D. Guo, M.R. Linford, and H. Zuilhof. Langmuir, **20**, 9108 (2004); (*b*) H.G. Huang, X. Lu, C.L. Xiang, T.L. Teo, Y.H. Lai, and G.Q. Xu. Chem. Phys. Lett. **398**, 11 (2004); (*c*) A. Fink, W. Widdra, W. Wurth, C. Keller, M. Stichler, A. Achleitner, G. Comelli, S. Lizzit, A. Baraldi, and D. Menzel. Phys. Rev. B, **64**, 045308 (2001); (*d*) X. Lu and M.C. Lin. Phys. Chem. Chem. Phys. **2**, 4213 (2000); (*e*) S.H. Xu, M. Keefe, Y. Yang, C. Chen, M. Yu, G.J. Lapeyre, E. Rotenberg, J. Denlinger, and J.T. Yates, Jr. Phys. Rev. Lett. **84**, 939 (2000); (*f*) S.H. Xu, Y. Yang, M. Keefe, G.J. Lapeyre, and E. Rotenberg. Phys. Rev. B, **60**, 11586 (1999); (*g*) F. Matsui, H.W. Yeom, A. Imanishi, K. Isawa, I. Matsuda, and T. Ohta. Surf. Sci. L413 (1998); (*h*) A.J. Dyson and P.V. Smith. Surf. Sci. **375**, 45 (1997); (*i*) L. Li, C. Tindall, O. Takaoka, Y. Hasegawa, and T. Sakurai. Phys. Rev. B, **56**, 4648 (1997); (*j*) C.S. Carmer, B. Weiner, and M. Frenklach. J. Chem. Phys. **99**, 1356 (1993); (*k*) M. Nishijima, J. Yoshinobu, H. Tsuda, and M. Onchi. Surf. Sci. **192**, 383 (1987); (*l*) J. Yoshinobu, H. Tsuda, M. Onchi, and M. Nishijima. Chem. Phys. Lett. **130**, 170 (1986).
16. (*a*) X. Lu, M. Zhu, X. Wang, and Q. Zhang. J. Phys. Chem. B, **108**, 4478 (2004); (*b*) Q. Liu and R. Hoffmann. J. Am. Chem. Soc. **117**, 4082 (1995).

© 2005 NRC Canada

Mechanism of the lithium–iodine exchange in an iodothiophene[1]

Hans J. Reich and Wesley L. Whipple

Abstract: Solutions of 2-lithio-5-methylthiophene (**4**) were characterized using DNMR techniques and shown to be a mixture of monomer and dimer in THF–Et_2O (3:2). The hypervalent iodine ate complex **5** ($Ar_2I^-Li^+$), a presumed intermediate in the Li–I exchange with 2-iodo-5-methylthiophene, was observed by ^{13}C and ^7Li NMR spectroscopy at low temperatures (–130 °C). At higher temperatures, the ate complex coalesced with 2-lithio-5-methylthiophene. A kinetic scheme was developed, which accounts for the exchange of the monomer **4M**, dimer **4D**, and 2-iodo-5-methylthiophene (**6**) with the ate complex **5**. The rates of the various exchanges were obtained through a DNMR analysis of the variable temperature ^{13}C and ^7Li NMR spectra, and the thermodynamic and activation parameters were calculated. The monomer **4M** and the ate complex **5** have similar reactivity as aryl donors in the Li–I exchange reaction, but **4M** is at least 1000 times as reactive as the dimer **4D** towards the iodide.

Key words: halogen–metal exchange, lithium iodinate, iodine ate complex, lithium reagent, aggregate reactivity.

Résumé : On a caractérisé des solutions de 2-lithio-5-méthylthiophène (**4**) en faisant appel à des techniques de RMN dynamique (RMND) et on a pu démontrer que, dans le THF–Et_2O (3 : 2), elles comprennent un monomère et un dimère. Faisant appel à la RMN du ^{13}C et du ^7Li à basse température (–130 °C), on a pu observer le complexe **5** de l'iodate hypervalent ($Ar_2I^-Li^+$), un intermédiaire supposé dans l'échange Li–I avec le 2-iodo-5-méthylthiophène. À des températures supérieures, il y a coalescence du complexe are avec le 2-lithio-5-méthylthiophène. On a développé un schéma cinétique qui permet de tenir compte de l'échange du monomère **4M**, du dimère **4D** et du 2-iodo-5-méthylthiophène (**6**) avec le complexe ate **5**. On a obtenu les vitesses des divers échanges par une analyse RMN des spectres RMN du ^{13}C et du ^7Li à des températures variables et on en a calculé les paramètres thermodynamiques et d'activation. Vis-à-vis des donneurs aryles, dans une réaction d'échange Li–I, les réactivités du monomère **4M** et du complexe ate **5** sont semblables; toutefois, vis-à-vis de l'iode, le monomère **4M** est au moins mille fois plus réactif que le dimère **4D**.

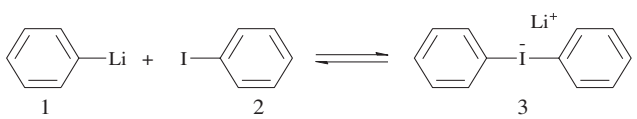
Mots clés : échange halogène–métal, iodate de lithium, complexe ate de l'iode, réactif de lithium, réactivité d'un agrégat.

[Traduit par la Rédaction]

Introduction

The lithium–metalloid exchange, independently discovered by Gilman et al. (1) and Wittig et al. (2) is an effective route for the formation of many organolithium reagents inaccessible by other methods. Understanding the mechanism of this process provides greater insight and predictability into the factors that influence reactivity. The reaction has commanded substantial research interest over the past 60 years (3*a*), where four-centered (4), SET (3*a*–3*c*, 5), S_N2 (6), and ate complex mechanisms (7*a*, 8) have been suggested. Investigation of the lithium–metalloid exchange identified ate complexes as permissible intermediates, including those of I (7*b*, 7*c*, 9), Te (7*c*–7*e*, 10*a*, 10*b*), Se (7*d*, 7*f*, 10*b*), Sn (7*g*, 11, 12), Si (13), and Hg (7*b*, 7*c*). Iodine ate complexes have also been detected as intermediates in the Li–Mg exchange (14). Both experimental (7*e*, 15) and computational (3*d*, 8) studies have addressed the ease of formation of various ate complexes. The relative rates of the lithium–metalloid exchanges follow the trend: I > Te >> Sn >> Br > Se >> S.

In previous reports of the lithium–iodine exchange of phenyllithium (**1**) with iodobenzene (**2**) we have kinetically and spectroscopically identified the stable hypervalent ate complex **3** as present in solution (7*b*, 7*c*, 7*e*). Direct involvement of **3** in the exchange process could not be proven, since analysis of the kinetic processes was complicated by the unfavorable equilibrium between phenyllithium monomer and dimer, and the degenerate exchange between **2** and **3**.



1 2 3

We report here our results on the solution structure of 5-methyl-2-thienyllithium (**4**) and its behavior in the lithium–iodine exchange using low-temperature, multinuclear NMR techniques. The use of **4**, with its favorable NMR properties, ease of handling, and considerably higher monomer to dimer ratio compared to PhLi, has allowed measurement of the rates and equilibria of exchange between monomer **4M** and

Received 25 April 2005. Published on the NRC Research Press Web site at http://canjchem.nrc.ca on 1 December 2005.

H.J. Reich[2] and W.L. Whipple. Department of Chemistry, University of Wisconsin, 1101 University Avenue, Madison, Wisconsin 53706, USA.

[1]This article is part of a Special Issue dedicated to organic reaction mechanisms.

[2]Corresponding author (e-mail: reich@chem.wisc.edu).

 doi: 10.1139/V05-173 © 2005 NRC Canada

dimer **4D** (eq. [1]), monomer and ate complex **5** (eq. [2]), and ate complex and 2-iodo-5-methylthiophene (**6**) (eq. [3]). It has also allowed an estimate of the maximum reactivity of the dimer with the iodide in the Li–I exchange (eq. [4]).

[1] $2\ \mathbf{4M} \underset{k_{-1}}{\overset{k_1}{\rightleftharpoons}} \mathbf{4D}$

$\Delta H_1^{\ddagger} = 6.4 \pm 0.3$ kcal/mol; $\Delta S_1^{\ddagger} = -2.3 \pm 2$ eu

$\Delta H_{-1}^{\ddagger} = 5.3 \pm 0.3$ kcal/mol; $\Delta S_{-1}^{\ddagger} = -13.6 \pm 2$ eu

$\Delta H_1 = 0.92 \pm 0.06$ kcal/mol; $\Delta S_1 = 11.2 \pm 0.3$ eu

$$K_1 = \frac{[\mathbf{4D}]}{[\mathbf{4M}]^2}$$

[2] $\mathbf{4M} + \mathbf{6} \underset{k_{-2}}{\overset{k_2}{\rightleftharpoons}} \mathbf{5}$

$\Delta H_2^{\ddagger} = 1.50 \pm 0.4$ kcal/mol; $\Delta S_2^{\ddagger} = -21.9 \pm 2$ eu

$\Delta H_{-2}^{\ddagger} = 10.4 \pm 0.4$ kcal/mol; $\Delta S_{-2}^{\ddagger} = 21.8 \pm 2$ eu

$\Delta H_2 = -10.2 \pm 0.3$ kcal/mol; $\Delta S_2 = -48.6 \pm 1.5$ eu

$$K_2 = \frac{[\mathbf{5}]}{[\mathbf{4M}]\,[\mathbf{6}]}$$

[3] $\mathbf{5} + \mathbf{6} \underset{k_{-3}}{\overset{k_3}{\rightleftharpoons}} \mathbf{6} + \mathbf{5}$

$\Delta H_3^{\ddagger} = 3.70 \pm 0.2$ kcal/mol; $\Delta S_3^{\ddagger} = -7.8 \pm 1$ eu

$\Delta H_{-3}^{\ddagger} = 3.70 \pm 0.2$ kcal/mol; $\Delta S_{-3}^{\ddagger} = -7.8 \pm 1$ eu

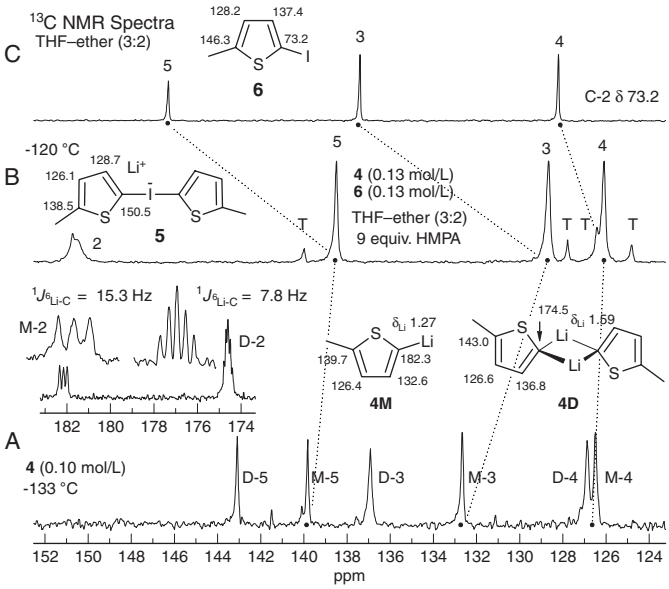
[4] $\mathbf{4D} + \mathbf{6} \underset{k_{-4}}{\overset{k_4}{\rightleftharpoons}} \mathbf{4M} + \mathbf{5}$

Results and discussion

The NMR study we set out to perform used four kinds of samples, all in THF–ether (3:2) solution (this mixed solvent system is close in donor strength to that of pure THF and allows the measurement of NMR spectra down to –135 °C). In each case variable temperature ^{6}Li, ^{7}Li, and ^{13}C NMR spectra were measured. They are:

1. Solutions of the lithium reagent **4** to define the aggregates (**4M** and **4D**) present (Figs. 1A and 2). The concentration and temperature dependence of the equilibrium constant (K_1) and the temperature dependence of the exchange rates k_1 and k_{-1} were determined from these samples (Figs. 3 and 4).

Fig. 1. ^{13}C NMR spectra in THF–ether (3:2). (A) 0.10 mol/L of **4** at –133 °C (the inset showing the C-2 signals is from a 0.2 mol/L ^{6}Li-labeled sample, where the dimer C-2 signal was processed by multiplying the FID with a Gaussian function before Fourier transformation (LB = –6.1, GB = 0.1). The coupling constants are believed accurate to ±0.2 Hz (D = **4D**, M = **4M**). (B) A 1:1 ratio of **4** and **6** with 9 equiv. of HMPA (T = 2-methylthiophene, protonation product). (C) The iodide **6**.



2. Solutions with a 1:1 ratio of lithium reagent **4** and iodide **6** with excess HMPA present (Fig. 1B). In such solutions K_2 becomes very large, leaving **5** as the only detectable species (7*a*, 7*b*) and allowing its NMR identification and characterization.
3. Solutions with an excess of lithium reagent over iodide (Fig. 5). Line-shape fitting of the ^{7}Li NMR spectra of these samples allow estimation of k_2 at each temperature, using as input the values of K_1, K_2, k_1, and k_3 obtained from samples 1 and 4.
4. Solutions with an excess of iodide **6** over lithium reagent **4** (Fig. 6). In these solutions **4M**, **5**, **6**, and, at temperatures above –85 °C, **4D**, are in rapid exchange and it is possible to measure the temperature dependence of the ate complex association constant K_2 from analysis of the averaged peak positions in the ^{13}C NMR spectra, using K_1 obtained from samples 1 and the chemical shifts of the individual species. Line-shape analysis of these samples also allowed measurement of k_3 and an estimate of k_4.

The solution structure of 2-lithio-5-methylthiophene

Previous studies of 2-thienyllithium reagents have included X-ray structures of the ether solvated tetramer of **4** (7*h*), several substituted lithiothiophenes,[3] and 2-lithiobenzothiophene (16*a*), as well as a report of the solution ^{13}C NMR spectrum of 2-lithiothiophene itself (17). We have recently

[3] Several single crystal X-ray structures have been reported in the Cambridge Structural Database as private communications (1999). 3-Dimethylaminomethyl-2-lithiothiophene dimer (LEDSES): A.L. Spek, M.T. Lakin, and R. den Besten. 3-Methoxy-2-lithiothiophene (HIGPOC): A.L. Spek and N. Veldman. 3-Bromo-2-lithiothiophene TMEDA dimer (HIGXUQ): A.L. Spek. 2-Lithiothiophene dimer (JUJXER): A.L. Spek and W.J.J. Smeets.

© 2005 NRC Canada

Fig. 2. Selected ^{13}C and ^{7}Li NMR spectra of a variable temperature study of 0.101 mol/L 5-methyl-2-thienyllithium (**4**) in THF–ether (3:2). These spectra were simulated to obtain k_1, k_{-1}, and K_1 (eq. [1]). Monomer (M), dimer (D).

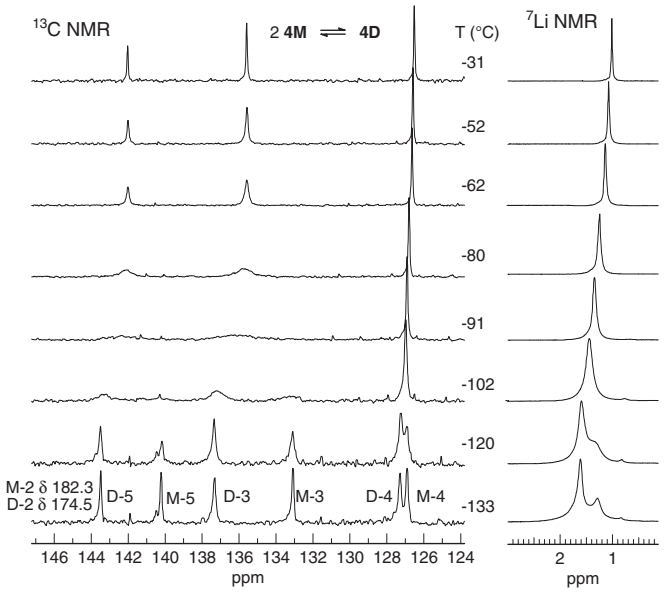
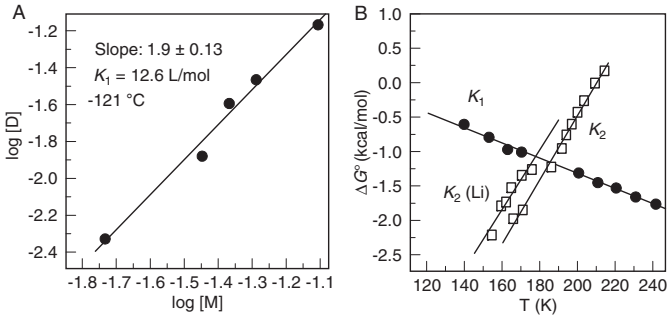


Fig. 3. (A) Concentration dependence of the **4M** and **4D** ratio in THF–ether (3:2) at –121 °C. (B) Temperature dependence of free energy ($\Delta G = RT \ln(K_{eq})$) for the monomer dimer equilibrium (K_1, eq. [1]) and the ate complex equilibrium (K_2, eq. [2]).



reported detailed NMR studies of a series of lithiothiophenes, including some with ortho chelating groups (7*i*).

Clean solutions of **4** were readily available since the precursor 2-methylthiophene is easily metalated with *n*-BuLi (17, 18), and the pure reagent can be crystallized from THF or ether (7*h*). Figure 1A reports the ^{13}C NMR spectrum of 95.5% ^{6}Li-labeled **4** (19) in THF–ether (3:2) at –121 °C. There are two sets of carbon signals, corresponding to two distinct lithium species (19*a*). Each showed fully resolved ^{13}C–^{6}Li scalar coupling of the ipso carbon signals at 182.3 ppm (1:1:1 triplet, ^{1}J = 15.3 Hz) and 174.5 ppm (1:2:3:2:1 pentet, ^{1}J = 7.8 Hz), respectively (19*b*). The assignment of the two species as monomer **4M** and dimer **4D** derives from the lithium–carbon coupling, as well as from a variable concentration study, which showed that the two species differ in aggregation state by a factor of two (slope of the log[M] vs. log[D] plot was 1.9 ± 0.13, K_1 = 12.6 (mol/L)$^{-1}$ at –128 °C, Fig. 3*a*) (7*j*, 7*k*, 16*b*). In addition,

Fig. 4. Temperature dependence of the free energy of activation (calculated from a form of the Eyring equation, $\Delta G^{\ddagger} = RT[23.76 + \ln(T/k_r)] = \Delta H^{\ddagger} - T\Delta S^{\ddagger}$) for the monomer–dimer exchange (k_1 (●) from line-shape analysis of the spectra in Fig. 2, eq. [1]), ate complex formation (k_2 (▲) from Fig. 6, eq. [2]), and ate complex – iodide exchange (k_3 (□) from Fig. 7, eq. [3]).

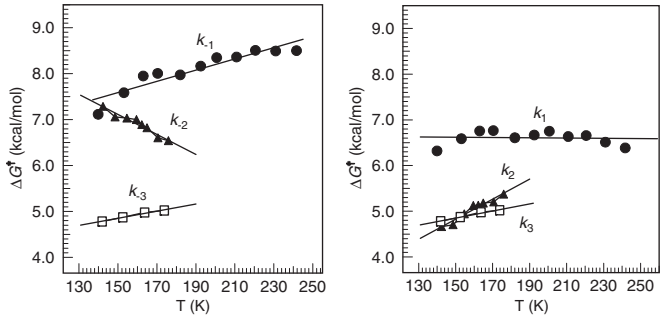
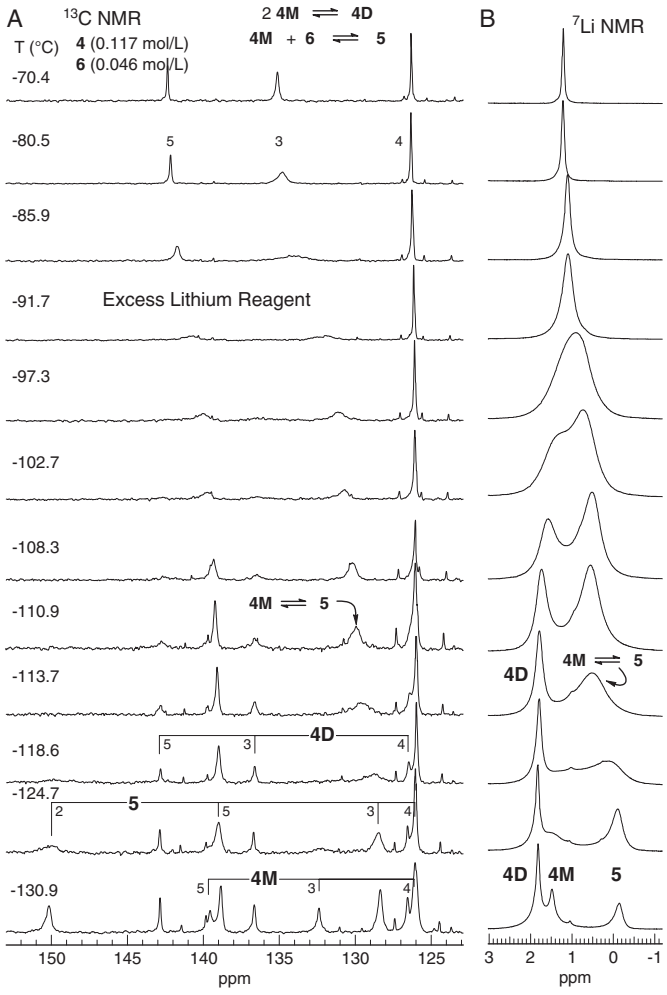


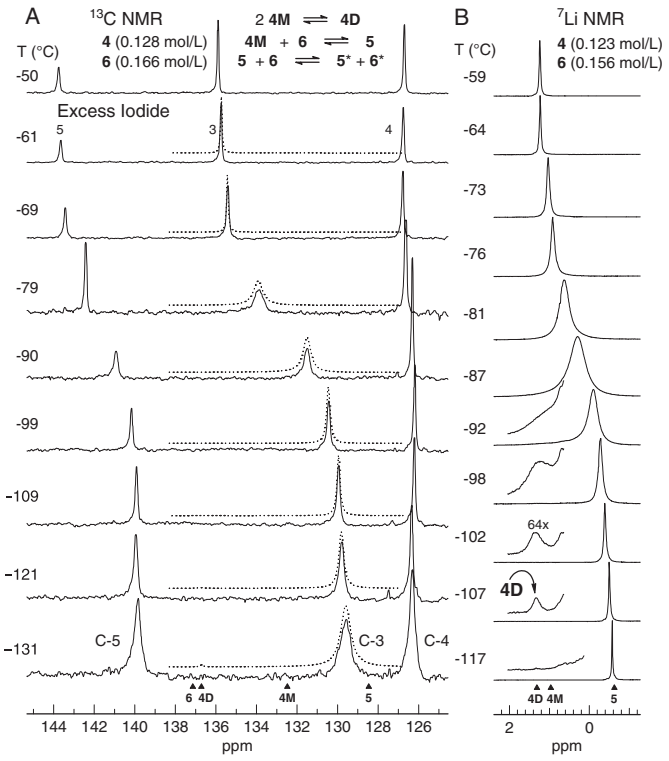
Fig. 5. Variable temperature (A) ^{13}C and (B) ^{7}Li NMR spectra of a solution of **4** (0.117 mol/L) and **6** (0.046 mol/L) in THF–ether (3:2).



experiments in various mixtures of THF and ether showed that the dimer signals increasingly predominated as the fraction of ether increased. The carbon assignments in the ^{13}C NMR spectra were based on identification of C-2 from the

© 2005 NRC Canada

Fig. 6. Variable temperature NMR spectra of solutions of **4** and **6** in THF–ether (3:2) with excess iodide. The two panels are from experiments with slightly different concentrations. (A) ^{13}C NMR spectra. The dotted spectra are simulations of the C-3 resonance, as described in the text. (B) ^{7}Li NMR spectra. The insets are vertical expansions showing the build-up and eventual coalescence of **4D** with the average of the other signals as temperature increased.



Li–C coupling, C-5 as a quaternary carbon by an INEPT experiment, on the literature assignments for 2-lithiothiophene (17), and on the correlation between equivalent carbons of **4M**, **4D**, **5**, and **6** provided by the coalescence experiments (Figs. 2, 5, and 6). Thus, the carbons of **6** could be readily assigned from shift parameters (20), and this allowed carbon signal assignments of all of the other compounds.

A variable temperature experiment of **4** is shown in Fig. 2. Each pair of ^{13}C and ^{7}Li NMR signals for **4M** and **4D** coalesced between –120 and –91 °C. Complete line-shape simulations of these spectra were used to determine the rates of interconversion for monomer and dimer. The relationship between the pseudo-first-order NMR rate constants (k_{MD} and k_{DM}) obtained from the simulation and the mechanistic rate constants k_1 and k_{-1} of eq. [1] is straightforward: k_{-1} is also a first-order rate constant (it is best to think of a first-order rate as the fraction of substrate converted per unit time), so $k_{-1} = k_{DM}$. The monomer to dimer conversion k_1 is a second-order rate constant (fractional conversion per unit time per molar concentration of reactant), and thus $k_{MD} = k_1[\mathbf{4M}]$. The activation parameters in eq. [1] were calculated from the temperature dependence of k_1 and k_{-1} (see Fig. 4). The simulation also gave the concentration of monomer and dimer as a function of temperature (for the four low temperature points from the areas of the two C-3 peaks, for the five high temperature points from the peak position of the averaged C-3 signals), and hence the thermodynamic parameters for the dimer–monomer equilibrium (Fig. 3B).

Lithium–iodine exchange of 2-lithio 5-methyl-thiophene

Solutions containing both **4** and **5** show complex DNMR behavior because of the presence of four species (**4M**, **4D**, **5**, and **6**) whose relative concentrations are strongly temperature dependent and which are all undergoing mutual exchange involving at least three different rate constants (k_1, k_2, and k_3). Figure 1 shows spectra of **4** and **6** and a 1:1 mixture of the two, the latter with 9 equiv. of hexamethylphosphoric triamide (HMPA) present, which has the effect of greatly increasing K_2 (7*a*, 7*b*). The presence of a new species in Fig 1B, the ate complex **5**, can be readily seen, since the ^{13}C signals for C-3, C-4, and C-5 are upfield of all three constituents, and so cannot simply be a dynamic average of them.

Examination of samples in THF–ether (3:2) with varying ratios of iodide and lithium reagent revealed that there were two limiting behaviors. With excess lithium reagent the signals of three of the components present (**4D**, **4M**, and **5**) could be decoalesced. There is not a detectable amount of **6** at the lower temperature limit of the solvent system (Fig. 5). On the other hand, when iodide was in excess there was (with a minor exception) a single, strongly temperature dependent set of ^{13}C and ^{7}Li signals throughout the accessible temperature range (Fig. 6).

The spectra of Fig. 5 can be interpreted as follows. At the lowest temperatures the signals of the ate complex **5** are decoalesced from those of the monomer **4M** and dimer **4D**. The formation constant (K_2) of **5** is high, and since there is excess lithium reagent, there is no detectable iodide **6**. Between –130 and –115 °C the signals of **5** and **4M** coalesce (eq. [2]). The signals of **4D** are not appreciably affected by this process. Between –110 and –90 °C the **4D** signals coalesce with the averaged signals of **5** and **4M**. Starting at ca. –110 °C, the shift of the equilibrium of eq. [2] (K_2) away from ate complex toward the iodide and lithium reagent becomes apparent as indicated by the downfield shift of the three visible signals (the C-3, C-4, and C-5 signals of **5** are all upfield of those of **4M**, **4D**, and **6**).

Figure 6 cannot be interpreted with only the eq. [1] and [2] processes, since the lowest temperature spectrum should show excess iodide **6** and the ate complex **5** in slow exchange, just as was seen for excess **4** in Fig. 5 (the process k_2 is slow on the NMR timescale at this temperature). We propose that here, as seen for the PhLi–PhI system (7*b*, 7*c*), there is another exchange process that averages the signals of **5** and **6**. The ate complex is behaving as a carbanion donor, and transferring an aryl group to the iodide to form a new ate complex (k_3, eq. [3]). When there is a stoichiometric excess of lithium reagent, there is no corresponding process that can average the lithium reagent and ate complex signals, and so the signals can be decoalesced (Fig. 5).

We will perform a quantitative analysis of the thermodynamics and kinetics of the Li–I exchange as revealed by the spectra of Figs. 5 and 6. First, we will determine the ate complex association constant K_2 from an analysis of chemical shifts and peak positions in the ^{13}C NMR spectra of Fig. 6 using the information on k_1 and K_1 gleaned from Fig. 2 and similar experiments. This allows us to extract the

© 2005 NRC Canada

Fig. 7. Exchange matrix used for the simulation of the ^{7}Li NMR spectra of Fig. 5B.

$$\begin{array}{c} \\ \mathbf{A}\ (\mathbf{5}) \\ \mathbf{D}\ (\mathbf{4D}) \\ \mathbf{M}\ (\mathbf{4M}) \end{array} \begin{array}{c} \begin{array}{ccc} \mathbf{A}\ (\mathbf{5}) & \mathbf{D}\ (\mathbf{4D}) & \mathbf{M}\ (\mathbf{4M}) \end{array} \\ \begin{bmatrix} i2\pi(\nu_A) - 1/T - \Sigma k_{AX} & k_{AD} & k_{AM} \\ k_{DA} & i2\pi(\nu_D) - 1/T - \Sigma k_{DX} & k_{DM} \\ k_{MA} & k_{MD} & i2\pi(\nu_M) - 1/T - \Sigma k_{MX} \end{bmatrix} \end{array} = E$$

$$k_{AD} = k_{-4}[\mathbf{4M}] \qquad k_{DA} = \frac{k_4[\mathbf{6}]}{2} \qquad k_{AM} = k_{-2}$$

$$k_{MA} = k_2[\mathbf{6}] \qquad k_{DM} = k_{-1} + \frac{k_4[\mathbf{6}]}{2} \qquad k_{MD} = k_1[\mathbf{4M}] + k_{-4}[\mathbf{5}]$$

Li–I exchange rate constant k_2 from the spectra of Fig. 5, and sets the stage for determining k_3 as well as estimating the maximum rate of exchange of the dimer **4D** with the iodide **6** (k_4).

Determination of the ate complex association constant (K_2)

We have used the chemical shift of the C-3 signal in the ^{13}C NMR spectra of an experiment like the one in Fig. 6A to determine the composition of the sample. At each temperature above coalescence (–87 to –59 °C) an iterative computer program was used to calculate the concentration of all species for a series of trial ate complex concentrations until the calculated averaged ^{13}C NMR chemical shift matched the experimental one. These calculations used the previously determined values of K_1 (eq. [1]), the concentrations of the component species, and the chemical shifts of each compound as input. The shifts of **4M**, **4D**, and **5** were found to be temperature independent and those of **6** were extrapolated from spectra of pure **6** taken at a series of temperatures.

Two additional data points were derived from the ^{7}Li NMR spectra. At –117, –107, –102, and –98 °C it was possible to detect the signal of **4D** (see insets, Fig. 6B). The area of this signal was determined at the two temperatures at which it is best defined (–102 and –107 °C), and these values were then used to calculate the concentrations of the other species using the known value of K_1.

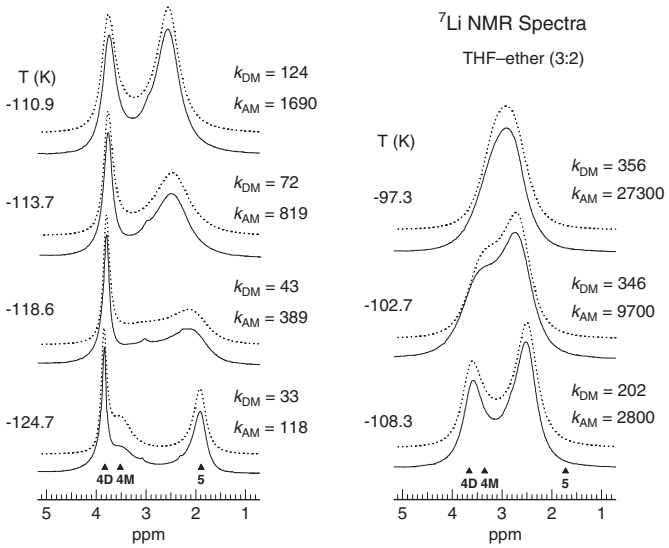
From the concentrations, K_2 can be calculated at each temperature and the thermodynamic parameters for the ate complex equilibrium determined (see eq. [2], Fig. 3B). The large negative entropy of formation of the ate complexes (–48.6 eu) is similar to that found for the formation of lithium diphenyliodinate **3** (–44 eu) (7*c*) and other systems (7*d*, 7*f*, 13). This loss of entropy derives from loss of translational and rotational motion for the component iodide and lithium reagent, as well as the extra THF molecules frozen by the very electrophilic free lithium cation of the ate complex (7*b*, 7*c*), compared to the strongly C-bound cation of the aryllithium reagent (7*l*).

Determination of the rate of Li–I exchange (k_2)

We next simulated the NMR spectra of Fig. 5 to determine values for k_2 and k_{-2}. The ^{13}C signals were rather noisy, and simulations were not very well defined. However, the ^{7}Li NMR signals had superb signal-to-noise and had the decisive advantage that the degenerate exchange of iodide and ate complex (eq. [3]) does not affect the ^{7}Li line shape, since this process leaves the lithium signal unchanged.

A significant problem for simulations of the ^{7}Li spectra is the quite variable quadrupolar T_1 relaxation rates (21), which could not be independently measured because of interference from dynamic effects. Since the lines were fifty to several hundred Hz wide in the crucial part of the simulation, we anticipated that errors in line width would not greatly affect the accuracy of the rate constants determined. We assigned inherent line widths of 4 Hz for **5**, 8 Hz for **4D**, and 10 Hz for **4M** based on the low temperature spectra and the behavior of other related aryllithium species. An iterative process was used to establish optimum populations and rates (see the Experimental section) using the exchange matrix shown in Fig. 7. The exchange matrix includes contributions from the reaction of dimer with iodide (k_4 process, eq. [4]). The values of k_{-1} in solutions containing **6** were actually smaller than those determined for solutions of just the lithium reagent. Since no detectable contribution from k_4 is present, it was set to zero, leaving only k_{DM} (k_{-1}) and k_{AM} (k_{-2}) to be adjusted (7*m*).

Fig. 8. Line-shape simulation of the variable temperature ^{7}Li NMR spectra of Fig. 5B (**4** (0.117 mol/L) and **6** (0.046 mol/L) in THF–ether (3:2)). Lower lines are experimental data, upper dotted lines are simulations using the rate constants shown and the exchange matrix of Fig. 7.



The simulations are presented in Fig. 8. An excellent match between experimental and calculated spectra was achieved, with k_{-1} within a factor of two of those values determined from solutions of **4** (Fig. 2) and K_2 values within a factor of four of those determined from analysis of the previous ^{13}C NMR shifts of Fig. 6 (see Fig. 4). There are a number of potential reasons for these discrepancies: the chemical shifts may have a slight temperature dependence, the assumption of T_1 values for the three lithium species may have been too crude, and there may have been small variations in solvent composition between experiments. Both K_1 and K_2 are very solvent sensitive. For example, K_1 decreased by a factor of 5.7 between 60% and 80% THF in ether at –117 °C. The values for k_2 and k_{-2} as a function of temperature are shown in an Eyring plot in Fig. 4, leading to the activation parameters reported in eq. [2].

Rate of exchange of ate complex with iodide (k_3)

We are now in a position to attempt a simulation of the ^{13}C NMR line shifts of Fig. 6, which involves, in addition to

© 2005 NRC Canada

Fig. 9. (A) Spectrum of a solution of **4** and **6** at –131 °C. (B) Optimal simulation. (C) Simulation with no contribution from the process of eq. [3] (k_3) (7*m*). See Fig. 10 for the definitions of k_{AI} and k_{AM}.

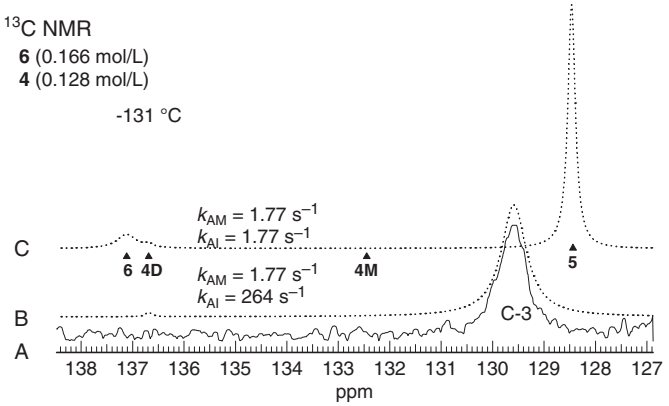


Fig. 10. Exchange matrix for the interactions between **4M**, **4D**, **5**, and **6**. See eqs. [1]–[4] for definitions of the rate constants.

$$\begin{array}{c} \\ \mathrm{A} \\ \mathrm{D} \\ \mathrm{M} \\ \mathrm{I} \end{array} \begin{bmatrix} \mathrm{A}\ (\mathbf{5}) & \mathrm{D}\ (\mathbf{4D}) & \mathrm{M}\ (\mathbf{4M}) & \mathrm{I}\ (\mathbf{6}) \\ i2\pi(\nu_A) - 1/T - \Sigma k_{AX} & k_{AD} & k_{AM} & k_{AI} \\ k_{DA} & i2\pi(\nu_D) - 1/T - \Sigma k_{DX} & k_{DM} & k_{DI} \\ k_{MA} & k_{MD} & i2\pi(\nu_M) - 1/T - \Sigma k_{MX} & k_{MI} \\ k_{IA} & k_{ID} & k_{IM} & i2\pi(\nu_I) - 1/T - \Sigma k_{IX} \end{bmatrix} = E$$

$$k_{AD} = \frac{k_{-4}[\mathbf{4M}]}{2} \qquad k_{DA} = \frac{k_4[\mathbf{6}]}{2}$$

$$k_{AM} = k_{-2} \qquad k_{MA} = k_2[\mathbf{6}]$$

$$k_{AI} = k_{-2} + \frac{k_3[\mathbf{6}]}{2} + \frac{k_{-4}[\mathbf{4M}]}{2}$$

$$k_{IA} = k_2[\mathbf{4M}] + k_3[\mathbf{5}]$$

$$k_{DM} = k_{-1} \qquad k_{MD} = k_1[\mathbf{4M}] + k_{-4}[\mathbf{5}]$$

$$k_{DI} = 0 \qquad k_{ID} = 0$$

$$k_{MI} = 0 \qquad k_{IM} = \frac{k_{-4}[\mathbf{4M}]}{2}$$

the eq. [1] and [2] processes, the bimolecular exchange between ate complex and iodide (k_3, eq. [3]). We used the values of k_1, k_2, K_1, and K_2 calculated from the thermodynamic and activation parameters in eqs. [1] and [2] to determine the NMR rates and populations of **4M**, **4D**, **5**, and **6** at each temperature. Neither the populations nor the k_1 and k_2 rate constants were allowed to vary in the simulation. Any excess broadening of the iodide **6** and ate complex **5** signals over that predicted by k_2 can then be assigned to k_3, the iodide – ate complex exchange of eq. [3]. This is illustrated in Fig. 9, which shows simulations of the –131 °C spectrum. At this temperature the iodide signal would be decoalesced if $k_{AI} = k_{AM}$ (Fig. 9C), i.e., if k_2 was the only mechanism for exchange. This can be compared with the simulation in Fig. 9B, which has the rate k_{AI} optimally adjusted to fit the actual spectrum.

The exchange matrix and the relationship between first-order NMR rate constants (k_{AD}, k_{AM}, k_{AI}, etc.) and their mechanistic equivalents (k_1, k_2, k_3, k_4, etc.) is shown in Fig. 10. This simulation is complicated by the fact that temperatures low enough for decoalescence cannot be achieved. In addition, values for k_3 and k_{-3} are calculated from k_2 and k_{-2} ($k_3 = (k_{IA} - k_2[\mathbf{4M}])/[\mathbf{5}]$, $k_{-3} = (2k_{AI} - k_{-2})/[\mathbf{6}]$), and so the limited accuracy of k_2 because of the small temperature range and scatter of the $\Delta G^{\ddagger}$ vs. T plot (Fig. 4) directly affects the accuracy of the k_3 values.

The simulation worked reasonably well (insets in Fig. 6A), although there were small errors in the chemical shift of the averaged signal, which is not surprising considering the accumulation of calculated values that comprise the input. The most likely source is small errors in the value of K_2 used to calculate the concentrations. Only at the four lowest temperatures in Fig. 6 were the spectra significantly affected by the value of k_3, so we report data only at these temperatures. Although there is significant broadening at intermediate temperatures (–87 and –81 °C), this is largely due to the monomer–dimer exchange (k_1) and is not very sensitive to k_3. Activation parameters are shown in eq. [3]. We did not perform experiments to verify that the k_3 process was first order in **6** by repeating this experiment with variable iodide concentrations. However, such an experiment was previously performed for a PhLi–PhI solution in THF–HMPA (7*b*), where first-order behavior in iodide was demonstrated by a DNMR study.

The data obtained show the astonishing result that the monomeric lithium reagent and the ate complex have comparable reactivity as donors in the Li–I exchange. In another test of ate complex reactivity, the reaction of PhLi–PhI with hexamethyldisiloxane in THF–HMPA, PhLi is at least a factor of 10^5 more reactive than $Ph_2I^-Li^+$ (7*a*). This estimate is based on the reduction in k_{obs} for the silylation reaction when excess PhI was added to a solution of PhLi in THF–HMPA. Of course, in this case the PhLi has been greatly activated by complexation to HMPA (by a factor of 10^3 or more) (7*j*), so a direct comparison is not very meaningful. We considered that the k_2 process might be approaching diffusion control, and thus suffer from rate compression, but diffusion-controlled processes at –102 °C in THF–ether should have rates of ca 1×10^9 s^{-1} $(mol/L)^{-1}$, about 10^3 times faster than the measured bimolecular rate (k_2). A more likely explanation is that the rate-limiting (or partial-limiting) step for the Li–I exchange (eq. [2]) is C—Li bond dissociation (CIP to SIP) or solvent association with or dissociation from the lithium cation. Barriers to dissociation of THF from lithium species can be substantially higher than the activation energies of the Li–I exchange measured here (7*n*, 22, 23). This is in principle testable (the Li–I exchange should have fractional or zero order in iodide) by repeating the experiment of Fig. 5 at various concentrations, to establish whether consistent rates would be obtained. Unfortunately, the concentration of iodide is not easily manipulated in solutions with excess lithium reagent, the only conditions where k_{-2} can be measured.

It is the interference by the process of eq. [3] that prevents us from demonstrating by DNMR techniques whether the ate complex is an obligatory intermediate in the Li–I exchange. This would require showing that the exchange rates of iodide and lithium reagent were the same and that the ate complex lifetime was correctly predicted from the lifetimes of the reaction partners. To achieve this, signals for all three components (**4M**, **5**, and **6**) must be visible in a sample so that lifetimes of all three can be simultaneously measured. As can be seen from Figs. 5 and 6, at no point can ^{13}C signals of all three species be seen. This is in part because at the low temperatures where rates are slow enough to observe individual signals, K_2 is so large that the concentrations of **4M** or **6** (whichever is stoichiometrically limiting) is too small to detect, and in part because k_3 is too large.

© 2005 NRC Canada

Rate of Li–I exchange for the dimer (k_4)

The observation that the ^{7}Li NMR signal of the dimer **4D** could be decoalesced from the averaged signal comprising the lithiums of **4M** and **5** in Fig. 6B shows that the dimer is not undergoing Li–I exchange (eq. [4]) under conditions where exchange of monomer is rapid. The ^{7}Li NMR signal of **4D** at –102 °C is 60 Hz wide. At the same temperature the ^{13}C NMR signal of **4D** in a sample containing only **4** is 80 Hz (Fig. 2), so there is no detectable broadening assignable to the Li–I exchange of dimer, the k_4 process. If we estimate that no more than 10 Hz of the 60 Hz line width of the lithium signal could be due to the k_4 process, then the NMR rate constant $k_{DA} \leq 31$ s^{-1} ($\pi\Delta\nu$), and the physical rate constant $k_4 = k_{DA}/[\mathbf{6}] \leq 670$ s^{-1} (mol/L)$^{-1}$. Since the rate of exchange of the iodide with monomer (k_2) is 6.7×10^6 s^{-1} (mol/L)$^{-1}$ at –102 °C (see eq. [2]), reaction of dimer with the iodide is at least a factor of 1000 slower than reaction of the monomer. Although many reactivity effects of organolithium reagents have been ascribed to aggregation phenomena, determination of quantitative and qualitative differences between reactivity of different aggregates of an organolithium species under the same conditions has rarely been reported (24, 25). This result shows that the common assumption that higher aggregates are less reactive than lower ones holds well in this monomer–dimer case, and that the differences can be quite large.

Summary

A DNMR investigation of 2-lithio-5-methylthiophene (**4**) showed this lithium reagent to be a mixture of monomer and 4-center dimer in THF–ether (3:2). Solutions of **4** and the corresponding iodide **6** undergo Li–I exchange on the NMR timescale. The ate complex **5**, a probable intermediate in the exchange, is formed with a high association constant at low temperature (–130 °C), but is largely dissociated at temperatures above –70 °C. A variable-temperature DNMR kinetic analysis showed that three exchange processes occurred on the NMR timescale, the monomer dimer exchange (eq. [1]), the Li–I exchange of the monomeric lithium reagent (eq. [2]), and direct exchange between the ate complex and the iodide (eq. [3]). The ate complex **5** is comparable in reactivity to the monomeric lithium reagent **4M** in the Li–I exchange process. The data obtained also allowed an estimate of the upper limit of a fourth process, the Li–I exchange of the dimer (eq. [4]). The bimolecular rate constants at –102 °C are shown in the following:

Rate constant	k ((mol/L)$^{-1}$ s^{-1})	k_{rel}
k_1 (eq. [1])	6.8×10^3	1/100
k_2 (eq. [2])	6.7×10^5	1.0
k_3 (eq. [3])	1.3×10^6	1.9
k_4 (eq. [4])	$<6.6\times10^2$	<1/1000

The lithium iodine exchange reaction has been mechanistically controversial since its discovery in 1938. The present DNMR investigation, together with other related papers (7*a*–7*c*), places aryl iodine ate complexes (**5**) firmly into the mechanistic picture in two roles: as a permissible intermediate in the exchange itself (our results do not make it an obligatory intermediate), and as a reactive partner in its own right in donating a thienyl anion to iodothiophene (eq. [3]). The latter observation suggests that ate complexes may be reactive partners in reactions when lithium reagents are prepared by Li–I exchange. The fact that solutions of iodide and lithium reagent are stable in samples where upwards of 10^9 Li–I exchanges have occurred during an experiment provides a strong argument that single electron transfer reactions involving aryl radical intermediates play no role in the reaction, since cage effects of this magnitude would seem impossible.

Experimental section

General

All glassware was dried in an oven at 110 °C for at least 2 h and flushed with N_2 for at least 5 min. All reactions were performed under an atmosphere of dry nitrogen.

Instrumentation

GC analyses were performed using a 12 m × 0.32 mm SE-30 capillary column, with He pressure of 6.0 psi (1 psi = 6.894 757 kPa), column flow rate (split ratio 300:1) of 3 mL/min, and column temperature of 90 °C. Retention times and response factors with respect to *n*-undecane are as follows: 2-iodo-5-methylthiophene (2.77 min, 2.39), 2-(methylthio)-5-methylthiophene (2.87 min, 1.99), *n*-undecane (2.67 min, 1.00). For a 1:1 molar solution of compound: $C_{11}H_{24}$, the response factor = (peak area $C_{11}H_{24}$)/(peak area compound).

^{13}C, ^{7}Li, and ^{6}Li NMR spectra were obtained on a Bruker AM-360 spectrometer operating at 90.56, 139.96, and 53.00 MHz, respectively. The NMR spectra were acquired unlocked and in non-deuterated solvents unless otherwise stated. For ^{13}C NMR, a 30° pulse of 5 μs repeated every 2.9 s was used. An exponential line broadening of 2–5 Hz was used, and a 64 K transform was carried out over a spectral width of 20 800 Hz. ^{13}C NMR chemical shifts are reported in ppm relative to TMS (δ 0.0), using THF as an internal reference. ^{7}Li NMR spectra were recorded over a spectral width of 1400 Hz (8K data points) using a 10 μs pulse and ^{6}Li NMR spectra over a spectral width of 2907 Hz (8K data points) with a pulse width of 10 μs and a recycle delay of 4 s. Both ^{7}Li and ^{6}Li NMR chemical shifts were referenced to external 0.30 mol/L LiCl in MeOH (δ 0.0 ≈ –100 °C) (19*c*). *n*-Bu-^{6}Li (95.5% enriched) was prepared by literature procedures (7*l*).

Probe temperatures were measured (decoupler turned off) by replacing the sample with an open tube containing the same solvent and the sensor of a RTD (platinum resistance) thermometer, which was designed to measure temperatures from –150 °C to 50 °C, and was calibrated using ice water (0.01 °C) and CO_2 (–78.5 °C). The accuracy of the resistance thermometer was checked with the melting points of toluene (–95.00 °C) and methylcyclohexane (–126.6 °C) and were found to be within 0.4 °C of the reported value. Samples were allowed to equilibrate for at least 8 min in the probe prior to tuning the spectrometer and acquiring the spectrum. Probe temperatures were confirmed following the acquisition of each spectrum.

DNMR simulations were performed with the Binsch DNMR program (26) and with WINDNMR (7*m*).

© 2005 NRC Canada

Solvents

THF and Et_2O were freshly distilled from sodium benzophenone ketyl prior to use. The THF still was recharged every 3 weeks to insure that no benzene (formed by cleavage of benzophenone) accumulated in the THF. Solutions of organolithium reagents were titrated by use of 1-propanol with 1,10-phenanthroline as the indicator (27). 2-Methylthiophene was commercially available.

Preparation of stock solutions of 2-lithio-5-methylthiophene (4)

To a solution of 2-methylthiophene (2.4 mL, 25 mmol) in 5 mL of THF at –78 °C was added 13.3 mL of a 1.88 mol/L solution of *n*-BuLi or *n*-Bu^{6}Li (25 mmol). The reaction mixture was warmed to 0 °C for 10 min, then cooled to –78 °C. Crystals formed in the centrifuge tube within 10 min. The supernatant was removed from the crystals, which were washed two times with 6 mL of THF, each time removing the excess solvent by cannula. The crystals were dissolved in ca. 15 mL of THF to give a solution of **4** in THF, which was determined to be 0.95 mol/L. The solution of **4** was stable for several months at –20 °C.

2-Iodo-5-methylthiophene (6)

To a solution of 2-methylthiophene (96.8 μL/mmol, 1.94 mL, 20 mmol) in 20 mL of THF at –78 °C was added a solution of *n*-BuLi (1.88 mol/L, 10.6 mL, 20 mmol). The solution of **4** was warmed to 0 °C and added dropwise to a suspension of 1,2-diiodoethane in THF at –78 °C. The mixture was stirred at –78 °C for 1 h, warmed to 0 °C for 2 h, and partitioned between 200 mL of Et_2O–pentane (1:1) and 150 mL of $NaHCO_3$. The organic layer (purple) was washed with 50 mL of 0.5 mol/L $Na_2S_2O_3$, 200 mL of water, 150 mL of brine, and passed through a cone of Na_2SO_4. Evaporation of the solvent gave a light brown liquid (4.34 g, 97%), which was purified by Kugelrohr distillation (bp 40–60 °C (1 mm Hg)) giving a colorless liquid. ^{1}H NMR ($CDCl_3$, 200 MHz) δ: 2.46 (d, J = 0.94 Hz, 3H), 6.45 (dq, J = 3.7, 0.9 Hz, 1H), 7.01 (d, J = 3.67 Hz, 1H). ^{13}C NMR (THF–Et_2O (60:40), –116 °C, 90.556 MHz) δ: 15.4, 73.2, 128.34, 137.4, 146.3 (28).

The preparation of NMR samples of 2-lithio-5-methylthiophene (4)

To a septum-capped 10 mm NMR tube under N_2 was added 0.05 mL of a 1.42 mol/L solution of 2-lithio-5-methylthiophene (**4**) and 1 mL of THF. The NMR tube containing the dilute solution of **4** was rolled so that all of the surface of the NMR tube and septum came in contact with the organolithium solution (to dry the NMR tube). The solution of **4** was removed from the NMR tube with a syringe. A solution of **4** in THF (1.42 mol/L, 0.20 mL, 0.288 mmol) was added to the NMR containing a static N_2 needle. THF (1.8 mL) and Et_2O (1.2 mL) was added to the tube and the solution was mixed with a vortex mixer. The contents of the tube were cooled to –78 °C and the septum was sealed with parafilm.

The determination of concentration for NMR samples

To the NMR solution was added Me_2S_2 and 25 μL (0.118 mmol) of *n*-undecane. The mixture was added to 10 mL of pentane and 1 to 2 drops of 30% NaOH and the mixture dried with Na_2SO_4. The organic solution was analyzed by GC to determine the relative concentrations of the components vs. *n*-undecane.

Table 1. Data for the plot of ln[monomer] vs. ln[dimer] at –121 °C.

[**4**] (mol/L)	Peak ratio (**4D**/**4M**)	[**4D**] (mol/L)	[**4M**] (mol/L)	K_1 ((mol/L)$^{-1}$)
0.21	1.845	0.0681	0.0783	12.5
0.12	1.332	0.0343	0.0515	12.9
0.094	1.190	0.0255	0.0429	13.9
0.062	0.739	0.0132	0.0357	10.4
0.028	0.510	0.0047	0.0185	13.8

Concentration dependence of 4

Seven samples of **4** in THF–ether (3:2) were prepared by appropriate dilution of a 0.78 mol/L sample of **4** in THF. Spectra (^{13}C, ^{7}Li) of each sample were taken at –121 °C. After the experiment, the concentration of **4** in each sample was determined by quenching with Me_2S_2 and GC analysis. The spectra from the five samples with the highest concentrations were integrated (C-3) by line-shape simulation. The data are shown in Table 1 and Fig. 3A.

Temperature dependence of 4

A 0.101 mol/L sample of **4** in THF–ether (3:2) was prepared and a series of ^{13}C and ^{7}Li NMR spectra were taken at accurately determined temperatures. Sample spectra are shown in Fig. 2. The spectra of the C-3 carbons were simulated. Line widths in the absence of exchange were determined from the solvent peaks. Below coalescence the line positions and populations of **4M** and **4D** were allowed to vary in the simulation. For determination of the thermodynamic parameters above coalescence, the populations were calculated from the chemical shift of the averaged peaks. Several experiments were performed to determine ΔH_1 and ΔS_1 at various concentrations: the ΔH_1 values varied from 0.8 to 1.4 kcal/mol and the ΔS_1 values from 10.5 to 14.5 eu, giving some measure of the reproducibility of these experiments. One significant variable may be accurately reproducing solvent composition for the NMR samples, since the K_1 values are very sensitive to the ratio of THF to ether.

For determination of the kinetic parameters, the populations during and above coalescence were calculated from the ΔH_1 and ΔS_1 values given in eq. [1]. Data used and derived from the simulations are shown in Table 2. Activation parameters were determined from the values of k_1 and k_{-1} and are shown in eq. [1].

The preparation of NMR samples of 4 containing 2-iodo-5-methylthiophene (6)

The sample preparation is the same as described in the previous section, except after the NMR tube was dried, Et_2O was added (22 °C) followed by **6**. The sample was mixed with a vortex mixer, cooled to –78 °C, then a solution of **4** in THF was added. The sides of the NMR tube were washed with the THF, which was added last.

© 2005 NRC Canada

Table 2. Data for DNMR simulation of the spectra in Fig. 2.

T (K)	[**4D**] (mol/L)	[**4M**] (mol/L)	k_{MD} (s^{-1})[a]	k_1 ($(mol/L)^{-1}$ s^{-1})[b]	k_{DM} (s^{-1})[c]	K_1 $((mol/L)^{-1})$[d]
139.9	0.0242	0.0526	20	386	22	8.7
153.1	0.0278	0.0457	57	1 246	47	13.3
163.0	0.0308	0.0394	116	2 931	74	19.8
170.4	0.0307	0.0396	293	7 400	189	19.6
182.0	0.0315[e]	0.0379[e]	1 654	43 600	995	21.9
192.5	0.0325[e]	0.0360[e]	3 859	107 000	2 134	25.1
200.7	0.0332[e]	0.0346[e]	6 405	175 000	3 350	27.7
210.9	0.0340[e]	0.0331[e]	19 260	582 000	9 380	31.0
220.6	0.0346[e]	0.0311[e]	36 820	1 180 000	16 900	35.8
231.0	0.0352[e]	0.0306[e]	101 000	3 300 000	43 950	37.6
241.7	0.0357[e]	0.0295[e]	248 300	8 410 000	102 600	41.0

[a]DNMR rate constant for conversion of monomer to dimer nuclei.
[b]$k_1 = k_{MD}/$[**4M**] (s^1 $(mol/L)^{-1}$).
[c]DNMR rate constant for the conversion of dimer to monomer nuclei $k_{-1} = k_{DM}$ (s^{-1}).
[d]$K_1 =$ [**4D**]/[**4M**]^2 $((mol/L)^{-1})$.
[e]These concentrations were calculated from ΔH_1 and ΔS_1 (eq. [1]).

Table 3. Input and output data for determination of K_2 in THF–ether (3:2).

T (K)	δ for **6**	δ obs	K_1 $((mol/L)^{-1})$	[**4D**] (mol/L)	[**4M**] (mol/L)	[**5**] (mol/L)	[**6**] (mol/L)	K_2 $((mol/L)^{-1})$
214.4	137.33	136.34	32.14	0.041 7	0.0360	0.0037	0.152	0.67
209.3	137.32	136.20	30.50	0.040 5	0.0394	0.0057	0.150	1.02
203.6	137.30	135.91	28.94	0.038 2	0.0365	0.0144	0.145	1.91
200.1	137.29	135.61	27.53	0.035 9	0.0361	0.0150	0.141	2.95
197.0	137.28	135.19	26.57	0.032 9	0.0352	0.0219	0.134	4.66
194.1	137.28	134.69	25.66	0.029 4	0.0338	0.0304	0.126	7.15
191.8	137.27	133.94	24.93	0.024 3	0.0312	0.0433	0.113	12.3
186.2	137.25	132.67	23.17	0.015 9	0.0262	0.0651	0.091	27.4
180.8	137.24	131.60	21.54	0.009 3	0.0207	0.0838	0.072	55.9
175.2	137.22	130.90	19.82	0.005 3	0.0163	0.0962	0.060	98.8
171.2		[a]	18.64	0.001 9	0.0101	0.109	0.047	229
166.2		[a]	17.11	0.000 78	0.0067	0.115	0.042	397

[a]Concentrations calculated from the fraction of dimer in the ^{7}Li NMR spectra.

Determination of the ate complex association constant (K_2)

A sample 0.156 mol/L in **6** and 0.123 mol/L in **4** was prepared using the previous procedure. ^{13}C and ^{7}Li NMR spectra were taken at 13 temperatures between –117 and –59 °C (Fig. 6). The ^{13}C NMR chemical shift of the averaged C-3 carbon in the spectra from –87 to –59 °C was used to determine the concentrations of **4M**, **4D**, **5**, and **6**. Input parameters were the values of the chemical shifts of the individual compounds (δ 132.6 for **4M**, δ 136.8 for **4D**, δ 128.7 for **5**, the shifts of **6** were temperature dependent and calculated using the formula δ = 0.002 815(T °C) + 137.500), the observed chemical shift in the averaged spectrum, the stoichiometric concentrations of **4** and **6**, and the value of K_1 calculated from ΔH_1 and ΔS_1. The input data were then used to iteratively calculate values for all concentrations using test values of K_2 until the average δ for all species matched observed δ for C-3. Data are presented in Table 3.

Two additional K_2 values were determined at –107 and –102 °C, where it is possible to detect the signal of **4D** (see Fig. 6B and insets). From the relative area of the dimer peak the concentrations of the other species could be determined by a similar iterative process. The area of this signal was determined at the two temperatures at which it is best defined (–102 and –107 °C), where **4D** corresponds to 1.4% and 0.6% of total peak area. These values were then used to calculate the concentrations of the other species using the known value of K_1.

Determination of ate complex association and dissociation rate constants (k_2 and k_{-2})

A sample 0.117 mol/L in **4** and 0.046 mol/L in **6** in THF–ether (3:2) was prepared by the general procedure, and ^{7}Li and ^{13}C NMR spectra were measured at a series of accurately measured temperatures (Fig. 5). The ^{7}Li signals were simulated as follows. The population of the exchanging species (**4M**, **4D**, **5**, and **6**) were calculated from the known concentrations and the values of K_1 and K_2 at each temperature, and values for k_1 and k_{-1} were calculated from the activation parameters of eq. [1]. These were used to start the simulation. The line width in the absence of exchange for the simulations was problematic, since it is likely to be both

© 2005 NRC Canada

Table 4. Data for the DNMR simulation of the ^{7}Li NMR spectra of Fig. 5B (determination of k_2 and k_{-2}).

T (K)	[**4D**] (mol/L)[a]	[**4M**] (mol/L)[a]	[**5**] (mol/L)[a]	[**6**] (mol/L)[a]	k_{DM} (s^{-1})[b]	k_{AM} (s^{-1})[b]	k_2 ((mol/L)$^{-1}$ s^{-1})[c]
148.5	0.0171	0.0370	0.0456	0.0004	12	127	3.70×10^5
154.6	0.0182	0.0358	0.0446	0.0014	29	369	3.32×10^5
159.5	0.0194	0.0354	0.0427	0.0032	52	849	3.16×10^5
162.2	0.0202	0.0353	0.0410	0.0049	109	1 750	4.12×10^5
164.9	0.0213	0.0353	0.0388	0.0073	181	3 100	4.68×10^5
170.5	0.0244	0.0361	0.0319	0.0142	336	12 200	7.61×10^5
175.9	0.0281	0.0372	0.0235	0.0225	356	27 300	7.67×10^5

[a]Calculated from K_1 (eq. [1]) and K_2(Li) at each temperature and fixed during the simulation (pop(dimer) = 2[dimer]).
[b]Determined by simulation NMR.
[c]$k_2 = k_{MA}/[\mathbf{6}]$.

Table 5. Input and output data for simulation of the ^{13}C NMR spectra in Fig. 6 (determination of k_3 and k_{-3}).

T (K)	[**4D**] (mol/L)[a]	[**4M**] (mol/L)[a]	[**5**] (mol/L)[a]	[**6**] (mol/L)[a]	k_{AI} (s^{-1})[b]	k_{-2} (mol/L)[c]	k_{-3} (mol/L)[d]	k_{IA} (s^{-1})[e]	k_2 (mol/L)[c]	k_3 (mol/L)[f]
141.9	0.0018	0.0035	0.127	0.0394	2.65×10^3	16.5	1.34×10^5	1.70×10^4	2.25×10^5	1.28×10^5
152.5	0.0015	0.0041	0.124	0.0426	7.31×10^3	230	3.38×10^5	4.24×10^4	3.50×10^5	3.32×10^5
163.7	0.0015	0.0086	0.117	0.0490	1.98×10^4	2 581	7.56×10^5	9.45×10^4	5.27×10^5	7.69×10^5
173.8	0.0041	0.0146	0.105	0.0606	5.62×10^4	17 570	1.57×10^6	1.96×10^5	7.31×10^5	1.76×10^6
183.0	0.0109	0.0222	0.084	0.0820	4.80×10^5	84 100	1.07×10^7	9.85×10^5	9.58×10^5	1.15×10^7

[a]Calculated from K_1 (eq. [1]) and K_2 (eq. [2]) at each temperature and fixed during the simulation (pop(dimer) = 2[dimer]).
[b]NMR rate for conversion of ate complex nuclei to iodide nuclei determined by line-shape simulation.
[c]Calculated from the activation parameters in eq. [2].
[d]Calculated: $k_{-3} = (2k_{AI} - k_{-2})/[\mathbf{6}]$.
[e]From line-shape fitting: $k_{IA} = k_{AI}$(Pop A)/(Pop I).
[f]Calculated: $k_3 = (k_{IA} - k_2[\mathbf{4M}])/[\mathbf{5}]$.

compound specific (different rates of quadrupolar relaxation for different lithium environments) and temperature sensitive. In the absence of actual information, the line widths were set at 4, 8, and 10 Hz for **5**, **4D**, and **4M**, respectively, based on values for several related species. The simulations were performed with the program WINDNMR (7*m*) using the exchange matrix of Fig. 7. The relative values of **4M** and **4D** fit well, but small changes in the relative populations of **5** were required for a good fit for all nuclei. Chemical shifts were assumed to be temperature independent (no actual measurements could be performed because dynamic broadening occurred at too low a temperature) and were set by fitting the spectrum at 142 K. After an optimal fit was achieved, we redetermined K_2 at each temperature, shown as K_2(Li) in Fig. 3B ($\Delta H_2 = -8.8 \pm 1$ kcal/mol, $\Delta S_2 = -43.3 \pm 1$ eu). New concentrations of all species were calculated with these parameters, and a final fitting was performed with the calculated concentrations frozen, modifying only k_{AI} and k_{AM}. Only the spectra from –124 to –97 °C provided good definition for the individual rates, and data for these temperatures are shown in Table 4 and Fig. 4.

Determination of rate constants for ate complex exchange with iodide (k_3, k_{-3})

The ^{13}C NMR spectra in Fig. 6A were simulated to extract values for the rate of **5/6** exchange. A sample was prepared 0.166 mol/L in **6** and 0.128 mol/L in **4** in THF–ether (3:2). In the simulations the population of all of the species was calculated from the values of K_1 and K_2 determined from ΔH_1 and ΔS_1, and values of k_1, k_{-1}, k_2, and k_{-2} were calculated from the values for the activation parameters in eqs. [1] and [2]. The exchange matrix is shown in Fig. 10, the numeric data in Table 5, and the simulated spectra in Fig. 6A.

Acknowledgement

We thank the National Science Foundation (NSF) for financial support.

References

1. H. Gilman, W. Langham, and A.L. Jacoby. J. Am. Chem. Soc. **61**, 106 (1939).
2. G. Wittig, U. Pockels, and H. Dröge, Chem. Ber. **71**, 1903 (1938).
3. (*a*) W.F Bailey and J.J. Patricia. J. Organomet. Chem. **352**, 1 (1988); (*b*) W.F. Bailey, T.T. Nurmi, J.J. Patricia, and W. Wang. J. Am. Chem. Soc. **109**, 2442 (1987); (*c*) E.C. Ashby and T.N. Pham. J. Org. Chem. **52**, 1291 (1987); (*d*) K.B. Wiberg, S. Sklenak, and W.F. Bailey. Organometallics, **20**, 771 (2001).
4. A.P Batalov. Zh. Obshch. Chim. **48**, 1607 (1978).
5. H.R. Ward. Acc. Chem. Res. **5**, 18 (1972).
6. H.R. Rogers and J. Houk. J. Am. Chem. Soc. **104**, 522 (1982).
7. (*a*) H.J. Reich, N.H. Phillips, and I.L. Reich. J. Am. Chem. Soc. **107**, 4101 (1985); (*b*) H.J. Reich, D.P. Green, and N.H. Phillips. J. Am. Chem. Soc. **111**, 3444 (1989); (*c*) H.J. Reich, D.P. Green, and N.H. Phillips. J. Am. Chem. Soc. **113**, 1414 (1991); (*d*) H.J Reich, B.Ö. Gudmundsson, D.P. Green, M.J. Bevan, and I.L. Reich. Helv. Chim. Acta, **85**, 3748 (2002); (*e*) H.J. Reich, D.P. Green, N.H. Phillips, J.P. Borst, and I.L. Reich. Phosphorus Sulfur Silicon Relat. Elem. **67**, 83 (1992);

© 2005 NRC Canada

(*f*) H.J. Reich, B.Ö. Gudmundsson, and R.R. Dykstra. J. Am. Chem. Soc. **114**, 7937 (1992); (*g*) H.J. Reich and N.H. Phillips. J. Am. Chem. Soc. **108**, 2102 (1986); (*h*) D.R. Powell, W.L. Whipple, and H.J. Reich. Acta Crystallogr. Sect. C, **C52**, 1346 (1996); (*i*) K.L. Jantzi, C.L. Puckett, I.A. Guzei, and H.J. Reich. J. Org. Chem. **70**, 7520 (2005); (*j*) H.J. Reich, D.P. Green, M.A. Medina, W.S. Goldenberg, B.Ö. Gudmundsson, R.R. Dykstra, and N.H. Phillips. J. Am. Chem. Soc. **120**, 7201 (1998); (*k*) H.J. Reich, W.S. Goldenberg, A.W. Sanders, K.L. Jantzi, and C.C. Tzschucke. J. Am. Chem. Soc. **125**, 3509 (2003); (*l*) H.J. Reich, J.P. Borst, R.R. Dykstra, and D.P. Green. J. Am. Chem. Soc. **115**, 8728 (1993); (*m*) DNMR simulations were performed with a version of the computer program WINDNMR: H.J. Reich. J. Chem. Ed. Software, **3D**, 2 (1996). Available from http://www.chem.wisc.edu/areas/reich/plt/windnmr.htm); (*n*) H.J. Reich and K.J. Kulicke. J. Am. Chem. Soc. **118**, 273 (1996).

8. G. Boche, M. Schimeczek, J. Cioslowski, and P. Piskorz. Eur. J. Org. Chem. 1851 (1998); J. Cioslowski, P. Piskorz, M. Schimeczek, and G. Boche. J. Am. Chem. Soc. **120**, 2612 (1998).
9. W.B. Farnham and J.C. Calabrese. J. Am. Chem. Soc. **108**, 2449 (1986).
10. (*a*) S. Ogawa, Y. Masutomi, N. Furukawa, and T. Erata. Heteroat. Chem. **3**, 423 (1992); (*b*) Y. Masutomi, N. Furukawa, and T. Erata. Heteroat. Chem. **6**, 19 (1995).
11. A.J. Ashe III, L.L. Lohr, and S.M. Al-Taweel. Organometallics, **10**, 2424 (1991).
12. A. Maercker, H. Bodenstedt, and L. Brandsma. Angew. Chem. Int. Ed. Engl. **31**, 1339 (1992).
13. A.H.J.F. de Keijzer, F.J.J. de Kanter, M. Schakel, R.F. Schmitz, and G.W. Klumpp. Angew. Chem. Int. Ed. Engl. **35**, 1127 (1996); A.H.J.F. de Keijzer, F.J.J. de Kanter, M. Schakel, V.P. Osinga, and G.W. Klumpp. J. Organomet. Chem. **548**, 29, (1997).
14. (*a*) V. Schulze, M. Brönstrup, V.P.W. Böhm, P. Schwerdtfeger, M. Schimeczek, and R.W. Hoffmann. Angew. Chem. Int. Ed. **37**, 824 (1998); (*b*) M. Müller, H.-C. Stiasny, M. Brönstrup, A. Burton, and R.W. Hoffmann. J. Chem. Soc. Perkin Trans. 2, 731 (1999).
15. T. Kanda, S. Kato, N. Kambe, Y. Kohara, and N. Sonoda. J. Phys. Org. Chem. **9**, 29 (1996).
16. (*a*) S. Harder, J. Boersma, L. Brandsma, J.A. Kanters, W. Bauer, R. Pi, P.v.R. Schleyer, H. Schöllhorn, and U. Thewalt. Organometallics, **8**, 1688 (1989); (*b*) W. Bauer, W.R. Winchester, and P.v.R. Schleyer. Organometallics, **6**, 2371 (1987).
17. R.R. Fraser, T.S. Mansour, and S. Savard. Can. J. Chem. **63**, 3505 (1985).
18. W.E. Truce and E. Wellish. J. Am. Chem. Soc. **74**, 5177 (1952).
19. For some organolithium aggregates, quadrupolar broadening is severe enough with ^{7}Li (92.6% natural abundance) that C–Li coupling cannot be resolved. The ^{6}Li analogs show little or no quadrupolar broadening and thus couplings are more easily seen. (*a*) G. Fraenkel, M. Henrichs, J.M. Hewitt, B.M. Su, and M.J. Geckle. J. Am. Chem. Soc. **102**, 3345 (1980); G. Fraenkel, A. Chow, and W.R. Winchester. J. Am. Chem. Soc. **112**, 6190 (1990); G. Fraenkel, S. Subramanian, and A. Chow. J. Am. Chem. Soc. **117**, 6300 (1995); (*b*) A.J. Jones, D.M. Grant, J.G. Russell, and G. Fraenkel. J. Phys. Chem. **73**, 1624 (1969); (*c*) G. Fraenkel and M.P. Hallden-Abberton. J. Am. Chem. Soc. **103**, 5657 (1981).
20. S. Gronowitz, I. Johnson, and A.B. Hörnfeldt. Chem. Scr. **7**, 76 (1975).
21. L.M. Jackman and L.M. Scarmoutzos. J. Am. Chem. Soc. **106**, 4627 (1984).
22. B.L. Lucht and D.B. Collum. J. Am. Chem. Soc. **116**, 6009 (1994).
23. G. Hilmersson and Ö. Davidsson. J. Org. Chem. **60**, 7660 (1995).
24. J.F. McGarrity, C.A. Ogle, Z. Brich, and H.-R. Loosli. J. Am. Chem. Soc. **107**, 1810 (1985).
25. (*a*) A. Streitwieser, S.S.-W. Leung, and Y.-J. Kim. Org. Lett. **1**, 145 (1999); (*b*) S.S.W. Leung and A. Streitwieser. J. Am. Chem. Soc. **120**, 10557 (1998).
26. D.S. Stephenson and G. Binsch. Quantum Chem. Prog. Exch. **10**, 365 (1978).
27. S.C. Watson and J.F. Eastham. J. Organomet. Chem. **9**, 165 (1967).
28. S. Hotta. J. Heterocycl. Chem. **38**, 923 (2001).

© 2005 NRC Canada

Influence of the number of water molecules on the mechanism of *N*-sulfinylaniline hydrolysis[1]

Elena V. Ivanova and Heidi M. Muchall

Abstract: The mechanism of the uncatalyzed hydrolysis of *N*-sulfinylaniline (Ph-N=S=O) has been studied with B3LYP/6-31+G(2d,2p) in the gas phase, with explicit treatment of water molecules. Hydrolysis involves water attack on sulfur, with a close to perpendicular alignment of a water molecule and the NSO plane in both prereaction complexes and transition states for the rate-determining step. Consequently, the distance of the weak S···O interaction, together with the efficiency of protonation of either nitrogen (attack across the N=S bond) or oxygen (attack across the S=O bond) atoms of the NSO group, determines the height of the activation barrier for hydrolysis. While the reaction with one water molecule is characterized by an unreasonably high enthalpy of activation, a cooperative effect from the weak interactions appears with the inclusion of a second water molecule, where both participate in the reaction, and the activation enthalpy drops significantly. The preference for attack across the S=O bond that is found in the reaction with one water molecule switches to a dominance of attack across the N=S bond in the reaction with three water molecules.

Key words: N-sulfinylaniline, hydrolysis, mechanism, density functional theory (DFT).

Résumé : Faisant appel à des calculs théoriques au niveau B3LYP/6-31+G(2d,2p), on a étudié le mécanisme de l'hydrolyse non catalysée du *N*-sulfinylaniline (Ph-N=S=O) en phase gazeuse, en faisant un traitement explicite des molécules d'eau. Dans l'étape cinétiquement déterminante, l'hydrolyse implique une attaque de l'eau sur le soufre, avec un alignement pratiquement perpendiculaire d'une molécule d'eau et du plan NSO tant dans les complexes préréactionnels que dans les états de transition. En conséquence, la distance de la faible interaction S···O ainsi que l'efficacité de la protonation de l'atome d'azote (attaque à travers la liaison N=S) ou de l'atome d'oxygène (attaque à travers la liaison S=O) du groupe NSO détermine la hauteur de la barrière d'activation de l'hydrolyse. Alors que la réaction avec une molécule d'eau est caractérisée par une enthalpie d'activation anormalement élevée, il semble se développer un effet de synergie avec les interactions faibles lors de l'inclusion d'une deuxième molécule d'eau alors que les deux participent à la réaction et que l'enthalpie d'activation diminue d'une façon significative. La préférence pour l'attaque à travers la liaison S=O qui caractérise la réaction avec une molécule d'eau se déplace vers une dominance pour une attaque à travers la liaison N=S dans la réaction avec trois molécules d'eau.

Mots clés : N-sulfinylaniline, hydrolyse, mécanisme, théorie de la densité fonctionnelle.

[Traduit par la Rédaction]

Introduction

Our interest in the electronic and molecular structures of NSO species (1, 2) is closely related to their reactivity. *N*-Sulfinylamines (R-N=S=O) were first prepared by Michaelis in 1890 (3) and their reaction with water was one of the first properties to be observed experimentally. While aromatic *N*-sulfinylamines are insoluble in water and hydrolized very slowly in it as well as in dilute acids, warm alkaline solutions or concentrated acids lead to their rapid hydrolysis (4). Aromatic *N*-sulfinylamines in particular are widely employed in synthetic organic chemistry, as they readily undergo a variety of cycloaddition reactions to yield N,S-heterocycles (Diels–Alder reactions as both dienes and dienophiles (5–7), 1,2-cycloadditions, and 1,3-dipolar additions (8, 9)). Common to all these reactions is the attack on the sulfur of the NSO group, and hydrolysis can be considered as the prototype reaction. Therefore, an understanding of the initial steps of the hydrolysis reaction mechanism of *N*-sulfinylaniline is fundamental to its exploitation in similar reactions involving *N*-sulfinylamines.

Scheme 1.

$$RNSO + H_2O \longrightarrow RNHS(O)OH \longrightarrow RNH_2 + SO_2$$

The mechanism for hydrolysis of *N*-sulfinylamines is believed to proceed through nucleophilic addition of a water molecule to the NSO group with the formation of sulfinamic acid, followed by the acid's fast decomposition to sulfur dioxide and a primary amine (Scheme 1) (10). Aromatic *N*-sulfinylamines are known to be somewhat resistant towards water, whereas aliphatic *N*-sulfinylamines hydrolyze more readily (4). For *N*-sulfinylaniline (Ph-N=S=O), kinetics studies using UV spectroscopy showed neutral hydrolysis to be a

Received 29 April 2005. Published on the NRC Research Press Web site at http://canjchem.nrc.ca on 29 November 2005.

E.V. Ivanova and H.M. Muchall.[2] Centre for Research in Molecular Modeling and Department of Chemistry and Biochemistry, Montreal, QC H4B 1R6, Canada.

[1]This article is part of a Special Issue dedicated to organic reaction mechanisms.

[2]Corresponding author (e-mail: muchall@alcor.concordia.ca).

 doi: 10.1139/V05-171 © 2005 NRC Canada

slow process (11, 12), with an induction period of approximately 4 h (12). The reaction is complicated by autocatalysis from aniline, formed as a product of the reaction, which explains the relatively low activation energy of 9.88 kcal mol^{-1} (1 cal = 4.184 J) in a water–1,4-dioxane (1:1) solution (11). In the presence of pyridine as a base or with a combination of pyridine and a carboxylic acid, the rate of reaction increases significantly (12). General base catalysis was proposed for the hydrolysis in the presence of pyridine, where the formation of a pyridine–water complex increases the nucleophilic properties of water and facilitates its interaction with the electrophilic sulfur atom. This is proposed to be the rate-determining step of hydrolysis. It is a third-order reaction, first-order in each *N*-sulfinylaniline, water, and pyridine, with an overall rate constant of 2.96×10^3 L^2 mol^{-2} s^{-1} and a low enthalpy of activation of 5.7 kcal mol^{-1} for the 20–40 °C temperature range.

For the combined catalysis by pyridine and a carboxylic acid, initial protonation of either nitrogen or oxygen atoms of the NSO group was predicted (12). This would lead to an increase in the net positive charge on the sulfur atom and promote the addition of a water molecule to the NSO group. This acid catalysis is not part of the discussion in the present paper.

While literature data on the hydrolysis of *N*-sulfinyl compounds are limited (11, 12), the hydrolysis of their cumulated analogs (isocyanates, R-N=C=O) was intensively studied, both experimentally (13–15) and computationally (16). Based on their structural similarities, one might expect similar reactivities for these two classes of compounds. And while the NCO group is more or less linear, whereas the NSO group is bent with a sulfur bond angle of 120.6° as determined from X-ray diffraction analysis (17), the similar solvent kinetic isotope effects $k(H_2O)/k(D_2O)$ of 1.65 for PhNCO (14) and 1.73 for PhNSO (12) seem to support the idea of similar reactivities and possibly similar mechanisms in the hydrolysis of these compounds.

A second-order dependence on water was found in the neutral hydrolysis of alkyl- and aryl-substituted isocyanates (13, 14, 16), where one molecule acts as a general acid and the other as a general base. This is closely related to the base-catalyzed hydrolysis of *N*-sulfinylaniline, if one water molecule is considered to take the role of the catalyst (pyridine). For the hydrolysis of 4-chlorophenyl isocyanate, however, a third-order dependence with respect to water concentration was reported (15). We therefore decided to explore the neutral hydrolysis of *N*-sulfinylaniline computationally to determine its mechanism and the number of water molecules involved.

Computational details

All geometry optimizations were performed with the Becke3 (18) – Lee, Young, and Parr (B3LYP) hybrid density functional (19) with the 6-31+G(2d,2p) basis set, using the GAUSSIAN 98 suite of programs (20). This computational level best reproduces the observed geometry (X-ray analysis) of *N*-sulfinylaniline (17), and the basis set superposition error (BSSE) (21) consists of less than 0.7 kcal mol^{-1} for the ternary complexes (counterpoise = 3, full geometry optimization).[3] All structures were optimized without constraints. The complexes and their transition states were studied in the gas phase, as it was found in similar studies of the hydrolysis of isocyanates (16) and amides (22) that the inclusion of the solvent as a dielectric continuum only leads to a small decrease in the activation barrier. Vibrational frequencies and zero-point vibrational energies (ZPVE) were obtained at the preceding level of theory. The identity of each transition state was additionally verified using the intrinsic reaction coordinate (IRC) method (23, 24). The total (E_{tot}) and ZPVE-corrected energies (E_{tot} + ZPVE), as well as the enthalpies of the complexes and their transition states, are summarized in Table 1. Throughout the paper, we will report only the enthalpy term at standard state, unless stated otherwise. We chose enthalpies over Gibbs free energies because an enthalpy is available (12) for comparison. Furthermore, the entropy contribution ($-T\Delta S$) to the Gibbs free energy barrier, on average 5.8 kcal mol^{-1}, is practically independent of the number of water molecules: it varies from 5.1 to 6.5 kcal mol^{-1} without apparent pattern for 1–5 H_2O. Net atomic charges were obtained within the quantum theory of atoms in molecules (QTAIM) (25) with the AIMPAC module PROAIM (26). The natural bond orbital (NBO) program (NBO 3.1) (27) was used to study the charge transfer in the complexes (28).

Results and discussion

Approach to the problem

While the NSO group is commonly considered a heterocumulene and, from ^{17}O NMR (29) and computational (2) studies, the S=O bond is best described as a four-electron bond not unlike the carbonyl C=O bond, the electronic structure of *N*-sulfinyl species can be represented as a set of resonance structures, shown in Scheme 2. Obviously, a change of substituent on nitrogen can change the reactivity of the NSO group; nevertheless, sulfur is the most positive centre and either nitrogen or oxygen is considered as the negative end of the bond dipole. We chose to study the computationally expensive *N*-sulfinylaniline (**1**) (instead of the more common approach to substitute the phenyl group for a smaller methyl group or the H atom (16)) because it is the only compound for which quantitative experimental data are available, and for comparison with the reactivities of aliphatic *N*-sulfinyl species in a subsequent paper.[4]

The calculated net atomic charges of **1** confirm the idea of sulfur being the most electrophilic atom of the NSO group (Fig. 1). Consequently, in a nucleophilic attack, the oxygen atom of the water molecule with a negative charge of

[3] We used the counterpoise correction method to verify the applicability of our chosen level of theory, and the BSSEs obtained with full geometry optimization for three structures are shown in Table 1. Our results of the study of other methods (HF and MP2) with various basis sets will be summarized elsewhere.

[4] A change in mechanism seems to be a common trait in the hydrolysis of NSO species with electron-donating substituents. For HNSO, the transition states for reaction with one water molecule are isoenthalpic, and the different mechanisms for CCl_3NSO hydrolysis do not seem to exhibit a dependence of preference on the number of water molecules. Manuscript in preparation.

© 2005 NRC Canada

Table 1. Calculated total and zero-point corrected energies, as well as enthalpies at 298 K (au) of **1**, water, the water dimer, and complexes **2**–**5** and their transition states for hydrolysis.

Species	E_{tot}	E_{tot} + ZPVE	H_{298}
1	–759.811591	–759.711892	–759.703552
H_2O	–76.441069	–76.419706	–76.415926
$(H_2O)_2$	–152.890084	–152.843858	–152.837139
2a	–836.255744	–836.133041	–836.120484
2a-TS	–836.199402	–836.079012	–836.068877
2b-TS	–836.193196	–836.073030	–836.062605
3a	–912.710720	–912.562579 (–912.561490)[a]	–912.547481
3a-TS	–912.665029	–912.520710	–912.508745
3b	–912.708424	–912.560220 (–912.559117)[a]	–912.545030
3b-TS	–912.661079	–912.517559	–912.505502
4a	–989.164674	–988.991597	–988.973598
4a-TS	–989.120910	–988.952285	–988.937976
4b	–989.162650	–988.989247 (–988.987225)[b]	–988.971435
4b-TS	–989.120013	–988.954007	–988.939706
4c	–989.158246	–988.985327	–988.967235
4c-TSa	–989.115485	–988.946429	–988.931412
4c-TSb	–989.112714	–988.943772	–988.928953
5c	–1142.068493	–1141.844795	–1141.821378
5c-TSb	–1142.028754	–1141.811961	–1141.792257

Note: Values in parentheses give counterpoise (CP) corrected energies.
[a]CP = 3 and BSSE = 0.7 kcal mol^{-1}.
[b]CP = 4 and BSSE = 1.3 kcal mol^{-1}.

Scheme 2.

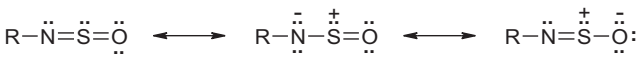
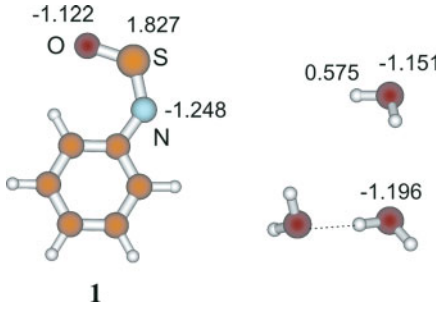


Fig. 1. Selected calculated charges of atoms of interest in *N*-sulfinylaniline (**1**), water, and the water dimer.



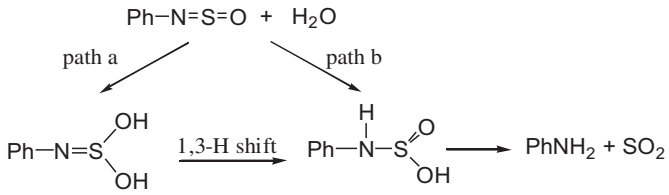
1

–1.151 au is expected to attack the sulfur atom. A proton can then be transferred to either the oxygen (attack across the S=O bond, path a) or the nitrogen (attack across the N=S bond, path b) atom of the NSO group (Scheme 3), similar to hydrogen isocyanate hydrolysis (16).

Reaction across the S=O bond includes two steps, the protonation of oxygen with formation of *N*-phenylsulfurimidic acid and a subsequent 1,3-hydrogen shift to form the intermediate *N*-phenylsulfinamic acid, which decomposes with formation of the final products, aniline and sulfur dioxide. Reaction across the N=S bond, on the other hand, is a one-step process that directly yields *N*-phenylsulfinamic acid.

Structures from the interaction across the S=O bond are denoted with the letter "**a**", those from the interaction across

Scheme 3.



the N=S bond with the letter "**b**". Structures with interactions across both S=O and N=S bonds are given the letter "**c**". The subscript "w" is used for the designation of atoms that belong to water molecules. In the description of complexes with multiple water molecules, "H_{w1}" determines a hydrogen atom of the water molecule that interacts with the oxygen atom of the S=O bond, and "H_{w2}", a hydrogen atom of the water molecule that interacts with the nitrogen atom of the N=S bond.

In the following, we examine how the preference for reaction across the N=S or S=O bond depends on the number of water molecules participating in the reaction. The complete reaction coordinate for the hydrolysis of **1** is presented for the participation of two water molecules.

Reaction of *N*-sulfinylaniline with one water molecule

Interaction with one water molecule is the simplest model in the study of the hydrolysis of *N*-sulfinylaniline (**1**). Even though the formation of a prereaction complex usually precedes the reaction, we were only able to locate complex **2a** with water situated on top of the S=O bond (Fig. 2). Our search for **2b** with water on top of the N=S bond produced numerous hydrogen-bonded complexes, but there does not

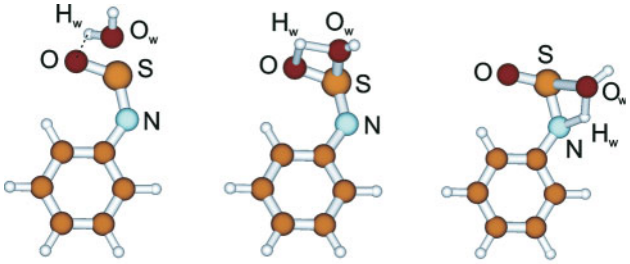
© 2005 NRC Canada

Table 2. Selected geometrical parameters (distances in pm, torsional angles in degrees) of *N*-sulfinylaniline (**1**) and its complexes with one, two, three, and five water molecules (**2**–**5**).

	1	**2a**	**3a**	**3b**	**4a**	**4b**	**4c**	**5c**
SO	148.1	148.7	149.2	147.7	149.2	147.4	148.7	148.5
		(+0.6)	(+1.1)	(–0.4)	(+1.1)	(–0.7)	(+0.6)	(+0.4)
NS	153.4	153.0	152.8	154.4	152.7	154.3	153.5	153.8
		(–0.4)	(–0.6)	(+1.0)	(–0.7)	(+0.9)	(+0.1)	(+0.4)
$S\cdots O_w$		319.0	314.6	377.9	297.9	296.2	284.0	271.8
$O\cdots H_{w1}$		240.4	192.0		195.9		197.6	189.2
$N\cdots H_{w2}$				199.4		194.7	236.4	196.9
$NSOO_w$		101.9	109.8	131.2	105.0	107.0	106.8	109.3
$NSOH_{w1}$		104.3	116.8		128.1		95.8	103.8
$OSNH_{w2}$				177.2		170.2	122.0	171.8

Note: Values in parentheses show the change in the distances upon complexation with respect to **1**.

Fig. 2. Optimized complex **2a** for the interaction of **1** with one water molecule, and transition states **2a-TS** and **2b-TS** for the addition of water across the S=O and the N=S bond of **1**, respectively. Weak interactions in the transition states are given with solid lines.



2a **2a-TS** **2b-TS**

seem to be a stationary point on the potential energy surface for **2b**.[5]

The intermolecular distance between the sulfur atom and the oxygen atom of water (O_w) in **2a** is 319.0 pm (Table 2), with the water molecule forming a close to perpendicular alignment with the plane of **1** (the $NSOO_w$ dihedral angle is 101.9°). Even though this distance is less than 325.0 pm, which is the accepted value for the sum of the van der Waals radii of oxygen and sulfur atoms (30), according to an analysis of the electron density within QTAIM, there is no interaction between these atoms.[5] The complex **2a** is stabilized by a hydrogen bond with an $O\cdots H_w$ distance of 240.4 pm and an OH_wO_w angle of 130.8°. This nonideal hydrogen bond geometry is in good agreement with the small stabilization energy of 0.6 kcal mol^{-1} upon complex formation (Table 3). The perpendicular attack on sulfur is in stark contrast to the in-plane attack of water on the carbon atom in HNCO (16).

The activation enthalpy for the reaction of **1** with one water molecule is very high with 31.8 and 35.7 kcal mol^{-1} for transition states **2a-TS** and **2b-TS**, respectively (Fig. 2 and Table 3). The barriers are calculated from the enthalpies of the reagents for lack of complex **2b** as a reference. The reaction across the S=O bond (path a) is favoured by 3.9 kcal mol^{-1}.

Reaction of *N*-sulfinylaniline with two water molecules

Introduction of a second water molecule allows the formation of a water dimer, which increases the nucleophilic properties of water towards the electrophilic sulfur. The negative charge on the oxygen atom of the original water molecule is increased by 0.045 au from –1.151 au in the monomer to –1.196 au in the dimer (Fig. 1). Unlike in the interaction with one water molecule, both prereaction complexes **3a** and **3b** were located (Fig. 3). This is also different from HNCO hydrolysis in that prereaction complexes of HNCO with water chains (dimers and trimers) were not found (16). Selected geometrical parameters of **3a** and **3b** are shown in Table 2. Stabilization in both complexes is achieved through an $S\cdots O_w$ interaction along with hydrogen bond formation. The $S\cdots O_w$ interaction is mostly due to the electrostatic attraction between sulfur and water oxygen atoms, combined with some charge transfer from the lone pair of O_w into the antibonding orbital of the N=S bond ($\pi^*_{N=S}$), found for **3a** from an NBO analysis.[5] As expected, complexation across the S=O bond primarily affects the S—O bond length, and complexation across the N=S bond mainly influences the N—S bond length. The lengthening of both bonds in their respective complexes to a similar degree coincides with the contraction of the second cumulated double bond (the changes in bond lengths from **1** are given in Table 2 for ease of comparison). But while **3a** exhibits the close to perpendicular arrangement between the plane of **1** and the water molecule complexed to sulfur that we also observed for **2a**, there is a much larger deviation from 90° found in **3b**. In addition, the $S\cdots O_w$ intermolecular distance in **3b** is significantly larger than that in **3a**, suggesting a nonideal arrangement of its constituent fragments. These findings are nicely in accord with those for complexation with one water molecule and offer an explanation as to why **2b** could not be located. The requirements of a perpendicular attack of O_w on sulfur and an in-plane $N\cdots H_wO$ hydrogen bond (the $OSNH_{w2}$ dihedral in **3b** is close to 180°, Table 2) prevent the formation of **2b** and render **3b** somewhat strained. This interpreta-

[5] A detailed analysis of hydrogen bonding and other weak interactions in the complexes and their transition states will be presented elsewhere. Manuscript in preparation.

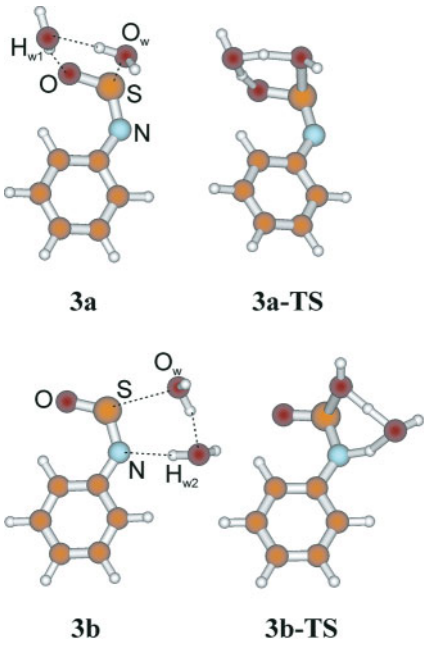
© 2005 NRC Canada

Table 3. Enthalpies (kcal mol^{-1}) of complex formation and of activation at 298 K for **1** with one, two, three, and five water molecules.

	Across S=O				Across N=S			
nH$_2$O	Complex	$-\Delta H_{bind}$	TS	$\Delta H^{\ddagger}$	Complex	$-\Delta H_{bind}$	TS	$\Delta H^{\ddagger}$
1	**2a**	0.6	**2a-TS**	32.4 (31.8)[b]	**2b**	[a]	**2b-TS**	— (35.7)[b]
2	**3a**	7.6	**3a-TS**	24.3	**3b**	6.0	**3b-TS**	24.8
3	**4a**	14.0	**4a-TS**	22.4	**4b**	12.6	**4b-TS**	19.9
	4c	10.0	**4c-TSa**	22.5	**4c**	10.0	**4c-TSb**	24.0
5	**5c**	24.0			**5c**	24.0	**5c-TSb**	18.3

[a]Complex not found.
[b]Based on the enthalpies of the reagents, **1** and water.

Fig. 3. Optimized complexes **3a** and **3b** for the interaction of **1** with the water dimer, and transition states **3a-TS** and **3b-TS**. Weak interactions in the transition states are given with solid lines.



tion is supported by the relative energies of **3a** and **3b**, with **3b** less stable by 1.6 kcal mol^{-1}. The formation of six-membered cycles reduces the strain that exists in the four-membered cycles of transition states **2a-TS** and **2b-TS** in the reaction of **1** with one water molecule. The full reaction coordinates for the reaction of *N*-sulfinylaniline (**1**) with two water molecules are given in Fig. 4 for water addition across the S=O bond (path a) and in Fig. 5 for addition across the N=S bond (path b).

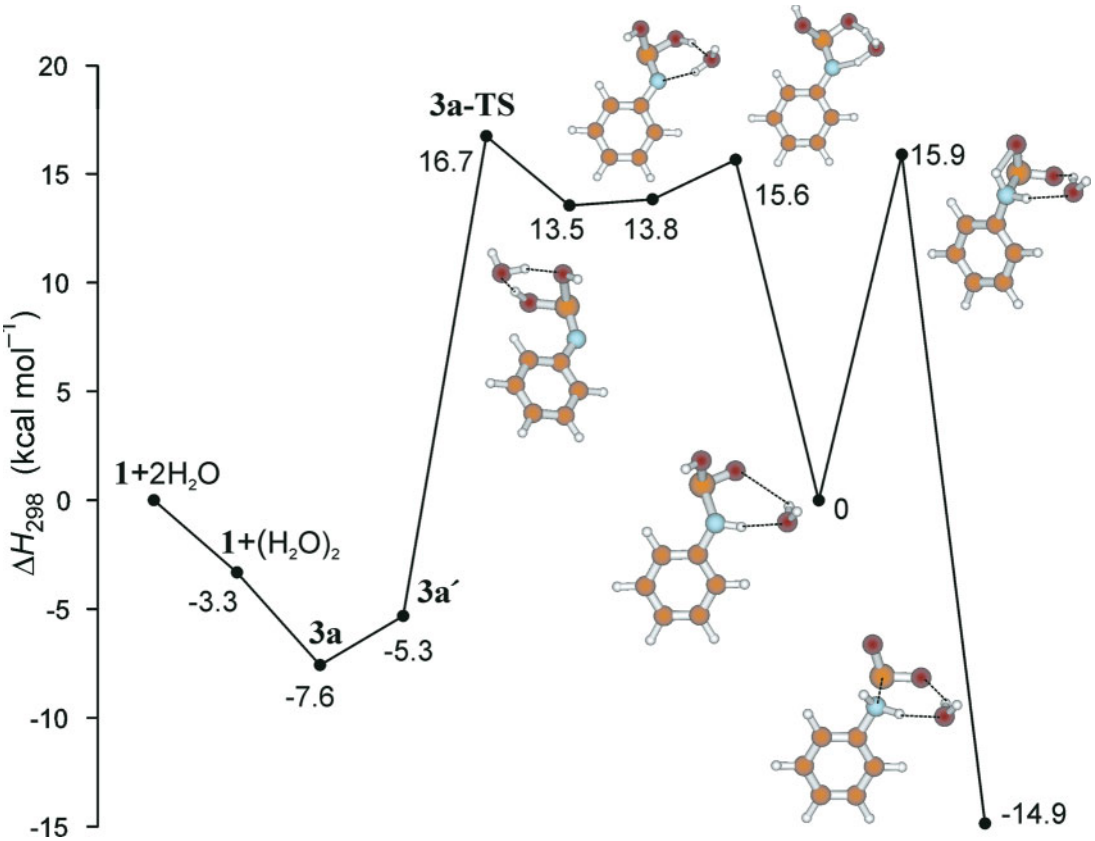
The formation of **3a** is favourable by 7.6 kcal mol^{-1} with a stabilization of 4.3 kcal mol^{-1} in addition to the 3.3 kcal mol^{-1} of energy gain due to water dimer formation. The experimental enthalpy of association in the water dimer was found to be –3.59 ± 0.5 kcal mol^{-1} at 373 K (31). As was proposed (12), hydration of sulfur with protonation of oxygen of **1** is indeed the rate-determining step of the reaction. The activation enthalpy is 24.3 kcal mol^{-1}, a value that includes 2.3 kcal mol^{-1} because of the loss of planarity in **1** (**1** in **3a** is planar whereas in both the complex **3a′** and the transition state **3a-TS**, CCNS and CNSO torsional angles are 6.1° and 23.6°, respectively). The torsions allow a decrease of the S···O$_w$ interatomic distance from 314.6 pm in **3a** to 299.4 pm in **3a′**, and this shortening of about 15 pm increases the strength of the interaction and facilitates the hydration of sulfur. Further along the reaction path, the water molecule in the primary reaction product (the complex of *N*-phenylsulfurimidic acid and water) changes its orientation, which allows it to abstract a proton from one hydroxyl group of *N*-phenylsulfurimidic acid and simultaneously protonate the acid's nitrogen atom. This "water-assisted" 1,3-hydrogen shift[6] requires only 1.8 kcal mol^{-1} and yields the complex of *N*-phenylsulfinamic acid and water in which the orientation of the water molecule cannot facilitate the protonation of nitrogen. Thus, the unassisted decomposition of *N*-phenylsulfinamic acid into the complex of aniline, sulfur dioxide, and water requires the large activation enthalpy of 15.9 kcal mol^{-1}. We find exactly the same value, 15.9 kcal mol^{-1}, for the enthalpy of activation for the decomposition of *N*-phenylsulfinamic acid in the absence of any water.[6]

The formation of **3b** is less favourable than that of **3a**, as previously discussed, and only shows a stabilization of 2.7 kcal mol^{-1} in addition to the stabilization from water dimer formation (Fig. 5). The reaction of the water dimer with **1** again is the rate-determining step and an activation enthalpy of 24.8 kcal mol^{-1} is required, which is only 0.5 kcal mol^{-1} higher than (and therefore comparable with) that for the reaction across the S=O bond. As in Fig. 4, this activation barrier includes 1.8 kcal mol^{-1} because of the torsion of the NSO group out of the plane of the aromatic ring (the CCNS and CNSO torsional angles of 46.0° and 7.9°, respectively, are similar in the complex **3b′** and in the transition state **3b-TS**). As in **3a′**, the S···O$_w$ interaction is strengthened through a decrease in the intermolecular distance by 37 pm, from 377.9 pm in **3b** to 340.9 pm in **3b′**. Unlike **3a-TS** in Fig. 4, **3b-TS** in Fig. 5 directly yields the

[6]We, of course, only present a subset of possibilities of hydrogen bond formation on the potential energy surface for reaction of *N*-sulfinylaniline (**1**) with two water molecules. We believe that the chosen structures explain the formation of the final products and in some cases show the importance of the explicit treatment of water along the reaction pathway. Thus, we exclude, for example, the nonassisted 1,3-hydrogen shift in *N*-phenylsulfurimidic acid.

© 2005 NRC Canada

Fig. 4. Enthalpy profile for the reaction of **1** with two water molecules (path a), attack across the S=O bond.



complex of *N*-phenylsulfinamic acid and water. Hydrogen bonding to the hydroxyl group of *N*-phenylsulfinamic acid allows for a reorientation of the water molecule that moves it into the ideal position for protonation of the nitrogen atom and facilitates the decomposition of the acid. In this water-assisted decomposition the activation barrier is decreased with respect to the nonassisted barrier in Fig. 4 by more than 10 kcal mol^{-1} to a mere 5.5 kcal mol^{-1}. This finding, as well as the assistance of water in the 1,3-hydrogen shift, which was discussed in the previous mechanism (path a, Fig. 4), demonstrates the importance of the explicit treatment of water molecules in these hydrolysis reactions, a conclusion that was drawn earlier in amide (32, 33) and isocyanate hydrolysis (16).

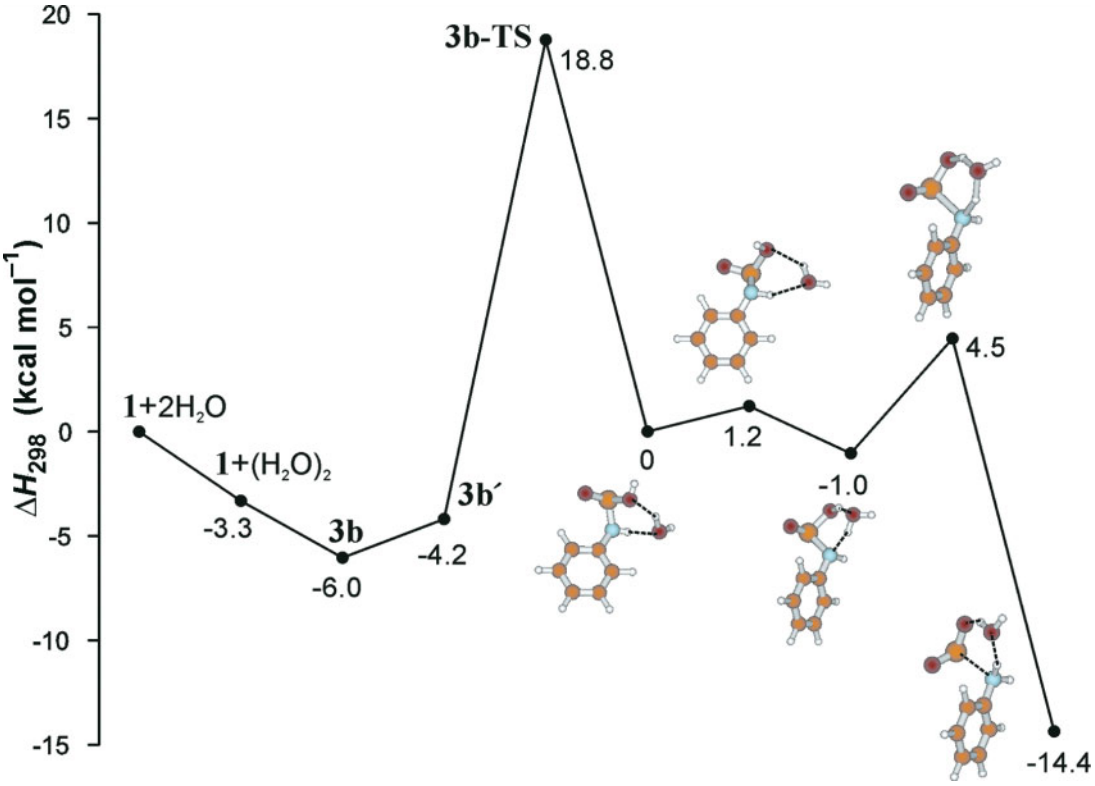
The increase in the number of water molecules from one to two allows a decrease in the activation barriers for the hydrolysis reaction of approximately 8–11 kcal mol^{-1} (from 32.4 in **2a-TS** to 24.3 kcal mol^{-1} in **3a-TS**, and from 35.7[7] in **2b-TS** to 24.8 kcal mol^{-1} in **3b-TS**). This is at least partially due to the relief of strain on going from four-membered cycles in **2a-TS** and **2b-TS** to the six-membered cycles in **3a-TS** and **3b-TS**, as was mentioned earlier. The N=S bond demonstrates a higher sensitivity to this effect because the hydroxyl group of the second water molecule now approaches **1** in the NSO plane (with a OSNH$_{w2}$ torsional angle of 177.2°, Table 2), where the nitrogen lone pair lies, confirming the idea of donor–acceptor directionality in hydrogen bond formation.

Our finding about the almost equal probability of both mechanisms owing to activation barriers of 24.3 kcal mol^{-1} for path a and 24.8 kcal mol^{-1} for path b seems quite different from the results for HNCO hydrolysis (16). Calculations in the gas phase and in a solvent field based on the polarizable continuum model (PCM) with MP2/6-31G(d,p), along with other methods, have shown that even though two water molecules are important for HNCO hydrolysis, in all cases studied (the presence of one, two, and three water molecules was considered), reaction across the N=C bond is favoured. With two water molecules, for example, the activation energy decreases from 28 kcal mol^{-1} for reaction across the C=O bond to 11 kcal mol^{-1} for reaction across the N=C bond (values reported in the paper are E_{tot} + ZPVE, given in kJ mol^{-1}, and based on the corrected energies of the reactants). In the presence of a solvent field this difference becomes much smaller though, 15 kcal mol^{-1} for reaction across C=O to 18 kcal mol^{-1} for reaction across N=C (single point energy calculations on the gas-phase optimized geometries). To be able to compare results more directly, we also report ZPVE corrected energies in Table 1. From these, we obtain an activation energy of 19.2 kcal mol^{-1} for reaction across S=O and 21.1 kcal mol^{-1} for that across N=S, both based on the corrected energies for **1** and two water mole-

[7] As previously discussed, this value is not based on the enthalpy of the prereaction complex, but rather on the enthalpies of the reactants, **1** and water.

© 2005 NRC Canada

Fig. 5. Enthalpy profile for the reaction of **1** with two water molecules (path b), attack across the N=S bond.



cules. Obviously, the direct comparison is limited by the different substituents (phenyl in **1** and hydrogen in HNCO), and further analysis of the difference between RNSO and RNCO hydrolysis will only be reported in our forthcoming paper on substituent effects in the reactivity of NSO species.[4]

Reaction of *N*-sulfinylaniline with three and five water molecules

Compared to the reaction of *N*-sulfinylaniline with one and two water molecules, water trimer complexation to **1** in **4a** and **4b** (Fig. 6) further increases the flexibility of the systems owing to formation of eight-membered cycles. As can be seen from Table 2, the lengths and, consequently, the strengths of the S=O and N=S bonds do not differ much in complexes of **1** with two (**3a**, **3b**) and three (**4a**, **4b**) water molecules. But inclusion of the third water molecule significantly strengthens the weak S···O$_w$ interaction. The effect is especially pronounced for complexation of the water trimer across the N=S bond. The S···O$_w$ intermolecular distance decreases by 81.7 pm, from 377.9 pm in **3b** to 296.2 pm in **4b** (Table 2). For complexation towards the S=O bond this effect is less pronounced, but still important, as the S···O$_w$ distance decreases by 16.7 pm going from **3a** to **4a**. Along with this, a contraction of the N···H$_{w2}$ hydrogen bond by 4.7 pm is found going from **3b** to **4b**. In contrast, comparing **3a** and **4a**, the O···H$_{w1}$ hydrogen bond distance increases by 3.4 pm.

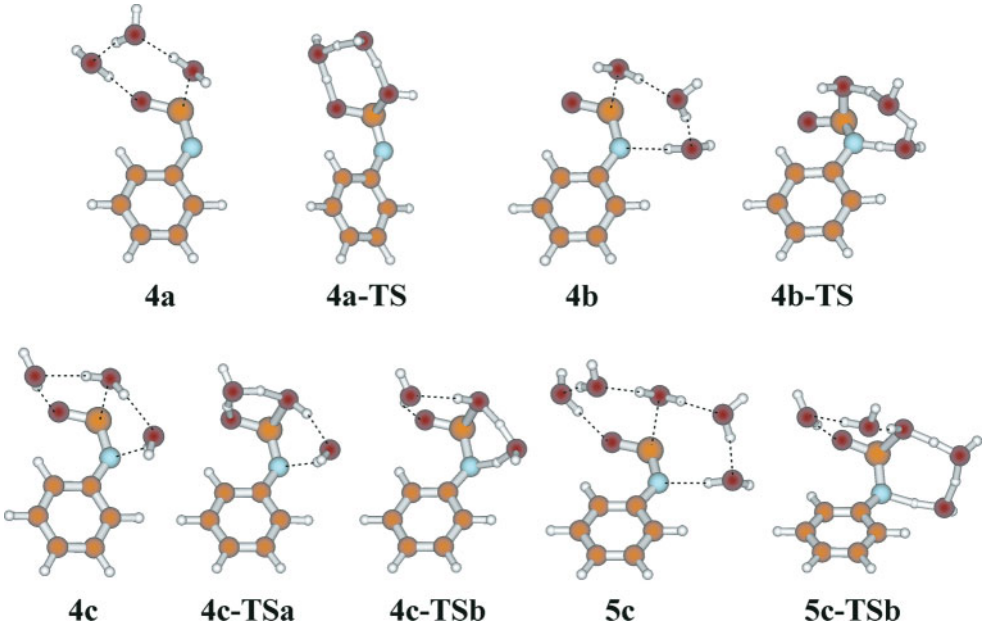
The strengthening of the S···O$_w$ intermolecular interaction in complexes **4a** and **4b** further decreases the activation barrier for hydrolysis by approximately 2–5 kcal mol^{-1} for the two pathways (from 24.3 in **3a-TS** to 22.4 kcal mol^{-1} in **4a-TS** for the reaction across the S=O bond, and from 24.8 in **3b-TS** to 19.9 kcal mol^{-1} in **4b-TS** for the reaction across the N=S bond, Table 3). The one-step mechanism, reaction across the N=S bond, is now favoured by 2.5 kcal mol^{-1}, as two requirements, "perpendicular" attack on sulfur (NSOO$_w$ torsional angle 107.0°) and in-plane protonation of nitrogen (OSNH$_{w2}$ torsional angle 170.2°), are fulfilled without apparent strain.

The two different attacks on the NSO group are combined in **4c**, where hydrogen bonding to both nitrogen and oxygen atoms of the NSO group assists in the strengthening of the S···O$_w$ interaction, which is 12.2 and 13.9 pm shorter than in **4a** and **4b**, respectively (Table 2). But both hydrogen-bonding interactions are weaker in **4c** than in either **4a** or **4b**. The increase in the O···H$_{w1}$ distance in **4c** from **4a** by 1.7 pm is considered to be insignificant, and this is reflected in the enthalpy barrier of 22.5 kcal mol^{-1} for reaction via **4c-TSa**, which is similar to the activation enthalpy of 22.4 kcal mol^{-1} for **4a-TS**. In contrast, the increase in the N···H$_{w2}$ intermolecular distance in **4c** from **4b** by 41.7 pm, together with a less favourable OSNH$_{w2}$ dihedral angle of 122.0° in **4c**, contributes to **4c-TSb** being less stable than **4b-TS** and increases the activation barrier by 4.1 kcal mol^{-1}.

As can be seen from Figs. 3 and 6, the structures for **4c-TSa** and **4c-TSb** are very similar to those obtained for reaction of **1** with two water molecules (**3a-TS** and **3b-TS**). The third water molecule in complex **4c**, and consequently in **4c-TS4a** and **4c-TSb**, might be seen as a bystander that does not directly react with **1**, yet it participates through hydrogen bond formation, which weakens both S=O and N=S bonds (Table 2). The elongation of these bonds from those in **1** is less efficient than in **3a** and **3b** and consists of 0.6 pm for the S=O and 0.1 pm for the N=S bond in **4c**, but the weak-

© 2005 NRC Canada

Fig. 6. Optimized structures **4a**–**4c** and **5c** for the interaction of **1** with three and five water molecules, and transition states **4a-TS**, **4b-TS, 4c-TSa, 4c-TSb**, and **5c-TSb** for hydrolysis.

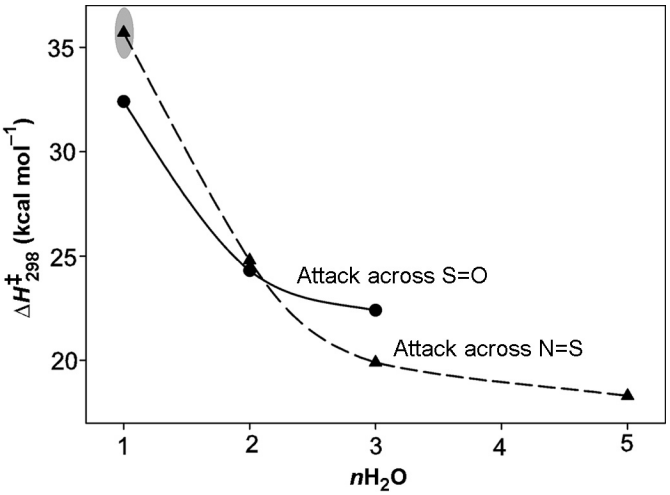


ening of the bonds of the NSO group is accompanied by a significant shortening of the S···O_w intermolecular distance in **4c** by 30.6 and 93.9 pm from **3a** and **3b**, respectively, which facilitates hydrolysis. This is reflected in a decrease in the activation barrier (by 2.2 kcal mol^{-1} in **4c-TSa** compared to **3a-TS**, and by 0.8 kcal mol^{-1} in **4c-TSb** compared to **3b-TS**).

Complex **5c** (Fig. 6) represents the combination of **4a**, **4b**, and **4c** in that both points of attack to the NSO group are connected as in **4c**, but the strain in **4c** is removed by the inclusion of water molecules, similar to **4a** and **4b**. The S···O_w intermolecular distance of 271.8 pm in **5c** is found to be the shortest among all complexes studied. The O···H_{w1} distance in **5c** is shorter than in both **4a** and **4c**, whereas the N···H_{w2} interaction is much shorter (by 39.5 pm) in **5c** than in **4c**, but longer by 2.2 pm compared to **4b**. The increase in the number of water molecules up to five further decreases the activation enthalpy for the hydrolysis reaction (only the reaction across the N=S bond was studied), but the barrier through **5c-TSb** is only 1.6 kcal mol^{-1} smaller than that in the corresponding reaction with three water molecules (**4c-TSb**).

Our results from the study of the influence of the number of water molecules in the hydrolysis of *N*-sulfinylaniline (**1**) are summarized in Fig. 7, which shows the decrease in the activation enthalpy with an increase in the number of water molecules for both pathways (reaction across the S=O and the N=S bond). For the reaction across N=S with one water molecule, the grey zone in Fig. 7, see the previous discussion.[7] The reaction barriers with one water molecule are prohibitively large, and therefore two water molecules are important for hydrolysis, as is suggested by the solvent isotope effect (12). Similar conclusions were drawn in the computational study of HNCO hydrolysis (16). However, there is a crossover in mechanism at this point, and participation of a third water molecule only benefits the reaction across the N=S bond, in contrast to HNCO hydrolysis (16). Such a third-order dependence on water concentration has been proposed for the hydrolysis of the related 4-chlorophenyl isocyanate (15). Figure 7 also suggests that the values for the enthalpy barriers are more or less converged for both pathways (with three water molecules for attack across S=O and five water molecules for that across N=S), and that larger numbers of water molecules need not be considered. The "converged" values for the activation enthalpy of about 23 kcal mol^{-1} for path a and 18 kcal mol^{-1} for path b are obviously still much higher than the experimentally determined values of 9.88 (11) and 5.7 kcal mol^{-1} (12). But as both experimental barriers were determined for a catalyzed hydrolysis (autocatalysis from aniline in the former case, pyridine catalysis in the latter), this is not surprising.

Fig. 7. Dependence of the activation barrier of the hydrolysis reaction on the number of water molecules. See text for the grey zone.



© 2005 NRC Canada

Conclusions

We have presented a computational study on complexes of *N*-sulfinylaniline (Ph-N=S=O, **1**) with one to three and five water molecules and on the mechanism of neutral hydrolysis of **1**. While the complex of **1** with one water molecule does not possess an interaction between the sulfur atom and the water oxygen atom, water chains of two, three, and five molecules lead to increasingly strong S···O interactions. In these complexes, water attacks on sulfur close to perpendicular to the NSO plane.

Two mechanisms have been investigated for reaction of **1** with one to three water molecules, hydration of the sulfur atom with protonation of either oxygen or nitrogen atoms of the NSO group. The full reaction coordinate was probed for hydrolysis with two water molecules, and S···O interaction with proton transfer from water is found to be the rate-determining step in both mechanisms. Unrealistically high activation barriers are found for reaction with one water molecule, and two water molecules are important for hydrolysis. This is in good agreement with the first-order dependence in both water and base that was observed for the base-catalyzed reaction, if one water molecule is considered to take the role of the base. Reaction across the S=O bond is preferred with one water molecule, whereas an increase in the number of water molecules leads to a change in mechanism. For two water molecules, both mechanisms are equally probable; for three water molecules, reaction across the N=S bond is favoured. As expected, the calculated enthalpies of activation for the neutral hydrolysis reaction are several kcal mol^{-1} larger than the experimentally determined barriers for the base-catalyzed reaction.

The results presented here have revealed differences between PhNSO and HNCO, the smallest member of the related isocyanates, in both complexation with water and mechanism for hydrolysis with an increasing number of water molecules. We are currently investigating this further with a study of substituent effects in *N*-sulfinylamine hydrolysis.

Acknowledgments

Calculations were performed at the Centre for Research in Molecular Modeling (CERMM), which was established with the financial support of the Concordia University Faculty of Arts and Science, the Ministère de l'Éducation du Québec (MEQ), and the Canada Foundation for Innovation (CFI). This work was supported by a research grant from the Natural Sciences and Engineering Research Council of Canada (NSERC).

References

1. H.M. Muchall. J. Phys. Chem. A, **105**, 632 (2001).
2. H.M. Muchall. ARKIVOC, 82 (2001).
3. A. Michaelis. Chem. Ber. **22**, 2228 (1889).
4. A. Michaelis and G. Junghans. Ann. Chem. **274**, 233 (1893).
5. P. Hanson and W.A. Stockburn. J. Chem. Soc. Perkin Trans. 2, 589 (1985).
6. P. Hanson and S.A.C. Wren. J. Chem. Soc. Perkin Trans. 2, 197 (1987).
7. P. Hanson and S.A.C. Wren. J. Chem. Soc. Perkin Trans. 1, 2089 (1990).
8. P. Rajagopalan and H.U. Daeniker. Angew. Chem. Int. Ed. Engl. **2**, 46 (1963).
9. G.R. Collins. J. Org. Chem. **29**, 1688 (1964).
10. A. Michaelis. Ber. **24**, 745 (1891).
11. T.L. Dawson. Ph.D. thesis, University of Kentucky, Lexington, Kentucky. 1960.
12. D.F. Mironova and O.Y. Konoplya. Ukr. Khim. Zh. (Russ. Ed.), **42**, 374 (1976).
13. A.F. Hegarty, C.N. Hegarty, and F.L. Scott. J. Chem. Soc. Perkin Trans. 2, 1166 (1975).
14. E.A. Castro, R.B. Moodie, and P.J. Sansom. J. Chem. Soc. Perkin Trans. 2, 739 (1985).
15. R.S. Satchell and R. Nyman. J. Chem. Soc. Perkin Trans. 2, 901 (1981).
16. G. Raspoet, M.T. Nguyen, M. McGarraghy, and A.F. Hegarty. J. Org. Chem. **63**, 6867 (1998).
17. R.M. Romano, C.O. Della Védova, and R. Boese. J. Mol. Struct. **475**, 1 (1999).
18. A.D. Becke. J. Chem. Phys. **98**, 5648 (1993).
19. C. Lee, W. Yang, and R.G. Parr. Phys. Rev. B, **37**, 785 (1988).
20. M.J. Frisch, G.W. Trucks, H.B. Schlegel, G.E. Scuseria, M.A. Robb, J.R. Cheeseman, V.G. Zakrzewski, J.A. Montgomery, Jr., R.E. Stratmann, J.C. Burant, S. Dapprich, J.M. Millam, A.D. Daniels, K.N. Kudin, M.C. Strain, O. Farkas, J. Tomasi, V. Barone, M. Cossi, R. Cammi, B. Mennucci, C. Pomelli, C. Adamo, S. Clifford, J. Ochterski, G.A. Petersson, P.Y. Ayala, Q. Cui, K. Morokuma, P. Salvador, J.J. Dannenberg, D.K. Malick, A.D. Rabuck, K. Raghavachari, J.B. Foresman, J. Cioslowski, J.V. Ortiz, A.G. Baboul, B.B. Stefanov, G. Liu, A. Liashenko, P. Piskorz, I. Komaromi, R. Gomperts, R.L. Martin, D.J. Fox, T. Keith, M.A. Al-Laham, C.Y. Peng, A. Nanayakkara, M. Challacombe, P.M.W. Gill, B. Johnson, W. Chen, M.W. Wong, J.L. Andres, C. Gonzalez, M. Head-Gordon, E.S. Replogle, and J.A. Pople. GAUSSIAN 98. Revision A.11 [computer program]. Gaussian, Inc., Pittsburgh, Penn. 2001.
21. S.F. Boys and F. Bernardi. Mol. Phys. **19**, 553 (1970).
22. S. Antonczak, M.F. Ruiz-López, and J.L. Rivail. J. Am. Chem. Soc. **116**, 3912 (1994).
23. C. Gonzalez and H.B. Schlegel. J. Chem. Phys. **90**, 2154 (1989).
24. C. Gonzalez and H.B. Schlegel. J. Phys. Chem. **94**, 5523 (1990).
25. R.F.W. Bader. Atoms in molecules: A quantum theory. Oxford University Press, Oxford. 1990.
26. R.F.W. Bader. AIMPAC module PROAIM [computer program]. Available from http://www.chemistry.mcmaster.ca/aimpac/ 1982.
27. E.D. Glendening, A.E. Reed, J.E. Carpenter, and F. Weinhold. QCPE Bull. **10**, 58 (1990).
28. A.E. Reed, L.A. Curtiss, and F. Weinhold. Chem. Rev. **88**, 899 (1988).
29. G. Cerioni, N. Culeddu, and A. Plumitallo. Tetrahedron, **49**, 2957 (1993).
30. F. Bernardi, I.G. Csizmadia, and A. Mangini. Organic sulfur chemistry. Theoretical and experimental advances. Vol. 19. Elsevier, Amsterdam, Oxford, New York, Tokyo. 1985. p. 195.
31. L.A. Curtiss, D.J. Frurip, and M. Blander. J. Chem. Phys. **71**, 2703 (1979).
32. Z. Wu, F. Ban, and R.J. Boyd. J. Am. Chem. Soc. **125**, 6994 (2003).
33. W. Liang, H. Li, X. Hu, and S. Han. J. Phys. Chem. A, **108**, 10219 (2004).

© 2005 NRC Canada

S_N2 and S_N2' reaction dynamics of cyclopropenyl chloride with halide ion — A direct ab initio molecular dynamics (MD) study[1]

Hiroto Tachikawa

Abstract: Direct ab initio molecular dynamics (MD) calculations have been carried out for the reaction of cyclopropenyl chloride with halide ion (F^-) ($F^- + (CH)_3Cl \rightarrow F(CH)_3 + Cl^-$) in gas phase. Both S_N2 and S_N2' channels were found as product channels. These channels are strongly dependent on the collision angle of F^- to the target $(CH)_3Cl$ molecule. The collision at one of the carbon atoms of the C=C double bond leads to the S_N2' reaction channel; whereas the collision at the methylene carbon atom leads to the S_N2 reaction channel. The reactions proceed via a direct mechanism without long-lived complexes. The reaction mechanism is discussed on the basis of the theoretical results.

Key words: S_N2 reaction, direct ab initio molecular dynamics, halogen exchange, reaction mechanism.

Résumé : On a effectué des calculs de dynamique moléculaire ab initio directs pour la réaction en phase gazeuse du chlorure de cyclopropényle avec l'ion fluorure (F^-) ($F^- + (CH)_3Cl \rightarrow F(CH)_3 + Cl^-$). On a trouvé que les voies S_N2 et S_N2' peuvent toutes les deux conduire au produit. Ces voies dépendent fortement de l'angle de collision du F^- sur la molécule cible $(CH)_3Cl$. Une collision sur un des atomes de carbone de la double liaison C=C conduit à une voie S_N2' alors qu'une collision sur l'atome de carbone méthylène conduit à une voie S_N2. La réaction se produit par le biais d'un mécanisme direct sans complexes de longue vie. On discute du mécanisme réactionnel sur la base des résultats théoriques.

Mots clés : réaction S_N2, calculs de dynamique moléculaire ab initio directs, échange d'halogène, mécanisme réactionnel.

[Traduit par la Rédaction]

Introduction

Bimolecular nucleophilic substitution (S_N2) reactions have been the focus of extensive theoretical and experimental works in recent years because of their central importance and basic reaction in organic and bioorganic chemistries (1, 2). In particular, the reaction of halide ion (X^-) plays an important role in several organic reactions.

For the reaction dynamics of the halogen exchange S_N2 reaction of a type, $X^- + RY \rightarrow RX + Y^-$ (X, Y = F, Cl, or Br), where R is an alkyl group. Hase and his co-workers (3, 4) have done extensive investigations by means of the classical trajectory method with ab initio fitted analytical potential energy functions. Several characteristic features for the halogen exchange S_N2 reactions have been elucidated from their results. However, the reactions previously investigated are only in the case of methyl halide (R = CH_3). There is no dynamics study on a more complicated system. This is due to the fact that dimension, which should be included in the calculation, will greatly increase as the number of atoms in the reaction system is increased. Therefore, the procedure of the fitting becomes more difficult and more complicated in a larger system.

In the present study, we have investigated a S_N2 reaction of cyclopropenyl chloride with halide ion (F^-), i.e., R = $(CH)_3$,

$$[1] \qquad F^- + (CH)_3Cl \rightarrow F(CH)_3 + Cl^-$$

by means of the direct ab initio molecular dynamics (MD) method. In this method, we do not need a fitting procedure of PES to an analytical function. Therefore, it is suitable to investigate a complex S_N2 reaction using the direct ab initio trajectory method. In previous papers, we have carried out direct ab initio MD calculations for the S_N2 reactions, $F^-(H_2O)_n + CH_3Cl$ (n = 0–1) (5–9) and $OH^- + CH_3Cl \rightarrow CH_3OH + Cl^-$ (10). Mechanism, collision energy dependence, and branching ratios of the product channels were predicted from the calculations. Also, it was suggested that the direct ab initio MD method is a powerful tool for investigating the reaction dynamics for the reactions with large degrees of freedom.

Figure 1 shows an illustration of the reaction scheme of cyclopropenyl chloride with halide ion (F^-). Cyclopropenyl chloride ($(CH)_3Cl$) is constructed of a three-membered ring with one double bond and a chlorine atom is substituted in the methylene (CH_2) group. Therefore, the reactive collisions of X^- ion take place in a σ attack S_N2 site, a π attack S_N2' (anti) site, and a π attack S_N2' (syn) site. For the reaction of F^-, three reaction channels will be expected: S_N2, S_N2' (anti), and S_N2' (syn).

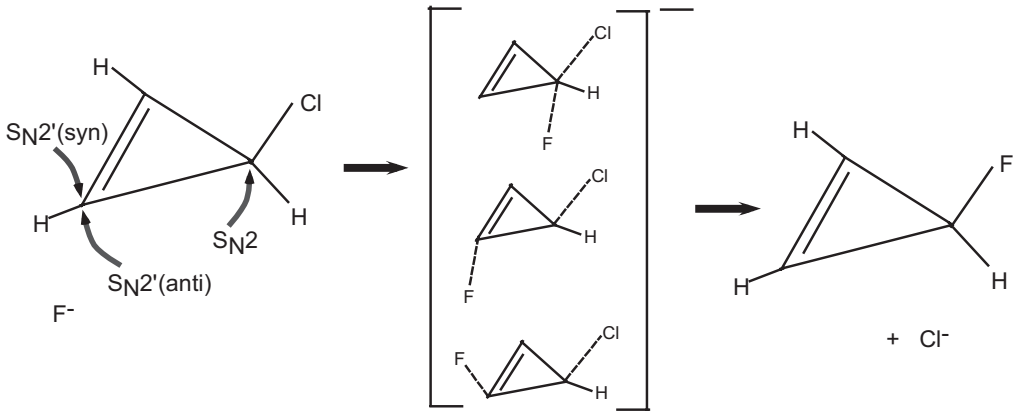
Received 14 April 2005. Published on the NRC Research Press Web site at http://canjchem.nrc.ca on 1 December 2005.

H. Tachikawa. Division of Materials Chemistry, Graduate School of Engineering, Hokkaido University, Sapporo 060-8628, Japan (e-mail: hiroto@eng.hokudai.ac.jp).

[1]This article is part of a Special Issue dedicated to organic reaction mechanisms.

 doi: 10.1139/V05-176 © 2005 NRC Canada

Fig. 1. Schematic illustration of the reaction of cyclopropenylchloride with F^- (F^- + $(CH)_3Cl$). Three reaction channels are possible for reactive collision.



From a theoretical point of view, Kim et al. (11) investigated the potential energy diagram for the symmetric S_N2 reaction

[2] $X^- + (CH)_3X \rightarrow X(CH)_3 + X^-$ (X = F, Cl, or Br)

by means of ab initio calculation. Their calculations indicated that there are double minima corresponding to pre- and late-complexes, while the transition state is lower in energy than the initial separation. The barrier height increases in the order S_N2' (anti) < S_N2' (syn) < S_N2 for X = F. For the symmetric S_N2 rxn. [2], static ab initio calculations have been thus carried out (11), and the energetics are well-elucidated. On the other hand, there is no dynamics study for rxn. [1] because the reaction has many degrees of freedom ($3N - 6 = 18$, where N is the number of atoms in the reaction system). Furthermore, the energetics for the asymmetric reaction, $X^- + (CH)_3Y \rightarrow X(CH)_3 + Y^-$ (X or Y = F, Cl, or Br), are not clearly understood.

In the present paper, a direct ab initio MD calculation (12–15) is carried out for rxn. [1] to elucidate the reaction mechanism and to obtain the dynamics feature. The reaction mechanism will be discussed on the basis of theoretical results. Note that this work is the first study to investigate the dynamics of rxn. [1].

Methods of calculation

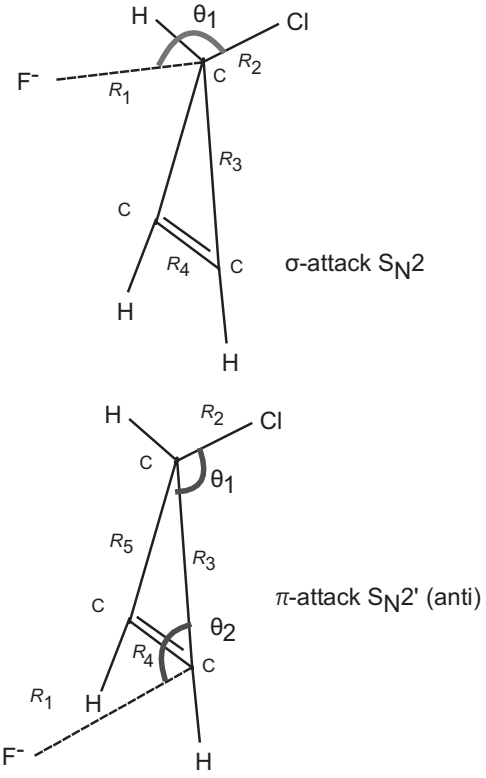
The Hartree–Fock (HF)/3-21+G(d) optimized geometry of $(CH)_3Cl$ was chosen as an initial structure. At the start of the trajectory calculation, atomic velocities of $(CH)_3Cl$ were adjusted to give a mean temperature of 10 K. Temperature of the reaction system is defined by

$$[3] \qquad T = \frac{1}{3kN}\left\langle \sum_i m_i v_i^2 \right\rangle$$

where N is number of atoms, v_i and m_i are the velocity and mass of the ith atom, and k is Boltzmann's constant.

Figure 2 shows the structure and geometrical parameters of the reaction system. We examined S_N2 and S_N2' (anti) collisions in the present work. At initial separations, i.e., F^- + $(CH)_3Cl$, the angles of F-$(CH)_3$-Cl (θ_1) were randomly generated from 0.0° to 180°. The distances between F^- and

Fig. 2. Geometrical parameters for the reaction system F^- + $(CH)_3Cl$.



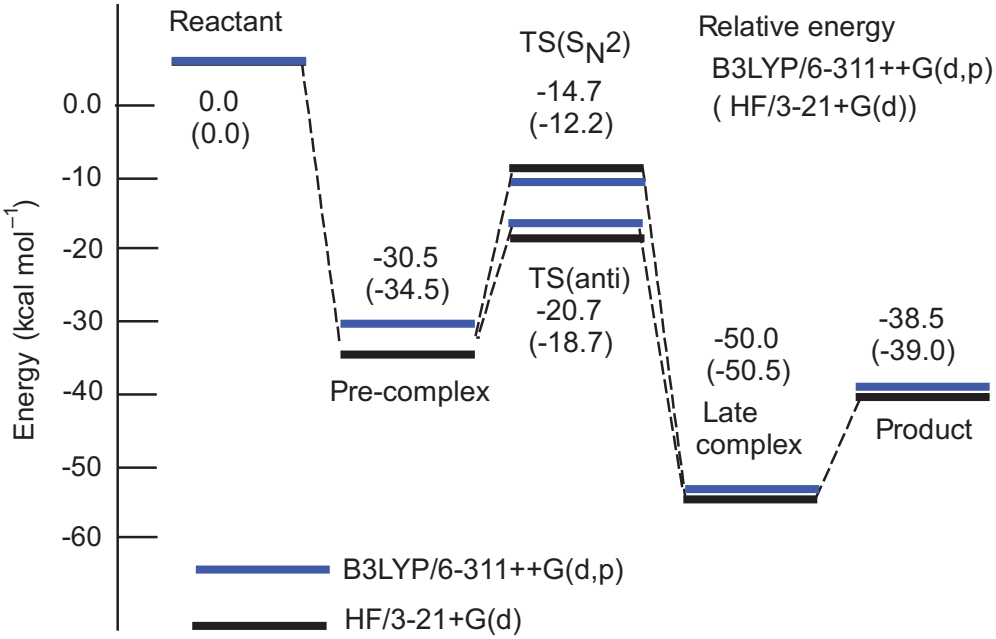
$(CH)_3Cl$ (R_1) were also generated within 8.0–10.0 Å. A total of 40 geometrical configurations were randomly generated, and 40 trajectories were analyzed for constant collision energy (E_{coll} = 5.0 kcal/mol, 1 cal = 4.184 J). The equations of motion for n atoms in the reaction system are given by

$$[4] \qquad \frac{dQ_j}{dt} = \frac{\partial H}{\partial P_j}$$
$$\frac{dP_j}{dt} = \frac{\partial H}{\partial Q_j} = \frac{\partial U}{\partial Q_j}$$

where j = 1–3N, H is the classical Hamiltonian, U is the potential energy of the reaction system, Q_j is the Cartesian co-

© 2005 NRC Canada

Fig. 3. Potential energy profile of the reaction $F^- + (CH)_3Cl \rightarrow (CH)_3F + Cl^-$, calculated at the B3LYP/6-311++G(d,p) and HF/3-21+G(d) levels. The values are relative energies (in kcal/mol) calculated at the B3LYP/6-311++G(d,p) level. The HF/3-21+G(d) values are given in parenthesis.



ordinate of the jth mode, and P_j is conjugated momentum. These equations were numerically solved by the standard fourth-order Runge–Kutta and sixth-order Adams–Moulton combined algorithm. No symmetry restriction was applied to the calculation of the gradients. The time step size was chosen as 0.2 fs, and a total of 5000 steps were integrated for each dynamics calculation. The drift of the total energy is confirmed to be less than 0.001% at all steps in the trajectory. The rotational quantum number of F^- at initial separation was assumed to be zero ($J = 0$). All static ab initio calculations were carried out using the GAUSSIAN03 program package (16).

Results and discussion

Potential energy diagram for the reaction

The potential energy diagram for rxn. [1] is illustrated in Fig. 3. The calculations are carried out at the B3LYP/6-311++G(d,p) level. The values obtained at the HF/3-21+G(d) level are also given for comparison. Zero level corresponds to the energy of the reactant at the initial separation between F^- and $(CH)_3Cl$. The precomplex, expressed by $F^-\cdots(CH)_3Cl$, was first formed in the entrance region. The binding energy of F^- to $(CH)_3Cl$ is calculated to be 30.5 kcal/mol at the B3LYP/6-311++G(d,p) level. From this point, the reaction is branched to two channels. These are the S_N2 and S_N2' (anti) channels. Both transition states (TS) for the two channels are lower in energy than that of the reactant. The energy levels of the TSs for S_N2 and S_N2' (anti) channels are calculated to be –14.7 and –20.7 kcal/mol relative to the reactant, respectively. These energy levels for S_N2 and S_N2' (anti) channels correspond to barrier heights of 15.8 and 9.8 kcal/mol relative to the precomplex, respectively.

After leaving the TS, the energy is suddenly decreased, and the reaction point reaches the late complex in the exit region. The late complex is expressed by $F(CH)_3\cdots Cl^-$, where one of the hydrogen atoms of $F(CH)_3$ orients the Cl^- ion. Finally, the reaction point reaches the product ($(CH)_3F + Cl^-$).

It should be noted that the energy diagram calculated at the HF/3-21+G(d) level resembles that of the B3LYP/6-311++G(d,p) level. The heat of reaction was calculated to be $-\Delta H = 39.0$ kcal/mol, which is in reasonable agreement with that of the higher level calculation (38.5 kcal mo1^{-1}). The energy levels for the TSs for S_N2 and S_N2' (anti) channels are –12.2 and –18.7 kcal/mol at the HF/3-21+G(d) level. The corresponding energies obtained were –14.7 and –20.7 kcal/mol at the B3LYP/6-311++G(d,p) level. Thus, the HF/3-21+G(d) calculation would give a reasonable multidimensional potential energy surface (PES) for the S_N2 reaction, $F^- + (CH)_3Cl \rightarrow F(CH)_3 + Cl^-$. At the very least, this level of theory is applicable to a qualitative argument for rxn. [1].

The relative energies for stationary points along the reaction $F^- + (CH)_3Cl$ are given in Table 1. Zero-point vibrational energies (ZPEs) are also considered in the relative energies (given in parenthesis). The relative energies for pre- and late-complexes and product state are similar to each other. It was found that the B3LYP calculation seems to slightly underestimate the barrier heights for rxn. [1] by comparison with the MP2 calculation.

The optimized structures at the stationary points of the $F^- + (CH)_3Cl$ reaction system are illustrated in Fig. 4. In the transition state for the S_N2 reaction channel denoted to TS(S_N2), the F^- ion is located at $R_1 = 2.360$ Å, while the C—Cl bond length is elongated to be $R_2 = 2.384$ Å. The angle for F-C-Cl was calculated to be 170°, implying that the structure at the transition state is close to collinear. The C—F and C—Cl bond lengths the transition state for the S_N2

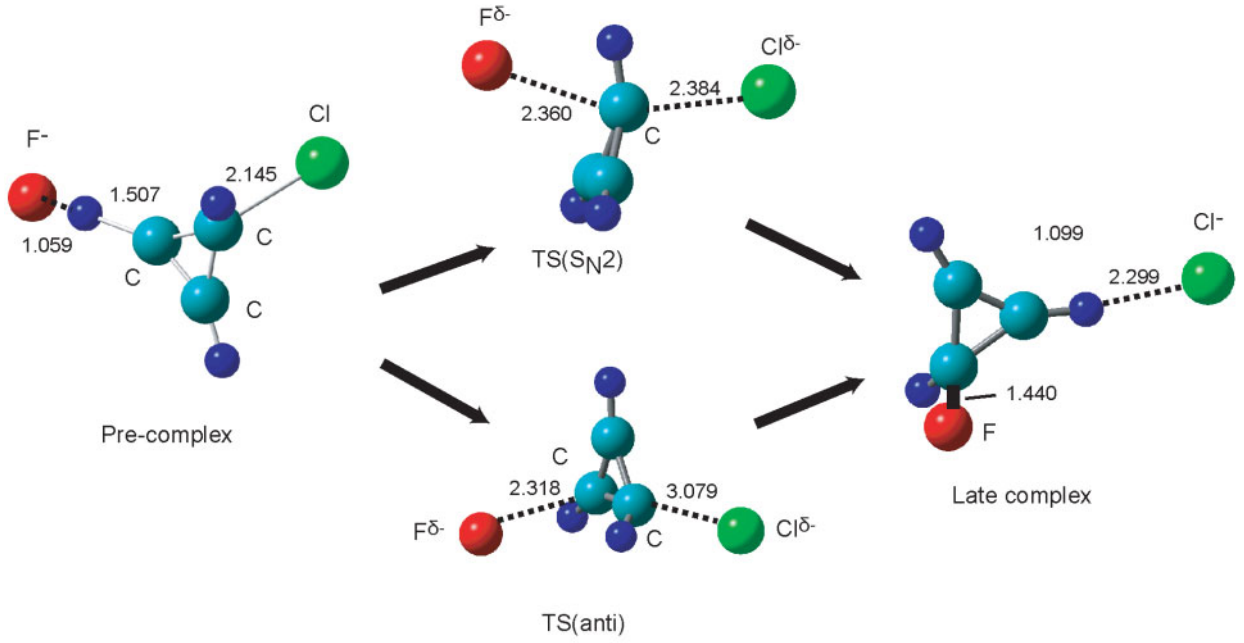
© 2005 NRC Canada

Table 1. Relative energies (in kcal/mol) for stationary points along the reaction coordinates of the F^- + $(CH)_3Cl$ reaction.

Stationary point	HF/3-21+G(d)	MP2/6-311+G(d,p)	B3LYP/6-311++G(d,p)
F^- + $(CH)_3Cl$	0.0 (0.0)	0.0 (0.0)	0.0 (0.0)
Precomplex	–34.5 (–36.2)	–28.3 (–29.5)	–30.5 (–32.3)
TS(S_N2)	–12.2 (–11.7)	–3.1 (–3.7)	–15.6 (–16.3)
TS(anti)	–18.8 (–19.9)	–13.8 (–13.8)	–20.7 (–21.3)
Late complex	–50.5 (–49.1)	–42.2 (–41.1)	–50.0 (–49.1)
Cl^- + $(CH)_3F$	–39.0 (–37.9)	–29.4 (–28.5)	–38.5 (–37.6)

Note: The energies corrected by ZPEs are given in parenthesis.

Fig. 4. The optimized structures of the F^- + $(CH)_3Cl$ reaction system at the stationary points. The bond lengths are calculated at the B3LYP/6-311++G(d,p) level.



(anti) channel were calculated to be 2.318 and 3.079 Å, respectively. At the pre- and late-complexes, the halide ions bind to a hydrogen atom of $(CH)_3X$ (X = F or Cl). Details of the static properties of the reaction system, such as the geometrical structures, vibrational frequencies, and intrinsic reaction coordinate (IRC), will be discussed in a forthcoming paper.[2]

S_N2 reaction dynamics — S_N2 channel

First, a sample trajectory for the S_N2 reaction channel is discussed in this section. Snapshots of the geometrical configuration for the S_N2 reaction are given in Fig. 5. At time zero, the F^- ion is located at 8.00 Å from the center-of-mass of $(CH)_3Cl$ (R_1 = 7.342 Å). The center-of-mass collision energy is 5.0 kcal/mol. The structural parameters of $(CH)_3Cl$ were calculated as follows: the C—Cl, C1—C2, and C2=C3 bond lengths are R_2 = 1.813 Å, R_3 = 1.4876 Å, and R_4 = 1.292 Å, respectively. The highest occupied molecular orbital (HOMO) is localized in the F^- ion.

At the start of the reaction, the F^- ion gradually approaches $(CH)_3Cl$, and arrives at the precomplex region at 198 fs. The distance of F^- from the C1 atom is R_1 = 3.672 Å. The C—Cl bond is elongated from R_2 = 1.813–1.902 Å. The HOMO of the reaction system is illustrated in Fig. 5: a 2p orbital of F^- interacts slightly with the lowest unoccupied MO (LUMO) of $(CH)_3Cl$.

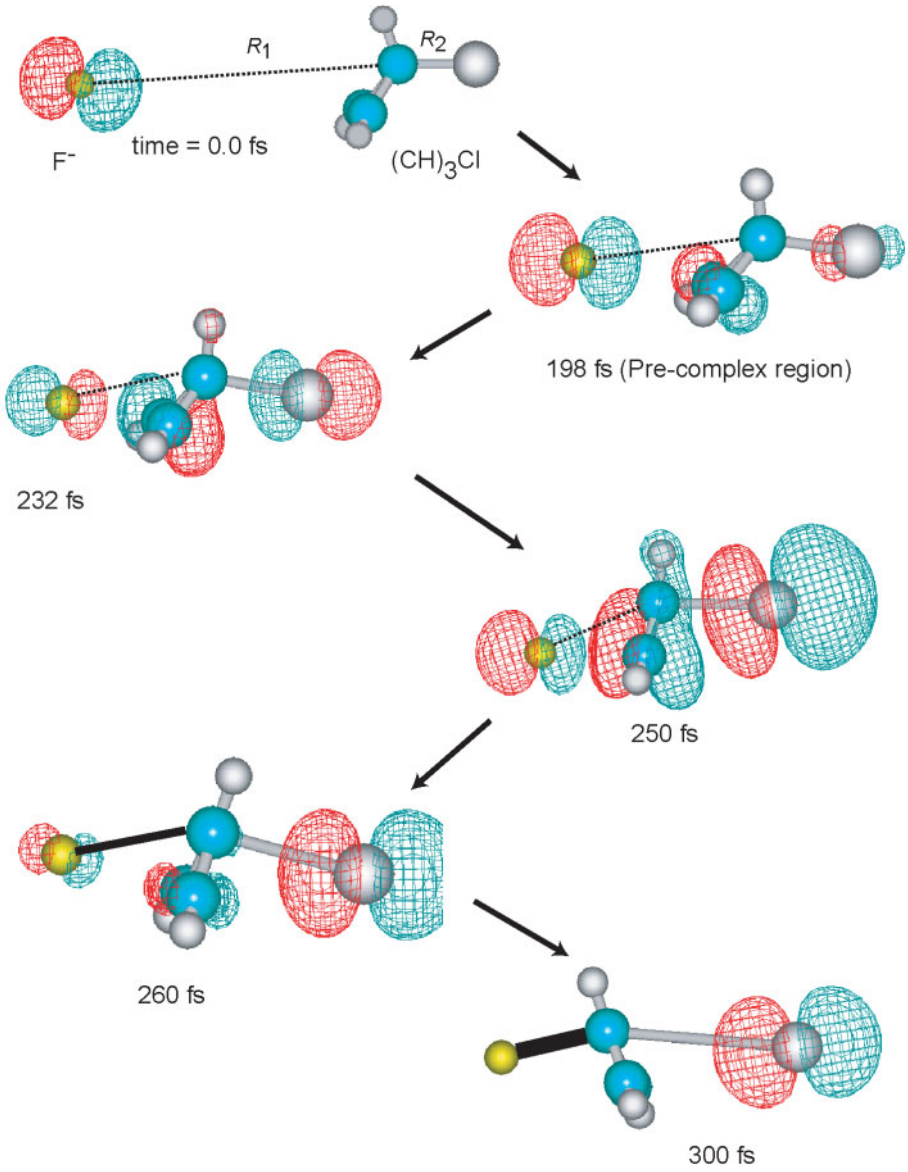
The trajectory passes the transition-state region at 230 fs. F^- collides the C=C double bond of $(CH)_3Cl$ at 232 fs, and the F^- distance is R_1 = 2.933 Å. The C—Cl bond length is further elongated, and the value is calculated at R_2 = 2.115 Å. The HOMO is delocalized over the complex.

At 250 fs, F^- is closer to the C1 atom. Distribution of HOMO on the Cl atom becomes larger. The geometrical parameters are R_1 = 2.761 Å and R_2 = 2.463 Å, while the C1—C2 and C2—C3 bond lengths are 1.363 and 1.331 Å, respectively, indicating that the double bond of the C2=C3 bond becomes a single bond as at 250 fs. Walden inversion of the carbon atom (C1) occurs at 260 fs and then it reaches the late complex at 300 fs. At the final stage, the products ($(CH)_3F$ and Cl^-) are formed, and Cl^- leaves rapidly from $(CH)_3F$. It was clearly found that the 2p orbital of F^- strongly interacts with C—Cl σ* orbital.

[2] H. Tachikawa. To be published.

© 2005 NRC Canada

Fig. 5. Snapshots of the conformations for the sample trajectory of the S_N2 reaction channel. The initial parameters are the distances, R_1 = 7.3424 Å, R_2 = 1.8133 Å, R_3 = 1.4876, and R_4 = 1.2915 Å. The center-of-mass collision energy (E_{coll}) is 5.0 kcal/mol. The 3-21+G(d) basis set was used for the reaction system. The time propagations for HOMO are illustrated by the iso surface.



To elucidate the reaction dynamics of F^- with $(CH)_3Cl$ in more detail, time propagation of the potential energy (PE), intra- and inter-molecular distances and angles are plotted in Fig. 6. This trajectory corresponds to that given in Fig. 5. The PE of the reaction system plotted as a function of reaction time is given in Fig. 6A. Parts B and C of Fig. 6 give the intermolecular distances (R_1 and R_2) and angles (θ_1), respectively.

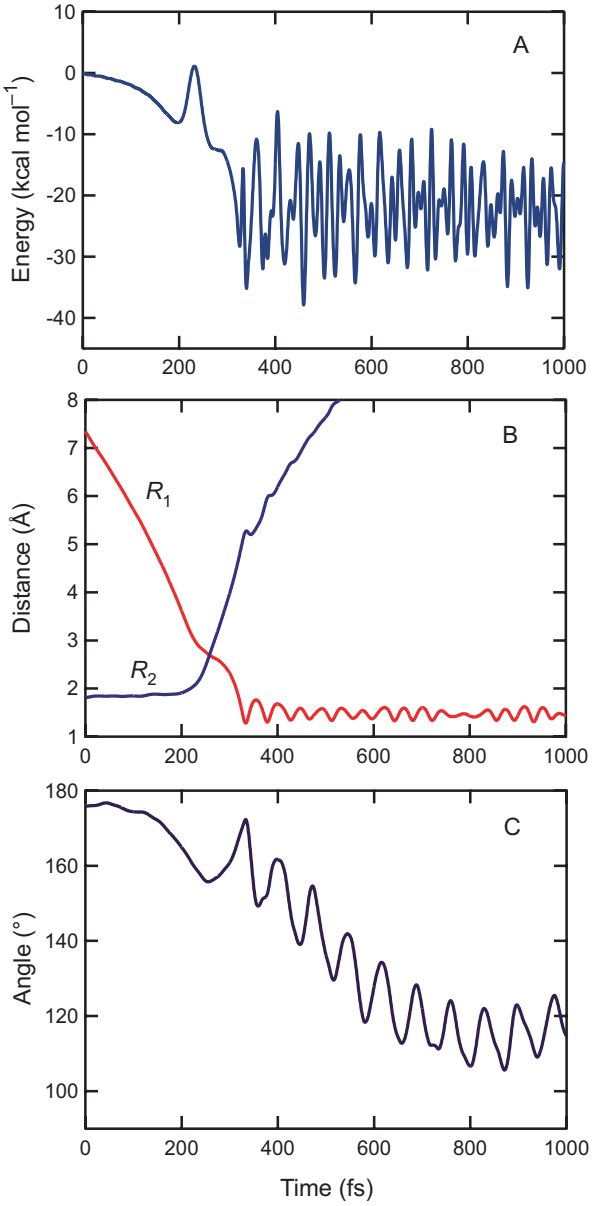
At time zero, F^- is located at R_1 = 7.342 Å from $(CH)_3Cl$. After starting of the reaction, PE gradually decreases as reaction time is increased, and it reaches –10.0 kcal/mol at 198 fs. This point corresponds to the precomplex region expressed by $F^-\cdots(CH)_3Cl$. The peak of PE is found at 232 fs. This peak is formed by the collision of F^- at the C=C double bond of $(CH)_3Cl$. However, the S_N2' reaction does not occur in the case of this trajectory because F^- collides at the center of the C=C bond, not at the carbon atom (C). Walden inversion and bond-forming and bond-breaking processes take place at 250–300 fs (transition-state region). The time propagation of R_1, R_2, and θ_1 around 200–300 fs shows explicit evidence of the S_N2 reaction. After the Walden inversion, the trajectory passes the late complex region (340 fs) and PE vibrates strikingly. This is due to the fact that the excess energy formed by the reaction is efficiently transferred into the C—F stretching mode of $(CH)_3F$. The translational energy of Cl^- is calculated to be 2.4 kcal/mol, which is 5.4% of the total available energy of the reaction. Almost all the energy of the reaction is transferred into the internal modes of $(CH)_3F$ in the case of this trajectory.

S_N2 reaction dynamics — S_N2' (anti) channel

A sample trajectory for the S_N2 (anti) reaction channel is

© 2005 NRC Canada

Fig. 6. Results of the sample trajectory for the S_N2 reaction channel. (A) Potential energy of the system, (B) inter- and intra-atomic distances (R_1 and R_2), and (C) angles vs. reaction time. The initial condition for the trajectory calculation is the same as that in Fig. 5.



discussed in this section. Snapshots of the geometrical configuration for the S_N2 (anti) reaction are given in Fig. 7. The F^- ion is located at R_1 = 6.228 Å at time zero. The center-of-mass collision energy is 5.0 kcal/mol. The HOMO is composed of a 2p orbital of the F^- ion.

At 140 fs, the distance of F^- from the C2 atom is R_1 = 3.626 Å and the C—Cl bond length is 1.895 Å. After that, the trajectory arrives at the precomplex region at 175 fs (R_1 = 2.659 Å and R_2 = 1.9273 Å). At 200 fs, the trajectory reaches the transition-state region. The HOMO of the system is composed of the C—F σ* orbital (LUMO) of $(CH)_3Cl$ and the HOMO of F^-. The F^- distance is R_1 = 1.522 Å at 235 fs, where the trajectory passes the late complex region. The C—Cl bond is largely elongated (R_2 = 2.934 Å).

From the present results, it is explicitly found that the bond forming of C—F and the bond breaking of C—Cl take place as a result of the approaching of F^- to $(CH)_3Cl$. The 2p orbital of F^- gradually interacts with the orbital of $(CH)_3Cl$. As a result of the collision of the F^- ion at the C2 atom of $(CH)_3Cl$, the Cl^- ion is dissociated from the $(CH)_3Cl$: namely, the S_N2' (anti) reaction takes place.

Time propagations of the potential energy, intra- and inter-molecular distances and angles are plotted in Fig. 8. At time zero, F^- is 8.0 Å from $(CH)_3Cl$. After the reaction has started, PE gradually decreases as reaction time is increased, and it reaches –10.0 kcal/mol at 190 fs. During this process, the R_1 distance linearly deceases as a function of reaction time, and the energy of the system decreases. This means that the approach of F^- to $(CH)_3Cl$ causes an energy lowering because of the attractive ion–dipole interaction. At 190 fs, PE reaches a minimum corresponding to the precomplex expressed by $F^-\cdots(CH)_3Cl$. The lifetime of the complex is very short (τ < 30 fs), and the trajectory rapidly reaches the TS. After TS, PE suddenly decreases to –38.0 kcal/mol at 220 fs. This point is located in the late-complex region. PE rapidly vibrates with an amplitude of ca.10 kcal/mol after the reaction. The relative translational energy between Cl^- and $(CH)_3F$ was calculated to be 8.4 kcal/mol, which is ca. 20% of the total available energy of the reaction.

The time propagations of the C—C bond lengths (R_3, R_4, and R_5) are plotted in Fig. 8C. Before reaction, the bond lengths are R_3 = R_5 = 1.487 Å and R_4 = 1.292 Å, indicating that R_4 is the C=C double bond at time zero. The C2—C3 bond is drastically changed from 1.292 to 1.50 Å around 200 fs. Also, at the same time, R_5 (= C1—C3) is suddenly changed from 1.478 to 1.300 Å. This indicates that the exchanges of single and double bonds are occurred in the transition-state region.

Discussion

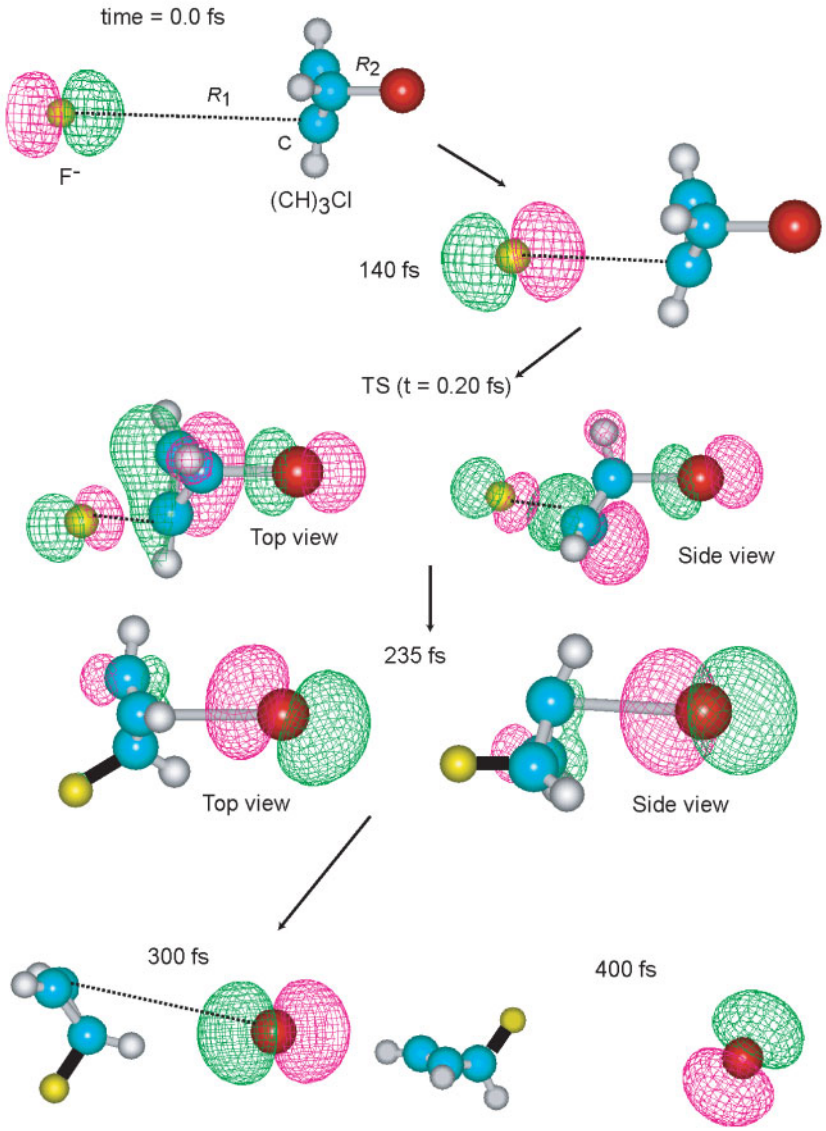
Summary

In the present study, direct ab initio MD calculations were carried out for rxn. [1] using the 3-21+G(d) basis set. Two reaction channels were examined: namely, S_N2 and S_N2' (anti) channels. The dynamics calculations showed that both reaction channels mainly occur by direct mechanism: namely, the trajectory quickly passes through the TS and the complex regions (pre- and late-complex regions). This is due to the fact that the reaction energy is significantly large (about 38 kcal/mol) and also, the basins of the complex regions are shallow for the product channel. Therefore, almost all trajectories proceed via direct mechanism.

The reaction channel is strongly dependent on the collision site of F^- around the $(CH)_3Cl$ molecule. Almost all trajectories lead to the S_N2' reaction channel, while specific collision gives the S_N2 reaction channel. This result originates from the lower activation barrier of the S_N2' (anti) channel. The branching ratios of reaction channels are roughly estimated from the results of the trajectory calculation: they are 0.2 for S_N2 and 0.8 for S_N2' (anti). However, the ratios were obtained from only 40 trajectories. To eluci-

© 2005 NRC Canada

Fig. 7. Snapshots of the conformations for the sample trajectory of the S_N2' (anti) reaction channel. The initial parameters are the distances, R_1 = 6.228 Å, R_2 = 1.815 Å, R_3 = 1.482, and R_4 = 1.291 Å. The center-of-mass collision energy (E_{coll}) is 5.0 kcal/mol. The 3-21+G(d) basis set was used for the reaction system. The time propagations for HOMO are illustrated by the iso surface.



date more accurate values, a larger number of trajectories will be required.[2]

In the present study, S_N2 and S_N2' (anti) channels were examined in low-collision energy (E_{coll} = 5 kcal/mol); whereas the S_N2' (syn) channel was not considered. This is due to the fact that the S_N2' (syn) channel has a high activation barrier and needs higher collision energy. In the forthcoming work, we will calculate the S_N2' (syn) channel.[2]

Comparison with previous studies

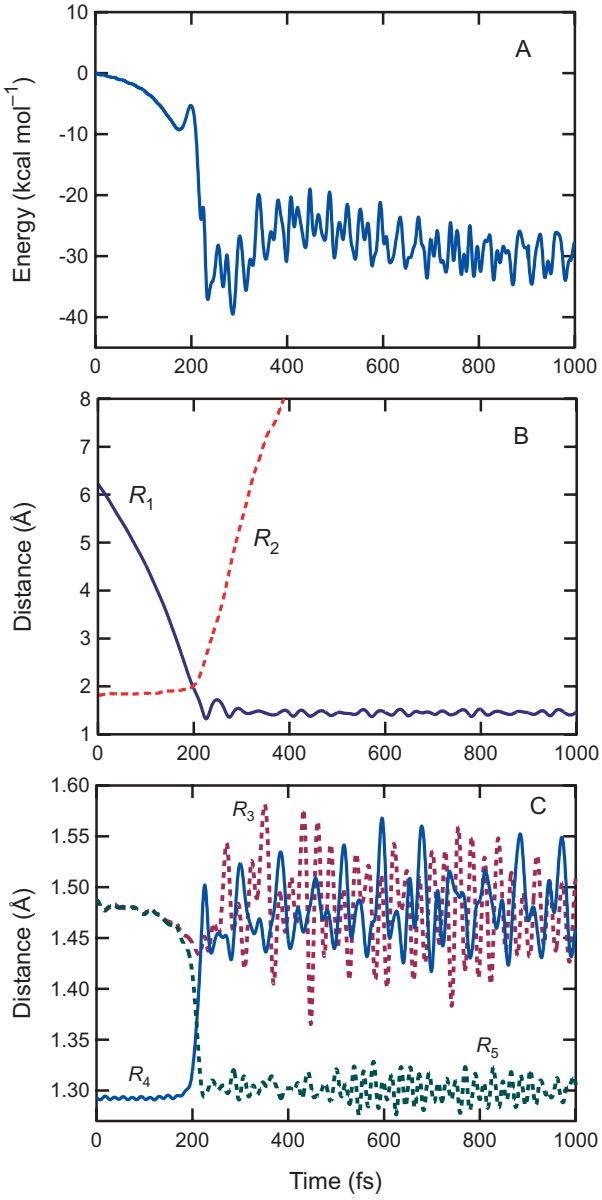
Recently, a PE diagram for the similar S_N2 reaction (rxn. [2]) was calculated by Kim et al. (11). Their calculations indicated that the energy level of the transition state for rxn. [2] is lower than that of the initial separation, which is in good agreement with the present calculation. The reaction they used is the symmetric system (X = Y), which is slightly different from the present system. However, the structures at the stationary points are very similar to those of the present calculations.

Concluding remarks

We have introduced several approximations to calculate the PES and to treat the reaction dynamics. First, we assumed a HF/3-21+G(d) multidimensional PES in the trajectory calculations throughout. As shown in the Results and discussion, the energy profile calculated at the HF/3-21+G(d) level is in good agreement with that of the B3LYP/6-311++G(d,p) level, and it reasonably reproduces the PES. Therefore, it is enough to discuss at least qualitatively the reaction dynamics for the F^- + $(CH)_3Cl$ reaction system. However, more accurate wave functions and accurate methods may provide a deeper insight into the dynamics.

© 2005 NRC Canada

Fig. 8. Results of the sample trajectory for the S_N2' (anti) channel. (A) Potential energy of the system, (B) inter- and intra-atomic distances (R_1 and R_2), and (C) C—C bond lengths (R_3, R_4, and R_5) vs. reaction time. The initial condition of the trajectory calculation is the same as that in Fig. 7.



Second, we calculated only 40 trajectories for constant collision energy (E_{coll} = 5.0 kcal/mol). The number of trajectories in the present work may be enough to discuss the at least qualitative feature of the dynamics. However, larger number of trajectories in wide range of collision energies would give a more detailed reaction mechanism. Despite several assumptions introduced here, the results enable us to obtain valuable information on the mechanism of the S_N2 and S_N2' (anti) reactions. The trajectory calculations for the random collisions are now in progress.[2]

Acknowledgments

The author is indebted to the Computer Center at the Institute for Molecular Science (IMS) for the use of the computing facilities. The author also acknowledges partial support from a Grant-in-Aid for Scientific Research (C) from the Japan Society for the Promotion of Science (JSPS).

References

1. For a selection of experimental works on the gas-phase S_N2 reaction, see: (*a*) W.N. Olmstead and J.I. Brauman. J. Am. Chem. Soc. **99**, 4219 (1997); (*b*) T. Su, R.A. Morris, A.A. Viggiano, and J.F. Paulson. J. Phys. Chem. **94**, 8426 (1990); (*c*) A.A. Viggiano, J.S. Paschkewitz, R.A. Morris, J.F. Paulson, A. Gonzalez-Lafont, and D.G. Truhlar. J. Am. Chem. Soc. **113**, 9404 (1991); (*d*) C.H. DePuy, S. Gronert, A. Mullin, and V.M. Bierbaum. J. Am. Chem. Soc. **112**, 8650 (1990); (*e*) S. Gronert, C.H. DePuy, and V.M. Bierbaum. J. Am. Chem. Soc. **113**, 4009 (1991); (*f*) S.T. Graul and M.T. Bowers. J. Am. Chem. Soc. **113**, 9696 (1991); (*g*) S.T. Graul and M.T. Bowers. J. Am. Chem. Soc. **116**, 3875 (1994); (*h*) S.L. Van Orden, R.M. Pope, and S.W. Buckner. Org. Mass Spectrom. **26**, 1003 (1991); (*i*) D.M. Cyr, L.A. Posey, G.A. Bishea, C.-C. Han, and M.A. Johnson. J. Am. Chem. Soc. **113**, 9697 (1991); (*j*) D.M. Cyr, G.A. Bishea, M.G. Scarton, and M.A. Johnson. J. Chem. Phys. **97**, 5911 (1992); (*k*) K. Giles and E.P. Grimsrud. J. Phys. Chem. **96**, 6680 (1992); (*l*) W.B. Knighton, J.A. Boghar, P.M. O'Connor, and E.P. Grimsrud. J. Am. Chem. Soc. **115**, 12079 (1993); (*m*) K.E. Sahlstrom, W.B. Knighton, and E.P. Grimsrud. J. Phys. Chem. A, **101**, 1501 (1997); (*n*) A.A. Viggiano, R.A. Morris, J.S. Paschkewitz, and J.F. Paulson. J. Am. Chem. Soc. **114**, 10477 (1992); (*o*) B.D. Wladkowski, K.F. Lim, W.D. Allen, and J.I. Brauman. J. Am. Chem. Soc. **114**, 9136 (1992); (*p*) A.A. Viggiano, R.A. Morris, T. Su, B.D. Wladkowski, S.L. Craig, M. Zhong, J.I. Brauman. J. Am. Chem. Soc. **116**, 2213 (1994); (*q*) S.L. Craig and J.I. Brauman. Science (Washington, D.C.), **276**, 1536 (1997); (*r*) A.A. Viggiano and R.A. Morris. J. Phys. Chem. **98**, 3740 (1994); (*s*) C. Li, P. Ross, J.E. Szulejko, and T.B. McMahon. J. Am. Chem. Soc. **118**, 9360 (1996); (*t*) S.L. Craig and J.I. Brauman. J. Phys. Chem. A, **101**, 4745 (1997); (*u*) V.F. DeTuri, P.A. Hintz, and K.M. Ervin. J. Phys. Chem. A, **101**, 5969 (1997); (*v*) J.V. Seeley, R.A. Morris, A.A. Viggiano, H. Wang, and W.L. Hase. J. Am. Chem. Soc. **119**, 577 (1997); (*w*) J.-L. Le Garrec, B.R. Rowe, J.L. Queffelec, J.B.A. Mitchell, and D.C. Clary. J. Chem. Phys. **107**, 1021 (1997); (*x*) M.L. Chabinyc, S.L. Craig, C.K. Regan, and J.I. Brauman. Science (Washington, D.C.), **279**, 1882 (1998); (*y*) P.M. Hierl, J.F. Paulson, and M.J. Henchman. J. Phys. Chem. **99**, 15655 (1995).
2. For a selection of theoretical studies of S_N2 reactions, see: (*a*) V.M. Ryaboy. *In* Advances in classical trajectory methods. Vol. 2. *Edited by* W.L. Hase. JAI Press, Greenwich, Connecticut. 1994. pp. 115–145; (*b*) S.R. Vande Linde and W.L. Hase. J. Phys. Chem. **94**, 2778 (1990); (*c*) S.C. Tucker and D.G. Truhlar. J. Am. Chem. Soc. **112**, 3338 (1990); (*d*) G.D. Billing. Chem. Phys. **159**, 109 (1992); (*e*) B.D. Wladkowski, W.D. Allen, and J.I. Brauman. J. Phys. Chem. **98**, 13532 (1994); (*f*) H. Wang, L. Zhu, and W.L. Hase. J. Phys. Chem. **98**, 1608 (1994); (*g*) H. Wang and W.L. Hase. J. Am. Chem. Soc. **117**, 9347 (1995); (*h*) W.-P. Hu and D.G. Truhlar. J. Am. Chem. Soc. **117**, 10726 (1995); (*i*) M.N. Glukhovtsev, A. Pross, and L. Radom. J. Am. Chem. Soc. **117**, 2024 (1995); (*j*) M.N. Glukhovtsev, A. Pross, and L. Radom. J. Am. Chem. Soc. **118**, 6273 (1996); (*k*) H. Wang and W.L. Hase. Chem. Phys. **212**,

© 2005 NRC Canada

247 (1996); (*l*) D.C. Clary and J. Palma. J. Chem. Phys. **106**, 575 (1996); (*m*) H. Wang, E.M. Goldfield, and W.L. Hase. J. Chem. Soc. Faraday Trans. **93**, 737 (1997); (*n*) P. Botschwina, M. Horn, S. Seeger, and R. Oswald. Ber. Bunsen–Ges. **101**, 387 (1997); (*o*) T. Baer and W.L. Hase. *In* Unimolecular reaction dynamics — Theory and experiments. Oxford University Press, New York. 1996.

3. For trajectory studies for the S_N2 reaction, see: (*a*) S.R. Vande Linde and W.L. Hase. J. Phys. Chem. **94**, 6148 (1990); (*b*) S.R. Vande Linde and W.L. Hase. J. Chem. Phys. **93**, 7962 (1990); (*c*) G.H. Peslherbe, H. Wang, and W.L. Hase. J. Chem. Phys. **102**, 5626 (1995); (*d*) Y.J. Cho, S.R. Vande Linde, L. Zhu, and W.L. Hase. J. Chem. Phys. **96**, 8275 (1992); (*e*) W.L. Hase and Y.J. Cho. J. Chem. Phys. **98**, 8626 (1993); (*f*) H. Wang, G.H. Peslherbe, and W.L. Hase. J. Am. Chem. Soc. **116**, 9644 (1994); (*g*) G.H. Peslherbe, H. Wang, and W.L. Hase. J. Am. Chem. Soc. **118**, 2257 (1996); (*h*) W.L. Hase. Science (Washington, D.C.), **266**, 998 (1994); (*i*) H. Wang and W.L. Hase. Int. J. Mass Spectrom. Ion Process. **167**, 573 (1997); (*j*) G. Li and W.L. Hase. J. Am. Chem. Soc. **121**, 7124 (1999); (*k*) H. Wang and W.L. Hase. J. Am. Chem. Soc. **199**, 3093 (1997); (*l*) S.L. Craig and J.I. Brauman. J. Phys. Chem. A, **101**, 4745 (1997); (*m*) L. Sun, W.L. Hase, and K. Song. J. Am. Chem. Soc. **123**, 5753 (2001).
4. For a selection of quantum-scattering studies for the S_N2 reaction, see: (*a*) D.C. Clary and J. Palma. J. Chem. Phys. **106**, 575 (1997); (*b*) S. Schmatz and D.C. Clary. J. Chem. Phys. **110**, 9483 (1999); (*c*) M.I. Hernandez, J. Campos-Martinez, P. Villarreal, S. Schmatz, and D.C. Clary. Phys. Chem. Chem. Phys. **1**, 1197 (1999).
5. H. Tachikawa. J. Phys. Chem. A, **105**, 1260 (2001).
6. H. Tachikawa. J. Phys. Chem. A, **104**, 497 (2000).
7. H. Tachikawa and M. Igarashi. Chem. Phys. Lett. **303**, 81 (1999).
8. M. Igarashi and H. Tachikawa. Int. J. Mass Spectrom. **181**, 151 (1998).
9. H. Tachikawa, M. Igarashi, and T. Ishibashi. Chem. Phys. Lett. **363**, 355 (2002).
10. H. Tachikawa, M. Igarashi, and T. Ishibashi. J. Phys. Chem. A, **106**, 10977 (2002).
11. C.K. Kim, H.G. Li, B.-S. Lee, C.K. Kim, H.W. Lee, and I. Lee. J. Org. Chem. **67**, 1953 (2002).
12. H. Tachikawa. Chem. Phys. Lett. **370**, 188 (2003).
13. H. Tachikawa and H. Kawabata. J. Phys. Chem. B, **107**, 1113 (2003).
14. H. Tachikawa, M. Igarashi, and T. Ishibashi. J. Phys. Chem. A, **107**, 7505 (2003).
15. H. Tachikawa. J. Phys. Chem. A, **108**, 7853 (2004).
16. M.J. Frisch, G.W. Trucks, H.B. Schlegel, G.E. Scuseria, M.A. Robb, J.R. Cheeseman, J.A. Montgomery, Jr., T. Vreven, K.N. Kudin, J.C. Burant, J.M. Millam, S.S. Iyengar, J. Tomasi, V. Barone, B. Mennucci, M. Cossi, G. Scalmani, N. Rega, G.A. Petersson, H. Nakatsuji, M. Hada, M. Ehara, K. Toyota, R. Fukuda, J. Hasegawa, M. Ishida, T. Nakajima, Y. Honda, O. Kitao, H. Nakai, M. Klene, X. Li, J.E. Knox, H.P. Hratchian, J.B. Cross, C. Adamo, J. Jaramillo, R. Gomperts, R.E. Stratmann, O. Yazyev, A.J. Austin, R. Cammi, C. Pomelli, J.W. Ochterski, P.Y. Ayala, K. Morokuma, G.A. Voth, P. Salvador, J.J. Dannenberg, V.G. Zakrzewski, S. Dapprich, A.D. Daniels, M.C. Strain, O. Farkas, D.K. Malick, A.D. Rabuck, K. Raghavachari, J.B. Foresman, J.V. Ortiz, Q. Cui, A.G. Baboul, S. Clifford, J. Cioslowski, B.B. Stefanov, G. Liu, A. Liashenko, P. Piskorz, I. Komaromi, R.L. Martin, D.J. Fox, T. Keith, M.A. Al-Laham, C.Y. Peng, A. Nanayakkara, M. Challacombe, P.M.W. Gill, B. Johnson, W. Chen, M.W. Wong, C. Gonzalez, and J.A. Pople. GAUSSIAN 03. Revision B.04 [computer program]. Gaussian, Inc., Pittsburgh, Penn. 2003.

© 2005 NRC Canada

Linear free energy relationship and kinetic isotope effects as measures for the transition-state variation — A case of the neophyl system[1]

Salai Cheettu Ammal and Hiroshi Yamataka

Abstract: Ab initio calculations at the MP2/6-31G* level and density functional theory (B3LYP/6-311+G**) calculations have been performed on acid-catalyzed ionizations of substituted neophyl alcohols to investigate whether a variation of the transition-state (TS) structure is reflected in the kinetic isotope effects (KIE) and linear free energy relationship. The effect of substituents on KIEs, TS structures, and activation and reaction energies was calculated. This study revealed that a curved Brønsted-type plot could arise for a single-step process from the variation of TS structure with the substituent, whereas the Hammett plots with a dual-parameter treatment can not detect such TS variation. The variation of KIEs at various positions of neophyl alcohol reflects the variation of TS structures in a manner consistent with the More O'Ferrall – Jencks type reaction diagram analyses.

Key words: transition-state variation, substituent effect, kinetic isotope effect, linear free energy relationship.

Résumé : On a effectué des calculs ab initio au niveau MP2/6-31G* et des calculs de théorie de la densité fonctionnelle (B3LYP/6-311+G**) sur les ionisations catalysées par les acides d'alcools néophyliques afin de déterminer si une variation dans la structure de l'état de transition (ET) se reflète dans les effets isotopiques cinétiques (EIC) et les relations linéaires d'énergie libre. On a calculé l'effet des substituants sur les EIC, les structures des ET et les énergies d'activation et de réaction. Sur la base de la variation de la structure de l'ET avec un substituant, cette étude révèle qu'une relation de type Brønsted incurvée peut apparaître pour un processus impliquant une seule étape; toutefois, les courbes de Hammett avec un traitement à double paramètre ne permettent pas de détecter de telles variations dans l'ET. La variation des EIC selon diverses positions de l'alcool néophylique sont un reflet des structures de l'ET d'une manière qui est en accord avec les analyses de diagrammes réactionnel de type More O'Ferral – Jencks.

Mots clés : variation de l'état de transition, effet de substituant, effet isotopique cinétique, relation linéaire d'énergie libre.

[Traduit par la Rédaction]

Introduction

Anchimeric assistance involving aryl groups in the solvolyses of β-arylalkyl systems has been the subject of numerous investigations (1). The solvolysis reaction of neophyl (2-phenyl-2-methylpropyl) derivatives is known to be the best example for this study because of its mechanistic simplicity. It is generally accepted that the solvolysis of neophyl derivatives proceeds through a discrete aryl-assisted (k_Δ) transition state (TS), which cascades downward to the tertiary carbenium ion (Scheme 1) (2, 3). The rate of this solvolysis reflects only the aryl-assisted ionization step, and is not complicated either by an internal return or by nucleophilic solvent assistance (3). A series of experimental studies on these reactions demonstrated that substituents in the phenyl ring have marked effects on the solvolysis rate (4, 5).

Linear free energy relationships (LFER), such as the Hammett and Brønsted equations, have been extensively used to analyze the reaction mechanism and to determine the structure of the TSs (6). According to the traditional interpretation, linear Hammett and Brønsted plots are expected for a series of reactions proceeding through similar TS structures. A curvature in the Brønsted-type plots has generally been attributed to a change in the rate-determining step (RDS) of a multistep reaction (7–12), and a curved Hammett plot has been taken as evidence either for a change in mechanism or a change in the RDS (13–16). Indeed, except for the S_N1/S_N2 and the E2 borderline cases of benzylic systems, where substituents on the central carbon readily change the structure of the three-centered or four-centered TS (15, 16), an unequivocal example of nonlinear Hammett plots due to a variation of the TS structure is rare. However, our recent computational studies on the ionization of substituted phenylethyl alcohols suggested that the variation of the TS

Received 27 April 2005. Published on the NRC Research Press Web site at http://canjchem.nrc.ca on 2 December 2005.

S.C. Ammal and H. Yamataka.[2] Department of Chemistry, Rikkyo University, Nishi-Ikebukuro, Toshima-ku, Tokyo 171–8501, Japan.

[1]This article is part of a Special Issue dedicated to organic reaction mechanisms.
[2]Corresponding author (e-mail: yamataka@rikkyo.ac.jp).

 doi: 10.1139/V05-209 © 2005 NRC Canada

Scheme 1.

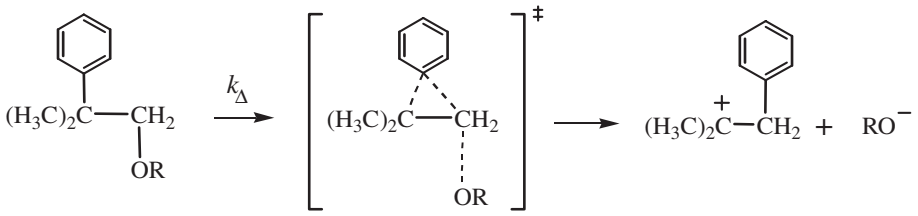


Table 1. Experimental kinetic isotope effects in the acetolysis of neophyl esters.

Labeled position	Substituent	Leaving group[a]	Temp. (°C)	$k/^*k$
α-^{14}C	*p*-OMe	OTs	50.0	1.117±0.009[b]
	p-H	OBs	75.0	1.093±0.003[c]
	p-Br	OBs	85.0	1.088±0.001[b]
β-^{14}C	*p*-H	OBs	75.0	1.014±0.001[c]
Ph1-^{14}C	*p*-OMe	OBs	40.0	1.006±0.001[d]
	p-H	OBs	75.0	1.023±0.001[e]
	p-Br	OBs	85.0	1.030±0.001[b]
α-D_2	*p*-OMe	OMs	25.0	1.248[f]
	p-CH_3	OMs	25.0	1.254[f]
	p-H	OMs	25.0	1.272[f]
		OBs	75.0	1.214±0.002[c]

[a]OTs is *p*-toluenesulfonate; OBs is *p*-bromobenzenesulfonate; OMs is methanesulfonate.
[b]Reference 19.
[c]Reference 21*a*.
[d]Reference 21*b*.
[e]Reference 21*c*.
[f]Reference 21*d*. The solvent used was 2,2,2-trifluoroethanol–water (70 wt%:30%).

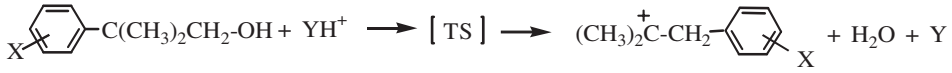
structure for a series of reactions could result in a nonlinear Brønsted-type plot, whereas the Hammett plot with a dual-parameter treatment could not detect such TS variation (17).

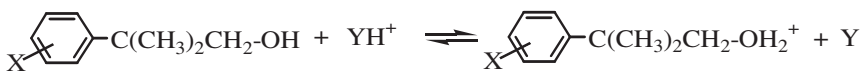
The concept of a variable TS has been of great use in explaining the mechanistic properties of organic reactions, and several methods have been proposed for detecting variations in TS structure. Kinetic isotope effects (KIEs) using a successive labeling technique are known to be the most effective tool for obtaining information on the variation of TS structures for a series of reactions (18–20). For the acetolysis of neophyl arenesufonates, KIEs were measured at four different positions in the molecule (α-^{14}C, α-D_2, β-^{14}C, and Ph1-^{14}C) as listed in Table 1 (19, 21). Model calculations of the KIEs by the BEBOVIB method allowed the authors to estimate the TS location and its variation with substituents on the reaction coordinate (19).

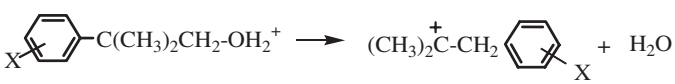
In the present study, the acid-catalyzed ionization of substituted neophyl alcohols (eq. [1*a*]) was examined computationally. This study was comprised of four phases. In the first phase, we studied to what extent the reactivity and the TS structure varies with substituents. Secondly, we examined how LFER can be used to study the effect of substituents on the reactivity and on the variation of the TS structure. In the third phase, KIEs at different positions were calculated to assess if they reflect the TS variations. Finally, the More O'Ferrall – Jencks type reaction map (22) was used to locate the position of the calculated TS and compare the results with the previous estimation based on the BEBOVIB calculations. The calculated results were compared with the experimental results whenever possible and also with the closely related 2-phenylethyl system at each stage.

Computational methods

All stable structures, including the substituted neophyl alcohols, protonated neophyl alcohols, TSs, and tertiary cations were fully optimized at the HF/6-31G*, B3LYP/6-31G*, B3LYP/6-311+G**, and MP2/6-31G* levels of theory with the GAUSSIAN 98 package of programs (23). Each stationary point was adequately characterized by normal coordinate analysis and thermochemical data was obtained

[1*a*] 

[1*b*] 

[1*c*] 

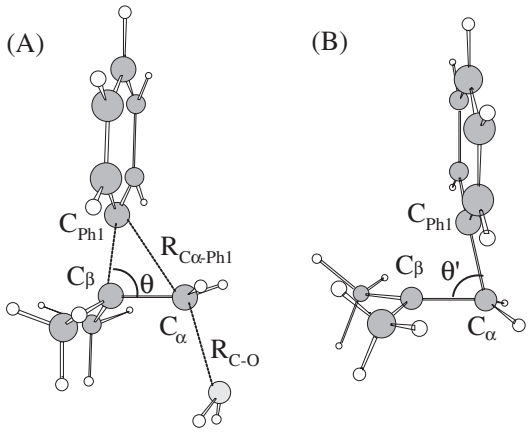
© 2005 NRC Canada

Table 2. Structural parameters, activation enthalpies, and reaction enthalpies for the parent as well as *p*-substituted neophyl alcohols obtained at different levels of theory.

		TS			Product cation		
X	Method	$R_{C\text{-}O}$	θ	Activation energy[a]	$R_{C\alpha\text{-}Ph1}$	$R_{C\beta\text{-}Ph1}$	Reaction energy[a]
p-OMe	HF/6-31G*	1.862	93.7	14.8 (14.6)	1.571	1.641	2.5 (–7.2)
	B3LYP/6-31G*	1.740	95.8	15.0 (16.5)	1.559	1.805	7.1 (–2.2)
	B3LYP/6-311+G**	1.716	97.1	13.7 (15.1)	1.552	1.892	–0.5 (–10.5)
	MP2/6-31G*	1.853	89.2	18.7 (19.8)	1.571	1.712	11.2 (2.3)
H	HF/6-31G*	1.951	91.9	17.7 (17.1)	1.547	2.206	9.4 (–2.3)
	B3LYP/6-31G*	1.990	87.6	19.0 (19.7)	1.555	2.077	15.1 (5.4)
	B3LYP/6-311+G**	1.862	92.0	16.9 (16.9)	1.556	2.122	6.7 (–3.9)
	MP2/6-31G*	1.957	85.8	22.3 (23.2)	1.572	1.838	20.0 (10.8)
p-NO_2	HF/6-31G*	2.106	88.8	28.7 (27.7)	1.543	2.334	21.0 (8.8)
	B3LYP/6-31G*	2.155	82.7	29.4 (29.5)	1.554	2.188	26.8 (16.2)
	B3LYP/6-311+G**	1.994	88.2	27.0 (26.9)	1.554	2.225	18.2 (6.5)
	MP2/6-31G*	1.989	84.9	31.3 (31.5)	1.572	1.865	31.3 (30.0)

Note: *R* refers to the bond length in angstoms and θ is the bond angle at C_α-C_β-C_{Ph1} in degrees.
[a]Enthalpies (free energies) in kcal/mol.

Fig. 1. Structures of (A) the TS and (B) the product cation of the parent compound.



from the harmonic frequencies. Natural bond orbital (NBO) analysis was also carried out using the NBO program, Version 3.1 (24) available in the GAUSSIAN 98 suite. Bond orders were calculated according to the conventional Pauling bond order – bond length expression (eq. [2]),

$$[2] \qquad R = R^0 - 0.3 \ln n$$

where *R* and R^0 refer to bond lengths with bond order *n* and 1.0, respectively (25).

Results and discussion

Effect of various methods and basis sets

Figure 1 shows the structures of the TS and the product cation for the parent compound. Unlike the phenylethyl alcohols, whose reactions gave symmetrical phenonium ions irrespective of the substituent (17), the reactions of neophyl alcohols gave rearranged tertiary carbocations. It is interesting to see that the product cation exhibits a strong interaction between the aromatic ring and the carbocation center. Our calculations show that the structures of these cations depend very much on the substituents as well as the computational method. Table 2 lists the selected structural parameters for the TS and the cations together with the activation and reaction energies calculated at different levels of theory for the parent as well as the *p*-OMe and *p*-NO_2 substituted substrates. The HF calculations indicate a large variation in the interaction of the aromatic ring with the tertiary carbocation center of the product cation when the substituent is changed from an electron-donating *p*-OMe ($R_{C\beta\text{-}Ph1}$ = 1.641 Å) to an electron-withdrawing *p*-NO_2 group ($R_{C\beta\text{-}Ph1}$ = 2.334 Å). On the other hand, the MP2 calculations show the least variation in C_β—Ph1 bond length (1.712 Å for *p*-OMe and 1.865 Å for *p*-NO_2). The structures calculated with different basis sets at the B3LYP level are quite similar. The structures of the TS (Table 2) also depend on the method of calculation. The activation and reaction energies calculated at B3LYP/6-311+G** are lower; whereas MP2 calculations predict higher energies. Substituent effects on the enthalpies and free energies are found to be very similar at all the levels of calculations employed. We use the enthalpy values and the results obtained from MP2/6-31G* calculations to discuss the effect of substitutions throughout. B3LYP/6-311+G** results are used whenever a direct comparison is made with the corresponding phenylethyl alcohols, since only the B3LYP results are available for this system (17).

Structure of the TS and product cation

Table 3 presents selected geometrical parameters of the substituted product cations and the TSs, together with a selected natural population. The structural parameters ($R_{C\beta\text{-}Ph1}$ and θ′) and the charge on the aromatic ring (q_{Ar}) for the substituted product cations shown in Table 3 clearly indicates that a strong interaction exists between the aromatic ring and the tertiary carbocation center. The interaction becomes weaker when the substituent on the phenyl ring is changed from an electron-donating to an electron-withdrawing group as seen in the C_β—Ph1 bond distance and the bond angle (θ′). Substituents did not change the structure of neophyl alcohol and protonated neophyl alcohol much; whereas substantial changes are observed in the structures of the TSs. The variation in the C—O bond length and the C_α-C_β-C_{Ph1} bond angle (θ) of the TS with different substituents clearly

© 2005 NRC Canada

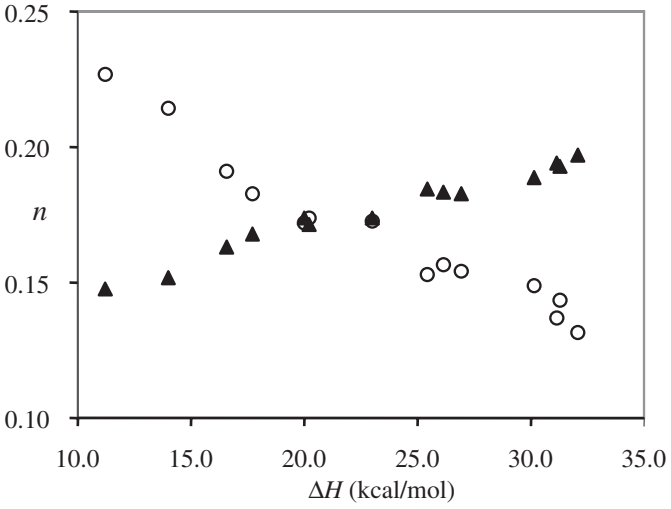
Table 3. Structural parameters of X-substituted product cations and TSs, together with selected natural population at reactants, TSs, and product cations calculated at the MP2/6-31G* level.

	TS			Product cation			q_{Ar}[a]			
X	$R_{C\text{-}O}$ ($n_{C\text{-}O}$)	$R_{C\alpha\text{-}Ph1}$ ($n_{C\alpha\text{-}Ph1}$)	θ	$R_{C\beta\text{-}Ph1}$	$R_{C\alpha\text{-}Ph1}$	θ′	Reactant	TS	Ion[b]	$\Delta q^{\ddagger}/\Delta q$[c]
p-OMe	1.875 (0.23)	2.099 (0.15)	88.4	1.712	1.571	69.1	0.080	0.172	0.500	0.22
p-OH	1.892 (0.21)	2.090 (0.15)	87.9	1.730	1.571	70.0	0.075	0.174	0.474	0.25
p-Me	1.927 (0.19)	2.069 (0.16)	86.7	1.805	1.571	73.6	0.074	0.180	0.401	0.32
m-Me	1.940 (0.18)	2.061 (0.17)	86.3	1.823	1.574	74.4	0.071	0.176	0.371	0.35
H	1.957 (0.17)	2.051 (0.17)	85.8	1.838	1.572	75.2	0.069	0.179	0.356	0.38
m-OH	1.954 (0.17)	2.055 (0.17)	86.0	1.826	1.572	74.6	0.066	0.170	0.357	0.36
p-Cl	1.955 (0.17)	2.050 (0.17)	85.8	1.815	1.569	74.1	0.063	0.174	0.372	0.36
m-Cl	1.991 (0.15)	2.033 (0.18)	84.8	1.870	1.570	76.8	0.058	0.175	0.316	0.45
p-CHO	1.984 (0.16)	2.034 (0.18)	84.9	1.858	1.571	76.2	0.058	0.172	0.322	0.43
m-CHO	1.989 (0.15)	2.035 (0.18)	84.9	1.870	1.569	76.8	0.061	0.181	0.326	0.45
p-CN	2.000 (0.15)	2.024 (0.19)	84.3	1.871	1.569	76.9	0.052	0.170	0.304	0.47
m-CN	2.023 (0.14)	2.017 (0.19)	83.9	1.910	1.568	78.8	0.052	0.177	0.280	0.55
m-NO_2	2.036 (0.13)	2.011 (0.20)	83.6	1.924	1.567	79.5	0.047	0.176	0.265	0.59
p-NO_2	2.009 (0.14)	2.018 (0.19)	84.0	1.865	1.572	76.5	0.047	0.160	0.287	0.47

Note: *R* refers to the bond length in angstoms, *n* is the Pauling bond order, and θ (C_α-C_β-C_{Ph1}) and θ′ (C_β-C_α-C_{Ph1}) are the bond angles in degrees.
[a]Group positive charge on the X-C_6H_4 moiety based on natural population analysis.
[b]Product cation.
[c]Change of the group positive charge between the reactant and the TS relative to that between the reactant and the phenonium ion.

indicated that the TS structure for a more electron-donating substituent is more reactantlike ($R_{C\text{-}O}$ = 1.88 Å and θ = 88° for *p*-OMe and $R_{C\text{-}O}$ = 2.01 Å and θ = 84° for *p*-NO_2). The group charge on the aromatic moiety (q_{Ar}) indicates a strong interaction between the aromatic ring and the cationic center in both the TSs and the product cations for all the substitutents. The charge becomes more positive in the reactant alcohol and in the product cation with a more electron-donating substituent, which is consistent with the nature of the substituent. In contrast, the group charge (q_{Ar}) is nearly constant for the TS. Here, an electron-donating substituent not only makes the aromatic moiety more positive but also shifts the TS more reactantlike, and the two effects are balanced in the charge distribution. The position of the TS along the reaction coordinate can be seen in the ratio of the change of the group charge on the aromatic ring on going from the reactant to the TS over the corresponding change between the reactant and the product cation ($\Delta q^{\ddagger}/\Delta q$); the ratio increases smoothly when the substituent becomes more electron-withdrawing. A clear picture of the TS variations can be seen in Fig. 2, where the C—O and C_α—C_{Ph1} bond orders were plotted against the reaction enthalpy. These results clearly indicate that the position of the TS indeed varies with the substituent and the variation is consistent with the Hammond postulate (26).

Fig. 2. Variation of the TS bond orders vs. the reaction enthalpy. Open circles refer to $n_{C\text{-}O}$ and closed triangles denote $n_{C\alpha\text{-}Ph1}$. Values are at the MP2/6-31G* level of theory.



Reaction energetics

Table 4 lists the activation and reaction enthalpies calculated for 14 different substituents at HF/6-31G*, B3LYP/6-31G*, MP2/6-31G*, and B3LYP/6-311+G** levels of theory. We used protonated water trimer as the proton source (YH^+ in eq. [1*a*]) for the initial protonation of alcohol, but the choice of the proton source does not affect the substituent effect. The effect of substitution is well-pronounced both in the activation and reaction enthalpies; a higher activation enthalpy leading to a more endothermic product for a more electron-withdrawing substituent is predicted at all levels. Correlation among the results at different methods gave excellent linear plots with slopes of nearly unity for both $\Delta H^{\ddagger}$ and ΔH. It is interesting to note that the plots of the relative equilibrium constants of substituted neophyl alcohols calculated at the B3LYP/6-311+G** level against those of substituted phenylethyl alcohols (17) (Fig. 3) gave a reasonably good straight line (R^2 = 0.989) with a slope of 0.66, even though the product in the equilibrium is the tertiary cation for the neophyl system; whereas it is the phenonium ion for the phenylethyl system. Owing to the stable nature of the tertiary carbocations, only a little or no interaction is generally assumed to exist between the phenyl group and the carbocation center in the cationic intermediates of neophyl alcohols and thus substituent effects on the cations are expected to be very small. However, our calculations clearly

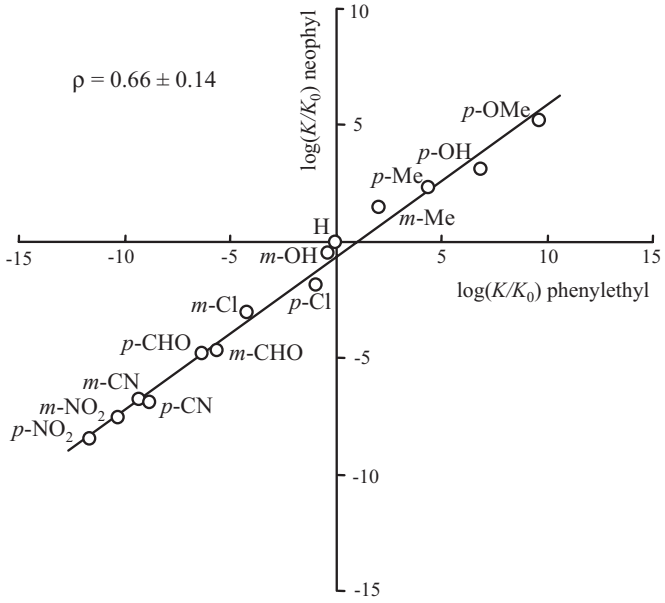
© 2005 NRC Canada

Table 4. Substituent effects on the activation and reaction enthalpies for rxn. [1].

Substituent	Activation enthalpy	Reaction enthalpy
p-OMe	14.8, *15.0* (18.5) [13.7]	2.5, *7.1* (11.2) [–0.5]
p-OH	16.1, *16.2* (20.0) [15.1]	5.5, *9.5* (14.0) [2.4]
p-Me	16.0, *16.8* (20.3) [14.9]	7.3, *11.9* (16.6) [3.5]
m-Me	16.7, *17.5* (20.9) [15.5]	8.2, *13.2* (17.7) [4.7]
H	17.7, *18.9* (22.3) [16.9]	9.4, *15.1* (20.0) [6.7]
m-OH	19.1, *19.3* (22.8) [17.5]	11.0, *15.3* (20.2) [7.3]
p-Cl	21.5, *22.0* (25.5) [19.5]	13.7, *18.1* (23.0) [9.3]
m-Cl	21.9, *23.2* (26.5) [20.3]	14.1, *19.9* (25.4) [10.8]
p-CHO	23.2, *24.9* (27.3) [22.7]	15.4, *21.7* (26.2) [13.2]
m-CHO	22.9, *24.6* (27.7) [22.5]	15.3, *21.5* (26.9) [13.1]
p-CN	26.6, *27.6* (30.4) [25.2]	19.1, *24.8* (30.1) [16.1]
m-CN	25.7, *27.4* (30.6) [24.9]	18.4, *24.8* (31.1) [16.0]
m-NO_2	26.5, *27.9* (31.1) [25.6]	19.4, *25.6* (32.1) [16.9]
p-NO_2	28.7, *29.4* (31.3) [27.0]	21.0, *26.8* (31.3) [18.2]

Note: Values are at the HF/6-31G*, *B3LYP/6-31G**, (MP2/6-31G*), and [B3LYP/6-311+G**] levels of theory and are in kcal/mol.

Fig. 3. log–log plot for the ionization constants of substituted neophyl alcohols against substituted phenylethyl alcohols.

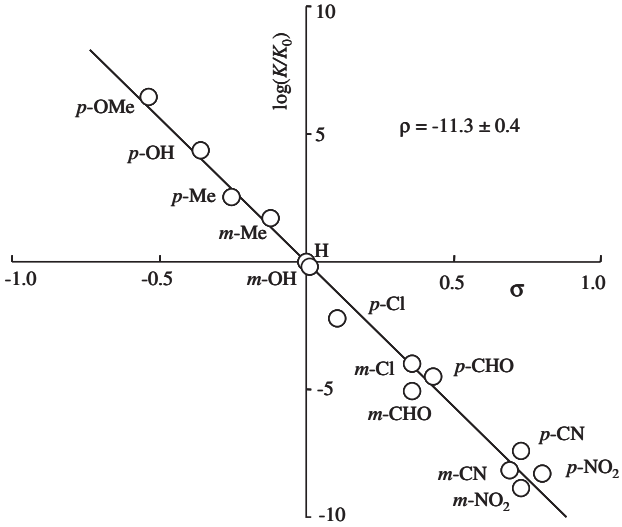


indicate that the substituent effect on the cations is quite significant because of the strong interaction between the tertiary carbocation center and the phenyl group, consistent with the structures of the cations as listed in Table 3.

Linear free energy relationship

The TSs of the present reactions are stabilized by the through-conjugation between the electron-donating substituents at the para position and the cationic reaction center. Substituent effects in such systems can be described by the well-known linear aromatic structure–reactivity relationship (LArSR, eq. [3]), often called the Yukawa–Tsuno equation, which is a multiparameter extension of the Hammett equation to quantify the role of enhanced resonance effects (27). In eq. [3], the term $\sigma^+ - \sigma^0$ measures the ability for π delocalization of π electron-donating substituents, and r^+ is a resonance-demand parameter characteristic of a given reaction.

Fig. 4. LArSR plot for the hydroxide transfer equilibrium of substituted neophyl alcohols and the corresponding product cations at 25 °C.



[3] $$\log(k/k_0) = \rho[\sigma^0 + r^+ (\sigma^+ - \sigma^0)]$$

The LArSR plots for the calculated acid-catalyzed ionization equilibrium of substituted neophyl alcohols are displayed in Fig. 4. We used the substituent constants (σ^0 and σ^+) derived from a series of gas-phase reactions (28). The figure shows that the LArSR treatment nicely correlates the substituent effect for the equilibrium process with a large ρ value of –11.3 at the MP2/6-31G* level (–9.9 at B3LYP/6-311+G**) and a r^+ value of 0.62. The exalted r^+ value and the large ρ value observed in the reactions of the substituted neophyl system were rationalized in terms of a direct π interaction between the aryl π system and the carbocation center at the transition state (5*b*). The ρ value obtained in the present case (9.9) is smaller than the ρ value obtained from our earlier calculations (17) on the phenylethyl alcohols (14.9 at B3LYP/6-311+G**), reflecting less positive charge developed on the aromatic ring of the neophyl product cations. On the other hand, the apparent r^+ value (0.62) is quite similar to that for the phenylethyl alcohol (r^+ = 0.65). This indicates that the relative importance of resonance to inductive stabilization by the substituents in the product tertiary cations is similar to that in the phenonium ions.

Figure 5 shows the LArSR plots for the ionization rate constants of substituted neophyl alcohols. The Hammett correlation gave a reasonably good straight line with r^+ = 0.27 and ρ = –8.9. We have previously reported the same r^+ value for the substituted phenylethyl alcohols (17). The similarity in these two reactions is most clearly illustrated in Fig. 6, which displays the log–log plots of the relative rate constants of substituted neophyl alcohols against those of substituted phenylethyl alcohols calculated at the B3LYP/6-311+G** level. The plots show an excellent linearity (R^2 = 0.999) with a slope of 0.89. The slope of less than unity was found, which indicates that the TS for the neophyl system is

© 2005 NRC Canada

Fig. 5. Substituent effects for the acid-catalyzed ionization of neophyl alcohol at 25 °C. Open circles represent $r^+ = 0.27$ and filled circles represent $r^+ = 0.62$.

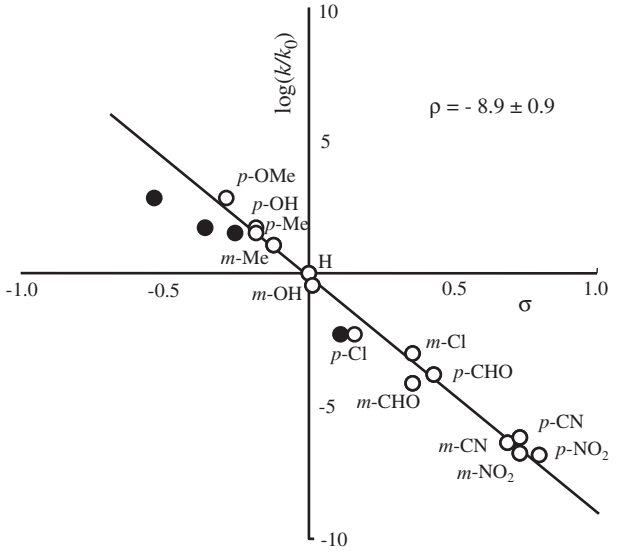
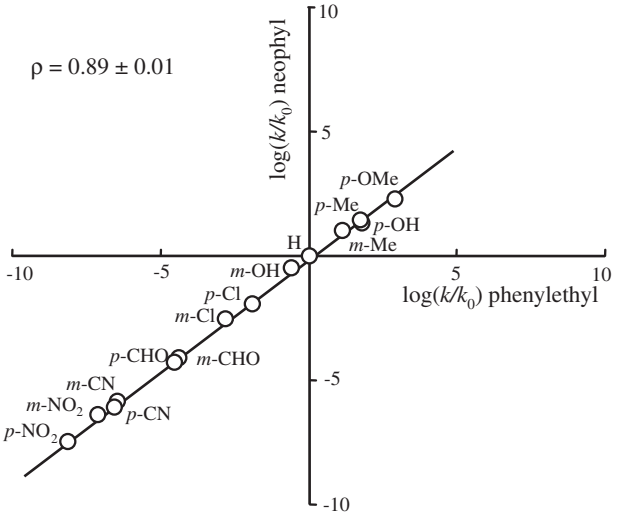


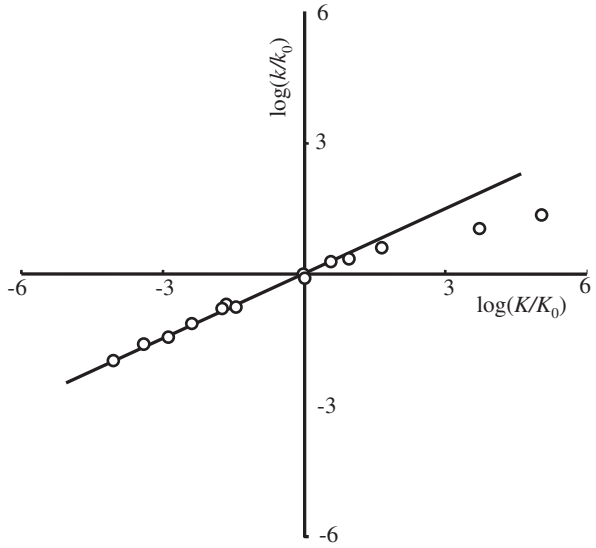
Fig. 6. log–log plot for the rate constants of substituted neophyl alcohols against substituted phenylethyl alcohols.



more reactantlike than the corresponding TS for the phenylethyl system for each substituent.

The Brønsted-type rate-equilibrium relation is applied to the elementary process of ionization of protonated neophyl alcohols to the product cations (eq. [1*c*]), and the substituent effects on the rate were plotted against those of the equilibrium in Fig. 7. A curved plot of the same type as that found for the phenylethyl alcohols (17) was obtained with a larger tangent slope for a reactant with a more electron-withdrawing substituent. The analysis of this curved Brønsted-type plot resulted in the formation of two distinct lines, each belonging to the least reactive compounds (*p*-NO_2, *m*-NO_2, *p*-CN, *m*-CN, *p*-CHO, *m*-Cl, and *m*-CHO) with a slope of 0.51 and the most reactive compounds (*p*-OMe, *p*-OH, *p*-Me, and *m*-Me) with a slope of 0.24. The biphase correlation arises from the variation of the TS structures with the substituents.

Fig. 7. Brønsted-type relation for the ionization of protonated neophyl alcohol to the product cation at 25 °C.



The following questions arise for the LFER treatments. First, why did the LArSR treatment on the rate process give linear plots, while the Brønsted-type plots gave a curved correlation? The linearity in the LArSR analysis was probably attained because the dual-parameter treatment masked a possible curvature of the plot. If the set of σ values obtained for the equilibrium (i.e., $r^+ = 0.62$) was used, a curved Hammett plot would be obtained, similar to that of the Brønsted-type plot in Fig. 7. Secondly, the LArSR treatment of the experimental kinetic data on the acetolysis of neophyl brosylates was reported to give a r^+ value of 0.58 (5*b*), a value closer to that calculated for the equilibrium (0.62). Then, why is the r^+ value for the gas-phase reaction (0.27) much smaller than that in solution? The reason is probably related to the large TS variations in the gas-phase reaction. Thus, the smaller r^+ value was obtained because the TS becomes more reactantlike, so the substituent effect becomes smaller for a strongly electron-donating substituent (*p*-OMe, *p*-OH). Such TS variation should in principle give curved Hammett plots, but as previously mentioned, the dual-parameter treatment in LArSR gave a straight line with a smaller r^+ value. Thus, caution should be paid when studying the reaction mechanism and its variation from LArSR analyses.

The different behavior in the LArSR analysis for the gas-phase and solution reactions probably arises from the larger TS variation with the substituent in the gas phase than in solution because of a large variation of the activation energy in the gas phase. The TS variation with the substituent in the solution phase could be minimized because of the multiple interaction mechanisms available in solution.

The fact that the Brønsted-type plot gave a curved correlation raises another point of interest. In the literature, curved or biphasic plots have often been taken as evidence for a shift of the rate-determining step in a multistep process. In other words, a single concerted mechanism has often been expected to give a straight-line correlation. However, the present study clearly indicated that such an argument may not be true in some cases and that a curved Brønsted plot can arise from variable TS.

© 2005 NRC Canada

Table 5. Kinetic isotope effects calculated at MP2/6-31G* for rxn. [1].

Labeled position	*p*-OMe	*p*-OH	*p*-Me	H	*p*-Cl	*p*-CHO	*p*-CN	*p*-NO_2
α-^{14}C	1.124	1.123	1.123	1.120	1.121	1.123	1.123	1.124
	1.041	*1.039*	*1.038*	*1.036*	*1.036*	*1.035*	*1.033*	*1.033*
α-D_2	1.011	1.015	1.027	1.035	1.034	1.055	1.062	1.061
	0.913	*0.911*	*0.909*	*0.909*	*0.907*	*0.906*	*0.905*	*0.904*
β-^{14}C	1.009	1.006	1.009	1.010	1.010	1.011	1.011	1.012
	1.004	*1.002*	*1.003*	*1.003*	*1.003*	*1.003*	*1.003*	*1.003*
Ph1-^{14}C	1.022	1.021	1.023	1.024	1.026	1.026	1.027	1.029
	1.006	*1.004*	*1.004*	*1.005*	*1.005*	*1.005*	*1.004*	*1.004*
γ-$^{14}C_2$	1.003	1.001	1.001	1.000	1.001	1.000	1.002	1.001
	1.003	*1.003*	*1.003*	*1.004*	*1.004*	*1.003*	*1.003*	*1.003*
γ-D_6	0.983	0.977	0.971	0.966	0.971	0.946	0.947	0.947
	1.036	*1.037*	*1.036*	*1.038*	*1.039*	*1.042*	*1.039*	*1.039*

Note: Numbers in italics are the EIEs for the protonation of alcohol (eq. [1*b*]).

Kinetic isotope effects and TS variation

Kinetic isotope effects have been used to provide experimental estimates of TS geometry and its variation. Table 5 presents the KIEs for the ionization reaction of substituted neophyl alcohols calculated from the isotopic shifts of vibrational frequencies at MP2/6-31G* after scaling with a factor of 0.94 (29) by using the Bigeleisen equation (30). Numbers shown in *italics* are the equilibrium IEs (EIEs) for protonation of the alcohols. The IEs were calculated at six different positions for the para-substituted compounds at 25 °C.

The protonation of the reactant alcohol induced a change in the reactant structure. For the parent compound, the protonation made the C_α—O bond longer (from 1.429 to 1.576 Å), the C_β—C_{Ph1} bond longer (from 1.526 to 1.533 Å), and the C_α-C_β-C_{Ph1} bond angle smaller (from 107.0° to 101.0°). The calculated EIE values are consistent with the structural variation; the carbon-14 EIE at the α position is larger than unity with larger values for the electron-donating substituents. The EIEs for the carbon isotopes at the β and γ positions were not significant. On the contrary, the α-D_2 EIEs became inverse because the protonation on the oxygen affects the strength and mode of frequencies related to α-D; the magnitude of a secondary deuterium IE is known to depend on the number of coordinates in which the deuterium atom is involved, and thus inverse deuterium IE on protonation arises (17, 31).

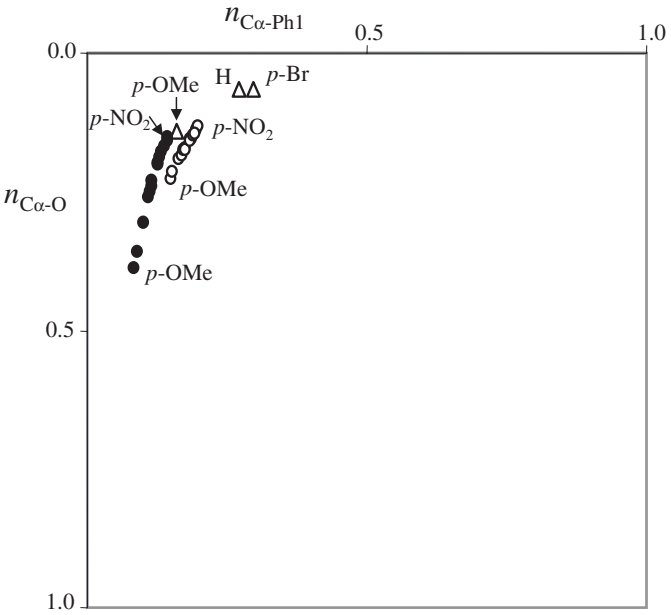
The KIEs were calculated with reference to the individual alcohols. They cannot be directly compared with the experimental data in solution, but the calculated trends may mirror the behavior in solution. The α-^{14}C, β-^{14}C, Ph1-^{14}C, and α-D_2 KIEs for neophyl brosylate were measured in AcOH at 75 °C as 1.093, 1.014, 1.023, and 1.214, respectively. In the acetolysis, *p*-methoxyneophyl tosylate gave a carbon-14 KIE at the α position of 1.117 at 50 °C, and the *p*-methoxyneophyl brosylate gave a Ph1 carbon-14 KIE of 1.006 at 40 °C (Table 1).

The calculated KIEs reasonably agree with the experimental values at all positions except for the α-D_2 KIEs. The variation of KIEs with the substituents at all positions should reflect the variation of the TS structures. The calculated α-^{14}C KIEs (1.120–1.124) are in the range of those reported for S_N2-type reactions (32), consistent with an S_N2-like, three-centered TS at the α-carbon. Since the magnitude of the KIE in this type of TS depends on the balance of the two reacting bonds ($C_\alpha\cdots C_{Ph1}$ and $C_\alpha\cdots OH_2$), large α-^{14}C KIEs suggest well-balanced TSs. A small variation of the α-^{14}C KIEs with the substituent is consistent with recent calculations, which showed that the magnitude of the α-C KIE changes little in such three-centered S_N2 TSs (33). The magnitude of the α-D_2 KIE is larger for an electron-withdrawing substituent, indicating that the total bonding at C_α is smaller at the TS (looser TS) because the change in the $C_\alpha\cdots O$ bond with the substituent is greater than the change in the $C_\alpha\cdots C_{Ph1}$ bond. When the phenyl group migrates from C_β to C_α, significant bonding change occurs at the β-carbon in the transition state, which should be reflected in the β-^{14}C KIE. The larger β-^{14}C KIE observed for the *p*-NO_2 substituent (1.012) indicates a later TS for the electron-withdrawing substituent. Although the isotope substitution at the γ-carbons gave almost null KIEs, distinct inverse deuterium KIEs were obtained at the γ position, which is consistent with the inductively electron-donating nature of deuterium. A more inverse γ-D_6 KIE for a more electron-withdrawing substituent is consistent with a more productlike TS for such a derivative. Finally, the Ph1-carbon-14 KIEs listed in Table 5 clearly indicate the change in the TS position along the reaction coordinate: a smaller Ph1-^{14}C KIE (1.022) for X = *p*-OMe and a larger value (1.029) for X = *p*-NO_2, reflecting a reactantlike TS for the electron-donating substituent.

The TS variation with the substituents can be displayed by the two-dimensional More O'Ferrall – Jencks diagram depicting the calculated C_α—O bond order against the C_α—C_{Ph1} bond order, as shown in Fig. 8. The lower left – upper right diagonal reflects the early late character of the transition structures, whereas the perpendicular diagonal represents variation from a loose (upper left corner) to a tight TS geometry (lower right corner). The diagram shows that in all cases the C_α—O bond cleavage goes ahead of the C_α—C_{Ph1} formation resulting in a carbocationic character developed at the α-carbon in the TS, and the sum of the two bond orders varies from 0.38 (*p*-OMe) to 0.33 (*p*-NO_2). The TS variation with substituent on the More O'Ferrall – Jencks diagram is fully consistent with the variation of the calculated KIEs.

© 2005 NRC Canada

Fig. 8. More O'Ferrall – Jencks diagram. Open triangles refer to the experimental values; open circles and filled circles correspond to the calculated values at MP2/6-31G* and B3LYP/6-311+G** levels, respectively.



The positions of the TSs for acetolyses of neophyl esters with three different substituents (*p*-OMe, H, and *p*-Br), which have previously been located based on the experimental KIEs and BEBOVIB calculations (19), are shown with triangles in Fig. 8. Comparison of the TS locations thus previously estimated and those calculated in the present study revealed that the results are in reasonable agreement with each other even though one is the TS position for the gas-phase reaction, and the other was estimated for reactions in solution. In particular, both methods predict loose TS structures regardless of substituent, and a more reactantlike TS for a more electron-donating substituent. This agreement suggests that the previously used method of combined experimental KIE measurements and BEBOVIB calculations is a useful method to estimate the TS location on the reaction coordinate.

Concluding remarks

The computational study on the ionization reaction of substituted neophyl alcohols revealed that substituents on the phenyl ring have marked effects on the reactivity and that the structure of the TS varies with substituent. The variations of activation and reaction enthalpies and of the TS structures with the substituent are consistent with the Leffler–Hammond postulate. The calculations gave a curved Brønsted-type plot, which arises from the variation of TS structure with the substituent. On the other hand, the Hammett correlation with a dual-parameter treatment (LArSR) gave reasonably good straight lines for both the rate and equilibrium of the gas-phase ionization process with different r^+ values (0.27 for the rate and 0.62 for the equilibrium process). The TS variation could not be detected by the Hammett plots because the dual-parameter treatment masked otherwise curved Hammett plots. The calculated KIE values are similar to the available experimental results and correlate very well with the TS structure variation with substituents. The position of the TSs on the More O'Ferrall – Jencks diagram obtained from the calculations supported the previous analysis based on the experimental KIEs and the BEBOVIB calculations.

Acknowledgements

The calculations were carried out in part at the Research Center for Computational Science, Okazaki National Research Institute. The study was supported by the Grant-in-Aid for Scientific Research from the Ministry of Education, Culture, Sports, Science and Technology, Japan and by the Rikkyo University Frontier project "Life's Adaptation Strategies to Environmental Changes".

References

1. C.J. Lancelot, D.J. Cram, and P.v.R. Schleyer. Carbonium ions. Wiley-Interscience, New York. 1972. Chap. 27.
2. S.G. Smith, A.H. Fainberg, and S. Winstein. J. Am. Chem. Soc. **83**, 618 (1961).
3. (*a*) D.D. Roberts. J. Org. Chem. **49**, 2521 (1984); (*b*) F.L. Schadt, T.W. Bentley, and P.v.R. Schleyer. J. Am. Chem. Soc. **98**, 7667 (1976); (*c*) M. Fujio, F. Sanematsu, Y. Tsuno, M. Sawada, and Y. Takai. Tetrahedron Lett. **29**, 93 (1988).
4. (*a*) S. Winstein and R. Heck. J. Am. Chem. Soc. **78**, 4801 (1956); (*b*) H. Tanida, T. Tsuji, H. Ishitobi, and T. Irie. J. Org. Chem. **34**, 1086 (1969); (*c*) V.J. Shiner, Jr. and R.C. Seib. J. Am. Chem. Soc. **98**, 862 (1976).
5. (*a*) M. Fujio, K. Funatsu, M. Goto, M. Mishima, and Y. Tsuno. Tetrahedron Lett. **43**, 307 (1987); (*b*) M. Fujio, M. Goto, M. Mishima, and Y. Tsuno. Bull. Chem. Soc. Jpn. **63**, 1121 (1990).
6. (*a*) J.E. Leffler and E. Grunwald. Rates and equilibria of organic reactions. Wiley, New York. 1963; (*b*) L.P. Hammett. Physical organic chemistry, reaction rates, equilibria, and mechanisms. 2nd ed. McGraw-Hill, New York. 1970; (*c*) J. Shorter. Correlation analysis on organic chemistry. Clarendon Press, Oxford. 1973; (*d*) C.R. Johnson. The Hammett equation. Cambridge University Press, New York. 1979.
7. (*a*) E.A. Castro, M. Cubillos, and J.G. Santos. J. Org. Chem. **59**, 3572 (1994); (*b*) E.A. Castro, M. Angel, P. Pavez, and J.G. Santos. J. Chem. Soc. Perkin Trans. 2, 2351 (2001); (*c*) E.A. Castro, M. Angel, D. Arellano, and J.G. Santos. J. Org. Chem. **66**, 6571 (2001); (*d*) E.A. Castro, M. Anduiar, P. Campodónico, and J.G. Santos. Int. J. Chem. Kinet. **34**, 309 (2002); (*e*) E.A. Castro, P. Pavez, and J.G. Santos. J. Org. Chem. **67**, 3129 (2002); (*f*) E.A. Castro, P. Pavez, and J.G. Santos. J. Org. Chem. **67**, 4494 (2002); (*g*) E.A. Castro, M. Angel, P. Campodónico, and J.G. Santos. J. Org. Chem. **67**, 8911 (2002).
8. A.S. Baynham, F. Hibbert, and M.A. Malana. J. Chem. Soc. Perkin Trans. 2, 1711 (1993).
9. (*a*) H.J. Koh, K.L. Han, and I. Lee. J. Org. Chem. **64**, 4783 (1999); (*b*) H.J. Koh, K.L. Han, H.W. Lee, and I. Lee. J. Org. Chem. **65**, 4706 (2000); (*c*) H.K. Oh, M.H. Ku, H.W. Lee, and I. Lee. J. Org. Chem. **67**, 3874 (2002).
10. E. Humeres, N.A. Debacher, M.M.D. Sierra, J.D. Franco, and A. Schutz. J. Org. Chem. **63**, 1598 (1998).
11. W.J. Spillane, P. McGrath, C. Brack, and A.B. O'Byrne. J. Org. Chem. **66**, 6313 (2001).
12. For cases where a nonlinear Brønsted plot was interpreted without invoking a shift of the rate-determining step of a step-

© 2005 NRC Canada

wise mechanism, see: (*a*) Y. Xu and P.E. Dietze. J. Am. Chem. Soc. **115**, 10722 (1993); (*b*) F. Terrier, G. Moutiers, L. Xiao, E. Lewguevel, and F. Guir. J. Org. Chem. **60**, 1748 (1995).
13. A. Pross. Adv. Phys. Org. Chem. **14**, 69 (1977).
14. (*a*) S. Hoz and M. Ban-Zion. J. Chem. Soc. Chem. Commun. 453 (1980); (*b*) F.G. Larkin, R.A. More O'Ferrall, and D.G. Murphy. Coll. Czech. Chem. Commun. **64**, 1833 (1999).
15. (*a*) C.G. Swain and W.P. Langsdorf, Jr. J. Am. Chem. Soc. **73**, 2813 (1951); (*b*) R.F. Hudson and G. Klopman. J. Chem. Soc. 1062 (1962); (*c*) P.R. Yang and W.P. Jencks. J. Am. Chem. Soc. **101**, 3288 (1979); (*d*) A.R. Stein, M. Tencer, E.A. Moffatt, R. Dawe, and J. Sweet. J. Org. Chem. **45**, 3540 (1980); (*e*) M. Fujio, M. Goto, T. Susuki, I. Akasaka, M. Mishima, and Y. Tsuno. Bull. Chem. Soc. Jpn. **63**, 1146 (1990).
16. (*a*) J.F. Bunnett, S. Sridharan, and W.P. Cavin. J. Org. Chem. **44**, 1463 (1979); (*b*) B.R. Cho, N.S. Kim, Y.K. Kim, and K.H. Son. J. Chem. Soc. Perkin Trans. 2, 1419 (2000).
17. S.C. Ammal, M. Mishima, and H. Yamataka. J. Org. Chem. **68**, 7772 (2003).
18. (*a*) A. Fry. Isotope effects in chemical reactions. *Edited by* C.J. Collins and N.S. Bowman. Van Nostrand Reinhold, New York. 1970. Chap. 6; (*b*) L. Melander and W.H. Saunders, Jr. Reaction rates of isotopic molecules. Wiley-Interscience, New York. 1980.
19. T. Ando, S.-G. Kim, K. Matsuda, H. Yamataka, Y. Yukawa, A. Fry, D. Lewis, L.B. Sims, and J.C. Wilson. J. Am. Chem. Soc. **103**, 3505 (1981).
20. (*a*) S. Schrøder and F. Jensen. J. Org. Chem. **62**, 253 (1997); (*b*) D.A. Singleton and M.J. Szymanski. J. Am. Chem. Soc. **121**, 9455 (1999); (*c*) M.P. Meyer, A.J. DelMonte, and D.A. Singleton. J. Am. Chem. Soc. **121**, 10865 (1999); (*d*) D.A. Singleton and C. Hang. J. Org. Chem. **65**, 895 (2000); (*e*) R.-r. Fang, Y. Gao, P. Ryberg, J. Eriksson, M. Kołodziejska-Huben, A. Dybała-Defratyka, S. Madhavan, R. Danielsson, P. Paneth, O. Matsson, and K.C. Westaway. Chem. Eur. J. **9**, 2696 (2003).
21. (*a*) H. Yamataka, S.-G. Kim, T. Ando, and Y. Yukawa. Tetrahedron Lett. 4767 (1973); (*b*) H. Tanida, T. Tsuji, H. Ishitobi, and T. Irie. J. Org. Chem. **34**, 1086 (1969); (*c*) Y. Yukawa, S.-G. Kim, and H. Yamataka. Tetrahedron Lett. 373 (1973); (*d*) V.J. Shiner, Jr. and C.R. Seib. J. Am. Chem. Soc. **98**, 862 (1976).
22. (*a*) R.A. More O'Ferrall. J. Chem. Soc. B, 274 (1970); (*b*) W.P. Jencks. Chem. Rev. **72**, 705 (1972); (*c*) W.P. Jencks. Acc. Chem. Res. **13**, 161 (1980).
23. M.J. Frisch, G.W. Trucks, H.B. Schlegel, G.E. Scuseria, M.A. Robb, J.R. Cheeseman, V.G. Zakrzewski, J.A. Montgomery, Jr., R.E. Stratmann, J.C. Burant, S. Dapprich, J.M. Millam, A.D. Daniels, K.N. Kudin, M.C. Strain, O. Farkas, V. Tomasi, M. Barone, R. Cossi, B. Cammi, C. Mennucci, C. Pomelli, S. Adamo, J. Clifford, J. Ochterski, G.A. Petersson, P.Y. Ayala, Q. Cui, K. Morokuma, D.K. Malick, A.D. Rabuck, K. Raghavachari, J.B. Foresman, J. Cioslowski, J.V. Ortiz, B.B. Stefanov, G. Liu, A. Liashenko, P. Piskorz, I. Komaromi, R. Gomperts, R.L. Martin, D.J. Fox, T. Keith, M.A. Al-Laham, C.Y. Peng, A. Nanayakkara, C. Gonzalez, M. Challacombe, P.M.W. Gill, B. Johnson, W. Chen, M.W. Wong, J.L. Andres, C. Gonzalez, M. Head-Gordon, E.S. Replogle, and J.A. Pople. GAUSSIAN 98. Revision A.6 [computer program]. Gaussian, Inc., Pittsburgh, Penn. 1998.
24. (*a*) A.E. Reed, R.B. Weinstock, and F. Weinhold. J. Chem. Phys. **83**, 735 (1985); (*b*) A.E. Reed, L.A. Curtiss, and F. Weinhold. Chem. Rev. **88**, 899 (1988); (*c*) E.D. Glendening, A.E. Reed, J.E. Carpenter, and F. Weinhold. NBO 3.1 [computer program]. University of Wisconsin, Madison, Wisconsin. 1990.
25. (*a*) L. Pauling. J. Am. Chem. Soc. **69**, 542 (1947); the coefficient of 0.30 in eq. [2] is a revised value (from 0.26) obtained by least-squares fit to data in ref. 25*b*; (*b*) L.E. Sutton (*Editor*). Tables of interatomic distances and configurations in molecules and ions. Special Publications Nos. 11 and 18. The Chemical Society (London), London. 1965 and 1958.
26. G.S. Hammond. J. Am. Chem. Soc. **89**, 2915 (1967).
27. (*a*) Y. Yukawa and Y. Tsuno. Bull. Chem. Soc. Jpn. **32**, 971 (1959); (*b*) Y. Yukawa, Y. Tsuno, and M. Sawada. Bull. Chem. Soc. Jpn. **39**, 2274 (1966); (*c*) Y. Tsuno and M. Fujio. Chem. Soc. Rev. **25**, 129 (1996); (*d*) Y. Tsuno and M. Fujio. Adv. Phys. Org. Chem. **32**, 267 (1999).
28. (*a*) M. Mishima, Mustanir, M. Fujio, and Y. Tsuno. Bull. Chem. Soc. Jpn. **69**, 2009 (1996); (*b*) C. Huh, C.H. Kang, H.W. Lee, H. Nakamura, M. Mishima, Y. Tsuno, and H. Yamataka. Bull. Chem. Soc. Jpn. **72**, 1083 (1999).
29. A.P. Scott and L. Radom. J. Phys. Chem. **100**, 16502 (1996).
30. (*a*) J. Bigeleisen and M.G. Mayer. J. Chem. Phys. **15**, 261 (1947); (*b*) J. Bigeleisen. J. Chem. Phys. **17**, 675 (1949).
31. W.E. Buddenbaum and V.J. Shiner, Jr. *In* Isotope effects on enzyme-catalyzed reactions. *Edited by* W.W. Cleland, M.H. O'Leary, and D.B. Northrop. University Park Press, Baltimore, Maryland. 1977. Chap. 1.
32. (*a*) M.L. Bender and D.F. Hoeg. J. Am. Chem. Soc. **79**, 5649 (1957); (*b*) G.J. Buist and M.L. Bender. J. Am. Chem. Soc. **80**, 4308 (1958).
33. O. Matsson, A. Dybala-Defratyka, M. Rostkowski, P. Paneth, and K.C. Westaway. J. Org. Chem. **70**, 4022 (2005).

© 2005 NRC Canada

A computational study of the 1,3-dipolar cycloaddition reaction mechanism for nitrilimines[1]

Robert C. Mawhinney, Heidi M. Muchall, and Gilles H. Peslherbe

Abstract: The [3+2] and [1+2] cycloaddition pathways between ethene and a series of 13 nitrilimines (R^1CNNR^2) have been examined by density functional theory [PBE0/6-311++G(2df,pd)] calculations. All reactions have low barriers ranging from 14.14 ($R^1 = CH_3$, $R^2 = H$) to 1.01 ($R^1 = R^2 = F$) kcal mol^{-1}, and large reaction exothermicities consistent with the transient nature of nitrilimines. The [3+2] and [1+2] transition-state structures are very similar, mainly differing in the relative orientation of their fragments and the newly forming C—C bond distance, and exhibit only minor deviations from the structures of the reactants. Both reaction pathways are concerted and asynchronous, but the [1+2] reaction has a greater degree of asynchronicity. Examination of the frontier molecular orbitals reveals that both the [3+2] and [1+2] barrier heights are related to two sets of orbital interactions, with the interaction between the lowest unoccupied molecular orbital π_5^{NN} of nitrilimine and the highest occupied molecular orbital of ethene in common. The second interaction in both cases is carbene-like. A relationship between the weights of the 1,3-dipolar resonance contribution in the various nitrilimines and the corresponding [3+2] barrier heights was not found, but a good correlation could be found between the [1+2] barrier heights and both the 1,3-dipolar and carbene contributions. Inspection of the potential energy surface in the vicinity of the two transition states for the reaction between unsubstituted nitrilimine and ethene suggests that the observed [3+2] product is a result of an initial carbene-like approach of the two fragments followed by a ridge bifurcation that leads to the [3+2] product minimum.

Key words: nitrilimines, 1,3-dipole, carbene, [3+2] cycloaddition, [1+2] cycloaddition, density functional theory (DFT).

Résumé : Les réactions de cycloaddition [3+2] et [1+2] entre l'éthène et une série de treize nitrilimines (R^1CNNR^2) ont été étudiées par calculs de théorie de la fonctionelle de densité [PBE0/6-311++G(2df,pd)]. Les réactions sont caratérisées par des barrières variant de 14,14 ($R^1 = CH_3$, $R^2 = H$) à 1,01 ($R^1 = R^2 = F$) kcal mol^{-1} et une forte exothermicité qui reflète la nature transitoire des nitrilimines. La structure des états de transition, très proche de celle des réactifs, est très semblable pour les réactions de cycloaddition [3+2] et [1+2] et ne diffère que par l'orientation relative des fragments et par la longueur de la liaison C—C qui se forme au cours de la réaction. Les deux chemins de réactions sont concertés et aynchrones, avec une asynchronicité plus prononcée pour la réaction [1+2]. Les orbitales moléculaires frontières démontrent que les barrières de réaction [3+2] et [1+2] sont reliées à deux groupes d'interactions orbitalaires qui ont en commun l'interaction entre la plus basse orbitale moléculaire inoccupée π_5^{NN} de la nitrilimine et la plus haute orbitale moléculaire occupée de l'éthène. La seconde interaction est de type carbène pour les deux réactions. Une corrélation entre la contribution de la forme de résonance 1,3-dipolaire des nitrilimines et les barrières de réaction [3+2] correspondantes n'a pu être trouvée. Par contre, une forte corrélation est observée entre les barrières de réaction [1+2] et les contributions 1,3-dipolaires et carbèniques. L'examen de la surface d'énergie potentielle à proximité des deux états de transition de la réaction entre la nitrilimine non-substituée et l'éthène suggère que le produit [3+2] résulte d'une approche initiale des deux fragments de type carbénique, suivie d'une bifurcation à la crête de la surface qui conduit au minimum d'énergie potentielle du produit [3+2].

Mots clés : nitrilimines, 1,3-dipolaire, carbène, cycloaddition [3+2], cycloaddition [1+2], théorie de la fonctionelle de densité.

Introduction

The addition of a 1,3-dipole, a system of three atoms over which four π electrons are distributed, to a dipolarophile, typically an alkene or alkyne, is the most commonly used synthetic method for forming five-membered heterocyclic molecules. The mechanism for these [3+2] reactions has been the subject of numerous articles and remains an open problem in physical organic chemistry (1–7). Originally, Huisgen (8–10) proposed a concerted, single-step mechanism with the two new bonds partially formed at the transition state, akin to that for the Diels–Alder cycloaddition. Shortly thereafter, an alternative two-step mechanism involving a biradical intermediate was presented by Firestone

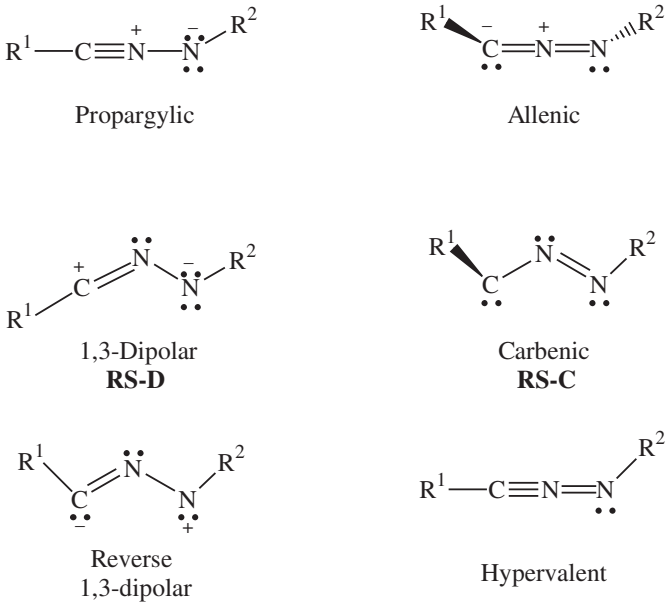
Received 23 June 2005. Published on the NRC Research Press Web site at http://canjchem.nrc.ca on 1 December 2005.

R.C. Mawhinney, H.M. Muchall,[2] and G.H. Peslherbe.[3] Centre for Research in Molecular Modeling and Department of Chemistry and Biochemistry, Concordia University, 7141 Sherbrooke Street West, Montreal, QC H4B 1R6, Canada.

[1]This article is part of a Special Issue dedicated to organic reaction mechanisms.
[2]Corresponding author (e-mail: muchall@alcor.concordia.ca).
[3]Corresponding author (e-mail: ghp@alcor.concordia.ca).

 doi: 10.1139/V05-179 © 2005 NRC Canada

Scheme 1.



(11–14). Since then, much work (1–7) has focused on distinguishing between the two mechanisms and, as Firestone originally alluded to (11), a duality of mechanism appears to exist. The majority of the initial explorations of Huisgen et al. (15–20) centered around the nitrilimine 1,3-dipole (R^1CNNR^2) for which the cycloaddition reactions are commonly believed to proceed via the concerted mechanism (7, 21, 22). Interestingly, no theoretical studies of an alternative pathway have been reported, even though this 1,3-dipole is at the heart of the original mechanism debate (9, 11, 23).

The nitrilimine 1,3-dipole is normally formed in situ as a transient, highly reactive species, which tends to dimerize, forming either dihydrotetrazines or bis(azo)ethenes, but in the presence of either electron-rich or electron-poor dipolarophiles, it readily undergoes [3+2] cycloadditions (24, 25). Stabilized nitrilimines also have been synthesized and they generally exhibit similar reactivity to their transient counterparts. Slight modifications of the substituents on the stabilized nitrilimine, though, have revealed that the philicity can be modified, with some nitrilimines acting strictly as nucleophiles and others as electrophiles (25, 26). A second important factor for the nitrilimine cycloaddition reactions is their regioselectivity, since the addition to unsymmetric dipolarophiles can result in two possible regioisomeric products. Nevertheless, nitrilimines appear to be highly selective with the newly formed bond to the carbon terminus typically with the less-substituted atom of the dipolarophile (24). Still, a recent study has revealed that changing the C-substituent of nitrilimine, from Br to H, results in an unexpected complete reversal in regioselectivity (27).

Employing resonance theory, Huisgen (28) explained the observed [3+2] reactivity in nitrilimines and related systems, and generalized the 1,3-dipole concept. For nitrilimines, several resonance structures have been invoked to explain their reactivity and electronic structure (Scheme 1) (28–31). In his original formulation, Huisgen (28) suggested that the electron sextet structures, the dipolar (**RS-D**) and carbenic (**RS-C**) forms, make only small contributions to the electronic structure of any 1,3-dipole owing to the lack of octet stabilization, but it was still this minor contribution that directed the course of reaction. In a recent study (32),[4] we evaluated the weights of various resonance contributions for a series of nitrilimines, using density functional methods combined with natural resonance theory (33–35), and found that the **RS-D** and **RS-C** structures were considerably more important than previously believed, and were even the dominant contributors in all systems studied. More interestingly, for some cases such as diaminonitrilimine ($R^1 = R^2 = NH_2$), **RS-C** was by far the primary resonance form.

The most fundamental of cycloadditions, a [1+2] reaction, occurs between carbenes and alkenes forming cyclopropanes (36, 37). Many carbenes are ambiphilic, reacting with both electron-rich and electron-poor alkenes, but varying the substituents can induce either electrophilic or nucleophilic behaviour exclusively (38). The mechanism for this fundamental reaction has been extensively studied (39–43), and theoretical studies suggest that the reaction between singlet carbenes and alkenes is a highly asynchronous yet concerted process, which was recently confirmed by kinetic isotope effect experiments (41). Given the significant carbene character contribution to the electronic structure in nitrilimines for certain substituents, it may be possible to observe [1+2] type reactivity.

In this paper we explore the [3+2] and [1+2] cycloaddition reaction pathways (Scheme 2) between ethene and nitrilimine, examining the effects of C-substitution, N-substitution, and symmetric C,N-disubstitution with CH_3, NH_2, OH, and F, and show that the [1+2] reaction path is an integral part of the early stages of the [3+2] mechanism. To the best of our knowledge, this is the first study of the [1+2] reaction in nitrilimines and the first attempt to examine systematically the effects of nitrilimine substituents on the [3+2] reaction.

Computational methods

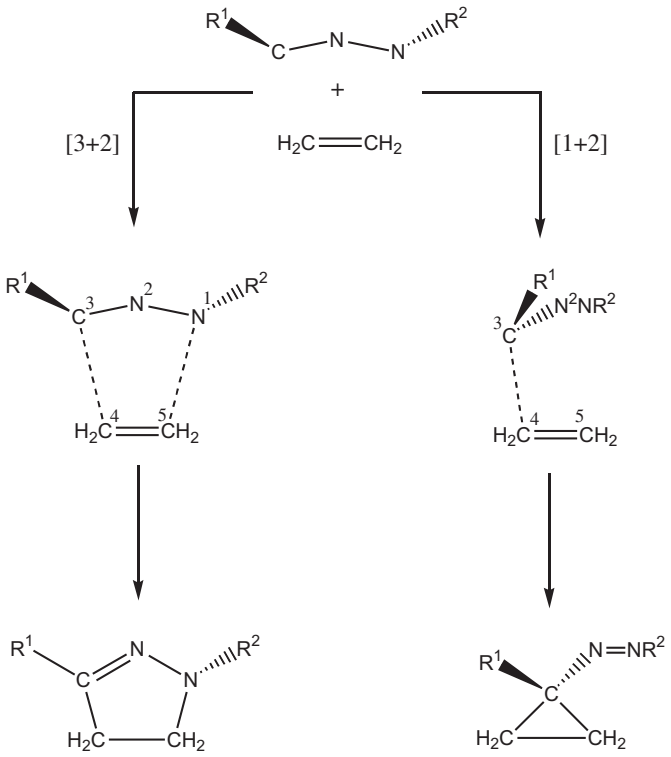
All calculations were carried out using the GAUSSIAN 98 suite of programs (44). The minima for all reactants and products, as well as transition-state (TS) stationary points, were obtained using the Perdew–Burke–Ernzerhof (PBE0) hybrid density functional (45–47) and a relatively large 6-311++G(2df,pd) basis set (48, 49). The nature of all stationary points was confirmed by vibrational analysis and the relative energies reported throughout include unscaled zero-point energy corrections. A stability analysis was performed on all stationary points to confirm that a lower energy broken-symmetry solution did not exist. Additionally, for reactions of the unsubstituted nitrilimine, biradical structures were explicitly searched for,[5] but in all calculations only closed shell structures could be obtained. Intrinsic reaction coordinate (IRC) calculations (50, 51), using mass-weighted

[4] R.C. Mawhinney, H.M. Muchall, and G.H. Peslherbe. To be submitted.

[5] Scans of the potential energy surface along the C5-C4-C3-N2 dihedral angle from 0° to 180°, in increments of 15°, and the C3—C4 distance from 2.7 to 2.0 Å, in increments of 0.1 Å, were performed using the unrestricted PBE0 level of theory and a mixed guess for the wave function to alleviate orbital symmetry.

© 2005 NRC Canada

Scheme 2.



Cartesian coordinates, were performed to confirm the relationship between TS structures and reactants and products.

Molecular geometries and energetics of cycloaddition reactions

Reactions of unsubstituted nitrilimine

Results for the [3+2] and [1+2] cycloaddition reactions between ethene and unsubstituted nitrilimine are collected in Table 1 and in the Supplemental material.[6] The results for the [3+2] reaction are in good agreement with a recent study at the B3LYP/6-31G(d) level of theory (7). The distances predicted by PBE0/6-311++G(2df,pd) are consistently smaller than the B3LYP values, by ca. 1% on average, but exhibit the same changes along the reaction coordinate. As expected, both methods predict a highly exothermic reaction and only a small barrier. With PBE0/6-311++G(2df,pd) the product is 5.1 kcal mol^{-1} more stable and the barrier is 0.38 kcal mol^{-1} lower than with B3LYP/6-31G(d).[7] In the earlier study, single point calculations at the CCSD(T)/6-311G(d,p) level, using B3LYP/6-31G(d) geometries, were also reported (7). Using the same approach with the PBE0/6-311++G(2df,pd) geometries, we find an even better agreement, with the above differences reduced to 0.3 and 0.06 kcal mol^{-1}, respectively. While there are no previous studies of the [1+2] cycloaddition reaction for comparison, the TS geometry involving the nitrilimine resembles those for the addition of dichlorocarbene and difluorocarbene to ethene (42) in that all cycloadditions are highly asynchronous.

The [3+2] reaction is kinetically favoured, with a reaction barrier that is ca. 4 kcal mol^{-1} smaller than that for the [1+2] reaction. The [1+2] and [3+2] TSs are remarkably similar with respect to geometrical changes from the reactants. The main differences are the C3—C4 distance (1.992 vs. 2.290 Å) and the C5-C4-C3-N2 dihedral angle (88.5° vs. –0.3°). The high asynchronicity of bond formation in the [1+2] TS is obvious, as both newly formed bonds have the same length in the product. Based on geometrical arguments, i.e., the ratio between the bond length in the product and the interatomic distance in the TS, bond formation is 76% complete for the C3—C4 and 60% complete for the C3—C5 bond at the TS. In the [3+2] TS structure, the C3—C4 distance is shorter than the N1—C5 distance, while the reverse is found in the product, demonstrating that the reaction is also significantly asynchronous, with the C3—C4 bond 66% formed and the N1—C5 bond 60% formed. While the N1—C5 bond in the [3+2] TS and the C3—C5 bond in the [1+2] TS are formed to the same extent, C3—C4 bond formation has proceeded further in the [1+2] TS, consistent with the Hammond postulate (52), where a later transition state is associated with a higher barrier and a less exothermic reaction (the relative energies for the two products (Δ^2-pyrazoline and azocyclopropane) are –60.5 and –35.5 kcal mol^{-1}, respectively).

Reactions of substituted nitrilimines

Naturally, all [3+2] products studied are more stable than their [1+2] counterparts and substitution increases the exothermicity of both reactions.[6] However, as observed for unsubstituted nitrilimine, both reaction paths have rather small barriers and fall under kinetic control (Table 1). To explore the effects of substitution, selected geometric parameters for the TS structures and relative barrier heights (E_a) for the two cycloaddition pathways are given in Table 1 for substituted nitrilimines. Three of the TSs for the [1+2] reaction path could not be located (see the following). Substitution does not dramatically affect the geometry of the CNN backbone from that observed in the parent nitrilimine (32)[4], consistent with an early TS. The C5-C4-C3-N2 dihedral angle in the [3+2] TSs is relatively unaffected, with only C-substitution by NH_2 causing any significant deviation from 0°, while in the [1+2] TSs it ranges from 95.6° ($R^1 = CH_3$, R^2 = H or CH_3) to 56.2° ($R^1 = R^2 = F$). The largest effect of substitution is on the newly forming C3—C4 bond, increasing the internuclear separation by as much as 0.245 Å in the [3+2] TSs and 0.252 Å in the [1+2] TSs. The increase in separation between the two fragments generally results in a smaller E_a. In the majority of cases, the [3+2] reaction remains kinetically favoured but, as also observed for the products,[6] substitution at N has a larger effect on the [1+2] reaction, lowering the E_a by as much as 8 kcal mol^{-1}. This results in two cases (R^1 = H, R^2 = OH and R^1 = H, R^2 = F) in which the [1+2] reaction is favoured and two cases (R^1 = H, $R^2 = NH_2$ and $R^1 = R^2 = F$), where the two barriers are within 1 kcal mol^{-1}.

[6] Supplementary data for this article are available on the Web site or may be purchased from the Depository of Unpublished Data, Document Delivery, CISTI, National Research Council Canada, Ottawa, ON K1A 0R6, Canada. DUD 4050. For more information on obtaining material refer to http://cisti-icist.nrc-cnrc.gc.ca/irm/unpub_e.shtml. Table S1 of the supplemental material contains selected product data.

[7] These differences are with respect to energies without zero-point energy corrections.

© 2005 NRC Canada

Table 1. Relative energies (kcal mol^{-1}), selected bond lengths (Å), and dihedral angles (°) of the transition states of [3+2] and [1+2] cycloaddition between ethene and substituted nitrilimines.

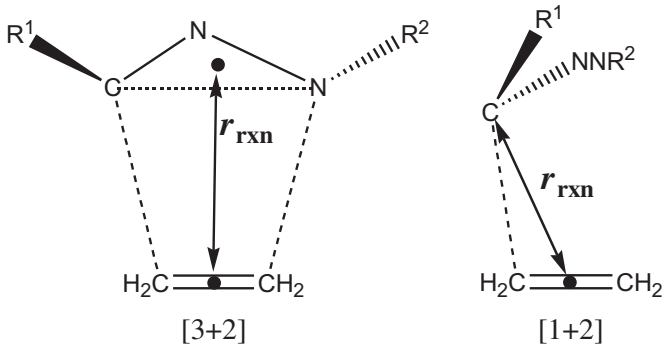
R^1	R^2	r_{C4-C5}	r_{C3-C4}	r_{C3-N2}	r_{N2-N1}	r_{N1-C5} or r_{C3-C5}	$\varphi_{C5-C4-C3-N2}$	E_a
[3+2] TS								
H	H	1.355	2.290	1.201	1.247	2.445	–0.3	8.40
CH_3	H	1.354	2.311	1.195	1.259	2.430	1.1	7.51
NH_2	H	1.349	2.345	1.234	1.261	2.449	5.3	4.47
OH	H	1.345	2.419	1.226	1.251	2.504	0.2	3.83
F	H	1.341	2.518	1.228	1.242	2.567	–2.1	2.30
H	CH_3	1.354	2.308	1.206	1.240	2.439	–1.0	8.12
H	NH_2	1.350	2.335	1.225	1.244	2.478	–0.3	7.00
H	OH	1.350	2.315	1.220	1.242	2.502	0.3	7.15
H	F	1.348	2.303	1.222	1.239	2.564	–0.1	6.26
CH_3	CH_3	1.352	2.336	1.199	1.250	2.436	0.4	6.94
NH_2	NH_2	1.351	2.273	1.280	1.255	2.456	7.7	4.73
OH	OH	1.348	2.322	1.268	1.237	2.502	1.8	4.23
F	F	1.338	2.456	1.282	1.217	2.690	–2.9	1.01
[1+2] TS								
H	H	1.356	1.992	1.225	1.246	2.516	88.2	12.54
CH_3	H	1.361	1.950	1.223	1.255	2.539	95.6	14.14
NH_2	H	Not obtained						
OH	H	1.354	2.031	1.252	1.253	2.606	71.4	9.32
F	H	1.348	2.115	1.244	1.245	2.652	68.4	5.72
H	CH_3	1.355	2.013	1.233	1.235	2.538	86.3	11.86
H	NH_2	1.347	2.129	1.247	1.229	2.605	83.7	7.70
H	OH	1.346	2.139	1.243	1.222	2.582	82.5	6.55
H	F	1.343	2.199	1.238	1.216	2.582	80.9	3.77
CH_3	CH_3	1.361	1.961	1.226	1.246	2.571	95.6	13.22
NH_2	NH_2	Not obtained						
OH	OH	Not obtained						
F	F	1.341	2.244	1.300	1.211	2.720	56.2	1.65

Note: Relative energies are with respect to reactants. Total energies are given in Table S2 of the Supplemental information.[6]

In all cases, the C3—C4 bond is formed to a larger extent than either the N1—C5 bond in the [3+2] TS or the C3—C5 bond in the [1+2] TS, demonstrating that both reactions remain asynchronous for substituted nitrilimines. The degree of asynchronicity, as measured by the difference in the extent of formation of the two new bonds, varies from 8% (R^1 = H, R^2 = F) to 2% (R^1 = F, R^2 = H) in the [3+2] TS and from 18% (R^1 = CH_3, R^2 = H or CH_3) to 10% (R^1 = H, R^2 = F) in the [1+2] TS. As expected, all [1+2] reactions are more asynchronous than their [3+2] analogs (41) and, like the reactions of the unsubstituted nitrilimine, the N1—C5 bond of the [3+2] TS and the C3—C5 bond of the [1+2] TS have virtually the same degree of formation, differing by no more than 2% with respect to one another. However, the extent of C3—C4 bond formation in the two TS structures is affected differently by substitution. In the majority of cases, the difference in % C3—C4 bond formation between the two TS structures is ca. 11%, but in four systems (R^1 = H, R^2 = NH_2; R^1 = H, R^2 = OH; R^1 = H, R^2 = F; and R^1 = R^2 = F) the difference is no more than 6%.

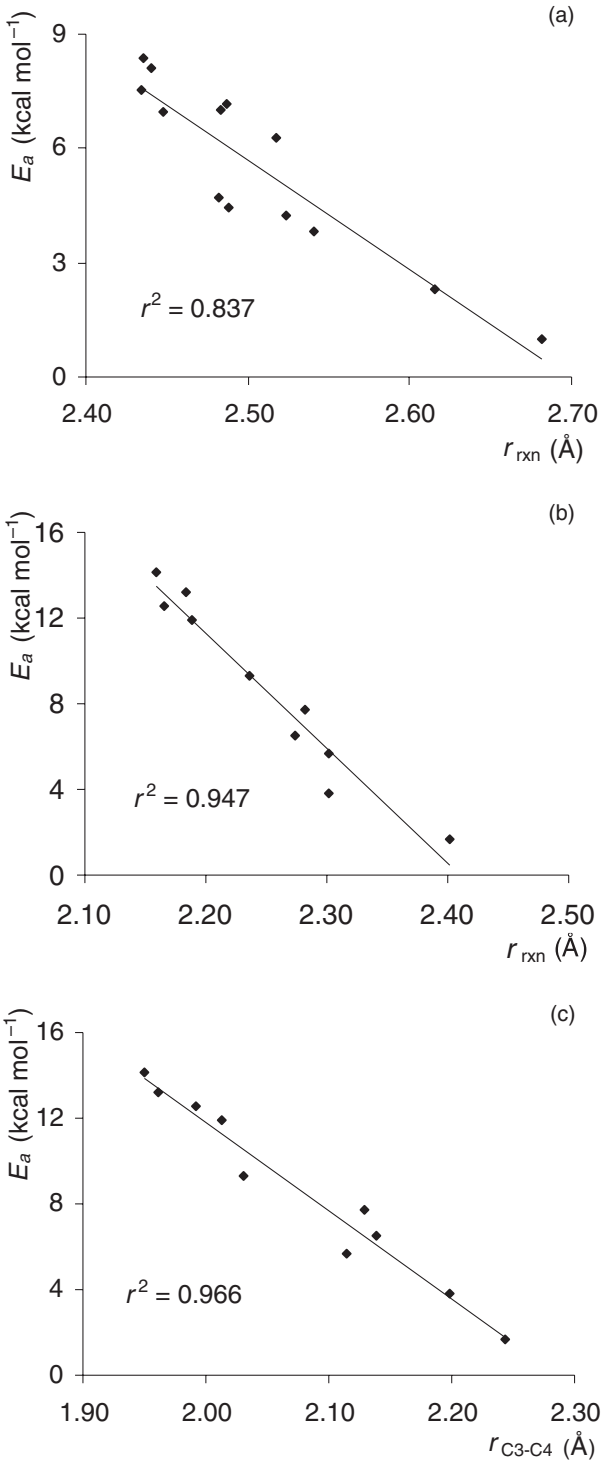
According to the Hammond postulate, the reaction rate should be related to the position of the transition state along the reaction coordinate (52). The reaction coordinate for carbene cycloadditions, as defined by Keating et al. (41), is the distance between the carbene carbon and the midpoint of the alkene double bond. Similarly, the reaction coordinate for the [3+2] cycloaddition reaction can be defined as the distance between the C3-N2-N1 incentre (the geometric midpoint of the C3-N2-N1 fragment) and the midpoint of the alkene bond. We will use these two approximate reaction coordinates, denoted r_{rxn} (Scheme 3), for the [3+2] and [1+2] reactions. The relationship between E_a and r_{rxn} for the various [3+2] and [1+2] reactions are shown in Fig. 1. For the [3+2] reaction, the linear correlation coefficient (r^2 = 0.837) suggests that r_{rxn} captures only part of the full reac-

Scheme 3.



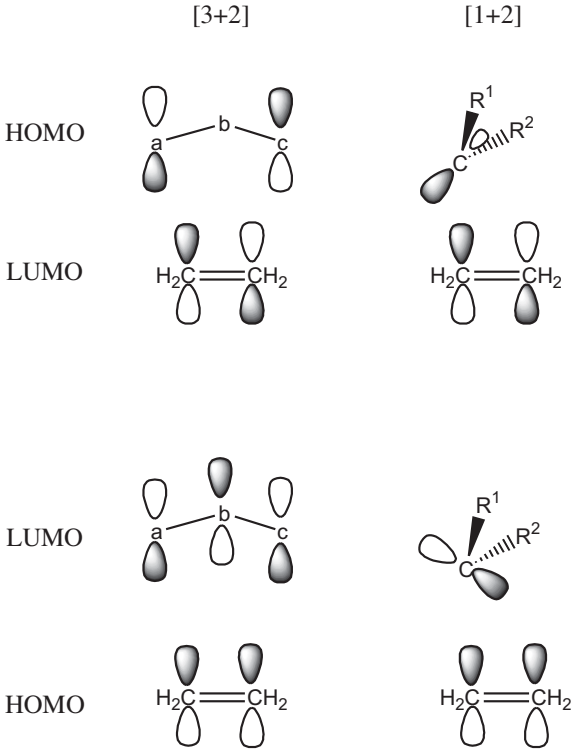
© 2005 NRC Canada

Fig. 1. The relationship between: (*a*) the [3+2] E_a and the corresponding r_{rxn} coordinate at the transition state; (*b*) the [1+2] E_a and the corresponding r_{rxn} coordinate at the transition state; and (*c*) the [1+2] E_a and the $r_{C3\text{-}C4}$ coordinate at the transition state. See Scheme 3 for the definitions of r_{rxn}.



tion coordinate, yet r_{rxn} is considerably more representative of the reaction than either $r_{N1\text{-}C5}$ or $r_{C3\text{-}C4}$, which correlate poorly with E_a (r^2 = 0.56 and 0.60, respectively). For the [1+2] reaction, the correlation coefficient (r^2 = 0.947) indicates that r_{rxn} captures the majority of the features of the full reaction coordinate. However, the correlation between E_a and $r_{C3\text{-}C4}$ is even better (r^2 = 0.966, Fig. 1*c*), suggesting that the [1+2] reaction is fully controlled by the approach of the nitrilimine carbon to only one ethene carbon atom.

Scheme 4.



Properties governing nitrilimine reactivity

According to the Hammond postulate (52), the low barrier heights and large reaction exothermicities indicate that both reactions are characterized by early transition states. This suggests that variations in reactivity largely depend on the properties of the reactants. Accordingly, in this section we examine the relationship between the properties of nitrilimines and their reactivity.

Frontier molecular orbitals

Frontier molecular orbital theory (FMO) has been extensively used to explain reactivity and regioselectivity in both [3+2] 1,3-dipolar (53, 54) and [1+2] carbene (55) cycloaddition reactions. Simplified representations of the important molecular orbital interactions between the HOMO (highest occupied molecular orbital) and LUMO (lowest unoccupied molecular orbital) of ethene and either a dipole (a-b-c) or a carbene (R^1-C-R^2) are given in Scheme 4. As noted in previous studies, the major effect of substitution is a change in orbital energy, while the orbital shapes retain the same qualitative features (54, 56). To identify the proper orbitals of nitrilimine involved in the two reactions, the four highest occupied and two lowest unoccupied Kohn–Sham orbitals of unsubstituted nitrilimine are shown in Fig. 2. All have pseudo-π symmetry (there is no strict σ–π separation in the C_1 symmetrical molecules) and can be characterized as either π^{CN} or π^{NN}. According to Scheme 4, the nitrilimine

© 2005 NRC Canada

orbitals involved in the [3+2] interactions are π_4^{NN} and π_5^{NN}, and those for the [1+2] interactions are π_4^{NN} and π_6^{CN}. Unlike carbenes, which are restricted to one occupied sp^2 orbital and one unoccupied p orbital on carbon, nitrilimines have two additional molecular orbitals (π_3^{CN} and π_5^{NN}) with the correct orientation for the [1+2] cycloaddition reaction. Therefore, π_5^{NN} may interact as LUMO and π_3^{CN} as HOMO with the corresponding ethene orbitals in a [1+2] fashion. These additional interactions, along with the typical [1+2] and [3+2] interactions for the addition of nitrilimine to ethene, are displayed in Scheme 5.

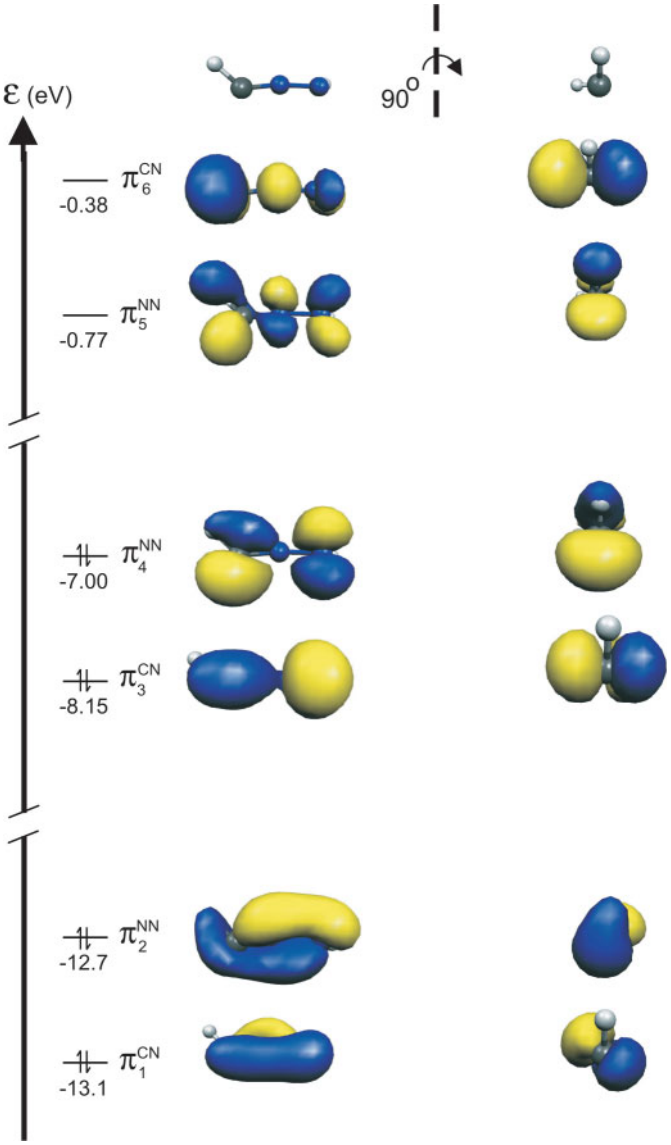
Both nitrilimines and carbenes are generally described as ambiphilic, reacting with both electron-rich and electron-poor alkenes, but varying substituents can induce either exclusive electrophilic or nucleophilic behaviour (24, 25, 37, 38). In FMO terms, electrophilic behaviour is attributed to systems where the $HOMO_{dipolarophile} - LUMO_{dipole}$ energy difference is smaller, nucleophilic behaviour to systems where the $HOMO_{dipole} - LUMO_{dipolarophile}$ energy difference is smaller, and ambiphilic behaviour corresponds to situations in which both energy differences are similar (53, 54). The energy differences associated with the four main orbital interactions (**A**–**D**, Scheme 5) between ethene and the various nitrilimines are given in Table 2. In the majority of cases, the smallest energy difference is $\Delta E_{\mathbf{B}}$, but in four systems (R^1 = OH, R^2 = H; R^1 = F, R^2 = H; R^1 = R^2 = OH; and R^1 = R^2 = F) $\Delta E_{\mathbf{C}}$ is lower, and only in one (R^1 = H, R^2 = F), $\Delta E_{\mathbf{D}}$ is the smallest. Despite the swap in the character of the lowest energy orbital interaction, the next lowest orbital energy difference is generally within ca. 1 eV and corresponds to an interaction of opposite character, consistent with the known ambiphilic reactivity of most nitrilimines (24). Exceptions where the two lowest energy interactions exhibit the same character appear for *N*-fluoro substituted nitrilimines (R^1 = H or F, R^2 = F).

The relative energy of a transition state for a reaction with a small barrier and large reaction exothermicity can be predicted from the relative energy of a weakly interacting complex. The original derivation of the equation for this interaction energy was given by Salem and contained three terms, representing closed shell interactions, coulombic interactions, and orbital overlap (57–59). In many implementations, though, the first two terms are commonly neglected and the relative energy of the complex is predicted from the orbital overlap alone (53, 54). The orbital interaction terms for a general [3+2] and [1+2] reaction with ethene (Scheme 4) are given in eqs. [1] and [2], respectively,

$$[1]\qquad \Delta E = \frac{[C_{HOMO(C4)}C_{LUMO(a)} + C_{HOMO(C5)}C_{LUMO(c)}]^2\ \beta^2}{\varepsilon_{HOMO(Ethene)} - \varepsilon_{LUMO(Dipole)}} + \frac{[C_{HOMO(a)}C_{LUMO(C4)} + C_{HOMO(c)}C_{LUMO(C5)}]^2\ \beta^2}{\varepsilon_{HOMO(Dipole)} - \varepsilon_{LUMO(Ethene)}}$$

$$[2]\qquad \Delta E = \frac{[C_{HOMO(C4)}C_{LUMO(C)} + C_{HOMO(C5)}C_{LUMO(C)}]^2\ \beta^2}{\varepsilon_{HOMO(Ethene)} - \varepsilon_{LUMO(Carbene)}} + \frac{[C_{HOMO(C)}C_{LUMO(C4)} + C_{HOMO(C)}C_{LUMO(C5)}]^2\ \beta^2}{\varepsilon_{HOMO(Carbene)} - \varepsilon_{LUMO(Ethene)}}$$

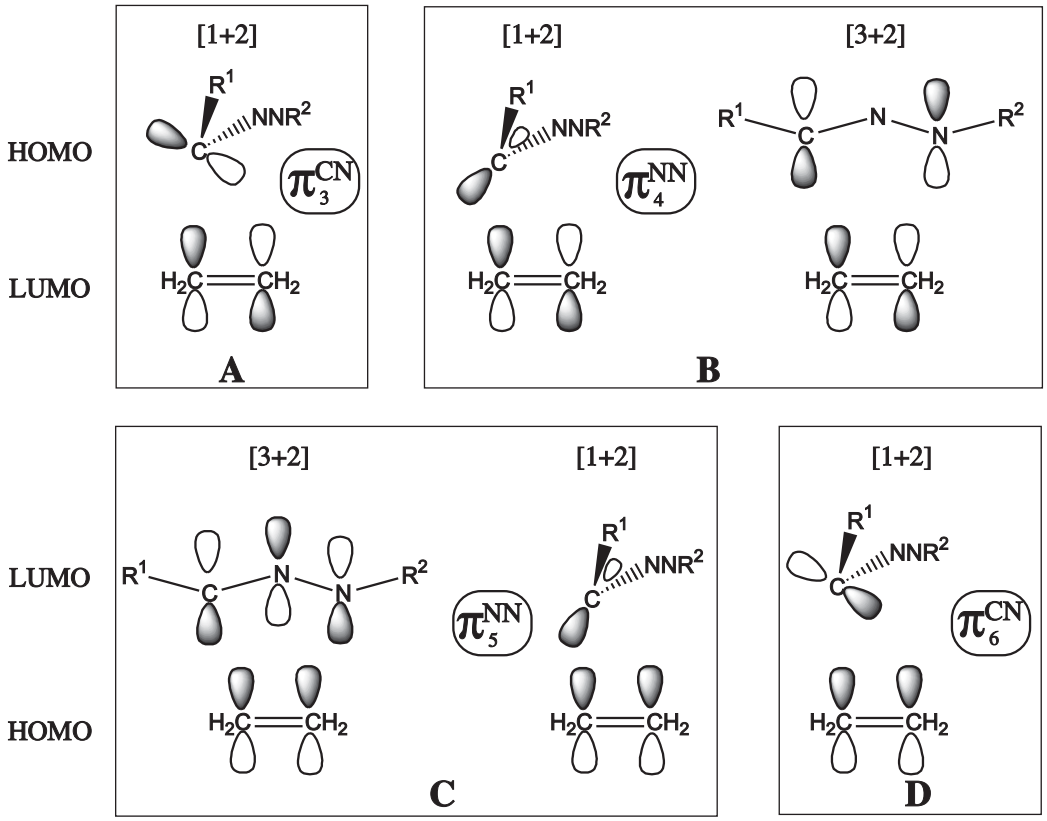
Fig. 2. Two representations of the six π-type molecular orbitals (0.05 au isosurface) of unsubstituted nitrilimine along with orbital energies.



where the denominator is the energy difference between the FMOs involved in the interaction and the numerator contains products of the atomic orbital coefficients at the centres where the two bonds are formed, and the resonance integral (β) is a measure of the interaction strength. These equations can readily be expanded to include additional orbital interactions. Since the ethene orbitals are the same throughout and the shapes of the nitrilimine orbitals are qualitatively similar (32), one may assume that the atomic orbital coefficients are relatively constant, and their products may be approximated by a general factor (*K*). Additionally, the distance between the interacting centres is moderately invariant (Table 1), and so β may also be considered constant. A similar approach has been used to explain the effects of substitution on the reactivity of phenylazide (54). Applying these approximations results in simplified eqs. [3] and [4] for the [3+2] and [1+2] interaction energies, respectively.

© 2005 NRC Canada

Scheme 5.



$$[3] \qquad \Delta E^{[3+2]} = K\beta^2\left[\frac{1}{\varepsilon_{\mathrm{HOMO(Ethene)}} - \varepsilon_{\mathrm{LUMO(Dipole)}}} + \frac{1}{\varepsilon_{\mathrm{HOMO(Dipole)}} - \varepsilon_{\mathrm{LUMO(Ethene)}}}\right]$$

$$[4] \qquad \Delta E^{[1+2]} = K\beta^2\left[\frac{1}{\varepsilon_{\mathrm{HOMO(Ethene)}} - \varepsilon_{\mathrm{LUMO(Carbene)}}} + \frac{1}{\varepsilon_{\mathrm{HOMO(Carbene)}} - \varepsilon_{\mathrm{LUMO(Ethene)}}}\right]$$

Following a systematic examination of the relationship between the barrier heights for both reaction types and all possible combinations of orbital interactions (Scheme 5), we present the best correlations in Figs. 3*a* and 3*b*. Naturally, for the [3+2] reaction, the barrier heights correlate with $1/\Delta E_{\mathbf{B}} + 1/\Delta E_{\mathbf{C}}$ ($r^2 = 0.728$). While a somewhat better correlation ($r^2 = 0.790$) is achieved for $1/\Delta E_{\mathbf{C}}$ alone, suggesting that π_5^{NN} plays a key role in [3+2] reactivity, the best correlation ($r^2 = 0.797$) involves $1/\Delta E_{\mathbf{C}}$ in conjunction with $1/\Delta E_{\mathbf{A}}$, formally a [1+2] orbital interaction (Fig. 3*a*, eq. [5]). The best correlation ($r^2 = 0.794$) for the [1+2] reaction barrier is for $1/\Delta E_{\mathbf{C}} + 1/\Delta E_{\mathbf{D}}$, both of which involve an unoccupied orbital of nitrilimine interacting with the HOMO of ethene (Fig. 3*b*, eq. [6]). As the relationships in eqs. [5] and [6] are linear, the differences in barrier heights (ΔE_a) between the [1+2] E_a and the [3+2] E_a can be approximated by eq. [7] for which results are plotted in Fig. 3*c*. Since the assumption of a constant numerator can not be expected to hold in the combined relationship, the correlation is slightly worse ($r^2 = 0.740$) than those for the individual relationships. None of the other potential combinations of individual relationships results in a reasonable correlation.

$$[5] \qquad E_a^{[3+2]} = m\left[\frac{1}{\varepsilon_{\mathrm{HOMO(Ethene)}} - \varepsilon_{\mathrm{LUMO}(\pi_5^{\mathrm{NN}})}} + \frac{1}{\varepsilon_{\mathrm{HOMO}(\pi_3^{\mathrm{CN}})} - \varepsilon_{\mathrm{LUMO(Ethene)}}}\right] + b$$

$$[6] \qquad E_a^{[1+2]} = m\left[\frac{1}{\varepsilon_{\mathrm{HOMO(Ethene)}} - \varepsilon_{\mathrm{LUMO}(\pi_5^{\mathrm{NN}})}} + \frac{1}{\varepsilon_{\mathrm{HOMO(Ethene)}} - \varepsilon_{\mathrm{LUMO}(\pi_6^{\mathrm{CN}})}}\right] + b$$

$$[7] \qquad \Delta E_a \approx \left[\frac{1}{\varepsilon_{\mathrm{HOMO(Ethene)}} - \varepsilon_{\mathrm{LUMO}(\pi_6^{\mathrm{NN}})}} + \frac{1}{\varepsilon_{\mathrm{HOMO}(\pi_3^{\mathrm{CN}})} - \varepsilon_{\mathrm{LUMO(Ethene)}}}\right] + b$$

© 2005 NRC Canada

Table 2. Interaction energies (ΔE, eV) between the "frontier" molecular orbitals of nitrilimine and ethene (lowest interaction energies are in boldface type).

R^1	R^2	ΔE_A[a]	ΔE_B[a]	ΔE_C[a]	ΔE_D[a]
H	H	–8.14	**–6.99**	–7.16	–7.55
CH_3	H	–7.56	**–6.24**	–7.44	–8.17
NH_2	H	–6.69	**–6.55**	–6.94	–9.02
OH	H	–7.43	–6.92	**–6.28**	–8.62
F	H	–8.29	–7.58	**–5.46**	–7.68
H	CH_3	–7.77	**–6.68**	–7.22	–7.67
H	NH_2	–8.36	**–6.20**	–7.21	–7.90
H	OH	–8.87	**–6.71**	–7.08	–6.75
H	F	–9.91	–7.64	–6.46	**–5.81**
CH_3	CH_3	–7.30	**–6.02**	–7.38	–8.07
NH_2	NH_2	–7.06	**–5.83**	–6.91	–7.91
OH	OH	–8.08	–6.74	**–6.32**	–7.50
F	F	–9.99	–8.33	**–4.90**	–5.85

Note: Ethene PBE0/6-311++G(2df,pd) orbital energies: –7.93 eV (HOMO) and –0.01 eV (LUMO).

[a] $\Delta E_A = \varepsilon_{[\pi_3^{CN}]_{nitrilimine}} - \varepsilon_{LUMO_{ethene}}$, $\Delta E_B = \varepsilon_{[\pi_4^{NN}]_{nitrilimine}} - \varepsilon_{LUMO_{ethene}}$; $\Delta E_C = \varepsilon_{HOMO_{ethene}} - \varepsilon_{[\pi_5^{NN}]_{nitrilimine}}$, $\Delta E_D = \varepsilon_{HOMO_{ethene}} - \varepsilon_{[\pi_6^{NN}]_{nitrilimine}}$ (see Scheme 5).

Resonance contributions

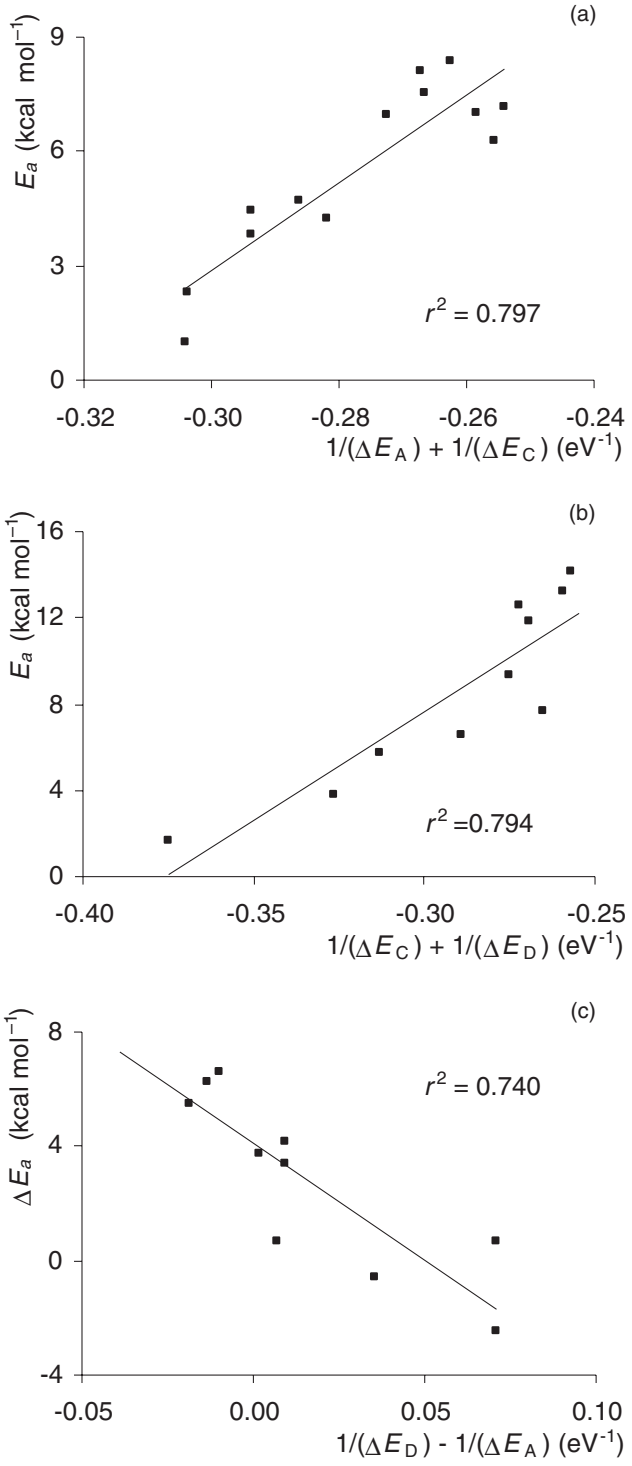
Huisgen (28) recognized early that any molecule that can be ascribed a 1,3-dipolar resonance structure could undergo a [3+2] reaction. Recently, we assessed the weights of the individual resonance contributions of nitrilimine and found that the 1,3-dipolar **RS-D** and the carbenic **RS-C** structures (Scheme 1) are the dominant contributors, consistent with the reactivity previously noted (32)[4].

Relationships between the 1,3-dipolar resonance contribution and the [3+2] E_a, and between the carbene resonance contributions and the [1+2] E_a, are given in Fig. 4 for the various nitrilimines. As expected, the carbene character of the different nitrilimines is well-correlated ($r^2 = 0.987$)[8] with the [1+2] barrier heights (Fig. 4*a*). On the other hand, there is no relationship ($r^2 = 0.319$) between the various [3+2] barrier heights and the 1,3-dipolar contribution (Fig. 4*b*), and even the slope of the trend line is opposite to that expected, suggesting that the 1,3-dipolar resonance structure is not a factor in the observed nitrilimine [3+2] reactivity. Interestingly, contributions from the 1,3-dipolar resonance form (**RS-D**) show a good correlation ($r^2 = 0.935$)[8] with the nitrilimine [1+2] barrier height (Fig. 4*c*), with the slope of the trend line opposite to that for the **RS-C** relationship, implying that an increase in 1,3-dipolar character disfavours the [1+2] pathway.

The nitrilimine cycloaddition mechanism

Considerable uncertainty still surrounds the 1,3-dipolar cycloaddition mechanism (1–4, 6). Two mechanisms have been proposed: (*i*) a concerted, single-step process with the two new bonds partially formed at the transition state (8–10, 60); and (*ii*) a two-step process with initial biradical formation followed by bond rotation and ring closure (11–13). The

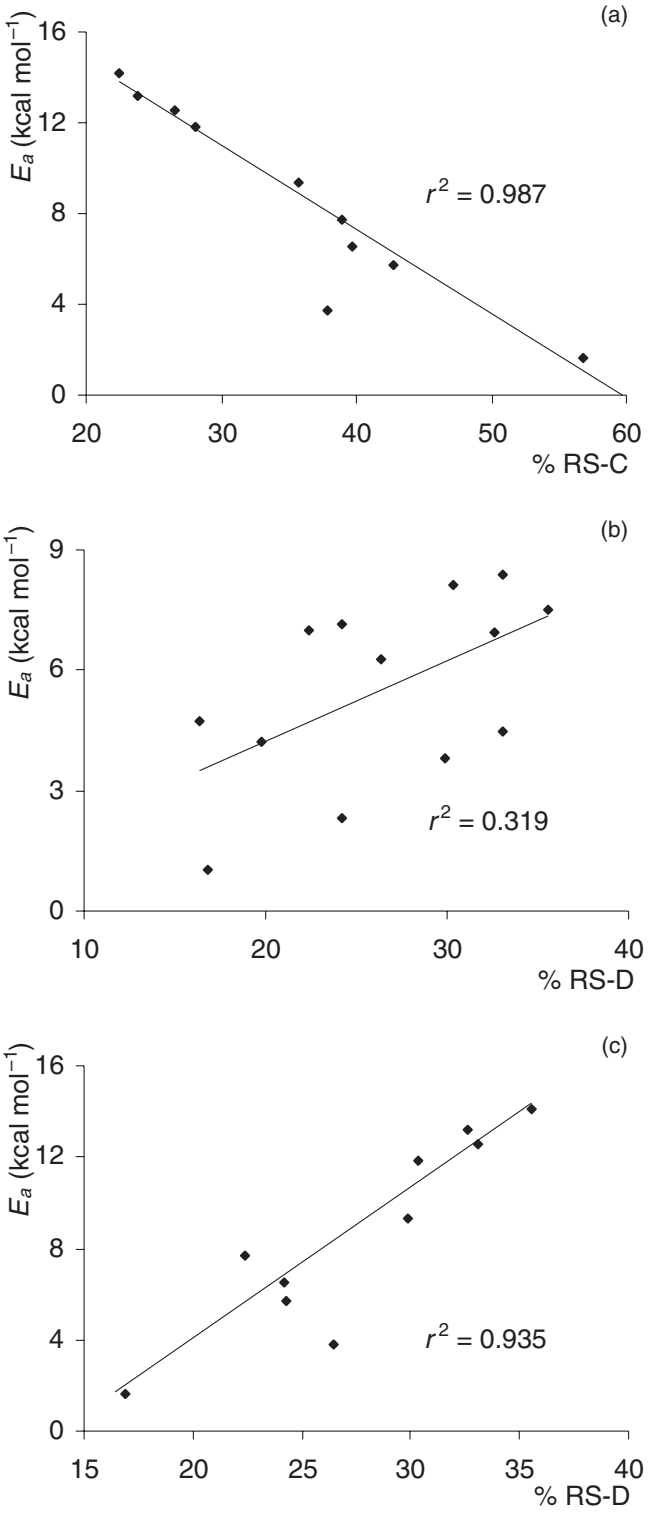
Fig. 3. The relationship between orbital interaction energy and reactivity: (*a*) the [3+2] E_a and the sum of the inverse of the **A** and **C** orbital interaction energies; (*b*) the [1+2] E_a and the sum of the inverse of the **C** and **D** orbital interaction energies; and (*c*) the difference in [1+2] and [3+2] E_a and the difference in the inverse of the **A** and **D** orbital interaction energies. Orbital interactions **A**, **C**, and **D** are defined in Scheme 5.



[8] These correlation coefficients do not include the outlying point, corresponding to *N*-fluoro substituted nitrilimine, which is believed to be a result of an anisotropic effect noted in the ^{13}C chemical shielding tensor (see footnote 10).

© 2005 NRC Canada

Fig. 4. The relationship between reactivity and % resonance contribution from natural resonance theory for: (*a*) the [1+2] E_a and the carbenic resonance (**RS-C**) contribution;[8] (*b*) the [3+2] E_a and the dipolar resonance (**RS-D**) contribution; and (*c*) the [1+2] E_a and the dipolar resonance (**RS-D**) contribution.[8] Resonance structures **RS-C** and **RS-D** are depicted in Scheme 1.



majority of 1,3-dipolar cycloaddition reactions are believed to proceed via a concerted mechanism (23), although there are now several reports of reactions with a biradical mechanism (1, 61–65).

For the nitrilimine [3+2] reaction, neither mechanism can be readily adopted. As previously mentioned, all calculated TS structures were stable with respect to a broken-symmetry solution to the wave function and no biradical TS could be located. Therefore, a biradical mechanism must be ruled out. From electronic structure considerations, we noted that [3+2] reactivity was not related to the changes in contributions from the 1,3-dipolar resonance structure, **RS-D** (Scheme 1), but was partially controlled by FMO interaction **A** (Scheme 5), formally a carbene-type orbital interaction, and an increase in the **RS-D** contribution resulted in higher [1+2] reaction barriers. Additionally, the fundamental differences between the two TS structures are the C3—C4 interatomic distance, which is slightly shorter in the [1+2] TS, and the C5-C4-C3-N2 dihedral angle. The difference in the dihedral angle between the two TS structures is linearly dependent ($r^2 = 0.842$) on the weight of the **RS-C** contribution, with the difference diminishing as the %**RS-C** increases. Considering that both reaction pathways evolve from the same starting point and the only difference is the orientation of approach (i.e., the C5-C4-C3-N2 dihedral angle), it is not surprising that the [3+2] reaction may involve some characteristics of a [1+2] reaction, especially in the early stages of the reaction. In the following, we suggest that the two reaction paths are not independent, but that the overall mechanism is a combination of the two pathways.

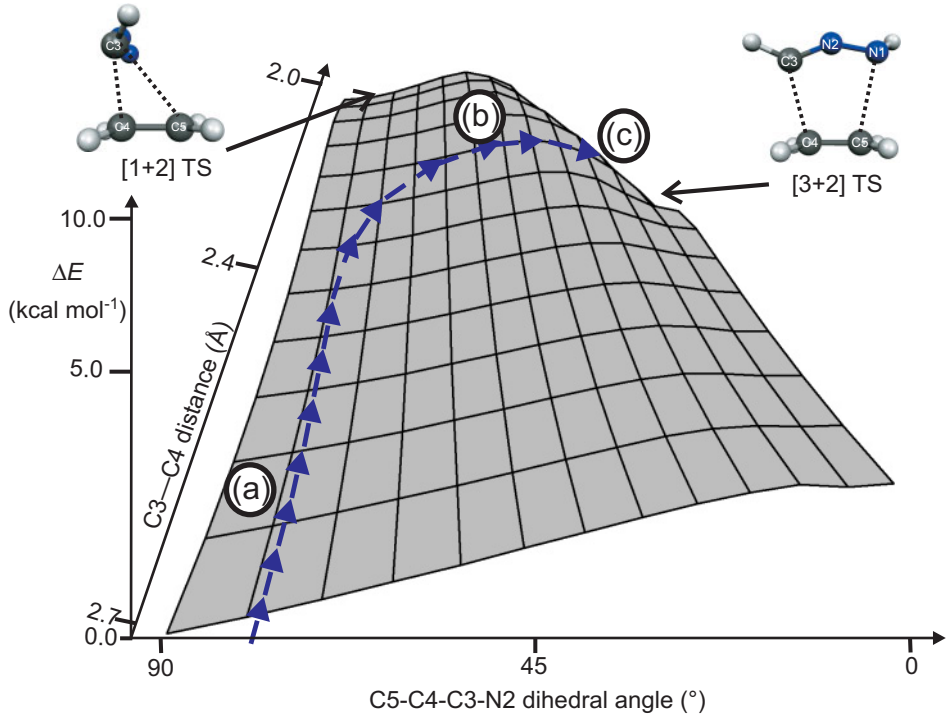
A relaxed potential energy scan was performed for the unsubstituted nitrilimine attacking ethene, varying the C5-C4-C3-N2 dihedral angle from 90° to 0° and the C3—C4 distance from 2.7 to 2.0 Å (Fig. 5). At large internuclear distances (2.7 Å), the [1+2] approach is favoured by 0.65 kcal mol^{-1} and there is a barrier to rotation of 0.85 kcal mol^{-1} at a dihedral angle of about 15°. As the C3—C4 distance decreases, the barrier to rotation steadily increases, while the location of the barrier shifts to larger dihedral angles. At a C3—C4 distance of 2.0 Å, corresponding to the distance at the [1+2] TS, the barrier to rotation is 1.29 kcal mol^{-1} at a dihedral angle of 50°. The [1+2] pathway is favoured up to about 2.3 Å. Beyond 2.3 Å, the [3+2] pathway steadily becomes more favourable as product formation begins, while the [1+2] approach results in an increase in energy until the TS at about 2.0 Å. Although the calculated energy differences are relatively small and generally within what may be considered the error limits of the model chemistry, it has been shown that the PBE0 functional is capable of reproducing experimental conformational equilibria that are a result of even smaller energy differences (66).

Obviously, many factors have been ignored, such as zero-point energy corrections and entropic factors, but both pathways should have comparable contributions since they are part of the same bimolecular process. Also, in the initial stages of reaction, the majority of approach trajectories (~90%)[9] result in the [1+2] pathway, highlighting the high statistical probability for this pathway. Therefore, as a general mechanism for nitrilimine cycloadditions, a statistically

[9] Only an initial dihedral angle range of ±20° leads to the [3+2] TS and all other dihedrals lead to the [1+2] TS.

© 2005 NRC Canada

Fig. 5. Relaxed potential energy surface in the vicinity of the two transition states for the reaction between unsubstituted nitrilimine and ethene. (*a*) Initial carbene-type approach, (*b*) ridge-bifurcation, and (*c*) formation of the [3+2] product.



and possibly thermodynamically favoured initial carbene-type attack occurs, up until a specific C3—C4 internuclear distance where the [3+2] reaction pathway becomes favoured, and a ridge-type bifurcation takes place with rotation about the C3—C4 bond axis (Fig. 5). The final product is typically still the thermodynamically, and for the most part kinetically, favoured Δ^2-pyrazoline, but the regio- and stereo-selectivity observed in the final product is a result of: (*i*) the initial carbene-type approach; and (*ii*) the position of the bifurcation region, which is a function of the difference in barrier heights for the two pathways (ΔE_a) and the magnitude of the rotation barrier. Recall that a [1+2] TS structure was not obtained for three systems ($R^1 = NH_2$, $R^2 = H$; $R^1 = R^2 = NH_2$; and $R^1 = R^2 = OH$). Inspection of the potential energy surface in the region of the [3+2] and [1+2] TSs for these systems reveals that there is no barrier to rotation, hence no ridge-inflection point, and therefore a [1+2] TS cannot be located. For diaminonitrilimine ($R^1 = R^2 = NH_2$), this is fully consistent with its description as a (possibly) stable carbene (32),[4,10] whose large nucleophilic character prevents its [1+2] addition to electron-rich alkenes.

Conclusion

Electronic structure calculations reveal that both the [3+2] and [1+2] cycloaddition pathways between ethene and a series of nitrilimines have low barriers and large reaction exothermicities, consistent with the transient nature of nitrilimines. In the majority of cases, the [3+2] reaction is preferred, but the [1+2] pathway can be favoured by varying the N-substituents. Both reactions proceed with concerted, asynchronous mechanisms, with the [1+2] pathway exhibiting a greater degree of asynchronicity. The geometries of the [1+2] and [3+2] TSs are similar and the fundamental difference lies in the orientation of the approaching reactants, i.e., the C5-C4-C3-N2 dihedral angle. The [3+2] reaction barrier is controlled by two orbital interactions, one of which is carbene-like in nature, and the [1+2] barrier is related to the interaction between the HOMO of ethene and the two unoccupied π orbitals of nitrilimine. The potential energy surface in the vicinity of the [3+2] and [1+2] TSs reveals that the initial phase of the reaction corresponds to a carbene-like attack of the nitrilimine, which after crossing a ridge-inflection region of the surface, eventually results in the formation of the [3+2] product. Further work is currently being carried out to examine the effects of ethene substitution and to design experiments that can confirm our proposed mechanism.

Acknowledgements

This research was supported by a Nouveaux Chercheurs-Équipe grant from the Fonds Québecois de Recherche sur la Nature et les Technologies (FQRNT). Calculations were performed at the Centre for Research in Molecular Modeling (CERMM), which was established with the financial support of the Concordia University Faculty of Arts and Science, the Ministère de l'Éducation du Québec (MEQ), and the Canada Foundation for Innovation (CFI). G.H.P. holds a Concordia University Research Chair.

References

1. S. Sakai and M.T. Nguyen. J. Phys. Chem. A, **108**, 9169 (2004).

[10]R.C. Mawhinney, H.M. Muchall, and G.H. Peslherbe. Submitted for publication.

© 2005 NRC Canada

2. V. Polo, J. Andres, R. Castillo, S. Berski, and B. Silvi. Chem. Eur. J. **10**, 5165 (2004).
3. M.J. Aurell, L.R. Domingo, P. Perez, and R. Contreras. Tetrahedron, **60**, 11503 (2004).
4. P. Perez, L.R. Domingo, A.J. Aurell, and R. Contreras. Tetrahedron, **59**, 3117 (2003).
5. G. Molteni and A. Ponti. Tetrahedron, **59**, 5225 (2003).
6. K. Sakata. J. Phys. Chem. A, **104**, 10001 (2000).
7. M.D. Su, H.L. Liao, W.S. Chung, and S.Y. Chu. J. Org. Chem. **64**, 6710 (1999).
8. R. Huisgen. Angew. Chem. Int. Ed. Engl. **2**, 633 (1963).
9. R. Huisgen. J. Org. Chem. **33**, 2291 (1968).
10. R. Huisgen. J. Org. Chem. **41**, 403 (1976).
11. R.A. Firestone. J. Org. Chem. **33**, 2285 (1968).
12. R.A. Firestone. J. Org. Chem. **37**, 2181 (1972).
13. R.A. Firestone. Tetrahedron, **33**, 3009 (1977).
14. R.A. Firestone. Heterocycles, **25**, 61 (1987).
15. R. Huisgen, M. Seidel, J. Sauer, J.W. McFarland, and G. Wallbillich. J. Org. Chem. **24**, 892 (1959).
16. R. Huisgen, R. Grashey, M. Seidel, R. Schmidt, H. Knupfer, and G. Wallbillich. Ann. Chem. **653**, 105 (1962).
17. R. Huisgen, H. Knupfer, R. Schmidt, M. Seidel, and R. Grashey. Ann. Chem. **658**, 169 (1962).
18. R. Huisgen, R. Grashey, M. Seidel, H. Knupfer, and R. Kunz. Chem. Ber. **97**, 1085 (1964).
19. R. Huisgen, K. Adelsberger, E. Aufderhaar, H. Knupfer, and G. Wallbillich. Monatsh. Chem. **98**, 1618 (1967).
20. R. Huisgen and E. Aufderhaar. Chem. Ber. **98**, 2185 (1965).
21. K. Marakchi, O.K. Kabbaj, N. Komiha, and M.L. Charibi. J. Fluorine Chem. **109**, 163 (2001).
22. A.F. Jalbout, Z. Jiang, H. Abou-Rachid, and N.N. Benkaddour. Spectrochim. Acta Part A, **60**, 603 (2004).
23. K.N. Houk, J. Gonzalez, and Y. Li. Acc. Chem. Res. **28**, 81 (1995).
24. J.T. Sharp. *In* The Chemistry of heterocyclic compounds 59: Synthetic applications of 1,3-dipolar cycloaddition chemistry toward heterocycles and Natural products. *Edited by* A. Padwa and W.H. Pearson. John Wiley and Sons, New York. 2002. pp. 473–537.
25. G. Bertrand and C. Wentrup. Angew. Chem. Int. Ed. Engl. **33**, 527 (1994).
26. F. Palacios, J. Pagalday, V. Piquet, F. Dahan, A. Baceiredo, and G. Bertrand. J. Org. Chem. **62**, 292 (1997).
27. F. Foti, G. Grassi, and F. Risitano. Synlett, 125 (2005).
28. R. Huisgen. Angew. Chem. Int. Ed. Engl. **2**, 565 (1963).
29. S.D. Kahn, W.J. Hehre, and J.A. Pople. J. Am. Chem. Soc. **109**, 1871 (1987).
30. M.W. Wong and C. Wentrup. J. Am. Chem. Soc. **115**, 7743 (1993).
31. K. Kuhler, R.T. Palmer, B.L. Wittkamp, and M.R. Hoffmann. THEOCHEM, **360**, 41 (1996).
32. R.C. Mawhinney, H.M. Muchall, and G.H. Peslherbe. Chem. Commun. (Cambridge), 1862 (2004).
33. E.D. Glendening and F. Weinhold. J. Comput. Chem. **19**, 593 (1998).
34. E.D. Glendening and F. Weinhold. J. Comput. Chem. **19**, 610 (1998).
35. E.D. Glendening, J.K. Badenhoop, and F. Weinhold. J. Comput. Chem. **19**, 628 (1998).
36. M.J. Jones and R.A. Moss. *In* Reactive intermediate chemistry. *Edited by* R.A. Moss, M.S. Platz, and M.J. Jones. John Wiley and Sons Inc., Toronto. 2004. pp. 273–328.
37. D. Bourissou, O. Guerret, F.P. Gabbai, and G. Bertrand. Chem. Rev. **100**, 39 (2000).
38. R.A. Moss. Acc. Chem. Res. **13**, 58 (1980).
39. N.G. Rondan, K.N. Houk, and R.A. Moss. J. Am. Chem. Soc. **102**, 1770 (1980).
40. S. Sakai. Int. J. Quantum Chem. **70**, 291 (1998).
41. A.E. Keating, S.R. Merrigan, D.A. Singleton, and K.N. Houk. J. Am. Chem. Soc. **121**, 3933 (1999).
42. J.J. Blavins, D.L. Cooper, and P.B. Karadakov. Int. J. Quantum Chem. **98**, 465 (2004).
43. D.C. Merrer and P.R. Rablen. J. Org. Chem. **70**, 1630 (2005).
44. M.J. Frisch, G.W. Trucks, H.B. Schlegel, G.E. Scuseria, M.A. Robb, J.R. Cheeseman, V.G. Zakrzewski, J.A. Montgomery, Jr., R.E. Stratmann, J.C. Burant, S. Dapprich, J.M. Millam, A.D. Daniels, K.N. Kudin, M.C. Strain, O. Farkas, J. Tomasi, V. Barone, M. Cossi, R. Cammi, B. Mennucci, C. Pomelli, C. Adamo, S. Clifford, J. Ochterski, G.A. Petersson, P.Y. Ayala, Q. Cui, K. Morokuma, N. Rega, P. Salvador, J.J. Dannenberg, D.K. Malick, A.D. Rabuck, K. Raghavachari, J.B. Foresman, J. Cioslowski, J.V. Ortiz, A.G. Baboul, B.B. Stefanov, G. Liu, A. Liashenko, P. Piskorz, I. Komaromi, R. Gomperts, R.L. Martin, D.J. Fox, T. Keith, M.A. Al-Laham, C.Y. Peng, A. Nanayakkara, M. Challacombe, P.M.W. Gill, B. Johnson, W. Chen, M.W. Wong, J.L. Andres, C. Gonzalez, M. Head-Gordon, E.S. Replogle, and J.A. Pople. GAUSSIAN 98. Revision A.11.4 [computer program]. Gaussian, Inc., Pittsburgh Penn. 2002.
45. J.P. Perdew, K. Burke, and M. Ernzerhof. Phys. Rev. Lett. **77**, 3865 (1996).
46. J.P. Perdew, K. Burke, and M. Ernzerhof. Phys. Rev. Lett. **78**, 1396 (1997).
47. J.P. Perdew, M. Ernzerhof, and K. Burke. J. Chem. Phys. **105**, 9982 (1996).
48. W.J. Hehre, R. Ditchfield, and J.A. Pople. J. Chem. Phys. **56**, 2257 (1972).
49. M.M. Francl, W.J. Pietro, W.J. Hehre, J.S. Binkley, M.S. Gordon, D.J. DeFrees, and J.A. Pople. J. Chem. Phys. **77**, 3654 (1982).
50. C. Gonzalez and H.B. Schlegel. J. Chem. Phys. **90**, 2154 (1989).
51. C. Gonzalez and H.B. Schlegel. J. Chem. Phys. **95**, 5853 (1991).
52. G.S. Hammond. J. Am. Chem. Soc. **77**, 334 (1955).
53. K.N. Houk, J. Sims, C.R. Watts, and L.J. Luskus. J. Am. Chem. Soc. **95**, 7301 (1973).
54. R. Sustmann. Pure Appl. Chem. **40**, 569 (1974).
55. R.A. Moss. Acc. Chem. Res. **22**, 15 (1989).
56. K.N. Houk, J. Sims, R.E. Duke, R.W. Strozier, and J.K. George. J. Am. Chem. Soc. **95**, 7287 (1973).
57. L. Salem. J. Am. Chem. Soc. **90**, 543 (1968).
58. L. Salem. J. Am. Chem. Soc. **90**, 553 (1968).
59. W.C. Herndon. Chem. Rev. **72**, 157 (1972).
60. R. Huisgen. Pure Appl. Chem. **53**, 171 (1981).
61. Y. Yoshioka, D. Yamaki, S. Kiribayashi, T. Tsunesada, M. Nishino, K. Yamaguchi, K. Mizuno, and I. Saito. Electron. J. Theor. Chem. **2**, 218 (1997).
62. Y. Yoshioka, D. Yamaki, S. Kubo, M. Nishino, K. Yamaguchi, K. Mizuno, and I. Saito. Electron. J. Theor. Chem. **2**, 236 (1997).
63. C. Di Valentin, M. Freccero, R. Gandolfi, and A. Rastelli. J. Org. Chem. **65**, 6112 (2000).
64. R. Sustmann, W. Sicking, and R. Huisgen. Chem. Eur. J. **9**, 2245 (2003).
65. R. Sustmann, W. Sicking, and R. Huisgen. J. Am. Chem. Soc. **125**, 14425 (2003).
66. R.C. Mawhinney, H.M. Muchall, and J. Lessard. Can. J. Chem. **81**, 1101 (2003).

© 2005 NRC Canada

Pople, Schneider, and Bernstein — A truly seminal treatise of NMR[1]

John D. Roberts

Abstract: The appearance of the authoritative and comprehensive book, *High-Resolution Nuclear Resonance Spectroscopy*, by John A. Pople, William G. Schneider, and Harold J. Bernstein in 1959 came at just the right time for chemists and other scientists to develop a clear vision of the wide breadth of applications of this critical emerging field and, in addition, to have the opportunity to learn the underlying basic theory in substantial detail.

Key words: Pople, Schneider, Bernstein, NMR theory, NMR applications.

Résumé : Le traité compréhensif de John A. Pople, William G. Schneider et Harold J. Bernstein, *High-Resolution Nuclear Resonance Spectroscopy* a fait autorité et son apparition en 1959 est arrivée juste au bon moment pour permettre aux chimistes et aux scientifiques de se faire une idée claire de l'étendue des applications de ce nouveau domaine critique alors en émergence et, de plus, d'avoir une opportunité d'apprendre en détail la théorie de base sous-jacente.

Mots clés : Pople, Schneider, Bernstein, théorie de la RMN, applications de la RMN.

[Traduit par la Rédaction]

Introduction

The progress of chemistry often occurs in spurts, especially as new ideas emerge or new understandings are achieved. Many such spurts are facilitated by especially significant books. Some of these books are of such nature to stay in print for many years; others are more ephemeral because they appear soon after a new field opens and although they may be especially timely when they first appear, before long they may be left behind as their impact leads to new applications and new insights. The first category includes such books as Lewis and Randall's *Thermodynamics* (1), Pauling and Wilson's *Quantum Mechanics* (2), Pauling's *Nautre of the Chemical Bond* (3), Sidgwick's *Organic Chemistry of Nitrogen* (4), and Hammett's *Physical Organic Chemistry* (5).

In 1952, while at MIT, I first was exposed to the possibilities of NMR in chemistry in a personal lecture by Richard A. Ogg of Stanford, but my level of comprehension of the physics involved was insufficient to take any action other than to note that Ogg's boundless enthusiasm surely meant that, for someone, NMR would be a winning research area. Two years later, William D. Phillips showed me actual spectra of organic compounds and what could be gleaned from them, especially such information as the rates of rotation about the C—N bond of *N*,*N*-dimethylformamide. That exposure led to an intense campaign to get a NMR spectrometer at Caltech to be under the general supervision of the organic group. Linus Pauling was unenthusiastic, because he thought such a spectrometer would be best supervised by more knowledgeable persons with experience in magnetic resonance and expertise in electronics. He relented when it was pointed out that NMR should be well-suited to investigate the borderline between resonance and tautomerism. Our installation was one of the very first Varian NMRs to be installed in an academic institution.

My initial plan was to determine the structure of diketene, a festering problem for many years, but Herbert S. Gutowsky (probably the first chemist to do extensive research on NMR with self-built instrumentation) got there first (6). A secondary goal was to determine the structure of Feist's acid, which was successful in confirming the material to be 3-methylene-1,2-cyclopropanedicarboxylic acid (7). But actually, my first paper using NMR was concerned with whether the very broad line observed for the N-H proton of pyrrole was the result of proton exchange or (as it turned out) ^{14}N quadrupolar interactions (8). I ran these and several hundred other NMR spectra over the next year with little clue as to the basics of how an NMR spectrometer actually worked. But as I caught on to more of it, my enthusiasm grew, and in the summer of 1958, an invitation to speak at a Reaction Mechanisms Conference at Bryn Mawr provided an opportunity to give a lecture on the subject to physical organic chemists. The response was so favorable, a missionary zeal quickly developed to write a book based on the lecture material.

It did not take long to realize that when one writes a book about an especially fast moving field, such as NMR, it is somewhat like writing in water. I experienced that feeling in 1959 with my book *Nuclear Magnetic Resonance* (9), even though my purpose of the book was simple: an alert to organic chemists of the possibilities of NMR in their area

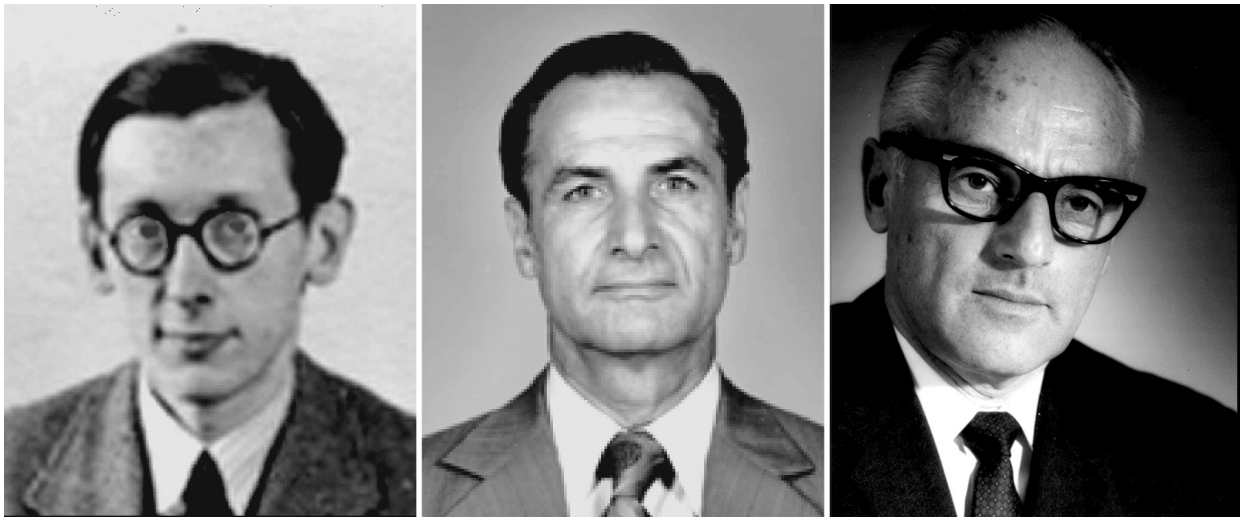
Received 30 March 2005. Published on the NRC Research Press Web site at http://canjchem.nrc.ca on 1 December 2005.

J.D. Roberts. Crellin Laboratory (164-30), California Institute of Technology, 1201 E. California Boulevard, Pasadena, CA 91125, USA (e-mail: robertsj@caltech.edu).

[1]This article is part of a Special Issue dedicated to organic reaction mechanisms.

 doi: 10.1139/V05-156 © 2005 NRC Canada

Fig. 1. (*a*) John A. Pople (10/31/1925 – 3/15/2004) was born in Somerset, UK, showed strong mathematical skills at a very early age, received a Ph.D. in mathematics at Cambridge in 1948, started in NMR in 1955, worked two summers at NRC in Ottawa with Schneider and Bernstein. His later interests were in quantum theory of molecular properties, he was knighted in 2003 and awarded the Nobel Prize in Chemistry in 1998. (Photo taken in the 1950s.) (*b*) William G. Schneider (6/1/1915 –) was born in Saskatchewan, took B.Sc. and M.S. at the University of Saskatchewan, received a Ph.D. in physical chemistry at McGill in 1941, worked as a postdoctoral fellow at Harvard (1941–1943), vice president and president (1965–1980) of the Pure Chemistry Division at NRC (1943–1980), and he was awarded the Order of Canada in 1977. (Photo taken in the 1950s from the NRC Archives.) (*c*) Harold J. Bernstein (8/26/1914 – 12/14/84) was born in Toronto and had his advanced education at the University of Toronto culminating with a Ph.D. in physical chemistry in 1938, postdoctoral scholar in Copenhagen (1938–1940), worked with NRC in chemistry from 1946 to his retirement in 1981. Following the publication of PSB, he gradually moved to research in Raman spectroscopy. (Photo taken in 1967 from the NRC Archives.)



and a hope of imparting simple general ideas of how it worked — at least at the level I knew it then. This book did, however, achieve two distinctions: (*a*) being the first advanced chemistry monograph with four-color illustrations, and (*b*) being the first book to publish the now ubiquitous problems in which students are given a NMR spectrum and an empirical formula and asked to deduce the molecular structure.

But the fact is that I was thoroughly upstaged shortly after publication, when still in 1959, a very different NMR book appeared on the scene, entitled *High-resolution Nuclear Magnetic Resonance* by John A. Pople, William G. Schneider, and Harold J. Bernstein (10). This book was itself to a degree ephemeral because of rapid experimental development of the field, but it still achieved a longer-term impact than otherwise might have been expected through its authoritative discussions of the basic theory of NMR, chemical shifts, spin–spin splitting, relaxation, and rate effects. One would presume that much of the theoretical part was written by John A. Pople, well-known for his work on applications of quantum mechanics to chemistry, who was then at the National Physical Laboratory at Teddington, UK. The extensive information on chemical applications was surely largely the work of William G. Schneider and Harold J. Bernstein at the National Research Council Canada (NRC) in Ottawa. The cooperative effort of the three authors says much for the acumen of NRC in getting into new areas of great promise.

The book by Pople, Schneider, and Bernstein (PSB, Fig. 1) was monumental. It was comprehensive and covered a wide range of applications using a wide range of NMR-active nuclei. At the same time, it supplied very authoritative, but not always user-friendly, theory for organic chemists. Many of those applications involved studies made by the authors at NRC. These included excellent and substantial work on the analysis of the shifts and couplings in a variety of organic heterocyclic compounds, such as pyridine, lutidine, quinoline, and isoquinoline, as well as substituted cyclohexanes. Hydrogen bonding was studied in considerable detail by changes in the chemical shifts of the acidic protons of carboxylic acids, as a function of concentration mostly in non-polar aprotic solvents. Related research was reported on the substantial changes in the proton shift of chloroform dissolved in aromatic solvents. Other important work involved changes in the relative keto–enol concentrations as a function of solvent.

Having already had some experience in organic chemical applications, I was especially interested in PSB's account of the theory of spin–spin splitting and how to extract spin–spin couplings from non-first-order spectra. When I wrote my NMR book, I was at the level of the dogma on shifts and spin–spin couplings that is taught in most elementary organic courses today. One of the principal tenets of the dogma relating to shifts was that electronegative substituents caused downfield proton shifts. Other tenets for spin–spin splitting included the notion that protons with the same chemical shift do not split one another (but not why), the $n+1$ rule for predicting proton–proton splittings, and also that proton–proton couplings are normally not significant when the protons are separated by more than three bonds. However, I did mention in my book the seemingly anoma-

© 2005 NRC Canada

lous AA′XX′ spectrum of 1,1-difluoroethene described by McConnell (11) and made it embarrassingly clear that I did not understand how it came about, although I was sufficiently interested to produce a higher resolution spectrum than the published one.

It should not be surprising that I was clearly an avid customer for PSB's methods for calculating spectral line positions. Although previously an advocate for organic chemists learning to apply Hückel MO theory to organic compounds (12), I needed a powerful catalyst for seeing the connection between the behavior of electrons in orbitals and of magnetic nuclei interacting with one another in a magnetic field. Fortunately, for my then colleague, Harden McConnell, this area of theory was like mother's milk and in a "*mano a mano*" struggle on July 4, 1956, he hoisted me over the energy barrier to use it. The ultimate result was a 105 page book (13) explaining in a way that I could understand a rather small number of pages of PSB. By the time I completed my manuscript, my copy of PSB was literally coming apart at the seams with the top of the pages deeply blackened, particularly in those areas covering the theory of NMR. Unfortunately, my manuscript was written and submitted just before it became commonplace to calculate and plot spectra as was done early on by Wiberg and Nist (14).

Others, such as Ray Lemieux (15) and Ted Schaefer (16) who achieved recognition of their own NMR research progress by way of the citation index approbations expressed strong appreciation for the contributions and inspiration provided to them by Schneider and Bernstein during the periods in which each worked at NRC.

The word *seminal* is used so much today in describing more or less new things in science that its real meaning is almost lost, but PSB's book sets a standard for the word by its timeliness, breadth, and depth of coverage at a crucial stage of NMR development. Furthermore, the book sparked the enthusiasm of chemists generally and it led them to demand more and better NMR spectrometers. The resulting market for machines turned out to be quite large and led to the early fierce and continuing competition among the instrument makers: Varian, Bruker, JEOL, and Nicolet (later GE) to provide customers with both routine and cutting-edge instrumentation representing the epitome of high technology.

Almost 60 years since the demonstration of NMR in the condensed phase (17, 18), the field is still growing almost explosively with applications in MRI (19), quantum computing (20), protein structure determinations (21), and optical detection of changes in force associated with excitation of nuclei in a magnetic field (22). The future of NMR is very bright indeed.

References

1. N. Gilbert and M.R. Lewis. Thermodynamics and the free energy of chemical substances. McGraw-Hill Book Company, New York. 1926.
2. L. Pauling and E.B. Wilson, Jr. Introduction to quantum mechanics, with applications to chemistry. McGraw-Hill Book Company, New York. 1935.
3. L. Pauling. The nature of the chemical bond and the structure of molecules and crystals. Cornell University Press, Ithaca, N.Y. 1939.
4. N.V. Sidgwick. The organic chemistry of nitrogen. Clarendon P., Oxford, UK. 1966.
5. L.P. Hammett. Physical organic chemistry. Reaction rates, equilibria and mechanisms. McGraw-Hill, New York. 1970.
6. A.R. Bader, H.S. Gutowsky, G.A. Williams, and P.E. Yankwich. J. Am. Chem. Soc. **78**, 2385 (1956).
7. A.T. Bottini and J.D. Roberts. J. Org. Chem. **21**, 1169 (1956).
8. J.D. Roberts. J. Am. Chem. Soc. **78**, 4495 (1956).
9. J.D. Roberts. Nuclear magnetic resonance: applications to organic chemistry. McGraw-Hill, New York. 1959.
10. J.A. Pople, W.G. Schneider, and H.J. Bernstein. High-resolution nuclear magnetic resonance. McGraw-Hill, New York. 1959.
11. H.M. McConnell, A.D. McLean, and C.A. Reilly. J. Chem. Phys. **23**, 1152 (1955).
12. J.D. Roberts. Notes on molecular orbital calculations. W.A. Benjamin, Inc., New York. 1961.
13. J.D. Roberts. An introduction to the analysis of spin–spin splitting in high-resolution nuclear magnetic resonance spectra. W.A. Benjamin, Inc., New York. 1961.
14. K.B. Wiberg and B.J. Nist. The interpretation of NMR spectra. W.A. Benjamin, Inc., New York. 1962.
15. R.U. Lemieux. Citation Classics, **26** (1980).
16. T. Schaefer. Citation Classics, **32** (1981).
17. E.M. Purcell, H.C. Torrey, and R.V. Pound. Phys. Rev. **69**, 37 (1946).
18. F. Bloch, W.W. Hansen, and M. Packard. Phys. Rev. **70**, 475 (1946).
19. C.A. Meriles, D. Sakellariou, A.H. Trabesinger, V. Demas, and V.A. Pines. Proc. Natl. Acad. Sci. U.S.A. **102**, 1840 (2005)
20. D.G. Cory, A.F. Fahmy, and T.F. Havel. Proc. Natl. Acad. Sci. U.S.A. **94**, 1634 (1997).
21. A. Bax. Protein Science, **12**, 1 (2003).
22. L.A. Madsen, G.M. Leskowitz, and D.P. Weitekamp. Proc. Natl. Acad. Sci. U.S.A. **101**, 2804 (2004).

© 2005 NRC Canada

Intramolecular general acid catalysis of sulfate transfer — Nucleophilic attack by oxyanions on the SO_3^- group[1]

Anthony J. Kirby, José Carlos Gesser, Florian Hollfelder, Jacks P. Priebe, and Faruk Nome

Abstract: The mechanism of hydrolysis of 8-*N*,*N*-dimethylaminonaphthyl sulfate closely resembles that of the corresponding phosphate monoester. Nucleophilic attack by water on the sulfate group of the zwitterion is catalyzed by the neighbouring dimethylammonium group, acting as a particularly efficient general acid through the intramolecular hydrogen bond. This hydrogen bond is present in both reactant and product, but is strongest in the transition state. Transfer of the sulfuryl group to oxygen nucleophiles, including water and carboxylate anions, shows steric and electrostatic effects, and a sensitivity to basicity which is low, but significantly higher than expected for uncatalyzed transfer of the SO_3^- group.

Key words: sulfate, sulfatase, intramolecular, general acid catalysis, promiscuity.

Résumé : Le mécanisme d'hydrolyse du sulfate de 8-*N*,*N*-diméthylaminonaphtyle ressemble fortement à celui du monophosphate correspondant. L'attaque nucléophile de l'eau sur le groupe sulfate du zwitterion est catalysée par le groupe diméthylammonium voisin qui agit comme un acide général particulièrement efficace par le biais de la liaison hydrogène intramoléculaire. Cette liaison hydrogène est présente tant dans le réactif que dans le produit, mais elle est encore plus forte dans l'état de transition. Le transfert du groupe sulfuryle vers les oxygènes nucléophiles, y compris l'eau et les anions carboxylates, est soumis à des effets stériques et électrostatiques et à une faible sensibilité à la basicité qui est toutefois supérieure à celle attendue pour un transfert non catalysé du groupe SO_3^-.

Mots clés : sulfate, sulfatase, intramoléculaire, catalyse acide générale, promiscuité.

[Traduit par la Rédaction]

Introduction

Interest in the biological chemistry of sulfate esters has grown rapidly in recent years, as it has become apparent that they are involved in a whole range of biological processes besides detoxification. These include molecular recognition and cell signaling, hormone regulation, and viral entry into cells (1, 2). The two types of enzyme involved in the metabolism of biological sulfates, the sulfatases and sulfotransferases, both catalyse the transfer of the SO_3 group between nucleophilic, typically oxygen, centres, but have evolved different mechanistic strategies. The sulfotransferases (1) generally use an "activated sulfate", PAPS, with a good, phosphate ester leaving group, to transfer SO_3 to a target nucleophile (Scheme 1), just as kinases use ATP to transfer the PO_3^- group to generate phosphate monoesters.

The sulfatases, by contrast, have evolved to transfer SO_3 from sulfate esters to a common, weak nucleophile, water, and like phosphatases, must activate both nucleophile and leaving group. Most attention, not surprisingly, has focused on their mechanistically ingenious use of a unique enzyme nucleophile, an OH group of a hydrated α-formylglycine residue (3, 4) (generated by post-translational oxidation of Ser or Cys). The sulfated enzyme intermediate is thus not an inconveniently stable alkyl sulfate (a potential alkylating agent) but a species **1** (Scheme 2), which rapidily eliminates sulfate to regenerate active enzyme.

The (presumably concerted) first step of this mechanism involves two key proton transfers. The nucleophilic OH group (more acidic by some 2 p*K* units than a serine OH) needs to be deprotonated, either in a preequilibrium or by a general base as part of the reaction. And the leaving group

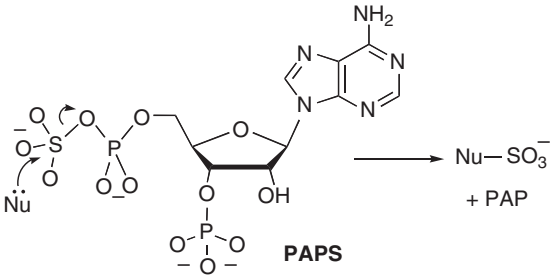
Received 11 April 2005. Published on the NRC Research Press Web site at http://canjchem.nrc.ca on 2 December 2005.

A.J. Kirby.[2] University Chemical Laboratory, University of Cambridge, Cambridge CB2 1EW, UK.
J.C. Gesser and F. Hollfelder. Department of Biochemistry, University of Cambridge, 80 Tennis Court Road, Cambridge CB2 1GA, UK.
J.P. Priebe and F. Nome.[3] Departamento de Química, Universidade Federal de Santa Catarina, Florianópolis, SC, 88040-900, Brazil.

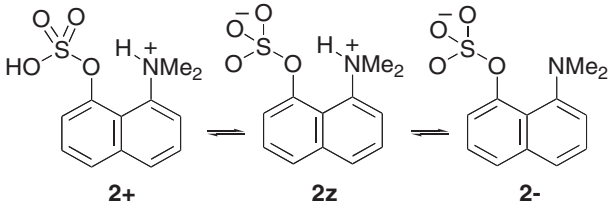
[1]This article is part of a Special Issue dedicated to organic reaction mechanisms.
[2]Corresponding author (e-mail: ajk1@cam.ac.uk).
[3]Corresponding author (e-mail: faruk@qmc.ufsc.br).

 doi: 10.1139/V05-172 © 2005 NRC Canada

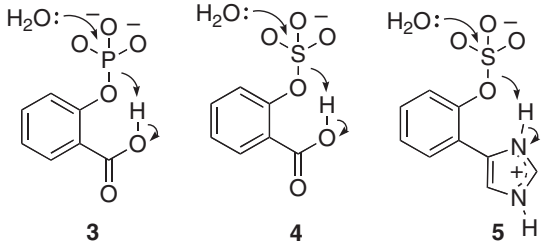
Scheme 1.



requires protonation by a general acid: sulfatases typically use the NH^+ groups of histidines and lysines (2). In this work we examine both reactions, using the model sulfate ester **2**, which has a built-in general acid that we expect from previous work to be catalytically efficient.

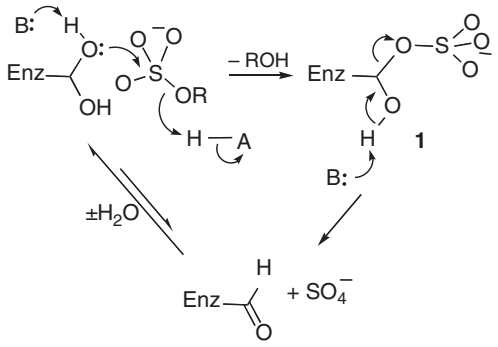


The similarities between the reactions of sulfate and phosphate monoesters $RO\text{-}SO_3^-$ and $RO\text{-}PO_3^{2-}$ are well-documented (and close enough that some phosphatases and sulfatases show significant crossover activity, as discussed in the following). Rates of hydrolysis depend strongly on the basicity of the leaving group, with slopes of linear plots of $\log k_{hyd}$ vs. pK_a of the conjugate acid ROH of the order of 1.2–1.3 in both cases. Cleavage of the bonds to the leaving group RO^- might therefore be expected to also be susceptible to relatively efficient general acid catalysis. Efficient catalysis by the COOH group was observed many years ago for salicyl phosphate **3** (5, 6) and sulfate **4** (7, 8). But catalysis of the hydrolysis of the sulfate group of **5** by the neighbouring imidazolium group (9), the best model for this part of the sulfatase mechanism, is typically inefficient (10), with the rate acceleration ascribed to intramolecular general acid catalysis only 49-fold (9).

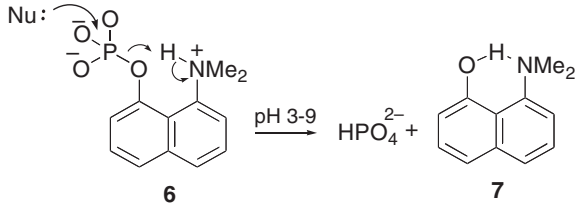


We have recently shown (11) that the phosphate monoester analogue **6** (closely analogous to the zwitterion **2z**) is hydrolyzed with highly efficient general acid catalysis by NH^+, supporting a rate acceleration of 2.4×10^5 at 60 °C. The key to efficient catalysis is the strong intramolecular hydrogen bond to the neighbouring dimethylammonium group (Scheme 3, Nu = H_2O). The attack of nucleophiles other than water is also catalyzed, and oxyanions are no less reactive than neutral amine nucleophiles of similar basicity. This

Scheme 2.



Scheme 3.



is remarkable since oxyanions do not normally react at a significant rate with the PO_3^{2-} group of reactive phosphate monoesters. Apparently, electrostatic repulsion among the reacting anions disappears when hydrolysis is catalyzed by a properly positioned *cationic* general acid (11). Since no data are available to characterize nucleophilic attack by oxyanions on sulfate monoesters, we have examined the spontaneous hydrolysis of **2z** and its catalysis by oxyanion nucleophiles, which are also potential general bases.

Methods and results

Materials

^1H NMR spectra were obtained on Bruker AW-200 and Varian Mercury Plus 400 MHz instruments using sodium 3-(trimethylsilyl)propionate as internal standard. IR spectra were obtained using KBr discs on PerkinElmer FT 16 PC and ABB BOMEM model FTLA 2000 instruments.

Melting points were measured on a hot stage Fisher-Johns MQAPF 301 instrument from Microquímica, and are uncorrected. pH values were measured at the end of each kinetic run using a Hanna pH200 digital pH meter, calibrated using standard buffer solutions (Carlo Erba, Milan, Italy) at pH 4.00, 7.00, and 10.00.

All solvents used in synthetic procedures were purified according to the best literature precedents (12, 13). Buffers and salts were used as supplied by Nuclear (São Paulo, Brazil), Vetec (Rio de Janeiro, Brazil), Carlo Erba (Milan, Italy), Merck (Darmstadt, Germany), and Aldrich (Milwaukee, Wisconsin), without further purification. 4-Nitrophenol (99%), DCl (37% in D_2O), and D_2O (99.9%) were supplied by Aldrich and Cambridge Isotope Laboratories (Andover, Massachusetts). 4-Nitrophenylsulfate and 8-*N*,*N*-dimethylaminonaphthyl sulfate (from the corresponding naphthol (14)) were synthesized as the potassium salts according to a literature method, modified in the latter case as follows.

© 2005 NRC Canada

Potassium 8-*N*,*N*-dimethylaminonaphthyl-1-sulfate (2)

A solution of 8-*N*,*N*-dimethylamino-1-naphthol (14) in pyridine was added in a single portion (15) to a cooled solution of the pyridine·SO_3 complex. After reaction and evaporation of the solvent, the syrupy residue was redissolved in water and the pH adjusted to 8.0–8.5 with KOH. The solid residue obtained by evaporation was triturated with dry acetonitrile and centrifuged (16). The supernatant was evaporated and the solid obtained dissolved in hot ethanol, cooled, and filtered under vacuum. Repetition of this procedure improved the purity of the product, but was always accompanied by a certain amount of hydrolysis to small amounts of the naphthol and inorganic sulfate. The compound used in the kinetic experiments was at least 96% pure. UV–vis λ_{max} (H_2O): 300 nm. ^{1}H NMR (400 MHz, D_2O) δ: 7.75 (d, 1H, J = 5.5 Hz), 7.54 (d, 1H, J = 5.5 Hz), 7.52 (d, 1H, J = 5.5 Hz), 7.44 (t, 1H, J = 5.5 Hz), 7.41 (t, 1H, J = 5.5 Hz), 7.15 (d, 1H, J = 5.5 Hz), 2.74 (s, 6H, NMe_2).

Kinetic measurements

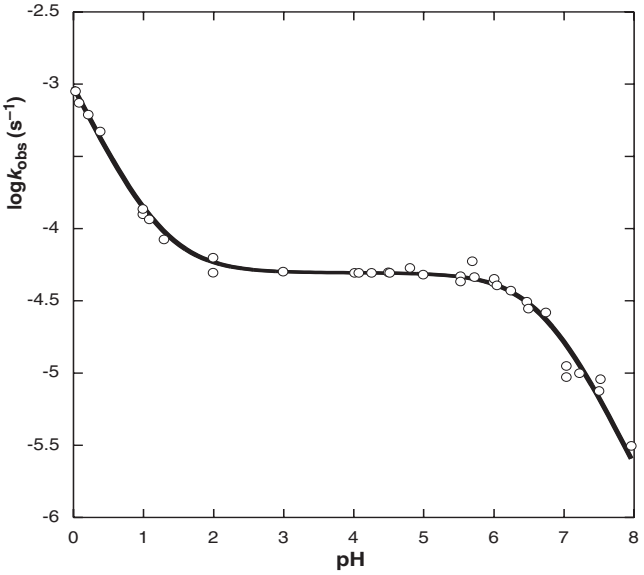
UV–vis spectra and kinetic runs were followed in the thermostatted cell compartment of a Varian Cary 50 spectrophotometer, and analysed on the dedicated microcomputer using the Cary WINUV 3.00 data acquisition and kinetics software program.

Kinetic measurements were carried out in aqueous solution, at 60 °C and ionic strength 1.0 mol/L (KCl), by following the appearance of 8-*N*,*N*-dimethylamino-1-naphthol, at three separate wavelengths (304, 316, and 320 nm). For the spectroscopic pK_a determination, baseline corrections (referred to 500 nm) allowed accurate assignment of isosbestic points. pH in the kinetic runs was maintained using HCl (at pH < 3.0) and the following buffers, generally at 0.01 mol/L: acetic acid – potassium acetate (pH 4–5.25), potassium phosphate (pH 5.5–7.5), and boric acid – borate (pH 7.75–9). For kinetic runs in D_2O at 60 °C, the pD was obtained by adding 0.25 to the meter reading (17). Reactions were initiated by adding 50 μL aliquots of a 1.25×10^{-3} mol/L stock solution of potassium 8-*N*,*N*-dimethylaminonaphthylsulfate to preheated buffer solution in 10 mm (3 mL) quartz cells, to give a final concentration of 2.5×10^{-5} mol/L. Reactions were followed by taking an average of 280 absorbance readings over at least three half-lives. Calculated rate constants showed standard errors of <1% over the three wavelengths for which data were collected. Observed rate constants for hydrolysis in HCl and DCl, and at pH 4.50 as a function of temperature (Tables S1–S3), are available as Supplemental material.[4]

Spectroscopic determination of the pK_a of 8-dimethylamino-1-napthyl sulfate (2)

Spectra were recorded at 25 °C, at 14 pH values between 4.0 and 10.0. Isosbestic points were observed at 270 and 300 nm, with λ_{max} at 290 nm at pH 4 and 330 nm at pH 10.0. The value obtained (6.98 ± 0.03) is similar to the kinetic pK_a of 6.70 ± 0.05 at 60 °C derived from the pH–rate profile for hydrolysis (Fig. 1). It is more than 2 units higher than expected for the system lacking the sulfate group, as discussed in the following.

Fig. 1. pH dependence of the rate of hydrolysis of 8-*N*,*N*-dimethylaminonaphthyl-1-sulfate (**2**) at 60 °C and ionic strength 1.0 mol/L. The points are experimental, and the curve calculated, using eq. [2] and the constants summarized in Table 2.



Hydrolysis of 8-*N*,*N*-dimethylaminonaphthyl-1-sulfate (2)

The pH–rate profile for the hydrolysis of **2** from pH 0 to 8.0 (Fig. 1) shows three distinct regions. (*i*) At pH < 2, the rate increases linearly with a_H, with a slope of –1, as expected for an acid-catalyzed reaction. (*ii*) A pH-independent reaction between pH 3.0–6.0 corresponds to the spontaneous hydrolysis of the ionic species **2z** present in this region, while the fall off in region (*iii*) at pH > 6.5 is consistent with the ionization of this species to form an unreactive conjugate base. The apparent pK_a at 60 °C is 6.70 ± 0.05.

Much precedent, from mechanistic work on the hydrolysis of simple aryl sulfates and on the phosphate monoester **6** under similar conditions, suggests the mechanisms outlined in Scheme 4, which translate into the kinetic expression of eq. [1]:

$$[1] \qquad k_{obs} = k_{2+}\chi_{2+} + k_{2z}\chi_{2z}$$

(The uncatalyzed reaction of the anion is not significant under the conditions used, as shown by the absence of reaction at high pH). Equation [1] can be simplified to eq. [2] because the pK_a of **2+** is expected to be of the order of –(4–6),[5] far from the pH region.

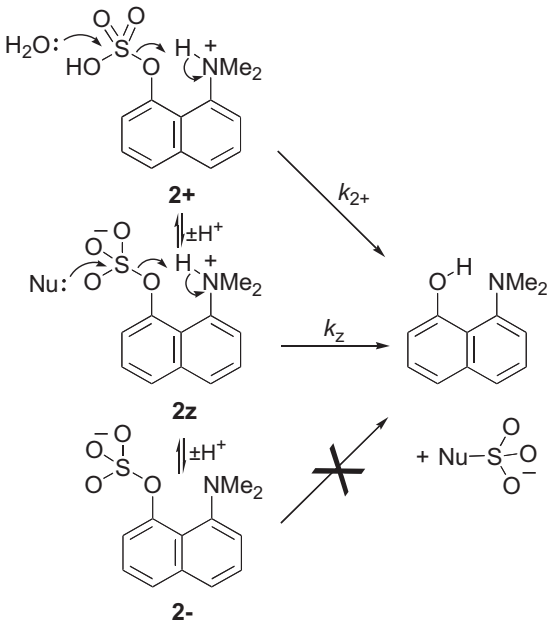
$$[2] \qquad k_{obs} = (k_H a_H + k_{2z}) \frac{a_H}{(a_H + K_{2z})}$$

[4] Supplementary data for this article are available on the Web site or may be purchased from the Depository of Unpublished Data, Document Delivery, CISTI, National Research Council Canada, Ottawa, ON K1A 0R6, Canada. DUD 4052. For more information on obtaining material refer to http://cisti-icist.nrc-cnrc.gc.ca/irm/unpub_e.shtml.

[5] Estimate based on a figure of ca. –3.5 for $MeOSO_3OH$ (J.P. Guthrie. Can. J. Chem. **56**, 2342 (1978)). The value will be lower for an aromatic sulfate, and reduced further by hydrogen bonding to the neighbouring NH^+. The value will be lower for an aromatic sulfate, and reduced further by hydrogen bonding to the neighbouring NH^+.

© 2005 NRC Canada

Scheme 4.



A least-squares fit to eq. [2] of the data shown in Table 1 gives the values of the rate and dissociation constants shown in Table 2: these define the calculated curve of Fig. 1.

Activation parameters

Activation parameters, based on the Eyring equation (18), were obtained for the spontaneous hydrolysis of the zwitterion **2z** from rate measurements at pH 4.55, done in triplicate at seven different temperatures in the range 60–90 °C. The correlation coefficient for the Arrhenius plot was 0.991. The results appear in Table 2, the data in Table S3.[4]

Solvent isotope effect

Rates of hydrolysis of **2** were compared in H_2O and D_2O in two regions of pH. In acid, between 0.52 and 1.06 mol/L, and at pH 4.55, in the pH-independent region where the reaction is the spontaneous hydrolysis of the zwitterion. Plotting k_{obs} vs. [LCl] in the acid region (for data see Tables S1 and S2)[4] gives good straight lines, with correlation coefficients of $r = 0.994$. The slopes give second-order rate constants for HCl–H_2O and DCl–D_2O of $1.67 \pm 0.10 \times 10^{-3}$ and $2.06 \pm 0.08 \times 10^{-3}$ $(mol/L)^{-1}$ s^{-1}, respectively, and thus an inverse isotope effect for the reaction in acid ($k_H/k_D = 0.81 \pm 0.08$). Rate constants at pH 4.55 were measured in triplicate: the values obtained ($k_{H_2O} = (4.95 \pm 0.20) \times 10^{-5}$ s^{-1} and $k_{D_2O} = (2.57 \pm 0.35) \times 10^{-5}$ s^{-1}, Table 2) give a kinetic isotope effect in this region ($k_{H_2O}/k_{D_2O} = 1.93 \pm 0.39$).

On the basis of the good linear free energy relationship ($r = 0.996$, slope = 1.346) among the rate constants for the hydrolysis of four simple aryl sulfates (extrapolated to 60 °C using Fendler's data (16)) and the pK_a of the leaving group, the rate of spontaneous hydrolysis of **2z** corresponds to that expected for a simple aryl sulfate with a leaving group (congugate acid) of $pK_a = 5.11$. The rate acceleration attributable to intramolecular general acid catalysis by the dimethylammonium group (based on a pK_a of 9.40 for 1-

Table 1. Observed rate constants for the hydrolysis of 8-*N*,*N*-dimethylaminonaphthyl-1-sulfate (**2**) at 60 °C and ionic strength 1.0 mol/L.

pH	k_{obs} (10^{-5} s^{-1})
–0.01	120.0
0.03	89.6
0.08	74.5
0.21	61.6
0.38	47.0
0.99	12.6
0.99	13.7
1.08	11.6
1.29	8.42
1.99	6.30
1.99	4.97
2.99	5.04
4.01	4.95
4.07	4.95
4.25	4.95
4.49	4.98
4.51	4.94
4.80	5.35
4.99	4.81
5.00	4.86
5.22	5.29
5.52	4.69
5.52	4.31
5.69	5.95
5.72	4.62
5.99	4.27
6.00	4.49
6.04	4.05
6.24	3.72
6.47	3.12
6.49	2.80
6.74	2.63
7.03	0.94
7.03	1.12
7.22	1.00
7.50	0.753
7.52	0.91
7.96	0.314

Table 2. Derived kinetic parameters for the hydrolysis of 8-*N*,*N*-dimethylaminonaphthyl-1-sulfate zwitterion **2z** at 60 °C and ionic strength 1.0 mol/L.

Kinetic parameter	Values for **2z**
k_H[a]	$9.05 \pm 0.60 \times 10^{-4}$ dm^3 mol^{-1} s^{-1}
k_{2z}[a]	$4.95 \pm 0.20 \times 10^{-5}$ s^{-1}
k_{2z} (D_2O)	$2.57 \pm 0.35 \times 10^{-5}$ s^{-1}
pK_{2z}	6.70±0.05
$\Delta H^{\ddagger}$	99.0±1.3 kJ dm^3 mol^{-1}
$\Delta S^{\ddagger}$ (60 °C)	–31.4±36.6 J K^{-1} mol^{-1}
k_{H_2O}/k_{D_2O} (pH 4.55)	1.93±0.39
k_{H_2O}/k_{D_2O} in acid[a]	0.81

[a]Defined in terms of eq. [2].

© 2005 NRC Canada

Table 3. Second-order rate constants for reactions of **2z** with nucleophiles.

Nucleophile[a]	pK_a[a]	k_2 (dm^3 mol^{-1} s^{-1})
Water	–1.74	8.9×10^{-7}
2-Chloroacetate	2.65	1.5×10^{-5}
Formate	3.52	3.8×10^{-5}
3-Chloropropionate	3.92	2.8×10^{-5}
Acetate	4.56	3.7×10^{-5}

[a]At 60 °C, under the conditions of the experiments.

naphthol (14)) is thus ca. 6×10^5 at 60 °C, and $>10^6$ at 25 °C.

Reactions with nucleophiles

The hydrolysis of **2z** is catalyzed by oxyanions in the plateau region. The data are shown in Table 3: rate enhancements of up to 78% are observed in the presence of 1 mol/L of nucleophile. These rate enhancements are clearly not specific ion effects because they depend on the basicity of the oxyanion, and to some extent on steric effects, as expected for nucleophilic reactions. The points for water and for acetate and substituted acetates (see the Discussion section) give an excellent Brønsted correlation, with $\beta_{nuc} = 0.26 \pm 0.01$.

Discussion

Hydrolysis of 2z

The estimated rate acceleration for the hydrolysis of the zwitterion **2z** is 6×10^5 at 60 °C, and the rate that is expected for a simple aryl sulfate ester with a leaving group (conjugate acid) of pK_a = 5.1 (16). The rate acceleration for the hydrolysis of the phosphate ester **6**, estimated in the same way, is 2.4×10^5 at 60 °C, and the rate that expected for a simple aryl phosphate ester with a leaving group (conjugate acid) of pK_a = 5.2. The close similarity of these figures suggests that the reactions of the two systems are also closely similar. In both cases, the efficiency of catalysis is reduced by the net stabilizing effect of the intramolecular hydrogen bond in the reactant (as revealed by the increase of >2 units in the pK_a of the dimethylammonium group of **2z**, and the similar but larger effect for **6**).[6] However, intramolecular general acid catalysis is still notably efficient, with **2z** hydrolyzed faster than the reaction of **5** by some three orders of magnitude, in water at 25 °C.

Other similarities are the absolute rates (**2z** is hydrolyzed just over 3 times more slowly at 60°) and the solvent deuterium isotope effects (k_{H_2O}/k_{D_2O}), which are identical ($k_H/k_D = 0.8 \pm 0.1$) for the acid-catalyzed reactions and low and normal for the plateau reactions ($k_H/k_D = 1.93 \pm 0.39$ for **2z**, 1.46 ± 0.04 for **6**). The activation parameters show the small differences typical for esters of these types, with entropies of activation small and negative for **2z** and small and positive for **6**. Thus, the enthalpy of activation for the hydrolysis of **2z** is similar to the value (24.7 kcal dm^3 mol^{-1}, 1 cal = 4.184 J) measured by Fendler and Fendler (16) for the hydrolysis of *o*-nitrophenyl sulfate. The low negative entropy of activation is similar within the experimental uncertainty to values (–17.4 and –18.5 eu) reported for 2,4- and 2,5-dinitrophenylsulfates (16, 19), and is consistent with a minimal net involvement of water (and perhaps a more significant release of (the more strongly) solvating water molecules from the phosphate dianion).

Mechanism

These close similarities in the hydrolysis reactions of **2z** and **6** clearly suggest that the mechanisms are also similar, and Scheme 4 is based on our conclusions for the phosphate ester. In neither system is there any significant reaction for the fully deprotonated form (**2**$^-$ in Scheme 4).

Hydrolysis in acid

C—O cleavage is not a serious possibility for an unactivated aromatic system, and for hydrolysis in acid there appears to be no convincing alternative to intramolecular general-acid-catalyzed attack of water on the neutral SO_3H group (Scheme 4, k_{2+}). The small inverse deuterium kinetic isotope effect is consistent with a reaction involving a preequilibrium proton transfer (20). A specific rate constant for the hydrolysis of **2+** can be estimated by assuming a pK_a for the sulfate S—OH group. Taking this pK_a to be –(5 ± 1), as previously discussed, gives an estimate for $\log(k_{2+}) = 1.93 \pm 1$ s^{-1}, corresponding to a rate acceleration of $1.8 \times 10^7 \pm 1$, of the same order of magnitude as that ($>10^8$-fold) estimated for catalysis by the same group of the hydrolysis of the cationic phosphoric acid ($PO(OH)_2$) form of **6**. The intramolecular hydrogen bond from NH^+ to the leaving group oxygen, which stabilizes the reactant **2z**, is expected, and appears to be, weak or nonexistent in the cation **2+** because the dimethylammonium group of the diethyl triester of **6** has a pK_a = 4.63, in the region expected for a naphthylammonium cation (21).

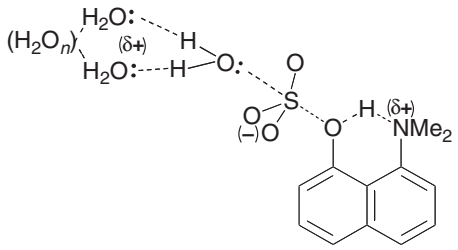
Spontaneous hydrolysis of the zwitterion 2z

The simple mechanism for the hydrolysis of **2z** (k_z with Nu = H_2O) suggested in Scheme 4 is also based on that described for the comparable, closely similar reaction of the phosphate ester **6** (11). It is expected to involve weak (but essential) bonding to the incoming nucleophile (see the following), thus accounting for the small negative entropy of activation. The involvement of the NH^+ group as a general acid will have no significant effect on the entropy term, since the proton transfer takes place within a strong hydrogen bond, which remains in place throughout the reaction. S—O cleavage can be presumed to be well-advanced, as appears invariably to be the case for the spontaneous cleavage of aryl sulfate monoesters. The solvent deuterium kinetic isotope effect ($k_{H_2O}/k_{D_2O} = 1.93 \pm 0.39$) is significant but small, as generally observed for reactions of derivatives of 8-dimethylamino-1-naphthol showing efficient intramolecular general acid catalysis (6, 11, 14, 21). (The closest comparison is with the hydrolysis of the methyl phosphodiester de-

[6]We expect this hydrogen bonding to result also in the lengthening of the S—OAr bond of **2z** that generally accompanies increased rates of cleavage (T.A.S. Brandao, J.P. Priebe, A.S. Damasceno, A.J. Bortoluzzia, A.J. Kirby, and F. Nome. J. Mol. Struct. **734**, 205 (2005); A.J. Kirby. Adv. Phys. Org. Chem. **29**, 87 (1994)), but have not been able to grow suitable crystals to confirm this prediction.

© 2005 NRC Canada

Scheme 5.

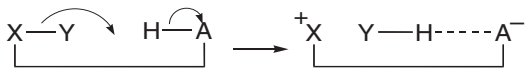


rived from **6** for which we find k_{H_2O}/k_{D_2O} = 1.72 ± 0.14.[7] This reaction involves a mechanism similar to k_z in Scheme 4, and the pK_a of the catalytic dimethylammonium group is also close to 7). The contribution to the solvent deuterium kinetic isotope effect from the in-flight proton of the general acid is small for reactions involving efficient intramolecular general acid catalysis because the transition state is typically early. (Perhaps also because the hydron transfer takes place within a hydrogen bond that is *strengthened* in the transition state, thus producing an inverse contribution to the overall observed isotope effect).[8]

The involvement (weak) of water as a nucleophile is not expected to contribute substantially to the observed solvent deuterium isotope effect, since k_{H_2O}/k_{D_2O} for the spontaneous hydrolysis of 4-nitrophenyl sulfate is only 1.26 (19). Thus, the kinetic parameters observed for the reaction of **2z** are consistent with the transition state shown in Scheme 5. The key to efficient catalysis is the strong intramolecular hydrogen bond, already present in the reactant state, stronger in the product naphthol **7**, and strongest in the transition state.

The key hydrogen bond

Phenomenologically, the key to efficient intramolecular general acid catalysis of X–Y cleavage (in the sense X^+Y^-) is the unique proton of a group HA, properly positioned and sufficiently acidic to form a strong hydrogen bond to the developing negative charge on Y^-.



The simplest experimental indication of a strong intramolecular hydrogen bond in a given system is a substantial increase in the pK_a of the relevant group HY in the product, associated with a proton exchange rate markedly slower than diffusion-controlled. (The pK_a of the dimethylammonium group of **2z** (6.98 at 25 °C) is raised substantially compared to the value of 4.83 at 28 °C observed (22) for *N*,*N*-dimethylammonium-1-naphthalene. We attribute this effect primarily to a relatively strong N—H···O—SO_3^- hydrogen bond: any electrostatic stabilization must be minor because a greater enhancement (pK_a of Me_2NH^+ raised to 7.75) is observed in the corresponding N—H···OMe system (23)).

The requirement that the proton of the general acid be unique defines the acid HA as necessarily monobasic: a COOH group complies, NH_n^+ does not if $n > 1$. Thus, only *N*,*N*-dialkylammonium groups show efficient general acid catalysis and much enhanced pK_as in peri-naphthylammonium systems. The low efficiency of the imidazolium group of **5**, for example, is presumably a consequence of the availability of the second exchangeable proton of the general acid. We note that special arrangements in many enzyme active sites ensure that the distal NH(+) of catalytic histidine imidazoles is not in rapid exchange with the medium.

Reactions with nucleophiles

The attack of nucleophilic amines on the SO_3^- group has been studied by several authors. Attack on sulfur competes with attack on phosphorus for phenyl phosphosulfate (24) and PAPS (25), and with attack on carbon for 4-nitrophenyl sulfate (26). The data for attack on sulfur consistently show a low sensitivity to the basicity of the nucleophile, with β_{nuc} = 0.20 for the reactions with 4-nitrophenyl sulfate. There is no good evidence for attack by oxyanions, though 0.8 mol/L KF occasions a 65% rate increase (and 0.8 mol/L KI an 80% rate decrease) in the rate of hydrolysis at 35 °C. Similarly the rate of hydrolysis of 2,4-dinitrophenyl sulfate increases linearly with fluoride concentration, by up to 17% for 1 mol/L NaF at 45 °C (16).

The hydrolysis of **2z** is catalyzed by oxyanions in the plateau region, with rate enhancements of up to 78% in the presence of 1 mol/L of nucleophile (Table 3). The second-order rate constants depend on the basicity of the oxyanion, and the four points for water, acetate, and substituted acetates (see the next section) give a good Brønsted correlation, with β_{nuc} = 0.26 ± 0.01. This is larger than the value of β_{nuc} = 0.20 observed for the reactions of amines with (the less reactive) 4-nitrophenyl sulfate, and consistent with relatively weak bonding to the nucleophile in the transition state, which is nevertheless somewhat tighter for the intramolecular general-acid-catalyzed reaction. A comparable effect in the same direction (0.20 compared with 0.13 or less for the intermolecular reactions) is observed for the reactions with nucleophiles of the corresponding phosphate ester **6** (11).

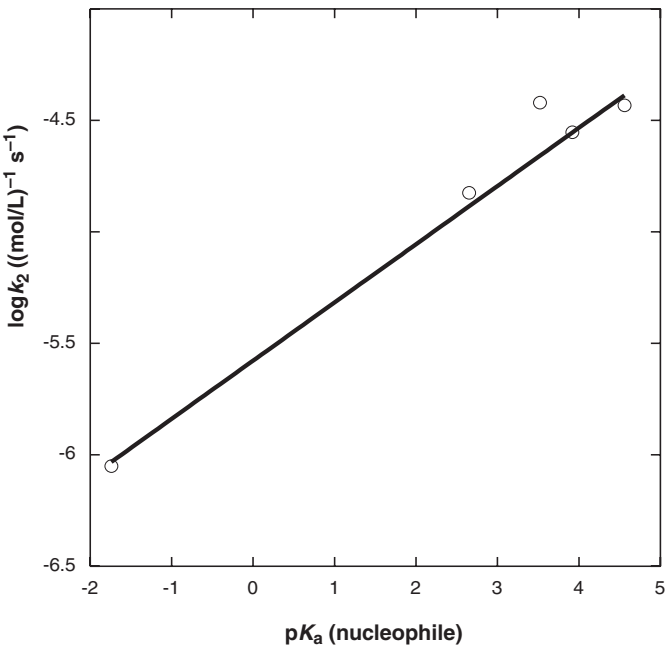
There is good, though largely indirect, evidence that the reactions of **2z** with nucleophiles involve nucleophilic, rather than general base catalysis of hydrolysis. (And good reason to expect S—O rather than C—O cleavage. Aromatic nucleophilic substitution involving the displacement of sulfate dianion by weak carboxylate nucleophiles is not expected from the unactivated aromatic ring system of **2**. And it would be much more strongly sensitive to the basicity of the nucleophile (β_{nuc} is typically 0.7–0.8 (27, 28)) than observed for the reactions of **2z**).

1. General base catalysis has never been reported for the reactions of nucleophiles with simple SO_3^- systems. Reactions of amines with 4-nitrophenyl sulfate (19) show steric effects and entropies of activation typical of nucleophilic, bimolecular processes, typically low sensitivity to the basicity of the nucleophile, and no solvent deuterium isotope effects. All the evidence is consistent with nucleophilic catalysis, albeit with a weak involvement of the committed nucleophile in the transition state typical of SO_3 group transfers.

[7] A.J. Kirby, D. da Silva, M.F. Lima, C.D. Roussev, and F. Nome. Unpublished work.
[8] We are grateful to a referee for this suggestion.

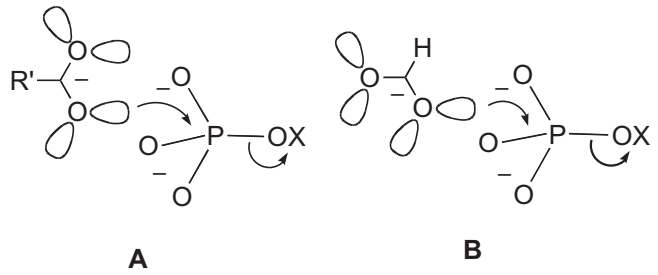
© 2005 NRC Canada

Fig. 2. Brønsted plot for the reactions of oxygen nucleophiles with **2z**. Data from Table 3. The least-squares line drawn is based on the four points for water and for acetate and substituted acetate anions (see the text).



2. The SO_3^- group of this system behaves *in detail* as expected for nucleophilic attack on a monoester $ROSO_3^-$ with a good leaving group.
3. Formate reacts faster than acetate with **2z**, showing a positive deviation from the Brønsted plot of Fig. 2; though from the observed Brønsted β of 0.26 formate should, other things being equal, and certainly for general base catalysis, react almost twice fast as acetate. This is not a unique observation: second-order rate constants for nucleophilic attack on PO_3^{2-} groups by acetate are generally smaller than for formate (11, 29), despite the higher basicity of acetate; so it is not unexpected that the same should apply to attack on the SO_3^- group. This behaviour can be understood in terms of a combination of steric and electrostatic effects, as follows: (*a*) There is no significant difference in basicity, and thus in intrinsic nucleophilic reactivity between the E and Z lone pairs of the carboxylate group (Scheme 6) (30). (*b*) If attack on PO_3^{2-} or SO_3^- involves a Z lone pair (**A** in Scheme 6) any steric effect of the acyl substituent R′ will be negligible, but the second O^- will inevitably come into close proximity to the negatively charged oxygens of the substrate phosphate or sulfate group. (*c*) The consequent repulsive electrostatic effect is avoided if reaction involves the E lone pair (**B** in Scheme 6), but then the steric requirements of the acyl substituent come into play. (*d*) Steric effects decrease in the order R′ > O^- > H. The balance of effects is evidently such that only formate reacts predominantly in mode **B**, and for this reason we have used only the points for water and for acetate and substituted acetate anions to calculate the Brønsted β for the reaction of **2z** (Fig. 2). For nucleophilic attack on neutral, e.g., C=O or alkyl carbon centres, no such electrostatic effect is involved, and acetate generally reacts faster as a nucleophile. These effects do not apply to general base catalysis for which acetate is reliably more reactive.

Scheme 6.



Thus, the evidence is strong that the reactions of **2z** with oxygen nucleophiles involve nucleophilic rather than general base catalysis. It is not, however, sufficient to rule out completely the possibility of a minor contribution from the latter mechanism.

Implications

This work is relevant to sulfate transfer in the context of enzyme evolution. In some cases, phosphatases and sulfatases belong to the same structural superfamily (31, 32) and some have been shown to be catalytically promiscuous. For example, *Escherichia coli* alkaline phosphatase also catalyses sulfate transfer at a measurable rate (33). Though some 10^{10} times slower (in terms of k_{cat}/K_M) than the native reaction, this corresponds to a rate enhancement of 10^9 compared to background for the promiscuous activity. Similarly, we find that arylsulfatase A has promiscuous phosphatase activity, with a rate acceleration $>10^{12}$ over background.[9] Duplication of a gene encoding a bifunctional catalyst could provide a modest advantage of the new activity, to be increased by further selection for higher promiscuous activity of the second gene copy. If catalytic promiscuity is a key to evolution (34–38), then catalytic "crossover" features, such as the effect of a properly positioned general acid on a family of reactions, are logical stepping stones in the process of molecular evolution of catalysis.

Acknowledgements

We are grateful to Programa de Apóio a Núcleos de Excelência (PRONEX), Conselho Nacional de Desenvolvimento Científico e Tecnológico (CNPq), Coordenação de Aperfeiçoamento de Pessoal de Nível Superior (Capes), and Fundação de Apoio a Pesquisa Científica e Tecnológica do Estado de Santa Catarina (FAPESC), all from Brazil and the Biotechnology and Biological Sciences Research Council of Great Britain (BBSRC), for financial assistance.

[9] L.F. Olguin-Contreras and F. Hollfelder. Unpublished results.

© 2005 NRC Canada

References

1. E. Chapman, M.D. Best, S.R. Hanson, and C.H. Wong. Angew. Chem. Int. Ed. **43**, 3526 (2004).
2. S.R. Hanson, M.D. Best, and C.H. Wong. Angew. Chem. Int. Ed. **43**, 5736 (2004).
3. C. Marquordt, Q.H. Fang, E. Will, J.H. Peng, K. von Figura, and T. Dierks. J. Biol. Chem. **278**, 2212 (2003).
4. J.H. Peng, B. Schmidt, K. von Figura, and T. Dierks. J. Mass Spectrom. **38**, 80 (2003).
5. M.L. Bender and J.M. Lawlor. J. Am. Chem. Soc. **85**, 3010 (1963).
6. R.H. Bromilow and A.J. Kirby. J. Chem. Soc. B, 149 (1972).
7. S.J. Benkovic. J. Am. Chem. Soc. **88**, 5511 (1966).
8. A.R. Hopkins, A.L. Green, and A. Williams. J. Chem. Soc. Perkin Trans. 2, 1279 (1983).
9. S.J. Benkovic. Biochemistry, **9**, 1390 (1970).
10. A.J. Kirby. Adv. Phys. Org. Chem. **17**, 183 (1980).
11. A.J. Kirby, M.F. Lima, D. da Silva, and F. Nome. J. Am. Chem. Soc **126**, 1350 (2004).
12. B.S. Furniss, A.J. Hannaford, P.W.G. Smith, and A.R. Tatchel. Vogel's textbook of practical organic chemistry. Longman, London. 1989.
13. W.L.F. Armarego and D.D. Perrin. Purification of laboratory chemicals. Butterworth-Heinemann, Oxford. 1998.
14. A.J. Kirby and J.M. Percy. J. Chem. Soc. Perkin Trans. 2, 907 (1989).
15. M.A. Ragan. Can. J. Chem. **56**, 2681 (1978).
16. E.J. Fendler and J.H. Fendler. J. Org. Chem. **33**, 3852 (1968).
17. T.H. Fife and T.C. Bruice. J. Phys. Chem. **65**, 1079 (1961).
18. H. Maskill. Structure and reactivity in organic chemistry. Oxford University Press, New York. 1999.
19. S.J. Benkovic and P.A. Benkovic. J. Am. Chem. Soc. **88**, 5504 (1968).
20. M.I. Page and A. Willams. Organic & bioorganic mechanisms. Addison Wesley Longman, Harlow. 1997.
21. N. Asaad and A.J. Kirby. J. Chem. Soc. Perkin Trans. 2, 1708 (2002).
22. N.F. Hall and H. Sprinkle. J. Am. Chem. Soc. **54**, 3469 (1932).
23. A. Awwal and F. Hibbert. J. Chem. Soc. Perkin Trans. 2, 152 (1977).
24. W. Tagaki and T. Eiki. Adv. Chem. Ser. **191**, 409 (1980).
25. C.T. Bedford, A.J. Kirby, C.J. Logan, and J.N. Drummond. Bioorg. Med. Chem. **3**, 167 (1995).
26. S.J. Benkovic and P.A. Benkovic. J. Am. Chem. Soc. **88**, 5504 (1966).
27. G. Moutiers, E. Le Guevel, C. Cannes, F. Terrier, and E. Buncel. Eur. J. Org. Chem. 3279 (2001).
28. A.H.M. Renfrew, J.A. Taylor, J.M.J. Whitmore, and A. Williams. J. Chem. Soc. Perkin Trans. 2, 2389 (1994).
29. D. Herschlag and W.P. Jencks. J. Am. Chem. Soc. **111**, 7587 (1989).
30. F.H. Allen and A.J. Kirby. J. Am. Chem. Soc. **113**, 8829 (1991).
31. M. Galperin, A. Bairoch, and E. Koonin. Protein Sci. **7**, 1829 (1998).
32. M.Y. Galperin and M.J. Jedrzejas. Proteins, **4**, 318 (2001).
33. P.J. O'Brien and D. Herschlag. J. Am. Chem. Soc. **120**, 12369 (1998).
34. A. Aharoni, L. Gaidukov, O. Khersonsky, S. McQ Gould, C. Roodveldt, and D.S. Tawfik. Nat. Genet. **37**, 73 (2005).
35. U.T. Bornscheuer and R.J. Kazlauskas. Angew. Chem. Int. Ed. **43**, 6032 (2004).
36. S.D. Copley. Curr. Opin. Chem. Biol. **7**, 265 (2003).
37. B.G. Miller and R.T. Raines. Biochemistry, **43**, 6387 (2004).
38. P.J. O'Brien and D. Herschlag. Chem. Biol. **6**, R91 (1999).

© 2005 NRC Canada

Dynamics of the transient species generated upon photolysis of diarylmethanes within zeolites — Deprotonation and oxidation reactions[1]

Suzanne Shea, Norman P. Schepp, Amy E. Keirstead, and Frances L. Cozens

Abstract: The oxidation of diarylmethanes is a multistep process involving initial formation of a radical cation, deprotonation of the radical cation to the radical, and oxidation of the radical to the carbocation. The dynamics and efficiency of the last two steps in this process, namely deprotonation and oxidation, in acidic zeolites and non-acid zeolites are examined in the present work as a function of the acidity of the diarylmethane radical cations and the oxidation potential of the diarylmethyl radicals. Our results indicate that rate constants for deprotonation strongly depend on the acidity of the radical cations, but not on the composition of the zeolites. In addition, oxidation of the radicals to the diarylmethyl cations is strongly dependent on both the oxidation potential of the radicals and the oxidizing ability of the zeolite. This dependence allows oxidation potentials of the zeolites to be estimated.

Key words: radical cations, carbocations, zeolites, laser flash photolysis.

Résumé : L'oxydation de diarylméthanes est un processus en plusieurs étapes qui implique la formation initiale d'un cation radical, une déprotonation du cation radical et une oxydation du radical en carbocation. On a étudié la dynamique et l'efficacité des deux dernières étapes de ce processus, soit la déprotonation et l'oxydation, dans des zéolites acides et des zéolites non acides, en fonction de l'acidité des cations radicaux diarylméthanes et du potentiel d'oxydation des radicaux diarylméthyles. Les résultats obtenus indiquent que les constantes de vitesse pour la déprotonation dépendent fortement de l'acidité des cations radicaux, mais pas sur la composition des zéolites. De plus, l'oxydation des radicaux en cations diarylméthyles est fortement dépendante à la fois sur le potentiel d'oxydation des radicaux et sur l'habilité des zéolites à oxyder. Cette dépendance permet d'évaluer les potentiels d'oxydation des zéolites.

Mots clés : cations radicaux, carbocations, zéolites, photolyse éclair au laser.

[Traduit par la Rédaction]

Introduction

Zeolites are crystalline aluminosilicate materials comprised of SiO_4 and AlO_4^- tetrahedra that are arranged in a three-dimensional array to form an open framework structure that consists of pores and channels whose size and shape vary widely (1–6). The presence of tetravalent aluminum gives rise to a net negative charge in the backbone, which must be balanced with a charge-balancing cation, typically alkali metals or protons. While the void cavities and channels of the zeolite are capable of accommodating molecular guests, zeolites are not simply inert vessels, but have been shown to participate as electron donors and acceptors in both thermal (7, 8) and photoinduced (9–14) electron transfer reactions. The high density of negative charge on the zeolite framework is thought to provide an environment well-suited for the generation of positively charged species and in fact, carbocations can be thermally generated within proton-exchanged zeolites (15). The redox properties of the zeolite are highly dependent on the nature of the charge-balancing cations (16), and it has been shown that proton-exchanged zeolites are much more powerful oxidizing agents than alkali cation-exchanged zeolites (17). These acidic solids have been the subject of extensive research because of their catalytic ability and wide use as industrial catalysts, particularly for the refinement of petroleum products (4, 18, 19).

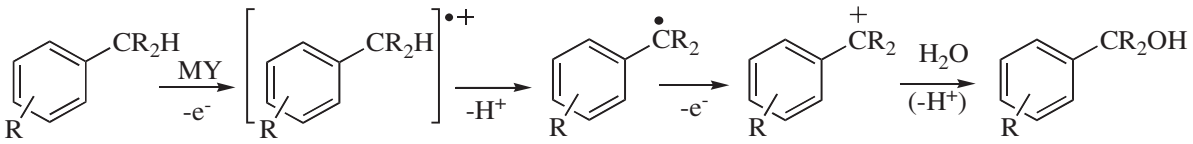
Zeolites have been shown to be good hosts for the study of cationic intermediates because of the stabilization provided by the internal electrostatic fields within the voids of the microporous solids and also by the confined environment, which provides protection of the cationic center from

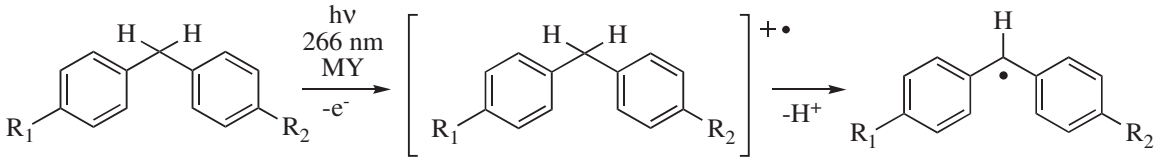
Received 4 May 2005. Published on the NRC Research Press Web site at http://canjchem.nrc.ca on 8 December 2005.

S. Shea, N.P. Schepp,[2] A.E. Keirstead, and F.L. Cozens.[3] Department of Chemistry, Dalhousie University, Halifax, NS B3H 4J3, Canada.

[1]This article is part of a Special Issue dedicated to organic reaction mechanisms.
[2]Corresponding author (e-mail: nschepp@dal.ca).
[3]Corresponding author (e-mail: fcozens@dal.ca).

 doi: 10.1139/V05-208 © 2005 NRC Canada

[1] 

[2] 

An_2CH_2: $R_1 = R_2 = OCH_3$ — $An_2CH_2^{+\bullet}$ — $An_2CH\bullet$

$AnPhCH_2$: $R_1 = H, R_2 = OCH_3$ — $AnPhCH_2^{+\bullet}$ — $AnPhCH\bullet$

Tol_2CH_2: $R_1 = R_2 = CH_3$ — $Tol_2CH_2^{+\bullet}$ — $Tol_2CH\bullet$

Ph_2CH_2: $R_1 = R_2 = H$ — $Ph_2CH_2^{+\bullet}$ — $Ph_2CH\bullet$

nucleophilic species (11, 20, 21). When a positively charged species is encapsulated within these solids, the whole lattice of the zeolite can act as a counteranion, insulating and protecting the carbocation from attack by external nucleophiles. This stabilization has been found to be dramatic in many cases in which the tight fit between the organic guest and the zeolite occurs (22). These characteristics, combined with the wide range of crystalline structures available and the ability to tailor the zeolite to the reaction of interest, have made zeolites the host of choice for many studies of organic cations (9, 17, 23). Organic radical cations formed within the zeolite framework have also been the subject of much interest. Photoionization reactions leading to radical cation formation have been shown to be easily carried out within zeolite frameworks, making zeolites convenient host materials to study the photoinduced formation of radical cations (10, 21).

It has long been known that arylmethanes can be oxidized when incorporated into acidic zeolites (17, 24, 25). The mechanism for this reaction is thought to involve initial one-electron oxidation to the arylmethane radical cation that then deprotonates to yield the corresponding arylmethyl radical. A second one-electron oxidation can occur to convert the radical to the carbocation, which is then trapped by water to give the arylmethyl alcohol (eq. [1]).

While several studies have appeared concerning the identification of radical cations and carbocations upon incorporation of arylmethane derivatives in acidic zeolites (26–28), little is known about the absolute kinetics of the individual reactions involved in the overall oxidation process. In addition, quantitative information regarding the effect of the acidity of the arylmethane radical cations and the oxidation potential of the arylmethyl radicals on the dynamics of these processes is not currently available. In the present work, we examine the intrazeolite behaviour of a series of diarylmethanes incorporated into both proton-exchanged (HY) and alkali cation-exchanged (NaY, KY, CsY) zeolites. Our results show that the dynamics of the deprotonation of the diarylmethane radical cations to diarylmethyl radicals strongly depends on radical cation acidity, and that oxidation of the diarylmethyl radicals to the corresponding diarylmethyl cations depends both on the oxidation potential of the radical and the oxidizing ability of the zeolite.

Results

Dianisylmethane (An_2CH_2) in NaY, KY, CsY, and HY

Laser flash photolysis (266 nm) of dianisylmethane in NaY under vacuum conditions resulted in the transient diffuse reflectance spectra shown in Fig. 1*a*. These spectra show the presence of absorption at 450 nm formed promptly within the laser pulse. With a time resolution of ca. 100 ns for the diffuse reflectance laser system, prompt formation of the band at 450 nm indicates that it was generated with a rate constant $>10^7$ s^{-1}. The band at 450 nm was not stable and decayed close to baseline (inset, Fig. 1*a*) over the 40 μs timescale of the experiment. Nonlinear least-squares analysis using a first-order rate expression[4] gave a rate constant ($k = 1.2 \times 10^5$ s^{-1}) for the decay of the 450 nm band. After saturation of the zeolite with molecular oxygen, the band at 450 nm was still observed (Fig. 1*b*) and its decay remained unchanged. In solution, the dianisylmethane radical cation ($An_2CH_2^{\cdot+}$) is known to have an absorption maximum at 450 nm and to be unaffected by oxygen (29, 30). Thus, the transient at 450 nm is assigned to $An_2CH_2^{\cdot+}$ (eq. [2], $R_1 = R_2 = OCH_3$).

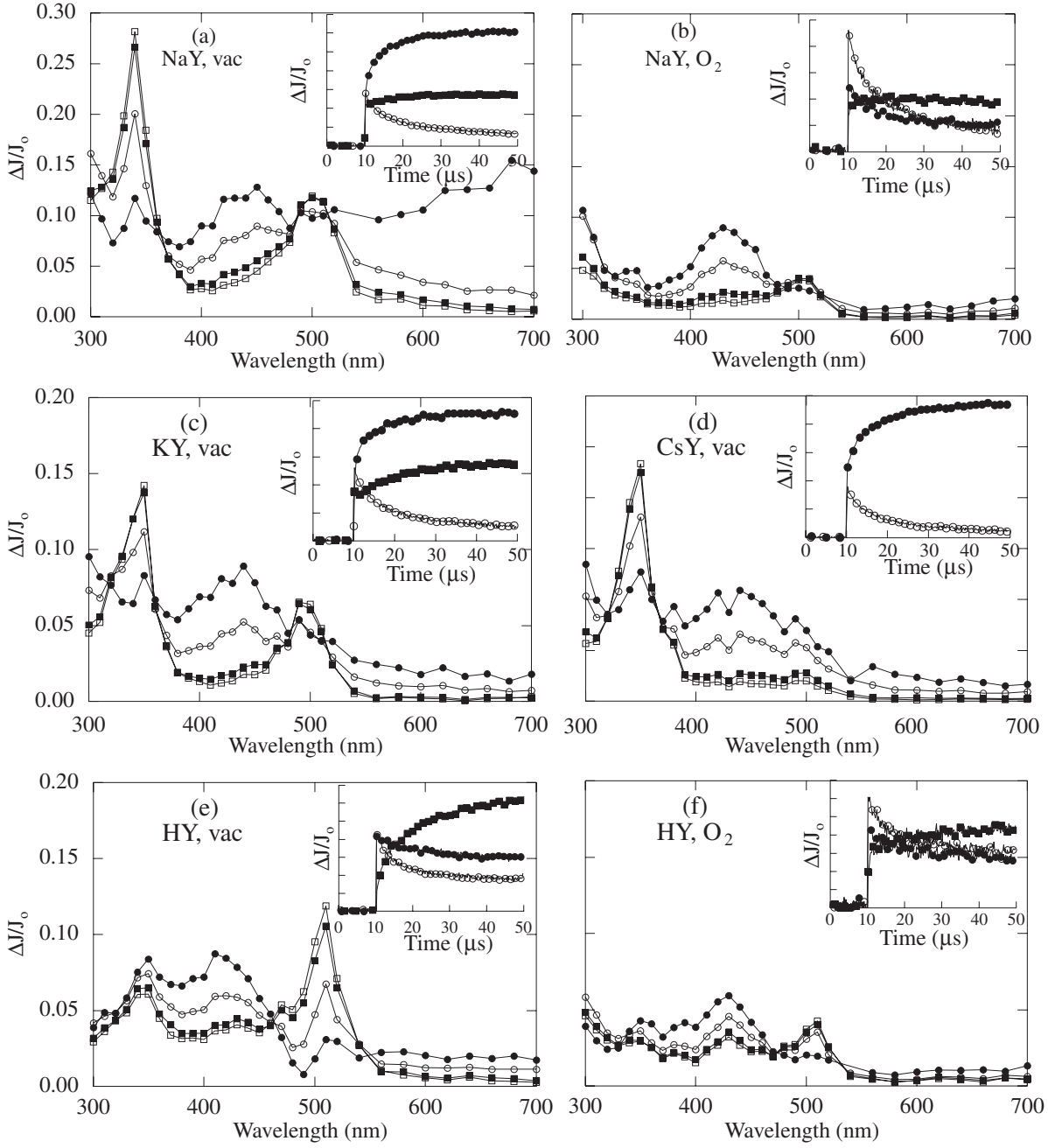
The radical cation is presumably formed by rapid photoionization of the incorporated dianisylmethane. Consistent with this mechanism is the observation of short-lived Na_3^{2+} clusters at wavelengths greater than 510 nm (Fig. 1*a*) produced when electrons are trapped by the counterbalancing sodium cations (10, 13, 31–33).

As $An_2CH_2^{\cdot+}$ decayed, a new transient species with a sharp absorption band at 340 nm grew in with a rate constant of 1.4×10^5 s^{-1}. Under vacuum conditions the transient responsible for this absorption did not decay over the timescale of the experiment, while the transient had a very short lifetime in the presence of oxygen (Fig. 1*b*). This transient is attributed to the dianisylmethyl radical ($An_2CH\cdot$), which in solution is known to have an absorption maximum at 340 nm (34) and to react rapidly with oxygen. Radical formation likely occurs by deprotonation (vide infra) of the initially

[4] See the Experimental section for explanation of data analysis.

© 2005 NRC Canada

Fig. 1. Transient diffuse reflectance spectra recorded 400 ns (●), 4.00 μs (○), 18.8 μs (■), and 32.0 μs (□) after 266 nm laser flash photolysis of An_2CH_2 in: (*a*) NaY under vacuum conditions; (*b*) NaY under oxygen conditions; (*c*) KY under vacuum conditions; (*d*) CsY under vacuum conditions; (*e*) HY under vacuum conditions; and (*f*) HY under oxygen conditions. Insets show kinetic traces collected at 340 nm (●), 440 nm (○), and 500 nm (■).



formed radical cation (eq. [2]), which is typically the dominant reaction of the $An_2CH_2^{\cdot+}$ in solution (29, 30). This mechanism for radical formation is supported by the similarity between the rate constants for the decay of $An_2CH_2^{\cdot+}$ at 450 nm (1.2×10^5 s^{-1}) and the growth of the radical at 340 nm (1.4×10^5 s^{-1}).

Close examination of the spectral data in Fig. 1*a* also shows some prompt absorption at 340 nm due to $An_2CH\cdot$ prior to the time-resolved growth. Thus, while most of the radicals were formed in a time-resolved manner after the laser pulse, a small fraction were generated more rapidly within the laser pulse with a rate constant $>10^7$ s^{-1}.

A fourth transient species with strong absorption at 500 nm is also present in the spectra in Fig. 1*a*. This transient was long-lived and did not decay under both vacuum and oxygen-saturated conditions over the longest timescale available on our laser system (10 ms). The location of the absorption band and the lack of sensitivity toward oxygen are consistent with the identification of the 500 nm transient as the dianisylmethyl cation (An_2CH^+) (34).

© 2005 NRC Canada

Like $An_2CH\cdot$, whose formation had a small prompt component and a larger time-resolved component, the formation of An_2CH^+ under vacuum conditions took place over two different time regimes. In this case, An_2CH^+ was mostly formed promptly within the laser pulse with a rate constant $>10^7$ s^{-1}, with the time-resolved component being comparatively small. The rate constant for the growth was measured to be 1.5×10^5 s^{-1}, which is similar to the rate constant for the decay of $An_2CH_2^{\cdot+}$. Under oxygen, both the prompt and time-resolved components of carbocation formation were still readily observable, but with substantially reduced intensity.

The results obtained upon laser flash photolysis of dianisylmethane in KY under vacuum conditions (Fig. 1*c*) were similar to those obtained for zeolite NaY. $An_2CH_2^{\cdot+}$ with absorption at 450 nm was formed promptly within the laser pulse and then decayed with a rate constant of 1.3×10^5 s^{-1}. Concomitant with this decay was a growth ($k = 1.4 \times 10^5$ s^{-1}) at 350 nm attributed to the formation of $An_2CH\cdot$. The long-lived An_2CH^+ was also observed at 500 nm and exhibited both prompt formation and a small amount of time-resolved growth ($k = 0.9 \times 10^5$ s^{-1}), similar to that seen in zeolite NaY.

In CsY, both $An_2CH_2^{\cdot+}$ and $An_2CH\cdot$ were again observed (Fig. 1*d*). The decay of the radical cation and the growth of the radical took place with similar rate constants of 1.4×10^5 s^{-1}. However, in this case, no distinct absorption at 500 nm was evident, indicating that An_2CH^+ was not generated in this zeolite.

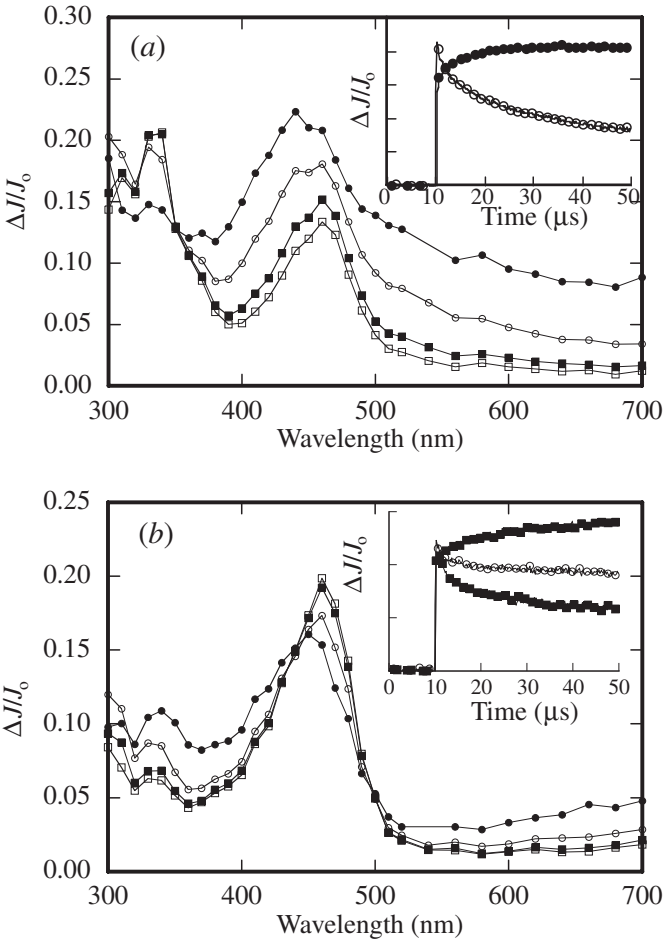
In the acidic zeolite HY, laser irradiation of dianisylmethane under hydrated vacuum conditions led to the formation of $An_2CH_2^{\cdot+}$ (Fig. 1*e*), which decayed with a rate constant of 1.2×10^5 s^{-1} that is similar to the rate constants previously measured in the alkali metal-exchanged Y zeolites. The decay of $An_2CH_2^{\cdot+}$ did not lead to a significant buildup of the radical $An_2CH\cdot$ at 350 nm. Instead, absorption at 510 nm owing to An_2CH^+ grew in with a rate constant of 0.9×10^5 s^{-1}. Some $An_2CH\cdot$ was formed promptly within the laser pulse. The radical was unusually reactive in HY and decayed with a rate constant of 1.1×10^5 s^{-1}, similar to the decay of $An_2CH_2^{\cdot+}$ and the growth of An_2CH^+.

The addition of oxygen to the dianisylmethane–HY composite did not significantly alter the transient diffuse reflectance spectra (Fig. 1*f*), which again showed $An_2CH_2^{\cdot+}$ decaying to give An_2CH^+ at 510 nm. The rate constants for decay of the radical cation and growth of the carbocation were not influenced by the presence of oxygen; however, the amount of An_2CH^+ formed was reduced to approximately half that observed under vacuum conditions.

Anisylphenylmethane ($AnPhCH_2$) in NaY, KY, CsY, and HY

The transient diffuse reflectance spectra obtained upon 266 nm laser irradiation of $AnPhCH_2$ in NaY under vacuum conditions showed the prompt formation of a transient with strong absorption at 440 nm (Fig. 2*a*) assigned to the anisylphenylmethane radical cation ($AnPhCH_2^{\cdot+}$) (29). The radical cation was not stable, but its decay was difficult to quantify because of the presence of residual absorption at 460 nm (vide infra) that also decayed slowly over the timescale of the experiment, as well as the presence of absorption due to Na^+-electron complexes. Analysis of the decay at 440 nm

Fig. 2. Transient diffuse reflectance spectra recorded 400 ns (●), 4.00 μs (○), 18.8 μs (■), and 32.0 μs (□) after 266 nm laser flash photolysis of $AnPhCH_2$ in: (*a*) NaY under vacuum conditions; and (*b*) HY under vacuum conditions. Insets show kinetic traces collected at 340 nm (●), 430 nm (○), and 460 nm (■).



was therefore carried out using a double first-order expression that led to a rate constant of 1.4×10^5 s^{-1} for the decay of $AnPhCH_2^{\cdot+}$. The spectra also feature an absorption band at 340 nm due to the anisylphenylmethyl radical ($AnPhCH\cdot$) (29, 34). The radical grew in with a rate constant of 1.8×10^5 s^{-1}. This is similar to the rate constant for the decay of $AnPhCH_2^{\cdot+}$, indicating that the radical was formed by deprotonation of $AnPhCH_2^{\cdot+}$ (eq. [2], $R_1 = H$, $R_2 = OCH_3$). Significant absorption was present at 340 nm immediately after the laser pulse. Thus, some prompt radical formation did occur prior to the time-resolved component.

After complete decay of $AnPhCH_2^{\cdot+}$, considerable absorption remained with a maximum at 460 nm. This matches well with the absorption spectrum of the anisylphenylmethyl cation ($AnPhCH^+$) (29). Due to the overlap in absorption of $AnPhCH_2^{\cdot+}$ and $AnPhCH^+$, it is difficult to determine if $AnPhCH^+$ was generated promptly within the laser pulse, or if its formation followed the decay of $AnPhCH_2^{\cdot+}$. Significant prompt formation likely did occur, as suggested by the shoulder at 460 nm in the diffuse reflectance spectrum recorded immediately after the laser pulse (Fig. 2*a*). The addition of oxygen to the sample did not significantly affect the

© 2005 NRC Canada

decay of the band at 440 nm, but the relative amount of residual absorption at 460 nm was reduced (see Supplemental material).[5] Absorption due to AnPhCH· at 340 nm was quenched upon addition of oxygen to the sample, which is consistent with the known reactivity of carbon-centered radicals.

Results similar to those described were obtained upon laser photolysis of $AnPhCH_2$ in both KY and CsY under vacuum conditions. The transient diffuse reflectance spectra again featured absorption of $AnPhCH_2^{\cdot+}$ that decayed on the timescale of the experiment and a band at 340 nm owing to AnPhCH· that exhibited a time-resolved growth. The rate constants for the decay of $AnPhCH_2^{\cdot+}$ and the growth of AnPhCH· in both KY and CsY were very similar (Table 1). The only major difference in the results obtained in these two zeolites was that substantial absorption at 460 nm due to the $AnPhCH^+$ was observed after the decay of $AnPhCH_2^{\cdot+}$ in KY, while $AnPhCH_2^{\cdot+}$ decayed to the baseline in CsY. Thus, $AnPhCH^+$ was generated in KY, but not in CsY.

In the acidic zeolite HY under hydrated vacuum conditions, the spectrum immediately after the laser pulse consisted of a strong band at 450 nm and a weaker band 340 nm (Fig. 2*b*). The band at 340 nm was quenched by oxygen and can be attributed to AnPhCH·. However, unlike the situation in the non-acidic zeolites where both prompt and time-resolved components were observed for the formation of AnPhCH·, only the prompt component was observed in HY. In addition, AnPhCH· was not stable in HY and decayed with a rate constant of 1.2×10^5 s^{-1}.

The absorption band at 450 nm did not decay, but instead increased in intensity as a function of time with a rate constant of 0.9×10^5 s^{-1} and shifted to 460 nm. These results indicate that both $AnPhCH_2^{\cdot+}$ and $AnPhCH^+$ were formed promptly within the laser pulse to give a composite band with a maximum at 450 nm. The small decrease in absorption at 420 nm on the side of the initially formed 450 nm composite band was presumably due to the decay of $AnPhCH_2^{\cdot+}$. The time-resolved increase leading to the final spectrum with a maximum at 460 nm is consistent with an additional time-resolved component for the formation of $AnPhCH^+$.

Upon the addition of oxygen to the sample, the absorption spectrum immediately after the laser pulse showed a strong band at 450 nm due to $AnPhCH^+$. A distinct shoulder at 410–430 nm was also evident, presumably because of $AnPhCH_2^{\cdot+}$. Under these conditions, there was no time-resolved growth of the carbocation at 450 nm; only a small decay due to the disappearance of $AnPhCH_2^{\cdot+}$ was observed.

Ditolylmethane (Tol_2CH_2) in NaY, KY, CsY, and HY

The transient diffuse reflectance spectra obtained upon laser irradiation of ditolylmethane in NaY under vacuum conditions (Fig. 3*a*) clearly show a sharp absorption band at 340 nm formed promptly within the laser pulse. This transient species, which reacted rapidly with oxygen, can be identified as the ditolylmethyl radical (Tol_2CH·) (34).

The ditolylmethane radical cation ($Tol_2CH_2^{\cdot+}$) has not been observed in solution, but its absorption spectrum should be similar to the 1,4-dimethylbenzene radical cation, which has a weak absorption band at 450 nm together with a stronger band at 305 nm in acetonitrile (35). A broad absorption centered at 460 nm is evident in Fig. 3*a*. However, this band is not likely due to the formation of $Tol_2CH_2^{\cdot+}$. In particular, the decay at 460 nm did not lead to the formation of the radical at 340 nm as would be expected if the band at 460 nm was due to $Tol_2CH_2^{\cdot+}$. In addition, the absorption band at 460 nm changed under oxygen conditions to give a transient with a narrow absorption band at 470 nm. The location and shape of this band is not consistent with the known spectrum of the $Tol_2CH_2^{\cdot+}$, but does agree well with the presence of the ditolylmethyl cation (Tol_2CH^+) (34). Thus, the broad absorption at 460 nm under vacuum conditions is most likely due to prompt formation of Tol_2CH^+, together with an oxygen sensitive transient such as sodium clusters (21) or the triplet excited state of ditolylmethane, which has broad absorption from 330 to 530 nm (36, 37). The inability to detect $Tol_2CH_2^{\cdot+}$ suggests that it is very unstable in NaY and undergoes deprotonation within the duration of the laser pulse to rapidly generate Tol_2CH·.

The absence of absorption due to $Tol_2CH_2^{\cdot+}$ was also evident in the spectra generated upon irradiation of ditolylmethane in KY. Only prompt formation of a sharp band at 340 nm owing to Tol_2CH· was observed, together with broad absorption due to trapped electrons or triplet ditolylmethane. In this zeolite, no substantial absorption due to Tol_2CH^+ at 470 nm was apparent. Thus, Tol_2CH^+ was not generated in KY. Results obtained in CsY were very similar to those in KY: only the prompt formation of Tol_2CH· was observed, with no evidence for the presence of $Tol_2CH_2^{\cdot+}$ or the formation of Tol_2CH^+.

Both Tol_2CH· and Tol_2CH^+ were readily observed upon laser irradiation of Tol_2CH_2 in HY (Fig. 3*b*). The absorption at 470 nm due to Tol_2CH^+ under vacuum conditions consisted of a large prompt component as well as a small time-resolved component. The rate constant for this delayed component was determined to be 0.9×10^5 s^{-1}. Tol_2CH· absorption at 340 nm was completely formed promptly within the laser pulse, with no time-resolved growth component. The radical was long-lived, but did show some decay over the timescale of the experiment. This decay could not be reliably analyzed because of the large residual absorption remaining 40 μs after the laser pulse. The time-resolved component of Tol_2CH^+ formation, together with absorption due to Tol_2CH·, was quenched under oxygen-saturated conditions, but prompt carbocation formation was still observed.

Diphenylmethane (Ph_2CH_2) in NaY, KY, CsY, and HY

The time-resolved diffuse reflectance spectra obtained upon laser flash photolysis (266 nm) of diphenylmethane in each of the four zeolites (NaY, KY, CsY, and HY) under vacuum conditions showed a strong absorption band centered at 330 nm (Figs. 4*a* (NaY) and 4*b* (HY)) because of the forma-

[5] Transient diffuse reflectance spectra of $AnPhCH_2$, Tol_2CH_2, and Ph_2CH_2 in NaY and HY under oxygen conditions and in KY and CsY under vacuum conditions are provided. Supplementary data for this article are available on the Web site or may be purchased from the Depository of Unpublished Data, Document Delivery, CISTI, National Research Council Canada, Ottawa, ON K1A 0R6, Canada. DUD 4051. For more information on obtaining material refer to http://cisti-icist.nrc-cnrc.gc.ca/irm/unpub_e.shtml.

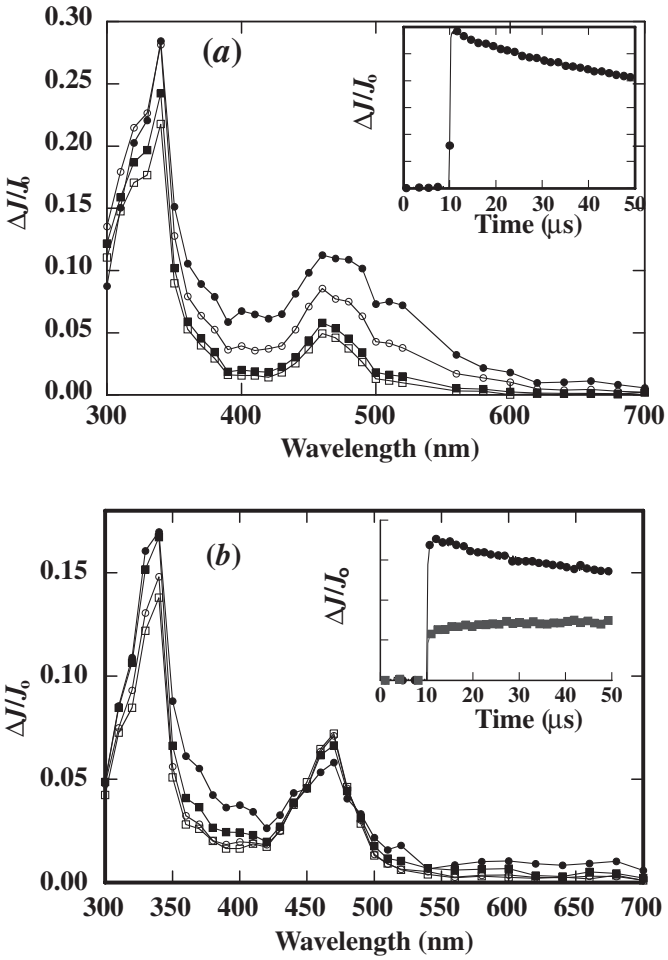
© 2005 NRC Canada

Table 1. Rate constants for the time-resolved decay of the diarylmethane radical cations (RC^{+}), growth of diarylmethyl radicals (R·), and growth of the diarylmethyl cations (C^{+}) in the acidic and non-acidic Y zeolites under vacuum conditions.

	k (10^5 s^{-1})[a,b]									
	NaY			KY			CsY		HY	
Substrate	RC^{+} decay	R· growth	C^{+} growth	RC^{+} decay	R· growth	C^{+} growth	RC^{+} decay	R· growth	RC^{+} decay	R· growth	C^{+} growth
An_2CH_2	1.2	1.4	1.5	1.3	1.4	0.9	1.4	1.4	1.2	No gr.[d]	0.9
$AnPhCH_2$	1.4	1.8	Overlap[e]	1.3	1.3	Overlap[e]	1.0	1.3	Overlap[e]	No gr.[d]	0.8
Tol_2CH_2	Not obs.[c]	No gr.[d]	No gr.[d]	Not obs.[c]	No gr.[d]	No gr.[d]	Not obs.[c]	No gr.[d]	Not obs.[c]	No gr.[d]	0.9

Note: Not observed (not obs.) and no growth (no gr.)
[a]Errors in the fitted data are typically small (±1%). However, due to the challenges associated with preparing zeolite samples in a reproducible manner, actual errors are closer to ±10%.
[b]All measurements were made at room temperature (22 ± 1 °C).
[c]Transient not observed.
[d]Transient formed promptly with no subsequent time-resolved growth.
[e]Time-resolved data obscured because of overlapping C^{+}/RC^{+} absorption bands.

Fig. 3. Transient diffuse reflectance spectra recorded 400 ns (●), 4.00 μs (○), 18.8 μs (■), and 32.0 μs (□) after 266 nm laser flash photolysis of Tol_2CH_2 in: (*a*) NaY under vacuum conditions; and (*b*) HY under vacuum conditions. Insets show kinetic traces collected at 340 nm (●) and 470 nm (■).



tion of the diphenylmethyl radical (Ph_2CH·) (34, 38). No absorption due to $Ph_2CH_2^{\cdot+}$ or Ph_2CH^{+} was evident in any of the four zeolites examined.

The transient diffuse reflectance spectra obtained in NaY and KY did include broad absorption stretching from ca. 400 to 700 nm that can be attributed to trapped electrons. In addition, an unexpected transient with absorption at 530 nm was observed in both KY and CsY. The transient species responsible for this absorption was quenched by oxygen. The absorption at 530 nm is not consistent with the presence of the diphenylmethane radical cation (λ_{max} for toluene radical cation ≈ 430 nm) (35) or the diphenylmethyl cation (λ_{max} = 435 nm) (34), but may be due to the diphenylmethane radical anion (λ_{max} = 530 nm) (39) generated by trapping of a photoionized electron by diphenylmethane, or by direct electron transfer from the framework to excited diphenylmethane.

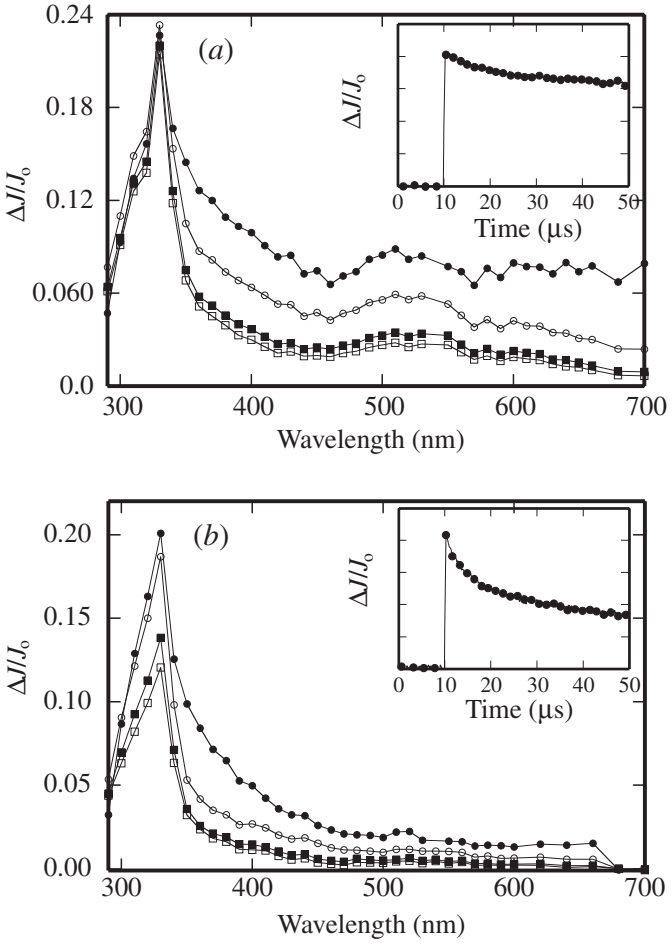
Discussion

Generation and deprotonation of diarylmethane radical cations

It is well-established that radical cations of organic mate-

© 2005 NRC Canada

Fig. 4. Transient diffuse reflectance spectra recorded 400 ns (●), 4.00 μs (○), 18.8 μs (■), and 32.0 μs (□) after 266 nm laser flash photolysis of Ph_2CH_2 in: (*a*) NaY under vacuum conditions; and (*b*) HY under vacuum conditions. Insets show kinetic traces collected at 340 nm (●).



rials incorporated within zeolites can be generated by direct irradiation of the precursor with the zeolite framework acting as the electron acceptor (10, 21). The results obtained in the present work provide either direct or indirect evidence that each of the four diarylmethanes do undergo photoionization within the cation-exchanged Y-zeolites. For An_2CH_2 and $AnPhCH_2$, direct evidence supporting photoionization comes from the observation of the absorption bands associated with their radical cations. For Tol_2CH_2 and Ph_2CH_2, the radical cations were not observed. However, prompt formation of the corresponding diarylmethyl radicals was observed, and the presence of these species can most reasonably be explained by initial formation of short-lived radical cations generated by photoionization of the neutral precursors, followed by rapid deprotonation ($>10^7$ s^{-1}) within the time duration of the laser pulse.

Diarylmethyl radicals were also observed upon direct 266 nm irradiation of An_2CH_2 and $AnPhCH_2$, but with these two substrates, most of the observed radicals were formed in a time-resolved manner with rate constants that ranged from 1.3×10^5 to 1.8×10^5 s^{-1} in NaY, KY, and CsY. These rate constants quite closely matched the rate constants for the decay of the radical cations, which provides good evidence that radical generation occurred by deprotonation of the radical cations. Some prompt formation of $An_2CH\cdot$ and $AnPhCH\cdot$ was observed upon irradiation of An_2CH_2 and $AnPhCH_2$ in the alkali-metal-exchanged zeolites. This suggests that radical cations generated by photoionization exist in at least two sites within the zeolites that exhibit considerably different deprotonation abilities (40, 41). One of these sites induces rapid deprotonation that leads to prompt radical growth, while the other induces a slower deprotonation.

It has previously been demonstrated that rate constants for deprotonation of arylmethyl radical cations in solution inversely correlate with thermodynamic stability of the radical cations (29). Thus, stabilized arylmethyl radical cations, such as those bearing electron-donating methoxy groups on the aromatic ring, undergo deprotonation reactions more slowly than nonstabilized radical cations. The relatively slow deprotonation recorded in the present work for $An_2CH_2^{\cdot+}$ and $AnPhCH_2^{\cdot+}$ radical cations compared to the fast deprotonation for $Tol_2CH_2^{\cdot+}$ and $Ph_2CH_2^{\cdot+}$ therefore agree well with expectations based on the relative stability of these radical cations.

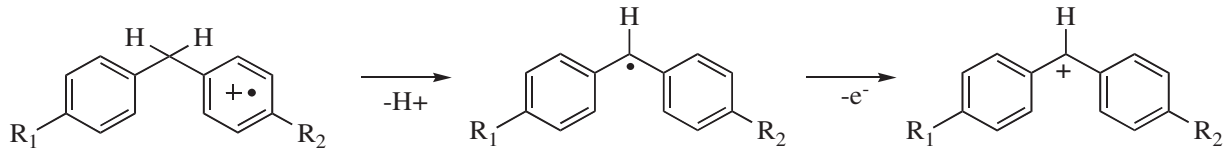
The absolute rate constants for the deprotonation reaction can in some cases be compared with those measured in solution. In particular, the rate constant for the conversion of $An_2CH_2^{\cdot+}$ to the dianisylmethyl radical in acetonitrile is approximately 2.5×10^5 s^{-1} (29), a value that is slightly greater than the rate constant of 1.1×10^5 s^{-1} in NaY. While competing processes may contribute to the decay of the radical cation, the differences in the rate constants from solution to NaY suggest that deprotonation in NaY is somewhat slower than in acetonitrile. It has also been demonstrated that the lifetime of $An_2CH_2^{\cdot+}$ in acetonitrile is very similar to the lifetime of $AnPhCH_2^{\cdot+}$ (29). The small difference measured in the present work between the decays of these two radical cations in zeolites is thus consistent with results obtained in solution.

While rate constants for the deprotonation of Tol_2CH_2 and Ph_2CH_2 radical cations have not been measured, previous results (42) have shown that the 1,4-dimethylbenzene radical cation is almost four orders of magnitude more reactive than the 4-methylanisole radical cation. Thus, replacing a methoxy group with a methyl group greatly decreases the lifetime of the radical cation. This is consistent with our inability to observe neither the ditolylmethane nor the diphenylmethane radical cations in the present work.

For $An_2CH_2^{\cdot+}$ and $AnPhCH_2^{\cdot+}$, which could be observed in all of the zeolites, the nature of the counterbalancing cation had little influence on the rate constant for the conversion of the radical cation to the radical. Thus, the increased Brønsted basicity associated with zeolites (11) as the counterion is changed from Na^+ to Cs^+ is not manifested in the radical cation decay kinetics, despite the evidence that deprotonation of the radical cations is a significant process.

In the strongly acidic HY zeolite, the diarylmethyl radicals that would be formed by deprotonation of diarylmethane radical cations should rapidly reprotonate, thus effectively shifting the radical cation – radical acid–base equilibrium to the radical cation side. Under these circumstances, the radical cations would be expected to have considerably longer lifetimes in HY compared with the nonacidic zeolites. Instead, $An_2CH_2^{\cdot+}$ decayed in HY with a rate

© 2005 NRC Canada

[3] 

constant that was very similar to its decay in the non-acidic alkali-metal-exchanged zeolites. Furthermore, no increase in the lifetimes of $Tol_2CH_2^{\cdot+}$ and $Ph_2CH_2^{\cdot+}$ was evident in HY, as these radical cations were still too short lived to be observed. The continued rapid decay of these radical cations, particularly in the case of $An_2CH_2^{\cdot+}$, is likely due to rapid oxidation of the diarylmethyl radicals in HY, which does not allow reprotonation of the radical to take place. This is discussed in further detail in the following.

Diarylmethyl cation formation

To discuss the mechanism for carbocation formation, it is useful to first summarize some relevant results and establish some revealing trends. First, in evacuated zeolites, formation of the diarylmethyl cations took place over one or two distinct time regimes, depending on the identity of the counterion and the structure of the substrate. A substantial fraction of An_2CH^+ in NaY and KY was formed promptly within the laser pulse with a rate constant $>10^7$ s^{-1}, and a smaller fraction was generated more slowly with rate constants similar to those for the decay of the radical cation and the growth of the radical. In HY, only time-resolved formation of An_2CH^+ was observed, while this carbocation was not detected in CsY. For $AnPhCH^+$, overlapping absorption of the radical cation and the carbocation made it difficult to evaluate the fraction of carbocation derived from prompt and time-resolved processes, but time-resolved formation was distinctly observed in HY. Only prompt formation of Tol_2CH^+ was observed in NaY, but a small amount of time-resolved formation was present in HY. No carbocation was observed upon irradiation of Ph_2CH_2 in any of the zeolites. Since the diphenylmethyl cation generated by other means is quite long-lived in HY (41), its absence upon irradiation of Ph_2CH_2 in HY in the present experiments suggests that it is not formed.

The results outlined above reveal several important trends about the conditions needed for delayed formation of the carbocations. First, in the non-acidic zeolites, only the most stable carbocation (An_2CH^+) showed time-resolved formation. In addition, this delayed formation of An_2CH^+ was observed in NaY and KY, but not in CsY. In the acidic HY, three carbocations (An_2CH^+, $AnPhCH^+$, and Tol_2CH^+) showed delayed formation, but the efficiency decreased upon going from the more stable An_2CH^+ to the less stable Tol_2CH^+. Thus, *these trends show that the presence of delayed carbocation formation depends both on the stability of the carbocation and the nature of the counterion.*

Trends concerning prompt carbocation formation can also be extracted from the results described above. Prompt carbocation formation was observed in NaY for An_2CH^+ and Tol_2CH^+ (and likely $AnPhCH^+$), but not for the less stable Ph_2CH^+. However, in KY only An_2CH^+ and $AnPhCH^+$ showed evidence for prompt carbocation formation. Thus, *prompt carbocation formation also depends both on the stability of the carbocation and the nature of the counterion.*

Second, under oxygenated conditions, the time-resolved growth of An_2CH^+ was almost completely quenched in NaY, and was considerably reduced in HY. Similarly, the delayed growth of $AnPhCH^+$ and Tol_2CH^+ observed in evacuated HY was no longer present under oxygen-saturated conditions. In addition, while prompt formation of An_2CH^+, $AnPhCH^+$, and Tol_2CH^+ in NaY continued to be observed in the presence of oxygen, there was a general reduction in intensity compared with non-oxygenated conditions. Thus, since carbocations themselves are not directly influenced by the presence of oxygen, *the quenching effect of oxygen strongly suggests that the precursor to the carbocation is a species such as a radical or triplet that is reactive toward oxygen.*

One mechanism for carbocation formation that agrees well with many of the trends and observations previously outlined involves zeolite-induced oxidation of the radical generated upon deprotonation of the diarylmethane radical cations (eq. [3]).

This mechanism is nicely consistent with the effect of changing counterion and substrate structure on the yield of the carbocations. In particular, the oxidizing ability of Y zeolites follows the order HY > NaY > KY > CsY (16), and this order matches the yield of time-resolved carbocation formation as a function of counterion. Furthermore, An_2CH^+ was generated under milder conditions than Tol_2CH^+, while Ph_2CH^+ was not detected even in the highly oxidizing HY zeolite. Since the oxidation potentials of the radicals increase in the order $An_2CH\cdot$ < $AnPhCH\cdot$ < $Tol_2CH\cdot$ < $Ph_2CH\cdot$ (Table 2), the mechanism in eq. [3] agrees well with the effect of substrate structure on carbocation formation.

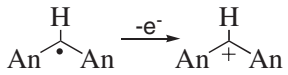
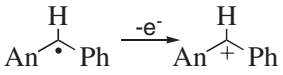
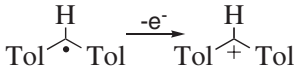
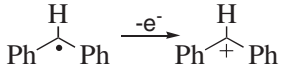
In addition, the efficiency of carbocation formation was substantially diminished upon addition of oxygen to the zeolite samples. Since neither the radical cations nor the carbocations are sensitive to oxygen, while the diarylmethyl radicals are quenched by oxygen, the observed decrease in the formation of the carbocation under oxygen conditions is consistent with the radicals being their immediate precursor.

If carbocation formation did take place via oxidation of the radical, a correlation would normally be expected between the decay of the radical and the growth of the carbocation. The current results show that such correlations are sometimes present: the radicals ($An_2CH\cdot$, $AnPhCH\cdot$, and $Tol_2CH\cdot$) in HY did decay as their corresponding carbocations grew in. However, a more typical correlation observed in the present work is that between the decays of the radical cations and the growths of the carbocations, particularly for the formation of An_2CH^+ in NaY, KY, and HY. As well, the radicals ($An_2CH\cdot$, $AnPhCH\cdot$, and $Tol_2CH\cdot$) observed in NaY under vacuum conditions were long-lived, and were not converted to their corresponding carbocations over the timescale of the experiments.

These results can be rationalized on the assumption that, in the inhomogeneous environment of the zeolites (40), the radicals may initially have been generated in or near sites that have substantially different oxidizing abilities. Thus, in

© 2005 NRC Canada

Table 2. Summary of time-resolved diarylmethyl cation (C^+) formation in Y zeolites by oxidation of diarylmethyl radicals, and oxidation potentials (vs. SCE in acetonitrile) for the diarylmethyl radicals.

Radical	E_{ox} ($R\cdot/R^+$ vs. SCE)	HY ($E_{red} \approx$ 0.23–0.35 V)[a]	NaY ($E_{red} \approx$ 0.04–0.16 V)[a]	KY ($E_{red} \approx$ 0.04–0.16 V)[a]	CsY ($E_{red} <$ 0.04 V)[a]
	≈0.04[b]	Time resolved	Time resolved	Time resolved	No C^+
	0.16[c]	Time resolved	Only prompt	Only prompt	No C^+
	0.23[d]	Time resolved	Only prompt	No C^+	No C^+
	0.35[d]	No C^+	No C^+	No C^+	No C^+

Note: Also included are estimates of reduction potentials of zeolites (vs. SCE, see text).

[a]Estimated as described in the text (vs. SCE).

[b]Oxidation potential not available. However, the oxidation potential for $An_2C^+CH_3$ has been measured as E_{ox} = –0.06 V vs. SCE in acetonitrile (43); replacing the methyl group in $An_2C^+CH_3$ with hydrogen to give An_2CH^+ should increase the oxidation potential by ca. 0.10 (44), leaving an oxidation potential for An_2CH^+ of ca. 0.04.

[c]Reference 45.

[d]Reference 46.

some cases, the radicals generated by deprotonation were created in a nonoxidizing environment and were not rapidly converted to the carbocations. These radicals may slowly migrate to an oxidizing site and eventually be oxidized to the carbocation, but this process would not be observed over the 40 μs timescale of our experiments, and the radicals would appear as long-lived. In other cases, the radicals were generated in an environment where they were oxidized as rapidly as they were formed. Under these conditions, deprotonation of the radical cations would be the rate-determining step, and the growth of the carbocations would match the decay of the radical cations.

The rapid oxidation of the radicals appeared to reach an extreme in the highly oxidizing HY zeolite. In zeolite, very little $An_2CH\cdot$ or $AnPhCH\cdot$ radicals were observed. Presumably, almost all these radicals were generated near highly oxidizing sites so that the majority of deprotonation events were coupled with an oxidizing event. Such rapid oxidation of radicals may also explain the higher than expected reactivity of the radical cations in HY. Instead of a radical cation – radical equilibrium being established in favour of the radical cation in the highly acidic medium, the radicals formed by deprotonation are immediately trapped by oxidation to the carbocation. Essentially, the radicals are diverted away from a reprotonation pathway by the presence of the oxidation pathway, and no equilibrium state is established.

As previously mentioned, prompt radical formation occurs to some extent by rapid deprotonation of a small fraction of the radical cations. If this situation was coupled with rapid oxidation of the radical, one would expect to observe prompt carbocation formation. This combination of rapid deprotonation and rapid oxidation provides a reasonable explanation for prompt carbocation formation upon irradiation of An_2CH_2 and $AnPhCH_2$ in NaY and KY and Tol_2CH_2 in NaY, KY, and HY. It is also possible that prompt carbocation formation is aided by a two-photon process whereby one photon generates the diarylmethane radical cation that rapidly deprotonates to give the radical, and a second photon within the same laser pulse is absorbed by the radical to give the excited radical (34). Since excited radicals are known to be more easily oxidized than ground-state radicals (47), this two-photon sequence would be expected to promote prompt carbocation formation.

Table 2 presents a qualitative summary to illustrate whether or not prompt and (or) time-resolved formation of the diarylmethyl cations was observed in the zeolites studied, and also includes oxidation potentials for the diarylmethyl radicals. Using the assumption that the rapid radical oxidations are exergonic, we can use the information in Table 2 to estimate "upper" and "lower" limits for the oxidizing ability of the cation- and proton-exchanged Y zeolites (22). Due to the possibility that prompt carbocation may be caused by two-photon ionization of the radicals, only the time-resolved formation of the diarylmethyl cations is used to signal that a particular zeolite is a sufficiently strong oxidant to induce oxidation of the radicals to carbocations. Time-resolved formation of the dianisylmethyl cation was observed in HY, NaY, and KY, but not in CsY. Given that the oxidation potential for $An_2CH\cdot \approx 0.04$ V,[6] we can estimate the reduction potentials for sites within HY, NaY, and KY that oxidize the radical to be >0.04 V, and <0.04 V for CsY. No obvious time-resolved growth of $AnPhCH^+$ was present in NaY or KY, thus limiting the oxidizing ability of these zeolites to <0.16 V. Time-resolved growth of Tol_2CH^+ was observed only in HY, which further indicates that the reduction potential for HY is >0.23 V. Finally, $Ph_2CH\cdot$ was not

[6]All oxidation potentials are vs. SCE in acetonitrile.

© 2005 NRC Canada

oxidized to Ph_2CH^+ in any of the zeolites, even HY. Thus, the reduction potential for HY should be <0.35 V.

Conclusions

The results clearly show that conversion of photogenerated diarylmethane radical cations to diarylmethyl radicals by deprotonation is an efficient process, with the dynamics of deprotonation depending on the acidity of the radical cations, but not the basicity of the zeolites. Subsequent conversion of the radicals to the diarylmethyl cations can also be rapid, but only when the oxidizing ability of the zeolite exceeds the oxidation potential of the radical. HY is the strongest oxidizing zeolite of the four Y zeolites used, with a reduction potential between 0.23 and 0.35 V. CsY is the poorest oxidant, with a reduction potential at least 0.20 V lower than HY.

Experimental

Materials

Faujasite zeolite NaY was commercially available from Aldrich (LZY52 molecular sieves, Si/Al = 2.4) and used as received. HY was prepared from NH_4^+Y (Aldrich) by calcining the zeolite at 500 °C to promote loss of NH_3. The cation-exchanged zeolites were prepared by washing the zeolites with their corresponding chloride salts. The % exchange was typically 97% for KY and 47% for CsY (16). The solvents used for the preparation of zeolite samples were spectroscopic grade (99.98%, Omnisolv, EMD Chemicals) and used as received.

Diphenylmethane was commercially available from Aldrich and was purified by distillation and column chromatography (silica, 70–270 mesh) prior to use. Dianisylmethane (bis(4-methoxyphenyl)methane), anisylphenylmethane (4-methoxyphenylphenylmethane), and ditolylmethane (bis(4-methylphenyl)methane) were prepared from their corresponding ketones (Aldrich) using the Huang–Minlon procedure (48). The products were purified on silica by column chromatography using hexane as the eluant. Melting point determinations and (or) gas chromatography (GC) were used to establish purity. All melting points and ^1H and ^{13}C NMR (Bruker 250 MHz using $CDCl_3$ as the solvent) matched literature values (49, 50).

Zeolite sample preparation

The zeolites were activated at 475 °C for at least 12 h before use; typically ~300 mg of zeolite was activated overnight and allowed to cool to room temperature in a dry environment. A solution of the diarylmethane (about 5 mg) dissolved in 15 mL of hexanes was rapidly added to 5 mL of hexanes containing the activated zeolite. The sample was magnetically stirred for 1 h after which time the sample was centrifuged and the solvent was decanted. Fresh solvent was added to wash the zeolite surface. The sample was stirred for another 30 min, centrifuged, and the solvent was decanted. The diarylmethane–zeolite complex was transferred to a dessicator and dried under vacuum of 10^{-2} torr (1 torr = 133.322 4 Pa) for at least 4 h. The samples were then transferred to 3 mm × 7 mm quartz sample cells, evacuated (10^{-3} torr) for several hours, and sealed prior to laser irradiation.

The amount of organic material incorporated into the zeolite was calculated from the difference between the initial amount of the diarylmethane and the amount that was recovered in the combined solutions measured by UV absorption. With hexane as the carrier solvent, it was found that >90% of the diarylmethanes were incorporated into the zeolite. In each case, the loading level for the diarylmethanes was $\langle S \rangle = 0.10 \pm 0.01$ (i.e., one molecule in every 10 supercages).

No color change was observed upon incorporation of the diarylmethanes into the alkali cation-exchanged zeolites, indicating that the substrates were not thermally converted to coloured carbocations within these zeolites. The thermal stability of An_2CH_2 and $AnPhCH_2$ within the alkali-exchanged zeolite NaY was studied in more detail by examining the material obtained after continuous extraction of An_2CH_2–NaY and $AnPhCH_2$–NaY composites prepared as previously described for the laser experiments. The extraction procedure involved placing the organic/zeolite composite in a filter thimble and subjecting the sample to continuous extraction using a Soxlet apparatus and refluxing CH_2Cl_2 for 7 days. GC analysis (Varian Saturn 11, 35 m capillary column crosslinked 5% phenylmethylsilicone) of the extracted material indicated that 80% of unreacted diarylmethanes was recovered (relative to the amount originally incorporated). No other materials were observed in the extracted material by GC, leading to the conclusion that the diarylmethanes were stable within the zeolites.

In HY, no colour change was observed upon incorporation of Tol_2CH_2 and Ph_2CH_2, again suggesting that these materials were thermally stable within the acidic zeolite. On the other hand, the zeolite samples displayed a pale pink colour upon incorporation of An_2CH_2 and $AnPhCH_2$. Steady-state diffuse reflectance of these samples showed absorption at 510 nm for the An_2CH_2–HY composite, and at 460 nm for the $AnPhCH_2$–HY composite, indicating that the coloration was due to thermal conversion of the substrates to their corresponding carbocations. The colour was completely removed upon exposure of the samples to atmospheric moisture because of quenching of the carbocations with water. After continuous extraction of these hydrated samples, An_2CH_2 or $AnPhCH_2$ were still the only compounds detected by GC. No evidence of the diarylmethanols or diarylketones, which would be formed by oxidation of the diarylmethanols, was found in the GC traces. Thus, while some decomposition took place in HY, the lack of substantial colour together with exclusive extraction of the unreacted diarylmethanes suggests that decomposition was minor. To ensure that no carbocations were present in the laser experiments, samples of An_2CH_2 and $AnPhCH_2$ in HY were initially prepared in the same way as previously described for the other samples, but then hydrated by exposure to the atmosphere to remove the coloration and reevacuated prior to laser irradiation. There was no further evidence for the presence of carbocations following this supplementary treatment.

Laser flash photolysis

The nanosecond laser flash photolysis system with diffuse

© 2005 NRC Canada

reflectance detection at Dalhousie University is of standard design and has been previously described (51). The samples, typically ~300 mg of zeolite, were contained in 3 mm × 7 mm laser cells made out of Suprasil quartz tubing and degassed at reduced pressure (10^{-3} torr) prior to photolysis. For the oxygen-quenching experiments, oxygen was passed through the sample for at least 30 min prior to photolysis. The excitation source was the fourth harmonic from a Continuum Nd:YAG NY-61 laser (266 nm, ≤8 ns/pulse, ≤15 mJ/pulse). Transient signals from a monochromator/photomultiplier system were initially captured by a Tektronix 620A digital oscilloscope and transferred to a Power Macintosh computer. The experiments are computer controlled using the Power Macintosh and software written using the Labview™ programming language.

Data analysis

The data analysis was based on the fraction of reflected light absorbed by the transient (reflectance change, $R = \Delta J/J_o$), where J_o is the reflectance intensity before excitation and ΔJ is the change in the reflectance after excitation. Zeolites are known to contain several different microenvironments, and as a result, time-resolved decays or growths of transients in zeolites frequently fit better to a multiple first-order rate equation ($R_t = R_\infty + \Delta R_1 e^{-k1t} + \Delta R_2 e^{k2t} + \ldots$) than to a single first-order rate equation ($R_t = R_\infty + \Delta R_1 e^{-k1t}$). In the present work, the growths and decays of transients sometimes fit very well to a simple first-order expression; other times, the data fit better to a double first-order expression, but were still well-described by a single first-order rate equation. Thus, for consistency across all time-resolved processes, all rate constant calculations, unless otherwise specified, were carried out by nonlinear squares fitting of the data to a single first-order rate equation.

Acknowledgments

We gratefully acknowledge the Natural Sciences and Engineering Research Council of Canada (NSERC) for financial support of this research.

References

1. M. Barrer. Zeolites and clay minerals as sorbents and molecular sieves. Academic Press, London. 1978.
2. D.W. Breck. Zeolite molecular sieves: Structure, chemistry and use. John Wiley and Sons, New York. 1974.
3. A. Dyer. An introduction to zeolite molecular sieves. John Wiley and Sons, Bath, UK. 1988.
4. J.A. Rabo. *In* ACS Monograph 171. American Chemical Society, Washington, D.C. 1976.
5. N.J. Turro. Pure Appl. Chem. **58**, 1219 (1986).
6. H. van Bekkum, E.M. Flanigen, and J.C. Jansen. Introduction to zeolite science and practice. Elsevier, Amsterdam. 1991.
7. H. Garcia, S. Garcia, J. Perez-Prieto, and J.C. Scaiano. J. Phys. Chem. **100**, 18158 (1996).
8. B.D. Flockhart, L. McLoughlin, and R.C. Pink. J. Catal. **25**, 305 (1972).
9. F.L. Cozens, H. Garcia, and J.C. Scaiano. J. Am. Chem. Soc. **115**, 11134 (1993).
10. K.K. Iu and J.K. Thomas. J. Phys. Chem. **95**, 506 (1991).
11. K.B. Yoon. Chem. Rev. **93**, 321 (1993).
12. F. Gessner and J.C. Scaiano. J. Photochem. Photobiol. A, **67**, 91 (1992).
13. M. O'Neill, F.L. Cozens, and N.P. Schepp. J. Phys. Chem. B, **105**, 12746 (2001).
14. S. Hashimoto. J. Chem. Soc. Faraday Trans. **93**, 4402 (1997).
15. F.L. Cozens, H. Garcia, and J.C. Scaiano. Langmuir, **10**, 2246 (1994).
16. F.L. Cozens, M.L. Cano, H. Garcia, and N.P. Schepp. J. Am. Chem. Soc. **120**, 5667 (1998).
17. M.L. Cano, A. Corma, V. Fornes, and H. Garcia. J. Phys. Chem. **99**, 4241 (1995).
18. B.W. Wojciechowski and A. Corma. Catalytic cracking, catalysis kinetics and mechanisms. Marcel Dekker, New York. 1984.
19. H. Choukroun, D. Brunel, and A. Germain. J. Chem. Soc. Chem. Commun. 6 (1986).
20. V. Ramamurthy, D.F. Eaton, and J.V. Caspar. Acc. Chem. Res. **25**, 299 (1992).
21. K.B. Yoon. *In* Handbook of zeolite science and technology. *Edited by* S.M. Auerbach, K.A. Carrado, and P.K. Dutta. Marcel Dekker, Inc., New York. 2003. p. 591.
22. V. Ramamurthy, J.V. Caspar, and D.R. Corbin. J. Am. Chem. Soc. **113**, 594 (1991).
23. P.L. Corio and S. Shih. J. Phys. Chem. **75**, 3475 (1971).
24. S.N. Khadzhiev, N.G. Yaralov, and Y.V. Shumorskii. React. Kinet. Catal. Lett. **24**, 297 (1984).
25. M.L. Poutsma. *In* Zeolite chemistry and catalysis. *Edited by* J.A. Rabo. American Chemical Society, Washington, D.C. 1976. p. 437.
26. H. Garcia, V. Marti, I. Casades, V. Fornes, and H.D. Roth. Phys. Chem. Chem. Phys. **3**, 2955 (2001).
27. T.M. Leu and E. Roduner. J. Catal. **228**, 397 (2004).
28. H. Garcia and H.D. Roth. Chem. Rev. **102**, 3947 (2002).
29. E. Baciocchi, T. Del Giacco, and F. Elisei. J. Am. Chem. Soc. **115**, 12290 (1993).
30. E. Baciocchi, T. Del Giacco, F. Elisei, and O. Lanzalunga. J. Am. Chem. Soc. **120**, 11800 (1998).
31. P.H. Kasai and J.R.J. Bishop. J. Phys. Chem. **77**, 2308 (1973).
32. J.A. Rabo, C.L. Angell, P.H. Kasai, and V. Schomaker. Discuss. Faraday. Soc. **41**, 328 (1966).
33. X. Liu and J.K. Thomas. Langmuir, **8**, 1750 (1992).
34. J. Bartl, S. Steenken, H. Mayr, and R.A. McClelland. J. Am. Chem. Soc. **112**, 6918 (1990).
35. K. Sehested, J. Holcman, and E.J. Hart. J. Phys. Chem. **81**, 1363 (1977).
36. M. Fujiwara and A. Yamasaki. J. Chem. Soc. Faraday Trans. **94**, 2525 (1998).
37. M. Fujiwara, A. Yamasaki, K. Mishima, and K. Toyomi. J. Chem. Phys. **109**, 1359 (1998).
38. A. Bromberg and D. Meisel. J. Phys. Chem. **89**, 2507 (1985).
39. T. Shida. Electronic absorption spectra of radical ions. Elsevier, New York. 1988.
40. J. Sivaguru, J. Shailaja, and V. Ramamurthy. *In* Handbook of zeolite science and technology. *Edited by* S.M. Auerbach, K.A. Carrado, and P.K. Dutta. Marcel Dekker, Inc., New York. 2003. p. 515.
41. F.L. Cozens, H. Garcia, and J.C. Scaiano. J. Am. Chem. Soc. **115**, 11134 (1993).
42. C. Russo-Caia and S. Steenken. Phys. Chem. Chem. Phys. **4**, 1478 (2002).
43. H. Ikeda, T. Nakamura, T. Miyashi, J.L. Goodman, K. Akiyama, S. Tero-Kubota, A. Houmam, and D.D.M. Wayner. J. Am. Chem. Soc. **120**, 5832 (1998).
44. D.D.M. Wayner, D.J. McPhee, and D. Griller. J. Am. Chem. Soc. **110**, 132 (1988).

© 2005 NRC Canada

45. L.J. Johnston and T. Kanigan. J. Am. Chem. Soc. **112**, 1271 (1990).
46. R. Popielarz and D.R. Arnold. J. Am. Chem. Soc. **112**, 3068 (1990).
47. B.R. Arnold, J.C. Scaiano, and W.G. McGimpsey. J. Am. Chem. Soc. **114**, 9978 (1992).
48. Huang-Minlon. J. Am. Chem. Soc. **68**, 2487 (1946).
49. Y. Makioka, S. Uebori, M. Tsuno, Y. Taniguchi, K. Takaki, and Y. Fujiwara. J. Org. Chem. **61**, 372 (1996).
50. H. Mayr, G. Lang, and A.R. Ofial. J. Am. Chem. Soc. **124**, 4067 (2002).
51. M. O'Neill, F.L. Cozens, and N.P. Schepp. J. Am. Chem. Soc. **122**, 6017 (2000).

© 2005 NRC Canada

Valence bond calculations on the transition state for the E2 reaction of fluoride ion with ethyl fluoride — Implications for the More O'Ferrall – Jencks diagram[1]

Wei Wu, Sason Shaik, and William H. Saunders, Jr.

Abstract: A valence bond self-consistent field (VBSCF) calculation has been carried out on the bimolecular elimination (E2) reaction of fluoride ion with ethyl fluoride. The transition state was first optimized at HF/6-31+G and the resulting orbitals were used in the VBSCF calculation. A transition-state hybrid consisting of four structures ($F^-H\text{-}CH_2\text{-}CH_2\text{-}F$, $F\text{-}HCH_2{=}CH_2F^-$, $F\text{-}H^-CH_2\text{-}CH_2\text{-}F$, and $F^-H\text{-}CH_2\text{-}CH_2{}^+F^-$) failed to give a reasonable energy. Incorporation of four charge-separated structures ($F^-H^+{-}CH_2\text{-}CH_2\text{-}F$, $F^-H^+{-}CH_2\text{-}CH_2{}^+F^-$, $F^-H^+CH_2{=}CH_2F^-$, and $F\text{-}H^-CH_2\text{-}CH_2{}^+F^-$) for a total of eight resulted in an energy slightly below Hartree–Fock. A full-space VBSCF calculation utilizing 50 structures showed that the eight structures give a sufficiently accurate wave function. The transition state is dominated by charge-separated structures, leading to a greater degree of charge separation than in either the reactant or product complex. Therefore, the transition state does not evolve synchronously from the reactants, and explicit allowance should be made for this fact when applying descriptions of the reaction path, such as that in the More O'Ferrall – Jencks diagram.

Key words: elimination reaction, E2, transition state, VBSCF calculation, XMVB programs.

Résumé : On a effectué des calculs de liaison de valence en champ autocohérent (VBSCF) sur la réaction d'élimination bimoléculaire (E2) de l'ion fluorure à partir du fluoroéthane. Dans une première étape, on a optimisé l'état de transition au niveau HF/6-31+G et on a utilisé les orbitales qui en ont résulté dans les calculs VBSCF. Un état de transition hybride formé des quatre structures ($F^-H\text{-}CH_2\text{-}CH_2\text{-}F$, $F\text{-}HCH_2{=}CH_2F^-$, $F\text{-}H^-CH_2\text{-}CH_2\text{-}F$ et $F^-H\text{-}CH_2\text{-}CH_2{}^+F^-$) ne permet pas d'obtenir une énergie raisonnable. L'incorporation des quatre structures à charges séparées ($F^-H^+{-}CH_2\text{-}CH_2\text{-}F$, $F^-H^+{-}CH_2\text{-}CH_2{}^+F^-$, $F^-H^+CH_2{=}CH_2F^-$ et $F\text{-}H^-CH_2\text{-}CH_2{}^+F^-$) pour un total de huit structures conduit à une énergie légèrement inférieure à celle prévue par des calculs de Hartree–Fock. Un calcul VBSCF à plein espace, faisant appel à 50 structures a permis de montrer que les huit structures conduisent à une fonction d'onde suffisamment exacte. L'état de transition est dominé par les structures à charges séparées et ceci conduit à un degré plus élevé de séparation de charge qui est plus élevé que dans le réactif ou dans le complexe du produit. De cette façon, l'état de transition n'évolue pas d'une façon synchrone avec les réactifs et on doit en conséquence faire des prévisions explicites pour ce fait lorsqu'on applique les descriptions de la voie réactionnelle, par exemple dans le diagramme de More O'Ferrall – Jencks.

Mots clés : réaction d'élimination, E2, état de transition, calcul de liaison de valence en champ autocohérent, programmes XMVB.

[Traduit par la Rédaction]

Introduction

The bimolecular elimination (E2) reaction

[1] $$B^- + H\text{-}CR_2\text{-}CR_2\text{-}X \rightarrow B\text{-}H + CR_2{=}CR_2 + X^-$$

has long been of interest to mechanistic chemists both for its own sake and as a model for other complex processes in which more than two bonds are undergoing changes in the course of the reaction. It was originally shown by Hanhart and Ingold (1) to be second order, first order in base and first order in substrate. Later works have pointed out that the bonding changes need not be synchronous, although they occur in a single elementary step. Proton transfer at the transition state may be more advanced than the C—X bond breakage, or vice versa (2–5). The possible variations in transition-state structure can be represented by means of a

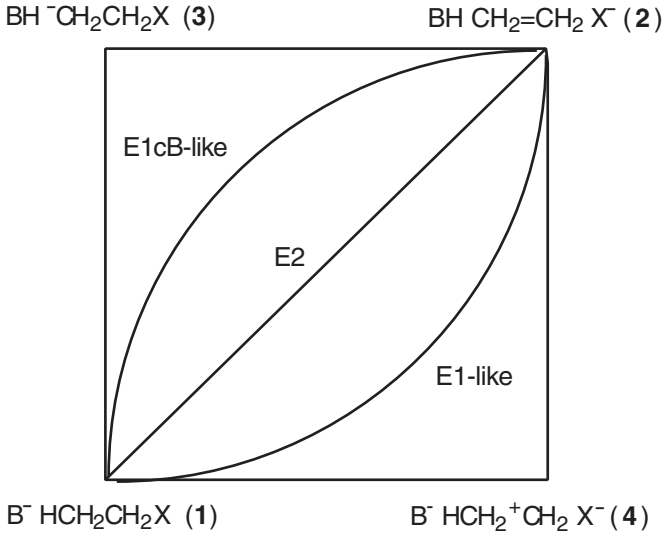
Received 22 February 2005. Published on the NRC Research Press Web site at http://canjchem.nrc.ca on 8 December 2005.

W. Wu. The State Key Laboratory for Physical Chemistry of Solid Surfaces and Institute of Physical Chemistry, Xiamen University, Xiamen 361005, P.R. China.
S. Shaik. Department of Organic Chemistry and the Lise Meitner-Minerva Center for Computational Quantum Chemistry, The Hebrew University, Jerusalem 91904, Israel.
W.H. Saunders, Jr.[2] Department of Chemistry, University of Rochester, Rochester, NY 14627, USA.

[1]This article is part of a Special Issue dedicated to organic reaction mechanisms.
[2]Corresponding author (e-mail: saunders@chem.rochester.edu).

 doi: 10.1139/V05-161 © 2005 NRC Canada

Fig. 1. More O'Ferrall – Jencks diagram.

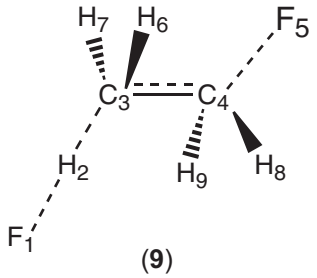


More O'Ferrall – Jencks diagram (6–8). In the diagram (Fig. 1) a completely synchronous process is represented by a diagonal line from reactants **1** to products **2**. A two-step (E1cB) process is represented by a straight line from reactants **1** to carbanionic intermediate **3** followed by a straight line from the intermediate to product **2**. An E1cB-like process is then represented by a line that curves toward **3** but does not go through it and proceeds on to **2** in a single step. Another two-step (E1) process goes from reactant to carbocation **4** and from there on to **2**. An E1-like concerted process is represented by a line that curves toward **4** but proceeds directly in a single step to **2**. Substituent effects and isotope effects have been extensively used in efforts to determine the locations on the diagram of the transition states for E2 reactions with various reactants under various reaction conditions (9).

An alternative description of the possibilities for E2 transition states was suggested by Pross and Shaik (10). They proposed a valence bond (VB) formalism in which the structures contributing to a transition-state hybrid are taken to be **5**–**8** ($F^{-}H\text{-}CH_2\text{-}CH_2\text{-}F$ (**5**), $F\text{-}HCH_2{=}CH_2F^{-}$ (**6**), $F\text{-}H^{-}CH_2\text{-}CH_2\text{-}F$ (**7**), and $F^{-}H\text{-}CH_2\text{-}CH_2{}^{+}F^{-}$ (**8**)). While these may appear to be the same as **1**–**4**, respectively, there is a crucial difference. **1** and **2** represent stable species, while **3** represents a stable species in an E1cB reaction and **4** represents a stable species in an E1 reaction. In contrast, **5**–**8** are hypothetical species with the transition-state geometry but the electron distributions of **1**–**4**, respectively. They represent, however, reasonable guesses for important contributors to the transition-state hybrid. Other structures are possible but were not considered in the initial qualitative model (10). With this idea in mind, we set out to perform quantitative valence bond self-consistent field (VBSCF) calculations on the E2 reaction of fluoride ion with ethyl fluoride.

Computational procedures

The first step was geometric optimization of the transition-state structure at the HF/6-31+G level utilizing the GAUSSIAN 98 (11) programs. A vibrational analysis showed that the structure was a stationary point with one imaginary frequency corresponding to the reaction coordinate. The choice of a relatively low level was dictated by the fact that the computation time in VB calculations rises very rapidly with an increase in the number of basis functions. Even with the further constraints described in the following, some VB calculations required 3 days or more on a dual-processor SGI Octane workstation. The number of active orbitals was further restricted by freezing all inner-shell electrons and those outer-shell electrons that occupy orbitals orthogonal to the active orbitals in the *xz* plane.



(**9**)

In structure **9**, the atoms directly involved in the reaction are F1, H2, C3, C4, and F5. These atoms are all in the *xz* plane. The nonreacting hydrogens can also be constrained to this plane by taking linear combinations: H6 + H7 and H8 + H9. Thus, all p_y orbitals are orthogonal to the reacting orbitals and can be frozen. The active electrons are then taken to be the eight electrons in the bonds undergoing change in the course of the reaction plus an unshared pair on each of the atoms F1 and F5 for a total of 12. The integrals from the Gaussian calculation are transformed to a VB set by utilizing the Xiamen programs (XMVB) (12, 13). The six active orbitals are chosen as those highest filled orbitals that contain no p_y contributions. The XMVB can then be used to optimize simultaneously each of the contributors to the hybrid and the hybrid itself. Each contributor can also be optimized separately if desired.

Results and discussion

Our first effort was to optimize a hybrid consisting of the structures **5**–**8**. The results are shown in Table 1. The individual contributors are all very high energy relative to the Hartree–Fock value, and the hybrid of all four is still more than 100 kcal/mol (1 cal = 4.184 J) above the Hartree–Fock value. In principle, a VBSCF calculation ought to give a lower energy than a comparable Hartree–Fock calculation because the VBSCF method takes implicit account of electron correlation. In the present case a very low energy cannot be expected because all but 12 of the electrons are frozen in their respective orbitals, which consequently are unable to adapt to changes in the active electrons. Even so, an energy more than 100 kcal/mol higher than the Hartree–Fock value is unacceptable.

There are evidently contributing structures beyond **5**–**8** that need to be considered. In our previous work on proton transfer processes (14, 19), we found that a triple ion structure of the type $X^{-}H^{+}X^{-}$ was necessary to describe the transition state. Ionic structures are known, in fact, to be very important for bonds involving halogens, and especially so

© 2005 NRC Canada

Table 1. Energies of F···H···CH_2==CH_2···F transition-state contributors and hybrids.

Structure	E (kcal/mol)[a]
5	212.3
6	215.0
7	244.1
8	161.7
5+6	205.3
5+6+7+8	137.1

[a]Energies are relative to the Hartree–Fock energy from the Gaussian calculation at HF/6-31+G.

Table 2. Energies of F···H···CH_2==CH_2···F transition-state charge-separated contributors and hybrids.

Structure	E (kcal/mol)[a]
10	64.9
11	34.3
5+6+10+11	30.5
5+6+7+8+10+11	21.4
12	30.6
13	185.7
5+6+7+8+10+11+12+13	–0.6
50 structures (full-space valence bond)	–9.5

[a]Energies are relative to the Hartree–Fock energy from the Gaussian calculation at HF/6-31+G.

for fluorine-containing bonds, where the mixing of the ionic structures leads to considerable stabilization via covalent–ionic resonance energies (15–18). Thus, **10** (F^-H^+-CH_2-CH_2-F) is an obvious choice, and we also added a structure with alternating charges (F^-H^+-CH_2-$CH_2^+F^-$ (**11**)). Indeed, these structures proved to be of considerably lower energy than **5**–**8**, and generate a hybrid with energy more than 100 kcal/mol below the hybrid of **5**–**8** (Table 2), even better than the energies we achieved in similarly complex processes — identity-reaction proton transfers from acids that yield resonance-stabilized anions (14).

To determine whether other significant structures were needed, we carried out a calculation on a complete set of 50 VB structures. There are five orbitals on five centers with six electrons, leading to 50 structures that are constructed as follows: (*i*) monoanionic structures, which involve a monoanion on a given site and two covalent bonds on the other sites — these covalent bonds have two possible ways of coupling the four electrons (Rumer structures) with five possible anionic sites, which lead to 10 structures; (*ii*) dianionic centers must have one cationic center and one covalent bond, leading to $[(5 \times 4)/2] \times 3 = 30$ structures; (*iii*) trianionic structures have two cationic centers, leading to a total of $(5 \times 4 \times 3)/6 = 10$ structures. This model gives an energy 9.5 kcal/mol lower than the Hartree–Fock value. Most of the structures possess high-energy features such as long bonds, adjacent charges of the same sign, or reversed charges (H^- and F^+), and thus make only very minor contributions to the hybrid; but eight of the fifty structures (**5**–**8** and **10**–**11**) along with two new ones ($F^-H^+CH_2$=CH_2F^- (**12**) and F-H^-CH_2-$CH_2^+F^-$ (**13**)) were of significant importance. Their weights total 0.986 out of 1.000 for the full 50 structures.

Table 3. Weights of contributors to the eight-structure hybrid of the F···H···CH_2==CH_2···F transition state.

Contributor	Weight
5	0.010
6	0.166
7	0.053
8	0.017
10	0.046
11	0.276
12	0.317
13	0.115

The eight-structure hybrid has a slightly lower energy than the Hartree–Fock values (Table 2). The weights of the individual contributors to this hybrid are recorded in Table 3. They compare well with the relative weights of the full calculation. Therefore, a sufficiently accurate wave function is deemed to be the one with eight structures. Note that the original structures **5**–**8** have a total weight of barely 25%, while the charge-separated structures **10**–**13** make up 75%. The transition structure is clearly not formed in a synchronous fashion of covalent bond switching but possesses a high degree of charge separation. Of course, since the charge-separated structures maintain large covalent–ionic resonance energies with the covalent structures (15–18), the charge separation does not mean that the transition state is ionic.

One may question whether this picture represents a real physical situation or is an artifact of the VB method. Table 4 compares charges calculated from the VB data[3] with Mulliken and NPA (natural population analysis) (20) charges calculated at MP2/6-31+G*//MP2/6-31+G*. While the charge alternation is somewhat stronger in the VB charges, the same pattern is clearly evident in the charges calculated at the correlation-corrected SCFMO level, with the NPA charges being closer to the VB charges. Structures optimized at the MP2/6-31+G* level have been found to give physically reasonable results for a variety of E2 reactions (21–23). Thus, there is no reason to doubt the reliability of the VB charges and the contributions of the charge-separated resonance structures that give rise to the charge distribution. The agreement is better than expected considering that all electrons are active in the SCFMO calculation but only 12 (one-third of the total) are active in the VB calculation.

Another question is why the VB calculation requires at least eight structures to describe the transition state when the More O'Ferrall – Jencks diagram requires only four. There are two reasons for this difference. The first is that even a normal covalent bond may require charge-separated contributors for an adequate description (15–18). Covalent contri-

[3]Supplementary data for this article are available on the Web site or may be purchased from the Depository of Unpublished Data, Document Delivery, CISTI, National Research Council Canada, Ottawa, ON K1A 0R6, Canada. DUD 4044. For more information on obtaining material refer to http://cisti-icist.nrc-cnrc.gc.ca/irm/unpub_e.shtml.

© 2005 NRC Canada

Table 4. Group charges in the F···H···CH_2==CH_2···F transition state.

Group	VB (HF/6-31+G)	Mulliken (MP2/6-31+G*)	NPA (MP2/6-31+G*)
F	–0.703	–0.654	–0.697
H	0.639	0.535	0.584
β-CH_2[a]	–0.454	0.267	0.389
α-CH_2[a]	0.444	0.267	0.350
F	–0.927	–0.780	–0.849

Note: VB = valance bond; NPA = natural population analysis.
[a]α refers to the carbon bearing the fluorine, and β refers to the carbon bearing the hydrogen in transit.

butors in a VB calculation have electron pairs shared equally between any two adjacent atoms. Thus, a polar bond, such as H-F or C-F, must include ionic contributors of the type H^+F^- or C^+F^- for a proper VB description. Even a homonuclear C=C bond, such as that in ethylene, requires two equivalent charge-separated contributors $H_2C^+C^-H_2$ in a VB calculation to correctly reproduce the properties of the molecule (24). This requirement can be thought of as allowing for the polarizability of the π bond. It is consequently not surprising that the E2 transition state requires charge-separated structures. The question is whether it requires them more than does the reactant or the product.

This question was examined by means of models of the reactant and product complexes. These models were set up under constraints intended to ensure that they were geometrically similar to the transition state. The F···H···C system was constrained to be linear, and planarity of the reacting bonds was enforced. For the reactant complex, the F···H bond length was fixed at 2.0 Å and the remaining parameters optimized except for the linearity of F···H···C. This gave a stationary point with no imaginary frequencies though probably not a global minimum. The C···F bond length in the product complex was fixed at 2.3 Å and the remaining parameters were optimized, again with the exceptions cited for the reactant complex. In this case, the species possessed one imaginary frequency, but no model with a reasonable C···F distance was a stationary point. The imaginary frequency corresponds to a vibration in which an essentially planar ethylene moiety twists about an axis through the C=C perpendicular to the plane of the carbons and hydrogens. FH and F^- remain almost stationary in this vibration. Thus, the model appears to be an ethylene interacting electrostatically with the leaving group and the conjugate acid.

The reactant and product complexes are compared with the transition state in Tables 5 and 6. Both show that the weights and group charges do not change monotonically from reactant to transition state to product. Charge-separated contributors (**8**, **10**–**13**) account for 68% of the reactant, 77% of the transition state, and 73% of the product. The prominence of **11** in the transition state is mainly responsible. The charges (Table 6) show even more clearly the degree of charge separation in the transition state. The proton in transit and the α-CH_2 are more positive and the β-CH_2 is more negative than in either the reactant or the product. The base has transferred 76% of its charge to the substrate, while the leaving group has acquired 88% of its final charge in the transition state. By these measures, the transition state is much closer to product than to reactant, and the positive charge on H-CH_2CH_2 is about 0.2 units greater than in the reactant, mainly due to the increased charge on the proton in transit. The large positive charge on the proton in transit and the large negative charge on the β-CH_2 are reminiscent of the behavior observed in proton transfers from acids that yield resonance-stabilized anions (14, 21, 25–28), which are the examples of the principle of nonperfect synchronization (29–31).

Table 5. Comparison of contributor weights for reactant complex, transition state, and product complex in the E2 reaction of F^- and C_2H_5F.

Contributor	Reactant complex wt.	Transition state wt.	Product complex wt.
5	0.319	0.010	0.000
6	0.0002	0.166	0.273
7	0.000	0.053	0.000
8	0.230	0.017	0.004
10	0.255	0.046	0.000
11	0.181	0.276	0.190
12	0.015	0.317	0.417
13	0.000	0.115	0.116

Table 6. Comparison of valance bond group charges for reactant complex, transition state, and product complex in the E2 reaction of F^- and C_2H_5F.

Group	Reactant complex	Transition state	Product complex
F	–1.000	–0.703	–0.611
H	0.451	0.639	0.607
β-CH_2	–0.436	–0.454	–0.306
α-CH_2	0.411	0.444	0.310
F	–0.383	–0.927	–1.000

The relevance of these observations to the More O'Ferrall – Jencks diagram is that the diagram takes no explicit account of such charge-localized transition states. While there is nothing about the diagram that excludes this possibility, it has in the past encouraged a tacit assumption that in atom or group transfers bond breaking and bond making occur synchronously. For example, calculations of isotope effects in elimination reactions often employ models in which total bonding to a given atom or group remains constant along the reaction coordinate (32, 33). The present results make it clear that one must be alert for evidence of nonperfect synchronization when considering transition states of elimination reactions or of proton transfers in general. Work is currently under way to determine the effect of the base and leaving group on the extent of charge localization in the transition state.

Acknowledgment

We thank Professor R.A. More O'Ferrall for helpful comments.

References

1. W. Hanhart and C.K. Ingold. J. Chem. Soc. 997 (1927).

© 2005 NRC Canada

2. R.L. Letsinger, A.W. Schnizer, and E. Bobko. J. Am. Chem. Soc. **73**, 5708 (1951).
3. D.J. Cram, F.D. Greene, and C.H. DePuy. J. Am. Chem. Soc. **78**, 790 (1956).
4. W.H. Saunders, Jr. and R.A. Williams. J. Am. Chem. Soc. **79**, 3712 (1957).
5. J.F. Bunnett. Angew. Chem. Int. Ed. Engl. **1**, 225 (1962).
6. R.A. More O'Ferrall. J. Chem. Soc. B, 274 (1970).
7. W.P. Jencks. Chem. Rev. **72**, 205 (1972).
8. W.P. Jencks. Chem. Rev. **85**, 517 (1985).
9. W.H. Saunders, Jr. and A.F. Cockerill. Mechanisms of elimination reactions. Wiley, New York. 1973.
10. A. Pross and S. Shaik. J. Am. Chem. Soc. **104**, 187 (1982).
11. M.J. Frisch, G.W. Trucks, H.B. Schlegel, G.E. Scuseria, M.A. Robb, J.R. Cheeseman, V.G. Zakrzewski, J.A. Montgomery, Jr., R.E. Stratmann, J.C. Burant, S. Dapprich, J.M. Millam, A.D. Daniels, K.N. Kudin, M.C. Strain, O. Farkas, J. Tomasi, V. Barone, M. Cossi, R. Cammi, B. Menucci, C. Pomelli, C. Adamo, S. Clifford, J. Ochterski, G.A. Petersson, P.Y. Ayala, Q. Cui, K. Morokuma, D.K. Malick, A.B. Rabuck, K. Raghavachari, J.B. Foresman, J. Cioslowski, J.V. Ortiz, B.B. Stefanov, G. Liu, A. Liashenko, P. Piskorz, I. Komaromi, R. Gomperts, R.L. Martin, D.J. Fox, T. Keith, M.A. Al-Laham, C.Y. Peng, A. Nanayakkara, C. Gonzalez, M. Challocombe, P.M.W. Gill, B.G. Johnson, W. Chen, M.W. Wong, J.L. Andres, M. Head-Gordon, E.S. Replogle, and J.A. Pople. GAUSSIAN 98 [computer program]. Gaussian Inc., Pittsburgh, Penn. 1998.
12. W. Wu, A. Wu, M. Mo, M. Lin, and Q. Zhang. Int. J. Quantum Chem. **67**, 287 (1998).
13. L. Song, Y.Q. Zhang, and W. Wu. J. Comput. Chem. **26**, 514 (2005).
14. N. Harris, W. Wu, W.H. Saunders, Jr., and S. Shaik. J. Am. Chem. Soc. **122**, 6754 (2000).
15. S. Shaik and A. Shurki. Angew. Chem. Int. Ed. **38**, 586 (1999).
16. S. Shaik, P. Maitre, G. Sini, and P.C. Hiberty. J. Am. Chem. Soc. **114**, 7861 (1992).
17. D. Lauvergnat, P.C. Hiberty, D. Danovich, and S. Shaik. J. Phys. Chem. **100**, 5715 (1996).
18. A. Shurki, P.C. Hiberty, and S. Shaik. J. Am. Chem. Soc. **121**, 822 (1999).
19. W. Wu, S. Shaik, and W.H. Saunders, Jr. J. Phys. Chem. A, **106**, 11616 (2002).
20. A.E. Reed, L.A. Curtiss, and F. Weinhold. Chem. Rev. **88**, 899 (1988).
21. W.H. Saunders, Jr. J. Org. Chem. **64**, 861 (1999).
22. W.H. Saunders, Jr. J. Org. Chem. **65**, 681 (2000).
23. W.H. Saunders, Jr. Croat. Chem. Acta, **74**, 575 (2001).
24. S. Shaik and P.C. Hiberty. Rev. Comput. Chem. **20**, 1 (2004).
25. W.H. Saunders, Jr. J. Am. Chem. Soc. **116**, 5400 (1994).
26. W.H. Saunders, Jr. and J.E. Van Verth. J. Org. Chem. **60**, 3452 (1995).
27. C.F. Bernasconi and P.J. Wenzel. J. Am. Chem. Soc. **118**, 10494 (1996).
28. C.F. Bernasconi, P.J. Wenzel, J.R. Keeffe, and S. Gronert. J. Am. Chem. Soc. **119**, 4008 (1997).
29. C.F. Bernasconi. Acc. Chem. Res. **20**, 301 (1987).
30. C.F. Bernasconi. Acc. Chem. Res. **25**, 9 (1992).
31. C.F. Bernasconi. Adv. Phys. Org. Chem. **27**, 119 (1992).
32. W.H. Saunders, Jr. Chem. Scr. **8**, 27 (1975).
33. W.H. Saunders, Jr. Chem. Scr. **10**, 82 (1976).

© 2005 NRC Canada

Elimination reactions — Calculation of rate constants from equilibrium constants and distortion energies by means of no barrier theory[1]

J. Peter Guthrie, Leonardo Leandro, and Vladimir Pitchko

Abstract: No barrier theory has been applied to the E2 reactions of five alkyl bromides with ethanolic ethoxide. The model used for these reactions is that the reaction proceeds from the encounter complex of base and alkyl halide to the product encounter complex of halide ion and alkene (and alcohol), and requires five simple processes, which combine to give the concerted elimination: transfer of a proton from carbon to base; a change in geometry at the carbon which loses a proton from sp^3 to sp^2; breaking the C-leaving group bond; a change in geometry at the carbon which loses the leaving group from sp^3 to sp^2; and a change in the length of the carbon–carbon bond. The free energy of activation can be calculated with an rms error of 2.58 kcal mol^{-1} (1 cal = 4.184 J).

Key words: Elimination, no barrier theory, rate constant, equilibrium constant.

Résumé : On a appliqué la théorie sans barrière à l'étude des réactions E2 de cinq bromures d'alkyles avec de l'éthanolate éthanolique. Le modèle utilisé pour ces réactions est celui d'une réaction qui se produit à partir d'un complexe de rencontre de la base et de l'halogénure d'alkyle et qui conduit au complexe de rencontre du produit avec l'ion halogénure, l'alcène (et l'alcool) et qui nécessite cinq processus simples qui se combinent pour conduit à une élimination concertée: le transfert d'un proton du carbone à la base; une modification de la géométrie au niveau du carbone qui perd un hydrogène et qui passe de sp^3 à sp^2; un changement de géométrie au niveau du carbone qui perd le groupe partant et qui passe de sp^3 à sp^2; la rupture de la liaison du carbone-groupe partant et un changement dans la longueur de la liaison carbone–carbone. On a calculé l'énergie libre d'activation avec une erreur de 2,58 kcal/mol (1 cal = 4,184 J).

Mots clés : élimination, théorie sans barrière, constante de vitesse, constante d'équilibre.

[Traduit par la Rédaction]

Introduction

The E2 elimination reaction is one of the type examples of a concerted process, with strict stereoelectronic requirements for a coplanar arrangement of both carbons, proton and leaving group, and a strong preference for anti vs. syn geometry. Some years ago we showed that this reaction could be described in terms of the multidimensional Marcus theory, using equilibrium constants and intrinsic barriers for the two limiting stepwise processes (solvolysis to give a carbocation–leaving group ion pair, and proton transfer to give a carbanion) (1). This treatment had the disadvantage of requiring two intrinsic barriers, which had to be evaluated from kinetics for simpler reactions. In addition, it was not clear how justified the essential assumption, of a transferable intrinsic barrier for C–Br cleavage with the same value for tertiary, secondary, and even primary alkyl halides, really was.

Recently we developed the no barrier theory (NBT), which permits the calculation of rate constants from equilibrium constants and certain distortion energies with no input of kinetic information. In the present manuscript we wish to report the application of this approach to the E2 elimination of simple alkyl halides in ethanol.

Theory and calculations

No barrier theory depends on the following postulates:

(1) Reactants[3] are in equilibrium with the starting material or product at each point along each reaction coordinate.
(2) For any process where only one elementary reaction coordinate changes, the energy will be a quadratic function of the corresponding reaction coordinate.
(3) Heterolytic bond cleavage constitutes an elementary reaction coordinate.

Received 11 May 2005. Published on the NRC Research Press Web site at http://canjchem.nrc.ca on 8 December 2005.

J.P. Guthrie,[2] L. Leandro, and V. Pitchko. Department of Chemistry, University of Western Ontario, London, ON N6A 5B7, Canada.

[1]This article is part of a Special Issue dedicated to organic reaction mechanisms.
[2]Corresponding author (e-mail: peter.guthrie@uwo.ca).
[3]Here we are using "reactants" to mean the molecular system involved in the chemical reaction at any point on the reaction hypersurface.

 doi: 10.1139/V05-160 © 2005 NRC Canada

(4) Proton transfer between two atoms constitutes an elementary reaction coordinate.
(5) For an anion to react at carbon, it must first undergo partial desolvation so that its reactive lone pair can be in van der Waals contact with the carbon.

For convenience in carrying out the calculations, all coordinates are defined to run from 0 at the starting material to 1 at the product.

To apply the theory to a reaction such as the E2 requires calculation of the energies of each of the corner intermediates where one, two, or more of the simple processes have gone to completion. These energies depend on equilibrium constants for any bond making, bond breaking, or proton transfer steps, any distortion energies (calculated relative to the equilibrium species with the same bonding arrangement), any hydrogen bond interactions or electrostatic interactions when species (molecules or ions) are brought together in the encounter complex, the entropic cost of the encounter complex formation, and any obligatory desolvation. Once all of these corner energies are in hand, the reaction energy hypersurface can be calculated and the transition state free energy can be determined.

Once the energies of the corners of the reaction hypercube are defined, the postulates allow the free energy hypersurface to be defined, at least approximately. The various sequences of calculations, which lead to the energy of a point on the hypersurface, lead to similar but not identical values, so we take the average as the best estimate.

From the postulates, the free energy surface for the reaction hypercube (a square for two dimensions, a cube for three, and an appropriate hypercube for higher dimensions) can be deduced. To calculate the energy at a point (v,w,x,y,z), an iterative process is used, where one dimension, e.g., v, is set, and the energies for the corresponding section through the reaction hypercube, which will be a hypercube with one less dimension, are calculated; for example, in this case: (v,0,0,0,0), (v,1,0,0,0), (v,0,1,0,0), … (v,1,1,1,1). The process is now repeated for this $n - 1$ dimensional hypercube, fixing another of the coordinates at the value for the desired point and calculating the corners of the corresponding ($n - 2$) dimensional hypercube. This iterative process is continued until one reaches a two-dimensional hypercube (a square) for which there are only two ways to calculate the energy of the point. Both are used and the average is taken. There are clearly many such alternative paths for a five-dimensional hypercube. At each stage the energy is calculated in each possible way and the average is taken.

To define the hypersurface, the energy of each corner must be calculated. The major contributions to the energy at most corners will be the distortion energy calculated by the ab initio or DFT method, relative to the equilibrium species with the same bonding arrangement. However, we also try to include all known interactions affecting the energy of the corner: ΔpK_a for proton transfers, hydrogen bonding interactions if present, electrostatic interactions if present, and desolvation if present. Desolvation must be taken into account whenever a potential bonding contact requires the loss of a strong interaction with solvent replaced by only a weak interaction with the reactant until a covalent bonding begins.

The limiting stepwise alternatives to the concerted E2 reaction are the S_N1 reaction leading to the carbocation and the E1cb reaction leading to the carbanion. On each energy hypersurface, eight of the corners are more or less distorted forms of the carbocation and eight are more or less distorted forms of the carbanion. Thus, the nature of the E2 reaction requires four equilibrium species to be considered for each reaction. These are as follows: the alkyl halide, the alkene, the carbocation from C-halide bond cleavage, and the carbanion (from loss of a proton on a carbon β to the halide). The carbanion is not a real intermediate because it would lose halide extremely rapidly if it were ever to form. The carbanion would also react, with essentially no barrier, to reabstract the proton from ethanol. The carbocation would react with the bromide ion with, in most cases, essentially no barrier to form the alkyl bromide; only in the cases of *tert*-butyl and 1-phenylethyl cations is there a small barrier to reaction with bromide. However, the carbanion is a conceptual intermediate in a stepwise E1cb version of the E2 and would be a real intermediate given adequate anion stabilizing substituents; the carbocation is a conceptual intermediate in a stepwise E1 version of the E2 and would be a real intermediate given adequate cation stabilizing substituents. The corner species corresponding to the ions will not generally have exactly the equilibrium geometry of the ion, but will have a mix of geometrical features from starting material and product. Nonetheless, one corner will be close to being the carbocation of the hypothetical stepwise reaction, and another one will be close to being the corresponding carbanion.

Equilibrium constants for elimination reactions

To begin the process of calculating the energy of all the corners of the reaction diagram, we require the overall equilibrium constants for the elimination reactions. For ethyl, isopropyl, and *tert*-butyl bromides these equilibrium constants have been reported (1). For 1-bromo-1-phenylethane and 1-bromo-2-phenylethane the free energies of the alkyl halides have not been reported, so values were obtained by computation using the G3MP2B3 method (2). The free energy of formation of styrene has been reported (3), although not the free energy of transfer to ethanol, which was calculated by the IPCM method.

The free energies of solvation were calculated using the IPCM method in Gaussian. This method gives ΔG_{solv} on the 1 mol/L (g) to 1 mol/L (aq) standard states. This can be converted to the free energy of transfer (ΔG_t), 1 atm (g) to 1 mol/L (aq) (1 atm = 101.325 kPa), by adding 1.90 kcal/mol (1 cal = 4.184 J). This method was used for all species except for H^+, Br^-, and H_2O. For H^+ we used either the Zhan and Dixon value for ΔG_t to water (–262.4 kcal/mol) (4), for the computational free energies with a free energy for gaseous H^+ (–6.28 kcal/mol) (5) based on the Sackur–Tetrode equation (6), or the conventional value for $\Delta G_f(aq)[H^+]$ (0.0) along with Marcus' (7) value for the free energy of transfer for H^+ from water to ethanol. For Br^- we used the NIST value for the conventional solvation energy in water (8) and the free energy of transfer from water to ethanol given by Marcus (7). We calculated ΔG_t (gas at 1 atm, ethanolic solution at 1 mol/L) for water from data given by Pemberton and Mash (9). From the total vapor pressure of a dilute solution of water in ethanol and the mol fraction of water in the vapor phase, we can calculate the

© 2005 NRC Canada

Table 1. Thermodynamic quantities for compounds discussed in this paper.

Compound	ΔH_f(g)	$S°$(g)	ΔG_f(g)	$\Delta G_t^{H_2O}$ [b]	ΔG_f(aq)	ΔG_t^{EtOH} [c]	ΔG_f(EtOH)
Compounds for which ΔG_f(EtOH) has not previously been reported[a]							
$PhCH(Br)CH_3$	6.60	93.69	29.21	–0.70	28.51	–0.55	28.66
$PhCH(OH)CH_3$	–33.80	91.98	–3.74	–2.21	–5.95		
$PhCH(^+)CH_3$						–42.57	76.08[d]
$PhCH_2CH_2Br$	8.08	81.44	29.55	–0.35	29.20	–0.40	29.15
$PhCH_2CH_2OH$	–30.18	95.59	–1.60	–0.33	–1.93	–0.53	–2.13
$PhCH_2CH_2^+$	241.03	81.44	261.87				113.60[d]
$PhCH=CH_2$	35.30±0.36[e]	82.48[e]	51.08[e]	0.69[e]	51.77±0.38[e]	–0.55	51.22
H^+							2.65[d]
Br^-							–20.50[d]
H_2O			–54.63[f]			–3.26[g]	–57.89
ΔG_f(ETOH) already reported							
CH_3CH_2Br							–8.29
$CH_2=CH_2$							17.28
$(CH_3)_2CHBr$							–8.79
$CH_3CH=CH$							15.19
$(CH_3)_3CBr$							–8.36
$(CH_3)_2C=CH$							12.35
HBr[h]							–17.85

[a]All at 25 °C; enthalpies and free energies are in kcal/mol, entropies are in cal/°/mol, standard states are the ideal gas at 1 atm and 1 mol/L aqueous solution with an infinitely dilute reference state. Unless otherwise noted, enthalpies of formation are derived from molecular orbital computations as described in the text, entropies are computational as described in the text, the free energies of formation in the gas phase are calculated from the corresponding enthalpies of formation and the standard entropies, the free energies of transfer are based on IPCM solvatation energy calculations as described in the text, and the free energies of formation in aqueous solution or ethanolic solution are calculated from the corresponding free energies of formation in the gas and the appropriate free energies of transfer.

[b]Free energy of transfer from gas at 1 atm to 1 mol/L aqueous solution, calculated by the IPCM/6-31+G* method with isodensity = 0.0004.

[c]Free energy of transfer from gas at 1 atm to 1 mol/L ethanolic solution, calculated by the IPCM/6-31+G* method with isodensity = 0.0004.

[d]Conventional ionic free energy: $\Delta G_f(aq)[H^+] = 0.0$.

[e]Reference 3.

[f]Reference 8 (pp. 2–38).

[g]Calculated from the data in ref. 9 as described in the text.

[h]Fully dissociated into H^+ and Br^-.

partial pressure of H_2O above the solution. From the mol fraction of water in the liquid phase, we can calculate the molar concentration of water. With the concentration of water in the liquid phase and the partial pressure of water above the solution in hand, we calculated the free energy of transfer at 303.15 and 323.15 K, the two temperatures studied by Pemberton and Mash, and then extrapolated to 298.15 K. The data and further details about the calculations are given in Appendix A and Table A1. All of the free energies of formation are found in Table 1.

In this way one calculates, from the free energies of formation in Table 1,

$$PhCH(Br)CH_3 + EtO^- \rightleftharpoons PhCH=CH_2 + Br^- + EtOH \qquad \Delta G° = -22.07$$

$$PhCH_2CH_2Br + EtO^- \rightleftharpoons PhCH=CH_2 + Br^- + EtOH \qquad \Delta G° = -22.56$$

Cation energies

The free energies of the ethyl, isopropyl and *tert*-butyl cations relative to the bromides were calculated after Abraham (10) as previously reported (1); energies for the phenylethyl cations were derived from DFT calculations as described below.

Free energies of the phenylethyl cations were calculated starting with the pK_R process for the corresponding alcohols. We have shown that for substituted benzyl alcohols, the relative values of pK_R can be calculated based on the gas-phase free energies using B3LYP/GTLarge//B3LYP/6-31G** and the free energies of solvation using IPCM/B3LYP/6-31G**. In other work we have shown that the pK_R values for a range of alcohols, alkyl, as well as benzyl, can be calculated using G3MP2B3 gas-phase free energies and IPCM/B3LYP/6-31G* free energies of solvation, with an rms error of 2.9 in pK_R, which can be reduced to 1.2 by scaling the solvation energies.[4] For 2-phenylethanol we calculated the gas-phase thermochemical quantities using G3MP2B3 and IPCM/B3LYP/6-31G* free energies of solvation. We have no basis for scaling the solvation energies in ethanol, and by analogy with cations in water, we must expect them to be in error by

[4]J.P. Guthrie. Manuscript in preparation.

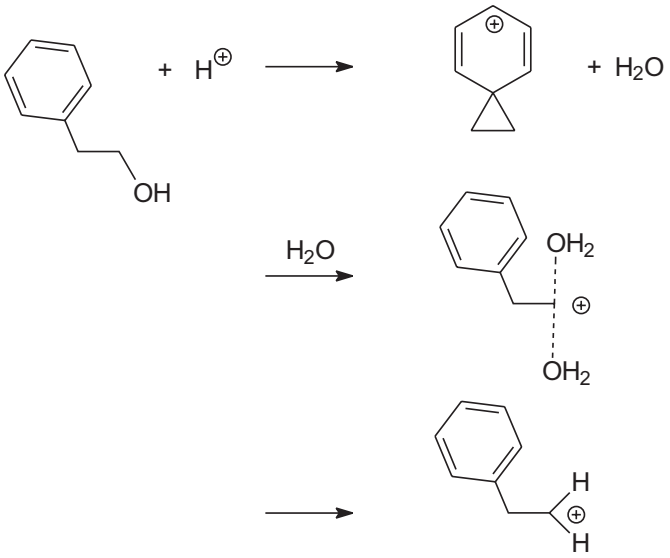
© 2005 NRC Canada

several kcal/mol. However, since the 2-phenylethyl cation is a high energy species, which will be quite far from the transition state, we expect that the transition state free energy will be insensitive to errors in the cation free energy.

We first calculated gas-phase thermodynamic quantities for each species. For 2-phenylethanol and 2-phenylethyl bromide the entropy value reported by Gaussian was corrected for the existence of multiple conformers (11). This correction was based on a conformational search using the GMXX routine in PCModel (12). The entropy of mixing given by PCModel includes contributions from indistinguishable rotamers, and thus, needs to be corrected to include only distinguishable conformations, including enantiomeric conformers. Then using the free energies of transfer of each species, we calculated the free energy of reaction in ethanol, and from the free energies of all species except the cation, this value can now be determined. This slightly roundabout procedure avoids most of the problems of multiple standard states for ionic species in solution. It is still necessary to be alert to the two conventions for free energies of formation in gas (ab initio where the assumed initial state is the nuclei and electrons infinitely separated in vacuum, and the thermochemical convention where the initial state has the elements in their standard state).

For 1-phenylethanol, $pK_R = -15.4$ has been reported by Amyes et al. (13). We have calculated the free energies of transfer for all species from gas to both water and ethanol and have taken the difference as the free energy of transfer from water to ethanol. There will be some cumulation of error, but one may hope there is also some cancellation of error from matching contributions on the left and right sides of the equilibrium equation. From the pK_R in water we calculated the corresponding free energy change in ethanol. From the free energies of all species except the cation we can now calculate the free energy of formation of the cation.

Free energies of formation for all species are contained in Table 1.



For 2-phenylethyl cation the situation was more complicated. The preferred form of the cation, both in the gas phase and in solution, is the phenonium ion. If the conformation is locked so that the phenyl cannot bridge, then the primary cation will not be a true intermediate because specific solvation by two equivalent solvent molecules would give the S_N2 transition state. (This was examined using water as solvent because water is smaller and more symmetrical than ethanol, which facilitates the calculations.) The ion needed as a starting point for calculating the cation corner of the reaction diagram would be the bare ion without specific solvation. We calculated the solvation energy of this hypothetical species by the continuum solvent approximation using the IPCM method:

[1] $\text{Ph-CH}_2\text{-CH}_2^+ + \text{H}_2\text{O} \rightleftharpoons \text{Ph-CH}_2\text{-CH}_2\text{-OH} + \text{H}^+$

$\Delta G^\circ = 55.20$ (EtOH)

From the calculated equilibrium free energy for rxn. [1] and the free energies of formation for the other species, already evaluated, we can calculate the free energy of formation for $\text{Ph-CH}_2\text{-CH}_2^+$ in ethanol as $\Delta G_f^\circ = 113.60$. Now with the free energies of formation in hand for all species in eq. [2] we can evaluate the standard free energy change in ethanol as $\Delta G^\circ = 63.95$.

[2] $\text{PhCH}_2\text{CH}_2\text{Br} \rightleftharpoons \text{Ph-CH}_2\text{-CH}_2^+ + \text{Br}^-$

We used the value estimated (1) by the procedure suggested by Abraham (10) to estimate the free energy of ion pair formation from ethyl cation and Br^-, i.e., $\Delta G_{ip} = -3.1$; this leads to a free energy change in ethanol for eq. [3] of 60.85.

[3] $\text{PhCH}_2\text{CH}_2\text{Br} \rightleftharpoons (\text{Ph-CH}_2\text{-CH}_2^+, \text{Br}^-)$

By analogous calculations, we deduce the free energy changes for rxns. [4]–[6]:

[4] $\text{PhCH(CH}_3)^+ + \text{H}_2\text{O} \rightleftharpoons \text{PhCH(CH}_3\text{)-OH} + \text{H}^+$

$\Delta G^\circ = 20.56$ (EtOH)

[5] $\text{PhCH(CH}_3\text{)-Br} \rightleftharpoons \text{PhCH(CH}_3\text{)}^+ + \text{Br}^-$

$\Delta G^\circ = 26.92$ (EtOH)

[6] $\text{PhCH(CH}_3\text{)-Br} \rightleftharpoons (\text{PhCH(CH}_3\text{)}^+, \text{Br}^-)$

$\Delta G^\circ = 23.82$ (EtOH)

Similarly we used the value estimated (1) by the procedure suggested by Abraham (10) for ion pair formation from isopropyl cation and Br^-, i.e., $\Delta G_{ip} = -3.1$; this leads to a free energy change for eq. [6] of 23.82.

Calculation of pK_a values for cations

For each cation we can define a pK_a for the loss of a proton to give the corresponding alkene. Since we now have the free energies of formation for each species in ethanol, it is straightforward to calculate the pK_a values. The values calculated are found in Table 2.

Calculation of pK_a values for alkyl bromides

For the anion equilibria we need the pK_a values for CH ionization. The starting point is toluene for which there is a reasonably good estimation of pK_a in water. Streitwieser and

© 2005 NRC Canada

Table 2. pK_a values for the alkyl bromides and cations in ethanol at 25 °C estimated as described in the text.

Compound	pK_a
$CH_3CH_2^+$	–33.44
$(CH_3)_2CH^+$	–23.84
$(CH_3)_3C^+$	–14.74
$PhCH(CH_3)^+$	–15.96
$PhCH_2CH_2^+$	–44.43
CH_3CH_2Br	54.0
$(CH_3)_2CHBr$	54.0
$(CH_3)_3CBr$	54.0
$PhCH(CH_3)Br$	53.0
$PhCH_2CH_2Br$	38.2

Ni (14) measured the rate of exchange and extrapolated to 25 °C, obtaining a rate constant for hydroxide of 7.4×10^{-17} $(mol/L)^{-1}$ s^{-1}. They used a rate constant for the reaction of water based on measurements of the bimolecular reaction in THF. This seems likely to be too low because water in THF will be far less acidic than water in water as a result of the absence of hydrogen bonding solvation for hydroxide. Instead, we used the rate constant for reorganization of water, following Richard (15), namely $k = 10^{11}$ s^{-1}. This leads to a $K_a = K_w$ $(k_{OH}/k_w) = 10^{-14}$ $[(7.4\times10^{-17})/10^{11}] = 7.4 \times 10^{-42}$, or p$K_a$ = 41.13. This is close to the value estimated by Bordwell for DMSO solution, namely 43 (16).

Cram (17) cites three studies of the relative rates of hydrogen isotope exchange in ethylbenzene relative to toluene; the relative rates are 0.14 (NH_3/NH_2K, 10°), 0.12 ($cC_6H_{11}NH_2/cC_6H_{11}NHK$, 50°), and 0.22 ($CH_3SOCH_3$/*t*-BuOK, 30°). Over a range of solvents the relative rate is 0.16 ± 0.5. It seems reasonable that the rate constant for the reverse reaction will be the same limiting value in both cases, so this will also be the ratio of acidity constants. This leads to a pK_a for the α-hydrogen of ethylbenzene of 41.13 – log(0.16) = 41.9 in water.

The effect of the β-bromine is estimated from the linear free energy relationships (LFER) for ionization of alcohols, taking $RCH_2OH \rightarrow RCH_2O^-$ as a model for $RCH_2CH_2R' \rightarrow RCH_2CH\text{-}R'$. The best model for the effect of solvent on the ρ* value for this reaction is a recent study of substituted acetic acids (18) in which it was found that the pK_a shift from acetic acid to chloroacetic acid was essentially the same in the two solvents. Based on this model we used the ρ* value for ionization of alcohols in water (ρ* = –1.32) (19) for the ionization of $PhCH_2CH_2X$. This leads to a predicted shift in pK_a of 1.32 × 2.84 = 3.75, and a pK_a for $PhCH_2CH_2Br$ of 38.2. The shift in pK_a from water to ethanol is taken as 5.7, as before (1). This leads to a pK_a for $PhCH_2CH_2Br$ of 43.9 in ethanol.

This value does not appear to be logically consistent with the pK_a for alkyl bromides of 47 used previously (1). It can be expected that the effect of a conjugated phenyl will be more than 3 pK_a units. The previously used value was based on Streitwieser's experimental values of cesium ion pair pK_a values in cyclohexylamine (20), which were reported to be equivalent to the pK_a values in methanol. This meant that they were very close to the desired pK_a values in ethanol. Given the more recent pK_a value for ethyl benzene deduced above, 43 in water, thus 48 in ethanol, a value of 51 for ethane in ethanol no longer looks reasonable. Instead, we started with Jorgensen's computational value for ethane (21) from which we deduced (1) a value of 54 for ethyl bromide (and isopropyl and *tert*-butyl bromides).

For the pK_a of $PhCH(CH_3)Br$ we started with the pK_a for ethyl bromide of 54 as estimated above. The effect of the β-phenyl is estimated using ρ* = –1.32 as 0.99, which leads to a pK_a for $PhCH(CH_3)Br$ in ethanol of 53. The pK_a values for all the alkyl bromides discussed are found in Table 2.

Electrostatic interactions

The "carbocation" corners are actually ion triples. The electrostatic interaction in such an ion triple is calculated from the relative positions of the charges, assuming a uniform dielectric constant, which is the same as the effective dielectric constant for a simple ion pair. The interaction is then scaled to ion-pair formation in ethanol, using the data for simple spherical ions. For KCl, the ion-pair association constant in ethanol (22) leads to $\Delta G_{ip} = -2.7$. This is the free energy for the formation of an ion pair from spherically symmetrical singly charged anion and cation. We partition this free energy into the statistical and electrostatic contributions using the equation (23) derived by Fuoss (24) and Eigen (25), picking an interaction distance to give $\Delta G_{overall} = \Delta G_{encounter} + \Delta G_{electrostatic} = -2.7$ kcal/mol in ethanol. The corresponding contributions can be calculated from the terms in this equation as $\Delta G_{encounter} = 1.44$ and $\Delta G_{electrostatic} = -4.14$. Simple electrostatic calculations are used to calculate the electrostatic interaction energy for the geometry in a cluster.

Desolvation energies

The free energy of transfer from water to ethanol for bromide ion is +18.2 kJ (4.35 kcal) (26), and from water to acetone (similar dielectric constant, no hydrogen bonding) it is +42 kJ (10.04 kcal) (26). From these we calculated that the free energy of transfer from ethanol to acetone is +5.69 kcal/mol. Taking the solvation number of bromide in ethanol as three (27), the loss of solvating ethanol would then be worth 1.90 kcal/mol.

The cost of losing a hydrogen bond from ethanol to ethanol can be estimated from the difference in the free energies of transfer for ethanol and dimethyl ether from ethanol to chloroform (slightly polar, non-hydrogen bond accepting solvent). These calculations are explained in Appendix B and Table B1. The difference in the free energy of transfer from ethanol to chloroform for ethanol and dimethyl ether is 1.74 kcal/mol, which is taken as the cost of losing one hydrogen bond from OH to solvent.

The total desolvation energy for EtOH:ethene:Br^- would then be 3.64 kcal/mol.

Hydrogen bonds

For all hydrogen bonds we used the Stahl–Jencks equation (28) to estimate the free energy of hydrogen bond formation. Corners with a carbanion hydrogen bonded to solvent will clearly have a strong hydrogen bond, but this is implicit in the pK_a values, which are estimated for the reactions in solu-

© 2005 NRC Canada

tion, thus including hydrogen bonding solvation. To use the Stahl–Jencks equation (28)

$$[7] \qquad \log K_{HB} = \tau\,(pK_a^{prosolv} - pK_a^{BH})\,(pK_a^{HA} - pK_a^{solv}) - \log[solv]$$

in ethanol we need to determine the τ parameter in ethanol. This would require either a study of hydrogen bonding equilibria, which has not been done, or an indirect calculation. The simplest approach is that of Funderberk and Jencks (29), who reported an electrostatic calculation. This approach derives τ from two quantities: the effect of a plus charge on pK_a for X-CH_2-Z vs. X-CH_2-ZH^+ and the attenuation factor for transmission of the substituent effects. We have found no data that allow the determination of the attenuation factor in ethanol; there are some data (see Appendix C and Table C1) for methanol (30) that suggest that the attenuation factor is similar to that in water. There is considerable scatter in the attenuation factors which can be calculated, but no basis for saying that the fall-off factor is different in methanol vs. water. If this is true, then it is reasonable to expect a very similar fall-off factor in ethanol.

What is the effect of a plus charge on pK_a in ethanol? The situation is more complicated than it might seem; see Appendix D and Table D1. The effect of a charge (in glycine) on the pK_a of a carboxylic acid is roughly the same in water or aqueous ethanol, at least up to 60% or 70% ethanol. One can also look at the effects of substituents in different solvents; see Table 3. The traditional expectation is that the substituent effects are larger in ethanol than in water. This is based on the studies of benzoic acids (31). However, some studies of the substituted acetic acids tell a different story; see XCH_2COOH data from Headley et al. (18). The sensitivity to the substituent effects is unaffected by solvent! A possible explanation is preferential solvent orientation, with the hydroxyl groups being close to the very polarized atoms of the substituted acetic acid, while the ethyl group of ethanol is close to the benzene ring in the benzoic acids. This would mean similar attenuation of field effects for all alcohol solvents in the acetic acid case, but much less attenuation in the benzoic acids, where the low dielectric constant volume between substituent and acid is greater in organic solvents.

The Funderburk–Jencks equation (29) is

$$[8] \qquad \tau = \frac{(\text{attenuation factor})^4}{pK_a^{ZH+CH_2XH} - pK_a^{ZCH_2XH}}$$

For the moment the available data suggest that using the Stahl–Jencks (28) parameters for water may the best approximation.

Experimental rate constants

The rate constants for the reactions of 1-phenylethylbromide and 2-phenylethylbromide were reported by McLennan (32). The rate constants determined at 50 °C in ethanol for the reaction of free ethoxide with the alkyl bromide were 1-Phenylethylbromide: $k = 7.95 \times 10^{-4}$ $(mol/L)^{-1}$ s^{-1} ($\Delta G^{\ddagger}$ = 23.58) and 2-Phenylethylbromide: $k = 45 \times 10^{-4}$ $(mol/L)^{-1}$ s^{-1} ($\Delta G^{\ddagger}$ = 22.46).

The free energies of activation calculated from these rate constants are likely to be very close to the desired free energies of activation at 25 °C. For a number of simple alkyl halides Ingold (33) gives Arrhenius *A* values in ethanol or aqueous ethanol, and these are consistently about 10^{11}. Such a value leads to $\Delta S^{\ddagger} = -10.36$. For a 25° change in reaction temperature $\Delta S^{\ddagger} = -10.36$ leads to a change of 0.26 in $\Delta G^{\ddagger}$, which is almost negligible for our purposes. Corrected values are: $\Delta G^{\ddagger}$ = 23.32 kcal/mol for 1-phenylethyl bromide and $\Delta G^{\ddagger}$ = 22.20 kcal/mol for 2-phenylethyl bromide in ethanol at 25 °C. The rate constants for ethyl, isopropyl, and *tert*-butyl bromides taken from the literature were as reported previously (1).

Table 3. Effect of substituents on pK_a values for carboxylic acids in various solvents.

	Substituted benzoic acids	Substituted acetic acids
Solvent	Hammett ρ	Taft ρ*
Water	1.054[a]	–0.75±0.05[b]
Methanol	1.47[c]	–0.78±0.02[b]
Ethanol		–0.76±0.11[b]
10% EtOH	1.092[a]	
50% EtOH	1.516[a]	
75% EtOH	1.672[a]	

[a]Reference 30.
[b]Reference 18.
[c]Reference 29.

Model used for the E2 reaction

The model, which is used in applying NBT to the E2 eliminations, is that the reaction proceeds from the encounter complex of base and alkyl halide to the product encounter complex of halide ion, alkene (and alcohol), and that the five simple processes that combine to give the concerted elimination are: transfer of a proton from carbon to base; change in geometry at the carbon, which loses a proton from sp^3 to sp^2; breaking the C-leaving group bond; change in geometry at the carbon, which loses the leaving group from sp^3 to sp^2; change in the length of the carbon–carbon bond.

Computer programs for calculations

To ease the burden of the number of calculations, which must be carried out to evaluate the relative energies of all corners (32 per reaction for a five-dimensional model), we have written computer programs, which: (*a*) examine the structures of the initial and final complexes and pick out the reaction dimensions; (*b*) construct structure files for each corner, and for the form of the starting material, product, cation or anion contained in that complex ready for the MO calculation of the energy; (*c*) extract results (distortion energies) from the set of output files; (*d*) calculate the corner energies involving all the effects included in the model; (*e*) search for the transition state.

Initial structures were generated and optimized using PCModel (12). All molecular orbital calculations were carried out using GAUSSIAN 98 (34) or GAUSSIAN 03 (35). Heats of formation or entropies were calculated using the G3MP2B3 (2) method in Gaussian; distortion energies were calculated at the B3LYP/6-31+G** level using DFT and the B3LYP (36, 37) method. Solvation energies were calculated at the IPCM/B3LYP/6-31G(d)//B3LYP/6-31G(d) level using the IPCM continuum solvation method (38).

© 2005 NRC Canada

Table 4. Distortion energies for the E2 reactions.

Corner	CH_3CH_2Br	$(CH_3)_2CHBr$	$(CH_3)_3CBr$	$PhCH(CH_3)Br$	$PhCH_2CH_2Br$
00000	0.000	0.000	0.000	0.613	0.766
10000	27.734	26.035	28.074	21.927	23.899
01000	4.749	5.056	1.072	6.281	8.732
00100	23.746	24.053	41.517	33.857	23.287
00010	29.721	36.768	24.206	24.512	32.172
00001	15.320	15.320	15.320	14.401	14.094
11000	39.301	40.818	42.140	40.158	39.717
10100	32.081	37.625	2.805	1.858	22.789
10010	5.238	3.256	42.513	39.162	8.254
10001	30.956	34.288	38.501	33.321	29.338
01100	7.660	8.579	45.501	45.194	3.830
01010	42.896	47.186	4.749	8.120	49.637
01001	10.877	10.724	6.128	10.264	16.239
00110	56.684	62.965	67.255	60.208	56.837
00101	37.994	38.607	58.676	50.863	35.696
00011	48.718	55.152	38.607	37.841	51.475
11100	28.907	31.588	28.122	27.768	26.121
11010	30.568	29.343	33.771	30.429	31.770
11001	30.133	32.129	33.982	32.459	31.904
10110	13.879	15.334	16.603	19.112	9.920
10101	30.300	40.546	8.780	9.632	23.152
10011	6.631	7.919	47.540	47.282	9.498
01110	42.590	47.186	45.347	44.735	38.453
01101	9.958	10.111	49.177	49.024	7.354
01011	49.943	52.701	5.668	8.426	62.506
00111	71.698	77.213	80.124	72.924	70.013
11110	17.144	17.077	16.814	15.626	15.473
11101	15.296	18.063	15.789	16.488	14.439
11011	17.407	16.565	20.481	17.848	19.610
10111	8.627	13.688	16.603	21.927	5.515
01111	44.735	47.339	43.509	43.356	43.356
11111	0.000	0.000	0.000	0.000	0.000

Note: The reaction is the ethoxide induced elimination of alkyl bromide in ethanol at 25 °C; distortion energies are in kcal/mol; if the reactive conformation of the starting alkyl bromide or product alkene is not the same as the lowest energy conformation, then these corners will have distortion energies. The dimensions are not defined in the same way for all compounds; the programs, which assign dimensions, do so in a logical but not necessarily a convenient (for humans) fashion. For ethyl, isopropyl, and 2-phenylethyl bromides, the dimensions are: *v*, C-Br bond breaking; *w*, proton transfer; *x*, C(H) geometry; *y*, C(Br) geometry; *z*, bond length. For *tert*-butyl and 1-phenylethyl bromides, the dimensions are: *v*, C-Br bond breaking; *w*, proton transfer; *x*, C(Br) geometry; *y*, C(H) geometry; *z*, bond length.

Results

To apply the model to a specific E2 reaction, we calculated the free energies of the various corner species: starting material, products, cation, and anion as previously described, and then the specific corner species by including all the interactions previously described. The distortion energies relative to the starting material, product, cation, and anion were calculated at the B3LYP/6-31+G** level, with geometries of the parent species altered according to the reaction dimensions, which had changed. For each distorted structure a partial optimization was carried out with the variables defining the reaction locked at the values specified for that structure. The distortion energies calculated are found in Table 4. These values, combined with the proton transfer equilibria, hydrogen bond equilibria, ion-pair equilibria, desolvation, etc., lead to the corner energies in Table 5. Finally searching the energy hypersurface defined by the corner energies and the postulates of NBT lead to the transition state energies and coordinates found in Table 6.

To examine the nature of the transition state, we projected the five-dimensional reaction diagram onto a two-dimensional diagram with the carbocation (really ion triple) and carbanion corners as the two intermediates to be considered. This requires a two-stage projection. Because of the nature of the reaction dimensions, the carbocation corner corresponds to (1,0,0,1,0) and the carbanion to (0,1,0,0,0); the initial state (0,0,0,0,0) is taken to be alkyl halide and ethoxide, and the product, (1,1,1,1,1) to be alkene, ethanol, and bromide. The carbanion is assumed to be approximately tetrahedral, while the carbocation is planar. The *x* and *z* dimensions are 0 for both intermediates and the product, so we first projected these dimensions onto a three-dimensional cube (*v*,*w*,*y*) and then projected *v* and *y* onto a new dimension corresponding to the progress towards the carbocation, while *w* represents progress towards the carbanion.

© 2005 NRC Canada

Table 5. Corner energies for the E2 reactions.

Corner	CH_3CH_2Br	$(CH_3)_2CHBr$	$(CH_3)_3CBr$	$PhCH(CH_3)Br$	$PhCH_2CH_2Br$
10000	68.16	55.46	41.65	37.82	77.72
01000	43.51	43.82	39.83	43.06	32.92
00100	23.75	24.05	41.52	33.24	22.52
00010	29.72	36.77	24.21	21.84	31.41
00001	15.32	15.32	15.32	13.79	13.33
11000	17.60	17.53	15.56	14.19	13.09
10100	72.15	66.69	16.46	17.84	76.28
10010	45.77	32.77	55.72	54.69	62.17
10001	71.29	63.62	51.98	49.13	83.07
01100	46.42	47.34	84.26	81.97	28.02
01010	81.66	85.95	43.51	44.90	73.83
01001	49.64	49.48	44.89	47.04	40.43
00110	56.68	62.96	67.25	59.60	56.07
00101	37.99	38.61	58.68	50.25	34.93
00011	48.72	55.15	38.61	34.76	50.71
11100	7.21	8.30	1.54	1.80	–0.92
11010	8.87	6.05	7.19	4.46	5.14
11001	8.43	8.84	7.40	6.49	5.28
10110	54.01	44.45	29.86	34.69	63.47
10101	70.30	69.53	22.34	25.52	76.57
10011	47.06	37.34	60.67	60.68	62.91
01110	81.35	85.95	84.11	81.52	62.65
01101	48.72	48.87	87.94	85.80	31.55
01011	88.70	91.46	44.43	45.21	86.70
00111	71.70	77.21	80.12	72.31	69.25
11110	–4.56	–6.21	–9.77	–10.35	–11.56
11101	–6.40	–5.23	–10.79	–9.48	–12.60
11011	–4.29	–6.72	–6.10	–8.54	–7.43
10111	48.67	42.72	29.77	37.42	58.98
01111	83.49	86.10	82.27	80.14	67.55
11111	–21.70	–23.29	–26.58	–25.97	–27.04

Note: The reaction is the ethoxide-induced elimination of alkyl bromide in ethanol at 25 °C; distortion energies are in kcal/mol; explanations as for Table 4.

Table 6. Observed and calculated free energies of activation for the E2 reactions of alkyl bromides with ethanolic ethoxide ion at 25 °C and transition state positions.

Compound	ΔG^*_{obs}	ΔG^*_{calc}	Dif.	*v*	*w*	*x*	*y*	*z*	*c*+	*c*–
CH_3CH_2Br	26.46	25.69	–0.76	0.406	0.609	0.469	0.141	0.344	0.274	0.609
$(CH_3)_2CHBr$	25.13	23.12	–2.01	0.422	0.609	0.297	0.250	0.359	0.336	0.609
$(CH_3)_3Br$	23.63	21.67	–1.96	0.391	0.531	0.313	0.281	0.281	0.352	0.531
$PhCH(Br)CH_3$	23.58	23.54	–0.04	0.438	0.375	0.344	0.563	0.188	0.376	0.344
$PhCH_2CH_2Br$	22.46	24.66	2.20	0.25	0.563	0.375	0.375	0.375	0.313	0.563

Note: *v*, *w*, *x*, *y*, *z* are the "simple process coordinates"; *c*+ is the projection of the transition-state position on the initial state to "carbocation" dimension; *c*– is the the projection of the transition-state position on the initial state to "carbanion" dimension; see the text for a discussion of these dimensions and projections.

The resulting positions of the transition states, projected onto a two-dimensional reaction diagram, are shown in Fig. 1. The results are mostly as expected: the transition state for 2-phenylethyl bromide has the least carbocation character and the most carbanion character; the transition state for *tert*-butyl and 1-phenylethyl bromide have the most carbocation character and the least carbanion character.

Discussion

The goal of this approach for calculating the rate constants is to use the equilibrium information and the usual models of physical organic chemistry to predict the rate constants without using any empirical kinetic information. A problem, which arises from time to time, is that we need

© 2005 NRC Canada

Fig. 1. Projected transition-state positions for the E2 reactions discussed here. (1,0) is the ion triple (ethoxide, carbocation, and bromide); (0,1) is the carbanion; (1,1) is the product complex. Projected coordinates calculated as described in the text and taken from Table 6.

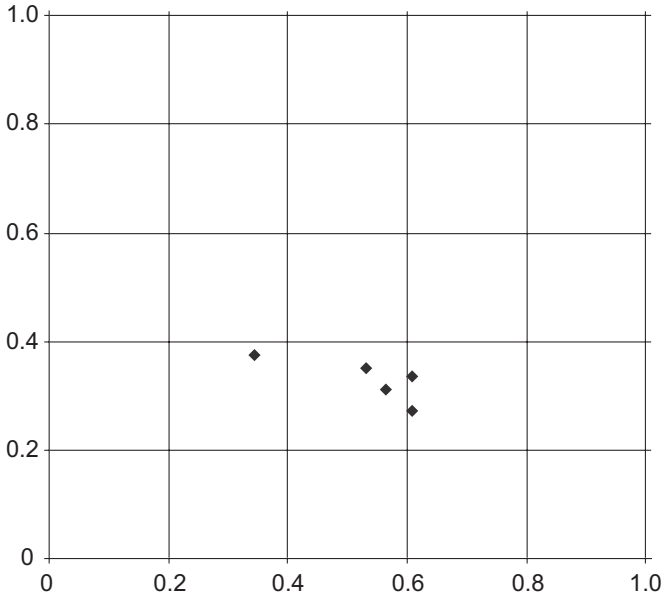
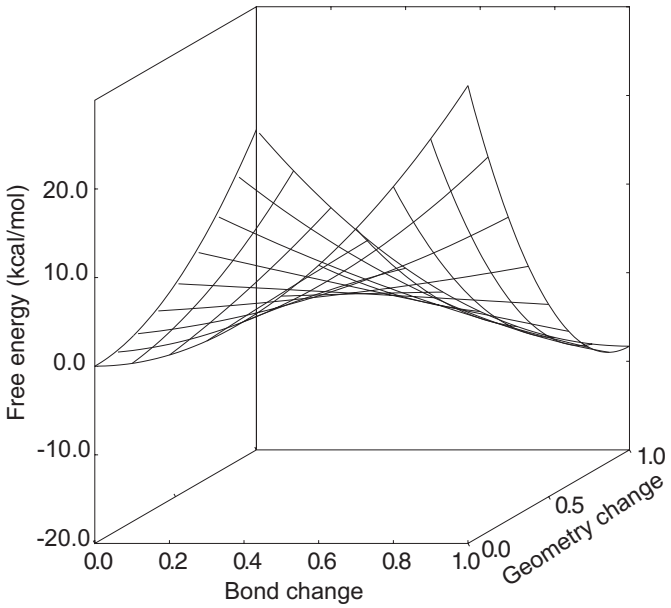


Fig. 2. A two-dimensional reaction diagram with the free energy orthogonal to the two reaction dimensions.



quantitative estimates for quantities normally talked about qualitatively. Such a problem arises when desolvation must be considered: it is generally accepted that ethoxide is strongly solvated and if one of the solvent molecules is lost and replaced by a weakly interacting molecule, then there will be a thermodynamic cost. What is not generally accepted is any general way to estimate this desolvation cost. Two kinds of desolvation arise in this work. There is a cost for having bromide and the OH of ethanol in contact with the product alkene; here we estimated the cost based on the free energies of transfer from a solvent capable of hydrogen bonding to one which is not. The energies involved are relatively small, so we should have satisfactory accuracy. Although bromide is not really a hydrogen bond acceptor, it will be better solvated by the more polar OH group of ethanol than the π cloud of an alkene. There is also a desolvation to consider when ethoxide is in contact with a C-H of an alkyl halide or a carbocation. We have based the estimates used in this work on the change in basicity of ethanol from water to DMSO, assuming this reflects the loss of three hydrogen bonds. If one were to use the very high pK_a of the CH of an alkyl bromide in the Stahl–Jencks equation, then a desolvation larger than 6.1 kcal/mol estimated previously would be obtained. This seems unrealistic because the ethoxide could at very low cost move slightly farther from the CH and lessen the interaction. Since this is a very low cost motion, it need not constitute an additional dimension. What is more problematic is the situation of ethoxide in "hydrogen bonding" contact with the β-CH of a carbocation. This hydrogen is, at equilibrium, a very strong acid, and thus, expected to form a strong hydrogen bond. However, when looking at the interaction of water with the β-CH of isopropyl cation (with the H oriented for hyperconjugation) the interaction is quite weak (G3MP2B3 calculations). The H_2O isopropyl cation complex has a noticeably elongated C—H bond 1.19 vs. 1.11 Å for the uncomplexed β-CH on the other methyl with the hyperconjugation orientation. Thus, even for a weak interaction there is noticeable elongation. This is in accord with the usual assumptions that hydrogen bonding involves partial proton transfer (normally to a slight extent only). For the situation of interest for this work, ethoxide in contact with a β-CH of a carbocation, this becomes a serious problem because a significant bond lengthening would be expected (if in fact the proton did not simply transfer) yet by the definition of a corner species the C—H bond length is locked at the initial value. This means that the hydrogen bond energy calculated by the Stahl–Jencks equation will be in error to some large but unknown extent. This poses a problem: on one hand if we regard the situation as ethoxide having lost a hydrogen bond to ethanol and forced to be in contact with a CH, then a desolvation of 6.1 kcal/mol is predicted; on the other hand we regard the situation as an ethoxide in contact with a quite acidic CH capable of forming a hydrogen bond then a complexation negative by several kcal/mol is predicted. There are reasons to believe both extremes are wrong, but at the moment apparently there is no way to make a better calculation. For the moment the best course of action seems to set the desolvation–hydrogen bonding to zero, at least between the two extremes. The saving thing is that the carbocation is in most cases a relatively high energy intermediate in ethanol and thus, the transition-state energy is relatively insensitive to errors in the energy of carbocation corners.

Despite these uncertainties in some of the quantities needed to calculate the rate constants by NBT, the overall predictions are quite good. The rms error in the free energy of activation for five E2 reactions is 1.63 kcal/mol; the reactions have $\Delta G^{\ddagger}$ values ranging from 22.20 to 26.46 kcal/mol, corresponding to the rate constants ranging from 3.3×10^{-4} to 2.5×10^{-7} $(mol/L)^{-1}$ s^{-1}.

It is surprising that the transition state positions are so similar for all the reactions considered in this work. There is

© 2005 NRC Canada

Fig. 3. Projection of the diagram in Fig. 2 onto the bond change — free energy plane to illustrate the crossover implied by our model.

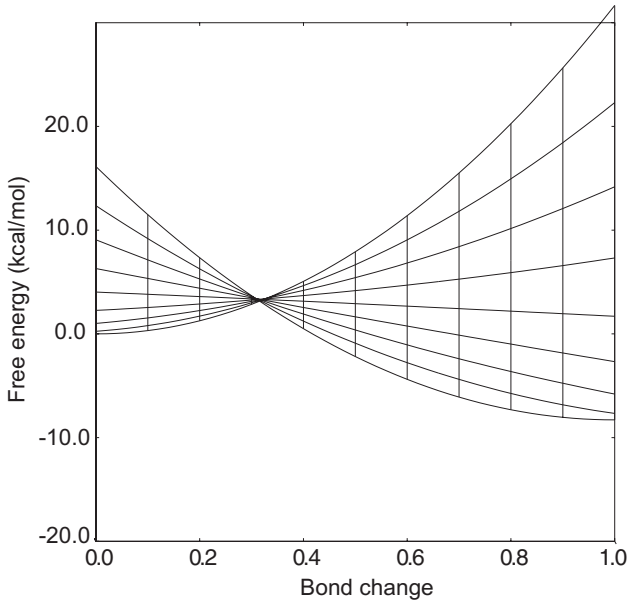
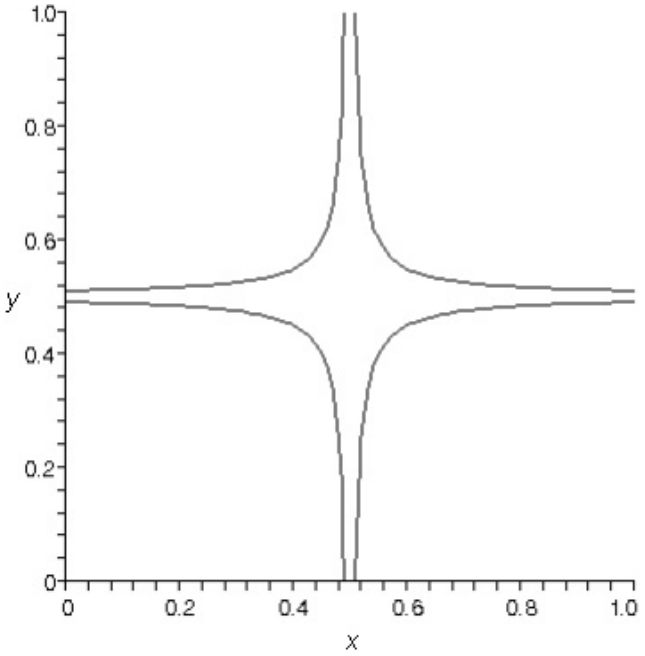


Fig. 4. Region of the reaction diagram with energy similar to that of the transition state (schematic with the transition state arbitrarily set at (0.5, 0.5)).



variation, which is in the expected directions, but the total variation is small. It should be kept in mind that the NBT model is designed to specify the transition-state energies and may not be well-suited to the specified transition-state positions. In particular, we expect that there will be a significant region of hyperspace with very similar energy centered in the transition state. This is most easily seen in a 2-dimensional case. Figure 2 shows a "two-dimensional" reaction diagram, with energy as a third dimension. The assumption of NBT is that for a proper choice of coordinates, when only one coordinate changes, the energy is a quadratic function of that coordinate, rising from a minimum at the lower energy end to the higher energy end. Thus, when the initial and final edge quadratics have the same energy, the energy along the orthogonal coordinate will be approximately constant. This can be seen by a projection as in Fig. 3 where we projected along the geometric distortion coordinate to make clear the crossover between the initial and final parabolas. Alternatively, by looking at a 2D diagram with only reaction coordinates as axes, it is expected that for the coordinates of the transition state there is an approximately cross-shaped region of the reaction coordinate space where energy will be essentially the same. This is illustrated in Fig. 4. A similar analysis for a 3D system shows that for each face there is one point where energy along the coordinate orthogonal to the face is essentially independent of that coordinate and there is a starlike region of hyperspace with essentially the same energy. Analogous situations obtain for the higher dimensional reaction coordinate diagrams, but such a diagram for a 5D reaction, such as the E2, is very difficult to present in an intelligible fashion.

A corollary of this analysis is that in addition to the traditionally assumed reaction path with all reaction dimensions changing at once as the path passes from the starting material through the center of the reaction diagram and through the transition state to the product, there are many alternative paths, which access the region of the transition-state energy by a lower dimensional path, then proceed through to the transition state and finish by another lower dimensional path.

The algorithm currently used to find the transition state finds the lowest energy point from which it is possible to proceed to either starting material or product without going higher in energy. There are typically hundreds or thousands of candidates, many of very similar energies, which are examined in turn; there is no guarantee that the traditionally pictured transition will be the one reported, and not one of very similar energies far along one of the arms of the star. Thus, the energy may be quite good, but the position may not be well-specified.

Acknowledgments

We thank the Natural Sciences and Engineering Research Council of Canada (NSERC) for financial support of this work. We thank Rana Ibrahim for technical assistance with the initial calculations for this project.

References

1. J.P. Guthrie. Can. J. Chem. **68**, 1643 (1990).
2. A. Baboul, L. Curtiss, P. Redfern, and K. Raghavachari. J. Chem. Phys. **110**, 7650 (1999).
3. J.P. Guthrie. Can. J. Chem. **70**, 1042 (1992).
4. C.G. Zhan and D.A. Dixon. J. Phys. Chem. **105**, 11534 (2001).
5. M. Liptak, K. Gross, P. Seybold, S. Felgus, and G. Shields. J. Am. Chem. Soc. **124**, 6421 (2002).
6. W.J. Moore. Physical chemistry. Prentice-Hall, Englewood Cliffs, N.J. 1962. p. 628.
7. Y. Marcus. Ion solvation. Wiley, New York. 1985.
8. D.D. Wagman, W.H. Evans, V.B. Parker, R.H. Schumm, I. Halow, S.M. Bailey, K.L. Churney, and R.L. Nuttall. J. Phys. Chem. Ref. Data, **11(Suppl. 2)**, 2 (1982).

© 2005 NRC Canada

9. R.C. Pemberton and C.J. Mash. J. Chem. Thermodyn. **10**, 867 (1978).
10. M.H. Abraham. J. Chem. Soc. Perkin Trans. 2, 1893 (1973).
11. J. Guthrie. J. Phy. Chem. A, **105**, 8495 (2001).
12. Serena Software. PCMODEL [computer program]. Serena Software, Bloomington, Ind. 1993.
13. T.L. Amyes, J.P. Richard, and M. Novak. J. Am. Chem. Soc. **114**, 8032 (1992).
14. A. Streitwieser and J.X. Ni. Tetrahedron Lett. **26**, 6317 (1985).
15. J. Richard, G. Williams, and J. Gao. J. Am. Chem. Soc. **121**, 715 (1999).
16. F.G. Bordwell. Acc. Chem. Res. **21**, 456 (1988).
17. D.J. Cram. Fundamentals of carbanion chemistry. Academic, New York. 1965.
18. A.D. Headley, S.D. Starnes, L.Y. Wilson, and G.R. Famini. J. Org. Chem. **59**, 8040 (1994).
19. S. Takahashi, L.A. Cohen, and H.K. Miller. J. Org. Chem. **36**, 1205 (1971).
20. A. Streitwieser and D.R. Taylor. Chem. Commun. 1248 (1970)
21. W.L. Jorgensen and J.M. Briggs. J. Am. Chem. Soc. **111**, 4190 (1989).
22. J. Hawes and R. Kay. J. Phys. Chem. **69**, 2420 (1965).
23. R.B. Jordan. Reaction mechanisms of inorganic and organometallic systems. Oxford University Press, New York. 1991.
24. R.M. Fuoss. J. Am. Chem. Soc. **80**, 5059 (1958).
25. M. Eigen. Z. Elektrochem. **64**, 115 (1960).
26. Y. Marcus, M. Kamlet, and R. Taft. J. Phys. Chem. **92**, 3613 (1988).
27. I. Watanabe. J. Mol. Liq. **65/66**, 245 (1995).
28. N. Stahl and W.P. Jencks. J. Am. Chem. Soc. **108**, 4196 (1986).
29. L. Funderburk and W. Jencks. J. Am. Chem. Soc. **100**, 6708 (1978).
30. F. Rived, M. Roses, and E. Bosch. Anal. Chim. Acta, **374**, 309 (1998).
31. A.J. Hoefnagel, M.A. Hoefnagel, and B.M. Wepster. J. Org. Chem. **43**, 4720 (1978).
32. D.J. McLennan. Tetrahedron Lett. 2317 (1971).
33. C.K. Ingold. Structure and mechanism in organic chemistry. Cornell University Press, Ithaca, N.Y. 1953.
34. M.J. Frisch, G.W. Trucks, H.B. Schlegel, G.E. Scuseria, M.A. Robb, J.R. Cheeseman, V.G. Zakrzewski, J.A. Montgomery, Jr., R.E. Stratmann, J.C. Burant, S. Dapprich, J.M. Millam, A.D. Daniels, K.N. Kudin, M.C. Strain, O. Farkas, J. Tomasi, V. Barone, M. Cossi, R. Cammi, B. Mennucci, C. Pomelli, C. Adamo, S. Clifford, J. Ochterski, G.A. Petersson, P.Y. Ayala, Q. Cui, K. Morokuma, D.K. Malick, A.D. Rabuck, K. Raghavachari, J.B. Foresman, J. Cioslowski, J.V. Ortiz, A.G. Baboul, B.B. Stefanov, G. Liu, A. Liashenko, P. Piskorz, I. Komaromi, R. Gomperts, R.L. Martin, D.J. Fox, T. Keith, M.A. Al-Laham, C.Y. Peng, A. Nanayakkara, M. Challacombe, P.M.W. Gill, B. Johnson, W. Chen, M.W. Wong, J.L. Andres, C. Gonzalez, M. Head-Gordon, E.S. Replogle, and J.A. Pople. GAUSSIAN 98. Revision A.9 [computer program]. Gaussian, Inc., Pittsburgh, Penn. 1998.
35. M.J. Frisch, G.W. Trucks, H.B. Schlegel, G.E. Scuseria, M.A. Robb, J.R. Cheeseman, J.A. Montgomery, Jr., T. Vreven, K.N. Kudin, J.C. Burant, J.M. Millam, S.S. Iyengar, J. Tomasi, V. Barone, B. Mennucci, M. Cossi, G. Scalmani, N. Rega, G.A. Petersson, H. Nakatsuji, M. Hada, M. Ehara, K. Toyota, R. Fukuda, J. Hasegawa, M. Ishida, T. Nakajima, Y. Honda, O. Kitao, H. Nakai, M. Klene, X. Li, J.E. Knox, H.P. Hratchian, J.B. Cross, C. Adamo, J. Jaramillo, R. Gomperts, R.E. Stratmann, O. Yazyev, A.J. Austin, R. Cammi, C. Pomelli, J.W. Ochterski, P.Y. Ayala, K. Morokuma, G.A. Voth, P. Salvador, J.J. Dannenberg, V.G. Zakrzewski, S. Dapprich, A.D. Daniels, M.C. Strain, O. Farkas, D.K. Malick, A.D. Rabuck, K. Raghavachari, J.B. Foresman, J.V. Ortiz, Q. Cui, A.G. Baboul, S. Clifford, J. Cioslowski, B.B. Stefanov, G. Liu, A. Liashenko, P. Piskorz, I. Komaromi, R.L. Martin, D.J. Fox, T. Keith, M.A. Al-Laham, C.Y. Peng, A. Nanayakkara, M. Challacombe, P.M.W. Gill, B. Johnson, W. Chen, M.W. Wong, C. Gonzalez, and J.A. Pople. GAUSSIAN 03. Revision B.04 [computer program]. Gaussian, Inc., Pittsburgh, Penn. 2003.
36. A.D. Becke. J. Chem. Phys. **98**, 5648 (1993).
37. C. Lee, W. Yang, and R.G. Parr. Phys. Rev. B, **37**, 785 (1988).
38. J. Foresman, T. Keith, K. Wiberg, J. Snoonian, and M. Frisch. J. Phys. Chem. **100**, 16098 (1996).

Appendix A

Table A1. Calculation of ΔG_t for water from water to ethanol at 25 °C.

T (K)	303.15	323.15	298.15
RT (kcal/mol)	0.603	0.643	0.593
x_{EtOH} (l)	0.981 53	0.981 53	
x_{EtOH} (g)	0.981 9	0.980 8	
p (kPa)	10.47 3	29.51	
x_{H_2O} (l)	0.018 47	0.018 47	
x_{H_2O} (g)	0.018 1	0.019 2	
p_{H_2O} (g, kPa)	0.189 6	0.567 7	
p_{H_2O} (g, atm)	0.001 871	0.005 6	
c_{H_2O} (l)	0.317	0.31	
ΔG_t (kcal/mol)	–3.09	–2.58	–3.23

Note: Densities of ethanol water mixtures were extrapolated from data in the *Handbook of chemistry and physics*, 85th ed. Linear extrapolation of ΔG_t from 30 and 50 °C gave the desired value at 25 °C. Data from ref. A1.

References

A1. R.C. Pemberton and C.J. Mash. J. Chem. Thermodyn. **10**, 867 (1978).

© 2005 NRC Canada

Appendix B

Experimental values for the partitioning of ethanol from gas to ethanol and from gas to chloroform (log L = 2.80 (B1)) were available, but values had to be estimated for dimethyl ether. The partitioning constant (log L) from gas to ethanol for diethyl ether could be calculated using Abraham's solvatochromic equation with coefficients from ref. B2 and the values for the solvatochromic parameters for diethyl ether from ref. B3. Since log L can be estimated by group additivity, a contribution for [CH_2] could be calculated from data for a series of normal hydrocarbons (B2). Subtracting this contribution (0.44) twice from the value for diethyl ether gave log L for dimethyl ether as 1.63. Similarly, a contribution for [CH_2] to log L from gas to chloroform could be calculated from data for hexane, octane, and cyclohexane as 0.54. Subtracting this contribution twice from the experimental value of log L for diethyl ether (3.05 (B1)) gave the desired value for dimethyl ether. It is now straightforward to calculate the partition constant from ethanol to chloroform for ethanol (log P = –0.93) and dimethyl ether (log P = 0.34), and thus, the free energies of transfer (ethanol, ΔG_t = 1.27; dimethyl ether, ΔG_t = –0.47) and finally the difference in the free energies of transfer, which is the cost of losing one hydrogen bond form OH to solvent. This was found to be 1.74 kcal/mol.

Table B1. Free energies of transfer from ethanol to chloroform.

Compound	$\log L^{EtOH}$	$\log L^{CHCl_3}$	$\log P^{EtOH>CHCl_3}$	$\Delta G_t^{EtOH>CHCl_3}$
EtOH	3.73[a]	2.8[b]	–0.93	1.27
Me_2O	1.63[c]	1.98[c]	0.34	–0.47

Note: At 25 °C; log L is concn. (mol/L) solute in solvent–concn. (mol/L) solute in gas phase; $\log P^{EtOH>CHCl_3}$ is concn. (mol/L) in $CHCl_3$–concn. (mol/L) in EtOH; $\Delta G_t^{EtOH>CHCl_3}$ is $-2.303RT$ log P; units for ΔG_t are kcal/mol. The cost of losing one hydrogen bond = 1.27 – (–0.47) = 1.74 kcal/mol.

[a]Experimental value, based on the vapor pressure of ethanol.

[b]Experimental value, ref. B1.

[c]Caculated as described in the text.

References

B1. M. Abraham, J. Platts, A. Hersey, A. Leo, and R. Taft. J. Pharm. Sci. **88**, 670 (1999).
B2. M. Abraham, G. Whiting, W. Shuely, and R. Doherty. Can. J. Chem. **76**, 703 (1998).
B3. M. Abraham. Chem. Soc. Rev. 73 (1993).

Appendix C

Available pK_a values permitting calculation of fall-off factors are given in Table B1. We first calculated the difference in pK_a upon introducing a substituent (δpK_a). Then we calculated the fall-off factor as the ratio of δpK_a with two intervening CH_2s to δpK_a with only one intervening CH_2. An alternative calculation is to take the square root of the ratio of δpK_a with three intervening CH_2s to δpK_a with only one intervening CH_2. Simple average values are: methanol, 0.47 ± 0.26; water, 0.33 ± 0.14. Although the average for methanol is larger, the range of values overlaps and the standard deviations are large. One cannot conclude that these values differ.

Table C1. Fall-off factors in water and methanol.

	Methanol				Water			
Acid	pK_a	δpK_a[a]	F[b]	F′[c]	pK_a	δpK_a[a]	F[b]	F′[c]
CH_3COOH	9.63	0.0			4.76			
$BrCH_2COOH$	8.06	1.57			2.86	1.90		
$ClCH_2COOH$	7.88	1.75			2.86	1.90		
$BrCH_2CH_2COOH$	9.00	0.63	0.40		4.02	0.74	0.38	
$ClCH_2CH_2COOH$	9.18	0.45	0.26		4.08	0.74	0.38	
$BrCH_2CH_2CH_2COOH$					4.58	0.18	0.24	0.30
$ClCH_2CH_2CH_2COOH$	9.29	0.34	0.76	0.44	4.52	0.24	0.32	0.36

Note: pK_a values from ref. C1.

[a]pK_a–pK_a for acetic acid.

[b]Fall-off factor: δpK_a for n CH_2s/(δpK_a for (n – 1) CH_2s).

[c]Fall-off factor: $\sqrt{}$(δpK_a for $(CH_2)_3$/δpK_a for CH_2).

References

C1. F. Rived, M. Roses, and E. Bosch. Anal. Chim. Acta, **374**, 309 (1998).

© 2005 NRC Canada

Appendix D

Data on the effect of a charge are hard to find, but one imperfect example is the pK_a for glycine dissociation in water and aqueous ethanol. The effect of changing solvent on the pK_a of glycine is smaller than that on the pK_a of benzoic acid, suggesting that there is no increase in the effect of a plus charge on changing solvent. The effect of changing solvent on the pK_a of glycine or acetic acid are very similar (the slopes of plots of pK_a vs. % ethanol are 0.022 for acetic acid, 0.016 for glycine, and 0.028 for benzoic acid); thus, the effect of a charged substituent is about the same.

Table D1. Effect of solvent on pK_a values for benzoic acid, acetic acid, and glycine.

Solvent: % ethanol	pK_a benzoic acid	pK_a glycine	pK_a acetic acid
0	4.18,[a] 4.21[b]	2.38,[a] 2.34[c]	4.76[d]
8		2.55[c]	
10	4.29,[a] 4.37[b]	2.47[a]	4.92[d]
16.4		2.66[c]	
20			5.17[d]
25.3		2.70[c]	
30	5.24[a]	2.68[a]	
34.4		2.88[c]	
40			5.57[d]
44.0		3.05[e]	
50	5.67,[a] 5.48[b]	3.03[a]	
54.1		3.38[c]	
60			6.10[d]
72	6.24[a]	3.21[a]	
75	6.29[b]		

Note: In the indicated solvent at 25 °C.
[a]Reference D1.
[b]Reference D2.
[c]Reference D3.
[d]Reference D4.

References

D1. M.S.K. Niazi and J. Mollin. Bull. Chem. Soc. Jpn. **60**, 2605 (1987).
D2. A.J. Hoefnagel, M.A. Hoefnagel, and B.M. Wepster. J. Org. Chem. **43**, 4720 (1978).
D3. A.K. Chattopadhyay and S.C. Lahiri. Electrochim. Acta, **27**, 269 (1982).
D4. H. Spivey and T. Shedlovsky. J. Phys. Chem. **71**, 2171 (1967).

© 2005 NRC Canada

On the displacement reactions of organic substances in water[1]

J.M.W. Scott

Abstract: The hydrolyses of a series of organic halides, nitrates, sulphonates, and perchlorates are examined from the standpoint of thermodynamics, kinetics, temperature dependence, isotope effects, the Kurz equation, and the Guthrie linear free energy relationship. The thermodynamics of several definite bimolecular displacements are also examined. Some mechanistic revisions are suggested to reach an improved accommodation with the experimental observations.

Key words: kinetics, thermodynamics, hydrolytic displacements, mechanism, ionic displacements, nucleofugality, linear free energy relationships.

Résumé : On a étudié la thermodynamique, la cinétique, l'influence de la température, les effets isotopiques, l'équation de Kurz et la relation linéaire d'énergie libre de Guthrie de l'hydrolyse d'une série d'halogénures, de nitrates, de sulfonates et de perchlorates organiques. On a aussi examiné des caractéristiques thermodynamiques de plusieurs déplacements bimoléculaires bien définis. On suggère quelques révisions mécanistiques pour mieux réfléter les observations expérimentales.

Mots clés : cinétique, thermodynamique, déplacements hydrolytiques, mécanisme, déplacements ioniques, nucléofugacité, relation linéaire d'énergie libre.

[Traduit par la Rédaction]

Prologue

"Because people are unwilling to challenge the expertise of their colleagues, or experts in other areas, the Old Guard can continue for many years to obstruct innovations they dislike. All experts may be equal, but some are more equal than others!" (M.J.S. Dewar in *A semiempirical life* (p. 180, 1992)).

"……. of all forms of mental activity, the most difficult to induce even in the minds of the young, who may be presumed not to have lost their flexibility, is the art of handling the same bundle of data as before, but placing them in a new system of relations with one another by giving them a different framework, all of which virtually means putting on a different thinking cap ……" (Herbert Butterfield in *The origins of modern science 1300–1800* (p. 1, 1957)).

"…. one cannot be a self respecting scientist without being a rebel" (Roger Penrose in *Nature's imagination* (Chap. 2, p. 12, 1995)).

Introduction and synopsis

The present review incorporates 17 sections with the purpose of scrutinizing the original Hughes–Ingold S_N1–S_N2 mechanistic description for displacements at a saturated carbon atom *in water*

Received 14 April 2005. Published on the NRC Research Press Web site at http://canjchem.nrc.ca on 8 December 2005.

J.M.W. Scott. 34 Poplar Avenue, St. John's, NL A1B 1C8, Canada. (e-mail: jmscott@mun.ca).

[1]This article is part of a Special Issue dedicated to organic reaction mechanisms.

[2]M.J. Blandamer, R.E. Robertson, and J.M.W. Scott. Unpublished material.

$$[1] \quad RX + 2H_2O \rightleftharpoons ROH + H_3O^+ + X^-$$

and includes displacements with charged nucleophiles in the same solvent. For a substantial range of structural alterations in (*a*) the organic group (R), (*b*) leaving group (X) of RX, and (*c*) the attacking nucleophile, the observed reactivity sequences intimate that the simple S_N1–S_N2 descriptions are inadequate and require revision.

The study of displacement reactions has generated a variety of concepts that are central to modern organic chemistry and studies in this area have continued to attract interest during the second half of the last century (1–24).[2] Mixed aqueous solvents have been the favoured media for kinetic studies of displacement reactions. In some cases the nonaqueous co-solvent may compete with the water as a nucleophile. The latter possibility complicates the kinetics particularly if the product-forming step is partly or wholly rate-determining. For the sake of simplicity, the present review largely confines attention to situations where the displacements occur in pure water and is only comprehensive from this particular viewpoint. The focus on aqueous systems is not meant to imply that the mechanisms of displacements in water are simple.

Section 1 examines the thermodynamics of the two reactions

$$[2] \quad CH_3X + 2H_2O \rightleftharpoons CH_3OH + H_3O^+ + X^-$$

$$[3] \quad CH_3X + OH^- \rightleftharpoons CH_3OH + X^-$$

with X = F, Cl, Br, and I in solvent water. The calculated equilibrium constants with the measured and calculated kinetic data for the eight reactions summarized by eqs. [2] and [3] suggest that the processes described by eq. [2] necessarily involve the intermediate production of the methyloxon-

 doi: 10.1139/V05-166 © 2005 NRC Canada

ium ion ($CH_3OH_2^+$) and that proton loss from this species is the *last step* in the hydrolysis. Indeed, eq. [2] as it stands omits the crucial fact that the product methanol will react with the hydronium ion to give the methyloxonium ion

$$[4] \quad CH_3OH + H_3O^+ \rightleftharpoons CH_3OH_2^+ + H_2O \ (K_e = 9.1 \times 10^{-3})$$

and consequently eq. [2] is a superficial account of an aqueous solution originally containing a methyl halide.

Section 2 examines the thermodynamics of the classical S_N2 displacements in water summarized by

$$[5] \quad Y^- + CH_3X \rightleftharpoons CH_3Y + X^-$$

where X = F, Cl, Br, and I: Y^- = F^-, Cl^-, Br^- and I^-, measured by Moelwyn-Hughes and several co-workers. A probing thermodynamic analysis of the rate measurements suggest that there is considerable evidence that the mechanism for these reactions is more complex than hitherto realized.

The mechanistic hypothesis that broaches the intermediacy of $CH_3OH_2^+$ for the reaction described by eq. [2] is elaborated in section 3 by analysing rxns. [2] and [3] for a wide range of leaving groups via the Kurz equation. These considerations vindicate the conclusions established in section 1 and concomitantly provide an improved understanding of the relative rates of solvolysis for a wide range of substrates in ordinary water and deuterium oxide often designated as the kinetic solvent isotope effect (KSIE) that is examined further in section 4. The small KSIE evinces no primary character and this observation is consistent with the nucleophilic water molecule, either light or heavy, shedding either its proton or deuteron to the solvent in a final fast step. Thus, the KSIE is consistent with the intermediacy of $CH_3OH_2^+$.

Solvolytic reactions in water give rise to activation energies that normally *decrease* with temperature. This observation may be discussed in thermodynamic terms involving genuine negative heat capacities of activation. However, there is alternative explanation in terms of kinetic complexity originally proposed by Albery and Robinson (21). The two contending interpretations are examined in sections 5 and 6 where it is concluded that the kinetic explanation has a slight edge. This judgment suggests that a more elaborate analysis of the raw experimental concentration–time data might be revealing. The revised analysis is reported in section 7 using numerical methods that were precluded when the raw data were initially measured. The amended analysis in sections 6 and 7 marginally favours reaction complexity as a source of the non-Arrhenius temperature dependence.

Section 8 presents some general observations concerning solvolytic reactivity as a function of the structure of the leaving group. This discussion is continued in section 9 with an examination of the Swain–Lohmann equation together with a modified version of this particular linear free energy relationship (LFER). The latter relationships show some unexpected and revealing similarities between the reactivity sequences of primary centres and those related to caged secondary substrates.

Section 10 examines and extends the Guthrie LFER that correlates rates of solvolysis of a series of methyl substrates (CH_3X with X variable) with the pK_a of HX. This correlation was confined originally to molecules yielding oxygenated anions on heterolysis. However, this LFER fails when the methyl halides are included.

Section 11 examines the Guthrie LFER for a wide range of halogen displacements at both carbon and inorganic (metallic) centres. The failure of the Guthrie LFER to embrace both oxygenated ions and halide ions as leaving groups in a single LFER possibly reflects internal return phenomena in the case of the halogen leaving groups. The kinetic data offers a measure of confirmation of the pK_a values calculated for the halogen acids by Myers.

Section 12 proffers an overview of the earlier discussions with respect to the reactivity of primary, secondary, and tertiary substrates in water. The various LFER correlations developed earlier provide reliable estimates of the solvolytic reactivity of several tertiary sulphonates in water.

Section 13 shifts the discussion to correlations between solvolytic reactivity and the gas-phase enthalpy of ionization of RX in cases where the immediate steric situation in the vicinity of the reacting carbon atom remains sensibly constant as the structure of the organic part of RX is altered e.g., structures such as RCH_2X. The various correlations detailed in the earlier sections give rise to an interesting array of conflicting reaction coordinate parameters. The discussion in section 13 shows that the degree of heterolysis of the RX bond in solution appears to *increase* as the enthalpy of ionization RX *decreases*. Previous quantum mechanical studies of varying degrees of sophistication to calculate the energy of heterolytic fission of RX in the gas phase are briefly considered.

Section 14 introduces a new LFER that relates to two series of molecules RX(1) and RX(2) with fixed leaving groups X(1) and X(2) and variable R groups. When X(1) = mesylate and X(2) = bromide, the new LFER underpins comment on the previous investigations by Hoffmann relating to the reactivity of these and other similar leaving groups.

Section 15 examines the possible origins of the curved Hammett plots that frequently characterize both solvolytic and definite S_N2 displacements, possibly proceeding by complex mechanisms.

Section 16 relates the Kurz analysis to secondary α-deuterium isotope effects involving such pairs as CH_3–CD_3, CH_3CH_2–CH_3CD_2, and $(CH_3)_2CH$–$(CH_3)_2CD$ with several leaving groups. Finally, section 17 offers some brief comments on the limitations of mechanistic organic chemistry.

1. The thermodynamics and kinetics of the reaction of the methyl halides with water and the lyate ion

The reactions of the methyl halides with water (w) and lyate (l) ion form the initial focus of the present contribution.

$$[6] \quad CH_3X + 2H_2O \underset{k_{bw}}{\overset{k_{fw}}{\rightleftharpoons}} CH_3OH + H_3O^+ + X^-$$

and

© 2005 NRC Canada

Table 1. Thermodynamic and kinetic data related to the hydrolysis and the lyate ion attack of the methyl halides.

Parameter	MeF	MeCl	MeBr	MeI
$\Delta H^{\ominus}$	–22.99	–18.04	–18.01	–14.99
$\Delta S^{\ominus}$	–2.35	13.14	17.98	21.12
$\Delta G^{\ominus}$	–22.28	–21.96	–23.37	–21.29
$K_{el}\times10^{-16}$	2.18	1.24	13.5	0.41
$\Delta H^{\ominus}$	–9.653	–4.703	–4.673	–1.653
$\Delta S^{\ominus}$	–21.676	–6.186	–1.346	1.749
$\Delta G^{\ominus}$	–3.190	–2.859	–4.271	–2.188
$K_{ew}\times10^{-2}$	2.18	1.25	13.5	0.40
$k_{fw}(21, 39)^a$	7.89×10^{-10}	2.39×10^{-8}	4.07×10^{-7}	7.35×10^{-8}
k_{bw}	3.62×10^{-12}	1.91×10^{-10}	3.01×10^{-10}	1.84×10^{-9}
$k_{fl}(9, 37, 42)^a$	5.85×10^{-7}	6.57×10^{-6}	1.46×10^{-4}	6.340×10^{-5}
k_{bl}	2.68×10^{-23}	5.3×10^{-22}	1.08×10^{-21}	1.58×10^{-19}

Note: MeX: X = F, Cl, Br and I: T = 298.15 K. $\Delta H_f^o(H_2O,liq)$ = –68.32 (29); $S(H_2O,liq)$ = 16.72 (29); $\Delta H_f^o(CH_3OH,sln)$ = –58.77 (30); $\Delta H_f^o(OH^-,sln)$ = –54.98 (29)); $S(CH_3OH,sln)$ = 30.29 (30); $S(OH^-,sln)$ = –2.61 (29). Enthalpies and the Gibbs function are reported in kcal and entropies in cal mol^{-1} K^{-1}. The units for the forward rate constants for k_{fw} are s^{-1} and for k_{fl}, L mol^{-1} s^{-1}. The units for the k_{bl} are the same as those for the forward reaction. The units for the back reaction in water are less obvious. The back reaction can be assumed to be a third-order reaction (Rate = $k_{bw}[MeOH][H_3O^+][X^-]$) with dimensions for k_{bw} of L^2 mol^{-2} s^{-1}. However, we argue in the text that the retro-hydrolysis takes place minimally by two second-order steps (see section 1). No attempt was made to assess the significance of the water concentration in calculating the reverse rate constants for the reactions in water.

[a]Some of the data in this table have been reprocessed with superior least-squares algorithms and this may account for any small differences from previously reported data.

$$[7]\qquad CH_3X + OH^- \underset{k_{bl}}{\overset{k_{fl}}{\rightleftharpoons}} CH_3OH + X^-$$

The pioneer studies of these displacements with R = CH_3, X = F, Cl, Br, and I (eq. [6]) were carried out by Moelwyn-Hughes (9 and refs. therein) alone and later with other authors. The Henry's Law constants (K_{hl}) that quantify the equilibria for the methyl halides

$$[8]\qquad CH_3X(aq) \overset{K_{hl}}{\rightleftharpoons} CH_3X(g)$$

have been measured by Glew and Moelwyn-Hughes (25) and these data are also important in the present context.

The kinetic studies launched by Moelwyn-Hughes have been repeated and extended by Robertson and numerous coworkers (6, 15)[2] using improved technology at the National Research Council in Ottawa and later at the University of Calgary. A remarkable body of data exist because of these efforts.[2] Other contributions by Albery and Robinson (21), Guthrie (23), Kurz (24), and Blandamer and Scott (22) are also important to the present considerations.

The thermochemistry of several methyl esters hydrolysing in pure water has been examined thoroughly by Guthrie (23): for earlier contributions see (26–28). The reactions of the methyl halides (CH_3X, X = F, Cl, Br, and I) with water and hydroxide ion were omitted from Guthrie's study, although the required thermochemical and kinetic data related to eqs. [6] and [7] were available at the time. A complete thermochemical account of the rxns. [6] and [7] can be calculated from the data assembled in Tables 1 and 2. The computed equilibrium constants (K_{ew}) for the reactions summarized by eq. [6] and the analogous quantities for eq. [7] (K_{el}) are also presented in Tables 1 and 2. Granted that the reactions of the methyl halides with water and the lyate ion are simple S_N2 displacements, i.e., a single transition state separates the reactants and products, then the values of k_{bw} and k_{bl} for the reverse reactions can be estimated from the measured forward rate constants (k_{fw} and k_{fl}) and the appropriate computed equilibrium constants (K_{ew} and K_{el}).

Several significant points emerge from these calculations. First, the second-order rate constants (k_{bl}) are relatively small and the related equilibrium constants (K_{el}) are correspondingly large. In contrast, the k_{bw} rate constants are comparable to the k_{fw} values and, necessarily, the equilibrium constants K_{ew} are relatively close to unity. Alternatively, the processes in which individual halide anions attack methyl alcohol are relatively slow reactions and, by inference, *cannot form any significant part of the* k_{bw} *process*. This means that the postulate previously advanced, namely that the *hydrolysis reaction* is a simple S_N2 process, is possibly in error. There is one further point to be made: eq. [6] is *an approximate description* of the reaction of the methyl halides with water because in the presence of hydronium ion from the hydrolysis some of the methanol will be converted into the methyloxonium ion (see eq. [11]). This important fact adds substance to the following discussion.

Second, the back reaction rate constants for the water and lyate, namely, k_{bw} and k_{bl} reactions *have different dimensions* if eq. [6] is considered sufficient to describe the water reaction completely. Thus, the back reaction for the former process is third order, whereas the back reaction with lyate ion is second order. Hence, k_{bw} and k_{bl} cannot be compared numerically. Generally speaking, the chemical literature concerned with kinetics regards third-order reactions with a good deal of scepticism because fruitful ternary collisions are improbable events. Granted that the grounds for this scepticism are valid, then the back reaction for water must be regarded as occurring minimally by two steps. There are

© 2005 NRC Canada

Table 2. Thermochemical data related to the aqueous solutions of methyl halides and halide ions.

X	F	Cl	Br	I
$S^{\ominus}(MeX)^a$	32.29 ± 1.2	33.15 ± 0.7	34.88 ± 0.52	38.38 ± 1.65
$S^{\ominus}(MeX)^b$	32.91	32.52	33.97	36.19
$S^{\ominus}(MeX)^c$	33.1	32.8	34.3	36.6
$\Delta H_f^o(MeX)^a$	–60.28 ± 0.44	–25.79 ± 0.4	–14.77 ± 0.39	–2.05 ± 0.61
$\Delta H_f^o(MeX)^c$	–60.2	–26.2	–15.2	–2.8
$\Delta H_{hl}(MeX)^d$	4.38 ± 0.44	5.16 ± 0.4	5.77 ± 0.39	5.39 ± 0.61
$S(X^-)^e$	–2.96 ± 0.57	13.39 ± 0.19	19.56 ± 0.24	26.6 ± 0.61
$S(X^-)^f$	–3.3	13.5	19.7	26.6
$\Delta H_f^o(X^-)^a$	–79.48 ± 0.16	–40.04 ± 0.02	–28.99 ± 0.08	13.25 ± 0.01

Note: Partington (31) states that selecting the "best values" for physical data is extremely difficult. No attempt has been made to flatter the data.

[a]Used in calculations for Tables 1, 4, and 5.

[b]Data from ref. 32.

[c]Data from ref. 33.

[d]Used in calculations for Tables 1, 4, and 5. Data are from an extensive analysis of the Henry's Law measurements reported in ref. 25. These measurements dominate the uncertainties presented here.

[e]Partly from ref. 29.

[f]Data from ref. 33 and partly from ref. 29.

at least a pair of second-order reversible two-step mechanisms that can be envisaged for the water back reaction. The first two-step mechanism involves the halide ion X^- attacking methanol liberating lyate ion

[9] $$CH_3OH + X^- \rightleftharpoons CH_3X + OH^- \text{ (slow)}$$

followed by the reaction of the generated lyate ion with hydronium ion.

[10] $$H_3O^+ + OH^- \rightleftharpoons 2H_2O \text{ (fast)}$$

The second two-step mechanism consists of a relatively rapid attack of hydronium ion on methanol

[11] $$CH_3OH + H_3O^+ \rightleftharpoons CH_3OH_2^+ + H_2O \text{ (fast)}$$

followed by

[12] $$CH_3OH_2^+ + X^- \rightleftharpoons CH_3X + H_2O$$ (fast relative to eq. [9])

A comparison of eqs. [9] and [10] vs. eqs. [11] and [12] reasonably favours the latter sequence because eq. [9] describes a very slow reaction: see k_{bl} in Table 1. On the other hand, eqs. [11] and [12] describe a proton transfer and an ion combination reaction, respectively: both these processes should be fast relative to a combination of eqs. [9] and [10].

These considerations reasonably lead to the conclusion that the *first* step of the retro-hydrolysis must involve the protonation of the alcohol to form the methyloxonium ion. If *protonation* is the first reaction of the reverse hydrolysis, the law of microscopic reversibility (4, 9, 18) in the form (18): "*The mechanism of a reversible reaction in the rearward direction is identical to the mechanism in the forward direction run backward*", predicates that *proton loss must be the last step* in the hydrolysis. This represents the first significant departure from the conventional description of these reactions, although Guthrie (23) suggests that the hydrolysis is a two-step reaction that proceeds via the methyloxonium ion ($CH_3OH_2^+$). On the other hand, Guthrie offers no reason for invoking the methyloxonium ion as an intermediate, and further, does not mention that his proposal requires that proton loss must be the *last step* in the hydrolysis.

Perhaps the tone of some of the previous remarks is too categorical in the sense that there are few places in the chemical literature where the detailed mechanism of a displacement at a primary centre by water, usually described as a typical example of an S_N2 process, is carefully delineated. There is a general tendency to consider that the exothermic character associated with the partial formation of a solvated proton in an S_N2 transition state provides an important driving force for fission of the carbon – leaving group bond (34). The thermodynamic argument previously presented does not substantiate this idea and it is at variance with the facts related to the synthesis of alkyl halides from the related alcohols under acid conditions. Of course, in favourable conditions the latter reaction may involve free carbocations generated via alkyloxonium ions. This is an uncongenial proposition in the case of methyl alcohol.

Here, the simple S_N2 description for the reaction of water with the methyl halides conceived in terms of the following three *concerted* events (*i*) carbon–oxygen bond formation between the attacking water molecule and the reacting carbon atom, (*ii*) proton transfer, and (*iii*) loss of the neutral or ionic leaving group, is *explicitly discarded.*

The retro-hydrolysis reaction is considered to occur in the following manner. The protonation of the alcohol is the first step

[13] $$CH_3OH + H_3O^+ \rightleftharpoons CH_3OH_2^+ + H_2O$$

There are two possible routes to the termination of the methyl halide synthesis from the methyloxonium ion and the halide ion: (*i*) the formation of the carbon–halogen bond and the loss of a water from the oxonium ion are postulated to be concerted processes or (*ii*) an intermediate exists between the methyloxonium ion and the fully formed methyl halide. The precursor of the latter might be either an ion pair or a Doering and Zeiss (35) intermediate. In the following scheme, the intermediate is specified as an ion pair, either intimate or solvent separated, merely for convenience: for

© 2005 NRC Canada

the present, the existence of an intermediate is a necessary feature required for future considerations. Thus, the remaining steps for the reverse hydrolysis are specified

[14] $X^- + CH_3OH_2^+ \rightleftharpoons X^-\cdots CH_3OH_2^+$

and

[15] $X^-\cdots CH_3OH_2^+ \rightleftharpoons CH_3X + H_2O$

Microscopic reversibility (see the previous section) demands that the mechanism for the hydrolysis is the reverse of rxns. [13]–[15], namely

[16] $$H_2O + CH_3X \underset{k_2}{\overset{k_1}{\rightleftharpoons}} H_2O\cdots CH_3^+\cdots X^- \underset{k_4}{\overset{k_3}{\rightleftharpoons}} CH_3OH_2^+ + X^- + H_2O \underset{k_6}{\overset{k_5}{\rightleftharpoons}} CH_3OH + H_3O^+ + X^-$$

There are two possible paths for the destruction of $H_2O\cdots CH_3^+\cdots X^-$. The first involves the complete ionization of the CH_3—X bond from the intermediate $H_2O\cdots CH_3^+\cdots X^-$ *without* the formation of a definite solvent-separated intermediate. The other arm of the bifurcation involves such an intermediate, specifically, $H_2O\cdots CH_3^+|H_2O|X^+$. This particular structure does not imply the eventual equivalence of the two water molecules, i.e., the inversion of the reacting carbon atom may still predominate if the inserted water molecule departs with the anion. Otherwise, it will be distributed between the leaving group and the carbon atom on the collapse of the intermediate. Thus, a mechanism that recognises the importance of solvent separation for the methyl compounds is possibly favoured, a point of view to be justified shortly.

The sequence of chemical events described by eq. [16] and the subsequent discussion will have a profound influence on the temperature dependence of the rate constants that characterize the aqueous displacement reactions leading to energies of activation that might show *either positive or negative temperature coefficients* that will be "mixed" with *bona fide* heat capacity changes: see sections 5 and 6, and refs. 6, 15, 21, and 22. The remainder of this contribution attempts to put the implications of eq. [16] on a firmer footing.

The k_5 and k_6 steps are, relatively speaking, well-established because the related equilibrium constant has been measured by Kurz and Saitz[3] ($pK_a = -2.04$). The other steps described by the rate constants k_1, k_2, k_3, and k_4 in eq. [16] are likely to be viewed less favourably and some further considerations originally presented by Kurz are important to our extended argument. The Kurz analysis is presented in section 3.

2. A thermodynamic analysis of some classical S_N2 displacements

The theoretical concept known as the S_N2 mechanism was originally established by the Ingold school (1, 8) and extended by others (2, 9, 11–13).This mechanism represents the conventional description of many displacement reactions in both organic and inorganic chemistry. More recently the S_N2 concept has been extended to gas-phase substitutions with notable success (17).

For carbon chemistry the isotopic exchange

[17] $CH_3I + I^{-*} \rightleftharpoons CH_3I^* + I^-$

exemplifies a prototypical example of such reactions in solution. The conventional wisdom postulates that this reaction is characterized by a symmetrical transition state (T.S.) with two identical partial bonds uniting the iodine atoms to the central carbon atom that is coplanar with the three symmetrically disposed hydrogens attached to it.

In contrast to the isotopic exchange reaction, displacements featuring a nucleophile and leaving group that differ, e.g., cyanide for the former reagent and iodide for the latter.

[18] $CH_3I + CN^- \rightleftharpoons CH_3CN + I^-$

These particular reagents attenuate the symmetries manifested for the displacement described by eq. [17]. The bonding of the departing and incoming reagents in this reaction is necessarily different, and concomitantly, the coplanarity of the hydrogen atoms with the reacting carbon atom is no longer assured. In the Marcus (36) theory of these reactions (13, 37, 38), the symmetry of the transition state is related to the thermochemical characteristics of the displacement, i.e., whether the reaction is either "uphill" (endoergonic), or "downhill" (exoergonic), or "on the level" (thermoneutral). The thermodynamic properties easily translate into structural information only for the symmetrical displacements that give rise to what are known as intrinsic barriers. For systems described by eq. [18], the collinearity of the reacting atoms in attacking and departing reagents with the reacting carbon atom is maintained, but the precise position of the hydrogen atoms attached to the carbon atom is uncertain.

Experimentally, when the concentrations of A and B are comparable, S_N2 displacements provide classic examples of second-order kinetics

[19] $$A + B \rightleftharpoons [T.S.] \underset{k_b}{\overset{k_f}{\rightleftharpoons}} C + D$$

The second-order rate constants k_f and k_b characterize the forward and back reactions with a *single* transition state separating the reactants and products. The Erying theory of reaction rates (39) requires the transition state to be in equilibrium with both the reactants, A and B, and the products, C and D.

When A = CH_3X (X = F, Cl, Br, and I) and B equals either OH^- or CN^-, these reactions are essentially irreversible, i.e., k_b is very small (see Table 1 and refs. 40 and 41). On the other hand, when B = F^-, Cl^-, Br^-, and I^-, the displacements summarized by eq. [19] are reversible in the sense that the rate constants can be measured for either the forward or reverse processes.

When [A] » [B] or vice versa, the reactions generalized by eq. [19] demonstrate pseudo-first-order kinetics with respect

[3] J. Kurz and R.M. Saitz. Private communication to R.E. Robertson. ca. 1979.

© 2005 NRC Canada

to the reagent present at the lower concentration. When the excess reagent is the solvent, a long-standing problem arises. In such cases, the solvent supplies both the reacting medium as well as the nucleophile, and the molecularity of the transition state for the displacement is ambiguous with respect to the solvent because alternative mechanisms are theoretically possible in which bond breaking and making are distinct kinetic processes: this is the so-called S_N1 mechanism. The focus in the present section is predominately concerned with those displacements that are traditionally regarded as displaying bimolecular transition states. Nonconcerted descriptions for traditional S_N2 displacements have been occasionally proposed. Such departures from the conventional wisdom (42, 43) have been subjected to critical scrutiny and, by and large, have been repudiated vigorously (33, 44, 45).

Albery and Robinson (21) described the hydrolysis reaction of *tert*-butyl chloride in water by the mechanism

$$[20] \quad A + B \underset{k_2}{\overset{k_1}{\rightleftharpoons}} I \xrightarrow{k_3} \text{Products}$$

and demonstrated that such a kinetic scheme would result in an observed activation energy that decreases with temperature. In more formal terms, a reaction proceeding by the mechanism presented in eq. [20] displays an apparent negative heat capacity of activation (6, 15). This particular description for the hydrolysis of *tert*-butyl chloride in which A represents the solvent water and B the substrate with [A] » [B] is certainly acceptable. However, the equation for the temperature dependence of the pseudo-first-order constants that describe the hydrolysis of *tert*-butyl chloride derived from the steady-state treatment of the kinetic scheme represented by eq. [20] also gives excellent fits for *several primary substrates* hydrolysing in water. This awkward and anomalous fact will be considered further in section 6.

The algebra related to the change of composition of systems reacting according to eq. [19] is standard fare in texts concerned with the basics of physical chemistry and monographs devoted to chemical kinetics. The mechanism represented by eq. [20] with one of either A or B in excess can be considered in terms of the steady-state theorem or without such approximations (21, 22).

The situation when the concentrations of species A and B are comparable and they react via a definite intermediate gives rise to *nonlinear differential equations* that require numerical integration (46). Some of the concentration–time data provided by such integrations that incorporate particular values of the rate constants k_1, k_2, and k_3 may provide acceptable numerical fits to the simple integrated second-order expressions (46). This sinister fact means that such fits may be actively misleading. More specifically, acceptable data fits to integrated second-order expressions do not necessarily confirm that a reaction is a simple S_N2 process.

Similarly, it has been shown (20) that the relationship that exists between the rate constants for racemization (k_r) and isotopic exchange (k_e), namely $k_r = 2k_e$ is a necessary but not a sufficient condition for the racemization and exchange processes to be characterized by the S_N2 displacement. The mechanism

$$[21] \quad (+)RX + X^- \underset{k_2}{\overset{k_\alpha}{\rightleftharpoons}} (T.S.) \underset{k_\alpha}{\overset{k_2}{\rightleftharpoons}} I \rightleftharpoons (T.S.) \rightleftharpoons (-)RX + X^-$$

$$[22] \quad RX + X^{-*} \underset{k_2}{\overset{k_\beta}{\rightleftharpoons}} (T.S.) \underset{k_\gamma}{\overset{k_2}{\rightleftharpoons}} I \rightleftharpoons (T.S.) \rightleftharpoons RX^* + X^-$$

where k_α, k_β, and k_γ are pseudo-first-order constants related to the second-order rate constant k_1 via the equations $k_\alpha = k_1[X^-]$, $k_\beta = k_1[RX]$, and $k_\gamma = k_1[X^-]$. The processes described by eqs. [21] and [22] involving the intermediate I also furnish the relationship $k_r = 2k_e$. Thus, this classical test does not guarantee that the simple S_N2 mechanism is operative. Readers are referred to the original paper (20) for further details.

The most important examples of simple S_N2 displacements are provided by the halide exchange reactions of the methyl halides

$$[23] \quad Y^- + CH_3X \overset{K_e}{\rightleftharpoons} CH_3Y + X^-$$

where $Y = F^-$, Cl^-, Br^-, and I^- and X = F, Cl, Br, and I (9, 40, 41). Granted that the 16 displacements all take place by the classical S_N2 mechanism, then the number of transition states implied by eq. [23] is *less* than the number of reactions. Thus, there are *four unique transition states* for the symmetrical exchanges ($Y^- = X^-$) that define four intrinsic barriers (13, 17, 38). On the other hand, there are only *six additional transition states* for the remaining 12 unsymmetrical displacements because the transition state for the process

$$[24] \quad X^- + CH_3Y \rightleftharpoons CH_3X + Y^-$$

is identical to that for the displacement described by eq. [23]. The thermodynamic quantities that characterize the 10 unique transition states, namely, $G^\ddagger$, $H^\ddagger$, $S^\ddagger$, and $C_p^\ddagger$ form the elements of a series of 4 × 4 Hermitian matrices $\lambda(i,j)(X^\ddagger)$ where $X = G, H, S$, and C_p. The entropy matrix is

$$[25] \quad \lambda(i,j)(S^\ddagger) = \begin{bmatrix} S^\ddagger(1,1) & S^\ddagger(1,2) & S^\ddagger(1,3) & S^\ddagger(1,4) \\ S^\ddagger(2,1) & S^\ddagger(2,2) & S^\ddagger(3,2) & S^\ddagger(2,4) \\ S^\ddagger(3,1) & S^\ddagger(3,2) & S^\ddagger(3,3) & S^\ddagger(3,4) \\ S^\ddagger(4,1) & S^\ddagger(4,2) & S^\ddagger(4,3) & S^\ddagger(4,4) \end{bmatrix}$$

with the conditions

$$[26] \quad S^\ddagger(i,i) \neq S^\ddagger(j,j) \text{ with } j = i = 1\text{–}4$$

and

$$[27] \quad S^\ddagger(i,j) = S^\ddagger(j,i) \text{ with } i \neq j = 1\text{–}4$$

Granted that the temperature dependence of the rates of the halide exchanges summarized by eq. [23] have been measured and other appropriate initial state thermodynamic data are available, then the formal requirements imposed on the matrix depicted in eq. [25] by the S_N2 mechanism specified by eqs. [26] and [27] can be tested.

© 2005 NRC Canada

Table 3. Thermodynamic parameters for halide displacements of the methyl halides (T = 298.15 K).

Reaction	$\Delta G^{\ddagger}$	$\Delta S^{\ddagger}$	$\Delta H^{\ddagger}$	C.C.
MeF + Cl^-	29.34 ± 0.14	–22.56 ± 1.53	22.62 ± 0.59	+0.999250
MeF + I^-	27.92 ± 0.10	–18.97 ± 1.88	22.26 ± 0.66	+0.997120
MeCl + F^-	26.78 ± 0.08	–0.77 ± 1.77	26.55 ± 0.61	+0.999425
MeCl + Br^-	26.01 ± 0.03	+4.90 ± 1.12	27.47 ± 0.36	+0.999813
MeCl + I^-	23.81 ± 0.04	–15.62 ± 0.88	19.16 ± 0.30	+0.999192
MeBr + F^-	27.69 ± 0.05	–10.46 ± 1.06	24.58 ± 0.36	+0.999530
MeBr + Cl^-	24.75 ± 0.03	–1.59 ± 0.89	24.27 ± 0.28	+0.999849
MeBr + I^-	21.76 ± 0.00	–13.86 ± 0.11	17.62 ± 0.03	+0.999982
MeI + F^-	27.22 ± 0.01	–7.98 ± 0.27	24.85 ± 0.09	+0.999985
MeI + Cl^-	24.90 ± 0.04	–12.97 ± 0.86	21.03 ± 0.29	+0.999353
MeI + Br^-	23.38 ± 0.01	–15.86 ± 0.54	18.65 ± 0.17	+0.999818
MeI + I^-	21.98 ± 0.00	–15.04 ± 0.13	17.50 ± 0.04	+0.999995

Note: $\Delta G^{\ddagger}$ and $\Delta H^{\ddagger}$ are in kcal mol^{-1} and $\Delta S^{\ddagger}$ in cal mol^{-1} K^{-1}. C.C. is the correlation coefficient.

For any particular substitution, the following equations define any corresponding element $S^{\ddagger}(i, j)$ of the matrix in eq. [25] related to the displacements represented by eq. [23].

$$[28]\quad \Delta S^{\ddagger}(CH_3X,Y^-sln) = S^{\ddagger}(CH_3X,Y^-sln) - S(CH_3X,sln) - S(Y^-sln)$$

$$[29]\quad \therefore S^{\ddagger}(CH_3,Y^-sln) = \Delta S^{\ddagger}(CH_3X,Y^-sln) + S(CH_3X,sln) + S(Y^-sln)$$

$$[30]\quad K_{hl} = p(CH_3X)/C(CH_3X,sln)$$

$$[31]\quad \Delta S_{hl} = S_g(CH_3X) - S(CH_3X,sln)$$

$$[32]\quad S(CH_3X,sln) = S_g(CH_3X) - \Delta S_{hl}$$

where $S(Y^-sln)$ is the aqueous entropy of the anion Y^-, $\Delta S^{\ddagger}(CH_3X,Y^-sln)$ is the entropy of activation for the anion Y^- attacking CH_3X, $S^{\ddagger}(CH_3X,Y^-sln)$ is the entropy of the related transition state, $S(CH_3X,sln)$ is the entropy of CH_3X in solution, and ΔS_{hl} is the entropy of escape for CH_3X from solution (sln) to the gas phase (g) determined from the temperature dependence of the Henry's Law constant K_{hl} defined in eq. [30]. The third law gas-phase entropies $S_g(CH_3X)$ at 298.15 K are well-established tabulated quantities (29, 30, 47–49) and need no further explanation here. The enthalpy equations related to the entropy expressions (eqs. [28]–[32]) can also be calculated from the data in refs. 29, 30, and 47–49.

The thermodynamic data also provide the means of calculating the equilibrium constants for the processes described by eqs. [23] and [24]. Granted that the off-diagonal processes are genuine S_N2 processes, the kinetic equilibrium constants $K_e = k_f/k_b$ can be compared with the values of the equilibrium constants calculated from purely thermochemical data.

Calculations related to experimental quantities

Gibbs energies, entropies, and enthalpies of activation

The temperature dependence of the rate constants for 11 of the 12 nonsymmetric exchanges have been measured in water by Moelwyn-Hughes and co-workers (9, 40, 41). Swart and LeRoux (50) have measured the temperature dependence of the reaction described by eq. [17] in water. These rate constants have been reanalysed via the Eyring (39) equation

$$[33]\quad k_r = \kappa kTK^{\ddagger}/\hbar \text{ or } K^{\ddagger} = k_r\hbar/kT \ (\kappa = 1)$$

in conjunction with the Eyring version of the van't Hoff equation

$$[34]\quad \ln K^{\ddagger} = -\Delta H^{\ddagger}/RT + \Delta S^{\ddagger}/R$$

on the assumption that the transmission coefficient (κ) in eq. [33] is unity and that over the temperature ranges studied, $\Delta H^{\ddagger}$ and $\Delta S^{\ddagger}$ are true constants. The data were fitted to eq. [34] with $\ln K^{\ddagger}$ as defined by eq. [33] as the ordinate and $1/T$ as the abscissa by a linear least-squares procedure providing $\Delta S^{\ddagger}/R$ from the intercept and $-\Delta H^{\ddagger}/R$ from the slope. The Gibbs energies of activation ($\Delta G^{\ddagger}$ at 298.15 K) were calculated from the extrapolated or interpolated value of $\ln K^{\ddagger}$ at 298.15 K from eq. [34] using

$$[35]\quad \Delta G^{\ddagger} = -RT \ln K^{\ddagger}$$

The errors for all the thermodynamic quantities, namely, $\Delta G^{\ddagger}$, $\Delta H^{\ddagger}$, and $\Delta S^{\ddagger}$, were calculated from the expressions specified in Margeneau and Murphy (51). These exercises were repeated by fitting the rate data to

$$[36]\quad k_r = (kT/\hbar)\exp(-\Delta H^{\ddagger}/RT + \Delta S^{\ddagger}/R)$$

by a weighted, nonlinear routine (52). There were no marked differences between the values of $\Delta G^{\ddagger}$, $\Delta H^{\ddagger}$, and $\Delta S^{\ddagger}$ and the probable errors in these quantities calculated by the two methods, and the correlation coefficients calculated for the linear regressions were all satisfactory. The thermodynamic kinetic data are reported in Table 3.

Initial state quantities

The determination of the initial state thermodynamic quantities from the Henry's Law studies proved more problematical than the quantities that characterize activation. The former were calculated from the temperature dependence of Henry's Law equilibrium constants K_{hl} (X = F, Cl, Br, and I)

$$[37]\quad CH_3X(sln) \overset{K_{hl}}{\rightleftharpoons} CH_3X(g)$$

measured by Glew and Moelwyn-Hughes (25). To avoid "cratic" terms for these measurements, a hypothetical ideal

© 2005 NRC Canada

standard state is required involving concentrations on the molar scale in both the gaseous and solution phases. However, because we are dealing with reversible chemical processes of simple stoichiometry, the standard state corrections to calculate $S(CH_3X,sln)$ are identical for both the forward (eq. [23]) and reverse (eq. [24]) chemical processes, and in the comparison of $S^{\ddagger}(i,j)$ and $S^{\ddagger}(j,i)$ they have no ultimate significance other than to meet the necessary requirements for the comparison with earlier reported quantities employed in the analysis presented and discussed in the following (see Table 2).

Moelwyn-Hughes and Glew fitted the four K_{hl}/T data sets for the methyl halides to the Valentiner equation

$$[38] \quad \ln K_{hl} = A/T + B \ln T + C$$

although the methodology used for this exercise was not revealed. The choice of an equation to describe the temperature dependence of either equilibrium constants or rate constants is arbitrary and this is very evident with the Henry's Law data (for a detailed discussion of such matters see the refs. in sections 5 and 6). Thus, although the fits to eq. [38] of the K_{hl} data for methyl fluoride are excellent for both linear and nonlinear regressions, they are relatively poor for the other methyl halides.

The calculation of $S^{\ddagger}$ and $H^{\ddagger}$ at 298.15 K requires ΔS_{hl} and ΔH_{hl} at this temperature and it was decided to adopt the following approach. The values from the Valentiner regressions were averaged with values calculated from three and five temperatures straddling 298.15 K using the two-parameter van't Hoff equation

$$[39] \quad \ln K_{hl} = -\Delta H_{hl}/RT + \Delta S_{hl}/R$$

The total K_{hl}/T data sets for the individual methyl halides were also fitted to various equations of the form of which eq. [38] is a particular example

$$[40] \quad \ln K_{hl} = A + Bf_1(T) + Cf_2(T)$$

The appropriate manipulations and differentiations with respect to T of eq. [40] give

$$[41] \quad \Delta H_{hl} = RT^2[Bf_1'(T) + Cf_2'(T)]$$

$$[42] \quad \Delta S_{hl} = R\{A + B[f_1(T) + Tf_1'(T)] + [Cf_2(T) + Tf_2'(T)]\}$$

The fits as judged by the Gauss criterion (55) proved to be relatively insensitive to the nature of $f_1(T)$ and $f_2(T)$. Values from the various possibilities represented by eqs. [40]–[42] for the four methyl halides adequately compared with those calculated with the other methods previously outlined via eqs. [39] and [40]. The Henry's Law data for methyl fluoride are apparently superior probably because of its higher volatility and low reactivity with water. The remaining methyl halides are more reactive with water (see Table 1) and become less volatile with increasing molecular weight, adding to the difficulty of precise measurements. The deviations for the averaged enthalpy and entropy functions characteristic of the Henry's Law measurements reported in Table 2 are based on all these calculations without reporting the numerical details of the various regressions used to obtain these quantities. There has been no attempt to hide the inadequacies in these data.

Discussion

For five reversible displacements the entropies of the transition states obtained from the appropriate calculations reveal that $S^{\ddagger}(i,j) \neq S^{\ddagger}(j,i)$ (see Table 4B). For $H^{\ddagger}(i,j)$ and $H^{\ddagger}(j,i)$ the picture alters; the data yield three cases where $H^{\ddagger}(i,j)$ and $H^{\ddagger}(j,i)$ fail to overlap and two cases where $H^{\ddagger}(i,j) \approx H^{\ddagger}(j,i)$ (see Table 4A). Thus, the combined score related to the $H^{\ddagger}$ and $S^{\ddagger}$ parameters is 80% suggesting that these reactions do not take place by the classical S_N2 mechanism. A comparison of the $\Delta H^{\ominus}$, $\Delta S^{\ominus}$, and $\Delta G^{\ominus}$ functions calculated from the kinetic data with that calculated from purely thermodynamic data show that the Gibbs energies are in reasonable agreement. In some cases compensations occur between $\Delta H^{\ominus}$ and $\Delta S^{\ominus}$ when the latter quantities differ from those calculated from kinetics, i.e., the kinetic and thermodynamic values of ΔG^{-} may agree although the quantities $\Delta H^{\ominus}$ and $\Delta S^{\ominus}$ fail to do so (see Table 5).

Although the experimental efforts by Moelwyn-Hughes and his co-workers related to the displacements and equilibria described, respectively, by eqs. [23] and [37] remain admirable, another sustained attack on the challenges these measurements represent might put the tentative conclusions drawn in the present section on a securer footing.

3. Kurz — The acidity of the protons in the attacking water molecule

Several years ago Kurz (24) pointed out that, if the reactions between a simple substrate RX with water and lyate ion are uncomplicated S_N2 displacements, then the ratio of the rate constants k_l/k_w provides a measure of the acidity of the hydrogens that form part of the attacking nucleophilic water molecule. The reactions summarized by eqs. [6] and [7] with halide and other anions as leaving groups are used to illustrate this idea. Kurz's treatment is not without conceptual difficulties, but, for the present, the basic premises of his work are accepted without qualification.

The Eyring theory (39) relates the rate constant k_w associated with eq. [6]

$$[43] \quad k_w = \kappa(w)(kT/\hbar)K_w^{\ddagger}$$

and the rate constant k_l associated with eq. [7]

$$[44] \quad k_l = \kappa(l)(kT/\hbar)K_l^{\ddagger}$$

where the symbols in eqs. [43] and [44] refer to the transmission coefficients $\kappa(w)$ and $\kappa(l)$, and k, T, and $\hbar$ have their conventional meanings. Expressing the quotients that define the equilibrium constants $K_w^{\ddagger}$ and $K_l^{\ddagger}$ in terms of concentrations rather than the more appropriate activities gives

$$[45] \quad k_w = \kappa(w)(kT/\hbar)\{[H_2O\text{-}CH_3\text{-}X]/[CH_3X][H_2O]\}$$

and

$$[46] \quad k_l = \kappa(l)(kT/\hbar)\{[HO\text{-}CH_3\text{-}X]/[CH_3X][OH^-]\}$$

Only the composition of the two transition states are represented in eqs. [45] and [46]; no attempt is made to specify the disposition of the charges in these symbolic expressions. The acidity constant of the transition state ($K_a^{\ddagger}$) produced

© 2005 NRC Canada

Table 4. (A) Transition-state enthalpies and (B) transition-state entropies for halide displacements of the methyl halides.

(A) Transition-state enthalpies.		
Reaction	$H^{\ddagger}$	Range
MeF + Cl^-	–77.70 ± 0.74	–76.97 to –78.44[a]
MeCl + F^-	–78.72 ± 0.74	–77.97 to –79.46[a]
MeF + I^-	–51.27 ± 0.79	–50.48 to –52.06[b]
MeI + F^-	–56.68 ± 0.64	–56.05 to –57.32[b]
MeCl + Br^-	–27.31 ± 0.54	–26.77 to –27.86[b]
MeBr + Cl^-	–30.54 ± 0.48	–30.06 to –31.02[b]
MeCl + I^-	–19.88 ± 0.50	–19.38 to –20.39[a]
MeI + Cl^-	–21.06 ± 0.68	–20.38 to –21.74[a]
MeBr + I^-	–10.40 ± 0.39	–10.00 to –10.79[b]
MeI + Br^-	–12.39 ± 0.64	–11.75 to –13.03[b]
(B) Transition-state entropies.		
Reaction	$S^{\ddagger}$	Range
MeF + Cl^-	+23.12 ± 1.96	25.07–21.16[b]
MeCl + F^-	+29.42 ± 1.99	31.41–27.43[b]
MeF + I^-	+39.92 ± 2.28	42.19–37.64[b]
MeI + F^-	+27.44 ± 1.77	29.21–25.68[b]
MeCl + Br^-	+57.61 ± 1.34	58.95–56.27[b]
MeBr + Cl^-	+46.68 ± 1.04	47.72–45.63[b]
MeCl + I^-	+44.13 ± 1.21	45.34–42.91[b]
MeI + Cl^-	+38.80 ± 1.87	40.67–36.93[b]
MeBr + I^-	+47.62 ± 0.70	48.32–46.92[b]
MeI + Br^-	+42.08 ± 1.75	43.84–40.33[b]

[a]Overlap.
[b]No overlap

Table 5. Thermodynamic data for methyl halide – halide ion equilibria calculated from kinetic and thermodynamic data.

Reaction	$\Delta G^{\ominus}$	$\Delta S^{\ominus}$	$\Delta H^{\ominus}$
MeF + Cl^-[a]	–0.33±0.76	–15.49±1.5	+14.95±0.62
MeF + Cl^-[b]	+2.56±0.84	–21.80±2.13	–3.94±0.73
MeCl + F^-[a]	+0.33±0.76	+15.49±1.51	+4.95±0.62
MeCl + F^-[b]	–2.56±0.84	+21.80±2.13	+3.94±0.73
MeF + I^-[a]	–1.00±1.00	–23.47±2.17	–8.00±0.77
MeF + I^-[b]	+0.69±0.10	–10.99±1.90	–2.59±0.67
MeI + F^-[a]	+1.00±1.00	+23.47±2.17	+8.00±0.77
MeI + F^-[b]	–0.69±0.10	+10.99±1.90	+2.59±0.67
MeCl + Br^-[a]	+1.29±0.63	–4.44±0.92	–0.03±0.63
MeCl + Br^-[b]	+1.26±0.04	+6.49±1.43	+3.19±0.46
MeBr + Cl^-[a]	–1.29±0.63	+4.44±0.92	+0.03±0.63
MeBr + Cl^-[b]	–1.26±0.04	–6.49±1.43	–3.19±0.46
MeCl + I^-[a]	–0.67±0.92	–7.98±1.86	–3.05±0.73
MeCl + I^-[b]	–1.08±0.06	–2.65±1.23	–1.88±0.42
MeI + Cl^-[a]	+0.67±0.92	+7.98±1.86	+3.05±0.73
MeI + Cl^-[b]	+1.08±0.06	+2.65±1.23	+1.88±0.42
MeBr +I^-[a]	–1.96±0.91	–3.54±1.81	–3.02±0.73
MeBr +I^-[b]	–1.62±0.01	+2.00±0.55	–1.03±0.17
MeI + Br^-[a]	+1.96±0.91	+3.54±1.81	+3.02±0.73
MeI + Br^-[b]	+1.62±0.01	–2.00±0.55	+1.03±0.17

[a]Calculated from thermodynamic data (see Table 2).
[b]Calculated from kinetic data (see Table 3).

Table 6. Rate and equilibrium data related to primary substrates.

RX	$-\log k_l$	$-\log k_w$	$pK_a^{\ddagger}$	$\log k_p^{\ddagger}$	$k_p^{\ddagger}\times10^2$
$MeClO_4$[a]	1.141	4.507	12.39	1.552	2.81
$(Me)_2SO_4$[b]	2.031	5.782	12.01	1.183	6.56
MeO_3SCH_3[c]	3.398	7.039	12.10	1.274	4.88
MeO_3SPh[d]	3.074	6.678	12.14	1.311	5.50
MeO_3SPh[e]	3.022	6.677	12.09	1.260	4.71
$MeNO_3$[f]	6.197	10.343	11.64	0.790	16.2
MeF[g]	6.232	10.847	11.10	1.545	55.2
MeCl[h]	5.181	9.366	12.02	1.188	6.48
MeBr[i]	3.845	8.134	11.45	0.609	24.60
MeI[j]	4.197	8.880	11.06	0.222	60.0
MeX[k,l]	0.575	4.831	11.49	0.653	22.2
EtOTos[m]	4.911	6.938	13.72	2.904	0.13
EtO_3SPh[n]	3.932	6.711	12.97	2.145	0.72

Note: In most cases, the data at 298.15 K has been recalculated from either the Arrhenius or Valentiner equations.[2] The k_w values have been divided by the molar concentration of water at 298.15 K.
[a]k_l (see ref. 54); k_w (see ref. 55).[2]
[b]k_l (see ref. 56); k_w.[2]
[c]k_l (see ref. 56); k_w.[2]
[d]k_l (see ref. 56); k_w.[2]
[e]k_w (see ref. 2); k_l (see ref. 2).
[f]k_l (see ref. 57); k_w(see ref. 58).
[g]k_l and k_w (see ref. 32).
[h]k_l (see ref. 59); k_w (60).[2]
[i]k_l (see ref. 59); k_w (60).[2]
[j]k_l (see ref. 59); k_w (21, 3960).[2]
[k]k_w and k_l (see ref. 61).
[l]Methyl-3-*N*-methylpyridinium sulphonate.
[m](11)k_w;[2] k_l(see ref. 62).
[n](12)k_w and k_l (see ref. 2).

when a water molecule attacks the CH_3X species is defined in the normal way

$$[47] \quad K_a^{\ddagger} = [HO\text{-}CH_3\text{-}X][H^+]/[H_2O\text{-}CH_3\text{-}X]$$

and, granted the condition that the transmission coefficients are equal, i.e., $\kappa(l) = \kappa(w)$, then some trivial manipulations that combine eqs. [45]–[47] at T = 298.15 K give

$$[48] \quad pK_a^{\ddagger} = 15.74 - \log(k_l/k_w)$$

Generally $k_l > k_w$, hence the magnitude of $pK_a^{\ddagger}$ calculated from eq. [48] is less than 15.74, which requires the hydrogens of the coordinated water molecule in the transition state to be *more acidic* than those in bulk water. This trend is in the direction anticipated for the protons of a water molecule bonded to a developing cationic centre. Data related to a series of methyl and ethyl substrates are presented in Table 6 and the calculated $pK_a^{\ddagger}$ values range from 13.72 for ethyl tosylate to 11.06 for methyl iodide. In comparison (63) with typical organic acids such as phenols ($pK_a \approx 8.0 \pm 2.0$) and carboxylic acids ($pK_a \approx 3.0 \pm 2.0$), the water hydrogens in the various transition states are weakly acidic. Indeed, if Kurz's model is valid, the acidity of the water hydrogens in the transition state is close to that of bulk water, and concomitantly, bonding between the nucleophilic water molecule and the reacting substrate is presumably weak in comparison with a fully formed methyloxonium ion. These qualitative considerations can be put on a more quantitative footing.

© 2005 NRC Canada

The range of acidity for the hydrogens of the nucleophile is from $pK_a = 15.76$ for a free water molecule to $pK_a = -2.04$ for the methyloxonium ion,[3] giving a total range of 17.80 pK_a units. The average $pK_a^{\ddagger}$ for the hydrolyses listed in Table 6 is 12.01, hence the average fractional movement of the reacting systems along the reaction coordinate is calculated to be: (15.76 – 12.01)/17.8 = 0.21. The latter value represents a reactantlike transition state *with respect to the attacking water molecule.* The magnitude of the reaction coordinate parameter estimated in this way differs from the values adopted by Albery and Kreevoy (13) in their Marcusian analysis of methyl transfers. These workers calculated reaction coordinate parameters that were larger than 0.21. The latter value is also uncomfortably small when compared to the Brönsted exponent of unity associated with the Guthrie LFER that indicates a productlike transition state with respect to the leaving group. Guthrie's work (23) will be examined in greater detail later. Obviously, there is no a priori rule or requirement for the extent of O—H bond breaking associated with the attacking water molecule to match the extent of C—X bond fission in the activated complex. *In any case, if intermediates are involved in a reaction, i.e., the reaction occurs in steps, such matters become extremely complex and the notion of a singular and simple reaction coordinate is less compelling*.

The classical studies of Hughes and Ingold (1–3, 8, 10) consider that values of k_l/k_w greater than unity are indicative of the S_N2 mechanism for the *hydrolysis reaction,* although the exact physical basis of this mechanistic test is not obvious. Indeed, the considerations presented by Kurz (24) might be regarded fairly as the first attempt to give a definite physical meaning to the ratio k_l/k_w. For many substrates, k_l cannot be measured because the magnitude of the rate constant characteristic of the hydrolysis reaction is large enough to swamp the reaction with lyate ion. However, if eq. [48] is to remain physically valid, the ratio k_l/k_w must remain finite within the framework of the current interpretation and must be numerically greater than unity. Nevertheless, Streitwieser (2) has tabulated such ratios as zero. Values of k_l/k_w less than unity would imply that a water molecule interacting with an incipient positive charge is less acidic than bulk water and, as such, is a physically uncongenial proposition.

The data in Table 6 related to the previous analysis display some odd features. Thus, although the reactivities of methyl perchlorate and methyl fluoride are separated by ca. six orders of magnitude for both water and the lyate ion, for each substrate, the acidities of the water hydrogens in their respective transition states are virtually identical. There is a modest trend for the acidity of the water protons to become higher as the *nucleophilicity* of the leaving group increases. This observation implies more "push" is required from the nucleophilic water molecule when the leaving group is a good nucleophile; this is an eminently reasonable proposition. The attack of water on ethyl tosylate produces the weakest acid. This observation is in accord with the conventional wisdom, namely, that α methylation *decreases* the importance of nucleophilic assistance in solvolytic displacements. Equation [48] is revealing with respect to some other features of the hydrolysis reaction.

The rate of proton transfer from acids to water is well-known to be a function of the strength of the acid from which the proton departs, and concomitantly, obeys an adequate Brönsted relationship, although the Brönsted exponent becomes smaller for very strong acids. However, the rates of proton loss ($k_p^{\ddagger}$) can be estimated safely to at least an order of magnitude from such a Brönsted correlation for weaker acids ($pK_a > 3.00$)

$$[49] \quad \log k_p^{\ddagger} = 10.95 \pm 0.12 - (1.01 \pm 0.02)pK_a \ (8,0.998)$$

Equation [49] was generated from data collected by Caldin (64) reported in Table 7. The numbers in parenthesis at the terminus of eq. [49] refer to the number of data point pairs and the related correlation coefficient, respectively. This mode of representation for these statistical quantities will be adopted in the rest of the review.

The correlation represented by eq. [49] is illustrated in Fig. 1 and it differs from the LFER reported by Grunwald (65), namely,

$$[50] \quad \log k_p^{\ddagger} = 11.74 - 0.54pK_a$$

that is restricted to stronger acids with pK_a values less than 3.00. Equations [48] and [49] may be combined to give

$$[51] \quad \log k_p^{\ddagger} = 1.01 \log(k_l/k_w) - 4.93$$

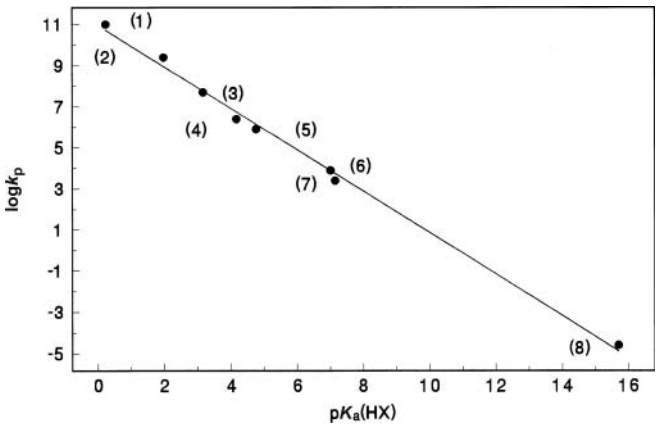
The $k_p^{\ddagger}$ rate constants calculated from eq. [49] are reported in the final column of Table 6 and give rise to half-

Table 7. Rates of proton transfer from various Brønsted acids.

Acid	pK_a[a]	$\log k_p$[b]
Water	15.7	–4.6
Hydrogen sulphide	7.0	3.9
Acetic acid	4.76	5.9
Benzoic acid	4.17	6.4
Hydrofluoric acid	3.17	7.7
Hydrogen sulphate	1.98	9.4
4-Nitrophenol	7.14	3.4
Trifluoroacetic acid	0.23	11.0

[a] pK_a data from refs. 63 and 64.
[b] Rate data from ref. 64.

Fig. 1. Brönsted linear free energy relationship between the rates of proton loss ($\log(k_p)$) and the pK_a of the acid. (1) CF_3COOH, (2) 4-NO_2-C_6H_4OH, (3) H_2SO_4, (4) HF, (5) PhCOOH, (6) CH_3COOH, (7) H_2S, (8) H_2O.



© 2005 NRC Canada

lives for proton transfer ($t_{1/2} = \ln 2/k_p^{\ddagger}$) that are several orders of magnitude longer than the lifetime of the transition state (ca. 1×10^{-13} s). Hence, the Kurz equation confirms the notion that *proton loss occurs later along the reaction coordinate* and does not necessarily coincide with the maxima in that coordinate, vindicating conclusions drawn on the basis of alternative evidence presented in section 1.

It should be noted Kurz (24) recognises that the lifetime of the transition state is insufficient to allow the hydrogens that form part of the attacking water molecule to be in true thermal acid–base equilibrium with the bulk solvent. Notwithstanding the latter limitation, the Kurz equation is in accord with the notion that the transfer of the proton in a hydrolysis reaction takes place from *a stronger acidic species generated later along the reaction coordinate*. This latter requirement is in accord with eq. [12] and evinces further credibility when the KSIE is examined. The KSIE is measured by the ratio $k(H_2O)/k(D_2O)$ (6, 66).

4. The rates of solvolysis in light and heavy water — The kinetic solvent isotope effect (KSIE)

Writing in 1964, Robertson (6) observed that the impetus for KSIE measurements was underpinned by the notion "... that there should be an indication of a primary isotope effect arising from nucleophilic interaction in the case of displacement by the S_N2 mechanism, but this would be absent for those molecules reacting by the S_N1 mechanism. Hence it was anticipated that the $k(H_2O)/k(D_2O)$ ratios would provide a new test for distinguishing between these two important mechanisms. No indication of such a difference was found for the hydrolysis of sulphonates and halides."

Typical measurements that confirm Robertson's final remark in the preceding quote are provided by the α methylated alkyl chlorides RCl (R = methyl, ethyl, 2-propyl, and *tert*-butyl). These reactants give ratios $k(H_2O)/k(D_2O)$ = 1.28, 1.26, 1.33, and 1.38 (66), respectively. The apparent insensitivity of the KSIE to the mechanistic categories postulated by the Ingold school (1, 8) prompted explanations of the observed ratios in terms of solvation differences for both the ground and transition states in the two isotopic solvents (see refs. 4, 6, and particularly 15).

The solvation hypothesis was developed in considerable detail by Swain and Thorton (4, 67). An alternative treatment was presented by Schowen (68) using isotopic fractionation factor theory. Schowen's calculations retained the conventional features of the original S_N2 and S_N1 mechanisms and provided theoretical ratios for the KSIE ranging from unity to 3.1 for the former route and from unity to 1.35 for the latter. These theoretical estimates suggest the magnitude of the experimental ratios imply the transition states for the S_N2 substrates are reactantlike and those for the S_N1 substrates productlike.

Two important points emerge from Schowen's analysis. First, the range of theoretical estimates confirms Robertson's expectations recorded in the previous quotation. Secondly, the experimental KSIE values for primary centres indicate that the nucleophilic water is reactantlike, or alternatively the KSIE does not reveal much incipient proton/deuteron formation. This agrees with conclusions reported in sections 1 and 3; however, this result for primary carbon centres is totally at variance with the Guthrie LFER (23) considered later.

The larger KSIE anticipated for S_N2 displacements reflects the notion that fission of one of the oxygen–hydrogen bonds of the attacking nucleophilic water molecule might be advanced in a simple S_N2 transition state. The previous discussion suggests that the heterolytic fission of the oxygen–hydrogen bond of the nucleophilic water molecule is the *last process* in the hydrolysis reaction. Because the pK_a values of the α methylated oxonium ions ROH_2^+ (R = methyl, ethyl, 2-propyl, and *tert*-butyl) are –2.04, –1.95, –1.86, and –3.7, respectively (69),[3] the rates of proton transfer from these acids estimated from eq. [50] will approach the theoretical limit. Such rapid kinetic events are unlikely to contribute to the observed rate constant that is *controlled by other much slower processes.*

Similar considerations must hold for other substrates that may react via more complicated schemes such as the Winstein mechanism (70)

$$\text{[52]}\quad RX \underset{k_2}{\overset{k_1}{\rightleftharpoons}} R^+X^-(\text{int}) \underset{k_4}{\overset{k_3}{\rightleftharpoons}} R^+||X^-(\text{ss}) \underset{k_6}{\overset{k_5}{\rightleftharpoons}} R^+ + X^-$$

$$\downarrow k_{1n} \qquad \downarrow k_{2n} \qquad \downarrow k_{3n} \qquad \downarrow k_{4n}$$

$$P \qquad P \qquad P \qquad P$$

The participants involved are intimate (int) and solvent separated (ss) ion pairs along with free carbocations. The rate constants k_r(r = 1–6) relate in pairs to the heterolytic equilibria implied by eq. [52] and the rate constants k_{nr}(r = 1–4) describe the irreversible nucleophilic components of the overall displacement leading to product P. Equation [52] does not alter the considerations previously presented, but merely describes alternative routes to alkyloxonium ions or carbocations more elaborate than those represented by eq. [12].

Robertson and co-workers (66) also measured changes in the enthalpy of activation $\delta_I\Delta H^{\ddagger}$ and the entropy of activation $\delta_I\Delta S^{\ddagger}$ that characterize ordinary water and deuterium oxide for several solvolytic substrates and these thermodynamic quantities demonstrate a respectable linear relationship (see Table 8 and Fig. 2). This observation is of no great significance by itself, however, when similar quantities that characterize the transfer of simple salts from water to heavy water ($\delta_I\Delta H$(sln) and $\delta_I\Delta S$(sln) (71)) are included in the plot, the values for transfer and activation reside in the *same region* of the coordinate system. The thermodynamic quantities derived from kinetic studies are intrinsically more complex because two transfers are involved, namely, the initial and transition states (15). In contrast, the paired ion transfers depend only on a single difference between G, H, and S for the ions in the two isotopic solvents. The initial state transfers for the methyl halides measured by Swain and Thornton (67) provide thermodynamic quantities that are in the same general region as those obtained from ion and kinetic transfers. The combination of the initial state and kinetic data so as to characterize the transition-state transfers would merely move the points along rather than away from the H,S vector.

For $B_{Ac}2$ solvolytic reactions that are partly characterized by rate-determining proton transfers (72), the related quantities $\delta_I\Delta H^{\ddagger}$ and $\delta_I\Delta S^{\ddagger}$ *are remote from regions of the plot that correspond to the displacements with which this review*

© 2005 NRC Canada

Table 8. Thermodynamic quantities related to transfers between light and heavy water.

Substance	Enthalpy ($\delta_I\Delta H$)	Entropy ($\delta_I\Delta S$)
Kinetic transfers (72) (KSIE)		
t-BuCl	818.0	2.24
$MeOC(CH_3)_2Cl$	624.0	1.54
$(CH_3)_2CBr_2$	629.0	1.47
$(CH_3)_2CBrCl$	676.0	1.58
Cyclo-C_4H_7Cl	502.0	1.05
Cyclo-C_5H_9Br	434.0	0.84
$C_6H_5CH_2Cl$	300.0	0.46
Saline transfers (73) (SIE)		
LiF	–155.0	–0.33
NaF	5.0	0.11
KF	60.0	0.21
LiCl	400.0	1.23
NaCl	560.0	1.51
KCl	615.0	1.63
LiBr	535.0	1.57
NaBr	695.0	1.76
KBr	750.0	1.91
LiI	675.0	1.93
NaI	835.0	2.03
KI	890.0	2.18
Neutral molecule transfers (73) (SIE)		
MeF	489.0	1.65
MeCl	140.0	0.40
MeBr	76.0	0.13
MeI	369.0	1.03
$B_{Ac}2$ mechanisms (KSIE) — Hydrolysis of carboxylic anhydrides (21)[a]		
Acetic	118.0	2.52
Propionic	–200.0	1.22
Succinic	338.0	3.15
Phthalic	460.0	3.23

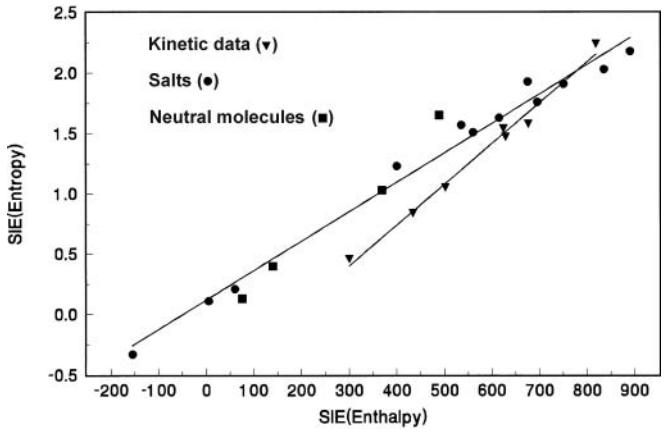
Note: Solvent isotope effect (SIE); kinetic solvent isotope effect (KSIE). The saline transfers refer to 25 °C and the methyl halides to 29.4 °C. The temperature for the kinetic transfers is less well-defined but will correspond to 0 °C < T < 25 °C. The units are cal/mol for the enthalpy function and cal mol^{-1} K^{-1} for the entropy. In Fig. 2, both the KSIE and SIE data are correlated on a single graph.

[a]These values for $\delta_I\Delta H$ and $\delta_I\Delta S$ are poorly correlated with the other data in the table (see related text).

is primarily concerned. The coincidence of the ion transfer and activation quantities is not definitive mechanistic information, but nevertheless, offers further confirmation that the proton transfer in the S_N hydrolyses occurs *after* the rate-determining step.

Neither the KSIE nor the Kurz analysis illuminates the extent and importance of the variation of nucleophilic assistance in the α-methylated substrates as previously defined in the way Robertson originally anticipated (6, 66). On the basis of more revealing investigations, current opinion (73) apparently casts doubt on the notion that *tert*-butyl substrates react via the classical S_N1 route involving the free *tert*-butyl carbocation. If this be the case, the possible significance of the *tert*-butyloxonium ion formation rather than the *tert*-butyl cation becomes an important question. Cases involving

Fig. 2. Correlation between enthalpy and entropy of transfer ($\delta_I\Delta H$ and $\delta_I\Delta S$) for ionic compounds (●), neutral molecules (■), and activation parameters (▼).



free carbocations do not necessarily require the intermediate formation of the related oxonium ion because the electrophilic attack of the carbocation on water and proton loss might be concerted processes. Further comment on these classical conundrums will be presented later. Clearly, the mechanism represented by eq. [12] is not at variance with the main features of the KSIE. Further evidence for the complexity exemplified by eq. [12] is revealed by the non-Arrhenius temperature dependence of the rates of hydrolysis of numerous simple halides and sulphonates. This well-established feature of hydrolyses in water (6, 15) and mixed aqueous solvents (7) will be examined in section 5.

5. The non-Arrhenius behaviour of solvolytic displacements — Heat capacities of activation

Moelwyn-Hughes (74) appears to have been the first author to focus sustained attention on the fact that solvolytic displacements in water do not obey the Arrhenius equation in the simple form

$$[53] \quad k = \exp(A(1) + A(2)/T)$$

The quantities k and T have their usual significance; $A(1)$ and $A(2)$ are empirical constants. The alternative and more usual version of this equation gives physical meaning to the constants $A(1)$ and $A(2)$

$$[54] \quad \ln k = -E_a/RT + \ln A$$

where E_a is the activation energy, the quantity A is usually interpreted as the product of a collision number Z and a probability factor P, i.e., $A = PZ$, and R is the gas constant.

Considerable experimental care is required to establish departures from eq. [53] or [54] and the related problems have been discussed by Robertson in an earlier review (6). An example of the level of precision and reproducibility obtained by the Robertson group is exemplified by some of the rate constants that characterize the hydrolysis of allyl bromide made by the author between 1957 and 1959 (75). The raw resistance – time data have been reexamined using various least-squares algorithms and the results from these computations are reported in Table 9. The measurements approach a

© 2005 NRC Canada

level of precision and reproducibility (0.03%) for solution kinetic data that was achieved by Shiner's group (70) by a more elaborate methodology.

The inadequacies of eq. [54] raise a whole range of theoretical and practical issues that have been thoroughly detailed elsewhere (6, 15, 77, 78). One solution to the mathematical representation of the non-Arrhenius dependence augments eq. [53] with the term $A(3)\ln T$ to give

$$[55] \quad \ln k = A(1) + A(2)/T + A(3)\ln T$$

Equation [55] is usually known as the Valentiner equation (77). A simple interpretation of the failure of eq. [54] emerges from eq. [55] and leads to the conclusion that a finite heat capacity of activation ($\Delta C_p^{\ddagger}$) exists between the reactants and the transition state. Alternatively, E_a is a function of temperature, and in terms of eq. [55], $\Delta C_p^{\ddagger}$ is finite but independent of temperature. For a broad range of substrates eq. [55] gives an adequate account of the *k*–*T* data sets, and empirically, $\Delta C_p^{\ddagger}$ was found to be negative (6, 7). This important fact was considered to signify a quasi-ionic transition state (6). The odd exception to the rule that $\Delta C_p^{\ddagger}$ is negative is exemplified by the rate constants that characterize the hydrolysis of 4-methoxybenzyl trifluoroacetate. This latter observation has its own particular explanation involving a mixed $S_N/B_{Ac}2$ mechanism (79).

Moelwyn-Hughes (80) has drawn an elaborate analogy between the solvolytic displacements considered as ionogenic reactions and the ionization of carboxylic acids

$$[56] \quad RCOOH + H_2O \rightleftharpoons RCOO^- + H_3O^+$$

The average heat capacity change that characterizes these important organic reactions is ca. –40 cal mol^{-1} K^{-1} (1 cal = 4.184 J). In a similar vein, Robertson (81) estimated the heat capacity change for the hypothetical model process from available thermochemical data

$$[57] \quad Ar(aq) \rightleftharpoons Cl^-(aq)$$

and found $\Delta C_p \approx -70$ cal mol^{-1} K^{-1}. These important models are considered to mimic an ionic solvolytic reaction and should not be overlooked. On the other hand, such analogies raise a variety of issues as to how quantities as complex as heat capacities behave along the reaction coordinate for reactions only vaguely related to the carboxylic acid equilibria. Furthermore, the model for the ionization of carboxylic acids represented by eq. [56] is neither unique nor necessarily correct (82–86). Until these matters are resolved, the felicity of the models proposed by Robertson and Moelwyn-Hughes for the non-Arrhenius behaviour of displacement reactions must remain in doubt. Indeed, some values of $\Delta C_p^{\ddagger}$ calculated from the appropriate *k*–*T* data sets are either uncomfortably large (87, 88) or essentially zero, e.g., the data reported in this communication for neopentyl methane sulphonate (see Appendix A). These observations suggest that the interpretations of finite negative $\Delta C_p^{\ddagger}$ values presented by Robertson and Moelwyn-Hughes based primarily on the importance of solvation may require revision, a possibility recognised and exploited by Albery and Robinson (21).

Table 9. Rate constants for the hydrolysis of allyl bromide at: (A) T = 25.005 °C and (B) T = 44.987 °C.

(A) T = 25.005 °C.

Run No.	A126T	A126B	A127T	A127B	Mean
$k\times10^{5a}$	1.6976	1.6990	1.6917	1.6961	1.6961
$SD\times10^{9}$	5.238	6.78	5.46	11.37	31.5
$k\times10^{5b}$	1.6653	1.6500	1.6637	1.6312	1.6526
$SD\times10^{8}$	7.62	10.8	7.11	12.9	15.8
$k\times10^{5c}$	1.6161	1.6063	1.5945	1.6382	1.6138
$SD\times10^{7}$	3.48	3.15	4.20	4.50	1.85
$k\times10^{5d}$	1.6976	1.6990	1.6917	1.6962	1.6961
$SD\times10^{9}$	5.34	7.96	5.46	11.40	31.6

(B) T = 44.987 °C.

Run No.	A104T	A104B	A105T	A105B	Mean
$k\times10^{4a}$	1.8855	1.8902	1.8907	1.8876	1.8885
$SD\times10^{8}$	7.83	13.77	23.09	9.57	24.0
$k\times10^{4b}$	1.9038	1.9217	1.9037	1.9062	1.9090
$SD\times10^{8}$	15.8	21.3	31.2	23.3	86.4
$k\times10^{4d}$	1.8234	1.7760	1.8149	1.8238	1.8105
$SD\times10^{6}$	2.78	2.48	2.08	2.68	2.36
$k\times10^{4d}$	1.8857	1.8901	1.8904	1.8876	1.8885
$SD\times10^{8}$	8.07	13.80	7.67	9.57	22.70

Note: k = rate constant in s^{-1}; SD = standard deviation. For details concerning the Robertson–Guggenheim method, see section 7. Attempts have been made to test the conclusions that might be drawn from this experimental data by producing synthetic resistance data at 298.155 K (≈25 °C) and 318.17 K (≈45 °C) with the pseudo-first-order constants (k) of 1.7×10^{-5} and 1.8885×10^{-4}, respectively. The concentration of the acid (HBr) at any time (C_t) is given by $C_t = C_o[1 - \exp(-kt)]$ for a true first-order process. The related expressions for the resistance as a function of time were: $1/R_t = 428.05C_t/(1000\kappa) - 157.87C_t^{3/2}/(1000\kappa)$ for 25 °C and $1/R_t = 552.00C_t/(1000\kappa) - 222.43C_t^{3/2}/(1000\kappa)$ for 45 °C. The numerical coefficients in these expressions for $1/R_t$ were calculated from information and data in Harned and Owen (76). The cell constant (κ) was given a value of unity. For $C_o = 1 \times 10^{-3}$, the analogues for footnotes *c* and *d* at 25 °C from the synthetic data differed from each other on average by 0.93% in contrast to the experimental data by 2.35%. For 45 °C, the corresponding data are 1.14% and 5.16%. Thus, the retardation of the rates along the $1/R_t$ vs. t curve is 2–5 times that anticipated on the basis of the approximation $C_t \approx 1/R_t$. This observation is regarded as indicative rather definitive. The Guggenheim algorithm applied to to the synthetic gave a value of k that differed from the input value by 0.35%–0.60%, which matches the reproducibility of the rate constants.

[a] Robertson–Guggenheim method (linear least-squares).

[b] Nonlinear least-squares (resistances measured in the first half-life).

[c] Nonlinear least-squares (resistances measured in the third half-life).

[d] Linear least-squares based on the infinity value from the calculation in footnote *c*.

6. The Albery–Robinson treatment of the non-Arrhenius temperature dependence of solvolytic displacements in water

In 1968 Albery and Robinson (21) reported an important study of the temperature dependence of the solvolysis of *tert*-butyl chloride in water. In their analysis of the non-Arrhenius temperature dependence, the solvation model was virtually discarded as the major source of these phenomena. To interpret the temperature dependence of the measured pseudo-first-order rate constants as a function of temperature for the hydrolysis of *tert*-butyl chloride, Albery and Robinson postulated that this reaction involved an unspecified intermediate "I"

© 2005 NRC Canada

Table 10. Data related to the Valentiner and Albery–Robinson temperature dependence equations.

Solvent	Valentiner equation			
	G.C.	$A(1)$	$A(2)$	$A(3)$
tert-Butyl chloride	2.168×10^{-3}	415.57697±2.496	–28408.64±110.7	–56.83256±0.373
Allyl chloride	3.60×10^{-6}	170.91295±0.3968	–18394.266±19.43	–21.56644±0.3968
Allyl bromide	3.35×10^{-6}	257.74021±0.7913	–21992.24±36.55	–34.213673±0.1174
Methyl Iodide	6.36×10^{-7}	224.5698±7.151	–22754.531±7.151	–28.903983±0.0205
Methyl 4-methylbenzenesulphonate	3.06×10^{-6}	134.03972±0.014	–15998.219±0.664	–16.168389±0.0021
Methyl bromide	4.08×10^{-6}	178.29445±0.6841	–19674.922±0.3397	–22.293587±0.1002

[58] $t\text{-BuCl} \underset{k_2}{\overset{k_1}{\rightleftharpoons}} \text{I} \xrightarrow{k_3} \text{Products}$

The application of the steady-state theorem to eq. [58], after some standard manipulations, gives for the observed rate constant k_o

$$[59] \quad k_o = k_1k_3/(k_2 + k_3)$$

The quantities k_1, k_2, and k_3 are, respectively, the three rate constants that characterize either first-or *pseudo*-first-order component reactions. If the temperature dependencies of the component rate constants k_n (n = 1–3) in eq. [59] are given by expressions identical to eq. [53] then

$$[60] \quad k_n = \exp(A_n(1) + A_n(2)/T)$$

Combining the three equations summarized by eq. [60] with eq. [59] provides an expression for the temperature dependence of k_o

$$[61] \quad k_o = \exp(A + B/T)/[1 + \exp(C + D/T)]$$

The constants A, B, C, and D of eq. [61] are functions of the six constants summarized by eq. [60] specified by the relationships: $A = A_1(1)$, $B = A_1(2)$, $C = A_2(1) - A_3(1)$, and $D = A_2(2) - A_3(2)$.

Both eqs. [55] and [56] give an adequate representation of all the data that relate to the temperature dependence of the hydrolysis of *tert*-butyl chloride measured in three separate locations (21, 89, 90). Indeed, there is little to choose between the details recorded in Table 10 for *tert*-butyl chloride and several other substrates chosen at random, where the two equations are statistically compared using the Gauss criterion (G.C.) (53, also see Appendix B). Further details of the results for the *tert*-butyl chloride hydrolysis are reported in Appendices B and C. Notwithstanding the excellent fits of these data to eq. [62], there are several important problems associated with this particular expression.

First, eq. [61] gives a satisfactory account of the temperature dependence of a whole range of substrates for which the kinetic scheme described by eqs. [58] and [59] would be considered as uncongenial (91), i.e., the mechanism represented by eq. [58] might be acceptable for tertiary substrates but not for reacting primary centres. Some of the data related to this comment are assembled in Table 10 where the Albery–Robinson equation appears to have a slight edge over eq. [60]. Secondly, eq. [61] demonstrates some odd properties when attempts are made to give physical meaning to the four constants that it contains. This important limitation was neglected by Albery and Robinson (21) in their original presentation and this problem is considered in greater detail in the following.

Dividing eq. [61] by the exponential term present in the denominator gives

$$[62] \quad k_o = \exp[(A - C) + (B - D)/T]/[1 + \exp -(C + D/T)]$$

Equation [62] is of the *same form* as eq. [61]. It follows that there are *two different numerical solutions* for the constants A, B, C, and D that provide identical fits for a particular k–T data set. These are: (*i*) A, B, C, and D and (*ii*) $A - C$, $B - D$, $-C$, and $-D$, respectively. There are no obvious reasons for preferring either solution corresponding to eqs. [61] and [62], respectively.

This anomaly is, at least, partly ameliorated by the observation that the expression for apparent heat capacity of activation

$$[63] \quad \Delta C_p^{\ddagger} = -(k_2k_3)^2[E(2) - E(3)]^2/RT^2(k_2 + k_3)^2$$

obtained by the appropriate differentiations of eq. [59] is always negative because the component expressions in eq. [63] are all necessarily positive. The apparent heat capacity is also independent of whether eq. [61] or [62] is employed to express the temperature dependence. The symbols in eq. [63] have their usual meanings and the activation energies $E(1)$, $E(2)$, and $E(3)$ are those associated with the k_1, k_2, and k_3 steps and are assumed to be true constants. However, although the structure of eq. [63] necessitates that $\Delta C_p^{\ddagger}$ is always negative, in contrast to the solvation model represented by eq. [55], this quantity is no longer independent of temperature because: (*i*) k_2 and k_3 are temperature dependent and (*ii*) eq. [63] contains a term in T^2 in the denominator.

The Albery–Robinson treatment of the non-Arrhenius temperature dependence of hydrolytic reactions has features in accordance with eq. [12] if certain conditions are met. These are: (*i*) the k_5 and k_6 rate constants are large and (*ii*) external return represented by the k_4 step is unimportant under the normal conditions of solvolysis, i.e., the substrate concentration is small. The constant k_4 describes a second-order process and because the methyloxonium ion is a very strong acid in water, then the maximum value of the term $[CH_3OH_2^+][X^-] \approx 1 \times 10^{-11}$ under the normal conditions of hydrolysis with the initial concentration of the substrate set at ca. 1×10^{-3} mol/L. Hence, the magnitude of k_4 must approach that for a diffusion-controlled reaction for external return to be significant. External return is signified by pseudo-first-order solvolytic rate constants that decrease systematically with time (1, 2, 8). Generally speaking, this feature was not detected in the systems investigated by Robertson and co-workers although the method of determin-

© 2005 NRC Canada

Table 10 (*concluded*).

Albery–Robinson equation				
G.C.	*A*	*B*	*C*	*D*
1.891×10^{-3}	–13062.15±253.7	40.66938±0.9657	–4944.060±350.9	15.80097±0.8297
2.477×10^{-6}	–12521.21±310.7	28.50059±1.120	–3486.229±21.23	9.986029±0.2026
3.190×10^{-6}	–12790.90±122.6	32.6176 ± 0.4639	–3577.697±56.76	11.10849±0.0839
4.87×10^{-7}	–14003.46±357.7	30.65874±1.217	–3991.416±425.6	10.72633±0.6563
1.60×10^{-6}	–12067.16±203.0	29.14935±0.802	–2592.759±45.70	8.031878±0.2679
3.12×10^{-6}	–13818.60±315.6	31.88790±1.139	–3255.250±51.29	9.716916±0.4660

ing the rate constants from the raw experimental data was not conducive to the detection of departures from simple first-order behaviour (6).[2] On the other hand, Hammett (92) has reported that the solvolysis of ethyl 4-methyl benzenesulphonate may not be a simple first-order process, and likewise, Moelwyn-Hughes and Glew (9, 32) use a relatively complex kinetic scheme to quantify composition changes as a function of time for the hydrolysis of methyl fluoride. These latter observations may have significance in the present context and are addressed further later.

The Albery–Robinson treatment of the non-Arrhenius temperature dependence of solvolytic rate constants represents an important innovation because attention is drawn to the possibility that observed rate constants may be complex and that this complexity may have profound implications as to the meaning of such quantities as $\Delta H^{\ddagger}$, $\Delta S^{\ddagger}$, and $\Delta C_p^{\ddagger}$ obtained from the temperature dependence of observed rate constants. Indeed, the latter suggestion may have a wider currency, explaining why activation energies in solution have rarely provided either unambiguous mechanistic information or fail to reflect structural changes in a systematic way, leading one distinguished author to describe temperature dependence studies as "a fetish" (93). However, the Albery–Robinson treatment, notwithstanding its novelty, interest, and utility, overlooks several approximations and it is important to examine the oversights associated with this model.

The Albery–Robinson kinetic scheme described by eq. [58] is more accurately represented (22, 94) by the following differential equation presented in matrix form (see Appendix D)

$$[64]\quad \begin{bmatrix} (D+k_1) & -k_2 & \\ -k_1 & (D+k_2+k_3) & \\ & k_3 & D \end{bmatrix} \begin{bmatrix} A \\ B \\ C \end{bmatrix} = 0$$

where the operator $D \equiv \mathrm{d}/\mathrm{d}t$ and B represents I in eq. [58]. The matrix represented by eq. [64] gives rise to the auxiliary cubic

$$[65]\quad \lambda[\lambda^2 + \lambda(k_1 + k_2 + k_3) + k_1k_3] = 0$$

When solved, eq. [65] gives rise to three roots: λ_1, λ_2, and λ_3, one of which is zero, here arbitrarily λ_3. The other two roots are defined by the quadratic part of eq. [65], and with their signs changed, define the two dynamic constants that describe the time evolution of the chemical system described by eq. [58].

The composition of the system with respect to the three components, namely, *A*, *B*, and *C* at any time "*t*", is given by the general expression

$$[66]\quad X_n = \alpha_{n1}\exp(-\lambda_1 t) + \alpha_{n2}\exp(-\lambda_2 t) + \alpha_{n3}$$

with n = 1–3. When $n = 1$, $X_n = A$, for $n = 2$, $X_n = B$ and for $n = 3$, $X_n = C$. The amplitude factors in eq. [66] α_{nr}, (n = 1–3 and r = 1–3) are functions of the initial concentration of *A*, namely A_o together with k_1, k_2, k_3, and the two dynamic constants, λ_1 and λ_2. If $\lambda_2 < \lambda_1$, then λ_2 will, generally speaking, dominate the time evolution of the system described by eq. [66]; concomitantly, λ_2 will correspond approximately to the measured rate constant.

If the temperature dependence of λ_2 approximates to the that of k_o, this possibility can be examined formally in three ways. The first approximation identifies λ_2 with k_o in the steady-state expression given in eq. [59]. A second approximation can be developed from the simple theory of quadratic equations. Some elementary considerations give

$$[67]\quad \lambda_1 + \lambda_2 = k_1 + k_2 + k_3$$

$$[68]\quad \lambda_1\lambda_2 = k_1k_3$$

Dividing eq. [67] by eq. [68] gives

$$[69]\quad 1/\lambda_1 + 1/\lambda_2 = (k_1 + k_2 + k_3)/k_1k_3$$

which, because $\lambda_1 > \lambda_2$, gives

$$[70]\quad \lambda_2 \approx k_1k_3/(k_1 + k_2 + k_3)$$

Equation [70] is clearly similar to the steady-state expression (eq. [59]), augmented by an extra term k_1 in the denominator. This equation will not be considered further here.

Finally, the ramifications of eqs. [67] and [68] can be investigated further with fewer approximations by defining apparent activation energies ($\Delta E(n)^{\ddagger}$) and heat capacities ($\Delta C_p(n)^{\ddagger}$) (n = 1 and *2*) via the Arrhenius version of the van't Hoff equation (22).

$$[71]\quad \partial\ln(\lambda_n)/\partial T = \Delta E(n)^{\ddagger}/RT^2$$

from which

$$[72]\quad \Delta C_p(n)^{\ddagger} = \partial\Delta E(n)^{\ddagger}/\partial T$$

Granted that the activation energies $E(1)$–$E(3)$ associated with steps k_1–k_3 are true constants, the appropriate differentiations of eqs. [67] and [68] with respect to temperature combined with eqs. [71] and [72] give

$$[73]\quad \lambda_1\Delta E(1)^{\ddagger} + \lambda_2\Delta E(2)^{\ddagger} = k_1E(1) + k_2E(2) + k_3E(3)$$

$$[74]\quad \Delta E(1)^{\ddagger} + \Delta E(2)^{\ddagger} = E(1) + E(3)$$

Further differentiation of eqs. [73] and [74] with respect to temperature gives

© 2005 NRC Canada

$$\lambda_1\Delta C_p(1)^{\ddagger} + \lambda_2\Delta C_p(2)^{\ddagger} + [\lambda_1\Delta E(1)^{\ddagger 2} + \lambda_2\Delta E(2)^{\ddagger 2}]/RT^2 = [k_1E(1)^2 + k_2E(2)^2 + k_3E(3)^2]/RT^2$$

or

[75] $$\lambda_1\Delta C_p(1)^{\ddagger} + \lambda_2\Delta C_p(2)^{\ddagger} = [k_1E(1)^2 + k_2E(2)^2 + k_3E(3)^2 - \lambda_1\Delta E(1)^{\ddagger 2} - \lambda_2\Delta E(2)^{\ddagger 2}]/RT^2$$

and

[76] $$\Delta C_p(1)^{\ddagger} + \Delta C_p(2)^{\ddagger} = 0$$

The simultaneous linear eqs. [73] and [74] can be solved to give $\Delta E(1)^{\ddagger}$ and $\Delta E(2)^{\ddagger}$ as functions of temperature and similarly, eqs. [75] and [76] can be solved to establish the behaviour of $\Delta C_p(1)^{\ddagger}$ and $\Delta C_p(2)^{\ddagger}$ with respect to temperature.

The preceding formalities emphasize the approximate nature of the original Albery–Robinson expressions represented by eqs. [59] and [61] and imply that little physical meaning can be attributed to the quantities *A*, *B*, *C*, and *D* obtained from *k*/*T* data fits to eq. [61]. Notwithstanding these limitations, the satisfactory *k*/*T* data fits to eq. [61] give a measure of credibility to the notion that an intermediate of the sort postulated in eq. [12] exists when simple solvolytic displacements take place in water unless opinion regards the solvation models originally presented by Robertson and Moelwyn-Hughes (90) to be more reasonable and attractive. Although the choice between these alternatives is not clear-cut, in our opinion, other evidence presented in the following ultimately favours the implications of the Albery–Robinson model, which, although weak in its details, remains as a potent mechanistic clue.

The formalities previously presented, particularly eq. [66] that contains two exponential terms rather than a single term, prompts a reexamination of the raw resistance – time data from which the solvolytic rate constants were established with the hope that such probings might reveal features previously overlooked. This exercise is briefly described in section 7.

7. A reexamination of the Robertson–Guggenheim method

The basic physical and chemical situation examined by the Robertson group (6, 15)[2] consists of a dilute aqueous solution of the substrate RX ($C_o \approx 1 \times 10^{-3} - 5 \times 10^{-4}$ mol/L) that reacts according to eq. [6], steadily increasing the concentration of ions in the solution. The reacting solution is at a fixed temperature controlled to better than ±0.005 K. The ions produced by the chemical reaction are monitored by measuring the electrical resistance (*R*) of the solution. For a fixed temperature, a given conductance cell, and a fixed electrolyte, the relationship between *R* and the concentration *C* of the ionic product is adequately quantified by a version of the Onsager equation (76)

[77] $$1/R = \alpha C + \beta C^{3/2}$$

where the two constants α and β depend on the conditions previously specified, namely the electrolyte, the solvent, the cell dimensions, and the temperature. In the following analysis, it is assumed that the ions from the autoprotolysis of the solvent water make no significant contribution to *R* and the electrolyte is strong.

If the reactant RX is converted to the products by a simple first-order process, then the concentration of the acid $C_t(HX)$ ($HX \equiv H_3O^+ + X^-$) is given by

[78] $$C_t(HX) = C_o(HX) + C_o(RX)[1 - \exp(-kt)]$$

where $C_o(HX)$ is the concentration of the acid product when the resistance measurements commence and $C_o(RX)$ is the concentration of the substrate at that time. Because of various manipulative problems, concentration determinations cannot commence immediately after the reactant and water are mixed. Hence, the concentration of the product acid is always finite when the resistance measurements commence.

If the linear term in *C* dominates eq. [77], a reasonable assumption because: (*i*) $|\beta| < |\alpha|$ and (*ii*) $C^{3/2} < C$ when $C <$ unity. With these approximations, eq. [78] can be recast in the approximate form

[79] $$1/R = B(1) - B(2)\exp(-kt)$$

where $B(1)$ and $B(2)$ are constants related to the constants in eq. [78] and α in eq. [77]. Resistance–time data can be fitted to eq. [79] using a suitable nonlinear least-squares algorithm generating the first-order rate constant (*k*) and the disposable constants $B(1)$ and $B(2)$. However, such a method of deriving *k* from the *R*–*t* data sets was not a practical proposition in the early days of Robertson's investigations. In consequence, the Guggenheim (95) algorithm was adopted in conjunction with large scale plots (ca. 48″(X) vs. 36″(Y)) to calculate *k* from the resistance–time data.

The Guggenheim method of evaluating *k* involves two sets of resistances: the first set is measured over the first half-life ($t_{1/2}$) of the reaction yielding $R_{t(1)}$, $R_{t(2)}$, $R_{t(3)}$... $R_{t(n)}$. The second set separated from the first set by an interval τ such that $\tau > 2t_{1/2}$ and is measured at the same time intervals as the first set over a period that corresponds roughly to the third half-life of the reaction. This yields the resistances $R_{t(1)+\tau}$, $R_{t(2)+\tau}$, $R_{t(3)+\tau}$... $R_{t(n)+\tau}$. For the resistances measured in the first half-life, eq. [79] gives

[80] $$1/R_t = B(1) - B(2)\exp(-kt)$$

and for those measured in the third half-life

[81] $$1/R_{t+\tau} = B(1) - B(2)\exp[-k(t + \tau)]$$

Subtracting eq. [80] from eq. [81] yields

[82] $$1/R_{t+\tau} - 1/R_t = B(2)\exp(-kt)[1 - \exp(-k\tau)]$$

Equation [82] can be regressed in either linear or nonlinear forms to establish *k* from the R_t,$R_{t+\tau}/t$ data sets. However, the use of this equation does not allow the observed resistances to be compared to a calculated set from the rate constant and times. The latter limitation can be circumvented in the following manner. Eliminating the term $B(2)\exp(-kt)$ between eqs. [80] and [81] generates a version of the Kedzy–Swinbourne equation (96–99)

[83] $$1/R_t - B(1) = [1/R_{t+\tau} - B(1)]/\exp(-k\tau)$$

that can be rearranged to give

[84] $$1/R_{t+\tau} = \exp(-k\tau)(1/R_t) + B(1)[1 - \exp(-k\tau)]$$

© 2005 NRC Canada

Thus, a regression of $1/R_{t+\tau}$ as Y vs. $1/R_t$ as X gives $\exp(-k\tau)$ as the slope and $B(1)[1 - \exp(-k\tau)]$ as the intercept. Because k is available from the Guggenheim least-squares analysis, τ can be calculated from the slope ($\exp(-k\tau)$). A linear least-squares is now possible for the complete data set $R_t, R_{t+\tau}/t, t + \tau$ because the times $t(1) + \tau$, $t(2) + \tau$... $t(n) + \tau$ can be absolutely characterized. A least-squares correlation of $1/R$ as Y with $\exp(-kt)$ as X according to eq. [79] yields $B(1)$ and $B(2)$ from which the resistances can be regenerated and compared with the observed values.

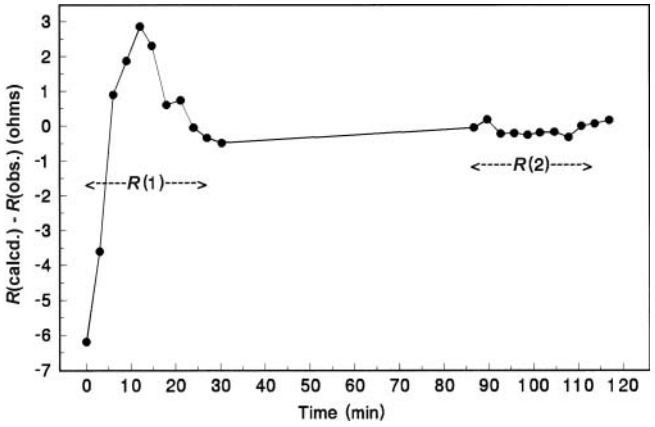
The preceding analysis has been applied to the raw resistance–time data for allyl bromide measured by the author between 1957–1959 and reported later with Robertson (75). This data set was selected because the hydrolysis of allyl bromide generated the most reproducible rate constants when *numerically* processed using eq. [82]. The reproducibility of not less than four rate constants measured at each of 13 temperatures averaged at 0.26 ± 0.09%. The measurements at 44.987 and 25.005 °C were selected for further analysis and the data from these calculations are reported in Table 9. The reported pseudo-first-order rate constants for each run were calculated in four ways: (*i*) a linear least-squares using eq. [82] using both sets of resistances in a numerical version of the Guggenheim algorithm; (*ii*) a nonlinear least-squares using the R_t values; (*iii*) a nonlinear least-squares using the $R_{t+\tau}$ values; and (*iv*) a linear least-squares technique using eq. [82] after the quantity $B(1)$ had been established on the basis of the regression in item (*iii*).

Both sets of data (T = 44.987 and 25.005 °C) show a reduction in the observed rate constants between the first half-life (R_t values) and the third half-life ($R_{t+\tau}$ values) of 4% that is approximately eight times the experimental error. Furthermore, the resistances regenerated from eq. [79] show systematic rather than random deviations (see Fig 3). These computed departures from strict first-order behaviour are in the anticipated direction when a more elaborate treatment of the Albery–Robinson mechanism is presented (see the previous paragraph), i.e., the double exponential expression (eq. [66]) that *might approximately describe* the production of acid with time would yield results in which the first-order rate constant becomes smaller with time. However, the present evidence is better regarded as indicative rather than compelling because other factors such as: (*i*) the linearization of eq. [77]; (*ii*) the possible nonlinearity of the conductance bridge; and finally, (*iii*) inadequate thermostatting might give rise to the effects these calculations establish.

Using the enthalpy of activation for the hydrolysis of allyl bromide (21.5 kcal mol^{-1} at 45 °C) in conjunction with the differential form of the Van't Hoff equation suggests that a temperature change of 0.37 K would be required at 45 °C to give a 4% retardation of the rate constant. This temperature drift is *well outside* that tolerated during the time–resistance measurements required for the rate constant determinations so item (*iii*) in the preceding paragraph can be safely discarded.

Sections 1–7 provide information that suggests that displacements at primary, secondary, and tertiary carbon atoms in water cannot be reconciled with the notion of simple S_N1 and S_N2 displacements. In the remaining sections, further influences of structure on reactivity are examined, particularly related to the nature of the leaving group or nucleofuge, a topic that hitherto has received less systematic attention.

Fig. 3. Deviations between calculated and observed resistances for run A82T related to the hydrolysis of allyl bromide.



8. Nucleofugality and mechanism

The purpose of the present section is to examine the solvolytic reactivity of a molecule (RX) in water as a function of anionic and neutral leaving groups. Generally speaking, the reactivity of RX has been primarily discussed in terms of the structure of the alkyl group (1–12). However, here, attention is focused on a wide variety of leaving groups associated with several organic structures, namely, the methyl, ethyl, allyl, 2-propyl, cyclohexyl, *tert*-butyl, 1-adamantyl, 2-adamantyl, benzyl, and 3- and 4-substituted benzyl structures. Such a range of solvolytic substrates is sufficient to embrace displacement reactions spanning the extremes of the classical S_N1–S_N2 mechanistic spectrum including the more elaborate descriptions represented by eqs. [16] and [52].

Leaving-group reactivity is intrinsically complex. Thus, it should be recognised at the outset that the order of reactivity manifested by RX as a function of X may not be independent of R. For instance, when X = Br or I the order of reactivity at 298.15 K is sometimes Br > I for R = methyl (60), ethyl,[2] allyl (75), and 2-propyl (6),[2] but for other structural environments, namely, R = *tert*-butyl (9) and 1-adamantyl (100, 101), the sequence I > Br is observed, an order that is considered here as "normal". This change in the order of reactivity of bromide and iodide leaving groups suggests the factors affecting nucleofugality are subtle, although the differences between bromide and iodide as nucleofuges are always small.

The *neutral* hydrolyses of carboxylate esters of strong carboxylic acids, e.g., trifluoroacetic acid, are also complex. Thus, most primary and secondary trifuoroacetate esters appear to react by an acyl-oxygen $B_{Ac}2$ path, whereas the tertiary esters heterolyse via an alkyl-oxygen S_N route. A reactive primary ester such as 4-methoxybenzyl trifluoroacetate demonstrates "mixed kinetics", reacting by both the $B_{Ac}2$ and S_N mechanisms (79, 102–105). On the other hand, *tert*-butyl trifluoroacetate appears to react predominately by the same mechanism as *tert*-butyl chloride, namely, via the alkyl-oxygen path (102–105). Thus, the entropies of activation at 25 °C for *tert*-butyl chloride and *tert*-butyl trifluoroacetate are both positive and similar in magnitude, 10.1 and 13.0 cal mol^{-1} K^{-1}, respectively. The secondary isotope ef-

© 2005 NRC Canada

fects (k(H)/k(D)) for the *tert*-butyl-d_9 compounds with chloride ion and trifluoroacetate ion as leaving groups are 2.2 and 2.6, respectively, and the KSIE ratios for these substrates are 1.22 and 1.38, respectively. The energy of activation for *tert*-butyl acetate is high (106) and this observation is consistent with an S_N route for this substrate.

The change in mechanism from $B_{Ac}2$ to S_N in the solvolytic behaviour with increasing homology for the simple α-methylated alkyl trifluoroacetates is presumably related to two energetic influences; the first, steric and the second, electronic. For a series of 4-substituted benzyl trifluoroacetates, the steric features are essentially constant for either mechanism. Hence, the changing electronic influences on each path as the ring substituent alters will dominate the observed reactivity sequence. The gas-phase enthalpy of ionization of a series of 4-substituted benzyl trifluoroacetates

[85] $ArCH_2OOCCF_3 \rightarrow ArCH_2^+ + CF_3COO^-$

should parallel those of the corresponding benzyl chlorides (105) (see section 13). On this basis, the reactivity sequence for the S_N mechanism should increase $CH_3O > CH_3 > H > Cl > NO_2$, and intuitively, that for the $B_{Ac}2$ mechanism should be in the opposite sense. A blend of these separate reactivity sequences is observed in practice, the mechanistic change occurring between the methoxy and methyl substrates. Thus, in two acetone water mixtures the four substrates with the substituents NO_2, Cl, H, and CH_3 in the 4-position react by the $B_{Ac}2$ mechanism and provide excellent Hammett plots with *positive* slopes. These correlations are presented in Fig. 4 and the data are recorded in Table 11. The numerical details related to the Fig. 4 are given in the following equations for: (*i*) acetone–water (~29%, *v*/*v*)

[86] $$\log k_o = 0.878 \pm 0.007\sigma - 3.284 \pm 0.003 \ (4,0.9993)$$

$$k(CH_3O, B_{Ac}2) = 3.75 \times 10^{-4}\ s^{-1} : k(CH_3O, S_N) = 2.68 \times 10^{-4}\ s^{-1}$$

and (*ii*) acetone–water (~5%, *v*/*v*)

[87] $$\log k_o = 0.643 \pm 0.01\sigma - 2.621 \pm 0.005 \ (4,0.9993)$$

$$k(CH_3O, B_{Ac}2) = 1.89 \times 10^{-3}\ s^{-1} : k(CH_3O, S_N) = 1.33 \times 10^{-3}\ s^{-1}$$

The $k(S_N)$ rate constants for 4-methoxybenzyl trifluoroacetate were obtained by calculating the $k(B_{Ac}2)$ rate constants by extrapolating the Hammett plots (eqs. [86] and [87]) with $\sigma(CH_3O) = -0.16$ and subtracting this value from k_o according to the equation

[88] $k_o = k(B_{Ac}2) + k(S_N)$

The change in reactivity of the 4-methoxybenzyl trifluoroacetate between the two acetone–water mixtures for the $k(S_N)$ process corresponds to a Grunwald–Winstein m value of 0.81. The latter value is consistent with an S_N process offering confirmation of the conclusions drawn from the behaviour of the α methylated substrates. The change in reactivity between the two acetone–water mixtures demonstrated for the $k(B_{Ac}2)$ rate constants is very close to that calculated for the S_N rate constants, and evidently, the Grunwald–Winstein m parameter is insensitive to the mechanistic shift $B_{Ac}2$ to S_N for 4-methoxybenzyl trifluoroacetate. The KSIE also confirms the conclusions drawn on the basis of the substituent effects on the benzyl trifluoroacetate solvolysis.

Fig. 4. Hammett LFER for a series of 4-substituted benzyl trifuoroacetates. Upper line solvent ca. 5% acetone – water; lower line solvent ca. 29% acetone – water.

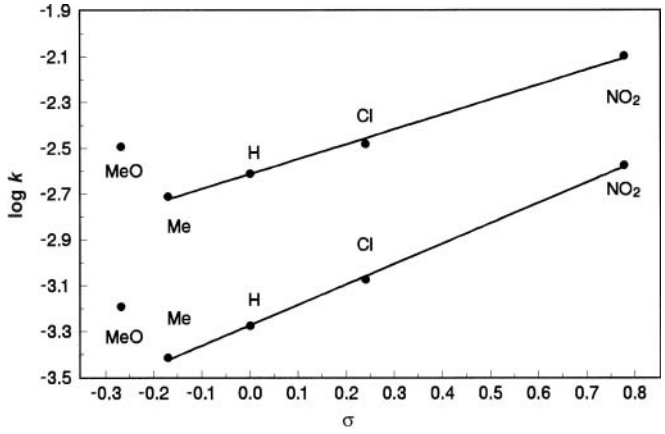


Table 11. Rates of hydrolysis of 4-substituted benzyl trifluoroacetates in acetone–water mixtures (T = 5.00 °C).

Substituent (σ)	log k^a	log k^b
MeO (–0.268)	–3.192	–2.493
Me (–0.17)	–3.415	–2.712
H (0.00)	–3.276	–2.611
Cl (0.24)	–3.075	–2.481
NO_2 (0.778)	–2.574	–2.097

Note: The data is from refs. 79 and 105.
[a]The solvent is 9.05×10^{-2} mol fraction acetone.
[b]The solvent is 1.2×10^{-2} mol fraction acetone.

Swain and Lohmann (4, 107) presented the first formal attempt to quantify leaving-group ability, but their work has attracted little attention and is notably absent in two fairly recent accounts of linear free energy relationships (108). Hoffmann (109) has used tosylate–bromide ratios as a mechanistic criterion, and there is a study by Bentley and Dewar (110) that also indirectly relates to the work of Hoffmann (109) and Swain and Scott (111). These contributions will be subsequently considered. In his discussion of the Swain–Lohmann LFER, Thornton (4) suggests that for anionic leaving groups X^- nucleofugality correlates with the pK_a of the acid HX. This hypothesis will be examined via the Guthrie LFER in section 10.

9. The Swain–Lohmann equation and derivative linear free energy relationships

The formalities of the Swain–Lohmann equation are similar to those adopted by Swain and Scott (111) in their development of an empirical scale of nucleophilicity represented

© 2005 NRC Canada

by the Swain–Scott LFER. To establish a scale of nucleofugality for the displacement

[89] $N + RX \rightleftharpoons RN + X$

it is necessary to define standard reagents and conditions. These are: (*i*) the leaving group X; (*ii*) the nucleophile N; (*iii*) the substrate RX; (*iv*) the solvent; and (*v*) the temperature. For the Swain–Lohmann equation, these are: Br^-, CH_3O^-, CH_3Br, CH_3OH, and 298.15 K, respectively. For a series of leaving groups X, the quantity *L* appropriate to each individual leaving group X is defined by the equation

[90] $$L = \log k(CH_3X) - \log k_o(CH_3Br) = \log[k(CH_3X)/k_o(CH_3Br)]$$

The broader influence of structure on leaving-group reactivity can now be examined via structural changes of N and R together with the same changes in the leaving group X that established the *L* scale via eq. [90]. Further options include the examination of the influence of solvent and temperature on the defined quantities.

Thus, for a selected N, R, solvent, and temperature, a series of second-order rate constants are generated when X is varied, which are then correlated with *L*. The resulting LFER is anticipated to be of the form

[91] $$\log[k(RX/N)/k(RBr/N)] = \gamma L$$

where γ is a constant characteristic of N, R, the temperature, and the solvent.

The *L* data are meagre and those given in Table 12 are selected from Thornton (4); apparently, the papers promised in Thornton's book (4) have failed to materialize, a point also raised by Bentley and Dewar (110). Other data for testing eq. [91] are provided by the rate constants that describe eqs. [6] and [7] for a series of methyl compounds reported in Table 6. A plot relating to the reactions with water and hydroxide ion as nucleophiles is shown in Fig. 5. A least-squares treatment of the two correlations for the water reactions gives

[92] $$\log k_w(CH_3X) = (0.993 \pm 0.078)L - 6.019 \pm 0.15 \quad (9,0.955)$$

and

[93] $$\log k_l(CH_3X) = (0.963 \pm 0.057)L - 3.900 \pm 0.13 \quad (8,0.977)$$

with aqueous hydroxide as the nucleophile. The correlation coefficients suggest that the relationships represented by eqs. [92] and [93] are only fair.

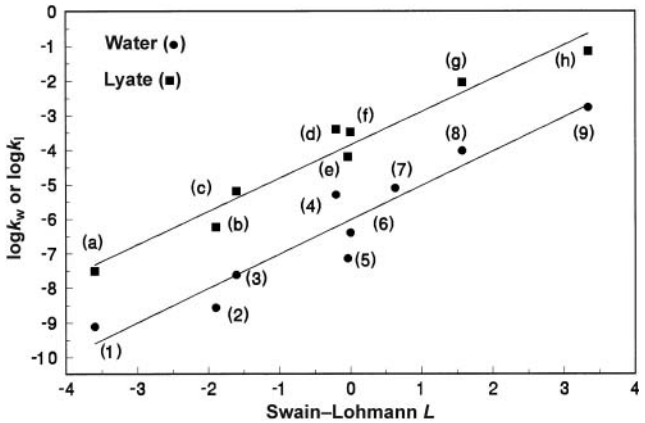
The Swain–Lohmann LFER is broad in scope because, as previously mentioned, the applications of the *L* values are, in principle, required to accommodate a variety of structural and environmental changes. Because our interest is confined to water, the Swain–Lohmann correlations are replaced here by what are designated to be the equivalent Hammett–Pfluger (115) forms. This tactic discards the notion of a standard data set, but retains a fixed solvent and temperature, namely, water and 298.15 K. The equivalent Hammett–Pfluger form is

Table 12. Rate data related to the Guthrie and Swain–Lohmann correlations.

Leaving group	$-\log k_w$[a]	pK_a[b]	*L*[c]	$-\log k_l$[d]
Chlorosulphate	1.783	–6.00	—	—
Triflate	1.760	–5.90	—	—
Perchlorate	2.763	–5.00	3.34	1.141
Methoxysulphate	4.082	–3.40	1.57	2.032
Benzenesulphonate	4.934	–2.80		
p-Nitropbenzenesulphonate	4.205	–4.00	—	—
m-Nitrobenzenesulphonate	4.278	–3.69	—	—
p-Bromobenzenesulphonate	4.711	–3.10	—	—
p-Methoxylbenzenesulphonate	5.226	–2.90	—	—
p-Methylbenzenesulphonate	5.098	–2.70	0.63	—
Methanesulphonate	5.295	–3.40	–2.05	3.398
Dimethylphosphate	8.200	0.76	—	—
Methylphosphate	9.660	1.50	—	—
Phosphoric acid	10.100	2.12	—	—
Fluoride[e]	9.103	3.17	–3.6	7.479
Chloride[e]	7.622	–2.18	–1.61	5.185
Bromide[e]	6.390	–4.70	0.00	3.480
Iodide[e]	7.134	–5.23	–0.04	4.196
Nitrate	8.559	–1.30	–1.90	6.223

[a]Hydrolysis rates (k_w): see Table 6 for references and also ref. 23. The k_w values in Table 6 are divided by the molar concentration of water.
[b]pK_a values are from ref. 23.
[c]*L* values are taken from ref. 4.
[d]Hydroxide rates (k_l): see Table 6.
[e]pK_as for halogen acids HX: for HF values see refs. 112 and 113; for HCl, HBr, and HI values see ref. 114.

Fig. 5. Correlations between the Swain–Lohmann *L* parameter and the rates of reaction of methyl substrates with hydroxide (upper curve) and water (lower curve). (a) and (1) MeF, (b) and (2) $MeNO_3$, (c) and (3) MeCl, (d) and (4) $MeSO_3Me$, (e) and (5) MeI, (f) and (6) MeBr, (g) and (7) Me_2SO_4, (h) and (8) $MeClO_4$, (9) 4-$CH_3C_6H_4SO_3CH_3$.



[94] $$\log k(RX) = \gamma \log k(R'X) + C$$

and all the rate constants for RX and R′X are confined to hydrolysis in pure water. The constants in eq. [94], namely, γ and *C*, are empirically defined by the two R groups, the leaving groups, the solvent, and the temperature. Here, the organic groups R′ and R are selected pairs from a range of structures previously mentioned. The least-squares lines for

© 2005 NRC Canada

a selection of such pairings are presented in the following in terms of eqs. [95]–[99]. The correlations are conservatively judged to be satisfactory and are an improvement to the correlations described by eqs. [92] and [93].

[95] $\log k(\mathrm{EtX}) = (0.997 \pm 0.025)\ \log k(\mathrm{CH_3X}) + 0.038 \pm 0.13\ (9,0.995)$

[96] $\log k(\mathrm{allylX}) = (1.140 \pm 0.08)\ \log k(\mathrm{CH_3X}) + 2.85 \pm 0.58\ (4,0.983)$

[97] $\log k(\mathrm{2\text{-}AdX}) = (1.416 \pm 0.06)\log k(\mathrm{CH_3X}) + 3.852 \pm 0.29\ (7,0.991)$

[98] $\log k(\mathrm{c\text{-}HexX}) = (1.001 \pm 0.057)\ \log k(\mathrm{2\text{-}PrX}) + 0.071 \pm 0.30\ (4,0.993)$

[99] $\log k(\mathrm{1\text{-}AdX}) = (0.959 \pm 0.040)\ \log k(t\text{-BuX}) - 1.862 \pm 0.13\ (6,0.993)$

Three of the correlations represented by eqs. [95], [97], and [99] are illustrated in Figs. 6, 7, and 8, respectively, and the related data are presented in Tables 13–16. The sources for the solvolytic data are reported in each table. For cases that required the extrapolation of rate data from measurements in mixed solvent systems at temperatures either lower or higher than the standard temperature, a brief outline of the least-squares and other numerical techniques employed to obtain a rate constant in water at 298.15 K is reported at the foot of Table 16. These details relate to the Grunwald–Winstein (118, 137–141, 143), Eyring, and Arrhenius equations, all in their respective linear forms. Some further comment on eqs. [95]–[99] is important to our general thesis.

The correlation represented by eq. [97] is notable in that the ordinate covers nearly 10 orders of magnitude. Equation [99] with R′ = *t*-Bu and R = 1-adamantyl embraces both anionic (Cl^-, Br^-, I^-, NO_3^-, CF_3COO^-) and neutral ($(CH_3)_2S$) leaving groups, the latter generated from the hydrolyses of the related sulphonium ions. As far as we are aware, eq. [99] provides the first real opportunity to predict the rates of hydrolysis for some tertiary sulphonates with fair precision, and this enhances a further discussion of Hofmann's ideas (109) presented later. Simple open-chain tertiary sulphonates are apparently very labile (109), and in consequence, these substances cannot be examined directly. Facile elimination appears to take precedence over substitution for these structures.

Some speculative comment of the mechanistic significance of eqs. [95]–[97] is in order. Presumably heterolytic fission of the 1- and 2-adamantyl substrates proceeds via front-side attack involving the solvent separation of intimate ion pairs. This conclusion has been confirmed by the elegant work of the Milton–Harris group (144, 145), who demonstrated that a series of 2-adamantyl-4-substituted-benzenesulphonates solvolysing in EtOH–H_2O mixtures yielded products that depend on the leaving group. Thus, the product ratios *R*, defined by *R* = ([2-AdOH][EtOH])/([2-AdOEt][H_2O]), alter with the pK_a of the acid related to the leaving group, becoming more selective as the pK_a decreases (see Fig. 9 and Table 17). Because rearside nucleophilic assistance is precluded for 2-adamantyl substrates, the *R* values indicate that

Fig. 6. Hammett–Pfluger version of the Swain–Lohmann equation for MeX and EtX substrates. The leaving groups are: (1) -Cl; (2) -I; (3) -Br; (4) $-SO_3CH_3$; (5) $4\text{-}CH_3C_6H_4SO_3$-; (6) $C_6H_5SO_3$-; (7) CH_3OSO_3-; (8) $-ClO_4$; (9) $ClSO_3$-.

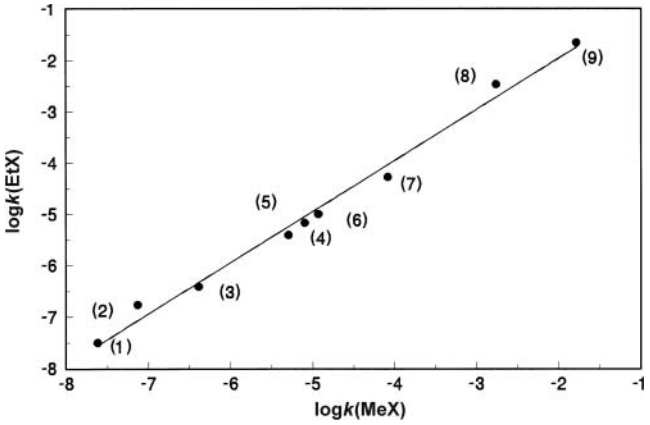


Fig. 7. Hammett–Pfluger version of the Swain–Lohmann equation for MeX and 2-AdX substrates. The leaving groups are: (1) $-NO_3$; (2) $4\text{-}CH_3C_6H_4SO_3$-; (3) $-SO_3CH_3$; (4) $4\text{-}BrC_6H_4SO_3$-; (5) $4\text{-}NO_2C_6H_4SO_3$-; (6) $-ClO_4$; (7) $-SO_3CF_3$.

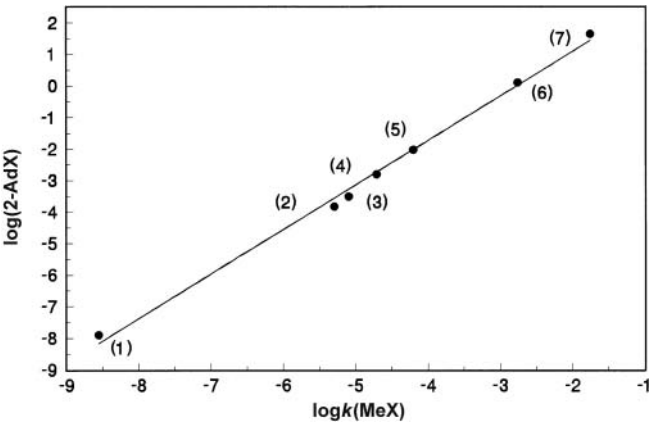
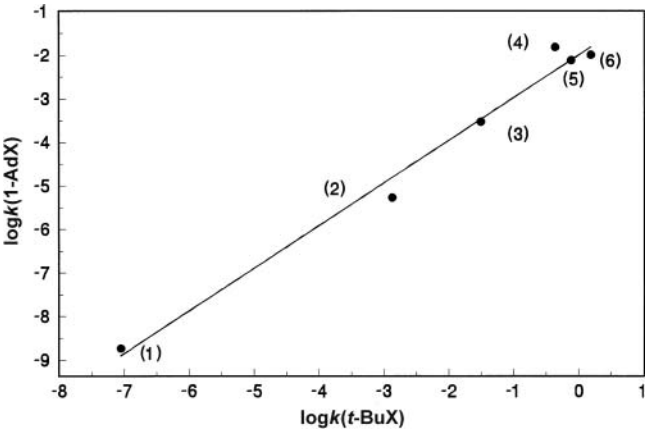


Fig. 8. Hammett–Pfluger version of the Swain–Lohmann equation for *t*-BuX and 1-AdX. The leaving groups are: (1) Me_2S; (2) CF_3COO-; (3) Cl-; (4) $-NO_3$; (5) Br-; (6) I.



© 2005 NRC Canada

Table 13. Rate data for the hydrolysis of allyl, 1-adamantyl, and 2-adamantyl derivatives (T = 298.15 K).

Leaving group	Allyl	1-AD	2-AD	pK_a[a]
Triflate			1.651[b]	–5.90
Trifluroacetate		–5.274[c]		0.23
Tosylate		1.064[d]	–4.1768[e]	2.70
Mesylate	–2.888[f]	0.701[g]	–3.827[h]	–1.92
			–3.817[i]	
Chloride	–5.917[j]	–3.529[k]		–2.18
Bromide	–4.770[j]	–2.114[k]		–4.70
Iodide	–5.387[j]	–1.996[k]		–5.23
Nitrate	–6.672[l]	–1.813[m]	–7.895[m]	–1.30
Nosylate			–2.022[n]	–4.00
Brosylate			–2.796[n]	–3.10
Perchlorate			0.115[o]	–5.00
4-Nitrobenzoate		–8.21[p]		3.43
Picrate		–1.609[g]		0.29
Dimethyl sulphide		–8.737[q]		

[a]See Table 12.
[b]References 116 and 117.
[c]References 118 and 119.
[d]References 120–122.
[e]References 73, 123, and 124.
[f]References 34 and 75.
[g]Reference 116.
[h]See footnote 4 in the text.
[i]References 124–126.
[j]Reference 75.[2]
[k]References 127 and 128.
[l]See footnotes 2 and 4 in the text.
[m]Reference 88.
[n]Reference 129.
[o]References 116 and 130.
[p]Reference 131.
[q]Reference 153.

Table 14. Data related to the solvolyis of tertiary butyl derivatives.

Leaving group	log$k$(t-BuX)	log$k$(1-AdX)[a]	pK_a
Fluoride	–6.269[b]	–8.13 ± 0.20[c]	3.452[d]
Chloride	–1.506[e]	–3.529	–2.176[f]
Bromide	–0.119[g,h]	–2.114	–4.699[f]
Iodide	0.186[g,h]	–1.996	–5.230[f]
Nitrate	–0.388[i]	–1.813	–1.300[j]
TFA	–2.884[k]	–4.231	–0.232[l]
Acetate	–7.345[m]	–9.21 ± 0.24[c]	4.755[n]
$S(Me)_2$	–7.052[o]	–8.767	—
Tosylate	3.13 ± 0.23[c]	1.221	–2.70[j]
Mesylate	3.15 ± 0.24[c]	1.235	–1.92[j]
4-Nitrobenzoate	–6.55 ± 0.22[c]	–8.21	3.34[l]
Picrate	0.231 ± 0.14[c]	–1.609	0.29[l]

[a]See Table 13 for references.
[b]Reference 34.
[c]Calculated from the appropriate equation: either [a] log$k$(t-BuX) = (1.027 ± 0.043) log$k$(1-AdX) + 1.884 ± 0.19 (6,0.9925) or [b] log$k$(1-AdX) = (0.959 ± 0.040) log$k$(t-BuX) – 1.862 ± 0.13 (6,0.9925).
[d]References 112 and 113.
[e]References 21, 89, and 90.
[f]Reference 114.
[g]References 9 and 133.
[h]Reference 9.
[i]Reference 134.
[j]Reference 23.
[k]References 102–105.
[l]Reference 63.
[m]Reference 106.
[n]References 63 and 135.
[o]See footnote 2 in the text.

Table 15. Rate data for ethyl, cyclohexyl, and 2-propyl substrates (T = 298.15 K).

Leaving group	Ethyl	2-Propyl	Cyclohexyl
Perchlorate	–2.461[a]		—
Chlorosulphate	–1.647[b]	—	—
Ethoxysulphate	–4.271[b]	—	—
Tosylate	–5.165[b]	–3.387[b]	–3.456[b]
Mesylate	–5.405[b]	–3.707[b]	–3.380[c]
Benzenesulphonate	–4.993[b]	–3.181[b]	—
Chloride	–7.499[c]	–6.675[b]	—
Bromide	–6.412[b]	–5.418[b]	–5.586[b]
Iodide	–6.767[b]	–5.554[b]	—
Nitrate	—	–7.326[b]	–7.175[b]

[a]Reference 136.
[b]See footnote 2 in the text.
[c]See Appendix C and footnote 5 in the text.

solvent-separated ion pairs such as 2-Ad$^+$|H_2O|X$^-$ and 2-Ad$^+$|EtOH|X$^-$ are important intermediates in the displacements of 2-adamantyl substrates.

Clearly, the LFER represented by eq. [97] covering nearly 10 orders of magnitude reasonably suggests that the heterolysis of the methyl substrates consists of chemical events analogous to those that characterize the heterolytic fission of 2-adamantyl substrates, i.e., the reaction of the methyl compounds probably involves *both backside and frontside* assistance in sequence. The notion that the several processes that must contribute to this description occur in a concerted manner involving termolecular and possibly higher order processes is uncongenial particularly for primary substrates.

The earlier sections of this paper concerned with the Kurz equation and the KSIE suggest that the hydrolyses at primary carbon centres are characterized by *weak* but definite nucleophilic assistance and solvent separation prior to heterolysis. Other centres, either secondary or tertiary, involve even less or no nucleophilic assistance with a further driving force represented by solvent separation of a partly heterolysed bond. It is conceivable that increased stability of the carbocation arising from internal electron delocalization, e.g., 4-methoxybenzyl chloride and related secondary and tertiary structures, might produce situations where the need for solvent insertion becomes less, and that cases where the heterolysis occurs without the intervention of front-side solvent separation may be a definite mechanistic category for the displacement process. This proposal offers a possible explanation of the curved Hammett plot using the σ or σ^+ substituent scales with the substituted benzyl chloride hydrolyses — the negative slope *decreases* as the substituent

[4]R.E. Robertson and E.C.F. Ko. Unpublished measurements.
[5]R.E. Robertson and J.M.W. Scott. Unpublished results.

© 2005 NRC Canada

Table 16. Grunwald–Winstein correlations (T = 298.14 K).

Substrate	N	m	log$k$(H_2O)	C.C.	logk_o
1-Ad mesylate	4	0.852±0.045	0.701±0.11	0.994	–2.275±0.028
2-Ad triflate	6	0.947±0.035	1.651±0.11	0.994	–1.658±0.108
2-Ad-4-TMABS[a]	7	0.948±0.011	–2.727±0.03	0.999	–6.036±0.016
1-Ad tosylate	8	0.992±0.017	1.064±0.07	0.998	–2.401±0.017
1-Ad$OOCCF_3$	5	0.739±0.059	–5.189±0.17	0.980	–7.771±0.098
2-AdClO_4	5	0.833±0.027	0.115±0.15	0.996	–2.742±0.059
1-Ad picrate	5	0.616±0.034	–1.609±0.06	0.991	–3.762±0.072
Cyclohexyl tosylate	5	0.807±0.054	–3.456±0.11	0.985	–6.276±0.104
tert-Butyl nitrate	2	0.897	–0.364		–3.497
2-Ad mesylate (*i*)[b]	7	1.074±0.021	–3.989±0.042	0.998	–7.741±0.045
2-Ad mesylate (*ii*)[b]	8	1.098±0.020	–3.933±0.037	0.998	–7.770±0.037
4-MeO-benzyl chloride (*i*)[c]	5	0.848±0.016	0.426±0.047	0.998	–2.537±0.029
4-MeO-benzyl chloride (*ii*)[c]	5	0.952±0.013	0.406±0.045	0.999	–2.921±0.025

Note: For details of the Grunwald–Winstein LFER, see refs. 118, 137–141. The "*Y*" values for mixtures of either MeOH–H_2O or EtOH–H_2O were interpolated using spline functions, which are particularly suited to this purpose (see ref. 139 for a suitable algorithm). The errors for m, logk_o, and log$k$(H_2O) (k(H_2O) is the rate extrapolated to pure water) were calculated by formulae given in ref. 51. The correlation coefficients (C.C.) were calculated from a formula given in ref. 140. The correlations as a whole are best described as adequate. The source of the N rate constants for each substrate is indicated in Tables 12–15. Rates were corrected to 298.15 K by either the Arrhenius or Eyring equations.

[a]2-Ad-4-TMABS is 2-adamantyl 4-trimethyammoniumbenzene sulphonate.

[b]The rate of hydrolysis has been measured by Robertson[2] (log k (298.15 K) = –3.9329; k = 1.489 × 10^{-4} s^{-1}. Correlations for 2-Ad mesylates (*i*) and (*ii*) give rate constants of 1.167 × 10^{-4} and 1.027 × 10^{-4} s^{-1}, respectively. The Grunwald Winstein LFER correlation for 2-adamantyl mesylate (*ii*) excludes the water point, but, in contrast the LFER for 2-adamantyl mesylate (*i*) includes the water point. Correlations (*i*) and (*ii*) give some idea of the errors incorporated into the data when the Grunwald–Winstein LFER is used to estimate the pure water rates. For 2-adamantyl mesylates this amounts to 2% to 3% in log k. With other more reactive substrates, the errors may be larger. More precise measurements in solvent mixtures richer in water in combination with measurements at temperatures lower than 298.15 K for more reliable extrapolations to pure water are desirable.

[c]Data are from ref. 142.

Fig. 9. Correlation of product selectivity with acid strength measured via σ^+.

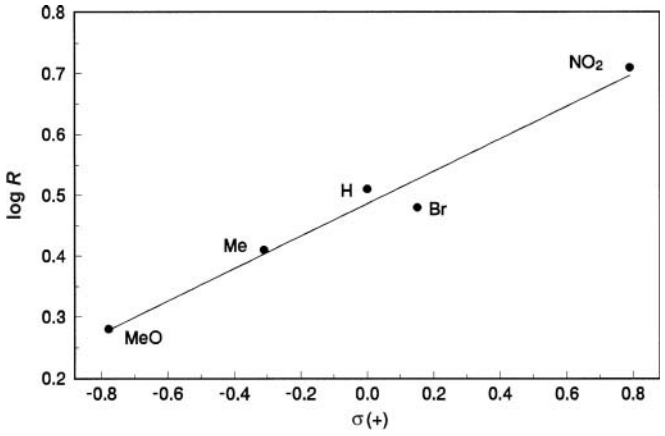


Table 17. Selectivity quantities related to the products obtained from the solvolysis of a series of 2-adamantyl 4-substituted benzenesulphonates.

X*	R[a]	log R	–log k[b]
MeO	1.94	0.28	5.226
Me	2.56	0.41	5.098
H	3.25	0.51	4.934
Br	3.05	0.48	4.711
NO_2	5.20	0.71	4.205

Note: X* is the 4-substituent.

[a]R = ([2-AdOH][EtOH])/([2-AdOEt][H_2O]) determined for the solvolysis of substrates in ethanol–water mixtures.

[b]k is the the first-order rate constant in water (T = 298.15 K) for the related methyl 4-substituted benzenesulphonates.[2] Note that the methyl esters become more reactive as the acid related to the leaving group becomes stronger and 2-adamanty esters react more selectively with the solvent.

constant becomes more *positive*. These matters will subsequently be elaborated.

The simple interpretation of the Kurz equation and eq. [97] adopted here has been independently considered and scrutinized by Albery and Kreevoy (13, 38) in an extension of the Marcus theory (36) of electron and proton transfers to methyl transfers.

[100] $Y + CH_3X \rightleftharpoons CH_3Y + X$

The analysis offered by these workers argues that the Kurz equation, as presented in section 3, cannot be used to accurately estimate the position of the transition state along the reaction coordinate for either the water or hydroxide reaction. The basis of this edictal conclusion is obscure but appears to have its origins in the notion that there are two conceivable values for the intrinsic barrier for the symmetrical exchange.

[101] $OH^- + CH_3OH \rightleftharpoons CH_3OH + OH^-$

One barrier supposedly involves the solvated lyate ion, the other, the desolvated version of the same molecular species. The special status reserved for the lyate ion is obscure, unless one of the paths embraces some sort of Grotthuss (146) chain phenomena that is absent in an alternative desolvation process.

© 2005 NRC Canada

Other simple anions involved in the Albery and Kreevoy (13) analysis might display similar phenomena, particularly fluoride, because HF is a weak acid and the fluoride leaving group is known to be susceptible to acid catalysis. In any case, the veracity of the conclusions derived from the Marcus theory applied to methyl transfers is contingent on the notion that a *single* barrier separates reactants and products. *The single barrier description is regarded here to be an hypothesis rather than a fact.* Indeed, the repudiation of the single barrier description for all S_N displacements in water is central to this paper, the present contentions originating from considerations detailed in sections 1–8.

Because data suitable for testing the Swain–Lohmann LFER are relatively scarce and the correlations represented by eqs. [92] and [93] are indifferent, an examination of the possibilities represented by Thornton's suggested correlation between nucleofugality and acid strength is more profitable. This proposal also draws further attention to the important contributions by Guthrie (23), Lewis et al. (37), and by Albery and Kreevoy (13). The interesting Brönsted LFER reported by Guthrie (23) will be considered next. Guthrie's failure to connect his work with the Swain–Lohmann LFER is both notable and puzzling because his work partly elucidates the fundamental factors that underpin the Swain–Lohmann LFER.

10. The Guthrie Brönsted LFER

In an important investigation, Guthrie (23) examined the thermodynamics and kinetics that characterize the hydrolysis of several methyl esters derived from a series of oxyacids. The study is significant on two counts. First, Guthrie critically scrutinized the existing pK_a data for a series of strong oxyacids (82). Second, Guthrie showed that the pseudo-first-order rate constants (k_w) that characterize the hydrolyses of the *methyl esters related to the oxyacids* measured at 298.15 K show an excellent Brönsted LFER (147, 148) (see Table 12 and Fig. 10).

$$[102]\quad \log k_w(CH_3X) = -7.922 \pm 0.092 - (1.008 \pm 0.025)pK_a(HX)\ (14,0.992)$$

The 14 leaving groups are those in Table 12 excluding the NO_3^- and halogen anions.

It is tempting to identify the close proximity of the Guthrie LFER exponent to unity with a productlike transition state for the oxygenated leaving groups. However, a careful analysis of the individual Gibbs energy terms that contribute to the ionization of the acid ($\Delta G^{\ominus}(i)$) together with the energy of activation ($\Delta G^{\ddagger}(RX)$) suggests the magnitude of the slope of the Guthrie LFER cannot be given a straightforward interpretation.

Thus, for the ionization of the acid

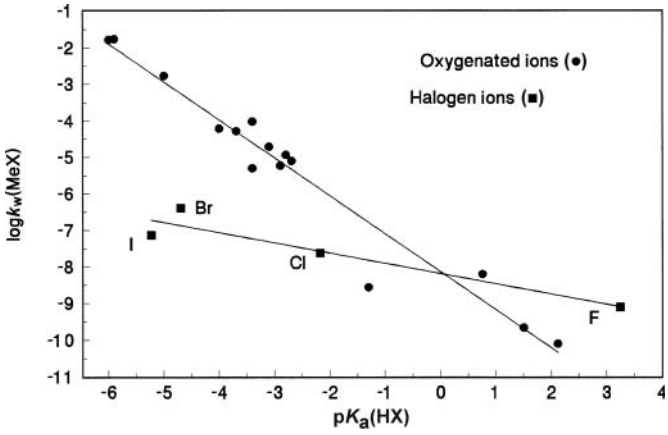
$$[103]\quad HX + H_2O \rightleftarrows H_3O^+ + X^-$$

the change in Gibbs energy ($\Delta G^{\ominus}(i)$) are given by:

$$[104]\quad \Delta G^{\ominus}(i) = G(H_3O^+) + G(X^-) - G(HX) - G(H_2O)$$

If δ_x is an operator denoting changes in the leaving group then

Fig. 10. Guthrie LFER for hydrolysis. The leaving groups are: oxygenated ions (●), halide ions (■).



$$[105]\quad \delta_x\Delta G^{\ominus}(i) = \delta_x G(X^-) - \delta_x G(HX)$$

because the terms $\delta_x G(H_3O^+) = \delta_x G(H_2O) = 0$. For the reaction

$$[106]\quad RX + 2H_2O \rightleftharpoons ROH + H_3O^+ + X^-$$

the variation of the free energy of activation with the leaving group X is given by

$$[107]\quad \delta_x\Delta G^{\ddagger}(RX) = \delta_x G^{\ddagger}(RX) - \delta_x G_i(RX)$$

granted that $\delta_x G(H_2O) = 0$. Hence, the Brönsted slope is a function of four quantities: $\delta_x G(X^-)$, $\delta_x G(HX)$, $\delta_x G^{\ddagger}(RX)$, and $\delta_x G_i(RX)$. This analysis demonstrates that the solvolytic Guthrie exponent is a complex quantity and its intricacy is increased when other acids that do not give oxygenated anions, e.g., the halogen acids, are included in the correlation.

This analysis may also explain why Guthrie was reluctant to draw any significant mechanistic conclusions from the magnitude of the exponent. Nevertheless, the latter quantity is suggestive that transition states that characterize the hydrolyses are productlike with respect to the leaving group for esters yielding oxygenated anions. However, a productlike leaving group conflicts with Schowen's (68) estimate based on the KSIE and with our extended discussion of the Kurz equation (see sections 3 and 4). Such paradoxes are possibly explained by the postulate, namely, that discordant reaction coordinate parameters signify that the reaction takes place by a mechanism involving more than one step.

Guthrie's failure to offer mechanistic comment on eq. [102] may also be a consequence of the harsh criticism levelled at such correlations by Abraham and McClellan (33, 44, 45), although a similar correlation of the Grunwald–Winstein Y quantities (118, 137–141) with the Gibbs energy of ionic solvation of potassium chloride in methanol–water mixtures presented by Hudson and Saville (149) curiously escapes their reproach.

Clearly, Guthrie's LFER (23) validates Thorton's hypothesis (4) for a *restricted* series of acids for which the conjugate bases are oxygenated anions, namely, that the nucleofugality of any leaving group X tracks the strength of the acid HX. Although both kinetic data for the hydrolysis of the methyl halides are available, (see Tables 3 and 12) and carefully cal-

© 2005 NRC Canada

Table 18. Kinetic data related to halide ion leaving groups.

Name/process	pK_a[a]	F	Cl	Br	I
HX(pK_a)[b]		3.15	–2.18	–4.70	–5.23
t-BuX(log *k*)[c]	(1.28±0.06) log *k* + 4.71±0.2	–6.269	–1.527	–0.119	0.186
1-AdX(log *k*)[d]	(1.35±0.06) log *k* + 7.43±0.6	–8.135	–3.523	–2.114	–1.816
A-log *k*[e]	(3.04±0.12) log *k* + 3.89±0.15	–9.206	–6.558	–5.360	–4.075
B-log *k*[f]	(4.15±0.61) log *k* + 25.53±0.34	–2.292	–0.602	0.146	0.568
C-log *k*[g]	(2.69±0.16) log *k* + 1.91±0.19	–1.886	0.220	0.792	1.36
D-log *k*[h]	(1.31±0.08) log *k* + 11.00±0.59	–7.12	–5.777	–5.187	–5.00

Note: HF (pK_a = 3.18 ± 0.11 (3.15)), HCl (pK_a = –2.41 ± 0.3 (–2.18)), HBr (pK_a = –4.36 ± 0.30 (–4.70)), HI (pK_a = –5.35 ± 0.3 (–5.23)). Values in parentheses are those calculated by Myers (114).

[a]Mean values of pK_a(HX) from the six inverted regressions (pK_a is the *y* variable and log *k* is the *x* variable) (X = F, Cl, Br, and I).

[b]See Myers (114).

[c]For *t*-BuX rate data see Table 14.

[d]For 1Ad-X rate data see Table 14.

[e]Hydrolysis of $Cr(H_2O)_5X^{2+}$ (A) (156, 157).

[f]Lyate ion halogen displacement (B), $Co(NH_3)_5X^{2+}$ (9).

[g]Lyate ion halogen displacement (C), $Co(NH_3)_5X^{2+}$(152).

[h]Hydrolysis of $Co(NH_3)_5X^{2+}$ (D) (154, 155).

culated pK_a(HX) values exist for the halogen acids HX, (X = F, Cl, Br and I) (112–114), Guthrie (23) excluded these acids from his correlation. This important omission is remedied in section 11.

11. The strength of the hydrohalic acids and the Guthrie LFER

The pK_a values for the halogen acids have been estimated via a thermodynamic cycle by Myers (114). Because the pK_a of hydrofluoric acid is known, Myers' calculation for the other three acids is partly calibrated. The cycle Myers used gave a value for hydrofluoric acid in acceptable accord with the experimental and readers are referred to his paper for details. The inclusion of the $k_w(CH_3X)$ rate constants and the related pK_a(HX) values for X = F, Cl, Br, and I, adds four points to the Guthrie LFER, but the new data are *poorly* represented by eq. [102]. The deviations from eq. [102] are large and *fall on a line of lower slope* (see Fig. 10). The order of reactivity of methyl bromide and iodide is incorrectly predicted on the basis of the pK_a values of HBr and HI, but, because the pK_a values of HBr and HI are close ($\Delta pK_a \approx 1$ unit), their predictive utility might be lost in the intricacy of the total displacement process. At the present juncture there is a more compelling question, namely, is the departure of the methyl halide leaving groups from the Guthrie LFER a consequence of either erroneous kinetic or equilibrium data?

To answer this question other kinetic data describing halogen displacements in water at 298.15 K for other reacting centres were sought and evaluated. Rate constants for the following reactions

[108] $t\text{-BuX} + 2H_2O \rightarrow t\text{-BuOH} + H_3O^+ + X^-$

[109] $\log k = (-0.773 \pm 0.038)pK_a - 3.66 \pm 0.15$ (4,0.995)

[110] $1\text{Ad-X} + 2H_2O \rightarrow 1\text{-AdOH} + H_3O^+ + X^-$

[111] $\log k = (-0.757 \pm 0.035)pK_a - 5.59 \pm 0.14$ (4,0.995)

[112] $[Co(NH_3)_5X]^{2+} + 2H_2O \rightarrow [Co(NH_3)_5OH]^{2+} + H_3O^+ + X^-$

[113] $\log k = (-0.327 \pm 0.013)pK_a - 1.275 \pm 0.052$ (4,0.9997)

[114] $[Co(NH_3)_5X]^{2+} + OH^- \rightarrow [Co(NH_3)_5OH]^{2+} + X^-$

[115] $\log k = (-0.327 \pm 0.013)pK_a - 1.275 \pm 0.052$ (4,0.997)

[116] $\log k = (-0.366 \pm 0.021)pK_a - 0.696 \pm 0.086$ (4,0.993)

[117] $[Cr(H_2O)_5X]^{2+} + 2H_2O \rightarrow [Cr(H_2O)_6]^{2+} + H_3O^+ + X^-$

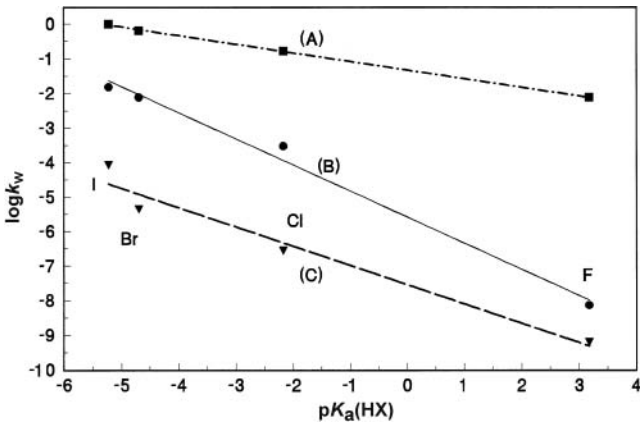
[118] $\log k = (-0.558 \pm 0.054)pK_a - 7.55 \pm 0.21$ (4,0.982)

with X = F, Cl, Br, and I are presented with their sources in Table 18. For the reaction described by eq. [114], two sets of data are reported in eqs. [115] and [116]. They are discordant, but no effort has been made to pursue the sources of this anomaly.

The hydrolyses and base attack rates have been correlated with the Myers' pK_a values in two ways: the pK_a quantities function as both the *dependent* and *independent* variable in the regressions. The least-squares lines quoted in the preceding are with the pK_a in the latter category and some representative samples of these correlations are presented in Fig. 11. From the six correlations in which the pK_a values are in the former category, six values of each of the four pK_a(HX) values can be calculated from the regressions. The mean values for each acid on this basis are reported in Table 18. These quantities are in satisfactory agreement with Myers' values and imply an average error equivalent to ≈300 cal in the four cycles. The six Guthrie correlations validate Myers' estimates of the pK_a values for the hydrogen halides. Further kinetic data for other leaving groups for which the pK_a values of the related acids can be measured are available for some of the reactions described by eqs. [108] and [110].

© 2005 NRC Canada

Fig. 11. Guthrie LFER for displacements of: (A) *tert*-butyl substrates; (B) chromium halides; and (C) cobalt halides. In graph (A) the log *k* axis is increased by five units for clarity of presentation. For details, see reactions [112], [114], and [117].

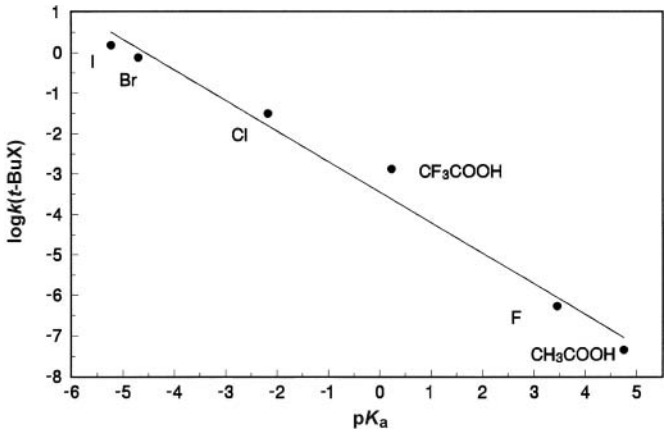


Thus, for the *tert*-butyl substrates the leaving groups embrace all the halide, acetate, and trifluoroacetate anions giving a Guthrie LFER,

[119] $\log k(t\text{-BuX}) = (-0.755 \pm 0.035)\mathrm{p}K_a - 3.44 \pm 0.14$ (6,0.991)

covering nearly 10 orders of magnitude on the abscissa. This correlation includes six acids (see Fig. 12) raising the number of acids for which the pK_a values that can be determined by conventional means to *three*. Thus, eq. [119] provides further confirmation of Myers' calculation and other insights into the details of the displacement reactions. For instance, the slope of the line represented by eq. [119] is enhanced relative to that for the methyl halides, suggesting that the tertiary centres produce a more ionic transition state in accord with the conventional wisdom. Paradoxically, the slope is still *less* than that for the hydrolysis of methyl esters giving rise to oxygenated anions. This observation suggests without compelling proof that the slopes of the Guthrie correlations are partly related to return phenomena, a hypothesis difficult to establish with certainty.

Fig. 12. Guthrie LFER for displacements of *tert*-butyl substrates.



The rate constants for *tert*-butyl fluoride and acetate involve large extrapolations to calculate the rate constants at 298.15 K. On the other hand, the extrapolations for the chloride, bromide, iodide, and trifluoroacetate are much smaller. The rate constants related to these four substrates give an excellent Guthrie LFER.

[120] $\log k = (-0.5606 \pm 0.0025)\mathrm{p}K_a - 2.745 \pm 0.009$ (4,0.99996)

This particular LFER offers convincing confirmation of Myers' estimates of the pK_a values for the halogen acids.

12. Primary, secondary, and tertiary substrates

General comment

The five Guthrie LFERs that accommodate the organic and inorganic halogen displacements described by eqs. [108] to [119] in section 11 confirm Myers' pK_a calculations for the hydrohalic acids. Consequently, the failure of the methyl halides to fit eq. [89] (see Figs. 10–12 and Table 18) does *not* appear to reside in erroneous estimates of the pK_a values for the hydrohalic acids. Instead, the deviations from the original Guthrie LFER (eq. [89]) offer a significant mechanistic clue that can be discussed in terms of two *modified* versions of the Winstein mechanism.

[121] $$\mathrm{W + RX \underset{k_2}{\overset{k_1}{\rightleftharpoons}} \underset{\text{(int)}}{W\text{-}R^+X^-} \underset{k_4}{\overset{k_3}{\rightleftharpoons}} \underset{\text{(ss)}}{W\text{-}R^+|W|X^-} \underset{k_6}{\overset{k_5}{\rightleftharpoons}} W\text{-}R^+ + X^- + H_2O \xrightarrow{\text{fast}} ROH + H_3O^+ + X^-}$$

$$k_8\uparrow\downarrow k_7$$

$$WR^+ + X^- + H_2O \xrightarrow{\text{fast}} ROH + H_3O^+ + X^-$$

and

[122] $$\mathrm{RX \underset{k_2}{\overset{k_1}{\rightleftharpoons}} \underset{\text{(int)}}{R^+X^-} \underset{k_4}{\overset{k_3}{\rightleftharpoons}} \underset{\text{(ss)}}{R^+|W|X^-} \underset{k_6}{\overset{k_5}{\rightleftharpoons}} R^+W + X^- + H_2O \xrightarrow{\text{fast}} ROH + H_3O^+ + X^-}$$

$$k_8\uparrow\downarrow k_7$$

$$R^+ + X^- + W \xrightarrow{\text{fast}} R^+W + H_2O + X^- \xrightarrow{\text{fast}} ROH + H_3O^+ + X^-$$

© 2005 NRC Canada

Equations [121] and [122] describe the mechanistic possibilities between the noncaged and caged substrates, respectively.

The rate constants k_7 and k_8 relate to the heterolyses of either nucleophilically assisted intimate ion pairs (eq. [121]) or intimate ion pairs (eq. [122]). The destruction of the two types of intimate and solvent-separated ion pairs might occur via the intermediate production of an oxonium ion followed by proton transfer to the solvent. Alternatively, the formation of the hydronium ion and the alcohol might proceed via a single concerted step, which has not been detailed in eqs. [121] and [122]. The two schemes described by these equations are sufficiently flexible to accommodate the departures from the Guthrie LFER evinced by the methyl halides. It should be clearly understood that the evidence for such complexity is indirect. There is no hope at present of establishing numerical values for the component rate constants in the schemes represented by eqs. [121] and [122].

There may be noncaged substrates for which backside attack is stereochemically possible but energetically superfluous, i.e., such substrates are candidates for the ionic displacement without backside nucleophilic assistance (eq. [122]). This mechanism is obviously similar to the classical S_N1 mechanism of heterolysis, taking place via an intimate ion pair noting that the leaving group may depart either with or without frontside solvent assistance.

If R(1) and R(2) refer to organic groups that heterolyse according to eqs. [121] and [122], respectively, then the basic hypothesis postulated here is that the structures W-$R(1)^+|W|X^-$ and $R(2)^+|W|X^-$ containing identical leaving groups show analogous properties and that the LFER represented by eq. [97] and illustrated in Fig. 7 substantiates such an analogy.

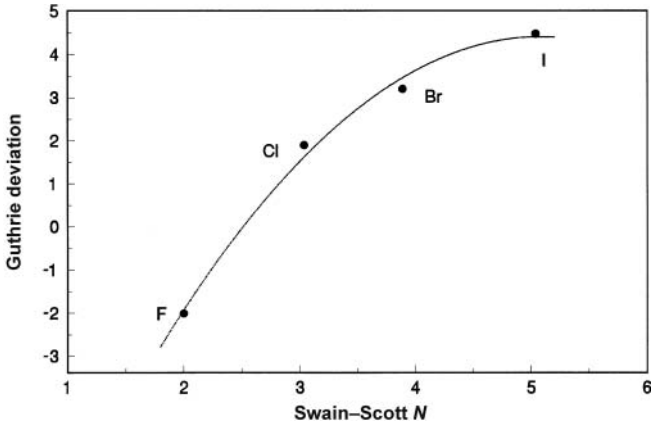
In water, leaving groups fall into four distinct categories: (*i*) poor nucleophiles and good leaving groups, e.g., sulphonates, perchlorates; (*ii*) poor nucleophiles and poor leaving groups, e.g., fluorides, acetates; (*iii*) good nucleophiles and good leaving groups, e.g., bromides, iodides; (*iv*) good nucleophiles and poor leaving groups, e.g., cyanides, thiosulphates.

Substrates for which rearside nucleophilic assistance is stereochemically possible and energetically significant are accommodated by the scheme represented by eq. [121]. Leaving groups (X) that are poor nucleophiles react by the k_1, k_2, and k_7 steps, i.e., return from the intimate ion pair is significant for all leaving groups. In cases where the nucleofuge combines good leaving group propensities with marked nucleophilic properties such as Br^- and I^-, all eight rate constants (k_1–k_8) may contribute to the observed rate, although there is little compelling evidence that external return at any stage is significant in water. In principle, external return requires second-order reactions that are obviously inhibited by low substrate concentrations.

Primary substrates

The large deviations from the original Guthrie LFER exhibited by the methyl halides noted in section 11 are attributed reasonably to the fact that the halogen anions, particularly iodide and bromide, are good nucleophiles and leaving groups. The deviations $\Delta\log k_r(CH_3X)$ from eq. [102] for X = F, Cl, Br, and I can be estimated from the expression

Fig. 13. Deviations of the methyl halides from the Guthrie LFER vs. Swain–Scott *N* values.



$$[123]\quad \Delta\log k_r(CH_3X) = \log k_o(CH_3X) + 7.92 + 1.008pK_a(HX)$$

where $\log k_o(CH_3X)$ is the observed rate constant for CH_3X and the other terms on the RHS of eq. [123] are derived from eq. [102]. The $\Delta\log k_r(CH_3X)$ quantities estimated from eq. [123] for the halogen leaving groups give a smooth correlation with the structurally related *N* values established from the Swain–Scott equation (111) (see Fig. 13).

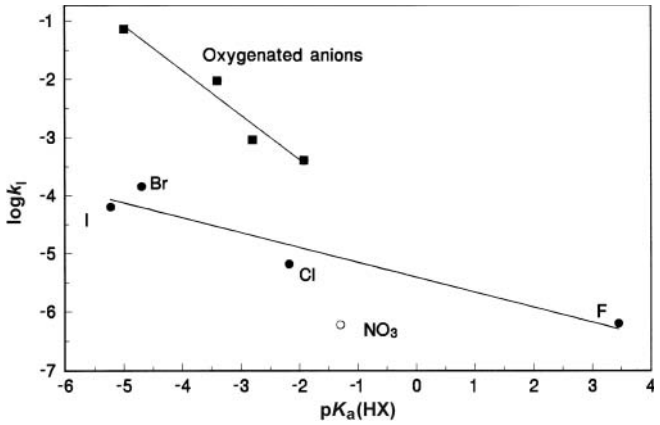
Finally, if the model represented by eq. [121] is correct, the observed rate constant for any system reacting according to this equation will be a complex function of the several component rate constants that describe this mechanism. Granted that an extended Albery–Robinson model for $\Delta C_p^{\ddagger}$ furnishes the major source of this quantity, then the sequence of rate constants k_n (n = 1–7) for the primary and other substrates will give rise to an apparent $\Delta C_p^{\ddagger}$ for these substances (15, 21, 22, 77, 94).

The data in Table 9 are sufficient to extend the Guthrie LFER to eq. [7]. Thus, the replacement of nucleophilic water by the hydroxide ion in the Guthrie LFER (see Fig. 14) also demonstrates the bifurcation evident for the water reactions, although the departure from the line defined by the oxygenated anions is now roughly half the extent observed with water. This is to be anticipated because, granted the hydroxide ion is a stronger nucleophile than water, then the deviations from the line for the oxygenated ions should be *less* because the *differences between the nucleophilic power of the attacking nucleophile and leaving group are presumably more balanced when hydroxide is the nucleophile*. This explanation is congruent with that offered to explain why the $pK_a^{\ddagger}$ calculated from the Kurz equation reached a minimum for methyl iodide, a substrate for which the leaving group combines substantial nucleophilic and leaving-group abilities.

These considerations can be examined in another way. The rate constants for both the attack of water and lyate ion are available for five methyl esters that yield oxygenated anions (see Table 6). The rate constants characteristic of these substrates when reacting with water and lyate ion display a respectable LFER.

© 2005 NRC Canada

Fig. 14. Guthrie LFER for lyate ion displacements.



[124] $\log k_w = (1.123 \pm 0.029) \log k_l - 1.576 \pm 0.099$ (5,0.998)

The four methyl halides provide an analogous but separate relationship.

[125] $\log k_w = (1.044 \pm 0.11) \log k_l - 2.485 \pm 0.52$ (4,0.978)

The overlapping slopes of [124] and [125] suggest the selectivities of water and hydroxide are close. However, a more telling observation is provided when eqs. [124] and [125] are considered together (see Fig. 15). All the methyl halides are *less* reactive with water than is predicted on the basis of their reactivity with lyate ion, i.e., the related methyl halide LFER plots *below* the LFER defined by the oxygenated anionic leaving groups. Presumably, this reflects the poor nucleophilicity of the oxygenated anions in comparison with the halide anions and suggests indirectly return phenomena are more prevalent when water reacts with the methyl halides, contrasting with esters related to the oxygenated anions. These observations are consistent with the larger (more positive) $\Delta C_p^{\ddagger}$ values observed for the sulphonates compared with halides as leaving groups. The separation of the lines in Fig. 15 is also reminiscent of the more marked separation shown in the Guthrie LFER in Fig. 10.

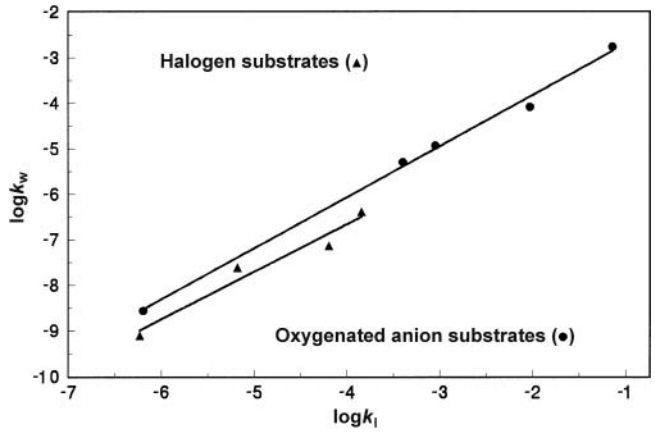
Hartshorn (10), following Winstein and co-workers, has pointed out that the rates of solvolyses of series of primary mesylates related to the methyl, ethyl, propyl, 2-methylpropyl, and neopentyl alcohols provide important mechanistic information. In both ethanol and water the reactivity (log *k*) of this series of substrates *decreases* with increasing homology and can be correlated with the Taft steric substituent constant E_s (108).

[126] $\log(k(\text{EtOH})) = 3.54 \pm 0.09 - (1.97 \pm 0.10)E_s$ (4,0.995)

[127] $\log(k(H_2O)) = -2.56 \pm 0.03 - (0.483 \pm 0.025)E_s$ (5,0.990)

[128] $\log(k(\text{TFA})) = (1.99 \pm 0.36)E_s + 0.836 \pm 0.32$ (5,0.907)

Fig. 15. A LFER for methyl substrates: upper and lower lines, respectively, relate to oxygenated and halide nucleofuges.



The Taft constants (E_s) were taken from a compilation by Shorter (108) and the data related to eqs. [126]–[128] are presented in Table 19. The coefficient of E_s increases by a factor of 4 in solvent ethanol compared to water. However, when the displacements are conducted in trifluoroacetic acid the coefficient of E_s *changes sign* and the reactivity *increases* with increasing homology, presumably, as a consequence of anchimeric assistance particularly in the case of the last two alkyl mesylates in the sequence. The *smaller influence* of the organic groups in water compared to ethanol suggests that the phenomena that underpin the behaviour observed in trifluoroacetic may contribute to the reactivity sequence observed in water. Thus, it is possible that the 2-methylpropyl and neopentyl mesylates react by two routes in water by a mixed mechanism, namely, by achimerically assisted and an unassisted displacement. This proposal offers a plausible explanation of the negligible $\Delta C_p^{\ddagger}$ for the neopentyl mesylate reported here. The details related to this observation are reported in Appendix B. Scott and co-workers (79) have discussed the details of an $S_N/B_{Ac}2$ mixed mechanism (see section 8). Unfortunately, the products from the hydrolysis of the 2-methylpropyl and neopentyl mesylates were not examined when the rate constants were established in water, and consequently, further confirmation of the mixed mechanism suggestion for the negligible $\Delta C_p^{\ddagger}$ for the hydrolysis of neopentyl mesylate awaits further verification.

Secondary substrates

The 2-adamantyl systems are important mechanistically for reasons reviewed by Bentley (144, 156). The rate ratios for the 2-adamantyl, cyclopentyl, cyclohexyl, and 2-propyl toslylates in solvents trifluoroacetic acid, ethanol, formic acid, and acetic acid are reported in Table 20A. The rate constants in water for various nucleofuges are also reported in Table 20B. In Table 20C the corresponding ratios for the same organic groups are reported for the nitrates, mesylates, and bromides in water. Granted that the nucleophilic properties of TFA are meagre, then the sequence of rate for these tosylates in this solvent are considered to reflect a limiting mechanism. The behaviour of the nucleophilic components of the ratios that are reported in parentheses for water and the other solvents and calculated according to Bentley's recipe (144) show that the values for water are similar to those

© 2005 NRC Canada

Table 19. Rate ratios for primary mesylates.

Methyl	Ethyl	Propyl	2-Methylpropyl	Neopentyl	Solvent
6.35	6.08	4.1	1.81	1.0	H_2O (363.15 K)[a]
4000	1750	—	80	1	EtOH[b]
1	13	93	3060	5790	TFA[b]
0.00	0.07	0.36	0.93	1.74	[c]

[a]See footnote 2 in the text.
[b]See Hartshorn (10).
[c]Taft steric constant E_s (see Shorter (108)).

Table 20. (A) Rate ratios related to secondary tosylates reacting in various solvents; (B) Rate constants for secondary substrates reacting in water at T = 298.15 K; (C) Bentley ratios for secondary substrates reacting in water.

(A) Rate ratios.

R group	R_a[a]	R_a(EtOH)	R_b[b]	R_b(CH_3COOH)	R_c[c]	R_c(HCOOH)	R_d[d]
2-Adamantyl	1.0		1.0		1.0		1.0
Cyclopentyl	6250.0	(2083.0)	280.0	(93.3)	37.0	(12.3)	3.0
Cyclohexyl	108.0	(360.0)	8.3	(27.7)	5.2	(17.6)	0.3
2-Propyl	910.0	(37900.0)	13.0	(541.0)	0.9	(37.5)	0.024

(B) Rate constants.

R group	k(RNO_3)	k(RBr)	k(R-Mesylate)	k(R-Tosylate)	I_p(R·)[e]
2-Adamantyl	1.27×10^{-8}	5.13×10^{-6}[f]	1.49×10^{-4}	6.65×10^{-5}	?
Cyclopentyl	5.08×10^{-7}	5.56×10^{-5}	5.46×10^{-3}	4.29×10^{-3}	7.79
Cyclohexyl	6.69×10^{-8}	2.59×10^{-6}	4.10×10^{-4}	3.50×10^{-4}	7.66
2-Propyl	4.72×10^{-8}	2.80×10^{-6}	1.96×10^{-4}	4.10×10^{-4}	7.98

(C) Bentley ratios.

R group	R_e(RNO_3)[g]	R_{ew}	R_f(RBr)[h]	R_{fw}	R_g(R-Mesylate)[i]	R_{gw}	R_h(R-Tosylate)[j]	R_{hw}
2-Adamantyl	1.00		1.0		1.0		1.0	
Cyclopentyl	40.0	(13.3)	10.8	(3.6)	36.7	(12.2)	64.4	(21.5)
Cyclohexyl	5.27	(17.6)	0.51	(1.7)	2.75	(9.2)	5.26	(17.5)
2-Propyl	3.72	(155)	0.55	(22.9)	1.31	(54.6)	6.16	(257)

Note: The importance of nucleophilicity measured by the quantity R_x(solvent)/R_d in part A and by R_{xw}/R_d recorded in part C, where x = a–h is demonstrated. The importance of nucleophilicity measured by the quantity R_{xy}/R_d is recorded in parentheses. For details, see ref. 144, and for data in water, see footnote 2 in the text.

[a]R_a = k(R-tosylate)/k(2-Ad-tosylate) in EtOH. R_a(EtOH) = R_a/R_d.
[b]R_b = k(R-tosylate)/k(2-Ad-tosylate) in CH_3COOH. $R_b(CH_3COOH) = R_b/R_d$.
[c]R_c = k(R-tosylate)/k(2-Ad-tosylate) in HCOOH. R_c(HCOOH) = R_c/R_d.
[d]R_d = k(R-tosylate)/k(2-Ad-tosylate) in trifluoroacetic acid.
[e]Units are in electron volts. For details, see ref. 144 and for data in water, see footnote 2 in the text.
[f]Mean value estimated from eqs. [97] and [180]: the agreement is fair.
[g]R_e = $k(RNO_3)/k(2\text{-}AdNO_3)$ in H_2O. $R_{ew} = R_e/R_d$.
[h]R_f = k(RBr)/k(2-AdBr) in H_2O. $R_{fw} = R_f/R_d$.
[i]R_g = k(R-mesylate)/k(2-Ad-mesylate) in H_2O. $R_{gw} = R_g/R_d$.
[j]R_h = k(R-tosylate)/k(2-Ad-tosylate) in H_2O. $R_{hw} = R_h/R_d$.

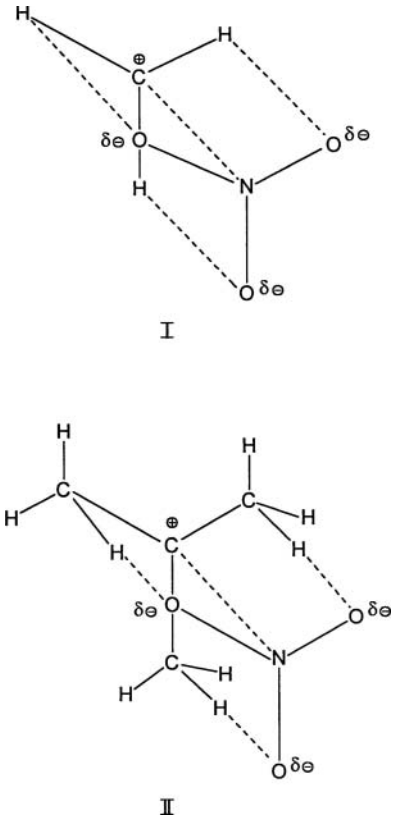
listed for acetic and formic acid. The other leaving groups, namely, nitrate, bromide, and mesylate have not been measured in trifluoroacetic acid, but the ratios for these leaving groups in water are comparable to the tosylates in water. The magnitudes of the nucleophilic components for the tosylates in water track the ionization potentials of the related organic radicals in the anticipated sense, i.e increased nucleophilic interaction accompanies an increase in the ionization potential of the radical. However, the rate constants themselves display the order cyclopentyl > 2-propyl > cyclohexyl, whereas the order of I_p(R·) is cyclohexyl < cyclopentyl < 2-propyl. The possible influence of return phenomena in the observed rate constant may be the source of this discrepancy. A wider range of data for different leaving groups in trifluoroacetic acid might be more revealing.

Tertiary substrates

The excellent LFER between *tert*-butyl and 1-adamantyl substrates in solvent water represented by eq. [99] involving the anionic leaving groups Cl, Br, I, TFA, NO_3 and the departure of the neutral molecule $(CH_3)_2S$ provides estimates of the rates of hydrolysis for other tertiary esters. Thus, the rates of *tert*-butyl tosylate, mesylate, picrate, and 4-nitrobenzoate can be established via eq. [99] from the corresponding known rates of related 1-adamantyl substrates. Similarly, the rates of hydrolysis of 1-adamantyl fluoride and acetate can

© 2005 NRC Canada

Fig. 16. Conformational possibilities for methyl nitrate and *tert*-butyl nitrate.



be calculated from the rates of the related *tert*-butyl compounds (see Table 14).

The Guthrie LFER for the *tert*-butyl substrates shows the same bifurcated behaviour as the methyl compounds between the halogen and the sulphonate esters. Tertiary butyl nitrate appears to be more reactive than might have been predicted on the basis of the relatively low reactivity of primary and secondary nitrates. The deviations of the nitrate esters from the Guthrie LFER may be a consequence of the stereochemistry and the symmetry of the incipient methyl, 2-propyl, and *tert*-butyl carbocations relative to the symmetry of the forming nitrate anion (see Fig. 16). The interactions of hydrogen atoms carrying increments of positive charge attached to the α-carbon for primary compounds interacting with suitably eclipsed negatively charged oxygen atoms of the nitrate anion would stabilize such structures. On the other hand, similar interactions for the *tert*-butyl cation might be repulsive rather than attractive. Such a lowering of the activation energy by intramolecular repulsions are likely to be less significant for the sulphonates because the S—O bond distances are larger than in similar structures containing nitrogen rather than sulphur.

The LFER represented by eq. [99] shows that the difference $\Delta G^{\ddagger}$(1-adamantyl) – $\Delta G^{\ddagger}$(*tert*-butyl) is, to a good first approximation, independent of the leaving group and has a constant value at ca. 2.600 kcal. This is in the opposite sense to the free energy change in the gas phase reported for

[129] $t\text{-Bu}^{+} + \text{1-AdBr} \rightleftharpoons t\text{-BuBr} + \text{1-Ad}^{+}$

quoted by Bentley and Carter (127) who give $\Delta G^{-} \approx -10$ kcal. Clearly, the relative stability of the 1-adamantyl and *tert*-butyl cations indicated by this equilibrium is not reflected in the kinetic behaviour of the related substrates reacting in water. The origin of the small constant difference between the 1-adamantyl and *tert*-butyl substrates is not easily interpreted on the basis of the thermodynamics associated with eq. [129], but may be associated again with return phenomena. For open chain as opposed to caged secondary and tertiary carbon centres, nucleophilic assistance in water may be a marginal matter. Less drastic steric strain energy influences may also contribute to the activation process for the open chain and caged substrates. The relative importance of such phenomena is not easily deduced from kinetic measurements alone in the case of the 1-adamantyl and *tert*-butyl derivatives.

13. Quantum mechanical and thermochemical calculations and their relation to solvolytic reactivity

Some general considerations

This section derives from studies by Evans (28), Franklin (157), Robertson (34), Dewar (138, 160–167), Streitwieser (2, 168–170), Martin (173, 177) and various members of is group (172, 174–176, 178, 179), Muller (180), Gold (181), Mason (182), and their respective co-workers.

Attention is directed primarily to measures of the extent of transition-state heterolysis for displacement processes for a series of primary reacting centres. The application of the Marcusian treatment to methyl transfers by Albery and Kreevoy (13) can be considered to scrutinize the same problem for several methyl substrates. This latter approach to organic reactivity probes transition-state structure via connections between Gibbs energies derived from rate and equilibrium constants. The same topic has been examined indirectly on a relative basis by Dewar and co-workers (110, 160) and Streitweiser (2, 168) for various arylmethyl substrates featuring a variety of leaving groups and solvent systems. Their approach correlates Gibbs energies of activation with what are essentially the energetics of gas phase heterolysis. The Guthrie LFER discussed in section 10 also illuminates this problem, although Guthrie himself eschewed comment (23).

In the middle of the last century Winstein and Marshall (183) drew attention to the relevance of the *internal properties* of molecules participating in solvolytic displacement reactions, particularly with respect to the reactivity of the α-methylated series that in the present context consists of substrates CH_3X, CH_3CH_2X, $(CH_3)_2CHX$, and $(CH_3)_3CX$ with X = either chloride or tosylate, reacting according to eq. [6]. These workers pointed out that the effect of each additional methyl group should increase the rate constant a 1000-fold for a limiting process. In water for X = Cl, the ratios are $1 : 3.2 : 8.9 : 1.24 \times 10^6$, with the ratio quoted for ethyl chloride less secure than those for the other substrates. From other data reported here with X = tosylate the ratios are $1 : 0.85 : 51.4 : 1.3 \times 10^8$. According to Ingold (1, 8) such sequences of reactivity with increasing α substitution signalize a shift towards the classical ionization mechanism

© 2005 NRC Canada

for the secondary and tertiary substrates. This simple conclusion must be regarded as tentative because of the observations reported here, particularly those in section 9. Nevertheless, the large increase in the rate constant between sPrX and *t*-BuX (X = chloride or tosylate) more than matches the change in reactivity suggested by Winstein and Marshall (183) for a limiting process.

In a contemporary study, Franklin (157) estimated the solvolytic rate constants of the *tert*-butyl halides (*t*-BuX, X = Cl, Br, and I) by simplifying techniques developed by the Evans–Polanyi group (28). The Gibbs energy of activation in solution ($\Delta G^{\ddagger}$) for an assumed S_N1 displacement was identified with the Gibbs energy of ionization (ΔG_s^i) of the alkyl halide in solution (sln).

$$[130]\quad RX(sln) \rightleftharpoons R^+(sln) + X^-(sln)$$

The quantity ΔG_s^i was calculated using a thermodynamic cycle (2, 34, 109, 157) yielding the expression

$$[131]\quad \Delta G^{\ddagger} \approx \Delta G_s^i = \Delta G(e) + \Delta G_g^i + \Delta G(s)$$

The terms $\Delta G(e)$, ΔG_g^i, and $\Delta G(s)$ refer to the Gibbs energies that characterize the processes: the transfer of the reactant from the solvent to the gas phase, the heterolysis of the reactant in the gas phase, and the Gibbs energy of solvation of the resulting anion and cation, respectively. Franklin (157) demonstrated that eq. [131] gave values of $\Delta G^{\ddagger}$ close to those calculated from the observed solvolytic rate constants (k_r) via the Eyring equation.

$$[132]\quad k_r = (kT/\hbar)\exp(-\Delta G^{\ddagger}/RT)$$

The various terms in eq. [132] having their usual meaning (see eqs. [43] and [44]).

The Franklin cycle provides a strategic route for the application of quantum mechanics (QM) to nucleophilic displacements at a saturated carbon atom adopting either the Dewar (PMO) or Huckel (HMO) molecular orbital (MO) methods including more advanced QM techniques (93, 110, 160, 161, 162–167, 169). The Franklin cycle also clarifies some shortcomings of the HMO and PMO (162) methods when employed in this and other contexts. These defects are augmented by approximations concerning the solvation of the ground and activated states and the details are developed in the following.

Expressing ΔG_g^i in eq. [131] in terms of the enthalpy and entropy functions gives

$$[133]\quad \Delta G_g^i = \Delta H_g^i - T\Delta S_g^i$$

Combining eqs. [133] and [131] yields

$$[134]\quad \Delta G^{\ddagger} = \Delta G(e) + \Delta H_g^i - T\Delta S_g^i + \Delta G(s)$$

Dewar and Sampson (160) and others (110, 179, 182), focused their attention on a series of arylmethyl substrates ($ArCH_2$-X, X = Cl, Br, I, and tosylate). If the operator δ_{Ar} denotes structural changes in the arylmethyl group, e.g., Ar = phenyl, 1-naphthyl, 2-naphthyl,…, etc., then operating on eq. [134] with δ_{Ar} gives

$$[135]\quad \delta_{Ar}\Delta G^{\ddagger} = \delta_{Ar}\Delta G(e) + \delta_{Ar}\Delta H_g^i - \delta_{Ar}T\Delta S_g^i + \delta_{Ar}\Delta G(s)$$

Dewar and Sampson make the following assumptions

$$[136]\quad \delta_{Ar}\Delta G^{\ddagger} \approx \delta_{Ar}\Delta H_g^i \approx \delta_{Ar}\Delta E_g^i \approx \delta_{Ar}\Delta E_{\pi}$$

where ΔE_{π} is the π electron energy difference between the arylmethyl carbocation and the related arylmethyl chloride. These approximations require that the two solvation terms and the entropy term in eq. [135] are zero, i.e., $\delta_{Ar}\Delta G(e) = 0$, $\delta_{Ar}T\Delta S_g^i = 0$, and $\delta_{Ar}\Delta G(s) = 0$.

The constancy of the solvation terms for such a series of arylmethyl carbocations has been queried by Mason (182), in terms of squared dependence on charge (q^2) and an inverse dependence on radius ($1/r$) demanded by the Born equation (184) for ionic solvation. This equation requires that the solvation of a *delocalized* single charge is *less* than that for a *localized* single charge, granted that the radii associated with the localized charge and each fragment of delocalized charge are identical.

To establish Mason's proposal, the arylmethyl carbocation is considered to consist of a framework of trigonal carbon atoms of equal radius with a single charge (q) fragmented into n fractional charges q_1, q_2, $q_3 ... q_n$ that are located at what are known as starred positions of the carbocation framework. Then, if these conditions are met, for any q_n, because $q_n < 1$, then $q_n^2 < q_n$. Hence, the sum of the squares of the fractional charges is less than the square of a single charge and by inference, the energy of solvation of the localized charge will be greater than for a fragmented single charge. The above reasoning justifies Mason's thesis. However, his analysis is not unique and other interpretations have been presented by Streitwieser and Nair (169) that, in essence, leave the approximations related to eq. [135] more or less intact.

The assumptions made between eqs. [135] and [136] frequently underpin reactivity studies interpreted by either QM or the classical electronic theory of organic chemistry. The justification of these manoeuvres has been formalized by Bell (186) in detail and less convincingly by Dewar (160, 161).

Such approximations include the possibility that the enthalpy and entropy terms that characterize the solvation of both ions and neutral molecules obey a version of the Barclay–Butler rule (34, 185). These correlations attenuate the variations of the Gibbs energies of solvation with structure either for ions or neutral substrates. Such cancellations occur via linear enthalpy–entropy correlations for both the ions and neutral molecules leaving the related Gibbs energy terms virtually constant as required by eq. [135]. Discussions of the influence solvation phenomena on more complex kinetic models (15, 22) and those represented by eqs. [121] and [122] have been, as far as we are aware, neglected.

Thermochemically, the problem of calculating the quantity ΔH_g^i as a function of the structure of the arylmethyl chloride involves three terms

$$[137]\quad \Delta H_g^i = D(ArCH_2\text{-}Cl) + I_p(ArCH_2^{\cdot}) + E_f(Cl^{\cdot})$$

© 2005 NRC Canada

that are: the bond dissociation energy (D(ArCH$_2$-Cl)) of the arylmethyl chloride, the ionization potential (I_p(ArCH$_2^{\cdot}$) of the arylmethyl radical, and the electron affinity (E_f(Cl$^{\cdot}$)) of the chlorine atom. Operating on eq. [137] with δ_{Ar},

$$[138]\quad \delta_{Ar}\Delta H_g^i = \delta_{Ar}D(\mathrm{ArCH_2\text{-}Cl}) + \delta_{Ar}I_p(\mathrm{ArCH_2^{\cdot}}) + \delta_{Ar}E_f(\mathrm{Cl^{\cdot}})$$

Clearly, $\delta_{Ar}E_f(\mathrm{Cl^{\cdot}}) = 0$, and hence, eq. [136] becomes

$$[139]\quad \delta_{Ar}\Delta G^{\ddagger} = \delta_{Ar}D(\mathrm{ArCH_2\text{-}Cl}) + \delta_{Ar}I_p(\mathrm{ArCH_2^{\cdot}})$$

that on integration gives

$$[140]\quad \Delta G^{\ddagger} = D(\mathrm{ArCH_2\text{-}Cl}) + I_p(\mathrm{ArCH_2^{\cdot}}) + C$$

Equation [140] demonstrates that *two variable thermochemical terms* contribute to ΔE_π in eq. [136]. Hence, these drastic simplifications to eq. [135] are equivalent to

$$[141]\quad \Delta G^{\ddagger} \approx \Delta E_\pi + C$$

where changes in ΔE_π with structure are rigorously defined by the RHS of eq. [139].

In terms of either PMO or HMO quantities eq. [141] can be recast

$$[142]\quad \Delta G^{\ddagger} = Q_f\beta + C$$

where Q_f is a structurally dependent numerical factor calculated from either the HMO or the PMO theories and β is a resonance integral: a "constant" disposable quantity in either the PMO or HMO contexts (180, 182, 192). The ΔE_π term can be calculated from more elaborate quantum mechanical algorithms without in any way compromising the thermodynamic analysis and the approximations previously presented.

Intuitively, eq. [142] might also be modified

$$[143]\quad \Delta G^{\ddagger} = \gamma\Delta H_g^i + C$$

with γ assumed to be in the range $0 < \gamma < 1$ with γ and C constants for a given series of displacements with a fixed leaving group, in a specified solvent at a fixed temperature. It is tacitly assumed that the organic group varies structurally in a systematic manner. In either of their respective contexts, the quantities γ and β are considered to provide measures of the ionic character of the displacement. Alternatively, γ and β may be considered as reaction coordinate parameters. The significance of the energetics of gas-phase heterolyses to the related displacements in solution has been briefly discussed elsewhere (2, 28, 79).

Dewar and Sampson's original PMO calculation of ΔE_π *lumps the two variable terms* on the RHS of eq. [140]. In their treatment, the Q_f parameter in eq. [142] is equal to $2a_{or}$, a quantity that relates to the linear coefficients of the nonbonding molecular orbitals (NBMO) for each arylmethyl carbocation or radical at their respective *extracyclic carbon atoms*. However, in thermodynamic terms the Dewar and Sampson calculation is in effect confined to the *first term* of eq. [140] because the unpaired electron in *all alternant arylmethyl radicals* occupies the NBMO of energy equal to α, the carbon Coulomb integral, a quantity common to both the HMO and PMO formalisms. Indeed, both theories assume the energy of the NBMO to be identical *for the carbons in all odd alternant radicals and carbocations.* This represents a major weakness of this approach because, experimentally, $\delta_{Ar}I_p(\mathrm{ArCH_2\cdot})$ is the dominant term in eq. [138], i.e., $\delta_{Ar}I_p(\mathrm{ArCH_2\cdot}) > \delta_{Ar}D(\mathrm{ArCH_2\text{-}Cl})$ (83, 193, 194) (see Table 21 and Figs. 17 and 18).

The ΔE_π values estimated by Dewar and Harget reported by Dewar and Bentley (110) presumably calculated by a self-consistent field (SCF) method, still account only for ca. 70% of the *measured* values of $\delta_{Ar}\Delta H_g^i$ for the benzyl, 1-naphthylmethyl, and 2-naphthylmethyl carbocations and further appraisal of such matters is presented at the end of this section.

In view of the last observation, a question of methodology now arises. The use of QM at any level of sophistication (17, 93, 110, 169, 187) to provide a quantitative understanding of chemical reactivity in the present and other contexts, e.g., aromatic substitution (163–167), invokes predominately *gas-phase* models at absolute zero to calculate the energy changes between either reactants and products or reactants and transition states with the further crucial assumption that the reactants and products are separated by a *single* barrier. These energy changes are then compared with reactivities observed *in solution* measured in terms of a Gibbs energy calculated from either rate or equilibrium constants established at a finite temperature. The first question that might be raised queries the calibre of the QM estimates *as gas-phase calculations*. Specifically, how well does the QM reproduce the *measured* gas-phase thermochemical quantities? If such computations are inadequate on their own terms, then, by the same token, their reliability with respect to understanding chemical reactivity *in solution at a finite temperature* is at least partly compromised. Some further comment related to this topic is presented at the end of this section.

Calculation of thermochemical quantities

The calculation of ΔH_g^i for a series of alkyl chlorides using eq. [137] requires values of D(R-Cl), I_p(R$^{\cdot}$), and E_f(Cl$^{\cdot}$). Such quantities for a particular series of alkyl halides are frequently unavailable. In cases where the corresponding values for D(R-Br) and D(R-I) are known, these can be used to estimate values for the chloride using the following analysis (see Table 22. A preliminary discussion of these matters was given by Scott and Winter and co-worker (79) that relates to more sustained approaches to such matters by Benson and co-worker (206, 207).

If X1 and X2 are two different leaving groups relating to the heterolytic process described by eq. [130] then

$$[144]\quad \Delta H_g^i(\mathrm{RX1}) = \Delta H_f^o(\mathrm{R^+}) + \Delta H_f^o(\mathrm{X1^-}) - \Delta H_f^o(\mathrm{RX1})$$

$$[145]\quad \Delta H_g^i(\mathrm{RX2}) = \Delta H_f^o(\mathrm{R^+}) + \Delta H_f^o(\mathrm{X2^-}) - \Delta H_f^o(\mathrm{RX2})$$

where the symbols in eqs. [144] and [145] have their conventional meanings.

Subtracting eq. [145] from eq. [144]

$$[146]\quad \Delta H_g^i(\mathrm{RX1}) - \Delta H_g^i(\mathrm{RX2}) = \Delta H_f^o(\mathrm{RX2}) - \Delta H_f^o(\mathrm{RX1}) + \Delta H_f^o(\mathrm{X1^-}) - \Delta H_f^o(\mathrm{X2^-})$$

© 2005 NRC Canada

Table 21. Data related to the gas-phase ionization and solvolysis of arylmethyl substrates (halides and sulphonates).

				$\Delta G^{\ddagger a}$					
$ArCH_2X$	$2a_{or}$	$S(q^2)$	ΔH_g^i	(I)[b]	(II)[b]	(III)[b]	(IV)[b]	(V)[b]	(VI)[b]
Benzyl	1.5118	0.3878	159	27.334	28.609	26.495	27.832	26.918	25.194
2-Naphthyl	1.4552	0.3495	154	26.906	—	—	27.123	25.063	23.560
2-Phenanthryl	1.4744	0.3507	155	26.965	—	—	27.177	25.022	23.489
3-Phenanthryl	1.4286	0.3153	150	26.595	28.378	26.031	26.250	23.999	22.715
2-Anthracyl	1.3720	0.3097	148	—	—	—	—	—	21.970
2-Pyrenyl	1.5118	0.3726	158	—	27.873	28.009	27.573	—	24.148
2-Triphenylyl	1.4552	0.3110	151	26.920	—	—	—	24.858	—
1-Naphthyl	1.3416	0.2900	145	26.403	27.996	25.636	25.990	23.399	22.343
1-Phenanthryl	1.3608	0.2819	145	26.595	—	—	23.386	23.617	—
9-Phenanthryl	1.3363	0.2971	147	26.506	28.187	25.990	26.154	23.330	22.228
6-Chrysyl	1.2810	0.2465	139	25.442	—	—	—	21.393	—
4-Pyrenyl	1.2865	0.2778	142	—	—	25.718	25.772	—	22.070
1-Pyrenyl	1.2060	0.1901	132	—	24.981	21.366	21.584	—	—
9-Anthracyl	1.0690	0.1939	128	—	23.944	19.238	—	—	—
1,2-Benz-10-anthracyl	1.1209	0.1849	129	—	—	—	—	—	—
1-Triphenylyl	1.4142	0.3093	149	—	—	—	—	—	—
1-Anthracyl	1.2344	0.2483	137	—	—	—	—	—	—

Note: $\Delta G^{\ddagger}$ calculated from the Eyring equation ($k_r = (kT/\hbar)\exp(-\Delta G^{\ddagger}/RT)$; see ref. 39). Solvolytic data taken from refs. 2, 110, 168, and 172–179 (also see Table 25 for temperatures. Temperatures for the calculation of $\Delta G^{\ddagger}$ are given at the end of each regression equation. The PMO quantities $S(q^2)$ and $2a_{or}$ were calculated by methods detailed in refs. 159 and 162. Details of the methodology used for the calculation of ΔH_g^i (see Table 23).

[a]Solvents: (I) 80% EtOH – H_2O – $ArCH_2Cl$, (II) 79.5% aqueous dioxane – $ArCH_2Cl$, (III) 50.7% aqueous dioxane – $ArCH_2Cl$, (IV) 6.1% H_2O, 51.4% HCOOH, 39.8% dioxane–$ArCH_2Cl$, (V) HCOOH, 0.38 mol/L H_2O–$ArCH_2Cl$, (VI) CH_3COOH–$ArCH_2OTs$, (VII) acetone – I^- attack – $ArCH_2Cl$, (VIII) 79.5% aqueous dioxane – $ArCH_2OTs$, (IX) 70% aqueous dioxane – $ArCH_2OTs$, (X) 60% aqueous dioxane – $ArCH_2OTs$, (XI) acetic acid – $ArCH_2OTs$, (XII) 79.5% aqueous dioxane – $ArCH_2OTs$, (XIII) 79.5% aqueous dioxane – $ArCH_2Cl$, (XIV) 79.5% aqueous dioxane – $ArCH_2Br$, (XV) 80% aqueous ethanol – $ArCH_2Cl$, (XVI) 80% aqueous ethanol – $ArCH_2Br$, 80% aqueous ethanol – $ArCH_2I$.

[b]The rate data for $\Delta G^{\ddagger}$ in solvents (I)–(VII) were taken from Table 12.4 of ref. 168.

[c]The data for $\Delta G^{\ddagger}$ in solvents (VIII)–(XVII) were taken from Tables I and II of ref. 110.

Fig. 17. Correlation of $D(ArCH_2\text{-}Cl)$ vs. the Dewar $2a_{or}$ PMO quantity.

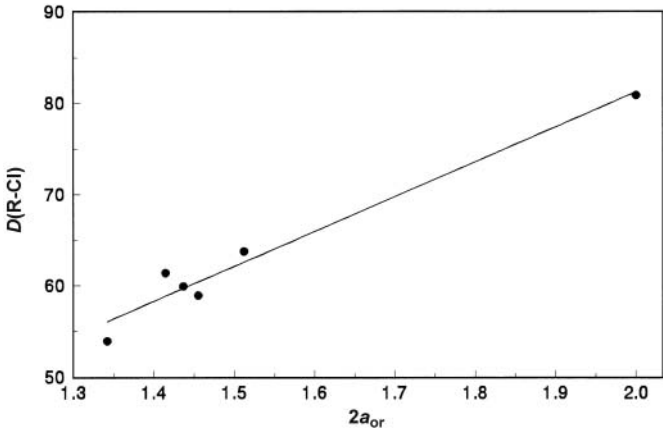
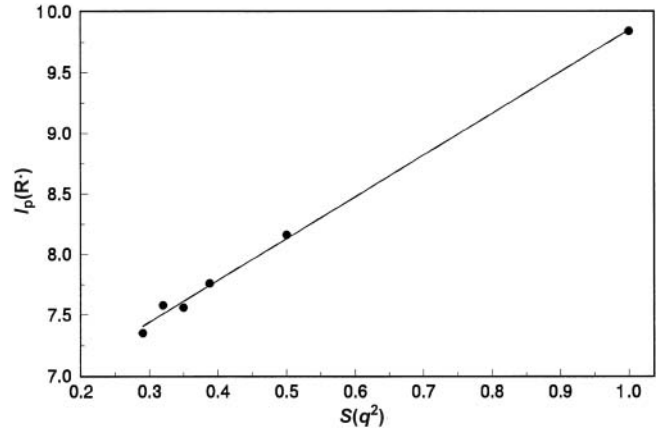


Fig. 18. Correlation of the Dewar $S(q^2)$ vs. the ionization potentials of a series of arylmethyl radicals.



that after a trivial manipulation provides

$$[147]\quad \Delta H_g^i(RX1) = \Delta H_g^i(RX2) + [\Delta H_f^o(RX2) - \Delta H_f^o(RX1)] + [\Delta H_f^o(X1^-) - \Delta H_f^o(X2^-)]$$

If the relationship

$$[148]\quad \delta_R \Delta H_g^i(RX1) = \delta_R \Delta H_g^i(RX2)$$

is to be an acceptable approximation, then, according to eq. [147], two conditions are required

$$[149]\quad \delta_R[\Delta H_f^o(RX2) - \Delta H_f^o(RX1)] = 0$$

and

$$[150]\quad \delta_R[\Delta H_f^o(X1^-) - \Delta H_f^o(X2^-)] = 0$$

Equation [150] is obviously true and integrating [149] gives

© 2005 NRC Canada

Table 21 (*concluded*).

(VII)[b]	(VIII)[c]	(IX)[c]	(X)[c]	(XI)[c]	(XII)[c]	(XIII)[c]	(XIV)[c]	(XV)[c]	(XVI)[c]	(XVII)[c]
21.803	24.278	23.450	22.643	25.193	24.287	30.115	27.289	27.331	25.320	25.679
21.352	23.280	22.514	21.790	23.572	23.485	29.806	27.549	26.900	24.984	25.365
21.421	23.202	22.524	21.725	23.926	23.455	29.907	27.570	26.963	24.964	
21.339	22.772	21.948	21.077	22.717	23.017	29.372	27.343	26.597	24.732	
—	—	—	—	—						
—	—	—	—	—						
—	—	—	—	—						
21.052	22.358	21.526	20.498	22.227	22.621	29.283	27.155	26.398	24.628	25.115
20.970	22.466	21.683	20.657	22.328						
20.970	—	—	—	—	22.639	29.332	27.345	26.510	24.707	—
—	—	—	—	—						
—	—	—	—	—						
20.288	—	—	—	—						
19.388	—	—	—	—						
19.579	—	—	—	—						
—	—	—	—	—						
—	21.177	—	—	—						

[151] $\Delta H_f^o(RX2) - \Delta H_f^o(RX1) = \text{constant}$

In the case of homolytic fission, the analogous equation to [144] is

[152] $D(RX1) - D(RX2) = [\Delta H_f^o(RX2) - \Delta H_f^o(RX1)] + \Delta H_f^o(X1^{\cdot}) - \Delta H_f^o(X2^{\cdot})$

that requires the similar conditions to those appropriate to eq. [146].

With X1 = Cl and X2 = Br, ΔH_f^o(RCl) and ΔH_f^o(RBr) are linearly related for various alkyl groups and the data that underpin these relationships for a series of alkyl chlorides, bromides, and iodides are reported in Table 22. For X1 = Cl and X2 = Br the empirical relationship is

[153] $\Delta H_f^o(RCl) = (0.9880 \pm 0.015)\Delta H_f^o(RBr) - 11.62 \pm 0.30$ (6,0.9990)

and similarly, when X1 = Cl and X2 = I

[154] $\Delta H_f^o(RCl) = (1.067 \pm 0.014)\Delta H_f^o(RI) - 24.33 \pm 0.18$ (6,0.9993)

Rearranging eq. [153] gives

[155] $(0.9880 \pm 0.015)\Delta H_f^o(RBr) - \Delta H_f^o(RCl) = 11.62 \pm 0.30$

and the similar manipulation of eq. [154] gives

[156] $(1.067 \pm 0.014)\Delta H_f^o(RI) - \Delta H_f^o(RCl) = 24.33 \pm 0.18$

The relationships [155] and [156] represent *the empirical versions* of eq. [151] and because the coefficients of ΔH_f^o(RI) and ΔH_f^o(RBr) are sufficiently close to unity in eqs. [155] and [156], these relationships can be combined

Table 22. Thermochemical data related to a series of alkyl halides.

Alkyl group	ΔH_f^o(RCl)	ΔH_f^o(RBr)	ΔH_f^o(RI)
Methyl	–20.63	–9.00	3.34
Allyl	–0.15	–11.80	22.9
Ethyl	–26.70	–15.30	–2.00
s-Propyl	–35.00	–23.20	–10.00
tert-Butyl	–43.80	–32.00	–17.60
n-Propyl	–31.00	–21.00	–7.30
Benzyl	8.14[a] (7.6)[b]	20.00	30.40

Note: Most of the data in Table 22 is from ref. 47.

[a]Extrapolated value. Skinner (189) gives 3.0 ± 1 based on a value of –7.8 kcal mol^{-1} for the heat of formation of the liquid benzyl chloride, which is discrepant with the value of –16.8 kcal mol^{-1} reported by Stull et al. (47). The vapour pressure data reported by Partington (190) correspond to a latent heat of evaporation for benzyl chloride of 11.2 kcal mol^{-1}, which is consistent with the values reported by Skinner (189) for the gaseous and liquid phases. Skinner (189) reports that the heat of formation of the benzyl radical is 38–46.5 kcal mol^{-1}, which is narrowed slightly by Walsh et al. (191) to 44.1 ± 3.1 kcal mol^{-1}. These data yield a value of 68 ± 4 kcal mol^{-1} for D(PhCH$_2$-Cl). The value reported by Shaik et al. (75 kcal mol^{-1}) (17) is well above the upper limit of this value. Shaik et al. give no references for the origins of the elevated value reported. The value calculated from ΔH_f^o(PhCH$_2$Cl) in Table 22 and ΔH_f^o(PhCH$_2^{\cdot}$) corresponds to that reported by Swarc and Taylor (192) is higher than the value obtained by Lossing et al. (193) using electron impact studies, which gave 60.4 kcal mol^{-1}. Two values for D(PhCH$_2$-Br) of 50.5 and 44.7 kcal mol^{-1} reported in refs. 194 and 193, respectively, give values for the chloride of 64.32 and 56.62 kcal mol^{-1} using eq. [157]. A further value for D(PhCH$_2$-Br) reported by Gellner and Skinner (195) based on the heat of hydrolysis of benzyl bromide treated in the same way gave 62.42 kcal mol^{-1}. Five measured values for D(PhCH$_2$-I) in combination with eq. [158] give 65.63 (196), 61.63 (193), 64.03 (197), and 69.83 (198) kcal mol^{-1} and 63.13 kcal mol^{-1} (195) for D(PhCH$_2$-Cl). The mean of these 10 values is 63.77 ± 3.41 kcal mol^{-1}. Values for the electron affinity of the chlorine atom (Cl$^{\cdot}$) vary widely: 93 (199), 83 (200), 83.26 (201), 87.3 (195), and 83.2 (114). The value reported in ref. 201 is adopted here. Values for the ionization potentials of the various radicals are predominately from Lossing and co-workers, reported and summarized in several articles (200, 202–205).

[b]Value in parenthesis calculated using the MNDO algorithm (188).

© 2005 NRC Canada

Table 23. Thermochemical and kinetic data at T = 298.15 K for a series of primary alkyl halides.

Organic group	D(RCl)	$\Delta G^{\ddagger}$(obs.)	$\Delta G^{\ddagger}$(calcd.)	I_p(R$^{\cdot}$)	ΔH^{i}_{g}(R-Cl)[a]
Methyl[b]	81.0	27.838	27.813	9.85	225 (0.00)
Allyl[c]	60.1	25.516	24.998	8.25	164 (0.15)
Ethyl	83.0	27.675	27.524	8.40	194 (0.04)
Cinnamyl	81.0	19.082	19.175	7.89	140 (0.36)
Propargyl	78.0	27.602	26.671	7.42	179 (0.08)
Benzyl[b]	63.8	24.086	24.105	7.76	159 (0.18)
4-Me-benzyl	62.2	22.014	22.078	7.46	151 (0.26)
3-Me-benzyl[c]	63.6	23.841	23.419	7.65	155 (0.21)
4-Cl-benzyl[c]	63.5	24.434	24.679	7.95	162 (0.16)
3-Cl-benzyl	63.2	25.231	25.510	8.21	168 (0.13)
4-MeO-benzyl	63.6	16.841	17.891	6.84	137 (0.40)
4-NO_2-benzyl[c]	62.5	26.359	26.733	8.11	180 (0.08)
3-NO_2-benzyl	61.5	26.121	26.244	8.56	174 (0.10)
4-CF_3-benzyl[c]	63.6	25.434	26.247	8.47	174 (0.10)
4-*t*-Bu-benzyl	63.6	22.902	22.429	7.46	151 (0.24)
4-Ph-benzyl[b]	60.9	—	—	7.32	151
1-Naphthylmethyl[b]	57.6	21.305[d]	20.796	7.35	145 (0.30)
2-Naphthylmethyl[b]	61.6	22.737[d]	23.080	7.56	154 (0.22)
2-Phenanthrylmethyl	62.3	22.701[d]	23.356	7.62	155 (0.21)
3-Phenanthrylmethyl	60.6	21.822[d]	22.195	7.49	150 (0.25)
2-Triphenylylmethyl	61.6	22.561[d]	22.370	7.55	151 (0.25)
1-Phenanthrylmethyl	58.2	20.817[d]	20.817	7.38	145 (0.30)
9-Phenanthrylmethyl	57.4	21.246[d]	21.228	7.43	147 (0.29)
6-Chrysylmethyl	55.4	19.580[d]	18.929	7.26	139 (0.37)
γ-Methylallyl	59.8	23.075	23.209	7.71	154 (0.13)

Note: Units for I_p(R$^{\cdot}$) are electron volts. Units for D(RCl) and ΔH^{i}_{g}(R-X) are kcal mol^{-1}. There are a variety of ways the existing thermochemical data can be used to estimate these quantities. These data were established via eqs. [160]–[162] using all the collected data. A data set restricted to *measured* values for the halogens (Cl, Br, and I) provides the following correlations for six alkyl groups, namely, methyl, allyl, benzyl, 1-naphthymethyl, 2-naphthylmethyl, and 4-phenylbenzyl, the bromides and iodides corrected to a value for the chloride by eq. [157] or [158]. The ionization potentials were calculated from the appropriate equation, either eq. [159] or [161]. $\Delta G^{\ddagger}$(obs.) is the observed Gibbs energy of activation and $\Delta G^{\ddagger}$(calcd.) is the calculated Gibbs energy of activation from eq. [168]. For sources of kinetic data for the unsubstituted and substituted benzyl chlorides see Table 26.

[a]Slopes in parenthesis calculated according to eq. [170].

[b]Values used to establish eqs. [160]–[162].

[c]Values were estimated from eq. [159].

[d]Calculated from log$k$(H_2O) = (0.8607 ± 0.0182) log$k$(HCOOH) + 0.924 ± 0.109 (see Table 24).

with the appropriate enthalpy difference between the halogen atoms to give the *approximate* relationships

[157] D(RCl) – D(RBr) ≈ 13.92 kcal

[158] D(RCl) – D(RI) ≈ 26.63 kcal

Equations [157] and [158] can be applied to experimental values for D($PhCH_2Br$) and D($PhCH_2I$) to estimate D($PhCH_2Cl$) and this is a tactic applicable to other alkyl groups. The values of D($PhCH_2Cl$) collected and calculated via eqs. [157] and [158] are reported in the extensive footnote to Table 22.

Changes in D($PhCH_2Cl$) as a consequence of substituents in the 3- and 4-positions in the benzene ring were calculated from data reported in texts authored by either Cotrell (208) or Trotman-Dickenson (209). These corrections are small and are within the errors reported for the heat of formation for the benzyl radical (see footnote *a* to Table 22). Swarc's group also provided further data for bond dissociation energies used here (210–212).

The ionization potentials for various radicals are those reported by Lossing's group (200, 202–205). In cases where data are absent for 3- and 4-substituted benzyl radicals, a correlation between existing values and the Hammett–Brown σ^+ substituent constants (215, 216) gives the relationship

[159] $I_p(R^{\cdot}) = (1.060 \pm 0.037)\sigma^+ + 7.782 \pm 0.017$ (10,0.987)

provided estimates for the unknown ionization potentials (see also Table 23).

The simple Dewar and Sampson (160) analysis for the calculation of ΔE_π gives an acceptable account of the *bond dissociation term* D(R-Cl) for six structures (see Table 23).

[160] $D(RCl) = (35.55 \pm 1.36)2a_{or} + 9.85 \pm 2.24$ (6,0.962)

and I_p(R$^{\cdot}$) for the related radicals is given by an equation indirectly related to the HMO/PMO methodology

[161] $I_p(R^{\cdot}) = (3.432 \pm 0.066)S(q^2) + 6.418 \pm 0.035$ (6,0.998)

© 2005 NRC Canada

Table 24. Kinetic data for the hydrolysis and formolysis of a series of 1°, 2°, and 3° alkyl chlorides (RCl: T = 298.15 K).

Alkyl group (R-)	$-\log k_a$(obs.)	$-\log k_w$(obs.)	$-\log k_w$(calcd.)
Benzyl	6.718[a]	4.869[b]	4.875
Allyl	8.149[c]	5.917[b]	6.037
4-Methylbenzyl	4.67[d]	3.350[b]	3.211
2-Propyl	8.656[c]	6.675[b]	6.473
tert-Butyl	2.98[c,d]	1.527[b]	1.839
α-Methylallyl	4.603[d]	3.157[b]	3.157
1-Phenylethyl	2.600[d]	1.330[d]	1.530
1-Chloro-1-phenylmethyl	4.229[c]	3.090[e]	2.853
3-Methylbenzyl	6.456[d]	4.689[d]	4.662
4-Chlorobenzyl	7.365[d]	5.124[d]	5.400
3-Chlorobenzyl	8.001[d]	5.708[d]	5.917
4-*tert*-Butylbenzyl	5.241[d]	4.000[d]	3.675

Note: k_a is the first-order rate in HCOOH and k_w is the first-order rate in H_2O. The units for k_a and k_w are s^{-1}. k_w(calcd.) is the calculated hydrolysis rate constant and $\log k_w$(calcd.) is calculated from eq. [*ii*]. Equation [*i*]: $\log k_w$(calcd.) = (0.8607 ± 0.0182) $\log k_a$ + 0.9236 ± 0.109 (6,0.998) was obtained from a linear least-squares regression using six of the results from this table. The complete data set gives eq. [*ii*]: $\log k_w$ = (0.8122 ± 0.0229) $\log k_a$ + 0.582 ± 0.140 (12,0.991); see also Fig. 19.

[a]Reference 168.
[b]See footnote 2 in the text.
[c]Reference 213.
[d]Reference 178.
[e]Estimated from data in footnote 2 of the text and ref. 214.

where the term $S(q^2)$ represents the sum of the squares of the charge distribution of either the arylmethyl carbocation or the related free radical. The charge distribution can be easily calculated using Dewar's PMO method (158, 159, 162). Equations [160] and [161] are illustrated in Figs. 17 and 18.

Changing the energy units of eq. [161] from ev to kcal followed by the addition of eq. [144] to the resulting expression and setting the electron affinity of the chloride atom at –83.26 kcal, gives an empirical relationship between ΔH_g^i and the PMO quantities $S(q^2)$ and a_{or}

$$[162] \quad \Delta H_g^i = 79.14S(q^2) + 71.11a_{or} + 74.58$$

For six chlorides (RCl) that cover a range of ca. 70 kcal in ΔH_g^i, the relationship between ΔH_g^i(calcd.) and ΔH_g^i(obs.) calculated via eq. [162] is

$$[163] \quad \Delta H_g^i(\text{calcd.}) = (1.007 \pm 0.019)\Delta H_g^i(\text{obs.}) - 1.11 \pm 3.22 \ (6,0.998)$$

with R = methyl, allyl, benzyl, 4-phenylbenzyl, 1-naphthylmethyl, and 2-naphthylmethyl.

The combined correlation between Dewar's PMO quantities ($S(q^2)$, $2a_{or}$) and ΔH_g^i represented by eq. [162] was used either by extrapolation or interpolation to estimate $\Delta H_g^i(ArCH_2\text{-}Cl)$ in cases where no measurements exist. These estimates are considered to be the best currently available and are recorded in Tables 21 and 23.

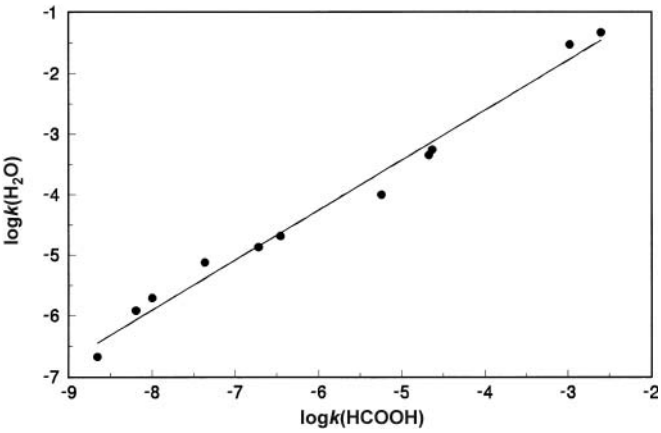
Slopes from the correlations between $\Delta G^‡$ and ΔH_g^i

The $\Delta H_g^i(ArCH_2\text{-}Cl)$ values provide an improved perspective from which the meaning of the slopes of the PMO or HMO correlations with $\Delta G^‡$ for a variety of arylmethyl substrate displacements (2, 110, 160, 162, 168, 179) can be evaluated. Similar comments apply to what Bentley and Dewar (110) designate as "Streitwieser Plots". The way the ΔH_g^i values are used here is relatively free of ambiguity compared with correlations with the purely theoretical quantities that are discussed further at the end of this section. Equation [143] may be tested against a wealth of solvolytic data for arylmethyl tosylates and halides collected in Table 21. The data in Table 21 include $\Delta G^‡$ from kinetic measurements for the classical S_N2 process in acetone

$$[164] \quad I^- + ArCH_2Cl \rightarrow ArCH_2I + Cl^-$$

usually known as the Finklestein reaction. Intuitively, the shift in mechanism from an ionic solvolytic displacement process to a definite second-order bimolecular displacement should lead to a reduction of the coefficient of ΔH_g^i, namely, γ in eq. [143], i.e., $\delta_{Ar}\Delta G^‡$ (S_N1) > $\delta_{Ar}\Delta G^‡$ (definite S_N2). This proposal anticipates that *less charge* is transferred from

Fig. 19. LFER between rates of formolysis and hydrolysis for a series of primary, secondary, and tertiary chlorides.



© 2005 NRC Canada

Table 25. Slopes of Streitwieser and related correlations.

Solvent and reaction	Substrate and temperature (T, K)	Slope	Intercept	N and C.C.[a]
80% EtOH – H_2O (S)[b]	$ArCH_2Cl$ (323.15)	0.0803±0.0085	14.6±1.3	9, 0.924
79.5% Aqueous dioxane (S)	$ArCH_2Cl$ (298.15)	0.1422±0.0208	6.46±3.04	7, 0.900
50.7% Aqueous dioxane (S)	$ArCH_2Cl$ (298.15)	0.2456±0.0288	–10.8±4.19	8, 0.920
HCOOH – 0.38 mol/L H_2O (S)	$ArCH_2Cl$ (298.15)	0.2452±0.0147	–12.5±2.21	9, 0.973
54.1% HCOOH – 6.1% H_2O – 9.8% dioxane (S)	$ArCH_2Cl$ (298.15)	0.1985±0.0207	–3.30±3.08	10, 0.916
Acetic acid (S)	$ArCH_2OTs$ (313.15)	0.1722±0.0172	–2.87±2.59	9, 0.913
Finklestein reaction acetone (S)	$ArCH_2Cl$ (298.15)	0.0711±0.0038	10.56±0.55	10, 0.975
79.5% Aqueous dioxane (DB)[c]	$ArCH_2Cl$ (313.15)	0.1321±0.0082	3.03±1.23	7, 0.980
70.0% Aqueous dioxane (DB)	$ArCH_2Cl$ (313.15)	0.1280±0.0098	2.88±1.49	6, 0.975
60.0% Aqueous dioxane (DB)	$ArCH_2Cl$ (303.15)	0.1458±0.0078	–0.670±1.17	6, 0.988
Acetic acid (DB)	$ArCH_2OTs$ (313.15)	0.1926±0.0211	5.90±3.20	6, 0.951
79.5% Aqueous dioxane (DB)	$ArCH_2OTs$ (323.15)	0.1134±0.007	6.09±1.20	6, 0.979
79.5% Aqueous dioxane (DB)	$ArCH_2Cl$ (352.35)	0.0619±0.0060	20.27±0.91	6, 0.961
79.5% Aqueous dioxane (DB)	$ArCH_2Br$ (352.35)	0.0388±0.0042	21.57±0.64	6, 0.951
80% EtOH – H_2O (DB)	$ArCH_2Cl$ (323.15)	0.0620±0.0048	17.40±0.71	6, 0.975
80% EtOH – H_2O (DB)	$ArCH_2Br$ (323.15)	0.0444±0.0050	18.17±0.75	6, 0.949
80% EtOH – H_2O (DB)	$ArCH_2I$ (323.15)	0.0395±0.0059	19.36±0.91	3, 0.976
80% EtOH – H_2O (SPA)[c]	$ArCH_2Cl$	0.558±0.128	13.38±3.34	4, 0.900
79.5% Aqueous dioxane (SPB)[d]	$ArCH_2Cl$	0.0385±0.0065	22.52±0.97	4, 0.943
80% EtOH – H_2O (SPC)[e]	$ArCH_2Cl$	0.0643±0.0070	17.07±1.05	4, 0.975
80% EtOH – H_2O (SPA)	$ArCH_2Cl$	0.778±0.14	5.24±3.75	4, 0.935
50.7% Aqueous dioxane (SPB)	$ArCH_2Cl$	0.0505±0.0102	18.47±1.53	4, 0.921
80% EtOH – H_2O (SPC)	$ArCH_2Cl$	0.0643±0.0070	17.07±1.05	4, 0.975
80% EtOH – H_2O (SPA)	$ArCH_2Cl$	3.85±0.20	–78.55±5.41	8, 0.982
0.38 mol/L H_2O – HCOOH (SPB)	$ArCH_2Cl$	0.2247±0.0018	–9.35±2.71	8, 0.960
80% EtOH – H_2O (SPC)	$ArCH_2Cl$	0.0570±0.0050	18.19±0.74	8, 0.954
80% EtOH – H_2O (SPA)	$ArCH_2Cl$	2.08±0.07	28.86±1.87	7, 0.994
6.1% H_2O – 54.1% HCOOH – 39.8% dioxane (SPB)	$ArCH_2Cl$	0.1168±0.0123	9.13±1.85	7, 0.944
80% EtOH – H_2O (SPC)	$ArCH_2Cl$	0.0565 ± 0.053	18.25 ± 0.80	7, 0.954
80% EtOH – H_2O (SPA)	$ArCH_2OTs$	3.09±0.22	–59.57±6.00	6, 0.978
Acetic acid (SPB)	$ArCH_2OTs$	0.1914±0.021	–5.71±3.29	6, 0.947
80% EtOH – H_2O (SPC)	$ArCH_2OTs$	0.0623±0.0048	17.36±0.72	6, 0.975
80% EtOH – H_2O (SPA)	$ArCH_2Cl$	0.846±0.112	–1.35±2.99	7, 0.916
Acetone/Finklestein reaction	$ArCH_2Cl$	0.0529±0.0041	13.32±0.62	7, 0.968
80% EtOH – H_2O (SPC)	$ArCH_2Cl$	0.0565±0.0053	18.26±0.80	7, 0.954

Note: The first 17 rows of this table relate to correlations between $\Delta G^{\ddagger}$(I)–$\Delta G^{\ddagger}$(XVII) and $\Delta H_g^i(ArCH_2X)$ from the data in Table 21. The subsequent rows in this table are in *groups of three* and provide a few examples of Streitwieser plots (see ref. 110). The first row in the group is a Streitwieser plot (SPA) between $\Delta G^{\ddagger}$(I) and $\Delta G^{\ddagger}$ for the solvent system specified in the next row. The second and third rows correlate $\Delta G^{\ddagger}$(I) and $\Delta G^{\ddagger}$ with ΔH_g^i again because the number of data point pairs is necessarily reduced, e.g., there are only *four* matching entries for $\Delta G^{\ddagger}$(I) and $\Delta G^{\ddagger}$(II) in Table 21.

[a] N is the number of the regression points and C.C. is the correlation coefficient.

[b] S data are from ref. 2.

[c] DB data are from Tables I and II of ref. 110.

[d] Streitwieser plot (SPA).

[e] Streitwieser plot vs. ΔH_g^i (SPB).

[f] Streitwieser plot of $\Delta G^{\ddagger}$(I) vs. ΔH_g^i (SPC) for rates in 80% EtOH–H_2O; the slopes differ because the number of data points from column $\Delta G^{\ddagger}$(I) differ in each regression. The mean slope is 0.060 ± 0.004. This particular calculation is repeated for each of the other solvents. The slopes differ because the number of substrates is not uniform in the other solvent systems. The mean of the six values is 0.060 ± 0.004. For all the data, the slope is 0.0803 ± 0.0085; cf. the first entry in this table. The slopes of the matching SPB plots involving the matching data from the related $\Delta G^{\ddagger}$(I–XVII) columns involving less than the complete data set are often in very poor agreement with the slopes from the complete data set. The Streitwieser plots present the elimination of ΔH_g^i between two simultaneous equations related to eq. [141] for two different solvent systems.

© 2005 NRC Canada

Table 26. Rate and thermodynamic data for a series of 3- and 4-substituted benzyl chlorides and tosylates.

X	σ^{+}[a]	log k[b,c]	log k[b,d]	log k[b]	log k[b]	ΔH_g^i[e]	log k[f]
4-H	0.00	–4.879	—	–4.858	—	159	–3.972
4-Me	–0.311	–3.338	—	–3.361	—	150	–2.466
3-Me	–0.066	–4.743	—	–4.635	—	155	–3.717
4-Cl	0.114	–5.147	–5.120	–5.105	—	162	—
3-Cl	0.399	—	—	–5.708	—	168	—
4-MeO	–0.778	—	—	0.472[g]	0.416[h]	137	0.500
4-NO_2	0.790	–6.573	–6.497	—	—	180	–5.630
3-NO_2	0.674	–6.361	—	—	—	174	—
4-CF_3	0.520	—	—	—	–5.857[i]	174	—
4-*t*-Bu	–0.256	—	—	–4.00	—	151	—
3-Br	0.410	—	—	—	—	169	–5.050
3-MeO	–0.05	—	—	—	—	160	–4.185
4-Br	0.15	—	—	—	—	164	–4.362

[a]Substituent X constants from ref. 137.
[b]The solvent was water and chloride was the leaving group (T = 298.15 K) for this data.
[c]Data are from footnote 2 in the text.
[d]Data are from refs. 219, 178, and 171.
[e]See Table 22. Average error on ΔH_g^i ca. ± 3.0 kcal mol^{-1}.
[f]The solvent was 76.6 mol% in water and tosylate was the leaving group (T = 298.45 K)[6] for this data.
[g]Data are from the Grunwald–Winstein LFER in two compositions of dioxane–water mixtures (177).
[h]Calculated from data in ref. 142 using the Grunwald–Winstein LFER in MeOH–H_2O mixtures giving log k = (0.848 ± 0.016)Y – 2.537 ± 0.029 (6,0.998), and in EtOH–H_2O mixtures giving log k = (0.952 ± 0.013)Y – 2.921 ± 0.025 (6,0.999).
[i]Calculated from data in footnote 2 in the text.

the conjugated aromatic system in definite bimolecular processes. Generally speaking, the least-squares correlations presented in Table 25 confirm this anticipated behaviour, noting that the correlation coefficients are not impressive. Nevertheless, the correlations generalized by eq. [143] definitely establish that the gas-phase heat of ionization is a significant quantity in determining the rate of heterolysis in both solvolytic and definite bimolecular displacements for the arylmethyl substrates listed in Tables 21 and 23.

The slopes (γ) related to eq. [143] are reported in Table 25. The maximum value of γ was observed in moist formic acid (γ = 0.25), confirming the conventional wisdom that this solvent facilitates heterolysis. However, the level of heterolysis assessed at 25% is remote from complete heterolytic fragmentation. The solvolysis of three arylmethyl iodides in 8O% EtOH–H_2O gives the minimum value of γ (0.040) that is *less* than that for the definitive bimolecular process, namely, the Finklestein reaction (γ = 0.053). However, the careful studies undertaken by Stein (217) and Boronius and Pataki (218) show that without a detailed examination of the concentration dependence of rate constants for displacement in acetone with respect to the attacking iodide ion, it is not possible to extract a meaningful value of the second-order rate constant for this reaction from a single determination of the second-order rate constant. Hence, the comparison of a series of Finklestein displacements with the solvolytic processes is less certain than the comparison of the solvolytic processes with each other.

The maximum of γ is observed in formic acid and becomes less in solvents of reduced ionizing power as measured by Grunwald–Winstein Y values. For various leaving groups under comparable conditions of solvent and temperature, the order of γ is tosylate (γ = 0.11) > chloride (γ = 0.062) > bromide (γ = 0.044) > iodide (γ = 0.040). These magnitudes are all much less than unity, suggesting all the displacements are remote from the complete heterolysis of the carbon – leaving group bond.

The slopes for the halide leaving groups increase regularly as the pK_a of the halogen acid increases. On this basis, the tosylate should be located between the chloride and bromide (see Table 13). However, return phenomena, presumably least for the tosylate, may influence the slopes of the $\Delta G^{\ddagger}$ vs. ΔH_g^i correlations. Bentley and Dewar (110) ignore this possibility, partly because their discussion is focused on the classical S_N1 and S_N2 (1, 8) descriptions of the displacements rather than the more elaborate schemes suggested here, e.g., eqs. [121] and [122].

Although toluenesulphonic acid is a weaker acid than hydrogen bromide, nevertheless, the organic tosylates (see section 9 and Table 12) react faster than bromides in both solvolytic and definite bimolecular displacements. The higher reactivity of the tosylates in comparison with the bromides is tentatively explained here on the basis of less return for the former than the latter leaving group (Table 26). This rationalization draws substance from the observation that $\Delta C_p^{\ddagger}$ is less negative for the sulphonates in water. This represents indirect evidence based on the Albery–Robinson revised interpretation of $\Delta C_p^{\ddagger}$ values discussed in section 6. The extended use of ΔH_g^i for arylmethyl chlorides to the other leaving groups, namely, bromides, iodides, and the sulphonates, is formally justified (see eqs. [132] and [133]. Thermochemical data for the alkyl sulphonates that would

[6]J.M.W. Scott. Unpublished data.

© 2005 NRC Canada

Table 27. Iodide–bromide rate ratios for various displacements (T = 298.15 K).

Substrate	Nucleophile	k(I)	k(Br)	Ratio	N
MeX[a,b]	H_2O	4.07×10^{-7}	7.35×10^{-8}	0.181	0.00
MeX[a,c]	OH^-	1.46×10^{-4}	6.34×10^{-5}	0.434	4.20
MeX[c,d]	CN^-	1.28×10^{-3}	5.94×10^{-4}	0.464	5.10
MeX[c,d]	$S_2O_3^{2-}$	3.82×10^{-2}	3.02×10^{-2}	0.791	6.36
MeX[c,d]	I^-	7.02×10^{-4}	4.8×10^{-4}	0.683	5.04
t-BuX[a,b]	H_2O	7.61×10^{-1}	1.53	2.02	0.00
1-AdX[a,b]	H_2O	7.69×10^{-3}	1.01×10^{-2}	1.31	0.00
2-PrX[a,b]	H_2O	3.82×10^{-6}	2.79×10^{-6}	0.73	0.00
AllylX[a,b]	H_2O	1.70×10^{-5}	4.10×10^{-6}	0.35	0.00
EtX[a,b]	H_2O	3.87×10^{-7}	1.71×10^{-7}	0.442	0.00
BenzylX[b,e]	80% aqueous alcohol	5.04×10^{-5}	2.88×10^{-5}	0.571	—
2-NaphthylX[b,e]	80% aqueous alcohol	8.50×10^{-5}	4.07×10^{-4}	0.478	—
1-NaphthylX[b,e]	80% aqueous alcohol	1.48×10^{-4}	6.94×10^{-5}	0.469	—

[a]This paper.
[b]Solvolytic rate constants units are s^{-1}.
[c]Second-order rate constants units are L mol^{-1} s^{-1}.
[d]From references cited in ref. 42.
[e]From ref. 110 (T = 323.15 K).

verify the assumed additivity phenomena are, unfortunately, not available.

The halide anomaly

Although ΔH_g^i(RX) correctly predicts the order of reactivity for a series of primary alkyl chlorides, the extension of this relationship to any particular series of alkyl halides, e.g., the series RX, (X = F, Cl, Br, and I), implies the order of reactivity should be: I > Br > Cl > F. However, the observed order often follows the sequence Br > I > Cl > > F, an experimental fact frequently ignored in monographs (5, 17), reviews (14), and texts (1, 8). This "abnormal order" for the bromide and iodide is characteristic of the hydrolysis of primary and secondary bromides and iodides in water[2] and the arylmethyl bromides and iodides in 80% aqueous ethanol reported by Bentley and Dewar (110). The same order also characterizes the reaction of hydroxide ion and several other charged nucleophiles with the methyl halides (42). It has been argued that this order of reactivity signifies mechanistic complexity (42) but this proposal was vigorously rejected (33, 44, 45). In contrast, the tertiary halides represented by the *tert*-butyl and 1-adamantyl halides appear to follow the order expected based on ΔH_g^i(RX), namely, I > Br > Cl > F. Here, this latter sequence is designated as normal and is also the order anticipated on the basis of the pK_a(HX) values for the halogen acids discussed earlier. Subsequently, we define the normal order as one strictly following the atomic numbers of the halogen atoms either in an increasing or decreasing mode as is appropriate. Several inorganic displacements previously detailed in section 11 also display the normal order (see Table 18).

Generally speaking, most displacements involving bromide and iodide as leaving groups characterized by second-order kinetics display rate constants for which the k(I)/k(Br) ratios are *less than unity*. The odd exception to this rule represented by the rate constants that quantify the reaction of fluoride ion with methyl iodide and bromide is notable (42). The second-order rates for the nucleophiles (N_r), represented by water, hydroxide, cyanide, iodide, chloride, and thiosulphate, provide a satisfactory Swain–Scott (42, 111) LFER for methyl bromide and methyl iodide.

$$[165]\quad \log k(CH_3I,N_r) = (1.18 \pm 0.05)\ \log k(CH_3Br,N_r) + 0.303 \pm 0.21\ (6,0.993)$$

The data for this correlation are presented in Table 27. Subtracting $\log k(CH_3Br,N_r)$ from both sides of eq. [165] gives

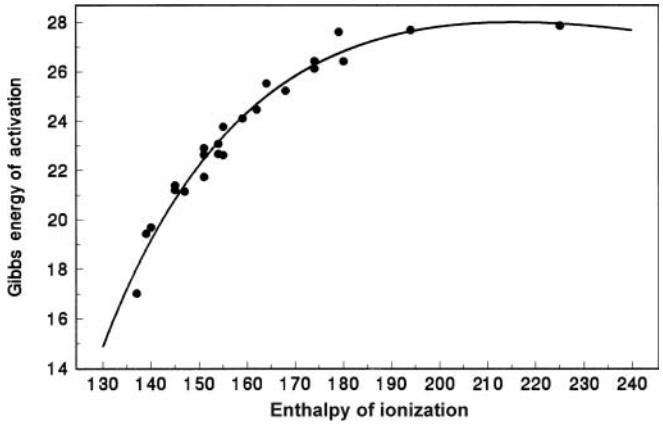
$$[166]\quad \log[k(CH_3I,N_r)/k(CH_3Br,N_r)] = (0.18 \pm 0.05)\ \log[k(CH_3Br,N_r)] + 0.303 \pm 0.21$$

Because the Swain–Scott nucleophilic constant N (or N_r) is defined in terms of $\log[k(CH_3Br,N_r)/k(CH_3Br,H_2O)]$, it follows from eq. [166] that the iodide–bromide ratios diminish with an increase in nucleophilic power as measured by N for methyl substrates. This particular observation suggests that *electron access* to the reacting carbon either from *external* or *internal* sources dominates the ratio. Furthermore, the electrostatic repulsion between the incoming nucleophile and the leaving group across the reacting carbon is likely to attenuate return phenomena. Hyperconjugative intramolecular electron release is important for the *tert*-butyl and 1-adamantyl iodides and bromides but presumably less so for the adamantyl substrates because the rigid structure of these compounds inhibits the change in geometry of the reacting carbon that facilitates hyperconjugation. The iodide–bromide ratio is larger for the former organic group. A small amount of rearside nucleophilic assistance that is necessarily absent in the case of the adamantyl compounds cannot be totally discounted in the case of the *tert*-butyl substrates.

The behaviour of bromide–iodide ratios for the arylmethyl systems is more difficult to understand. The *slopes* of the $\Delta G^{\ddagger}$ vs. ΔH_g^i for the arylmethyl halides ($ArCH_2X$, X = Cl, Br, and I, Cl > Br > I) show a *normal* halogen order, but this does not correlate with the reactivity sequence for a fixed arylmethyl system, which is Br > I > Cl. The slopes of the Swain–Scott LFER that are related to a definite bimolecular process are in a normal sequence: Cl < Br < I (42), but se-

© 2005 NRC Canada

Fig. 20. Correlation between the rates of hydrolysis for a series of primary chlorides (RCl) and the enthalpy of ionization of RCl.



lectivity and reactivity fail to correlate here too, reactivity being in the order Br > I > Cl. This contrasts with more recent product studies elsewhere for displacement reactions in which there is a good match between selectivity and reactivity (220, 221). However, the interpretations related to the latter study (221) do not appear to conflict with the main thesis of this contribution.

Nonlinear relationships between $\Delta G^{\ddagger}$ and ΔH_g^i

Nonlinear expressions that relate $\Delta G^{\ddagger}$ to ΔH_g^i can be developed to describe the hydrolytic reactivity for a more extended series of primary organic substrates ranging from methyl chloride to 4-methoxybenzyl chloride (see Table 23). This reaction series embraces a range of just under 100 kcal in ΔH_g^i on the abscissa (see Fig. 20).

The $\Delta G^{\ddagger}$ values for these substrates produce a fairly smooth curve that can be fitted to *empirical* equations either of the form $\Delta G^{\ddagger} = f(\Delta H_g^i)$ or $\ln(k) = f(\Delta H_g^i)$. A suitable empirical function that adequately relates $\Delta G^{\ddagger}$ to ΔH_g^i is

$$[167] \quad \Delta G^{\ddagger} = A(1) + A(2)/(\Delta H_g^i + 1) + A(3)/(\Delta H_g^i + 1)^2$$

A linear least-squares fit of the available data for the chlorides reported in Table 23 and and illustrated in Fig. 19 gives

$$[168] \quad \Delta G^{\ddagger} = 1.3377 \times 10^4/(\Delta H_g^i + 1) - 1.4461 \times 10^6/(\Delta H_g^i + 1)^2 - 2.94625$$

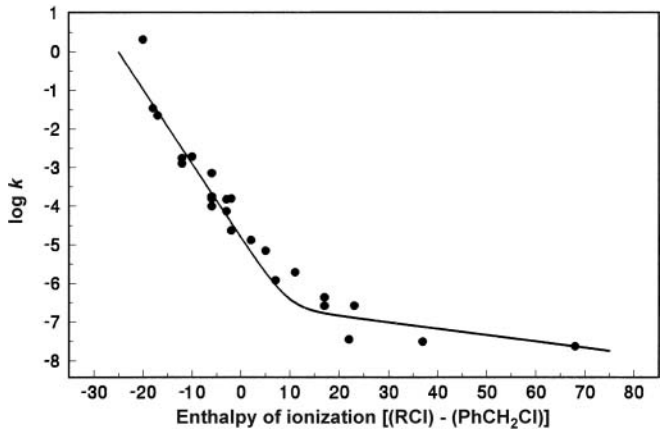
The observed and calculated values from eq. [168] give an adequate linear correlation

$$[169] \quad \Delta G^{\ddagger}(\text{calcd.}) = (0.970 \pm 0.024)\Delta G^{\ddagger}(\text{obs.}) + 0.698 \pm 0.577 \ (24, 0.985)$$

The slope at any point on the curve represented by eq. [167] can be obtained from the differential coefficient $\partial\Delta G^{\ddagger}/\partial\Delta H_g^i = \gamma$ and this quantity can be assigned the same meaning it has in eq. [143].

$$[170] \quad \partial\Delta G^{\ddagger}/\partial\Delta H_g^i = \gamma = -[A(2)/(\Delta H_g^i + 1)^2 + 2A(3)/(\Delta H_g^i + 1)^3]$$

Fig. 21. Alternative correlation of the rates of hydrolysis for a series of primary chlorides (RCl) and the relative enthalpies of ionization of RCl (RCl – $PhCH_2Cl$).



When the differential coefficient in eq. [170] is unity, $\Delta H_g^i \approx 111$ kcal. The slope for the most reactive substrate, namely, 4-methoxybenzyl chloride, is ≈0.40 ($\Delta H_g^i = 138$ kcal). On the basis of eqs. [168] and [170] none of the primary reactants between methyl chloride and 4-methoxybenzyl chloride approach a limiting (S_N1) mechanism when probed by this simple-minded criterion. On the other hand, eqs. [168] and [170] demonstrate that the reacting carbon becomes increasingly more electron deficient at some point on the reaction coordinate as ΔH_g^i is reduced — an eminently reasonable proposition.

The previous analysis (eqs. [144]–[158]) shows that the ΔH_g^i values for the chlorides can be used to correlate with $\Delta G^{\ddagger}$ for other leaving groups. For a series of organic methanesulphonates, the slope of the $\Delta G^{\ddagger}$ vs. ΔH_g^i plot for any particular alkyl methanesulphonate suggests the transition state is more ionic than for the corresponding chloride. This provides further evidence that the reacting carbon atom for sulphonate esters is more electron deficient than in the case of the related chlorides, a conclusion matching the findings of Bentley and Dewar (110) and Guthrie (23) established in other ways previously discussed. There is also an indirect link with Hoffmann's (109) use of the bromide–tosylate ratios as a basis for mechanistic diagnosis that will be examined in the next section.

A previously mentioned second tactic develops a definite correlation between ΔH_g^i and the rate of hydrolysis for a series of primary chlorides described by the bifurcated mechanism that forms part of the series of chemical events represented by eq. [121]. The equation

$$[171] \quad k_o \approx K_e(k_3 + k_7)$$

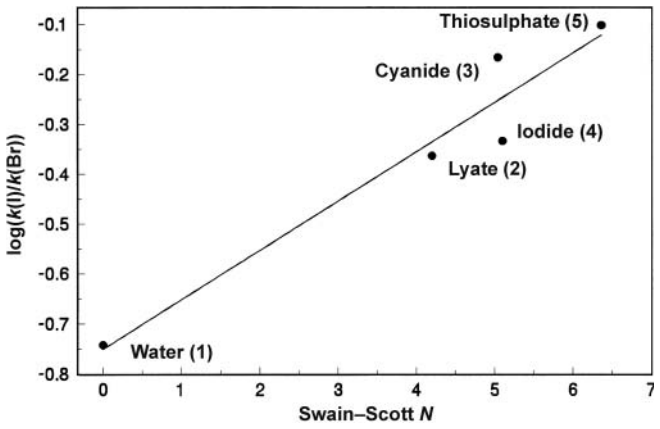
represents a simplified version of this scheme. The assumption that the two terms $K_e k_3$ and $K_e k_7$ related to ΔH_g^i exponentially gives

$$[172] \quad k_o = A(1)\exp(-A(2)\Delta H_g^i) + A(3)\exp(-A(4)\Delta H_g^i))$$

The fit of the experimental of the rate data to eq. [172] for a series of primary chlorides reacting in water listed in Table 23 to this expression via a grid search routine for $A(n)$ (n = 1–4) gave

© 2005 NRC Canada

Fig. 22. Variation of k(iodide)/k(bromide) ratios for a series of displacements in water. (1) Water, (2) lyate ion, (3) cyanide ion, (4) iodide ion, (5) thiosulphate ion.



$$[173]\quad \ln k_o = \ln[11.62\ \exp(-0.463\Delta H_g^i) + 13.10\ \exp(-0.0774\Delta H_g^i)]$$

and is illustrated in Fig. 21. A linear least-squares correlation between the observed rates and calculated from eq. [173] to base 10 gives

$$[174]\quad \log k_o(\text{calcd.}) = (1.010 \pm 0.031)\ \log k_o(\text{obs.}) - 0.186 \pm 0.155\ (24,0.977)$$

that is slightly inferior to eq. [168]. The fit to eq. [173] suggests that two distinct processes combine to give the observed rate constant as ΔH_g^i changes resulting in a mixed kinetics situation similar to that described for the substituted benzyl trifluoroacetates (see section 8, particularly, eq. [88]). A similar treatment underpins the discussion of curved Hammett plots in section 15 (Fig. 22).

It should be pointed out that the classical bifurcation for displacement reactions was between the S_N1 and S_N2 mechanisms. This split is accommodated here by the appropriate parts of eqs. [122] and [121]. Such a shift would involve processes *with and without backside assistance*. Equation [170] refers to a mechanism *with or without frontside assistance*. It is possible that actual substitutions as structure changes alter the ease of heterolysis and involve a meld of both these paths when rearside attack is unhindered. Such a mechanism is too complex to warrant further discussion.

Alternative quantum mechanical calculations

The present section briefly examines the use of more elaborate quantum mechanical energy calculations that relate to solvolytic displacements instead of energies estimated via either the HMO and PMO methods. We note that the primitive HMO and PMO methodologies depend on the application of the *aufbau* principle involving bonding, nonbonding, and antibonding orbitals. This principle apparently discards the fundamental tenet that all electrons within a given atom or molecule are identical. We would like to tackle the problems addressed here in a more rigorous manner that Ogilvie (222) demands, but the details of these techniques are not revealed. Our attitude to these matters has been briefly reported elsewhere (223).

Table 28. Data related to more advanced quantum mechanical methods.

Aryl group	$\Delta\Delta E_\pi$[a]	$\Delta\Delta E_\pi$[b]	ΔH_g^i[c]	ΔH_g^i[d]	ΔE_ω[e]
Benzyl	0.00	0.00	159	—	1.578
1-Naphthyl	17.84	10.99	145	—	1.805
2-Naphthyl	10.56	7.17	154	—	1.642
2-Anthracyl	18.57	—	148	—	1.734
2-Phenanthryl	13.29	10.12	155	—	1.644
3-Phenanthryl	13.38	11.53	150	—	1.712
9-Phenanthryl	22.39	14.15	146	—	1.796
2-Pyrenyl	10.56	—	158	—	1.594
4-Pyrenyl	25.12	—	142	—	1.838
1-Anthyracyl	—	17.53	137	—	—
4-MeO-Benzyl	—	—	138	145	—
4-Me-Benzyl	—	—	151	151	—
3-Me-Benzyl	—	—	157	152	—
4-Cl-Benzyl	—	—	163	158	—
3-Cl-Benzyl	—	—	169	161	—
4-CF_3-Benzyl	—	—	176	170	—
1-Phenanthryl	—	—	145	—	1.808
3-Triphenylyl	—	—	152	—	1.681
6-Chrysyl	—	—	140	—	1.838
1-Pyrenyl	—	—	132	—	1.999

[a]Reference 170.
[b]Reference 110.
[c]This paper.
[d]Reference 188.
[e]Reference 168.

Fry and co-workers (188) have calculated the heats of formation of a series of substituted benzyl chlorides and the related substituted benzyl carbocations using the MINDO algorithm. These quantities can be combined with the heat of formation of the chloride ion at 58.3 kcal mol^{-1} to give ΔH_g^i(MINDO) for the processes

$$[175]\quad \text{X-C}_6\text{H}_4\text{CH}_2\text{Cl} \rightarrow \text{X-C}_6\text{H}_4\text{CH}_2^+ + \text{Cl}^-$$

with X = 4-H, 4-CH_3O, 4-CH_3, 3-CH_3, 4-Cl, 3-Cl, and 4-CF_3, which when compared with thermochemical values ΔH_g^i(T) gives

$$[176]\quad \Delta H_g^i(\text{MINDO}) = (0.629 \pm 0.058)\Delta H_g^i(\text{T}) + 55.7 \pm 9.9\ (7,0.957)$$

Both Bentley and Dewar (110) and Streitwieser et al. (170) report energies of stabilization relative to the benzyl cation for series of arylmethyl cations. Streitwieser's data (170) correlate with the thermochemical data

$$[177]\quad \Delta\Delta E_\pi = (1.13 \pm 0.13)\Delta H_g^i(\text{T}) - 186.0 \pm 19.5\ (9,0.913)$$

and similar data reported by Bentley and Dewar (110) give

$$[178]\quad \Delta\Delta E_\pi = (0.665 \pm 0.104)\Delta H_g^i(\text{T}) - 109.6 \pm 15.5\ (6,0.89)$$

Streitwieser (168) has also reported a correction to the simple HMO levels presented as ΔE_ω, which give a satisfactory correlation with ΔH_g^i(T).

© 2005 NRC Canada

Table 29. Data related to the Hoffmann linear free energy relationship (T = 298.15 K).

Organic group	log$k$(RBr)	log$k$($ROSO_2CH_3$)	log$k$(calcd.)	Ratio	RCl	RNO_3
Ethyl	–6.412	–5.405	–5.055	10.16	—	—
Propyl	–6.565	–5.539	–5.242	10.62	—	—
3-Me-2-Butyl	–4.100	–2.964	–2.234	13.68	—	—
2-Adamantyl	*–5.190*	–3.827	–3.564	23.07	*–6.643*	–7.895
2-Propyl	–5.148	–3.707	–3.513	27.61	–6.675	–7.326
Methyl	–6.890	–5.295	–5.639	39.36	–7.622	–8.559
4-Nitrobenzyl	*–5.371*	*–3.741*	–3.785	42.66	–6.535	–7.413
Benzyl	*–3.780*	–1.973	–1.843	64.12	–4.869	–5.305
4-Chlorobenzyl	*–4.022*	*–2.205*	–2.139	65.61	–5.144	–5.595
3-Methylbenzyl	*–3.544*	*–1.690*	–1.555	71.45	–4.689	–4.967
Allyl	–4.770	*–2.888*	–3.051	76.21	–5.917	–6.672
2-Methylbenzyl	*–2.829*	*–0.845*	–0.683	96.38	–3.903	–4.000
4-Methylbenzyl	*–2.308*	*–0.252*	–0.047	113.76	–3.350	—
3-Chlorobenzyl	—	—	—	—	–5.708	—
4-Methoxybenzyl	—	—	—	—	0.499	—
Cyclopentyl	–5.568	–3.380	–4.025	154.17	—	–7.175
Cyclohexyl	–4.754	–2.263	–3.032	309.74	—	–6.294
tert-Butyl	–0.119	*+2.680*	+2.624	629.51	–1.506	–0.364
1-Adamantyl	–2.114	+0.701	+0.190	653.13	–3.529	–1.813

Note: Italicized values interpolated and extrapolated from other Hoffmann linear free energy relationships. See section 14 of the text. log$k$($ROSO_2CH_3$) = (1.220 ± 0.038) log(RBr) + 2.77 ± 0.18 (17,0.985).

[179] $\Delta H_g^i(T) = (-64.16 \pm 1.48)\Delta E_\omega - 260.0 \pm 2.58$ (13,0.994)

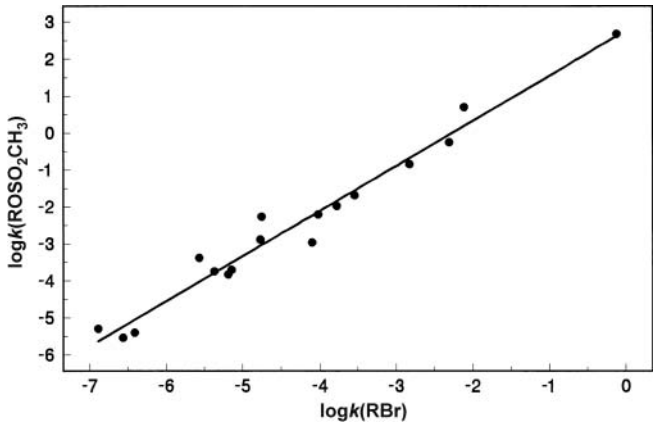
This is not surprising because the dependent and independent variables in eq. [176] have similar origins. It should be pointed out here that the calibration from measured thermochemical data that allow the calculation of $\Delta H_g^i(T)$ for the arylmethyl systems of interest covers 70% of the total range of this quantity. Attention is also drawn to the observation that the slopes of eqs. [177] and [178] both demonstrate considerable departures from unity. Clearly, in all cases, the more advanced methods correctly predict trends but require scaling to reproduce the experimentally based thermochemical values. The data for these correlations are reported in Table 28.

14. The Hoffmann criterion — A new linearfree energy relationship

Hoffmann's (109) use of the rate constant ratios k(R-tosylate)/k(R-Br) as mechanistic criteria can also be scrutinized in terms of a LFER similar to those examined in section 9. Instead of fixing two R groups and varying the leaving groups, as discussed in section 9, the two leaving groups are fixed and the organic groups are varied over primary, secondary, and tertiary organic structures. The Streitwieser Plots examined in section 13 involving tosylates and chlorides represent similar correlations, although in this particular LFER the substrates are confined to primary carbon centres.

The rate data for the bromide and tosylate leaving groups reacting in water are relatively meagre in comparison with the k(R-mesylate)/k(R-Br) ratios. Hence, the LFER is developed here in terms of the mesylate and bromide rate constants and the data are recorded in Table 29. The minor kinetic differences between tosylate and mesylate as leaving groups are considered inconsequential for these displacements in the present context. The data recorded in Table 29 give rise to

Fig. 23. Hoffmann LFER between the rates of hydrolysis for a series of organic methanesulphonates and chlorides.



[180] log$k$(R-mesylate) = (1.220 ± 0.038) log$k$(R-Br) + 2.77 ± 0.18 (17,0.985)

Equation [180] is illustrated in Fig. 23 and embraces over six orders of magnitude on each axis. Available data for other leaving groups when paired with bromide give

[181] log$k$(R-NO_3) = (1.085 ± 0.028) log$k$(R-Br) – 1.332 ± 0.12 (12,0.993)

and

[182] log$k$(R-Cl) = (0.847 ± 0.040) log$k$(R-Br) – 1.689 ± 0.19 (7,0.988)

© 2005 NRC Canada

The Hoffmann criterion proposes that the ratio k(R-mesylate)/k(R-Br) is "large" for limiting (S_N1) displacements and smaller for those with S_N2 character. However, because structural changes are treated as "continuous" in physical approaches to the reactivity of organic substances, the Hoffmann ratios that are related to the LFER represented by eq. [180] are constitutionally unsuited for making *sharp mechanistic distinctions* (72, 181).

The subtraction of log$k$(RBr) from both sides of eq. [180] gives

$$[183] \quad \log[k(\text{R-mesylate})/k(\text{R-Br})] = 0.220\ \log k(\text{R-Br}) + 2.77$$

Thus, the focal quantity related to Hoffmann's discussion here, namely, the ratio k(R-mesylate)/k(R-Br), rather than k(R-tosylate)/k(R-Br), is trivially an increasing function of the reactivity of the bromide if the coefficient of log$k$(R-Br) is greater than zero and vice versa if the coefficient is less than zero. Equation [183] is clearly in the former category.

On the basis of thermodynamic considerations, the mesylate–bromide ratio should reach a limiting value that is a function of the Gibbs energy differences related to: (*i*) the gas-phase heterolysis of the paired alkyl mesylates and bromides; (*ii*) the solvation difference between the mesylate and bromide anions; and (*iii*) initial state differences. To a first approximation, items (*i*)–(*iii*) are all expected to be constant for the classical S_N1 mechanism (see section 13, particularly eq. [131] and ref. 34). For cases where the mechanism is not limiting and kinetic complexity is prevalent, e.g., the Winstein scheme and analogous alternatives (see eqs. [52], [121], and [122]), the simple thermodynamic differences previously listed *would only contribute to part of the observed ratio.* Indeed, Hoffmann's mechanistic analysis is limited to that appropriate to a simple classical S_N1 reaction as originally envisaged by the Ingold (1, 8) school. Any return processes, either internal or external, invalidate the meaning of the rate ratio in Hoffmann's terms. Return processes are likely to favour the bromide in comparison with the mesylate anion because these ions are good and poor nucleophiles, respectively. Hence, the increasing ratio for the faster reacting substrates probably reflects reduced return phenomena combined with an increased tendency towards a more limiting (S_N1) process for both the mesylates and the bromides as the relative reactivity of the latter substrate increases.

The problem of mesylate–bromide ratios has also been considered indirectly by Bentley and Dewar (110) within the framework of the simple Ingold S_N1–S_N2 dichotomy and this is considered in section 13. These workers anticipate the order for increasing carbocation character for a series of arylmethyl halides to be I > Br > Cl. However, this is in the opposite order they observed based on an analysis linked to the simple Ingold mechanistic dichotomy that is based on the γ quantities mentioned in section 13. For the arylmethyl halides, the latter quantities are in the order γ(Cl) > γ(Br) > γ(I) indicating that the extent of heterolysis increases in the order I < Br < Cl rather than the opposite sequence suggested by Bentley and Dewar (110). Again, no kinetic complexity was attributed to the observed rate constants and the possible significance of return phenomena either internal or external to their work was overlooked for all the leaving groups they considered.

15. Curved Hammett plots

Curved plots frequently characterize attempts to apply the Hammett LFER to the rate constants that characterize solvolytic and definite bimolecular nucleophilic displacements of substituted benzyl substrates (see, particularly, refs. 2, 216, and 217). The solvolysis of the 3- and 4-substituted dimethylphenylcarbinyl chlorides (215) and the α-phenylethyl chlorides (70) represent a notable exception to this observation. The former displacements underpin and define the σ^+ scale that is apparently uncluttered with either differential solvation phenomena or significant mechanistic changes — a proposition evident from the observation that the σ^+ quantities give a satisfactory Hammett plot with the ionization potentials of the substituted benzyl radicals measured in the *gas phase* (200, 202–205) (see eq. [159]). Thus, displacements at these activated secondary and tertiary carbon centres are presumably dominated by internal energy changes on activation rather than solvation, although the conditions $\delta_{Ar}[\Delta G^{\ddagger}(ArCH_3)_2CCl)] \approx 0.3\delta_{Ar}[I_p(ArCH^{\cdot})]$ and $\delta_{Ar}[\Delta G^{\ddagger}(Ar(CH_3)_2CCl)] \approx \delta_{Ar}[\Delta G^{\ddagger}(Ar(CH_3)HCCl)]$ respectively hint that something less than a limiting mechanism is operative for both series of substrates (see section 13). This contrasts with the solvolytic rate constants that characterize displacements involving primary benzyl systems, which inevitably give curved Hammett plots with correlations employing either the σ^+ or σ substituent constants.

Curved Hammett plots for benzyl displacements are often explained (2, 224) in terms of the differential influence of the substituents on concerted bond-making and bond-breaking processes in the transition state. Such bonding changes result in concave up plots with the minimal reactivity usually coinciding with the unsubstituted substrate. Negative substituents located at the 3- and 4-ring positions are postulated to facilitate bond breaking relative to hydrogen, whereas positive substituents in the same locations expedite bond formation relative to the standard atom. Thus, the observed rate constants reflect a meld of two distinct influences by the 3- and 4-substituents on the bonding in a bimolecular transition state.

Nevertheless, there are alternative possibilities that can be offered to explain the curvature of Hammett correlations. It is possible that the observed rate constants for these displacements are a function of two or more rate constants (e.g., eq. [58]) and that these quantities correlate *individually and accurately* with the appropriate Hammett substituent constants. This proposal can be examined further for the mechanism described by eq. [58] using either the steady-state expression eq. [59] or eqs. [67] and [68]. Here the second, more rigorous, of these alternatives is preferred and the equations basic to this mechanism are repeated here for convenience: $\lambda_1 + \lambda_2 = k_1 + k_2 + k_3$ and $\lambda_1\lambda_2 = k_1k_3$.

The differentiations necessary to develop the formalities of the Hammett analysis are simplified by conducting the mathematical manipulations in terms of natural rather than decadic logarithms with the central premise that the individual processes in eq. [58] obey a linear Hammett LFER. This means that each k_n (n = 1–3) using either the σ or σ^+ scales

© 2005 NRC Canada

gives rise to ρ_n values (n = 1–3) defined by the equations summarized by

$$[184] \quad \frac{\partial \ln k_n}{\partial \sigma} = \rho_n = \text{constant } (n = 1\text{–}3)$$

Two slopes ($\boldsymbol{P}_r$, r = 1 or 2) of the Hammett correlation related to eq. [58] are defined in terms of the dynamic constants λ_1 and λ_2

$$[185] \quad \frac{\partial \ln \lambda_r}{\partial \sigma} = \boldsymbol{P}_r \quad (r = 1 \text{ or } 2)$$

At this point in the mathematical analysis it is not immediately obvious which of either $\boldsymbol{P}_1$ or $\boldsymbol{P}_2$ is related to the experimental observations, so the formalities are conducted assuming that $\boldsymbol{P}_1$ and $\boldsymbol{P}_2$ have parity until all of the pertinent expressions have been derived. The appropriate differentiations with respect to σ of eqs. [67] and [68] lead to relationships between $\boldsymbol{P}_1$ and $\boldsymbol{P}_2$ to rate constants that characterize the mechanism described by eq. [58].

Differentiating eqs. [67] and [68] with respect to σ provides the linear system

$$[186] \quad \lambda_1 \boldsymbol{P}_1 + \lambda_2 \boldsymbol{P}_2 = k_1\rho_1 + k_2\rho_2 + k_3\rho_3$$

$$[187] \quad \boldsymbol{P}_1 + \boldsymbol{P}_2 = \rho_1 + \rho_3$$

Simultaneously solving [186] and [187] for $\boldsymbol{P}_1$ and $\boldsymbol{P}_2$ on the assumption that $\lambda_2 < \lambda_1$ (see the previous paragraph) gives

$$[188] \quad \boldsymbol{P}_1 = [k_1\rho_1 + k_2\rho_2 + k_3\rho_3 - \lambda_1(\rho_1 + \rho_3)]/(\lambda_1 - \lambda_2)$$

$$[189] \quad \boldsymbol{P}_2 = [k_1\rho_1 + k_2\rho_2 + k_3\rho_3 - \lambda_2(\rho_1 + \rho_3)]/(\lambda_2 - \lambda_1)$$

Because $k_n = f(\sigma)$ and $\lambda_r = f(k_n)$, the slope of the Hammett plot given by either eqs. [188] or [189] is not constant but depends on σ. In short, the related Hammett plot must be curved.

Differentiating [186] and [187] with respect to σ to obtain the second differential gives

$$[190] \quad \lambda_1(\boldsymbol{P}_1)^2 + \lambda_2(\boldsymbol{P}_2)^2 + \frac{\lambda_1 \partial \boldsymbol{P}_1}{\partial \sigma} + \frac{\lambda_2 \partial \boldsymbol{P}_2}{\partial \sigma} = k_1(\rho_1)^2 + k_2(\rho_2)^2 + k_3(\rho_3)^2$$

$$[191] \quad \frac{\partial \boldsymbol{P}_1}{\partial \sigma} + \frac{\partial \boldsymbol{P}_2}{\partial \sigma} = 0$$

For either a maximum or minimum in the log$k$(obs.) or here in the $\ln\lambda_1$ or $\ln\lambda_2$ vs. σ coordinate system, $\boldsymbol{P}_1 = 0$ and $\boldsymbol{P}_2 = 0$, and hence, the first two expressions on the LHS of eq. [190] are zero. Additionally, the three terms on the RHS of eq. [190] are necessarily positive because $k_n > 0$ and $\rho_n^2 > 0$ (n = 1–3). The time evolution of the chemical system described by eq. [58] is given by eq. [66]. This expression involves two exponential terms containing λ_1 and λ_2. Generally speaking, the smaller dynamic constant, arbitrarily λ_2 (see eq. [70]), will dominate the changes of concentration with time. Hence, $\boldsymbol{P}_2$ and the differential of $\boldsymbol{P}_2$ with respect to σ provide the information to fix the behaviour of the Hammett plots related to the mechanism described by eq. [58]. Simultaneously solving eqs. [190] and [191] gives

$$[192] \quad \frac{\partial \boldsymbol{P}_1}{\partial \sigma} = [k_1(\rho_1)^2 + k_2(\rho_2)^2 + k_3(\rho_3)^2]/(\lambda_1 - \lambda_2) \; (>0 \rightarrow \text{minimum})$$

$$[193] \quad \frac{\partial \boldsymbol{P}_2}{\partial \sigma} = [k_1(\rho_1)^2 + k_2(\rho_2)^2 + k_3(\rho_3)^2]/(\lambda_2 - \lambda_1) \; (<0 \rightarrow \text{maximum})$$

The differential coefficient in eq. [193] is *negative* corresponding to a maxima in the logλ_2 vs. σ coordinate system. Such unusual behaviour has been observed recently by Kevil et al. (225) for the methanolysis of a series of benzyl tosylates and is suggestive of the mechanism represented by eq. [58] for these displacements. However, this analysis will not explain the more usual observation for substitutions at a saturated carbon atom in which either the Hammett correlations show a definite minima or steadily increasing slope (more positive) with increasing σ. This behaviour is exemplified by the hydrolysis of a series of substituted benzyl chlorides and tosylates (see Table 26). The data for the two former reaction series are presented in Table 26 and the related Hammett plots are illustrated in Figs. 24 and 25.

Fig. 24. Curved Hammett LFER for the hydrolysis of a series of benzyl tosylates in acetone–water mixtures.

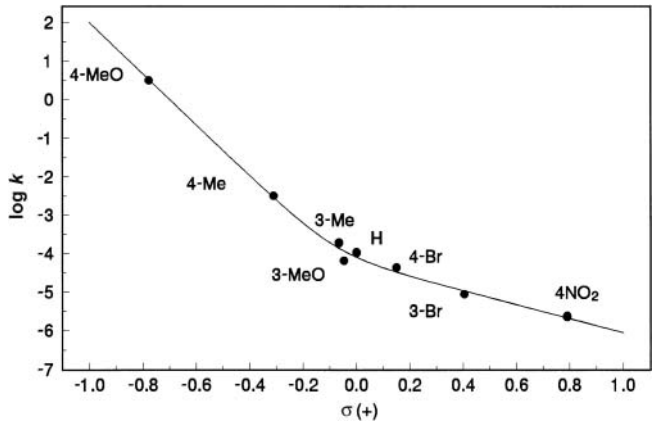
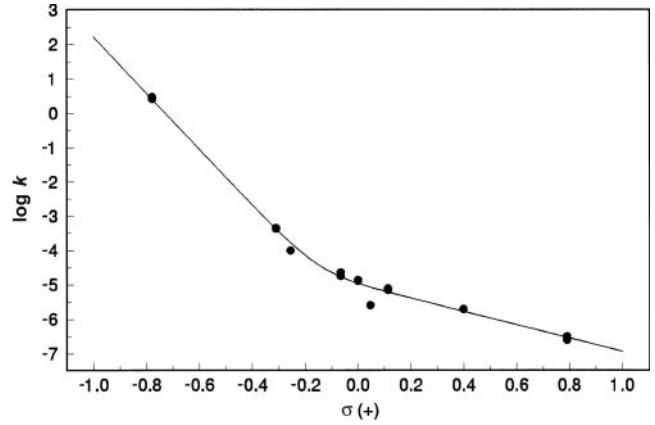


Fig. 25. Curved Hammett LFER for the hydrolysis of a series of benzyl chlorides.



© 2005 NRC Canada

Clearly, the mechanism represented by eq. [58] fails to quantify the curved Hammett profiles.

A Hammett plot with either a definite minimum or a continuously increasing slope as σ increases requires a revised model. The observed profile can be understood in terms of a bifurcated mechanism such as

$$[194]\qquad \begin{array}{l} \qquad\qquad\qquad\qquad\qquad\qquad \overset{\text{fast}}{\text{W-R}^+ + \text{X}^- \rightarrow}\ \text{Route } R(1) \\ \text{RX} + \text{W} \underset{k_2}{\overset{k_1}{\rightleftharpoons}} \text{W-R}^+\text{X}^- \begin{array}{l} \nearrow k_3 \\ \searrow k_4 \end{array} \\ \qquad\qquad\qquad\qquad\qquad\qquad \overset{\text{fast}}{\text{W-R}^+|\text{W}|\text{X}^- \rightarrow}\ \text{Route } R(2) \end{array}$$

In this scheme, the nucleophilically assisted ion pair can react directly to give an oxonium ion route ($R(1)$) or via a solvent separated ion pair ($R(2)$). It is important to note here that the mechanism represented by eq. [194] will add a positive component to the apparent heat capacity of activation for which there is a well-established similar example (79) that involves a bifurcation between S_N and $B_{Ac}2$ mechanisms. Other bifurcations are possible within the framework of the Winstein scheme, but we favour the sequences in eq. [194] for the benzyl chlorides and tosylates in Table 26.

The matrix formulation (see Appendix D) of the rate equations associated with the mechanism described by eq. [194] is

$$[195]\qquad \begin{bmatrix} (D + k_1) & -k_2 & & \\ -k_1 & (D + k_2 + k_3 + k_4) & & \\ & -k_3 & D & \\ & -k_4 & & D \end{bmatrix} \begin{bmatrix} A \\ B \\ P(1) \\ P(2) \end{bmatrix} = 0$$

where the operator $D \equiv \mathrm{d}/\mathrm{d}t$. Equation [195] gives rise to the auxiliary quartic equation

$$[196]\qquad \lambda^2[\lambda^2 + \lambda(k_1 + k_2 + k_3 + k_4) + k_1k_3 + k_1k_4] = 0$$

and the related dynamic constants λ_1 and λ_2, aside from the two trivial roots of zero, relate to the component rate constants of the bifurcated mechanism in eq. [194] by

$$[197]\qquad \lambda_1 + \lambda_2 = k_1 + k_2 + k_3 + k_4$$

$$[198]\qquad \lambda_1\lambda_2 = k_1k_3 + k_1k_4$$

In this case, the repetition of the analysis elaborated in eqs. [67], [68], and [184]–[191] is superfluous. The differentiation of eq. [198] twice with respect to σ suffices to establish the required conditions for $\boldsymbol{P}_1$ and $\boldsymbol{P}_2$, namely,

$$[199]\qquad \frac{\partial \boldsymbol{P}_1}{\partial \sigma} + \frac{\partial \boldsymbol{P}_2}{\partial \sigma} = k_3k_4(\rho_4 - \rho_3)^2/(k_3 + k_4)^2$$

Equation [199] confirms that the second differentials related to $\boldsymbol{P}_1$ and $\boldsymbol{P}_2$, in contrast to those in eq. [191] can, in principle, be positive, whereas in the case of eq. [191], the requirement that the first differential corresponding to the smaller dynamic constant is impossible. Hence, the curved Hammett plots provide indirect evidence that the hydrolysis reactions are complex. It should be emphasized that the preceding treatment of curved Hammett profiles remains true for the mechanisms considered under all situations, whereas previous analysis appears to be confined to steady-state treatments (216).

Two groups of rate data are consistent with eq. [194], namely, the solvolysis of a series of benzyl tosylates measured by Kochi and Hammond (226) in acetone–water mixtures and the hydrolysis of a series of benzyl chlorides measured by several groups reported in Table 26. In both cases, the rate data can be fitted to a simplified equation of the form

$$[200]\qquad \log k_o = \log[10^{(a(1)+b(1)x)} + 10^{(a(2)+b(2)x)}]$$

that relates to eq. [167] in an earlier section and eq. [194]. The quantity k_o is the observed rate constant, x is the Hammett σ^+ substituent constant, and the quantities $a(1)$, $b(1)$, $a(2)$, and $b(2)$ are empirical constants. In the case of the rate data reported in Table 26 for a series of substituted benzyl chlorides and tosylates, the empirical constants were established by a grid search routine.

For the benzyl tosylate rate data, the numerical constants are: $a(1) = -4.641$, $b(1) = -6.639$, $a(2) = -4.237$, and $b(2) = -1.813$. The correlation between the observed and calculated (k_c) rate constants from eq. [200] using the values for $a(1)$, $b(1)$, $a(2)$, and $b(2)$ gives

$$[201]\qquad \log k_c = (0.9934 \pm 0.0168)\ \log k_o(-0.037 \pm 0.071)\ (18,0.9950)$$

Similarly, for the benzyl chloride rate data, the constants are $a(1) = -5.950$, $b(1) = -8.170$, $a(2) = -4.999$, and $b(2) = -1.930$. The equation corresponding to [201] is

$$[202]\qquad \log k_c = (0.9856 \pm 0.0153)\ \log k_o(-0.024 \pm 0.072)\ (16,0.9963)$$

The curves calculated from the derived empirical constants along with the experimental points are illustrated in Figs. 24 and 25. Both sets of data give adequate fits to eq. [200] supporting the bifurcated mechanism described by eq. [194].

The two differing coefficients of σ^+, namely $b(1)$ and $b(2)$, for the individual curve fits for both the benzyl chlorides and tosylates are suggestive of mechanistic shifts, the more negative values suggesting pathways involving a more electron-deficient carbon atom. The smaller (more negative) coefficients of σ^+ are comparable to the slope of the Hammett correlation for the solvolysis of the dimethylcarbinyl chlorides (215)

$$[203]\qquad \log k_o = (-4.48 \pm 0.02)\sigma^+ - 3.90 \pm 0.01\ (9,0.998)$$

and that of the α-phenylethyl chlorides (70),

$$[204]\qquad \log k_o = (-6.41 \pm 0.02)\sigma^+ - 2.28 \pm 0.11\ (8,0.992)$$

but these comparisons are not clear-cut because of drastic solvent changes that are involved in the comparison.

The steady-state treatment related to eq. [194] for k_o for the removal of the substrate RX gives

$$[205]\qquad k_o = k_1(k_3 + k_4)/(k_2 + k_3 + k_4)$$

The smaller of the two dynamic constants correlates with k_o. Synthetic data generated by solving eq. [188] to give the products $\boldsymbol{P}(1)$ and $\boldsymbol{P}(2)$ as a function time can be processed

© 2005 NRC Canada

Table 30. α-Deuterium secondary isotope effects and related transition-state acidities for primary substrates.

Hydrogen substrate	$pK_a^{\ddagger a}$	$\delta_I\Delta G^{\ddagger}$(obs.)[b]	$\delta_I\Delta G^{\ddagger}$(calcd.)[c]	Δ^d
Methyl chloride	12.02	19.900	15.403	–4.50
Methyl bromide	11.45	23.800	24.390	+0.59
Methyl iodide	11.06	32.400	30.539	–1.86
Methyl mesylate	12.10	12.600	14.142	+1.54
Methyl sulphate	12.01	4.800	15.561	+10.76
Methyl perchlorate	12.39	16.500	9.570	–6.93
Methyl nitrate	11.64	21.600	21.394	–0.21
Ethyl tosylate	13.72	–12.000	–11.399	+0.60

[a] $pK_a^{\ddagger}$ is the transition-state acidity constant (see section 3).
[b] $\delta_I\Delta G^{\ddagger}$(obs.) is the observed isotope effect (eq. [207]); Units in calories. Data is from ref. 55.
[c] $\delta_I\Delta G^{\ddagger}$(calcd.) is the calculated isotope effect according to the least-squares correlation (eq. [206]).
[d] $\Delta = \delta_I\Delta G^{\ddagger}$(calcd.) – $\delta_I\Delta G^{\ddagger}$(obs.).

to yield a pseudo-first-order rate constant (k_o) that, generally speaking, closely matches the smaller of the dynamic constants λ_2 rather than k_o given by eq. [205], i.e., the more elaborate analyses via eqs. [67] and [68] for eq. [58] and eqs. [197] and [198] for eq. [194] are more reliable.

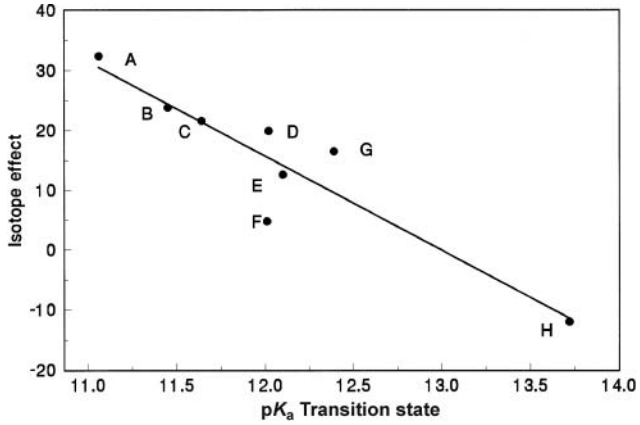
16. Secondary hydrogen–deuterium isotope effects

Secondary isotope effects have contributed to an understanding of solvolytic displacements (2, 4, 55, 70, 227–230). Here we offer brief comment on α-deuterium effects for primary and secondary displacements in the light of the Kurz (24) analysis that clarifies the meaning of the k_l/k_w ratios discussed in section 3. Kurz considers that this ratio gives a measure of the acidity of the protons that are components of the attacking water molecule (see eq. [48]).

It is reasonable to assume that increasing interaction of the attacking water molecule with the incipient positive carbon centre will be paralleled by increasing acidity of the water protons. The α-deuterium effects are usually interpreted in terms of the "tightness" of a S_N2 transition state that is anticipated to be a function of the nucleophilicity of both the nucleofuge and the nucleophilicity of the attacking nucleophile. According to the conventional wisdom, the tightness, when translated into vibrational terms, influences the out-of-plane vibrations of the α-hydrogens that are postulated to dominate the magnitude of the ratio, $k(H)/k(D)$. Thus, "tighter" transition states are to be anticipated with leaving groups that combine enhanced leaving group and nucleophilic properties. In this role, the bromide and iodide ions are surely preeminent: both are good nucleophiles and good leaving groups. Hence, the transition-state water molecules are expected to display enhanced acidity for these leaving groups and this speculation is born out in practice. Indeed, there is a definite trend between the isotope effect and $pK_a^{\ddagger}$ for the eight structures in Table 30, the isotope effect passing from inverse ($k(H)/k(D) < 1$) to normal ($k(H)/k(D) > 1$) as the nucleophilicity of the nucleofuge decreases.

$$[206]\quad \delta_I\Delta G^{\ddagger} = (-15.77 \pm 1.8)pK_a^{\ddagger} + 204.9 \pm 21.8\ (8,0.92)$$

Fig. 26. Correlation isotope effects with $pK_a^{\ddagger}$ (also see section 3). (A) CH_3I, (B) CH_3Br, (C) CH_3NO_3, (D) CH_3Cl, (E) $CH_3SO_3CH_3$, (F) $(CH_3)_2SO_4$, (G) CH_3ClO_4, (H) 4-CH_3-$C_6H_4SO_3CH_2CH_3$.



Departures from eq. [206] that are evident in Fig. 26 are probably a consequence of the difficulty of normalizing the isotope effects to a common temperature. This is accomplished here and elsewhere (230) by the expression

$$[207]\quad \delta_I\Delta G^{\ddagger} = -(RT/n)\{\ln[k(H)/k(D)]\}$$

an equation that is, at best, a compromise. The symbols R, T, k, H, and D in eq. [207] have their usual connotation and "n" specifies the number of deuterium atoms attached to the reacting α-carbon, three, two, and one for the methyl, ethyl, and 2-propyl derivatives, respectively. It should be noted that Halevi (230) reports data with the negative sign in eq. [207] dropped.

When the $pK_a^{\ddagger}$ reaches 15.74, according to eq. [206], $k(H)/k(D) = 1.07 \pm 0.01$ for a single deuterium. This ratio corresponds to the acidity of the nucleophilic water molecule being identical to that of bulk water at 298.15 K, suggesting that nucleophilic assistance at this value of $pK_a^{\ddagger}$ has become negligible. A further increase in the α-deuterium isotope effect beyond 1.07 ± 0.01 for other alkyl groups more reactive than methyl possibly corresponds to further loosening of the RX bond that, in the case of *p*-methylbenzyl chloride and nitrate, lead to normal ratios $k(H)/k(D) = 1.06$ and 1.08 per deuterium, respectively (229), in good agreement with the calculated limiting value from

© 2005 NRC Canada

eq. [206]. These are suggestive of the mechanism given in eq. [122], but the evidence for this proposal is not definitive.

The extension of the Kurz analysis to displacements at a secondary carbon centre is not possible at the present time because the rate constants for lyate ion attack on secondary substrates have not been measured in water. The k(H)/k(D) ratios for the α-deuterated 2-propyl group linked to halide and sulphonic acid leaving groups are normal (70) and in the terminal parts of the limiting region and beyond, i.e., 1.05–1.13. Halevi (230) regards these ratios to be characteristic of a predominately "dissociative" displacement. However, there are problems with this conclusion. The rates of the 2-propyl sulphonates and the nitrate and the related 2-adamantyl derivatives are almost equal in water, the former esters being only marginally more reactive (see Tables 13, 14, and 21B. The small enhancement manifested by the 2-propyl esters can be attributed to a meagre measure of nucleophilic assistance necessarily absent in the case of the adamantyl compounds. However, the extent of such assistance, measured by Bentley's ratio $R(H_2O)/R$(TFA) (144) suggests a level of interaction in the case of the open chain secondary compounds well beyond the actual difference in reactivity between the open chain and hindered substrates and is at variance with the large normal isotope effects previously mentioned. There is a hint here that suggests that the 2-propyl substrates heterolyse via the intervention of an intimate ion pair that is predominately removed by the *frontside* rather than *backside* attack of a water molecule and that this sequence of chemical events represents a significant and possible mechanistic category.

17. Conclusions

The aim of the present contribution has been to highlight facts and issues that are at variance with the notion that simple displacements in water, particularly those associated with primary carbon atoms, are adequately described by the S_N2 mechanism. The theoretical discussions of related matters by Dewar and Carrion (231) and Wolfe and co-workers (17) do not seem to clarify these issues. Indeed, it would appear that the intricacies in solution are not necessarily reflected in gasphase phenomena, although simple gas-phase phenomena definitely offer a measure of illumination of reactivity in the condensed phase. An appropriate general philosophy towards mechanistic studies has been presented aptly by Hirsch (232): "It is a basic tenet that a mechanism can never be proven. In order for a mechanism to be accepted the experimental observations must rule out all other conceivable mechanisms. If we accept the premise that the current approach to the analysis of reaction mechanism is itself a cohesive and viable model, we recognise therefore the limitation of this approach is the ability of human beings to conceive possible mechanisms."

Acknowledgements

The author wishes to thank Professor M.J. Blandamer and Professor R.E. Robertson retired from the University of Leicester, Leicester, UK and the University of Calgary, Calgary, Alberta, respectively, for their continued interest. Dr. Robertson is also thanked for permission to report some unpublished data. Several colleagues and students at Memorial University are also thanked for their continued interest, particularly, Dr. Peter Golding and the late Dr. June Winter. The author would also like to thank one of his referees for sustained advice.

References

1. C.K. Ingold. *In* Structure and mechanism in organic chemistry. G. Bell, London. 1953.
2. A. Streitwieser, Jr. *In* Solvolytic displacement reactions. McGraw-Hill, New York. 1962.
3. C. Bunton. *In* Nucleophilic substitution at a saturated carbon atom. Elsevier, London. 1963.
4. E.R. Thornton. *In* Solvolysis mechanisms. Ronald Press, New York. 1964. Chap. 5.
5. R.F. Hudson. *In* Structure and mechanism in organophosphorus chemistry. Academic Press, London and New York. 1965. Chap. 4.
6. R.E. Robertson. *In* Progress in physical organic chemistry. Vol. 4. John Wiley and Sons, New York. 1967. p. 213.
7. G. Kohnstam. *In* Advances in physical organic chemistry. Vol. 5. Academic Press, New York. 1967. p. 121.
8. C.K. Ingold. *In* Structure and mechanism in organic chemistry. 2nd. ed. G. Bell, London. 1969.
9. E.A. Moelwyn-Hughes. *In* Chemical statics and kinetics of solutions. Academic Press, New York. 1971.
10. S.R. Hartshorn. *In* Aliphatic nucleophilic substitution. Cambridge University Press, Cambridge, UK. 1973. p. 124
11. J. Milton Harris. *In* Adances in physical organic chemistry. Vol. 11. Academic Press, New York. 1974. p. 89.
12. T.W. Bentley and P.v.R. Schleyer. *In* Advances in physical organic chemistry. Vol. 14. Academic Press, New York. 1977. p. 1.
13. W.J. Albery and M.M. Kreevoy. *In* Advances in physical organic chemistry. Vol. 16. Academic Press, New York. 1978. p. 87.
14. S.S. Shaik. *In* Progress in physical organic chemistry. Vol. 15. John Wiley and Sons, New York. 1985. p. 197.
15. M.J. Blandamer, R.E. Robertson, and J.M.W. Scott. *In* Progress in physical organic chemistry. Vol. 15. John Wiley and Sons, New York. 1985. p. 149.
16. J. Milton Harris and S.P. McManus (*Editors*). Nucleophilicity. American Chemical Society, Washington, D.C. 1987.
17. S.S. Shaik, H.B. Schlegel, and S. Wolfe. *In* Theoretical aspects of physical organic chemistry — the S_N2 Mechanism. Wiley Interscience, Washington, D.C. 1987; New York. 1992.
18. E.L. Eliel. *In* Steric effects in organic chemistry. *Edited by* M.S.Newman. John Wiley and Sons Inc., New York. 1956.
19. R.E. Robertson and J.M.W. Scott. Can. J. Chem. **50**, 167 (1972).
20. J.M.W. Scott and D. Summers. Can. J. Chem. **76**, 643 (1999).
21. W.J. Albery and B.H. Robinson. Trans. Faraday Soc. **65**, 980 (1969).
22. M.J. Blandamer and J.M.W. Scott. J. Phys. Chem. **92**, 6264 (1988).
23. J.P. Guthrie. Can. J. Chem. **56**, 2342 (1978).
24. J.L. Kurz. Acc. Chem. Res. **5**, 1 (1972).
25. D.N. Glew and E.A. Moelwyn-Hughes. Discuss. Faraday Soc. **15**, 150 (1952).
26. R.A. Ogg. Trans. Faraday Soc. **31**, 1385 (1935).
27. R.A. Ogg. J. Am. Chem. Soc. **61**, 1946 (1939).
28. A.G. Evans. Trans. Faraday Soc. **42**, 719 (1946).
29. J.D. Cox, D.D. Wagman, and V.A. Medvedev. *In* CODATA Key values for thermodynamics. Hemisphere Publishing Corp., New York. 1989.

© 2005 NRC Canada

30. F.D. Rossini, D.D. Wagman, W.H. Evans, S. Levine, and I. Jaffe. Selected values of chemical thermodynamic properties. Circular of the National Bureau of Standards 500. US Government Printing Office, Washington, D.C. 1952.
31. J.R. Partington. *In* An advanced treatise on physical chemistry. Vol. 1. Longmans Green, London. 1953.
32. D. Glew and E.A. Moelwyn-Hughes. Proc. Roy. Soc. **A211**, 254 (1952).
33. M.H. Abraham and D.J. McLennan. J. Chem. Soc. Perkin Trans. 2, 873 (1977).
34. R.E. Robertson, R.L. Heppolette, and J.M.W. Scott. Can. J. Chem. **37**, 8034 (1959).
35. W.v.E. Doering and H.H. Zeiss. J. Am. Chem. Soc. **75**, 4733 (1953).
36. R.A. Marcus. J. Chem. Phys. **72**, 891 (1968).
37. E.S. Lewis, T.A. Douglas, and M.L. McLaughlin. *In* Nucleophilicity. *Edited by* J. Milton Harris and S.P. McManus. American Chemical Society, Washington, D.C. 1987. Chap. 3
38. W.J. Albery. *In* Annual review of physical chemistry. Vol. 16. Annual Reviews, Palo Alto, California. 1978. p. 87.
39. H. Eyring, K.J. Laidler, and S. Glasstone. *In* The theory of rate processes. McGraw-Hill, New York. 1941.
40. R.H. Bathgate and E.A. Moelwyn-Hughes. J. Chem. Soc. 2642 (1959).
41. R.H. Bathgate and E.A. Moelwyn-Hughes. J. Chem. Soc. 7119 (1965).
42. J.M.W. Scott. Can. J. Chem. **48**, 3807 (1970).
43. R.A. Sneen. Acc. Chem. Res. **6**, 46 (1973).
44. M.H. Abraham. J. Chem. Soc. Perkin Trans. 2, 1893 (1973).
45. D.J. McLennan. Aust. J. Chem. **31**, 1897 (1978).
46. S. Ralph, J.M.W. Scott, and D. Summers. Int. J. Chem. Kinet. **19**, 553 (1986).
47. D.R. Stull, E.F. Westrum, and G.C. Sinke. *In* The chemical thermodynamics of organic compounds. John Wiley, New York. 1969.
48. R.C. Weast (*Editor*). CRC Handbook of Chemistry and Physics. 64th ed. CRC Press Inc., Boca Raton, Florida. 1983.
49. R.D. Harrison (*Editor*). Book of data. Sixth impression. Longman Group Ltd., London. 1980.
50. E.R. Swart and L.J. LeRoux. J. Chem. Soc. 406 (1957).
51. H. Margenau and G.M. Murphy. *In* The mathematics of physics and chemistry. 2nd ed. Van Nostrand, New York. 1956.
52. W.E. Wentworth. J. Chem. Ed. **42**, 96 (1965).
53. W.S. Dorn and D.D. McCracken. Numerical methods with Fortran IV case studies. Wiley, New York. 1977. p. 351.
54. J. Koskikallio. Acta. Chem. Scand. **23**, 1477 (1969).
55. A. Annesa, R.E. Robertson, and J.M.W. Scott. Can. J. Chem. **53**, 3106 (1975).
56. S. Hartman and R.E. Robertson. Can. J. Chem. **38**, 2033 (1960).
57. S. Jokinen, E. Lukkonen, J. Ruostesuo, J. Virtanen, and J. Koskikallio. Acta Chem. Scand. **25**, 3367 (1971).
58. J.S. McKinley-Mckee and E.A. Moelwyn-Hughes. Trans. Faraday Soc. **48**, 247 (1952).
59. E.A. Moelwyn-Hughes. Proc. Roy. Soc. **A196**, 540 (1949).
60. R.L. Heppolette and R.E. Robertson. Proc. Roy. Soc. **A252**, 273 (1959).
61. A.B. Ash, P. Blumbergs, C.L. Stevens, H.O. Michel, B.E. Blackey, Jr., and J. Epstein. J. Org. Chem. **34**, 1070 (1969).
62. R.E. Davis, R. Nehring, W.J. Blume, and C.R. Chuang. J. Am. Chem. Soc. **91**, 92 (1969).
63. H.C. Brown, D.H. McDaniel, and O. Hafliger. *In* Determination of organic structures by physical methods. *Edited by* E.A. Braude and F.C. Nachod. Academic Press, New York. 1955.
64. E.F. Caldin. *In* Fast reactions in solution. Blackwell, Oxford. 1964. Chap. 12.
65. E. Grunwald. *In* Progress in physical organic chemistry. Vol. 3. John Wiley and Sons, New York. 1965. p. 137.
66. R.E. Robertson and P.M. Laughton. *In* Solvent interactions. *Edited by* J.F. Coetzee and C.D. Richtie. Marcel Dekker, New York. 1969. p. 399.
67. C.G. Swain and E.R. Thornton. J. Am. Chem. Soc. **84**, 822 (1962).
68. R. Schowen. *In* Progress in physical organic chemistry. Vol. 9. John Wiley and Sons, New York. 1972. p. 303.
69. E.M. Arnett. *In* Progress in physical organic chemistry. Vol. 1. John Wiley and Sons, New York. 1963. p. 223.
70. V.J. Shiner. *In* Isotope effects in chemical reactions. *Edited by* C.J. Collins and N.S. Bowman. Van Nostrand, New York. 1970. p. 90.
71. E.M. Arnett and D.R. McKelvey. *In* Solvent interactions. *Edited by* J.F. Coetzee and C.D. Richtie. Marcel Dekker, New York. 1969. p. 343.
72. J.G. Martin and J.M.W. Scott. Can. J. Chem. **46**, 2887 (1968).
73. F.L. Schadt, P.v.R. Schleyer, and T.W. Bentley. J. Am. Chem. Soc. **98**, 7668 (1976).
74. E.A. Moelwyn-Hughes. J. Chem. Soc. 779 (1938).
75. R.E. Robertson and J.M.W. Scott. J. Chem. Soc. 1596 (1961).
76. H.S. Harned and B.B. Owen. *In* The physical chemistry of electrolyte solutions. American Chemical Society Monograph. Reinhold, New York. 1957.
77. M.J. Blandamer, J. Burgess, R.E. Robertson, and J.M.W. Scott. Chem. Rev. **82**, 259 (1982).
78. M.J. Blandamer. *In* Chemical equilibria in solution. Ellis Horwood, London. 1992.
79. J. Barron, J.M.W. Scott, and J.G. Winter. Can. J. Chem. **53**, 1975 (1975).
80. E.A. Moelwyn-Hughes. Discuss. Faraday Soc. 91 (1937).
81. R.E. Robertson. Can. J. Chem. **33**, 1536 (1955).
82. R. Stewart. *In* The proton: applications to organic chemistry. Academic Press, New York. 1985. Chap. 2.
83. M.J. Blandamer, J. Burgess, P.P. Duce, R.E. Robertson, and J.M.W. Scott. Can. J. Chem. **59**, 2845 (1981).
84. M.J. Blandamer, R.E. Robertson, and J.M.W. Scott. J. Chem. Soc. Perkin Trans. 2, 447 (1981).
85. M.J. Blandamer, R.E. Robertson, and J.M.W. Scott. J. Am. Chem. Soc. **104**, 1136 (1982).
86. M. Eigen. Angew. Chem. Int. Ed. Engl. **3**, 1 (1964).
87. K.M. Koshy, R.K. Mohanty, and R.E. Robertson. Can. J. Chem. **55**, 1314 (1977).
88. R.K. Mohanty and R.E. Robertson. Can. J. Chem. **55**, 1319 (1977).
89. P.A. Adams and J.G. Sheppard. J. Chem. Soc. Faraday Trans. 1, **76**, 2114 (1980).
90. R.E. Robertson, S. Sugamori, and E.A. Moelwyn-Hughes. J. Chem. Soc. 1965 (1965).
91. M.J. Blandamer, P.D. Golding, J.M. MacNeil, R.E. Robertson, and J.M.W. Scott. J. Am. Chem. Soc. **103**, 2415 (1981).
92. L.P. Hammett. *In* Physical organic chemistry. 2nd ed. McGraw-Hill, New York. 1970.
93. M.J.S. Dewar. *In* The molecular orbital theory of organic chemistry. McGraw-Hill, New York. 1969.
94. M.J. Blandamer, E. Ralph, R.E. Robertson, and J.M.W. Scott. J. Chem. Soc. Faraday Trans. **79**, 1289 (1989).
95. E.A. Guggenheim. Phil. Mag. **2**, 538 (1926).
96. J.H. Espenson. *In* Chemical kinetics and reaction mechanisms. McGraw-Hill, New York. 1995. Chap. 2.

© 2005 NRC Canada

97. F.J. Kedzy, J. Kaj, and A. Bruylants. Bull. Soc. Chim. Belg. **67**, 687 (1958).
98. E.S. Swinbourne. J. Chem. Soc. 2371 (1960).
99. P.C. Mangelsdorf. J. Appl. Phys. **30**, 442 (1959).
100. P.v.R. Schleyer and R.D. Nicholas. J. Am. Chem. Soc. **83**, 2700 (1961).
101. T.W. Bentley, G.E. Carter, and K. Roberts. J. Org. Chem. **49**, 5183 (1984).
102. J.G. Martin and J.M.W. Scott. Chem. Ind. (London), 1665 (1967).
103. J.G. Martin and J.M.W. Scott. Can. J. Chem. **46**, 2887 (1968).
104. D.J. Barnes, M. Cole, S. Lobo, J.M.W. Scott, and J.G. Winter. Can. J. Chem. **50**, 2175 (1972).
105. J.G. Winter and J.M.W. Scott. Can. J. Chem. **50**, 1886 (1972).
106. K.R. Adam, J. Lander, and V.R. Stimson. Aust. J. Chem. **15**, 467 (1962).
107. K.H. Lohmann. Ph.D. thesis, Massachusetts Institute of Technology (MIT), Cambridge, Massachusetts. 1959.
108 (*a*). J. Shorter. *In* Correlation analysis of organic reactivity. Research Studies Press, Baldock, Hertfordshire, UK. 1982 p. 101; (*b*) J. Shorter. Correlation analysis in organic chemistry. Clarendon Press, Oxford. 1973.
109. H.M.R. Hoffmann. J. Chem. Soc. 6748, (1965); 6753 (1965); 6762 (1965).
110. M.D. Bentley and M.J.S. Dewar. J. Am. Chem. Soc. **90**, 3991 (1970).
111. C.G. Swain and C.B. Scott. J. Am. Chem. Soc. **75**, 141 (1953).
112. R.A. Robinson and R.H. Stokes. *In* Electrolyte solutions. Butterworth, London. 1959. p. 390.
113. H.H. Broene and T. DeVries. J. Am. Chem. Soc. **67**, 1644 (1947).
114. R.T. Myers. J. Chem. Ed. **12**, 793 (1976).
115. L.P. Hammett and H.L. Pfluger. J. Am. Chem. Soc. **55**, 4079 (1933).
116. T.W. Bentley and K. Roberts. J. Org. Chem. **50**, 4823 (1985).
117. D.N. Kevill and S.W. Anderson. J. Org. Chem. **50**, 3330 (1985).
118. E. Kosower. *In* An introduction to physical organic chemistry. John Wiley and Sons, New York. 1968.
119. T.W. Bentley and K. Roberts. J. Chem. Soc. Perkin Trans. 2, 1055 (1989).
120. T.W. Bentley, G.E. Carter, and K. Roberts. J. Org. Chem. **49**, 5186 (1984).
121. D.N. Kevill, K.C. Kolwyck, and L. Weitl. J. Am. Chem. Soc. **92**, 7300 (1970).
122. D.T. Stoelting and V.J. Shiner, Jr. J. Am. Chem. Soc. **115**, 1695 (1993).
123. T.W. Bentley, C.T. Bowen, D.H. Morton, and P.v.R. Schleyer. J. Am. Chem. Soc. **103**, 5466 (1981).
124. T.W. Bentley, C.T. Bowen, H.C. Brown, and F.J. Chloupek. J. Org. Chem. **46**, 39 (1981).
125. T.W. Bentley and G.E. Carter. J. Org. Chem. **48**, 579 (1983).
126. T.W. Bentley and C.T. Bowen. J. Chem. Soc. Perkin Trans. 2, 557 (1978).
127. T.W. Bentley and G.E. Carter. J. Am. Chem. Soc. **104**, 5741 (1982).
129. C.A. Bunton. *In* Nucleophilicity. *Edited by* J. Milton Harris and S.P. McManus, American Chemical Society, Washington, D.C. 1987. Chap. 29.
130. D.N. Kevill, M.S. Bahuri, and S.W. Anderson. J. Am. Chem. Soc. **106**, 289 (1984).
131. T.W. Bentley, M. Christl, and S.J. Norman. J. Org. Chem. **56**, 6238 (1991).
132. D.N. Kevill and S.W. Anderson. J. Am. Chem. Soc. **108**, 289 (1986).
133. J. Biordi and E.A. Moelwyn-Hughes. J. Chem. Soc. 4291 (1961).
134. J.W. Baker and D.M. Easty. J. Chem. Soc. 1193 (1952).
135. D. Barnes and J.M.W. Scott. Can. J. Chem. **51**, 421 (1973).
136. J.L. Kurz, J. Lee, M.E. Love, and S. Rhodes. J. Am. Chem. Soc. **108**, 2960 (1986).
137. E. Grunwald and J.E. Leffler. *In* Rates and equilibria of organic reactions. John Wiley and Sons, New York. 1963.
138. C. Reichardt. *In* Solvents and solvent effects in organic chemistry. 2nd ed. VCH Verlagsgesellschaft mbH, Weinheim, Germany. 1988.
139. R.L. Burden and J.D. Faires. *In* Numerical analysis. 3rd ed. Prindle Weber & Schmidt, Boston. 1985.
140. R.G. Mortimer. *In* Mathematics for physical chemistry. Macmillan Publishing Co. Inc., New York. 1981.
141. E. Grunwald. *In* Thermodynamics of molecular species. John Wiley and Sons Inc., New York. 1997. Chap. 5.
142. T.W. Bentley, S. Koo, and S.J. Norman. J. Org. Chem. **56**, 1605 (1991).
143. E. Amis. *In* Solvent effects on reaction rates and mechanisms. Academic Press Inc., New York. 1966. Chap. 6. p. 162.
144. T.W. Bentley. Annu. Rep. Chem. Soc. **71**, 111 (1974).
145. J.M. Harris, A. Becker, J.F. Becker, and F.A. Walden. J. Am. Chem. Soc. **96**, 4484 (1974).
146. W.J. Hamer. *In* The structure of electrolyte solutions. *Edited by* W.J. Hamer. John Wiley, New York. 1959. Chap 15.
147. J.N. Bronsted and K. Pederson. Z. Phys. Chem. Stoechiom. Verwandtschftsl. **108**, 185 (1924).
148. R.P. Bell. *In* Correlation analysis in chemistry. *Edited by* N.B. Chapman and J. Shorter. Plenum Press, New York. 1978. Chap. 2.
149. R.F. Hudson and B. Saville. J. Chem. Soc. 4114 (1955).
150. T.W. Swaddle and E.L. King. Inorg. Chem. **4**, 532 (1965).
151. F.A. Guthrie and E.L. King. Inorg. Chem. **3**, 916 (1964).
152. R.G. Wilkins. *In* Study of kinetics and mechanism of reactions of transition complexes. Allyn and Bacon Inc., Boston. 1974.
153. D.N. Kevill and S.W. Anderson. J. Am. Chem. Soc. **108**, 1579 (1986).
154. C.H. Langford. Inorg. Chem. **4**, 265 (1965).
155. C.H. Langford and H.B. Gray. *In* Ligand substitution processes. W.J. Benjamin, New York. 1965.
156. J.M. Harris, A. Becker, J.F. Becker, and F.A. Walden. J. Am. Chem. Soc. **96**, 4484 (1974).
157. J. Franklin. Trans. Faraday Soc. **48**, 443 (1952).
158. M.J.S. Dewar. J. Am. Chem. Soc. **74**, 3341 (1952); 3345, (1952); 3350, (1952); 3353, (1952); 3355, (1952); 3357 (1952).
159. H.C. Longuet-Higgins. J. Chem. Phys. **18**, 275 (1950).
160. M.J.S. Dewar and R.J. Sampson. J. Chem. Soc. 2946 (1957); 2952 (1957).
161. M.J.S. Dewar. *In* Advances in chemical physics. Vol. 8. John Wiley, New York. 1965. p. 65.
162. M.J.S. Dewar and R.C. Dougherty. *In* The PMO theory of organic chemistry. Plenum Press, New York. 1975.
163. P.M.G. Bavin and M.J.S. Dewar. J. Chem. Soc. 164 (1956).
164. M.J.S. Dewar and E.W.T. Warford. J. Chem. Soc. 3570 (1956).
165. M.J.S. Dewar, T. Mole, D.S. Urch, and E.W.T. Warford. J. Chem. Soc. 3572 (1956).
166. M.J.S. Dewar, T. Mole, and E.W.T. Warford. J. Chem. Soc. 3576 (1956).

© 2005 NRC Canada

167. M.J.S. Dewar, T. Mole, and E.W.T. Warford. J. Chem. Soc. 3581 (1956).
168. A.J. Streitwieser, Jr. *In* Molecular orbital theory for organic chemists. John Wiley and Sons Inc., New York. 1961.
169. A.J. Streitweiser and P.M. Nair. Tetrahedron, **5**, 149 (1959).
170. A. Streitweiser, H.A. Hammond, R.H. Jagow, R.M. Williams, R.G. Jesaitis, C.J. Chang, and J.R. Wolf. J. Am. Chem. Soc. **92**, 5141 (1970).
171. K.M. Koshy, R.E. Robertson, and W.M.J. Strachan. Can. J. Chem. **51**, 2958 (1973).
172. J. van Rysselberg. Ph.D. thesis, Free University of Brussels, Brussels, Belgium. 1954.
173. P.J.C. Fierens, H. Hannaert, J. van Rysselberg, and R.H. Martin. Helv. Chim. Acta, **38**, 2009 (1955).
174. L. Wilputte Steinert. Ph.D. thesis, Free University of Brussels, Brussels, Belgium. 1954.
175. L. Wilputte Steinert and P.J.C. Fierens. Bull. Soc. Chim. Belg. **64**, 308 (1955).
176. P.J.C. Fierens, A. Halleux, and H. Hannaert. Bull. Soc. Chim. Belg. **64**, 203 (1955).
177. R.H. Martin, P.J.C. Fierens, and M. Planchen. Helv. Chim. Acta, **42**, 517 (1959).
178. P.J.C. Fierens. Ph.D. thesis, Free University of Brussels, Brussels, Belgium. 1955.
179. J. Berkowitch. Ph.D. thesis, Free University of Brussels, Brussels, Belgium. 1956.
180. P. Muller, D. Milim, W.Q. Feng, R. Hourit, and E.W. Della. J. Am. Chem. Soc. **114**, 6169 (1992).
181. V. Gold. J. Chem. Soc. 4633 (1956).
182. S.F. Mason. J. Chem. Soc. 808 (1958).
183. S. Winstein and H. Marshall. J. Am. Chem. Soc. **74**, 1120 (1952).
184. M. Born. Z. Phys. **1**, 45 (1920).
185. I.M. Barclay and J.A.V. Butler. Trans. Faraday Soc. **34**, 1445 (1938).
186. R.P. Bell. *In* The proton in chemistry. 2nd. ed. Cornell University Press, Ithaca, New York. 1973. p. 81.
187. A.J. Streitwieser. *In* Progress in physical organic chemistry. Vol. 1. John Wiley and Sons, New York. 1962. p. 1.
188. R. Karaman, J.T.L. Huang, and J.L. Fry. J. Org. Chem. **56**, 188 (1991).
189. H.A. Skinner. *In* Modern aspects of thermochemistry. Royal Institute of Chemistry report No. 3. 1958.
190. J.R. Partington. *In* An advanced treatise on physical chemistry. Vol. 2. Longmans Green, London. 1953.
191. R. Walsh, D.M. Golden, and S.W. Benson. J. Am. Chem. Soc. **88**, 650 (1966).
192. M. Swarc and J.W. Taylor. J. Chem. Phys. **22**, 270 (1954).
193. F.P. Lossing, K.U. Ingold, and I.H.S. Henderson. J. Chem. Phys. **22**, 621 (1954).
194. M. Swarc and M. Ladacki. Proc. Roy. Soc. **A219**, 341 (1953).
195. O.H. Gellner and H.A. Skinner. J. Chem. Soc. 1145 (1949).
196. M. Swarc. Chem. Rev. **47**, 75 (1950).
197. M. Gazith and R.M. Noyes. J. Am. Chem. Soc. **77**, 6091 (1955).
198. W.S. Graham, R.J. Nichol, and A.R. Ubbelode. J. Chem. Soc. 115 (1955).
199. E.A. Moelwyn-Hughes. *In* Physical chemistry. Pergamon Press, London. 1957. p. 551.
200. P. Kebarle. *In* Ions and ion pairs in organic reactions. Vol. 1. *Edited by* M. Swarc. John Wiley, New York. 1972.
201. A.J. Gordon and R.A. Ford. *In* The chemist's companion. Wiley-Interscience, New York. 1972. p. 83.
202. J. Franklin. *In* Carbonium ions. Vol. 1. *Edited by* G.A. Olah and P.v.R. Schleyer. John Wiley Interscience, New York. 1968.
203. A.G. Harrison, P. Kebarle, and F.P. Lossing. J. Am. Chem. Soc. **83**, 777 (1961).
204. A.G. Harrison and F.P. Lossing. J. Am. Chem. Soc. **82**, 1052 (1960).
205. J.B. Farmer and F.P. Lossing. Can. J. Chem. **33**, 861 (1955).
206. S.W. Benson. *In* Thermochemical kinetics. John Wiley, New York. 1968.
207. S.W. Benson and J.H. Buss. J. Chem. Phys. **29**, 546 (1958).
208. T. Cotrell. *In* Strength of chemical bonds. Butterworths, London. 1958.
209. A. Trotman-Dickenson. *In* Gas kinetics. Butterworths, London. 1955.
210. M. Swarc. J. Chem. Phys. **16**, 128 (1948).
211. M. Swarc. Discuss. Faraday Soc. **14**, 248 (1953).
212. M. Swarc and A.H. Sehon. Annu. Rev. Phys. Chem. **8**, 439 (1957).
213. A.G. Evans and S.G. Hamann. Trans. Faraday Soc. **45**, 25 (1951).
214. G. Kohnstam. *In* The transition state. Chemical Society, London. 1962. p. 179.
215. H.C. Brown and L.M. Stock. *In* Advances in physical organic chemistry. Vol. 1. *Edited by* V. Gold. Academic Press Inc., New York. 1963. p. 35.
216. O. Exner. *In* Advances in linear free energy relationships. *Edited by* N.B. Chapman and J. Shorter. Plenum Press, New York and London. 1972. p. 1.
217. A.J. Stein. J. Org. Chem. **41**, 519 (1976).
218. P. Boronius and L. Pataki. J. Am. Chem. Soc. **92**, 4518 (1970).
219. J.B. Hyne and R. Wills. J. Am. Chem. Soc. **85**, 3650 (1963).
220. E. Buncel and H. Wilson. J. Chem. Ed. **64**, 475 (1987).
221. A. Pross, H. Aronovitch, and R. Koren. J. Chem. Soc. Perkin Trans. 2, 197 (1978).
222. J.F. Ogilvie. J. Chem. Ed. **67**, 280 (1990).
223. J.M.W. Scott. J. Chem. Ed. **69**, 600 (1992).
224. C.G. Swain and W.P. Langsdorf. J. Am. Chem. Soc. **73**, 2813 (1951).
225. D.N. Kevill, M.J. D'Souza, and H. Ren. Can. J. Chem. **76**, 751 (1998).
226. J.K. Kochi and G.S. Hammond. J. Am. Chem. Soc. **75**, 3445 (1953).
227. J.A. Llewellyn, R.E. Robertson, and J.M.W. Scott. Can. J. Chem. **38**, 222 (1960).
228. K.T. Leffek, J.A. Llewellyn, and R.E. Robertson. Can. J. Chem. **38**, 1505 (1960).
229. K.M. Koshy and R.E. Robertson. J. Am. Chem. Soc. **96**, 914 (1974).
230. E.A. Halevi. *In* Progress in physical organic chemistry. Vol. 1. John Wiley and Sons, New York. 1963. p. 109.
231. M.J.S. Dewar and F. Carrion. J. Am. Chem. Soc. **106**, 3531 (1984).
232. J.A. Hirsch. *In* Concepts in theoretical organic chemistry. Allyn and Bacon Inc., Boston. 1974. Footnote to Chap. 7. p. 147.

© 2005 NRC Canada

Appendix A. Valentiner equation analysis (neopentyl methanesulphonate).

[A1] $\ln k = A(1) + A(2)/T + A(3) \ln T$

Coeffficients of eq. [A1]: $A(1) = -12\,943.215 \pm 47.75$, $A(3) = -3.53 \times 10^{-4} \pm 0.1395$, $A(2) = +27.911\,781 \pm 0.9534$.

Table A1. Observed and calculated first-order rate constants for the hydrolysis of neopentyl mesylate from the Valentiner equation.

T (°C)	k_o	k_c
44.016	2.582×10^{-6}	2.5000×10^{-6}
54.968	9.743×10^{-6}	9.7612×10^{-6}
55.002	9.726×10^{-6}	9.8012×10^{-6}
59.721	1.682×10^{-5}	1.7144×10^{-5}
65.009	3.172×10^{-5}	3.1491×10^{-5}
65.882	3.392×10^{-5}	3.4753×10^{-5}
72.979	7.612×10^{-5}	7.6023×10^{-5}
75.015	9.612×10^{-5}	9.4605×10^{-5}
78.089	1.316×10^{-4}	1.3098×10^{-4}
81.549	1.885×10^{-4}	1.8764×10^{-4}
85.015	2.688×10^{-4}	2.6710×10^{-4}
87.249	3.327×10^{-4}	3.3417×10^{-4}
90.001	4.376×10^{-4}	4.3869×10^{-4}
94.960	7.019×10^{-4}	7.0906×10^{-4}
95.006	7.059×10^{-4}	7.1218×10^{-4}
44.991	2.867×10^{-6}	2.8367×10^{-6}
54.874	9.604×10^{-6}	9.6631×10^{-6}
59.936	1.767×10^{-5}	1.7601×10^{-5}
62.531	2.347×10^{-5}	2.3767×10^{-5}
65.000	3.168×10^{-5}	3.1495×10^{-5}
69.742	5.355×10^{-5}	5.3470×10^{-5}
74.995	9.628×10^{-5}	9.4504×10^{-5}
75.298	9.787×10^{-5}	9.7609×10^{-5}
80.025	1.619×10^{-4}	1.6047×10^{-4}
81.584	1.889×10^{-4}	1.8851×10^{-4}
85.326	2.769×10^{-4}	2.7589×10^{-4}
89.983	4.414×10^{-4}	4.3835×10^{-4}
90.138	4.419×10^{-4}	4.4506×10^{-4}
94.977	7.046×10^{-4}	7.1089×10^{-4}
97.499	8.860×10^{-4}	9.0301×10^{-4}

Note: Gauss criterion = 4.10880×10^{-6}.

Table A2. Thermodynamic parameters characterizing the hydrolysis of neopentyl mesylate.

T (K)	$\Delta H^{\ddagger}$	$\Delta S^{\ddagger}$	k_c
273.15	273.15	–4.89	3.484×10^{-9}
298.15	25.126	–5.06	1.852×10^{-7}
323.15	25.076	–5.22	5.323×10^{-6}
348.15	25.026	–5.37	9.445×10^{-5}
373.15	24.976	–5.51	1.140×10^{-3}

Note: Heat capacity = –1.99 cal mol^{-1} K^{-1}.

Appendix B. Valentiner equation analysis (*tert*-butyl chloride).

[B1] $\ln k = A(1) + A(2)/T + A(3) \ln T$

Coefficients for eq. [B1]: $A(1) = 4.155\,769\,7 \times 10^{2} \pm 2.496$, $A(2) = -2.840\,864\,0 \times 10^{4} \pm 1.107 \times 10^{2}$, $A(3) = -5.683\,256\,0 \times 10^{1} \pm 3.729 \times 10^{-1}$.

Table B1. Observed and calcuated first-order rate contants for the hydrolysis of *tert*-butyl chloride from the Valentiner equation.

T (°C)	k(obs.)	k(calcd.)
0.070	7.237×10^{-4}	7.1259×10^{-4}
1.940	9.949×10^{-4}	9.8050×10^{-4}
3.010	1.174×10^{-3}	1.1733×10^{-3}
4.010	1.396×10^{-3}	1.3848×10^{-3}
5.961	1.896×10^{-3}	1.9029×10^{-3}
6.310	2.010×10^{-3}	2.0126×10^{-3}
8.016	2.609×10^{-3}	2.6389×10^{-3}
9.019	3.051×10^{-3}	3.0868×10^{-3}
11.012	4.145×10^{-3}	4.1923×10^{-3}
12.025	4.829×10^{-3}	4.8849×10^{-3}
13.040	5.665×10^{-3}	5.6833×10^{-3}
15.016	7.488×10^{-3}	7.5924×10^{-3}
16.060	8.845×10^{-3}	8.8242×10^{-3}
18.012	1.154×10^{-2}	1.1632×10^{-2}
19.008	1.324×10^{-2}	1.3360×10^{-2}
20.013	1.519×10^{-2}	1.5340×10^{-2}
22.020	2.008×10^{-2}	2.0118×10^{-2}
24.510	2.795×10^{-2}	2.7919×10^{-2}
25.310	2.976×10^{-2}	3.0957×10^{-2}
25.110	3.018×10^{-2}	3.0170×10^{-2}
26.950	4.034×10^{-2}	3.8142×10^{-2}
28.020	4.395×10^{-2}	4.3613×10^{-2}
29.930	5.630×10^{-2}	5.5176×10^{-2}
31.970	7.133×10^{-2}	7.0525×10^{-2}
32.660	7.274×10^{-2}	7.6528×10^{-2}
34.990	1.013×10^{-1}	1.0036×10^{-1}
36.100	1.169×10^{-1}	1.1390×10^{-1}
40.940	1.971×10^{-1}	1.9408×10^{-1}
43.340	2.505×10^{-1}	2.5002×10^{-1}
46.730	3.556×10^{-1}	3.5329×10^{-1}
48.380	4.116×10^{-1}	4.1598×10^{-1}
1.020	8.418×10^{-4}	8.4019×10^{-4}
2.004	9.925×10^{-4}	9.9282×10^{-4}
3.996	1.379×10^{-3}	1.3839×10^{-3}
5.005	1.618×10^{-3}	1.6326×10^{-3}
6.030	1.941×10^{-3}	1.9272×10^{-3}
7.019	2.241×10^{-3}	2.2576×10^{-3}
8.110	2.684×10^{-3}	2.6824×10^{-3}
10.013	3.569×10^{-3}	3.6047×10^{-3}
11.010	4.191×10^{-3}	4.1974×10^{-3}
13.006	5.602×10^{-3}	5.6631×10^{-3}
14.010	6.491×10^{-3}	6.5666×10^{-3}
16.000	8.667×10^{-3}	8.7613×10^{-3}
16.996	9.964×10^{-3}	1.0096×10^{-2}
18.040	1.169×10^{-2}	1.1694×10^{-2}

© 2005 NRC Canada

Table B1 (*concluded*)

T (°C)	k(obs.)	k(calcd.)
19.780	1.488×10^{-2}	1.4879×10^{-2}
20.530	1.646×10^{-2}	1.6482×10^{-2}
23.710	2.522×10^{-2}	2.5188×10^{-2}
24.990	2.963×10^{-2}	2.9746×10^{-2}
24.910	2.961×10^{-2}	2.9440×10^{-2}
26.880	3.808×10^{-2}	3.7855×10^{-2}
27.560	4.050×10^{-2}	4.1231×10^{-2}
28.260	4.549×10^{-2}	4.4990×10^{-2}
30.000	5.383×10^{-2}	5.5716×10^{-2}
32.450	7.076×10^{-2}	7.4743×10^{-2}
33.550	8.625×10^{-2}	8.5050×10^{-2}
35.000	9.542×10^{-2}	1.0059×10^{-1}
38.610	1.530×10^{-1}	1.5089×10^{-1}
42.500	2.298×10^{-1}	2.2924×10^{-1}
44.900	2.964×10^{-1}	2.9394×10^{-1}
47.570	3.804×10^{-1}	3.8446×10^{-1}
49.750	4.641×10^{-1}	4.7572×10^{-1}

Note: Gauss criterion = $2.168\ 27\times10^{-3}$.

Table B2. Thermodynamic parameters characterizing the hydrolysis of *tert*-butyl chloride.

T (K)	$\Delta H^{\ddagger}$	$\Delta S^{\ddagger}$	k
273.15	25.059	+18.96	7.040×10^{-4}
298.15	22.187	+8.90	2.975×10^{-2}
323.15	19.314	–0.36	4.868×10^{-1}
348.15	16.441	–8.92	3.888
373.15	13.568	–16.89	1.788×10^{1}

Note: Heat capacity = –114.91 cal mol^{-1} K^{-1}. The Gauss criterion (G.C.) is given by G.C. = $[\Sigma d^2/(N-P)]^{1/2}$ where Σd^2 = sum of the squares of deviations for N data point pairs and P is the number of parameters being determined. For example, $P = 3$ for the Valentiner equation (eq. [B1]) and $P = 4$ in the case of the Albery–Robinson equation (eq. [B2]: $k_o = \exp[(A-C)+(B-D)/T]/[1+\exp-(C+D/T)]$). This expression is also given in ref. B1, but is not designated as the Gauss criterion there, although Wentworth's paper is based on Deming's book (B2), which in turn is totally derivative of Gauss' work.

References

B1. W.E. Wentworth. J. Chem. Ed. **42**, 96 (1965).
B2. W.E. Deming. *In* Statistical adjustment of data. Dover, New York. 1958.

Appendix C. Albery–Robinson fit for tertiary butyl chloride.

[C1] $k_o = \exp(A + B/T)/[1 + \exp(C + D/T)]$

[C2] $k_o = \exp[(A - C) + (B - D)/T]/[1 + \exp -(C + D/T)]$

Fig. C1. Fit of observed data for *t*-BuCl to Albery-Robinson eqs. [C1] and [C2].

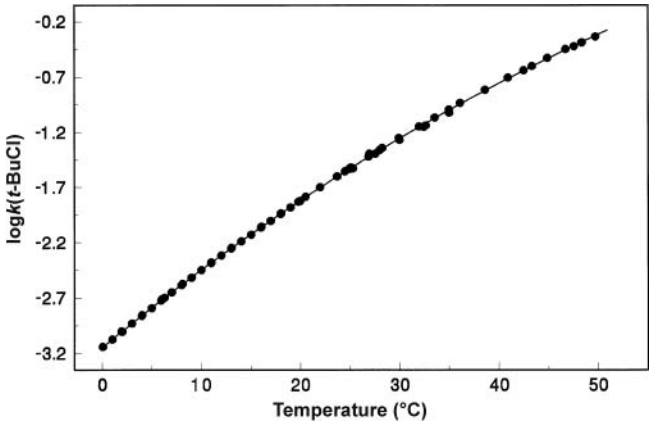


Table C1. First solution.

T (K)	k(obs.)	k(calcd.)
273.22	7.237×10^{-4}	7.210×10^{-4}
275.09	9.949×10^{-4}	9.861×10^{-4}
276.16	1.174×10^{-3}	1.177×10^{-3}
277.16	1.396×10^{-3}	1.385×10^{-3}
279.11	1.896×10^{-3}	1.897×10^{-3}
279.46	2.010×10^{-3}	2.005×10^{-3}
281.17	2.609×10^{-3}	2.624×10^{-3}
282.17	3.051×10^{-3}	3.067×10^{-3}
284.16	4.145×10^{-3}	4.160×10^{-3}
285.18	4.829×10^{-3}	4.846×10^{-3}
286.19	5.665×10^{-3}	5.638×10^{-3}
288.17	7.488×10^{-3}	7.533×10^{-3}
289.21	8.845×10^{-3}	8.758×10^{-3}
291.16	1.154×10^{-2}	1.155×10^{-2}
292.16	1.324×10^{-2}	1.328×10^{-2}
293.16	1.519×10^{-2}	1.525×10^{-2}
295.17	2.008×10^{-2}	2.002×10^{-2}
297.66	2.795×10^{-2}	2.783×10^{-2}
298.46	2.976×10^{-2}	3.087×10^{-2}
298.26	3.018×10^{-2}	3.008×10^{-2}
300.10	4.034×10^{-2}	3.806×10^{-2}
301.17	4.395×10^{-2}	4.354×10^{-2}
303.08	5.630×10^{-2}	5.512×10^{-2}
305.12	7.133×10^{-2}	7.048×10^{-2}
305.81	7.274×10^{-2}	7.649×10^{-2}
308.14	1.013×10^{-1}	1.003×10^{-1}
309.25	1.169×10^{-1}	1.138×10^{-1}
314.09	1.971×10^{-1}	1.937×10^{-1}
316.49	2.505×10^{-1}	2.492×10^{-1}
319.88	3.556×10^{-1}	3.515×10^{-1}
321.53	4.116×10^{-1}	4.134×10^{-1}
274.18	8.418×10^{-4}	8.473×10^{-4}
275.16	9.925×10^{-4}	9.983×10^{-4}
277.16	1.379×10^{-3}	1.385×10^{-3}
278.17	1.618×10^{-3}	1.630×10^{-3}
279.19	1.941×10^{-3}	1.921×10^{-3}
280.18	2.241×10^{-3}	2.247×10^{-3}
281.27	2.684×10^{-3}	2.667×10^{-3}
283.17	3.569×10^{-3}	3.579×10^{-3}

© 2005 NRC Canada

Table C1 (*concluded*).

T (K)	k(obs.)	k(calcd.)
284.17	4.191×10^{-3}	4.165×10^{-3}
286.17	5.602×10^{-3}	5.618×10^{-3}
287.17	6.491×10^{-3}	6.514×10^{-3}
289.16	8.667×10^{-3}	8.695×10^{-3}
290.16	9.964×10^{-3}	1.002×10^{-2}
291.20	1.169×10^{-2}	1.161×10^{-2}
292.94	1.488×10^{-2}	1.479×10^{-2}
293.69	1.646×10^{-2}	1.639×10^{-2}
296.87	2.522×10^{-2}	2.509×10^{-2}
298.15	2.963×10^{-2}	2.965×10^{-2}
298.07	2.961×10^{-2}	2.935×10^{-2}
300.04	3.808×10^{-2}	3.777×10^{-2}
300.72	4.050×10^{-2}	4.115×10^{-2}
301.42	4.549×10^{-2}	4.492×10^{-2}
303.16	5.383×10^{-2}	5.566×10^{-2}
305.61	7.076×10^{-2}	7.470×10^{-2}
306.71	8.625×10^{-2}	8.501×10^{-2}
308.16	9.542×10^{-2}	1.005×10^{-1}
311.77	1.530×10^{-1}	1.507×10^{-1}
315.66	2.298×10^{-1}	2.286×10^{-1}
318.06	2.964×10^{-1}	2.927×10^{-1}
320.73	3.804×10^{-1}	3.823×10^{-1}
322.91	4.641×10^{-1}	4.724×10^{-1}

Note: Gauss criterion = $2.074\,83\times10^{-4}$, sum of deviations = $1.891\,37\times10^{-3}$. [C1] $k_o = \exp(A + B/T)/[1 + \exp(C + D/T)]$. Coefficients of eq. [C1]: $A = -1.306\,215\times10^{4} \pm 2.537\times10^{2}$, $B = 4.066\,938\times10^{1} \pm 9.657\times10^{-1}$, $C = -4.944\,060\times10^{3} \pm 3.509\times10^{2}$, D = $1.580\,097\times10^{1} \pm 8.297\times10^{-1}$.

Table C2. Second solution.

T (K)	k(obs.)	k(calcd.)
273.22	7.237×10^{-4}	7.210×10^{-4}
275.09	9.949×10^{-4}	9.861×10^{-4}
276.16	1.174×10^{-3}	1.177×10^{-3}
277.16	1.396×10^{-3}	1.385×10^{-3}
279.11	1.896×10^{-3}	1.897×10^{-3}
279.46	2.010×10^{-3}	2.005×10^{-3}
281.17	2.609×10^{-3}	2.624×10^{-3}
282.17	3.051×10^{-3}	3.067×10^{-3}
284.16	4.145×10^{-3}	4.160×10^{-3}
285.18	4.829×10^{-3}	4.846×10^{-3}
286.19	5.665×10^{-3}	5.638×10^{-3}
288.17	7.488×10^{-3}	7.533×10^{-3}
289.21	8.845×10^{-3}	8.758×10^{-3}
291.16	1.154×10^{-2}	1.155×10^{-3}
292.16	1.324×10^{-2}	1.328×10^{-2}
293.16	1.519×10^{-2}	1.525×10^{-2}
295.17	2.008×10^{-2}	2.002×10^{-2}
297.66	2.795×10^{-2}	2.783×10^{-2}
298.46	2.976×10^{-2}	3.087×10^{-2}
298.26	3.018×10^{-2}	3.008×10^{-2}
300.10	4.034×10^{-2}	3.806×10^{-2}
301.17	4.395×10^{-2}	4.354×10^{-2}
303.08	5.630×10^{-2}	5.512×10^{-2}
305.12	7.133×10^{-2}	7.048×10^{-2}
305.81	7.274×10^{-2}	7.649×10^{-2}

Table C2 (*concluded*).

T (K)	k(obs.)	k(calcd.)
308.14	1.013×10^{-1}	1.003×10^{-1}
309.25	1.169×10^{-1}	1.138×10^{-1}
314.09	1.971×10^{-1}	1.937×10^{-1}
316.49	2.505×10^{-1}	2.492×10^{-1}
319.88	3.556×10^{-1}	3.515×10^{-1}
321.53	4.116×10^{-1}	4.134×10^{-1}
274.18	8.418×10^{-4}	8.473×10^{-4}
275.16	9.925×10^{-4}	9.983×10^{-4}
277.16	1.379×10^{-3}	1.385×10^{-3}
278.17	1.618×10^{-3}	1.630×10^{-3}
279.19	1.941×10^{-3}	1.921×10^{-3}
280.18	2.241×10^{-3}	2.247×10^{-3}
281.27	2.684×10^{-3}	2.667×10^{-3}
283.17	3.569×10^{-3}	3.579×10^{-3}
284.17	4.191×10^{-3}	4.165×10^{-3}
286.17	5.602×10^{-3}	5.618×10^{-3}
287.17	6.491×10^{-3}	6.514×10^{-3}
289.16	8.667×10^{-3}	8.695×10^{-3}
290.16	9.964×10^{-3}	1.002×10^{-2}
291.20	1.169×10^{-2}	1.161×10^{-2}
292.94	1.488×10^{-2}	1.479×10^{-2}
293.69	1.646×10^{-2}	1.639×10^{-2}
296.87	2.522×10^{-2}	2.509×10^{-2}
298.15	2.963×10^{-2}	2.965×10^{-2}
298.07	2.961×10^{-2}	2.935×10^{-2}
300.04	3.808×10^{-2}	3.777×10^{-2}
300.72	4.050×10^{-2}	4.115×10^{-2}
301.42	4.549×10^{-2}	4.492×10^{-2}
303.16	5.383×10^{-2}	5.566×10^{-2}
305.61	7.076×10^{-2}	7.470×10^{-2}
306.71	8.625×10^{-2}	8.501×10^{-2}
308.16	9.542×10^{-2}	1.005×10^{-2}
311.77	1.530×10^{-1}	1.507×10^{-1}
315.66	2.298×10^{-1}	2.286×10^{-1}
318.06	2.964×10^{-1}	2.927×10^{-1}
320.73	3.804×10^{-1}	3.823×10^{-1}
322.91	4.641×10^{-1}	4.724×10^{-1}

Note: Gauss criterion = $2.074\,83\times10^{-4}$, sum of deviations = $1.891\,37\times10^{-3}$. [C2] $k_o = \exp[(A - C) + (B - D)/T]/[1 + \exp -(C + D/T)]$. Coefficients of eq. [C2]: $A - C = -8.118\,089\times10^{3} \pm 5.929\times10^{2}$, $B - D = 2.486\,841\times10^{1} \pm 1.738$, $-C = 4.944\,060\times10^{3} \pm 3.509\times10^{2}$, $-D = -1.580\,097\times10^{1}\times10^{-1} \pm 8.297\times10^{-1}$.

Appendix D.

Readers unfamiliar with the matrix approach to the system of linear differential equations that describe the system

[D1] $$A \underset{k_2}{\overset{k_1}{\rightleftharpoons}} B \xrightarrow{k_3} C$$

can find a rudimentary treatment of the time evolution of this system in Hammett's book (D1). There is a minor error in the stoichiometric mass balance expression (eq. [76], p. 74) that should read

[D2] $$A + B + C = A_o$$

© 2005 NRC Canada

where A, B, and C are the concentrations of the chemical species A, B, and C at any time "t"; A_o is the concentration of A at zero time. The relationship

[D3] $dA/dt + dB/dt + dC/dt = 0$

is obtained by differentiating eq. [D2] with respect to time. Equation [D3], when combined with other relationships reported by Hammett, provides the differential equation for the species B

[D4] $d^2B/dt^2 + (k_1 + k_2 + k_3)dB/dt + k_1k_3B = 0$

Hammett solves this equation, but the particulars of the solution are more transparent via the matrix method reported in section 6 of this paper (eq. [D5]).

[D5] $$\begin{bmatrix} (D + k_1) & -k_2 & \\ -k_1 & (D + k_2 + k_3) & \\ & k_3 & D \end{bmatrix} \begin{bmatrix} A \\ B \\ C \end{bmatrix} = 0$$

Evaluating the determinant defined by the matrix in eq. [D5] gives for operator part of this equation

[D6] $D(D^2 + (k_1 + k_2 + k_3)D + k_1k_3)$

Clearly, the *quadratic component* of this equation when operating on either A, B, or C yields three differntial equations, one of which is identical to eq. [D4] involving species B.

The complete version of [D6] operating on B is

[D7] $(D^3 + (k_1 + k_2 + k_3)D^2 + k_1k_3D)B = 0$

The corresponding differential equations for A and C are identical in form to eq. [D7].

To solve eq. [D7], let

[D8] $B = \exp(\lambda t)$

Since $DB = dB/dt = \lambda B$, $D^2B = d^2B/dt^2 = \lambda^2B$, and $D^3 = d^3B/dt^3 = \lambda^3B$, substituting the first, second and third differentials in eq. [D7] gives $[\lambda^3 + (k_1 + k_2 + k_3)\lambda^2 + k_1k_3\lambda] \exp(\lambda t) = 0$.

Dividing by $\exp(\lambda t)$ (noting $\exp(\lambda t) \neq 0$) gives the cubic *auxiliary equation*

[D9] $\lambda^3 + (k_1 + k_2 + k_3)\lambda^2 + k_1k_3\lambda = 0$

If the roots of the cubic are respectively λ_1, λ_2, and λ_3 with the latter root set arbitrarily to zero (λ is a factor of eq. [D9]), then the other two negative roots of the residual quadratic *with their signs changed* define the dynamic constants that describe the time evolution of the chemical system represented by eq. [D1]. The dynamic contants are functions of k_1, k_2, and k_3. If $k_1 + k_2 + k_3 = P$ and $k_1k_3 = Q$, then $\lambda_1 = [P + (P^2 - 4Q)^{1/2}]/2$ and $\lambda_2 = [P - (P^2 - 4Q)^{1/2}]/2$.

The solution for A, B, and C as functions of time are linear combinations of exponential functions of the three roots

[D10] $X_n = \alpha_n \exp(-\lambda_1 t) + \alpha_{rn} \exp(-\lambda_2 t) + \alpha_{rn}$

where the final term on the RHS of eq. [D10] relates to the root $\lambda = 0$. The quantities X_n (n = 1–3) refer to the concentrations of A, B, and C any time t, respectively. The constants or amplitudes α_{nr} (n = 1–3, r = 1–3) may be evaluated from the various boundary conditions that characterize the chemical system represented by eq. [D1]. This matter is not pursued further here. There are other more sophisticated versions of this part of the exercise using linear and matrix algebra, which are presented in Ritchie's monograph (D2). Further relevant information can be found in books by Hollingsworth (D3), Leon (D4), and Caunt (D5); refs. D6 and D7 also contain useful material.

References

D1. L.P. Hammett. *In* Physical organic chemistry. 2nd ed. McGraw-Hill, New York. 1970. pp. 73–75.

D2. C.D. Ritchie. *In* Physical organic chemistry. Marcel Decker, New York. 1975.

D3. C.A. Hollingsworth. *In* Vectors, matrices and group theory for scientists and engineers. McGraw-Hill, New York. 1967.

D4. S.J. Leon. *In* Linear algebra with applications. MacMillan, New York. 1980.

D5. G.W. Caunt. *In* An introduction to the infinitesimal calculus with applications to mechanics and physics. Clarendon Press, Oxford. 1949.

D6. N.M. Rodiguin and E.N. Rodiguina. *In* Consecutive chemical reactions. Van Nostrand Inc., New York. 1964.

D7. H. Margenau and G.M. Murphy. *In* The mathematics of physics and chemistry. 2nd ed. Van Nostrand, New York. 1956.

Appendix E.

Table E1. Rates of hydrolysis for cyclohexane methane sulphonate (P. Barnard, R.E. Robertson, and J.M.W. Scott).

Temperature (K)	$k_c \times 10^4$	$k_o \times 10^4$
293.164	2.158	2.164, 2.182, 2.175, 2.175
303.146	7.938	7.876, 7.855, 7.881, 7.869, 7.858, 7.817, 7.858, 7.863
303.141	7.933	7.892, 7.877, 7.913, 7.895
308.173	14.82	15.13, 15.11, 15.26

Note: Observed rate constant (k_o); $k_c = (kT/\hbar)[\exp(-\Delta H^{\ddagger}/RT) \exp(\Delta S^{\ddagger}/R))]$. Regression of $\ln(k_o/T) - \ln(k/\hbar)$ vs. $1/T$ where k_o is the measured first-order rate constant and T, k, and $\hbar$ have their conventional meanings. The regression provides $\Delta H^{\ddagger}$ as the slope and $\Delta S^{\ddagger}$ as the intercept. Correlation coefficient = 0.999 64. $\log(k_c)$ at 25 °C = –3.380. $\Delta H^{\ddagger}$ = 22 451 ± 74 cal mol^{-1} and $\Delta S^{\ddagger}$ = 1.30 ± 0.24 cal mol^{-1} K^{-1}.

Table E2. Rates of hydrolysis of ethyl chloride (R.L. Heppolette and R.E. Robertson. Unpublished results).

Temperature (K)	$k_c \times 10^5$	$k_o \times 10^5$
353.16	1.849	1.841, 1.840, 1.839, 1.841
363.16	4.782	4.828, 4.818, 4.818, 4.828, 4.828
373.14	11.75	11.71, 11.70, 11.69, 11.68, 11.69

Note: See Table E1 for details of the regression. Correlation coefficient = 1.00 010. $\log(k_c)$ = –7.499 (at 25 °C). $\Delta H^{\ddagger}$ = 23511 ± 42 cal mol^{-1}; $\Delta S^{\ddagger}$ = –13.96 ± 0.11 cal mol^{-1} K^{-1}.

© 2005 NRC Canada

A multinuclear solid-state magnetic resonance study of silver nitrate triphenylphosphine

Se-Woung Oh, Guy M. Bernard, Roderick E. Wasylishen, Robert McDonald, and Michael J. Ferguson

Abstract: Variable-temperature solid-state ^{31}P, ^{15}N, and ^{2}H NMR spectroscopy, X-ray diffraction, and differential scanning calorimetry studies of the 1:1 adduct of silver nitrate and triphenylphosphine ($AgNO_3 \cdot PPh_3$) reveal a solid–solid phase transition at 300 K. The principal components of the phosphorus and nitrogen chemical shift tensors for both phases are determined from NMR spectra of MAS and stationary samples. In addition, the indirect spin-spin coupling between phosphorus and the naturally occurring isotopes of silver (^{107}Ag and ^{109}Ag) are resolved. Experimental ^{2}H NMR line shapes for silver nitrate perdeuterated triphenylphosphine are those characteristic of rigid phenyl groups at temperatures above and below the phase-transition temperature. Powder and single-crystal X-ray diffraction data for $AgNO_3 \cdot PPh_3$ obtained at 193, 295, and 313 K are reported; data obtained at 193 and 295 K are almost identical, but are significantly different from those obtained at 313 K and from an earlier single-crystal X-ray diffraction investigation performed at 298 K. All X-ray studies found that $AgNO_3 \cdot PPh_3$ crystallizes in the monoclinic form, space group $P2_1/c$.

Key words: 1:1 silver nitrate triphenylphosphine adduct, solid-state NMR, X-ray diffraction, phase transition.

Résumé : Des études à températures variables de spectroscopie RMN du ^{31}P, du ^{15}N et du ^{2}H à l'état solide, de diffraction des rayons X et de calorimétrie à balayage différentiel sur une adduit 1 : 1 de nitrate d'argent et de triphénylphosphine, $AgNO_3 \cdot PPh_3$, mettent en évidence l'existence d'une transition de phase solide-solide à 300 K. En se basant sur les spectres RMN d'échantillons stationnaires et à l'angle magique de spin, on a déterminé les principaux composants des tenseurs de déplacement chimique du phosphore et de l'azote pour les deux phases. De plus, on a résolu le couplage spin-spin indirect entre le phosphore et les isotopes naturels de l'argent, ^{107}Ag et ^{109}Ag. Aux températures supérieures et inférieures à la température de transition, les formes expérimentales des raies RMN du ^{2}H de l'adduit nitrate d'argent/triphénylphosphine perdeutérée sont caractéristiques de groupes phényles rigides. On rapporte aussi des données de diffraction des rayons X obtenues sur des poudres et sur des cristaux uniques de $AgNO_3 \cdot PPh_3$, à 193, 295 et 313 K; les données obtenues à 193 et 295 K sont presque identiques, mais elles diffèrent beaucoup de celles obtenues à 313 K ainsi que de celles obtenues antérieurement dans une étude de diffraction des rayons X effectuée à 298 K. Toutes les études de diffraction des rayons X indiquent que le $AgNO_3 \cdot PPh_3$, cristallise dans la forme monoclinique, groupe d'espace $P2_1/c$.

Mots clés : adduit 1 : 1 de nitrate d'argent et de triphénylphosphine, RMN à l'état solide, diffraction des rayons X, transition de phase.

[Traduit par la Rédaction]

Introduction

The versatility of silver in coordination chemistry has prompted numerous structural studies (1, 2). For example, silver nitrate can form a variety of adducts with phosphorus-containing ligands (2, 3); the phosphine-to-silver ratio may vary from one to four depending on the nature of the ligand and on the stoichiometric ratios used in the syntheses (4). In the case of triphenylphosphine, structures for the 1:1, 2:1, 3:1, and 4:1 adducts are available from earlier single-crystal X-ray diffraction (XRD) studies (3, 4).

In an early solid-state ^{31}P magic-angle spinning (MAS) NMR study, Barron et al. (4) investigated all four adducts of $AgNO_3 \cdot (PPh_3)_n$, $n = 1$–4. For the 1:1 adduct, they observed a broad doublet, centred at $\delta_{iso} = 11.7$ ppm, with a splitting of approximately 780 Hz that arises from indirect spin-spin

Received 20 April 2005. Published on the NRC Research Press Web site at http://canjchem.nrc.ca on 2 December 2005.

S.-W. Oh,[1] G.M. Bernard, and R.E. Wasylishen.[2] Department of Chemistry, Gunning/Lemieux Chemistry Centre, University of Alberta, Edmonton, AB T6G 2G2, Canada.
R. McDonald and M.J. Ferguson. X-Ray Crystallography Laboratory, Department of Chemistry, University of Alberta, Edmonton, AB T6G 2G2, Canada.

[1]Present address: Department of Chemistry, Mokpo National University, Muan, Chonnam 534-729, Republic of Korea.
[2]Corresponding author (e-mail: roderick.wasylishen@ualberta.ca).

 doi: 10.1139/V05-174 © 2005 NRC Canada

coupling (J) of ^{31}P to both ^{107}Ag and ^{109}Ag, which are spin-1/2 nuclei with similar magnetogyric ratios and natural abundances.

Several years ago, we examined ^{31}P NMR spectra of the 1:1 adduct of solid $AgNO_3 \cdot PPh_3$ and observed well-resolved doublets resulting from indirect spin-spin coupling to ^{107}Ag (^1J = 707 Hz) and to ^{109}Ag (^1J = 813 Hz);[3] as expected, the ratio of the spin-spin coupling corresponds to the ratio $\gamma(^{107}Ag)/\gamma(^{109}Ag)$. However, we were puzzled by the presence of additional peaks in our spectra, occurring at different chemical shifts. These peaks exhibited the same splitting pattern as those attributed to the 1:1 adduct. Also, the relative intensities of the two sets of ^{31}P NMR peaks seemed irreproducible. Initially, we ascribed the additional peaks to the presence of a polymorph (5–8) of the 1:1 adduct. However, all attempts to consistently isolate a "pure" polymorph by preparing the sample in various solvent systems under a variety of conditions (e.g., darkness) failed. Our earlier work was performed using rotors restricted to a maximum MAS frequency (ν_{rot}) of 4 kHz. Recently, we reinvestigated $AgNO_3 \cdot PPh_3$ with the goals of understanding our earlier irreproducible results and of obtaining unambiguous ^{31}P NMR spectra from which the chemical shift (CS) tensors could be determined. For the latter study, our NMR measurements were made using rotors that allowed spinning frequencies in excess of 4 kHz. This work indicates that the intensity of the additional peaks depends on the degree of heating arising from sample spinning. Here we present a comprehensive solid-state NMR study of the 1:1 adduct of $AgNO_3 \cdot PPh_3$, corroborated with the results of differential scanning calorimetry (DSC), as well as single-crystal and powder X-ray diffraction experiments.

Experimental

Sample preparation

The 1:1 adduct of $AgNO_3 \cdot PPh_3$ was prepared as reported in the literature (3). Because the adduct may be light sensitive, all synthetic work was undertaken in a dark room. Triphenylphosphine (1.2 g, 4.5 mmol), recrystallized from methanol, was dissolved in 50 mL of methanol, which had been heated to 313 K, and mixed with a solution containing 1.0 g (5.9 mmol) of silver nitrate in 5 mL of acetonitrile and 20 mL of methanol. The mixture was stirred for 2 min and allowed to stand overnight at room temperature. The precipitate that formed was washed five times with 1 mL of methanol after decantation, dried at room temperature, and placed in an evacuated desiccator for 1 h. The colourless solid was recrystallized using either methanol, acetonitrile, or methylene chloride at room temperature. Perdeuterated $AgNO_3 \cdot PPh_3$ was prepared from $AgNO_3$ and tri(phenyl-d_5)phosphine (Sigma-Aldrich Canada Ltd., Oakville, Ontario, 99% ^2H) as previously described. Nitrogen-15 enriched $AgNO_3$ was obtained by reacting 0.6 g Ag powder (Alfa Aesar, Ward Hill, Massachusetts) in ^{15}N-labelled nitric acid (1 mL; Sigma-Aldrich Canada Ltd., Oakville, Ontario, 98% ^{15}N, 40 wt% solution in water). After the reaction was complete, 1 mL of distilled water was added to the solution, which was then filtered and dried in an oven at 393 K to yield $Ag^{15}NO_3$ (0.75 g). $Ag^{15}NO_3 \cdot PPh_3$ was prepared from $Ag^{15}NO_3$ and triphenyphosphine as previously described for the natural abundance sample.

Solid-state NMR spectroscopy

Phosphorus-31 NMR spectra of stationary and MAS samples of $AgNO_3 \cdot PPh_3$ were acquired on Chemagnetics CMX Infinity 200 (B_0 = 4.70 T) as well as Bruker Avance 300 (B_0 = 7.05 T) and 500 (B_0 = 11.75 T) NMR spectrometers with cross-polarization (CP) from ^1H under the Hartmann–Hahn match condition (9). Samples were packed in 7.5 or 4 mm o.d. rotors for spectra acquired on the Chemagnetics and Bruker spectrometers, respectively. Proton 90° pulse widths of 4.5 or 3.5 μs, a contact time of 2 ms, and a pulse delay of 60 s were used to acquire most ^{31}P NMR spectra. Some ^{31}P NMR spectra were acquired with single-pulse excitation and ^1H decoupling on the Bruker Avance 300 NMR spectrometer using a 90° pulse width of 4 μs and a pulse delay of 1 h. Phosphorus-31 NMR chemical shifts were referenced with respect to 85% aqueous phosphoric acid (H_3PO_4) by setting the isotropic peak of external solid ammonium dihydrogen phosphate ($NH_4H_2PO_4$) to 0.81 ppm (10).

Nitrogen-15 NMR spectra of stationary and MAS samples of $AgNO_3 \cdot PPh_3$ were acquired with CP at 20.3 MHz on the CMX Infinity 200 NMR spectrometer using the same acquisition parameters as for the ^{31}P NMR experiments apart from a 6.0 ms contact time. Nitrogen-15 NMR chemical shifts were referenced with respect to external neat ammonia ($^{15}NH_3$(l)) at 293 K by setting the isotropic peak of solid ammonium nitrate ($^{15}NH_4NO_3$) to 23.80 ppm at room temperature (10). Another common nitrogen NMR reference (CH_3NO_2(l)) appears at 381.9 ppm relative to the nitrogen signal of NH_3(l).[4]

Principal components of the phosphorus and nitrogen CS tensors are assigned using the convention $\delta_{11} \geq \delta_{22} \geq \delta_{33}$, representing the directions of least, intermediate, and greatest shielding, respectively. For convenience, CS tensors are discussed in terms of their isotropic chemical shifts ($\delta_{iso} = (\delta_{11} + \delta_{22} + \delta_{33})/3$), their span ($\Omega = \delta_{11} - \delta_{33}$), and their skew ($\kappa = 3(\delta_{22} - \delta_{iso})/\Omega$) (11). Spectra of stationary samples were simulated using WSOLIDS, a program written in this laboratory (12).

Deuterium NMR spectra of stationary perdeuterated $AgNO_3 \cdot PPh_3$ were acquired on the CMX Infinity 200 NMR spectrometer with a 5 mm double resonance solenoid probe using the quadrupolar-echo pulse sequence ($90^\circ_x - \tau - 90^\circ_y - \tau$ – acq) (13–16) with a ^2H 90° pulse of 3 μs, τ = 20 μs, and a pulse delay of 60 s. Samples were packed into a 5 mm o.d. glass container. Perdeuterated poly(methyl methacrylate) was used to optimize experimental conditions. Prior to Fourier transformation (FT), the initial points of the free-induction decay (FID) were deleted to ensure that the first point was at the top of the echo (10).

Variable-temperature (VT) solid-state ^{31}P, ^{15}N, ^2H, and ^{207}Pb NMR experiments were performed on the Chemagnetics CMX Infinity 200 NMR spectrometer. The temperature was varied from 247 to 319 K and calibrated using the

[3] G.H. Penner, R.D. Curtis, S. Kroeker, and R.E. Wasylishen. Unpublished results.
[4] R.E. Wasylishen. Unpublished results.

© 2005 NRC Canada

Table 1. Crystallographic data for the 1:1 adduct of silver nitrate and triphenylphosphine.

	This work[a]	This work[a]	This work[b]	Reference 3	This work[b]
Temp. (K)	193	295	295	298	313
Crystal system	Monoclinic	Monoclinic	Monoclinic	Monoclinic	Monoclinic
Space group	$P2_1/c$	$P2_1/c$	$P2_1/c$	$P2_1/c$	$P2_1/c$
a (Å)	10.2221(16)	10.2430(14)	10.233(7)	10.659(2)	10.690(6)
b (Å)	18.497(3)	18.521(3)	18.495(17)	18.558(4)	18.607(12)
c (Å)	9.1925(14)	9.1373(12)	9.127(9)	9.045(1)	9.094(7)
β (°)	91.053(3)	90.596(3)	90.50(7)	100.393(7)	100.31(5)
Z	4	4	4	4	4
ρ_{calcd} (g cm^{-3})	1.652	1.656	1.661	1.631	1.612
R_1[c]	0.0664	0.0535		0.049	

[a]Determined by X-ray diffraction on a single crystal. Refinement of F_o^2 for all reflections (all of these having $F_o^2 \geq -3\sigma(F_o^2)$). Weighted R factors (wR_2) and all goodnesses-of-fit (S) are based on F_o^2; conventional R factors (R_1) are based on F_o, with F_o set to zero for negative F_o^2. The observed criterion of $F_o^2 > 3\sigma(F_o^2)$ is used only for calculating R_1, and is not relevant to the choice of reflections for refinement. R factors based on F_o^2 are statistically about twice as large as those based on F_o, and R factors based on all data will be even larger.
[b]Determined by powder X-ray diffraction.
[c]$R_1 = \Sigma[|F_o| - |F_c|]/\Sigma|F_o|$.

isotropic ^{207}Pb NMR peak of lead(II) nitrate (17–19). For this calibration, a mixture containing 15% lead nitrate and 85% $AgNO_3{\cdot}PPh_3$ was packed into a 7.5 mm o.d. rotor. Lead-207 NMR chemical shifts were referenced by setting the isotropic peak of solid lead(II) nitrate, acquired at 294 K with ν_{rot} = 1.0 kHz, to –3505.5 ppm (17).

Proton spin-lattice relaxation times (T_1) were indirectly estimated through the observation of the ^{31}P NMR peak intensities in a CP experiment (20, 21), using the progressive saturation FT technique (22). Peak intensities were obtained with various inter-pulse delays, to a maximum of 5400 s. To establish a steady state before measuring the signal intensity, two FIDs preceded the one that was measured.

Differential scanning calorimetry

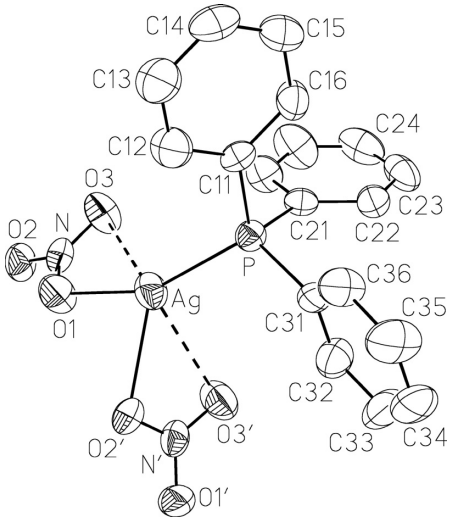
DSC was performed with a Pyris DSC1 from PerkinElmer Instruments, Inc. Approximately 6.5 mg of sample was used for the measurements with a scanning rate of 5 K/min; data were collected between 293 and 323 K.

X-ray diffraction

A single crystal of $AgNO_3{\cdot}PPh_3$ recrystallized from methanol, dimensions 0.20 mm × 0.17 mm × 0.08 mm, was selected for the single-crystal XRD experiments. Diffraction data were obtained with a Bruker PLATFORM/SMART 1000 CCD diffractometer (Mo Kα, λ = 0.710 73 Å graphite monochromator), operating at 193 or 295 K. For data acquired at 193 K, 10 098 reflections were collected in the range 5.24° < 2θ < 53.24° of which 3613 were independent. For the data acquired at 295 K, 8097 reflections were collected in the range 5.24° < 2θ < 52.86° of which 3553 were independent. The structure was solved by direct methods using DIRDIF-99 (23) and refined with SHELXL-93 (24).

Powder X-ray diffraction data were collected at 295 and 313 K on an Inel powder diffractometer equipped with a CPS 120 position-sensitive detector and Cu Kα$_1$ radiation (Si standard). Programs used for data collection and analysis were those supplied by Inel. Cell parameters were refined by least-squares methods on 24–40 reflections in the X-ray powder pattern with the program UnitCell (25). Calculated intensities were obtained using the program PowderCell (26).

Fig. 1. Perspective view of the 1:1 adduct of silver nitrate triphenylphosphine showing the atom labelling scheme and including interactions with the nearest-neighbour symmetry-related nitrate ion; the structure was obtained at 295 K. Non-hydrogen atoms are represented by Gaussian ellipsoids at the 50% probability level. The hydrogen atoms are not shown.



Results and discussion

Solid-state NMR spectra of MAS samples

Phosphorus

To facilitate the discussion of the NMR spectra the structure of $AgNO_3{\cdot}PPh_3$, as determined by single-crystal X-ray crystallography at 295 K (vide infra), is shown in Fig. 1 (see also Tables 1 and 2). On the basis of the crystal structure, one site is expected for the ^{31}P NMR spectra of MAS samples; however, spectra acquired at room temperature generally consisted of eight peaks attributed to two peaks (see Fig. 2 for a typical spectrum), four peaks centred at 13.2 ppm and four centred at 12.0 ppm. These are hereinafter referred to as sites I and II, respectively. Four peaks are expected for a single phosphorus NMR site of $AgNO_3{\cdot}PPh_3$,

© 2005 NRC Canada

Table 2. Bond distances (Å) and angles (°) for silver nitrate triphenylphosphine.

	This work	This work	Reference 3
Temp. (K)	193	295	298
Bond lengths (Å)			
Ag—P	2.3757(15)	2.3573(15)	2.369(6)
Ag—O1	2.277(4)	2.257(4)	2.438(7)
Ag—O2′	2.472(5)	2.454(4)	2.363(7)
Ag—O3	3.110(5)	3.036(5)	2.628(7)
Ag—O3′	2.867(5)	2.865(4)	2.916(7)
N—O1	1.261(7)	1.259(6)	1.238(9)
N—O2	1.258(6)	1.233(6)	1.270(9)
N—O3	1.254(6)	1.240(6)	1.227(9)
P—C11	1.833(6)	1.811(5)	1.813(11)
P—C21	1.829(6)	1.811(6)	1.816(11)
P—C31	1.831(6)	1.823(6)	1.828(11)
Bond angles (°)			
P-Ag-O1	153.86(12)	154.87(12)	136.5(2)
P-Ag-O3	110.66(9)	111.67(9)	117.2(2)
P-Ag-O3′	99.48(10)	99.40(10)	95.7(2)
O1-Ag-O3	44.68(14)	45.40(13)	49.7(2)
O1-Ag-O3′	94.91(16)	96.42(16)	127.6(2)
O3-Ag-O3′	100.93(4)	102.07(4)	110.0(2)
Ag-P-C11	119.5(2)	118.97(19)	116.6(3)
Ag-P-C21	107.61(19)	107.68(18)	109.6(3)
Ag-P-C31	114.26(19)	114.21(18)	115.1(3)
C11-P-C21	103.2(3)	103.8(2)	104.4(5)
C11-P-C31	106.0(3)	106.0(3)	105.7(5)
C21-P-C31	104.9(3)	104.9(3)	104.3(5)
O1-N-O2	119.1(5)	119.5(5)	120.3(5)
O1-N-O3	120.9(5)	120.1(5)	119.9(5)
O2-N-O3	120.0(5)	120.4(5)	119.7(5)

Note: Data were obtained by X-ray diffraction experiments on single crystals. See Fig. 1 for the atom labelling scheme.

a pair of doublets arising from indirect spin-spin coupling to ^{107}Ag and ^{109}Ag with 51.8% and 48.2% natural abundance, respectively (27, 28). Another interesting observation was that the intensities of the peaks centred at 13.2 ppm, relative to those centred at 12.0 ppm, increase with MAS frequency. This was observed for all samples of $AgNO_3{\cdot}PPh_3$, regardless of the solvent used to prepare the sample.

Sample heating resulting from MAS is well-known (17, 18, 29, 30); the effect, arising from friction between the rotor and the bearing gas, has been described by Doty and Ellis (31). Hence, the possibility that the spinning-frequency dependence of the ^{31}P NMR spectra arises from a solid–solid phase transition induced by sample heating was considered; this has been previously observed for other samples (32, 33).

To investigate the temperature dependence of the ^{31}P NMR signals for $AgNO_3{\cdot}PPh_3$, spectra were acquired from 247 to 319 K (Fig. 3*a*). At 319 K, only the peaks centred at 13.2 ppm were observed, while only those centred at 12.0 ppm were observed at 247 K. These observations suggest that sites I and II correspond to different phases of solid $AgNO_3{\cdot}PPh_3$, and that the solid–solid phase transition occurs between 286 and 306 K. The isotropic phosphorus chemical

Fig. 2. Isotropic region of the ^{31}P NMR spectrum of $AgNO_3{\cdot}PPh_3$ acquired with CP at room temperature; ν_{rot} = 4.6 kHz and B_0 = 7.05 T. The solid and dashed lines, respectively, indicate contributions to the spectra from sites I and II.

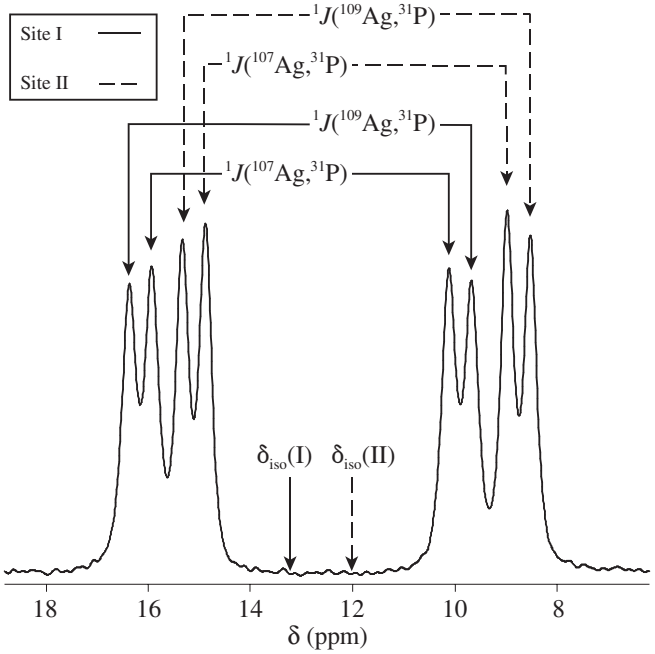
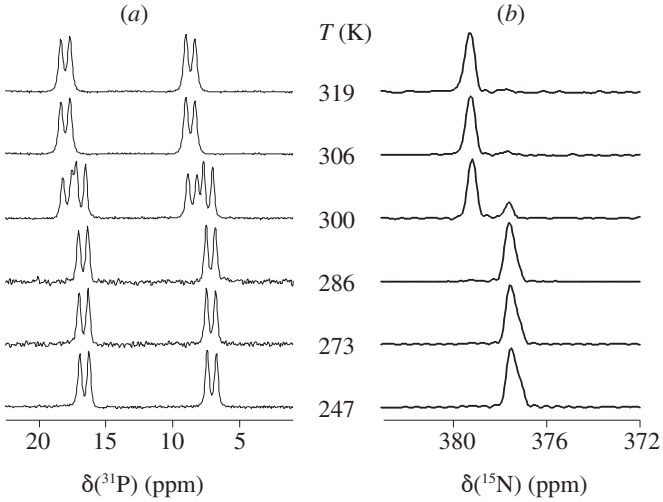


Fig. 3. (*a*) Phosphorus-31 and (*b*) nitrogen-15 NMR spectra of MAS samples of $AgNO_3{\cdot}PPh_3$ acquired with CP at various temperatures; B_0 = 4.70 T and ν_{rot} = 3.0 kHz. Because splittings due to ^2J(Ag,N) are not resolved, a single peak is observed for each site in the ^{15}N spectra.



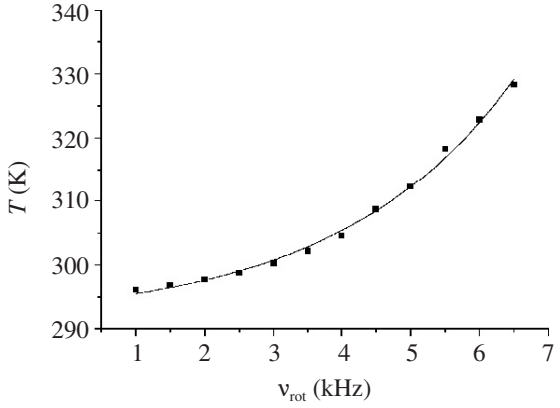
shifts for both phases vary slightly with temperature, but the values of $^1J(^{109}Ag,^{31}P)$ and $^1J(^{107}Ag,^{31}P)$ for the two phases are independent of temperature over the range examined. In the discussion that follows, the high- and low-temperature phases, corresponding to sites I and II, respectively, will be referred to as phases I and II.

Nitrogen

To corroborate the conclusions reached from the ^{31}P NMR experiments, ^{15}N NMR spectra of MAS samples of

© 2005 NRC Canada

Fig. 4. Internal temperature of a sample packed in a 7.5 mm Chemagnetics probe as a function of ν_{rot}, based on ^{207}Pb NMR chemical shifts for $Pb(NO_3)_2$. The solid line is a fit of the experimental points according to T (K) = 3.0 exp(ν_{rot}/2500) + 291.2, with R^2 = 0.9960.



$Ag^{15}NO_3{\cdot}PPh_3$ were acquired at various temperatures (see Fig. 3*b*). These experiments confirm that the peaks at 377 and 379 ppm correspond to the high- and low-temperature phases, respectively, and that a phase transition occurs in the 286–306 K range. The temperature and the spinning-frequency dependence of the ^{15}N NMR spectra are similar to those observed for ^{31}P NMR, apart from the ratio of phase I to phase II for spectra acquired at 300 K. This is attributed to the fact that these spectra were acquired near the phase-transition temperature. VT ^{15}N NMR has been used previously to investigate the thermal behaviour of other nitrates. For example, ^{15}N NMR chemical shift data were determined for the five solid phases of ammonium nitrate using VT ^{15}N NMR spectroscopy of MAS and stationary samples (33–35).

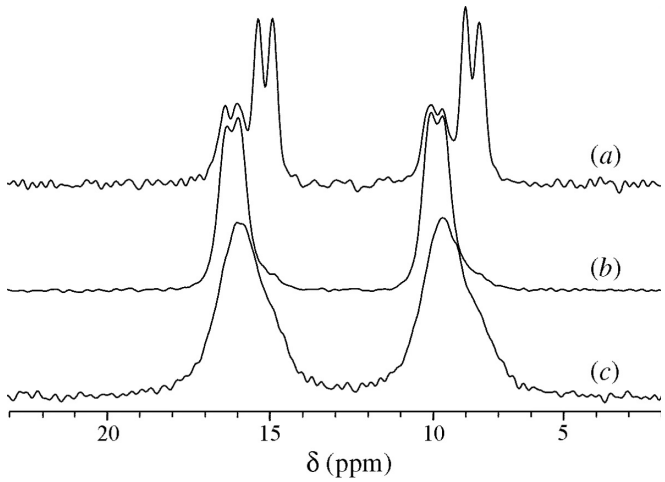
Temperature calibration

To determine the internal temperature of the samples during MAS, ^{207}Pb NMR spectra of a mixture of lead(II) nitrate and $AgNO_3{\cdot}PPh_3$ were acquired as a function of MAS frequency; the internal temperature was calculated from the ^{207}Pb chemical shifts (Fig. 4). These experiments confirm that the temperature of the sample, when in the rotor, changes approximately exponentially as the MAS frequency increases. A sample in a 7.5 mm Chemagnetics rotor spinning at 3 kHz in a laboratory at 295 K was heated to approximately 300 K.

Deuterium isotope effect

Phosphorus-31 NMR spectra of a perdeuterated sample of $AgNO_3{\cdot}PPh_3$ were also acquired. These spectra exhibit the same splitting patterns and similar spinning-frequency dependence as those for the natural abundance sample, but the isotropic ^{31}P NMR chemical shifts of all peaks were shifted by approximately 0.8 ppm to lower frequency upon substitution of hydrogen for deuterium in $AgNO_3{\cdot}PPh_3$. Substitution of a heavier isotope of a given atom has long been known to induce chemical shifts, usually to lower frequency, in the resonance frequencies of neighbouring nuclei (36, 37). The magnitude of these isotope shifts depends on the ratio of the masses of the substituted nuclei, the chemical shift range of the observed nucleus, and the number of intervening bonds between the site of isotopic substitution and the observed nucleus; for multiple isotopic substitution, the effect is usually additive (38–40). Isotope shifts are usually obtained from samples dissolved in isotropic solutions, but there have been a few reports of solid-state NMR measurements (41–45). Perdeuterated $AgNO_3{\cdot}PPh_3$ has six ^2H nuclei 3-bonds distant, six ^2H nuclei 4-bonds distant, and three ^2H nuclei 5-bonds distant from the phosphorus atom. Each deuterium may contribute to the overall isotope shift in the ^{31}P NMR resonance of perdeuterated $AgNO_3{\cdot}PPh_3$; however, determining their individual contributions is not possible unless the phenyl rings are selectively ^2H enriched.

Fig. 5. Effect of sample grinding on the solid-state ^{31}P NMR spectra of $AgNO_3{\cdot}PPh_3$. Trace (*a*) is that obtained from a sample that was packed into a rotor without grinding; trace (*b*) is that from a sample that was not subjected to intense grinding; and trace (*c*) is that obtained from a sample following intense grinding for 90 s. All spectra were acquired at room temperature with CP at ν_{rot} = 3.0 kHz and B_0 = 4.70 T.



Effect of sample grinding

For solid-state NMR experiments, grinding samples prior to packing in an NMR rotor is common practice. We found that the peaks in the ^{31}P NMR spectra of $AgNO_3{\cdot}PPh_3$ were broadened when the solid sample was ground using a mortar and a pestle (Fig. 5). When the sample was ground mildly, peaks corresponding to phase I were obtained at room temperature, but lowering the temperature resulted in a single site, corresponding to phase II. This behaviour is identical to that observed when spinning the sample at high frequencies, suggesting that the transition is induced by sample heating during grinding. Solid-solid phase transitions induced by grinding have been previously reported (46, 47). In their solid-state NMR investigation of poly(L-alanine) at various temperatures, Wildman et al. (46) attributed a phase transition induced by grinding to mechanical shear forces rather than to sample heating. However, contrary to the results of these studies, more intense grinding of $AgNO_3{\cdot}PPh_3$ gave rise to a broad peak spread between those assigned for phases I and II, with maximum intensity at the resonance frequency of the high-temperature phase (Fig. 5*c*). These broad peaks, suggesting the presence of an amorphous

© 2005 NRC Canada

phase, persist when the sample is cooled. A DSC scan of such a sample indicates that there is no phase transition at the expected temperature (~300 K). A stable amorphous phase induced by grinding for CS-891, a testosterone inhibitor, has been reported (48).

Further investigations of the solid–solid phase transition in $AgNO_3 \cdot PPh_3$

DSC

To investigate the phase transition indicated by the ^{31}P and ^{15}N NMR experiments, DSC measurements were performed. A broad endothermic peak was observed from the DSC scans of natural abundance or perdeuterated $AgNO_3 \cdot PPh_3$, confirming a solid–solid phase transition. This transition was observed at approximately 301 K (onset temperature at 300 K) for $AgNO_3 \cdot PPh_3$ at natural abundance. This is consistent with the observation of two NMR sites in the ^{31}P and ^{15}N NMR spectra of MAS samples acquired at room temperature and with the fact that such a sample spinning at 3.0 kHz is heated to 300 K. DSC measurements on a perdeuterated sample of $AgNO_3 \cdot PPh_3$ also indicate a phase transition, but at a higher temperature, 310 K (onset temperature at 309 K). The higher transition temperature for the perdeuterated sample is attributed to the deuterium isotope effect, and has been observed for many other compounds (49). For example, the hexagonal-to-cubic phase transition for norbornane-d_4 is elevated by 25 K compared to the temperature for this transition in the natural abundance sample (50).

X-ray diffraction

XRD data for $AgNO_3 \cdot PPh_3$ collected on single crystals at 193 and 295 K are given in Tables 1 and 2. These data were collected on the same crystal, but when the temperature was increased to 298 K, the single crystal crumbled. All attempts to grow a single crystal in our laboratory at or above 298 K failed. Hence, the cell parameters were investigated via powder XRD; cell parameters determined by this method at 295 and 313 K are also listed in Table 1. The latter temperature was selected since NMR and DSC experiments indicate that $AgNO_3 \cdot PPh_3$ is definitely in the high-temperature phase at this temperature. Also listed in Tables 1 and 2 are the single-crystal structure data reported by Stein and Knobler (3), collected at 298 K.

Cell parameters determined via powder XRD at 295 K are, within error, in agreement with those determined from a single crystal at the same temperature. Likewise, powder XRD data collected at 313 K are similar to those obtained by Stein and Knobler from their analysis of a single crystal at 298 K (3); small differences between the latter two structures are consistent with changes in cell parameters induced by temperature (51). Both powder and single-crystal XRD data indicate that $AgNO_3 \cdot PPh_3$ exists in the same space group for the two phases, with similar cell parameters apart from a much greater value for the angle β in the high-temperature phase. Both methods also indicate that the high-temperature phase has a lower density, as expected. The structure obtained at 298 K by Stein and Knobler (3) is consistent with the NMR and DSC data obtained for the high-temperature phase previously discussed — the phase-transition temperature obtained via DSC is thought to be slightly elevated, a consequence of super heating (52). However, we can not discount the possibility that these authors obtained the structure for a polymorph of $AgNO_3 \cdot PPh_3$ that we were unable to isolate.

Our X-ray diffraction data for the low-temperature phase indicate that two nitrate anions are in proximity to each silver atom (see Fig. 1). The minor differences in the crystal structures of $AgNO_3 \cdot PPh_3$ obtained at 193 and 295 K (Tables 1 and 2) are consistent with temperature effects on crystal structures (51); there are significant differences, however, between the structure determined at 295 K and that determined at 298 K by Stein and Knobler (3). For example, the Ag—O1 and Ag—O3 bonds are 0.1 Å shorter and 0.4 Å longer, respectively, for the structure obtained in our laboratory. The P-Ag-O and O-Ag-O bond angles are also significantly different in the structures obtained here and in ref. 3. The X-ray diffraction data consistently shows that, regardless of phase, $AgNO_3 \cdot PPh_3$ exists in the space group $P2_1/c$ with four molecules per unit cell. Note that the four molecules in the unit cell are related by symmetry, explaining why single ^{31}P and ^{15}N NMR sites are observed for a single phase of $AgNO_3 \cdot PPh_3$.

Proton spin-lattice relaxation times

While optimizing experimental conditions for the ^{31}P and ^{15}N CP experiments, we noticed that the ^1H T_1s are much longer when $AgNO_3 \cdot PPh_3$ is in phase II rather than in phase I. Values for T_1 were estimated using the progressive saturation technique (22) from $T_1 = -t/\ln(0.5)$ where t was the time preceding the ^1H 90° pulse that gave rise to the peak that had 50% of the maximum intensity; the latter was obtained with $t >> T_1$ (53). This experiment shows that $T_1(I) \approx 65$ s and $T_1(II) \approx 300$ s. The significance of these differences is discussed in the following section.

Deuterium NMR

The phase transition previously discussed, as well as the difference between the ^1H T_1s for $AgNO_3 \cdot PPh_3$ in phases I and II, may be associated with the onset of motion of the phenyl rings of $AgNO_3 \cdot PPh_3$ at elevated temperatures (54). Since solid-state ^2H NMR spectroscopy is a sensitive probe of internal motion (10, 54), the technique has been applied to investigate the phenyl-ring dynamics of compounds such as phenylpropylammonium chloride (55), phenylalanine (56, 57), or the insulin fragment Gly-Phe-Phe (58). Rotation of phenyl rings about its C_{ipso}—P bond can occur either by small-step diffusion or by π flips (54). Both types of rotation are predicted to result in significant changes in the ^2H NMR line shape compared to that expected in the absence of motion. As well, the ^2H NMR line shapes arising from rapid π flips are significantly different from those arising from small-step diffusion (54). To investigate the dynamics of the phenyl rings of $AgNO_3 \cdot PPh_3$, ^2H NMR spectra of a perdeuterated sample were acquired at temperatures ranging from 293 to 364 K. At temperatures below 350 K, the ^2H NMR spectra are typical of those previously observed for rigid phenyl groups (54, 56, 57). Simulation of the line shape indicates that the quadrupolar coupling (C_Q) is 176 ± 5 kHz and that the asymmetry in the electric field gradient (η_Q) is 0.03. A spectrum obtained at 364 K contains small

© 2005 NRC Canada

Table 3. Phosphorus NMR chemical shift tensor parameters and ^1J(Ag,P) for phases I and II of silver nitrate triphenylphosphine.

	Natural abundance		Perdeuterated	
Parameter	Phase I	Phase II	Phase I	Phase II
δ_{11} (ppm)	41.5±0.5	37.1±0.5	—	—
δ_{22} (ppm)	16.6±0.6	15.8±0.6	—	—
δ_{33} (ppm)	–18.5±0.5	–16.9±0.5	—	—
δ_{iso} (ppm)	13.2±0.2	12.0±0.2	12.5±0.2	11.2±0.2
Ω (ppm)	60±1	54±1	—	—
κ	0.17±0.02	0.21±0.02	—	—
θ_{11} (°)	60±5	66±5	—	—
θ_{22} (°)	85±5	61±5	—	—
θ_{33} (°)	30±5	40±5	—	—
$^1J(^{107}Ag,^{31}P)$ (Hz)	±707±14	±719±14	±711±14	±718±14
$^1J(^{109}Ag,^{31}P)$ (Hz)	±815±14	±830±14	±813±14	±828±14
$\Delta^{31}P(^{2/1}H)$ (ppm)[a]	—	—	–0.7±0.2	–0.8±0.2

Note: Spectra for both phases were obtained at room temperature, see text.
[a] $\Delta^{31}P(^{2/1}H) = \delta_{iso}[AgNO_3{\cdot}^{31}P(C_6D_5)_3] - \delta_{iso}[AgNO_3{\cdot}^{31}P(C_6H_5)_3]$.

inner singularities with a splitting of 32 kHz, consistent with the onset of π flips about the P—C_{ipso} bond (54).

DSC measurements indicate that a phase transition occurs at approximately 310 K for perdeuterated $AgNO_3{\cdot}PPh_3$, and the ^{1}H T_1s are very different for phases I and II. The much shorter ^{1}H T_1 value for phase I is probably a consequence of motion of the phenyl groups, yet there is no indication of significant motion of the phenyl rings from the ^{2}H NMR line shapes obtained near the phase-transition temperature. Small-angle torsional oscillations about the P—C_{ipso} bond may result in shorter ^{1}H T_1 values, but this motion would be difficult to detect by ^{2}H NMR (54). As well, it is possible that the phenyl rings do undergo π flips about the P—C_{ipso} bond, but on a timescale that is significantly greater than C_Q^{-1}, approximately 5×10^{-6} s (54).

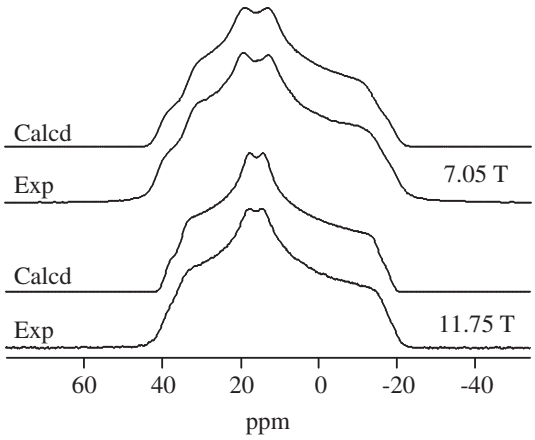
Characterization of phosphorus and nitrogen chemical shift (CS) tensors

Phosphorus CS tensors

Phosphorus-31 NMR spectra of a stationary sample of the low- and high-temperature phases of $AgNO_3{\cdot}PPh_3$ were acquired at room temperature at B_0 = 4.7, 7.05, and 11.75 T. Spectra obtained for the low-temperature phase are shown in Fig. 6; those for the high-temperature phase are similar. In the absence of external heat sources, such as that arising from MAS, transitions from phases I to II occur very slowly at 295 K. Hence, spectra for both phases were acquired at this temperature after the sample had been either heated or cooled overnight to obtain the desired phase; to verify that only one phase was contributing to the given spectrum, spectra of MAS samples (ν_{rot} = 1.5 kHz) were acquired immediately before and after acquisition of the spectra of stationary samples.

The line shapes of the ^{31}P NMR spectra (Fig. 6) arise from the anisotropy in the magnetic shielding, as well at the direct and indirect $^{107/109}$Ag–P spin-spin interactions, R_{DD} and J_{iso}, respectively (10, 59). Seven independent parameters must be determined to describe these spectra (10, 60–62): the three principal components of the CS tensor, two

Fig. 6. Experimental and calculated ^{31}P NMR spectra of a stationary sample of phase II of $AgNO_3{\cdot}PPh_3$, acquired at 295 K. Fifty-eight and sixty-eight transients, respectively, were added for spectra acquired at 7.05 and 11.75 T.



polar angles describing the orientation of the dipolar vector in the principal axis system of the CS tensor, as well as the $^{107/109}$Ag,^{31}P direct and indirect spin-spin coupling constants. Values for δ_{iso} and J_{iso} were determined from spectra of MAS samples and R_{DD} was estimated (59) from the Ag—P bond length determined at 295 and 298 K (3) (Table 2). The remaining four parameters were determined by simulation of the NMR spectra of stationary samples; spectra were obtained at more than one applied magnetic field to ensure that spectral features were properly assigned (10). The phosphorus CS tensor data for each phase, derived from the simulations, are given in Table 3. The orientation dependence of the dipolar interaction (59) yields θ_{ii} (i = 1, 2, or 3), the angle formed by the CS tensor component δ_{ii} with the Ag—P bond (62–65). However, calculated line shapes are invariant to rotation of the CS tensor about the dipolar vector, since in such cases the angles formed by the tensor components with the dipolar vector are unchanged. Hence, experimentally one determines the orientation of the tensor components relative

© 2005 NRC Canada

to the dipolar vector, but not the orientation of the CS tensor in the molecular framework. The θ_{ii}, listed in Table 3, indicate that the principal components of the phosphorus CS tensors for $AgNO_3{\cdot}PPh_3$ in phases I or II approximately straddle the Ag—P bond.

Comparison of the phosphorus CS tensor principal components for $AgNO_3{\cdot}PPh_3$ with those for triphenylphosphine (PPh_3) suggests that coordination of the PPh_3 ligand with silver nitrate has a moderate effect on the phosphorus CS tensor. That for triphenylphosphine is axially symmetric with $\delta_{11} = \delta_{22} = 9$ ppm and $\delta_{33} = -42$ ppm; the latter component is along the C_3 symmetry axis (66). The nonaxial symmetry of the phosphorus CS tensor for $AgNO_3{\cdot}PPh_3$ is a consequence of the nonsymmetrical environment about the phosphorus nucleus of $AgNO_3{\cdot}PPh_3$. A direct comparison of the CS tensor components would require knowledge of the CS tensor orientation for $AgNO_3{\cdot}PPh_3$, but the shielding clearly has not undergone a large change upon coordination of PPh_3 with Ag. For example, the spans and isotropic values for the phosphorus CS tensors for PPh_3 and $AgNO_3{\cdot}PPh_3$ are similar. This is in contrast to numerous ^{31}P NMR studies of phosphorus–metal complexes (67) that indicate that the phosphorus nucleus is sensitive to metal coordination (27, 68, 69). For example, the three phosphorus CS tensors for the PPh_3 groups of $Rh(PPh_3)_3Cl$ are distinct, with spans ranging from 150 to 271 ppm (70), compared to a span of 51 ppm for triphenyl phosphine (66).

Nitrogen CS tensors

The nitrogen CS tensor data for the two phases of $AgNO_3{\cdot}PPh_3$ obtained from analyses of ^{15}N NMR spectra for stationary samples (not shown) are summarized in Table 4. The principal components of the nitrogen CS tensors for the two phases are similar, although the span is greater and the skew is less for phase II than for phase I. Because of the small values of $R(^{107/109}Ag,^{15}N)$, we are unable to determine orientations for the principal components of the nitrogen CS tensors relative to the dipolar vector, but previous NMR studies and first-principles calculations indicate that nitrogen CS tensors for nitrates are axially symmetric with the direction of greatest shielding perpendicular to the plane of the anion (33, 71, 72). The nitrogen CS tensor principal components for $AgNO_3{\cdot}PPh_3$ are similar to those for the nitrogen nucleus of silver nitrate (71) and for other nitrates (33, 67, 72). This insensitivity of the nitrogen shielding tensor to coordination with silver is not surprising, since the nitrogen atom is not directly involved in coordination with Ag. The nonaxial symmetry observed here is a consequence of the nonsymmetric environment about the nitrogen atom of $AgNO_3{\cdot}PPh_3$.

Conclusions

In this study we have found that two ^{31}P NMR sites with variable relative intensities in high-resolution ^{31}P NMR spectra of solid silver nitrate triphenylphoshine at ambient temperature are a consequence of a solid–solid phase transition at 299 ± 2 K. This phase transition has been confirmed by multinuclear magnetic resonance measurements, DSC, and X-ray diffraction. There are only minor differences in the crystal structures determined by X-ray diffraction experiments conducted at 193 and 295 K, both of which correspond to phase II. Powder XRD data for phase I, obtained at 313 K, are consistent with the structure reported by Stein and Knobler (3); this structure is significantly different from that obtained at 295 K. In the course of our study we characterized nitrogen and phosphorus chemical shift tensors for $AgNO_3{\cdot}PPh_3$ in both solid phases. In the ^{31}P and ^{15}N NMR spectra, the NMR signals arising from the low-temperature phase are more shielded than those for the high-temperature phase. The proton T_1s are longer when $AgNO_3{\cdot}PPh_3$ is in phase II rather than phase I. Although the shorter T_1 for the former must be a consequence of motion of the phenyl rings at the higher temperature, this motion is not directly evident from the ^2H NMR line shapes. Replacement of the phenyl group hydrogen atoms by deuterium results in a 0.8 ppm shift to low frequency in the ^{31}P NMR peaks. Finally, we noticed that grinding samples of $AgNO_3{\cdot}PPh_3$ may cause line broadening in solid-state NMR spectra, apparently because of the formation of an amorphous phase, which persists over a long period of time and over a range of temperatures.[5]

This work has shown that many factors, such as temperature and sample preparation, must be considered when studying transition-metal complexes. The ability to obtain pure phases of $AgNO_3{\cdot}PPh_3$ through the selection of the appropriate temperature has been demonstrated.

Table 4. Nitrogen chemical shift tensor parameters for phases I and II of silver nitrate triphenylphosphine.

Parameter	Phase I	Phase II
δ_{11} (ppm)	449±0.5	457±0.5
δ_{22} (ppm)	438±0.6	434±0.6
δ_{33} (ppm)	249±0.5	242±0.5
δ_{iso} (ppm)	379±0.2	377±0.2
Ω (ppm)	200±1	215±1
κ	0.89±0.02	0.79±0.02

Note: Spectra for both phases were obtained at room temperature, see text.

Addendum

Since submitting this manuscript, Xu and Harris (73) reported the observation of a solid–solid phase transition in sodium acetate induced by magic angle spinning.

Acknowledgements

We thank members of the solid-state NMR group at the University of Alberta for many helpful comments and Fu Chen for obtaining some NMR spectra. Some preliminary

[5] Supplementary data for this article are available on the Web site or may be purchased from the Depository of Unpublished Data, Document Delivery, CISTI, National Research Council Canada, Ottawa, ON K1A 0R6, Canada. DUD 4053. For more information on obtaining material refer to http://cisti-icist.nrc-cnrc.gc.ca/irm/unpub_e.shtml. CCDC 280719 and 280720 contain the crystallographic data for this manuscript. These data can be obtained, free of charge, via www.ccdc.cam.ac.uk/conts/retrieving.html (Or from the Cambridge Crystallographic Data Centre, 12 Union Road, Cambridge CB2 1EZ, UK; fax +44 1223 336033; or deposit@ccdc.cam.ac.uk).

© 2005 NRC Canada

work on this project was undertaken by Glenn Penner, Ron Curtis, and Scott Kroeker; we are grateful to these researchers. We also thank Darlene Mahlow of the microanalytical laboratory at the University of Alberta for obtaining the DSC data. We acknowledge the financial support of the Natural Sciences and Engineering Research Council of Canada (NSERC). REW acknowledges the Government of Canada for a Canada Research Chair in Physical Chemistry and SWO is grateful to Mokpo National University, Republic of Korea, for an award under the Professors' training program (2001).

References

1. R.J. Lancashire. *In* Comprehensive coordination chemistry. Vol. 5. Late transition elements. *Edited by* G. Wilkinson, R.D. Gillard, and J.A. McCleverty. Pergamon Press, Oxford. 1987. p. 775.
2. C.E. Holloway, W.A. Nevin, and M. Melnik. J. Coord. Chem. **31**, 191 (1994).
3. R.A. Stein and C. Knobler. Inorg. Chem. **16**, 242 (1977).
4. P.F. Barron, J.C. Dyason, P.C. Healy, L.M. Englehardt, B.W. Skelton, and A.H. White. J. Chem. Soc. Dalton Trans. 1965 (1986).
5. J.D. Dunitz and J. Bernstein. Acc. Chem. Res. **28**, 193 (1995).
6. T.L. Threlfall. Analyst (Cambridge, U.K.), **120**, 2435 (1995).
7. J. Bernstein, R.J. Davey, and J.-O. Henck. Angew. Chem. Int. Ed. **38**, 3440 (1999).
8. D. Braga and F. Grepioni. Chem. Soc. Rev. **29**, 229 (2000).
9. A. Pines, M.G. Gibby, and J.S. Waugh. J. Chem. Phys. **56**, 1776 (1972).
10. D.L. Bryce, G.M. Bernard, M. Gee, M. Lumsden, K. Eichele, and R.E. Wasylishen. Can. J. Anal. Sci. Spectrosc. **46**, 46 (2001).
11. J. Mason. Solid State Nucl. Magn. Reson. **2**, 285 (1993).
12. K. Eichele and R.E. Wasylishen. WSOLIDS NMR simulation package [computer program]. University of Alberta, Edmonton, Alberta. 2001.
13. J.H. Davis, K.R. Jeffrey, M. Bloom, M.I. Valic, and T.P. Higgs. Chem. Phys. Lett. **42**, 390 (1976).
14. M. Bloom, J.H. Davis, and M.I. Valic. Can. J. Phys. **58**, 1510 (1980).
15. H.W. Spiess and H. Sillescu. J. Magn. Reson. **42**, 381 (1981).
16. P.M. Henrichs, J.M. Hewitt, and M. Linder. J. Magn. Reson. **60**, 280 (1984).
17. L.C.M. van Gorkom, J.M. Hook, M.B. Logan, J.V. Hanna, and R.E. Wasylishen. Magn. Reson. Chem. **33**, 791 (1995).
18. A. Bielecki and D.P. Burum. J. Magn. Reson. Ser. A, **116**, 215 (1995).
19. G. Neue, C. Dybowski, M.L. Smith, M.A. Hepp, and D.L. Perry. Solid State Nucl. Magn. Reson. **6**, 241 (1996).
20. P.E. Pfeffer, W.V. Gerasimowicz, and E.G. Piotrowski. Anal. Chem. **56**, 734 (1984).
21. P. Tekely and M.R. Vignon. J. Polym. Sci. Part C: Polym. Lett. **25**, 257 (1987).
22. R. Freeman and H.D.W. Hill. J. Chem. Phys. **54**, 3367 (1971).
23. P.T. Beurskens, G. Beurskens, R. de Gelder, S. Garcia-Granda, R. Israel, R.O. Gould, and J.M.M. Smits. The DIRDIF-99 program system [computer program]. Crystallography Laboratory, University of Nijmegen, Nijmegen, The Netherlands. 1999.
24. G.M. Sheldrick. SHELXL-93 [computer program]. University of Göttingen, Göttingen, Germany. 1993.
25. T.J.B. Holland and S.A.T. Redfern. Mineral. Mag. **61**, 65 (1997).
26. W. Kraus and G. Nolze. PowderCell for Windows. Version 2.4 [computer program]. Federal Institute for Materials Research and Testing, Berlin, Germany. 2000.
27. J.H. Nelson. Concepts Magn. Reson. **14**, 19 (2002).
28. S. Attar, N.W. Alcock, G.A. Bowmaker, J.S. Frye, W.H. Bearden, and J.H. Nelson. Inorg. Chem. **30**, 4166 (1991).
29. B. Wehrle, F. Aguilar-Parrilla, and H.-H. Limbach. J. Magn. Reson. **87**, 584 (1990).
30. G.-J.M.P. van Moorsel, E.R.H. van Eck, and C.P. Grey. J. Magn. Reson. Ser. A, **113**, 159 (1995).
31. F.D. Doty and P.D. Ellis. Rev. Sci. Instrum. **52**, 1868 (1981).
32. T. Bjorholm and H.J. Jakobsen. J. Magn. Reson. **84**, 204 (1989).
33. K.L. Anderson-Altmann and D.M. Grant. J. Phys. Chem. **97**, 11096 (1993).
34. M.G. Gibby, R.G. Griffin, A. Pines, and J.S. Waugh. Chem. Phys. Lett. **17**, 80 (1972).
35. R.E. Wasylishen. Spectrochim. Acta Part A, **40**, 115 (1984).
36. N.F. Ramsey. Phys. Rev. **87**, 1075 (1952).
37. T.F. Wimett. Phys. Rev. **91**, 476 (1953).
38. C.J. Jameson and H.-J. Osten. J. Chem. Phys. **81**, 4293 (1984).
39. C.J. Jameson and H.-J. Osten. Annu. Rep. NMR Spectrosc. **17**, 1 (1986).
40. C.J. Jameson. *In* Encyclopedia of nuclear magnetic resonance. Vol. 4. *Edited by* D.M. Grant and R.K. Harris. John Wiley and Sons, Chichester. 1996. p. 2638.
41. H. Benedict, C. Hoelger, F. Aguilar-Parrilla, W.P. Fehlhammer, M. Wehlan, R. Janoschek, and H.H. Limbach. J. Mol. Struct. **378**, 11 (1996).
42. T.C. Stringfellow, G. Wu, and R.E. Wasylishen. J. Phys. Chem. B, **101**, 9651 (1997).
43. K. Eichele, R.E. Wasylishen, and J.H. Nelson. J. Phys. Chem. A, **101**, 5463 (1997).
44. H. Benedict, H.-H. Limbach, M. Wehlan, W.-P. Fehlhammer, N.S. Golubev, and R. Janoschek. J. Am. Chem. Soc. **120**, 2939 (1998).
45. T. Dziembowska, K. Ambroziak, Z. Rozwadowski, W. Schilf, and B. Kamieński. Magn. Reson. Chem. **41**, 135 (2003).
46. K.A.H. Wildman, D.-K. Lee, and A. Ramamoorthy. Biopolymers, **64**, 246 (2002).
47. K.A.H. Wildman, E.E. Wilson, D.-K. Lee, and A. Ramamoorthy. Solid State Nucl. Magn. Reson. **24**, 94 (2003).
48. S. Yada, M. Ohya, Y. Ohuchi, T. Hamaura, N. Wakiyama, F. Usui, A. Kusai, and K. Yamamoto. Int. J. Pharm. **255**, 69 (2003).
49. N.G. Parsonage and L.A.K. Stavely. Disorder in crystals. Oxford University Press, Oxford. 1978.
50. R.E. Wasylishen, S. Peiris, and D.R. Arnold. Chem. Phys. Lett. **114**, 31 (1985).
51. M.F.C. Ladd and R.A. Palmer. Structure determination by X-ray crystallography. 2nd ed. Plenum Press, New York. 1985.
52. P. Papon, J. Leblond, and P.H.E. Meijer. The physics of phase transitions. Concepts and applications. Springer, Berlin. 2002.
53. M.L. Martin, J.-J. Delpuech, and G.J. Martin. Practical NMR spectroscopy. Heyden, London. 1980.
54. R.G. Griffin, K. Beshah, R. Ebelhäuser, T.H. Huang, E.T. Olejniczak, D.M. Rice, D.J. Siminovitch, and R.J. Wittebort. *In* The time domain in surface and structural dynamics. *Edited by* G.J. Long and F. Grandjean. Kluwer Academic Publishers, Dordrecht. 1988. Chap. 7.
55. M.L.H. Gruwel and R.E. Wasylishen. Z. Naturforsch. A, **47**, 1073 (1992).
56. C.M. Gall, J.A. DiVerdi, and S.J. Opella. J. Am. Chem. Soc. **103**, 5039 (1981).
57. T. Hiraoki, A. Kogame, N. Nishi, and A. Tsutsumi. J. Mol. Struct. **441**, 243 (1998).
58. A. Naito, T. Iizuka, S. Tuzi, W.S. Price, K. Hayamizu, and H. Saitô. J. Mol. Struct. **355**, 55 (1995).

© 2005 NRC Canada

59. R.E. Wasylishen. *In* Encyclopedia of nuclear magnetic resonance. Vol. 3. Advances in NMR. *Edited by* D.M. Grant and R.K. Harris. John Wiley and Sons, Chichester. 1996. p. 1685.
60. D.M. Grant. *In* Encyclopedia of nuclear magnetic resonance. Vol. 2. *Edited by* D.M. Grant and R.K. Harris. John Wiley and Sons, Chichester. 1996. p. 1298.
61. R.E. Wasylishen, R.D. Curtis, K. Eichele, M.D. Lumsden, G.H. Penner, W.P. Power, and G. Wu. *In* Nuclear magnetic shieldings and molecular structure. *Edited by* J.A. Tossell. Kluwer Academic Publishers, Dordrecht. 1993. p. 297.
62. M.J. Duer. *In* Physical organometallic chemistry. Vol. 2. John Wiley and Sons, Chichester. 1999. Chap. 6.
63. K. Eichele and R.E. Wasylishen. J. Magn. Reson. A, **106**, 46 (1994).
64. H. van Willigen, R.G. Griffin, and R.A. Haberkorn. J. Chem. Phys. **67**, 5855 (1977).
65. K.W. Zilm and D.M. Grant. J. Am. Chem. Soc. **103**, 2913 (1981).
66. G.H. Penner and R.E. Wasylishen. Can. J. Chem. **67**, 1909 (1989).
67. T.M. Duncan. Principal components of chemical shift tensors: A compilation. 2nd ed. Farragut Press, Chicago. 1994.
68. P.S. Pregosin and R.W. Kunz. NMR Basic Princ. Prog. **16**, 1 (1979).
69. S. Berger, S. Braun, and H.-O. Kalinowski. NMR spectroscopy of non-metallic elements. John Wiley and Sons, Chichester. 1997. Chap. 7.
70. A. Naito, D.L. Sastry, and C.A. McDowell. Chem. Phys. Lett. **115**, 19 (1985).
71. R.A. Santos, P. Tang, W.-J. Chien, S. Kwan, and G.S. Harbison. J. Phys. Chem. **94**, 2717 (1990).
72. P.J. Barrie, C.J. Groombridge, J. Mason, and E.A. Moore. Chem. Phys. Lett. **219**, 491 (1994).
73. M. Xu and K.D.M. Harris. J. Am. Chem. Soc. **127**, 10832 (2005).

© 2005 NRC Canada

The detrimental effect of orotic acid substitution in the peptide nucleic acid strand on the stability of PNA_2:NA triple helices

Robert H.E. Hudson and Filip Wojciechowski

Abstract: We have investigated the incorporation of C6 derivatives of uracil into polypyrimidine peptide nucleic acid oligomers. Starting with uracil-6-carboxylic acid (orotic acid), a peptide nucleic acid monomer compatible with Fmoc-based synthesis was prepared. This monomer then served as a convertible nucleobase whereupon treatment of the resin-bound methyl orotate containing hexamers with hydroxide or amines cleanly converted the ester to an orotic acid or orotamide-containing peptide nucleic acid. Peptide nucleic acid hexamers containing the C6-modified nucleobase hybridized to both poly(riboadenylic acid) and poly(deoxyriboadenylic acid) via triplex formation. Complexes formed with poly(riboadenylic acid) were more stable than those formed with poly(dexoyriboadenylic acid), as measured by temperature-dependent UV spectroscopy. However, both of these complexes were destabilized relative to the complexes formed by an unmodified peptide nucleic acid oligomers. Internal or doubly substituted hexamers are destabilized more strongly than a terminally substituted one, and the type of substitution (carboxamide, ester, carboxylic acid) affects the overall triplex stability. These results clearly show that incorporation of a C6-substituted uracil into polypyrimidine PNA is detrimental to triplex formation. We have also extended this chemistry to incorporate uracil-5-methylcarboxylate into a peptide nucleic acid hexamer. After on-resin conversion of the C5 ester to the 3-(*N*,*N*-dimethylamino)propylamide, significant stabilization of the triplex formed with poly(riboadenylic acid) was observed, which illustrates the compatibility of C5 substitution with peptide nucleic acid directed triple helix formation.

Key words: peptide nucleic acid, triple helix, orotic acid, orotamide, PNA.

Résumé : On a étudié l'incorporation de dérivés en C6 de l'uracile dans la polypyrimidine, des oligomères du peptide de l'acide nucléique. Utilisant l'acide uracile-6-carboxylique (acide orotique) comme produit de départ, on a préparé un monomère compatible avec une synthèse à base de dérivés Fmoc. Ce monomère a ensuite été utilisé comme nucléobase convertible qui, par traitement des hexamères contenant de l'orotate de méthyle lié à une résine de l'hydroxyde ou par des amines, conduit à la formation propre d'un peptide de l'acide nucléique qui contient de l'acide orotique ou un orotamide. Les peptides d'hexamères contenant de la nucléobase modifiée par un dérivé en C6 donnent, par le biais de la formation d'un triplex, une hybridisation tant avec l'acide poly(riboadénylique) qu'avec l'acide poly(désoxyriboadénylique). Sur la base des résultats de spectroscopie UV mesurés en fonction de la température, on a observé que les complexes formés à partir de l'acide poly(riboadénylique) sont plus stables que ceux formés à partir de l'acide poly(désoxyriboadénylique). Toutefois, ces deux complexes sont déstabilisés par rapport aux complexes formés à partir d'oligomères non modifiés du peptide de l'acide nucléique. Les hexamères internes ou doublement substitués sont encore plus déstabilisés que les hexamères substitués en position terminale; de plus, le type de substitution (carboxamide, ester ou acide carboxylique) affecte aussi la stabilité globale du triplex. Ces résultats montrent clairement que l'incorporation d'uraciles substitués en C6 dans une polypyrimidine de l'acide polynucléique est nuisible à la formation de triplex. On a aussi étendu cette chimie à l'introduction d'un uracile 5-carboxylate de méthyle dans un peptide hexamère de l'acide nucléique. Après une conversion sur la résine de l'ester en position C5 en un 3-(*N*,*N*-diméthylamino)propylamide, on a observé une stabilisation importante du triplex formé avec de l'acide poly(riboadénylique); ce qui illustre la compatibilité d'une substitution en C5 avec un peptide de l'acide nucléique en vue de former une hélice triple.

Mots clés : peptide de l'acide nucléique, triple hélice, acide orotique, orotamide, acide polynucléique.

[Traduit par la Rédaction]

Received 9 May 2005. Published on the NRC Research Press Web site at http://canjchem.nrc.ca on 2 December 2005.

R.H.E. Hudson[1] and F. Wojciechowski. Department of Chemistry, The University of Western Ontario, London, ON N6A 5B7, Canada.

[1]Corresponding author (e-mail: rhhudson@uwo.ca).

 doi: 10.1139/V05-180 © 2005 NRC Canada

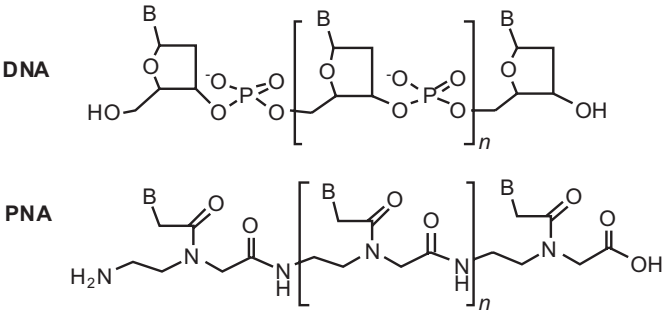
Introduction

Modified nucleobases have been intensively studied in the field of nucleic acids (NAs) for a plethora of reasons (reviewed in 1, 2). Inclusion of modified nucleobases in RNA and DNA provides a route to modulation of the hybridization properties (stability, selectivity), artificial expansion of the genetic code, incorporation of reporter groups, inclusion of reactive sites for conjugation or further chemistry, and the ability to undertake fundamental studies on the forces stabilizing nucleic acid complexes, to name but a few current areas of interest. The study of modified or unnatural nucleobases combined with oligonucleotide analogues containing backbone structural alterations is a less well-developed area (3). However, the intersection of these two types of modifications is fertile ground, in general, for the synthesis and investigation of oligomers with tunable properties.

In some of our previous work, we have exploited established chemistry to incorporate modified nucleobases into peptide nucleic acid (PNA) (4). Peptide nucleic acid is an oligonucleotide mimic based on a polyamide backbone, which is structurally compatible with the formation of helical complexes with natural DNA or RNA (Fig. 1) (5). Due to its modular nature, it is relatively straightforward to incorporate modifications into the *N*-(2-aminoethyl)glycine backbone, the methylene carbonyl linker, or the nucleobase, either separately or in concert. Thus, the first generation of peptide nucleic acid is a convenient scaffold for surveying the effects of changes in these portions of the molecule. Modification of the nucleobases has the advantage of being able to introduce a diversity of functional groups (e.g., charged, hydrophilic, lipophilic) or sites for conjugation or further chemistry that do not interfere with the base-pairing face. Additionally, nucleobase modifications can be done without introducing chirality. Avoiding changing any of the $-CH_2-$ groups in the backbone and linker region is key to a modification that circumvents the additional synthetic complexity, challenges to maintaining the integrity of the chiral center during synthesis/deprotection, and possible consequences to hybridization (6).

The introduction of modified nucleobases into oligonucleotides usually involves time-consuming and laborious synthesis of a variety of individual nucleobase-modified monomers each requiring a multistep synthesis. A clever solution to this drawback is to perform a post-synthetic step on an oligomer containing a convertible nucleobase (7). Herein, we describe the efficient synthesis of a methyl orotate (MO) PNA monomer, its smooth incorporation into an oligomer and straightforward on-resin derivatization to various oligomers. To our knowledge orotic acid or orotamides have not been incorporated into oligonucleotides, therefore their effects on PNA cannot be predicted by analogy. To gain some insight on the possible consequences of exchanging a thymine nucleobase for an orotic acid derivative, a qualitative molecular modeling exercise was undertaken. Working from existing structural information, the modeling suggested each of PNA:DNA duplexes (8), PNA:RNA duplexes (9), and

Fig. 1. Structures of DNA and PNA.



PNA_2:DNA triple helical complexes (10) could possibly accommodate C6 substitution, although each structure showed some deformation from the starting conformation.[2] Given the plasticity of PNA conformations, we decided to experimentally investigate all three types of complexes, and the results for triple helices are reported herein. As a point of comparison, we have also prepared an oligomer possessing a carboxamide substitution at C5 of uracil. In DNA chemistry, substituents at the C5 position of uracil are known to occupy the major grove and are generally tolerated (2).

Experimental

General

All chemicals were obtained from commercial sources and were of ACS reagent grade or higher and were used without further purification, unless noted. Solvents for solution-phase chemistry were obtained from Caledon Laboratories Ltd. (Georgetown, Ontario) and were dried by passing through columns packed with activated alumina (Innovative Technology, Inc., Newburyport, Massachusetts). Reagents for peptide synthesis were obtained from NovaBiochem (San Diego, California) and synthesis grade solvent from Caledon Laboratories. ^{1}H NMR spectra were recorded at 400.085 MHz and chemical shifts were referenced to the residual proton of the deuterated solvent, and ^{13}C NMR spectra were recorded at 100.609 MHz were referenced to the ^{13}C NMR signal of the solvent used. The reported melting points are uncorrected.

Methyl orotate (2)

Orotic acid monohydrate (24.0 g, 138 mmol) was suspended in methanol (3.0 L) and HCl gas (60 g) was bubbled into the suspension. Reflux was maintained for 24 h after which time the suspension had cleared. The volume was reduced by two-thirds, and cooled for 5 h below 0 °C. The white crystals were collected by filtration and washed with cold methanol to yield 21.3 g (91%). TLC (EtOAc–MeOH, 80:20): R_f 0.58; mp 249–251 °C. ^{1}H NMR (400 MHz, DMSO, ppm) δ: 11.40 (s, 1H), 11.16 (s, 1H), 6.03 (s, 1H), 3.83 (s, 3H). ^{13}C NMR (100 MHz, DMSO, ppm) δ: 163.5, 160.5, 150.5, 141.1, 103.5, 53.4.

[2] HyperChem 5.1 was used to modify a central thymine or uracil nucleobase in a trimer that was excised from existing structures. The nucleobase was modified to possess a 6-carboxamide group and was geometrically optimized using the MM+ force field, while the remainder of the structure was held fixed.

© 2005 NRC Canada

***tert*-Butyl (methyl orotate-1-yl)acetate (3)**

Methyl orotate (18.9 g, 111.0 mmol) was suspended in dry DMF (600 mL) and K_2CO_3 (15.34 g, 111.0 mmol) was added and the mixture was stirred under N_2 at room temperature for 30 min. *tert*-Butyl bromoacetate (18.0 mL, 122.0 mmol) was added dropwise over 1 h and the suspension was vigorously stirred for 48 h under an atmosphere of nitrogen. The mixture was filtered and solvent removed in vacuo, the residue was extracted with ethyl acetate (4 × 250 mL) and water (100 mL). The combined organic phase was washed with brine, dried (Na_2SO_4), filtered, and concentrated in vacuo. The material contained a small amount of dialkylated product, which could be removed by recrystallization from absolute ethanol to yield 19.3 g (61%) of a white solid. TLC (EtOAc–MeOH, 90:10): R_f 0.76; mp 186–188 °C. ^{1}H NMR (400 MHz, DMSO, ppm) δ: 11.85 (s, 1H), 6.13 (s, 1H), 4.60 (s, 2H), 3.80 (s, 3H), 1.40 (s, 9H). ^{13}C NMR (100 MHz, DMSO, ppm) δ: 167.1, 162.2, 161.5, 151.0, 143.8, 105.6, 81.8, 53.7, 46.2, 27.6. HR-MS (EI) calcd. for $C_{12}H_{16}N_2O_6$: 284.1009; found: 284.1009.

(Methyl orotate-1-yl)acetic acid (4)

Compound **3** (7.0 g, 24.6 mmol) was suspended in 80 mL of CH_2Cl_2 and cooled to 0 °C, the mixture was stirred under nitrogen, and Et_3SiH (3.9 mL, 24.4 mmol) was added. TFA (80 mL) was added dropwise over 30 min, with stirring under nitrogen. The solution was stirred for 1 h while in an ice bath and then allowed to warm to room temperature for 3 h. The mixture was evaporated to dryness in vacuo and the remaining volatiles were removed by successive co-evaporations with CH_2Cl_2 (3×) and diethyl ether (1×). The white solid was triturated with a mixture of 30 mL of CH_2Cl_2 and 60 mL of diethyl ether and cooled below 0 °C for 12 h; filtration gave 5.04 g (89%) of a white solid. TLC (EtOAc–MeOH–AcOH, 80:15:5): R_f 0.35; mp 206 to 207 °C. ^{1}H NMR (400 MHz, DMSO, ppm) δ: 11.84 (s, 1H), 6.13 (s, 1H), 4.62 (s, 2H), 3.80 (s, 3H). ^{13}C NMR (100 MHz, DMSO, ppm) δ: 169.6, 162.3, 161.6, 151.5, 144.0, 105.5, 53.70, 45.8. HR-MS (EI) calcd. for $C_{12}H_8N_2O_6$: 228.0382; found: 228.0377.

***tert*-Butyl *N*-[2-Fmoc-aminoethyl]-*N*-[(methyl orotate-1-yl)acetyl]glycinate (5)**

Compound **4** (4.0 g, 17.5 mmol) and HOBt hydrate (2.68 g, 17.53 mmol) were dissolved in 20 mL DMF and stirred for 10 min while kept under a nitrogen atmosphere. DCC (3.61 g, 17.5 mmol) was added and the mixture was stirred on ice for 30 min. The free Fmoc-backbone *tert*-butyl ester (**2**) (6.95 g, 17.53 mmol) was dissolved in 5 mL CH_2Cl_2 and added to the mixture. The reaction mixture was stirred for 24 h at room temperature, extracted with EtOAc (4 × 150 mL) and phosphate buffer (pH ~ 4.5, 2 × 50 mL), and the combined organic phase was washed with sodium bicarbonate (2 × 50 mL) and brine (50 mL), dried (Na_2SO_4), filtered, and concentrated in vacuo. The solid was recrystallized from a mixture of 10 mL of MeOH and 25 mL of isopropanol, and isolated by filtration to give 7.44 g (70%) of a white solid. TLC (EtOAc–MeOH, 90:10): R_f 0.74; mp (dec.) 171–173 °C. ^{1}H NMR (400 MHz, DMSO-d_6, ppm) δ: 11.79 (br s, 1H), 7.88 (d, 2H, J = 7.4 Hz), 7.66 (d, 2H, J = 6.9 Hz), 7.40 (t, 2H, J = 7.3 Hz), 7.31 (t, 2H, J = 7.5 Hz), 6.09 (br s, 1H), 5.05 (s, ma., 1.2H) and 4.86 (s, mi., 0.8H), 4.36–4.18 (m) and 3.90 (s, ma.) (5H), 3.75 (s, 3H), 3.39–3.07 (m, 4H). ^{13}C NMR (100.6 MHz, DMSO-d_6, ppm) δ: 167.9, 167.4, 162.2, 161.6, 156.3, 151.1, 144.7, 143.9, 140.8, 127.6, 127.1, 125.1, 120.1, 80.9, 65.5, 53.5, 48.9, 46.8, 44.6, 41.8, 27.7. HR-MS (ESI-TOF) calcd. for sodium adduct $C_{31}H_{34}N_4O_9Na$: 629.2225; found: 629.2217.

***N*-[2-Fmoc-aminoethyl]-*N*-[(methyl orotate-1-yl)acetyl]glycine (6)**

Compound **5** (5.20 g, 8.57 mmol) was suspended in 30 mL of CH_2Cl_2 and cooled to 0 °C and the mixture was stirred under nitrogen, and Et_3SiH (1.37 mL, 8.57 mmol) was added. TFA (30 mL) was added dropwise over 30 min while stirring on ice under an atmosphere of nitrogen. The solution was stirred for an additional hour while in the ice bath and then allowed to warm to room temperature while stirring was continued for an additional 4 h, after which TLC analysis showed complete consumption of the starting material. The mixture was evaporated to dryness in vacuo and the remaining volatiles were removed by repeated co-evaporation with CH_2Cl_2 and diethyl ether. The white solid was triturated with a mixture of 30 mL of CH_2Cl_2 and 60 mL of diethyl ether and cooled below 0 °C for 12 h. The product was isolated by filtration to give 3.87 g (82%) of a white solid. TLC (EtOAc–MeOH–AcOH, 80:15:5): R_f 0.30; mp (dec.) 157 to 158 °C. ^{1}H NMR (400 MHz, DMSO, ppm) δ: 11.81 (br s, 1H), 7.89 (d, 2H, J = 7.4 Hz), 7.66 (d, 2H, J = 6.8 Hz), 7.40 (t, 2H, J = 7.4 Hz), 7.32 (t, 2H, J = 7.4 Hz), 6.07 (br s, 1H), 5.05 (s, ma., 1.2H) and 4.86 (s, mi., 0.8H), 4.34–4.20 (m) and 3.93 (s, ma.) (5H), 3.74 (s, 3H), 3.37–3.08 (m, 4H). ^{13}C NMR (100 MHz, DMSO, ppm) δ: 170.4, 167.4, 162.3, 161.7, 156.5, 151.2, 144.8, 144.0, 140.8, 127.7, 127.1, 125.2, 120.2, 105.2, 65.6, 53.6, 48.0, 47.1, 46.8, 45.0, 44.6. HR-MS (ESI-TOF) calcd. for sodium adduct $C_{27}H_{26}N_4O_9Na$: 573.1599; found: 573.1595.

5-Hydroxymethyluracil (7)

Triethylamine (42.0 mL, 0.30 mol) was added to a suspension of uracil (22.4 g, 0.20 mol) and paraformaldehyde (18.0 g, 0.60 mol) in 600 mL of water. The solution turned clear when heated to 65 °C and was allowed to stir for 12 h at 65 °C. The water was removed under vacuum until approximately 50 mL of volume remained. To the residue was added 60 mL of 95% ethanol and the solution was allowed to stand for 30 min at room temperature and further cooled at 4 °C. The white precipitate was collected by filtration and was washed with 95% ethanol. The procedure of concentrating the filtrate and precipitation with 95% ethanol was repeated three times and the combined mass was 25.3 g (89%) of a white solid. TLC ($CHCl_3$–MeOH, 80:20): R_f 0.15; mp (dec.) 360 °C. ^{1}H NMR (400 MHz, DMSO, ppm) δ: 11.06 (s, 1H), 10.71 (s, 1H), 7.23 (s, 1H), 4.84 (s, 1H), 4.08 (s, 2H). ^{13}C NMR (100 MHz, DMSO, ppm) δ: 163.0, 151.5, 138.5, 112.8, 56.0.

5-Formyluracil (8)

Hydroxymethyluracil (21.50 g, 151.30 mmol) was dissolved in 800 mL of water by heating to approximately 90 °C. The solution was then cooled to 45 °C, $K_2S_2O_8$ (75.0 g, 277.4 mmol) and $AgNO_3$ (0.80 g, 4.71 mmol) were

© 2005 NRC Canada

added, and the product began to slowly precipitate. The reaction was stirred for a further 20 min at 40 °C and then cooled to room temperature over 15 min while stirring was continued. The suspension was then placed at 4 °C, the off-white crystals were collected by filtration, and rinsed with 50 mL of cold water to yield 17.65 g (83%) of the title compound; mp 302–304 °C. ^{1}H NMR (400 MHz, DMSO, ppm) δ: 11.89 (s, 1H), 11.49 (s, 1H), 9.72 (s, 1H), 8.12 (s, 1H). ^{13}C NMR (100 MHz, DMSO, ppm) δ: 186.8, 162.6, 150.6, 149.4, 110.2.

Uracil-5-carboxylic acid (9)

5-Formyluracil (4.30 g, 30.70 mmol) was dissolved in 350 mL of water by heating to reflux. To this solution was added $K_2S_2O_8$ (8.30 g, 30.70 mmol) and $AgNO_3$ (50 mg, 0.29 mmol), and the reaction was stirred while cooling to 65 °C over 30 min. A precipitate formed upon concentrating the volume to 50 mL. This mixture was cooled to 4 °C to promote the precipitation, and the product was subsequently collected by filtration. The title compound was purified by suspending it in 125 mL of water, adding 4 mol/L NaOH until a clear solution was obtained, and reprecipitating the compound by dropwise addition of concd. HCl until pH 2.0. Cooling the mixture to 4 °C followed by filtration yielded 3.34 g (70%) of a white solid; mp (dec.) 286–288 °C. ^{1}H NMR (400 MHz, DMSO, ppm) δ: 12.73 (s, 1H), 11.99 (s, 2H), 8.25 (s, 1H). ^{13}C NMR (100 MHz, DMSO, ppm) δ: 165.2, 163.5, 150.4, 150.2, 101.2.

Uracil-5-methylcarboxylate (10)

Uracil-5-carboxylic acid (2.50 g, 16.00 mmol) was suspended in methanol (150 mL) and HCl gas was bubbled into the suspension. The HCl was generated by the dropwise combination of 40 mL of concd. H_2SO_4 and 40 mL of concd. HCl. Once the mixture was saturated with HCl, it was refluxed for 12 h and then the solvent was removed in vacuo. The product was then recystallized from methanol to yield 2.34 g (86%) of a white solid. TLC (EtOAc–MeOH, 90:10): R_f 0.52; mp (dec.) 267 to 268 °C. ^{1}H NMR (400 MHz, DMSO, ppm) δ: 11.61 (s, 1H), 11.31 (s, 1H), 8.12 (s, 1H), 3.67 (s, 3H). ^{13}C NMR (100 MHz, DMSO, ppm) δ: 163.2, 160.1, 150.6, 149.7, 102.9, 51.4. HR-MS (EI) calcd. for $C_6H_6N_2O_4$: 170.0328; found: 170.0324.

***tert*-Butyl (uracil-5-methylcarboxylate-1-yl)acetate (11)**

Uracil-5-methylcarboxylate (2.06 g, 12.11 mmol) was dissolved in dry DMF (40 mL), and K_2CO_3 (1.67 g, 12.11 mmol) was added. *tert*-Butyl bromoacetate (1.79 mL, 12.11 mmol) was added dropwise to the stirred mixture and stirring was continued for 24 h while the reaction mixture was kept under an atmosphere of nitrogen. The reaction mixture was filtered to remove the undissolved potassium carbonate and then the solvent was removed in vacuo. The residue was extracted with ethyl acetate (3 × 75 mL) and water (25 mL). The combined organic layers were then washed with brine, dried (Na_2SO_4), filtered, and concentrated in vacuo. The crude product was recrystallized from methanol to yield 2.14 g (62%) of a white solid. TLC (EtOAc–MeOH, 90:10): R_f 0.71; mp 179 to 180 °C. ^{1}H NMR (400 MHz, $CHCl_3$, ppm) δ: 8.69 (s, 1H), 8.19 (s, 1H), 4.43 (s, 2H), 3.86 (s, 3H), 1.47 (s, 9H). ^{1}H NMR (400 MHz, DMSO, ppm) δ: 11.79 (s, 1H), 8.59 (s, 1H), 4.53 (s, 2H), 3.71 (s, 3H), 1.40 (s, 9H). ^{13}C NMR (100 MHz, $CHCl_3$, ppm) δ: 165.6, 163.2, 158.8, 152.3, 149.6, 105.3, 84.1, 52.5, 49.9, 28.0. HR-MS (EI) calcd. for $C_{12}H_{16}N_2O_6$: 284.1009; found: 284.1009.

(Uracil-5-methylcarboxylate-1-yl)acetic acid (12)

Compound **11** (1.61 g, 5.66 mmol) and Et_3SiH (0.75 mL, 4.70 mmol) were suspended in 20 mL DCM, cooled to 0 °C, and 15 mL of TFA was added dropwise. The reaction was stirred for 1 h on ice and an additional 2.5 h at room temperature. The mixture was evaporated to dryness in vacuo and the remaining volatiles were removed by co-evaporation with CH_2Cl_2 and diethyl ether. The compound was triturated with a mixture of approximately 5 mL of CH_2Cl_2 and 80 mL of diethyl ether and cooled to 0 °C overnight. Filtration and drying under vacuum gave 1.22 g (94%) of a white solid. TLC (EtOAc–MeOH–AcOH, 80:15:5): R_f 0.16; mp 227–229 °C. ^{1}H NMR (400 MHz, DMSO, ppm) δ: 11.68 (s, 1H), 8.59 (s, 1H), 4.55 (s, 2H), 3.70 (s, 3H). ^{13}C NMR (100 MHz, $CHCl_3$, ppm) δ: 169.2, 163.0, 159.5, 153.4, 150.2, 103.4, 51.6, 49.2. HR-MS (EI) calcd. for $C_{12}H_8N_2O_6$: 228.0382; found: 228.0375.

***tert*-Butyl *N*-[2-Fmoc-aminoethyl]-*N*-[(uracil-5-methylcarboxylate-1-yl)acetyl]glycinate (13)**

Compound **12** (0.210 g, 0.92 mmol), HOBt hydrate (0.141 g, 0.92 mmol), and DCC (0.190 g, 0.92 mmol) were dissolved in 3 mL of DMF and stirred under nitrogen for 15 min. The free amine form of the Fmoc-backbone *tert*-butyl ester (0.365 g, 0.92 mmol) was dissolved in a minimal amount of DMF and added to the mixture along with Hünings base (0.169 mL, 0.97 mmol). The reaction was stirred for 24 h at room temperature and extracted with EtOAc, sodium bicarbonate, phosphate buffer (pH ~ 4.5), and brine. The combined organic phases were dried (Na_2SO_4), filtered, and concentrated in vacuo. The solid was purified by flash chromatography (DCM–MeOH gradient) to yield 0.298 g (55%) of a white solid. TLC (EtOAc–MeOH, 90:10): R_f 0.67; mp (dec.) 135–137 °C. ^{1}H NMR (400 MHz, DMSO, ppm) δ: 8.43 (s, ma., 0.6H), 8.34 (s, mi., 0.4H), 7.89 (d, 2H, J = 7.4 Hz), 7.68 (m, 2H), 7.40 (t, 2H, J = 7.4 Hz), 7.32 (t, 2H, J = 7.4 Hz), 7.24 (m, 1H), 4.85 (s, ma., 1.2H) and 4.86 (s, mi., 0.8H), 4.34–4.16 (m) and 3.98 (s, ma.) (5H), 3.68 (s, 3H), 3.28–3.02 (m, 4H). ^{13}C NMR (100 MHz, DMSO, ppm) δ: 167.9, 166.8, 163.0, 159.5, 156.1, 153.7, 150.1, 143.9, 140.8, 127.6, 127.1, 125.1, 120.1, 103.2, 81.0, 65.5, 51.5, 50.0, 48.8, 48.3, 46.7, 27.7. HR-MS (ESI-TOF) calcd. for sodium adduct $C_{31}H_{34}N_4O_9Na$: 629.2225; found: 629.2254.

***N*-[2-Fmoc-aminoethyl]-*N*-[(uracil-5-methylcarboxylate-1-yl)acetyl]glycine (14)**

Compound **13** (0.250 g, 0.41 mmol) and Et_3SiH (59.0 uL, 0.37 mmol) were suspended in 2 mL DCM, cooled to 0 °C, 3 mL of TFA was added dropwise, and the reaction was stirred for 1 h in an ice bath and 2.0 h at room temperature. The mixture was evaporated to dryness in vacuo and the remaining volatiles were removed by co-evaporation sequentially with CH_2Cl_2 and diethyl ether. The solid was slurried in CH_2Cl_2–diethyl ether, cooled to 0 °C for 12 h, and subse-

© 2005 NRC Canada

Table 1. Mass spectral characterization of PNA oligomers.

		Found		Calcd.			
Entry	Formula	$[M + H]^+$	M^+	$[M + H]^+$	M^+	Method	Resolution
7	$C_{74}H_{101}N_{27}O_{26}$	1784.6012		1784.7489		MALDI	M
8	$C_{75}H_{101}N_{27}O_{28}$		1829.25		1828.79	ESI	A
9	$C_{75}H_{101}N_{27}O_{28}$		1829.10		1828.79	ESI	A
10	$C_{76}H_{101}N_{27}O_{30}$	1872.7588		1872.7286		MALDI	M
11	$C_{74}H_{99}N_{27}O_{28}$		1814.69		1814.77	ESI	A
12	$C_{74}H_{99}N_{27}O_{28}$		1814.65		1814.77	ESI	A
13	$C_{74}H_{97}N_{27}O_{30}$	1844.5623		1844.6973		MALDI	M
14	$C_{79}H_{111}N_{29}O_{27}$	1898.8276		1898.8283		ESI	M
15	$C_{79}H_{111}N_{29}O_{27}$		1899.14		1898.93	ESI	A
16	$C_{84}H_{121}N_{31}O_{28}$	2012.7640		2012.9076		MALDI	M
17	$C_{76}H_{104}N_{28}O_{28}$		1858.14		1857.84	ESI	A
18		ND		ND			
19	$C_{75}H_{101}N_{27}O_{28}$		1828.59		1828.79	ESI	A
20	$C_{79}H_{111}N_{29}O_{27}$		1898.63		1898.93	ESI	A

Note: Abbreviations in use: monoisotopic mass determination (M), average mass determination (A), and not determined (ND).

quently filtered to give 0.187 g (83%) of a white solid. TLC (EtOAc–MeOH–AcOH, 80:15:5): R_f 0.11; mp (dec.) 146 to 147 °C. ^{1}H NMR (400 MHz, DMSO, ppm) δ: 8.43 (s, ma., 0.6H), 8.35 (s, mi., 0.4H), 7.89 (d, 2H, J = 7.3 Hz), 7.68 (d, 2H, J = 7.7 Hz), 7.40 (t, 2H, J = 7.4 Hz), 7.32 (t, 2H, J = 7.3 Hz), 4.86 (s, ma., 1.0H) and 4.86 (s, mi., 0.6H), 4.33–4.17 (m) and 3.98 (s, ma.) (5H), 3.68 (s, 3H), 3.30–3.09 (m, 4H). ^{13}C NMR (100 MHz, DMSO, ppm) δ: 170.33, 166.79, 162.99, 159.52, 156.35, 153.67, 150.06, 143.87, 140.73, 127.61, 127.07, 125.12, 120.11, 103.18, 65.49, 51.53, 48.31, 47.78, 46.88, 46.72, 46.22. HR-MS (ESI-TOF) calcd. for sodium adduct $C_{27}H_{26}N_4O_9Na$: 573.1599; found: 573.1597.

Synthesis of PNA oligomers

PNA hexamers were synthesized on a 5 or 10 μmol scale using the standard FastMoc module on an Applied Biosystems 433A synthesizer employing NovaSyn TGR (Rink amide) resin.

Cleavage from resin

To 6 mg (~1 μmol) of the appropriate resin-bound oligomer (**8**–**10**), in a peptide vessel, was added a 1 mL solution containing ice-cold TFA–Et_3SiH (0.975:0.025), the vessel was purged with nitrogen and the mixture was shaken for 2 h. The solution was emptied into a 5 mL flask and the resin was rinsed with 0.5 mL of TFA. The combined TFA was evaporated with a stream of nitrogen and 3 mL of cold ether was added. Upon 1 h of cooling, the ether was decanted and a white precipitate was collected. The solid was dissolved in 0.1% TFA–H_2O, filtered, and purified under RP-HPLC.

Hydrolysis of methyl orotate oligomers

To 6 mg (~1 μmol) of the appropriate resin-bound oligomer (**8**–**10**), in a microfuge tube (Eppendorf), was added 50 μL of THF and 100 μL of 1 mol/L NaOH. The tubes were allowed to stand for 30 min and heated to 50 °C for a further 30 min. The resin was transferred to a peptide vessel, rinsed with H_2O, THF, and DCM. The resin was dried in vacuo and cleavage and release of the orotic-acid-containing oligomers was performed as previously described.

On resin aminolysis of oligomers containing C5 or C6 esters

To 6 mg (~1 μmol) of the appropriate resin bound oligomer (**1**–**3**, **19**), in a glass vial, was added 1 mL of the appropriate amine, the vial was purged with nitrogen, capped and allowed to stir for 6 h at 55 °C. The resin was transferred to a peptide vessel and rinsed with DCM. Cleavage and release of the orotamide-containing oligomers was performed as previously described.

Purification of PNAs

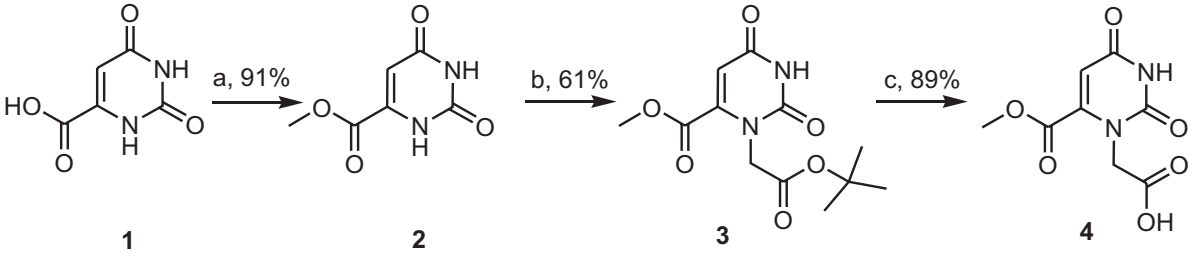
Crude PNA, isolated as previously described, was redissolved in 0.1% TFA in water (approximately 4 mg/mL) and purified by reversed phase HPLC using a 250 mm × 4.6 mm, C18-bonded phase, 100 pore, 5 μm particle size column. A binary gradient elution was used 0–5 min, 100% A; 5–20 min, 100% to 80% A; 20–40 min, 80% to 70% A, wherein solvent A is 0.1% TFA in water and solvent B is 0.1% TFA in MeCN.

Characterization of base-modified PNAs

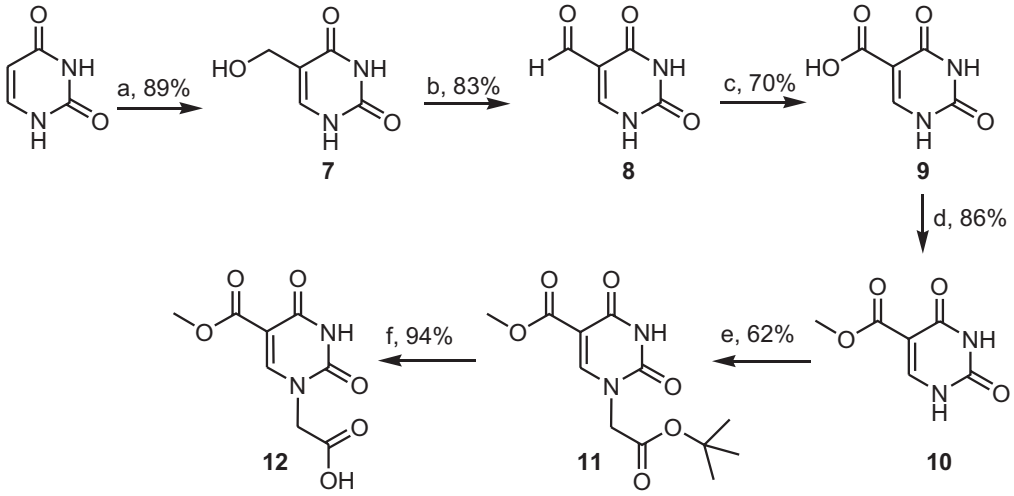
Mass spectral analysis of oligomers was done at the Dr. Don Rix Protein Identification and UWO Biological Mass Spectrometry Laboratory. Electrospray ionization time-of-flight mass spectrometry (ESI-TOF MS) was done with mass calibration provided by Glu-fibrinopeptide 1 (m/z (+2) = 785.842, monoisotopic mass), myoglobin (M^+ = 16951.499, average mass), or histatin 5 (M^+ = 3034.515, monoisotopic mass). Matrix-asisisted laser desorption ionization time-of-flight mass spectrometry (MALDI-TOF MS) was performed using α-cyano-4-hydroxycinnamic acid as the matrix, and calibration for monoisotopic masses was provided by angio-

© 2005 NRC Canada

Scheme 1. Reagents and conditions: (*a*) HCl(g)–MeOH, reflux for 24 h; (*b*) K_2CO_3, DMF, $BrCH_2CO_2$-*t*-Bu, 24 h; (*c*) CF_3COOH, DCM, Et_3SiH, 1 h at 0 °C, 3 h at room temperature.



Scheme 2. Reagents and conditions: (*a*) $(HCHO)_n$, 0.5 mol/L Et_3N, H_2O, 12 h at 65 °C; (*b*) $K_2S_2O_8$, $AgNO_3$, H_2O; (*c*) $K_2S_2O_8$, $AgNO_3$, H_2O; (*d*) HCl(g)–MeOH, reflux for 12 h; (*e*) K_2CO_3, DMF, $BrCH_2CO_2$-*t*-Bu, 24 h; (*f*) CF_3COOH, DCM, Et_3SiH, 1 h at 0 °C, 2.5 h at room temperature.



tensin I ($[M + H]^+$ = 1296.687), renin substrate ($[M + H]^+$ = 1758.933), or ACTH clip 18–39 ($[M + H]^+$ = 2465.199) (Table 1).

Binding analysis

Poly(riboadenylic acid) (poly(rA)) and poly(deoxyriboadenylic acid) (poly(dA)) were purchased from Sigma (Milwaukee, Wisconsin). Thermal denaturation of PNA:NA complexes (~2 μmol/L in nucleobases) were measured at 260 nm with a temperature ramp of 0.5 °C/min. A minimum of two independent samples were run in triplicate and the T_m was estimated by the first derivative method. Identical ionic conditions (150 mmol/L NaCl, 10 mmol/L Na_2HPO_4, 1 mmol/L EDTA at pH 7.0) were used for both the thermal denaturation studies and the determination of binding stoichiometry by the method of continuous variations. The error associated with the reported T_m values is ±0.5 °C.

Binding stoichiometry was determined by linear least-squares fitting of the curves. For the example, the two lines: $y = 0.2935x + 0.4744$ and $y = 0.3028x + 0.064$ fit the experimental data and gives the binding stoichiometry (calcd. 0.66; found: $0.69\chi_{PNA}$).

Results and discussion

Synthesis of PNA monomers

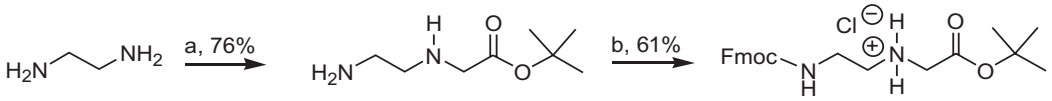
Our initial approach to incorporate C6 derivatives of uracil into PNA involved the synthesis of individual orotamide monomers for discrete incorporation into oligomers. This approach proved to be inefficient and, ultimately, synthetically intractable (4). We therefore decided to pursue the post-synthetic modification strategy based on a methyl orotate containing oligomer, thus exploring its feasibility as a convertible nucleobase. Synthesis of the methyl orotate monomer was achieved in five steps with an overall yield of 28%, compounds **2**–**6** were easy to handle and purified by recrystallization or trituration.

The nucleobase submonomer was approached by the standard Fisher esterification of orotic acid **1**, which gave methyl orotate **2** in high yield. The methyl ester was chosen as a simple, orthogonal protecting group to the Fmoc-protected amine and the acid labile *tert*-butyl group for carboxyl protection. The alkylation of **2** with *tert*-butyl bromoacetate and potassium carbonate gave **3** and acidolysis of the *tert*-butyl ester gave (methyl orotate-1-yl)acetic acid (**4**, Scheme 1). The alkylation at N1 of methyl orotate was confirmed by 2D NMR (gHMBC) spectroscopy. Compound **3** showed coupling from the methylene protons of CH_2-COO-*t*-Bu (singlet at δ 4.60) to both C6 (δ 143.8) and C2 (δ 151.0), while no coupling to C4 (δ 162.2) was observed.

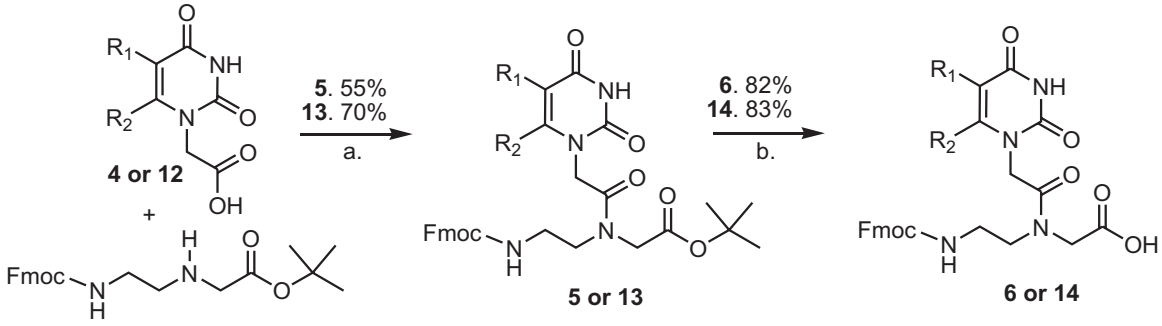
The synthesis of uracil-5-methylcarboxylate, as shown in Scheme 2, began with 5-hydroxymethyluracil, which is easily synthesized in high yield by the well-known reaction of uracil with formaldehyde (11). The oxidation of 5-hydroxymethyluracil to the carboxylic acid may be achieved in one step, but we found that 5-formyluracil cleanly precip-

© 2005 NRC Canada

Scheme 3. Reagents and conditions: (*a*) $ClCH_2CO_2$-*t*-Bu, DCM, 4 h at 0 °C, 12 h at ambient; (*b*) Fmoc-NHS, DIPEA, 0–20 °C, 4 h.



Scheme 4. Reagents and conditions: (*a*) DCC, HOBt, DMF, 24 h; (*b*) CF_3COOH, DCM, Et_3SiH.



4. R_1= CO_2CH_3 R_2=H
12. R_1= H R_2=CO_2CH_3

5. R_1= CO_2CH_3 R_2=H
13. R_1= H R_2=CO_2CH_3

6. R_1= CO_2CH_3 R_2=H
14. R_1= H R_2=CO_2CH_3

itated during the course of the reaction using potassium persulfate and catalytic silver nitrate by a modified procedure of Ziegler and Brossmer (12). The 5-formyluracil may subsequently be dissolved in boiling water and subjected to another round of oxidation with potassium persulfate and catalytic silver nitrate to give the carboxylic acid. Next Fisher esterfication, alkylation, and acidolysis as previously described gave (uracil-5-methylcarboxylate-1-yl)acetic acid, compound **12**. Although the C5-methyl carboxylate nucleoside has been prepared by carbonylation of 5-iodo-2-deoxyuridine (15), the stepwise process previously described is preferable to us because it is technically very simple, may be done on a large (multigram) scale in good chemical yields, and furnishes intermediates that are useful for other studies (4). Once the C5-ester had been installed, compound **10** was alkylated at N1 to give **11** and the regiochemistry for this reaction was confirmed by 2D NMR (gHMBC) spectroscopy. Compound **11** showed coupling from the methylene protons of CH_2-COO-*t*-Bu (singlet at δ 4.43) to both C6 (δ 149.6) and C2 (δ 152.3), as well as CH(6) (singlet at δ 8.19) to the methylene carbon (δ 49.9).

Next, the Fmoc backbone was prepared by a modified procedure of Thomson et al. (14) (Scheme 3). An excess of ethylenediamine was alkylated with *tert*-butyl chloroacetate, followed by aqueous work up. The product, *tert*-butyl *N*-(2-aminoethyl) glycinate, was then reacted with Fmoc-NHS for 4 h, extracted and carefully acidified with 1 equiv. of HCl in ether (5 mol/L) to give the Fmoc backbone HCl salt (Scheme 3). In the condensation to the nucleobase-1-yl-acetic acid, the Fmoc backbone HCl salt was neutralized by extraction against sodium bicarbonate and used as the free base.

Condensation of **4** and **12** to the neutralized Fmoc backbone was achieved with DCC–HOBt, and subsequent acidolysis of the *tert*-butyl ester gave the target methyl orotate monomer **6** and uracil-5-methylcarboxylate monomer **14** (Scheme 4). Both the methyl orotate and uracil-5-methylcarboxylate monomers were used in the solid-phase peptide synthesis of oligomers.

Synthesis of PNA oligomers

Incorporation of the methyl orotate (*MO*) monomer into PNA hexamers was done using a Rink amide resin using standard conditions for Fmoc-based oligomerization chemistry. Hexamers were synthesized containing thymine and terminally, internally, or doubly substituted MO derivatives **8**–**10**. The methyl orotate monomer, and the subsequently incorporated methyl orotate unit, was found to be completely compatible with the solid-phase synthesis; no saponification, transesterification, or other loss of the methyl ester functional group was found.

The amide linkage to the resin allowed for reaction of resin bound oligomers **8**–**10** with hydroxide or an amine. Standard acidolysis with TFA–Et_3SiH released the oligomers from the resin to give methyl orotate **8**–**10**, orotic acid **11**–**13**, or orotamide **14**–**17** containing PNAs (Table. 2). Hydrolysis of resin-bound methyl orotate oligomers was performed using NaOH in THF–H_2O. The orotic acid oligomers were released from the resin by acidolysis and RP-HPLC showed one major peak with minimal byproducts. Aminolysis of methyl orotate allows for the introduction of various substituted amides, and incorporation of 3-(*N*,*N*-dimethylamino)propylamide or ethanolamide was accomplished by treating the resin with neat amine at 55 °C for 6 h, and cleavage form the resin was performed as described. For example, resin-bound oligomer **10** was converted to **16** as previously described (Fig. 2A), isolated as the only major product by RP-HPLC (Fig. 2B), and identified by mass spectrometry (Fig. 2C).

Synthesis of uracil-5-methylcarboxylate and uracil-5-carboxamide containing oligomers (**19**, **20**) proceeded in a similar fashion. The uracil-5-methylcarboxylate (*UM*) was introduced into the internal position of a hexamer Ac-TTT*UM*TTK-NH_2 (**19**) and converted to the 3-(*N*,*N*-

© 2005 NRC Canada

Fig. 2. (A) $(CH_3)_2N(CH_2)_3NH_2$, 55 °C, 6 h. (B) RP-HPLC trace of crude oligomer **16**. (C) MALDI-MS of purified **16** (calcd. mass MH^+: 2012.9076; observed MH^+: 2012.7640).

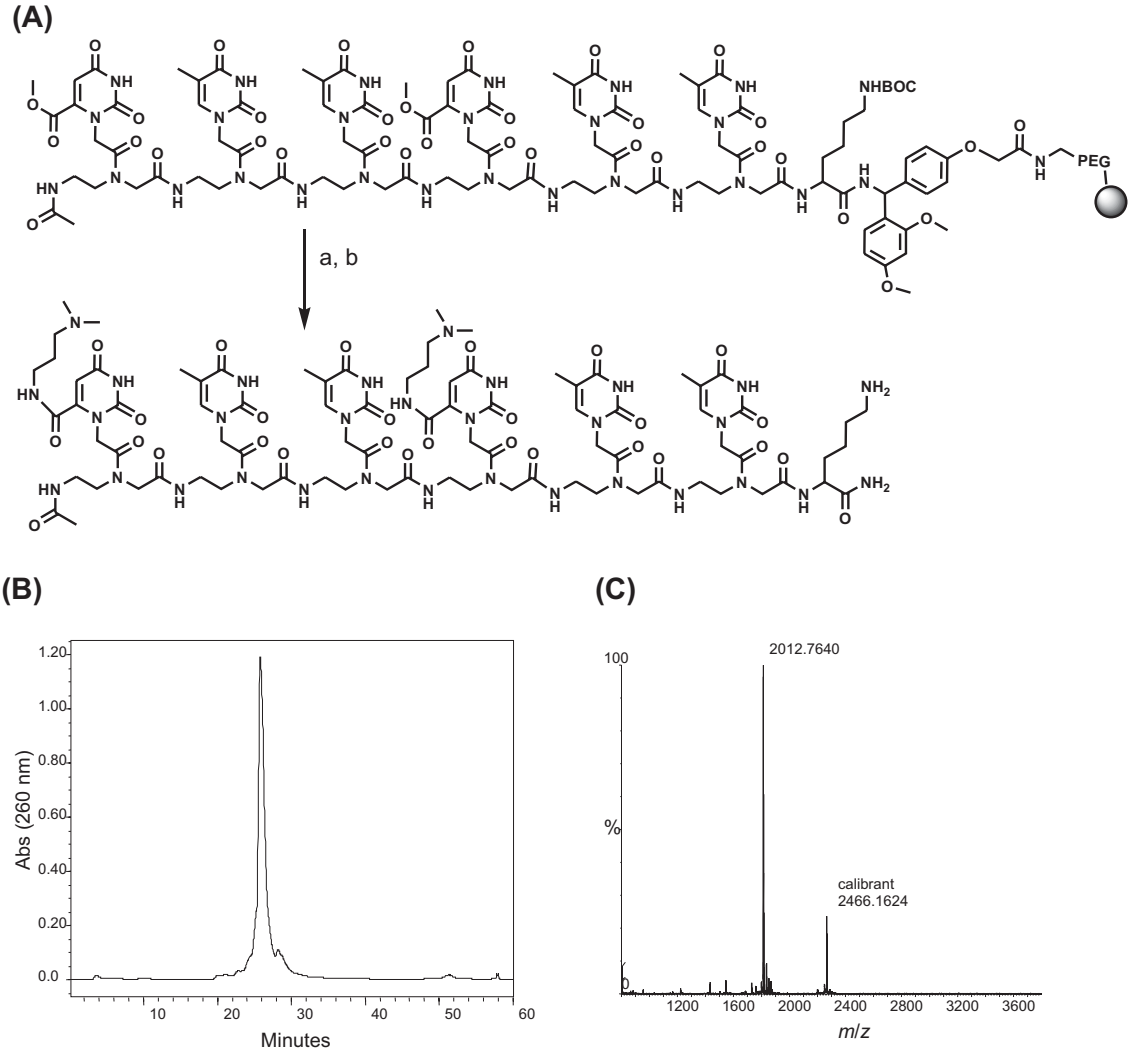


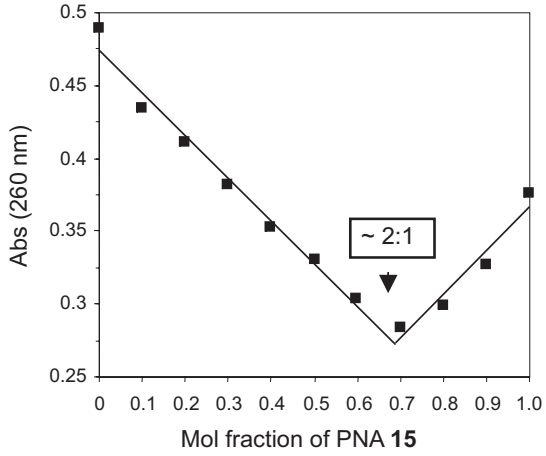
Table 2. Summary of T_m values for triplex complexes formed between PNA hexamers **7**–**18** and poly(rA) or poly(dA).

Entry	PNA	T_m(RNA)	T_m(DNA)	ΔT_m(RNA)	ΔT_m(DNA)
7	Ac-TTTTTTK-NH_2	62.0	57.0	—	—
8	Ac-*MO*TTTTTK-NH_2	47.2	35.8	–14.8	–21.2
9	Ac-TTT*MO*TTK-NH_2	22.5	25.5	–39.5	–31.5
10	Ac-*MO*TT*MO*TTK-NH_2	28.0	17.0	–34.0	–40.0
11	Ac-*OA*TTTTTK-NH_2	46.0	35.0	–16.0	–22.0
12	Ac-TTT*OA*TTK-NH_2	18.3	24.3	–43.7	–32.7
13	Ac-*OA*TT*OA*TTK-NH_2	23.5	—	–38.5	—
14	Ac-*OM*TTTTTK-NH_2	56.5	47.2	–3.5	–9.8
15	Ac-TTTT*OM*TTK-NH_2	34.0	28.0	–28.0	–29.0
16	Ac-*OM*TT*OM*TTK-NH_2	—	30.0	—	–27.0
17	Ac-TTTOM_eTTK-NH_2	33.5	29.5	–28.5	–27.5
18	Ac-TTT*C*TTK-NH_2	19.0	—	–43.0	—
19	Ac-TTT*UM*TTK-NH_2	59.0	—	–3.0	—
20	Ac-TTT*UA*TTK-NH_2	70.0	—	+8.0	—

Notes: Abbreviations in use for modified nucleobases: methyl orotate (MO), orotic acid (OA), uracil-6-{*N*-[3-(*N*′,*N*′-dimethylamino]propyl}carboxamide (OM), uracil-6-(*N*-2-hydroxyethyl)carboxamide (OM_e), uracil-5-methylcarboxylate (UM), uracil-5-{*N*-[3-(*N*′,*N*′-dimethylamino]propyl}carboxamide (UA), lysine (K), acetyl (Ac).

© 2005 NRC Canada

Fig. 3. Job plot of poly(rA) and the orotamide hexamer **15** (single internal substitution) in 150 mmol/L NaCl, 10 mmol/L Na_2HPO_4, and 1 mmol/L EDTA at pH 7.0 buffer.



dimethylamino)propylamide giving oligomer Ac-TTT*UA*TTK-NH_2 (**20**).

Hybridization studies of PNA containing C5 and C6 derivatives of uracil

The hybridization of methyl orotate, orotic acid, and orotamide substituted hexamers **8**–**17** and C5-substituted ester and amide **19** and **20** was studied by temperature-dependent UV absorbance. The binding stoichiometry for the modified oligomers containing C5 and C6 carboxamides with poly(rA) was determined by the method of continuous variation, commonly referred to as Job plots (15). This analysis revealed a 2:1 ratio, which is consistent with triplex formation (Fig. 3, shown for orotamide). Presumably, this triplex is composed of an antiparallel Watson–Crick (16) binding domain and a parallel Hoogsteen (17) binding domain as seen for covalently linked bisPNAs (10). The use of unlinked binding domains is useful in this case because an antiparallel orientation between the two domains is not enforced and the oligomers are free to adopt the most favourable binding arrangement. If the C6 derivatives had been found to benefit triplex formation, elucidation of the strand orientation would be more relevant (vide infra).

The thermal stability (T_m) of triplex formation was evaluated near physiological ionic conditions (150 mmol/L NaCl, 10 mmol/L Na_2HPO_4, 1 mmol/L EDTA at pH 7.0). The hexamers were hybridized to poly(rA) or poly(dA) in a 2:1 ratio at a concentration of ~2 umol/L per nucleobase. The compounds were all well-behaved and showed a monophasic hyperchromic shift. The introduction of C6-modified residues into the hexamers (**8**–**17**) caused a drop in T_m in all cases as compared to an unmodified PNA control sequence (Ac-TTTTTTK-NH_2, **7**), as summarized in Table 2. Single modified residues located at the N terminus of the sequence (**8**, **11**, **14**) were better tolerated than at an internal position (**9**, **12**, **15**). The N-terminal modifications show a trend that can be rationalized predominately on electrostatic interactions. For instance, the introduction of an orotamide, with a pendant positively charged group, at the N terminus of the hexamers had only a weakly destabilizing effect. Complexes formed with hexamers containing an N-terminal methyl orotate (uncharged group) or orotic acid (negatively charged group) suffered a much greater destabilization. The greatest destabilization of complexes formed with both RNA or DNA contained the orotic acid insert, thus implying that electrostatic interactions are important. Single substitution internal to the sequence (**9**, **12**, **15**, **17**) and doubly substituted oligomers (terminal and internal: **10**, **13**, **16**) had a large detrimental effect. Such large effects for internal substitution suggest that the substituents exert a significant steric effect. For comparison, the internal substituted orotic acid hexamer **12** has a decrease in T_m that is comparable to the oligomers containing a mismatch: (Ac-TTT***C***TTK-NH_2, **18**, ΔT_m = −43 °C). Even the putative beneficial effect of a pendant positive charge (**15**, **16**) is insufficient to recover the binding affinity of the hexamers.

In stark contrast, our preliminary results show that the PNA containing an internal uracil-5-carboxamide stabilizes triple-helix formation with complementary RNA (Table 2, **20**). This result parallels those found in the chemistry of DNA and RNA, but in PNA the stabilization is larger in magnitude. The introduction of a single internal C5 carboxamide with a pendant positively charged group into an oligodeoxynucleotide has been shown to have a very modest effect on thermal stability (at 100 mmol/L NaCl) for duplexes formed with complementary DNA or RNA (18, 19), although larger effects were observed under low-salt conditions (20). The stabilization in these cases was attributed to increased base stacking through a five-membered ring formed by H bonding of the amide hydrogen with the C4 carbonyl of uracil and (or) by the pendant cationic charge (19). Other studies with oligonucleotides capable of forming triple helices demonstrated a destabilization of the complex when the polypyrimidine oligonucleotide possessed a single internal C5-carboxamide-modified uracil (18, 21). Granted, these are different sequence contexts and different structural backbones, thus comparisons between PNA and NA systems need to be made cautiously. In addition, for the triplex system described herein, each PNA strand carries a modification, so that each complex has a total of two modified residues; whereas the studies referenced on duplexes possess a single modified residue. However, it is noteworthy that the introduction of a single internal modification bearing a pendant positively charged group into the PNA strand is more stabilizing to the triplex formed than incorporation of a backbone modification based on lysine (22), but not as significant as a positively charged nucleobase analog that makes a specific H-bonding interaction with the complementary base — the so-called G-clamp (23). Such pendant positive charges incorporated into PNA via the nucleobases may benefit the binding affinity, sequence discrimination (24), accelerate hybridization and strand invasion (25–27), and favourably affect the intracellular accumulation (28) for in vivo applications.

In summary, we have described the synthesis of a methyl orotate and uracil-5-methylcarboxylate monomers that are effective convertible nucleobases, compatible with an on-resin conversion strategy. Incorporation of the esters into oligomers allows for aminolysis in high yield and purity. However the C6-modified PNA_2:NA triple helices do not tolerate this substitution, while the C5-carboxamide substitution stabilized triplex formation. We are extending these investiga-

© 2005 NRC Canada

tions to the duplexes formed between methyl orotate PNA sequences and DNA or RNA to determine if this substitution is tolerated better. Furthermore, the C5-substituted oligomers merit further investigation for the effect of various charged, lipophilic or hydrophilic groups on their hybridization properties.

Acknowledgements

The authors thank the Natural Sciences and Engineering Research Council of Canada (NSERC) and the Academic Development Fund at the University of Western Ontario for support of this work. Professor G. Lajoie, Dr. Amanda Doherty-Kirby, Paula Pittock, and Heidi (Yin Yin) Liao are thanked for their expert assistance with mass spectral characterization of the polyamides.

References

1. G.R. Revandkar and T.S. Rao. *In* Comprehensive natural products: DNA and aspects of molecular biology. Vol. 7. *Edited by* E.T. Kool. Elsevier Sciences Ltd., Oxford, UK. 2002. Chap. 2.
2. I. Luyten and P. Herdewijn. Eur. J. Med. Chem. **33**, 515 (1998).
3. For PNA: K.N. Ganesh and P.E. Nielsen. Curr. Org. Chem. **4**, 931 (2000).
4. R.H.E. Hudson, R.D. Viirre, Y.H. Liu, F. Wojciechowski, and A.K. Dambenieks. Pure Appl. Chem. **76**, 1591 (2004).
5. P.E. Nielsen, M. Egholm, R.H. Berg, and O. Buchardt. Science (Washington, D.C.), **254**, 1497 (1991).
6. S. Sforza, G. Gianna, A. Dossena, A. Dossena, R. Corradini, and R. Marchelli. Chirality, **14**, 591 (2002), and refs. cited therein.
7. A.M. MacMillan and G.L. Verdine. J. Org. Chem. **55**, 5931 (1990).
8. M. Eriksson and P.E. Nielsen. Nat. Struct. Biol. **3**, 410 (1996).
9. S.C. Brown, S.A. Thomson, J.M. Veal, and D.G. Davis. Science (Washington, D.C.), **265**, 777 (1994).
10. L. Betts, J.A. Josey, J.M. Veal, and S.R. Jordan. Science (Washington, D.C.), **270**, 1828 (1995).
11. R.E. Cline, R.M. Fink, and K. Fink. J. Am. Chem. Soc. **81**, 2521 (1959).
12. D. Ziegler and R. Brossmer. Tetrahedron Lett. **43**, 5253 (1966).
13. A. Ono, N. Haginoya, M. Kiyokawa, N. Minakawa, and A. Matsuda. Bioorg. Med. Chem. Lett. **4**, 361 (1994).
14. S.A. Thomson, J.A. Josey, R. Cadilla, M.D. Gaul, C.F. Hassman, M.J. Luzzio, A.J. Pipe, K.L. Reed, D.J. Ricca, R.W. Wiethe, and S.A. Noble. Tetrahedron, **51**, 6179 (1995).
15. P. Job. Ann. Chim. **9**, 113 (1928).
16. J.D. Watson and F.H. Crick. Nature (London), **171**, 737 (1953).
17. K. Hoogsteen. Acta Crystallogr. **16**, 907 (1963).
18. A. Matsuda, Y. Ueno, Y. Nomura, A. Ono, and N. Haginoya. Bioconjugate Chem. **8**, 271 (1997).
19. Y. Normura, Y. Ueno, and A. Matsuda. Nucleic Acids Res. **25**, 2784 (1997).
20. T. Ito, Y. Ueno, Y. Komatsu, and A. Matsuda. Nucleic Acids Res. **31**, 2514 (2003).
21. Y. Ueno, M. Mikawa, and A. Matsuda. Bioconjugate Chem. **9**, 33 (1998).
22. G. Haaima, A. Lohse, O. Buchardt, and P.E. Nielsen. Angew. Chem. Int. Ed. Engl. **35**, 1939 (1996).
23. K.G. Rajeev, M.A. Maier, E.A. Lesnik, and M. Manoharan. Org. Lett. **4**, 4395 (2002).
24. H. Kuhn, V.V. Demidov, M.D. Frank-Kamenetskii, and P.E. Nielsen. Nucleic Acids Res. **26**, 582 (1998).
25. M.C. Griffith, L.M. Risen, M.J. Greig, E.A. Lesnik, K.G. Sprankle, R.H. Griffey, J.S. Kiely, and S.M. Frier. J. Am. Chem. Soc. **117**, 831 (1995).
26. M. Iyer, J.C. Norton, and D.R. Corey. J. Biol. Chem. **270**, 14712 (1995).
27. K. Kaihatsu, D.A. Braasch, A. Cansizoglu, and D.R. Corey. Biochemistry, **41**, 11118 (2002).
28. P. Sazani, S.-H. Kang, M.A. Maier, C. Wei, J. Dillman, J. Summerton, M. Manoharan, and R. Kole. Nucleic Acids Res. **29**, 3965 (2001).

© 2005 NRC Canada

Chemoselective thioacetalization with odorless 2-(1,3-dithian-2-ylidene)-3-oxobutanoic acid as a 1,3-propanedithiol equivalent

Haifeng Yu, Dewen Dong, Yan Ouyang, and Qun Liu

Abstract: Odorless 2-(1,3-dithian-2-ylidene)-3-oxobutanoic acid (**1c**) was prepared and investigated in the thioacetalization of carbonyl compounds as a 1,3-propanedithiol equivalent. The results showed that the thioacetalization of various carbonyl compounds **2** with **1c** proceeded smoothly and afforded the corresponding dithioacetals **3** in high yields (up to 99%) in the presence of acetyl chloride at room or reflux temperatures. Moreover, the thioacetalization exhibited high chemoselectivity between aldehydes and ketones.

Key words: chemoselectivity, 2-(1,3-dithian-2-ylidene)-3-oxobutanoic acid, α-oxo ketene dithioacetal, 1,3-propanedithiol equivalent, thioacetalization.

Résumé : On a préparé l'acide inodore 2-(1,3-dithian-2-ylidène)-3-oxoburanoîque (**1c**) et on a évalué son utilité comme équivalent du propane-1,3-dithiol dans la thioacétalisation de composés carbonyles. Les résultats ont montré que la thioacétalisation des divers composés **2** à l'aide de **1c** en présence de chlorure d'acétyle, à la température ambiante, s'effectue sans problème et conduit aux dithioacétals **3** avec des rendements élevés (99 %). De plus, la thiacétalisation présente une chimiosélectivité élevée entre les aldéhydes et les cétones.

Mots clés : chimiosélectivité, acide 2-(1,3-dithian-2-ylidène)-3-oxoburanoîque, dithioacétal d'α-oxocétène, équivalent du propane-1,3-dithiol, thioacétalisation.

[Traduit par la Rédaction]

Introduction

Thioacetals play very important roles in organic synthesis since they are widely used as protecting groups for carbonyl compounds and applied as umpolung reagents in a diverse array of organic transformations (1, 2).

To date, there are many approaches developed for the synthesis of thioacetals from carbonyl compounds or *O*,*O*-acetals with thiols employing various acid catalysts such as protic acids, Lewis acids, and solid acids (3, 4). Unfortunately, the conventional methods suffer from the use of volatile, foul-smelling, low molecular weight thiols that can lead to serious safety and environment problems. To resolve these drawbacks, some attempts have been made to develop odorless substitutes for these obnoxious thiols. As a result, a range of odorless or faint smell thiols have been prepared by increasing the alkyl chain length of thiol or introducing a trialkylsilyl group into the benzene ring of benzyl mercaptan and benzenethiol (5). Alternatively, incorporation of 1,3-propanedithiol functions within linear or cross-linked copolymeric reagents have been realized and applied in organic synthetic chemistry (6). However, the multistep process of preparation, the high cost of catalysts, and the toxicity of some precursors limit the further utilization of such thiol reagents or their equivalents. From the green chemistry point of view, the development of practically odorless and less volatile substitutes for such thiols is still of great importance and necessity.

Recently, we developed a novel thioacetalization with nonthiolic odorless cyclic ketene dithioacetals, e.g., 2-(2-chloro-1-(1-chloroethenyl)-2-propenylidene)-1,3-dithiane (**1a**) and 3-(1,3-dithian-2-ylidene)pentane-2,4-dione (**1b**) (Fig. 1), as 1,3-propanedithiol equivalents (7). We demonstrated that the reaction of carbonyl compounds with **1a** is an acid-assisted, self-catalyzed thioacetalization running through the formation of the intermediate **1b** (7*a*). The thioacetalization of **1b**, achieved under mild acidic conditions with high chemoselectivity (7*b*), encouraged us to believe that a wide range of cyclic ketene dithioacetals might be used as dithiol equivalents. There are many reports, including some review articles, regarding synthesis and application of α-oxo ketene dithioacetals (8). The decomposition reaction of α-oxo ketene dithioacetals had a different course depending on the reagent structure (9). For example, 2-(1,3-dithian-2-ylidene)-3-oxobutanoic acid (**1c**) undergoes iododecarboxylation rather than iododeacylation after treatment with iodine in

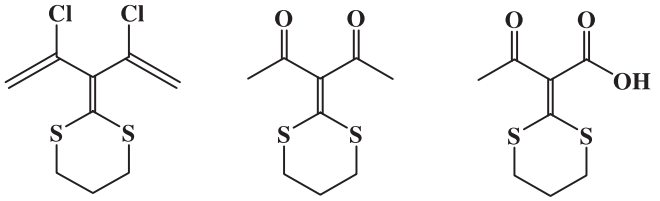
Received 18 January 2005. Published on the NRC Research Press Web site at http://canjchem.nrc.ca on 13 December 2005.

H. Yu, D. Dong,[1] Y. Ouyang, and Q. Liu.[2] Department of Chemistry, Northeast Normal University, Changchun, 130024, P.R. China.

[1]Corresponding author (e-mail: dongdw663@nenu.edu.cn).
[2]Corresponding author (e-mail: liuqun@nenu.edu.cn).

 doi: 10.1139/V05-184 © 2005 NRC Canada

Fig. 1. Odorless cyclic ketene dithioacetals.



EtOH–H_2O, affording the same intermediate obtainable with **1b** (9*a*). With the aim of obtaining efficient and practical reagents for general application, we investigated the thioacetalization reaction of a range of selected carbonyl compounds **2** with **1c**.

Results and discussion

According to the literature, we prepared ethyl 2-(1,3-dithian-2-ylidene)-3-oxobutanoate (10) from ethyl 3-oxobutanoate, carbon disulfide, 1,3-dibromopropane, and K_2CO_3 in nearly quantitative yield (99%), then we converted it into the 2-(1,3-dithian-2-ylidene)-3-oxobutanoic acid (**1c**) via a hydrolysis process (9*a*, 11). It is worth noting that **1c** is an odorless solid, stable under ambient atmosphere, which is associated with some advantages such as a simple synthetic procedure, mild conditions, high yield, and commercial starting materials without a foul smell.

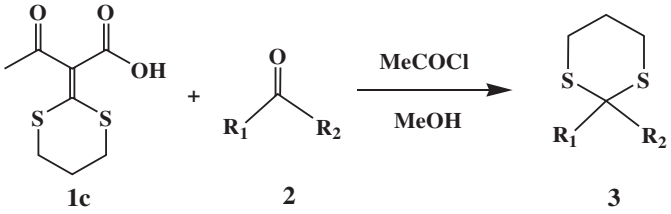
Since our previous experience has revealed that it is a convenient way to achieve the thioacetalization of a range of aldehydes and ketones in the presence of a mixture of acetyl chloride and methanol (7*b*), in the present work the same mixture was adopted for studying the thioacetalization of various carbonyl compounds **2** with **1c** (Scheme 1).

The thioacetalization of piperonal (**2a**) with **1c**, initially carried out under reflux, showed that the reaction was completed within 30 min affording the corresponding dithioacetal **3a** in 89.3% yield. Significantly, this reaction proceeded much faster in comparison to the reaction reported in our previous work (7). So, we repeated the reaction at room temperature. To our delight, **2a** was transformed into **3a** in 92.7% yield within 2 h. It is worth mentioning that only a very faint smell of thiol was perceived during both the reaction and work-up process, in agreement with practically no release of 1,3-propanedithiol.

We next investigated the thioacetalization of aromatic, aliphatic, and heterocyclic aldehydes and ketones (**2a**–**2w**) with **1c** in the presence of acetyl chloride in methanol at both room and reflux temperatures. With a constant feed molar ratio of acetyl chloride : **1c** : **2** of 3:2:2, all the reactions proceeded smoothly under mild acidic conditions. Table 1 summarizes some reaction data. The results confirm the general value of **1c** as a key reagent for the thioacetalization reaction.

A range of aromatic and aliphatic aldehydes and aliphatic ketones (**2a**–**2p**) were rapidly converted into their corresponding dithioacetals (**3a**–**3p**) in very high yields at both room and reflux temperatures. The reflux condition allowed a shorter reaction time, nevertheless, some thermosensitive substrates could benefit from the use of room temperature. In the cases of entries 23 and 24 in Table 1, the yield was increased by 25% when the reaction of thermo- and acid-sensitive furan-2-carbaldehyde (**2l**) proceeded at room temperature rather than at reflux. Generally, it is difficult to cleanly realize the thioacetalization of **2l** with the use of conventional acid catalysts (12). Several research groups reported high-yield thioacetalizations of **2l** by using thionyl chloride treated silica gel (12), trimethylsilyl chloride (13), and lithium tetrafluoroborate (14) as the catalyst, respectively. Our thioacetalization of **2l** can be considered a useful alternative procedure.

Scheme 1. Thioacetalization of carbonyl compounds **2** with **1c**.



In contrast with **2a**–**2p**, the aromatic ketones **2q**–**2u** could not be thioacetalized at room temperature, but they gave their corresponding dithioacetals in high yields after prolonged reflux. The aromatic sterically hindered benzophenone (Table 1, entry 37) was the slowest to react with an excess of **1c** (feed molar ratio of acetyl chloride : **1c** : **2** = 3:4:2).

To exploit the differences in the thioacetalization rate of aldehydes and aliphatic ketones and aromatic ketones, for the selective protections we carried out some competitive reactions under the above reaction conditions (Table 1, entries 38 and 39). The reaction of **2b**–**2q**–**1c** with a 1:1:1 molar ratio performed at reflux temperature (Table 1, entry 38) afforded the thioacetal **3b** in 92.4% yield, while the ketone **2q** was almost completely recovered (97.2%), **3q** not even being detectable. Similar results were obtained in the case of **2p**–**2q**–**1c** with a 1:1:1 molar ratio (Table 1, entry 39), where **2p** was converted into thioacetal **3p** in 91.2% yield, while **2q** remained intact. The reported thioacetalization procedure thus showed a high chemoselectivity, providing selective protection of an aromatic aldehyde or an aliphatic ketone in the presence of an aromatic ketone.

The mechanism of the thioacetalization reaction was investigated with the help of a supporting reaction. The mixture of **1c** (1.0 mmol), **2a** (1.0 mmol), and acetyl chloride (1.5 mmol) in methanol (10 mL) was stirred at room temperature and interrupted after 50 min by neutralizing with 10% aq. $NaHCO_3$. With this procedure, decarboxylated product 1-(1,3-dithian-2-ylidene)propan-2-one (**4**) and dithioacetal **3a** were obtained in 79.3% and 14.6% yields, respectively, while unreacted **2a** (81.3%) was recovered. Compound **4** was also obtained in our previous work and assumed to be an intermediate (7*a*, 7*b*). These results indicate that **1c** undergoes decarboxylation much more easily than deacylation under the acidic conditions applied. The novelty of the reagent **1c** is in the fact that the thioacetalization of aldehydes and aliphatic ketones could proceed at room temperature with high yields. On the basis of the previously mentioned experimental results together with our previous work (7), a mechanism for the thioacetalization reaction of various carbonyl compounds with **1c** in methanol is proposed in

© 2005 NRC Canada

Table 1. Thioacetalization of carbonyl compounds **2** with **1c**.

Entry	Substrate **2**	R_1	R_2	Product **3**	Temp.[a]	Time (min)	Yield[b] (%)	Reference
1	**2a**	3,4-O_2CH_2Ph	H	**3a**	A	25	89.3	4*c*, 7
2	**2a**	3,4-O_2CH_2Ph	H	**3a**	B	120	92.7	
3	**2b**	Ph	H	**3b**	A	25	91.8	3*a*, 3*c*, 7
4	**2b**	Ph	H	**3b**	B	120	92.5	
5	**2c**	4-MePh	H	**3c**	A	30	96.5	7, 14
6	**2c**	4-MePh	H	**3c**	B	120	96.2	
7	**2d**	4-MeOPh	H	**3d**	A	30	92.3	4*e*, 7
8	**2d**	4-MeOPh	H	**3d**	B	120	94.1	
9	**2e**	4-HOPh	H	**3e**	A	25	88.9	3*a*, 3*c*, 7
10	**2e**	4-HOPh	H	**3e**	B	120	91.2	
11	**2f**	4-ClPh	H	**3f**	A	25	88.9	4*c*, 4*i*, 14
12	**2f**	4-ClPh	H	**3f**	B	120	98.5	
13	**2g**	4-FPh	H	**3g**	A	30	96.5	7
14	**2g**	4-FPh	H	**3g**	B	120	97.2	
15	**2h**	$PhCH_2$	H	**3h**	A	40	91.2	4*f*, 7
16	**2h**	$PhCH_2$	H	**3h**	B	180	91.7	
17	**2i**	4-NO_2Ph	H	**3i**	A	60	97.4	4*f*, 7
18	**2i**	4-NO_2Ph	H	**3i**	B	180	96.9	
19	**2j**	PhCHCH	H	**3j**	A	50	82.5	4*f*, 7, 12
20	**2j**	PhCHCH	H	**3j**	B	180	87.7	
21	**2k**	*n*-C_4H_9	H	**3k**	A	30	89.7	[3]
22	**2k**	*n*-C_4H_9	H	**3k**	B	130	91.5	
23	**2l**	2-Furyl	H	**3l**	A	25	61.4	12–14
24	**2l**	2-Furyl	H	**3l**	B	120	87.2	
25	**2m**	2-Thiophen	H	**3m**	A	25	99.1	4*i*, 7
26	**2m**	2-Thiophen	H	**3m**	B	120	99.3	
27	**2n**	*n*-C_4H_9	Me	**3n**	A	45	90.5	14
28	**2n**	*n*-C_4H_9	Me	**3n**	B	300	92.1	
29	**2o**	$(CH_2)_4$		**3o**	A	50	90.7	7, 14
30	**2o**	$(CH_2)_4$		**3o**	B	360	91.5	
31	**2p**	$(CH_2)_5$		**3p**	A	45	93.4	4*h*, 7, 14
32	**2p**	$(CH_2)_5$		**3p**	B	300	94.7	
33	**2q**	Ph	Me	**3q**	A	240	96.9	3*c*, 4*f*, 7
34	**2r**	4-H_2NPh	Me	**3r**	A	300	90.2	7
35	**2s**	4-NO_2Ph	Me	**3s**	A	300	93.3	7
36	**2t**	4-ClPh	Me	**3t**	A	240	95.8	7
37	**2u**	Ph	Ph	**3u**	A	480	94.2[c]	3*c*, 4*c*
38	**2b+2q**			**3b**	A	25	92.4 (97.2)[d]	
39	**2p+2q**			**3p**	A	45	91.2 (91.8)[d]	

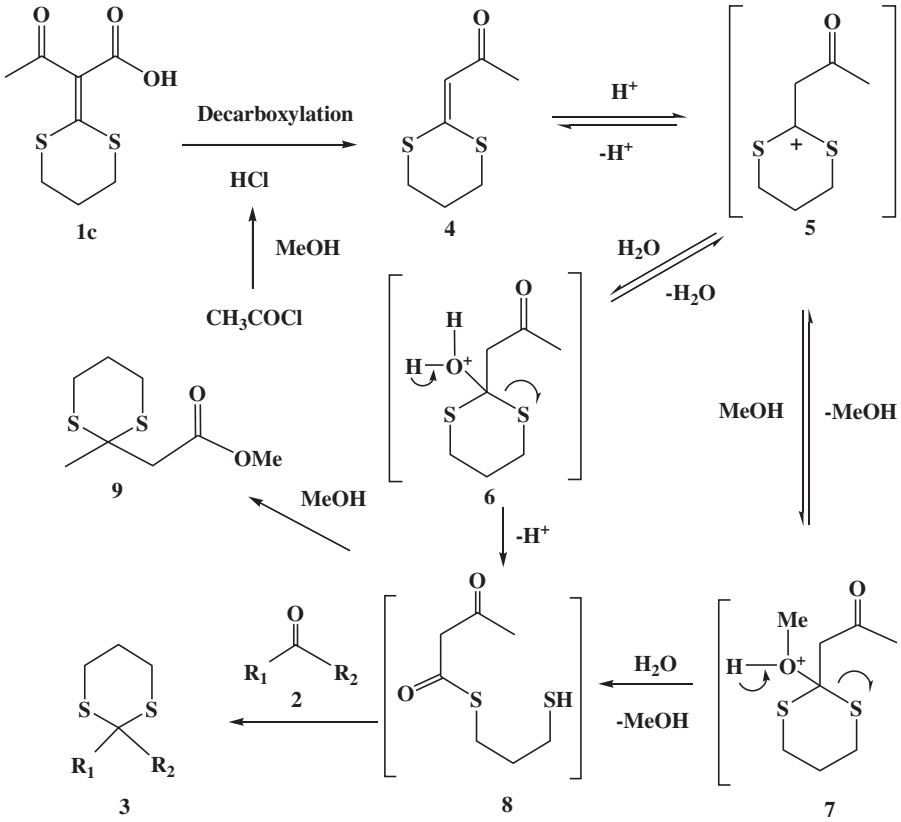
[a]Reflux temperature (A), room temperature (B).
[b]Yields after silica gel chromatography.
[c]Obtained with a feed molar ratio of acetyl chloride : **1c** : **2** of 3:4:2.
[d]Recovery of the intact compound **2q**.

Scheme 2. The reaction process starts with the generation of HCl from the esterification between acetyl chloride and methanol, which catalyzes the decarboxylation of **1c** to give **4**. Through the addition of a proton to the carbon–carbon double bond, **4** is converted into the carbocation **5**, stablized by the electron-donating effect of two sulfur atoms, then into **6** or **7** with H_2O or methanol, respectively, and finally by cleavage of the ring into **8**, which reacts with the carbonyl compound **2** to give the corresponding dithioacetal **3**. An indirect evidence of the formation of **8** is the production of the dithiane **9** (7*b*), obtained in the present work most likely from the inter- or intra-molecular transformation of **8**.

[3] Spectral properties of 2-butyl-1,3-dithiane (**3k**): IR (KBr, cm^{-1}): 2954, 2929, 2899, 1421, 1378, 1275, 1181, 908. ^1H NMR (500 MHz, $CDCl_3$) δ: 0.90 (3H, t, *J* = 7.0 Hz), 1.29–1.36 (2H, m), 1.45–151 (2H, m), 1.72–1.84 (2H, m), 1.86–1.89 (1H, m), 2.10–2.13 (1H, m), 2.80–2.91 (4H, m), 4.04 (1H, t, *J* = 7.0 Hz). ^{13}C NMR (500 MHz, $CDCl_3$) δ: 14.15, 22.60, 26.30, 29.00, 30.77 (2C), 35.41, 47.90.

© 2005 NRC Canada

Scheme 2. Proposed mechanism for the thioacetalization of carbonyl compounds **2** with **1c**.



In summary, odorless 2-(1,3-dithian-2-ylidene)-3-oxobutanoic acid (**1c**) has been investigated as a 1,3-propanedithiol equivalent in thioacetalization. In the presence of **1c**, a wide range of carbonyl compounds, aldehydes, and ketones have been converted into the corresponding dithioacetals **3** in high yields. The thioacetalization reaction is characterized by a simple procedure, mild conditions, high yields, and high chemoselectivity towards aldehydes and aliphatic ketones with respect to aromatic ketones.

Experimental

All reagents were purchased from commercial sources. The products were purified by column chromatography over silica gel. ^{1}H NMR spectra were recorded at 25 °C on a Varian INOVA500 (500 MHz) spectrometer in $CDCl_3$ and with TMS as the internal standard. IR spectra (KBr) were recorded on a Magna-560 FT IR spectrophotometer. Elemental analyses were measured on a PE-2400 analyzer (PerkinElmer).

General procedure for thioacetalization of aldehydes and ketones 2 with 1c

Preparation of **3a** as a typical procedure: the mixture of **1c** (218 mg, 1 mmol), **2a** (150 mg, 1 mmol), and CH_3COCl (0.11 mL, 1.5 mmol) in MeOH (10 mL) was stirred under reflux. As monitored by TLC, compound **1c** was consumed within 10 min; whereas aldehyde **2a** disappeared after 25 min. The reaction mixture, allowed to cool to room temperature, was neutralized with 10% aq. $NaHCO_3$ and extracted with diethyl ether (3 × 10 mL). The combined organic extracts were dried over anhydr. $MgSO_4$, filtered, and concentrated under reduced pressure to yield the crude product. The purification by silica gel chromatography (eluent: petroleum ether – EtOAC, 75:1) gave the dithioacetal **3a** in 89.3% yield.

Acknowledgements

Financial support of this research by the National Natural Science Foundation of China (20272008, 20572013) and the Key Project of the Ministry of Education of China (03059, 105061) is greatly acknowledged.

References

1. (*a*) P.J. Kocienski. Protecting groups. Thieme, Stuttgart. 1994; (*b*) T.W. Greene and P.G.M. Wuts. Protective groups in organic synthesis. 3rd ed. John Wiley and Sons, New York. 1999.
2. (*a*) J.E. Lynch and E.L. Eliel. J. Am. Chem. Soc. **106**, 2943 (1984); (*b*) K. Utimoto, A. Nakamura, and S. Molsubara. J. Am. Chem. Soc. **112**, 8189 (1990); (*c*) W.K. Kim, S.C. Park, H. Lee, and C.G. Cho. Tetrahedron Lett. **41**, 5111 (2000); (*d*) B. Breit. Angew. Chem. Int. Ed. **37**, 453 (1998); (*e*) A.B. Smith III, S.M Pitram, M.J. Gaunt, and S.A. Kozmin. J. Am. Chem. Soc. **124**, 14516 (2002).
3. (*a*) B. Ku and D.Y. Oh. Synth. Commun. **19**, 433 (1989); (*b*) P.C.B. Page, J.C. Prodger, and D. Westwood. Tetrahedron, **49**, 10355 (1993); (*c*) H. Tani, K. Masumoto, T. Inamasu, and H. Suzuki. Tetrahedron Lett. **32**, 2039 (1991); (*d*) L.F. Tietze, B. Weigand, and C. Wulff. Synthesis, 69 (2000); (*e*) T. Aoyama, T. Tashio, and M. Kodomari. Synlett, 2307 (2004).
4. (*a*) L. Garlaschelli and G. Vidari. Tetrahedron Lett. **31**, 5815 (1990); (*b*) H.K. Patney. Tetrahedron Lett. **32**, 2259 (1991);

© 2005 NRC Canada

(*c*) P. Kumar, R.S. Reddy, A.P. Singh, and B. Pandey. Synthesis, 67 (1993); (*d*) V.G. Saraswathy and S. Sankararaman. J. Org. Chem. **59**, 4665 (1994); (*e*) R.V. Anand, P. Saravanan, and V.K. Singh. Synlett, 415 (1999); (*f*) H. Firouzabadi, N. Iranpoor, and H. Hazarkhani. J. Org. Chem. **66**, 7527 (2001); (*g*) S. Muthusamy, S.A. Babu, and C. Gunanathan. Tetrahedron Lett. **42**, 359 (2001); (*h*) S. Samajdar, M.K. Basu, F.F. Becker, and B.K. Banik. Tetrahedron Lett. **42**, 4425 (2001); (*i*) A. Kamal and G. Chouhan. Tetrahedron Lett. **43**, 1347 (2002); (*j*) H. Firouzabadi, N. Iranpoor, and K. Amani. Synthesis, 59 (2002); (*k*) A. Kamal and G. Chouhan. Tetrahedron Lett. **44**, 3337 (2003).

5. (*a*) M. Node, K. Kumura, K. Nishide, S. Ohsugi, and T. Miyamoto. Tetrahedron Lett. **42**, 9207 (2001); (*b*) K. Nishide, T. Miyamoto, K. Kumura, S.I. Ohsugi, and M. Node. Tetrahedron Lett. **43**, 8569 (2002); (*c*) K. Nishide, S.I. Ohsugi, M. Fudesaka, S. Kodama, and M. Node. Tetrahedron Lett. **43**, 5177 (2002).
6. (*a*) V. Bertini, F. Lucchesini, M. Pocci, and A. De Munno. Tetrahedron Lett. **39**, 9263 (1998); (*b*) V. Bertini, F. Lucchesini, M. Pocci, and A. De Munno. J. Org. Chem. **65**, 4839 (2000); (*c*) V. Bertini, M. Pocci, F. Lucchesini, S. Alfei, and A. De Munno. Synlett, 864 (2003).
7. (*a*) Q. Liu, G. Che, H. Yu, Y. Liu, J. Zhang, Q. Zhang, and D. Dong. J. Org. Chem. **68**, 9148 (2003); (*b*) H. Yu, Q. Liu, Y. Yin, Q. Fang, J. Zhang, and D. Dong. Synlett, 999 (2004); (*c*) J. Liu, Q. Liu, H. Yu, Y. Ouyang, and D. Dong. Synth. Commun. **34**, 4545 (2004).
8. (*a*) R.K. Dieter. Tetrahedron, **42**, 3029 (1986); (*b*) H. Junjappa, H. Ila, and C.V. Asokan. Tetrahedron, **46**, 5423 (1990); (*c*) M. Kolb. Synthesis, 171 (1990); (*d*) H. Ila, H. Junjappa, and O. Barun. J. Organomet. Chem. **624**, 34 (2001); (*e*) H. Ila, H. Junjappa, and P.K. Mohanta. *In* Progress in heterocyclic chemistry. Vol. 13. *Edited by* G.H. Gribble and L.T. Gilchrist. Pergamon Press, Oxford. 2001. Chap. 1. pp. 1–24.
9. (*a*) Y. Zhao, Q. Liu, R. Sun, Q. Zhang, and X. Xu. Synth. Commun. **34**, 463 (2004); (*b*) Y. Zhao, Q. Liu, R. Sun, and Y. Chi. Chem. J. Chin. Univ. **25**, 297 (2004); (*c*) S. Zhang, Q. Liu, Z. Zhu, C. Zhang, and H. Huang. Chem. J. Chin. Univ. **15**, 1155 (1994); (*d*) Y. Zhao, Q. Liu, R. Sun, X. Xu, and L. Pan. Chem. J. Chin. Univ. **23**, 1901 (2002).
10. (*a*) E.B. Choi, I.K. Youn, and C.S. Pak. Synthesis, 792 (1988); (*b*) S. Zhang, Q. Liu, Z. Zhu, C. Zhang, and H. Huang. Chem. J. Chin. Univ. **15**, 1155 (1994).
11. H. Yu, Y. Xiao, Q. Liu, Y. Chi, and Q. Zhang. Chem. J. Chin. Univ. **25**, 673 (2004).
12. Y. Kamitori, M. Hojo, R. Masuda, T. Kimura, and T. Yoshida. J. Org. Chem. **51**, 1427 (1986).
13. M. Medarde, A.C. Ramos, R. Pelaez-Lamaie de Clairac, E. Caballero, and A.S. Feliciano. J. Chem. Soc. Perkin Trans. 1, 45 (1994).
14. K. Kazahaya, S. Tsuji, and T. Sato. Synlett, 1640 (2004).

© 2005 NRC Canada

Ionic liquid promoted simple and efficient synthesis of β-enamino esters and β-enaminones from 1,3-dicarbonyl compounds — One-pot, three-component reaction for the synthesis of substituted pyridines

Ganesan Karthikeyan and Paramasivan T. Perumal

Abstract: A facile enamination of 1,3-dicarbonyl compounds with amines has been developed that affords good to excellent yields of β-enamino esters and β-enaminones using Brønsted acidic ionic liquid 1-methylimidazolium trifluoroacetate ([Hmim]$^+$Tfa$^-$) at room temperature. This methodology has been extended for the synthesis of substituted pyridines in excellent yield by a one-pot, three-component reaction of 1,3-dicarbonyl compounds, ammonium acetate, and alkynone in the presence of [Hmim]$^+$Tfa$^-$.

Key words: ionic liquid, β-enaminones, β-enamino esters, 1,3-dicarbonyl compounds, amines, pyridines.

Résumé : Opérant à la température ambiante et utilizant le trifluoroacétate de 1-méthylimidazolinum, [Hmim]$^+$Tfa$^-$, un liquide ionique agissant comme acide de Brønsted, on a mis au point une méthode facile d'énamination des composés 1,3-dicarbonyles par les amines qui fournit des rendements allant de bons à excellents en β-énaminoesters et β-énaminones. Cette méthode a été étendue à la synthèse de pyridines substituées réalisée avec d'excellents rendements par une réaction monotope à trois composants formés de composés 1,3-dicarbonyles, d'acétate d'ammonium et d'alkynone, en présence de [Hmim]$^+$Tfa$^-$.

Mots clés : liquide ionique, β-énaminones, β-énaminoesters, composés 1,3-dicarbonyles, amines, pyridines.

[Traduit par la Rédaction]

β-Enamino esters and β-enaminones are important precursors for the synthesis of biologically active compounds such as amino acids (1), γ-aminols (1*d*), peptides (2), and heterocyclic compounds (3).

The most common route for the synthesis of these compounds involves the direct condensation of β-dicarbonyl compounds with amines at reflux in benzene–toluene with azeotropic removal of water (4). Recently, K_{10}clay/ultrasound (5*a*), silica-supported microwave irradiaton (5*b*), $NaAuCl_4$ (5*c*), $Bi(TFA)_3$ (5*d*), and $Zn(ClO_4)_2{\cdot}6H_2O$ (5*e*) have been used for the condensation of 1,3-dicarbonyl compounds with amines. However, these methods have not been entirely satisfactory owing to such drawbacks as low yields, long reaction time, nonreusable catalyst, and use of hazardous solvents such as benzene and chlorinated solvents.

Several improved methods have been reported for the Bohlmann–Rahtz pyridine synthesis (6) from β-enaminones. Recently Bagley and co-workers (7) have reported one-pot, three-component reactions for the synthesis of pyridines in toluene at reflux temperature by generating the enaminone from the corresponding β-ketoesters for in situ heteroannulation in the Bohlmann–Rahtz reaction. In these studies we set out to test similar methodology using an ionic liquid for the mild preparation of enaminones and their in situ heteroannulation reaction for the Bohlmann–Rahtz pyridine synthesis.

Room-temperature ionic liquids (RTILs) consisting of imidazolium cations have gained popularity as an alternative to conventional organic solvents (8). They are highly polar yet noncoordinating and dissolve a wide range of organic and organometallic compounds. Ionic liquids were shown to enhance reaction rates in a range of reactions (9), including acid-catalysed processes (10). Chloroaluminate ionic liquids have been reported as both solvents and Lewis acid catalysts for Diels–Alder reactions and the Friedel–Crafts reaction. However, chloroaluminate ionic liquids are sensitive to water, and lead to undesired side reactions due to the release of HCl. Several Brønsted acidic ILs are synthesized and used as catalysts and solvents for esterification and pinacol–benzopinacol rearrangement (11).

In continuation of our research interest in the application (12) of RTILs in organic synthesis, we report a facile, high-yielding protocol for the condensation of 1,3-dicarbonyl compounds with amines using 1-methylimidazolium tri-

Received 19 April 2005. Published on the NRC Research Press Web site at http://canjchem.nrc.ca on 13 December 2005.

G. Karthikeyan and P.T. Perumal.[1] Department of Organic Chemistry, Central Leather Research Institute, Adyar, Chennai, 600 020, India.

[1]Corresponding author (e-mail: ptperumal@hotmail.com).

 doi: 10.1139/V05-186 © 2005 NRC Canada

fluoroacetate ([Hmim]$^+$Tfa$^-$) at room temperature. The ionic liquids were prepared according to the procedures reported in the literature (13).

In our initial search for optimal reaction conditions, we explored the condensation of benzoyl acetone with aniline in [Hmim]$^+$Tfa$^-$, [Hmim]$^+$Tsa$^-$, and a neat solution. The results are summarized in Table 1.

Encouraged by these results, several β-diketones were condensed with amines giving the β-enaminones in excellent yields at room temperature. The results are summarized in Table 2.

Anilines and aliphatic amines reacted efficiently to produce the corresponding β-enaminones in excellent yields. Although an earlier report (10*d*) shows that anilines with strong electron-withdrawing groups, such as 4-nitro aniline, are unreactive, we have shown that they produce the corresponding β-enaminone in good yield (Table 2, entry 6). The stereochemistry of the compounds is Z because of the intramolecular H-bonding. The (Z)-s-cis configuration shown for β-enaminones and β-enamino esters was confirmed from their ^{1}H NMR. The characteristic signals of the vinylic proton (δ 4.5–5.1 ppm) and NH signals (δ 8.3–11.3 ppm) corroborate the proposed structure.

In the case of 1,2-diaminoethane, 2 equiv. of the 1,3-dicarbonyl compound were used giving bisenaminones in 80% yield (Table 2, entry 7). In the case of aryl alkyl dicarbonyl compounds, we observed the regioselective amination of the aliphatic carbonyl group. In addition, when the 1,1,1-trifluoro-pentan-2,4-dione (**1b**) reacted with benzylamine (Table 2, entry 8) only enaminones derived from the regioselective amination of the less reactive carbonyl-bound methyl group were observed.

The scope and generality of this method was also expanded for the condensation of β-ketoesters with amines to produce β-enamino esters. The results are summarized in Table 3.

Several β-ketoesters were subjected to condensation with amines to get the β-enamino esters in excellent yields at room temperature. Due to steric hindrance, the condensation of ethyl benzoyl acetate with benzylamine requires 60 °C heating to produce the corresponding β-enamino esters in 75% yield.

Finally, the reusability of ionic liquid was studied and we found that the ionic liquid could be reused at least four times without significant loss of activity (Table 4).

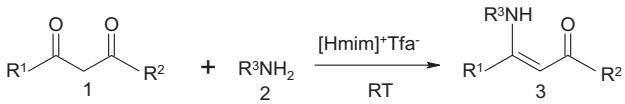
Next, we extended this methodology for a one-pot, three-component reaction of 1,3-dicarbonyl compounds, ammonium acetate, and alkynone in [Hmim]$^+$Tfa$^-$ to synthesize various substituted pyridines. The results are summarized in Table 5.

Ethyl acetoacetate reacts with ammonium acetate and 4-phenyl-3-butyn-2-one in the presence of [Hmim]$^+$Tfa$^-$ at room temperature to give ethyl 2,6-dimethyl-4-phenylpyridine-3-carboxylate in 80% yield. When methyl acetoacetate or acetyl acetone was reacted with 4-(trimethylsilyl)but-3-yn-2-one, the corresponding protodesilylated pyridines **6b** and **6d** were obtained in 90% and 92% yield.

Conclusion

In summary, this paper describes a novel and efficient protocol for the synthesis of β-enamino esters and β-enaminones from 1,3-dicarbonyl compounds and amines. The advantage of this methodology lies in its operational simplicity and relatively shorter reaction time. This method also avoids the use of hazardous solvents such as benzene and azeotropic distillation conditions. The ionic liquid used can be recycled up to four times without an appreciable fall in yield, indicating that this protocol will be useful for the synthesis of natural products involving the intermediacy of β-enamino esters and β-enaminones. The one-pot, three-component reaction for the synthesis of substituted pyridines was achieved without using hazardous solvents, such as toluene or dichloromethane, at room temperature in excellent yields.

Table 1. Condensation of benzoyl acetone with aniline under various mediums.



Entry	Medium	Time (h)	Yield (%)
1	[Hmim]$^+$Tfa$^-$	0.25	95
2	[Hmim]$^+$Tsa$^-$	4	75
3	Neat	24	40

Experimental

IR spectra were recorded as solids in KBr pellets on a PerkinElmer FT IR spectrometer. ^{1}H NMR spectra were recorded on a 500 MHz Joel spectrometer using TMS as the internal standard. ^{13}C NMR spectra were recorded on a 125 MHz spectrometer in $CDCl_3$, and chemical shifts are given in δ relative to the solvent peak. Mass spectra were recorded on a Joel DX-303 mass spectrometer. Analytical TLC was performed on precoated sheets of silica gel G of 0.25 mm thickness containing PF 254 indicator (Merck, Darmstadt). Column chromatography was performed with silica gel (60–120 mesh, S.d Fine, Boisar).

Typical experimental procedure for the preparation of β-enaminones 3a–3k and β-enamino esters 5a–5e

To a solution of 1,3-dicarbonyl compounds (1 mmol) in [Hmim]$^+$Tfa$^-$ (1 mL) was added amines (1.5 mmol). The reaction mixture was stirred at room temperature for the appropriate time (Tables 1 and 2). After completion of the reaction as indicated by TLC, the reaction mixture was diluted with distilled water (20 mL) and extracted with diethyl ether (3 × 15 mL). The combined organic layer was dried over anhydr. Na_2SO_4, filtered, and concentrated under reduced pressure. The crude product was purified by filtration on a short silica gel column pretreated with Et_3N.

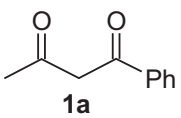
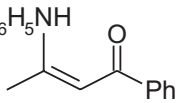
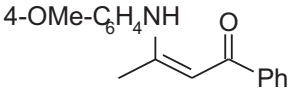
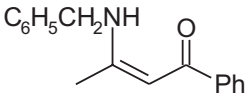
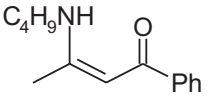
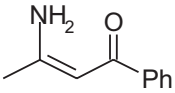
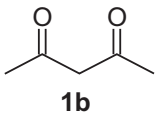
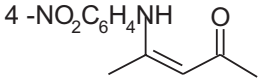
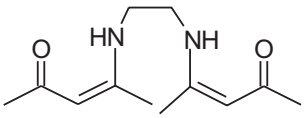
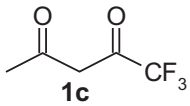
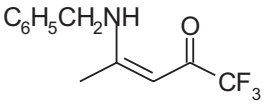
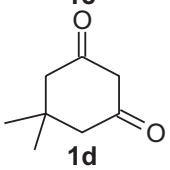
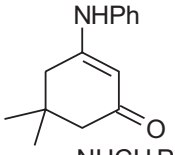
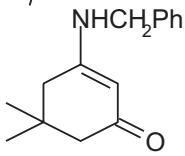
The aqueous layer was extracted with ether to remove residual reactants. Then the aqueous layer was collected and concentrated under reduced pressure at 70 °C to recover the IL, and was recycled.

Typical experimental procedure for the preparation of pyridines (6a–6e)

A solution of 1,3-dicarbonyl compounds (1 mmol), alkynone (1.2 mmol), and ammonium acetate (5 mmol) in

© 2005 NRC Canada

Table 2. Ionic liquid promoted condensation of 1,3-dicarbonyl compounds with amines.

Entry	1,3-Dicarbonyl	Amine	Time (h)	Product (**3a-3j**)[a]	Yield (%)[b]
1	 **1a**	$C_6H_5NH_2$	0.25		95
2	**1a**	4-OMe-$C_6H_4NH_2$	0.25		92
3	**1a**	$C_6H_5CH_2NH_2$	0.25		98
4	**1a**	$C_4H_9NH_2$	0.5		84
5	**1a**	$CH_3COO^-NH_4^+$	4		85
6	 **1b**	4 -$NO_2C_6H_4NH_2$	24		65[c]
7	**1b**	$H_2NCH_2CH_2NH_2$	0.25		80
8	 **1c**	$C_6H_5CH_2NH_2$	2		80
9	 **1d**	$C_6H_5NH_2$	1		82
10	**1d**	$C_6H_5CH_2NH_2$	0.5		85

[a]All the products were identified by IR, NMR, and MS.
[b]Isolated yield.
[c]Reaction was carried out at 80 °C.

[Hmim]$^+$Tfa$^-$ was stirred at room temperature for 24 h. After completion of the reaction as indicated by TLC, the reaction mixture was diluted with distilled water (20 mL) and extracted with diethyl ether (3 × 15 mL). The combined ether extracts were dried over anhydr. Na_2SO_4, filtered, and concentrated under reduced pressure. The crude product was purified by column chromatography to give pyridines **6a**–**6e**.

Spectral data

(2Z)-3-Anilino-1-phenylbut-2-en-1-one (3a)

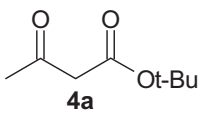
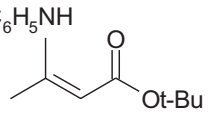
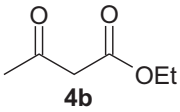
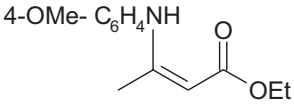
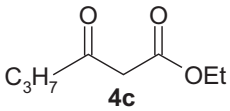
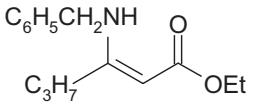
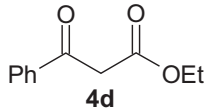
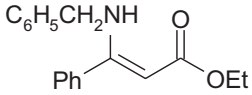
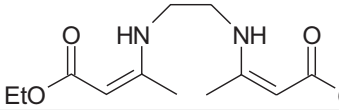
IR (KBr, cm^{-1}): 1622, 1550. ^{1}H NMR (500 MHz, $CDCl_3$) δ: 2.14 (s, 3H), 5.89 (s, 1H), 7.15–7.26 (m, 3H), 7.35–7.47 (m, 5H), 7.91–7.96 (m, 2H), 11.7 (bs, 1H, NH). ^{13}C NMR (125 MHz, $CDCl_3$) δ: 20.5, 94.3, 124.8, 125.8, 127.1, 128.4, 129.2, 131.0, 138.7, 140.0, 162.3, 188.7. MS (EI) *m*/*z* (%): 268 (20) [M$^+$], 105 (100). Anal. calcd. for $C_{16}H_{15}NO$: C 80.98, H 6.37, N 5.90; found: C 80.71, H 6.20, N 5.78.

(2Z)-3-[(4-Methoxyphenyl)amino]-1-phenylbut-2-en-1-one (3b)

IR (KBr, cm^{-1}): 1614, 1550. ^{1}H NMR (500 MHz, $CDCl_3$) δ: 2.05 (s, 3H), 3.80 (s, 3H), 5.85 (s, 1H), 6.87–6.90 (m, 2H), 7.08–7.11 (m, 2H), 7.40–7.46 (m, 3H), 7.98–7.92 (m, 2H), 10.7 (bs, 1H, NH). ^{13}C NMR (125 MHz, $CDCl_3$) δ: 20.3, 55.5, 93.6, 114.4, 126.7, 127.1, 128.3, 130.8, 131.4,

© 2005 NRC Canada

Table 3. Ionic liquid promoted condensation of β-ketoesters with amines.

Entry	1,3-Dicarbonyl	Amine	Time (h)	Product (**5a**-**5e**)[a]	Yield (%)[b]
1	 **4a**	$C_6H_5NH_2$	0.25		90
2	 **4b**	4-OMe-$C_6H_4NH_2$	0.25		95
3	 **4c**	$C_6H_5CH_2NH_2$	1		82
4	 **4d**	$C_6H_5CH_2NH_2$	8		75[c]
5	**4b**	$H_2NCH_2CH_2NH_2$	5		80

[a]All the products were identified by IR, NMR, and MS.
[b]Isolated yield.
[c]Reaction was carried out at 60 °C.

Table 4. Results obtained with recycled ionic liquid – $[Hmim]^+Tfa^-$.

Entry	Product	Run	Yields (%)
1	**3a**	1	90
2	**3a**	2	89
3	**3a**	3	89
4	**3a**	4	87

140.2, 157.9, 163.2, 188.4. MS (EI) *m/z* (%): 268 (20) [M^+], 105 (100). Anal. calcd. for $C_{17}H_{17}NO_2$: C 76.38, H 6.41, N 5.24; found: C 76.62, H 6.30, N 4.98.

(2Z)-3-(Benzylamino)-1-phenylbut-2-en-1-one (3c)

IR (KBr, cm^{-1}): 1618, 1554. ^1H NMR (500 MHz, $CDCl_3$) δ: 2.06 (s, 3H), 4.54 (d, 2H), 5.75 (s, 1H), 7.23–7.44 (m, 8H), 7.87–7.89 (m, 2H), 11.7 (bs, 1H, NH). ^{13}C NMR (125 MHz, $CDCl_3$) δ: 9.6, 47.1, 92.7, 126.9, 127.0, 127.6, 128.2, 128.9, 130.6, 137.8, 140.3, 165.0, 188.1. MS (EI) *m/z* (%): 251 (30) [M^+], 105 (100). Anal. calcd. for $C_{17}H_{17}NO$: C 81.24, H 6.82, N 5.57; found: C 80.12, H 6.97, N 5.45.

(2Z)-3-(Butylamino)-1-phenylbut-2-en-1-one (3d)

IR (neat, cm^{-1}): 1612, 1579. ^1H NMR (500 MHz, $CDCl_3$) δ: 0.90 (t, 3H, J = 7.4 Hz), 1.34–1.41 (sex, 2H), 1.50–1.56 (pent, 2H), 1.88 (s, 3H), 1.96 (s, 3H), 3.17–3.21 (q, 2H, J = 6.85 Hz), 4.91 (s, 3H), 10.83 (bs, 1H, NH). ^{13}C NMR (125 MHz, $CDCl_3$) δ: 13.7, 18.8, 20.0, 28.7, 32.1, 42.7, 95.0, 123.9, 125.5, 129.3, 161.0, 186.4. MS (EI) *m/z* (%): 251 (30) [M^+], 77 (100). Anal. calcd. for $C_{14}H_{19}NO$: C 77.38, H 8.81, N 6.45; found: C 77.29, H 8.91, N 6.34.

(2Z)-3-Amino-1-phenylbut-2-en-1-one (3e)

IR (KBr, cm^{-1}): 1612, 1579. ^1H NMR (500 MHz, $CDCl_3$) δ: 2.0 (s, 3H), 5.75 (s, 1H), 7.4 (m, 3H), 7.8 (m, 2H), 10.1 (brs, NH, 1H). ^{13}C NMR (125 MHz, $CDCl_3$) δ: 22.97, 95.2, 123.9, 125.5, 129.3, 161.0, 185.63. MS (EI) *m/z* (%): 161 (60) [M^+], 160 (100). Anal. calcd. for $C_{10}H_{11}NO$: C 74.51, H 6.88, N 8.69; found: C 74.49, H 6.80, N 8.74.

(3Z)-4-(4-Nitrophenyl)pent-3-en-2-one (3f)

IR (KBr, cm^{-1}): 1618, 1554. ^1H NMR (500 MHz, $CDCl_3$) δ: 1.85 (s, 3H), 1.92 (s, 3H), 5.80 (s, 1H), 6.82 (m, 2H), 7.02–6.99 (m, 2H), 10.4 (brs, NH, 1H). ^{13}C NMR (125 MHz, $CDCl_3$) δ: 18.5, 28, 96.3, 14.7, 116.2, 126.9, 132.2, 147.6, 156.2, 185.0. MS (EI) *m/z* (%): 220 (45) [M^+], 85 (100). Anal. calcd. for $C_{11}H_{12}N_2O_3$: C 59.99, H 5.49, N 12.72; found: C 60.20, H 5.61, N 12.85.

(3Z)-4-[(2-{[(1Z)-1-Methyl-3-oxobut-1-enyl]amino}ethyl)-amino]pent-3-en-2-one (3g)

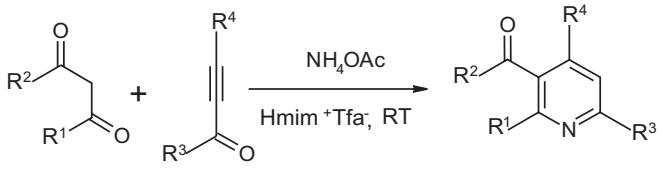
IR (KBr, cm^{-1}): 1609, 1576. ^1H NMR (500 MHz, $CDCl_3$) δ: 1.88 (s, 6H), 1.94 (s, 6H), 3.3 (t, 4H), 4.97 (s, 2H), 10.8 (bs, 2H, NH). ^{13}C NMR (125 MHz, $CDCl_3$) δ: 18.8, 28.9, 43.6, 96.2, 162.9, 195.6. MS (EI) *m/z* (%): 225 (67.4) [M^+], 182.4 (71.7), 83.1 (100). Anal. calcd. for $C_{12}H_{20}N_2O_2$: C 64.26, H 8.99, N 12.49; found: C 64.17, H 9.14, N 12.54.

(3Z)-4-(Benzylamino)-1,1,1-trifluoropent-3-en-2-one (3h)

IR (KBr, cm^{-1}): 1612, 1579. ^1H NMR (500 MHz, $CDCl_3$) δ: 2.09 (s, 3H), 4.54 (d, 2H), 5.39 (s, 1H), 7.25–7.39 (m, 5H), 11.421 (s, br, 1H). ^{13}C NMR (125 MHz, $CDCl_3$) δ: 19.5, 47.6, 89.9, 127.0, 128.1, 129.2, 136.0, 169.7, 175 (q, J = 32 Hz). MS (EI) *m/z* (%): 249 (41) [M + 2], 82.7 (100). Anal. calcd. for $C_{12}H_{12}F_3NO$: C 59.26, H 4.97, F 23.43, N 5.76; found: C 59.38, H 5.15, F 23.59, N 5.63.

© 2005 NRC Canada

Table 5. Synthesis of pyridines in a one-pot, three-component reaction.



R^1 = OEt, OMe, R^3 = CH_3, Ph 80%–94%

R^2 = Me, Ph R^4 = Ph, $SiMe_3$, H

	1,3-Dicarbonyl		Alkynones			
Entry	R^1	R^2	R^3	R^4	Product[a]	Yield (%)[b]
1	CH_3	OEt	CH_3	Ph	**6a**	80
2	CH_3	OMe	CH_3	$SiMe_3$	**6b** (R^4 = H)	90
3	CH_3	OMe	Ph	H	**6c**	94
4	CH_3	CH_3	CH_3	$SiMe_3$	**6d** (R^4 = H)	92
5	CH_3	CH_3	CH_3	Ph	**6e**	82

[a]All the products were identified by IR, NMR, and MS.
[b]Isolated yield.

3-Anilino-5,5-dimethylcyclohex-2-en-1-one (3i)

IR (KBr, cm^{-1}): 1618, 1554. ^1H NMR (500 MHz, $CDCl_3$) δ: 1.05 (s, 6H), 2.17 (s, 2H), 2.34 (s, 2H), 5.54 (s, 1H), 7.00 (bs, 1H, NH), 7.10–7.13 (m, 3H), 7.28–7.32 (m, 2H). ^{13}C NMR (125 MHz, $CDCl_3$) δ: 28.3, 32.8, 43.5, 50.4, 98.3, 123.9, 125.5, 129.3, 138.3, 161.0, 198.1. MS (EI) *m/z* (%): 215 (45) [M^+], 159 (79), 85 (100). Anal. calcd. for $C_{14}H_{17}NO$: C 78.1, H 7.96, N 6.51; found: C 78.24, H 7.85, N 6.59.

3-Benzylamino-5,5-dimethylcyclohex-2-en-1-one (3j)

IR (KBr, cm^{-1}): 1620, 1554. ^1H NMR (500 MHz, $CDCl_3$) δ: 1.05 (s, 6H), 2.17 (s, 2H), 2.36 (s, 2H), 4.50 (d, 2H), 5.52 (s, 1H), 7.00 (bs, 1H, NH), 7.10–7.13 (m, 3H), 7.28–7.32 (m, 2H). ^{13}C NMR (125 MHz, $CDCl_3$) δ: 28.3, 32.8, 43.4, 47.14, 50.4, 98.3, 123.9, 125.5, 129.3, 161.0, 198.1. MS (EI) *m/z* (%): 229 (40) [M^+], 85 (100). Anal. calcd. for $C_{15}H_{19}NO$: C 78.56, H 8.35, N 6.11; found: C 78.64, H 8.27, N 6.22.

tert-*Butyl (2Z)-3-anilinobut-2-enoate (5a)*

IR (KBr, cm^{-1}): 3416, 1640, 1610. ^1H NMR (500 MHz, $CDCl_3$) δ: 1.50 (s, 9H), 1.95 (s, 3H), 4.60 (s, 1H), 7.05–7.23 (m, 3H), 7.22–7.35 (m, 2H), 10.4 (bs, 1H, NH). ^{13}C NMR (125 MHz, $CDCl_3$) δ: 02.3, 28.8, 78.5, 87.8, 124.3, 124.5, 128.9, 139.5, 158.1, 170.3. MS (EI) *m/z* (%): 233 (6) [M^+], 77 (30), 59 (100). Anal. calcd. for $C_{14}H_{19}NO_2$: C 72.97, H 8.21, N 6.08; found: C 72.82, H 8.34, N 6.20.

Ethyl (2Z)-3-[(4-methoxyphenyl)amino]but-2-enoate (5b)

IR (KBr, cm^{-1}): 3251, 1646, 1612. ^1H NMR (500 MHz, $CDCl_3$) δ: 1.26 (t, 3H, *J* = 6.9 Hz), 1.86 (s, 3H), 3.78 (s, 3H), 4.13 (q, 2H, *J* = 6.9 Hz), 4.63 (s, 1H), 6.87–6.82 (m, 2H), 7.02–6.99 (m, 2H), 10.7 (bs, 1H, NH). ^{13}C NMR (125 MHz, $CDCl_3$) δ: 14.7, 20.1, 55.5, 58.7, 84.7, 114.2, 126.9, 132.2, 157.5, 160.1, 170.5. MS (EI) *m/z* (%): 235 (20) [M^+], 59 (100). Anal. calcd. for $C_{13}H_1NO_3$: C 66.36, H 7.28, N 5.95; found: C 66.22, H 7.40, N 5.83.

Ethyl (2Z)-3-(benzylamino)hex-2-enoate (5c)

IR (KBr, cm^{-1}): 3250, 1643, 1612. ^1H NMR (500 MHz, $CDCl_3$) δ: 0.98 (s, 3H), 1.26 (t, 3H, *J* = 6.9 Hz), 1.61 (m, 2H), 2.55 (t, 2H), 4.13 (q, 2H, *J* = 6.9 Hz), 4.43 (q, 2H, *J* = 6.9 Hz), 5.35 (s, 1H), 7.05–7.23 (m, 3H), 7.22–7.35 (m, 2H), 10.4 (bs, 1H, NH). ^{13}C NMR (125 MHz, $CDCl_3$) δ: 14.17, 14.85, 23.3, 36.1, 45.38, 60.15, 94.79, 127.29, 128.56, 127.17, 138.47, 166.27. MS (EI) *m/z* (%): 247 (20) [M^+]. Anal. calcd. for $C_{15}H_{21}NO_2$: C 72.84, H 8.56, N 5.66; found: C 70.5, H 8.68, N 5.83.

Ethyl (2Z)-3-(benzylamino)-3-phenylacrylate (5d)

IR (neat, cm^{-1}): 1646, 1612. ^1H NMR (500 MHz, $CDCl_3$) δ: 1.26 (t, 3H, *J* = 6.9 Hz), 4.43 (q, 2H, *J* = 6.9 Hz), 5.35 (s, 1H), 7.2–7.4 (m, 8H), 7.87–7.89 (m, 2H), 10.6 (bs, 1H, NH). ^{13}C NMR (125 MHz, $CDCl_3$) δ: 14.8, 45.30, 58.0, 86.2, 127.0, 127.12, 127.17, 127.39, 128.07, 136.54, 138.32, 166.65, 167.86. MS (EI) *m/z* (%): 281 (40) [M^+], 59 (100). Anal. calcd. for $C_{18}H_{19}NO_2$: C 76.84, H 6.81, N 4.98; found: C 76.97, H 6.69, N 5.19.

Ethyl (2Z)-3-[(2-{[(1Z)-3-ethoxy-1-methyl-3-oxoprop-1-enyl]amino}ethyl)amino]but-2-enoate (5e)

IR (KBr, cm^{-1}): 1648, 1605. ^1H NMR (500 MHz, $CDCl_3$) δ: 1.20–1.23 (t, 2 × 3H, *J* = 6.85 Hz), 1.88 (s, 6H), 3.32–3.33 (t, 4H, *J* = 3.4 Hz), 4.03–4.07 (q, 4H, *J* = 6.9 Hz), 4.45 (s, 2H), 8.61 (s, 2H, NH). ^{13}C NMR (125 MHz, $CDCl_3$) δ: 14.6, 19.3, 43.8, 58.5, 83.61, 161.3, 170.6. MS (EI) *m/z* (%): 284 (20) [M^+], 81 (100). Anal. calcd. for $C_{14}H_{24}N_2O_4$: C 59.13, H 8.51, N 9.85; found: C 59.22, H 8.43, N 9.70.

Ethyl 2,6-dimethyl-4-phenylnicotinate (6a)

R_f 0.43 (20% EtOAc in petroleum ether). IR (neat, cm^{-1}): 1725, 1580. ^1H NMR (500 MHz, $CDCl_3$) δ: 0.94–0.97 (t,

© 2005 NRC Canada

3H, J = 7.45 Hz), 2.59 (s, 3H), 2.65 (s, 3H), 4.04–4.09 (q, 2H, J = 7.45 Hz), 7.00 (s, 1H), 7.31–7.39 (m, 5H). ^{13}C NMR (125 MHz, $CDCl_3$) δ: 13.6, 24.3, 27.7, 61.3, 121.3, 125.9, 127.9, 128.51, 128.57, 138.7, 148.7, 155.1, 158.6, 169.04. MS (EI) *m/z* (%): 255 (95) [M^+], 210 (90), 115 (100). Anal. calcd. for $C_{16}H_{17}NO_2$: C 75.27, H 6.71, N 5.49; found: C 75.41, H 6.83, N 5.40.

Methyl 2,6-dimethylnicotinate (6b)

R_f 0.3 (20% EtOAc in petroleum ether). IR (neat, cm^{-1}): 1720. ^{1}H NMR (400 MHz, $CDCl_3$) δ: 2.57 (s, 3H), 2.73 (s, 3H), 3.89 (s, 3H), 7.05–7.07 (s, 1H, J = 8 Hz), 8.08–8.10 (s, 1H, J = 8 Hz). ^{13}C NMR (100 MHz, $CDCl_3$) δ: 13.6, 24.3, 40.0, 120.8, 124.9, 139.1, 159.1, 161.0, 166.6. MS (EI) *m/z* (%): 179 (60) [M^+], 151 (100). Anal. calcd. for $C_{10}H_{13}NO_2$: C 67.02, H 7.31, N 7.82; found: C 66.91, H 7.44, N 7.89.

Methyl 2-methyl-4-phenylnicotinate (6c)

R_f 0.4 (20% EtOAc in petroleum ether). IR (neat, cm^{-1}): 1720. ^{1}H NMR (400 MHz, $CDCl_3$) δ: 2.58 (s, 3H), 3.89 (s, 3H), 7.05–7.07 (s, 1H, J = 8 Hz), 8.08–8.10 (s, 1H, J = 8 Hz), 7.31–7.39 (m, 5H). ^{13}C NMR (125 MHz, $CDCl_3$) δ: 25.1, 45.1, 121.3, 125.9, 127.9, 128.51, 128.57, 138.7, 148.7, 155.1, 158.6, 162.5, 169.04. MS (EI) *m/z* (%): 227 (80) [M^+], 115 (100). Anal. calcd. for $C_{14}H_{13}NO_2$: C 73.99, H 5.77, N 6.16; found: C 74.17, H 5.71, N 6.22.

1-(2,6-Dimethylpyridin-3-yl)ethanone (6d)

R_f 0.4 (20% EtOAc in petroleum ether). IR (neat, cm^{-1}): 1686. ^{1}H NMR (400 MHz, $CDCl_3$) δ: 2.57 (s, 3H), 2.73 (s, 3H), 7.05–7.07 (s, 1H, J = 8 Hz), 8.08–8.10 (s, 1H, J = 8 Hz). ^{13}C NMR (100 MHz, $CDCl_3$) δ: 13.6, 24.3, 40.0, 120.8, 124.9, 139.1, 159.1, 161.0, 166.6. MS (EI) *m/z* (%): 149 (60) [M^+]. Anal. calcd. for $C_9H_{11}NO$: C 72.46, H 7.43, N 9.39; found: C 72.58, H 7.50, N 9.42.

1-(2,6-Dimethyl-4-phenylpyridin-3-yl)ethanone (6e)

R_f 0.34 (20% EtOAc in petroleum ether). IR (neat, cm^{-1}): 1686. ^{1}H NMR (400 MHz, $CDCl_3$) δ: 2.55 (s, 3H), 2.75 (s, 3H), 7.00 (s, 1H), 7.31–7.39 (m, 5H). ^{13}C NMR (125 MHz, $CDCl_3$) δ: 23.3, 24.3, 27.7, 121.3, 125.9, 127.9, 128.51, 128.57, 138.7, 148.7, 155.1, 158.6, 169.04. MS (EI) *m/z* (%): 225 (60) [M^+], 115 (100). Anal. calcd. for $C_{15}H_{15}NO$: C 79.97, H 6.71, N 6.22; found: C 80.16, H 6.79, N 6.33.

Acknowledgement

One of the authors (G.K.) thanks the Council of Scientific and Industrial Research, New Delhi for the financial support.

References

1. (*a*) K. Tomioka, K. Ando, Y. Takemasa, and K. Koga. J. Am. Chem. Soc. **106**, 2718 (1984); (*b*) G.I. Georg and J. Kant. Tetrahedron Lett. **29**, 403 (1988); (*c*) W.D. Lubell, M. Kitamura, and R. Noyori. Tetrahedron: Asymmetry, **2**, 543 (1991); (*d*) G. Bartoli, C. Cimarelli, E. Marcantoni, G. Palmieri, and M. Petrini. J. Org. Chem. **59**, 5328 (1994).
2. L.G. Beholtz, P. Benovsky, D.L. Ward, N.S. Barta, and J.R. Stille. J. Org. Chem. **62**, 1033 (1997).
3. (*a*) A.-Z.A. Elassar and A.A. El-khair. Tetrahedron, **59**, 8463 (2003); (*b*) C. Agami, L. Dechoux, and S. Hebbe. Tetrahedron Lett. **43**, 2521 (2002); (*c*) H.A Stefani and E. de Avila. Synth. Commun. **32**, 2041 (2002); (*d*) H.M.C. Ferraz, F.L.C. Pereira, F.S. Letie, M.R.S. Nunes, and M.E. Payret-Arrua. Tetrahedron, **55**, 10915 (1999).
4. (*a*) P.G. Baraladi, D. Simoni, and S. Manfredini. Synthesis, 902 (1983); (*b*) D.F. Martin, G.A. Janusonis, and B.B. Martin. J. Am. Chem. Soc. **83**, 73 (1961); (*c*) H.M.C. Ferraz, E.O. Oliceira, M.E. Payret-Arrua, and C.A. Brandt. J. Org. Chem. **60**, 7357 (1995); (*d*) J.A. Kloek and K.L. Leschinsky. J. Org. Chem. **43**, 1460 (1978); (*e*) V.A. Soloshonok and V. Kukhar. Tetrahedron, **52**, 6953 (1996); (*f*) N. Lflemme, P. Dallemange, and S. Rault. Synthesis, 1740 (2002).
5. (*a*) C.J. Valduga, A. Squizani, H.S. Braibante, and M.E.F. Braibante. Synthesis, 1019 (1998); (*b*) B. Rechsteiner, F. Texier-Boullet, and J. Hamekin. Tetrahedron Lett. **34**, 5071 (1993); (*c*) A. Arcadi, G. Bianchi, S. Di Giuseppe, and F. Marinelli. Green Chem. 64 (2003); (*d*) A.R. Khosropour, M.M. Khodaei, and M. Kookhazhdeh. Tetrahedron Lett. **45**, 1725 (2004); (*e*) G. Bartoli, M. Boscp, M. Locatelli, E. Marcantoni, P. Melchiorre, and L. Sambri. Synlett, 239 (2004).
6. (*a*) M.C. Bagley, J.W. Dale, and J. Bower. Synlett, 1149 (2001); (*b*) M.C. Bagley, J.W. Dale, D.D. Hughes, M. Ohnesorge, N.G. Phillips, and J. Bower. Synlett, 1523 (2001); (*c*) M.C. Bagley, C. Brace, J.W. Dale, M. Ohnesorge, N.G. Phillips, X. Xiong, and J. Bower. J. Chem. Soc. Perkin Trans. 1, 1663 (2002).
7. (*a*) M.C. Bagley, J.W. Dale, and J. Bower. Chem. Commun. (Cambridge), 1682 (2002); (*b*) X. Xiong, M.C. Bagley, and K. Chapaneri. Tetrahedron Lett. **45**, 6121 (2004); (*c*) M.C. Bagley, K. Chapaneri, J.W. Dale, X. Xiong, and J. Bower. J. Org. Chem. **70**, 1389 (2005).
8. (*a*) T. Welton. Chem. Rev. **99**, 2071 (1999); (*b*) P. Wasserchеid and K. Wilhelm. Angew. Chem. Int. Ed. **39**, 3772 (2000); (*c*) R. Sheldon. Chem. Commun. 2399 (2001).
9. R.S. Varma and V.V. Namboodivi. Chem. Commun. (Cambridge), 543 (2001).
10. J. Howart, K. Hanlon, D. Fayne, and P. McCormac. Tetrahedron Lett. **38**, 3097 (1997).
11. (*a*) A.C. Cole, J.L. Jensen, I. Ntai, K.L.T. Tran, K.J. Weaver, D.C. Forbes, and J.H. Davis, Jr. J. Am. Chem. Soc. **124**, 5962 (2002); (*b*) H.P. Zhu, F. Yang, J. Tang, and M.Y. He. Green Chem. **5**, 38 (2003).
12. (*a*) G. Karthikeyan and P.T. Perumal. Synlett, 2249 (2003); (*b*) G. Karthikeyan and P.T. Perumal. J. Heterocycl. Chem. **41**, 1039 (2004).
13. G. Zhao, T. Jiang, H. Gao, B. Han, J. Huang, and D. Sun. Green Chem. **6**, 75 (2004).

© 2005 NRC Canada

The mechanism of 1,3-dipolar cycloaddition reactions of cyclopropanes and nitrones — A theoretical study

D. Wanapun, K.A. Van Gorp, N.J. Mosey, M.A. Kerr, and T.K. Woo

Abstract: The 1,3-dipolar cycloaddition reaction of cyclopropanes and nitrones to give tetrahydro-1,2-oxazine has been studied with density functional theory calculations at the B3LYP/6-31+G(d,p) level of theory. Realistic substituents were modelled including those at the 2-, 3-, 4-, and 6-positions of the final oxazine ring product. The strained σ bond of the cyclopropane was found to play the role of an alkene in a conventional [3+2] dipolar cycloaddition. Two distinct, but similar, reaction mechanisms were found — an asymmetric concerted pathway and a stepwise zwitterionic pathway. The reaction barriers of the two pathways were nearly identical, differing by less than ~1 kcal/mol, no matter what the substituents were. The effect of a Lewis acid catalyst was examined and found to have a very large effect on the calculated barriers through coordination to the carbonyl oxygen atoms of the diester substituents on the cyclopropane. The reaction barrier was found to decrease by as much as ~19 kcal/mol when using a BF_3 molecule as a model for the Lewis acid catalyst. Solvent effects and the nature of the regiospecificity of the reaction were also examined. Trends in the calculated barriers for the reaction were in good agreement with available trends in the reaction rates measured experimentally.

Key words: 1,3-dipolar cycloaddition, cyclopropane, nitrone, tetrahydro-1,2-oxazines, ab initio quantum chemistry, mechanism.

Résumé : Faisant appel à des calculs de la théorie de la densité fonctionnelle au niveau B3LYP/6-31+G(d,p), on a étudié la réaction d'addition 1,3-dipolaire des cyclopropanes et des nitrones qui conduit à la formation de tétrahydro-1,2-oxazines. On a effectué des études modèles réalistiques de substituants, y compris ceux dans les positions 2, 3, 4 et 6 du cycle oxazine du produit final. On a trouvé que les liaisons σ tendues du cyclopropane jouent le rôle d'un alcène dans une cycloaddition dipolaire [3+2] conventionnelle. On a trouvé deux mécanismes distincts, mais similaires, soit une voie asymétrique concertée et une voie zwitterionique par étape. Les barrières à la réaction pour les deux voies sont presque identiques, ne différant que par moins qu'une kcal/mol, quelle que soit la nature du substituant. On a examiné l'effet catalytique d'un acide de Lewis et on a trouvé un effet très important sur les barrières calculées en raison d'une coordination des atomes d'oxygène du carbonyle des substituants esters sur le cyclopropane. On a trouvé que la barrière diminue par une valeur allant jusqu'à environ 19 kcal/mol lorsqu'on a utilisé une molécule de BF_3 comme modèle d'un catalyseur acide de Lewis. On a aussi étudié les effets de solvant et la nature de la régiospécificité de la réaction. Les tendances dans les barrières calculées pour la réaction sont en bon accord avec les tendances disponibles dans les vitesses de réactions qui ont été mesurées expérimentalement.

Mots clés : cycloaddition 1,3-dipolaire, cyclopropane, nitrone, tétrahydro-1,2-oxazines, chimie quantique ab initio, mécanisme.

[Traduit par la Rédaction]

Introduction

The tetrahydro-1,2-oxazine heterocycle forms the central feature of several natural products possessing antitumor and antibiotic properties, such as FR900482 (1–3) and FR66979 (4), shown in Fig. 1. These natural products have received great interest from the synthetic community for their potential as therapeutic drugs. The tetrahydro-1,2-oxazine heterocycle has also been used recently in the synthesis of a pyrrolidine ring in a synthetically challenging fused 6/5/5/5 ring system that forms the tetracyclic core of nakadomarin A (5). However, the preparations of the heterocyclic core are not abundant (6), making alternative methods for the synthesis of the tetrahydro-1,2-oxazine ring desirable. Recently, a new and flexible synthesis of the 1,2-oxazine ring has been developed involving the reaction of nitrones with

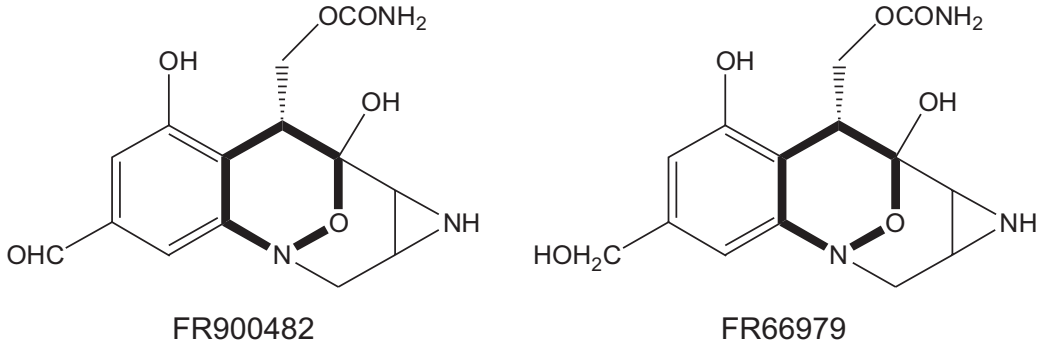
Received 16 June 2005. Published on the NRC Research Press Web site at http://canjchem.nrc.ca on 13 December 2005.

D. Wanapun, K.A. Van Gorp, N.J. Mosey, M.A. Kerr, and T.K. Woo.[1,2] Department of Chemistry, The University of Western Ontario, London, ON N6A 5B7, Canada.

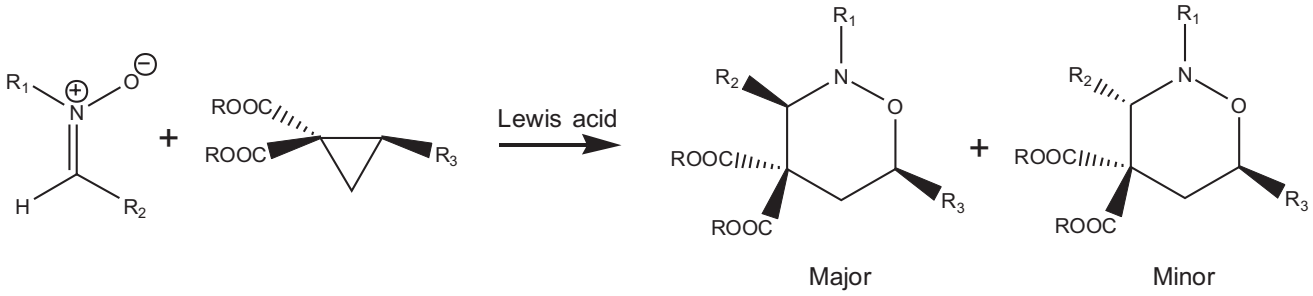
[1]Present address: Department of Chemistry, University of Ottawa, D'Iorio Hall, 10 Marie-Curie, Ottawa, ON K1N 6N5, Canada.
[2]Corresponding author (e-mail: twoo@uottawa.ca).

 doi: 10.1139/V05-182 © 2005 NRC Canada

Fig. 1. Structures of FR900482 and FR66979, both containing a tetrahydro-1,2-oxazine heterocycle highlighted in bold.



Scheme 1.



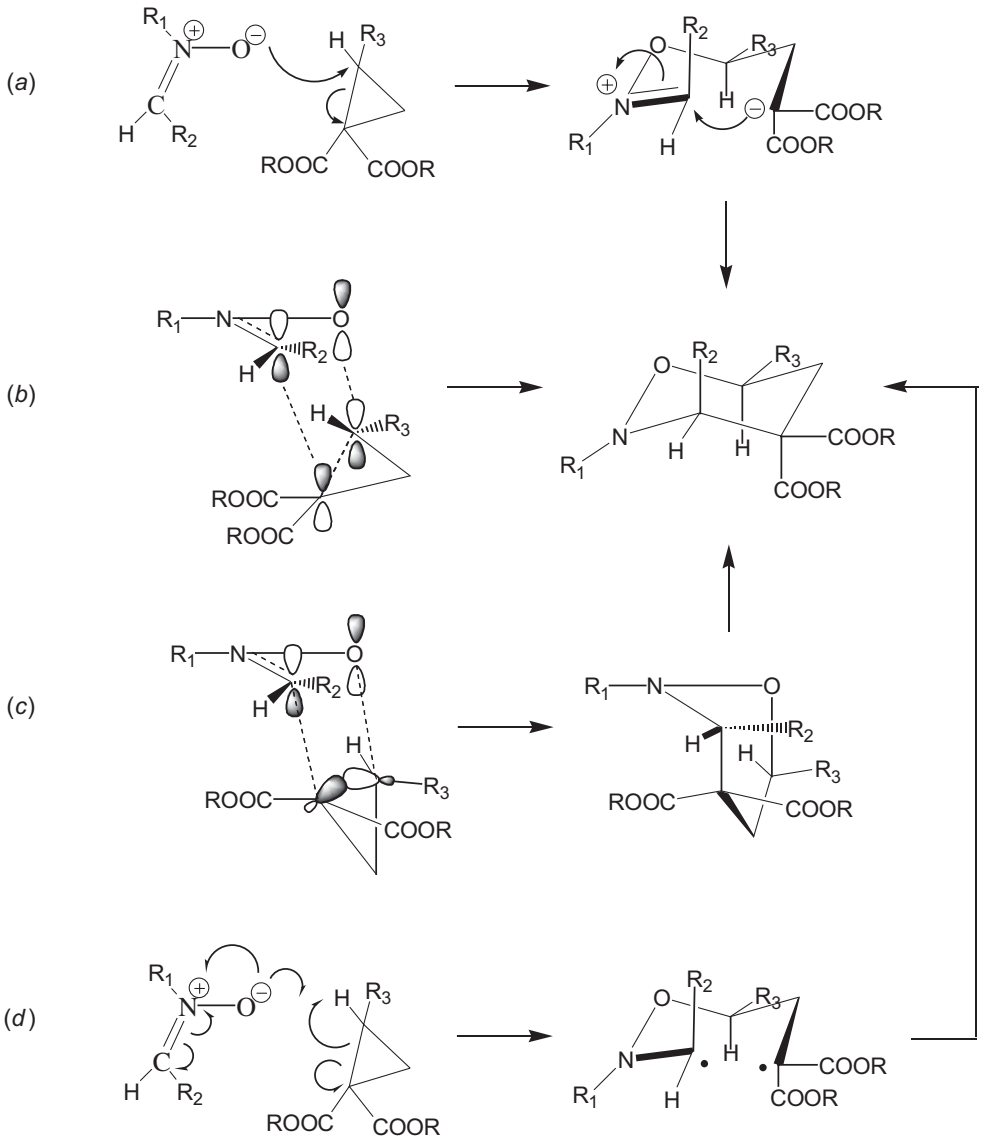
cyclopropane rings that bear electron-withdrawing ester substituents (5, 7–10). This reaction, which is shown in Scheme 1, was the first report of a cycloaddition reaction between a nitrone and a cyclopropane. The synthetic utility of the reaction is evident with the formidable tetrahydro-1,2-oxazine heterocycle being prepared in excellent yields under relatively mild conditions and with virtually complete diastereoselectivity. More recently, an effective three-component, one-pot protocol has been developed where the nitrone is generated in situ allowing for a diversity-oriented synthesis of tetrahydro-1,2-oxazines (8). It was found that electron-withdrawing groups (EWGs) are required on the cyclopropane for the reaction to proceed and, to date, 1,1-cyclopropanediesters have been utilized almost exclusively. Additionally, the presence of electron-donating groups, such as phenyl or vinyl, vicinal (R3 in Scheme 1) to the diester moiety on the cyclopropane enhances the activity of the reaction. The reaction also requires the presence of a Lewis acid catalyst, the best of which, in terms of activity and yield, was found to be $Yb(OTf)_3$. The reaction is regiospecific, with the sole regioisomer being that with the oxygen atom lying distal to the diester moiety in the product 1,2-oxazine ring.

1,3-Dipolar cycloadditions are amongst the most important synthetic reactions for generating heterocycles (11–14). The predictability of cycloaddition reactions based on steric and electronic considerations in the transition-state structure allows for the selective synthesis of complex heterocyclic structures (15). Consequently, a detailed understanding of the mechanism of the reaction will improve the predictability and the synthetic utility of the reaction. Three distinct reaction mechanisms were proposed originally (7) and are depicted in Schemes 2*a*–2*c*. The first pathway, labeled "*a*" in Scheme 2, involves the stepwise formation of the products through the initial formation of the C—O bond to yield a zwitterionic intermediate with a negative charge on the carbon atom bearing the ester groups and the positive charge on the nitrogen followed by formation of the C—C bond to yield the products. The second pathway, labeled "*b*", involves concerted bond formation through a chairlike conformation to form the products in a single step. This pathway is analogous to that of the reaction of nitrones with alkenes. The third pathway also involves concerted bond formation between the nitrone and cyclopropane ring; however, this time the strained σ bond of the cyclopropane ring is involved and the transition-state species is in a half-chair geometry. Another possible pathway, not mentioned by the initial work of Young and Kerr (7), for 1,3-dipolar cycloadditions is a stepwise mechanism involving a diradical intermediate (Scheme 2*d*) that was proposed by Firestone in the 1970s (16). To date, however, no convincing experimental evidence has been reported that supports the diradical mechanism (17), and it is now a general consensus that 1,3-dipolar cycloadditions do not react through a diradical pathway (18). A recent computational study of the reaction of a nitrone with ethene further supports this picture (17).

As mentioned in the preceding paragraph, the reaction of nitrones with substituted cyclopropanes can be described as a 1,3-dipolar cycloaddition. In general, this class of reactions provides an efficient means of forming heterocyclic components of larger systems, such as that of FR-900482 previously described. 1,3-Dipolar cycloadditions have also been well-studied through computational and theoretical means (19–22), including those of nitrones with alkenes (23–30). Such previous work is relevant to the current study since it has been proposed that the strained bonds in the

© 2005 NRC Canada

Scheme 2.



cyclopropane rings exhibit substantial π character (31). Although the specific details of these studies will not be discussed here, it is important to consider several general observations that have been reported in these studies that can be applied to this system. In general, density functional theory (DFT) has been employed as a relatively accurate, cost-effective method for the study of these systems (24). From a mechanistic point of view most ab initio calculations favour or assume a concerted pathway for the addition of nitrones to alkenes (21). Although the regio- and stereochemistry of the products of the reaction of nitrones with alkenes is quite complicated and dependent upon substituent effects, it has been found that the origins of the regio- and stereo-selectivity can often be adequately described by frontier molecular orbital (FMO) theory (32–34). In cases where such analysis is inadequate, more sophisticated models have been used that take into account secondary orbital interactions (21) and closed-shell repulsions (35) between the two reactant species, or alternative reactivity concepts based on hard and soft acid–base principles such as local and global hardness (25).

In this work we apply quantum chemistry to examine the mechanism of the 1,3-dipolar cycloaddition reaction between nitrones and cyclopropanes. The goal is to provide a detailed mechanistic account of the reaction that will hopefully provide key information that will assist in future experimental efforts to optimize the reaction. Specifically, the effect of the diester substitution and the R3 substitution on the reactant cyclopropane on the reaction has been probed. Up to two BF_3 molecules have been used to study the role of the Lewis acid catalyst that is required for the reaction to be observed. Using a continuum solvation model, solvent effects on the reaction have been examined. Finally, we have examined the nature of the regiospecificity of the reaction. The computational methods used throughout this study are introduced in the next section. This section is followed by a discussion of the results of the calculations that have been performed and finishes with conclusions.

© 2005 NRC Canada

Table 1. Relative energies (kcal/mol) for the reaction of **N1** with cyclopropane **C1** and dimethyl 1,1-cyclopropanedicarboxylate (**C2**) calculated using several different basis sets.

	B3LYP/6-31G(d,p)		B3LYP/6-31+G(d,p)		B3LYP/6-31++G(d,p)		B3LYP/6-311++G(d,p)	
Species	ΔE	ΔG^a	ΔE	ΔG^a	ΔE	ΔG^a	ΔE	ΔG^a
N1 + C1	0.00	0.00	0.00	0.00	0.00	0.00	0.00	0.00
CN1‡	57.41	67.77	60.37	71.00	60.49	71.08	60.38	71.08
P1	–36.26	–24.72	–30.13	–18.24	–30.06	–18.17	–28.68	–16.81
N1 + C2	0.00	0.00	0.00	0.00	0.00	0.00	0.00	0.00
CN2‡	43.31	55.27	47.00	59.34	47.05	59.41	47.03	59.37
SW2-A‡	42.74	55.59	46.98	59.47	47.13	59.67	47.26	59.76
SW2-B	17.41	30.65	22.98	36.47	22.86	36.32	23.28	36.58
SW2-C‡	23.31	36.50	27.57	40.99	27.85	41.28	29.23	42.52
P2	–31.43	–17.96	–24.21	–10.35	–24.16	–10.28	–23.27	–9.41

Note: Energies are relative to the free nitrone and cyclopropane.
[a]Gas-phase relative free energy at 298 K and 1 atm.

Methods

Computational details

All energies and geometry optimizations of the stationary points (reactants, products, transition states, and intermediates) were performed using Kohn–Sham DFT (36, 37) at the B3LYP level of theory (38, 39) using the Jaguar 5.0 program (40) unless otherwise stated. The results from a basis set study using the 6-31G(d,p), B3LYP/6-31+G(d,p), 6-31++G(d,p), and 6-311++G(d,p) basis sets are summarized in Table 1 for the reaction of a nitrone with both an unsubstituted and substituted cyclopropane. The data in Table 1 reveals that the relative energies of the transition states, intermediates, and products converge with the 6-31+G(d,p) basis set, and using a larger basis set, results in minimal changes in these properties. Thus, the 6-31+G(d,p) basis set was used for this study as it provided the best balance of accuracy and computational efficiency. To search for the biradical pathway, a procedure similar to that in our previous work on diradical dimetallenes (41) was followed where unrestricted DFT was employed with mixing of the HOMO and LUMO in the initial guess of the wave function to generate open shell electronic structures.

Due to the conformational flexibility of the substituents on some of the cyclopropanes studied, a comprehensive conformer search was carried out on the reactants, intermediates, and products using the following protocol. First, a conformational search was performed at the semiempirical PM3 (42) level of theory using the default Monte Carlo based conformational search engine of the Spartan 2002 molecular modeling package (43). The three lowest energy and distinct structures obtained at the PM3 level were then optimized at the B3LYP/6-31+G(d,p) level. The structures and energies reported here are the lowest energy structures resulting from this procedure. Frequency calculations were performed on all stationary points to confirm that minimum energy structures had no imaginary frequencies and that transition states had only one imaginary frequency. All of the energies include unscaled zero point energy corrections. Intrinsic reaction coordinate (IRC) calculations were performed for the reactions involving cyclopropane, 1,1-cyclopropane-dimethylester, and 2-methyl-1,1-cyclopropane-dimethylester using the GAUSSIAN 98 program (44). For other reactions, it is reasonable to assume that the transition states located correspond to analogous pathways as those found in the aforementioned IRC calculations based on the comparison of geometries, relative energies, and bond orders of the stationary points.

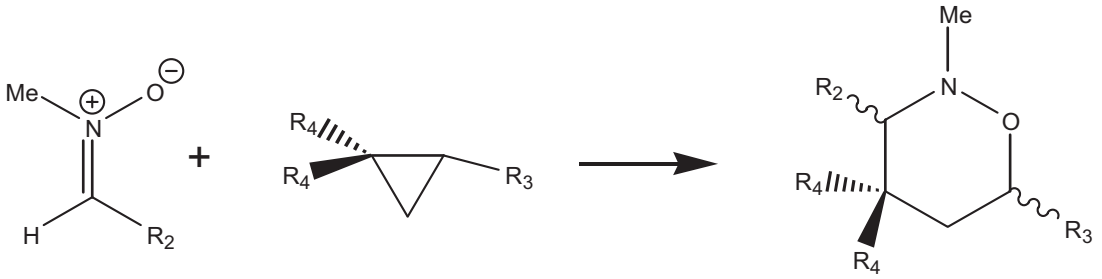
The natural bond orbital (NBO) analysis (45) was performed with the NBO program that is distributed with Jaguar 5.0. The use of Kohn–Sham orbitals, both virtual and occupied, for qualitative chemical analysis in molecular orbital arguments has been previously shown to be suitable (46, 47). Solvent effects on the relative energetics of the various reaction pathways were taken into account through the polarizable continuum model of Friesner and co-workers (48) as implemented in the Jaguar 5.0 package. The default values of Jaguar were used for the solvent dielectric constants and probe radii. Frequency calculations with the continuum solvation model performed on both minima and transition states revealed that the structures had many more low frequency (<40 cm^{-1}) vibrational modes compared with their gas-phase counterparts. Additionally, the structures often possessed several superfluous imaginary vibrational frequencies that could not be eliminated after many optimization attempts with adjusted convergence parameters. The small vibrational modes have a large impact on the calculated vibrational free energy term that can result in large errors when comparing relative free energies of species. Although a cut-off frequency can be applied, one must ensure all compared species have the same number and nature of frequencies removed or again, large errors can ensue when comparing energies. For these reasons, we have opted to report the relative free energies of solvation that do not include any vibrational, rotational, and translational thermal or entropic corrections. The relative free energies of solvation reported, however, do include the zero point vibrational energy corrections, which are not significantly effected by the low vibrational modes, such that these values can be most directly compared with the ΔE values reported for the gas phase.

Model systems

The typical approach to the development of model systems for use in a computational study is to decrease the size of the system as much as possible through the removal of all substituents that are not absolutely necessary to achieve the goals of the study. As such, a completely hydrogen substi-

© 2005 NRC Canada

Scheme 3.



N1 + C1 → P1	R_2 = H	R_3 = H	R_4 = H
N1 + C2 → P2	R_2 = H	R_3 = H	R_4 = COOMe
N1 + C3 → P3	R_2 = H	R_3 = Me	R_4 = COOMe
N1 + C4 → P4	R_2 = H	R_3 = vinyl	R_4 = COOMe
N1 + C5 → P5	R_2 = H	R_3 = phenyl	R_4 = COOMe
N2 + C2 → P6	R_2 = Me	R_3 = H	R_4 = COOMe

tuted nitrone was used initially as a model reactant. However, reactions of this nitrone with the 1,1-cyclopropanedicarboxylic acid reactant lead to proton transfer between the nitrone and the carboxylic acid groups, which is also observed in experiment (8). Replacing the hydrogen bonded to the nitrogen of the nitrone with a methyl group prevented the proton transfer and was also a more realistic model. This model, shown in Scheme 3, is referred to as methyl nitrone **N1** and was used in all calculations performed in this study.

Results and discussion

The discussion section begins with a minimally substituted model system, where the reactant cyclopropane is unsubstituted. Substituent effects are examined in the following two sections. More specifically, the role of the diester moiety on the cyclopropane is studied, followed by the nature of the R3 substitution on the cyclopropane. Solvent effects are briefly discussed in the next section, followed by a more detailed examination of the role of the Lewis acid catalyst. The last section details the nature of the regiospecificity that was experimentally observed.

Throughout this discussion an unconventional naming scheme has been employed to reflect both the nature of the pathway and the reactant species involved. Although it is common practice to simply identify species with a numerical digit, it is hoped that the nomenclature system used here will ease in the identification of the species that is being discussed. The reactant nitrones and cyclopropanes are labeled **N*x*** and **C*x***, respectively, with *x* representing the specific nitrone or cyclopropane (see Scheme 3). The names of the other stationary points have three parts to them. The nature of the pathway is expressed in the first part of the name for the transition states and intermediates — either **CN** for a concerted pathway or **SW** for a stepwise pathway. The second part of the name is a numeric digit (*n*) used to identify the unique combination of R2 and R3 substituents. These are shown in the product labels "**P*n***" in Scheme 3. For example, the concerted reaction that gives rise to the product **P4**, goes through a concerted transition state **CN4**‡, where the superscript double dagger denotes a transition-state structure. For the stepwise pathways a third portion of the name exists that consists of an alphabetical character that corresponds to the position of the stationary point beyond the reactants towards the products. For example, **SW2-A**‡ refers to first transition state for the stepwise reaction of methyl nitrone to dimethyl 1,1-cyclopropanedicarboxylate. The label "**A**" refers to the fact that this transition state is the first stationary point following the reactants. **SW2-B** refers to the intermediate for the stepwise pathway. The intermediate is the second stationary point along the reaction coordinate past the reactants and, hence, "**B**". Additions to this naming scheme for the calculations that model the solvent, the Lewis acid, and regiochemistry will be introduced in the respective sections ahead.

Reaction of methyl nitrone with unsubstituted cyclopropane

We began our study by investigating the reaction of **N1** with the unsubstituted cyclopropane ring **C1**. The goal here is to examine the intrinsic reactivity of these two species in the absence of any substituents for later comparison with more realistic models. Attempts were made to locate intermediates and transition states corresponding to all four of the proposed mechanisms depicted in Scheme 2, including the diradical pathway. However, the only pathway that was found is one that is consistent with a concerted addition through a half-chair geometry (reaction c in Scheme 2). The transition-state structure (**CN1**‡) is shown in Fig. 2*a*, and the relative energies for this reaction pathway are detailed in Table 2. The electronic barrier for the reaction is 60.4 kcal/mol, while the estimated free energy barrier at 298 K and 1 atm is 71.0 kcal/mol (1 atm = 10.325 kPa). The large reaction barriers are consistent with the fact that the reaction involving unsubstituted reactants is not observed.

Examination of the geometry of the transition-state structure reveals that **CN1**‡ can be characterized as a half-chair

© 2005 NRC Canada

Fig. 2. Optimized structures of the selected stationary points at the B3LYP/6-31+G(d,p) level. For the transition-state structures **CN2**‡ and **SW2-A**‡, the values shown in parenthesis () and square brackets [ ] refer to the structures optimized with a continuum solvation model using dichloroethane and methanol, respectively, as solvents.

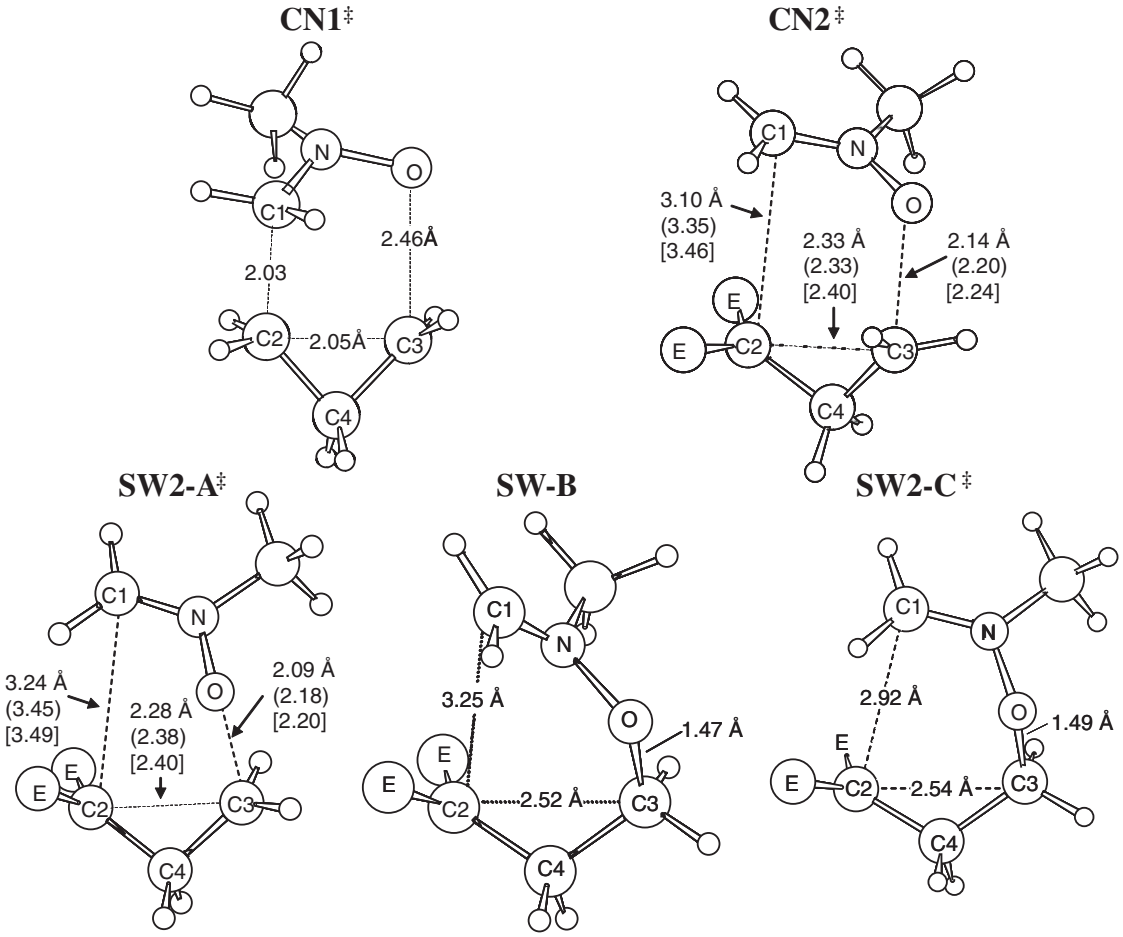


Table 2. Relative energies (kcal/mol) and bond orders for the reaction of **N1** and cyclopropane **C1**.

	Energies		Wiberg bond orders			
Species	ΔE	ΔG^a	C1—C2	C2—C3	C3—O	C1—N
N1 + C1	0.00	0.00	0.00	1.00	0.00	1.55
CN1‡	60.37	71.00	0.53	0.48	0.30	1.27
P1	–30.13	–18.24	1.01	0.01	0.91	0.98

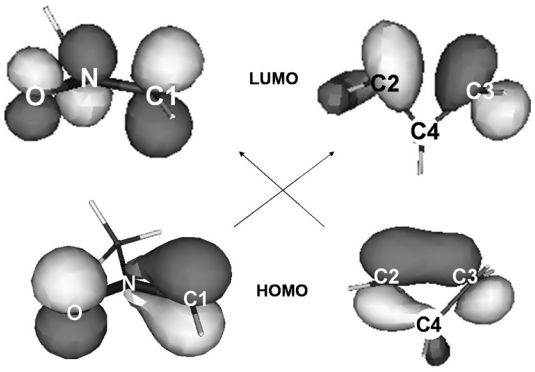
Note: Energies are relative to **N1 + C1**.
[a]Gas-phase relative free energy at 298 K and 1 atm.

conformation. For example, the C4-C3-C2-O dihedral angle in **CN1**‡ of 182° is very close to the value of 180° found in an ideal half-chair geometry. The C4-C3-C2-C1 dihedral angle of 160.0° and the N-O-C1-C4 dihedral angle of 132.3° are close enough to the ideal values of 180.0° and 125.3°, respectively, to be classified as half-chair geometries.

It is possible to further characterize this transition state through an examination of the bond orders and lengths at stationary points along the reaction path. Relevant Wiberg bond orders are listed in Table 2 along side the relative energies. The C1—C2 and O—C3 bond orders in the transition state (**CN1**‡) have values of 0.53 and 0.30, respectively, which indicates that these bonds are both partially formed. Also, the C2—C3 bond order (0.48) shows evidence of dissociation, and the C1—N bond order (1.27) illustrates that the double bond is being decreased to a single bond. The bond lengths for the C1—C2 and O—C3 bonds, which are shown in Fig. 2*a*, are typical for partially formed bonds of this nature. The initial C2—C3 bond length was found to increase from a value of 1.51 Å in the reactant to a value of 2.05 Å in the transition state, which is indicative of bond dissociation. The C1—N transition-state bond length of 1.35 Å is larger than the reactant value of 1.31 Å, signifying that the bond is converting to a single bond. The bond order and bond length results complement each other and indicate that the process is in fact a synchronous concerted mechanism.

© 2005 NRC Canada

Fig. 3. Frontier molecular orbitals of the two reactant species fragments in their respective geometries in transition state **CN1**‡. For nitrone, ε_{LUMO} = –0.083969 and ε_{HOMO} = –0.235387 au. For cyclopropane, ε_{LUMO} = –0.047419 and ε_{HOMO} = –0.220461 au. All isosurfaces are plotted at a value of 0.07 au.



Further characterization of the pathway can be obtained through examination of the FMO interactions (15, 34). Isosurface plots of the frontier molecular orbitals of the two reactant species in their respective transition-state geometries are shown in Fig. 3 along with their respective orbital energies. It is possible to identify the HOMO of the cyclopropane as a strained σ bond between the C2 and C3 atoms, while the LUMO of this fragment is its antibonding counterpart. The HOMO of the nitrone fragment is a nonbonding orbital with a nodal plane approximately centered on the nitrogen atom, while the LUMO consists of π-antibonding interactions along the C1—N and N—O bonds. Drawing the analogy between the strained σ-bonding frontier orbitals of cyclopropane to the π-bonding orbitals of an alkene, it is apparent that the frontier molecular orbitals of the reactants have the proper symmetry to take part in a classic, concerted 1,3-dipolar cycloaddition reaction. The energy difference between the LUMO of the nitrone and the HOMO of the cyclopropane is 0.14 au, while the energy difference between the LUMO of the cyclopropane and the HOMO of the nitrone is 0.19 au. Thus, on the basis of a smaller HOMO–LUMO difference, the dominant orbital interaction involves the LUMO of the nitrone and the HOMO of the cyclopropane. Since the LUMO of the nitrone is clearly polarized toward the C atom, one would expect the formation of the C1—C2 bond to lead the reaction. This is consistent with the slightly larger C1—C2 bond order of 0.53 as compared with the C3—O bond order of 0.30 in the transition state (**CN1**‡).

The reaction of **N1** with the unsubstituted cyclopropane ring **C1** occurs via a concerted mechanism. Moreover, analysis of the geometry, bond orders, and frontier molecular orbitals of the transition state (**CN1**‡) reveals that the reaction can be further characterized as a classic [3+2] synchronous concerted cycloaddition.

Reaction of methyl nitrone with 1,1-cyclopropanedimethyl ester

Experimentally, the cycloaddition reaction requires EWGs on the cyclopropane to proceed under normal reaction conditions, and to date 1,1-cyclopropanediesters have been used almost exclusively (7). In this section the reaction of **N1** with 1,1-cyclopropanedimethyl ester (**C2**) to yield the product (**P2**) will be examined. Two pathways were found — a concerted mechanism and a stepwise mechanism. An intrinsic reaction coordinate calculation starting from each transition-state structure verified that these structures connect the reactants to the products and that the two pathways are in fact distinct. In what follows, the concerted pathway will be examined in detail, followed by an examination of the stepwise pathway.

Concerted pathway

The first pathway is a concerted process as it involves progression over a single transition-state structure (**CN2**‡), shown in Fig. 2*b*, linking the reactants to the products. Energetics and bond orders of the stationary points involved in the concerted pathway and the stepwise pathway are detailed in Table 3. The concerted pathway has a gas-phase free energy barrier of 59.3 kcal/mol at 298 K and 1 atm, which is significantly less than the barrier for the reaction of **N1** with the unsubstituted cyclopropane, which possessed a free energy barrier of 71.0 kcal/mol.

Analysis of the geometric details of this transition state indicate that the two reactant species have the correct relative orientations to be characterized as an approximate half-chair conformation with the C4-C3-C2-O (148.1°), C4-C3-C2-C1 (160.8°), and N-O-C1-C4 (152.3°) dihedral angles all slightly deviated from the ideal values of 180.0°, 180.0°, and 125.3°, respectively. However, the C1—C2 and O—C3 bond distances are not indicative of a synchronous concerted process where both bonds form simultaneously. The C1—C2 bond length of 3.10 Å in the transition state is too large for significant bond formation, while the O—C3 bond length of 2.14 Å is approximately 15% shorter than that observed in the synchronous concerted transition-state structure (**CN1**‡). Thus, the O—C3 bond is preferentially forming over the C1—C2 bond, and the transition-state structure is suggestive of an asynchronous concerted process. Calculated bond orders also support this picture, with the C1—C2 bond order in the transition state being negligible at 0.05, with the O—C3 bond order being 0.33. The double bond character of the C1—N bond does not significantly change in the transition state, which differs from that of the unsubstituted transition state (**CN1**‡).

A FMO analysis of the reaction is also consistent with an asynchronous bond formation. The HOMO and LUMO of each of the two reactant fragments in their respective transition-state geometries are shown in Fig. 4 along with the energies of these orbitals. The effect of ester groups is to lower the LUMO level of the cyclopropane and to polarize the LUMO away from C2 towards the C3 atom. Conversely, the HOMO of the cyclopropane is polarized in the opposite direction. Favourable overlap appears to be possible for both HOMO–LUMO pairs between the two species and the formation of the O—C3 and C1—C2 bonds is sterically unimpeded. The orbital energies demonstrate that the HOMO(nitrone)–LUMO(cyclopropane) gap has a value of only 0.087 au; whereas the HOMO(cyclopropane)–LUMO(nitrone) is significantly larger with a value of 0.186 au. As a result, donation from the HOMO of the nitrone to the LUMO of the cyclopropane, both orbitals of which are polarized toward the oxygen atom and C3, is

© 2005 NRC Canada

Table 3. Relative energies (kcal/mol) and bond orders for the reaction of **N1** with various dimethyl 1,1-cyclopropanedicarboxylates (**C*n***, where n = 3–5).

	Energies		Wiberg bond orders			
Species	ΔE	ΔG^a	C1—C2	C2—C3	C3—O	C1—N
N1 + C2	0.00	0.00	0.00	0.91	0.00	1.55
CN2‡	47.00	59.34	0.05	0.27	0.33	1.58
SW2-A‡	46.98	59.47	0.06	0.27	0.36	1.59
SW2-B	22.98	36.47	0.12	0.01	0.85	1.54
SW2-C‡	27.57	40.99	0.12	0.02	0.82	1.60
P2	–24.21	–10.35	0.97	0.01	0.91	0.98
N1 + C3	0.00	0.00	0.00	0.90	0.00	1.55
CN3‡	41.06	53.23	0.05	0.17	0.32	1.58
SW3-A‡	41.79	55.21	0.04	0.20	0.32	1.59
SW3-B	20.40	33.91	0.11	0.01	0.82	1.54
SW3-C‡	25.33	38.83	0.13	0.02	0.79	1.60
P3	–22.20	–8.26	0.97	0.01	0.90	0.94
N1 + C4	0.00	0.00	0.00	0.87	0.00	1.55
CN4‡	39.49	51.93	0.10	0.12	0.33	1.55
SW4-A‡	40.70	52.56	0.04	0.17	0.26	1.57
SW4-B	22.80	36.14	0.11	0.01	0.82	1.56
SW4-C‡	28.01	41.53	0.07	0.02	0.78	1.54
P4	–24.16	–10.50	0.97	0.01	0.89	0.94
N1 + C5	0.00	0.00	0.00	0.87	0.00	1.55
CN5‡	36.77	49.29	0.07	0.09	0.33	1.60
SW5-A‡	37.86	50.31	0.03	0.10	0.31	1.57
SW5-B	21.93	35.29	0.12	0.01	0.82	1.55
SW5-C‡	26.84	40.27	0.08	0.02	0.78	1.54

Note: Energies are relative to **N1 + C*n***.
[a]Gas-phase relative free energy at 298 K and 1 atm.

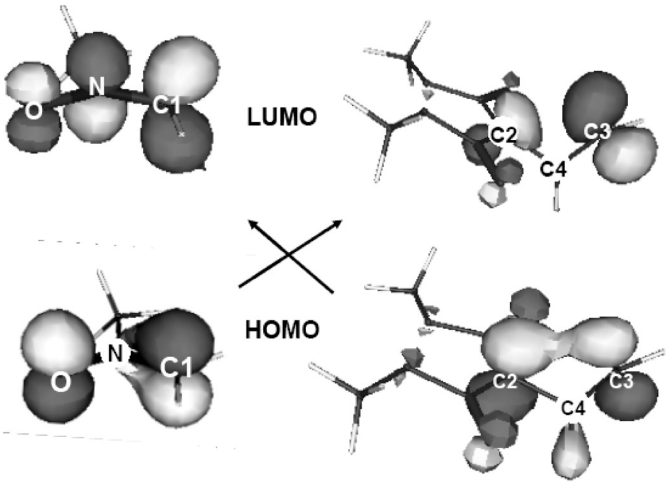
favoured. This is consistent with the observed asynchronous pathway in which the O—C3 bond forms first.

Stepwise pathway

The second pathway for the addition of **N1** to 1,1-cyclopropanedimethylethyl (**C2**) occurs in a stepwise fashion. Geometric details of the transition states and the intermediate for the stepwise pathway are shown in Figs. 2*c*–2*e*, while the bond orders and relative energetics are listed in Table 3. As shown in Fig. 5, the stepwise pathway involves the progression of the reactants over an initial transition state (**SW2-A**‡) to form an intermediate (**SW2-B**), which then proceeds over a second transition state (**SW2-C**‡), to form the product (**P2**).

Examination of the first transition state (**SW2-A**‡) shows that the geometry around the C2, C3, and O atoms is similar to the transition state **CN2**‡ located for the asynchronous concerted pathway. The only exception to this is the C1—C2 distance, which is slightly longer at 3.24 Å compared with 3.10 Å in **CN2**‡. Analysis of the bond orders at this transition state indicates partial formation of the C3—O bond (0.36), as well as initial dissociation of the C2—C3 bond (0.27). The C1—C2 bond order has a value of 0.06, confirming that there is no significant bonding interaction between these two atoms. These bond orders are remarkably similar to the bond orders found in the asynchronous concerted transition state (**CN2**‡). Similarly, the electronic and free energy barriers associated with this transition state of $\Delta E^{\ddagger}$ = 47.0 and $\Delta G^{\ddagger}$ = 59.5 kcal/mol, respectively, are almost identical to the **CN2**‡ barriers of $\Delta E^{\ddagger}$ = 47.0 and $\Delta G^{\ddagger}$ = 59.3 kcal/mol.

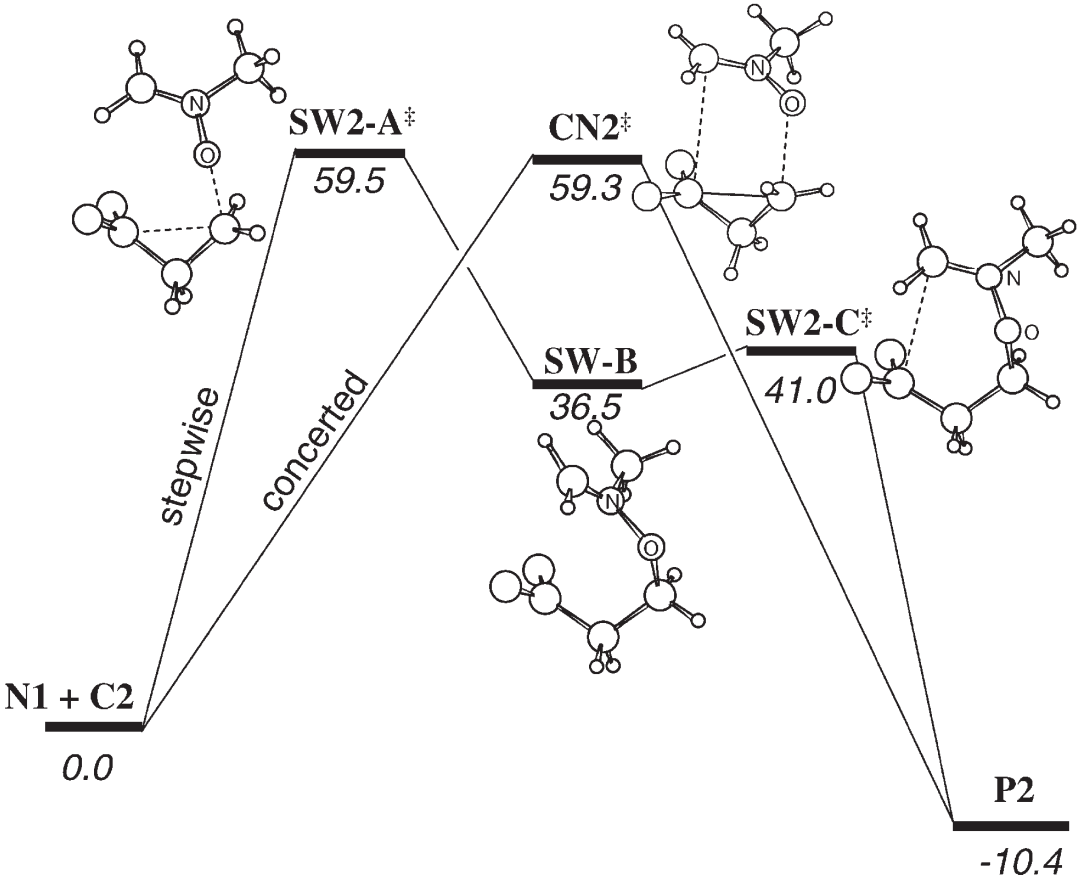
Fig. 4. Frontier molecular orbitals of the two reactant species fragments in their respective geometries in transition state **CN2**‡. For nitrone, ε_{LUMO} = –0.047957 and ε_{HOMO} = –0.234643 au. For cyclopropane, ε_{LUMO} = –0.147346 and ε_{HOMO} = –0.233880 au. All isosurfaces are plotted at a value of 0.07 au.



Once the system passes over the transition state it proceeds to a stable minimum energy structure (**SW2-B**) that is 36.5 kcal/mol higher in energy than the separated reactants. This intermediate can be described as a zwitterionic

© 2005 NRC Canada

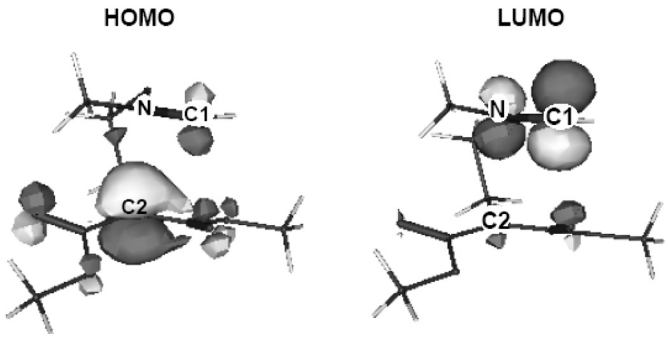
Fig. 5. Reaction profile comparing the concerted and stepwise reaction pathways for the reaction of **N1** with **C2**. Numbers in italics represent the gas-phase free energy at 298 K and 1 atm relative to the free nitrone and cyclopropane.



imminium species as depicted in rxn. *a* of Scheme 2. As shown by the bond distances and the calculated bond orders, the O—C3 bond has fully formed, the C2—C3 σ bond of the reactant cyclopropane has completely dissociated, while the C1=N double bond remains unchanged from that of the original nitrone fragment. The HOMO and LUMO orbitals of **SW2-B** visualized in Fig. 6 are consistent with the characterization of this intermediate as zwitterionic. The isosurface plot of the HOMO reveals a lone pair orbital that is localized on C2; whereas the LUMO can be described as a π* orbital between the C1 and N atoms.

To form the product (**P2**), the intermediate proceeds over a second transition state (**SW2-C**‡) that only lies 4.5 kcal/mol higher in free energy than the preceding intermediate. Interestingly, the C1—C2 and C1—N bond orders in the transition state remain unchanged from those in the intermediate, suggesting that the origin of this barrier does not directly involve the formation of the C1—C2 bond and breakage of the C1=N double bond. Following the IRC trajectory from the intermediate **SW2-B** to the transition state **SW2-C**‡ suggests that the barrier is associated with rotation about the N—O bond. The reduction of the C1-N-O-C3 dihedral angle from 136° in **SW2-B** to 102° in **SW2-C**‡ facilitates reduction of the C1—C2 bond distance from 3.52 to 2.92 Å. Only in the later stages of the IRC trajectory from the transition state (**SW2-C**‡) to the product does the C1—C2 bond order increase and the C1—N bond order decrease.

Fig. 6. Isosurface plots of the HOMO and LUMO molecular orbitals of the stepwise zwitterionic intermediate, **SW2-B**. All isosurfaces are plotted at a value of 0.07 au.

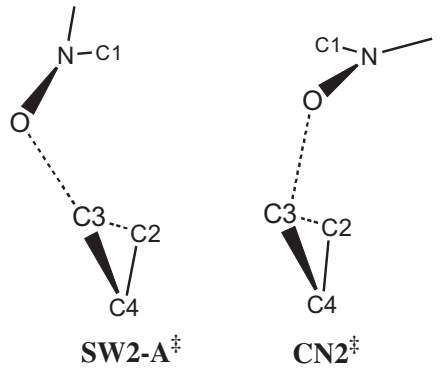


Comparison of the pathways

Several similarities exist between the concerted and stepwise reaction pathways, most notably the remarkable similarity in the energetic barrier and bond orders of the concerted transition state (**CN2**‡) and the first stepwise transition state (**SW2-A**‡). Bond orders of the transition states (**CN2**‡ and **SW2-A**‡), which show that the only bond in the process of breaking is the C2—C3 bond, one can conclude that the origin of the barrier for both pathways is the dissociation of the C2—C3 bond of the cyclopropane moiety. The foremost geometric difference between the two transition

© 2005 NRC Canada

Fig. 7. Comparison of the structures of the transition states for the stepwise zwitterionic and asynchronous concerted pathways that highlights their foremost differences.



SW2-A‡ **CN2**‡

states is the orientation of the nitrone moiety relative to the plane of the cyclopropane ring as depicted in Fig. 7. The C2-C4-C3-O dihedral angle can be used to quantify this difference in the two transition states. In **CN2**‡ this dihedral angle is –40°; whereas it is +37° in **SW2-A**‡. In the stepwise pathway, the nitrone moiety is twisted such that a weak intermediate forms instead of the C1—C2 bond forming directly as in the concerted pathway. Thus, although the two pathways are distinct, one can characterize the difference as only conformational in nature.

Substitution at the R3 position of the cyclopropane

Kerr and Young (7) have investigated the presence of phenyl, styryl, and vinyl substituents vicinal to the diester moiety on the cyclopropane or, in the labeling convention of this work, substitution at the R3 position of Scheme 3. Only qualitative reaction times were recorded in their experiments, but it was found that these substitutions at the R3 position resulted in greatly reduced reaction times. We have computationally examined the effect of replacing R3 = H with R3 = Me, vinyl, and phenyl. Relative energetics for the reactions of **N1** with these substituted dimethyl 1,1-cyclopropanedicarboxylates — **C3** (R3 = Me), **C4** (R3 = vinyl), and **C5** (R3 = phenyl) — are detailed in Table 3. In all cases, both concerted and stepwise reaction pathways were found. Although an IRC calculation was only performed for the reaction of **N1** with **C3** (R3 = Me), we are reasonably certain that all of the pathways located are consistent with the asynchronous concerted and stepwise pathways described in the previous section through comparison of the geometries, relative energies, and bond orders of the stationary points.

Addition of the R3 substituent resulted in a significant decrease in the free energy barriers for each of the substituents studied. The phenyl substitution had the strongest effect, followed in sequence by the vinyl and methyl substitutions. More specifically, for the concerted pathway, the free energy barrier was lowered by 10.1, 7.4, and 6.1 kcal/mol for the R3 = Ph, vinyl, and Me substitutions, respectively, compared with the reaction involving **C2**. These computed values are consistent with the experimental results that the phenyl substitution resulted in a lower reaction time than the vinyl substitution (7). Substitution at the R3 position is expected to stabilize the carbocationic character of the C3 atom in the transition states as the C2—C3 bond of the cyclopropane breaks. The trends in the C2—C3 bond orders for both the concerted and first stepwise transition states are in agreement with this picture. For example, for **CN2**‡ with R3 = H, the C2—C3 bond order is 0.27. Upon substitution with R3 = Me, vinyl, and phenyl this is reduced to 0.17, 0.12, and 0.09, respectively. This trend in the C2—C3 bond orders matches that of the reaction barriers for the concerted reaction. A similar trend is observed for the bond orders involving the first stepwise transition states. It is worth noting that regardless of the substituent at the R3 position, the energetic barriers for the concerted and stepwise reaction pathways are remarkably close — each within 2 kcal/mol of one another. This provides further evidence of the similarity between the asynchronous concerted and the stepwise zwitterionic cycloaddition pathways, in the sense that they are influenced equally by the substituents. Similarily, it is notable that the free energy barrier of the second transition state (**SWn-C**‡) is in all cases 5 kcal/mol or less, suggesting that the intermediate **SWn-B** is very short lived and would not be isolatable.

Solvent effects

Experimentally, the reactions were often performed in dichloromethane or, when heating was required, 1,2-dichloroethane was used as a solvent. Toluene was also a suitable solvent and was used when the nitrone was formed in situ from hydroxylamines and aldehydes (8). More polar solvents were found to be less suitable. We have employed a continuum solvation model (48) to examine solvation effects on the quantum mechanical potential energy surface. The reaction of **N1** with **C2** was examined in a low polarity solvent (1,2-dichloroethane, $\varepsilon \sim 10$), and a more polar solvent (methanol, $\varepsilon \sim 33$). In both solvents, the concerted and stepwise reaction pathways were found with stationary points that are similar in structure to those in the gas phase. Important geometric parameters for the concerted and first stepwise transition-state structures are shown in Figs. 2*b* and 2*c*, respectively, with the values for dichloroethane shown in parenthesis and the values for methanol shown in square brackets. In these structures, the solvation model results in a modest elongation (<6%) of all the bonds that are being formed or broken. Relative free energies of solvation of the pathways in both solvents are summarized in Table 4, with species solvated in methanol suffixed with the label **(M)** and those solvated in dichloroethane suffixed with **(D)**. As mentioned in the computational details section, the relative free energies of solvation reported here do not include any vibrational, rotational, or translation free energy corrections and are best compared to the reported internal energies (ΔE) for the gas-phase reactions.

One might expect that a polar solvent would favour the zwitterionic pathway more than the concerted pathway because of the greater charge separation in the former. The calculated results are in agreement with this picture. In the gas phase, the barrier difference between zwitterionic and concerted pathways is only 0.02 kcal/mol in favour of the zwitterionic pathway. In 1,2-dichloroethane this preference increases to 1.7 kcal/mol and in methanol it increases to 2.9 kcal/mol. In all cases, the solvent model modestly increases the barriers compared with the gas phase. This can be attributed to the favourable free energy of solvation of the reactant nitrone, which can be characterized as zwitterionic.

© 2005 NRC Canada

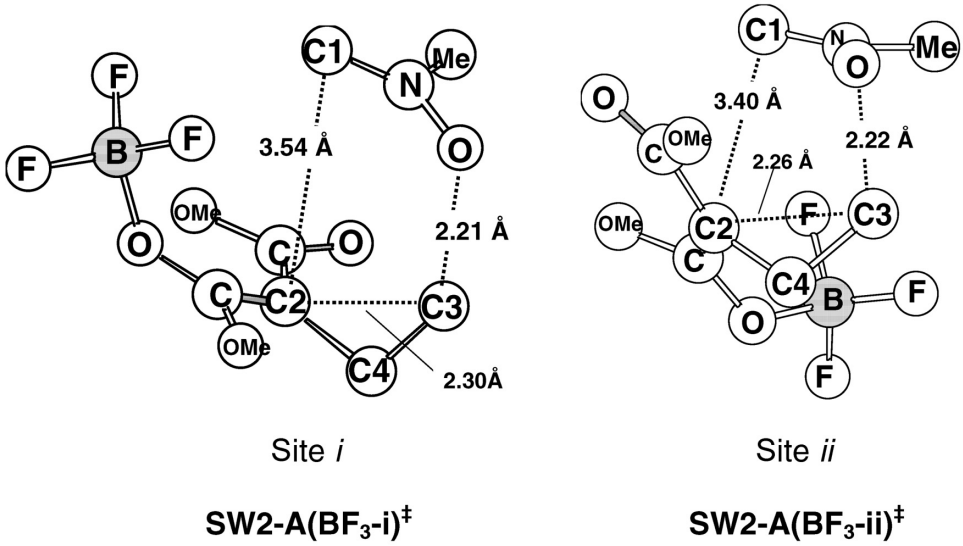
Table 4. Relative energies (kcal/mol) and bond orders of the rate-determining step for the reaction of **N1** with **C2** in dichloroethane (**D**) and methanol (**M**).

		Wiberg bond orders			
Species	ΔG^a	C1—C2	C2—C3	C3—O	C1—N
N1(D) + C2(D)	0.00	0.00	0.91	0.00	1.61
CN2(D)‡	48.65	0.02	0.24	0.29	1.62
SW2-A(D)‡	46.94	0.03	0.26	0.30	1.62
P2(D)	–15.32	0.97	0.01	0.90	0.98
N1(M) + C2(M)	0.00	0.00	0.90	0.00	1.62
CN2(M)‡	50.04	0.02	0.24	0.29	1.63
SW2-A(M)‡	47.19	0.03	0.27	0.29	1.62
P2(M)	–14.06	0.97	0.01	0.90	0.98

Note: Energies are relative to solvated **N1** + **C2**.

[a]Relative free energy of solvation including vibrational zero point energy corrections, but not including vibrational, rotational, or translational free energy corrections.

Fig. 8. Transition-state structure **SW2-A‡** with model Lewis catalyst (BF_3) coordinated on site *i* (left) and *ii* (right).



The thermodynamics of the overall reaction are more strongly affected by the solvent model than the reaction barriers. In the gas phase, the overall reaction energy is ΔE = –24.2 kcal/mol, which compares with ΔE = –15.3 kcal/mol in dichloroethane and ΔE = –14.1 kcal/mol in methanol. The decrease in reaction energy as the solvent polarity increases can be attributed to the fact that the reactant nitrone is zwitterionic and has a more polarizable π system; whereas the oxazine product is not zwitterionic and lacks a π system.

Lewis acid catalysis

Experimentally, the reaction of nitrones with cyclopropane diesters has only been observed in the presence of a Lewis acid catalyst. It was proposed that the Lewis acid induces polarization of the C2—C3 bond by coordinating to the carbonyl oxygen of the ester group on the cyclopropane ring (7). The most often used and effective Lewis acid is ytterbium triflate ($Yb(OTf)_3$). Here we explore the influence of a Lewis acid on the reaction using a much smaller and computationally tractable model Lewis acid, trifluoroborane (BF_3). The BF_3 molecule was assumed to coordinate to the diester moiety and coordination at numerous sites was tested, followed by a Monte Carlo conformational search of these coordination motifs.

The naming scheme used so far must now be expanded upon to incorporate the addition of a Lewis acid catalyst. Coordination of a single BF_3 molecule was found to occur in one of two distinct sites, which will be referred to as site "*i*" and site "*ii*". The two sites are shown in Fig. 8 for a stepwise transition state to be discussed ahead. An additional descriptor **(BF_3-i)** will be added to the structure name to denote coordination to site *i*, while **(BF_3-ii)** will be used to denote coordination at site *ii*. For example, the transition state **CN2‡** with the Lewis acid bound to site *i* becomes **CN2(BF_3-i)‡** and the stepwise intermediate **SW2-B** with the Lewis acid bound to site *ii* becomes **SW2-B(BF_3-ii)**. It should be noted that for **C2** the two coordination sites are actually identical. Thus, one molecule of BF_3 coordinated to **C2** will be referred to as **C2(BF_3)**. The effect of two molecules of BF_3 acting simultaneously was also studied, and is identified by descriptor **($2BF_3$)**.

Coordination of a single BF_3 molecule to **C2** results in a significant decrease in the reaction barriers, as one would expect. Kerr and Young (7) have suggested that the coordi-

© 2005 NRC Canada

Table 5. Relative energies (kcal/mol) and bond orders for the reaction of **N1** with one and two molecules of BF_3 coordinated to **C2**.

	Energies		Wiberg bond orders			
Species	ΔE	ΔG^a	C1—C2	C2—C3	C3—O	C1—N
N1 + C2 + BF_3	6.68	–5.35	0.00	0.91	0.00	1.55
N1 + C2(BF_3)	0.00	0.00	0.00	0.92	0.00	1.55
CN2($BF_{3\text{-}i}$)‡	35.18	47.67	0.02	0.23	0.28	1.61
SW2-A($BF_{3\text{-}i}$)‡	36.61	49.17	0.02	0.24	0.31	1.61
P2($BF_{3\text{-}i}$)	–23.23	–8.90	0.96	0.01	0.92	0.98
P2 + BF_3	–19.33	–15.38	0.97	0.01	0.91	0.98
CN2($BF_{3\text{-}ii}$)‡	32.97	46.36	0.02	0.25	0.29	1.61
SW2-A($BF_{3\text{-}ii}$)‡	31.80	45.19	0.02	0.26	0.29	1.61
P2($BF_{3\text{-}ii}$)	–22.70	–8.41	0.96	0.01	0.92	0.98
N1 + C2($2BF_3$)	0.00	0.00	0.00	0.91	0.00	1.55
CN2($2BF_3$)‡	28.16	39.78	0.01	0.20	0.26	1.61
SW2-A($2BF_3$)‡	27.49	39.67	0.01	0.25	0.27	1.62
P2($2BF_3$)	–20.26	–5.95	0.95	0.01	0.91	0.99

Note: Energies are relative to the free **N1 + C2** with coordinated BF_3 molecule(s).
[a]Gas-phase relative free energy at 298 K and 1 atm.

nation of the Lewis acid to the carbonyl groups of the ester substituents would further enhance the electron-withdrawing nature of the substituents as to further polarize the C2—C3. Calculated ESP charges on the C2 and C3 atoms in the free cyclopropane indeed show an observable charge polarization in the C2—C3 bond. The uncoordinated **C2** molecule is calculated to have ESP charges on the C2 and C3 atoms of –0.58 and –0.21 *e*, respectively; whereas upon coordination of the BF_3 molecule the charges become –0.72 and –0.13 *e*, indicating a stronger polarization of the C2—C3 bond.

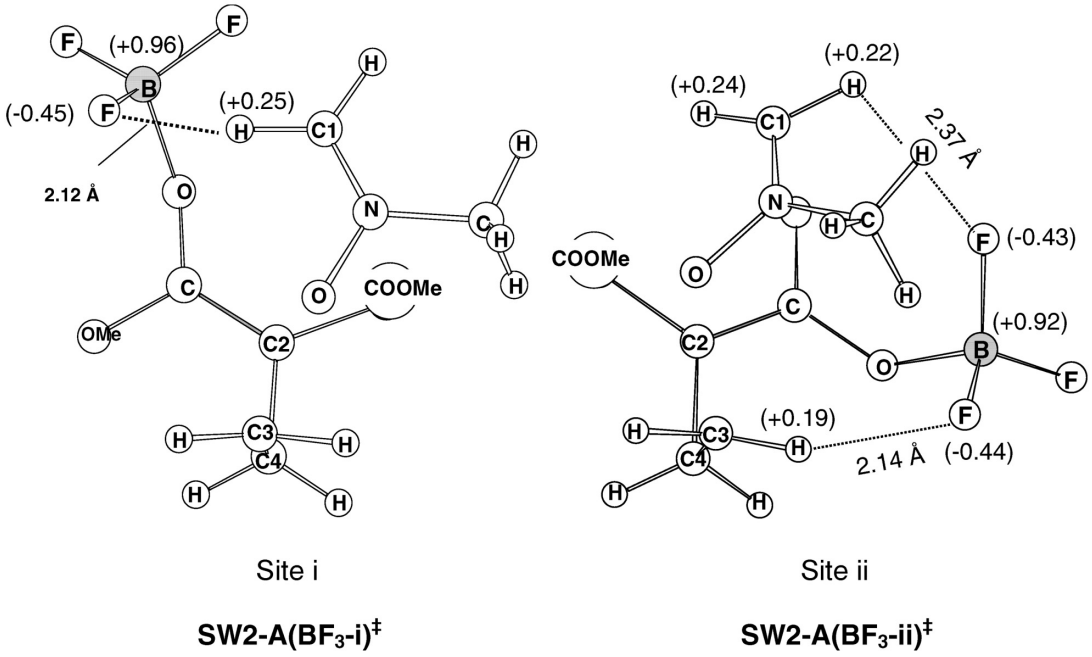
The calculated energetics of the reaction with the model Lewis acid (BF_3) are given in Table 5 relative to the free nitrone and cyclopropane–BF_3 complex. Both the concerted and the stepwise pathways were successfully located. The presence of the BF_3 promotes the transition state of the concerted pathway to be more asynchronous. This is supported by the geometrical parameters of the transition state (**CN2(BF_3-i)‡**), where the C1—C2 and O—C3 bond distances are 3.45 and 2.25 Å, respectively. The transition-state structures of the stepwise pathways (**SW2-A(BF_3-i)‡** and **SW2-A(BF_3-ii)‡**) are depicted in Fig. 8. The addition of a single BF_3 molecule results in a significant (11.8 (site *i*) and 14.0 (site *ii*) kcal/mol) decrease in the energetic barrier for the concerted pathway compared with the equivalent reaction without the coordinated Lewis acid. For the stepwise pathway, the decrease in the first barriers are 10.4 (site *i*) and 15.2 (site *ii*) kcal/mol. Thus, for the stepwise pathway, the site *ii* pathway is markedly more favourable than the site *i* pathway by 4.8 kcal/mol. A steric preference for the site *i* pathway, which one might expect, was not present. Rather, the preference appears to be due to the formation of what may be characterized as weak hydrogen bonds involving the fluorine atoms of the BF_3 moiety. For the site *ii* coordination two such hydrogen bonds are formed as compared with the site *i* coordination of the BF_3 molecule. These stabilizing interactions are highlighted in Fig. 9 for the transition states **SW2-A(BF_3-i)‡** and **SW2-A(BF_3-ii)‡**. The H—F bond distances are long for hydrogen bonds (>2.1 Å) and consequently, labeling these interactions as hydrogen bonds may be debatable. Nevertheless, the calculated ESP charges (also shown in Fig. 9) suggest that these "bonds" minimally involve a favourable electrostatic interaction between the atoms. Although the hydrogen bonding is interesting, it and the site *ii* coordination preference are not likely to be a general feature of other Lewis acids. On the other hand, the coordination observed here does suggest that the Lewis acid has a very strong influence on the reaction and such interactions may be important in steering the reaction, particularly the relative stereochemistry of the R2 and R3 groups in the product.

Coordination of a second BF_3 molecule to the ester substituents of the cyclopropane further decreases the calculated cycloaddition barriers. The relevant energetics are tabulated in Table 5. With two BF_3 molecules coordinated, the concerted free energy barrier is 39.8 kcal/mol, and the first stepwise barrier is 39.7 kcal/mol. This compares with an energetic barrier of 59.3 kcal/mol for both the concerted and stepwise pathways without any coordinated Lewis acid. This is a substantial ~20 kcal/mol decrease. Compared to the site *ii* coordination of a single BF_3 molecule, addition of a second BF_3 molecule modestly lowers the barriers by approximately 5 kcal/mol. Although reaction conditions that have been reported are not such that it is likely that two Lewis acid molecules would be coordinated to a single cyclopropane, the two BF_3 molecules used here do model the likely scenario that a single Lewis acid, such as $Yb(OTf)_3$ or MgI_2, binds to the ester groups in a bidentate manner.

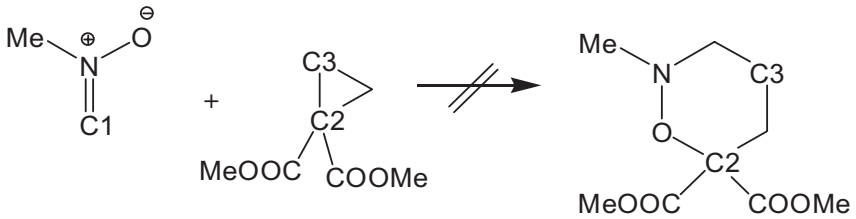
It should be noted that in some previous theoretical studies (49, 50) of nitrone cycloadditions with alkenes, it has been suggested that in the reaction the addition of a Lewis acid catalyst changes the mechanism from a classic cycloaddition to a stepwise reaction that is more akin to a Michael addition followed by cyclization. In those studies, the stepwise mechanisms are similar to the stepwise path-

© 2005 NRC Canada

Fig. 9. H–F interactions between fluorine atoms in BF_3 and H atoms of the reactantants for **SW2-A(BF_3-i)**‡ and **SW2-A(BF_3-ii)**‡. Values in paranthesis are calculated ESP charges in units of electron charge.



Scheme 4.



ways located in the present case. Thus, one could similarly classify the stepwise pathways found in this study as Michael additions followed by cyclization. On the other hand, both stepwise and concerted pathways were found, with or without the Lewis acid catalyst. Additionally, with or without the catalyst, the intermediate in the stepwise pathways is transient, with the barrier to form the products being very small (<5 kcal/mol). To be consistent with the current literature on the reaction, the term cycloaddition has been chosen for this work.

Regioselectivity of the cycloaddition

The cycloaddition reaction of nitrones to 1,1-cyclopropanediesters is found to be regiospecific with the oxygen atom of the reacting nitrone always lying distal to the diester substituent in the product as shown in Scheme 1 (7). An example of the cycloaddition reaction leading to the regioisomer that is not observed is shown in Scheme 4. The regiochemistry of the reaction was explained (7) by considering that significant charge separation occurs within the substituted cyclopropane ring due to the electron-withdrawing effect of the ester groups. The carbon atom bearing the ester substituents becomes negative while the carbon bearing the R3 substituent undergoes an increase in positive charge and, hence, becomes a preferred site for attack by the negatively charged oxygen of the nitrone.

To investigate the nature of the regiochemistry, the reaction of **N1** with **C2** to give the unobserved regioisomer (**(U)P2**) has been examined (Scheme 4). For lack of better words, we will refer to this as the "incorrect" pathway. Only a stepwise reaction pathway could be located for the formation of the unobserved regioproduct (**(U)P2**) that involves an initial transition state (**(U)SW2-A**‡), zwitterionic intermediate (**(U)SW2-B**), and second transition state (**(U)SW2-C**‡). The most striking feature of **(U)SW2-A**‡ (not shown) is that the oxygen atom of the nitrone is not involved in the initial attack on the cyclopropane. Rather, the carbon atom of the nitrone initially attacks cyclopropane as can be seen by examining the calculated bond orders of **(U)SW2-A**‡ in Table 6. This contrasts the concerted and stepwise pathways leading to the correct regioisomer, where the oxygen of the nitrone initially attacks the cyclopropane.

The calculated energetics suggest that the observed regioisomer is favoured both kinetically and thermodynamically. Relative energies of important stationary points along the reaction pathway are given in Table 6 for the incorrect

© 2005 NRC Canada

Table 6. Relative energies (kcal/mol) and bond orders giving rise to the unobserved regioisomer.

	Energies		Wiberg bond orders			
Species	ΔE	ΔG^a	O—C2	C2—C3	C3—C1	C1—N
N1 + C2	0.00	0.00	0.00	0.91	0.00	1.55
(U)SW2-A‡	53.07	65.97	0.13	0.39	0.41	1.33
(U)P2	–18.51	–4.96	0.92	0.01	1.00	0.98
N2 + C2	0.00	0.00	—[b]	0.91	—[b]	1.52
SW6-A‡	47.96	59.59	—	0.24	—	1.57
P6	–14.40	0.95	—	0.01	—	0.97
(U)SW6-A‡	57.99	70.48	0.39	0.36	0.13	1.30
(U)P6	–16.80	–2.14	1.00	0.01	0.92	0.96
N1 + C2(BF_3)	0.00	0.00	0.00	0.91	0.00	1.55
(U)SW2-A($BF_{3\text{-ii}}$)‡	50.90	62.63	0.07	0.28	0.41	1.31

Note: Energies are relative to the free **N1 + C2**.
[a]Gas-phase relative free energy at 298 K and 1 atm.
[b]For the unobserved pathway, the O—C2 and C3—C1 bonds form, but these are not applicable for the observed pathway in which the O—C3 and C1—C2 bonds form instead.

pathway. These values can be compared with Table 3, which shows the equivalent data for the "correct" regioisomer. Again the first transition state is rate-determining, and the calculated free energy barrier is found to be 63.2 kcal/mol. This compares with the 59.3 and 59.5 kcal/mol barriers for the correct concerted and stepwise pathways, respectively. In other words, the calculated barrier for the correct regioisomer is only favoured by about 3 kcal/mol. Thermodynamically, the observed product (**P2**) is found to be 5.4 kcal/mol more stable than the unobserved product ((**U**)**P2**) on the gas-phase B3LYP/6-31+G(d,p) free energy surface at 298 K and 1 atm.

The calculated kinetic preference for the observed regioisomer is perhaps surprisingly small with a barrier difference of only 3 kcal/mol. Thus, the affect of more realistic reactant models on the calculated thermodynamic and kinetic preference for the correct regioisomer has been examined. It is interesting that the carbon atom, not the oxygen atom, of the nitrone leads the initial attack of the δ+ C3 atom in the cyclopropane in the incorrect pathway. As it turns out, the ESP charges on the C1 and O atoms of the nitrone N1 are nearly identical, at –0.54 and –0.55 *e*, respectively. Therefore, from an electrostatic perspective, both centers have similar potential to act as nucleophiles. It is therefore notable that the model nitrone (**N1**) is unsubstituted at the R2 position (i.e., R2 = H); whereas all nitrones experimentally described were substituted at this position. Thus, the stepwise reaction pathway was studied using the nitrone **N2** with R2 = Me for both the observed and unobserved regioisomer pathways. It was found that the transition state for the incorrect regioisomer is 10.5 kcal/mol higher in free energy than the transition state for the correct pathway. Examination of the ESP charges of the substituted **N2** reveals that the charges on the C1 and O atoms are –0.11 and –0.53 *e*, respectively. Therefore, Me substitution at the R2 position makes the C1 atom significantly less negative and therefore less effective than the oxygen center of the nitrone to interact with a positively charged C3 center. Similarly, from a FMO perspective, methyl substitution has the effect of polarizing the HOMO of the nitrone away from the C1 atom (15). Surprisingly, the product (**P6**) of the observed pathway is 3.1 kcal/mol higher in energy than its regioisomer ((**U**)**P6**). This result is opposite to that of the reaction between **N1** and **C2**, where the correct pathway gives a more thermodynamically stable product. It also contradicts the experimental results, which show that the reaction is regiospecific. Analysis of the geometries of the two products shows there is a steric interaction between the R2 = Me substituent and the diester groups in **P6**; whereas in (**U**)**P6**, this steric interaction is relieved because the C1 atom lies vicinal to the diester groups. We note that this steric relief is only available when the R3 substituent is hydrogen and that the majority of experimental results have utilized a electron-donating group in the R3 position. Nevertheless, these results suggest that with some substitution patterns, the thermodynamic product may indeed be the oxazine ring with the oxygen atom lying adjacent to the diester groups.

The influence of a Lewis acid on the regiochemistry has been examined. The reaction of **N1** and **C2** with a single BF_3 molecule coordinated to it, as previously described, has been calculated. As previously described the coordination of a model Lewis acid results in a large ~14 kcal/mol decrease in the free energy barrier for the correct pathway. On the other hand, addition of a coordinated BF_3 molecule only decreases the barrier for the unobserved regioisomer by 3.3 kcal/mol. Thus, without the Lewis acid, the difference in the free energy barrier for the observed and unobserved reactions is only 3 kcal/mol; whereas the difference is more than 17 kcal/mol with the Lewis acid. As a result, the coordination of a Lewis acid to the cyclopropane results in a stronger kinetic preference for the observed regioisomer.

Conclusions

The mechanism of the 1,3-dipolar cycloaddition of nitrones with cyclopropane has been examined with quantum chemical DFT calculations. With realistic substituents, two very similar, but distinct reaction pathways were found. The first can be characterized as an asynchronous concerted mechanism involving a transition state that has an approximate half-chair conformation and where the oxygen atom of the nitrone leads the attack on the cyclopropane. The second is a stepwise mechanism involving a zwitterionic imminium intermediate, again with the oxygen atom of the nitrone

© 2005 NRC Canada

leading the attack of the cyclopropane. The intermediate is short lived as the barrier to form the product from this intermediate is very small in all cases. For both pathways, the origin of the barrier is the breaking of the C—C σ bond of the cyclopropane. Substituents that promote this process will provide an enhancement of the reaction rates. Substituent effects were examined and the influence on the calculated barriers matches the available experimental data on the observed reaction rates.

The influence of a Lewis acid catalyst on the reaction was also examined, using a small model for the catalyst (BF_3) that was coordinated to a carbonyl oxygen of the ester groups in the cyclopropane. The effect of the Lewis acid on the calculated barriers was found to be dramatic as one might expect, since experimentally the reaction is not observed without the catalyst. For example, the barriers were found to decrease by as much as 20 kcal/mol with coordination of two BF_3 molecules. This provides additional evidence that the Lewis acid's role during the reaction is indeed to further polarize the C—C bond of the cyclopropane via coordination to the ester substituents.

Solvation effects were briefly examined with a polarizable continuum model. Two solvents were used: 1,2-dichloroethane and methanol. In both solvents the reaction barriers were slightly increased; whereas the overall exothermicity of the reaction was significantly decreased. Both effects were more prominent in the more polar solvent.

The nature of the regiochemistry was also examined. Experimentally, it was found that the oxygen atom of the reacting nitrone exclusively ends up lying distal to the diester substituent in the product oxazine ring. The calculations show that there is both a kinetic and thermodynamic preference for the observed regioisomer. This preference was found to be significantly enhanced in the presence of a Lewis acid and with substitution at the R2 position of the reactant nitrone.

The 1,3-dipolar cycloaddition reactions of nitrones and cyclopropanes represents a new and important synthetic route for generating tetrahydro-1,2-oxazine rings that have been difficult to synthesize in the past. The computational study presented here provides a detailed account of the mechanism for this reaction and provides the basis for future work on optimizing the reaction.[3] Of particular interest is the relative stereochemistry of the R2 and R3 substituents in the product tetrahydrooxazine ring. In almost all cases the reaction is highly diastereoselective with the major product containing the R2 and R3 substituents in a cis relationship in the oxazine ring. However, recently it was found that by using MgI_2 as the Lewis acid catalyst an observable amount of the trans isomer could be isolated (9). The synthetic utility of the cycloaddition reaction would be greatly expanded if one could control the stereochemistry of the reaction. A computational study in this direction is currently underway.

Acknowledgements

This work was supported by the Natural Sciences and Engineering Research Council of Canada (NSERC), the University of Western Ontario, and Shared Hierarchical Academic Research Computing Network (SHARCNet) of Canada. Computing resources were made available by the Canadian Foundation for Innovation, the Ontario Innovation Trust, SHARCNet of Canada, and the Academic Development Fund at the University of Western Ontario.

References

1. T.C. Judd and R.M. Williams. Angew. Chem. Int. Ed. **41**, 4683 (2002).
2. T. Kato, E. Itoh, T. Yoshino, and S. Terashima. Tetrahedron, **53**, 10229 (1997).
3. M. Suzuki, J. Kambe, H. Tokuyama, and T. Fukuyama. Angew. Chem. Int. Ed. **41**, 4686 (2002).
4. H. Terano, S. Takase, J. Hosoda, and M. Kohsaka. J. Antibiot. **42**, 145 (1989).
5. I.S. Young, J.L. Williams, and M.A. Kerr. Org. Lett. **7**, 953 (2005).
6. P.G. Tsoungas. Heterocycles, **57**, 1149 (2002).
7. I.S. Young and M.A. Kerr. Angew. Chem. Int. Ed. **115**, 3131 (2003).
8. I.S. Young and M.A. Kerr. Org. Lett. **6**, 139 (2004).
9. M.D. Ganton and M.A. Kerr. J. Org. Chem. **69**, 8554 (2004).
10. M.P. Sibi, Z. Ma, and C.P. Jasperse. J. Am. Chem. Soc. **127**, 5764 (2005).
11. K.V. Gothelf. *In* Cycloaddition reactions in organic synthesis. *Edited by* S. Kobayashi and K.A. Jorgensen. Wiley-VCH, Weinheim, Germany. 2002. p. 211.
12. S. Kanemasa. *In* Cycloaddition reactions in organic synthesis. *Edited by* S. Kobayashi and K.A. Jorgensen. Wiley-VCH, Weihneim, Germany. 2002. p. 249
13. R. Huisgen. *In* Advances in cycloaddition. *Edited by* D.P. Curran. JAI Press Inc., Greenwich, Conn. 1988. p. 1.
14. A. Padwa (*Editor*). 1,3-Dipolar cycloaddition chemistry. Wiley, New York. 1984.
15. A. Rauk. Orbital interaction theory of organic chemistry. 2nd ed. Wiley-Interscience, New York. 2001.
16. R.A. Firestone. J. Org. Chem. **37**, 2181 (1972).
17. C. Di Valentin, M. Freccero, R. Gandolfi, and A. Rastelli. J. Org. Chem. **65**, 6112 (2000).
18. K.N. Houk, J. Gonzalez, and Y. Li. Acc. Chem. Res. **28**, 81 (1995).
19. K.V. Gothelf and K.A. Jorgensen. Chem. Rev. **98**, 863 (1998).
20. F.P. Cossio, L. Morao, H. Jiao, and P.v.R. Scheleyer. J. Am. Chem. Soc. **121**, 6737 (1999).
21. K.N. Houk and K. Yamaguchi. *In* 1,3-Dipolar cycloaddition chemistry. *Edited by* A. Padwa. Wiley, New York. 1984. p. 407.
22. M. Sana, G. Leroy, G. Dive, and M.T. Nguyen. THEOCHEM, **89**, 142 (1982).
23. M.A. Silva and J.M. Goodman. Tetrahedron, **58**, 3667 (2002).
24. P. Merino, J. Revuelta, T. Tejero, U. Chiacchio, A. Rescifina, and G. Romeo. Tetrahedron, **59**, 3581 (2003).
25. R. Herrera, A. Nagarajan, M. Morales, F. Mendez, H.A. Jimenez-Vazquez, L. Gerardo Zepeda, and J. Tamariz. J. Org. Chem. **66**, 1252 (2001).
26. P. Merino, S. Anoro, F.L. Merchan, and T. Tejero. Heterocycles, **53**, 861 (2000).

[3] Supplementary data for this article are available on the Web site or may be purchased from the Depository of Unpublished Data, Document Delivery, CISTI, National Research Council Canada, Ottawa, ON K1A 0R6, Canada. DUD 4054. For more information on obtaining material refer to http://cisti-icist.nrc-cnrc.gc.ca/irm/unpub_e.shtml.

© 2005 NRC Canada

27. L.R. Domingo. Eur. J. Org. Chem. 2265 (2000).
28. C. DiValentin, M. Freccero, R. Gandolfi, and A. Rastelli. J. Org. Chem. **65**, 6112 (2000).
29. M. Carda, R. Portoles, J. Murga, S. Uriel, J.A. Marco, L.R. Domingo, R.J. Zaragoze, and H. Roper. J. Org. Chem. **65**, 7000 (2000).
30. J. Liu, S. Niwayama, Y. You, and K.N. Houk. J. Org. Chem. **63**, 1064 (1998).
31. T.T. Tidwell. *In* The chemistry of the cyclopropyl group. *Edited by* Z. Rappoport. Wiley, New York. 1987. p. 565.
32. W. Carruthers. Cycloaddition reactions in organic synthesis. Pergamon Press, Oxford. 1990.
33. K.N. Houk, Y.M. Chang, R.w. Strozier, and P. Caramella. Heterocycles, **7**, 793 (1977).
34. I. Fleming. Frontier orbitals and organic chemical reactions. Wiley, New York. 1976.
35. R. Sustmann, W. Sicking, and M. Felderhoff. Tetrahedron, **46**, 783 (1990).
36. P. Hohenburg and W. Kohn. Phys. Rev. B, **136**, 864 (1964).
37. W. Kohn and L.J. Sham. Phys. Rev. A, **140**, 1133 (1965).
38. A.D. Becke. J. Chem. Phys. **98**, 5648 (1993).
39. C. Lee, W. Yang, and R.G. Parr. Phys. Rev. B, **37**, 785 (1988).
40. Schrödinger, LLC. Jaguar 5.0 [computer program]. Schrödinger LLC, Portland, Oregon. 2002.
41. N.J. Mosey, K.M. Baines, and T.K. Woo. J. Am. Chem. Soc. **124**, 13306 (2002).
42. J.J.P. Stewart. J. Comput. Chem. **10**, 209 (1989).
43. Wavefunction, Inc. Spartan '02 [computer program]. Wavefunction Inc., Irvine, California. 2002.
44. M.J. Frisch, G.W. Trucks, H.B. Schegel, G.E. Scuseria, M.A. Robb, J.R. Cheeseman, V.G. Zakrzewski, J.A. Montgomery, Jr., R.E. Stratmann, J.C. Burant, S. Dapprich, J.M. Millam, A.D. Daniels, K.N. Kudin, M.C. Strain, O. Farkas, V. Tomasi, V. Barone, M. Cossi, R. Cammi, B. Mennucci, C. Pomelli, C. Adamo, S. Clifford, J. Ochterski, G.A. Petersson, P.Y. Ayala, Q. Cui, K. Morokuma, D.K. Malick, A.D. Rabuck, K. Raghavachari, J.B. Foresman, J. Cioslowski, J.V. Ortiz, A.G. Baboul, B.B. Stefanov, G. Liu, A. Liashenko, P. Piskorz, I. Komaromi, R. Gomperts, R.L. Martin, D.J. Fox, T. Keith, M.A. Al-Laham, C.Y. Peng, A. Nanayakkara, C. Gonzalez, M. Challacombe, P.M.W. Gill, B.G. Johnson, W. Chen, M.W. Wong, J.L. Andres, M. Head-Gordon, E.S. Replogle, and J.A. Pople. GAUSSIAN 98. Revision A.9 [computer program]. Gaussian, Inc., Pittsburgh, Penn. 1998.
45. E.D. Glendening, A.E. Reed, J.E. Carpenter, and F. Weinhold. NBO Version 5.0 [computer program]. University of Wisconsin, Madison, Wisconsin. 2001.
46. E.J. Baerends and O.V. Gritsenko. J. Phys. Chem. A, **101**, 5383 (1997).
47. R. Stowasser and R. Hoffmann. J. Am. Chem. Soc. **121**, 3414 (1999).
48. B. Marten, K. Kim, C. Cortis, R.A. Friesner, R.B. Murphy, M.N. Ringnalda, D. Sitkoff, and B. Honig. J. Phys. Chem. **100**, 11775 (1996).
49. L.R. Domingo. Eur. J. Org. Chem. 2265 (2000).
50. J. Tanaka and S. Kanemasa. Tetrahedron, **57**, 899 (2001).

© 2005 NRC Canada

Synthesis and structural characterization of zinc complexes of the imido–amido phosphate anions $OP[(NHR)_{3-x}(NR)]^{x-}$ (R = Me, *t*-Bu; *x* = 1–3) and $EP[(NH\text{-}t\text{-}Bu)_2(N\text{-}t\text{-}Bu)]^-$ (E = S, $NSiMe_3$)

Andrea F. Armstrong, Tristram Chivers, Mark Krahn, and Masood Parvez

Abstract: The reaction of $OP(NH\text{-}t\text{-}Bu)_3$ with 1 equiv. of $ZnMe_2$ generates the dimeric eight-membered ring $\{MeZn[(\mu\text{-}NH\text{-}t\text{-}Bu)(\mu\text{-}N\text{-}t\text{-}Bu)P(NH\text{-}t\text{-}Bu)(\mu\text{-}O)]\}_2$ (**5**) and the cubane $\{[MeZn]_3[OP(N\text{-}t\text{-}Bu)_3][OP(NH\text{-}t\text{-}Bu)_3]\}$ (**6**), which contains the first known trisimidophosphate trianion. A related complex $\{Zn[ZnMe]_2[OP(N\text{-}t\text{-}Bu)(NH\text{-}t\text{-}Bu)_2][OP(N\text{-}t\text{-}Bu)_3]\}$(**7**) is obtained by the reaction of $OP(NH\text{-}t\text{-}Bu)_3$ with $ZnMe_2$ in a 2:3 molar ratio. The treatment of $OP(NHMe)_3$ with 1 equiv. of $ZnMe_2$ produces the oxide-templated cluster $\{Zn_4(\mu_4\text{-}O)[OP(NMe)(NHMe)_2]_4[OP(NMe)_2(NHMe)]\}_2$ (**8**). Each half of this centrosymmetric dimer contains a tetrahedral arrangement of four 4-coordinate Zn^{2+} ions surrounding the central $\mu_4\text{-}O^{2-}$ anion. The reaction of $SP(NH\text{-}t\text{-}Bu)_3$ with $ZnMe_2$ in a 1:1 molar ratio generates the dimer $\{MeZn(\mu\text{-}S)(\mu\text{-}N\text{-}t\text{-}Bu)P(NH\text{-}t\text{-}Bu)_2\}_2$ (**10**), which has a ladder-type structure. When a 2:1 molar ratio of the same reagents is employed, the bis(*N*,*S*)-chelated complex $\{Zn[(\mu\text{-}S)(\mu\text{-}N\text{-}t\text{-}Bu)P(NH\text{-}t\text{-}Bu)_2]_2\}$ (**11**) is obtained. The monomeric *N*,*N′*-chelated complex $\{MeZn[(\mu\text{-}N\text{-}t\text{-}Bu)(\mu\text{-}NSiMe_3)P(NH\text{-}t\text{-}Bu)_2]\}$ (**12**) results from the reaction of $Me_3SiNP(NH\text{-}t\text{-}Bu)_3$ with 1 equiv. of dimethylzinc. All new compounds have been characterized by multinuclear (^1H, ^{13}C, and ^{31}P) NMR spectroscopy and, in the case of **5**, **6**, **7**, **8**, and **10**, by X-ray structural determinations.

Key words: zinc, phosphate, imido ligands, sulfur.

Résumé : La réaction du $OP(NH\text{-}t\text{-}Bu)_3$ avec un équivalent de $ZnMe_2$ conduit à la formation du cycle dimère à huit chaînons $\{MeZn[(\mu\text{-}NH\text{-}t\text{-}Bu)(\mu\text{-}N\text{-}t\text{-}Bu)P(NH\text{-}t\text{-}Bu)(\mu\text{-}O)]\}_2$ (**5**) et du cubane $\{[MeZn]_3[OP(N\text{-}t\text{-}Bu)_3][OP(NH\text{-}t\text{-}Bu)_3]\}$ (**6**) qui contient le premier trisimidophosphate connu. Le complexe apparenté $\{Zn[ZnMe]_2[OP(N\text{-}t\text{-}Bu)(NH\text{-}t\text{-}Bu)_2][OP(N\text{-}t\text{-}Bu)_3]\}$ (**7**) est obtenu lors de la réaction du $OP(NH\text{-}t\text{-}Bu)_3$ avec du $ZnMe_2$ dans un rapport de 2 : 3. Le traitement du $OP(NHMe)_3$ avec un équivalent de $ZnMe_2$ conduit à la formation de l'agrégat avec gabarit d'oxyde $\{Zn_4(\mu_4\text{-}O)[OP(NMe)(NMe)_2]_4[OP(NMe)_2(NHMe)]\}_2$ (**8**). Chacune des moitiés de ce dimère centrosymétrique comprend un arrangement tétraédrique de quatre ions Zn^{2+} tétracoordinés qui entourent l'anion $\mu_4\text{-}O^{2-}$ central. La réaction du $SP(NH\text{-}t\text{-}Bu)_3$ avec du $ZnMe_2$ dans un rapport molaire de 1 : 1 génère la formation du dimère $\{MeZn(\mu\text{-}S)(\mu\text{-}N\text{-}t\text{-}Bu)P(NH\text{-}t\text{-}Bu)_2\}_2$ (**10**) dont la structure est en échelle. Quand on utilize un rapport 2 : 1 des même réactifs, on obtient le complexe bis-*N,S*-chélaté $\{Zn[(\mu\text{-}S)(\mu\text{-}N\text{-}t\text{-}Bu)P(\mu\text{-}NH\text{-}t\text{-}Bu)_2]_2\}$ (**11**). Le complexe *N,N′*-chélaté monomère $\{MeZn[(\mu\text{-}N\text{-}t\text{-}Bu)(\mu\text{-}NSiMe_3)P(NH\text{-}t\text{-}Bu)_2]\}$ (**12**) résulte de la réaction du $Me_3SiNP(NH\text{-}t\text{-}Bu)_3$ avec un équivalent de diméthylzinc. Tous les nouveaux composés ont été caractérisés par spectroscopie RMN (^1H, ^{13}C et ^{31}P) et dans les cas des composés **5**, **6**, **7**, **8** et **10**, par diffraction des rayons X.

Mots clés : zinc, phosphate, ligands imido, soufre.

Introduction

The preparation and structural characterization of imido analogues of common phosphorus oxoanions is an active area of main group chemistry (1, 2). The imido group $[NH]^{2-}$ is formally isoelectronic with the oxo $[O]^{2-}$ substituent;[2] partial or complete replacement of the oxygen atoms in an oxoanion such as orthophosphate $[PO_4]^{3-}$ by NH ligands generates a series of polyimido anions that are isoelectronic with phosphate. The introduction of an alkyl or aryl substituent on nitrogen is expected to result in polyimido anions whose metal complexes will exhibit significantly different structures and chemical properties compared with those of $[PE_4]^{3-}$ (E = O, NH). In addition, one or more of the oxo substituents in a polyimido phosphate can be replaced by a heavier chalcogen, such as sulfur, to create

Received 26 April 2005. Published on the NRC Research Press Web site at http://canjchem.nrc.ca on 13 December 2005.

A.F. Armstrong, T. Chivers,[1] M. Krahn, and M. Parvez. Department of Chemistry, University of Calgary, Calgary, AB T2N 1N4, Canada.

[1]Corresponding author (e-mail: chivers@ucalgary.ca).

[2]The original definition of "isoelectronic" (isosteric) compounds restricts the term to species having the *same number of atoms* and the same number of electrons (I. Langmuir. J. Am. Chem. Soc. **41**, 1543 (1919)). Thus, according to this definition, N^{3-} is isoelectronic with O^{2-}. However, nitrides are compositionally different to oxides as a result of the different charges on the anions.

 doi: 10.1139/V05-183 © 2005 NRC Canada

ligands with different coordinating properties as a result of the presence of both hard (N) and soft (S) binding sites.

In recent years, we have thoroughly investigated the reactivities of the triamidophosphates $OP(NH\text{-}t\text{-}Bu)_3$ (**1a**) (3, 4), $SP(NHR)_3$ (**2**, R = alkyl, aryl) (4, 5), and $Me_3SiNP(NH\text{-}t\text{-}Bu)_3$ (**3**) (3, 6) toward alkyllithium reagents. The mono- and di-lithium salts $\{Li[(\mu\text{-}N\text{-}t\text{-}Bu)(\mu\text{-}O)P(NH\text{-}t\text{-}Bu)_2]\}_3\cdot THF$ (**4**) and the double cubane $\{Li_2[OP(NH\text{-}t\text{-}Bu)(N\text{-}t\text{-}Bu)_2]\}_2\cdot 4THF$, isoelectronic with $[H_2PO_4]^-$ and $[HPO_4]^{2-}$, respectively, are readily obtained by treatment of **1a** with *n*-BuLi. However, complete deprotonation of **1a** to give the trianion $[OP(N\text{-}t\text{-}Bu)_3]^{3-}$ could not be achieved (3, 4). The mono- and di-anions $[OP(N\text{-}t\text{-}Bu)_x(NH\text{-}t\text{-}Bu)_{3-x}]^{x-}$ (x = 1 or 2) are also produced from the reactions of **1a** with $AlMe_3$ or $LiAlH_4$ (7).

Similar reactivity was observed for the thiophosphates $SP(NHR)_3$ (**2a** (R = *t*-Bu), **2b** (R = *i*-Pr)) (4, 5). The mono- and di-lithium salts of **2b** ($\{Li[(\mu\text{-}N\text{-}i\text{-}Pr)(\mu\text{-}S)P(NH\text{-}i\text{-}Pr)_2]\}_2\cdot 2THF$) and $\{[Li(TMEDA)]_2[SP(NH\text{-}i\text{-}Pr)(N\text{-}i\text{-}Pr)_2]\}_2$ have been isolated and characterized, as has a mixed monolithium–dilithium derivative of **2a**; attempts to generate $[SP(N\text{-}i\text{-}Pr)_3]^{3-}$ resulted in sulfur extrusion. Trilithiation can be achieved, however, by replacement of the alkyl substituents by more electron-withdrawing *para*-tolyl groups; in this case, the trisimidothiophosphate $\{Li_3[SP(N\text{-}p\text{-}tol)_3]\}$ is readily obtained (4).

In sharp contrast to the somewhat limited reactivities of the chalcogen systems **1a** and **2** toward *n*-BuLi, both symmetrical and unsymmetrical tetraimidophosphates, $\{Li_3[P(NPh)_4]\}$ (8) and $\{Li_3[P(NR)_3(NSiMe_3)]\}$ (3) (R = *t*-Bu, Cy), respectively, are readily prepared by the reaction of the corresponding iminophosphorane $(RNH)_3PNR$ with 3 equiv. of *n*-butyllithium.

Zinc phosphates are the second-largest family of the well-known metal phosphate open-framework materials and have applications as both catalysts and molecular sieves. These materials are generally prepared under hydro- or solvothermal conditions; the three-dimensional structures of the products are highly dependent upon reaction conditions such as temperature and time, and the presence and shape of a templating agent (9–11). Consequently, it is of interest to explore the possibility of preparing a series of zinc imidophosphates. While the steric bulk of the imido groups is expected to hinder aggregation resulting in the formation of much smaller oligomers than the extended networks that are characteristic of metal-phosphate complexes (12), it remains to be seen whether these systems will exhibit similar dependencies on reaction conditions as do the zinc phosphates. In addition, it is germane to examine the modes of coordination of these multidentate ligands for comparison with their behaviour in the lithium derivatives (3–6). In an attempt to shed light upon these and other points, we have investigated the reactions of the triamidophosphates $OP(NHR)_3$ (R = Me, *t*-Bu), $SP(NH\text{-}t\text{-}Bu)_3$, and $Me_3SiNP(NH\text{-}t\text{-}Bu)_3$ towards dimethylzinc.

Experimental

Reagents and general procedures

All experiments were carried out under an argon atmosphere using standard Schlenk techniques. Toluene, *n*-hexane, and diethyl ether were dried over Na/benzophenone, distilled, and stored over molecular sieves prior to use. Dimethylzinc (1.0 and 2.0 mol/L solutions in toluene) was used as received from Aldrich. $Me_3SiNP(NH\text{-}t\text{-}Bu)_3$ (3), $OP(NHR)_3$ (R = Me, *t*-Bu) (4), and $SP(NH\text{-}t\text{-}Bu)_3$ (5) were prepared according to the literature procedures.

Instrumentation

^1H, ^7Li, ^{13}C, and ^{31}P NMR spectra were collected on a Bruker DRX-400 spectrometer with chemical shifts reported relative to Me_4Si in $CDCl_3$ (^1H and ^{13}C), LiCl in D_2O (^7Li), and 85% H_3PO_4 in D_2O (^{31}P). All spectra were collected at 22 °C, with the exception of compound **10** (spectra recorded at –30 °C). Infrared spectra were recorded as Nujol mulls on KBr plates using a Nicolet Nexus 470 FT IR spectrometer in the range 4000–400 cm^{-1}. Mass spectra were recorded on a Bruker Esquire 3000 ESI ion trap mass spectrometer. Elemental analyses were provided by the Analytical Services Laboratory, Department of Chemistry, University of Calgary.

Preparation of $\{MeZn[(\mu\text{-}NH\text{-}t\text{-}Bu)(\mu\text{-}N\text{-}t\text{-}Bu)P(NH\text{-}t\text{-}Bu)(\mu\text{-}O)]\}_2$ (5) and $\{[MeZn]_3[OP(N\text{-}t\text{-}Bu)_3][OP(NH\text{-}t\text{-}Bu)_3]\}$ (6)

A solution of $ZnMe_2$ (0.70 mL, 2.0 mol/L, 1.40 mmol) in toluene was added to a slurry of $OP(NH\text{-}t\text{-}Bu)_3$ (0.366 g, 1.39 mmol) in toluene (20 mL) at 22 °C, resulting in a clear solution after 10 min. The reaction mixture was heated at 60 °C for 4 h; the solvent was then removed under vacuum to give a white powder (0.417 g). $^{31}P\{^1H\}$ NMR (C_6D_6) δ: 46.8, 28.6, 24.3 (minor), 13.2 (minor), 11.3, 10.2, 9.3 (br), 8.1 (s).

Recrystallization of the product (72 mg) from toluene yielded colourless crystals of **5** (35 mg, 0.051 mmol, 21% based on $ZnMe_2$). $^{13}C\{^1H\}$ NMR (solid state, 12 kHz) δ: 53.03 (s, N*C*Me_3), 52.28 (s, μ-HN*C*Me_3), 49.79 (s, HN*C*Me_3), 34.52 (s, N*C*Me_3), 32.05 (s, μ-HN*C*Me_3), 31.44 (s, HN*C*Me_3), –11.63 (s, MeZn). $^{31}P\{^1H\}$ NMR (C_6D_6) δ: 9.3 (br), 8.1 (s). $^{31}P\{^1H\}$ NMR (solid state, 5 kHz) δ: 7.4 (s). Anal. calcd. for $C_{38}H_{64}N_6O_2P_2Zn_2$: C 45.73, H 9.45, N 12.31; found: C 45.53, H 9.68, N 12.36.

Recrystallization of the product (51 mg) from Et_2O yielded colourless crystals of **6** (14 mg, 0.018 mmol, 32% based on $ZnMe_2$). ^1H NMR (C_6D_6) δ: 2.30 (br, 3H, N*H*), 1.38 (s, 9H, NC*Me*$_3$), 1.33 (s, 27H, NHC*Me*$_3$), 1.09 (s, 18H, NC*Me*$_3$), –0.12 (s, 9H, $MeZn^+$). $^{31}P\{^1H\}$ NMR (C_6D_6) δ: 46.8, 10.2. Anal. calcd. for $C_{27}H_{66}N_6O_2P_2Zn_2$: C 42.39, H 8.70, N 10.99; found: C 42.02, H 8.93, N 11.21.

Preparation of $\{Zn[MeZn]_2[OP(N\text{-}t\text{-}Bu)(NH\text{-}t\text{-}Bu)_2][OP(N\text{-}t\text{-}Bu)_3]\}$ (7)

A solution of $ZnMe_2$ (5.34 mL, 1.0 mol/L, 5.34 mmol) in toluene was added dropwise to a solution of $OP(NH\text{-}t\text{-}Bu)_3$ (0.937 g, 3.56 mmol) in toluene (25 mL) at 22 °C. The toluene solution was refluxed at 113 °C for 18 h yielding a clear, colourless solution. The volume was reduced to 10 mL and after 1 day at 22 °C, colourless crystals of **7** had formed (0.601 g, 0.802 mmol, 45%). IR (cm^{-1}): 3279 (ν(N-H)). ^1H NMR (C_6D_6) δ: 2.05 (br s, N*H*), 1.75–1.18 (numerous resonances, NC*Me*$_3$), 0.29 (s, Zn*CH*$_3$). $^{31}P\{^1H\}$ NMR (C_6D_6) δ: 22.0 (s), 14.6 (s), 13.1 (s) (1:1:1), and additional minor reso-

© 2005 NRC Canada

nances; solid state (10 kHz) δ: 22.0 (s), 13.5 (s). MS (ESI^+): 549 ($M^+ - 199$).

Preparation of $\{Zn_4(\mu_4\text{-}O)[OP(NMe)(NHMe)_2]_4[OP(NMe)_2(NHMe)]\}_2$ (8)

A solution of $ZnMe_2$ (1.18 mL, 1.0 mol/L, 1.18 mmol) in toluene was added dropwise to a solution of $OP(NHMe)_3$ (0.162 g, 1.18 mmol) in toluene (25 mL) at 22 °C. The toluene solution was heated at reflux for 24 h. The volume of the solution was reduced to one-half and the concentrate was placed in the freezer. After 7 days at –15 °C, colourless crystals of **8**·C_7H_8 were recovered (0.144 g, 0.0718 mmol, 49% based on $ZnMe_2$). IR (cm^{-1}): 3323 (ν(N-H)). ^1H NMR (C_6D_6) δ: 2.25 (s, NH*Me*), 2.22 (s, NH*Me*), 2.20 (s, NH*Me*), 2.16 (s, NH*Me*) (1:1:1:1), 1.36 (br s, N*Me*). $^{31}P\{^1H\}$ NMR (C_6D_6) δ: 37.9 (s), 28.2 (s) (relative intensities ~1:3), and additional minor resonances; solid state (13 kHz) δ: 38.7 (s), 27.6 (s). Anal. calcd. for $C_{37}H_{116}N_{30}O_{12}P_{10}Zn_8$: C 22.15, H 5.83, N 20.94; found: C 22.02, H 6.05, N 19.96.

Preparation of $[MeZn(\mu\text{-}S)(\mu\text{-}N\text{-}t\text{-}Bu)P(NH\text{-}t\text{-}Bu)_2]_2$ (10)

A solution of $ZnMe_2$ (0.83 mL, 2.0 mol/L, 1.66 mmol) in toluene was added slowly to a slurry of $SP(NH\text{-}t\text{-}Bu)_3$ (0.461 g, 1.65 mmol) in toluene (20 mL) at 22 °C. The clear solution was stirred for 18 h; the solvent was then removed under vacuum to give **10** as a white powder (0.468 g, 0.652 mmol, 79%). ^1H NMR (C_6D_6) δ: 2.15 (br, N*H*), 1.48 (s, 9H, N), 1.31 (d, $^4J(^1H\text{-}^{31}P)$ = 6.8 Hz, 18H, NHC*Me*$_3$), –0.1 (s, 3H, *Me*Zn^+). $^{13}C\{^1H\}$ NMR (C_6D_6) δ: 53.90 (d, *C*Me_3, $^2J(^{13}C\text{-}^{31}P)$ = 44.4 Hz), 51.63 (d, *C*Me_3, $^2J(^{13}C\text{-}^{31}P)$ = 19.3 Hz), 33.40 (d, C*Me*$_3$, $^3J(^{13}C\text{-}^{31}P)$ = 27.7 Hz), 30.41 (d, C*Me*$_3$, $^3J(^{13}C\text{-}^{31}P)$ = 136.5 Hz). $^{31}P\{^1H\}$ NMR (C_6D_6) δ: 39.3 (s). Anal. calcd. for $C_{26}H_{62}N_6P_2S_2Zn_2$: C 43.68, H 9.03, N 11.76; found: C 44.33, H 9.28, N 11.87.

Preparation of $\{Zn[(\mu\text{-}S)(\mu\text{-}N\text{-}t\text{-}Bu)P(NH\text{-}t\text{-}Bu)_2]_2\}$ (11)

A solution of $ZnMe_2$ (0.58 mL, 2.0 mol/L, 1.16 mmol) in toluene was added slowly to a slurry of $SP(NH\text{-}t\text{-}Bu)_3$ (0.648 g, 2.32 mmol) in toluene (20 mL) at 22°C. The resulting clear solution was stirred for 18 h; the solvent was then removed under vacuum to give **11** as an analytically pure white powder (0.710 g, 1.14 mmol, 98%). ^1H NMR (C_6D_6) δ: 2.12 (br, 2H, N*H*), 1.44 (s, 9H), 1.32 (s, 18H, C*Me*$_3$). $^{13}C\{^1H\}$ NMR (C_6D_6) δ: 54.06 (d, *C*Me_3, $^2J(^{13}C\text{-}^{31}P)$ = 43.5 Hz), 51.82 (d, *C*Me_3, $^2J(^{13}C\text{-}^{31}P)$ = 9.9 Hz), 34.18 (d, C*Me*$_3$, $^3J(^{13}C\text{-}^{31}P)$ = 38.7 Hz), 31.67 (d, C*Me*$_3$, $^3J(^{13}C\text{-}^{31}P)$ = 17.1 Hz). $^{31}P\{^1H\}$ NMR (C_6D_6) δ: 42.0 (s). Anal. calcd. for $C_{24}H_{58}N_6P_2S_2Zn$: C 46.33, H 9.40, N 13.51; found: C 45.30, H 10.64, N 13.48.

Preparation of $\{MeZn[(\mu\text{-}N\text{-}t\text{-}Bu)(\mu\text{-}NSiMe_3)P(NH\text{-}t\text{-}Bu)_2]\}$ (12)

A solution of $ZnMe_2$ (0.53 mL, 2.0 mol/L, 1.06 mmol) in toluene was added slowly to a pale yellow solution of $Me_3SiNP(NH\text{-}t\text{-}Bu)_3$ (0.357 g, 1.07 mmol) in hexane (20 mL) at 22 °C, resulting in an opaque yellow mixture. After 3 h, the solvent was removed under vacuum to give **12** as a yellow paste (0.400 g, 0.966 mmol, 91%). Washing with organic solvents did not improve the physical appearance of this highly soluble paste, which was shown to be pure **12** on the basis of spectroscopic and analytical data. ^1H NMR (C_6D_6) δ: 1.75 (br, N*H*), 1.22 (s, 27H, C*Me*$_3$), 0.27 (s, 9H, Si*Me*$_3$), –0.24 (s, 3H, *Me*Zn). $^{13}C\{^1H\}$ NMR (C_6D_6) δ: 51.14 (d, *C*Me_3, $^2J(^{13}C\text{-}^{31}P)$ = 8.9 Hz), 50.41 (d, *C*Me_3, $^2J(^{13}C\text{-}^{31}P)$ = 11.9 Hz), 34.06 (d, C*Me*$_3$, $^3J(^{13}C\text{-}^{31}P)$ = 34.2 Hz), 32.42 (d, C*Me*$_3$, $^3J(^{13}C\text{-}^{31}P)$ = 15.5 Hz), 4.61 (d, Si*Me*$_3$, $^3J(^{13}C\text{-}^{31}P)$ = 12.5 Hz), –15.0 (s, Zn*Me*). $^{31}P\{^1H\}$ NMR (C_6D_6) δ: 9.1 (s). Anal. calcd. for $C_{16}H_{41}N_4PSiZn$: C 46.42, H 9.98, N 13.53; found: C 46.50, H 10.05, N 13.86.

X-ray analyses

Colourless crystals of **5**, **6**, **7**, **8**·C_7H_8, and **10** were coated with Paratone 8277 oil and mounted on a glass fibre. All measurements were made on a Nonius Kappa CCD diffractometer using graphite-monochromated molybdenum–K_α radiation. Crystallographic data are summarized in Table 1. The structures were solved by direct methods (13) and refined by full-matrix least-squares methods with SHELXL-97 (14). Hydrogen atoms were included at geometrically idealized positions and were not refined; the non-hydrogen atoms were refined anisotropically. Thermal ellipsoid plots were created using Diamond version 2.1 (15). Additional data are available in the Supporting information.[3]

Results and discussion

Reactions of $OP(NHR)_3$ with $ZnMe_2$ — Formation and structures of $\{MeZn[(\mu\text{-}NH\text{-}t\text{-}Bu)(\mu\text{-}N\text{-}t\text{-}Bu)P(NH\text{-}t\text{-}Bu)O]\}_2$ (5), $\{[MeZn]_3[OP(N\text{-}t\text{-}Bu)_3][OP(NH\text{-}t\text{-}Bu)_3]\}$ (6), and $\{Zn[ZnMe]_2[OP(N\text{-}t\text{-}Bu)(NH\text{-}t\text{-}Bu)_2][OP(N\text{-}t\text{-}Bu)_3]\}$ (7)

Initial attempts to conduct a thorough investigation of the reactivity of $ZnMe_2$ towards $OP(NHR)_3$ (**1a** (R = *t*-Bu), **1b** (R = Me), **1c** (R = Ad)) were confounded by the subtle dependence of these reactions upon both temperature and time. A mixture of products was observed by ^{31}P NMR spectroscopy in all cases. Both the number and relative intensities of the resonances observed were strongly influenced by minor changes in the reaction conditions so that reproducible results were difficult to obtain, except for the reaction of **1a** with 1 equiv. of dimethylzinc at 60 °C. The solid-state ^{31}P NMR spectrum of the white powder produced in this reaction contains a single broad signal centred at 7 ppm. In solution at 22 °C, eight ^{31}P NMR resonances of various intensities and linewidths were observed, suggesting the presence of multiple products. A variable-temperature NMR experiment showed that the linewidths, relative intensities, and indeed the number of resonances present are dependent upon temperature, indicating that this system is highly dynamic in solution and suggesting that different modes of ag-

[3] Supplementary data for this article are available on the Web site or may be purchased from the Depository of Unpublished Data, Document Delivery, CISTI, National Research Council Canada, Ottawa, ON K1A 0R6, Canada. DUD 4056. For more information on obtaining material refer to http://cisti-icist.nrc-cnrc.gc.ca/irm/unpub_e.shtml. CCDC 269284–269287 contain the crystallographic data for this manuscript. These data can be obtained, free of charge, via www.ccdc.cam.ac.uk/conts/retrieving.html (or from the Cambridge Crystallographic Data Centre, 12 Union Road, Cambridge CB2 1EZ, UK; fax +44 1223 336033; or deposit@ccdc.cam.ac.uk).

© 2005 NRC Canada

Table 1. Crystallographic data.

	5	**6**	**7**	**8**	**10**
Formula	$C_{26}H_{64}N_6P_2O_2Zn_2$	$C_{27}H_{66}N_6P_2O_2Zn_2$	$C_{26}H_{62}N_6O_2P_2Zn_3$	$C_{23}H_{62}N_{15}O_6P_5Zn_4$	$C_{13}H_{32}N_3PSZn$
fw (g)	685.51	764.97	748.87	1049.20	358.82
Space group	*P*1	*Pna*2$_1$	*Pca*2$_1$	*C*2/*c*	*P*2$_1$/*c*
a (Å)	9.764(2)	22.936(5)	19.286(7)	17.5081(2)	11.854(3)
b (Å)	9.854(2)	10.445(2)	17.059(11)	23.6571(3)	9.678(2)
c (Å)	11.230(2)	16.213(3)	22.530(11)	21.4354(4)	17.108(6)
α (°)	64.54(3)	90	90	90	90
β (°)	71.01(3)	90	90	101.3377(5)	107.818(15)
γ (°)	72.64(3)	90	90	90	90
V (Å^3)	906.4(3)	3884.2	7412(7)	8705.1(2)	1868.5(9)
Z	1	4	8	4	2
T (K)	173(2)	173(2)	173(2)	173(2)	173(2)
λ (Å)	0.71073	0.71073	0.71073	0.71073	0.71073
d_{calcd} (g cm^{-3})	1.256	1.121	1.342	1.601	1.275
μ (mm^{-1})	1.441	1.340	2.042	2.410	1.505
F(000)	368	1400	3168	4336	768
R^a	0.035	0.0355	0.1198	0.040	0.0411
$R_w{}^b$	0.093	0.0799	0.3503	0.107	0.0763

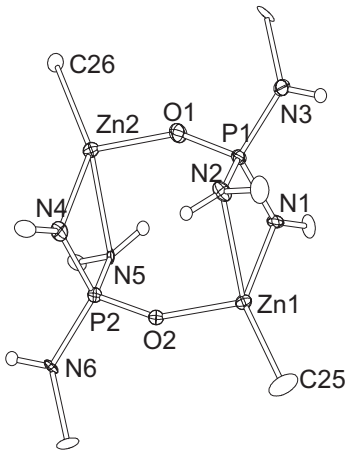
[a] $R = [\Sigma||F_o| - |F_c||]/[\Sigma |F_o|]$ for reflections with $I > 2.00\sigma(I)$.
[b] $R_w = \{[\Sigma w(F_o^2 - F_c^2)^2]/[\Sigma w(F_o^2)^2]\}^{1/2}$ for all reflections.

gregation can occur for these products, even in the noncoordinating solvent d_8-toluene.

Recrystallization of the white powder from toluene resulted in the isolation of colourless crystals, which were characterized by X-ray crystallography and multinuclear NMR spectroscopy; crystal data are compiled in Table 1. An X-ray structure, depicted in Fig. 1, showed the crystals to consist of the monoanion [OP(N-*t*-Bu)(NH-*t*-Bu)$_2$]$^-$ with a methylzinc counterion. The complex {MeZn[(μ-NH-*t*-Bu)(μ-N-*t*-Bu)P(NH-*t*-Bu)(μ-O)]}$_2$ (**5**) exists as a centrosymmetric dimer. Each of the methylzinc cations is chelated by a *t*-BuNH and a *t*-BuN group of one monoanion, with a Zn—O bond serving to both link the zinc atom to the second monoanion and to complete the tetrahedral coordination sphere of the Zn atom. The second *t*-BuNH group on each phosphorus centre is not coordinated to either of the methylzinc cations.

Selected bond lengths and bond angles for **5** are summarized in Table 2. Three different P—N bond lengths and two distinct Zn—N distances are observed: the Zn(1)—N(1) bond length (1.980(9) Å) is substantially shorter than the Zn(1)—N(2) distance (2.430(8) Å), reflecting the greater strength of the zinc–imido linkage. Similarly, the P(1)—N(1) bond distance (1.590(8) Å) is considerably shorter than the P(1)—N(2) single-bond distance of 1.705(8) Å. The fact that N(3) is not coordinated to an electropositive zinc centre results in a shorter, stronger P—N bond (P(1)—N(3) 1.627(9) Å) than that observed for the coordinated N(2) atom. The Zn—O distances in **5** are slightly longer than those typically observed in zinc phosphates, with an average value of 2.001(7) Å, cf., mean values of 1.936(4) Å in the histidine complex [Zn(HPO$_4$)·(C$_6$H$_9$N$_3$O$_2$)] (9) and 1.933(2) Å in the aminobenzene-templated system [Zn(HPO$_3$)$_2$·C$_6$N$_2$H$_{10}$] (11). As expected, the bond angle at the sp^2 nitrogen atom (∠P(1)-N(1)-Zn(1), 102.5(5)°) is larger than the corresponding angle involving the sp^3 amido nitrogen atom (∠P(1)-N(2)-Zn(1), 83.1(3)°), though both angles markedly deviate from ideal values, presumably owing to steric repulsions among the three *tert*-butyl groups attached to the nitrogen atoms.

Fig. 1. Thermal ellipsoid plot of **5** (30% probability ellipsoids). Only α-carbon atoms of the *t*-Bu groups are shown.



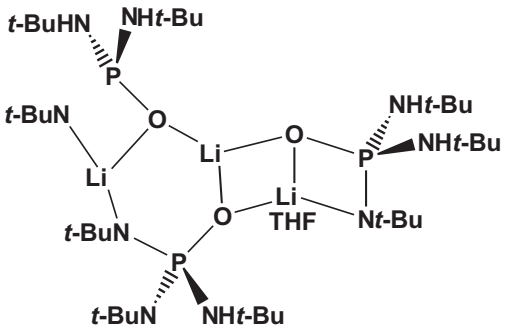
The structure of **5** is a sharp contrast to the trimeric structure adopted by the lithium salt {Li[(μ-N-*t*-Bu)(μ-O)P(NH-*t*-Bu)$_2$]}$_3$·THF (**4**) (4), which contains the same monoanion. The Li$^+$ cations in **4** are coordinated only by the oxo- and N-*t*-Bu ligands, while the NH-*t*-Bu groups are exocyclic. Whereas **5** is centrosymmetric, the trimer **4** displays C_1 symmetry, due in part to the presence of a molecule of THF coordinated to one Li$^+$ cation. Some of these structural differences can be attributed to the high polarity of Li-E (E = N or O) units and their consequent propensity for aggregation to form ladder-type motifs.

The solid-state ^{31}P and ^{13}C NMR data for **5** were consistent with the X-ray structure; a major ^{31}P resonance is observed at 7.4 ppm, and three distinct ^{13}C signals for the

© 2005 NRC Canada

Table 2. Selected bond lengths (Å) and bond angles (°) for **5**.

Bond lengths (Å)	
P(1)—O(1)	1.495(7)
P(1)—N(2)	1.705(8)
Zn(1)—O(1)	2.000(7)
Zn(1)—N(1)	1.980(9)
Zn(1)—C(25)	1.970(10)
P(1)—N(1)	1.590(8)
P(1)—N(3)	1.627(9)
Zn(1)—O(2)	2.001(7)
Zn(1)—N(2)	2.430(8)
Bond angles (°)	
P(1)-N(1)-Zn(1)	102.5(5)
P(1)-N(2)-Zn(1)	83.1(3)
P(1)-O(1)-Zn(2)	152.2(4)
O(1)-Zn(2)-C(26)	109.6(4)
P(1)-O(1)-Zn(2)	154.2(4)
O(1)-P(1)-N(1)	122.5(5)
N(1)-Zn(1)-O(2)	107.7(3)
N(3)-P(1)-O(1)	106.8(4)
N(2)-P(1)-N(3)	110.7(4)

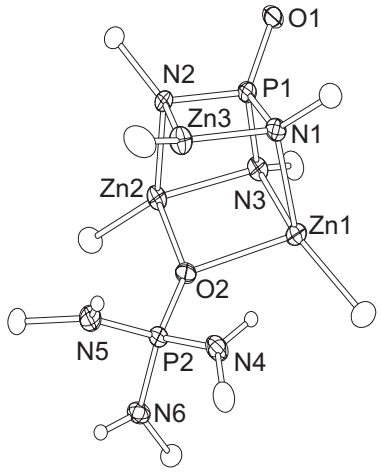


4

inequivalent C*Me*$_3$ groups occur at 34.52, 32.05, and 31.44 ppm. In C_6D_6 solution, however, the ^{31}P NMR spectrum consists of a sharp singlet at 8.1 ppm and a broader resonance at 9.3 ppm, possibly owing to an equilibrium between the dimer **5** and the corresponding monomer {[MeZn][(N-*t*-Bu)P(O)(NH-*t*-Bu)$_2$]}. A variable-temperature NMR experiment showed that, at low temperature (–50 °C), the 8.1 ppm species is predominant, while the intensity of the resonance at 9.3 ppm increases at higher temperatures, consistent with the proposed monomer–dimer equilibrium. The apparently facile dissociation of **5** into the corresponding monomer is somewhat surprising in light of its relatively strong Zn—O linkages (vide supra). Interestingly, the solid-state ^{31}P NMR spectrum of **5** also displays a minor resonance at 9.8 ppm, which may be attributable to the presence of a small amount of the monomer.

When the product of the reaction of OP(NH-*t*-Bu)$_3$ with 1 equiv. of $ZnMe_2$ at 60 °C was recrystallized from diethyl ether rather than toluene, colourless crystals of a different product were obtained. An X-ray structure (Fig. 2) identified this compound as {[MeZn]$_3$[OP(N-*t*-Bu)$_3$][OP(NH-*t*-Bu)$_3$]}

Fig. 2. Thermal ellipsoid plot of **6** (30% probability ellipsoids). Only α-carbon atoms of the *t*-Bu groups are shown.



(**6**), which is comprised of the trianion [OP(N-*t*-Bu)$_3$]$^{3-}$ and three MeZn$^+$ counterions, with a neutral molecule of **1a** coordinated to two of the zinc centres. The formation of this previously unobserved trianion was somewhat unexpected given the lack of success encountered in attempts to generate [OP(N-*t*-Bu)$_3$]$^{3-}$ using organolithium reagents (4). In addition, the presence of unreacted OP(NH-*t*-Bu)$_3$ concomitant with the formation of this trianion is rather surprising; the generation of a mixture of mono- and di-anions would seem more probable.

In the solid state, **6** exists as a distorted PN_3Zn_3O cube, with the phosphorus and nitrogen atoms of the [OP(N-*t*-Bu)$_3$]$^{3-}$ trianion contributing four of the vertices, while the remaining positions are occupied by the three zinc cations and the oxygen atom O(2) of the neutral OP(NH-*t*-Bu)$_3$ molecule. While O(2) is coordinated to two of the methylzinc cations, the =P(NH-*t*-Bu)$_3$ fragment is pendant from the cube. Selected bond lengths and bond angles for **6** are given in Table 3. The oxo ligand of the trianion is exo to the cluster, with a P(1)—O(1) bond distance of 1.475(2) Å, cf., 1.474(3) Å in **1a** (4). In contrast, the P(2)—O(2) bond length is significantly longer (1.519(2) Å) because of coordination of this oxygen atom to two zinc atoms. The increase in this P=O distance has little effect on the P—N bond lengths in the neutral fragment; the average P(2)—N distance is 1.631(3) Å, cf., 1.637(3) Å in **1a** (4). The mean P—N bond length in the trianion is significantly longer (1.689(3) Å), since the nitrogen atoms in this moiety are four-coordinate.

Two of the zinc centres are four-coordinate, with two Zn—N bonds, one Zn—O linkage, and a methyl substituent, while the third zinc cation exhibits only a weak Zn—O contact (2.648(2) Å) and is thus considered three-coordinate. The zinc–oxygen distances for the two four-coordinate zinc atoms are Zn(1)—O(2) = 2.333(2) Å and Zn(2)—O(2) = 2.314(2) Å. These Zn—O distances are substantially longer than the mean values of 1.980(4) Å found in zinc-di(oxo)cyclodiphosph(V)azane systems (16), or the distances reported for the polymeric di(*tert*-butyl)phosphates {Zn[O$_2$P-(O-*t*-Bu)$_2$]$_2$[H$_2$N(CH$_2$)$_6$NH$_2$]}$_n$ and {Zn[O$_2$P(O-*t*-Bu)$_2$]$_2$}$_n$ (range: 1.914(8)–1.929(6) Å) (17). The mean Zn—N dis-

© 2005 NRC Canada

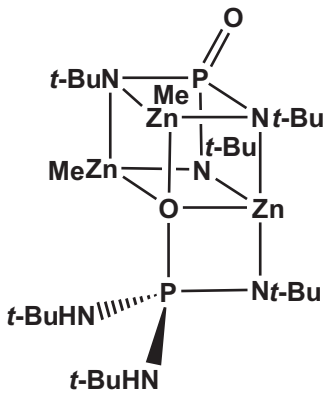
Table 3. Selected bond lengths (Å) and bond angles (°) for **6**.

Bond lengths (Å)	
P(1)—O(1)	1.476(2)
P(1)—N(2)	1.696(2)
P(2)—O(2)	1.519(2)
P(2)—N(5)	1.627(3)
Zn(1)—N(1)	2.091(2)
Zn(2)—N(2)	2.079(3)
Zn(1)—O(2)	2.333(2)
P(1)—N(1)	1.686(2)
P(1)—N(3)	1.684(3)
P(2)—N(4)	1.642(3)
P(2)—N(6)	1.625(3)
Zn(1)—N(3)	2.046(2)
Zn(2)—N(3)	2.074(2)
Zn(2)—O(2)	2.314(2)
Bond angles (°)	
N(1)-P(1)-N(2)	98.1(1)
N(2)-P(1)-N(3)	99.1(1)
N(1)-Zn(1)-O(2)	89.62(9)
N(2)-Zn(2)-N(3)	76.54(9)
N(3)-Zn(2)-O(2)	86.29(9)
Zn(1)-O(2)-Zn(2)	86.26(7)
N(1)-P(1)-N(3)	99.4(1)
N(1)-Zn(1)-N(3)	76.82(9)
N(3)-Zn(1)-O(2)	86.46(9)
N(2)-Zn(2)-O(2)	89.11(9)
N(1)-Zn(3)-N(2)	77.52(9)

tance for the three-coordinate zinc cation Zn(3) is 2.040(2) Å, cf., 2.073(2) Å for the four-coordinate zinc centres. The mean ∠N-P-N bond angle is 98.9(1)° while the ∠N-Zn-N and ∠N-Zn-O bond angles range from 76.54(9)° to 89.62(9)°.

A ^{31}P NMR spectrum of **6** in C_6D_6 solution displayed two sharp singlets at 46.8 and 10.2 ppm, which are assigned to the $[OP(N\text{-}t\text{-}Bu)_3]^{3-}$ trianion and the neutral $OP(NH\text{-}t\text{-}Bu)_3$ ligand, respectively. Three resonances are observed in the ^{1}H NMR spectrum with relative intensities of 3:1:2, attributed to the three NH-*t*-Bu groups of the coordinated molecule of **1a** (27H) and the inequivalent N-*t*-Bu ligands of the trianion (9H and 18H), while a single broad resonance at –0.12 ppm is assigned to the methylzinc cations. These NMR data are consistent with the solid-state structure of **6**.

When the reaction of **1a** with dimethylzinc was carried out in a 2:3 molar ratio in boiling toluene, the ^{31}P NMR spectrum of the resulting white powder indicated the formation of a mixture of products. However, recrystallization from toluene produced a single compound identified as $\{Zn[ZnMe]_2[OP(N\text{-}t\text{-}Bu)(NH)_2][OP(N\text{-}t\text{-}Bu)_3]\}$ (**7**) by X-ray crystallography. Although the structure could not be satisfactorily refined (R_1 = 0.12) because of poor diffraction of the crystals and disorder of the *tert*-butyl substituents, the atom connectivities of **7** were established. Complex **7** is closely related to **6** in that its primary structural feature is a PN_3Zn_3O cube; however, in place of the neutral $OP(NH\text{-}t\text{-}Bu)_3$ ligand of **6**, complex **7** contains a monoanion $[OP(N\text{-}t\text{-}Bu)(NH\text{-}t\text{-}Bu)_2]^-$ that is *N*,*O* chelated to a Zn^{2+} dication. The oxo substituent of this monoanion is coordinated to all three zinc centres, all of which are four-coordinate: the Zn^{2+} dication is also coordinated to nitrogen donors, while the other zinc atoms are also bound to two nitrogen atoms and a methyl substituent.



7

The solid-state ^{31}P NMR spectrum of **7** consists of two singlets at 22.0 and 13.5 ppm, consistent with the X-ray structure. In C_6D_6 solution, the ^{31}P NMR spectrum exhibits three major resonances at 22.0, 14.6, and 13.1 ppm, suggesting that more than one mode of aggregation occurs in solution; consistently, the solution ^{1}H NMR spectrum of **7** contains numerous resonances in the N-*t*-Bu region.

The contrasting structures of **5**, **6**, and **7** suggest that there are two different pathways possible for the reaction of dimethylzinc with $OP(NH\text{-}t\text{-}Bu)_3$. Complex **6** is clearly a precursor of **7**; in a separate experiment, it was shown by ^{31}P NMR spectroscopy that crystalline **6** can, in fact, be converted to **7** by thermal elimination of methane under reduced pressure (Scheme 1). At the same time, **5** is clearly not a precursor of **6**, despite the fact that the first step in the formation of both **5** and **6** is likely the monodeprotonation of $OP(NH\text{-}t\text{-}Bu)_3$. In the case of **6**, the second step of the reaction results in the double deprotonation of one of the ligands.

The different coordination modes of the two ligands within both **6** and **7** are also noteworthy. The oxo unit of one ligand (the trianion) remains exo to the cubane, while the other oxygen atom plays an integral role in cluster formation, as it is coordinated to either two or three zinc centres in **6** and **7**, respectively. Additionally, two distinct modes of coordination for the $[OP(N\text{-}t\text{-}Bu)(NH\text{-}t\text{-}Bu)_2]^-$ monoanion are observed in these complexes, with *N*,*O* chelation displayed in **7**, whereas *N*,*N*′ chelation prevails in **5**; similar *N*,*N*′ coordination also occurs for the trianionic ligands in **6** and **7**, but in those two instances the oxo substituent remains noncoordinated.

Formation and X-ray structure of $\{Zn_4(\mu_4\text{-}O)[OP(NMe)(NHMe)_2]_4[OP(NMe)_2(NHMe)]\}_2$ (8)

Following the successful generation of the trisimidophosphate trianion $[OP(N\text{-}t\text{-}Bu)_3]^{3-}$ utilizing dimethylzinc, similar reactions with tris(methylamido)phosphate $OP(NHMe)_3$ (**1b**) were investigated to determine the effect of the replacement of the bulky *tert*-butyl groups of **1a** with the much smaller NMe units on the size of the zinc imidophosphate clusters formed. The reaction of dimethylzinc with **1b** in a

© 2005 NRC Canada

Scheme 1. Thermal conversion of **6** to **7**.

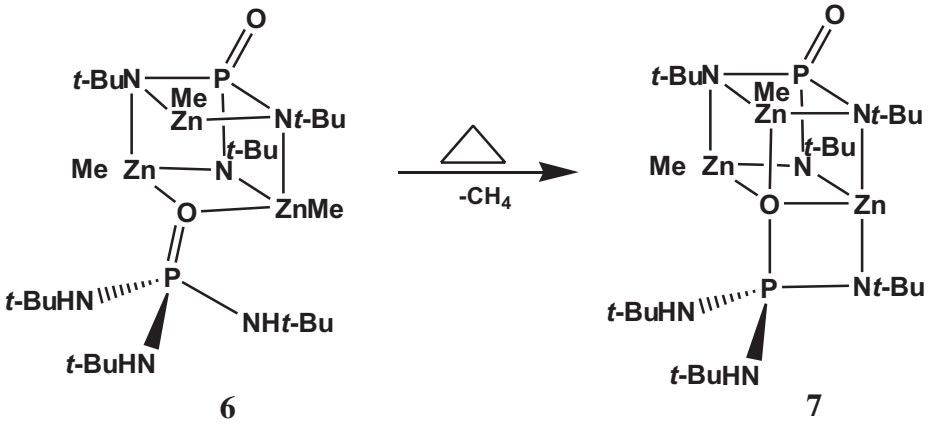
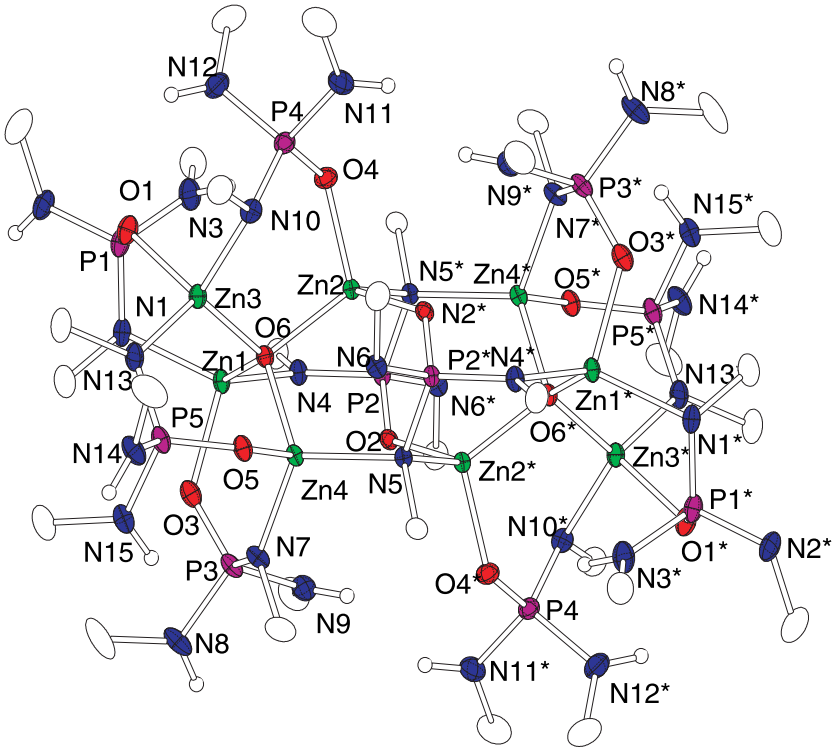


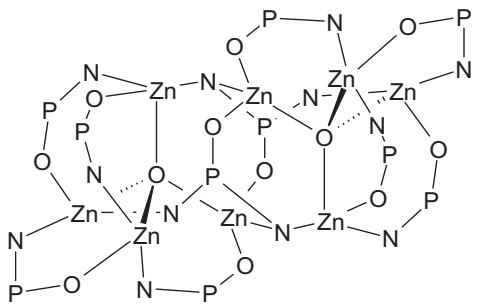
Fig. 3. Thermal ellipsoid plot of **8** (30% probability ellipsoids). Hydrogen atoms of methyl groups are omitted.



1:1 ratio in boiling toluene led to the isolation of colourless crystals of the oxide-templated complex $\{Zn_4(\mu_4\text{-}O)[OP(NMe)(NHMe)_2]_4[OP(NMe_2)(NHMe)]\}_2$ (**8**) in 49% yield.

An X-ray structure of **8** revealed that this complex is a centrosymmetric dimer, which crystallizes with a molecule of toluene in its lattice. A thermal ellipsoid plot is shown in Fig. 3, while the framework of the cluster is pictorially represented in Fig. 4. Each monomeric unit consists of four Zn^{2+} ions, four $[OP(NMe)(NHMe)_2]^-$ monoanions, one $[OP(NMe_2)(NHMe)]^{2-}$ dianion, and one oxide ligand; in each half of the cluster there is a tetrahedral core of four 4-coordinate Zn^{2+} ions that surround a central $\mu_4\text{-}O^{2-}$ anion. The four monoanions bridge four edges of the Zn_4 tetrahedron. The two halves of the molecule are joined together by the two $[OP(NMe_2)(NHMe)]^{2-}$ dianions, while the NHMe

Fig. 4. Structural framework of **8**. All methyl groups and noncoordinated NHMe groups are omitted for clarity.



© 2005 NRC Canada

group of each dianion does not participate in cluster bonding. Three of the four Zn^{2+} ions (Zn(1), Zn(2), and Zn(4)) interact with the two dianions and thus participate in linking together the two halves of the dimer. As a result of these linkages, there are numerous six-, eight-, ten-, and twelve-membered rings in the structure. The Zn and O atoms reside near the centre of the cluster, while the methyl groups of the phosphate anions point away from the central core.

The X-ray structure described in the preceding section is expected to give rise to five resonances in the ^{31}P NMR spectrum of **8**. However, a solution ^{31}P NMR spectrum in d_6-benzene revealed two dominant resonances at 37.9 and 28.2 ppm in an approximately 1:4 ratio, while the solid-state spectrum exhibited only two singlets centred at 38.7 and 27.6 ppm. These observations are tentatively attributed to the similar chemical environments experienced by the four crystallographically inequivalent $[OP(NMe)(NHMe)_2]^-$ monoanions, which result in the appearance of only one resonance for those four phosphorus atoms, along with a second resonance attributed to the $[OP(NMe)_2(NHMe)_2]^{2-}$ dianion. The solution ^1H NMR spectrum of **8** exhibits four singlets of equal intensities at 2.25, 2.22, 2.20, and 2.16 ppm, assigned to the four different environments of the NHMe groups, while a single broad resonance centred at 1.36 ppm is observed for the indistinguishable NMe substituents. While no NH resonance could be detected in the ^1H NMR spectrum, the NHMe fragments were clearly identified by a sharp N-H stretch (3323 cm^{-1}) in the IR spectrum of **8**.

The formation of the much larger cluster **8**, as compared with complexes **5**, **6**, and **7**, is a direct consequence of the decrease in steric bulk of the NR groups, which allows for more extensive aggregation. Roesky and co-workers (18, 19) have reported the synthesis of a zinc complex of *tert*-butylphosphonic acid, $[Zn_2(THF)_2(EtZn)_6Zn_4(\mu_4\text{-}O)(t\text{-}BuPO_3)_8]$ (**9**), with a structure similar to that of **8**: complex **9** contains a central $Zn_4(\mu_4\text{-}O)$ core, with the *tert*-butylphosphonate ligands radiating outwards from the centre of the dodecanuclear cluster. Selected bond lengths and bond angles for **8** are summarized in Table 4. The phosphorus–μ_2-O bond lengths range from 1.498(3) to 1.532(2) Å (cf., 1.499(5)–1.527(5) Å in **9**). The zinc–μ_4-O distance is also similar to those of **9** (1.957(2)–2.026(2) Å in **8**; 1.948(4)–2.073(4) Å in **9**); however, the Zn—μ_2-O distances are significantly longer in **8** than those in **9** (1.964(2)–2.055(1) Å vs. 1.891(5)–1.990(5) Å, respectively).

The origin of the μ_4-oxygen atom of **8** remains uncertain. It has been suggested that the presence of oxide in **9** results from the dehydration of *tert*-butylphosphonic acid induced by diethylzinc (19). However, this explanation is clearly not applicable to the reaction of $ZnMe_2$ with $OP(NHMe)_3$. Possible sources of the oxide ligand in the current case include (*a*) P=O bond cleavage during the course of the reaction, (*b*) the contamination of the reagent **1b** by water, or (*c*) the presence of "adventitious" water during the recrystallization process, as suggested for related systems (17, 20). As ^{31}P NMR studies of the reaction mixtures gave no evidence for P=O bond cleavage, and the IR spectrum of **1b** showed that it was anhydrous, the most probable source of the oxide unit is the introduction of moisture during the recrystallization process.

Table 4. Selected bond lengths (Å) and bond angles (°) for **8**.

Bond lengths (Å)	
Zn(1)—N(4)	1.971(3)
Zn(1)—N(1)	1.999(3)
Zn(1)—O(3)	2.005(3)
Zn(1)—O(6)	2.026(2)
Zn(2)—O(4)	1.969(3)
Zn(2)—O(2)[a]	1.964(2)
Zn(2)—O(6)	1.957(2)
Zn(2)—N(5)	2.045(2)
Zn(3)—N(13)	1.958(3)
Zn(3)—O(6)	1.989(2)
Zn(3)—N(10)	1.992(3)
Zn(3)—O(1)	2.055(2)
Zn(4)—O(6)	1.974(2)
Zn(4)—N(7)	1.986(3)
Zn(4)—O(5)	2.045(2)
Zn(4)—N(5)[a]	2.079(2)
P(1)—O(1)	1.515(2)
P(1)—N(1)	1.605(3)
P(1)—N(2)	1.633(3)
P(1)—N(3)	1.650(3)
P(2)—O(2)	1.532(2)
P(2)—N(4)	1.602(3)
P(2)—N(6)	1.646(3)
P(2)—N(5)	1.667(3)
P(3)—O(3)	1.498(3)
P(3)—N(7)	1.607(3)
P(3)—N(8)	1.652(3)
P(3)—N(9)	1.660(3)
P(4)—O(4)	1.522(2)
P(4)—N(10)	1.598(3)
P(4)—N(11)	1.639(3)
P(4)—N(12)	1.649(4)
P(5)—N(13)	1.589(4)
P(5)—O(5)	1.515(2)
P(5)—N(14)	1.640(3)
P(5)—N(15)	1.671(3)
Bond angles (°)	
N(4)-Zn(1)-N(1)	124.56(11)
N(13)-P(5)-N(15)	117.63(16)
N(4)-Zn(1)-O(3)	106.27(10)
N(14)-P(5)-N(15)	100.88(16)
N(14)-P(5)-N(15)	100.88(16)
N(1)-Zn(1)-O(3)	98.83(11)
P(1)-O(1)-Zn(3)	121.67(14)
N(4)-Zn(1)-O(6)	109.48(10)
P(2)-O(2)-Zn(2)[a]	133.13(12)
N(1)-Zn(1)-O(6)	108.6(1)
P(3)-O(3)-Zn(1)	130.67(16)
O(3)-Zn(1)-O(6)	107.51(9)
P(4)-O(4)-Zn(2)	125.79(14)
O(6)-Zn(2)-O(2)[a]	111.28(8)
P(5)-O(5)-Zn(4)	126.97(13)
O(6)-Zn(2)-O(4)	111.61(9)
Zn(2)-O(6)-Zn(4)	109.04(10)
O(2)[a]-Zn(2)-O(4)	105.71(9)
Zn(2)-O(6)-Zn(3)	104.22(9)

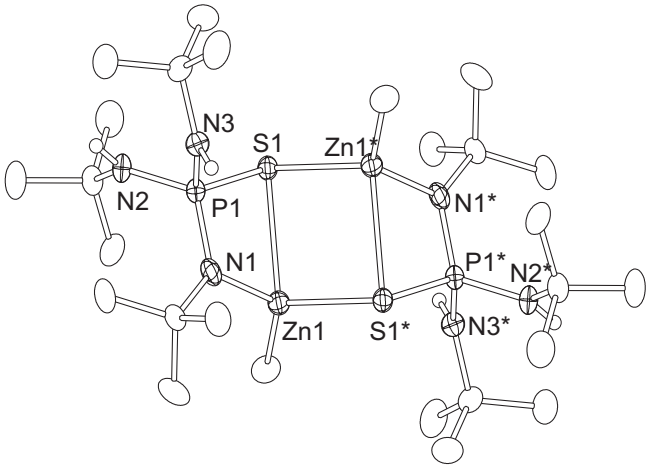
© 2005 NRC Canada

Table 4 (*concluded*).

Bond angles (°)	
O(6)-Zn(2)-N(5)	118.42(9)
Zn(4)-O(6)-Zn(3)	110.93(10)
O(2)[a]-Zn(2)-N(5)	103.71(9)
Zn(2)-O(6)-Zn(1)	110.67(9)
O(4)-Zn(2)-N(5)	105.07(10)
O(1)-P(1)-N(2)	110.45(15)
N(1)-P(1)-N(2)	107.12(16)
O(1)-P(1)-N(3)	104.80(15)
P(4)-N(10)-Zn(3)	116.75(15)
N(1)-P(1)-N(3)	110.10(16)
N(2)-P(1)-N(3)	108.71(16)
O(2)-P(2)-N(4)	108.48(12)
O(2)-P(2)-N(6)	114.66(13)
N(4)-P(2)-N(6)	109.53(14)
O(2)-P(2)-N(5)	105.23(12)
N(4)-P(2)-N(5)	114.35(13)
N(6)-P(2)-N(5)	104.66(13)
O(3)-P(3)-N(7)	110.36(15)
O(3)-P(3)-N(8)	107.33(16)
Zn(4)-O(6)-Zn(1)	108.18(9)
Zn(3)-O(6)-Zn(1)	113.71(10)
P(1)-N(1)-Zn(1)	113.64(16)
N(13)-Zn(3)-O(6)	117.01(10)
N(13)-Zn(3)-O(6)	117.01(10)
N(13)-Zn(3)-N(10)	112.50(11)
O(6)-Zn(3)-N(10)	111.18(10)
N(13)-Zn(3)-O(1)	105.55(11)
O(6)-Zn(3)-O(1)	109.56(9)
P(2)-N(4)-Zn(1)	116.69(15)
N(10)-Zn(3)-O(1)	99.34(10)
P(2)-N(5)-Zn(2)	105.20(13)
N(10)-Zn(3)-Zn(2)	75.03(8)
O(1)-Zn(3)-Zn(2)	106.81(7)
P(2)-N(5)-Zn(4)[a]	114.87(13)
O(6)-Zn(4)-N(7)	120.77(10)
Zn(2)-N(5)-Zn(4)[a]	103.58(10)
O(6)-Zn(4)-O(5)	101.62(8)
N(7)-Zn(4)-O(5)	101.59(10)
O(6)-Zn(4)-N(5)[a]	114.13(9)
N(7)-Zn(4)-N(5)[a]	114.42(10)
P(3)-N(7)-Zn(4)	120.41(16)
O(5)-Zn(4)-N(5)[a]	99.70(9)
O(1)-P(1)-N(1)	115.53(16)
N(7)-P(3)-N(8)	114.25(16)
O(3)-P(3)-N(9)	114.75(15)
N(7)-P(3)-N(9)	108.98(15)
N(8)-P(3)-N(9)	101.00(16)
O(4)-P(4)-N(10)	110.00(14)
O(4)-P(4)-N(11)	107.17(15)
N(10)-P(4)-N(11)	116.08(16)
O(4)-P(4)-N(12)	112.26(15)
N(10)-P(4)-N(12)	108.23(16)
N(11)-P(4)-N(12)	103.01(17)
O(5)-P(5)-N(13)	109.46(14)
O(5)-P(5)-N(14)	115.83(14)
N(13)-P(5)-N(14)	108.36(16)
O(5)-P(5)-N(15)	104.78(14)

[a] $-x + 1/2, -y + 1/2, -z$.

Fig. 5. Thermal ellipsoid plot of **10** (30% probability ellipsoids). Only hydrogen atoms bonded to nitrogen atoms are shown.



Preparation and characterization of [MeZn(μ-S)(μ-N-*t*-Bu)P(NH-*t*-Bu)$_2$]$_2$ (10) and {Zn[(μ-S)(μ-N-*t*-Bu)P(NH-*t*-Bu)$_2$]$_2$} (11)

The reaction of SP(NH-*t*-Bu)$_3$ with 1 equiv. of dimethylzinc produces {MeZn(μ-S)(μ-N-*t*-Bu)P(NH-*t*-Bu)$_2$}$_2$ (**10**) in 78% yield. An X-ray structure (Fig. 5) revealed that in the solid state, **10** exists as a centrosymmetric dimer in which each ligand is *N*,*S* chelated to a MeZn$^+$ cation, with Zn—S bonds linking the two halves together into a step-shaped ladder motif. Each zinc atom is thus four-coordinate, with two Zn—S linkages, one Zn—C bond, and a Zn-N-*t*-Bu unit. Selected bond lengths and bond angles for **10** are given in Table 5. As expected, the mean P—N distances involving the pendant NH-*t*-Bu groups (1.650(2) Å) are longer than the P-N(*t*-Bu) linkage (1.592(2) Å). The substantial difference between the Zn(1)—N(1) (2.007(2) Å) and Zn(1)—S(1) (2.5849(9) Å) bond lengths, combined with the tetrahedral geometries of the phosphorus and zinc atoms, gives the four-membered PNSZn rings a distorted diamondoid shape. The Zn_2S_2 ring is closer to square-shaped, with bond angles of 97.10(3)° and 82.90(3)° at the zinc and sulfur centres, respectively. Two distinct Zn—S distances are observed with the shorter bond (2.4627(9) Å) linking the two monomeric units and contributing to the distortion of the ring.

The dimeric laddering arrangement exhibited by **10** has been observed for other complexes of imidophosphate monoanions. The lithium derivatives {Li[(μ-N-*t*-Bu)(μ-NSiMe$_3$)P(NH-*t*-Bu)$_2$]}$_2$ (6) and {Li[(μ-N-*i*-Pr)(μ-S)P(NH-*i*-Pr)$_2$]}$_2$·2THF (5) both display this connectivity. The latter thiophosphate complex and **13** both exist in the trans conformation to minimize steric repulsions between the bulky *tert*-butyl substituents. The different mode of coordination of the heteroleptic imidophosphate ligand to zinc in **10** compared with that in **5** may be attributed, in part, to the greater affinity of zinc for the softer sulfur centre, resulting in *N*,*S* chelation, while *N*,*N*′ coordination is observed for the *O*-containing ligand in **5**. This, in turn, results in significantly different modes of oligomerization for these two dimers. It should be noted that the first transition-metal complexes of the monoanion [SP(N-*t*-Bu)(NH-*t*-Bu)$_2$]$^-$ have been reported recently (21); interestingly, both *N*,*S* and *N*,*N*′ chelation were observed in a single Ni(II) complex.

© 2005 NRC Canada

Table 5. Selected bond lengths (Å) and bond angles (°) for **10**.

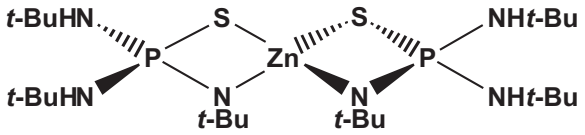
Bond lengths (Å)	
P(1)—N(1)	1.592(2)
P(1)—N(3)	1.651(2)
Zn(1)—S(1)	2.4627(9)
P(1)—N(2)	1.648(2)
P(1)—S(1)	2.0501(11)
Zn(1)—C(1)	1.966(3)
Bond angles (°)	
S(1)-Zn(1)-S(1)[a]	97.10(3)
S(1)-P(1)-N(1)	101.66(9)
S(1)-P(1)-N(3)	108.51(9)
N(2)-P(1)-N(3)	100.42(12)
N(1)-Zn(1)-C(1)	121.18(10)
S(1)-Zn(1)-N(1)	82.90(3)
Zn(1)-N(1)-P(1)	106.22(12)
N(1)-P(1)-N(2)	110.49(13)
S(1)-Zn(1)-C(1)	121.18(10)
N(1)-Zn(1)-S(1)	75.19(7)

[a]Symmetry transformations used to generate equivalent atoms: $-x + 1, -y + 1, -z$.

The ^{31}P NMR spectrum of **10** in C_6D_6 at 22 °C exhibits resonances at 41.1 and 39.6 ppm in an approximately 1:3 ratio, rather than the expected single peak; multiple resonances are observed in the ^{1}H NMR spectrum. Variable-temperature ^{31}P NMR spectra were recorded at temperatures ranging from –30 to +40 °C. At higher temperatures, the minor signal at 41.1 ppm was observed to increase in intensity, while at lower temperatures this resonance became less intense and was not observed below –15 °C. This suggests that an equilibrium exists between the dimer **10** and the corresponding monomer. The ^{1}H and ^{13}C NMR spectra of **10** at –30 °C showed the expected resonances for two inequivalent *tert*-butyl environments in a 2:1 ratio, as well as a singlet assigned to the two equivalent $MeZn^+$ cations. Thus the low-temperature NMR spectra are consistent with the presence of a single species consistent with the solid-state structure of **10**.

When the reaction of $SP(NH\text{-}t\text{-}Bu)_3$ with dimethylzinc was carried out in a 2:1 molar ratio, a white powder was recovered and characterized by multinuclear NMR spectroscopy and CHN analysis. The ^{31}P NMR spectrum of this product contained a singlet at 42.0 ppm, while the ^{1}H and ^{13}C NMR spectra revealed two *tert*-butyl resonances with relative intensities of 1:2. No resonance for a $MeZn^+$ cation was observed. These NMR data are consistent with the formation of $\{Zn[(\mu\text{-}S)(\mu\text{-}N\text{-}t\text{-}Bu)P(NH\text{-}t\text{-}Bu)_2]_2\}$ (**11**) in which a Zn^{2+} cation is *N*,*S* chelated by two monoanions. A peak at *m*/*z* 607 ($M - Me^+$) is observed in the ESI mass spectrum of **11**.

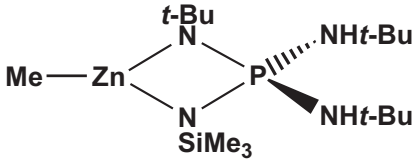
In contrast to the diverse reaction pathways and complex product mixtures in the reactions of $OP(NHR)_3$ with $ZnMe_2$, only monodeprotonation is observed in the corresponding reaction of $SP(NH\text{-}t\text{-}Bu)_3$. The lower reactivity of **2a** toward $ZnMe_2$ is unexpected, as previous studies have shown this thiophosphate to be much more reactive toward alkyllithium reagents than is the oxo analogue **1a** (3–5).



11

Preparation and characterization of {MeZn[(μ-N-*t*-Bu)-(μ-NSiMe$_3$)P(NH-*t*-Bu)$_2$]} (12)

The reaction of $(t\text{-}BuNH)_3PNSiMe_3$ with 1 equiv. of dimethylzinc generates $\{MeZn[(\mu\text{-}N\text{-}t\text{-}Bu)(\mu\text{-}NSiMe_3)P(NH\text{-}t\text{-}Bu)_2]\}$ (**12**) as a yellow oil, which has been characterized by multinuclear NMR spectroscopy and CHN analysis. The ^{1}H NMR spectrum of **12** exhibits only three resonances with relative intensities of 9:3:1 assigned to the *t*-Bu groups, the $SiMe_3$ substituent, and the $MeZn^+$ cation, respectively. Although the signals from the μ-N-*t*-Bu and NH-*t*-Bu groups are not resolved in the ^{1}H NMR spectrum, the ^{13}C NMR spectrum shows two distinct sets of *t*-Bu resonances in an approximately 1:2 ratio. A singlet is observed at 9.1 ppm in the ^{31}P NMR spectrum. Thus, the NMR data indicate a *N*,*N*′-chelated structure for **12**.



12

The reaction of **3** with $ZnMe_2$ in a 2:1 molar ratio produces a 1:1 mixture of **12** and unreacted **3**, indicating that dimethylzinc in only sufficiently basic to effect monodeprotonation of **3**. This result was somewhat surprising, given that **3** can be triply deprotonated by reactions with *n*-BuLi at room temperature; conversely, the trisamidophosphate **1a** can only be dilithiated regardless of reaction conditions, whereas reactions with dimethylzinc lead to the formation of triply deprotonated species such as **6** and **7**.

Conclusions

The reactivity of the triamidophosphates $EP(NHR)_3$ (E = O, S, $NSiMe_3$; R = alkyl) toward dimethylzinc markedly decreases on moving from oxygen to the heavier chalcogen sulfur. The higher basicity of the oxo ligand results in a tendency for coordination to numerous metal centres. Both the oxygen and sulfur systems display temperature-dependent solution dynamics. A further decrease in reactivity is observed when the chalcogen atom is replaced by an $NSiMe_3$ group; the only product observed is the monomer $\{[MeZn][(\mu\text{-}N\text{-}t\text{-}Bu)(\mu\text{-}NSiMe_3)P(NH\text{-}t\text{-}Bu)_2]\}$, presumably because the steric bulk of the alkylimido groups impedes aggregation. Curiously, the reactivities of these triamidophosphates towards *n*-butyllithium decrease in the reverse order; threefold deprotonation of $OP(NHR)_3$ occurs only in reactions with dimethylzinc. The reactions of other organometallic reagents such as $MgBu_2$ with these triamidophosphates is worthy of investigation for comparison with the results observed for *n*-BuLi and $ZnMe_2$.

© 2005 NRC Canada

Acknowledgments

We thank the University of Calgary and the Natural Sciences and Engineering Research Council of Canada (NSERC) for funding. The advice of Dr. Dana J. Eisler in the structure solutions of **5** and **6** is gratefully acknowledged.

References

1. T. Chivers. Top. Curr. Chem. **229**, 143 (2003).
2. G.M. Aspinall, M.C. Copsey, A.P. Leedham, and C.A. Russell. Coord. Chem. Rev. **227**, 217 (2002).
3. A. Armstrong, T. Chivers, M. Krahn, M. Parvez, and G. Schatte. Chem. Commun. (Cambridge), 2332 (2002).
4. T. Chivers, M. Krahn, G. Schatte, and M. Parvez. Inorg. Chem. **42**, 3994 (2003).
5. T. Chivers, M. Krahn, M. Parvez, and G. Schatte. Chem. Commun. (Cambridge), 1992 (2001).
6. A. Armstrong, T. Chivers, M. Parvez, and R.T. Boeré. Inorg. Chem. **43**, 3453 (2004).
7. P. Blais, T. Chivers, M. Krahn, and G. Schatte. J. Organomet. Chem. **646**, 107 (2002).
8. J.F. Bickley, M.C. Copsey, J.C. Jeffery, A.P. Leedham, C.A. Russell, D. Stalke, A. Steiner, T. Stey, and S. Zacchini. Dalton Trans. 989 (2004).
9. J. Fan, C. Slebodnick, R. Angel, and B.E. Hanson. Inorg. Chem. **44**, 552 (2005).
10. Z.-E. Lin, J. Zhang, S.-T. Zheng, and G.-Y. Yang. Z. Anorg. Allg. Chem. **631**, 148 (2005).
11. A. Kirkpatrick and W.T.A. Harrison. Solid State Sci. **6**, 593 (2004).
12. See, for example: S. Oliver, A. Kuperman, and G.A. Ozin. Angew. Chem. Int. Ed. **37**, 47 (1998).
13. A. Altomare, M. Cascarano, C. Giacovazzo, and A. Guagliardi. J. Appl. Crystallogr. **26**, 343 (1993).
14. G.M. Sheldrick. SHELXL-97 [computer program]. University of Göttingen, Göttingen, Germany. 1997.
15. K. Brandenberg. Diamond 2.1c [computer program]. Crystal Impact GbR, Bonn, Germany. 1999.
16. G.R. Lief, D.F. Moser, L. Stahl, and R.J. Staples. J. Organomet. Chem. **689**, 1110 (2004).
17. C.G. Lugmair, T.D. Tilley, and A.L. Rheingold. Chem. Mater. **9**, 339 (1997).
18. Y. Yang, J. Pinkas, M. Noltemeyer, H.-G. Schmidt, and H.W. Roesky. Angew. Chem. Int. Ed. **38**, 664 (1999).
19. G. Anantharaman, V. Chandrasekhar, M.G. Walawalker, H.W. Roesky, D. Vidovic, J. Magull, and M. Noltemeyer. Dalton Trans. 1271 (2004).
20. W.T.A. Harrison, M.L.F. Phillips, A.V. Chavez, and T.M. Nenoff. J. Mater. Chem. **9**, 3087 (1999).
21. K.A. Rufanov, B. Ziemer, and M. Meisel. Dalton Trans. 3808 (2004).

© 2005 NRC Canada

Enhancing image quality of scanning electrochemical microscopy by improved probe fabrication and displacement

Renkang Zhu and Zhifeng Ding

Abstract: Scanning electrochemical microscopy (SECM) is a powerful tool for its wide applications in determining charge transfer kinetics, imaging chemical reactions and topography, as well as fabricating microstructures at various interfaces and (or) surfaces. Imaging applications, in particular, rely on the natures of SECM probes and the scanning systems to move them in the vicinity of interfaces. While progress has been made in new approaches to tip fabrication, there are few reports on the improvement of the tip positioning system to enhance SECM image quality. We have recently built an advanced SECM setup using a closed-loop scanning system and improved probe fabrication and characterization procedures. Here we will describe this development, as well as the application of these techniques to greatly improve the quality of SECM images. Video micrograph, cyclic voltammograms, and SECM approach curves (current vs. tip–substrate distance) were chosen to characterize probe quality and to determine the ratio of electrode diameter to glass sheath diameter. The SECM setup has a resolution and repeatability of 20 nm in three dimensions (*x*, *y*, and *z*) and can locate and relocate areas of interest precisely after a coarse image. Interdigitated electrode arrays of platinum and gold were first imaged. Image resolution revealed by sharpness of Pt band edges was enhanced by using a 2 μm diameter electrode. Pt or Au band height was found to be around 80–200 nm by fitting the approach curves to the theoretical ones. Imaging conditions such as delay time for a large step size between two succeeding data points were optimized. To test its thermal and temporal stability, the system was then used to image letters, which were printed on a transparency with font bold Courier New and font size 2. Minor drifts were found during the image process up to the experimental length of 8 h and 45 min. Letter thickness was found to be 1.0–1.2 μm. A silicon substrate with an array of square pits spaced apart on 10 μm centers was finally imaged. Good quality images were obtained at various tip–substrate distances even though the squares were just as small, if not smaller, than the tip. The samples were also imaged by AFM for comparison.

Key words: scanning electrochemical microscopy, atomic force microscopy, microelectrode fabrication, closed-loop imaging, probe approach curve.

Résumé : La microscopie électrochimique à balayage (MECB) est un puissant outil avec de nombreuses applications dans la détermination de la cinétique de transfert de charge, dans l'imagerie et la topographie des réactions chimiques ainsi que dans la fabrication de microstructures à diverses interfaces et (ou) surfaces. En particulier, les applications en imagerie reposent sur la nature de sondes de MECB et de systèmes de balayage pour les amener dans les environs des interfaces. Même si des progrès ont été réalisés dans de nouvelles approches pour fabriquer des électrodes pointus (pointes), il y a eu peu de publications sur les améliorations des systèmes de positionnement des pointes afin d'améliorer la qualité des images de MECB. On a récemment construit un ensemble élaboré de MECB qui utilise un système de balayage à circuit fermé, des méthodes améliorées de fabrication des sondes et de méthode de caractérisation. Dans ce travail, on décrit les développements mentionnés dessus ainsi que l'application de ces techniques afin d'améliorer considérablement les images de MECB. Afin de caractériser la qualité des sondes et pour déterminer le rapport du diamètre de l'électrode par rapport au diamètre de la gaine de verre, on a choisi un micrographe vidéo, des voltampérogrammes et les courbes d'approche de la MECB (courant en fonction de la distance entre la pointe et le substrat). La résolution et la répétabilité de l'arrangement de MECB est de 20 nm dans les trois dimensions *x*, *y* et *z* et il est possible de localiser et de relocaliser les zones d'intérêt avec précision à partir d'une image grossière. Dans un premier temps, on a déterminé des images d'arrangements d'électrodes d'or et de platine interdigitées. La résolution de l'image mise en évidence par la netteté des arêtes de la bande du platine a été améliorée en utilisant une électrode de 2 μm de diamètre. En ajustant les courbes d'approche aux courbes théoriques, on a trouvé que la hauteur des bandes du platine ou de l'or est d'environ 80 à 200 nm. On a optimisé les conditions d'obtention des images, par exemple, pour le temps d'attente pour une montée importante entre deux points successifs de données. Afin d'évaluer la stabilité thermique et temporelle du système, on l'a ensuite utilisé pour produire des images de lettres qui avaient été imprimées

Received 16 May 2005. Published on the NRC Research Press Web site at http://canjchem.nrc.ca on 16 December 2005.

R. Zhu and Z. Ding.[1] Department of Chemistry, The University of Western Ontario, London, ON N6A 5B7, Canada.

[1]Corresponding author (e-mail: zfding@uwo.ca).

 doi: 10.1139/V05-189 © 2005 NRC Canada

sur une diapositive avec police Courrier New en gras et une taille de 2. On a observé des déplacements mineurs lors de l'obtention de l'image, jusqu'à 8 h et 45 min. On a trouvé que l'épaisseur de la lettre était de 1,0 à 1,2 μm. Enfin, on a obtenu l'image d'un substrat de silicium comportant un arrangement de puits carrés éparpillés sur des centres de 10 μm. On a obtenu des images de bonne qualité à des distances variables entre la pointe et le substrat, même si les carrés étaient de la même taille que la pointe, si non plus gros. Pour fins de comparaison, on a aussi obtenu des images par AFM.

Mots clés : microscopie électrochimique à balayage, microscopie de forces atomiques, fabrication de microélectrodes, imagerie en circuit fermé, courbe d'approche de la sonde.

[Traduit par la Rédaction]

Introduction

In recent years, scanning electrochemical microscopy (SECM) (1–3) has shown great applications in the area of chemical and biochemical kinetics (4–16), chemical activity imaging (17–34), and micrometer scale structuring (32, 35–43) at liquid–liquid, liquid–solid, and liquid–membrane interfaces. The most significant advantage offered by SECM is its capability of probing chemical information of interfacial electron and ion transfer processes at the interfaces. Consequently, there is great interest in the development and application of SECM, as over 600 publications have appeared to date. While SECM is a powerful tool for these studies, two challenges remain: speed and resolution. These link to the nature of the available SECM probes (also named as tips, ultramicroelectrodes (UME)) and the techniques used to displace them in the vicinity of the interfaces (3).

The SECM probe is usually a platinum disk insulated by a glass sheath. A constant potential is applied to the electrode to quickly drive an electrochemical reaction of one redox species (the mediator) in a bulk solution. The measured current has to be constant (steady-state current), which is determined by hemispherical diffusion of the reactant at a fixed concentration to the electrode with a diameter of less than 25 μm. When the tip is brought down toward a substrate, this constant current is perturbed by the substrate at close proximity through either blockage of the diffusion (on an insulator, negative feedback) or dominant regeneration of the reacted species from the tip (on a conductor, positive feedback) (3). To better detect the feedback, the probe should get closer to the substrate. The edge of the glass sheath has to be machined down to a small size (sharpened to a tip) to avoid touching a tilted substrate. A small ratio of the outermost glass diameter to Pt disk diameter (RG) is very critical. On the other hand, the disk diameter and then the global tip diameter (outermost diameter), determine the resolution of SECM directly as the feedback reflects the perturbation from a substrate domain as small as the electrode. The reduction of the electrode size, however, further increases the workload and the difficulty in making the electrode. A lot of efforts are therefore needed to fabricate submicron or nanometer scale tips, aiming at high-resolution SECM (36, 44–47). For instance, it is very time-consuming and difficult to prepare a 2 μm diameter electrode with a small RG. We present here our improved procedure to make 2 μm diameter UMEs. The condition for sealing Pt wires was optimized and the workload to sharpen an UME was reduced by pulling the glass tubing. The rate for breaking the glass sheath and accidentally cutting the Pt disk was decreased to a minimum by employing a used computer hard disk drive.

It is possible to map out the surface topography and (or) chemical reactions by monitoring the current perturbation when the tip is rastered above a plane close to the substrate. It is obvious that the quality of SECM images is determined by how accurately the tip is positioned and the current is measured.

In fact, tip displacement in SECM is mostly driven by a piezoelectric device where the move is a function of the applied voltage to piezoelements (48). In some reports, the tip was displaced by a stepper motor (34, 49). While piezoelectric tube or disc scanners are widely applied in other scanning probe microscopy (SPM), an inchworm motor stage for three orthogonal dimensions is typically used in SECM due to its long traveling range (more than 25 mm), rigid stiffness, high stability, and minor creep, an effect of relaxation to a steady state after a fast movement. However, an inchworm scanning system suffers from two other common problems as those of other SPM techniques do: nonlinearity and hysteresis. Nonlinearity is a variation of the travel distance with the same increment of applied voltage. For instance, an image of a circular object will look like an oval if the linearity in the x direction is different from that in the y direction. The case will become much worse if each move is nonlinear to the voltage. Hysteresis is the deviation between curves of extension-voltage and retraction-voltage, i.e., the traveling distance is direction dependent. Both factors deform the images. In most SPM techniques, hysteresis and nonlinearity are compensated for by a scan in a single direction and a calibration array for a specific scanning system generated with a well-characterized sample. It is more difficult to calibrate an inchworm motor in this way because more parameters, such as direction, speed, step size, etc., should be considered (48).

Note that the operation of the inchworm scanning system as previously depicted employs an open-loop mode, where a voltage is applied to command a move without measuring the real travel that occurred. The controller in the system is only a voltage generator. Encoder-counting circuitry in the controller and a linear encoder integrated in the inchworm motor constitute a closed-loop operation, where the system applies a voltage to the motor, measures the actual motion, and eventually adjusts the position. Closed-loop operation gives the additional features of setting a zero point, stepping, moving to a targeted position, maintaining the position, as well as relocating the original position. The resolution of the system is the same as that of the encoder. We report here a

© 2005 NRC Canada

new SECM facility built with a closed-loop scanning system, which allows for bidirectional repeatability of ±20 nm linearly and easy programming through graphic user interfaces (GUI). Nonlinearity and hysteresis are minimized with the instrument. The scanning system not only receives motor control instructions from a computer, but also sends back the information on position and motor status. Other instrumentation details will be described in the Experimental section. Several samples were imaged with the setup to show how the system enhanced the SECM image quality. They included platinum and gold interdigitated electrode arrays (IDEAs) with alternative 20 μm digit width and interdigit space, printed letters in bold font New Courier and font size 2, and a platinum-coated silicon substrate with an array of square pits spaced apart on 10 μm centers. The IDEAs and the platinum-coated silicon substrate were also imaged for comparison, using a commercial atomic force microscope (AFM).

It is worth noting that SECM instrumentation was well-documented in a review by Wipf in the SECM monograph (48). However, the incorporation of a closed-loop scanning system into the SECM technique remains scarce. Only recently has the closed-loop system been introduced to the *z* direction by Denuault and co-workers (50). We believe that the new instrument, with added advantages, will benefit SECM research and its applications to various fields.

Experimental section

Chemicals

Electrolyte solutions consisted of 0.9 mmol/L ferrocenemethanol (Fc, 97%, Aldrich, Mississauga, Ontario) as the mediator and 0.1 mol/L sodium perchlorate hydrate (99.99%, Aldrich) as the supporting electrolyte. Concentrated nitric acid (Caledon Laboratories Ltd., Georgetown, Ontario) was diluted to 1:1 (*v*/*v*) with water. Distilled water (Milli-Q, Millipore, Bedford, Massachusetts, 18.2 MΩ resistivity) was used to prepare all aqueous solutions.

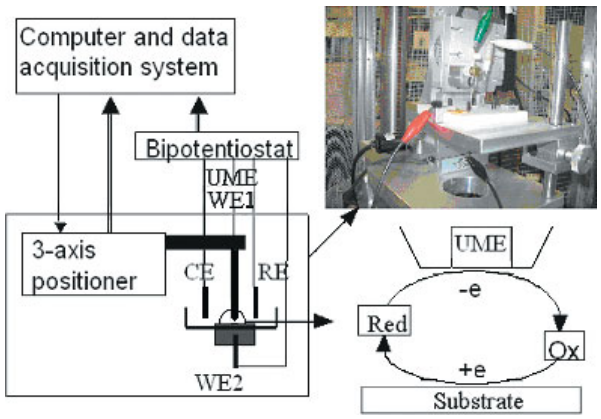
Samples

Pt- or Au-coated IDEAs were purchased from ABTECH Scientific, Inc. (Richmond, Virginia). A 100 nm thick layer of metals was sputtered on the Schott D263 borosilicate glass substrate metallized with 100 Å Ti in a monolithic configuration. Each IDEA electrode had 25 digital pairs with a 20 μm digit width, a 20 μm interdigit space, and a digit length of 3 mm. Letters, "SECM", "CHEM", and "UWO" were printed on a transparency (3M, London, Ontario) in bold font Courier New and in font size 2 with an HP 2200 Laser jet printer (HP, Mississauga, Ontario). A platinum-coated silicon substrate with an array of square pits spaced apart on 10 μm centers is the calibration reference from Digital Instruments (Santa Barbara, California).

Electrode fabrication

Platinum UMEs of 25 μm diameter were prepared by sealing nominal diameter Pt wire (Goodfellow Metals, Cambridge, UK) into glass capillary (o.d.: 2 mm; i.d.: 1 mm; length: 10 cm, Sutter instrument) as described elsewhere (36). We have modified the preparation procedure as described in the following. One end of the glass capillary was pulled by a heating coil puller (PP-83, Narishige, Japan) and was sealed by a Bunsen lamp. A corn shape inside the pulled capillary favourably fitted the inserted Pt wire to keep it straight. The thinner glass wall at the pulled end not only enhanced the quality of sealing the glass onto the Pt wire but also reduced the workload of sharpening the glass sheath.

Fig. 1. An illustrative scheme of the home-built SECM instrument. The inset is the zoom-in assembly of the electrochemical cell and the SECM probe mounted on the positioning system.



To prepare 2.0 μm diameter Pt tip UMEs, 2 μm diameter Pt wire (Goodfellows Metals, Cambridge, UK), known as Wollaston wire, was loaded into a similar pulled capillary but with an open-end. The support silver coating on the wire was etched out by briefly dipping the assembly in 1:1 (*v*/*v*) water – nitric acid. Exposed Pt wire was sealed in the glass capillary after washing out the residue acid with copious water and drying the inside by vacuum pumping and heating simultaneously.

All the tip surfaces were polished in succession by polishing pads (Buehler Ltd., Bluff, Ilinois) coated with alumina having diameters of 3.0, 0.3, and 0.05 μm, respectively. The glass sheath was sharpened by 3.0 and 0.05 μm diameter diamond pads. The RG is 6–8 for the 2 μm diameter Pt UME and 4 for the 25 μm diameter Pt UME. A used hard drive disk was used as polishing wheel, which was spun at high speed and had minor planer vibration.

The quality of these probes was monitored by cyclic voltammetry in the electrolyte solution, video micrography (TE-300, Nikon, Japan), as well as the SECM approach curves. In the cyclic voltammetry experiments, an electrochemical analyzer (CH 832A, CH Instruments, Austin, Texas) was used. A three-electrode system was employed, where the UME in question was the working electrode, a Pt wire 0.75 mm in diameter was used as the counter electrode, and a saturated Ag/AgCl (CH Instruments) electrode was the reference electrode.

Custom-built SECM instrument

The custom-built SECM instrument is schematically shown in Fig. 1. Indeed, the instrument is composed of three major parts: the electrochemical system, the positioning system, and the active data acquisition system. In general practice, a potential was applied to the SECM probe and a current was measured by the electrochemical system. The positioning and data acquisition systems were used to dis-

© 2005 NRC Canada

place the probe and record the current and position data simultaneously. The electrochemical and positioning systems were built together in a Faraday cage to isolate external electrical noise. At this time, our SECM setup can be operated in approach curve and constant-height imaging modes. In the approach curve experiments, UME current was monitored when the probe was brought closer to the specimen. In constant-height imaging mode, the current was recorded vs. lateral coordinates when the electrode was scanned in a plane at a fixed height in the vicinity of the substrates. Details on SECM instrumentation have been previously described (48). Here we outline some important aspects in our microscope.

Electrochemical system

A 3 mL cell circular in cross section was machined on a 4 cm × 4 cm Teflon block with a thickness of 0.8 cm. Substrates were mounted at the bottom opening of the cell and exposed a 5 mm diameter area. The cell block was clamped onto a very stable supporter, where the horizontal plane of the sample was adjusted to minimize the substrate tilt. Unless otherwise stated, three-electrode configuration was utilized, as described in the CV experiments. All electrochemical measurements were performed on an electrochemical analyzer (CH 832A, CH Instruments), which combined a bipotentiostat with an internal waveform generator. Note that it is possible for us to apply another potential with the instrument to the substrate for future SECM study as shown in the inset of Fig. 1.

Positioning system

Our positioning system was a FREEDOM^{TM} 1500-3 nano robot system purchased from EXFO Burleigh Products Group Inc. (Canada), which consisted of an EXFO 8200 controller and three Burleigh TSE-820 linear stages for the displacement in *x*, *y*, and *z* directions. The positioning speed could be adjusted to as high as 1.5 mm/s. The 8200 controller generates desired motion waveforms and supplies power to drive the motors and to control the encoders simultaneously. The 8200 can not only receive motor control instructions from a system controller (typically a personal computer), but also send position and motor status information. The controller allowed us to move an absolute target value, set a motor speed and a step size, and read the current motor position. Each TSE-820 linear stage was based on a 25 mm travel, 75 mm × 75 mm footprint, crossed roller bearing stage driven by a compact inchworm motor integrated with a 20 nm resolution encoder. The integral encoder was connected with a Heidenhain model EXE-650B electronic box that converts the analog signals into digital signals that are compatible with the controller. The *z* axis supported by a vertical bracket was also equipped with an adjustable spring-loaded counterbalance (TS-CB, Burleigh) to minimize gravity loads resting directly on the inchworm motor. The SECM probe was held in a groove by a screw and a Teflon Lucite washer on a custom-built holder mounted on the *z*-axis stage as shown in the inset of Fig. 1.

Active data acquisition system

This part consisted of a computer loaded with home-made virtual instruments (VIs) programmed in LabVIEW (Version 7, National Instruments, Austin, Texas), a general purpose interface bus (GPIB) board (PCI-GPIB, National Instruments) to communicate with the 8200 controller, and a 16 bit DAQ card (PCI-6052E, National Instruments) with a connection board (BNC-2090, National Instruments) to record current output from the electrochemical workstation. All SECM experiments were driven and automated by the custom-built LabVIEW VIs. In our LabVIEW VI programming, various controller implementations written in C++ language were called from the C++ library into a thin front end GUI, a Microsoft technology named Active X interface that accelerated the operation speed. Programming was very straightforward. After the input of parameters such as scan range, pixel and delay between action steps, the SECM VIs generated a loop consisting of iterations to move an absolute distance in one direction at a time (only call the C++ interface for target positioning), and then to measure the electrochemical current and record the positions simultaneously. The data were displayed in situ. For instance, approach curves were obtained by plotting the current vs. the displacement in the *z* direction. Images were acquired by plotting the current vs. lateral motion. A spreadsheet file was saved after each experiment for further analysis.

SECM experiments

The redox potential value, determined by CV in the bulk electrolyte solution, to oxidize the mediator, ferrocenemethanol, was held at 0.35 V vs. Ag/AgCl. The biased SECM probe was slowly brought (at a speed of 1 μm/s) to a specimen, until a normalized positive feedback current of 2 or a normalized negative feedback current of 0.3 was achieved. The distance between this engaged tip and the substrate was adjusted by withdrawing or pushing an absolute distance. Images were obtained by scanning the tip laterally above the substrate. Interesting spots (small areas) in images were zoomed in by relocating the tip and rescanning the substrate in closed loops. All experiments were conducted in air under an ambient temperature of 20 ± 2 °C.

Data analysis

Theoretical approach curves were obtained based on previous studies (4, 51, 52) and our simulation using FluxExpert software at the Swiss Federal Institute of Technology in Lausanne (EPFL). The height of the gold bands on the IDEAs was extracted from the approach curves by differentiating the distances corresponding to the normalized current (positive feedback) above the band and that above the glass (negative feedback). Similarly, the heights of the printed letters were obtained by reading the distance differences corresponding to the appropriate normalized currents on the negative feedback approach curve.

AFM image

AFM images were carried out in air on Alpha-SNOM (WiTec, Ulm, Germany), using a contact mode. The AFM probes had a spring constant of 2.8 N/m.

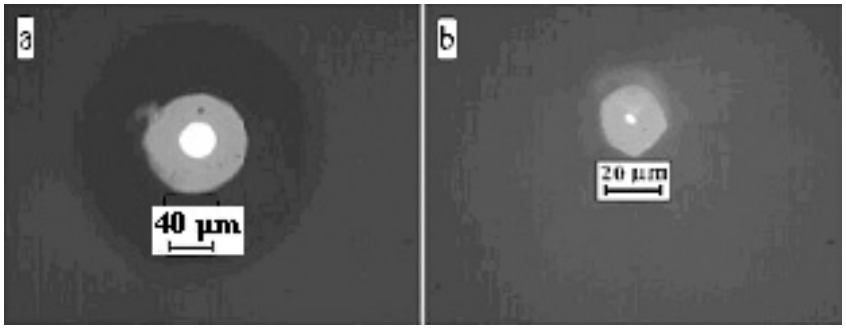
Results and discussion

Characterization of SECM probes (UMEs)

Video micrographs, cyclic voltammograms, and SECM

© 2005 NRC Canada

Fig. 2. Typical video micrographs of (*a*) a 25 μm diameter electrode with a RG value of about 3 and (*b*) a 2 μm ultramicroelectrode with a RG value of 8.



approach curves were used to characterize the prepared UMEs, which were finely polished and sharpened.

Video micrographs

Figure 2 illustrates representative micrographs of the two types of microelectrodes (25 and 2 μm in diameter) monitored after intensive polishing and sharpening. RG, the ratio of the glass sheath radius to the Pt disk radius, was determined via a high-magnification optical microscope. RG values for the 25 μm microelectrodes used in the experiments of this report can easily go to 3 to 4 with our modified fabrication procedure (Fig. 2*a*). It is known that the smaller the RG, the greater the feedback the SECM probe will give (3). This is because the reduced glass sheath will decrease the case where the electrode edge touches a substrate, especially a tilted one. The touching, in fact, compromises the expected feedback response from the probe. The prepared 2 μm diameter electrode showed a quasi-disk shape (Fig. 2*b*). In the following, these UMEs are defined as 2 μm "effective diameter" probes, assuming that there is no large difference between the oval shape and the disk shape in very small sizes. The RG for these electrodes can reach 6–8. The micrographs of both electrodes show a very smooth surface. There was little shade at the edge of the Pt disk, showing a good sealing of the glass sheath surround the disk.

Cyclic voltammograms

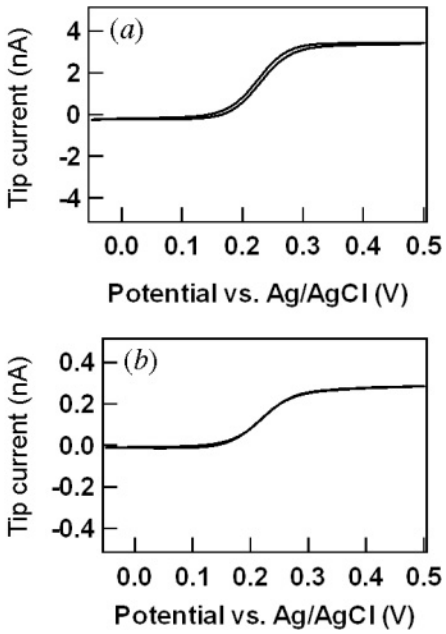
Cyclic voltammetry of a 0.9 mmol/L ferrocenemethanol solution containing 0.1 mol/L TEAP as the supporting electrolyte was carried out on each of the electrodes to test their electrochemical behavior. The electrochemical active group, ferrocene (Fc), in ferrocenemethanol is oxidized to ferrocenium (Fc^+) when the applied potential at the electrode is scanned in a positive direction.

$$[1] \qquad Fc - e^- \rightarrow Fc^+$$

The redox couple (Fc^+/Fc) has a fast electron transfer rate at an UME and shows a steady-state voltammogram (Fig. 3) because of its hemispherical diffusion to the electrode (53). The size of the 25 μm UME was confirmed by calculating its radius (*a*) from the measured steady-state current or diffusion-limiting current on the voltammogram (Fig. 3*a*) via eq. [2],

$$[2] \qquad a = \frac{i_{T,\infty}}{4nFDc^0}$$

Fig. 3. Representative cyclic voltammograms recorded at (*a*) a 25 μm diameter UME and (*b*) a 2 μm diameter UME. The solution in the electrochemical cell contained 0.9 mmol/L ferrocenemethanol and 0.1 mol/L KCl. The scan rate was 10 mV/s.



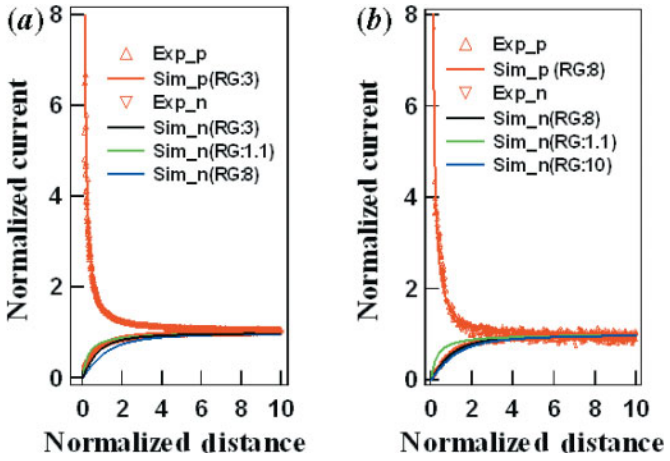
where $i_{T,\infty}$ is the steady-state limiting current of the UME far from a substrate (several UME diameters), n is the number of electrons transferred in eq. [1], F is the Faraday constant, D and c^0 are the diffusion coefficient and concentration of ferrocenemethanol, respectively. The diffusion coefficient here was taken as 7.8×10^{-6} cm^2/s from a previous report (54). The electrochemically determined result of $a = 13$ μm agrees well with that measured on the micrographs. From the voltammogram of the 2 μm diameter UME shown in Fig. 3*b*, the effective radius was 1.0 μm, a result calculated from eq. [2]. Both voltammograms show a flat steady-state current. The forward and backward current–potential curves almost overlapped, indicating a very small capacitive current and therefore a good electric isolation on the sides of UME disks (44).

Approach curves

UMEs were further checked by recording SECM approach curves of the UMEs toward a conductor or an insulator substrate (Fig. 4). In fact, an UME was biased with a potential at 0.35 V in the same solution as in Fig. 3, and the

© 2005 NRC Canada

Fig. 4. Respective approach curves toward a 2 mm diameter Pt disk electrode and a glass microscope slide for a (*a*) 25 μm diameter UME with RG = 3 and (*b*) a 2 μm diameter UME with RG = 8. The electrochemical cell is the same as described in Fig. 3. The applied potential at the UMEs was 0.35 V and the approach speed was 1 μm/s. The current shown here was normalized by the infinite tip current ($i_{T,\infty}$) when the UME was far away from the substrate, whereas the distance was normalized by the electrode radius. Simulated negative approach curves with RG values of 4, 8, and 10 for both substrates are plotted for comparison.



diffusion-limiting current was monitored vs. the distance between the electrode and the substrate while it was driven toward the substrates by a *z*-inchworm motor. Figure 4*a* illustrates two expected approach curves for a 25 μm diameter SECM tip: (*i*) the steady-state current decreased when the SECM tip moved toward a glass slide (negative feedback) because the insulator blocked the diffusion of ferrocenemethanol to the tip and the reaction shown in eq. [1] slowed down; (*ii*) the diffusion-limiting current increased when the UME approached a 25 μm diameter Pt disk electrode (positive feedback) because the reaction below at the Pt substrate regenerated the ferrocenemethanol to the tip and most importantly, the electrochemical reaction was faster than the normal diffusion.

[3] $Fc^+ + e^- \rightarrow Fc$ (fast)

The detail of this reaction governed by the Nernst equation at open circuit has been described elsewhere (24, 55). Note that the substrate also blocked the diffusion. However, the fast regeneration of Fc (eq. [3]) dominated. Normalized current ($i_T/i_{T,\infty}$) of 8 and 0.1 at both SECM tips was attained for positive and negative feedback, respectively, as shown in Fig. 4. Relative small RG in the probe fabrication avoided contacting the tip glass sheath with substrates eventually tilted and enabled the UMEs to get closer to the substrate. Shao and Mirkin (51) and Amphlett and Denuault (52) have demonstrated that RG affects SECM approach curves for insulating substrates more obviously than those for conductive substrates. RG values estimated from video micrographs were therefore confirmed by fitting experimental approach curves with theoretical ones generated by solving the diffusion problems with different RG values in this system based on previous publications (51, 52) and the simulation using FluxExpert software. While the experimental approach curves are practically coincident with theoretical ones for RG = 10, 8, and 4 in positive feedback mode (with Pt substrates), the curves for the negative feedback differentiate from simulated ones with different RG values as illustrated in Fig. 4. An extracted RG value of 3 agrees well with that estimated from video micrographs. Similar responses were observed from a 2 μm diameter SECM tip as shown in Fig. 4*b*. A RG value of 8 was determined from the theoretical curves for negative feedback.

Imaging Pt and Au IDEAs

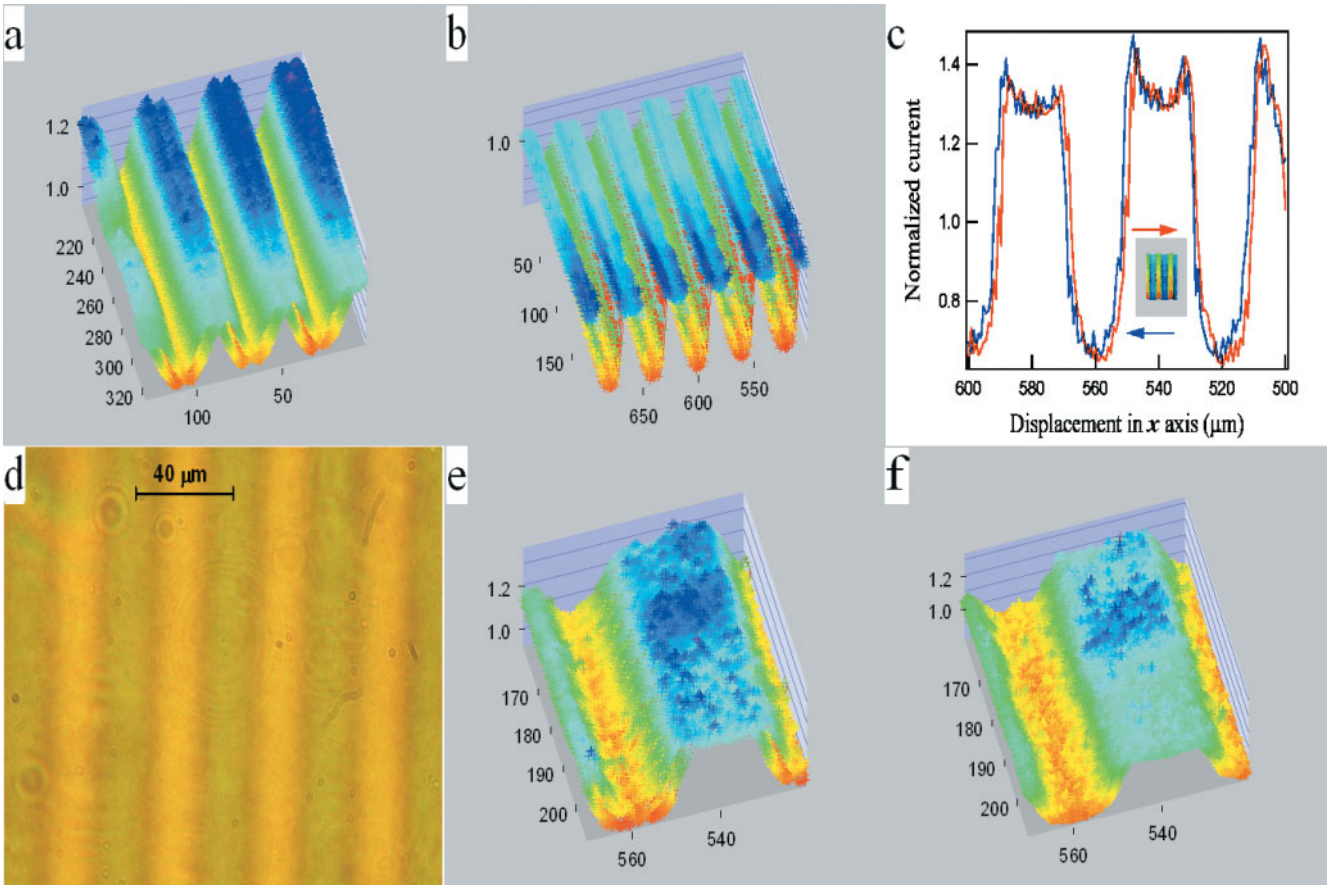
Well-characterized UMEs were first used to image Pt and Au IDEAs consisting of 25 digital pairs with 20 μm digit width, 20 μm interdigit space, and a digit length of 2985 μm. 0.35 V was applied to a UME tip immersed in a solution containing 0.9 mmol/L ferrocenemethanol and 0.1 mol/L KCl.

Tip size effect

A 25 μm UME tip was driven slowly toward a Pt array until a normalized current of 4 was achieved. The tip was withdrawn 6.0 μm before starting to image. This avoided a potential crash of the electrode against the substrate because of the tilt surface. Notice that the tip-to-substrate distance cannot be calculated by reading the distances from the approach curves as shown in Fig. 4*a* because the tip diameter is larger than the Pt bandwidth. The UME was then rastered in the *x*,*y* plane above the IDEA by the closed-loop inchworm positioner system, and the tip current was recorded to obtain SECM images (Fig. 5*a*). Data acquisition followed a zigzag scan pattern, i.e., the image was composed of alternative forward and backward line scans in the *x* direction. It took only 11 min to obtain this 130 μm × 130 μm (with 256 × 256 pixels) image because of this time-saving dual direction scanning. The step size was then 510 nm. The *x*,*y* position coordinate data recorded by the closed-loop system was examined. Real step size was found to be 510 and 490 nm alternatively. Note that the anodic current for ferrocenemethanol was monitored in Fig. 5. Normalized current would be more than 1 if the UME tip was above a Pt band. In contrast, the current would be less than 1 when it was positioned above a glass spacer. As shown by its cross section, the resolution can be evaluated by examining the sharpness of the rise and fall of the tip current when the probe was crossing the edges from a glass spacer to a Pt band or vice versa. The resolution shown in Fig. 5*a* is quite low because of the large size of the electrode. Quantitative analysis was therefore difficult to do in this case. However, the image clearly shows the alternative structure of the Pt bands and their glass spacers. The sharp contrast and the repeatability of the image match those of a micrograph magnified at 400 times (Fig. 5*d*). Images obtained by using this closed-loop system show a good quality. When the UME size was reduced to 2 μm in diameter, sharper rises and falls of the normalized current than those obtained with the 25 μm UME were observed at the Pt band edges as shown in Fig. 5*b*, indicating a higher resolution. The starting tip-to-substrate distance was set at 2.78 μm. It is evident that SECM resolution is dependent on the tip size. Further analysis of the resolution can be carried out by examining the cross section of the image (Fig. 5*c*). It is interesting to note

© 2005 NRC Canada

Fig. 5. Surface plots of tip current recorded at (*a*) a 25 μm diameter UME and (*b*) a 2 μm diameter UME during an image scan of a Pt IDEA in the area of 130 μm × 130 μm and 200 μm × 200 μm, respectively. Graph (*c*) shows two line scans in a length of 50 μm, from left to right (red) and from right to left (blue). In fact, the lines were extracted from an image that magnified a small area of 100 μm × 100 μm in image (*b*) as shown in the inset. An optical micrograph at a magnification of 400 times is shown in graph (*d*). Figures (*e*) and (*f*) illustrate step-size effect on SECM images of an area of 50 μm × 50 μm obtained on a 2 μm UME, with pixels 128 × 128 and 256 × 256, respectively. The UME tips were biased at 0.35 V and the IDEA was at open circuit. The tip-to-substrate distance (*d*) for (*a*) was set by first approaching the tip to a Pt band on the IDEA until the normalized current of 4 was reached and then withdrawing an extra distance of 6 μm. For graphs (*b*), (*c*), (*e*), and (*f*), the *d* was set at 2.78, 2.78, 3.30, and 2.92 μm, respectively. Inchworm speed for all three axes was set at 1000 μm/s. The solution was 0.90 mmol/L ferrocenemethanol and 0.1 mol/L KCl. The current shown here was normalized by the infinite tip current ($i_{T,\infty}$) when the UME was far away from the substrate, whereas the distance was normalized by the electrode radius. The scale of the *x*,*y* position was in μm units.



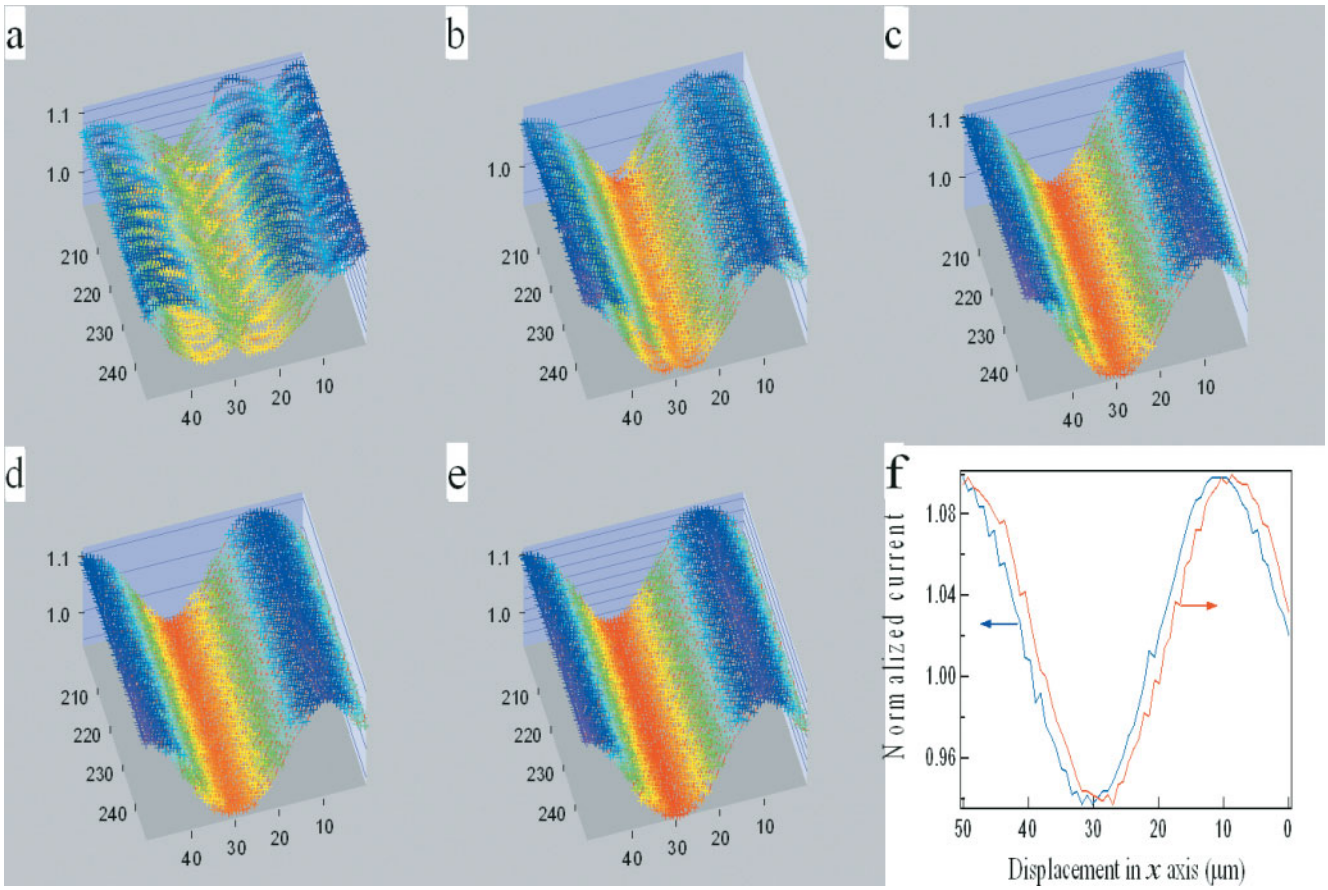
that the line scans tell us more detail about the band structures. For instance, the feedback current above the two edges of the Pt bands is higher than that above the center of the bands. This higher current corresponds to a shorter tip-to-substrate distance, i.e., the edges are thicker than the center. This can be well-understood by looking closely at the approach curve for the positive feedback. Interesting areas were zoomed in to show details as illustrated in the inset of Fig. 5*c*. In addition, a fine step size for imaging is helpful to enhance the image quality. For example, a sharper current rise and fall were observed in imaging an area of 50 μm × 50 μm with 256 × 256 pixels (equivalent to a step size of 195 nm) than in imaging the same area but with of 128 × 128 pixels (step size of 390 nm), as illustrated in Figs. 5*e* and 5*f*.

Overcoming hysteresis

Looking closer at the surface plot shown in Fig. 5*a*, the cross section reveals a double alternative wave, a systematic deviation between forward and backward scans in the *x* direction at the imaging conditions previously indicated. The hysteresis was worse especially when a large step size was taken (Fig. 6*a*). It is unlikely that this hysteresis came from natural behaviors of a closed-loop positioning system at a resolution of 20 nm because the tip position was measured by the capacitive sensor and was forced to adjust until the programmed targets were attained. Imaging conditions with a 25 μm diameter electrode, such as scan range, inchworm speed, as well as delay time (dt) between two succeeding data points on the scan line etc., were further adjusted and optimized with the home-made LabVIEW VIs. In fact, a 50 μm × 50 μm area of the Pt IDEA was located to image each time when one condition was changed. With the help of the closed-loop system, the UME tip was easily relocated to the original point by simply setting the coordinates of this point as the target position. The image quality was then inspected through SECM surface plots. For instance, the dt optimizing process is demonstrated in Fig. 6, where the tip-

© 2005 NRC Canada

Fig. 6. SECM images demonstrating optimization processes for delay time (dt), an interval taken between the two succeeding data points. (*a*) dt = 0 ms (data acquisition rate depended on the CPU dedicated to the LabVIEW VI; (*b*) dt = 20 ms; (*c*) dt = 40 ms; (*d*) dt = 50 ms; and (*e*) dt = 60 ms. (*f*) Forward and reverse line scans extracted from image (*e*) are shown. The UME diameter was 25 μm. An exact 50 μm × 50 μm area of the Pt IDEA was located and relocated again and again via the closed-loop system to keep other imaging conditions identical. The starting tip-to-substrate distance was set in the same way as in Fig. 5*a*. Pixels were at 64 × 64, equivalent to a step size of 780 nm. The electrochemical parameters were the same as described in Fig. 5.



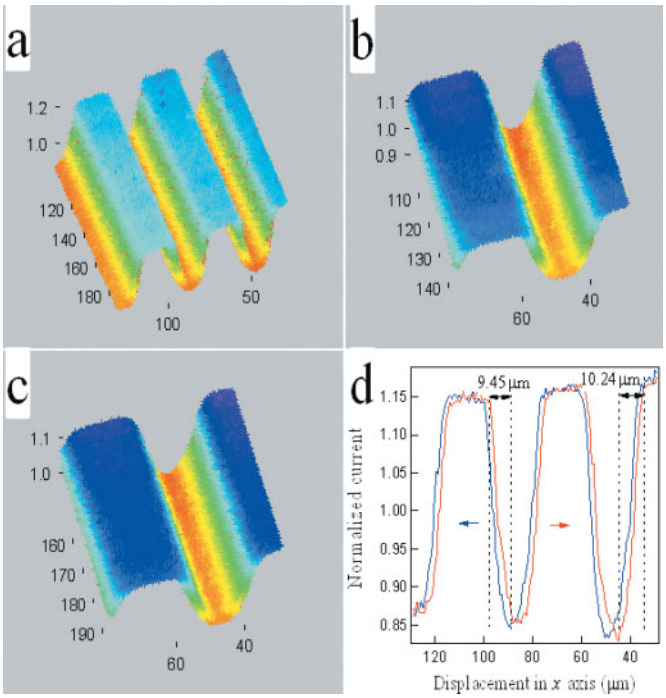
to-substrate distance was set as in Fig. 5*a*. When the dt was set at 0, the forward and backward scans deviated almost 10 μm (Fig. 6*a*), and the SECM image showed much wider Pt bands and their glass spacers, almost twice larger than the real ones. Note that the data acquiring speed at this dt totally depended on the computer processing unit (CPU) dedicated to the system in which the software and the hardware, including an inchworm motor, its capacitive sensor, and its controller as well, should have recorded the current after finishing several cycles of moving, judging, and adjusting the tip position to reach a target position. Real dt was probably within 1 ms at dt = 0 and was too short for the system to fulfill the task. The hysteresis became worse if the travel distance between the two succeeding data points is longer. In addition, the diffusion-limiting current might not reach a steady state immediately after positioning the tip. This explains that current signal, shown in Fig. 6*a*, was a little noisy. Delay time was then set to 20, 40, 50, and 60 ms, respectively, and the same area was imaged again and again (Figs. 6*b*–6*e*). The longer the dt, the less the hysteresis. The deviation became small and constant if the dt was larger than 50 ms. The remaining hysteresis was caused by the asymmetry of the glass sheath around the Pt disk. For instance, in the case of this experiment, the Pt disk located on the right slightly from the central axis of the global electrode. Positive feedback from the Pt bands was monitored earlier in forward scan (the direction of the red arrow, left to right) than that in the reverse scan (the direction of the blue arrow, right to left) as illustrated by the cross sections in Fig. 6*f*, which were extracted from the image in Fig. 6*d*. We will come back to this point later in examining the SECM images of a gold IDEA. Effects on the image quality such as scan range and inchworm speed were also investigated. It turned out that the dt was mostly related to the hysteresis previously observed.

A gold IDEA with the same structure as the platinum one was also imaged by a 2 μm diameter probe (Fig. 7). When the probe was approaching the IDEA this time, a negative feedback was observed as shown in Fig. S1 in the Supporting information[2] of this report. The negative feedback

[2] Supplementary data for this article are available on the Web site or may be purchased from the Depository of Unpublished Data, Document Delivery, CISTI, National Research Council Canada, Ottawa, ON K1A 0R6, Canada. DUD 3630. For more information on obtaining material refer to http://cisti-icist.nrc-cnrc.gc.ca/irm/unpub_e.shtml.

© 2005 NRC Canada

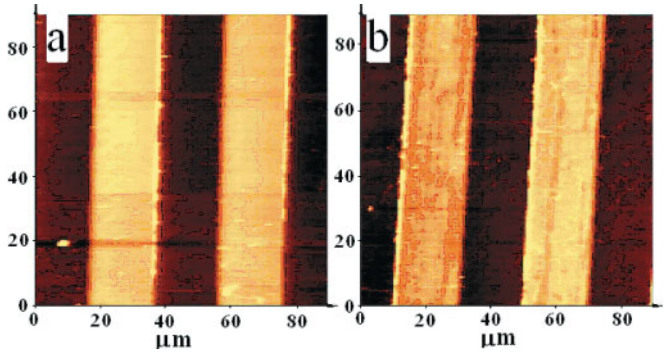
Fig. 7. SECM images of a gold IDEA acquired by a 2 μm UME. Image (*a*) shows an area of 100 μm × 100 μm covering 2.5 Au bands. Images (*b*) and (*c*) demonstrate 1.5 Au bands in an area of 50 μm × 50 μm. Graph (*d*) shows a forward (red) and a reverse (blue) line scan of image (*a*). All images were conducted with 128 × 128 pixels. The starting tip-to-substrate distance was set at 2.82 μm. Other imaging conditions are the same as in Fig. 5.



indicated that the electrode approached to an interdigit. The tip-to-substrate distance was set at 2.82 μm, and the probe was scanned in the constant-height mode to obtain images. Two and a half Au bands imaged in an area of 100 μm × 100 μm were well-resolved in Fig. 7*a*. The digit and interdigit width was measured and both were found to be 20 μm, which agreed well with their specification from the manufacturer. Two parts of the one and a half bands on the right in Fig. 7*a* were rescanned (magnified) in an area of 50 μm × 50 μm, as shown in Figs. 7*b* and 7*c*. These again demonstrated the quality of the SECM images using the closed-loop positioning system.

Lee et al. (18) investigated a gold IDEA with combined SECM and scanning optical microscopy in a constant-distance feedback mode. They showed that a topographic image of Au band edges is affected by the substrate tilt. We extracted both the forward and backward scan lines, which are shown in Fig. 7*d*. A similar phenomenon was observed both in forward and backward scans: the upward (from the glass to the Au band) edge width (10.24 μm) is larger than that of the downward (from the Au band to the glass) (9.45 μm) because of the substrate tilt. In addition, slight hysteresis because of the asymmetry of the glass sheath around the Pt disk was also observed. In the case of Fig. 7*d*, the disk is located further to the right. The positive feedback from the Au bands responded earlier in forward scans than in the backward scans. This was also observed in the SECM

Fig. 8. Topographical AFM images of (*a*) the Pt IDEA and (*b*) the Au IDEA.



images of the previous Pt IDEA scanned by a 25 μm diameter electrode, as shown in Fig. 6*f*.

Figure 8 shows topographical images for the Pt and Au IDEAs for a comparison with the previous SECM images. The AFM images correlate well with those from SECM. This demonstrates the enhanced quality of images on our SECM setup.

Measuring Pt and Au band height

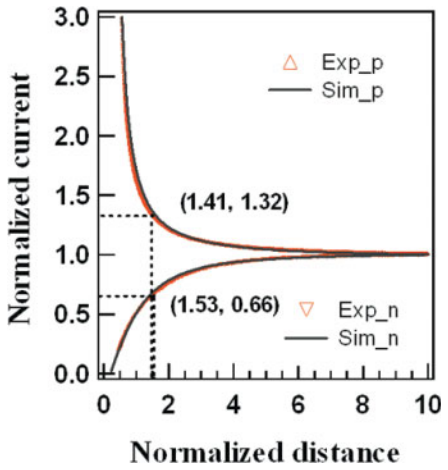
Two average tip currents (1.32 and 0.66) were measured when the tip was above the center of a Pt digit and above the center of an interdigit (Fig. 5*c*). The distance from the tip to the digit (1.41 μm) and the distance from the tip to the interdigit (1.53 μm), corresponding to the two currents, respectively, were read from the approach curves for positive feedback (above the conductor) and negative feedback (above the insulator). The Pt band height is then the difference of the two distances (120 nm), which agrees with the 100 nm indicated in the specification from the manufacturer and that from AFM measurements. This measuring procedure is outlined in Fig. 9. As described in the Tip size effect section, higher currents at the band edges were observed (Fig. 5*c*), and therefore larger heights were expected. The height at the edges of the Pt bands was found to be 130–270 nm in the same measuring manner. Similarly, the cross section extracted from the image in Fig. 7*a* is shown in Fig. 7*d*. The Au bands look flatter than the Pt ones. However, the band thickness was determined to be around 200 nm.

High-resolution images of printed letters

To further demonstrate the advantages of the closed-loop scan system, such as high repeatability, high resolution, and low hysteresis, some letters printed on a transparency and in very small font size were imaged. The sample was fixed in the electrochemical cell described in the Experimental section, which contained a solution of 0.90 mmol/L ferrocenemethanol and 0.10 mol/L KCl. A 2 μm diameter UME biased at a potential of 0.35 V was first brought to the transparency body to attain a normalized current of 0.5, corresponding to a tip-to-substrate distance of 1.0 μm. Both the transparency substrate and the printed letters were found to behave like an insulator because a negative feedback was observed everywhere. The tip-to-substrate distance was set at 1.5 μm by withdrawing the tip an extra distance of 0.5 μm. At this fixed height, the tip was rastered above the letters to

© 2005 NRC Canada

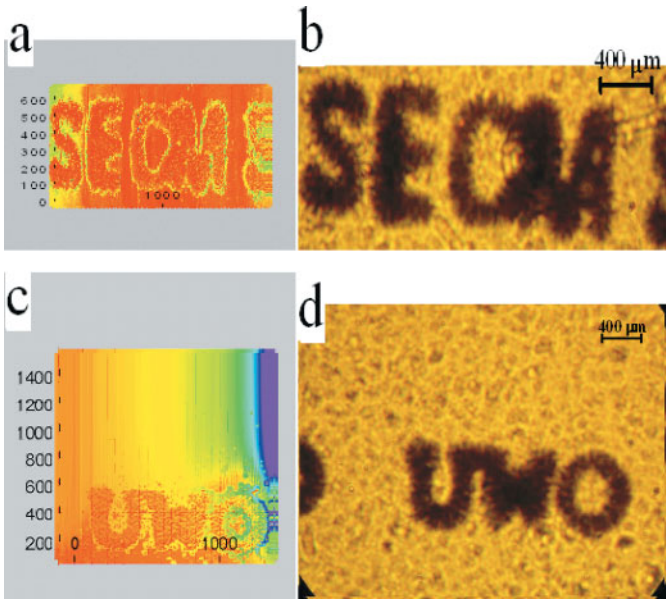
Fig. 9. Respective approach curves toward (*a*) a Pt digit and (*b*) an interdigit with a 2 μm diameter UME for RG = 8. The electrochemical cell is the same as described in Fig. 5. The applied potential at the UMEs was 0.35 V and the approach speed was 1 μm/s. Simulated approach curves are also plotted.



obtain images (Fig. 10). A large area was first scanned to find the letters. The UME was then relocated to a desired position and rastered over desired letters. Figure 10*a* shows a SECM image of the letters SECM printed with bold font Courier New and in font size 2. An area as large as 700 μm × 2000 μm was imaged with a step size of 5 μm. Knowing that the tip to substrate was fixed relative to the transparency substrate and the printed letters protruded out of the substrate plane, a more negative feedback above the letters was expected because the letters with a shorter distance blocked more redox species diffusing to the UME. This can be further demonstrated by the current profile of a line across the image. From the theoretical approach curve for negative feedback on an insulator, a height of 1.2 μm for the letters can be estimated by differentiating the distances of tip-to-letter and tip-to-transparency, corresponding to the tip currents above the letter and above the transparency, respectively. The image quality in terms of contrast, sharpness, etc. is even better than that of an optical micrograph at a magnification of 400× (Fig. 10*b*). No deformation was observed due to the closed-loop control.

The letters UWO, printed in bold font Courier New and font size 2, were imaged in addition. The same imaging procedure was followed. In fact, a very high-resolution image (1024 × 1024 pixels) for an area of 1500 μm × 1500 μm was acquired ambitiously (Fig. 10*c*). It took about 8 h and 44 min to finish this image. A clear picture of the letters was obtained and the image quality matched to that of a video micrograph (Fig. 10*d*). Capacitive sensors integrated in the three inchworm motors measured the traveling distance precisely and lead the system to attain the target movement in each step. Thermal and temporal drafts were minor according to the sharpness of letter edges shown in Fig. 10*c*. This proved again that the present closed-loop scanning system has a superior repeatability, high resolution, very low hysteresis, and high stability as well. The letter height was estimated to be 1.0 μm from the approach curve. While high quality SECM images can be obtained by the closed-loop scanning system, the effect caused by tilted substrates is still

Fig. 10. (*a*) SECM image of the letters SECM printed in bold font Courier New and font size 2 on a transparency, with a step size of 5.00 μm. (*b*) Optical micrograph corresponding to letters in (*a*). (*c*) SECM image of the letters UWO printed in bold font Courier New and font size 2 on a transparency, with a step size of 1.46 μm. (*d*) Optical micrograph corresponding to the letters in (*c*). The UME size was 2 μm in diameter. The tip was engaged by approaching the transparency body unitl the normalized current of 0.50 was attained. A distance of 1.0 μm was withdrawn before starting to image. The tip-to-substrate distance was determined to be 1.5 μm. Other imaging conditions are the same as in Fig. 5.



observed, especially when a large area was imaged. This is because a so-called constant-height mode was employed. The regular variation of the tip-to-substrate distance because of the tilt can be easily distinguished with original sample topography and should be accounted for during the examination of SECM images. The letters CHEM printed in the same size and font were then imaged individually. Less tilt effect was observed as demonstrated in Fig. 11.

Imaging a sample with small topography structures

Finally, SECM was used to image a platinum-coated silicon substrate with an array of square pits spaced apart on 10 μm centers. A 2 μm diameter UME poised at a potential of 0.35 V was brought to the sample immersed in a solution containing 0.90 mmol/L ferrocenemethanol as the mediator and 0.1 mol/L KCl as the supporting electrolyte. A slight positive feedback approach curve was obtained, showing that reaction expressed by eq. [3] became much slower than that on a Pt band electrode. An effective reaction constant (0.1 cm/s) can be extrapolated by fitting the approach curve with theoretical curves obtained by Mirkin and Bard and coworkers (4, 56). This is possibly because the Pt coating is very thin and the sample does not behave as a conductor. The tip-to-substrate position was set by approaching the tip to the silicon specimen until a normalized current of 1.5 was reached and then withdrawing an extra distance. Images of various areas on the specimen in different sizes are demon-

© 2005 NRC Canada

Fig. 11. SECM image of the letters CHEM printed in bold font New Courier and font size 2 on a transparency, with a step size of 3.90 μm. The letters (*a*) C, (*b*) H, (*c*) E, and (*d*) M were imaged individually to minimize the effect of the substrate tilt. The UME size was 2 μm in diameter. The tip was engaged by approaching the transparency body until the normalized current of 0.50 was attained. A distance of 1.9 μm was withdrawn before starting to image. The starting tip-to-substrate distance was determined to be 2.4 μm from the approach curve. Other imaging conditions are the same as in Fig. 5.

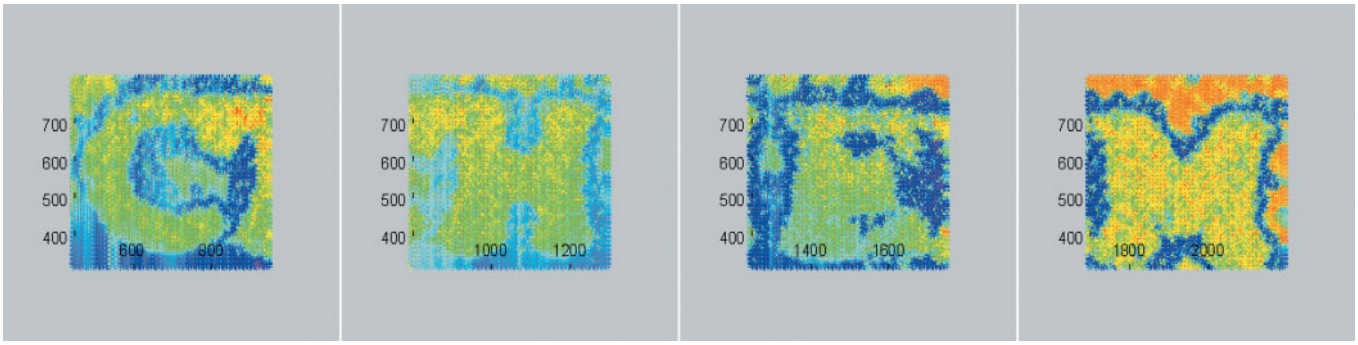
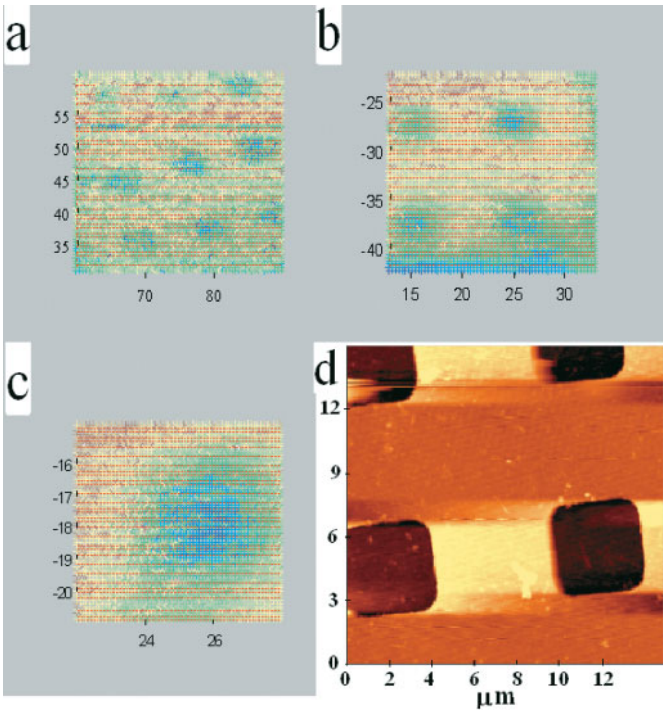


Fig. 12. The silicon structures of a DI calibration reference imaged by a 2 μm diameter UME to demonstrate (*a*) an area of 30 μm × 30 μm, (*b*) an area of 20 μm × 20 μm, (*c*) and a single square. Pixels were at 64 × 64. The tip was brought to the silicon body until the normalized current of 1.5 was attained. A distance of 1.50, 1.36, and 0.86 μm was withdrawn before starting to image in (*a*), (*b*), and (*c*), respectively. Other imaging conditions are the same as in Fig. 5. An AFM image is shown in (*d*).



strated in Fig. 12. Clear square structures were observed. In fact, a less positive feedback was observed when the tip moved from the substrate body to a square because the tip–substrate distance above a square was larger than that above the body and less ferrocene molecules regenerated at the substrate could be detected. The edge-to-edge distance of two neighboring squares, equivalent to center-to-center distance, was determined to be 10 μm from Figs. 12*a* and 12*b*, which agrees very well with the specification from the manufacturer. The squares on the substrate were estimated to be 4 μm × 4 μm from the SECM images. It was a challenge to map them with a 2 μm diameter UME, whose size is barely smaller than that of the squares. A typical AFM image of the calibration reference is shown in Fig. 12*d*, which agree well with our SECM images.

Note that the shape of the SECM tip is probably related to the observed lateral size when the probe size is close to that of the squares on the substrate. The size of the squares is expected to be affected. This phenomenon is common in scanning probe microscopy such as atomic force microscopy. The shape of the tip and sample in the SECM experiments is what might be seen in the final images. That is why the observed squares were somehow deformed. However, these considerations are not well-described in previous reports and are not completely understood.

Conclusions

This work improves the fabrication of ultramicroelectrodes of various sizes, especially of 2 μm diameter electrodes. Application of a pulled glass tubing optimized the sealing of glass around the Pt disk and reduced the workload for sharpening the electrode to a small RG. Normalized currents of 8 and 0.1 for positive and negative feedback, respectively, can be easily attained with SECM probes having a RG value of 3–8. Video micrographs, cyclic voltammetry, and SECM approach curves were complementary to each other and were routinely used for characterization of the prepared electrodes. Electrochemical behavior and RG values can be verified in this manner.

Open-loop imaging procedures in conventional SECM instruments are problematic in obtaining an authentic image, especially when a large area is mapped and (or) a fast scan rate is used. Frequent trivial calibration is essential to correct any image deformation that occurs. The case is even worse when both forward and reverse scans are used for imaging purposes. Images lack integrity because of the alternative deviation of scans in two directions. The present work illustrates that a closed-loop system can be used to correct for these nonlinearity and hysteresis effects.

© 2005 NRC Canada

An advanced scanning electrochemical microscope has been built, for the first time, using a closed-loop scanning system. This new generation of SECM system consists of a bipotentiostat capable of measuring a current as small as 1 pA, a scanning stage of three inchworm motors integrated with a capacitive sensor, an Active-X controller, and an active data acquisition system for experimental control, fast data acquisition of the data, and in situ display and analysis of the data. SECM approach curves and images can be carried out with user-friendly, home-built LabVIEW VIs in which parameters such as scan range and step size (pixels) can be adjusted. The strategy for moving the probe in each step is to stand in a closed-loop of positioning, sensing and adjusting until attaining a target distance. The scanning system has a superior repeatability of 20 nm as well as a high resolution of 20 nm in the whole scan range of 25 mm × 25 mm × 25 mm. This new instrument opens a wide avenue for SECM image studies on reactions at various substrates, without requiring a calibration of the scanning system. The microscope provides real information on three-dimensional displacement of the probe and avoids artifacts on the size and shape of chemically active spots.

In the case of Pt and Au IDEAs, SECM images clearly showed the alternative Pt bands and glass spacers. Image quality can match that of an optical micrograph. In addition, reduction of tip size from 25 μm in diameter to 2 μm leads to a higher resolution image. It is noted that enough time delay to fulfill the closed-loop in each scan step is necessary to obtain an optimal image. Information on detained band structures was revealed. Pt band height was found to be 80–120 nm, deducting from tip – Pt band and tip – glass spacer distances the corresponding normalized current in the approach curves, and band height for Au was measured to be 200 nm. Another advantage of the present SECM is the capability to locate, relocate, and zoom into the area of interest.

In the case of printed letters on a transparency in font Courier New and font size 2, responses of the negative feedback on an insulator were obtained above both letters and the transparency substrate. More negative feedback was observed when a 2 μm diameter UME was displaced from the transparency substrate to the letters in a constant-height image mode. This is because letters have a certain height (1.0 μm) and therefore provide more of a block to the diffusion of ferrocene molecules diffusing to the tip. In addition, the SECM setup was used exhaustively for imaging letters as long as 8 h and 40 min. No much thermal and temporal draft was observed.

For the silicon substrate with an array of square pits spaced apart on 10 μm centers, it was fortuitous that a 2 μm diameter UME, only a little smaller than the the squares in a size 4 μm × 4 μm, was able to map the array. In fact, small positive feedback was observed due to a slow electrochemical reaction when a 2 μm diameter electrode was brought to the substrate immersed in a solution of 0.9 mmol/L ferrocenemethanol as the mediator. By properly relocating the original position of the probe and adjusting the imaging parameters, a single square, though it looked like a hole, was imaged. Tip shape plays an important role in imaging. A smaller probe is needed to obtain the real structure information.

We are confident that SECM image quality is enhanced by improving UME fabrication and introducing a closed-loop scanning system. More operation modes can be added on, such as constant-distance mode, constant-current mode, etc. It is anticipated that instrumentation of this kind will further broaden the applicability and the reliability of SECM for the study of the various (bio)chemical processes at interfaces and (or) surfaces.

Acknowledgments

We appreciate the financial support for this research from the Natural Sciences and Engineering Research Council of Canada (NSERC, New Discovery and Equipment Grants), Canada Foundation for Innovation (CFI), Ontario Innovation Trust (OIT), the Premier's Research Excellence Award (PREA), and the University of Western Ontario (Academic Development Fund (ADF) and the Start-up Fund). ZFD is grateful to the Swiss Federal Institute of Technology in Lausanne (EPFL) for a visiting professorship in Professor Hubert Girault's group during the summer of 2003. We thank Dr. Bernie Quinn for her constructive discussions and suggestions on the fabrication of ultramicroelectrodes. Technical assistance from John Vanstone, Sherrie McPhee, Mary Lou Hart, and Marty Scheiring is gratefully acknowledged. We are in debt to Drs. David Shoesmith, Peter Norton, Mark Workentin, and Milan Kovar for their kind help and fruitful discussions. Thanks are owed to Dr. Jacques Josserand at EPFL for his expertise on using FluxExpert software to fit approach curves.

References

1. J. Kwak and A.J. Bard. Anal. Chem. **61**, 1794 (1989).
2. J. Kwak and A.J. Bard. Anal. Chem. **61**, 1221 (1989).
3. A.J. Bard. *In* Scanning electrochemical microscopy. *Edited by* A.J. Bard and M.V. Mirkin. Marcel Dekker, Inc., New York. 2001. p. 1.
4. C. Wei, A.J. Bard, and M.V. Mirkin. J. Phys. Chem. **99**, 16033 (1995).
5. Z.F. Ding, B.M. Quinn, and A.J. Bard. J. Phys. Chem. B, **105**, 6367 (2001).
6. S. Amemiya and A.J. Bard. Anal. Chem. **72**, 4940 (2000).
7. S. Amemiya, Z.F. Ding, J. Zhou, and A.J. Bard. J. Electroanal. Chem. **483**, 7 (2000).
8. M. Tsionsky, A.J. Bard, and M.V. Mirkin. J. Am. Chem. Soc. **119**, 10785 (1997).
9. J. Mauzeroll and A.J. Bard. Proc. Natl. Acad. Sci. U.S.A. **101**, 7862 (2004).
10. B. Liu, S.A. Rotenberg, and M.V. Mirkin. Anal. Chem. **74**, 6340 (2002).
11. C. Cai, B. Liu, M.V. Mirkin, H.A. Frank, and J.F. Rusling. Anal. Chem. **74**, 114 (2002).
12. A.L. Barker, P.R. Unwin, S. Amemiya, J. Zhou, and A.J. Bard. J. Phys. Chem. B, **103**, 7260 (1999).
13. D. Mandler and P.R. Unwin. J. Phys. Chem. B, **107**, 407 (2003).
14. J. Zhang and P.R. Unwin. J. Phys. Chem. B, **105**, 11052 (2001).
15. S. Cannan, J. Zhang, F. Grunfeld, and P.R. Unwin. Langmuir, **20**, 701 (2004).
16. F. Li, Y. Chen, P. Sun, M. Zhang, Z. Gao, D. Zhan, and Y. Shao. J. Phys. Chem. B, **108**, 3295 (2004).
17. F.R. Fan and A.J. Bard. Proc. Natl. Acad. Sci. U.S.A. **96**, 14222 (1999).
18. Y. Lee, Z.F. Ding, and A.J. Bard. Anal. Chem. **74**, 3634 (2002).

© 2005 NRC Canada

19. D.O. Wipf and A.J. Bard. Anal. Chem. **64**, 1362 (1992).
20. B. Liu, W. Cheng, S.A. Rotenberg, and M.V. Mirkin. J. Electroanal. Chem. **500**, 590 (2001).
21. W. Feng, S.A. Rotenberg, and M.V. Mirkin. Anal. Chem. **75**, 4148 (2003).
22. J.V. MacPherson, C.E. Jones, A.L. Barker, and P.R. Unwin. Anal. Chem. **74**, 1841 (2002).
23. J.V. MacPherson and P.R. Unwin. Anal. Chem. **73**, 550 (2001).
24. C.G. Zoski, N. Simjee, O. Guenat, and M. Koudelka-Hep. Anal. Chem. **76**, 62 (2004).
25. O.D. Uitto and H.S. White. Pharm. Res. **20**, 646 (2003).
26. S.B. Basame and H.S. White. Abstracts of the 214th ACS National Meeting, Las Vegas, Nevada, 7–11 September, ANYL. 1997.
27. S.B. Basame and H.S. White. J. Phys. Chem. **99**, 16430 (1995).
28. N. Casillas, S. Charlebois, W.H. Smyrl, and H.S. White. J. Electrochem. Soc. **141**, 636 (1994).
29. W.B. Nowall, D.O. Wipf, and W.G. Kuhr. Anal. Chem. **70**, 2601 (1998).
30. M. Nishizawa, T. Kaya, K. Takoh, K. Nishimura, Y. Takii, and T. Matsue. Proc. Electrochem. Soc. **2001–18**, 315 (2001).
31. Y. Takii, K. Takoh, M. Nishizawa, and T. Matsue. Electrochim. Acta, **48**, 3381 (2003).
32. G. Wittstock. Fresenius' J. Anal. Chem. **370**, 303 (2001).
33. G. Wittstock and T. Wilhelm. Anal. Sci. **18**, 1199 (2002).
34. B.B. Katemann, A. Schulte, and W. Schuhmann. Chem. Eur. J. **9**, 2025 (2003).
35. A.J. Bard, G. Denuault, C. Lee, D. Mandler, and D.O. Wipf. Acc. Chem. Res. **23**, 357 (1990).
36. A.J. Bard, F.R.F. Fan, and M.V. Mirkin. Electroanal. Chem. **18**, 243 (1994).
37. A.J. Bard, O.E. Huesser, and D.H. Craston. *In* US Patent 4 968 390, 16 November 1990.
38. D. Mandler and A.J. Bard. J. Electrochem. Soc. **136**, 3143 (1989).
39. E.M. El-Giar, R.A. Said, G.E. Bridges, and D.J. Thomson. J. Electrochem. Soc. **147**, 586 (2000).
40. F. Ge, R.C. Tenent, and D.O. Wipf. Anal. Sci. **17**, 27 (2001).
41. C. Kranz, M. Ludwig, H.E. Gaub, and W. Schuhmann. Adv. Mater. **7**, 38 (1995).
42. C. Combellas, F. Kanoufi, D. Mazouzi, and A. Thiebault. J. Electroanal. Chem. **556**, 43 (2003).
43. F. Kanoufi, C. Combellas, and M.E.R. Shanahan. Langmuir, **19**, 6711 (2003).
44. C.G. Zoski. Electroanalysis, **14**, 1041 (2002).
45. F.-R.F. Fan and C. Demaille. *In* Scanning electrochemical microscopy. *Edited by* A.J. Bard and M.V. Mirkin. Marcel Dekker, Inc., New York. 2001. p. 75.
46. J.V. Macpherson and P.R. Unwin. Anal. Chem. **72**, 276 (2000).
47. B.B. Katemann and W. Schuhmann. Electroanalysis, **14**, 22 (2002).
48. D.O. Wipf. *In* Scanning electrochemical microscopy. *Edited by* A.J. Bard and M.V. Mirkin. Marcel Dekker, Inc., New York. 2001. p. 17.
49. M. Etienne, A. Schulte, and W. Schuhmann. Electrochem. Commun. **6**, 288 (2004).
50. B. Gollas, P.N. Bartlett, and G. Denuault. Anal. Chem. **72**, 349 (2000).
51. Y. Shao and M.V. Mirkin. J. Phys. Chem. B, **102**, 9915 (1998).
52. J.L. Amphlett and G. Denuault. J. Phys. Chem. B, **102**, 9946 (1998).
53. A.J. Bard and L.R. Faulkner. Electrochemical methods, fundamentals and applications. 2nd ed. John Wiley and Sons, New York. 2001.
54. W.J. Miao, Z.F. Ding, and A.J. Bard. J. Phys. Chem. B, **106**, 1392 (2002).
55. D.O. Wipf and A.J. Bard. J. Electrochem. Soc. **138**, 469 (1991).
56. E.F. Fabrizio, T.M. McEvoy, P. Jassel, J. Lozano, K.J. Stevenson, and A.J. Bard. J. Electroanal. Chem. **554–555**, 99 (2003).

© 2005 NRC Canada

A new method for evaluation of the mobility of silica-grafted alkyl chains by suspension-state ^{1}H NMR

Mahnaz Derakhshan, Hamid R. Ansarian, M. Mizanur Rahman, Toshihiko Sakurai, Makoto Takafuji, and Hirotaka Ihara

Abstract: Although molecular mobility is usually probed by measurement of the T_1 relaxation time, it is not the case for methylene groups of grafted acyl chains because each methylene group has a different mobility and hence, a different T_1 relaxation time depending on the distance from the junction between organic molecule and nonorganic particle. Therefore, we devised a very simple method that can semiquantitatively determine the extent of mobility in the grafted acyl chains. Silica-supported poly(octadecylacrylate) (Sil-ODA$_n$), polymeric octadecylsilyl silica (polymeric ODS), and monomeric octadecylsilyl silica (monomeric ODS) were studied by comparing the intensity of NMR peaks from grafted molecules with the same amount of nongrafted molecules. In the case of Sil-ODA$_n$, with a gradual increase in temperature, the intensity of the proton signals (^{1}H NMR) of the octadecyl moieties (mainly methylene groups) rose dramatically. This dramatic rise was at the same temperature as that of an endothermic peak detectable in its DSC thermogram, indicating a relatively complete solid to liquid phase transition. Sil-ODA$_n$, as the stationary phase in RP-HPLC, showed analogous temperature dependencies of the separation factor between naphthacene and triphenylene (as a simple indicator of shape selectivity). Using this method we determined the liquid phase percentage (LPP) in Sil-ODA$_n$, polymeric ODS, and monomeric ODS at various temperatures. We suggest LPP as a semiquantitative index of mobility for grafted organic layers.

Key words: comb-shaped polymer, nanocomposite, alkyl chain mobility, NMR, liquid chromatography.

Résumé : Même si la mobilité moléculaire est généralement étudiée par une mesure du temps de relaxation T_1, cette méthode ne peut s'appliquer aux groupes méthylènes liés à des chaînes acyles en raison du fait que chaque groupe méthylène présente une mobilité et, en conséquence, un temps de relaxation T_1 différent suivant la distance entre la jonction entre la molécule organique et la particule non organique. On a donc mis au point une méthode très simple qui permet de déterminer semi-quantitativement le degré de mobilité des chaînes acyles greffées. On a étudié du poly(acrylate d'octadécyle) supporté sur de la silice (Sil-ODA$_n$), de l'octadécylsilylsilice polymère (ODS polymère) et de l'octadécylsilylsilice monomère (ODS monomère) en comparant l'intensité des pics de RMN de molécules greffées avec ceux obtenus avec la même quantité de molécules non greffées. Dans le cas du (Sil-ODA$_n$), en RMN du ^{1}H, l'intensité des signaux des protons des portions octadécyles, qui sont composées principalement de groupes méthylènes, augmente d'une façon dramatique avec une augmentation graduelle de la température. Cette augmentation dramatique se produit à la même température qu'un pic endothermique décelé dans son thermogramme de calorimétrie à balayage différentiel, ce qui indique qu'il se produit une transition relativement complète de la phase solide à la phase liquide. Si on utilise le Sil-ODA$_n$ comme phase stationnaire en chromatographie liquide à haute performance « RP », on observe le même type de dépendance entre la température et le facteur de séparation entre le naphtacène et le triphénylène, utilisé comme simple indicateur de la forme de la sélectivité. Utilisant cette méthode, on a déterminé le pourcentage de phase liquide (PPL) dans le Sil-ODA$_n$, l'ODS polymère et l'ODS monomère, à diverses températures. On suggère un indice semi-quantitatif de la mobilité des phases organiques greffées.

Mots clés : polymère en forme de peigne, nanocomposite, mobilité d'une chaîne alkyle, RMN, chromatographie liquide.

[Traduit par la Rédaction]

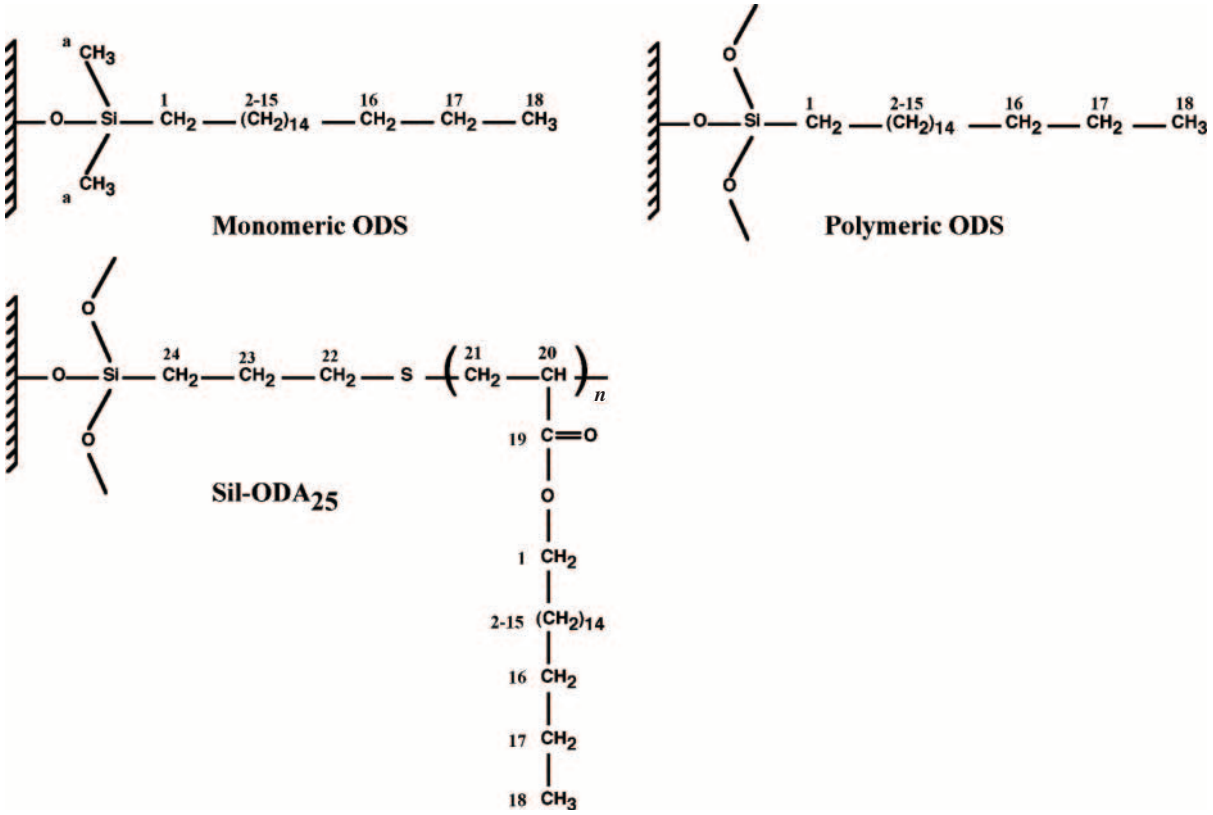
Received 17 March 2005. Published on the NRC Research Press Web site at http://canjchem.nrc.ca on 16 December 2005.

M. Derakhshan, M.M. Rahman, T. Sakurai, M. Takafuji, and H. Ihara.[1] Department of Applied Chemistry and Biochemistry, Kumamoto University, Kumamoto 860-8555, Japan.
H.R. Ansarian. SVB Laboratory, Kumamoto University, Kumamoto 860-8555, Japan.

[1]Corresponding author (e-mail: ihara@gpo.kumamoto-u.ac.jp).

 doi: 10.1139/V05-197 © 2005 NRC Canada

Fig. 1. The structures of the silica-supported stationary phases discussed in this paper: silica-supported polyoctadecylacrylate (Sil-ODA$_n$), polymeric octadecylsilyl silica (polymeric ODS), and monomeric octadecylsilyl silica (monomeric ODS).



Introduction

Much effort has gone into the characterization of various kinds of grafted polymers on nonorganic compounds to disclose mechanisms of their function. Perhaps the most popular one is the characterization of various stationary phases applicable in reverse-phase high performance chromatography (RP-HPLC) (1–10). Identifying the structure–function relationship of these silica-supported organic materials, as well as other organic–inorganic hybrid materials, enhances our knowledge of their underlying mechanisms of function, and enables scientists to make and use such products more effectively.

Monomeric octadecylsilyl silica (monomeric ODS) and polymeric octadecylsilyl silica (polymeric ODS) are two popular stationary phases for RP-HPLC. Polymeric ODS has the benefit of higher immobilization compared with monomeric ODS, but its potential to self-assemble is still perturbed because of the short rigid covalent bonds of Si-O-Si either between the alkylsilane and silica surface or between two alkylsilanes (cross-polymerization). Silica-supported poly(octadecylacrylate) (Sil-ODA$_n$) differs from conventionally modified silicas because octadecyl moieties are not directly bonded to the silica surface, so they can form an ordered structure. In this study we have tried to evaluate and compare the mobility of octadecyl chains among these three stationary phases at different temperatures. Previously we studied poly(octadecylacrylate) (ODA$_n$) grafted on porous silica particles, which proved advantageous for use as a stationary phase for geometrical detection with a strong temperature dependency (11–15). This prominent temperature dependency in the separation behaviour of grafted ODA$_n$ was coincident with an endothermic peak detectable by DSC. This unique behaviour of Sil-ODA$_n$, poly(octadecyacrylate) grafted on silica, was supposed to be due to a dramatic increase in the mobility of the grafted polymer. Suspension-state ^{1}H NMR was performed at different temperatures to identify the mobility of the alkyl chains of Sil-ODA$_n$, polymeric ODS, and monomeric ODS. Our efforts, as discussed in this paper, eventually led us to a simple method for determining the mobility of grafted organic molecules on the surface of nonorganic particles. We hope this study will be useful for providing more effective methods in the characterization of polymers grafted on nonorganic materials by NMR spectroscopy. The chemical composition of the stationary phases mentioned are shown in Fig. 1.

Experimental

Sample preparation

Reagents

Silica particles (120-S5, diameter 5 μm, pore size 120 Å, specific surface area 300 m^2 g^{-1}) were purhased from YMC (Kyoto, Japan), and all other materials were from Sigma-Aldrich (Tokyo, Japan) or Fluka Chemica-Biochemica (Tokyo, Japan).

Synthesis of Sil-ODA$_{25}$

Sil-ODA$_n$ was prepared by radical telomerization of octadecyl acrylate (ODA) with 3-mercaptopropyltrimethoxysilane (MPS), followed by immobilization onto sil-

© 2005 NRC Canada

ica, mostly according to our previously reported method (15). The preparation procedure was as follows: ODA and MPS (30:1 molar ratio) were dissolved in ethanol and azobisisobutyronitrile (20 mol% for the mercapto group) was added to the ethanol solution at 80 °C. The mixture was stirred for 6 h at 80 °C under an atmosphere of N_2 gas. The resulting white precipitate was gathered by filtration, washed successfully with methanol and acetone, and dried in vacuo.

The structure and polymerization degree was determined by NMR spectroscopy. ^{1}H NMR shifts of ODA_n were as follows: δ 0.8 ppm ($SiCH_2$), δ 1.9 ppm ($CHCO$), δ 3.6 ppm ($SiOCH_3$), and δ 4 ppm ($C(=O)OCH_2$). The average degree of polymerization was determined to be 25 by the proton ratio at 3.6 and 4.0 ppm.

Then ODA_{25} was readily immobilized onto porous silica by mixing in toluene at reflux temperature for 24 h. YMC 120-S5 was used as the porous silica. The white powder was gathered after filtration and several consecutive washings with toluene and chloroform. After vacuum drying the amount of carbon and hydrogen were determined to be 18.3% and 3.2% by elemental analysis. Successive washing with chloroform (as a good solvent for ODA_{25}) showed no significant change in the elemental analysis results. Coverage of Sil-ODA_{25} by octadecyl moieties was calculated to be 3 μmol m^{-2} and 726 μmol g^{-1}.

Synthesis of polymeric ODS

The same silica particles (YMC 120-S5) were mixed with octadecyltrichlorosilane at reflux temperature in toluene for 24 h. There was no effort made for a controlled inclusion of water in the reaction. The white powder was gathered after washing with chloroform and toluene several times. After vacuum drying the amount of carbon and hydrogen were determined to be 23.3% and 4.3% according to elemental analysis. Successive washing with chloroform showed no significant change in the elemental analysis results. Coverage of polymeric ODS by octadecyl moieties was calculated to be 4.9 μmol m^{-2} and 1078 μmol g^{-1}.

Synthesis of monomeric ODS

YMC 120-S5 particles were mixed with dimethyloctadecylchlorosilane at reflux temperature in toluene for 24 h. The white powder was gathered after filtration and frequently washed with chloroform and toluene. After vacuum drying the amount of carbon and hydrogen was determined to be 13.8% and 2.7% based on elemental analysis. Successive washing with chloroform showed no significant change in the elemental analysis results. Coverage of monomeric ODS by octadecyl moieties was calculated to be 2.5 μmol m^{-2} and 638 μmol g^{-1}.

NMR spectroscopy

All NMR spectra were measured by a Varian ^{UNITY}INOVA AS400 at a static magnetic field of 9.4 T using a GHX Varian AS400 nanoprobe for suspension-state ^{1}H NMR. All NMR parameters mentioned in this paper are compatible with the terminology of the Varian ^{UNITY}INOVA. A spin rate of 2000–3500 Hz for suspension-state ^{1}H NMR was used.

Suspension-state ^{1}H NMR

Three suspensions were made by adding 10 mg of each of Sil-ODA_{25}, polymeric ODS, and monomeric ODS to 100 μL of methanol-*d* (CD_3OD) including 0.03% tetramethylsilane (TMS) and 0.05% hexamethyldisilane (HMS). Hexamethyldisilane was added as a reference for signal intensity, but the protons of CD_3OD proved better for this purpose. All samples were prepared at the same time using one single ampoule of CD_3OD. Forty microliters of each suspension was transferred to the nanotube for measurement. Suspension-state ^{1}H NMR spectra were measured at the temperatures: 20, 25, 30, 35, 40, 45, and 50 °C using the GHX Varian AS400 nanoprobe. The parameters used for measurement were delay time = 10 s, pulse width = 30°, number of transients = 32, and spectral width = 6000 Hz. For assigning peaks, after determining the 90° pulse width, DQCOSY (correlation spectroscopy) was performed and the chemical shifts of the terminal methyl and methylene of the octadecyl groups were determined. Shimming was adjusted for each temperature using a standard semiautomatic method. Delay time was chosen to be long enough to avoid saturation in order to have reliable NMR intensities for the quantitative measurements. Baseline correction was performed on all spectra before measuring the under-peak areas.

Solution-state ^{1}H NMR

A solution was made of 1 mg of octadecyl acrylate in 100 μL of hot methanol-*d*. Forty microliters of the solution was transferred to a nanotube for measurement. The amount of 1 mg was chosen in a way that represented the approximate amount of alkyl chains relative to their correspondent grafted samples in suspension-state ^{1}H NMR because the NMR intensity of methylene groups in the nongrafted solution state was meant to be compared with the grafted suspension state. The NMR measurements were performed at 50 °C. The same parameters used in suspension-state ^{1}H NMR were used for these measurements.

Chromatography

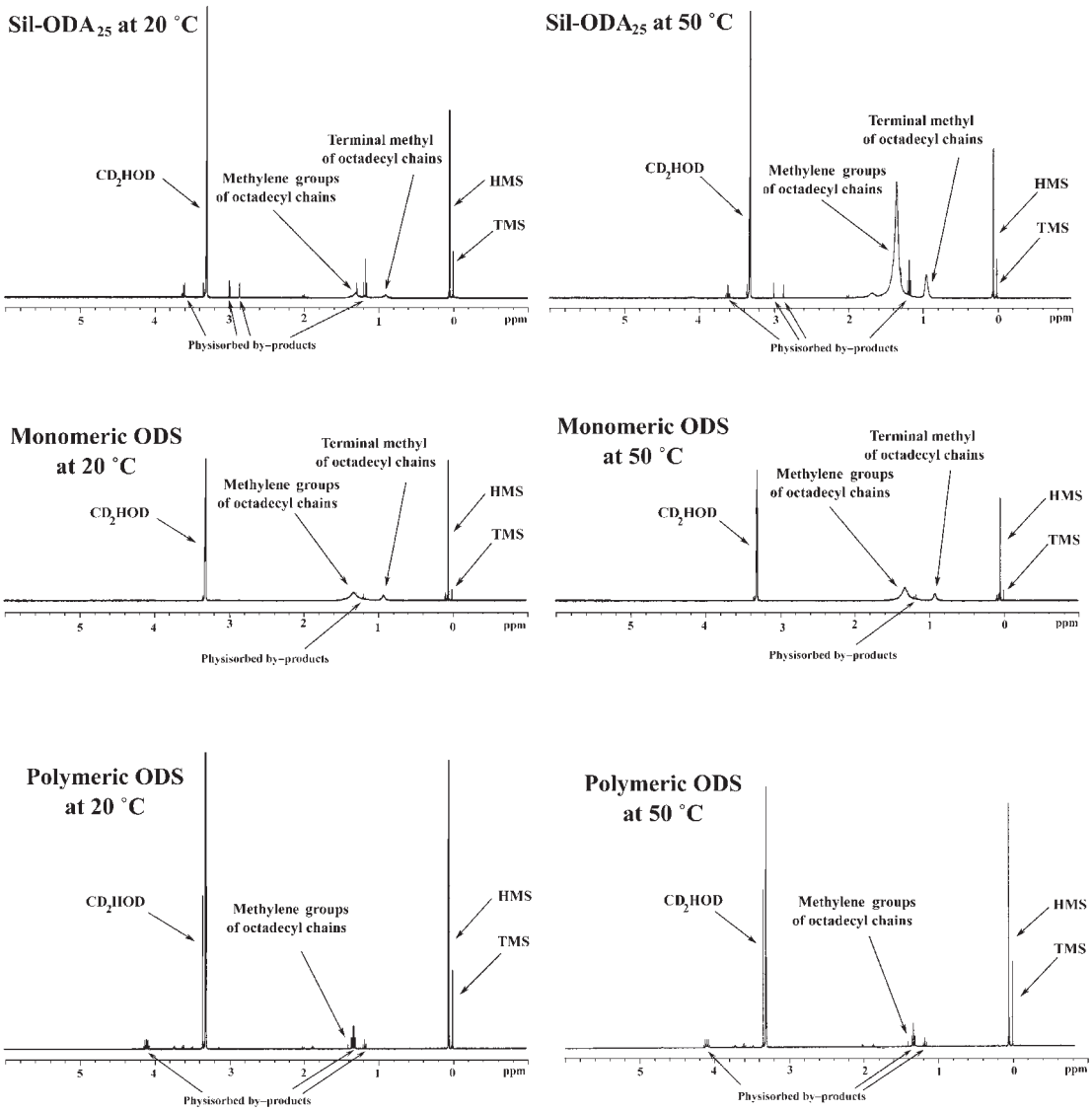
The polymeric ODS column (Shodex C18P 4E) was purchased from Shodex (Tokyo, Japan). The monomeric ODS (Inersil) was purchased from G.L. Sciences (Tokyo, Japan). Sil-ODA_n was packed into stainless steel columns (4.6 mm i.d. × 250 mm) using a hexanol–chloroform (1:1) mixture. Methanol–water (9:1) was used as the mobile phase at a flow rate of 1 mL min^{-1}. The chromatograph included a Gulliver 980 PU pump, a JASCO photodiode array detector (UVIDEC-100-IV), and a NESLAB column Jacket (Newington, New Hampshire). Five microliters of the sample dissolved in methanol were injected through a Reodyne model 7125 injector. Indicators of shape selectivity, naphthacene and triphenylene, were purchased from Sigma-Aldrich (Schnelldorf, Germany). The separation factor ($\alpha_{naphthacene-triphenylene}$) was defined as the ratio of the retention factor of naphthacene to the retention factor of triphenylene. The retention factors (k') were determined by the equation $(t_e - t_0)/t_0$, where t_e and t_0 are the retention times of the sample and the void volume mark, respectively.

Differential scanning calorimetery

DSC was performed using a heating rate of 1 °C min^{-1} with Seiko I and E SSC-580 and DSC-10 instruments.

© 2005 NRC Canada

Fig. 2. (*a*) Suspension-state ^{1}H NMR of Sil-ODA$_{25}$, monomeric ODS, and polymeric ODS.



Results and discussion

Surface coverage

The molar amount of octadecyl moieties per 1 g of silica (R, μmol g^{-1}) can be calculated as follows

$$[1] \qquad R = 10^6(P_C/100)/12n$$

where P_C is the percentage of the carbon element according to elemental analysis, and n is the corresponding number of carbon atoms per one octadecyl moiety, which in polymeric and monomeric ODS is 18, and in Sil-ODA$_{25}$ is equal to 21 (Fig. 1).

On the other hand, because the molecular mass of a grafted octadecyl moiety is 253 Da, the weight % of the grafted phase (P_w) in each case can be calculated as follows

$$[2] \qquad P_w = (253 \times 10^{-4})R(n/18)$$

Furthermore, surface coverage (N, μmol m^{-2}) can be calculated as follows

$$[3] \qquad N = R/\{S[(100 - P_w)/100]\} = 10^6P_C/[12nS(100 - P_w)]$$

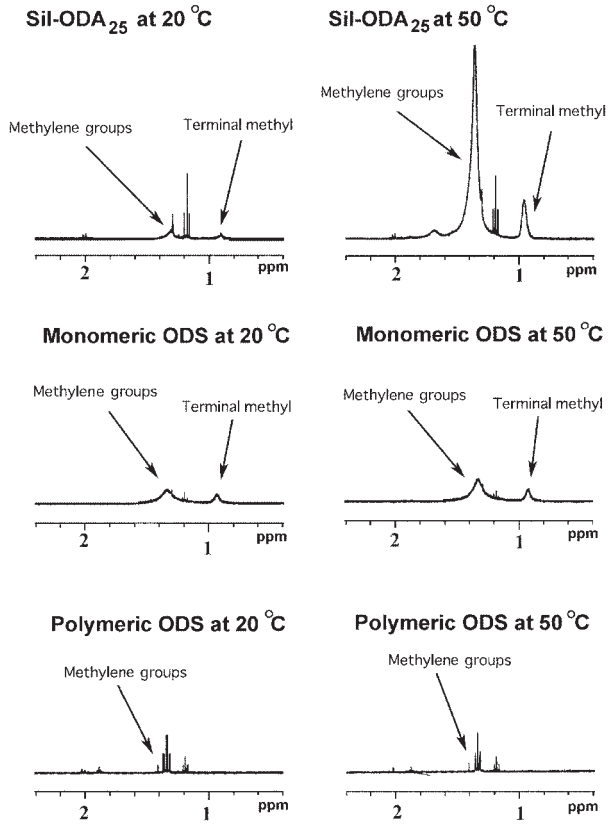
where S is the surface area per 1 g of nonmodified silica.

^{1}H NMR spectroscopy

Although molecular mobility is usually probed by the measurement of the T_1 relaxation time, this was not the case for our study because the NMR peaks of several methylene groups (with different mobilities and hence, different T_1 relaxation times) were superimposed. There are three methods for the measurement of T_1: inversion recovery, progressive saturation, and saturation recovery. Here we provide a detailed discussion about how the peculiarity of relaxation in grafted alkyl chains makes the inversion recovery method unreliable. Our reasoning undermines the very assumption that the relaxation of grafted alkyl chains has an averaged relaxation time constant. Therefore, the reliability of other methods that are based on that assumption will be spontaneously ruled out.

© 2005 NRC Canada

Fig. 2 (*concluded*). (*b*) Intensity of the NMR peaks of methylene groups in the case of Sil-ODA$_{25}$ increases dramatically as temperature rises. However, monomeric ODS shows only a slight increase as temperature rises, and polymeric ODS shows almost no increase.



In a common inversion recovery experiment, the magnetization vector is inverted with a 180° pulse, then the magnetization vector ($\mathbf{M}_z$) begins to relax exponentially during a given period of time:

$$[4] \qquad \mathbf{M}_z = \mathbf{M}_0\ (1 - 2e^{-t/T_1})$$

Finally, a monitoring 90° pulse is used to measure the correspondent peak height. The peak height (H) as a function of the given delaying time is supposed to behave exponentially with the same exponential time as T_1.

$$[5] \qquad H = H_{max}(1 - 2e^{-t/T_1})$$

In the process of measuring T_1, a software program solves eq. [5] by matching the array of measurements to the most fitting exponential curve. But if an actual NMR peak is the result of several NMR peaks, each with a distinct exponential time (like that of methylene groups in the case of grafted alkyl chains), the equation of peak height will be:

$$[6] \qquad H = H_a + H_b + H_c + \cdots + H_n$$
$$H = H_{max-a}(1 - 2e^{-t/T_{1a}}) + H_{max-b}\ (1 - 2e^{-t/T_{1b}})$$
$$+ H_{max-c}(1 - 2e^{-t/T_{1c}}) + \cdots + H_{max-n}(1 - 2e^{-t/T_{1n}})$$

The important point is that the sum of two or several exponential functions does not remain exponential. Therefore, the NMR peak height of the methylene groups as a function of delaying time, in the case of grafted polymers, no longer behaves exponentially. In other words, the relaxation function cannot be expressed by an averaged T_1.

$$[7] \qquad H_{max-a}(1 - 2e^{-t/T_{1a}}) + H_{max-b}(1 - 2e^{-t/T_{1b}})$$
$$+ H_{max-c}(1 - 2e^{-t/T_{1c}}) + \cdots \neq H_{max}(1 - 2e^{-t/T_{1avg}})$$

Therefore, we turned to a rather new, but very simple approach that determines the percentage of octadecyl moieties with liquid-type mobility in each case. The form of the motionally averaged Hamiltonian depends very strongly on the type and the timescale of the molecular motion and hence, on the phase of matter (16). In suspension-state NMR, only those molecules or parts of molecules with very fast rotational motions are detectable. Motion most be in a range that can average out dipolar coupling and chemical shift anisotropy until the related NMR peaks become narrow enough to be detected. Those molecules or those parts of molecules that have a low mobility scale will give such a broad peak (because of the dipolar coupling and the chemical shift anisotropy contribution) that they cannot be detected.

The suspension-state ^{1}H NMR spectra were obtained for Sil-ODA$_{25}$, polymeric ODS, and monomeric ODS at variable temperatures from 20 to 50 °C. Neither half-height width (line width) of the methylene groups nor the spin–spin relaxation time (T_2) showed any significant change with temperature. Figure 2*a* shows the ^{1}H NMR spectra of the three samples at 20 and 50 °C. As shown in Fig. 2*b*, the intensity of the NMR peaks representing the terminal methyl and methylene groups of the octadecyl moieties increases significantly in Sil-ODA$_{25}$. If there was any transition from the liquid crystalline phase to the isotropic phase, a fixed intensity with a declining line width (or an increasing T_2) would be expected.

For the monomeric ODS, the intensity of the NMR peaks representing the terminal methyl and methylene groups increased slightly, but for the polymeric ODS only the peaks of the methylene groups were detectable when a very high vertical scale was used for graphical presentation.

As all the three samples were washed carefully with toluene and chloroform, the small sharp peaks detected in the ^{1}H NMR spectra should be regarded as those of the physisorbed by-products of the grafting reactions. Interestingly, the amount of physisorbed by-products of polymeric ODS or Sil-ODA$_{25}$ was higher than that of monomeric ODS, a fact that indicates the presence of more closed spaces in the nano-architecture of polymeric ODS and Sil-ODA$_{25}$. As shown in Fig. 3, the intensity of the NMR signals from the methylene groups of Sil-ODA$_{25}$ increases distinctly around an endothermic peak in DSC. Peak-top temperature was measured to be 38.4 °C for Sil-ODA$_{25}$ in the presence of methanol. To make suspension-state NMR intensities comparable with the solution state in different samples and at different temperatures, they were weighted according to the following formula (justification will be discussed in the next section):

$$[8] \qquad I_{susp} = (I_m/I_D)/(4 \times 10^{-3}R) = 250[I_m/(I_D R)]$$

I_{susp} (μmol^{-1}) is the calculated normalized intensity (the relative intensity of the suspension-state ^{1}H NMR signal per

© 2005 NRC Canada

Fig. 3. Normalized relative ^{1}H NMR–NMR intensities of the methylene groups of Sil-ODA$_{25}$ increase distinctly around 38 °C, which is just around the peak-top temperature of its DSC thermogram.

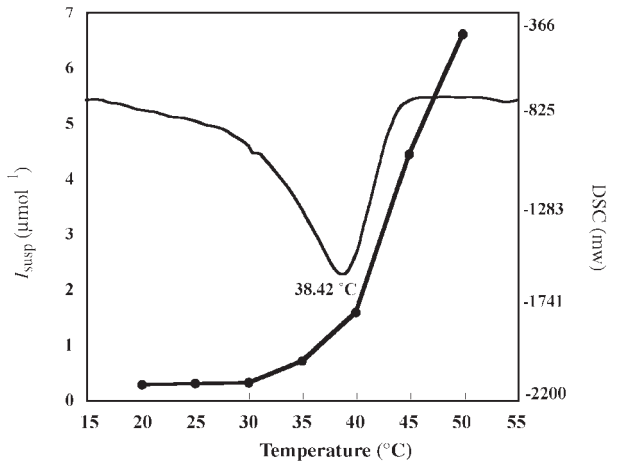
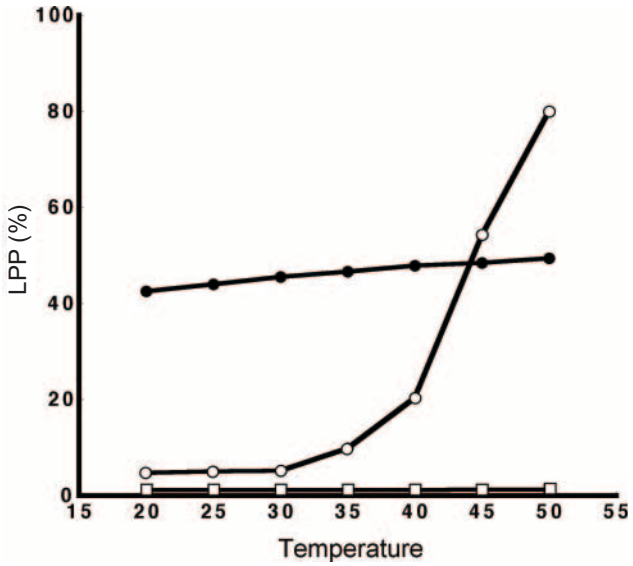


Fig. 4. Temperature dependencies of the liquid phase percentages (LPP) of the methylene groups of Sil-ODA$_n$ (○), monomeric ODS (●), and polymeric ODS (□).



1 μmol of grafted octadecyl moieties) shown in Fig. 4, I_m is the under-peak area of the methylene peak, I_D is the intensity of a few protons belonging to methanol-*d*, and *R* is the amount of grafted octadecyl moiety per 1 g of modified silica.

The intensity of the signals can be affected by time to time instrumental conditions, namely tuning of the observation channel. Considering the fact that instrumental conditions affect the intensities of I_m and I_D equally, and using one single ampoule of methanol-*d* for all measurements, the value of I_m/I_D can be assumed to be independent from instrumental conditions. At this stage, the value of I_m/I_D represents all octadecyl moieties with liquid-type mobility. Finally, dividing this value with $4 \times 10^{-3}R$ will give us a normalized value for comparison among different experiments.

Table 1. Summarized characterizations of Sil-ODA$_{25}$, monomeric ODS, and polymeric ODS.

Stationary phase	Temperature (°C)	I_{susp}	I_{sol}	LPP
Sil-ODA$_{25}$	20	0.37	7.84	4.76
Sil-ODA$_{25}$	50	6.28	7.84	80.04
Monomeric ODS	20	3.34	7.84	42.07
Monomeric ODS	50	3.88	7.84	49.43
Polymeric ODS	20	0.09	7.84	1.14
Polymeric ODS	50	0.09	7.84	1.23

The term 4×10^{-3} is included because the NMR signal of only 4 mg of the modified silica was measured in each suspension-state ^{1}H NMR spectroscopy.

On the other hand, normalized NMR intensities of octadecyl chains in the solution state (I_{sol}, μmol^{-1}), in order to be comparable with the suspension state, were calculated according to the following formula:

$$[9] \quad I_{sol} = (I_m/I_D)/[(0.4 \times 10^{-3}/\mathrm{MW}) \times 10^6] = (I_m \times \mathrm{MW})/(400 \times I_D)$$

Again the value of I_m/I_D can be assumed to be independent from instrumental conditions. At this stage, the value of I_m/I_D represents all octadecyl moieties. Finally, dividing this value with 0.4×10^3 MW will give us a normalized value for comparison among different experiments. MW is the molecular weight of each monomer and the term 0.4×10^3 is included because the NMR signal of only 0.4 mg of each monomer was measured in each solution-state ^{1}H NMR spectroscopy. The term 10^6 is included because I_{sol} is meant to be the normalized NMR intensity per 1 μmol of each monomer.

Determination of the liquid phase percentage (LPP)

By comparing the standardized NMR intensities of the methylene groups per 1 μmol of grafted odtadecyl chains (I_{susp}) and the standardized NMR intensities of the methylene groups per 1 μmol of nongrafted octadecyl chains (I_{sol}), we can determine the percentage of octadecyl chains with liquid scale mobility, the liquid phase percentage (LPP), at each temperature (Table 1) according to the following simple formula:

$$[10] \quad \mathrm{LPP} = (I_{susp}/I_{sol})100$$

The temperature dependency of LPP is shown in Fig. 4.

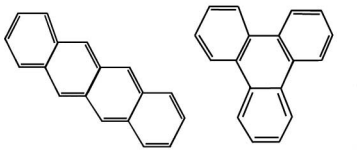
Chromatography

We used $\alpha_{\text{naphthacene–triphenylene}}$ as a quantitative index of the ability to detect the linearity of compounds. As shown in Fig. 5, naphthacene and triphenylene have equal molecular weights, but naphthacene is apparently more linear than triphenylene (its length to breadth ratio is higher than that of triphenylene), so $\alpha_{\text{naphthacene–triphenylene}}$ can be regarded as a quantitative index of shape selectivity. Figure 6 shows the temperature dependencies of $\alpha_{\text{naphthacene–triphenylene}}$ in the three stationary phases.

Although comparing separation factors between two stationary phases based on their LPP is not reliable (because mobility is not the only factor that affects performance of a stationary phase), it has been shown that the shape selectiv-

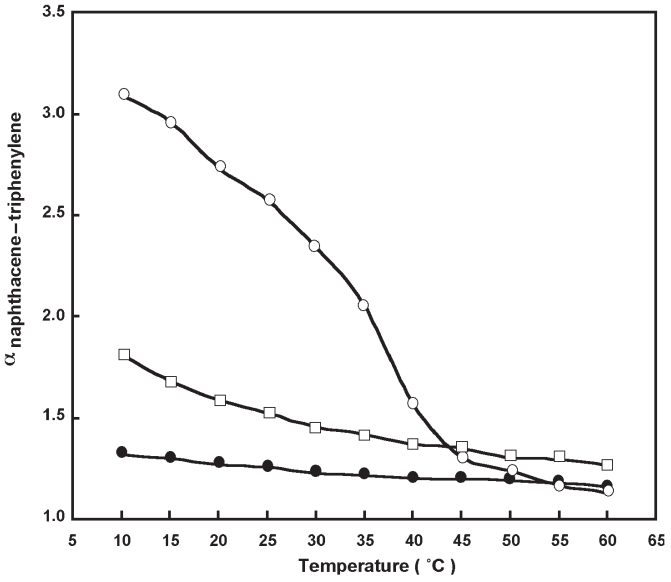
© 2005 NRC Canada

Fig. 5. The structures of napthacene and triphenylene. Naphthacene and triphenylene have similar molecular weights but different shapes, therefore the separation factor ($\alpha_{naphthacene-triphenylene}$) can show the ability of each stationary phase to detect molecular shapes.



Naphthacene Triphenylene

Fig. 6. Temperature dependencies of $\alpha_{naphthacene-triphenylene}$ in Sil-ODA$_n$ (○), monomeric ODS (●), and polymeric ODS (□). The shape selectivity of Sil-ODA$_n$ is highest at low temperatures, but decreases dramatically as the temperature increases from 20 to 50 °C.



ity of silica-grafted alkyl chains in each stationary phase is considerably correlated with their mobility as the temperature changes. As shown in Figs. 4 and 6, a dramatic increase in mobility of the alkyl chains in Sil-ODA$_{25}$ is coincident with a dramatic decrease of its molecular shape selectivity, but in ODS a gradual increase in mobility is concomitant with a gradual decrease in shape selectivity.

Conclusion

These comparative methods, based on suspension-state ^{1}H NMR, can be used for categorizing the scale of mobility (liquid scale or solid scale) of the polymers grafted on silica or any other supporting particles. This phase characterization is important for a better understanding of the function of organic layers grafted onto nonorganic particles.

Acknowledgement

This research was supported in part by a Grant-in-Aid for scientific research from the Ministry of Education, Culture, Sports, Science and Technology of Japan.

References

1. H. Ihara, T. Sagawa, K. Nakashima, K. Mitsushi, Y. Goto, J. Chowdhury, and S. Sakaki. Chem. Lett. **2**, 128 (2000).
2. E. Ruiz-Hitzky. Chem. Rec. **3**, 88 (2003).
3. L.D. White and C.P. Tripp. J. Colloid Interface Sci. **232**, 400 (2000).
4. C.P. Tripp and M.L. Hair. Langmuir, **12**, 3952 (1996).
5. M. Turowski, T. Morimoto, K. Kimata, H. Monde, T. Ikegami, K. Hosoya, and N. Tanaka. J. Chromatogr. A, **911**, 177 (2001).
6. P.B. Wright, E. Lamb, J.G. Dorsey, and R.G. Kooser. Anal. Chem. **64**, 785 (1992).
7. R. Bailey and R.M. Cassidy. Anal. Chem. **64**, 2277 (1992).
8. K.K. Unger, N. Becker, and P. Roumeliotis. J. Chromatogr. **251**, 115 (1976).
9. K. Karch, I. Sebestian, and I. Halasz. J. Chromatogr. **122**, 3 (1976).
10. M.J. Stevens. Langmuir, **15**, 2773 (1999).
11. H. Ihara, T. Sagawa, Y. Goto, and S. Nagaoka. Polymer, **40**, 2555 (1999).
12. H. Ihara, Y. Goto, T. Sakurai, M. Takafuji, T. Sagawa, and S. Nagaoka. Chem. Lett. **12**, 1252 (2001).
13. M.A.J. Chowdhury, H. Ihara, T. Sagawa, and C. Hyrayama. J. Chromatogr. A, **877**, 71 (2000).
14. M.A.J. Chowdhury, R.I. Boysen, and H. Ihara. J. Phys. Chem. B, **106**, 11936 (2002).
15. H. Ihara, H. Tanaka, S. Nagaoka, and C. Hirayama. J. Liq. Chromatogr. **19**, 2367 (1996).
16. M. Levitt. *In* Spin dynamics. John Wiley and Sons Ltd, New York. 2001. pp. 169–222.

© 2005 NRC Canada

Triazene derivatives of (1,*x*)-diazacycloalkanes. Part V.[1] Synthesis and characterization of 4-ethyl-3-({6-ethyl-3-[2-aryl-1-diazenyl]hexahydro-1-pyrimidinyl}methyl)-1-[2-aryl-1-diazenyl)hexahydropyrimidines from the reaction of diazonium salts with mixtures of formaldehyde and 1,3-diaminopentane

Reid Tingley, M. Brad Peori, Ryan Church, and Keith Vaughan

Abstract: A new series of bistriazenes has been synthesized from a general reaction of diazonium salts with a mixture of 1,3-diaminopentane (DYTEK® EP diamine) and formaldehyde, which affords the 4-ethyl-3-({6-ethyl-3-[2-aryl-1-diazenyl]hexahydro-1-pyrimidinyl}methyl)-1-[2-aryl-1-diazenyl]hexahydropyrimidines (**1**). Each of the molecules of type **1** is built up of two equivalent 3-(aryldiazenyl)-6-ethylhexahydro-1-pyrimidinyl groups attached to a central methylene group. The importance of this study is in part due to the fact that the formaldehyde–1,3-diaminopentane system has not previously been investigated. All new compounds have been characterized by IR and NMR spectroscopy, with elemental analysis for selected compounds; one example from the series has been unequivocally characterized by X-ray crystallography. Although analysis of the NMR spectra is made somewhat difficult because of broadness and coalescence of signals due to the rotational dynamics of the N—N single bonds, it is possible to fully assign the proton spectra of all compounds and to detect 94% of all carbon signals. The fine structure within the proton spectra illustrate the diastereotopic nature of the methylene group protons because of the presence of a stereocenter in each hexahydropyrimidine ring. The general conclusion of this study is that alkanediamines with three carbon atoms in the spacer link between the nitrogen atoms give rise to the linear bicyclic molecules of type **1**, **2**, and **3**, in contrast to the case of ethylenediamine (spacer link has two carbon atoms), which affords molecules of type **7** that exemplify the bridged bicyclic bistriazene structure. The new compounds of series **1** represent an extension of a broad ranging study of the synthesis of new bistriazene derivatives of (1,*x*)-diazacycloalkanes.

Key words: triazene, diazonium coupling, hexahydropyrimidine, diaminopentane, diazacycloalkanes, stereocenter, diastereotopic protons.

Résumé : On a effectué la synthèse d'une nouvelle série de bistriazènes par le biais d'une réaction générale des sels de diazonium avec un mélange de 1,3-diaminopentane (DYTEK® EP diamine) et de formaldéhyde qui conduit à la formation de 4-éthyl-3-({6-éthyl-3-[2-aryldiazén-1-yl]hexahydropyrimidin-1-yl}méthyl)-1-[2-aryldiazén-1-yl]hexahydropyrimidines (**1**). Chacune des molécules du type **1** correspond à l'addition de deux équivalents de groupes 3-(aryldiazényl)-6-éthylhexahydropyrimidin-1-yle à un groupe méthylène central. L'importance de cette étude réside en partie dans le fait que le système formaldéhyde–1,3-diaminopentane n'avait pas été étudié antérieurement. Tous les nouveaux composés ont été caractérisés par spectroscopies IR et RMN et par analyse élémentaire de composés choisis; un exemple de la série a été caractérisé sans équivoque par diffraction des rayons X. Même si l'analyse des spectres RMN est rendue assez difficile en raison de la largeur et de la coalescence des bandes provoquée par la dynamique rotationnelle des liaisons simples N—N, il a été possible de faire une attribution complète des spectres du proton de tous les composés et de détecter 94 % des signaux dus au carbone. La structure fine observée dans les spectres du proton illustre la nature diastéréotopique des protons du groupe méthylène qui découle de la présence d'un centre stéréogène dans chacun des cycles hexahydropyrimidines. La conclusion générale de cette étude est que les alcanediamines comportant trois atomes de carbone comme lien qui sépare les atomes d'azote conduisent à des molécules bicycliques linéaires des types **1**, **2** ou **3**, en opposition avec ce qui a été observé dans le cas de l'éthylènediamine (lien comportant deux atomes

Received 27 June 2005. Published on the NRC Research Press Web site at http://canjchem.nrc.ca on 16 December 2005.

R. Tingley, M.B. Peori, R. Church, and K. Vaughan.[2] Department of Chemistry, Saint Mary's University, Halifax, NS B3H 3C3, Canada.

[1]For part IV in this series, see: Can. J. Chem. **83**, 1071 (2005).
[2]Corresponding author (e-mail: keith.vaughan@smu.ca).

 doi: 10.1139/V05-192 © 2005 NRC Canada

de carbone) qui conduit à des molécules du type **7**, un exemple de structure bistriazène bicyclique pontée. Les nouveaux composés de la série **1** représentent une extension d'une étude de grande envergure sur la synthèse de nouveaux dérivés bistriazène des (1,*x*)-diazacycloalcanes.

Mots clés : triazène, couplage de diazonium, hexahydropyrimidine, diaminopentane, diazacycloalcanes, centre stéréogène, protons diastéréotopiques.

[Traduit par la Rédaction]

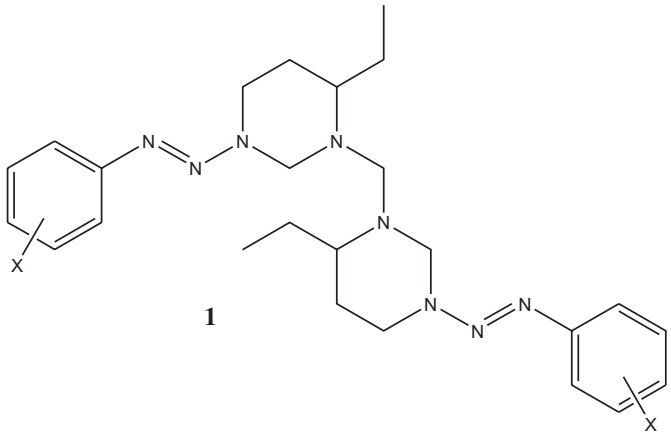
Introduction

A triazene is any molecule containing three contiguous nitrogen atoms with one N=N double bond, i.e., N=N-N. Triazenes have been studied extensively as versatile tools for organic synthesis (1), as multifunctional linkers in the solid-phase synthesis of heterocyclic libraries (2), as antitumour agents (3), specifically recently in the treatment of brain tumours (4), and in natural product synthesis (5). The term "bistriazene" has been coined to describe any molecule that contains two triazene units in the same molecule, with a link or spacer in between the triazene moieties. A typical example of a bistriazene is the bis[aryldiazenyl]ethylenediamine ($ArN{=}N\text{-}N(Me)CH_2CH_2N(Me)\text{-}N{=}NAr$) available from diazonium coupling with *N*,*N*′-dimethylethylenediamine (6). Recent progress in the synthesis of bistriazenes has been reviewed (7).

This paper reports the synthesis and characterization of a series of 4-ethyl-3-({6-ethyl-3-[2-aryl-1-diazenyl]hexahydro-1-pyrimidinyl}methyl)-1-[2-aryl-1-diazenyl]hexahydropyrimidines (**1a**–**1m**), which have been obtained by the reaction of a series of diazonium salts with a mixture of 1,3-diaminopentane (DYTEK® EP diamine) and formaldehyde. This work complements a recent study (8) of the synthesis of the bistriazene series **2** and **3**, which were synthesized in a similar manner from 1,3-propanediamines. The molecular scaffold of the new series (**1**) has been established unequivocally by the solution of an X-ray structure of the *p*-bromo derivative (**1g**) (9).

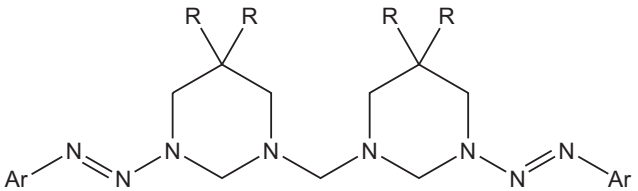
Fundamental to the appreciation of the importance of this new work is to consider the previous work dealing with the reaction of alkanediamines with formaldehyde. Krassig (10) conducted extensive work on these condensation reactions, but Evans (11) was the first to find spectroscopic evidence for the formation of hexahydropyrimidine (**4**) from 1,3-diaminopropane and formaldehyde. However, isolation of compound **4** in a free state was hindered by its apparent proclivity to form oligomers (10, 11). Later studies demonstrated that the unlikely end-product of the reaction of 1,3-diaminopropane with formaldehyde is in fact 1-formyl-3-methylhexahydropyrimidine (**5**) (12). The most comprehensive work in this field is the study by Dale and Sigvartsen (13), who investigated the reactions of ethylenediamine, 1,3-diaminopropane, 1,4-diaminobutane, and 1,5-diaminopentane with formaldehyde and identified novel heterocycles as products in all cases. However, none of the previous studies have included the reaction of 1,3-diaminopentane (**6**) with formaldehyde, which gives the present work a certain degree of importance in the study of new heterocycles.

One focus of research in this laboratory is the synthesis of novel bistriazenes from the reaction of diazonium salts with mixtures of formaldehyde and alkanediamines. Previously, we found that such reaction with ethylenediamine affords the bridged bicyclic bistriazene (**7**) (14); this structure was clearly established by X-ray crystallography (15). When this study was extended to the cyclohexanediamine–formaldehyde system, the products were found to be of a linear bicyclic structure (**8**), which has also been established by X-ray analysis (16). Clearly, there is a crossover in molecular architecture going from ethylenediamine to cyclohexanediamine, and our recent studies have shown that this crossover also occurs when going from ethylenediamine to propanediamine, as evident from the formation of the linear bicyclic compounds in series **2** and **3** (8). This trend is continued in the present study, which reports the synthesis of the linear bicyclic bistriazene series (**1a**–**1m**) from the reaction of a series of diazonium salts with mixtures of 1,3-diaminopentane and formaldehyde.



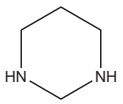
1

(a) X = *p*-CN
(b) X = *p*-NO_2
(c) X = *p*-CO_2Me
(d) X = *p*-CO_2Et
(e) X = *p*-$COCH_3$
(f) X = *p*-$CONH_2$
(g) X = *p*-Br
(h) X = *p*-Cl
(i) X = *p*-CH_3
(j) X = *p*-OCH_3
(k) X = H
(l) X = *o*-CN
(m) X = *o*-Br

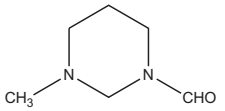


2 R = H
3 R = CH_3

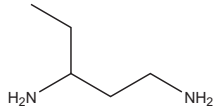
© 2005 NRC Canada



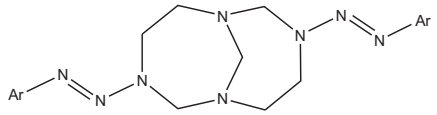
4



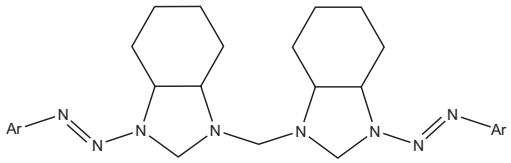
5



6



7



8

Experimental

All reagents were reagent grade materials purchased from the Aldrich Chemical Co. Ltd. (Oakville, Ontario), and were used without further purification. DYTEK® EP diamine is the Aldrich trade name for 1,3-diaminopentane. Melting points were determined on a Fisher-Johns melting point apparatus and are uncorrected. Infrared spectra were obtained using Nujol mulls, unless otherwise stated, on a PerkinElmer 299 spectrophotometer or with a Brucker Vector 22 spectrometer. ^{1}H and ^{13}C NMR spectra were obtained using either the Anasazi Instruments 60 MHz EFT spectrometer at Saint Mary's University, or the Bruker 250 MHz spectrophotometer at the Atlantic Regional Magnetic Resonance Centre at Dalhousie University in Halifax, Nova Scotia. Chemical shifts were recorded in $CDCl_3$ or d_6-DMSO solutions at 20 °C and are relative to TMS as the internal standard. Elemental analysis was carried out at the Canadian Microanalytical Laboratory, Delta, British Columbia.

4-Ethyl-3-({6-ethyl-3-[2-aryl-1-diazenyl]hexahydro-1-pyrimidinyl}methyl)-1-[2-aryl-1-diazenyl]hexahydropyrimidines (1)

General procedure

The appropriate arylamine (0.010 mol) was dissolved in 3 mol/L hydrochloric acid (20 mL) with heating if necessary to obtain a clear solution, and this solution was cooled in an ice–salt bath. The arylamine hydrochloride solution was diazotized at 0–5 °C with a solution of sodium nitrite (0.011 mol) in water and the resulting mixture was stirred in the cold for 0.5 h after which any insoluble impurities were removed by vacuum filtration. The mixture was brought to pH 7 using a saturated solution of sodium bicarbonate at which point 37% aqueous formaldehyde solution (5 mL) was added. An appropriate amount of 1,3-diaminopentane (0.010 mol) was slowly added to the solution, which was allowed to stir in the cold for a further 0.5 h. Occasionally, a slight precipitate was evident during the period of the addition, but it was not removed. The mixture was then adjusted to alkaline pH with additional saturated sodium bicarbonate solution, whereupon the product precipitated out of solution. Solid precipitates were isolated by vacuum filtration and purified by recrystallization from an appropriate solvent (see Tables 1 and 2). Oils were recovered by extraction into dichloromethane (3 × 20 mL aliquots), dried over anhydr. $MgSO_4$, and rotoevaporated under vacuum. This procedure afforded the following products.

*4-Ethyl-3-({6-ethyl-3-[2-(*p*-cyanophenyl)-1-diazenyl]hexahydro-1-pyrimidinyl}methyl)-1-[2-(*p*-cyanophenyl)-1-diazenyl]-hexahydropyrimidine (**1a**)*

Yield: 95%; off-white needles, mp 144–147 °C (hexanes – ethyl acetate). IR ν_{max} (cm^{-1}): 2222 (CN), 843 (OOP). Anal. calcd. for $C_{27}H_{34}N_{10}$ (%): C 65.1, H 6.8, N 28.1; found: C 65.2, H 6.9, N 28.3.

*4-Ethyl-3-({6-ethyl-3-[2-(*p*-nitrophenyl)-1-diazenyl]hexahydro-1-pyrimidinyl}methyl)-1-[2-(*p*-nitrophenyl)-1-diazenyl]hexahydropyrimidine (**1b**)*

Yield: 80%; red oil. IR ν_{max} (cm^{-1}): 1529, 1353 (NO_2), 854 (OOP).

*4-Ethyl-3-({6-ethyl-3-[2-(*p*-methoxycarbonylphenyl)-1-diazenyl]hexahydro-1-pyrimidinyl}methyl)-1-[2-(*p*-methoxycarbonylphenyl)-1-diazenyl]hexahydropyrimidine (**1c**)*

Yield: 15%; amorphous, mp 105–108 °C (hexanes – ethyl acetate). IR ν_{max} (cm^{-1}): 1709 (C=O), 866 (OOP).

*4-Ethyl-3-({6-ethyl-3-[2-(*p*-ethoxycarbonylphenyl)-1-diazenyl]hexahydro-1-pyrimidinyl}methyl)-1-[2-(*p*-ethoxycarbonylphenyl)-1-diazenyl]hexahydropyrimidine (**1d**)*

Yield: 95%; golden yellow prisms, mp 120–123 °C (hexanes – ethyl acetate). IR ν_{max} (cm^{-1}): 1707 (C=O), 861 (OOP). Anal. calcd. for $C_{31}H_{44}N_8O_4$ (%): C 62.8, H 7.4, N 18.9; found: C 62.7, H 7.0, N 18.5.

*4-Ethyl-3-({6-ethyl-3-[2-(*p*-acetylphenyl)-1-diazenyl]hexahydro-1-pyrimidinyl}methyl)-1-[2-(*p*-acetylphenyl)-1-diazenyl]-hexahydropyrimidine (**1e**)*

Yield: 62%; brown prisms, mp 144–147 °C (ethyl acetate). IR ν_{max} (cm^{-1}): 1732 (C=O), 845 (OOP). Anal. calcd. for $C_{29}H_{40}N_8O_2$ (%): C 65.4, H 7.5, N 21.05; found: C 65.7, H 7.4, N 21.1.

*4-Ethyl-3-({6-ethyl-3-[2-(*p*-carboxamidophenyl)-1-diazenyl]hexahydro-1-pyrimidinyl}-methyl)-1-[2-(*p*-carboxamidophenyl)-1-diazenyl]hexahydropyrimidine (**1f**)*

Yield: 95%; off-white small prisms, mp 91–94 °C (hexanes – ethyl acetate – toluene). IR ν_{max} (cm^{-1}): 3174, 3341 (NH), 1645 (C=O), 856 (OOP). Anal. calcd. for $C_{27}H_{38}N_{10}O_2$ (%): C 60.7, H 7.1, N 26.2; found: C 60.8, H 7.2, N 26.7.

*4-Ethyl-3-({6-ethyl-3-[2-(*p*-bromophenyl)-1-diazenyl]-hexahydro-1-pyrimidinyl}methyl)-1-[2-(*p*-bromophenyl)-1-diazenyl]hexahydropyrimidine (**1g**)*

Yield: 88%; pale beige prisms, mp 100–102 °C (hexanes – ethyl acetate). IR ν_{max} (cm^{-1}): 827 (OOP). Anal. calcd. for $C_{25}H_{34}N_8Br_2$ (%): C 49.5, H 5.6, N 18.5; found: C 49.3, H 5.7, N 18.2.

© 2005 NRC Canada

Table 1. ^{1}H NMR data in $CDCl_3$ relative to TMS for the 4-ethyl-3-({6-ethyl-3-[2-aryl-1-diazenyl]hexahydro-1-pyrimidinyl}methyl)-1-

Compound No.	X	Aromatic (8H)	H_a,H_b (2H)	H_c,H_d (4H)
1a	*p*-CN	7.46 (d, *J* = 7.5 Hz), 7.59 (d, *J* = 7.5 Hz)	3.20 (d, *J* = 10.2 Hz), 3.51 (d, *J* = 10.2 Hz), 3.36 (s)	4.84 (m)
1b	*p*-NO_2	7.48 (d, *J* = 8.7 Hz), 8.19 (d, *J* = 8.7 Hz)	3.37 (br)	4.86 (br m)
1c	*p*-CO_2Me	7.49 (d, *J* = 8.5 Hz), 8.05 (d, *J* = 8.6 Hz)	3.42 (br)	4.83 (br m)
1d	*p*-CO_2Et	7.44 (d, *J* = 7.0 Hz), 8.00 (d, *J* = 7.9 Hz)	3.21 (d, *J* = 10.1 Hz), 3.38 (s), 3.54 (d, *J* = 10.1 Hz)	4.705 (d, *J* = 13.3 Hz), 4.82 (s), 4.925 (d, *J* = 13.3 Hz)
1e	*p*-$COCH_3$	7.45 (d, *J* = 6.8 Hz), 7.93 (d, *J* = 6.8 Hz)	3.21 (d, *J* = 10.5 Hz), 3.37 (s), 3.54 (d, *J* = 10.4 Hz)	4.70 (d, *J* = 11.5 Hz), 4.82 (s), 4.925 (d, *J* = 11.5 Hz)
1f	*p*-$CONH_2$	7.48 (d, *J* = 8.6 Hz), 7.80 (d, *J* = 8.6 Hz)	Not observed	4.8 (v br)
1g	*p*-Br	7.28 (d, *J* = 8.8 Hz), 7.43 (d, *J* = 8.5 Hz)	3.23 (d, *J* = 10.5 Hz), 3.39 (s), 3.54 (d, *J* = 10.5 Hz)	4.68 (t, *J* = 13.3 Hz), 4.84 (t, *J* = 13.3 Hz)
1h	*p*-Cl	7.3 (m)	3.4 (br m)	4.75 (m)
1i	*p*-CH_3	7.12 (d, *J* = 7.0 Hz), 7.32 (d, *J* = 7.0 Hz)	3.26 (d, *J* = 10.4 Hz), 3.43 (s), 3.59 (d, *J* = 10.4 Hz)	4.665 (dd, *J* = 8.9, 13 Hz), 4.835 (dd, *J* = 10.5, 13 Hz)
1j	*p*-OCH_3	6.86 (d, *J* = 8.8 Hz), 7.38 (d, *J* = 8.8 Hz)	3.2–3.6 (m)	4.5–4.9 (br m)
1k	H	7.0–7.5 (m)	3.17 (d, *J* = 4.0 Hz), 3.34 (d, *J* = 2.6 Hz), 3.42 (s)	4.75 (m)
1l	*o*-CN	7.02–8.03 (m)	3.40 (t)	4.85 (br m)
1m	*o*-Br	7.05 (br t, *J* = 5.6 Hz), 7.28–7.37 (m), 7.60 (d, *J* = 7.6 Hz)	Not observed (hidden by H_2O)	4.7–4.9 (br)

*4-Ethyl-3-({6-ethyl-3-[2-(*p*-chlorophenyl)-1-diazenyl]-hexahydro-1-pyrimidinyl}methyl)-1-[2-(*p*-chlorophenyl)-1-diazenyl]hexahydropyrimidine (**1h**)*

Yield: 76%; lustrous yellow rhomboids, mp 117–119 °C (hexanes – ethyl acetate). IR ν_{max} (cm^{-1}): 832 (OOP). Anal. calcd. for $C_{25}H_{34}N_8Cl_2$ (%): C 58.0, H 6.6, N 21.7; found: C 58.1, H 6.6, N 21.7.

*4-Ethyl-3-({6-ethyl-3-[2-(*p*-tolyl)-1-diazenyl]hexahydro-1-pyrimidinyl}methyl)-1-[2-(*p*-tolyl)-1-diazenyl]hexahydropyrimidine (**1i**)*

Yield: 19%; red prisms, mp 116–119 °C (hexanes). IR ν_{max} (cm^{-1}): 823 (OOP). Anal. calcd. for $C_{27}H_{40}N_8$ (%): C 68.07, H 8.40, N 23.53; found: C 68.13, H 8.67, N 23.60.

*4-Ethyl-3-({6-ethyl-3-[2-(*p*-methoxyphenyl)-1-diazenyl]-hexahydro-1-pyrimidinyl}methyl)-1-[2-(*p*-methoxyphenyl)-1-diazenyl]hexahydropyrimidine (**1j**)*

Yield: 71%; oil. IR ν_{max} (cm^{-1}): 834 (OOP).

*4-Ethyl-3-({6-ethyl-3-[2-phenyl-1-diazenyl]hexahydro-1-pyrimidinyl}methyl)-1-[2-phenyl-1-diazenyl]hexahydropyrimidine (**1k**)*

Yield: 30%; mp 98–101 °C. IR ν_{max} (cm^{-1}): 758 (OOP). Anal. calcd. for $C_{25}H_{36}N_8$ (%): H 8.04, N 25.0; found: H 8.3, N 24.5.

*4-Ethyl-3-({6-ethyl-3-[2-(*o*-cyanophenyl)-1-diazenyl]hexahydro-1-pyrimidinyl}methyl)-1-[2-(*o*-cyanophenyl)-1-diazenyl]hexahydropyrimidine (**1l**)*

Yield: 50%; amorphous, mp 64–70 °C (hexanes – ethyl acetate). IR ν_{max} (cm^{-1}): 2223 (CN), 759 (OOP).

*4-Ethyl-3-({6-ethyl-3-[2-(*o*-bromophenyl)-1-diazenyl]hexahydro-1-pyrimidinyl}methyl)-1-[2-(*o*-bromophenyl)-1-diazenyl]hexahydropyrimidine (**1m**)*

Yield: 31%; white prisms, mp 112 to 113 °C (hexanes – ethyl acetate). IR ν_{max} (cm^{-1}): 756 (OOP). Anal. calcd. for $C_{25}H_{34}N_8Br_2$ (%): C 49.5, H 5.6, N 18.5; found: C 49.4, H 5.6, N 18.3.

^{1}H NMR spectroscopic data for compounds **1a**–**1m** are shown in Table 1; Table 2 is a list of the ^{13}C NMR spectroscopic data for these compounds. Proton and carbon labels relevant to these tables are shown in Fig. 1.

Results and discussion

The reaction of 1,3-diaminopentane (DYTEK® EP diamine, **6**) with arene diazonium salts in the presence of formaldehyde results in the formation of a series of 4-ethyl-3-({6-ethyl-3-[2-aryl-1-diazenyl]hexahydro-1-pyrimidinyl}methyl)-1-[2-aryl-1-diazenyl]hexahydropyrimidines (**1a**–**1m**) in moderate to excellent yields (20%–100%). These products represent a novel series of new bistriazenes and also represent new derivatives of the hexahydropyrimidine heterocyclic system. Also, the dimeric character of these molecules is novel because of the bis(hexahydropyrimidinyl)methane structure. The bistriazene series **1** is a new extension of our broad-ranging study of triazene derivatives of (1,*x*)-diazacycloalkanes; previously, we reported the synthesis of new aryldiazenylpiperazines (17), bis(aryldiazenyl)piperazines (18), aryldiazenylhomopiperazines (19), bis(aryldiazenyl)-homopiperazines (19), and a series of aryldiazenylhexahydropyrimidines (8).

© 2005 NRC Canada

[2-aryl-1-diazenyl]hexahydropyrimidines **1a**–**1m**) (see Fig. 1 for proton labels).

H_e (2H)	H_f,H_g,H_j (8H)	H_h,H_i (4H)	H_k (6H)	X
2.75 (br m)	1.41–2.04 (m)	3.865 (m), 4.03 (m)	0.97 (t, J = 7.2 Hz)	—
2.8 (br)	1.4–2.0 (m)	4.0 (br m)	0.98 (t, J = 7.8 Hz)	—
2.8 (br)	1.4–2.0 (m)	4.0 (br)	0.997 (br t, J = 7.1 Hz)	3.93 (O-CH_3)
2.74 (br m)	1.41–1.91 (m)	3.86 (m), 4.0 (m)	0.96 (t, J = 7.3 Hz), 0.97 (t, J = 7.5 Hz)	1.38 (t, J = 7.0 Hz, 6H), 4.35 (q, J = 7.1 Hz, 4H)
2.75 (br)	1.39–2.03 (m)	3.85 (m), 4.03 (m)	0.97 (t, J = 7.3 Hz), 0.96 (t, J = 7.3 Hz)	2.57 (s)
2.75 (br)	1.4–2.03 (m)	4.0 (br)	0.97 (t, J = 7.5 Hz)	—
2.75 (septet, J = 3.8 Hz)	1.39–1.92 (m)	3.80 (dq, J = 4.9, 9.0 Hz), 3.96 (dq, J = 4.6, 11.0 Hz)	0.96 (t, J = 7.3 Hz), 0.97 (t, J = 7.3 Hz)	—
2.8 (br m)	1.3–2.0 (m)	3.8 (br m)	0.93 (t, J = 6.8 Hz)	—
2.75 (m)	1.39–1.57 (m), 1.69–1.89 (m)	3.77–3.80 (m, 2H), 3.94 (dq, J = 3.5, 10.1 Hz, 2H)	0.972 (t, J = 7.3 Hz), 0.977 (t, J = 7.3 Hz)	2.33 (s, CH_3-Ar)
2.8 (m)	1.3–2.0 (m)	3.9 (m)	0.95 (t, J = 7.5 Hz), 0.97 (t, J = 7.0 Hz)	3.8 (s, O-CH_3)
2.83 (br m)	1.59 (br septet, J = 6.5 Hz)	3.86 (br m)	0.94 (br t, J = 6.9 Hz)	—
2.83 (br m)	1.4–2.1 (m)	4.02 (br)	0.97 (t, J = 6.8 Hz)	—
2.72 (br)	1.38–2.08 (m)	3.76 (br), 4.02 (br)	0.89 (br t, J = 6.55 Hz)	—

The structure of the new compounds of series **1** has been established by a variety of spectroscopic methods, but a crucial piece of evidence providing unequivocal corroboration is the X-ray crystal structure of one compound in the series, that of compound **1g**, the *p*-bromo derivative. An ORTEP perspective diagram of **1g** is shown in Fig. 2; full details of the X-ray structure of **1g** have been published (9). Compound **1g** crystallizes in two polymorphic forms; both polymorphs display crystallographic disorder within the hexahydropyrimidine rings. Another feature evident in the ORTEP diagram (Fig. 2) is the chirality of the two stereocentres; C9 has the R configuration whereas C14 has the S configuration. Thus, it is clear that the molecule of **1g** is the meso compound, and we can infer that all the compounds of series **1** have this configuration.

The structure of other members of series **1** can be deduced by spectroscopic correlation, as well as elemental analysis. The IR spectra of the compounds of series **1** are consistent with the presence of the functional group (X) in the aryl moiety, and the out-of-plane bending vibrations in the region 750–850 cm^{-1} confirm the ortho- or para-substitution. The ^1H NMR spectral data of the compounds of series **1** are shown in Table 1 and are consistent with the proposed structures. However, many of the signals are broadened and not fully resolved for several possible reasons. For example, the protons of the methylene groups H_f, H_g, and H_j (see Fig. 1 for proton and carbon labels) are overlapping in a broad multiplet in the range 1.4–2.0 ppm. Also, the proton signals of the methylene groups H_h and H_i are consistently broadened, possibly owing to the rotational dynamics of the N—N bond in the triazene moieties; it is well-known that the restricted rotation around the N—N bond in the triazene causes broadening of signals in the NMR spectrum (20). Nevertheless, some of the spectra of these triazenes show remarkable fine structure, which can be interpreted to support the assigned structures. A good example is the spectrum of the *p*-tolyl-derivative (**1i**), which shows some evidence for the existence of two rotamers in $CDCl_3$ solution. Also, many of the complex features of the proton spectrum of **1i** (and others in the series) indicate the presence of sets of diastereotopic protons (e.g., H_c and H_d) arising from the presence of the stereocentre at C5.

Thus, the signal from the terminal methyl groups (H_k) in **1i** is clearly a doublet of triplets integrating for 6H; the triplet splitting arises from coupling to the adjacent methylene protons (H_j), but the doubling of the triplets is interpreted as arising from two different rotamers of the molecule. A set of multiplets in the range 1.39–1.89 ppm, integrating for 8H, is assigned to the overlapping methylene protons H_f, H_g, and H_j. At 2.75 ppm, a multiplet for 2H is assigned to the two equivalent methine protons (H_e), which couple to the neighbouring hydrogens H_f, H_g, and H_j. Multiple signals at 3.77–3.80 and 3.94 ppm are assigned to the diastereotopic methylene protons H_h and H_i; the multiplicity, when resolved, is eight lines (doublets of doublets of doublets) owing to the combination of geminal coupling and vicinal coupling to protons H_f and H_g. The signals of the diastereotopic protons (H_c and H_d) each appear as a doublet of doublets at 4.665 and 4.835 ppm, owing to the combination of geminal coupling and long range coupling to H_e. The signal from the single central methylene group (H_a and H_b) is complex, showing five lines, which appear to consist of a doublet of doublets plus a singlet in the middle. This is interpreted as arising from a combination of geminal coupling of the

© 2005 NRC Canada

Table 2. ^{13}C NMR data in $CDCl_3$ relative to TMS for the 4-ethyl-3-({6-ethyl-3-[2-aryl-1-diazenyl]hexahydro-1-pyrimidinyl}methyl)-1-[2-aryl-1-diazenyl]hexahydropyrimidines (**1a–1m**) (see Fig. 1 for carbon labels).

Compound No.	X	Instrument[a]	Aromatic	C1[b]	C2[b]	C3[b]	C4[b]	C5[b]	C6[b]	C7	X
1a	*p*-CN	B	119.6, 121.0 133.1, 154.2	—	67.0	64.8 (w)	42.1	59.0	26.05	11.1	108.2 (CN)
1b	*p*-NO_2	B	119.8, 123.7 132.3, 145.0	75.0 (br)	65.2	62.3	42.2	58.5	26.0	11.0	—
1c	*p*-CO_2Me	A	120.3, 126.8 130.6, 154.4	—	66.9 (w)	64.0 (br)	43.0 (w)	58.6 (br)	25.6	11.0	51.7 (OMe) 166.8 (C=O)
1d	*p*-CO_2Et	A	120.3, 127.2 130.5, 154.4	—	68.0 (w)	60.8	43.5 (br)	58.8	25.8	10.9	14.4 (Me) 60.6 (O-CH_2) 166.6 (C=O)
1e	*p*-$COCH_3$	B	120.5, 129.5 134.1, 154.5	—	—	—	42.8	58.7	26.4	11.1	25.4 (Me) 197.4 (C=O)
1f	*p*-$CONH_2$	A	120.7, 129.1 131.9, 153.2	—	67.3 (w)	62.5 (w)	43.7	58.1 (br)	24.4	10.4	168.6 (C=O)
1g	*p*-Br	A	118.7, 122.1 131.7, 149.6	74.8	66.4	63.9	42.9	58.6	25.6	11.0	—
1h	*p*-Cl	A	121.7, 128.7 130.7, 149.5	72.1	66.5	63.8	44.1	58.6	25.5	10.4	—
1i	*p*-CH_3	A	120.7, 129.4 135.1, 148.8	72.4	64.0	63.8	42.7 (br)	58.6 (53.9)	27.7 (br)	10.6	21.0 (Me)
1j	*p*-OCH_3	A	114.1, 121.7 144.6, 158.0	79.4	72.4	64.1	31.5	61.6	27.2	10.6	52.5 (O-Me)
1k	H	A	120.7, 125.9 128.8, 151.0	72.3	66.3 (w)	63.7 (w)	42.5 (w)	58.8 (53.8)	25.5	10.6	—
1l	*o*-CN	A	117.7, 125.1 133.0, 152.8	—	68.0 (br)	62.0 (w)	43.0 (br)	58.4 (br)	25.9 (br)	10.9	107.5 (CN)
1m	*o*-Br	A	118.2, 119.9, 125.6 127.5, 132.8, 147.8	75.0 (w)	66.6 (w)	63.7 (br)	42.9 (br)	58.5	26.4	10.9	—

[a]Anasazi 60 MHz (A); Bruker AC 250 MHz (B).
[b]Weak (w); broad (br).

© 2005 NRC Canada

Fig. 1. Proton and carbon labels for interpretation of the ^{1}H NMR data in Table 1 and ^{13}C NMR data in Table 2.

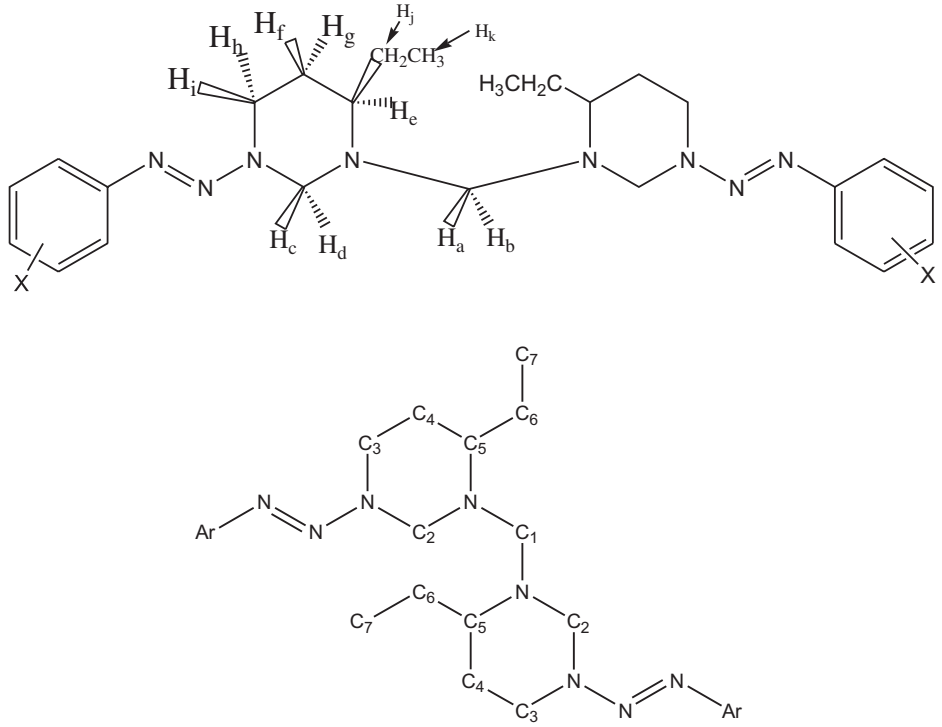
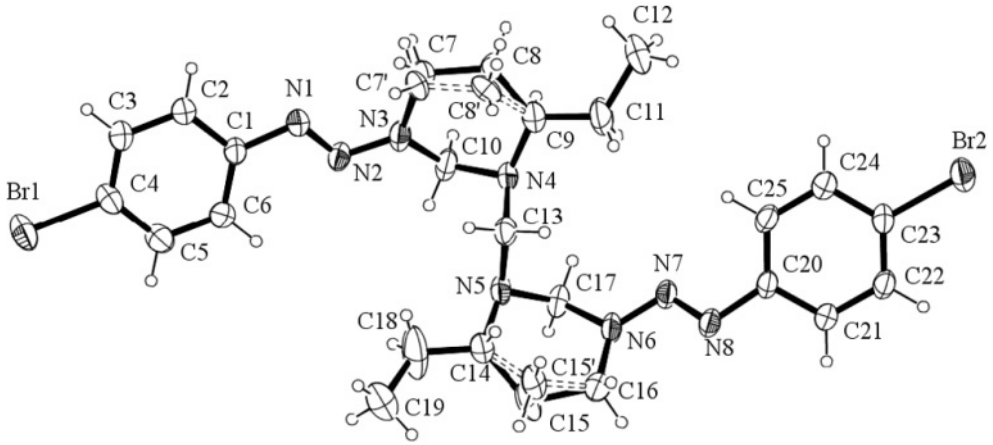


Fig. 2. ORTEP view of the molecule of 4-ethyl-3-({6-ethyl-3-[2-(*p*-bromophenyl)-1-diazenyl]hexahydro-1-pyrimidinyl}methyl)-1-[2-(*p*-bromophenyl)-1-diazenyl]hexahydropyrimidine (**1g**) showing the thermal ellipsoids at 30% probability level.



diastereotopic protons H_a and H_b and rotational isomerism of the triazene. The singlet + doublet of doublets set is also clearly seen in the spectra of compounds **1a**, **1d**, **1e**, and **1g**.

Further characterization of the triazenes of series **1** by ^{13}C NMR spectroscopy was complicated by the rotational dynamics of the triazene moiety. The carbon signals are broadened to the extent that they are often not detected at normal concentrations. However, by making very concentrated solutions of the compounds in $CDCl_3$, the ^{13}C NMR spectra were recorded with the in-house SMU 60MHz Anasazi spectrometer set for 512 scans per spectrum. In this way, it was possible to detect most of the carbon signals from all of the compounds in series **1a**–**1m**; the results are presented in Table 2. The success of detecting the various carbon atoms largely depends on the proximity of the carbon atom to the triazene group within the molecule; the carbon atoms closest to the triazene are most affected by the rotational dynamics. Thus, the extreme methyl carbon (C7; see Fig. 1)is readily observed at ca. 11 ppm in all compounds, as is the methylene carbon C6 at ca. 26 ppm. The carbon signal of C4 is observed in most compounds at ca. 43 ppm, but is shifted to 31.5 ppm in compound **1j**, which has an electron-releasing group in the aryl ring. The electron-withdrawing effect of the N atom attached to C5 causes this signal to shift downfield to ca. 59 ppm, but this signal shows signs of doubling because of the presence of more than one rotational isomer. Carbons C2 and C3, which are directly attached to the triazene moiety, are the most elusive signals to observe as broad, weak signals at variable frequency, C2 at 65–72 ppm and C3 at 61–64 ppm. The bridging methylene

© 2005 NRC Canada

carbon C1 is observed as a weak signal in the range 72–79 ppm.

In the previous part of this study (8*a*), the bistriazenes of types **2** and **3** were characterized, but it was observed that there is a wide range of stability of the compounds of series **2** and **3**. This range of stability is also evident in the new compounds of series **1**. Several of the compounds, notably **1b**, **1c**, **1j**, and **1l**, started to decompose within a short time of being isolated, so that characterization of these products was restricted to immediate IR and NMR spectroscopic analysis. The low yields of some products, particularly **1c** and **1i**, may be partially attributable to the instability of the compounds. Several of the more stable products displayed a limited shelf life when stored for a couple of years; samples that were fine powders when fresh are now glass, such as **1e** and **1h**. Others like **1a**, **1d**, **1f**, and **1g** show little if any sign of decay. Compounds **1e** and **1h** are somewhat fickle in this regard; crude samples that were stored for over 2 years show definite signs of decomposition, whereas purified samples of the same compounds show no sign of decomposition. It is possible that the stability of these bis[{6-ethyl-}3-(aryldiazenyl)hexahydropyrimidin-1-yl]methanes is prolonged in the crystalline state compared with the amorphous state, but we have not undertaken a systematic study of this question.

An important issue regarding the synthesis of compounds of series **1** is the question of the manner of their formation. Central to this question is the previously reported work relating to the reaction of 1,3-diaminopropanes and formaldehyde, which was reviewed in the Introduction to this paper. Several groups have studied the reaction of alkanediamines with formaldehyde, but surprisingly there has been no previous work on the reaction of formaldehyde with 1,3-pentanediamine. However, it seems likely that the initial reaction of these molecules will produce the 4-ethylhexahydropyrimidine (**9**) (eq. [1]).

[1] **6** + CH_2O $\xrightarrow{-H_2O}$ **9**

Further condensation–dimerization of **9** with formaldehyde could theoretically lead to any of the three dimeric isomers 6-ethyl-1-[(6-ethylhexahydro-1-pyrimidinyl)methyl]hexahydropyrimidine (**10**), 4-ethyl-1-[(6-ethylhexahydro-1-pyrimidinyl)methyl]hexahydropyrimidine (**11**), or 4-ethyl-1-[(4-ethylhexahydro-1-pyrimidinyl)methyl]hexahydropyrimidine (**12**), which differ in the location of the ethyl groups relative to the bridging methylene group (C1) (eq. [2]).

The observed product **1** is readily formed by diazonium coupling to the preferred isomer (**10**) (eq. [3]).

Effectively, the diazonium coupling reaction serves as a tool for trapping otherwise unstable amines from solution; it could also mean in this case that the dimer (**10**) is more reactive than either of the isomers (**11** or **12**). The X-ray structure evidence (9) of the *p*-bromo derivative (**1g**) is the unequivocal evidence for the structure and by inference is evidence for the mechanism of formation of **1** via **10**. An alternative pathway for formation of **1** would involve diazonium coupling with the monomeric perhydropyrimidine (9), followed by condensation. However, such a pathway would likely lead to mixtures of products that we have not observed. Although intermediate **10** should exist as a mixture of diastereomers, it would appear that only the meso form is involved in the formation of the meso form of product **1**.

Oligomers of hexahydropyrimidine, analogous to the proposed intermediate (**10**), are reported to be thermally unstable (13). Although the mechanism of decomposition is unclear, there may be a connection between this previous work and the observation in the present work that the bistriazenes of type **1** are not universally stable. The instability of compounds of type **1** is also evident from attempts to record their mass spectra under electron ionization conditions; no molecular ions were observed under EI, thus inhibiting our ability to obtain accurate mass measurement of their molecular ions.

[2] **9** + **9** + CH_2O $\xrightarrow{-H_2O}$ **10** + **12** + **11**

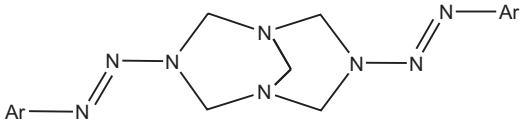
© 2005 NRC Canada

[3] **10** $\xrightarrow[-2H^+]{2\ ArN_2^+}$ **1**

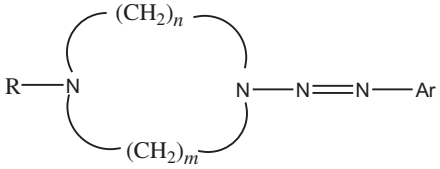
Conclusion

It appears from our on-going studies that the interaction of a diazonium salt with a mixture of formaldehyde and an alkanediamine ($NH_2(CH_2)nNH_2$) gives rise to two distinct types of oligomer. Bistriazenes of types **7** (14) and **13** (21) are examples of the bridged bicyclic bistriazene, whereas the compounds of series **2** and **3** (8) exemplify the linear bicyclic bistriazene. The new compounds of series **1**, reported here, clearly belong to the linear bicyclic class, providing further evidence that there is a crossover in the molecular architecture going from ethylenediamine (two-carbon spacer) to propanediamine (three-carbon spacer). This type of crossover was also observed in the transition from ethylenediamine to cyclohexanediamine in structure **8** (16).

This paper is part V in a series that describes the synthesis of a variety of triazenes and bistriazenes that fit the general classification of 1-aryldiazenyl-(1,*x*)-diazacycloalkanes described by the general structure **14**, where *m* = 1 or 2 and *n* = 2–5. The new compounds of series **1** fit to the general structure **14**, where *m* = 1 and *n* = 3. Previously, we reported new triazenes derived from piperazine (17, 18) (*m* = *n* = 2) and homopiperazine (19) (*m* = 2, *n* = 3). It is worth pointing out that the hexahydropyrimidine rings in **1**, **2**, and **3** represent the isomeric heterocycle to the piperazine ring system, and that the compounds of series **1** are isomeric with those of series **3**.



13



14

In future papers in this series, we will report more examples of the linear bicyclic bistriazene derived from other diamines, such as 1,4-diaminobutane, 1,5-diaminopentane, and 2-methyl-1,2-diaminopropane. Evidently, the linear bicyclic bistriazene reported here in the new compounds of series **1** appears to be the normal type of molecular architecture in this field of chemistry.

Acknowledgements

The authors are grateful to the Natural Sciences and Engineering Research Council of Canada (NSERC) for a Discovery Grant to the principal author (KV) and to Human Resources at Saint Mary's University for a Student Employment Experience Program (SEEP) Award (2003) to Reid Tingley. Financial support, to Ryan Church, was also provided by the Student Employment Experience Program 2003–2004 (SEEP) at Saint Mary's University. We are also grateful to the Atlantic Region Magnetic Resonance Centre at Dalhousie University for providing NMR spectra; in particular, we would like to thank Dr. Mike Lumsden for assistance with interpretation of the NMR spectral data.

References

1. D.B. Kimball and M.M Haley. Angew. Chem. Int. Ed. **41**, 3338 (2002); D.B. Kimball, R. Herges, and M.M. Haley. J. Am. Chem. Soc. **124**, 1572 (2002).
2. S. Brase. Acc. Chem. Res. **37**, 805 (2004).
3. T.A. Connors, P.M. Goddard, K. Merai, W.C.J. Ross, and D.E.V. Wilman. Biochem. Pharmacol. **25**, 241 (1976); G. Daidone, D. Raffa, B. Maggio, M.V. Raimondi, F. Plescia, and D. Schillachi. Eur. J. Med. Chem. **39**, 219 (2004).
4. E.S. Newlands, G.R.P. Blackledge, J.A. Slack, C. Goddard, C.J. Brindley, L. Holder, and M.F.G. Stevens. Cancer Treat. Rep. **69**, 801 (1985).
5. K.C. Nikolau, C.N.C. Boddy, S. Brase, and N. Wissinger. Angew. Chem. Int. Ed. **38**, 2097 (1999).
6. D.L. Hooper, I.R. Pottie, M. Vacheresse, and K. Vaughan. Can. J. Chem. **76**, 125 (1998).
7. K. Vaughan. Org. Prep. Proced. Int. **33**, 59 (2001).
8. S. Moser, R. Church, M.B. Peori, and K. Vaughan. Can. J. Chem. **83**, 1071 (2005); M.B. Peori, K. Vaughan, and V. Bertolasi. J. Chem. Crystallogr. **35**, 297 (2005).
9. R. Tingley, V. Bertolasi, and K. Vaughan. J. Chem. Crystallogr. **35**, 821 (2005).
10. H. Krassig. Makromol. Chem. **17**, 77 (1955).
11. R.F. Evans. Aust. J. Chem. **20**, 1643 (1967).
12. M.M. Bagga, B. Everett, and I.G. Hinton. Chem. Commun. (Cambridge), 259 (1987).
13. J. Dale and T. Sigvartsen. Acta Chem. Scand. **45**, 1064 (1991).
14. M.B. Peori, K. Vaughan, and D.L. Hooper. J. Org. Chem. **63**, 7437 (1998).
15. K. Biradha, M.B. Peori, K. Vaughan, and M.J. Zaworotko. J. Chem. Crystallogr. **29**, 145 (1999).
16. J.F. Glister, K. Vaughan, and V. Bertolasi. J. Chem. Crystallogr. **34**, 175 (2004).
17. V.R. Little and K. Vaughan. Can. J. Chem. **82**, 1294 (2004).
18. V.R. Little, R. Tingley, and K. Vaughan. Can. J. Chem. **83**, 471 (2005).
19. S.L. Moser and K. Vaughan. Can. J. Chem. **82**, 1725 (2004).
20. M. Barra, S. Srivastava, and E. Brockman. J. Phys. Org. Chem. **17**, 1057 (2004); B.T. Golding, T.J. Kemp, R. Narayanaswamy, and B.W. Waters. J. Chem. Res. (S), 130 (1984).
21. R.D. Singer, K. Vaughan, and D.L. Hooper. Can. J. Chem. **64**, 1567 (1986).

© 2005 NRC Canada

Effective and regioselective iodination of arenes using iron(III) nitrate in the presence of tungstophosphoric acid

Mohammad Jafarzadeh, Kamal Amani, and Farzad Nikpour

Abstract: An easy, cheap, and effective method for iodination of various aromatic compounds takes place with molecular iodine and iron nitrate nonahydrate as the oxidant in the presence of a catalytic amount of tungstophosphoric acid in dichloromethane, with good yield and high regioselectivity under very mild conditions.

Key words: iodination, arenes, iodine, iron(III) nitrate, tungstophosphoric acid.

Résumé : On a mis au point une méthode facile, peu coûteuse et efficace de procéder à l'iodation de divers composés aromatiques; elle fait appel à de l'iode moléculaire et du nonahydrate du nitrate de fer qui agit comme agent oxydant en présence de quantités catalytiques d'acide tungstophosphorique dans le dichlorométhane et elle donne de bons rendements et une régiosélectivité élevée dans des conditions très douces.

Mots clés : iodation, arènes, iode, nitrate de fer(III), acide tungstophosphorique.

[Traduit par la Rédaction]

Introduction

Heteropoly acids (HPAs) and their salts are useful acid and oxidation catalysts for various reactions and there are already many practical applications (1–3). One of the most interesting aspects may be the fact that they can be used in various kinds of reaction media or fields. Furthermore, they can be active solid acid catalysts and can provide unique reaction fields such as a pseudoliquid that is a "catalytically active solid solvent". HPA catalysts will find more green and sustainable applications in the future (4). Solid HPAs possess purely Brønsted acidity and are stronger than the usual mineral acids such as H_2SO_4, HCl, HNO_3, $HClO_4$, CF_3SO_3H, etc. (5, 6), and than conventional solid acids such as SiO_2–Al_2O_3, H_3PO_4–SiO_2, HX, HY, and H-ZSM-5 zeolites, Amberlyst-15, and Nafion-H (7). Among HPAs, polytungstic acids are the most widely used catalysts because of their high acid strengths, thermal stabilities, and low reducibility. Tungstophosphoric acid ($H_3PW_{12}O_{40}$) is a inexpensive, reusable, heterogeneous, and easily available catalyst (8, 9).

Iodoaromatic compounds are useful synthetic reagents for fine organic synthesis. They are valuable, versatile synthetic intermediates and have found wide applications in medicine and biochemistry (10, 11). The direct iodination of arenes with molecular iodine under mild conditions requires an oxidizing agent to activate the low reactivity of iodine. The oxidants such as oleum (12*a*), $Pb(OAc)_4$ (12*b*), diiodine pentoxide (12*c*), CrO_3 (12*d*), sodium perborate (12*e*), hydrogen peroxide (12*e*), $KMnO_4$ (12*f*), MnO_2 (12*f*), tetrabutylammonium disulfate (12*g*), sodium periodate (12*h*), sodium iodate (12*h*), ceric ammonium nitrate(CAN) (12*i*), F-TEDA-BF_4(1-fluoro-4-chloromethyl-1,4-diazoniabicyclo[2.2.2]-octane bis(tetrafluoroborate)) (12*j*, 12*k*), urea–H_2O_2 (12*l*), etc., were reported. Recently, silica-supported $Bi(NO_3)_3{\cdot}5H_2O$ and $Fe(NO_3)_3{\cdot}9H_2O$ (silfen) were used as mild oxidizing agents for the iodination of active arenes (12*m*, 12*n*). However, most of the described reactions in the literature require one or some of the following conditions: an excess of the reagent or strong oxidizing agent, hazardous toxic solvents such as acetonitrile at elevated temperature, the use of expensive catalysts that need to be prepared prior to use, corrosive mineral acids, expensive Lewis acids, the use of corrosive and moisture-sensitive iodine monochloride, iodine vapor irritant in solvent free conditions and mostly waste remains.

Here, we describe an improved, simple, and eco-friendly method for regioselective iodination of arenes with iodine and iron(III) nitrate nonahydrate as the oxidant in the presence of a catalytic amount of tungstophosphoric acid at room temperature with good yields (Scheme 1).

Results and discussion

Effect of catalyst

Iron(III) nitrate nonahydrate, an abundant, inexpensive, nontoxic, and commercially available reagent can be used as an oxidant in the presence of a catalytic amount of dehy-

Received 23 May 2005. Published on the NRC Research Press Web site at http://canjchem.nrc.ca on 23 December 2005.

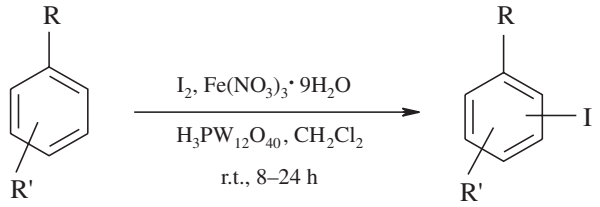
M. Jafarzadeh,[1,2] K. Amani, and F. Nikpour. Department of Chemistry, Kurdistan University, Sanandaj, Iran.

[1]Present address: No. 54, Omid Ave., Khorshidkola St., Babol, 47147-13597, Iran.

[2]Corresponding author (e-mail: mjafarzadeh1027@yahoo.com).

 doi: 10.1139/V05-187 © 2005 NRC Canada

Scheme 1. Iodination of arenes with iron nitrate in the presence of tungstophosphoric acid at room temperature.



Yield 9%–92%

R = OCH_3, CH_3, OH, NH_2, $NHCOCH_3$
R' = OCH_3, CH_3, NO_2, Br, H

drated heteropoly acids. Primarily, iodination of anisole, as a model compound, was performed in the presence of several HPAs and some other solid acids in dichloromethane at room temperature for 8 h (GC results are presented in Table 1). The result shows that in the absence of the catalyst, the reaction proceeds with low yield, but in the presence of HPAs, this conversion proceeded efficiently under similar reaction conditions. In this reaction, anisole was converted to *p*-iodoanisole in good yield and excellent regioselectivity (100%) without the formation of diiodinated derivatives. To show that tungstophoric acid is more effective than other HPAs and solid acids, we chose $H_3PW_{12}O_{40}$, which is a very efficient and environmentally friendly catalyst (6), for further iodination studies.

Heterogeneous acid-catalyzed systems

Heteropoly acids and solid acids are not dissolved in dichloromethane, thus the iodination reaction takes place in heterogeneous conditions. The acid catalysis of heteropoly compounds in the solid state is classified into "surface-type" and "bulk-type" catalysis. Catalytic reactions involving polar molecules (here, anisole) occur not only at the surface, but also in the bulk solid HPAs. This shows good parallelism between catalytic activity (bulk-type) and acidity (surface-type) (13). Under bulk-type conditions, all of the acid sites are available to the reactant and therefore high catalytic activity could be expected. Cs and NH_4 salts (scarcely soluble in polar solvents) usually show only surface-type catalysis. However, solid HPAs containing a cation of low ionic radii to charge ratio (H^+) readily absorb small polar molecules and tend to exhibit pseudoliquid behaviour (bulk-type), and are soluble in polar solvents. The diffusion of reactant molecules in the solid is faster than the reaction; the solid bulk forms a pseudoliquid phase in which the catalytic reaction can proceed (14). Therefore, the heteropoly salts containing Cs, NH_4, and Fe (Table 1, entries 6–9) showed less catalytic activity than HPAs containing W and Mo (Table 1, entries 3–5).

On the other hand, although Keggin-type HPAs ($H_3PM_{12}O_{40}$, M = W, Mo) are much stronger acids than the Dawson-type HPAs ($H_6P_2Mo_{18}O_{62}$) (6), but Dawson-type heteropoly acids, because of their amorphous shape (ellipsoidal shape of the polyanion), show higher catalytic acivity than Keggin-type HPAs, and this is because of their crystalline shape (spherical shape) (14). Consequently, we can see a low selectivity in the iodination of anisole in the presence of $H_6P_2Mo_{18}O_{62}$. The formation of the resulting by-product is due to the amorphous shape and high catalytic activity in Dawson-type HPAs (Table 1, entry 10). Also, solid acids show only surface-type activity, so their catalytic activities are less than those of $H_3PM_{12}O_{40}$ (M = W, Mo) (Table 1, entries 11–13). One of the most desirable properties for a catalyst is the ease of its recovery. We have found that $H_3PW_{12}O_{40}$ can be easily recovered and recycled simply by filtering (by diethyl ether) and drying (Table 1, entry 14). The recovery had only slightly decreased their catalytic activity (because of the reduction of tungsten atoms) without structural degradation.

Table 1. Iodination of anisole with $Fe(NO_3)_3{\cdot}9H_2O$ in the presence of various heteropoly acids and other solid acids in CH_2Cl_2 at room temperature for 8 h.

Entry	Catalyst	Conv. (%)	GC yield (%)[a]
1	None	36	36
2	$H_3PW_{12}O_{40}$[b]	78	77
3	$H_3PW_{12}O_{40}$	100	99
4	$H_3PMo_{12}O_{40}$	92	92
5	$H_3PW_{12}O_{40}$:$H_3PMo_{12}O_{40}$[c]	97	96
6	$Cs_{2.5}H_{0.5}PW_{12}O_{40}$	83	82
7	$Cs_{2.5}H_{0.5}PMo_{12}O_{40}$	75	75
8	$(NH_4)_2HPW_{12}O_{40}$	72	71
9	$Fe_{0.85}H_{0.45}PMo_{12}O_{40}$	80	79
10	$H_6P_2Mo_{18}O_{62}$	82	74, 7[d]
11	Montmorillonite-K10[e]	85	85
12	Amberlyst-15H$^+$[e]	89	89
13	Silica gel[e]	83	82
14	$H_3PW_{12}O_{40}$[f]	88	>86

Note: Reaction conditions: anisole (1 mmol), I_2 (0.6 mmol), $Fe(NO_3)_3{\cdot}9H_2O$ (0.4 mmol), catalyst (0.1 mmol), CH_2Cl_2 (1 mL).
[a]Product: 4-IC_6H_4OMe.
[b]Catalyst: 0.05 mmol.
[c]HPW and HPMo in equal molar ratio.
[d]By-product: 2-IC_6H_4OMe.
[e]One gram of solid acid was used.
[f]Catalyst: after recovery and reuse.

Effect of oxidant

We also investigated other metal nitrates for the iodination of anisole under similar reaction conditions in dichloromethane at room temperature for 8 h (GC results are presented in Table 2). The results revealed that in the absence of the oxidant (Table 2, entry 1), and also with an excess of the catalyst (tungstophosphoric acid) (Table 2, entry 2), the iodination reaction did not proceed after 8 h. Therefore, we have concluded that in the presence of oxidant, most of the metal nitrates were effective oxidants for this reaction, but iron(III) and bismuth(III) nitrates gave better results. These results were expected regarding their reduction potential.

Effect of solvent

The iodination of anisole was also conducted in different solvents at room temperature for 8 h (GC results are presented in Table 3). The results show that in the absence of solvent (Table 3, entry 1) the iodination reaction proceeds with low yield after 1 h at room temperature. The iodination

© 2005 NRC Canada

Table 2. Iodination of anisole with various metal nitrates in the presence of $H_3PW_{12}O_{40}$ in CH_2Cl_2 at room temperature for 8 h.

Entry	Metal nitrates	Conv. (%)	GC yield (%)[a]
1	None	0	0
2	None[b]	0	0
3	$Mn(NO_3)_3{\cdot}4H_2O$	3	2
4	$Fe(NO_3)_3{\cdot}9H_2O$	100	99
5	$Bi(NO_3)_3{\cdot}5H_2O$	97	96
6	$Ce(NO_3)_3{\cdot}6H_2O$	25	24
7	$(NH_4)_2[Ce(NO_3)_6]$ (CAN)	69	68
8	$Cu(NO_3)_2{\cdot}3H_2O$	78	77
9	$Ni(NO_3)_2{\cdot}6H_2O$	58	57

Note: Reaction conditions: anisole (1 mmol), I_2 (0.6 mmol), metal nitrate (0.4 mmol), $H_3PW_{12}O_{40}$ (0.1 mmol), CH_2Cl_2 (1 mL).
[a]Product: 4-IC_6H_4OMe.
[b]Catalyst: 0.5 mmol.

reaction also proceeds with the use of microwave irradiation (using a common household microwave oven) under solvent-free conditions for 2 min with the power set at 200 W (Table 3, entry 2). The microwave-assisted method has been accepted as a method for dramatically reducing reaction time, and for increasing isolated yields of products compared with the conventional method, but unfortunately this technique is not a selective tool. The results (Table 3, entries 3–6) show that the efficiency and the yield of the reaction in chlorinated solvents is much more than other solvents at room temperature. We chose dichloromethane for further studies.

On the other hand, HPAs do not dissolve in nonpolar solvents (chlorinated solvents), thus the iodination reaction takes place in a heterogeneous system. HPAs have very high solubility in polar solvents such as water, lower alcohols, ketones, ethers, esters, etc. They absorb a large amount of polar solvents not only on the surface, but also in the bulk of crystalline HPA, forming heteropoly acid solvates (14). Consequently, a homogeneous system exists. Therefore, the iodination reaction in ethyl acetate and MeOH takes place in homogeneous conditions (Table 3, entries 11 and 12). The formation of a by-product can result from high catalytic activity in homogeneous conditions. For relatively polar solvents, we can expect heterogeneous bulk-type (pseudoliquid) catalysis conditions (Table 3, entries 7–10).

According to the results obtained from effects of catalyst, metal nitrate, and solvent, our method is suitable for the iodination of arenes. The aromatic compounds were converted to the corresponding monoiodoaromatic compounds at room temperature in good yields with excellent regioselectivities for 8–24 h. The results of this study are shown in Table 4.

The iodination occurred at a less sterically hindered position. As anticipated, *o*-iodination occurred only when the para position was occupied. In the present method, the formation of a nitro derivative was not observed in spite of increasing reaction time. Our investigation showed that the electron-releasing substituents increased the rate of reaction and yield; however, the electron-attracting groups decreased the rate of reaction and yield of iodination. Aromatic compounds, such as acetanilide, aniline, and phenol, were converted to the corresponding monoiodoproducts in good

Table 3. Iodination of anisole with $Fe(NO_3)_3{\cdot}9H_2O$ in the presence of $H_3PW_{12}O_{40}$ in various solvents at room temperature for 8 h.

Entry	Solvent	Conv. (%)	GC yield (%)[a]
1	0[b]	35	>33
2	0[c]	100	58, 40[d]
3	CH_2Cl_2	100	>99
4	$ClCH_2CH_2Cl$	99	>97
5	$CHCl_3$	94	93
6	CCl_4	94	92
7	Et_2O	33	32
8	THF	32	31
9	DMF	13	12
10	DMSO	31	30
11	Ethyl acetate	98	61, 37[d]
12	MeOH	46	28, 18[d]

Note: Reaction conditions: anisole (1 mmol), I_2 (0.6 mmol), $Fe(NO_3)_3{\cdot}9H_2O$ (0.4 mmol), $H_3PW_{12}O_{40}$ (0.1 mmol), solvent (1 mL).
[a]Product: 4-IC_6H_4OMe.
[b]Solventless for 1 h.
[c]Solventless for 2 min and microwave irradiation (200 W).
[d]By-product: 2-IC_6H_4OMe.

yields (Table 4, entries 6–9). Xylenes and toluene were converted to iodo derivatives in relatively good yields (Table 4, entries 10–12), but activated naphthalenes were converted to diiodinated derivatives (Table 4, entries 13 and 14). Finally, this method is only suitable and effective for activated aromatic compounds.

Conclusion

The present method is very simple, cheap, effective, and selective for iodination of electron-rich aromatic compounds, which when carried out under mild conditions and ambient temperature by tungstophosphoric acid, is an effective, readily available, recoverable, reusable, and low-cost catalyst.

Experimental

Chemicals were purchased from Fluka and Merck. Organic solvents were purified and dried by the procedures extracted from *Vogel's textbook of practical organic chemistry* (5th ed. John Wiley and Sons, New York. 1991). $H_3PW_{12}O_{40}$, $H_3PMo_{12}O_{40}$, $Cs_{2.5}H_{0.5}PMo_{12}O_{40}$, and $(NH_4)_2HPW_{12}O_{40}$ were purchased from Merck and were purified by extraction with Et_2O from aqueous solutions of the acids, and dried and dehydrated by evacuating at 150–300 °C for 1 to 2 h. These HPAs can be prepared according to the known procedures (15). Some solid HPAs and their salts, such as $Cs_{2.5}H_{0.5}PW_{12}O_{40}$, $Fe_{0.85}H_{0.45}PMo_{12}O_{40}$, and $H_6P_2Mo_{18}O_{62}$, were prepared according to the reported methods (16) in our laboratory.

General reaction procedure

To iodine (0.6 mmol, 0.152 g) in dichloromethane (1 mL), iron nitrate (0.4 mmol, 0.161 g) and then $H_3PW_{12}O_{40}$ (0.1 mmol, 0.288 g) were added. After 10 min, arene (1 mmol) was added and the reaction mixture was stirred at room temperature for 8–24 h. The completion of the reaction

© 2005 NRC Canada

Table 4. Iodination of various arenes with $Fe(NO_3)_3{\cdot}9H_2O$ catalyzed by $H_3PW_{12}O_{40}$ in CH_2Cl_2 at room temperature.

Entry	Substrate	Time (h)	Product	Yield (%)[a]
1	C_6H_5OMe	8	4-IC_6H_4OMe	92
2	1,3-$(MeO)_2C_6H_4$	2	4-I-1,3-$(MeO)_2C_6H_3$	76[b]
			2-I-1,3-$(MeO)_2C_6H_3$	23[b]
3	2-MeC_6H_4OMe	10	4-I-2-MeC_6H_3OMe	90
4	4-MeC_6H_4OMe	13	2-I-4-MeC_6H_3OMe	75
5	2-BrC_6H_4OMe	24	4-I-2-BrC_6H_3OMe	46
6	$C_6H_5NHCOMe$	12	4-$IC_6H_4NHCOMe$	78
7	$C_6H_5NH_2$	12	4-$IC_6H_4NH_2$	82
8	2-$NO_2C_6H_4NH_2$	24	4-I-2-$NO_2C_6H_3NH_2$	9
9	C_6H_5OH	10	4-IC_6H_4OH	79
10	1,2-$(Me)_2C_6H_4$	20	4-I-1,2-$(Me)_2C_6H_3$	40
11	1,4-$(Me)_2C_6H_4$	24	2-I-1,4-$(Me)_2C_6H_3$	34
12	C_6H_5Me	12	4-IC_6H_4Me	59
13	1-$MeOC_{10}H_7$	6	4-I-1-$MeOC_{10}H_6$	84[b]
			2-I-1-$MeOC_{10}H_6$	16[b]
14	2-$MeOC_{10}H_7$	6	1-I-2-$MeOC_{10}H_6$	76[b]
			3-I-2-$MeOC_{10}H_6$	10[b]

Note: Reaction conditions: substrate (1 mmol), I_2 (0.6 mmol), $Fe(NO_3)_3{\cdot}9H_2O$ (0.4 mmol), $H_3PW_{12}O_{40}$ (0.1 mmol), CH_2Cl_2 (1 mL).
[a]Isolated yield.
[b]GC yield.

was monitored by TLC and GC. After the usual work-up of the reaction mixture with Na_2SO_3 (25 mL, 5%), the crude product was extracted with CH_2Cl_2 (3 × 25 mL). The organic phase was dried over $MgSO_4$ and filtered, the crude product was purified by column chromatography on silica gel (petroleum ether – ethyl acetate, 5:1). All products are well-known in the literature. The products were identified by the comparison of their mp and IR data with those reported for the authentic samples in the literature.

Acknowledgments

The authors are thankful to Dr. Roushan Khoshnavazi and Fariba Maleki for useful discussions and their encouragement. We are also thankful to the Kurdistan University Research Council for the partial support of this work.

References

1. (*a*) M. Misono. Catal. Rev. Sci. Eng. **29**, 269 (1987); (*b*) M. Misono. Catal. Rev. Sci. Eng. **30**, 339 (1987).
2. M. Misono and N. Mizuno. Chem. Rev. **98**, 199 (1998).
3. I.V. Kozhevnikov. Chem. Rev. **98**, 171 (1998).
4. M. Misono, I. Ono, G. Koyano, and A. Aoshima. Pure Appl. Chem. **72**, 1305 (2000).
5. R.S. Drago, J.A. Dias, and T.O. Maier. J. Am. Chem. Soc. **119**, 7702 (1997).
6. M.N. Timofeeva. Appl. Catal. A, **256**, 19 (2001).
7. M. Misono, N. Mizuno, and T. Okuhara. Adv. Catal. **41**, 113 (1996).
8. F. Cavani. Catal. Today, **41**, 73 (1998).
9. J. Liu, J. Li, and X. Wang. Inorg. Chem. Commun. **4**, 372 (2001).
10. R.H. Seevers and R.E. Counsell. Chem. Rev. **82**, 575 (1982).
11. E.B. Merkushev. Synthesis, 923 (1988).
12. (*a*) J. Arotsky, R. Butler, and A.C. Darby. J. Chem. Soc. C, 1480 (1970); (*b*) B. Krassowska-Swiebocka, P. Lulinski, and L. Skulski. Synthesis, 926 (1995); (*c*) L.C. Brazdil and C.J. Cutler. J. Org. Chem. **61**, 9621 (1996); (*d*) P. Lulinski and L. Skulski. Bull. Chem. Soc. Jpn. **70**, 1665 (1997); (*e*) P. Beinker, J.R. Hanson, N. Meindl, and I.C.R. Medina. J. Chem. Res. Synop. 204 (1998); (*f*) P. Lulinski and L. Skulski. Bull. Chem. Soc. Jpn. **72**, 115 (1999); (*g*) S.G. Yang and Y.H. Kim. Tetrahedron Lett. **40**, 6051 (1999); (*h*) P. Lulinski and L. Skulski. Bull. Chem. Soc. Jpn. **73**, 951 (2000); (*i*) M.I. Rodriguez-Franco, I. Dorronsora, A.I. Hernandez-Higueras, and G. Antequera. Tetrahedron Lett. **42**, 863 (2001); (*j*) S. Stavber, P. Kralj, and M. Zupan. Synlett, 598 (2002); (*k*) S. Stavber, P. Kralj, and M. Zupan. Synthesis, 1513 (2002); (*l*) P. Lulinski, A. Kryska, M. Sosnowski, and L. Skulski. Synthesis, 441 (2004); (*m*) V.M. Alexander, A.C. Khandekar, and S.D. Samant. Synlett, 1895 (2003); (*n*) R.D. Tilve, V.M. Alexander, and B.M. Khadilkar. Tetrahedron Lett. **43**, 9457 (2002).
13. A. Corma. Chem. Rev. **95**, 559 (1995).
14. M. Misono. Chem. Commun. 1141 (2001).
15. (*a*) C. Rocchiccioli-Deltcheff, M. Fournier, R. Franck, and R. Thouvenot. Inorg. Chem. **22**, 207 (1983); (*b*) T. Okuhara, H. Watanabe, T. Nishimura, K. Inumara, and M. Misono. Chem. Mater. **12**, 2230 (2000).
16. (*a*) T. Okuhara, T. Nishimura, H. Watanabe, and M. Misono. J. Mol. Catal. **74**, 247 (1992); (*b*) S. Tatematsu, T. Hibi, T. Okuhara, and M. Misono. Chem. Lett. 865 (1984); (*c*) L. McKean and M.T. Pope. Inorg. Chem. **13**, 747 (1974).

© 2005 NRC Canada

Thermodynamics of organic mixtures containing amines. IV. Systems with aniline

Juan Antonio González, Ismael Mozo, Isaías García de la Fuente, and José Carlos Cobos

Abstract: Binary mixtures of aniline with benzene, toluene, alkane, alkanol, or *N*,*N*-dialkylamide have been investigated in the framework of the DISQUAC model. The reported interaction parameters change regularly with the molecular structure of the mixture components. The model consistently describes a set of thermodynamic properties including liquid–liquid equilibria, vapor–liquid equilibria, and molar excess enthalpies. The two latter properties for ternary systems are well-represented by DISQUAC using binary parameters only (i.e., neglecting ternary interactions). A comparison of DISQUAC results and those obtained from the UNIFAC (Dortmund version) and ERAS models is also shown. The experimental molar excess enthalpies for binary and ternary mixtures are better described by DISQUAC than by UNIFAC. ERAS fails when representing molar excess enthalpies of those binary systems including methanol or ethanol. This may be due to the existence of strong dipolar interactions among aniline molecules as well as to effects related to the equation of state term, evaluated comparing molar excess enthalpies, and molar excess internal energies at constant volume. The study of the aniline systems in terms of the concentration–concentration structure factor also underlines the importance of dipolar interactions in solutions with alkanes or alcohols, which may be due to the high polarizability of the aniline molecule.

Key words: thermodynamics, mixtures, aniline, dipolar interactions, structural effects.

Résumé : Étude de mélanges binaires d'aniline en présence de benzène, de toluène, d'alcane, d'alcanol et de *N*,*N*-dialkylamide dans le contexte du modèle DISQUAC. Les paramètres d'interaction qui ont été rapportés varient régulièrement en fonction de la structure moléculaire des composés des mélanges. Le modèle décrit d'une façon consistante un ensemble de propriétés thermodynamiques, y compris les équilibres liquide–liquide, les équilibres vapeur–liquide et les enthalpies molaires en excès. Pour les systèmes ternaires, ces deux dernières propriétés sont bien représentées par le modèle DISQUAC en n'utilisant que des paramètres binaires, c'est-à-dire en négligeant les interactions ternaires. On présente aussi une comparaison des résultats obtenus avec le modèle DISQUAC et de ceux obtenus avec les modèles UNIFAC (version Dortmund) et ERAS. Les enthalpies molaires en excès des mélanges binaires ou ternaires sont mieux représentées par DISQUAC que par UNIFAC. Le modèle ERAS n'arrive pas à représenter les enthalpies molaires en excès de ces systèmes binaires, y compris le méthanol ou l'éthanol. Ce résultat peut être dû à l'existence de fortes interactions dipolaires entre les molécules d'aniline ainsi qu'aux effets reliés aux termes de l'équation d'état, qui est évalué en comparant les enthalpies molaires en excès, et les énergies internes molaires en excès à volume constant. L'étude des systèmes de l'aniline en termes de facteur de structure concentration-concentration met aussi en évidence l'importance des interactions dipolaires en solutions dans des alcanes ou des alcools qui peuvent être dus à la grande polarisabilité de la molécule d'aniline.

Mots clés : thermodynamique, mélanges, aniline, interactions dipolaires, effets de structure.

[Traduit par la Rédaction]

Introduction

Amines are a very interesting class of compounds. Primary and secondary linear amines are weakly self-associated (1–5). Solutions of tertiary amines with aliphatic hydrocarbons, and particularly with homomorphic alkanes, are nearly ideal (6). Therefore, different effects can be studied through mixtures including amines. Such investigations may contribute to the development of chemical theories of solutions, and are also useful to obtain information on the interactions between amines and other molecules characterized by different functional groups, for example, in biological systems.

Mixtures containing aniline show very interesting features. Except in dilute regions, aniline does not mix with alkanes at 298.15 K (7). Systems with 1-alkanols are characterized by quite large positive deviations from Raoult's law. For example, at equimolar composition and 298.15 K, the molar excess enthalpy (H^E) of the aniline + 1-propanol system is 783 J mol^{-1} (8). Primary or secondary linear amines or tertiary amine + 1-alkanol mixtures behave quite differently. At the

Received 7 October 2004. Published on the NRC Research Press Web site at http://canjchem.nrc.ca on 22 December 2005.

J.A. González,[1] I. Mozo, I. García de la Fuente, and J.C. Cobos. G.E.T.E.F. Dpto Termodinámica y Física Aplicada, Facultad de Ciencias, Universidad de Valladolid, Valladolid, 47071 Spain.

[1]Corresponding author (e-mail: jagl@termo.uva.es).

 doi: 10.1139/V05-190 © 2005 NRC Canada

same conditions as above, H^E(hexylamine + 1-propanol) = –2561 J mol^{-1} (9), H^E(dipropylamine + 1-butanol) = –2432 J mol^{-1} (10), and H^E(triethylamine + 1-propanol) = –1413 J mol^{-1} (11). Therefore, these mixtures show rather large negative deviations from Raoult's law (12, 13). All this makes the study of systems with aniline very interesting, which have been investigated using different models. For example, the aniline + toluene mixture has been treated in terms of the Mecke–Kempter theory (14). The UNIQUAC association solution model (15) has been applied to correlate and (or) predict thermodynamic properties of this class of binary–ternary mixtures (16–18). For technical applications, in the framework of the UNIFAC model (Dortmund version) (19, 20), interaction parameters for contacts between the aniline group and other different groups are available.

As a continuation of our studies on mixtures containing amines (12, 13, 21–23), the first purpose of this article is to extend the purely physical model DISQUAC (24), based on the rigid lattice model developed by Guggenheim (25), to mixtures containing aniline. The solvents considered are: benzene, toluene, alkanes, alkanols, dimethylformamide (DMF), and dimethylacetamide (DMA). In previous studies, we showed that DISQUAC rather accurately represents thermodynamic properties, such as vapour–liquid equilibria (VLE), molar excess Gibbs energies (G^E), H^E, or molar excess heat capacity at constant pressure (C_P^E), of any class of system, independently of its deviation from Raoult's law (12, 13, 26–30). For mixtures with large positive deviations from this law (28–30), DISQUAC also properly describes liquid–liquid equilibria (LLE). From a practical point of view, the model provides reliable predictions on VLE and H^E for ternary systems (31–33), improving UNIFAC predictions (32, 33). Our second purpose is to gain insight into the interactions and structural effects present in solutions with aniline. As in terms of DISQUAC, the excess molar volume (V^E) is assumed to be zero, here we also apply, to some selected systems, the so-called ERAS model (34). As it is known, ERAS combines the real association solution model (35, 36) with a physical term, Flory's equation of state (37), and simultaneously provides information on H^E and V^E. Amine + alkane (4, 22) systems and 1-alkanol + primary or secondary linear amines, or + triethylamine (4, 9, 12, 13, 38–42) mixtures have been successfully characterized using ERAS. To complete our study, we also analysed the experimental database and investigated the mixture structure in terms of the concentration–concentration structure factor ($S_{CC}(0)$) (43). We have shown elsewhere (44, 45) that DISQUAC is a reliable tool to describe this important property.

THEORY

DISQUAC

In the framework of DISQUAC, mixtures of aniline with an organic solvent are regarded as possessing the following four types of surface: (*i*) type n, NH_2 in aniline; (*ii*) type p, C_6H_5 in aniline or toluene; (*iii*) type a, aliphatic (CH_3, CH_2, CH in *n*-alkanes, toluene, methylcyclohexane, alkanols, or *N*,*N*-dialkylamides); (*iv*) type s (s = b, C_6H_6 in benzene; s = c, *c*-CH_2 or *c*-CH in cycloalkanes; s = h, OH in alkanols; s = m, N-CO in *N*,*N*-dialkylamides).

Assessment of geometrical parameters

When DISQUAC is applied, the total molecular volumes (r_i), surfaces (q_i), and the molecular surface fractions (α_i) of the compounds present in the mixture are calculated additively on the basis of the group volumes (R_G) and surfaces (Q_G) recommended by Bondi (46). As volume and surface units, the volume R_{CH_4} and surface Q_{CH_4} of methane are taken arbitrarily (47). For the NH_2 group, r_{NH_2} = 0.61565 and q_{NH_2} = 0.6000. For the CH group, r_{CH} = 0.39603 and q_{CH} = 0.19655. The geometrical parameters for the remaining groups referred to in this work are given elsewhere (47–50).

General equations

The main features of DISQUAC are: (*i*) the partition function is factorized into two terms, in such a way that the excess functions are calculated as the sum of two contributions: a dispersive (DIS) term that represents the contribution from the dispersive forces and a quasichemical (QUAC) term that arises from the anisotropy of the field forces created by the solution molecules. Thus,

$$[1] \qquad G^E = G^{E,COMB} + G^{E,DIS} + G^{E,QUAC}$$

$$[2] \qquad H^E = H^{E,DIS} + H^{E,QUAC}$$

(*ii*) The interaction parameters are assumed to be dependent on the molecular structure. (*iii*) The value $z = 4$ for the coordination number is used for all the polar contacts. This represents one of the most important shortcomings of the model, and is partially removed via the hypothesis of considering structure dependent interaction parameters. In eq. [1], the combinatorial term ($G^{E,COMB}$) is represented by the Flory–Huggins equation (47, 48).

The temperature dependence of the interaction parameters has been expressed in terms of the DIS and QUAC interchange coefficients (49) ($C_{st,l}^{DIS}$ and $C_{st,l}^{QUAC}$), where s ≠ t = a, b, c, h, m, n, p, and l = 1 (Gibbs energy, $C_{st,1}^{DIS/QUAC} = g_{st}^{DIS/QUAC}(T_o)/RT_o$); l = 2 (enthalpy, $C_{st,2}^{DIS/QUAC} = h_{st}^{DIS/QUAC}(T_o)/RT_o$); l = 3 (heat capacity, $C_{st,3}^{DIS/QUAC} = c_{pst}^{DIS/QUAC}(T_o)/R$). T_o = 298.15 K is the scaling temperature and R is the gas constant.

Modified UNIFAC (Dortmund version)

Modified UNIFAC (19) differs from the original UNIFAC (51) by the combinatorial term and the temperature dependence of the interaction parameters.

The equations to calculate G^E and H^E are obtained from the fundamental equation for the activity coefficient (γ_i) of component i:

$$[3] \qquad \ln\gamma_i = \ln\gamma_i^{COMB} + \ln\gamma_i^{RES}$$

where $\ln\gamma_i^{COMB}$ is the combinatorial term and $\ln\gamma_i^{RES}$ is the residual term. The equations are given elsewhere (12).

Assessment of geometrical and interaction parameters

In modified UNIFAC, a new main group $ACNH_2$, different to that of linear primary or secondary amines, is defined for the representation of the thermodynamic properties of aniline + organic solvent mixtures. In this model, the geo-

© 2005 NRC Canada

Table 1. Dispersive (DIS) and quasichemical (QUAC) interchange coefficients $C^{DIS}_{sn,l}$ and $C^{QUAC}_{sn,l}$ (l = 1, Gibbs energy; l = 2, enthalpy; l = 3, heat capacity) for (s,n) contacts in aniline + organic solvent mixtures.

Solvent	Contact	$C^{DIS}_{sn,1}$	$C^{DIS}_{sn,2}$	$C^{DIS}_{sn,3}$	$C^{QUAC}_{sn,1}$	$C^{QUAC}_{sn,2}$	$C^{QUAC}_{sn,3}$
Benzene or toluene	(b,n) or (p,n)	3.7	–2.8	–4	1.25	10	4
n-Alkane	(a,n)	2	0.65		6	11.5	
Cyclohexane	(c,n)	1.85	0.82		6	11.5	
Methanol	(h,n)	1.4	–8.95	7	0.5	4.35	5
Ethanol	(h,n)	–0.5	–8.4	7	1.5	4.35	5
1-Propanol	(h,n)	–3	4	7	3	–3.5	5
≥1-Butanol	(h,n)	–3.75	4.5	7	3	–3.5	5
2-Propanol	(h,n)	–1.5[a]	–8.3	7	3	5	5
2-Butanol	(h,n)	–0.5	–6.7	7	3	5	5
DMF	(h,m)	–6.5	–15.8		1	–1	
DMA	(h,m)	2[a]	9.9		1	–1	

Note: type a, CH_3, CH_2, CH, in *n*-alkanes, toluene, methylcyclohexane, alkanols, or *N*,*N*-dialkylamides; type b, C_6H_6; type c, *c*-CH_2 or *c*-CH in cycloalkanes; type h, OH in alkanols; type m, N-CO in *N*,*N*-dialkylamides; type n, NH_2 in aniline; type p, C_6H_5 in toluene or aniline.

[a]Estimated value.

metrical parameters, the relative van der Waals volumes, and the relative van der Waals surfaces are not calculated from molecular parameters as in the original UNIFAC, but fitted together with the interaction parameters to the experimental values of the thermodynamic properties considered. The geometrical and interaction parameters were taken from the literature and used without modifications (19, 20).

ERAS

The excess functions are split into two additive terms, which arise from hydrogen-bonding effects (the so-called chemical contribution, X^E_{chem}) and nonpolar van der Waals' interactions including free volume effects (the so-called physical interactions, X^E_{phys}). The excess functions are written as:

$$[4] \qquad X^E = X^E_{phys} + X^E_{chem}$$

where $X^E = H^E$, V^E, or G^E. The resulting expressions for these functions are given elsewhere (12).

Moreover, it is assumed that only consecutive linear association occurs, which is described by a chemical equilibrium constant (K_A) independent of the chain length (m) of the associated species, according to the equation

$$[5] \qquad A_m + A \xleftrightarrow{K_A} A_{m+1}$$

with m ranging from 1 to ∞. The cross-association between two self-associated species, A_m and B_n, is represented by

$$[6] \qquad A_m + B_n \xleftrightarrow{K_{AB}} A_mB_n$$

The association constants (K_{AB}) of eq. [6] are also assumed to be independent of the chain length. Equations [5] and [6] are characterized by Δh^*_i, the enthalpy for the reactions that corresponds to the hydrogen-bonding energy, and by the volume change (Δv^*_i) related to the formation of the linear chains.

X^E_{phys} is derived from Flory's equation of state (37), which is assumed to be valid not only for pure components but also for the mixture (9, 38).

Estimation of the model parameters

DISQUAC interaction parameters

The general procedure applied in the estimation of the interaction parameters has been explained in detail elsewhere (28). Some remarks are given in the following.

Aniline + benzene system

This mixture is characterized by the contacts (b,n), (p,n), and (b,p). The (b,p) contact is represented by DIS parameters only, which are neglected in view of the low values of the excess functions of the benzene + toluene system (e.g., at equimolar composition and 298.15 K; H^E = 68 J mol^{-1} (52)). On the other hand, and for the sake of simplicity, we assumed that the (b,n) and (p,n) contacts are represented by the same interaction parameters, i.e., only the $C^{DIS/QUAC}_{bn,l}$ coefficients must be determined (Table 1). In our previous work on sulfolane (28), alkanol (53), dimethylsulfoxide (54), and amides (44, 45, 50) + benzene or + toluene, we have already shown that for solute (characteristic group X) + benzene or + toluene mixtures ($C^{QUAC}_{bx,l} = C^{QUAC}_{px,l}$), while the DIS parameters are quite close.

Aniline + n-*alkane or + cyclohexane systems*

The mixtures with *n*-alkanes are built by three contacts: (a,p), (p,n), and (a,n). The (a,p) contacts are represented by DIS parameters only. Here, the values used are: $C^{DIS}_{ap,1}$ = 0.332 and $C^{DIS}_{ap,2}$ = 0.57 (53). As $C^{DIS/QUAC}_{bn,l} = C^{DIS/QUAC}_{pn,l}$ and these parameters are known (see the previous section), only the interchange coefficients for the (a,n) contacts must be fitted. This is somewhat difficult because these systems show miscibility gaps (7). DISQUAC is a mean field theory and LLE calculations are developed under the basic and wrong assumption that G^E is an analytical function close to the critical point. The instability of a system is given by $(\partial^2 G^M/\partial x_1^2)_{P,T}$ ($G^M = G^E + G^{ideal}$) and represented by the critical exponent $\gamma > 1$ in the critical exponents theory (55). According to this theory, mean field models (γ = 1) provide LLE curves that are too high at the upper critical solution temperature (UCST) and too low at the lower critical solution temperature (LCST) (55). Thus, one must keep the

© 2005 NRC Canada

Table 2. ERAS parameters at 298.15 K for pure compounds.

Compound	K_i	V_i (cm^3 mol^{-1})	V_i^* (cm^3 mol^{-1})	P_i^* (J cm^{-3})	Δh_i^* (J mol^{-1})	Δv_i^* (cm^3 mol^{-1})
Methanol	986[a]	40.73[b]	32.13[c]	443.6[c]	–25.1[d]	–5.6[d]
Ethanol	317[a]	58.67[b]	47.11[c]	426.4[c]	–25.1[d]	–5.6[d]
1-Propanol	197[a]	75.16[b]	61.22[c]	433.9[c]	–25.1[d]	–5.6[d]
1-Butanol	175[a]	91.97[b]	75.70[c]	422.7[c]	–25.1[d]	–5.6[d]
Aniline	14.8[e]	91.53[f]	79.77[e]	541[e]	–15[e]	–12[e]
n-Hexane	0	131.57[g]	99.52[g]	424.2[g]	0	0
n-Decane	0	195.94[g]	155.75[g]	447[g]	0	0

[a]References 4 and 38.
[b]Reference 4.
[c]Reference 38.
[d]Values widely used (4, 9, 38, 91, 92).
[e]This work.
[f]Reference 82.
[g]Reference 93.

$C_{an,l}^{DIS/QUAC}$ coefficients between certain limits to provide not very high calculated UCSTs. The same occurs, e.g., for sulfolane (28), alkoxyethanol (29), crown ether (30), or amide (44, 45, 50) + alkane mixtures. Final parameters are collected in Table 1.

The aniline + cyclohexane system is characterized by the following contacts: (c,p), (p,n), and (c,n). For the (c,p) contacts the values used for the interchange coefficients are $C_{cp,1}^{DIS} = 0.332$ and $C_{cp,2}^{DIS} = 0.65$ (31). The interaction parameters for the (p,n) contacts are known, so only those for the (c,n) contacts must be fitted (Table 1). Calculations were carried out assuming that $C_{an,l}^{QUAC} = C_{cn,l}^{QUAC}$. This general rule is valid for many other solutions, such as sulfolane (28), alkoxyethanol (29), amide (44, 45, 50), linear oxaalkane (56), linear alkanone (57), linear organic carbonate (58), alkanoic acid anhydride (59), chloroalkane (60), linear carboxylic acid (61), alkanol (62–67), + *n*-alkane, or + cyclohexane mixtures. On the other hand, as the aniline + cyclohexane also shows a miscibility gap, similar considerations to those previoiusly stated are still valid.

Aniline + alkanol or + N,N-*dialkylamide systems*

Solutions with alkanols are built by five types of contacts: (a,h), (a,n), (a,p), (p,h), and (h,n). The $C_{ah,l}^{DIS/QUAC}$ and $C_{ph,l}^{DIS/QUAC}$ (l = 1–3) coefficients, different for contacts involving the OH group in 1-alkanols or 2-alkanols, have been previously determined from data on VLE, LLE, SLE (solid–liquid equilibria), H^E, and C_P^E for 1-alkanol or 2-alkanol + *n*-alkane or + toluene systems (13, 49, 53, 62–64). Therefore, only the interaction parameters for the (h,n) contacts must be fitted (Table 1).

Mixtures including amides are also formed by five contacts: (a,m), (a,n), (a,p), (p,m), and (m,n). The $C_{am,l}^{DIS/QUAC}$ and $C_{pm,l}^{DIS/QUAC}$ (l = 1, 2) coefficients have been determined in a previous study from thermodynamic properties of *N*,*N*-dialkylamide + *n*-alkane or + toluene systems (50). The $C_{mm,l}^{DIS/QUAC}$ values (l = 1–3) fitted in this work for the (m,n) contacts are listed in Table 1.

Adjustment of ERAS parameters

For pure compounds, the reduction parameters of volume and pressure (V_i^* and P_i^*, i = A, B) are collected in Table 2. The parameters adjustable to H^E and (or) V^E data are K_i, Δh_i^*, and Δv_i^* (values for aniline or 1-alkanols) and K_{AB}, Δh_{AB}^*, Δv_{AB}^*, and X_{AB} (binary parameters for aniline + *n*-alkane or for 1-alkanol + aniline systems). X_{AB} is the energetic interaction parameter characterizing the difference of dispersive intermolecular interactions between molecules A and B in the solution and in the pure components, and is the only adjustable parameter of the physical part of H^E and V^E (4, 9, 38).

The determination of K_i, Δh_i^*, and Δv_i^* for aniline is somewhat difficult because only a few H^E data at very high T are available (68). Our parameters are listed in Table 2. These H^E data were also used to determine the binary X_{AB} parameters of such systems (Table 3).

K_i, Δh_i^*, and Δv_i^* for 1-alkanols are known from H^E and V^E data for the corresponding mixtures with alkanes (Table 2). The remaining parameters K_{AB}, Δh_{AB}^*, Δv_{AB}^*, and X_{AB} for 1-alkanol + aniline systems (Table 3) were adjusted using the available data in the literature for H^E (8, 69–72) and V^E (73–75) for such solutions.

Results

DISQUAC results

These results are compared with experimental data for LLE, VLE G^E and H^E in Tables 4–8 and in Figs. 1–6. DISQUAC is useful for describing the thermodynamic properties of the studied mixtures. Here, we show three severe tests of the model: (*i*) LLE curves are calculated using the same parameters as for VLE and H^E. It should be considered as a success that immiscibility is predicted in the right temperature and composition region (Table 4, Fig. 1). As usual, the calculated curves for LLE and H^E are not as flat as the experimental curves close to the UCST (Figs. 1 and 4; refs. 29, 30, 44, 45, 50, 58, 59, 62, 63). (*ii*) DISQUAC correctly predicts H^E for ternary systems involving aniline. As in other applications (32, 33), deviations between experimental data and calculated values for ternary mixtures and for the constituent binaries are of the same order (Tables 6 and 8), which suggests that ternary interactions can be neglected when calculating H^E of these ternary systems. Their mean deviation, defined as

© 2005 NRC Canada

Table 3. ERAS parameters at temperature T for some mixtures containing aniline (this work) or other isomeric amines.

System	T (K)	K_{AB}	Δh^*_{AB} (J mol^{-1})	Δv^*_{AB} (cm^3 mol^{-1})	X_{AB} (J cm^{-3})
Aniline + n-C_6	363.15	0	0	0	78
Aniline + n-C_{10}	363.15	0	0	0	70
Methanol + aniline	298.15	60	–40.5	–20	2
Ethanol + aniline	298.15	28	–30.5	–18	4
1-Propanol + aniline	298.15	28	–25.5	–16.6	6
1-Butanol + aniline	298.15	28	–25.5	–16.6	18
Methanol + hexylamine[a]	298.15	2500	–42.4	–10.6	5
1-Propanol + hexylamine[a]	298.15	1500	–36	–9.1	5
Methanol + dipropylamine[b]	298.15	2450	–42.4	–12.2	5
1-Propanol + dipropylamine[b]	298.15	825	–34.5	–11.2	5

[a]Reference 42.
[b]Reference 39.

Table 4. Critical points, temperatures (T_c), and compositions (x_{1c}) for aniline(1) + alkane(2) mixtures calculated using DISQUAC (DQ) with interaction parameters from Table 1.

	x_{1c}		T_c (K)		
Solvent	Exp.	DQ	Exp.	DQ	Ref
Cyclohexane		0.338	304.4	304.5	94
n-Hexane		0.451	339	336.1	95
	0.504		342.7		96
n-Heptane	0.578	0.506	343.11	346.5	7
Methylcyclohexane[a]	0.528	0.412	313.8	327.3	97
n-Octane		0.558	345.15	355.2	98

[a]Treated as n-alkane (58).

$$\mathrm{Mdev}(H^E) = \sum \frac{\mathrm{dev}(H^E)}{N_S}$$

where N_S is the number of systems and dev(H^E) is given in the footnote of Table 8, is 0.061 (N_S = 6), in agreement with the value 0.058 calculated for the 163 mixtures previously studied (32, 33). The UNIQUAC association solution model using only binary parameters improves results for the ternary mixtures considered here. For example, the mean absolute deviation (in J mol^{-1}) is 11, 15, and 24.5 for methanol + aniline + benzene (18), 1-propanol + aniline + benzene (8), and for 2-butanol + aniline + benzene (76) systems, respectively. DISQUAC provides, in the same order, 14, 43, and 91 J mol^{-1}. A part of the observed differences between the results from the DISQUAC and UNIQUAC association solution models may be due to in this one the binary parameters are obtained from a direct fitting to H^E of the constituent binaries. The few VLE ternary data available in the literature are also well-represented by DISQUAC (Table 7). The mean deviation in pressure is ≈1.6%. For the other 39 systems examined in a previous study, this deviation was 2.2%. (*iii*) DISQUAC can be applied to those mixtures showing large positive deviations from Raoult's law (aniline + alkane), or to those mixtures showing large negative deviations from this law (aniline + DMF). It is remarkable that for systems containing alcohols or amides, the QUAC interchange coefficients are usually constant along each homologous series. This behaviour has been also found when investigating other solutions in terms of DISQUAC (12, 13, 26, 29, 30, 44, 45, 49, 50, 62, 64–66). The different values of $C^{QUAC}_{hn,l}$ (l = 1, 2) for aniline + methanol or + ethanol may be ascribed to the different character (higher dielectric constant, stronger self-association) of these alcohols when compared to the longer ones. A similar trend has been found when developing the DISQUAC treatment of alkanol + aromatic compound (53), 1-alkanol + CCl_4 (77), + linear primary or secondary amine (12), + triethylamine (13), or + amide (44, 45, 50), or the study of 1-alkanol + aromatic compound or + CCl_4 using Barker's theory (78, 79).

Comparison between DISQUAC and UNIFAC results

UNIFAC provides similar results to those from the DISQUAC model for VLE of binary and ternary mixtures (Tables 5 and 7). However, H^E is poorly represented in terms of UNIFAC (Tables 6 and 8). The same occurs for the temperature dependence of the thermodynamic properties. For example, UNIFAC predicts UCST = 363 K for the aniline + n-heptane system (experimental value (7), 343.11 K; DISQUAC result, 346.5 K). At 298.15 K, for the aniline(1) + toluene(2) mixture, UNIFAC yields for the excess heat capacity at constant pressure, $C^E_P(x_1 = 0.5) = 2.7$ J mol^{-1} K^{-1}. This value is rather high, as this system is characterized by $C^E_P \approx 0$ (14). DISQUAC provides $C^E_P(x_1 = 0.5) = -1$ J mol^{-1} K^{-1} and positive values at high mole fractions of aniline in agreement with the experimental data (14). The Mecke–Kempter model gives $C^E_P(x_1 = 0.329) = -0.63$ J mol^{-1} K^{-1}, this value calculated assuming that aniline is a moderately associated liquid (14).

ERAS results

Results for H^E from the ERAS model for some aniline mixtures are collected in Table 6. At 298.15 K and equimolar composition, ERAS gives V^E(aniline + 1-propanol) = –0.53 cm^3 mol^{-1} and V^E(aniline + 1-butanol) = –0.39 cm^3 mol^{-1}. The experimental values are –0.515 (73) and –0.365 cm^3 mol^{-1} (74), respectively.

The ERAS parameters of pure aniline (K_A and Δh^*_{AB}) are in good agreement with the values determined (24.2 (at 323.15 K) and –15.4 kJ mol^{-1}, respectively) in the frame-

© 2005 NRC Canada

Table 5. Molar excess Gibbs energies (G^E) at equimolar composition and at temperature T for aniline(1) + organic solvent(2) mixtures.

			G^E (J mol^{-1})			$\sigma_r(P)^b$			
Solvent	T (K)	N^a	Exp.[c]	DQ[d]	UNIF[e]	Exp.[c]	DQ[d]	UNIF[e]	Ref.
Benzene	298.15	28	374	419	493	0.007	0.026	0.061	99
	318.15	25	448	399	481	0.006	0.045	0.013	99
	343.15	11	531	379	465	0.005	0.068	0.032	100
		11	403			0.009	0.041	0.034	101
	392.45	10	458	364	435	0.007	0.041	0.014	102
Toluene	293.15	9	1090	606	621	0.031	0.34	0.35	103
	303.15	10	669	591	616	0.021	0.088	0.09	103
	313.15	11	746	576	611	0.011	0.071	0.069	103
	313.15	11	723			0.020	0.084	0.068	104
	363.15	16	802	515	582	0.005	0.15	0.12	105
Methanol	293.15	13	515	515	520	0.004	0.008	0.010	106
	338.15	13	592	599	587	0.007	0.011	0.008	106
	385.15	13	601	621	562		0.013	0.021	106
Ethanol	313.15	13	644	627	689	0.004	0.018	0.027	107
	350.81	13	629	614	641	0.001	0.010	0.006	107
	386.66	13	574	571	554	0.002	0.004	0.011	107
1-Pentanol	373.15	9	570	477	529	0.003	0.035	0.014	108
2-Butanol	293.51	5	962	899	799	0.018	0.058	0.12	109
DMF	298.15		–718	–735					110

[a]Number of data points.

[b] $$\sigma_r(P) = \left\{ \frac{1}{N} \sum \left[\frac{P_{exp} - P_{calcd}}{P_{exp}} \right]^2 \right\}^{1/2}$$.

[c]Experimental value.
[d]DISQUAC value calculated with interaction parameters from Table 1.
[e]UNIFAC value using parameters from the literature (19, 20).

Table 6. Molar excess enthalpies (H^E) at equimolar composition and at temperature T for aniline(1) + organic solvent(2) mixtures.

			H^E (J mol^{-1})			dev(H^E)[b]			
Solvent	T (K)	N^a	Exp.[c]	DQ[d]	UNIF[e]	Exp.[c]	DQ[d]	UNIF/ERAS[e]	Ref.
Benzene	298.15	15	751	757	657	0.002	0.015	0.096	111
		10	720			0.013	0.044	0.085	112
		19	748			0.013	0.036	0.081	113
		6	815			0.012	0.048	0.128	114
	303.15	14	742	743	664	0.010	0.013	0.091	115
	308.15	13	768	727	670	0.014	0.068	0.083	113
		6	737			0.010	0.064	0.060	114
	323.15	16	779	672	681	0.011	0.167	0.117	113
Toluene	298.15	6	1009	1037	771	0.001	0.028	0.19	116
			937				0.067	0.156	117
	303.15		1020	1032	784				14
	308.15	6	918	1024	794				116
	323.15		1040	996	808				14
	353.15		1060	915	770				14
	373.15		1080	853	706				14
n-Pentane	363.15	21	2105	2203	3406	0.004	0.033	0.418	68
n-Hexane	339.65	15	2888	2323	2774	0.040	0.225	0.105	118
	363.15	13	2295	2386	3653	0.003	0.032	3.81 (0.029)	68
n-Octane	363.15	15	2583	2690	4049	0.002	0.039	0.357	68
n-Decane	363.15	21	2814	2936	4354	0.001	0.053	0.436 (0.035)	68
Cyclohexane	308.15	6	1460	2075	1881	0.005	0.376	0.244	116
		12	1880			0.002	0.069	0.069	119
		12	1868			0.016	0.10	0.047	120
	323.15	12	2055	2135	2070	0.002	0.036	0.061	119
			2090						121

© 2005 NRC Canada

Table 6 (*concluded*).

Solvent	T (K)	N^a	H^E (J mol^{-1}) Exp.[c]	DQ[d]	UNIF[e]	dev(H^E)[b] Exp.[c]	DQ[d]	UNIF/ERAS[e]	Ref.
	363.15	12	2226	2248	2662	0.001	0.023	0.131	68
Methanol	298.15	16	–170	–178	–147	0.039	0.065	0.085 (0.267)	69
Ethanol	298.15	20	360	318	540	0.002	0.142	0.414 (0.178)	70
1-Propanol	298.15	18	783	783	754	0.006	0.031	0.030 (0.069)	8
1-Butanol	298.15	16	1020	1017	942	0.003	0.014	(0.047)	71
		19	945			0.003	0.060	0.018	72
2-Propanol	298.15	16	1130	1117	767	0.001	0.025	0.262	122
2-Butanol	298.15	15	1548	1530	956	0.0007	0.046	0.293	76
DMF	298.15	21	–2946	–2896		0.008	0.022		123
DMA	298.15	17	–352	–352		0.019	0.068		124

[a]Number of data points.

[b]$\mathrm{dev}(H^E) = \left\{ \frac{1}{N} \sum \left[\frac{H^E_{exp} - H^E_{calcd}}{H^E_{exp}(x_i = 0.5)} \right]^2 \right\}^{1/2}$.

[c]Experimental value.

[d]DISQUAC value calculated with interaction parameters from Table 1.

[e]UNIFAC value using parameters from the literature (19, 20), or ERAS result (in parenthesis) obtained using parameters from Tables 2 and 3.

Table 7. Vapor–liquid equilibria (VLE) for some ternary systems containing aniline.

System	T (K)	N^a	$\sigma_r(P)^b$ DQ[c]	UNIF[d]	Ref.
Aniline + cyclohexane + benzene	343.15	10	0.022	0.008	125
Aniline + methylcyclohexane + toluene	353.15	7	0.018	0.003	126
	363.15	9	0.014	0.007	126
	373.17	9	0.012	0.015	126

[a]Number of data points.

[b]$\sigma_r(P) = \sigma_r(P) = \left\{ \frac{1}{N} \sum \left[\frac{P_{exp} - P_{calcd}}{P_{exp}} \right]^2 \right\}^{1/2}$.

[c]DISQUAC values calculated with interaction parameters from Table 1.

[d]UNIFAC values using parameters from the literature (19, 20).

Table 8. Molar excess enthalpies (H^E) at 298.15 K, minimum (min) and maximum (max), for alkanol + aniline + benzene systems.

System[a]	N^b	H^E_{min} (J mol^{-1}) Exp.[d]	DQ[e]	UNIF[f]	H^E_{max} (J mol^{-1}) Exp.[d]	DQ[e]	UNIF[f]	dev(H^E)[c] DQ[e]	UNIF[f]	Ref.
Methanol + aniline + C_6H_6	53	–170	–168	–189	868	868	799	0.094	0.312	18
Methanol + C_6H_6	19				622	624	598	0.019	0.037	127
Ethanol + aniline + C_6H_6	58	218	272	389	1075	1131	1035	0.043	0.063	70
Ethanol + C_6H_6	20				761	753	720	0.012	0.088	127
1-Propanol + aniline + C_6H_6	56	612	655	556	1271	1330	1104	0.038	0.094	8
1-Propanol + C_6H_6	25				950	953	827	0.019	0.086	127
1-Butanol + aniline + C_6H_6	52	766	790	660	1389	1484	1192	0.055	0.094	71
1-Butanol + C_6H_6	25				1044	1059	921	0.026	0.076	127
2-Propanol + aniline + C_6H_6	57	866	873	810	1510	1698	1002	0.079	0.218	122
2-Propanol + C_6H_6	24				1288	1302	827	0.022	0.21	127
	17				1291			0.020	0.24	128

© 2005 NRC Canada

Table 8 (*concluded*).

System[a]	N^b	H^E_{min} (J mol^{-1}) Exp.[d]	DQ[e]	UNIF[f]	H^E_{max} (J mol^{-1}) Exp.[d]	DQ[e]	UNIF[f]	dev(H^E)[c] DQ[e]	UNIF[f]	Ref.
2-Butanol + aniline + C_6H_6	48	868	887	893	1805	1908	1107	0.055	0.249	76
2-Butanol + C_6H_6	8				1590	1636	927	0.025	0.31	129
	18				1603			0.021	0.31	130

[a]Values at equimolar composition for the constituent binaries of the alkanol + benzene systems are also included. For other related binaries, see Table 6.
[b]Number of data points.
[c]$\mathrm{dev}(H^E) = \left\{ \frac{1}{N} \sum \left[\frac{H^E_{exp} - H^E_{calcd}}{H^E_{exp}(x_i = 0.5)} \right]^2 \right\}^{1/2}$.
[d]Experimental value.
[e]DISQUAC values calculated with interaction parameters from Table 1.
[f]UNIFAC values using parameters from the literature (19, 20).

Fig. 1. Liquid–liquid equilibria (LLE) curves for aniline(1) + alkane(2) mixtures. Experimental results: methylcyclohexane (97) (■); *n*-heptane (7) (●). DISQUAC calculations (solid lines).

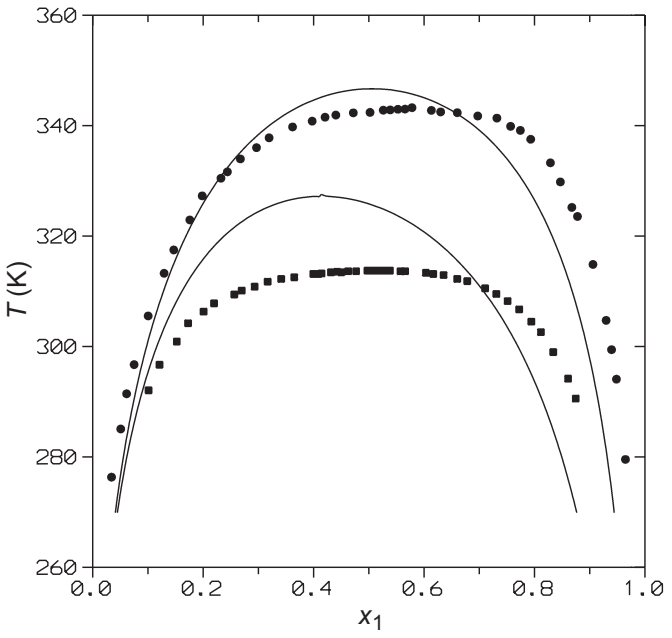
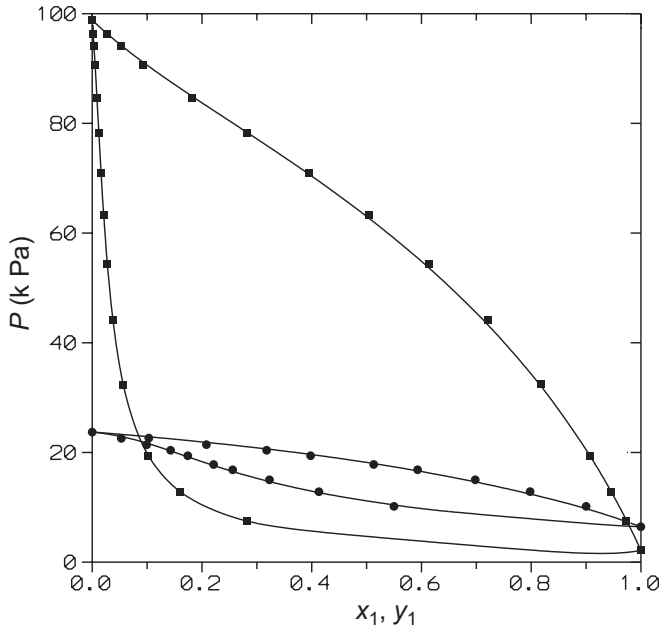


Fig. 2. Vapor–liquid equilibria (VLE) curves for aniline(1) + 1-alkanol(2) mixtures. Experimental results: 1-pentanol (T = 373.15 K (108)) (●); ethanol (T = 350.81 K (107)) (■). DISQUAC calculations (solid lines).



work of the UNIQUAC association solution model (see, e.g., 8, 16, 18, 76). In terms of the Mecke–Kempter model the self-association enthalpy of aniline is –8.4 kJ mol^{-1} (14). The ERAS parameters derived in this work are supported by the predicted enthalpy of vaporization (51.7 kJ mol^{-1}), which is close to the experimental value (55.8 kJ mol^{-1} (80)).

Regarding the ERAS parameters for the studied mixtures, we note: (*i*) The large X_{AB} values for the systems with *n*-alkane remark the importance of the physical interactions in these solutions. It should be kept in mind that, typically, the X_{AB} values are in the range between 2 and 20 J cm^{-3} (9). (*ii*) From the comparison of the K_{AB} and Δh^*_{AB} values with those for other 1-alkanol + linear amine mixtures (Table 3), it is possible to conclude that interactions between dissimilar molecules are much weaker in aniline systems. (*iii*) In contrast, Δv^*_{AB} is lower for solutions involving aniline (Table 3), which suggests that structural effects are more important in this class of mixtures (see the following).

We note that H^E is better represented by DISQUAC for mixtures with methanol or ethanol (Table 6). In addition, ERAS yields for the aniline + methanol system a G^E curve skewed to low mol fractions of the alcohol, while the experimental one is rather symmetrical. Therefore, it is possible to conclude that ERAS overestimates the self-association of the alcohol in systems containing methanol or ethanol.

Discussion

The inmiscibility of aniline with alkanes at room temperature (7) is characteristic of systems where strong polar inter-

© 2005 NRC Canada

Fig. 3. Molar excess enthalpies (H^E) for aniline(1) + aromatic compound(2) mixtures. Experimental results: benzene (T = 303.15 K (115)) (●); toluene (T = 298.15 K (116)) (■). DISQUAC calculations (solid lines).

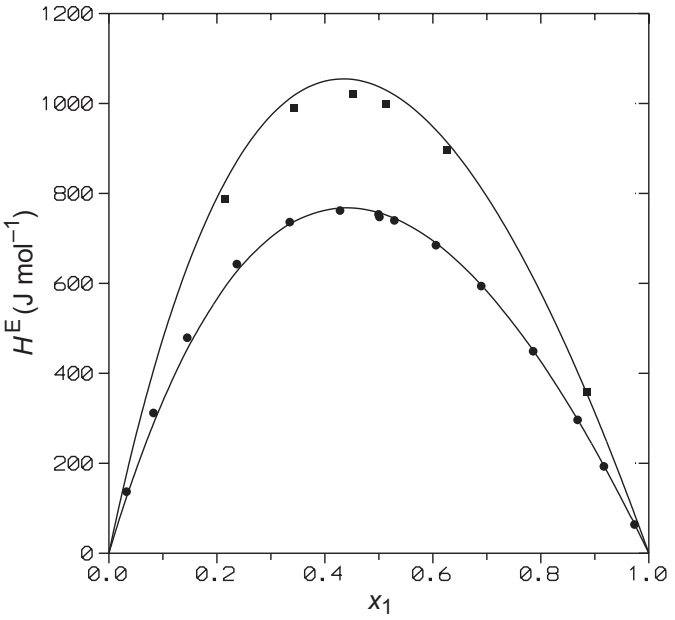


Fig. 4. Molar excess enthalpies (H^E) at 363.15 K for aniline(1) + alkane(2) mixtures. Experimental results (68): cyclohexane (▲); *n*-hexane (●); *n*-decane (■). DISQUAC calculations (solid lines).

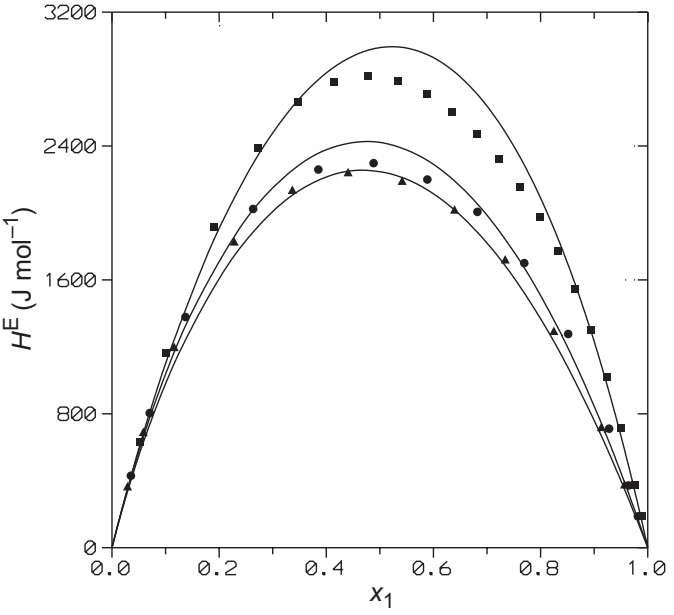


Fig. 5. Molar excess enthalpies (H^E) at 298.15 K for aniline(1) + 1-alkanol(2) mixtures. Experimental results: methanol (69) (●); ethanol (70) (▲); 1-propanol (8) (■). DISQUAC calculations (solid lines); ERAS results (dashed lines).

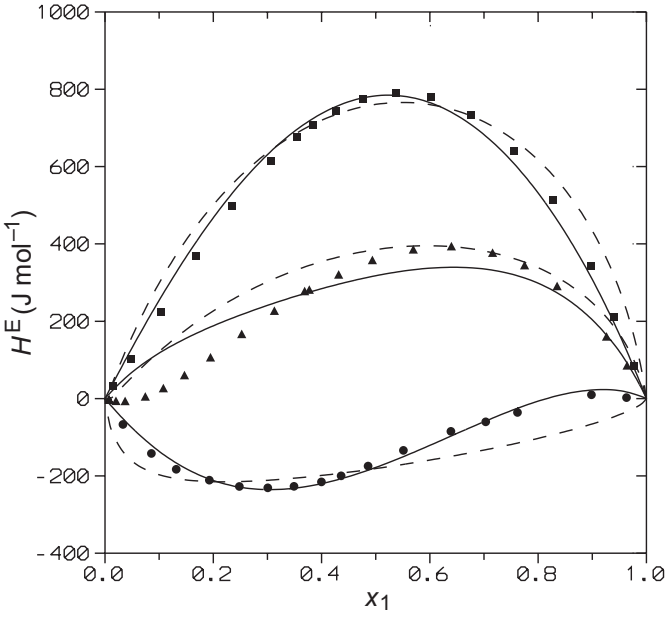
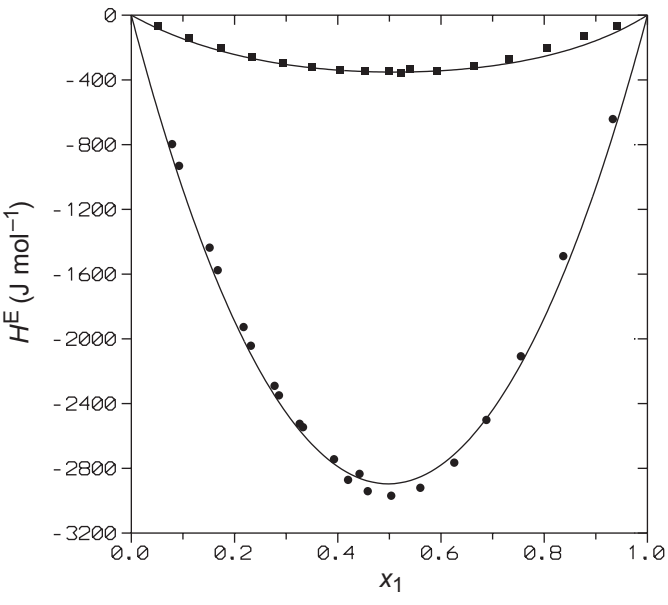


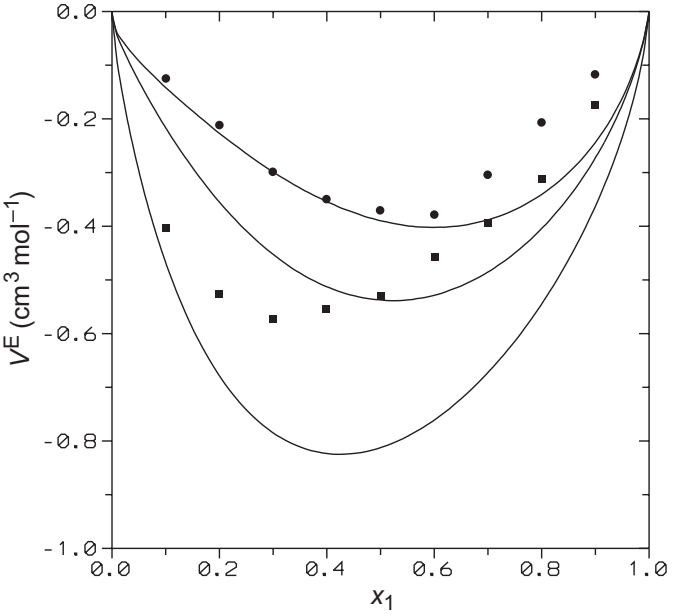
Fig. 6. Molar excess enthalpies (H^E) at 298.15 K for aniline(1) + *N*,*N*-dialkylamide(2) mixtures. Experimental results: DMF (123) (●); DMA (124) (■). DISQUAC calculations (solid lines).



actions between like molecules exist, and is found, e.g., in sulfolane (28), alkoxyethanol (29), 1-methyl pyrrolidin-2-one (44), dimethylformamide (50), or dimethylsulfoxide (54) + alkane mixtures. Such interactions may be roughly evaluated in terms of $\Delta\Delta_{vap}H_m$, (27, 56, 81), the difference between the standard enthalpy of vaporization ($\Delta_{vap}H_m$, (data taken from refs. 80 and 82) of a given component with a characteristic group X and that of the homomorphic alkane. Therefore, $\Delta\Delta_{vap}H_m$(aniline) = 18.2 > $\Delta\Delta_{vap}H_m$(cyclohexylamine) = 10.36 > $\Delta\Delta_{vap}H_m$(hexylamine) = 8.52 > $\Delta\Delta_{vap}H_m$(dipropylamine) = 3.46 > $\Delta\Delta_{vap}H_m$(triethylamine) = –1.77 (all values in kJ mol^{-1}). The large $\Delta\Delta_{vap}H_m$ value for aniline suggests that the high polarizability of the aromatic ring of this amine enhances the interactions between aniline mole-

© 2005 NRC Canada

Fig. 7. Excess molar volumes (V^E) at 298.15 K for aniline(1) + 1-alkanol(2) mixtures. Experimental results: 1-propanol (73) (■); 1-butanol (74) (●). ERAS calculations (solid lines), including results for the system with methanol.



cules. Therefore, the strength of the interactions among amine molecules decreases in the sequence: aniline > cyclohexylamine > hexylamine > dipropylamine > triethylamine. This may explain some of the features previously mentioned, or that at equimolar composition and 298.15 K, H^E(hexylamine + n-C_7) = 1064 J mol^{-1} (83) > H^E(dipropylamine + n-C_7) = 454 J mol^{-1} (84).

For linear primary or secondary amines + 1-alkanol mixtures, V^E is large and negative. At 298.15 K and equimolar composition, V^E(hexylamine + 1-propanol) = –1.147 cm^3 mol^{-1} (42) and V^E(dipropylamine + 1-propanol) = –1.550 cm^3 mol^{-1} (39). This has been interpreted in terms of strong interactions between dissimilar molecules, which is supported by large and negative H^E values (see Table A1 of the Appendix), as well as by solid–liquid equilibria measurements (85, 86). However, taking into account the rather large positive H^E of aniline + 1-alkanol (≠methanol, ethanol) systems, the corresponding negative V^E values suggest that important structural effects exist in these solutions. So, the V^E curve for aniline + 1-propanol is very skewed towards high mole fractions of the alcohol (Fig. 7), the smaller compound, indicating that free volume effects exist.

To evaluate the importance of the equation of state term, it is interesting to calculate the excess internal energy at constant volume U_V^E, for some aniline + 1-alkanol systems. Neglecting terms in higher order in V^E (55, 87), U_V^E is displayed as

$$[7] \qquad U_V^E = H^E - \frac{\alpha_P V^E}{\kappa_T}$$

where α_P and κ_T are the isobaric thermal expansion coefficient and the isothermal compressibility factor of the mixture, respectively. Due to the lack of experimental data, these quantities were calculated as (88, 89)

$$[8] \qquad M = \phi_1 M_1 + \phi_2 M_2$$

In this equation, M is the value of α_P or κ_T for the mixture, M_i is the value of these magnitudes for the pure compound i (i = 1, 2) and

$$\phi_i = \frac{x_i V_i}{x_1 V_1 + x_2 V_2}$$

The results are: U_v^E(aniline + 1-propanol) = 985 J mol^{-1} and U_v^E(aniline + 1-butanol) = 1158 J mol^{-1}. Using V^E = –0.81 cm^3 mol^{-1}, the value calculated from the ERAS model, U_v^E(aniline + methanol) = 160 J mol^{-1}. Therefore, the poor results obtained from ERAS for these mixtures may be ascribed, at least in part, to effects related to the equation of state term that are not properly described by the model. In contrast, 1-alkanol + primary or secondary linear amine mixtures are much better represented by ERAS because thermodynamic properties of these solutions are mainly determined by strong interactions between dissimilar molecules (see Table A1 of the Appendix) (42).

The concentration–concentration structure factor ($S_{CC}(0)$) (43), is defined as

$$[9] \qquad S_{CC}(0) = \frac{RT}{\left(\frac{\partial^2 G^M}{\partial x_1^2}\right)_{P,T}} = \frac{x_1 x_2}{D}$$

with

$$[10] \qquad D = \frac{x_1 x_2}{RT}\left(\frac{\partial^2 G^M}{\partial x_1^2}\right)_{P,T} = 1 + \frac{x_1 x_2}{RT}\left(\frac{\partial^2 G^E}{\partial x_1^2}\right)_{P,T}$$

D is a function closely related to thermodynamic stability (55, 90). For ideal mixtures, $G^{E,id} = 0$, $D^{id} = 1$, and $S_{CC}(0) = x_1 x_2$. As stability conditions require, $S_{CC}(0) > 0$, and if the system is close to phase separation, $S_{CC}(0)$ must be large and positive (∞, when the mixture presents a miscibility gap). In contrast, if compound formation between components appears, $S_{CC}(0)$ must be very low (0, in the limit). So, if $S_{CC}(0) > x_1 x_2$, i.e., $D < 1$, the dominant trend in the system is the separation of the components (homocoordination), and the mixture is less stable than the ideal. If $0 < S_{CC}(0) < x_1 x_2 = S_{CC}(0)^{id}$, i.e., $D > 1$, the fluctuations in the system have been removed, and the dominant trend in the solution is compound formation (heterocoordination). In this case, the system is more stable than ideal. The $S_{CC}(0)$ function clearly shows the features examined. The large and positive values of $S_{CC}(0)$ for aniline + alkane mixtures (Table 9) indicate strong homocoordination between aniline molecules. Systems with 1-alkanols are also characterized by homocoordination ($S_{CC}(0) > S_{CC}^{ideal}$, Table 9). This even occurs for the solution containing methanol, which shows $H^E < 0$ at equimolar composition (Table 6) (and $U_V^E > 0$). In contrast, interactions between dissimilar molecules are more important in the propylamine + 1-propanol mixture, as the $S_{CC}(0)$ results underline (Fig. 8 (12)). On the other hand, systems involving 1-propanol or longer 1-alkanols are characterized

© 2005 NRC Canada

Table 9. Concentration–concentration structure factor ($S_{CC}(0)$) at equimolar composition and temperature T for some aniline + organic solvent mixtures.

Solvent	T (K)	$S_{CC}(0)$ Exp.[a]	$S_{CC}(0)$ DQ[b]	Ref.
n-Heptane	373.15		8.53	
Benzene	298.15	0.344	0.375	99
	392.45	0.349	0.321	102
Methanol	293.15	0.404	0.398	106
	338.15	0.409	0.407	106
	385.15	0.382	0.401	106
Ethanol	313.15	0.477	0.433	107
	350.81	0.422	0.400	107
	386.66	0.378	0.367	107
1-Propanol	298.15		0.461	
	385.15		0.316	
1-Butanol	298.15		0.493	
	385.15		0.321	
1-Pentanol	298.15		0.504	108
	373.15	0.394	0.335	
2-Propanol	298.15		0.567	
DMF	298.15		0.154	
	343.15		0.187	
DMA	298.15		0.227	

[a]Experimental value.
[b]DISQUAC values calculated with interaction parameters from Table 1.

by TS^E (= $H^E - G^E$) > 0 (Table A1 of the Appendix). The interactions present in such solutions may be then be assumed to be of the dipole–dipole type. Mixtures with methanol or ethanol show $TS^E < 0$ (Table A1 of the Appendix). To obtain more information on the studied systems, we have also examined the temperature dependence of $S_{CC}(0)$, which is well-represented by DISQUAC (Table 9). We note that $S_{CC}(0)$ seems to decrease rather weakly with increasing T (Table 9). In the framework of the quasichemical theory developed by Guggenheim (25), Cobos (43) has shown that

$$[11] \qquad \frac{\partial S_{CC}(0)}{\partial T} = \frac{S^2_{CC}(0)}{T} \frac{\partial^2 (U^E_v/RT)}{\partial x_1^2}$$

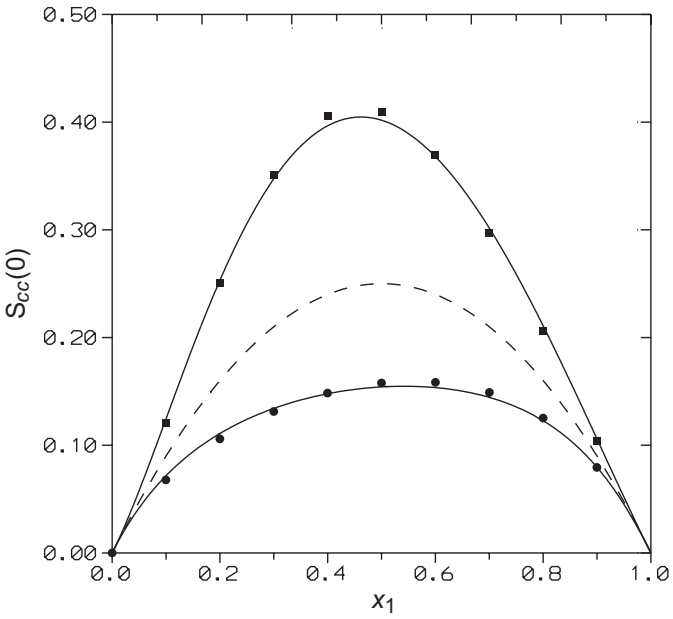
For the investigated mixtures,

$$U^E_V > 0, \quad \frac{\partial^2 (U^E_v/RT)}{\partial x_1^2} < 0$$

and $S_{CC}(0)$ should decrease with T. For the system containing methanol, $S_{CC}(0)$ remains practically constant, reflecting a rather flat U^E_V curve. This weak temperature dependence of $S_{CC}(0)$ implies that low C^E_P values should be expected, a characteristic of systems where dipole–dipole, or dipole-induced dipole interactions are present ((14); see the results for the solution with benzene, Table 9). This newly underlines the importance of the high polarizability of the aniline molecule (Table A1 of the Appendix).

We note that $S_{CC}(0)$(2-propanol) > $S_{CC}(0)$(1-propanol) (Table 9), in agreement with the fact that dipolar interactions between 2-alkanol molecules are stronger than between those of 1-alkanols.

Fig 8. Concentration–concentration structure factors ($S_{CC}(0)$) for amine(1) + 1-alkanol(2) mixtures. Experimental results: propylamine(1) + 1-propanol (T = 302.95 K (131)) (■); aniline(1) + methanol(2) (T = 338.15 K (106)) (●). DISQUAC calculations (solid lines); ideal mixture (dashed line).



Finally, it should be mentioned that for the mixture with *N*,*N*-dialkylamides DISQUAC predicts $S_{CC}(0) < S^{ideal}_{CC}(0)$, remarking that heterocoordination here plays the dominant role, particularly for the DMF system.

Conclusions

DISQUAC accurately represents a whole set of thermodynamic properties: LLE, VLE, G^E, H^E, and $S_{CC}(0)$ of the investigated binary mixtures. The model also correctly predicts VLE and H^E of ternary systems involving aniline.

Solutions with alkane or alkanol are characterized by strong homocordination between aniline molecules. Structural effects, not represented properly by the ERAS model, are also present in systems with alcohols. Mixtures with *N*,*N*-alkylamides are characterized by heterocoordination.

Acknowledgements

This work was supported by the Consejería de Educación y Cultura of Junta de Castilla y León, under project VA080/04. I.M. acknowledges the grant received from the Consejería de Educación de la Junta de Castilla y León y del Fondo Social Europeo.

References

1. H. Wolff and G. Gamer. J. Phys. Chem. **76**, 871 (1972).
2. H. Landeck, H. Wolff, and R. Götz. J. Phys. Chem. **81**, 718 (1977).
3. I. Cibulka, K. Tamura, and I. Nagata. Fluid Phase Equilib. **39**, 39 (1988).
4. H. Funke, M. Wetzel, and A. Heintz. Pure Appl. Chem. **61**, 1429 (1989).

© 2005 NRC Canada

5. H. Wolff, H. Landeck, H.-P. Frerichs, and E. Wolff. Fluid Phase Equilib. **109**, 245 (1995).
6. K. Sosnkowska-Kehiaian, R. Hryniewicz, and H.V. Kehiaian. Bull. Acad. Pol. Sci. Ser. Sci. Chim. **17**, 185 (1969).
7. H. Matsuda, K. Ochi, and K. Kojima. J. Chem. Eng. Data, **48**, 184 (2003).
8. I. Nagata. Thermochim. Acta, **208**, 73 (1992).
9. A. Heintz, P.K. Naicker, S.P. Verevkin, and R. Pfestorf. Ber. Bunsen-Ges. Phys. Chem. **102**, 953 (1998).
10. F. Sarmiento, M.I. Paz Andrade, J. Fernández, R. Bravo and M. Pintos. J. Chem. Eng. Data, **30**, 321 (1985).
11. M. Bender, J. Hauser, and A. Heintz. Ber. Bunsen-Ges. Phys. Chem. **95**, 801 (1991).
12. J.A. González, I. García de la Fuente, and J.C. Cobos. Fluid Phase Equilib. **168**, 31 (2000).
13. J.A. González, I. García de la Fuente, and J.C. Cobos. Can. J. Chem. **78**, 1272 (2000).
14. H.V. Kehiaian and K. Sosnkowska-Kehiaian. Trans. Faraday Soc. **62**, 838 (1965).
15. I. Nagata. Fluid Phase Equilib. **19**, 153 (1985)
16. I. Nagata. Thermochim. Acta, **244**, 21 (1994).
17. I. Nagata. Thermochim. Acta, **186**, 123 (1991).
18. I. Nagata and M. Sano. Fluid Phase Equilib. **72**, 147 (1992).
19. J. Gmehling, J. Li, and M. Schiller. Ind. Eng. Chem. Res. **32**, 178 (1993).
20. J. Gmehling, J. Lohmann, A. Jakob, J. Li, and R. Joh. Ind. Eng. Chem. Res. **37**, 4876 (1998).
21. N. Riesco, S. Villa, J.A. González, I. García de la Fuente, and J.C. Cobos. Fluid Phase Equilib. **202**, 345 (2002).
22. S. Villa, J.A. González, I. García de la Fuente, N. Riesco, and J.C. Cobos. J. Solution Chem. **31**, 1019 (2002)
23. N. Riesco, J.A. González, S. Villa, I. García de la Fuente, and J.C. Cobos. Phys. Chem. Liq. **41**, 309 (2003).
24. H.V. Kehiaian. Fluid Phase Equilib. **13**, 243 (1983); Pure Appl. Chem. **57**, 15 (1985).
25. E.A. Guggenheim. Mixtures. Oxford University Press, London. 1952.
26. J.A. González, I. García de la Fuente, and J.C. Cobos. J. Chem. Soc. Faraday Trans. **93**, 3773 (1997).
27. J.A. González, I. García de la Fuente, and J.C. Cobos. Phys. Chem. Chem. Phys. **1**, 275 (1999).
28. J.A. González and U. Domanska. Phys. Chem. Chem. Phys. **3**, 1034 (2001).
29. J.A. González, J.C. Cobos, F.J. Carmona, I. García de la Fuente, V.R. Bhethanabotla, and S.W. Campbell. Phys. Chem. Chem. Phys. **3**, 2856 (2001).
30. U. Domanska and J.A. González. Fluid Phase Equilib. **205**, 317 (2003).
31. J.A. González, J. Carmona, N. Riesco, I. García de la Fuente, and J.C. Cobos. Thermochim. Acta, **326**, 53 (1999).
32. J.A. González, J. Carmona, N. Riesco, I. García de la Fuente, and J.C. Cobos. Can. J. Chem. **79**, 1447 (2001).
33. J.A. González, I. Mozo, I. García de la Fuente, and J.C. Cobos. Ind. Eng. Chem. Res. **43**, 7622 (2004).
34. A. Heintz. Ber. Bunsen-Ges. Phys. Chem. **89**, 172 (1985).
35. C.B. Kretschmer and R. Wiebe. J. Chem. Phys. **22**, 1697 (1954).
36. H. Renon and J.M. Prausnitz. Chem. Eng. Sci. **22**, 299 (1968); H.V. Kehiaian. Bull. Acad. Pol. Sci. **16**, 171 (1968).
37. P.J. Flory. J. Am. Chem. Soc. **87**, 1833 (1965).
38. A. Heintz and D. Papaioannou. Thermochim. Acta, **310**, 69 (1998).
39. S. Villa, N. Riesco, I. García de la Fuente, J.A. González, and J.C. Cobos. Fluid Phase Equilib. **190**, 113 (2001).
40. S. Villa, N. Riesco, I. García de la Fuente, J.A. González, and J.C. Cobos. Fluid Phase Equilib. **198**, 313 (2002).
41. S. Villa, N. Riesco, I. García de la Fuente, J.A. González, and J.C. Cobos. J. Solution Chem. **32**, 179 (2003).
42. S. Villa, N. Riesco, I. García de la Fuente, J.A. González, and J.C. Cobos. Fluid Phase Equilib. **216**, 123 (2004).
43. J.C. Cobos. Fluid Phase Equilib. **133**, 105 (1997).
44. J.A. González, U. Domanska, and J. Lachwa. Can. J. Chem. **81**, 1451 (2003).
45. J.A. González, I. García de la Fuente, and J.C. Cobos. J. Mol. Liq. **115**, 93 (2004).
46. A. Bondi. Physical properties of molecular crystals, liquids and glasses. Wiley, New York. 1968.
47. H.V. Kehiaian, J.-P.E. Grolier, and G.C. Benson. J. Chim. Phys. **75**, 1031 (1978).
48. J.A. González, I. García de la Fuente, J.C. Cobos, C. Casanova, and A. Ait-Kaci. Fluid Phase Equilib. **112**, 63 (1995).
49. J.A. González, I. García de la Fuente, J.C. Cobos, and C. Casanova. Ber. Bunsen-Ges. Phys. Chem. **95**, 1658 (1991).
50. J.A. González, J.C. Cobos, and I. García de la Fuente. Fluid Phase Equilib. **224**, 169 (2004).
51. A. Fredenslund, R.L. Jones, and J.M. Prausnitz. AIChE J. **21**, 1086 (1975).
52. K.-Y. Hsu and H.L. Clever. J. Chem. Thermodyn. **7**, 435 (1975).
53. J.A. González, I. García de la Fuente, J.C. Cobos, and C. Casanova. Fluid Phase Equilib. **93**, 1 (1994); J.A. González, I. García de la Fuente, and J.C. Cobos. Can. J. Chem. **76**, 1418 (1998).
54. J.A. González, S. Villa, N. Riesco, I. García de la Fuente, and J.C. Cobos. Phys. Chem. Liq. **41**, 583 (2003).
55. J.S. Rowlinson and F.L. Swinton. Liquids and liquid mixtures. 3rd ed. Butterworths, London. 1982.
56. H.V. Kehiaian, M.R. Tiné, L. Lepori, E. Matteoli, and B. Marongiu. Fluid Phase Equilib. **46**, 131 (1989).
57. H.V. Kehiaian, S. Porcedda, B. Marongiu, L. Lepori, and E. Matteoli. Fluid Phase Equilib. **63**, 231 (1991).
58. J.A. González, I. García de la Fuente, J.C. Cobos, C. Casanova, and H.V. Kehiaian. Thermochim. Acta, **217**, 57 (1993).
59. M. Aboy, S. Villa, N. Riesco, J.A. González, I. García de la Fuente, and J.C. Cobos. J. Chem. Eng. Data, **47**, 950 (2002); H.V. Kehiaian, J.A. González, I. García, R. Escarda, J.C. Cobos, and C. Casanova. Fluid Phase Equilib. **69**, 91 (1991).
60. H.V. Kehiaian and B. Marongiu. Fluid Phase Equilib. **40**, 23 (1988).
61. J.A. González, I. García de la Fuente, J.C. Cobos, and C. Casanova. Fluid Phase Equilib. **99**, 19 (1994); **135**, 1 (1997).
62. J.A. González, I. García de la Fuente, J.C. Cobos, and C. Casanova. J. Solution Chem. **23**, 399 (1994); U. Domanska and J.A. González. Fluid Phase Equilib. **123**, 167 (1996).
63. J.A. González, I. García de la Fuente, and J.C. Cobos. Ber. Bunsen-Ges. Phys. Chem. **101**, 219 (1997).
64. J.A. González, I. García de la Fuente, and J.C. Cobos. Fluid Phase Equilib. **123**, 39 (1996).
65. J.A. González, I. García de la Fuente, J.C. Cobos, and U. Domanska. Fluid Phase Equilib. **119**, 81 (1996).
66. J.A. González, I. García de la Fuente, and J.C. Cobos. Thermochim. Acta, **278**, 57 (1996).
67. J.A. González, I. García de la Fuente, and J.C. Cobos. Ber. Bunsen-Ges. Phys. Chem. **100**, 1746 (1996).
68. G. Avedis, B. Meents, and J. Gmehling. J. Chem. Thermodyn. **27**, 939 (1995).
69. K. Nakanishi and H. Tohuara. J. Chem. Thermodyn. **18**, 657 (1986).

© 2005 NRC Canada

70. I. Nagata and M. Sano. Thermochim. Acta, **200**, 475 (1992).
71. I. Nagata. J. Chem. Thermodyn. **25**, 1281 (1993).
72. J.P. Chao and M. Dai. J. Chem. Thermodyn. **21**, 337 (1989).
73. M.A. Saleh, M. Alauddin, and S. Begum. Phys. Chem. Liq. **39**, 453 (2001).
74. M.A. Wahab, M.A. Islam, M.A. Ali, and M.A. Mottaleb. Phys. Chem. Liq. **14**, 189 (2003).
75. N.G. Tsierkezos, M.R. Polaidogou, and I.E. Molinou. J. Chem. Eng. Data, **45**, 272 (2000).
76. I. Nagata. Thermochim. Acta, **232**, 19 (1994).
77. J.A. González, I. García de la Fuente, J.C. Cobos, and C. Casanova. Thermochim. Acta, **237**, 261 (1994).
78. J.R. Goates, R.L. Snow, and J.B. Ott. J. Phys. Chem. **66**, 1301 (1962).
79. B. Dacre and G.C. Benson. Can. J. Chem. **42**, 278 (1962).
80. V. Majer and V. Svoboda. Enthalpies of vaporization of organic compounds. Blackwell, Oxford. 1985.
81. J.A. González, I. García de la Fuente, and J.C. Cobos. Fluid Phase Equilib. **154**, 11 (1999).
82. J.A. Riddick, W.B. Bunger, and T.K. Sakano. Organic solvents, techniques of chemistry. Vol. 2. *Edited by* A. Weissberger. Wiley, New York. 1986.
83. R. Pfestorf, D. Kuchenbecker, and K Quitzsch. Z. Phys. Chem. (Leipzig), **263**, 233 (1982).
84. M.I. Paz Andrade and F. Sarmiento. Int. Data Ser. Selec. Data Mixtures Ser. A, 110 (1984).
85. U. Domanska and M. Gloskowska. J. Chem. Eng. Data, **49**, 101 (2004).
86. U. Domanska and M. Gloskowska. Fluid Phase Equilib. **216**, 135 (2004).
87. H. Kalali, F. Kohler, and P. Svejda. Fluid Phase Equilib. **20**, 75 (1985).
88. G. Douheret, C. Moreau, and A. Viallard. Fluid Phase Equilib. **22**, 277 (1985).
89. J. Zielkiewicz. Phys. Chem. Chem. Phys. **2**, 2925 (2002).
90. A.B. Bhatia and D.E. Thorton. Phys. Rev. B, **21**, 3004 (1970).
91. R. Garriga, P. Pérez, and M. Gracia. Ber. Bunsen-Ges. Phys. Chem. **101**, 1466 (1997).
92. J.A. González, M. Surgocinska, and U. Domanska. Fluid Phase Equilib. **200**, 349 (2002).
93. J.A. González, S. Villa, N. Riesco, I García de la Fuente, and J.C. Cobos. Can. J. Chem. **81**, 319 (2003).
94. E.H. Buchner and D. Kleyn. Recl. Trav. Chim. Pays–Bas, **43**, 143 (1924).
95. C. Drucker. Recl. Trav. Chim. Pays–Bas, **42**, 552 (1923).
96. K. Ochi, M. Momose, and K. Kojima. Can. J. Chem. Eng. **71**, 982 (1993).
97. H. Matsuda, M. Fujita, and K. Ochi. J. Chem. Eng. Data, **48**, 1076 (2003).
98. A.W. Francis. Critical solution temperatures, advances in chemistry series. American Chemical Society, Washington, D.C. 1961.
99. D.D. Keshpande and M.V. Pandya. Trans. Faraday Soc. **63**, 2149 (1967).
100. S.M. Hosseini and G. Schneider. Z. Phys. Chem. (Frankfurt/Main), **36**, 137 (1963).
101. A.R. Martin and B. Collie. J. Chem. Soc. (London), 2658 (1932).
102. G. Kortuem and H.-J. Freier. Monatsh Chem. **85**, 693 (1954).
103. F. Billes and G.Y. Varsanyi. Acta Chim. Acad. Sci. Hung. **35**, 147 (1963).
104. J. Heinrich. Coll. Czech. Chem. Commun. **40**, 787 (1975).
105. G. Schneider. Z. Phys. Chem. (Frankfurt/Main), **24**, 165 (1960).
106. P.J. Maher and B.D. Smith. J. Chem. Eng. Data, **25**, 61 (1980).
107. P.J. Maher and B.D. Smith. J. Chem. Eng. Data, **24**, 16 (1979).
108. J. Surovy and J. Dojcansky. Chem. Zvesti, **20**, 313 (1974).
109. M. Roland. Bull. Soc. Chim. Belg. **37**, 117 (1928).
110. R.S. Ramadevi, P. Venkatesu, M.V. Prabhakara Rao, and M. Ramakrishna. Thermochim. Acta, **277**, 133 (1996).
111. I. Nagata and K. Tamura. J. Chem. Thermodyn. **24**, 613 (1992).
112. D.D. Keshpande and M.V. Pandya. Trans. Faraday Soc. **61**, 1858 (1965).
113. G. Pannetier and L. Abello. Bull. Soc. Chim. Fr. 2048 (1965).
114. R.K Nigam, P.P. Singh, and K.C. Singh. Can. J. Chem. **57**, 2211 (1979).
115. I. Velasco, S. Otín, and C. Gutiérrez Losa. Int. Data Ser. Selec. Data Mixtures Ser. A, **1**, 8 (1979).
116. R.K Nigam, P.P. Singh, and K.C. Singh. Thermochim. Acta, **35**, 1 (1980).
117. D.D. Keshpande and M.V. Pandya. Trans. Faraday Soc. **65**, 1456 (1969).
118. A.N. Campbell and E.M. Kartzmark. Can. J. Chem. **47**, 619 (1969).
119. G.L. Nicolaides and C.A. Eckert. J. Chem. Eng. Data, **23**, 152 (1978).
120. W. Woycicki. J. Chem. Thermodyn. **18**, 317 (1986).
121. K. Sosnkowska-Kehiaian and H.V. Kehiaian. Bull Acad. Pol. Sci. Ser. Sci. Chim. **14**, 573 (1966).
122. I. Nagata and K. Miyazaki. J. Chem. Thermodyn. **24**, 1175 (1992).
123. R.S. Ramadevi, P. Venkatesu, M.V. Prabhakara Rao, and M. Ramakrishna. Fluid Phase Equilib. **114**, 189 (1996).
124. G. Chandra Sekhar, M.V. Prabhakara Rao, D.H.L. Prasad, and Y.V.L. Ravi Kumar. Thermochim. Acta, **402**, 99 (2003).
125. C. Podder. Z. Phys. Chem. (Frankfurt/Main), **39**, 79 (1963).
126. G. Schneider. Z. Phys. Chem. (Frankfurt/Main), **27**, 171 (1961).
127. H.C. Van Ness and M.M. Abbott. Int. Data Ser. Selec. Data Mixtuers Ser. A, **1**, 1 (1976).
128. I. Nagata, H. Asano, and K. Fujiwara. Fluid Phase Equilib. **1**, 211 (1978).
129. I. Brown, W. Fock, and F. Smith. J. Chem. Thermodyn. **1**, 273 (1969).
130. I. Nagata and K. Tamura. Fluid Phase Equilib. **41**, 127 (1988).
131. E. Kristof, I. Orszag, and F. Ratkovics. J. Chem. Thermodyn. **13**, 557 (1981).

© 2005 NRC Canada

Appendix A

Table A1. Molar excess functions at equimolar composition and 298.15 K for different mixtures.

System	G^E (J mol^{-1})	Ref.	H^E (J mol^{-1})	Ref.	TS^E (J mol^{-1})
1-Propanol + n-C_7	1291	A1	597	A2	–694
Methanol + C_6H_6	1241	A3	622	A4	–619
1-Propanol + C_6H_6	1007	A3	951	A4	–56
Methanol + hexylamine	–787[a]		–3200	A5	–2413
1-Propanol + hexylamine	–313[a]		–2561	A5	–2248
1-Propanol + dipropylamine	–325	A6	–2269[b]		–1944
Methanol + triethylamine	247[a]		–1871	A7	–2118
1-Propanol + triethylamine	78[a]		–1413	A8	–1491
Methanol + aniline	527[a]		–170	A9	–697
1-Propanol + aniline	689[a]		783	A10	94

[a]DISQUAC value.
[b]Values estimated from vapor–liquid equilibria (VLE) measurements at different temperatures (A6).

References

A1. H.C. Van Ness, C.A. Soczek, G.L. Peloquin, and R.L. Machado. J. Chem. Eng. Data, **12**, 217 (1967).
A2. M. Keller, J. Schnable, and A. Heintz. Fluid Phase Equilib. **110**, 231 (1995).
A3. Sh.-Ch. Hwang and R.L. Robinson. J. Chem. Eng. Data, **32**, 319 (1977).
A4. H.C. Van Ness and M.M. Abbott. Int. Data Ser. Selec. Data Mixtures Ser. A, 1 (1976).
A5. A. Heintz, P.K. Naicker, S.P. Verevkin, and R. Pfestorf. Ber. Bunsen-Ges. Phys. Chem. **102**, 953 (1998).
A6. S. Villa, R. Garriga, P. Pérez, M. Gracia, J.A. González, I. García de la Fuente, and J.C. Cobos. Fluid Phase Equilib. **231**, 211 (2005).
A7. A. Chand and D.V. Fenby. J. Chem. Eng. Data, **22**, 289 (1977).
A8. M. Bender, J. Hauser, and A. Heintz. Ber. Bunsen-Ges. Phys. Chem. **95**, 801 (1991).
A9. K. Nakanishi and H. Tohuara. J. Chem. Thermodyn. **18**, 657 (1986).
A10. I. Nagata. Thermochim. Acta, **208**, 73 (1992).

© 2005 NRC Canada

Microwave- and ultrasound-assisted semisynthesis of natural methoxylated propiophenones from isomeric mixture of phenylpropenes in minutes[1]

Bhupendra P. Joshi, Anuj Sharma, and Arun K. Sinha

Abstract: A rapid and practical semisynthesis of natural methoxylated propiophenones (**3a**–**3f**) is realized by reacting stereo- and regio-isomeric mixture of phenylpropenes (**1a**–**1f**) with a catalytic amount of palladium chloride – sodium formate in formic acid, methanol, and water (2:1:2) into single product phenylpropanes (**2a**–**2f**) followed by its oxidation with 2,3-dichloro-5,6-dicyanobenzoquinone (DDQ) in wet dioxane, containing a few drops of formic acid. Conventional, ultrasound, and microwave heating were compared through these studies.

Key words: focused microwave, ultrasound, phenylpropene, propiophenone, DDQ.

Résumé : On a mis au point une semi-synthèse rapide et pratique des propiophénones méthoxylées naturelles (**3a**–**3f**) en faisant réagir des mélanges stéréo- et régio-isomères de phénylpropènes (**1a**–**1f**) avec une quantité catalytique de chlorure de palladium – formiate de sodium dans l'acide formique, le méthanol et l'eau (2 : 1 : 2) qui conduisent à des phénylpropanes isolés sous la forme de produits uniques (**2a**–**2f**) qui ont été isolés par du 2,3-dichloro-5,6-dicyanobenzoquinone (DDQ) dans du dioxane humide contenant quelques gouttes d'acide formique. Dans toutes les études mentionnées ci-dessus, on a comparé les méthodes de chauffage traditionnelle, aux ultrasons et aux micro-ondes.

Mots clés : micro-onde focalisée, ultrason, phénylpropène, propiophénone, DDQ.

[Traduit par la Rédaction]

Introduction

Methoxylated propiophenones (1) are isolated from a large number of medicinally important plants and possess a wide range of biological (2–5) activities such as choleretic (2), antiplatelet activating factor (anti-PAF) (3), antifungal (4), and hypolipidemic (5) activities. In addition, methoxylated propiophenones are utilized as intermediates for the production of various bioactive molecules (6) and are also used as modifiers in flavour and perfumery formulations (7).

Various methods are reported for the preparation of propiophenones (C_6–C_3). These methods fundamentally fall under three categories: (*a*) combination of a C_6 unit with a C_3 unit, (*b*) combination of a C_6–C_1 unit with a C_2 unit, and (*c*) semisynthetic route from an already existing C_6–C_3 unit. The methods in category (*a*) include reactions of substituted benzene with phenyllithium – lithium propionate (8) and Zn-Cu–Pd$(PPh_3)_4$–CO (9). Similarly, Friedel–Crafts propionylation (6) of an aromatic ring with a Lewis acid (10) also falls under this category and remains a well-exploited method. Propionylation of a methoxylated aromatic ring, however, suffers from some degree of demethoxylation (11) with Lewis acids such as aluminium chloride (12). The methods in category (*b*) include the reaction of substituted benzaldehydes (13–15), benzonitrile (16), or benzoic acids (17, 18) with cyanohydrin – vinyl ether (13), chlorotrimethylsilane–KCN (14), Grignard (15), isobutylmagnesium bromide (16), thionyl chloride – $Cd(C_2H_5)_2$ (17), or propionic acid – iron(II) salt (18), respectively. Overall, all of the synthetic methods in categories (*a*) and (*b*) are limited by expensive starting material, maintenance of anhydrous conditions, and environmentally hostile reagents (19).

In this regard, the methods in category (*c*) hold a better semisynthetic approach (20, 21) than categories (*a*) and (*b*) because the former utilizes an already existing C_6–C_3 unit in the form of substituted phenylpropenes for the formation of methoxylated propiophenones. Hence, only slight modifications in the structure are desired, which may not require harsh conditions if a suitable choice of substrate and reagent is made.

Received 17 June 2005. Published on the NRC Research Press Web site at http://canjchem.nrc.ca on 22 December 2005.

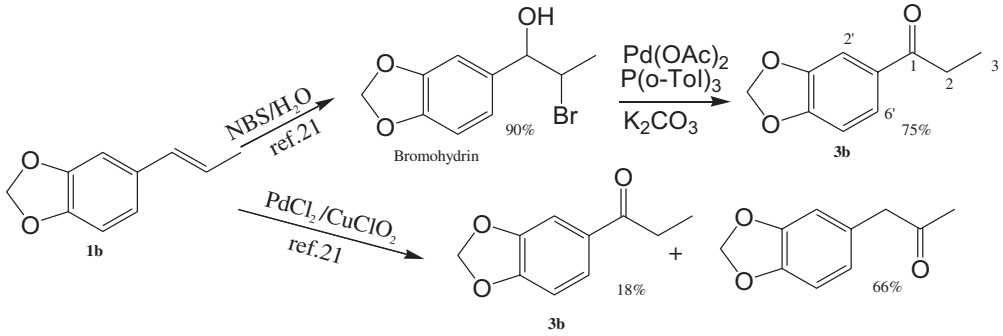
B.P. Joshi, A. Sharma, and A.K. Sinha.[2] Natural Plant Products Division, Institute of Himalayan Bioresource Technology, Palampur, HP 176061, India.

[1]IHBT communication No. 0307.

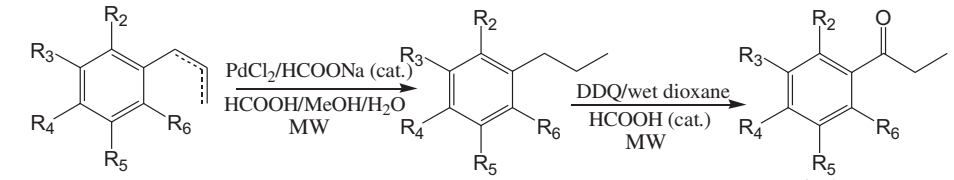
[2]Corresponding author (e-mail: aksinha08@rediffmail.com).

 doi: 10.1139/V05-185 © 2005 NRC Canada

Scheme 1.



Scheme 2.



(a) $R_2=R_4=R_5=OMe$; $R_3=R_6=H$ (b) $R_3=R_4=OCH_2O$; $R_2=R_5=R_6=H$ (c) $R_3=R_4=R_5=OMe$; $R_2=R_6=H$
(d) $R_3=R_4=OMe$; $R_2=R_5=R_6=H$ (e) $R_4=OMe$; $R_2=R_3=R_5=R_6=H$ (f) $R_3=OMe$; $R_4=OH$; $R_2=R_5=R_6=H$

Phenylpropenes are readily available natural phenylpropanoids (22)[3] whose structures and economical prices make them excellent precursors for the semisynthesis of a large number of products (23, 24) including propiophenones. Some methoxylated propiophenones (20, 21) (**3a** and **3b**) have already been synthesized from phenylpropenes utilizing either *N*-bromosuccinimide – H_2O – palladium acetate or $PdCl_2$–$CuCl$–O_2 (Scheme 1). However, the extension of these semisynthetic methods for a large-scale preparation of propiophenones is not viable due to a longer reaction time (20), the maintenance of anhydrous conditions, and the use of expensive reagents (21). In addition, phenylpropenes are usually available from natural sources as an isomeric (22) mixture, and their purification into a pure single isomer is tedious (25). Consequently, chemical modification of any isomer of phenylpropenes results in the formation of side products owing to the presence of its other two isomers (23).[4]

Against this backdrop, we report microwave- (26) and ultrasound-assisted (27) rapid and practical semisynthesis of methoxylated propiophenones (**3a**–**3f**) where toxic (28) *cis*-phenylpropenes with their stereo- and regio-isomeric mixtures (**1a**–**1f**) were first hydrogenated into a single product phenylpropane (**2a**–**2f**). This method thus eliminated the possibility of the formation of side products arising from the isomeric nature of phenylpropenes. These phenylpropanes (**2a**–**2f**) were then oxidized to provide bioactive propiophenones (**3a**–**3f**) (Scheme 2). The above microwave- and ultrasound-assisted reactions were also conducted under conventional conditions to compare all three methods viz. microwave, ultrasound, and conventional methods to establish the superiority of the microwave-assisted reactions.

Experimental

Melting points were determined with a Metler FP80 micromelting point apparatus and are uncorrected. Column chromatography was performed on silica gel (60–120 mesh size). ^1H (300 MHz) and ^{13}C (75.4 MHz) NMR spectra were recorded in $CDCl_3$ on a Bruker Avance-300 spectrometer. A CEM Discover® focused microwave (2450 MHz, 300 W) and a Sonics ultrasonicator (20 kHz, 750 W) were used for all the given reactions. GC and HR-ES-MS were determined using Shimadzu-2010 and Micromass Q-TOF Ultima spectrometers, respectively.

Representative experimental for conversion of stereo- and regio-isomeric mixtures of phenylpropenes (1a–1f) into phenylpropane (2a–2f)

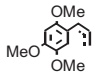
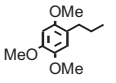
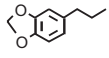
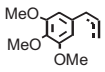
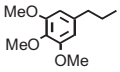
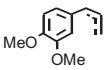
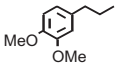
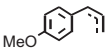
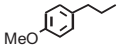
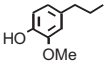
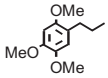
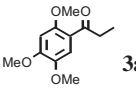
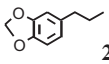
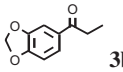
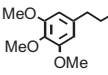
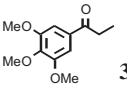
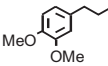
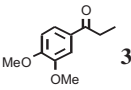
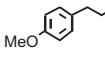
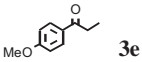
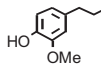
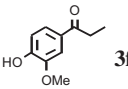
A homogeneous mixture containing $PdCl_2$ (0.01 g) and sodium formate (0.01 g) was prepared by completely mixing both in a mortar. To this powdered mixture, the isomeric

[3] A large number of methoxylated phenylpropenes are found in high concentration (22) up to 90% in many essential oil-bearing plants, but generally exist as an isomeric mixture of three isomers namely trans (α), cis (β), and γ-isomers whose purification into a pure single isomer is tedious by column chromatography (25). On the other side, *cis*-phenylpropenes (e.g., *cis*-2,4,5-trimethoxyphenylpropene) are proven carcinogenic and toxic (26), which overall restrict the market potential of an essential oil rich in cis isomer, therefore, utilization of a stereo- and regio-isomeric mixture of phenylpropene (**1a**–**1f**) is an added benefit for phenylpropenes towards the formation of useful products including propiophenones (**3a**–**3f**).

[4] For example, the oxidation of *cis*- and (or) *trans*-phenylpropenes provides phenylaldehyde; however, contamination of γ-phenylpropene will lead to phenylacetaldehyde (23).

© 2005 NRC Canada

Table 1. Comparative analysis among microwave, ultrasound, and conventional reactions for the formation of phenylpropanes (**2a–2f**) and propiophenones (**3a–3f**) from phenylpropenes (**1a–1f**).

			Microwave[a]		Ultrasonic[b]		Conventional[c]	
S. No.	Substrate[d]	Product	Time (min)	Yield (%)	Time (min)	Yield (%)	Time[e] (min)	Yield (%)
1	 **1a**	 **2a**	10	94	60	84	300	79
2	 **1b**	 **2a**	10	89	60	81	300	76
3	 **1c**	 **2c**	10	93	60	84	300	78
4	 **1d**	 **2d**	10	94	60	86	300	77
5	 **1e**	 **2e**	10	92	60	82	300	79
6	 **1f**	 **2f**	10	96	60	89	300	84
7	 **2a**	 **3a**	16	69	20	64	480	59
8	 **2b**	 **3b**	16	73	20	70	480	64
9	 **2c**	 **3c**	16	71	20	65	480	58
10	 **2d**	 **3d**	16	81	20	78	480	70
11	 **2e**	 **3e**	16	66	20	61	480	58
12	 **2f**	 **3f**	16	56	20	53	480	47

[a]CEM monomode synthesizer at temp. 110–120 °C, power 150–250 W.
[b]Sonics with pulse length 9 s, 75% duty, pause after every 10 min.
[c]At reflux temp.
[d]Dotted lines over the phenylpropenes represent an isomeric mixture of cis, trans, and allyl isomers.
[e]The mentioned reaction period required for maximum yield.

mixture of substituted phenylpropene **1a–1f** (2.9 mmol) and an 8–10 mL reagent mixture of HCOOH–MeOH–H_2O (2:1:2) was added. The mixture was then either irradiated using a focused monomode microwave system (in a round bottom flask fitted with a reflux condenser at 110–120 °C, power 150–250 W) for 10 min, or ultrasonicated (power 560 W) for 60 min, or refluxed for 300 min using the conventional method. After completion of the reaction, the catalyst[5] was removed by filtration and the filtrate was evaporated. The residue was partitioned between ethyl acetate (70 mL) and water (15 mL), and the ethyl acetate layer was washed with water (2 × 10 mL), $NaHCO_3$ (10%), brine (10 mL), dried over Na_2SO_4, and filtered. The filtrate was evaporated, and the obtained residue was purified by column chromatography (hexane – ethyl acetate, 9:1) to afford phenylpropane **2a–2f** in 89%–96% yield (Table 1).

1-(2′,4′,5′-Trimethoxyphenyl)propane (2a) (23)

Liquid. ^{1}H NMR ($CDCl_3$) δ: 6.81 (1H, s, H-6′), 6.32 (1H, s, H-3′), 3.84, 3.82, 3.78 (each 3H, s, three -OCH_3),

[5]After reaction, palladium chloride was filtered and was reused for the hydrogenation reaction, and was found to be active even after three cycles of reuse with a mere 5% loss in the activity.

© 2005 NRC Canada

2.42 (2H, t, *J* = 7.7 Hz, H-1), 1.64 (2H, m, H-2), 0.93 (3H, t, *J*= 7.2 Hz, H-3). ^{13}C NMR ($CDCl_3$) δ: 151.4 (C-2′), 147.4 (C-4′), 142.7 (C-5′), 122.7 (C-1′), 114.3 (C-6′), 98.0 (C-3′), 56.5, 56.2, 55.0 (2′-OCH_3, 4′-OCH_3, 5′-OCH_3), 31.6 (C-1), 23.3 (C-2), 13.7 (C-3).

1-(3′,4′-Dioxymethylenephenyl)propane (2b) (29a)

Liquid. ^{1}H NMR ($CDCl_3$) δ: 6.79 (3H, m, H-2′, H-5′, H-6′), 5.94 (2H, s, -OCH_2O-), 2.56 (2H, t, *J* = 7.8 Hz, H-1), 1.66 (2H, m, H-2), 0.99 (3H, t, *J* = 7.3 Hz, H-3). ^{13}C NMR ($CDCl_3$) δ: 147.5 (C-3′), 145.4 (C-4′), 136.5 (C-1′), 121.4 (C-6′), 108.9 (C-5′), 107.9 (C-2′), 100.6 (-OCH_2O-), 37.5 (C-1), 24.8 (C-2), 13.6 (C-3).

1-(3′,4′,5′-Trimethoxyphenyl)propane (2c)

Liquid. ^{1}H NMR ($CDCl_3$) δ: 6.46 (2H, s, H-2′, H-6′), 3.89 (9H, s, three -OCH_3), 2.55 (2H, t, *J* = 7.8 Hz, H-1), 1.66 (2H, m, H-2), 0.96 (3H, t, *J* = 7.2 Hz, H-3). ^{13}C NMR ($CDCl_3$) δ: 151.2 (C-3′, C-5′), 140.5 (C-1′), 136.8 (C-4′), 107.2 (C-2′, C-6′), 60.9 (4′-OCH_3), 56.7 (3′-OCH_3, 5′-OCH_3), 31.3 (C-1), 23.9 (C-2), 13.4 (C-3). HR-EI-MS (positive) *m*/*z*: 211.2826. Anal. calcd. for $C_{12}H_{19}O_3$: 211.2821.

1-(3′,4′-Dimethoxyphenyl)propane (2d) (29b)

Liquid. ^{1}H NMR ($CDCl_3$) δ: 6.76 (3H, m, H-2′, H-5′, H-6′), 3.82, 3.79 (each 3H, s, two OCH_3), 2.50 (2H, t, *J* = 7.7 Hz, H-1), 1.61 (2H, m, H-2), 0.92 (3H, t, *J* = 7.2 Hz, H-3). ^{13}C NMR ($CDCl_3$) δ: 148.8 (C-3′), 147.1 (C-4′), 135.3 (C-1′), 120.2 (C-6′), 112.7 (C-5′), 111.6 (C-2′), 55.7 (3′-OCH_3), 55.6 (4′-OCH_3), 37.6 (C-1), 24.6 (C-2), 13.7 (C-3).

1-(4′-Methoxyphenyl)propane (2e)

Liquid. ^{1}H NMR ($CDCl_3$) δ: 7.29 (2H, d, *J* = 8.07 Hz, H-2′, H-6′), 7.03 (2H, d, *J* = 8.07 Hz, H-3′, H-5′), 3.98 (3H, OCH_3), 2.71 (2H, t, *J* = 7.6 Hz, H-1), 1.77 (2H, m, H-2), 1.06 (3H, t, *J* = 7.1 Hz, H-3). ^{13}C NMR ($CDCl_3$) δ: 157.9 (C-4′), 134.7 (C-1′), 129.7 (C-2′, C-6′), 114.1 (C-3′, C-5′), 55.1 (4′-OCH_3), 37.2 (C-1), 24.7 (C-2), 13.8 (C-3). HR-EI-MS (positive) *m*/*z*: 151.2298. Anal. calcd. for $C_{10}H_{16}O$: 151.2294.

1-(4′-Hydroxy-3′-methoxyphenyl)propane (2f) (29c)

Liquid. ^{1}H NMR ($CDCl_3$) δ: 6.80 (2H, m, H-2′, H-6′), 6.62 (1H, d, *J* = 8.3 Hz, H-5′), 6.01 (1H, s, -OH), 3.91 (3H, s, -OCH_3), 2.48 (2H, t, *J* = 7.9 Hz, H-1), 1.58 (2H, m, H-2), 0.96 (3H, t, *J* = 7.3 Hz, H-3). ^{13}C NMR ($CDCl_3$) δ: 146.5 (C-3′), 143.7 (C-4′), 134.6 (C-1′), 121.4 (C-6′), 114.4 (C-5′), 111.4 (C-2′), 55.8 (-OCH_3), 37.7 (C-1), 24.9 (C-2), 13.8 (C-3).

General procedure for the preparation of methoxylated propiophenones 3a–3f from the oxidation of phenylpropanes 2a–2f with 2,3-dichloro-5,6-dicyanobenzoquinone (DDQ)

A mixture of substituted phenylpropane **2a–2f** (2.4 mmol), DDQ (4.8–5.24 mmol), and HCOOH (1 to 2 drops) in wet dioxane (30 mL, water–dioxane 1:9) was irradiated using focused microwave irradiation (in a round bottom flask fitted with a reflux condenser at 110–120 °C, power 150–250 W) for 25 min, or ultrasonicated (power 560 W) for 20 min, or refluxed for 240 min under conventional method. The precipitated hydroquinone ($DDQH_2$) was filtered, and the red-coloured filtrate was evaporated and subsequently chromatographed on silica gel (hexane – ethyl acetate, 7:3) to provide methoxylated propiophenone **3a–3f** in 56%–81% yield (Table 1).

1-(2′,4′,5′-Trimethoxyphenyl)propan-1-one (3a)

White solid; mp 108 to 109 °C (lit. value (6*b*) mp 108–110 °C). ^{1}H NMR ($CDCl_3$) δ: 7.45 (1H, s, H-6′), 6.77 (1H, s, H-3′), 3.96, 3.93–3.89 (each 3H, s, three OCH_3), 2.99 (2H, q, *J* = 6.9 Hz, H-2), 1.18 (3H, t, *J* = 6.9 Hz, H-3). ^{13}C NMR ($CDCl_3$) δ: 201.1 (C-1), 155.5 (C-2′), 153.9 (C-4′), 143.3 (C-5′), 118.9 (C-1′), 112.6 (C-6′), 96.7 (C-3′), 56.1 (4′-OCH_3, 5′-OCH_3), 55.9 (2′-OCH_3), 36.9 (C-2), 8.4 (C-3).

1-(3′,4′-Dioxymethylenephenyl)propan-1-one (3b)

White solid; mp 35 to 36 °C (lit. value (30*a*) mp 38 to 39 °C). ^{1}H NMR ($CDCl_3$) δ: 7.60 (1H, d, *J* = 8.1 Hz, H-6′), 7.50 (1H, s, H-2′), 6.86 (1H, d, *J* = 8.1 Hz, H-5′), 6.34 (2H, s, -OCH_2O-), 2.91 (2H, q, *J* = 6.9 Hz, H-2), 1.25 (3H, t, *J* = 6.9 Hz, H-3). ^{13}C NMR ($CDCl_3$) δ: 199.1 (C-1), 151.8 (C-4′), 148.2 (C-3′), 132.1 (C-1′), 122.4 (C-6′), 110.1 (C-2′), 109.7 (C-5′), 100.5 (-OCH_2O-), 31.4 (C-2), 8.6 (C-3).

1-(3′,4′,5′-Trimethoxyphenyl)propan-1-one (3c)

White solid; mp 52 to 53 °C (lit. value (17) mp 51.5–52.5 °C). ^{1}H NMR ($CDCl_3$) δ: 7.23 (2H, s, H-2′, H-6′), 3.90 (9H, s, three OCH_3), 2.95 (2H, q, *J* = 7.2 Hz, H-2), 1.22 (3H, t, *J* = 7.2 Hz, H-3). ^{13}C NMR ($CDCl_3$) δ: 199.5 (C-1), 153.1 (C-3′, C-5′), 141.4 (C-4′), 137.6 (C-1′), 105.4 (C-2′, C-6′), 60.8 (4′-OCH_3), 56.3 (3′-OCH_3, 5′-OCH_3), 31.8 (C-2), 8.4 (C-3).

1-(3′,4′-Dimethoxyphenyl)propan-1-one (3d)

White solid; mp 59 to 60 °C (lit. value (30*b*) mp 59 to 60 °C). ^{1}H NMR ($CDCl_3$) δ: 7.62 (1H, d, *J* = 8.0 Hz, H-6′), 7.56 (1H, s, H-2′), 6.88 (1H, d, *J* = 8.0 Hz, H-5′), 3.96 (6H, s, two OCH_3), 2.97 (2H, q, *J* = 7.2 Hz, H-2), 1.23 (3H, t, *J* = 7.2 Hz, H-3). ^{13}C NMR ($CDCl_3$) δ: 200.0 (C-1), 153.4 (C-4′), 149.3 (C-3′), 130.5 (C-1′), 122.9 (C-6′), 110.4 (C-2′), 110.3 (C-5′), 56.5 (3′-OCH_3, 4′-OCH_3), 31.7 (C-2), 9.0 (C-3).

1-(4′-Methoxyphenyl)propan-1-one (3e) (30c)

Liquid. ^{1}H NMR ($CDCl_3$) δ: 7.58 (2H, d, *J* = 8.05 Hz, H-2′, H-6′), 6.85 (2H, d, *J* = 8.05 Hz, H-3′, H-5′), 3.90 (3H, s, OCH_3), 2.93 (2H, q, *J* = 7.2 Hz, H-2), 1.18 (3H, t, *J* = 7.2 Hz, H-3). ^{13}C NMR ($CDCl_3$) δ: 199.2 (C-1), 163.2 (C-4′), 130.4 (C-1′), 129.9 (C-2′, C-6′), 113.5 (C-3′, C-5′), 55.3 (4′-OCH_3), 31.2 (C-2), 8.2 (C-3).

1-(4′-Hydroxy-3′-methoxyphenyl)propan-1-one (3f)

White solid; mp 61 to 62 °C (lit. value (2) mp 63 °C). ^{1}H NMR ($CDCl_3$) δ: 7.58 (2H, m, H-2′, H-6′), 6.95 (1H, d, *J* = 8.4 Hz, H-5′), 6.08 (1H, s, Ar-OH), 3.92 (3H, s, three OCH_3), 2.96 (2H, q, *J* = 6.9 Hz, H-2), 1.23 (3H, t, *J* = 6.9 Hz, H-3). ^{13}C NMR ($CDCl_3$) δ: 199.7 (C-1), 151.3 (C-3′), 147.8 (C-4′), 130.9 (C-1′), 123.7 (C-6′), 112.1 (C-5′), 111.9 (C-2′), 55.2 (OCH_3), 31.7 (C-2), 8.4 (C-3).

© 2005 NRC Canada

Table 2. Catalytic transfer hydrogenation of 2,4,5-trimethoxyphenylpropene (**1a**) into 2,4,5-trimethoxyphenylpropane (**2a**) using $PdCl_2$ as catalyst.

	Catalytic transfer hydrogenating agents			
Entry	Reagents and solvents	Catalyst	CEM Discover microwave irradiation[a] time (min)	Yield[b] (%)
1	HCOOH (excess)	$PdCl_2$	80	20
2	HCOOH (excess) – NaOH (10%)	$PdCl_2$	65	15
3	HCOOH (excess) – isopropanol	$PdCl_2$	50	35
4	HCOOH (excess) – ethylene glycol	$PdCl_2$	50	38
5	HCOOH (excess) – methanol	$PdCl_2$	50	54
6	HCOOH (excess) – MeOH – water (2:1:2)	$PdCl_2$	40	82
7	HCOOH (excess) – MeOH – water (2:1:2) (HCOONa, cat.)	$PdCl_2$	9	94
8	HCOOH (excess) – MeOH – water (2:1:2) (HCOOK, cat.)	$PdCl_2$	9	94
9	HCOOH (excess) – MeOH – water (2:1:2) ($HCOONH_4$, cat.)	$PdCl_2$	9	93
10	HCOOH (excess) – MeOH – water (2:1:2) (HCOONa, cat.)	Pd/C	30	25
11	HCOOH (excess) – MeOH – water (2:1:2) (HCOONa, cat.)	$PdCl_2$	15[c]	67
12	HCOOH (excess) – MeOH – water (2:1:2) (HCOONa, cat.)	$PdCl_2$	6[c]	79

[a]CEM monomode Discover synthesizer at temp. 110–120 °C, power 150–250 W.
[b]Yields based on GC (Shimadzu).
[c]The reaction was performed using a domestic microwave oven at power 300 and 900 W (entries 11 and 12, respectively) resulting in either unreacted starting material (entry 11) or evaporation of the product (entry 12).

Results and discussion

In recent years, there has been a tremendous shift in the use of microwave (26) and ultrasound (27) irradiation in organic reactions owing to the shorter reaction time, higher yields, operational simplicity, and most importantly, the fact that it is a more eco-friendly process compared with conventional heating. As per our ongoing interest in semisynthesis of phenylpropanoids, we decided to prepare 2,4,5-trimethoxypropiophenone (**3a**), a hypolipidemic (5) active compound, from abundantly available toxic (28) 2,4,5-trimethoxyphenylpropene (**1a**) through catalytic transfer hydrogenation (31) (CTH) of **1a** in the first step to form 2,4,5-trimethoxyphenylpropane (**2a**), which would then be oxidized by addition of the suitable oxidant in the next step to form **3a**. For catalytic transfer hydrogenation, a stereo- and regioisomeric mixture of phenylpropene **1a** was treated with $PdCl_2$ in formic acid (98%) as a hydrogen transferring agent for 80 min under focused monomode (32) microwave (CEM Discover® synthesizer); but only 20% of product **2a** formed (Table 2, entry 1), the rest being a number of side products. Similarly, a combination of HCOOH and NaOH (33) did not improve the yield of the product (Table 2, entry 2). The addition of isopropanol (34) or high boiling ethylene glycol (31*a*, 35) to formic acid also did not improve the yield of product **2a** (Table 2, entries 3 and 4). Later on, hydrogenating a mixture comprising $PdCl_2$–HCOOH in methanol was found suitable, and **2a** was obtained up to 54% yield (Table 2, entry 5). Prompted by reports on water–methanol assisted yield enhancement of products (36), we decided to utilize a combination of methanol and water as solvents in this reaction. After a lot of experimentation, a 2:1:2 mixture of HCOOH–MeOH–H_2O in catalytic amounts of $PdCl_2$ for 40 min under microwave proved to give the optimum results, and provided an 82% yield of **2a** (Table 2, entry 6). Later on, we realized that the addition of a catalytic amount of either sodium formate, potassium formate, or ammonium formate,[6] along with this hydrogenating system, was important in increasing the yield of the product (**2a**) up to 94% with a drastic reduction in reaction time up to 9 min under focused monomode (32) microwave (Table 2, entries 7–9). For comparison, the same reaction performed in a domestic microwave oven provided the product (**2a**) in 79% yield and the loss in yield may be due to the easy evaporation of the product in the domestic microwave oven (Table 2, entries 11 and 12).

In the next step, comprising oxidation of phenylpropane **2a** into **3a**, several common oxidizing reagents (37) such as pyridinium chlorochromate and potassium permanganate were tried, but none of the oxidants was found to be effective and a number of side products were obtained with little or no product **3a**. Use of excess potassium permanganate – copper sulphate (10 mol equiv. of reactant **2a**) under ultrasound and microwave irradiation (38) was also unfruitful. Similarly, under various conditions, chromium(IV) oxide (37*b*, 39) also failed to convert **2a** into **3a**, although a yellow-colored solid was obtained; NMR studies revealed it to be 2-propyl-5-methoxy-1,4-benzoquinone (40). The reason for the failure of all the above general oxidants (37–39) was believed to be due to the substituent effect of methoxy groups present at the 2, 4, and 5 positions of phenylpropane, while oxidation of unsubstituted phenylpropane into propiophenones is well-reported with potassium permanganate (38*c*).

Later on, 2,3-dichloro-5,6-dicyanobenzoquinone (DDQ) (41) was found to be an appropriate oxidant for successfully converting **2a** into **3a**. Initially, **2a** was reacted with 1.25–

[6]Ammonium formate itself is a well-known hydrogen-transferring agent for reduction of various functional groups (31, 32) including carbon–carbon double bonds; however, a large excess of ammonium formate (10 equiv.) and its sublimation on the walls of the vessels somewhat limit its use.

© 2005 NRC Canada

1.5 equiv. of DDQ in the presence of various organic solvents such as methanol, ethanol, THF, and dioxane. Dioxane along with 3 to 4 mL of water (42), considered most suitable, provided **3a** only up to 47% along with 11% of α-asarone (23).[7] An increased amount of DDQ, varying from 2 to 2.2 equiv., provided a little more improvement in the yield (58%) of **3a**, but no more improvement in the yield resulted from a further addition of DDQ. Interestingly, the addition of a few drops of HCOOH (98%) in this reaction mixture increased the yield of propiophenone **3a** up to 69% (Scheme 2) within 16 min under focused microwave irradiation.

After choosing DDQ as the reagent, we decided to carry out both hydrogenation of **1a** into **2a** and oxidation of **2a** into **3a** in one pot. One-pot synthesis has recently attracted interest, providing a simple and efficient entry to compounds by amalgamating two or more operations into a single step. Hence, after performing hydrogenation of **1a** into **2a** for 10 min, DDQ was added in the same reaction pot and irradiated under microwave irradiation intermittently for 20 min. We had thought that HCOOH, besides acting as hydrogen source, would not interfere in the DDQ-assisted oxidation of phenylpropane **2a** into propiophenone **3a** in the same pot, as the importance of an acidic (42) medium in DDQ-assisted oxidation is well-understood. Unfortunately, the conversion of **2a** into **3a** resulted in a poor yield (up to 22%). This implied that oxidation could not occur completely in one pot probably owing to the presence of $PdCl_2$, which would keep on reacting with formic acid to release hydrogen, thus hampering the abstraction of the benzylic proton of **2a** with DDQ for the formation of **3a**. Hence, we decided to remove $PdCl_2$ by mere filtration in the first step before the addition of the oxidant (DDQ) in the same pot. Although product **3a** was formed in this case, the yield was still no higher than 34% and there was no further increase in the yield by either lengthening the reaction period or changing the amount of DDQ. This implied that the hydrogenating solvent mixture must have interfered in the oxidation of **2a** into **3a**, which is otherwise performed effectively in dioxane in the two-step methodology. Finally, all this prompted us to change the one-pot two-step methodology, and retain the two-step methodology by performing the hydrogenation in methanol and oxidation in a dioxane medium.

After the success of these reactions for the conversion of **1a** into **2a** followed by the oxidation of **2a** into **3a**, the same methodology was employed for the oxidation of other natural methoxylated phenylpropenes **1b**–**1f**, which successfully provided the corresponding propiophenones **3b**–**3f** in moderate yields (56%–81%). To make a comparative analysis, these reactions (hydrogenation and oxidation) were performed under ultrasonication as well as refluxed under conventional heating and the results are shown in Table 1. The results clearly show that microwave activation afforded better yields of **3a**–**3f** with shorter reaction time than those obtained under other classical or sonication methods. Moreover, the reactions using microwave are more environment friendly than conventional heating in terms of a reduced reaction time and the use of less solvent for the reaction.

Conclusion

In conclusion, we have realized a microwave and ultrasound-assisted rapid and mild semi-synthetic approach towards preparation of a number of natural bioactive methoxylated propiophenones (**3a**–**3f**) from abundantly available stereo- and regio-isomeric mixtures of phenylpropenes (**1a**–**1f**) via phenylpropanes (**2a**–**2f**). Moreover, such a comparative analysis among microwave, ultrasound, and conventional methodologies, to the best of our belief, is disclosed for the first time. Overall, this is an environment friendly process with none of the steps requiring maintenance of anhydrous conditions or hazardous chemicals. The intermediates (**2a**–**2f**) may have general utilities in the convenient synthesis of many other phenylpropanoids (26*d*, 27*c*).

Acknowledgments

AS and BP are indebted to the Council for Scientific and Industrial Research (CSIR), Delhi for the award of a Senior Research Fellowship (SRF). The authors gratefully acknowledge the Director of the Institute of Himalayan Bioresource Technology, Palampur, for his kind cooperation and encouragement.

References

1. (*a*) J. Mėndez. Phytochemistry, **19**, 1557 (1980); (*b*) M.G.A. Hassan. Phytochemistry, **25**, 2417 (1986); (*c*) J.B. Harborne and H. Baxter. *In* Phytochemical dictionary: A handbook of bioactive compounds from plants. Taylor & Francis Ltd., Washington, D.C. 1993; (*d*) B.V. de O. Santos and M.C. de O. Chaves. Biochem. Syst. Ecol. **25**, 539 (1999); (*e*) J. Hu and X. Feng. Planta Med. **66**, 662 (2000); (*f*) V.A. Facundo and S.M. Morais. Biochem. Syst. Ecol. **31**, 111 (2003).
2. O.P. Suri, R.S. Bindra, N.K. Satti, and R.K. Khajuria. Indian J. Chem. Sect. B, **26B**, 587 (1987).
3. C. Lariucci, L.I.B. Homar, P.H. Ferri, and L.S. Santos. Anais Assoc. Bras. Quim. **44**, 22 (1995).
4. A.Z. Susana, N.L. Silvia, D.P. Germán, L.F. Ricardo, B.S. Carina, M.F. Lorena, A.G. Fernando, M.R. Ana, and D.E. Ricardo. J. Nat. Prod. **62**, 1353 (1999).
5. (*a*) A. Cruz, L. Gardu, M. Salazar, E. Martínez, H.A. Jiménez-Vázquez, F. Diaz, G. Chamorro, and J. Tamariz. Arzneim. Forsch. Drug Res. **51**, 535 (2001); (*b*) Z. Chilmonczyk, D. Siluk, R. Kaliszan, B. Łozowicka, J. Popławski, and S. Filipek. Pure Appl. Chem. **73**, 1445 (2001).
6. (*a*) C.W. Perry. US Patent 3 769 350, 30 October 1973; (*b*) T. Högberg, S. Bengtsson, T. de Paulis, L. Johansson, P. Ström, H. Hall, and S.O. Ögren. J. Med. Chem. **33**, 1155 (1990); (*c*) D. Francisco, C. Leticia, F. Rosa, T. Joaquin, L. Fernando, C. German, and M. Heber. Org. Prep. Proced. Int. **23**, 133 (1991); (*d*) A. Cruz, L. Garduño, M. Salazar, E. Martínez, F. Díaz, G. Chamorro, and J. Tamariz. Med. Chem. Res. **10**, 587 (2001).
7. A. Steffen. *In* Perfume and flavor chemicals: Aroma chemicals. Vols. I and II. Allured Publishing Corporation, Carol Stream, Ill. 1994.

[7] DDQ is a well-known dehydrogenating agent used to provide carbon–carbon double bonds in anhydrous (41) conditions and also used as an oxidizing agent to provide benzylic ketones in aqueous (45) conditions. However, formation of dehydrogenated product, α-asarone (11%), during oxidation of **2a** with DDQ and dioxane in wet conditions is a surprise finding.

© 2005 NRC Canada

8. R. Levine, M.J. Karten, and W.M. Kadunce. J. Org. Chem. **40**, 1770 (1975).
9. Y. Tamaru, H. Ochiai, Y. Yamada, and Z. Yoshida. Tetrahedron Lett. **24**, 3869 (1983).
10. (*a*) S.R. Stauffer, C.J. Coletta, R. Tedesco, G. Nishiguchi, K. Carlson, J. Sun, B.S. Katzenellenbogen, and J.A. Katzenellenbogen. J. Med. Chem. **43**, 4934 (2000); (*b*) P. Salehi, M.K. Mohammad, A.Z. Mohammad, and S. Sara. Bull. Chem. Soc. Jpn. **76**, 1863 (2003).
11. (*a*) R.H. Prager and Y.T. Tan. Tetrahedron Lett. **8**, 3661 (1967); (*b*) T. Horie, H. Tominaga, Y. Kawamura, T. Hada, N. Ueda, Y. Amano, and S. Yamamoto. J. Med. Chem. **34**, 2169 (1991).
12. B.H. Lipshutz, P. Mollard, S.S. Pfeiffer, and W. Chrisman. J. Am. Chem. Soc. **124**, 14282 (2002).
13. M. Makosza and T. Goetzen. Org. Prep. Proced. Int. **5**, 203 (1973).
14. M.L. Edwards, D.M. Stemerick, and P.S. Sunkara. J. Med. Chem. **33**, 1948 (1990).
15. J.S. Henk, J.M.V. Frank, A.F. Jim, and B.P.A.W. Joannes. J. Nat. Prod. **61**, 1110 (1998).
16. H.L. Haller and P.S. Schaffer. J. Am. Chem. Soc. **61**, 2175 (1939).
17. C.D. Gutsche and F.A. Hoyer. J. Am. Chem. Soc. **72**, 4285 (1950).
18. C. Granito and H.P. Schultz. J. Org. Chem. **28**, 879 (1963).
19. (*a*) H. Nakamura, Y. Kashiwara, and K. Arata. Bull. Chem. Soc. Jpn. **76**, 1071 (2003); (*b*) R. Sigrid, L.R. Christophe, R. Nicolas, and J. Dubac. Tetrahedron Lett. **44**, 2037 (2003).
20. V. Lander and P. Schreier. Flavour Fragrance, J. **6**, 21 (1991).
21. J. Tsuji, H. Nagashima, and K. Sato. Tetrahedron Lett. **23**, 3085 (1982).
22. K. Bauer, D. Garbe, and H. Surburg. *In* Common fragrance and flavor materials: Preparation, properties and uses. 4th ed. Wiley-VCH Verlag GmbH, Weinheim, Germany. 2001.
23. A. Patra and A.K. Mitra. J. Nat. Prod. **44**, 668 (1981).
24. P.Z. Bezoukian. *In* Perfumery and flavoring synthetics. Allured Publishing Corp. Wheaton, Ill. 1986.
25. B.D. Gates and J.S. Swenton. Tetrahedron Lett. **33**, 2127 (1992).
26. (*a*) M. Larhed and A. Hallberg. Drug Discovery Today, **6**, 406 (2001); (*b*) N.E. Leadbeater and H.M. Torenius. J. Org. Chem. **67**, 3145 (2002); (*c*) A.K. Sinha, B.P. Joshi, and R. Acharya. Chem. Lett. **32**, 780 (2003); (*d*) A.K. Sinha, B.P. Joshi, and R. Dogra. US Patent 6 544 390, 8 April 2003; (*e*) A. Sharma, B.P. Joshi, and A.K. Sinha. Bull. Chem. Soc. Jpn. **77**, 2231 (2004); (*f*) N. Kaval, W. Dehaen, P. Mátyus, and E. Van der Eycken. Green Chem. **6**, 125 (2004); (*g*) V. Pathania, A. Sharma, and A.K. Sinha. Helv. Chim. Acta, **88**, 811 (2005).
27. (*a*) S.R. Soudagar and S.D. Samant. Ultrason. Sonochem. **2**, S15 (1995); (*b*) L.H. Thompson and L.K. Doraiswamy. Ind. Eng. Chem. Res. **38**, 1215 (1999); (*c*) B.P. Joshi, A. Sharma, and A.K. Sinha. Tetrahedron, **61**, 3075 (2005).
28. S.C. Kim, A. Liem, B.C. Stewart, and J.A. Miller. Carcinogensis, **20**, 1303 (1999).
29. (*a*) M.T. Bogert and G. Powell. J. Am. Chem. Soc. **53**, 2747 (1931); (*b*) W.J. Horton and E.G. Paul. J. Am. Chem. Soc. **79**, 2264 (1957); (*c*) M. Ogata, M. Hoshi, S. Urano, and T. Endo. Chem. Pharm. Bull. **48**, 1467 (2000).
30. (*a*) I. Hirao. J. Pharm. Soc. Jpn. **73**, 1224 (1954); (*b*) C.W. Perry, M.V. Kalnins, and K.H. Deitcher. J. Org. Chem. **37**, 4371 (1972); (*c*) C.R. Noller and R. Adams. J. Am. Chem. Soc. **46**, 1889 (1924).
31. (*a*) K.J. Barakat, B.K. Banik, D.R. Wagle, M.S. Manhas, and A.K. Bose. J. Org. Chem. **64**, 5746 (1999); (*b*) Z. Paryzek, H. Koenig, and B. Tabaczka. Synthesis, **13**, 2023 (2003).
32. B.L. Hayes. *In* Microwaves: Chemistry at the speed of light. CEM Publishing, Matthews, N.C. 2002.
33. A. Sharma, B.P. Joshi, and A.K. Sinha. Chem. Lett. **32**, 1186 (2003).
34. S.U. Sonavane and R.V. Jayaram. Synlett, **1**, 146 (2004).
35. H.S.P. Rao and S. Jothilingam. J. Org. Chem. **68**, 5392 (2003).
36. (*a*) J.M. Khurana and P. Sharma. Bull. Chem. Soc. Jpn. **77**, 549 (2004); (*b*) S. Bhar and S. Guha. Tetrahedron Lett. **45**, 3775 (2004).
37. (*a*) R. Rathore, N. Saxena, and S. Chandrasekaran. Synth. Commun. **16**, 1493 (1986); (*b*) J. Muzart. Tetrahedron Lett. **27**, 3139 (1986).
38. (*a*) M. Mačiarova, Š. Toma, and A. Heribanová. Tetrahedron, **56**, 8561 (2000); (*b*) A. Shaabani, and D.G. Lee. Tetrahedron Lett. **42**, 5833 (2001); (*c*) A. Shaabani, A. Bazgir, F. Teimouri, and D.G. Lee. Tetrahedron Lett. **43**, 5165 (2002).
39. R. Rangarajan and E.J. Eisenbraun. J. Org. Chem. **50**, 2435 (1985).
40. A.A.L. Gunatilaka, J.M. Berger, R. Evans, J.S. Miller, J.H. Wisse, K.M. Neddermann, I. Bursuker, and D.G.I. Kingston. J. Nat. Prod. **64**, 2 (2001).
41. (*a*) P.P. Fu and R.G. Harvey. Chem. Rev. **78**, 317 (1978); (*b*) D. Walker and J.D. Hiebert. Chem. Rev. **67**, 153 (1967); (*c*) A.G. Gonzalez, Z.E. Aguiar, J.G. Luis, and A.G. Ravelo. J. Nat. Prod. **52**, 1231 (1989); (*d*) F.D. Ramdayal, D.J. Kiemle, and R.T. Lalonde. J. Org. Chem. **64**, 4607 (1999).
42. A.G. Gonzalez, Z.E. Aguiar, J.G. Luis, and A.G. Ravelo. J. Nat. Prod. **52**, 1231 (1989).

© 2005 NRC Canada

Enhancement of aqueous solubility of itraconazole by complexation with cyclodextrins using supercritical carbon dioxide

Ibrahim Shehatta, Ali Hassan Al-Marzouqi, Baboucarr Jobe, and Ali Dowaidar

Abstract: The formation of inclusion complexes between itraconazole, a highly hydrophobic drug, and α-, β-, γ-, and hydroxylpropyl-β-cyclodextrin (HP-β-CD) were assessed using phase-solubility techniques. The solubility of itraconazole increased as a function of cyclodextrin concentration showing an AL phase diagram indicating the formation of soluble complexes with 1:1 stoichiometry. The Gibbs free energies of transfer of the drug from aqueous solution to the cavity of cyclodextrin are negative and increase in magnitude with increasing cyclodextrin concentration. The solubility of itraconazole, as well as the stability constant of its complex with HP-β-CD, are found to be affected by the pH of the medium. The HP-β-CD cavity was found to have a greater affinity for the unionized itraconazole than the protonated one. It was found that the interaction between the drug and the cyclodextrin is weakened as the medium becomes more apolar by the addition of methanol. Also, the size of the cavity of the cyclodextrins plays an important role in the association process. Furthermore, the thermodynamic parameters of the complexation process were calculated, by monitoring the isothermic solubility diagrams of itraconazole–HP-β-CD and itraconazole–β-CD at various temperatures, to gain information on the driving forces for the formation of inclusion complexes. Drug formulations of itraconazole were prepared by complexation of the drug into different cyclodextrins using supercritical carbon dioxide in a static mode. The effects of cyclodextrins on the prepared inclusion complexes were studied and characterized by differential scanning calorimetry.

Key words: cyclodextrin, itraconazole, inclusion complex, solubility, stability constant.

Résumé : Faisant appel à des techniques de solubilité de phase, on a évalué la formation de complexes d'inclusion entre l'itraconazole, un médicament fortement hydrophobe, et les α-, β- et γ-cyclodextrines et la hydroxypropyl-β-cyclodextrine (HP-β-CD). La solubilité de l'itraconazole augmente en fonction de la concentration de cyclodextrine en présentant un diagramme de phase AL qui indique la formation de complexes de stoechiométrie 1 : 1. Les énergies libres de Gibbs de transfert du médicament de la phase aqueuse à la cavité de la cyclodextrine sont négatives et leur valeur augmente en amplitude avec une augmentation de la concentration de cyclodextrine. On a observé que la solubilité de l'itraconazole ainsi que la constante de stabilité de son complexe avec la HP-β-CD sont affectées par le pH du milieu. On a trouvé que l'affinité de la cavité de la HP-β-CD pour l'itraconazole non ionisé est plus élevée que pour la forme protonée. On a trouvé que l'interaction entre le médicament et la cyclodextrine est affaiblie quand le milieu devient plus apolaire par addition de méthanol. De plus, la taille de la cavité des cyclodextrines joue un rôle important dans le processus d'association. De plus, dans le but d'obtenir des informations relatives aux facteurs influençant la formation des complexes d'inclusion, on a calculé les paramètres thermodynamiques du processus de complexation en évaluant les diagrammes de solubilité isothermes de l'itraconazole–HP-β-CD et de l'itraconazole–β-CD à diverses températures. Utilisant du bioxyde de carbone hypercritique en un mode statique, on a préparé des formulations d'itraconazole par complexation du médicament dans différentes cyclodextrines. On a étudié les effets des cyclodextrines sur les complexes d'inclusion préparés et on les a caractérisés par calorimétrie à balayage différentiel.

Mots clés : cyclodextrine, itraconazole, complexe d'inclusion, solubilité, constante de stabilité.

[Traduit par la Rédaction]

Introduction

Itraconazole is a broad-spectrum antifungal agent (1–3). However, some difficulties are encountered in preparing the pharmaceutical formulation of oral or injectable solutions owing to the very poor aqueous solubility of the drug at physiological pH conditions, leading to a minimal bioavailability (4). Itraconazole is a weak base (pK_a = 4.0) and

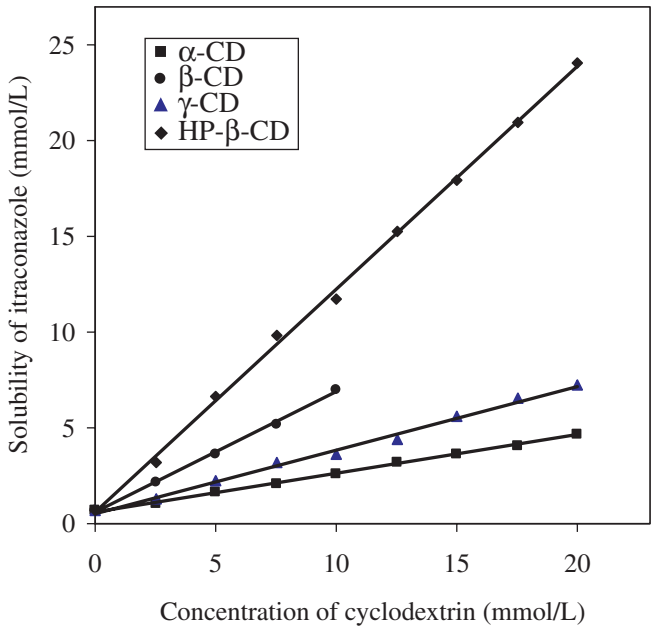
Received 20 November 2004. Published on the NRC Research Press Web site at http://canjchem.nrc.ca on 23 December 2005.

I. Shehatta. Department of Chemistry, Faculty of Science, Mansoura University, Mansoura, Egypt.
A.H. Al-Marzouqui,[1] B. Jobe, and A. Dowaidar. Department of Chemical & Petroleum Engineering, UAE University, Al-Ain, P.O. Box 17555, United Arab Emirates.

[1]Corresponding author (e-mail: hassana@uaeu.ac.ae).

 doi: 10.1139/V05-181 © 2005 NRC Canada

Fig. 1. Phase-solubility diagrams of itraconazole in phosphate buffer (pH 7.4) solution in the presence of different concentrations of α-CD (■), β-CD (●), γ-CD (▲), and HP-β-CD (◆) at 298.15 K.



poorly soluble in aqueous solutions (less than 1 μg/mL at pH values ranging from 1 to 12.7) (5). To overcome this problem, efforts must be made to improve the aqueous solubility of itraconazole.

The commercially available itraconazole capsules are highly effective for the treatment of superficial fungal maladies and disseminated infections. For good absorption, the itraconazole capsule should be administrated with food where gastric secretion is stimulated, leading to a low pH in the stomach allowing for drug dissolution and thereby improving bioavailability. Unfortunately, itraconazole is not effective for the treatment of AIDS and cancer patients. This is due to the inhibition or neutralization of gastric secretion, common in AIDS patients, leading to a decrease in the bioavailability of itraconazole. For insoluble drugs, the formulations involve the use of solvents, surfactants, microemulsion dosage forms, and (or) pH adjustment for ionizable drugs. However, these formulations are often found to cause some adverse reactions and to reduce the efficacy and safety of the drug. To enhance the efficacy and safety of antifungal drugs, another approach has been applied in which a cyclodextrin is used as a drug carrier.

Cyclodextrins are cyclic oligosaccharides consisting of six or more D(+)-glucopyranose units. They are linked to each other by α(1→4) bonds to form macrocyclic rings having the shape of a truncated hollow cone. The interiors, which are the sites for the guest molecules, are largely hydrophobic. Due to their ability to form inclusion complexes with lipophilic drugs and consequently changing their physicochemical and biopharmaceutical properties, cyclodextrins have great potential to be used as pharmaceutical excipients (6). Drug–cyclodextrin complexes have shown to improve the aqueous solubility, dissolution rates, chemical stability, and bioavailability of various drug molecules that are poorly soluble in water. In addition, the complexation may also mask unpleasant odors or tastes (7–9).

Table 1. Values of the Gibbs free energy of transfer of itraconazole from aqueous solution to the hydrophobic cavity of various cyclodextrins at 298.15 K.

	$-\Delta_{trans}G°$ (kJ mol^{-1})			
[CD] (mol/L)	α-CD	β-CD	γ-CD	HP-β-CD
0.0025	0.85	2.72	1.52	3.74
0.0050	2.01	4.03	2.80	5.53
0.0075	2.69	4.94	3.74	6.51
0.0100	3.20	5.68	4.07	6.95
0.0125	3.71	—	4.53	7.61
0.0150	4.05	—	5.12	8.00
0.0175	4.34	—	5.50	8.40
0.0200	4.67	—	5.76	8.74

As a continuation of our previous work (10–18), the present work is undertaken to improve the solubility of itraconazole and thereby its bioavailability characteristics by complexation with cyclodextrins. Four different types of cyclodextrins (α-, β-, γ-, and hydroxypropyl-β-cyclodextrin (HP-β-CD)) were used. The thermodynamic parameters of itraconazole complexed with HP-β-CD and β-CD are calculated from the temperature dependence of the stability constant. Itraconazole–CD inclusion complexes are prepared using supercritical carbon dioxide (SC CO_2), which is a nontoxic, nonhazardous solvent. Properties of supercritical fluids (SCFs) can be changed from gaslike to liquidlike values by simply adjusting the pressure and temperature.

Experimental

Materials and reagents

Itraconazole was generously donated by the College of Pharmacy at Oregon State University. α-, β-, HP-β- and γ-CDs were obtained from Sigma-Aldrich Chemical Co. (Milwaukee, Wisconsin). All cyclodextrins were subjected to a thermogravimetric (TG) analysis to find the degree of hydration, which was considered in the calculations of their concentrations. The phosphate buffer solutions (pH 7.4) were prepared by adding appropriate amounts of orthophosphoric acid (0.2 mol/L) to trisodium phosphate (0.2 mol/L). All chemicals were reagent grade (Merck, Darmstadt) and were used as received. All solutions were prepared using deionized water (specific conductivity <2 μS cm^{-1}) and were used within 24 h. Bidistilled water was purified by using a Millipore Super Q system and was also degassed prior to the preparation of the solutions. The homogeneity of the initial solutions was assured by sonification for 15 min in an ultrasonic bath.

Solubility study

Solubility measurements were performed as described by Higuchi and Connors (19). Excess amounts of itraconazole were added to 10 mL of phosphate buffer solutions (pH 7.4) containing various concentrations of the cyclodextrins. The suspensions formed were sonicated for 15 min and then shaken for 3 days in a water bath (40 °C). After equilibrium was attained an aliquot was filtered through a Millipore

© 2005 NRC Canada

Table 2. Stability constant ((mol/L)$^{-1}$) and thermodynamic parameters (kJ mol^{-1}) for the association of itraconazole with various cyclodextrins in phosphate buffer (pH 7.4).

Parameter	Temp. (K)	α-CD	β-CD	γ-CD	HP-β-CD
K	288.15	—	1249±111	—	1703±128
	293.15	—	1064±92	—	1353±113
	298.15	284±27	885±71[a]	453±34	1168±101
	303.15	—	735±59	—	898±73
	308.15	—	639±56	—	773±63
$-\Delta G°$	298.15	14.01±0.24	16.82±0.20	15.16±0.19	17.51±0.22
$-\Delta H°$	298.15	—	25.29±0.65	—	29.44±1.37
$-T\Delta S°$	298.15	—	8.47±0.68	—	11.93±1.39

[a]A value of 785 (mol/L)$^{-1}$ was reported earlier for the stability constant of itraconazole–β-CD inclusion complex at 298.15 K (31).

membrane (0.45 μm). The filtered solutions were appropriately diluted, and the amount of dissolved itraconazole was determined via absorbance measurements in matched quartz cells using a Shimadzu UV-2101PC UV–vis scanning spectrophotometer at 265 nm. Previous determinations showed that the CDs did not interfere with the spectrophotometric measurements.

Preparation of inclusion complexes using supercritical carbon dioxide

The supercritical fluid experimental apparatus consisted of a 260 mL capacity syringe pump and controller system (ISCO 260D) and an ISCO series 2000 SCF extraction system (SFX 220) consisting of a dual-chamber extraction module with two 10 mL stainless steel vessels as discussed previously (17, 18). Temperature and pressure within the vessels were measured and could be independently adjusted. Inclusion experiments with SC CO_2 were performed using the SCF experimental apparatus similar to the procedures of Van Hees et al. (20). The 10 mL cell was filled with a physical mixture of itraconazole–cyclodextrin at a drug to cyclodextrin molar ratio of 1:2 (0.125 mmol drug : 0.25 mmol cyclodextrin). The system was pressurized and heated to the desired pressure and temperature and left in a static mode for 3 h. At the end of the process, the pressure in the cell was suddenly dropped to atmospheric pressure. The contents of the cell were ground and homogenized in a mortar.

Thermal analysis

Thermal characteristics of the products were determined using a differential scanning calorimeter (DSC 7, PerkinElmer) with a nitrogen flow rate of 40 mL/min and a heating rate of 10 °C/min from 50 to 250 °C.

Results and discussion

Effect of cyclodextrins on the aqueous solubility of itraconazole

The phase-solubility diagrams of itraconazole in different cyclodextrins were constructed by plotting the total dissolved itraconazole against the total concentration of the respective cyclodextrin. Figure 1 shows that all the studied cyclodextrins were able to increase the poor aqueous solubility of itraconazole. The aqueous solubility of the drug increased linearly as a function of the cyclodextrin concentration. Therefore, in the CD concentration range studied, the solubility diagrams can be classified as A_L type following the Higuchi and Connors classification (19). This would lead to the conclusion that soluble complexes were formed between the drug and the host substances. In aqueous solutions of itraconazole–CD complexes, the free drug molecules are in equilibrium with the drug molecules entrapped within the cavity. Thus, as the concentration of CD is increased, more itraconazole molecules will transfer from the aqueous solution to the hydrophobic cavity of CD. Therefore, one can expect that more itraconazole will dissolve in aqueous CD solutions than in pure water, and consequently, the solubility of itraconazole would increase when the concentration of CD is increased.

Table 3. Stability constant and the standard Gibbs free energy of complexation between itraconazole and HP-β-CD in the presence of various methanol concentrations at 298.15 K.

% (*v*/*v*) Methanol	K (mol/L)$^{-1}$	$-\Delta G°$ (kJ mol^{-1})
0	1168±101	17.51±0.22
5	1043±88	17.23±0.21
10	902±73	16.87±0.20
20	662±57	16.10±0.22
30	455±34	15.17±0.19
40	213±20	13.29±0.23

The Gibbs free energies of transfer of itraconazole from aqueous solution to the cavity of CD (Table 1) were calculated from the following equation:

$$[1] \qquad \Delta_{trans}G° = -RT \ln(S/S_o)$$

where S and S_o are the solubilities of itraconazole in the presence and absence of CD, respectively. As evident from Table 1, the $\Delta_{trans}G°$ values are negative and increase in magnitude with increasing CD concentration. This indicates that CD is a more favorable environment for itraconazole than water. Moreover, the interaction between itraconazole and CD increases as the CD content is increased. With regard to the linear solubility diagrams, a 1:1 itraconazole–CD formulation was suggested for the complex in the aqueous solutions of all the studied cyclodextrins (slope of the solubility diagram was smaller than 1 for each CD).

The apparent stability constants (K) were calculated from eq. [2] using the slope of the solubility diagrams.

$$[2] \qquad K = \text{slope}/S_o(1 - \text{slope})$$

© 2005 NRC Canada

As shown in Fig. 1 and Table 2, there were noticeable differences among the CDs, with respect to both the solubilization efficiency and the stability of their complexes with itraconazole. The apparent 1:1 stability constants for the complex of itraconazole with the studied cyclodextrins (Table 2) were within the range of 200–5000 $(mol/L)^{-1}$, suggesting that these cyclodextrins are suitable candidates for the improvement of bioavailability of poorly water-soluble drugs such as itraconazole (21).

Effect of temperature

Since the stability constant is related to the Gibbs free energy ($\Delta G°$) of complexation, which has contributions from enthalpic ($\Delta H°$) and entropic ($\Delta S°$) terms, the estimation of these thermodynamic parameters may provide additional insight into the driving forces for complexation. Generally, a change in thermodynamic properties during CD complexation is an intricate phenomenon, resulting from changes in van der Waals interaction energy, hydrogen bonding, and hydrophobic interactions between the guest and cyclodextrin.

The thermodynamic parameters for inclusion processes were determined from the temperature dependence of the stability constants using van't Hoff plots ($\ln(K)$ vs. $1/T$). These plots for itraconazole–HP-β-CD and itraconazole–β-CD complexes were linear (plots not presented here) with correlation coefficients ≥0.99 within the temperature range considered in the present study, indicating that the changes in the heat capacity could be safely neglected.

The standard Gibbs free energy change of the binding was calculated using the following relation:

$$[3] \qquad \Delta G° = -RT \ln K = \Delta H° - T\Delta S°$$

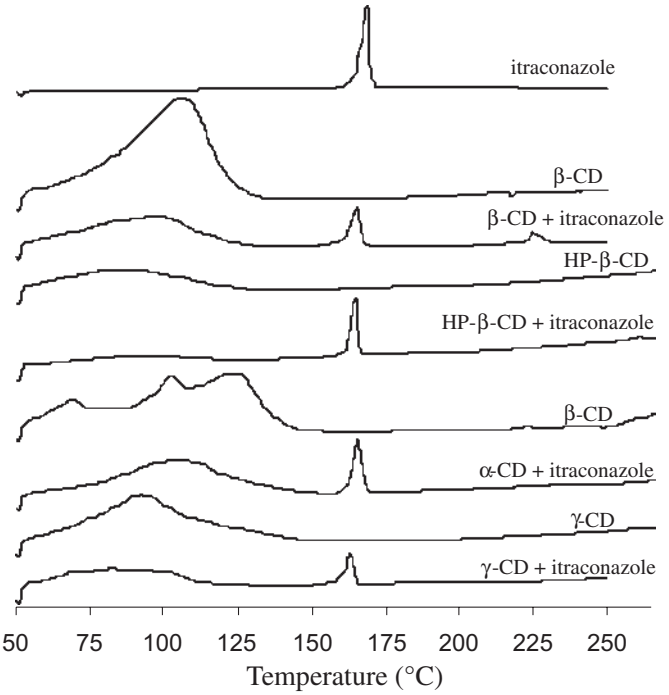
where $\Delta H°$ and $\Delta S°$ can be deduced from the slope and intercept of the van't Hoff plots, respectively. The stability constants of itraconazole–HP-β-CD and itraconazole–β-CD at 288, 293, 298, 303, and 308 K, as well as the corresponding thermodynamic parameters ($\Delta G°$, $\Delta H°$, and $\Delta S°$) are listed in Table 2. In view of the values shown in Table 2, it appears that

(1) the K values decrease with increasing temperature because the formation of the complexes is exothermic ($\Delta H° < 0$);
(2) the negative value of $\Delta G°$ suggests that complexation is thermodynamically favored; and
(3) the drug binds to CD with a favorable enthalpic term ($\Delta H° < 0$) and an unfavorable entropic term ($\Delta S° < 0$).

Effect of pH

The influence of pH on the apparent stability constant of the itraconazole–HP-β-CD inclusion complex, as a representative example, and on the efficacy of the solubility-enhancing effect was studied. A decrease in pH resulted in a decrease in the apparent stability constant (K = 1168 $(mol/L)^{-1}$ at a pH of 7.4; whereas at a pH of 2, K = 310 $(mol/L)^{-1}$) indicating that for the itraconazole–HP-β-CD complex K was larger in the less protonated form (pK_a = 4.0). Thus, the inclusion process with itraconazole was more favorable than that with itraconazoleH$^+$. At pH 2, the slope of the phase-solubility diagram and the S_o value (the solubility of itraconazole in the absence of CD) were larger than the corresponding values for a solution with pH of 7.4. At the lower pH, itraconazole, which is a basic drug, is present in the protonated form and is more water-soluble (has a weaker interaction with CD) than the unionized form of itraconazole (22, 23). This is in accordance with the fact that when the drug aqueous solubility increases, the K value decreases as a result of decreasing hydrophobicity of the drug (24).

Fig. 2. DSC curves of pure itraconazole, pure cyclodextrins, and itraconazole–CD (1:2) complexes prepared by the SC CO_2 method at 130 °C, 3 h of static mode, and 45 MPa.



Effect of solvent

To evaluate the effect of the medium on apolar host–guest associations, the K values of itraconazole–HP-β-CD were determined at 298.15 K in the presence of different methanol concentrations. Methanol was selected owing to its low affinity for binding with CD (25), thus making it a poor competitor for CD compared with itraconazole. Therefore, all the effects observed in the presence of methanol can be attributed only to a change in the solvophobic characteristics of the medium.

As illustrated in Table 3, the change in the Gibbs free energy decreased negatively as the hydrophobicity of the medium increased owing to the increase in percentage of methanol. This reveals a clear contribution of the hydrophobic effect as a driving force of complexation. Therefore, water is the best solvent for inducing strong association between apolar binding partners, and this property is essential for sustaining all functions of life.

Obviously, on the basis of the previous discussion one can conclude that the formation of a complex between itraconazole and CD is hydrophobically driven. On the other hand, although the hydrophobic interaction is characterized (26) by $\Delta H° \approx 0$ and $\Delta S° > 0$, the derived enthalpy and entropy changes (Table 2) do not agree with those expected for the classical hydrophobic interaction. Similar results (27, 28) were obtained for association between guest molecules and

© 2005 NRC Canada

an apolar cavity in water. These processes are exothermic and enthalpy driven ($|\Delta H°| > T|\Delta S°|$). This suggests that forces other than hydrophobic interactions significantly contribute to the stabilization of itraconazole–CD complexes. Such processes have been considered as nonclassical hydrophobic interactions. The favorable $\Delta H°$ values may be a result of the van der Waals interaction ($\Delta H° < 0$ and $\Delta S° < 0$) of the host and guest molecules. Another contribution to the favorable $\Delta H°$ values comes from the changes in the behavior of water associated with the host and guest molecules, the replacement of the incorporated water molecules (unstable) from the CD cavity by the drug and (or) the conformational change of CD (29). Lewis and Hansen (30) attributed the large enthalpy change to the formation of hydrogen bonds between water molecules displaced from the cyclodextrin cavity, which become bulk water and form hydrogen bonds. The unfavorable entropy change results from the greater ordering of the displaced water molecules from the cyclodextrin cavity.

Effect of cyclodextrin size

Because the cyclodextrin cavity has a fixed size, only the compounds with a similar molecular size and an appropriate structure could be included into the cavity. Other compounds with larger or smaller size or inappropriate structure could only achieve partial inclusion, causing decreased solubilization.

The stability of inclusion complexes between itraconazole and different cyclodextrins was in the following order: HP-β-CD > β-CD > γ-CD > α-CD (Table 2). This fact emphasizes the importance of the size–fit relation between the host and the guest in the complexation process. Also, the side chain substitutions of β-CD have a remarkable effect on the binding of itraconazole.

The K value of itraconazole–β-CD complexes is in good agreement with the literature value (K = 785 $(mol/L)^{-1}$) (31). The interaction of itraconazole with α- and γ-CDs was weak, as expressed by the lower K values (284 and 453 $(mol/L)^{-1}$, respectively), compared with β-CD. Higher stability constants were observed for β-CD and its substituted derivative, confirming that itraconazole interacts more strongly with these CDs than with α- or γ-CDs. Obviously the higher stability constants reflect a favorable positioning of the guest molecule inside the cavity of the CD host molecule (32). Therefore, the itraconazole structure is not compatible with the internal cavity of α- or γ-CD. These cavities are too small to allow penetration or too large to allow a close fit, respectively. Interaction of itraconazole with β- and HP-β-CD is more sterically favorable than with α- or γ-CD. Diaz et al. (33) reached similar conclusions for drug–CD complexation. The highest stability constant was found for the inclusion complex between itraconazole and HP-β-CD. This may be due to the fact that alkyl chains may provide additional hydrophobic binding sites, thus interacting with hydrophobic portions of itraconazole outside the cyclodextrin cavity (34).

Analysis of inclusion complexes prepared by supercritical carbon dioxide

Our previous results showed that the solubility of itraconazole in SC CO_2 is a function of temperature and pressure, and the maximum solubility (96.86 μg/g of CO_2) was obtained at 130 °C and 45 MPa (18). Although inclusion complexes were prepared using SC CO_2 at different temperatures and pressures, the maximum inclusion yield was obtained at 130 °C and 45 MPa (CO_2 density = 0.70321 g/mL). Therefore, the results presented here are for this optimum condition.

Preliminary studies showed that increasing the exposure time ensured a higher inclusion yield. Therefore, 3 h was selected as the exposure time in this investigation. Van Hees et al. (20) also mentioned that such a long exposure time is required to ensure a better inclusion yield for piroxicom–β-cyclodextrin inclusion complexes.

DSC curves for pure itraconazole, pure cyclodextrins, as well as itraconazole–CD (1:2) products obtained by physical mixing and the SC CO_2 method at 130 °C (3 h of exposure and 45 MPa) are shown in Fig. 2. Pure itraconazole showed a sharp melting endotherm at 165.2 °C. Pure β-CD showed two peaks: a broad endothermal effect, ranging between 50 and 150 °C corresponding to the dehydration of β-CD and a second peak at 219 °C characteristic of pure β-CD, which was also observed by other authors (35). In the product obtained by the SC CO_2 method, the endothermal peak for β-CD disappeared and a new peak with a different shape appeared at about 226 °C (approximately 7 °C higher than that of β-CD), which is most likely attributed to the formation of an inclusion complex. The endothermic peak corresponding to pure itraconazole, although reduced in size, was observed, indicating an incomplete inclusion of the drug in the cyclodextrin cavity.

The formation of an inclusion complex depends on the extent of the solubility of cyclodextrin and itraconazole in CO_2. As mentioned previously, the solubility of itraconazole in CO_2 is very low (96.86 μg/g of CO_2) and cyclodextrin is also expected to have a low solubility in CO_2, since it is a large polar molecule. The composition of mixtures in the cell containing CO_2, cyclodextrin, and itraconazole at 130 °C and 45 MPa was estimated to be between 93 and 95 wt% CO_2 for different cyclodextrin mixtures. However, this amount of CO_2 would only dissolve a small portion of itraconazole and cyclodextrin present in the cell, resulting in incomplete inclusion of itraconazole by cyclodextrin. This is in agreement with the DSC curves shown in Fig. 2 and the UV analysis of the inclusion complexes, which indicated an inclusion yield of about 8.28% for the case of the β-cyclodextrin–itraconazole system (18). The inclusion yield could be enhanced by increasing the wt% of CO_2 in the mixture or by the addition of a solvent, which enhances the solubility of the cyclodextrin and itraconazole in CO_2. The later option is now under investigation.

Pure HP-β-CD showed one broad endothermal peak, ranging between 50 and 150 °C, corresponding to the dehydration of HP-β-CD. No peak corresponding to pure HP-β-CD was observed. In the product obtained by the SC CO_2 method a small peak appeared at about 260.5 °C, which is probably attributed to the formation of an inclusion complex.

DSC curves for the products containing α- or γ-CD prepared by the SC CO_2 method did not show any new peaks, indicating no drug–CD interactions and thus no formation of inclusion complexes. This is expected, since the structure of itraconazole is not compatible with the internal cavity of α- or γ-CD, as was observed by the lower solubility and stabil-

© 2005 NRC Canada

ity constants of itraconazole with α- and γ-CD compared with β- and HP-β-CD. As mentioned earlier, this can be explained by the fact that the cavity of α-CD is too small to allow penetration and the cavity of γ-CD is too large to allow a close fit with itraconazole. Although the solubility and stability constant of itraconazole with HP-β-CD are higher than those of itraconazole with β-CD, DSC curves show a smaller inclusion complex in the product containing HP-β-CD. This is unexplained up to now and other analytical techniques (i.e., UV spectroscopy for determination of inclusion yield) are underway to explain this discrepancy.

Conclusions

Phase-solubility techniques were used to assess the formation of inclusion complexes between itraconazole and four different cyclodextrins (α-, β-, γ-, and HP-β-CD). The stability constant and thermodynamic parameters of the complexation process were calculated. The effects of cyclodextrin size and side chains, temperature, pH, and solvent on drug–cyclodextrin interactions were studied. The results showed that each cyclodextrin significantly improves the solubility of itraconazole in aqueous solutions according to the order HP-β-CD > β-CD > γ-CD > α-CD. Moreover, the inclusion process with itraconazole is more favorable than that with itraconazoleH^+, and the formation of the inclusion complex between itraconazole and CD is hydrophobically driven.

Itraconazole–cyclodextrin formulations were prepared by complexation of the drug into different cyclodextrins using SC CO_2. The solvent-free inclusion complexes obtained by this method were characterized by differential scanning calorimetry. No inclusion complexes were indicated by the DSC curves for drug formulations containing α- or γ-CD, while inclusion complexes were observed for drug formulations containing β- and HP-β-CD. The DSC curves showed higher inclusion in the product containing β-CD than that containing HP-β-CD. Itraconazole produced using SC CO_2 should provide minimal side effects in the human body since this method has no toxic solvent residuals. The SC CO_2 method will be tested at other conditions (varying exposure time and drug:cyclodextrin ratio). Efficacy, safety, and pharmacokinetics of the new inclusion complexes obtained by SC CO_2 will be investigated in both in vitro and in vivo. This method will also be tested on other drugs.

Acknowledgements

The authors are grateful to the Research Affairs at the United Arab Emirates University for financial support of this project under the contract No. 02/12-7-02. We are also thankful to the College of Pharmacy at Oregon State University, Corvallis, Oregon for providing itraconazole powder.

References

1. J. Heykants, A. Van Peer, V. Van de Velde, P. Van Rooy, W. Meuledermans, K. Lavrijsen, R. Woestenborghs, J. Van Custem, and G. Cauwenbergh. Mycoses, **32**, 67 (1989).
2. J. Van Cutsen. Mycoses, **32**, 14 (1989).
3. R. Negroni and A.I. Archavala. Arch. Med. Res. **24**, 387 (1993).
4. A. Van Peer, R. Woestsnborghs, J. Heykants, R. Gasparini, and G. Gauwenbergh. Eur. J. Clin. Pharmacol. **36**, 423 (1989).
5. S. Kapsi and J. Ayres. Int. J. Pharm. **229**, 193 (2001).
6. V. Stella and R. Rajeweski. Pharm. Res. **14**, 556 (1997).
7. W. Saenger. Angew. Chem. Int. Ed. Engl. **19**, 344 (1980).
8. T. Szejtle. Cyclodextrin and their inclusion complexes. Academiai Kiado, Budapest, Hungary. 1982.
9. S.P. Jones, D.J.W. Grant, J. Hadgraft, and G.P. Parr. Acta Pharm. Technol. **30**, 213 (1984).
10. M. Bastos, L.E. Briggner, I. Shehatta, and I. Wadsö. J. Chem. Thermodyn. **22**, 1181 (1990).
11. D. Hallen, A. Schon, I. Shehatta, and I. Wadsö. J. Chem. Soc. Faraday Trans. **88**, 2859 (1992).
12. I. Shehatta. React. Funct. Polym. **28**, 183 (1996).
13. I. Shehatta and M. Ibrahim. Can. J. Chem. **79**, 1431 (2001).
14. M. Ibrahim, I. Shehatta, and Al-Naiyle. J. Pharm. Biomed. Anal. **28**, 217 (2001).
15. I. Shehatta. Monatsh. Chem. **133**, 1239 (2002).
16. I. Shehatta, M.S. Ibrahim, and M.R. Sultan. Can. J. Chem. **80**, 1313 (2002).
17. A. Hassan, Y. Tang, and J. Ayres. Drug Dev. Ind. Pharm. **30**, 1029 (2004).
18. A.H. Al-Marzouqi, I. Shehatta, B. Jobe, and A. Dowaidar. J. Pharm. Sci. In press.
19. T. Higuchi and K.A. Connors. Adv. Anal. Chem. Instrum. **4**, 117 (1965).
20. T. Van Hees, G. Piel, B. Evrard, X. Otte, L. Thunus, and L. Delattre. Pharm. Res. **16**, 1864 (1999).
21. T.L. Blanco, J. Vila-Jato, F. Otero, and S. Anguianco. Drug. Dev. Ind. Pharm. **17**, 943 (1991).
22. K.H. Fromming and J. Szejtli. Cyclodextrins in pharmacy. Kluwer Academic, Dordrecht, The Netherlands. 1994.
23. T. Loftsson and M.E. Brewster. J. Pharm. Sci. **85**, 1017 (1996).
24. T. Loftsson and M.E. Brewster. Pharm. Technol. Eur. **9**, 26 (1997).
25. A. Mounoz de la Pena, T.T. Ndou, J.B. Zung, K.L. Greene, D.H. Live, and I.M. Warner. J. Am. Chem. Soc. **113**, 1572 (1991).
26. C. Tanford. The hydrophobic effect: Formation of micelles and biological membranes. 2nd ed. John Wiley & Sons, New York. 1980.
27. E. Junquera and E. Aicart. J. Phys. Chem. B, **101**, 7163 (1997).
28. M. Valero, S.B. Costa, J.R. Ascenso, M.M. Velazquez, and L.J. Rodriguez. J. Inclusion Phenom. Macrocyclic Chem. **35**, 663 (1999).
29. M.I. Bender and M. Komiyama. Bioorganic chemistry. Vol. 1. *Edited by* Van Tamelen. Academic Press, New York. 1977.
30. E.A. Lewis and L.D. Hansen. J. Chem. Soc. Perkin Trans. 2, 2081 (1973).
31. H. Van Doorne, E.H. Bosch, and C.F. Lerk. Pharm. Weekbl. Sci. Ed. **10**, 80 (1988).
32. D. Duchene, F. Glomot, and C. Vaution. *In* Cyclodextrins and their industrial uses. *Edited by* D. Duchene. Les editions de Sante, Paris. 1986.
33. D. Diaz, M.J.B. Bernard, J.G. Mora, and C.M.E. Llanos. Pharm. Dev. Technol. **3**, 395 (1998).
34. V. Zia, R.A. Rajewski, and V.J. Stella. Pharm. Res. **17**, 936 (2000).
35. P. Mura, E. Adragna, A. Rabasco, J. Moyano, J. Perez-Martinez, M. Arias, and J. Gines. Drug Dev. Ind. Pharm. **25**, 279 (1999).

© 2005 NRC Canada

Gas-phase reactions of atomic lanthanide cations with methyl chloride — Periodicities in reactivity[1]

Xiang Zhao, Gregory K. Koyanagi, and Diethard K. Bohme

Abstract: Room temperature reactions of lanthanide atomic cations (excluding Pm^+) with CH_3Cl are surveyed systematically in the gas phase using an inductively coupled plasma/selected-ion flow tube (ICP/SIFT) tandem mass spectrometer. Reaction rate coefficients are reported along with product distributions in He at 0.35 Torr (1 Torr = 133.3224 Pa) and 295 K. Cl atom transfer is the predominant reaction channel observed with all 14 lanthanide cations, but minor CH_3Cl addition also occurs with the late lanthanide cations Dy^+, Ho^+, Er^+, Tm^+, and Yb^+. The reaction efficiency for Cl atom transfer is shown to be governed by the energy required to promote an electron to achieve a d^1s^1 excited electronic configuration in which two non-f electrons are available for bonding: it decreases as the promotion energy increases and the periodic trend in reaction efficiency along the lanthanide series matches the periodic trend in the corresponding electron-promotion energy. This behaviour is consistent with a C—Cl bond insertion mechanism of the type proposed previously for insertion reactions of Ln^+ cations with hydrocarbons and methyl fluoride. Direct Cl atom abstraction by a harpoonlike mechanism was excluded because of an observed noncorrelation of reaction efficiency with IE(Ln^+). A remarkable Arrhenius-like correlation is observed for the dependence of reactivity on promotion energy: the early and late lanthanide cations exhibit characteristic temperatures of $(1.4 \pm 0.2) \times 10^4$ and $(4.5 \pm 0.3) \times 10^3$ K, respectively. A rapid second Cl atom transfer occurs with $LaCl^+$, $CeCl^+$, $GdCl^+$, $TbCl^+$, and $LuCl^+$, but there was no evidence for a third chlorine atom abstraction with any of the $LnCl_2^+$ cations. Both $LnCl^+$ and $LnCl_2^+$ add up to five methyl chloride molecules under the experimental operating conditions of the ICP/SIFT tandem mass spectrometer.

Key words: lanthanide cations, Cl atom transfer, electron promotion, methyl chloride.

Résumé : Faisant appel à un spectromètre de masse en tandem avec plasma à couplage induit/tube d'écoulement d'ion choisi (« ICP/SIFT »), on a étudié d'une façon extensive les réactions en phase gazeuse et à la température ambiante du CH_3Cl avec les cations atomiques des lanthanides, à l'exception du Pm^+. On a mesuré les coefficients des vitesses réactionnelles ainsi que les distributions des produits dans He, à 0,35 Torr (1 Torr = 133,3224 Pa) et à 295 K. On a observé que le transfert d'un atome de chlore est la voie réactionnelle prédominante pour les quatorze cations de lanthanides, mais il se produit aussi une faible addition de CH_3Cl avec les derniers cations de lanthanides, Dy^+, Ho^+, Er^+, Tm^+ et Yb^+. On a démontré que l'efficacité de la réaction de transfert de l'atome de chlore est gouvernée par l'énergie requise pour faire passer un électron à la configuration électronique excitée d^1s^1 dans laquelle deux électrons non-f sont disponibles pour créer une liaison: elle diminue avec une augmentation de l'énergie nécessaire pour atteindre ce niveau et la tendance périodique observée dans l'efficacité de la réaction dans la série des lanthanides suit bien la tendance dans l'énergie correspondante nécessaire pour la promotion de l'électron. Ce comportement est en accord avec le type de mécanisme d'insertion dans une liaison C—Cl qui a été suggéré antérieurement pour les réactions d'insertion des cations de Ln^+ dans les hydrocarbures et le fluorure de méthyle. On a exclu un mécanisme de type harpon avec enlèvement direct d'un atome de chlore en raison du manque de corrélation qui a été observé pour la dépendance de la réactivité sur l'énergie de promotion: les cations du début et de la fin de la série des lanthanides des températures caractéristiques de $(1{,}4 \pm 0{,}2) \times 10^4$ et $(4{,}5 \pm 0{,}3) \times 10^3$ K, respectivement. Un deuxième transfert rapide d'un atome de chlore se produit avec le $LaCl^+$, le $CeCl^+$, le $GdCl^+$, le $TbCl^+$ et le $LuCl^+$, mais on n'a pas trouvé de données pouvant supporter un troisième transfert d'un atome de chlore à partir d'un cation quelconque de $LnCl_2^+$. Le $LnCl^+$ et le $LnCl_2^+$ ajoutent chacun jusqu'à cinq molécules de chlorure de méthyle dans les conditions expérimentales d'opération du spectromètre de masse en tandem ICP/SIFT.

Mots clés : cations de lanthanides, transfert d'atomes de chlore, promotion d'un électron, chlorure de méthyle.

[Traduit par la Rédaction]

Received 5 May 2005. Published on the NRC Research Press Web site at http://canjchem.nrc.ca on 16 December 2005.

X. Zhao, G.K. Koyanagi, and D.K. Bohme.[2] Department of Chemistry, Centre for Research in Mass Spectrometry and Centre for Research in Earth and Space Science, York University, Toronto, ON M3J 1P3, Canada.

[1]This article is part of a Special Issue dedicated to Professor P. Kebarle.

[2]Corresponding author (e-mail: dkbohme@yorku.ca).

 doi: 10.1139/V05-198 © 2005 NRC Canada

Introduction

Recent laboratory measurements have shown that the unique electronic configurations of lanthanide cations lead to unique trends in the kinetics of chemical bond activation by these cations across the periodic table. As early as 1988, Shilling and Beauchamp (1) proposed that electron promotion from the $4f^n6s^1$ ground state to the $4f^{n-1}5d^16s^1$ excited state was required for these cations to be effective in C—H and C—C bond activation and insertion. A plethora of investigations into lanthanide ion chemistry followed, in part to further characterize this requirement, but also motivated by general interests in the gas-phase and solution chemistry of lanthanides (2). Reactions of Ln^+ cations now have been investigated systematically with various inorganic and organic molecules, including hydrogen (3), oxygen (4), nitrous oxide (4), alkanes and cycloalkanes, alkenes (1, 5, 6), alcohol (7–9), benzene and substituted benzenes (10, 11), phenol (12), orthoformates (10, 13), ferrocene, and iron pentacarbonyl (14). Generally these studies show that the reactivity of Ln^+ varies along the 4f series often in a manner that appears to be determined by the accessibility, through electron promotion, of excited electronic configurations of the Ln^+ cations with two unpaired non-f electrons. Results with N_2O (4), O_2 (4), and CH_3F (15) have also revealed intriguing Arrhenius-like dependencies of the reactivity of the Ln^+ cation on the electron promotion energy, which exhibit different characteristic temperatures for the early and late lanthanide cations.

Here we present a survey of gas-phase reactions of all the lanthanide cations (except Pm^+, which does not have a stable isotope) using inductively coupled plasma/selected-ion flow tube (ICP/SIFT) tandem mass spectrometry (4, 16, 17). The aim of this work is to expand on our previous studies of gas-phase reactions of lanthanide cations with CH_3F (15). We are not aware of any previous studies of reactions of atomic lanthanide cations with chlorinated hydrocarbons.

Experimental section

The experiments were performed with the ICP/SIFT tandem mass spectrometer that has been described in detail previously (4, 16, 17). The atomic ions were generated within an atmospheric pressure argon plasma at 5500 K fed with a vaporized solution containing the lanthanide salt. The ions emerging from the ICP were injected through a differentially pumped sampling interface into a quadrupole mass filter and after mass analysis, introduced through an aspiratorlike interface into flowing helium carrier gas at 0.35 Torr (1 Torr = 133.3224 Pa) and 295 ± 2 K. After experiencing about 10^5 collisions with He atoms, the ions were allowed to react with CH_3Cl added into the flow tube.

The lanthanide ions emerging from the plasma initially have a Boltzmann internal energy distribution characteristic of the plasma temperature. However, these emerging hot populations are expected to be downgraded during the approximately 20 ms duration before entry into the reaction region in the flow tube. Energy degradation can occur by radiative decay as well as by collisions with argon atoms and the 10^5 collisions with He before entry into the reaction region. The extent to which quenching of any electronically excited states of the lanthanide cations that may be formed within the ICP is complete is uncertain and could be inferred only indirectly from the observed decays of primary ion signals. The observed semilogarithmic decays of the reacting lanthanide cations were invariably linear, often over as much as four decades of ion depletion, and so were indicative of single-state populations. This was also the case in our earlier studies with methyl fluoride (15). The many collisions with Ar and He between the source and the reaction region should ensure that the atomic ions reach a translational temperature equal to the tube temperature of 295 ± 2 K prior to entering the reaction region.

Reactant and product ions were sampled at the end of the flow tube with a second quadrupole mass filter and were measured as a function of added reactant. The resulting profiles provide information about reaction rate coefficients and product–ion distributions. Rate coefficients for primary reactions were determined with an uncertainty estimated to be less than ±30% from the semilogarithmic decay of the reactant ion intensity as a function of added reactant.

Methyl chloride was introduced into the reaction region of the SIFT as a dilute mixture in helium (~10%). The methyl chloride was obtained commercially and was of high purity (Matheson Gas Products, Whitby, Ontario, 99.5%).

Results and discussion

The reactions of 14 lanthanide cations were investigated with CH_3Cl. Both the primary and higher order reactions were monitored. Results obtained for the reactions of La^+, Gd^+, Dy^+, and Lu^+ are shown in Fig. 1. Table 1 summarizes the measured rate coefficients, reaction efficiencies, and product distributions. The reaction efficiency is taken to be equal to the ratio k/k_c, where k is the experimentally measured rate coefficient and k_c is the capture or collision rate coefficient. k_c was computed using the algorithm of the modified variational transition-state/classical trajectory theory developed by Su and Chesnavich (18) with $\alpha(CH_3Cl) = 4.72 \times 10^{-24}$ cm^3 (19) and $\mu_D(CH_3Cl) = 1.896$ D (19).

Only Cl atom transfer (rxn. [1*a*]) and adduct formation (rxn. [1*b*]) were observed as primary reaction channels.

$$[1a] \quad Ln^+ + CH_3Cl \rightarrow LnCl^+ + CH_3$$

$$[1b] \quad \rightarrow Ln^+(CH_3Cl)$$

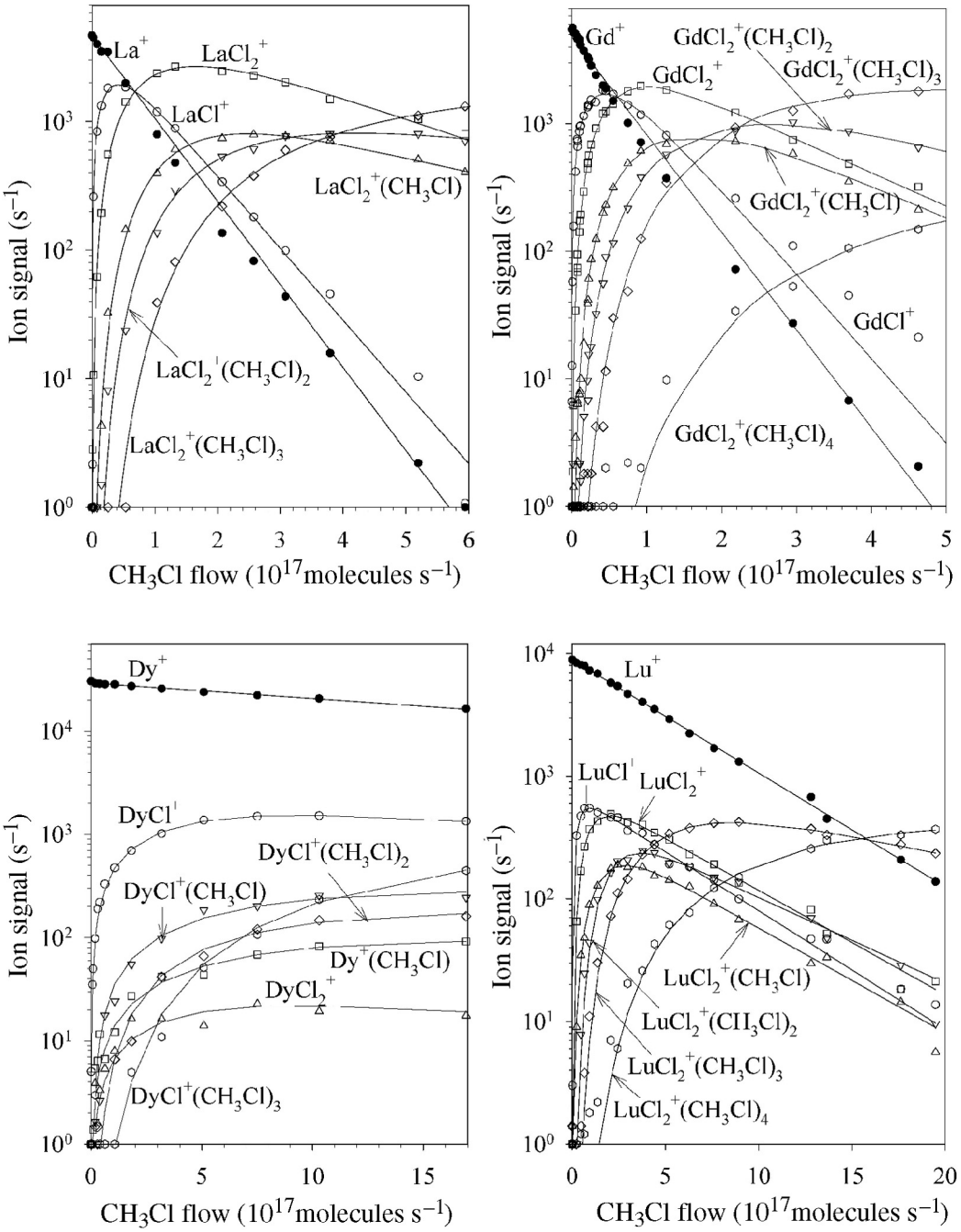
Adduct formation is a minor channel (≤30%) and was observed to compete only with the late Ln^+ cations Dy^+, Ho^+, Er^+, Tm^+, and Yb^+. As expected from the much lower first ionization energy of the lanthanides (IE(Ln)), all <6.3 eV, than that for CH_3Cl (11.29 eV) (20), electron transfer was not observed with any of the Ln^+ cations. The C—H bond activation channel (rxn. [1*c*]) is not competitive because it is quite endothermic since $D(H\text{-}CH_2Cl) >> HA(Ln^+)$, the H-atom affinity of the atomic lanthanide ions. $D(H\text{-}CH_2Cl) = 100.2 \pm 0.6$ kcal mol^{-1} (19), whereas, for example, $HA(La^+) = 57.1 \pm 2.8$ kcal mol^{-1} and $HA(Lu^+) = 48.8 \pm 3.6$ kcal mol^{-1} (21).

$$[1c] \quad Ln^+ + CH_3Cl \rightarrow LnH^+ + CH_2Cl$$

A fast ($k \geq 1.4 \times 10^{-10}$ cm^3 molecule^{-1} s^{-1}) second chlorine atom abstraction (rxn. [2]) was observed with $LaCl^+$ (25), $CeCl^+$ (28), $GdCl^+$ (16), $TbCl^+$ (14), $DyCl^+$ (1.4), $HoCl^+$ (2.3), and $LuCl^+$ (17), where the rate coefficient is

© 2005 NRC Canada

Fig. 1. Composite of ICP/SIFT results for the reactions of the lanthanide metal ions La^+, Gd^+, Dy^+, and Lu^+ with CH_3Cl in helium buffer gas at 0.35 ± 0.01 Torr (1 Torr = 133.3224 Pa) and 295 ± 2 K.



given in parentheses in units of 10^{-10} cm^3 $molecule^{-1}$ s^{-1}. These rate coefficients were obtained by curve fitting of the ion profiles for $LnCl^+$ and are less accurate than those for the primary reactions (the first few have values above k_c). The remaining $LnCl^+$ cations react with CH_3Cl with rate coefficients equal to or less than that measured for the first abstraction. No third Cl atom abstraction was observed with any of the $LnCl_2^+$ cations.

[2] $LnCl^+ + CH_3Cl \rightarrow LnCl_2^+ + CH_3$

CH_3Cl addition according to rxn. [3] was also observed for almost all of the lanthanide chloride cations. These addition reactions are expected to be termolecular with He buffer – gas atoms acting as the stabilizing third body.

[3] $LnCl_m^+(CH_3Cl)_n + CH_3Cl \rightarrow LnCl_m^+(CH_3Cl)_{n+1}$ $(m = 0–2)$

Secondary and higher order CH_3Cl addition was observed for $LnCl^+$ = $YbCl^+$ (m = 1, n = 0 to 1), $PrCl^+$, $DyCl^+$ (m = 1, n = 0–2), $NdCl^+$, $SmCl^+$, $EuCl^+$, $HoCl^+$ (m = 1, n = 0–3), $PrCl^+$ (m = 1, n = 1–4), and $LnCl_2^+$ = $LaCl_2^+$ (m = 2, n = 0–2), $CeCl^+$, $PrCl^+$, $GdCl_2^+$, $HoCl_2^+$, $LuCl_2^+$ (m = 2, n = 0–3). Table 1 includes a listing of all the higher order prod-

© 2005 NRC Canada

Table 1. First rate coefficients (in 10^{-10} cm^3 molecule^{-1} s^{-1}), reaction efficiencies (k/k_c), and higher order product ions measured for reactions of atomic cations Ln^+ with CH_3Cl in helium at 0.35 ± 0.01 Torr (1 Torr = 133.3224 Pa) and 295 ± 2 K.

M^+	k^a	$k_c{}^b$	k/k_c	Primary products	PD[c]	Higher order product ions
La^+	11	17.2	0.62	$LaCl^+$	100	$LaCl_2^+$, $LaCl_2^+(CH_3Cl)_{1–3}$
Ce^+	9.5	17.2	0.55	$CeCl^+$	100	$CeCl_2^+$, $CeCl_2^+(CH_3Cl)_{1–4}$
Pr^+	2.3	17.2	0.13	$PrCl^+$	100	$PrCl_2^+$, $PrCl^+(CH_3Cl)_{1–5}$, $PrCl_2^+(CH_3Cl)_{1–4}$
Nd^+	1.9	17.2	0.11	$NdCl^+$	100	$NdCl^+(CH_3Cl)_{1–4}$
Sm^+	1.1	17.0	0.064	$SmCl^+$	100	$SmCl(CH_3Cl)_{1–4}$
Eu^+	0.33	17.0	0.019	$EuCl^+$	100	$EuCl^+(CH_3Cl)_{1–4}$
Gd^+	10	17.0	0.59	$GdCl^+$	100	$GdCl_2^+$, $GdCl_2^+(CH_3Cl)_{1–4}$
Tb^+	3.0	16.9	0.18	$TbCl^+$	100	$TbCl_2^+$, $TbCl_{1,2}^+(CH_3Cl)_{1–4}$
Dy^+	0.23	16.9	0.013	$DyCl^+$	~97	$DyCl_2^+$, $DyCl^+(CH_3Cl)_{1–3}$
				Dy^+CH_3Cl	~3	
Ho^+	0.16	16.9	9.5×10^{-3}	$HoCl^+$	~90	$HoCl_2^+$, $HoCl_{1,2}^+(CH_3Cl)_{1–4}$
				Ho^+CH_3Cl	~10	
Er^+	0.13	16.9	7.7×10^{-3}	$ErCl^+$	92	$ErCl_2^+$, $ErCl_2^+(CH_3Cl)$
				Er^+CH_3Cl	8	$Er^+(CH_3Cl)_{2,3}$
Tm^+	≤0.01	16.8	$\leq6.0\times10^{-4}$	$TmCl^+$	~70	—
				Tm^+CH_3Cl	~30	—
Yb^+	≤0.01	16.8	$\leq6.0\times10^{-4}$	$YbCl^+$	70	$YbCl^+(CH_3Cl)_{1,2}$
				Yb^+CH_3Cl	30	$Yb^+(CH_3Cl)_{2,3}$
Lu^+	1.2	16.7	0.072	$LuCl^+$	100	$LuCl_2^+$, $LuCl_2^+(CH_3Cl)_{1–4}$

Note: Products and product distributions are also included along with calculated collision rate coefficients (k_c, in 10^{-10} cm^3 molecule^{-1} s^{-1}, see text) and reaction efficiencies (k/k_c).

[a]Measured reaction rate coefficient with an estimated accuracy of ±30%.

[b]Calculated capture rate coefficient (see text).

[c]PD = product distribution expressed as a percentage.

uct ions that were observed. The higher order chemistry initiated by La^+, Gd^+, Dy^+, and Lu^+ can be tracked in Fig. 1.

Periodicities in reaction efficiencies

The primary CH_3Cl reaction efficiencies of the 14 Ln^+ cations change dramatically along the 4f row. The efficiencies of the reactions of La^+ (0.62), Ce^+ (0.55), and Gd^+ (0.59) are all higher than 0.50, and it is interesting to note that these cations all have two non-f electrons in their electronic ground state. In contrast, the efficiencies of the reactions of the early lanthanide cations Sm^+ (0.064) and Eu^+ (0.019) are ≤0.1 and those of the late lanthanide cations Dy^+ (0.013), Ho^+ (9.5×10^{-3}), Er^+ (7.7×10^{-3}), Tm^+ ($\leq 6.0 \times 10^{-4}$), and Yb^+ ($\leq 6.0 \times 10^{-4}$) are all <0.02, near or below the detection limit. An overview of the variation in reaction efficiency across the lanthanide series is included in Fig. 2.

Thermodynamics of Cl atom abstraction

Cl atom abstraction was observed with all the lanthanide cations. Rate coefficients measured for Cl atom abstraction are in the range $\leq 1.0 \times 10^{-12}$ cm^3 molecule^{-1} s^{-1} (for Tm^+ and Yb^+) to 1.1×10^{-9} cm^3 molecule^{-1} s^{-1} (for La^+). Assuming that only exothermic or thermoneutral reaction can be observed under our experimental operating conditions, we estimate that the chlorine atom affinity ($ClA(Ln^+)$) is higher than $ClA(CH_3)$ = 83.7 kcal mol^{-1} (19) for all the lanthanide cations investigated. Unfortunately, no Cl atom affinities appear to be available for any lanthanide cations, either from theory or from experiment. The lower limit of 83.7 kcal mol^{-1} for the 14 lanthanide cations investigated therefore represents the first such determination.

Mechanism for Cl atom abstraction by Ln^+

Two mechanisms have been proposed for the reactions of lanthanide cations with fluorinated hydrocarbons (22): a harpoonlike abstraction and C—F bond insertion. The first mechanism involves the transfer of an electron within the encounter complex $LnFR^+$, perhaps at long range, from the lanthanide cation to the fluorinated substrate. This favors the homolytic cleavage of the C—F bond to form LnF^+ according to rxn. [4]. The reaction efficiency predicted by this mechanism should correlate with the second ionization energy of Ln ($IE(Ln^+)$) as has been proposed by Cornehl et al. (22) in their attempt to account for their measured reaction rates with fluoromethane, 1,1-difluoroethane, fluorobenzene, and hexafluorobenzene.

$$[4] \qquad Ln^+ + R\text{-}F \rightarrow [Ln^+\cdots F\text{-}R \rightarrow Ln^{2+}\text{-}F^-\cdots R] \rightarrow LnF^+ + R$$

In the C—F bond insertion mechanism, a cyclic ion complex is initially formed, which is then transformed through a three-centre transition state into a complex in which Ln^+ is

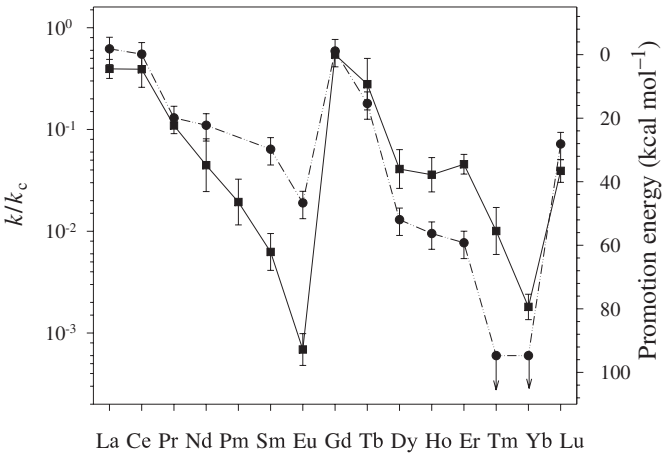
© 2005 NRC Canada

Table 2. Ln^+ ground-state valence configurations, term symbols, the promotion energies to first $5d^16s^1$ configuration, and the ionization energies of Ln^+.

Ln^+ species	Ln^+ ground-state valence configuration	Ln^+ term symbol[a]	Promotion energy to first $5d^16s^1$ configuration[a] (kcal mol^{-1})	IE Ln^+[b] (eV)
La^+	$5d^2$	$^3F_2$	4.5±3.0	11.06
Ce^+	$4f^15d^2$	$^4H_{7/2}{}^0$	4.6±5.7	10.85
Pr^+	$4f^36s^1$	$(9/2,1/2)_4{}^0$	22.3±0.8	10.55
Nd^+	$4f^46s^1$	$^6I_{7/2}$	34.8±8.3	10.72
Pm^+	$4f^56s^1$	$^7H_2{}^0$	46.4±7.2	11.07
Sm^+	$4f^66s^1$	$^8F_{1/2}$	62.1±5.8	11.07
Eu^+	$4f^76s^1$	$^9S_4{}^0$	92.8±5.0	11.25
Gd^+	$4f^75d^16s^1$	$^{10}D_{5/2}{}^0$	0.0	12.10
Tb^+	$4f^96s^1$	$(15/2,1/2)_8{}^0$	9.3±8.1	11.52
Dy^+	$4f^{10}6s^1$	$(8,1/2)_{17/2}$	36.0±6.1	11.67
Ho^+	$4f^{11}6s^1$	$(15/2,1/2)_8{}^0$	37.8±5.4	11.80
Er^+	$4f^{12}6s^1$	$(6,1/2)_{13/2}$	34.5±3.1	11.93
Tm^+	$4f^{13}6s^1$	$(7/2,1/2)_4{}^0$	55.5±7.4	12.05
Yb^+	$4f^{14}6s^1$	$^2S_{1/2}$	79.4±4.0	12.17
Lu^+	$4f^{14}6s^2$	$^1S_0$	36.6±3.6	13.90

[a]See ref. 24.
[b]See ref. 25.

Fig. 2. Reaction efficiency (closed circle for CH_3Cl and left ordinate axis) and the energy required to promote an electron and leave the Ln^+ cation in a d^1s^1 configuration (solid square and right ordinate axis) plotted along the lanthanide row of elements. There is an apparent correlation between reaction efficiency and electron promotion energy.



inserted into the R—F bond. The inserted complex can then eliminate the LnF^+ and R species. This mechanism requires that at least two Ln^+ electrons reside in non-f valence orbitals. The reaction efficiency predicted by this mechanism should correlate with the $4f^n6s^1$ to $4f^{n-1}5d^16s^1$ promotion energy (E_p). Our previous measurements of reactions of lanthanide cations with CH_3F provide reactivity correlations that demonstrate a preference for the C—F bond insertion mechanism, which also has been shown to apply to hydrocarbon activation by Ln^+ (1).

The experimental results reported here clearly show that the ability of Ln^+ to abstract a chlorine atom from methyl chloride does not correlate well with the second IE of the lanthanide (see Table 2 and Fig. 3). So we cannot assign a harpoonlike Cl abstraction mechanism to these reactions with CH_3Cl on the basis of such a correlation.

Our experimental results indicate that La^+ ($5d^2$) with two non-f valence electrons exhibits the highest efficiency for Cl atom abstraction followed closely by Gd^+ ($4f^75d^16s^1$) and Ce^+ ($4f^15d^2$) all of which also have two non-f valence electrons. The reactivities of the remaining Ln^+ cations (except Lu^+), all of which have available only one non-f electron (s^1), are all less and decrease along the early and late lanthanide series. So apparently the s electron at most plays a small role in determining these reactivities. Indeed, as shown in Figs. 2 and 4, these decreasing reactivities correlate well with the variation in the electron-promotion energy of Ln^+ required to achieve a $4f^{n-1}5d^16s^1$ configuration. Thus, f to d electron promotion appears crucial for the efficient occurrence of Cl atom transfer. This correlation indicates that two non-f electrons are required for Cl atom abstraction from CH_3Cl and that the reaction occurs via a C—Cl bond insertion mechanism. We note that the trend exhibited in Fig. 4 is remarkably similar to that presented by Cornehl et al. (23) for reactions of Ln^+ cations with saturated and unsaturated hydrocarbons and to that we have reported for reactions of Ln^+ with methyl fluoride (15) for which a C—X (X = C, H, or F) bond insertion mechanism also has been advanced. The small amounts of $Ln^+(CH_3Cl)$ adduct ions observed with the late lanthanide cations may be collisionally stabilized remnants of the inserted reaction intermediate. It is interesting to see that Lu^+, although having two electrons in non-f orbitals ($4f^{14}6s^2$), has a much lower reaction efficiency compared with La^+, Ce^+, and Gd^+; this can be attributed to the closed 6s and 4f subshells of Lu^+.

Inspection of our results for the addition of another Cl atom to $LnCl^+$ in a second reaction with CH_3Cl indicates that the second Cl atom transfers are fast ($k > 1.4 \times 10^{-10}$ cm^3 molecule^{-1} s^{-1}) with those Ln^+ cations with low

© 2005 NRC Canada

Fig. 3. The dependence of the efficiencies for Cl atom abstraction in reactions of Ln^+ with CH_3Cl on the second ionization energy of Ln ($IE(Ln^+)$).

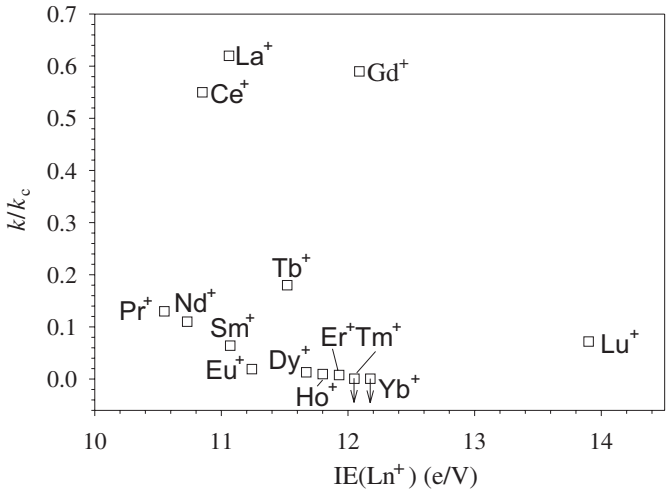
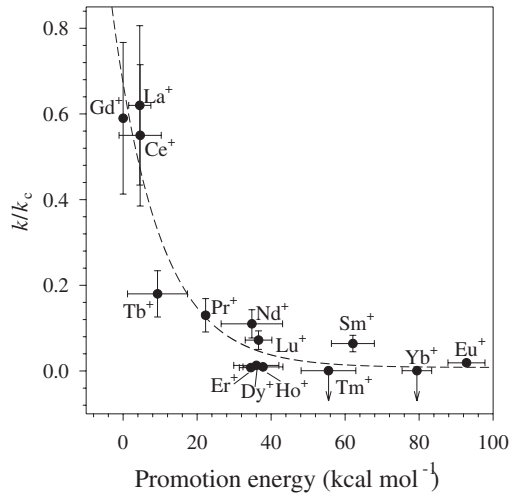


Fig. 4. Correlation of reaction efficiency for Cl atom abstraction from CH_3Cl with the energy E_p required to promote an electron and leave the Ln^+ cation in a d^1s^1 configuration. The dashed curve represents a fit with $k/k_c = 0.0081 + 0.66 \exp(-0.078E_p)$.



promotion energies (E_p < 9.3 kcal mol^{-1}) and slow (k < 5.4 × 10^{-11} cm^3 molecule^{-1} s^{-1}) with those Ln^+ cations with high promotion energies (E_p > 92.8 kcal mol^{-1}). Such a reactivity pattern again is not inconsistent with an insertion mechanism that requires two unpaired valence electrons.

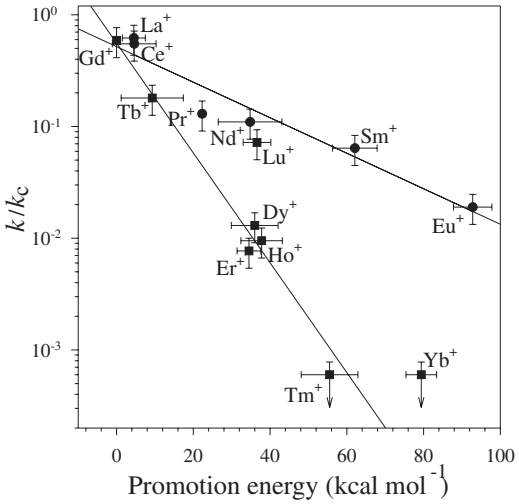
Arrhenius-like plots

Figure 5 demonstrates, in an Arrhenius-like plot, that the reaction efficiency of the Ln^+ reactions with CH_3Cl, here measured at constant temperature (295 K), exhibits an exponential dependence on the promotion energy according to eq. [5].

$$[5] \qquad k/k_c = \exp(-XE_p)$$

A remarkable aspect of these results is the distinct difference in this dependence between the early and late lanthanide ions. If interpreted as $1/RT_{eff}$, the slopes of the

Fig. 5. Correlation of reaction efficiency with the electron promotion energy that is proposed to be required for Ln^{2+}—Cl^- bond formation in the reactions of early and late Ln^+ ions with CH_3Cl. Lu^+ clearly is an exception to the trend observed for the late Ln^+ ions. The slopes of these van't Hoff-like plots provide characteristic temperatures of (1.4 ± 0.2) × 10^4 and (4.5 ± 0.3) × 10^3 K for Cl atom abstraction with the early and late lanthanide cations, respectively.



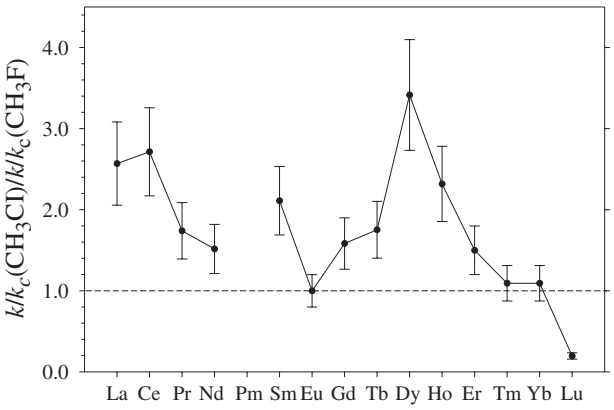
semilogarithmic plots in Fig. 5 indicate "characteristic temperatures" of (1.4 ± 0.2) × 10^4 and (4.5 ± 0.3) × 10^3 K for Cl atom abstraction with the early and late lanthanide cations, respectively. The indicated accuracy is the standard error derived from the fit. The exact physical meaning of these characteristic temperatures is not completely clear, but we postulate, as we have done before for reactions of Ln^+ with CH_3F (15), that the difference in characteristic temperature can be attributed to an energy associated with the electron promotion. Electron promotion in the early lanthanide ions involves an unpaired f electron while that in the late lanthanide ions involves a paired f electron. Thus, electron promotion in the late lanthanide ions involves electron–electron repulsion and so can be expected to be more effective and exhibit a lower characteristic temperature. It is noteworthy that the characteristic temperatures obtained for the Cl atom abstraction from CH_3Cl with the early and late lanthanide cations are similar to those for F atom abstraction from CH_3F, (1.80 ± 0.24) × 10^4 and (4.4 ± 0.2) × 10^3 K, respectively (15). This would be expected since F atom abstraction from CH_3F also requires the electronic excitation of Ln^+ by electron promotion (15).

Comparison of the reactivities of lanthanide cations towards CH_3Cl and CH_3F

A comparison of the reactivities that we have measured previously with CH_3F (15) shows that all the lanthanide cations, except for Lu^+, react more efficiently with CH_3Cl than with CH_3F; Fig. 6 indicates that values for $k/k_c(CH_3Cl)/k/k_c(CH_3F)$ range from 1.0 (for Eu^+) to 3.4 (for Dy^+). This can be attributed to at least two causes. The Cl—CH_3 bond is much weaker than the F—CH_3 bond (the bond dissociation energies for Cl—CH_3 and F—CH_3 are 83.7 and 112.9 kcal mol^{-1}, respectively (19)), and this makes

© 2005 NRC Canada

Fig. 6. Comparison of the reaction efficiencies of the reactions of Ln^+ with CH_3F and CH_3Cl.



the Cl abstraction more exothermic than the F atom abstraction, which reduces the kinetic barrier. Also, the electrostatic interaction between Ln^+ and CH_3Cl is stronger than that between Ln^+ and CH_3F since CH_3Cl has a much higher polarizability (4.72×10^{-24} cm^3 compared with 2.97×10^{-24} cm^3 for CH_3F (19)) and a slightly higher dipole moment (1.896 D vs. 1.858 D (19)), and this also lowers the kinetic barrier with respect to the initial energy of the reactants.

The T_{eff} ($(4.5 \pm 0.3) \times 10^3$ K) for the reactions of the late lanthanide cations with CH_3Cl obtained in Fig. 5 is close to the value for CH_3F ($(4.4 \pm 0.2) \times 10^3$ K) (15), while the T_{eff} ($(1.4 \pm 0.2) \times 10^4$ K) for the reactions of the early lanthanide cations with CH_3Cl is close to, but distinctly below, the value for CH_3F ($(1.80 \pm 0.24) \times 10^4$ K) (15). This may imply that stronger carbon–halogen bonds result in higher values for T_{eff}, but the effect on the reaction efficiency for the late lanthanide cations is much weaker than that for the early lanthanide cations.

We have previously found (15) that Lu^+ is quite reactive with CH_3F ($k/k_c = 0.37$) even though it has a $4f^{14}6s^2$ ground electronic configuration and a high s to d promotion energy (36.6 kcal mol^{-1}). We suggested that this apparent anomaly might be explained by the overlap of the $6s^2$ orbital with the antibonding orbital of methyl fluoride. This will weaken the F—CH_3 bond sufficiently to enable F atom transfer without the need for s to d promotion. In this work, Lu^+ was found to be much less reactive towards CH_3Cl ($k/k_c = 0.072$) compared with CH_3F. This may imply that the orbital levels of $6s^2$ of Lu^+ and the antibonding orbital of CH_3Cl do not match for overlapping so that the promotion energy governs the reactivity in this case.

Conclusions

Lanthanide cations have been observed to react with methyl chloride at room temperature predominantly by Cl atom transfer. The efficiency of this transfer correlates with the energy required to promote an electron to achieve a d^1s^1 excited electronic configuration in which two non-f electrons are available for bonding. The efficiency decreases as the promotion energy increases and the periodic trend in reaction efficiency along the lanthanide series matches the periodic trend in the corresponding electron promotion energy. This behavior is consistent with a C—Cl bond insertion mechanism of the type previously proposed for C—F, C—H, and C—C bond activation reactions of Ln^+ cations with alkanes and alkenes (23). Direct Cl atom abstraction by a harpoonlike mechanism can be excluded on the basis of an observed noncorrelation of reaction efficiency with IE(Ln^+). A remarkable Arrhenius-like correlation is observed for the dependence of reactivity on promotion energy: the early and late lanthanide cations exhibit characteristic temperatures of $(1.4 \pm 0.2) \times 10^4$ and $(4.5 \pm 0.3) \times 10^3$ K, respectively. A rapid, second Cl atom transfer occurs with $LaCl^+$, $CeCl^+$, $GdCl^+$, $TbCl^+$, and $LuCl^+$, but there was no evidence for a third chlorine atom abstraction with any of the $LnCl_2^+$ cations. Both $LnCl^+$ and $LnCL_2^+$ can sequentially add up to five methyl chloride molecules under the experimental operating conditions of the ICP/SIFT tandem mass spectrometer.

Acknowledgments

Continued financial support from the Natural Sciences and Engineering Research Council of Canada (NSERC) is greatly appreciated. Also, we acknowledge support from the National Research Council of Canada, the Natural Sciences and Engineering Research Council, and MDS SCIEX in the form of a Research Partnership grant. As holder of a Canada Research Chair in Physical Chemistry, Diethard K. Bohme acknowledges the contributions of the Canada Research Chair Program to this research.

References

1. J.B. Schilling and J.L. Beauchamp. J. Am. Chem. Soc. **110**, 15 (1988).
2. D.K. Bohme. The encyclopedia of mass spectrometry. Vol. 4. Elsevier Ltd., London, UK. 2005. pp. 638–648.
3. J.L. Elkind, L.S. Sunderlin, and P.B. Armentrout. J. Phys. Chem. **93**, 3151 (1989).
4. G.K. Koyanagi and D.K. Bohme. J. Phys. Chem. A, **105**, 8964 (2001).
5. Y. Huang, M.B. Wise, D.B. Jacobson, and B.S. Freiser. Organometallics, **6**, 346 (1987).
6. J.K. Gibson. J. Phys. Chem. **100**, 15688 (1996).
7. M. Azzaro, S. Breton, M. Decouzon, and S. Geribaldi. Int. J. Mass Spectrom. Ion Processes, **128**, 1 (1993).
8. S. Geribaldi, S. Breton, M. Decouzon, and M. Azzaro. J. Am. Soc. Mass. Spectrom. **7**, 1151 (1996).
9. J.M. Carretas, J. Marcalo, and A. Pires de Matos. Int. J. Mass Spectrom. **234**, 51 (2004).
10. J.K. Gibson and R.G. Haire. Radiochimica Acta, **89**, 709 (2001).
11. W.W. Yin, A.G. Marshall, J. Marcalo, and A. Pires de Matos. J. Am. Chem. Soc. **116**, 8666 (1994).
12. J.M. Carretas, A. Pires de Matos, J. Marcalo, M. Pissavini, M. Decouzon, and S. Geribaldi. J. Am. Soc. Mass. Spectrom. **9**, 1035 (1998).
13. N. Marchande, S. Breton, S. Geribaldi, J.M. Carretas, A. Pires De Matos, and J. Marcalo. Int. J. Mass Spectrom. **195/196**, 139 (2000).
14. M. da Conceicao Vieira, J. Marcalo, and A. Pires de Matos. J. Organomet. Chem. **632**, 126 (2001).
15. G.K. Koyanagi, X. Zhao, V. Blagojevic, M.J.Y. Jarvis, and D.K. Bohme. Int. J. Mass Spectrom. **241**, 189 (2005).

© 2005 NRC Canada

16. G.K. Koyanagi, V.V. Lavrov, V. Baranov, D. Bandura, S. Tanner, J.W. McLaren, and D.K. Bohme. Int. J. Mass Spectrom. **194**, L1 (2000).
17. G.K. Koyanagi, V.I. Baranov, S.D. Tanner, and D.K. Bohme. J. Anal. At. Spectrom. **15**, 1207 (2000).
18. T.C. Su and W. J. Chesnavich. J. Chem. Phys. **76**, 5183 (1982).
19. D.R. Lide (*Editor*). CRC handbook of chemistry and physics. 80th ed. CRC Press, Boca Raton, Florida. 2001.
20. K. Kimura, S. Katsumata, Y. Achiba, T. Yamazaki, and S. Iwata. *In* Handbook of HeI photoelectron spectra of fundamental organic compounds. Japan Scientific Soc. Press, Tokyo. 1981.
21 P.B. Armentrout. Int. J. Mass Spectrom. **227**, 289 (2003).
22. H.H. Cornehl, G. Hornung, and H. Schwarz. J. Am. Chem. Soc. **118**, 9960 (1996).
23. H.H. Cornehl, C. Heinemann, D. Schroder, and H. Schwarz. Organometallics, **14**, 992 (1995).
24. Z.B. Goldschmidt. Handbook on the physics and chemistry of rare earths. North-Holland Publishing Co, Amsterdam. 1978. p. 79.
25. C.E. Moore. Nat. Stand. Ref. Data Ser. Nat. Bur. Stand. **34**, 1 (1970).

© 2005 NRC Canada

The water elimination from the ethyl acetate radical cation — Answers from theory to a longstanding mechanistic problem[1]

Richard Lee, Paul J.A. Ruttink, Peter C. Burgers, and Johan K. Terlouw

Abstract: Previous experimental studies of the water elimination from ionized ethyl acetate (**EA-1**) and its enol, CH_2=C(OH)$OC_2H_5^{\cdot+}$ (**EA-2**), provide no mechanistic proposals, but note that the reaction is complex because all hydrogen atoms and both oxygen atoms participate. Loss of H_2O is the predominant process observed for the metastable ions, yielding ionized methyl vinyl ketone, $CH_3C(=O)CH=CH_2^{\cdot+}$ (**MVK**), as the product ion. Metastable keto-alcohol ions $CH_3C(=O)CH_2CH_2OH^{\cdot+}$ (**HB-1**) also abundantly lose H_2O, yielding **MVK** at the thermochemical threshold. Using the CBS-QB3 model chemistry and complementary RRKM calculations, we have examined plausible mechanisms for the water elimination from metastable ions **EA-1/2** and **HB-1**. Our calculations support the proposal that (*i*) ions **HB-1** dissociate into **MVK** at the thermochemical threshold via a 1,4-H shift and a consecutive [1,2]-hydroxycarbene shift, and (*ii*) ions **EA-1/2** undergo a three-step isomerization reaction into **HB-1**, which serves as the precursor for the ensuing water elimination. It is further shown that synergy between theory and experiment leads to a complex, yet transparent, mechanistic picture of the isomerization and dissociation behaviour of ionized ethyl acetate, which accounts for the labelling results.

Key words: tandem mass spectrometry, CBS-QB3 model chemistry, reaction mechanism, hydroxycarbene shift.

Résumé : Les études expérimentales antérieures sur l'élimination d'eau à partir d'acétate d'éthyle ionisé (**EA-1**) et de son énol, CH_2=C(OH)$OC_2H_5^{\cdot+}$ (**EA-2**) ne permettent pas de faire des propositions relatives au mécanisme, mais indiquent que la réaction est complexe parce que tous les atomes d'hydrogène ainsi que les deux atomes d'oxygène participent. La perte de H_2O est le processus prédominant qui est observé avec les ions métastables et elle conduit à la formation de méthylvinylcétone ionisée, $CH_3C(=O)CH=CH_2^{\cdot+}$ (**MVK**), comme produit ionique. Au seuil thermodynamique, les ions du céto-alcool métastable, $CH_3C(=O)CH_2CH_2OH^{\cdot+}$ (**HB-1**) perdent aussi abondamment de l'eau pour conduire à la formation de **MVK**. Utilisant la modélisation chimique CBS-QB3 et des calculs RRKM complémentaires, on a examiné divers mécanismes plausibles pour l'élimination d'eau à partir des ions métastables **EA-1/2** et **HB-1**. Les résultats de ces calculs confirment la proposition à l'effet que (*i*) au seuil thermodynamique, les ions **HB-1** se dissocient en **MVK** par le biais d'un déplacement 1,4 d'hydrogène et un déplacement [1,2]-hydroxycarbène consécutif et (*ii*) les ions **EA-1/2** subissent une réaction d'isomérisation en trois étapes qui conduit au **HB-1** qui sert de précurseur pour l'élimination d'eau qui suit. On a aussi démontré qu'une synergie entre la théorie et les expériences conduisent à une proposition de mécanisme, transparente malgré sa complexité, pour l'isomérisation de l'acétate d'éthyle ionisé et le comportement de sa dissociation qui permet de tenir compte des résultats de marquage.

Mots clés : spectroscopie de masse en tandem, modélisation chimique CBS-QB3, mécanisme réactionnel, déplacement d'hydroxycarbéne.

[Traduit par la Rédaction]

Introduction

Since the inception of electron ionization (EI) mass spectrometry as a powerful method for the structure analysis of organic molecules in the mid 1950s, the gas-phase ion chemistry of ethyl acetate has been studied extensively. Two dissociations of the ethyl acetate radical cation ($CH_3C(=O)OCH_2CH_3^{\cdot+}$, **EA-1**) have received particular attention: **EA-1** $\rightarrow C_2H_5O_2^+ + C_2H_3^{\cdot}$ and **EA-1** $\rightarrow C_4H_6O^{\cdot+} + H_2O$. Peaks at *m*/*z* 61 and 70 resulting from these rearrangement reactions prominently feature in the conventional EI mass spectrum of the ester, as shown in Fig. 1*a*.

Received 27 April 2005. Published on the NRC Research Press Web site at http://canjchem.nrc.ca on 14 January 2006.

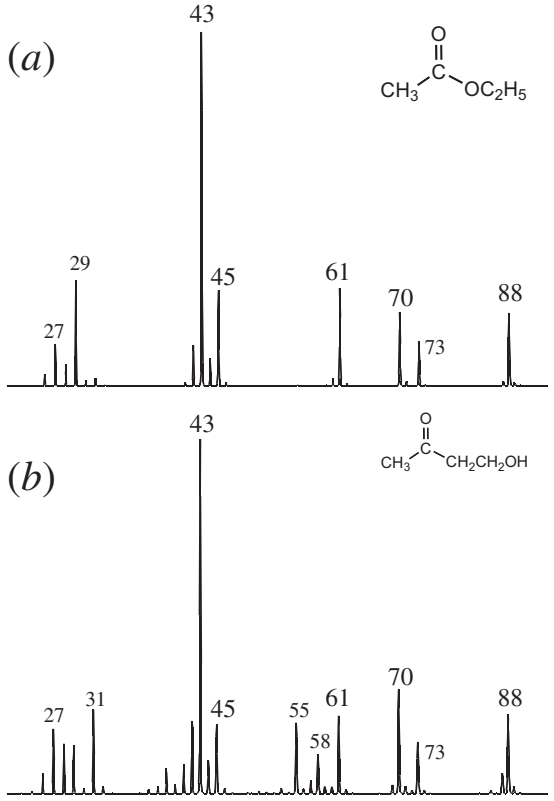
Dedicated to Paul Kebarle in recognition of his seminal contributions to the field of gas-phase ion chemistry.

R. Lee and J.K. Terlouw.[2] Chemistry Department, McMaster University, 1280 Main St. W., Hamilton, ON L8S 4M1, Canada.
P.J.A. Ruttink. Theoretical Chemistry Group, Department of Chemistry, Utrecht University, 3584 CH Utrecht, The Netherlands.
P.C. Burgers. Department of Neurology, Erasmus Medical Center, 3015 GE Rotterdam, The Netherlands.

[1]This article is part of a Special Issue dedicated to Professor P. Kebarle.
[2]Corresponding author (e-mail: terlouwj@mcmaster.ca).

 doi: 10.1139/V05-199 © 2005 NRC Canada

Fig. 1. (*a*) 70 eV EI mass spectra of ethyl acetate and (*b*) its 4-hydroxy-2-butanone isomer.

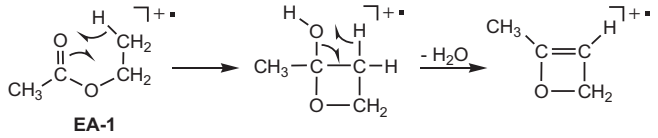


In 1962, Godbole and Kebarle (1) using deuterium labeling found that the acetyl methyl group remained intact during the formation of $C_2H_5O_2^+$, while hydrogen atoms were randomly transferred from the ethyl group. In 1977, Benoit et al. (2) concluded that the *m*/*z* 61 product ion is carbonyl-protonated acetic acid ($CH_3C(OH)_2^+$), rather than its higher energy isomer ($CH_3C(=O)OH_2^+$) (3), and that the keto ester ion **EA-1** may isomerize to its more stable (4) enol form ($CH_2=C(OH)OCH_2CH_3^{\cdot+}$, **EA-2**) prior to dissociation. Dissociation into $CH_3C(OH)_2^+$ has become a textbook example of a "McLafferty + 1" rearrangement (5). The first step of the proposed mechanism (5) leads to the distonic ion $[CH_3C(OH)OCH_2CH_2]^{\cdot+}$ (**EA-3**) via a 1,5-H shift in **EA-1**. A consecutive 1,3-H shift from the terminal CH_2 group to the ether O atom in **EA-3** then initiates the C_2H_3 loss. We will examine this proposal in more detail in the Results and discussion.

The elimination of H_2O into ions $C_4H_6O^{\cdot+}$ (*m*/*z* 70) has been studied in much greater detail (6–8) than the $C_2H_3^{\cdot}$ loss, but its mechanism is still shrouded in mystery. Loss of water represents the unimolecular reaction of lowest energy requirement for ionized ethyl acetate (7, 8). In line with this, it is the predominant process observed for metastable (9) ions **EA-1** dissociating in the μs time frame: loss of $C_2H_3^{\cdot}$ competes unfavourably as its metastable peak is only 0.02 as intense as that for the H_2O loss process (7).

The reaction was first studied by Yeo (6) in 1970. He studied both metastable ions and ions dissociating in the source and found that deuteriums on the ethyl group more readily end up in the neutral water fragment than do the deuteriums on the acetyl group. The degree of hydrogen exchange becomes greater as the lifetime of the precursor ion increases, which is when the internal energy content of the ion becomes lower. Yeo proposed that the intra- and inter-alkyl H–H exchange reactions take place from the *unrearranged* keto ion **EA-1** and that the actual mechanism for H_2O loss involves ring closure of **EA-1** into the 2-hydroxy-2-methyloxetane ion, as depicted in Scheme 1.

Scheme 1.



The cyclic ion would then undergo H_2O elimination yielding ionized 2-methyloxetene, the four-membered ring – closed form of ionized methyl vinyl ketone ($CH_3C(=O)CH=CH_2^{\cdot+}$, **MVK**). Yeo formulated this proposal some 20 years before the role of distonic ions as stable key intermediates was fully established (10). A more plausible formulation of the cyclization step in his mechanism would involve formation of the distonic ion **EA-3** as the first step (as in the mechanism for $C_2H_3^{\cdot}$ loss discussed previously), followed by cyclization. We further note that Yeo's proposal remains speculative because there is no experimental evidence for the proposed product ion structure.

In 1981, Holmes et al. (7) investigated the H_2O loss from **EA-1** and its independently generated enol **EA-2**, employing most of the presently available methodology for the detailed study of unimolecular ionic dissociations (11). These included metastable ion (MI) and collision-induced dissociation (CID) mass spectra, appearance energy (AE) measurements using electron ionization (EI), thermochemical data (12), and analysis of D- and ^{18}O-labelled isotopologues. Shortly thereafter, Baer and co-workers (8) used photoionization (PI) to study the energetics of the five primary dissociations of **EA-1**; in addition, they studied the rate of the H_2O elimination using photoion–photoelectron coincidence (PIPECO) experiments in conjunction with RRKM/QET calculations.

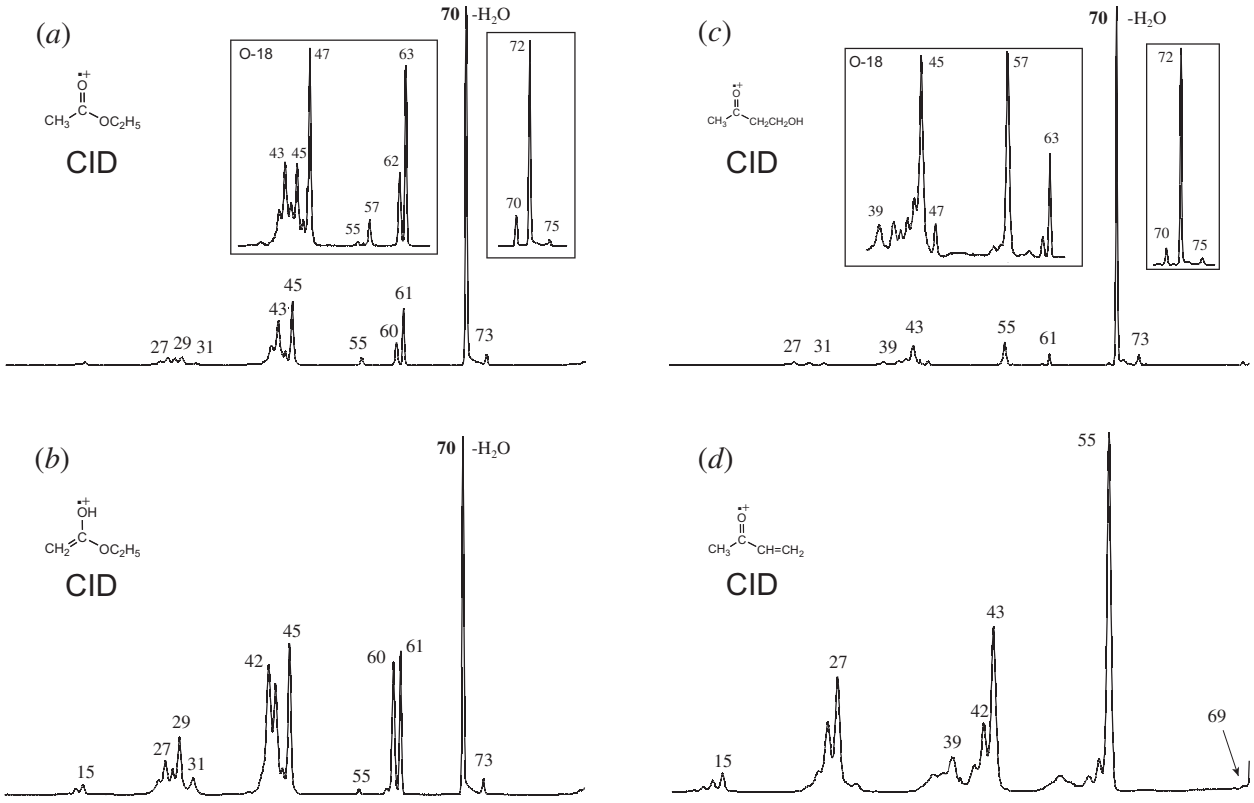
Although these two papers contain a wealth of experimental observations on the gas-phase ion chemistry of ethyl acetate, they do not provide a clear mechanistic picture of the H_2O loss. The most important results and conclusions pertaining to the H_2O elimination are the following:

(*i*) Holmes et al. (7) found that metastable enol ions **EA-2** also abundantly lose H_2O and deduce from their D- and ^{18}O-labelling experiments that the reaction probably occurs via the reacting configuration(s) of the less stable keto tautomer **EA-1**. The isomers have different CID spectra (see Figs. 2*a* and 2*b* of this study), but this does not imply that keto ions cannot partially tautomerize: the CID spectrum of **EA-1** is not necessarily that of a *single* ionic species.

(*ii*) Analysis of ^{18}O-labelled ions (7) showed that for ion source decompositions and all metastable ion observation times, the keto and enol O atoms in both **EA-1** and **EA-2** are similarly preferentially lost: ion source, 65%; metastable ions, 70%–90%. It is likely that this process has a lower energy requirement than the H_2O loss that involves the ester O atom. This is because (*i*) the associated kinetic energy release (9) is lower than that for the

© 2005 NRC Canada

Fig. 2. CID mass spectra of the radical cations of (*a*) ethyl acetate, (*b*) its enol, and (*c*) the 4-hydroxy-2-butanone isomer (**HB-1**). Partial spectra of $CH_3C(=O)^{18}OC_2H_5$ and $CH_3C(=O^{18})CH_2CH_2OH$ are shown in the insets of (*a*) and (*c*), respectively. (*d*) Represents the CID mass spectrum of the *m/z* 70 product ion generated by the loss of water from metastable ion **HB-1**.



ester O atom and (*ii*) the degree of exchange becomes increasingly less important at longer ion lifetimes, which is just the opposite of the H atom exchange results (6, 7). These data indicate that there is a significant barrier to O atom migration, whereas the H atoms have no significant barrier for exchange but do so at a slow rate because of circuitous (high entropy) pathways (7, 8).

(*iii*) From their analysis of the CID spectra of various $C_4H_6O^{+}$ isomers (13), Holmes et al. (7) concluded that $CH_3C(=O)CH=CH_2^{\cdot+}$ (**MVK**) is generated by H_2O loss from either metastable ions **EA-1** and **EA-2** or those fragmenting in the ion source. They further noted that the CID results do not exclude that a *minor* fraction of the ions would be $CH_2=C(OH)CH=CH_2^{\cdot+}$, the enol of **MVK** that is 13 kcal mol^{-1} lower in energy than **MVK** (11*a*). They entertained this possibility because their AE measurements on **EA-1** yielded an apparent $\Delta_f H^0_{298}$ = 190 kcal mol^{-1} for the $C_4H_6O^{+}$ ion, which lies below the proposed value for **MVK** (195 kcal mol^{-1}) (13*a*).

(*iv*) Baer and co-workers (8) note that this enthalpy difference is on the border line of being significant. They conclude from their experiments on **EA-1** that **MVK** ions (for which they derive $\Delta_f H^0_{298}$ = 194 kcal mol^{-1}) are also generated at threshold. They further conclude that **EA-1** isomerizes to a more stable structure prior to dissociating, possibly the enol ion **EA-2**.

In the summary of their paper Baer and co-workers state: "we know the energy of the isomerized molecular ion, but not its structure; we suspect that the transition state is cyclic; and we believe that the product ion is **MVK**. With all this information it should be possible to derive a mechanism and determine the structure of the molecular ion. However, as was already pointed out by Holmes et al. the loss of H_2O is a very complicated reaction." Yeo's mechanistic proposal of Scheme 1 is mentioned in these studies but not discussed.

At the time these studies were published, the use of ab initio MO calculations as a complementary tool in studying structures and reactions of gas-phase organic ions was only in its infancy. However, theory steadily progressed, and in 1989 a review of structures and reactions of gas-phase ions (10*b*) stated that the computational results of Heinrich et al. (14) on ionized methyl acetate offer some hope that the chemistry of ionized ethyl acetate may some day be understood. A hydrogen-bridged radical cation (15) (CH_3-CH=O···H···OCH=$CH_2^{\cdot+}$) was suggested to play a key role in the water elimination from **EA-1**. It was also stressed that ab initio calculations are required to solve this problem but that, considering the size of the system and the number of possible intermediates, this would be a formidable task.

Fortunately, the following decade witnessed a development in methodology and computing power short of a revolution, enabling computational chemistry to become a key player in the field of gas-phase ion chemistry (11). The G-3 variant of the Gaussian methods of Pople and co-workers (16) and the CBS-QB3 variant of the complete basis set methods of Petersson and co-workers (17) provide absolute enthalpies of chemical accuracy for medium-sized ions and neutrals. This makes both model chemistries attractive for a study of the gas-phase ion chemistry of ethyl acetate. During the past 5 years we have successfully used the CBS-QB3

© 2005 NRC Canada

method in mechanistic studies of organophosporus ester ions (18) and proton-transport catalysis in various organic radical cations (19). We therefore decided to use this CBS variant, which uses density functional geometries and frequencies in the calculations, as the primary computational tool in probing the elusive mechanism for the H_2O elimination from metastable ions **EA-1** and **EA-2**.

It will be shown that synergy between theory and experiment leads to a complex yet transparent mechanistic proposal for the H_2O elimination into **MVK**, which satisfies the energetic constraints imposed by experiment and accounts for the labelling results.

Results and discussion

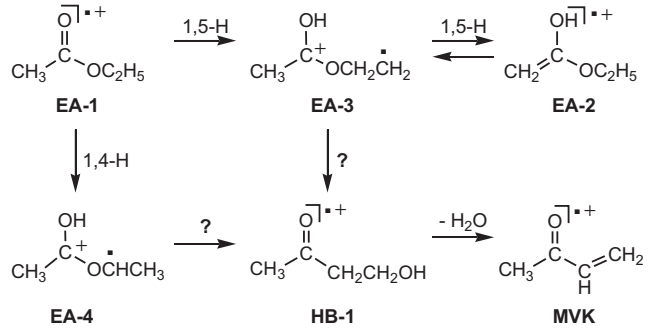
Experimental and theoretical preliminaries

In our computational quest of plausible mechanisms for the H_2O elimination from **EA-1** and **EA-2** we focussed on the behaviour of the *metastable* ions. For such ions the experiments (7, 8) stipulate that none of the stable intermediates or connecting transition states of a viable calculated mechanism should lie significantly higher in energy than the thermochemical threshold for the formation of **MVK** + H_2O. The experimental and calculated enthalpies for this threshold are close (137 ± 3 and 139 kcal mol^{-1}, respectively, see Table 1). The experimental value suffers from a rather large uncertainty because the heat of formation of neutral methyl vinyl ketone has not been measured with great precision. The computed enthalpies of the stable structures (minima) presented in Tables 1 and 2 of this study are expected to be reliable to 2 kcal mol^{-1} (17, 18*a*); for the uncertainty in computed barrier heights we affix ±4 kcal mol^{-1} as a conservative estimate (18*a*).

As mentioned in the Introduction, Holmes et al. (7) in their detailed experimental study do not propose a mechanism for the water loss from **EA-1/2**. However, they do make the intriguing suggestion that the isomeric 4-hydroxy-2-butanone ion ($CH_3C(=O)CH_2CH_2OH^{\cdot+}$, **HB-1**) is a participating structure in the complex behaviour of the keto and enol ions of ethyl acetate. This suggestion is based upon their observations that metastable ions **HB-1** readily lose H_2O, with a small kinetic energy release, and that the source generated ions **HB-1** (see Fig. 1*b*) also generate *m*/*z* 61 ions $CH_3C(OH)_2^+$. The CID mass spectrum of **HB-1** (see Fig. 2*c*) also displays a *m*/*z* 61 peak, supporting the idea that **EA-1/2** and **HB-1** can (inter)convert via a fairly low energy route. There is no mechanistic proposal for the loss of H_2O from **HB-1** but, as will be discussed in the next section, there is little doubt that the product ion generated is **MVK** and that the reaction occurs at the thermochemical threshold.

We decided to further explore the idea that ions **EA-1/2** can access the potential energy surface (PES) that describes the water elimination from **HB-1**. Ions **EA-1** may well undergo a facile isomerization into distonic ions **EA-3** or **EA-4** as depicted in Scheme 2. Ion **EA-3** could in principle connect to the PES of **HB-1** via a well-documented skeletal rearrangement, the [1,3]-hydroxycarbene shift (10*b*). In this rearrangement the CH_3-C-OH moiety of **EA-3** migrates, via a cyclic transition state, to the radical position, yielding $[CH_3C(OH)CH_2CH_2O]^{\cdot+}$, a 1,5-hydrogen-shift isomer of **HB-1**.

Scheme 2.



Our computational results for this reaction sequence are presented in the energy level diagram of Fig.3*a*, which will be discussed in detail in a following section. Here we note that the barrier for the hydroxycarbene shift is too high to account for the loss of water at the thermochemical threshold.

In the same vein, ion **EA-4** could undergo a [1,2]-hydroxycarbene shift (10*b*), leading to $[CH_3C(OH)C(H)(CH_3)O]^{\cdot+}$, a 1,5-hydrogen-shift isomer of $CH_3C(=O)CH(OH)CH_3^{\cdot+}$ (ionized acetoin). This reaction does not play a role in the water elimination either, since (*i*) the isomerization barrier is not sufficiently low and (*ii*) low energy acetoin ions do not lose H_2O but rather dissociate into $CH_3C(H)OH^+$ + $CH_3C{=}O^{\cdot}$, via a remarkable hidden rearrangement (20). However, as will be discussed in a following section in conjunction with the energy diagram of Fig. 3*b*, this rearrangement sheds light on another intriguing aspect of the ion chemistry of ethyl acetate (8). This concerns the formation of the prominent *m*/*z* 45 $C_2H_5O^+$ ions in the CID mass spectra of **EA-1/2**, shown in Figs. 2*a* and 2*b*.

Despite these negative answers from theory, we further pursued the idea that the water loss from **EA-1/2** occurs via the PES of **HB-1** and considered the distonic ion **EA-3** to be the most likely intermediate for the conversion. This indeed proved to be the case: as shown in the calculated energy diagram of Fig. 4*a*, **EA-3** can rearrange into **HB-1** via a two-step low energy route. This finding and its implication on the interpretation of the labelling results will be discussed in a following section. However, we will first deal with our mechanistic proposal for the water elimination from **HB-1** which, as we shall see, involves a [1,2]-hydroxycarbene shift (10*b*) as the key step of the reaction.

The water elimination from ionized 4-hydroxy-2-butanone (HB-1)

Before we discuss our mechanistic proposal for the water loss from **HB-1**, we will first briefly review the experimental observations. The spectrum of metastable ions **HB-1** displays a single narrow peak at *m*/*z* 70, indicating that loss of H_2O represents the reaction of lowest energy requirement. The kinetic energy release derived from the *m*/*z* 70 peak at half-height ($T_{0.5}$) is only 7 meV (7), indicating that the water elimination may well occur at the thermochemical threshold. The CID mass spectrum of the resulting $C_4H_6O^{\cdot+}$ product ion, generated from metastable ions **HB-1**, is shown in Fig. 2*d*. Comparison of this spectrum with that of $CH_3C(=O)CH{=}CH_2^{\cdot+}$ (**MVK**) and other isomeric $C_4H_6O^{\cdot+}$ ions (7, 13) leaves little doubt that **MVK** is the product ion

© 2005 NRC Canada

Table 1. Energetic data for dissociation reactions of the radical cations of ethylacetate and 4-hydroxy-2-butanone derived from CBS-QB3 calculations and experimental observations.

Ionic/neutral species	CBS-QB3 *E*(total) (0 K)	CBS $\Delta_f H^0_0$	CBS $\Delta_f H^0_{298}$	Exp. $\Delta_f H^0_{298}$	Ref.
$CH_3C(=O)OCH_2CH_3^{\cdot+}$ (**EA-1b**)	–306.83503	131.9	126.3	125±1	8
$CH_3C(=O)OCH_2CH_3$	–307.20745	–101.8	–107.7	–106.1	12*a*
$CH_3C(=O)CH=CH_2^{\cdot+}$ + H_2O			**139.2**[a]	**137±3**	[b]
$CH_3C(=O)CH=CH_2$	–230.83494	–22.3	–26.2[a]	–27.4	12*b*
$CH_3C(=O)CH=CH_2^{\cdot+}$	–230.47885	201.1	197.4[a]	195	[b]
$CH_2=C(OH)CH=CH_2^{\cdot+}$	–230.49955	188.2	184.1	182	13*a*
2-Methyloxetene ion (Scheme 1)	–230.47852	201.3	197.2		
$CH_3C\text{-}O\text{-}CH=CH_2^{\cdot+}$	–230.44607	221.6	218.1		
$CH_3C{=}O^+$ + $CH_3CH_2O^{\cdot}$			**154.5**	**155**	
$CH_3C{=}O^+$ + $CH_2CH_2OH^{\cdot}$			**151.9**	**150**	
$CH_3C(H)OH^+$ + $CH_3C{=}O^{\cdot}$			**139.7**	**140**	
$CH_3C{=}O^+$	–152.68582	159.8	158.0	157	[c]
$CH_3C(H)OH^+$	–153.87250	145.7	142.2	142.4	[d]
$CH_2CH_2OH^{\cdot}$	–154.10928	–2.9	–6.1[e]	–7	12*d*
$CH_3CH_2O^{\cdot}$	–154.10513	–0.3	–3.5[f]	–3.6	12*d*
$CH_3C{=}O^{\cdot}$	–152.94202	–1.0	–2.5	–2.4	12*d*
$CH_3C(OH)_2^+$ + $CH_2{=}CH^{\cdot}$			**146.4**	**147**	
$CH_2{=}C(OH)_2^{\cdot+}$ + $CH_2{=}CH_2$			**135.0**	**132.5**	
CH_3COOH + $CH_2{=}CH_2^{\cdot+}$			**152.2**	**152.5**	
$CH_3C(OH)_2^+$	–229.06154	78.3	74.7[g]	75	[h]
$CH_2=C(OH)_2^{\cdot+}$	–228.40494	40.0	121.8[i]	120	12*a*
CH_3COOH	–228.76536	–101.2	–104.3	–103.3	12*a*
$CH_2{=}CH^{\cdot}$	–77.74299	72.7	71.7	71.6	12*d*
$CH_2=CH_2^{\cdot+}$	–78.02908	258.4	256.5	254.8	12*a*
$CH_2=CH_2$	–78.41664	15.3	13.2	12.5	12*a*
$CH_3C(OH){=}CH_2^{\cdot+}$ + $CH_2{=}O$			**135.7**	**137.4**	
$CH_3C(OH)=CH_2^{\cdot+}$	–192.47686	167.0	163.0	163.4	[j]
$CH_2=O$	–114.34411	–26.4	–27.3	–26.0	12*a*

Note: *E*(total) in Hartrees; all other components, including the ZPE scaled by 0.99, are in kcal mol^{-1}.
[a]Refers to the anti conformer; the ionic and neutral syn conformers are 0.5 kcal mol^{-1} higher in energy.
[b]Ionic $\Delta_f H^0_{298}$ based upon IE_a = 9.65 ± 0.02 eV and $\Delta_f H^0_{298}$ (neutral ketone) = –27.4 ± 2.6 kcal mol^{-1} as quoted in ref. 12*b*.
[c]Derived from PA (ketene) = 197.3 kcal mol^{-1} (12*b*) and $\Delta_f H^0_{298}$ (ketene) = –11.4 ± 0.6 kcal mol^{-1} (12*a*).
[d]From PA (acetaldehyde) = 183.7 kcal mol^{-1} (12*c*) and $\Delta_f H^0$ (aldehyde) = –39.6 ± 0.1 kcal mol^{-1} (12*a*).
[e]Refers to the U-shaped conformer; the S conformer is 0.6 kcal mol^{-1} higher in energy.
[f]2A′ state.
[g]Value of the lowest energy syn/anti (position hydroxylic Hs relative to CH_3 group) conformer.
[h]From PA (acetic acid) = 187.3 kcal mol^{-1} (12*c*) and $\Delta_f H^0_{298}$ (acid) = –103.3 ± 0.1 kcal mol^{-1} (12*a*).
[i]Lowest energy conformer.
[j]Upper limit (see ref. 21*d* for details).

generated from **HB-1**. We note in particular that the peak at *m/z* 69 (loss of H$^{\cdot}$) in the spectrum of Fig. 2*d* is barely visible (<1% of the base peak at *m/z* 55). Since loss of H$\cdot$ represents (7, 13*a*) a major collision-induced dissociation of the enol ion of **MVK** ($CH_2=C(OH)CH=CH_2^{\cdot+}$), it is unlikely that this more stable isomer (see Table 1) is cogenerated from **HB-1** to any significant extent.

Our CID mass spectrum of the $C_4H_6O^{\cdot+}$ ion generated from metastable ethyl acetate ions is identical with that of Fig. 2*d*. This reinforces the conclusion of the PI study of Baer and co-workers (8) that the water elimination from **EA-1** yields **MVK** at the thermochemical threshold. Their derived $\Delta_f H^0_{298}$ value of 194 ± 2 kcal mol^{-1} is close to its experimental estimate of 195 ± 3 kcal mol^{-1} (see Table 1). On the other hand (see the Introduction), Holmes et al. (7) invoked the co-generation of the enol ion because the $\Delta_f H^0_{298}$ ($C_4H_6O^{\cdot+}$) they derived from their AE (EI) measurements (190 kcal mol^{-1}) lies 5 kcal mol^{-1} below the experimental estimate for **MVK**. We note that the AE values from the PI and EI studies are virtually the same (10.31 ± 0.1 eV), and that the discrepancy between the derived $\Delta_f H^0_{298}$ values arises from differences in the thermochemical treatment of the appearance energies (8).

The ambiguities in defining appearance energies and their conversion into $\Delta_f H^0_{298}$ values of the reaction products has been a matter of considerable debate (21). Here we note that applying the Traeger–McLoughlin correction term (21*a*) ($\Delta H_{cor} = \Delta H_{298}$ (**MVK** + H_2O) – 1.48 kcal mol^{-1}) raises the

© 2005 NRC Canada

Table 2. Enthalpies of formation derived from CBS-QB3 calculations of stable isomers and connecting transition states involved in the water loss from (*a*) the ethyl acetate (EA) radical cation and (*b*) the 4-hydroxy-2-butanone (HB) radical cation.

(*a*) Ethyl acetate (EA) radical cation.

Ionic species[a]	B3LYP/CBSB7 *E*(total)	CBS-QB3 (0 K) *E*(total)	ZPE	$\Delta_f H_0^0$	$\Delta_f H_{298}^0$
EA-1a (Figs. 3*a*/4*a*)	–307.43701	–306.83417	71.2	132.4	126.5
EA-1b (Fig. 3*b*)	–307.43573	–306.83503	71.4	131.9	126.3
EA-2a (Fig. 5)	–307.46197	–306.86357	72.8	114.0	108.0
EA-2b (Fig. 3*a*)	–307.45361	–306.85647	72.6	118.3	112.4
EA-2c (Fig. 3*a*)	–307.45268	–306.85569	72.7	118.9	113.0
EA-3a (Figs. 3*a*/4*a*)	–307.45414	–306.85760	71.7	117.7	112.2
EA-3b (Figs. 3*a*/4*a*)	–307.45000	–306.85448	72.6	119.7	113.9
EA-3c (Fig. 3*a*)	–307.45252	–306.85565	71.8	118.9	113.3
EA-4a (Fig. 3*b*)	–307.45513	–306.85827	71.4	117.3	111.7
EA-4b (Fig. 3*b*)	–307.46221	–306.86186	71.4	115.1	109.5
EA-4c (Fig. 3*b*)	–307.45945	–306.85995	71.4	116.3	110.7
EA-5 (Fig. 3*a*)	–307.42616	–306.82834	70.1	136.1	131.1
EA-6a (Fig. 3*a*)	–307.41941	–306.82415	69.3	138.6	133.6
EA-6b (Fig. 5)	–307.41997	–306.82469	68.2	138.4	133.6
TS EA-1a → 3b	–307.43426	–306.83666	69.4	130.9	124.5
TS EA-3a → 3b	–307.39355	–306.83688	70.2	130.7	125.1
TS EA-3a → 5	–307.42543	–306.82502	69.7	138.1	132.8
TS EA-5 → HB-1b	–307.41738	–306.82077	69.8	140.8	135.3
TS EA-3b → 6a	–307.41335	–306.81679	66.0	143.2	138.1
TS EA-6a → 6a[b]	–307.41768	–306.82381	68.8	138.2	133.6
TS EA-3a → 3c	–307.43466	–306.83390	70.7	132.5	126.9
TS EA-3c → 2b	–307.42637	–306.83177	70.1	133.8	127.1
TS EA-3a → HB-5b	–307.39355	–306.79996	71.9	153.9	147.3
TS EA-1b → 4a	–307.42702	–306.83023	68.9	134.9	128.8
TS EA-4a → 4b	–307.44507	–306.84473	70.2	125.8	120.0
TS EA-4b → 4c	–307.43112	–306.83260	70.1	133.4	127.4
TS EA-4c → 2c	–307.41198	–306.81925	69.4	141.8	135.4
TS EA-4c → AC-2a	–307.39971	–306.80465	70.8	151.0	144.8
TS AC-2a → AC-1a	–307.41178	–306.81565	68.9	144.1	137.9
AC-1a (Fig. 3*b*)	–307.44905	–306.84929	71.2	122.9	117.6
AC-1b (Fig. 5)	–307.45270	–306.85452	71.4	119.7	114.2
AC-2a (Fig. 3*b*)	–307.42693	–306.82804	71.8	136.3	130.3
TS AC-1b → HB-3c	–307.40616	–306.81321	68.6	145.5	139.3

(*b*) 4-Hydroxy-2-butanone (HB) radical cation.

Ionic species[a]	B3LYP/CBSB7 *E*(total)	CBS-QB3 (0 K) *E*(total)	ZPE	$\Delta_f H_0^0$	$\Delta_f H_{298}^0$
HB-1a (Figs. 3*a*/4*b*)	–307.44506	–306.83754	72.6	130.3	124.2
HB-1b (Fig. 4*b*)	–307.43634	–306.82849	71.5	136.0	130.3
HB-2a (Fig. 4*b*)	–307.44923	–306.85337	72.1	120.4	114.5
HB-2b (Fig. 4*b*)	–307.45479	–306.85769	72.1	117.7	111.7
HB-2c (Fig. 4*b*)	–307.45761	–306.85799	72.9	117.5	111.5
HB-2d (Scheme 3)	–307.45709	–306.85622	72.9	118.6	112.6
HB-3a (Fig.4*b*)	Collapses to **HB-3b** (see Fig. 4*b*)				
HB-3b (Fig. 4*b*)	–307.43867	–306.84450	71.5	126.0	120.1
HB-3c (Scheme 3)	–307.42725	–306.83376	71.3	132.7	126.9
HB-4 (Fig. 4*b*)	–307.43067	–306.83034	69.2	134.7	130.0
HB-5a (Fig. 3*a*)	–307.43519	–306.83329	71.7	133.0	126.7
HB-5b (Fig. 3*a*)	–307.42527	–306.82318	71.8	139.3	133.2
HB-6 (Fig. 5)	–307.49397	–306.89424	73.0	94.7	88.9
TS HB-1a → 1b	–307.42771	–306.82407	71.6	138.7	132.5
TS HB-1b → 2a	–307.43400	–306.83444	70.1	132.3	125.9
TS HB-2a → 2b	–307.44918	–306.84645	71.9	116.3	113.6
TS HB-2b → 2c	–307.45295	–306.85634	72.0	113.6	112.0
TS HB-2c → 3b	–307.43004	–306.83772	71.9	130.2	123.8
TS HB-3b → 4	–307.41736	–306.81619	69.9	143.6	138.0

© 2005 NRC Canada

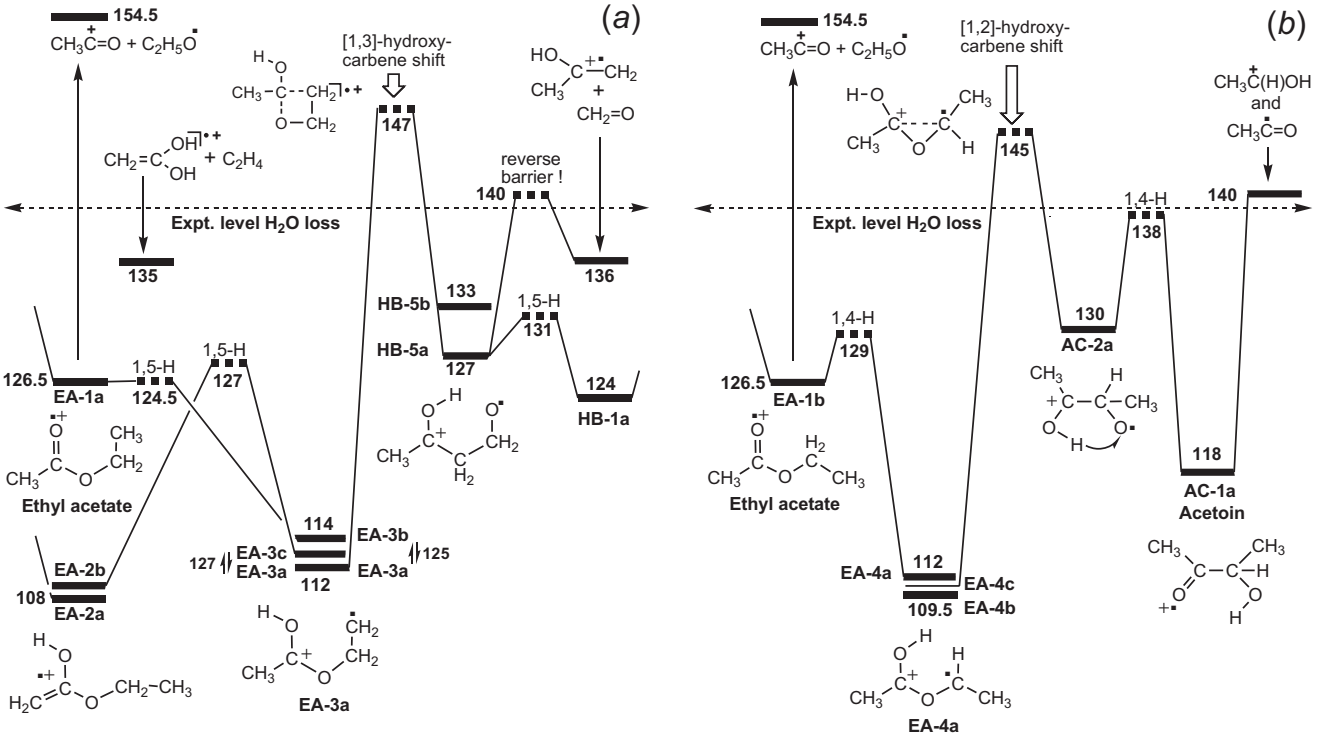
Table 2 (*concluded*).

(*b*) 4-Hydroxy-2-butanone (HB) radical cation.

Ionic species[a]	B3LYP/CBSB7 *E*(total)	CBS-QB3 (0 K) *E*(total)	ZPE	$\Delta_f H_0^0$	$\Delta_f H_{298}^0$
TS HB-3b → 6	–307.40840	–306.81415	69.7	144.9	138.8
TS HB-2d → 3c	–307.42347	–306.83107	71.9	134.4	128.0
TS HB-3b → 3c	–307.42011	–306.82905	70.7	135.6	129.6
TS HB-1a → 5a	–307.42702	–306.82607	68.7	137.4	131.0
TS HB-5a → diss.[c]	–307.40780	–306.81181	69.7	146.4	140.2

[a] *E*(total) in Hartrees; all other components, including the ZPE scaled by 0.99, are in kcal mol^{-1}.
[b] The transition state for the O equilibration (see Fig. 4*a*).
[c] This TS represents the reverse barrier for the dissociation into $CH_3C(H)OH^+$ (see Fig. 3*a*).

Fig. 3. Energy level diagrams derived from CBS-QB3 calculations for the isomerization of ionized ethyl acetate (AE-1) into the distonic ions (*a*) EA-3 and (*b*) EA-4, and the subsequent [1,3]- and [1,2]-hydroxycarbene shift. The numbers refer to $\Delta_f H_{298}^0$ values in kcal mol^{-1}.



$\Delta_f H_{298}^0$ ($C_4H_6O^{+\cdot}$) value derived by Holmes et al. by 5.3 to 195 kcal mol^{-1} (using the ΔH_{298} values available from the CBS-QB3 calculations). Note that ΔH_{cor} is negative and this negative number is subtracted from the measured AE, thereby raising the derived $\Delta_f H_{298}^0$. This correction holds rigorously if all the available internal energy of the precursor ion is used for dissociation, which is, the products are formed at 0 K. The actual thermal content of the products is not known and hence, the correction term only provides an upper limit to the derived enthalpy.

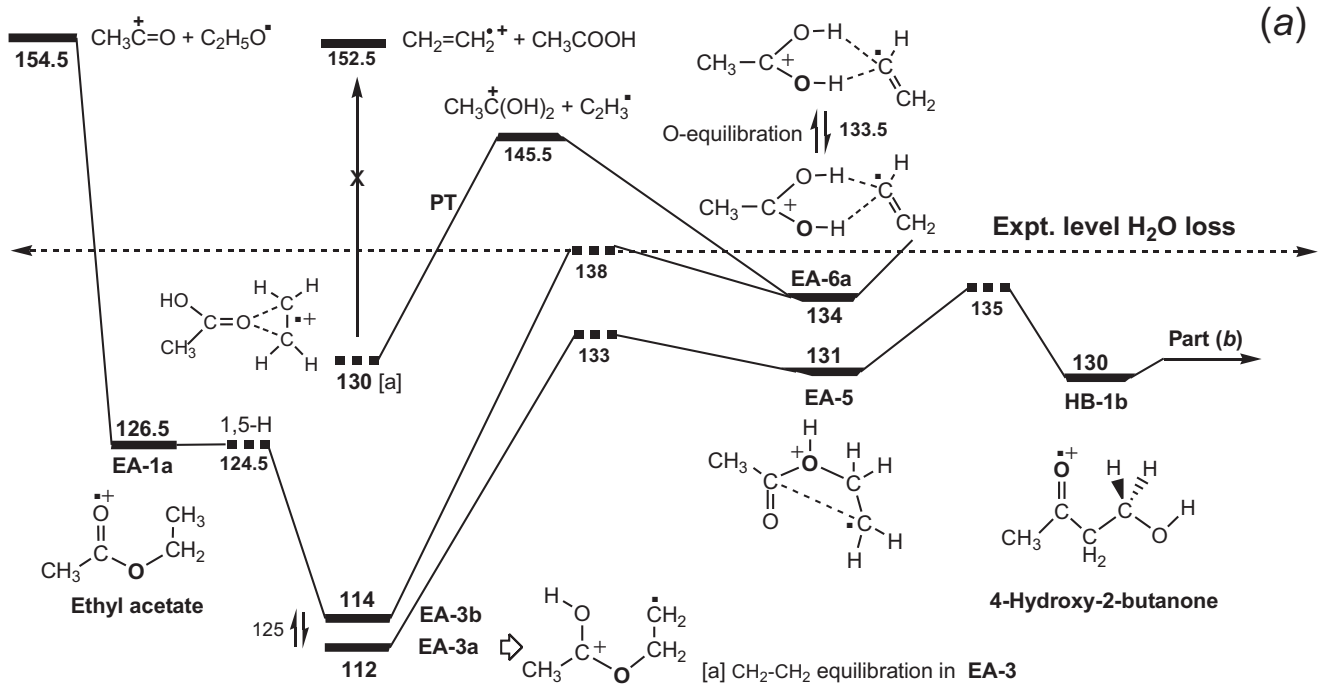
Interestingly, the same situation obtains for the water loss from **HB-1**. The available AE (9.78 eV)[3] leads to a $\Delta_f H_{298}^0$ ($C_4H_6O^{+\cdot}$) value of only 190.3 kcal mol^{-1};[4] when the above correction term is applied, the number increases to 195.6 kcal mol^{-1} and becomes compatible with the formation of **MVK**.

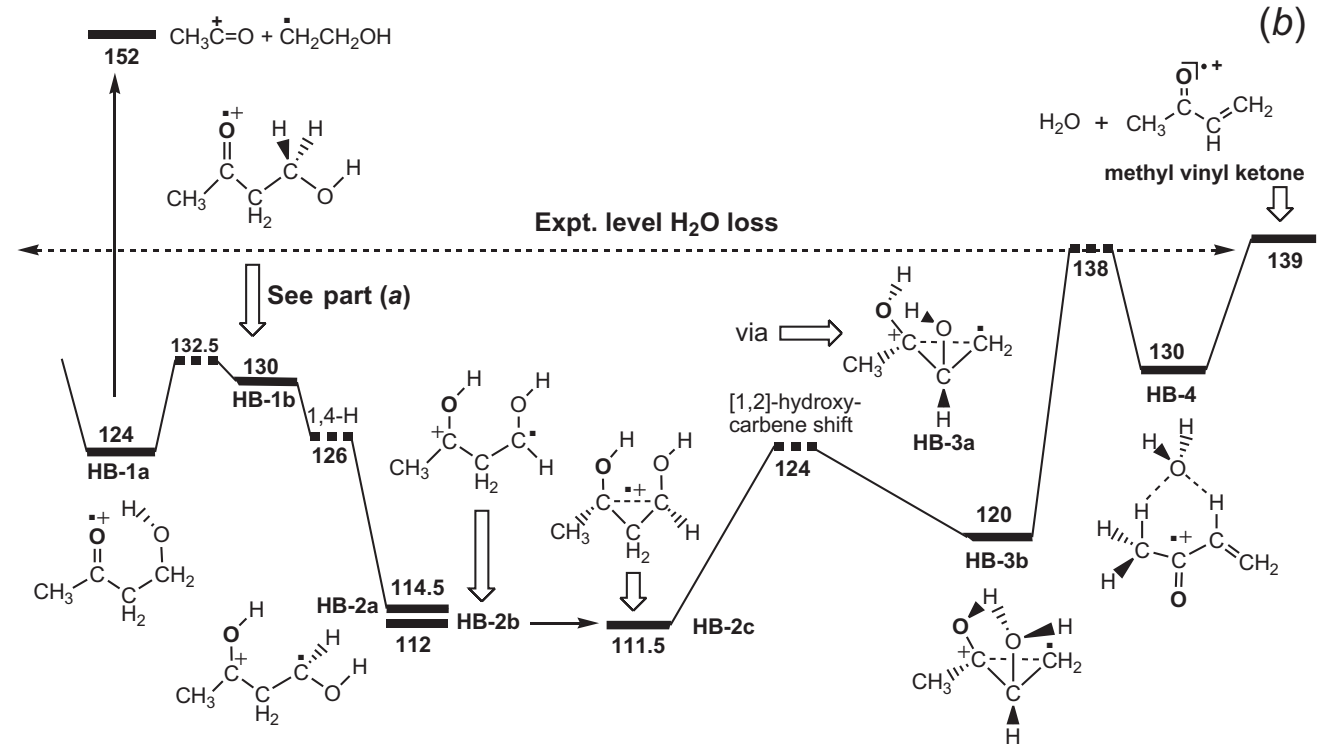
The previous observations lead us to conclude that the water elimination from both **HB-1** and **EA-1** yields **MVK** at the thermochemical threshold. Further, the MI spectrum of the ^{18}O-labelled isotopologue $CH_3C(=O^{18})CH_2CH_2OH^{+\cdot}$ reveals that the H_2O molecule lost from metastable ions **HB-1** largely (~95%) consists of the hydroxyl ^{16}O atom. The inset of the CID mass spectrum of Fig. 2*c* shows that this is also true for stable ions undergoing collision-induced dissociation, although it should be noted that the larger part (~70%) of the dominating peak for water loss in the CID spectrum is of metastable origin. This also applies to the *m*/*z* 70 peak in the CID mass spectrum of **EA-1**, but now the water loss (see inset of Fig. 2*a*) largely (~90%) involves the keto ^{16}O atom. For both isomers the kinetic energy release ($T_{0.5}$ value) associated with the major loss of $H_2{}^{16}O$ from the labelled isotopomers is significantly lower than that of the minor

[3] From unpublished EI results of the late Dr. F.P. Lossing (J.L. Holmes. Personal communication. 2005).
[4] Using $\Delta_f H_{298}^0$ (4-hydroxy-2-butanone) = –93 kcal mol^{-1} from a Benson additivity (12*e*) estimate. Our CBS-QB3 value is –93.4 kcal mol^{-1}.

© 2005 NRC Canada

Fig. 4. Energy level diagram derived from CBS-QB3 calculations describing the water elimination from metastable ethyl acetate ions (**EA-1**). Part (*a*) describes the isomerization of **EA-1** into ionized 4-hydroxy-2-butanone (**HB-1**); part (*b*) presents the mechanisms by which ions **HB-1** lose H_2O. The numbers refer to $\Delta_f H^0_{298}$ values in kcal mol^{-1}.



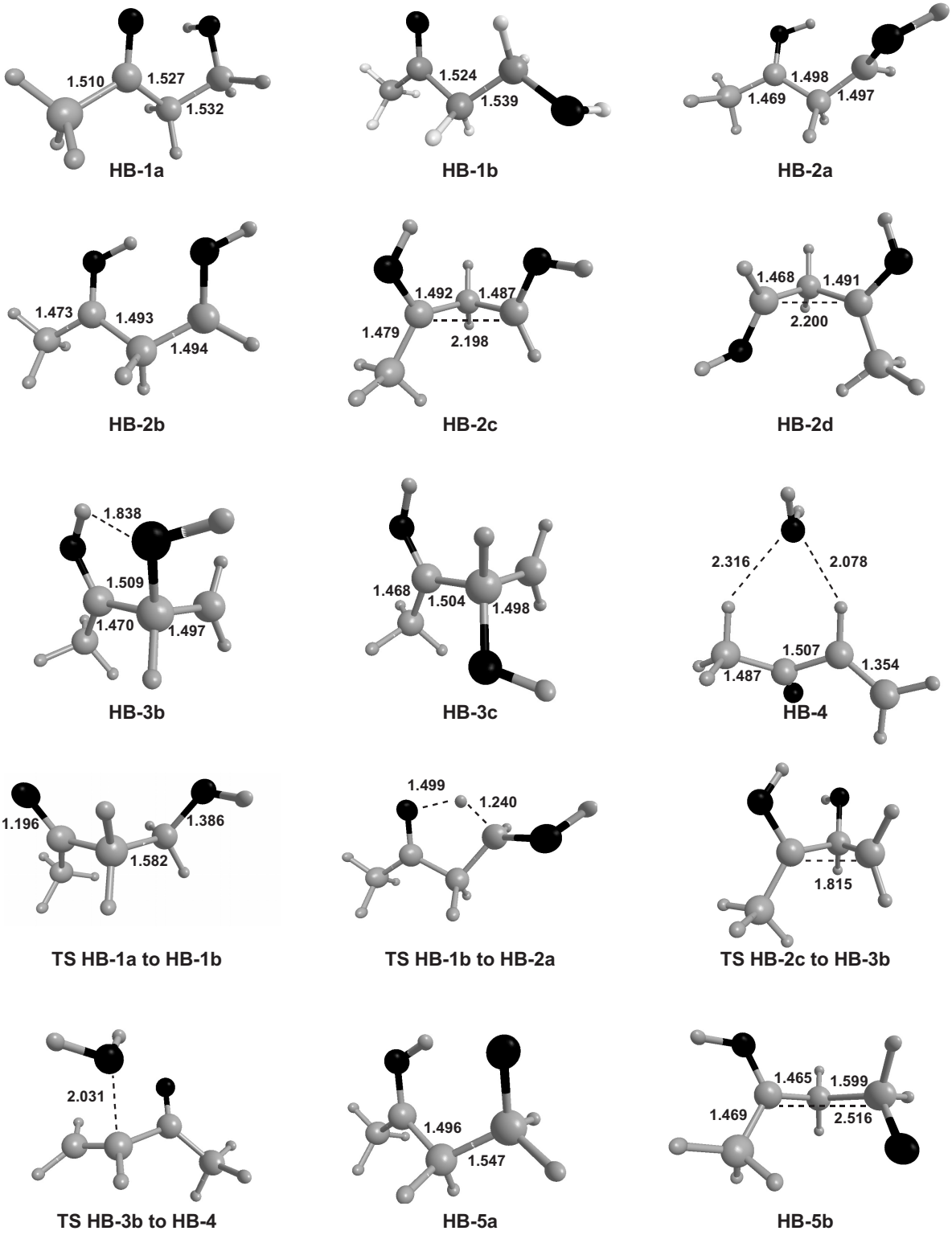


$H_2{}^{18}O$ loss: 8.6 vs. 13.0 meV for **EA-1** (7) and 5.5 vs. 11.5 meV for **HB-1** (this work). This observation suggests that the $H_2{}^{18}O$ loss from **EA-1** and **HB-1** involves an oxygen equilibration reaction whose energy requirement is somewhat higher than the atom specific water loss. As we shall see, the mechanistic proposal of Fig. 4 provides a rationale for these labelling results.

Our mechanistic proposal for water loss from metastable ions **HB-1** is presented in the bottom part of the energy diagram of Fig. 4. Starting from the lowest energy conformer

© 2005 NRC Canada

Fig. 5. The CBS-QB3 optimized geometries for ionized 4-hydroxy-2-butanone (**HB-1**) and ethyl acetate (**EA-1**) isomers, and selected transition states.

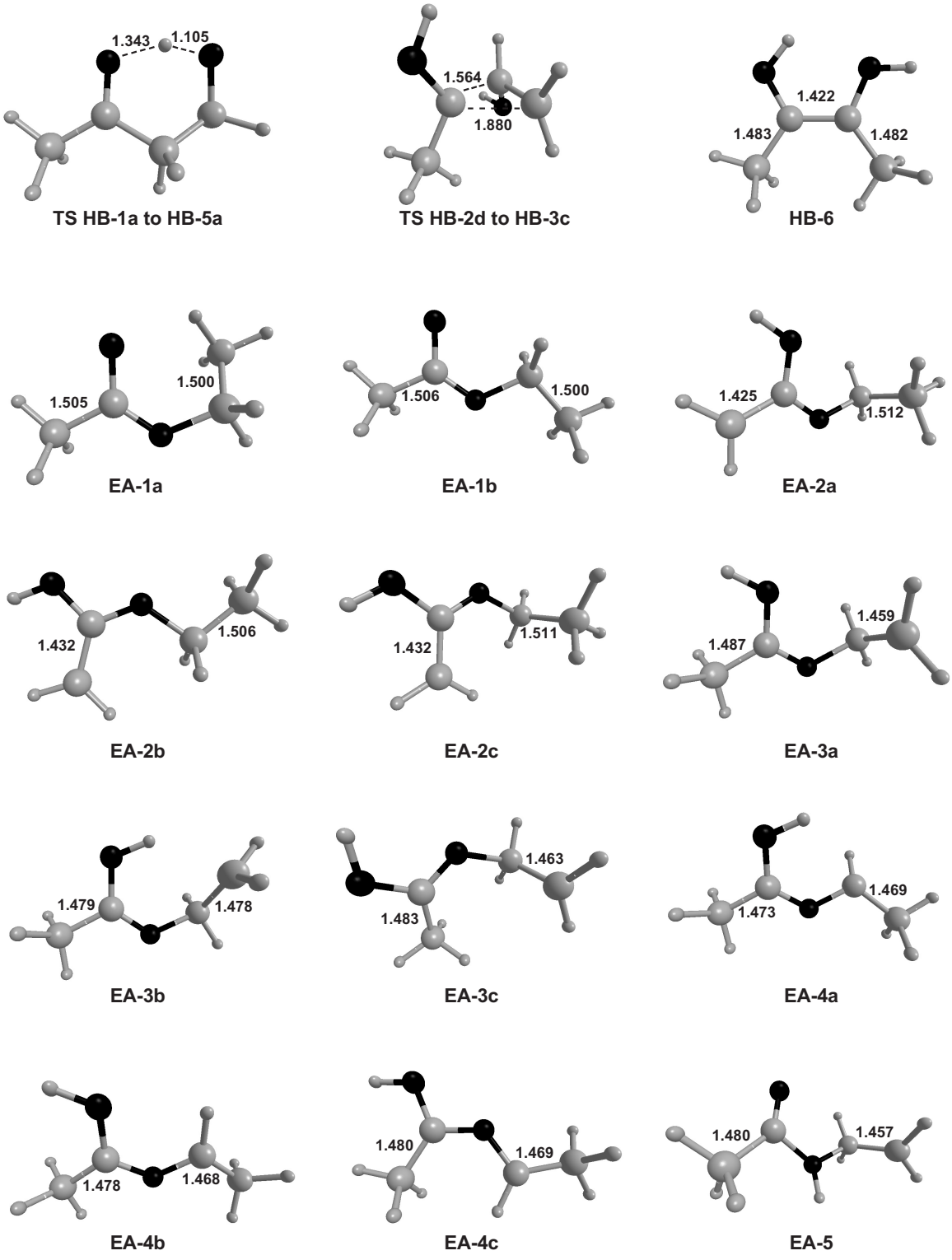


HB-1a, a facile rotation of the CH_2OH moiety yields conformer **HB-1b**, which forms the connection with the PES of ethyl acetate in the top part of the energy diagram. Ion **HB-1b** then rearranges into the very stable distonic ion **HB-2a** via a 1,4-H shift. The TS for this shift is undoubtedly not high but the calculated value is clearly too low; this point is further discussed in the Theoretical methods section.

Ion **HB-2a** may undergo a facile rotation of its HCOH moiety to yield the slightly more stable conformer **HB-2b**, which has a planar structure. However, its HCOH and

© 2005 NRC Canada

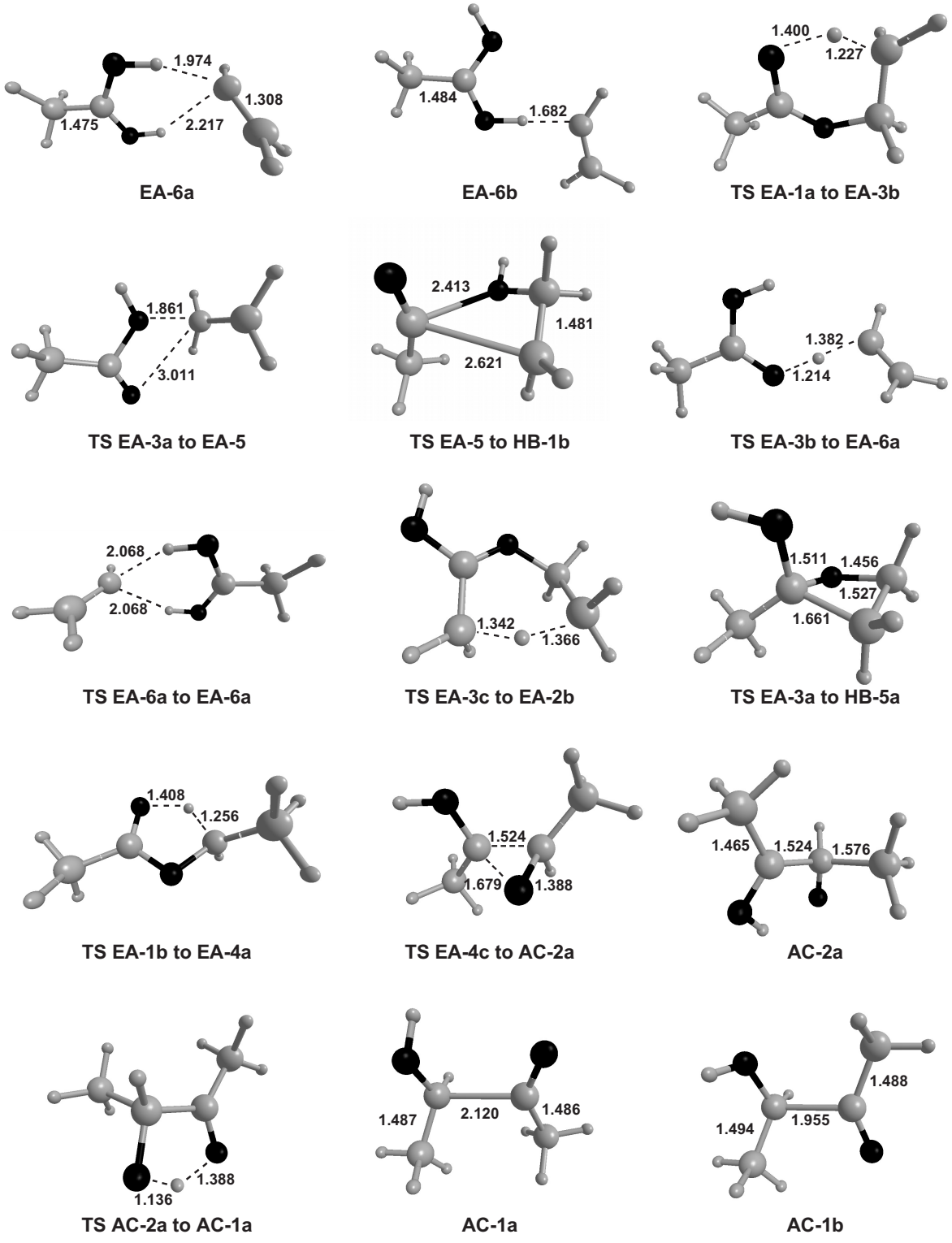
Fig. 5 (*continued*).



CH_3COH moieties can slightly move out of the plane (with a negligible energy requirement, see Table 2*b*) to form **HB-2c**, which (also see Fig. 5) can be viewed as a one-electron long bonded species. Contraction of its one-electron bond was expected to initiate the isomerization of **HB-2c** into **HB-3a** (see Fig. 4*b*) via a [1,2]-hydroxycarbene shift (10*b*). However, **HB-3a** does not appear to be a minimum on the PES: all attempts to optimize its geometry yielded its conformer **HB-3b** in which the hydroxyl groups are bridged in such a way that an ensuing loss of water into **MVK** can easily be envisaged. We were able to locate the transition state connecting **HB-2c** and **HB-3b** and it appears to lie at only 124 kcal mol^{-1}, well below the threshold for the water elimination. **HB-3b** does not

© 2005 NRC Canada

Fig. 5 (*concluded*).

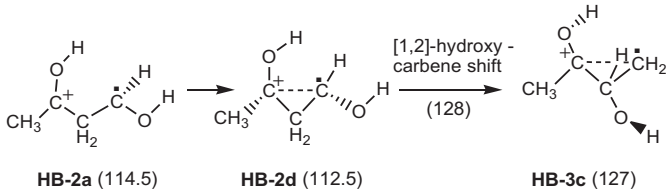


directly lose water but rather it isomerizes (TS at 138 kcal mol^{-1}) into an ion–dipole type complex between **MVK** and H_2O (**HB-4**), which then dissociates into its components at the thermochemical threshold.

We note that other conformers of **HB-2b** may also undergo a [1,2]-hydroxycarbene shift, as illustrated in Scheme 3 for **HB-2a**. However, the stable **HB-3** conformers then generated cannot immediately lose water but must first isomerize via rotation(s) into **HB-3b**. We have examined several of these pathways but they all appear to have a slightly higher energy requirement than the direct route (**HB-2b** → **HB-3b**) depicted in Fig. 4*b*.

© 2005 NRC Canada

Scheme 3.



Three points deserve further comment:

(*i*) The minor loss of $H_2{}^{18}O$ from $CH_3C(=O^{18})CH_2CH_2OH^{+}$ could be ascribed to a partial equilibration of **HB-3b** with its 1,2-H shift isomer $CH_3C(OH)=C(OH)CH_3^{+}$ (**HB-6**): the associated TS (see Table 2*b*) lies at 139 kcal mol^{-1}, i.e., at the threshold for the water elimination.

(*ii*) The H_2O molecule in **HB-4** is not expected to promote enolization of the ketone moiety by proton transport catalysis (19). This is because the proton affinity (PA) of water (164 kcal mol^{-1}) is much lower than the (calculated) topical PAs at $^{\cdot}CH_2$ and C=O in the deprotonated ketone $^{\cdot}CH_2C(=O)CH=CH_2$, 187 and 200 kcal mol^{-1}, respectively.

(*iii*) A McLafferty type rearrangement in **HB-1** would yield enol ions $CH_3C(OH)=CH_2^{\cdot+}$ at *m*/*z* 58 by loss of CH_2=O. As seen from Table 1, the minimum energy requirement for this reaction is only 136 kcal mol^{-1}, i.e., lower than that for the loss of water. However, our calculations indicate that the formaldehyde loss involves a reverse barrier of 4 kcal mol^{-1} (see Fig. 3 and Table 2*b*), which makes the energy requirements for the losses of formaldehyde and water comparable. Yet, neither the MI nor the CID spectrum (see Fig. 2*c*) of **HB-1** displays a signal at *m*/*z* 58!

Standard RRKM calculations for the formaldehyde loss from **HB-5a** and the water loss from **HB-3b** indicate that the internal energy needed for the formaldehyde loss in the metastable time frame is lower than that for the water loss. However, this model is misleading because it does not take into account that both isomers communicate with the much more stable isomers **HB-2a**–**HB-2c** via low barriers (see Fig. 4). This leads to a rapid interconversion of the various isomeric ions involved in the competing losses of formaldehyde and water.

The extended RRKM model as described by Baer et al. (22) (also see the Theoretical methods section) does account for the competition between the two dissociation channels. Calculations based on this model revealed that equilibration via the low-lying distonic ions **HB-2a**–**HB-2c** leads to a much lower yield (by a factor of 140) of the *m*/*z* 58 product ion formed by loss of formaldehyde compared with the yield of *m*/*z* 70 **MVK** ions formed by loss of water. As a result, loss of formaldehyde from **HB-1** cannot effectively compete with its water loss.

The water elimination from ionized ethyl acetate (EA-1)

As discussed in the previous section, 4-hydroxy-2-butanone ions **HB-1** lose water via the mechanism presented in the bottom part of the energy diagram of Fig. 4. The top part of this diagram (Fig. 4*a*) shows that ionized ethyl acetate can undergo a three-step isomerization reaction into **HB-1**, which may then serve as the precursor for its subsequent water elimination. The first step involves the conversion of **EA-1** into its stable distonic isomer **EA-3** via a facile 1,5-H shift. This reaction involves a conformer of ionized ethyl acetate (**HB-1a**) and it yields a conformer of the distonic ion (**EA-3b**). Rotation of its hydroxyl group via a low-lying transition state converts **EA-3b** into **EA-3a**. Next, the O—CH_2 bond in **EA-3a** stretches and breaks while the methylene group moves to the hydroxyl O atom to make a new bond, yielding distonic ion **EA-5**. Ion **EA-5**, akin to the well-documented (23) distonic $C_2H_6O^{\cdot+}$ isomer H_2O^{+}-CH_2-$CH_2^{\cdot}$, lies in a shallow potential well and requires only 4 kcal mol^{-1} to further rearrange into a conformer of ionized 4-hydroxy-2-butanone (**HB-1b**). This rearrangement can be viewed as a 1,3-acetyl shift.

This three-step isomerization route of **EA-1** into **HB-1** takes place at energies below that required for the water loss and it thus satisfies the energetic constraints imposed by experiment. It further converts the ^{18}O-labelled **EA-1** isotopologue $CH_3C(=O)^{18}OC_2H_5^{\cdot+}$ into the **HB-1** isotopologue $CH_3C(=O^{18})CH_2CH_2OH^{\cdot+}$, which (see Fig. 4*b*) is expected to specifically lose $H_2{}^{16}O$. This too is in agreement with the experimental observations, albeit that a small fraction of high energy metastable ions (~5%) appears to lose $H_2{}^{18}O$. The loss of $H_2{}^{18}O$ from both labelled isotopologues probably results from a weakly competing oxygen equilibration reaction rather than a different dissociation pathway. Two equilibration mechanisms are feasible: (*i*) the equilibration of **HB-3b** with its 1,2-H shift isomer **HB-6** mentioned in the previous section and (*ii*) the route **EA-3b** → **EA-6a** depicted in Fig. 4*a*. The transition-state energies for the two processes are very close but the first route is kinetically less attractive because the equilibration **HB-3** ↔ **HB-6** is associated with a very large activation energy (44 kcal mol^{-1} relative to **HB-6**) and a tight transition state. This makes it unlikely that this equilibration can effectively compete with the dissociation **HB-3** → **HB-4** → **MVK** + H_2O, even at elevated energies. The dynamic picture is more favourable for the second route, which converts **EA-3b** by elongation of its O—CH_2 bond into the hydrogen-bridged radical cation **EA-6a**. As depicted in Fig. 4*a*, **EA-6a** can undergo a facile exchange of its vinyl moiety via a low-lying transition state, which makes its oxygen atoms equivalent.

We further note that elongation of the O—CH_2 bond in other conformers of **EA-3** leads to various **EA-6** conformers, including **EA-6b** whose structure is shown in Fig. 5, which are similar in energy and may dissociate into $CH_3C(OH)_2^{+}$ + $C_2H_3^{\cdot}$ at elevated energies. Elongation of the O—CH_2 bond in **EA-3** can also lead to ion–dipole complexes of ionized ethylene and acetic acid. Such species can be formed from **EA-3** at fairly low internal energies, as seen in Fig. 4*a* where the symmetrical ion–dipole structure at 130 kcal mol^{-1} represents the transition state for switching the acetic acid dipole molecule between the methylene moieties of ionized ethylene (see the Deuterium labelling section). This switching reaction makes the C and H atoms of the ethyl group in **EA-1** equivalent and accounts in part for the H–D exchange reactions of D-labelled isotopologues of **EA-1** as will be discussed later in this paper. At elevated energies, the ion–dipole complexes do not dissociate into

© 2005 NRC Canada

$C_2H_4^{\cdot+}$ + CH_3COOH. Instead, proton transfer (PT) occurs from the ionized ethylene moiety to the acetic acid dipole, which allows the energetically more favourable dissociation into $CH_3C(OH)_2^+$ + $C_2H_3^{\cdot}$ to take place.

In this context we note that the PI study by Baer and co-workers (8) reports an AE of 10.67 ± 0.08 eV for the dissociation of **EA-1** into $CH_3C(OH)_2^+$ (*m/z* 61) + $C_2H_3^{\cdot}$. From the experimental enthalpies of Table 1 and using ΔH_{cor} = 4.7 kcal mol^{-1}, we derive a thermochemical AE of 10.75 eV. These results indicate that this dissociation takes place virtually at the thermochemical threshold, i.e., it has no reverse activation barrier. As previously discussed, loss of $C_2H_3^{\cdot}$ from **EA-1** (see Fig. 4*a*) may be envisaged to occur from the hydrogen-bridged ion **EA-6** or by proton transfer from ethylene – acetic acid ion–dipole complexes, rather than by a formal 1,3-H shift as mentioned in the Introduction.

The [1,3]-hydroxycarbene shift in the distonic ion $[CH_3C(OH)OCH_2CH_2]^{\cdot+}$ (EA-3)

The energy level diagram of Fig. 3*a* describes the communication of ionized ethyl acetate with its enol (**EA-2**), which will be addressed in the next section. It also shows the energetics associated with a [1,3]-hydroxycarbene shift in distonic ion **EA-3**. This isomerization leads to **HB-1** via its 1,5-hydrogen-shift isomer **HB-5** and it could in principle provide an alternative pathway for the loss of water. The energy requirement for this rearrangement precludes this possibility: Fig. 3*a* shows that TS **EA-3** → **HB-5** lies some 10 kcal mol^{-1} above the threshold for the dissociation of the incipient **HB-5** ions into $CH_3C(OH)=CH_2^{\cdot+}$ (*m/z* 58) + CH_2=O by direct bond cleavage. The fact that this dissociation is not observed in either the MI, the CID, or the conventional mass spectrum of **EA-1** implies that the [1,3]-hydroxycarbene shift does not even occur. This is not surprising considering the discussion of the previous section, where it was shown that ions **EA-3** are able to undergo several isomerization and dissociation reactions at energies well below that required for the [1,3]-hydroxycarbene shift.

The energy diagram of Fig. 3*a* also shows that the mechanism proposed by Yeo (Scheme 1) can be refuted: his proposed intermediate is not a minimum on the PES but rather corresponds to the high lying TS **EA-3b** → **HB-5b** associated with the [1,3]-hydroxycarbene shift. Interestingly, our calculations (see Table 1) indicate that the cyclic product ion structure proposed in his scheme (ionized 2-methyloxetene) has the same heat of formation as its ring-opened isomer **MVK**.

Another simple mechanism for water loss from ionized ethyl acetate that complies with the finding that its keto oxygen atom is preferentially lost, would involve a double H transfer to its keto oxygen atom. This reaction would generate an ionized oxycarbene via the sequence **EA-1** (1,4H) → **EA-4** (1,4H) → CH_3-C-O-$CH=CH_2^{\cdot+}$ + H_2O. Ionized oxycarbenes are well-documented species in the gas phase, which may be as stable as their keto or aldehyde counterparts (24). However, CH_3-C-O-$CH=CH_2^{\cdot+}$ appears to be much higher in energy than CH_3-C(=O)-$CH=CH_2^{\cdot+}$, by 21 kcal mol^{-1} (see Table 1) and so its formation, certainly as a product ion in the metastable time frame, can effectively be ruled out.

Table 3. Relative abundances for the loss of water from selected D-labelled isotopologues of ionized ethyl acetate and its enol.

Compound		H_2O:HDO:D_2O	Calculated[a]
$CD_3C(=O)OCD_2CH_3$	Source	39:52:09	11:53:36
	m*[b]	17:58:25	
$CH_3C(=O)OCD_2CD_3$	Source	00:13:86	11:53:36
	m*	06:44:50	
$CD_3C(=O)OCH_2CH_3$	Source	100:00:00	36:53:11
	m*	59:35:06	
$CH_2=C(OH)OCD_2CD_3$	Source	02:56:44	11:53:36
	m*	07:51:42	
$CD_2=C(OH)OCH_2CH_3$	Source	95:05:00	53:43:04
	m*	73:26:01	

[a]Assuming complete loss of positional identity.
[b]Metastable ions 2ffr ZAB or MS902.

Figure 3*a* also shows that the thermochemical energy requirement for the dissociation **EA-1/2** → $CH_2=C(OH)_2^{\cdot+}$ (*m/z* 60) + C_2H_4 is lower than that for the loss of H_2O. However, metastable ions **EA-1/2** do not lose C_2H_4, indicating that the associated dissociative rearrangement, possibly a 1,3-H shift in **EA-2**, has a high activation energy. As seen in Figs. 2*a* and 2*b*, this dissociation becomes prominent upon collisional activation. A double collision experiment confirmed that the *m/z* 60 ions in the CID spectra are ions $CH_2=C(OH)_2^{\cdot+}$, not $CH_3COOH^{\cdot+}$.

Deuterium-labelling experiments — The relationship between ionized ethyl acetate (EA-1) and its enol (EA-2), and identification of the rate-determining step for the loss of H_2O

Table 3 provides selected deuterium-labelling results taken from refs. 6 and 7. Metastable ions fragmenting in the second field free region (2ffr) of the ZAB and MS902 instruments do so at the same average rate so that the data are comparable (7). From the results of Table 3, it can be deduced that there are two H/D equilibration reactions.

In the first reaction, which is so fast that it readily occurs for ions dissociating in the source, the H atoms of the ethyl chain become positionally equivalent (see the results for $CD_3C(=O)OCD_2CH_3$). A complete exchange of these H atoms would yield a H_2O:HDO:D_2O ratio of 33:67:00, which is close to the observed ratio of 39:52:09. Reversible rearrangement of **EA-1** into **EA-3** followed by isomerization into the ion–dipole complex $CH_3C(OH)=O\cdots C_2H_4^{\cdot+}$, as previously discussed, accounts for this exchange reaction.

In the longer lived metastable ions, the H atoms of the acetyl group also participate in the exchange reactions, almost to the statistical limit. This can be rationalized by invoking a slow but reversible isomerization of **EA-3** into the enol ion **EA-2**. It leads to exchange of the H atoms of the acetyl group with those of the methyl H atoms of the ethyl group and together with the above fast exchange reaction, an (almost) complete equilibration of all H atoms now takes place. This would imply that metastable ethyl acetate ions consist of an (almost) equilibrated mixture of the keto, distonic, and enol isomers.

© 2005 NRC Canada

Our calculations (see Fig. 3*a*) indicate that ions **EA-2** and **EA-3** are lower in energy than **EA-1** and that they can be produced at energies just above the formation of **EA-1**. This makes it very likely that metastable ions **EA-1** primarily exist as enol ions **EA-2** and distonic ions **EA-3**. This is in good agreement with a Fourier transform ion cyclotron resonance study by Kiminkinen et al. (25), who concluded that the long-lived (timescale > 1 s) radical cation of ethyl acetate exists as its enol form in the gas phase. Their experiments further indicated, in agreement with our calculations, that the energy barriers for isomerization of **EA-1** to the distonic ion **EA-3** and of **EA-3** to the enol ion **EA-2** must be near or below the enthalpy of formation of **EA-1**, and that this radical cation is kinetically unstable.

As expected from this scenario, the enol ion also shows fast H/D equilibration reactions of the ethyl side chain (see Table 3). Earlier work (7) has noted that enol ions dissociating in the source rearrange irreversibly to the distonic ion, i.e., $CH_2{=}C(OH)OCD_2CD_3^{\cdot+} \rightarrow CH_2DC^{+}(OH)OCD_2CD_2^{\cdot}$. As previously discussed, the latter ion can then access the ion–dipole complex $CH_2DC(OH){=}O\cdots C_2D_4^{\cdot+}$ and fall back to the distonic form leading to equilibration of the OH hydrogen and the four C_2D_4 deuterium atoms. Again, in the metastable time frame, almost complete equilibration of all H and D atoms occurs.

The labelled ion $CD_3C(=O)OCH_2CH_3^{\cdot+}$ shows a H_2O/HDO loss ratio of 1.69, while the D_2O/HDO loss ratio for the inversely labelled compound $CH_3C(=O)OCD_2CD_3$ is 1.25, and so an H/D isotope effect is operative. According to the energy diagram of Fig. 4*b*, the final step is rate-determining. This step is a H transfer, and so we propose that the isotope effect can be connected with this step.

From the data in Table 3 we can calculate that for the metastable ions loss of H_2O is 36% specific for the keto ions and 41% specific for the enol ions: the final entry in Table 3, for example, can be broken down into a 41% specific H_2O loss and random H_2O, HDO, and D_2O losses of 32%, 26%, and 1%, respectively. This small increase in specificity may well indicate that the starting enol ions fragment at a slightly higher internal energy than the keto ions. This is corroborated by the finding that the kinetic energy release ($T_{0.5}$) for loss of water is slightly larger for the enol ion than for the keto ion (7). The larger $T_{0.5}$ value cannot be taken as showing that a rate-determining isomerization precedes fragmentation of the enol ion, paralleling the behaviour of the acetamide system (26).

Baer and co-workers (8) note that the measured activation energy for loss of H_2O from ionized ethyl acetate (0.3 eV) is too small to allow the molecular ion to be metastable, unless it rearranges into a more stable form. By modelling their experimentally derived *k* vs. *E* curve with standard RRKM calculations, Baer and co-workers concluded that the rearranged form has a $\Delta_f H^0_{298}$ of 110 kcal mol^{-1}, which can be associated with **EA-2**, **EA-3**, or **HB-2**. The slow rate constant is the result of the participation of all the low energy isomers leading to a large density of states of the dissociating ions.

The [1,2]-hydroxycarbene shift in the distonic ion $[CH_3C(OH)OCHCH_3]^{\cdot+}$ (EA-4)

Using the energy diagram of Fig. 3*b* as a guide, we note that the distonic ion **EA-4** is readily accessible from **EA-1** via a low energy 1,4-H shift. The ion can communicate with **EA-2** via its conformer **EA-4c**, but the TS for the associated 1,4-H shift (see Table 2*a*) is ca. 8 kcal mol^{-1} higher in energy than that for the enolization of its slightly less stable distonic isomer **EA-3** (see Fig. 3*a*).

The energy diagram of Fig. 3*b* further shows that conformer **EA-4c** may serve as the immediate precursor for a [1,2]-hydroxycarbene shift that connects **EA-1** with the PES of the acetoin radical cation ($CH_3C(=O)CH(OH)CH_3^{\cdot+}$, **AC-1**). This rearrangement, whose transition state lies ca. 6 kcal mol^{-1} above the level for the water loss, does not contribute to the loss of water because low energy acetoin ions exclusively dissociate into $CH_3C(H)OH^+ + CH_3C{=}O^{\cdot}$. This reaction involves a remarkable hidden rearrangement — metastable ions $CH_3C(=O^{18})CH(OH)CH_3^{\cdot+}$ generate $CH_3C(H)^{18}OH^+$ and $CH_3C(H)^{16}OH^+$ in a 1:1 ratio — and a mechanism involving the hydrogen-bridged radical cation ($CH_3C(=O^{18})\cdots H\cdots O{=}C(H)CH_3^{\cdot+}$) as the key intermediate has been proposed (20).

Metastable ions **EA-1** do not dissociate into $CH_3C(H)OH^+ + CH_3C{=}O^{\cdot}$, but the reaction becomes important upon collisional activation, as seen from the prominent *m*/*z* 45 peak in the CID mass spectrum of Fig. 2*a*. From the inset of Fig. 2*a*, it is seen that this peak shifts almost completely to *m*/*z* 47 in the CID spectrum of $CH_3C(=O)^{18}OCH_2CH_3$. This observation is in line with the expectation that the energy-rich acetoin ions ($CH_3C(=O)CH(^{18}OH)CH_3^{\cdot+}$) resulting from the [1,2]-hydroxycarbene shift will not rearrange but immediately dissociate.

Baer and co-workers (8) have reported the experimental AE for this reaction (10.70 ± 0.1 eV). They note that this value is too high to account for the threshold generation of the above products and suggest that the reaction may have a significant reverse activation barrier. From the evaluated experimental enthalpies of Table 1 and using ΔH_{cor} = 4.7 kcal mol^{-1}, we derive a thermochemical AE of 10.46 eV, implying that a reverse barrier of ca. 5.5 kcal mol^{-1} may indeed be present. Our calculations support this proposal: the barrier for the [1,2]-hydroxycarbene shift (see Fig. 3*b*) lies 5 kcal mol^{-1} above the dissociation level $CH_3C(H)OH^+ + CH_3C{=}O^{\cdot}$.

As previously mentioned, metastable acetoin ions do not lose water. Nevertheless, our CBS-QB3 calculations indicate that **AC-1** can communicate with **HB-3b** of Scheme 3 at the threshold for the water loss. The barrier for the isomerization of conformer **AC-1b** into **HB-3c** lies at 139 kcal mol^{-1}, while TS **HB-3c** → **3b** lies at 130 kcal mol^{-1} (Tables 2*a* and 2*b*). Thus, the overall energy requirement for this rearrangement of **AC-1** is very close to that of the products formed by its direct bond cleavage into $CH_3C(H)OH^+$ (140 kcal mol^{-1}, see Table 1). However, the dynamical situation for these two reactions is very different. The rearrangement has a tight transition state, whereas the dissociation, which has no reverse activation energy, corresponds to a loose transition state. A standard RRKM calculation predicts that the excess energy needed for the rearrangement to take place in the metastable time window (10 μs) exceeds 5 kcal mol^{-1}. This is caused by the large activation energy associated with the rearrangement. For the direct bond cleavage reaction we have used the model derived from the statistical adiabatic channel theory (27). Here the excess energy

© 2005 NRC Canada

needed is less than 1 kcal mol^{-1} because the acetyl radical lost has a large dipole moment (2.5 D at the B3LYP/CBSB7 level of theory). Therefore, low energy acetoin ions **AC-1** prefer the direct dissociation pathway above rearrangement into **HB-3c** and the subsequent loss of water. In the same vein, the rearrangement **HB-3b** → **AC-1** → $CH_3C(H)OH^+$ + $CH_3C{=}O^{\cdot}$ does not occur, as demonstrated by the complete shift of the *m*/*z* 45 peak to *m*/*z* 47 in the CID spectrum of ^{18}O-labelled **HB-1** (see the inset of Fig. 2*c*).

Summary

Our computational study, in concert with previous and present experimental work, leads to the following mechanistic proposal for the loss of water from ionized ethyl acetate in the metastable time frame. As shown in Scheme 4, the mechanism involves seven steps. These are: (1) a 1,5-hydrogen shift in ionized ethyl acetate yielding its distonic isomer **EA-3**; (2) an ethylene shift in **EA-3** generating another distonic ion (**EA-5**); (3) a 1,3-acetyl shift in **EA-5** yielding a conformer of ionized 4-hydroxy-2-butanone (**HB-1**); (4) a 1,4-hydrogen shift in **HB-1** yielding its distonic isomer **HB-2**; (5) a 1,2-hydroxycarbene shift in **HB-2**. This step leads to **HB-3**, a one-electron long bonded species whose hydroxyl groups are bridged. (6) A formal 1,4-hydrogen shift in which the bridging hydrogen moves to the adjacent hydroxyl group to form the water molecule of the ion–dipole complex **HB-4**. This step is rate-determining and may account for the kinetic H/D isotope effect. (7) Dissociation into ionized methyl vinyl ketone and a water molecule.

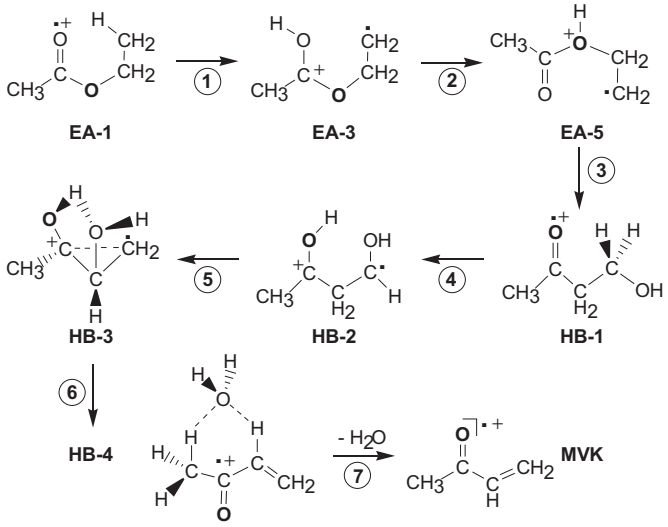
Each step is a simple transformation in itself, and all consecutive steps yield a transparent picture of the seemingly complex dissociation behaviour of ionized ethyl acetate. Our mechanism satisfies the energetic constraints imposed by experiment and provides a rationale for the ^{18}O- and D-labelling results.

Experimental and theoretical methods

The experiments were performed with the VG Analytical ZAB-R mass spectrometer of BEE geometry (B, magnet; E, electric sector) (28). MI mass spectra were recorded in the second field free region (2ffr); CID mass spectra were recorded in the 2 and 3ffr using oxygen as the collision gas (transmittance, T = 70%). The CID mass spectra of the 2ffr metastable peaks were obtained in the 3ffr using O_2 as the collision gas. For these experiments the maximum available accelerating voltage (10 kV) was used. CID spectra of reference ions having a translational energy close to that of the product ions resulting from (MI or CID) dissociations in the 2ffr were also obtained in the 3ffr. All spectra were recorded using a PC-based data system developed by Mommers Technologies Inc. (Ottawa, Ontario).

Ethyl acetate, methyl vinyl ketone, and 4-hydroxy-2-butanone were of research grade (Aldrich) and used without further purification. The ^{18}O-labelled ester $CH_3C(=O)^{18}OCH_2CH_3$ was synthesized on a microscale by esterification of acetic acid with $C_2H_5{}^{18}OH$ (MSD Canada); samples of $CH_3C(=O^{18})OCH_2CH_3$ and $CH_3C(=O^{18})CH_2CH_2OH$ were prepared by exchange of the carbonyl oxygen of the unlabelled precursors with $H_2{}^{18}O$ (Prochem 90 atom%) under slightly acidic conditions.

Scheme 4.



The calculations were performed with the CBS-QB3 model chemistry (17) using Gaussian 2003, Rev C.02 (29) and (for selected transition state searches) GAMESS-UK (30). In this model chemistry, the geometries of minima and connecting transition states are obtained from B3LYP density functional theory in combination with the 6-311G(2d,d,p) basis set (also denoted as the CBSB7 basis set). The resulting total energies and enthalpies of formation for minima and connecting transition states (TS) in the ethyl acetate (**EA**), acetoin (**AC**), and 4-hydroxy-2-butanone (**HB**) systems of ions are presented in Tables 2*a* and 2*b*. Computational and experimental enthalpies for various dissociation products are presented in Table 1. We have also used the G3 model chemistry (16*b*) to calculate the enthalpies of the species of Table 1: agreement with the results of the CBS-QB3 method (and experiment) was quite satisfactory, within ±1 to 2 kcal mol^{-1}.

Spin contaminations were within an acceptable range. The correct identity of transition states was verified (where not trivially evident) by means of intrinsic reaction coordinate (IRC) calculations using the algorithm implemented in Gaussian 2003.

For several facile isomerization reactions, including **EA-1a** → **EA-3a** in Fig. 4, the CBS-QB3 energy of the TS is calculated to be slightly lower than that of the least stable of the connecting isomers. This may happen since transition states are more sensitive to correlation effects than minima and the ZPE also tends to favour transition states.

However, the TS connecting **HB-1b** and **HB-2a** (see Fig. 4 and Table 2*b*) is calculated to lie much lower in energy: 4.5 kcal mol^{-1} below that of **HB-1b**. Here, the discrepancy between the B3LYP/CBSB7 energies and the final CBS-QB3 results is probably due to the fact that the B3LYP and the MP2 parts of the CBS-QB3 calculation disagree about the geometry of the transition state. We have compared the contributions to the CBS-QB3 energy for **HB-1b** and two transition states relating to this isomer. It was found that for **HB-1b** and TS **HB-1a** → **1b** the various contributions are

© 2005 NRC Canada

nearly the same, but this is not case for TS **HB-1** $\rightarrow$ **2a**. Here, the ΔE(MP2) contribution is much larger and the effect is enhanced in the ΔE(CBS) component, which is based on the MP2 energies. In contrast, the ΔE(MP4) contribution for this TS is smaller. This analysis suggests that for this transition state the MP2 method is not reliable enough to give satisfactory results.

Figure 5 displays the optimized geometries for the principal species. The complete set of computational results is available from the authors upon request.

RRKM theory (22) was used to calculate microcanonical rate constants. The harmonic frequencies and rotational constants were taken from the B3LYP/CBSB7 part of the CBS-QB3 calculations. The internal energies were calculated from the CBS-QB3 heats of formation at 0 K.

The extended RRKM model used is that described by Baer and Hase (22). Here several reaction steps are combined to get an overall rate constant. As will be discussed in a separate publication (in preparation) this procedure also makes it possible to compare the yields of various dissociation products.

Acknowledgements

J.K.T and R.L thank the Natural Sciences and Engineering Research Council of Canada (NSERC) for financial support. P.J.A.R thanks the Netherlands Organization for Scientific Research (NWO) for making available the SGI TERAS computer of SARA (Amsterdam).

References

1. E.W. Godbole and P. Kebarle. Trans. Faraday Soc. **58**, 1897 (1962).
2. F.M. Benoit, A.G. Harrison, and F.P. Lossing. Org. Mass Spectrom. **12**, 78 (1977).
3. C.G. de Koster, J.K. Terlouw, K. Levsen, H. Halim, and H. Schwarz. Int. J. Mass Spectrom. Ion Processes, **61**, 87 (1984).
4. J.L. Holmes and F.P. Lossing. J. Am. Chem. Soc. **102**, 1591 (1980).
5. F.W. McLafferty and F. Turecek. Interpretation of mass spectra. 4th ed. University Science Books, Mill Valley, California. 1993. p. 81.
6. A.N.H. Yeo. J. Chem. Soc. Chem. Commun. 1154 (1970).
7. J.L. Holmes, P.C. Burgers, and J.K. Terlouw. Can. J. Chem. **59**, 1805 (1981).
8. L. Fraser-Monteiro, M.L. Fraser-Monteiro, J. Butler, and T. Baer. J. Phys. Chem. **86**, 752 (1982).
9. (*a*) J.L. Holmes and J.K. Terlouw. Org. Mass. Spectrom. **15**, 383 (1980); (*b*) J.L. Holmes *In* Encyclopedia of mass spectrometry. Vol. 1. *Edited by* P.B. Armentrout. Elsevier, Amsterdam. 2004. p. 91.
10. (*a*) S. Hammerum. Mass Spectrom. Rev. **7**, 123 (1988); (*b*) P.C. Burgers and J.K. Terlouw. *In* Specialist periodical reports: mass spectrometry. Vol. 10. *Edited by* M.E. Rose. The Royal Society of Chemistry, London. 1989. Chap. 2.
11. J.L. Holmes and J.K. Terlouw. *In* Encyclopedia of mass spectrometry. Vol. 4. *Edited by* N.M.M. Nibbering. Elsevier, Amsterdam. 2005. p. 287.
12. (*a*) S.G. Lias, J.E. Bartmess, J.F. Liebman, J.L. Holmes, R.O. Levin, and W.G. Maillard. J. Phys. Chem. Ref. Data, **17**(Suppl. 1). 1988; (*b*) W.G. Mallard (*Editor*). NIST Chemistry WebBook [online]. The National Institute of Standards and Technology, Gaithersburg, Maryland. Available from http://webbook.nist.gov/chemistry [accessed April 2005]. 2003; (*c*) E.P.L. Hunter and S.G. Lias. J. Phys. Chem. Ref. Data, **27**, 413 (1998); (*d*) Y.-R. Luo. Handbook of dissociation energies in organic compounds. CRC Press, Boca Raton, Florida. 2003; (*e*) N. Cohen and S.W. Benson. Chem. Rev. **93**, 2419 (1993).
13. (*a*) J.K. Terlouw, W. Heerma, J.L. Holmes, and P.C. Burgers. Org. Mass. Spectrom. **15**, 582 (1980); (*b*) C. Dass and M.L. Gross. Org. Mass. Spectrom. **25**, 24 (1990).
14. N. Heinrich, J. Schmidt, H. Schwarz, and Y. Apeloig. J. Am. Chem. Soc. **109**, 1317 (1987).
15. P.C. Burgers and J.K. Terlouw. *In* Encyclopedia of mass spectrometry. Vol. 4. *Edited by* N.M.M. Nibbering. Elsevier, Amsterdam. 2005. p. 173.
16. (*a*) L.A. Curtiss, K. Raghavachari, G.W. Trucks, and J.A. Pople. J. Chem. Phys. **98**, 1293 (1993); (*b*) L.A. Curtiss, K. Raghavachari, P.C. Redfern, V. Rassolov, and J.A. Pople. J. Chem. Phys. **109**, 7764 (1998); (*c*) A.G. Baboul, L.A. Curtiss, and P.C. Redfern. J. Chem. Phys. **110**, 7650 (1999).
17. (*a*) J.W. Ochterski, G.A. Petersson, and J.A. Montgomery, Jr. J. Chem. Phys. **104**, 2598 (1996); (*b*) J.A. Montgomery, Jr., M.J. Frisch, J.W. Ochterski, and G.A. Petersson. J. Chem. Phys. **112**, 6532 (2000).
18. (*a*) L.N. Heydorn, Y. Ling, G. de Oliveira, J.M. Martin, C.L. Lifshitz, and J.K. Terlouw. Z. Physik. Chem. (Muenchen), **215**, 141 (2001); (*b*) L.N. Heydorn, P.C. Burgers, P.J.A. Ruttink, and J.K. Terlouw. Int. J. Mass Spectrom. Ion Processes, **228**, 759 (2003).
19. C.Y. Wong, P.J.A. Ruttink, P.C. Burgers, and J.K. Terlouw. Chem. Phys. Lett. **387**, 204 (2004), and refs. cited therein.
20. D. Suh, P.C. Burgers, and J.K. Terlouw. Int. J. Mass Spectrom. Ion Processes, **144**, L1 (1995).
21. (*a*) J.C. Traeger and R.G. McLoughlin. J. Am. Chem. Soc. **103**, 3647 (1981); (*b*) J.C. Traeger, R.G. McLoughlin, and A.J.J. Nicholson. J. Am. Chem. Soc. **104**, 5318 (1982); (*c*) J.L. Holmes, F.P. Lossing, and P.M. Mayer. J. Am. Chem. Soc. **113**, 9723 (1991); (*d*) F. Turecek and C.J. Cramer. J. Am. Chem. Soc. **117**, 12243 (1995); (*e*) H. Ervasti, P.C. Burgers, and P.J.A. Ruttink. Eur. J. Mass Spectrom. **10**, 791 (2004).
22. (*a*) T. Baer, W.A. Brand, T.L. Bunn, and J.J. Butler. Faraday Discuss. Chem. Soc. **75**, 45 (1983); (*b*) T. Baer and W.L. Hase. Unimolecular reaction dynamics. Oxford University Press, New York. 1996.
23. (*a*) J.K. Terlouw, W. Heerma, and G. Dijkstra. Org. Mass Spectrom. **16**, 326 (1981); (*b*) D.J. McAdoo and C.E. Hudson. Org. Mass Spectrom. **21**, 779 (1986).
24. R. Flammang, M.T. Nguyen, G. Bouchoux, and P. Gerbaux. Int. J. Mass Spectrom. **202**, A8 (2000).
25. L.K.M. Kiminkinen, L.C. Zeller, and H.I. Kenttämaa. Chem. Commun. (Cambridge), 466 (1992).
26. M.A. Trikoupis, P.J.A. Ruttink, P.C. Burgers, and J.K. Terlouw. Eur. J. Mass Spectrom. **10**, 801 (2004).
27. P.J.A. Ruttink. J. Phys. Chem. **91**, 703 (1987).
28. H.F. van Garderen, P.J.A. Ruttink, P.C. Burgers, G.A. McGibbon, and J.K. Terlouw. Int. J. Mass Spectrom. Ion Processes, **121**, 159 (1992).
29. M.J. Frisch, G.W. Trucks, H.B. Schlegel, G.E. Scuseria, M.A. Robb, J.R. Cheeseman, J.A. Montgomery, Jr., T. Vreven, K.N. Kudin, J.C. Burant, J.M. Millam, S.S. Iyengar, J. Tomasi, V. Barone, B. Mennucci, M. Cossi, G. Scalmani, N. Rega, G.A. Petersson, H. Nakatsuji, M. Hada, M. Ehara, K. Toyota, R. Fukuda, J. Hasegawa, M. Ishida, T. Nakajima, Y. Honda, O. Kitao, H. Nakai, M. Klene, X. Li, J.E. Knox, H.P. Hratchian,

© 2005 NRC Canada

J.B. Cross, V. Bakken, C. Adamo, J. Jaramillo, R. Gomperts, R.E. Stratmann, O. Yazyev, A.J. Austin, R. Cammi, C. Pomelli, J.W. Ochterski, P.Y. Ayala, K. Morokuma, G.A. Voth, P. Salvador, J.J. Dannenberg, V.G. Zakrzewski, S. Dapprich, A.D. Daniels, M.C. Strain, O. Farkas, D.K. Malick, A.D. Rabuck, K. Raghavachari, J.B. Foresman, J.V. Ortiz, Q. Cui, A.G. Baboul, S. Clifford, J. Cioslowski, B.B. Stefanov, G. Liu, A. Liashenko, P. Piskorz, I. Komaromi, R.L. Martin, D.J. Fox, T. Keith, M.A. Al-Laham, C.Y. Peng, A. Nanayakkara, M. Challacombe, P.M.W. Gill, B. Johnson, W. Chen, M.W. Wong, C. Gonzalez, and J.A. Pople. Gaussian 03. Revision C.02 [computer program]. Gaussian, Inc., Wallingford, Connecticut. 2004.

30. GAMESS-UK is a package of ab initio programs written by M.F. Guest, J.H. van Lenthe, J. Kendrick, K. Schoffel, and P. Sherwood, with contributions from R.D. Amos, R.J. Buenker, H.J.J. van Dam, M. Dupuis, N.C. Handy, I.H. Hillier, P.J. Knowles, V. Bonacic-Koutecky, W. von Niessen, R.J. Harrison, A.P. Rendell, V.R. Saunders, A.J. Stone, D.J. Tozer, and A.H. de Vries. The package is derived from the original GAMESS code. M. Dupuis, D. Spangler, and J. Wendolowski. GAMESS, Program No. QG01. NRCC software catalogue 1. Vol. 1. 1980.

© 2005 NRC Canada

Predicting ion rearrangement reactions — The energetics of the internal S_N2 reaction in gas-phase proton-bound molecular pairs[1]

Julie A.D. Grabowy and Paul M. Mayer

Abstract: A common rearrangement reaction for gas-phase proton-bound molecular pairs corresponds to an internal S_N2 reaction that results in the loss of a small neutral molecule. For pairs $(RCN)(ROH)H^+$, the energies of the two transition states (TS_a and TS_b) and the intermediate complex (IC) in the isomerization reaction (relative to the proton-bound pair, in kJ mol^{-1}) can be estimated using the following relationships: $E(TS_a) = 87 - 9(n) - 0.33(\Delta PA)$, $E(IC) = 83 - 9(n) - 0.33(\Delta PA)$, and $E(TS_b) = 107 - 9(n) - 0.10(\Delta PA)$, where 87, 83, and 107 kJ mol^{-1} are the values for $(CH_3CN)(CH_3OH)H^+$. Here, n is the number of stablizing alkyl groups on the central S_N2 carbon and ΔPA is the difference between the proton affinity of the migrating moiety and that for the base system (in this case, CH_3CN). For the analogous pairs $(ROH)(R'OH)H^+$, only the first value in each expression is different (98, 94, and 121 kJ mol^{-1}, respectively, calculated for $(CH_3OH)_2H^+$).

Key words: proton-bound molecular pairs, isomerization, internal S_N2 reaction, energetics, metastable ions.

Résumé : Les réactions S_N2 internes qui résultent de la perte d'une petite molécule neutre sont des réactions de réarrangements communes en phase gazeuse pour des paires moléculaires liées par un proton. Pour les paires $(RCN)(ROH)H^+$, il est possible d'évaluer les énergies des deux états de transition (ET_a et ET_b) et le complexe intermédiaire (CI) dans la réaction d'isomérisation (relatives à la paire liée par un proton, en kJ mol^{-1}) en utilisant les relations suivantes: $E(ET_a) = 87 - 9(n) - 0{,}33(\Delta PA)$, $E(CI) = 83 - 9(n) - 0{,}33(\Delta PA)$ et $E(ET_b) = 107 - 9(n) - 0{,}10(\Delta PA)$, dans lesquelles les valeurs 87, 83 et 107 kJ mol^{-1} sont les valeurs pour $(CH_3CN)(CH_3OH)H^+$, n est le nombre de groupes alkyles stabilisants sur l'atome de carbone central de la réaction S_N2 et ΔPA est différence entre les affinités protoniques de la portion qui migre et celle du système basique, dans ce cas le CH_3CN. Pour les paires analogues $(ROH)(R'OH)H^+$, seule la première valeur de chaque expression diffère, soit 98, 94 et 121 kJ mol^{-1} respectivement pour $(CH_3OH)_2H^+$.

Mots clés : paires moléculaires liées par un proton, isomérisation, réaction S_N2 interne, énergie, ions métastables.

[Traduit par la Rédaction]

Introduction

The search for meaningful trends in chemical reactivity and their correlation with molecular parameters is one of the fundamental goals of chemistry. One well-established mechanism for the reaction of gas-phase and solution ions is the bimolecular nucleophilic substitution or S_N2 reaction (1). This type of reaction has been used to study the role of steric and solvent effects (2), and structure–reactivity correlations (3) in chemical reactivity. While the S_N2 reaction has been studied extensively in solution, interpretation of the results is often complicated by the effects of solvation. It is these solvent effects that result in the large difference between the rates and mechanisms of gas-phase and solution-phase S_N2 reactions. Both experimental and theoretical studies have shown that a gas-phase S_N2 reaction can be characterized by a double-well potential energy surface (PES) with a central barrier separating two ion–molecule complexes (4–9); this discovery is in sharp contrast with the PES derived for an S_N2 reaction occurring in solution, which consists of a transition state that directly connects reactants and products (Fig. 1). In aqueous solution, the ion–dipole attraction (responsible for the two minima shown in the gas-phase PES) is nullified by the energy required to partially desolvate the ion, resulting in a unimodal energy profile with a large central barrier.

One class of gas-phase ions that undergo a unimolecular rearrangement that is similar to the above mentioned S_N2 reaction is the family of proton-bound pairs of alcohols and nitriles $(RCN)(ROH)H^+$ and $(ROH)(R'OH)H^+$ (where R represents substituents). The mass spectrometry of these proton-bound pairs has been extensively studied in this laboratory (10–14) and by Fridgen and McMahon (15, 16) and Audier et al. (17). A feature common to each system is an isomerization reaction (leading to a kinetically unstable isomer that loses water) that competes on the microsecond timescale with the cleavage of the hydrogen bond. The competition between the two reaction channels indicates that a

Received 22 March 2005. Published on the NRC Research Press Web site at http://canjchem.nrc.ca on 20 December 2005.

It is with great pleasure that we honour Paul Kebarle for his many outstanding contributions to mass spectrometry and gas-phase ion chemistry.

J.A.D. Grabowy and P.M. Mayer.[2] Chemistry Department, University of Ottawa, Ottawa, ON K1N 6N5, Canada.

[1]This article is part of a Special Issue dedicated to Professor P. Kebarle.

[2]Corresponding author (email: pmmayer@uottawa.ca).

 doi: 10.1139/V05-196 © 2005 NRC Canada

Scheme 1.

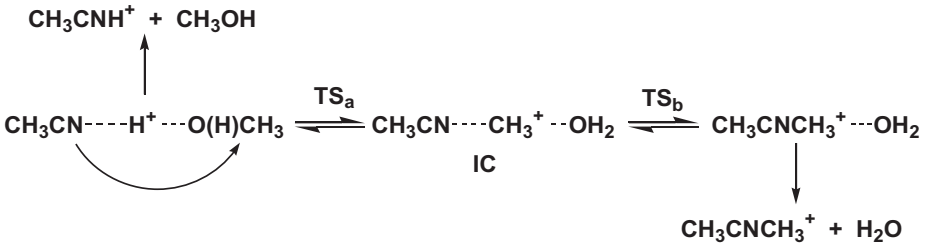


Fig. 1. Schematic energy profiles highlighting the differences between gas-phase and solution-phase S_N2 reactions.

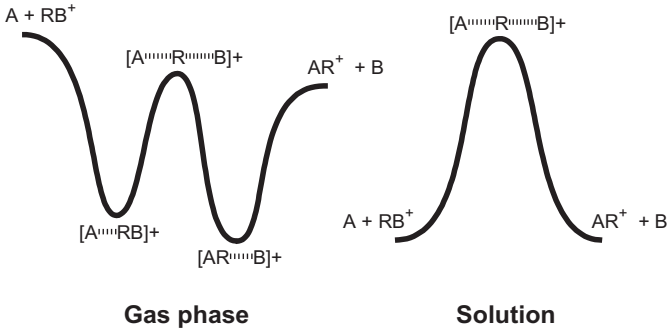
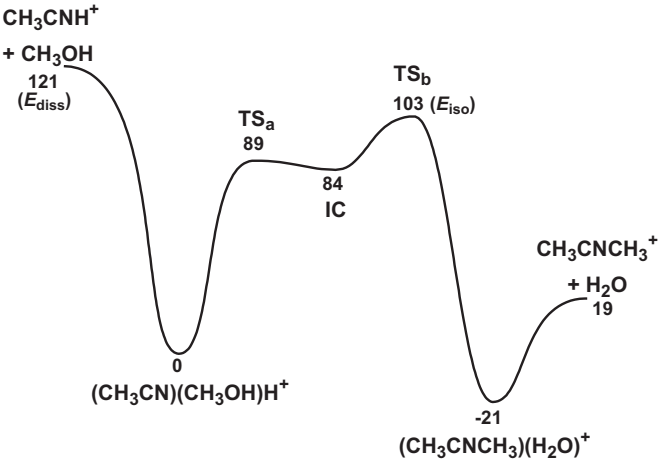


Fig. 2. MP2/6-31+G(d) potential energy diagram for the unimolecular process of the proton-bound pair consisting of acetonitcrile and methanol. The structures of TS_a, TS_b, and IC are illustrated in Scheme 1 and can be found in a previous publication (12). The labels E_{diss} and E_{iso} refer to the two energy levels used in the peak height intensity ratio vs. ΔE modeling.



fine balance exists between the relative energy barriers for dissociation and isomerization. The isomerization mechanism is outlined in Scheme 1 and a typical PES is shown in Fig. 2 for $(RCN)(ROH)H^+$ (12). The mechanism and surface are analogous to that for $(ROH)(R'OH)H^+$. Computationally, it has been found that methyl substitution of the central carbon of the intermediate complex (IC) will stabilize this ion and the transition states TS_a and TS_b (12). RRKM modelling of the kinetics on the reaction surface has shown that even though it is lower in energy, TS_a can play an important role in determining the fraction of ions that undergo isomerization (14).

Empirical relationships exist indicating that the key factor in determining the strength of the hydrogen bonds in these ions (18, 19) is the difference in proton affinity (PA) of the two molecules. The present work addresses the unimolecular S_N2 reaction by first examining the relationship between the energetics and relative peak intensities in tandem mass spectra and then by deriving empirical formulae for predicting the energies of the IC and transition states, thereby allowing the entire potential energy surface to be mapped out without experimental or computational input.

Experimental and computational procedures

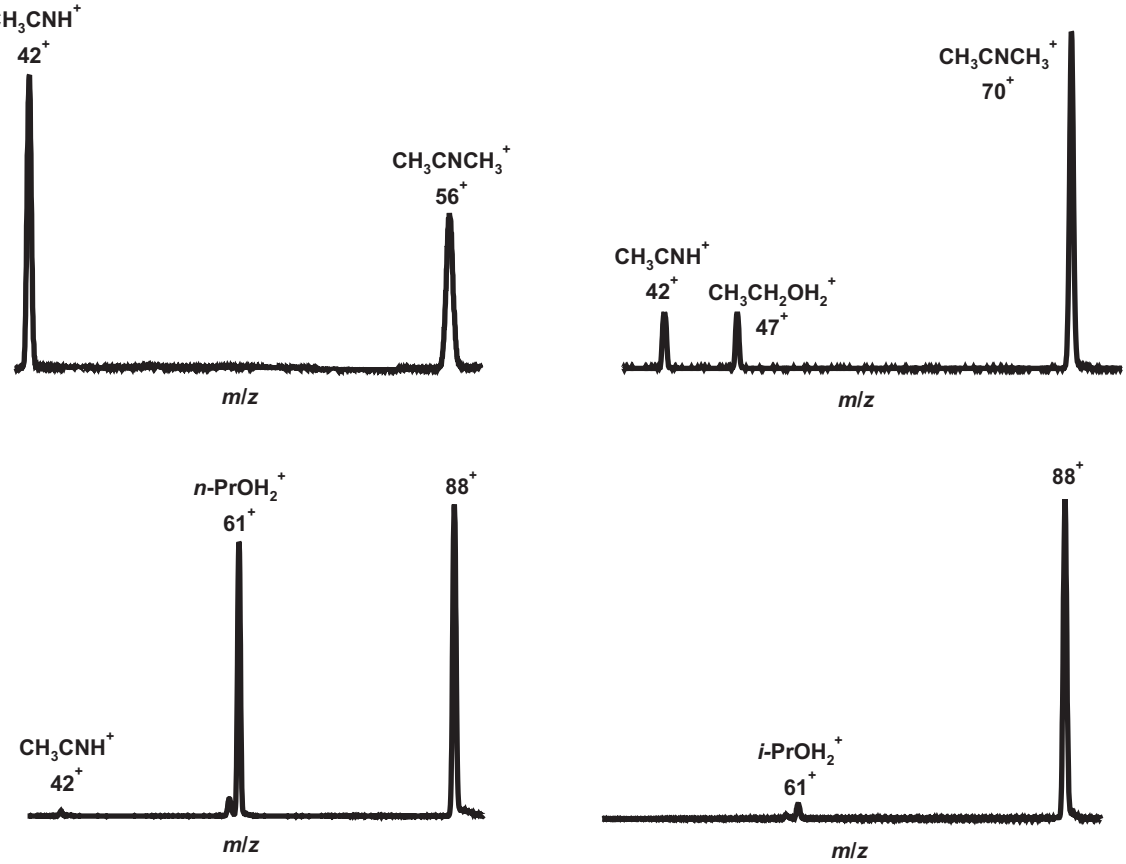
The experiments were performed on a modified VG ZAB-2HF mass spectrometer, which incorporates a magnetic sector followed by two electrostatic analysers (BEE geometry) (20). Protonated cluster ions were generated in the chemical ionization ion source of the instrument. The pressures in the ion source chamber, read with an ionization gauge located above the ion source diffusion pump, were typically between 10^{-5} and 10^{-4} Torr (1 Torr = 133.3224 Pa) (the pressure in the ion source itself being approximately two orders of magnitude higher). The accelerating voltage was held constant at 8 kV. Metastable ion (MI) mass spectra were recorded in the usual manner in the second field-free region (2FFR) of the mass spectrometer (21). All chemicals were commercially obtained and used without further purification.

Standard ab initio molecular orbital calculations (22) were performed using the Gaussian 98 suite of programs (23). Geometries were optimized at the MP2/6-31+G(d) level of theory as previous work from this group has shown that relative energies on these surfaces are adequately described at this level of theory (24). Vibrational frequency analysis was performed to verify transition states and equilibrium structures. Transition-state structures were further confirmed by the intrinsic reaction coordinate (IRC) method in Gaussian 98. The zero-point energies were scaled by a factor of 0.967 recommended by Scott and Radom (25). Readers are directed to Supplemental data[3] available from this journal for the full list of calculated relative energies for TS_a, IC, and TS_b used in this study.

[3] Supplementary data for this article are available on the Web site or may be purchased from the Depository of Unpublished Data, Document Delivery, CISTI, National Research Council Canada, Ottawa, ON K1A 0R6, Canada. DUD 4059. For more information on obtaining material refer to http://cisti-icist.nrc-cnrc.gc.ca/irm/unpub_e.shtml.

© 2005 NRC Canada

Fig. 3. Representative MI mass spectra of the proton-bound pairs (*a*) $(CH_3CN)(CH_3OH)H^+$, (*b*) $(CH_3CN)(CH_3CH_2OH)H^+$, (*c*) $(CH_3CN)(CH_3CH_2CH_2OH)H^+$, and (*d*) $(CH_3CN)((CH_3)_2CHOH)H^+$.



Microcanonical rate constants were calculated using the RRKM expression (26)

$$k(E) = \frac{\sigma}{h}\frac{N^{\ddagger}(E - E_0)}{\rho(E)}$$

where σ is the reaction symmetry number, h is Planck's constant, $N^{\ddagger}(E - E_0)$ is the sum-of-states for the transition state, and $\rho(E)$ is the density of states of the reacting ion. Sums and densities of states were calculated using the direct count algorithm of Beyer and Swinehart (27).

Results and discussion

General mechanistic features

The mechanism outlined in Scheme 1 has features that are common with and distinct from the gas-phase bimolecular S_N2 reaction. The most obvious similarity is TS_b, which resembles the transition state in Fig. 1. The main distinctions are in the initial isomerization step from the proton-bound pair to the IC via TS_a. It has been shown that the bimolecular reaction of CH_3CNH^+ with neutral methanol skips the proton-bound pair and forms the IC directly before crossing TS_b (15). The long lifetime (and lower internal energy) of metastable ions means that any IC formed will rearrange back to the proton-bound pair prior to dissociation.

Peak intensity ratio vs. ΔE

Characteristic MI mass spectra for the acetonitrile–alcohol proton-bound pairs involving methanol, ethanol, and 1- and 2-propanol are shown in Fig. 3 (these spectra have been previously published (10–12)). It is tempting to simplify the potential energy surfaces from that shown in Fig. 2 to single-well surfaces whose product channels are simple hydrogen bond cleavage and isomerization through the high energy transition state TS_b leading to water loss. This simplification makes sense when the rate constants for the fundamental process in Fig. 2 are compared (Fig. 4). The $k(E)$ vs. E curves in Fig. 4 suggest that the IC will not have a significant lifetime and may be considered, to a first approximation, as kinetically irrelevant. With this simplification, there should be a relationship between the ratios of the intensities of the peaks in the MI mass spectra for the two processes and the relative barrier heights, similar to the commonly used kinetic method (28)

$$\ln\left(\frac{k_{diss}}{k_{iso}}\right) = \ln\left(\frac{I_{diss}}{I_{iso}}\right) = \ln\left(\frac{A_{diss}}{A_{iso}}\right) - \frac{\Delta E}{RT}$$

where k_{diss} and k_{iso} are the rate constants for the dissociation and isomerization of the proton-bound pair, I_{diss} and I_{iso} are the ion peak intensities measured in the mass spectrum of metastable proton-bound pairs, A_{diss} and A_{iso} are the pre-exponential factors, ΔE is the difference between the calculated barrier heights to dissociation and isomerization

© 2005 NRC Canada

Fig. 4. RRKM rate constants ($k(E)$) of the four elementary processes in the S_N2 mechanism for $(CH_3CN)(CH_3OH)H^+$. k_1 = dissociation of $(CH_3CN)(CH_3OH)H^+$ to $CH_3CNH^+ + CH_3OH$, k_2 = $(CH_3CN)(CH_3OH)H^+$ to IC via TS_a, k_3 = IC to $(CH_3CN)(CH_3OH)H^+$ via TS_a, and k_4 = IC to $(CH_3CNCH_3)(H_2O)^+$ via TS_b.

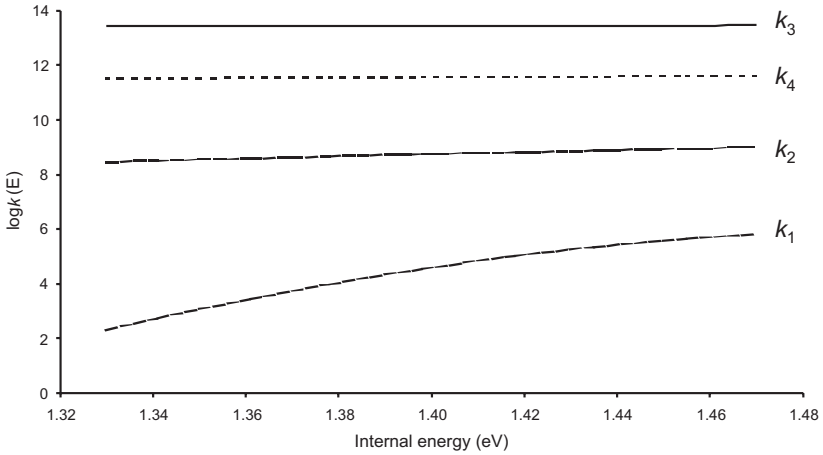
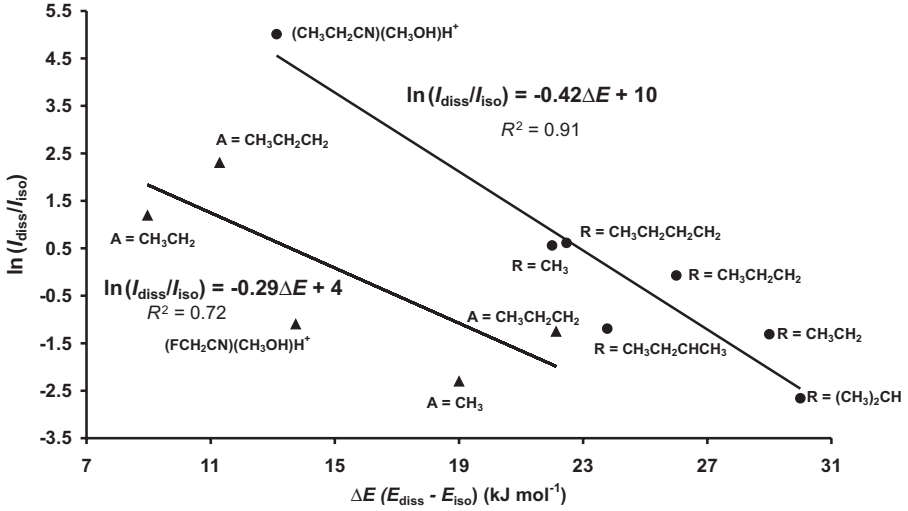


Fig. 5. Plot of $\ln(I_{diss}/I_{iso})$ vs. ΔE for the following proton-bound pairs: $(CH_3CN)(ROH)$ (●), unless otherwise noted and $(ClCH_2CN)(AOH)$ (▲), unless otherwise noted.



(which consist of the difference between the energy of the proton-bound pair and the lowest energy dissociation products (E_{diss}) and the high energy transition state, $TS_b(E_{iso})$), R is the gas constant, and T is the temperature. By plotting the natural logarithm of the ratio of peak intensities ($\ln(I_{diss}/I_{iso})$) against the difference in the calculated barrier heights, a linear relationship is obtained (Fig. 5). The equation of the line was determined to be $\ln(I_{diss}/I_{iso}) = -0.42\Delta E + 10$. This relationship is based upon the calculated relative energies for the proton-bound pairs of acetonitrile with methanol, ethanol, 1-propanol, 2-propanol, 1-butanol, and 2-butanol, but extends to proton-bound pairs involving propionitrile, suggesting that this equation can be used to determine the barrier height ratio between the two channels for any alkylnitrile–alcohol pair. Thus, by measuring the relative peak intensities in the MI mass spectra of proton-bound pairs involving alkylnitriles and alcohols, the difference in the barrier heights for the two dissociation channels may be obtained (Table 1). Coupled with the empirical expression for E_{diss} (19), E_{iso} can be extracted (Table 1). The slope ($1/RT$) of 0.42 mol kJ^{-1} yields a temperature of 286 K. This "effective" temperature has been discussed in relation to the kinetic method (28) and has been found to be related to the internal energy content of dissociating proton-bound pairs (29).

The single-well approximation breaks down when halogenated nitriles are examined. MP2/6-31+G(d) calculations for $(ClCH_2CN)(CH_3OH)H^+$ (14) showed that chloro substitution lowered the relative energy of TS_a, but left TS_b unaffected, resulting in a more abundant isomerization reaction compared with $(CH_3CN)(CH_3OH)H^+$. Plotting $\ln(I_{diss}/I_{iso})$ vs. ΔE for the proton-bound pairs $(ClCH_2CN)(AOH)H^+$ and $(FCH_2CN)(CH_3OH)H^+$ (where A = CH_3, CH_3CH_2, $CH_3CH_2CH_2$, and $(CH_3)_2CH$)) results in a displaced line with $\ln(I_{diss}/I_{iso}) = -0.29\Delta E + 4$. The lower PAs of the halogenated alkyl nitriles (745.7 kJ mol^{-1} for $ClCH_2CN$ vs. 779.2 kJ mol^{-1} for CH_3CN) make it easier for them to migrate to the backside of the alcohol moiety, resulting in a lower energy for TS_a (14). This slope yields an effective temperature of 414 K, which means that these dissociating

© 2005 NRC Canada

Table 1. Isomerization energies (corresponding to TS_b) determined from mass spectrometric peak intensity ratios for the proton-bound pairs between the indicated nitrile and alcohols.

Proton-bound pair	I_{diss} (kJ mol^{-1})	I_{iso} (kJ mol^{-1})	ΔE (kJ mol^{-1})	E_{diss}[a] (kJ mol^{-1})	E_{iso} (kJ mol^{-1})
CH_3CH_2CN					
Methanol	100.00	0.67	12	115	103
Ethanol	100.00	12.67	19	120	102
1-Propanol	100.00	40.00	22	123	101
2-Propanol	1.00	100.00	35	125	90
1-Butanol	81.56	100.00	24	124	99
2-Butanol	0.67	100.00	36	120	84
2-Methylpropanol	5.33	100.00	31	125	94
1,1-Dimethylethanol	0.67	100.00	36	123	87
$CH_3CH_2CH_2CN$					
Methanol	100.00	0.00	—	114	—
Ethanol	100.00	2.67	15	119	104
1-Propanol	100.00	11.33	19	122	103
2-Propanol	2.67	100.00	32	124	91
1-Butanol	100.00	52.00	22	123	100
2-Butanol	1.57	100.00	34	121	87
2-Methylpropanol	26.67	100.00	27	124	97
1,1-Dimethylethanol	2.00	100.00	33	124	91
$(CH_3)_2CHCN$					
Methanol	100.00	0.00	—	112	—
Ethanol	100.00	0.67	12	118	106
1-Propanol	100.00	2.33	15	121	106
2-Propanol	6.67	100.00	30	122	92
1-Butanol	100.00	8.67	18	121	103
2-Butanol	13.73	100.00	29	122	93
2-Methyl-1-propanol	100.00	94.00	24	122	99
2-Methyl-2-propanol	2.67	100.00	32	125	92

Note: All reactions lead to H_2O loss and involve the nitrile migrating to the backside of the protonated alcohol. Values in kJ mol^{-1}.

[a]Derived employing the relationship $E_{diss} = -0.26|\Delta PA| + 125$ kJ mol^{-1} (19).

ions may have a broader internal energy distribution than those for the alkyl nitriles discussed earlier.

Clearly, two main factors in determining the energetics of the species in this rearrangement reaction are the stabilization of the charge in TS_b and the proton affinity of the migrating moiety. These two parameters are employed in the following to produce more general relationships for the energetics of the S_N2 rearrangement.

Empirical relationships

The preceding discussion clearly illustrates the relationship between the peak intensities observed in mass spectra and the barrier heights calculated with theory. Although this method for extracting energetics is simple to use, it has the drawback that only the energy of TS_b is found and that considerable mass spectrometric and theoretical work must be done to establish the linear relationships to begin with. More desirable would be the ability to predict the relative energies of TS_a, TS_b, and IC without the use of mass spectrometry or theory. The MP2/6-31+G(d) relative energies of TS_a, TS_b, and IC for the proton-bound pairs were calculated for $(CH_3CN)(ROH)H^+$, $(CH_3CH_2CN)(CH_3OH)H^+$, $(ClCH_2CN)(AOH)H^+$, and $(FCH_2CN)(CH_3OH)H^+$ (where R = CH_3, CH_3CH_2, $CH_3CH_2CH_2$, $(CH_3)_2CH$, $CH_3CH_2CH_2CH_2$, $CH_3CH_2CHCH_3$ and A = CH_3, CH_3CH_2, $CH_3CH_2CH_2$, $(CH_3)_2CH$)). Using $(CH_3CN)(CH_3OH)H^+$ as the base system, the data provides the following empirical corrections to the relative energies of TS_a, TS_b, and IC.

$$E(TS_a) = 87 - 9(n) - 0.33(\Delta PA)$$
$$E(IC) = 83 - 9(n) - 0.33(\Delta PA)$$
$$E(TS_b) = 107 - 9(n) - 0.10(\Delta PA)$$

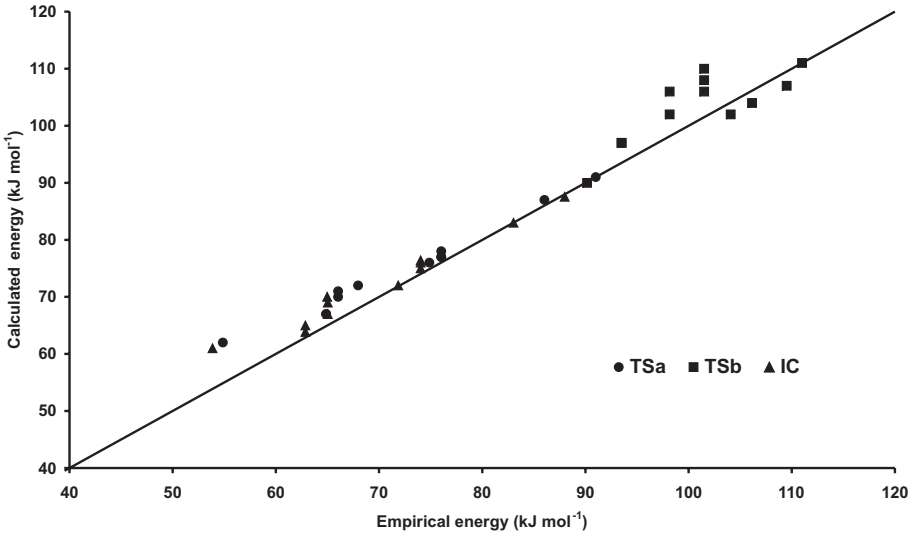
Similar results are obtained when the family of alcohol proton-bound pairs are investigated (here the base system is $(CH_3OH)_2H^+$). For these ions, one alcohol migrates to the back of the protonated alcohol resulting in the formation of an isomer consisting of a protonated ether bound to H_2O.

$$E(TS_a) = 98 - 9(n) - 0.33(\Delta PA)$$
$$E(IC) = 94 - 9(n) - 0.33(\Delta PA)$$
$$E(TS_b) = 121 - 9(n) - 0.10(\Delta PA)$$

PA effects were probed in the latter series using $(CF_3OH)(CH_3OH)H^+$ and $(CF_3OH)(CH_3CH_2OH)H^+$ and alkyl substitution with $(CH_3OH)(ROH)H^+$ (where R = CH_3,

© 2005 NRC Canada

Fig. 6. Plot of the MP2/6-31+G(d) calculated relative energies for TS_a, TS_b, and IC vs. those obtained from the empirical relationships outlined in the text. The line represents perfect agreement.



CH_3CH_2, $CH_3CH_2CH_2$, $(CH_3)_2CH$). The first number in each equation is the energy calculated for the reference proton-bound pair, namely $(CH_3CN)(CH_3OH)H^+$ and $(CH_3OH)_2H^+$. The *n* term represents the number of alkyl substituents on the central S_N2 carbon (e.g., *n* = 0, 1, and 2 for methyl, ethyl/1-propyl, and 2-propyl, respectively), and the 9 kJ mol^{-1} was deduced by comparing the relative energies for TS_a, TS_b, and IC among pairs having a constant migrating group (i.e., $(CH_3CN)(ROH)H^+$ and $(CH_3OH)(ROH)H^+$). The ΔPA term is the difference between the proton affinities of the migrating moieties (e.g., for $(ClCH_2CN)(CH_3OH)$, ΔPA = PA (CH_3CN) – PA $(ClCH_2CN)$). The *n* term is identical for the equations owing to the fact that alkyl substitution of the alcohol results in alkyl substitution of the charge-bearing site in all three species, the central carbon in the S_N2 process (see Scheme 1). In the proton-bound pair, however, this alkyl substitution is not at the charge-bearing site (the proton), but remote from it. Thus, TS_a, TS_b, and IC are stabilized to a greater extent than the original proton-bound pair by approximately 9 kJ mol^{-1} per alkyl group. This is comparable to that found in covalently bound ions. Let us consider alkyl substitution on $CH_3CH_2OH^{+\cdot}$ (ΔH_f = 775 kJ mol^{-1}). If the H on the charge-bearing oxygen is replaced with a methyl group to form the methyl ethyl ether ion $(CH_3CH_2OCH_3^{+\cdot})$, the heat of formation decreases by 54 kJ mol^{-1} to 721 kJ mol^{-1}. Similarly, if a methyl group hydrogen is replaced instead to form the *n*-propanol ion, the heat of formation decreases by only 44 kJ mol^{-1} to 731 kJ mol^{-1}, a difference of 10 kJ mol^{-1} with the previous case. So it can be reasonably inferred that substituents that stabilize or destabilize charge in conventional ions will also do so to the same extent in the species in this S_N2 mechanism.

The second parameter that influences the relative energy of TS_a, TS_b, and IC is the proton affinity of the migrating molecule. A slightly larger proton affinity effect is observed for TS_a and IC than for TS_b. To rearrange to IC via TS_a the migrating molecule must break a hydrogen bond, whereas for the second transition state (TS_b), no migration is involved. The larger the proton affinity of the migrating species, the stronger the hydrogen bond to the proton and thus the higher the energy barrier. For example, the relative energies of TS_a, TS_b, and IC for $(CH_3OCH_2CN)(CH_3OH)H^+$ are 82, 106, and 78 kJ mol^{-1}, respectively. The differences between these values and those for the $(CH_3CN)(CH_3OH)H^+$ base system are 5, 1, and 5 kJ mol^{-1}, in agreement with the predictions from the empirical equations of 7, 2, and 7 kJ mol^{-1} (the PA of CH_3OCH_2CN is 758.1 kJ mol^{-1}) (30). In general, there is excellent agreement between the original calculated MP2/6-31+G(d) relative energies and those derived from the empirical equations described earlier (Fig. 6).

Table 2. Calculated relative energies of TS_a, TS_b, and IC for four base system proton-bound pairs involving the listed migrating molecule and methanol. The S_N2 reaction leads to water loss in each case.

Migrating molecule	PA[a] (kJ mol^{-1})	TS_a (kJ mol^{-1})	IC (kJ mol^{-1})	TS_b (kJ mol^{-1})
CH_3OH	754.3	98	94	121
CH_3CN	779.2	87	83	107
CH_3CHO	768.5	86	82	112
CH_3NO_2	754.6	80	63	99

Note: Values in kJ mol^{-1} and are relative to the proton-bound pair.
[a]Reference 30.

Base systems for other proton-bound pairs between different migrating molecules and methanol (all resulting in H_2O loss) are listed in Table 2. Note that the empirical formulae can only be used within a particular family of proton-bound molecular pairs (e.g., any nitrile with any alcohol or any nitroalkane with any alcohol). The relative energy values for TS_a, TS_b, and IC can be used in conjunction with the correction factors described earlier to provide a wide range of isomerization energies.

Conclusions

A relationship has been demonstrated between relative peak intensities measured in metastable ion mass spectra and calculated barrier heights to dissociation and isomerization

© 2005 NRC Canada

reactions in gas-phase proton-bound pairs. A series of empirical relationships have been derived for the energetics of S_N2 reaction surfaces involving alcohol–alcohol and alcohol–acetonitrile proton-bound pairs. The relative energies of the species involved in the isomerization reactions are lowered by charge-stabilizing substituents at the S_N2 carbon. The PA of the migrating molecule in the mechanism can cause the relative energy of the first barrier and the intermediate complex in the mechanism to be raised or lowered. By calculating the first member in a family of proton-bound pairs, the three empirical equations can be used to determine the energetics of other members of the series. The family of nitroalkane proton-bound pairs have been recently studied in our group and they have been found to also undergo the internal S_N2 rearrangement to lose nitrous acid (HONO, subject of a future publication). It is reasonable to conclude that all proton-bound pairs obey the S_N2-type mechanism, the observation of the products simply being determined by the energetics.

Acknowledgement

PMM thanks the Natural Sciences and Engineering Research Council of Canada (NSERC) for continued funding.

References

1. S.S. Shaik, H.B. Schlegel, and S. Wolfe. Theoretical aspects of physical organic chemistry: The S_N2 mechanism. John Wiley and Sons, New York. 1992.
2. C.K. Regan, S.L. Craig, and J.I. Brauman. Science, **295**, 2245 (2002).
3. B.D. Wladkowski, J.L. Wilbur, and J.I. Brauman. J. Am. Chem. Soc. **116**, 2471 (1994).
4. (*a*) J.I. Brauman, W.N. Olmstead, and C.A. Lieder. J. Am. Chem. Soc. **96**, 4030 (1974); (*b*) W.N. Olmstead and J.I. Brauman. J. Am. Chem. Soc. **99**, 4219 (1976); (*c*) W.N. Olmstead and J.I. Brauman. J. Am. Chem. Soc. **99**, 4219 (1977); (*d*) M.J. Pellerite and J.I. Brauman. J. Am. Chem. Soc. **102**, 5993 (1980); (*e*) M.J. Pellerite and J.I. Brauman. J. Am. Chem. Soc. **105**, 2672 (1983); (*f*) B.D. Wladkowski, K.F. Lim, W.D. Allen, and J.I. Brauman. J. Am. Chem. Soc. **114**, 9136 (1992); (*g*) M.L. Chabinyc, S.L. Craig, C.K. Regan, and J.I. Brauman. Science (Washington, D.C.), **279**, 1882 (1998); (*h*) S.L. Craig and J.I. Brauman. J. Am. Chem. Soc. **121**, 6690 (1999); (*i*) J. Ren and J.I. Brauman. J. Phys. Chem. A, **106**, 3804 (2002).
5. (*a*) D.K. Bohme and L.B. Young. J. Am. Chem. Soc. **92**, 7354 (1970); (*b*) K. Tanaka, G.I. Mackay, J.D. Payzant, and D.K. Bohme. J. Am. Chem. Soc. **96**, 4027 (1974).
6. (*a*) C. Li, P. Ross, J.E. Szulejko, and T.B. McMahon. J. Am. Chem. Soc. **118**, 9630 (1996); (*b*) T.D. Fridgen and T.B. McMahon. J. Phys. Chem. A, **107**, 668 (2003); (*c*) B. Bogdanov and T.B. McMahon. Int. J. Mass Spectrom. **241**, 205 (2005).
7. (*a*) J.K. Laerdahl and E. Uggerud. Int. J. Mass Spectrom. **214**, 277 (2002); (*b*) J.K. Laerdahl and E. Uggerud. Org. Biomol. Chem. **1**, 2935 (2003).
8. S. Wolfe, D.J. Mitchell, and H.B. Schlegel. J. Am. Chem. Soc. **103**, 7694 (1981).
9. S. Gronert, A.E. Fagin, K. Okamoto, S. Mogali, and L.M. Pratt. J. Am. Chem. Soc. **126**, 12977 (2004).
10. P.M. Mayer. J. Phys. Chem. A, **103**, 3687 (1999).
11. R.A. Ochran, A. Annamalai, and P.M. Mayer. J. Phys. Chem. A, **104**, 8505 (2000).
12. R.A. Ochran and P.M. Mayer. Eur. J. Mass Spectrom. **7**, 267 (2001).
13. J.A.D. McCormack and P.M. Mayer. Int. J. Mass Spectrom. **207**, 183 (2001).
14. R.A. Ochran and P.M. Mayer. Int. J. Mass Spectrom. **227**, 471 (2003).
15. T.D. Fridgen, J.D. Keller, and T.B. McMahon. J. Phys. Chem. A, **105**, 3816 (2001).
16. T.D. Fridgen and T.B. McMahon. J. Phys. Chem. A, **106**, 9648 (2002).
17. H.E. Audier, C. Monteiro, P. Mourgues, and D. Robin. Rapid Commun. Mass Spectrom. **3**, 84 (1989).
18. J.W. Larson and T.B. McMahon. J. Am. Chem. Soc. **104**, 6255 (1982).
19. P.M. Mayer. J. Phys. Chem. A, **103**, 5905 (1999).
20. J.L. Holmes and P.M. Mayer. J. Phys. Chem. **99**, 1366 (1995).
21. K.L. Busch, G.L. Glish, and S.A. McLuckey. Mass spectrometry/mass spectrometry. VCH Publishers, New York. 1988.
22. W.J. Hehre, L. Radom, P.v.R. Schleyer, and J.A. Pople. Ab initio molecular orbital theory. John Wiley and Sons, New York. 1986.
23. M.J. Frisch, G.W. Trucks, H.B. Schlegel, G.E. Scuseria, M.A. Robb, J.R. Cheeseman, V.G. Zakrzewski, J.A. Montgomery, Jr., R.E. Stratmann, J.C. Burant, S. Dapprich, J.M. Millam, A.D. Daniels, K.N. Kudin, M.C. Strain, O. Farkas, J. Tomasi, V. Barone, M. Cossi, R. Cammi, B. Mennucci, C. Pomelli, C. Adamo, S. Clifford, J. Ochterski, G.A. Petersson, P.Y. Ayala, Q. Cui, K. Morokuma, D.K. Malick, A.D. Rabuck, K. Raghavachari, J.B. Foresman, J. Cioslowski, J.V. Ortiz, B.B. Stefanov, G. Liu, A. Liashenko, P. Piskorz, I. Komaromi, R. Gomperts, R.L. Martin, D.J. Fox, T. Keith, M.A. Al-Laham, C.Y. Peng, A. Nanayakkara, C. Gonzalez, M. Challacombe, P.M.W. Gill, B. Johnson, W. Chen, M.W. Wong, J.L. Andres, C. Gonzalez, M. Head-Gordon, E.S. Replogle, and J.A. Pople. Gaussian 98. Rev. A.7 [computer program]. Gaussian Inc., Pittsburgh, Penn. 1998.
24. P.M. Mayer. Chem. Phys. Lett. **314**, 311 (1999).
25. A.P. Scott and L. Radom. J. Phys. Chem. **100**, 16502 (1996).
26. T. Baer and W.L. Hase. Unimolecular reaction dynamics, theory and experiments. Oxford University Press, New York. 1996.
27. T. Beyer and D.R. Swinehart. Commun. ACM, **16**, 379 (1973).
28. (*a*) S.A. McLuckey, D. Cameron, and R.G. Cooks. J. Am. Chem. Soc. **130**, 1313 (1981); (*b*) X. Cheng, Z. Wu, and C. Fenselau. J. Am. Chem. Soc. **115**, 4844 (1993); (*c*) Z. Wu and C. Fenselau. Rapid Commun. Mass Spectrom. **8**, 777 (1994); (*d*) B.A. Cerda and C. Wesdemiotis. J. Am. Chem. Soc. **118**, 11884 (1996); (*e*) B.A. Cerda, S. Hoyau, G. Ohanessian, and C. Wesdemiotis. J. Am. Chem. Soc. **120**, 2437 (1998); (*f*) B.A. Cerda and C. Wesdemiotis. Int. J. Mass Spectrom. **185/186/187**, 107 (1999); (*g*) X. Zheng and R.G. Cooks. J. Phys. Chem. A, **106**, 9939 (2002); (*h*) A.G. Harrison. Mass Spectrom. Rev. **16**, 201 (1997).
29. L. Drahos and K. Vekey. J. Mass Spectrom. **34**, 79 (1999).
30. P.J. Linstrom (*Editor*). NIST Chemistry WebBook, NIST Standard Reference Database Number 69 [online]. Available from http://webbook.nist.gov/chemistry/. National Institute of Standards and Technology, Gaithersburg, Maryland. 2000.

© 2005 NRC Canada

Electrospray ionization Fourier transform mass spectrometry of polycyclic aromatic hydrocarbons using silver(I)-mediated ionization[1]

E. Peter Maziarz III, Gary A. Baker, and Troy D. Wood

Abstract: Here, a methodology employing doped Ag(I) salt as an in situ cationization reagent for efficient ionization of nonpolar molecules within a conventional electrospray ionization source is described. The effectiveness of Ag(I)-mediated ionization is demonstrated using ESI Fourier transform mass spectrometry for the rapid detection and identification of priority pollutant polyaromatic hydrocarbon (PAH) species. In contrast to earlier coordination ESI-MS reports employing silver salts, argentated species are *not* typically observed for PAH species. Instead, oxidation of the PAH occurs to produce only the $[PAH]^{+\cdot}$ odd-electron molecular parent ion, simplifying spectral analysis. In addition, the method demonstrates linear quantitative performance. The Ag(I) reagent provides quantifiable PAHs (not ordinarily amenable to ESI-MS) from 64 ppb, and suggests the immediate potential for sampling and on-line monitoring of complex, real world, and otherwise intractable environmental samples. Finally, the high mass accuracy of ESI Fourier transform mass spectrometry further allows unequivocal identification of molecular formulas within PAH mixtures.

Key words: electrospray ionization, nonpolar, hydrocarbons, polyaromatic, Fourier transform mass spectrometry.

Résumé : Dans ce travail, on décrit une méthodologie utilisant un sel de Ag(I) dopé comme réactif de cationisation in situ pour effectuer une ionisation efficace des molécules non polaires dans une source à ionisation par électronébulisation conventionnelle. L'efficacité de l'ionisation favorisée par le Ag(I) est démontrée en utilisant un spectromètre de masse à ionisation par électronébulisation (SM-IEN) à transformée de Fourier pour effectuer la détection rapide et l'identification d'espèces prioritaires de polluants de la famille des hydrocarbures polyaromatiques (HPA). En comparaison avec les rapports antérieurs de coordination SM-IEN utilisant des sels d'argent, on n'observe généralement pas d'espèces argentées avec les HPA. On observe plutôt une oxydation des HPA qui ne conduisent qu'à l'ion moléculaire parent à électron célibataire, $[HPA]^{+\cdot}$, ce qui simplifie l'analyse des spectres. De plus, la méthode a démontré une performance quantitative linéaire. Le réactif de Ag(I) fournit des valeurs quantifiables de HPA à partir de 64 ppb, ce qui n'est généralement pas le cas avec la SM-IEN; ceci suggère que la méthode présente un potentiel immédiat pour l'échantillonnage et l'évaluation en ligne d'échantillons environnementaux complexes, provenant de situations réelles et autrement inextricables. Enfin, l'exactitude de la spectroscopie de masse avec ionisation par électronébulisation à transformée de Fourier permet de faire une identification sans équivoque des formules moléculaires des composés formant des mélanges de HPA.

Mots clés : ionisation par électronébulisation, non polaire, hydrocarbures, polyaromatique, spectrométrie de masse à transformée de Fourier.

[Traduit par la Rédaction]

Introduction

Electrospray ionization (ESI) has established itself as a versatile means for generating intact, gas-phase molecular or pseudomolecular ions (e.g., $(M + nH)^{n+}$) from nonvolatile analyte species with little or no fragmentation (1–4). Further benefits of ESI include the ability to multiply charge macromolecules at relatively low mass-to-charge ratios (generally $m/z < 2000$) to obtain direct mass information on species present, minimal consumption of solvent and other consumables, high ionization efficiency, and the ability to couple high-resolution separation techniques such as capil-

Received 3 March 2005. Published on the NRC Research Press Web site at http://canjchem.nrc.ca on 20 December 2005.

E.P. Maziarz III[2] and G.A. Baker.[3] Department of Chemistry, Natural Sciences Complex, University at Buffalo, The State University of New York, Buffalo, NY 14260-3000, USA.
T.D. Wood.[4] Department of Chemistry, Natural Sciences Complex, University at Buffalo, The State University of New York, Buffalo, NY 14260-3000, USA and Department of Molecular and Cellular Biophysics, Roswell Park Cancer Institute, Elm and Carlton Streets, Buffalo, NY 14263, USA.

[1]This article is part of a Special Issue dedicated to Professor P. Kebarle.
[2]Present address: Bausch & Lomb Healthcare, 1400 N. Goodman St., P.O. Box 450, Rochester, NY 14603-0450, USA.
[3]Present address: Michelson Resource, Bioscience Division, B-4, Mail Stop: J586, Los Alamos National Laboratory, Los Alamos, NM 87545, USA.
[4]Corresponding author (e-mail: twood@acsu.buffalo.edu).

 doi: 10.1139/V05-195 © 2005 NRC Canada

lary electrophoresis (CE), capillary electrochromatography (CEC), and capillary HPLC. Thus, ESI has been considered an ideal ionization source for polar species including peptides, proteins, and oligonucleotides.

It is appropriate in this special issue honoring Paul Kebarle to note his important contributions toward gaining a greater fundamental understanding of the ESI process. Kebarle's group proposed the electrophoretic mechanism for droplet charging in the ESI process from experimental evidence (5, 6). This result was of importance because it indicated that analyte ions were preformed in the spray and supported the charged droplet model proposed by Iribarne and Thomson (7). A consequence of the electrophoretic charge separation mechanism in ESI is that charge balance requires a conversion of ions to electrons. The Kebarle group provided evidence of this in using zinc and stainless steel ESI emitters that produced Zn^{2+} (the amount of which corresponded to the amount required to carry the electrospray current) and Fe^{2+}, respectively (8). Kebarle and co-workers (9, 10) also explored the corona discharge phenomenon, and in particular provided experimental verification of the quantitative prediction for the onset voltage of charged-droplet emission. In addition, Tang and Kebarle's paper (11) on the influence of conductivity of the solution on total electrospray current yield and analyte ion yield provided important insight into why ESI produces decreased sensitivity at higher analyte concentrations. A detailed account by Kebarle and Tang (12) on these early advances in understanding the mechanism of ESI is available in a now classic review paper, with a more recent update by Kebarle (13).

In spite of the many fine features of ESI for analysis of biological molecules, analysis of nonpolar analytes has been limited. Two different approaches have shown promise in the analysis of nonpolar analytes by ESI. The first, developed by Bayer and co-workers (14–16), is known as coordination ion spray mass spectrometry (CIS-MS) in which minute amounts of a silver salt are injected into a nebulizer spray. This renders slightly polar or nonpolar molecules such as terpenes, sugars, aromatics, vitamins, or protected peptides amenable to ESI-MS. In these reports, substances were detected primarily as the silver coordination complexes $[M + Ag]^+$ (14–16). This method has been recently extended to hydrocarbons, including nonpolar hydrocarbons (17) and polar aromatic hydrocarbons (18). A second promising approach has been to exploit the oxidation–reduction behavior inherent in ESI noted by Kebarle and co-workers (8); in a series of papers, Van Berkel and co-workers (19–35) have shown that electrochemical effects of ESI can be exploited to enable detection of low polarity analytes.

Borrowing from these two approaches, here we report on the analysis of nonpolar polyaromatic hydrocarbons (PAHs) by ESI-FTMS. In this method, $[PAH]^{+\cdot}$ radical cations are produced upon exposure to Ag(I) salt. The suppression of silver-attached species (and conversion to the corresponding radical cations) is attributable to an electrospray-assisted oxidation of the PAH species or by dissociation of argentated PAH species in the ESI source. PAHs were chosen to test this methodology because they are ubiquitous environmental pollutants representing a family of molecules lacking sites for protonation (36). Interest in the direct analysis of PAHs in mixtures has increased in recent years stemming from concerns over their mutagenic and carcinogenic properties, coupled with the fact that these environmental pollutants originate from a wide variety of natural and anthropogenic sources. The technique demonstrates linear MS response for PAHs from ca. 64 ppb to the low ppm range. The high mass accuracy of Fourier transform mass spectrometry (FTMS) further allows identification of analytes within a multicomponent mixture of PAHs. Recently, the combination of ESI-FTMS, which is known for its utility in biomolecule characterization (37–48), has been shown to be an extremely useful technique in the characterization of complex mixtures of relatively nonpolar compounds, including hydrocarbons (49–55), humic acids (56–59), and fulvic acids (60–65). More recently, field desorption ionization has been coupled to FTMS for hydrocarbon analysis (52, 66, 67). The current results suggest the potential for ESI-FTMS for quantification and molecular identification analysis of even nonpolar molecules such as PAHs.

Experimental section

ESI-FTMS instrumentation

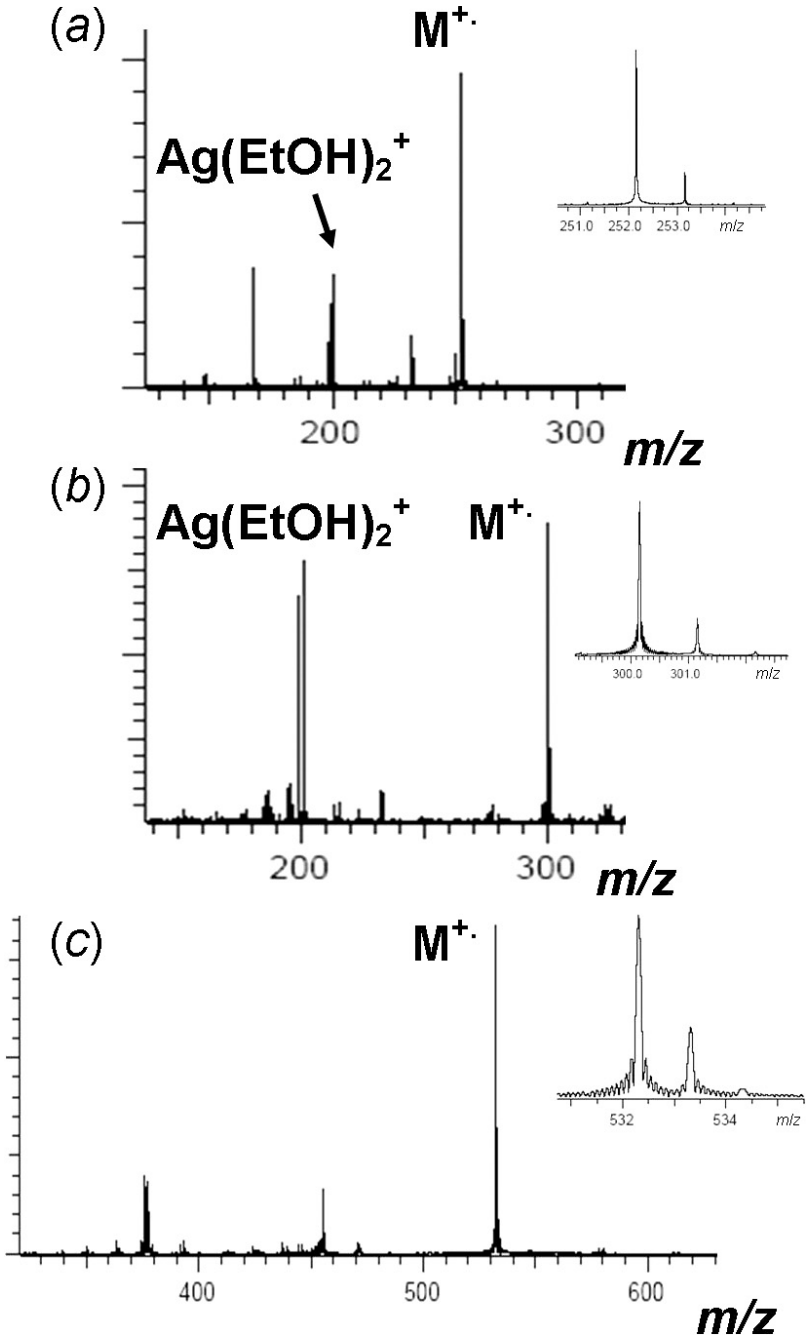
All experiments were performed on a Bruker (Billerica, Massachusetts) BioApex 30es Fourier transform mass spectrometer. The instrument design and a description of the 3.0 T magnet and pumping system used here have been reported elsewhere (68). This instrument is equipped with an Analytica of Branford (Branford, Connecticut) ESI source that contains an rf-only hexapole ion guide that is used to externally accumulate ions. A Cole-Palmer (Vernon Hills, Illinois) series 74900 infusion pump was used to continuously inject analyte samples into the ESI source at a rate of 1 μL min^{-1}. A second Cole-Palmer 74900 pump was used to inject a solution containing silver nitrate. The analyte sample solution and the silver nitrate solution were placed in separate Hamilton syringes connected to Teflon tubing, and the two solutions were mixed in a model MT1CS6 0.25 mm bore microvolume tee (Valco, Houston, Texas). The tee was connected to the stainless steel needle of the ESI outlet with a short segment of the Teflon tubing. Nitrogen countercurrent drying gas (300 °C) at a flow rate of 5–7 L min^{-1} was used to desolvate droplets produced by the ESI source. A potential between –2.9 and –3.2 kV (relative to the grounded needle) was applied to the metal-capped glass capillary. Ions were injected into the Infinity cell (2.0 V trapping potential unless otherwise noted) using the patented Sidekick method (69). Frequency-sweep excitation from m/z 100 to 2800 was applied at an amplitude of ~44–63 V_{pp} and detection was in direct mode (500 kHz Nyquist bandwidth) from 128K data sets (10 scans per experiment). The data sets were apodized with a Gaussian function, Fourier transformed, and displayed in magnitude mode.

Sample preparation

The following materials were used in these experiments. Silver nitrate solution was prepared as a 10 mmol/L stock solution in methanol–ethanol (50:50, HPLC grade, Mallinckrodt), then diluted to 1%–5% of this concentration (0.1–0.5 mmol/L) in methanol–ethanol (50:50) when used for the ESI experiments. The use of silver nitrate for ioniz-

© 2005 NRC Canada

Fig. 1. Representative ESI mass spectra of PAH samples by silver(I)-mediated ionization: (*a*) perylene, (*b*) coronene, and (*c*) rubrene. Insets represent the isotopic pattern observed for $[PAH]^{+\cdot}$.



ing hydrocarbon polymers in laser desorption has been known for some time (70). The PAHs pyrene, perylene, anthracene, coronene, and rubrene (Aldrich, Milwaukee, Wisconsin) were all prepared initially as stock solutions in ethanol. Final solutions used in ESI experiments were produced from serial dilution of these intial stock solutions. All reagents and solvents were used as received and without further purification.

Results and discussion

Characterization of the PAHs by Ag(I)-mediated ESI

As shown in Fig. 1, the mixing of Ag(I) salt with the PAH analyte does not generally result in production of argentated species $[PAH + Ag]^+$, as is typically observed in ESI-MS when silver salt is added to samples containing polar molecules (14–16). Instead, it is clear that the ESI mass spectra are dominated by the production of odd-electron radical parent ions ($[PAH]^{+\cdot}$). For example, in Fig. 1*a*, Ag(I)-mediated ESI-MS of perylene shows exclusively $[PAH]^{+\cdot}$ and no $[PAH + Ag]^+$; a similar result is found using Ag(I)-mediated ESI-MS of coronene (Fig. 1*b*). In both of these mass spectra, peaks at *m*/*z* 185 and 187, corresponding to the silver-cationized $Ag(CH_3OH)(C_2H_5OH)^+$, and at *m*/*z* 199 and 201, corresponding to the silver-cationized $Ag(C_2H_5OH)_2^+$, are observed. These ions clearly result from the cationization

© 2005 NRC Canada

of small solvent clusters by silver. In the ESI-MS of coronene, a doublet at ~2% relative to the odd-electron radical cation is observed at *m/z* 407/409, consistent with argentated coronene $[PAH + Ag]^+$.

A simple explanation for the production of odd-electron radical parent ions ($[PAH]^{+\cdot}$) is that a single electron transfer event occurs in which an electron from the PAH molecule is transferred to the Ag(I), thereby reducing it to silver metal, as shown in eq. [1].

$$[1] \quad PAH + Ag(I) \rightarrow PAH^{+\cdot} + Ag(0)$$

This is sensible because the ionization potential of Ag (7.57 eV) is above that of the PAHs used in this study, whose ionization energy (IE) values are: anthracene, 7.44 eV; pyrene, 7.43 eV; perylene, 6.96 eV; coronene, 7.29 eV; rubrene, 6.41 eV (71). Macha et al. (72) have indicated such an electron-transfer process can occur in matrix-assisted laser desorption ionization (MALDI) between nonpolar hydrocarbons, and such nonpolar matrixes are valuable for MALDI of high boiling point crude oil fractions (73). However, an alternative ionization route (eqs. [2*a*] and [2*b*]) proposed by Ng et al. (17) in silver-assisted ESI of PAHs may be more likely here.

$$[2a] \quad [Ag + 2PAH]^+ \rightarrow PAH + [PAH + Ag]^+$$

$$\rightarrow PAH + Ag(I)$$

$$[2b] \quad \rightarrow PAH^{+\cdot} + Ag(0)$$

Their proposed mechanism was supported by the presence of $[Ag + 2PAH]^+$ in the mass spectra (17). While such species are not indicated in the silver-assisted ESI of PAHs reported here, it is worth noting that all of the present results were collected at nozzle-skimmer potential differences above 100 V, in contrast to the report by Ng et al. (17). Furthermore, Ng et al. noted that $[PAH + Ag]^+$ tended to dominate the odd-electron radical cations ($[PAH]^{+\cdot}$) at low (20–60 V) nozzle-skimmer potential differences. Here, $[PAH]^{+\cdot}$ dominates in Figs. 1*a* and 1*b* as well as in Fig. 1*c* at *m/z* 532 in the ESI mass spectrum of rubrene (Fig. 1*c*), although ~3% relative abundance argentated species $[PAH + Ag]^+$ at *m/z* 639/641 (Fig. 1*c*) is also observed, as is the silver-cationized $Ag(C_2H_5OH)_2^+$. Varying the concentration of silver nitrate in the range 0.1–0.5 mmol/L has virtually no effect on the observed ion abundances for the analytes, probably owing to the large molar excess of Ag(I) relative to PAH.

Quantification of PAHs

Having identified the odd-electron radical cations in the ESI mass spectra as the ionic species produced after exposure to Ag(I), the linearity of ESI-FTMS response as a function of PAH concentration was examined. Linearity in ESI-FTMS response for individual biomolecules has been demonstrated over approximately three orders of magnitude (68, 74, 75). Miyabayshi et al. (50) reported linearity in quantitation for *total* hydrocarbon content in a complex crude oil sample containing over 500 distinguishable molecular formulas. A calibration curve of MS response (determined from the peak height (76) of the odd-electron radical cation, $M^{+\cdot}$) vs. perylene concentration was constructed using three replicate measurements; the results are shown in Table 1. As indicated in Table 1, ESI-FTMS response is linear ($R^2 = 0.9794$) with perylene concentration over a range of 64 ppb to 3.2 ppm, fit to the equation $y = 8.4 \times 10^4 x - 4.0 \times 10^5$. At perylene concentrations above 3.2 ppm, the peak height begins to deviate strongly from the calibration curve. This saturation effect has been previously reported with ESI-FTMS (68), and may be due to saturation of ESI ionization efficiency or from number of trapped ions in the FTMS trap. Coefficients of variation (CV) in the $[PAH]^{+\cdot}$ ICR magnitudes were calculated to determine the relative precision of the ion signal measurements using eq. [3].

Table 1. Calibration curve of ESI-FTMS response vs. perylene concentration.

Concentration (ppb)	$M^{+\cdot}$ peak height	SD $M^{+\cdot}$ peak height	%CV
64	5.8×10^5	1.0×10^5	18
160	1.6×10^6	5.7×10^4	3.5
320	2.7×10^6	2.2×10^5	8.1
1600	1.0×10^7	1.8×10^6	18
3200	2.8×10^7	4.7×10^6	17

Table 2. Calibration curve of ESI-FTMS response vs. coronene concentration.

Concentration (ppb)	$M^{+\cdot}$ peak height	SD $M^{+\cdot}$ peak height	%CV
76	3.4×10^5	1.6×10^4	4.8
190	1.1×10^6	7.6×10^4	7.0
380	6.8×10^6	8.0×10^5	12
1900	2.6×10^7	9.6×10^6	3.7
3800	4.3×10^7	1.2×10^6	2.8

$$[3] \quad CV = (SD/I) \times 100\%$$

where SD refers to the standard deviation in the ion ICR magnitude measurements and *I* refers to the mean ion ICR magnitude. CVs ranged from 3.5% to 18%, consistent with earlier ESI-FTMS results for biomolecules (68, 74, 75). Further experiments using Ag(I)-mediated ionization for PAHs using other mass analyzers are warranted and currently underway.

In a similar fashion, a calibration curve of MS response (determined from the peak height of the odd-electron radical cation, $M^{+\cdot}$) vs. coronene concentration was constructed (three replicate measurements) and the results are shown in Table 2. As indicated, ESI-FTMS response is linear ($R^2 = 0.9833$) with coronene concentration over a range of 76 ppb to 3.8 ppm, fit to the equation $y = 1.2 \times 10^5 x - 8.2 \times 10^5$. CVs are generally slightly better (2.8%–12%) than those observed with perylene. At coronene concentrations above 3.8 ppm, the signal intensity levels off and the calibration curve begins to deviate strongly from linear behavior, as was discussed earlier.

High mass accuracy of Ag(I)-mediated ESI-FTMS

FTMS, using a variety of ionization sources, has a long-standing history of identifying hydrocarbons from com-

© 2005 NRC Canada

Fig. 2. ESI mass spectrum of a five-component PAH sample (anthracene, pyrene, perylene, coronene, and rubrene) by silver(I)-mediated ionization. Peaks labeled with an asterisk are silver-cationized.

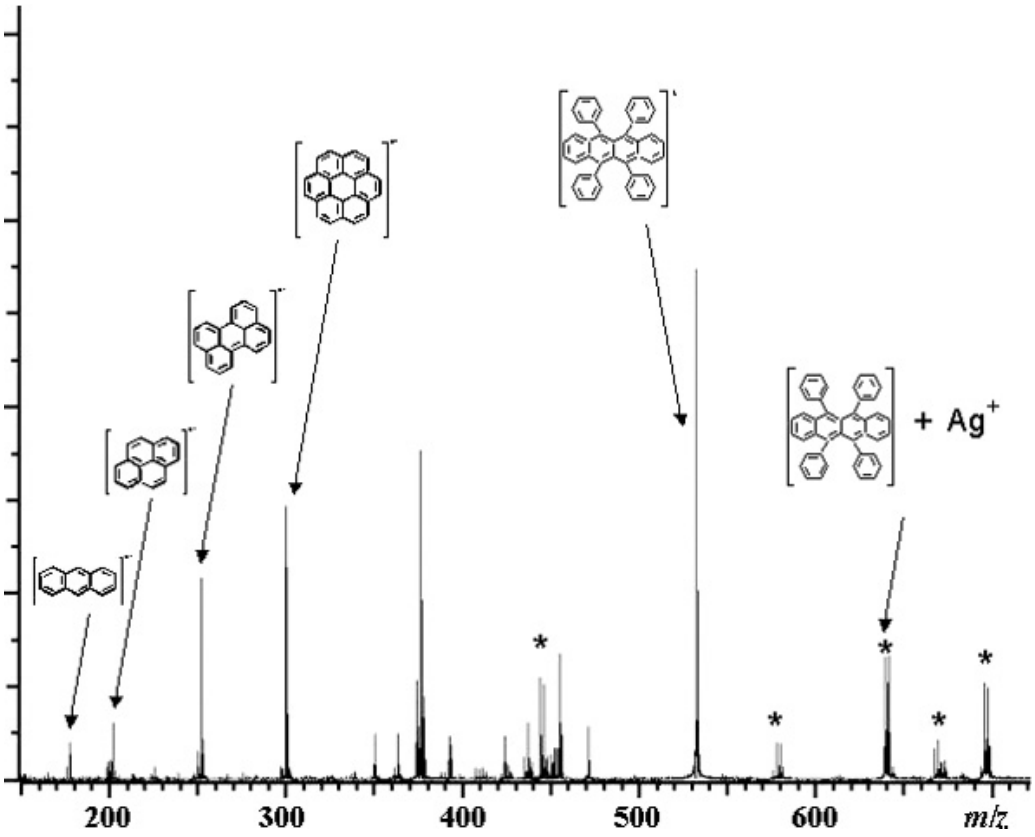


Table 3. High mass accuracy measurements by ESI-FTMS of PAH components using Ag(I)-mediated ionization.

Molecular species, $M^{+\cdot}$	Reference mass (amu)	Experimental mass (amu)	Error (ppm)
Anthracene, $C_{14}H_{10}$	178.0777	178.0776	0.3
Pyrene, $C_{16}H_{10}$	202.0777	202.0778	0.4
Perylene, $C_{20}H_{12}$	252.0934	252.0941	2.5
Coronene, $C_{24}H_{12}$	300.0934	300.0931	1.2
Rubrene, $C_{42}H_{28}$	532.2186	532.2188	0.5

plex mixtures because of its inherent high mass accuracy, on the order of a few ppm (49–55, 77–81). Here, a mixture of five PAHs (anthracene, pyrene, perylene, coronene, and rubrene, 3 μmol/L each in methanol–ethanol (50:50)) was exposed to 0.1 mmol/L $AgNO_3$ solution at the mixing tee to produce the spectrum shown in Fig. 2. As noted previously, Ag(I) mediates oxidation of the PAHs to produce $[PAH]^{+\cdot}$ odd-electron molecular parent ions for each of the compounds. From the isotope pattern, several peaks due to silver cationization are observed (as denoted in Fig. 2), but of the sample analytes, only rubrene produces an $[PAH + Ag]^+$, as shown by the *m/z* 639 and 641 doublet. High mass accuracy measurements of the five $[PAH]^{+\cdot}$ using external calibration is given in Table 3. As can be noted from Table 3, mass accuracy of the $[PAH]^{+\cdot}$ ions ranges from 0.3 to 2.5 ppm, consistent with FTMS performance. The peaks at 372.0908 and 374.1078 Da are closely matched to hydrocarbons with the molecular formulae $C_{30}H_{12}$ (–7.0 ppm error) and $C_{30}H_{14}$ (–4.6 ppm error), respectively. Even though these species differ in mass by 2 Da, examination of the ion intensities suggests these peaks are very unlikely to be silver-cationized species. Further, peaks at 348.0939 and 350.1130 Da are tentatively identified as the molecular formulae $C_{28}H_{12}$ (1.5 ppm error) and $C_{28}H_{14}$ (10.9 ppm error), respectively. Other low ICR magnitude peaks at 361.0999, 363.1219, and 393.1258 Da are also observed. The exact mass difference between the species at 361.0999 and 393.1259 Da is 32.0260 Da, consistent with the mass of neutral methanol, which is used in the ESI solvent. However, their odd nominal masses indicate the presence of an odd number of nitrogen atoms, and it is not clear chemically how these might have been formed from neat PAH samples unless the nitrate from silver nitrate is somehow being incorporated into the molecular structure.

Conclusions

The methodology shown here demonstrates the applicability of using Ag(I) salt as an in situ ionization reagent for nonpolar molecules (PAHs) in a conventional ESI source. The effectiveness of Ag(I)-mediated cationization is demonstrated using ESI Fourier transform mass spectrometry for the detection and identification of priority pollutant polyaromatic hydrocarbon (PAH) species. In contrast to earlier coordination ESI-MS reports employing silver salts, argentated species are generally *not* observed for PAH spe-

© 2005 NRC Canada

cies, but instead radical cations ($[PAH]^{+\cdot}$) are produced. The high mass accuracy of FTMS used as the detector allows for identification of PAH molecular formulas. The low detection limits and linear response of the FTMS with solution concentration of PAH suggests the potential for quantitative analysis, although in complex, real-world environmental samples this will need to be tested because the presence of other analytes may significantly influence ion yield for the analyte of interest. In addition, if coupled to a miniaturized mass spectrometer such as an ion trap equipped with ESI (82), Ag(I)-mediated cationization of PAHs might be well-suited for on-line determination of PAHs from environmental water and soil samples.

Acknowledgments

We would like to congratulate Professor Kebarle on an outstanding career and to thank him in particular for all of his contributions to understanding the ESI mechanism; without his inspiration, this manuscript would never have been possible. Acknowledgment is made to the donors of the Petroleum Research Fund, administered by the American Chemical Society, the American Society for Mass Spectrometry (Research Award sponsored by the Exxon Education Foundation), and the State University of New York at Buffalo for support of this research.

References

1. J.B. Fenn, M. Mann, C.K. Meng, S.F. Wong, and C.M. Whitehouse. Science (Washington, D.C.), **246**, 64 (1989).
2. J. Fernandez de la Mora, G.J. Van Berkel, C.G. Enke, R.B. Cole, M. Martinez-Sanchez, and J.B. Fenn. J. Mass Spectrom. **35**, 939 (2000).
3. R.B. Cole (*Editor*). Electrospray ionization mass spectrometry: fundamentals, instrumentation and applications. John Wiley and Sons, Inc., New York. 1997. pp. 577.
4. R.D. Smith, J.A. Loo, R.A. Ogorzalek Loo, M. Busman, and H.R. Udseth. Mass Spectrom. Rev. **10**, 359 (1991).
5. M.G. Ikonomou, A.T. Blades, and P. Kebarle. Anal. Chem. **62**, 957 (1990).
6. M.G. Ikonomou, A.T. Blades, and P. Kebarle. Anal. Chem. **63**, 1989 (1991).
7. J.V. Iribarne and B.A. Thomson. J. Chem. Phys. **64**, 2287 (1976).
8. A.T. Blades, M.G. Ikonomou, and P. Kebarle. Anal. Chem. **63**, 2109 (1991).
9. M.G. Ikonomou, A.T. Blades, and P. Kebarle. J. Am. Soc. Mass Spectrom. **2**, 492 (1991).
10. F.M. Wampler III, A.T. Blades, and P. Kebarle. J. Am. Soc. Mass Spectrom. **4**, 289 (1993).
11. L. Tang and P. Kebarle. Anal. Chem. **63**, 2709 (1991).
12. P. Kebarle and L. Tang. Anal. Chem. **65**, 972A (1993).
13. P. Kebarle. J. Mass Spectrom. **35**, 804 (2000).
14. C. Rentel, S. Strohschein, K. Albert, and E. Bayer. Anal. Chem. **70**, 4394 (1998).
15. C. Rentel, P. Gfrorer, and E. Bayer. Electrophoresis, **20**, 2329 (1999).
16. E. Bayer, P. Gfrorer, and C. Rentel. Angew. Chem. Int. Ed. **38**, 992 (1999).
17. K.M. Ng, N.L. Ma, and C.W. Tsang. Rapid Commun. Mass Spectrom. **17**, 2082 (2003).
18. S.G. Roussis and R. Proulx. Rapid Comm. Mass Spectrom. **18**, 1761 (2004).
19. G.J. Van Berkel, S.A. McLuckey, and G.L. Glish. Anal. Chem. **64**, 1586 (1992).
20. G.J. Van Berkel and F.M. Zhou. Anal. Chem. **66**, 3408 (1994).
21. G.J. Van Berkel, K.G. Asasno, and S.A. McLuckey. J. Am. Soc. Mass Spectrom. **5**, 689 (1994).
22. F. Zhou, G.J. Van Berkel, and B.T. Donovan. J. Am. Chem. Soc. **116**, 5485 (1994).
23. F.M. Zhou and G.J. Van Berkel. Anal. Chem. **67**, 3643 (1995).
24. G.J. Van Berkel and F.M. Zhou. Anal. Chem. **67**, 3958 (1995).
25. G.J. Van Berkel and F.M. Zhou. Anal. Chem. **67**, 2916 (1995).
26. G.J. Van Berkel and F.M. Zhou. J. Am. Soc. Mass Spectrom. **7**, 157 (1996).
27. S.L. Zhou, A.G. Edwards, K.D. Cook, and G.J. Van Berkel. Anal. Chem. **71**, 769 (1999).
28. H.T. Deng and G.J. Van Berkel. Anal. Chem. **71**, 4284 (1999).
29. H.T. Deng and G.J. Van Berkel. Electroanalysis, **11**, 857 (1999).
30. G.J. Van Berkel, G.E. Giles, J.S. Bullock, and L.J. Gray. Anal. Chem. **71**, 5288 (1999).
31. G.J. Van Berkel. J. Am. Soc. Mass Spectrom. **11**, 951 (2000).
32. G.J. Van Berkel, K.G. Asano, and P.D. Schnier. J. Am. Soc. Mass Spectrom. **12**, 853 (2001).
33. V. Kertesz and G.J. Van Berkel. J. Mass Spectrom. **36**, 204 (2001).
34. G.J. Van Berkel, K.G. Asano, and V. Kertesz. Anal. Chem. **74**, 5047 (2002).
35. G.J. Van Berkel, V. Kertesz, M.J. Ford, and M.C. Granger. J. Am. Soc. Mass Spectrom. **15**, 1755 (2004).
36. T. Yoshikawa, L.P. Ruhr, W. Flory, D. Giamalva, D.F. Church, and W.A. Pryor. Toxicol. Appl. Pharmacol. **79**, 218 (1985).
37. M.V. Buchanan and R.L. Hettich. Anal. Chem. **65**, 245A (1993).
38. C.L. Holliman, D.L. Rempel, and M.L. Gross. Mass Spectrom. Rev. **13**, 105 (1994).
39. F.W. McLafferty. Acc. Chem. Res. **27**, 379 (1994).
40. E.R. Williams. Anal. Chem. **70**, 179A (1998).
41. A.G. Marshall, C.L. Hendrickson, and G.S. Jackson. Mass Spectrom. Rev. **17**, 1 (1998).
42. S.A. Lorenz, E.P. Maziarz III, and T.D. Wood. Appl. Spectrosc. **53**, 18A (1999).
43. C.L. Hendrickson and M.R. Emmett. Annu. Rev. Phys. Chem. **50**, 517 (1999).
44. A.G. Marshall. Int. J. Mass Spectrom. **200**, 331 (2000).
45. N.L. Kelleher. Chem. Biol. **7**, R37 (2000).
46. J. Bergquist, M. Palmblad, M. Wetterhall, P. Hakansson, and K.E. Markides. Mass Spectrom. Rev. **21**, 2 (2002).
47. A.P. Null and D.C. Muddiman. J. Mass Spectrom. **36**, 589 (2001).
48. L.K. Zhang, D. Rempel, B.N. Pramanik, and M.L. Gross. Mass Spectrom. Rev. **24**, 286 (2005).
49. K. Miyabayashi, K. Suzuki, T. Taranishi, Y. Naitro, K. Tsujimoto, and M. Miyhake. Chem. Lett. 172 (2000).
50. K. Miyabayashi, Y. Naito, M. Miyake, and K. Tsujimoto. Eur. Mass Spectrom. **6**, 251 (2000).
51. M.P. Barrow, L.A. McDonnell, X.D. Feng, J. Walker, and P.J. Derrick. Anal. Chem. **75**, 860 (2003).
52. T.M. Schaub, C.L. Hendrickson, K.N. Qian, J.P. Quinn, and A.G. Marshall. Anal. Chem. **75**, 2172 (2003).
53. K. Miyabayashi, Y. Naito, K. Tsujimoto, and M. Miyake. Int. J. Mass Spectrom. **235**, 49 (2004).
54. C.A. Hughey, R.P. Rodgers, A.G. Marshall, C.C. Walters, K.N. Quian, and P. Mankiewicz. Org. Geochem. **35**, 863 (2004).
55. M.P. Barrow, J.V. Headley, K.M. Peru, and P.J. Derrick. J. Chromatogr. A, **1058**, 51 (2004).

© 2005 NRC Canada

56. A. Fievre, T. Solouki, A.G. Marshall, and W.T. Cooper. Energy Fuels, **11**, 554 (1997).
57. A.C. Stenson, W.M. Landing, A.G. Marshall, and W.T. Cooper. Anal. Chem. **74**, 4397 (2002).
58. E.B. Kujawinski. Environ. Forensics, **3**, 207 (2002).
59. R.W. Kramer, E.B. Kujawinski, and P.G. Hatcher. Environ. Sci. Technol. **38**, 3387 (2004).
60. T. Solouki, M.A. Freitas, and A. Alomary. Anal. Chem. **71**, 4719 (1999).
61. A. Alomary, T. Solouki, H.H. Patterson, and C.S. Cronan. Environ. Sci. Technol. **34**, 2830 (2000).
62. E.B. Kujawinski, P.G. Hatcher, and M.A. Freitas. Anal. Chem. **74**, 413 (2002).
63. E.B. Kujawinski, M.A. Freitas, X. Zang, P.G. Hatcher, K.B. Green-Church, and R.B. Jones. Org. Geochem. **33**, 171 (2002).
64. A.C. Stenson, A.G. Marshall, and W.T. Cooper. Anal. Chem. **75**, 1275 (2003).
65. E.B. Kujawinski, R. Del Vecchio, N.V. Blough, G.C. Klein, and A.G. Marshall. Mar. Chem. **92**, 23 (2004).
66. T.M. Schaub, H.B. Linden, C.L. Hendrickson, and A.G. Marshall. Rapid Commun. Mass Spectrom. **18**, 1641 (2004).
67. T.M. Schaub, C.L. Hendrickson, J.P. Quinn, R.P. Rodgers, and A.G. Marshall. Anal. Chem. **77**, 1317 (2005).
68. H.R. Padley, S. Bashir, and T.D. Wood. Anal. Chem. **69**, 2914 (1997).
69. P. Caravatti. US Patent 4 924 089, 8 May 1990.
70. M.S. Kahr and C.L. Wilkins. J. Am. Soc. Mass Spectrom. **4**, 453 (1993).
71. S.G. Lias. *In* NIST Chemistry WebBook, NIST Standard Reference Database Number 69. *Edited by* P.J. Linstrom and W.G. Mallard. National Institute of Standards and Technology, Gaithersburg, Md. 2001.
72. S.F. Macha, T.D. McCarley, and P.A. Limbach. Anal. Chim. Acta, **397**, 235 (1999).
73. C. Robins and P.A. Limbach. Rapid Commun. Mass Spectrom. **17**, 2839 (2003).
74. E.F. Gordon and D.C. Muddiman. Rapid Commun. Mass Spectrom. **13**, 164 (1999).
75. S.A. Lorenz, M.A. Moy, A.R. Dolan, and T.D. Wood. Rapid Commun. Mass Spectrom. **13**, 2098 (1999).
76. Z. Liang and A.G. Marshall. Anal. Chem. **62**, 70 (1990).
77. P.F. Greenwood, M.G. Strachan, G.D. Willett, and M.A. Wilson. Org. Mass Spectrom. **25**, 353 (1990).
78. C.S. Hsu, Z. Liang, and J.E. Campana. Anal. Chem. **66**, 850 (1994).
79. S. Guan, A.G. Marshall, and S.E. Scheppele. Anal. Chem. **68**, 46 (1996).
80. R.P. Rodgers, E.N. Blumer, M.A. Freitas, and A.G. Marshall. Anal. Chem. **71**, 5171 (1999).
81. R.P. Rodgers, E.N. Blumer, M.A. Freitas, and A.G. Marshall. J. Forensic Sci. **46**, 268 (2001).
82. Z. Takats, K.J. Koch, and R.G. Cooks. Anal. Chem. **73**, 4522 (2001).

© 2005 NRC Canada

Fragmentation pathways of negative ions produced by electrospray ionization of acyclic dicarboxylic acids and derivatives[1]

J. Stuart Grossert, Paul D. Fancy, and Robert L. White

Abstract: Fragmentation pathways have been studied on the monoanions formed during electrospray ionization of a wide range of aliphatic dicarboxylic acids and their monoesters. All negative ion spectra were obtained from alcoholic or aqueous methanolic solutions without buffers or adjustment of pH, using either a Finnigan LCQ ion trap or a VG-Micromass Quattro triple quadrupole mass spectrometer. Fragmentation pathways were studied using collision-induced dissociation and isotopic-labelling techniques. Two primary fragmentation pathways of the dicarboxylic acid monoanions were observed, namely decarboxylation of the non-ionized carboxyl group and loss of water from this group. The fragmentations were strongly dependent on the chain lengths of the diacids. In the case of a monoester anion, loss of a molecule of alcohol paralleled the loss of water from the diacid monoanion. Losses of water or alcohol were shown to lead to formation of reactive ynolate anions ($HOOC(CH_2)_xC{\equiv}CO^-$, x = 3–9), which in the ion trap spectrometer engaged in complex ion – molecule reactions consistent with the chemistry of these anions. For the longer chains ($x > 6$), the interactions between the ionized and non-ionized carboxyl groups led to readily formed ion–neutral complexes, which are described as a neutral molecule (ROH, R = H or alkyl) held by a pair of molecular tweezers.

Key words: ESI-MS/MS on negative ions, fragmentation pathways of acyclic carboxylic acid monoanions, ion–molecule reactions in an ion trap mass spectrometer, hydrogen–deuterium exchange in a gas-phase anion–neutral complex.

Résumé : Faisant appel à un spectromètre de masse Finnigan LCQ à piège d'ion ou VG-Micromass Quattro quadripolaire triple, on a étudié les voies de fragmentation des monoanions qui se forment lors de l'ionisation par électronébulisation d'un large éventail d'acides dicarboxyliques aliphatiques et de leurs monoesters. On a obtenu tous les spectres d'ions négatifs à partir de solutions alcooliques ou méthanoliques aqueuses, sans tampon ou ajustement de pH. On a étudié les voies de fragmentation en faisant appel à des techniques de dissociation induite par des collisions et par marquage isotopique. On a observé deux voies primaires de fragmentation des monoanions des acides dicarboxyliques, soit la décarboxylation du groupe carboxyle qui n'est pas ionisé et une perte d'eau à partir de ce groupe. Les fragmentations dépendent fortement des longueurs de chaînes des diacides. Dans le cas d'un anion d'un monoester, la perte d'une molécule d'alcool est parallèle à celle de la perte d'une molécule d'eau à partir du monoanion du diacide. On a montré que la perte d'eau ou la perte d'alcool conduit à la formation d'anions ynolates réactifs, $HOOC(CH_2)_xC{\equiv}CO^-$, x = 3–9 qui, dans le spectromètre à piège d'ion participe à une série complexe de réactions ion–molécule qui est en accord avec la chimie de ces anions. Pour les chaînes plus longues ($x > 6$), les interactions entre les groupes carboxyles ionisés et non ionisés conduisent à la formation facile de complexes ion – entité neutre qui sont décrits comme une molécule neutre (ROH, R = H ou alkyle) retenu par des pinces moléculaires.

Mots clés : ESI-MS/MS d'ions négatifs, voies de fragmentations de monoanions d'acides dicarboxyliques acycliques, réactions ion–molécule dans un piège à ion d'un spectromètre de masse, échange hydrogène–deutérium dans un complexe anion–produit neutre en phase gazeuse.

[Traduit par la Rédaction]

Introduction

The importance of negative ion mass spectrometry has increased since the advent of chemical ionization (CI) and fast atom bombardment (FAB) methods (1–3). More recently, the proliferation of mass spectrometers equipped with electrospray ionization (ESI) and quadrupole, ion trap, or time-of-flight mass analyzers has allowed negative ions to be studied as easily as positive ions. Using ESI-MS, negative ions are easily generated from solutions of molecules

Received 5 May 2005. Published on the NRC Research Press Web site at http://canjchem.nrc.ca on 9 January 2006.

This paper is dedicated to Professor Paul Kebarle in recognition of his outstanding contributions to chemistry.

J.S. Grossert,[2] P.D. Fancy, and R.L. White.[3] Department of Chemistry, Dalhousie University, Halifax, NS B3H 4J3, Canada.

[1]This article is part of a Special Issue dedicated to Professor P. Kebarle.

[2]Corresponding author (e-mail: J.S.Grossert@Dal.ca).
[3]Corresponding author (e-mail: Robert.White@Dal.ca).

 doi: 10.1139/V05-214 © 2005 NRC Canada

containing readily ionizable functional groups (4). The approach has been applied successfully to fatty acids (5, 6), peptides (7–11), and pharmaceuticals containing carboxylic acids (12).

Fragmentation pathways examined by collision-induced dissociation (CID) using linked-scan methods at high collision energies (2) or more recently, at low collision energies (8, 9), have provided evidence from which structural information about the ions can be deduced. Bowie and co-workers (8–10), in particular, have shown that CID experiments at low collision energies on deprotonated peptide ions, generated by ESI, complement the results obtained from studies of protonated peptides. Although CID spectra of negative ions are easily obtained using modern mass spectrometers, work on the fragmentation pathways of negative ions remains limited, compared with that on positive ions.

In earlier studies on the fragmentation of carboxylate anions (2, 13, 14), CID experiments at high collision energies showed that different pathways exist for anions formed by O–H deprotonation and enolate anions formed by α-C–H deprotonation of aliphatic carboxylic acids. It appeared that the pathway for loss of water from the anion of carboxylic acids was via the enolate anion and an ion–neutral complex, followed by the formation of an ynolate anion and water (see the following). However, protons were observed to exchange on collisions, complicating the interpretation of the spectra. Further details of the mechanism for the loss of water from a carboxylate anion emerged from the work of Jensen et al. (15) who found that the ion $[CH_3(CH_2)_5CD_2COO]^-$ prepared in a FAB source on collisional activation cleanly lost D_2O (>90%), whereas the corresponding 2,3-dideutero compound lost HOD. These authors presented evidence to support the concept that a carboxylate anion could be converted into the corresponding enolate anion, which can fragment into a complex of a hydroxide anion and a ketene from which water can be lost (eq. [1]).

$$[1] \quad RCD_2COO^- \rightarrow R^-CDCOOD \rightarrow [RCD{=}C{=}O + OD]^- \rightarrow RC{\equiv}CO^- + D_2O$$

Loss of water as the only fragmentation pathway of deprotonated saturated fatty acids was shown by MS/MS studies at low collision energies using a SCIEX API III triple quadrupole spectrometer having an ESI source (5). This was achieved by varying the orifice voltage and the collision gas thickness, with increases above the optimum producing no other reaction pathway.

Another approach to studying the loss of water from the anions derived from fatty acids used resonant electron capture mass spectrometry and high-energy CID (16). These experiments led, via an unobserved radical anion, either to the carboxylate anion or to an anion on the chain. Studies on the labelled carbanion ($[CH_3(CH_2)_{13}CD_2COOH–H/D]^-$) showed losses of both H_2O and HOD, indicating a selective rearrangement process, but the ions in these experiments appear to be different from those described in the previous FAB experiments (15).

A recent survey of the MS/MS spectra of over 100 carboxylic acids, including some dicarboxylic acids, attempted to correlate structures with the loss of carbon dioxide (12). The work was focused on analytical applications and did not describe other possible fragmentations. Other ESI-MS studies on a wide range of dicarboxylic acids were limited to the formation of halide ion complexes (17) and to the effects of solvents on ionization (6); neither work reported on fragmentations of dicarboxylic acid anions. The work by Aplin et al. (6) showed predominantly monoanion formation; dianions were formed as the most abundant ion only when $\geq C_{12}$ dicarboxylic acids were dissolved in MeOH–water (1:1). Preferred monoanion formation by the diacids having shorter chain lengths was attributed to stabilization by intramolecular hydrogen bonding between the ionized and non-ionized carboxyl groups (6), analogous to the cluster ions formed between aliphatic carboxylic acids (14, 18). Similarly, the high proton affinities of diamines (19–22) and diols (23), as well as the acidities of diols (24), have been attributed to the stabilization of gas-phase ions by intramolecular hydrogen bonding between an ionized and a non-ionized functional group. Furthermore, the fragmentation of protonated lysine has been interpreted on the basis of considerable hydrogen bonding between a proton and the two amino groups (25).

Understanding the mass spectral fragmentation pathways of ions generated by electrospray ionization is important for the structural characterization of polyfunctional compounds such as peptides (7–9), drug metabolites (12), and products of bacterial metabolism (26). In the present investigation, we focus on low-energy fragmentation mechanisms as a function of chain length for a series of monoanions from dicarboxylic acids and some diacid monoesters. The gas-phase ions studied show interactions among remote functional groups in an acyclic chain (24, 27). Moreover, they point to the importance of considering interactions between ionized and nonionized carboxyl groups in studying the fragmentation pathways of more complex polyfunctional ions, such as the anions derived from aminodicarboxylic and hydroxydicarboxylic acids as well as from peptides.

Experimental

All acid samples were obtained from Sigma-Aldrich (Oakville, Ontairo) or Acros Organics (Nepean, Ontario), unless otherwise specified; 2,2,9,9-tetradeuterosebacic (decanedioic) (99.3% d_4) and [1-^{13}C]- and [5-^{13}C]-glutamic acids were from CDN isotopes (Montreal, Quebec); [4-^{13}C]aspartic acid was from MSD isotopes (Montreal, Quebec); α-methyl aspartate and glutarate were from CHEM-IMPEX (Wood Dale, Illinois). The isotopic purity of the 2,2,9,9-tetradeuterosebacic acid was checked by ESI-MS and found to be as indicated by the manufacturer. The side chain methyl ester of aspartic acid was available from a previous study (28).

Negative ion ESI spectra were obtained by flow injection analysis (20 μL min^{-1}) of the aliphatic dicarboxylic acids and their derivatives dissolved in HPLC grade methanol, or in aqueous methanol (1:1), at concentrations ranging from 0.2 to 1 mg mL^{-1}. Regular mass spectra and MS/MS spectra at low collision energies were obtained on either a Finnigan LCQ Duo ion trap or a Micromass Quattro triple quadrupole mass spectrometer. Spectra from the LCQ were run with the ESI needle at 4000 V and the capillary at 200 °C. Nitrogen was used as the nebulizing gas, with helium as the damping and collision gas in the trap under regular conditions. CID

© 2005 NRC Canada

Table 1. Primary fragmentations by MS/MS of $[M - H]^-$ ions from dicarboxylic acids and some monoesters having C-3 to C-12 chain lengths.

Precursor ion (*m/z*)	Collision energy (%)[a]	Fragment ions *m/z*, (rel. inten.)	Neutral loss(es)
103,[b] $[C_3H_3O_4]^-$	24	59 (100)	CO_2
117,[b] $[C_4H_5O_4]^-$	25	99 (32), 73 (100)	H_2O, CO_2
131,[b] $[C_5H_7O_4]^-$	25	113 (62), 87 (100)	H_2O, CO_2
145,[b] $[C_6H_9O_4]^-$	24	127 (80), 101 (40), 83 (100)	H_2O, CO_2, (H_2O+CO_2)
159,[b] $[C_7H_{11}O_4]^-$	24	141 (31), 115 (3), 97 (100)	H_2O, CO_2, (H_2O+CO_2)
173,[b] $[C_8H_{13}O_4]^-$	24	155 (5), 129 (1), 111 (100)	H_2O, CO_2, (H_2O+CO_2)
187,[b] $[C_9H_{15}O_4]^-$	24	169 (8), 143 (1), 125 (100)	H_2O, CO_2, (H_2O+CO_2)
201,[b] $[C_{10}H_{17}O_4]^-$	24	183 (76), 139 (100)	H_2O, (H_2O+CO_2)
229,[b] $[C_{12}H_{21}O_4]^-$	24	211 (100), 167 (20)	H_2O, (H_2O+CO_2)
145,[c] $[C_6H_9O_4]^-$	22	113 (100)	MeOH
215,[d] $[C_{11}H_{19}O_4]^-$	22	183 (100), 139 (32)	MeOH, $(MeOH+CO_2)$
199,[e] $[C_{12}H_{23}O_2]^-$	40	181 (100)	H_2O

[a]Collision energies expressed as an arbitrary percentage using the LCQ ion trap MS.
[b]Monoanions from malonic (C_3), succinic (C_4), glutaric (C_5), adipic (C_6), pimelic (C_7), suberic (C_8), azelaic (C_9), sebacic (C_{10}), and dodecanedioic (C_{12}) acids.
[c]Monoanion from glutaric acid monomethyl ester.
[d]Monoanion from sebacic acid monomethyl ester.
[e]Dodecanoic acid anion added for comparison with the diacid monoanions.

experiments are reported in arbitrary percentage units from the Xcalibur software in which an energy of 16% began to produce fragmentation of most ions studied, but an energy of 40% typically reduced the intensity of the ion being fragmented to almost zero. In a few experiments noted in the text, a voltage was applied to promote source-induced collisions. In the case of the Quattro MS, the bath and nebulizer gases were nitrogen at optimized flow rates, the source temperature was set between 90 and 100 °C, the electrospray needle was at 3000 V, and the source cone voltage varied between 10 and 40 V, depending on the spectrum being acquired. CID experiments were carried out using argon collision gas at energies reported in eV (laboratory frame). The argon was at a pressure to reduce the main beam by 50%–80%. Spectra from the LCQ ion trap were averaged and processed using the supplied Xcalibur software; in the case of the Quattro MS, 10–30 spectra were combined, background-subtracted, and smoothed using MassLynx software.

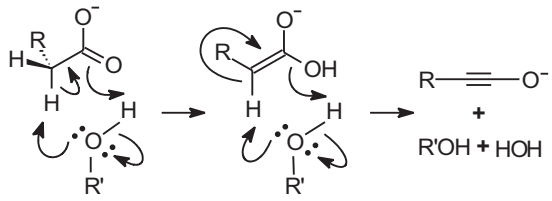
Results and discussion

Acyclic monocarboxylic acids

Using either the LCQ or the Quattro MS, electrospray ionization of a methanolic solution of dodecanoic (lauric) acid readily led to full-scan mass spectra showing the deprotonated molecule ($CH_3(CH_2)_{10}COO^-$). In the LCQ ion trap MS, loss of water from this ion was observed in the MS/MS spectrum only at a relatively high collision energy (see Table 1), about 70% greater than the energy needed to fragment the monoanions of dicarboxylic acids. Using the Quattro MS, neither loss of water nor any other fragmentation was observed from $CH_3(CH_2)_{12}COO^-$, even at collision energies up to 40 eV.

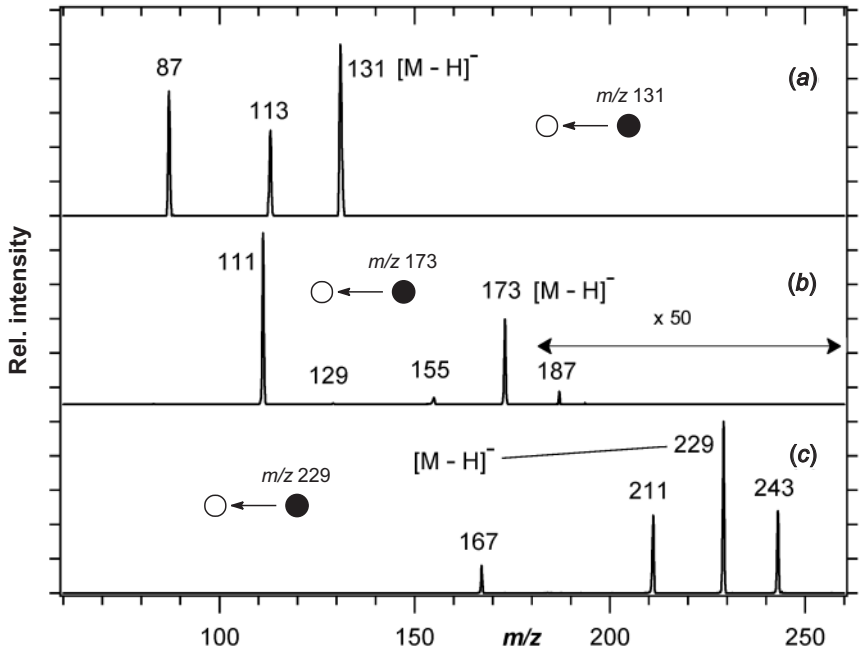
Previously, loss of water from carboxylic acid anions has been observed in negative ion CI and high-energy CID studies by Bowie (2) and in lower energy CID experiments conducted by Kerwin et al. (5) using electrospray ionization on a SCIEX API III MS. The latter authors noted that increased fragmentation could be brought about by increasing the collision gas pressure, which suggests that ion–molecule collisions are important for the conversion of carboxylate anions to the enolate anions needed for the loss of water to be observed. From our later experiments on the LCQ MS (vide infra), it became apparent that collisions in the trap occur not only with the helium damping gas, but also with solvent molecules. These collisions of ions with solvent molecules could facilitate other reaction pathways in the trap and lead to a variety of ions that might not have been expected. Accordingly, we suggest that elimination of water from a carboxylate anion in the LCQ ion trap is a process involving an ion – solvent molecule complex, as outlined in Scheme 1, and is not induced simply by collisions of an ion with an inert gas. The reactions proposed in Scheme 1 are directly comparable to those outlined in eq. [1], except that they are bimolecular and solvent assisted. In the Quattro MS, the solvent molecules are pumped away in the source volume and very few, if any, would penetrate into the chamber holding the quadrupole mass analyzers and the collision cell. Finally, we have no evidence that the direct loss of carbon dioxide from the laurate anion to form a carbanion occurred in either mass spectrometer nor is this pathway likely under the conditions employed in these spectrometers (29).

Scheme 1.



© 2005 NRC Canada

Fig. 1. MS/MS fragment ion spectra (LCQ ion trap, methanol) of the monoanions from (*a*) glutaric (*m/z* 131, 25% rel. CID), (*b*) suberic (*m/z* 173, 24% CID), and (*c*) dodecanedioic acids (*m/z* 229 = **f**, 24% CID; *m/z* 211 = **g**; *m/z* 243 = adduct ion **fm**).



Acyclic dicarboxylic acids

The negative ion ESI mass spectra collected for the series of C_3–C_{12} dicarboxylic acids dissolved in methanol showed a major ion at an *m/z* value corresponding to $[M - H]^-$, indicating facile anion formation from a weakly acidic solution (4) and the ionization of only one of the two acidic groups in the dicarboxylic acid during electrospray ionization. No evidence of dianion formation was apparent in any of the spectra. For dianion formation to occur, a second ionization step would require much higher energy to overcome the stabilization provided by intramolecular hydrogen bonding in the monoanion (6). This hydrogen bonding between the ionized carboxyl group and the proton of the second carboxyl group (the most acidic hydrogen in the molecule) is possible only if the chain is long enough and if the monoanion adopts a coiled conformation placing the two functional groups in close proximity. The concept of coiled conformations in the gas phase leading to stabilizing interactions between ionized and non-ionized functional groups is well-documented (19–21, 24).

Intermolecular interactions leading to the association of ionized and non-ionized carboxylic acids have been studied using CI-MS (18). In ESI-MS, a low source cone voltage allows intermolecular adducts to remain intact. For dodecanedioic acid, a regular Quattro MS scan (10 V on the source cone) showed that the intermolecular proton-bound anion dimer ($[C_{24}H_{43}O_8]^-$) was present at *m/z* 459 at about 10% of the intensity of the unsolvated monoanion at *m/z* 229. For glutaric and adipic acids, similar intermolecular dimers were observed by using the Quattro MS but not by using the LCQ MS. The low relative abundances of these dimer anions indicates the greater importance of intramolecular vs. intermolecular interactions.

General trends in fragmentation patterns of dicarboxylic acid monoanions

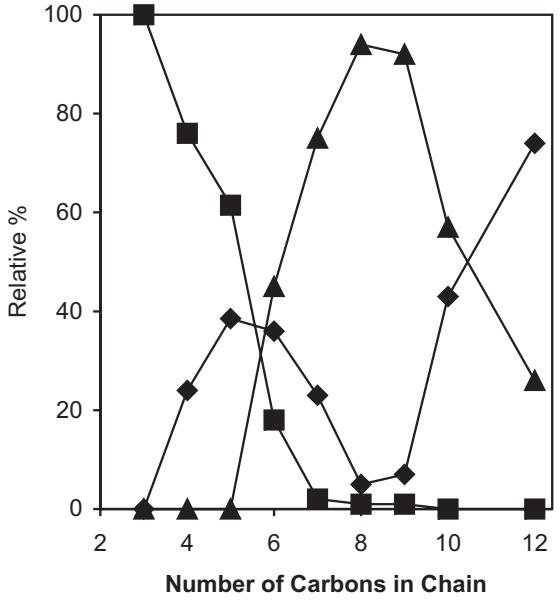
Typical MS/MS spectra, using the LCQ ion trap MS, of dicarboxylic acid monoanions from glutaric (C_5), suberic (C_8), and dodecanedioic (C_{12}) acids are shown in Fig. 1 as representative examples of the series examined. For the purpose of comparison with Fig. 1*c*, MS/MS spectra from the Quattro MS of the monoanion from dodecanedioic acid has been included in the Supplementary data for this paper.[4]

At the same nominal collision energies in the LCQ MS, the independent and combined losses of water and carbon dioxide were strongly dependent on chain length (Fig. 2). An overview of the results is given in Table 1. Except for malonic acid, a primary fragmentation resulting in loss of water was evident in the spectrum of each dicarboxylic acid. For shorter chain diacids ($\leq C_6$), decarboxylation was a competing primary process, decreasing in importance with increasing chain length and becoming negligible for diacids $\geq C_7$. For diacids $\geq C_6$, the combined loss of ($H_2O + CO_2$) was observed, becoming the dominant process at intermediate chain lengths (i.e., C_6–C_{10}). Loss of water was the dominant process for the C_{12} diacid. The strong dependence of the fragmentation pathways on the chain length of the dicarboxylic acids suggested a close relationship between chain length and mechanism. Mechanistic information was obtained by studying a selected range of compounds, by using

[4] Supplementary data for this article are available on the Web site or may be purchased from the Depository of Unpublished Data, Document Delivery, CISTI, National Research Council Canada, Ottawa, ON K1A 0R6, Canada. DUD 4060. For more information on obtaining material refer to http://cisti-icist.nrc-cnrc.gc.ca/irm/unpub_e.shtml.

© 2005 NRC Canada

Fig. 2. Fragmentation patterns of $[M - H]^-$ ions from acyclic dicarboxylic acids vs. chain length (LCQ MS), with the intensity of each fragmentation being relative to the sum of the three fragmentation processes ($-CO_2$ (■), $-H_2O$ (◆), $-(H_2O + CO_2)$ (▲)).



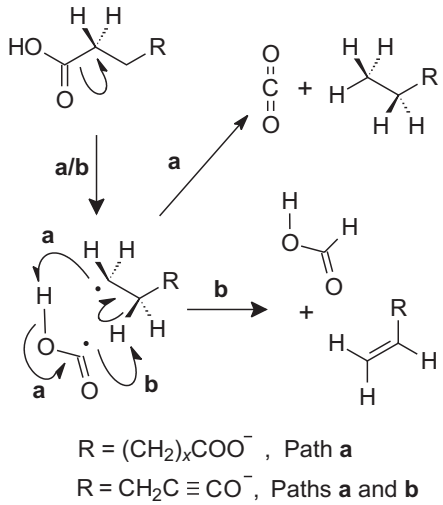
fragment ion, precursor ion and neutral loss scans on the Quattro MS, as well as by using compounds labelled at specific atoms with ^{13}C or deuterium.

Decarboxylations of short-chain dicarboxylate monoanions

The malonate anion has the shortest chain of the ions examined. Malonic acid solutions produced only peaks at *m/z* 103 and 59; no precursor ions and only fragment ions were observed at 24% collision energy, whereas precursor ions from the anions of all the other acids were present at this collision energy. The fragmentation of *m/z* 103 is explicable in terms of a simple bond heterolysis to yield carbon dioxide and the enolate anion of acetic acid.

The greater separation between the carboxyl groups in the diacids having more than three carbon atoms decreased the likelihood that decarboxylation would occur by simple bond heterolysis. Furthermore, the monoanion from a dicarboxylic acid contains both an ionized and a non-ionized carboxyl group, either one of which could in principle lose carbon dioxide. Distinction between the groups was readily achieved using aspartic and glutamic acids. Negative ions, localized at the more acidic α-carboxyl group, were generated from aqueous methanol. On CID, they showed losses of 18 u (water) and 44 u (carbon dioxide); in the case of Asp, 17 u (ammonia) was lost also. Clear evidence supporting decarboxylation of the α- or the side-chain carboxyl group came from aspartic (Asp) and glutamic (Glu) acids labelled with ^{13}C. Fragmentation of the $[M - H]^-$ ion at *m/z* 147 from [1-^{13}C]glutamate gave a series of fragment ions analogous to those observed for unlabelled glutamate. Each ion in the CID mass spectrum of [1-^{13}C]glutamate was, however, one mass unit higher, indicating retention of the ^{13}C label during all fragmentation processes. In the CID spectra of [4-^{13}C]aspartic acid and [5-^{13}C]glutamic acid, losses of 17 and 18 u from the $[M - H]^-$ ion were consistent with losses of ammonia and water, respectively, and retention of the ^{13}C label in the side chain. For these samples, a loss of 45 u from the $[M - H]^-$ ion signified that ^{13}C was associated with the $^{13}CO_2$ being formed upon fragmentation, clearly associating decarboxylation with the non-ionized side-chain carboxyl group. This result is complementary to that obtained in the positive ion CID mass spectra of acidic amino acids where the α-carboxyl group is lost by sequential losses of water and carbon monoxide (25, 30, 31).

Scheme 2.



The spectra obtained point to the elimination of carbon dioxide being a unimolecular process, which must be initiated by homolytic cleavage of a C—C bond, followed by hydrogen atom abstraction by the resulting carbon radical, as outlined in Scheme 2*a*. A consequence of this proposed mechanism is that its facility depends on the strength of the C—C bond being cleaved and conceivably this is a function of the chain length of the dicarboxylic acid monoanions. However, it may also be that other reaction pathways simply become more important as the chain length increases. Support for the process being unimolecular and involving a tightly held radical pair comes from the fact that the anion from deuterated glutaric acid (R-COOD) cleanly retained the deuterium label on decarboxylation with no sign of scrambling. Evidence that the structures of product anions from these eliminations must be carboxylates of acyclic monoacids could be deduced from the fact that these ions could not be further fragmented in the collision cell of the Quattro MS. The elimination of carbon dioxide could be mechanistically analogous to the thermal decomposition of formic acid into dihydrogen and carbon dioxide (32). Further details of the decarboxylation process are presented in the next section.

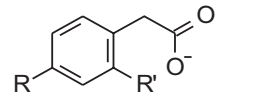
Using the Quattro mass spectrometer, a full range of fragment, precursor, and neutral loss scans was made for the fragmentation of the adipic acid monoanion ($[C_6H_9O_4]^-$, in methanol), the shortest chain anion to show combined losses of both water and carbon dioxide. Fragment ion spectra on the anion at *m/z* 145 showed essentially no fragmentation at a collision energy of 5 eV (lab. frame); however, at 10 eV fragmentation was observed (*m/z* 127, 101, and 83). In all cases from 10 to 30 eV, the loss of carbon dioxide predominated and a neutral loss scan showed the loss of 44 u from

© 2005 NRC Canada

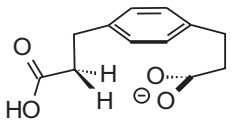
ions at both *m*/*z* 145 and 127. On the contrary, water was only lost from the ion at *m*/*z* 145 (loss of water discussed in a later section). The fragment ion at *m*/*z* 101 could not be fragmented further, which is consistent with it being the anion of a monocarboxylic acid (vide supra). The fragment ion observed at *m*/*z* 127 could be fragmented further into two ions at *m*/*z* 83 and 81. The loss of both 44 u (carbon dioxide) and 46 u (formic acid) from the ion (*m*/*z* 127) can be rationalized by postulating the structures and fragmentation pathways outlined in Scheme 2 (the alkyne oxide structure is justified later). Again, the initial step is a bond homolysis to give a radical pair that can further react in either of two ways, leading to two different fragment ions and two neutral species. This competitive fragmentation was only observed in a few cases by using the Quattro MS and it appears that loss of carbon dioxide is generally preferred.

Fragmentations of conformationally and structurally constrained diacids

To probe conformational effects on the primary fragmentation pathways, MS/MS spectra of the monoanions from 1,2- and 1,4-phenylenediacetic acids ($HOOCCH_2C_6H_4CH_2COO^-$, **a** and **b** respectively, *m*/*z* 193), were studied using the LCQ MS. Both anions **a** and **b** cleanly lost two molecules of carbon dioxide, but the ions at *m*/*z* 193, 149, and 105 (only ions in the spectra) under the same nominal collision energies (16%) had ratios of 100:475:160 for **a** and 100:82:12 for **b**. Thus, the ortho compound showed more facile decarboxylation than the para compound. The facile loss of carbon dioxide from these molecules is consistent with the mechanism proposed for this process in Scheme 2*a*, the phenyl ring providing stabilization for the intermediate carbon-centred radical. The loss of the second molecule of carbon dioxide from ions **a** and **b** would lead to a carbanion stabilized by the benzene ring (29), an interesting process but one which is not directly relevant to the fragmentations of the acyclic diacid monoanions.



a: R = H, R' = CH_2COOH
b: R = CH_2COOH, R' = H



c

The spacing between the two carboxyl groups in 1,2-phenylenediacetic acid is comparable to that in the C_5–C_7 aliphatic diacids. The anions of these latter diacids readily lost water on CID, whereas, under comparable conditions, neither **a** nor **b**, the anions from the phenylenediacetic acids, did. The orientations of the carboxyl groups in 1,2-phenylenediacetic acid are more conformationally restricted than those in the aliphatic diacids and even though loss of water from anions **a** or **b** is structurally possible, the pathway for the loss of carbon dioxide must enjoy a lower critical energy than that for the loss of water.

As a further example of the behaviour of anions with less conformational mobility than those of the acyclic diacids, the MS/MS spectrum of the monoanion from 1,4-phenylenedipropionic acid (**c**, *m*/*z* 221, LCQ ion trap) was recorded. The spectrum of this anion was more complex, as might reasonably be expected for a species with more degrees of freedom than **a** or **b** and in which the ionized and non-ionized carboxyl groups can interact. While elimination of one molecule of carbon dioxide (*m*/*z* 177) was the major loss, this was less facile than for either **a** or **b** since a higher relative collision energy (24%) was needed. The fact that loss of carbon dioxide from anion **c** is more difficult than the loss from either **a** or **b** is consistent with the mechanism for this process as laid out in Scheme 2 in which a radical site is stabilized by the phenyl ring. Loss of the second molecule of carbon dioxide from **c** to give an ion at *m*/*z* 133 was also disfavoured (rel. intensities of ions at *m*/*z* 221, 203, 177, and 133 were 100:30:200:12). Loss of a molecule of water (*m*/*z* 203) from anion **c** was clearly apparent. The fragmentation behaviour of **c** (LCQ ion trap, 24% rel. CID) is comparable to that of the monoanion from glutaric acid (C_5, Table 1). This observation has further mechanistic implications that are discussed later.

To examine the participation of protons α to carboxyl groups in fragmentation pathways, the spectra of the monoanion from 2,2,6,6-tetramethylheptanedioic acid were acquired. This has the same chain length as pimelic acid (C_7), which showed essentially no loss of carbon dioxide (Table 1), but rather a loss of water, followed by a loss of carbon dioxide, the combined loss being the major fragmentation process. By contrast, the tetramethylpimelic acid showed essentially only loss of carbon dioxide (LCQ ion trap, 28% rel. CID), thus establishing decarboxylation as a perfectly viable process for a diacid monoanion having a chain length of seven carbon atoms. However, the presence of the α protons in pimelic acid opens up an alternative reaction pathway with a lower critical energy; this process was studied in more detail using acyclic diacids and some monomethyl esters.

Loss of water from diacid monoanions and methanol from diacid monomethyl ester anions

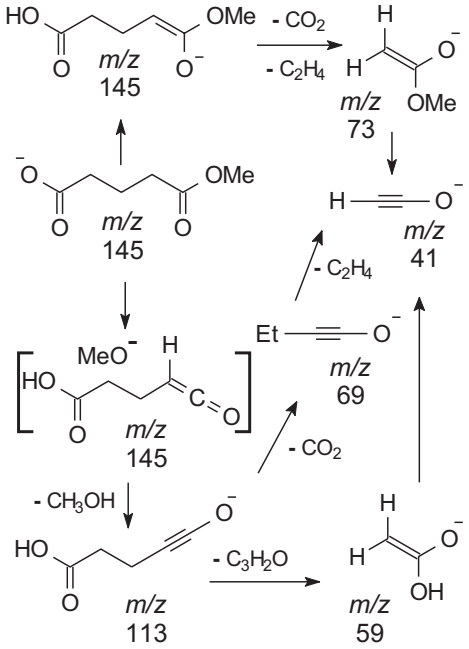
By way of comparison with results from the LCQ ion trap MS (summarized in Table 1 and Fig. 2), fragment ion spectra using the Quattro MS were obtained from the monoanions of sebacic and dodecanedioic acids, as well as from the monomethyl esters of glutaric and sebacic acids. The monoanions of the dicarboxylic acids ($HOOC(CH_2)_nCOO^-$) and dicarboxylic acid monoesters ($MeOOC(CH_2)_nCOO^-$) showed analogous MS/MS behaviour, losing water or methanol, respectively, to generate the same fragment ion.

The fragment ion spectra (not shown) on the monoanion of sebacic acid (**d**, *m*/*z* 201) and the anion from the monomethyl ester of sebacic acid (**e**, *m*/*z* 215) using the Quattro MS both showed additional peaks only at *m*/*z* 183 and 139. Fragmentation was very facile, since fragment ions were observed at collision energies of 10 and 5 eV (lab. frame), respectively, the absolute intensity of both peaks reaching a maximum around 15 eV and thereafter decreasing as the collision energy was increased to 30 eV. Similar MS/MS spectra were obtained from the monoanion of dodecanedioic acid (**f**, *m*/*z* 229).[4] For each of these longer chain monoanions, the losses of water and methanol were accompanied by a combined loss of water–methanol and carbon dioxide. No other fragmentation pathways were indicated by the MS/MS spectra.

The spectra from the anion of the monomethyl ester of glutaric acid showed a prominent loss of methanol at a colli-

© 2005 NRC Canada

Scheme 3.

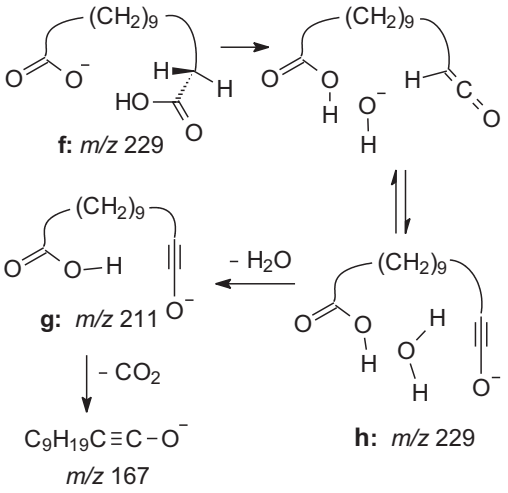


sion energy in the Quattro MS as low as 5 eV (lab. frame). No decarboxylation of the ester anion was observed, but fragment, parent, and neutral loss spectra[4] obtained on the Quattro MS could be interpreted in terms of a rich set of other fragmentation pathways. The pathways proposed in Scheme 3 are fully consistent with the ion chemistry outlined in this work, together with that already published (2). The deprotonated molecule observed at *m/z* 145 fragmented in two ways, the major pathway being loss of methanol to give *m/z* 113 and the minor pathway giving an ion at *m/z* 73. The major ion at *m/z* 113 also fragmented into major (*m/z* 69 and 41) and minor (*m/z* 59 and 41) pathways. The minor ion at *m/z* 73 lost methanol on further fragmentation to give an ion at *m/z* 41. The loss of 72 u (*m/z* 145 → 73) must result from the loss of $C_3H_4O_2$ since the ion at *m/z* 73 contains the elements of CH_4O (32 u) and C_2HO (*m/z* 41). The loss of $C_3H_4O_2$ corresponds to the elements of CO_2 and C_2H_4 and we suggest that this loss is a synchronous process since there was no evidence in the various spectra for a stepwise process. These two stable neutral species would assist in promoting the fragmentation process (*m/z* 145 → 73).

The CID spectra of the anions from both the α- and side-chain methyl esters of Asp and Glu also showed a prominent loss of 32 u (MeOH), but no loss of water or carbon dioxide. As previously noted, these spectra show the specific loss of methanol from the ester group, which can be extrapolated to serve as a probe for the regiochemistry of the dehydration reactions in the diacid monoanions occurring at the non-ionized carboxyl group.

The facile losses of water from a dicarboxylic acid monoanion and methanol from the anion of a dicarboxylic acid monomethyl ester (at collision energies as low as 10 and 5 eV, respectively) contrast strongly with the difficult loss of water from the anions of monocarboxylic acids. In the latter, the process required high collision energies in the LCQ MS and was not observed in the Quattro MS. The different fragmentation behaviour for monocarboxylic and dicarboxylic acids suggests that intramolecular interactions of the ionized and non-ionized carboxyl groups facilitate the losses of water or methanol; this is undoubtedly a consequence of the coiled conformation that these ions adopt (19–21, 24). These fragmentations are therefore not examples of charge-remote fragmentations occurring under conditions of low-energy CID (27, 33, 34).

Scheme 4.

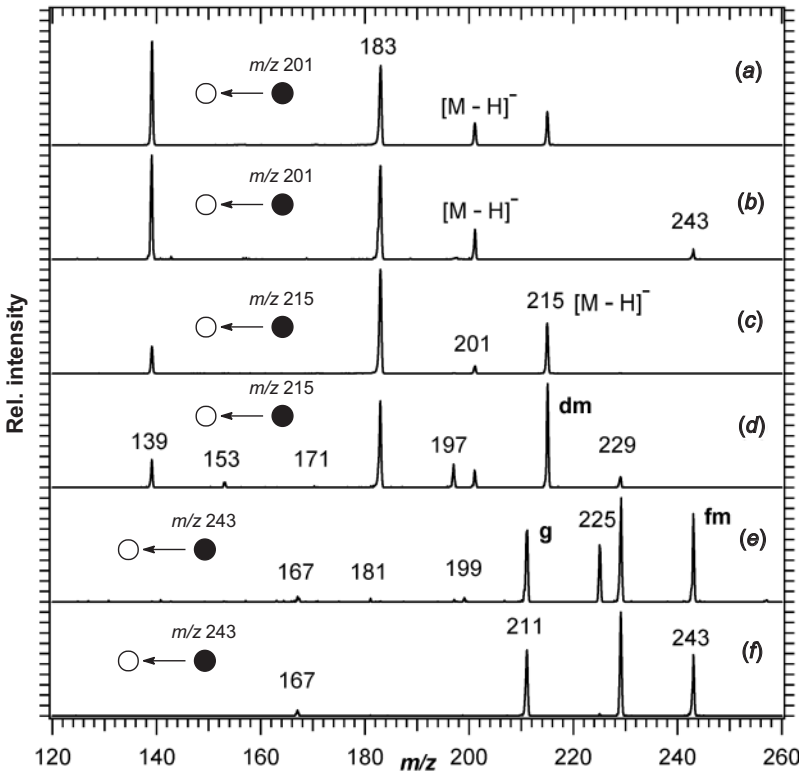


Given the very low CID energies at which fragment ions formed from the monoanions of sebacic acid (**d**), sebacic acid monomethyl ester (**e**), and dodecanedioic acid (**f**), these spectra also provided an important clue to the structures of the various fragment and adduct (see the next section) ions arising from **d**, **e**, and **f**, namely, that at least some fraction of each ion must have the structure of an ion–molecule complex. Mechanistic proposals incorporating such cluster ions are outlined in Scheme 4, which features ions derived from **f**; several points are noteworthy. The facile loss of water or methanol from **d**, **f**, or **e** ultimately arises from intramolecular interactions between the ionized and non-ionized carboxyl groups, which in turn must be a function of the chain length, longer chains allowing for more conformational flexibility so that the two groups can interact closely. The initial dehydration product of a non-ionized carboxyl group will be a ketene-containing cluster ion, but these can readily undergo proton transfer to the alkyne oxide cluster ion (**h**). Ethynol, isolated in a mass spectrometer, was first described almost 20 years ago (35) and alkynols have been extensively studied photochemically. They are stronger acids than carboxylic acids (36, 37), which provides good support for the ionic structures outlined in Scheme 4.

Other coiled conformers of these anions are undoubtedly present, but were not included to keep Scheme 4 reasonably uncluttered. In principle, the proton exchange processes for the conversion **f** → **h** outlined in Scheme 4 are reversible and could occur in electrospray ion sources. However, we note that we have found no evidence for deuterium exchange in the electrospray source (vide infra), and all details of the processes are therefore not at this time clear. However, we believe that all the evidence we have accumulated requires that at least some of the ions observed in either the Quattro or LCQ ion trap MS at, for example, *m/z* 229, have a struc-

© 2005 NRC Canada

Fig. 3. MS/MS fragment ion spectra from the LCQ MS for the (*a*) monoanion from sebacic acid (**d**, *m*/*z* 201) in methanol (24%, CID), (*b*) ion **d** (*m*/*z* 201) in 2-propanol solution (24% CID), (*c*) monoanion from sebacic acid monomethyl ester (**e**, *m*/*z* 215, methanol, 20% CID), (*d*) adduct ion **dm** (*m*/*z* 215) from sebacic acid monoanion in methanol, acquired at 20 V SID, 22% CID, (*e*) adduct ion **fm** (*m*/*z* 243) from dodecanedioic acid monoanion in methanol, acquired at 0 V SID, 24% CID, (*f*) adduct ion at *m*/*z* 243 from dodecanedioic acid monoanion in methanol, acquired at 30 V SID, 24% CID.



ture such as **h**. This would explain the very low collision energies needed to facilitate loss of water or alcohol from anions such as **d**, **e**, or **f**.

Ion–molecule reactions in the LCQ ion trap MS

When studying the spectra of the dicarboxylic acid monoanions using the LCQ MS, it became apparent that, in some cases, ion–molecule reactions were occurring as a result of solvent molecules in the ion trap, leading to more complex spectra than were obtained from the Quattro MS. The first indication of these reactions came from the MS/MS spectrum of the deprotonated molecule of sebacic acid in methanol ($HOOC(CH_2)_8COO^-$, **d**, *m*/*z* 201, Fig. 3*a*), which showed not only loss of water as an intense peak (*m*/*z* 183) and the combined loss of water plus carbon dioxide (*m*/*z* 139), but also a peak at *m*/*z* 215 from adduct ion **dm**, corresponding to [**d** – H_2O + MeOH]. Similarly, if the solvent was 2-propanol (Fig. 3*b*), a peak at *m*/*z* 243 from adduct ion **dp**, [**d** – H_2O + *i*-PrOH], was observed, in addition to the same fragment ions that were observed when the solvent was methanol. The peaks from these two solvent-derived adduct ions could be found in the full-scan mass spectra (not shown) by increasing the in-source collision (SID) energy from 0 to 20 V. It should be noted that others have previously described similar reactions between ions and solvent molecules in ion traps (38).

The mass spectra obtained on the anion from the monomethyl ester of sebacic acid ($MeOOC(CH_2)_8COO^-$, **e**, *m*/*z* 215, LCQ ion trap) showed behaviour comparable to that of the free acid. The MS/MS spectrum from a methanolic solution of **e** is shown in Fig. 3*c* and is very similar to the spectrum from **d** (Fig. 3*a*), with the fragment ion (*m*/*z* 183) being prominent. The ion **ew**, [**e** – MeOH + H_2O], observed at *m*/*z* 201 must arise from ion–molecule reactions between water present in the ion trap and the fragment ions seen at *m*/*z* 183, a phenomenon observed routinely when acquiring spectra for the present work. When the spectrum of **e** was run in 2-propanol,[4] an adduct ion **ep** (*m*/*z* 243, [**e** – MeOH + *i*-PrOH]) was also found, as was observed in the case of **d** (Fig. 3*b*).

The MS/MS spectrum from the adduct ion **dm** is shown in Fig. 3*d*. It was initially expected that the ion **dm** would have the same structure as that of the monoester ion **e** (both *m*/*z* 215), but on comparison of the MS/MS spectra shown in Figs. 3*c* and 3*d*, it is apparent that this is not the case. The spectrum in Fig. 3*d* shows that the adduct ion **dm** can lose either water (*m*/*z* 197) or methanol (*m*/*z* 183), with the addition of a molecule of methanol to *m*/*z* 197 leading to the peak observed at *m*/*z* 229 and the addition of a molecule of water to *m*/*z* 183 leading to the peak observed at *m*/*z* 201. Similar complex behaviour was shown by the adduct ion **dp** (*m*/*z* 243), formed when sebacic acid was dissolved in

© 2005 NRC Canada

Table 2. LCQ ion trap MS/MS spectra on adduct ions **dm**, **dp**, **fm**, **fp**, and **ep** derived from anions formed during electrospray ionization of sebacic acid (**d**), dodecanedioic acid (**f**), and monomethyl sebacate (**e**).

	Fragment ions (*m/z*) from adduct ions (*m/z*)				
Ionic species	**dm** (215)[a,b]	**dp** (243)[a,b]	**fm** (243)[a,b]	**fp** (271)[a,b]	**ep** (243)[a,b,c]
[**k** + HOH][d]	201	201[b]	229[b]	229	201
[**k** + *i*-PrOH – HOH][d]	—	225[b]	—	—	—
[**k** + MeOH – HOH][d]	197	—	225[b]	—	—
[**k**][d]	183[b]	183[b]	211[b]	211	183[b]
[**k** + MeOH – CO_2][d]	171	—	199	—	—
[**k** + MeOH – HOH – CO_2][d]	153	—	181	—	—
[**k** – CO_2][d]	139	139	167	—	139

Note: Methanol (**m**) or 2-propanol (**p**) solvent; LCQ conditions: 0 V SID, 22%–24% CID; for MS/MS spectra of adduct ions **dm** and **fm** (MeOH), see Figs. 3*d* and 3*e*.

[a]Ion selected for MS/MS fragmentation.

[b]Major ions observed.

[c]Ions also observed at *m/z* 167 = [211 – CO_2] and at *m/z* 211 = [**k** + *i*-PrOH – 32], which gave adduct ions at *m/z* [211 + 18] and [211 + 60].

[d]**k** = reactive fragment ion derived from sebacic acid, [**d** – H_2O]; from dodecandioic acid, [**f** – H_2O]; from monomethyl sebacate, [**e** – MeOH].

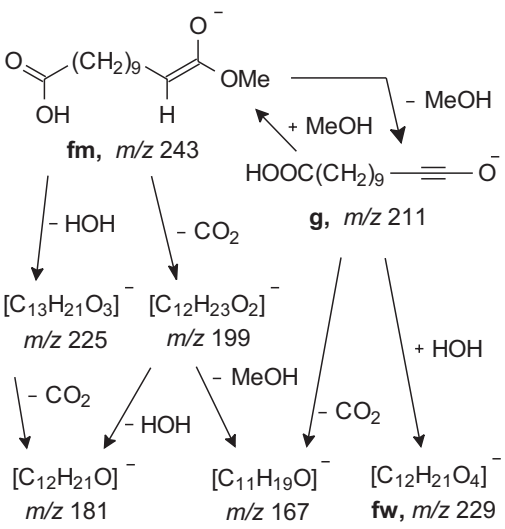
2-propanol.[4] The spectra of these adduct ions will be discussed in more detail later.

Some results from dodecanedioic acid were similar to those from sebacic acid. In addition to the fragment ions described previously, such as **g** (*m/z* 211, [**f** – H_2O]), the MS/MS spectrum from the monoanion $HOOC(CH_2)_{10}COO^-$ (**f**, Fig. 1*c*) also showed an abundant adduct ion **fm** (*m/z* 243, [**g** + MeOH]). By facilitating in-source fragmentation (40 V SID) on the LCQ MS, the MS/MS spectrum on *m/z* 211 (**g**) was acquired. At 0% CID (not shown) two additional peaks, corresponding to **fw** = [**g** + H_2O] at *m/z* 229 and **fm** (*m/z* 243 $[C_{13}H_{23}O_4]^-$) were notable. Therefore, the anion **g** must be a reactive species that combines with weakly acidic HX reagents (water or methanol) during the lifespan of the ion in the trap. When the experiment was repeated with the application of collision energy to the trap (40 V SID, 24% CID), the adduct ions were observed, but the base peak was now the fragment ion corresponding to [**g** – CO_2] (*m/z* 167, spectrum not shown). This loss of carbon dioxide is consistent with anion **g** containing a non-ionized carboxyl group.

In contrast to the results from sebacic acid, when the adduct ion from dodecanedioic acid observed at *m/z* 243 was formed with or without in-source fragmentation voltage in the LCQ MS, two different MS/MS spectra (Figs. 3*e* and 3*f*) were obtained. At 0 V SID (24% CID) the spectrum (Fig. 3*e*) paralleled that of **dm** (Fig. 3*d*), but at 30 V SID (24% CID), the spectrum (Fig. 3*f*) paralleled that from the monoester anion (**e**, Fig. 3*c*), suggesting that ions (*m/z* 243) of two different structures lead to the MS/MS spectra shown in Figs. 3*e* and 3*f*.

The reactivity of the fragment ions observed at *m/z* 183 (from **d** or **e**, Figs. 3*a* and 3*b*) and *m/z* 211 (**g**, from **f**, Fig. 1*c*) with water or alcohols, within their residence time in the ion trap, is consistent with the behaviour of a structure containing an alkyne oxide functionality. Addition of a species in the form of HX to an alkyne oxide is facile (36), and addition products with water, methanol or 2-propanol were observed in all cases. It is reasonable to assume that the structures of these addition products are enolate anions. As already mentioned, the fragmentation patterns of these ions were studied further using MS/MS on the LCQ MS and methanol solvent (Figs 3*d*–3*f*). When the solvent was

Scheme 5.

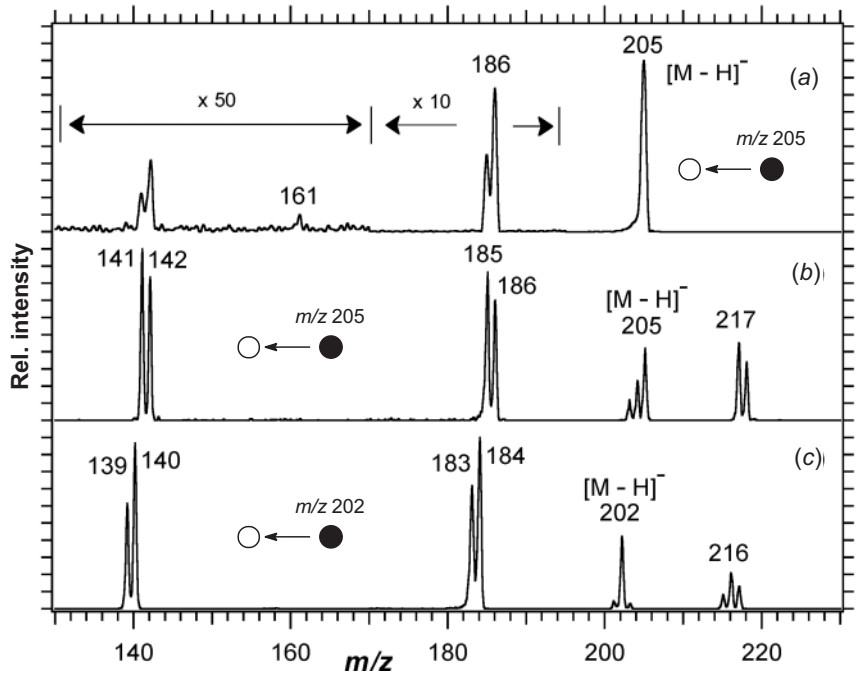


2-propanol, the adduct ions were generally of lower intensity and their spectra were therefore less detailed, but were reproducible. A summary of the MS/MS spectra of the adduct ions is presented in Table 2. A useful feature of the fragmentation of anion **dm** (*m/z* 215) was the low-intensity peak at *m/z* 171 for the loss of carbon dioxide (Fig. 3*d*); a similar fragmentation (*m/z* 199) was observed from **fm** (*m/z* 243, Fig 3*e*). This loss, a major feature in the MS/MS spectra of monoanions of the short-chain diacids, became progressively less important as the chain length increased and was not seen in the spectra of **d** or **f** from the LCQ MS. However, loss of carbon dioxide was present when ions of different structures from **d** or **f** were fragmented; it was also present as a low-intensity signal in the MS/MS spectrum of **f** from the Quattro MS.[4] We suggest that this fragmentation provides evidence for the structures of the adduct ions **dm** and **fm** having both a non-ionized carboxyl group and a charge-bearing enolate anion group. This is shown in Scheme 5, which is illustrated using species arising from fragmentation of anion **f**.

Although a reasonable structure for the adduct ion **fm** is proposed in Scheme 5, it does not allow for a simple expla-

© 2005 NRC Canada

Fig. 4. MS/MS fragment ion spectra for the (*a*) monoanion from 2,2,9,9-tetradeuterosebacic acid (**i**, *m*/*z* 205, MeOH, Quattro MS, 15 V cone, 20 eV CID), (*b*) monoanion from 2,2,9,9-tetradeuterosebacic acid (**i**, *m*/*z* 205, MeOH, LCQ ion trap MS, 24% CID), (*c*) monoanion from sebacic acid (**j**, *m*/*z* 202, MeOD, LCQ ion trap MS, 28% CID).



nation of all the features found in the spectrum shown in Fig. 3*e*. For example, the loss of 18 u (H_2O, *m*/*z* 225) is a prominent ion in this spectrum. It is tempting to suggest that a molecule of water is lost from the non-ionized carboxyl group, yet the spectrum reproducibly contains a low-intensity peak at *m*/*z* 181. If the carboxyl group has lost a molecule of water, it cannot also decarboxylate, which suggests that the ion **fm** (*m*/*z* 243) has rearranged or comes from more than one structure. It is difficult to explain the loss of both water and carbon dioxide from the structure given for **fm** in Scheme 5, but this structure can obviously rearrange as seen from the spectrum shown in Fig. 3*f*. Thus, the adduct ion observed at *m*/*z* 243 and labelled **fm** must represent several structures. The MS/MS spectrum of **fp** (Table 2), the adduct ion formed when dodecanedioic acid was dissolved in 2-propanol, was of low intensity but showed ions comparable to the major ones in the spectrum of **fm** (Table 2). Comparable MS/MS spectra to that of **fm** were seen when sebacic acid was dissolved in methanol (**dm**, Fig. 3*d*) or 2-propanol (**dp**, Table 2);[4] again, the adduct ion was able to lose either a molecule of alcohol or water (Table 2).

The MS/MS spectrum of the anion **e** (*m*/*z* 215) from monomethyl sebacate in methanol is shown in Fig. 3*c*. Any adduct ion with methanol would also be observed at *m*/*z* 215 and could not be distinguished from the anion itself under these conditions. However, the 2-propanol solution clearly gave an adduct ion at *m*/*z* 243 and details of the MS/MS spectra of this ion have been provided (Table 2).[4] Again, as noted in Table 2, structures for some lower intensity ions cannot be explained readily, but most major ions were directly comparable to those formed when sebacic acid was dissolved in 2-propanol.

We believe that the ion–molecule reactions occurring in the LCQ ion trap provide important evidence that loss of water from the longer chain diacid monoanions (or alcohol from monoester anions) leads to the formation of ynolate anions such as **g**. However, the reactions of these ynolate anions are not only simple addition processes, but also appear to involve rearrangements that depend on the operating conditions of the electrospray source and the ion trap. A study of these rearrangements would be interesting but is beyond the scope of the present work.

Studies on fragmentation pathways using deuterium-labelled compounds

Further evidence for the role of both the α-hydrogen atoms and ion–molecule complexes (Scheme 4) in the neutral loss of water was obtained by studying fragment ion spectra from the monoanion of 2,2,9,9-tetradeuterosebacic acid (**i**). This anion, observed at *m*/*z* 205, cleanly and reproducibly fragmented in the Quattro MS to give peaks at both *m*/*z* 186 and 185, in a ratio of ca. 2:1 (Fig. 4*a*). These ions correspond to the loss of HOD and DOD, respectively, and they fragmented further by losing carbon dioxide to give peaks at *m*/*z* 142 and 141. The observed 2:1 ratio is consistent with an equal distribution of two deuterium labels over three positions. This result must mean that the ketene and alkyne oxide cluster ions (Scheme 4) have sufficient time to interconvert before fragmenting in the collision cell. The collision cell of the Quattro MS allows for multiple collisions at the collision gas pressures employed. The information gained from the fragment ion spectra was supported by precursor ion and neutral loss scans.

When this tetradeuterated sebacic acid was studied using the LCQ ion trap MS, the MS/MS spectrum from **i** (24%

© 2005 NRC Canada

nominal CID energy) is shown in Fig. 4*b*. The phenomena observed are similar to those observed in the Quattro MS in that both HOD and DOD were lost from **i**, followed by a further loss of carbon dioxide. However, as discussed in the previous section, the ion trap is a reactive milieu and the addition of methanol (major) and water (minor) to both ions at *m*/*z* 185/186 was observed also. The other major difference between the results from the two spectrometers lies in the intensity ratios of the fragment ions observed at *m*/*z* 185/186 and *m*/*z* 141/142. The intensity ratio of *m*/*z* 185/186 in the Quattro was 0.5, but was 1.2 in the ion trap, indicating a process in the ion trap leading to greater loss of the deuterium label. The similar relative intensities of the peaks in the pairs at *m*/*z* 141/142 and *m*/*z* 185/186 suggest that the isotopic exchange process in the LCQ ion trap is faster than decarboxylation. It was intriguing to observe that, unlike all other ions studied, the MS/MS spectrum of anion **i** in the LCQ ion trap at 0% CID energy did not give a single peak for the precursor ion (*m*/*z* 205), but reproducibly showed another ion (*m*/*z* 204) at 15% of the precursor ion intensity. Therefore, some proton–deuterium exchange with the solvent in the trap was occurring, even with no added collisional excitation energy.

When the tetradeutero anion **i** was studied by CID on the Quattro MS, only intramolecular deuterium exchange processes are possible for the deuterated ions similar to the alkyne oxide **h** and the ketene cluster ions shown in Scheme 4. A similar process would occur in the LCQ ion trap, but in this instrument, other exchange processes with the solvent (e.g., between deuterated ions, comparable to **h** and **g**) occur also. Therefore, the spectra in Figs. 4*a* and 4*b* should be different. From the spectra (Figs. 4*a* and 4*b*) only two deuterium atoms are lost, indicating that exchange in both spectrometers is limited to one end of the anion **i**, consistent with processes shown in Schemes 4 and 5.

Complementary results were obtained when sebacic acid was dissolved in MeOD to generate an anion monodeuterated on the non-ionized carboxyl group ($DOOC(CH_2)_8COO^-$, **j**, *m*/*z* 202). This ion fragmented in the LCQ ion trap MS to give peaks at *m*/*z* 184 and 183, corresponding to the loss of both HOH and HOD, in a ratio of ca. 1.4:1 as shown in Fig. 4*c*. Since the ion trap MS also contains both deuterated and undeuterated solvent molecules (vide infra), this fragment ion spectrum is more complex than that of the sebacic acid monoanion **g**, although all the observed peaks can be explained by postulating the addition of MeOD, MeOH, HOD, or H_2O to the ions giving the pair peaks seen at *m*/*z* 184/183; loss of carbon dioxide from these ions leads to the peaks at *m*/*z* 140/139. An analogous spectrum (not shown) was obtained from $DOOC(CH_2)_{10}COO^-$.

Acquiring full-scan spectra (not shown) on the LCQ MS from a solution of the monomethyl ester of sebacic acid in MeOD produced a major ion at *m*/*z* 215 ($MeOOC(CH_2)_8COO^-$, **e**) and showed little evidence of deuterium exchange, except for a minor ion at *m*/*z* 202, which could be attributed to a small amount of diacid impurity ($DOOC(CH_2)_8COO^-$, **j**). The presence of a small amount of diacid in the sample of monoester was seen also in other full-scan spectra, including those taken on the Quattro MS. Other minor ions observed in the full-scan spectra on the LCQ MS were at *m*/*z* 229, 230, and 231. The various ions observed in these full-scan spectra on the LCQ MS were studied by MS/MS fragment ion scans. An important result from these spectra was the fragment ion spectrum (not shown) on *m*/*z* 215 (22% CID) which, in addition to the expected fragment ions at *m*/*z* 183 and 139, also gave an ion at *m*/*z* 216 with some 40% of the intensity of the ion at *m*/*z* 215. The intensity of this deuterated ion could be increased by increasing the collision energy and it must arise from addition of residual MeOD in the trap with the ion at *m*/*z* 183, as described previously. MS/MS scans on *m*/*z* 216 under the same conditions gave a minor ion at *m*/*z* 215 together with an ion at *m*/*z* 217, again at about 40% of the intensity of the ion at *m*/*z* 216. Since there was no evidence for direct, in-source deuterium exchange in **e**, it appears that any formation of an enolate anion leads rapidly only to other species. In addition, the formation of an enolate anion is not directly reversible during in-trap CID, but as observed previously (Figs. 3*e* and 3*f*) it appears that this can be brought about by application of in-source SID.

To examine whether enolate anions could be formed from more acidic species using ESI-MS under neutral solvent conditions, we examined the behaviour of methanolic solutions of dimethyl and diethyl malonate using the LCQ ion trap MS. In both cases enolate anions (*m*/*z* 131 and 159, respectively) were formed readily and both ions easily (16% relative collision energy) lost a molecule of alcohol. This fragmentation can be interpreted as leading to the formation of an alkynyl oxide anion (eq. [2]), in agreement with the major fragmentation observed in earlier work using high-energy collisions (39).

$$[2] \quad {}^-CH(COOR)_2 \rightarrow [(ROOC)CH{=}C{=}O + OR]^- \rightarrow (ROOC)C{\equiv}CO^- + ROH$$

Thus, the fact that enolate anions do not appear to be forming by deprotonation processes in the case of anions such as **e** simply reflects unfavourable energetics, compared with other accessible fragmentation pathways.

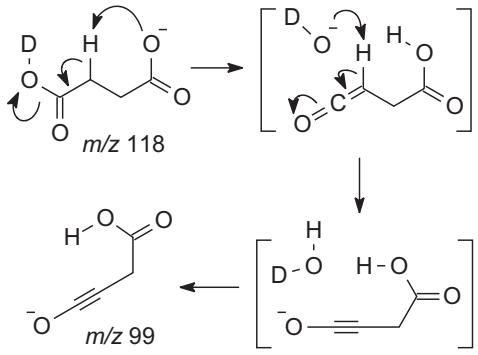
In contrast to the complex fragmentation behaviour exhibited by anions such as **d** and **f** from longer chain diacids, the short chain diacids in MeOD gave simple spectra. For example, the monoanion from succinic acid (C_4) in MeOH (seen at *m*/*z* 117) gave only two fragment ions, namely *m*/*z* 99 and 73 (Table 1). In MeOD, the anion at *m*/*z* 118 cleanly fragmented to give *m*/*z* 99 and 74. No adduct ions were observed, which could be explained by the fact that an ynolate anion in this case would be internally stabilized by the non-ionized carboxyl group, as shown in Scheme 6. In the case of adipic acid (C_6), the chain is now long enough that the anion exhibits very similar behaviour (in both MeOH and MeOD) to monoanions such as **d** (C_{10} chain). The difference between the six- and ten-carbon chains is that in the case of the latter anions the direct loss of carbon dioxide becomes a minor process (Table 1).

Conclusions

We have found no evidence for the formation of dianions in the spectra of the dicarboxylic acids, in either the LCQ ion trap or the Quattro MS (6, 40). All spectra in the present study were run in methanol, 2-propanol, or methanol–water

© 2005 NRC Canada

Scheme 6.



solutions without the addition of salts or bases. At low source cone voltages on the Quattro MS, the expected cluster ions of the diacids and their deprotonated molecules, $[2M - H]^-$, were readily observed (18). As previously discussed, stabilization of anions in the gas phase by interaction with another functional group is important (19–21, 24). In the present work this is illustrated by the exclusive formation of monoanions from dicarboxylic acids. Typically, most smaller ions would carry only a single charge, but most of the ions described in this work are undoubtedly stabilized by intramolecular interactions between the ionized and non-ionized carboxyl groups and dianion formation would thus be less favourable.

When subjected to CID, the pattern of reactivity of the monoanions from the series of dicarboxylic acids turned out to be complex, showing a strong dependence on chain length. Loss of carbon dioxide from a non-ionized carboxyl group is important for ions of structure $HOOC(CH_2)_xCOO^-$ only when $x \leq 4$. When $x > 4$, then the loss of carbon dioxide is preceded by an initial loss of water. For larger molecules, fragment ions that are formed by loss of water in the LCQ ion trap MS also form adduct ions. The properties of the anions that have lost water are consistent with structures in the form $HOOC(CH_2)_xC{\equiv}CO^-$, x = 3–7 or 9, based on the fact that the MS/MS spectra of the parent anions in the LCQ ion trap MS consistently showed low-intensity peaks for solvent adduct ions (see Fig. 1). These signals were absent in the spectra of the short-chain dicarboxylic acid monoanions.

The experiments that showed the loss of water or alcohol (ROH) from ions of structure $ROOC(CH_2)_xCOO^-$, x = 8 or 10, are noteworthy. The facility with which this process occurs points to a process with a very low critical energy. The remarkable results from the tetradeuterated anion **i**, $[HOOCCD_2(CH_2)_6CD_2COO^-]$, mean that the elimination of water cannot be a direct, simple process, but rather should be interpreted as involving a tightly held ion–molecule complex with a structure such as **h** (see Scheme 4) and having sufficient lifetime to permit exchange of the deuterium label during the multiple collisions of its passage through the Quattro collision cell. Perhaps the most appropriate structural description of the ion–molecule complex is that of a neutral molecule being held by a pair of molecular tweezers, which implies an adequate chain length of the starting diacid. A measure of the length of chain needed for the loss of water can be gauged from the MS/MS spectra of the phenylenediacetate ions (**a** and **b**) and the phenylenedipropanoate ion (**c**). In the case of the first two ions only carbon dioxide, but no water, was lost and the molecular geometry in **b** (1,4-disubstituted) is such that the ionized and non-ionized carboxyl groups are too far apart to interact. By contrast, in **c** interaction is possible and loss of both carbon dioxide and water was observed.

The lack of deuterium exchange when the monodeuterated anion **j**, $[DOOC(CH_2)_8COO^-]$, was studied points to the unimportance of enolate anion formation in the electrospray ionization process of these compounds. Finally, limited studies on the complex series of ion–molecule reactions occurring in the LCQ ion trap have provided good evidence for the formation of alkyne oxides in the form of $HOOC(CH_2)_xC{\equiv}CO^-$, x = 3–9. It has also become apparent from current work that the processes described in this work are dominant in the fragmentation of monoanions from both amino- and hydroxy-substituted diacids; the amino or hydroxy groups of these species appear to play a minor role in the fragmentation processes (Grossert, Fancy, and White, to be published).

Acknowledgements

We thank the Natural Sciences and Engineering Research Council of Canada (NSERC) for financial support (to RLW), Dalhousie University for access to the facilities of the Maritime Mass Spectrometry Laboratories (maintained by Xiao Feng), and Drs K. Bateman, L. Ramaley, and N. Schepp for helpful comments.

References

1. C.H. DePuy. Int. J. Mass Spectrom. **200**, 79 (2000).
2. J.H. Bowie. Mass Spectrom. Rev. **9**, 349 (1990).
3. W.P.M. Maas and N.M.M. Nibbering. Org. Mass Spectrom. **25**, 154 (1990).
4. B.A. Mansoori, D.A. Volmer, and R.K. Boyd. Rapid Commun. Mass Spectrom. **11**, 1120 (1997).
5. J.L. Kerwin, A.M. Wiens, and L.H. Ericsson. J. Mass Spectrom. **31**, 184 (1996).
6. R.T. Aplin, M.G. Moloney, R. Newby, and E. Wright. J. Mass Spectrom. **34**, 60 (1999).
7. A.G. Harrison. J. Mass Spectrom. **39**, 136 (2004).
8. C.S. Brinkworth and J.H. Bowie. Rapid Commun. Mass Spectrom. **17**, 2215 (2003).
9. J.H. Bowie, C.S. Brinkworth, and S. Dua. Mass. Spectrom. Rev. **21**, 87 (2002).
10. P. Boontheung, C.S. Brinkworth, J.H. Bowie, and R.V. Baudinette. Rapid Commun. Mass Spectrom. **16**, 287 (2002).
11. Z.-Z. Chen, S.-B. Chen, Y. Chen, Y.-M. Li, J. Chen, and Y.-F. Zhao. Rapid Commun. Mass Spectrom. **16**, 790 (2002).
12. M.L. Bandu, K.R. Watkins, M.L. Bretthauer, C.A. Moore, and H. Desaire. Anal. Chem. **76**, 1746 (2004).
13. R.A.J. O'Hair, S. Gronert, C.H. DePuy, and J.H. Bowie. J. Am. Chem. Soc. **111**, 3105 (1989).
14. J.J. Grabowski and X. Cheng. J. Am. Chem. Soc. **111**, 3106 (1989).
15. N.J. Jensen, G.W. Haas, and M.L. Gross. Org. Mass Spectrom. **27**, 423 (1992).
16. V.G. Voinov, H. Van den Heuvel, and M. Claeys. J. Mass Spectrom. **37**, 313 (2002).
17. M.R. Kumar, S. Prabhakar, M.K. Kumar, T.J. Reddy, and M. Vairamani. Rapid Commun. Mass Spectrom. **18**, 1109 (2004).

© 2005 NRC Canada

18. L.G. Wright, S.A. McLuckey, R.G. Cooks, and K.V. Wood. Int. J. Mass Spectrom. Ion Phys. **42**, 115 (1982).
19. J.C. Poutsma, E.J. Andriole, T. Sissung, and T.H. Morton. Chem. Commun. (Cambridge), 2040 (2003).
20. D.H. Aue and M.T. Bowers. *In* Gas phase ion chemistry. Vol. 2. *Edited by* M.T. Bowers. Academic Press, New York. 1979. Chap. 9. pp. 1–51.
21. R. Yamdagni and P. Kebarle. J. Am. Chem. Soc. **95**, 3504 (1973).
22. D.H. Aue, H.M. Webb, and M.T. Bowers. J. Am. Chem. Soc. **95**, 2699 (1973).
23. Q.-F. Chen and J.A. Stone. J. Phys. Chem. **99**, 1142 (1995).
24. C.A. Crowder and J.E. Bartmess. J. Am. Soc. Mass Spectrom. **4**, 723 (1993).
25. A.G. Harrison and T. Yalcin. Int. J. Mass Spectrom. Ion Processes, **165/166**, 339 (1997).
26. S. Satyanarayana, J.S. Grossert, S.F. Lee, and R.L. White. Amino Acids, **21**, 221 (2001).
27. C. Seto, J.S. Grossert, D.S. Waddell, J.M. Curtis, and R.K. Boyd. J. Am. Soc. Mass Spectrom. **12**, 571 (2001).
28. R.L. White, K.C. Smith, and A.C. DeMarco. Can. J. Chem. **72**, 1645 (1994).
29. S.T. Graul and R.R. Squires. J. Am. Chem. Soc. **112**, 2506 (1990).
30. A.G. Harrison. Int. J. Mass Spectrom. **210/211**, 361 (2001).
31. N.N. Dookeran, T. Yalcin, and A.G. Harrison. J. Mass Spectrom. **31**, 500 (1996).
32. J.R. Hyde and M. Poliakoff. Chem. Commun. (Cambridge), 1482 (2004).
33. M.L. Gross. Int. J. Mass Spectrom. **200**, 611 (2000).
34. C. Cheng and M.L. Gross. Mass Spectrom. Rev. **19**, 398 (2000).
35. B. van Baar, T. Weiske, J.K. Terlouw, and H. Schwarz. Angew. Chem. Int. Ed. Engl. **25**, 282 (1986).
36. Y. Chiang, A.J. Kresge, and V.V. Popik. J. Am. Chem. Soc. **117**, 9165 (1995).
37. A.J. Kresge. Acc. Chem. Res. **23**, 43 (1990).
38. Z. Guan and J.M. Liesch. J. Mass Spectrom. **36**, 264 (2001).
39. R.N. Hayes and J.H. Bowie. Org. Mass Spectrom. **21**, 425 (1986).
40. L.-S. Wang, C.-F. Ding, X.-B. Wang, and J.B. Nicholas. Phys. Rev. Lett. **81**, 2667 (1998).

© 2005 NRC Canada

An overview of organic molecule soft ionization using vacuum ultraviolet laser radiation[1]

Y.J. Shi and R.H. Lipson

Abstract: The utility of coherent vacuum ultraviolet (VUV) single-photon ionization (SPI) combined with time-of-flight mass spectrometry (TOF-MS) for organic molecule detection by parent mass is explored in this short review. Nonresonant tripling in phase-matched Xe–Ar gas mixtures was used to generate photons at a fixed energy of 10.5 eV. Representative organic molecules with different functional groups were examined, including aliphatic and aromatic alkanes, alkenes, alkynes, alkanols, ethers, amines, aldehydes, ketones, carboxylic acids, and esters. In almost every case, the intensity of the resultant parent molecular ion peak detected by TOF-MS was found to be superior to that obtained using 70 eV electron impact (EI), and comparable to that obtained with 12 eV EI. In those instances when fragmentation reactions did occur, the resultant ions were similar to those found using EI but with significantly reduced mass spectral intensities. It was still possible to establish one dominant fragmentation pathway that could be used for molecular identification even if the parent molecular ion was not the strongest feature in the spectrum, for example, in the case of alcohols, alcohol clusters, and alcohol–ether adducts. Several of the fragment ions were metastably broadened. Not surprisingly, their known appearance energies or estimated reaction enthalpies were very similar to the fixed photon energy used. The success of using VUV for organic molecule soft ionization is attributed to the low photon energy that removes predominantly a π- or non-bonding electron from the functionalized species. As most organic compounds have ionization potentials in the 10.5 eV region, this approach is expected to be near universal.

Key words: vacuum ultraviolet laser, single photon ionization, organic molecule detection, soft-ionization, mass spectrometry.

Résumé : Dans cette courte revue, on examine l'utilité d'une ionisation par un photon unique dans l'ultraviolet lointain cohérent combinée avec un spectromètre de masse à temps d'envol (SM-TDE) pour la détection de molécules organiques à l'aide de la masse parente. Le triplage non résonant de mélanges de gaz Xe–Ar en phase a été utilisé pour générer des photons d'énergie fixe de 10,5 eV. Des molécules organiques représentatives portant divers groupes fonctionnels ont été examinées, y compris des alcanes, des alcènes, des alcynes, des alcools, des éthers, des amines, des aldéhydes, des cétones, des acides carboxyliques et des esters aliphatiques et aromatiques. Dans pratiquement tous les cas, il a été trouvé que l'intensité du pic de l'ion moléculaire parent qui en résulte telle que détectée par SM-TDE est supérieure à celle obtenue en utilisant un impact électronique (IE) de 70 eV, et qu'elle est comparable à celle obtenue avec un IE de 12 eV. Dans les cas où des réactions de fragmentation se sont produites, les ions qui en résultent sont semblables à ceux observés avec un IE, mais les intensités des masses spectrales sont de beaucoup réduites. Il est toujours possible d'établir une voie de fragmentation dominante qui pourrait être utilisée pour l'identification moléculaire, même si l'ion moléculaire parent n'est pas la caractéristique la plus forte du spectre, par exemple, dans le cas des alcools, des agrégats d'alcools et des adduits alcool-éther. Plusieurs fragments ioniques sont élargis par leurs ions métastables. Il n'est pas surprenant que leurs énergies d'apparition connues ou les enthalpies réactionnelles évaluées soient très semblables à celle de l'énergie photonique fixe utilisée. Le succès obtenu en utilisant l'ionisation douce des molécules organiques à l'aide d'ultraviolet lointain est attribué à la faible énergie photonique qui élimine principalement un électron π ou non liant des espèces fonctionnalisées. Comme les potentiels d'ionisation de la plupart des molécules organiques se situent autour de 10,5 eV, il semble que cette approche pour être universelle.

Mots clés : laser ultraviolet lointain, ionisation photonique unique, détection de molécules organiques, ionisation douce, spectrométrie de masse.

[Traduit par la Rédaction]

Received 17 November 2004. Published on the NRC Research Press Web site at http://canjchem.nrc.ca on 14 January 2006.

Y.J. Shi.[2] Department of Chemistry, University of Calgary, 2500 University Drive NW, Calgary, AB T2N 1N4, Canada.
R.H. Lipson. Department of Chemistry, University of Western Ontario, London, ON N6A 5B7, Canada.

[1]This article is part of a Special Issue dedicated to Professor P. Kebarle.
[2]Corresponding author (e-mail: shiy@ucalgary.ca).

 doi: 10.1139/V05-193 © 2005 NRC Canada

Introduction

Several ionization schemes have been developed for mass spectrometry of gas-phase organic molecules. Electron impact (EI) and chemical ionization (CI) (1, 2) predominate. While claims for each have been made for some degrees of "soft ionization", that is, ionization without parent ion fragmentation, more often than not, the base peaks are due to fragment ions. Indeed, a considerable portion of the mass spectrometry literature is concerned with the mechanisms and energetics of fragment ion formation, as these species can be used as markers to identify the parent precursor. It follows that any technique that can provide a direct measure of the parent mass would be a valuable addition to the arsenal of tools available to analytical chemistry.

In this paper, we explore the utility and universality of organic molecule soft single-photon ionization (SPI) and detection using the combination of coherent vacuum ultraviolet (VUV) radiation and time-of-flight mass spectrometry (TOF-MS). VUV SPI is generally considered to be a "soft" ionization method because only modest amounts of excess energy are deposited in the resulting photoions. Furthermore, efficient ionization can occur with relatively low laser intensities, minimizing the probability of multiphoton absorption. This technique works for all compounds whose ionization potentials lie below the VUV photon energy (in most experiments, less than 10.5 eV). As VUV SPI is nonresonant, spectral tuning or prior knowledge of the electronic properties of the molecular species is not required. Furthermore, although the absolute photoionization cross sections are difficult to measure, it is known that they tend to differ little from one another for molecules, compared to resonant multiphoton ionization. This makes quantitative measurements using VUV SPI much more feasible. This burgeoning field has been previously reviewed (3–6).

In our initial experiments, derivatives of the common *O*-alkyl dithiocarbonate (xanthate) salts used in mineral sulphide flotation were examined. We showed conclusively that VUV SPI (7) coupled with TOF-MS (8) could readily identify the components of gas-phase xanthate mixtures by parent mass with detection sensitivity in the femtomole (picomolar) regime (9). More recently, we used VUV laser – TOF-MS to determine the gas-phase distributions of hydrogen-bonded alcohol clusters and alcohol–ether clusters formed above their respective liquids (10).

In this work, TOF mass spectra of various representative aliphatic and aromatic compounds were recorded using a fixed 118.2 nm (10.5 eV) "laser" generated by nonresonantly tripling the UV output of a Nd:YAG laser in phase-matched Xe–Ar mixtures. The resultant TOF mass spectra are compared with those obtained by conventional 70 eV EI, and where possible, lower energy 12 eV EI. Needless to say, not every possible organic compound could be examined. Furthermore, our choice of species in these experiments was limited to those with ionization potentials below 10.5 eV, and to gases or liquids with sufficiently high enough vapour pressures to be detected in the gas phase. Still, strong evidence is provided here that such an experimental approach is a powerful and general tool for identification of organic molecules with a wide variety of functional groups by parent mass.

Experimental

The experimental arrangement used to record 118.2 nm VUV laser – TOF mass spectra of various organic compounds is identical to that described in detail elsewhere (10–12). Briefly, coherent VUV radiation at 118.2 nm was generated by nonresonantly tripling the 355 nm (UV) third harmonic output of a Nd:YAG laser in a phase-matched 1:10 Xe–Ar gas mixture at a total pressure of ~100 Torr (1 Torr = 133.3224 Pa). A dispersive MgF_2 lens was inserted into the optical path after the Xe–Ar gas cell to minimize the possibility of ion formation by a multiphoton process involving the 118.2 nm beam and one or more 355 nm UV photons. The vapour of organic compounds mixed with 1 atm (1 atm = 101.325 kPa) of ultra pure helium was introduced into a vacuum chamber through a 1.0 mm diameter pinhole of a pulsed nozzle operating at 10 Hz. Ions, produced by VUV SPI, were mass dispersed in the 1 m long field-free flight tube of a linear TOF mass spectrometer, and detected by a two-stage microchannel plate (MCP). Although the mass resolving power of the TOF mass spectrometer ($m/\Delta m$) is designed to be >500, the typical mass resolution obtained from our mass spectra is 120. This lower mass resolution is attributed to the fact that an unskimmed pulsed jet was used for sample delivery that increases the spatial distribution of the sample. In addition, at the fixed VUV wavelength used for soft ionization, it is quite possible that the generated molecular ions could end up in a number of internal energy states, resulting in a wider velocity distribution. These factors, however, were not felt to distract from the goals of this work and technically, could be rectified with some modification of the apparatus.

Results

TOF mass spectra of various aliphatic and aromatic compounds with different functional groups were recorded with the fixed short wavelength VUV laser to determine the extent of fragmentation and any characteristic patterns.

Aliphatic compounds

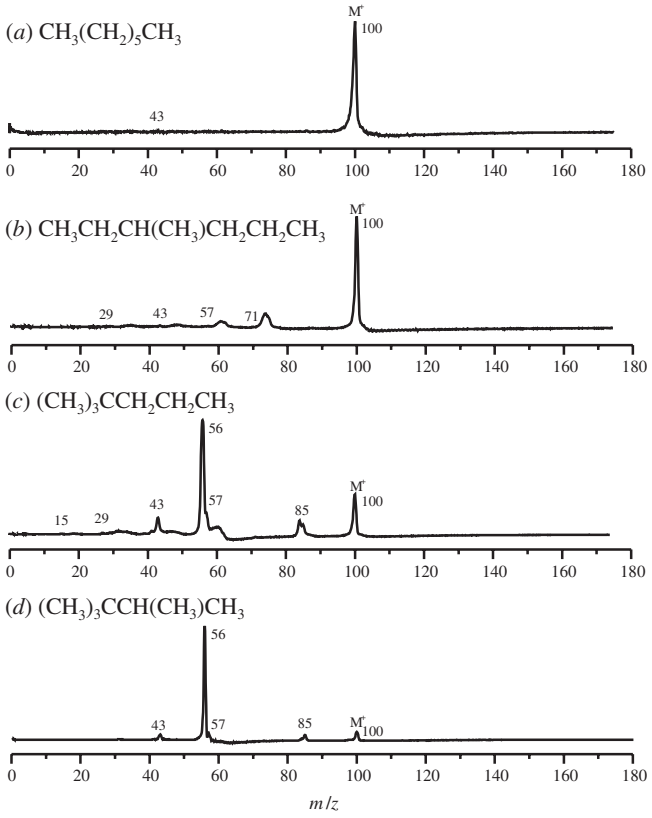
Alkanes

Four isomeric heptanes (*n*-heptane, 3-methylhexane, 2,2-dimethylpentane, and 2,2,3-trimethylbutane) were examined to determine the effect of branching on the degree of fragmentation resulting from VUV SPI. The resultant TOF mass spectrum for *n*-heptane (ionization potential, IP = 9.93 eV (13)) is shown in Fig. 1*a*. The base peak at m/z = 100 in the mass spectrum is due to the parent ion. The 10.5 eV SPI spectra of *n*-octane (14) and *n*-hexane (15) exhibit similar behaviour. The very weak feature at m/z = 43 in Fig. 1*a* is attributed to the propyl cation ($C_3H_7^+$).

Both the 70 eV (16) and 12.1 eV (17) EI mass spectra of *n*-heptane have been studied in detail. A photoionization study using incoherent VUV sources has also been reported (18). A comparison summary between VUV SPI and EI methods for *n*-heptane and all other compounds examined in

© 2005 NRC Canada

Fig. 1. Vacuum ultraviolet (VUV) (118.2 nm) single-photon ionization (SPI) – time-of-flight (TOF) mass spectra of *n*-heptane and its isomers: (*a*) *n*-heptane, (*b*) 3-methylhexane, (*c*) 2,2-dimethylpentane, and (*d*) 2,2,3-trimethylbutane. The features indicated by M^+ correspond to parent ion peaks.



this work is given in Table 1. The ion intensity distribution in Fig. 1*a* is opposite to that obtained by 70 eV EI. Since *n*-alkanes do not possess a natural focal point for ionization, EI nonselectively ionizes a C-C σ electron (19) leading to random cleavage down the chain, producing, in the case of *n*-heptane, ion fragments at *m*/*z* = 85, 71, 57, 43, and 29. The actual mechanism is more complex than the description above. ^{13}C and ^{2}H isotope labelling experiments suggest that the behaviour of isolated $C_nH_{2n+2}^{+\cdot}$ radicals can be rationalized in terms of a radical bound to an incipient carbonium ion (20, 21). Depending on the size of the alkane, isomerization reactions of the incipient carbonium ion can compete effectively with direct cleavage. For example, in the case of *n*-heptane ions, there is only a 22% probability that direct C_4H_9 scission will produce $C_3H_7^+$. On the other hand, there is a 72% chance that C_2H_5 will be lost from $C_7H_{16}^{+\cdot}$ to produce a $C_5H_{11}^+$ intermediate that then eliminates ethylene to form $C_3H_7^+$. A minor pathway (6% probability) also exists where methyl radicals are lost to produce a $C_6H_{13}^+$ intermediate followed by loss of C_3H_6 to form an ion with *m*/*z* = 43, which is the strongest peak in the mass spectrum of *n*-heptane using EI. However, only one fragment at *m*/*z* = 43 can be discerned just above the noise when using VUV SPI, while all other fragment mass peaks disappear.

It is well-known that branching in alkanes causes a decrease in the parent ion signal and characteristic increases in the intensities of the $C_nH_{2n+1}^+$ and $C_nH_{2n}^+$ homologous ion series through cleavage and charge retention at the branched carbon. Typically, the loss of the largest alkyl group is favoured. Furthermore, as the electron energy in the ionization is decreased, the higher mass fragments begin to predominate, as does the probability of alkene formation. Similar trends are found for the more branched alkanes examined in this work, as illustrated in Figs. 1*b*–1*d*, corresponding to the VUV SPI TOF mass spectra of 3-methylhexane, 2,2-dimethylpentane, and 2,2,3-trimethylbutane, respectively. Still, the parent ion mass in the VUV laser SPI TOF mass spectrum of 3-methylhexane is the base peak, compared to an abundance of 2% by 70 eV EI. Unless otherwise cited, the parent ion abundance data using 70 eV EI of all molecules studied in this work comes from the NIST Chemistry WebBook (13).

The base peaks in the VUV SPI mass spectra of the more highly branched 2,2-dimethylpentane and 2,2,3-trimethylbutane are both due to the $C_4H_8^+$, 2-methyl-1-propene ion, at *m*/*z* = 56. This feature is characteristic of dimethyl substitution at the 2-position in the low-energy 12 eV EI mass spectra of alkanes (17). The fragment ions, their corresponding *m*/*z* values, their assignments and relative intensities for alkanes and other organic molecules examined in this paper are listed in Table 2. A series of $C_nH_{2n+1}^+$ fragment ions, with *m*/*z* at 15, 29, 43, 57, 71, and 85, were observed in Figs. 1*b*–1*d*. This cleavage series appear to be metastably broadened, corresponding to fragmentation taking place in the flight tube of the mass spectrometer. Such observations can be rationalized for these two isomers as the enthalpies of reaction ($\Delta H°$) leading to the formation of these ions, $C_nH_{2n+2} \rightarrow C_{n-m}H_{2(n-m)+1}^+ + C_mH_{2m+1}$, are comparable to the energy of the ionizing photon used (22, 23), particularly if the ions formed are tertiary in nature. The parent ion abundances for these branched alkanes are 35% and 7%, respectively. Although these abundances are relatively low, it should be appreciated that the parent ions are essentially absent in the 70 eV EI mass spectra. Instead, their base peak is the very stable $(CH_3)_3C^+$ tertiary butyl carbocation at *m*/*z* = 57. Similar trends have also been seen in branched hexanes (15).

Cyclohexane (IP = 9.80 eV (24)) was also examined. Its 10.5 eV VUV laser SPI TOF mass spectrum is presented in Fig. 2*a*. The lowest energy feature in the cyclohexane dispersive photoelectron spectrum is attributed to ionization from the degenerate $4e_g$ molecular orbitals, which have both σ (C-C) and π (CH_2) character (25, 26). The strongest feature in the VUV laser SPI TOF mass spectrum is due to the parent ion at *m*/*z* = 84, in agreement with an earlier work (15). The weak fragment at *m*/*z* = 56 is attributed to the loss of ethylene from the parent molecule ($[M - C_2H_4]^+$), while the small peak at *m*/*z* = 42 is assigned to the loss of propene ($[M - C_3H_6]^+$). The broad peak at *m*/*z* = 59 is not readily assigned.

While the cyclohexane parent ion peak is strong in the 70 eV EI mass spectrum, the dominant feature is the fragment peak at *m*/*z* = 56 owing to the loss of ethylene. Strong parent ion peaks are not uncommon in cycloalkanes because ring fragmentation requires breaking two C—C bonds. Nevertheless, VUV SPI appears to be superior in this regard.

© 2005 NRC Canada

Table 1. The parent ion abundances of different aliphatic and aromatic compounds by 118.2 nm (10.5 eV) VUV laser SPI–TOF-MS, 12 eV EI-MS, and 70 eV EI-MS.

		Parent ion abundances (%)		
Compound	Molecular weight[a]	10.5 eV SPI	12 eV EI	70 eV EI
Alkanes				
n-Heptane	100	100	100	13
3-Methylhexane	100	100	[b]	2
2,2-Dimethylpentane	100	35	[b]	[c]
2,2,3-Trimethylbutane	100	7	[b]	[c]
Cyclohexane	84	100	[b]	74
Alkenes and alkynes				
1-Hexene	84	100	[b]	29
Cyclohexene	82	100	[b]	34
1-Hexyne	82	21	[b]	1
Alcohols				
1-Pentanol	88	0.9	[c]	0.4
2-Pentanol	88	8	2	[c]
3-Pentanol	88	11	2	[c]
2-Methyl-butan-2-ol	88	2	[c]	[c]
Cyclohexanol	100	22	10	3
Ethers				
Diethyl ether	74	100	100	23
Methyl *tert*-butyl ether	88	6	[c]	[c]
Tetrahydrofuran	72	100	[b]	29
Alkyl amines				
1-Butylamine	73	100	100	7
Diethylamine	73	100	100	19
Triethylamine	101	100	100	19
Alkanals				
n-Butanal	72	100	100	74
n-Pentanal	86	100	17	6
n-Hexanal	100	100	11	1
Alkanones				
2-Pentanone	86	100	[b]	20
3-Pentanone	86	100	[b]	17
Cyclohexanone	98	100	[b]	33
Alkanoic acids and alkyl alkanoates				
n-Heptanoic acid	130	100	6	0.7
Methyl butanoate	102	100	[b]	4
Aromatic hydrocarbons				
Benzene	78	100	[b]	100
Toluene	92	100	[b]	62
o-Xylene	106	100	[b]	42
Aromatic aldehydes, ketones, and esters				
Benzaldehyde	106	100	[b]	95
Acetophenone	120	100	[b]	29
Methyl benzoate	136	100	[b]	39

[a]Atomic mass units.
[b]Data not available.
[c]Not observed.

Alkenes and alkynes

The VUV SPI mass spectrum of 1-hexene (IP = 9.46 eV (24, 27)) is shown in Fig. 2*b*. The ionization threshold corresponds predominately to the loss of an electron from the π π orbital of the double bond (28). In this work, the parent molecular ion at m/z = 84 is the base peak, while the strongest feature in the 70 eV EI spectrum is assigned to $C_4H_8^+$ at m/z = 56. The parent ion abundance by 70 eV EI is considerably

© 2005 NRC Canada

Table 2. Fragment masses, their assignments, and their abundances relative to the base peaks in the VUV laser SPI–TOF mass spectra of different organic molecules.

Compound	Fragment masses, their assignments, and relative abundances (%)
n-Heptane	43 ($C_3H_7^+$, 0.91)
3-Methylhexane	29 ($C_2H_5^+$, 0.74), 43 ($C_3H_7^+$, 1.6), 57 ($C_4H_9^+$, 1.3), 71 ($C_5H_{11}^+$, 0.58)
2,2-Dimethylpentane	15 (CH_3^+, 0.59), 29 ($C_2H_5^+$, 1.4), 43 ($C_3H_7^+$, 14), 56 ($C_4H_8^+$, 100), 57 ($C_4H_9^+$, 19), 85 ($C_6H_{13}^+$, 10)
2,2,3-Trimethylbutane	43 ($C_3H_7^+$, 4.8), 56 ($C_4H_8^+$, 100), 57 ($C_4H_9^+$, 6.6), 85 ($C_6H_{13}^+$, 4.2)
Cyclohexane	42 ($C_3H_6^+$, 0.85), 56 ($C_4H_8^+$, 2.1)
1-Hexene	27 ($C_2H_3^+$, 1.7), 28 ($C_2H_4^+$, 0.51), 41 ($C_3H_5^+$, 3.3), 42 ($C_3H_6^+$, 6.3), 55 ($C_4H_7^+$, 3.8), 56 ($C_4H_8^+$, 6.7)
Cyclohexene	54 ($C_4H_6^+$, 0.90), 67 ($C_5H_7^+$, 0.93)
1-Hexyne	39 ($C_3H_3^+$, 1.2), 41 ($C_3H_5^+$, 2.5), 43 ($C_3H_7^+$, 2.1), 54 ($C_4H_6^+$, 4.8), 67 ($C_5H_7^+$, 100), 81 ($C_6H_9^+$, 14)
1-Pentanol	45 ($C_2H_5O^+$, 7.9), 57 ($C_4H_9^+$, 7.4), 70 ($C_5H_{10}^+$, 100)
2-Pentanol	44 ($C_2H_4O^+$, 52), 45 ($C_2H_5O^+$, 8.8), 57 ($C_4H_9^+$, 5.4), 70 ($C_5H_{10}^+$, 100), 73 ($C_4H_9O^+$, 28)
3-Pentanol	58 ($C_3H_6O^+$, 100), 59 ($C_3H_7O^+$, 45)
2-Methyl-2-butanol	58 ($C_3H_6O^+$, 23), 59 ($C_3H_7O^+$, 100), 70 ($C_5H_{10}^+$, 10), 73 ($C_4H_9O^+$, 68)
Cyclohexanol	57 ($C_3H_5O^+$, 7.0), 67 ($C_5H_7^+$, 0.90), 71 ($C_4H_7O^+$, 0.41), 82 ($C_6H_{10}^+$, 100)
Diethyl ether	29 ($C_2H_5^+$, 1.8), 31 (CH_3O^+, 7.2), 45 ($C_2H_5O^+$, 2.2), 59 ($C_3H_7O^+$, 1.3)
Methyl *tert*-butyl ether	73 ($C_4H_9O^+$, 100)
Tetrahydrofuran	45 ($C_2H_5O^+$, 1.6)
1-Butylamine	30 (CH_4N^+, 26)
Diethylamine	58 ($C_3H_8N^+$, 67)
Triethylamine	86 ($C_5H_{12}N^+$, 87)
n-Butanal	47 (?, 3.6), 59 (?, 1.2)
n-Pentanal	47 (?, 0.96), 58 ($C_3H_6O^+$, 53)
n-Hexanal	44 ($C_2H_4O^+$, 0.77), 45 ($C_2H_5O^+$, 0.017), 56 ($C_4H_8^+$, 12), 58 ($C_3H_6O^+$, 26), 72 ($C_4H_8O^+$, 42), 82 ($C_6H_{10}^+$, 50)
2-Pentanone	43 ($C_2H_3O^+$, 0.30), 58 ($C_3H_6O^+$, 2.2), 71 ($C_4H_7O^+$, 0.81)
3-Pentanone	56 ($C_3H_4O^+$, 2.9), 57 ($C_3H_5O^+$, 3.2)
Cyclohexanone	42 ($C_3H_6^+$, 0.45), 55 ($C_3H_3O^+$, 0.51)
n-Heptanoic acid	60 ($C_2H_4O_2^+$, 7.8), 70 ($C_5H_{10}^+$, 93), 73 ($C_3H_5O_2^+$, 10), 122 (?, 18)
Methyl butanoate	43 ($C_3H_7^+$, 1.1), 74 ($C_3H_6O_2^+$, 24)

less (only 29% of the base peak). A small feature at m/z = 168 in the VUV SPI mass spectrum is attributed to the 1-hexene dimer. At this time however, details about the structure or formation of this ion are uncertain.

Weak fragments corresponding to $C_nH_{2n}^+$ (n = 2, 3, and 4 at m/z = 28, 42, and 56) and $C_nH_{2n-1}^+$ (n = 2, 3, and 4 at m/z = 27, 41, and 55) are evident in Fig. 2*b*. The broader peaks at higher m/z values relative to the sharper features are attributed to metastable ion decomposition in the mass spectrometer flight tube. This is consistent with reaction enthalpies for $C_6H_{12} \rightarrow C_nH_{2n}^+ + C_{6-n}H_{12-2n}$, which are estimated to be comparable to the ionization photon energy used in this work. The fragment ions observed are common for alkenes that are known to exhibit allylic cleavage. The intensities of the fragment peaks are similar, which indicates that the double bond can easily migrate within the molecule after ionization. This conclusion is supported by an earlier VUV laser ionization study of 1-octene, 2-octene, and 4-octene (14), where the fragmentation patterns and intensities observed for those compounds are similar to the findings here.

The VUV TOF mass spectrum of cyclohexene is shown in Fig. 2*c* and once again, the base peak is due to the parent ion at m/z = 82. The ionization process is also due to loss of a π electron (29) (IP = 8.94 eV (26)). The feature at m/z = 67 is due to loss of a methyl radical from the parent molecule to form the C_5H_7 diene radical cation, and is the base peak in the 70 eV EI mass spectrum of the parent compound. Its formation is ascribed to a hydrogen abstraction mechanism that transfers the unpaired electron to an allylic radical site prior to methyl loss. The weak feature at m/z = 54 is another characteristic fragment for cyclohexene, which arises from a retro Diels–Alder reaction that forms the $C_4H_6^+$ diene radical cation and ethylene. The two broad peaks at m/z = 58 and 69 in Fig. 2*c* remain unassigned.

The lowest energy ionization of 1-hexyne (IP = 10.07 eV (30)) yields a photoelectron from a π orbital of the triple bond (31). As shown in Fig. 2*d*, the base peak obtained by VUV SPI corresponds to $[M - CH_3]^+$ at m/z = 67, similar to that obtained by high energy EI (32). VUV SPI however, considerably enhances the intensity of the parent peak (21%) compared with that observed using 70 eV EI where the relative abundance of the parent ion is only 1%. A strong feature is observed by VUV SPI at m/z = 81 (14%) that corresponds to a well-known fragmentation mode for terminal alkynes; namely the loss of the terminal H atom. The remaining fragment ions at m/z = 39, 41, 43, and 54, owing to the $C_3H_3^+$ (propargyl ion), $C_3H_5^+$ (allyl carbocation), $C_3H_7^+$ (propyl cation), and $C_4H_6^+$ (1-butyne fragment), respectively, are also observed in the EI spectrum, but are considerably depressed using VUV laser soft ionization.

© 2005 NRC Canada

Fig. 2. 118.2 nm VUV SPI–TOF mass spectra of: (*a*) cyclohexane, (*b*) 1-hexene, (*c*) cyclohexene, and (*d*) 1-hexyne. The features indicated by M^+ correspond to parent ion peaks.

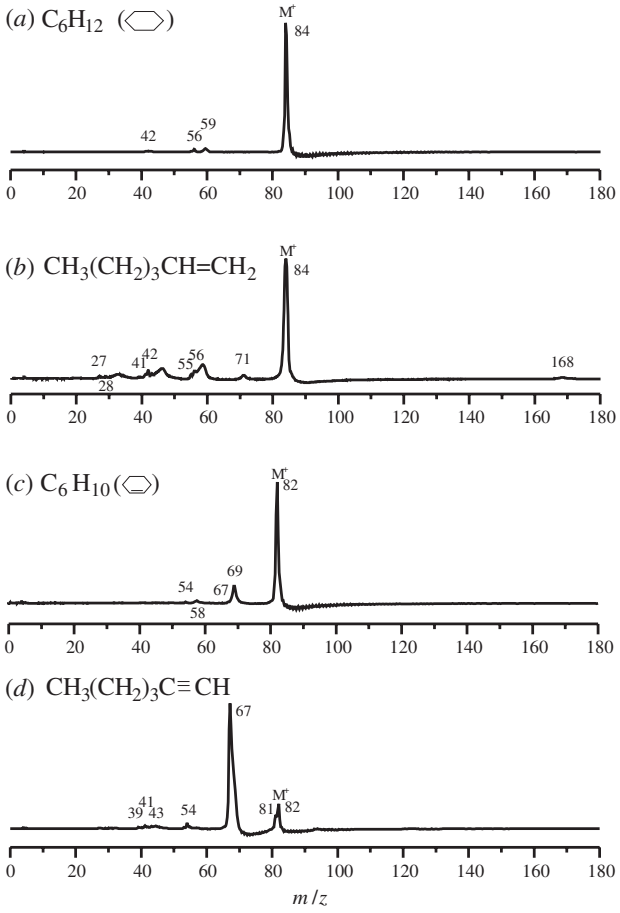
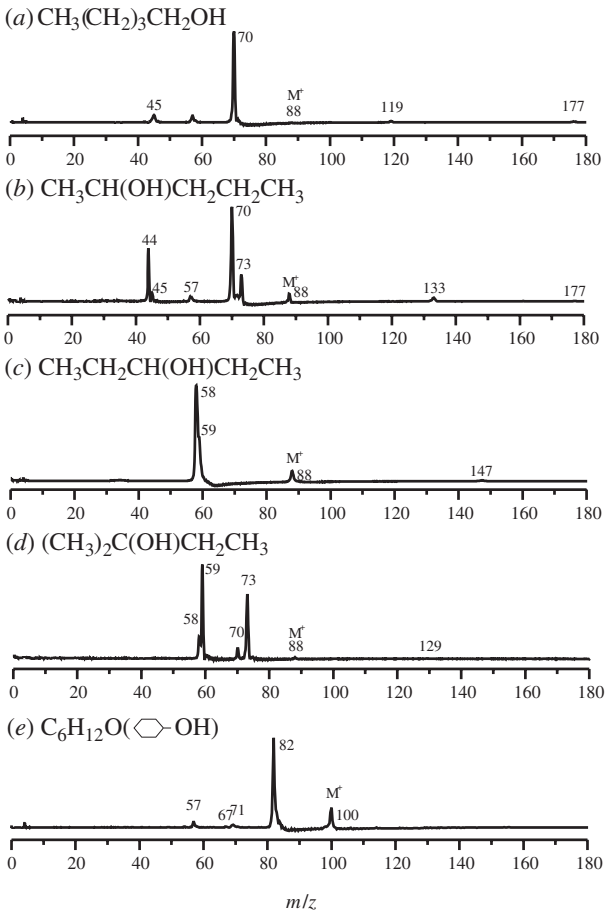


Fig. 3. 118.2 nm VUV SPI–TOF mass spectra of alkanols: (*a*) 1-pentanol, (*b*) 2-pentanol, (*c*) 3-pentanol, (*d*) 2-methyl-butan-2-ol, and (*e*) cyclohexanol. The features indicated by M^+ correspond to parent ion peaks.



Alkanols

In this work, four isomeric pentanols were examined: 1-pentanol, IP = 10.42 eV; 2-pentanol, IP = 9.78 eV; 3-pentanol, IP = 9.76 eV; and 2-methyl-butan-2-ol, IP = 10.16 eV; their VUV SPI mass spectra are shown in Figs. 3*a*, 3*b*, 3*c*, and 3*d*, respectively. Calculations have shown that the molecular orbitals of the larger alcohols are considerably more delocalized than those of their smaller alkyl counterparts (33). Thus, while the main effect associated with the lowest ionization potential of an alcohol is often viewed as the removal of an oxygen lone-pair electron, the actual amount of atomic oxygen character is only ~54%.

The parent ion peak at m/z = 88 was observed for all four isomeric alcohols, albeit weakly. The relative intensities of this feature are 0.9%, 8%, 11%, and 2% for 1-pentanol, 2-pentanol, 3-pentanol, and 2-methyl-butan-2-ol, respectively. In contrast, only 1-pentanol exhibits a parent ion peak by 70 eV EI, with an abundance that is 0.4% of the base peak at m/z = 42. In a low-energy 12 eV EI study, parent ions were observed for 2- and 3-pentanol, (abundance ~ 2%), but not for the other isomers (17, 34). Interestingly, in an earlier 118.2 nm VUV laser ionization – mass spectrometric study of 1-pentanol and 1-, 2-, and 3-octanol (14), only 1-octanol was found to exhibit a very weak parent ion peak.

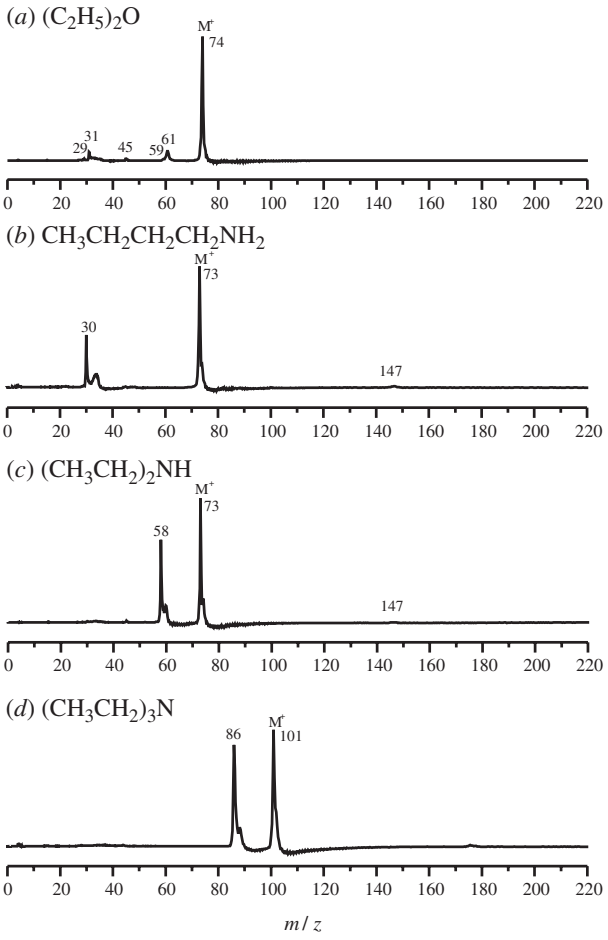
Base peak formation at m/z = 70 in our mass spectra of 1-pentanol and 2-pentanol is due to parent molecule dehydration $[M - H_2O]^+$, which is a common fragmentation mode for alcohols having five carbons or more. In contrast, α cleavage appears to be more important for 3-pentanol and 2-methyl-butan-2-ol. The strongest fragment ion from the former compound at m/z = 58 is attributed to the loss of ethane (C_2H_6 (35)), while a feature at m/z = 59 for the latter is due to the loss of the ethyl radical C_2H_5 resulting from α cleavage. More α-cleavage ion peaks are observed for 2-pentanol at m/z = 73 ($[M - CH_3]^+$) and m/z = 45 ($[M - C_3H_7]^+$), for 3-pentanol at m/z = 59, and for 2-methyl-butan-2-ol at m/z = 73. Two fragment ions observed at m/z = 45 and 57 for 1-pentanol are assigned to $C_2H_5O^+$ and $C_4H_9^+$, respectively. The peak at m/z = 44 for 2-pentanol is due to the $C_2H_4O^+$ ion.

Alkanols are also known to dissociate further in a manner analogous to olefins (36), to yield $C_nH_{2n}^+$ and $C_nH_{2n-1}^+$ ions. However, unlike previous mass spectrometric studies using VUV laser radiation (14), these features are not evident in our TOF mass spectra.

Several heavier mass peaks are present for all four pentanols, which suggests the presence of dimers and associated fragments. Van Bramer and Johnston (14) made a similar observation and suggestion for 1-pentanol, but did not

© 2005 NRC Canada

Fig. 4. 118.2 nm VUV SPI–TOF mass spectra of ether and amines: (*a*) diethyl ether, (*b*) 1-butylamine, (*c*) diethylamine, and (*d*) triethylamine. The features indicated by M^+ correspond to parent ion peaks.



exclude the possibility of impurities. Our group has used VUV lasers to map out the nascent gas-phase distributions of hydrogen-bonded clusters above liquid ethanol, methanol, and butanol (10), and in this regard, clusters are almost certainly being detected. For example, the feature at m/z = 119 for 1-pentanol can be assigned to $[M_2 - C_4H_9]^+$, the one at m/z = 133 to $[M_2 - C_3H_7]^+$ for 2-pentanol, the one at m/z = 147 to $[M_2 - C_2H_5]^+$ for 3-pentanol, and the one at m/z = 129 to $[M_2 - C_2H_7O]^+$ for 2-methyl-butan-2-ol. The features at m/z = 177 for 1- and 2-pentanol are attributed to the protonated alcohol dimer HM_2^+.

The VUV SPI mass spectrum of cyclohexanol (shown in Fig. 3*e*) also exhibits a base peak at m/z = 82 corresponding to water loss. The parent ion peak at m/z = 100 is the second strongest feature with a relative intensity of 22%. Two fragment ions at m/z = 57 and 71 are due to the loss of C_3H_7 and C_2H_5 from the parent molecule, respectively, while a weak feature at m/z = 67 is tentatively assigned to the loss of a methyl group from the dehydrated parent ion. These results can be compared with those obtained by 70 eV EI where the parent ion abundance is 3% relative to the base peak at m/z = 57, and to those in the 12 eV EI spectrum where the parent ion peak is 10% as intense as the base feature at m/z = 82.

Ethers

Three ethers were chosen for study: diethyl ether (Fig. 4*a*, IP = 9.51 eV), methyl *tert*-butyl ether (MTBE, IP = 9.24 eV), and tetrahydrofuran (IP = 9.40 eV). In each case, the first photoionization threshold is expected to involve an electron with predominately lone-pair character centred on the oxygen atom.

The base peak of the VUV laser TOF mass spectrum of diethyl ether is due to the parent ion mass at m/z = 74. A similar result was obtained using 12 eV EI (17), while the parent ion peak in the 70 eV EI mass spectrum is only 23% of the base peak at m/z = 31.

The main fragments observed for diethyl ether by 10.5 eV SPI are similar to those seen with 12 eV EI, and follow the expected trend for *n*-alkyl ethers. The spectrum exhibits a series of $C_nH_{2n+1}O^+$ oxonium ions at m/z = 31 (CH_3O^+), m/z = 45 ($C_2H_5O^+$), and m/z = 59 ($C_3H_7O^+$). The $C_2H_5^+$ ion at m/z = 29 formed from α cleavage is also observed. The peak at m/z = 61 is attributed to metastably broadened $C_3H_7O^+$ ions. The CH_3O^+ feature is also metastably broadened. It is noted that the intensities of all fragment ions of diethyl ether using VUV SPI are depressed significantly as compared with those in the 70 eV EI mass spectrum.

It is not particularly surprising that the parent ion peak for MTBE (mass spectrum not shown) at m/z = 88 is found to be relatively weak since the neutral contains a tertiary alkyl group. Its intensity is only 6% of the base peak at m/z = 73 which is attributed to α cleavage of a methyl group. Still, it should be appreciated that the parent ion is not observed at all by 12 eV (17) or 70 eV EI. The m/z = 73 feature is also the base peak in both the 12 eV and 70 eV EI mass spectra, but VUV SPI appears to give a much cleaner spectrum that contains only the base peak at m/z = 73 and the parent ion peak. MTBE is the main ether additive to gasoline and may accumulate in the atmosphere through automobile exhaust. Butcher et al. (37) has reported the real-time determination of aromatics and oxygenates in automobile exhaust using SPI – ion trap mass spectrometry (IT-MS). Their 118 nm SPI mass spectrum of MTBE also showed a predominant fragment peak at m/z = 73, along with two very weak fragment peaks at m/z = 56 and 57.

The strongest feature in the VUV laser TOF mass spectrum of tetrahydrofuran (not shown) is due to the parent ion at m/z = 72. A weak feature observed at m/z = 45 is assigned to $C_2H_5O^+$. The ion signal at m/z = 116 is tentatively assigned to its dimer fragment ($[M_2 - C_2H_4]^+$). In the 70 eV EI mass spectrum, the parent ion intensity is only 29% of the base peak at m/z = 42 ($C_3H_6^+$), where $C_nH_{2n}^+$ fragments are attributed to be formed following parent ion dehydration.

Alkyl amines

One primary amine (1-butylamine, IP = 8.71 eV (38), Fig. 4*b*), one secondary amine (diethylamine, IP = 8.01 eV (38), Fig. 4*c*), and one tertiary amine (triethylamine, IP = 7.50 eV (38), Fig. 4*d*) were considered in this category. The lowest ionization potential of these compounds represents the energy required to remove a near nonbonding $3a_1$ electron associated with the N atom (38).

As seen in Fig. 4*b*, the parent ion peak is the strongest feature in the VUV SPI mass spectrum of 1-butylamine. Similar results were previously obtained using 10.5 eV laser

© 2005 NRC Canada

photons to *n*-heptylamine and *n*-octylamine (14). Our study on two other alkylamines (diethylamine and triethylamine) shows that their VUV SPI mass spectra also exhibit the parent ion peak as the base peak. These results indicate that alkylation on the nitrogen atom has relatively little effect.

Like the 12 eV EI mass spectrum for 1-butylamine (39), the α-cleavage ion $[M - C_3H_7]^+$ at m/z = 30 is relatively strong using VUV SPI. Metastable decomposition is experimentally evident even though a thermodynamic estimate for the enthalpy of reaction for $C_4H_{11}N \rightarrow C_3H_7 + CH_4N^+$ (40) is ~0.75 eV lower than the photon energy used. With 70 eV EI, the α-cleavage ion is the base peak, while the relative intensity of the parent ion peak is only 7%. The β-cleavage ions ($[M - CH_3]^+$) are the only fragment ions observed in this work for the other two amines and in both cases, these features are metastably broadened. Here, the reaction enthalpy of diethylamine to form the β-cleavage fragment ion is estimated to be lower than the 10.5 eV (41) photon used. However, for the triethylamine, the appearance energy of the $[M - CH_3]^+$ ion has been determined to be 11.48 eV (42), which suggests that the UV light used to generate the VUV photons is participating in the ionization scheme. The 12 eV EI mass spectra for both compounds (39) are similar to those obtained by VUV SPI, whereas the 70 eV spectra are congested with additional fragment ion peaks, and the parent ion abundances are ~19%. These results indicate that in this work, for the alkylamines considered, ammonia elimination is not favoured compared to water elimination for alcohols, which dominates over α cleavage. In the previous study of the heavier *n*-heptyl amines and *n*-octyl amines using VUV SPI (14), however, a series of $[M - C_nH_{2n+1}]^+$ ions ($[M - NH_3]^+$ and ammonium NH_4^+) at m/z = 18 were all observed.

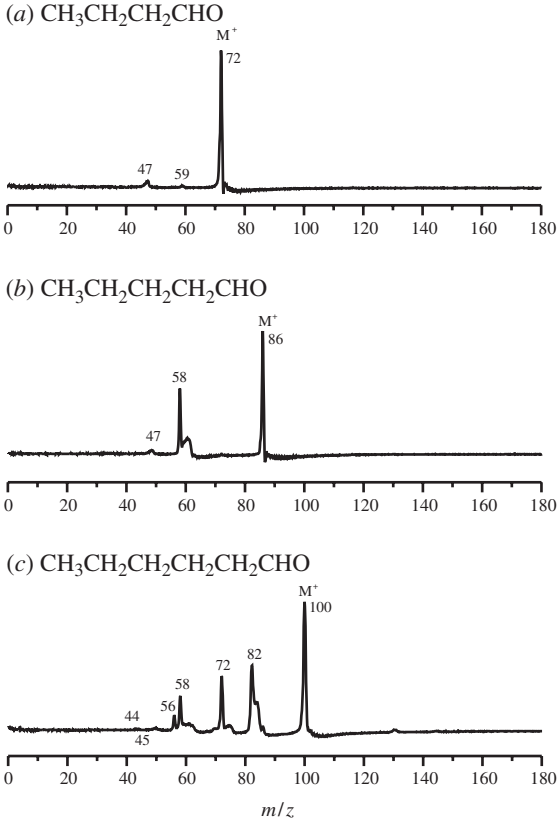
Similar to alcohols, both 1-butylamine and diethyl amine spectra show a weak, protonated HM_2^+ dimer peak at m/z = 147. Not unexpectedly, however, a protonated dimer ion peak was not observed for triethylamine, since it has no hydrogen atom directly bonded to its nitrogen atom.

On the basis of the nitrogen rule, a compound with an odd number of nitrogen atoms must have an odd-valued molecular weight. Thus, unlike conventional 70 eV EI mass spectrometry, amine identification should be relatively straightforward using VUV SPI for parent ion formation.

Alkanals

VUV SPI mass spectra were obtained for *n*-butanal (vertical IP = 9.73 eV (43)), *n*-pentanal (IP = 9.65 eV (44)), and *n*-hexanal (IP = 9.62 eV (44)). The resultant spectra can be inspected in Figs. 5*a*, 5*b*, and 5*c*, respectively. The ionized electron originates from the lone-pair orbital on the oxygen atom in the plane of the carbon chain, and perpendicular to the carbon–oxygen bond (45). In all three TOF mass spectra, the base peak corresponds to the parent ion, which therefore, to the best of our knowledge, represents the softest ionization ever achieved for aldehydes. The same three molecules have been studied using SPI by the same type of laser sources (14, 37). There, only *n*-butanal yielded a base peak at the m/z = 72. The pentanal parent ion intensity (m/z = 86) was 52% of the base peak at m/z = 58 ($[M - C_2H_4]^+$), and the hexanal parent ion (m/z = 100) was 57% of the base peak at m/z = 72, also due to $[M - C_2H_4]^+$ (14).

Fig. 5. 118.2 nm VUV SPI–TOF mass spectra of alkanals: (*a*) *n*-butanal, (*b*) *n*-pentanal, and (*c*) *n*-hexanal. The features indicated by M^+ correspond to parent ion peaks.



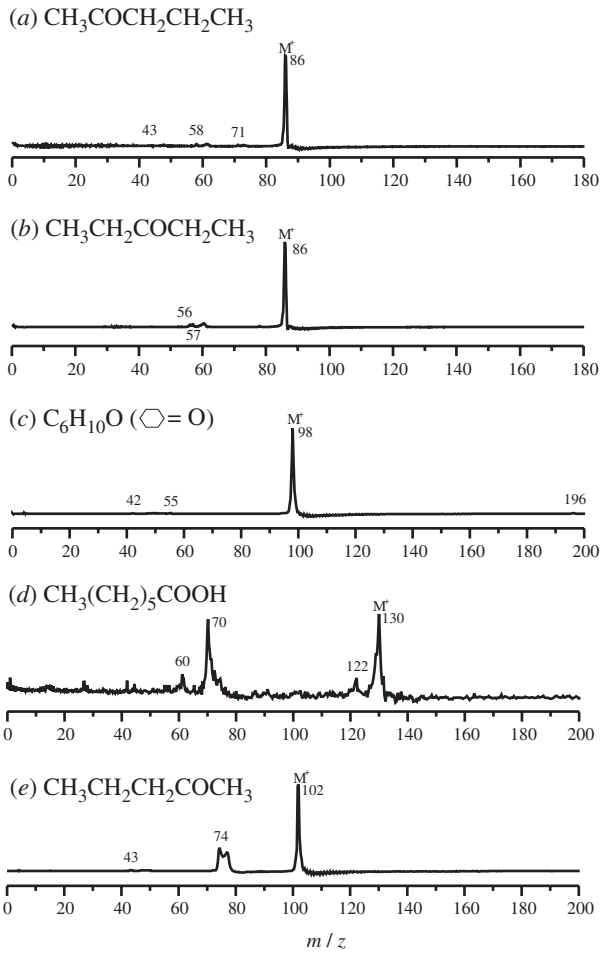
In the 12 eV EI mass spectrum of butanal, the parent ion generates the base peak, while the relative intensities of the parent ion signals for pentanal and hexanal drop to 17% and 11%, respectively (46). A mass spectrum using 70 eV EI shows a relative abundance of 74% for the butanal parent ion, although it is not the base peak, while the parent ions for *n*-pentanal and *n*-hexanal are only 6% and 1%, respectively, of the McLafferty ion ($C_2H_4O^+$) (47) base peak at m/z = 44.

The number of fragment peaks increases with the length of the alkyl chain using VUV SPI. For *n*-hexanal, but not butanal or pentanal, the dehydrated species $[M - H_2O]^+$ is seen at m/z = 82 in addition to the $[M - C_nH_{2n}]^+$ ions at m/z = 72 (n = 2) and 58 (n = 3). The McLafferty and McLafferty + 1 ions are also weakly observed at m/z = 44 and 45, respectively, as is the McLafferty complimentary ion ($C_4H_8^+$) at m/z = 56. The McLafferty fragment ion intensities are the reverse of what is observed by 70 eV EI, but are consistent with the trend obtained with 12 eV electrons (48).

The strongest fragment ions in the aldehyde mass spectra are metastably broadened, which is consistent with the reaction enthalpies listed in ref. 46 (ΔH ~ 10.5 eV). The exception is *n*-butanal where the formation of $[M - C_nH_{2n}]^+$ ions requires >11 eV energy (46) and therefore, are not observed experimentally. In each spectrum a feature at m/z = 47 is observed that remains unassigned, although an impurity or elimination of protonated ethanol from the parent molecule can not be discounted at this time. This peak was not ob-

© 2005 NRC Canada

Fig. 6. 118.2 nm VUV SPI–TOF mass spectra of (*a*) 2-pentanone, (*b*) 3-pentanone, (*c*) cyclohexanone, (*d*) *n*-heptanoic acid, and (*e*) butanoic acid, methyl ester. The features indicated by M^+ correspond to parent ion peaks.



served by 12 eV or 70 eV EI, or in previous VUV laser studies.

Alkanones

The VUV SPI mass spectra were recorded for 2-pentanone (IP = 9.39 eV (49), Fig. 6*a*) and 3-pentanone (IP = 9.32 eV (49), Fig. 6*b*). Ionization is expected to remove a lone-pair electron from the highest occupied molecular orbitals of aliphatic ketones that are predominantly composed of oxygen atomic orbitals. The proportion of atomic character, however, is expected to decrease with increasing alkyl chain length (41, 50, 51).

The parent ion feature at m/z = 86 is the base peak for both ketones in their VUV SPI mass spectra, and the fragment ions are weak. The mass spectrum of 2-pentanone shows two α-cleavage ions at m/z = 43 $[M - C_3H_7]^+$ and m/z = 71 $[M - CH_3]^+$, and a McLafferty ion at m/z = 58. These bands are metastably broadened, which is reasonable given the known appearance energies of these ions (50, 52). The only exception is the $[M - C_3H_7]^+$ ion, which has an appearance energy of 11.54 eV. This suggests that the UV fundamental used to generate the coherent VUV light is also involved in the ionization process. Similar fragmentation patterns have been obtained using 12 eV EI, but the relative intensity of the features at m/z = 43, 58, and 71 are considerably higher at 22%, 17%, and 12%, respectively (17). In the 70 eV EI mass spectrum, the fragment at m/z = 43 becomes the base peak, and the relative intensity of the parent ion is 20%.

The symmetrical 3-pentanone exhibits only one α-cleavage feature at m/z = 57 ($[M - C_2H_5]^+$), and a feature at m/z = 56, which is assigned to $C_3H_4O^+$. Both appear to be metastably broadened, a reasonable result given that the appearance energy of the heavier fragment is 9.90 eV (53). The intensity of the parent ion peak in the 70 eV EI spectrum of 3-pentanone is only 17% of the base peaks at m/z = 57 and 29 [$C_2H_5^+$].

The VUV SPI mass spectrum of cyclohexanone (Fig. 6*c*, IP = 9.16 eV) is also very clean, with the strongest feature due to the parent ion at m/z = 98. Again, photoionization involves an electron from a nonbonding orbital on the oxygen atom that is destabilized by interactions with σ orbitals associated with the alkyl ring (54). Weak fragment peaks at m/z = 42 (relative intensity: 0.45%) and 55 (0.51%) result from rearrangement processes after fragmentation. The former is attributed to the $C_3H_6^+$ ion due to loss of C_2H_4 and CO after ionization, while the latter is assigned to $C_3H_3O^+$ formed as a result of the loss of one C_3H_7 radical. In the 70 eV EI mass spectrum, the feature due to $C_3H_3O^+$ forms the base peak, while the relative parent ion intensity is 33%. A feature due to the cyclohexanone dimer at m/z = 196 is also present in our VUV laser TOF mass spectrum.

Alkanoic acids and alkyl alkanoates

The overall signal intensity of the VUV laser – TOF mass spectrum of *n*-heptanoic acid (shown in Fig. 6*d*) is weak owing to the low vapour pressure of the compound (boiling point = 222.2 °C (55)). The lowest energy ionization event from an alkyl carboxylic acid is expected to involve an electron with primarily lone-pair character on the oxygen atom of the carbonyl group of the acid moiety (56). The base peak observed by VUV SPI is due to the parent ion at m/z = 130. The strongest fragment ion is the McLafferty complementary ion at m/z = 70, while the McLafferty ion at m/z = 60 is weaker. The overlapping peak near m/z = 73 is assigned to the $[M - C_4H_9]^+$ β-cleavage ion. These ions and their relative intensities agree very well with an earlier VUV laser study (14), except for an additional feature at m/z = 102 owing to $[M - C_2H_4]^+$, which is not observed in this work.

The 12 eV (57) and 70 eV EI mass spectra are considerably more congested, with the McLafferty ion at m/z = 60 in both cases providing the base peak. There, the relative intensities of molecular ion peaks are ~6% and 0.7%, respectively.

The VUV SPI mass spectrum of methyl butanoate (IP = 10.07 eV (49)) exhibits a strong parent ion peak at m/z = 102 (Fig. 6*e*). Electron ionization here most likely involves the oxygen of the carbonyl group (58), although fragmentation reactions are expected to involve both the keto and enol forms of the resultant gas-phase parent molecular ion (59). The main fragment peak at m/z = 74 is the McLafferty ion, which appears to be metastably broadened. The result is consistent with the known appearance energy of the ion (10.08 eV) (60). A signal at m/z = 43, just discernible above

© 2005 NRC Canada

the noise, is due to $C_3H_7^+$. The McLafferty ion is not significant, but its complementary ion becomes the origin for the base peaks of butyl ethanoate and larger esters using 12 eV EI mass spectrometry (17). Similarly, the parent ion abundance of methyl butanoate formed by ionization with 70 eV electrons falls to only 4% of the base peak at m/z = 74. Interestingly, however, while methyl butanoate has not been examined previously by VUV SPI mass spectrometry, single-photon ionization data for propyl propionate and butyl butyrate exhibit only weak parent ions peaks (0.4% and 12%, respectively) (14).

Aromatic compounds

Aromatic hydrocarbons

Three aromatic hydrocarbons, benzene (IP = 9.24 eV, Fig. 7*a*), methylbenzene (toluene, IP = 8.83 eV), and 1,2-dimethylbenzene (*o*-xylene, IP = 8.56 eV), were studied in this category. In all three cases, ionization removes a π electron from the aromatic ring orbital, which has e_{1g} symmetry for benzene (D_{6h} point group), and b_1 symmetry for toluene and *o*-xylene (C_{2v}) (61, 62). A single parent ion peak dominates each SPI mass spectrum. These three molecules have also been studied by Butcher et al. (37) using 118 nm SPI–IT-MS, where the parent ion peak is the base peak for all three compounds. The relative abundances of the base peaks as a percentage of the total ion signals were 100, 100, and 90 for benzene, toluene, and *o*-xylene, respectively.

The absence of any fragmentation for benzene is not particularly surprising as this aromatic ring is very stable. Even in the 70 eV EI mass spectrum, while some fragment ions are observed, the parent ion with m/z = 78 is the base peak. In the case of both toluene and *o*-xylene, the base peak in the 70 eV EI mass spectrum is due to the formation of the tropylium ion ($C_7H_7^+$) at m/z = 91, while the parent ion abundances are 62% and 42% for toluene and *o*-xylene, respectively.

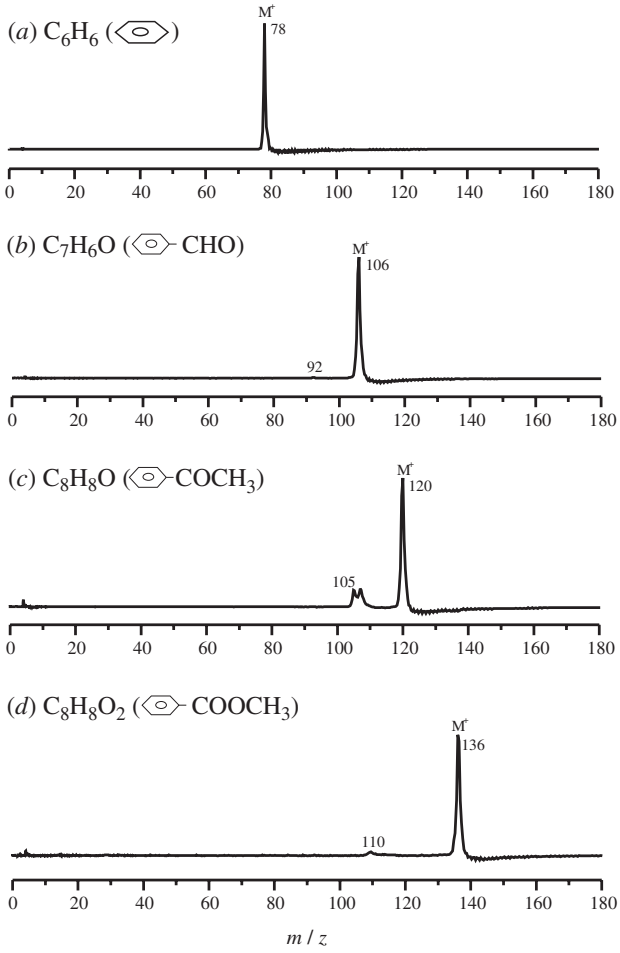
Formation of the tropylium rearrangement product is sensitive to the internal energy of the parent molecular ion first formed. In this context, 10.5 eV VUV SPI is particularly effective in minimizing the formation of $C_7H_7^+$, as its appearance potential for both methyl substituted benzenes is >11 eV (63).

Aromatic aldehydes, ketones, and esters

VUV SPI mass spectra of benzaldehyde (IP = 9.5 eV), acetophenone (IP = 9.28 eV), and methyl benzoate (IP = 9.32 eV) are shown in Figs. 7*b*, 7*c*, and 7*d*, respectively. Photoelectron spectroscopy has been particularly effective in establishing whether the lowest energy ionization involves a predominately nonbonding electron associated with the oxygen of the carbonyl group, or a π electron from the aryl ring. The dominant electron character is thought to be nonbonding for benzaldehyde (64) and acetophenone (65), but π type for the ester (66).

Each spectrum is relatively clean in that the molecular parent ions form the base peaks (m/z = 106 for benzaldehyde, m/z = 120 for acetophenone, and m/z = 136 for methyl benzoate). The result for benzaldehyde is consistent with a previous study (37). The metastably broadened feature in the acetophenone spectrum at m/z = 105 is assigned to the α-cleavage ion $[M - CH_3]^+$ (67), while the weak bands at m/z = 92 and 110 in the benzaldehyde and methyl benzoate spectra, respectively, are unassigned. The parent ion compounds are seen by 70 eV EI and in the case of benzaldehyde this feature is 95% of the base peak at m/z = 77 ($C_6H_5^+$). For the other two species the 70 eV EI base peak is due to the formation of $C_7H_5O^+$ at m/z = 105, while the relative parent ion abundances are 29% and 39% for acetophenone and methyl benzoate, respectively.

Fig. 7. 118.2 nm VUV SPI–TOF mass spectra of aromatic compounds: (*a*) benzene, (*b*) benzaldehyde, (*c*) acetophenone, and (*d*) benzoic acid, methyl ester. The features indicated by M^+ correspond to parent ion peaks.



Discussion and conclusions

While a complete survey of all organic compounds is obviously not possible, the choices presented in this work, and the range of functional groups examined clearly demonstrate that VUV SPI TOF mass spectrometry is superior to electron-based ionization methods for generating parent molecular ions. In those cases where fragmentation reactions were observed, the ions produced were similar to those generated by EI, but were almost always much weaker in intensity.

It could be argued that a considerable amount of useful structural information is lost through such dramatic mass spectral simplification. For example, in the case of aromatic compounds such as benzaldehyde, acetophenone, and methyl

© 2005 NRC Canada

benzoate, the important fragment ion at m/z = 77 indicating the existence of a benzene ring is not observed in the VUV laser SPI TOF mass spectra of all three compounds. Isomeric distinction is also impossible. However, since VUV laser SPI enhances the intensity of parent ions and relatively high mass fragment ions, it should be a useful ionization technique for tandem mass spectrometry. Also, VUV SPI TOF mass spectrometry is expected to be particularly valuable for the analysis of mixtures of similar compounds whose fragmentation patterns by higher energy EI techniques are similar, and where parent ion formation is either very weak or absent.

It was found when using a 10.5 eV photon source that many metastable parent molecular ion decomposition reactions compete effectively with direct soft ionization. Overall, however, these reactions did not detract significantly from the primary goal of this work, namely, parent ion mass identification. In fact, these observations suggest that using *tunable* coherent VUV radiation generated by nonresonant tripling or two-photon resonance enhanced four-wave mixing may in fact be an ideal method of establishing accurate appearance energies of these fragment ions.

Some fragment ions were observed in the TOF mass spectra despite having appearance energies >10.5 eV because our experiment was carried out with the residual UV 355 nm (~3.5 eV) fundamental beam propagating colinearly with the coherent VUV light after nonresonant tripling. Although the focal length of the MgF_2 lens used to focus the VUV light into the supersonic jet is strongly wavelength dependent, the UV intensity in the VUV focal region may be sufficient to initiate multiphoton ionization. One possible solution to this problem involves placing either a prism, an off axis lens, or a monochromator before the analyte ionization region, although optical alignment and light loss may then become issues. These issues are being explored in our lab.

The success of VUV laser SPI for organic molecule identification by parent mass is attributed to two main factors. The first is that almost all organic compounds have IPs that lie in the VUV spectral region, and therefore, the approach described in this work is near universal. The second reason is that except for alkanes, the first ionization threshold of most functionalized organic molecules involves a chromophore having either π- or non-bonding character. As a result, ionization is not expected to significantly perturb the structural framework of the molecule. The lower energy IP trends for aliphatic and aromatic compounds containing nitrogen and sulphur moieties are well-known (68). Thus, VUV SPI may be useful for biomolecule characterization as routine methods emerge to deliver these species, intact, into the gas phase.

It has been demonstrated that modern desorption techniques such as secondary ion mass spectrometry (SIMS) and matrix-assisted laser desorption and ionization (MALDI) have the ability to achieve a softer ionization. However, as the sputtering or desorption processes also lead to ionization, there is little control over the ionization efficiency. Furthermore, most of the desorbed material using SIMS and MALDI are neutrals rather than ions. Typically, the ion to neutral ratios are in the range of 10^{-3} to 10^{-5}. A significant enhancement in sensitivity can be expected if these neutral species are post ionized. In this aspect, VUV laser radiation is expected to be a potentially powerful post ionization source that could improve the sensitivity of these mass spectrometric techniques.

Acknowledgements

Funding from the Natural Sciences and Engineering Research Council of Canada (NSERC) and the University of Western Ontario is gratefully acknowledged. The authors thank Diane Lacey for her experimental contributions.

References

1. M.S.B Munson and F.H. Field. J. Am. Chem. Soc. **88**, 2621 (1966).
2. F.H. Field. Acc. Chem. Res. **1**, 42 (1968).
3. R.H. Lipson and Y.J. Shi. *In* Ultraviolet spectroscopy and UV lasers. *Edited by* P. Misra and M.A. Dubinskii. Marcel Dekker Inc., NewYork. 2001. pp. 131–190, and refs. cited therein.
4. D.J. Butcher. Microchem. J. **62**, 354 (1999).
5. S.E. Van Bramer and M.V. Johnston. Appl. Spectrosc. **46**, 255 (1992).
6. J.H. Arps, C.H. Cen, M.P. McCann, and I. Datskou. Appl. Spectrosc. **43**, 1211 (1989).
7. R.H. Lipson. Physics in Canada, **55**, 223 (1999).
8. W.C. Wiley and I.H. McLaren. Rev. Sci. Instrum. **26**, 1150 (1955).
9. Y.J. Shi, X.K. Hu, D.M. Mao, S.S. Dimov, and R.H. Lipson. Anal. Chem. **70**, 4534 (1998).
10. Y.J. Shi, S. Consta, A.K. Das, B. Mallik, D. Lacey, and R.H. Lipson. J. Chem. Phys. **116**, 6990 (2002); G.S. Fanougakis, Y.J. Shi, S. Consta, and R.H. Lipson. J. Chem. Phys. **119**, 6597 (2003); S. Lam, Y.J. Shi, N.J. Mosey, T.K. Woo, and R.H. Lipson. J. Chem. Phys. **121**, 10006 (2004).
11. S.S. Dimov, R.H. Lipson, T. Turgeon, J.A. Vanstone, P. Wang, and D.S. Yang. J. Chem. Phys. **100**, 8666 (1994).
12. R.H. Lipson, S.S. Dimov, P. Wang, Y.J. Shi, D.M. Mao, X.K. Hu, and J.A. Vanstone. Instrum. Sci. Technol. **28**, 85 (2000).
13. W.G. Mallard (*Editor*). NIST Chemistry WebBook [online]. Available from http://webbook.nist.gov/chemistry/. National Institute of Standards and Technology, Gaithersburg, Maryland. 2005.
14. S.E. Van Bramer and M.V. Johnston. J. Am. Soc. Mass Spectrom. **1**, 419 (1990).
15. R.J.J.M Steenvoorden, P.G. Kistemaker, A.E. De Vries, L. Michalak, and N.M.M. Nibbering. Int. J. Mass Spectrom. Ion Processes, **107**, 475 (1991).
16. A. Lavanchy, R. Houriet, and T. Gäumann. Org. Mass Spectrom. **13**, 410 (1976).
17. A. Maccoll. Org. Mass Spectrom. **21**, 601 (1986).
18. M. Bobeldijk, P.G. Kistemaker, and J.J. Boon. Int. J. Mass Spectrom. Ion Processes, **110**, 179 (1991).
19. K. Fukui, H. Kato, and T. Yonezawa. Bull. Chem. Soc. Jpn. **33**, 1197 (1960).
20. A. Lavanchy, R. Houriet, and T. Gäumann. Org. Mass Spectrom. **14**, 79 (1979).
21. J.F. Wendelboe, R.D. Bowen, and D.H. Williams. J. Am. Chem. Soc. **103**, 2333 (1981).
22. A. Maccoll. Org. Mass Spectrom. **17**, 1 (1982).
23. F.P. Lossing and A. Maccoll. Can. J. Chem. **54**, 990 (1976).
24. J.L. Holmes and F.P. Lossing. Org. Mass Spectrom. **26**, 537 (1991).

© 2005 NRC Canada

25. S. Ikuta, K. Yoshihara, T. Shiokawa, M. Jinno, Y. Yokoyama, and S. Ikeda. Chem. Lett. 1237 (1973).
26. K. Kimura, S. Katsumata, Y. Achiba, T. Yamazaki, and S. Iwata. *In* Handbook of HeI photoelectron spectra of fundamental organic molecules. Japan Scientific Societies Press, Tokyo; Halsted Press, New York. 1981.
27. P. Masclet, D. Grosjean, G. Mouvier, and J. Dubois. J. Electron Spectrosc. Relat. Phenom. **2**, 225 (1973).
28. D.A. Krause, J.W. Taylor, and R.F. Fenske. J. Am. Chem. Soc. **100**, 718 (1978).
29. D.C. Clary, A.A. Lewis, D. Morland, J.N. Murrell, and E. Heilbronner. J. Chem. Soc. Faraday Trans. 2, **70**, 1889 (1974).
30. G. Bieri, F. Burger, E. Heilbronner, and J.P. Maier. Helv. Chim. Acta, **60**, 2213 (1977).
31. G. Carlier, J.E. Dubois, P. Masclet, and G. Mouvier. J. Electron Spectrosc. Relat. Phenom. **7**, 55 (1975).
32. M.Th. Praet. Org. Mass Spectrom. **4**, 65 (1970).
33. J.B. Peel and G.D. Willett. Aust. J. Chem. **28**, 2357 (1975).
34. R.D. Bowen and A. Maccoll. Org. Mass Spectrom. **19**, 379 (1984).
35. S. Hammerum, K.F. Donchi, and P.J. Derrick. Int. J. Mass Spectrom. Ion Processes, **47**, 347 (1983).
36. R.A. Friedel, J.L. Shultz, and A.G. Sharkey, Jr. Anal. Chem. **28**, 926 (1956).
37. D.J. Butcher, D.E. Douglas, and G.E. Hurst. Anal. Chem. **71**, 489 (1999).
38. K. Watanabe and J.R. Mottl. J. Chem. Phys. **26**, 1773 (1957).
39. R.D. Bowen and A. Maccoll. Org. Mass Spectrom. **20**, 331 (1985).
40. T.J. Burkey, A.L. Castelhano, D. Griller, and F.P. Lossing. J. Am. Chem. Soc. **105**, 4701 (1983).
41. F.P. Lossing, Y.-T. Lam, and A. Maccoll. Can. J. Chem. **59**, 2228 (1981).
42. V.F. Plotnikov, G.M. Bogolyubov, I.A. Maretina, and A.A. Petrov. Zh. Org. Khim. **5**, 1137 (1969).
43. Th.M. El-Sherbini, S.H. Allam, M.D. Migahed, and A.M. Dawoud. Z. Naturforsch A, **36**, 1334 (1981).
44. F.S. Ashmore and A.R. Burgess. J. Chem. Soc. Faraday Trans. 2, **74**, 734 (1978).
45. K. Kimura, S. Katsumata, T. Yamazaki, and H. Wakabayashi. J. Electron Spectrosc. Relat. Phenom. **6**, 41 (1975).
46. A. Maccoll and M.N. Mruzek. Org. Mass Spectrom. **21**, 251 (1986).
47. F.W. McLafferty. Anal. Chem. **31**, 82 (1959).
48. A. Maccoll. Org. Mass Spectrom. **23**, 381 (1988).
49. K. Watanabe, T. Nakayama, and J.R. Mottl. J. Quant. Spectrosc. Radiat. Transfer, **2**, 369 (1962).
50. E. Murad and M.G. Inghram. J. Chem. Phys. **40**, 3263 (1964).
51. M.J.S. Dewar and S.D. Worley. J. Chem. Phys. **50**, 654 (1969).
52. J.C. Traeger. Org. Mass Spectrom. **20**, 223 (1985).
53. G. Mouvier and R. Hernández. Org. Mass Spectrom. **10**, 958 (1975).
54. D. Chadwick, D.C. Frost, and L. Weiler. Tetrahedron Lett. **47**, 4543 (1971).
55. D.R. Lide (*Editor*). CRC handbook of chemistry and physics. 81st ed. (2000–2001). CRC Press, Boca Raton, Florida. 2000.
56. I. Watanabe, Y. Yokoyama, and S. Ikeda. Bull. Chem. Soc. Jpn. **46**, 1959 (1973).
57. A. Maccoll. Int. J. Mass Spectrom. Ion Processes, **86**, 227 (1988).
58. I. Howe and D.H. Williams. J. Am. Chem. Soc. **90**, 5461 (1968).
59. J.L. Holmes and F.P. Lossing. Org. Mass Spectrom. **14**, 512 (1979).
60. J.L. Holmes and F.P. Lossing. J. Am. Chem. Soc. **102**, 1591 (1980).
61. M. Klessinger. Angew. Chem. Int. Ed. Engl. **11**, 525 (1972).
62. M.H. Palmer, W. Moyes, M. Spiers, and J.N.A. Ridyard. J. Mol. Struct. **49**, 105 (1978).
63. M.E. Akopyan and F.I. Vilesov. High Energy Chem. **2**, 89 (1968).
64. J.W. Rabalais and R.J. Colton. J. Electron Spectrosc. Relat. Phenom. **1**, 83 (1972).
65. T. Kobayashi and S. Nagakura. Bull. Chem. Soc. Jpn. **47**, 2563 (1974); R. Egdell, J.C. Green, and C.N.R. Rao. Chem. Phys. Lett. **33**, 600 (1975); G. Centineo, I. Fragala, G. Bruno, and S.J. Spampinato. J. Mol. Struct. **44**, 203 (1978).
66. J. Meeks, A. Wahlborg, and S.P. McGlynn. J. Electron Spectrosc. Relat. Phenom. **22**, 43 (1981).
67. R.G. McLoughlin and J.C. Traeger. Org. Mass Spectrom. **14**, 434 (1979).
68. C.N.R. Rao. Indian J. Chem. **13**, 950 (1975).

© 2005 NRC Canada

A study of the isomerization and dissociation of formal [acetone–methanol]$^{+\cdot}$ ion–molecule complexes[1]

Xian Wang and John L. Holmes

Abstract: The energy barrier for the keto–enol isomerization of the isolated acetone ion to its distonic (enol) isomer lies above its lowest dissociation limit and so the spontaneous isomerization can never be observed. Keto–enol isomerizations can be catalyzed within appropriate ion–molecule complexes. The present study involved two systems, $[(CH_3)_2C{=}O\cdots H^+\cdots O(H)CH_2^{\cdot}]$ (ion **1**) and $[(CH_3)_2C{=}O\cdots H^+\cdots {}^{\cdot}OCH_3]$ (ion **2**), in both stable and metastable adducts. When acetone is bound to $^{\cdot}CH_2OH$ though a proton bridge, shown as ion **1**, an enol acetone ion is produced. This reaction results from a proton attaching to the acetone, which then gives an $H^{\cdot}$ atom back to the radical site by a 1,6-H transfer, involving a transition state of low energy requirement. In contrast, when the acetone is protonated and bound to the radical $CH_3O^{\cdot}$ (ion **2**), the above rearrangement does not take place. The metastable complex ion **2** loses a methyl radical, producing a new $[C_3H_7O_2]^+$ isomer of structure $[CH_3C^+(O)\cdots(H)OCH_3]$. Tandem mass spectrometry combined with ab initio calculations were used to investigate the two systems. Potential energy surface diagrams were obtained by calculations at the MP2/6-31+G(d) level of theory to aid further elucidation of the reaction mechanisms.

Key words: ion–molecule complexes, keto–enol mechanisms, ion rearrangements and structures.

Résumé : La barrière d'énergie pour l'isomérisation céto–énolique de l'ion acétone isolé vers son isomère énolique (distonique) se trouve au-dessus de sa plus basse limite de dissociation et on n'observe donc jamais d'isomérisation spontanée. Les isomérisations céto–énoliques peuvent être catalysées à l'intérieur de complexes ion-molécule appropriés. La présente étude implique deux systèmes, $[(CH_3)_2C{=}O\cdots H^+\cdots O(H)CH_2^{\cdot}]$ (ion **1**) et $[(CH_3)_2C{=}O\cdots H^+\cdots {}^{\cdot}OCH_3]$ (ion **2**) chacun dans les adduits stables et métastables. Quand l'acétone est liée au $^{\cdot}CH_2OH$ par un proton agissant comme pont telle que représentée dans l'ion **1**, il y a production de l'ion énolique de l'acétone. Cette réaction résulte du fait qu'un proton se lie à l'acétone qui redonne ensuite l'atome $H^{\cdot}$ au site radicalaire par le biais d'un transfert 1,6 d'hydrogène impliquant un état de transition de bas niveau d'énergie. Au contraire, lorsque l'acétone est protonée et liée au radical $CH_3O^{\cdot}$, tel que représentée dans l'ion **2**, ce réarrangement ne se produit pas. Le complexe ionique métastable **2** perd un radical méthyle conduisant à la formation d'un nouvel isomère $[C_3H_7O_2]^+$ de structure $[CH_3C^+(O)\cdots(H)OCH_3]$. On a utilisé la spectrométrie de masse en tandem combinée à des calculs ab initio pour étudier les deux systèmes. Afin d'élucider les mécanismes réactionnels, on a déterminé les diagrammes de surface d'énergie potentielle par des calculs au niveau MP2/6-31+G(d) de la théorie.

Mots clés : complexes ion–molécule, mécanismes céto–énolique, réarrangements et structures d'ions.

Introduction

Keto–enol isomerization is a well-known process in solution in which the keto species is readily isomerized by acid or base catalysis into the corresponding enol (1). In the gas phase, isolated ketone or aldehyde radical cations do not enolize spontaneously. High-energy barriers that exceed the ions' first dissociation threshold effectively prevent this reaction (2). For example, experiments and theoretical calculations show that the acetone radical cation in the gas phase is 58 kJ/mol (3, 4) less stable than its enol isomer, and the energy barrier for the required intra-ionic 1,3-H shift lies 74 kJ/mol higher than the dissociation threshold of the lowest energy reaction (5, 6).

$$(CH_3)_2C{=}O^{+\cdot} \rightarrow CH_3CO^+ + CH_3^{\cdot}$$

Therefore, acetone cations undergo dissociation rather than enolization.

Recent studies have shown, however, that within an ion–molecule complex, i.e., in which an ion is electrostatically bound to a neutral molecule, the isomerization barrier of the ion can be greatly reduced by the presence of the neutral

Received 29 April 2005. Published on the NRC Research Press Web site at http://canjchem.nrc.ca on 14 January 2006.

X. Wang and J.L. Holmes.[2] Chemistry Department, University of Ottawa, 10 Marie-Curie, Ottawa, ON K1N 6N5, Canada.

[1]This article is part of a Special Issue dedicated to Professor P. Kebarle.
[2]Corresponding author (e-mail: jholmes@science.uottawa.ca).

 doi: 10.1139/V05-200 © 2005 NRC Canada

substrate. Significant mechanisms for such isomerizations have been identified and named "proton transport catalysis" (PTC), the "H-atom transfer" mechanism (ATM), (also known as the quid-pro-quo mechanism), and the "spectator" mechanism. The PTC processes involve H^+ transport between the partners.

$$HAB^{+\cdot} + M \rightarrow [AB^{\cdot}\cdots{}^{+}HM] \rightarrow ABH^{+\cdot} + M$$

The PTC mechanism has to meet a necessary criterion that has been established by the calculations of Chalk and Radom (7), namely that when the proton can return to two sites in the radical (see above), the proton affinity (PA) of the catalyst must lie between the PA values for the radical and heteroatom sites.

The keto–enol isomerization of the acetone cation is a good subject for catalyzed isomerizations and has been investigated by many groups. Trikoupis et al. (8–10) have reported that benzonitrile and acetone itself convert ionized acetone into its enol isomer in a chemical ionization (CI) source of a sector mass spectrometer. Mourgues et al. (11) have studied the isomerization using a variety of substrates having a wide range of PA values, using FT-ICR experimental conditions in which only bimolecular reactions are observed. A disadvantage of this latter method is that the initially formed ion–substrate complex has a high internal energy, equal to or greater than the dissociation energy of the complex. It therefore investigates only those processes, e.g., H^+-transport, that can take place at such an elevated energy. The method cannot therefore study the many stable equilibrium structures that lie in potential wells far below the energy of the biomolecular adduct.

We have employed an alternative strategy in which we explicitly make ions of structure(s) corresponding to adduct isomers that occupy deep potential wells. In such an experiment, a variety of stable or metastable isomeric species are made in which a formal H^+ or $H^{\cdot}$ transfer may already be in place. Detailed studies of the complete potential energy surface (PES) for acetaldehyde and methanol ion–molecule pairs have been described (12, 13). On the PES of the $[CH_3CHO/{}^{\cdot}CH_2OH_2{}^{+}]$ system, the adduct ion structure, $[CH_3CHO\cdots H^+\cdots O(H)CH_2{}^{\cdot}]$, corresponds to the ground state of the ion–molecule complex made by a bimolecular process. Calculations show that in this proton-bridged stable structure, the proton is attached to the acetaldehyde, rather than to ${}^{\cdot}CH_2OH$, in keeping with the PA of CH_3CHO (at O) being greater than that for the ${}^{\cdot}CH_2OH$ radical at oxygen. This complex ion ($CH_3CHO\cdots H^+\cdots O(H)CH_2{}^{\cdot}$) lies in a well on the PES and its metastable dissociation produces an unexpected product, the vinyl alcohol ion $CH_2CHOH^{+\cdot}$. This shows that there is a rearrangement, prior to the loss of CH_3OH. Because it is a metastable ion (MI) process, the isomerization must involve a low internal energy. Isotopic labelling experiments and ab initio calculations were then employed for mechanistic studies and ion structure assignments. In the previous study (12) of $[CH_3CHO/{}^{\cdot}CH_2OH_2{}^{+}]$, the chemistry proceeded via protonated acetaldehyde attached to a ${}^{\cdot}CH_2OH$ radical, and yielded ionized vinyl alcohol and a methanol molecule, $[CH_2CHOH^{+\cdot}\cdots OHCH_3]$, via a $H^+/H^{\cdot}$ transfer mechanism. In contrast, if the protonated acetaldehyde is instead attached to a methoxyl radical, $[CH_3CHOH^+\cdots{}^{\cdot}OCH_3]$, the enol ion is not produced and the precursor ion directly dissociates to the keto ion and methanol.

The stable ion–molecule complexes of desired structure were generated in the mass spectrometer by selecting the appropriate fragment ions in the CID mass spectra of proton-bound molecular pairs (14).

In a previous study, the reaction mechanism was established for a methanol ion associated with the simpler keto molecule, acetaldehyde. The present work was to investigate whether the above mechanism was a general one that could apply to larger polyatomic keto species and so we here describe the behaviour of $[\text{acetone–methanol}]^{+\cdot}$ ion–molecule complexes, having structures $[(CH_3)_2C{=}O\cdots H^+\cdots O(H)CH_2{}^{\cdot}]$ (ion **1**) and $[(CH_3)_2C{=}O\cdots H^+\cdots{}^{\cdot}OCH_3]$ (ion **2**). The mechanisms of rearrangements and dissociations of ions **1** and **2** have been explored by experiment and by computation, and the PESs for these two systems will be discussed in the Results and discussion section of this paper.

Experimental and theoretical section

All experiments were carried out on a modified ZAB-3F tandem mass spectrometer (15) with BEE geometry (VG Analytical, Manchester, UK). MI and collision-induced dissociation (CID) mass spectra of selected proton-bound pairs were acquired, and the desired ion–molecule complex was produced by CID of the proton-bound ion in the second field-free region (2FFR) of the mass spectrometer. MI and CID dissociations of the ion–molecule complex were observed in the third field-free region (3FFR). The ion accelerating voltage on the proton-bound pairs was 8 kV. In the 2FFR and 3FFR helium was used as the collision gas for the CID experiments. All spectra were recorded with the ZABCAT program developed by Mommers Technologies (Ottawa, Ontario) (15).

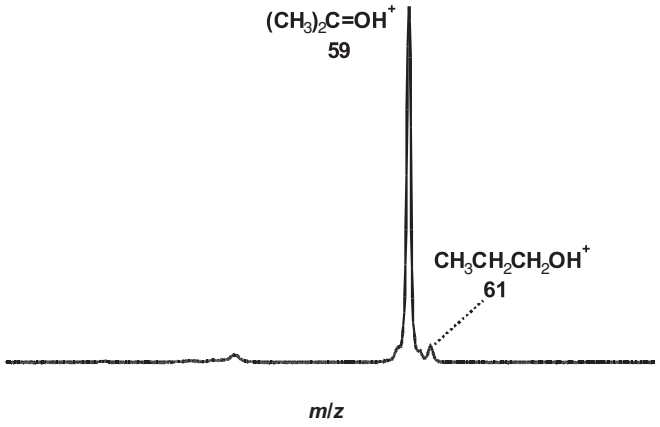
The proton-bound dimer of acetone and propanol was generated by admitting the mixed reagents $CH_3CH_2CH_2OH$ and $(CH_3)_2C{=}O$ into a high pressure ion source at a total observed pressure of ca. 8×10^{-5} mbar (1 bar = 100 kPa), indicating an ion pressure of 0.5 mbar (16). The proton-bound dimer $(CH_3)_2C{=}O\cdots H^+\cdots O(H)CH_2CH_2CH_3$ (*m*/*z* 119) was mass-selected by the magnet and dissociated by collision in the second field-free region. The fragment ion $[(CH_3)_2C{=}OH^+\cdots O(H)CH_2{}^{\cdot}]$ (*m*/*z* 90) resulted from the loss of $CH_3CH_2{}^{\cdot}$ from the precursor ion (*m*/*z* 119) and it was transmitted into the third field-free region to observe its MI and CID characteristics.

A similar experiment was used for the acetone – dimethyl ether proton-bound dimer, $(CH_3)_2C{=}O\cdots H^+\cdots O(CH_3)_2$ (*m*/*z* 105), to collisionally generate the ion $[(CH_3)_2C{=}OH^+\cdots{}^{\cdot}OCH_3]$ (*m*/*z* 90) by the specific loss of $CH_3{}^{\cdot}$ from the ether moiety. An experiment with $(CD_3)_2C{=}O\cdots H^+\cdots O(CH_3)_2$ (*m*/*z* 111) showed that it was an ether methyl group that was specifically lost following collisional activation. Dimethyl ether was introduced through the gas inlet at an observed pressure of 5×10^{-5} mbar, producing ca. 0.3 mbar in the high pressure ion source.

The molecules $(CH_3)_2C{=}O$, $CH_3CH_2CH_2OH$, $(CH_3)_2O$, and the isotopically labelled compounds, $(CD_3)_2C{=}O$, $CH_3CH_2CD_2OH$, and $CH_3CH_2{}^{13}CH_2OH$, were used to generate various isotopomeric ion–molecule pairs. The

© 2005 NRC Canada

Fig. 1. MI mass spectrum of the proton-bound pair $(CH_3)_2C{=}O{\cdots}H^+{\cdots}O(H)CH_2CH_2CH_3$ (*m/z* 119).



unlabeled chemicals were purchased from Aldrich and all the labelled samples, of 99.5%–99.9% isotopic purity, were obtained from CDN Isotopes (Montreal, Quebec) and were used without further purification.

The GAUSSIAN 98 programs were used to perform standard ab initio molecular orbital calculations to investigate the potential energy surface. Optimized geometries and the energies of all minima and transition states were calculated at the MP2/6-31+G(d) level of theory. Zero-point energies obtained from calculations of vibrational frequencies at the same level of theory were scaled by a factor of 0.943 (17).

Results and discussion

Experimental observations for ion 1 $[(CH_3)_2C{=}0{\cdots}H^+{\cdots}O(H)CH_2^{\cdot}]$ and ion 2 $[(CH_3)_2C{=}0{\cdots}H^+{\cdots}{}^{\cdot}OCH_3]$

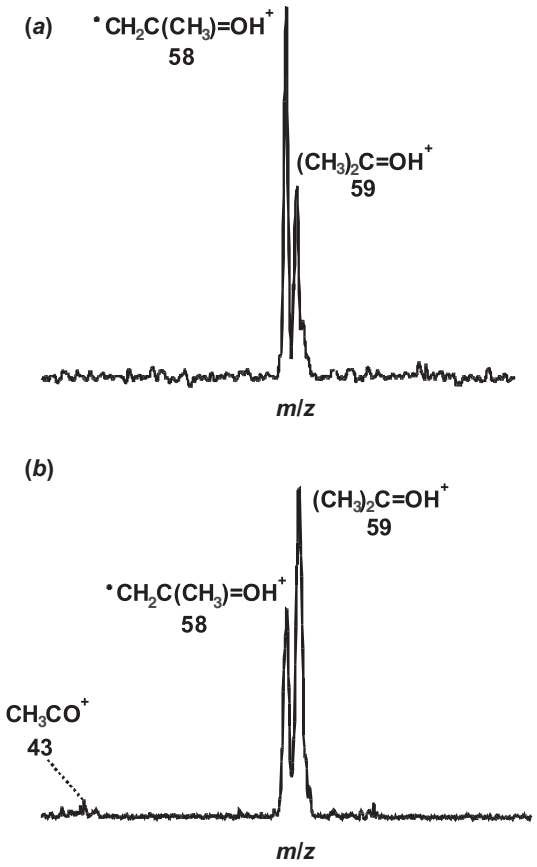
Ion 1

An ion of structure **1** was obtained by the collision-induced loss of a $CH_3CH_2^{\cdot}$ radical from the proton-bound dimer $(CH_3)_2C{=}O{\cdots}H^+{\cdots}O(H)CH_2CH_2CH_3$ (*m/z* 119), ion **P1**. The PA of acetone (812.0 kJ/mol) (18) is greater than that of propanol (786.5 kJ/mol) (18), and so the proton is preferentially attached to the alcohol thus resembling protonated acetone electrostatically bound to a propanol molecule, i.e., $(CH_3)_2C{=}OH^+{\cdots}O(H)CH_2CH_2CH_3$. Its MI mass spectrum has *m/z* 59 (100%), $(CH_3)_2C{=}OH^+$, as the most intense peak and a small signal for protonated propanol (*m/z* 61, 5%) as shown in Fig. 1. These are the only MI processes, showing that no rearrangement of the proton-bound dimer can likely take place at internal energies up to those for MI dissociations. In its CID mass spectrum, in addition to the above major peaks, there is now a small signal for $CH_3CH_2^{\cdot}$ loss (*m/z* 76, <<1%).

[1] $(CH_3)_2C{=}OH^+{\cdots}O(H)CH_2CH_2CH_3$ (*m/z* 119) $\rightarrow [(CH_3)_2C{=}OH^+{\cdots}O(H)CH_2^{\cdot}]$ (*m/z* 90, Ion **1**) + $CH_3CH_2^{\cdot}$ (CID)

The MI spectrum of ion **1** (Fig. 2*a*) contains two peaks: protonated acetone, $(CH_3)_2C{=}OH^+$ (*m/z* 59, 53%), and as base peak (*m/z* 58), which was shown to be the distonic acetone ion ($^{\cdot}CH_2C(CH_3) = OH^+$, see the following discussion).

Fig. 2. (*a*) MI mass spectrum of $[(CH_3)_2C{=}OH^+{\cdots}O(H)CH_2^{\cdot}]$ (*m/z* 90). (*b*) CID mass spectrum of $[(CH_3)_2C{=}OH^+{\cdots}O(H)CH_2^{\cdot}]$ (*m/z* 90).

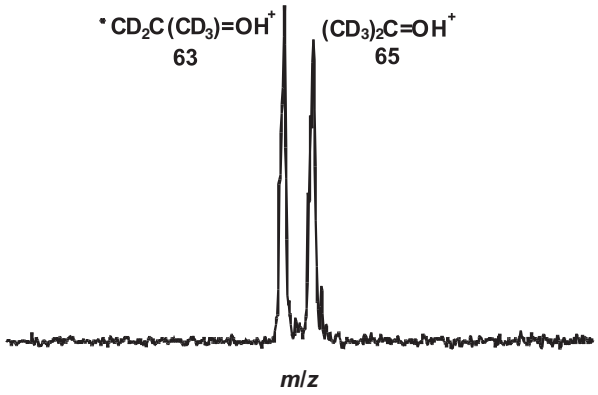


In the CID mass spectrum of ion **1** (Fig. 2*b*), the intensity of the peak at *m/z* 59 ($(CH_3)_2C{=}OH^+$) is increased and is now the base peak. The formation of $(CH_3)_2C{=}OH^+$ is thus collision sensitive, being a simple bond cleavage in ion **1**. The observation that a metastable ion peak is insensitive to collision gas signifies that the mass selected ion has undergone a rearrangement to an isomeric species over an energy barrier close to the lowest energy fragmentation for that ion. In cases where this energy barrier is lower or nonexistent, the collision sensitivity of the peak is correspondingly greater. If the MI peak is for a simple bond cleavage in the mass selected ion, the collision sensitivity is greatest and often produces the base peak in a CID mass spectrum (19). Ion **1** keeps the proton-bridged form of the precursor proton-bound pair (*m/z* 119), and so it is represented as $[(CH_3)_2C{=}OH^+{\cdots}O(H)CH_2^{\cdot}]$. This is also in keeping with the PA of $(CH_3)_2C{=}O$ at O (812.0 kJ/mol) being higher than the PA of $^{\cdot}CH_2OH$ (695.0 kJ/mol). However, note that the peak at *m/z* 58 ion is *not* collision sensitive, indicating that ion **1** rearranges before it fragments by this route.

The dissociation channel that leads to the enol form of ionized acetone is energetically the most favourable process. If the ion *m/z* 58 has the enol structure, the dissociation threshold energy is at 459 kJ/mol (from $\Delta_f H[^{\cdot}CH_2C(CH_3){=}OH^+]$ = 661 kJ/mol and $\Delta_f H[CH_3OH]$ = –202 kJ/mol) (20). This is lower than the dissociation limit (470 kJ/mol) for the formation of protonated acetone *m/z* 59 (from $\Delta_f H[(CH_3)_2C{=}OH^+]$ = 489 kJ/mol and $\Delta_f H[^{\cdot}CH_2OH]$ = –19 kJ/mol) (20). If the *m/z*

© 2005 NRC Canada

Fig. 3. MI mass spectrum of $[(CD_3)_2C{=}OH^+\cdots O(H)CD_2^{\cdot}]$ (**1-d$_8$**, *m/z* 98).



58 ion had the keto structure, the threshold energy for this dissociation would be much higher, at 517 kJ/mol (from $\Delta_f H[(CH_3)_2C{=}O^{+\cdot}]$ = 719 kJ/mol and $\Delta_f H[CH_3OH]$ = −202 kJ/mol) (20), and would be unable kinetically to compete with the simple bond cleavage to *m/z* 59. That the enol ion is produced is fully supported by the results of isotopic labelling.

The deuterium-labelled ion–molecule pairs, $[(CH_3)_2C{=}OH^+\cdots O(H)CD_2^{\cdot}]$ (**1-d$_2$** (*m/z* 92)), $[(CD_3)_2C{=}OH^+\cdots O(H)CD_2^{\cdot}]$ (**1-d$_8$** (*m/z* 98)), and $[(CD_3)_2C{=}OD^+\cdots O(H)CD_2^{\cdot}]$ (**1-d$_9$** (*m/z* 99)), were examined to help assign the structure of the *m/z* 58 ion to that of the enol of acetone. The MI mass spectrum of **1-d$_8$** (*m/z* 98) (Fig. 3) shows intense peaks at *m/z* 63 and *m/z* 65, corresponding to the ions $^{\cdot}CD_2C(CD_3){=}OH^+$ and $(CD_3)_2C{=}OH^+$, respectively. No peak at *m/z* 64 was observed; had the keto ion been the product, it would have resulted in *m/z* 64 ($(CD_3)_2C{=}O^{+\cdot}$) being observed instead. The relative abundance of the two product ions for the labelled complexes differs from that for the unlabelled ion **1** owing to an isotope effect in the H transport in the isomerization process. In general, the rate constant for k_{isom} (H) has been found to be greater than k_{isom} (D), resulting in smaller distonic acetone peaks in the mass spectra of labelled ions. The MI mass spectra of **1-d$_2$** (*m/z* 92) and **1-d$_9$** (*m/z* 99) showed only two dissociation reactions, again resulting from the explicit formation of distonic acetone and protonated acetone. These two ions carry different labels for the hydroxyl or methyl H atoms of the radical site, indicating that the H atoms from $^{\cdot}CH_2OH$ were not found in the product ions. Thus, there was no H/D mixing involved in the ion dissociations. The rearrangement process is described as follows. Before the ion–molecule complex **1**, $[(CH_3)_2C{=}OH^+\cdots O(H)CH_2^{\cdot}]$, dissociates to the distonic acetone ion and methanol, a H$^{\cdot}$ atom from $CH_3C(CH_3){=}OH^+$ is transferred to the $^{\cdot}CH_2OH$ radical via a 1,6-H shift. This process involves a low energy barrier, shown as TS1 on the PES of ion **1** (see Fig. 4 and the discussion of the computations).

Ion 2

The MI mass spectrum of the proton-bound acetone – dimethyl ether ion pair, $(CH_3)_2C{=}O\cdots H^+\cdots O(CH_3)_2$ (*m/z* 105) (**P2**), showed two major peaks, namely protonated acetone (*m/z* 59) and protonated dimethyl ether (*m/z* 47), indicating that the ion keeps its original structure prior to dissociation. A minor $CH_3^{\cdot}$ loss peak (*m/z* 90) is produced by collision-induced dissociation; this reaction is shown in eq. [2].

$$[2]\quad (CH_3)_2C{=}O\cdots H^+\cdots O(CH_3)_2\ (m/z\ 105) \rightarrow [(CH_3)_2C{=}OH^+\cdots{}^{\cdot}OCH_3]\ (m/z\ 90,\ \text{Ion } \mathbf{2}) + CH_3^{\cdot}\ (\text{CID})$$

The lost methyl radical could come from either molecule, and so deuterium labelling was used to identify the methyl groups, e.g., $(CD_3)_2C{=}O\cdots H^+\cdots O(CH_3)_2$ (**P2-d$_6$**) and $(CD_3)_2C{=}O\cdots D^+\cdots O(CH_3)_2$ (**P2-d$_7$**), which lost only $^{\cdot}CH_3$ in their CID mass spectra, showing that only an ether methyl group is involved.

Compared with its isomer **1**, where the radical is located on the carbon atom, ion **2** carries the radical on methoxyl group owing to a removal of a radical from the oxygen atom. Their MI dissociation profiles are different. For example, the MI mass spectrum of $[(CD_3)_2C{=}OH^+\cdots OCH_3]$ (**2-d$_6$**, *m/z* 96) showed that there are three competing dissociation channels, giving protonated acetone (*m/z* 65), the acetone ion (*m/z* 64), and $CD_3^{\cdot}$ loss (*m/z* 78) (see Fig. 5).

The smaller peak *m/z* 58 in the MI mass spectrum of unlabeled ion **2** must be the acetone cation, not the enol ion, even though the latter is more energetically favoured than protonated acetone (see the Discussion for ion **1**), showing no rearrangement of ion **2** to its enol form. The deuterium-labelling results indicate that the lost methyl group comes exclusively from the acetone moiety and that H/D atoms in ion **2** have retained their original positions before it fragments, i.e., no H/D mixing between the two moieties in the complex. Surprisingly, the methyl loss peak is collision insensitive, indicating that it does not arise from a simple C—C bond cleavage. It was concluded from the computations that the product ion from the methyl lost from ion **2** is an ion–molecule complex of the acetyl ion and methanol, $[CH_3C^+(O)\cdots O(H)CH_3]$, an ion that comprises a new member of the $[C_3H_7O_2]^+$ isomers. The detailed path for the generation of the ion $[CH_3C^+(O)\cdots O(H)CH_3]$ is discussed in the Calculations section. To date, the other three identified ion $[C_3H_7O_2]^+$ structures were characterized, which are $[CH_3OCH{=}OCH_3]^+$ and the proton-bound complex of acetaldehyde and formaldehyde, $CH_3CHO\cdots H^+\cdots OCH_2$, by McLafferty and Proctor (21), and protonated ethyl formate, $CH_3CH_2OC^+(H)OH$, by Larson and McMahon (22).

Theoretical calculations

The two ion–molecule complexes, $[(CH_3)_2C{=}OH^+\cdots O(H)CH_2^{\cdot}]$ and $[(CH_3)_2C{=}OH^+\cdots{}^{\cdot}OCH_3]$, display different chemistries in their mass spectra. Thus, these two systems do not communicate with each other, presumably because a high energy barrier prevents them from freely interconverting in the metastable ion dissociation time frame. Calculations were performed to produce a PES for each ion and to investigate the mechanisms of the isomerizations and fragmentations. The energies (in kJ/mol) shown on the PES are relative to the calculated energy of the stable complex IV of distonic acetone and methanol, $[^{\cdot}CH_2C(CH_3) = OH^+\cdots O(H)CH_3]$, obtained at the MP2/6-31+G(d) level of theory, and are given in Table 1. Intrinsic reaction coordinate (IRC) calculations have been used to follow the reaction paths from all transition states to identify intermediates. IRCs were also used to

© 2005 NRC Canada

Fig. 4. The 0 K potential energy surface of the $[(CH_3)_2C{=}OH^+\cdots O(H)CH_2^{\cdot}]$ system at MP2/6-31+G(d).

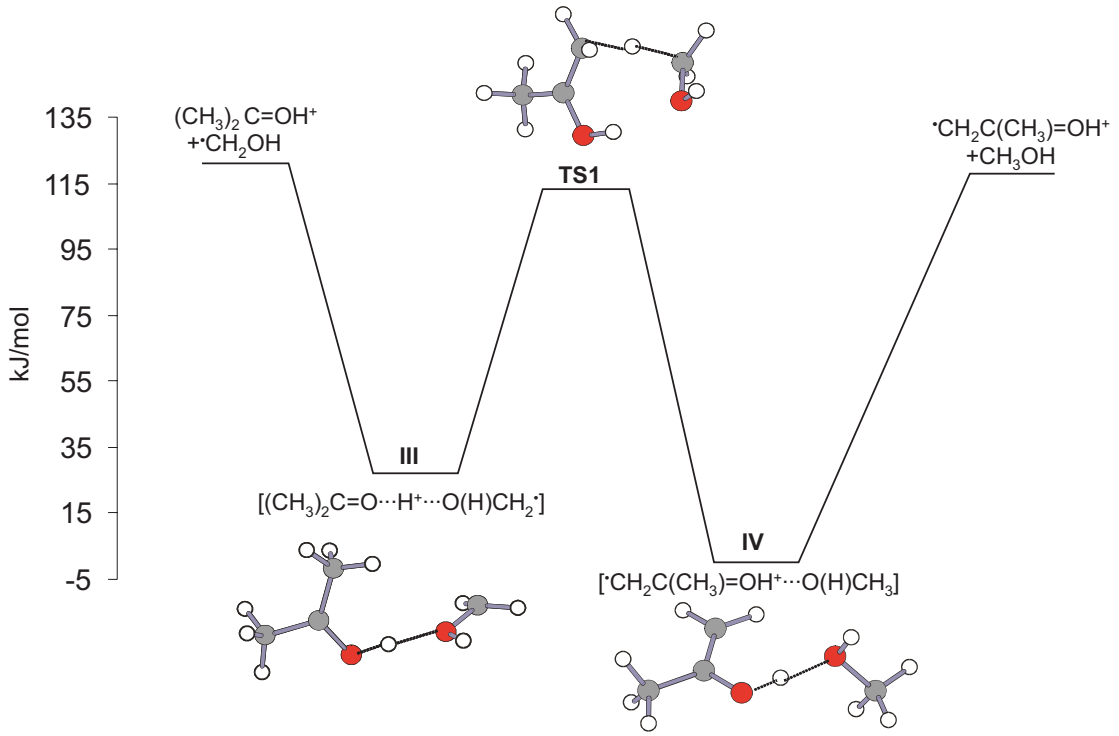
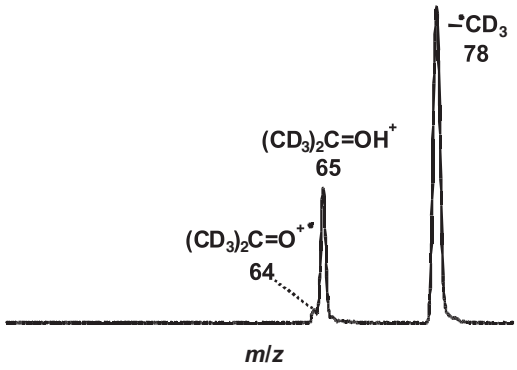


Fig. 5. MI mass spectrum of $[(CD_3)_2C{=}OH^+\cdots OCH_3]$ (**2-d$_6$**, *m/z* 96).



test whether a transition state is the correct structure that connects two minimum wells.

The $[(CH_3)_2C{=}O\cdots H^+\cdots O(H)CH_2^{\cdot}]$ system

The 0 K potential energy profile is shown in Fig. 4. The optimized structure of ion **1** is indeed $[(CH_3)_2C{=}O\cdots H^+\cdots O(H)CH_2^{\cdot}]$. In the stable species III, the proton is closer to the keto oxygen than to the hydroxyl oxygen of the radical, the two bond lengths being 1.031 Å for $(CH_3)_2C{=}O$-H and 1.565 Å for $^{\cdot}CH_2O(H)$-H (see Fig. 6*a*). This is in keeping with the PA of $(CH_3)_2C{=}O$ being greater than that for $^{\cdot}CH_2OH$ at oxygen. Ion III rearranges to the stable complex IV, distonic acetone ion and methanol, $[^{\cdot}CH_2C(CH_3){=}OH^+\cdots O(H)CH_3]$, via a cyclic transition state (TS1). This rearrangement requires only ca. 113 kJ/mol and the TS1 lies below the dissociation threshold of III to protonated acetone and the hydroxylmethyl radical (120 kJ/mol). The energy for the isolated ionized acetone ion to isomerize to its enol form is at 213 kJ/mol (6, 23), above the heat of formation of the latter and lies well above the dissociation limit for the keto ion's loss of $CH_3^{\cdot}$ (139 kJ/mol) (23). Note that TS1, the seven-membered ring intermediate structure, would be favoured by entropy considerations. Complex IV then dissociates to produce the enol ion and a methanol molecule, the dissociation limit for which is 117 kJ/mol. This process involves the low energy barrier TS1 and is the competing dissociation channel with an energy lower than that for the production of protonated acetone (*m/z* 59), and thus distonic acetone (*m/z* 58) gives rise to the most intense peak in the MI mass spectrum of ion **1**. Thus, the initial acetone molecule has been ionized and isomerized to its enol ion form by the transferring of H^+ and $H^{\cdot}$ from the substrate in which the free radical site functions as a good $H^{\cdot}$ or H^+ acceptor, facilitating the enolization of acetone.

The $[(CH_3)_2C{=}O\cdots H^+\cdots{}^{\cdot}OCH_3]$ system

Ion **2** is shown as the stable complex I on the 0 K PES (Fig. 7). In this proton-bound complex, acetone is more strongly associated with the proton because the PA of acetone (812 kJ/mol) is significantly higher than that of $CH_3O^{\cdot}$ (658 kJ/mol). A simple bond cleavage produces $(CH_3)_2C{=}OH^+$ (*m/z* 59) and $CH_3O^{\cdot}$ at a dissociation threshold of 155 kJ/mol. The ion I, $[(CH_3)_2C{=}OH^+\cdots{}^{\cdot}OCH_3]$, is able to rearrange to a complex of the acetone ion and methanol, stable complex II $[(CH_3)_2C{=}O^{+\cdot}\cdots HOCH_3]$. However, no transition-state structure has been found to connect these two minima. The same problem has been encountered when calculating the transition state between the stable $[CH_3CHOH^+\cdots{}^{\cdot}OCH_3]$ complex and of CH_3CHOH^+ with CH_3OH on the PES for the acetaldehyde–methanol ion complex (12, 13, 24). Similarly, here, with the complex II, $[(CH_3)_2C{=}O^{+\cdot}\cdots HOCH_3]$, the O atom of CH_3OH is associ-

© 2005 NRC Canada

Table 1. Calculated electronic energies (in Hartrees), incorporating a scaled zero-point energies and relative energies, E_{rel} (in kJ/mol), at 0 and 298 K for the different structures.

	0 K		298 K	
Structure	MP2/6-31+G(d)	E_{rel}	MP2/6-31+G(d)	E_{rel}[a]
I	–307.442602	69	–307.432051	69
II	–307.423063	120	–307.411855	122
III	–307.458494	27	–307.447603	29
IV	–307.468849	0	–307.458509	0
V	–307.427055	110	–307.413557	118
VI	–307.447685	56	–307.437100	56
VII	–307.429401	104	–307.418488	105
TS0	–307.373164	251	–307.363053	251
TS1	–307.425812	113	–307.416873	109
TS3	–307.408672	158	–307.398900	157
TS4	–307.406161	165	–307.395807	165
TS5	–307.419918	128	–307.408595	131
$(CH_3)_2C{=}OH^+ + {}^{\cdot}CH_2OH$	–307.423212	120	–307.412746	120
${}^{\cdot}CH_2C(CH_3){=}OH^+ + CH_3OH$	–307.423780	118	–307.413405	118
$(CH_3)_2C{=}OH^+ + CH_3O^{\cdot}$	–307.409759	155	–307.399554	155
$(CH_3)_2C{=}O^{+\cdot} + CH_3OH$	–307.402802	173	–307.392064	174
$[CH_3C^+(O)\cdots O(H)CH_3] + CH_3^{\cdot}$	–307.421890	123	–307.409611	128

[a]The relative energies (at 298 K) can be also normalized using the established energies of a selected product pair, e.g., $\Delta_f H[{}^{\cdot}CH_2C(CH_3){=}OH^+] + \Delta_f H[CH_3OH]$ = 459 kJ/mol, and so adding 341 kJ/mol (= 459 kJ/mol – 118 kJ/mol) to all values achieves this.

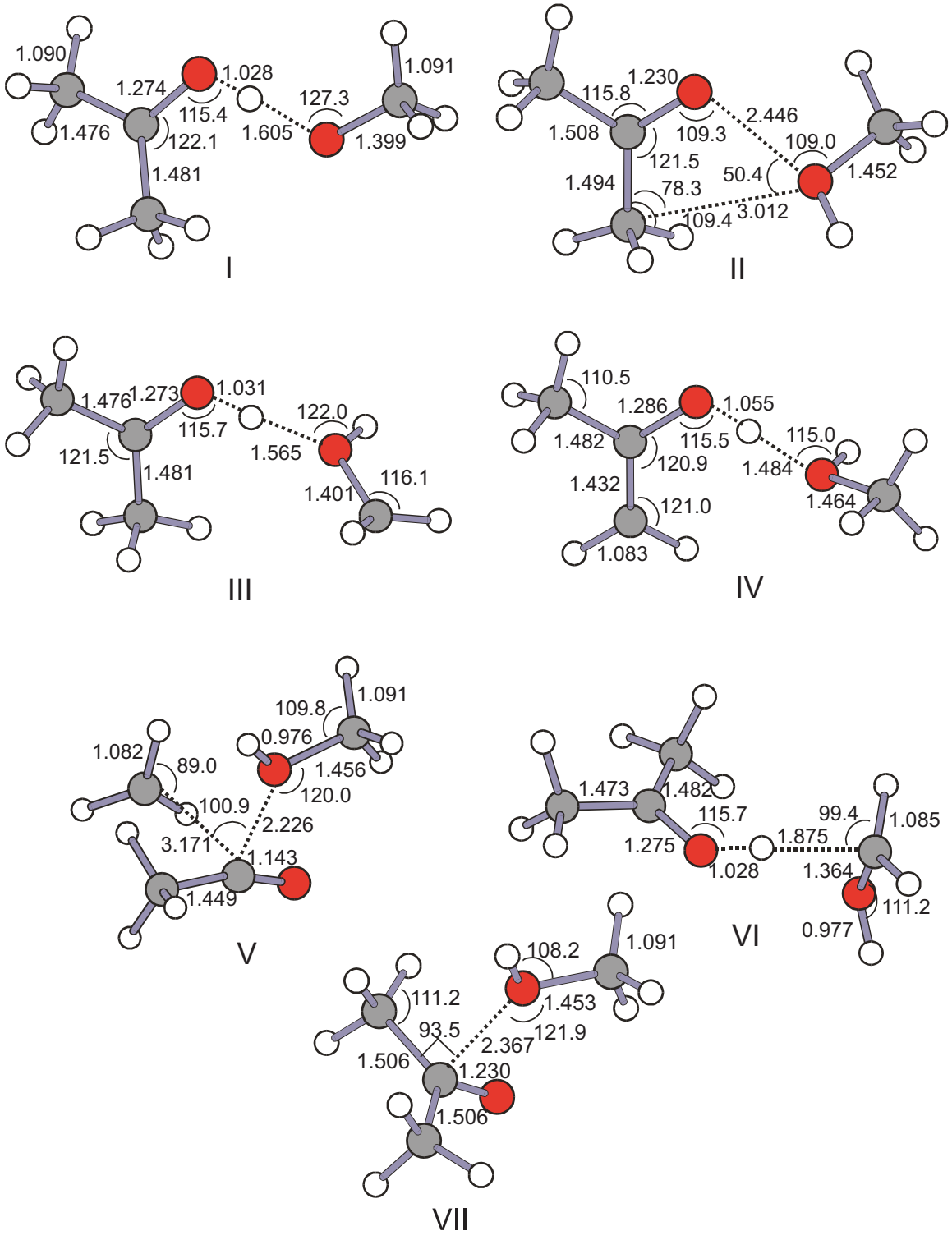
ated with the carbonyl O and methyl C of $(CH_3)_2C{=}O^{+\cdot}$ in the form of a four-membered ring structure. The computational difficulty arises when I converts to II, the charge centre migrates from the proton to the acetone C atom and a $H^{\cdot}$ atom moves to $CH_3O^{\cdot}$. A minimum energy crossing point (MECP) has been suggested by Ruttink and co-workers (8) and by Haranczyk et al. (13), which is defined as the geometry corresponding to the minimum energy complex for the intersection of the two discontinuous PES. Because the acetone ion (*m*/*z* 58) is observed in the MI mass spectrum of ion **2**, this transition state (TS2) should be below the dissociation limits of the precursor ion–molecule complex I (at 155 kJ/mol). Complex II can also fragment to the acetone ion (*m*/*z* 58) and methanol.

Another competing dissociation channel of ion **2** is the generation of $(CH_3)_2C{=}OH^+$ (*m*/*z* 59) and a ${}^{\cdot}CH_2OH$ radical, a reaction that is energetically more favourable than the simple bond dissociation to $(CH_3)_2C{=}OH^+$ and $CH_3O^{\cdot}$ because the heat of formation of ${}^{\cdot}CH_2OH$ (–19 kJ/mol) (20) is lower than that of $CH_3O^{\cdot}$ (16 kJ/mol) (20). This reaction involves an ion rearrangement from complex II to ion VI, $[(CH_3)_2C^+(=OH)\cdots O(H)CH_2^{\cdot}]$. The latter is an isomer of complex III, $[(CH_3)_2C{=}OH^+\cdots O(H)CH_2^{\cdot}]$. In structure VI, $CH_2OH^{\cdot}$ is bound to $(CH_3)_2C{=}OH^+$ through a C(of ${}^{\cdot}CH_2OH$)···H···O(of acetone) bridge, different from the O···H···O proton bridge in complex III. In TS3, the H atom moves from the methyl group of methanol to carbonyl O. TS3 between complex II and VI lies at 158 kJ/mol, close to the dissociation threshold of complex I (155 kJ/mol). Thus, the two reactions can compete in terms of their energy requirements.

The MI mass spectrum of ion **2** shows as a base peak the loss of methyl from the acetone moiety, and the mechanism explored by the calculations is as follows. Interconversion between complex II and its isomer, i.e., complex VII, takes place via transition state TS4 (165 kJ/mol). In complex VII, the methanol is perpendicular to the acetone plane and separated by an elongated C···O bond of 2.367 Å between the two species. Note that in ion VII the rearrangement of the methanol molecule leads to stabilization of the charge on the carbonyl C atom, facilitating the ensuing methyl loss. In TS5, the extension of the C—C bond in acetone leads to the elimination of a methyl radical, leaving a new complex of an acetyl ion and methanol, $[CH_3C^+(O)\cdots(H)OCH_3]$. The geometry of this ion is shown in Fig. 8. The dissociation limit for **2** to produce $[CH_3C^+(O)\cdots(H)OCH_3]$ and $CH_3^{\cdot}$ is 128 kJ/mol at 298 K (Table 1). Heats of formation of new products can be calculated by normalizing the computed relative energies (at 298 K) using the well-established experimental energies of a selected product pair, e.g., $\Delta_f H[{}^{\cdot}CH_2C(CH_3){=}OH^+] + \Delta_f H[CH_3OH]$ = 459 kJ/mol (20); adding 341 kJ/mol to all relative energies achieves this (see Table 1). The heat of formation of the product ion $[CH_3C^+(O)\cdots(H)OCH_3]$ (322 kJ/mol) is obtained by subtracting $\Delta_f H[{}^{\cdot}CH_3]$ = 147 kJ/mol from the dissociation limit for the ion (469 kJ/mol (= 128 kJ/mol + 341 kJ/mol)). Thus, the binding energy in this ion to the products $CH_3CO^+ + CH_3OH$ is 129 kJ/mol, using $\Delta_f H[CH_3C^+O]$ = 653 kJ/mol (18) and $\Delta_f H[CH_3OH]$ = –202 kJ/mol (18). The relatively high energy of the electrostatic bond in this ion is similar to that of -O···H^+···O- (~130 kJ/mol) in proton-bound pairs (25), although this ion does not contain a proton bridge. It follows therefore that the attachment of methanol to ionized acetone (shown as complex VII) results in a remarkable weakening of the H_3C—C bond from 81 kJ/mol in the isolated ion ($\Delta_f H[(CH_3)_2CO^{+\cdot}]$ = 719 kJ/mol) (20) to only 26 kJ/mol (the

© 2005 NRC Canada

Fig. 6. (*a*) Optimized geometries of the stable complexes at MP2/6-31+G(d). (*b*) Optimized geometries of the transition states at MP2/6-31+G(d).

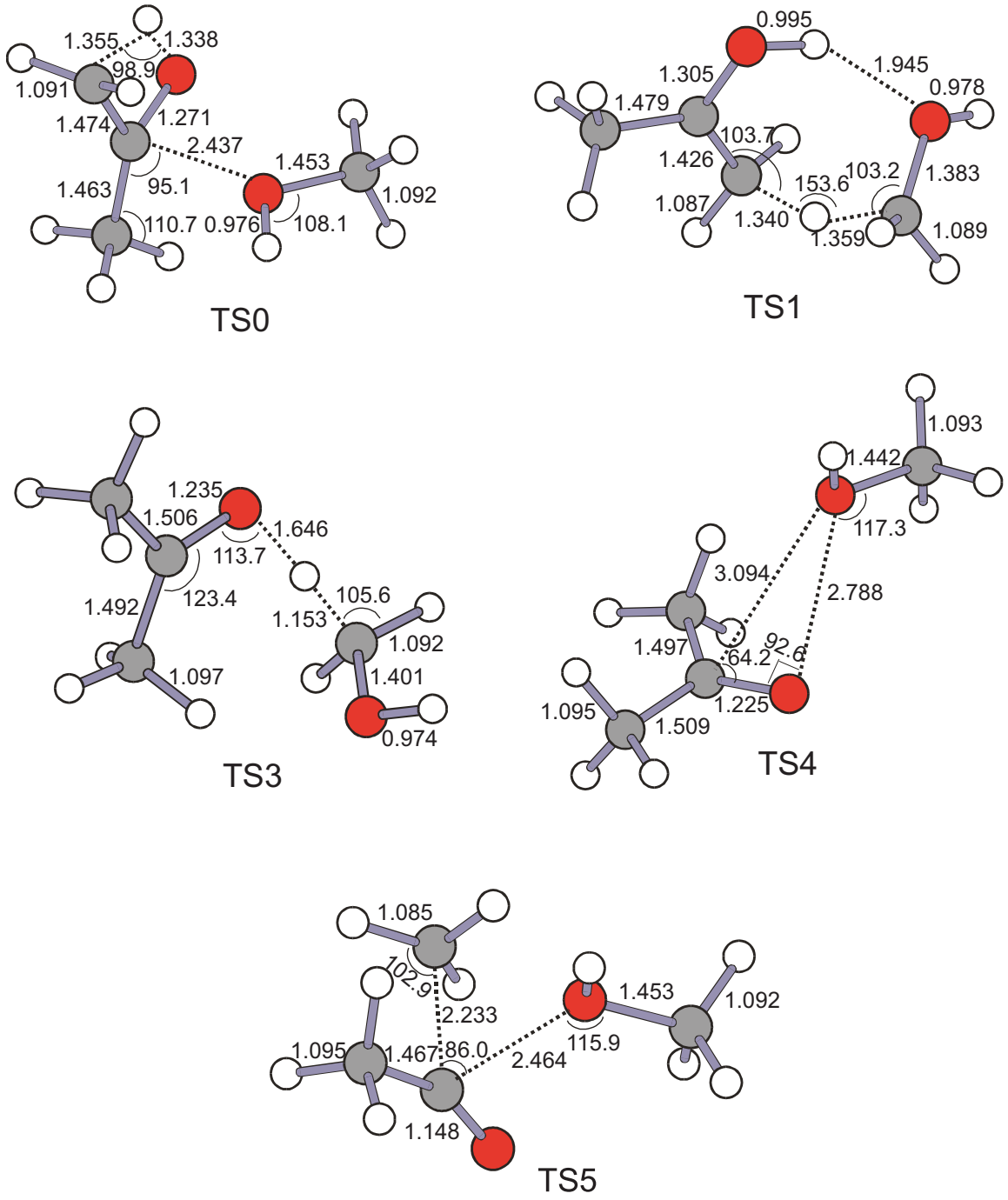


298 K energy difference between TS5 and ion VII) in the complex, and this results from the high stability of the $[CH_3C^+(O)\cdots(H)OCH_3]$ product ion.

The flat transition state of this reaction (TS5) lies at 128 kJ/mol in Fig. 7, but the overall energy-determining barrier for this process is TS4 at 165 kJ/mol. As previously mentioned, these three reactions for the production of protonated acetone (*m*/*z* 59), the acetone ion (*m*/*z* 58), and the methyl loss product at *m*/*z* 75 are all MI processes and so they have closely similar energy requirements. The PES of ion **2** shows that the major energy barriers for these three reactions lie within a small energy range of 18 kJ (the highest

© 2005 NRC Canada

Fig. 6 (*concluded*).



energy limit, 173 kJ/mol; the lowest energy limit, 155 kJ/mol), which ensures the observation of all three products in the MI time frame.

Another transition-state energy has been calculated, that for TS0, by which complex VII, the acetone ion and methanol, converts to ion IV, the distonic acetone ion and methanol. TS0 lies at a rather high energy (251 kJ/mol). In the metastable time frame of the mass spectrometer, a reaction requiring such a high relative internal energy is usually not competitive and therefore is not observed. This is confirmed by the experimental observation that ion **2** does not isomerize to an enol form.

Conclusions

In summary, the proton-bound complex of acetone and $CH_2OH^{\cdot}$ (ion **1**) isomerizes into the enol ion, i.e., distonic acetone, attached to a methanol molecule. In contrast, ion **2** does not produce the enol ion. It simply dissociates into the keto ion, i.e., ionized acetone and the methanol neutral counterpart.

[3] $[(CH_3)_2C{=}O\cdots H^+\cdots O(H)CH_2^{\cdot}]$

$\rightarrow [^{\cdot}CH_2C(CH_3){=}OH^+\cdots O(H)CH_3]$

© 2005 NRC Canada

Fig. 7. The 0 K potential energy surface of the $[(CH_3)_2C{=}OH^+\cdots{}^{\cdot}OCH_3]$ system at MP2/6-31+G(d).

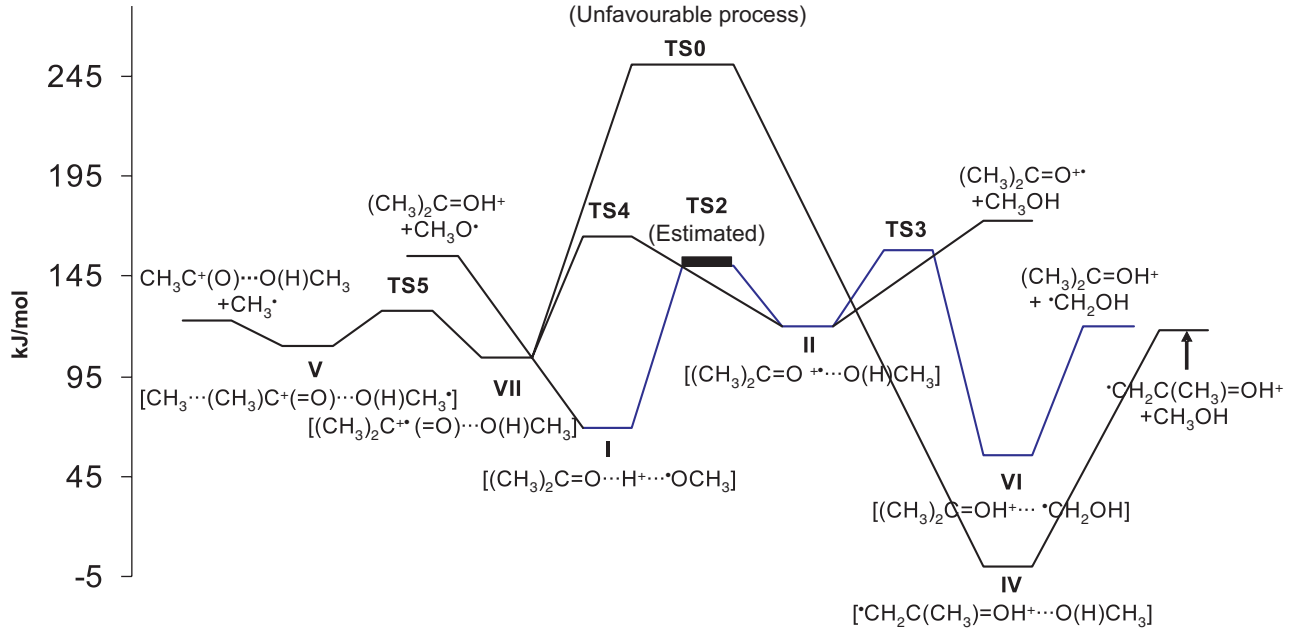
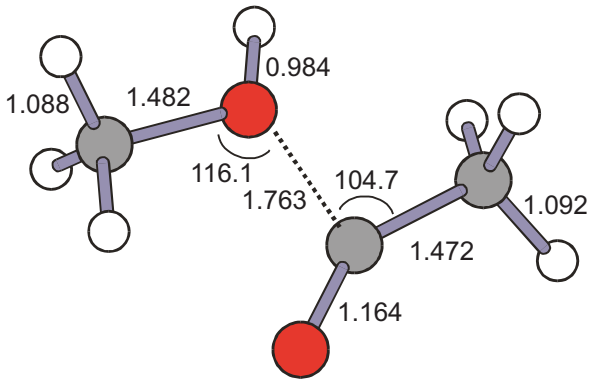


Fig. 8. Geometry of $[CH_3C^+(O)\cdots O(H)CH_3]$.

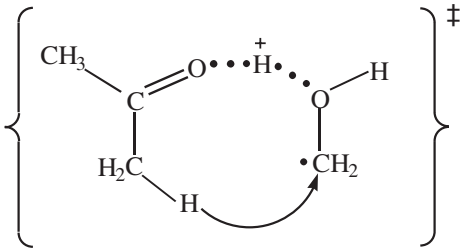


[4] $[(CH_3)_2C{=}O\cdots H^+\cdots{}^{\cdot}OCH_3]$

$\rightarrow [(CH_3)_2C{=}O^{+\cdot}\cdots HOCH_3]$

These observations are in keeping with the chemistries of $[CH_3CHO\cdots H^+\cdots O(H)CH_2^{\cdot}]$ and $[CH_3CHO\cdots H^+\cdots{}^{\cdot}OCH_3]$. We believe that the first reaction proceeds because the charge and radical sites are on separate groups in ion **1**. In rxn. [3], a proton is given to a keto group and the radical moiety takes back an $H^{\cdot}$ atom. The ketone is thus readily converted to its enol ion form. The key transition state (TS1, shown in Fig. 9) transfers an $H^{\cdot}$ atom back to the methyl hydroxyl radical by an *$H^{\cdot}$ atom transfer mechanism*. The important result from ion **1** is that the enol ion results from proton transfer to acetone, which then gives an $H^{\cdot}$ atom back to the $^{\cdot}CH_2OH$ radical by a 1,6-H transfer, producing the enol ion. In contrast, when the protonated acetone is attached to the radical $CH_3O^{\cdot}$ (ion **2**) the above rearrangement does not take place. Ion **2** cannot communicate with ion **1** on their PES. A high barrier prevents the complex of the acetone ion with methanol (complex VII) from rearranging to distonic acetone and methanol (complex IV, see Fig. 7).

Fig. 9. 1,6-Hydrogen shift for TS1.



Radom's rule predicts that PTC cannot facilitate the isomerization either because the PA of methanol (755 kJ/mol) is lower than PA values of $^{\cdot}CH_2(CH_3)C{=}O$ at the O atom (811 kJ/mol) and the C site (769 kJ/mol). Instead, ion **2** dissociates to a stable complex of an acetyl ion with methanol. The energy barriers calculated at the MP2/6-31+G(d) level of theory for all the MI processes fully support the experimental observations.

Acknowledgements

The authors acknowledge the Natural Sciences and Engineering Research Council of Canada (NSERC) for continuing financial support. Special thanks go to Dr. Paul M. Mayer for his assistance with the computations.

References

1. R. Keeffe and A.J. Kresge. *In* The chemistry of enols. *Edited by* Z. Rappoport. Wiley, Chichester. 1990. p. 399.
2. F. Turecek. *In* The chemistry of enols. *Edited by* Z. Rappoport. Wiley, Chichester. 1990. p. 95.
3. F. Turecek and C.J. Cramer. J. Am. Chem. Soc. **117**, 12243 (1995).
4. D. Lee, C.K. Kim, B.S. Lee, I. Lee, and B.C. Lee. J. Comput. Chem. **18**, 56 (1997).
5. D.H. Williams. Acc. Chem. Res. **10**, 280 (1977).

© 2005 NRC Canada

6. P.C. Burgers and J.L. Holmes. Org. Mass Spectrom. **17**, 123 (1982).
7. A.J. Chalk and L. Radom. J. Am. Chem. Soc. **121**, 1574 (1999).
8. M.A. Trikoupis, P.C. Burgers, P.J.A. Ruttink, and J.K. Terlouw. Int. J. Mass Spectrom. **217**, 97 (2002).
9. M.A. Trikoupis, P.C. Burgers, P.J.A. Ruttink, and J.K. Terlouw. Int. J. Mass Spectrom. **210/211**, 489 (2001).
10. M.A. Trikoupis and J.K. Terlouw. J. Am. Chem. Soc. **120**, 12131 (1998).
11. P. Mourgues, J. Chamot-Rooke, G. van der Rest, H. Nedev, H.E. Audier, and T.B. McMahon. Int. J. Mass Spectrom. **210/211**, 429 (2001).
12. X. Wang and J.L. Holmes. Int. J. Mass Spectrom. **242**, 75 (2005).
13. M. Haranczyk, P.C. Burgers, and P.J.A. Ruttink. Int. J. Mass Spectrom. **220**, 53 (2002).
14. Y.-P. Tu and J.L. Holmes. J. Am. Chem. Soc. **122**, 3695 (2000).
15. J.L. Holmes and P.M. Mayer. J. Phys. Chem. **99**, 1366 (1995).
16. E. Rennie and P.M. Mayer. J. Chem. Phys. **120**, 10561 (2004).
17. A.P. Scott and L. Radom. J. Phys. Chem. **100**, 16502 (1996).
18. E.P.L. Hunter and S.G. Lias. J. Phys. Chem. Ref. Data, **27**, 413 (1998).
19. J.L. Holmes. *In* The encyclopedia of mass spectrometry. *Edited by* P.B. Armentrout. Elsevier, Amsterdam. 2003. pp. 91–98.
20. S.G. Lias, J.E. Bartmess, J.G. Liebman, J.L. Holmes, R.D. Levin, and W.G. Mallard. J. Phys. Chem. Ref. Data, **17**(Suppl. 1), 1 (1988).
21. F.W. McLafferty and C.J. Proctor. Org. Mass Spectrom. **18**, 272 (1983).
22. J.W. Larson and T.B. McMahon. J. Am. Chem. Soc. **104**, 6255 (1982).
23. J.L. Holmes and F.P. Lossing. J. Am. Chem. Soc. **102**, 1591 (1980).
24. G. van der Rest, H. Nedev, J. Chamot-Rooke, P. Mourgues, T.B. McMahon, and H.E. Audier. Int. J. Mass Spectrom. **202**, 161 (2000).
25. T.D. Fridgen and T.B. McMahon. J. Phys. Chem. A, **106**, 1576 (2002).

© 2005 NRC Canada

Gas-phase ion chemistry of Ti(O-*i*-Pr)$_4$[1]

Luciano A. Xavier and José M. Riveros

Abstract: The positive and negative gas-phase ion chemistry of Ti(O-*i*-Pr)$_4$ was investigated at low pressures by FT-ICR. The fragment ion, (*i*-PrO)$_3$Ti-O$^+$=C(H)Me, reacts with the parent neutral by proton transfer and by a nucleophilic addition–elimination reaction. The nature of the fragment ion and the ensuing ion–molecule reactions clearly indicate that Ti(O-*i*-Pr)$_4$ exists as a monomer in the gas phase. In the negative ion mode, F$^-$ was found to react easily with Ti(O-*i*-Pr)$_4$ to yield the pentacoordinated complex FTi(O-*i*-Pr)$_4^-$ ion. This hypervalent Ti species undergoes a series of sequential fragmentations induced by IR multiphoton excitation. The first step is unusual because two channels are observed by IRMPD: one involves loss of HF, and the other loss of *i*-PrOH. The subsequent dissociation processes are characterized by progressive elimination of propene giving rise to a number of different titanaoxirane-containing anions with the general formula [(η^2-CMe$_2$O)Ti(OH)$_{3-n}$(*i*-PrO)$_n$]$^-$. FTi(O-*i*-Pr)$_4^-$ was also observed to undergo multiple alkoxide–fluoride exchanges with BF_3 leading to the eventual formation of TiF_5^-.

Key words: titanium tetraisoproxide, gas-phase ion chemistry, hypervalent Ti, ion–molecule reactions, IRMPD.

Résumé : On a étudié la chimie en phase gazeuse des ions positifs et négatifs du Ti(O-*i*-Pr)$_4$ en opérant à basse pression et en faisant appel à la spectrométrie de masse à résonance cyclotronique ionique avec transformée de Fourier (SM-RCI-TF). Le fragment ionique (*i*-PrO)$_3$Ti-O$^+$=C(H)Me réagit avec une molécule parente neutre par un transfert de proton et par une réaction nucléophile d'addition–élimination. La nature de l'ion fragment et les réactions subséquentes ion–molécule indiquent clairement que le Ti(O-*i*-Pr)$_4$ existe sous la forme de monomère en phase gazeuse. Dans le mode d'ion négatif, on a trouvé que l'ion F$^-$ réagit facilement avec le Ti(O-*i*-Pr)$_4$ pour conduire à la formation de l'ion complexe pentacoordiné FTi(O-*i*-Pr)$_4^-$. Cette espèce hypervalente du titane subit une série de fragmentations en séquence induites par une excitation multiphotonique infrarouge. La première étape est inhabituelle parce qu'on observe deux voies par photodissociation multiphotonique par infrarouge (DMPIR): une implique une perte de HF et l'autre une perte de *i*-PrOH. Les processus subséquents de dissociation sont caractérisés par une élimination progressive de propène qui conduit à la formation d'un certain nombre d'anions différents contenant du titanaoxirane de formule générale [(η^2-CMe$_2$O)Ti(OH)$_{3-n}$(*i*-PrO)$_n$]$^-$. On a aussi observé que le FTi(O-*i*-Pr)$_4^-$ subit de multiples échanges alcoolate–fluorure avec le BF_3 qui conduisent à la formation éventuelle de TiF_5^-.

Mots clés : isopropylate de titane, chimie ionique en phase gazeuse, titane hypervalent, réactions ion–molécule, photodissociation multiphotonique par infrarouge (DMPIR).

[Traduit par la Rédaction]

Introduction

Metal alkoxides (M(OR)$_n$) are recognized as excellent and versatile precursors for deposition of metal oxides by chemical vapor deposition (CVD) and for the synthesis of advanced materials and ceramics (1–3). For example, titanium tetraisopropoxide (Ti(O-*i*-Pr)$_4$) has been extensively characterized as a precursor for deposition of titanium dioxide (4), and the titanium alkoxides have found a wide range of applications in the design of multifunctional materials by sol-gel processes (5–9).

Thermal decomposition of titanium isopropoxide yields TiO_2 via rxns. [1] and [2],

[1] $$Ti(O\text{-}i\text{-}Pr)_4 \rightarrow TiO_2 + 4CH_3CH{=}CH_2 + 2H_2O$$

[2] $$Ti(O\text{-}i\text{-}Pr)_4 \rightarrow TiO_2 + 2CH_3CH{=}CH_2 + 2i\text{-}PrOH$$

whereas sol-gel processes of Ti alkoxides are based on hydrolysis of the alkoxy groups. The latter reaction proceeds by progressive replacement of the R groups as shown in rxn. [3].

[3] $$Ti(OR)_4 + H_2O \rightarrow Ti(OR)_3(OH) + ROH$$

Although complete hydrolysis eventually leads to TiO_2, there are also competing reactions initiated by the partially hydrolyzed Ti(OR)$_{4-n}$(OH)$_n$ species that can result in condensation products as shown in rxns. [4] and [5] (10–12).

Received 29 April 2005. Published on the NRC Research Press Web site at http://canjchem.nrc.ca on 10 January 2006.

Dedicated to Professor Paul Kebarle for his pioneering work on the solvation of ions in the gas phase.

L.A. Xavier and J.M. Riveros.[2] Institute of Chemistry, University of São Paulo, Av. Lineu Prestes 748, Cidade Universitária, São Paulo, CEP 05508-900, Brazil.

[1]This article is part of a Special Issue dedicated to Professor P. Kebarle.

[2]Corresponding author (e-mail: jmrnigra@iq.usp.br).

 doi: 10.1139/V05-202 © 2005 NRC Canada

[4] $Ti(OR)_3(OH) + Ti(OR)_4 \rightarrow (RO)_3Ti\text{-}O\text{-}Ti(OR)_3 + ROH$ (Alkoxolation)

[5] $Ti(OR)_3(OH) + Ti(OR)_3(OH) \rightarrow (RO)_3Ti\text{-}O\text{-}Ti(OR)_3 + H_2O$ (Oxolation)

Understanding the detailed mechanisms of these processes is of paramount importance because of the possibility of tailoring the structure of materials (13–15). A variety of oxytitanium species are presumably key intermediates in the chemistry of these systems, but they have not been well-characterized. Oxytitanium species are also of interest because of: (*a*) their possible role in chemical vapor deposition processes aimed at preparing catalytic materials (16); (*b*) the increasing catalytic, ferroelectric, and nanostructure capabilities found for titanate-type compounds (17–20); and (*c*) the mechanisms of growth and nucleation of TiO_2 nanoparticles (12).

Some insight into the underlying basic chemistry involved in sol-gel reactions and in metal organic chemical vapor deposition can be gained by probing the gas-phase behavior of simple processes involving titanium alkoxides. This approach was pioneered by Traldi and co-workers (21) in their study of model acid- and base-induced hydrolysis of $Si(OEt)_4$ in the gas phase. By comparison, little is known about the gas-phase ion chemistry of titanium alkoxides or of other titanium-containing substrates. The question of the nuclearity of the different $Ti(OR)_4$ species in the gas phase is particularly intriguing. There is strong evidence that $Ti(OMe)_4$ and $Ti(OEt)_4$ form polynuclear species in the solid state, but $Ti(O\text{-}i\text{-}Pr)_4$, a liquid at room temperature, is suspected to be mostly monomeric because of steric inhibition by the bulky substituents (22). A recent study by desorption chemical ionization mass spectrometry (23) reveals that $Ti(O\text{-}i\text{-}Pr)_4$ yields substantial amounts of the molecular ions $[M]^{-\cdot}$ and $[M_2]^{-\cdot}$ in the negative ion mode, and the fragment binuclear ion $[M_2\text{-}O\text{-}i\text{-}Pr]^+$ in the positive ion mode. By comparison, the mass spectrum of $Ti(OMe)_4$ obtained by the same technique does not exhibit any mononuclear Ti-containing ions. On the other hand, electrospray ionization of very dilute solutions of $Ti(O\text{-}i\text{-}Pr)_4$ and $Ti(OBu)_4$ in methanol reveals the formation of ions resulting from polycondensation reactions following solvent exchange of the *i*-PrO and BuO ligands (24).

In this report, we describe some basic aspects of (*a*) the positive ion chemistry derived from the main mononuclear fragment ion of $Ti(O\text{-}i\text{-}Pr)_4$ and (*b*) the negative ion chemistry resulting from nucleophilic attack of F^-, and the sequential IR multiphoton dissociation of the hypervalent anionic adduct $[FTi(O\text{-}i\text{-}Pr)_4]^-$. This study follows our early investigation of the ion–molecule reactions of the fragment ions of $Si(OR)_4$ (R = Me, Et) and $Ge(OMe)_4$ with their neutral precursors (25, 26), as well as the ion–molecule reactions of a number of anionic nucleophiles with these same substrates (27, 28). Much of the motivation for this type of work stems from the increasing interest in the gas-phase ion chemistry of organometallics (29) and our very limited knowledge about the gas-phase behavior of Ti-containing substrates when compared with that of silicon (30) or germanium derivatives (31).

Experimental

Experiments were carried out in our FT-ICR spectrometer interfaced to an IonSpec Omega Fourier transform data system. The general characteristics of this spectrometer for studying gas-phase ion reactivity have been illustrated in several publications from these laboratories (32–35). The spectrometer operates with a water-cooled 9 in. (1 in. = 25.4 mm) electromagnet that is normally set at 1.0 T and contains a ~15.6 cm^3 cubic cell with center holes drilled on both transmitter plates that allow for laser light to go through the cell. The vacuum chamber housing the ICR cell is provided with two opposing ZnSe windows that act as entry and exit ports for IR laser radiation.

$Ti(O\text{-}i\text{-}Pr)_4$ (Strem Chemicals, Newburyport, Massachusetts) was handled in an inert atmosphere and introduced in the spectrometer through an inlet system and high vacuum tubing leading to the ICR cell heated to about 100 °C. Volatile impurities and free *i*-PrOH were removed by repeated freeze–pump–thaw cycles. Typical times for seasoning the vacuum system and obtaining good quality and reproducible spectra (free of *i*-PrOH) were in the order of 4 h. The partial pressures of $Ti(O\text{-}i\text{-}Pr)_4$ used in this work were in the range of (2–6.5) × 10^{-8} Torr (1 Torr = 133.3224 Pa) as measured by an ion gauge located just before the turbomolecular pump.

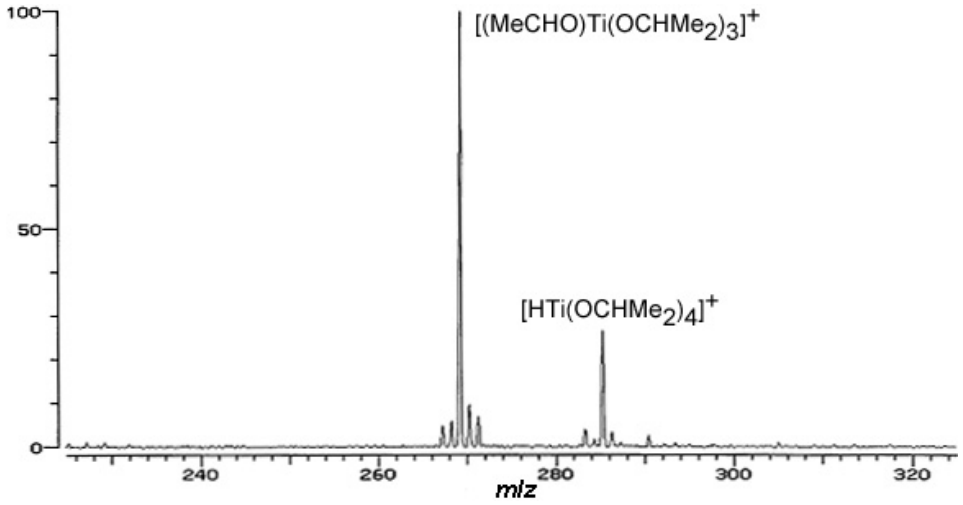
Positive ions were generated by 21 eV electron ionization during a 50 ms electron beam pulse. The subsequent ion–molecule reactions were studied by isolating the ion of interest through a combination of single frequency and swept frequency ejection pulses, and by varying the trapping time prior to ion detection. In the case of Ti-containing ions, the isolation process retained the full Ti isotopic composition.

Negative ion–molecule reactions were investigated following the formation of fluoride ions by electron impact on NF_3 (Pennwalt Ozark-Mahoning, Folcroft, Pennsylvania) with 80 ms pulses at pressures around 3.8 × 10^{-8} Torr (ion gauge reading). The electron energy was maintained at 1.5 eV and the trapping voltage at –1.9 V. A radio-frequency field of ~7 MHz was applied to one of the trapping plates during ~140 ms to eject trapped thermal electrons from the cell. $Ti(O\text{-}i\text{-}Pr)_4$ was then introduced in the cell to a final pressure of 9 × 10^{-8} Torr. Under these conditions, the fluoride ions react completely in less than 2 s. At these electron energies, no negative ions were observed to originate directly from neat $Ti(O\text{-}i\text{-}Pr)_4$.

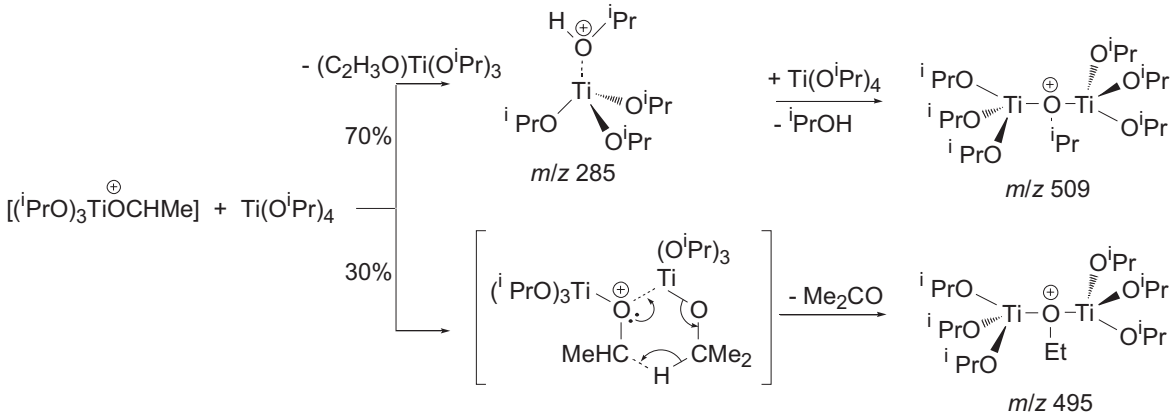
Infrared multiphoton dissociation experiments were carried out after selective isolation of the ion of interest. In the case of the stepwise photodissociation experiments, each primary photoproduct was reisolated after ~300 ms of irradiation time. A grating tunable CW CO_2 laser (model 48G-1, Synrad, Mukilteo, Washington) was used as the IR source in the multiphoton dissociation experiments. The laser was typically operated on the P(20) line of the 10.6 μ band at 944 cm^{-1}. Varying the width of a 10 kHz modulation pulse from a Hewlett-Packard pulse generator allowed for external control of the laser power level. The laser power measured at the exit window of the vacuum system of the spectrometer was typically 1–3 W. An electromechanical shutter placed in front of the laser was used to control the irradiation time, and a pulse from the IonSpec data system determined the

© 2005 NRC Canada

Fig. 1. The 21 eV mass spectrum of Ti(O-*i*-Pr)$_4$, obtained in our FT-ICR spectrometer at 70 ms trapping time, reveals a single fragment ion. No other ions are observed at lower *m*/*z* values.



Scheme 1.



trigger and aperture times of the shutter. Sequential IRMPD can be studied conveniently with this arrangement by using several laser pulses programmed for different delay times. This arrangement is similar to a procedure previously described in the literature (36).

Results and discussion

Mass spectrum of Ti(O-*i*-Pr)$_4$ and positive ion–molecule reactions

Figure 1 shows the positive ion mass spectrum of Ti(O-*i*-Pr)$_4$ obtained in our FT-ICR at 21 eV, trapping time of 70 ms, and a pressure of 6×10^{-8} Torr. This spectrum reveals essentially a single fragment ion, namely (*i*-PrO)$_3$Ti-O$^+$=CHMe, with its cluster of Ti isotopic peaks centered at *m*/*z* 269 corresponding to the ion containing the most abundant ^{48}Ti isotope. At these short trapping times, the protonated species, [Ti(O-*i*-Pr)$_4$]H$^+$ (*m*/*z* 285 for the ^{48}Ti ion), is already noticeable and results from an ion–molecule reaction of the fragment ion with the parent molecule. From the isotopic distribution for the protonated species, it is unclear whether Ti(O-*i*-Pr)$_4$ yields traces of the molecular ion. However, the present mass spectrum yields unequivocal evidence of monomeric Ti(O-*i*-Pr)$_4$ in the gas phase and differs significantly from the polynuclear Ti-containing fragment ions observed in the desorption chemical ionization mass spectrum (23) and the polycondensation ions revealed in the ESI spectrum of Ti(O-*i*-Pr)$_4$ (24).

An interesting observation of the mass spectrum of Ti(O-*i*-Pr)$_4$ obtained by electron ionization is the fact that the fragment ion originates from the cleavage of a carbon–carbon bond. This is quite unlike the case observed in the mass spectrum of the group 14 (E = Si, Ge, Sn) derivatives where the preferential cleavage always occurs on an E—L (L = ligand) bond to give rise to very stable EL$_3^+$ ions (31).

Two ion–molecule reactions are observed to occur upon isolation of the (*i*-PrO)$_3$Ti-O$^+$=C(H)Me ion as shown in Scheme 1. The most important one leads to protonated Ti(O-*i*-Pr)$_4$, and the second one to a condensation product of *m*/*z* 495 for the isotopomer containing ^{48}Ti$_2$. The condensation product ((*i*-PrO)$_3$Ti-O$^+$(Et)-Ti(O-*i*-Pr)$_3$) results from an addition–elimination reaction in which neutral Me$_2$CO is presumably expelled. The mechanism shown in Scheme 1 provides a rationale for the elimination of acetone, but no further evidence is available to favor this neutral product over the isomeric EtCHO.

The protonated species ([Ti(O-*i*-Pr)$_4$]H$^+$) undergoes further reaction with the parent molecule to yield a nucleophilic

© 2005 NRC Canada

Scheme 2.

$$[(^{i}PrO)_4Ti]H^+ + (^{i}PrO)_4Ti \rightarrow [(^{i}PrO)_3TiO(^{i}Pr)\cdots Ti^+(O^{i}Pr)_3\cdots(^{i}PrOH)] \rightarrow (^{i}PrO)_3TiO^+(^{i}Pr)Ti(O^{i}Pr)_3 + {}^{i}PrOH$$

displacement reaction (Scheme 2) to yield the putative ion $(i\text{-PrO})_3\text{Ti-O}^+(i\text{-Pr})\text{-Ti(O-}i\text{-Pr})_3$ for which the most intense isotopic peak corresponds to *m/z* 509. No further reactions are observed at longer reaction times, a fact that is consistent with the proposed structures for the *m/z* 509 and 495 ions.

The positive ion chemistry of the $(i\text{-PrO})_3\text{Ti-O}^+\text{=CHMe}$ ion with its parent substrate, as well as the secondary reaction of $[\text{Ti(O-}i\text{-Pr})_4]H^+$, bear strong resemblance to the ion chemistry previously reported for Si(OEt)_4 (25). In the Si case, the main fragment ion ($(\text{EtO})_3\text{Si-O}^+\text{=CH}_2$) was shown to react with the parent neutral to yield the corresponding protonated Si(OEt)_4 and $(\text{EtO})_3\text{Si-O}^+\text{(Me)-Si(OEt)}_3$. Likewise, the $[\text{Si(OEt)}_4]H^+$ ion was found to undergo a displacement reaction similar to that outlined in Scheme 2.

Negative ion–molecule reactions

One of our main interests in the titanium alkoxides was to explore nucleophilic type reactions to establish the relative reactivity of the Ti center compared with that of an S_N2 reaction at the C centers of the alkoxide groups. Fluoride was chosen as our model reagent because it is a strong gas-phase nucleophile and it is a weaker base than the simple alkoxides. Some early work by Nibbering and co-workers (37) reported the ion–molecule reactions of $\text{EtO}^-\text{(HOMe)}$ with $\text{Ti(O-}i\text{-Pr})_4$ and showed that reactions proceed exclusively and rapidly by ligand exchange to yield the solvated alkoxide ions $i\text{-PrO}^-\text{(HOMe)}$ and $i\text{-PrO}^-\text{(HOEt)}$. The mechanistic details of these reactions were not explored, and the possible participation of a pentacoordinated Ti adduct was not observed experimentally.

Reaction of F^- with $\text{Ti(O-}i\text{-Pr})_4$ under our experimental conditions proceeds readily by addition to form the pentacoordinated Ti species (*m/z* 303 for the ^{48}Ti isotopomer) as shown in eq. [6].

$$[6] \qquad F^- + \text{Ti(O-}i\text{-Pr})_4 \rightarrow [\text{FTi(O-}i\text{-Pr})_4]^-$$

This reaction leading to a hypervalent Ti adduct is analogous to what has been observed as the main reaction channel in the alkoxide derivatives of Si (27) and Ge (28) and confirms the fact that the Ti center is much more prone to nucleophilic attack than the C center. This pentacoordinated Ti anion is expected to have a near trigonal bipyramid geometry with the fluorine occupying an apical position in the most stable isomer. This proposed geometry is based on the calculations reported for related hypervalent species such as FSi(OMe)_4^- (35), FGe(OMe)_4^- (28), and SiCl_4F^- and GeCl_4F^- (38). These calculations and earlier studies on hypervalent Si anions (39) suggest that the electronegative fluorine ligand prefers the apical position in these trigonal bipyramid structures.

The fluoride binding energy of $\text{Ti(O-}i\text{-Pr})_4$ is a matter of some interest because there is little thermochemical data for hypervalent species of Ti. For comparison purposes, it is interesting to point out that the relative fluoride affinity of TiF_4 has been established on the basis of gas-phase ionic equilibrium reactions studied by high-temperature mass spectrometry (40, 41). Because of the uncertainties in the absolute values for the fluoride affinities of the reference substrates used in the experiments, namely AlF_3 and VF_3, the $\text{TiF}_4\cdots\text{F}^-$ can be estimated to be larger than 80 kcal mol^{-1} (1 cal = 4.184 J). The fluoride affinity of $\text{Ti(O-}i\text{-Pr})_4$ is probably somewhat less than this value because the fluoride affinity has been found to increase with a larger number of very electronegative substituents (like F) in species like Si and Ge (38, 42). Our previous ab initio calculations estimated a fluoride affinity of 60 kcal mol^{-1} for the prototype Ge(OH)_4 substrate, and of 79 kcal mol^{-1} for GeF_4 (28). Thus, these numbers suggest that the fluoride affinity of $\text{Ti(O-}i\text{-Pr})_4$ is very high and very likely in excess of 50 kcal mol^{-1}.

Scheme 3.

$$[\text{FTi(O}^{i}\text{Pr)}_4]^- + n\text{h}\upsilon_{IR} \xrightarrow{80\%} \text{HF} + [(\text{CMe}_2\text{O})\text{Ti(O}^{i}\text{Pr)}_3]^-$$

$$[\text{FTi(O}^{i}\text{Pr)}_4]^- + n\text{h}\upsilon_{IR} \xrightarrow{20\%} {}^{i}\text{PrOH} + [\text{FTi(OCMe}_2)(\text{O}^{i}\text{Pr)}_2]^-$$

Dissociation of $[\text{FTi(O-}i\text{-Pr})_4]^-$

Further information on structural features of the pentacoordinated $[\text{FTi(O-}i\text{-Pr})_4]^-$ ion can be gained from dissociation experiments as recently illustrated for a number of silane adducts (43). This is particularly true in the present case because no competing reactions are observed with respect to direct addition of the nucleophile (rxn. [6]). As in previous studies from these laboratories (26, 28), we chose to study the dissociation induced by IR multiphoton dissociation (IRMPD). The use of a low power CW CO_2 laser in IRMPD is a very soft technique for ion dissociation (44, 45) that can be particularly useful when the ion of interest has a strong absorption band that overlaps with the operating range of the laser. Neutral $\text{Ti(O-}i\text{-Pr})_4$ displays a very strong absorption in the IR at 988 cm^{-1} that is downshifted to 940 cm^{-1} for associated $\text{Ti(O-}i\text{-Pr})_4$ species (46). The strong absorption in this region has been identified to both the C-O and Ti-O stretches, and thus provides a convenient feature for vibrational multiphoton excitation.

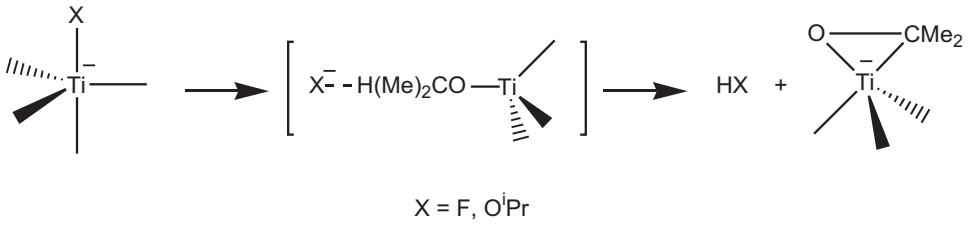
Initial IR multiphoton dissociation experiments of the isolated $[\text{FTi(O-}i\text{-Pr})_4]^-$ ion with our CO_2 laser revealed the facile formation of two primary dissociation products as shown in Scheme 3 with their respective yields.

There are two interesting aspects about the results of these experiments: (*a*) the nature of the product ions and the mechanism of their formation and (*b*) the energetics associated with the processes. Scheme 4 outlines a simple mechanism that can account for the dissociation pathways observed. In this scheme, progressive vibrational excitation is envisioned to loosen up the pentacoordinated complex to yield either an F^- or an $i\text{-PrO}^-$ ion–molecule complex followed by proton abstraction by the nascent base to yield the photoproducts shown in Scheme 4.

The resulting product ions are assumed to take the titanaoxirane structure shown in Scheme 4 rather than an

© 2005 NRC Canada

Scheme 4.



open structure corresponding to a carbanion or a substituted alkoxide ion. This assumption is based on our previous work on the related $FSi(OMe)_2(cyc\text{-}OCH_2)^-$ species (47) for which the cyclic oxirane structure was found to be more stable than either the carbanion or alkoxide form. Although the characterization of titanaoxiranes has been elusive, these species have been claimed to be stable and key intermediates in titanium-mediated reductive coupling reactions (48).

The second interesting aspect of Scheme 4 is the photophysical and energetic aspects of the two dissociation channels. IRMPD processes promoted by low power CW CO_2 lasers typically occur when the stepwise IR photon absorption produces ions with internal energies above their dissociation threshold. For "small" ions, dissociation typically takes place through the lowest energy channel because further vibrational pumping is normally slower than the unimolecular dissociation rate constant. Thus, and as a rule of thumb for these cases, competitive reactions can be promoted by CW CO_2 lasers in the special case where activation energies for two or more reaction channels differ at most by the energy of a single IR photon from the laser (~3 kcal mol^{-1} in this case). Thus, we can conclude that the activation energies for the two processes in Scheme 4 are probably within 3 kcal mol^{-1} of each other, and that elimination of HF is the lowest dissociation channel.

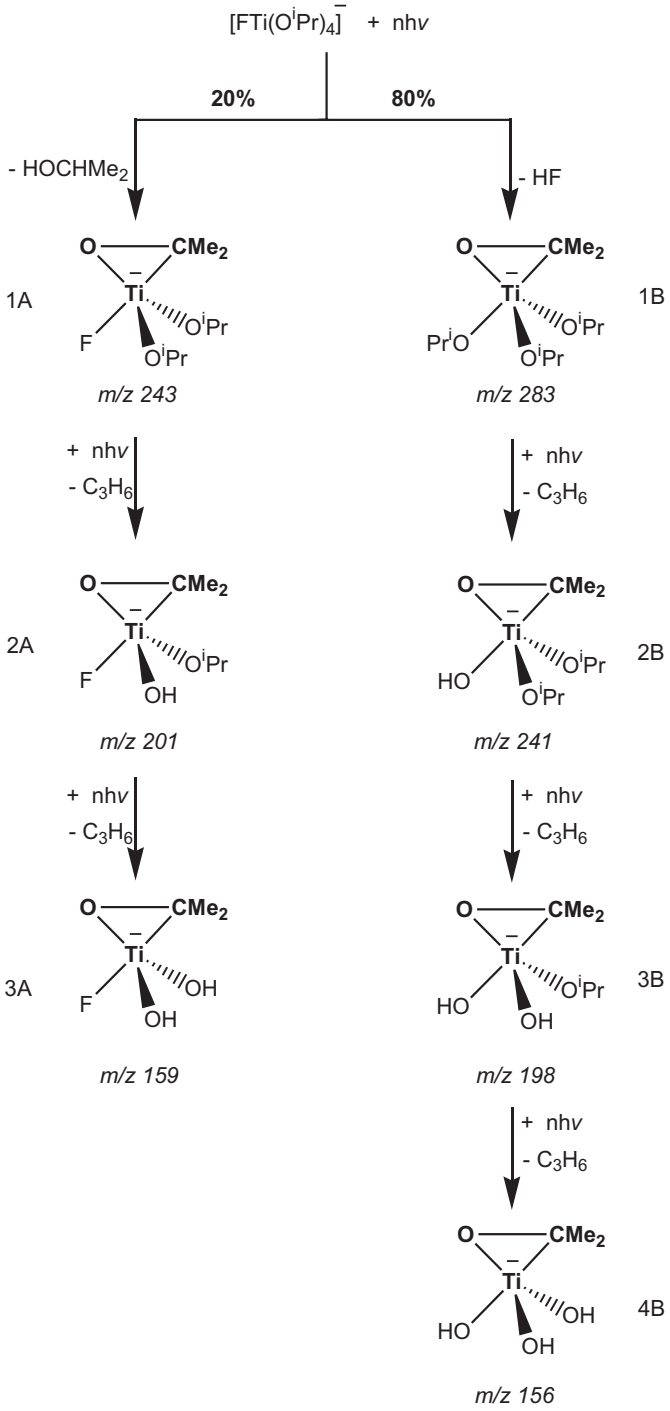
Each one of the primary photoproducts shown in Scheme 4 was further investigated by isolating these ions typically after 300–400 ms of laser irradiation time. A full range of sequential dissociation processes induced by IR multiphoton excitation was observed for both photoproducts as shown in full detail in Scheme 5 with the ions identified by the *m*/*z* value of the ^{48}Ti isotopomer.

The sequential loss of propene in the consecutive IRMPD processes is an interesting case in which the ions progressively "peel off" an olefin. The mechanism for these consecutive elimination processes is envisioned to proceed initially by ring opening of the titanaoxirane moiety followed by proton abstraction. Elimination of propene is then followed by ring closure again to yield a titanaoxirane species, $[(i\text{-}PrO)_2Ti(cyc\text{-}CMe_2O)OH]^-$, that is expected to be more stable than the open $(i\text{-}PrO)_2Ti(CMe_2OH)O^-$ species. Scheme 6 illustrates the proposed mechanism for the representative case of **1A** forming **2A**, and likewise **1B** leading to **2B**.

It is clear that this same mechanism can account for all the secondary dissociation processes. The fact that further dissociation is not observed for ions **3A** and **4B** is a strong indication that the ions retain a titanaoxirane structure, and thus no *i*-PrO groups are left to promote olefin elimination.

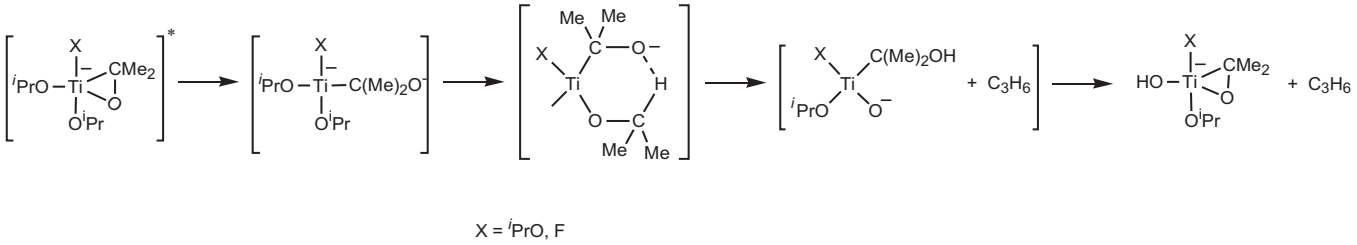
The anions produced in the sequential IRMPD processes correspond to different types of titanols. These species are of

Scheme 5.



© 2005 NRC Canada

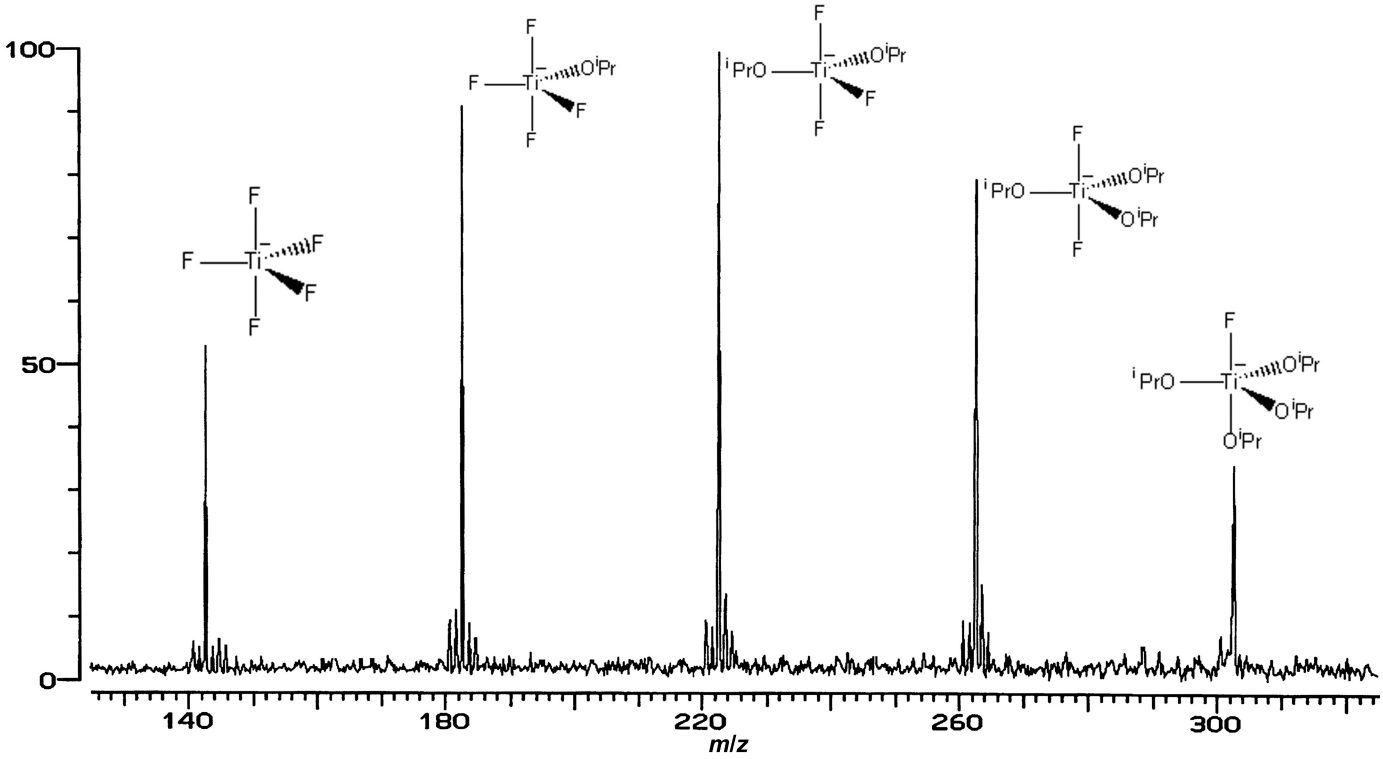
Scheme 6.



Scheme 7.



Fig. 2. FT-ICR spectrum obtained after a 2 s reaction between $[FTi(O\text{-}i\text{-}Pr)_4]^-$ and 1×10^{-8} Torr (1 Torr = 133.3224 Pa) of BF_3, showing progressive substitution of the alkoxy groups by fluorine.



great interest because titanols are intermediates in the reactions that lead to the formation of TiO_2 nanoparticles (12). Attempts to bracket the acidity of these species were not successful because of the difficulties in finding neutral substrates of well-known gas-phase acidities that could be easily introduced via a pulsed valve in our system. The use of a pulsed valve for these experiments is necessary because of the characteristics of our cell and spectrometer. However, work is under way to estimate the acidity of these species by theoretical calculations using the general methodology recently illustrated for the gas-phase acidity of tetrahedral oxyacids (49) to compare with those obtained for related silanols (50).

Reaction of $[FTi(O\text{-}i\text{-}Pr)_4]^-$ with BF_3

It has long been known that alkoxy ligands in $Ti(OR)_4$ undergo rapid exchange with halides from a Lewis acid such as $TiCl_4$ (51). A more recent investigation of these exchange reactions suggests that these reactions proceed via an oxo (from the O-*i*-Pr ligand) bridge between the two Ti centers followed by a halide migration (52). Alkoxy–fluoride exchanges were reported to occur in our previous studies of pentacoordinated Si (47) and Ge (28) anions with BF_3 acting as the Lewis acid. We therefore decided to investigate the behavior of the $[FTi(O\text{-}i\text{-}Pr)_4]^-$ ion in similar reactions.

$[FTi(O\text{-}i\text{-}Pr)_4]^-$ was found to undergo rapid exchange reactions with BF_3 as shown in rxn. [7].

[7] $$[FTi(O\text{-}i\text{-}Pr)_4]^- + BF_3 \rightarrow [F_2Ti(O\text{-}i\text{-}Pr)_3]^- + i\text{-}PrOBF_2$$

These exchange reactions proceed rapidly for all the different $[F_{1+n}Ti(O\text{-}i\text{-}Pr)_{4-n}]^-$ species (with $n = 0$–4), and Fig. 2 reproduces the spectrum obtained after 2 s of reaction where

© 2005 NRC Canada

all the different exchange species are present, leading eventually to the formation of TiF_5^-. The proposed mechanism for these reactions involves initial transfer of *i*-PrO^- to BF_3 in the collision complex followed by F^- transfer from the B center to the Ti center (see Scheme 7).

This exchange reaction is driven by the increasing stability of the Ti hypervalent species upon fluorine substitution.

Conclusions

We have shown that the 21 eV electron ionization mass spectrum of Ti(O-*i*-Pr)$_4$ yields a single fragment ion and that this mass spectrum is consistent with a monomeric Ti species in the gas phase. The monomeric character is also reinforced by the ion–molecule reactions of the (*i*-PrO)$_3$Ti-O$^+$=C(H)Me fragment ion. Furthermore, the addition–elimination reaction of the fragment ion and the secondary reaction of protonated Ti(O-*i*-Pr)$_4$ are identical to those observed in Si(OEt)$_4$, and indicate strong similarities between the ion chemistry of silicon and titanium alkoxides.

The pentacoordinated [FTi(O-*i*-Pr)$_4$]$^-$ ion has been shown to be an interesting starting species for the synthesis of a number of titanol ions by sequential IR multiphoton dissocation processes. In fact, this represents a facile approach for generating species that are of great interest in sol-gel processes and will be further investigated in the future. Furthermore, these alkoxy-containing hypervalent Ti complexes have been shown to undergo a number of alkoxide–fluoride exchanges in the presence of a suitable Lewis acid and open up new ways of generating a variety of pentacoordinated Ti anions in the gas phase.

Acknowledgments

The authors wish to thank the Brazilian Research Council (CNPq), the Millennium Institute of Complex Materials, and the São Paulo Science Foundation (FAPESP).

References

1. L.G. Hubert-Pfalzgrag. New J. Chem. **11**, 663 (1987).
2. D.C. Bradley. Chem. Rev. **89**, 1317 (1989).
3. D.C. Bradley. Polyhedron, **13**, 1111 (1994).
4. See, for example: C.J. Taylor, D.C. Gilmer, D.G. Colombo, G.D. Wilk, S.A. Campbell, J. Roberts, and W.L. Gladfelter. J. Am. Chem. Soc. **121**, 5220 (1999), and refs. therein.
5. C. Sanchez and F. Ribot. New J. Chem. **18**, 1007 (1994).
6. P.D. Moran, J.R. Bartlett, G.A. Bowmaker, J.L. Woolfrey, and R.P. Cooney. J. Sol-Gel Sci. Technol. **15**, 251 (1999).
7. P. Innocenzi, A. Martucci, L. Armelao, S. Licoccia, and M.L. Di Vona. Chem. Mater. **12**, 517 (2000).
8. G. Schottner. Chem. Mater. **13**, 3422 (2001).
9. O. Soppera, C. Croutxe-Barghorn, and D.J. Lougnot. New. J. Chem. **25**, 1006 (2001).
10. J. Blanchard, M. In, B. Schaudel, and C. Sanchez. Eur. J. Inorg. Chem. 1115 (1998).
11. R. Mehrotra and A. Singh. Chem. Soc. Rev. **25**, 1 (1996).
12. G. Oskam, A. Nellore, R.L. Penn, and P.C. Searson. J. Phys. Chem. B, **107**, 1734 (2003).
13. M.Z.C. Hu, J.T. Zielke, C.H. Byers, J.S. Lin, and M.T. Harris. J. Mater. Sci. **35**, 1957 (2000).
14. S. Weymann-Schildknetch and M. Henry. J. Chem. Soc. Dalton Trans. 2425 (2001).
15. N.V. Golubko, M.I. Yanovskava, I.P. Romm, and A.N. Ozerin. J. Sol-Gel Sci. Technol. **20**, 245 (2001).
16. P. Serp, P. Kalck, and R. Feurer. Chem. Rev. **102**, 3085 (2002).
17. T. Ohya, A. Nakayama, T. Ban, Y. Ohya, and Y. Takahashi. Chem. Mater. **14**, 3082 (2002).
18. J.A. Rodriguez, A. Etxeberria, L. Gonzalez, and A. Maiti. J. Chem. Phys. **117**, 2699 (2002).
19. X.M. Sun, X. Chen, and Y.D. Li. Inorg. Chem. **41**, 4996 (2002).
20. C.J. Barbe, R. Graf, K.S. Finnie, M. Blackford, R. Trautman, and J.R. Bartlett. J. Sol-Gel Sci. Technol. **26**, 457 (2003).
21. R. Campostrini, G. Carturan, B. Pelli, and P. Traldi. J. Non-Cryst. Solids, **108**, 143 (1989).
22. D.C. Bradley, R.C. Mehrotra, and P.D. Gaur. Metal alkoxides. Academic Press, New York. 1978. p. 68.
23. S.R. Damo, K.-C. Lam, A. Rheingold, and M.A. Walters. Inorg. Chem. **39**, 1635 (2000).
24. S. Cristoni, L. Armelao, S. Gross, E. Tondello, and P. Traldi. Rapid Commun. Mass Spectrom. **14**, 662 (2000).
25. M.L.P. da Silva and J.M. Riveros. Int. J. Mass Spectrom. Ion Processes, **165/166**, 83 (1997).
26. L.A. Xavier and J.M. Riveros. Int. J. Mass Spectrom. **179/180**, 223 (1998).
27. M.L.P. da Silva and J.M. Riveros. J. Mass Spectrom. **30**, 733 (1995).
28. N.H. Morgon, L.A. Xavier, and J.M. Riveros. Int. J. Mass Spectrom. **195/196**, 363 (2000).
29. R. Damrauer. Organometallics, **23**, 1462 (2004).
30. R. Damrauer and J.A. Hankin. Chem. Rev. **95**, 1137 (1995).
31. J.M. Riveros. *In* The chemistry of organic germanium, tin and lead compounds. Vol. 2. Part 1. *Edited by* Z. Rappoport. John Wiley and Sons, Ltd., Chichester, UK. 2002. pp. 359–397.
32. H.V. Linnert and J.M. Riveros. Int. J. Mass Spectrom. Ion Processes, **140**, 163 (1994).
33. N.H. Morgon, H.V. Linnert, T. Giroldo, and J.M. Riveros. J. Phys. Chem. **100**, 18048 (1996).
34. P.R.P Moraes, H.V. Linnert, M. Aschi, and J.M. Riveros. J. Am. Chem. Soc. **122**, 10133 (2000).
35. L.A. Xavier, N.H. Morgon, J.J. Menegon, and J.M. Riveros. Int. J. Mass Spectrom. **219**, 485 (2002).
36. D.S. Tonner and T.B. McMahon. Anal. Chem. **69**, 4735 (1997).
37. H. van der Wel, N.M.M. Nibbering, J.C. Sheldon, R.N. Hayes, and J.H. Bowie. J. Am. Chem. Soc. **109**, 5823 (1987).
38. C. Hao, J.D. Kaspar, C.E. Check, K.C. Lobring, T.M. Gilbert, and L.S. Sunderlin. J. Phys. Chem. A, **109**, 2026 (2005).
39. M.S. Gordon, L.P. Davis, and L.W. Burggraf. *In* Advances in gas phase ion chemistry. Vol. 1. *Edited by* N. Adams and L.M. Babcock. JAI Press, Greenwich, Connecticut. 1992. pp. 203–223.
40. V. Boltalina, A.Y. Borshchevskii, and L.N. Sidorov. Russ. J. Phys. Chem. **66**, 1223 (1992).
41. W.G. Mallard (*Editor*). NIST Chemistry WebBook [online]. NIST Standard Reference Database Number 69. National Institute of Standards and Technology, Gaithersburg, Maryland. Available from http://webbook.nist.gov/chemistry/. March 2005.
42. I.H. Krouse, H.A. Lardin, and P.G. Wenthold. Int. J. Mass Spectrom. **227**, 303 (2003).
43. I.H. Krouse and P.G. Wenthold. Organometallics, **23**, 2573 (2004).
44. J.M. Riveros. *In* The encyclopedia of mass spectrometry. Vol. 1. *Edited by* P.B. Armentrout. Elsevier, Amsterdam. 2003. pp. 262–271.
45. S.A. McLuckey and D.E. Goeringer. J. Mass Spectrom. **32**, 461 (1997).

© 2005 NRC Canada

46. P.D. Moran, G.A. Bowmaker, R.P. Cooney, K.S. Finnie, J.R. Bartlett, and J.L. Woolfrey. Inorg. Chem. **37**, 2741 (1998).
47. N.H. Morgon, A.B. Argenton, M.L.P. da Silva, and J.M. Riveros. J. Am. Chem. Soc. **119**, 1708 (1997).
48. S.O. Agustsson, C. Hua, U. Englert, T. Marx, L. Wesemann, and C. Ganter. Organometallics, **21**, 2993 (2002).
49. J.R. Rustad, D.A. Dixon, J.D. Kubicki, and A.R. Felmy. J. Phys. Chem. A, **104**, 4051 (2000).
50. R. Damrauer, R. Simon, and M. Krempp. J. Am. Chem. Soc. **103**, 4431 (1991).
51. H. Weingarten and J.R. Van Wazer. J. Am. Chem. Soc. **87**, 724 (1965).
52. P. Arnal, R.J.P. Corriu, D. Leclercq, P.H. Mutin, and A. Vioux. Chem. Mater. **9**, 694 (1997).

© 2005 NRC Canada

A collisionally activated dissociation (CAD) and computational investigation of doubly and singly charged DMSO complexes of Cu^{2+} [1]

John A. Stone, Timothy Su, and Dragic Vukomanovic

Abstract: The singly and doubly charged Cu(II)–DMSO complexes formed by electrospray have been examined by CAD and computation. The CAD spectra were obtained as a function of collision energy. The doubly charged ions, $[Cu(DMSO)_n]^{2+}$, were observed only for $n \geq 2$. For $n = 3$, dissociation leads mainly to $[Cu(DMSO)_2]^+ + DMSO^+$, with only a trace of $[Cu(DMSO)_2]^{2+}$. Although $[Cu(DMSO)]^{2+}$ was never detected, computation shows that the $n = 1$ complex exists in a potential well. Loss of $DMSO^+$ is computed to be exothermic for $n = 1$–3, the exothermicity decreasing as n increases. The singly charged complexes in the ESI spectra were $[CuX(DMSO)_n]^+$ (X = Cl, Br, NO_3, HSO_4, $n = 1$ or 2). The CAD spectra showed competition between electron transfer from anion to metal followed by loss of X and loss of $DMSO^+$. Experiment and computation show that for $[CuX(DMSO)]^+$, loss of X is the preferred decomposition at low collision energy. NBO analysis shows that electron transfer to Cu from DMSO decreases in $[Cu(DMSO)_n]^{2+}$ as n increases, the bonding becoming more electrostatic and less covalent. In $[CuX(DMSO)_n]^+$, the negative charge on X is much less than unity with most of the difference appearing on the DMSO ligand(s).

Key words: copper–DMSO complexes, electrospray, CAD, structures.

Résumé : Faisant appel à des calculs théoriques et aux spectres de décomposition par activation collisonnelle (DAC), on a étudié les complexes Cu(II)–DMSO portant une ou deux charges qui se forment par électronébulisation. On n'observe la présence d'ions doublement chargés, $[Cu(DMSO)_n]^{2+}$ qui si $n \geq 2$. Pour $n = 3$, la dissociation conduit principalement à la formation de $[Cu(DMSO)_2]^+ + DMSO^+$ et à seulement une trace de $[Cu(DMSO)_2]^{2+}$. Même si la présence de $[Cu(DMSO)_2]^{2+}$ n'a jamais été détectée, les calculs montrent que le complexe avec $n = 1$ se trouverait dans un puits de potentiel. On a calculé que la perte de $DMSO^+$ est exothermique pour $n = 1$ à 3 et que le caractère exothermique diminue avec une augmentation de la valeur de n. Dans les spectres de masse avec électronébulisation ionique (ENI), la structure générale des complexes ne portant qu'une charge est $[CuX(DMSO)_n]^+$ dans laquelle X = Cl, Br, NO_3, HSO_4 et $n = 1$ ou 2. Les spectres de décomposition par activation collisionnelle montrent qu'il existe une compétition entre le transfert d'électron de l'anion au métal, suivi d'une perte de X et la perte de $DMSO^+$. Les données expérimentales et les calculs montrent que pour $[CuX(DMSO)]^+$, la perte de X est la décomposition privilégiée à de faibles énergies de collision. Une analyse de l'orbitale de liaison naturelle (OLN) montre que le transfert d'électron du DMSO au cuivre diminue dans le $[Cu(DMSO)_n]^{2+}$ quand la valeur de n augmente alors que la liaison devient plus électrostatique et moins covalente. Dans le $[CuX(DMSO)_n]^+$, la charge négative sur X est de beaucoup inférieure à l'unité et presque toute la différence apparaît sur le(s) ligand(s) DMSO.

Mots clés : complexes cuivre–DMSO, électronébulisation, décomposition par activation collisionnelle (DAC), structures.

[Traduit par la Rédaction]

Introduction

Liquid DMSO is an excellent solvent for metal cations but a poor solvent for anions. The oxygen atom carries a negative charge while the methyl groups are positive so that coordination with a metal cation is through oxygen, while the interaction with an anion is with the methyl groups (1, 2). Since DMSO is a valuable and widely used solvent, it is not surprising that its solvation properties on the microscale in the gas phase have been the subject of study by mass spectrometry. High-pressure mass spectrometry showed that the enthalpy of association of a singly charged metal cation with DMSO was approximately twice that of a singly charged anion of the same size (1, 3). The advent of electospray ioniza-

Received 26 April 2005. Published on the NRC Research Press Web site at http://canjchem.nrc.ca on 21 January 2006.

Dedicated to Paul Kebarle in honor of his 50 years of trail blazing in many areas of ion–molecule chemistry.

J.A. Stone.[2] Department of Chemistry, Queen's University, Kingston, ON K7L 3N6, Canada.
T. Su and D. Vukomanovic. Department of Chemistry and Biochemistry, University of Massachusetts Dartmouth, N. Dartmouth, MA 02747-2300, USA.

[1]This article is part of a Special Issue dedicated to Professor P. Kebarle.
[2]Corresponding author (e-mail: stonej@chem.queensu.ca).

 doi: 10.1139/V05-201 © 2005 NRC Canada

tion (ESI) allowed the facile formation of DMSO complexes of multiply charged metal cations. Complexes of metal di- and tri-cations are readily formed by ESI using neat DMSO, or aqueous solutions containing DMSO, together with a low concentration of an appropriate metal salt (4–11). When water comprises the majority of the solvent, the complexes $[M(DMSO)_n]^{2+}$ rather than hydrated cations such as $[M(H_2O)_n]^{2+}$ and $[M(H_2O)_m(DMSO)_n]^{2+}$ may be obtained even though the DMSO is at a concentration only in the millimolar range. This can usually be accomplished by a judicious selection of low electric fields in the intermediate pressure region between cone and lens (9). $[M(DMSO)_n]^{2+}$ (n = 2 or 3) in such spectra is usually accompanied by the ions $[M(CH_3SO)(DMSO)_{n-1}]^{2+}$ formed by collisionally activated dissociation (CAD) in the source (8, 9, 12).

[1] $$[M(DMSO)_n]^{2+} \rightarrow [M(CH_3SO)(DMSO)_{n-1}]^{2+} + CH_3$$

Shvartsburg and Wilkes (8) found that of all the DMSO complexes of the divalent metals that they studied, only those of Cu^{2+} could definitely be said not to show loss of methyl by eq. [1]. In addition only a trace of $[Cu(DMSO)_2]^{2+}$ was found, but no $[Cu(DMSO)]^{2+}$. The low intensity and (or) absence of these two ions and the absence of methyl loss was attributed to the very high second ionization energy of Cu (20.3 eV) favoring charge transfer to the DMSO ligand and subsequent Coulombic explosion (eq. [2]) rather than methyl loss from the higher complexes, the usual precursors of such ions.

[2] $$[M(DMSO)_n]^{2+} \rightarrow [M(DMSO)_{n-1}]^{+} + DMSO^{+}$$

Verification of this unique behavior of copper and a search for a possible explanation is warranted and in this paper we report on a more extended study of the ions observed in the ESI spectra of aqueous solutions containing cupric salts and DMSO. The Cu(II)–DMSO complexes observed were not only the doubly charged $[Cu(DMSO)_n]^{2+}$, but also the singly charged $[Cu(X)(DMSO)_n]^{+}$, where X^- (NO_3^-, Cl^-, Br^-, HSO_4^-) is the counterion of the cupric salt. We have determined the dependence of product formation on the collision energy in the CAD of mass selected ions. The results of ab initio calculations to determine ion structures and the energetics of ligand association are found to be consistent with the energy dependence of the CAD spectra.

Experimental

ESI spectra were obtained using a triple sector mass spectrometer (quadrupole/hexapole/quadrupole, Quattro, Fisons, UK) in the manner previously described (9, 13–15). Aqueous solutions containing 1.0×10^{-2} mol/L DMSO or DMSO-d_6 and 1.0×10^{-3} mol/L of a cupric salt (nitrate, chloride, bromide, or sulfate) were infused using a syringe pump at a flow rate of 5 μL min^{-1}. The metal capillary potential, optimized for the various positive ion spectra of interest, was in the range +2.5 to +3.0 kV, and the counter electrode was in the range +50 to +100 V. Optimization for maximum intensity of individual ions depended on the adjustment of the electric field in the intermediate pressure region of the source between the sampling cone and the grounded skimmer lens. The temperature of the desolvation chamber through which dry nitrogen flowed was 80 °C.

CAD spectra were obtained using argon as the collision gas. The energies of the incident ions were determined by the potential difference between the grounded skimmer lens and the collision cell. The potential of the latter (V_{lab}) was used in the range 0 to –40 V with respect to ground. Collision energies are quoted as centre of mass (c of m) energies determined as

$$E_{cm} = -V_{lab}\left(\frac{m_{ion}M_{argon}}{m_{ion} + M_{argon}}\right)$$

Computations were carried out using the Gaussian 03W suite of programs (16). The calculations required for the large complexes and the limited available computing capacity enforced the use of the density functional method at the B3LYP/6-31+G(d,p) level for both optimization and energy calculations. No negative frequencies were present in any of the optimized structures. No scaling factors were employed in calculating the energies (17). The atomic charges were calculated with the natural bond orbital (NBO) program that is a constituent part of the Gaussian G03W suite of programs.

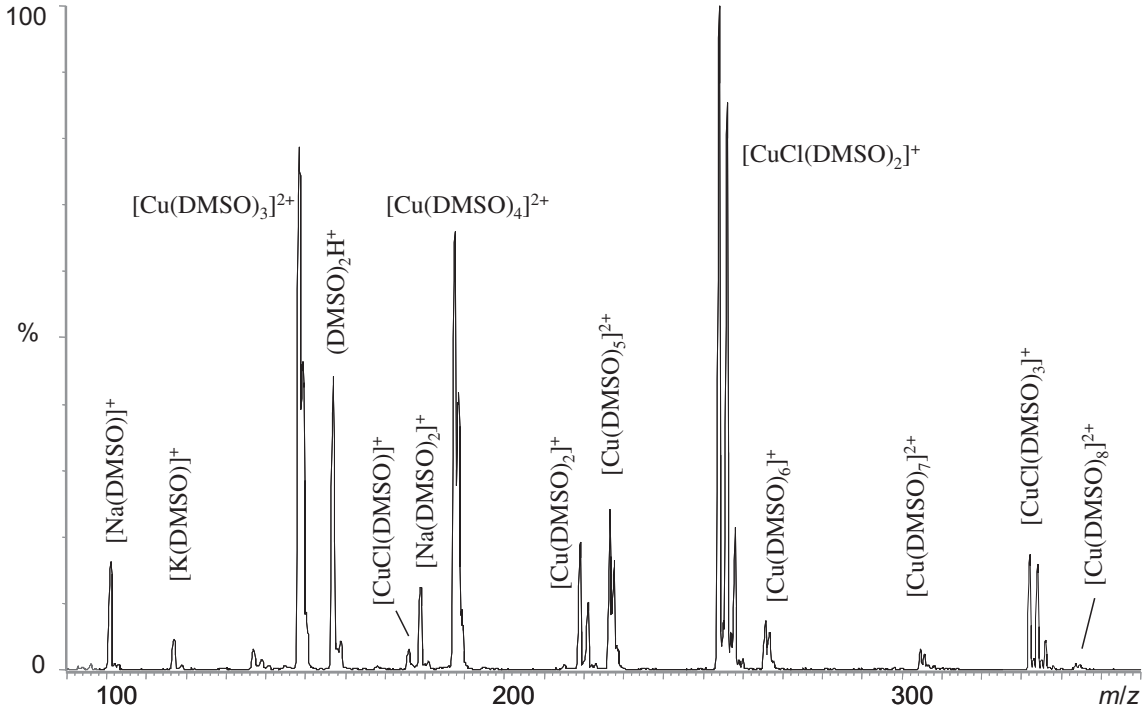
Results and discussion

Figure 1 shows a typical ES spectrum obtained with a cupric ion – DMSO aqueous solution, in this case using $CuCl_2$ as the source of the cation. The cone voltage was 22 V. The isotopic patterns of copper (^{63}Cu:^{65}Cu = 60:31) and chlorine (^{35}Cl:^{37}Cl = 75:25) aid peak identification, and doubly and singly charged ions are distinguished by the respective 1 and 2 m/z unit peak separation in the isotopic clusters. The use of DMSO-d_6 and CAD experiments provided additional confirmation. Two main series of peaks, both due to Cu(II) complexes, are present, viz. the doubly charged $[Cu(DMSO)_n]^{2+}$ with n ranging from 3 to 8, and the singly charged $[CuCl(DMSO)_n]^{+}$ with n in the range 1 to 3. No $[Cu(DMSO)_2]^{2+}$ or $[Cu(DMSO)]^{2+}$ is observed in the spectrum, but higher complexes of very low intensity containing as many as 11 DMSO molecules were observed that are beyond the m/z scale of the figure. The only other copper-containing peak of significance is at m/z 219 owing to the Cu(I) complex, $[Cu(DMSO)_2]^{+}$. When $CuBr_2$ replaced $CuCl_2$ in the electrosprayed solution, the only difference in the spectrum was the presence of $[CuBr(DMSO)_n]^{+}$ rather than $[CuCl(DMSO)_n]^{+}$. Similarly $Cu(NO_3)_2$ formed $[CuNO_3(DMSO)_n]^{+}$ and $CuSO_4$ formed $[Cu(HSO_4)(DMSO)_n]^{+}$. It is noticeable that there are no ions with water as a ligand, even though the solvent in the infused solution was 99.9% water.

The two series of Cu(II) ions, $[Cu(DMSO)_n]^{2+}$ and $[CuX(DMSO)_n]^{+}$ (X = Cl, Br, NO_3, HSO_4), were collisionally activated and the resulting spectra were studied as a function of collision energy. The CAD spectra described in this paper were obtained at an argon collision gas pressure of $1.0 \pm 0.1 \times 10^{-4}$ Torr (1 Torr = 133.3224 Pa) in a 7 cm long hexapole collision cell. Even at this low pressure some ions may experience multiple collisions and product ions may also be collisionally activated and decompose (18). Two products that were present in many of the CAD sprectra of the doubly charged complexes were the Cu(I) ions

© 2005 NRC Canada

Fig. 1. ESI mass spectrum of an aqueous solution containing 1.0×10^{-3} mol/L $CuCl_2$ and 1.0×10^{-2} mol/L DMSO.



$[Cu(DMSO)_2]^+$ and $[Cu(DMSO)]^+$. The CAD spectra of these ions were therefore examined to assess the contributions from their dissociations to the product ions observed in other spectra. In the following sections the copper complexes and products that are shown in the figures are those containing ^{63}Cu, ^{32}S and where appropriate, ^{35}Cl. CAD spectra of other isotopomers were always obtained for conformation of ion identities.

CAD of $[Cu(DMSO)_2]^+$ and $[Cu(DMSO)]^+$

The ions formed as a function of collision energy from $[Cu(DMSO)_2]^+$ and $[Cu(DMSO)]^+$ are shown in Figs. 2*a* and 2*b*, respectively. $[Cu(DMSO)_2]^+$ has one major, $[Cu(DMSO)]^+$, and one minor, $[Cu(CH_3SO)(DMSO)]^+$, product at low collision energy.

[3] $[Cu(DMSO)_2]^+ \rightarrow [Cu(DMSO)]^+ + DMSO$

[4] $[Cu(DMSO)_2]^+ \rightarrow [Cu(CH_3SO)(DMSO)]^+ + CH_3$

Loss of methyl, as described by eq. [1] for multiply charged metal – DMSO complexes, is therefore not dependent on a high metal cation charge. The yield of $[Cu(CH_3SO)(DMSO)]^+$ shows little dependence on collision energy, but the apparent minimum at ~4.5 eV shows the possibility of two pathways for the reaction of eq. [4], one at low energy and one at high energy. The extremely low abundances of Cu^+ and $[Cu(CH_3SO)]^+$ that appear at the higher collision energies originate from the further decomposition of $[Cu(DMSO)]^+$, as demonstrated by its decline in relative abundance and by the CAD results in Fig. 2*b* for $[Cu(DMSO)]^+$. The very small yield of $CH_3SCH_2^+$ is observed for $[Cu(DMSO)_2]^+$ but not for $[Cu(DMSO)]^+$. $[Cu(DMSO)_2]^+$ is a very stable ion since even at 6 eV collision energy, only 10% has decomposed.

The major lowest energy process in the activated dissociation of $[Cu(DMSO)]^+$ is loss of methyl (eq. [5]), while at higher energies the product, $[Cu(CH_3SO)]^+$, decomposes further to either $Cu^+ + CH_3SO$ or $CH_3SO^+ + Cu$ (eqs. [6] and [7]).

[5] $[Cu(DMSO)]^+ \rightarrow [Cu(CH_3SO)]^+ + CH_3$

[6] $[Cu(CH_3SO)]^+ \rightarrow Cu^+ + CH_3SO$

[7] $[Cu(CH_3SO)]^+ \rightarrow Cu + CH_3SO^+$

The formation of $[Cu(CH_3)]^+$ (eq. [8]) at very low energy is competitive with the formation of CH_3SO^+, which is surprising since, as seen later, computation shows it as a high energy product.

[8] $[Cu(DMSO)]^+ \rightarrow [Cu(CH_3)]^+ + CH_3SO$

CAD of $[Cu(DMSO)_n]^{2+}$

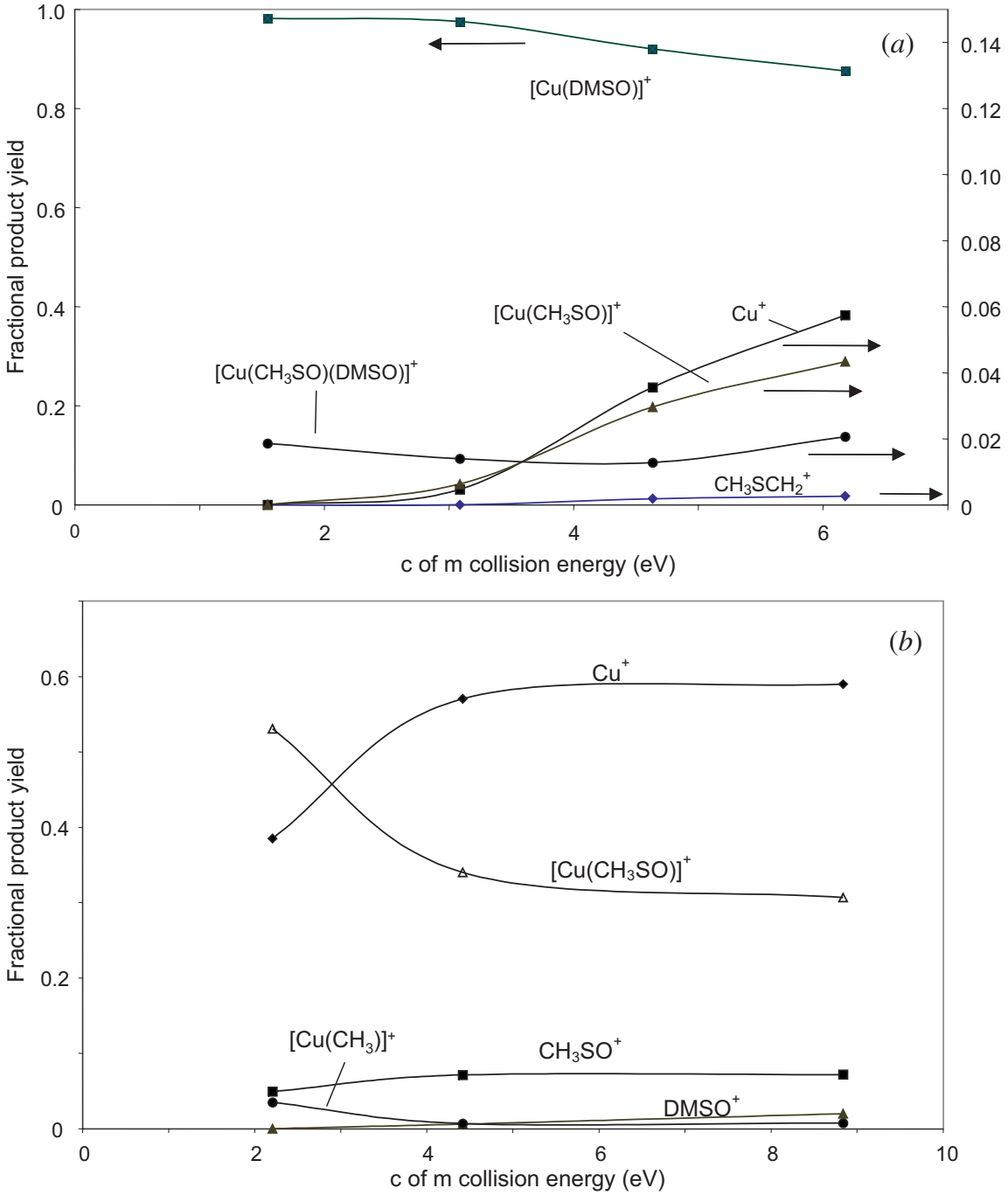
Loss of one or more ligands with no loss of charge was the only CAD reaction for $[Cu(DMSO)_n]^{2+}$ complexes with $n \geq 4$. The CAD spectrum of $[Cu(DMSO\text{-}d_6)_4]^{2+}$, obtained at a collision energy of 0.1 eV, showed only the loss of DMSO (eq. [9]). In particular, in agreement with Shvartsburg and Wilkes (8), loss of methyl with retention of charge (eq. [1]) was not observed, and all other product ions observed at higher collision energies from $[Cu(DMSO)_n]^{2+}$ ($n \geq 4$) could be ascribed to the further decomposition of $[Cu(DMSO)_3]^{2+}$.

[9] $[Cu(DMSO)_4]^{2+} \rightarrow [Cu(DMSO)_3]^{2+} + DMSO$

The CAD spectrum of $[Cu(DMSO\text{-}d_6)_3]^{2+}$ (*m*/*z* 157.5), obtained at a collision energy of 4.5 eV, is shown in Fig. 3*a*. There is excellent agreement with the spectrum obtained by Shvartsburg and Wilkes (8) at the slightly higher energy of 4.74 eV. In particular, there was an extremely weak signal for $[Cu(DMSO\text{-}d_6)_2]^{2+}$ (*m*/*z* 115.5), which is too small to be

© 2005 NRC Canada

Fig. 2. Fractional product yields in the CAD spectra of (*a*) $[Cu(DMSO)_2]^+$ and (*b*) $[Cu(DMSO)]^+$ as a function of collision energy.

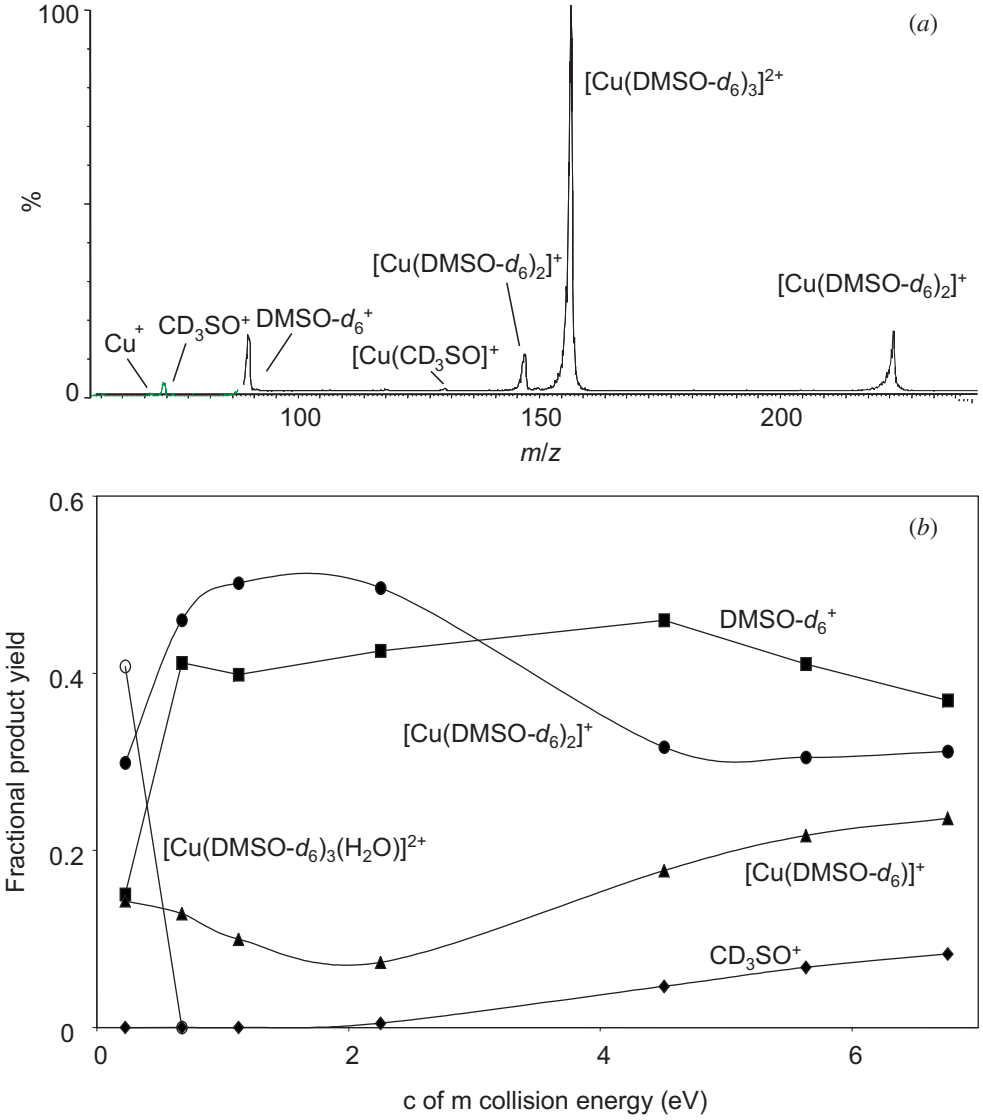


shown in the figure. The major products, $[Cu(DMSO\text{-}d_6)_2]^+$, $[Cu(DMSO\text{-}d_6)]^+$, and DMSO-d_6^+, are all singly charged. There are small yields of $[Cu(CD_3SO)]^+$, CD_3SO^+, and Cu^+. No $[Cu(DMSO\text{-}d_6)]^{2+}$ (*m*/*z* 73.5) is present in the spectrum and this ion was never observed in any CAD spectrum at any collision energy. Stace and co-workers (19), using the pick-up technique, an alternative method of producing gas-phase metal cation complexes, and a wide variety of N and O potential ligands, found no Cu^{2+} ions solvated by a single DMSO molecule either in the spectra or in the CAD spectra of the isolated higher solvates. The conclusion is that $[Cu(DMSO)]^{2+}$ is not experimentally observable in the gas phase with the present ESI technique. This does not mean that it is not a stable entity. As the initial doubts and final observation of $[Cu(H_2O)]^{2+}$ has demonstrated, it is unwise to make bold statements regarding the possibility or impossibility of the existence of a species (18–25). As shown later, calculation does suggests that the monoligated ion may be viable.

The evolution of the intensities of the major products from $[Cu(DMSO\text{-}d_6)_3]^{2+}$ as a function of collision energy is shown in Fig. 3*b*. The intensities of $[Cu(CD_3SO)]^+$, CD_3SO^+, and Cu^+ that were too small to quantitate can be ascribed to the further decomposition of the singly charged products $[Cu(DMSO\text{-}d_6)_n]^+$ (n = 1 or 2) as detailed earlier. At very low energy, background water adds to the precursor ion giv-

© 2005 NRC Canada

Fig. 3. (*a*) CAD spectrum of $[Cu(DMSO\text{-}d_6)_3]^{2+}$ at 4.5 eV collision energy. (*b*) Fractional product yields in the CAD spectra of $[Cu(DMSO\text{-}d_6)_3]^{2+}$ as functions of collision energy.



ing $[Cu(H_2O)(DMSO\text{-}d_6)_3]^{2+}$, but the addition is absent above 0.5 eV, as expected for the product of an association reaction. This water addition leads to a geometry with four ligands about the central Cu^{2+}, each coordinated through oxygen. DFT calculation shows that the preferred geometry for both $[Cu(H_2O)_4]^{2+}$ and $[Cu(NH_3)_4]^{2+}$ is planar tetragonal, a fifth ligand preferring hydrogen bonding in an outer shell rather than occupying a vacant axial position (26). The same tetragonal geometry should be present in $[Cu(H_2O)(DMSO\text{-}d_6)_3]^{2+}$ and also presumably in $[Cu(DMSO\text{-}d_6)_4]^{2+}$.

The initial activated decomposition of $[Cu(DMSO\text{-}d_6)_3]^{2+}$ involves electron transfer from one ligand to the metal, followed by dissociation (eq. [10]), both the products, $[Cu(DMSO\text{-}d_6)_2]^+$ and DMSO-d_6^+, appearing in high yield.

$$[10] \quad [Cu(DMSO\text{-}d_6)_3]^{2+} \rightarrow [Cu(DMSO\text{-}d_6)_2]^+ + DMSO\text{-}d_6^+$$

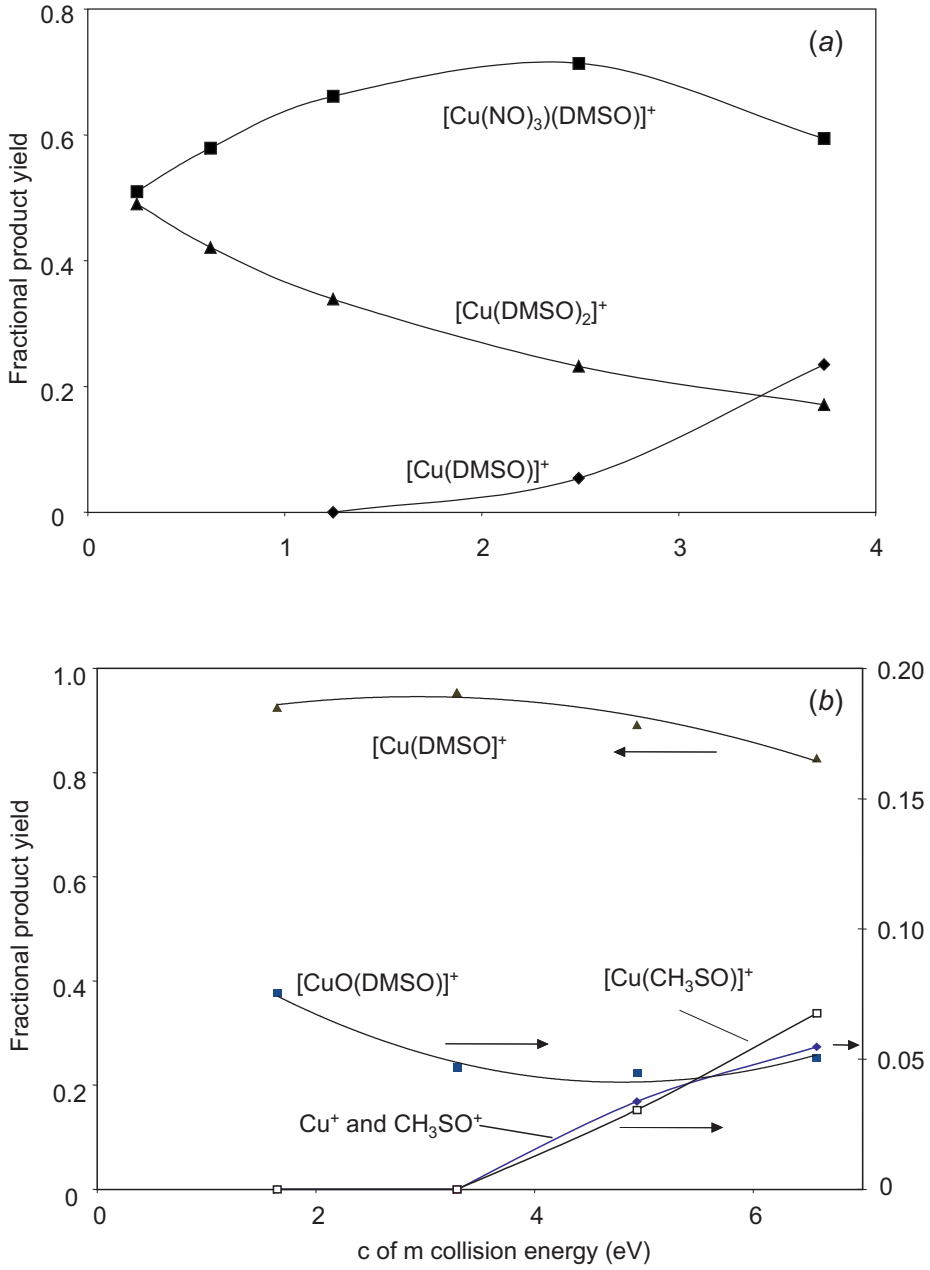
The loss of two DMSO-d_6 ligands from $[Cu(DMSO\text{-}d_6)_3]^{2+}$, giving $[Cu(DMSO\text{-}d_6)]^+$, appears to have two components since there is a shallow minimum in yield at 2 eV. The increasing yield at higher energies complements the decrease in $[Cu(DMSO\text{-}d_6)_2]^+$, but the origin of the low energy contribution is not known. The increasing yield of CD_3SO^+ at the higher energies must arise from the further decomposition of DMSO-d_6^+ since as described earlier, the decomposition of $[Cu(DMSO\text{-}d_6)_2]^+$ and $[Cu(DMSO\text{-}d_6)]^+$ yield approximately equal intensities of Cu^+ and CD_3SO^+. Cu^+, seen in the CAD spectrum of $[Cu(DMSO\text{-}d_6)_3]^{2+}$ in Fig. 3*a*, was too low in intensity to appear in Fig. 3*b*, and was never more than 15% of that of CD_3SO^+ at even the highest collision energy.

The collisionally assisted dissociation of singly charged Cu(II) complexes

The complexes investigated were: $[Cu(NO_3)(DMSO)_n]^+$, $[CuCl(DMSO)_n]^+$, $[CuBr(DMSO)_n]^+$ (n = 1 or 2), and $[Cu(HSO_4)(DMSO)]^+$. All these are Cu(II) complexes that are singly charged because of the presence of an anionic ligand. When the anion is retained in a singly charged cop-

© 2005 NRC Canada

Fig. 4. Fractional product yields in the CAD spectra of (*a*) $[Cu(NO_3)(DMSO)_2]^+$ and (*b*) $[Cu(NO_3)(DMSO)]^+$ as functions of collision energy.



per-containing product ion in a CAD spectrum then no metal reduction has occurred, but if no anion is present then the complex contains Cu(I). The CAD spectra show the competition between reductive and nonreductive processes. Spectra were obtained as functions of collision energy for all ions except $[Cu(HSO_4)(DMSO)]^+$, whose intensity was too low for all but a qualitative examination.

Figure 4*a* shows the results obtained for $[Cu(NO_3)(DMSO)_2]^+$ and the results obtained for $[Cu(NO_3)(DMSO)]^+$ are shown in Fig. 4*b*. At all energies there is competition in the decomposition of $[Cu(NO_3)(DMSO)_2]^+$ between loss of NO_3 (eq. [11]) and loss of DMSO (eq. [12]).

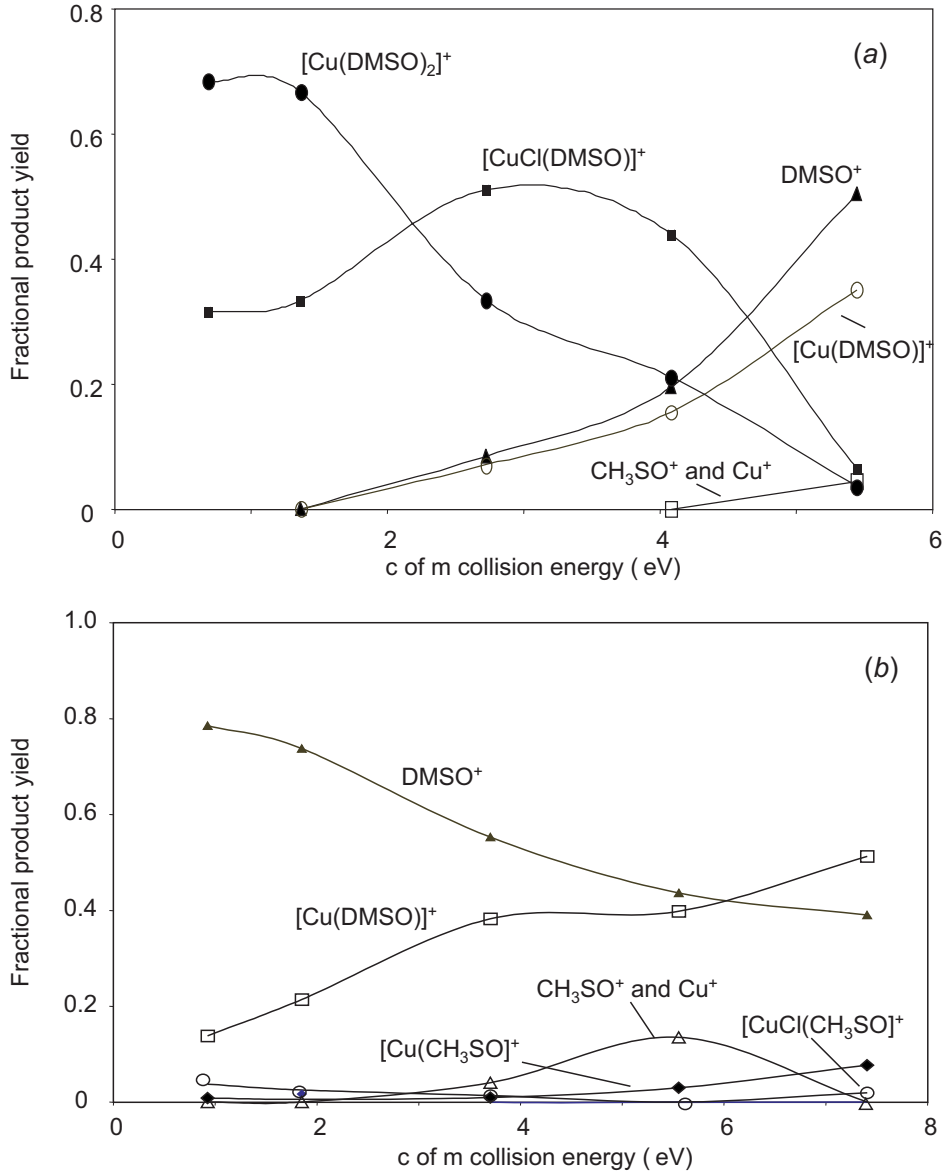
[11] $[Cu(NO_3)(DMSO)_2]^+ \rightarrow [Cu(DMSO)_2]^+ + NO_3$

[12] $[Cu(NO_3)(DMSO)_2]^+ \rightarrow [Cu(NO_3)(DMSO)]^+ + DMSO$

Equation [11] describes a reduction of copper from Cu(II) to Cu(I), while in eq. [12] the oxidation state of the metal remains Cu(II). Extrapolation of the results suggests that, at very low energy, loss of NO_3 is the favored mode. With increased collision energy, loss of DMSO rather than NO_3 becomes dominant. At the highest energy, the appearance of $[Cu(DMSO)]^+$ shows loss of both DMSO and NO_3. This ion can arise from the decomposition of both $[Cu(DMSO)_2]^+$ (vide supra) and $[Cu(NO_3)(DMSO)]^+$. Both may be occurring since the CAD products of $[Cu(NO_3)(DMSO)]^+$ shown in Fig. 4*b* demonstrate that $[Cu(DMSO)]^+$ is the major product at all collision energies (eq. [13]), and it was shown ear-

© 2005 NRC Canada

Fig. 5. Fractional product yields in the CAD spectra of (*a*) $[CuCl(DMSO)_2]^+$ and (*b*) $[CuCl(DMSO)]^+$ as functions of collision energy.



lier that $[Cu(DMSO)]^+$ is the major product from $[Cu(DMSO)_2]^+$. There is a small competing, nonreductive process, the loss of NO_2 (eq. [14]), a reaction verified by the use of DMSO-d_6. Further decomposition of $[Cu(DMSO)]^+$ gives the usual products, $[Cu(CH_3SO)]^+$, CH_3SO^+, and Cu^+.

[13] $[Cu(NO_3)(DMSO)]^+ \rightarrow [Cu(DMSO)]^+ + NO_3$

[14] $[Cu(NO_3)(DMSO)]^+ \rightarrow [CuO(DMSO)]^+ + NO_2$

$[CuCl(DMSO)_2]^+$ behaves in a similar but more pronounced manner than $[Cu(NO_3)(DMSO)_2]^+$ in that reductive loss of the halogen is much preferred over loss of DMSO at the lowest energy (Fig. 5*a*).

At intermediate energies, as for $[Cu(NO_3)(DMSO)_2]^+$, loss of DMSO becomes the preferred reaction. Both $[CuCl(DMSO)]^+$ and $[Cu(DMSO)_2]^+$ decompose further, the products being $DMSO^+$ and $[Cu(DMSO)]^+$. The decomposition of $[CuCl(DMSO)]^+$ as a function of energy is shown in Fig. 5*b*. Of particular note is the absence of Cl in any of the ions with the exception of the appearance of a trace of $[CuCl(CH_3SO)]^+$ at the highest energy. The major process at all but the highest energy is the loss of CuCl following electron transfer from the DMSO ligand (eq. [15]).

[15] $[CuCl(DMSO)]^+ \rightarrow CuCl + DMSO^+$

When $CuBr_2$ was the cupric salt employed, $[CuBr(DMSO)_2]^+$ was produced in good yield in the ESI spectrum, but $[CuBr(DMSO)]^+$ was present with low intensity. Loss of Br from $[CuBr(DMSO)_2]^+$ was the only reaction at collision energies up to 2 eV and even at 5 eV, loss of DMSO to give $[CuBr(DMSO)]^+$, the only other reaction, constituted less than 10% of the products. Loss of Br from $[CuBr(DMSO)_2]^+$ was more facile than loss of Cl from $[CuCl(DMSO)_2]^+$, presumably because of the lower electron affinity of the halogen and its lower energy of association with copper. The intensity of $[CuBr(DMSO)]^+$ was too low in the ESI spectrum for a quantitative study, but qualitative

© 2005 NRC Canada

results showed that loss of Br constituted >95% of the reaction at the highest collision energy.

The intensity of $[Cu(HSO_4)(DMSO)]^+$ was very low and it was only possible to obtain sufficient signal for qualitative CAD experiments at collision energies above 3.6 eV. By comparing results obtained at 3.6 and 5.4 eV, it appears that the lowest energy decomposition pathway was OH transfer to the metal together with loss of SO_3 (eq. [16]) and at higher energy, losses of HSO_4 and $CuHSO_4$ were evident.

$$[16] \quad [Cu(HSO_4)(DMSO)]^+ \rightarrow [Cu(OH)(DMSO)]^+ + SO_3$$

Ab initio calculations

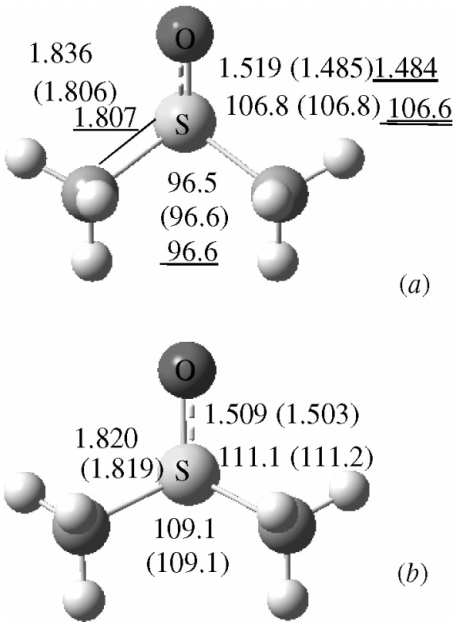
The optimized geometries and energies of most of the complexes and some of the major CAD products were calculated using the B3LYP functional with the 6-31+G(d,p) basis set. Metal cations coordinate with DMSO at oxygen (2, 9, 27, 28). This was verified for Cu^{2+} by optimizing the structure of $[Cu(DMSO)]^{2+}$ from a variety of initial configurations. Only one potential minimum was found, that with Cu-O coordination. All initial geometries for the complexes studied were therefore set up with that geometry, and no other initial geometries were examined. Each optimized structure was at a minimum on the potential energy surface.

DMSO and $DMSO^+$

The structure of DMSO is shown in Fig. 6*a*. For comparison, experimental results and those from higher levels of theory are also shown. Typke and Dakkouri (29) have presented an extensive study of the structural parameters for DMSO from both ab initio calculations with different levels of theory and have also reevaluated extant experimental data. The results obtained with the B3PW91/6-311++G(3df,3pd) method were found to be in best agreement with experiment. Figure 6*a* shows that our B3LYP/6-31+G(d,p) results slightly overestimate the experimental S—O and C—S bond lengths but show excellent agreement for bond angles. The dipole moment of DMSO is calculated to be 4.41 D at an angle of 12° to the O—S bond in the direction of the methyls. The experimental dipole moment is 3.9 D. The angle is considerably smaller than the value of 25 ± 1° obtained by both B3LYP and MP2 methods with a variety of basis sets (2). Since limitation of computational capacity prevented the use of higher levels of calculation for the large metal cation – DMSO complexes of interest in this study, higher level calculations for DMSO were not appropriate.

The association of DMSO with Cu^{2+} was expected to transfer some electron density from the ligand to the metal and therefore, for reference, the geometry of $DMSO^+$ is shown in Fig. 6*b*. Ionization causes a shortening of the O—S bond from 1.519 to 1.509 Å and of the S—C bond from 1.836 to 1.820 Å. The C—H bond lengths remain constant at 1.092 ± 0.001 Å. Of significance are the accompanying increases in the bond angles, < O-S-C increases by 4.3° and < C-S-C by 12.6°. The geometry about S is assuming a more planar character than in DMSO. The angle between the S—O bond and the C-S-C plane is 116° in DMSO, in agreement with Typke and Dakkouri's value of 115.4° (29), and this increases to 128° in $DMSO^+$. The structure of $DMSO^+$ is in good agreement with that computed previously at the

Fig. 6. Structures obtained at B3LYP/6-31+G(d,p) of (*a*) DMSO (values underlined are evaluated experimental results given in ref. 29) and (*b*) $DMSO^+$. The values in brackets in both structures are computational results at the B3LYP/6-311+G(d,p) level from ref. 31. Distances are in angstroms and angles are in degrees.



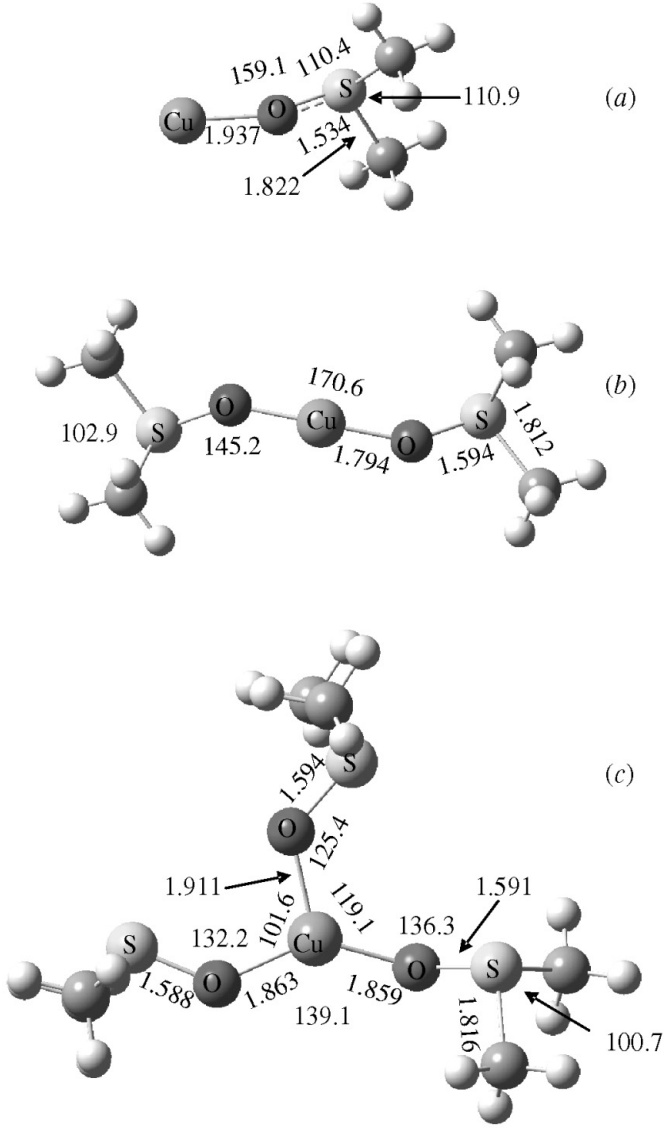
B3LYP/6-311++G(d,p) level (30), and the structures of both DMSO and $DMSO^+$ are almost identical with those obtained using B3LYP/6-311+G(d,p) (31). The latter values are shown in Fig. 6.

Doubly charged Cu(II) complexes — $[Cu(DMSO)_n]^{2+}$

Figure 7 shows the structures of $[Cu(DMSO)_n]^{2+}$ (n = 1–3). When DMSO is coordinated with Cu^{2+} in $[Cu(DMSO)]^{2+}$, the S—O bond is lengthened by 0.015 Å and the S—C bonds are decreased by 0.014 Å (Fig. 7*a*). The Cu is situated trans to the two methyl groups. The angles about S are almost identical (< O-S-C = 110.4° and < C-S-C = 110.9°) and compared to DMSO, the angle between the S—O bond and the C-S-C plane is increased to 128°. These angles are essentially the same as those of $DMSO^+$, but the S—O distances and to a lesser extent the S—C distances are considerably different. The Cu-O-S angle is 159.1°, which may be compared to the M-O-S angles in doubly charged $[M(DMSO)]^{2+}$ for closed shell cations: Mg (153.9° at the B3LYP/6-31G(d) level (9)), and Zn (129.8°), Ca (167.9°), Mg (152.8°), and Be (166.8°) at the B3LYP/6-31+G(d) level (27). El-Nahas (27) has suggested that nonlinear M-O-S geometry denotes the presence of charge transfer, whereas a linear geometry is consistent with a purely electrostatic interaction. Since the dipole moment of DMSO is not colinear with the O—S bond and since a purely electrostatic interaction would involve the dipole, then the M-O-S bond would not be expected to be 180°, whether or not the bond was purely electrostatic. If Cu^{2+} were interacting only with the DMSO molecular dipole then < Cu-O-S would be 168°, significantly larger than the computed 159.1°. Not only the dipole but the higher multipoles and the polarizability must

© 2005 NRC Canada

Fig. 7. Structures of (*a*) $[Cu(DMSO)]^{2+}$, (*b*) $[Cu(DMSO)_2]^{2+}$, and (*c*) $[Cu(DMSO)_3]^{2+}$. Distances are in angstroms and angles are in degrees.



also be taken into consideration for a pure electrostatic interaction. The Cu—O distance of 1.937 Å is larger than that for the analogous DMSO complexes of Zn^{2+} and Mg^{2+}. El-Nahas obtained a Zn—O distance of 1.819 Å at the B3LYP/6-31+G(d) level (27) and a value of 1.806 Å was obtained at the B3LYP/6-31G(d) level for Mg—O (9). These M—O distances are in the same order as the metal cation radii: Cu^{2+} (0.62 Å), Zn^{2+} (0.60 Å), and Mg^{2+} (0.49 Å).

Figure 7*b* shows the structure of the diligated cupric ion, $[Cu(DMSO)_2]^{2+}$. The most remarkable feature of this structure is that the Cu—O distance has decreased to 1.794 Å from the 1.937 Å in $[Cu(DMSO)]^{2+}$. It is usual, as was seen for the analogous Mg^{2+}–DMSO complexes (9) and for other symmetrical complexes of divalent metal cations (31–33), that the presence of a second identical ligand increases the metal–ligand bond length. Copper, however, is unusual, both the Cu^+ and the Cu^{2+} complexes with both H_2O and NH_3 have, respectively, smaller computed Cu—O and Cu—N distances in the diligated than in the monoligated complex (20, 22). The O-Cu-O angle in $[Cu(DMSO)_2]^{2+}$ is 170.6°. For comparison, the lowest energy form of $[M(H_2O)_2]^{2+}$ has a linear conformation for M = Mg (9, 33), but for M = Ca, Sr, Ba, and Ra, the angles are much less than 180° (33). The DMSO groups in $[Cu(DMSO)_2]^{2+}$ are identical but staggered, with a S-O-O-S dihedral angle of 101.7° and the C-Cu-C angle defined by proximate carbons from the two ligands of 143.1°.

The three oxygen atoms and copper in $[Cu(DMSO)_3]^{2+}$ are almost coplanar, as shown by the sum of the three O-Cu-O angles (359.7°) (Fig. 7*c*). However, the individual angles (101.6°, 119.1°, and 139.1°) are very different. This difference is reflected in the significant differences in the Cu—O distances (1.859, 1.863, and 1.911 Å). An unsuccessful attempt was made to find an energy minimum for a structure with three equal Cu—O distances. An initial starting geometry with equal Cu—O bond lengths of 1.870 Å optimized to the same asymmetric structure shown in the figure. The geometry around the central metal ion in both $[Cu(H_2O)_3]^{2+}$ and $[Cu(NH_3)_3]^{2+}$ is similar to that of $[Cu(DMSO)_3]^{2+}$, being almost planar with one Cu—X bond significantly longer than the other two (26). With all three ligands (DMSO, H_2O, and NH_3) the largest X-Cu-X angle is diametrically opposed to the longest Cu—X bond.

As the number of DMSO ligands in $[Cu(DMSO)_n]^+$ increases, the geometry of the CH_3SCH_3 group changes monotonically. The C-S-C angle decreases from 110.9° for n = 1 to 100.8° for n = 3. At the same time, the S—C bond length decreases from 1.822 to 1.814 Å. The trend is towards, but the values are still significantly different from, those of neutral DMSO. Figure 7 shows that the O—S distance is most influenced by the metal cation. The shortest, and nearest to the value for DMSO, occurs for n = 1. The distances for n = 2 and 3 are considerably larger. It was expected that the O—S distance would vary inversely with the Cu—O distance, but this is not the case.

Singly charged Cu(I) complexes — $[Cu(DMSO)_n]^+$

The structures of $[Cu(DMSO)_n]^+$ (n = 1 or 2) are shown in Fig. 8. Comparison with Fig. 7 shows that the computed Cu—O bond in $[Cu(DMSO)]^+$ is shorter than that in $[Cu(DMSO)]^{2+}$ by 0.08 Å, while the O—S bond is longer by 0.035 Å. When the second ligand is added to $[Cu(DMSO)]^+$, the Cu—O bond increases slightly by 0.005 Å, which contrasts with the observation of a decrease in the Cu—X (X = O or N) bond length for $Cu(H_2O)_2^+$ and $Cu(NH_3)_2^+$. Both these ions have linear X-Cu-X geometry, whereas O-Cu-O in $[Cu(DMSO)_2]^+$, which has C_1 geometry, is slightly bent with an angle of 173.8°. The two identical DMSO groups are staggered with a S-O-O-S dihedral angle of 108.5° and a C-Cu-C angle defined by the proximate carbons of the two ligands of 52.9°.

Singly charged Cu(II) complexes — $[CuX(DMSO)_n]^+$

Figure 9 shows the optimized structure of $CuCl^+$ and the structures of its DMSO adducts $[CuCl(DMSO)]^+$ and $[CuCl(DMSO)_2]^+$. The Cu—Cl distance is greater in CuCl than in $[CuCl(DMSO)]^+$ by 0.041 Å, but when a second DMSO is present in the complex, the Cu—Cl distance is

© 2005 NRC Canada

Fig. 8. Structures of the Cu(I) ions (*a*) $[Cu(DMSO)]^+$ and (*b*) $[Cu(DMSO)_2]^+$. Distances are in angstroms and angles are in degrees.

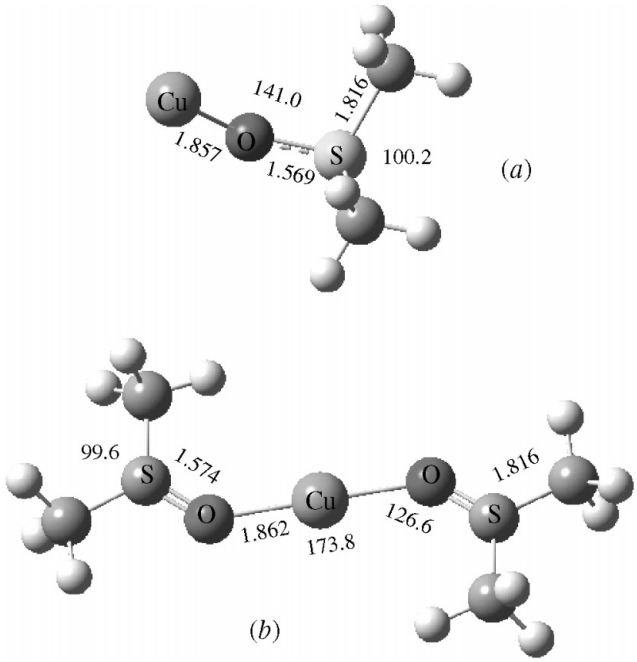
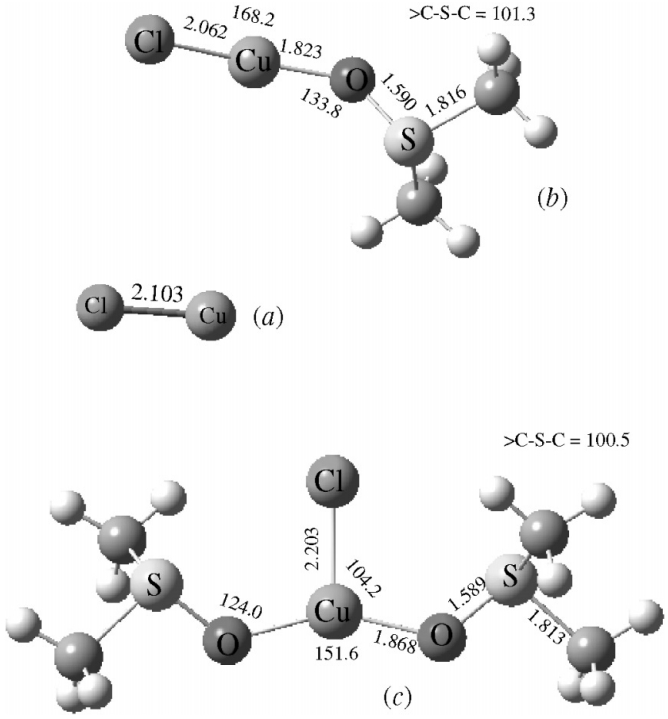


Fig. 9. Structures of (*a*) CuCl, (*b*) $[CuCl(DMSO)]^+$, and (*c*) $[CuCl(DMSO)_2]^+$. Distances are in angstroms and angles are in degrees.



greater than in Cu—Cl by 0.100 Å, presaging the preferred loss of neutral Cl in the CAD spectrum. The geometry of $[CuCl(DMSO)]^+$ has some similarities to that of the diligated $[Cu(DMSO)_2]^{2+}$, especially in the Cl-Cu-O angle, which is 168.2° compared to 170.6° for O-Cu-O, and the O—S distance, 1.590 compared to 1.594 Å. The geometries of the CH_3SCH_3 groups are also very similar.

When a second DMSO is added to $[CuCl(DMSO)]^+$, the two ligands have identical structures, but unlike in $[Cu(DMSO)_2]^+$ and $[Cu(DMSO)_2]^{2+}$, the O—S bonds are in the cis position rather than trans. This positioning allows each bond dipole ($O^{\delta-}$–$S^{\delta+}$) to interact favorably with Cl, whereas in the absence of the halogen, the two dipoles repel and the bonds occupy the trans position.

The nitrate anion is planar and symmetric with a N—O bond length of 1.265 Å (Fig. 10*a*). No potential minimum could be found for monodentate coordination of nitrate with Cu^{2+}; the only minimum is for bidentate coordination in which the NO_3 symmetry is broken in the planar $[CuNO_3]^+$ (Fig. 10*b*). The N—O distance for the two coordinating oxygens increases by 0.048 Å, while the third N—O bond, diametrically opposed to Cu, decreases by 0.088 Å. All atoms in $[CuNO_3(DMSO)]^+$, with the exception of those of the methyl groups, are coplanar (Fig. 10*c*). The NO_3 group remains bidentate, but the two Cu—O bonds are not equal in length; one is larger and the other smaller than the Cu—O distance in $[CuNO_3]^+$. The bond cis to O—S has increased by 0.046 Å and the other has decreased by 0.032 Å. This orientation of NO_3 relative to DMSO again shows the interaction between the O—S bond dipole and the anion. Comparison of the interatomic distances and angles for $[CuNO_3(DMSO)]^+$ and $[CuCl(DMSO)]^+$ shows very minor changes in the Cu(DMSO) moiety; the Cu—O distance is 0.009 Å smaller with nitrate, and all other parameters are the same within 1%.

The structure of $[CuNO_3(DMSO)_2]^+$ (Fig. 10*d*) has four coplanar oxygens surrounding Cu, the two DMSO oxygens being closer to the metal by 0.064 Å. The N—Cu distance is greater than in either $[CuNO_3(DMSO)]^+$ or $[CuNO_3]^+$ as NO_3 reverts towards the structure of the free anion. Both coordinating nitrate oxygens are identically positioned and as for $[CuCl(DMSO)_2]^+$, the two DMSO ligands are oriented so that interaction between the S—O dipole and the anion is favored, allowing long-range interaction between an O of the nitrate and the electropositive S of the DMSO.

Figure 11 shows that HSO_4^- behaves as a ligand very much like NO_3^- when in association with Cu^{2+}. It is bidentate in $[Cu(HSO_4)]^+$, the presence of the copper decreasing two of the S—O distances and increasing the other two. The O—H bond increases by 0.023 Å and the O-S-O angles change, the angle defined by copper decreasing by 19.6° and the opposite one increasing by 8.4°. The presence of DMSO as a second ligand leads to asymmetry in the bidentate bonding, as was seen for the nitrate analogue. One Cu—O increases by 0.071 Å and the other decreases by 0.013 Å. Again, as for complexes containing either Cl or NO_3, the structure (Fig. 11*d*) of $[Cu(HSO_4)(DMSO)]^+$ shows that the cis orientation of DMSO with the HSO_3 group is determined by bond dipole interactions.

NBO analysis

The ground state of Cu has the $4s^13d^{10}$ configuration, Cu^+ has a closed shell $4s^03d^{10}$ configuration, and Cu^{2+} has an open $4s^03d^9$ configuration. In any Cu(I) complex, charge transfer from ligand to Cu^+ is demonstrated by electron den-

© 2005 NRC Canada

Fig. 10. Structures of (*a*) NO_3^-, (*b*) $CuNO_3^+$, (*c*) $[CuNO_3(DMSO)]^+$, and (*d*) $[CuNO_3(DMSO)_2]^+$. Distances are in angstroms and angles are in degrees.

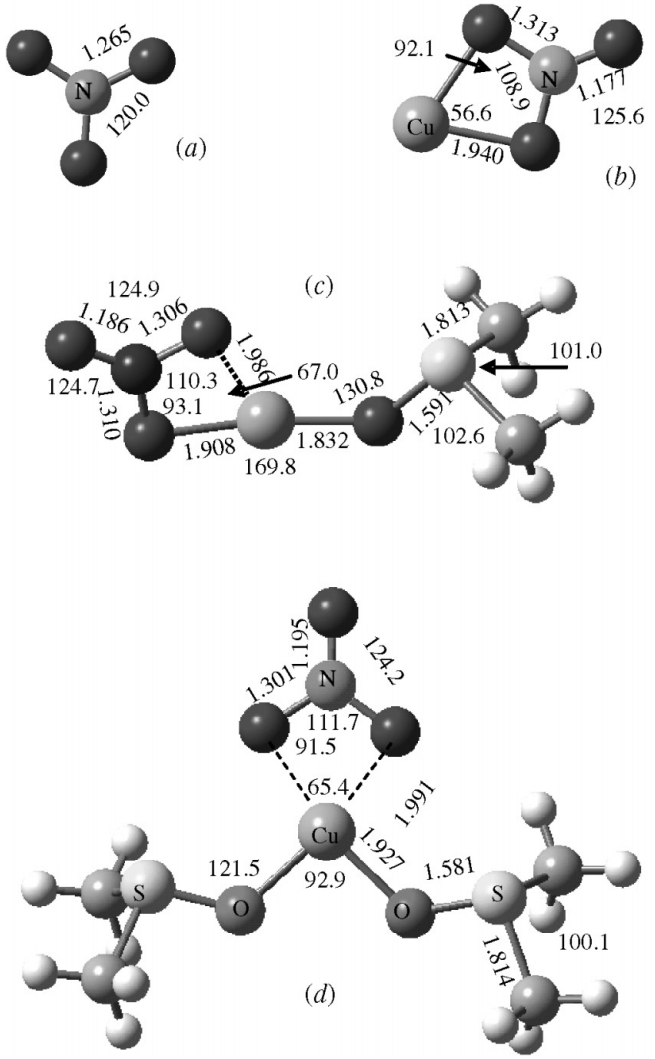
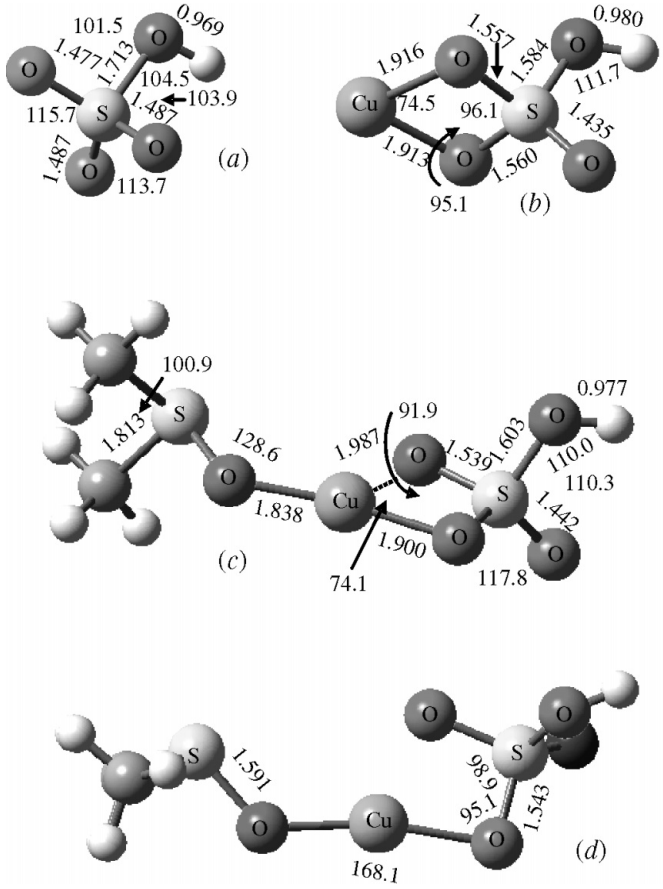


Fig. 11. Structures of (*a*) HSO_4^-, (*b*) $[Cu(HSO_4)]^+$, (*c*) $[Cu(HSO_4)(DMSO)]^+$, and (*d*) another view of (*c*). Distances are in angstroms and angles are in degrees.



sity in the 4s orbital, and charge transfer in a Cu(II) complex is demonstrated by increased population in either or both the 3d and 4s orbitals. The results of NBO calculations for DMSO, $DMSO^+$, and the complexes are shown in Table 1. Listed are the natural charges on copper as well as the populations of its 4s and 3d orbitals, the charges on the S, O, and methyl groups of the DMSO ligands, the charge associated, where applicable, with the anion, and the spin populations on the atoms of some of the odd electron ions.

The reason DMSO preferentially coordinates through O with metal cations is the large S—O bond dipole. The large negative charge of –0.968*e* on O is accompanied by the even larger positive charge of 1.207*e* on S. The two methyl groups combined have the small charge of –0.239*e*. When DMSO is ionized the effect is seen in substantial changes in all parts of the molecule. The change is greatest for O, which becomes more positive by 0.427*e* and least for S, 0.186*e*. The majority of the odd electron spin density is on O. The charge on the methyls increases by 0.387*e* so that they collectively switch from being negative to being positive.

In $[Cu(DMSO)_n]^{2+}$ the positive charge attributed to Cu increases as *n* increases, from 1.103*e* for *n* = 1 to 1.396*e* for *n* = 3. Charge transfer from all ligands to the metal cation therefore decreases as the number of ligands increases, implying that the interaction is becoming less covalent and more electrostatic in nature. Almost one unit of electronic charge has been transferred in $[Cu(DMSO)]^{2+}$ from ligand to metal, the majority increasing the 3d population to almost its maximum value of 10, with little entering the 4s orbital. The electron transfer from H_2O to Cu^{2+} in $[Cu(H_2O)]^+$ was also found to be mainly into 3d (population 9.36e) with only 0.04e into 4s (34). For $[Cu(DMSO)_n]^{2+}$ (*n* = 2 or 3) there is significant electron density in the 4s orbital and the population of the 3d orbital is much less than 10e, electron transfer into 3d being comparable to that into 4s. The charge distribution in DMSO when complexed with Cu^{2+} is very different to that of $DMSO^+$, where much of the electron density is lost from the O atom. In $[Cu(DMSO)]^{2+}$ the most marked change is shown by S and the methyls. These become more positive by 0.247 and 0.543*e*, respectively, while O becomes more positive by only 0.106*e*. As the number of DMSO ligands increases, the charge distribution of each ligand tends towards that of neutral DMSO.

© 2005 NRC Canada

Table 1. Natural charges (*e*) and Cu 4s and 3d orbital populations.

Complex	q_{Cu}	4s[a]	3d[a]	q_O[b]	q_S[b]	q_X[c]	q_{methyl}[d]
DMSO				–0.968	1.207		–0.239
$DMSO^+$				–0.541 (0.597)[e]	1.393 (0.292)[e]		0.148
$[Cu(DMSO)]^{2+}$	1.103 (0.12)[e]	0.05	9.84	–0.862 (0.40)[e]	1.454 (0.37)[e]		0.305
$[Cu(DMSO)_2]^{2+}$	1.226 (0.46)[e]	0.31	9.45	–0.986 (0.44)[e]	1.266 (0.10)[e]		0.214
$[Cu(DMSO)_3]^{2+}$	1.396 (0.60)[e]	0.25	9.32	–1.039[f] (0.36)[e]	1.213[f] (0.01)[e]		0.082
$[Cu(DMSO)]^+$	0.892	0.20	9.90	–1.101	1.262		–0.053
$[Cu(DMSO)_2]^+$	0.785	0.44	9.76	–1.047	1.214		–0.119
$CuCl^+$	1.065	0.22	9.69			–0.065	
$[CuCl(DMSO)]^+$	1.091	0.41	9.46	–1.026	1.234	–0.327	0.028
$[CuCl(DMSO)_2]^+$	1.275	0.32	9.36	–1.034	1.230	–0.613	–0.054
$CuNO_3^+$	1.278	0.15	9.55			–0.278	
$[CuNO_3(DMSO)]^+$	1.379	0.27	9.33	–0.904	1.345	–0.760	–0.744
$[CuNO_3(DMSO)_2]^+$	1.343	0.31	9.31	–1.026	1.218	–0.643	0.108
$Cu(HSO_4)^+$	1.350	0.14	9.52			–0.350	
$[Cu(HSO_4)(DMSO)]^+$	1.352	0.27	9.35	–1.049	1.230	–0.544	

[a]Orbital populations of Cu.
[b]Charges on O and S in DMSO.
[c]Total charge on Cl, NO_3, or HSO_4.
[d]Total charge on methyls of all DMSO ligands.
[e]Unpaired spin.
[f]Average values.

All the $[Cu(DMSO)_n]^{2+}$ are odd-electron species and the location of the unpaired electron in each complex may be obtained by the difference in the populations of the α and β electrons on each atom. These differences are shown in Table 1. In $[Cu(DMSO)]^{2+}$ the spin is almost equally located on the O and S atoms, with only 12% on Cu consistent with the metal having an almost completely filled 3d shell. In $[Cu(DMSO)_2]^{2+}$ the spin is almost equally located on the copper and the oxygens, with only 5% on each of the two sulfurs. With three DMSO ligands, 60% of the spin is on the metal, 35% is on the three oxygens, and only 1% is on the three sulfurs. These spin locations are in accord with the earlier conclusion that as the number of ligands increases, the interaction becomes more electrostatic in nature with decreasing charge transfer.

In contrast to $[Cu(DMSO)_n]^{2+}$, the singly charged $[Cu(DMSO)_n]^+$ show electron transfer to the 4s orbital for both $n = 1$ and 2. The positive charge on Cu is decreased by $0.108e$ ($n = 1$) and $0.215e$ ($n = 2$), but in both cases there is also electron transfer from the 3d to the 4s orbital, implying sd hybridization is important for both complexes. Such transfer has been reported for $[Cu(H_2O)_n]^+$ and for $[Cu(NH_3)_n]^+$ obtained at the B3LYP/cc-pVDZ level; however, the effect and the total charge transferred to the metal were found to be attenuated for $n = 3$ and 4 (22). Another similarity of DMSO with H_2O and NH_3 as ligands, and in contrast to the behaviour of all the ligands with Cu^{2+}, is that the positive charge on Cu for the diligated complex is less than it is for the monoligated ion.

Surprisingly, the NBO charge on copper shows little change when Cl^- is coordinated to Cu in both $[Cu(DMSO)]^{2+}$ and $[Cu(DMSO)_2]^{2+}$, even though the negative charge on Cl is very low ($–0.327e$). The presence of the negatively charged anion results in increased negative charges on the DMSO ligand. Comparison of the charges on the S and O atoms of DMSO in $[Cu(DMSO)]^{2+}$ with those for $[CuCl(DMSO)]^+$ illustrates this statement. While the positive charge on copper decreases by only 0.012 and the charge on Cl is only $–0.327e$, the charges on O, S, and the two methyl groups have become more negative by $0.164e$, $0.220e$, and $0.277e$, respectively. A similar comparison of $[CuCl(DMSO_2]^+$ and $[Cu(DMSO)_2]^{2+}$ shows that the charge associated with Cu is slightly greater ($0.049e$) with a Cl^- ligand, only $–0.387e$ is transferred from the anion, but 85% of the transfer is to the DMSO ligands.

Table 2. Enthalpy changes for Cu^{2+}–DMSO complexes.

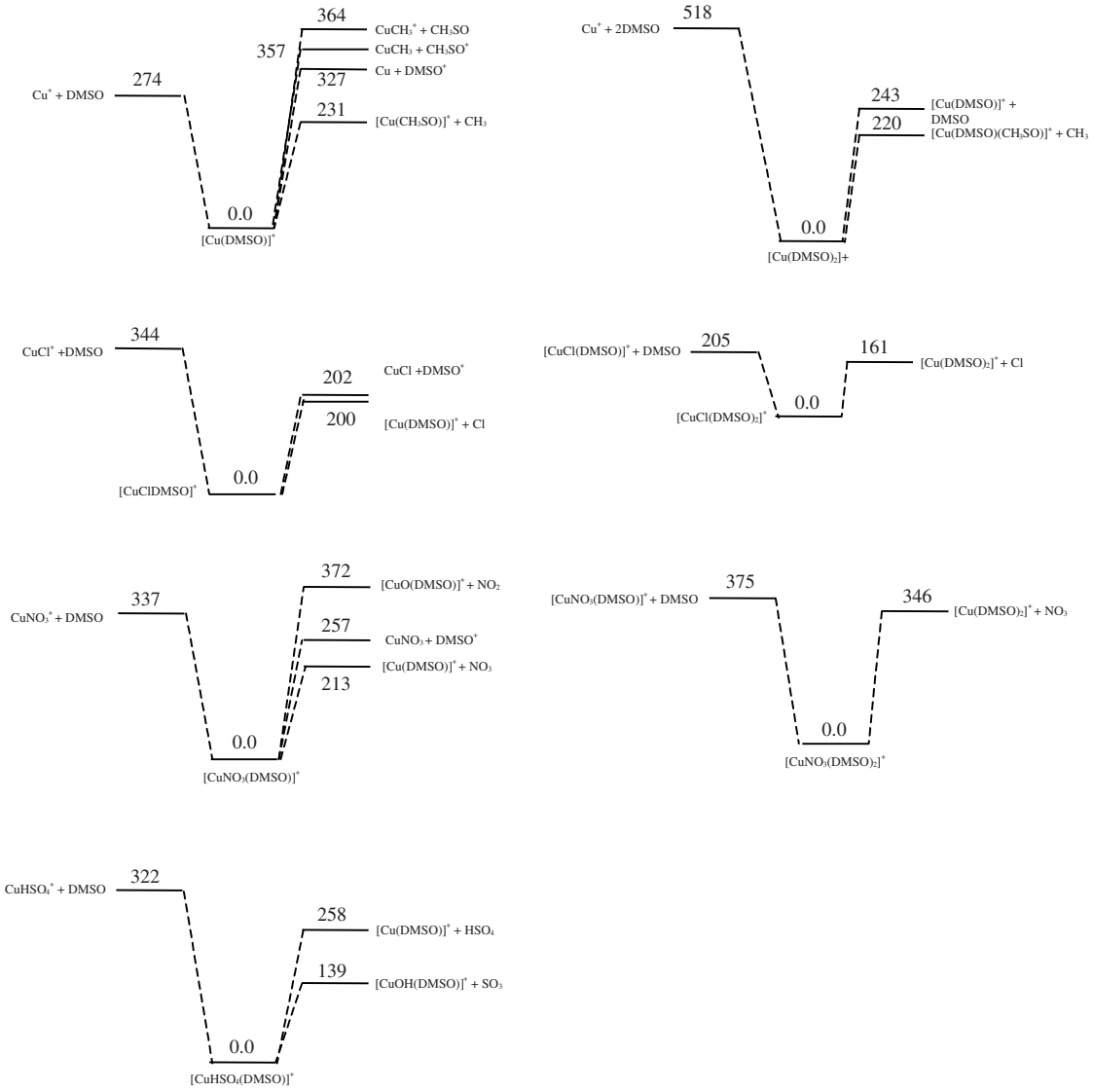
Reaction	H^0_{298} (kJ mol^{-1})
$Cu^{2+} + DMSO = [Cu(DMSO)]^{2+}$	–975
$[Cu(DMSO)]^{2+} + DMSO = [Cu(DMSO)_2]^{2+}$	–421
$[Cu(DMSO)_2]^{2+} + DMSO = [Cu(DMSO)_3]^{2+}$	–258
$[Cu(DMSO)_3]^{2+} = [Cu(DMSO)_2]^+ + DMSO^+$	–35.6
$[Cu(DMSO)_2]^{2+} = [Cu(DMSO)]^+ + DMSO^+$	–50.2
$[Cu(DMSO)]^{2+} = Cu^+ + DMSO^+$	–197
$[Cu(DMSO)_3]^{2+} = [Cu(CH_3SO)(DMSO)_2]^{2+} + CH_3$	294

Enthalpy changes for association and dissociation reactions

Harmonic frequency calculations were performed for all the structures shown in the figures and for a few other ions and molecules. It was thus possible to obtain from the Gaussian program the standard enthalpies of formation for precursor ions and ion and neutral products pertinent to the CAD experiments. The standard enthalpy changes for the association reactions forming $[Cu(DMSO)_n]^{2+}$ and for the dissociation by electron transfer from DMSO to metal are shown in Table 2. The enthalpy changes for the formation of

© 2005 NRC Canada

Fig. 12. Standard enthalpy levels (kJ mol^{-1}) of products relative to those of the precursor ions in the CAD spectra of singly charged Cu(I) and Cu(II) complexes.



and the activated dissociations of the singly charged complexes are given in Fig. 12.

When possible, computational results should always be compared with experimental results, and vice versa. Unfortunately only one experimental thermodynamic measurement for the association of DMSO with a copper ion has been reported. Deng and Kebarle (35), using high-pressure mass spectrometry, determined the enthalpy of association of Cu^+ with two molecules of DMSO from a ladder of relative free energies obtained with many ligands (L) for the reaction $CuL_2^+ = Cu^+ + 2L$. The high level theoretical $\Delta H^0 = -441$ kJ mol^{-1}, computed by Bauschlicher and co-workers (36) for L = NH_3 together with computed entropies at the HF/3-21G* level, enabled the scale of free energies to be converted to a scale of enthalpies, leading to the value of –472 kJ mol^{-1} for DMSO. Our computed enthalpy change for L = DMSO is –518 kJ mol^{-1}. For L = NH_3 at the B3LYP/6-31G+(d,p) level of computation we obtain $\Delta H^0 =$ –485 kJ mol^{-1}. Our values for both DMSO and NH_3 are approximately 45 kJ mol^{-1} more negative than the values reported by Deng and Kebarle. This constitutes an acceptable agreement considering the reported difficulties encountered with computations involving even simple Cu^+ complexes (37). The enthalpy of association of the second DMSO molecule with $[Cu(DMSO)]^+$ (–237 kJ mol^{-1}) is 16% less negative than that for the first. A decrease in binding energy for the second ligand compared with the first is usually, but not always, the case for most metal cations (33, 36, 38–40).

$[Cu(DMSO)_n]^{2+}$

The enthalpy changes for the association of one, two, and three DMSO molecules and the enthalpy changes for dissociative charge transfer to a DMSO ligand for each of the $[Cu(DMSO)_n]^{2+}$ complexes is shown in Table 2. The association of Cu^{2+} with one DMSO ligand is 975 kJ mol^{-1} exothermic. The exothermicity decreases to 421 kJ mol^{-1} for the second ligand and further still to 258 kJ mol^{-1} for the third. There are no experimental data with which to compare

© 2005 NRC Canada

these values, but several computational studies are extant for other metal cations. In a B3LYP/6-311+G(d,p) calculation, we found the enthalpy change for the association of the closed shell cation Mg^{2+} with DMSO to be –611 kJ mol^{-1} (9). El-Nahas (27) computed the energies of association of Be^{2+}, Mg^{2+}, Ca^{2+}, and Zn^{2+} with formaldehyde, acetone, and DMSO by both ab initio and DFT methods and concluded that DFT overestimates the stability in comparison to CCSD with the same basis set by 40–80 kJ mol^{-1}. The binding energy of $[Zn(DMSO)]^{2+}$ was –715 kJ mol^{-1}. The energy of association of the triply charged Sc^{3+} with DMSO was –1394 kJ mol^{-1}, as expected much higher than that of Cu^{2+} (31).

Electron transfer from ligand to metal cation (eq. [10]) was the major CAD reaction for $[Cu(DMSO)_3]^{2+}$ and is computed to be exothermic by 35.6 kJ mol^{-1}. A Coulomb barrier must ensure the stability of $[Cu(DMSO)_3]^{2+}$ against this process. $[Cu(DMSO)_2]^{2+}$ was observed in the ESI spectrum of the cupric–DMSO aqueous solutions, but $[Cu(DMSO)]^{2+}$ was not. $[Cu(DMSO)_2]^{2+}$ exists in a potential minimum that is higher in energy by 50.2 kJ mol^{-1} than $[Cu(DMSO)]^{+}$ + $DMSO^{+}$ and must be protected by a Coulomb barrier. The potential minimum for $[Cu(DMSO)]^{2+}$ is 197 kJ mol^{-1} higher than for the charge-separated products (Cu^{+} and $DMSO^{+}$). A large enough Coulombic barrier may not be present to afford sufficient stability for the ion to be observed experimentally by the technique of collisionally exciting and hence desolvating more highly solvated doubly charged complexes. The ion might possibly be observed by charge-stripping mass spectrometry commencing with $[Cu(DMSO)]^{+}$, as has been demonstrated for the formation of $[Cu(H_2O)]^{2+}$ and $[Cu(NH_3)]^{2+}$ from $[Cu(H_2O)]^{+}$ and $[Cu(NH_3)]^{+}$, respectively (41).

As noted by Shvartsburg and Wilkes (8) and as observed in this work, unlike most metal dication – DMSO complexes, $[Cu(DMSO)_3]^{2+}$ shows no evidence of methyl loss in its CAD spectrum. Methyl loss is computed to be endothermic by 294 kJ mol^{-1}, a high value that must make competition with dissociative electron transfer to DMSO impossible.

Enthalpy changes for the formation of the CAD products of singly charged Cu(II) complexes

Figure 12 shows the relative standard enthalpy levels of the major CAD products of $[CuX(DMSO)_n]^{+}$. The order of the levels for each complex is, in general, consistent with that observed or surmised by extrapolation of the curves in the energy resolved spectra. For example, it was surmised from Fig. 4 that $[Cu(NO_3)(DMSO)_2]^{+}$ would preferentially lose NO_3 rather than DMSO at low collision energy. Figure 12 is in accord, loss of NO_3 is favored by 29.7 kJ mol^{-1}. $[Cu(NO_3)(DMSO)]^{+}$ is an exception in that the relative enthalpy levels are inconsistent with the spectrum. Although loss of NO_3 is correctly predicted to be the lowest energy path, neither formation of $CuNO_3$ + $DMSO^{+}$ nor of $CuNO_3^{+}$ + DMSO are observed. However the formation of $[CuO(DMSO)]^{+}$ + NO_2, which requires 34.7 kJ mol^{-1} more than the formation of $CuNO_3^{+}$ + DMSO, does occur. Loss of DMSO from $[CuCl(DMSO)_2]^{2+}$ requires 43.5 kJ mol^{-1} more than loss of Cl and becomes the major CAD product above 2 eV collision energy due only to the further decomposition of $[Cu(DMSO)_2]^{+}$ (Fig. 5).

All these results show that electron transfer from X, the less endothermic path for Cu(II) reduction in $[CuX(DMSO)_n]^{+}$ (n = 1 and 2), is energetically favored over the alternate electron transfer from DMSO.

Conclusions

The ESI spectra of dilute aqueous solutions of a cupric salt and DMSO contain Cu(II)–DMSO complexes in two forms. The doubly charged $[Cu(DMSO)_n]^{2+}$ are present as major ions, with n = 3 and 4 prominent, but ions with n up to 11 are observed. $[Cu(DMSO)_2]^{2+}$ is present but with very low intensity, and no $[Cu(DMSO)]^{2+}$ is found under any experimental conditions. In CAD experiments, $[Cu(DMSO)_n]^{2+}$ ($n \geq 4$) decomposes only by loss of neutral DMSO. The only significant primary products of collisional activation of $[Cu(DMSO)_3]^{2+}$ are the Cu(I) ion $[Cu(DMSO)_2]^{+}$ and $DMSO^{+}$. No $[Cu(DMSO)_2]^{2+}$ or $[Cu(DMSO)]^{2+}$ formed by loss of neutral ligand(s) is observed. Computation shows that each of these ions exists at a minimum on the potential energy surface, which may mean that it might be possible to form them with useful intensities by alternate methods. Although the loss of a methyl radical is a ubiquitous process for other doubly charged metal complexes, $[M(DMSO)_3]^{2+}$, no loss of methyl was observed for $[Cu(DMSO)_3]^{2+}$. This is presumably because the endothermicity of methyl loss (294 kJ mol^{-1}) is significantly higher than the Coulomb barrier for dissociative electron transfer from DMSO that is exothermic by 35.6 kJ mol^{-1}.

The second type of Cu(II)–DMSO complex is singly charged and has the form $[CuX(DMSO)_n]^{+}$, where X^{-} is the anion of the cupric salt (Cl^{-}, Br^{-}, NO_3^{-}, or HSO_4^{-}). The CAD spectra, obtained as a function of collision energy, show that for $[CuX(DMSO)_n]^{+}$ (n = 1 or 2) and all X, dissociation by charge retention and charge reduction compete. At the lowest collision energy, electron transfer from X^{-} to Cu^{2+} and loss of neutral X (Cl, Br, NO_3, HSO_4) is the preferred reaction, while at higher collision energy, electron transfer from DMSO to Cu^{2+} can compete. The computed structures of $[CuX(DMSO)_n]^{+}$ (n = 1 or 2) show that the interaction between X and the $S^{\delta+}$–$O^{\delta-}$ dipole influences the orientation of the DMSO ligands and introduces symmetry in the n = 2 complexes.

References

1. T.F. Magnera, G. Caldwell, J. Sunner, S. Ikuta, and P. Kebarle. J. Am. Chem. Soc. **106**, 6140 (1984).
2. U. Onthong, I. Bako, T. Radnai, K. Hermansson, and M. Probst. Int. J. Mass Spectrom. **223–224**, 263 (2003).
3. J. Sunner and P. Kebarle. J. Am. Chem. Soc. **106**, 6135 (1984).
4. A.T. Blades, P. Jayaweera, M.G. Ikonomou, and P. Kebarle. J. Chem. Phys. **92**, 900 (1990).
5. A.T. Blades, P. Jayaweeram, M.G. Ikonomou, and P. Kebarle. Int. J. Mass Spectrom. Ion Processes, **101**, 325 (1990).
6. A.T. Blades, P. Jayaweera, M.G. Ikonomou, and P. Kebarle. Int. J. Mass Spectrom. Ion Processes, **102**, 251 (1990).
7. P. Jayaweera, A.T. Blades, M.G. Ikonomou, and P. Kebarle. J. Am. Chem. Soc. **112**, 2542 (1990).
8. A.A. Shvartsburg and J.G. Wilkes. J. Phys. Chem. A, **106**, 4543 (2002).

© 2005 NRC Canada

9. J.A. Stone, T. Su, and D. Vukomanovic. Int. J. Mass Spectrom. **216**, 219 (2002).
10. A.A. Shvartsburg. J. Am. Chem. Soc. **124**, 12343 (2002).
11. P.T. Szabo and Z. Kele. Rapid Commun. Mass Spectrom. **15**, 2415 (2001).
12. A.A. Shvartsburg, J.G. Wilkes, J.O. Lay, and K.W.M. Siu. Chem. Phys. Lett. **350**, 216 (2001).
13. C. Seto and J.A. Stone. Int. J. Mass Spectrom. Ion Processes, **175**, 263 (1998).
14. J.A. Stone and D. Vukomanovic. Int. J. Mass Spectrom. **185/186/187**, 227 (1999).
15. C. Seto and J.A. Stone. Int. J. Mass Spectrom. **192**, 289 (1999).
16. M.J. Frisch, G.W. Trucks, H.B. Schlegel, G.E. Scuseria, M.A. Robb, J.R. Cheeseman, J.A. Montgomery, Jr., T. Vreven, K.N. Kudin, J.C. Burant, J.M. Millam, S.S. Iyengar, J. Tomasi, V. Barone, B. Mennucci, M. Cossi, G. Scalmani, N. Rega, G.A. Petersson, H. Nakatsuji, M. Hada, M. Ehara, K. Toyota, R. Fukuda, J. Hasegawa, M. Ishida, T. Nakajima, Y. Honda, O. Kitao, H. Nakai, M. Klene, X. Li, J.E. Knox, H.P. Hratchian, J.B. Cross, C. Adamo, J. Jaramillo, R. Gomperts, R.E. Stratmann, O. Yazyev, A.J. Austin, R. Cammi, C. Pomelli, J.W. Ochterski, P.Y. Ayala, K. Morokuma, G.A. Voth, P. Salvador, J.J. Dannenberg, V.G. Zakrzewski, S. Dapprich, A.D. Daniels, M.C. Strain, O. Farkas, D.K. Malick, A.D. Rabuck, K. Raghavachari, J.B. Foresman, J.V. Ortiz, Q. Cui, A.G. Baboul, S. Clifford, J. Cioslowski, B.B. Stefanov, G. Liu, A. Liashenko, P. Piskorz, I. Komaromi, R.L. Martin, D.J. Fox, T. Keith, M.A. Al-Laham, C.Y. Peng, A. Nanayakkara, M. Challacombe, P.M.W. Gill, B. Johnson, W. Chen, M.W. Wong, C. Gonzalez, and J.A. Pople. Gaussian 03. Version 6.0 [computer program]. Gaussian, Inc., Pittsburgh, Penn. 2003.
17. A.P. Scott and L. Radom. J. Phys. Chem. **100**, 16502 (1996).
18. J.A. Stone. Org. Mass Spectrom. **2**8 1119 (1993).
19. R.R. Wright, N.R. Walker, S. Firth, and A.J. Stace. J. Phys. Chem. A, **105**, 54 (2001).
20. A.M. El-Nahas, N. Tajima, and K. Hirao. Chem. Phys. Lett. **318**, 333 (2000).
21. A.M. El-Nahas. Chem. Phys. Lett. **329**, 176 (2000).
22. A.M. El-Nahas, N. Tajima, and K. Hirao. THEOCHEM, **469**, 201 (1999).
23. J.A. Stone and D. Vukomanovic. Chem. Phys. Lett. **346**, 419 (2001).
24. A.A. Shvartsburg and K.W.M. Siu. J. Am. Chem. Soc. **123**, 10071 (2001).
25. D. Schroder, H. Schwarz, J. Wu, and C. Wesdemiotis. Chem. Phys. Lett. **343**, 258 (2001).
26. A. Berces, T. Nakuda, P. Margl, and T. Ziegler. J. Phys. Chem. **103**, 9693 (1999).
27. A.M. El-Nahas. Chem. Phys. Lett. **365**, 251 (2002).
28. A.M. El-Nahas, C. Xiao, and F. Hagelberg. Int. J. Mass Spectrom. **237**, 47 (2004).
29. V. Typke and M. Dakkouri. J. Mol. Struct. **599**, 177 (2001).
30. G. Bouchoux, H.T. Le, and M.T. Nguyen. J. Phys. Chem. A, **105**, 11128 (2001).
31. A.M. El-Nahas. Chem. Phys. Lett. **345**, 325 (2001).
32. M. Pavlov, P.E.M. Siegbahn, and M. Sandstrom. J. Phys. Chem. **102**, 219 (1998).
33. E.D. Glendening and D. Feller. J. Phys. Chem. **100**, 4790 (1996).
34. C. Xiao, F. Hagelberg, and A.M. El-Nahas. J. Phys. Chem. A, **40**, 5322 (2004).
35. H. Deng and P. Kebarle. J. Am. Chem. Soc. **120**, 2925 (1998).
36. S.R. Langhoff, C.W. Bauschlicher, H. Partridge, and M. Sodupe. J. Phys. Chem. **95**, 10677 (1991).
37. B.J. Lynch and D.G. Truhlar. Chem. Phys. Lett. **361**, 251 (2002).
38. R.G. Keesee and A.W. Castleman. J. Phys. Chem. Ref. Data, **15**, 1011 (1986).
39. C.W. Bauschlicher, M. Sodupe, and H. Partridge. J. Phys. Chem. **96**, 4453 (1991).
40. C.W. Bauschlicher, M. Sodupe, and H. Partridge. J. Chem. Phys. **96**, 4453 (1992).
41. D. Schröder, H. Schwarz, J. Wu, and C. Wesdemiotis. Chem. Phys. Lett. **343**, 258 (2001).

© 2005 NRC Canada

Activation of methane by gaseous platinum(II) ions PtX^+ (X = H, Cl, Br, CHO)[1]

Detlef Schröder and Helmut Schwarz

Abstract: The gas-phase reactions of methane with the platinum(II) ions PtX^+ with X = H, Cl, Br, and CHO are studied by mass spectrometry. The PtX^+ ions are generated by electrospray ionization of methanolic solutions of hexachloroplatinic acid and hexabromoplatinic acid, respectively. Small to moderate intramolecular kinetic isotope effects determined for the C—H(D) bond activation of CH_2D_2 suggest that the activation of methane by gaseous PtX^+ cations is subject to thermochemical control by the product channels. In addition, the $PtCl_2^+$ cation is also able to activate methane, whereas $PtCl_3^+$ is unreactive under the conditions chosen.

Key words: gas-phase reactions, mass spectrometry, methane activation, platinum bromide, platinum chloride.

Résumé : Faisant appel à la spectrométrie de masse, on a étudié les réactions en phase gazeuse du méthane avec les ions du platine(II), PtX^+ dans lesquels X = H, Cl, Br et CHO. On a généré les ions PtX^+ par électronébulisation ionique de solutions méthanoliques respectivement d'acide hexachloroplatinique et d'acide d'hexabromoplatinique. Les effets isotopiques cinétiques intramoléculaires allant de faibles à modérés qui ont été observés pour l'activation de la liaison C—H(D) en CH_2D_2 suggèrent que l'activation du méthane par des cations gazeux de PtX^+ est sujette à un contrôle thermochimique par les canaux conduisant aux produits. De plus, le cation $PtCl_2^+$ peut aussi activer le méthane alors que le cation $PtCl_3^+$ n'est pas réactif dans les conditions choisies.

Mots clés : réactions en phase gazeuse, spectrométrie de masse, activation du méthane, bromure de platine, chlorure de platine.

[Traduit par la Rédaction]

Introduction

Platinum can certainly be regarded as the catalytically most active element, as it is capable of mediating a wide variety of reactions, such as hydrogenation as well as dehydrogenation, combustion processes, and the oxidation of ammonia (1, 2). In addition to heterogeneous catalysis, platinum compounds occupy an outstanding position in homogeneous catalysis. In the present context, the Shilov systems are particularly relevant in which platinum(II) species permit the activation of hydrocarbons under ambient conditions (3–6). Accordingly, a number of gas-phase studies on the chemistry of transition metals also dealt with platinum in either neutral or ionic form (7). Small platinum clusters ($Pt_m^{-/0/+}$), for example, whether they are neutral or either anionic or cationic can activate methane to afford the corresponding carbenes $Pt_mCH_2^{-/0/+}$ concomitant with liberation of molecular hydrogen (8–14). Likewise, several covalently bound platinum ions such as $PtCH_2^+$, PtO^+, and PtO_2^+ react with methane under thermal conditions (11, 15, 16). Under fortunate circumstances, these gas-phase studies may even allow predictions for the mechanistic schemes operative in applied catalysis (7, 17–19).

With good reasons, however, it has been argued that gaseous platinum ions such as Pt^+, PtO^+, or PtO_2^+ cannot be regarded as useful models for the catalytically active intermediates in real-life scenarios, as the metal does not occur in its most common oxidation states, i.e., Pt^0, Pt^{II}, Pt^{IV}, and Pt^{VI}. A more appropriate model for the Shilov systems would be, for example, mononuclear platinum halide cations PtX^+ (X = Cl, Br) with or without additional ligand or solvent molecules. Accordingly, we have already previously attempted to generate PtX^+ ions, but failed to achieve reasonable yields of these ions with several types of mass spectrometric approaches. Thus, direct ionization of gaseous PtX_2 is hampered by the high temperatures required for evaporation, higher valent platinum halides are too corrosive for the instrument, and all attempts to generate PtX^+ in ion–molecule reactions of mass-selected Pt^+ with appropriate reagents RX failed (R = CH_3, CH_2X, CHX_2, CX_3, etc.) in that

Received 10 May 2005. Published on the NRC Research Press Web site at http://canjchem.nrc.ca on 21 January 2006.

Dedicated to Paul Kebarle in recognition of his fundamental contributions to many fields of mass spectrometry and gas-phase ion chemistry.

D. Schröder[2] and H. Schwarz.[3] Institut für Chemie der Technischen Universität Berlin, Strasse des 17. Juni 135, D-10623 Berlin, Germany.

[1]This article is part of a Special Issue dedicated to Professor P. Kebarle.
[2]Corresponding author (e-mail: Detlef.Schroeder@tu-berlin.de).
[3]Corresponding author (e-mail: Helmut.Schwarz@mail.chem.tu-berlin.de).

 doi: 10.1139/V05-217 © 2005 NRC Canada

if C—X bond activation takes place at all, it is associated with electron transfer leading to neutral PtX and the corresponding carbenium ion. We note in passing that this finding implies a fairly large ionization energy of PtX, thereby also explaining the difficulties encountered with the generation of PtX^+ (X = Cl, Br). An exception is the reaction of Pt^+ with Cl_2, which affords $PtCl^+$ as ionic product (20), but the usage of molecular chlorine as a reagent is not suitable in the instrumentation available to us.

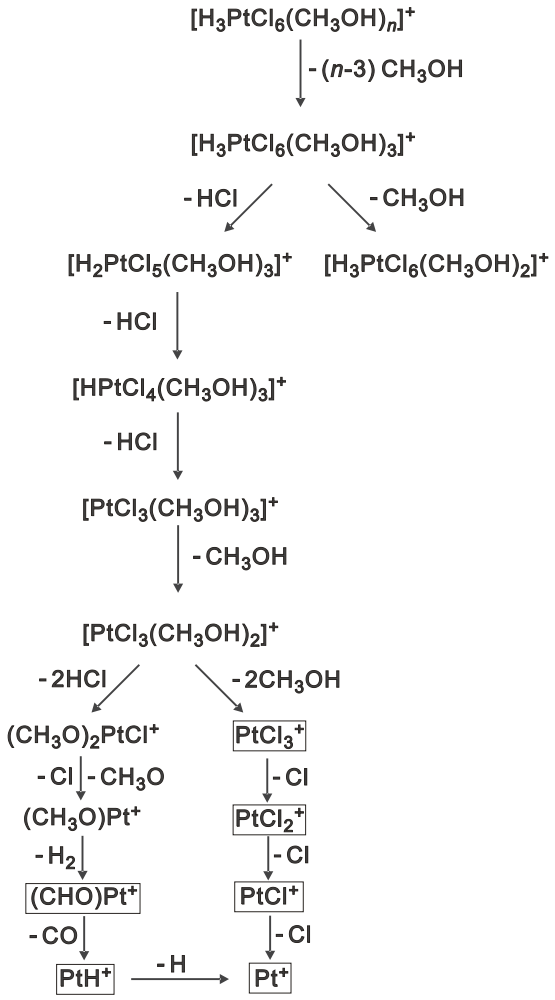
Here, we report a facile and conceptually straightforward route for the generation of PtX^+ cations by means of electrospray ionization (ESI) (21) of transition-metal salts in dilute solution (22, 23), which provides the ions of interest in yields sufficient for subsequent reactivity studies.

Experimental details

The experiments were performed with a VG BIO-Q instrument that consists of an ESI source followed by a mass spectrometer of QHQ configuration (quadrupole, Q; hexapole, H) as described elsewhere (24, 25). In the experiments, mmolar solutions of H_2PtCl_6 in methanol were introduced via a syringe pump (flow rate 5 μL/min) to the fused silica capillary of the ESI source. Nitrogen was used as nebulizing and drying gas at a source temperature of 80 °C. As both platinum as well as chlorine have several isotopes and moreover, depending on the ESI conditions, more or less broad distributions of several ionic species are formed, particular care has to be taken in mass selection to avoid isobaric overlaps. In the case of $PtCl^+$, for example, only the $^{194}Pt^{35}Cl^+$ cation with *m*/*z* 229 is of sufficient purity and intensity for MS/MS experiments, whereas all other $PtCl^+$ isotopes formed under these conditions suffer from isobaric interferences; note that $^{194}Pt^{35}Cl^+$ is inherently accompanied by about 1% of $^{192}Pt^{37}Cl^+$. In the MS/MS studies, the first as well as the second mass analyzer were kept at mass resolutions $m/\Delta m > 500$ to warrant proper mass selection of the reactant ions and an appropriate accuracy in the mass analysis of the ionic products.

For collision-induced dissociation (CID) and ion–molecule reactions, the ions of interest were mass-selected using Q1, interacted with an appropriate neutral gas (ca. 3×10^{-4} mbar, 1 bar = 100 kPa) in the hexapole collision cell, while scanning Q2 to monitor the product ions formed. CID experiments were performed with xenon at various collision energies (E_{Lab} = 0–20 eV), and reactivity studies were conducted at a collision energy nominally set to E_{Lab} = 0 eV. As pointed out previously (24), the VG Bio-Q does not allow direct extraction of quantitative energetic information from these kinds of experiments because of some limitations of the commercial instrument. Even at E_{Lab} = 0 eV, for example, nonnegligible ion decay is observed for weakly bound ions, which is in part attributed to the presence of a collision partner not only in the hexapole, but also in the focusing regions between the mass analyzers. To a first approximation, however, the reactions observed can be ascribed to thermally activated processes, rather than collisionally driven reactions (26–28).

Scheme 1.



Results and discussion

Under mild conditions of ionization, electrospray of a dilute solution of hexachloroplatinic acid (H_2PtCl_6) in methanol–water (1:1) affords cations of the type $[H_3PtCl_6(CH_3OH)_n]^+$ with n = 4–6, which can be regarded as the protonated acid solvated by several methanol molecules. With increasingly harsher ionization conditions, sequential losses of solvent molecules take place as commonly observed in ESI (22, 29). However, for the ion $[H_3PtCl_6(CH_3OH)_3]^+$ formal degradation of the metal halide core via expulsion of HCl can also take place as shown by CID of the mass selected ion (-CH_3OH:-HCl ≈ 2:1). This route continues to be dominant until formation of $[PtCl_3(CH_3OH)_3]^+$ from which homolytic bond cleavages concomitant with the loss of open-shell fragments lead to several Pt-containing ions in yields sufficient for further reactivity studies. The formation of PtH^+ finally occurring under harsh ESI conditions can be rationalized by consecutive fragmentation of $PtOCH_3^+$ and (or) $PtCHO^+$ via β-hydrogen transfer (30–34) concomitant with liberation of formaldehyde and carbon monoxide, respectively. In Scheme 1, a simplified view of the consecutive fragmentation sequences from $[H_3PtCl_6(CH_3OH)_n]^+$ to diatomic PtX^+ species and

© 2005 NRC Canada

Table 1. Reactions of mass-selected PtX^+ cations with methane.

Reaction	Products	x_i[a]	k_{rel}	ϕ_i[b] (%)
$Pt^+ + CH_4$	$PtCH_2^+ + H_2$	100	40	35
$PtH^+ + CH_4$	$PtCH_3^+ + H_2$	100	50	45
$PtCHO^+ + CH_4$			<1[c]	
$PtCl^+ + CH_4$	$PtCH_3^+ + HCl$	100	70	65
$PtCl_2^+ + CH_4$	$ClPtCH_3^+ + HCl$	100	60	55
$PtBr^+ + CH_4$	$BrPtCH_2^+ + H_2$	15	100	90
	$PtCH_3^+ + HBr$	85		
$PtCl_3^+ + CH_4$			<1	

[a]Branching ratio x_i with $\Sigma x_i = 100$.
[b]Reaction efficiencies (ϕ_i) derived from $k_r(Pt^+) = 4.8 \times 10^{-10}$ cm^3 s^{-1} (11–13).
[c]H–D exchange was observed with deuterated methane.

Table 2. Apparent H–D kinetic isotope effects (KIEs) in the reactions of mass-selected PtX^+ cations with [D_2]-methane.

Reaction	Products	KIE[a]
$Pt^+ + CH_4$	$PtCH_2^+ + H_2$	1.70±0.04[b,c], 1.6±0.1[c,d]
$PtH^+ + CH_4$	$PtCH_3^+ + H_2$	1.11±0.05[b,c]
$PtCl^+ + CH_4$	$PtCH_3^+ + HCl$	1.16±0.04
$PtCl_2^+ + CH_4$	$ClPtCH_3^+ + HCl$	1.38±0.04
$PtBr^+ + CH_4$	$BrPtCH_2^+ + H_2$	1.25±0.08[b,c]
	$PtCH_3^+ + Hbr$	1.03±0.03

[a]Determined from the ratios of the isotopologs.
[b]For dehydrogenation, the KIE is determined by assuming a statistical distribution, where the latter assumption is self-consistently confirmed by comparison of the modeled and measured ratios of H_2, HD, and D_2 losses.
[c]In the case of dehydrogenation, the fact that a single KIE per deuterium atom involved can be used to model the ratios of H_2, HD, and D_2 formation further supports the proposed H–D equilibration prior to product formation and moreover, implies that both H(D) atoms involved participate in the rate-determining barrier to a similar extent; also see ref. 11.
[d]KIE found for thermalized Pt^+ in independent ICR experiments; see ref. 11.

even Pt^+ is provided as derived from the evolution of the ion intensities as a function of cone voltage as well as a number of CID experiments. Nevertheless, note that for the pathways shown some alternatives may exist, e.g., the combined elimination of two radicals ($Cl^·$ and $CH_3O·$) in the sequence from $(CH_3O)_2PtCl^+$ to CH_3OPt^+ may also involve elimination of the more stable neutral molecules HCl and CH_2O. Thus, even though the details of ion formation in the course of the ESI process may be quite complex, the key aspect in the present context is that this method of ionization allows the generation of gaseous platinum(II) species in yields fully sufficient for reactivity studies.

The ions of interest, namely, $PtCl_n^+$ (n = 0–3), $PtCHO^+$, and PtH^+, were then mass-selected by means of the first quadrupole Q1, reacted with several neutral reagents admitted to the hexapole collision cell at a collision energy nominally set to 0 eV, and the product ions were detected by scanning the second quadrupole analyzer Q2. Likewise, the platinum bromide cation $PtBr^+$ was generated by ESI of a diluted solution of hexabromoplatinic acid. Given the enormous interest in metal-mediated C—H bond activations (3–7), the first and obvious choice as a neutral reagent is methane, and it is indeed found that most of the ions investigated efficiently react with methane (Table 1). In the multipole mass spectrometer used in the present experiments, a direct measurement of absolute rate constant is difficult. However, the amount of conversion of the different precursor ions at given static pressures of the neutral reagent can be used for the determination of relative rate constants (k_{rel}) (26–28, 35). In the present case, the well-studied reaction of bare Pt^+ with methane (9–17) may further be used as a reference for the conversion of the relative into absolute rate constants (k_r); hence, reaction efficiencies (ϕ), defined as the ratio of k_r and the gas-kinetic collision rate (k_c) calculated from capture theory (36), can also be derived.

Bare Pt^+ reacts with methane via a formal oxidative addition to first afford the insertion product $H\text{-}Pt^+\text{-}CH_3$ and subsequently $PtCH_2^+$ and molecular hydrogen associated with a change of the formal oxidation state from Pt^I in atomic Pt^+ to Pt^{III} in the platinum carbene cation. In contrast, the reactions of the PtX^+ cations studied here occur as a formal substitution concomitant with loss of neutral HX, thereby retaining the oxidation state Pt^{II} in reactants and products. Likewise, formal substitution is observed with $PtCl_2^+$, whereas the $PtCl_3^+$ cation does not react with methane to a notable amount, even though of all ions studied here platinum has the highest formal valence in $PtCl_3^+$. A direct conclusion about the reaction mechanisms cannot be inferred from this observation, however, because the lack of reactivity towards CH_4 may be either due to thermochemical or kinetic reasons. While $PtCHO^+$ also does not react with CH_4, occurrence of H/D exchange with labeled methane indicates that activation itself is feasible. Absence of products other than the reactants, such as $PtCH_3^+ + CH_2O$, for example, is therefore most likely because of a lack of thermochemical driving force. For $PtBr^+$, oxidative addition is inferred to a small extent, as indicated by the side reaction leading to dehydrogenation concomitant with the formation of the bromo platinum carbene cation $BrPtCH_2^+$.

As another probe for reactivity, the reactions with partially deuterated methane (CH_2D_2) were investigated for which the ratio of isotopologous products can be regarded as a direct measure for the intramolecular kinetic isotope effect associated with C—H(D) bond activation (Table 2). Analysis of the isotope patterns results in comparably small kinetic isotope effects (KIEs; here, defined as KIE = k_H/k_D) and moreover, H–D equilibration is observed for the reaction of PtH^+ with CH_2D_2 in that H_2, HD, as well as D_2 are lost as neutral molecules. The experimentally found isotope patterns can be modeled with the KIEs given in Table 2 by taking into account the corresponding statistical weights (11).

For the reaction of $PtCl^+$ with methane, the thermochemical data derived by Armentrout and co-workers (13, 20) also provide more detailed energetic insight. Thus, the bond dissociation energy $D(Pt^+—Cl)$ = 2.55 ± 0.15 eV (20) in conjunction with $D(H—CH_3)$ = 4.48 ± 0.01 eV and $D(H—Cl)$ = 4.43 ± 0.01 eV from supplementary thermochemical data (37), as well as $D(Pt^+—CH_3)$ = 2.67 ± 0.08 eV (13), imply a total exothermicity of 0.07 ± 0.17 eV for bond activation of methane according to rxn. [1].

[1] $PtCl^+ + CH_4 \rightarrow PtCH_3^+ + HCl$

[2] $PtH^+ + CH_4 \rightarrow PtCH_3^+ + H_2$

© 2005 NRC Canada

In contrast, activation of methane by PtH^+ according to rxn. [2] is predicted to bear a slight endothermicity of 0.13 ± 0.09 eV (13, 20), which is, nevertheless, within the margin of ion–molecule reactions occurring under thermal conditions (38). Note, however, that the formation of PtH^+ under the harsh conditions of electrospray ionization can also be associated with some excess energy content in the cations mass-selected from the ESI source (27). Nevertheless, the near thermoneutrality of the reactions in conjunction with the low KIEs observed with partially labeled methane indicate that the bond activation of methane by PtX^+ cations is primarily subject to thermochemical control of the exit channels, as also predicted by theory for the reaction of bare Pt^+ with methane (12, 13, 15). As far as the reaction mechanism is concerned, the present results do not permit a distinction whether or not oxidative addition to an $XPt(H)(CH_3)^+$ intermediate is operative in the course of the formal substitution reactions. Furthermore, theoretical studies of related systems have predicted quite low reaction barriers for the direct electrophilic substitution of methane by PtX species, thus a route with parallel H—X as well as Pt—C bond formation, without involving a change of the metal's oxidation state (39–41). In fact, with regard to the low kinetic isotope effect observed, the mechanism of the gas-phase processes described here is most likely difficult to assess by experimental means for the time being, and instead adequate theoretical studies might provide more detailed insight.

Given the facile activation of methane by most of the PtX^+ cations investigated, the reactions of $PtCl^+$ with some other substrates were explored briefly. Thus, $PtCl^+$ reacts with molecular hydrogen to afford PtH^+ according to rxn. [3] for which an exothermicity of 0.25 ± 0.16 eV is predicted from literature thermochemistry (13, 20, 37). With a larger hydrocarbon substrate such as propane, single and multiple C—H bond activations (rxns. [4*a*] and [4*b*]), as well as a small amount of C—C bond cleavage (rxn. [4*c*]), are observed with a branching ratio of [4*a*]:[4*b*]:[4*c*] ≈ 5:90:5.

$$[3] \quad PtCl^+ + H_2 \rightarrow PtH^+ + HCl$$

$$[4a] \quad PtCl^+ + C_3H_8 \rightarrow PtC_3H_7^+ + HCl$$

$$[4b] \quad \rightarrow PtC_3H_5^+ + HCl + H_2$$

$$[4c] \quad \rightarrow PtC_2H_3^+ + HCl + CH_4$$

Similarly, multiple C—H bond activation prevails in the reaction of mass-selected $PtCl^+$ with isomeric butenes, which afford $PtC_4H_5^+$ as the major product ion. Likewise, PtH^+ as well as $PtBr^+$ react with these hydrocarbons via multiple dehydrogenation, indicating the high reactivity of gaseous Pt^{II} cations for the activation of hydrocarbons.

Conclusions

Electrospray ionization can be used for the efficient generation of reactive PtX^+ cations in the gas phase, which are difficult to produce by other means. Reactivity studies of mass-selected PtX^+ reveal that these species are able to activate hydrocarbons including methane. Thermochemical considerations as well as the kinetic isotope effects associated with the C—H(D) bond activation of CH_2D_2 suggest that the reactions are subject to thermochemical control by the product channels. In a more general perspective, the present gas-phase studies imply that cationic species might also play a distinct role in C—H bond activation of alkanes in the condensed phase, for example, as in the system $Pt^{(II)}$–H_2SO_4–CH_4 developed by Periana et al. (42).

Acknowledgments

Financial support by the Deutsche Forschungsgemeinschaft, the Sonderforschungsbereich 546, the Fonds der Chemischen Industrie, and the Degussa AG is gratefully acknowledged.

References

1. J.H. Lunsford. Catal. Today, **63**, 165 (2000).
2. P. Gélin and M. Primet. Appl. Catal. B, **39**, 1 (2002).
3. A.E. Shilov. Activation of saturated hydrocarbons by transition metal complexes. Reidel, Dordrecht. 1984.
4. J.A. Labinger and J.E. Bercaw. Nature (London), **417**, 507 (2002).
5. M. Lersch and M. Tilset. Chem. Rev. **105**, 2471 (2005).
6. J.A. Labinger. J. Mol. Catal. A, **220**, 27 (2004).
7. D.K. Böhme and H. Schwarz. Angew. Chem. **117**, 2388 (2005); Angew. Chem. Int. Ed. **44**, 2336 (2005).
8. A. Kaldor and D.M. Cox. Pure Appl. Chem. **62**, 79 (1990).
9. K.K. Irikura and J.L. Beauchamp. J. Am. Chem. Soc. **113**, 2769 (1991).
10. K.K. Irikura and J.L. Beauchamp. J. Phys. Chem. **95**, 8344 (1991).
11. R. Wesendrup, D. Schröder, and H. Schwarz. Angew. Chem. **106**, 1232 (1994); Angew. Chem. Int. Ed. Engl. **33**, 1174 (1994).
12. U. Achatz, C. Berg, S. Joos, B.S. Fox, M.K. Beyer, G. Niedner-Schatteburg, and V.E. Bondybey. Chem. Phys. Lett. **320**, 53 (2000).
13. X.G. Zhang, R. Liyanage, and P.B. Armentrout. J. Am. Chem. Soc. **123**, 5563 (2001).
14. K. Koszinowski, D. Schröder, and H. Schwarz. J. Phys. Chem. A, **107**, 4999 (2003).
15. M. Pavlov, M.R.A. Blomberg, P.E.M. Siegbahn, R. Wesendrup, C. Heinemann, and H. Schwarz. J. Phys. Chem. **101**, 1567 (1997).
16. M. Brönstrup, D. Schröder, I. Kretzschmar, H. Schwarz, and J.N. Harvey. J. Am. Chem. Soc. **123**, 142 (2001).
17. M. Aschi, M. Brönstrup, M. Diefenbach, J.N. Harvey, D. Schröder, and H. Schwarz. Angew. Chem. **110**, 858 (1998); Angew. Chem. Int. Ed. **37**, 829 (1998).
18. M. Diefenbach, M. Brönstrup, M. Aschi, D. Schröder, and H. Schwarz. J. Am. Chem. Soc. **121**, 10614 (1999).
19. K. Koszinowski, D. Schröder, and H. Schwarz. Organometallics, **22**, 3809 (2003).
20. R. Liyanage, M.L. Styles, R.A.J. O'Hair, and P.B. Armentrout. J. Phys. Chem. A, **107**, 10303 (2003).
21. J.B. Fenn, M. Mann, C.K. Meng, S.F. Wong, and C.M. Whitehouse. Science (Washington, D.C.), **246**, 64 (1989).
22. P. Jawaweera, A.T. Blades, M.G. Ikonomou, and P. Kebarle. J. Am. Chem. Soc. **112**, 2452 (1990).
23. M. Peschke, A.T. Blades, and P. Kebarle. J. Am. Chem. Soc. **122**, 10440 (2000).
24. D. Schröder, T. Weiske, and H. Schwarz. Int. J. Mass Spectrom. **219**, 729 (2002).
25. N.G. Tsierkezos, D. Schröder, and H. Schwarz. J. Phys. Chem. A, **107**, 9575 (2003).

© 2005 NRC Canada

26. D. Schröder, H. Schwarz, S. Schenk, and E. Anders. Angew. Chem. **115**, 5241 (2003); Angew. Chem. Int. Ed. **42**, 5087 (2003).
27. D. Schröder, M. Engeser, M. Brönstrup, C. Daniel, J. Spandl, and H. Hartl. Int. J. Mass Spectrom. **228**, 743 (2003).
28. D. Schröder, M.C. Holthausen, and H. Schwarz. J. Phys. Chem. B, **108**, 14407 (2004).
29. M. Kohler and J.A. Leary. Int. J. Mass Spectrom. Ion Processes, **162**, 17 (1997).
30. C.J. Cassady, B.S. Freiser, S.W. McElvany, and J. Allison. J. Am. Chem. Soc. **106**, 6125 (1984).
31. C.J. Cassady and B.S. Freiser. J. Am. Chem. Soc. **107**, 1566 (1985).
32. C.J. Cassady and B.S. Freiser. J. Am. Chem. Soc. **107**, 1573 (1985).
33. D. Schröder and H. Schwarz. Angew. Chem. **102**, 925 (1990); Angew. Chem. Int. Ed. Engl. **29**, 910 (1990).
34. A. Fiedler, D. Schröder, H. Schwarz, B.L. Tjelta, and P.B. Armentrout. J. Am. Chem. Soc. **118**, 5047 (1996).
35. C. Trage. Dissertation, Technische Universität Berlin, Berlin. 2005. p. D83.
36. T. Su. J. Chem. Phys. **88**, 4102 (1988); **89**, 5355 (1988).
37. J. Berkowitz, G.B. Ellison, and D. Gutman. J. Phys. Chem. **98**, 2744 (1994).
38. G. Bouchoux, D. Leblanc, and M. Sablier. Int. J. Mass Spectrom. **210/211**, 189 (2001), and refs. cited therein.
39. P.E.M. Siegbahn and R.H. Crabtree. J. Am. Chem. Soc. **118**, 4442 (1996).
40. J. Kua, X. Xu, R.A. Periana, and W.A. Goddard III. Organometallics, **21**, 511 (2002).
41. Also see: J. Schwarz, D. Schröder, H. Schwarz, C. Heinemann, and J. Hrušák. Helv. Chim. Acta, **79**, 1110 (1996).
42. R.A. Periana, D.J. Taube, S. Gamble, H. Taube, T. Satoh, and H. Fujii. Science (Washington, D.C.), **280**, 560 (1998).

© 2005 NRC Canada

Carbonate, carbamate, urea, and guanidine as model species for functional groups in biological molecules — A combined density functional theory and mass spectrometry examination of polysodiation and gas-phase dissociation[1]

Tujin Shi, Junfang Zhao, P.Y. Iris Shek, Alan C. Hopkinson, and K.W. Michael Siu

Abstract: Electrospray mass spectrometric analyses of carbonate, carbamate, urea, and guanidine in the presence of sodium ions results in polysodiated complexes of the type, $[M - (n - 1)H + nNa]^+$, where M is the species analyzed and $n = 2$ and (or) 3. These complexes are unusual in their high sodium contents and their attractive structures. The $[M - H + 2Na]^+$ complexes fragment to produce $[Na_2NH_2]^+$, Na^+, and a product ion resulting from the loss of NH_3. The $[M - 2H + 3Na]^+$ complexes dissociate to give a number of fragment ions, including $[Na_3O]^+$, $[Na_2OH]^+$, $[NaOCNNa]^+$, $[Na_2NH_2]^+$, $[Na_3CN_2]^+$, and Na^+, depending on the elemental composition of M. These dissociation reactions were examined both experimentally by mass spectrometry and theoretically by density functional theory. Reaction profiles as calculated at B3LYP/6-311G** for disodiated carabamate, urea, and guanidine, and for all the bases in trisodiated form are given. Both experimental and theory show $[Na_3CO_3]^+$ to have high stability towards collisional activation and to preferentially dissociate to give $[Na_3O]^+$ and CO_2, rather than Na^+ and Na_2CO_3.

Key words: carbonate, carbamate, urea, guanidine, electrospray, collision-induced dissociation, density functional theory, sodium ion binding energies.

Résumé : Les analyses par spectrométrie de masse avec ionisation par électronébulisation des carbonates, des carbamates, de l'urée et de la guanidine en présence d'ions sodium conduit à la formation de complexes polysodés du type $[M - (n - 1)H + nNa]^+$ dans lesquels M est l'espèce analysée et $n = 2$ et (ou) 3. Ces complexes sont inhabituels en raison de leur teneur élevée en sodium et leurs structures intéressantes. Les complexes $[M - H + 2Na]^+$ se fragmentent pour conduire à la formation de $[Na_2NH_2]^+$, Na^+ et un ion qui résulte de la perte de NH_3. Les complexes $[M - 2H + 3Na]^+$ se dissocient pour donner, suivant la composition élémentaire de M, un certain nombre de fragments ioniques, dont le $[Na_3O]^+$, le $[Na_2OH]^+$, le $[NaOCNNa]^+$, le $[Na_2NH_2]^+$, le $[Na_3CN_2]^+$ et le Na^+. On a étudié ces réactions de dissociation tant d'une façon expérimentale par spectrométrie de masse que d'une façon théorie par la théorie de la densité fonctionnelle. On rapporte les profils de réaction calculés au niveau B3LYP/6-311G** pour le carbamate, l'urée et la guanidine sous la forme disodée et pour toutes les bases sous la forme trisodée. Les résultats tant expérimentaux que théoriques montrent que le $[Na_3CO_3]^+$ est très stable vis-à-vis des activations par collision et qu'il se dissocie d'une façon privilégiée pour donner du $[Na_3O]^+$ et du CO_2 plutôt que du Na^+ et du Na_2CO_3.

Mots clés : carbonate, carbamate, urée, guanidine, électronébulisation, dissociation induite par une collision, théorie de la densité fonctionnelle, énergie de fixation de l'ion sodium.

[Traduit par la Rédaction]

Introduction

The sodium ion is ubiquitous in biology. It plays many roles and has many important functions; these include regulating metabolism and signaling through trans-membrane concentration gradients, and stabilizing the structure of proteins and membranes (1–4). To carry out its regulatory and structural functions, the sodium ion must interact with the appropriate peptides or proteins. This interaction is specific and can be quite complex as peptides and proteins are

Received 12 June 2005. Published on the NRC Research Press Web site at http://canjchem.nrc.ca on 21 January 2006.

In honour of Paul Kebarle, in recognition of his major contributions in the areas of mass spectrometry, gas-phase ion chemistry, and thermochemistry.

T. Shi, J. Zhao, P.Y.I. Shek, A.C. Hopkinson, and K.W.M. Siu.[2] Department of Chemistry and Centre for Research in Mass Spectrometry, York University, 4700 Keele Street, Toronto, ON M3J 1P3, Canada.

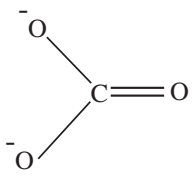
[1]This article is part of a Special Issue dedicated to Professor P. Kebarle.
[2]Corresponding author (e-mail: kwmsiu@yorku.ca).

 doi: 10.1139/V05-204 © 2005 NRC Canada

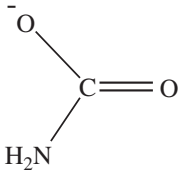
multifunctional molecules with several to many potential binding sites. By contrast, nonspecific sodium binding, resulting in the complexes $[M - (n - 1)H + nNa]^+$ (where M = the peptide or protein), is often observed when a peptide or protein is analyzed using electrospray mass spectrometry (MS), especially in the presence of sodium hydroxide or a sodium salt (5–8). Rodriquez et al. (6, 7) postulated that these polysodiated ions are formed in the lens region of the mass spectrometer as a result of gas-phase reactions: the relative yield of the $[M - (n - 1)H + nNa]^+$ complexes increases with increasing collision energy in the lens region, in accordance with the interpretation of their gas-phase origin. It was shown that substitution reactions are a consequence of amidic and carboxylic protons being replaced by Na^+. Indeed, hexaglycine forms a series of $[M - (n - 1)H + nNa]^+$ complexes; the complex with the largest n, $[M - 6H + 7Na]^+$, has all its five amidic protons and one carboxylic proton replaced by six Na^+ with the seventh Na^+ "ionizing" the peptide (8). Na^+ substitution for amidic protons has also been observed in dinucleotides containing guanine and thymine (9).

Ion affinities, properties that reveal intrinsic binding strengths unencumbered by solvation, are often measured with mass spectrometry (10). Sodium ion affinities of amino acids have been reported (11–17). Kebarle and co-workers (12) were the first to report the Na^+ affinity of diglycine, measured using the threshold collision-induced dissociation (CID) technique. This work was followed by others that examined more complex peptides.

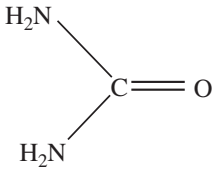
Here we report a combined mass spectrometric and density functional theory examination of the polysodiation of four model species — carbonate (CN), carbamate (CM), urea (UR), and guanidine (GU) — that mimic functional groups on peptides and the nucleobases, guanine, cytosine, and thymine. Polysodiation results in novel and attractive structures that dissociate to give interesting, highly sodiated products.



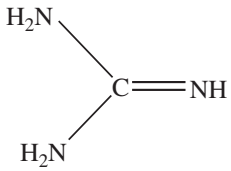
CN



CM



UR



GU

Experimental section

Mass spectrometry

Experiments were performed on MDS SCIEX (Concord, Ontario) triple-quadrupole mass spectrometers, API III and a prototype of the API 3000. Samples were 50 μmol/L model species and 200 μmol/L sodium nitrate at typically pH 12 (adjusted with sodium hydroxide) in water–methanol (50:50). All chemicals and solvents were available from Sigma-Aldrich (St. Louis, Missouri). Sample solutions were introduced into the ion source via pneumatically assisted electrospray at a typical flow rate of 3 μL/min. The lens voltages, including the orifice voltage, were optimized to produce optimal abundance of $[M - (n - 1)H + nNa]^+$ ($n \leq 3$) complexes. MS/MS experiments were performed by mass selecting the precursor ions using the first quadrupole mass analyzer (Q1), colliding them with argon (API III) or nitrogen (API 3000) in the second quadrupole (Q2), and mass analyzing with the third quadrupole (Q3). Energy-resolved CID experiments were performed under on-average, single-collision conditions on only the API III.

Computations

Density functional theory calculations were implemented with Gaussian 98 (18). Geometry optimization and energy calculations were performed using the B3LYP exchange correlation functional (19–21) with the 6-311G** triply split valence basis set (22–25). All stationary points were characterized by harmonic vibrational frequency calculations. Connections between transition states and corresponding minima were verified using the intrinsic reaction coordinate (IRC) method developed by Gonzalez and Schlegel (26, 27). Relative enthalpies at 0 K (ΔH_0°) are reported and used to compare relative energies. Natural population atomic (NPA) charges were determined using the natural bond orbital analysis of Reed, Weinhold, and co-workers (28–31). Cartesian coordinates and electronic energies for key structures are available as Supplementary material.[3]

Results and discussion

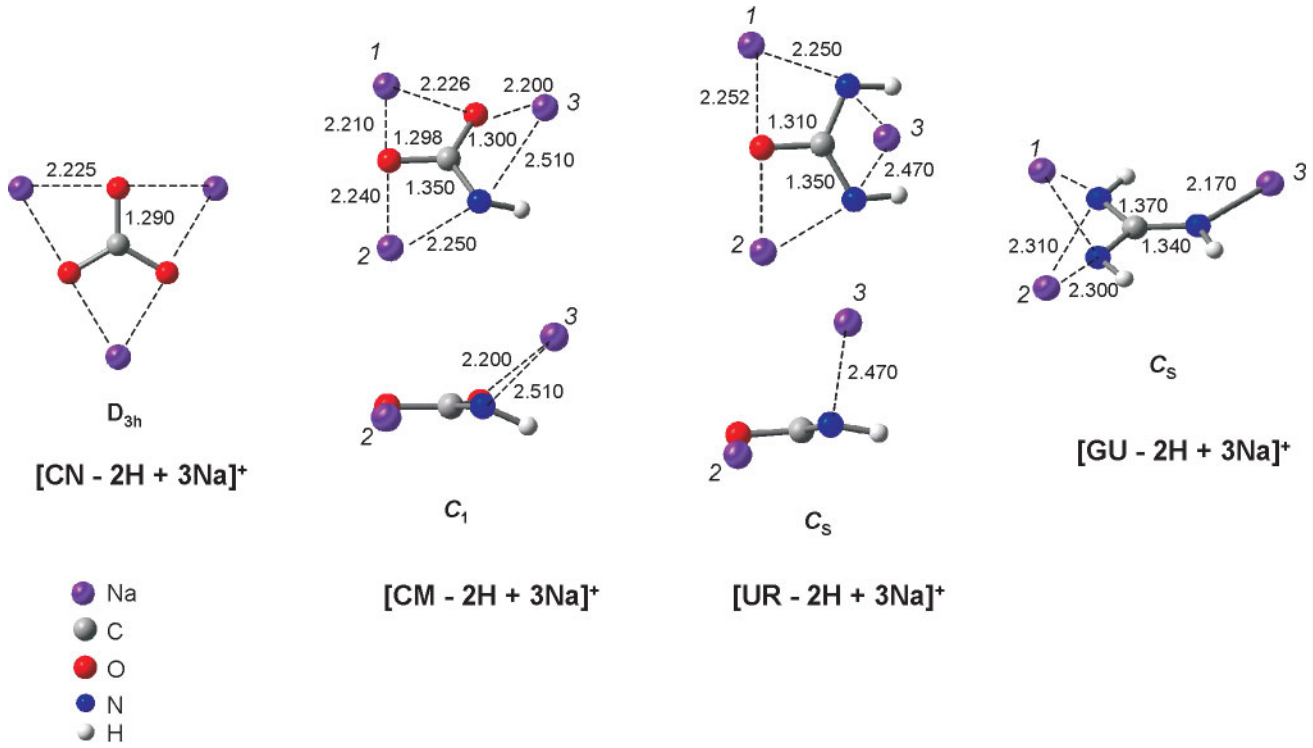
Polysodiated complexes

Electrospraying a solution of the model species in the presence of Na^+ produces abundant sodiated complexes. The relative abundances of the $[M - (n - 1)H + nNa]^+$ complexes for $n = 2$ and 3 increase with collision energy in the lens region, which is in accordance with previous observations (6–8) and is in direct support of a gas-phase origin of these polysodiated complexes. In short, the electrosprayed ions react with sodium hydroxide or sodium salt in the ion source and (or) the lens region of the mass spectrometer, which results in substitution of a carboxylic or amidic proton by a Na^+, in addition to ionization via direct sodiation (6–8). The

[3] Supplementary data for this article are available on the Web site or may be purchased from the Depository of Unpublished Data, Document Delivery, CISTI, National Research Council Canada, Ottawa, ON K1A 0R6, Canada. DUD 4065. For more information on obtaining material refer to http://cisti-icist.nrc-cnrc.gc.ca/irm/unpub_e.shtml.

© 2005 NRC Canada

Fig. 1. The optimized structures of $[M - 2H + 3Na]^+$ for M = carbonate (CN), carbamate (CM), urea (UR), and guanidine (GU) calculated at the B3LYP/6-311G** level. Bond distances are in angstroms. Italicized numbers are referred to in the text for distinguishing sodium atoms.



maximum number of sodium atoms incorporated observed in this study is three, which results in sodium binding to each O and N atom in the four model species — carbonate, carbamate, urea, and guanidine. Three of the four resulting $[M - 2H + 3Na]^+$ complexes have high degrees of symmetry resulting in interesting structures (Fig. 1).

$[CN - 2H + 3Na]^+$ has several unusual geometric and electronic structural features. It is planar with each sodium equidistant from two oxygen atoms, i.e., the ion has D_{3h} symmetry. The atoms in Na-O-Na are essentially collinear (angle 179.7°) and the Na—O distances are 2.225 Å; these compare with an angle of 180° and a Na—O distance of 1.980 Å in the triatomic molecule Na_2O. NPA analysis gave charges of +0.95 on the sodium atoms, –0.95 on the oxygen atoms, and +1.00 on the carbon. There are three occupied π orbitals in the valence shell, an a_2''-type and doubly degenerate e_2''-types. The latter have nodes passing through the carbon atom and the contribution from the carbon atom to the a_2'' orbital is 0.80 *e*; hence the majority of the π-electron density is on the oxygen and sodium atoms on the perimeter. $[CN - 2H + 3Na]^+$ has remarkable stability, as will be discussed in terms of Na^+ binding energies, and it is tempting to suggest that this stability is attributable to the presence of some aromatic character.

$[CM - 2H + 3Na]^+$ belongs to the C_1 point group. The O, C, and N atoms are close to being coplanar. Na_1 and Na_2 are just below the "plane". The hydrogen atom is also below, whereas Na_3 is above, the plane. Interestingly, the three Na atoms carry an identical charge of +0.94, almost identical to the charge on Na in $[CN - 2H + 3Na]^+$. $[UR - 2H + 3Na]^+$ has C_s geometry. The plane of symmetry contains the O, C, and Na_3 atoms. The O, C, and the two N atoms are essentially coplanar, in a plane that is perpendicular to the C_s plane. Na_1 and Na_2 have a charge of +0.93 and lie just below the former plane, whereas Na_3 (+0.95 charge) lies above it. $[GU - 2H + 3Na]^+$ also has C_s geometry with the plane of symmetry containing the C, the three H, the three N, and Na_3 atoms. Na_1 lies above, whereas Na_2 lies below, this plane. Both Na_1 and Na_2 carry a charge of +0.92; Na_3 is almost identically charged at +0.93.

Table 1. Na^+ binding energies (kcal/mol) as calculated at B3LYP/6-311G**.

Molecule	Monosodiated	Disodiated	Trisodiated
Carbonate	NA[a]	NA	79.4
Carbamate	NA	47.4	63.6
Urea	43.7	51.8	58.2
Guanidine	42.8	52.7	62.2

[a]NA = not detected experimentally and not calculated.

$[M + Na]^+$ and $[M - H + 2Na]^+$ complexes

Under appropriate conditions, fairly abundant $[M + Na]^+$ complexes were observed for urea and guanidine. The CID of these complexes is uninteresting, as the only product ion observed was Na^+. In all these structures, the charge on Na was calculated to be +0.94 ± 0.01. Na^+ binding energies were calculated to be 43.7 and 42.8 (see Table 1). Possible alternative pathways to dissociation, loss of NH_3 (see later), although not observed here, were calculated to have barriers of 50.8 and 48.9 kcal/mol for M = UR and GU, respectively.

Abundant $[M - H + 2Na]^+$ complexes were observed for carbamate, urea, and guanidine. CID of these complexes re-

© 2005 NRC Canada

Fig. 2. Dissociation of [UR – H + 2Na]$^+$. (*a*) Energy-resolved CID plots; the inset shows low-energy details; (*b*) CID spectrum at a laboratory collision energy of 10 eV; and (*c*) reaction profiles. Bond distances are in angstroms, relative energies are ΔH°_0 in kcal/mol, and transition states are indicated as such by ‡.

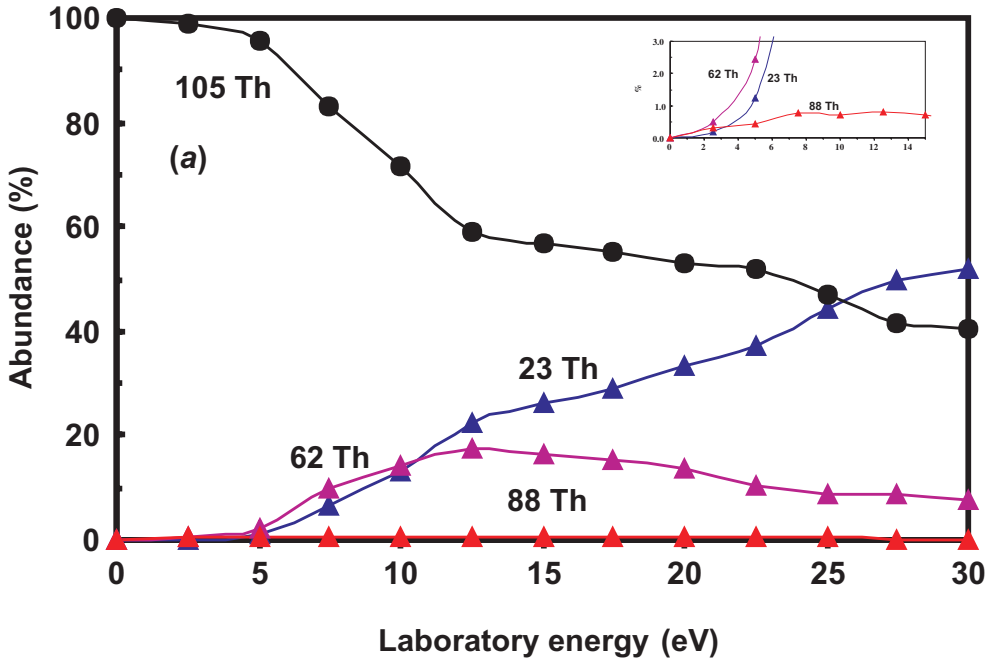
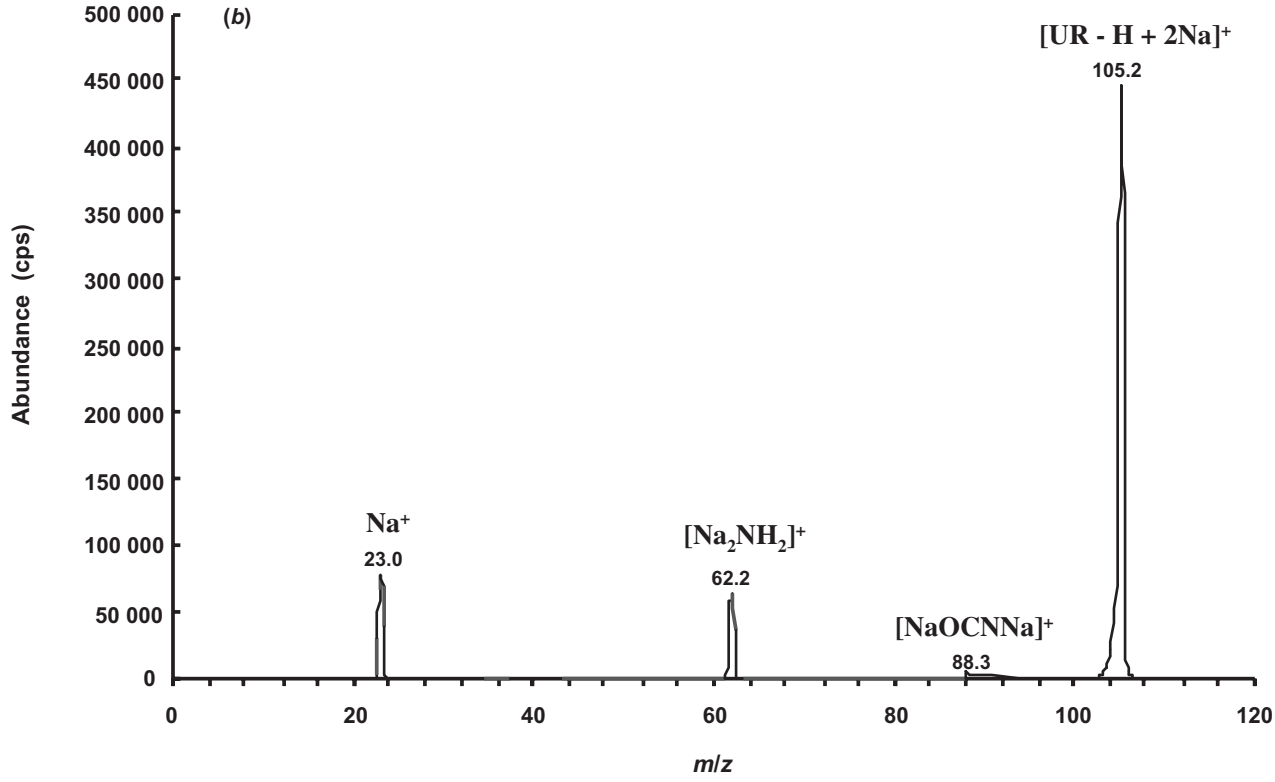


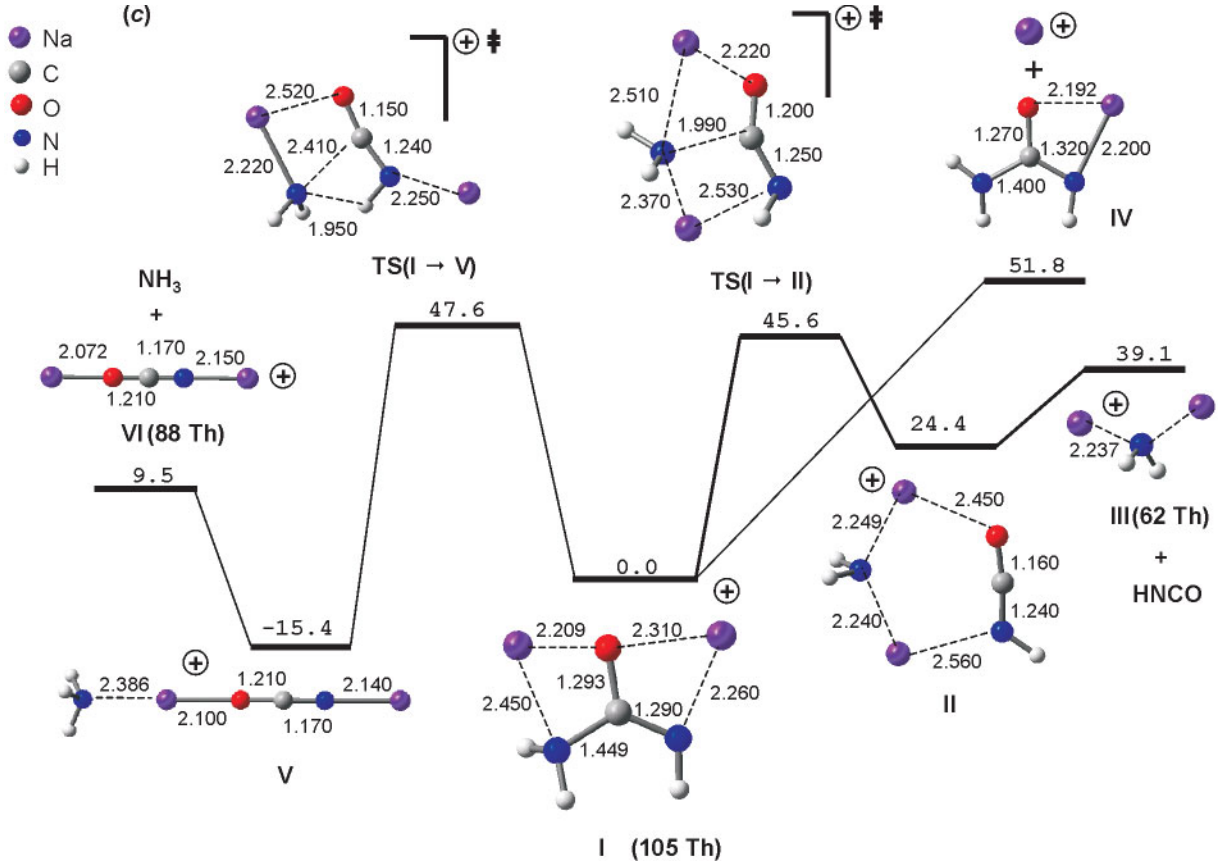
Fig. 2 (*b*).



sults in the observation of Na^+ (23 Th), $[Na_2NH_2]^+$ (62 Th), and a product ion resulting from the loss of NH_3. The last reaction is not observed in carbamate as it contains only two hydrogen atoms. Figure 2*a* shows the energy-resolved CID results for [UR – H + 2Na]$^+$; the CID spectrum at a laboratory collision energy of 10 eV is shown in Fig. 2*b*. The dissociation reaction to give $[Na_2NH_2]^+$ appears to require the least amount of energy, followed by that to give $[NaOCNNa]^+$. This latter product ion at 88 Th, resulting from elimination of NH_3, has a low abundance (<1%) under all energies. Na^+ is formed at slightly higher energies and becomes the dominant product at high collision energy (see

© 2005 NRC Canada

Fig. 2 (*c*).



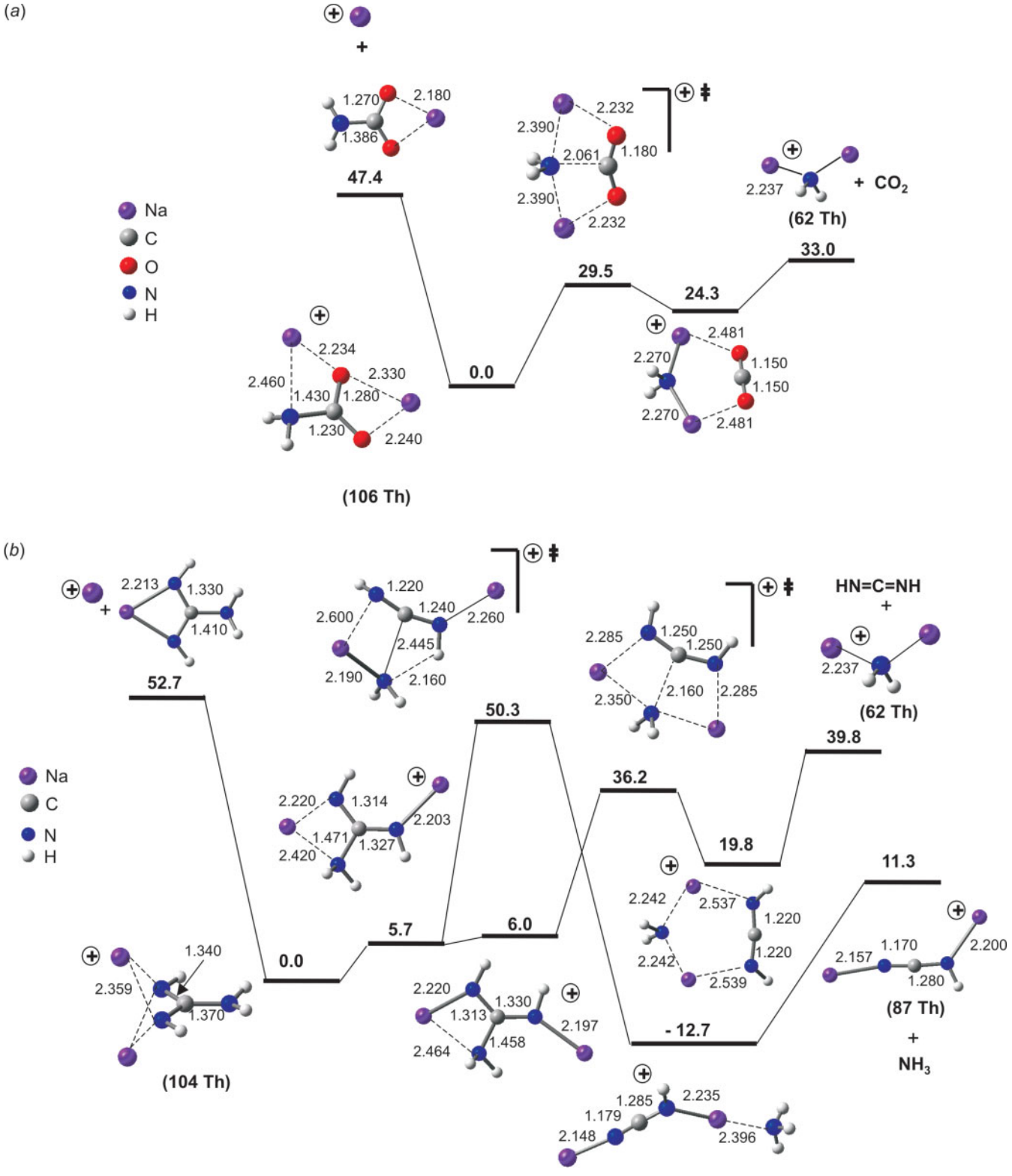
the inset in Fig. 2*a* for details). The abundance of the $[Na_2NH_2]^+$ ion maximizes at about 12.5 eV and decreases substantially at higher energies. By contrast, the abundance of Na^+ increases with increasing collision energy, initially more steeply between 5 and 12.5 eV, and then more gently between 12.5 and 30 eV. These observations are indicative that $[Na_2NH_2]^+$ dissociates to Na^+ at laboratory energies above 12.5 eV.

Figure 2*c* shows the reaction profiles for the dissociation of $[UR - H + 2Na]^+$ (structure **I**). Formation of $[Na_2NH_2]^+$ initially requires a Na^+ transfer resulting in both Na being bound to $-NH_2$ to give structure **II**, an ion–neutral complex in which $[Na_2NH_2]^+$ is solvated by HNCO. Separation of the parts yields **III**, $[Na_2NH_2]^+$, and HNCO. The transition state (**TS(I→II)**) lies 45.6 kcal/mol (1 cal = 4.184 J) above **I** and is higher than the products of dissociation. Fragmentation of **I** to Na^+ and structure **IV** does not have a transition state; the endothermicity of this reaction is 51.8 kcal/mol. Elimination of NH_3 from **I** requires transfer of the -NH proton to $-NH_2$ to give **V**, which is $[NaOCNNa]^+$ solvated by NH_3. Separating the ion–neutral complex results in ion **VI** and NH_3. The transition state (**TS(I→V)**) lies 47.6 kcal/mol above **I**. Of the three reaction pathways, formation of $[Na_2NH_2]^+$ has the lowest activation energy, which is in qualitative agreement with the experimental results shown in Fig. 2*a*.[4] Formation of Na^+, the process shown to have the highest energy experimentally, requires only an additional 6.2 kcal/mol (~0.3 eV) and is calculated to be 8.1 kcal/mol higher than the dissociation energy of $[UR + Na]^+$. The sodium ion affinity of $NaNH_2$ is 60.3 kcal/mol, higher than the sodium ion affinity of **IV**, by only 8.5 kcal/mol. Under high CID energies (>12.5 eV), dissociation of $[Na_2NH_2]^+$ is apparent. By contrast, the sodium ion affinity of NaOCN is 52.9 kcal/mol, which is lower than the affinity of $NaNH_2$ by 7.4 kcal/mol. In addition, the products **VI** and NH_3 lie 38.1 kcal/mol below the critical transition state (**TS(I→V)**), which leads to their formation. This value is considerably larger than the difference of 6.5 kcal/mol between the energy of products **III**, $[Na_2NH_2]^+$, plus HNCO, and **TS(I→II)**, the corresponding critical transition state. This means that nascent $[NaOCNNa]^+$ is probably a lot hotter than nascent $[Na_2NH_2]^+$. This higher internal energy content, coupled with the comparatively lower sodium ion affinity of NaOCN relative to that of $NaNH_2$, means that $[NaOCNNa]^+$ must dissociate readily to yield Na^+ at a low collision energy (even $[Na_2NH_2]^+$ dissociates at energy > 12.5 eV), and accounts for its low abundance in all collision energies examined (Fig. 2*a*).

[4] The energy-resolved CID results show that the $[Na_2NH_2]^+$ abundance becomes nonzero at ~2 eV. Our data analyses are qualitative because, although the experiments were carried out under on-average single collision conditions, there were multiple collisions that led to an apparent decrease of the critical energy. In addition, the experiments were carried out at 298 K, which also led to a decrease in the critical energy. A factor that led to an increase in the critical energy was the kinetic shift, a consequence of the limited observation window in the MS/MS experiment.

© 2005 NRC Canada

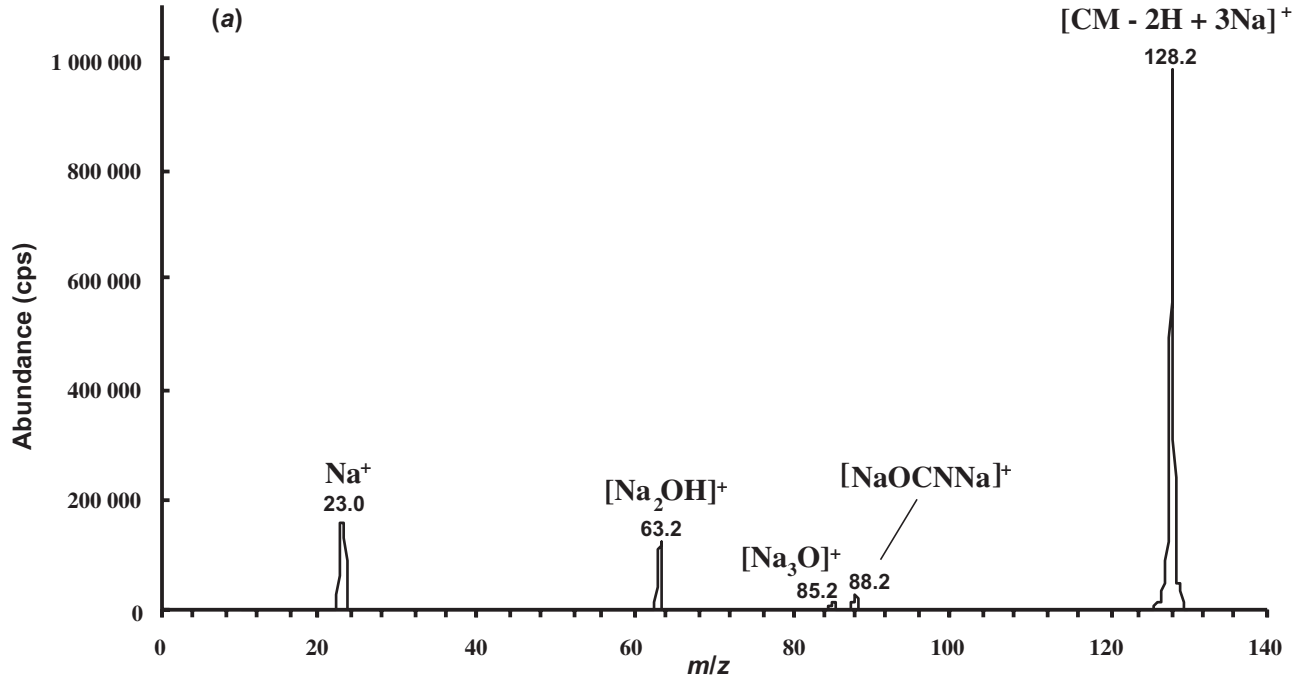
Fig. 3. Reaction profiles of (*a*) $[CM - H + 2Na]^+$ and (*b*) $[GU - H + 2Na]^+$.



Reaction profiles for $[CM - H + 2Na]^+$ and $[GU - H + 2Na]^+$ are shown in Fig. 3. The profile for $[CM - H + 2Na]^+$ (Fig. 3*a*) is the simplest of all three $[M - H + 2Na]^+$ complexes, as $[CM - H + 2Na]^+$ contains only two hydrogen atoms and thus cannot lose NH_3. As in $[UR - H + 2Na]^+$, the first step in forming $[Na_2NH_2]^+$ is an Na^+ transfer resulting in both Na atoms being bound to $-NH_2$ to give an ion–neutral complex in which $[Na_2NH_2]^+$ is solvated by CO_2. Dissociation of this complex yields the products $[Na_2NH_2]^+$ and CO_2. However, in contrast to $[UR - H + 2Na]^+$, formation of

© 2005 NRC Canada

Fig. 4. Dissociation of $[CM - 2H + 3Na]^+$. (*a*) CID spectrum at a laboratory collision energy of 12.5 eV; (*b*) energy-resolved CID plots; the inset shows low-energy details; and (*c*) reaction profiles. Bond distances are in angstroms, relative energies are ΔH°_0 in kcal/mol, and transition states are indicated as such by ‡.



$[Na_2NH_2]^+$ proceeds with an activation energy that is lower than the endothermicity of the reaction at 33.0 kcal/mol. This is considerably lower than the endothermicity (39.1 kcal/mol) and the activation energy (45.6 kcal/mol) of the analogous reaction in $[UR - H + 2Na]^+$. Dissociation of $[CM - H + 2Na]^+$ to give Na^+ requires 47.4 kcal/mol, which is also lower in energy than the analogous reaction in $[UR - H + 2Na]^+$ by 4.4 kcal/mol.

Relative to the profiles of $[CM - H + 2Na]^+$ and $[UR - H + 2Na]^+$, that of $[GU - H + 2Na]^+$ (Fig. 3*b*) is the most complicated. Contributing to this complexity is the lowest energy structure of $[GU - H + 2Na]^+$, which has the two Na bound to only two (nitrogen) atoms, as opposed to those of $[CM - H + 2Na]^+$ and $[UR - H + 2Na]^+$ that have Na^+ binding to three atoms. Both the formation of $[Na_2NH_2]^+$ and elimination of NH_3 in $[GU - H + 2Na]^+$ require, as a first step, transfer of one Na^+ from the two -NH groups to the $-NH_2$ group, which initially has no Na^+. Transfer of the second Na^+ leads to an ion–neutral complex, the dissociation of which gives $[Na_2NH_2]^+$ and HN=C=NH. Alternatively, transfer of a hydrogen eventually results in elimination of NH_3. As in the other profiles, formation of Na^+ from the complex requires the highest energy of 52.7 kcal/mol.

$[M - 2H + 3Na]^+$ complexes

As alluded to earlier, abundant $[M - 2H + 3Na]^+$ ions were observed at relatively energetic collision energies in the lens region. Collision-induced dissociations of the trisodiated ions have a lot in common and yield the following product ions: $[Na_3O]^+$ (85 Th), except for GU, which has no oxygen atom; $[Na_2OH]^+$ (63 Th), except for CN, which has no hydrogen (in the trisodiated complex), and GU, which has no oxygen atom; $[NaOCNNa]^+$ (88 Th), except for CN, which has no nitrogen, and GU, which has no oxygen atom; $[Na_2NH_2]^+$ (62 Th), except for CN, which has neither nitrogen nor hydrogen atom, and CM, which has only one hydrogen atom; $[Na_3CN_2]^+$ (109 Th), except for CN and CM, both of which contain fewer than two nitrogen atoms; and Na^+ (23 Th). A representative CID spectrum of $[CM - 2H + 3Na]^+$ at 12.5 eV is shown in Fig. 4*a*. Energy-resolved CID results show that dissociation to the product ions ($[Na_2OH]^+$ and $[NaOCNNa]^+$) require the lowest critical energies (Fig. 4*b*). As the abundance of Na^+ is much higher than those of any other product ions (see inset), estimation of the Na^+ critical energy relative to $[Na_2OH]^+$ and $[NaOCNNa]^+$ is more difficult; it is probably comparable to or slightly larger than those of the two disodiated fragment ions. These two ions can also subsequently fragment to give Na^+ at collision energies beyond 15 eV.

Figure 4*c* shows the energy profiles for the various dissociation pathways of $[CM - 2H + 3Na]^+$ (structure **VII**). Dissociation to give $[Na_2OH]^+$ (63 Th) requires first migration of the hydrogen from N to O to form complex **VIII**, and then a sodium moving in the opposite direction to form complex **IX**. This latter complex dissociates to yield $[Na_2OH]^+$ (structure **X**) and NaNCO. Alternatively, **IX** can dissociate to give $[NaOCNNa]^+$ (88 Th), ion **VI**, and NaOH. It is noteworthy that both product combinations lie below the critical transition state **TS(VII→VIII)**, which lies 54.1 kcal/mol above **VII**. This means that the dissociations to $[Na_2OH]^+$ and $[NaOCNNa]^+$ have an identical reaction barrier. The abundance of $[Na_2OH]^+$ is expected to be higher than that of $[NaOCNNa]^+$, as the product combination containing the former, at 40.7 kcal/mol, is lower lying than that containing the latter, at 50.8 kcal/mol. This prediction is consistent with experimental results shown in Fig. 4*b*. Elimination of Na^+ from structure **VII** results in product **XI**; the endothermicity of the reaction is 63.6 kcal/mol, larger than the critical bar-

© 2005 NRC Canada

Fig. 4 (*b*).

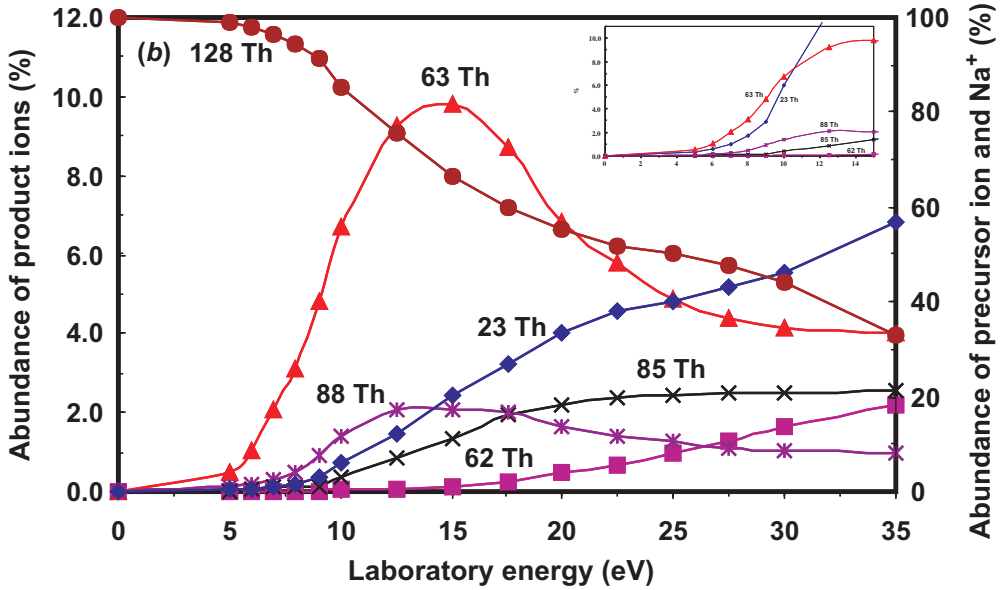
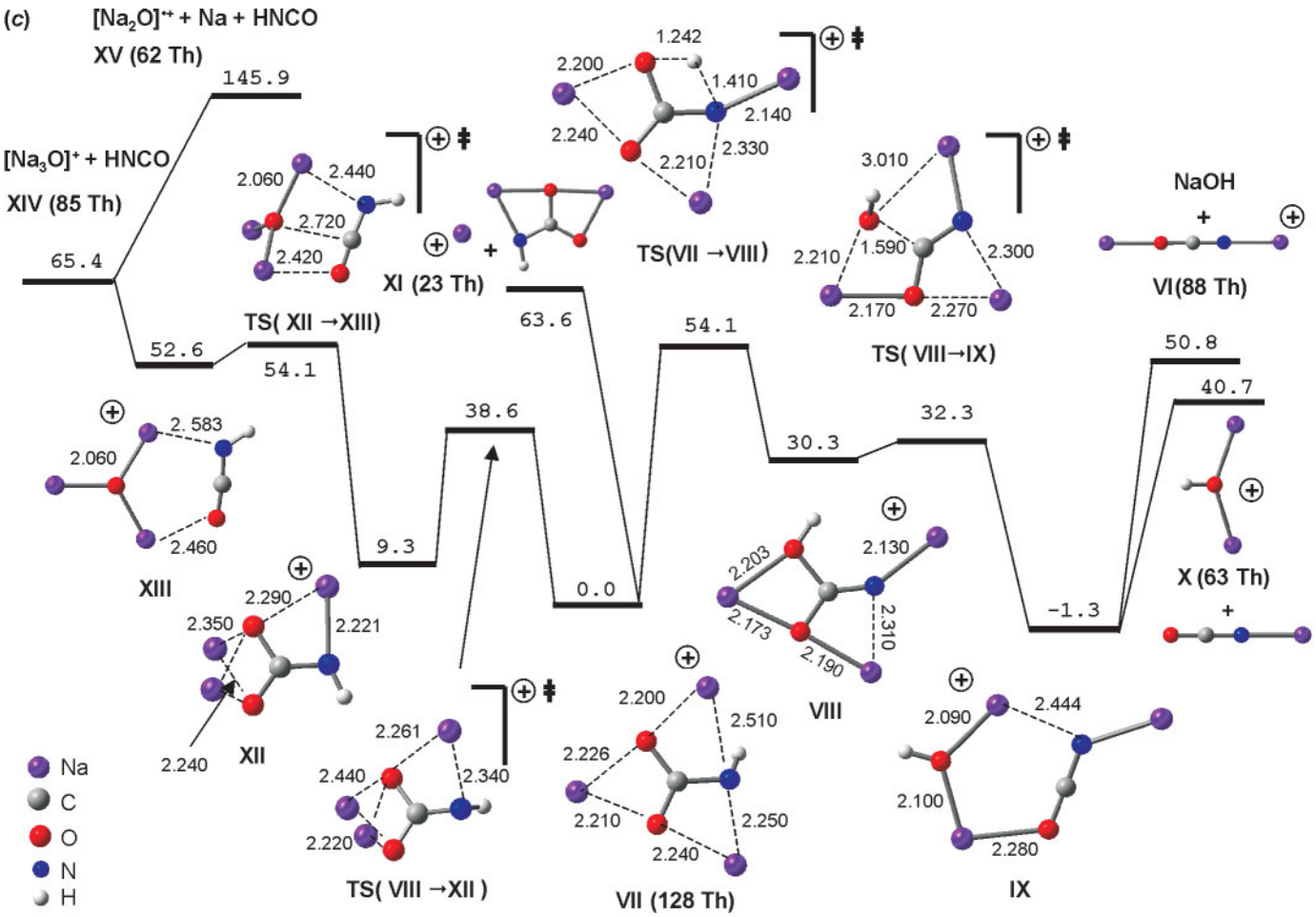


Fig. 4 (*c*).

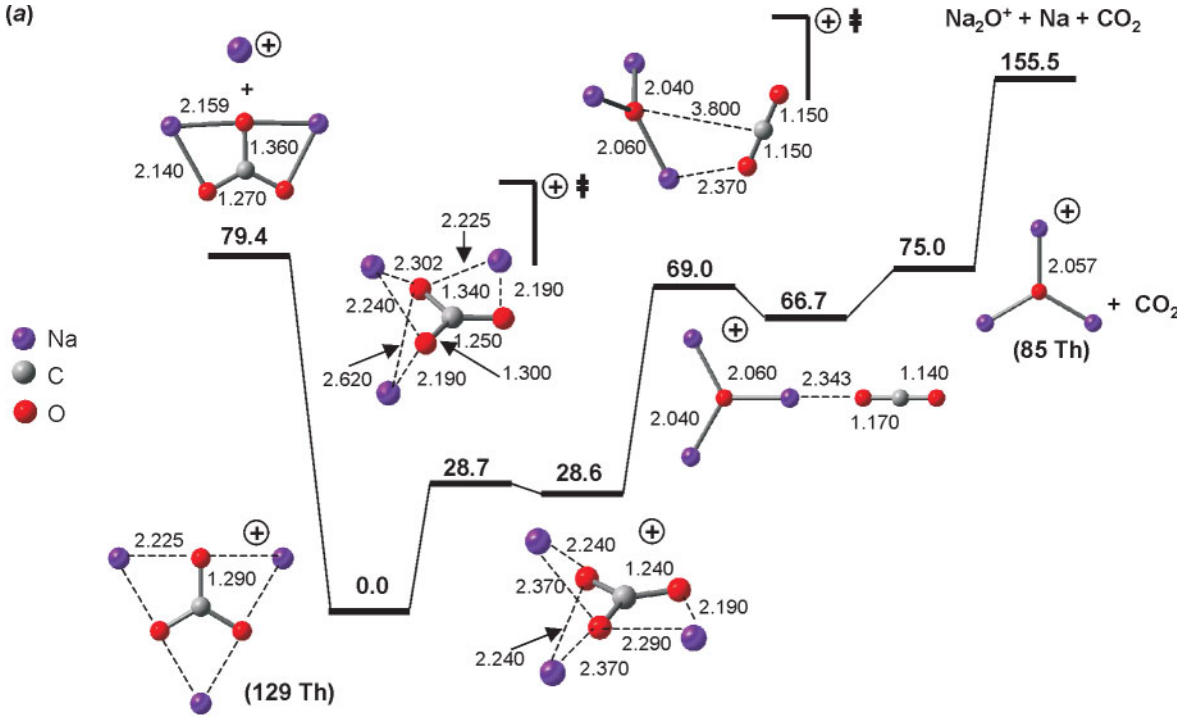


rier against the dissociations to $[Na_2OH]^+$ and $[NaOCNNa]^+$ by 9.5 kcal/mol. Dissociation to yield $[Na_3O]^+$ (85 Th), **XIV**, and HNCO requires eventual transfer of all three sodium onto a single oxygen atom. This reaction is endothermic by 65.4 kcal/mol, the largest barrier for the processes examined. These relative energetics are all in accordance with experimental results (Fig. 4*b*).

Reaction profiles for the other three $[M - 2H + 3Na]^+$

© 2005 NRC Canada

Fig. 5. Reaction profiles of (*a*) [CN – 2H + 3Na]$^+$, (*b*) [UR – 2H + 3Na]$^+$, and (*c*) [GU – 2H + 3Na]$^+$.



complexes are shown in Fig. 5. The [CN – 2H + 3Na]$^+$ complex gives the simplest profile (Fig. 5*a*) as it contains only carbon, oxygen, and sodium atoms. As observed in [CM – 2H + 3Na]$^+$, formation of $[Na_3O]^+$ (85 Th) requires transfer of all three sodium onto a single oxygen atom, resulting in an ion–neutral complex in which $[Na_3O]^+$ is solvated by CO_2. Dissociation of this ion–neutral complex yields the separated products, $[Na_3O]^+$ and CO_2. The activation energy for formation of $[Na_3O]^+$ and CO_2 is lower than the endothermicity of the reaction at 75.0 kcal/mol. Elimination of Na from $[Na_3O]^+$ to give $[Na_2O]^+$ is endothermic by 80.5 kcal/mol. Elimination of Na$^+$ from [CN – 2H + 3Na]$^+$ is endothermic by 79.4 kcal/mol.

The reaction profile of [UR – 2H + 3Na]$^+$ (Fig. 5*b*) is considerably more complicated, but it has similarities with those of [CM – H + 2Na]$^+$ and [CM – 2H + 3Na]$^+$. Formations of $[Na_2NH_2]^+$ (62 Th) and [NaOCNNa]$^+$ (88 Th) require an intermediate analogous to complex **IX**, which then dissociates to give either $[Na_2NH_2]^+$ and NaNCO, 34.8 kcal/mol above the lowest energy structure of [UR – 2H + 3Na]$^+$, or [NaOCNNa]$^+$ and $NaNH_2$, 42.3 kcal/mol above the same. By contrast, formation of $[Na_3O]^+$ and HN=C=NH requires a relatively large energy of 61.2 kcal/mol, which, however, is lower than the 75.0 kcal/mol required for the formation of $[Na_3O]^+$ and CO_2 from [CN – 2H + 3Na]$^+$, and the 65.4 kcal/mol required for the formation of $[Na_3O]^+$ and HNCO from [CM – 2H + 3Na]$^+$. Formation of $[Na_2OH]^+$ (63 Th) also proceeds via an intermediate analogous to complex **IX** in the dissociation of [CM – 2H + 3Na]$^+$. In addition, migration of the hydrogen from N to O involves the highest transition state.

Similar to those of [CM – 2H + 3Na]$^+$ and [UR – 2H + 3Na]$^+$, dissociation of [GU – 2H + 3Na]$^+$ (Fig. 5*c*) proceeds via an ion–neutral complex that can be viewed as either $[Na_2NH_2]^+$ solvated by NaN=C=NH or [NaN=C-N(H)Na]$^+$ (87 Th). Dissociation of the complex yields the two sets of separated products; these reactions have an identical barrier of 54.6 kcal/mol, encountered in the migration of a sodium ion. Elimination of Na$^+$ has the largest barrier at 62.2 kcal/mol.

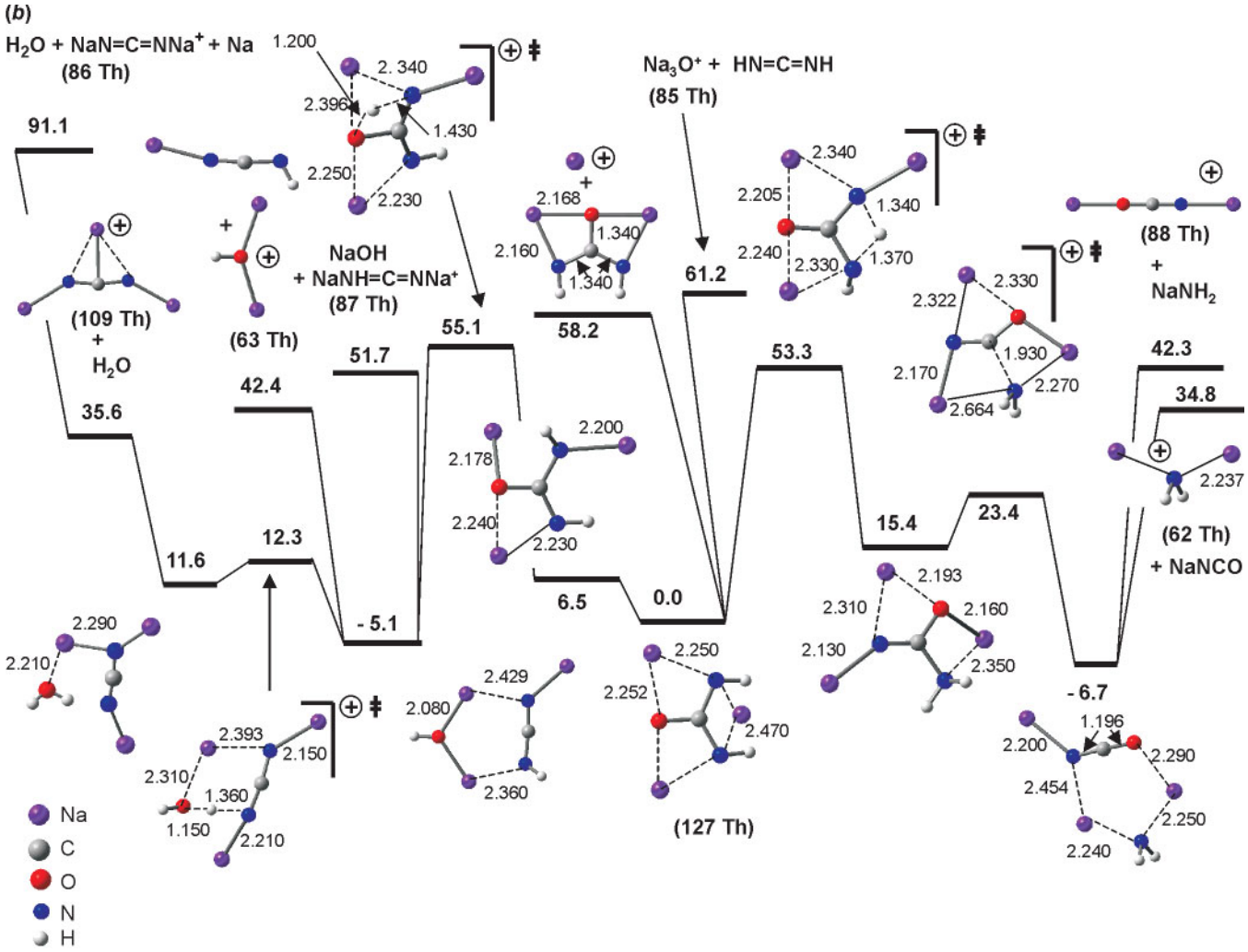
Additional interesting fragment ions

An interesting fragment is $[Na_3CN_2]^+$ (109 Th) ion, formed after elimination of water and ammonia, respectively, from trisodiated UR and GU. Details of its DFT-predicted structure are shown in Fig. 6. The ion has C_{2v} symmetry. The dissociation products Na$^+$ and NaN=C=NNa lie 55.1 kcal/mol above $[Na_3CN_2]^+$. Electrospraying the amino acids, arginine, lysine, and serine in the presence of Na$^+$ also produces abundant [M – 2H + 3Na]$^+$. CID of these ions produce the fragment ion $[Na_3CO_2]^+$ (113 Th),[5] whose DFT-predicted structure is also shown in Fig. 6. This ion also has C_{2v} symmetry. The dissociation products are $[Na_3O]^+$ (85 Th) and CO; this compares with the products $[Na_3O]^+$ and CO_2 formed in the dissociation of $[Na_3CO_3]^+$. Thus, $[Na_3O]^+$ turns out to be a rather common polysodiated fragment ion. Dissociation requires first transfer of Na$^+$ such that all three Na are bound to the same O atom, resulting in an ion–neutral complex of $[Na_3O]^+$ solvated by CO_n (where n = 1 or 2). Separation of the parts produces $[Na_3O]^+$ and CO_n. Although the rearrangement reactions involve a number of steps, the transition states are low lying, and the over-

[5] Full details will be presented elsewhere.

© 2005 NRC Canada

Fig. 5 (*b*).



all reaction is limited by only the endothermicities (39.4 kcal/mol for $n = 1$ and 79.4 kcal/mol for $n = 2$). The high value for the latter dissociation underlines the remarkable stability of the cyclic (possibly aromatic) $[Na_3CO_3]^+$ ion.

Dissociation to Na^+ and ligand

One of the unusual features of these sodiated complexes is that the energy required for dissociation to Na^+ and ligand *increases* with an increasing number of sodium atoms. Table 1 gives the Na^+ binding energies as calculated at B3LYP/6-311G**. These binding energies increase by approximately 10 kcal/mol for each additional sodium atom present. For example, for guanidine, the values are: monosodiated, 42.8; disodiated, 52.7; and trisodiated, 62.2 kcal/mol. The interaction between Na and GU is essentially electrostatic. In $[GU + Na]^+$, the binding is between Na^+ and neutral GU. By contrast, in $[GU - H + 2Na]^+$, the binding is between $2Na^+$ and $[GU - H]^-$; in other words, each Na^+ is attracted by 0.5 negative charge. Similarly, in $[GU - 2H + 3Na]^+$, the binding is between $3Na^+$ and $[GU - 2H]^{2-}$, or each Na^+ is attracted by 0.67 negative charge. Thus, it makes sense that binding energy increases with the extent of sodiation. Examination of any one column of data in Table 1 reveals that complexes with a fixed number of sodium atoms have similar Na^+ binding energies, consistent with the electrostatic nature of sodium binding. The one notable exception is $[Na_3CO_3]^+$, where the Na^+ binding energy is ~20 kcal/mol higher than those for the other trisodiated ions.

Conclusions

$[M - (n - 1)H + nNa]^+$ complexes ($n = 1$–3) of carbonate, carbamate, urea, and guanidine are observed in electrospray experiments. Na^+ binding energies follow the order monosodiated < disodiated < trisodiated with almost monotonic increases of ~10 kcal/mol with additional sodiation. The $[M - 2H + 3Na]^+$ complexes have particularly interesting structures in which the positive charge is almost evenly distributed among the sodium atoms. Collision-induced dissociations lead to a number of common, polysodiated fragment ions that can, in turn, fragment to give Na^+. The smallest polysodiated ion observed is $[Na_3O]^+$, which is also formed from $[Na_3CO_2]^+$, itself a fragment ion of singly charged trisodiated amino acids. The $[M - H + 2Na]^+$ complexes fragment to give $[Na_2NH_2]^+$ and Na^+. A number of fragment ions are common to both types

© 2005 NRC Canada

Fig. 5 (*c*).

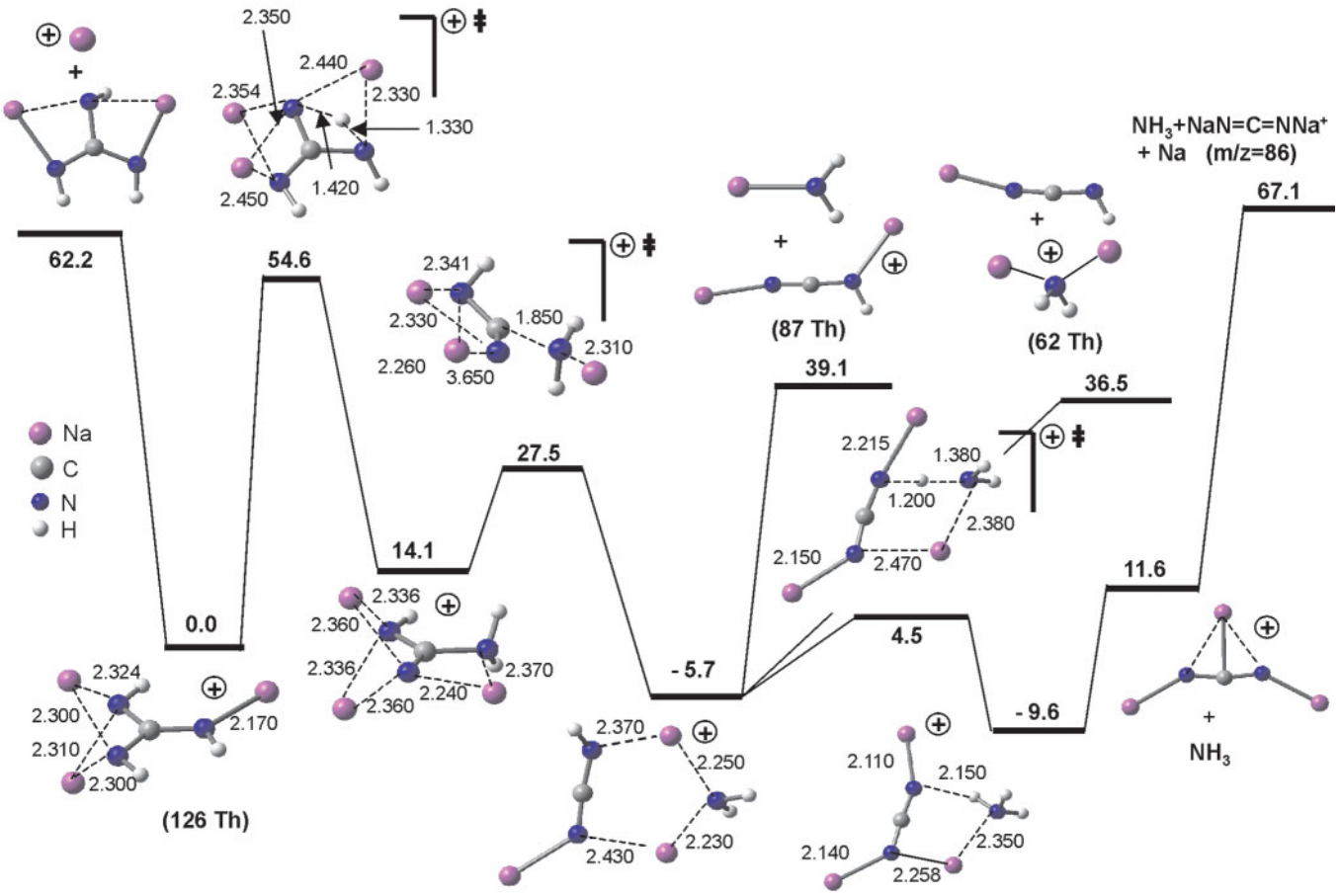
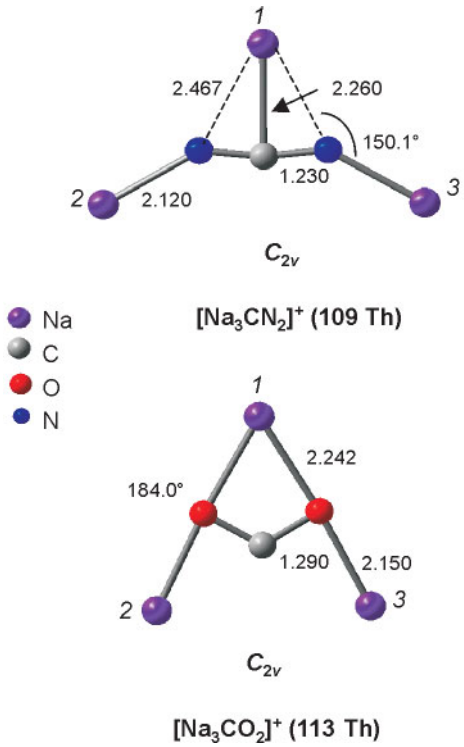


Fig. 6. Structural details of $[Na_3CN_2]^+$ and $[Na_3CO_2]^+$. Bond distances are in angstroms.



of complexes. Results of density functional theory calculations are consistent with mass spectrometric results.

Acknowledgements

This work was supported by the Natural Sciences and Engineering Research Council of Canada (NSERC), MDS SCIEX, and York University.

References

1. S.J. Lippard and J.M. Berg. Principles of bioinorganic chemistry. University Science Books, Mill Valley, California. 1994.
2. W. Kaim and B. Schwederski. Bioinorganic chemistry: Inorganic elements in the chemistry of life. Wiley, New York. 1994.
3. D.J. Aidley and P.R. Stanfield. Ion channels: Molecules in action. Cambridge University Press, Cambridge. 1996.
4. J.A. Cowan. Inorganic biochemistry: An introduction. 2nd ed. Wiley-VCH, New York. 1997.
5. G. Neubauer and R.J. Anderegg. Anal. Chem. **66**, 1056 (1994).
6. C.F. Rodriquez, R. Fournier, I.K. Chu, A.C. Hopkinson, and K.W.M. Siu. Int. J. Mass Spectrom. **192**, 303 (1999).
7. C.F. Rodriquez, X. Guo, T. Shoeib, A.C. Hopkinson, and K.W.M. Siu. J. Am. Soc. Mass Spectrom. **11**, 967 (2000).
8. R.N. Grewal, H. El Aribi, J.C. Smith, C.F. Rodriquez, A.C. Hopkinson, and K.W.M. Siu. Int. J. Mass Spectrom. **219**, 89 (2002).

© 2005 NRC Canada

9. E.S. Baker, J. Gidden, A. Ferzoco, and M.T. Bowers. Phys. Chem. Chem. Phys. **6**, 2786 (2004).
10. M.T. Rodgers and P.B. Armentrout. Mass Spectrom. Rev. **19**, 215 (2000).
11. G. Bojesen, T. Breindahl, and U.N. Andersen. Org. Mass Spectrom. **28**, 1448 (1993).
12. J.S. Klassen, S.G. Anderson, A.T. Blades, and P. Kebarle. J. Phys. Chem. **100**, 14218 (1996).
13. U.N. Andersen and G. Bojesen. J. Chem. Soc. Perkins Trans. 2, **2**, 323 (1997).
14. B.A. Cerda, S. Hoyau, G. Ohanessian, and C. Wesdemiotis. J. Am. Chem. Soc. **120**, 2437 (1998).
15. W.Y. Feng, S. Gronert, and C. Lebrilla. J. Am. Chem. Soc. **121**, 1365 (1999).
16. W.Y. Feng, S. Gronert, and C. Lebrilla. J. Phys. Chem. A, **107**, 405 (2003).
17. M.M. Kish, G. Ohanessian, and C. Wesdemiotis. Int. J. Mass Spectrom. **227**, 509 (2003).
18. M.J. Frisch, G.W. Trucks, H.B. Schlegel, G.E. Scuseria, M.A. Robb, J.R. Cheeseman, V.G. Zakrzewski, J.A. Montgomery, Jr., R.E. Stratmann, J.C. Burant, S. Dapprich, J.M. Millam, A.D. Daniels, K.N. Kudin, M.C. Strain, O. Farkas, J. Tomasi, V. Barone, M. Cossi, R. Cammi, B. Mennucci, C. Pomelli, C. Adamo, S. Clifford, J. Ochterski, G.A. Petersson, P.Y. Ayala, Q. Cui, K. Morokuma, P. Salvador, J.J. Dannenberg, D.K. Malick, A.D. Rabuck, K. Raghavachari, J.B. Foresman, J. Cioslowski, J.V. Ortiz, A.G. Baboul, B.B. Stefanov, G. Liu, A. Liashenko, P. Piskorz, I. Komaromi, R. Gomperts, R.L. Martin, D.J. Fox, T. Keith, M.A. Al-Laham, C.Y. Peng, A. Nanayakkara, M. Challacombe, P.M.W. Gill, B. Johnson, W. Chen, M.W. Wong, J.L. Andres, C. Gonzalez, M. Head-Gordon, E.S. Replogle, and J.A. Pople. Gaussian 98. Rev. A. 11 [computer program]. Gaussian, Inc., Pittsburgh, Penn. 2001.
19. A.D. Becke. Phys. Rev. A, **A38**, 3098 (1988).
20. A.D. Becke. J. Chem. Phys. **98**, 5648 (1993).
21. C. Lee, W. Yang, and R.G. Parr. Phys. Rev. B, **B37**, 785 (1988).
22. W.J. Hehre, R. Ditchfield, and J.A. Pople. J. Chem. Phys. **56**, 2257 (1972).
23. P.C. Hariharan and J.A. Pople. Chem. Phys. Lett. **16**, 217 (1972).
24. J. Chandrasekhar, J.G. Andrade, and P.v.R. Schleyer. J. Am. Chem. Soc. **103**, 5609 (1981).
25. T. Clark, J. Chandrasekhar, G.W. Spitznagel, and P.v.R. Schleyer. J. Comput. Chem. **4**, 294 (1983).
26. C. Gonzalez and H.B. Schlegel. J. Chem. Phys. **90**, 2154 (1989).
27. C. Gonzalez and H.B. Schlegel. J. Chem. Phys. **94**, 5523 (1990).
28. A.E. Reed, R.B. Weinstock, and F. Weinhold. J. Chem. Phys. **83**, 735 (1985).
29. A.E. Reed and F. Weinhold. J. Chem. Phys. **83**, 1736 (1985).
30. A.E. Reed, L.A. Curtiss, and F. Weinhold. Chem. Rev. **88**, 899 (1988).
31. A.E. Reed and P.v.R. Schleyer. J. Am. Chem. Soc. **112**, 1434 (1990).

© 2005 NRC Canada

Do electrospray mass spectra reflect the ligand binding state of proteins in solution?[1]

Belal M. Hossain, Douglas A. Simmons, and Lars Konermann

Abstract: Electrospray ionization (ESI) mass spectrometry (MS) has become a popular tool for monitoring ligand–protein and protein–protein interactions. Due to the "gentle" nature of the ionization process, it is often possible to transfer weakly bound complexes into the gas phase, thus making them amenable to MS detection. One problem with this technique is the potential occurrence of fragmentation events during ESI. Also, some analytes tend to cluster together during ionization, thus forming nonspecific gas-phase assemblies that do not represent solution-phase complexes. In this work, we implemented a hydrogen–deuterium exchange (HDX) approach that can reveal whether or not the free and (or) bound constituents of a complex observed in ESI-MS reflect the binding situation in solution. Proteins are subjected to ESI immediately following an isotopic labeling pulse; only ligand-free and ligand-bound protein ions that were formed directly from the corresponding solution-phase species showed different HDX levels. Using myoglobin as a model system, it is demonstrated that this approach can readily distinguish scenarios where the heme–protein interactions were disrupted in solution from those where dissociation of the complex occurred in the gas phase. Experiments on cytochrome c strongly suggest that dimeric protein ions observed in ESI-MS reflect aggregates that were formed in solution.

Key words: electrospray mass spectrometry, ligand–protein interaction, noncovalent complex, hydrogen–deuterium exchange, protein folding.

Résumé : La spectrométrie de masse (SM) avec ionisation par électronébulisation (IEN) est devenue un outil populaire pour étudier les interactions ligand–protéine et protéine–protéine. En raison de la nature douce du processus d'ionisation, il est souvent possible de transférer des complexes à faiblement liés dans la phase gazeuse et de les rendre ainsi d'être détectés en SM. Un problème lié à cette technique tient au fait qu'elle est susceptible de provoquer des fragmentations au cours de l'IEN. De plus, quelques analytes ont tendance à former des agrégats durant l'ionisation et ceci conduit à la formation d'assemblages en phase gazeuse qui ne sont pas spécifiques et qui ne représentent pas les complexes de la phase en solution. Dans ce travail, on a mis au point une approche impliquant un échange hydrogène–deutérium (HDX) qui permet de mettre en évidence si les constituants libres et (ou) liés d'un complexe observé en SM-IEN représentent ou pas la situation de liaison en solution. Les protéines sont soumises à l'IEN immédiatement après avoir subi une pulsation de marquage isotopique; seuls les ions ne contenant pas ligand et les protéines liées au ligand qui se sont formés directement à partir des espèces correspondantes de la phase en solution présenteront des niveaux de HDX différents. Utilisant la myoglobine comme système modèle, on a démontré que cette approche permet de distinguer facilement le scénario dans lequel les interactions hème–protéine ont été rompues en solution de celui où la dissociation du complexe s'est produite en phase gazeuse. Des expériences avec le cytochrome c suggèrent fortement que les ions dimères de protéine observés dans les SM-IEN sont un reflet d'agrégats qui se seraient formés en solution.

Mots clés : spectrométrie de masse avec ionisation par électronébulisation, interaction ligand–protéine, complexe monovalent, échange hydrogène–deutérium, repliement d'une protéine.

[Traduit par la Rédaction]

Introduction

Noncovalent ligand–protein interactions are involved in virtually all biological processes, and they play a central role in numerous drug action mechanisms. Ligands that may bind to a given protein receptor include metal ions, prosthetic groups, nucleic acids, saccharides, peptides, and other proteins. Experimental methods capable of detecting and mapping these interactions are of considerable interest (1–6). The use of electrospray ionization (ESI) mass spectrometry (MS) for experiments of this kind is a particularly promising approach (7, 8). The "gentle" nature of the ESI process al-

Received 25 February 2005. Published on the NRC Research Press Web site at http://canjchem.nrc.ca on 27 January 2006.

B.M. Hossain, D.A. Simmons,[2] and L. Konermann.[3] Department of Chemistry, The University of Western Ontario, London, ON N6A 5B7, Canada.

[1]This article is part of a Special Issue dedicated to Professor P. Kebarle.
[2]Present address: Department of Chemistry, Cambridge University, Lensfield Road, CB2 1EW, UK.
[3]Corresponding author (e-mail: konerman@uwo.ca).

 doi: 10.1139/V05-194 © 2005 NRC Canada

lows the transfer of intact biological complexes into the gas phase, thus making them amenable to MS detection. Systems that have been studied in this way range from metal–protein complexes to cell organelles and whole virus particles (9–16). The advantages of ESI-MS as a tool for monitoring ligand–protein interactions include speed, sensitivity, ease of use, and the ability to provide direct information on the binding stoichiometry. Due to its "mix-and-measure" nature, this approach is very attractive for the high-throughput screening of compound libraries in the context of drug discovery (17). Difficult sample preparation steps, such as chemical immobilization or fluorescence labeling, are not required.

The use of ESI-MS for studying ligand–protein interactions requires the composition of the observed ions to be the same as that of the corresponding solution-phase complexes. For many ligand–protein systems, this is indeed the case. This is evident from the agreement of dissociation constants measured by solution-phase methods with those obtained from gas-phase ion abundance ratios (13, 18–20). However, it is undisputed that the ion abundance ratio can be affected by a number of processes that may occur during ESI. Charge-balancing redox reactions taking place within the emitter capillary can result in significant pH changes, which may induce complex disruption immediately prior to ion formation (19, 21, 22). Dissociation events in the gas phase can occur during or after desolvation, e.g., by collisions with background gas molecules (19, 23). Generally, it is thought that complexes stabilized by ionic and polar noncovalent bonds are more likely to survive the ESI process than those held together by hydrophobic interactions (17, 24, 25). Despite this widely accepted notion, there are electrostatically stabilized complexes that are not particularly amenable to ESI-MS detection (26) and, conversely, some hydrophobically bound systems that do not get disrupted during ESI (27, 28). Clustering events taking place during ESI can lead to the formation of nonspecific aggregates in the gas phase, i.e., complexes that did not exist in solution prior to ionization (25, 29, 30). Clustering is expected to occur especially at high ligand to protein concentration ratios (31). A detailed account of all these processes, and their implications for the detectability of noncovalent complexes, has recently been given by Kebarle and co-workers (32).

The preceding discussion shows that the presence or absence of noncovalent complex ions in an ESI mass spectrum does not always allow conclusions to be drawn regarding specific solution-phase interactions. Several strategies have been devised to circumvent this problem. One alternative is the use of MS-based methods that do not rely on the preservation of specific interactions in the gas phase (20, 33–37). However, these techniques are often considerably more complicated and labor-intensive than the direct ESI-MS approach. Another possibility is the use of reference systems that can serve as internal standards for tuning the conditions of the ESI-MS experiment. An obvious limitation of this method is that appropriate reference systems may not always be available, especially when studying ligand–protein complexes that are biochemically not well characterized.

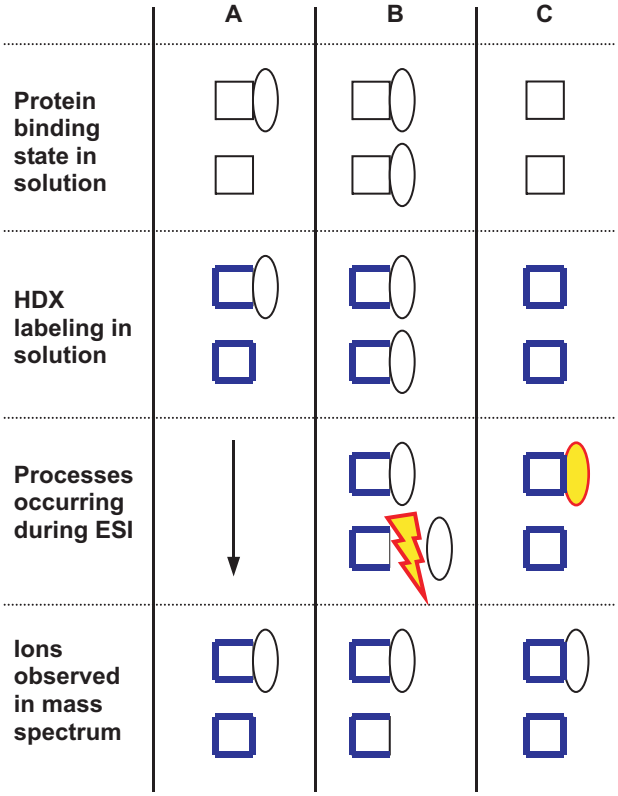
In this study, we propose a new strategy to determine whether the ligand binding state of a protein in solution is correctly represented by its ESI mass spectrum. For a spectrum that shows ions corresponding to both free and ligand-bound protein, we considered three scenarios. (A) The mass spectrum accurately reflects the binding state of the protein in solution. The free, as well as the ligand-bound protein ions observed in ESI-MS, originate from the corresponding solution-phase species. (B) All the proteins in solution are ligand-bound, but a certain percentage of these complexes gets disrupted during ESI. (C) The protein does not bind the ligand in solution. Instead, ligand-bound protein ions in the mass spectrum represent nonspecific complexes resulting from clustering processes during ionization. Various combinations of these scenarios are possible, but for the sake of simplicity, we restricted the discussion to these three cases. In the following, they will be referred to as "scenario A", "scenario B", and "scenario C", respectively.

For the method used here, proteins in solution were exposed to a hydrogen–deuterium exchange (HDX) pulse-labeling step immediately prior to ESI. HDX techniques are widely used for exploring the folding and dynamics of proteins in solution (8, 38, 39). Exposure of a protein to D_2O can lead to HDX of all the hydrogens in N—H, O—H, and S—H bonds, including those in amide groups, side chains, and on the chain termini. However, rapid exchange will only occur at the sites that are exposed to the solvent and not involved in hydrogen bonds. The mass shifts resulting from these exchanges can easily be monitored by ESI-MS (8, 38). Ligand–protein interactions will generally decrease the extent of HDX. This effect can result from (*i*) the steric protection of exchangeable sites owing to the presence of the ligand, (*ii*) the formation of intermolecular hydrogen bonds, and (*iii*) the fact that ligand-bound proteins often adopt more tightly folded solution-phase conformations than their ligand-free counterparts (40, 41). For pulsed HDX studies it has to be ensured that the intrinsic HDX rate constant is large enough to allow significant labeling during the brief exposure of the protein to the deuterated solvent. This can be achieved by controlling the pD of the labeling solution. For pD values in the range of 9 to 10, labeling of unprotected sites occurs in the millisecond time range (42, 43).

Figure 1 illustrates how pulsed HDX can be used to distinguish the "well-behaved" case, A, from the artifactual scenarios B and C. In scenario A, the extent of HDX for ligand-bound protein is lower than for free protein. In case B, the HDX level is the same for all protein molecules in the sample. This labeling behavior is unaffected by the dissociation events taking place during ESI, thus resulting in ligand-bound gas-phase proteins that exhibit the same exchange behavior as their ligand-free counterparts. Similarly, the clustering events taking place in scenario C are not expected to modify the HDX levels, such that the exchange behavior of free and ligand-bound protein ions are identical. In summary, the observation of identical HDX levels for free and ligand-bound protein ions indicates the occurrence of either dissociation or clustering events during ESI. In cases where the ESI mass spectrum correctly reflects the solution-phase binding equilibrium, the HDX levels observed for the free and ligand-bound protein should be different. The

© 2005 NRC Canada

Fig. 1. Schematic representation of the experimental approach used in this work. Pulsed HDX can be used to determine whether ligand-free and ligand-bound protein ions observed in ESI-MS represent the corresponding solution-phase species. Thick blue lines indicate regions on the protein that have undergone HDX. Three scenarios are considered: (A) Both ligand-bound and ligand-free protein ions observed in ESI-MS are formed directly from the corresponding solution-phase species. (B) Ligand-free protein ions are the product of dissociation events taking place during ESI. (C) Ligand-bound protein ions are the product of clustering processes taking place during ESI. Without isotope exchange, the mass spectra obtained for the three scenarios would be indistinguishable (last row). With labeling, however, only scenario A will result in different HDX levels for ligand-free and ligand-bound protein ions.



proposed method is expected to be applicable if the interconversion between the free and bound forms of the protein is slow compared to the duration of the labeling pulse. This study demonstrates the validity of this concept by applying it to a number of model systems.

Experimental

Chemicals

Ammonium-d_4 deuteroxide, acetic acid-OD (Isotec, Inc., Miamisburg, Ohio), deuterium oxide (Cambridge Isotope Laboratories, Inc., Andover, Massachusetts), acetic acid, ammonium hydroxide (Fisher Scientific, Nepean, Ontario), acetonitrile (Caledon Laboratories, Georgetown, Ontario), ammonium acetate (Fluka, Buchs, Switzerland), and bradykinin (Bachem, King of Prussia, Pennsylvania) were used without further purification. Horse ferrimyoglobin and cytochrome c (Sigma, St. Louis, Missouri) were dialyzed against 20 mmol/L ammonium acetate in water and subsequently acidified to pH 3.0 with acetic acid. Ammonium hydroxide and (or) acetonitrile were then added to obtain the protein solutions used in the experiments. pH and pD values were measured with an AB15 pH meter (Fisher Scientific, Nepean, Ontario). Reported pD values were corrected for isotope effects based on the relation pD = pH meter reading + 0.4 (44).

Pulsed HDX

ESI-MS with on-line pulsed HDX was carried out by employing a continuous-flow rapid-mixing setup similar to that used for earlier studies from our laboratory (45). Briefly, two syringes, containing aqueous protein solution at pH 9.3 and D_2O-containing labeling solution at pD 9.3, respectively, were advanced simultaneously by syringe pumps (Harvard Apparatus, South Natick, Massachusetts). Solutions expelled from the two syringes were combined at a mixing tee that emptied into a 1 cm long fused silica capillary (TSP075150, 75 μm i.d., Polymicro Technologies, Phoenix, Arizona) where isotope labeling took place. This labeling capillary was connected to the ESI source of the mass spectrometer. The residence time of the solution within the capillary (labeling time) was 26 ms at a total flow rate of 100 μL/min. Other flow rates used for this work were 20 and 150 μL/min, corresponding to labeling times of 130 and 17 ms, respectively. Mass spectra were recorded on an API 365 triple quadrupole mass spectrometer (SCIEX, Concord, Ontario). Ions were generated by pneumatically assisted ESI in positive ion mode at a sprayer voltage of 6 kV. Approximately 500 scans at a dwell time of 1 ms per data point were averaged for each HDX experiment.

Isotope back-exchange and mixing efficiency

In ESI-MS-based HDX experiments, it is common to observe some back-exchange in the ion source, i.e., deuterons on the protein can exchange with hydrogens originating from residual water vapor. The approach used here requires that the solution-phase labeling of the protein be preserved as much as possible, and it is therefore important to minimize the extent of back-exchange. Previous studies have reported that back-exchange can be suppressed by continuously purging the ion source region with dry air (46, 47). Figure 2 provides a quantitative assessment of this effect for the conditions of the current study, using the peptide bradykinin (Arg-Pro-Pro-Gly-Phe-Ser-Pro-Phe-Arg, monoisotopic mass 1059.57) as a test compound. The isotope distribution of unlabeled bradykinin is shown in Fig. 2A. All 17 labile hydrogens in bradykinin are accessible to the solvent and should be readily exchangeable (46). For pulse-labeling of this peptide, syringe 1 (5 μL/min) contained 250 μmol/L bradykinin in water at pH 9.3 and syringe 2 (95 μL/min) contained D_2O at pD 9.3. Figure 2B shows the mass spectrum of singly charged bradykinin recorded after 26 ms of labeling, without air purging of the ion source; whereas the external air flow was activated for the spectrum depicted in Fig. 2C. It is evident that air purging causes the peak cluster to shift to higher m/z values. Based on the D_2O content of

© 2005 NRC Canada

Fig. 2. Partial ESI mass spectra, showing singly charged bradykinin ions: (A) bradykinin in water without isotope labeling; (B) bradykinin after solution-phase isotope labeling for 26 ms, ion source not purged; (C) as (B), except that the ion source was purged with dry air. The monoisotopic peak of the fully exchanged peptide in panels B and C (marked with an asterisk) is shifted 18 mass units compared with that of the unlabeled peptide in A. This mass shift corresponds to 17 exchangeable sites plus 1 charge carrier. Bar diagrams represent theoretical isotope distributions for hydrogen exchange probabilities of 0 (A), 0.81 (B), and 0.89 (C).

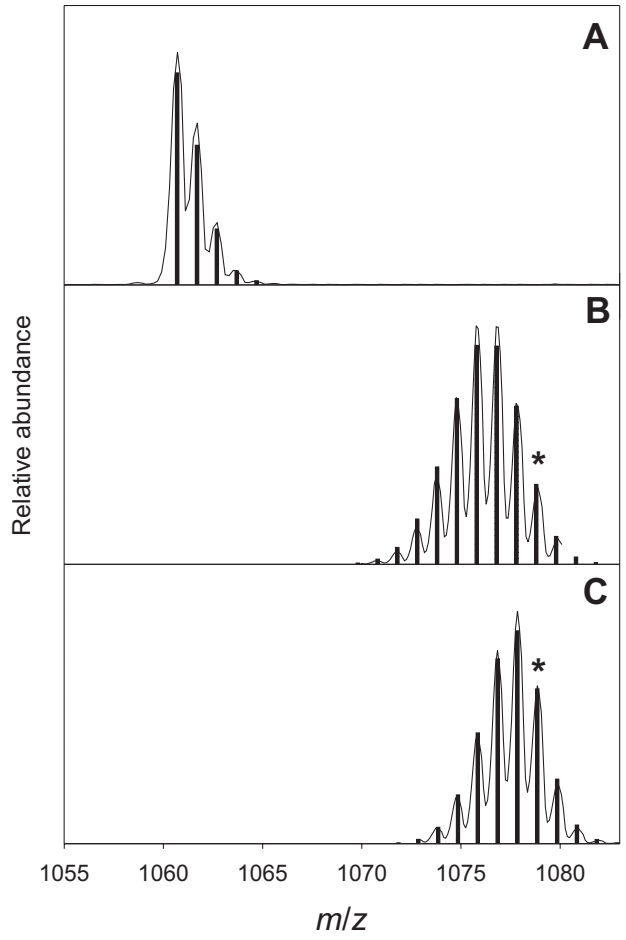
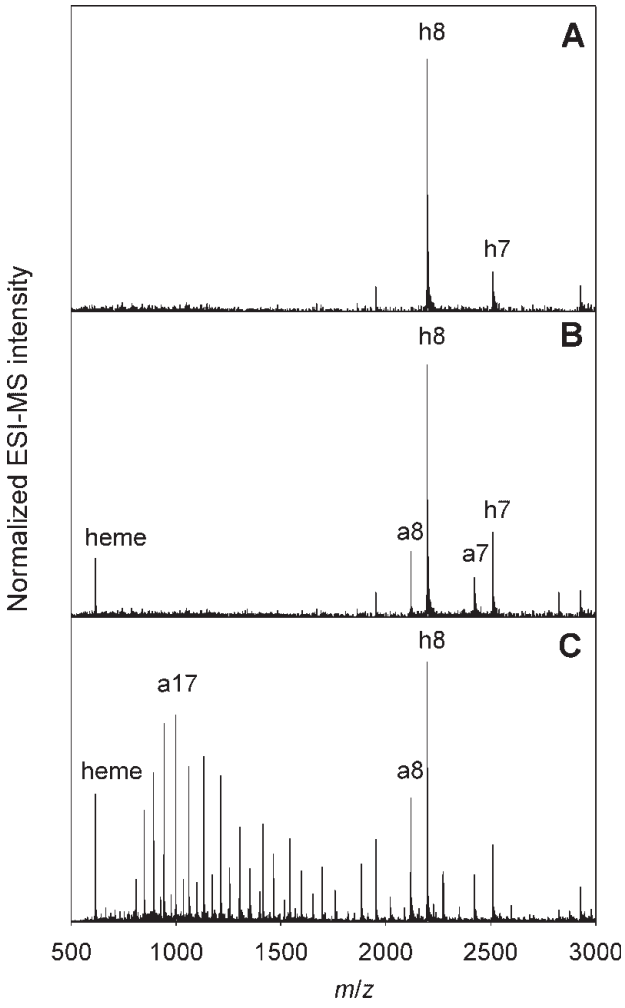


Fig. 3. ESI mass spectra of myoglobin at pH 9.3 recorded under different conditions: (A) myoglobin in water, orifice-skimmer voltage 20 V; (B) like (A), but recorded under harsher desolvation conditions (orifice-skimmer voltage 100 V); (C) myoglobin in water–acetonitrile (73:27 *v*/*v*), orifice-skimmer voltage 20 V. Notation: h and a indicate holomyoglobin and apomyoglobin (hMb and aMb), respectively. Numbers represent the charge states of protein ions, e.g., h8 ≡ hMb^{8+} ≡ (holomyoglobin + 8H)$^{8+}$.



the labeling solution, the exchange probability for each of the 18 exchangeable sites on singly charged bradykinin (17 labile hydrogens and 1 charge carrier) should be 0.95. The bar diagrams in Fig. 2 represent simulated isotope distributions for different exchange probabilities. The best match with the experimental data in Fig. 2B is obtained for a probability of 0.81. In contrast, the data in Fig. 2C are best described by a labeling probability of 0.89. This result shows that air purging leads to a significant suppression of back-exchange. Therefore, all the subsequent protein HDX experiments for this work were carried out by using the source conditions of Fig. 2C. It is noted that the data in Fig. 2C also demonstrate an efficient mixing of the labeling setup. Incomplete mixing would result in a much lower average exchange probability. In addition, the broad isotope distributions expected under those conditions would not be describable by the modeling approach used here. Efficient mixing was also demonstrated at elevated solution flow rates, corresponding to labeling times down to 7 ms (data not shown).

Results and discussion

Myoglobin ESI mass spectra

Myoglobin is one of the most common model systems for studying ligand–protein interactions (11). Native myoglobin contains a heme group which is seated in a hydrophobic binding pocket where it makes numerous contacts with the protein, including ligation of the heme iron with His93 (48). The intact heme–protein complex is readily observable in ESI-MS, as long as gentle declustering conditions are used in the ion-sampling interface of the mass spectrometer. Figure 3A shows a spectrum of myoglobin recorded in aqueous solution at pH 9.3, using an orifice-skimmer voltage of 20 V.

© 2005 NRC Canada

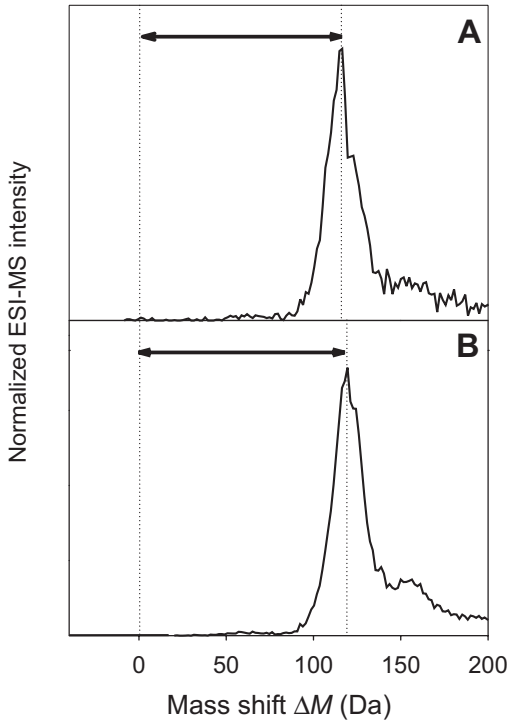
The spectrum exclusively shows ions corresponding to the intact heme–protein complex (holo-myoglobin, hMb), whereas heme-free protein (apo-myoglobin, aMb) is not observed. Figure 3B shows a spectrum recorded under the same solvent conditions, but at an orifice-skimmer voltage of 100 V. It can be seen that some fraction of proteins loose their heme group in the gas phase by collision-induced dissociation, such that both aMb and hMb ions are observed in the spectrum (23). Also shown is a spectrum of myoglobin recorded at pH 9.3 in the presence of 27% acetonitrile, using gentle declustering conditions (orifice-skimmer voltage 20 V, Fig. 3C). Owing to the presence of the organic cosolvent, the protein is partially denatured and adopts several aMb and hMb solution-phase conformations that are in equilibrium with each other. The different protein conformations give rise to various charge-state distributions. In general, highly charged protein ions represent more unfolded solution-phase structures (8). Our group recently conducted a detailed study of the solution-phase conformational dynamics of myoglobin under the solvent conditions of Fig. 3C (45). For the current work, it is important to note that Fig. 3C represents a situation where the aMb and hMb ions observed in the spectrum are thought to reflect the presence of the corresponding solution-phase species (Fig. 1, scenario A). In contrast, Fig. 3B represents fully intact solution-phase complexes that undergo partial dissociation during ESI (Fig. 1, scenario B).

Pulse-labeling experiments on myoglobin

The total number of exchangeable hydrogens in hMb is 263, 148 of which are located along the amide backbone, 110 on the amino acid side chains, 3 on the termini, and 2 on the heme propionates. Figure 4 shows the HDX data obtained for native myoglobin that has undergone partial dissociation in the ion source of the mass spectrometer, i.e., under the conditions of Fig. 3B. After 26 ms of labeling at pD 9.3 in D_2O–H_2O (95:5 *v*/*v*), the measured mass shifts for aMb and hMb are (116 ± 1) and (120 ± 1) Da, respectively. When taking into account the presence of two additional exchangeable sites on the hMb heme group, these exchange levels are indistinguishable within error limits. This result confirms the validity of the proposed labeling strategy for an example of scenario B. It is likely that the majority of the exchange events under the conditions of Fig. 4 are due to side chain hydrogens, since most of the amides in native myoglobin are protected by the presence of an α-helical hydrogen bonding network.

Figures 5A and 5B depict the results obtained in an experiment analogous to that in Fig. 4. However, the solution in this case contained 27% acetonitrile, and the orifice-skimmer voltage was reduced to 20 V. As discussed previously, aMb ions observed under these conditions are expected to originate from heme-free proteins in solution (scenario A). The extent of HDX after 26 ms of labeling is dramatically higher for aMb than for hMb. The mass shifts observed for the two ionic species are (196 ± 1) and (92 ± 1) Da, respectively. The different HDX levels are consistent with the known fact that the removal of the heme group induces the polypeptide chain to adopt a partially disordered structure that is more conducive to rapid HDX (40, 45, 49). The lower extent of HDX for hMb in this experiment compared with the data in Fig. 4 is attributed to the reduced D_2O concentration in the labeling solution, caused by the presence of acetonitrile.

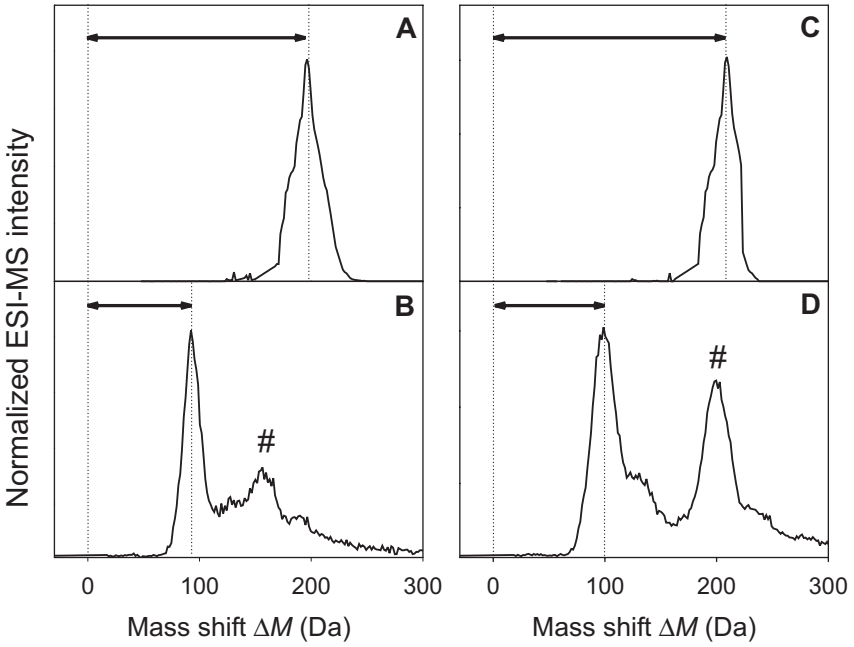
Fig. 4. Ions of (A) aMb and (B) hMb in the 8+ charge state, observed after pulse-labeling the protein at pD 9.3 for 26 ms. The mixing ratio of deuterated to non-deuterated solution during labeling was 95:5. No organic cosolvents were used for this experiment, aMb ions in panel (A) are the product of collision-induced dissociation in the gas phase (orifice-skimmer voltage 100 V). To allow a direct comparison of the HDX level (visualized by double-headed arrows), the *x*-axes were converted from m/z to mass shift (ΔM), according to $\Delta M = (m/z \times 8) - (0.95 \times 2 \times 8) - (0.05 \times 1 \times 8) - M_0$. M_0 is the mass of the unlabeled protein, 16 952 Da for aMb and 17 568 Da for hMb.



To assess the effects of labeling pulse length, the same experiment was repeated at a lower flow rate. The data in Figs. 5C and 5D corresponding to a pulse duration of 130 ms show mass shifts of (209 ± 1) and (99 ± 1) Da for the dominant aMb and hMb signals, respectively. The main conclusion to be drawn from the data in Fig. 5 is that the pulse-labeling strategy used here can clearly pinpoint a situation where the ligand-binding state of a protein in solution is directly represented by its ESI mass spectrum. The interconversion of free and ligand-bound proteins in this case is slow enough to differentiate the two forms, even when the time resolution of the experiment is reduced. Interestingly, the occurrence of interconversion processes is directly evident in our experimental data. The satellite peaks in Figs. 5B and 5D (marked with "#") are attributed to protein molecules that underwent a transition from aMb to hMb during labeling. Such a process necessarily leads to EX1 characteristics that are accompanied by peak splitting in ESI-MS. The intensity increase of the satellite peak observed for longer labeling times is fully consistent with this scenario (45, 50, 51).

© 2005 NRC Canada

Fig. 5. Ions of (A) aMb and (B) hMb in the 8+ charge state, observed after pulse-labeling the protein at pD 9.3 for 26 ms. The solvent used in this case contained 27% acetonitrile, leading to partial denaturation of the protein in solution (orifice-skimmer voltage 20 V). The data shown in (C) and (D) are analogous to those in (A) and (B), except that the labeling time was increased to 130 ms. The appearance of a satellite peak, marked with "#", is discussed in the text. Mass axis conversion was performed as for the preceding figure.

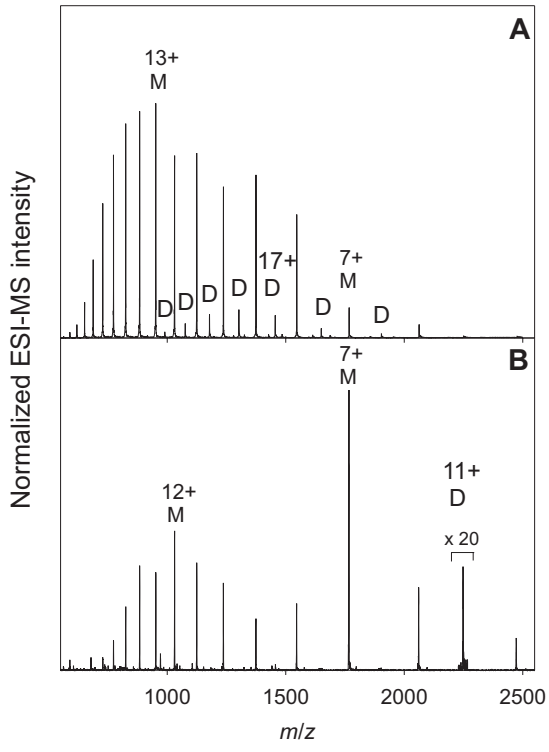


Dimerization of cytochrome c

When studying noncovalent protein–protein complexes by ESI-MS, it is fairly common to not only observe ions of the expected quaternary structures, but also larger assemblies (52, 53). The origin of these larger structures is not always clear. On one hand, it is possible that they represent weakly bound solution-phase complexes that may go undetected by other methods. Another possible scenario is the occurrence of clustering processes during ESI (scenario C) (25, 29, 30). The extent of clustering during ESI shows a strong dependence on protein concentration (32), but a similar dependence might be expected for the formation of protein aggregates in solution (54). To illustrate this issue using a very simple model system, we chose to apply our labeling approach to cytochrome c (MW 12 360 Da), a commonly studied model protein that possesses 198 exchangeable hydrogens (55). It has previously been reported that the mass spectra of cytochrome c recorded under acidic conditions and at elevated protein concentrations show noncovalently bound protein dimers (56, 57). This observation is corroborated by the data in Fig. 6A, which were recorded at a protein concentration of 1 mmol/L. Previous studies in the literature have not thoroughly addressed the question of whether these complexes represent clusters formed during ESI or assemblies that were formed in solution. Unfortunately, the acidic conditions used for acquiring the data in Fig. 6A are not conducive to rapid HDX (42). However, dimeric species are also observed at more basic pH and in the presence of acetonitrile, albeit with a very low ion abundance (Fig. 6B).

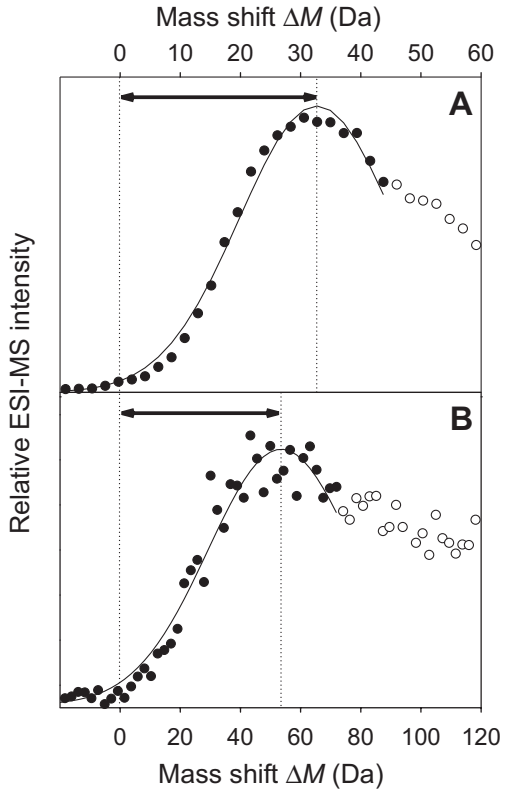
Figure 7 shows the results of pulsed HDX experiments obtained under the solvent conditions analogous to those used for Fig. 6B, with a labeling time of 17 ms. To maintain a high protein concentration after labeling, the mixing ratio was changed from 95:5 to 1:1. The analysis of the HDX data

Fig. 6. ESI mass spectra of cytochrome c recorded at a protein concentration of 1 mmol/L. (A) Aqueous solution containing 10% acetonitrile and 2% glacial acetic acid. (B) Aqueous solution containing 47% acetonitrile at pH 9.3. Peaks corresponding to monomeric and dimeric protein ions are marked with M and D, respectively, and some charge states are indicated. Note that the region around the dimeric 11+ signal in panel B has been magnified by a factor of 20 for better visualization.



© 2005 NRC Canada

Fig. 7. Ions of (A) monomeric and (B) dimeric cytochrome c in the 11+ charge state, observed after pulse-labeling the protein at pD 9.3 for 17 ms. The mixing ratio of deuterated to non-deuterated solution during labeling was 1:1 (final protein concentration 1 mmol/L). Solid lines are Gaussian fits to the low mass portion of the peaks. The high mass portion (indicated by open symbols) could not be considered for the analysis owing to extensive tailing. The *x*-axes were converted from *m*/*z* to mass shift (ΔM), according to $\Delta M = (m/z \times 11) - (0.5 \times 2 \times 11) - (0.5 \times 1 \times 11) - M_0$, with M_0 = 12 360 Da (A) and $M_0 = 2 \times 12\,360$ Da (B).



obtained under these conditions was complicated by the fact that the overall mass shifts obtained were relatively small. Moreover, the low intensity of the dimer ions resulted in data with poor signal-to-noise ratio, and the measured peaks showed considerable tailing. A Gaussian fitting procedure, based on a strategy developed in earlier HDX studies (47), was employed to estimate the mass shifts incurred by the two types of ions. If the protein dimer ions were a product of clustering events during ESI (scenario C), the mass shift observed for the dimer should be exactly twice that of monomeric cytochrome c. Interestingly, a comparison of the two data sets in Fig. 7 reveals that this is *not* the case. Based on the mass shift of (33 ± 2) Da that is observed for the monomeric ions in Fig. 7A, the dimer mass would have to be shifted by ca. 66 Da to be compatible with scenario C. However, the measured value of (54 ± 3) Da is significantly lower, thus suggesting that the dimer ions are derived from an aggregated species in solution. In other words, our data imply that cytochrome c follows scenario A under the conditions of this experiment. This interpretation is compatible with the known tendency of many proteins to undergo partial aggregation under mildly denaturing solution-phase conditions, especially at elevated concentrations (54).

Conclusions

The use of ESI-MS as a tool for studying noncovalent ligand–protein interactions is an extraordinarily powerful approach. However, there still is a need to gain a better understanding of factors that can potentially lead to disparities between the solution-phase and gas-phase composition of these complexes. As a first step, it is important to identify cases in which such disparities exist. The pulse-labeling approach proposed in this work provides a tool that can distinguish the "undisturbed" transfer of proteins and ligand–protein complexes into the gas phase from scenarios that involve the occurrence of dissociation or clustering processes. It appears that this technique works best when studying interactions of protein receptors with ligands that would be expected to (*i*) induce major conformational changes, and (or) (*ii*) cause a significant degree of steric shielding upon binding in solution. Basic pD conditions were chosen for the current work to ensure intrinsic HDX rate constants in the millisecond range. The use of near-neutral solutions reduces the extent of HDX, thus leading to less clear-cut labeling signatures for the different scenarios. In cases where the solution-phase interconversion of free and bound forms of the protein is slow, it is possible to compensate the lower HDX rate by extending the duration of the labeling pulse. When studying systems where both the protein of interest and its ligand(s) can undergo extensive HDX, it is beneficial to study the HDX behavior of individual constituents by tandem mass spectrometry. We are currently applying this approach to various multiprotein assemblies. It is hoped that those studies will provide novel insights into the processes that occur upon transferring macromolecular complexes from solution into the gas phase.

Acknowledgments

We thank Jingxi Pan and Derek J. Wilson for assistance during the experiments and for helpful discussions. Financial support was provided by the Natural Sciences and Engineering Research Council of Canada (NSERC), the Canada Foundation for Innovation (CFI), the province of Ontario, and the Canada Research Chairs Program.

References

1. S. Li, C.M. Armstrong, N. Bertin, H. Ge, S. Milstein, M. Boxem, P.-O. Vidalain, J.-D.J. Han, A. Chesneau, T. Hao, D.S. Goldberg, N. Li, M. Martinez, J.-F. Rual, P. Lamesch, L. Xu, M. Tewari, S.L. Wong, L.V. Zhang, G.F. Berriz, L. Jacotot, P. Vaglio, J. Reboul, T. Hirozane-Kishikawa, Q. Li, H.W. Gabel, A. Elewa, B. Baumgartner, D.J. Rose, H. Yu, S. Bosak, R. Sequerra, A. Fraser, S.E. Mango, W.M. Saxton, S. Strome, S. van den Heuvel, F. Piano, J. Vandenhaute, C. Sardet, M. Gerstein, L. Doucette-Stamm, K.C. Gunsalus, J.W. Harper, M.E. Cusick, F.P. Roth, D.E. Hill, and M. Vidal. Science, **303**, 540 (2004).
2. B. Titz, M. Schlesner, and P. Uetz. Expert Rev. Proteomics, **1**, 111 (2004).
3. A.-C. Gavin, M. Bösche, R. Krause, P. Grandi, M. Marzioch, A. Bauer, J. Schultz, J.M. Rick, A.-M. Michon, C.-M. Cruciat, M. Remor, C. Höfert, M. Schelder, M. Brajenovic, H. Ruffner, A. Merino, K. Klein, M. Hudak, D. Dickson, T. Rudi, V. Gnau, A. Bauch, S. Bastuck, B. Huhse, C. Leutwein, M.-A. Heurtier,

© 2005 NRC Canada

R.R. Copley, A. Edelmann, E. Querfurth, V. Rybin, G. Drewes, M. Raida, T. Bouwmeester, P. Bork, B. Seraphin, B. Kuster, G. Neubauer, and G. Superti-Furga. Nature (London), **415**, 141 (2002).
4. J.M. McDonnell. Curr. Opin. Chem. Biol. **5**, 572 (2001).
5. M. Auer, K.J. Moore, F.J. Meyer-Almes, R. Guenther, A.J. Pope, and K.A. Stoeckli. Drug Discovery Today, **3**, 457 (1998).
6. P. Gribbon and A. Sewing. Drug Discovery Today, **8**, 1035 (2003).
7. P. Kebarle and M. Peschke. Anal. Chim. Acta, **406**, 11 (2000).
8. I.A. Kaltashov and S.J. Eyles. Mass Spectrom. Rev. **21**, 37 (2002).
9. B. Ganem, Y.-T. Li, and J.D. Henion. J. Am. Chem. Soc. **113**, 6294 (1991).
10. B. Ganem, Y.-T. Li, and J.D. Henion. J. Am. Chem. Soc. **113**, 7818 (1991).
11. V. Katta and B.T. Chait. J. Am. Chem. Soc. **113**, 8534 (1991).
12. J.A. Loo. Int. J. Mass Spectrom. **200**, 175 (2000).
13. J.M. Daniel, S.D. Friess, S. Rajagopalan, S. Wendt, and R. Zenobi. Int. J. Mass Spectrom. **216**, 1 (2002).
14. A.J.R. Heck and R.H.H. Van den Heuvel. Mass Spectrom. Rev. **23**, 368 (2004).
15. B. Bothner and G. Siuzdak. ChemBioChem, **5**, 258 (2004).
16. A.A. Rostom, P. Fucini, D.R. Benjamin, R. Juenemann, K.H. Nierhaus, F.U. Hartl, C.M. Dobson, and C.V. Robinson. Proc. Natl. Acad. Sci. U.S.A. **97**, 5185 (2000).
17. M. Wigger, J.R. Eyler, S.A. Benner, W. Li, and A.G. Marshall. J. Am. Soc. Mass Spectrom. **13**, 1162 (2002).
18. T.J.D. Jorgensen, P. Roepstorff, and A.J.R. Heck. Anal. Chem. **70**, 4427 (1998).
19. W. Wang, E.N. Kitova, and J.S. Klassen. Anal. Chem. **75**, 4945 (2003).
20. S.M. Clark and L. Konermann. Anal. Chem. **76**, 7077 (2004).
21. G.J. Van Berkel, F. Zhou, and J.T. Aronson. Int. J. Mass Spectrom. Ion Processes, **162**, 55 (1997).
22. L. Konermann, E.A. Silva, and O.F. Sogbein. Anal. Chem. **73**, 4836 (2001).
23. B.A. Collings and D.J. Douglas. J. Am. Chem. Soc. **118**, 4488 (1996).
24. A. Schmidt and M. Karas. J. Am. Soc. Mass Spectrom. **12**, 1092 (2001).
25. C.V. Robinson, E.W. Chung, B.B. Kragelund, J. Knudsen, R.T. Aplin, F.M. Poulsen, and C.M. Dobson. J. Am. Chem. Soc. **118**, 8646 (1996).
26. M.R. Mauk, A.G. Mauk, Y.-L. Chen, and D.J. Douglas. J. Am. Soc. Mass Spectrom. **13**, 59 (2002).
27. Y. Li, F. Heitz, C. Le Grimellec, and R.B. Cole. Rapid Commun. Mass Spectrom. **18**, 135 (2003).
28. R. Gupta, S.M. Hamdan, N.E. Dixon, M.M. Sheil, and J.L. Beck. Protein Sci. **13**, 2878 (2004).
29. D.L. Zechel, L. Konermann, S.G. Withers, and D.J. Douglas. Biochemistry, **37**, 7664 (1998).
30. R. Juraschek, T. Dulcks, and M. Karas. J. Am. Soc. Mass Spectrom. **10**, 300 (1999).
31. W. Wang, E.N. Kitova, and J.S. Klassen. J. Am. Chem. Soc. **125**, 13630 (2003).
32. M. Peschke, U.H. Verkerk, and P. Kebarle. J. Am. Soc. Mass Spectrom. **15**, 1424 (2004).
33. D.C. Schriemer. Anal. Chem. **76**, 441A (2004).
34. S.M. Clark and L. Konermann. Anal. Chem. **76**, 1257 (2004).
35. P.A. Wabnitz and J.A. Loo. Rapid Commun. Mass Spectrom. **16**, 85 (2002).
36. K.D. Powell, S. Ghaemmaghami, M.Z. Wang, L. Ma, T.G. Oas, and M.C. Fitzgerald. J. Am. Chem. Soc. **124**, 10256 (2002).
37. M.M. Zhu, D.L. Rempel, Z. Du, and M.L. Gross. J. Am. Chem. Soc. **125**, 5252 (2003).
38. L. Konermann and D.A. Simmons. Mass Spectrom. Rev. **22**, 1 (2003).
39. M.M.G. Krishna, L. Hoang, Y. Lin, and S.W. Englander. Methods (San Diego, Calif.), **34**, 51 (2004).
40. R.S. Johnson and K.A. Walsh. Protein Sci. **3**, 2411 (1994).
41. D. Baker and W.A. Eaton. Curr. Opin. Struct. Biol. **14**, 67 (2004).
42. Y. Bai, J.S. Milne, L. Mayne, and S.W. Englander. Proteins: Struct. Funct. Genet. **17**, 75 (1993).
43. H. Roder, G.A. Elöve, and S.W. Englander. Nature (London), **335**, 700 (1988).
44. P.K. Glasoe and F.A. Long. J. Am. Chem. Soc. **64**, 188 (1960).
45. D.A. Simmons, S.D. Dunn, and L. Konermann. Biochemistry, **42**, 5896 (2003).
46. V. Katta and B.T. Chait. J. Am. Chem. Soc. **115**, 6317 (1993).
47. D.A. Simmons and L. Konermann. Biochemistry, **41**, 1906 (2002).
48. S.V. Evans and G.D. Brayer. J. Mol. Biol. **213**, 885 (1990).
49. D. Eliezer, J. Yao, H.J. Dyson, and P.E. Wright. Nat. Struct. Biol. **5**, 148 (1998).
50. A. Miranker, C.V. Robinson, S.E. Radford, and C.M. Dobson. FASEB J. **10**, 93 (1996).
51. D.M. Ferraro, N.D. Lazo, and A.D. Robertson. Biochemistry, **43**, 587 (2004).
52. W.J.H. van Berkel, R.H.H. van den Heuvel, C. Versluis, and A.J.R. Heck. Protein Sci. **9**, 435 (2000).
53. D.A. Simmons, D.J. Wilson, G.A. Lajoie, A. Doherty-Kirby, and L. Konermann. Biochemistry, **43**, 14792 (2004).
54. F.M. Hughson, P.E. Wright, and R.L. Baldwin. Science (Washington, D.C.), **249**, 1544 (1990).
55. T.D. Wood, R.A. Chorush, F.M. Wampler, D.P. Little, P.B. O'Connor, and F.M. McLafferty. Proc. Natl. Acad. Sci. U.S.A. **92**, 2451 (1995).
56. J.C. Jurchen and E.R. Williams. J. Am. Chem. Soc. **125**, 2817 (2003).
57. K. Breuker and F.W. McLafferty. Angew. Chem. Int. Ed. **42**, 4900 (2003).

© 2005 NRC Canada

Combining H–D exchange and ESI-FAIMS-MS for detecting gas-phase conformers of equine cytochrome c[1]

Randy W. Purves, Barbara Ells, David A. Barnett, and Roger Guevremont

Abstract: Conformers of equine cytochrome c were investigated in the gas phase using a combination of high-field asymmetric waveform ion mobility spectrometry (FAIMS) and hydrogen–deuterium (H–D) exchange. Electrospray generated ions of equine cytochrome c were exposed to a low concentration of D_2O vapour while being transported by a flow of nitrogen through a FAIMS device. During this transport period of about 250 ms in the FAIMS analyzer, the various conformers of multiply charged ions of cytochrome c were simultaneously undergoing H–D exchange and being separated from each other. The extent of H–D exchange was calculated from the observed *m*/*z* of conformers after exposure to D_2O vapour in FAIMS. The complementary nature of these two methods resulted in observations supporting a greater number of conformers (e.g., at least 11 conformers were identified for the +16 charge state) than would be expected by analyzing the FAIMS data and the H–D exchange data independently.

Key words: FAIMS, H–D exchange, mass spectrometry, protein conformations, electrospray ionization.

Résumé : On a étudié les conformères du cytochrome c équin en phase gazeuse en utilisant une combinaison d'échange d'hydrogène et de deutérium et de spectrométrie de la mobilité ionique, de forme d'onde asymétrique et à haut champ (« FAIMS »). Les ions générés par électronébulisation du cytochrome c équin sont exposés à une faible concentration de vapeur de D_2O pendant qu'ils sont entraînés par un courant d'azote à travers un analyseur FAIMS. Au cours de la période de 250 ms de ce transport dans l'analyseur FAIMS, les divers conformères des ions du cytochrome c à charges multiples subissent des échanges H–D simultanés et se séparent les uns des autres. On a calculé le degré d'échange H–D à partir des valeurs *m*/*z* observées pour les conformères après leur exposition à la vapeur de D_2O dans l'analyseur FAIMS. La nature complémentaire de ces deux méthodes permet de faire des observations qui suggèrent l'existence d'un beaucoup plus grand nombre de conformères (par exemple, on a identifié au moins 11 conformères pour l'état de charge +16) que le nombre attendu sur la base d'une analyse des données FAIMS et des données d'échange H–D prises indépendamment.

Mots clés : « FAIMS », échange H–D, spectrométrie de masse, conformations de protéines, ionisation par électronébulisation.

[Traduit par la Rédaction]

Introduction

The ability to produce intact ions from large molecules (1, 2) has led to the development of several methods for studying biomolecular ions in the gas phase (3, 4). These methods have been divided into two categories (5): chemically reactive and nonreactive. Chemically reactive studies, including hydrogen–deuterium (H–D) exchange (4, 6–10), examine the reactivity of different conformations. Nonreactive studies, including drift tube ion mobility spectrometry (DTMS) (3, 4, 11, 12), use collisions with inert species to derive ion collision cross sections, and indirectly, conformational information. Compiling data from gas-phase methods having independent mechanisms of operation may bring to light new information. Additional benefits are derived from combining complementary methods experimentally, where ions separated by a first mechanism are subjected to further investigation using the second, orthogonal technique. For example, a combination of DTMS and H–D exchange was used to investigate electrosprayed ions of equine cytochrome c (5). This study showed two different H–D exchange levels for the +8 to +10 charge states (one each for either a compact or a diffuse conformer), whereas for charge states +11 through +18, a single exchange level was observed.

Recently, high-field asymmetric waveform ion mobility spectrometry (FAIMS) has emerged as an effective method for separating conformers in the gas phase at room temperature and atmospheric pressure (13–15). The FAIMS separa-

Received 22 April 2005. Published on the NRC Research Press Web site at http://canjchem.nrc.ca on 27 January 2006.

R.W. Purves,[2] B. Ells, D.A. Barnett, and R. Guevremont. Ionalytics Corporation, M50-IPF, 1200 Montreal Road, Ottawa, ON K1A 0R6, Canada.

[1]This article is part of a Special Issue dedicated to Professor P. Kebarle.
[2]Corresponding author (e-mail: randy.purves@thermo.com).

 doi: 10.1139/V05-215 © 2005 NRC Canada

tion mechanism is based on changes in the mobilities of ions at high electric fields relative to low fields (16–19). Recent studies have helped elucidate several of the experimental parameters that impact sensitivity and separation in FAIMS (20–23). The importance of the bath gas composition on the FAIMS separation (20) and in particular, on separation of protein conformers (24–26), is only beginning to be studied.

The first FAIMS conformational studies showed that multiple peaks within the compensation voltage (CV) spectra of the individual charge states of bovine ubiquitin were attributable to different conformations (13, 14). Further work with this protein (15) showed that FAIMS provided information that pointed to the existence of a greater number of conformers for the elongated charge states than have been previously reported using either DTMS (27) or H–D exchange in an FTICR (8, 9). In a recent study (28), FAIMS was used in combination with pH and solvent studies to investigate conformers of β_2-microglobulin and a mutant variant of this protein, and concluded that FAIMS could potentially be used to study the role played by different conformers in disease.

Although FAIMS and DTMS are related techniques based on ion mobility, there are several key differences between them. Several of these differences are critical to the discussion of the present work and are therefore summarized in the following.

Transit time

The electric fields that are used for separating ions in a FAIMS device are applied perpendicular to the flow of gas that carries the ions through the device. Since the ions are transported through the device by a flow of gas, all of the ions spend equal time in transit through the device. For the FAIMS device used in this study, the transit time is ~250 ms. In DTMS, the applied electric fields are used to transport the ions through a drift tube and consequently, ions will spend different times in the device. In general, the ion drift times in DTMS are short relative to the transit time through a FAIMS device.

Ion heating

The strong electric fields (E/N) used in a FAIMS device result in heating of an ion. The heating of an ion in a strong electric field is a function of the electric field strength, the ion drift velocity, and the mass of the molecules of the bath gas. The heating of an ion is an inverse function of the mass of the ion since the drift velocity decreases as the mass of the ion increases (when the charge is constant). The effect of heating on protein conformation is discussed later in this report. In most DTMS experiments, the electric fields are weak and ion heating is minimal. However, in DTMS where the ion source is decoupled from the drift tube, ion conformation can be manipulated by changing the energy used to inject ions into the drift tube (29).

Changes to ion structure during analysis

The CV is used to separate ions in a FAIMS device. At a given CV, only ions that are stable within the device at that CV are transferred through the device; all other ions are lost to the walls of the device. Consequently, if an ion changes structure during transit through the FAIMS device, the resulting ion may be transmitted at a new CV. This ion will be lost to the walls and will not be observed in the spectrum. This is analogous to an ion changing m/z during transit through a quadrupole mass analyzer. With DTMS, a change in structure (resulting in a change in the low field ion mobility) would result in a shift in the drift time; however, the ion would still be observed in the spectrum.

Continuous vs. discrete

Ion separation in FAIMS is electrically controlled. Ions can be selectively and continuously transmitted through the FAIMS device and introduced into a mass spectrometer for further investigation. With DTMS, ions will pass through the drift tube as discrete, transient ion packets.

Ion transmission

An ion focusing mechanism exists in cylindrical FAIMS devices. Ion focusing helps minimize ion losses to the walls of the device caused by diffusion and space charge repulsion (30), thereby resulting in high ion transmission efficiency. With DTMS, there is no mechanism for preventing the spread of ions owing to diffusion and space charge repulsion during transit through the drift tube. Ion spreading is minimized by reduction of ion drift times.

For use in protein conformational studies, the FAIMS device offers several benefits (many of which have been described earlier) and is an ideal technique for use in combination with other gas-phase methods. For example, an energy loss method (31, 32) in a triple quadrupole MS has been applied to obtain cross sections of bovine ubiquitin (13, 15) and bradykinin (33) conformers separated by FAIMS. In these examples, the energy loss method for determination of ion collision cross sections is readily applicable to FAIMS separated conformers, but would provide very little information if the mixture was not resolved prior to the measurement. Recently, further studies of ubiquitin were reported where conformers of ubiquitin were separated by FAIMS and the H–D characteristics of individual FAIMS-separated species were studied in an FTICR instrument (34). The objective was to establish the relationship (if any) between gas-phase collision cross section and the degree of H–D exchange of a gas-phase protein ion.

An experiment is described herein where conformers of equine cytochrome c undergo ion separation and H–D exchange simultaneously while being transported through the FAIMS device. Equine cytochrome c was selected for this experiment because several gas-phase H–D exchange studies of this protein have been described in the literature (5, 7, 35, 36).

Experimental

The ESI-FAIMS-MS instrument used in this study has been described previously (13, 15). In brief, gas-phase ions were produced using ESI and passed through a desolvation region before entering the FAIMS device. The annular region in FAIMS was 2.0 mm along the length of the device and adjustable near the ion outlet by translating the inner electrode (distance was set to ~2.5 mm). A nitrogen (Air Products, Nepean, Ontario) curtain gas, which was passed through a charcoal–molecular sieve filter, entered the desolvation region at a flow rate of 2 L/min. The gas flow

© 2005 NRC Canada

rate was adjusted using a mass flow meter (MKS type 179A, MKS Instruments, Andover, Massachusetts) that was controlled using an MKS type 1179A mass flow controller (MKS Instruments). A portion of the curtain gas carried the ions through the FAIMS device (i.e., carrier gas) at a flow rate of ~0.5 L/min (dictated by the gas throughput of the mass spectrometer). The remainder of the gas flowed out of the desolvation region towards the ESI needle (i.e., desolvation gas).

For H–D exchange experiments, a syringe containing 99.9% purity D_2O (Cambridge Isotope Laboratories, Andover, Massachusetts) was inserted into the curtain gas line (via a Tee, after the filter) such that D_2O vapour from the headspace of the syringe was entrained into the gas stream. The pressure of D_2O in the gas stream was not measured, however, H–D exchange experiments were repeated and the amount of exchange for each conformer was reproducible. Since the ions were carried through FAIMS by the flow of gas, the ion transit time (and reaction time for H–D exchange) was determined only by the gas flow rate and was equal for every species (charge states and conformers) investigated here. The reaction time for all experiments (and all types of ions) was the same (~250 ms). Since the curtain gas contained D_2O, the possibility of a limited amount of H–D exchange occurring external to the FAIMS device cannot be eliminated. However, since the ions spend only a short time external to the FAIMS device (relative to 250 ms), this contribution is not expected to be significant.

A 750 kHz asymmetric waveform generator was used and the dispersion voltage (i.e., maximum peak voltage, DV) was –4200 V for all experiments. The "OR" power supply from the mass spectrometer was used to apply the compensation voltage so that the LCTune™ (PE Sciex, Concord, Ontario) software synchronized the scanning function with the data acquisition. A separate DC power supply was used to control the OR voltage on the mass spectrometer. Ions transmitted by the FAIMS device were detected using an API 300 triple quadrupole mass spectrometer (PE Sciex, Concord, Ontario). Total ion current compensation voltage (TIC-CV) spectra were generated by collecting mass spectra (steps of 0.1 amu with a 25 ms dwell time) over specified *m/z* ranges at each CV value (in steps of 0.035 V). Ion-selected (IS)-CV spectra were acquired by monitoring a specific *m/z* value as the CV was ramped. Mass spectra, acquired at fixed values of CV, are a sum of 10 scans.

For the determination of the *m/z* of maximum ion intensity, the mass spectrum generated at each CV value was smoothed to reduce noise and improve the reliability of the measurement. The *m/z* value was recorded on the figures to an accuracy of ±0.1 amu. Mass spectra whose intensities were too low to obtain reliable measurements were omitted.

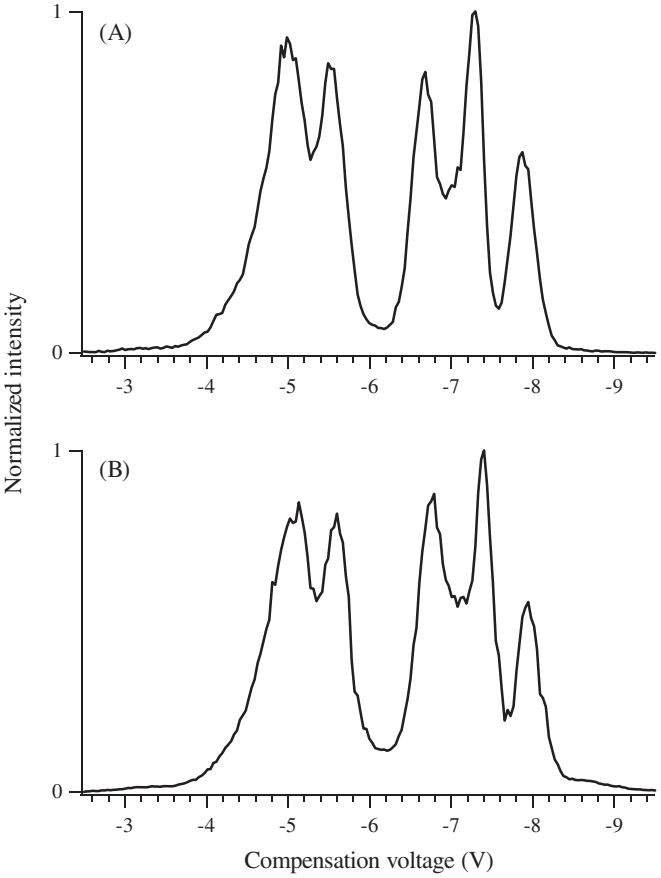
Equine cytochrome c was purchased from the Sigma Chemical Company (St. Louis, Missouri) and used without further purification. Solutions of equine cytochrome c were prepared at a concentration of 2 μmol/L in a solvent of water–methanol (1:1, *v/v*) and either 0.2% or 1% acetic acid.

Results and discussion

High charge states

A solution acidified to 1% acetic acid was used to favour the formation of the higher charge states of equine cytochrome c during the electrospray process. Figure 1 shows two CV spectra obtained for the +17 charge state. Figure 1A is an IS-CV spectrum (*m/z* 728.1) acquired with no D_2O present in the nitrogen gas stream. Experiments were carried out at the CV of maximum transmission for each of the five peaks to ensure that each peak was attributable to (at least) one different conformer and was not the result of adducts, multimers, or impurities (14). All of the peaks in the CV spectra presented in this document were treated similarly. Figure 1B is a total ion current (TIC) CV spectrum summing all ions between *m/z* 728.0 and 734.0, collected using the same experimental conditions as Fig. 1A except that D_2O was present in the nitrogen gas stream. The presence of water in the nitrogen carrier gas has been reported to have adverse effects on the performance of the FAIMS device (30), including significant changes in the CV value and complete loss of ion transmission in extreme cases. A comparison of Figs. 1A and 1B reveals that the level of D_2O used in this study did not significantly alter the appearance of the CV spectrum, and only a very small shift toward higher magnitude CV values was observed. Additionally, proton transfer reactions were not observed to substantially change the distribution of conformers of this charge state. Figures 1A and 1B indicate the presence of at least five conformers for the +17 charge state of equine

Fig. 1. (A) CV spectrum of the +17 charge state of equine cytochrome c (*m/z* 728.1) with no D_2O present in the nitrogen curtain gas and (B) TIC-CV spectrum (*m/z* 728.0–734.0) acquired with D_2O present.



© 2005 NRC Canada

cytochrome c. The observation of multiple conformers for this charge state is consistent with H–D exchange studies reported by McLafferty et al. (36) using an FTICR-MS, where the existence of five conformational states for the elongated charge states (+11 through +18) were shown.

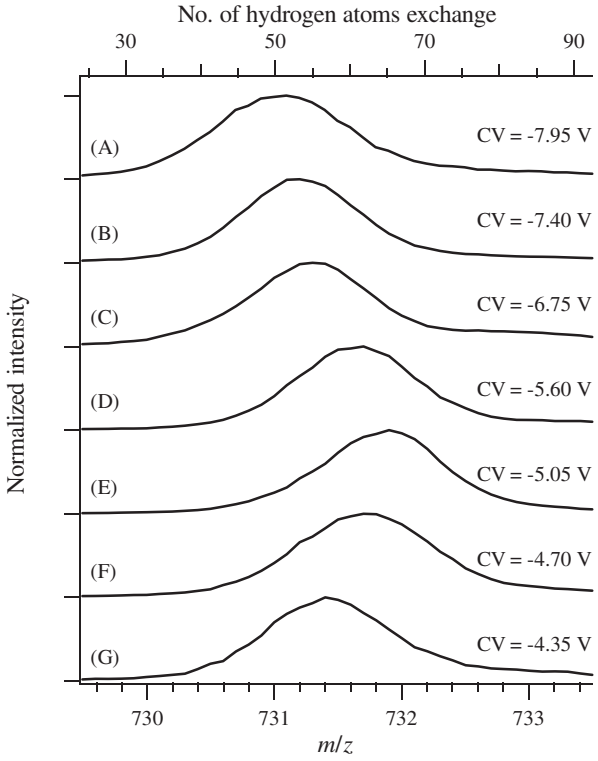
All of the mass spectra acquired in generating Fig. 1B were summed to effectively eliminate the separation by the FAIMS device and to allow an examination of only the H–D exchange data obtained in this experiment. The resulting mass spectrum (not shown) consisted of a single, broad peak centred at *m*/*z* 731.5, representing an average of 58 H–D exchanges among all conformers of this charge state. Individual mass spectra (i.e., at each CV value) were examined to determine the degree of H–D exchange of each conformer, and to determine if additional conformers could be identified using an experimental combination of FAIMS and H–D exchange. Mass spectra acquired at seven CV values, including each of the five peak maxima in Fig. 1B, are shown in Figs. 2A–2G. Although the low resolution of the quadrupole mass spectrometer made mass separation of the distribution of isotopomeric subspecies of a conformer impossible, the average mass of this ensemble was determined with an accuracy of about 0.2 *m*/*z*. Significant differences in the mass spectra are observed in going from the most negative (Fig. 2A) to the least negative CV (Fig. 2G).

The *m*/*z* values of the maximum intensity in the mass spectra were used to estimate average hydrogen atom exchange levels (top axis in Fig. 2). For example, the conformer of the +17 charge state, transmitted through FAIMS at CV –7.95 V (trace A in Fig. 2), was *m*/*z* shifted from 728.1 (without H–D exchange) to about 731.1 (with H–D exchange), corresponding to about 51 exchanges (top axis in Fig. 2). For conformers of the +17 charge state, the number of hydrogen atoms that were exchanged for deuterium ranged from about 50 to 65. The extent of exchange in this experiment was limited by the fixed exchange time using the FAIMS device (i.e., ~250 ms ion transit time) and the D_2O pressure range tolerable to FAIMS. Thus, the relationship between the maximum number of hydrogen atoms that could be exchanged for deuterium and the observed exchange levels were not available. Consequently, comparisons of the absolute exchange levels observed in this experiment with levels reported in previous studies (in which the exchange essentially went to completion) were not possible.

Figure 2 also shows that the use of the experimental combination of FAIMS and H–D exchange provides an opportunity to detect additional conformers. In particular, the traces in Figs. 2E–2G are mass spectra obtained between CV –4 and –5 V, corresponding to CV values to the left of the major peak (centred at about CV = –5 V) in Fig. 1. The gradually sloping trace in Fig. 1, between CV –4 and –5 V, suggests the possibility of several coexisting unresolved species. The three mass spectra collected in this range (Figs. 2E–2G) show different levels of deuterium incorporation, further establishing the presence of at least two overlapping conformers within this region of CV.

Individual mass spectra were examined at incremental CV values to determine the *m*/*z* value of maximum intensity (and thus, the hydrogen atom exchange level) across the CV range shown in Fig. 1B. This data is summarized for the +17 charge state of equine cytochrome c in Fig. 3A. The solid line in the figure represents the normalized intensity for the summation of all isotopomers of the +17 ion (same plot as Fig. 1B) and the individual data points (represented by "x" in the figure) indicate the *m*/*z* value (in 0.1 amu steps) of the maximum intensity in each mass spectrum. The figure shows that the CV of transmission appears to be independent of the hydrogen atom exchange level. In other words, the physical properties of the ions that lead to separation by FAIMS are quite distinctly different from the physical properties of the ions that determine the level of H–D exchange (34).

Fig. 2. Mass spectra (*m*/*z* 729.5–733.5) acquired with D_2O present in the nitrogen curtain gas. (A) CV = –7.95 V, (B) CV = –7.40 V, (C) CV = –6.75 V, (D) CV = –5.60 V, (E) CV = –5.05 V, (F) CV = –4.70 V, and (G) CV = –4.35 V.

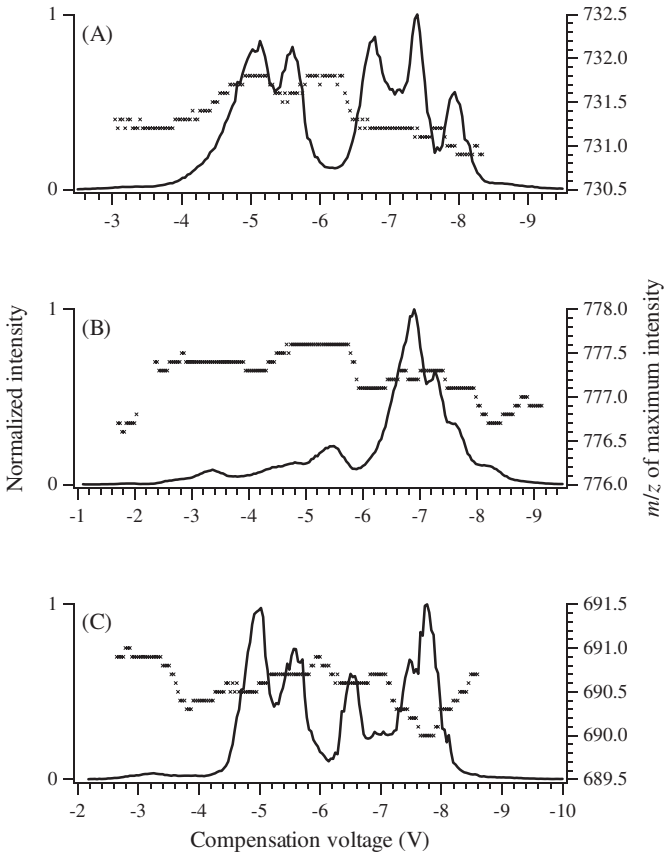


The independence of the FAIMS CV value and the level of H–D exchange provides an experimental combination that leads to new information. For example, the presence of additional conformers that did not appear as separate peaks in the CV spectrum could be deduced from the data in Fig. 3A. In Fig. 3A, the level of H–D exchange increases (*m*/*z* shifts to a higher value) at the valley between two more intense conformers(CV ~ –6 V), indicating the presence of a low abundance conformer at this CV. The H–D exchange level also revealed that the low abundance ions transmitted near a CV of –3.5 V were not part of the tail of the peak centred at CV = –5 V, but were from a different conformer.

The hydrogen atom exchange level changes rapidly as a function of CV in some cases. A steep slope (e.g., near a CV of –6.5 V) in the H–D exchange level is consistent with the presence of only two conformers each having distinctly different levels of H–D exchange, whereas a gradual slope

© 2005 NRC Canada

Fig. 3. Hydrogen atom exchange level as a function of CV for high charge states of equine cytochrome c. TIC-CV spectra of the (A) +17 (*m*/*z* 728.0–734.0), (B) +16 (*m*/*z* 773.0–780.0), and (C) +18 (*m*/*z* 687.0–693.0) charge states. The *m*/*z* value of the maximum intensity in each mass spectrum (right vertical axis) collected at incremental CV values (given by x) is superimposed on the figure.



(e.g., between CV –4 and –5 V) suggests that two or more conformers coexist with relatively similar levels of H–D exchange. The relative abundance of the conformer transmitted at CV ~ –3.5 V is much lower than the conformer transmitted at CV ~ –5 V and would have little effect on the measured *m*/*z* at intermediate CV values. Therefore, the H–D exchange data illustrates that there must be at least one additional conformer present in the region between CV = –3.5 and –5 V. The use of combined data analysis (as described earlier) has resulted in the detection of at least eight conformers for the +17 charge state of equine cytochrome c.

Other high charge states of equine cytochrome c (i.e., +14 to +21) were examined in a similar manner using a solution containing 1% acetic acid. Figures 3B and 3C show data for the +16 and +18 charge states, respectively. The solid line in Fig. 3B shows the normalized intensity for the +16 charge state (*m*/*z* 773.0–780.0) plotted as the CV was scanned from –1 to –9.5 V. The individual data points (x) in the figure represent the *m*/*z* of the maximum intensity in the mass spectra acquired at each CV value. The CV spectrum shows at least eight peaks (CV ~ –1.9 (low abundance), –3.4, –4.8, –5.5, –6.9, –7.3, –7.6, and –8.2 V), each of which was confirmed in separate experiments (not shown) to represent at least one different conformer of the +16 charge state. The combination of FAIMS with the H—D exchange data enables at least three additional conformers to be detected (i.e., at CV~ –4.1, –6.0, and –9.0 V). Thus, the data in Fig. 3B supports the assignment of at least 11 conformers for the +16 charge state. Figure 3C shows a plot of the normalized intensity (solid line, *m*/*z* 687.0–693.0) and the *m*/*z* of the maximum intensity (individual data points, x) plotted as the CV was ramped from –2 to –10 V, for the +18 charge state of equine cytochrome c. As was observed for both the +16 and +17 charge states, the CV of transmission appears to be independent of the number of hydrogen atoms exchanged. In addition to conformers identified by the FAIMS device at CV values of ~–3.2, –4.9, –5.6, –6.5, –7.0, –7.5, and –7.7 V, the presence of additional conformers at CV values of ~–4.0, –5.9, and at least one at –8.5 V can be derived from the H–D exchange information. Thus, the presence of at least 10 conformers for the +18 charge state can be extracted from Fig. 3C.

The number of conformers detected for the +16, +17, and +18 charge states of equine cytochrome c (at least 11, 8, and 10, respectively) are significantly higher than reported previously. For these charge states, results using H–D exchange (36) showed five conformational states, whereas DTMS studies (5, 37) showed only one ion cross section value for charge states +11 through +18. In acquiring the DTMS data, however, the authors indicated that they favoured a single conformer with the injection process (5).

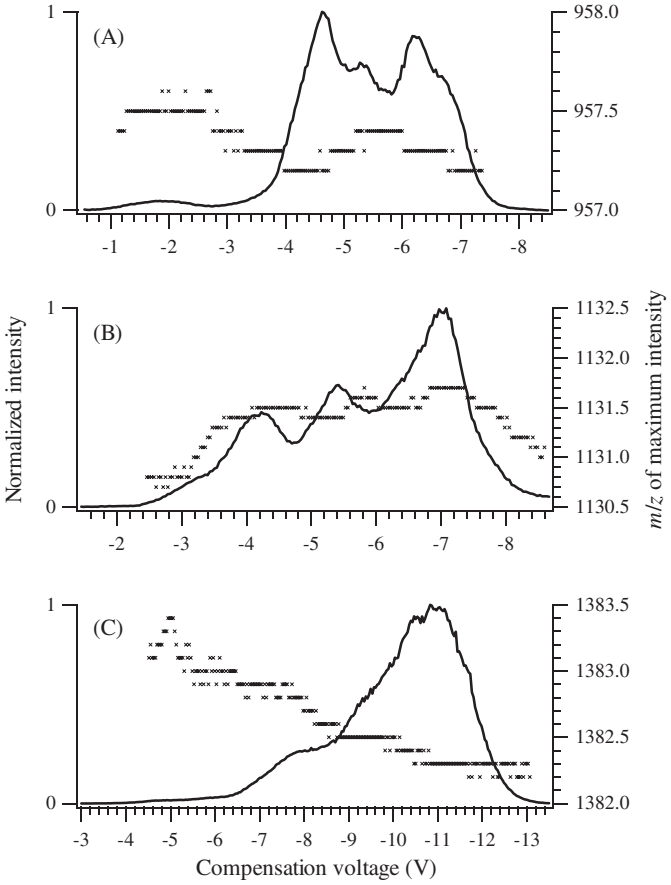
Low charge states

Low charge states of equine cytochrome c (i.e., +7 through +13) were examined using a solution of 0.2% acetic acid. In the mass spectra of the +7 and +8 charge states, the intensity of the sodiated peak relative to the protonated peak was significant (these ions were not separated by FAIMS). After H–D exchange, the wide *m*/*z* distributions of the sodiated and protonated peaks of these charge states overlapped, thereby making the determination of the amount of hydrogen atom exchange extremely difficult. Consequently, plots for these charge states have been omitted from this discussion. This limitation could be overcome by performing H–D exchange in an ion-trapping device after the FAIMS separation (34).

The data acquired using a combination of FAIMS and H–D exchange is described for three of the low charge states in Fig. 4. Figures 4A–4C show plots of the TIC-CV spectrum for the +13 (*m*/*z* 955.5–959.5), +11 (*m*/*z* 1129.0–1133.0), and +9 (*m*/*z* 1380.0–1385.0) charge states, respectively. Again, the *m*/*z* of maximum intensity is superimposed on each of the figures (shown as x). Figure 4A shows that conformers of the +13 charge state experienced similar hydrogen atom exchange levels (only a range of 0.4 amu). Nonetheless, there are several stepwise changes that occur, indicating small, but distinguishable differences. For this charge state, the experimental combination of the two techniques did not result in strong evidence to support the detection of additional conformers (likely because of the limited range of exchange for this charge state). Conversely, the data in Fig. 4B shows that the experimental combination of FAIMS and H–D exchange enabled the detection of addi-

© 2005 NRC Canada

Fig. 4. Hydrogen atom exchange level as a function of CV for low charge states of equine cytochrome c. TIC-CV spectra of the (A) +13 (*m*/*z* 955.5–959.5), (B) +11 (*m*/*z* 1129.0–1133.0), and (C) +9 (*m*/*z* 1380.0–1385.0) charge states. The *m*/*z* value of the maximum intensity in each mass spectrum (right vertical axis) collected at incremental CV values (given by x) is superimposed on the figure.



tional conformers. In particular, the presence of at least five more conformers (i.e., CV ~ –3.0, –5.9, –6.4, and at least two more conformers at CV values more negative than –7.0 V) were observed in addition to the three conformers detected by FAIMS alone (i.e., CV ~ –4.2, –5.4, –7.0 V). The +9 charge state (Fig. 4C) is different from the other charge states discussed thus far in that the number of hydrogen atoms exchanged appears to gradually decrease as the CV becomes more negative. In addition, the TIC-CV spectrum shows only two main peaks, however, the shoulders on the main peak at CV ~ –9.4 and –10.5 V are reproducible. Although the presence of only four conformers is confirmed (i.e., CV ~ –5.0, –7.5, –9.5, and –11.0 V), the data suggests that this charge state is composed of additional conformers with similar H–D exchange levels that were only partially separated using the FAIMS device.

In addition to examining hydrogen atom exchange levels within charge states, a comparison of the exchange levels between different charge states can also be made. For the six charge states shown in Figs. 3 and 4, the greatest amount of exchange was observed for the +9 charge state (i.e., range from 71 to 81) and the lowest amount was observed for the +18 charge state (i.e., range from 42 to 60). The maximum amount of average hydrogen atom exchange observed for all of the charge states in Figs. 3 and 4 in decreasing order was: +9 (81), +11 (77), +13 (76), +16 (66), +17 (65), +18 (60). The decrease in the number of hydrogen atoms exchanged with increasing charge state is consistent with previous work by McLafferty et al. (36).

Influence of DV on conformation

The high electric fields (E/N) used in FAIMS will cause "heating" of a protein conformer because of the high velocities that the ions experience as they move through the bath gas. This heating could cause the ion to adopt new structures. The two-temperature kinetic theory of gaseous ion transport (38, 39) uses the effective temperature (T_{eff}) to characterize the total random energy of the ions, which consists of a thermal part and a field part (40). Since the applied electric field in FAIMS changes with time, an expression for the average effective temperature ($\overline{T}_{eff}$) in a FAIMS device was used and is given as (15, 40)

$$[1] \qquad \overline{T}_{eff} = T\left[1 + \frac{M\overline{v}_d^2}{3RT}\right]$$

where T is the gas temperature, M is the molar mass of the gas, R is the ideal gas constant, and $\overline{v}_d$ is the average velocity of the ion as given by

$$[2] \qquad \overline{v}_d = N_0 K_0 \left(\frac{\overline{E}}{N}\right)$$

Here, N_0 is Loschmidt's constant, K_0 is the reduced mobility, $\overline{E}$ is the average electric field in the FAIMS separation region, and N is the number density of the bath gas at ambient conditions. The maximum value of E (and hence v_d) can also be used in eqs. [1] and [2] to calculate the maximum effective temperature (T^{m}_{eff}) when the waveform is at its peak value. Previous calculations (15) of the values of $\overline{T}_{eff}$ and T^{m}_{eff} for conformers of bovine ubiquitin showed increases of ion temperature of ~7 and 31 K, respectively, at the highest DV used (DV = –4400 V).

To illustrate the effects of heating, calculations of the effective temperature were carried out for the +16 charge state. Experimental values of K_0 for several charge states (including +16) of equine cytochrome c were determined using an ion mobility spectrometer containing nitrogen gas (41). Based on this data, the reduced mobility value at room temperature for the +16 charge state (required in eq. [2]) was ~0.9 $cm^2\ V^{-1}\ s^{-1}$. At the DV (i.e., DV = –4200 V) used in this study, the calculated values of $\overline{T}_{eff}$ and T^{m}_{eff} were 10 and 47 K, respectively.

Previous work with DTMS has shown that gas-phase heating occuring via transport of an ion at high E/N can modify conformer structure. An increase of ion injection energy during introduction of a protein into the drift tube of a low-pressure IMS was shown to unfold compact conformers to less compact conformations (3, 29). In addition, the FAIMS-energy loss method showed that the measured cross section of a compact conformer increased as the energy drop into the second quadrupole of the mass spectrometer was increased (13). From these studies, the compact conformers

© 2005 NRC Canada

that are observed for the lower charge states appear to be most susceptible to structural changes induced by heating.

The effect of heating on protein conformation in the FAIMS device will require further investigation. Consider the situation in which heating leads to a change of conformation of an ion during its transit through the FAIMS device. The resulting CV spectrum is expected to be modified relative to a spectrum in which all ions retain their structure during the separation. As described in the Introduction, if an ion changes conformation during transit through the FAIMS device, and the CV of the ion changes, this ion will no longer be stable within the FAIMS device. The ion will be lost to the walls of the FAIMS device and not observed in the CV spectrum. In this example, a particular conformer can only be observed if the CV of transmission does not significantly change during transport through FAIMS. For this reason, and because of a relatively low value of the average $\overline{T}_{\text{eff}}$ of about 10 K in the present work, evidence of field-induced changes of conformation are not apparent in this work. This will be investigated further when instruments capable of higher voltages become available.

This study has illustrated that a relatively simple experiment in which ions simultaneouly undergo H–D exchange and separation in FAIMS, offers new opportunity for the study of protein ions. Further work is required to help identify the chemical (interaction with the bath gas) or mechanical (shape, flexibility) properties of the ions that contribute to the nonlinear behavior of K_h/K upon which the FAIMS separation is based. This knowledge may offer insight into ion structure. The extent to which FAIMS operational parameters, such as using strong electric fields for ion heating and using trace modifiers in the FAIMS carrier gas, can be used to probe structure, also requires investigation.

Conclusions

An experimental combination of FAIMS and H–D exchange was employed to investigate gas-phase conformers of equine cytochrome c. The ions exposed to low concentrations of D_2O vapour in the FAIMS bath gas simultaneously undergo H–D exchange and separation during transport through the FAIMS analyzer. In general, the CV of ion transmission was found to be independent of the number of hydrogen atoms exchanged. The experimental combination of these complementary techniques enabled a greater number of conformers to be detected (i.e., at least 11 conformers for the +16 charge state) than have previously been reported for equine cytochrome c using gas-phase techniques.

References

1. J.B. Fenn, M. Mann, C.K. Meng, S.F. Wong, and C.M. Whitehouse. Science (Washington, D.C.), **246**, 64 (1989).
2. M. Karas and F. Hillenkamp. Anal. Chem. **60**, 2299 (1988).
3. C.S. Hoaglund-Hyzer, A.E. Counterman, and D.E. Clemmer. Chem. Rev. **99**, 3037 (1999).
4. M.F. Jarrold. Annu. Rev. Phys. Chem. **51**, 179 (2000).
5. S.J. Valentine and D.E. Clemmer. J. Am. Chem. Soc. **119**, 3558 (1997).
6. B.E. Winger, K.J. Light-Wahl, A.L. Rockwood, and R.D. Smith. J. Am. Chem. Soc. **114**, 5897 (1992).
7. D. Suckau, Y. Shi, S.C. Beu, M.W. Senko, J.P. Quinn, F.M. Wampler III, and F.W. McLafferty. Proc. Natl. Acad. Sci. U.S.A. **90**, 790 (1993).
8. C.J. Cassady and S.R. Carr. J. Mass Spectrom. **31**, 247 (1996).
9. M.A. Freitas, C.L. Hendrickson, M.R. Emmett, and A.G. Marshall. Int. J. Mass Spectrom. **187**, 565 (1999).
10. M.K. Green and C.B. Lebrilla. Mass Spectrom. Rev. **16**, 53 (1997).
11. D.E. Clemmer, R.R. Hudgins, and M.F. Jarrold. J. Am. Chem. Soc. **117**, 10141 (1995).
12. P. Dugourd, R.R. Hudgins, D.E. Clemmer, and M.F. Jarrold. Rev. Sci. Instrum. **68**, 1122 (1997).
13. R.W. Purves, D.A. Barnett, B. Ells, and R. Guevremont. J. Am. Soc. Mass Spectrom. **11**, 738 (2000).
14. R.W. Purves, R. Guevremont, and D. Barnett. Int. J. Mass Spectrom. **197**, 163 (2000).
15. R.W. Purves, D.A. Barnett, B. Ells, and R. Guevremont. J. Am. Soc. Mass Spectrom. **12**, 894 (2001).
16. I.A. Buryakov, E.V. Krylov, E.G. Nazarov, and U.K. Rasulev. Int. J. Mass Spectrom. Ion Processes, **128**, 143 (1993).
17. B.L. Carnahan and A.S. Tarassov. US Patent 5 420 424, 30 May 1995.
18. R.W. Purves, R. Guevremont, S. Day, C.W. Pipich, and M.S. Matyjaszczyk. Rev. Sci. Instrum. **69**, 4094 (1998).
19. R.W. Purves and R. Guevremont. Anal. Chem. **71**, 2346 (1999).
20. A. Shvartsburg, K. Tang, and R.D. Smith. Anal. Chem. **76**, 7366 (2004).
21. A. Shvartsburg, K. Tang, and R.D. Smith. J. Am. Soc. Mass Spectrom. **16**, 2 (2005).
22. A. Shvartsburg, K. Tang, and R.D. Smith. J. Am. Soc. Mass Spectrom. **16**, 1447 (2005).
23. A. Shvartsburg, K. Tang, and R.D. Smith. J. Am. Soc. Mass Spectrom. **15**, 1487 (2004).
24. R. Guevremont, R.W. Purves, and D.A. Barnett. US Patent 6 639 212, 28 October 2003.
25. R. Guevremont, R.W. Purves, and D.A. Barnett. US Patent 6 774 360, 10 August 2004.
26. R. Guevremont, R.W. Purves, D.A. Barnett, and B. Ells. PCT Patent W0 03/067237, 2003.
27. J.A. Taraszka, J. Li, and D.E. Clemmer. J. Phys. Chem. B, **104**, 4545 (2000).
28. A.J.H. Borysik, P. Read, D.R. Little, R.H. Bateman, S.E. Radford, and A.E. Ashcroft. Rapid Commun. Mass Spectrom. **18**, 2229 (2004).
29. D.E. Clemmer and M.F. Jarrold. J. Mass Spectrom. **32**, 577 (1997).
30. R. Guevremont and R.W. Purves. Rev. Sci. Instrum. **70**, 1370 (1999).
31. T. Covey and D.J. Douglas. J. Am. Soc. Mass Spectrom. **4**, 616 (1993).
32. Y. Chen, B.A. Collings, and D.J. Douglas. J. Am. Soc. Mass Spectrom. **8**, 681 (1997).
33. R.W. Purves, D.A. Barnett, B. Ells, and R. Guevremont. Rapid Commun. Mass Spectrom. **15**, 1453 (2001).
34. E.W. Robinson and E.R. Williams. J. Am. Soc. Mass Spectrom. **16**, 1427 (2005).
35. T.D. Wood, R.A. Chorush, F.M. Wampler III, D.P. Little, P.B. O'Connor, and F.W. McLafferty. Proc. Natl. Acad. Sci. U.S.A. **92**, 2451 (1995).
36. F.W. McLafferty, Z. Guan, U. Haupts, T.D. Wood, and N.L. Kelleher. J. Am. Chem. Soc. **120**, 4732 (1998).
37. K.B. Shelimov, D.E. Clemmer, R.R. Hudgins, and M.F. Jarrold. J. Am. Chem. Soc **119**, 2240 (1997).

© 2005 NRC Canada

38. L.A. Viehland and E.A. Mason. Ann. Phys. **91**, 499 (1975).
39. L.A. Viehland and E.A. Mason. Ann. Phys. **110**, 287 (1978).
40. E.A. Mason and E.W. McDaniel. Transport properties of ions in gases. John Wiley and Sons, Inc., New York. 1988.
41. R. Guevremont, K.W.M. Siu, and L. Ding. *In* Proceedings of the 45th ASMS Conference on Mass Spectrometry and Allied Topics, Palm Springs, California. 1–5 June 1997. 1997. p. 374.

© 2005 NRC Canada

Structural and sequence effects in the fragmentation of protonated tripeptides containing tyrosine[1]

Alex G. Harrison

Abstract: The fragmentation reactions of a variety of protonated tripeptides containing tyrosine in the three possible positions have been studied by energy-resolved collision-induced dissociation mass spectrometry. The primary fragmentation reactions involve cleavage of the N-terminal and (or) C-terminal amide bond with the relative importance of the two cleavages depending strongly on the identity and position of the amino acid residues in the tripeptide. The results are interpreted in terms of the a_1–y mechanism for cleavage of the N-terminal amide bond and the b_x–y_z mechanism for cleavage of the C-terminal amide bond and, indeed, provide support for these mechanisms. However, it appears likely that, for protonated H-Val-Tyr-Pro-OH, the neutral accompanying formation of the y_1 (protonated proline) ion is a cyclic dipeptide (cyclo-Val-Tyr) rather than the oxazolone predicted by the b_x–y_z mechanism.

Key words: tyrosine-containing peptides, fragmentation mechanisms, tandem mass spectrometry.

Résumé : Faisant appel à la spectrométrie de masse avec dissociation induite par une collision et résolue en énergie, on a étudié les réactions de fragmentation d'une variété de tripeptides protonés contenant de la tyrosine dans les trois positions possibles. Les réactions primaires de fragmentation implique un clivage de la liaison amide N-terminale et (ou) C-terminale; l'importance relative de ces deux modes de clivage dépend fortement de l'identité et la position des résidus d'acides aminés dans le tripeptide. On interprète les résultats en fonction du mécanisme a_1–y pour le clivage de la liaison amide N-terminale et en fonction du mécanisme b_x–y_z pour le clivage de la liaison amide C-terminale et les résultats expérimentaux supportent ces mécanismes. Toutefois, il semble probable que, pour le H-Val-Tyr-Pro-OH, le produit neutre qui accompagne la formation de l'ion y_1 (proline protonée) est un dipeptide cyclique (cyclo-Val-Tyr) plutôt que l'oxazolone à laquelle on s'attend sur la base du mécanisme b_x–y_z.

Mots clés : peptides contenant de la tyrosine, mécanismes de fragmentation, spectrométrie de masse en tandem.

[Traduit par la Rédaction]

Introduction

With the introduction of the soft ionization techniques of electrospray ionization (ESI) (1–3) and matrix-assisted laser desorption–ionization (MALDI) (4, 5) tandem mass spectrometry (6, 7) of protonated peptides has become an important method for determining the amino acids present, as well as their sequence, in peptides. As a result of many studies, the main fragmentation reactions occurring on collision-induced dissociation (CID) of protonated peptides are well-established (8–11), at least in a qualitative sense, as illustrated in Scheme 1. However, in many cases the factors that determine relative fragment ion abundances are not clearly understood. Upon low-energy CID the fragment ion spectrum typically consists of a series of b, a, and y ions arising from amide bond cleavage in the protonated peptide; these fragment ions normally provide the necessary information for amino acid identification and sequencing.

It has been shown (12, 13) that the y ions are protonated amino acids (y_1) or truncated peptides (y_n). The b ions originally were considered to be acyclic acylium ions (8, 10, 11); however, extensive experimental and theoretical studies (14–20) have shown that, in many cases, at least the lower mass b_n (n = 2 or 3) ions have a cyclic protonated oxazolone structure arising by nucleophilic attack of the next-nearest carbonyl function as the amide bond is being cleaved. When there are strong nucleophilic side-chain groups, alternative cyclic structures may be formed by attack of the side-chain nucleophile as amide bond cleavage occurs; this appears to be the case for protonated peptides containing lysine (21–24), arginine (23, 25), or histidine (26–28). As a result, b_1 ions normally are not seen unless cyclization occurs involving the side-chain nucleophile. The a ions frequently arise by loss of CO from the b ions (14, 15, 28, 29), although other pathways do exist. Despite the extensive studies, relatively little is known concerning the structural and sequence factors that determine the propensity for b, a, and y ion formation. The present study has examined the fragmentation reactions of a variety of protonated peptides containing tyrosine in an effort to obtain information on the structural and

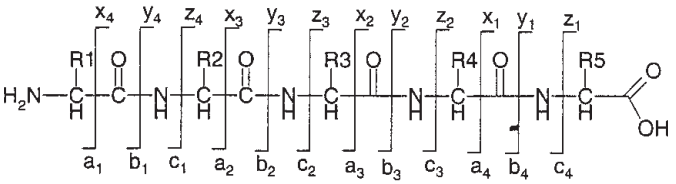
Received 19 April 2005. Published on the NRC Research Press Web site at http://canjchem.nrc.ca on 28 January 2006.

A.G. Harrison. Department of Chemistry, University of Toronto, 80 St. George Street, Toronto, Ont M5S 3H6, Canada. (e-mail: aharriso@chem.utoronto.ca).

[1]This article is part of a Special Issue dedicated to Professor P. Kebarle.

 doi: 10.1139/V05-206 © 2005 NRC Canada

Scheme 1.



sequence effects that influence the fragmentation of the protonated species upon low-energy collisional activation.

Experimental

Collision-induced dissociation studies were carried out using an electrospray / quadrupole mass spectrometer (VG Platform, Micromass, Manchester, UK) with CID in the interface region between the atmospheric pressure source and the quadrupole mass analyzer, so-called cone voltage CID. It has been clearly established (30–34) that by varying the field in this interface region, energy-resolved mass spectra (35) similar to those obtained by variable low-energy CID in quadrupole cells can be obtained. The results of these cone voltage CID studies are presented in the following as breakdown graphs expressing the percentage of total ion signal as a function of the cone voltage, a measure of the field in the interface region. Ionization was by electrospray with the sample dissolved at micromolar concentration in CH_3CN – 1% aqueous formic acid (1:1). The sample was introduced into the ion source at a flow rate of 30 μL min^{-1} with nitrogen as both nebulizing and drying gas.

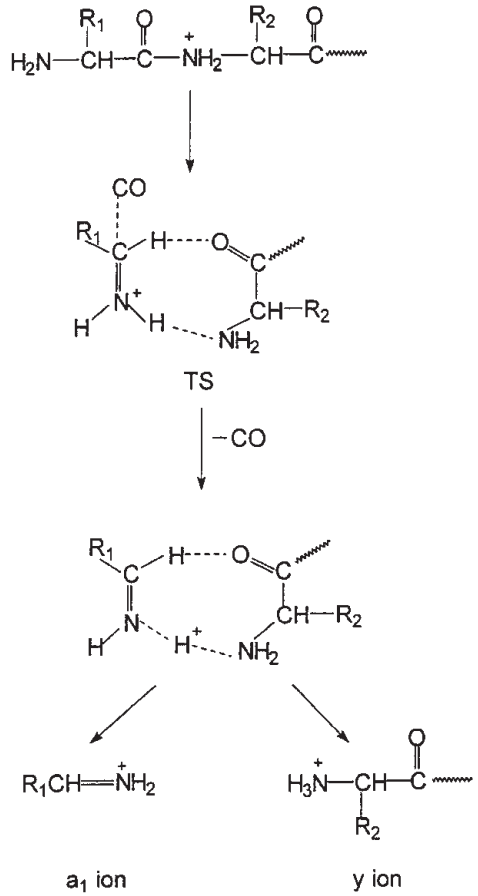
All peptide samples were obtained from Bachem Biosciences (King of Prussia, Pennsylvania) and were used as received.

Results and discussion

The major fragmentation reactions of protonated peptides frequently involve cleavage of an amide bond. For tripeptides there are two amide bonds that can be cleaved, the N-terminal and the C-terminal amide bond. Although not definitively established, it appears most likely that amide bond cleavage occurs from the amide–nitrogen protonated species. Ab initio calculations have shown that protonation at the amide nitrogen leads to considerable weakening of the amide bond, while protonation at the amide oxygen results in strengthening of the amide bond (36–38). For peptides not containing strongly basic residues there is general agreement that the most basic site is the N-terminal amino group, although usually there are other stable structures only slightly higher in energy (39–41). It also has been clearly established (12, 42, 43) that, at least for simple peptides, the proton added in the ionization process is mobile and can readily migrate to an amide nitrogen at internal energies below that required for fragmentation, the so-called mobile proton model (26, 44).

The detailed mechanisms of amide bond cleavage are not firmly established. For cleavage of the N-terminal amide bond there is substantial evidence (45–47) that fragmentation occurs by way of the a_1–y mechanism outlined in Scheme 2, which involves, at least at low internal energies, elimination of CO to form a proton-bound complex of an

Scheme 2.



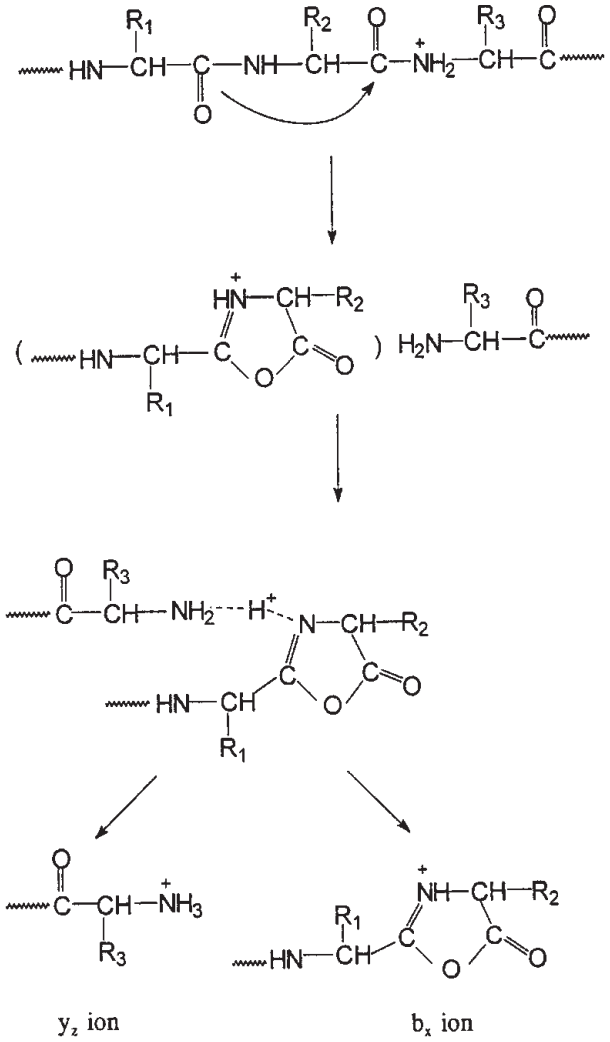
imine and an amino acid/peptide. On fragmentation of this complex the proton preferentially resides with the species (imine or amino acid or peptide) with the higher proton affinity resulting in the formation of an iminium ion and (or) a protonated amino acid or truncated peptide. Again, there is substantial evidence (47–51) that cleavage of amide bonds, other than the N-terminal amide bond, occurs by way of the b_x–y_z mechanism outlined in Scheme 3 for a tripeptide. At least at low internal energies, this mechanism involves formation of a proton-bound complex of a cyclic oxazolone and an amino acid (or a truncated peptide for larger peptides). On fragmentation of this complex, the proton would be expected to reside with the species of higher proton affinity resulting, for a tripeptide, in formation of a protonated oxazolone (b_2 ion) and (or) a protonated amino acid (y_1 ion). The results of the present study will be interpreted in terms of these mechanisms and, indeed, provide support for the detailed pathways outlined in Schemes 2 and 3.

H-Tyr-Aaa-Bbb-OH

Figure 1 shows the breakdown graph obtained for protonated H-Tyr-Gly-Gly-OH. At the lowest collision energies the b_2 ion (C-terminal amide bond cleavage) and the a_1 ion (N-terminal amide bond cleavage) are of similar intensity with very minor formation of the y_2 ion. It appears that the two possible amide bond cleavage reactions have similar critical reaction energies. As the collision energy increases the a_1 ion dominates the CID mass spectrum indicating that

© 2005 NRC Canada

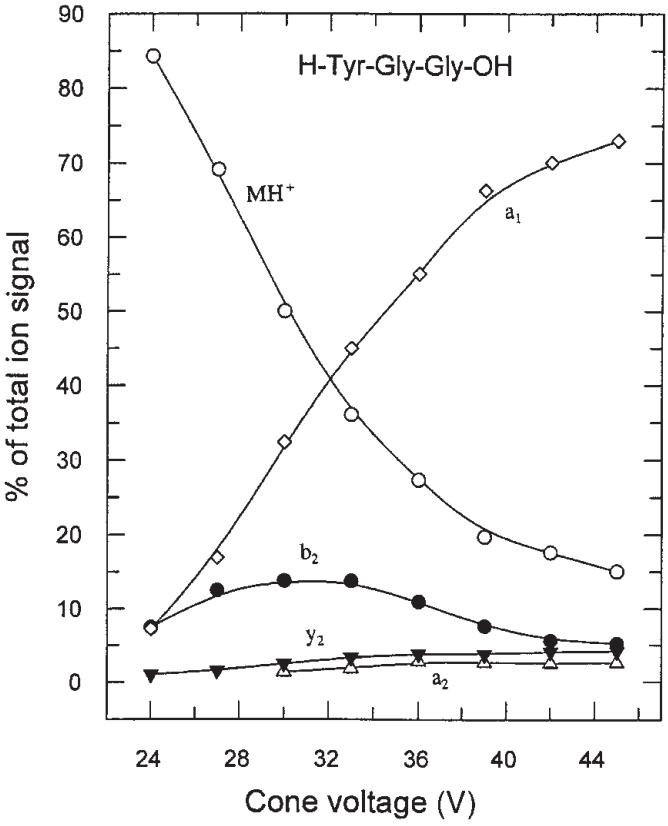
Scheme 3.



cleavage of the N-terminal amide bond is entropically favoured in comparison with cleavage of the C-terminal amide bond. The proton affinity of $HOC_6H_4CH_2CH{=}NH$ has been calculated (46) to be 225.1 kcal mol^{-1} (1 cal = 4.184 J), which is considerably greater than the value of ca. 219 kcal mol^{-1} for the proton affinity of diglycine (estimated from the gas-phase basicity, GB(diglycine) = 210.8 kcal mol^{-1} (52)). Thus, it is not surprising that, in terms of Scheme 2, the a_1 ion is favoured rather than the y_2 ion on cleavage of the N-terminal amide bond.

Figure 2 presents the breakdown graph for protonated H-Tyr-Gly-Val-OH. The b_2 ion is more prominent than for H-Tyr-Gly-Gly-OH (Fig. 1) presumably because neutral H-Val-OH, derived by cleavage of the C-terminal amide bond, is more stable than H-Gly-OH. The a_1 ion dominates the breakdown graph at higher collision energies. It arises both by cleavage of the N-terminal amide bond and, most likely, by further fragmentation of the b_2 ion. The cleavage reaction $b_2 \rightarrow a_1$ has been noted previously (18); the fragmentation mechanism proposed by Siu and co-workers (53, 54) is presented in Scheme 4. The formation of the a_1 ion from the b_2 ion is in competition with fragmentation of b_2 to a_2 by loss of CO.

Fig. 1. Breakdown graph for protonated H-Tyr-Gly-Gly-OH. In this and the following figures MH^+ represents the protonated peptide subject to collisional activation.



The breakdown graph obtained for protonated H-Tyr-Ala-Gly-OH is shown in Fig. 3. The replacement of H by CH_3 as the side chain on the central amino acid residue has made the formation of the b_2 ion (C-terminal amide bond cleavage) the dominant primary fragmentation reaction (compare with Fig. 1). In this respect one notes that the proton affinity of 2-aminomethyl-5-oxazolone has been calculated to be 217.6 kcal mol^{-1}, while that of 2-aminomethyl-4-methyl-5-oxazolone has been calculated to be 220.5 kcal mol^{-1} (50). The main pathway to the a_1 ion, which dominates the breakdown graph at higher collision energies, appears to be by fragmentation of the b_2 ion (Scheme 4), although at higher collision energies formation of a_1 by cleavage of the N-terminal amide bond may be occurring. The b_2 ion also shows minor fragmentation to the a_2 ion by loss of CO.

Figure 4 shows the breakdown graph for protonated H-Tyr-Val-Gly-OH. The b_2 ion is the dominant low-energy fragmentation product (C-terminal amide bond cleavage), although there is some formation of the y_2 ion (N-terminal amide bond cleavage) at higher collision energies. The b_2 ion fragments primarily to the a_2 ion which, in turn, fragments to form both the a_1 ion (tyrosine iminium ion) and the internal valine iminium ion at *m/z* 72. The mechanism proposed (55) for fragmentation of a_2 ions to iminium ions, outlined in Scheme 5, involves formation of a proton-bound complex of two imines; on decomposition of this complex one would expect the proton to preferentially reside with the species of higher proton affinity. In this respect we note the

© 2005 NRC Canada

Fig. 2. Breakdown graph for protonated H-Tyr-Gly-Val-OH.

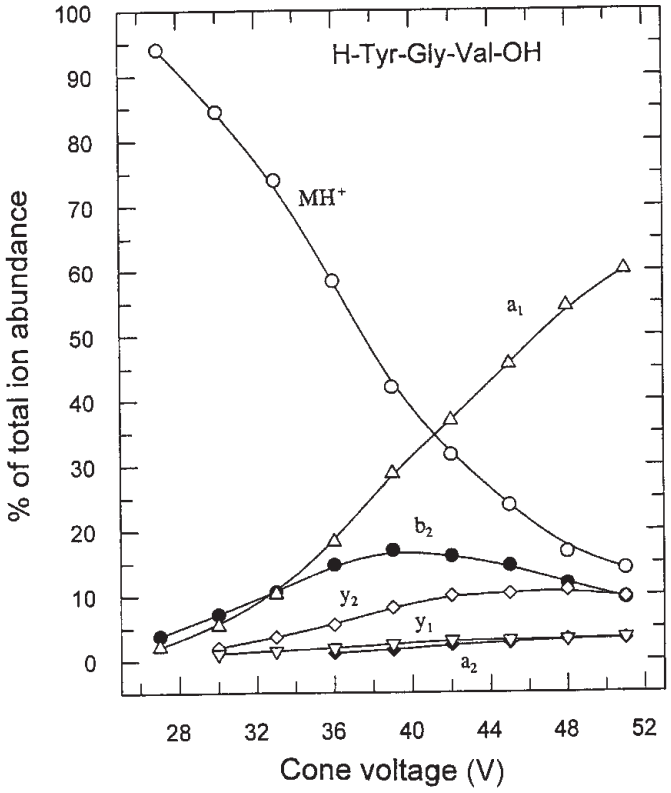
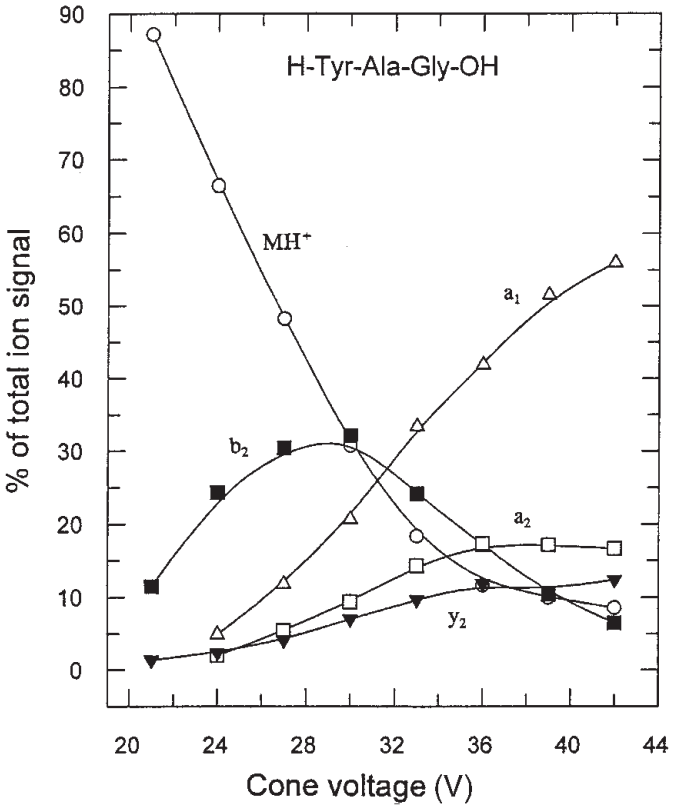
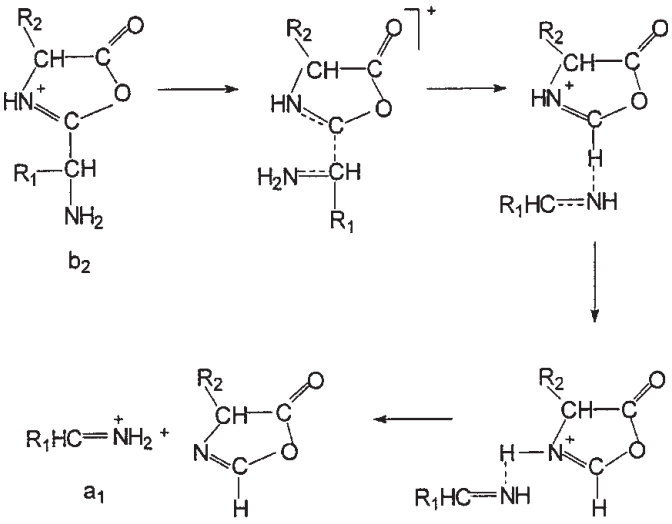


Fig. 3. Breakdown graph for protonated H-Tyr-Ala-Gly-OH.

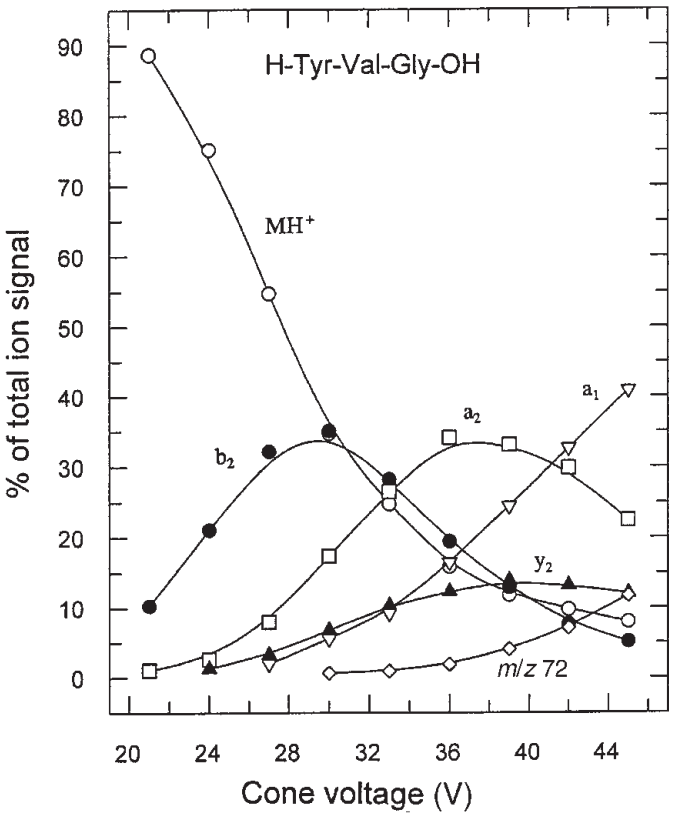


Scheme 4.



calculated (46) proton affinities, PA($HOC_6H_4CH_2CH{=}NH$) = 225.1 kcal mol^{-1} and PA($(CH_3)_2CHCH{=}NH$) = 221.7 kcal mol^{-1}; in line with these relative proton affinities, the tyrosine iminium ion (*m/z* 136) is more abundant than the valine iminium ion (*m/z* 72).

Fig. 4. Breakdown graph for protonated H-Tyr-Val-Gly-OH (*m/z* 72 represents the internal valine iminium ion).



H-Aaa-Tyr-Bbb-OH

The breakdown graphs for protonated H-Gly-Tyr-Ala-OH, H-Val-Tyr-Val-OH, and H-Leu-Tyr-Leu-OH (Figs. 5–7) are similar in showing that the major primary fragmentation reaction involves cleavage of the C-terminal amide bond to form predominantly the appropriate b_2 ion. In each case the

© 2005 NRC Canada

Scheme 5.

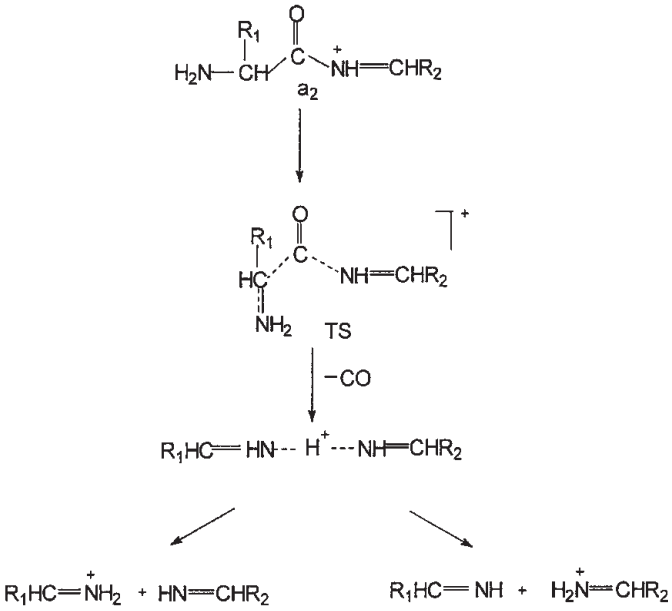
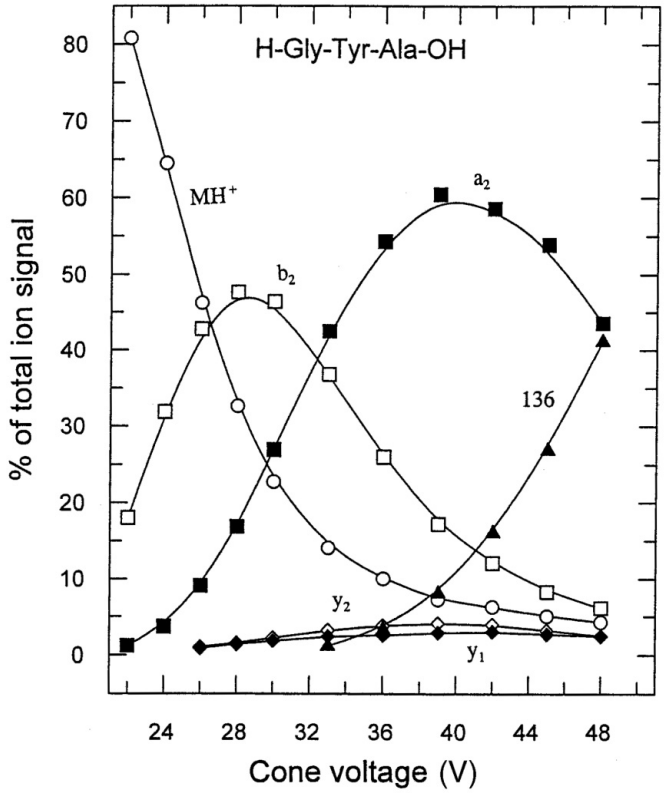


Fig. 5. Breakdown graph for protonated H-Gly-Tyr-Ala-OH (136 represents the internal tyrosine iminium ion).



b_2 ion fragments primarily by loss of CO to give the a_2 ion. The Gly-Tyr a_2 ion fragments (Scheme 5) to give only the internal tyrosine iminium ion (*m/z* 136) because the calculated (46) proton affinity of $HOC_6H_4CH_2CH{=}NH$ (225.1 kcal mol^{-1}) is considerably greater than the proton affinity of $CH_2{=}NH$ (207.2 kcal mol^{-1}). However, the Val-Tyr and Leu-Tyr a_2 ions fragment to both possible iminium ions;

Fig. 6. Breakdown graph for protonated H-Val-Tyr-Val-OH (136 represents the internal tyrosine iminium ion, 72 the valine iminium ion).

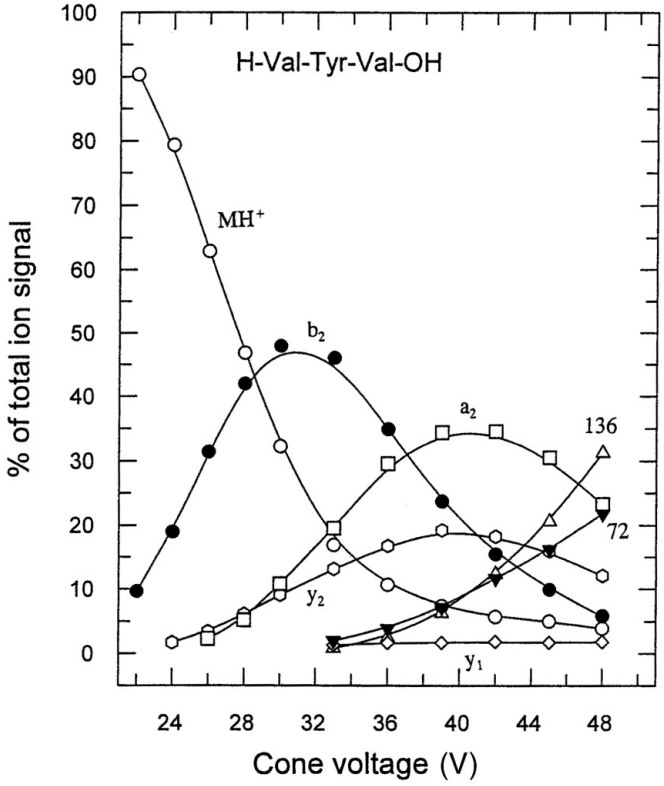
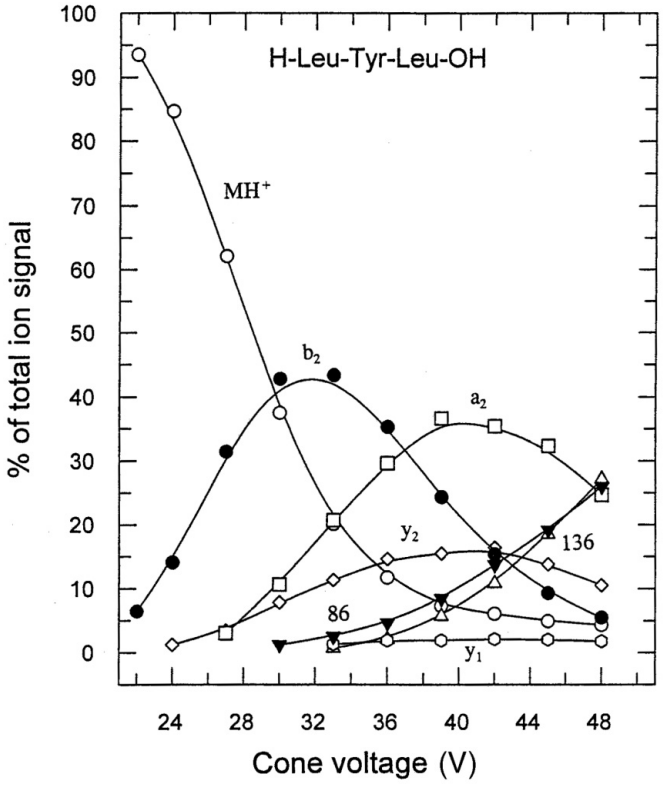


Fig. 7. Breakdown graph for protonated H-Leu-Tyr-Leu-OH (136 represents the internal tyrosine iminium ion, 86 the leucine iminium ion).



© 2005 NRC Canada

Fig. 8. Breakdown graph for protonated H-Val-Tyr-Pro-OH (136 represents the internal tyrosine iminium ion, 72 the valine iminium ion).

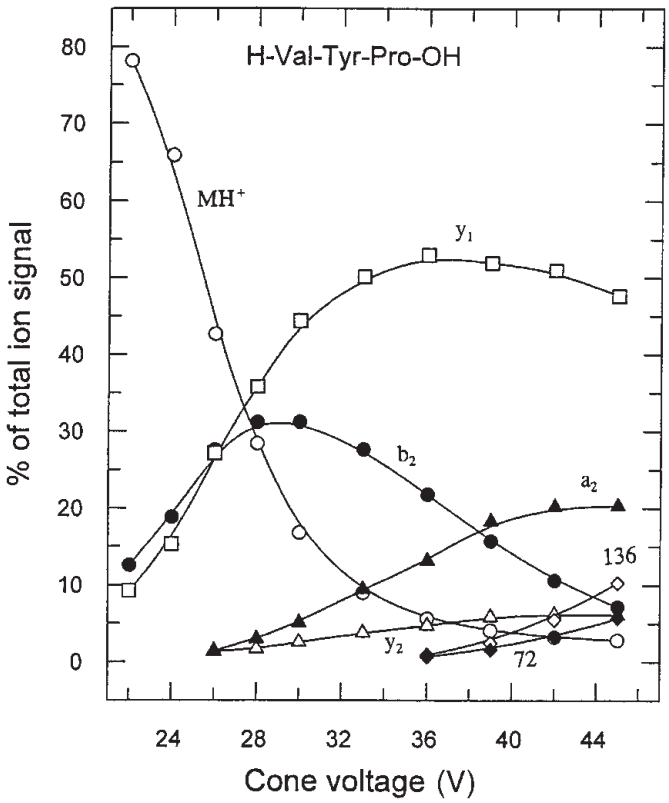
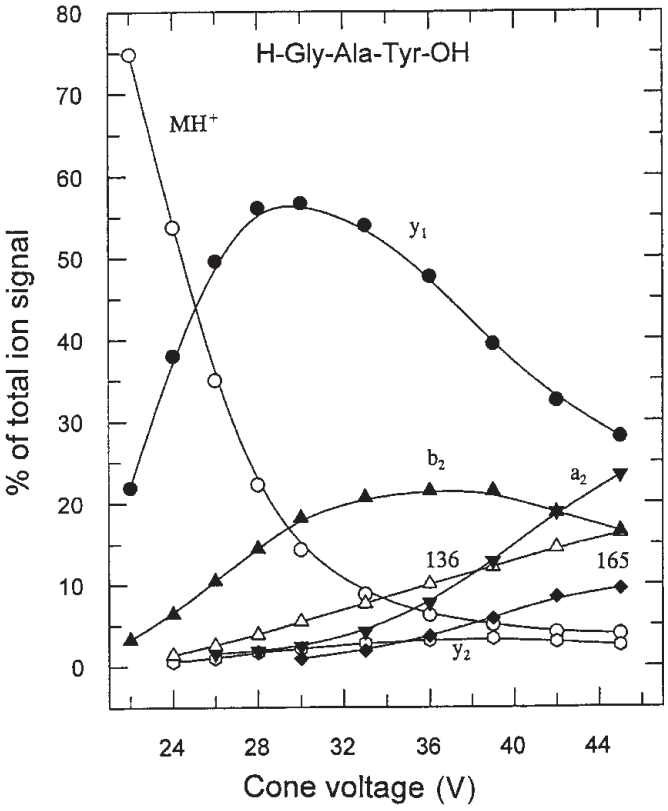


Fig. 9. Breakdown graph for protonated H-Gly-Ala-Tyr-OH (136 represents the tyrosine iminium ion, 165 represents y_1-NH_3).



in both cases the a_1 iminium ion may arise, in part, by initial cleavage of the N-terminal amide bond and, indeed, significant ion signals are observed for the corresponding y_2 ion in both systems.

Protonated Val-Tyr-Pro-OH (Fig. 8) shows a different behaviour in that the b_2 and y_1 ions are of approximately equal abundance at low collision energies indicating dominant cleavage of the C-terminal amide bond. The equal formation of the b_2 and y_1 ions is somewhat surprising in terms of the b_x–y_z mechanism outlined in Scheme 3. The oxazolone derived from Gly-Phe (2-aminomethyl-4-benzyl-5-oxazolone) has been calculated (49) to have a proton affinity of 224.2 kcal mol^{-1}; the proton affinity of the oxazolone derived from Val-Tyr would be expected to be higher than this value. There is some uncertainty in the proton affinity of proline with values ranging from 220 to 226 kcal mol^{-1} having been reported (52, 56–60). The most recent experimental value (60) is 221.3 kcal mol^{-1} in agreement, within expected error, with the value of 220.8 kcal mol^{-1} calculated by Maksić and Kovačević (56); it appears likely that the recent determinations by the kinetic method of 225.7 (58) and 224.9 kcal mol^{-1} (59) are too high for reasons unknown. It thus appears likely that the proton affinity of proline is significantly less than that of the oxazolone derived from Val-Tyr; given this difference, the pathway of Scheme 3 would predict a more abundant formation of the b_2 ion than the y_1 ion. However, there is substantial evidence from neutral fragment reionization (61) studies that, in the fragmentation of protonated H-Leu-Gly-Pro-OH, the neutral accompanying the y_1 ion (proline·H^+) is a cyclic peptide (cyclo-Leu-Gly) rather than an oxazolone (16). Calculations (62) have shown that the proton affinities of cyclic peptides are much lower than the proton affinities of the isomeric oxazolones. For example, the calculated proton affinity of cyclo-Leu-Gly has been calculated to be 210 kcal mol^{-1} (62), while the proton affinity of the isomeric 2-aminomethyl-4-isobutyl-5-oxazolone has been calculated to be 223.7 kcal mol^{-1} (49). Consequently, if a cyclic peptide is formed in concert with cleavage of the C-terminal amide bond in fragmentation of H-Val-Tyr-Pro-OH, formation of the y_1 ion will be strongly favoured. Thus, it appears likely that for H-Val-Tyr-Pro-OH a protonated oxazolone is formed as a b_2 ion, but that the neutral accompanying formation of the y_1 ion is a cyclic peptide (cyclo-Val-Tyr) not an oxazolone. It appears that this dichotomy of mechanism may be peculiar to tripeptides with a C-terminal proline for reasons that are unknown. Certainly, if a similar mechanism was operative for formation of y_1 ions from H-Leu-Tyr-Leu-OH, one would expect a much grater abundance of the y_1 ion since the proton affinity of leucine (217–219 kcal mol^{-1} (52, 56, 57)) is not greatly less than that of proline.

H-Aaa-Bbb-Tyr-OH

Figure 9 presents the breakdown graph for protonated H-Gly-Ala-Tyr-OH. The major primary fragment ion is the y_1 ion (protonated tyrosine) with a more minor yield of the b_2 ion. Clearly, fragmentation has involved almost entirely cleavage of the C-terminal amide bond. The proton affinity of tyrosine is 221 to 222 kcal mol^{-1} (52, 56, 57), while that

© 2005 NRC Canada

Fig. 10. Breakdown graph for protonated H-Gly-Leu-Tyr-OH (86 represents the internal leucine iminium ion).

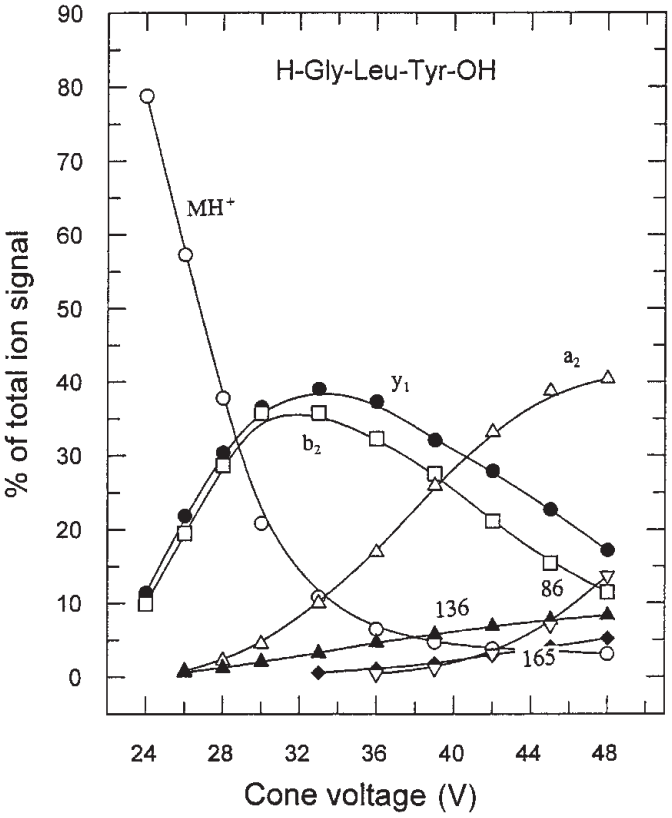
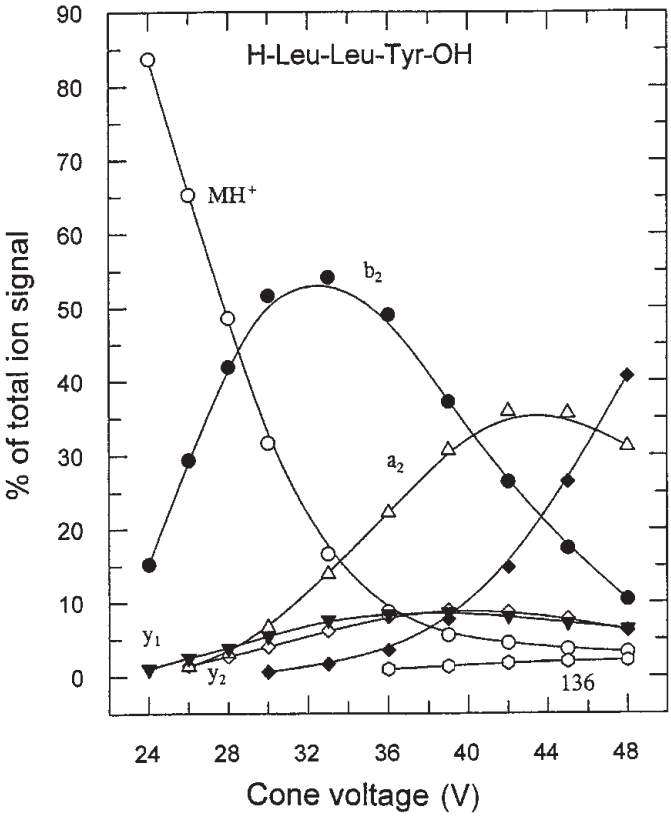


Fig. 11. Breakdown graph for protonated H-Leu-Leu-Tyr-OH.



of the oxazolone (2-aminomethyl-4-methyl-5-oxazolone) has been calculated to be 220.5 kcal mol^{-1} (49). Within combined uncertainties, these proton affinities can be considered to be the same; however, the results of Fig. 9 suggest that the proton affinity of tyrosine is, indeed, greater than that of the oxazolone. The y_1 ion shows further fragmentation to *m/z* 165 (loss of NH_3) and to *m/z* 136 (loss of H_2O + CO) at higher collision energies, both of which are known fragmentation products of protonated tyrosine (63, 64). The b_2 shows fragmentation to the a_2 ion at higher collision energies.

When the central alanine is replaced by leucine, the breakdown graph (Fig. 10) shows that the b_2 and y_1 ions are formed in essentially equal abundance at low collision energies, although the sum of the b_2 ion and its main a_2 fragmentation product are more dominant at higher collision energies. The proton affinity of the oxazolone (2-aminomethyl-4-isobutyl-5-oxazolone) has been calculated to be 223.7 kcal mol^{-1} (49) compared to a proton affinity of 221 to 222 kcal mol^{-1} (52, 56, 57) for tyrosine. Within combined uncertainties these two proton affinities could be considered to be the same, in line with the similar abundances of the b_2 and y_1 ions at low collision energies. The a_2 ion shows fragmentation to the internal leucine iminium ion at higher collision energies.

Figure 11 shows the breakdown graph obtained for protonated H-Leu-Leu-Tyr-OH. The N-terminal leucine has increased the proton affinity of the oxazolone (compared with Gly-Leu) to the extent that the b_2 ion is now the dominant primary fragmentation product with only minor formation of the y_1 ion. Again dominant cleavage of the C-terminal amide bond is observed. The b_2 ion shows extensive fragmentation by loss of CO to form the a_2 ion, which fragments further at high collision energies to form the leucine iminium ion (*m/z* 86) originating from either or both of the leucine residues of the peptide.

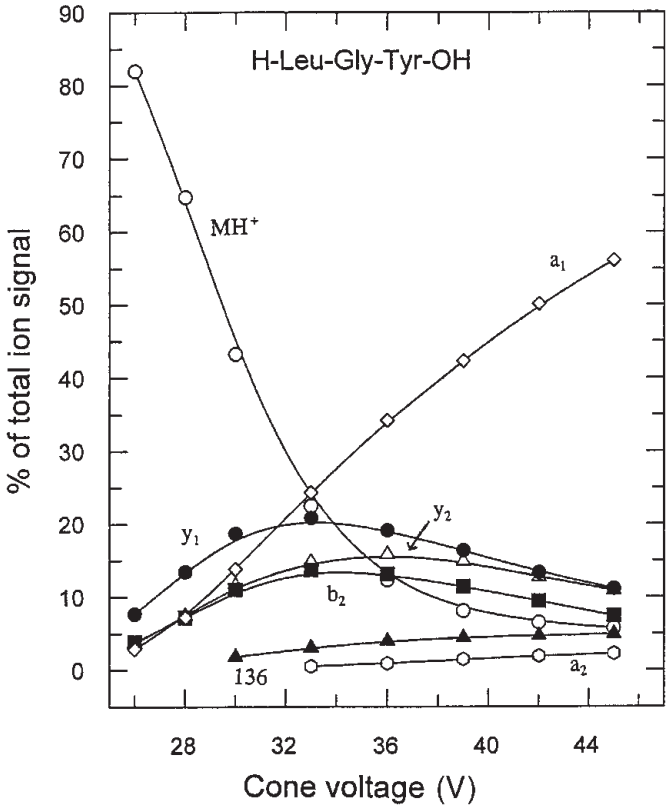
Figure 12 presents the breakdown graph for protonated H-Leu-Gly-Tyr-OH. The switching of the positions of the first two residues (compare with Fig. 10) has substantially changed the fragmentation modes observed. In contrast to H-Gly-Leu-Tyr-OH, where cleavage of the C-terminal amide bond dominated and formed the y_1 and b_2 ions in approximately equal yields, cleavage of the C-terminal amide bond for H-Leu-Gly-Tyr-OH results in more prominent formation of the y_1 ion than the b_2 ion. There also is significant cleavage of the N-terminal amide bond resulting in formation of the y_2 and a_1 ions (Scheme 2) with the latter dominating the breakdown graph at higher collision energies. The a_1 ion also may arise, in part, by further fragmentation of the b_2 ion. The enhanced cleavage of the N-terminal amide bond presumably reflects the stability of the leucine iminium (a_1) ion.

Conclusions

The fragmentation reactions of a variety of protonated tripeptides containing tyrosine have been studied and the energy evolution of the fragmentation reactions occurring elucidated by energy-resolved CID studies. Depending on the identity and location of the amino acid residues contained in the peptide, N-terminal and (or) C-terminal amide bond

© 2005 NRC Canada

Fig. 12. Breakdown graph for protonated H-Leu-Gly-Tyr-OH.



cleavage occurs as primary fragmentation. The results are rationalized in terms of the a_1–y mechanism (Scheme 2) for N-terminal amide bond cleavage and the b_x–y_z mechanism (Scheme 3) for C-terminal amide bond cleavage and, indeed, provide support for these mechanisms. The one exception is C-terminal amide bond cleavage for protonated H-Val-Tyr-Pro-OH, where it appears likely that the neutral accompanying formation of the y_1 (protonated proline) ion is a cyclic dipeptide (cyclo-Val-Tyr) rather than the oxazolone predicted by Scheme 3.

Acknowledgement

The financial support of the Natural Sciences and Engineering Research Council of Canada (NSERC) is gratefully acknowledged.

References

1. C.M. Whitehouse, R.N. Dreyer, M. Yamashita, and J.B. Fenn. Anal. Chem. **57**, 675 (1985).
2. R.B. Cole (*Editor*). Electrospray ionization mass spectrometry. Fundamentals, Instrumentation and Applications. Wiley, New York. 1997.
3. B.N. Pramanik, A.K. Ganguly, and M.L. Gross (*Editors*). Applied electrospray mass spectrometry. Marcel Dekker, New York. 2002.
4. M. Karas and F. Hillenkamp. Anal. Chem. **60**, 2299 (1988).
5. R.C. Beavis and B.T. Chait. Methods Enzymol. **270**, 519 (1996).
6. F.W. McLafferty (*Editor*). Tandem mass spectrometry. Wiley, New York. 1983.
7. K.L. Busch, G.L. Glish, and S.A. McLuckey. Mass spectrometry/mass spectrometry: Techniques and applications of tandem mass spectrometry. VCH, New York. 1988.
8. P. Roepstorff and J. Fohlman. Biomed. Mass Spectrom. **11**, 601 (1984).
9. K. Biemann. Biomed. Environ. Mass Spectrom. **16**, 99 (1988).
10. K. Biemann. Methods Enzymol. **193**, 455 (1990).
11. I.A. Papayannopoulos. Mass Spectrom. Rev. **14**, 49 (1995).
12. D.R. Mueller, M. Eckersley, and W. Richter. Org. Mass Spectrom. **23**, 217 (1988).
13. M.M. Cordero, J.J. Houser, and C. Wesdemiotis. Anal. Chem. **65**, 1594 (1993).
14. T. Yalcin, C. Khouw, I.G. Csizmadia, M.R. Peterson, and A.G. Harrison. J. Am. Soc. Mass Spectrom. **6**, 1165 (1995).
15. T. Yalcin, I.G. Csizmadia, M.R. Peterson, and A.G. Harrison. J. Am. Soc. Mass Spectrom. **7**, 293 (1996).
16. M.J. Nold, C. Wesdemiotis, T. Yalcin, and A.G. Harrison. Int. J. Mass Spectrom. Ion Processes, **164**, 137 (1997).
17. B. Paizs, G. Lendvay, K. Vékey, and S. Suhai. Rapid Commun. Mass Spectrom. **13**, 525 (1999).
18. A.G. Harrison, I.G. Csizmadia, and T.-H. Tang. J. Am. Soc. Mass Spectrom. **11**, 427 (2000).
19. C.F. Rodriquez, T. Shoeib, I.K. Chu, K.W.M. Siu, and A.C. Hopkinson. J. Phys. Chem. A, **104**, 5355 (2000).
20. B. Paizs and S. Suhai. Rapid Commun. Mass Spectrom. **16**, 375 (2002).
21. T. Yalcin and A.G. Harrison. J. Mass Spectrom. **31**, 1237 (1996).
22. I.P. Csonka, B. Paizs, G. Lendvay, and S. Suhai. Rapid Commun. Mass Spectrom. **15**, 1437 (2001).
23. J.M. Farrugia, R.A.J. O'Hair, and G.E. Reid. Int. J. Mass Spectrom. **210/211**, 71 (2001).
24. M.M. Kish and C. Wesdemiotis. Int. J. Mass Spectrom. **227**, 191 (2003).
25. J.H. Farrugia and R.A.J. O'Hair. Int. J. Mass Spectrom. **222**, 229 (2002).
26. V.H. Wysocki, G. Tsaprailis, L.L. Smith, and L.A. Breci. J. Mass Spectrom. **35**, 1399 (2000).
27. J.M. Farrugia, T. Taverner, and R.A.J. O'Hair. Int. J. Mass Spectrom. **209**, 99 (2001).
28. G. Tsaprailis, H. Nair, W. Zhong, K. Kuppannan, V.H. Wysocki, and J.H. Futrell. Anal. Chem. **76**, 2083 (2004).
29. K. Ambihapathy, T. Yalcin, H.-W. Leung, and A.G. Harrison. J. Mass Spectrom. 1**32**, 209 (1997).
30. A.G. Harrison. Rapid Commun. Mass Spectrom. **13**, 1663 (1999).
31. W.D. van Dongen, J.I.T. van Wijk, B.M. Green, W. Heerma, and J. Haverkamp. Rapid Commun. Mass Spectrom. **13**, 1712 (1999).
32. A.G. Harrison. J. Mass Spectrom. **34**, 1253 (1999).
33. J. Makowiecki, A. Tolonen, J. Uusitalo, and J. Jalonen. Rapid Commun. Mass Spectrom. **15**, 1506 (2001).
34. C. Buré and C. Lange. Current Org. Chem. **7**, 1613 (2003).
35. S.A. McLuckey and R.G. Cooks. *In* Tandem mass spectrometry. *Edited by* F.W. McLafferty. Wiley, New York. 1983. p. 203.
36. A.L. McCormack, Á. Somogyi, A.R. Dongré, and V.H. Wysocki. Anal. Chem. **65**, 2859 (1993).
37. Á. Somogyi, V.H. Wysocki, and I. Mayer. J. Am. Soc. Mass Spectrom. **5**, 704 (1994).
38. K. Vékey and A. Gömöry. Rapid Commun. Mass Spectrom. **10**, 1485 (1996).
39. J. Wu and C.B. Lebrilla. J. Am. Chem. Soc. **115**, 3230 (1993).
40. K. Zhang, D.A. Zimmerman, and C.J. Cassady. J. Am. Chem. Soc. **115**, 10812 (1993).

© 2005 NRC Canada

41. K. Zhang, C.J. Cassady, and A. Chung-Phillips. J. Am. Chem. Soc. **116**, 11512 (1994).
42. R.S. Johnson, D. Krylov, and K.A. Walsh. J. Mass Spectrom. **30**, 386 (1995).
43. A.G. Harrison and T. Yalcin. Int. J. Mass Spectrom. Ion Processes, **165**, 339 (1997).
44. A.R. Dongré, J.L. Jones, Á. Somogyi, and V.H. Wysocki. J. Am. Chem. Soc. **118**, 8365 (1996).
45. B. Paizs and S. Suhai. Rapid Commun. Mass Spectrom. **15**, 651 (2001).
46. B. Paizs, M. Schnoelzer, U. Warnken, S. Suhai, and A.G. Harrison. Phys. Chem. Chem. Phys. **6**, 2691 (2004).
47. B. Paizs and S. Suhai. Mass Spectrom. Rev. **24**, 508 (2005).
48. B. Paizs and S. Suhai. Rapid Commun. Mass Spectrom. **16**, 395 (2002).
49. B. Paizs and S. Suhai. Rapid Commun. Mass Spectrom. **16**, 1699 (2002).
50. B. Paizs, S. Suhai, and A.G. Harrison. J. Am. Soc. Mass Spectrom. **14**, 1454 (2003).
51. B. Paizs and S. Suhai. J. Am. Soc. Mass Spectrom. **15**, 103 (2004).
52. E.P.L. Hunter and S.G. Lias. J. Phys. Chem. Ref. Data, **27**, 413 (1998).
53. H. El Aribi, C.F. Rodriquez, D.R.P. Almeida, Y. Ling, W.W.-N. Mak, A.C. Hopkinson, and K.W.M. Siu. J. Am. Chem. Soc. **125**, 9229 (2003).
54. H. El Aribi, G. Orlova, C.F. Rodriquez, D.R.P. Almeida, A.C. Hopkinson, and K.W.M. Siu. J. Phys. Chem. B, **108**, 18743 (2004).
55. A.G. Harrison, A.B. Young, M. Schnoelzer, and B. Paizs. Rapid Commun. Mass Spectrom. **18**, 1635 (2004).
56. Z.B. Maksić and B. Kovačević. Chem. Phys. Lett. **307**, 497 (1999).
57. A.G. Harrison. Mass Spectrom. Rev. **16**, 201 (1997).
58. C. Alfonso, F. Modeste, P. Breton, F. Fournier, and J.-C. Tabet. Eur. J. Mass Spectrom. **6**, 443 (2000).
59. A.F. Kuntz, A.W. Boynton, G.A. David, K.E. Colyer, and J.C. Poutsma. J. Am. Soc. Mass Spectrom. **13**, 72 (2002).
60. G. Bouchoux and J.-Y. Salpin. Eur. J. Mass Spectrom. **9**, 391 (2003).
61. M.J. Polce, Š. Beranová, M.J. Nold, and C. Wesdemiotis. J. Mass Spectrom. **31**, 1073 (1996).
62. M.J. Nold, B. Cerda, and C. Wesdemiotis. J. Am. Soc. Mass Spectrom. **10**, 1 (1999).
63. N.N. Dookeran, T. Yalcin, and A.G. Harrison. J. Mass Spectrom. **31**, 500 (1996).
64. H. El Aribi, G. Orlova, A.C. Hopkinson, and K.W.M. Siu. J. Phys. Chem. A, **108**, 3844 (2004).

© 2005 NRC Canada

An investigation of the ion–molecule interactions of protonated glycine with ammonia by high pressure mass spectrometry and ab initio calculations[1]

Ronghu Wu and Terry B. McMahon

Abstract: The thermochemistry of gas-phase ion molecule interactions and the structures of various clusters between protonated glycine ($GlyH^+$), glycine, and ammonia have been studied by high pressure mass spectrometry (HP-MS) and ab initio calculations. For the association reactions of $GlyH^+$ with NH_3, $Gly(NH_3)H^+$ with NH_3, and $(Gly)_2H^+$ with NH_3, the enthalpy changes experimentally determined are –23.2, –18.3, and –19.1 kcal mol^{-1} (1 cal = 4.184 J), respectively. For all clusters investigated, the measured binding enthalpies are in excellent agreement with those obtained from ab initio calculations at the B3LYP/6-311+G(d,p) level of theory. Different isomers of each of these clusters have been obtained and the corresponding binding energies have been computed. The potential energy surface for isomerization of the clusters of protonated glycine with ammonia has also been computed at the same level. For this cluster, the three most stable isomers all involve a proton transfer from protonated glycine to ammonia. According to the calculated potential energy surface, the barrier between **GN4**, the least stable isomer, and the most stable isomer (**GN1**) is 11.5 kcal mol^{-1} at 298 K. Thus, this isomerization will be facile given the exothermicity of the association reaction. Therefore, a statistical distribution of isomers will be present under thermal equilibrium conditions. Single point energy calculations at the MP2(full)/6-311++G(2d,2p)//B3LYP/6-311+G(d,p) level of theory reveal that the isomer **GN2** in which glycine has a zwitterionic structure has the same energy as the most stable non-zwitterionic isomer **GN1**. NH_4^+ evidently may stabilize the zwitterionic structure of glycine. In contrast, $N_2H_7^+$ and $GlyH^+$ are not as effective in stabilizing the zwitterionic structure of glycine. This likely results from the more localized charge in NH_4^+ giving rise to stronger hydrogen bonds with the carboxylate moiety of zwitterionic glycine. This conjecture is supported by the computational results.

Key words: high pressure mass spectrometry, glycine, gas-phase ion thermochemistry, ab initio calculations, cluster structure.

Résumé : Faisant appel à des calculs ab initio et à la spectrométrie de masse à haute pression (SM-HP), on a étudié la thermochimie des interactions ion–molécule en phase gazeuse et les structures de divers agrégats entre la glycine protonée ($GlyH^+$), la glycine et l'ammoniac. On a déterminé expérimentalement les changements d'enthalpie des réactions de $GlyH^+$ avec NH_3, de $Gly(NH_3)H^+$ avec NH_3 et de $(Gly)_2H^+$ avec NH_3 qui sont respectivement de –23,2, –18,3 et –19,1 kcal mol^{-1} (1 cal = 4,184 J). Pour tous les agrégats étudiés, les enthalpies de liaison mesurées sont en excellent accord avec celles obtenues par des calculs ab initio au niveau B3LYP/6-311+G(d,p) de la théorie. Divers isomères de chacun de ces agrégats ont été obtenus et on a calculé les énergies de liaison correspondantes. On a aussi calculé au même niveau la surface d'énergie potentielle pour l'isomérisation des agrégats de la glycine protonée avec l'ammoniac. Pour cet agrégat, les trois isomères les plus stables impliquent tous un transfert de proton de la glycine protonée à l'ammoniac. Sur la base de la surface d'énergie potentielle calculée, la barrière entre **GN4**, l'isomère le moins stable, et l'isomère le plus stable, **GN1**, est de 11,5 kcal mol^{-1} à 298 K. Cette isomérisation sera donc facile compte tenu du caractère exothermique de cette réaction d'association. Dans des conditions d'équilibre thermique, on retrouvera donc une distribution statistique des isomères. Des calculs d'énergie ponctuelle au niveau MP2(complet)//6-311++G(2d,dp)//B3LYP/6-311+G(d,p) de la théorie révèlent que l'énergie de l'isomère **GN2**, dans lequel la glycine assume une structure zwitterionique, est la même que celle de l'isomère non zwitterionique **GN1** le plus stable. Le cation NH_4^+ peut évidemment stabiliser la structure zwitterionique de la glycine. À l'opposé, les cations $N_2H_7^+$ et $GlyH^+$ ne stabilisent pas d'une façon efficace la structure zwitterionique de la glycine. Ceci résulte probablement du fait que la charge du NH_4^+ est plus localisée, ce qui conduit à des liaisons hydrogènes plus fortes avec la portion carboxylate de la glycine zwitterionique. Cette hypothèse est supportée par des résultats de calculs théoriques.

Received 27 April 2005. Published on the NRC Research Press Web site at http://canjchem.nrc.ca on 28 January 2006.

This manuscript is dedicated to Paul Kebarle, an outstanding scientist, an excellent mentor, and a great friend, in honour of his 50 years of research in mass spectrometry.

R. Wu and T.B. McMahon.[2] Department of Chemistry, University of Waterloo, Waterloo, ON N2L 3G1, Canada.

[1]This article is part of a Special Issue dedicated to Professor P. Kebarle.
[2]Corresponding author (e-mail: mcmahon@uwaterloo.ca).

 doi: 10.1139/V05-205 © 2005 NRC Canada

Mots clés : spectrométrie de masse à haute pression, glycine, thermochimie ionique en phase gazeuse, calculs ab initio, structure d'agrégats.

[Traduit par la Rédaction]

Introduction

Amino acids are among the most fundamental of the biochemical building blocks. They form polymeric chains known as peptides and polypeptides which, in turn, form proteins. Twenty amino acids make up the standard genetic code and are known as proteinogenic or standard amino acids. Glycine is the smallest and simplest of these proteinogenic amino acids and all other amino acids can be regarded as derivatives of glycine substituted by different side chains (1). There have been many studies of the structures of glycine and protonated glycine and their interaction with other ions or molecules, especially by theoretical methods. As early as 1977, Vishveshwara and Pople (2) studied the possible minima on the potential energy surface of glycine by ab initio methods using, by today's standards, relatively small basis sets (RHF/4-31G). Jensen and Gordon (3) later investigated the glycine structure using MP2/6-31G*//HF/6-31G* methods and a total of eight structures corresponding to minima on the potential energy surface (PES) were found. Subsequently, protonated glycine and the complexes of glycine with Li^+ and Na^+ were also investigated by these authors (4) An extensive computational investigation of protonated glycine has been performed by Zhang and Chung-Phillips (5) in which they carried out geometry optimizations to find many N-protonated and O-protonated species at the MP2 level of theory. The most stable isomer was found to be one in which a proton is attached to the most basic site, the amino nitrogen. Campbell et al. (6) used the experimental lone-pair ionization energies to infer experimentally that the nitrogen should be the most favorable protonation site. The proton affinity of glycine has been determined to be 208.2 kcal mol^{-1} from equilibrium measurements of the thermocemistry of proton transfer between glycine and reference bases (7). It has also been assigned as 211.6 kcal mol^{-1} based on kinetic method experiments (8), as well as 215.4 (9) and 213.5 kcal mol^{-1} (10) by proton-transfer reaction bracketing experiments. Recently, the interactions between protonated glycine and ammonia (11) and either one or two water molecules have been calculated (12). For the water clusters, no proton transfer to H_2O occurs; however, in the ammonia clusters, proton transfer to NH_3 is suggested to be favorable.

The high pressure mass spectrometry (HP-MS) technique has played an extremely important role in developments in gas ion thermochemistry. Among the important thermochemical data produced are: proton affinities, gas-phase acidities, ionization energies, electron affinities, hydrogen bond energies, Lewis acid affinities, and metal cation affinities (13). HP-MS has also been a powerful tool for the study of ion–molecule association reactions leading to cluster formation (14–18) and investigations of the solvation of ionic species (19–23). The exact binding enthalpy and entropy changes can be directly obtained by measuring equilibrium constants as a function of temperature. When combined with ab initio calculations, the HP-MS energetic measurements lead as well to significant structural insights that permit an in-depth understanding of potential energy surfaces for complex ion–molecule interactions. Meot-Ner and Field (24) used high pressure mass spectrometry to study the solvation of protonated amino acids some 30 years ago but, until very recently, there have been very few reported investigations concerning the interaction between amino acids and common solvents, including such basic and simple systems as the interaction between protonated glycine and water or ammonia.

In the current study, the binding enthalpy and entropy changes of the clusters of protonated glycine with one and two ammonia molecules, and of the protonated glycine dimer with one ammonia molecule have been determined by HP-MS. By using ab initio calculations, various isomers of these clusters have been revealed and the potential energy surface for the interconversion of these isomers has been elucidated. The calculated binding energetics agree extremely well with the experimental values. At the same time, very interesting structural information for the various isomers has been obtained.

Experimental and computational

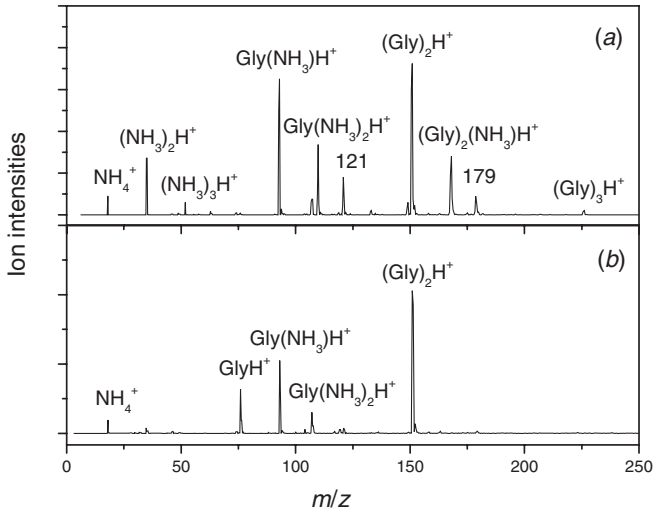
Experimental

All experiments were carried out on a high pressure mass spectrometer constructed at the University of Waterloo and whose general design has been described in detail elsewhere (25–27). The instrument used in the present work is configured around a double-focusing reversed geometry (B-E) magnetic sector mass spectrometer (VG ZAB-2F) mated to the home-built high pressure ion source. Experiments were carried out in positive ion mode with an ion energy of 4 keV.

Gas mixtures were prepared in a 2.54 L reservoir using N_2 as the bath gas at a pressure of 500–1200 Torr (1 Torr = 133.3224 Pa). The partial pressure of ammonia was typically in the range of 0.5–50 Torr, depending upon the ion signal intensities desired for the particular equilibrium to be examined. A small amount of CCl_4 was added to the reservoir to increase the signal intensity at long ion source residence times by slowing the rate of ion diffusion to the source walls. The gas mixture was flowed into the ion source to a total pressure of 3–7 Torr. A solid sample of glycine (>99.7%, EM Science) was placed directly inside the high-pressure source. When the high-pressure source is heated, glycine vapor forms inside. Ionization is initiated by energetic electrons, from an electron gun external to the ion source, focused onto the 100 μm electron entrance aperture of the ion source. Chemical ionization processes then lead to formation of the desired ions in the high-pressure source. The electron gun can function in either continuous or pulsed modes. In continuous mode, mass spectra can be obtained such as those shown in Fig. 1, which illustrate the effect of changing temperature and partial pressure in the ion source.

© 2005 NRC Canada

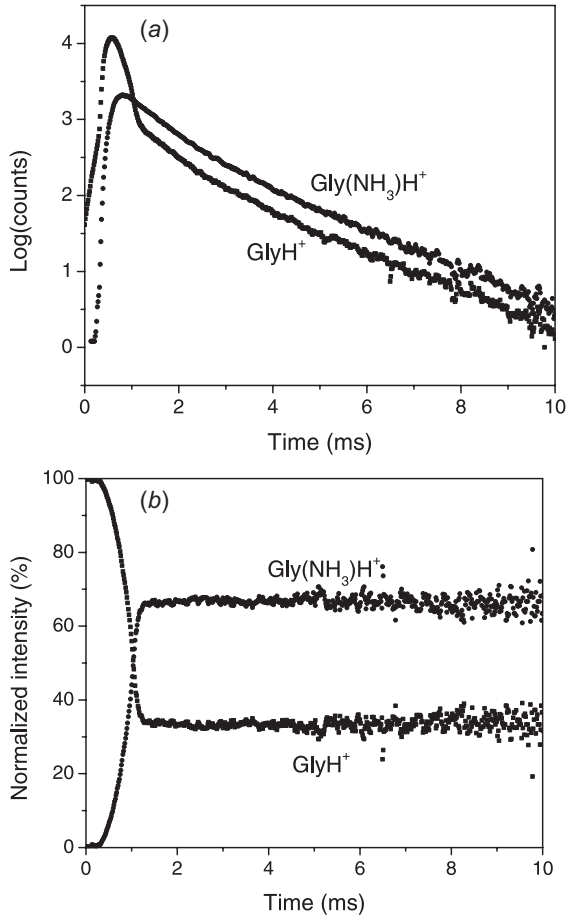
Fig. 1. Mass spectra of protonated glycine and ammonia. (*a*) 2.86 Torr NH_3 (1 Torr = 133.3224 Pa) in a 2.54 L reservoir with a total pressure of 1011 Torr. The temperature of the ion source was 375 K. (*b*) 0.94 Torr NH_3 and a total reservoir pressure of 912 Torr at 435 K. The ion source pressure was 5 Torr in each case.



In Fig. 1*a*, the ion source temperature is 375 K and the pressure of ammonia in the source is 14 mTorr. The two strongest peaks in the spectrum are the protonated dimer of glycine and the cluster of protonated glycine with one ammonia molecule, with additional significant peaks corresponding to $Gly(NH_3)_2H^+$ and $(Gly)_2(NH_3)H^+$. The protonated trimer of glycine also appears as a very small peak at *m*/*z* 226. In addition, peaks owing to the protonated monomer, dimer, and trimer of ammonia are also evident in the mass spectrum. The peaks at *m*/*z* 121 and 179 are likely due to weakly bound adducts of $Gly(NH_3)H^+$ and $(Gly)_2H^+$ with the abundant bath gas, N_2. The mass spectrum of Fig. 1*b* was obtained at an ion source temperature of 435 K and an ammonia ion source pressure of 5 mTorr. The strongest peak is still $(Gly)_2H^+$, but the peak owing to $(Gly)_3H^+$is no longer present, even though the amount of glycine in the gas phase should be greater because of the increased ion source temperature. This indicates that the abundance of species present is determined, not only by the amount of ammonia and glycine in the gas phase, but also by the equilibrium constant for the association reaction at a given temperature. The intensities of NH_4^+, $GlyH^+$, and $Gly(NH_3)H^+$ are also significant.

The ion intensities obtained from the continuous ionization mode mass spectra do not necessarily reflect equilibrium ion abundances owing to the fact that it may take equilibrium some time to be established after initial ionization. To obtain equilibrium abundances, the electron gun is operated in pulsed mode. Mass-selected ion intensity temporal profiles are monitored using a PC-based multichannel scaler data acquisition system, typically configured between 10 and 30 μs dwell time per channel. A total of 1024 channels were acquired, and at least 3000 electron gun pulses were accumulated. For example, the temporal profiles for protonated glycine and the adduct of protonated glycine with ammonia are shown in Fig. 2*a*. At sufficiently long time after the ionization pulse, these decaying intensities become

Fig. 2. (*a*) Variation of ion intensities with time for protonated glycine and its ammonia cluster; 0.66 Torr NH_3 (1 Torr = 133.3224 Pa) in a 2.54 L reservoir with a total pressure of 1180 Torr. The temperature of the ion source was 430 K and the pressure was 5 Torr. (*b*) Normalized intensities for the data shown in (*a*).



parallel, indicating that equilibrium has been reached. The corresponding association reaction is described by eq. [1], and the associated equilibrium constant is given by eq. [2].

$$[1] \qquad GlyH^+ + NH_3 \leftrightarrows Gly(NH_3)H^+$$

$$[2] \qquad K_{eq} = \frac{I_{GLY(NH_3)(H^+)}}{I_{GlyH^+}} \frac{1}{P_{NH_3}}$$

This is seen even more clearly in Fig. 2*b* where the two ion intensities are normalized and, after equilibrium is established, the normalized ion abundances are constant. The equilibrium constants can be calculated from the relative ionic abundance and the partial pressure of ammonia. The relative ionic abundance is simply the constant ratio of intensities, measured by the HP-MS experiment, at sufficiently long reaction time in the ion intensity temporal profiles. The partial pressure of ammonia is readily determined from the known partial pressure of ammonia added to the gas mixture in the gas sample reservoir and the measured total pressure in the ion source. This pressure can be easily changed over several orders of magnitude by simply changing the partial pressure of ammonia in the gas sample reservoir. As the

© 2005 NRC Canada

Table 1. Experimental values of enthalpy and entropy changes of the association reactions measured by HP-MS.

Reaction	ΔH (kcal mol^{-1})	ΔS (cal mol^{-1} K^{-1})
$GlyH^+ + NH_3 \leftrightarrow Gly(NH_3)H^+$	–23.2±1.0	–26.9
$Gly(NH_3)H^+ + NH_3 \leftrightarrow Gly(NH_3)_2H^+$	–18.3±1.0	–28.4
$(Gly)_2H^+ + NH_3 \leftrightarrow (Gly)_2(NH_3)H^+$	–19.1±1.0	–30.5

temperature is changed, K_{eq} can be determined at each temperature. Then, as given by the van't Hoff equation (eq. [3]), the enthalpy change (ΔH) and the entropy change (ΔS) for the reaction can be obtained from a plot of K_{eq} vs. reciprocal temperature.

$$[3] \qquad \ln(K_{eq}) = -\frac{\Delta H}{RT} + \frac{\Delta S}{R}$$

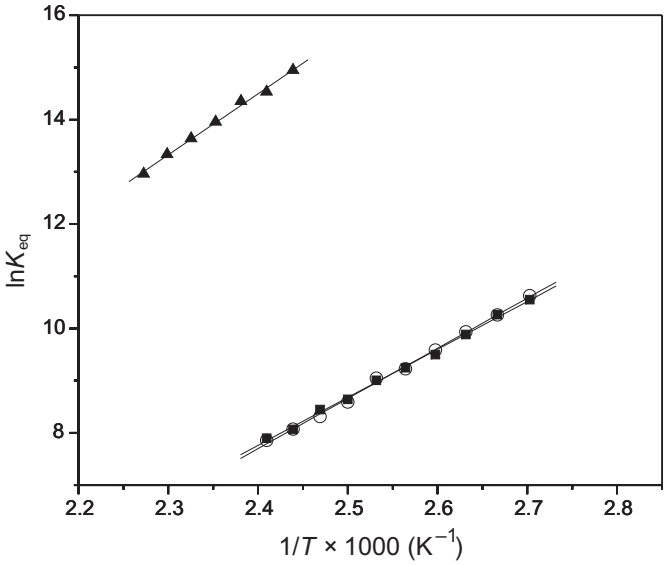
Ab initio calculations

Ab initio calculations have been carried out using the Gaussian 03 program (28). The structures of the protonated glycine and its clusters with ammonia and (or) glycine were calculated at the density functional theory level, employing the B3LYP exchange-correlation functional and the 6-311+G(d,p) basis set. The calculations of the potential energy surfaces for the transformation of the isomers of protonated glycine clusters with ammonia and the protonated glycine dimer have also been carried out using the same method. Vibrational frequencies were calculated for all structures using the harmonic approximation to verify that no imaginary frequencies were present for species determined to be local and global minima on the potential energy surface. For the transition states obtained, only one imaginary frequency is found and, by examination of these imaginary frequencies, every transition state could be confirmed to be directly related to the corresponding reactant and product. Zero point energies and thermal energy corrections at 298 K were also obtained. Basis set superposition error (BSSE) was computed after the geometry optimization using the counterpoise correction method (29).

The entropies of the association reactions were also computed at the B3LYP/6-311+G(d,p) level. The use of the harmonic approximation for calculation of vibrational frequencies introduces some uncertainty in the calculation of vibrational entropies because of the anharmonic nature of the intermolecular vibrational modes of ion–molecule complexes. The relative free energies of the isomers of several of the cluster species reported in this work dictate that in an equilibrium mixture of these species a significant population of more than one isomer will be present. As such, for comparison with the experimental energetics, the calculated entropies should also include a term for the entropy of mixing of these isomers.

To obtain somewhat more accurate interaction enthalpies, single point energies have also been computed for the local minima at the MP2(full)/6-311++G(2d,2p)//B3LYP/6-311+G(d,p) level. The enthalpies derived from these MP2 calculations do not include BSSE corrections. All values of enthalpy changes reported include appropriate zero point energy and thermal energy corrections.

Fig. 3. van't Hoff plots for the association reactions: $GlyH^+ + NH_3 \leftrightarrows Gly(NH_3)H^+$ (▲); $Gly(NH_3)H^+ + NH_3 \leftrightarrows Gly(NH_3)_2H^+$ (■); $(Gly)_2H^+ + NH_3 \leftrightarrows (Gly)_2(NH_3)H^+$ (○).



Results and discussion

Equilibrium measurements and computational energetics

The experimental van't Hoff plots for the three association reactions investigated (eqs. [1], [4], and [5]) are shown in Fig. 3, and the thermochemical data extracted from these van't Hoff plots are summarized in Table 1.

$$[4] \qquad Gly(NH_3)H^+ + NH_3 \leftrightarrows Gly(NH_3)_2H^+$$

$$[5] \qquad (Gly)_2H^+ + NH_3 \leftrightarrows (Gly)_2(NH_3)H^+$$

For the association reaction of protonated glycine with ammonia (eq. [1]), the measured enthalpy and entropy changes are –23.2 kcal mol^{-1} and –26.9 cal mol^{-1} K^{-1}, respectively. The computed enthalpy change for the formation of the most stable isomer (**GN1**) obtained at the B3LYP/6-311+G(d,p) level of –25.8 kcal mol^{-1} is somewhat greater than the measured value. When enthalpy changes are taken from the single point energies determined at the MP2(full)/6-311++G(2d,2p)//B3LYP/6-311+G(d,p) level, this value is reduced to –24.4 kcal mol^{-1} for both the **GN1** and **GN2** structures, in excellent agreement with the experimental value. The calculated entropy changes for formation of **GN1** and **GN2** are –27.8 and –30.9 cal mol^{-1} K^{-1}, respectively, again in very good agreement with the experimentally determined value.

For the association reaction of $Gly(NH_3)H^+$ with ammonia (eq. [4]), the measured enthalpy and entropy changes are –18.3 kcal mol^{-1} and –28.4 cal mol^{-1} K^{-1}, respectively. Sim-

© 2005 NRC Canada

ilarly, the experimental data for the association reaction of the protonated glycine dimer with ammonia (eq. [5]) give enthalpy and entropy changes of –19.1 kcal mol^{-1} and –30.5 cal mol^{-1} K^{-1}, respectively. The computed enthalpy changes from the single point energies at the MP2(full)/6-311++G(2d,2p)//B3LYP/6-311+G(d,p) level for the formation of the corresponding most stable isomers (**GNN1** and **GGN1**) of –18.2 and –19.2 kcal mol^{-1}, respectively, are also in excellent agreement with the experimental data. The corresponding values computed at the lower B3LYP/6-311+G(d,p) level of –17.7 and –19.5 kcal mol^{-1} are only slightly different than the measured values. After correction with BSSE, these data become slightly lower than the measured values. It is well-known that the BSSE correction often introduces an underestimation of the binding energies when the basis set used is not large enough and when the structure computed is sufficiently loose such as those previously reported (30, 31). The computed entropy changes for formation of the corresponding most stable isomers in eqs. [4] and [5] are found to be –28.7 and –28.5 cal mol^{-1} K^{-1}, respectively, again in very good agreement with analogous measured values. Note that this discussion is limited to computed values for the most stable isomers involved in each of these equilibria. A more detailed discussion follows in which many other structures are reported and their implication in the potential energy surface for the reactions is discussed.

Kebarle and co-workers (32, 33) and Meot-Ner (34) have previously reported extensive data for strong hydrogen-bonded dimers (BH^+A), where B is a nitrogen base, and they have shown that a good correlation exists between the binding enthalpy and the proton affinity difference (ΔPA) between the two bases (A and B) involved in the hydrogen bond. The binding enthalpy is found to decrease as the difference between the proton affinities of A and B increases. This may be understood in terms of the occurrence of a partial proton transfer from BH^+ to A within the cluster in the hydrogen bond formation between BH^+ and A. Partial proton transfer will thus be facilitated when BH^+ becomes a more efficient proton donor, which will result either when the proton affinity of neutral B decreases or when A becomes more efficient proton acceptor, i.e., when the proton affinity of A increases. This general trend has also been confirmed in several further investigations (35–38). Viewed in the light of this trend, since the neutral dimer of glycine will have a higher proton affinity than glycine itself, the proton affinity difference between glycine dimer and ammonia will be larger than that between glycine and ammonia and therefore, the binding enthalpy of protonated glycine dimer to ammonia (–19.1 kcal mol^{-1}) will be less than that of protonated glycine to ammonia (–23.2 kcal mol^{-1}). This is, in fact, exactly what was experimentally and computationally observed here.

Computed structures and energetics of clusters

$Gly(NH_3)H^+$

As a first step in determining the computational binding energetics of the protonated glycine–ammonia cluster, various possible stable isomers of protonated glycine were explored. The three most stable species found at the B3LYP/6-311+G(d,p) level are shown in Fig. 4. **G1** is found to be the most stable isomer in which the proton is bound to the amine nitrogen and an intramolecular hydrogen bond is formed between one of the acidic hydrogens of the resulting ammonium group and the carbonyl oxygen. The second most stable structure is **G2**, which lies 4.6 kcal mol^{-1} higher in energy than the most stable isomer that is also amine protonated, but in this case with an intramolecular hydrogen bond between an ammonium hydrogen and the hydroxyl oxygen. A similar structure had also been found previously (5, 11). Protonation on the carbonyl oxygen results in a much higher energy structure (**G3**), which has no intramolecular hydrogen bonding. If rotation about the C—O bond syn to the amino group takes place, an intramolecular proton transfer occurs and **G3** collapses to **G1**. Thus, according to these computed data, **G1** will constitute more than 99% of the protonated glycine species present throughout the temperature range of our experiments. Therefore, **G1** has been used as the basis for all computations of the energetics of eq. [1].

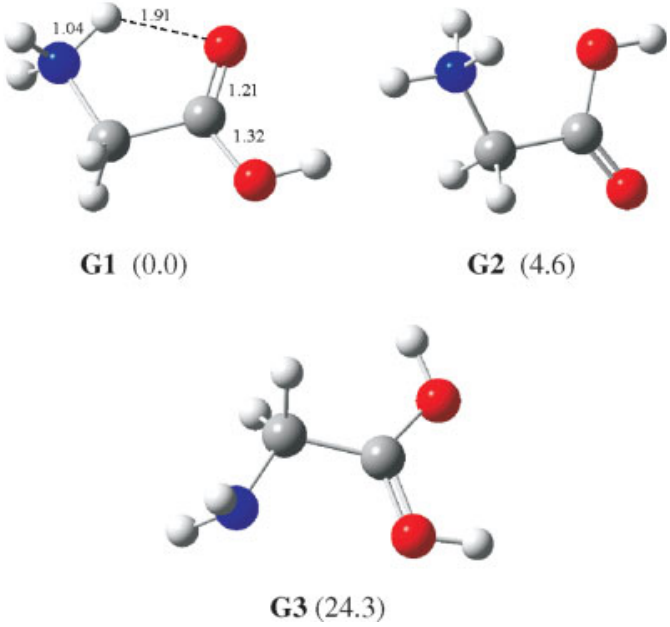
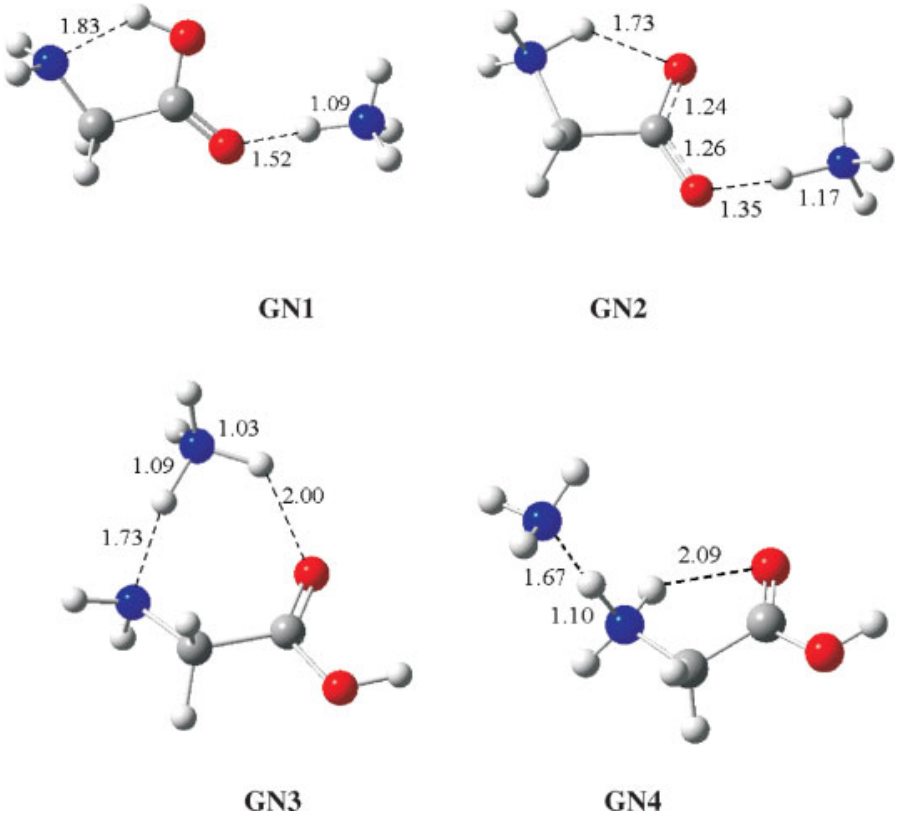


Fig. 4. The different isomers of protonated glycine calculated at the B3LYP/6-311+G(d,p) level. The relative energies are given in parentheses (kcal mol^{-1}, 1 cal = 4.184 J).

The four most stable isomers found for the 1:1 cluster ($Gly(NH_3)H^+$) are shown in Fig. 5. For the first three of these isomers (**GN1, GN2** and **GN3**), a proton transfer from protonated glycine to ammonia has occurred, despite the fact that the proton affinity of glycine is some 8 kcal mol^{-1} greater than that of ammonia (39). This results in species that can be more appropriately regarded as glycine-solvated ammonium ions. The corresponding computed binding enthalpies are 25.8, 24.9, and 24.3 kcal mol^{-1} for **GN1** through **GN3**, respectively, at the B3LYP/6-311+G(d,p) level, and 24.4, 24.4, and 23.7 kcal mol^{-1}, respectively, using the MP2(full)/6-311++G(2d,2p)//B3LYP/6-311+G(d,p) calculation. A similar finding has been reported in the literature (11). The isomer **GN1** can be thought of as being derived from separated protonated glycine and ammonia by two proton transfers. The first of these can be viewed as an intermolecular proton transfer from the hydroxyl group of the protonated glycine to ammonia and the second as an intra-

© 2005 NRC Canada

Fig. 5. The different isomers of the cluster of protonated glycine and one ammonia obtained at the B3LYP/6-311+G(d,p) level.



molecular proton transfer from the protonated amino group to the carboxyl oxygen. The resulting structure is an ammonium ion solvated by neutral glycine at the carbonyl oxygen.

The isomer **GN2** similarly is derived from separated reactants by proton transfer; however, in this case, only a single transfer occurs from the hydroxyl oxygen of protonated glycine to ammonia. This leads to the novel structure of a gas-phase ammonium ion solvated by a gas-phase zwitterionic glycine molecule at one of its carboxylate oxygens. The two C—O bond lengths in this structure are very similar (1.24 and 1.26 Å), in contrast to the values of 1.21 and 1.32 Å found in **G1** for the bonds to the carboxyl and hydroxyl oxygens, respectively. The hydrogen bonding in **GN2** appears to be particularly favorable. The bond length of 1.35 Å between the ammonium hydrogen and carboxylate oxygen is significantly reduced by 0.17 Å relative to the analogous bond in **GN1**, while the length of the N—H bond involved increases only by 0.08 Å. In addition, the intramolecular hydrogen bond also appears to be significantly enhanced, decreasing by 0.18 Å, from 1.91 Å in **G1** to 1.73 Å in **GN2**. In the cases of both isomers **GN1** and **GN2**, attempts were made to locate analogous structures in which the intermolecular proton transfer from protonated glycine to ammonia did not occur. All such attempts were unsuccessful, however, indicating that this intermolecular proton transfer is a virtually barrierless process.

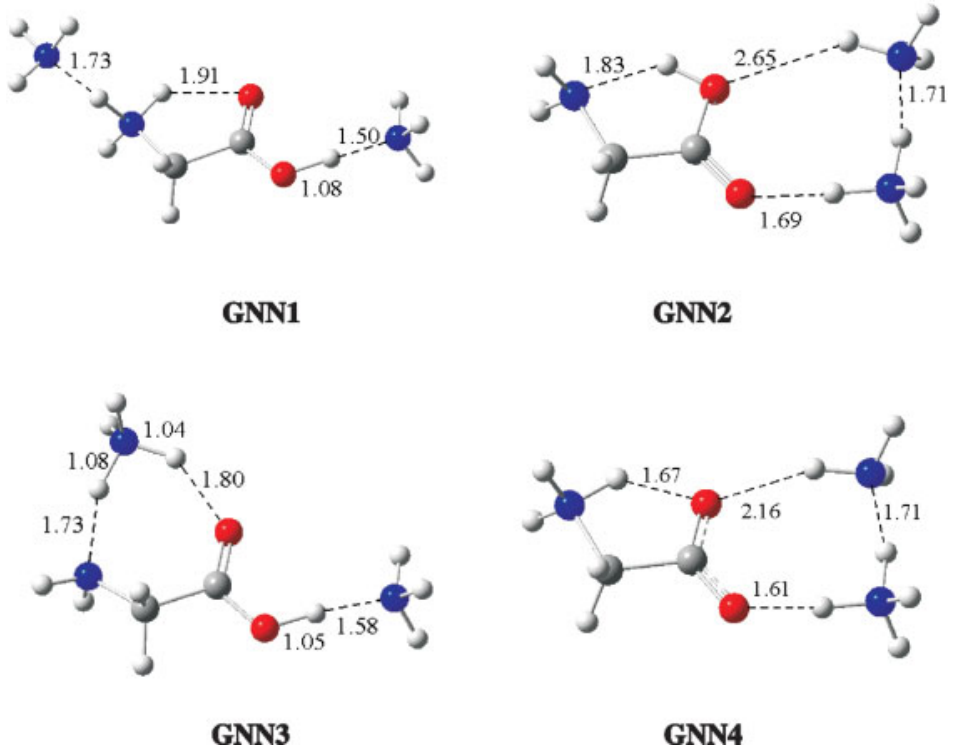
The isomer **GN3** is derived from separated reactants by a single proton transfer from the protonated amino group of protonated glycine to ammonia. At the same time, two intermolecular hydrogen bonds are formed, one between the two nitrogens and a second between another ammonium hydrogen and the carbonyl oxygen of glycine. The two hydrogen bond lengths of 1.73 and 2.00 Å to the amine nitrogen and carbonyl oxygen, respectively, are together longer than the combination of intermolecular and intramolecular hydrogen bonds in **GN1** and **GN2**.

Isomer **GN4** is perhaps what might initially have been regarded as being the most intuitively logical species derived from protonated glycine and ammonia. Its binding enthalpy is, however, more than 2 kcal mol^{-1} less favorable than that in **GN1**. Here ammonia functions as a hydrogen bond acceptor, forming an intermolecular hydrogen bond of 1.67 Å to a hydrogen of the protonated amine group of protonated glycine. At the same time, the intramolecular hydrogen bond length from the protonated amino group to the carboxyl oxygen increases to 2.09 Å from the original 1.91 Å in isolated protonated glycine. This is the only isomer, among these four most stable species, in which no intermolecular proton transfer occurs.

Presuming a Boltzmann distribution of possible isomers, the dominant species present throughout our experimental temperature range would be **GN1** (78%) and **GN2** (16%) with smaller amounts of **GN3** (2%) and **GN4** (4%) present using the enthalpy data from the MP2(full)/6-311++G(2d,2p)//B3LYP/6-311+G(d,p) calculation and entropies from the B3LYP/6-311+G(d,p) calculation. Assuming such a statistical mixture and average entropy change, including the entropy of mixing term, becomes –27.7 cal mol^{-1} K^{-1}, essentially unchanged from the value determined for the most stable isomer. In addition, the question can also be posed of the possibility of facile interconversion of these isomers to arrive at a statistical distribution. This question will be ad-

© 2005 NRC Canada

Fig. 6. The different isomers of the cluster of protonated glycine and two ammonia molecules obtained at the B3LYP/6-311+G(d,p) level of theory.



dressed in the following section in a discussion of the potential energy surface for the **GN** species.

Gly(NH$_3$)$_2$H$^+$

The four most stable structures found for the cluster of protonated glycine and two ammonia molecules are shown in Fig. 6. In the most stable isomer (**GNN1**), two ammonia molecules act as hydrogen bond acceptors interacting with both the protonated amine and hydroxyl hydrogen of the protonated glycine moiety. In contrast to the most stable isomers of Gly(NH$_3$)H$^+$, no proton transfer to ammonia is observed. However, from the shorter OH···N hydrogen bond length (1.50 Å) compared with the NH···N hydrogen bond length (1.73 Å), it appears that the hydrogen bond strength to the hydroxyl hydrogen may be stronger than that to the amino hydrogen. This would indicate that the positive charge density at the hydrogen of the carboxylic acid group is likely greater than that of a single hydrogen of the ammonium moiety in protonated glycine. The calculated binding enthalpy of 18.2 kcal mol^{-1} is nearly identical to the measured value and, similarly, the calculated entropy change for addition of the second ammonia molecule (–28.7 cal mol^{-1} K^{-1}) is also very close to the measured value of –26.9 cal mol^{-1} K^{-1}.

The second most stable isomer (**GNN2**) has a binding enthalpy of 18.0 kcal mol^{-1}, very similar to that of the most stable isomer (**GNN1**). It should be noted, however, that at the B3LYP/6-311+G(d,p) level, this species is the most stable isomer. **GNN2** might be thought of as being derived from **GN1** by the addition of a second ammonia molecule hydrogen bonded to the ammonium ion already interacting with a neutral glycine molecule at the carboxyl oxygen. In effect, this resembles an asymmetric $N_2H_7^+$ species interacting with neutral glycine primarily via a hydrogen bond to the carboxyl oxygen (1.69 Å) but with a weaker, secondary intermolecular hydrogen bond to the hydroxyl oxygen (2.65 Å). The intramolecular hydrogen bond between the hydroxyl hydrogen and amino nitrogen is identical in length (1.83 Å) to that in **GN1** from which it is derived.

The binding enthalpy of **GNN3** is computed to be 1.5 kcal mol^{-1} less than that of the most stable isomer at the MP2(full)/6-311++G(2d,2p)//B3LYP/6-311+G(d,p) level. Given its remarkable structural similarity, it seems clear that it is derived from **GN3** by the interaction of ammonia as a hydrogen bond acceptor at the hydroxyl hydrogen of the glycine moiety. In **GNN3** a proton transfer has once again occurred from protonated glycine to the first ammonia molecule leading to the doubly hydrogen-bonded configuration in which NH_4^+ hydrogen bonds to both the amino nitrogen and carbonyl oxygen of neutral glycine. The only significant structural change in this configuration relative to **GN3** is the contraction of the NH···O hydrogen bond from 2.00 to 1.80 Å. This is likely the result of the increased negative charge density at the carbonyl oxygen caused by the interaction of the hydroxyl hydrogen of the carboxyl group with the second ammonia molecule, giving a partial proton transfer and hence increased negative charge density at both oxygens of the carboxyl group. This latter hydrogen bond in **GNN3** is slightly longer (1.58 Å) than the analogous hydrogen bond in **GNN1** (1.50 Å), likely because of the partial proton transfer to the carbonyl oxygen in the adjacent double hydrogen bond to NH_4^+.

In exactly the same way that **GNN2** can be thought of as being derived from **GN1**, **GNN4** can be considered to be derived from **GN2**. The most significant difference between

© 2005 NRC Canada

Table 2. Calculated values of enthalpy (298 K) and entropy changes of the association reactions related to different isomers.

	B3LYP/6-311+G(d,p)			MP2(full)/6-311++G(2d,2p)//B3LYP/6-311+G(d,p)
Isomer	ΔH (kcal mol^{-1})	ΔH with BSSE (kcal mol^{-1})	ΔS (cal mol^{-1} K^{-1})	ΔH (kcal mol^{-1})
GN1	–25.8	–25.4	–27.8	–24.4
GN2	–24.9	–24.6	–30.9	–24.4
GN3	–24.3	–23.4	–32.9	–23.7
GN4	–22.8	–21.7	–27.2	–22.4
GNN1	–17.7	–15.5	–28.7	–18.2
GNN2	–18.0	–16.8	–30.2	–18.0
GNN3	–16.5	–14.4	–33.3	–16.7
GNN4	–14.3	–13.1	–36.4	–15.2
GG1	–29.1	–28.6	–34.2	–29.7
GG2	–27.0	–26.0	–35.7	–28.4
GG3	–26.5	–25.9	–37.2	–28.0
GGN1	–19.5	–18.0	–28.5	–19.2
GGN2	–19.6	–17.4	–28.5	–19.0
GGN3	–16.7	–15.3	–24.9	–16.9
GGN4	–17.2	–15.0	–27.3	–16.8

GNN4 and **GNN2** is the fact that in the former an intramolecular proton transfer has occurred to yield a zwitterionic glycine neutral, which is now hydrogen bonded to the asymmetric $N_2H_7^+$ species. Although the number of hydrogen bonds (4) is nominally the same in **GNN4** as in **GNN2**, the hydrogen bond lengths in **GNN4** are notably shorter at 1.61, 1.71, 2.16, and 1.67 Å, meaning that they are stronger overall than the corresponding bonds in **GNN2**. The ~3.0 kcal mol^{-1} higher energy of **GNN4** is thus the result of the higher energy of zwitterionic neutral glycine relative to the molecular form. Viewed in terms of cationic interactions with the molecular form of neutral glycine, it thus appears that the interaction with NH_4^+ is much better able to promote the isomerization to zwitterionic neutral glycine (**GN1** → **GN2**) than is $N_2H_7^+$ (**GNN2** → **GNN4**).

Given the values of ΔH and ΔS for eq. [4] summarized in Table 2, it would be predicted that, under thermal equilibrium conditions, the population of **GNN1** and **GNN2** would be 75% and 25%, respectively, with **GNN3** and **GNN4** having very minor contributions throughout our entire experimental temperature range. A calculation of the average entropy change, including entropy of mixing, gives a value of ΔS of –28.5 cal mol^{-1} K^{-1}. The experimental ΔH and ΔS values for eq. [4] are in excellent agreement with the values computed for **GNN1** and **GNN2**, the dominant species observed.

(Gly)$_2$H$^+$

As demonstrated previously (27), the three most stable isomers of the protonated dimer of glycine may contribute to a statistical population at HP-MS temperatures. The structures and energetics obtained in the present work agree very well with the previous study (27). These three isomers are shown in Fig. 7. The thermochemical data for **GG1**–**GG3** represent the enthalpy and entropy changes associated with the reaction of protonated glycine (**G1**) with the most stable conformer of neutral glycine (eq. [6]) (27).

[6] $(Gly)H^+ + Gly \leftrightarrows (Gly)_2H^+$

The most stable isomer (**GG1**) is a direct analogue of **GN1** in which a nitrogen-protonated glycine has replaced the ammonium ion in an interaction with the carbonyl oxygen of neutral glycine. At the same time, there are intramolecular hydrogen bonds in both the glycine and protonated glycine moieties with the bond length in the former being identical to that in the analogous **GN1** structure. It is of interest to compare the enthalpy of binding of 29.7 kcal mol^{-1} with that for the analogous reaction leading to **GN1** (eq. [1]) of 24.4 kcal mol^{-1}. As noted as a general phenomenon in previous studies, the greater hydrogen bond energy in **GG1** relative to **GN1** can be understood from the 7.9 kcal mol^{-1} lower proton affinity of ammonia relative to glycine.

The **GG2** structure is the analogue of **GN3** in which one hydrogen of a nitrogen-protonated base interacts with the neutral glycine molecule via a hydrogen bond to the amino nitrogen of neutral glycine, while a secondary hydrogen bond is formed between another hydrogen of the protonated-nitrogen base and the carbonyl oxygen of the neutral glycine. In addition, an intramolecular hydrogen bond interaction within the protonated glycine moiety results in a hydrogen bond length of 2.16 Å. This dimer species has a binding enthalpy of 28.4 kcal mol^{-1}, 1.3 kcal mol^{-1} less than that in **GG1**.

GG3 is very similar in structure to **GG1**, with the exception that an intramolecular proton transfer from the hydroxyl hydrogen of the carboxyl group to the amino nitrogen has occurred in the neutral glycine moiety, such that the structure of neutral glycine becomes zwitterionic. This is again reminiscent of the difference between **GN1** and **GN2**. The intermolecular hydrogen bond length of 1.50 Å is less than the corresponding value of 1.61 Å in **GG1**, a result of the increased negative charge density on the carboxylate oxygens following the intramolecular proton transfer. The binding energy of 28.0 kcal mol^{-1} at the MP2(full)/6-311++G(2d,2p)//B3LYP/6-311+G(d,p) level is only 1.7 kcal mol^{-1} less than that in the more stable **GG1**.

These calculated values for the binding enthalpy in the protonated glycine dimer are all very close to those previ-

© 2005 NRC Canada

Fig. 7. The different isomers of the cluster of protonated glycine dimer obtained at the B3LYP/6-311+G(d,p) level of theory.

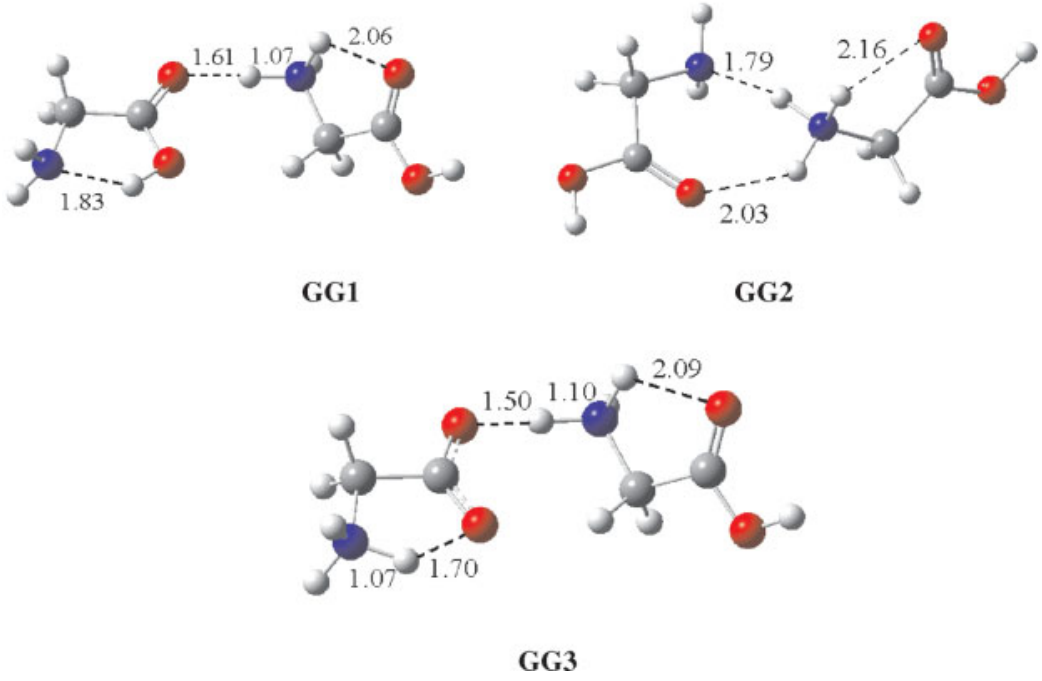
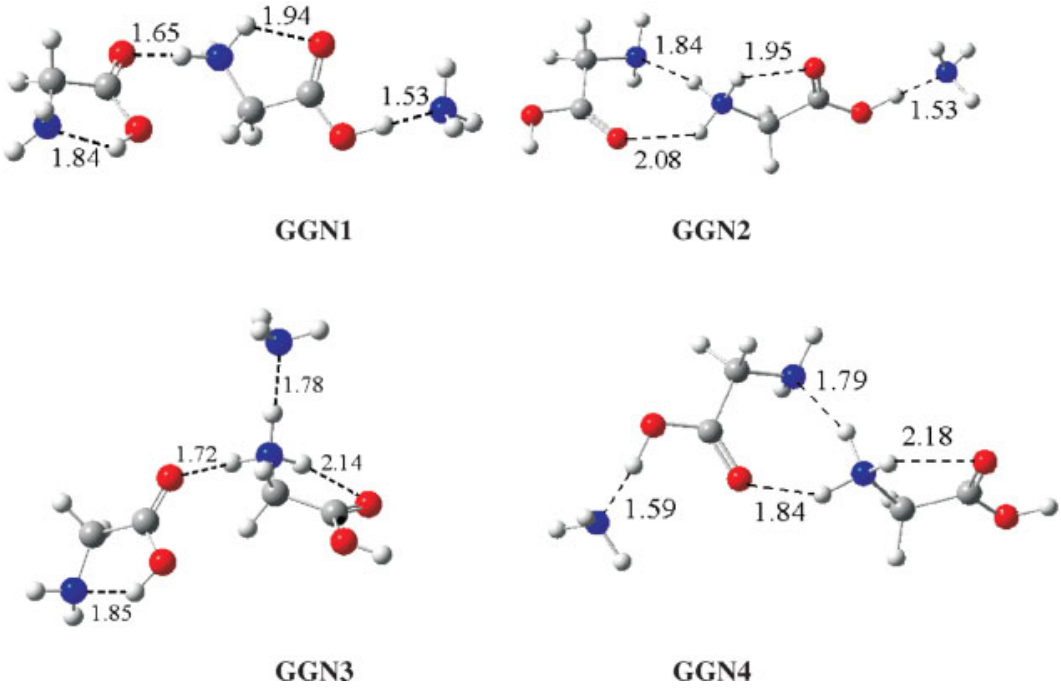


Fig. 8. The different isomers of the cluster of protonated glycine dimer with one ammonia obtained at the B3LYP/6-311+G(d,p) level of theory.



ously computed in this laboratory at the MPW1PW91/6-31+G(*d*) level of 29.2, 27.7, and 27.5 kcal mol^{-1} for **GG1**, **GG2**, and **GG3**, respectively. The experimentally determined binding enthalpy of 27.2 kcal mol^{-1} obtained from HP-MS experiments is in reasonable agreement with the computed values (27). In addition, as discussed in the following, no barrier for proton transfer between **GG1** and **GG3** is found at 298 K. The following discussion of binding of ammonia to $(Gly)_2H^+$ is based on structures **GG1** and **GG2**.

$(Gly)_2(NH_3)H^+$

The four most stable structures located for $(Gly)_2(NH_3)H^+$ species are shown in Fig. 8. Two of these (**GGN1** and **GGN3**) can be considered to be derived from **GG1**, while

© 2005 NRC Canada

the remaining two are derived from **GG2**. In none of these species does any proton transfer occur, consistent with the much greater proton affinity of the neutral glycine dimer relative to that of ammonia. In the most stable isomer (**GGN1**), ammonia forms a strong hydrogen bond to the hydroxyl hydrogen of the carboxyl group within the protonated glycine moiety with a hydrogen bond length of 1.53 Å. This is similar to the bond length found in the analogous hydrogen-bonding situation in **GNN1**. The computed enthalpy of binding is 19.2 kcal mol^{-1} at the MP2(full)/6-311++G(2d,2p)// B3LYP/6-311+G(d,p) level. In **GGN3**, ammonia forms a hydrogen bond with one of the hydrogens at the protonated amino group of glycine with a hydrogen bond length of 1.78 Å. This species can also be considered to be an analogue of **GNN1**, at its other ammonia binding site, where the corresponding hydrogen bond length from the amino proton to ammonia is 1.73 Å. The computed enthalpy of binding in **GGN3** of 16.9 kcal mol^{-1} is considerably less than that in **GGN1**, however, the calculated entropies of association for the two isomers are essentially identical, –28.5 and –28.4 cal mol^{-1} K^{-1}, respectively, for **GGN1** and **GGN3**.

The two structures derived from **GG2** both involve hydrogen bonds to ammonia at a hydroxyl hydrogen of either the protonated glycine or neutral glycine moieties. **GGN2** results from binding of ammonia as a hydrogen bond acceptor at the hydroxyl hydrogen of the protonated amino acid entity with a hydrogen bond length of 1.53 Å, essentially identical to that found in **GGN1**. The binding enthalpy of 19.0 kcal mol^{-1} is only 0.2 kcal mol^{-1} less than that in **GGN1**. The interaction of ammonia with **GG2** at the hydroxyl hydrogen of the neutral glycine moiety yields **GGN4**, which is a new structural motif. Somewhat surprisingly, the new hydrogen bond length of 1.59 Å is only slightly greater than that in **GGN2**. The enthalpy of binding is, however, considerably less at 16.8 kcal mol^{-1}. It is of interest to note that when ammonia interacts with **GG2** to form a hydrogen bond with the hydroxyl group of the protonated glycine entity, the intramolecular hydrogen bond length between the protonated amine and carbonyl oxygen decreases from 2.16 Å in **GG2** to 1.95 Å in **GGN2**. Similarly, when ammonia forms a hydrogen bond with the hydroxyl hydrogen of the neutral glycine moiety, the intermolecular hydrogen bond length for the bond between an amino hydrogen of the protonated amine and the carbonyl oxygen of the neutral glycine moiety decreases from 2.03 Å in **GG2** to 1.84 Å in **GGN4**. The shortening and strengthening of these two hydrogen bonds is the direct result of the increased negative charge density on the two carbonyl oxygens induced by partial proton transfer to the bound ammonia.

Based on the calculated energetics, a statistical mixture would contain 53% **GGN1**, 38% **GGN2**, 7% **GGN3**, and 2% **GGN4**. The measured enthalpy of the association reaction is 19.1 kcal mol^{-1}, which is essentially identical to the computed values for **GGN1** and **GGN2**. In addition, the calculated entropy changes for the association reaction for **GGN1** and **GGN2** are each the same (–28.5 cal mol^{-1} K^{-1}) and in excellent agreement with the experimentally determined value of –30.5 cal mol^{-1} K^{-1}. Including the entropy of mixing term, an average entropy change of –27.2 cal mol^{-1} K^{-1} is obtained, again in good agreement with the experimental value. Since, as shown in the following, **GG1** and **GG2** can readily interconvert at our experimental temperatures, it is likely that the experimental measurement does constitute a statistical mixture of **GGN1** and **GGN2**.

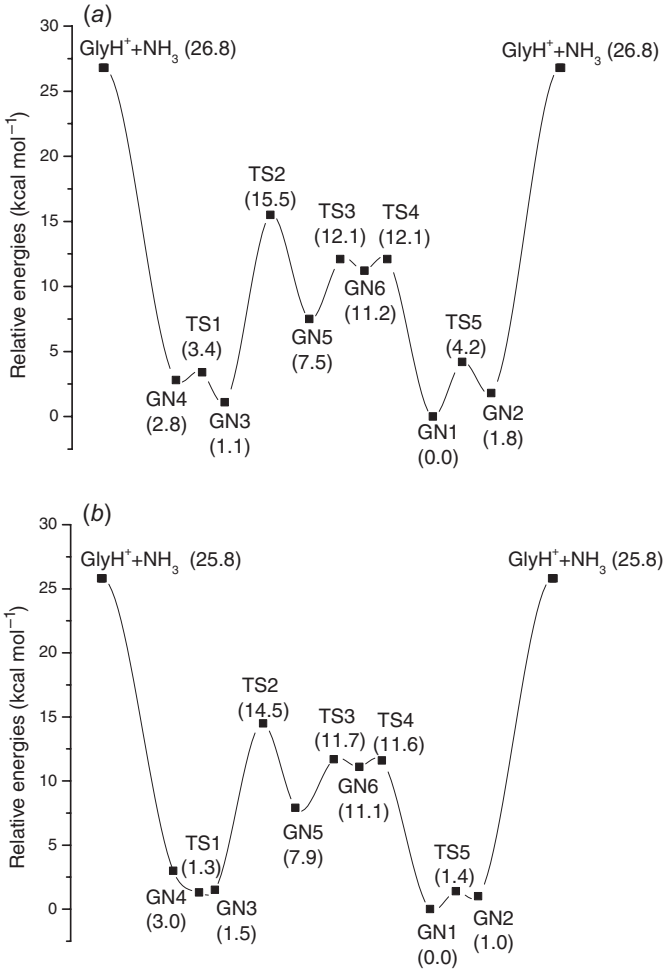


Fig. 9. (*a*) Vibrationless potential energy surface (0 K) for the isomerization of protonated glycine – ammonia clusters calculated at the B3LYP/6-311+G(d,p) level. The relative 0 K electronic energies of each stationary point are given in parentheses (kcal mol^{-1}, 1 cal = 4.184 J). (*b*) Potential energy surface including zero point energy contributions (ZPC) and thermal energy correction at 298 K. The relative enthalpies of each stationary point at 298 K are given in parentheses (kcal mol^{-1}). (*c*) The structures of each stationary point.

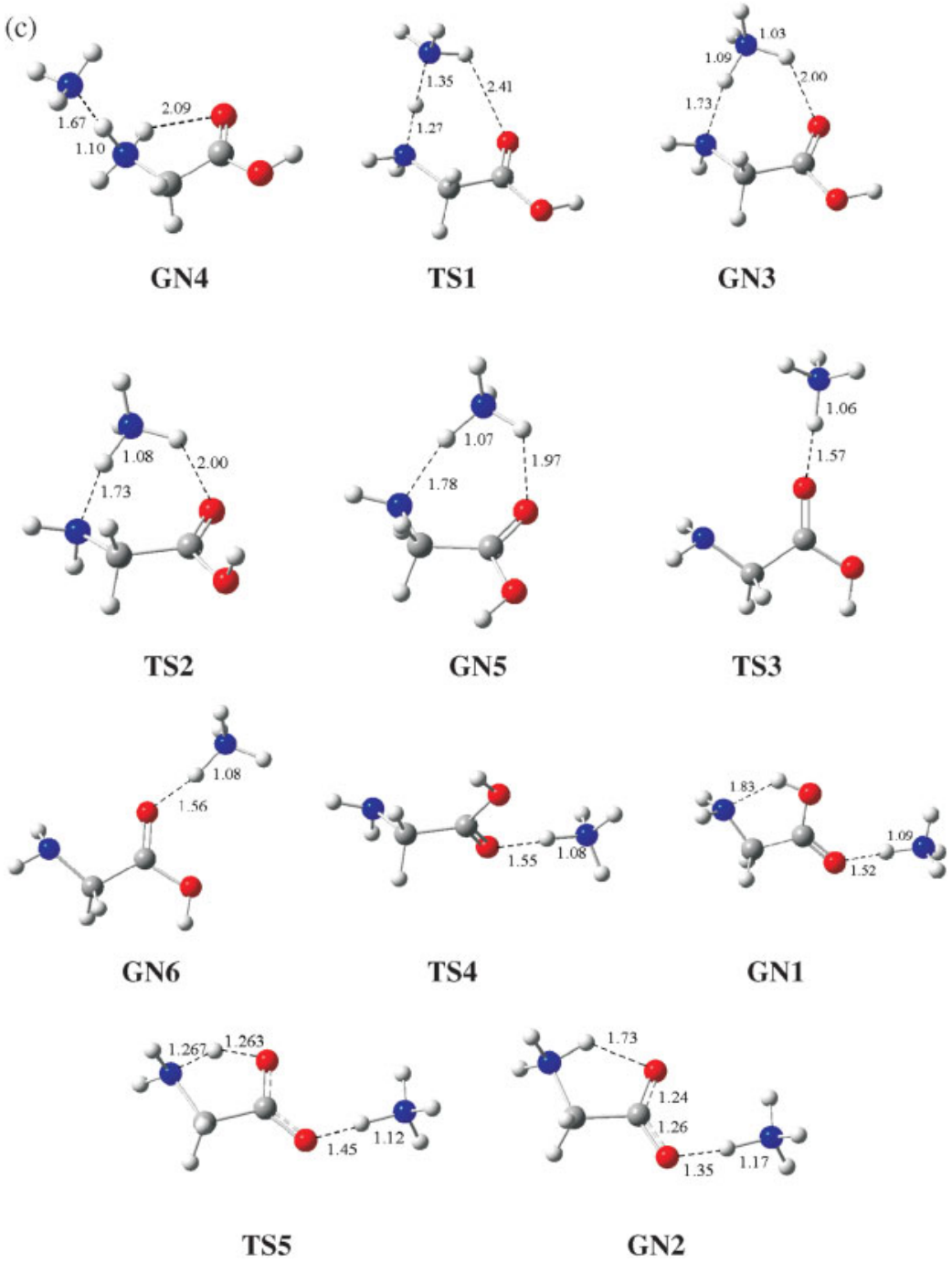
Potential energy surfaces for isomerization

Gly(NH$_3$)H$^+$

Even though the ab initio calculations reveal stable minima corresponding to several different stable isomers of each of the cluster species investigated here are possible, the question remains as to whether all such species are energetically accessible under the experimental conditions employed. To answer this question an exhaustive search of the potential energy surface for several key cluster ions was undertaken to examine their interconversion. These potential energy surfaces for isomer transformation have been investigated at the B3LYP/6-311+G(d,p) level. The results of such

© 2005 NRC Canada

Fig. 9 (*concluded*).



a search for the potential energy surface of the cluster of protonated glycine with ammonia are shown in Fig. 9. Figure 9*a* shows a vibrationless 0 K potential energy surface, based on differences in electronic energies, for interconversion of the various $Gly(NH_3)H^+$ cluster species, while Fig. 9*b* shows the potential energy surface using 298 K enthalpy differences that include zero point energy contributions and thermal energy corrections at 298 K. This surface is somewhat different than that at 0 K, and the energy of one transition state (**TS1**) becomes lower in energy than either of the two minimum energy structures to which it is linked. However, this constitutes a more accurate representation of the actual experimental situation. The structures of every stationary point located are shown in Fig. 9*c*, including two new energy minima (**GN5** and **GN6**) and five transition states (**TS1** through **TS5**).

Two different approaches of NH_3 to the **G1** form of protonated glycine might be envisaged, either at the protonated amino group or at the hydroxyl hydrogen. In the former case, ammonia acts as a hydrogen bond acceptor and **GN4** is formed. Alternatively, in the approach at the hydroxyl hydrogen, a barrierless proton transfer occurs leading to **GN2**, which, through the intramolecular proton transfer via **TS5**, can also rearrange to the most stable **GN1**. In

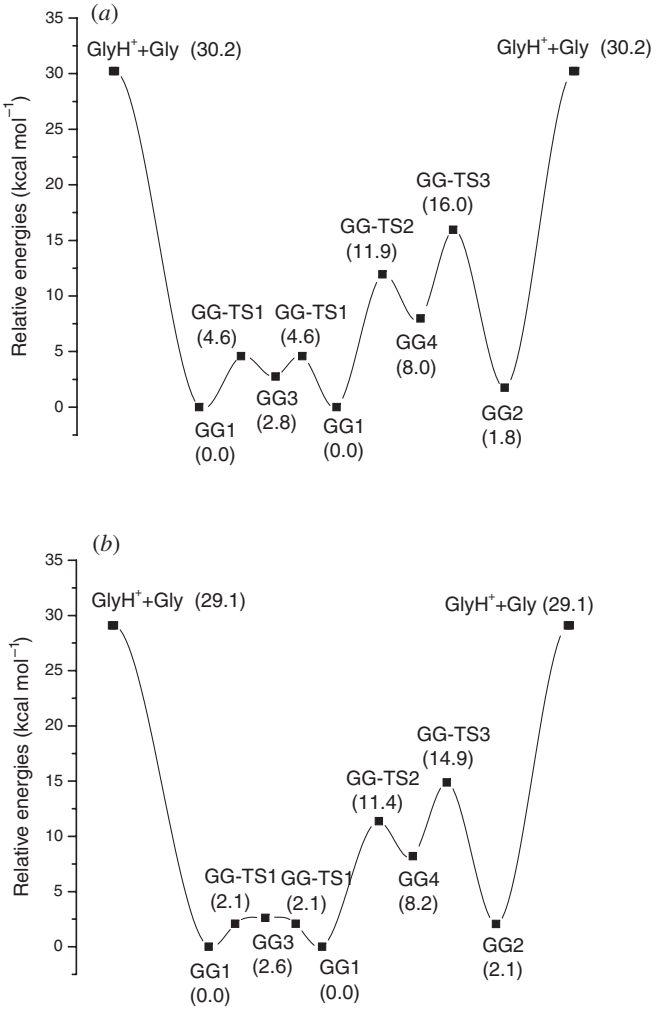
© 2005 NRC Canada

the first case, **GN4** may undergo an intermolecular proton transfer to ammonia and form an additional hydrogen bond via **TS1** to arrive at **GN3**. Although transition state **TS1** lies 0.6 kcal mol^{-1} above **GN4** at 0 K, at 298 K it is 1.7 kcal mol^{-1} lower in energy than **GN4** and even 0.2 kcal mol^{-1} lower in energy than the rearranged **GN3**. This thus constitutes an extremely facile transformation. The conversion of **GN3** to **GN1** involves additional higher energy intermediates. Rotation about the C—OH bonds leads to a slight shift of the NH_4^+ moiety toward the carbonyl oxygen, transforming **GN3** into the new species **GN5** via **TS2**. As the hydrogen bond between the ammonium ion and the amino nitrogen is broken, a rotation about the O···H-N hydrogen bond transforms **GN5** to **GN6** via **TS3**. **GN5** and **GN6** are 7.9 and 11.1 kcal mol^{-1}, respectively, higher in energy than the most stable isomer **GN1**, while the barrier at **TS2** is 13.0 and 6.6 kcal mol^{-1}, respectively, higher in energy than either **GN3** or **GN5**, which it separates. **TS3**, separating **GN5** and **GN6**, lies 3.2 kcal mol^{-1} higher in energy than the former and 0.6 kcal mol^{-1} above the latter. Finally, **GN6** may find the global minimum (**GN1**) via rotation about the C—C bond through **TS4**, which permits formation of the intramolecular hydrogen bond between the hydroxyl hydrogen and the amino nitrogen. This process has a very small barrier, with the energy of **TS4** lying only 0.5 kcal mol^{-1} above **GN6**. Thus, at the temperature of the HP-MS experiments conducted here, the complete potential energy surface will be explored leading to a statistical distribution of isomeric species.

(Gly)$_2$H$^+$

Both **GG1** and **GG2** can be considered to be formed directly, without barrier, from separated protonated glycine (**G1**) and neutral glycine by intermolecular hydrogen bond formation between a protonated amino group hydrogen of **G1** and either the carbonyl oxygen or amino nitrogen of neutral glycine. The potential energy surface for interconversion of protonated glycine dimer isomers, computed at the B3LYP/6-311+G(d,p) level of theory, is shown in Fig. 10. The vibrationless 0 K potential energy surface, based on differences in electronic energies, is given in Fig. 10*a*, and the 298 K surface, based on enthalpy differences including zero point energy contributions and thermal energies, is given in Fig. 10*b*. The transformation of **GG1** to **GG3** involves a barrier at **GG-TS1** of 4.6 kcal mol^{-1} at 0 K, which falls to 2.1 kcal mol^{-1} at 298 K, at which point this transition state lies lower in energy than **GG3** by 0.5 kcal mol^{-1}. While **GG2** had previously been considered to be the most stable of the isomers of protonated glycine dimer (40), in fact it lies 2.1 kcal mol^{-1} higher in energy than **GG1** at 298 K at the B3LYP/6-311+G(d,p) level of theory and 1.3 kcal mol^{-1} higher at the MP2(full)/6-311++G(2d,2p)//B3LYP/6–311+G(d,p) level. The interconversion of **GG1** and **GG2** involves an additional stable intermediate and two transition states. Starting from **GG1**, the intramolecular hydrogen bond in the neutral glycine moiety is broken, accompanied by rotation about the neutral C—C bond, to give **GG-TS2** lying 11.4 kcal mol^{-1} higher in energy. From this transition state, the C—C bond rotation continues, accompanied by an angular deformation of the intermolecular O···H-N hydrogen bond, to arrive at **GG4**, 8.2 kcal mol^{-1} higher in energy than

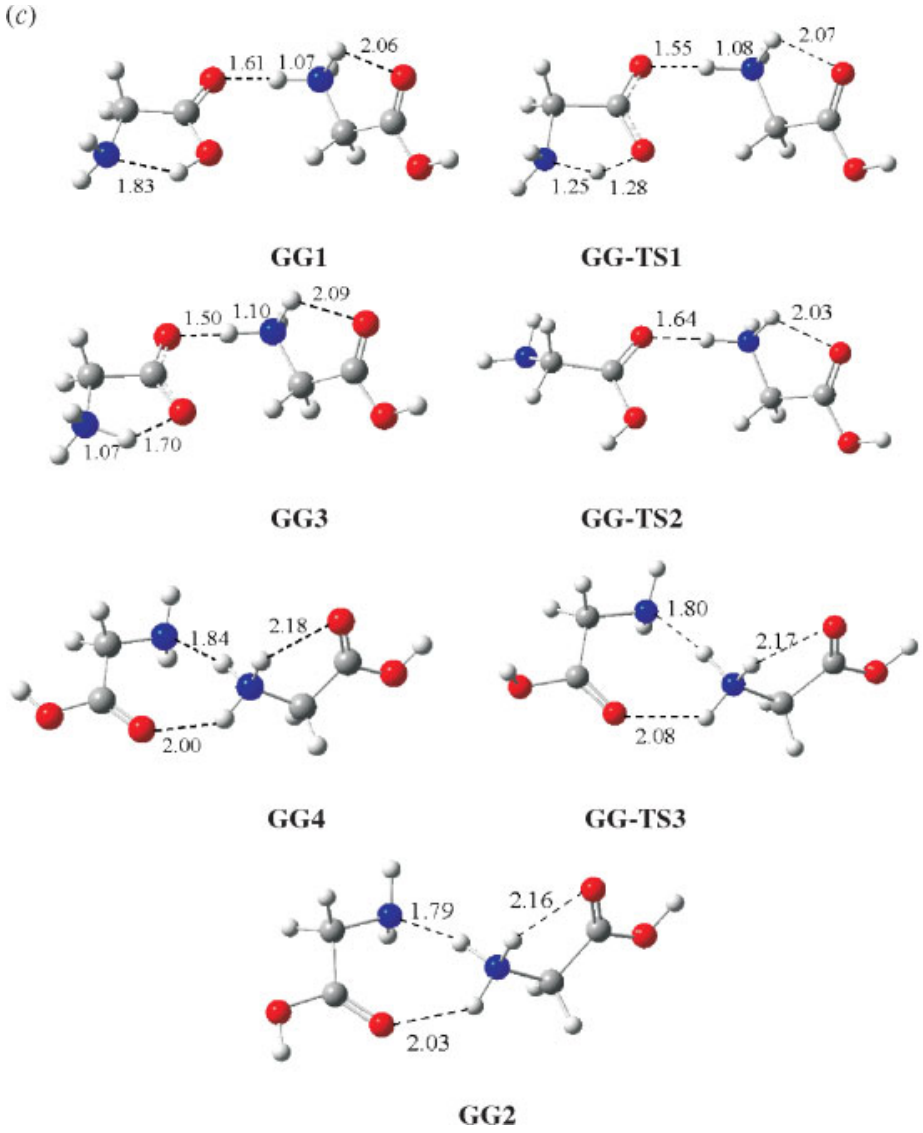
Fig. 10. (*a*) Vibrationless potential energy surface (0 K) for isomerization of the protonated glycine dimer at 0 K calculated at the B3LYP/6-311+G(d,p) level. The relative electronic energies of each stationary point are given in parentheses (kcal mol^{-1}, 1 cal = 4.184 J). (*b*) Potential energy surface including zero point energy contributions (ZPC) and thermal energy corrections at 298 K. The relative enthalpies at 298 K of each stationary point are given in parentheses (kcal mol^{-1}). (*c*) The structures of each stationary point.



GG1. Rotation about the C—OH bond in the neutral glycine moiety gives rise to **GG-TS3**, which is 14.9 kcal mol^{-1} higher in energy than **GG1** and which then collapses to **GG2**. The protonated glycine dimer has also recently been studied by infrared photodissociation spectroscopy (IRPD) (41) in the 3000–4000 cm^{-1} range. The experimental IRPD spectrum has only two peaks, with the strongest peak at 3584 cm^{-1} presumably associated with the stretching vibration of the free OH group in the protonated glycine moiety. A second, weaker peak at 3372 cm^{-1} was assigned to the free NH asymmetric stretch at the ammonium nitrogen of a **GG2** dimer structure. However, the free NH symmetric stretch and the stretching vibration of bonded NH are also possible at this position. In addition, in **GG1**, the symmetric stretch of the free NH at the ammonium nitrogen is 3375 cm^{-1}, and the stretching vibrational frequency of free

© 2005 NRC Canada

Fig. 10 (*concluded*).



OH is 3599 cm^{-1} at the B3LYP/6-311+G(d,p) level, which, after a scaling of 0.965, is also in the correct range. Thus, on the basis of these two peaks, it is not possible to assign the structure unambiguously as **GG1** or **GG2**. Again, it is to be anticipated that, either by direct association or by rearrangement, a statistical population of G**G1** and **GG2** can be achieved.

Gly(NH$_3$)$_2$H$^+$

Detailed calculations of the potential energy surface for Gly(NH$_3$)$_2$H$^+$ species were not carried out. However, structure **GNN1** would appear to be readily accessible without a barrier from direct association of **GN2** with ammonia. Similarly, structure **GNN2** could be presumed to be directly accessed via barrierless association of **GN1** with ammonia. The higher energy structure **GNN3** can be likely formed reasonably readily from **GNN1** via a transition state analogous to **TS1** on the Gly(NH$_3$)H$^+$ potential energy surface. Similarly, the transformation of **GNN2** to **GNN4** should proceed via a low-lying transition state resembling **TS5**. Thus, it seems highly likely that the Gly(NH$_3$)$_2$H$^+$ system can freely explore all four of the stable minima calculated here.

(Gly)$_2$(NH$_3$)H$^+$

Extensive calculations of the potential energy surface for (Gly)$_2$(NH$_3$)H$^+$ species similarly were not carried out. Structures **GGN1** and **GGN3** should be formed without a barrier from direct association of **GGN1** with ammonia. Similarly, structures **GGN2** and **GGN4** could be presumed to be directly accessed via barrierless association of **GG2** with ammonia. The interconversion of these four species should also be reasonably facile via transition states resembling those on the (Gly)$_2$H$^+$ potential energy surface. Thus, it also seems highly likely that the (Gly)$_2$(NH$_3$)H$^+$ system can freely explore all four of the stable minima calculated here.

Zwitterionic structure of glycine

In the gas phase, neutral glycine, as well as all other amino acids, are known to exist in the non-zwitterionic form. The non-zwitterionic form of glycine is computed to

© 2005 NRC Canada

be 22 ± 2 kcal mol^{-1} lower in energy than the zwitterionic form at the *thermodynamically calibrated* BAC/MP4/6-31G(d,P)/6-31G(*d*) level of theory (42), although the existence of an actual stable minimum for the zwitterionic form seems unlikely because of facile proton transfer. Two water molecules can make the zwitterionic form of glycine a local minimum on the potential energy surface, but this hydrated zwitterion is still about 12 kcal mol^{-1} higher in energy than the non-zwitterionic analogue (43). For amino acids interacting with metal ions, two different structural motifs can be envisaged, either a charge-solvated structure in which the amino acid is non-zwitterionic or alternatively, a salt bridge structure in which the amino acid is zwitterionic. Alkali cation attachment does have the effect of stabilizing the salt bridge structure relative to the charge-solvated analogue but, for example, upon sodium ion attachment the relative energy of the salt bridge structure of glycine, is still 1–3 kcal mol^{-1} higher than the charge-solvated structure according to the calculations (4, 44–47). Hodyau and Ohanessian (44) carried out a systematic series of calculations of the interaction of glycine with all alkali metal cations (Li^+ to Cs^+) in the gas phase and found that the most stable alkali cation – glycine species always had a non-zwitterionic structure. The most stable non-zwitterionic structure was lower in energy, by from 1.4 to 3.3 kcal mol^{-1}, than the salt bridge form for the Li^+ to Cs^+ adducts. For Na^+, the most stable non-zwitterionic isomer had a relative energy lower by either 1.4 or 2.7 kcal mol^{-1} than the zwitterionic one using either a MP2/6-31G* or MP2/6-311+G (2d,2p)//MP2/6-31G* calculation, respectively, including correction for BSSE. Similarly, a B3LYP/DZVP calculation gives the energy of the most stable non-zwitterionic isomer to be 2.5 kcal mol^{-1} lower than the salt bridge structure in Na^+(Gly) (46).

For the structures of ammonia adducts of protonated glycine investigated here, structures **GN1**–**GN3** involve neutral glycine interacting with NH_4^+, while **GN4** is a true adduct of neutral ammonia with an intermolecular hydrogen bond at the protonated nitrogen of glycine. However, the **GN2** adduct involves NH_4^+ interacting with a zwitterionic glycine molecule and this species is comparable in stability to the most stable of the non-zwitterionic forms (**GN1**). It is likely that the identical energies of **GN1** and **GN2** calculated at the MP2(full)/6-311++G(2d,2p)//B3LYP/6-311+G(d,p) level are more accurate than the B3LYP/6-311+G(d,p) results, since the agreement between the experimental and calculated values for each of the three adducts investigated in the present work is better at the former computational level. Thus, it appears that the interaction of NH_4^+ is very effective in stabilizing the zwitterionic structure of glycine. In comparison to NH_4^+, the $N_2H_7^+$ and $GlyH^+$ ions are not as effective in stabilizing the zwitterionic structure of glycine, as evidenced by the greater energetic difference between structures **GG3** and **GG1** (1.7 kcal mol^{-1}) and between **GNN4** and **GNN2** (2.8 kcal mol^{-1}). This is likely due to the fact that the positive charge on each of the hydrogens of NH_4^+ is quite substantial, so that a very strong hydrogen bond with the anionic carboxylate moiety in zwitterionic glycine can be formed. In contrast, the charges on the possible hydrogen-bonding sites of $N_2H_7^+$ and $GlyH^+$ are substantially less, which makes them less able to stabilize the zwitterionic form of glycine very effectively. According to the Mulliken population analysis calculated at the B3LYP/6-311+G(d,p) level, when atomic charges on the hydrogens are summed with those on the heavy atoms, in **GG1** the sum of charges on the nitrogen of $GlyH^+$ is 0.664, and that in **GG3** becomes 0.639. The charge on the nitrogen in NH_4^+ in **GN1** is 0.973, while that in **GN2** is dramatically less at 0.787, which indicates that NH_4^+ effectively shares the partial negative charge on the carboxylate group of the zwitterionic glycine.

It is of interest to compare the interactions of NH_4^+ and Na^+ with glycine. The binding energy of Na^+ to glycine has been determined by four different experimental methods as either 36.3 ± 1.4 (48), 38.5 ± 1.9 (49), 39.7 ± 1.4 (50), or 36.6 ± 2.3 kcal mol^{-1} (51). Based on the data from the present work and the known proton affinity difference between glycine and ammonia of 7.8 kcal mol^{-1}, the binding energy between neutral glycine and NH_4^+ can be determined to be 31.0 kcal mol^{-1}, which is some 5–9 kcal mol^{-1} lower than the binding energy between glycine and Na^+. However, if the calculation is based upon supposing, albeit naively, that the $Gly(NH_3)H^+$ cluster structure is derived from association of NH_4^+ with the most closely corresponding neutral conformer, then, using the calculated energetic differences between glycine conformers, the binding energy for NH_4^+ to glycine to yield the **GN1** conformer is 32.7 kcal mol^{-1}. Thus, to arrive at **GN2** in a similar fashion, it is necessary to presume a zwitterionic glycine neutral species. As noted earlier, such a structure is not found to be a stable minimum, but if the result from ref. 42 is taken in which the zwitterionic form was given as 22 ± 2 kcal mol^{-1} higher in energy than the most stable conformer, the binding energy for NH_4^+ to zwitterionic glycine to yield **GN2** is about 54 kcal mol^{-1}. Such a strong interaction energy is not surprising given that this is effectively a polyatomic cation – polyatomic anion interaction.

Conclusions

Gas-phase ion–molecule interactions involving glycine and ammonia have been studied by high pressure mass spectrometry. The association reaction of protonated glycine with ammonia yields the enthalpy and entropy changes of –23.2 kcal mol^{-1} and –26.9 cal mol^{-1} K^{-1}, respectively. The subsequent addition of a second molecule of ammonia to the product ion thus formed results in corresponding thermochemical values of –18.3 kcal mol^{-1} and –28.4 cal mol^{-1} K^{-1}. Finally, addition of ammonia to the protonated dimer of glycine gives enthalpy and entropy changes of –19.1 kcal mol^{-1} and –30.5 cal mol^{-1} K^{-1}, respectively. These interactions have also been examined by computational methods and several different isomers for each of the cluster species involved in these equilibria have been located at the B3LYP/6-311+G(d,p) level of theory, and binding enthalpies and entropies have been obtained for each possible isomer. The potential energy surface for the interconversion of the isomers of the protonated glycine clusters with ammonia has been calculated by the same method. Single point energy calculations have been carried out at the MP2(full)/6-311++G(2d,2p)//B3LYP/6-311+G(d,p) level of theory, which yield binding energies that are in excellent agreement with the experimentally measured values.

© 2005 NRC Canada

For the $Gly(NH_3)H^+$ cluster, the three most stable isomers all involve a proton transfer from protonated glycine to ammonia to yield various glycine-solvated ammonium ion structures. Calculations of the potential energy surface for this system show that the highest barrier on the surface lies 14.5 kcal mol^{-1} above the global minimum energy structure. Given that the exothermicity of formation of the minimum energy structure is ~10 kcal mol^{-1} greater than this, the entire surface, involving six stable minima and five transition states, can be fully sampled during the association–dissociation equilibrium process. One of the stable isomers on this surface (**GN2**) involves NH_4^+ bound to glycine in a zwitterionic form and this adduct is found to be one of two isoenergetic species that constitute the global minimum structure at the MP2(full)/6-311++G(2d,2p)//B3LYP/6-311+G(d,p) level.

The global minimum energy isomer for the cluster of protonated glycine with two ammonia molecules is found to be one in which a protonated glycine moiety acts as a double hydrogen bond donor to bind one ammonia molecule at the protonated amino site and a second at the hydroxyl hydrogen site of the carboxylic acid functionality. Thus, in this species, no proton transfer occurs. However, a nearly isoenergetic structure of this composition also exists, derived from the most stable $Gly(NH_3)H^+$ cluster in which a $N_2H_7^+$ moiety interacts with neutral glycine as a double hydrogen bond donor with resulting interactions at both the carbonyl and hydroxyl oxygens. A third, intramolecular hydrogen bond also exists in this species between the hydroxyl hydrogen and the amino nitrogen.

The most stable form of the protonated dimer of glycine involves an intermolecular hydrogen bond between a hydrogen of the protonated amino functionality and the carbonyl oxygen of the neutral glycine. This is supplemented by one intramolecular hydrogen bond between a second hydrogen of the protonated amino group and the carbonyl oxygen of this molecule and a second between the hydroxyl hydrogen of the neutral glycine moiety and the amino nitrogen of the same molecule. Correspondingly, the most stable isomer of the adduct of the protonated dimer of glycine and ammonia is one in which ammonia forms a strong hydrogen bond with the remaining free hydroxyl hydrogen of the protonated glycine moiety. An only slightly less stable isomer of this adduct also exists, derived from the second most stable protonated dimer of glycine.

For each of the clusters examined, the measured enthalpies are in excellent agreement with the corresponding calculated values of the most stable isomers obtained at the MP2(full)/6-311++G(2d,2p)//B3LYP/311+G(d,p) level of theory. Considering the calculated differences in binding energies of the various isomers, the most stable isomers would be predicted to be the dominant species under our experimental conditions.

In this work, NH_3 has served as a model compound to probe the interaction of important functional groups and protonated glycine as a model for amino acids and other biomolecules. Continuing investigations from this laboratory will extend such studies to other systems of biochemical and biological significance. In particular, the study of isomerizations on the potential energy surfaces for these species may serve as an aid to the understanding of biological structure and function.

Acknowledgements

The generous financial support of this work by the Natural Sciences and Engineering Research Council of Canada (NSERC) is gratefully acknowledged. RW acknowledges helpful discussions with T.D. Fridgen, R. Nieckarz, P. Ng, and R. Marta of the University of Waterloo.

References

1. T. Wieland and M. Bodanszky. The world of peptides. Springer-Verlag, Berlin. 1991.
2. S. Vishveshwara and J.A. Pople. J. Am. Chem. Soc. **99**, 2422 (1977).
3. J.H. Jensen and M.S. Gordon. J. Am. Chem. Soc. **113**, 7913 (1991).
4. J.H. Jensen. J. Am. Chem. Soc. **114**, 9533 (1992).
5. K. Zhang and A. Chung-Phillips. J. Comput. Chem. **19**, 1862 (1998).
6. S. Campbell, J.L. Beauchamp, M. Rempe, and D.L. Lichtenberger. Int. J. Mass Spectrom. Ion Processes, **117**, 83 (1992).
7. M. Meot-Ner, E.P. Hunter, and F.H. Field. J. Am. Chem. Soc. **101**, 686 (1979).
8. Z. Wu and C. Fenselau. J. Am. Soc. Mass Spectrom. **3**, 863 (1992).
9. J. Wu and C.B. Lebrilla. J. Am. Chem. Soc. **115**, 3270 (1993).
10. K. Zhang, D.M. Zimmerman, A. Chung-Philips, and C.J. Cassidy. J. Am. Chem. Soc. **115**, 10812 (1993).
11. B. Balta, M. Basma, V. Aviyente, C. Zhu, and C. Lifshitz. Int. J. Mass Spectrom. **201**, 69 (2000).
12. H.Q. Ai and Y.X. Bu. J. Chem. Phys. **120**, 2208 (2004).
13. T.B. McMahon. Int. J. Mass Spectrom. **200**, 187 (2000).
14. M. Meot-Ner. Acc. Chem. Res. **17**, 186 (1984).
15. G. Caldwell, T.F. Magnera, and P. Kebarle. J. Am. Chem. Soc. **106**, 959 (1984).
16. C. Li, P. Ross, J.E. Szulejko, and T.B. McMahon. J. Am. Chem. Soc. **118**, 9360 (1996).
17. K. Normann and T.B. McMahon. J. Am. Chem. Soc. **118**, 2449 (1996).
18. C.D. Deakyne and M. Meot-Ner. J. Am. Chem. Soc. **121**, 1546 (1999).
19. M. Meot-Ner, P. Hamlet, E.P. Hunter, and F.H. Field. J. Am. Chem. Soc. **102**, 6393 (1980).
20. J.S. Klassen, A.T. Blades, and P. Kebarle. J. Am. Chem. Soc. **116**, 12075 (1994).
21. J.S. Klassen, A.T. Blades, and P. Kebarle. J. Phys. Chem. **99**, 15509 (1995).
22. B. Bogdanov, H.J. Lee, and T.B. McMahon. Int. J. Mass. Spectrom. **210**, 387 (2001).
23. B. Bogdanov and T.B. McMahon. Int. J. Mass. Spectrom. **219**, 593 (2002).
24. M. Meot-Ner and F.H. Field. J. Am. Chem. Soc. **96**, 3168 (1974).
25. J.E. Szulejko, J.J. Fisher, T.B. McMahon, and J. Wronka. Int. J. Mass Spectrom. Ion Processes, **83**, 147 (1988).
26. J.E. Szulejko and T.B. McMahon. Int. J. Mass Spectrom. Ion Processes, **109**, 279 (1991).
27. S.A. Raspapov and T.B. McMahon. J. Mass Spectrom. **40**, 1536 (2005).

© 2005 NRC Canada

28. M.J. Frisch, G.W. Trucks, H.B. Schlegel, G.E. Scuseria, M.A. Robb, J.R. Cheeseman, J.A. Montgomery, Jr., T. Vreven, K.N. Kudin, J.C. Burant, J.M. Millam, S.S. Iyengar, J. Tomasi, V. Barone, B. Mennucci, M. Cossi, G. Scalmani, N. Rega, G.A. Petersson, H. Nakatsuji, M. Hada, M. Ehara, K. Toyota, R. Fukuda, J. Hasegawa, M. Ishida, T. Nakajima, Y. Honda, O. Kitao, H. Nakai, M. Klene, X. Li, J.E. Knox, H.P. Hratchian, J.B. Cross, C. Adamo, J. Jaramillo, R. Gomperts, R.E. Stratmann, O. Yazyev, A.J. Austin, R. Cammi, C. Pomelli, J.W. Ochterski, P.Y. Ayala, K. Morokuma, G.A. Voth, P. Salvador, J.J. Dannenberg, V.G. Zakrzewski, S. Dapprich, A.D. Daniels, M.C. Strain, O. Farkas, D.K. Malick, A.D. Rabuck, K. Raghavachari, J.B. Foresman, J.V. Ortiz, Q. Cui, A.G. Baboul, S. Clifford, J. Cioslowski, B.B. Stefanov, G. Liu, A. Liashenko, P. Piskorz, I. Komaromi, R.L. Martin, D.J. Fox, T. Keith, M.A. Al-Laham, C.Y. Peng, A. Nanayakkara, M. Challacombe, P.M.W. Gill, B. Johnson, W. Chen, M.W. Wong, C. Gonzalez, and J.A. Pople. Gaussian 03. Revision B.04 [computer program]. Gaussian, Inc., Pittsburgh, Penn. 2003.
29. S.F. Boys and F. Bernardi. Mol. Phys. **19**, 553 (1970).
30. P. Tarakeshwar and K.S. Kim. J. Phys. Chem. A, **103**, 9116 (1999).
31. R.H. Wu, S. Vaupel, P. Nachtigall, and B. Brutschy. J. Phys. Chem. A, **108**, 3338 (2004).
32. W.R. Davidson, J. Sunner, and P. Kebarle. J. Am. Chem. Soc. **101**, 1675 (1979).
33. Y.K. Lau, K. Nishizawa, A. Tse, R.S. Brown, and P. Kebarle. J. Am. Chem. Soc. **103**, 6291 (1981).
34. M. Meot-Ner. J. Am. Chem. Soc. **106**, 1257 (1984).
35. R. Yamdagni and P. Kebarle. J. Am. Chem. Soc. **95**, 3504 (1973).
36. Y.K. Lau and P. Kebarle. Can. J. Chem. **59**, 151 (1981).
37. M. Meot-Ner. J. Am. Chem. Soc. **106**, 1265 (1984).
38. M. Meot-Ner. J. Phys. Chem. **91**, 417 (1987).
39. W.G. Mallard (*Editor*). NIST Chemistry WebBook. NIST standard reference database 69 [online]. Available from http://webbook.nist.gov. National Institute of Standards and Technology, Gaithersburg, Maryland. 2005.
40. W.D. Price, P.D. Schnier, and E.R. Williams. J. Phys. Chem. B, **101**, 664 (1997).
41. H.B. Oh, C. Lin, H.Y. Hwang, H. Zhai, K. Breuker, V. Zabrouskov, B.K. Carpenter, and F.W. McLafferty. J. Am. Chem. Soc. **127**, 4076 (2005).
42. E. Kassab, J. Langlet, E. Evleth, and Y. Akacem. J. Mol. Struct: THEOCHEM, **531**, 267 (2000).
43. J.H. Jensen and M.S. Gordon. J. Am. Chem. Soc. **117**, 8159 (1995).
44. S. Hodyau and G. Ohanessian. Chem. Eur. J. **4**, 1561 (1998).
45. T. Wyttenbach, M. Witt, and M.T. Bower. Int. J. Mass Spectrom. **183**, 243 (1999).
46. T. Wyttenbach, M. Witt, and M.T. Bower. J. Am. Chem. Soc. **122**, 3458 (2000).
47. S. Hodyau, J.P. Pelicier, F. Rogalewicz, Y. Hoppilliard, and G. Ohanessian. Eur. J. Mass Spectrom. **7**, 303 (2001).
48. A. Gapeev and R.C. Dunbar. Int. J. Mass Spectrom. **228**, 825 (2003).
49. M.M. Kish, G. Ohanessian, and C. Wesdemiotis. Int. J. Mass Spectrom. **227**, 509 (2003).
50. R.M. Moision and P.B. Armentrout. J. Phys. Chem. **106**, 10350 (2002).
51. J.S. Klassen, S.G. Anderson, A.T. Blades, and P. Kebarle. J. Phys. Chem. **100**, 14218 (1996).

© 2005 NRC Canada

Gas-phase experiments on the chemistry and coordination of Zn(II) by aprotic solvent molecules[1]

Bridgette J. Duncombe, Lijlijana Puškar, Bohan Wu, and Anthony J. Stace

Abstract: Experiments have been performed in the gas phase on a series of doubly charged zinc–ligand complexes to elucidate their solvation structure and available fragmentation pathways. Production of such complexes was achieved by the formation of neutral argon–ligand clusters followed by the subsequent addition of a single zinc atom using a pickup technique. Multiply charged ions were then produced by electron impact within a high resolution, double-focusing mass spectrometer. Studies have been undertaken on a number of zinc(II) – aprotic solvent complexes including those consisting of argon and carbon dioxide in association with the zinc cation. Investigation of these novel metal–solvent clusters took the form of recorded parent ion intensity distributions and the measurement of fragmentation patterns promoted via collision-induced dissociation (CID). Discussion of the intensity distributions is presented in terms of the solvation of Zn(II) by each solvent, drawing on existing theoretical and experimental data from the gaseous and condensed phases. Investigation of collision-induced dissociation processes includes identifying charge transfer reactions in each solvated system, and analysis of the results in terms of kinetic energy release as well as possible mechanisms for fragmentation pathways.

Key words: zinc, clusters, dications, gas phase, solvation.

Résumé : Dans le but d'élucider leur structure de solvatation et les voies qui leur sont disponibles pour la fragmentation, on a effectué des expériences en phases gazeuses sur une série de complexes zinc–ligand doublement chargés. La production de tels complexes a été réalisée par la formation d'agrégats argon–ligand neutres, suivie d'une addition subséquente d'un seul atome de zinc en utilisant la technique du « ramassage ». On a ensuite produit les ions à multiples charges par une ionisation électronique dans un spectromètre de masse à double focalisation, à haute résolution. On a entrepris des études sur un certain nombre de complexes de zinc(II) – solvants aprotiques, y compris ceux formés d'argon et de dioxyde de carbone en association avec le cation zinc. L'examen de ces nouveaux agrégats métal–solvant a pris la forme de distributions enregistrées de l'intensité de l'ion précurseur et la mesure des patrons de fragmentation qui résultent d'une dissociation induite par une collision (DIC). On présente une discussion des distributions de l'intensité en fonction de la solvatation du Zn(II) par chaque solvant en se basant sur des données théoriques et expérimentales existantes pour les phases gazeuses et condensées. L'étude des processus de dissociation induits par une collision inclut l'identification des réactions de transfert de charge dans chaque système solvaté et une analyse des résultats en termes d'énergie cinétique émise ainsi que des mécanismes possibles pour les voies de fragmentation.

Mots clés : zinc, agrégats, dications, phase gazeuse, solvatation.

[Traduit par la Rédaction]

Introduction

Gas-phase studies of multiply charged metal ion solvation have been extremely fruitful over the past decade (1). Two principal methods, notably *electrospray* (2–4) and *pick-up*, have been used with considerable success to investigate a wide range of systems. The pick-up method, first utilized by Scoles and co-workers (5) to investigate the solvation of molecules within argon clusters, is now routinely used to produce a wide variety of heterogeneous clusters. It is, however, within our group that the pick-up technique has been utilized, with considerable success, for the production of multiply charged metal–ligand complexes (6–15).

Although the intensities of solvated multiply charged metal ions formed via the pick-up technique can be relatively low, there are a number of advantages in using this method of preparation when compared with electrospray or laser vaporization. A wide variety of solvent entities can be used, including species that are frequently involved in matrix isolation experiments rather than complexation. For example, carbon dioxide and argon would fall into the latter group. Furthermore, a wide variety of metals can be studied,

Received 26 May 2005. Published on the NRC Research Press Web site at http://canjchem.nrc.ca on 3 February 2006.

B.J. Duncombe,[2] L. Puškar, B. Wu,[2] and A.J. Stace.[2,3] Department of Chemistry, School of Life Sciences, University of Sussex, Falmer, Brighton BN1 9QJ, UK.

[1]This article is part of a Special Issue dedicated to Professor P. Kebarle.

[2]Present address: School of Chemistry, The University of Nottingham, University Park, Nottingham NG7 2RD, UK.
[3]Corresponding author (e-mail: Anthony.Stace@nottingham.ac.uk).

 doi: 10.1139/V05-203 © 2005 NRC Canada

frequently in oxidation states that are not easily accessible in the condensed phase i.e., gold(II) (11).

In the experiments reported here the pick-up technique has been used to prepare a range of Zn(II) complexes in association with aprotic solvents. In addition to recording ion intensities, we also report on the fragmentation patterns and chemistry of individual complexes. Below a critical size, many of the Zn(II)–molecule combinations are found to exhibit extensive chemical reactivity, driven primarily by charge transfer from the metal cation to a molecule.

Experimental Section

The experiments described herein were performed using instrumentation that has been described in detail in earlier publications (7, 12). In brief, argon carrier gas at a pressure of 30–50 psi (1 psi = 6.894757 kPa) was seeded with the desired solvent, which then underwent adiabatic expansion through a pulsed, 200 μm diameter conical nozzle, leading to the formation of neutral mixed argon–solvent clusters. Most of the solvents used in this study were in the liquid state and were held in a stainless steel reservoir through which the carrier gas passed. It was frequently found necessary to keep the reservoir in an ice bath to reduce the vapour pressure of the solvent concerned such that it remained constant over the average time of a single experimental period lasting approximately 10 h. In the case of carbon dioxide, a premixed cylinder of Ar–CO_2 in the ratio 99:1 was used. Collimation of the beam took place downstream from the nozzle with a 1 mm diameter skimmer before passing into the pick-up region. In this next section of the apparatus, zinc pieces (Aldrich, Gillingham, UK) held in a pyrolytic boron nitride crucible (Sintec, Halblech, Germany) were heated in an effusion cell (model EC-40-63-21, DCA Instruments, Turku, Finland) to a temperature of 320–340 °C, as measured with a standard C-type thermocouple. These conditions were found to be sufficient to produce zinc vapour of approximately 10^{-2} mbar (1 bar = 100 kPa) partial pressure. The metal vapour flowed into the path of the molecular beam where the mixed argon–solvent clusters "picked-up" a metal atom to produce neutral clusters of varying composition, including $Zn(L)_N(Ar)_M$, $Zn(L)_N$, and $Zn(Ar)_M$. If the temperature of the oven was too high, the molecular beam intensity diminished because of scattering by zinc atoms. A shutter positioned at the exit of the oven acted as a guide to the relative intensity of zinc–ligand signals within a series, such that parent ion intensity distributions were recorded by taking the difference in intensity between the shutter being open and closed.

Zinc has five naturally occurring isotopes, of which three, ^{64}Zn, ^{66}Zn, and ^{68}Zn, have relatively high intensities, and when recording parent ion intensity distributions and reaction pathways, complexes containing these isotopes were used. On entering the ion source of a reverse geometry Vacuum Generators ZAB-E mass spectrometer, the clusters were ionized using high-energy electron impact (70–100 eV). The positively charged clusters were then accelerated at 5 kV through the first field free region (FFR) into the magnetic sector of the mass spectrometer where they were selected according to their mass to charge ratio. The ion clusters then passed through the second FFR into a gas cell that allowed the controlled introduction of a collision gas. Collision-induced dissociation (CID) was promoted by the introduction of air (at a background pressure of ~1×10^{-6} mbar), and the m/z values of any ionic fragments were identified by passing the ion beam through an electrostatic analyser (ESA). This particular linked-scanning technique is normally referred to as a MIKE (mass-analysed ion kinetic energy) scan (16). Although the loss of neutral ligands from a multiply charged metal–solvent complex is of interest, it is the appearance or absence of charge transfer pathways that can frequently yield more useful information on the structure and composition of parent ions.

When doubly charged species are produced in the ion source, they appear with twice the kinetic energy of mass coincident singly charged ions. Accordingly, when charge transfer occurs to produce two singly charged daughter ions, these are transmitted at kinetic energies double that of a mass coincident singly charged species formed in the ion source. With the ion source operating at 5 kV, it was necessary to scan the ESA such that ions with kinetic energies between 0 and 10 keV were transmitted through to the detector to identify all possible charge transfer products. Singly charged ions created by charge transfer are frequently accompanied by an extensive release of kinetic energy, which appears as a consequence of repulsion between the two separating positively charged daughter ions (Coulomb explosion). Thus, peaks associated with charge transfer processes are often much broader than neutral loss peaks, which makes identification easier, but accurate mass assignment difficult. Ion detection was via a Daly scintillation detector linked to a lock-in amplifier (SR850, Stanford Research Systems, Sunnyvale, California), which provided phase-sensitive detection referenced with respect to the train of nozzle pulses.

Results and discussion

Experiments have been undertaken on the solvation properties of Zn(II) with a variety of aprotic solvents (loosely defined as solvents that are unable to hydrogen bond). In previous studies, parent ion intensity distributions have acted as a guide as to the coordination of a central metal ion by surrounding ligand molecules. Several factors control the size distribution, with the method of preparation being of particular significance. As a consequence of the expansion process, clusters of the form Ar_ML_N are probably present in the seeded beam for $N + M \leq 200$. Cluster size plays a significant role in the pick-up of metal as the collision between a "hot" atom and a "cold" cluster probably results in a phase transition (cluster melting) accompanied by the evaporation of a large number of argon atoms and some solvent molecules. However, it cannot be assumed that the neutral metal atom becomes surrounded by solvent molecules, rather that a variety of interactions including metal–solvent, solvent–solvent, and metal–argon will determine where the metal atom "resides" at this point in the preparation process.

Final composition and structure of the multiply charged metal–solvent complexes are most strongly influenced by the final step in the production process, namely electron impact (EI) ionization. This is a complicated process and with increasing electron energy a wide variety of reaction channels exist, creating a diverse range of ionized and neutral products (17). Using a simple analysis of the ionization en-

© 2005 NRC Canada

ergies of the constituents of the neutral cluster undergoing EI, it can be seen that since the first ionization energies of most metals are below those of a typical solvent species studied, it is to be expected that the metal will be preferentially ionized. However, for multiple ionization, the route to forming $[M(L)_N]^{Z+}$ is not so obvious. The first ionization energy of a solvent species is usually lower than the second ionization energy of the metal or any argon atoms left within the cluster, therefore, the solvent molecule would be expected to be preferentially ionized in any sequential double ionization step. However, for most small clusters ($N < \sim 30$) this should result in Coulomb explosion and the appearance of two singly charged entities. Hence, the formation of $[M(L)_N]^{Z+}$ species is most likely to be a single electron event centred on the metal atom.

In relation to the ionization process, there are a number of observations that are of significance: since no species of the form $[M(L)_N Ar_M]^{Z+}$ are detected, this gives credence to the belief that argon atoms act as a heat sink to dispose of any thermal energy that appears as a consequence of the metal–cluster collision in the pick-up process. The pivotal role played by argon is confirmed by the fact that similar experiments performed using helium fail to produce multiply charged metal–ligand complexes. Ions of the form $[M(Ar)_M]^{Z+}$ produced via the pick-up technique have been detected for a number of transition metals M (14), but their initial formation is presumably as a consequence of a collision with a large cold argon cluster, and their stability is due to a combination of a high first ionization energy on the part of argon (15.75 eV) and its moderate polarizability. However, in competition with a solvent molecule, which would probably have a much stronger electrostatic interaction with the metal cation, the formation of metal–solvent complexes would be preferred over containing a metal atom combined with argon.

The signal intensities of $[M(L)_N]^{Z+}$ ions are frequently quite low ($\sim 10^{-12}$ A) and a comparison of relative ion intensity would suggest that many more ionization and (or) fragmentation events lead to singly charged species. However, there are examples of systems where singly and doubly charged metal-containing ions have been found to have comparable intensities (cf. Cu(I) and Cu(II)) (18). Since electron impact ionization is such a violent process, multiply charged ions will have high internal energies with contributions from electronic as well as vibrational excitation. However, the ions are approximately 10^{-4} s "old" before detection and as such can undergo radiative decay and (or) evaporation of molecules to reduce their internal energy content (1). Since on leaving the ion source there is no mechanism available to promote ion growth, the system can be classed as being *nonequilibrium* (1). The rate of evaporative or radiative decay will be dependent on the intrinsic stability of the cluster ion. Thus, ions with high internal energies and (or) low binding energies will have rapid rates of decay (1). As a consequence, anomalies or magic numbers (clusters of greater intensity, hence stability) are to be found in cluster ion distributions, that is, as a function of time and under collision-free conditions, stable ions gain in intensity relative to less stable neighbours (1).

Thus, parent ion intensity is influenced by experimental parameters such that the distribution is weighted towards small N, which is a common feature of many cluster ion experiments. In the case of multiply charged ions, however, very small values of N are either not seen or are of very low intensity, as to stabilize the multiple charge with respect to charge transfer the presence of at least a partial solvent shell is required (18). Nevertheless, intensity distributions can be insightful as to the factors that influence a specific metal–solvent system. A number of quantities can be identified from mass spectral measurements: a minimum stable size N_{min}, the parent ion with greatest intensity I_{max}, and N_{crit}, the minimum number of ligands needed to prevent a complex from decomposition via charge transfer.

Zn(II) – carbon dioxide and Zn(II)–acetone complexes

Although there is currently no experimental evidence for $[Zn(CO_2)_N]^{2+}$ complexes in the condensed phase, data are available on other (atomic) transition metals interacting with CO_2 in a matrix (19, 20). Low temperature (under 60 K) Fourier transform infrared (FT IR) studies in CO_2 matrices show that along the first row transition metals the mode of bonding changes such that the insertion of a metal atom into a C—O bond can occur. Previous gas-phase pick-up experiments involving such metal cations as Cu(II), Ag(II), Au(II), and Mg(II), show that although carbon dioxide is an atypical ligand, it is very proficient at stabilizing doubly charged cations in the gas phase (12, 13, 18, 21). Much of this stability is derived from the high ionization energy of the molecule, which helps to prevent charge transfer between the ligand and the metal cation.

The fact that carbon dioxide can bond in so many different ways, viz. η^1-C, η^1-O, η^2-O,O, or η^2-C,O, has led to a great deal of theoretical interest in bonding with both atomic and cationic first row transition metals (22–24). Sodupe et al. (22) point out that the interaction of a metal ion with carbon dioxide can best be described as electrostatic. The molecule has no permanent dipole moment; consequently, the interaction can be seen as a charge-quadrupole interaction, such that linear η^1-O (end-on) coordination can be expected. However, there is undoubtedly a charge-induced dipole interaction, which because it depends on z^2 could make a dominant contribution to bonding with metal dications. However, recent experiments with Al(III) have shown carbon dioxide to be far less successful with trications (25). Calculations found the ionic charge transfer structures $M^{2+}CO_2^-$ to be much higher in energy than M^+CO_2 configurations; however, the negative charge on CO_2 would cause the molecule to bend, which in turn would weaken any end-on structure with a metal dication. Obviously, similar considerations do not apply to the complexes studied here.

Figure 1 shows the relative parent ion intensity distributions recorded for complexes of zinc(II) with carbon dioxide. The series show a clear maximum at $N = 3$, although the drop in intensity at $N = 4$ for the ^{64}Zn and ^{66}Zn isotopes is minimal. A further important feature is that a single carbon dioxide molecule is able to stabilize the zinc(II) ion; however, the intensity of the ion is comparatively low. Figure 2 shows similar data for Zn(II)–acetone complexes where, for the three main isotopes, the relative intensities follow a similar pattern to that seen for zinc(II) – carbon dioxide: a maximum at $N = 3$, followed by a slight decline at $N = 4$. Unlike the zinc – carbon dioxide system, it was not possible to lo-

© 2005 NRC Canada

Fig. 1. Relative intensities of $[Zn(CO_2)_N]^{2+}$ complexes plotted as a function of size (N).

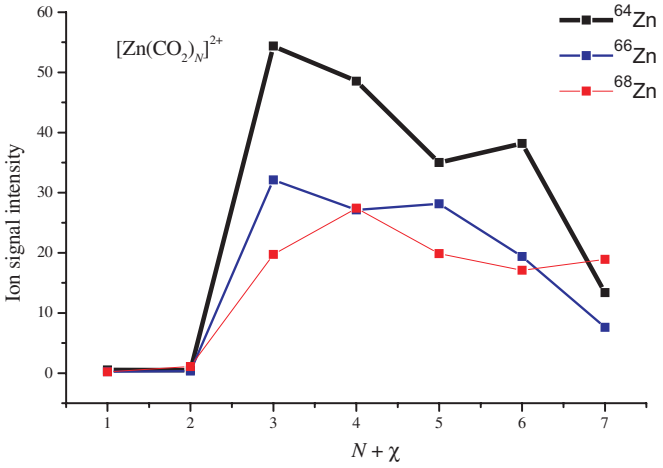
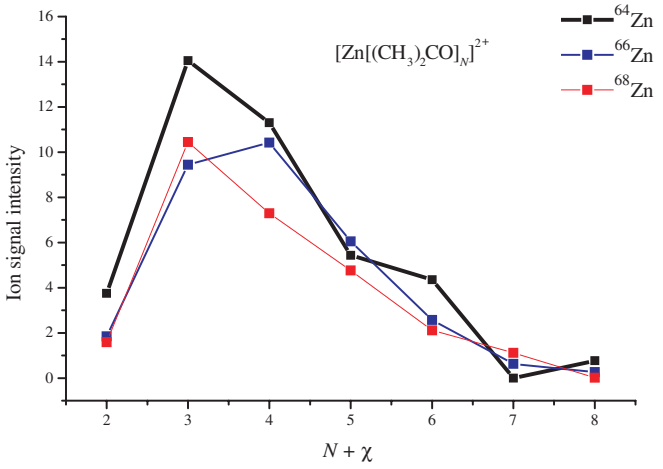


Fig. 2. Relative intensities of $[Zn[(CH_3)_2CO]_N]^{2+}$ complexes plotted as a function of size (N).



cate an ion corresponding to $[Zn(CH_3COCH_3)_1]^{2+}$, which is in contrast with recent calculations (26). El-Nahas (26) has used ab initio and DFT methods to analyse a number of metal dications interacting with aprotic solvents, including the $[Zn(CH_3COCH_3)_1]^{2+}$ system, and it was found that the complex formed a stable structure that was bent at the oxygen atom. This behaviour was attributed to substantial charge transfer occurring between the acetone molecule and the Zn^{2+} ion, and the author argued that, in the absence of such a step, the structure would be linear. Kebarle and co-workers (27) also used theory to examine $[Zn(CH_3COCH_3)_N]^{2+}$ cations. With DFT (B3LYP/6-311++G(d,p)), the optimized geometries for $[Zn(CH_3COCH_3)_1]^{2+}$ and $[Zn(CH_3COCH_3)_2]^{2+}$ were found, in each case, to be bent at the oxygen atom. It was concluded that electrostatic bonding would be strengthened by the large dipole moment and high polarizability, whilst the electron-donating ability of the lone pair on oxygen would result in ligand-to-metal charge transfer strengthening the cation–oxygen bond. Thus, with regard to the measurements presented here, it is quite possible that $[Zn(CH_3COCH_3)_1]^{2+}$ is present, but that it has an intensity that is too low to be detected in our experiment. Problems of this nature have been identified in previous work (28).

In the only other experimental study of zinc dications solvated by acetone, Kebarle and co-workers (27) used electrospray to generate $[Zn(CH_3COCH_3)_{5-7}]^{2+}$ complexes and determined enthalpies and entropies by establishing an equilibrium in the gas phase. They concluded that the transition to an outer shell occurred at the fifth molecule (i.e., 4+1 structure), and coincided with a pronounced decrease in enthalpy difference caused, in part, by the inability of acetone to form a hydrogen-bonded network. However, it was not possible to undertake experiments at smaller values of N (<5) as the temperature needed to establish equilibrium, was outside the range of the apparatus. Thus, although the maximum at $N = 3$ seen in the data presented here would seem slightly low, it is possible that the maximum reflects the high charge density present on the small zinc ion. The strong ion–dipole and ion-induced dipole interactions will pull the ligands in close to the cation and the effects of ligand–ligand repulsion will begin to have an influence at small values of N. The results presented in Figs. 1 and 2 show a sharp reduction in intensity with increasing N. Such behaviour is to be expected, as the molecules involved have no mechanism for inducing a strong secondary solvent network of the type previously seen for protic solvent systems. In the case, for example, of $[Mg(CH_3OH)_N]^{2+}$, a significant plateau in the parent ion distribution was observed and thought to be related to the formation of an extended network of charge-enhanced hydrogen bonds (7).

To investigate further the interaction between carbon dioxide and zinc(II), collision-induced fragmentation studies were undertaken. Figure 3 shows a selection of results taken from MIKE scans from which the following fragmentation patterns could be identified:

$$[1] \quad [Zn(CO_2)_N]^{2+} \rightarrow [Zn(CO_2)_{N-K}]^{2+} + K CO_2$$

$$[2] \quad \rightarrow Zn^+(CO_2)_{N-K-1} + CO_2^+ + K CO_2$$

$$[3] \quad \rightarrow Zn^+O(CO_2)_{N-K-2} + CO_2^+ + CO + K CO_2$$

Several features of these MIKE scans should be noted. For $N = 1$, there is no neutral loss, whilst for $N = 2$–4, neutral loss leads to $[Zn(CO_2)_1]^{2+}$, which supports the argument that this latter species is stable (cf. Fig. 1). For $N = 5$ and 6, neutral loss proceeds all the way to $[Zn(CO_2)_2]^{2+}$. For small N, charge transfer processes have significant intensity (relative to neutral loss) and moreover, the charge transfer peaks are comparatively narrow. Previous experiments have noted similar behaviour when ligands with high ionization energies are used to prepare complexes. Of significance is the observation that collisions promote not only direct charge transfer (rxn. [2]), but also reactivity in the form of rxn. [3]; however, the latter is a minor pathway relative to rxn. [2]. For $N = 1$ and 2, reactive charge transfer leads to ZnO^+, a process that is undoubtedly driven, in part, by the high stability of this ion. For $N = 2$–6, the most intense charge transfer product is Zn^+CO_2 whilst, for N in the range 3–6, the most prominent reaction product is OZn^+CO_2. These charge trans-

© 2005 NRC Canada

Fig. 3. Fragmentation patterns recorded following the collisional activation of $[Zn(CO_2)_N]^{2+}$ complexes for N = 3, 4, and 5.

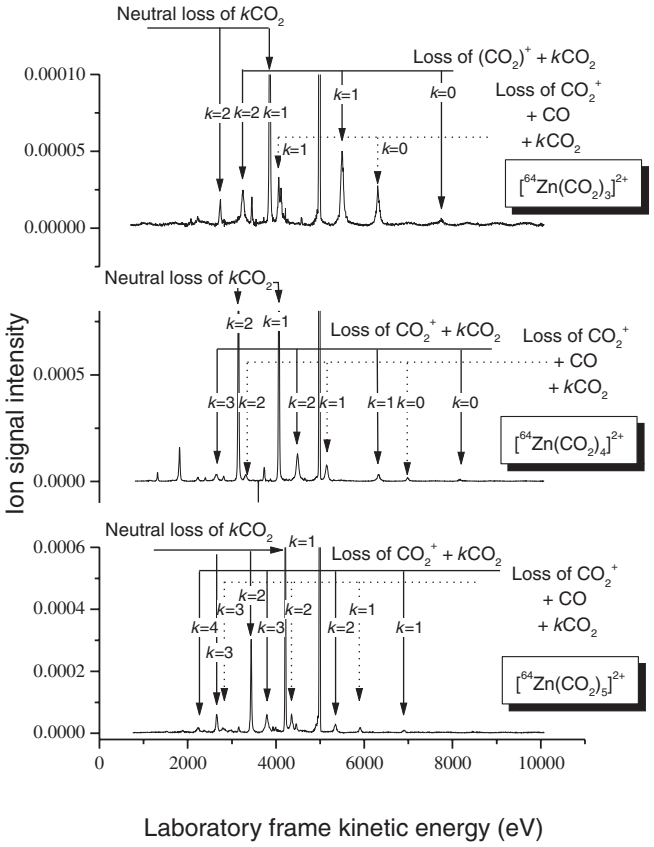
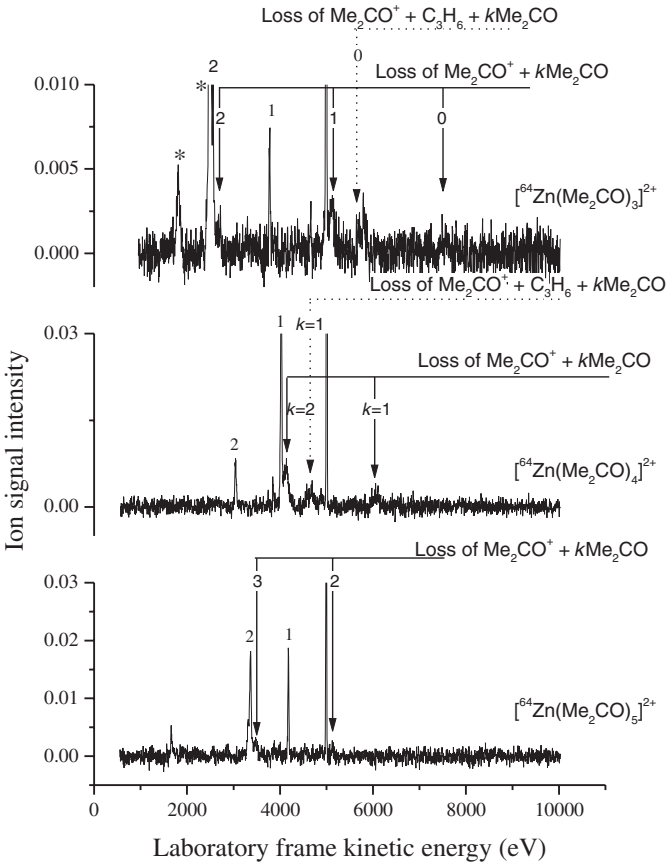


Fig. 4. Fragmentation patterns recorded following the collisional activation of $[Zn[(CH_3)_2CO]_N]^{2+}$ complexes for N = 3, 4, and 5.



fer pathways have some significance when attempting to recognize the mode of bonding between carbon dioxide and zinc(II). If the interaction were considered to be purely electrostatic, then the ion-induced dipole interaction would favour η^1-O (end-on) coordination. Side-on coordination would be unlikely as metal–ligand repulsion between filled d orbitals on the metal and the π electrons of CO_2 would be significant in such a geometry. Calculations show that, for singly charged ions of the early transition metals (Sc^+, Ti^+, and V^+), insertion into the C—O bond leading to OM^+CO formation is exothermic owing to the strength of the M^+—O bond formed (22). Therefore, it is important to identify whether or not the $[Zn(CO_2)_N]^{2+}$ complexes formed here have isomers of the form $[(O)_MZn(CO_2)_{N-M}(CO)_M]^{2+}$ (where $M \geq 1$), which would naturally lead to the loss of CO fragments (rxn. [3]). Alternatively, this reaction could be driven by a combination of collisional activation and charge transfer, with the possibility that the process is aided by a significant fraction of charge being transferred prior to the collision, with the result that the O—C bond is weakened.

As stated earlier, we are not aware of any data in the literature on Zn^{2+}-CO_2; however, calculations have been undertaken on the isoelectronic ion Cu^+-CO_2 (22). It should be borne in mind that although isoelectronic, the size of the metal ion is determined largely by its charge (z) such that aspects of bonding influenced by charged density would not be fully accounted for. The relative energies of the products of rxns. [4] and [5] are –105.02 and +421.33 kJ mol^{-1} when compared with the ground-state asymptote $Cu^+ + CO_2$ (22).

[4] $\quad Cu^+ + CO_2 \rightarrow Cu^+OCO$

[5] $\quad \rightarrow OCu^+CO$

However, the binding energies (D_0) for the product species are 101.67 and 162.76 kJ mol^{-1}, respectively. This difference is due to the electrostatic interaction for OCu^+CO being larger than Cu^+CO_2 since CO_2 does not have a permanent dipole moment (22). Thus, although the binding energy for the product from rxn. [5] is larger, the barrier to its formation is sufficiently high that the most stable configuration is η^1-O end-on CO_2 coordination in the form of the product of rxn. [4]. Further support in the case of linear $[ZnCO_2]^{2+}$ comes from recognition that the strength of the ion–dipole interaction depends on z^2. The most likely cause of rxn. [3] is the charge transfer loss of CO_2^+ accompanied by the fragmentation of CO_2 to lose neutral carbon monoxide and some carbon dioxide molecules; a process which is aided, in part, by the comparatively high bond dissociation energy of Zn^+O (161 ± 5 kJ mol^{-1} (29)). This mechanism is supported by the fact that the loss of carbon monoxide is always associated with charge transfer. In contrast, if $[(O)_MZn(CO_2)_{N-M}(CO)_M]^{2+}$ isomers were present, then neutral loss of CO or CO_2 + CO might be expected.

© 2005 NRC Canada

Figure 4 shows MIKE scans recorded following the collisional activation of $[^{64}Zn(Me_2CO)_N]^{2+}$ complexes where $N = 3$–5. The asterisks on several of the peaks in the scan for $[^{64}Zn(Me_2CO)_3]^{2+}$ denote coincidental nonmetal-containing ions, which were verified by repeating the scans, firstly, without collision gas and secondly at a low oven temperature. Compared with the results presented earlier and with neutral loss signals, the intensities of collision-induced charge transfer fragments from zinc(II)–acetone complexes were found to be relatively low. However, it was still possible to identify the following fragmentation pathways:

[6] $$[Zn(Me_2CO)_N]^{2+} \rightarrow [Zn(Me_2CO)_{N-K}]^{2+} + KMe_2CO$$

[7] $$\rightarrow Zn^+ (Me_2CO)_{N-K-1} + Me_2CO^+ + KMe_2CO$$

[8] $$\rightarrow Zn^+CH_3(Me_2CO)_{N-K-2} + Me_2CO^+ + OCH_3 + KMe_2CO$$

Although the breadth of the charge transfer peak that accompanies rxn. [8] does not allow an unambiguous assignment, loss of a methyl group is the most facile fragmentation route found in gas-phase acetone ions. An alternative route might be the formation of ZnO^+ in association with one or more acetone molecules. This route is clearly seen in the case of Zn–CO_2, but in those circumstances, there is no less exothermic alternative. In addition, the Zn^+—CH_3 bond strength has been calculated to be 240 kJ mol^{-1}, which is considerably higher than that found for Zn^+—O (30).

It should be noted from Fig. 4 that neutral loss of two acetone molecules from $[^{64}Zn(Me_2CO)_3]^{2+}$ leaves $[^{64}Zn(Me_2CO)_1]^{2+}$, which clearly contradicts the findings of the parent ion intensity distribution shown in Fig. 1. However, it is also obvious from Fig. 3 that the intensity of the fragment ion is extremely low, which would make its presence in a normal mass spectrum hard to detect. With respect to the charge transfer processes shown in Fig. 3, there are a number of conclusions to be made. First, electron transfer (rxn. [7]) is the preferred charge transfer process. The reactive charge transfer process (rxn. [8]) is probably assisted by the strength of the Zn^{2+}—O interaction, which results in ligand-to-metal electron donation, thus causing the C—CH_3 bond to weaken. It is noticeable that for $N = 5$ (and presumably for all $N > 5$), rxn. [8] is not present, which is again an indication of the low probability of this process.

Theoretical and experimental evidence presented by other groups (26, 27) points to the interaction of zinc(II) ion with acetone being more than just electrostatic in nature. Emphasis has been placed on the bent geometry (Zn-Ô-C) being an indication that factors other than electrostatic interactions play a role in bonding. Ion–dipole, ion-induced-dipole interaction (electrostatic model) would presumably prefer a linear geometry to maximize the interaction of the charge on the zinc(II) ion and dipole on acetone. A bent geometry can be rationalized in terms of an increased alignment between an empty sd hybridized orbital on zinc with the lone pair on oxygen such that charge transfer is made easier; however, full alignment is not possible because of repulsion between Zn^{2+} and the hydrogen atoms on the methyl groups. Kebarle and co-workers (27) calculated the atomic charge on Zn^{2+} as 1.65 for the addition of one Me_2CO. It is an indication of the complex nature of the zinc–acetone interaction that on addition of a second ligand, these authors also found that no further charge was transferred to the zinc ion and that the geometry became slightly more linear, seemingly to increase the electrostatic contribution to the bonding. It is also clear that an effective reduction in charge will lead to a drop in magnitude of the electrostatic interaction with increasing N. This means that, along with ligand–ligand repulsion, the bonding of further ligands is weaker than would be expected from a purely electrostatic model, and thus the parent ion intensity distribution decays rapidly with increasing N.

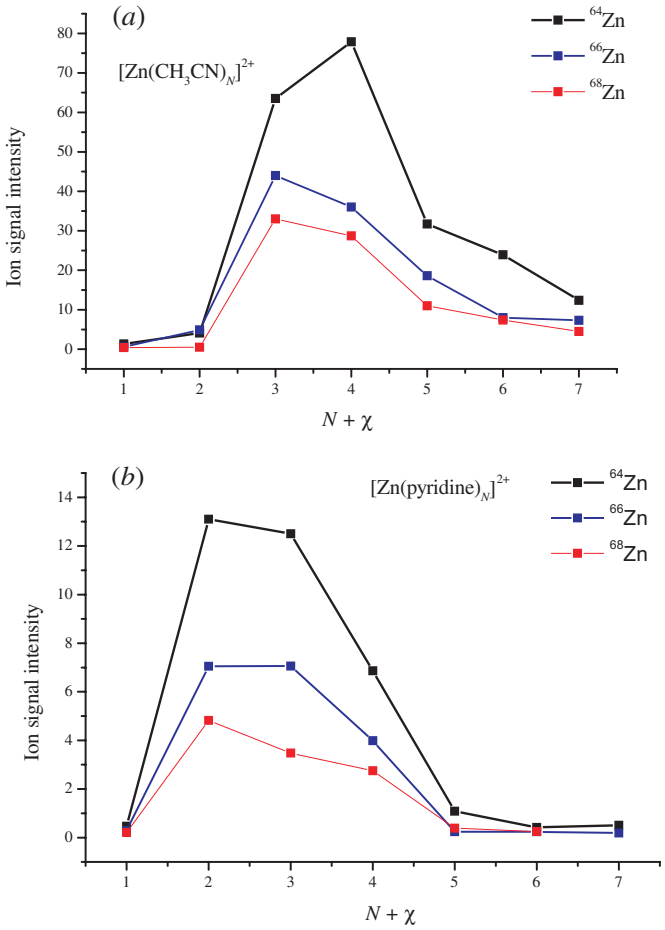


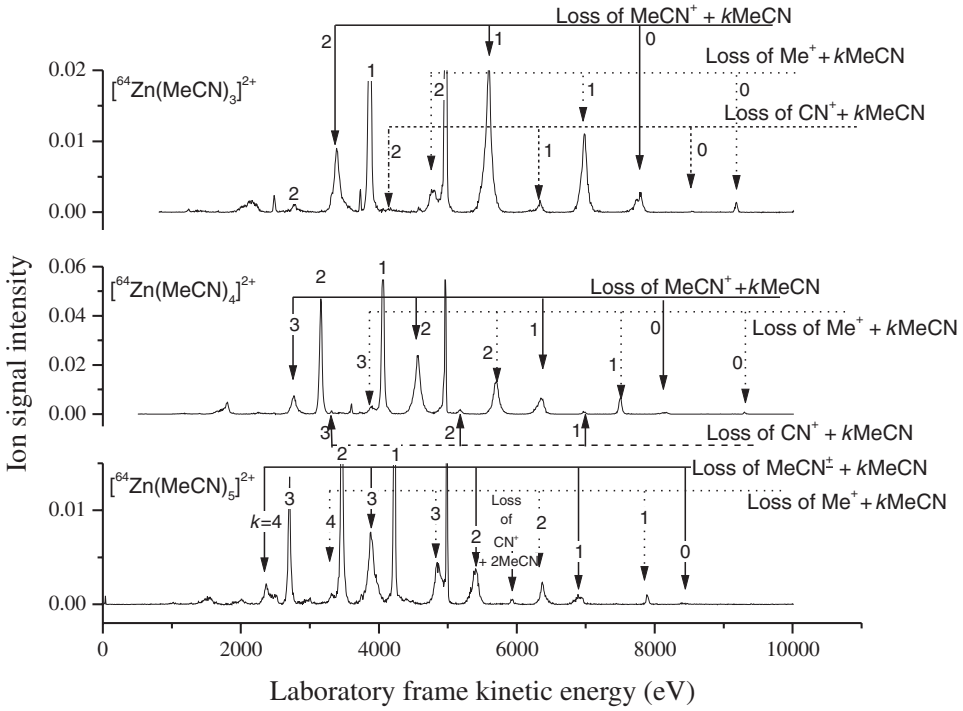
Fig. 5. (*a*) Relative intensities of $[Zn(CH_3CN)_N]^{2+}$ complexes plotted as a function of size (N). (*b*) Relative intensities of $[Zn(pyridine)_N]^{2+}$ complexes plotted as a function of size (N).

Zn(II)–acetonitrile and Zn(II)–pyridine complexes

Figure 5 shows parent ion intensity distributions recorded for $[Zn(MeCN)_N]^{2+}$, with $1 \le N \le 7$, and $[Zn(Py)_N]^{2+}$ for the three most intense isotopes of zinc. As seen before, a discrepancy exists between the three major isotopes of zinc as to the maximum in the parent ion intensity distribution recorded for zinc(II)–acetonitrile complexes. For ^{64}Zn, the most intense isotope, it is $N = 4$, whilst for ^{66}Zn and ^{68}Zn it is $N = 3$. It is suggested from these distributions that the primary solvation shell has the form $[Zn(MeCN)_4]^{2+}$, which compares favourably with the results from other studies on

© 2005 NRC Canada

Fig. 6. Fragmentation patterns recorded following the collisional activation of $[Zn(MeCN)_N]^{2+}$ complexes for N = 3, 4, and 5.



metal dication $[M(MeCN)_N]^{2+}$ systems (12, 13, 18). For the zinc(II)–pyridine complexes, the maximum intensity peak is at N = 2 for all isotopes; however, the relative intensity does not decline significantly for N = 3, which suggests that these two particular parent ions may be stable relative to others within the distribution. It should also be noted that $[Zn(Py)_1]^{2+}$ is a kinetically stable entity, which we have not found for other transition metals (31, 32). Shvartsburg et al. (33) have studied the fragmentation patterns of a number of gas-phase complexes between acetonitrile and divalent metal ions, including zinc(II). This group used electrospray ionization to produce the ions, and for zinc(II)–acetonitrile complexes also found a single acetonitrile molecule was sufficient to stabilize zinc(II) with respect to charge transfer.

To elucidate the fragmentation channels available to the $[Zn(MeCN)_N]^{2+}$ system, collision-induced dissociation studies were undertaken and the results are shown in Fig. 6. Overall, the following fragmentation channels were found:

[9] $[Zn(MeCN)_N]^{2+} \rightarrow [Zn(MeCN)_{N-K}]^{2+} + K\text{MeCN}$

[10] $\rightarrow Zn^+(MeCN)_{N-K-1} + MeCN^+ + K\text{MeCN}$

[11] $\rightarrow Zn^+CN(MeCN)_{N-K-1} + Me^+ + K\text{MeCN}$

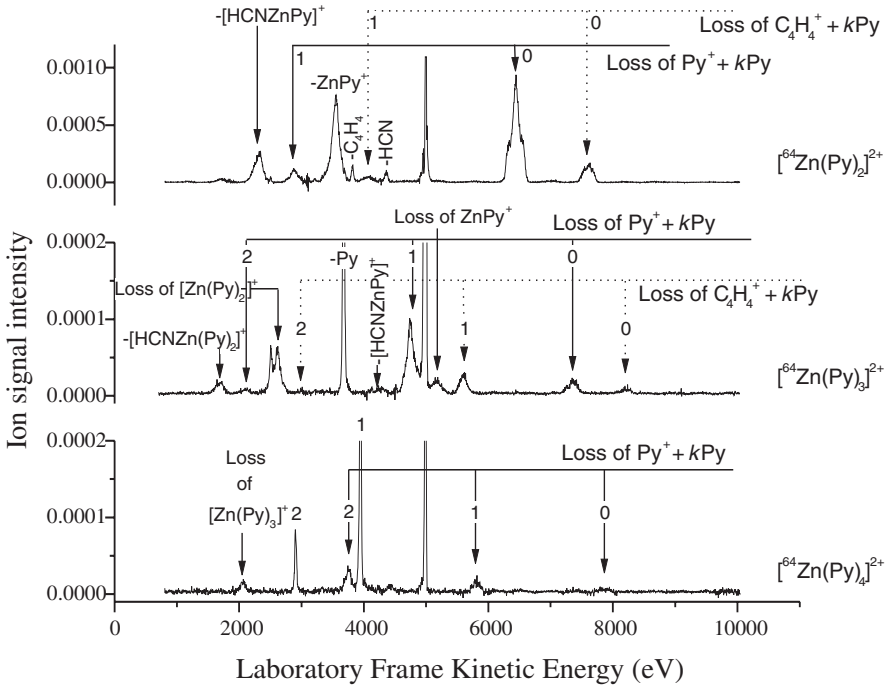
[12] $\rightarrow Zn^+CH_3(MeCN)_{N-K-1} + CN^+ + K\text{MeCN}$

For the two smallest complexes (N = 1 and 2, not shown in Fig. 6), charge transfer processes dominate the observed fragmentation patterns; however, as Fig. 6 shows, such processes also make a significant contribution to the range of fragmentation pathways recorded at larger values of N. Equations [9]–[12] summarize the diversity of processes identified from the results. For N = 2 and 3, the final product of neutral loss via rxn. [9] is $[Zn(MeCN)_1]^{2+}$; for all other values of N neutral loss leads to $[Zn(MeCN)_2]^{2+}$. Of the three charge transfer pathways identified above, the most intense product arises from straight electron transfer (see the following). For N = 2–5, this pathway leads predominantly to the appearance of $Zn^+(MeCN)_1$; for N = 7 the most intense product increases in size to $Zn^+(MeCN)_2$. For N = 2–5, rxn. [11] yields $[ZnCN(MeCN)_1]^+$ as the dominant charge transfer product. When compared with rxns. [10] and [11], rxn. [12] is a minor charge transfer pathway; however, it is also a process that has not previously been identified in earlier studies of $[M(MeCN)_2]^{2+}$ complexes (33, 34). An unusual feature of the latter process is that its presence appears to be restricted to selected values of N. For N = 1 and 2, the dominant charge transfer pathways are rxns. [10] and [11]; as N increases to between 3 and 5, all three charge transfer processes appear and finally, by the time N = 7, rxns. [10] and [11] are again the only charge transfer pathways observed. The dominant product from rxn. [12] is always Zn^+CH_3 and, as noted above, the high Zn^+—C bond strength, probably drives the appearance of this ion. The size constraint on the appearance of this ion would suggest that the reaction pathway is strongly influenced by the geometric arrangement of participating ligands; either in the form of access to the metal cation on the part of CH_3 (bearing in mind that the methyl group is unlikely to be the primary site for coordination to the metal ion), or through the configuration required for an intracluster reaction.

The mass resolution that can be achieved for charge transfer reactions, such as those shown in Fig. 6, is limited; therefore, it is not possible to distinguish between CN and HCN as possible products in rxn. [11]. However, previous studies by Kohler and Leary (34) and Shvartsburg et al. (33) on

© 2005 NRC Canada

Fig. 7. Fragmentation patterns recorded following the collisional activation of $[Zn(pyridine)_N]^{2+}$ complexes for N = 3, 4, and 5.



acetonitrile clustered with a wide range of doubly and triply charged metal cations, show evidence of rxn. [11]. Cleavage of the C—C bond being attributed to the electron-withdrawing properties and high second ionization enthalpy of zinc, such that the acetonitrile ligand is polarized through the metal–nitrogen interaction weakening the C—C bond (34). Both Kohler and Leary (34) and Shvartsburg et al. (33) have also identified a proton transfer reaction that accompanies rxn. [10], but we are unable to detect (resolve) this feature. More recently, Shvartsburg (35) has studied a similar range of reactions in metal trications complexed with acetonitrile.

In their study of the $[Zn(MeCN)_N]^{2+}$ system, Shvartsburg et al. (33) reported that only complexes up to N = 4 underwent charge transfer and above this dissociation occurred solely via acetonitrile evaporation. It was reasoned that unlike $[Zn(H_2O)_N]^{2+}$, the threshold size for charge transfer had to be lower owing to the smaller range over which intermolecular forces can occur because of a lack of hydrogen bonding (33). Although there is clear evidence for charge transfer in kinetic energy scans recorded from complexes containing up to seven acetonitrile molecules, the largest product ion observed is $Zn^+(MeCN)_4$. This suggests one of two possibilities: either the doubly charged precursor loses neutral molecules until it reaches a critical size needed to promote charge transfer, or charge transfer occurs in complexes larger than N = 4, and the process of Coulomb explosion then promotes the lose of additional, neutral molecules. The latter process has certainly been observed in large multiply charged molecular clusters (36).

There have been several recent electrospray studies of gas-phase metal(II)–pyridine complexes (31, 32). The pick-up technique has previously been used to prepare a number of different metal(II)–pyridine systems including Mg (13), Mn (37), Ag (12), Au, and Cu (18). Shvartsburg (32) has used electrospray to study pyridine complexed with doubly charged cations of the metals Ca, Mg, Mn, Fe, Co, and Cu. A number of charge transfer processes were observed including electron, proton transfer and two π-ring cleavage processes, although these latter two processes were not observed for the $[Cu(Py)_N]^{2+}$ system (32).

To elucidate the fragmentation channels available to $[Zn(Py)_N]^{2+}$ complexes, collision-induced dissociation studies were undertaken for several values of N and the results are summarized in Fig. 7. In general, the following fragmentation channels were found:

[13] $$[Zn(Py)_N]^{2+} \rightarrow [Zn(Py)_{N-K}]^{2+} + K\text{Py}$$

[14] $$\rightarrow Zn^+(Py)_{N-K-1} + Py^+ + K\text{Py}$$

[15] $$\rightarrow Zn^+CN(H)(Py)_{N-K-1} + C_4H_{4,5}{}^+ + K\text{Py}$$

Once again, Fig. 7 shows that the fragmentation channels available vary significantly with the size of the complex. No neutral loss is found for N = 1; however, for all other ions studied (N = 3–6), fragmentation is dominated by the loss of neutral pyridine and terminates with the appearance of $[Zn(Py)_2]^{2+}$, which could be taken as evidence that the latter is a particularly stable complex. This observation would also appear to support the data shown in Fig. 7. All of the ions studied underwent electron transfer. For N = 1, this led naturally to reduction of zinc(II) to the bare zinc(I) ion, whilst for N = 2–5, the most prominent charge transfer pathway led to the appearance of $Zn^+(Py)_1$. Shvartsburg (32) concluded that for N = 3, proton transfer is prevalent over electron transfer; however, owing to the width of the charge transfer peaks in the MIKE scan for $[Zn(Py)_3]^{2+}$, it is not possible to reach a similar conclusion.

© 2005 NRC Canada

It would appear from the data that rxn. [15], the heterolytic cleavage reaction leading to $C_4H_{4,5}^+$ is present only for $N = 2$ and 3, where the complementary peaks $Zn^+CN(H)Py_M$ can also seen in each of the MIKE scans shown in Fig. 7. Once again, the widths of the peaks prevent the resolution of Zn^+CNPy from $Zn^+CN(H)Py$.

It is known from studies in aqueous solution that the CN^- ion forms strong complexes with Zn^{2+} (38) in which binding occurs via the carbon atom. However, the lone pair on nitrogen leads to bridging in crystalline complexes such as $Zn(CN)_2$ (38). Density functional theory calculations on complexes of singly charged metal cations with pyridine, including Cu^+–pyridine (isoelectronic with the Zn^{2+}–pyridine system) favour in-plane bonding to the nitrogen of pyridine over a π-electron interaction within the carbon ring (39). The evidence from gas-phase experiments suggests that the cyanide ion is also bonded via the nitrogen atom; however, collisional excitation coupled with charge transfer imparts a considerable amount of energy to a complex. Therefore, it is quite feasible that rearrangement does occur and that, as suggested by Shvartsburg (32) and Kohler and Leary (31), the cyanide negative ion is actually bound via carbon to zinc(II).

Zn(II) with carbon disulfide, thiophene, and 2-methyl thiophene

A survey of the Cambridge Structural Database showed that 50% of all zinc-containing crystal structures had four-coordination and of these approximately 20% had sulfur-donating ligands (40). Although it was possible to prepare singly charged zinc–sulphur complexes with carbon disulfide, thiophene, and 2-methyl thiophene in the gas phase, it was not possible to isolate any equivalent doubly charged species. Further experiments are underway to investigate this behaviour.

Zn(II)–argon complexes

Figure 8 shows an intensity distribution recorded for $[ZnAr_N]^{2+}$ complexes plotted as a function of N. As noted earlier, it is not always possible to derive agreement between all of the different isotopic combinations, however, the general trend would suggest that $[ZnAr_5]^{2+}$ is a stable combination. Figure 9 shows the consequences of size-selected $[ZnAr_N]^{2+}$ being subjected to collisional activation. In comparison to some of the earlier examples, the difference in ionization energy between Zn^+ and argon is comparatively small (~2.2 eV), which means that first, the dimer ion $[ZnAr]^{2+}$ is stable and secondly, the kinetic energy release values determined from the MIKE scans are all low. The dominant charge transfer process for the examples shown is

$$[16] \quad [ZnAr_N]^{2+} \rightarrow Zn^+Ar + (N-2)Ar + Ar^+$$

which is probably influenced by the underlying stability of Zn^+Ar. An estimated kinetic energy release for the dominant charge transfer process seen following the CID of $[ZnAr_3]^{2+}$ is ~0.14 eV. An exception to rxn. [16] is $[ZnAr_5]^{2+}$, which gives rise to an unusual feature seen at ~2424 eV. This result is reproducible and possibly arises from a combination of charge transfer leading to $Zn^+ + Ar^+ + 4Ar$ to give the two outer peaks via Coulomb explosion, plus a central low energy feature owing to electron capture from the collision gas to give $Zn^+ + 5Ar$. Since it is not possible to assign the sequence in which atoms and (or) ions leave the complex following collisional activation, an accurate kinetic energy release cannot be calculated from the usual two-body equation.

Fig. 8. Relative intensities of $[ZnAr_N]^{2+}$ complexes plotted as a function of size (N).

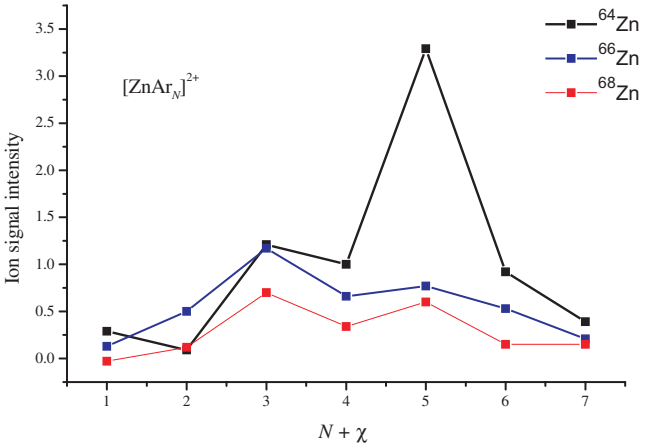
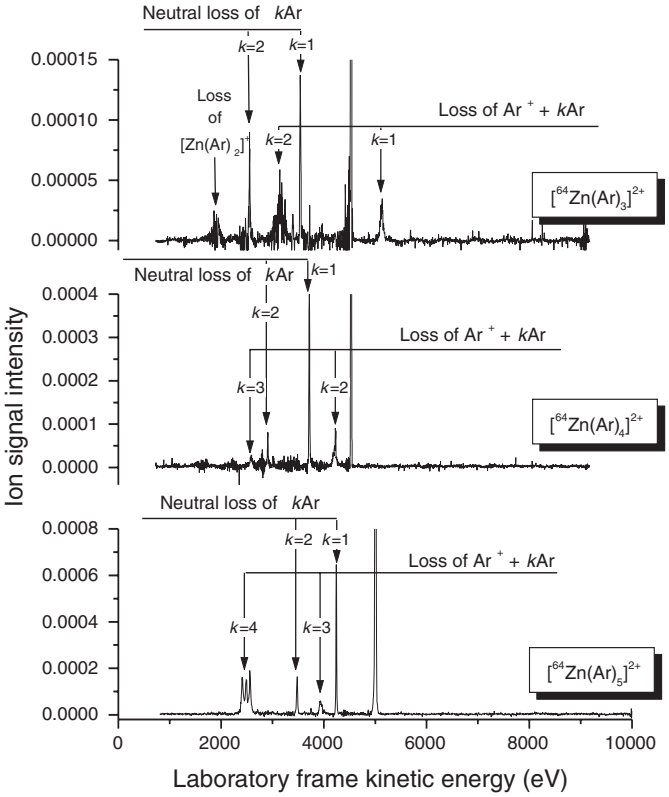


Fig. 9. Fragmentation patterns recorded following the collisional activation of $[ZnAr_N]^{2+}$ complexes for $N = 3$, 4, and 5.

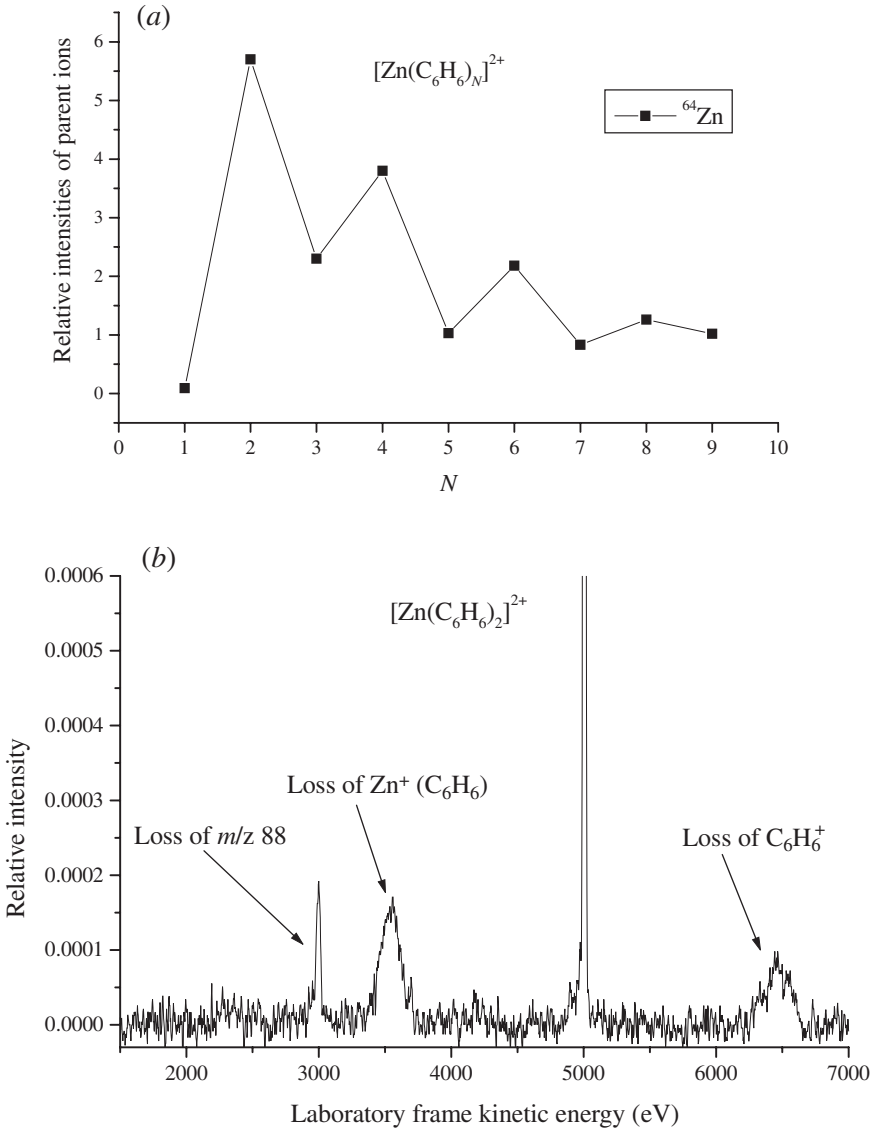


Zn(II)–benzene complexes

Figure 10*a* shows a plot of the relative intensities of $[Zn(C_6H_6)_N]^{2+}$ complexes as a function of N. As seen in a

© 2005 NRC Canada

Fig. 10. (*a*) Relative intensities of $[Zn(C_6H_6)_N]^{2+}$ complexes plotted as a function of size (*N*). (*b*) Fragmentation pattern recorded following the collisional activation of the $[Zn(C_6H_6)_2]^{2+}$ complex.



number of earlier examples (12, 18), the most intense ion is $[Zn(C_6H_6)_2]^{2+}$, which has been attributed to the formation of a stable sandwich structure. Figure 10*b* shows the result of a CID experiment on $[Zn(C_6H_6)_2]^{2+}$, which is interesting for a number of reasons. Firstly, there is no evidence for the loss of neutral benzene; this confirms the result give in Fig. 10*a*, which is that the dimer dication is unstable. Secondly, there are peaks corresponding to the formation of $[ZnC_6H_6]^+$ and $C_6H_6^+$ via one or more charge reduction processes. The peak at ~6400 eV, which is due to the appearance of $[ZnC_6H_6]^+$, has a composite structure similar to that analysed recently in a detailed study of charge reduction mechanisms.[4] There are two mechanisms that can lead to the formation of this ion: electron transfer from the ligand to the metal and electron capture from the collision gas (air). The large potential energy difference associated with the first mechanism leads to a substantial release of kinetic energy and, as a consequence, the peaks are dish-shaped. In this particular example, that energy difference is represented by the first IE of Zn(I) minus the IE of benzene and is ~8.5 eV. In the second mechanism, the energy available for partitioning to kinetic energy is far less as it is given by the difference between the first IE of Zn(I) and the IE of the collision gas ($\sim N_2$), which is ~2 eV. As a consequence, the peak profiles are much narrower and Gaussian-like.

The peak at ~3500 eV could be taken as being due to $C_6H_6^+$ in the form of the complementary charge transfer product to $Zn^+C_6H_6$; however, this may not be the case for two reasons. First, it is unusual in charge transfer studies of multiply charged metal complexes to have a nonmetallic ion with intensity comparable to that of the metallic ion. Secondly, given the large amount of (potential) kinetic energy available, a dish-shaped peak might have been expected. An alternative pathway leading to a benzene cation with a small

[4] B. Wu, B.J. Duncombe, and A.J. Stace. Unpublished results.

© 2005 NRC Canada

release of kinetic energy arises from electron capture and the fact that the IE of benzene (9.24 eV) is lower than that of zinc at 9.37 eV. As noted before, such a mechanism would leave the single charged $[Zn(C_6H_6)_2]^+$ ion with ~2.5 eV and the most stable state, based on ionization energy data, would have the charge residing on a benzene molecular ion. Any excess energy would then promote the loss of both neutral zinc and the extra benzene molecule to leave $C_6H_6^+$ with a kinetic energy of ~1 eV (FWHM).

Conclusion

The chemistry and coordination of a number of zinc(II) – aprotic solvent complexes have been studied using ligands that coordinate primarily through either an oxygen or nitrogen atom. Within this group, charge transfer, promoted by collisional activation, led to extensive chemical reactivity. In a number of cases, chemical bonds with high dissociation energies, for example those of CO_2, were observed to break. Contributing factors to the ease of reactivity were seen as: (*i*) the degree of electron transfer taking place between the metal dication and the molecules concerned, which might lead to a weakening of bonds; (*ii*) the stability of the product metal-containing ion, and the formation of Zn^+CH_3 from $[Zn(CH_3CN)_N]^{2+}$ was seen as a good example of the latter. This particular fragment had not been observed in any of the earlier studies of metal cations with acetonitrile. Even though extensive evidence of complexes between zinc(I) and sulfur-donor ligands was found, attempts to identify similar complexes containing Zn(II) failed completely. Such behaviour contrasts with that seen in the condensed phase where there is an extensive range of stable Zn(II)–sulfur complexes. This is clearly not a failure of the pick-up technique, since it succeeds in generating the singly charged ions. It would appear that, using the ligands selected, Zn(II)–sulfur complexes are not stable in isolation.

Acknowledgements

The authors would like to thank the Engineering and Physical Sciences Research Council (EPSRC) for financial support and for the award of a studentship to BJD; BW would like to acknowledge the award of a Madame Chen Zhili scholarship and thank Nottingham University for financial support.

References

1. A.J. Stace. J. Phys. Chem. A, **106**, 7993 (2002).
2. A.T. Blades, P. Jayaweera, M.G. Ikonomou, and P. Kebarle. J. Chem. Phys. **92**, 5900 (1990).
3. M. Peschke, A.T. Blades, and P. Kebarle. J. Phys. Chem. A, **102**, 9978 (1998).
4. M. Peschke, A.T. Blades, and P. Kebarle. Int. J. Mass Spectrom. **185/186/187**, 685 (1999).
5. T. Gough, M. Mengel, P. Rowntree, and G. Scoles. J. Chem. Phys. **83**, 4958 (1985).
6. C.A. Woodward, M.P. Dobson, and A.J. Stace. J. Phys. Chem. **100**, 5605 (1996).
7. C.A. Woodward, M.P. Dobson, and A.J. Stace. J. Phys. Chem. A, **101**, 2279 (1997).
8. M.P. Dobson and A.J. Stace. J. Chem. Soc. Chem. Commun. 1533 (1996).
9. M.P. Dobson and A.J. Stace. Int. J. Mass Spectrom. **165**, 5 (1997).
10. A.J. Stace, N.R. Walker, and S. Firth. J. Am. Chem. Soc. **119**, 10239 (1997).
11. N.R. Walker, R.R. Wright, P.E. Barran, and A.J. Stace. Organometallics, **18**, 3569 (1999).
12. N.R. Walker, R.R. Wright, and A.J. Stace. J. Am. Chem. Soc. **121**, 4837 (1999).
13. N.R. Walker, M.P. Dobson, R.R. Wright, P.E. Barran, J.N. Murrell, and A.J. Stace. J. Am. Chem. Soc. **122**, 11138 (2000).
14. N.R. Walker, R.R. Wright, P.E. Barran, H. Cox, and A.J. Stace. J. Chem. Phys. **114**, 5562 (2001).
15. H. Cox, G. Akibo-Betts, R.R. Wright, N.R. Walker, S. Curtis, B. Duncombe, and A.J. Stace. J. Am. Chem. Soc. **125**, 233 (2003).
16. R.G. Cooks, J.H. Beynon, R.M. Caprioli, and G.R. Lester. Metastable ions. Elsevier, Amsterdam. 1973.
17. T.D. Märk. *In* Gaseous ion chemistry and mass spectrometry. *Edited by* J.H. Futrell. John Wiley and Sons, New York. 1986.
18. R.R. Wright, N.R. Walker, S. Firth, and A.J. Stace. J. Phys. Chem. A, **105**, 54 (2001).
19. J. Mascetti and M. Tranquille. J. Phys. Chem. **92**, 2177 (1988).
20. F. Galan, M. Fouassier, M. Tranquille, J. Mascetti, and I. Pápai. J. Phys. Chem. A, **101**, 2626 (1997).
21. N.R. Walker, R.R. Wright, P.E. Barran, J.N. Murrell, and A.J. Stace. J. Am. Chem. Soc. **123**, 4223 (2001).
22. M. Sodupe, V. Branchadell, M. Rosi, and C.W. Bauschlicher, Jr. J. Phys. Chem. A, **101**, 7854 (1997).
23. R. Caballol, E. Sánchez Marcos, and J.-C. Barthelat. J. Phys. Chem. **91**, 1328 (1987).
24. H.-J. Fan and C.-W. Liu. Chem. Phys. Lett. **300**, 351 (1999).
25. L. Puškar, K. Tomlins, B. Duncombe, H. Cox, and A.J. Stace. J. Am. Chem. Soc. In press.
26. A.M. El-Nahas. Chem. Phys. Lett. **365**, 251 (2002).
27. M. Peschke, A.T. Blades, and P. Kebarle. J. Am. Chem. Soc. **122**, 10440 (2000).
28. A.J. Stace, N.R. Walker, R.R. Wright, and S. Firth. Chem. Phys. Lett. **329**, 173 (2000).
29. D.E. Clemmer, N.F. Dalleska, and P.B. Armentrout. J. Chem. Phys. **95**, 7263 (1991).
30. B.S. Freiser (*Editor*). Organometallic ion chemistry. Kluwer Academic Publishers, Dordrecht. 1996.
31. M. Kohler and J.A. Leary. J. Am. Soc. Mass Spectrom. **8**, 1124 (1997).
32. A.A. Shvartsburg. Chem. Phys. Lett. **376**, 6 (2003).
33. A.A. Shvartsburg, J.G. Wilkes, J.O. Lay, and K.W.M. Siu. Chem. Phys. Lett. **350**, 216 (2001).
34. M. Kohler and J.A. Leary. Int. J. Mass Spectrom. Ion Processes, **162**, 17 (1997).
35. A.A. Shvartsburg. J. Am. Chem. Soc. **124**, 7910 (2002).
36. N.G. Gotts, P.G. Lethbridge, and A.J. Stace. J. Chem. Phys. **96**, 408 (1992).
37. G. Akibo-Betts, P.E. Barran, and A.J. Stace. Chem. Phys. Lett. **329**, 431 (2000).
38. F.A. Cotton and G. Wilkinson. Advanced inorganic chemistry. John Wiley and Sons, New York. 1988.
39. M.T. Rodgers, J.R. Stanley, and R. Amunugama. J. Am. Chem. Soc. **122**, 10969 (2000).
40. C.W. Bock, A. Kaufman Katz, and J.P Glusker. J. Am. Chem. Soc. **117**, 3754 (1995).

© 2005 NRC Canada

The gas-phase acidities of the elemental hydrides are functions of electronegativity and bond length[1]

John E. Bartmess and Robert J. Hinde

Abstract: The gas-phase Brønsted acidities of the group 1, group 2, and main group elemental hydrides (XH_n) are shown to be a combined function of the bond length, electronegativity, and position in the periodic table, via a separation of the acidity into coulombic and electronic reorganization enthalpy parts. The Coulombic acidity is defined as the enthalpy to separate unit positive and negative charges from the neutral acid's X—H bond length to infinity; the reorganization enthalpy is the difference between that and the measured acidity, and represents the enthalpy required to reorganize the electrons of the neutral acid, creating an ion pair at the original bond distance. Predictions are made for the gas-phase Brønsted acidities of several elemental hydrides for which this quantity is not known.

Key words: acidity, gas phase, coulomb, elements, hydride.

Résumé : On démontre que les acidités de Brønsted des hydrures de formule générale XH_n des éléments du groupe 1, du groupe 2 et du groupe principal sont une fonction qui combine la longueur de liaison, l'électronégativité et la position dans le tableau périodique par le biais d'une séparation de l'acidité en deux parties impliquant des enthalpies de réorganisation coulombique et électronique. L'acidité coulombique est définie comme l'enthalpie qui sépare une unité de charges positive et négative de la liaison X—H d'un acide neutre de la longueur de liaison jusqu'à l'infini; l'enthalpie de réorganisation est la différence entre ceci et l'acidité mesurée et elle représente l'enthalpie nécessaire pour réorganiser les électrons de l'acide neutre en créant une paire d'ions à la distance originale de la liaison. On fait des prédictions relatives aux acidités de Brønsted de plusieurs hydrures d'éléments pour lesquels cette valeur n'est pas connue.

Mots clés : acidité, phase gazeuse, coulomb, éléments, hydrure.

[Traduit par la Rédaction]

Gas-phase acidities of neutral species have traditionally been analyzed in terms of (and the values often obtained from) the thermochemical cycle of Scheme 1, involving the homolytic bond dissociation enthalpy of the generic acid AH, the electron affinity of $A^{\cdot}$, and the ionization energy of the hydrogen atom (1). This cycle has been used to explain observed variations in the acidities of the main group elemental hydrides, wherein the electron affinity is the principal factor in determining the acidities across a row of the periodic table, and the bond dissociation energy the major factor determining the acidities down a column (2).

[1] $$\Delta_{acid}H(AH) = BDE(A\text{-}H) + IE(H^{\cdot}) - EA(A^{\cdot})$$

Although Scheme 1 is mathematically rigorous, chemical intuition suggests that there should be some relationship between acidities and electronegativity, and thus perhaps a different method of deriving such acidities. We present here an empirical alternative, using only the relatively low-level quantities of bond lengths, electronegativities, and position in the periodic table. The Coulombic acidity, $\Delta_{CA}H(AH)$, is here defined as the absolute value of the enthalpy change for separating the acidic proton of an acid AH from its anionic conjugate base A^-, from the distance corresponding to the A—H bond length in the neutral acid to infinity, without any electronic reorganization. This then would be a measure of the gas-phase acidity if only Coulombic forces were involved (3). Coulomb's law along with the necessary physical constants (4) yields:

[2] $$\Delta_{CA}H(AH) = 332.1/d(A\text{—}H) + RT$$

where the Coulombic acidity, $\Delta_{CA}H(AH)$, is in units of kcal/mol (1 cal = 4.184 J) and the bond length d(A—H) is in angstroms. The constant 332.1 kcal-Å/mol represents the Coulombic acidity at $T = 0$ K for a standard 1.0 Å bond. This falls in the middle of the scale of known gas-phase ΔH_{acid} values, which range from 294 kcal/mol for $(n\text{-}C_4F_9SO_2)_2NH$ to 420 kcal/mol for ethane (5).

If $\Delta_{CA}H(AH)$ is subtracted from the measured or calculated enthalpy of acidity, $\Delta_{acid}H(AH)$, defined by Scheme 1 (5), the resulting electronic reorganization enthalpy ($\Delta_{ER}H$, eq. [3]) represents the energetics of creating the A^-H^+ pair of ions, without having to pay the enthalpy

Received 3 May 2005. Published on the NRC Research Press Web site at http://canjchem.nrc.ca on 1 February 2006.

This paper is in honor of Professor Paul Kebarle, whose body of research has influenced almost all of JEB's own efforts.

J.E. Bartmess[2] and R.J. Hinde. Department of Chemistry, University of Tennessee, Knoxville TN 37996-1600, USA.

[1]This article is part of a Special Issue dedicated to Professor P. Kebarle.

[2]Corresponding author (e-mail: bartmess@utk.edu).

 doi: 10.1139/V05-218 © 2005 NRC Canada

Scheme 1.

$$\begin{array}{ccc} & \Delta_{acid}H(AH) & \\ AH & \rightarrow & A^- + H^+ \\ \downarrow \text{BDE(A-H)} & & \uparrow \text{-EA}(A^\cdot) \\ A^\cdot + H^\cdot & \rightarrow & A^\cdot + H^+ + e^- \\ & \text{IE}(H^\cdot) & \end{array}$$

$$\Delta_{acid}H(AH) = \text{BDE(A-H)} + \text{IE}(H^\cdot) - \text{EA}(A^\cdot)$$

[3] $$\Delta_{ER}H(\text{A-H}) = \Delta_{acid}H(AH) - \Delta_{CA}H(AH)$$

price for separating them so that they do not influence each other's structure via their electric field. It also can be taken as the energy to relax both the atomic and electronic structures (save for the departed proton) from those in the acid to those in the anion.

Experimental data and calculations

Values of experimental bond lengths for the elemental hydrides were compiled from standard sources (6–10). Equilibrium bond lengths (r_e) were the selected ones; when only r_0 values were available, notably for the group 14 hydrides, the r_e values were estimated to be 0.01 Å shorter than the r_0 value. This is consistent with experimental data for H_2, NH_3, H_2O, HCl, PH_3, and H_2Se (6, 10), and with computational approaches (10, 11). For the third through fifth rows, many experimental values were either absent or of considerable uncertainty. The only available experimental bond length for CaH_2, for example, is from a crystal structure, and that is the average of two disparate values in the crystal. For use in the estimation of these missing values, bond lengths obtained from a variety of computational methods are also presented in Table 1. The Gaussian 98 (12) program was utilized, with some of the basis sets taken from the online compilation (13).

It has been noted that correlated computational methods tend to consistently give bond lengths that are longer than those found experimentally, especially for X—H bonds (14–17). As seen in Table 1, for the elemental hydrides under consideration here, the MP2(full)/6-31G(d) geometries used in the Gn methods (18) deviate from experimental values almost exclusively in the direction of being too long. Highly electronegative or electropositive elements seem to deviate the most from agreement, with the alkali metal hydrides being the worst. For the compounds shown, the rms deviation is 0.024 Å. The worst case, KH at 0.075 Å too long, yields a $\Delta_{CA}H$ 5 kcal/mol numerically smaller than that from the experimental bond length. If this trend holds true for the various computational geometries used from the literature, the theoretical ΔH_{ER} values will be slightly too large.

In Table 1, the values overall closest to the experimental ones are from the B3LYP/6-311G(3df,3pd) calculations. These are used to estimate missing experimental values for the first three rows. The 3-21G** basis set, although likely too small for accuracy in itself, is included because it extends to elements in the fourth row, and thus can be used as guidance for estimations there. Computational values for bond lengths of fifth row elements are from a variety of methods in the literature, and from a basis set with the heavy atom modeled with (or using) the CRENBL ECP basis set and pseudopotential (13) and the hydrogen as 3-21G**. This latter choice is also carried through for the fourth row elements, where it is found to deviate by less than 0.05 Å from experimental bond lengths for the main group elements. Gas-phase enthalpies of acidity were obtained via Scheme 1, save that a few were from equilibrium data anchored to values from Scheme 1 (5). Again, there are a number of elemental hydrides for which experimental $\Delta_{acid}H$ values are not available. For MgH_2 and AlH_3, we have computed $\Delta_{acid}H(AH)$ at T = 298 K from a series of ab initio CCSD(T)/aug-cc-pVxZ calculations (x = D, T, Q), which are then extrapolated to the complete basis set limit (19). For HF, HCl, H_2O, and H_2S, this method of computation reproduces the experimentally obtained acidities to within 0.5 kcal/mol, comparable to the experimental error (19).

From the data for these quantities given in Tables 1 and 2, values of $\Delta_{CA}H$ and $\Delta_{ER}H$ are derived as per eqs. [2] and [3]. To examine the generality of the concepts developed here, we have also examined the corresponding experimental and computational data for the elemental monohydrides, as given in Table 3.

Results

The values obtained for $\Delta_{ER}H$ in Table 2 range from 9 kcal/mol for FH to 211 kcal/mol for CsH, with an anomalous value of –48 kcal/mol for H_2 (which is discussed separately in the following). Are these values of a reasonable magnitude? Gas-phase basicities likewise involve loss of a proton with no Coulombic cost of charge separation (rxn. [4]), only the energetics of bond breaking. That experimental basicity scale ranges from 42.5 kcal/mol for He (giving HeH^+) to 248 kcal/mol for NaOH (5). The magnitudes of the values obtained for the reorganization enthalpies are thus reasonable in this light.

[4] $$BH^+ \rightarrow B + H^+$$

Examination of the $\Delta_{ER}H$ values in Table 2 reveals a distinct periodic trend: $\Delta_{ER}H$ decreases across a row of the periodic table, and increases down a column. The smallest positive $\Delta_{ER}H$ is for HF. This is reasonable in that HF is the elemental hydride with the largest difference in electronegativity between the hydrogen and the heavy atom. The electrons in HF are thus already well on the way to being reorganized toward the products of F^- and H^+, and relatively little further reorganization is necessary. The other extreme, of very large $\Delta_{ER}H$ values for the alkali hydrides, reflect the opposite polarization of charge. Considerable energy is required to move electrons to an electropositive element.

The negative $\Delta_{ER}H$ for H_2 appears anomalous. The Coulombic acidity of H_2 is the weakest in Table 2, weaker even than the experimental acidity, owing to the very short bond length engendered by the 1s—1s bonding in H_2. The negative $\Delta_{ER}H$ in this case would seem to imply that H_2 should exist as H^-H^+ rather than H—H at the equilibrium bond length, a situation clearly at odds with observations. However, it has been noted (20) that the H—H bond requires

© 2005 NRC Canada

Table 1. Bond lengths (in angstroms) of elemental hydrides.

	d(A—H)[a]							
Acid	Exptl.	MP2(fu)/6-31G(d)	MP2(fu)/3-21G**	B3LYP/3-21G**	B3LYP/6-311G**(3df,3pd)	B3LYP/6-311G	CCSD(T)/cc-pvtz	Other computational
H_2	0.7414	0.7375	0.7382	0.7464	0.7440	0.7427	0.7427	
LiH	1.5947	1.6396	1.6319	1.6213	1.5930	1.5894	1.6078	
BeH_2	(1.325)	1.3329	1.3313	1.3344	1.3267	1.3250	1.3339	
BH_3	1.1800[b]	1.1910	1.1854	1.1949	1.1890	1.1879	1.1914	
CH_4	1.0856[b]	1.0894	1.0802	1.0895	1.0907	1.0878	1.0890	
NH_3	1.0118	1.0168	1.0014	1.0123	1.0159	1.0136	1.0140	
OH_2	0.9579	0.9686	0.9506	0.9662	0.9619	0.9603	0.9594	
FH	0.9169	0.9339	0.9138	0.9323	0.9199	0.9186	0.9170	
NaH	1.8874	1.9181	1.8963	1.8640	1.8870	1.8752	1.9232	
MgH_2	(1.700)	1.7213	1.7109	1.7110	1.7042	1.7010	1.7116	
AlH_3	(1.581)	1.5888	1.5811	1.5935	1.5831	1.5790	1.5853	
SiH_4	1.4711[b]	1.4825	1.4756	1.4896	1.4839	1.4793	1.4831	
PH_3	1.4200	1.4140	1.4062	1.4246	1.4235	1.4179	1.4184	
SH_2	1.3356	1.3395	1.3293	1.3479	1.3480	1.3418	1.3409	
ClH	1.2746	1.2800	1.2674	1.2849	1.2871	1.2808	1.2773	
KH	2.242	2.3178	2.3444	2.3052	2.2436	2.2398		
CaH_2	(2.040)	2.1235	2.1461	2.1335	2.0499	2.0483	2.0879	
GaH_3	(1.560)	1.5762	1.5570	1.5600	1.5672	1.5663	1.5623	1.586[c]
GeH_4	1.5151[b]	1.5421	1.5219	1.5325	1.5347	1.5334	1.5229	
AsH_3	1.5108	1.5357	1.5119	1.5331	1.5251	1.5240	1.5096	
SeH_2	1.4600	1.4806	1.4567	1.4767	1.4717	1.4697	1.4584	
BrH	1.4144	1.4356	1.4091	1.4260	1.4263	1.4236	1.4131	
RbH	2.367		2.4792	2.4515[d]				
SrH_2	(2.2)		2.3206	2.3056[d]				2.201[c]
InH_3	(1.7)		1.7623	1.7854[d]				1.734[e]
SnH_4	1.7008[b]		1.7314	1.7497[d]				
SbH_3	1.7039		1.7196	1.7482[d]				
TeH_2	1.658		1.6690	1.6901[d]				
IH	1.6092		1.6235	1.6416[d]				
CsH	2.4938			2.5211[d]				
BaH_2	(2.1)			2.2923[d]				2.314[c]
TlH_3	(1.76)			1.8368[d]				1.756[e]
PbH_4	(1.77)			1.8400[d]				1.767[e]
BiH_3	(1.82)			1.8897[d]				1.826[e]
PoH_2	(1.73)			1.7896[d]				1.835[f]
AtH								
C_2H_4	1.0760	1.0826						
HC≡CH	1.0550	1.0618						

[a]Experimental bond lengths (6–9). Values in parentheses are estimated from computational values as per the text.
[b]Estimated r_e value by reducing the r_0 value by 0.01 Å.
[c]Reference 34.
[d]H is stated basis set; heavy atom is CRENBL ECP basis set and pseudopotential (13).
[e]Reference 35, QCI calculations.
[f]Reference 36, second-order CI/CASSCF calculations.

about a 5% ionic contribution to the "pure" covalent bond predicted by electronegativity to explain the bond length and enthalpy; this may be the reason for this unusual result. In addition, a plot of the homolytic bond dissociation energies of the elemental hydrides (5) against the reciprocal of the X—H bond length yields a moderately linear (r = 0.96, sd = 8.4 kcal/mol) correlation, with H_2 as an outlier. Its bond dissociation energy is 62 kcal/mol stronger than expected from its bond length. One additional possibility is that the electronegativity value is not applicable in this case, although it would require an X of <1.94 or a bond length of >0.84 Å to make $\Delta_{ER}H$ (H_2) positive. We emphasize that this "anomalous" $\Delta_{ER}H$ is really a problem with the $\Delta_{CA}H$ being too weak, not the $\Delta_{ER}H$ being too strong.

© 2005 NRC Canada

Table 2. Coulombic acidity and electron reorganization enthalpy of elemental hydrides.

Acid	$\Delta_{CA}H^a$	$\Delta_{acid}H^b$	$\Delta_{acid}H^c$	$\Delta_{ER}H^d$	$X_A{}^e$
H_2	448.5	400.4±0.01	*406.7*	–48.1	2.25
LiH	208.7	356.0±0.1	*348.8*	147.3	0.97
BeH_2	*251.2*	387.4±3.0	*389.8*	136.2	1.54
BH_3	282.0	*411.8*[f]	*411.3*	*129.8*	2.04
CH_4	307.0	416.7±0.8	*417.3*	109.7	2.48
NH_3	328.9	404.3±0.3	*403.0*	75.4	3.04
OH_2	347.1	390.7±0.1	*390.1*	43.6	3.68
FH	362.8	371.6±0.2	*371.4*	8.8	4.30
NaH	176.6	345.1±0.3	*340.2*	168.6	0.91
MgH_2	*195.9*	360.7±2.4	*361.1*	*164.8*	1.37
AlH_3	*210.8*	*373.2*[f]	*371.4*	*162.4*	1.83
SiH_4	226.3	372.8±0.8	*372.2*	146.5	2.28
PH_3	236.1	363.7±1.6	*365.8*	127.6	2.41
SH_2	249.2	350.7±0.9	*350.1*	101.5	2.86
ClH	261.1	333.4±0.01	*332.3*	72.3	3.34
KH	148.7	344.4±5.0	*339.2*	195.7	0.73
CaH_2	*162.2*	353.1[c]	*353.1*	*190.9*	1.08
GaH_3	*211.2*	*367.2*[c]	*367.2*	*156*	2.01
GeH_4	219.8	358.9±1.3	*362.9*	139.1	2.33
AsH_3	220.4	357.5±2.1	*359.6*	137.1	2.38
SeH_2	228.1	341.5±0.7	*342.6*	113.4	2.79
BrH	235.4	323.5±0.05	*324.7*	88.1	3.20
RbH	140.9	343.4±0.5		202.5	0.69
SrH_2	*152*	*354*		*202*[g]	1.00
InH_3	*196*	*384*[h]		*183*[g]	1.76
SnH_4	195.9	350.5±2.1		154.7	2.21
SbH_3	195.5	*349*[h]		154[g]	2.22
TeH_2	200.9	331.1±1.1		130.2	2.57
IH	207	314.3±0.02		107.3	2.95
CsH	133.8	344.6±0.1		210.8	0.62
BaH_2	*159*	*375*[h]		*216*[g]	0.88
TlH_3	*189*	*364*[h]		*175*[g]	1.96
PbH_4	*188*	*333*[h]		*145*[g]	2.41
BiH_3	*183*	*337*[h]		*154*[g]	2.28
PoH_2	*193*	*323*[h]		*130*[g]	2.65
AtH	—	—		*104*[g]	3.05
$CH_2{=}CH_2$	315.4	409.4		94.0	2.73[i]
HC≡CH	307.2	378.0		70.8	3.16[i]

Note: Values in italics are derived wholly or in part from ab initio computations and the correlations described in the text. All energetics are kcal/mol at 298 K.

[a]Coulombic acidity from eq. [2].
[b]Experimental enthalpy of acidity (5).
[c]G3(MP2) enthalpy of acidity.
[d]Electron reorganization enthalpy (eq. [3]).
[e]Mulliken–Jaffé electronegativity (23).
[f]ΔH_{acid} (BH_3) is calculated at the B3LYP/aug-cc-pVTZ level as per ref. 19. The triplet ground state for BH_2^- is used; the singlet is calculated as 0.7 kcal/mol higher in energy.
[g]Extrapolated from X_A with eqs. [6]–[10]; up to ±10 kcal/mol uncertain.
[h]Unknown experimentally. Value is from eq. [2] combined with eqs. [6]–[10].
[i]Calculated from an inversion of eq. [6].

Table 3. Coulombic acidity and electron reorganization enthalpy of elemental monohydrides.

Acid	d(A—H)[a]	$\Delta_{CA}H^b$	$\Delta_{acid}H^c$	$\Delta_{ER}H^d$	$\Delta_{promo}H^e$
H_2	0.7414	448.5	400.4	–48.1	
LiH	1.5947	208.9	356	147.1	
BeH	1.3426	248.0	*371.5*[f]	*123.5*	
BH	1.2324	270.1	387.7	117.6	8.7
CH	1.1199	297.1	365.1	68.0	28.4
NH	1.0362	321.1	*404.9*[f]	*83.8*	
OH	0.9677	343.8	382.6	38.8	
FH	0.9169	362.8	371.3	8.5	
NaH	1.8874	176.6	345.1	168.5	
MgH	1.7297	192.6	*350.0*[f]	*157.4*	
AlH	1.6478	202.1	371.7	169.6	7.7
SiH	1.5201	219.1	353.1	134.0	19.9
PH	1.4223	234.1	367.7	133.6	
SH	1.3409	248.3	350.4	102.1	
ClH	1.2746	261.2	333.4	72.2	
KH	2.2420	148.7	344.1	195.4	
CaH	2.0025	166.4	352.8	186.4	
GaH	1.6630	200.3	369.6	169.3	5.7
GeH	1.5880	209.7	348.3	138.6	19.2
AsH	1.5394	216.3	359.4	143.1	
SeH	1.4750	225.8	339.9	114.1	
BrH	1.4144	235.4	323.5	88.1	
RbH	2.3670	140.9	343.4	202.5	
SrH	2.1456	155.4	350.5	195.1	
InH	1.838	181.3	362.5	181.2	
SnH	1.8215	182.9	343.0	160.1	16.5
SbH	1.7226	193.4	345.1	151.7	
TeH	1.741	191.4	333.2	141.8	
IH	1.6092	207.0	314.3	107.3	
CsH	2.4938	133.8	344.6	210.8	
BaH	2.2318	149.4			
TlH	1.87	178.2	351.3	173.1	
PbH	1.8388	181.2	347.5	166.3	
BiH	1.805	184.6			

[a]Experimental bond lengths in angstroms (6).
[b]Coulombic acidity from eq. [2] (kcal/mol).
[c]Experimental enthalpy of acidity (kcal/mol) (5).
[d]Electronic reorganization enthalpy (kcal/mol, eq. [3]).
[e]Term energy for first excited state of the atomic anion corresponding to the multiplicity of the monohydride acid.
[f]Anion unbound; acidity is from G3(MP2) calculations.

If the $\Delta_{ER}H$ values are plotted as a function of the Mulliken–Jaffé electronegativity (21–23), the main group hydrides and the alkali metal hydrides yield excellent (r = 0.979 and 0.999, respectively) correlations, as shown in Fig. 1. This electronegativity scale is based on the equation of Mulliken (21), involving ionization energies and electron affinities, but with more recent values of those quantities used to obtain the numeric electronegativity, and separate values for different hybridization states (23). For the main group compounds with eight valence electrons:

$$[5] \qquad \Delta_{ER}H(\mathrm{AH}) = -67.2 \times X_A + 295.6 \text{ kcal/mol}$$

$$r = -0.9778$$

where X_A is the Mulliken–Jaffé electronegativity of atom A (23). The largest deviation from eq. [5] is that of methane at 19 kcal/mol, and the average deviation is 8.2 kcal/mol. Other electronegativity scales, such as the Allred–Rochow (24), Sanderson (25), and Pauling (20) scales, yield similar,

© 2005 NRC Canada

Fig. 1. Electronic reorganization enthalpy (kcal/mol) vs. Mulliken–Jaffé electronegativity, all elemental hydrides. Lines are least-squares fit to a row or column.

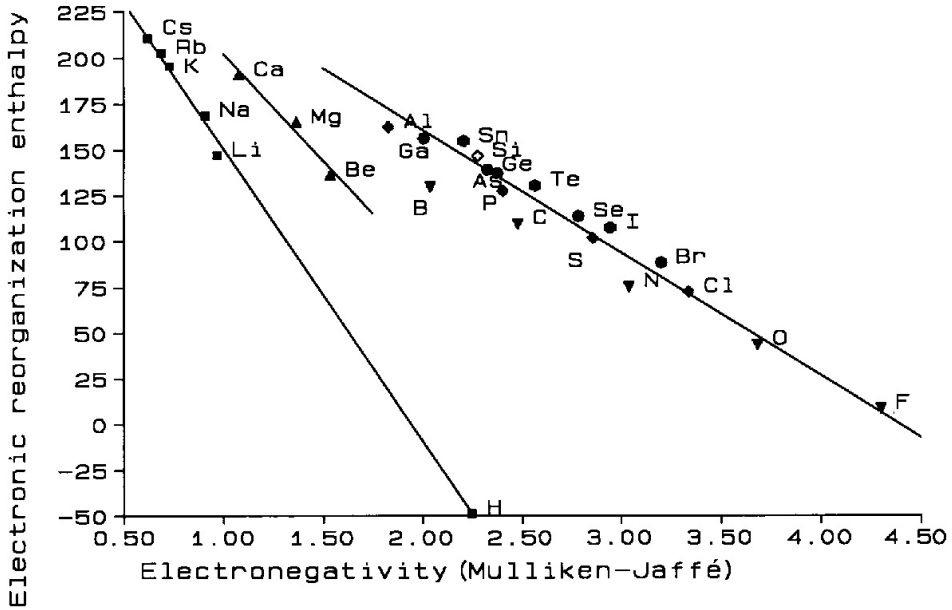
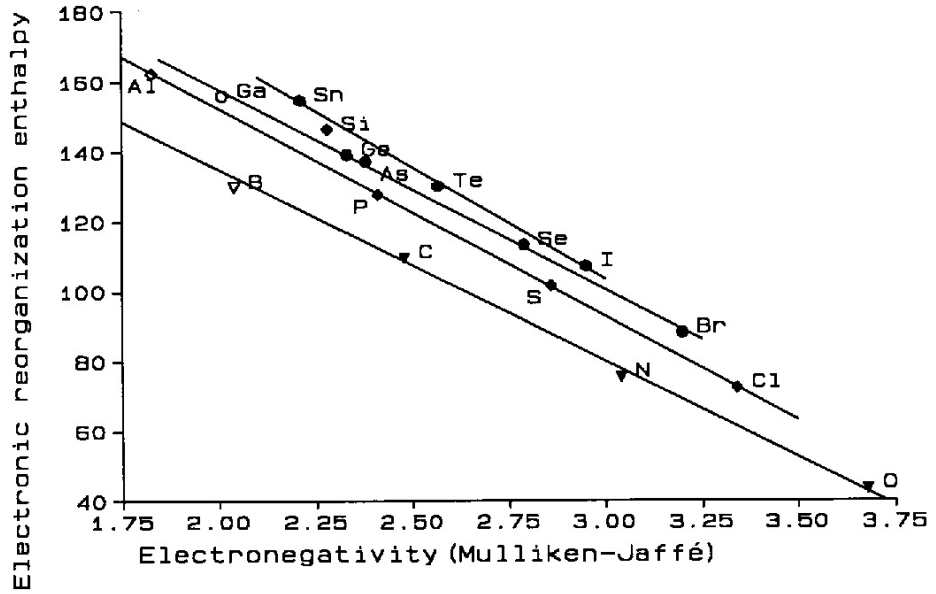


Fig. 2. Electronic reorganization enthalpy (kcal/mol) vs. Mulliken–Jaffé electronegativity for the main-group hydrides. Lines are least-squares fit to a row. Open symbols are in part computational and are not included in the least-squares fit. Fluorine is on the first row line, but off-scale for reasons of legibility.



though not quite as good, correlations, with r values of 0.95 or higher.

Closer examination of the main group compounds (shown in Fig. 2) reveals that the correlation between $\Delta_{ER}H$ and electronegativity X_A is even stronger when each row of the periodic table is considered individually

[6] CH_4 through HF: $\Delta_{ER}H = (-54.8 \pm 1.5) \times X + (244 \pm 5)$ $r = -0.9992$, sd = 1.5

[7] SiH_4 through HCl: $\Delta_{ER}H = (-68.1 \pm 6.3) \times X + (298 \pm 17)$ $r = -0.9913$, sd = 4.2

[8] SiH_4 without SiH_4: $\Delta_{ER}H = (-59.5 \pm 0.8) \times X + (271 \pm 2)$ $r = -0.9999$, sd = 0.3

[9] GeH_4 through HBr: $\Delta_{ER}H = (-63.3 \pm 4.4) \times X + (290 \pm 11)$ $r = -0.993$, sd = 0.6

[10] SnH_4, TeH_2, HI: $\Delta_{ER}H = (-64.0 \pm 2.2) \times X + (296 \pm 6)$ $r = -0.9994$, sd = 0.7

where $\Delta_{ER}H$ is in kcal/mol and the correlated data are confined to experimental values.

© 2005 NRC Canada

It is evident that SiH_4 deviates from eq. [8], being 11 kcal/mol more weakly acidic than predicted by this correlation. There is no obvious chemical reason for silane being special. The deviation must lie in the measured geometry, acidity, or electronegativity. The silyl anion and radical are both clearly pyramidal (26), so it is not a matter of using the wrong hybridization state in choosing the electronegativity (23). The experimental bond length agrees with computations. To put the measured $\Delta_{ER}H$ on the line of eq. [8] requires either $X = 2.1$, or a strengthening of the measured acidity by 11 kcal/mol. An error of the latter size seems unlikely, considering the internal consistency of the experimental gas-phase acidity scale (5), and its agreement with the value from Scheme 1 for silane. It is noteworthy, however, that the difference between the Mulliken–Jaffé electronegativity for tetrahedral Si ($X_{Si} = 2.28$) and the Pauling electronegativity for the same element and hybridization state ($X_{Si} = 1.90$) is the greatest for any main group element listed in the Bratsch tables (23). A smaller X_{Si} value would put the silane point closer to the least-squares line.

Both the slopes and intercepts of eqs. [6]–[10] show periodic trends: the acids in rows lower in the periodic table are more sensitive to electronegativity in determining their $\Delta_{ER}H$ value. The intercepts of these equations indicate weaker intrinsic $\Delta_{ER}H$ at zero electronegativity, as one goes lower in the table. Because electronegativity also follows periodic trends, this implies that perhaps a somewhat higher power function might be more applicable. However, we believe that the precision of both the experimental data and the electronegativities does not support further extension of this.

In contrast, the alkali metal hydrides (and hydrogen), with two valence electrons, fall on a separate line from the main group elements, and $\Delta_{ER}H$ is stronger than expected relative to the main group. Proton loss for these group 1 hydrides involves an s orbital, as opposed to the p shell of the main group species, so a different correlation is not surprising. The group 2 acids BeH_2, MgH_2, and CaH_2 fall between the group 1 and main group lines. It is therefore clear that orbital occupation is another variable that affects the gas-phase acidities of the elemental hydrides. The greater sensitivity of $\Delta_{ER}H$ of the group 1 and 2 acids to electronegativity than for the main group species, may reflect the proximity of the bonding s orbital to the nucleus, compared with the participation of the more distant p electrons for the main group elements.

There are several elemental hydrides for which the experimental gas-phase acidity is not known and for which reliable computational approaches fail because the necessary basis sets are unavailable, or because relativistic effects are important. Using eq. [3] in combination with eqs. [2] and [7], [9], or [10] yields predictions in Table 2 for these unknown gas-phase acidities including those of SrH_2, InH_3, SbH_3, and the row 5 species BaH_2, TlH_3, PbH_4, BiH_3, and PoH_2. Because of the uncertainty in even the order of bond length in the row 5 acids, as noted earlier, the derived acidities are expected to be uncertain by at least ±10 kcal/mol.

Likewise, a rearrangement of eqs. [2] and [5] allows prediction of an effective group electronegativity for hydrocarbon fragments from known bond lengths and gas-phase acidities. For -CH=CH_2 and -C≡CH, as seen in Table 2, derived electronegativities of 2.73 and 3.16, respectively, are obtained. The first value is somewhat larger than that of the sp^3 carbon at 2.48, but the value for -C≡CH places the electronegativity of an sp carbon between that of N and O, as expected (27). From the Pauling definition of electronegativity in eq. [11], we can utilize currently available

$$[11] \quad |X_A - X_B| = 0.208[D(A—B) - D(A—A) + D(B—B)/2]^{1/2}$$

thermochemistry (5) to obtain Pauling electronegativities for the groups -CH_2CH_3, -CH=CH_2, and -C≡CH of 2.56, 2.58, and 2.93, respectively, relative to $X_F = 4.0$ (28). Wells (29) reports group electronegativities for these of 2.3, 3.0, and 3.3, but the derivation of these values is not clear. Taft and co-workers (30) give polar σ values of 0.16, 0.17, and 0.28 for the groups based on calculated charge densities on the acidic hydrogen in the acids, implying again that ethenyl is only slightly more electronegative than ethyl, but ethynyl considerably more so. Boyd and Boyd (31) present group electronegativity values of 2.55, 2.58, and 2.66. The Mulliken–Jaffé electronegativities (23) for these hybridization states are 2.48, 2.66, and 2.99, relative to $X_F = 4.30$. Guillermin et al. (32) likewise comment on these points.

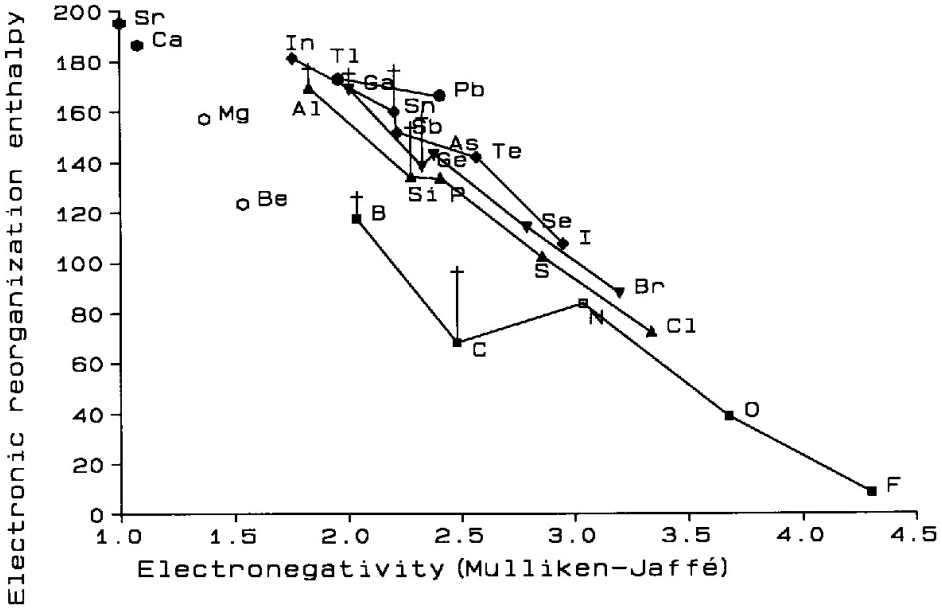
For the elemental monohydrides (in Table 3 and Fig. 3), it is evident that while there is a general correlation with electronegativity, there is considerably more scatter here than for the saturated hydrides. A complicating factor with these monohydride acidities is that the most thermochemically stable monohydride acid and atomic conjugate base can have different spin states, i.e., CH is a ground-state doublet while C^- is a quartet, with the anion doublet state 28 kcal/mol higher in energy. The group 13 and 14 monohydrides are all such cases. Such a multiplicity change during a proton transfer can result in an appreciable barrier and a concomitant lack of reactivity (34). Also, several of the atomic anions (N^-, Be^-, Mg^-) are not bound with respect to electron loss; values for these are obtained computationally at the G3(MP2) (18) level, and are shown as open symbols in Fig. 3. Finally, the electronegativities used here are hybridization state dependent (23), and it is not clear whether the hybridization of the acid or conjugate base should be used. We thus take Fig. 3 as indicating semiquantitative agreement at best with the general concept presented here. The monohydride $\Delta_{ER}H$ values are in general within a few kcal/mol of the saturated hydride ones, save that CH is notably 41 kcal/mol weaker than methane.

This correlation of acidity with bond length and electronegativity is an empirical one, unlike the rigorous thermochemical cycle in Scheme 1. Is there a physical rationale for this? We argue that for a limited series of structurally related compounds, such as the elemental hydrides here, it is not unreasonable that a longer bond should be proportionately weaker, in the homolytic sense. As noted earlier, excluding H_2, this holds to within a standard deviation of 7.1 kcal/mol for these species.

Likewise, the Mulliken definition of electronegativity involves an average of the electron affinity and ionization energy of the species involved. Thus, qualitatively both bond dissociation energies and electron affinities are related to the quantities used here. It appears that there are canceling ef-

© 2005 NRC Canada

Fig. 3. Reorganization enthalpy (kcal/mol) vs. Mulliken–Jaffé electronegativity, all elemental monohydrides. Open symbols denote computational values for unbound anions. Species of a row are connected. Vertical lines to a cross show the effect of promotion of the anion to the same multiplicity state as the acid.



fects in the differences between Scheme 1 and eqs. [2] and [6]–[10].

The gas-phase acidities of sp^3 carbon acids, all of which have the same nominal C—H bond length and electronegativity, are spread across a range of values 122 kcal/mol wide, from ethane to $(C_4F_7SO_2)_2CH_2$ (5). The correlations found here are thus not general ones, but valid only for the elemental hydrides, where the additional effects of resonance, polarity, and polarizability arising from the substituents on the central atom are not present or cancel out. Nevertheless, within this chemically related family of molecules, the gas-hase acidities can be shown to be simply and intuitively related to molecular geometry, atomic electronegativity, and position in the Periodic table.

Acknowledgments

We thank the National Institute of Standards and Technology for support of this work, and Professors George Schweitzer and William Herndon for helpful discussions.

References

1. E.C. Baughn. J. Chem. Soc. 1403 (1940).
2. J.I. Brauman and L.K. Blair. J. Am. Chem. Soc. **93**, 3911 (1971).
3. K.E. Laidig and A. Streitwieser, Jr. J. Comp. Chem. **17**, 1771 (1996).
4. E.R. Cohen and B.N. Taylor. J. Res. Nat. Bur. Stand. **92**, 85 (1987).
5. W.G. Mallard and P.J. Linstrom (*Editors*). NIST Chemistry WebBook, NIST Standard Reference Database Number 69 [online]. National Institute of Standards and Technology, Gaithersburg, Md. Available from http://webbook.nist.gov/chemistry/. June 2005.
6. K.P. Huber and G. Herzberg. *In* Molecular spectra and molecular structure. IV. Constants of diatomic molecules. 2nd ed. Van Nostrand Reinhold Co., New York. 1979.
7. K.-H. Hellwege (*Editor*). Landolt–Börnstein numerical data and functional relationships in science and technology II/6: Molecular constants. Springer-Verlag, Berlin. 1974.
8. O. Madelung (*Editor*). Landolt–Börnstein numerical data and functional relationships in science and technology II/15: Structure data of free polyatomic molecules. Springer-Verlag, Berlin. 1987.
9. W. Martienssen (*Editor*). Landolt–Börnstein numerical data and functional relationships in science and technology II/23: Structure data of free polyatomic molecules. Springer-Verlag, Berlin. 1995.
10. M.D. Harmony. Acc. Chem. Res. **25**, 321 (1992).
11. F. Pawlowski, P. Jorgensen, J. Olsen, F. Hegelund, T. Helgaker, J. Gauss, K.L. Bak, and J.F. Stanton. J. Chem. Phys. **116**, 6482 (2002).
12. M.J. Frisch, G.W. Trucks, H.B. Schlegel, G.E. Scuseria, M.A. Robb, J.R. Cheeseman, V.G. Zakrzewski, J.A. Montgomery, Jr., R.E. Stratmann, J.C. Burant, S. Dapprich, J.M. Millam, A.D. Daniels, K.N. Kudin, M.C. Strain, O. Farkas, J. Tomasi, V. Barone, M. Cossi, R. Cammi, B. Mennucci, C. Pomelli, C. Adamo, S. Clifford, J. Ochterski, G.A. Petersson, P.Y. Ayala, Q. Cui, K. Morokuma, D.K. Malick, A.D. Rabuck, K. Raghavachari, J.B. Foresman, J. Cioslowski, J.V. Ortiz, A.G. Baboul, B.B. Stefanov, G. Liu, A. Liashenko, P. Piskorz, I. Komaromi, R. Gomperts, R.L. Martin, D.J. Fox, T. Keith, M.A. Al-Laham, C.Y. Peng, A. Nanayakkara, C. Gonzalez, M. Challacombe, P.M.W. Gill, B. Johnson, W. Chen, M.W. Wong, J.L. Andres, C. Gonzalez, M. Head-Gordon, E.S. Replogle, and J.A. Pople. Gaussian 98. Revision A.7 [computer program]. Gaussian, Inc., Pittsburgh, Penn. 1998.
13. Molecular Science Computing Facility, Environmental and Molecular Sciences Laboratory (EMSL). Extensible Computational Chemistry Environment Basis Set Database. Version 02/25/04. EMSI Gaussian basis sets [online]. Pacific North-

© 2005 NRC Canada

west Laboratory, Richland, Washington. Available from http://www.emsl.pnl.gov/forms/basisform.html.
14. D. Cremer, E. Kraka, and Y. He. J. Mol. Struct. **567–568**, 275 (2001).
15. Y. He and D.J. Cremer. J. Phys. Chem. A, **104**, 7679 (2000).
16. D. Cremer, A. Wu, A. Larsson, and E. Kraka. J. Mol. Model. **6**, 396 (2000).
17. J. Sánchez Márquez and M. Fernández Núñez. J. Mol. Struct: THEOCHEM, **624**, 239 (2003).
18. L.A. Curtiss, P.C. Redfern, K. Raghavachari, V. Rassolov, and J.A. Pople. J. Chem. Phys. **110**, 4703 (1999).
19. R.J. Hinde. J. Phys. Chem. A, **104**, 7580 (2000).
20. L. Pauling. The nature of the chemical bond. Cornell University Press, Ithaca, N.Y. 1939. Chap. 2.
21. R.S. Mulliken. J. Chem. Phys. **2**, 782 (1934).
22. J. Hinze, M.A. Whitehead, and H.H. Jaffé. J. Am. Chem. Soc. **85**, 148 (1968).
23. S.G. Bratsch. J. Chem. Educ. **65**, 34 (1988).
24. A.L. Allred and E.G. Rochow. J. Inorg. Nucl. Chem. **5**, 264 (1958); **5**, 269 (1958).
25. R.T. Sanderson. J. Am. Chem. Soc. **105**, 2259 (1983).
26. M.R. Nimlos and G.B. Ellison. J. Am. Chem. Soc. **108**, 6522 (1986).
27. A.D. Walsh. Discuss. Faraday Soc. **2**, 18 (1947).
28. The literature experimental value for $\Delta_f H^0$(HC≡CCl) appears to be at least 16 kcal/mol too positive, based on group additivity and G3(MP2) calculations: E. Kloster-Jensen, C. Pascual, and C.J. Vogt. Helv. Chim. Acta, **53**, 2109 (1970).
29. P.R. Wells. Prog. Phys. Org. Chem. **6**, 111 (1968).
30. S. Marriott, W.F. Reynolds, R.W. Taft, and R.D. Topsom. J. Am. Chem. Soc. **106**, 959 (1984).
31. R.J. Boyd and S.L. Boyd. J. Am. Chem. Soc. **114**, 1652 (1992).
32. J.-C. Guillermin, E.H. Ruiague, J.-F. Gal, P.-C. Maria, O. Mó, and M. Yáñez. Chem. Eur. J. **11**, 2145 (2005).
33. G.A. Janaway and J.I. Brauman. J. Phys. Chem. A, **104**, 1795 (2000).
34. M. Kaupp, P.v.R. Schleyer, H. Stoll, and H.J. Preuss. Chem. Phys. **94**, 1360 (1991)
35. P. Schwerdtfeger, G.A. Heath, M. Dolg, and M.A. Bennett. J. Am. Chem. Soc. **114**, 7518 (1992).
36. K. Sumathi and K. Balasubramanian. J. Chem. Phys. **92**, 6604 (1990).

© 2005 NRC Canada

The bond dissociation energies of SO_3—X^- (X = F, Cl, Br, and I)[1]

Changtong Hao, Thomas M. Gilbert, and Lee S. Sunderlin

Abstract: The gas-phase strengths of the SO_3—X^- bonds (X = Cl, Br, and I) have been determined to be 222 ± 13, 179 ± 11, and 161 ± 9 kJ/mol, respectively, by measuring thresholds for collision-induced dissociation in a flowing afterglow-tandem mass spectrometer. An upper limit of $D(SO_3—F^-) \leq 488 \pm 19$ kJ/mol was also determined. The periodic trends in the halide affinities of SO_3 closely parallel those for SO_2 and other Lewis acids. Bond strengths computed using the B3LYP, MP2, QCISD(T), and other models with several basis sets are generally lower than experiment.

Key words: bond dissociation energies, computational chemistry, Lewis acids, superacids, halide affinities.

Résumé : Utilisant un spectromètre de masse en tandem à écoulement postluminescence, on a mesuré les seuils de dissociation induite par une collision et on en déduit que les forces, en phase gazeuse, des liaisons SO_3—X^- (X = Cl, Br et I) sont respectivement de 222 ± 13, 179 ± 11 et 161 ± 9 kJ/mol. On a aussi déterminé que la limite supérieure de $D(SO_3—F^-)$ est ≤ 488 ± 19 kJ/mol. Les tendances périodiques dans les affinités des halogénures pour le SO_3 sont parallèles à celles pour le SO_2 et pour d'autres acides de Lewis. Les forces des liaisons calculées par les méthodes B3LYP, MP2, QCISD(T) et d'autres modèles en utilisant plusieurs ensembles de bases sont généralement inférieures aux valeurs expérimentales.

Mots clés : énergies de dissociation de liaison, calculs théoriques, acides de Lewis, superacides, affinités pour les halogénures.

[Traduit par la Rédaction]

Introduction

The thermodynamic properties of halosulfuric acids ($HXSO_3$, X = F, Cl, Br, and I) in solution have been studied in detail and are well-known (1–3). The halosulfuric acids can be thought of as strong acids (HX) modified to superacids by the attraction between the Lewis acid SO_3 and the halide X^- (4, 5). While they are important catalysts in solution (1, 5), information about these superacids and their conjugate bases (the halosulfonate anions) in the gas phase is limited. Larson and McMahon (6) estimated a fluoride affinity for SO_3 of 326 ± 42 kJ/mol. Viggiano et al. (7) estimated an electron affinity for SO_3F of 4.8 eV based on bracketing experiments; they later (8) revised this number to 5.2 eV and calculated a value of 5.53 eV using the G2 model. Structures of SO_3F^- (9) and SO_3Cl^- (10) were determined by X-ray crystallography; the solid-state anions show lower symmetries and shorter bond lengths than calculated gas-phase structures (8). Steudel and Otto (4) carried out ab initio calculations on chlorosulfonate and fluorosulfonate anions as part of a study of superacids.

In 1985, Caldwell and Kebarle (11) measured the gas-phase SO_2—X^- bond enthalpies for X = Cl, Br, and I, while Larson and McMahon measured $D(SO_2—F^-)$ and $D(SO_3—F^-)$ (6). This work is an example of how systematic measurement of gas-phase energetics, a field largely pioneered by Kebarle after his development of high-pressure mass spectrometry (12), can be used to understand chemical interactions. Measurements of the dissociation energies of SO_3—X^- (X = Cl, Br, I) would allow new comparisons to the previous gas-phase data and solution-phase results. In this paper, the energetics of halosulfonate anions SO_3X^- (X = F, Cl, Br, I) are examined experimentally and computationally.

Experimental

Bond dissociation energies (BDEs) were measured using the energy-resolved collision-induced dissociation (CID) technique (13–16) in a flowing afterglow-tandem mass spectrometer (MS) (17). The instrument consists of an ion source region, a flow tube, and the tandem MS. The DC discharge ion source used in these experiments is typically set at 2000 V with 2 mA of emission current. The flow tube is a 92 cm × 7.3 cm i.d. stainless steel pipe that operates at a buffer gas pressure of 0.35 Torr (1 Torr = 133.3224 Pa), a flow rate of 200 standard $cm^3\ s^{-1}$, and an ion residence time of 100 ms. The buffer gas is helium with up to 10% argon added to stabilize the DC discharge.

To make SO_3F^- for this study, SF_6 and fuming H_2SO_4 (20%–30% SO_3) were added to the ion source. Dissociative

Received 6 May 2005. Published on the NRC Research Press Web site at http://canjchem.nrc.ca on 1 February 2006.

Dedicated to Paul Kebarle in appreciation of his many contributions to ion chemistry.

C. Hao, T.M. Gilbert, and L.S. Sunderlin.[2] Department of Chemistry and Biochemistry, Northern Illinois University, DeKalb, IL 60115, USA.

[1]This article is part of a Special Issue dedicated to Professor P. Kebarle.

[2]Corresponding author (e-mail: sunder@niu.edu).

 doi: 10.1139/V05-216 © 2005 NRC Canada

Table 1. Calculated and experimental spectroscopic parameters of SO_3 and SO_3X^- (X = halogen).

Species	SO_3		SO_3F^-		SO_3Cl^-		SO_3Br^-	SO_3I^-
Reference	Calcd.[a]	Exp.[b]	Calcd.[a]	Exp.[b]	Calcd.[a]	Exp.[b]	Calcd.[a]	Calcd.[b]
Rotational constant	0.3357		0.1701		0.1699		0.1696	0.1693
	0.1678 (×2)		0.1587 (×2)		0.0845 (×2)		0.0512 (×2)	0.0362 (×2)
Vibrational frequencies	441	495	353 (×2)	424 (×2)	254 (×2)	312 (×2)	198	158
	496 (×2)	529 (×2)	476	571	267	381	221 (×2)	195 (×2)
	1016	1068	537 (×2)	619 (×2)	506 (×2)	553 (×2)	500 (×2)	493 (×2)
	1328 (×2)	1391 (×2)	635	862	552	601	543	529
			1003	1142	988	1042	982	974
			1232 (×2)	1302 (×2)	1230 (×2)	1300 (×2)	1225 (×2)	1220 (×2)

Note: Rotational constants and vibrational frequenciess are in cm^{-1}. (×2) indicates a degeneracy of 2.
[a]B3LYP/6-311+G(d) values from this work.
[b]Reference 19.

electron impact on SF_6 gives F^-, which adds to SO_3 to give SO_3F^-. Similarly, C_2Cl_4, CBr_4, and I_2 were added as Cl^-, Br^-, and I^- ion sources to make SO_3Cl^-, SO_3Br^-, and SO_3I^-. The C_2Cl_4 and H_2SO_4 precursors were cooled in an ice bath to improve control of the vapor flow.

The tandem MS includes a quadrupole mass filter, an octopole ion guide, a second quadrupole mass filter, and a detector contained in a stainless steel box that is partitioned into five interior chambers. Differential pumping on the five chambers ensures that further collisions of the ions with the buffer gas are unlikely after ion extraction. During CID experiments, the ions are extracted from the flow tube and focused into the first quadrupole for mass selection. The reactant ions are then focused into the octopole, which passes through a reaction cell that contains an unreactive collision gas. Ar and Xe were used for SO_3F^- and SO_3I^-, respectively. Ar, Kr, and Xe were used on SO_3Cl^- and SO_3Br^-; the effect of using different collision gases is discussed in the following. After the dissociated and unreacted ions pass through the reaction cell, the second quadrupole is used for mass analysis. The detector is an electron multiplier operating in pulse-counting mode.

The energy threshold for CID is determined by modeling the cross section for product formation as a function of the reactant ion kinetic energy in the center-of-mass (CM) frame (E_{cm}). The octopole is used as a retarding field analyzer to measure the reactant ion beam energy zero. The ion kinetic energy distribution for the present data is typically Gaussian with a full-width at half-maximum of 0.7–2.1 eV (1 eV = 96.5 kJ/mol). The octopole offset voltage measured with respect to the center of the Gaussian fit gives the laboratory kinetic energy (E_{lab}) in eV. Low offset energies are corrected for truncation of the ion beam (18). To convert to the CM frame, the equation $E_{cm} = E_{lab}m(m + M)^{-1}$ is used, where m and M are the masses of the neutral and ionic reactants, respectively. All experiments were performed with both mass filters at low resolution to improve ion collection efficiency and reduce mass discrimination. For SO_3Cl^- and SO_3Br^-, the two major isotopic peaks were used simultaneously, and average atomic masses were used for all elements in determining the energy scale conversions.

The total cross section for a reaction (σ_{total}) is calculated using eq. [1], where I is the intensity of the transmitted reactant ion beam, I_o is the intensity of the incoming beam ($I_o = I + \Sigma I_i$), I_i is the intensity of each product ion, n is the number density of the collision gas, and l is the effective collision length (13 ± 2 cm). Individual product cross sections (σ_i) are equal to $\sigma_{total}(I_i/\Sigma I_i)$.

$$[1] \qquad I = I_o \exp(-\sigma_{total} nl)$$

Threshold energies are derived by fitting the data to a model function given in eq. [2], where $\sigma(E)$ is the cross section for formation of the product ion at CM energy E, E_T is the desired threshold energy, σ_o is the scaling factor, n is an adjustable parameter, and i denotes rovibrational states having energy E_i and population g_i ($\Sigma g_i = 1$). Doppler broadening and the kinetic energy distribution of the reactant ion are also accounted for in the data analysis, which is done using the CRUNCH program written by Armentrout and coworkers (18).

$$[2] \qquad \sigma(E) = \sigma_o \Sigma_i g_i (E + E_i - E_T)^n / E$$

Collisionally activated metastable complexes can have sufficiently long lifetimes that they do not dissociate on the experimental timescale (ca. 50 μs). Such kinetic shifts are accounted for in the CRUNCH program by RRKM lifetime calculations. Reactant and product vibrational frequencies are needed to determine both the RRKM lifetimes and the reactant internal energy distribution.

Complete experimental fundamental vibrational frequency sets are available for the neutral SO_3 molecule and the SO_3F^- and SO_3Cl^- anions (19–21). However, they are unavailable for the SO_3Br^- and SO_3I^- species, such that the dissociation modeling described earlier cannot be performed using solely experimental data. Furthermore, the values for the ionic species are from condensed-phase experiments, and are likely to differ from gas-phase values. Therefore, vibrational harmonic frequencies and rotational constants were calculated using the B3LYP hybrid density functional method with the 6-311+G(*d*) basis set to give a consistent set of frequencies for all analyses of CID data. The calculated and experimental frequencies are given in Table 1. Other work on similar molecules suggests that the closely related B3LYP/6-311+G(d,p) approach gives generally good agreement with experiment without scaling (22), but for the systems studied here, the calculated values are too high (by 7%, 17%, and 14% for SO_3, SO_3F^-, and SO_3Cl^-, respectively). Because the derived thermochemistry is most sensitive to the *ratio* of the reactant and product frequencies,

© 2005 NRC Canada

unscaled computational results were used for all molecules. Uncertainties in the derived thresholds owing to possible inaccuracies in the calculated spectroscopic constants were estimated by multiplying the entire sets of frequencies by 0.8 and 1.2, and by multiplying the time window for dissociation by 10 and 0.1. The effect of this scaling on the calculated thresholds is less than 2 kJ/mol for all the anions in this study. The neutral SO_3 product polarizability also has a minor effect on the derived thresholds; the B3LYP/ 6-311+G(d,p) value of 3.90 Å^3 is used in this work.

An ion not sufficiently energized by one collision with the target gas may gain enough energy in a second collision to exceed the dissociation threshold. This effect is eliminated by linear extrapolation of the data taken at several pressures to a zero pressure cross section before fitting the data (23).

The reagents C_2Cl_4, CBr_4, I_2, and fuming H_2SO_4 were obtained from Acros (Pittsburgh, Pennsylvania). He, Ar, and SF_6 were obtained from BOC (Murray Hill, New Jersey), and Xe was obtained from Spectra Gases (Irvington, New Jersey). All reagents were used as received.

Computational details

Computational work for this project was performed using the Gaussian program suite (24). All molecular structures were initially optimized without symmetry constraints, and plausible alternative structures, such as geometries with O-bonded halogens, were tested. These studies showed that C_{3v} structures are minima for SO_3X^-, and the D_{3h} structure is the minimum for SO_3. Thus, in most further calculations, symmetry was enforced. The nature of all stationary point structures was determined by analytical frequency analysis, which also provided zero-point energies (ZPEs). The ZPEs were not scaled when used to correct the raw energy values except in the G3X and CBS-Q calculations. Several basis sets were used. The 6-311+G(*d*) basis set (25) and the smaller LANL2DZpd basis set (26, 27), which uses the LANL effective core potential, were used for all of the molecules involved in this study. Other calculations employed the larger aug-cc-pVTZ basis set (28) for S, O, F, Cl, and Br, and the SDB-aug-cc-pVTZ basis set (29) (which uses the SDB effective core potential) for I. Several single-energy models, including MP2 (30), CCD (31), QCISD (32), QCISD(T), CCSD(T) (33), and B3LYP (34), as well as the CBS-Q (35), G3(MP2) (36), and G3X (37) composite models, were used to predict bond dissociation energies. Not all of these methods are available for the heavier halogens, and some possible calculations were beyond the available computational resources, so not every method was used with each basis set.

Results and discussion

Experimental bond dissociation energies

CID of all species studied in this work gives loss of X^- (X = F, Cl, Br, and I) as the only dissociation pathway. Appearance curves for dissociation of SO_3F^-, SO_3Cl^-, SO_3Br^-, and SO_3I^- are given in Figs. 1–4. The eq. [2] fitting parameters are given in Table 2, and the fits are shown in the figures. The effects of reactant and product internal energy are included in the fitting procedure; therefore, the dissociation thresholds correspond to BDEs at 0 K. The final uncertainties in the BDEs are derived from the standard deviation of the thresholds determined for individual data sets, the uncertainty in the reactant internal energy, the effects of kinetic shifts, and the uncertainty in the energy scale (±0.15 eV lab). These results are given in Table 3.

Fig. 1. Cross section for collision-induced dissociation of SO_3F^- as a function of energy in the center-of-mass frame. The solid and dashed lines represent convoluted and unconvoluted fits to the data, as discussed in the text.

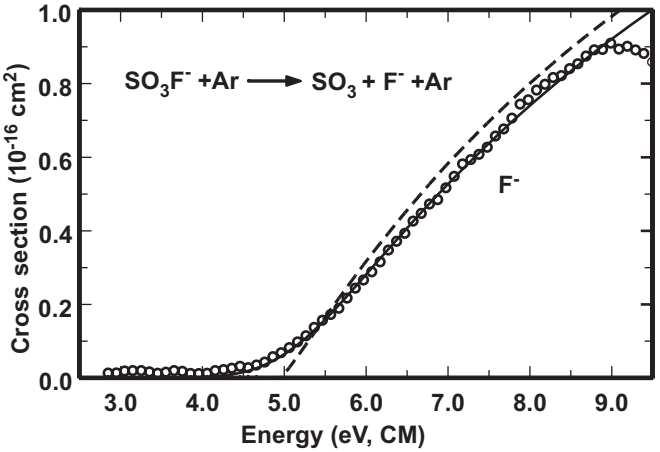


Fig. 2. Cross section for collision-induced dissociation of SO_3Cl^- as a function of energy in the center-of-mass frame. The solid and dashed lines represent convoluted and unconvoluted fits to the data, as discussed in the text.

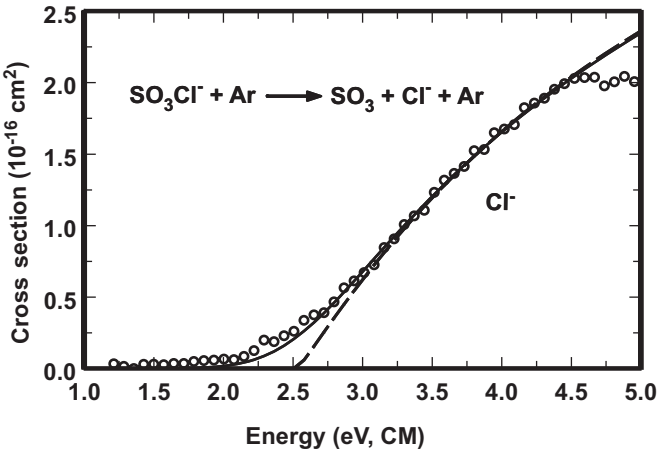


Table 2. Fitting parameters for CID.

Anion	E_T (eV)	n	Collision gas
SO_3F^-	5.06±0.20	1.23±0.22	Ar
SO_3Cl^-	2.53±0.10	1.10±0.04	Ar
	2.35±0.05	1.19±0.08	Kr
	2.30±0.14	1.11±0.09	Xe
SO_3Br^-	2.08±0.10	1.01±0.09	Ar
	1.95±0.09	1.07±0.09	Kr
	1.85±0.11	1.10±0.18	Xe
SO_3I^-	1.67±0.09	1.10±0.12	Xe

Note: See text for discussion of fitting parameters.

© 2005 NRC Canada

Table 3. O_3S—X^- (X = F, Cl, Br, I) bond dissociation enthalpies in kJ/mol.

Anion	Exp. (0 K)	B3LYP/ LANL2DZpd	B3LYP/6-311+G(d)	B3LYP/ aug-cc-pVTZ	MP2/ LANL2DZpd	MP2/6-311+G(d)	MP4/6-311+G(d)	CCD/6-311+G(d)
SO_3F^-	≤488±19, 326±42[c]	327	332	344	301	324	—	348
SO_3Cl^-	222±13	177	178	184	171	179	179	190
SO_3Br^-	179±11	158	159	159	154	154	—	159
SO_3I^-	161±9	137	138	137[e]	126	126	—	126

[a]CCD/6-311+G(d) geometry and unscaled B3LYP/6-311+G(d) ZPE corrections.
[b]QCISD/6-311+G(d) geometry and unscaled B3LYP/6-311+G(d) ZPE corrections.
[c]298 K value from ref. 6.
[d]298 K results from ref. 4.
[e]Iodine basis set is SDB-aug-cc-pVTZ.

Fig. 3. Cross section for collision-induced dissociation of SO_3Br^- as a function of energy in the center-of-mass frame. The solid and dashed lines represent convoluted and unconvoluted fits to the data, as discussed in the text.

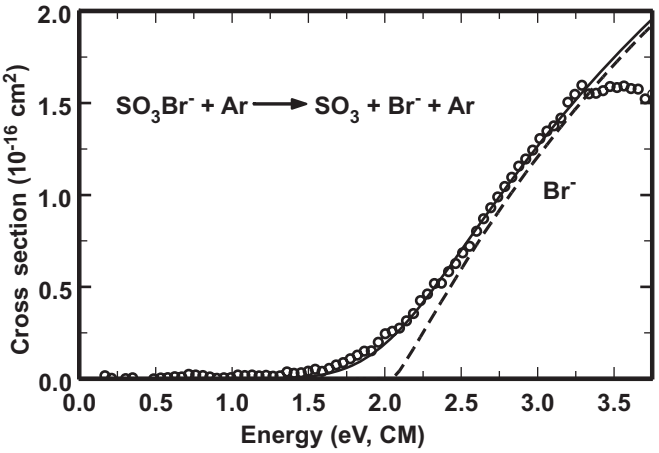
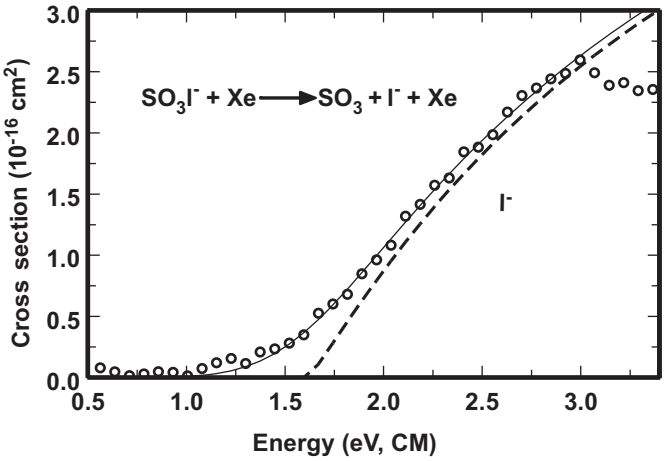


Fig. 4. Cross section for collision-induced dissociation of SO_3I^- as a function of energy in the center-of-mass frame. The solid and dashed lines represent convoluted and unconvoluted fits to the data, as discussed in the text.



The relative locations of the solid and dashed lines are different in these four figures, but the reasons are straightforward. The dashed lines (unconvoluted fits) represent the cross sections expected if the reactant ions had no internal energy and no translational energy broadening, and the activated ions always dissociated if given sufficient energy. The solid lines (convoluted fits) include the effect of ion internal energy, translational broadening, and delayed dissociation, as discussed earlier. For SO_3I^-, the main effect is the internal energy of the ion (0.20 eV on average), which shifts the solid line to the left. For SO_3F^-, the higher BDE leads to a significantly larger kinetic shift, nearly canceling the effect of the internal energy.

Several collision gases (Ar, Kr, and Xe) were used with SO_3Cl^- and SO_3Br^-, and the results are listed in Table 2. The CID threshold of SO_3Br^- with Ar collision gas is 0.13 eV higher than with Kr, and 0.23 eV higher than with Xe gas. SO_3Cl^- has a similar trend with the three collision gases. While this could conceivably be due to the experimental uncertainties, it is probably a systematic effect: previous cases have been noted where the heavier, more polarizable collision gas Xe (which is more likely to form a complex with the CID target and efficiently transfer energy from translational into internal degrees of freedom) gives lower thresholds that are more consistent with known thermochemistry (14, 38, 39). This is not always the case (40); systems with strong bonds and low densities of states (few atoms and high vibrational frequencies) are more likely to show this collision gas effect. Since the SO_3Cl^- and SO_3Br^- systems appear to show a moderate threshold shift of this type, SO_3F^- is likely to have a greater one. However, collecting reliable data on SO_3F^-–Xe collisions requires a very narrow Gaussian ion translational energy distribution. This has proven challenging so far; efforts to improve the experimental procedure for this molecule continue. Thus, the results with Xe collision gas are reported as final values for the three heavier systems, and the SO_3F^-–Ar results should be viewed as an upper limit on the actual threshold energy, $D(SO_3$—$F^-) \leq 488 \pm 19$ kJ/mol. The Larson–McMahon value of 326 ± 42 kJ/mol should therefore be taken as the best current experimental determination of this value.

Computed geometries

The optimized geometries are very similar for all models employed. Calculated bond lengths using B3LYP with the aug-cc-pVTZ (SDB-aug-cc-pVTZ for I) basis set are given in Table 4. The calculated S—O bond distance in SO_3 is 0.02 Å larger than the experimental value (41). The addition of halogen ions to SO_3 makes the S—O bonds 0.020–0.022 Å longer, in addition to pyramidalizing the geometry. The X-ray structures (9, 10) of crystals containing SO_3Cl^-

© 2005 NRC Canada

CCSD(T)/6-311+G(d)[a]	QCISD/LANL2DZpd	QCISD/6-311+G(d)	QCISD(T)/6-311+G(d)[b]	QCISD(T)/aug-cc-pVTZ	CBS-Q	G3 (MP2)	G3X
333	360	338	329	354	377[d], 372	365	368
186	221	187	185	190	202[d], 198	195	197
159	190	159	158	—	—	174	173
130	161	127	129	—	—	—	—

Table 4. Geometries of SO_3X^-.

Species	*r*(S—O) (Å)	*r*(S—X) (Å)	∠O-S-O (°)	∠O-S-X (°)	Ref.
SO_3	1.418 (×3)	—	120 (×3)	—	41
	1.44 (×3)	—	120 (×3)	—	This work
SO_3F^-	1.455	1.555	117.4	104.5	9
	1.424 (×2)		113.5 (×2)	102.8 (×2)	
	1.461 (×3)	1.670	115.8 (×3)	102 (×3)	This work
SO_3Cl^-	1.419	2.051	115.2	103.1	10
	1.445		113.0	103.1	
	1.453		115.7	104.7	
	1.46 (×3)	2.256	116.1 (×3)	101.6 (×3)	This work
SO_3Br^-	1.461 (×3)	2.448	116.2 (×3)	101.4 (×3)	This work
SO_3I^-	1.462 (×3)	2.683	116.2 (×3)	101.5 (×3)	This work

Note: This work, calculated using B3LYP/aug-cc-pVTZ for all elements except SDB-aug-cc-pVTZ for I. Degeneracies are given in parentheses.

and SO_3F^- show anions that are slightly distorted by lattice effects, with S—O bond lengths averaging 0.03 Å less than the B3LYP/aug-cc-pVTZ values (Table 4). The S—X bond length increases in the order F < Cl < Br < I. The calculated S—X distances are significantly longer than the X-ray diffraction values, a difference attributed to lattice effects (8). The calculated O-S-X angle varies from 101.5° for SO_3F^- to 102.0° for SO_3I^-.

Computational bond dissociation energies

BDEs calculated at various levels of theory are summarized in Table 3. All the computational results predict BDEs smaller than experiment, although the differences decrease with the size of the halide. The computational results parallel the experimental trend in that BDEs increase in the order I < Br < Cl < F.

Comparison of BDEs predicted using the B3LYP model and increasingly large basis sets suggests that the differences between theory and experiment do not result from basis set incompleteness for this hybrid density functional approach (Table 3). Only the BDEs of SO_3F^-, where the value calculated using the aug-cc-pVTZ basis set is 12 kJ/mol higher than that from the 6-311+G(*d*) basis set and 16 kJ/mol higher than that from the LANL2DZpd basis set, show any sizable basis set effect. For the other three anions, the predicted BDEs differ little with basis set size.

However, the ab initio perturbational models show signs of basis set incompleteness. For example, the QCISD/LANL2DZpd results match the experiment well, but changing to the larger triple-ζ 6-311+G* basis set led to poorer agreement (Table 3). Consequently, we employed the G3X and CBS-Q composite models to approximate full configuration interaction and large basis set calculations, even though they could not be used for SO_3Br^- (CBS-Q) and SO_3I^- (G3 methods). These models lessen the problem of basis set incompleteness by providing corrections to lower level calculations. The G3X methods are comparable to QCISD(T)/G3Large computations, while the CBS-Q method approximates a QCISD(T)/6-311++G(3d2f,2df,2p) calculation.

As can be seen, the composite approaches predict BDEs nearer experimental values than do the single-energy methods. The G3 models perform particularly well for SO_3Br^-, with the G3X prediction of 173 kJ/mol lying within 6 kJ/mol of the experimental result of 179 ± 11 kJ/mol. The agreement for SO_3Cl^- is less good, but the composite energies lie within 2σ of the experimental value. The Larson–McMahon value for SO_3F^- of 326 ± 42 kJ/mol is somewhat lower than, but consistent with, most of the computational results (330–380 kJ/mol); the composite model values lie within 1σ of the experimental value.

That some difference in BDEs between experiment and theory remains for SO_3X^- suggests that we have not yet determined and compensated for all the sources of error in the methodologies. The computational models may still be inadequate in terms of basis set and (or) configuration interaction. In this regard, we have found no evidence that a

© 2005 NRC Canada

Table 5. Bond dissociation energies of X^-—A (X = F, Cl, Br, and I).

X^-—A	SO_3	SO_2[a]	HCOOH[b]	CH_3OH[c]	HOH[c]	HI[d]	HBr[d]	HCl[d]	HF[d]	PX_3[e]	$AlCl_3$[f]
F^-	326±42[g]	227	190	124	97	301	272	251	162	168	506
Cl^-	222±13[h]	93	114	59	55	129	123	100	91	90	321
Br^-	179±11[h]	81	70			106	87	82	71	66	
I^-	161±9[h]	60	52	47	42	71	67	60	63	55	

[a]From ref. 45.
[b]From ref. 44.
[c]From ref. 43.
[d]From ref. 11.
[e]From ref. 46.
[f]Reference 47.
[g]Reference 6.
[h]This work.

multireferential description of the bond-breaking process is required. Moreover, scans of the potential energy surface for dissociation show no barrier in excess of the endothermicity for all four halogens. Thus, it seems unlikely this represents a source of error. The effect of collision gas described earlier points to issues of efficient energy transfer in the anions; it may be there is some residual inefficiency of collisional energy transfer, even with Xe. Such an effect has been observed for extremely strongly bound ions such as SbF_6^-.[3]

Periodic trends

The trend in the halide affinities correlates with the large difference between the electronegativities (or radii) of fluorine and chlorine, and much smaller differences between the electronegativities of chlorine, bromine, and iodine (11, 42, 43). Caldwell and Kebarle (11, 43) collected an extensive set of measurements of the binding energies of three or four halide ions to different ligands, and other studies have added to this work (44–46). Representative experimental data are shown in Table 5. Several trends can be noted in this data. The average L—Cl^- bond (L = ligand) is 0.48 ± 0.07 times as large as the average L—F^- bond. The corresponding D(L—Br^-)/D(L—Cl^-) ratio is 0.75 ± 0.08, and the D(L—Br^-)/D(L—Cl^-) ratio is 0.75 ± 0.07. In this regard, the properties of SO_3 appear to be typical.

SO_3 is a much stronger Lewis acid with respect to halide anions than SO_2, but it is not the strongest. For example, the fluoride and chloride affinities of $AlCl_3$ are determined to be 506 ± 0.7 and 321 ± 0.6 kJ/mol (47).

Conclusions

The gas-phase strengths of the S—X^- bonds in SO_3X^- (X = Cl, Br, and I) have been determined by measuring thresholds for collision-induced dissociation in a flowing afterglow-tandem mass spectrometer. The experimental BDEs increase in the order I < Br < Cl < F. The trend in halide affinities correlates with a large difference between the electronegativities of fluorine and chlorine, and smaller differences between the electronegativities of chlorine, bromine, and iodine. All computational BDEs in this study are systematically lower than the experimental values, with the G3(MP2) and G3X composite models giving predictions closest to experimental results.

Acknowledgments

We acknowledge the taxpayers of the State of Illinois and the US Department of Education (Grant P116Z020095) for their support of the NIU Computational Chemistry Laboratory. We thank Peter Armentrout, Mary Rodgers, and Kent Ervin for use of the CRUNCH software for data analysis.

References

1. F.A. Cotton, G. Wilkinson, C.A. Murillo, and M. Bochmann. Advanced inorganic chemistry. 6th ed. John Wiley and Sons, New York. 1999. Chap. 12.
2. B.S. Yiin and D.W. Margerum. Inorg. Chem. **29**, 1559 (1990).
3. B.S. Yiin and D.W. Margerum. Inorg. Chem. **27**, 1670 (1989).
4. R. Steudel and A.H. Otto. Eur. J. Inorg. Chem. **11**, 2379 (2000).
5. G.A. Olah, G.K. Surya Prakash, and J. Sommer. Superacids. Wiley, New York. 1985.
6. J.W. Larson and T.B. McMahon. J. Am. Chem. Soc. **107**, 766 (1985).
7. A.A. Viggiano, M.J. Henchman, F. Dale, C.A. Deakyne, and J.F. Paulson. J. Am. Chem. Soc. **114**, 4299 (1992).
8. S.T. Arnold, T.M. Miller, and A.A. Viggiano. Int. J. Mass. Spectrom. **218**, 207 (2002).
9. Z. Zak and M. Kosicka. Acta Crystallogr. Sect. B, **B34**, 38 (1978).
10. T. Laube. J. Am. Chem. Soc. **126**, 10904 (2004).
11. G. Caldwell and P. Kebarle. Can. J. Chem. **63**, 1399 (1985).
12. P. Kebarle. Int. J. Mass Spectrom. **200**, 313 (2000).
13. F. Muntean and P.B. Armentrout. J. Chem. Phys. **115**, 1213 (2001).
14. P.B. Armentrout. J. Am. Soc. Mass Spectrom. **13**, 419 (2002).
15. P.B. Armentrout. Top. Curr. Chem. **225**, 233 (2003).
16. S.G. Anderson, A.T. Blades, J. Klassen, and P. Kebarle. Int. J. Mass Spectrom. Ion Processes, **141**, 217 (1995).
17. K. Do, T.P. Klein, C.A. Pommerening, and L.S. Sunderlin. J. Am. Soc. Mass Spectrom. **8**, 688 (1997).
18. (*a*) K.M. Ervin and P.B. Armentrout. J. Chem. Phys. **83**, 166 (1985); (*b*) M.T. Rodgers, K.M. Ervin, and P.B. Armentrout. J. Chem. Phys. **106**, 4499 (1997).
19. K. Nakamoto. Infrared and Raman spectra of inorganic and coordination compounds part A: Theory and applications in inorganic chemistry. 5th ed. John Wiley and Sons, New York. 1997.
20. E. Steger, I.C. Ciurea, and S.A. Fadini. Spectrochim. Acta, **25**, 1649 (1969).

[3] C. Hao and L.S. Sunderlin. Unpublished results.

© 2005 NRC Canada

21. E. Steger, I.C. Ciurea, and S.A. Fadini. Z. Anorg. Allg. Chem. **350**, 225 (1967).
22. E.G. Robertson and D. McNaughton. J. Phys. Chem. A, **107**, 642 (2003).
23. (*a*) S.K. Loh, D.A. Hales, L. Lian, and P.B. Armentrout. J. Chem. Phys. **90**, 5466 (1989); (*b*) R.H. Schultz, K.C. Crellin, and P.B. Armentrout. J. Am. Chem. Soc. **113**, 8590 (1991).
24. M.J. Frisch, G.W. Trucks, H.B. Schlegel, G.E. Scuseria, M.A. Robb, J.R. Cheeseman, J.A. Montgomery, Jr., T. Vreven, K.N. Kudin, J.C. Burant, J.M. Millam, S.S. Iyengar, J. Tomasi, V. Barone, B. Mennucci, M. Cossi, G. Scalmani, N. Rega, G.A. Petersson, H. Nakatsuji, M. Hada, M. Ehara, K. Toyota, R. Fukuda, J. Hasegawa, M. Ishida, T. Nakajima, Y. Honda, O. Kitao, H. Nakai, M. Klene, X. Li, J.E. Knox, H.P. Hratchian, J.B. Cross, V. Bakken, C. Adamo, J. Jaramillo, R. Gomperts, R.E. Stratmann, O. Yazyev, A.J. Austin, R. Cammi, C. Pomelli, J.W. Ochterski, P.Y. Ayala, K. Morokuma, G.A. Voth, P. Salvador, J.J. Dannenberg, V.G. Zakrzewski, S. Dapprich, A.D. Daniels, M.C. Strain, O. Farkas, D.K. Malick, A.D. Rabuck, K. Raghavachari, J.B. Foresman, J.V. Ortiz, Q. Cui, A.G. Baboul, S. Clifford, J. Cioslowski, B.B. Stefanov, G. Liu, A. Liashenko, P. Piskorz, I. Komaromi, R.L. Martin, D.J. Fox, T. Keith, M.A. Al-Laham, C.Y. Peng, A. Nanayakkara, M. Challacombe, P.M.W. Gill, B. Johnson, W. Chen, M.W. Wong, C. Gonzalez, and J.A. Pople. Gaussian 03. Revision C.02 [computer program]. Gaussian, Inc., Wallingford, Conn. 2004.
25. (*a*) R. Krishnan, J.S. Binkley, R. Seeger, and J.A. Pople. J. Chem. Phys. **72**, 650 (1980); (*b*) T. Clark, J. Chandrasekhar, and P.v.R. Schleyer. J. Comput. Chem. **4**, 294 (1983).
26. (*a*) P.J. Hay and W.R. Wadt. J. Chem. Phys. **82**, 270 (1985); (*b*) W.R. Wadt and P.J. Hay. J. Chem. Phys. **82**, 284 (1985); (*c*) P.J. Hay and W.R. Wadt. J. Chem. Phys. **82**, 299 (1985).
27. C.E. Check, T.O. Faust, J.B. Bailey, B.J. Wright, T.M. Gilbert, and L.S. Sunderlin. J. Phys. Chem. A, **105**, 8111 (2001).
28. (*a*) T.H. Dunning, Jr. J. Chem. Phys. **90**, 1007 (1989); (*b*) R.A. Kendall, T.H. Dunning, Jr., and R.J. Harrison. Chem. Phys. **96**, 6796 (1992); (*c*) D.E. Woon and T.H. Dunning, Jr. J. Chem. Phys. **98**, 1358 (1993); (*d*) A.K. Wilson, D.E. Woon, K.A. Peterson, and T.H. Dunning, Jr. J. Chem. Phys. **110**, 7667 (1999).
29. (*a*) J.M.L. Martin and A. Sundermann. J. Chem. Phys. **114**, 3408 (2001); (*b*) A. Bergner, M. Dolg, W. Kuechle, H. Stoll, and H. Preuss. Mol. Phys. **80**, 1431 (1993).
30. (*a*) M. Head-Gordon, J.A. Pople, and M.J. Frisch. Chem. Phys. Lett. **153**, 503 (1988); (*b*) M.J. Frisch, M. Head-Gordon, and J.A. Pople. Chem. Phys. Lett. **166**, 275 (1990); (*c*) M.J. Frisch, M. Head-Gordon, and J.A. Pople. Chem. Phys. Lett. **166**, 281 (1990); (*d*) M. Head-Gordon and T. Head-Gordon. Chem. Phys. Lett. **220**, 122 (1994); (*e*) S. Saebo and J. Almlof. Chem. Phys. Lett. **154**, 83 (1989).
31. J.A. Pople, R. Krishnan, H.B. Schlegel, and J.S. Binkley. Int. J. Quantum Chem. **XIV**, 545 (1978).
32. J.A. Pople, M. Head-Gordon, and K. Raghavachari. J. Chem. Phys. **87**, 5968 (1987).
33. (*a*) J. Gauss and C. Cramer. Chem. Phys. Lett. **150**, 280 (1988); (*b*) E.A. Salter, G.W. Trucks, and R.J. Bartlett. J. Chem. Phys. **90**, 1752 (1989).
34. A.D. Becke. J. Chem. Phys. **98**, 5648 (1993).
35. J.W. Ochterski, G.A. Petersson, and J.A. Montgomery, Jr. J. Chem. Phys. **104**, 2598 (1996).
36. L.A. Curtiss, P.C. Redfern, K. Raghavachari, V. Rassolov, and J.A. Pople. J. Chem. Phys. **110**, 4703 (1999).
37. L.A. Curtiss, P.C. Redfern, K. Raghavachari, and J.A. Pople. J. Chem. Phys. **114**, 108 (2001).
38. (*a*) N. Aristov and P.B. Armentrout. J. Phys. Chem. **90**, 5135 (1986); (*b*) P.B. Armentrout. *In* Advances in gas phase ion chemistry. Vol.1. *Edited by* N.G. Adams and L.M. Babcock. JAI Press, Greenwich, Conn. 1992. p. 83.
39. I.H. Krouse and P.G. Wenthold. Inorg. Chem. **42**, 4293 (2003).
40. B.W. Walker, C.E. Check, K.C. Lobring, C.A. Pommerening, and L.S. Sunderlin. J. Am. Soc. Mass Spectrom. **13**, 469 (2002).
41. A.H. Clark and B. Beagley. Trans. Faraday Soc. **67**, 2216 (1971).
42. J.W. Larson and T.B. McMahon. J. Am. Chem. Soc. **109**, 6230 (1987).
43. G. Caldwell and P. Kebarle. J. Am. Chem. Soc. **106**, 967 (1984).
44. B.W. Walker and L.S. Sunderlin. Int. J. Mass Spectrom. **184**, 183 (1999).
45. K.C. Lobring, C.E. Check, and L.S. Sunderlin. Int. J. Mass Spectrom. **222**, 221 (2003).
46. T.E. Heil, C.E. Check, K.C. Lobring, and L.S. Sunderlin. J. Phys. Chem. A, **106**, 10043 (2002).
47. Y.V. Pervova, M.V. Korobov, and L.N. Sidorov. Russ. J. Phys. Chem. **66**, 1199 (1992).

© 2005 NRC Canada

TRIBUTE

Most of Paul Kebarle's research was due to his early venture into unique, near atmospheric pressure ionization conditions, with a mass spectrometer. He and his co-workers designed and home built this apparatus for studies of reactions in gas phase radiation chemistry. However, they soon discovered that the created conditions were also suited for other much more interesting work. Due to the slow diffusion of the ions to the walls of the ion source at these pressures, the ions had a lot of time to react with any trace gases that were also present in the ion source. The time was also long enough for many of the reactions to reach equilibrium. They soon realized that the determinations of ion–molecule reaction equilibria was of far greater importance than the initially planned studies in radiation chemistry.

Results from measurements of ion equilibria in solution, compiled in the form of acid–base dissociation constants, stability constants for ion–ligand complexes, and electrochemical oxidation–reduction potentials, represent the quantitative backbone of chemistry in solution. Also very notable is the use of equilibrium data in modern biochemistry, such as determinations of the stability constants of protein–Zn^{2+} ions in metalloenzymes such as carbonic anhydrase. The same type of fundamental reactions, proton transfer, ion–ligand association, ion–solvent molecule(s) association, and electron transfer, can occur also in the gas phase. Recognizing the great importance of such determinations, Paul and co-workers, in a series of papers starting in 1965, showed that the equilibria involving a variety of reactions can be determined reliably with the new mass spectrometer. For the first time, comparison of the gas-phase data with those for the same reactions in solution were possible and these showed, in most cases, similar trends. However, the free energy change ($\Delta G^0 = RT \ln K$), with change of substituent, was about 10 times larger in the gas phase than in solution (water). Quite often, there were also reversals of the order. Thus, in the gas phase, substituted acetic acids experienced a larger increase of acidities when Cl was the substituent rather than F, while the opposite is the case in solution. The reverse order observed in aqueous solution must be due to a solvent effect. These results showed that many of the properties that had been attributed in conventional texts to the reactant ions alone, were actually strongly dependent also on the solvent. The presence of specific solvent effects could be further examined by the determinations in the gas phase of the stepwise solvation of the ions involved. Thus, for A^- ions and water as solvent the equilibria:

$$A^- + H_2O = A(H_2O)^- \ (0,1)$$

$$A(H_2O)^- + H_2O = A(H_2O)_2^- \ (1,2)$$

$$A(H_2))_{n-1}^- + H_2O = A(H_2O)_n \ (n-1,n)$$

could be determined. Summation of the $\Delta G^0_{n-1,n}$ values leads then to the solvation energy, $\Delta G^0_{0,n}(A^-)$, and when n is large, the $\Delta G^0_{0,n}$ values for given ions can predict the total solvation energies of the ion in the given solvent.

The uniqueness and fundamental importance of the results based on gas-phase ion–molecule equilibria was immediately recognized by experimentalists, and particularly by the practitioners of ion cyclotron resonance (ICR) mass spectrometry who found that ICR also can provide equilibrium data for certain types of reactions. A number of theoretical chemists, such as M. Newton, E. Clementi, A. Pullman, B. Pullman, P. Kollman, G. Diercksen, L.C. Allen, P.v.R. Schleyer, P. Kollman, J. Pople, L. Radom, and others, who were involved in ab initio calculations, also found the new experimental gas-phase data of great interest. The gas-phase ion–molecule reactions provided the energy changes for closed shell even electron compounds and these were also best suited for the theoretical calculations. In the early 1970s, ab initio calculations used small basis sets. The gas-phase thermochemical data showed that much larger basis sets and electron correlation corrections had to be used to obtain agreement with the experiment. Early developers of Monte Carlo modeling of ion hydration, such as E. Clementi and co-workers, F.F. Abraham and M.R. Mruzick, and J. Jortner, also made use of the detailed stepwise ion hydration data to develop pair potential functions needed for the modeling of ion–solvent molecule assemblies.

Prominent workers in physical organic chemistry, such as E. Grunwald, F. Bordwell, E.M. Arnett, W. Doering, R.W. Taft, and G. Olah, also recognized the value of the data and became involved in interactions with the gas phase researchers or even switched to gas-phase determinations, such as R.W. Taft.

Physical and analytical chemists, such as K.S. Pitzer, I.M. Kolthoff, and G. Zundel, as well as electrochemists, such as B.E. Conway, J.O.M. Bockris, and Y. Marcus, began using and reporting the data in the specialized electrochemical literature.

The combined output of Kebarle's laboratory and others led to thermochemical data for gas phase ions and ion–molecule reactions involving many thousands of compounds. These data are now compiled by the US National Institute of Standards and Technology (NIST), in printed databases on gas-phase ion thermochemistry now also available on the Web. They are used in many areas of research.

Paul's research is remarkable because he and his co-workers not only developed the method and did the determinations, but also actively entered different areas to which the data could be applied and managed to solve outstanding, unresolved problems. Contributions were made to several areas: (*i*) ion chemistry in the D region of the ionosphere; (*ii*) the solvation of ions in different solvents; (*iii*) applications in physical organic and organic chemistry; (*iv*) binding energies of ion–ligand complexes. Multiply charged metal ions and particularly transition metal ions are difficult to produce in the gas phase. Kebarle and co-workers were the first to show that these ions are readily produced with electrospray and design an equilibrium chamber attached to a mass spectrometer with which the ion–ligand equilibrium constants could be determined; (*v*) applications to analytical mass spectrometry and particularly atmospheric chemical ionization (APIMS); and (*vi*) mechanisms and electrospray mass spectrometry.

Paul's contributions were recognized by the following awards: Fellow, New York Academy of Sciences (1965); Fellow of the Chemical Institute of Canada (1969); Fellow of the Royal Society of Canada (1978); Elected Member of the Sigma Xi Research Society (1980); Award for Excellence in Chemistry, Province of Alberta (1980); member of the Board of Directors of the American Society for Mass Spectrometry (1982–1984); University of Alberta McCalla Professor (1984); the Medal of the Canadian Institute of Chemistry (1986); the J. Gordin Kaplan Award for Excellence in Research, University of

© 2005 NRC Canada

Alberta (1989); first recipient of the Lossing Award of the Canadian Society of Mass Spectrometry (1994); the Frank H. Field and Joe L. Franklin Award for Outstanding Achievement in Mass Spectrometry, American Chemical Society (1994); and a Special Issue of the *International Journal of Mass Spectrometry and Ion Processes* with an Honor Biography, dedicated to Paul Kebarle (Vol. 109, 1 November 1991).

Paul has authored 165 publications in various chemistry journals and five invited chapters in books.

Paul was born in Bulgaria. He was to enter his father's business. However, the nationalization of business by the Communist regime at that time changed this. Paul managed to leave Bulgaria via Czechoslovakia and then managed to make it to the Eidgenössiche Technische Hochschule (ETH) in Zurich, Switzerland, where he obtained his undergraduate degree in chemistry in 1952. This was followed by a Ph.D. at the University of British Columbia (UBC) in Vancouver, British Columbia, where he also met his wife Beverly Harris. Post doctoral work with Fred Lossing at the National Research Council of Canada (NRC) in Ottawa (1956–1958), made Paul a real mass spectrometrist and led to his appointment at the University of Alberta where he has stayed ever since.

John S. Klassen

© 2005 NRC Canada

HOMMAGE

L'œuvre scientifique de Paul Kebarle est en grande partie le fruit d'une série d'essais réalisés tôt dans sa carrière avec un spectromètre de masse, dans des conditions uniques d'ionisation à pression quasi atmosphérique. C'est avec l'aide de ses collègues qu'il met au point le spectromètre conçu pour étudier des réactions en chimie sous rayonnement en phase gazeuse. Toutefois, ils découvrent rapidement que les conditions créées se prêtent également très bien à d'autres travaux beaucoup plus intéressants. En effet, sous de telles pressions, ils observent que la diffusion ralentie vers les parois de la source d'ions permet aux ions de réagir avec les gaz avoisinants. De plus, ils notent que la plupart des réactions avaient même le temps d'atteindre un état d'équilibre. Paul et ses collègues constatent rapidement que la détermination des équilibres des réactions ions–molécules est de plus grande importance que les études en chimie sous rayonnement prévues originalement.

Les résultats des mesures de l'équilibre ionique en phase aqueuse — compilés à partir des constantes de dissociation des acides et des bases, les constantes de stabilité pour les complexes ions–ligands et les potentiels électrochimiques d'oxydoréduction — constituent la base quantitative de la chimie en solution. Un fait aussi remarquable est l'utilisation des données d'équilibre dans la biochimie contemporaine, par exemple pour déterminer les constantes de stabilité de l'interaction protéines–ions Zn^{2+} dans les métalloenzymes, tels que l'anhydrase carbonique. Le même type de réactions fondamentales — transfert de protons, association ions–ligands, association ions–molécules de solvant et transfert d'électrons — peut également se produire en phase gazeuse. Reconnaissant la grande importance de telles déterminations, Paul et ses collègues montrent, à l'aide d'une série d'articles, dont le premier est publié en 1965, que l'équilibre qui met en jeu diverses réactions peut être déterminé, d'une manière fiable, avec le nouveau spectromètre de masse. Ils comparent ensuite les données en phase gazeuse avec celles en phase aqueuse pour une même réaction, une première dans ce domaine, et remarquent des tendances réactionnelles comparables dans la plupart des cas. Toutefois, ils observent aussi que le changement d'énergie libre ($\Delta G^0 = RT \ln K$), avec le changement de substituant, est environ dix fois plus important en phase gazeuse qu'en phase aqueuse et que, très souvent, il y a un renversement de l'ordre. Ainsi, en phase gazeuse, les acides acétiques substitués subissent une augmentation plus marquée de l'acidité lorsque le chlore est l'agent de substitution, plutôt que le fluor; le contraire est observé en solution. Or, l'ordre inversé observé en phase aqueuse doit nécessairement provenir de l'effet du solvant. Cette constatation leur permet de confirmer que de nombreuses propriétés traditionnellement attribuables uniquement aux ions participant à la réaction sont en réalité aussi fortement tributaires du solvant. De plus, les effets particuliers de certains solvants peuvent être examinés plus en détail par la détermination, en phase gazeuse, de la solvatation progressive des ions mis en jeu. Ainsi, pour les ions A^- et l'eau comme solvant, l'équilibre se caractérise de la façon suivante :

$$A^- + H_2O = A(H_2O)^- \ (0,1)$$

$$A(H_2O)^- + H_2O = A(H_2O)_2^- \ (1,2)$$

$$A(H_2))_{n-1}^- + H_2O = A(H_2O)_n \ (n-1,n)$$

La sommation des valeurs $\Delta G^0_{n-1,n}$ mène ensuite à l'énergie de solvatation, $\Delta G^0_{0,n}(A^-)$, et lorsque la valeur de n est élevée, les valeurs $\Delta G^0_{0,n}$ pour les ions en cause peuvent être utilisées pour calculer les énergies de solvatation totales d'un ion en présence d'un solvant donné.

Les expérimentalistes ont immédiatement reconnu l'importance distinctive et fondamentale des résultats tirés des équilibres ions–molécules en phase gazeuse. Plus particulièrement, les utilisateurs du spectromètre de masse à résonnance cyclotronique ionique (ICR) ont remarqué que l'ICR pouvait également fournir des données sur les équilibres pour certains types de réaction. Bon nombre de chimistes théoriciens, dont M. Newton, E. Clementi, A. Pullman, B. Pullman, P. Kollman, G. Diercksen, L.C. Allen, P.v.R. Schleyer, P. Kollman, J. Pople et L. Radom, qui ont participé aux calculs dès le début, ont également reconnu l'intérêt manifeste des nouvelles données expérimentales en phase gazeuse. Par ailleurs, les réactions ions–molécules en phase gazeuse ont fourni les changements d'énergie pour les composés à couches fermées d'électrons appariés et celles-ci convenaient également mieux aux calculs théoriques. Au début des années 1970, les calculs se faisaient à l'aide d'un nombre restreint d'ensembles de base. Les données thermochimiques en phase gazeuse ont démontré qu'un bien plus grand nombre d'ensembles de base et de corrections de corrélation des électrons devait être utilisé afin d'obtenir une bonne corrélation avec les résultats expérimentaux. Les pionniers de la méthode de Monte Carlo pour l'analyse de l'hydratation ionique, y compris E. Clementi et ses collègues, F.F. Abraham et M.R. Mruzick, et J. Jortner, ont aussi utilisé les données détaillées d'hydratation progressive des ions pour élaborer les fonctions du potentiel d'appariement nécessaires à la modélisation des assemblages ions–molécules de solvant.

D'éminents chercheurs du domaine de la chimie organique physique (p. ex. E. Grunwald, F. Bordwell, E.M. Arnett, W. Doering, R.W. Taft et G. Olah) ont attesté le mérite de ces données en collaborant avec des spécialistes de la recherche en phase gazeuse; certains, dont R.W. Taft, ont même réorienté leurs travaux de recherche vers la détermination en phase gazeuse.

Des chercheurs spécialisés en chimie physique et chimie analytique, tels que K.S. Pitzer, I.M. Kolthoff et G. Zundel, ainsi que des électrochimistes, tels que B.E. Conway, J.O.M. Bockris et Y. Marcus, se sont également intéressés à ces données en les utilisant dans leurs recherches et dans la littérature spécialisée du domaine de l'électrochimie.

Les travaux de recherche du laboratoire de Kebarle et ceux des autres spécialistes du domaine ont permis l'obtention de données thermochimiques sur des ions en phase gazeuse et des réactions ions–molécules pour plusieurs milliers de composés. Le National Institute of Standards and Technology des États-Unis (NIST) compile ces données sous la forme de bases de données en format imprimé sur la thermochimie des ions en phase gazeuse. Maintenant accessibles sur le Web, ces données sont utilisées dans de nombreux domaines de recherche.

La contribution de Paul est d'autant plus remarquable que ses collègues et lui ont non seulement mis au point la méthode et effectué les déterminations, mais aussi activement tiré parti des différents domaines capables d'exploiter et de gérer ces données afin de dénouer des problèmes de longue date jusque-là non résolus. Ses contributions se manifestent dans plusieurs domaines : (*i*) la chimie des ions dans la région

© 2005 NRC Canada

D de l'ionosphère; (*ii*) la solvatation des ions dans différents solvants; (*iii*) les applications dans le domaine de la chimie organique physique et de la chimie organique; (*iv*) les énergies de liaison des complexes ions-ligands (il est difficile de produire des ions métalliques multiples et plus particulièrement des ions de métaux de transition en phase gazeuse; Paul et ses collègues ont été les premiers à démontrer que ces ions sont facilement produits par électronébulisation, et ont mis au point une chambre d'équilibre fixée à un spectromètre de masse avec laquelle ils ont pu déterminer les constantes d'équilibres des complexes ions–ligands); (*v*) les applications dans le domaine de la spectrométrie analytique de masse, en particulier dans l'ionisation chimique à pression atmosphérique (APIMS); (*vi*) les mécanismes de la spectrométrie de masse avec électronébulisation.

De nombreuses distinctions lui ont été décernées pour ses diverses contributions : membre de la New York Academy of Sciences (1965); membre de l'Institut de chimie du Canada (1969); membre de la Société royale du Canada (1978); membre élu de la Sigma Xi Research Society (1980); prix d'excellence en chimie (Alberta) (1980); membre du conseil d'administration de l'American Society for Mass Spectrometry (1982–1984); McCalla Professor à l'Université de l'Alberta (1984); médaille de l'Institut de chimie du Canada (1986); prix J. Gordin Kaplan pour l'excellence en recherche, Université de l'Alberta (1989); premier lauréat du prix Lossing de la Société canadienne de spectrométrie de masse (1994); prix Frank H. Field and Joe L. Franklin pour réalisations exceptionnelles en spectrométrie de masse, American Chemical Society (1994). En outre, un numéro spécial de l'*International Journal of Mass Spectrometry and Ion Processes* a consacré une biographie honorifique à Paul Kebarle (vol. 109, le 1er novembre 1991).

Paul a rédigé 165 publications destinées à des revues du domaine de la chimie, ainsi que cinq chapitres pour des livres spécialisés.

Paul est né en Bulgarie. Alors qu'il est appelé à œuvrer au sein de l'entreprise de son père, la nationalisation de ce commerce par le régime communiste lui fait changer ses plans. Paul quitte la Bulgarie en passant par la Tchécoslovaquie pour se rendre à l'École polytechnique fédérale de Zurich (Suisse), où il reçoit le grade de premier cycle en chimie en 1952. Il obtient ensuite un doctorat de l'Université de la Colombie-Britannique (UBC) à Vancouver. C'est aussi là qu'il rencontre sa femme Beverly Harris. Il fait ensuite un stage postdoctoral sous la supervision de Fred Lossing du Conseil national de recherches du Canada (CNRC), à Ottawa (1956–1958), et devient véritable spécialiste en spectrométrie de masse, avant de décrocher un poste à l'Université de l'Alberta, poste qu'il occupe encore aujourd'hui.

John S. Klassen

© 2005 NRC Canada

Theoretical, thermal, and coordination chemistry of the amphoteric thiazate (NSO^-)[1] ion

D. Scott Bohle, Chen-Hsiung Hung, and Bryan D. Smith

Abstract: The isomers of thiazate (NSO^-) have a rich chemistry that is examined theoretically and experimentally for their thermal and coordination characteristics. The intramolecular isomerization of NSO^- to monothionitrite (ONS^-) is predicted (B3LYP/6-311+G*) to have a substantial barrier, greater than 418 kJ mol^{-1}. Thus, thiazates are expected to be relatively thermally stable towards isomerization, and DSC indicates that KNSO undergoes a two stage irreversible thermolytic decomposition only beginning at 132 °C with ΔH = –116.3 kJ mol^{-1}. As a ligand, the thiazate can adopt a range of geometries in response to the metal's oxidation state and ligand sphere. For example, in Ru(TTP)(NO)(NSO) the ligand has a markedly bent Ru-N-S geometry, and when contrasted with other structurally characterized thiazate coordination compounds, it is concluded that in addition to σ donation the thiazate binds to metals in an amphoteric manner because of either a forward or reverse OSN $\rightarrow$ M π donation similar to transition metal nitrosyl, amido, and imido complexes.

Key words: thiazate, isomerization, thermolysis, amphoteric ligand, coordination chemistry.

Résumé : Les isomères du thiazate (NSO^-) offrent une chimie riche qu'on a examinée d'un point de vue expérimental et théorique dans le but de déterminer leurs caractéristiques thermiques et de coordination. Selon des calculs théoriques (B3LYP/6-311+G*) l'isomérisation intramoléculaire du NSO^- en monothionitrite (ONS^-) doit présenter une barrière importante, supérieure à 418 kJ mol^{-1}. On s'attend donc à ce que les thiazates soient thermiquement relativement stables vis-à-vis l'isomérisation et la calorimétrie à balayage différentiel indique que le KNSO subit une décomposition thermolytique irréversible en deux étapes qui ne commence qu'à 132 °C, avec un ΔH = –116,3 kJ mol^{-1}. Comme ligand, le thiazate peut adopter une grande variété de géométries en réponse à l'état d'oxydation du métal et à la sphère du ligand. Par exemple, dans le Ru(TTP)(NO)(NSO), le ligand adopte une géométrie Ru-N-S très tendue et, quand on le met en opposition à d'autres composés de coordination du thiazate dont la structure a été caractérisée, on en conclut que, en plus d'une donation σ, le thiazate se lie aux métaux d'une façon amphotère qui est due une donation π OSN $\rightarrow$ M (ou l'inverse) semblable celle des complexes nitrosyles, amido et imido des métaux de transition.

Mots clés : thiazate, isomérisation, thermolyse, ligand amphotère, chimie de coordination.

[Traduit par la Rédaction]

The remarkably complex family of thiazyl anions, collectively described by the formula $[N_xS_yO_z]^{-n}$, include two comparatively simple isomeric species with $x = y = z = 1$, the thiazate anion (NSO^-) and monothionitrite (ONS^-). Although many alkyl derivatives RNSO (2–4) and RSNO (5) are known, discrete, well-characterized ionic solids of the parent anions have only recently been described (6, 7). There is now an emerging structural (7–9), coordination (10), and theoretical (11–14) basis for understanding the chemistry of these triatomic anions. In general, the chemistry of the thiazate anion is much more developed owing to the comparative ease of synthesis and thermal stability. Surprisingly, a convenient synthesis of potassium thiazate was only described in 1979 (6). Metathesis of the potassium for a range of other cations has led to a number of new salts with considerable solubility in organic solvents (8, 15).

What is still needed for the thiazate anion is a correlation of the various theoretical descriptions with the observed thermal reactivity and coordination chemistry. In this paper we describe: (1) the thermal chemistry of KNSO as characterized by DSC; (2) theoretical predictions for the ground-state structures, frequencies, and isomerization transition-state geometries with density functional and second-order Møller–Plesset levels of theory; and (3) a framework for understanding the coordination chemistry particularly in reference to Ru(TTP)(NO)(NSO). Some of these results have been briefly described before (10).

Received 20 June 2005. Published on the NRC Research Press Web site at http://canjchem.nrc.ca on 24 January 2006.

D.S. Bohle.[2] Department of Chemistry, McGill University, 801 Sherbrooke St. W., Montreal, QC H3A 2K6, Canada. **C.-H. Hung and B.D. Smith.** Department of Chemistry, University of Wyoming, Laramie, WY 82071-3838, USA.

[1]Other names for thiazate include thionylimide and sulfinylnitrilo. The IUPAC name for the NSO^- ion is nitridooxosulfate(2–) (1); however, in this report thiazate will be used exclusively.

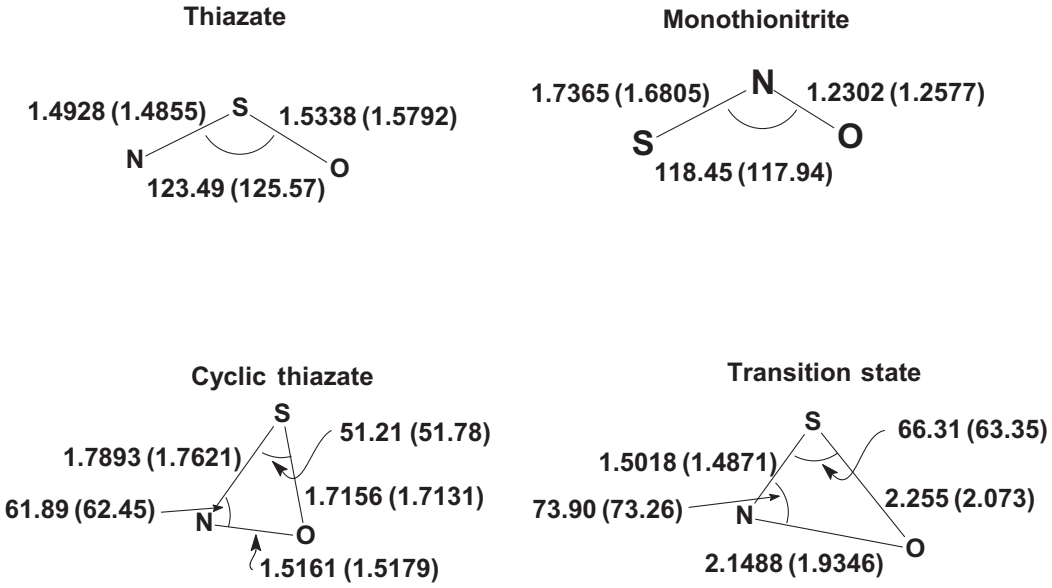
[2]Corresponding author (e-mail: Scott.Bohle@mcgill.ca).

Experimental

The general instrumental and synthetic methods have been described in a prior report (16). For the differential calorimetry studies described herein a TA-2010 DSC calibrated with indium metal and fitted with an nitrogen-purged sample

 doi: 10.1139/V05-191 © 2005 NRC Canada

Fig. 1. Optimized ground-state structures for thiazate, monothionitrite, and cyclic thiazate, as well as the transition-state structure for the thiazate monthionitrite isomerization. Bond lengths are given in angstroms and bond angles in degrees. The first value corresponds to the density functional result (B3LYP/6-311+G*), and the value in the brackets corresponds to the MP2/6-311+G* result.



chamber was used for the routine thermal analyses. Potassium thiazate (6) and Ru(TTP)(NO)Cl (10) were prepared by literature methods. All reactions and transformations were performed under an inert atmosphere.

The calculations described here were performed using GAUSSIAN 98 (17) implemented on a Silicon Graphics Iris Indigo workstation. Full optimizations were initially performed at the restricted Hartree–Fock (HF) level using the polarized split valence 6-31G* basis sets before the final optimizations with density functional theory using Becke's three-parameter functional (18) and triple split contracted basis sets (6-311+G*).

After determination of the ground-state geometries for the thiazate and monothionitrite isomers, the transition state for their conversion was determined using the synchronous transit-guided quasi-Newton algorithm developed by Peng and Schlegel (19). The optimized transition states were tested by stepping through the internal reaction coordinate to verify that the saddle separated the minima described by the isomeric structures.

Preparation of Ru(TTP)(NO)(NSO)

Ru(TTP)(NO)Cl (150 mg, 0.18 mmol) in 25 mL dry dichloromethane was treated with KNSO (80 mg, 0.8 mmol) at room temperature for 2 h. The solution was filtered and dried in vacuo. The resulting purple solid was recrystallized three times from dichloromethane–hexanes and dried in vacuo to afford **3** (144 mg, 92% yield) as a fine purple crystalline solid. UV–vis (in CH_2Cl_2, λ_{max}, nm) (log ε ((mol/L)$^{-1}$ cm^{-1})): 416 (5.40), 572 (3.96), 606 (sh). IR (KBr, cm^{-1}): ν(NO) 1829.3 (s), ν_{as}(NSO) 1255 (s), ν_s(NSO) 1075 (w), δ(NSO) 515 (w). ^{1}H NMR (22 °C, $CDCl_3$, ppm) δ: 8.90 (s, 8H, H_β), 8.07 (d, $^3J_{HH}$ = 7.7 Hz, 4H, H_m), 8.00 (d, $^3J_{HH}$ = 8.6 Hz, 4H, $H_{m'}$), 7.48 (t, $^3J_{HH}$ = 9.0 Hz, 8H, H_o, $H_{o'}$), 2.62 (s, 12H, *p*-CH_3). Elemental anal. calcd. for $C_{48}H_{36}N_6SO_2Ru$: C 66.88, H 4.21, N 9.75; found: C 66.70, H 4.49, N 9.50. The ^{1}H NMR and IR spectra were identical to the corresponding spectra of Ru(TTP)(NO)(NSO) prepared by treating Ru(TTP)(NS)Cl with $AgNO_2$ (10).

Results and discussion

Thermal analysis

A range of alkali metal thiazate salts have recently been prepared and structurally characterized by Mann and Jansen (9). These salts melt between 125 and 190 °C and reportedly decompose on further heating between 210 and 225 °C. We have reexamined this thermal behavior with differential scanning calorimetry to more exactly define the nature of these transformations and the nature of their reversibility. The first exothermic transition for potassium thiazate initiates at 132 °C and has exothermic maxima at 154 and 178 °C. These temperatures correspond well to the darkening first described by Armitage and Brand (6) at 135 °C and the suggested melting described by Mann and Jansen (9). However, the net transformation up to this temperature is irreversible and exothermic, both indicating decomposition rather than a phase transition. Further heating above 200 °C leads to the evolution of an unknown with an exothermic maximum at 262 °C. The integrated total exothermic release is ΔH = –1095.8(5) J g^{-1} or –116.3(3) kJ mol^{-1} for all processes between 132 and 278 °C. It has been reported that heating potassium thiazate leads to nitrogen evolution (9).

Ab initio calculations

To more fully understand both the thermal behavior of thiazates and their coordination chemistry we have reexamined the ground states of thiazate, monothionitrite, and a cyclic isomeric thiazate, as well as the transition state corresponding to isomerization by O-atom transfer from S to N. Prior studies have examined thiazate with a range of theoretical methods including CNDO/2 (12), MNDO (13), HF (13), HF/CPF (20), and MP2 (11). In addition, the gas-phase structures of thiazate salts of metals of the groups 1, 2, and

© 2005 NRC Canada

Table 1. Theoretically optimized and experimentally determined geometries for thiazate, monothionitrite, and the isomerization transition state.

Specific salt and (or) level of theory	N—S (Å)	S—O (Å)	N-S-O (°)	Ref.
Thiazate				
KNSO	(1.442(5))[a,b]		123.7(5)	9
RbNSO	(1.465(4))[a,b]		121.1(4)	9
$[NMe_4][NsO]$[b]	1.431(8)	1.438(7)	126.8(4)	8
η^2-LiNSO//MP2/6-31G*	1.489	1.532	115.6	14
η^2-NaNSO//MP2/6-31G*	1.487	1.524	118.6	14
η^2-HBeNSO//MP2/6-31G*	1.499	1.539	106.8	14
η^1-HBeNSO//MP2/6-31G*	1.509	1.472	120.1	14
η^1-HBeOSN//MP2/6-31G*	1.445	1.691	120.3	14
$[NSO^-]$//HF/double-ζ	1.587	1.430	111	13
$[NSO^-]$//HF/6-31+G*	1.4615	1.4885	122.4	4
$[NSO^-]$//MP2/6-31G*	1.459	1.484	123.0	11
$[NSO^-]$//MP2/6-31+G*	1.462	1.489	122.4	11
$[NSO^-]$//HF/CGTO[c]	1.467	1.495	121.4	20
$[NSO^-]$//HF/CGTO[d]	1.471	1.497	121.0	20
$[NSO^-]$//CPF/CGTO[e]	1.467	1.495	121.4	20
$[NSO^-]$//MP2/6-311+G*	1.486	1.579	125.57	This work
$[NSO^-]$//B3LYP/6-311+G*	1.493	1.534	123.49	This work
Specific salt and (or) level of theory	N—S (Å)	N—O (Å)	S-N-O (°)	Ref.
Monothionitrite				
[PNP][SNO][f]	1.695(4)	1.214(5)	120.5(3)	7
$[SNO^-]$//HF/double-ζ	1.587	1.208	120	13
$[SNO^-]$//MP2/6-31G*	1.715	1.195	118.0	11
$[SNO^-]$//MP2/6-31+G*	1.706	1.196	118.4	11
$[SNO^-]$//HF/CGTO[c]	1.706	1.194	118.8	20
$[SNO^-]$//HF/CGTO[d]	1.713	1.195	118.1	20
$[SNO^-]$//CPF/CGTO[e]	1.706	1.194	118.8	20
$[SNO^-]$//MP2/6-311+G*	1.681	1.258	117.94	This work
$[SNO^-]$//B3LYP/6-311+G*	1.737	1.230	118.45	This work
Specific salt and (or) level of theory	N—S (Å)	N—O (Å)	S—O (Å)	Ref.
Cyclic thiazate[g]				
cy-$[SNO^-]$//MP2/6-31G*	1.799	1.440	1.685	11
cy-$[SNO^-]$//MP2/6-31+G*	1.760	1.460	1.669	11
cy-$[SNO^-]$//MP2/6-311+G*	1.762	1.518	1.713	This work
cy-$[SNO^-]$//B3LYP/6-311+G*	1.789	1.516	1.716	This work
Transition state[g]				
sp-$[SNO^-]$//MP2/6-311+G*	1.487	1.935	2.073	This work
sp-$[SNO^-]$//B3LYP/6-311+G*	1.502	2.149	2.255	This work

[a]Powder diffraction structure.
[b]Probably N/O disorder. Value listed corresponds to either a mixture of N—S and O—S distances or best fit.
[c]Huzinaga primitive Gaussian-type orbitals.
[d]Huzinaga primitive Gaussian-type orbitals with *f* polarization functions.
[e]Huzinaga primitive Gaussian-type orbitals with *d* and *f* functions.
[f]$[PNP]^+$ is the bis(triphenylphosphino)imide cation.
[g]cy- is So's (11) designation for the cyclic NSO structure, while sp is the desigination for the saddle-point for the isomerization barrier.

13 derivatives have also been recently described (14). Prior attempts to examine thiazate to monothionitrite isomerization have only used an estimated structure for the transition state in one case (13), and a very constrained three-membered ring that corresponds to a local minimum and not a saddle point in the other (11).

To improve our understanding of these anions and their relative energetics we have recalculated all three ground-state structures and the transition energy surface with both MP2 and density functional theory with large triple-ζ quality basis sets. Optimized ground- and transition-state structures, corresponding to their gas-phase structures as isolated anions, are shown in Fig. 1. These results are contrasted in Table 1 with the relevant crystallographic data for these anions. For the thiazate anion all crystallographic determinations have been hampered by disorder of the nitrogen and oxygen. While this is clear and not readily resolvable for the structures of KNSO and RbNSO determined by powder diffrac-

© 2005 NRC Canada

Table 2. Absolute energies for the optimized geometries for the gas phase thiazate, monothionitrite, and the isomerization transition state.

	Energy (Hartrees)				ΔE (kJ mol^{-1})			
Theory/basis set	Thiazate	Monothionitrite	cy-NSO	sp-NSO	$E_{SNO^-} - E_{NSO^-}$	$E_{TS} - E_{NSO^-}$	$E_{cy} - E_{NSO^-}$	Ref.
MP2/6-31G*	–527.22747	–527.21306	–527.10139	—	37.8	—	331.0	11
MP2/6-31+G*	–527.26955	–527.24456	–527.13980	—	65.79	—	340.7	11
MP2/6-311+G*	–527.34597	–527.33150	–527.21565	–527.14487	37.99	519.2	342.2	This work
B3LYP/6-311+G*	–528.21666	–528.21503	–528.09635	–528.03650	4.31	473.0	315.9	This work
HF/double-ς					–351.6			13
HF/CGTO[a]					–15.40			20
HF/CGTO[b]					–19.79			20
CPF/CGTO[c]					69.91			20

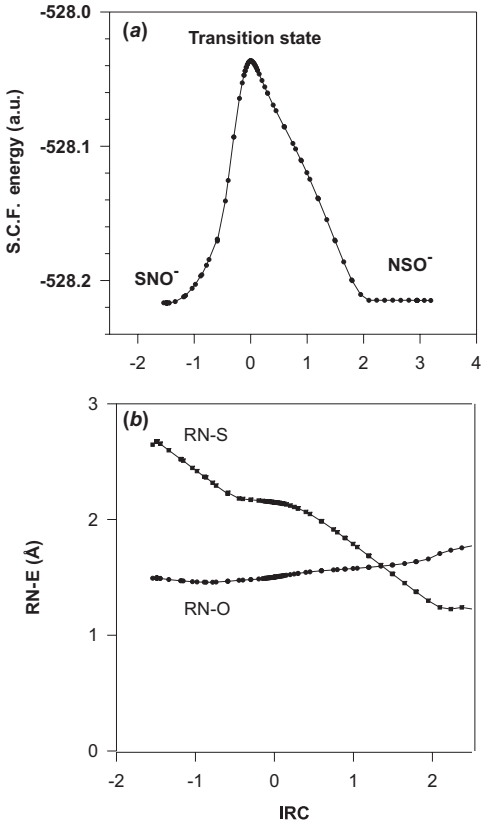
Note: cy refers to cyclic local minimum as reported by So (11); sp is the saddle point found in this paper.
[a]Huzinaga primitive Gaussian-type orbitals (GTOs).
[b]Huzinaga primitive GTOs with *f* polarization functions.
[c]Huzinaga primitive GTOs with *d* and *f* functions.

tion (9), the single crystal structure of tetramethylammonium thiazate also suffers from this, with the basis for assigning the oxygen and nitrogen atoms to the peaks found in the Fourier difference syntheses being the small differences in the two S—E (E = N and O) bond lengths. Nevertheless, in all of these studies the relatively large bond angle at the sulfur is not only reliably determined, it is much larger than most theoretically predicted angles. The optimized geometries, contrasted in Table 1 with prior theoretical reports, illustrate a number of trends: (1) for the anion, incorporation of diffuse and polarizable functions leads to lengthening of both bonds, and increases in the bond angle to values close to those experimentally observed; (2) inclusion of even approximate methods to account for configuration interaction leads to substantial alterations in optimized geometries; (3) coordination of *both ends of the thiazate* to a Lewis acid results in lengthening of both bonds and a decrease in the bond angle; and (4) coordination of HBe^+ to *either the N or the O of thiazate* leads to lengthening of the bond length of the element–sulfur bond, which is bound to the Lewis acid. A note of caution needs to be sounded about the calculations of the Lewis acid adducts of thiazate (14); the optimized gas-phase structures with η^2-NSO geometries do not correspond to what is found in the lattice of the potassium and rubidium salts (9). It has recently been shown that related nitrogen oxide anions exhibit Hartree–Fock instability and that an effective method to model this is with Becke's three-parameter hybrid functionals (21). The choice of basis set in our calculations stems from the well-known difficulty in calculations of anions with limited basis sets. In general the best models for these systems include polarization functions on all heavy atoms and preferably on the hydrogen atoms as well (22–24).

There is only one structurally characterized monothionitrite that we are aware of, and this corresponds to an ordered structure with a short N—O bond and relatively long N—S bond (7). Most theoretically calculated structures have significantly shorter N—O bonds and more compact bond angles. While our results with a 6-311+G* basis sets result in optimized geometries with longer N—O bonds, even this relatively large basis set returns an angle 2° less than the experimental value at both the MP2 and B3LYP levels of theory.

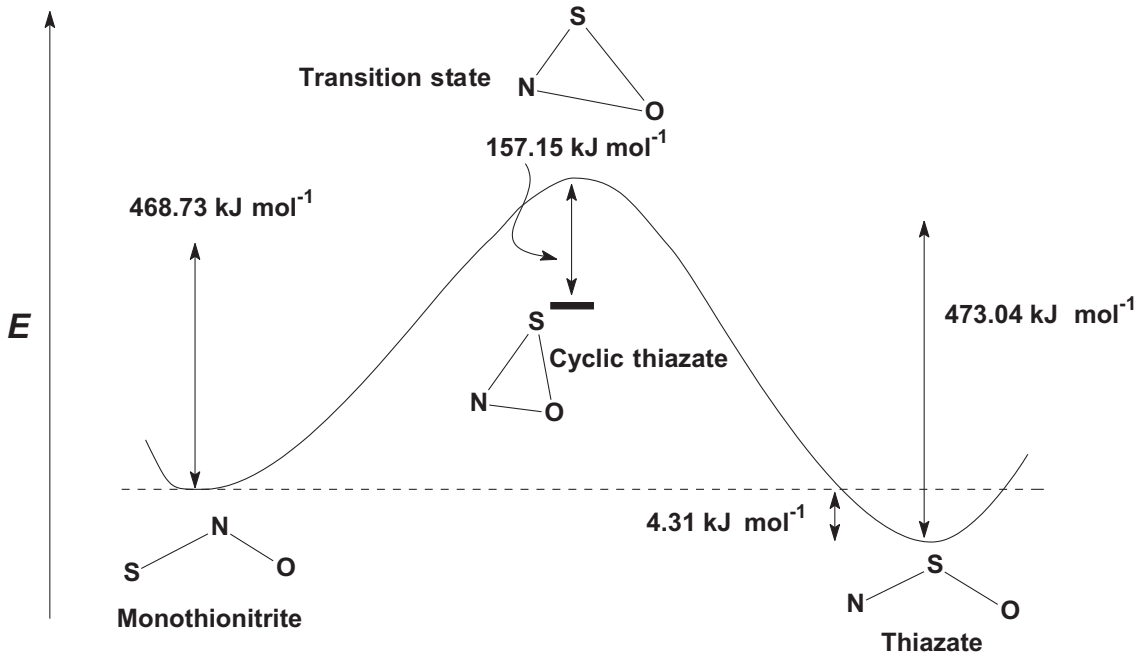
The absolute energies shown in Table 2 for all available optimized geometries reflects many of these same trends. At relatively low levels of theory the monothionitrite isomer is markedly more stable, but this is reversed for the CPF and MP2 levels of theory. Although the energy differences are basis set dependent, the B3LYP calculation gives a very small (4.31 kJ mol^{-1}) difference in gas-phase energies between NSO^- and SNO^-. The transition state connecting these two isomers has been located by finding the saddle point with a quasi-Newton synchronous transit algorithm (19). In Fig. 2, plots of energy vs. the internal reaction coordinate

Fig. 2. Internal reaction coordinate (IRC) diagrams for thiazate anion transformations (B3LYP/6-311+G*). (*a*) Shows the calculated energy as a function of the internal reaction coordinate. (*b*) Shows the variation of N—O and N—S separations as a function of IRC.



© 2005 NRC Canada

Fig. 3. Calculated energy relationships for the thiazate anions (B3LYP/6-311+G*).



(IRC) and key atomic separations are shown. These plots clearly demonstrate that stepping along the IRC leads to a smooth correlation of each isomer to the saddle point, and that for the isomerization of thiazate along this pathway the transition state retains strong N≡S bond character. Prior to N—S bond rupture or weakening, there is substantial S—O bond deformation and elongation. We have also found that a cyclic thiazate, first described by So (11), is also present near these structures. Its geometry (Fig. 1) corresponds to a local minimum in these calculations, and it is ca. 167.4 kJ mol^{-1} less than the transition state.

To visualize these relationships we have plotted a schematic view of their energies in Fig. 3. Although the cyclic thiazate is much lower in energy, it is not an intermediate in the $NSO^- \rightarrow SNO^-$ transformation, since the IRC profile in Fig. 2 never approaches this geometry. To verify this conclusion we have calculated the potential energy surface near the cyclic thiazate structure, and a contour plot of these results is shown in Fig. 4. The expansion shown in Fig. 4*b* for the region where the two potential energy wells for the SNO^- and cyclic thiazate anion intersect, demonstrates that there is a cusp between the two surfaces and that this region does not contain saddle points, which correlates cyclic thiazate with SNO^-. Similar results are also found for the region connecting the potential energy surfaces of the cyclic thiazate and the thiazate anions. Thus, there is an orbital crossover separating cyclic thiazate from the other isomers, and that its thermal formation is prohibited, most likely owing to the conservation of orbital symmetry. Although this is not a thermally allowed process, it may be achievable by photochemical methods or by bimolecular pathways.

Finally, we note that the theoretical and experimental frequencies for these anions, collected in Table 3, indicate the close match in experiment and theory presented here. Unfortunately, the values for the bands of [PNP][SNO] are obscured by the cation and were thus not reported (7). However, even though it is difficult to comment on the values for the SNO^- calculations, the extensive sets of results for the thiazate anion both illustrate the utility of B3LYP theory in these calculations and suggest that the values for the other thiazate isomers are probably close to these calculated values. Density functional theory also comes closest to the experimental vibrational frequencies for $[NMe_4][NSO]$, where MP2 is consistently 60 cm^{-1} too high. This case is especially diagnostic owing to the soft nature of the cation, which delocalizes cation–anion ionic bonding in the salt.

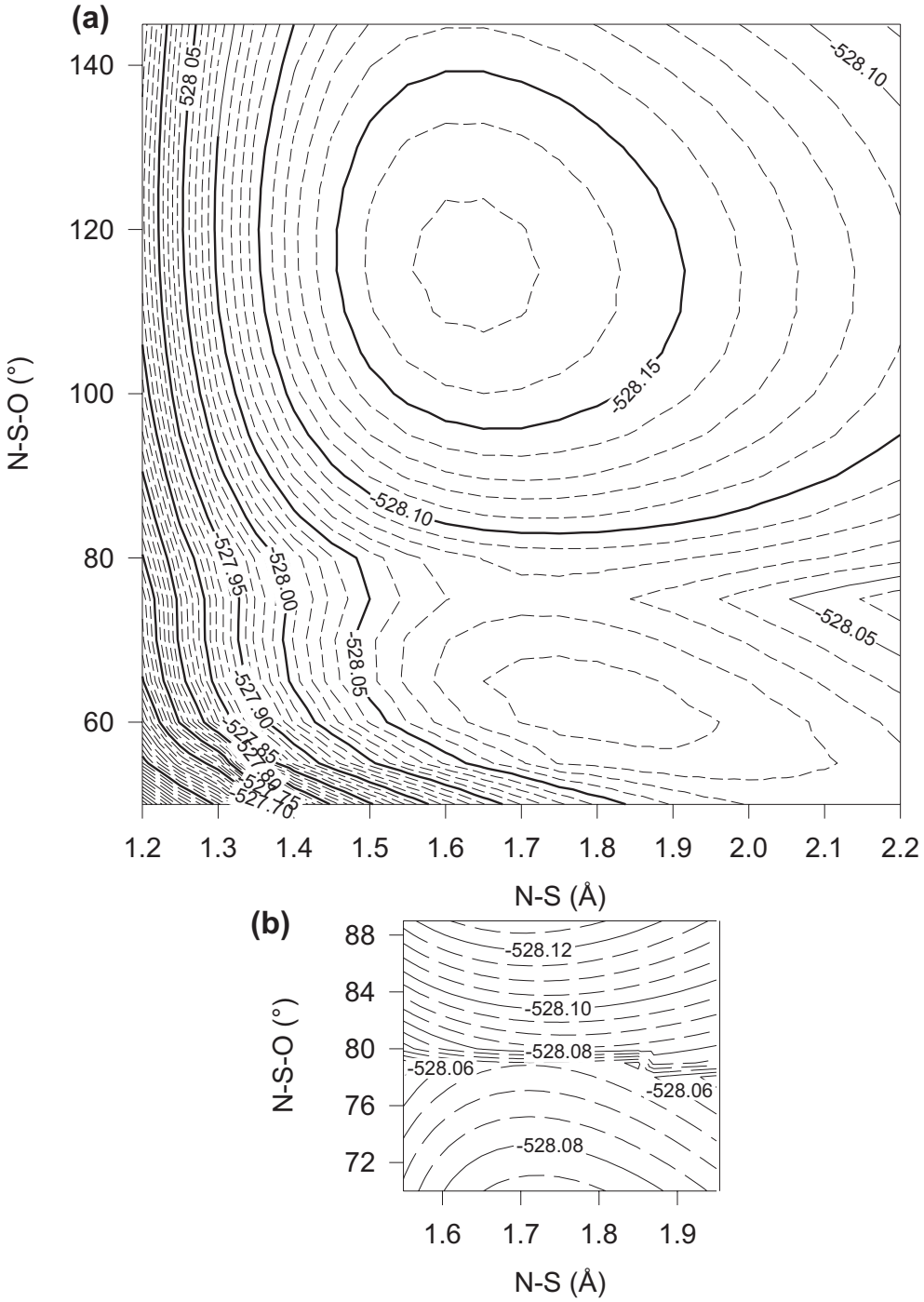
Thiazate coordination chemistry

Substituted thiazates (RNSO) are potent dieneophiles and react exothermically at low temperatures in a [4+2] fashion across the N=S bond (25). The organic, electronic, and spectroscopic properties of these species have been recently reviewed in detail (4), but little comment was made concerning their metal adducts, that is when R = transition metal. RSNO form strong π adducts with low valent transition metals, and this has been shown in the reactions of *p*-tolylNSO with d^8 and d^{10} centers to give η^2-arylthiazate complexes such as the structurally characterized $OsCl(NO)(\eta^2\text{-}p\text{-tolylNSO})(PPh_3)_2$ and $Ni(\eta^2\text{-}p\text{-tolylNSO})(PPh_3)(CN\text{-}t\text{-Bu})$, where the thiazates are bound through the N and the S (26, 27). However, when there are bulky ligands such as tris(isopropyl)phosphine in $Rh[\eta^1\text{-}(p\text{-tolylNSO})](CO)(P\text{-}i\text{-}Pr_3)_2$, then the RNSO ligand can also bind in an η^1 manner through the sulfur (28). Finally, thiazates with electron-donating substituents (R = AsR_2' and PR_2') have been shown to bind through the group 15 element to the transition metal (13, 15).

For the thiazate anion, however, only one coordination mode is known. This is the terminal N-bound ligand for which a range of complexes (Table 4) have been structurally characterized. The most frequently used method to prepare these complexes is by metathesis of a suitable metal-bound X group with a thiazate salt, often an alkali metal salt. Another variation on this approach is to couple the metathesis to an oxidative addition, for example, with the use of

© 2005 NRC Canada

Fig. 4. Contour plot for the potential energy surface near the cyclic thiazate region. Energies calculated with B3LYP/6-311+G* with an N—O bond length of 1.5161 Å, the N—O separation in the thiazate anion. Energies given in au (Hartrees) with the N—S separation in angstroms and the S-N-O angle in degrees. Plot (*a*) shows global surface with the minimum near N—S = 1.7 Å and S-N-O = 110°, corresponding to the monothionitrite anion and the minimum near near N—S = 1.8 Å and S-N-O = 65°, corresponding to cyclic thiazate. Plot (*b*) is an expanded detail of the cusp region where the two potential surfaces for each well cross to give a discontinuity.



$Hg(NSO)_2$. Here the other by-product is elemental mercury (30, 33). For late-transition-metal thionitrosyl complexes, there are two cases where O-atom transfer results in a thiazate complex. In the first example of a thiazate complex, when $IrCl_2(CO)(NS)(PPh_3)_2$ is treated with dioxygen the result is the thiazate complex $IrCl_2(NSO)(CO)(PPh_3)_2$ (34, 35). More recently we described the result of O-atom transfer from nitrite to thionitrosyl when Ru(TTP)(NS)Cl is treated with $AgNO_2$ (eq. [1]) (10). Finally, there is a report of O-atom transfer to an unspecified acceptor in the reaction of NSO_2^- to give the thiazate complex $Rh(CO)(NSO)(PPh_3)_2$ (31). However, it has subsequently been shown that the salt used in this reaction is most likely Cs[NSO] (36).

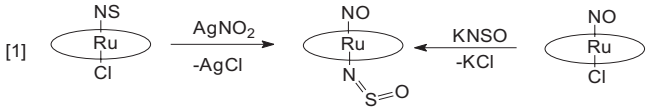
Our interest in this topic began with an effort to prepare a

© 2005 NRC Canada

Table 3. Theoretical and experimental vibrational frequencies for thiazate, monothionitrite, and cyclicthiazate.

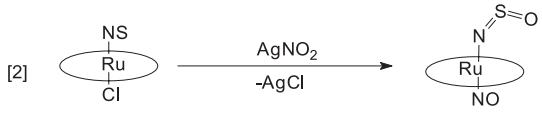
Specific salt and (or) level of theory	$\nu(NSO)_{asym}$ (cm^{-1})	$\nu(NSO)_{sym}$ (cm^{-1})	$\delta(NSO)$ (cm^{-1})	Ref.
Thiazate				
NaNSO	1283	999	528	9
KNSO	1276	994	519	9
RbNSO	1271	986	507	9
CsNSO	1272	992	511	9
$[NMe_4][NSO]^a$	1268	992	496	8
η^2-LiNSO//MP2/6-31G*	1274	1039	[b]	14
η^2-NaNSO//MP2/6-31G*	1286	1052	[b]	14
η^2-HBeNSO//MP2/6-31G**	1237	1062	[b]	14
η^2-HMgNSO//MP2/6-31G**	1249	1042	[b]	14
η^2-H_2AlNSO//MP2/6-31G**	1215	1056	[b]	14
$[NSO^-]$//MP2/6-31G*	1443	1139	574	11
$[NSO^-]$//MP2/6-311+G*	1322	1040	471	This work
$[NSO^-]$//B3LYP/6-311+G*	1250	945	473	This work
Specific salt and (or) level of theory	$\nu(SNO)_{asym}$ (cm^{-1})	$\nu(SNO)_{sym}$ (cm^{-1})	$\delta(SNO)$ (cm^{-1})	Ref.
Monothionitrite				
$[PNP][SNO]^b$	[c]	[c]	[c]	7
$[SNO^-]$//MP2/6-31G*	1765	811	547	11
$[SNO^-]$//MP2/6-311+G*	1321	827	531	This work
$[SNO^-]$//B3LYP/6-311+G*	1420	713	477	This work
Level of theory	ν_1 (cm^{-1})	ν_2 (cm^{-1})	ν_3 (cm^{-1})	Ref.
Cyclic thiazate[d]				
cy-$[SNO^-]$//MP2/6-31G*	1060	764	380	11
cy-$[SNO^-]$//MP2/6-311+G*	886	681	592	This work
cy-$[SNO^-]$//B3LYP/6-311+G*	873	667	492	This work

[a] $[PNP]^+$ is bis(triphenylphosphine)iminium cation.
[b] Mode mixed into ring mode with chelated metal.
[c] Not reported.
[d] cy- is So's (11) designation for the cyclic NSO structure.



diamagnetic d^6 Ru(II) porphyrin complex with a trans arrangement of nitrosyl and thionitrosyl ligands. These complexes would be isoelectronic with the known osmium octaethylporphyin dinitrosyl complexes, which have only been spectroscopically characterized (37, 38). Our synthetic approach was via O-atom transfer from an N-bound nitrite ligand is a well-known synthetic approach for the preparation of ferrous porphyrin complexes with bent nitrosyl ligands (39). However, attempts to prepare a putative Ru(TTP)-(NS)(NO_2) complex as an intermediate, which would then be trapped out with excess nitrite or trimethylphosphine, resulted only in the formation of Ru(TTP)-(NO)(NSO), typically in yields greater than 60%. This complex can also be prepared by the direct metathesis of Ru(TTP)(NO)Cl with KNSO, as described in the Experimental section.

Prior to its complete identification by convergent syntheses and X-ray crystallography, we also prepared a series of ^{15}N-substituted derivatives by both (2) treating Ru(TTP)-(^{15}NS)Cl with $Ag^{14}NO_2$ (eq. [2]) and Ru(TTP)(^{14}NS)(Cl) with $^{15}NO_2^-$ (eq. [3]). IR spectra of the resulting products, summarized in Table 5, indicate that ^{14}N/^{15}N isotopic substitution in the nitrosyl ligand leads to a shift of 36.5 cm^{-1}, which is extremely close to that predicted from a simple Hook's law calculation of 37.8 cm^{-1}. However, incorporation of ^{15}N into the thionitrosyl, prepared from $^{15}NH_4Cl$ and $^{15}N_3S_3Cl_3$, lead to an isotopic shift of only 22.6 cm^{-1} in the product, significantly less than the shift expected for a thionitrosyl ligand of 30.1 cm^{-1}. For example, ^{15}N/^{14}N isotopic exchange in the thionitrosyl ligand in Ru(TTP)(NS)Cl leads to a shift of 36 cm^{-1}, which is in closer agreement with the result predicted by a simple harmonic oscillator model. The observed shifts in Table 5 are in accord with those predicted from the ab initio calculations for the thiazate. That is, while $[NMe_4][^{14}NSO]$ has bands at 1268, 992, and 496 cm^{-1} (8), the force constants calculated at the B3LYP/6-311+G* level predict that in $^{15}NSO^-$ the bands will be at 1224.0, 941.6, and 466.9 cm^{-1}, and will thus shift by 25.7, 3.3, and 6.1 cm^{-1}, respectively, for the three bands. These isotopic shifts fit very well with the observed shifts in for Ru(TTP)(NO)(^{15}NSO) (Table 5).



Unambiguous identification of the ligand sphere in Ru(TTP)(NO)(NSO) came from a single crystal X-ray diffraction structure (10). The well-ordered structure has a lin-

© 2005 NRC Canada

Table 4. Structural and vibrational data for selected thiazate complexes.

Complex	M—N (Å)	N—S (Å)	S—O (Å)	M-N-S (°)	N-S-O (°)	τ M-N-S-O (°)	$\nu(NSO)_a$ (cm^{-1})	$\nu(NSO)_s$ (cm^{-1})	δ(NSO) (cm^{-1})	Ref.
$(Cp)_2Ti(NSO)_2$	2.010(4)	1.483(4)	1.450(6)	150.8(3)	119.1(3)	2.2	1235	1075	525	29
(Cp)(CpMe)Zr $(NSO)_2$	2.121(4)	1.469(4)	1.435(4)	159.8(2)	120.0(2)	16.0				30
Ru(TTP)(NO)(NSO)	2.021(4)	1.467(4)	1.460(5)	140.9(3)	122.8(3)	–6.3	1235s	1075s	515w	This work
$Rh(CO)(NSO)(PPh_3)_2$[a]	1.989(9)	1.480(12)	1.509(10)	135.1(8)	122.5(5)	4.8	1240	1040	580	31
cis-$Pt(NSO)_2(PMe_3)_2$[b]	2.049(10)	1.465(14)	1.442(18)	132.6(8)	121.4(8)	–4.4	1245s	1061m	567w	32
	2.049(11)	1.492(13)	1.456(19)	129.5(1)	123.3(8)		1230vs	1047vs		
cis-$Pt(NSO)_2(PPh_3)_2$							1243vs	1092m	547w	32
							1228s	1062m		
trans-$Pt(NSO)_2(PPh_3)_2$	1.994(6)	1.472(7)	1.455(8)	133.3(3)	120.7(5)	–0.8	1218	1099	590	33
$[NMe_4][NSO]$[c]	—	1.431(8)	1.438(7)	—	126.8(4)		1268	992	496	34
NSO^-[d]	—	1.493	1.534	—	123.49		1250	945	473	This work

[a]NSO/CO disorder.
[b]Two rows correspond to the two ligands.
[c]Some O/S disorder.
[d]Theory (B3LYP/6-311+G*).

ear nitrosyl (Ru-N-O = 170.3(4)°), which is trans to an N-bound thiazate ligand, which in turns adopts a cis–cis geometry and is bent towards a meso carbon. The porphyrin exhibits a very slight S_4 ruffling with the mean average displacement from the best fit plane for the 24 ring atoms being 0.0401 Å. The ruthenium is displaced 0.12 Å out of the plane toward the nitrosyl ligand. Most of these structural features are shared by other Ru(TTP)(NO)X complexes (16).

The contrast of the thiazate geometry in Ru(TTP)-(NO)(NSO) with other thiazate complexes and the anion (Table 4) is striking. Upon binding to a transition metal there is a very modest lengthening of the N—S and S—O bonds, although the combination of the inherently large esds for these atoms with the disorder problem described previously for the reference structures, limits further interpretation of these data. However, the contrast with the theoretical results indicates that sharp changes occur in thiazate geometry upon binding to a metal. Not only is there a severe contraction in the N—S and S—O bonds, there is a marked decrease in the N-S-O angle. This latter trend is also seen in the contrast of the experimental data. Coordination to a metal leads to a slight decrease in the $\nu(NSO)_{asym}$ and increases in $\nu(NSO)_{sym}$ and δ(NSO). The asymmetric and symmetric stretching modes are dominated by the N—S and S—O bond stretches, respectively, and this suggests population of an orbital that is antibonding with respect to N—S and bonding with respect to S—O. This point will be discussed later in this paper.

The contrasts in the metric parameters in Table 4 for the complexes themselves are also revealing. Clearly the most sensitive parameter is the angle at the nitrogen (M-N-S), where the observed range is 160°–130°. Inspection suggests that there is a rough correlation of the angle with the relative electron densities at the metal; earlier transition metals bind thiazate in a more linear fashion, while the later transition metals bind it in a slightly more bent configuration. However, there is also a dependence on the trans ligand, which is exemplified by the platinum PMe_3 results where the thiazates are cis to one another but trans to a strong phosphine donor; here the thiazates are more strongly bent than in the related PPh_3 complex where the two thiazates are trans to one another and less bent. In the structurally characterized ruthenium and rhodium examples in Table 4, the thiazates are trans to strong π-accepting ligands.

In general the geometry the thiazate adopts appears to be responsive to the metal's environment, and thus NSO^- is in a small class of ligands such as NO, N_2R, and PR_2. These amphoteric ligands have geometries that respond to the metal's electronic structure in distinct ways (40). For thiazate the data base is too small to draw conclusive trends from the emerging data; however, the theoretical results previously presented allow us to pose a theoretical framework for the origin of these trends.

The best way to understand the electronic structure of the thiazate is to consider the frontier molecular orbitals (Fig. 5). The C_s geometry of the thiazate anion results in

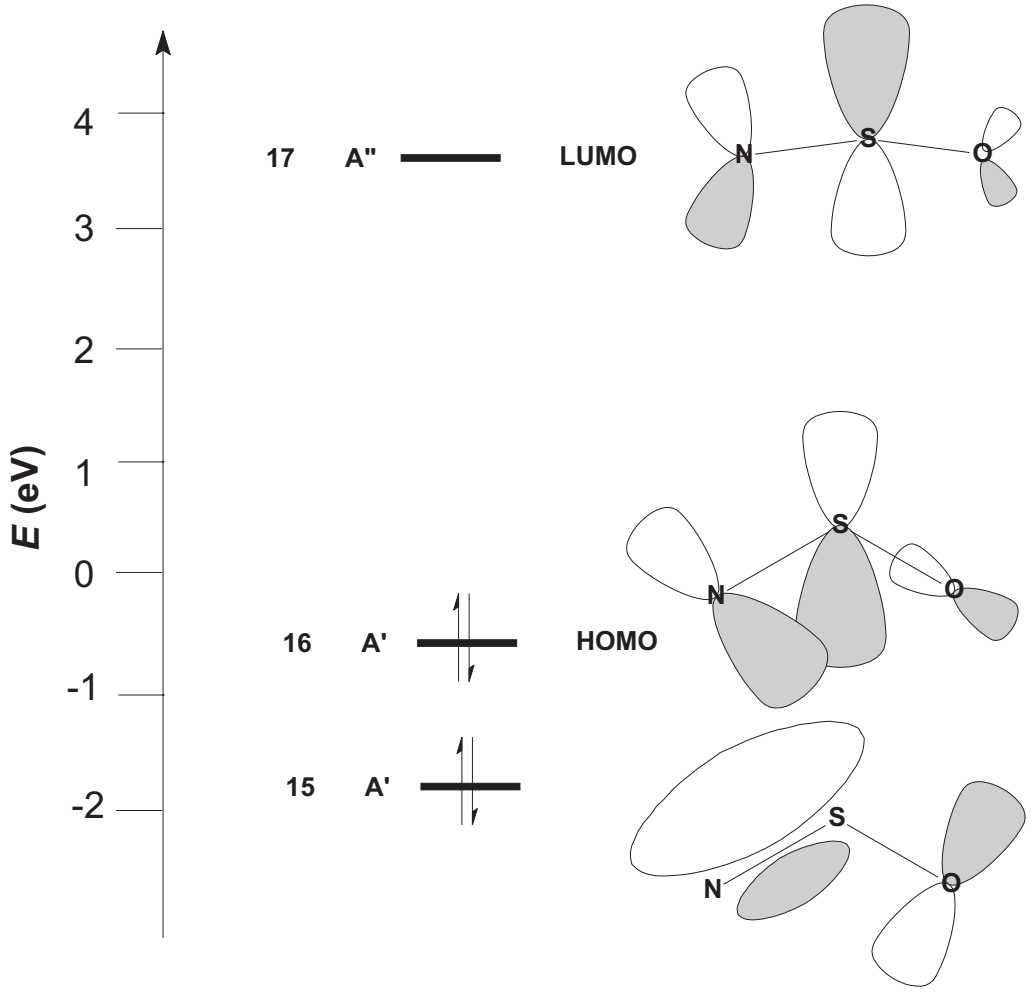
© 2005 NRC Canada

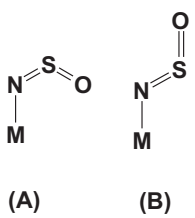
Table 5. Experimental and theoretical isotopic shifts for NO, NS, and NSO complexes.

Compound Ru(TTP)(L)(L′)		Experimental		Theory	
L	L′	Band (assignment)	ν(^{14}NX){^{15}N shift} (cm^{-1})	Calculated harmonic oscillator shift (cm^{-1})	Ab initio (B3LYP/6-311+G*)[a]
NO	Cl	ν(NO)	1845{37.1}[b]	33.1	2491.72{44.7}
			1830{35.2}[b]	32.8	2491.72{44.7}
NS	Cl	ν(NS)	1271{36}	30.1	1504.77{35.4}
NO	NSO	ν(NO)	1829.2{36.5}	32.8	2491.72{44.7}
		$\nu(NSO)_a$	1255{22.6}	—	1249.7{25.7}
		$\nu(NSO)_s$	1075{2}	—	944.9{3.3}
		δ(NSO)	515{6}	—	473.0{6.1}

[a]For the NO^+, NS^+, and NSO^- ions.
[b]Solid state splitting giving rise to two bands in the KBr pellet.

Fig. 5. Frontier molecular orbitals for the free thiazate anion.





(A) (B)

orbitals with either A′ (in plane) or A′′ (out of plane) symmetry. The A′ set are a mixture of nonbonding lone pairs, σ bonding, and π_x bonding from NS^- and O. This can be readily seen in the HOMO shown in Fig. 5; orbital 16 is a mix of predominantly p_xN, nS, and a minor amount of S—O antibonding. The largest lobe for this orbital is on the bent side of the anion, so the σ bonding to the transition metal will clearly favor the geometry **A** where the anion bends towards the metal and has a M-N-S-O torsion angle of 0°,

© 2005 NRC Canada

rather than the trans arrangement with a M-N-S-O torsion angle of 180°, shown in **B**. For the η^1-RNSO species this orbital is most likely responsible for the strong σ bonding leading to the η^1-S(O)(=NR) geometry (28). Orbital 15 with A′ symmetry is slightly lower in energy. This orbital has a substantial p_xN contribution, and its proximity in energy and extent suggests that it may engage in forward π donation to the metal. This is most likely an important factor in the observed trends in M-N-S angles (Table 4), especially for the electron-deficient metals, cf. the M(IV) d^0 examples where empty metal-based dπ orbitals with the correct symmetry can accept electrons from orbitals 16 and 15 of the thiazate. A strong interaction here will tend to linearize the M-N-S angle. Forward π donation will decrease bonding electron density between the nitrogen and the sulfur, while at the same time decreasing the occupation of orbitals antibonding with respect to the S—O bond.

The thiazate ligand is also a potential π-acceptor ligand if there is substantial overlap between filled dπ metal orbitals and the A″ LUMO. In this case any electron donation into this orbital will be both antibonding with respect to both the N—S and S—O bonds. Occupation of this orbital will lead to an increase in the electron density at the sulfur and nitrogen, and results in a decrease of both the O-S-N and S-N-M bond angles.

Conclusion

This paper establishes the structural and electronic basis for the amphoteric character of the thiazate ligand. Surprisingly, although organothiazates are potent dienophiles, there are no reports describing this reaction for a coordinated thiazate. One prediction based on the electronic structural model developed in this report is that those metal centers that have more linear M-N-S thiazate ligands are expected to promote dienophile addition through lowering of the energy of the NSO^- HOMO in a manner similar to electron-withdrawing organic substitutents. Thus, early transition-metal thiazate complexes may be synthons for a range of other new nitrogen–sulfur containing ligands prepared in situ. Alternatively, thiazate complexes of more electron-rich centers, such as those found for the already characterized later transition metals, may attenuate this same dieneophile reactivity or it may lead to unusual examples of inverse electron demand from the diene/thiazate cycloaddition. In either case, there clearly are a range of new horizons for thiazate complexes, and we note that very little is known about their coordination sphere reactivity.

Acknowledgements

We gratefully acknowledge the Natural Sciences and Engineering Research Council of Canada (NSERC) for support in form of a Discovery Grant and the Air Force Office of Scientific Research, Grants F49620-96-1-0417 and 98-1-0461, for their financial support of this research.

References

1. G.J. Leigh. Nomenclature of inorganic chemistry. Blackwell Scientific Publications, Oxford. 1990.
2. C. Bottinger. Chem Ber. **11**, 1407 (1878).
3. R. Bussas, G. Kresze, H. Munsterer, and A. Schwobel. Sulfur Rep. **2**, 215 (1983).
4. R.M. Romano and C.O. Della Vedova. J. Mol. Struct. **522**, 1 (2000).
5. (*a*) S.S.K. Oae. Org. Prep. Proced. Int. **15,** 165 (1983); (*b*) N. Arulsamy, D.S. Bohle, J.A. Butt, P.A. Jordan, and E.S. Sagan. J. Am. Chem. Soc. **121**, 7115 (1999).
6. D.A. Armitage and J.C. Brand. J. Chem. Soc. Chem. Commun. 1078 (1979).
7. F. Seel, R. Kuhn, G. Simon, M. Wagner, B. Krebs, and M.Z. Dartmann. Z. Naturforsch. B, **40B**, 1607 (1985).
8. S. Mann and M. Jansen. Z. Naturforsch. B, **49B**, 1503 (1994).
9. S. Mann and M. Jansen. Z. Anorg. Allg. Chem. **621**, 153 (1995).
10. D.S. Bohle, C.-H. Hung, A.K. Powell, B.D. Smith, and S. Wocadlo. Inorg. Chem. **36**, 1992 (1997).
11. S.P. So. Inorg. Chem. **28**, 2888 (1989).
12. K.K. Pandey and D. Birdi. Indian J. Pure Appl. Phys. **28**, 435 (1990).
13. T. Chivers, A.B.F. Dasilva, O. Treu, and M. Trsic. J. Mol. Struct. **162**, 351 (1987).
14. T. Pasinszki, T. Veszpremi, and M. Feher. Chem. Phys. Lett. **250**, 466 (1996).
15. (*a*) T. Chivers, K.S. Dhathathreyan, C. Lensink, and J.F.C. Richardson. Inorg. Chem. **27**, 1570 (1988); (*b*) W. Heilemann and R. Mews. Chem. Ber. **121**, 461 (1988).
16. D.S. Bohle, C.-H. Hung, and B.D. Smith. Inorg. Chem. **37**, 5798 (1998).
17. M.J. Frisch, G.W. Trucks, H.B. Schlegel, G.E. Scuseria, M.A. Robb, J.R. Cheeseman, V.G. Zakrzewski, J.A. Montgomery, R.E. Stratmann, J.C. Burant, S. Dapprich, J.M. Millam, A.D. Daniels, K.N. Kudin, M.C. Strain, O. Farkas, J. Tomasi, V. Barone, M. Cossi, R. Cammi, B. Mennucci, C. Pomelli, C. Adamo, S. Clifford, J. Ochterski, J.A. Petersson, P.Y. Ayala, Q. Cui, K. Morokuma, D.K. Malick, A.D. Rabuck, K. Raghavachari, J.B. Foresman, J. Cioslowski, J.V. Ortiz, B.B. Stefanov, G. Liu, A. Liashenko, P. Piskorz, I. Kamaromi, R. Gomperts, R.L. Martin, D.J. Fox, T. Keith, M.A. Al-Laham, C.Y. Peng, A. Nanayakkara, C. Gonzalez, M. Challacombe, P.M.W. Gill, B.G. Johnson, W. Chen, M.W. Wong, J.L. Andres, M. Head-Gordon, E.S. Replogle, and J.A. Pople. GAUSSIAN 98 [computer program]. Gaussian, Inc., Pittsburgh, Penn. 1998.
18. A.D. Becke. J. Chem. Phys. **98**, 5648 (1993)
19. D. Peng and H.B. Schlegel. Israel J. Chem. **33**, 449 (1993).
20. C. Ehrhardt and R Ahlrichs. Chem. Phys. **108**, 417(1986).
21. H.-H. Tsai, T.P. Hamilton, J.-H.M. Tsai, J.G. Harrison, and J.S. Beckman. J. Phys. Chem. **100**, 6942 (1996).
22. M.J. Frisch, J.A. Pople, and J.S. Binkley. J. Chem. Phys. **80**, 3265 (1984).
23. R. Krishnan, J.S. Binkley, R. Seeger, and J.A. Pople. J. Chem. Phys. **72**, 650 (1980).
24. T. Clark, J. Chandrasekhar, G.W. Spitznagel, and P.v.R. Schleyer. J. Comput. Chem. **4**, 294 (1983).
25. D.L. Boger and S.M. Weinreb. Hetero Diels–Alder methodology in organic synthesis. Vol. 47. Academic Press, San Diego. 1987.
26. A.F. Hill, G.R. Clark, C.E.F. Rickard, W.R. Roper, and M. Heberhold. J. Organomet. Chem. **401**, 357 (1991).
27. D. Wilhelm, E. Wenschuh, U. Baumeister, and H. Hartung. Z. Anorg. Allg. Chem. **620**, 2114 (1994).
28. K. Vrieze and G.v. Koten. Recl. Trav. Chim. Pays–Bas, **99**, 145 (1980).

© 2005 NRC Canada

29. M. Herberhold, F. Neumann, G. Sussfink, and U. Thewalt. Inorg. Chem. **26**, 3612 (1987).
30. H. Plenio, H.W. Roesky, F.T. Edelmann, and M. Noltemeyer. J. Chem. Soc. Dalton Trans. 1815 (1989).
31. H.W. Roesky, K.K. Panday, B. Krebs, and M. Dartmann. J. Chem. Soc. Dalton Trans. 2271 (1984).
32. I.P. Parkin, A.M.Z. Slawin, D.J. Williams, and J.D. Woollins. Polyhedron, **8**, 835 (1989).
33. R. Short, M.B. Hursthouse, T.G. Purcell, and J.D. Woollins. J. Chem. Soc. Chem. Commun. 407 (1987).
34. K.K. Pandey and U.C. Agarwala. Indian J. Chem. Sect. A, **20**, 906 (1981).
35. K.C. Jain, K.K. Pandey, and U.C. Agarwala. Indian J. Chem. Sect. A, **20**, 1022 (1981).
36. T. Chivers, K.J. Schmidt, D.D. McIntyre, and H.J. Vogel. Can. J. Chem. **67**, 1788 (1989).
37. A. Antipas, J.W. Buchler, M. Gouterman, and P.D. Smith. J. Am. Chem. Soc. **100**, 3015 (1978).
38. J.W. Buchler and P.D. Smith. Chem. Ber. **109**, 1465 (1976).
39. W.R. Scheidt and M.K. Ellison. Acc. Chem. Res. **32**, 350 (1999).
40. J.P. Collman, L.S. Hegedus, J.R. Norton, and R.G. Finke. Principles and applications of organotransition metal chemistry. University Science Books, Mill Valley, Calif. 1987.

© 2005 NRC Canada

Thermodynamics of electrolytes in mixed solvent media — Application of the Pitzer ion interaction approach

Bijan Das

Abstract: Although for a long time considerable attention has been paid to the application of the Pitzer ion interaction approach to describe the thermodynamic properties of a variety of aqueous electrolyte solutions, such studies in mixed solvent media are still scarce. The present paper discusses the application of the Pitzer ion interaction approach in the case of electrolyte solutions in mixed solvent media. In particular, a comprehensive equation for the thermodynamic properties of hydrochloric acid in dioxane–water mixtures within the temperature range 273.15 to 323.15 K has been generated in the ion interaction (Pitzer) equation form on the basis of electrochemical cell measurements of the hydrochloric acid available in the literature. It was necessary to set varying values of the exponential coefficients α_1 and α_2 of the standard Pitzer model in different mixed solvent media to achieve a satisfactory fit. The present model quantitatively reproduces the experimental cell electromotive forces over the entire concentration and temperature range used for the experiments. The Pitzer ion interaction approach is, thus, proved to be a very valuable method for the correlation and prediction of thermodynamic properties of electrolytes in mixed solvent media. The implications of the Pitzer ion interaction parameters ($\beta^{(0)}$, $\beta^{(1)}$ $\beta^{(2)}$, and C^{ϕ}) have also been discussed in terms of interionic forces. The present study also stresses the need for additional emf measurements to help interpolation through the dioxane composition.

Key words: Pitzer's equations, Pitzer ion interaction parameter, activity coefficients, emf, hydrochloric acid.

Résumé : Même si l'approche de l'interaction ionique de Pitzer a reçu beaucoup d'attention, depuis longtemps, pour décrire les propriétés thermodynamiques de diverses solutions d'électrolytes aqueux, il existe peu d'études semblables dans des solvants mixtes. Dans ce travail, on discute de l'application de l'interaction ionique de Pitzer dans le cas de solutions d'électrolytes dans des solvants mixtes. En particulier, en se basant sur des mesures de cellules électrochimiques de l'acide chlorhydrique disponibles dans la littérature, on a développé une équation générale de la forme de celle de l'interaction ionique de Pitzer pour décrire les propriétés thermodynamiques de l'acide chlorhydrique dans des mélanges d'eau et de dioxane, à des températures allant de 273,15 à 323,15 K. Afin d'obtenir de bonnes corrélations dans divers milieux de solvants mixtes, il a été nécessaire d'attribué des valeurs diverses aux coefficients exponentiels α_1 et α_2 du modèle standard de Pitzer. Le présent modèle reproduit quantitativement les valeurs expérimentales de forces électromotrices de cellules pour la plage entière de concentrations et de températures utilizées dans cette étude. On a donc démontré que l'approche d'interaction ionique de Pitzer peut être très utile pour établir des corrélations et pour prédire les propriétés thermodynamiques d'électrolytes dans divers solvants mixtes. En se basant sur les forces interioniques, on discute aussi des implications des paramètres d'interactions ioniques de Pitzer $\beta^{(0)}$, $\beta^{(1)}$, $\beta^{(2)}$ et $C^{(\phi)}$. La présente étude met aussi en relief l'importance de pouvoir disposer de mesures additionnelles de f.é.m. si on veut pouvoir interpoler à toutes les compositions de dioxane.

Mots clés : équations de Pitzer, paramètre d'interaction ionique de Pitzer, coefficients d'activité, f.é.m., acide chlorhydrique.

[Traduit par la Rédaction]

Introduction

At present, the most frequently used model to describe the thermodynamic properties of a variety of aqueous electrolyte solutions is the ion interaction or virial coefficient approach developed by Pitzer and his scientific school in the early 1970s (1–4). The Pitzer model extended the Debye–Hückel method, using a virial expansion to account for the ionic strength dependence of the short-range forces in binary and ternary ion interactions. The model is applicable to solutions of high ionic strength as well. Moreover, these equations can be used in iterative calculations since the ion interaction parameters are expressed as explicit functions of ionic strength and need very few parameters to estimate properties of both single and mixed electrolytes. The Pitzer model finds extensive application for the correlation and prediction of thermodynamic properties of electrolyte solutions (5–15). Many publications (5, 16–18) have shown that this model results in excellent predictions of thermodynamic quantities. An important compilation of the ion interaction parameters of a

Received 25 May 2005. Published on the NRC Research Press Web site at http://canjchem.nrc.ca on 28 January 2006.

Bijan Das. Department of Chemistry, North Bengal University, Darjeeling 734 430, India. (e-mail: bijan_dasus@yahoo.com).

 doi: 10.1139/V05-222 © 2005 NRC Canada

large number of electrolytes in aqueous solutions is available in ref. 5. Although for a long time attention has been paid to the application of the Pitzer ion interaction approach in aqueous electrolyte solutions (5–18), such studies in nonaqueous or in mixed solvent media are still scarce (19, 20), and the theory is not as developed as in the case of aqueous systems.

It is the twofold purpose of this research to obtain the Pitzer ion interaction parameters required to represent as compactly and as accurately as possible the literature experimental data (21–24) on the cell electromotive forces of hydrochloric acid in dioxane–water mixtures over a wide range of concentrations and temperatures using the Pitzer ion interaction model, with a view of testing the applicability of Pitzer equations in mixed solvent media and interpreting the resulting Pitzer parameters in terms of interionic forces.

Working equations for the model

We will be using the ion interaction model of Pitzer (1–4) as the basic framework for the mathematical description of the thermodynamic properties as functions of molality and temperature.

In the Pitzer ion interaction model, the pertinent equations for the osmotic coefficient (ϕ) and the activity coefficient (γ) for single electrolyte solutions can be expressed as

$$[1] \qquad \phi = 1 + \left|z_M z_X\right| f^{\phi} + \frac{2\nu_M\nu_X}{\nu} mB^{\phi} + \frac{2(\nu_M\nu_X)^{3/2}}{\nu} m^2C^{\phi}$$

and

$$[2] \qquad \ln\gamma = \left|z_M z_X\right| f^{\gamma} + \frac{2\nu_M\nu_X}{\nu} mB^{\gamma} + \frac{2(\nu_M\nu_X)^{3/2}}{\nu} m^2C^{\gamma}$$

where ν_M and ν_X are the numbers of ions in the formula and z_M and z_X give their respective charges in electronic units; also $\nu = \nu_M + \nu_X$, and m is the conventional molality. The other quantities have the form

$$[3] \qquad f^{\phi} = -A_{\phi}\left[\frac{I^{1/2}}{1 + bI^{1/2}}\right]$$

$$[4] \qquad f^{\gamma} = f^{\phi} + (2/b)A_{\phi}\ln(1 + bI^{1/2})$$

$$[5] \qquad B^{\phi} = \beta^{(0)} + \beta^{(1)}e^{-x_1} + \beta^{(2)}e^{-x_2}$$

$$[6] \qquad B^{\gamma} = 2\beta^{(0)} + \frac{2\beta^{(1)}}{x_1^2}[1 - e^{-x_1}(1 + x_1 - 0.5x_1^2)] + \frac{2\beta^{(2)}}{x_2^2}[1 - e^{-x_2}(1 + x_2 - 0.5x_2^2)]$$

$$[7] \qquad x_1 = \alpha_1 I^{1/2}$$

$$[8] \qquad x_2 = \alpha_2 I^{1/2}$$

Here, I is the ionic strength of solution and the term b is an empirical parameter equal to 1.2 $mol^{-1/2}$ $kg^{1/2}$, which is assumed to be the same throughout the calculation (2), α_1 and α_2 are two numerical parameters whose assigned values are discussed in the following, and A_{ϕ} is the Debye–Hückel coefficient for the osmotic function and is given by

$$[9] \qquad A_{\phi} = \frac{1}{3}\left(\frac{2\pi N_0 d_s}{1000}\right)^{1/2}\left(\frac{e^2}{\varepsilon kT}\right)^{3/2}$$

where N_0 is Avogadro's number, k is the Boltzmann constant, d_s is the density of solvent, ε is the relative permittivity of solvent, and T is the temperature in absolute scale. For SI units, ε is multiplied by $4\pi\varepsilon_0$, with ε_0 the permittivity of free space.

Experimental electromotive force (emf) data from the literature

In the present analysis, the experimental data on the electromotive forces of HCl in dioxane–water mixtures were taken from the literature reported by the Harned group (21–24) in the late 1930s. These authors obtained HCl activities from electromotive force measurements of the cells

$$[10] \qquad H_2|HCl(m),\ \text{dioxane}\ (x),\ H_2O|AgCl,Ag$$

with m being the molality of HCl and x being the weight % of dioxane in dioxane–water mixtures. Harned and coworkers (21–24) gave quadratic expressions for the cell emf (E) as functions of temperature (t) at the experimental molal concentrations (m) used. $E(t,m)$ calculated with these quadratic expressions for the experimental m and t are thus the closest to the experimental data as can be achieved.

The values of the activity coefficients (γ) can be computed by employing the equation of the cell

$$[11] \qquad \ln\gamma = \frac{E - E^0}{2k} + \ln m$$

where E^0 is the standard potential of the cell and k equals RT/F.

The literature sources of these data along with the concentration and temperature ranges are listed in Table 1.

Results and discussion

The numerical values of A_{ϕ} were computed using the temperature-dependent values of the density (d_s) and the relative permittivity (ε) of the mixed solvent media obtained from the literature (25) and these were used in the present analysis. However, for the convenience of using the A_{ϕ} values at any temperature in the temperature interval under study, we presented the calculated temperature dependence of A_{ϕ} in the polynomial form with temperature as a variable

$$[12] \qquad A_{\phi} = p_0 + p_1(T - 298.15\text{K}) + p_2(T - 298.15\text{K})^2 + p_3(T - 298.15\text{K})^3$$

where p_0 is equal to A_{ϕ} at 298.15 K. The temperature-independent coefficients (p_0, p_1, p_2, and p_3) were calculated by the least-squares method and are presented in Table 2.

In the vast majority of cases involving the application of the ion interaction model, α_1 is taken (5) to be 2.0 $kg^{1/2}$ $mol^{-1/2}$ and in some cases (26, 27) a value of 1.4 $kg^{1/2}$ $mol^{-1/2}$ gives a better fit when only this parameter is necessary. In cases where both α_1 and α_2 are required, the values α_1 = 1.4 $kg^{1/2}$ $mol^{-1/2}$ and α_2 = 12.0 $kg^{1/2}$ $mol^{-1/2}$ fitted the experimental thermodynamic properties very well (5). However,

© 2005 NRC Canada

Table 1. Literature sources of experimental electromotive forces used for the calculation of Pitzer ion interaction parameters of HCl in dioxane–water mixtures at different temperatures.

% Dioxane	Temperature range (K)	Molality m (mol kg^{-1}) From	To	Literature source	Year	Ref.
20	273.15–323.15	0.005	3.0	Harned and Donelson	1938	21
45	273.15–323.15	0.003	3.0	Harned and Donelson	1938	22
70	273.15–323.15	0.001	1.5	Harned et al.	1938	23
82	278.15–318.15	0.001	0.5	Harned and Walker	1939	24

Table 2. Constants for the temperature-dependent parameters and the standard deviations (σ).

Parameter	Constant	20% Dioxane	45% Dioxane	70% Dioxane	82% Dioxane
A_ϕ	p_0	0.5784	1.1585	3.7268	9.4125
	$10^3 p_1$	1.4201	3.5329	11.025	18.564
	$10^6 p_2$	6.6822	14.711	47.204	108.80
	$10^9 p_3$	2.8903	43.488	67.619	–691.72
	$10^5\sigma$	4.14	15.0	75.2	659
$\beta^{(0)}$	q_0	0.2389	0.4342	1.7514	9.5253
	$10^5 q_1$	–5.5056	51.132	298.43	1530.8
	$10^6 q_2$	–6.0719	–4.0785	12.509	312.73
	$10^9 q_3$	24.021	29.627	14.782	–8.5266
	$10^5\sigma$	2.29	4.28	1.39	330
$\beta^{(1)}$	q_0	0.57771	2.0046	12.868	66.312
	$10^3 q_1$	2.4302	6.1625	46.708	156.5
	$10^5 q_2$	2.7489	7.4145	29.908	–99.748
	$10^8 q_3$	4.4417	24.903	55.658	–188.41
	$10^3\sigma$	4.30	80.5	535	1140
$\beta^{(2)}$	q_0	—	—	–14.026	–588.38
	q_1	—	—	–0.2067	–5.0132
	$10^3 q_2$	—	—	2.2412	–751.1
	$10^5 q_3$	—	—	2.2933	–3345.4
	σ			0.1913	5.27
C^ϕ	$10^3 q_0$	–4.7362	–23.390	–337.0	–6678.2
	$10^3 q_1$	–9.0043	–24.278	–98.770	–1461.6
	$10^7 q_2$	15.946	16.303	–4.1444	–4983.8
	$10^9 q_3$	–3.7115	–5.4634	2.7960	–986.11
	$10^6\sigma$	7.97	3.41	67.5	2300
E^0	q_0	0.20310	0.16366	0.06573	–0.04016
	$10^4 q_1$	–7.5307	–11.143	–17.542	–22.992
	$10^6 q_2$	–3.7432	–3452.4	–3.3260	–17.000
	$10^{10} q_3$	1.2659	–6.5105	3.7621	–5083.3
	$10^6\sigma$	4.81	2.52	15.2	753

Pitzer and Silvester (28) found that $\alpha_1 = 2.0$ kg$^{1/2}$ mol$^{-1/2}$ and $\alpha_2 = 50$ kg$^{1/2}$ mol$^{-1/2}$ were nearly optimum for 3–2 and 2–3 electrolytes. Reardon (29) has also considered $Al_2(SO_4)_3$ with the same set of values of α_1 and α_2. Rard (30), on the other hand, gives alternate sets of values for $Lu_2(SO_4)_3$. The commonly used values for these two parameters do not give an acceptable fit for the system under study. In the present treatment, therefore, the following values for these numerical parameters were used: $\alpha = 2.3$ kg$^{1/2}$ mol$^{-1/2}$ for the 20% dioxane–water system, $\alpha = 2.8$ kg$^{1/2}$ mol$^{-1/2}$ for the 45% mixture, $\alpha_1 = 3.7$ kg$^{1/2}$ mol$^{-1/2}$ and $\alpha_2 = 36$ kg$^{1/2}$ mol$^{-1/2}$ for the 70% mixture, and $\alpha_1 = 6.4$ kg$^{1/2}$ mol$^{-1/2}$ and $\alpha_2 = 87$ kg$^{1/2}$ mol$^{-1/2}$ for the 82% mixture, and these were assumed to be independent of temperature. In fact, a series of values of α_1 (or α_1 and α_2, as the case may be) were tested for each solvent mixture. While the optimum values of the parameters varied a little from one temperature to the other for a given solvent mixture, the above values fitted all cases

© 2005 NRC Canada

very well. It is important to keep this in mind when employing the present model to other studies.

The parameters β^{ϕ} and β^{γ}, which describe the interaction of pairs of oppositely charged ions, represent measurable combinations of the second virial coefficients $\beta^{(0)}$, $\beta^{(1)}$, and $\beta^{(2)}$. These two parameters are functions of ionic strength (I). The single electrolyte third virial coefficients (C^{ϕ} and C^{γ}) account for the short-range interaction of ion triplets and are important only at high concentrations. These two are related by

$$[13] \quad C^{\gamma} = \frac{C^{\phi}}{2\left|z_M z_X\right|^{1/2}}$$

Isothermal least-squares fits of the experimental emf data using eq. [2] in conjunction with eq. [11] clearly demonstrated that the simple three-parameter ion interaction model (involving $\beta^{(0)}$, $\beta^{(1)}$, and C^{ϕ}) is capable of satisfactorily describing the results for HCl activity in 20% and 45% dioxane–water mixtures where ionic association is not expected (see later discussion). For the other two mixed solvent media comprising 70% and 82% dioxane, HCl ion association is appreciable (also see later discussion), and it has been observed that the quality of fit can be improved significantly only if we include the parameter $\beta^{(2)}$ in the Pitzer equation.

For the mixed solvent media containing 20% and 45% of dioxane, the ion interaction parameters along with the standard potentials (E^0) were obtained from the experimental emf data by the least-squares method. For the other two systems exhibiting ionic association, however, the standard potentials were first evaluated following the method described in the literature (31) using the appropriate form of the Debye–Hückel term consistent with the Pitzer formalism employed here. The required ionization constants of HCl in these mixtures were taken from the conductometric study of Owen and Waters (32).

The temperature dependence of the Pitzer ion interaction parameters ($\beta^{(0)}$, $\beta^{(1)}$, $\beta^{(2)}$, and C^{ϕ}) and the standard potentials (E^0) have been conveniently described by an arbitrary form of $f(T)$ as given below:

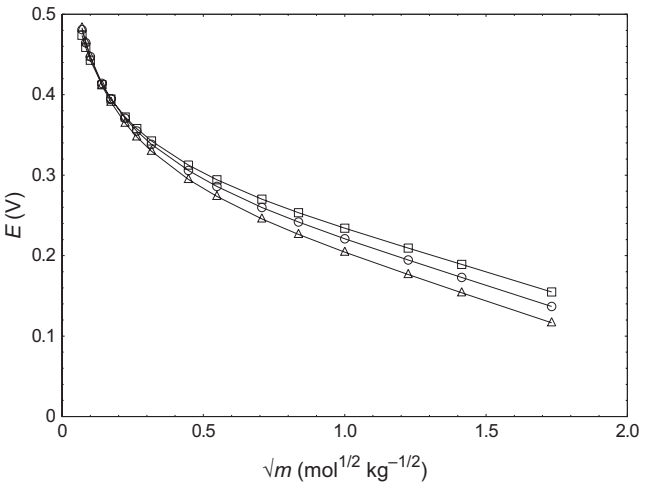
$$[14] \quad f(T) = q_0 + q_1\,(T - 298.15\text{K}) + q_2\,(T - 298.15\text{K})^2 + q_3\,(T - 298.15\text{K})^3$$

where q_0 is equal to $f(T)$ at 298.15 K, and q_0 through q_3 are temperature-independent constants.

Parameters resulting from the least-squares calculations along with their standard deviations (σ) are listed in Table 2.

The parameter $\beta^{(2)}$ is not always necessary; it is taken to be zero for nonassociated electrolytes. One needs to include this parameter in the second virial coefficient to fit the unusual behavior of electrolytes with ionic association. Special attention was given to the problem of calculating the $\beta^{(2)}$ parameter. Earlier, Pitzer and Mayorga (3) observed the peculiar behavior of the activity coefficients of 2–2 valence type electrolytes. This phenomenon was discussed by these authors in terms of various theories, some of which assume formation of ion pairs in such solutions while others do not. Bjerrum and Silskab (33) showed that an ionic association could be expected on the basis of purely electrostatic forces

Fig. 1. Comparison of the experimental values of the electromotive forces (E) of HCl in a 20% dioxane–water mixture with those calculated from the present correlation. Experimental values: 273.15 K (□), 298.15 K (○), 323.15 K (Δ). Calculated values: lines.



for 2–2 electrolytes, even in water. In some cases, the existence of ion pairs in aqueous solutions was proven by spectroscopic or ultrasonic data. Various authors (34) treated their experimental data for bivalent sulfates by using the ion association model. Although this approach fit the experimental data well, there were serious disadvantages that led one to seek a simpler method of correlation. The $\beta^{(2)}$ parameter was designed by Pitzer and Mayorga (3) to apply the Pitzer ion interaction approach to 2–2 aqueous electrolyte solutions characterized by a partial ionic association of M^{2+} and X^{2-} ions. These authors suggested that there were many advantages in representing the thermodynamic properties (activity and osmotic coefficients) of 2–2 electrolytes by introducing an appropriate second virial coeffcient containing $\beta^{(2)}$ parameter into the Pitzer equation instead of including the parameters determined by a chemical association model. Such a modified equation has been successfully applied for the calculation of thermodynamic quantities for single 2–2 electrolyte solutions, for mixed electrolytes involving one component of the 2–2 type (3), and also for other valence-type electrolytes (e.g., 2–3, 3–2, etc.) with significant ionic association. Various authors (35–38) demonstrated that the experimental data for 2–2 electrolytes could be treated without the assumption of an ionic association equilibrium, provided one avoids the Debye–Hückel approximation of linearization of the exponential term in the Boltzmann distribution. However, the equations now become so complex that one has only a few numerical results for a particular ionic model. Thus, it was desirable to deal with the development of equations that were simpler, but which still adequately reflect the thermodynamic behavior of electrolyte solutions. Therefore, the principal aim of the present study was the development of the Pitzer ion interaction approach for activity coefficients of HCl in dioxane–water mixtures.

Figures 1–4 compare the calculated cell potentials for HCl from the present study with the available experimental data in dioxane–water mixtures at some selected temperatures. The corresponding standard deviations of fit of the cell elec-

© 2005 NRC Canada

Fig. 2. Comparison of the experimental values of the electromotive forces (E) of HCl in a 45% dioxane–water mixture with those calculated from the present correlation. Experimental values: 273.15 K (□), 298.15 K (○), 323.15 K (Δ). Calculated values: lines.

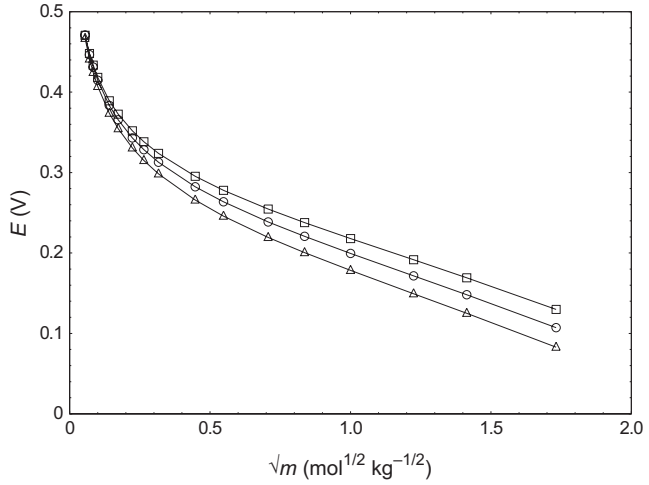
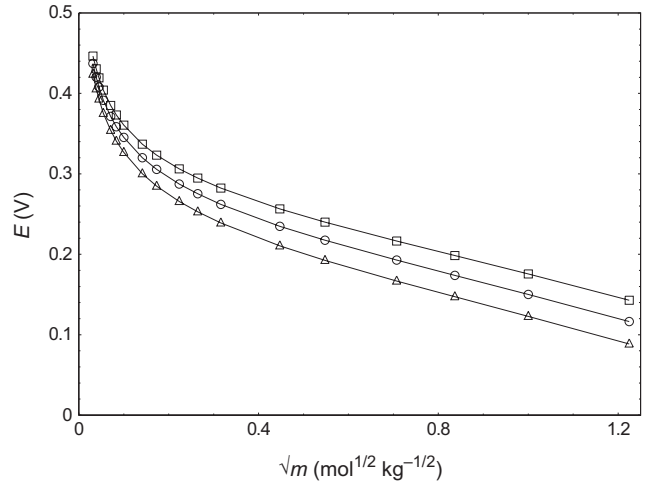


Fig. 3. Comparison of the experimental values of the electromotive forces (E) of HCl in a 70% dioxane–water mixture with those calculated from the present correlation. Experimental values: 273.15 K (□), 298.15 K (○), 323.15 K (Δ). Calculated values: lines.



tromotive forces obtained using the ion interaction parameters evaluated in this study to the experimental values have been included in Table 3. From the standard deviations recorded in this table, as well as from an inspection of these figures, it is directly evident that the ion interaction parameters reported here reproduce the experimental results excellently throughout the entire composition range.

The negative values of the ion interaction parameter $\beta^{(2)}$ observed in 70% and 82% dioxane–water mixtures indicate ionic association of HCl in these mixed solvent media. Greater ionic association with increasing temperature or with increasing amounts of dioxane in the mixture is reflected in the more negative values of $\beta^{(2)}$ at higher temperatures or in a mixture richer in organic solvent. This is in good agreement with the findings from an earlier conductivity study (32).

Fig. 4. Comparison of the experimental values of the electromotive forces (E) of HCl in a 82% dioxane–water mixture with those calculated from the present correlation. Experimental values: 278.15 K (□), 298.15 K (○), 318.15 K (Δ). Calculated values: lines.

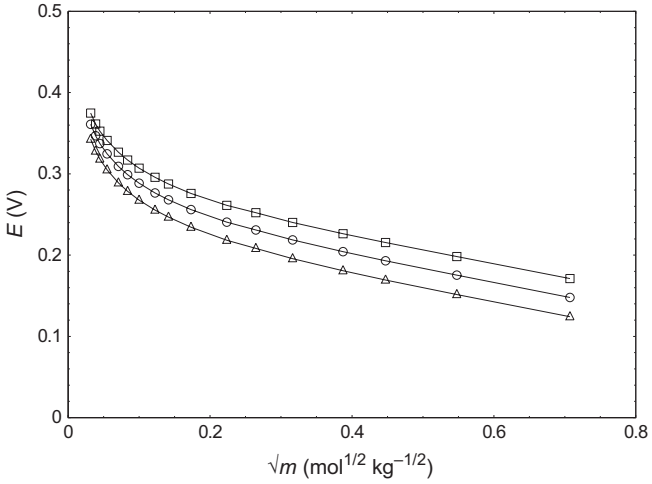


Table 3. Standard deviations (σ) for estimated vs. experimental electromotive forces for HCl in dioxane–water mixtures.

	Standard deviation			
T (K)	20% Dioxane	45% Dioxane	70% Dioxane	82% Dioxane
273.15	1	2	2	
278.15				6
283.15	1	2	2	
288.15				5
293.15	1	1	2	
298.15	1	1	2	5
303.15	1	1	2	
308.15				5
313.15	1	1	2	
318.15				5
323.15	1	2	3	

Note: $10^4\sigma$ values have been tabulated.

The third virial coefficients (C^{ϕ}), which account for ion triplet interaction, are found to be negative for HCl in the mixed solvent media investigated over the temperature interval 273.15–323.15 K. The very small negative values in 20% and 45% dioxane–water mixtures indicate the possible absence of ion association in those solutions (2). The large negative values for C^{ϕ} in the remaining two mixtures over the entire temperature range, on the other hand, suggest some tendency towards ion-pair formation for this electrolyte. Moreover, the more the dioxane content of the mixed solvent media at a given temperature or the higher the temperature for a given mixture, the more negative are the values for the third virial coefficients. This clearly indicates greater ionic association with increasing temperature or with increasing amounts of dioxane in the mixture.

© 2005 NRC Canada

Table 4. Association constants (K_A) and $\beta^{(2)}$ values for HCl in 70% and 82% dioxane–water mixtures.

	70% Dioxane		82% Dioxane	
Temperature (K)	K_A	$\beta^{(2)}$	K_A	$\beta^{(2)}$
288.15	9.1	–11.758	3922	–579.904
298.15	12.5	–14.292	4950	–588.380
308.15	14.6	–15.846	6098	–889.382
318.15	16.6	–17.080	9346	–1256.716

Note: Association constants derived from ref. 32.

Thus, the values of the parameters $\beta^{(2)}$ and C^{ϕ} point to the same conclusion concerning the ion association behaviour of HCl in dioxane–water mixtures.

It is thus apparent that the solvent mixtures comprising 20% and 45% dioxane behave differently from the other two that are richer in dioxane as far as the ion association of HCl is concerned. Although a three-parameter Pitzer equation is sufficient to describe the data for 20% and 45% mixtures, a four-parameter equation capable of taking into account the ion association is essential for 70% and 82% mixtures. That is, effectively we have only two sets of Pitzer parameters in the nonassociating regime and two sets in the associating regime. An attempt to perform interpolation to other dioxane percentages with these limited sets of parameters (except $\beta^{(2)}$) did not yield satisfactory fits; for two sets of $\beta^{(2)}$ values, no such attempt could be made. It is, thus, at this stage not possible to perform an interpolation of the Pitzer ion interaction parameters over the solvent composition essentially because of the availability of the emf data in a limited number of mixtures. More extensive emf measurements in a large number of dioxane–water mixtures is required for a meaningful interpolation of the data. However, the present analysis clearly demonstrates the medium effect on the ion interaction parameters, although correlating equations are yet to be developed pending further measurements on the cell [10] both in the nonassociating and associating regimes.

In the limit of infinite dilution it has been shown that (3) $\beta^{(2)}$ becomes equal to $-K_A/2$, where K_A is the association constant for HCl in the relevant dioxane–water mixture. The dissociation constants for HCl are available in 70% and 82% mixtures from the conductometric study of Owen and Waters (32). No accurate estimate can be made of the results in 20% and 45% dioxane solutions, although these investigators judge that the dissociation constant is of the order of unity in the latter and hence HCl may be treated as completely dissociated in 20% and 45% solutions. The association constant values for HCl obtained from ref. 32, along with the $\beta^{(2)}$ values at 288.15, 298.15, 308.15, and 318.15 K in 70% and 82% mixtures, are given in Table 4. It is evident from this table that the above relationship between $\beta^{(2)}$ and the association constant does not hold true in the present case. The failure of this relationship has also been observed by Rard (30) for $Lu_2(SO_4)_3$ in aqueous medium.

Finally, it can be concluded that the present set of ion interaction parameters would be useful to predict the emf as well as the activity and osmotic coefficients of hydrochloric acid in dioxane–water mixtures over a wide concentration and temperature range. This analysis thus yields a set of parameters from which these important and useful thermodynamic properties can be reproduced. Thus, the Pitzer ion interaction approach is proved to be a valuable method for correlation and prediction of thermodynamic properties of electrolytes in mixed solvent media also. Although correlating equations to perform interpolation of the Pitzer ion interaction parameters over the solvent composition are yet to be developed pending further measurements on the cell [10] both in the nonassociating and associating regimes, the present study amply served the twofold purpose to obtain the Pitzer parameters required to represent as compactly and as accurately as possible the literature experimental data on the cell electromotive forces of hydrochloric acid in dioxane–water mixtures over a wide range of concentration and temperature with a view to test the applicability of Pitzer equations in mixed solvent media and to interpret the resulting Pitzer parameters in terms of interionic forces.

Acknowledgement

The author thanks the University of North Bengal for supporting the research described in this article.

References

1. K.S. Pitzer. J. Phys. Chem. **77**, 268 (1973).
2. K.S. Pitzer and G. Mayorga. J. Phys. Chem. **77**, 2300 (1973).
3. K.S. Pitzer and G. Mayorga. J. Solution Chem. **3**, 359 (1974).
4. K.S. Pitzer and J.J. Kim. J. Am. Chem. Soc. **96**, 5701 (1974).
5. K.S. Pitzer. *In* Activity coefficients in electrolyte solutions. 2nd ed. *Edited by* K.S. Pitzer. CRC Press, Boca Raton, Florida. 1991. Chap. 3.
6. H.T. Mocharle, S. Manohar, and G. Atkinson. J. Solution Chem. **21**, 345 (1992).
7. Th. Koennecke, V. Neck, Th. Fanhaenel, and J.I. Kim. J. Solution Chem. **26**, 561 (1997).
8. K.S. Pitzer, R.N. Roy, and P. Wang. J. Phys. Chem. B, **101**, 4120 (1997).
9. K.S. Pitzer and B. Das. Geochim. Cosmochim. Acta, **62**, 915 (1998).
10. K.S. Pitzer, P. Wang, J.A. Rard, and S.L. Clegg. J. Solution Chem. **28**, 265 (1999).
11. B. Das and K.S. Pitzer. J. Solution Chem. **28**, 283 (1999).
12. B. Das and K.S. Pitzer. Indian J. Chem. **38A**, 1261 (1999).
13. B. Das, R.N. Roy, K.S. Pitzer, D.R. Gregory, and S.A. Keifer. J. Solution Chem. **29**, 289 (2000).
14. B. Das and K.S. Pitzer. J. Solution Chem. **30**, 489 (2001).
15. B. Das. J. Solution Chem. **33**, 33 (2004).
16. C.E. Harvie, N. Moller, and J.H. Weare. Geochim. Cosmochim. Acta, **48**, 723 (1984).
17. R.T. Pabalan and K.S. Pitzer. *In* Activity coefficients in electrolyte solutions. 2nd ed. *Edited by* K.S. Pitzer. CRC Press, Boca Raton, Florida. 1991. Chap. 7.
18. R.T. Pabalan and K.S. Pitzer. Geochim. Cosmochim. Acta, **52**, 2393 (1988).
19. K. Nasirzadeh, N. Papaiconomou, R. Neueder, and W. Kunz. J. Solution Chem. **33**, 227 (2004).
20. J.Z. Yang and W.G. Xu. J. Solution Chem. **34**, 71 (2005).
21. H.S. Harned and J.G. Donelson. J. Am. Chem. Soc. **60**, 339 (1938).
22. H.S. Harned and J.G. Donelson. J. Am. Chem. Soc. **60**, 2128 (1938).
23. H.S. Harned, J.G. Donelson, and C. Calmon. J. Am. Chem. Soc. **60**, 2133 (1938).

© 2005 NRC Canada

24. H.S. Harned and F. Walker. J. Am. Chem. Soc. **60**, 48 (1939).
25. H.S. Harned and B.B. Owen. *In* The physical chemistry of electrolyte solutions. Reinhold, New York. 1950. pp. 544–546.
26. H.F. Holmes and R.E. Mesmer. J. Solution Chem. **15**, 495 (1986).
27. H.F. Holmes, R.H. Busey, J.M. Simonson, D.G. Archar, and R.H. Wood. J. Chem. Thermodyn. **19**, 863 (1987).
28. K.S. Pitzer and L.F. Silvester. J. Phys. Chem. **82**, 1239 (1978).
29. E. Reardon. J. Phys. Chem. **92**, 6426 (1988).
30. J.A. Rard. J. Solution Chem. **19**, 525 (1990).
31. H.S. Harned, F. Walker, and C. Calmon. J. Am. Chem. Soc. **61**, 44 (1939).
32. B.B. Owen and W. Waters. J. Am. Chem. Soc. **60**, 2371 (1938).
33. N. Bjerrum and K.D.V. Silskab. Mats. Fys. Medd. **7**, 9 (1926).
34. K.S. Pitzer. J. Chem. Soc. Faraday Trans. 2, **68**, 101 (1972), and refs. cited therein.
35. T.H. Gronwall, V.K. LaMer, and K. Sandved. Phys. Z. **29**, 358 (1928).
36. E.A. Guggenheim. Trans. Faraday Soc. **55**, 1714 (1959).
37. A.W. Gardner and E. Gluekauf. Proc. R. Soc. London Ser. A, **321**, 515 (1971).
38. J.C. Rasaiah. J. Chem. Phys. **56**, 3071 (1972).

© 2005 NRC Canada

Synthesis and characterization of alkyl- and acyl-substituted oxime–phosphazenes

Erol Çil, Mustafa Arslan, and Ahmet Orhan Görgülü

Abstract: Two oxime–cyclophosphazenes were prepared from the hexakis(4-formylphenoxy)cyclotriphosphazene (**2**) and hexakis(4-acetylphenoxy)cyclotriphosphazene (**8**). The reactions of these oximes with ethyl bromide, allyl bromide, propanoyl chloride, and acriloyl chloride were studied. Hexasubstituted compounds were obtained from the reactions of hexakis{4-[(hydroxyimino)methyl]phenoxy}cyclotriphosphazene (**3**) with ethyl bromide (**4**), allyl bromide (**5**), and propanoyl chloride (**6**), however, the oxime groups on **3** rearranged to nitrile (**7**) in the reaction of **3** with acriloyl chloride. Hexasubstituted compounds were also obtained from the reactions of hexakis{4-[(1)-*N*-hydroxyethaneimidoyl]phenoxy}cyclotriphosphazene (**9**) with allyl bromide (**11**) and propanoyl chloride (**12**). Tetra- and penta-substituted products were obtained from the reactions of **9** with ethyl bromide (**10**) and acriloyl chloride (**13**), respectively. All products were generally obtained in high yields. The structures of the compounds were defined by elemental analysis, IR, ^{1}H, ^{13}C, and ^{31}P NMR spectroscopy.

Key words: hexachlorocyclotriphosphazene, phosphazene, oxime, oxime derivatives, oxime–phosphazenes.

Résumé : On a préparé deux oximes de cyclophosphazènes à partir de l'hexakis(4-formylphénoxy)cyclotriphosphazène (**2**) et de l'hexakis(4-acétylphénoxy)cyclotriphosphazène (**8**). On a étudié les réactions de ces oximes avec le bromure d'éthyle, le bromure d'allyle, le chlorure de propanoyle et le chlorure d'acryloyle. Les réactions de l'hexakis{4-[(hydroxyimino)méthyl]phénoxy}cyclotriphosphazène (**3**) avec le bromure d'éthyle (**4**), le bromure d'allyle (**5**) et le chlorure de propanoyle (**6**) conduit à la formation de produits hexasubstitués; toutefois, par réaction avec le chlorure d'acryloyle, les groupes oximes du composé **3** se réarrangent en nitrile (**7**). On a aussi obtenu des produits hexasubstitués lors des réactions de l'hexakis{4-[(1)-*N*-hydroxyéthaneimidoyl]phénoxy}cyclotriphosphazène (**9**) avec le bromure d'allyle (**11**) et le chlorure de propanoyle (**12**). Les réactions du composé **9** avec le bromure d'éthyle (**10**) et le chlorure d'acryloyle (**13**) conduisent respectivement à des produits tétra- et pentasubstitués. Tous les produits ont généralement été obtenus avec des rendements élevés. Les structures des composés ont été définies par des analyses chimiques et par les spectroscopies IR et RMN du ^{1}H, ^{13}C et ^{31}P.

Mots clés : hexachlorocyclotriphosphazène, phosphazène, oxime, dérivés d'oximes, oxime de phosphazène.

[Traduit par la Rédaction]

Introduction

The linear, cyclo- and poly-phosphazenes are the best known and most intensively studied phosphorus–nitrogen compounds (1–5). These compounds are reported to possess interesting biomedical properties and promising applications (6–9). Phosphazene polymers bearing flouroalkoxy or aryloxy groups stimulated considerable interest in the past as biologically inert, water insoluble polymers for blood vessel or heart valve construction (10). Cyclophosphazene derivatives, substituted with aziridine groups, were investigated as biomedical products because of their strong antitumor activity (11). Antimicrobial and biological effects of some phosphazenes on bacterial and yeast cells have been studied (12–14). On the other hand, it is known that phosphorus and nitrogen compounds are effective flame retardants for fibre materials (15). Some other applications include model compounds for polyphosphazenes, starting materials for the preparation of cyclolinear and (or) cyclomatrix phosphazene substrates, commercial polymers with carbon backbones containing pending cyclophosphazene groups, inorganic hydraulic fluids and lubricants, biologically important substrates such as anticancer agents, insect chemosterilants, pesticides and fertilizers, supports for catalysts, dyes, and crown ether phase-transfer catalysts for nucleophilic substitution reactions, core substrates for dendrimers, thermal initiators for anionic polymerization reactions, and photosensitive materials (16).

The literature contains reports on the synthesis of different linear, cyclic or polyphosphazenes (17–27). There are also a large number of literature reports on reactions of the functional groups on phosphazene substituents (10, 28). Typical of these include coupling reactions of trimeric phosphazene azides with aryloxy, alkoxy, and dialkylamino cosubstituents (29), *N*-vinylic phosphazenes with azodicarboxylic and

Received 19 July 2005. Published on the NRC Research Press Web site at http://canjchem.nrc.ca on 28 January 2006.

E. Çil,[1] M. Arslan, and A.O. Görgülü. Chemistry Department, Firat University, TR-23169 Elazig, Turkey.

[1]Corresponding author (e-mail: cilerol@yahoo.com).

 doi: 10.1139/V05-223 © 2005 NRC Canada

acetylenic esters (30), polymers from 4-formylphenoxy (31, 32), from maleic (33), and from 3,4-methylenedioxyphenoxy substituents (34).

In this paper we have prepared oxime–cyclophosphazenes from hexakis(4-formylphenoxy)cyclotriphosphazene and hexakis(4-acetylphenoxy)cyclotriphosphazene, and studied their reactions with alkyl and acyl halides such as ethyl bromide, allyl bromide, propanoyl chloride, and acriloyl chloride.

Experimental

General remarks

Solvents and other liquids used in the experimental works were dried by conventional methods. Hexachlorocyclotriphosphazene ($N_3P_3Cl_6$) (**1**) was recrystallized from hexane. Other chemicals were used as purchased. Hexakis(4-formylphenoxy)cyclotriphosphazene (**2**) and hexakis(4-acetylphenoxy)cyclotriphosphazene (**8**) were prepared as described by Carriedo et al. (25). The reactions of ($N_3P_3Cl_6$) with the phenols were carried out under dry nitrogen.

The IR spectra were recorded on an ATI Unicam Mattson 1000 FT IR spectrometer. ^1H, ^{13}C, and ^{31}P NMR spectra were recorded using a Bruker DPX-300 spectrometer operating at 300.13, 75.46, and 121.49 MHz, respectively. The ^1H and ^{13}C NMR chemical shifts were measured using $SiMe_4$ as an internal standard and the ^{31}P chemical shifts were measured using 85% H_3PO_4 as an external standard. Chemical shifts downfield from the standard were assigned positive δ values. Microanalysis was carried out by a LECO 932 CHNS-O apparatus.

Synthesis of compound 2

A mixture of **1** (10.34 g, 29.74 mmol), 4-hydroxybenzaldehyde (22.05 g, 180.56 mmol), and K_2CO_3 (50.00 g, 361.76 mmol) was stirred in THF (250 mL) at 0 °C and then was reacted at ambient temperature for 48 h. The solvent was removed under vacuum. The residue was extracted with CH_2Cl_2 (4 × 75 mL). After the solvent was removed, a white solid (**2**) formed in 92% (23.57 g) yield.

Synthesis of compound 3

A mixture of **2** (20.00 g, 23.21 mmol) and hydroxylaminehydrochloride (10.00 g, 143.90 mmol) was refluxed in pyridine (15 mL) for 3 h. After the reaction was complete, the mixture was allowed to cool and was slowly poured into water (100 mL) and reprecipitated twice from water. The white solid (**3**) was washed with alcohol and dried at 50 °C in a vacuum. Yield: 83% (18.33 g).

Reaction of 3 with ethyl bromide

A solution of 0.40 mL (0.74 g, 6.79 mmol) ethyl bromide in acetone (10 mL) was slowly added dropwise to a stirred and cooled (0–5 °C) mixture of **3** (0.80 g, 0.84 mmol) and K_2CO_3 (2.00 g, 14.47 mmol) in acetone (30 mL). The reaction was carried out at room temperature for 1 h and then was refluxed for 24 h. After the reaction was complete, the mixture was slowly poured into water (50 mL) and reprecipitated twice from water. The white solid (**4**) was recrystallized from chloroform. Yield: 59% (0.55 g).

Reaction of 3 with allyl bromide

A solution of 0.50 mL (0.7 g, 5.77 mmol) allyl bromide in acetone (10 mL), **3** (0.80 g, 0.84 mmol), and K_2CO_3 (1.60 g, 11.57 mmol) in acetone (30 mL) was used for the preparation of **5** as for **4**. The reflux period was 48 h. The white solid (**5**) was recrystallized from alcohol. Yield: 84% (0.85 g).

Reaction of 3 with propanoyl chloride

A solution of 0.40 mL (0.42 g, 4.58 mmol) propanoyl chloride in acetone (10 mL), **3** (0.60 g, 0.63 mmol), and Et_3N (2 mL) in acetone (30 mL) was used for the preparation of **6** as for **4**. The reaction was carried out at room temperature for 12 h. The white solid (**6**) was recrystallized from alcohol. Yield: 74% (0.60 g).

Reaction of 3 with acriloyl chloride

A solution of 0.40 mL (0.44 g, 4.86 mmol) acriloyl chloride in acetone (10 mL), **3** (0.60 g, 0.63 mmol), and Et_3N (2 mL) in acetone (30 mL) was used for the preparation of **7** as for **4**. The reaction was carried out at room temperature for 12 h. The orange colour solid (**7**) was washed with alcohol. Yield: 94% (0.50 g).

Synthesis of compound 8

A mixture of **1** (7.00 g, 20.13 mmol), 4-hydroxyacetophenone (16.72 g, 122.80 mmol), and K_2CO_3 (34.00 g, 245.99 mmol) was refluxed in acetone (250 mL) for 3 h. The solvent was evaporated in vacuum and the residue was extracted with CH_2Cl_2 (4 × 75 mL). After the evaporation of the solvent in vacuum, a white solid (**8**) formed in 87% (16.50 g) yield.

Synthesis of compound 9

Hydroxylaminehydrochloride (4.50 g, 64.75 mmol) and **8** (10.00 g, 10.57 mmol) were used for the preparation of **9** as for **3**. After the reaction was complete, the mixture was allowed to cool and the mixture was slowly poured into water (100 mL) and reprecipitated twice from water. The white solid (**9**) was obtained in 99% (10.89 g) yield.

Reaction of 9 with ethyl bromide

A solution of 0.40 mL (0.59 g, 5.43 mmol) ethyl bromide in acetone (10 mL), **9** (0.60 g, 0.58 mmol), and K_2CO_3 (2.00 g, 14.47 mmol) in acetone (30 mL) was used for the preparation of **10** as for **4**. The oily product (**10**) was obtained and dried under vacuum for 48 h. Yield: 62% (0.41 g).

Reaction of 9 with allyl bromide

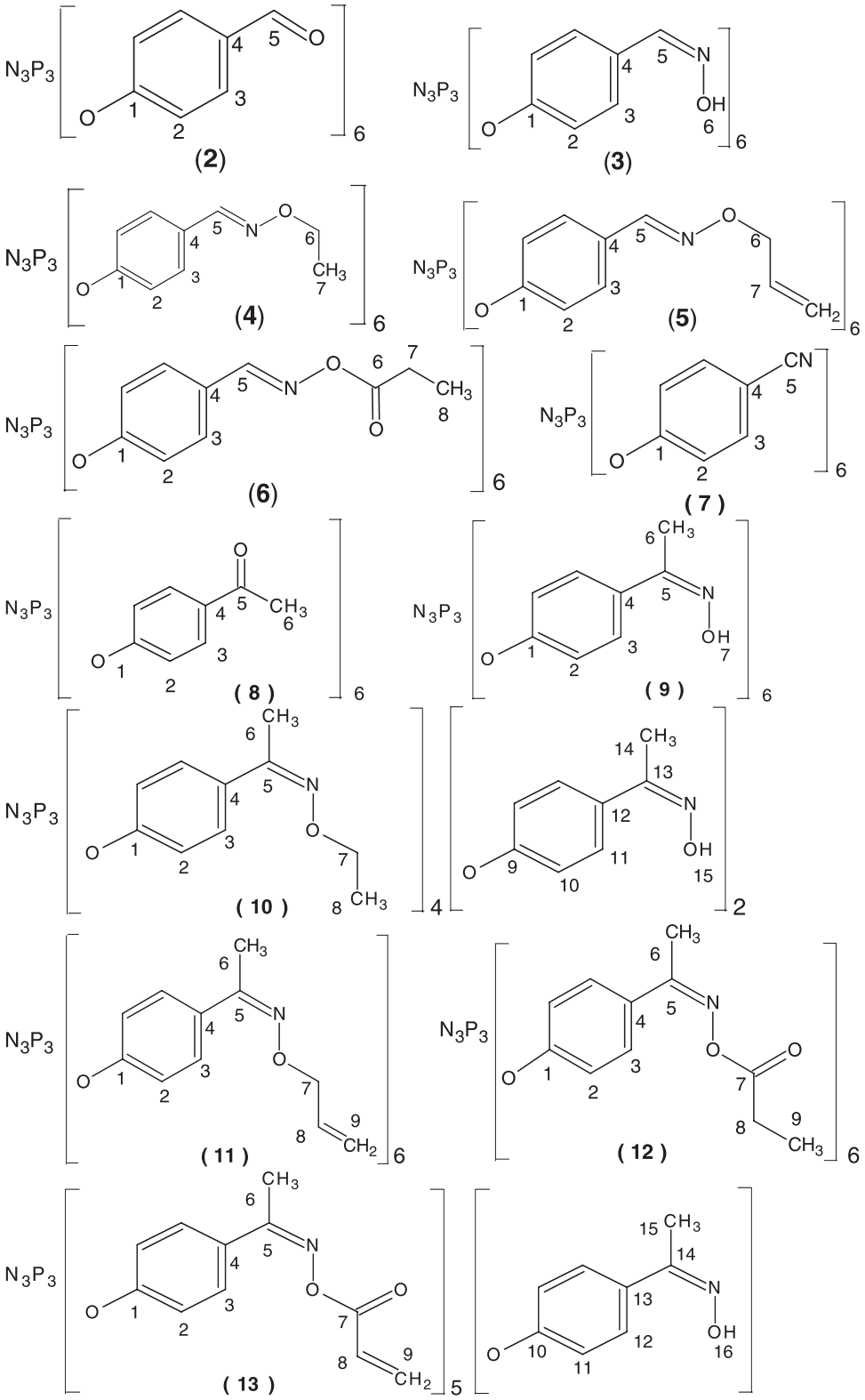
A solution of 0.40 mL (0.55 g, 4.56 mmol) allyl bromide in acetone (10 mL), **9** (0.60 g, 0.58 mmol), and K_2CO_3 (2.00 g, 14.47 mmol) in acetone (30 mL) was used for the preparation of **11** as for **4**. The reflux period was 48 h. The oily product (**11**) was obtained and dried under vacuum for 48 h. Yield: 89% (0.65 g).

Reaction of 9 with propanoyl chloride

A solution of 0.40 mL (0.42 g, 4.60 mmol) propanoyl chloride in acetone (10 mL), **9** (0.60 g, 0.58 mmol), and K_2CO_3 (2.00 g, 14.47 mmol) in acetone (30 mL) was used for the preparation of **12** as for **4**. The oily product (**12**) was

© 2005 NRC Canada

Scheme 1. The structures of compounds **2**–**13**.



obtained and dried under vacuum for 24 h. Yield: 89% (0.70 g).

Reaction of 9 with acriloyl chloride

A solution of 0.40 mL (0.44 g, 4.86 mmol) acriloyl chloride in acetone (10 mL), **9** (0.60 g, 0.58 mmol), and Et_3N (2 mL) in acetone (30 mL) was used for the preparation of **13** as for **4**. The reaction was carried out at room temperature for 24 h. The yellowish solid (**13**) was washed with alcohol three times. Yield: 59% (0.45 g).

© 2005 NRC Canada

Results and discussion

The reaction of **1** with 6 equiv. of 4-hydroxybenzaldehyde and 4-hydroxyacetophenone in the presence of K_2CO_3 in THF gave hexakis(4-formylphenoxy)cyclotriphosphazene (**2**) and hexakis(4-acetylphenoxy)cyclotriphosphazene (**8**). Oxime compounds hexakis{4-[(hydroxyimino)methyl]phenoxy}cyclotriphosphazene (**3**) and hexakis{4-[(1)-*N*-hydroxyethaneimidoyl]phenoxy}cyclotriphosphazene (**9**) were synthesized from the reactions of **2** and **8** with hydroxylaminehydrochloride in pyridine, respectively.

Hexasubstituted oxime derivatives were obtained from the reactions of oxime compound **3** with ethyl bromide, allyl bromide, and propanoyl chloride in acetone (in the presence of K_2CO_3 for ethyl and allyl bromide, of Et_3N for propanoyl and acriloyl chloride) via replacement of all the oxime protons with ethyl, allyl and propanoyl groups. However, the oxime groups on **3** rearranged to nitrile (**7**) in the reaction of **3** with acriloyl chloride via the dehydration of oximes (35, 36). Compound **7** was previously synthesized by Carriedo (25). $N_3P_3(OC_6H_4\text{-}CN)_6$ was directly obtained from the reaction of $N_3P_3Cl_6$ with 4-cyanophenol and characterized by elemental analysis and ^1H, ^{13}C, and ^{31}P NMR spectra (25). The analysis results of **7** are in good accordance with the literature values (25). Similar compounds, $N_3P_3(OPh)_5(OC_6H_4\text{-}CN\text{-}p)$ and $N_3P_3(OC_6H_4\text{-}R\text{-}4)_5(OC_6H_4\text{-}CN\text{-}4)$ (R = H or *t*-Bu), were synthesized by Allcock et al. (37) and Carriedo et al. (38), respectively. Hexasubstituted derivatives were obtained from the reactions of **9** with allyl bromide and propanoyl chloride. Tetra- and penta-substituted products were obtained from the reactions of **9** with ethyl bromide and acriloyl chloride in acetone (in the presence of K_2CO_3 for ethyl bromide, of triethylamine for acriloyl chloride), respectively.

The structures of the compounds were defined by elemental analysis, IR, and ^1H, ^{13}C, and ^{31}P NMR spectroscopy (structures **2**–**13** are shown in Scheme 1). Physical properties and analytical data for **2**–**13** are given in Table 1. Compounds **2**–**13** were synthesized in high yields except **4**, **10**, and **13**. The solvents used for the purification of compounds **7**, **10**, and **11** could not be removed completely as observed by ^1H and ^{13}C NMR spectra. Thus, the presence of these trace amounts of solvent affect the elemental analysis, in particular the carbon value.

The characteristic stretching peaks in the IR spectra of the phosphazenes have been assigned as in Table 2. The P=N stretching vibrations, which are observed between 1173 and 1208 cm^{-1}, are characteristic of cyclophosphazenes. Compared to **1**, which appeared at 1218 cm^{-1}, these peaks are shifted to longer wavelengths for **2**–**13**. The OH stretching vibrations in the IR spectra of **3**, **9**, **10**, and **13** indicate the oxime compounds. While **3** and **9** are initial oximes, all hydrogen atoms of the OH groups of **10** and **13** could not be replaced by the alkyl and acyl substituents.

The NMR data for **2**–**13** are presented in Tables 3–5. The ^{31}P NMR shifts of **2**–**13** change between 8.05 and 17.21 ppm. Although there is only one peak in the ^{31}P NMR spectra of **1**, **2**, **4**, **5**, **7**, **8**, **10**, **12**, and **13** at 20.12, 8.33, 7.49, 9.49, 7.51, 8.05, 9.07, 8.80, and 8.73 ppm, respectively, two peaks, with very weak second signals, are observed at δ 17.21, 17.26, δ 8.33, 8.21, δ 9.04, 9.01, and δ 9.01 and 8.98 ppm for **3**, **6**, **9**, and **11**, respectively. It is assumed that the weak peaks due to the cyn and anti isomerism of the -C=N- groups. The effects of the cyn and anti isomerism are also observed in the ^{13}C NMR spectra of **3**, **6**, and **11** (Table 5). This data demoinstrates that compounds **3**, **6**, **9**, and **11** consist of a mixture of two isomers, but others have one isomer. Although there are the different phosphorus environments in the molecules of **10** and **13**, the main peak is observed as a singlet. It is understood that the phosphorus peaks are not affected by these changes because the substituted groups are far off the phosphorus atoms.

The ^1H and ^{13}C NMR data also confirm the structures of **2**–**13** (Scheme 1). In the ^1H NMR spectra (Table 4), the OH protons are observed at 10.17, 11.25, 11.30, and 11.25 ppm for **3**, **9**, **10**, and **13**, respectively. It is understood from the integral intensities that there are six OH protons in **3** and **9**, which are original oxime–phosphazenes, two OH protons in **10**, one OH proton in **13**. This observation for **10** and **13** indicates that alkyl or acyl groups have not replaced all OH protons in **3** and **9**. The aldehyde proton for **2** appears at

Table 1. Physical properties and analytical data for **2**–**13**.

Compound	Yield (%)	Atom	Found	Calcd.
2	92	C	58.52	58.55
		H	3.39	3.51
		N	4.51	4.88
3	83	C	53.43	53.00
		H	3.75	3.81
		N	12.98	13.25
4	59	C	58.16	57.91
		H	5.33	5.40
		N	11.02	11.26
5	84	C	60.10	60.45
		H	5.11	5.07
		N	10.40	10.57
6	74	C	56.21	55.95
		H	4.63	4.70
		N	9.21	9.79
7	94	C	58.29	59.80
		H	2.96	2.87
		N	13.33	14.94
8	87	C	60.93	60.96
		H	4.50	4.48
		N	4.40	4.44
9	99	C	55.67	55.66
		H	4.69	4.67
		N	11.98	12.17
10	62	C	56.42	58.58
		H	5.42	5.62
		N	9.48	10.98
11	89	C	60.76	62.11
		H	5.44	5.69
		N	8.92	9.88
12	89	C	57.27	57.77
		H	5.19	5.29
		N	8.38	9.10
13	59	C	58.28	57.93
		H	4.45	4.48
		N	9.27	9.65

© 2005 NRC Canada

Table 2. Characteristic IR vibrations (in cm^{-1}) for **2–13**.

Compound	ν_{OH}	$\nu_{C\text{-}Har.}$	$\nu_{C\text{-}Hal.}$	$\nu_{C=O}$	$\nu_{P=N}$	$\nu_{N\text{-}O\text{-}C}$	$\nu_{P\text{-}O\text{-}C}$
2	—	3040, 3100	2732, 2820	1706	1184	—	962
3	3340	3044, 3086	2903, 2980	—	1187	—	949
4	—	3059, 3100	2881, 2981	—	1179	1054	954
5	—	2976, 3087	2868, 2981	—	1179	1039	950
6	—	3060, 3097	2883, 2991	1764	1182	1070	973
7	—	3065, 3103	2951, 2997	—	1188	—	950
8	—	3067, 3105	2927, 3002	1685	1188	—	949
9	3460	3058, 3109	2913, 2981	—	1208	—	960
10	3309	2978, 3065	2886, 2931	—	1183	1048	956
11	—	2981, 3078	2864, 2920	—	1183	1036	959
12	—	3058, 3104	2937, 2981	1765	1186	1068	953
13	3410	3038, 3068	2860, 2927	1755	1173	1020	958

Table 3. ^{31}P NMR data for **1–13**.

Compound	Main compound (ppm)	Minor isomer (ppm)
1	20.12	—
2	8.33	—
3	17.21	17.26
4	7.49	—
5	9.49	—
6	8.33	8.21
7	7.51	—
8	8.05	—
9	9.04	9.01
10	9.07	—
11	9.01	8.98
12	8.80	—
13	8.73	—

Table 4. ^{1}H NMR data for **2–13**.

Compound	^{1}H NMR
2	7.10 (d) : H^2 ($^4J_{POCCH}$ = 8.50), 7.60 (d) : H^3 ($^5J_{POCCCH}$ = 8.56), 9.90 (s) : H^5; H^2:H3:H^5 = 2:2:1
3	6.86 (d) : H^2 ($^4J_{POCCH}$ = 8.45), 7.28(d) : H^3 ($^5J_{POCCCH}$ = 8.50), 7.96 (s) : H^5, 10.17 (s) : H^6, 7.20 : H^2 (is.), 7.77 : H^3 (is.); H^2:H^3:H^5:H^6 = 2:2:1:1
4	6.88 (d) : H^2 ($^4J_{POCCH}$ = 8.54), 7.38 (d) : H^3 ($^5J_{POCCCH}$ = 8.61), 7.97 (s) : H^5, 4.08 (q) : H^6, 1.16 (t) : H^7
5	6.88 (d) : H^2 ($^4J_{POCCH}$ = 8.47), 7.38 (d) : H^3 ($^5J_{POCCCH}$ = 8.55), 8.03 (s) : H^5, 4.55 (d) : H^6 (J = 5.59), 5.90 (m) : H^7, 5.10 (d) : H^8_{cis} (J = 10.23), 5.25 (d) : H^8_{trans} (J = 16.28)
6	7.05 (d) : H^2, 7.61 (d) : H^3, 8.60 (s) : H^5, 1.10 (t) : H^8, 2.50 (k): H^7
7	7.15 (d) : H^2, 7.85 (d) : H^3
8	7.05 (d) : H^2, 7.85 (d) : H^3, 2.45 (s) : H^6; H^2:H^3:H^6 = 2:2:3
9	6.85 (d) : H^2, 7.50 (d) : H^3, 2.10 (s) : H^6, 11.25 (s) : H^7; H^2:H^3:H^6:H^7 = 2:2:3:1
10	11.30 (s) : H^{15}, 6.90 : H_2, H^{10}, 7.55 : H_3, H^{11}, 4.15 (q) : H^7, 2.15 (s) : H^6, H^{14}, 1.25 (t) : H^8
11	6.88 (d) : H^2, 7.50 (d) : H^3, 6.00 (m) : H^8, 5.20 (d) : H^9_{cis}, 5.35 (d) : H^9_{trans}, 4.65 (d) : H^7, 2.15 (s) : H^6
12	7.00 (d) : H^2, 7.65 (d) : H^3, 2.60 (q) : H^8, 2.30 (s) : H^6, 1.15 (s) : H^9
13	11.25 (s) : H^{16}, 7.00 : H^2, H^{11}, 7.80 : H^3, H^{12}, 6.1 (d) : H^9_{cis}, 6.30–6.60 (m) : H^8, H^9_{trans}, 2.3 (s) : H^6, 2.10 (s) : H^{15}

Note: For numbering see Scheme 1; coupling constants J (Hz). Acetone-d (for **3–5**), $CDCl_3$-d (for **2**) and DMSO-d (for **6–13**) were used as solvents in NMR analyses. Isomer (is), singlet (s).

9.90 ppm. The azomethine protons for **3–6** are observed at 7.96 (H^5), 7.97 (H^5), 8.03 (H^5), and 8.60 (H^5) ppm, respectively. The aromatic protons for all the compounds appear between 6.85 and 7.85 ppm.

The detailed ^{13}C NMR spectral data are given in Table 5. The aldehyde carbon atom for **2** and ketone carbon atom for **8** are observed at 190.83 and 197.00 ppm, respectively, at the lowest downfield of the carbon atoms. Compared to **3**

© 2005 NRC Canada

Table 5. ^{13}C NMR data for **2–13**.

Compound	^{13}C NMR
2	121.60 : C^2, 131.40 : C^3, 134.14 : C^4, 154.80 : C^1, 190.83 : C^5
3	121.50 : C^2, 121.33 : C^2 (is), 129.00 : C^3, 129.37 : C^3 (is), 131.00 : C^4, 131.00 : C^4 (is), 148.19 : C_5, 151.70 : C^1
4	14.46 : C^7, 69.81 : C^6, 121.57 : C^2, 128.62 : C^3, 130.46 : C^4, 147.35 : C^5, 151.63 : C^1
5	151.63 : C^1, 147.93 : C^5, 134.92 : C^7, 130.20 : C^4, 128.72 : C^3, 121.57 : C^2, 117.33 : C^8, 75.29 : C^6
6	9.22 : C^8, 25.85 : C^7, 121.89 : C^2, 121.58 : C^2 (is), 128.13 : C^4, 130.27 : C^3, 134.93 : C^3 (is), 152.16 : C^1, 155.86 : C^5, 172.03 : C^6
7	152.88 : C^1, 135.07 : C^3, 121.99 : C^2, 118.85 : C^4, 109.37 : C^5
8	27.04 : C^6, 120.96 : C^2, 131.20 : C^3, 134.54 : C^4, 153.27 : C^1, 197.00 : C^5
9	11.90 : C^6, 120.93 : C^2, 127.36 : C^3, 134.64 : C^4, 150.39 : C^1, 152.51 : C^5
10	153.08 : C^{13}, 152.48 : C^5, 150.53 : C^9, 150.27 : C^1, 134.60 : C^{12}, 133.72 : C^4, 127.58 : C^{11}, 127.33 : C^3, 120.93 : C^2, C^{10}, 69.53 : C^7, 15.05 : C^8, 12.63 : C^{14}, 11.82 : C^6
11	12.69 : C^6, 74.88 : C^7, 74.57 : C^7 (is), 117.75 : C^9, 117.47 : C^9 (is), 120.99 : C^2, 120.53 : C^2 (is), 127.69 : C^3, 133.53 : C^4, 134.97 : C^8, 150.67 : C^1, 153.67 : C^5, 152.34 : C^5 (is)
12	9.29 : C^9, 14.19 : C^6, 26.12 : C^8, 121.16 : C^2, 128.94 : C^3, 132.25 : C^4, 151.68 : C^1, 161.91 : C^5, 171.88 : C^7
13	163.38 : C^7, 162.89 : C^5, 152.55 : C^{14}, 151.73 : C^1, 150.22 : C^{10}, 134.77 : C^4, 133.31 : C^{13}, 132.03 : C^9, 129.02 : C^3, 127.43 : C^8, 126.94 : C^{12}, 121.16 : C^2, 120.96 : C^{11}, 14.35 : C^6, 11.82 : C^{15}

Note: For numbering see Scheme 1. Acetone-*d* (for **3–5**), $CDCl_3$-*d* (for **2**), and DMSO-*d* (for **6–13**) were used as solvents in NMR analyses. Isomer (is).

and **9**, the azomethine carbon atoms in the substituted moiety of the molecules are shifted to the lower downfield for compound **6**, **11**, **12**, and **13**, except **4**, **5**, and **10** in which the alkyl groups release an electron to the molecule. But the azomethine resonances do not change or change very little in the nonsubstituted moieties of **10** and **13**. In addition, the ^{13}C NMR data clearly show that compound **10** is referred to as the geminal isomer. There are essentially two different sets of carbon atoms within the geminal structures, but three sets within the nongeminal structures for the tetrasubstituted cyclotriphosphazenes. The resonances of two sets of carbon atoms were observed in the ^{13}C NMR spectrum of **10**. These results indicate the geminal structure. A triplet and a doublet are expected in the ^{31}P NMR spectra of geminal structures for tetrasubstituted cyclotriphosphazene (**10**), but the main peak was observed as a singlet. These results show that the phosphorus signals are not affected from the binding groups because the substituents at the end of the molecule are far from the phosphorus atoms.

Conclusion

Hexasubstituted compounds were obtained from the reactions of hexakis{4-[(hydroxyimino)methyl]phenoxy}cyclotriphosphazene (**3**) with ethyl bromide, allyl bromide, and propanoyl chloride; however, the oxime groups on **3** rearranged to nitrile in the reaction of **3** with acriloyl chloride. Hexasubstituted compounds were also obtained from the reactions of hexakis{4-[(1)-*N*-hydroxyethaneimidoyl]phenoxy}cyclotriphosphazene (**9**) with allyl bromide and propanoyl chloride. The tetrasubstituted product, which is a geminal isomer, and pentasubstituted products were obtained from the reactions of **9** with ethyl bromide and acriloyl chloride, respectively.

Acknowledgement

We thank the Firat University Research Fund for support (project no. FUBAP 923).

References

1. H.R. Allcock. Phosphorus–nitrogen compounds. Academic Press, New York. 1972.
2. C. Diaz, I. Izquierdo, F. Mendizabal, N. Yutronic. Inorg. Chim. Acta, **294**, 20 (1999).
3. A. Kılıç, S. Begeç, B. Çetinkaya, T. Hökelek, Z. Kılıç, N. Gündüz, and M. Yıldız. Heteroat. Chem. **7**, 249 (1996).
4. G.A. Carriedo, F.J.G. Alonso, P.G. Elipe, E. Brillas, and L. Julia. Org. Lett. **3**, 1625 (2001).
5. H.R. Allcock, C.T. Morrissey, W.K. Way, and N. Winograd. Chem. Mater. **8**, 2730 (1996).
6. H.R. Allcock. *In* Inorganic and organometallic polymers. *Edited by* H.R. Allcock, M. Zeldin, and K.J. Wynne. ACS Symposium Series 360. 1988. Chap. 19.
7. C.T. Laurencin, H.J. Koh, T.X. Neenan, H.R. Allcock, R. Langer. J. Biomed. Mater. Res. **21**, 1231 (1987).
8. H.R. Allcock, S.R. Pucher, R.J. Fitzpatrick, and K. Rashid. Biomaterials, **13**, 857 (1992).
9. G. Giavaresi, M. Tschon, V. Borsari, J.H. Daly, J.J. Liggat, M. Fini, V. Bonazzi, A. Nicolini, A. Carpi, M. Morra, C. Cassinelli, and R. Giardino. Biomedicine and Pharmacotherapy, **58**, 411 (2004).
10. G. Fantin, M. Fogagnolo, M. Gleria, A. Medici, F. Minto, and P. Pedrini. Tetrahedron, **52**, 9535 (1996).
11. K. Brandt, R. Kruszynski, T.J. Bartczak, and I.P. Czomperlik. Inorg. Chim. Acta, **322**, 138 (2001).
12. A.I. Ozturk, O. Yılmaz, S. Kırbag, and M. Arslan. Cell. Biochem. Funct. **18**, 117 (2000).
13. V. Konar, O.Yılmaz, A.I. Ozturk, S. Kırbag, and M. Arslan. Bioorg. Chem. **28**, 214 (2000).
14. O. Yılmaz, F. Aslan, A.I. Ozturk, N. Vanlı, S. Kırbag, and M. Arslan. Bioorg. Chem. **30**, 303 (2002).
15. C.W. Allen. J. Fire Sci. **11**, 320 (1993).
16. M. Gleria and R.D. Jaeger. J. Inorg. Organomet. Polym. **11**, 1(2001).
17. M.T.R. Laguna, M.P. Tarazona, G.A. Carriedo, F.J.G. Alonso, J.I. Fidalgo, and E. Saiz. Macromolecules, **35**, 7505 (2002).
18. E. Çil, M. Arslan, F. Aslan, and A.I. Ozturk. Phosphorus Sulfur Silicon Relat. Elem. **178**, 1037 (2003).
19. A.I. Ozturk, F. Aslan, E. Cil, M. Arslan, and A. Kılıç. Phosphorus Sulfur Silicon Relat. Elem. **178**, 2097 (2003).

© 2005 NRC Canada

20. M. Arslan, F. Aslan, and A.I. Ozturk. Heteroat. Chem. **14**, 138 (2003).
21. F. Aslan, A.I. Ozturk, and M. Arslan. Heteroat. Chem. **14**, 413 (2003).
22. C.V. Diaz and I.G. Izquierdo. Polyhedron, **18**, 1479 (1999).
23. R. Bertani, G. Facchin, and M. Gleria. Inorg. Chim. Acta, **165**, 73 (1989).
24. A. Kılıç, S. Beğeç, Z. Kılıç, and T. Hokelek. J. Mol. Struct. **516**, 255 (2000).
25. G.A. Carriedo, L.F. Catuxo, F.J.G. Alonso, P.G. Elipe, P.A. Gonzalez, and G. Sanchez. J. Appl. Polym. Sci. **59**, 1879 (1996).
26. H.R. Allcock and M.L. Turner. Macromolecules, **26**, 3 (1993).
27. G.A. Carriedo, L.F. Catuxo, F.J.G. Alonso, P.G. Elipe, and P.A. Gonzalez. Macromolecules, **29**, 5320 (1996).
28. U. Belluco, R. Bertani, R.A. Michelin, M. Mozzan, F. Zingales, and M. Gleria. Inorg. Chim. Acta, **229**, 13 (1995).
29. M.B. McIntosh, T.J. Hartle, and H.R. Allcock. J. Am. Chem. Soc. **121**, 884 (1999).
30. F. Palacios, C. Alonso, G.G. Rubialesa, and J.M. Ezpeleta. Tetrahedron, **60**, 2469 (2004).
31. W. Yuan, L. Zhu, X. Huang, S. Zheng, and X. Tang. Eur. Polym. J. **41**, 1867 (2005).
32. W. Yuan, X. Tang, X. Huang, and S. Zheng. Polymer, **46**, 1701 (2005).
33. G. Fontana, F. Minto, M. Gleria, G. Facchin, R. Bertani, and G. Favero. Eur. Polym. J. **32**, 1273 (1996).
34. T. Muraki, M. Ueta, E. Ihara, and K. Inoue. Polym. Degrad. Stab. **84**, 87 (2004).
35. N. Coşkun and N. Arıkan. Tetrahedron, **55**, 11943 (1999).
36. H.J.P. Lijser, F.H. Fardoun, J.R. Sawyer, and M. Quant. Org. Lett. **4**, 2325 (2002).
37. H.R. Allcock, T.X. Neenan, and W.C. Kossa. Macromolecules, **15**, 693 (1982).
38. G.A. Carriedo, L.F. Catuxo, F.J.G. Alonso, and P.G. Elipe. J. Organomet. Chem. **503**, 59 (1995).

© 2005 NRC Canada

$SnCl_4$–I_2 mediated regioselective 6-endo- and 5-exo-cyclization of *ortho*-allylenols

K.C. Majumdar, A. Biswas, and P.P. Mukhopadhyay

Abstract: 3-Allyl-4-hydroxycoumarins and 4-allyl-3-hydroxycoumarins are obtained in 90%–92% yields by the thermal [3,3] sigmatropic rearrangement of the corresponding ethers. 3-Allyl-4-hydroxy-6-methylpyrone is obtained from the direct alkylation of 4-hydroxy-6-methylpyrone with allyl halide. These substrates on treatment with $SnCl_4$–I_2 at 25 °C give a mixture of both *5*-exo- and 6-endo-cyclization products. However, regioselective formation of 5-exo products is observed when the reactions are conducted at lower temperatures (0–5 °C, kinetically controlled), while the reaction at a higher temperature (50 °C, thermodynamically controlled) affords regioselectively 6-endo cyclization products.

Key words: stannic chloride, iodine, claisen rearrangement, 6-endocyclization, 5-exocyclization, kinetically controlled reaction, thermodynamically controlled reaction.

Résumé : On a obtenu les 3-allyl-4-hydroxycoumarines et les 4-allyl-3-hydroxycoumarines avec des rendements de 90 % à 92 % par un réarrangement sigmatropique [3,3] thermique des éthers correspondants. On a obtenu la 3-allyl-4-hydroxy-6-méthylpyrone par alkylation directe de la 4-hydroxy-6-méthylpyrone avec un halogénure d'allyle. Le traitement de ces substrats avec du $SnCl_4$–I_2, à 25 °C, conduit à un mélange des deux produits cyclisation, 5-exo- et 6-endo-. Toutefois, on observe la formation sélective des produits 5-exo- quand les réactions sont effectuées à des températures plus basses, 0 à 5 °C (contrôle cinétique) alors que la réaction à une température plus élevée, 50 °C (contrôle thermodynamique) conduit régiosélectivement aux produits de cyclisation 6-endo-.

Mots clés : chlorure stannique, iode, réarrangement de Claisen, cyclisation 6-endo, cyclisation 5-exo, réaction cinétiquement contrôlée, réaction sous contrôle thermodynamique.

[Traduit par la Rédaction]

Introduction

Coumarins fused with other heterocyclic rings are known to have interesting biological and photodynamic properties (1). This has encouraged a flurry of research activities with regard to methodologies for the preparation of these compounds. Thus, a number of protocols have been reported (2) for the synthesis of various 3,4-fused furo- and pyranocoumarins as some members belonging to these two families have shown (3) useful levels of biological activity. 4-Hydroxy-6-methyl-2-pyrone and its derivatives are known to act as specific inhibitors of human leukocyte elastase (4) and also as anticoagulant agents (5).

Recently, we have reported *N*-iodosuccinimide (NIS) mediated heterocyclization of *ortho*-cyclohex-2′-enyl phenols (6) and 3-cyclohex-2′-enyl-4-hydroxycoumarin (7) in acetonitrile at 0–5 °C in almost quantitative yield. We have also reported heterocyclization using pyridine hydrotribromide (8), mercuric acetate (9), and hexamethylenetetramine hydrotribromide (10). However, no study on the temperature dependence of these reactions was conducted. NIS has been used for 6-endo heterocyclization of different substrates via an iodonium intermediate. Recently (11), $SnCl_4$–I_2 has been found to be a convenient and practical reagent for providing positive iodine. This prompted us to undertake a study on the heterocyclization of 3-allyl-4-hydroxycoumarin, 4-allyl-3-hydroxycoumarin, and 3-allyl-4-hydroxy-6-methylpyrones. Herein we report the results.

The starting materials 3-allyl-4-hydroxycoumarins (12) (**4a**–**4e**) and 4-allyl-3-hydroxycoumarins (13) (**5a**, **5b**) were obtained in 90%–92% yield by the thermal rearrangement of the corresponding allyl ethers in refluxing chlorobenzene (132 °C) for 8 h. 3-Allyl-4-hydroxy-6-methylpyrones (**6**) were prepared from the direct alkylation of 4-hydroxy-6-methylpyrones (**1e**) with allyl halide (**2a**). The ethers **3a**–**3g** were in turn prepared by the reaction of substrates **1a**–**1d** with allylic halides (**2a**, **2b**) in refluxing acetone in the presence of anhydr. K_2CO_3 (Scheme 1).

Results and discussion

Substrate **4a** was treated with $SnCl_4$–I_2 in dichloromethane or acetonitrile at 25 °C for 6 h to give a mixture of two products. The mixture on separation afforded kinetically controlled 2,3-dihydro-2-iodomethylfuro[3,2-*c*]coumarin (**7a**, 65%) as the major product and thermodynamically controlled 3-iodo-2,3,4-trihydropyrano[3,2-*c*]coumarin (**8a**, 25%) as the minor product (Scheme 2). The other substrates (**4b**–**4e**, **5a**, **5b**, and **6**) were also similarly treated to give a mixture of products, which were separated by chromatogra-

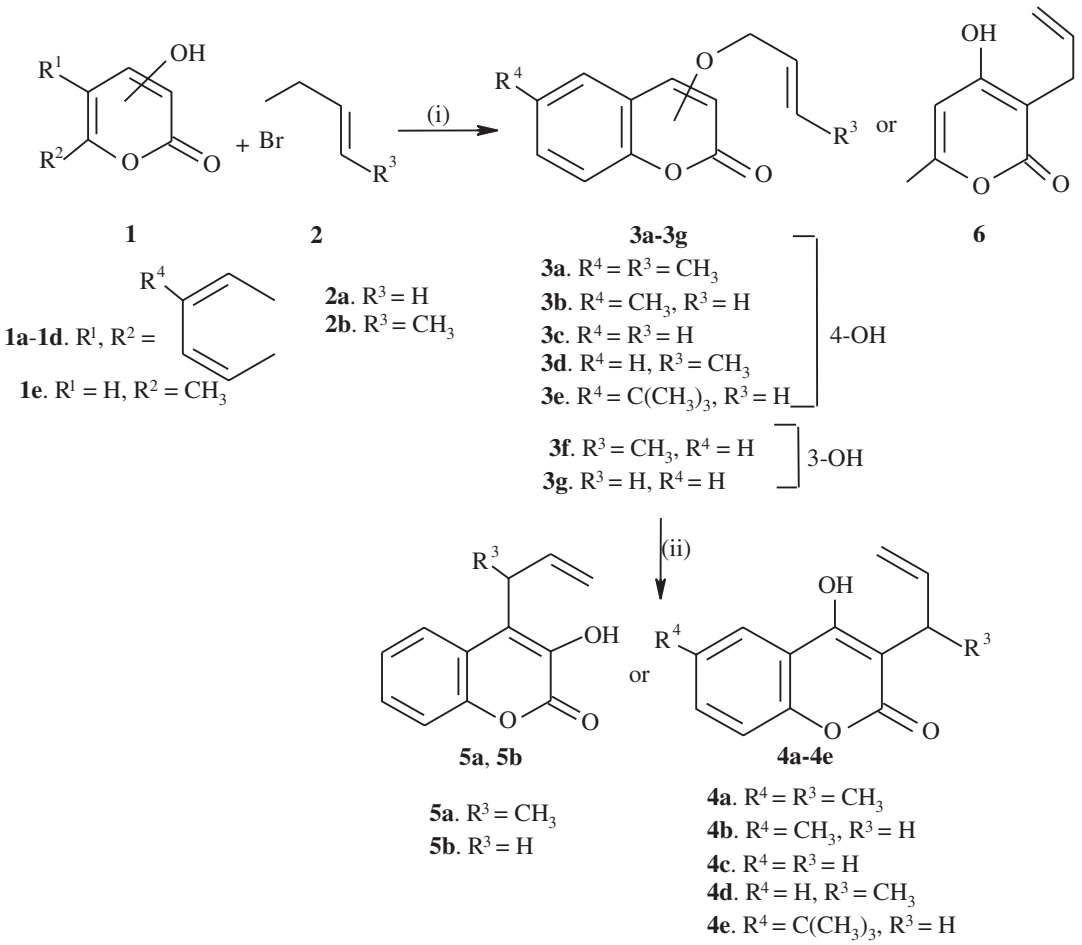
Received 28 February 2005. Published on the NRC Research Press Web site at http://canjchem.nrc.ca on 3 February 2006.

K.C. Majumdar,[1] A. Biswas, and P.P. Mukhopadhyay. Department of Chemistry, University of Kalyani, Kalyani 741 235, West Bengal, India.

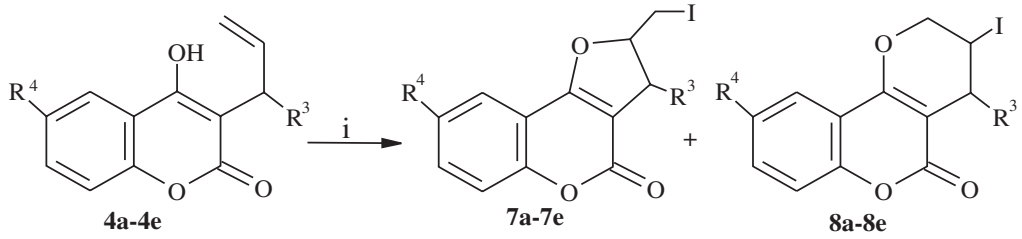
[1]Corresponding author (e-mail: kcm_ku@yahoo.co.in and kcm@klyuniv.ernet.in).

 doi: 10.1139/V05-212 © 2005 NRC Canada

Scheme 1. Reagents and conditions: (*i*) Me_2CO, KCO_3, reflux, 6–8 h; (*ii*) chlorobenzene, reflux, 8 h.



Scheme 2. Reagents and conditions: (*i*) $SnC1_4$–I_2, $CHC1_2$, r.t., stirring, 6 h.



phy (Table 1). However, if the reaction mixture obtained at 25 °C in acetonitrile was heated to 50 °C. only the six-membered ring products (**8a**–**8e**, **10a**, **10b**, **12**) were obtained. The five-membered ring products (**7a**–**7e**, **9a**, **9b**, **11**) when heated at 50 °C also afforded exclusively the six-membered ring products (**8a**–**8e**, **10a**, **10b**, **12**).

These reactions were then conducted at different temperatures to ascertain the effect of temperature on the selectivity of the heterocyclization. Substrate **4a** was allowed to react with $SnCl_4$–I_2 at 0–5 °C in dichloromethane or acetonitrile for 2 h and to our surprise we obtained a single product (**7a**, kinetically controlled) in almost quantitative yield. The other substrates (**4b**–**4e**, **5a**, **5b**, **6**), when treated under the same reaction conditions also afforded the single products **7b**–**7e**, **9a**, **9b**, and **11** in 85%–92% yields. The same reaction was then conducted in acetonitrile at 50 °C for 1 h to give a thermodynamically controlled six-membered heterocyclic product (**8a**, 72%) without formation of the five-membered product that we obtained when the reaction was conducted at 0–5 °C. In all other cases (**4b**–**4e**, **5a**, **5b**, **6**), the six-membered ring products (**8b**–**8e**, **10a**, **10b**, **12**) were exclusively obtained in 65%–72% yield at 50 °C. The reactions were also conducted in various solvents. Dichloromethane and acetonitrile were found to provide a clean reaction for the exclusive formation of the five-membered ring and acetonitrile gave the best result for the synthesis of six-membered cyclic products (Table 1).

A literature search revealed that $SnCl_4$–I_2 has been used for the cyclization of *ortho*-allyl phenols by Orito et al. (11). The formation of five-membered and six-membered products has been explained in terms of substituent effects. In the present study we have successfully demonstrated the

© 2005 NRC Canada

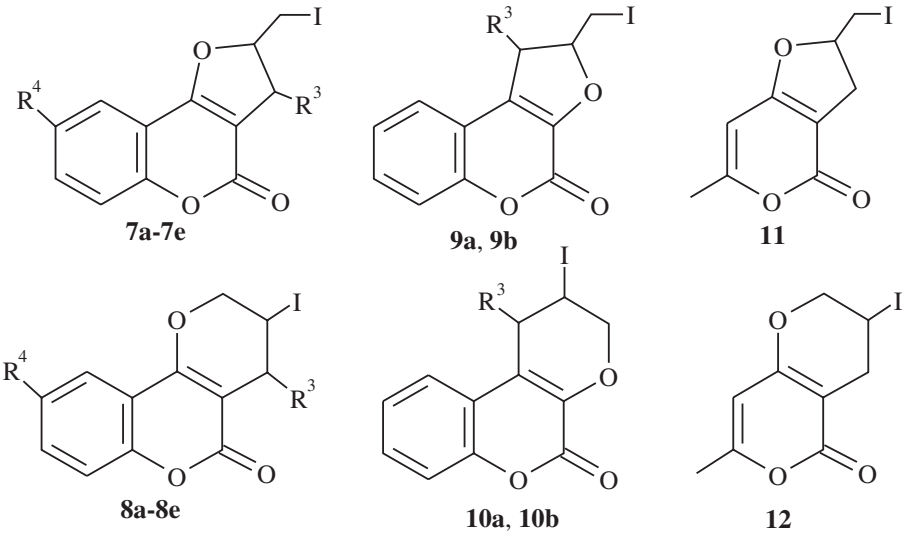


Table 1. Yield of 5-exo and 6-endo products in different reaction conditions.

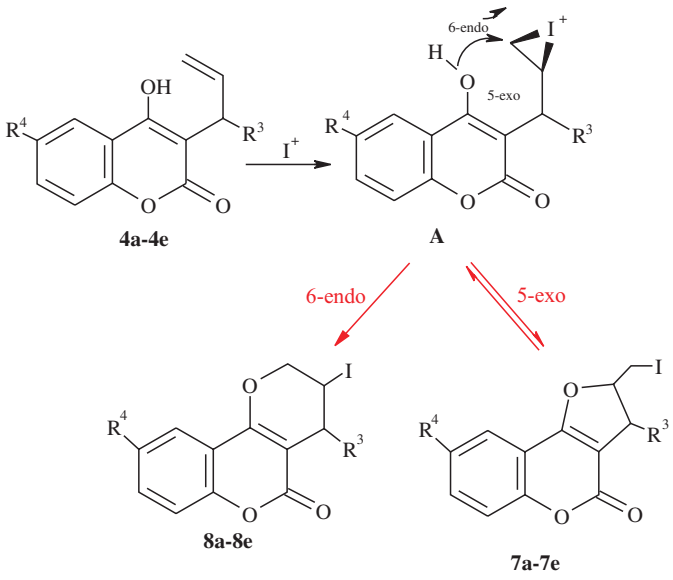
Substrate	Reaction condition	6-endo (yield in %)		5-exo (yield in %)	
4a	A		25		65
	B	**8a**	—	**7a**	90
	C		70[a]		—
4b	A		30		60
	B	**8b**	—	**7b**	86
	C		72[a]		—
4c	A		30		62
	B	**8c**	—	**7c**	90
	C		66[a]		—
4d	A		28		62
	B	**8d**	—	**7d**	85
	C		70[a]		—
4e	A		22		65
	B	**8e**	—	**7e**	92
	C		65[a]		—
5a	A		32		58
	B	**10a**	—	**9a**	85
	C		72[a]		—
5b	A		30		60
	B	**10b**	—	**9b**	88
	C		70[a]		—
6	A		28		64
	B	**12**	—	**11**	90
	C		68[a]		—

Note: Reaction conditions: A = $SnCl_4$–I_2 added at room temp. in CH_2Cl_2 solution and stirring for 6 h. B = $SnCl_4$–I_2 added at 0–5 °C in CH_2Cl_2 solution and stirring for 2 h. C = $SnCl_4$–I_2 added at 50 °C in CH_3CN solution and stirring for 1 h at the same temperature.

[a]Yield given represents isolated yield. In the case of reaction at 50 °C, five-membered products were obtained with additional amounts (5%–10%) of by-products arising out of the addition of iodine to the olefinic double bond were also detected.

temperature-dependent regioselectivity (kinetic and thermodynamic control) for the formation of five- and six-membered heterocyclic compounds.

Scheme 3.



The key step of the synthesis that we report here is based on the intramolecular cyclization allowed by the activation of an olefinic double bond by means of an iodonium intermediate (**A**). The intramolecular ring closure may occur via a 5-exo-trig at 0–5 °C (kinetically controlled) and by a 6-endo-trig at 50 °C (equilibrium controlled) to give five-membered and six-membered heterocyclic rings, respectively (Scheme 3). As the five-membered ring products (**7a**–**7e**, **9a**, **9b**, **11**) are converted to the six-membered ring products (**8a**–**8e**, **10a**, **10b**, **12**) at 50 °C, we can say that the thermodynamic mixture must be formed through the reversible conversion of the five-membered ring to the six-membered ring via a common intermediate (**A**), i.e., the five-membered ring is in reversible equilibrium with the iodonium ion intermediate (**A**).

Thus, we have been able to demonstrate the selectivity in the formation of five- and six-membered oxygen heterocyclic rings by the combined Claisen rearrangement fol-

© 2005 NRC Canada

lowed by temperature-dependent ring closure methodology. The reagent $SnCl_4$–I_2 used for this protocol is quite cheap and easily accessible compared with other reagents for similar cyclizations (12). This offers a facile synthesis for potentially bioactive heterocycles.

Experimental

Melting points were determined in a open capillary and are uncorrected. IR spectra were recorded on a PerkinElmer L 120-000A spectrometer (ν_{max} in cm^{-1}) and solid samples were recorded in KBr disks. UV absorption spectra were recorded in EtOH on a Shimadzu UV-2401PC spectrophotometer (λ_{max} in nm). ^1H NMR (300 and 500 MHz) and ^{13}C NMR (75.5 and 125 MHz) spectra were recorded on Bruker DPX-300 and Bruker DPX-500 spectrometers in $CDCl_3$ (chemical shifts in δ) with TMS as internal standard. Elemental analyses and mass spectra were recorded on a LECO 932 CHNS analyser and on a JEOL JMS600 instrument, respectively. ^1H NMR and ^{13}C NMR spectra were recorded at the Indian Institute of Chemical Biology, Kolkata, India and the Bose Institute, Kolkata, India. Silica gel (60–120 mesh, Spectrochem, India) was used for chromatographic separation. Silica gel G (E-Merck, India) was used for TLC. Petroleum ether refers to the fraction boiling between 60 and 80 °C.

General procedure for the alkylation of compounds 1a–1e

A mixture of 4-hydroxy coumarin or 4-hydroxy-6-methyl-2-pyrone or 3-hydroxy coumarin **1a**–**1e** (5 mmol), appropriate halides **2a** and **2b** (5 mmol), and anhydr. K_2CO_3 (3 g) was refluxed in dry acetone (150 mL) for 6–8 h. The reaction mixture was then cooled, filtered, and the solvent was removed. The residual mass was subjected to column chromatography over silica gel. Compounds **3a**–**3g** and **6** were obtained when the column was eluted with petroleum ether – ethyl acetate (9:1).

Compounds **3b**–**3d**, **3f**, and **3g** were reported earlier (12, 13).

Compound 3a

White solid, mp 124–126 °C; yield: 82%. UV (EtOH, nm) λ_{max}: 311, 279, 268, 229. IR (KBr, cm^{-1}) ν_{max}: 1439, 1574, 1707. ^1H NMR ($CDCl_3$, 300 MHz) δ: 1.8 (d, J = 6 Hz, 3H, CH_3), 2.41 (s, 3H, ArCH_3), 4.60 (d, J = 6 Hz, 2H, -OCH_2), 5.66 (s, 1H, COCH), 5.72–5.80 (m, 1H, CH_3CH), 5.90–5.99 (m, 1H, -OCH_2CH), 7.19–7.62 (m, 3H, ArH). MS *m*/*z*: 230 (M^+). Anal. calcd. for $C_{14}H_{14}O_3$ (%): C 73.03, H 6.13; found: C 73.21, H 6.28.

Compound 3e

White solid, mp 133–135 °C; yield: 80%. UV (EtOH, nm) λ_{max}: 310, 278, 268, 230. IR (KBr, cm^{-1}) ν_{max}: 1437, 1572, 1706. ^1H NMR ($CDCl_3$, 300 MHz) δ: 1.36 (s, 9H, C(CH_3)$_3$), 4.71 (d, J = 6 Hz, 2H, -OCH_2), 5.41–5.54 (m, 2H, =CH_2), 5.68 (s, 1H, COCH), 6.04–6.17 (m, 1H, CH=CH_2), 7.24–7.82 (m, 3H, ArH). MS *m*/*z*: 258 (M^+). Anal. calcd. for $C_{16}H_{18}O_3$ (%): C 74.40, H 7.02; found: C 74.22, H 7.24.

Compound 6

White solid, mp 154–156 °C; yield: 90%. UV (EtOH, nm) λ_{max}: 290, 208. IR (KBr, cm^{-1}) ν_{max}: 1589, 1624, 1668, 3251. ^1H NMR ($CDCl_3$, 300 MHz) δ: 2.22 (s, 3H, CH_3), 3.24 (d, J = 6.0 Hz, 2H, CH_2), 5.05–5.19 (m, 2H, =CH_2), 5.86–5.99 (m, 1H, CH_2=CH), 6.15 (s, 1H, =CH). MS *m*/*z*: 166 (M^+). Anal. calcd. for $C_9H_{10}O_3$ (%): C 65.05, H 6.06; found: C 65.31, H 5.84.

General procedure for rearrangement of compounds 3a–3g

The starting ether (**3a**–**3g**, 2 mmol) was refluxed in chlorobenzene (4 mL) in an oil bath for 8 h. The chlorobenzene was removed in vacuo and the residual mass was chromatographed over silica gel. Elution of the column with petroleum ether (60–80 °C) removed the residual chlorobenzene and then a white solid was obtained by eluting the column with petroleum ether – ethyl acetate (9:1).

Compounds **4b**–**4d** and **5a** and **5b** were reported earlier (12*a*, 13).

Compound 4a

White solid, mp 162–164 °C; yield: 92%. UV (EtOH, nm) λ_{max}: 315, 285, 273, 229. IR (KBr, cm^{-1}) ν_{max}: 1564, 1611, 1693, 3218. ^1H NMR ($CDCl_3$, 300 MHz) δ: 1.39 (d, J = 7 Hz, 3H, CHCH_3), 2.40 (s, 3H, ArCH_3), 4.02–4.07 (m, 1H, CH_3CH), 5.51–5.61 (m, 2H, =CH_2), 6.35–6.46 (m, 1H, CH_2=CH), 7.18–7.56 (m, 3H, ArH). MS *m*/*z*: 230 (M^+). Anal. calcd. for $C_{14}H_{14}O_3$ (%): C 73.03, H 6.13; found: C 73.19, H 6.02.

Compound 4e

White solid, mp 142–144 °C; yield: 90%. UV (EtOH, nm) λ_{max}: 314, 284, 273, 230. IR (KBr, cm^{-1}) ν_{max}: 1580, 1618, 1695, 3250. ^1H NMR ($CDCl_3$, 300 MHz) δ: 1.36 (s, 9H, C(CH_3)$_3$), 3.49 (d, J = 6.4 Hz, 2H, CH_2), 5.28–5.43 (m, 2H, =CH_2), 6.97–6.11 (m, 1H, CH_2=CH), 7.24–7.81 (m, 3H, ArH). MS *m*/*z*: 258 (M^+). Anal. calcd. for $C_{16}H_{18}O_3$ (%): C 74.40, H 7.02; found: C 74.59, H 6.86.

General procedure for the cyclization of compounds 4a–4e and 5a, 5b, and 6

$SnCl_4$ (0.13 mL, 2 mmol) and I_2 (512 mg, 2 mmol) were added to a CH_2Cl_2 (10 mL) solution of the compounds **4a**–**4e** or **5a**, **5b**, or **6** (2 mmol) at room temperature. The mixture was then magnetically stirred for 6 h. The mixture was treated with ice-cold water (40 mL), and then washed with 5% $Na_2S_2O_3$ (2 × 20 mL) and water (2 × 20 mL) and dried over Na_2SO_4. The final residual mass after removal of the solvent was subjected to column chromatography over silica gel and the cyclic products were separated out.

Compound 7a

White solid, mp 130–132 °C; yield: 65%. UV (EtOH, nm) λ_{max}: 334, 277, 233. IR (KBr, cm^{-1}) ν_{max}: 1461, 1688, 2958. ^1H NMR ($CDCl_3$, 300 MHz) δ: 1.49 (d, J = 7.0 Hz, 3H, CH_3), 2.45 (s, 3H, ArCH_3), 3.35–3.49 (m, 3H, -CH_2I and CH_3CH), 4.54 (dt, J = 7.0, 5.0 Hz, 1H, -OCH), 7.29–7.99 (m, 3H, ArH). ^{13}C NMR ($CDCl_3$, 75.5 MHz) δ: 5.4 (d), 19.6 (q), 20.8 (q), 40.1 (d), 89.7 (t), 98.8 (s), 117.1 (d), 123.7 (s), 125.3 (d), 133.5 (d), 135.5 (s), 151.6 (s), 167.4 (s), 175.2 (s).

© 2005 NRC Canada

MS *m*/*z*: 356 (M^+). Anal. calcd. for $C_{14}H_{13}O_3I$ (%): C 47.21, H 3.68; found: C 47.09, H 3.82.

Compound 7b

White solid, mp 127–129 °C; yield: 62%. UV (EtOH, nm) λ_{max}: 332, 261, 217. IR (KBr, cm^{-1}) ν_{max}: 1445, 1700, 2920. ^1H NMR ($CDCl_3$, 300 MHz) δ: 2.42 (s, 3H, ArCH_3), 2.94 (dd, *J* = 15.5, 6.0 Hz, 1H, =CCH_2), 3.31 (dd, *J* = 15.5, 10.2 Hz, 1H, =CCH_2), 3.45 (dd, *J* = 10.2, 6.0 Hz, 1H, -CH_2I), 3.50 (dd, *J* = 10.2, 5.0 Hz, 1H, -CH_2I), 5.11–5.21 (m, 1H, -OC*H*), 7.27–7.44 (m, 3H, Ar*H*). MS *m*/*z*: 342 (M^+). Anal. calcd. for $C_{13}H_{11}O_3I$ (%): C 45.61, H 3.22; found: C 45.69, H 3.34.

Compound 7c

White solid, mp 138–140 °C; yield: 60%. UV (EtOH, nm) λ_{max}: 326, 261, 217. IR (KBr, cm^{-1}) ν_{max}: 1440, 1690, 2910. ^1H NMR ($CDCl_3$, 300 MHz) δ: 2.96 (dd, *J* = 15.5, 6.0 Hz, 1H, =CCH_2), 3.33 (dd, *J* = 15.5, 10.2 Hz, 1H, =CCH_2), 3.45 (dd, *J* = 10.2, 6.0 Hz, 1H, -CH_2I), 3.51 (dd, *J* = 10.2, 6.0 Hz, 1H, -CH_2I), 5.13–5.23 (m, 1H, OC*H*), 7.27–7.68 (m, 4H, Ar*H*). MS *m*/*z*: 328 (M^+). Anal. calcd. for $C_{12}H_9O_3I$ (%): C 43.90, H 2.74; found: C 43.80, H 2.61.

Compound 7d

White solid, mp 121–123 °C; yield: 62%. UV (EtOH, nm) λ_{max}: 326, 311, 260, 217. IR (KBr, cm^{-1}) ν_{max}: 1450, 1685, 2920. ^1H NMR ($CDCl_3$, 300 MHz) δ: 1.47 (d, *J* = 7.0 Hz, 3H, CH_3), 3.38–3.56 (m, 3H, -CH_2I and CH_3C*H*), 4.66 (dt, *J* = 7.0, 5.0 Hz, 1H, -OC*H*), 7.28–7.68 (m, 4H, Ar*H*). MS *m*/*z*: 342 (M^+). Anal. calcd. for $C_{13}H_{11}O_3I$ (%): C 45.61, H 3.22; found: C 45.72, H 3.29.

Compound 7e

White solid, mp 132–134 °C; yield: 65%. UV (EtOH, nm) λ_{max}: 332, 277, 233. IR (KBr, cm^{-1}) ν_{max}: 1469, 1695, 2960. ^1H NMR ($CDCl_3$, 300 MHz) δ: 1.38 (s, 9H, C(CH_3)$_3$), 2.97 (dd, *J* = 14.5, 6.4 Hz, 1H, =CCH_2), 3.26 (dd, *J* = 14.5, 9.5 Hz, 1H, =CH_2), 3.43 (dd, *J* = 10.6, 6.4 Hz, 1H, CH_2I), 3.48 (dd, *J* = 10.6, 5.1 Hz, 1H, -CH_2I), 5.03–5.12 (m, 1H, -OC*H*), 7.35–7.82 (m, 3H, Ar*H*). MS *m*/*z*: 258 (M^+). Anal. calcd. for $C_{16}H_{17}O_3I$ (%): C 50.02, H 4.46; found: C 50.19, H 4.61.

Compound 9a

White solid, mp 92–94 °C; yield: 58%. UV (EtOH, nm) λ_{max}: 320, 297, 285, 233. IR (KBr, cm^{-1}) ν_{max}: 751, 1455, 1732, 2958. ^1H NMR ($CDCl_3$, 300 MHz) δ: 3.17 (dd, *J* = 17.0, 7.0 Hz, 1H, =CCH_2), 3.39 (dd, *J* = 10.2, 8.5 Hz, 1H, -CH_2I), 3.51 (dd, *J* = 17.0, 10.0 Hz, 1H, =CCH_2), 3.54 (dd, *J* = 10.2, 4.0 Hz, 1H, -CH_2I), 5.08–5.18 (m, 1H, -OC*H*), 7.28–7.47 (m, 4H, Ar*H*). ^{13}C NMR ($CDCl_3$, 75.5 MHz) δ: 7.8 (d), 35.4 (t), 82.5 (t), 116.7 (d), 118.1 (s), 123.3 (d), 124.8 (d), 128.4 (s), 128.9 (d), 142.5 (s), 151.5 (s), 154.1 (s). MS *m*/*z*: 328 (M^+). Anal. calcd. for $C_{12}H_9O_3I$ (%): C 43.93, H 2.76; found: C 43.79, H 2.62.

Compound 9b

White solid, mp 124–126 °C; yield: 60%. UV (EtOH, nm) λ_{max}: 320, 299, 285, 232. IR (KBr, cm^{-1}) ν_{max}: 759, 1455, 1721, 2960. ^1H NMR ($CDCl_3$, 300 MHz) δ: 1.54 (d, *J* = 7.0 Hz, 3H, CH_3), 3.46–3.67 (m, 3H, -CH_2I and CH_3C*H*), 4.64 (dt, *J* = 7.0, 7.5 Hz, 1H, -OC*H*), 7.28–7.46 (m, 4H, Ar*H*). ^{13}C NMR ($CDCl_3$, 75.5 MHz) δ: 7.0 (d), 20.4 (q), 38.8 (d), 87.4 (t), 117.3 (d), 117.8 (s), 123.1 (d), 125.1 (d), 129.0 (s), 129.1 (d), 141.6 (s), 152.1 (s), 154.5 (s). MS *m*/*z*: 342 (M^+). Anal. calcd. for $C_{13}H_{11}O_3I$ (%): C 45.64, H 3.24; found: C 45.49, H 3.41.

Compound 11

White solid, mp 112–114 °C; yield: 64%. UV (EtOH, nm) λ_{max}: 362, 245, 218. IR (KBr, cm^{-1}) ν_{max}: 1247, 1429, 1669, 2921. ^1H NMR ($CDCl_3$, 300 MHz) δ: 2.27 (s, 3H, CH_3), 2.78 (dd, *J* = 15.2, 6.7 Hz, 1H, =CCH_2), 3.16 (dd, *J* = 15.2, 9.8 Hz, 1H, =CCH_2), 3.39 (d, *J* = 5.6 Hz, 2H, -CH_2I), 4.95–5.04 (m, 1H, -OC*H*), 5.94 (s, 1H, =C*H*). MS *m*/*z*: 292 (M^+). Anal. calcd. for $C_9H_9O_3I$ (%): C 37.01, H 3.11; found: C 37.23, H 3.29.

Compound 8a

White solid, mp 166–168 °C; yield: 25%. UV (EtOH, nm) λ_{max}: 335, 294, 274, 232. IR (KBr, cm^{-1}) ν_{max}: 813, 1258, 1719. ^1H NMR ($CDCl_3$, 300 MHz) δ: 1.37 (d, *J* = 6.8 Hz, 3H, CH_3), 2.44 (s, 3H, ArCH_3), 3.38–3.42 (m, 1H, CH_3C*H*), 4.55–4.62 (m, 3H, -OCH_2C*H*I), 7.24–7.94 (m, 3H, Ar*H*). ^{13}C NMR ($CDCl_3$, 75.5 MHz) δ: 19.6 (t), 20.9 (q), 23.9 (q), 29.1 (d), 69.3 (d), 99.3 (s), 116.8 (d), 121.9 (s), 125.3 (d), 134.2 (d), 134.9 (s), 151.1 (s), 161.9 (s), 176.6 (s). MS *m*/*z*: 356 (M^+). Anal. calcd. for $C_{14}H_{13}O_3I$ (%): C 47.21, H 3.68; found: C 47.09, H 3.82.

Compound 8b

White solid, mp 146–148 °C; yield: 30%. UV (EtOH, nm) λ_{max}: 333, 294, 274, 231. IR (KBr, cm^{-1}) ν_{max}: 758, 1257, 1726. ^1H NMR ($CDCl_3$, 300 MHz) δ: 2.44 (s, 3H, CH_3), 3.01 (dd, *J* = 16.0, 8.8 Hz, 1H, =CCH_2), 3.31 (dd, *J* = 16.0, 4.8 Hz, 1H, =CCH_2), 4.44–4.49 (m, 2H, -OCH_2), 4.56–4.63 (m, 1H, C*H*I), 7.27–7.95 (m, 3H, Ar*H*). ^{13}C NMR ($CDCl_3$, 75.5 MHz) δ: 13.9 (t), 21.1 (q), 30.6 (t), 74.3 (d), 95.7 (s), 117.2 (d), 122.2 (s), 125.5 (d), 134.5 (d), 135.4 (s), 151.5 (s), 162.6 (s), 177.4 (s). MS *m*/*z*: 242 (M^+). Anal. calcd. for $C_{13}H_{11}O_3I$ (%): C 45.64, H 3.24; found: C 45.79, H 3.11.

Compound 8c

White solid, mp 136–138 °C; yield: 30%. UV (EtOH, nm) λ_{max}: 343, 296, 271, 231. IR (KBr, cm^{-1}) ν_{max}: 764, 1251, 1717. ^1H NMR ($CDCl_3$, 300 MHz) δ: 3.02 (dd, *J* = 16.0, 8.7 Hz, 1H, =CCH_2), 3.32 (dd, *J* = 16.0, 4.6 Hz, 1H, =CCH_2), 4.45–4.50 (m, 2H, -OCH_2), 4.57–4.65 (m, 1H, C*H*I), 7.37–8.19 (m, 4H, Ar*H*). ^{13}C NMR ($CDCl_3$, 75.5 MHz) δ: 13.6 (t), 30.8 (t), 74.1 (d), 95.6 (s), 117.2 (d), 122.3 (s), 125.2 (d), 125.7 (d), 133.1 (d), 152.9 (s), 162.4 (s), 176.9 (s). MS *m*/*z*: 328 (M^+). Anal. calcd. for $C_{12}H_9O_3I$ (%): C 43.93, H 2.76; found: C 43.79, H 2.92.

Compound 8d

White solid, mp 150–152 °C; yield: 28%. UV (EtOH, nm) λ_{max}: 328, 298, 273, 231. IR (KBr, cm^{-1}) ν_{max}: 756, 1259, 1720. ^1H NMR ($CDCl_3$, 300 MHz) δ: 1.38 (d, *J* = 6.8 Hz, 3H, CH_3), 3.39–3.43 (m, 1H, C*H*CH_3), 4.55–4.63 (m, 3H, -OCH_2C*H*I), 7.29–8.18 (m, 4H, Ar*H*). MS *m*/*z*: 242 (M^+). Anal. calcd. for $C_{13}H_{11}O_3I$ (%): C 45.64, H 3.24; found: C 45.49, H 3.41.

© 2005 NRC Canada

Compound 8e

White solid, mp 152–154 °C; yield: 22%. UV (EtOH, nm) λ_{max}: 331, 295, 274, 232. IR (KBr, cm^{-1}) ν_{max}: 756, 1261, 1713. ^{1}H NMR ($CDCl_3$, 300 MHz) δ: 1.38 (s, 9H, $C(CH_3)_3$, 2.97 (dd, J = 16.0, 8.5 Hz, 1H, $=CCH_2$), 3.26 (dd, J = 16.0, 4.6 Hz, 1H, $=CCH_2$), 4.46–4.51 (m, 2H, $-OCH_2$), 4.56–4.59 (m, 1H, CHI), 7.24–7.81 (m, 3H, ArH). MS *m*/*z*: 384 (M^+). Anal. calcd. for $C_{16}H_{17}O_3I$ (%): C 50.02, H 4.46; found: C 50.21, H 4.58.

Compound 10a

White solid, mp 150–152 °C; yield: 32%. UV (EtOH, nm) λ_{max}: 357, 311, 290, 234. IR (KBr, cm^{-1}) ν_{max}: 754, 1296, 1724. ^{1}H NMR ($CDCl_3$, 300 MHz) δ: 3.24 (dd, J = 18.0, 8.5 Hz, 1H, $=CCH_2$), 3.49 (dd, J = 18.0, 5.8 Hz, 1H, $=CCH_2$), 4.26 (dd, J = 9.3, 10.8 Hz, 1H, $-OCH_2$), 4.49–4.54 (m, 1H, CHI), 4.55 (dd, J = 10.8, 5.2 Hz, 1H, $-OCH_2$), 7.29–7.45 (m, 4H, ArH). ^{13}C NMR ($CDCl_3$, 75.5 MHz) δ: 13.2 (t), 33.2 (t), 71.9 (d), 116.7 (d), 118.9 (s), 122.1 (d), 122.4 (s), 124.7 (d), 129.0 (d), 138.0 (s), 149.2 (s), 156.6 (s). MS *m*/*z*: 328 (M^+). Anal. calcd. for $C_{12}H_9O_3I$ (%): C 43.93, H 2.76; found: C 43.72, H 2.59.

Compound 10b

White solid, mp 178–180 °C; yield: 30%. UV (EtOH, nm) λ_{max}: 358, 311, 290, 234. IR (KBr, cm^{-1}) ν_{max}: 754, 1285, 1724. ^{1}H NMR ($CDCl_3$, 300 MHz) δ: 1.48 (d, J = 7.0 Hz, 3H, CH_3), 3.56–3.59 (m, 1H, CH_3CH), 4.37–4.48 (m, 3H, OCH_2CHI), 7.28–7.43 (m, 4H, ArH). ^{13}C NMR ($CDCl_3$, 75.5 MHz) δ: 21.2 (t), 22.5 (q), 37.5 (d), 68.2 (d), 117.4 (d), 119.2 (s), 122.6 (d), 124.9 (d), 125.9 (s), 128.9 (d), 137.1 (s), 149.8 (s), 156.8 (s). MS *m*/*z*: 342 (M^+). Anal. calcd. for $C_{13}H_{11}O_3I$ (%): C 45.64, H 3.24; found: C 45.79, H 3.11.

Compound 12

White solid, mp 98–100 °C; yield: 28%. UV (EtOH, nm) λ_{max}: 292, 258, 234, 215. IR (KBr, cm^{-1}) ν_{max}: 977, 1261, 1451, 1582, 1713. ^{1}H NMR ($CDCl_3$, 300 MHz) δ: 2.25 (s, 3H, CH_3), 2.87 (dd, J = 16.0, 7.0 Hz, 1H, $=CCH_2$), 3.17 (dd, J = 16.0, 5.0 Hz, 1H, $=CCH_2$), 4.31–4.40 (m, 2H, $-OCH_2$), 4.47–4.52 (m, 1H, ICHCHI), 6.06 (s, 1H, $=CH$). MS *m*/*z*: 292 (M^+). Anal. calcd. for $C_9H_9O_3I$ (%): C 37.01, H 3.11; found: C 37.19, H 3.31.

Acknowledgements

We thank the Council of Scientific and Industrial Research (CSIR, New Delhi) for financial assistance. A. Biswas and P.P. Mukhopadhyay are grateful to CSIR (New Delhi) for a Senior Research fellowship. We also thank Department of Science and Technology (New Delhi) for providing a UV–vis spectrophotometer and a FT-IR spectrometer under the DST-FIST program.

References

1. (*a*) A. Murakami, G. Gao, M. Omura, M. Yano, C. Ito, H. Furukawa, D. Takahasi, K. Koshimizu, and H. Ohigashi. Bioorg. Med. Chem. Lett. **10**, 59 (2000); (*b*) S.R. Rajski and R.M. Williams. Chem. Rev. **98**, 2723 (1998); (*c*) J.P. Ali, A.P. Jackson, A.J. Howells, and A. Maxwell. Biochemistry, **32**, 2717 (1993).
2. (*a*) F. Risitano, G. Grassi, F. Foti, and C. Billardo. Tetrahedron Lett. **42**, 3503 (2001); (*b*) T. Nemeto, T. Oshima, and M. Shibasaki. Tetrahedron Lett. **41**, 9569 (2000); (*c*) L. Santana, E. Uriarte, L. Dalla Via, and O. Gia. Bioorg. Med. Chem. Lett. **10**, 135 (2000); (*d*) C. Jia, D. Piao, T. Kitamura, and Y. Fujiwara. J. Org. Chem. **65**, 7516 (2000); (*e*) G. Appendino, G. Cravotto, L. Toina, R. Annunziata, and G. Palmisano. J. Org. Chem. **59**, 5556 (1994); (*f*) K.C. Majumdar, R.N. De, A.T. Khan, S.K. Chattopadhyay, K. Dey, and A. Patra. J. Chem. Soc. Chem. Commun. 777 (1988); (*g*) K.C. Majumdar, P. Chatterjee, and S. Saha. Tetrahedron Lett. **39**, 7147 (1998).
3. For an extensive bibliography, see: J. Wu, Y. Liao, and Z. Yang. J. Org. Chem. **66**, 3642 (2001).
4. (*a*) W.C. Groutas, W.R. Abrams, R.T. Carrol, M.K. Moi, K.E. Miller, and M.T. Margolis. Experientia, **40**, 361 (1984); (*b*) W.C. Groutas, M.A. Stanga, M.J. Brubaker, T.L. Huang, M.K. Moi, and R.T. Carrol. J. Med. Chem. **28**, 1106 (1985); (*c*) R.W. Spencer, L.J. Copp, and J.R. Pfister. J. Med. Chem. **28**, 1828 (1985); (*d*) L. Cook, B. Ternai, and P. Ghosh. J. Med. Chem. **30**, 1017 (1987).
5. (*a*) K. Rehse, W. Schinkel, and U. Siemann. Arch. Pharm. (Weinheim, Ger.), **313**, 344 (1980); (*b*) K. Rehse and W. Schinkel. Arch. Pharm. (Weinheim, Ger.), **316**, 845 (1983); (*c*) K. Rehse and W. Schinkel. Arch. Pharm. (Weinheim, Ger.), **316**, 988 (1983); (*d*) K. Rehse and F. Brandt. Arch. Pharm. (Weinheim, Ger.), **316**, 1030 (1983).
6. K.C. Majumdar and P.K. Basu. Synth. Commun. **32**, 3719 (2002).
7. K.C. Majumdar and S. Sarkar. Tetrahedron, **58**, 8501 (2002).
8. (*a*) K.C. Majumdar, U.K. Kundu, and S.K. Ghosh. Org. Lett. **4**, 2629 (2002); (*b*) K.C. Majumdar and A.K. Kundu. Can. J. Chem. **73**, 1727 (1995); (*c*) K.C. Majumdar, P.K. Choudhury, and M. Nethaji. Tetrahedron Lett. **35**, 5927 (1994).
9. (*a*) K.C. Majumdar, R.N. De, and S. Saha. Tetrahedron Lett. **31**, 1207 (1990); (*b*) K.C. Majumdar and U. Das. Can. J. Chem. **74**, 1592 (1996).
10. K.C. Majumdar, P. Chatterjee, and A.K. Kundu. Synth. Commun. **26**, 893 (1996).
11. K. Orito, T. Hatakeyama, M. Takeo, H. Suginome, and M. Tokuda. Synthesis, 23 (1997).
12. (*a*) R. Jagdish Kumar, G.L.D. Krupadanam, and G. Srimannarayana. Synthesis, 535 (1990); (*b*) K.C. Majumdar, A.T. Khan, and S.K Chattopadhyay. Indian J. Chem. **29B**, 483 (1990).
13. K.C. Majumdar, A.T. Khan, and S.K. Chattopadhyay. Heterocycles, **29**, 1573 (1989).

© 2005 NRC Canada

Dihydropyrimidinones containing boronic acids

Johanna M. Blacquiere, Oana Sicora, Christopher M. Vogels, Miroslava Čuperlović-Culf, Andreas Decken, Rodney J. Ouellette, and Stephen A. Westcott

Abstract: The addition of formylphenylboronic acid derivatives to urea and ethyl acetoacetate proceeds in the absence of an additional Lewis acid catalyst to give the corresponding dihydropyrimidinones (Biginelli products) in good yields. Novel boron-containing dihydropyrimidinones have been investigated for their ability to act as anticancer agents against the breast cancer cell line MCF7.

Key words: anticancer, Biginelli compounds, boronic acids, breast cancer, dihydropyrimidinones.

Résumé : L'addition de dérivés de l'acide formylphénylboronique sur l'urée et l'acétoacétate d'éthyle se produit, même en l'absence d'un catalyseur acide de Lewis additionnel, pour conduire à la formation de dihydropyrimidinones (produits de Biginelli), avec de bons rendements. On a examiné les propriétés antitumorales des nouvelles dihydropyrimidinones contenant du bore en faisant appel à des cellules de cancer du sein de la souche MCF7.

Mots clés : antitumorale, composés de Biginelli, acides boroniques, cancer du sein, dihydropyrimidinones.

[Traduit par la Rédaction]

Introduction

Compounds containing boronic acids [$RB(OH)_2$] or boronate esters [$RB(OR')_2$] have found remarkable utility in Suzuki–Miyaura cross-coupling reactions (1) and as molecular recognition sensors (2). Interest in these compounds also arises from their potent biological activities (3). For instance, boronic-amino acid derivatives (Fig. 1*a*) are strong inhibitors of human arginase II, whose primary function appears to be in L-arginase homeostasis (3*b*). Indeed, related α-aminoboronic acid derivatives are well-known for their ability to act as serine protease inhibitors (3*c*). Serine proteases are a diverse group of proteolytic enzymes whose numerous physiological functions include digestion, growth, differentiation, and apoptosis. Proteases are also vital in the generation of most disease processes. As a result, a considerable amount of research has focussed on these potentially valuable compounds. Analogous amino acids containing boron have been investigated for their use in boron neutron capture therapy (BNCT) for the treatment of cancer (4). BNCT is a bimodal form of therapy that depends on selectively depositing boron-10 atoms into the cancerous tumor prior to irradiation by slow neutrons. 4-Dihydroxyborylphenylalanine (Fig. 1*b*) has shown promise in the treatment of brain tumours (4*b*). Likewise, substituted C_2B_{10} carborane cages have been attached to the sides of single-wall carbon nanotubes. The nanotubes have been used as an attractive nanovehicle for delivering boron to tumour cells in BNCT (4*f*). More relevant to this study, however, is the recent observation that novel boronic-chalcone derivatives (Fig. 1*c*) display considerable activity against human breast cancer cell lines (5).

The Biginelli reaction is a simple and convenient method of preparing dihydropyrimidinones (DHPMs) from the three-component condensation of aliphatic or aromatic aldehydes, acetylacetonate esters, and urea. The original reaction reported by Pietro Biginelli in 1893 was conducted in boiling ethanol using a catalytic amount of concentrated aqueous hydrochloric acid (6*a*). The major drawback of this classical Biginelli reaction is the low to moderate yields, particularly for substituted aromatic or aliphatic aldehydes (6*b*–6*d*). As a result, a considerable amount of research has focussed on using Lewis acid catalysts to improve the efficiency of the Biginelli DHPM synthesis (7). DHPMs are an interesting class of compounds that have extensive pharmacological properties owing, in part, to their similarity to the well-known Hantzsch dihydropyridine calcium channel modulators (8). Of relevance to the present study is the observation that certain DHPMs also display significant anticancer activities (9). For instance, monastrol (Fig. 2) is known to specifically inhibit mitotic kinesin Eg5 and is considered a lead compound in the search for a new anticancer drug (8*a*).

As part of our ongoing investigation into making novel

Received 22 June 2005. Published on the NRC Research Press Web site at http://canjchem.nrc.ca on 3 February 2006.

J.M. Blacquiere, C.M. Vogels, and S.A. Westcott.[1] Department of Chemistry, Mount Allison University, Sackville, NB E4L 1G8, Canada.
A. Decken.[2] Department of Chemistry, University of New Brunswick, Fredericton, NB E3B 5A3, Canada.
O. Sicora, M. Čuperlović-Culf,[3] **and R.J. Ouellette.** Institut de recherche médicale Beauséjour, Pavillion Hôtel-Dieu, 35 Providence, Moncton, NB E1C 8X3, Canada.

[1]Corresponding author (e-mail: swestcott@mta.ca).
[2]Corresponding author regarding X-ray crystallography (e-mail: adecken@unb.ca).
[3]Corresponding author regarding biological studies (e-mail: miroslavac@health.nb.ca).

 doi: 10.1139/V05-211 © 2005 NRC Canada

Fig. 1. Bioactive boron compounds.

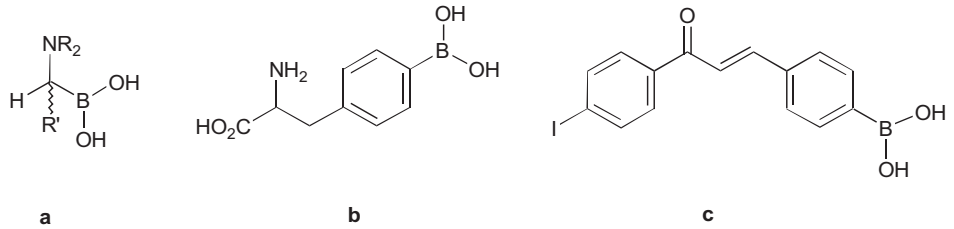
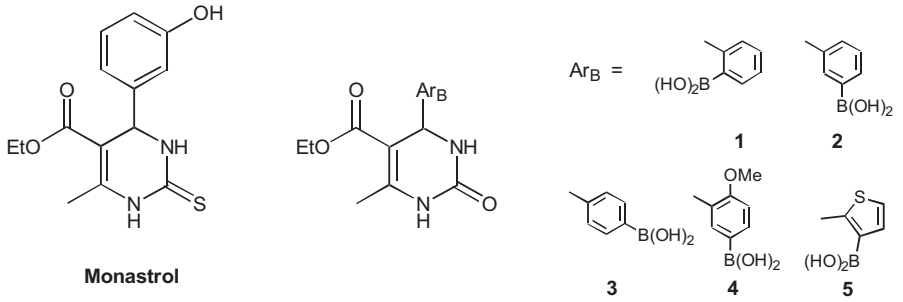


Fig. 2. Monastrol and new boron-containing Biginelli DHPMs.



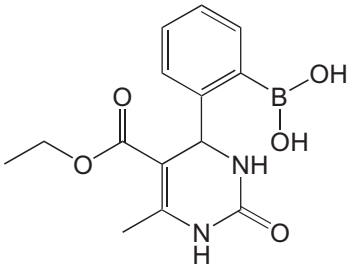
boron compounds (10), and considering the wealth of bioactivities found in aminoboronic acid derivatives, we decided to examine the synthesis and the anticancer properties of Biginelli products derived from formylphenylboronic acids. Initial results are presented herein.

Experimental

General

Reagents and solvents used were obtained from Aldrich Chemicals. ^{1}H and ^{13}C NMR spectra were recorded on a Varian 200 Mercury NMR spectrometer. ^{11}B NMR spectra were recorded on a JEOL JNM-GSX270 FT NMR spectrometer. ^{1}H NMR chemical shifts are reported in ppm and referenced to residual protons in deuterated solvent at 200 MHz. ^{11}B NMR chemical shifts are referenced to external $F_3B{\cdot}OEt_2$ at 87 MHz. ^{13}C NMR chemical shifts are referenced to solvent carbon resonances as internal standards at 50 MHz. Multiplicities are reported as singlet (s), doublet (d), triplet (t), quartet (q), multiplet (m), broad (br), and overlapping (ov). Infrared spectra were obtained using a Mattson Genesis FT-IR spectrometer and reported in cm^{-1}. Elemental analyses were performed by Guelph Chemical Laboratories Ltd. (Guelph, Ontario).

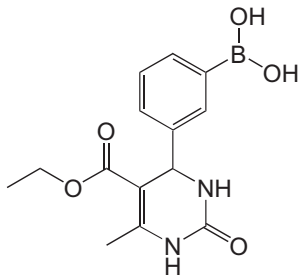
Synthesis



Compound **1**

Compound 1

2-Formylphenylboronic acid (500 mg, 3.3 mmol), ethyl acetoacetate (541 mg, 4.1 mmol), and urea (248 mg, 4.1 mmol) were added together with CH_3CN (12 mL). The reaction mixture was heated at reflux for 24 h, cooled to room temperature, and the solvent removed under vacuum. The mixture was dissolved in MeOH (5 mL) and passed through a silica plug (1 cm). The solvent was removed under vacuum and the resulting solid dried. Yield: 607 mg (60%); mp 192 to 193 °C. FT-IR (Nujol): 3398 (m), 3321 (s), 2920 (s), 2856 (m), 1689 (s), 1643 (s), 1568 (w), 1444 (m), 1371 (m), 1338 (m), 1313 (m), 1228 (m), 1097 (m). ^{1}H NMR (DMSO-d_6) δ: 0.99 (t, J = 7 Hz, 3H, CH_3CH$_2$), 2.26 (s, 3H, CH_3), 3.88 (m, 2H, CH$_3$CH_2), 5.45 (d, J = 2 Hz, 1H, PhCH), 7.03 (br s, 1H, NH), 7.14–7.45 (ov m, 4H, Ar), 8.19 (s, 2H, B(OH)$_2$), 9.18 (br s, 1H, NH). ^{13}C NMR (DMSO-d_6) δ: 14.7, 18.4, 54.4, 59.8, 100.2, 126.3, 127.0, 130.4, 134.0, 135.6 (br, CB), 148.8, 149.0, 152.1, 166.1. ^{11}B NMR (THF) δ: 29 (br). Anal. calcd. for $C_{14}H_{17}O_5N_2B$ (%): C 55.29, H 5.63, N 9.21; found: C 55.23, H 5.15, N 9.64.



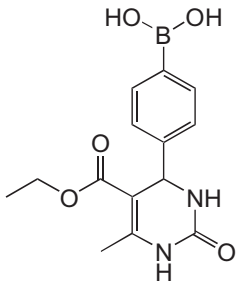
Compound **2**

Compound 2

3-Formylphenylboronic acid (502 mg, 3.3 mmol), ethyl acetoacetate (539 mg, 4.1 mmol), and urea (249 mg, 4.1 mmol) were added together with CH_3CN (12 mL). The reaction mixture was heated at reflux for 46 h, cooled to room temperature, and the solvent removed under vacuum.

© 2005 NRC Canada

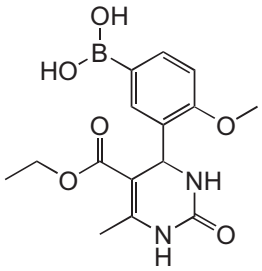
The mixture was dissolved in MeOH (5 mL) and passed through a silica plug (1 cm). The solvent was removed under vacuum and the resulting solid dried. Yield: 769 mg (76%); mp 198–202 °C. FT-IR (Nujol): 3280 (m), 3271 (m), 2951 (s), 2935 (s), 2910 (s), 2856 (s), 1697 (s), 1657 (m), 1462 (m), 1375 (m), 1232 (m), 1103 (m). ^{1}H NMR (DMSO-d_6) δ: 1.06 (t, J = 7 Hz, 3H, CH_3CH$_2$), 2.21 (s, 3H, CH_3), 3.93 (q, J = 7 Hz, 2H, CH$_3$CH_2), 5.10 (d, J = 3 Hz, 1H, PhCH), 7.23 (ov m, 2H, Ar and NH), 7.66 (ov m, 3H, Ar), 7.96 (s, 2H, B(OH)$_2$), 9.10 (br s, 1H, NH). ^{13}C NMR (DMSO-d_6) δ: 14.7, 18.5, 55.0, 59.8, 100.0, 128.0, 128.8, 133.0, 133.7, 134.9 (br, CB), 144.6, 148.8, 152.7, 166.0. ^{11}B NMR (THF) δ: 27 (br). Anal. calcd. for $C_{14}H_{17}O_5N_2B$ (%): C 55.29, H 5.63, N 9.21; found: C 54.88, H 5.20, N 9.04.



Compound **3**

Compound 3

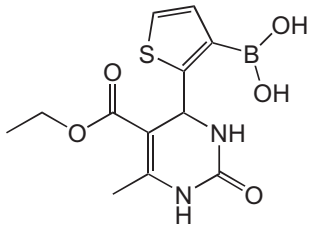
4-Formylphenylboronic acid (501 mg, 3.3 mmol), ethyl acetoacetate (540 mg, 4.1 mmol), and urea (247 mg, 4.1 mmol) were added together with CH_3CN (10 mL). The reaction mixture was heated at reflux for 55 h, cooled to room temperature, and solvent was removed under vacuum. The resulting solid was washed with H_2O (40 mL) and ether (20 mL). Yield: 818 mg (82%); mp 214–218 °C. FT-IR (Nujol): 3253 (s), 3109 (s), 2939 (s), 2848 (s), 1695 (s), 1610 (m), 1416 (m), 1369 (m), 1331 (s), 1294 (m), 1238 (s), 1090 (m), 773 (m), 708 (m). ^{1}H NMR (DMSO-d_6) δ: 1.09 (t, J = 7 Hz, 3H, CH_3CH$_2$), 2.24 (s, 3H, CH_3), 3.97 (q, J = 7 Hz, 2H, CH$_3$CH_2), 5.14 (d, J = 3 Hz, 1H, PhCH), 7.16 (d, J = 7 Hz, 2H, Ar), 7.65–7.96 (ov m, 3H, NH and Ar), 8.02 (s, 2H, CB(OH)$_2$), 9.13 (br s, 1H, NH). ^{13}C NMR (DMSO-d_6) δ: 14.7, 18.5, 54.6, 59.9, 99.8, 126.0, 134.7 (br, CB), 134.9, 147.2, 149.0, 152.8, 166.0. ^{11}B NMR (THF) δ: 27 (br). Anal. calcd. for $C_{14}H_{17}O_5N_2B$ (%): C 55.29, H 5.63, N 9.21; found: C 55.32, H 5.97, N 8.84.



Compound **4**

Compound 4

3-Formyl-4-methoxyphenylboronic acid (501 mg, 2.8 mmol), ethyl acetoacetate (453 mg, 3.4 mmol), and urea (205 mg, 3.4 mmol) were added together with CH_3CN (11 mL). The reaction mixture was heated at reflux for 41 h, cooled to room temperature, and the solvent removed under vacuum. The mixture was dissolved in wet MeOH (5 mL) and passed through a silica plug (1 cm). The solvent was removed under vacuum and the resulting solid dried. Yield: 601 mg (65%); mp 196–199 °C. FT-IR (Nujol): 3319 (s), 3253 (m), 2919 (s), 2854 (s), 1705 (s), 1668 (s), 1601 (m), 1460 (m), 1394 (m), 1365 (s), 1335 (m), 1292 (m), 1246 (s), 1099 (m), 771 (w). ^{1}H NMR (DMSO-d_6) δ: 0.98 (t, J = 7 Hz, 3H, CH_3CH$_2$), 2.24 (s, 3H, CH_3), 3.76 (s, 3H, CH_3O), 3.86 (q, J = 7 Hz, 2H, CH$_3$CH_2), 5.45 (d, J = 2 Hz, 1H, PhCH), 6.91 (d, J = 8 Hz, 1H, Ar), 7.17 (br s, 1H, NH), 7.49 (d, J = 2 Hz, 1H, Ar), 7.66 (dd, J = 8, 2 Hz, 1H, Ar), 7.80 (s, 2H, B(OH)$_2$), 9.04 (br s, 1H, NH). ^{13}C NMR (DMSO-d_6) δ: 14.6, 18.5, 49.9, 55.9, 59.6, 98.1, 110.7, 125.7 (br, CB), 131.3, 134.4, 135.8, 149.4, 152.8, 159.0, 166.1. ^{11}B NMR (DMF) δ: 28 (br). Anal. calcd. for $C_{15}H_{19}O_6N_2B\cdot 1H_2O$ (%): C 51.15, H 6.02, N 7.96; found: C 51.82, H 5.91, N 7.89.



Compound **5**

Compound 5

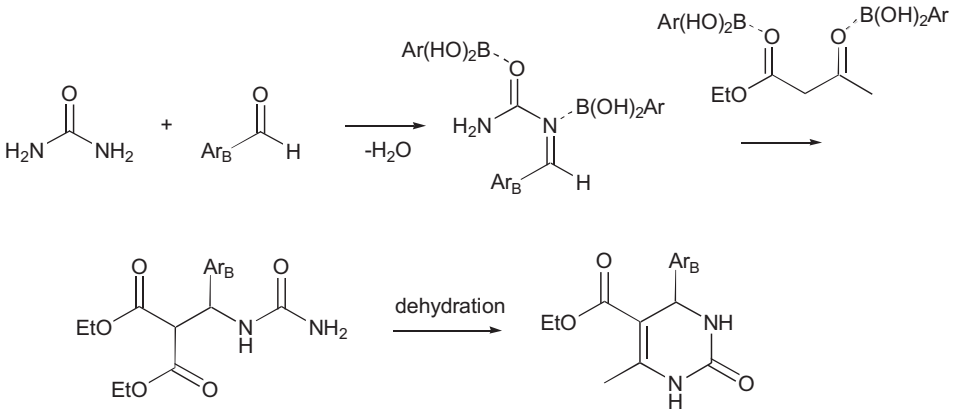
2-Formyl-3-thiopheneboronic acid (500 mg, 3.2 mmol), ethyl acetoacetate (507 mg, 4.0 mmol), and urea (239 mg, 4.0 mmol) were added together with CH_3CN (10 mL). The reaction mixture was heated at reflux for 41 h, cooled to room temperature, and the solvent was removed under vacuum. The solid was washed with H_2O (5 mL) and dried. Yield: 597 mg (60%); mp 158–160 °C. FT-IR (Nujol): 3392 (m), 3338 (m), 3288 (m), 3232 (m), 3109 (m), 2951 (s), 2926 (s), 2856 (s), 1699 (s), 1686 (s), 1460 (m), 1421 (m), 1365 (m), 1342 (m), 1319 (m), 1290 (m), 1236 (s), 1099 (m), 1068 (m), 897 (w), 777 (m), 713 (w). ^{1}H NMR (DMSO-d_6) δ: 1.03 (t, J = 7 Hz, 3H, CH_3CH$_2$), 2.23 (s, 3H, CH_3), 3.94 (q, J = 7 Hz, 2H, CH$_3$CH_2), 5.81 (d, J = 2 Hz, 1H, PhCH), 7.06 (br s, 1H, NH), 7.21 (s, 2H, Ar), 8.20 (s, 2H, B(OH)$_2$), 9.33 (br s, 1H, NH). ^{13}C NMR (DMSO-d_6) δ: 14.7, 18.4, 49.6, 59.9, 100.7, 123.6, 133.5 (br, CB), 134.1, 149.8, 152.5, 158.6, 165.9. ^{11}B NMR (THF) δ: 27 (br). Anal. calcd. for $C_{12}H_{15}O_5N_2BS$ (%): C 46.48, H 4.88, N 9.03; found: C 46.54, H 4.75, N 9.06.

X-ray crystallography

Crystals of **1** and **5** were grown from satd. CH_3CN solutions at 20 °C. Single crystals were coated with Paratone-N oil, mounted using a glass fibre, and frozen in the cold stream of the goniometer. A hemisphere of data were collected on a Bruker AXS P4/SMART 1000 diffractometer using ω and θ scans with a scan width of 0.3° and exposure times of 30 s (**1**) and 10 s (**5**). The detector distances were 5 cm. The data were reduced (11*a*) and corrected for absorption (11*b*). The structures were solved by direct methods and

© 2005 NRC Canada

Scheme 1. Proposed pathway for the self-mediated synthesis of boronic acid containing DHPMs.



refined by full-matrix least-squares on F^2 (11*c*). All nonhydrogen atoms were refined anisotropically. Hydrogen atoms were located in Fourier difference maps and refined isotropically.

Biological studies

Cell culture

MCF7 (human breast cancer) cell line was obtained from American Type Culture Collection and grown in optimal medium (DMEM supplemented with 10% FBS, 2 mmol/L L-glutamin and 50 μg/mL gentamicin).

Cell growth inhibition assay

Cells were seeded in 96-well plates at a concentration of 1×10^5 cells/mL in 100 μL of complete media and incubated for 24 h at 37 °C in a 5% CO_2 atmosphere to allow for cell adhesion. The stock solutions of compounds **1**–**3** and **5** were made in EtOH. Compound **4** was not soluble in EtOH and therefore not tested. Stock solutions of compounds **1** and **3** were prepared at 20 mg/mL. Compound **2** and **5** stock solutions were prepared as 33.3 and 7.7 mg/mL, respectively. The stock solutions were first sterilized and then diluted with EtOH to final concentrations between 20 and 0.07 μg/μL for compounds **1** and **3**, 33.3 and 0.1 μg/μL for compound **2**, and 7.7 and 0.06 μg/μL for compound **5**. Solutions of compound **1** and **3** were diluted 10× in fresh medium and testing was performed with 100 μL of solution added to 100 μL of fresh medium. Compound **2** was diluted 3.33× in fresh medium and testing was done with 20 μL of solution added to 180 μL of fresh medium. Compound **5** was diluted 7.7× in fresh medium and from this dilution 100 μL was added to 100 μL of medium. All assays were performed in quadruplicate tests. The control group for each compound contained only EtOH in the medium in the same concentration as in the compound solutions. The cells were incubated in the solution for 24 h, and the evaluation of cell proliferation was performed by the MTT colorimetric assay.

MTT colorimetric assay

MTT solution (8 μL, 4 mg/mL in PBS, Sigma Chemical Co.) along with 50 μL of fresh, complete media was added to each well and plates were incubated for 3 h. Following incubation, the purple formazan precipitate in each well was solubilized in 120 μL lysis buffer (5% Triton X-100, 0.37% HCl in isopropanol). Absorbance was measured using a SpectroMax microplate reader (Molecular Devices) at 570 nm. The reduction of cell proliferation was determined as a fraction of the absorbance values for each drug treatment (*T*) and the mean absorbance of the nondrug control (*C*) and calculated using the expression $1 - (T/C) \times 100\%$.

IC_{50} determination

Stock solutions of selected compounds were freshly prepared. The nine step dilutions were prepared in EtOH as described earlier. The final range of concentrations used was 1 mg/mL to 3 μg/mL. Approximate IC_{50} values were obtained graphically using Excel Software from the control-corrected values of the MTT colorimetric assay.

Results and discussion

In this study, we have found that commercially available aldehydes containing boronic acids add to ethyl acetylacetonate ester and urea in *the absence of an additional Lewis acid* to give moderate to high yields of the desired boron-containing Biginelli products (Fig. 2). It appears that the boronic acid group in the aldehydes acts to mediate this reaction, presumably in a manner similar to that reported for other Lewis acid catalyzed Biginelli reactions (12). The Lewis acidic boron atom presumably activates the transient imine nitrogen, the carbonyl oxygens of the urea, and the β-keto ester through coordination (Scheme 1). An excellent review by Ishihara and Yamamoto (13*a*) describes the use of arylboron compounds as Lewis acid catalysts in organic transformation. Although other Lewis acids, such as LiBr, could also be used to facilitate this reaction, no significant improvement in product yields were observed.

All new compounds have been characterized by a number of physical methods including multinuclear NMR spectroscopy. A broad peak at around 30 ppm in the ^{11}B NMR spectra suggests that the boron atom lies in a three-coordinate environment in solution (14), even for the ortho derivatives **1** and **5**. This result is somewhat surprising in light of boron's propensity to form coordinate bonds with Lewis basic atoms (15). Previous studies have shown that compounds containing boronic acids can be extremely difficult to characterize in terms of elemental composition, owing to the ease with which they partially dehydrate to the corresponding trimeric and oligomeric anhydrides (16). Compounds **1** and **5** have

© 2005 NRC Canada

Table 1. Crystallographic data collection parameters for **1** and **5**.

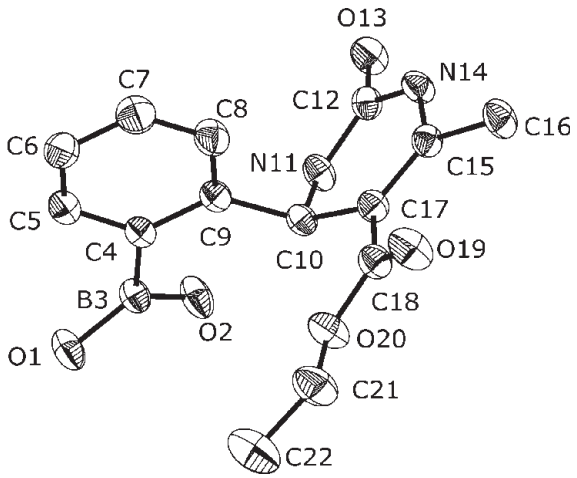
Complex	**1**	**5**
Chemical formula	$C_{14}H_{17}BN_2O_5$	$C_{12}H_{15}BN_2O_5S$
Formula weight	304.11	310.13
Crystal system	Monoclinic	Monoclinic
Space group	*P*2(1)/*n*	*P*2(1)/*n*
a (Å)	11.5282(7)	10.9913(8)
b (Å)	11.9687(7)	12.0270(9)
c (Å)	11.6176(7)	11.6959(8)
β (°)	109.433(1)	108.788(1)
V (Å^3)	1 511.65(16)	1463.73(18)
Z	4	4
ρ_{calcd} (mg m^{-3})	1.336	1.407
Crystal dimensions (mm)	0.50 × 0.40 × 0.20	0.45 × 0.40 × 0.30
Temperature (K)	198(1)	198(1)
Radiation (λ = 0.71073 Å)	Mo Kα	Mo Kα
μ (mm^{-1})	0.101	0.243
Total reflections	10 256	9964
Independent reflections	3 377	3233
No. of variables	267	250
R_{int}	0.0195	0.0186
θ range (°)	2.16–27.48	2.21–27.48
Largest difference peak/hole (e Å^{-3})	0.551/–0.290	0.415/–0.187
S (GoF) on F^2	1.111	1.094
$R1^a$ ($I > 2\sigma(I)$)	0.0437	0.0375
w$R2^b$ (all data)	0.1304	0.1104

[a] $R1 = \Sigma||F_o| - |F_c||/\Sigma|F_o|$.
[b] $wR2 = (\Sigma[w(F_o^2 - F_c^2)^2]/\Sigma[F_o^4])^{1/2}$, where $w = 1/[\sigma^2(F_o^2) + (0.0787P)^2 + (0.2917P)]$ (**1**) and $w = 1/[\sigma^2(F_o^2) + (0.0691P)^2 + (0.2521P)]$ (**5**), where $P = (\max(F_o^2, 0) + 2F_c^2)/3$.

therefore been characterized by X-ray diffraction studies and crystallographic data[4] are given in Table 1. The molecular structure of **1** is shown in Fig. 3 and compound **5** is shown in Fig. 4. The B—O bond distances of B(3)—O(1) (1.370(2) Å) and B(3)—O(2) (1.356(2) Å) for **1** and B(3)—O(1) (1.367(2) Å) and B(3)—O(2) (1.359(2) Å) for **5** are typical for those observed in related structures where the boron is three coordinate (17). Likewise, the sum of the angles around boron for **1** are 360.0(1)° and 360.1(1)° for **5**, indicating that both boron atoms are three coordinate. Bond distances and angles for the six-membered ring are similar to those reported for analogous compounds (18).

As mentioned previously, DHPMs are biologically active compounds and several, such as monastrol, are potent anticancer agents. With this in mind, we have examined four new boron Biginelli compounds for their potential antitumour activity. Breast cancer is the most common form of cancer among women and is the second leading cause of cancer-related death in women of the western world. The identification of an optimal treatment for breast cancer is therefore of crucial importance. In this context, the most often utilized method for the initial testing of potential drug activity is performed on breast cancer cell lines (19*a*). MCF7 cell lines have been used frequently as standards for various cell culture testing experiments (19*b*, 19*c*).

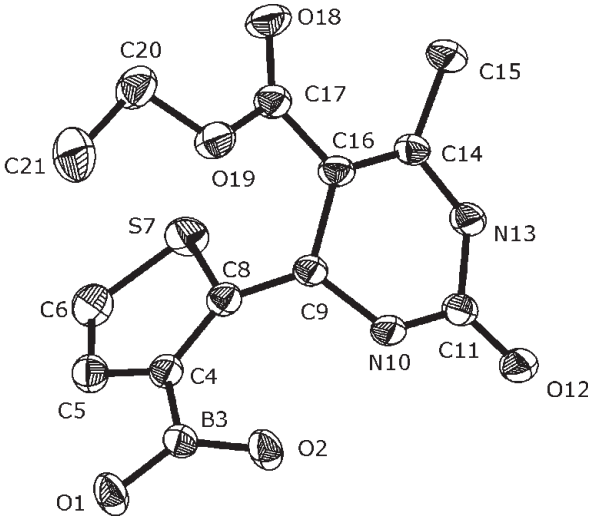
Fig. 3. The molecular structure of **1** with probability ellipsoids drawn at 30% and hydrogen atoms omitted for clarity. Selected bond lengths (Å) and angles (°): O(1)—B(3) 1.370(2), O(2)—B(3) 1.356(2), B(3)—C(4) 1.583(2), C(12)—O(13) 1.233(2); O(2)-B(3)-O(1) 117.5(1), O(2)-B(3)-C(4) 120.0(1), O(1)-B(3)-C(4) 122.5(1), C(12)-N(14)-C(15) 124.2(1), C(10)-N(11)-C(12) 125.5(1), O(13)-C(12)-N(14) 119.6(1).



[4] Supplementary data for this article are available on the journal Web site (http://canjchem.nrc.ca) or may be purchased from the Depository of Unpublished Data, Document Delivery, CISTI, National Research Council Canada, Ottawa, ON K1A 0S2, Canada. DUD 4068. For more information on obtaining material refer to http://cisti-icist.nrc-cnrc.gc.ca/irm/unpub_e.shtml. CCDC 275770 and 275771 contain the crystallographic data for this manuscript. These data can be obtained, free of charge, via www.ccdc.cam.ac.uk/conts/retrieving.html (Or from the Cambridge Crystallographic Data Centre, 12 Union Road, Cambridge CB2 1EZ, UK; fax +44 1223 336033; or deposit@ccdc.cam.ac.uk).

© 2005 NRC Canada

Fig. 4. The molecular structure of **5** with probability ellipsoids drawn at 30% and hydrogen atoms omitted for clarity. Selected bond lengths (Å) and angles (°): B(3)—O(2) 1.359(2), B(3)—O(1) 1.367(2), B(3)—C(4) 1.568(2), O(12)—C(11) 1.234(2); O(2)-B(3)-O(1) 118.2(1), O(2)-B(3)-C(4) 118.8(1), O(1)-B(3)-C(4) 123.1(1), C(11)-N(13)-C(14) 124.2(1), C(11)-N(10)-C(9) 126.5(1), O(12)-C(11)-N(13) 119.7(1).



Initial studies of boron compounds were tested against the MCF7 breast cancer cell line. When the boron compounds **1**–**5** were dissolved in DMSO, a significant decrease in activity was observed the longer these compounds stayed in this media. This result suggests that DMSO may be reacting with, and deactivating, the compounds and is not surprising as the strongly coordinating DMSO solvent can interact with the three-coordinate boron atom. Indeed, we have found that addition of excess DMSO to these compounds gave a number of identified products. Unfortunately, the insolubility of compound **4** in other media precluded testing at this time. All four compounds (**1**–**3** and **5**) tested in EtOH, however, have shown some level of activity against the cells at their highest concentrations (Fig. 5). Unfortunately, the low solubility of compounds **1**–**3** prevented further investigation at higher concentrations, therefore the respective IC_{50} concentrations are unattainable. The thiophene derivative **5** was significantly more active with respect to the other compounds. The reduction of cell proliferation caused by **5** is given as the average % reduction of the cell proliferation of MCF7 cells relative to the EtOH treated controls (Table 2). The effect of the compound at low concentrations is negligible but becomes significant above ca. 15 μg/mL. The estimated IC_{50} value relative to the control group (cells exposed to EtOH only) for compound **5** is ca. 0.46 mmol/L (140 μg/mL). Although the IC_{50} value determined is relatively large, these initial studies show that the thiophene derivative **5** has potential as an agent against the breast cancer cell line. Further in vitro studies are underway to address the activity of this compound against other breast cancer cell lines.

Conclusion

We have prepared new boron-containing DHPMs in moderate yields, and reactions proceed without the need of an additional Lewis acid catalyst. These initial compounds have also been examined for their ability to inhibit the MCF7 breast cancer cell line. Although compounds **1**–**4** suffered from poor solubilities, tests with the thiophene derivative **5** showed considerable promise. Future work in this area will focus on making more soluble thiophene derivatives as well as boron-containing DHPMs derived from thiourea, the results of which will be published in due course.

Fig. 5. Averaged optical density values for the four compounds at different concentrations. Values are corrected for differences in EtOH concentrations.

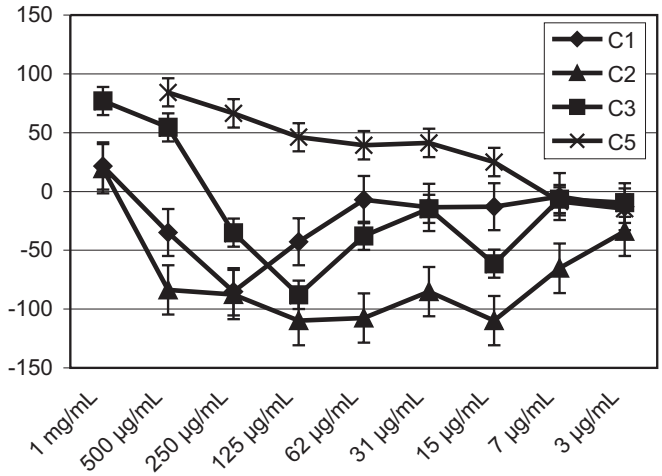


Table 2. % Reduction of cell proliferation of MCF7 cells exposed to a range of concentrations for compound **5**.

Concentration (μg/mL)	% Reduction
500	84.2
250	66.5
125	46.2
62	39.3
31	41.3
15	25.0
7	–8.4
3	–14.7

Acknowledgements

Thanks are extended to the American Chemical Society-Petroleum Research Fund (Grant No. 37824-B1; SAW), Mount Allison University, the Natural Sciences and Engineering Research Council of Canada (NSERC), the Canada Research Chairs Program, the Canadian Foundation for Innovation/Atlantic Innovation Fund for financial support, Merck Frosst Canada and Co., and Pfizer Inc. for a Summer Undergraduate Research Fellowship (JMB). We also thank Dan Durant (Mount Allison University) and Roger Smith (Mount Allison University) for expert technical assistance and anonymous reviewers for helpful comments.

References

1. N. Miyaura and A. Suzuki. Chem. Rev. **95**, 2457 (1995).
2. W. Ni, H. Fang, G. Springsteen, and B. Wang. J. Org. Chem. **69**, 1999 (2004).

© 2005 NRC Canada

3. (*a*) W. Yang, X. Gao, and B. Wang. Med. Res. Rev. **23**, 346 (2003); (*b*) E. Cama, D.M. Colleluori, F.A. Emig, H. Shin, S.W. Kim, N.N. Kim, A.M. Traish, D.E. Ash, and D.W. Christianson. Biochemistry, **42**, 8445 (2003), (*c*) M.L. Stolowitz, C. Ahlem, K.A. Hughes, R.J. Kaiser, E.A. Kesicki, G. Li, K.P. Lund, S.M. Torkelson, and J.P. Wiley. Bioconjugate Chem. **12**, 229 (2001); (*d*) C. Morin. Tetrahedron, **50**, 12521 (1997); (*e*) G.S. Weston, J. Blazquez, F. Baquero, and B.K. Shoichet. J. Med. Chem. **41**, 4577 (1998).
4. (*a*) G.W. Kabalka, B.C. Das, and S. Das. Tetrahedron Lett. **42**, 7145 (2001); (*b*) A.H. Soloway, W. Tjarks, B.A. Barnum, F.-G. Rong, R.F. Barth, I.M. Codogni, and J.G. Wilson. Chem. Rev. **98**, 1515 (1998); (*c*) H. Yanagië, H. Kobayashi, Y. Takeda, I. Yoshizaki, Y. Nonaka, S. Naka, A. Nojiri, H. Shinnkawa, Y. Furuya, H. Niwa, K. Ariki, H. Yasuhara, and M. Eriguchi. Biomed. Pharmacother. **56**, 93 (2002); (*d*) K.J. Winberg, M. Persson, P.-U. Malmström, S. Sjöberg, and V. Tolmachev. Nucl. Med. Biol. **31**, 425 (2004); (*e*) J.F. Valliant, K.J. Guenther, A.S. King, P. Morel, P. Schaffer, O.O. Sogbein, and K.A. Stephenson. Coord. Chem. Rev. **232**, 173 (2002); (*f*) Z. Yinghuai, A.T. Peng, K. Carpenter, J.A. Maguire, N.S. Hosmane, and M. Takagaki. J. Am. Chem. Soc. **127**, 9875 (2005); (*g*) K. Vyakaranam, G. Rana, N.S. Hosmane, and B.F. Spielvogel. Met.-Based Drugs, **8**, 145 (2001); (*h*) K. Vyakaranam, G. Rana, B.F. Spielvogel, and N.S. Hosmane. Inorg. Chem. Commun. 4, 629 (2001); (*i*) G. Rana, K. Vyakaranam, S.C. Ledger, S.L. Delaney, J.A. Maguire, and N.S. Hosmane. Appl. Organomet. Chem. **17**, 361 (2003); (*j*) N.S. Hosmane. Pure Appl. Chem. **75**, 1219 (2003); (*k*) N.S. Hosmane and J.A. Maguire. Eur. J. Chem. 3989 (2003).
5. S.K. Kumar, E. Hager, C. Pettit, H. Gurulingappa, N.E. Davidson, and S.R. Khan. J. Med. Chem. **46**, 2813 (2003).
6. (*a*) C.M. Vogels, L.G. Nikolcheva, D.W. Norman, H.A. Spinney, A. Decken, M.O. Baerlocher, F.J. Baerlocher, and S.A. Westcott. Can. J. Chem. **79**, 1115 (2001); (*b*) A.M. Irving, C.M. Vogels, L.G. Nikolcheva, J.P. Edwards, X.-F. He, M.G. Hamilton, M.O. Baerlocher, F.J. Baerlocher, A. Decken, and S.A. Westcott. New. J. Chem. **27**, 1419 (2003); (*c*) S. Gronowitz, T. Dalgren, J. Namtvedt, C. Roos, B. Sjöberg, and U. Forsgren. Acta Pharm. Suec. **8**, 377 (1971).
7. (*a*) Bruker AXS Inc. SAINT 6.02 [computer program]. Madison, Wisconsin. 1997–1999; (*b*) G.M. Sheldrick. SADABS [computer program]. Bruker AXS Inc., Madison, Wisconsin. 1999; (*c*) G.M. Sheldrick. SHELXTL 5.1 [computer program]. Bruker AXS Inc., Madison, Wisconsin. 1997.
8. (*a*) P. Biginelli. Gazz. Chim. Ital. **23**, 360 (1893); (*b*) P. Wipf and A. Cunningham. Tetrahedron Lett. **36**, 7819 (1995); (*c*) K. Folkers and T.B. Johnson. J. Am. Chem. Soc. **56**, 1180 (1934); (*d*) G. Sabitha, G.S.K.K. Reddy, Ch.S. Reddy, and J.S. Yadav. Synlett, 858 (2003).
9. (*a*) N.-Y. Fu, Y.-F. Yuan, Z. Cao, S.-W. Wang, J.-T. Wang, and C. Peppe. Tetrahedron, **58**, 4801 (2002); (*b*) I. Cepanec, M. Litvić, A. Bartolinčić, and M. Lovrić. Tetrahedron, **61**, 4275 (2005); (*c*) J. Lu and H. Ma. Synlett, 63 (2000); (*d*) G. Maiti, P. Kundu, and C. Guin. Tetrahedron Lett. **44**, 2757 (2003); (*e*) R. Varala, M.M. Alam, and S.R. Adapa. Synlett, 67 (2003); (*f*) G. Jenner. Tetrahedron Lett. **45**, 6195 (2004); (*g*) J.S. Yadav, B.V.S. Reddy, R. Srinivas, C. Venugopal, and T. Ramalingam. Synthesis, 1341 (2001); (*h*) B.C. Ranu, A. Hajra, and U. Jana. J. Org. Chem. **65**, 6270 (2000); (*i*) K.A. Kumar, M. Kasthuraiah, C.S. Reddy, and C.D. Reddy. Tetrahedron Lett. **42**, 7873 (2001).
10. (*a*) A.K. Bose, M.S. Manhas, S. Pednekar, S.N. Ganguly, H. Dang, W. He, and A. Mandadi. Tetrahedron Lett. **46**, 1901 (2005); (*b*) A. Dondori, A. Massi, E. Minghini, S. Sabbatini, and V. Bertolasi. J. Org. Chem. **68**, 6172 (2003); (*c*) A. Dondori, A. Massi, S. Sabbatini, and V. Bertolasi. J. Org. Chem. **67**, 6979 (2002); (*d*) G.C. Rovnyak, S.D. Kimball, B. Beyer, G. Cucinotta, J.D. DiMarco, J. Gougoutas, A. Hedberg, M. Malley, J.P. McCarthy, R. Zhang, and S. Moreland. J. Med. Chem. **38**, 119 (1995).
11. (*a*) T.U. Mayer, T.M. Kapoor, S.J. Haggarty, R.W. King, S.L. Schreiber, and T.J. Mitchison. Science, **286**, 971 (1999); (*b*) C.O. Kappe. Eur. J. Med. Chem. **35**, 1043 (2000); (*c*) X. Fei, J.-Q. Wang, K.D. Miller, G.W. Sledge, G.D. Hutchins, and Q.-H. Zheng. Nucl. Med. Biol. **31**, 1033 (2004).
12. (*a*) S. Tu, F. Fang, C. Miao, H. Jiang, Y. Feng, D. Shi, and X. Wang. Tetrahedron Lett. **44**, 6153 (2003); (*b*) E.H. Hu, D.R. Silder, and U.H. Dolling. J. Org. Chem. **63**, 3454 (1998).
13. (*a*) K. Ishihara and H. Yamamoto. Eur. J. Org. Chem. 527 (1999); (*b*) R.L. Giles, J.A.K. Howard, L.G.F. Patrick, M.R. Probert, G.E. Smith, and A. Whiting. J. Organomet. Chem. **680**, 257 (2003).
14. H. Nöth and B. Wrackmeyer. *In* Nuclear magnetic resonance spectroscopy of boron compounds. Springer-Verlag, Berlin. 1978.
15. (*a*) H. Höpfl, M. Sánchez, V. Barba, N. Farfán, S. Rojas, and R. Santillan. Inorg. Chem. **37**, 1679 (1998); (*b*) A.N.J. Moore and D.D.M. Wayner. Can. J. Chem. **77**, 681 (1999); (*c*) M. Sánchez, O. Sánchez, H. Höpfl, M.-E. Ochoa, D. Castillo, N. Farfán, and S. Rojas-Lima. J. Organomet. Chem. **689**, 811 (2004); (*d*) Y. Kanekiyo, R. Naganawa, and H. Tao. Chem. Commun. (Cambridge), 1006 (2004); (*e*) S. Arimori, M.G. Davidson, T.M. Fyles, T.G. Hibbert, T.D. James, and G.I. Kociok-Köhn. Chem. Commun. (Cambridge), 1604 (2004); (*f*) T. Beringhelli, G. D'Alfonso, D. Donghi, D. Maggioni, P. Mercandelli, and A. Sironi. Organometallics, **23**, 5493 (2004); (*g*) K.E. Secor and T.E. Glass. Org. Lett. **6**, 3727 (2004); (*h*) N. Christinat, R. Scopelliti, and K. Severin. Chem. Commun. (Cambridge), 1158 (2004); (*i*) H. Höpfl. J. Organomet. Chem. **581**, 129 (1999); (*j*) H. Höpfl. Struct. Bonding (Berlin), **103**, 1 (2002); (*k*) M. Sánchez, H. Höpfl, M.-E. Ochoa, N. Farfán, R. Santillan, and S. Rojas-Lima. Chem. Eur. J. **8**, 612 (2002).
16. (*a*) V. Martichonok and J.B. Jones. J. Am. Chem. Soc. **118**, 950 (1996); (*b*) T. Lee, R. Sakowicz, V. Martichonok, J.K. Hogan, M. Gold, and J.B. Jones. Acta Chem. Scand. **50**, 697 (1996).
17. (*a*) R.B. Coapes, F.E.S. Souza, M.A. Fox, A.S. Batsanov, A.E. Goeta, D.S. Yufit, M.A. Leech, J.A.K. Howard, A.J. Scott, W. Clegg, and T.B. Marder. J. Chem. Soc. Dalton Trans. 1201 (2001); (*b*) W. Clegg, M.R.J. Elsegood, F.J. Lawlor, N.C. Norman, N.L. Pickett, E.G. Robbins, A.J. Scott, P. Nguyen, N.J. Taylor, and T.B. Marder. Inorg. Chem. **37**, 5289 (1998); (*c*) P. Nguyen, R.B. Coapes, A.D. Woodward, N.J. Taylor, J.M. Burke, J.A.K. Howard, and T.B. Marder. J. Organomet. Chem. **652**, 77 (2002); (*d*) P. Nguyen, R.B. Coapes, A.D. Woodward, N.J. Taylor, J.M. Burke, J.A.K. Howard, and T.B. Marder. J. Organomet. Chem. **652**, 77 (2002); (*e*) J.M. Burke, M.A. Fox, A.E. Goeta, A.K. Hughes, and T.B. Marder. Chem. Commun. (Cambridge), 2217 (2000); (*f*) C.J. Carmalt, W. Clegg, A.H. Cowley, F.J. Lawlor, T.B. Marder, N.C. Norman, C.R. Rice, O.J. Sandoval, and A.J. Scott. Polyhedron, **16**, 2325 (1997); (*g*) C. Zheng, B.F. Spielvogel, R.Y. Smith, and N.S. Hosmane. Z. Kristallogr. New Cryst. Struct. **216**, 341 (2001).
18. (*a*) A. Dondoni, A. Massi, E. Minghini, S. Sabbatini, and V. Bertolasi. J. Org. Chem. **68**, 6172 (2003); (*b*) C.O. Kappe, G. Uray, P. Roschger, W. Lindner, C. Kratky, and W. Keller. Tetrahedron, **48**, 5473 (1992); (*c*) C.O. Kappe, W.M.F. Fabian,

© 2005 NRC Canada

and M.A. Semones. Tetrahedron, **53**, 2803 (1997); (*d*) S.-J. Tu, F. Fang, C.-B. Miao, H. Jiang, and D.-Q. Shi. Chin. J. Chem. **21**, 706 (2003); (*e*) K. Lewandowski, P. Murer, F. Svec, and J.M.J. Frechet. J. Comb. Chem. **1**, 105 (1999); (*f*) J.C. Barrow, P.G. Nantermet, H.G. Seinick, K.L. Glass, K.E. Rittle, K.F. Gilbert, T.G. Steele, C.F. Homnick, R.M. Freidinger, R.W. Ransom, P. Kling, D. Reiss, T.P. Broten, T.W. Schorn, R.S.L. Chang, S.S. O'Malley, T.V. Olah, J.D. Ellis, A. Barrish, K. Kassahun, P. Leppert, D. Nagarathnam, and C. Forray. J. Med. Chem. **43**, 2703 (2000).

19. (*a*) M. Lacroix and G. Leclercq. Breast Cancer Res. Treat. **83**, 249 (2004); (*b*) H.D. Soule, J. Vazquez, A. Long, S. Albert, and M. Brennan. J. Nat. Cancer Inst. **51**, 1409 (1973); (*c*) L.-H. Wang, X.-Y., X. Zhang, and K. Mihalic. Nat. Med. (N.Y.), **10**, 40 (2004).

© 2005 NRC Canada

A convenient solid-phase synthesis methodology for preparing peptide-derived molecular imaging agents — Synthesis, characterization, and in vitro screening of Tc(I) – chemotactic peptide conjugates

Karin A. Stephenson, Sangeeta Ray Banerjee, Nicole McFarlane, Douglas R. Boreham, Kevin P. Maresca, John W. Babich, Jon Zubieta, and John F. Valliant

Abstract: A versatile solid-phase synthesis strategy for preparing peptide–chelate conjugates was developed. The methodology was optimized using a series of ligands, designed to bind Tc(I)/Re(I), and a chemotactic peptide fMFL, which was exploited as a model targeting vector. The peptide derivatives were prepared in parallel using a conventional automated peptide synthesizer in multi-milligram quantities, which provided sufficient material to perform complete characterization, radiolabelling, and in vitro screening studies. Because of the robust nature of the metal–chelate complexes, the Re complex of a chelate–peptide conjugate was prepared on the resin using the same methodology employed to prepare the free ligand conjugates. As such, the reported methodology is amenable to the preparation of libraries of novel Tc radiopharmaceutical ligands and their corresponding Re reference standards in which several factors, including peptide sequence, site of derivatization, and both the type and length of the spacer, can be easily varied.

Key words: radiopharmaceuticals, technetium, rhenium, peptides, solid-phase synthesis.

Résumé : On a développé une stratégie versatile de synthèse en phase solide de produits conjugués peptide–chélate. On a optimisé la méthodologie en utilisant une série de ligands qui ont été développés pour se lier au Tc(I)/Re(I) et au peptide chimiotactique fMFL qui a été exploité comme vecteur modèle de ciblage. On a préparé les dérivés peptidiques en parallèle en faisant appel à un synthétiseur automatique conventionnel de peptides à des niveaux de plusieurs milligrammes, ce qui fournissait des quantités suffisantes de matériel pour en faire une caractérisation complète, un marquage radiochimique et des études in vitro. En raison du fait que les complexes métal–chélate sont très robustes, un complexe du Re d'un produit conjugué chélate peptide a été préparé sur la résine en faisant appel à la même méthodologie qui avait été utilisée pour préparer les conjugués libres du ligand. De cette façon, la méthodologie qui a été mise au point peut être amener à la préparation de librairies de nouveaux ligands radiopharmaceutiques du Tc et des produits de référence du Re dans lesquels il est possible de faire varier plusieurs facteurs, y compris la séquence peptidique, le site de formation du dérivé ainsi que le type et la longueur du groupe d'écartement.

Mots clés : radiopharmaceutiques, technitium, rhénium, peptides, synthèse en phase solide.

[Traduit par la Rédaction]

Introduction

Small peptides have been shown to be highly effective targeting agents for delivering radionuclides to specific receptors, including those associated with tumours, infection, and thrombosis (1–8). Peptides are able to reach their target rapidly, thus avoiding the need to use radionuclides with excessively long half-lives, and they typically clear from nontarget tissues quickly, which improves image contrast and quality (1, 9). Peptides can be prepared in a cost-effective manner via automated solid-phase synthesis, and they can be designed to target practically any receptor (10–12).

The traditional strategy for linking radiometals to peptides involves appending a bifunctional chelate (BFC) to either the N or C termini of the peptide. This was typically performed in solution (1, 6), which can lead to numerous side products, particularly if lysine residues are present in the peptide. To avoid the poor regioselectivity of this approach, which often results in the need to employ extensive HPLC purification to isolate the desired product (13), several groups began to exploit the advantages of solid-phase synthesis (SPS) to prepare peptide–ligand conjugates directly on polymer supports

Received 3 August 2005. Published on the NRC Research Press Web site at http://canjchem.nrc.ca on 3 February 2006.

K.A. Stephenson, N. McFarlane, D.R. Boreham, and J.F. Valliant.[1] Departments of Chemistry and Medical Physics & Applied Radiation Sciences, McMaster University, Hamilton, ON L8S 4M1, Canada.
S.R. Banerjee and J. Zubieta. Department of Chemistry, Syracuse University, Syracuse, NY 13244-4100, USA.
K.P. Maresca and J.W. Babich. Molecular Insight Pharmaceuticals Inc., Cambridge, MA 02142, USA.

[1]Corresponding author (e-mail: valliant@mcmaster.ca).

 doi: 10.1139/V05-224 © 2005 NRC Canada

(14, 15). Using this approach, orthogonal protecting groups can be employed, and large excesses of reagents can be used to drive reactions to completion while byproducts are removed by simple filtration (10, 15–17). SPS of this type is amenable to automation and can therefore be used to prepare libraries of compounds (18–21).

Current SPS methods used to prepare peptide-targeted radiotracers derived from ^{99m}Tc (the most widely used radionuclide in diagnostic medicine (22–24)) typically involve conjugating a ligand to the N-terminus of the resin-bound peptide. For instance, Hoffman and co-workers (25) prepared a series of bombesin derivatives using N_3S triamide chelates linked to the N-terminal amino acid through different spacer groups. Egli et al. (26) attached a protected histidine derivative to the N-terminus of neurotensin as a way of tagging the peptide with the $[^{99m}Tc(CO)_3]^+$ core. More recently, two strategies for incorporating ligands within the backbone of the peptide have been reported. Blower and co-workers (15) prepared a derivative of Fmoc-lysine that contained a hydrazine substituent as a way of incorporating a ^{99m}Tc binding ligand within peptides. We recently reported the synthesis of amino acid derived chelates for Tc(I), which can also be incorporated regioselectively into the backbone of a peptide (17, 27). A unique feature of this system is that the Re complex can be prepared in parallel with the free ligand, owing to the stability of the low spin d^6 Re(I) complex.

This paper describes a new approach for preparing peptide–Tc ligand conjugates. The reported method is attractive in that a chelate can be attached at any position within the backbone of the peptide and not simply to the terminal amino or acid groups. Specifically, the approach involves using an on-resin orthogonal protecting group strategy, where a Tc(I) chelate is linked to a specific lysine residue. This methodology will ultimately be useful for creating libraries of tracers as a means of rapidly identifying new radiopharmaceuticals.

Experimental section

Unless otherwise stated, all reagents and solvents were ACS grade or higher and used without further purification. Polystyrene-based *N*-α-9-fluorenylmethoxycarbonyl (Fmoc)-glycine loaded SASRIN resin (0.69 mmol/g, 1% divinylbenzene, 200–400 mesh) was obtained from Bachem Inc. Fmoc-protected amino acids were purchased from NovaBiochem Inc., Bachem Inc., and Advanced ChemTech Inc. Fluorescein-labelled fNLFNTK was purchased from Molecular Probes Inc. (product No. F-1314).

Peptides were analyzed by electrospray mass spectrometry using a Micromass Quattro Ultima instrument in positive ion mode. Samples were dissolved in 50:50 ACN–H_2O prior to analysis. FT IR spectra were acquired on a Bio-Rad FTS-40 FT IR spectrometer. Analytical HPLC on nonradioactive compounds was performed using a Varian Pro Star model 330 PDA detector, model 230 solvent delivery system, and a C-18 Microsorb column (4.6 × 250 mm, 300 Å – 5 μm). Semipreparative HPLC on nonradioactive compounds was carried out using a Varian Pro Star HPLC fitted with a model 320 UV detector, a model 215 solvent delivery system, and a C-18 Microsorb column (10 × 250 mm, 300 Å – 5 μm). The elution protocol for both analytical and semipreparative experiments was a linear gradient of from 25% acetonitrile containing 0.1% TFA to 50% acetonitrile containing 0.1% TFA over 15 min. The flow rates were 1.0 and 4.2 mL/min for the analytical and semipreparative experiments, respectively. All HPLC experiments were monitored at λ = 254 and 214 nm. Radio–HPLC experiments were performed on a Varian Prostar HPLC equipped with an autosampler (model 410), a UV–vis detector (model 345), an NaI radiometric detector, Prostar Pumps (model 210), and a Vydac C18 25 cm × 4.6 mm column (5 μm pore size) fitted with a 2 cm guard column. The mobile phase consisted of the following: solvent A = pH 2–2.5 triethylammonium phosphate buffer (7 mL NEt_3, 4 mL concd. H_3PO_4 in 1000 mL water); solvent B = CH_3OH. The method employed a gradient run over 30 min at a flow rate of 1 mL/min. The gradient ramped from 5% to 100% B, beginning at 3 min and ending at 20 min.

Solid-phase peptide synthesis

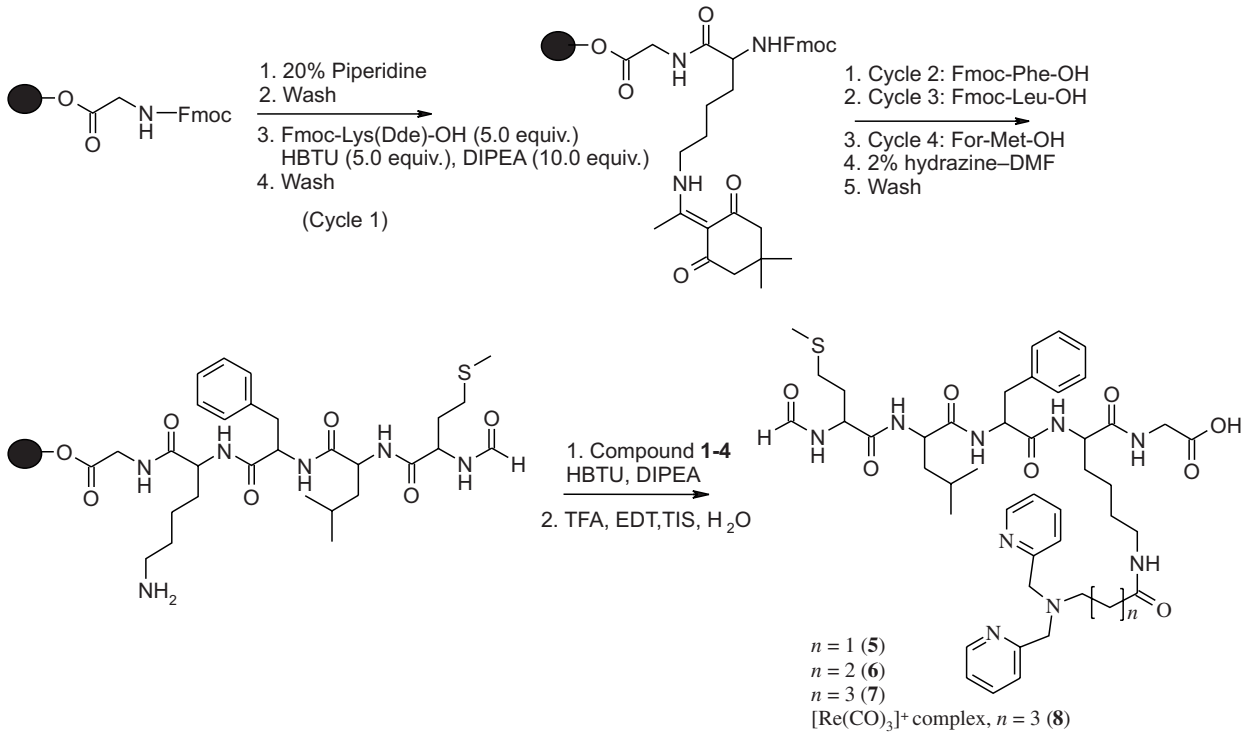
Fmoc-glycine loaded SASRIN resin (150 mg/well, 0.69 mmol/g) was added to four wells of an Advanced ChemTech 348 automated synthesizer, suspended in DMF (2 mL/well), and shaken at 600 rpm for 1 min. The wells were subsequently filtered, suspended in THF (2 mL/well), shaken at 600 rpm for 1 min, and drained for 90 s. The THF wash was repeated two more times. The DMF wash was then repeated a final two times to complete the general wash cycle. This procedure was used between every deprotection and coupling step. Fmoc deprotection was accomplished through the addition of a 20% *v*/*v* piperidine–DMF solution to the active vessels (2 mL/well) and shaking for 5 min at 600 rpm. Following filtration, the process was repeated, but with shaking for 10 min. The deprotected resin-bound amino acid was washed using the general wash procedure and subsequently coupled to the next Fmoc-protected amino acid using a standard HBTU coupling technique. A "cycle", according to Scheme 1, consists of Fmoc deprotection, a wash, and coupling the specified amino acid, followed by an additional wash.

Coupling reactions initially involved adding DMF (200 μL) to the active vessels followed by a fivefold excess of the protected amino acid as a 0.5 mol/L solution in DMF. Five equivalents of HBTU as a 0.5 mol/L solution in DMF were then added, followed by a 10-fold excess of DIPEA as 2.0 mol/L solution in DMF. The reaction block was subsequently shaken for 80 min at 600 rpm. Following filtration, the resin was washed using the general washing procedure prior to the start of the next cycle. Dde deprotection was accomplished through the addition of a 2% *v*/*v* hydrazine–DMF solution to the active vessels (2 mL/well) and shaking for 5 min at 600 rpm. Following filtration, the process was repeated, with shaking for 10 min. The free ε amine was then subjected to the general wash cycle and coupled to the desired chelate using the HBTU protocol described above, which was followed with a final wash.

Peptides were cleaved from the resin using a cocktail of TFA containing (*v*/*v*/*v*) EDT (2%), water (2%), and TIS (2%). The cleavage cocktail, cooled to 0 °C, was added to the resin, and the mixture was allowed to warm to room temperature over 60 min. The suspension was filtered into

© 2005 NRC Canada

Scheme 1. Synthesis of compounds **5**–**8**.



cold diethyl ether, and the resulting heterogeneous solution was centrifuged at 3000 rpm and –5 °C for 10 min. The resulting pellet was washed with cold ether (3 × 25 mL), dissolved in distilled–deionized water, and lyophilized, yielding a white solid.

Preparation of fMLFK(4m-Tc(CO)$_3^+$)G (9)

Technetium-99m was obtained in saline from a commercial ^{99}Mo/^{99m}Tc generator (Cardinal Health), and $[^{99m}Tc(CO)_3(H_2O)_3]^+$ was prepared using the commercially available Isolink kits (Mallinckrodt). Compound **7** (0.1 mg, 0.11 μmol) and 370 MBq (10 mCi) $[^{99m}Tc(CO)_3(H_2O)_3]^+$ were combined and heated at 75 °C for 60 min. After cooling to room temperature, the product was purified by HPLC (R_t = 12.1 min).

Ligand challenge experiments

Compound **9** in methanol (50 μL) and PBS buffer (1 mL, pH 7.2) was added to 0.1 mol/L solutions of cysteine in PBS buffer (pH 7.2) and histidine in PBS buffer (pH 7.2). The solutions were incubated at 37 °C for 24 h.

Leukocyte preparation

Whole human blood (10–15 mL) was collected in vacutainer tubes (Becton Dickinson) containing sodium heparin. The red blood cells were lysed using a modified ammonium chloride method (1 part whole blood to 23 parts 0.145 mol/L ammonium chloride solution containing 1.5 mmol/L potassium bicarbonate and 0.1 mmol/L EDTA). Tubes were incubated at room temperature for 15 min and then centrifuged in a Beckman Coulter Allegra 6R centrifuge at 900 rpm (400 g) for 7 min at 5 °C. The supernatant was removed, and the pellet of leukocytes were subsequently resuspended in Hank's Balanced Salt Solution (HBSS), containing 0.1% BSA, 10 mmol/L HEPES, and 1.5 mmol/L $CaCl_2$ (HBSS+). The cells were spun for 7 min at 400 g at 5 °C, the supernatant was removed, and the pellet was resuspended in HBSS+. Cell counts were performed using a hemacytometer and a Beckman Coulter Z2 Coulter particle count and size analyzer. Cell concentrations were adjusted to 2×10^6 mL^{-1}.

Flow cytometry

Samples were run on a Beckman Coulter EPICS XL, equipped with an argon laser (488 nm excitation wavelength). Fluorescence was measured using a 525 ± 15 nm band pass filter. The flow cytometer was calibrated with fluorescein isothiocyanate (FITC)-labeled beads (Quantum 26 beads, Bangs Laboratories, Inc, Fishers, Indiana) prior to sample analysis. The fluorescence intensity of the standard was provided by the manufacturer in units of molecules of equivalent soluble fluorochrome (MESF) and ranged from 5300 to 468 800. A linear fit of MESF vs. mean channel number of the beads was used to convert all subsequent mean channel values to MESF values.

Equilibrium-binding assay

The equilibrium-binding assay was used to determine the number of formyl peptide receptors (FPRs) on the surface of the neutrophils and the dissociation constant (K_d) of the fluorescein-labeled fNLFNTK (Molecular Probes) by preparing a saturated binding curve of peptide concentrations vs. fluorescence intensity (28, 29). Peptide stock solutions were made by dissolving the peptide derivative in DMSO and then diluting with HBSS+ to the desired concentrations, ensuring the concentration of DMSO was less than 0.1%. Cells at 1×10^6 mL^{-1} were equilibrated with 0.25, 0.50, 1.0, 3.0, 5.0, 10.0, and 20.0 nmol/L solutions of the peptide de-

© 2005 NRC Canada

rivative (L) in duplicate. The samples were incubated for 2 h at 4 °C in the dark and then run on the flow cytometer. Granulocytes were gated on the basis of forward and side scatter parameters using Expo 32 ADC software (Beckman Coulter). All samples were repeated in the presence of 30 μmol/L fMLF to account for nonspecific binding. The number of receptor–ligand complexes per cell (*B*) was determined using the following equation, where Q is a normalization factor used by Waller and *F* is the total fluorescence per cell:

$$B\,(\text{in ligand bound per cell}) = F\left(\frac{\text{MESF}}{\text{cell}}\right)\times \text{Q}$$

The level of nonspecific binding did not vary significantly with concentration of labeled peptide; thus, an average value of nonspecific binding was subtracted from the total fluorescence per cell, *F*, when determining the number of receptor–ligand complexes. The total number of *N*-formyl peptide receptors, R_{tot}, and the equilibrium dissociation constant, K_d, were evaluated by minimizing the squared residual of the equilibrium solution using a one-site binding model. The values of R_{tot} and K_d for each donor were solved simultaneously.

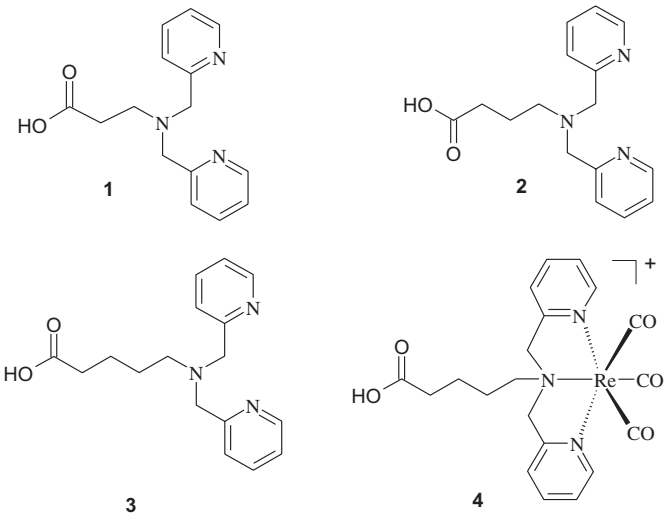
Results and discussion

The aim of this study was to develop a versatile bioconjugation strategy in which Tc ligands could be linked to peptides using a conventional automated peptide synthesizer. The method entailed incorporating lysine into the backbone of a peptide in such a manner that the ε-nitrogen could be selectively liberated and a Tc chelate added while the peptide was still linked to the resin. Using this approach, a number of important structural features, including the position and nature of the chelate, can be easily varied.

The blocking group selected for the ε-nitrogen of lysine was the 1-(4,4-dimethyl-2,6-dioxocyclohexyldiene)ethyl (Dde) protecting group, which is stable to the conditions used in typical Fmoc solid-phase synthesis, and which can be selectively liberated without affecting Boc protecting groups (30–32). The planned approach is amenable to any bifunctional chelating system containing a pendent acid group; however, for the work described here a series of dipyridyl amine ligands with linker arms of varying length were employed (Fig. 1) (17). These ligands form stable complexes with Tc(I), and their Re(I) complexes are sufficiently robust that the metal complex can be incorporated into peptides using the same methodology employed for the free ligand (33–37).

To develop the approach, the chemotactic peptide fMLFKG, which binds to the formyl peptide receptor (FPR) expressed on granulocytes, was used as a model system. Labelled versions of fMLF have shown potential utility for imaging sites of infection and inflammation (38–47). fMLF bioconjugates have traditionally been prepared in solution by conjugating hydrazine-type ligands (HYNIC) to the ε amine of fMLFK. This approach is not easily amenable to preparing libraries of fMLF derivatives, which would accelerate the process of identifying the appropriate derivative for clinical applications.

Fig. 1. Tc(I)/Re(I) ligands and the Re(I) complex of **3**.



The peptide fMLFK(Dde)G was prepared on an Advanced ChemTech 348 synthesizer using standard Fmoc–HBTU protecting groups – coupling protocols (Scheme 1). The Dde protecting group was removed by employing 2% hydrazine in DMF, and the reaction time was optimized using ninhydrin to ensure complete deprotection (48). Following removal of the Dde protecting group, the bifunctional chelates (**1**–**3**) were coupled to the resin-bound peptides using HBTU and DIPEA, and reaction times were again monitored to ensure complete coupling (48). The time required (80 min) for conversion to the desired product did not differ from standard amino acid coupling procedures.

Peptide conjugates **5**–**7** were cleaved from the resin using a cleavage cocktail containing 94% TFA, 2% triisopropylsilane, 2% ethanedithiol, and 2% water. Nitrogen was bubbled through the cocktail at 0 °C prior to and during use, to help prevent oxidation of methionine. Peptides were precipitated by trituration with cold diethyl ether and centrifuged, and the resulting pellet was washed with cold ether to remove any trace of the cleavage cocktail. Precipitates were then dissolved in distilled water and lyophilized to yield white solids.

Peptides **5**–**7** were analyzed using electrospray mass spectrometry (ESMS), and in each case the observed molecular ion was consistent with the mass of the desired compound (Table 1). Analytical HPLC and LC–MS studies of each peptide indicated the presence of two peaks in a 3:1 ratio, corresponding to the same *m*/*z* values. Previous studies in our group and by others showed that the two peaks in the HPLC chromatogram are the result of epimerization of methionine, which is promoted by the electron-withdrawing nature of the formyl group (17, 49). Notwithstanding, the two isomers were readily separated using semipreparative HPLC.

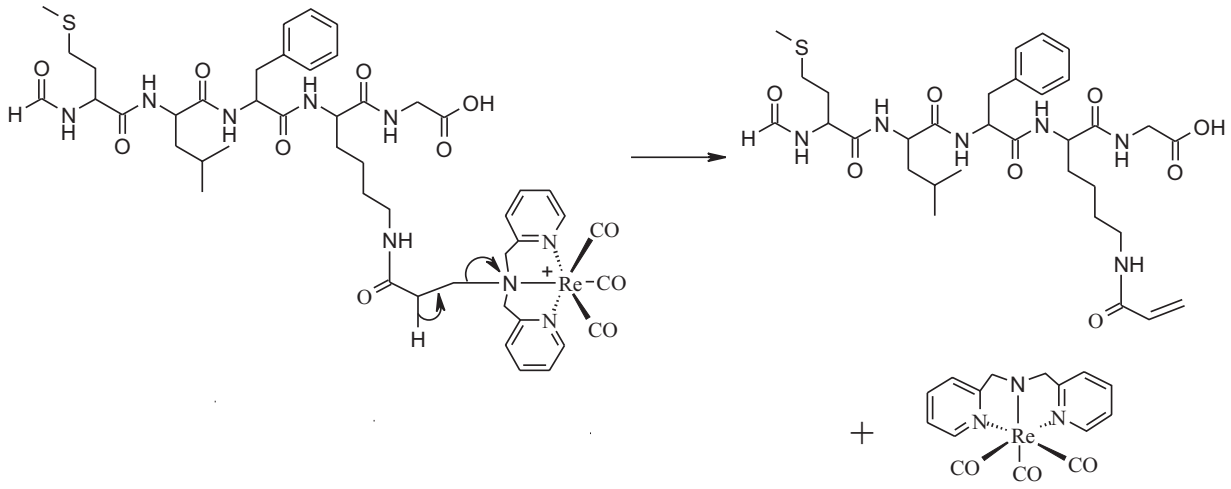
One of the advantages of using M(I) (M = Tc, Re) ligands for methods involving solid-phase synthesis is the ability to prepare the Re complex in parallel with compounds containing the free ligand. Preparation of Re complexes is vitally important as they are needed for proper characterization of the ^{99m}Tc-analogues and for performing in vitro screening studies. For the method described here, the Re complex of **7**

© 2005 NRC Canada

Table 1. HPLC and ESMS data for compounds **5**–**8**.

Compound number	Elution time (min)	Found *m/z*	Calcd. *m/z*	Yield (%)	νCO (cm^{-1})
5	6.6	876.4	876.1	34	—
6	6.5	890.5	890.1	35	—
7	6.9	904.5	904.1	33	—
8	8.7	1174.4	1174.3	30	1933, 2041

Fig. 2. Proposed mechanism for the degradation of an Re(I)–peptide conjugate.

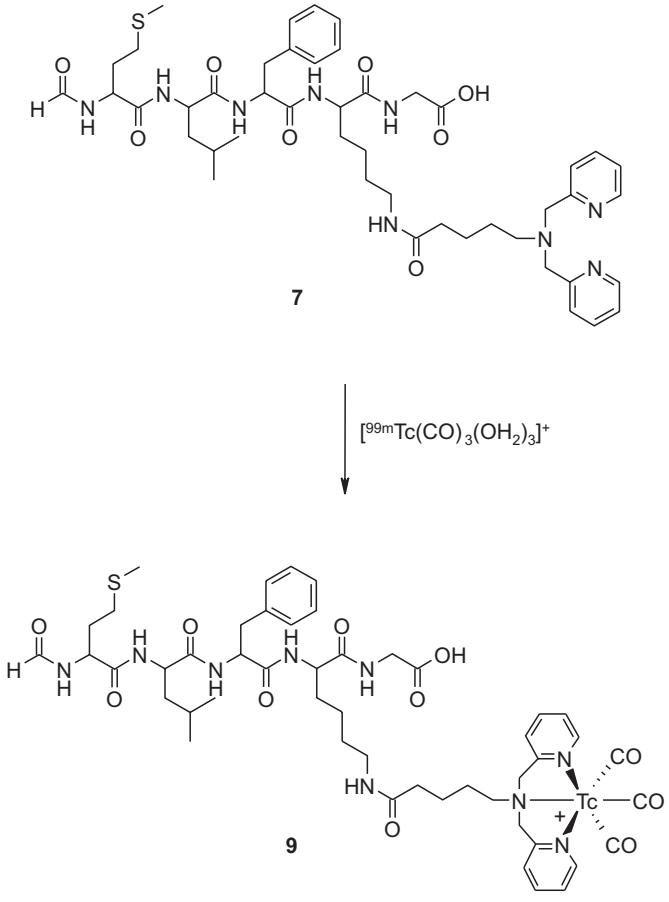


(**8**) was prepared successfully in parallel with the synthesis of compounds **5**–**7**, without modifying the basic strategy. After cleavage of the conjugate from the resin using the same cocktail described above, the product was isolated in comparable yields to the free ligands. Mass spectrometry clearly indicated the presence of the desired product (**8**), while IR showed two distinct metal CO stretches (1933 and 2041 cm^{-1}), which are consistent with values reported for analogous Re complexes (17, 33–37).

As an aside, attempts to prepare the peptide containing the Re(I) complex of **1** lead to a complex mixture of products according to HPLC. MS analysis of the precipitate formed after the addition of ether to the reaction mixture indicated the presence of the target compound, along with several degradation products. The likely cause of these impurities is elimination to form an αβ-unsaturated amide, which concomitantly results in liberation of a neutral metal complex (Fig. 2). By-products of this nature were not observed for the other ligands.

To ensure the products from the solid-phase synthesis can be radiolabeled, compound **7** (100 μg) was combined with 370 MBq (10 mCi) of $[^{99m}Tc(CO)_3(OH_2)]^+$, which was prepared using the commercially available Isolink kit (Scheme 2). After 60 min at 75 °C, the desired product **9** was isolated by HPLC in greater than 98% radiochemical purity in 63% radiochemical yield. Analytical HPLC of the purified product is shown in Fig. 3. The stability of the purified peptide **9** towards metal substitution was tested using a large excess of cysteine and histidine. The peptide and the two amino acids were heated at 37 °C for 24 h, whereupon HPLC analysis showed that the product was intact in both cases and that the radiochemical purities remained above 95% (Fig. 4).

Scheme 2. Synthesis of fMLFK(4m-$Tc(CO)_3^+$)G (**9**).



© 2005 NRC Canada

Fig. 3. γ-HPLC radio chromatogram (mV vs. time (min)) for purified **9**.

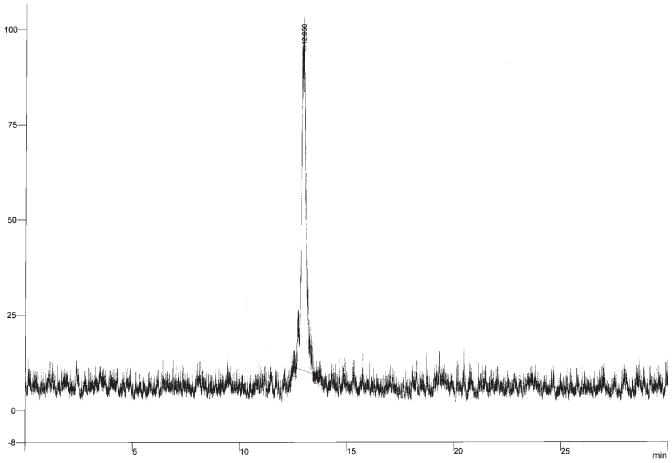
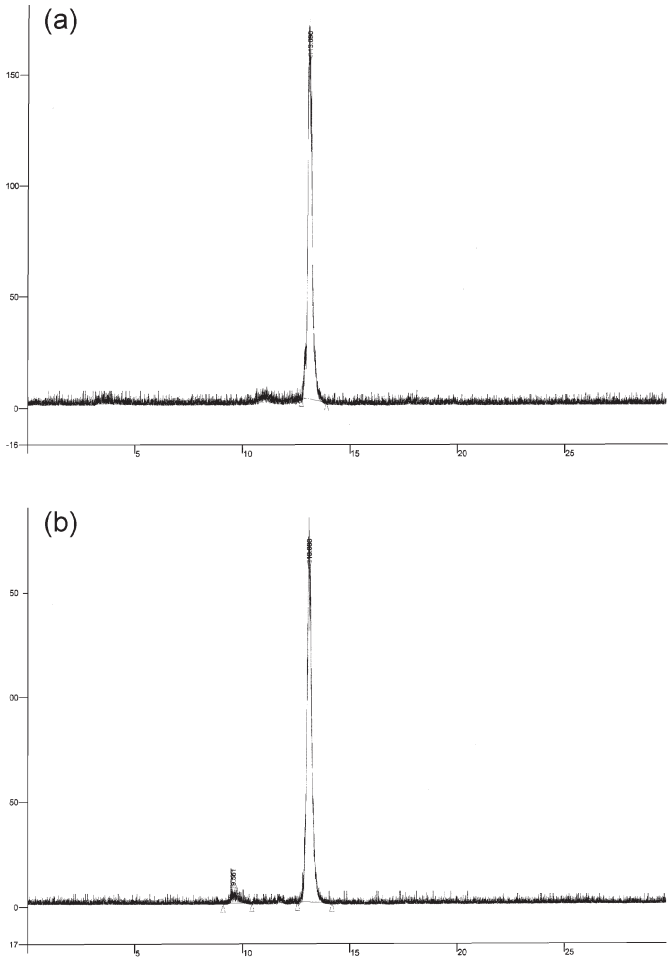


Fig. 4. γ-HPLC radio chromatograms (mV vs. time (min)) of the (*a*) cysteine and (*b*) histidine challenges of **9** after 24 h at 37 °C.



With the above methodology in hand it is possible to generate diverse libraries of compounds. The next step is to select the appropriate in vitro screening method that will indicate what compounds are the most promising for more advanced biological studies. In the example presented here, the ability of peptides **5–8** to bind to the FPR receptor was determined using flow cytometry. Flow cytometry is an attractive tool for screening novel molecular imaging agents because it is amenable to automation, which means that libraries can be evaluated rapidly, and it affords the opportunity to investigate specific cell populations. To evaluate the fMLF derivatives, human white blood cells were incubated with 1.0 nmol/L fluorescein-labelled fNLFNTK and varying amounts of the competitor in duplicate for 2 h at 0 °C in the dark. fMLF, which was used as a reference standard, exhibited a K_d that was in good agreement with the value reported in the literature (28, 50). Conjugates **5–8** had dissociation constants (Table 2) in the low nanomolar range, which is similar to the value for fMLF, thus demonstrating that incorporation of the ligand or Re complex does not have a negative impact on the ability of the peptides to bind the FPR.

Table 2. Dissociation constants (K_d) for compounds **5–8**.

Compound Number	Peptide sequence	K_d (nmol/L)
	fMLF	32±3
5	fMLFK(2M)G	21±6
6	fMLFK(3M)G	52±3
7	fMLFK(4M)G	55±8
8	fMLFK(4M-Re(CO)$_3^+$)G	67±6

Conclusions

The reported strategy offers a new alternative to existing solid-phase synthetic methodologies for preparing peptide-based radiotracers. The ligands and their rhenium complexes employed in this study can be incorporated into the backbone of peptides using traditional automated solid-phase synthesis methods. For instruments that have multiple reaction wells, the free ligand and Re–peptide conjugates can be prepared in parallel. The peptide derivatives described here were prepared in parallel in multi-milligram quantities, which provided sufficient material to allow for complete characterization, radiolabelling, and in vitro screening studies to be performed from the products of a single run of the synthesizer. The reported methodology can be used to prepare libraries of compounds in which several factors, including peptide sequence, site of derivatization, nature of the chelate, and both the type and length of the spacer can be varied, which will decrease the time and effort required to identify lead compounds.

Acknowledgements

We would like to acknowledge the Ontario Research and Development Challenge Fund (ORDCF) and the Natural Sciences and Engineering Research Council of Canada (NSERC) for funding and for providing a scholarship for KAS.

References

1. S.M. Okarvi. Med. Res. Rev. **24**, 357 (2004).
2. S.M. Okarvi. Nucl. Med. Commun. **20**, 1093 (1999).
3. J. Fichna and A. Janecka. Bioconjugate Chem. **14**, 3 (2003).

© 2005 NRC Canada

4. A. Signore, A. Annovazzi, M. Chianelli, F. Corsetti, C. Van de Wiele, R.N. Watherhouse, and F. Scopinaro. Eur. J. Nucl. Med. **28**, 1555 (2001).
5. R.E. Weiner and M.L. Thakur. Sem. Nucl. Med. **31**, 296 (2001).
6. S. Liu and D.S. Edwards. Chem. Rev. **99**, 2235 (1999).
7. S. Liu, D.S. Edwards, and J.A. Barrett. Bioconjugate Chem. **8**, 621 (1997).
8. D. Blok, R.I.J. Feitsma, P. Vermeij, and E.J.K. Pauwels. Eur. J. Nucl. Med. **26**, 1511 (1999).
9. W.C. Eckelman. Eur. J. Nucl. Med. **22**, 249 (1995).
10. W.C. Chan and P.D. White. FMOC solid-phase peptide synthesis, a practical approach. Oxford University Press, New York. 2000.
11. G.B. Fields and R.L. Noble. Int. J. Pept. Protein Res. **35**, 161 (1990).
12. P. Seneca. Solid-phase synthesis and combinatorial technologies. Wiley-Interscience, Toronto. 2000.
13. M.L. Thakur. Nucl. Med. Commun. **16**, 724 (1995).
14. J. Gariépy, S. Rémy, X. Zhang, J.R. Ballinger, E. Bolewska-Pedyczak, M. Rauth, and S.K. Bisland. Bioconjugate Chem. **13**, 679 (2002).
15. W.E.P. Greenland, K. Howland, J. Hardy, I. Fogelman, and P.J. Blower. J. Med. Chem. **46**, 1751 (2003).
16. R.B. Merrifield. J. Am. Chem. Soc. **85**, 2149 (1963).
17. K.A. Stephenson, J. Zubieta, S.R. Banerjee, M.K. Levadala, L. Taggart, L. Ryan, N. McFarlane, D.R. Boreham, K.P. Maresca, J.W. Babich, and J.F. Valliant. Bioconjugate Chem. **15**, 128 (2004).
18. N.W. Hird. Drug Discovery Today, **4**, 265 (1999).
19. B.A. Bunn. The combinatorial index. Academic Press, San Diego. 1998.
20. A. Nefzi, J.M. Ostresh, J. Yu, and R.A. Houghten. J. Org. Chem. **69**, 3603 (2004).
21. M. Cano and S. Balasubramanian. Drugs Future, **28**, 659 (2003).
22. J.R. Dilworth and S.J. Parrot. Chem. Soc. Rev. **27**, 43 (1998).
23. S.S. Jurisson and J.D. Lydon. Chem. Rev. **99**, 2205 (1999).
24. K. Schwochau. Angew. Chem. Int. Ed. Engl. **33**, 2258 (1994).
25. C.J. Smith, H. Gali, G.L. Sieckman, C. Higginbotham, W.A. Volkert, and T.J. Hoffman. Bioconjugate Chem. **14**, 93 (2003).
26. A. Egli, R. Alberto, L. Tannahill, R. Schibli, U. Abram, A. Schaffland, R. Waibel, D. Tourwe, L. Jeannin, K. Iterbeke, and P.A. Schubiger. J. Nucl. Med. **40**, 1913 (1999).
27. K.A. Stephenson, S.R. Banerjee, T. Besanger, O.O. Sogbein, M.K. Levadala, N. McFarlane, J.A. Lemon, D.R. Boreham, K.P. Maresca, J. Brennan, J.W. Babich, J. Zubieta, and J.F. Valliant. J. Am. Chem. Soc. **126**, 8598 (2004).
28. A. Waller, D. Pipkorn, K.L. Sutton, J.J. Linderman, and G.M. Omann. Cytometry, **45**, 102 (2001).
29. J.F. Hoffman, M.L. Keil, T.A. Riccobene, G.M. Omann, and J.L. Linderman. Biochemistry, **35**, 13 047 (1996).
30. B.W. Bycroft, W.C. Chan, S.R. Chhabra, and N.D. Hone. J. Chem. Soc. Chem. Commun. 778 (1993).
31. S. Peluso, P. Dumy, C. Nkubana, Y. Yokokowa, and M. Mutter. J. Org. Chem. **64**, 7114 (1999).
32. B. Rohwedder, Y. Mutti, P. Dumy, and M. Mutter. Tetrahedron Lett. **39**, 1175 (1998).
33. L. Wei, S. Banerjee, M.K. Levadala, J.W. Babich, and J. Zubieta. Inorg. Chem. Commun. (Cambridge), **6**, 1099 (2003).
34. L. Wei, S.R. Banerjee, M.K. Levadala, J.W. Babich, and J. Zubieta. Inorg. Chim. Acta, **357**, 1499 (2004).
35. M.K. Levadala, S.R. Banerjee, K.P. Maresca, J.W. Babich, and J. Zubieta. Synthesis, **11**, 1759 (2004).
36. S.R. Banerjee, M.K. Levadala, N. Lazarova, L. Wei, J.F. Valliant, K.A. Stephenson, J.W. Babich, K.P. Maresca, and J. Zubieta. Inorg. Chem. **41**, 6417 (2002).
37. S.R. Banerjee, L. Wei, M.K. Levadala, N. Lazarova, V.O. Golub, C.J. O'Conner, K.A. Stephenson, J.F. Valliant, J.W. Babich, and J. Zubieta. Inorg. Chem. **41**, 5795 (2002).
38. J.W. Babich, W. Graham, S.A. Barrow, S.C. Dragotakes, R.G. Tompkins, R.H. Rubin, and A.J. Fischman. J. Nucl. Med. **34**, 2176 (1993).
39. J.W. Babich, W. Graham, S.A. Barrow, and A.J. Fischman. Nucl. Med. Biol. **22**, 643 (1995).
40. J.W. Babich, W.G. Coco, S. Barrow, A.J. Fischman, F.J. Femia, and J. Zubieta. Inorg. Chim. Acta, **309**, 123 (2000).
41. J.W. Babich, H. Solomon, M.C. Pike, D. Kroon, W. Graham, M.J. Abrams, R.G. Tompkins, R.H. Rubin, and A.J. Fischman. J. Nucl. Med. **34**, 1964 (1993).
42. K.E. Baidoo, U. Scheffel, M. Stathis, P. Finley, S.Z. Lever, Y. Zhan, H.N.J. Wagner. Bioconjugate Chem. **9**, 208 (1998).
43. A.J. Fischman, D. Rauh, H. Solomon, J.W. Babich, R.G. Tompkins, D. Kroon, H.W. Strauss, and R.H. Rubin. J. Nucl. Med. **34**, 2130 (1993).
44. A.J. Fischman, M.C. Pike, D. Kroon, A.J. Fucello, D. Rexinger, C. TenKate, R. Wilkinson, R.H. Rubin, and H.W. Strauss. J. Nucl. Med. **32**, 483 (1991).
45. A. Pollak, A.E. Goodbody, J.R. Ballinger, G.S. Duncan, L.L. Tran, R. Dunn-Dufault, K. Meghji, F. Lau, T.W. Andrey, I. Boxen, and M. Sumner-Smith. Nucl. Med. Commun. **17**, 132 (1996).
46. C.J. Van Der Laken, O.C. Boerman, W.J.G. Oyen, M.T.P. Van De Ven, D.S. Edwards, J.A. Barrett, J.W.M. Van Der Meer, and F.H.M. Corstens. J. Nucl. Med. **38**, 1310 (1997).
47. K. Verbeke, A. Verbeke, H. Vanbilloen, and A. Verbruggen. Nucl. Med. Biol. **29**, 585 (2002).
48. V.K. Sarin, S.B. Kent, J.P. Tam, and R.B. Merrifield. Anal. Biochem. **117**, 147 (1981).
49. D.V. Greathouse, R.L. Goforth, T. Crawford, P.C.A. Van Der Wel, and J.A. Killian. J. Pept. Res. **57**, 519 (2001).
50. H.J.J.M. Rennen, O.C. Boerman, W.J.G. Oyen, and F.H.M. Corstens. Curr. Med. Chem.: Anti-Inflamm. Anti-Allergy Agents, **1**, 63 (2002).

© 2005 NRC Canada

Fluorescence quenching of Safranine T by inorganic anions in Tween micelles

Stephanie A. Moore, Sarah E. Moore, Karen M. Glenn, Subhash C. Bhattacharya, and Rama M. Palepu

Abstract: The fluorescence quenching of the dye Safranine T by various inorganic anions such as $[Fe(CN_6)]^{-3}$, $[Fe(CN_6)]^{-4}$, I^-, Br^-, NO_2^-, and N_3^- in aqueous solution and in nonionic micellar solutions of Tweens (Tween 20, Tween 40, and Tween 80) was studied. The Stern–Volmer quenching constants and quenching rate constants were evaluated. Compared to the quenching efficiency in aqueous media, that of the micellar media was found to be lower, except when iodide ion was used as a quencher. With the exception of the iodide ion, it has been established that collisional quenching plays a major role in the photophysical process. In the case of the iodide ion, both static and collisional quenching processes play a major role, owing to the complexation of iodide ion with Tween micelles. The Stern–Volmer quenching constants were found to be dependent on the ionic strength of the medium.

Key words: fluorescence, static quenching, Tweens, Stern–Volmer constant, micellar media.

Résumé : Opérant en solutions aqueuses et dans des solutions micellaires non-ioniques de Tween (Tween 20, Tween 40 et Tween 80), on a étudié le piégeage de la fluorescence du colorant safranine T par divers anions inorganiques, tels que $[Fe(CN)_6]^{-3}$, $[Fe(CN)_6]^{-4}$, I^-, Br^-, NO_2^- et N_3^-. On a évalué les constantes de piégeage et les constantes de vitesse de piégeage de Stern–Volmer. Comparées aux constantes de piégeage en milieu acide, on a trouvé que les constantes dans les milieux micellaires sont plus faibles, excepté dans le cas où l'ion iodure est utilisé comme piège. À l'exception de l'ion iodure, on a pu établir que le piégeage par collision joue un rôle prépondérant dans le processus photophysique. Dans le cas de l'ion iodure, les processus tant statique et collisionnel jouent tous les deux un rôle important en raison de la complexation de l'ion iodure par les micelles de Tween. On a trouvé que les constantes de piégeage de Stern–Volmer dépendent de la force ionique du milieu.

Mots clés : fluorescence, piégeage statique, Tween, constante de Stern–Volmer, milieu micellaire.

[Traduit par la Rédaction]

Introduction

Cationic organic dyes are an important class of compounds that are employed as laser dyes, dyes for textiles, and initiators for photopolymerization (1–3). Knowledge of the reaction mechanism involving the excited dyes used as photo-initiators is important in order to understand the processes occurring in the early stages of photo-induced polymerization (4, 5).

The photophysical properties of many dyes are influenced by surfactant micelles and reverse micelles (6–12). Studies of these systems are important for understanding the photophysical–photochemical activities of dyes in organized media. The fluourescence quenching of dyes or photoactive compounds by neutral or charged species in organized assemblies has been done to characterize these assemblies (13–19). With regards to fluorescence quenching in micellar media, there are two factors that affect the mutual encounter of the probe and the quencher molecules. These factors are: (*i*) the partitioning of the fluorescent probe and the quencher between the micellar and the aqueous phases and (*ii*) the dynamic distribution of these species during the quenching process.

The quenching of the dye Safranine T (ST) in different nonionic micellar and reverse micellar media using transition metal ions as quenchers was studied earlier (20–22). The results indicated the absence of charge interactions between the probe and the quencher, but collisional quenching interplay without electron transfer was found to occur. For further correlation, the cationic fluorescent probe ST with anionic quenchers could be informative. With this objective, the fluorescence quenching of ST in Tween micelles using I^-, Br^-, N_3^-, NO_2^-, $[Fe(CN_6)]^{-4}$, and $[Fe(CN_6)]^{-3}$ as quenchers is investigated in the present study.

Received 4 May 2005. Published on the NRC Research Press Web site at http://canjchem.nrc.ca on 3 February 2006.

S.A. Moore, S.E. Moore, K.M. Glenn, and R.M. Palepu.[1] Department of Chemistry, St. Francis Xavier University, Antigonish, NS B2G 2W5, Canada.
S.C. Bhattacharya.[2] Department of Chemistry, Jadavpur University, Kolkata 700 032 India.

[1]Corresponding author (e-mail: rpalepu@stfx.ca).
[2]Corresponding author (e-mail: sbjuchem@yahoo.com).

 doi: 10.1139/V05-225 © 2005 NRC Canada

Table 1. Stern–Volmer constants (K_{sv}) and bimolecular rate constants (k_q) for the quenching of the fluorescence of ST by inorganic anions in aqueous and micellar media at 298 K.

	K_{SV} (dm^3 mol^{-1})				$k_q \times 10^{-9}$ (dm^3 mol^{-1} s^{-1})			
Quencher ions	Aqueous	TW 20	TW 40	TW 80	Aqueous	TW 20	TW 40	TW 80
$[Fe(CN)_6]^{-3}$	45.0	23.8	21.4	19.1	30.8	16.3	14.7	13.1
$[Fe(CN)_6]^{-4}$	34.0	18.2	16.6	8.1	23.3	12.5	11.4	5.5
Br^-	8.0	1.72	1.61	1.57	5.5	1.2	1.1	1.1
NO_2^-	6.3	3.65	3.42	2.76	4.3	2.5	2.3	1.9
N_3^-	11.9	5.23	4.80	4.20	8.2	3.6	3.3	2.9

Note: Concentration of Tweens 25 mmol dm^{-3}; lifetime of ST, τ = 1.46 ns (ref. 15); viscosity values: 0.92, 0.90, and 1.02 cP for Tweens 20, 40, and 80, respectively.

Tweens are nonionic surfactants composed of a fixed length of 20 polyethylene oxide polar head groups, a sorbitan moiety, and a variable-length polymethylene chain (monolaurate, monopalmitate, and monooleate in Tween 20, Tween 40, and Tween 80, respectively).

Experimental details

ST (Merck) was recrystallized from ethanol–water mixtures before use. Tween 20, Tween 40, and Tween 80 were Aldrich products. Their light-sensitive characteristics within the region of interest were checked by absorption and emission measurements. Doubly distilled conductivity water was used for solution preparation. BDH (AR grade) salts $K_4[Fe(CN)_6]$, $K_3[Fe(CN)_6]$, KI, KBr, $NaNO_2$, and NaN_3 were used as quenchers.

The fluorescence of ST was measured using a spectrofluorometer (Spex Fluoro Max-3) with a slit width of 2.0 nm. The excitation and emission wavelengths are 520 and 586 nm, respectively. The concentration of ST used in the aqueous and micellar solutions was of the order of 10^{-5} mol dm^{-3}. The quencher concentrations were varied in the range of 0.1–0.9 mol dm^{-3} for Br^- and 1–50 mmol dm^{-3} for the other anions. The fluorescence spectra of the dye at a constant surfactant concentration with different quencher concentrations were recorded. Different sets of surfactant concentrations, varying from 10 to 50 mmol dm^{-3}, were used. Also, the quenching of ST by various anions was investigated as a function of ionic strength. The ionic strength of the solution was varied with sodium chloride. All the measurements were repeated at least three times, and the accuracy in calculated parameters was within ±0.5%.

Results and discussion

The inorganic ions $[Fe(CN_6)]^{-3}$, $[Fe(CN_6)]^{-4}$, I^-, Br^-, NO_2^-, and N_3^- were found to have quenched the fluorescence of ST in the aqueous Tween 20, Tween 40, and Tween 80 micellar media. Figure 1 illustrates the quenching process of ST as a function of concentration of ferrocyanide as quencher. The values of the Stern–Volmer quenching constants (K_{SV}) were obtained using the Stern–Volmer equation

$$[1] \qquad \frac{F_0}{F} = 1 + K_{SV}[Q]$$

where F_0 and F are the fluorescence intensities without and with quencher and [Q] is the concentration of the quencher.

Fig. 1. Quenching of Safranine T fluorescence in 50 mmol/L Tween 20 solution where [ferrocyanide] = (1) 0.0 mmol dm^{-3}; (2) 1.0 mmol dm^{-3}; (3) 2.0 mmol dm^{-3}; (4) 3.0 mmol dm^{-3}; (5) 5.0 mmol dm^{-3}; (6) 6.0 mmol dm^{-3}; (7) 7.0 mmol dm^{-3}; (8) 8.0 mmol dm^{-3}; and (9) 9.0 mmol dm^{-3}, respectively.

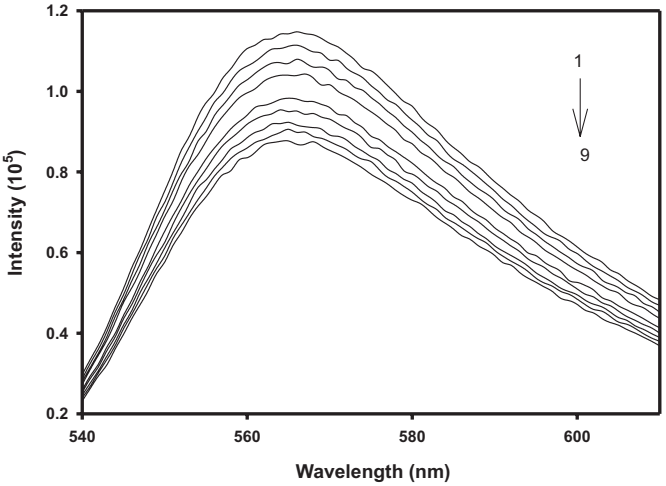


Table 2. Stern–Volmer constants (K_{sv}), fraction of inaccessible fluorophore (f_b), and r^2 values for the quenching of ST by iodide ions in Tween micellar media at 25 °C.

	K_{sv}	f_b	r^2
Tween 20	303±18	0.513±0.011	0.998
Tween 40	232±6	0.481±0.005	0.999
Tween 80	169±12	0.216±0.025	0.998

By employing single-photon counting techniques, the singlet state lifetime (τ_0) of ST in water was found to be 1.46 ns (20). The rate constants for quenching (k_q) were calculated from the relationship $K_{sv} = k_q\tau_0$, employing the value of 1.46 ns for τ_0. The results of the present study are given in Tables 1 and 2. The lifetime of ST is expected to be influenced by the presence of micelles. El-Kemary et al. (23) reported a value of 2.30 ns in methanol and a value of 2.81 ns for methanol – Triton X100 solutions. Therefore, the rate constants obtained in this study may tend to be slightly higher than the true values. The quenching efficiency of various anions was assessed from the relative magnitude of the Stern–Volmer constant (K_{sv}). Nonequivalent quenching manifestations of the inorganic ions were observed. The effi-

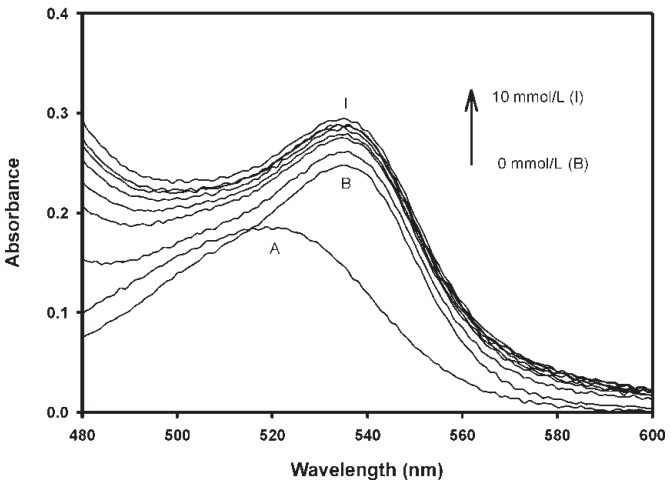
© 2005 NRC Canada

Table 3. Hydrated radius of different quencher ions, and free energy change, calculated from Rehm and Weller's equation.

		$-\Delta G^0$ (eV)			
Quencher ion	Radius (nm)	Water	Tween 20	Tween 40	Tween 80
$[F_e(CN)_6]^{-4}$	0.402	3.53	3.67	3.67	3.94
I^-	0.300	3.78	3.96	3.94	4.2
Br^-	0.300	4.26	4.42	4.42	4.66
N_3^-	0.300	5.05	5.21	5.26	5.45
NO_2^-	0.300	3.33	3.49	3.49	3.73

Note: K_{eq} values for I^- with Tween 20: 288 ± 10; Tween 40: 377 ± 13; and Tween 80: 259 ± 9.

Fig. 2. (A) Absorption spectrum of ST in water (1×10^{-5} mol/L); (B) absorption spectrum of ST in 35 mmol/L Tween 40 solution in the presence of varying concentrations of KI (0–10 mmol/L).



ciencies of the quencher ions in aqueous medium follow the order $[Fe(CN_6)]^{-3} > [Fe(CN_6)]^{-4} > I^- > Br^- > N_3^- > NO_2^-$. In micellar media, however, the quenching efficiencies follow the order $I^- > [Fe(CN_6)]^{-3} > [Fe(CN_6)]^{-4} > N_3^- > NO_2^- > Br^-$.

The quencher ions, except for the iodide ion, have no effect on the absorption spectrum of ST in aqueous and micellar media. In aqueous media the iodide ion has no effect on the absorption spectrum of ST. In aqueous Tween micellar media, however, there is an enhancement in the absorbance with bathochromic spectral shift (Fig. 2). This is indicative of complex formation between the iodide ion and the Tween micelles. The equilibrium constants for the complex formation were calculated by employing Lang's equation (24) from the absorption spectral data. The values are reported as a note below Table 3.

The reduction potential of ST is –0.467 V, calculated with reference to a standard hydrogen electrode (SHE) (20). Knowing the excitation energy (ΔE_{00}) of ST, the reduction potential of the first excited singlet state of ST can be calculated. A value of 2.68 eV was obtained for ΔE_{00}, and a value of 2.21 V was computed as the reduction potential of ST in the excited state. The reduction potentials of the $[Fe(CN_6)]^{-3}/[Fe(CN_6)]^{-4}$, I_2/I^-, Br_2/Br^-, $NO_2^-/N_2O_2^-$, and N_3^-/N_2 couples are 0.36, 0.62, 1.08, 0.15, and 1.87 V, respectively (25). The reduction of the dye in the excited state by the quenchers via an electron-transfer (ET) mechanism was therefore energetically feasible (Fig. 3).

In the case of $[Fe(CN)_6]^{-3}$, the quencher ion is in its maximum oxidized state; therefore, quenching of the fluorescence of ST should not take place by an electron-transfer mechanism. As mentioned earlier, the quenching efficiency trends of the anions (except for the iodide ion) are the same in aqueous and in micellar media.

Earlier studies (20) reported that the dye ST can reside at the micellar interface, penetrating it only partially. The poor solubility of ST in the nonpolar hydrocarbon media is indicative of its nonresidency in the hydrophobic micellar interior. In polar nonaqueous media, such as ethanol, ethylene glycol, and formamide, a sharp but red-shifted spectra is produced when compared with water. In very weak polar solvents, such as 1,4-dioxane, a broad spectrum with a minor red shift is obtained. In micellar media, a reasonable red shift is also observed. The spectral change in polar nonaqueous and micellar media supports the suggestion that ST resides on the outer surface of the micelles, particularly in the palisade layer, which consists of the ethylene oxide residues of the Tween micelles. There is a distribution of the dye between the aqueous bulk and the micellar outer surface. The quenching process is therefore believed to occur in both regions.

For an interpretation of the fluorescence quenching in terms of the electron-transfer mechanism for the quenchers $[Fe(CN_6)]^{-4}$, I^-, Br^-, NO_2^-, and N_3^-, the free energy change (ΔG) for the process may be evaluated from the following equations (26, 27):

$$[2] \qquad \log_{10} k_q = \log_{10} k_{diff} - \frac{\Delta G}{2.303RT}$$

where

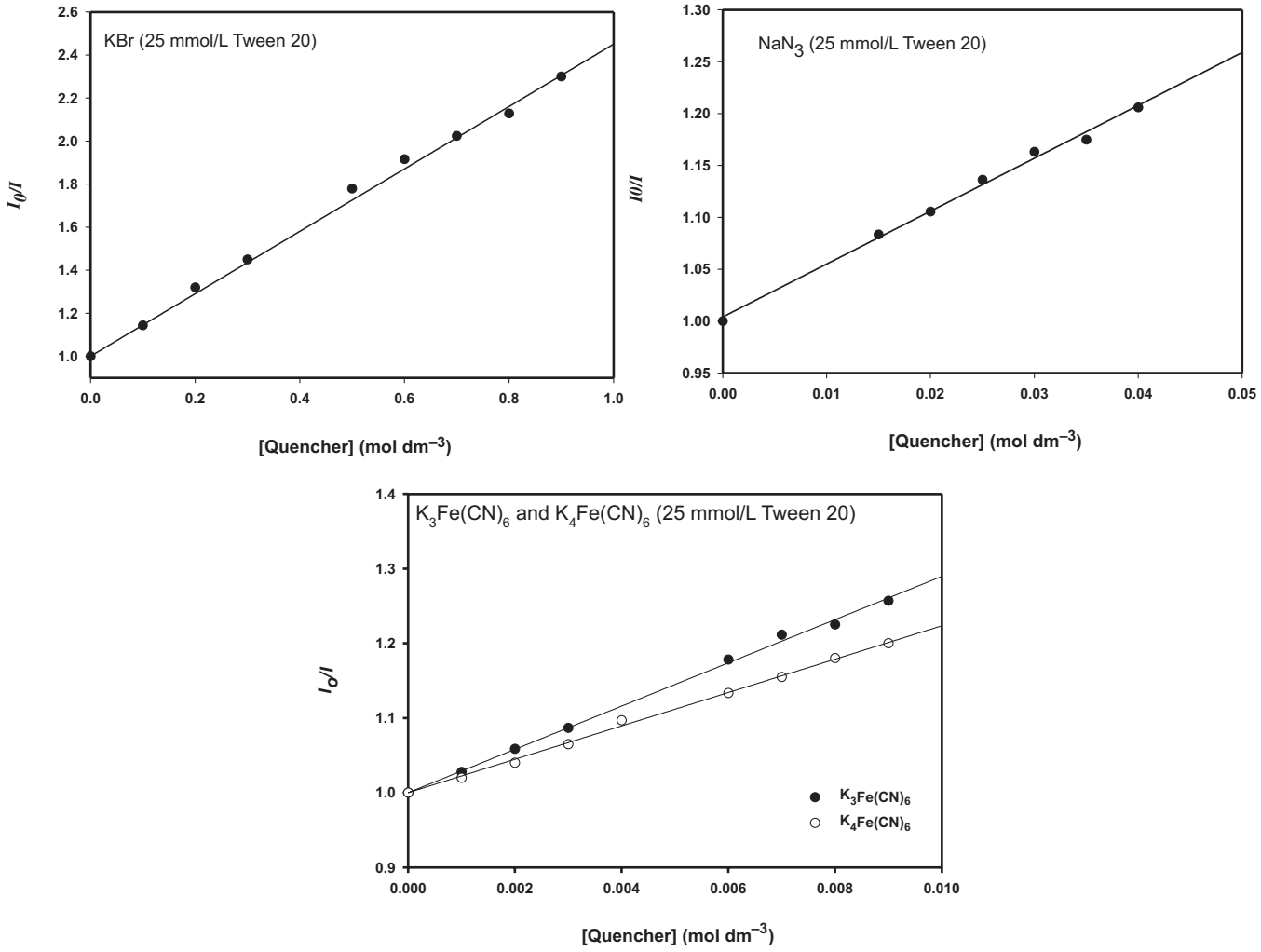
$$[3] \qquad \Delta G = \left\{ E(D^+/D) - E(A/A^-) - \frac{e^2}{\epsilon a} \right\} - \Delta E_{00}$$

The values of $E(D^+/D)$ and $E(A/A^-)$ represent reduction potentials of the donor and acceptor, respectively, $e^2/\epsilon a$ is the free energy change gained by bringing two radical ions to encounter distance a in the solvent of dielectric constant ϵ, and k_{diff} is the rate constant for the diffusion *interaction* between the reacting species.

Plots of log k_q vs. ΔG (not shown) were nonlinear for both aqueous and micellar media for the quenching of the fluores-

© 2005 NRC Canada

Fig. 3. Stern–Volmer plots of fluorescence quenching of ST in micellar media by various inorganic anions.



cence of ST. Therefore, an electron-transfer mechanism can be ruled out for this quenching process.

Although the quencher $[Fe(CN)_6]^{-3}$ is in its maximum oxidation state, its quenching efficiency is similar to the other ions in their reduced states. This suggests that the transfer of electrons from the quencher to ST is not solely responsible for the quenching process. It is likely that the collisional quenching plays a major role in this process. In micellar media, the probability of a collision of quenchers with dye molecules decreases as a result of the barrier provided by the organised interfacial layer of micelles, as represented by the viscosity coefficients of the micellar medium (Table 1). The collisional quenching is also supported by the decreased k_q value in micellar media, except for the iodide ion.

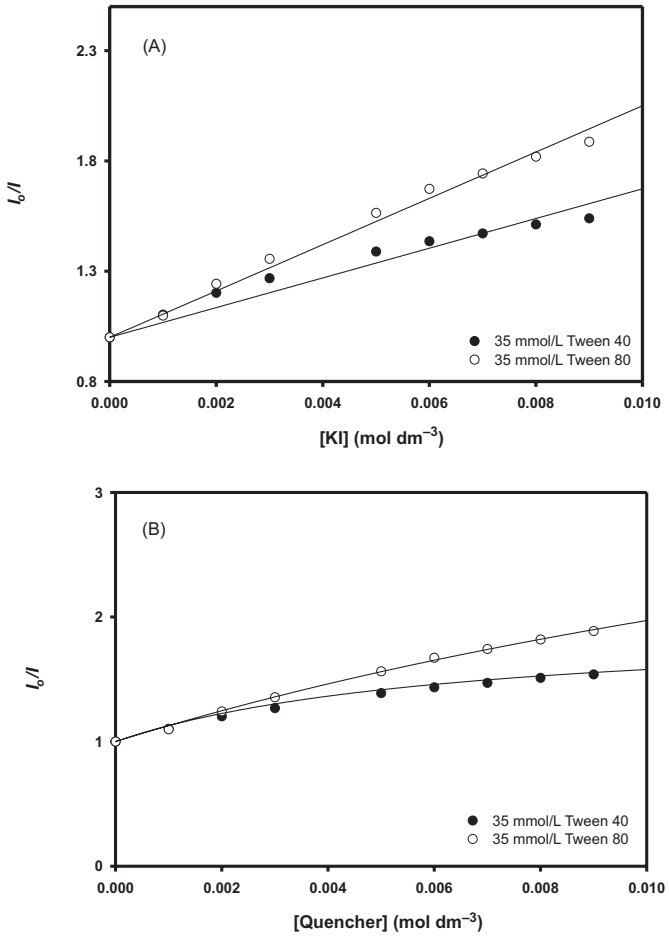
The counterions K^+ (for the ferro, ferri cyanide, iodide, and bromide salts) and Na^+ (for the nitrite and azide salts) played no role in the quenching process. The dye ST underwent collisional quenching by the inorganic ions. The efficiency order of these ions did not follow the order of their hydrated radius. The valency and ionic charges also did not correlate with the effects. It is not easy to rationalize why the collisional quenching effect for Br^- is weaker. One explanation could be the difference in the degree of fruitful collisions by the different ions. Since ST is distributed between the aqueous bulk and the micellar interface, the quenching process is the result of the effects in these two regions. The ionic size and the charge determine the access of the ions to these two regions and essentially guide the overall quenching process. Except for the case of I^-, the effect of the quenchers in aqueous media is greater than the effect in the micellar media because the dye takes shelter at the micellar interface, which has a lower fluidity. This lower fluidity is caused by hydration of the polyethylene oxide head groups of the nonionic surfactant molecules. Therefore, the ionic quencher molecules have relatively low access to the dye, resulting in a lower quenching effect. Also, the K_{sv} values decrease with increasing concentrations of Tween micelles.

Quenching of the fluorescence of ST by the iodide ion does not obey the Stern–Volmer equation (Fig. 4A), indicating that a single type of quenching does not apply in the present case. The experimental results are therefore analysed by employing a modified Stern–Volmer equation, as follows:

$$[4] \qquad \frac{F_0}{F} = \frac{1 + K_{sv}[Q]}{1 + f_b K_{sv}[Q]}$$

© 2005 NRC Canada

Fig. 4. Stern–Volmer plots of quenching of ST fluorescence in (A) Tween 40 and 80; (B) curve fit according to eq. [4].



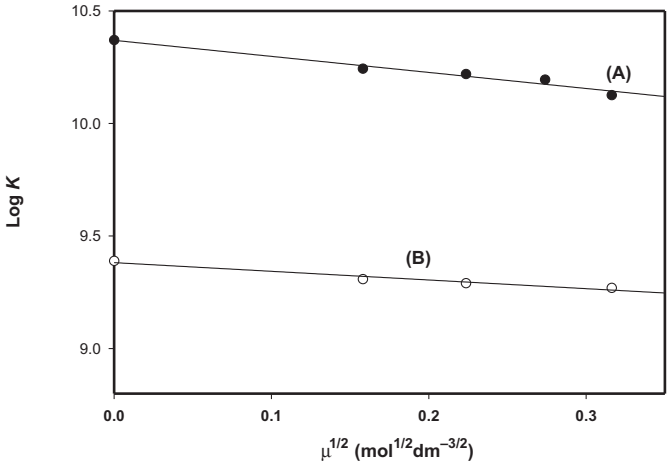
where f_b is the fraction of fluorophore inaccessible to quencher. The modified equation is based on the scenario that a fraction of either the quencher or the probe population is inaccessible to the other population (28, 29). In the present study, since the quencher ions are involved in the complexation with the Tween micelles, the application of the modified Stern–Volmer equation is justified. Plots of the data vs. the predicted values using eq. [4] are presented in Fig 4B. The resulting constants derived from the fit to eq. [4], along with correlation coefficient values (r^2), can be found in Table 2.

Since both the fluorophore and the quencher are ionic species, and since they have opposite charges, it is expected that the quenching phenomenon will be dependent on the ionic strength of the medium (μ). Following the Bronsted–Bjerrum equation (30),

$$[5] \qquad \log_{10} k = \log_{10} k^0 + 1.02 z_A z_B \sqrt{\mu}$$

where z_A and z_B represent the charge of cation and anion, respectively. The rate of quenching and the K_{sv} values therefore decrease with an increase in ionic strength. In the absence of lifetime values (τ_o) as a function of electrolyte concentrations, the validity of eq. [3] cannot be verified at the present time. However, it is expected that the k and, therefore, K_{sv} values will decrease with increasing ionic strength. In the present study the values of K_{sv} decreased in all cases with increasing ionic strength. Representative plots of $\log_{10} k$ vs. $\mu^{1/2}$ are given in Fig. 5. The approximate values of k were calculated using the lifetime τ_0 as 1.46 ns. As predicted by eq. [3], the rate constants decreased with an increase in ionic strength.

Fig. 5. Effect of ionic strength on the K_{sv} values: (A) 50 mmol/L Tween 20 and $[Fe(CN)_6]^{-4}$; (B) 50 mmol/L Tween 40 and NO_2^-.



Conclusions

(1) Inorganic ions such as $[Fe(CN_6)]^{-3}$, $[Fe(CN_6)]^{-4}$, I^-, Br^-, NO_2^-, and N_3^- quench the fluorescence of ST in aqueous media.
(2) In nonionic Tween micellar media, the quenching effects of the above ions on the fluorescence of ST are significantly weaker. The effect of I^- is significantly different from the other ions.
(3) The quenching phenomenon is not guided by the transfer of electrons from the quencher to the dye molecule, but is controlled by collisional quenching.
(4) For the iodide ion, the modified Stern–Volmer equation, based on the inaccessibility of a fraction of fluorophore (f_b), is employed to calculate the K_{sv} values.
(5) The Stern–Volmer constants are found to be dependent on both the concentration of the Tween micelles and the ionic strength of the solution.

Acknowledgements

RMP is grateful to the Natural Sciences and Engineering Research Council of Canada (NSERC) for a Discovery Grant. SCB acknowledges St. Francis Xavier University for a James Chair visiting professorship. SAM, SEM, and KMG acknowledge Undergraduate Summer Research Awards from NSERC.

References

1. A.D. Kettey. J. Radiat. Curing, **9**, 35 (1982).
2. H.J. Timpe, S. Jockusch, and K. Koerner. *In* Radiation curing in polymer science and technology. Vol. 2. *Edited by* J.P. Fouassier and J.F. Rabek. Elsevier, London. 1993. p. 575.

© 2005 NRC Canada

3. S. Jockusch, H.J. Timpe, W. Schnabel, and N.J. Turro. J. Phys. Chem. A, **101**, 440 (1997).
4. C.M. Previtali, S.G. Bertolotti, M.G. Neumann, I.A Pastre, A.M. Rufs, and M.V. Encias. Macromolecules, **27**, 7454 (1994).
5. E. Kustermann, H.J. Timpe, K. Gabert, and H. Schulert. Wiss. Z. Techn. Hochsch. Leuna Merseburg, **29**, 287 (1987).
6. S.C. Bhattacharya, H. Das, and S.P. Moulik. J. Photochem. Photobiol. A, **74**, 239 (1993).
7. S. Nandi and S.C. Bhattacharya. J. Mol. Liq. **89**, 223 (2000).
8. S.C. Bhattacharya, H. Das, and S.P. Moulik. J. Photochem. Photobiol. A, **79**, 109 (1994).
9. B.B. Bhowmik, S. Roy, and K.K. Rohatgi-Mukherjee. Indian J. Chem. **25A**, 714 (1986).
10. N. Sarkar, K. Das, A. Datta, S. Das, and D. Bhattacharya. J. Phys. Chem. **100**, 10 523 (1996).
11. M.V. Encinas and E.A. Lissi. Chem. Phys. Lett. **91**, 55 (1982).
12. P. Roy, S.C. Bhattacharya, and S.P. Moulik. J. Photochem. Photobiol. A, **105**, 69 (1997).
13. M. Almgren, J.E. Lofroth, and J.V. Stam. J. Phys. Chem. **90**, 4431 (1986).
14. B. Medhage, M. Almgren, and J. Alsin. J. Phys. Chem. **97**, 7753 (1993).
15. J.E. Lofroth and M. Almgren. J. Phys. Chem. **86**, 1636 (1982).
16. P. Lianos and R. Zana. J. Phys. Chem. **84**, 3339 (1980).
17. J. Guharey and P.K. Sengupta. Biochem. Biophys. Res. Commun. **219**, 388 (1996).
18. P. Hansson, B. Jonsson, C. Strom, and O. Soderman. J. Phys. Chem. B, **104**, 3496 (2000).
19. S. Nandi and S.C. Bhattacharya. Colloids Surf. A, **186**, 179 (2001).
20. S.C. Bhattacharya, H. Das, and S.P. Moulik. J. Photochem. Photobiol. A, **84**, 39 (1994).
21. P. Roy, S.C. Bhattacharya, and S.P. Moulik. J. Photochem. Photobiol. A, **105**, 69 (1997).
22. S.K. Ghosh, P.K. Khatna, and S.C. Bhattacharya. Int. J. Mol. Sci. **4**, 562 (2003).
23. M.A. El-Kemary, R.A. Khedr, and S. El-Din Etaiw. Spectrochim. Acta, **58**, 3011 (2002)
24. R.P. Lang. J. Am. Chem. Soc. **84**, 1185 (1965).
25. D.H. Harris. Quantitative chemical analysis. Freeman, New York. 2002.
26. J.R. Lackowicz. Principles of fluorescence spectroscopy. Plenum, New York. 1983.
27. D. Rehm and A. Weller. Isr. J. Chem. **8**, 259 (1970).
28. P. Ray, S.C. Bhattacharya, and S.P. Moulik. J. Photochem. Photobiol. A, **116**, 85 (1998).
29. D.T. Cramb and S.C. Beck. J. Photochem. Photobiol. A, **134**, 87 (2000).
30. K.J. Laidler. Chemical kinetics. 3rd. ed. Harper and Row, New York. 1987.

© 2005 NRC Canada

Synthesis, characterization, and single crystal X-ray structures of $[Co^{III}(acacen)(thioacetamide)_2]ClO_4$ and $[Co^{III}((BA)_2en)(thioacetamide)_2]PF_6$ — Solvatochromic properties of $[Co^{III}(acacen)(thioacetamide)_2]ClO_4$

Mehdi Amirnasr, Vratislav Langer, Nahid Rasouli, Mehdi Salehi, and Soraia Meghdadi

Abstract: The *trans*-$[Co^{III}(acacen)(ta)_2]ClO_4$ (**1**) and *trans*-$[Co^{III}((BA)_2en)(ta)_2]PF_6$ (**2**) complexes, where H_2acacen = bis(acetylacetone)ethylenediimine, $H_2(BA)_2$en = bis(benzoylacetone)ethylenediimine, and ta = thioacetamide, have been synthesized by a solid-state method, and characterized by elemental analyses, IR, UV–vis, and ^{1}H NMR spectroscopy. The crystal and molecular structures of **1** and **2** were determined by X-ray crystallography. Both compounds crystallize in the monoclinic space group *P*2/*n*. The ClO_4 and PF_6 ions are both disordered, ClO_4 on a twofold axis in **1** and PF_6 on an inversion center in **2**. Also bridging N-CH_2-CH_2-N is disordered in both compounds. The octahedral coordination of Co(III) is slightly distorted in both cases. The thioacetamide ligands are S-bonded and occupy the axial position. The IR, UV–vis, and ^{1}H NMR spectra of the two complexes and their solvatochromic properties are also discussed. The longest wavelength absorption that appears at 517 nm for **1** and at 528 nm for **2** in chloroform is solvent dependent, and is assigned as a metal-mediated ligand-to-ligand charge transfer (LLCT).

Key words: solid-state synthesis, thioactamide, Co(III) (Schiff base), crystal structure, solvatochromism, metal-mediated LLCT.

Résumé : Utilisant une méthode en phase solide, on a synthétisé les complexes *trans*-$[Co^{III}(acacen)(ta)_2]ClO_4$ (**1**) et *trans*-$[Co^{III}((BA)_2en)(ta)_2]PF_6$ (**2**) dans lesquels H_2acacen = bis(acétylacétone)éthylènediimine, $H_2(BA)_2$en = bis(benzoylacétone)éthylènediimine et ta = thioacétamide, et on les a caractérisés par le biais d'analyses élémentaires, de spectroscopies IR, UV–vis et RMN du ^{1}H. On a déterminé les structures cristallines et moléculaires des composés **1** et **2** par diffraction des rayons X. Les deux composés cristallisent dans le groupe d'espace monoclinique *P*2/*n*. Les ions ClO_4 et PF_6 sont tous les deux désordonnés, le ClO_4 sur un axe binaire dans **1** et le PF_6 sur un centre d'inversion dans **2**. Le chaînon N-CH_2-CH_2-N qui agit comme pont est aussi désordonné dans les deux composés. La coordination tétraédrique du Co(III) est légèrement déformée dans les deux cas. Les ligands thioacétamides sont liés par le soufre et occupent une position axiale. On discute aussi des spectres IR, UV–vis et RMN du ^{1}H des deux complexes et de leurs propriétés solvatochromiques. La bande d'absorption de plus grande longueur d'onde qui apparaît, dans le chloroforme, à 517 nm pour le composé **1** et à 528 nm pour le composé **2**, dépend du solvant et elle est attribuée à un transfert de charge de ligand à ligand aidée par le métal.

Mots clés : synthèse à l'état solide, thioacétamide, base de Shiff du Co(III), structure cristalline, solvatochromie, transfert de charge de ligand à ligand aidée par le métal.

[Traduit par la Rédaction]

Introduction

Cobalt(III) is normally considered a hard metal center that favors coordination to second-row atoms like oxygen and nitrogen. This is clearly evident from numerous Co(III) complexes bearing ambidentate ligands such as thiocyanate (1), selenocyanate (2), formamide, acetamide (3), methanesulfinamide, and methanesulfinate (4). However, when other ligands on the metal center tend to make the metal softer, bonding to soft donor atoms like S is favored. For instance,

Received 2 July 2005. Published on the NRC Research Press Web site at http://canjchem.nrc.ca on 10 February 2006.

M. Amirnasr,[1] N. Rasouli, M. Salehi, and S. Meghdadi. Department of Chemistry, Isfahan University of Technology, Isfahan 84156-83111, Iran.
V. Langer. Chalmers University of Technology, Department of Chemical and Biological Engineering, SE-412 96 Gothenburg, Sweden.

[1]Corresponding author (e-mail: amirnasr@cc.iut.ac.ir).

 doi: 10.1139/V05-207 © 2005 NRC Canada

the S-bonded form of the complex $[Co(CN)_5SCN]^{3-}$, which is the primary product of the reduction of $Co(NH_3)_5NCS^{2+}$ by $Co(CN)_5^{3-}$, is the stable linkage isomer (2).

Schiff base ligands also play an effective role in the modification of the electronic structure of metal centers. Co(II) Schiff base complexes are among the most versatile compounds that are of potential interest in many different areas such as catalysis (5, 6), modeling of antiviral agents (7), and oxygen-binding biomolecules (8). This remarkable diversity of functions is achieved by suitable modification of their basic electronic structure. Several elegant theoretical studies have been carried out to elucidate the electronic structure of Co(II) Schiff base complexes and to rationalize their reactivity (9, 10). The Schiff base ligand may modify the electron density on the metal center in such a way that the coordination of a soft atom like S of thioacetamide to cobalt is favored. In the course of our studies on the structural and electronic effects that may influence the reactivity of cobalt Schiff base complexes (11) we report the synthesis, characterization, and X-ray crystal structure of *trans*-$[Co^{III}(acacen)(ta)_2]ClO_4$ (**1**) and *trans*-$[Co^{III}((BA)_2en)(ta)_2]PF_6$ (**2**). The structures of **1** and **2** are the first reported structures of Co(acacen) and Co($(BA)_2$en) complexes containing S-donor axial ligands.

Experimental

Caution! Transition-metal complex perchlorate salts are known to be hazardous and must be treated with care, especially in the presence of organic solvents.

Materials and methods

The Schiff base ligands, bis(acetylacetone)ethylenediimine (H_2acacen) and bis(benzoylacetone)ethylenediimine ($H_2(BA)_2$en), and their cobalt(II) complexes were prepared as described in the literature (12). Silica gel 60 (70–230 mesh, Merck) was used as the solid-state reaction media. All other chemicals were commercial reagent grade and used as received from Aldrich and Merck. Elemental analyses were performed by using a Heraeus CHN-O-RAPID elemental analyzer.

Electronic absorption spectra were recorded on a JASCO V-570 spectrophotometer. Fourier transform IR spectroscopy on KBr pellets was performed on a JASCO-680 Plus instrument. ^{1}H NMR spectra were obtained on a Bruker Avance DRX500 (500 MHz) spectrometer. Proton chemical shifts are reported in part per million (ppm) relative to an internal standard of Me_4Si.

Synthesis

trans-*[Co^{III}(acacen)$(ta)_2$]ClO_4 (1)*

A homogenized mixture of 951 mg (3 mmol) of $[Co^{II}$(acacen)], 900 mg (12 mmol) of thioacetamide, and 1.2 g of silica gel in a porcelain dish was heated at 80 °C for 30 min. The color changed from orange to dark purple. The reaction mixture was then cooled to room temperature and treated with 50 mL of chloroform. A solution of 368 mg (3 mmol) sodium perchlorate in 3 mL methanol was then added and the mixture was stirred for 10 min and finally filtered off. The filtrate was left in the open air and slow evaporation of the solvent at room temperature gave a dark violet microcrystalline powder. The powder was then dissolved in chloroform and the resulting solution was filtered off. An equal volume of toluene was added to the filtrate and left undisturbed at room temperature. Dark violet crystals suitable for X-ray crystallography were obtained after 2 days. The crystals were isolated by filtration and washed with a mixture of chloroform–toluene (1:9, *v*/*v*) and dried in vacuo. Yield: 340 mg (64%). IR (KBr, cm^{-1}) ν_{max}: 3323 (m, N-H), 1515 (s, C=N), 1318 (m, C-N), 708 (m, C=S), 1116 (s, ClO_4). ^{1}H NMR (500 MHz, $CDCl_3$) δ: 2.02 (s, $6H_a$, CH_3), 2.20 (s, $6H_b$, CH_3), 2.37 (s, $6H_c$, CH_3), 3.5 (s, $4H_d$, H_2C-CH_2), 5.05 (s, $2H_e$, C*H*), 8.73 (s, $2H_g$, N*H*), 10.22 (s, $2H_f$, N*H*). Anal. calcd. for $C_{16}H_{28}N_4O_6ClS_2Co$: C 36.20, H 5.30, N 10.50; found: C 36.20, H 5.40, N 9.80.

trans-*[Co^{III}($(BA)_2$en)$(ta)_2$]PF_6 (2)*

A homogenized mixture of 203 mg (0.5 mmol) of $[Co^{II}((BA)_2en)]$, 113 mg (1.5 mmol) of thioacetamide, and 900 mg of silica gel in a porcelain dish was heated at 80 °C for 60 min. The bright orange color of the mixture turned dark orange. The reaction mixture was then cooled to room temperature, transferred to a 100 mL beaker, and treated with a mixture of 50 mL of dichloromethane and 20 mL ethyl acetate. After adding 37.5 mg (0.5 mmol) of additional thioacetamide, the reaction mixture was stirred in open air for an extra 6 h. A solution of 98 mg (0.6 mmol) of NH_4PF_6 in 10 mL ethyl acetate was then added and the reaction mixture was stirred for an additional 30 min and finally filtered off. After adding 15 mL of carbon tetrachloride to the filtrate, the resulting solution was left in open air, and slow evaporation of the solvent at room temperature gave dark cherry red crystals. Yield: 420 mg (60%). The product was recrystallized by slow evaporation of its solution in a mixture of ethyl acetate – benzene – dibutyl ether – carbon tetrachloride (15:1:3:18, *v*/*v*) at room temperature and dark cherry red crystals suitable for X-ray crystallography were obtained after 4 days. The crystals were isolated by filtration and washed with a mixture of ethyl acetate – carbon tetrachloride (1:9, *v*/*v*) and dried in vacuo. IR (KBr, cm^{-1}) ν_{max}: 3386 (m, N-H), 1515 (s, C=N), 1311 (m, C-N), 699 (m, C=S), 852 (s, PF_6). ^{1}H NMR (500 MHz, $CDCl_3$) δ: 2.23 (s, $6H_a$, CH_3), 2.39 (s, $6H_c$, CH_3), 3.73 (s, $4H_d$, H_2C-CH_2), 5.78 (s, $2H_e$, C*H*), 7.44–7.83 (m, 10H, Ar), 8.04 (s, $2H_g$, N*H*), 10.59 (s, $2H_f$, N*H*). Anal. calcd. for $C_{26}H_{32}N_4O_2S_2PF_6Co$: C 44.57, H 4.57, N 8.00; found: C 43.0, H 4.70, N 8.00.

X-ray crystallography

Data were collected on a Siemens SMART CCD diffractometer equipped with LT-2A low temperature device, using graphite-monochromated Mo Kα (λ = 0.710 73 Å) radiation. A full sphere of reciprocal lattice was scanned by 0.3° steps in ω with a crystal-to-detector distance of 3.97 cm. Preliminary orientation matrices were obtained from the first frames using SMART (13). The frames were integrated using the preliminary orientation matrices, which were updated every 100 frames. Final cell parameters were obtained by the refinement on the positions of 6923 (for **1**) and 8192 (for **2**) reflections with $I > 10\sigma(I)$, after integration of all the frames using SAINT (13). The data were empirically corrected for absorption and other effects using SADABS (14). The structures were solved by direct methods and refined by the full-

© 2005 NRC Canada

Table 1. Crystal data and structure refinement for *trans*-[Co^{III}(acacen)$(ta)_2$]ClO_4 (**1**) and *trans*-[Co^{III}($(BA)_2$en)$(ta)_2$]PF_6 (**2**).

Empirical formula	$C_{16}H_{28}ClCoN_4O_6S_2$ (**1**)	$C_{16}H_{32}CoF_6N_4O_2PS_2$ (**2**)
Formula weight	530.92	700.58
Crystal system	Monoclinic	Monoclinic
Space group	*P*2/*n*	*P*2/*n*
a (Å)	13.409 9(4)	11.308 3(1)
b (Å)	11.772 1(3)	11.168 3(1)
c (Å)	16.109 4(4)	12.470 6(1)
β (°)	109.306 (1)	94.19 3(1)
V (Å^3)	2 400.07(11)	1 570.7 5(2)
Z	4	2
D_c (Mg m^{-3})	1.469	1.481
Crystal size (mm)	0.20 × 0.20 × 0.08	0.50 × 0.26 × 0.22
Radiation (λ, Å)	Mo Kα, 0.710 73	Mo Kα, 0.710 73
θ range (°)	2.19–30.53	1.82–32.87
T (K)	183(2)	173(2)
μ (mm^{-1})	1.038	0.796
F(000)	1 104	720
Index ranges	$-19 \le h \le 19$, $-15 \le k \le 16$, $-22 \le l \le 22$	$-17 \le h \le 16$, $-16 \le k \le 16$, $-18 \le l \le 18$
Reflections collected	30 332	26 822
Independent reflections	7 335 (R_{int} = 0.040 8)	5 621 (R_{int} = 0.025 1)
Completeness of data	99.7%, θ = 30.53°	99.9%, θ = 30.00°
Absorption correction	Multi-scan	Multi-scan
Max and min transmission	0.921 6 and 0.819 3	0.844 3 and 0.691 5
Refinement method	Full-matrix least-squares on F^2	Full-matrix least-squares on F^2
Data/restraints/parameters	7 335/119/358	5 621/66/236
Goodness-of-fit on F^2	1.021	1.038
Final *R* indices [$I > 2\sigma(I)$]	R_1 = 0.042 3, wR_2 = 0.102 8	0.033 1, wR_2 = 0. 090 5
R indices (all data)	R_1 = 0.067 3, wR_2 = 0.116 8	0.040 8, wR_2 = 0.096 3
Largest diff. peak and hole (e Å^{-3})	0.721 and –0.570	0.716 and –0.294

matrix least-squares method on F^2 data using the SHELXTL (15). All non-H atoms were refined anisotropically. Oxygen atoms of both perchlorate ions, which are disordered on the twofold axis with occupancy factors of 0.5, were refined with restraints to form regular tetrahedrons. Also PF_6 ion was found to be disordered on an inversion center and refined with geometrical restraints. The H atoms were constrained to idealized geometries and refined isotropically. The crystallographic and refinement data are summarized in Table 1.

Results and discussion

Synthesis

The cobalt(III) complexes (**1** and **2**) were prepared by air oxidation of a homogenized mixture of the corresponding cobalt(II) (Schiff base) complex and thioacetamide, in the presence of silica gel at 80 °C. The solid reaction mixture was heated in an oven for 30 min during which the color changed from orange to dark purple for **1** and from red orange to dark orange for **2**. In addition to providing a suitable reaction medium to ensure that the reactive molecules achieve contact with each other, silica gel is apparently effective in adsorbing the water molecules that are loosely coordinated to Co(II) in [Co^{II}(Schiff base)] complexes. It is also likely that the nitrogen atom of thioacetamide binds more tightly to the Lewis acid sites of silica gel, therefore facilitating the coordination of thioacetamide through its S atom.

It has been postulated that the tendency of a given [Co^{II}(Schiff base)] complex towards oxidation is dependent on the available charge density on cobalt (10). For example, the [Co^{II}(acacen)] complex is more readily oxidized in air than [Co^{II}(salen)]. The common explanation for this property is that the presence of the extended conjugation system in the salen ligand reduces the charge density at oxygen and reduces the reactivity of [Co^{II}(salen)] towards oxidation. It is interesting to note that the oxidation process in the preparation of **1** from [Co^{II}(acacen)] occurs within a short period, while it takes a bout 12 h in the synthesis of **2** from [Co^{II}($(BA)_2$en)]. This would be expected considering the presence of two additional phenyl rings and extended conjugation in the bis(benzoylacetone)ethylenediimine Schiff base complex.

Structures of *trans*-[Co(acacen)$(ta)_2$]ClO_4 (1) and *trans*-[Co($(BA)_2$en)$(ta)_2$]PF_6 (2)

A view of the cations of **1** and **2** can be seen in Figs. 1 and 2, respectively. The atom labeling scheme used is presented in the figures with the unlabeled atoms being related

© 2005 NRC Canada

Fig. 1. Numbering scheme with thermal ellipsoids at 30% probability level. The disordered section N1-C1B-C2B-N2 with higher occupancy (0.686) is shown.

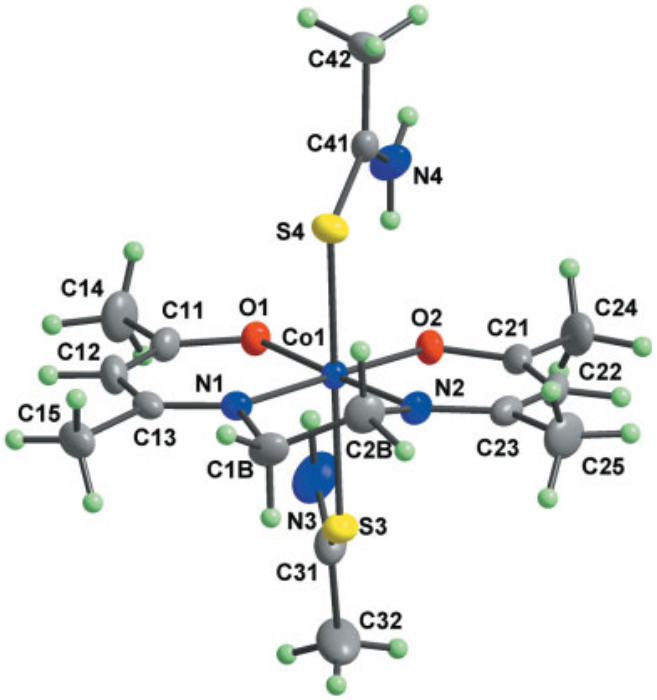
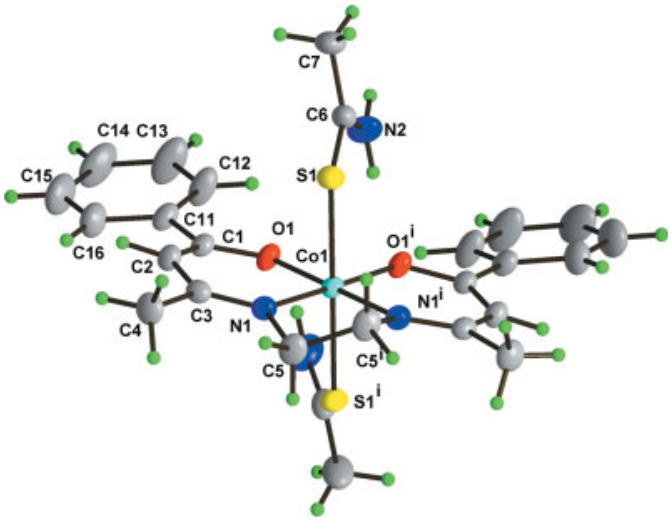


Fig. 2. Numbering scheme with thermal ellipsoids at 30% probability level. The disordered section N1-C5-C5^{i}-N1^{i} with higher occupancy (0.80) is shown. Symmetry code: $-x + 3/2$, y, $-z + 1/2$ (i).



to the labeled atoms by a twofold axis upon which the cobalt cation in **2** resides. Selected bond lengths and angles are listed in Table 2. In both cases, the octahedral coordination of Co(III) is slightly distorted, the Schiff base ligand (ONNO ligand) coordinates the cobalt ion in four equatorial positions, and the two thioacetamide molecules occupy the two axial positions of the octahedral complexes.

The Co—O and Co—N bond distances of the acacen and $(BA)_2$en ligands in the equatorial plane of **1** and **2** are symmetric within the limits of the experimental error. In *trans*-[Co^{III}(acacen)(ta)$_2$]ClO$_4$ (**1**), Co—O(1) = 1.8992(15) Å, Co—O(2) = 1.9023(15) Å, Co—N(1) = 1.9018(17) Å, Co—N(2) = 1.8967(18) Å, which compare well with the Co—O and Co—N distances found in *trans*-[Co(acacen)(piperidine)$_2$]NCS (Co—O$_{av}$ = 1.897 Å, Co—N$_{av}$ = 1.902 Å) (16) and *trans*-[Co(3-Cl-acacen)(NH$_3$)$_2$]BPh$_4$ (Co—O = 1.881(4) Å, Co—N = 1.8918(9) Å) (7). In *trans*-[Co^{III}((BA)$_2$en)(ta)$_2$]PF$_6$ (**2**), Co—O(1) = Co—O(1)i = 1.9004(9) Å, Co—N(1) = Co—N(1)i = 1.9010(10) Å, which compare well with the Co—O and Co—N distances found in *trans*-[Co((BA)$_2$en)(morpholine)$_2$]ClO$_4$ (Co—O$_{av}$ = 1.897 Å, Co—N$_{av}$ = 1.902 Å) (17). The average cobalt–sulfur bonds in the axial positions are different in **1** and **2** (Co—S$_{av}$ = 2.3013(6) Å in **1** and 2.3169(3) Å in **2**) and are in good agreement with the Co—S distances in cobalt–thiourea (e.g., [Co(NioxH)$_2$(Thio)$_2$]$_2$SiF$_6$, Co—S = 2.300–2.318 Å) complexes (18).

The C—S and C—N bond distances for the axial thioacetamide ligands, C(31)—S(3) = 1.675(3) Å, C(41)—S(4) = 1.682(2) Å, C(31)—N(3) = 1.305(4) Å, C(41)—N(4) = 1.288(3) Å in **1**, and C(6)—S(1) = 1.6944(16) Å, C(6)—N(2) = 1.298(2) Å in **2**, agree with those reported for the related complexes (17) and are close to the C=S double

Table 2. Bond lengths (Å) and angles (°) for complexes **1** and **2**.

Bond lengths (Å)		Bond angles (°)	
***trans*-[Co^{III}(acacen)(ta)$_2$]ClO$_4$ (1)**			
Co(1)—N(1)	1.9018(17)	O(1)-Co(1)-N(2)	178.03(8)
Co(1)—N(2)	1.8967(18)	O(1)-Co(1)-N(1)	95.45(7)
Co(1)—O(1)	1.8992(15)	N(2)-Co(1)-N(1)	86.16(8)
Co(1)—O(2)	1.9023(15)	O(1)-Co(1)-O(2)	82.84(7)
Co(1)—S(3)	2.2919(6)	N(2)-Co(1)-O(2)	95.59(8)
Co(1)—S(4)	2.3107(6)	N(1)-Co(1)-O(2)	177.46(7)
S(3)—C(31)	1.675(3)	O(1)-Co(1)-S(3)	95.43(5)
S(4)—C(41)	1.682(2)	N(2)-Co(1)-S(3)	85.76(6)
N(3)—C(31)	1.305(4)	N(1)-Co(1)-S(3)	87.81(6)
N(4)—C(41)	1.288(3)	O(2)-Co(1)-S(3)	90.48(5)
		O(1)-Co(1)-S(4)	91.78(5)
		N(2)-Co(1)-S(4)	87.17(6)
		N(1)-Co(1)-S(4)	86.79(6)
		O(2)-Co(1)-S(4)	95.13(5)
		S(3)-Co(1)-S(4)	171.37(3)
***trans*-[Co^{III}((BA)$_2$en)(ta)$_2$]PF$_6$ (2)**			
Co(1)—N(1)	1.9010(10)	N(1)i-Co(1)-O(1)	178.83(4)
Co(1)—N(1)i	1.9010(10)	O(1)-Co(1)-N(1)	94.85(4)
Co(1)—O(1)	1.9004(9)	N(1)i-Co(1)-N(1)	86.22(6)
Co(1)—O(1)i	1.9004(9)	O(1)-Co(1)-O(1)i	84.09(5)
Co(1)—S(1)i	2.3169(3)	N(1)i-Co(1)-O(1)i	94.85(4)
Co(1)—S(1)	2.3169(3)	N(1)-Co(1)-O(1)i	178.83(4)
S(1)—C(6)	1.6944(16)	O(1)-Co(1)-S(1)i	94.36(3)
N(2)—C(6)	1.298(2)	N(1)i-Co(1)-S(1)i	85.13(3)
		N(1)-Co(1)-S(1)i	91.45(3)
		O(1)i-Co(1)-S(1)i	89.13(3)
		O(1)-Co(1)-S(1)i	89.13(3)
		N(1)i-Co(1)-S(1)	91.45(3)
		N(1)-Co(1)-S(1)	85.12(3)
		O(1)i-Co(1)-S(1)	94.36(3)
		S(1)i-Co(1)-S(1)	175.309(19)

© 2005 NRC Canada

Table 3. Selected torsion angles (°) for compounds **1** and **2**.

1		**2**	
ϕ_1 (C11-C12-C13-N1)	1.5(4)	ϕ_1 (C1-C2-C3-N1)	7.4(2)
ϕ_2 (O1-C11-C12-C13)	–0.1(4)	ϕ_2 (O1-C1-C2-C3)	–6.4(2)
ϕ_3 (C21-C22-C23-N2)	3.7(4)	ϕ_3 ($C1^i$-$C2^i$-$C3^i$-$N1^i$)	7.4(2)
ϕ_4 (O2-C21-C22-C23)	–1.8(4)	ϕ_5 (N1-C5-$C5^i$-$N1^i$)	–44.7(4)
ϕ_5 (N1-C1B-C2B-N2)	–41.0(9)	ϕ_6 (O1-C1-C11-C12)	–18.98(18)

bond (1.6854(10) Å) and C—N single bond (1.3126(12) Å) in free thioacetamide (19).

All angles around the Co center deviate significantly from 90° indicating a rectangular distortion. The ligand-cobalt-ligand bond angles in the equatorial plane consist of two that are larger than 90° (O(1)-Co(1)-N(1) = 95.45(7)° and N(2)-Co(1)-O(2) = 95.59(8)° in **1** and O(1)-Co(1)-N(1) = (N(1)i-Co(1)-O(1)i = 94.85(4)° in **2**), and two smaller angles (O(1)-Co-O(2) = 82.84(7)° and N(1)-Co-N(2) = 86.16(8)° in **1** and O(1)-Co-O(1)I = 84.09(5)° and N(1)-Co-N(1)i = 86.22(6)° in **2**) (Table 2), which are close to the corresponding values in *trans*-[Co(acacen)(piperidine)$_2$]NCS (94.1(1)°, 95.2(1)°, 84.6(1)°, 86.2(1)°) (16) and *trans*-[Co((BA)$_2$en)(morpholine)$_2$]ClO_4 (93.89(1)°, 94.26(11)°, 86.10(9)°, 85.87(11)°) (17).

The trans angles of 178.03(8)° and 177.46(7)° in **1** and 178.83(4)° in **2** are indicative of a slight tetrahedral distortion of the basal coordination of Co(III), which in the case of perfect planarity have values of 180°. This distortion is also reflected by the torsion angles of ~2° in the six-membered rings of basal coordination in **1** and ~6 ° in **2** (Table 3), and the angle between the best least-squares planes (Co1-O1-C11-C12-C13-N1 and Co1-O2-C21-C22-C23-N2) in **1** being 5.61(9)°, and (Co1-O1-C1-C2-C3-N1 and Co1-$O1^i$-$C1^i$-$C2^i$-$C3^i$-$N1^i$) in **2** being 0.08(4)°.

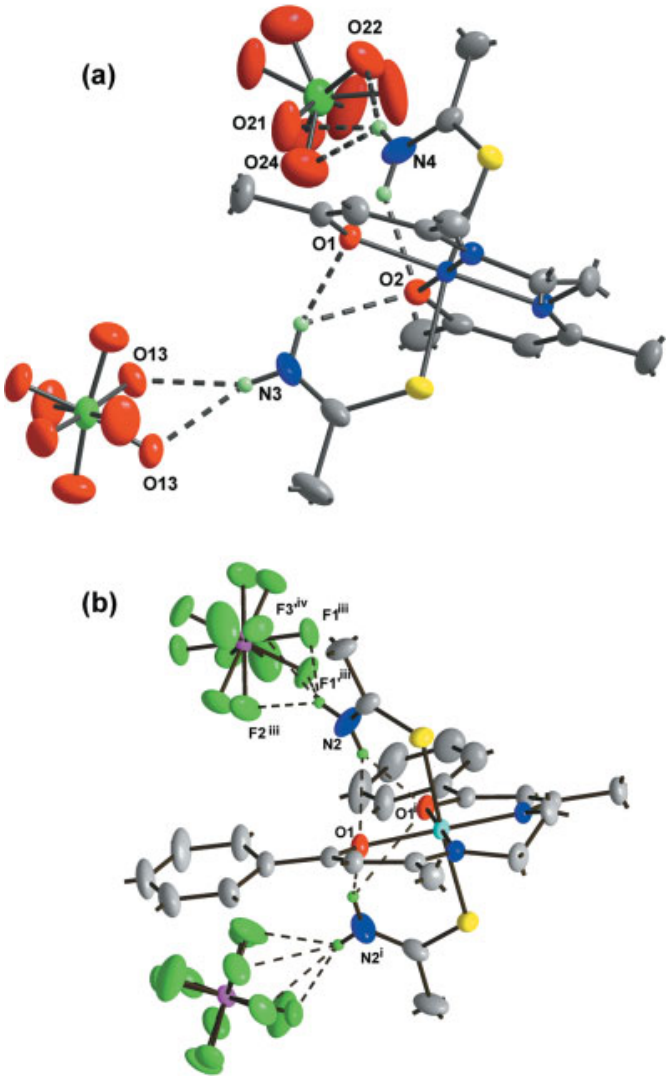
The (N-H) atoms of the axial thioacetamide ligands are involved in hydrogen bonding with the oxygen atoms of ClO_4^- (in **1**) and PF_6^- (in **2**) anions and the equatorial Schiff base ligand (Fig. 3). As a result, the two axial thioacetamide ligands are tilted away from the *Z* axis by ~9° in **1** (S(3)-Co(1)-S(4) = 171.37(3)°) and ~5° in **2** (S(1)-Co(1)-S(1)i = 175.309(19)°). Some features of this hydrogen bonding are also observed in the IR and ^{1}H NMR spectra of the compound (vide infra). The geometry of the hydrogen bonds is given in Table 4.

Spectral studies

Thioamides are potential ambidentate ligands that can coordinate to the transition-metal ions through either the sulfur or the nitrogen atoms. Thioacetamide exists as the two resonance structures presented in Scheme 1. When N-bonded, **I** is the dominant structure and as a result the C—N stretching frequency is lowered while the C=S stretching frequency is raised relative to the free thioacetamide. In the S-bonded complex, **II** is the dominant structure and consequently the C—N stretching frequency is raised while the C=S stretching frequency is lowered relative to the free thioacetamide.

Yet another possibility for the S-bonded form is structure **I** in which the CS group acts as a thione. The shift in the vibrational frequencies and the bond lengths of C—N and C=S indicate which of the thione or thiolate structures is the major contributor to the ligand–metal coordination.

Fig. 3. (*a*) Hydrogen bonds in **1**. Both perchlorate ions are disordered on the twofold axis. Hydrogens not taking part in the bonding scheme were omitted for clarity. (*b*) Hydrogen bonds in **2** (for details and symmetry codes see Table 4). Both PF_6 ions are disordered on the inversion center. The main sections with occupancy 0.702(5) and the other with occupancy 0.298(5) (atom labels with a prime) are shown. Atomic displacement ellipsoids are shown at 30% probability level. Hydrogens not taking part in the bonding scheme were omitted for clarity.



Except for the aromatic region, the IR spectral pattern is essentially the same for **1** and **2**. The fairly strong band appearing at 1305 cm^{-1} in the IR spectrum of free thioacetamide, due to ν(CN) (20), shifts to 1318 cm^{-1} in **1** and 1311 cm^{-1} in **2**, respectively. The ν(CS), appearing at

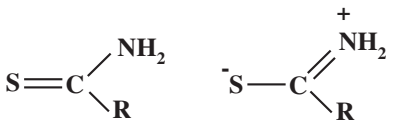
© 2005 NRC Canada

Table 4. The hydrogen bonds for compounds (*a*) **1** and (*b*) **2**.

(*a*) *trans*-[Co^{III}(acacen)(ta)$_2$]ClO_4 (**1**).				
D-H···A	*d*(D-H) (Å)	*d*(H···A) (Å)	*d*(D···A) (Å)	<(DHA) (°)
N(3)-H(3A)···O(13)	0.88	2.18	3.014(5)	158.3
N(3)-H(3A)···O(13)#1	0.88	2.13	2.963(4)	157.1
N(3)-H(3B)···O(1)	0.88	1.98	2.747(3)	144.9
N(3)-H(3B)···O(2)	0.88	2.54	3.103(3)	122.2
N(4)-H(4A)···O(22)	0.88	2.17	3.020(6)	161.8
N(4)-H(4A)···O(24)	0.88	2.47	3.150(8)	134.0
N(4)-H(4A)···O(21)#2	0.88	2.23	2.997(5)	145.3
N(4)-H(4B)···O(2)	0.88	1.97	2.731(3)	143.4
C(2B)-H(2B1)···S(4)	0.99	2.86	3.252(6)	104.5
C(42)-H(42A)···O(22)	0.98	2.60	3.353(6)	134.1
(*b*) *trans*-[Co^{III}((BA)$_2$en)(ta)$_2$]PF_6 (**2**).				
D-H···A	*d*(D-H) (Å)	*d*(H···A) (Å)	*d*(D···A) (Å)	<(DHA) (°)
N(2)-H(2A)···F(1)iii	0.88	2.27	2.994(2)	38.9
N(2)-H(2A)···F(3′)iv	0.88	2.28	3.124(6)	161.1
N(2)-H(2A)···F(2)iii	0.88	2.40	3.162(3)	144.6
N(2)-H(2A)···F(1′)iii	0.88	2.39	3.056(5)	132.5
N(2)-H(2B)···O(1)i	0.88	1.91	2.7144(16)	150.9
N(2)-H(2B)···O(1)	0.88	2.64	3.1031(18)	113.6

Note: Symmetry transformations used to generate equivalent atoms: $-x + 1/2$, y, $-z + 1/2$ (#1), $-x - 1/2$, y, $-z + 1/2$ (#2), $-x + 3/2$, y, $-z + 1/2$ (i), $-x + 1$, $-y$, $-z$ (ii), x, $y + 1$, z (iii), $-x + 1$, $-y + 1$, $-z$ (iv).

Scheme 1.



(I) **(II)**

708 cm^{-1} in free thioacetamide, appears at 708 cm^{-1} in **1** and 699 cm^{-1} in **2**, respectively. The small increase in ν(CN) and the small decrease in ν(CS) of the coordinated thioacetamide is consistent with a metal sulfur coordination of the thione form, and conform with the X-ray molecular structure. The N—H stretching vibrational band of NH_2 appears at 3323 and 3386 cm^{-1} in **1** and **2**, respectively. This band is relatively broad and appears at a lower frequency in the IR spectrum of **1** because of the formation of strong hydrogen bonds with the oxygen atoms of the perchlorate anions and the equatorial Schiff base ligand.

The ν(C=N) of the equatorial Schiff base ligands that appears at about 1540 cm^{-1} in the IR spectra of the free ligands is shifted to a lower frequency by ~25 cm^{-1} and appears at 1515 cm^{-1} in the IR spectra of the two complexes. The stretching vibrations of ClO_4^- (1116 cm^{-1}) and PF_6^- (852 cm^{-1}) anions are observed in the corresponding regions (21).

The ^1H NMR spectrum of **1** in $CDCl_3$ is shown in Fig. 4 (assignment as in Scheme 2). The signals at 2.02 and 2.20 ppm are assigned to two sets of CH_3 protons, H_a and H_b, respectively. The four ethylenediamine protons (H_d) appear as a singlet at 3.50 ppm. The singlet at 5.05 ppm corresponds to the H_e protons of acacen. The six methyl protons (H_c) of the axial thioacetamide ligands appear as a singlet at 2.37 ppm.

The amide protons are usually observed at δ 5–8.5 ppm (22). The free thioacetamide in $CDCl_3$ shows two NH proton resonances at 7.27 and 7.75 ppm. Upon coordination, these two signals move to lower fields. Since the two N-H protons of the coordinated thioacetamide (H_f and H_g) are involved in different hydrogen-bonding patterns (Fig. 3, Table 4), the two protons will presumably appear at considerably different chemical shifts if the hydrogen bonding retains its character in solution. This is most probably the origin of observing a higher chemical shift for the H_f proton (10.22 ppm), which is more strongly involved in an intramolecular hydrogen bonding relative to the H_g proton (8.73 ppm).

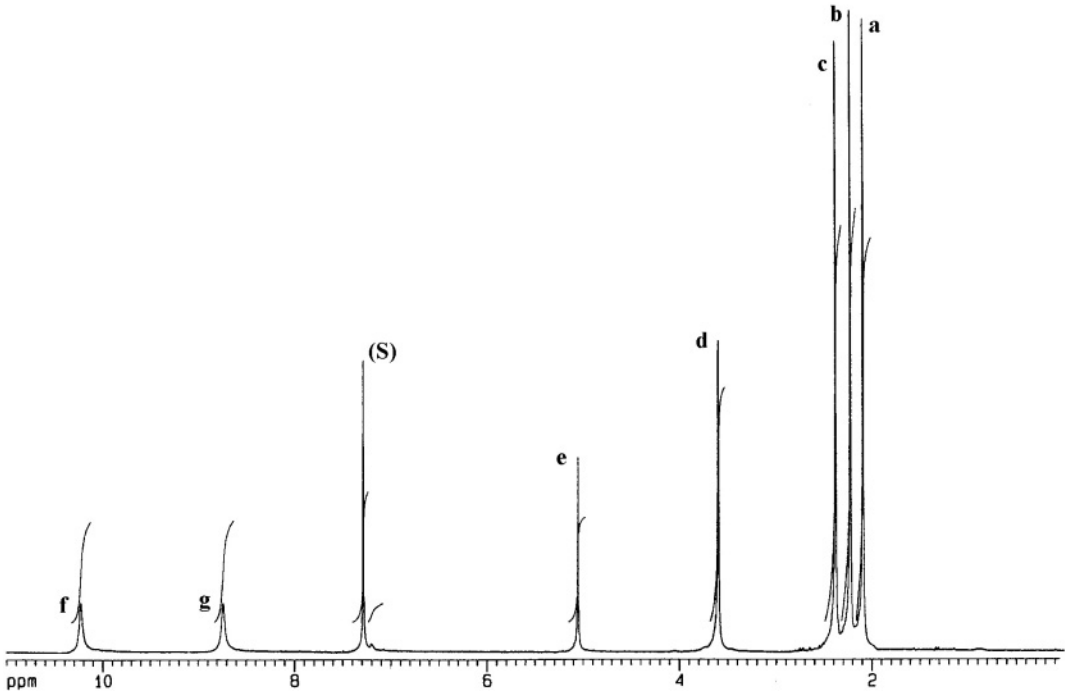
The ^1H NMR spectrum of **2** in $CDCl_3$ shows a pattern similar to that of **1** except for the signals due to the aromatic protons of the two phenyl rings that appear in the 7.44–7.83 ppm region. Other protons are also slightly shifted downfield as expected from the electron-withdrawing character of the rings. The signal at 2.23 ppm is assigned to the six methyl protons (H_a) of the equatorial ligand. The six methyl protons (H_c) of the axial thioacetamide ligands appear as a singlet at 2.39 ppm. The signal at 3.73 ppm is assigned to the four ethylenediamine protons (H_d) and the singlet at 5.78 ppm corresponds to the H_e protons of the equatorial ligand. The NH_2 protons (H_g and H_f) of the coordinated thioacetamide appear as singlets at 8.04 and 10.59 ppm, respectively.

UV–vis and solvatochromism studies

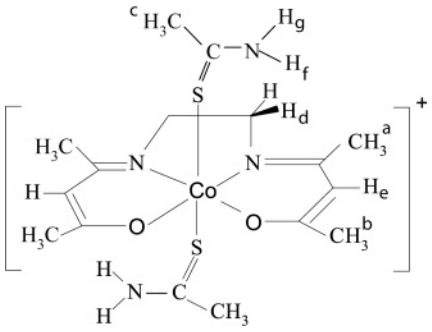
The absorption spectrum of *trans*-[Co^{III}(acacen)(ta)$_2$]ClO_4 in chloroform features a band with a true maximum at 518 nm. Based on the relatively high ε (3654 $(mol/L)^{-1}$ cm^{-1}) of this band it may be assigned to a combination of d–d and CT transitions. The position of this band is solvent dependent and shows negative solvatochromic shifts in a dozen organic solvents of various polarities (Table 5). This change

© 2005 NRC Canada

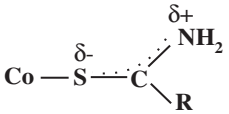
Fig. 4. ^{1}H NMR spectrum of *trans*-[Co^{III}(acacen)$(ta)_2$]ClO_4 in $CDCl_3$ at 298 K. The spectrum is labeled as to peak assignment discussed in the text.



Scheme 2.



Scheme 3. Co–thioacetamide fragment with a high contribution to the ground state.



does not agree with the change in the polarity of the solvent. Therefore, it can be considered to correspond to the net of several solvent effects such as polarity, basicity, and H-bond accepting ability. The solvents can be divided into two groups based on the degree of solvatochromic shift. Solvents with dielectric constants below 20.7 (Nos. 1–6), exhibit small solvatochromic shifts of the band (14 nm) and relatively large ϵ. It is reasonable to assume that the first coordination sphere of the bis(thioacetamide) complex remains intact in these solvents. The structural integrity of the complex in solution is confirmed by its ^{1}H NMR spectrum in $CDCl_3$ (Fig. 4). The larger shift is observed in the solvent potentially capable of forming stronger hydrogen bonds with the NH_2 protons of the coordinated thioacetamide. This observation may be rationalized based on the assumption that the CT band is mainly of LLCT character and the electronic transition occurs from the p_π(C=S) of the coordinated thioacetamid to a π^* of acacen chelate, mediated by the central Co atom. A stronger hydrogen bonding stabilizes the ground state of the complex (Scheme 3) and has an unfavorable effect on the S $\rightarrow$ Co $\rightarrow$ acacen charge transfer transition and shifts the band to a higher energy.

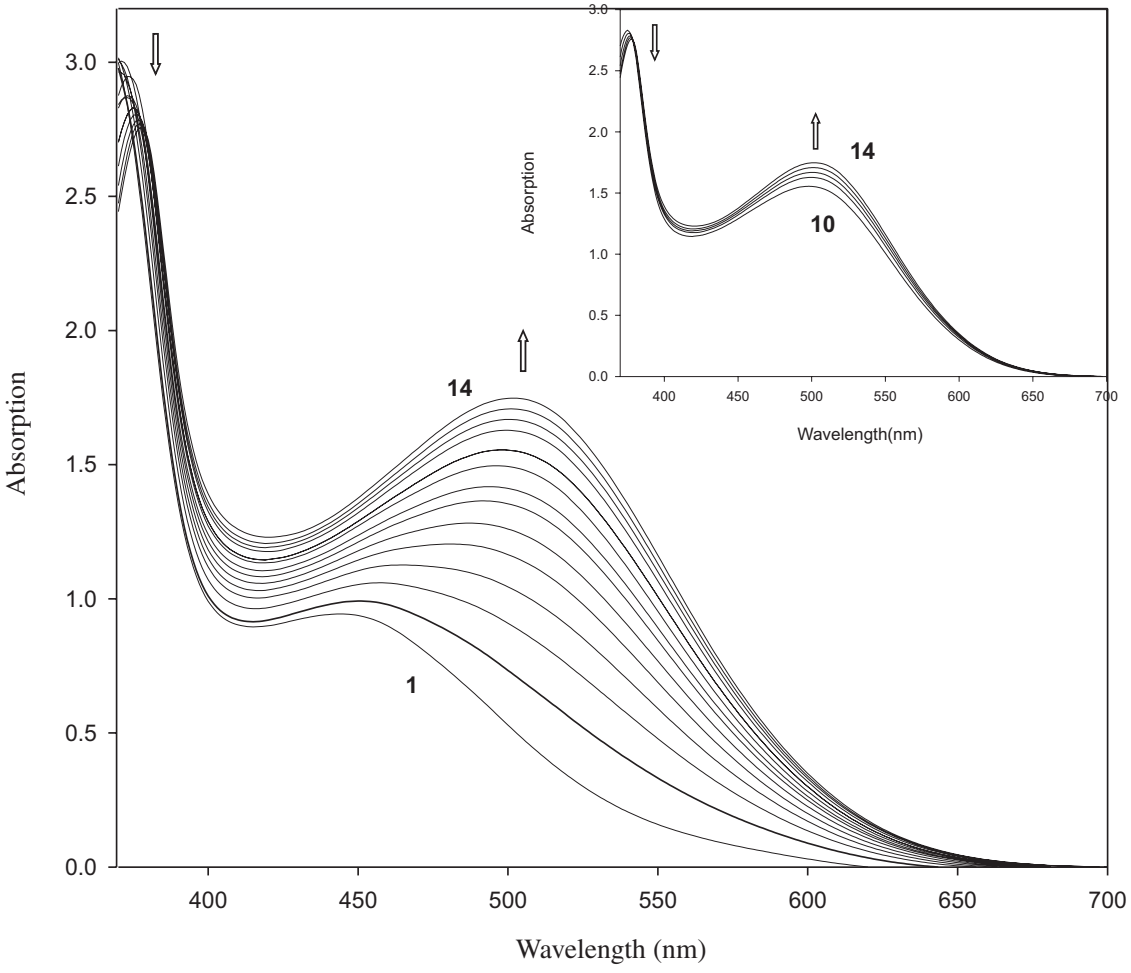
In solvents of high dielectric constant and those that can coordinate to the metal center such as methanol, acetonitrile, DMSO, and water, there is a drastic change in both the position (up to 72 nm) and ϵ of the band. This hints at the possibility of a substitution process in which the two axial thioacetamide ligands are replaced by solvent molecules. Additional evidence for the substitution of the axial ligands comes from the ^{1}H NMR of the complex in DMSO-d^6 and CD_3OD. The appearance of a signal centered at about 7.2 ppm, which can be attributed to the NH_2 protons of the free thioacetamide, is supportive of a dissociation process leading to the free ligand. A further clue to this point is obtained from the electronic absorption spectral changes of the methanolic solution of the complex in the presence of excess thioacetamide. This is achieved by adding increasing amounts of thioacetamide to a solution of *trans*-[Co^{III}(acacen)$(ta)_2$]ClO_4 in methanol and monitoring the absorption spectral changes (Fig. 5). The absorption maximum moves from 450 nm in pure methanol to 510 nm (a red shift of about 60 nm) after adding excess (56 times molar ratio) thioacetamide. While no isosbestic points are observed during the first nine additions, an isosbestic point at 382 nm appears from then on and persists to the final stages of the reaction (Fig. 5. inset). These results indicate the existence of a two-step reversible equilibrium in methanolic solution

© 2005 NRC Canada

Table 5. Electronic absorption data for *trans*-[Co^{III}(acacen)$(ta)_2$]ClO_4 (**1**) and *trans*-[Co^{III}($(BA)_2$en)$(ta)_2$]PF_6 (**2**) in solvents of various polarities.

			1		**2**	
Sample	Solvent	Dielectric constant	λ_{max} (nm)	ϵ ((mol/L)$^{-1}$ cm^{-1})	λ_{max} (nm)	ϵ ((mol/L)$^{-1}$ cm^{-1})
1	Chloroform	4.8	518	3654	528	3059
2	Dichloromethane	8.9	518	3189	528	2955
3	1,4-Dioxane	2.2	512	3621	518	3450
4	Ethyl acetate	6.0	510	3636	524	3441
5	Acetone	20.7	508	2593	518	2440
6	2-Butanone	18.5	504	2670	516	2170
7	Acetonitrile	37.5	489	1621	500(sh)	1473
8	Tetrahydrofurane	7.6	487	1199	496(sh)	1142
9	Ethanol	24.6	462	1463	474(sh)	1424
10	Dimethyl sulfoxide	46.6	458	910	468(sh)	1472
11	Methanol	32.7	454	1149	465(sh)	967
12	Water	80.3	446	677	455(sh)	672

Fig. 5. The electronic absorption spectral traces of *trans*-[Co^{III}(acacen)$(ta)_2$]ClO_4 in methanol upon addition of thioacetamide at 298 K. The inset shows the spectral traces of samples 10–14 with the isosbestic point at 382.



involving association–dissociation of the thioacetamide ligand as presented in eq. [1].

[1*a*] *trans*-[Co^{III}(acacen)$(ta)_2$]$^+$ + Sol $\rightleftharpoons$ *trans*-[Co^{III}(acacen)(ta)(Sol)]$^+$ + ta

[1*b*] *trans*-[Co^{III}(acacen)(ta)(Sol)]$^+$ + Sol $\rightleftharpoons$ *trans*-[Co^{III}(acacen)$(Sol)_2$]$^+$ + ta

The molar absorption coefficient ϵ (3160 (mol/L)$^{-1}$ cm^{-1}) and the λ_{max} (510 nm) in the final solution are close to those measured in chloroform. Considering the microscopic reversibility principle, the dissociation of the axial thioaceta-

© 2005 NRC Canada

mide ligands in methanol and other coordinating solvents is evident.

As a typical pseudooctahedral low-spin d^6 complex, *trans*-$[Co^{III}(acacen)(ta)_2]^+$ contains the thioacetamide ligand that can function as a CT donor ligand for ligand-to-metal charge transfer (LMCT). The acacen is a π-donor and π-acceptor ligand that can contribute to a metal-to-ligand charge transfer transition (MLCT). The relatively high ϵ of the band at 517 nm in a chloroform solution of **1** and the solvatochromic properties of the complex are in agreement with the LLCT assignment of the longest wavelength absorption, which is mediated by the metal center. Some Co-centered character is also possible. This is in analogy to certain low-spin d^6 complexes such as Mo(diphos)(CO)(NO)(dtc) (23) and several d^8, Ni(diimine)(dithiolate) (24), and d^{10}, $Zn(phen)(C_6H_5S)_2$ (25) and $Zn(SC_6H_4\text{-}CH_3\text{-}p)_2$(dic), complexes (26).

The spectral properties of **2** fully support these conclusions (Table 5). The first transition in the electronic spectrum of *trans*-$[Co((BA)_2en)(ta)_2]PF_6$ in chloroform solution appears at a longer wavelength (528 nm) relative to that observed for *trans*-$[Co(acacen)(ta)_2]ClO_4$ (518 nm). This is a direct consequence of increasing the π-acceptor character of the equatorial Schiff base ligand by the two additional phenyl rings in $(BA)_2$en, which facilitates the metal-mediated LLCT. The π–π* intraligand transition of the Schiff base is also red-shifted. While the first electronic absorption of **1** in methanol is well-resolved (λ = 454 nm), it is obscured by the π–π* intraligand transition in **2** and appears as a shoulder to the π–π* transition, which tails down to 450 nm. The overall solvatochromic behavior of complex **2** in different solvents is similar to that of **1** and can be used as further evidence for the LLCT nature of the first absorption band in the electronic spectra of these complexes.

Conclusions

The preparation and detailed crystallographic and spectroscopic characterization of *trans*-$[Co^{III}(acacen)(ta)_2]ClO_4$ (**1**) and *trans*-$[Co((BA)_2en)(ta)_2]PF_6$ (**2**) have been carried out.[2] The thioacetamide ligands are S-bonded and occupy the axial positions. The donor ability of thioacetamide falls below that of common solvents: MeOH, CH_3CN, Me_2SO, and H_2O. The compounds exhibit a long wavelength LLCT, mediated by the metal center. The observed solvatochromism is explained by the effect that solvents of low dielectric constant have on the LLCT and a facile replacement of the thioacetamide ligands by the coordinating solvents.

Acknowledgements

We gratefully acknowledge Professor Peter C. Ford of the University of California, Santa Barbara for insightful discussions. M.A. wishes to thank the IUT Research Council for partial support of this research under Grant 1 CHC 812.

References

1. D.A. Buckingham, I.I. Creaser, and A.M. Sargeson. Inorg. Chem. **9**, 655 (1970).
2. D.F. Gutterman and H.B. Gray. J. Am. Chem. Soc. **93**, 3364 (1971).
3. R.L. Angel, D.P. Fairlie, and W.G. Jackson. Inorg. Chem. **29**, 20 (1990).
4. D.P. Fairlie, W.G. Jackson, and K.H. Thompson. Inorg. Chem. **29**, 3145 (1990).
5. K. Kervinen, H. Korpi, M. Leskelä, and T. Repo. J. Mol. Catal. A: Chem. **203**, 9 (2003).
6. A. Kumar, G.S. Mishra, and A. Kumara. J. Mol. Catal. A: Chem. **201**, 179 (2003).
7. A. Bottcher, T. Takeuchi, K.I. Meade, H.B. Gray, D. Cwikel, M. Kapon, and Z. Dori. Inorg. Chem. **36**, 2498 (1997).
8. Y. Nishida and S. Kida. Coord. Chem. Rev. **27**, 275 (1979).
9. A. Ceulemans, M. Dendooven, and L.G. Vanquickenborn. Inorg. Chem. **24**, 1159 (1985).
10. N.J. Henson, P.J. Hay, and A. Redondo. Inorg. Chem. **38**, 1618 (1999).
11. M. Amirnasr and R. Vafazadeh. Int. J. Chem. Kinet. **34**, 387 (2002).
12. P.J. McCarthy, R.J. Hovey, K. Ueno, and A.E. Martell. J. Am. Chem. Soc. **77**, 5820 (1955).
13. SMART and SAINT [computer programs]. Siemens Analytical X-ray Instruments Inc., Madison, Wisconsin. 1995.
14. G.M. Sheldrick. SADABS. Version 2.03 [computer program]. University of Göttingen, Göttingen, Germany. 2002.
15. G.M. Sheldrick. SHELXTL. Version 6.10 [computer program]. Bruker AXS Inc., Madison, Wisconsin. 2001.
16. M. Amirnasr and R. Vafazadeh. Scientia Iranica, **4**, 35 (1997).
17. M. Amirnasr, R. Vafazadeh, and A. Mahmoudkhani. Can. J. Chem. **80**, 1196 (2002).
18. Yu.A. Simonov, N.V. Gerbeleu, M. Gdaniec, P.N. Bourosh, E.B. Koropchanu, and O.A. Bologa. Russ. J. Coord. Chem. **27**, 341 (2001).
19. T.W. Hambley, D.E. Hibbs, P. Turner, S.T. Howard, and M.B. Hursthouse. J. Chem. Soc. Perkin Trans. 2, 235 (2002).
20. R. Knudsen, O. Sala, and Y. Hase. J. Mol. Struct. **321**, 197 (1994).
21. K. Nakamoto. Infrared and Raman spectra of inorganic and coordination compounds part II: Application in coordination, organometallic, and bioinorganic chemistry. 5th ed. Wiley-Interscience, New York. 1997.
22. R.M. Silverstein and F.X. Webster. Spectroscopic identification of organic compounds. 6th ed. John Wiley and Sons Inc., New York. 1997.
23. H. Kunkely and A. Vogler. Inorg. Chem Commun. **7**, 767 (2004).
24. C.-T. Chen, S.-Y. Liao, K.-J. Lin, C.-H. Chen, and T.-Y.J. Lin. Inorg Chem. **38**, 2734 (1999).
25. W.F. Wacholtz and J.T. Mague. Acta Crystallogr. Sect. C, **C57**, 1400 (2001).
26. V.W.W. Yam, Y.L. Pui, K.K. Cheung, and N. Zhu. New J. Chem. **26**, 536 (2002).

[2] Supplementary data for this article are available on the Web site or may be purchased from the Depository of Unpublished Data, Document Delivery, CISTI, National Research Council Canada, Ottawa, ON K1A 0R6, Canada. DUD 4067. For more information on obtaining material refer to http://cisti-icist.nrc-cnrc.gc.ca/irm/unpub_e.shtml. CCDC 261132 and 261133 contain the crystallographic data for this manuscript. These data can be obtained, free of charge, via www.ccdc.cam.ac.uk/conts/retrieving.html (Or from the Cambridge Crystallographic Data Centre, 12 Union Road, Cambridge CB2 1EZ, UK; fax +44 1223 336033; or deposit@ccdc.cam.ac.uk).

© 2005 NRC Canada

Ab initio study of the decomposition of formamidine

M.H. Almatarneh, C.G. Flinn, and R.A. Poirier

Abstract: The decomposition of formamidine yielding hydrogen cyanide and ammonia has been investigated by ab initio calculations. Optimized geometries for reactants, transition states, and products were determined at the HF/6-31G(d) and MP2/6-31G(d) levels of theory. Energies were also determined at the G1, G2, G2MP2, G3, G3B3, G3MP2, and G3MP2B3 levels of theory. The role of water in the decomposition reaction of formamidine was examined. Intrinsic reaction coordinate (IRC) analysis was carried out for all transition states. Activation energies, enthalpies and free energies of activation were also calculated for each reaction pathway. G3 level of theory predicts the gas-phase decomposition of formamidine to have a high activation energy of 259.1 kJ mol^{-1}. Adding one water molecule catalyses the reaction by forming a cyclic hydrogen-bonded transition state, reducing the barrier to 169.4 kJ mol^{-1} at the G3 level. Addition of a second water, which acts as a "solvent" molecule, further reduces the barrier to 151.1 kJ mol^{-1} at the G3 level. These values are still high and explain why rather extreme conditions are necessary to achieve this reaction experimentally. Thermodynamic properties (ΔE, ΔH, and ΔG) for each reaction pathway studied were also calculated. The G3 heats of reaction (ΔE) of the gas-phase decomposition of formamidine, its complex with one water molecule, and its complex with two water molecules are 0.9, 2.2, and –5.1 kJ mol^{-1}, respectively. The G3 heat of reaction for the gas-phase decomposition to yield separated products is 22.3 kJ mol^{-1}. Free energies of reaction and of activation in aqueous solution were calculated with PCM using the KLAMT cavity model. At MP2 the formamidine reaction is found to be exergonic in aqueous solution and to favour formation of the separated products (NH_3 + HCN). The solvent model predicts a significant lowering of the free energy of activation (16–18 kJ mol^{-1}) for the unimolecular reaction and 21–42 kJ mol^{-1} for the water-mediated reaction in aqueous solution relative to the gas phase.

Key words: decomposition reaction, formamidine, Hartree–Fock, post Hartree–Fock, Gaussian-n theories, IRC, solvation models, PCM, KLAMT.

Résumé : Faisant appel à des calculs ab initio, on a étudié la décomposition de la formamidine qui conduit à la formation de cyanure d'hydrogène et d'ammoniac. On a déterminé les géométries optimisées des réactifs, des états de transition et des produits aux niveaux HF/6-31G(d) et MP2/6-31G(d) de la théorie. On a aussi déterminé les énergies aux niveaux G1, G2, G2MP2, G3, G3B3, G3MP2 et G3MP2B3 de la théorie. On a réalisé une analyse de tous les états de transition par le biais des coordonnées intrinsèques de la réaction. On a aussi calculé les énergies d'activation, les enthalpies et les énergies libres d'activation de chaque voie réactionnelle. Au niveau G3 de la théorie, les prédictions suggèrent que l'énergie d'activation de la décomposition de la formamidine en phase gazeuse est élevée et se situe à 259,1 kJ mol^{-1}. Au niveau G3, l'addition d'une molécule d'eau catalyse la réaction, avec formation d'un état de transition comportant une liaison hydrogène cyclique, et la barrière est réduite à 169,4 kJ mol^{-1}. Toujours au niveau G3, l'addition d'une deuxième molécule d'eau qui agit comme solvant réduit à nouveau la barrière à 151,1 kJ mol^{-1}. Ces valeurs sont toujours élevées et elles expliquent pourquoi il est nécessaire d'utiliser des conditions extrêmes pour effectuer cette réaction expérimentalement. On a aussi calculé les propriétés thermodynamiques (ΔE, ΔH et ΔG) pour chaque voie réactionnelle étudiée. Au niveau G3, chaleurs de réaction (ΔE) de décomposition en phase gazeuse de la formamidine, de son complexe avec une molécule d'eau et de son complexe avec deux molécules d'eau sont respectivement de 0,9, 2,2 et –5,1 kJ mol^{-1}. Au niveau G3, la chaleur de réaction pour la décomposition en phase gazeuse conduisant à des produits séparés est de 22,3 kJ mol^{-1}. On a calculé les énergies libres de réaction et d'activation en solution aqueuse « PCM », en utilisant le modèle de cavité de « KLAMT ». Au niveau MP2, on a trouvé que, en solution aqueuse, la réaction de la formamidine est exogernique et qu'elle favorise la formation de produits séparés (NH_3 + HCN). Le modèle du solvant permet de prédire que, pour la réaction en solution par rapport à la réaction en phase gazeuse, il y aura une diminution significative de l'énergie libre d'activation, de l'ordre de 16 à 18 kJ mol^{-1} pour la réaction unimoléculaire et de 21 à 42 kJ mol^{-1} pour la réaction catalysée par l'eau.

Received 7 June 2005. Published on the NRC Research Press Web site at http://canjchem.nrc.ca on 7 February 2006.

M.H. Almatarneh, C.G. Flinn, and R.A. Poirier.[1] Department of Chemistry, Memorial University of Newfoundland, St. John's, NF A1B 3X7, Canada.

[1]Corresponding author (e-mail: rpoirier@mun.ca).

 doi: 10.1139/V05-233 © 2005 NRC Canada

Mots clés : réaction de décomposition, formamidine, Hartree–Fock, post Hartree–Fock, théories à n Gaussiennes, IRC, modèles de solvatation, PCM, KLAMT.

[Traduit par la Rédaction]

Introduction

Amidine compounds are of interest because of their medical and biochemical importance, having many biological and pharmaceutical uses (1). Formamidine is the simplest of the amidine class and has been found to exhibit antibiotic, antifungal, and anaesthetic properties. Amidines play a significant role in the biosynthesis of other biologically important compounds, such as purines, imidazoles, and the catabolism of histidine (1). Due to its small size, formamidine has been a prime target of both experimental and theoretical investigation. In addition to serving as a model for hydrogen-transfer reactions in bases of nucleic acids, formamidine has been extensively studied theoretically since it forms hydrogen-bonded complexes with itself and other molecules such as water.

The intramolecular 1,3-sigmatropic hydrogen rearrangement and intermolecular hydrogen transfers have been studied theoretically for various formamidine systems (2–9) including formamide–formamidine (10–17) and formamidine – formic acid (18, 19). Since most hydrogen transfers occur in aqueous solution, one must consider the role of water molecules in hydrogen transfer. Water can act not only as a solvent but also as a catalyst by both donating and accepting a hydrogen to promote long-range hydrogen transfer (water-mediated pathway).

Tautomerization by intramolecular hydrogen transfer involving formamidine and its complexes with one, two, and three water molecules was studied by Zhang et al. (20) using ab initio and density functional methods. They reported the importance of hydrogen-bonded water molecules that lowered the barrier to tautomerization. Nguyen et al. (6) investigated double hydrogen transfer in formamidine dimers using ab initio methods. The barrier for the prototropic tautomerization in these systems is reduced by about 84 kJ mol^{-1} at the Hartree–Fock level of theory when the hydrogen transfer is mediated by a water molecule. The solvent effect on the potential energy surface for double hydrogen transfer in formamidine dimers has also been studied (21). Solvent effects on the potential energy surface have also been investigated for formamidine hydrogen bonded to a water molecule using the chemical molecular dynamic simulation method (22).

Since biological activity depends greatly on the molecular conformation, Tortajada et al. (23) have investigated the relative stabilities of the E(trans) and Z(cis) conformers of formamidine and the relative stabilities of the complexes of both conformers with different monocations. They found that the (E) conformer of formamidine is 7.5 kJ mol^{-1} more stable than the Z conformer at both G2MP2 and G2 levels of theory. Dynamics and kinetic isotope effects for tautomerization of the formamidine-monohydrated complex using direct semiempirical dynamic calculation and the G2 level of theory was studied by Kim (24). Primary and solvent kinetic isotope effects in the water-mediated tautomerization of formamidine using an ab initio direct dynamic study was investigated by Bell and Truong (25).

A number of reactions of formamidine have been considered to be model reactions for more complex molecules with structural similarities to formamidine, such as single hydrogen transfer in bases of nucleic acids (6, 8, 26) as well as double hydrogen-transfer reactions. Recently, the deamination of the more stable E-isomer of formamidine with OH^-, H_2O, and H_3O^+ to yield formamide has been studied by Flinn et al. (26). This investigation was undertaken as a precursor to a study of the deamination of the DNA base cytosine. The E(trans) isomer of formamidine forms part of the cytosine structure, notably in the region of cytosine where the deamination of cytosine to uracil can take place. Cytosine is the most unstable of the DNA bases, deaminating spontaneously to uracil with an activation energy of 117 ± 4 kJ mol^{-1} (27). The mechanism for the deamination of formamidine was investigated using high level ab initio methods. Flinn et al. (26) found that deamination with OH^- yields a tetrahedral intermediate with a much lower activation energy barrier than for the reaction with H_2O and H_3O^+ using G2 theory.

Amidine is also known to undergo decomposition at elevated temperatures, yielding hydrogen cyanide and ammonia. Some experimental results suggest that the decomposition of amidine is an unimolecular process (28). The unimolecular decomposition mechanism of formamidine to give ammonia and hydrogen cyanide has been investigated by Andres et al. (28, 29) at the HF level of theory using the 4-31G basis set. They determined the activation energy to be 333 kJ mol^{-1} and the energy of reaction to be 0.04 kJ mol^{-1} for the formation of the NH_3–HCN complex. A potential energy hypersurface was established. The first step was the isomerization of the E(trans) to Z (cis) isomer followed by a 1,3-shift of the hydrogen bonded to the imino nitrogen to the amino nitrogen accompanied by the cleavage of the bond between the carbon and the amino nitrogen. At present, no computational studies of water-mediated or solution-phase decomposition of formamidine to yield hydrogen cyanide and ammonia have been reported. In this work, a detailed study of the unimolecular and the water-mediated (mono- and di-hydrated complexes) decomposition of formamidine, both in the gas phase and in solution, is presented. Because of the size of the system, it is possible to perform the calculations at high levels of theory, such as the Gaussian-n theories, which are known to give reliable energetics. The role played by water as a catalyst as well as its role as solvent on the energetics and mechanism of this reaction were also investigated. The results serve as a benchmark for similar reactions in solution for more complex systems, few of which have been studied in depth computationally.

Computational method

The MUNgauss (30) computational program was used for most of the geometry optimizations at HF/6-31G(d) for reactants, products, and transition state structures. All other calculations were performed with either Gaussian 98 (31) or

© 2005 NRC Canada

Table 1. Thermodynamic properties for the decomposition reaction of formamidine (in kJ mol^{-1}) at 298.15 K.

	Formamidine[a]			Formamidine[b]			Formamidine–H_2O[b]			Formamidine–$2H_2O$[b]		
Level of theory	ΔE	ΔH	ΔG[c]	ΔE	ΔH	ΔG[d]	ΔE	ΔH	ΔG[e]	ΔE	ΔH	ΔG[f]
HF/6-31G(d)	36.9	23.5	–20.2	5.0	–2.5	–15.6	6.9	–1.2	–10.5	1.6	–7.7	–21.3
Solution[g]			–18.5			4.8						
			–25.1			3.1						
MP2/6-31G(d)	26.9	13.5	–30.5	–11.4	–18.2	–30.3	–9.9	–17.6	–24.9	–5.5	–14.8	–30.2
Solution[g]			–23.2			–20.5						
			–35.5			–23.3						
G1	22.1	28.8	–14.3	–0.8	4.8	–9.0	–1.1	3.5	–6.5	–8.5	–2.7	–17.0
G2	23.2	29.8	–13.3	2.6	8.2	–5.6	3.3	7.9	–2.1	–2.8	2.9	–11.4
G2MP2	23.5	30.1	–13.0	3.7	9.3	–4.5	4.3	8.9	–1.1	–1.9	3.9	–10.4
G3	22.3	29.0	–14.1	0.9	6.5	–7.3	2.2	6.7	–3.2	–5.1	0.6	–13.7
G3B3	21.0	27.8	–15.6	1.7	6.6	–5.0	3.5	7.0	0.0	–5.1	0.0	–11.5
G3MP2	20.8	27.5	–15.6	0.4	6.0	–7.8	1.7	6.2	–3.7	–5.2	0.6	–13.7
G3MP2B3	19.8	26.6	–16.9	1.6	6.5	–5.1	3.4	6.9	–0.1	–4.9	0.2	–11.3

[a]For the formation of separated products.
[b]For the formation of the HCN–NH_3–$n H_2O$ complex (n = 0–2).
[c]ΔS values range from 0.145 to 0.148 kJ mol^{-1} K^{-1}.
[d]ΔS values range from 0.039 to 0.046 kJ mol^{-1} K^{-1}.
[e]ΔS values range from 0.017 to 0.033 kJ mol^{-1} K^{-1}.
[f]ΔS values range from 0.035 to 0.052 kJ mol^{-1} K^{-1}.
[g]Values are reported in order; the PCM–KLAMT model was used for single point calculation and for optimized structures. In all cases $\Delta G = \Delta\Delta G$ (thermal correction) + ΔG_{solv}.

Gaussian 03 (32). The geometries of all reactants, transition states, and products were fully optimized at the restricted HF and second-order Møller–Plesset (MP2) levels of theory using the 6-31G(d) and 6-31+G(d) basis sets. Energies have also been calculated using the Gaussian-n theories, G1, G2, G2MP2, G3, G3B3, G3MP2, and G3MP2B3. B3LYP/6-31+G density functional theory calculations were also performed. Intrinsic reaction coordinate (IRC) analysis was carried out for all transition states. Free energies of reaction and activation in aqueous solution for the unimolecular decomposition reaction of formamidine were calculated with the polarizable continuum model (PCM) as implemented in Gaussian03. The choice of cavity in PCM is important because the computed energies and properties depend on the cavity size. By default, the PCM model builds up the cavity using the united atom (UA) model, i.e., by putting a sphere around each solute heavy atom; hydrogen atoms are enclosed in the sphere of the atom to which they are bonded. The three UA models that are available in Gaussian03 are not suitable for reactions involving hydrogen transfers and hence were not used. In this study, the PCM solvent calculations were performed using the KLAMT cavity. All free energy calculations involving solvation were performed using both gas- and solution-phase structures optimized at the RHF/6-31G(d) and MP2/6-31G(d) levels. Other cavities were also investigated (UFF and PAULING), but it was impossible to obtain all the optimized structures for these models. Single point calculations based on gas-phase optimized geometries using UFF and PAULING cavities gave results that were very close to the KLAMT cavity.

Results and discussion

The results for the decomposition reaction of formamidine and its mono- and di-hydrated complexes in the gas phase and in aqueous solution are given in Tables 1–3.

Thermodynamic results for the decomposition of formamidine

The thermodynamic properties for the decomposition reaction of formamidine are listed in Table 1. The reaction for the decomposition of formamidine is found to be endothermic at the Gaussian-n theories (with enthalpies of 26.6–30.1 kJ mol^{-1}) and less endothermic for the formation of the NH_3–HCN complex (4.8–9.3 kJ mol^{-1}). These results do not differ by more than 4.5 kJ mol^{-1}, which is within the expected error of the Gaussian-n theories. The HF/6-31G(d) enthalpies are consistently in better agreement with the Gaussian-n theories than the MP2/6-31G(d) enthalpies. The difference between the enthalpy for the formation of the complex and the formation of separated products (–22.5 kJ mol^{-1} at G3) represents the stability of the NH_3–HCN complex. Adding a single water molecule has little effect on the enthalpy of reaction (6.5 vs. 6.7 kJ mol^{-1} at G3). Addition of the second water molecule has a larger effect on the enthalpy of reaction, which is now only slightly endothermic (0.6 kJ mol^{-1} at G3). The decomposition reaction of formamidine with separated products is more exergonic than the formation of the HCN–NH_3 complex. This difference is simply due to the increase in the entropy for the formation of the separated products. Except for the HF solution results, all other levels of theory predict the reaction to be exergonic, where formation of the separated species (HCN + NH_3) is favoured over formation of the complex (HCN–NH_3)

Activation energy, enthalpy and free energies of activation for the decomposition of formamidine

The gas-phase unimolecular decomposition of formamidine

The geometries for the reactant, transition state, and products for the unimolecular gas-phase decomposition of formamidine are shown in Scheme 1 along with the atom-numbering scheme.

© 2005 NRC Canada

Table 2. Activation energies, enthalpies of activation, and free energies of activation for the decomposition reaction of formamidine (in kJ mol^{-1}) at 298.15 K.

	Formamidine			Formamidine–H_2O			Formamidine–$2H_2O$		
Level of theory	ΔE_{act}	$\Delta H^{\ddagger}$	$\Delta G^{\ddagger a}$	ΔE_{act}	$\Delta H^{\ddagger}$	$\Delta G^{\ddagger b}$	ΔE_{act}	$\Delta H^{\ddagger}$	$\Delta G^{\ddagger c}$
HF/6-31G(d)	331.5	314.3	315.3	244.0	226.7	246.4	217.4	203.3	219.7
Solution[d]			296.1			212.5			
			299.0			204.6			
MP2/6-31G(d)	274.1	255.4	255.7	173.1	152.8	169.9	156.2	139.6	152.6
Solution[d]			236.1			157.6			
			237.9			148.9			
G1	253.5	252.7	253.8	165.3	158.0	178.3	146.9	141.0	158.0
G2	257.6	256.8	257.9	168.8	161.5	181.9	151.4	145.5	162.5
G2MP2	257.2	256.3	257.4	168.8	161.5	181.9	151.6	145.6	162.7
G3	259.1	258.2	259.4	169.4	162.1	182.4	151.1	145.2	162.2
G3B3	256.6	256.1	256.6	164.9	158.6	174.7	145.5	140.9	154.5
G3MP2	257.9	257.1	258.2	172.7	165.4	185.8	154.7	148.8	165.8
G3MP2B3	255.4	254.9	255.4	168.1	161.8	177.8	148.7	144.0	157.7

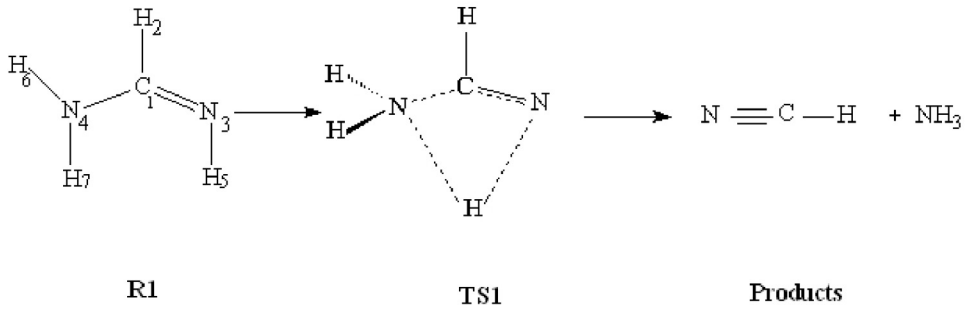
[a]$\Delta S^{\ddagger}$ values range from –0.001 to –0.004 kJ mol^{-1} K^{-1}.
[b]$\Delta S^{\ddagger}$ values range from –0.041 to –0.068 kJ mol^{-1} K^{-1}.
[c]$\Delta S^{\ddagger}$ values range from –0.04 to –0.06 kJ mol^{-1} K^{-1}.
[d]Values are reported in order; the PCM–KLAMT model was used for single point calculation and for optimized structures. In all cases $\Delta G = \Delta\Delta G$ (thermal correction) + ΔG_{solv}.

Table 3. Activation energies, enthalpies of activation, and free energies of activation (in kJ mol^{-1}) at 298.15 K for the intermolecular hydrogen transfers in formamidine–$2H_2O$ (TS4a, TS4b, and TS5).

	TS4a			TS4b			TS5		
Level of theory	ΔE_{act}	$\Delta H^{\ddagger}$	$\Delta G^{\ddagger}$	ΔE_{act}	$\Delta H^{\ddagger}$	$\Delta G^{\ddagger}$	ΔE_{act}	$\Delta H^{\ddagger}$	$\Delta G^{\ddagger}$
HF/6-31G(d)	211.3	195.0	215.0	206.6	190.2	210.6	236.5	233.1	246.7
MP2/6-31G(d)	142.1	121.5	137.3	135.6	114.7	130.8	156.2	139.6	152.6
G1	134.1	126.3	147.2	128.4	120.3	141.7	155.9	150.4	164.7
G2	136.8	129.0	149.9	132.3	124.2	145.6	160.4	154.9	169.2
G2MP2	136.7	128.9	149.8	132.3	124.3	145.6	160.6	155.0	169.3
G3	137.0	129.2	150.1	132.3	124.2	145.6	160.2	154.6	168.9
G3B3	129.6	123.4	138.4	124.2	117.9	133.2	145.5	140.9	154.5
G3MP2	142.5	134.7	155.6	138.1	130.0	151.4	163.7	158.2	172.5
G3MP2B3	134.9	128.7	143.7	129.8	123.4	138.7	148.7	144.0	157.7

Note: $\Delta S^{\ddagger}$ values range from –0.05 to –0.07 kJ mol^{-1} K^{-1} for TS4a; $\Delta S^{\ddagger}$ values range from –0.05 to –0.07 kJ mol^{-1} K^{-1} for TS4b; $\Delta S^{\ddagger}$ values range from –0.03 to –0.05 kJ mol^{-1} K^{-1} for TS5.

Scheme 1.



R1 TS1 Products

Vibrational analysis for the two structures in Fig. 1 shows that the C_s structure, used in a previous study (28), has one imaginary frequency, and the nearly planar C_1 structure to be a minimum. From these results, the equilibrium structure with C_1 symmetry was considered as the starting point for this reaction in this study.

The IRC analysis of TS1 for the gas-phase decomposition reaction of formamidine is shown in Fig. 2. The formamidine decomposition transition state can be described in terms of two bond ruptures (N3—H5 and N4—C1) and one bond formation (N4—H5). The transition state structure is highly strained, with an N3-C1-N4 angle of 106.7° com-

© 2005 NRC Canada

Scheme 2.

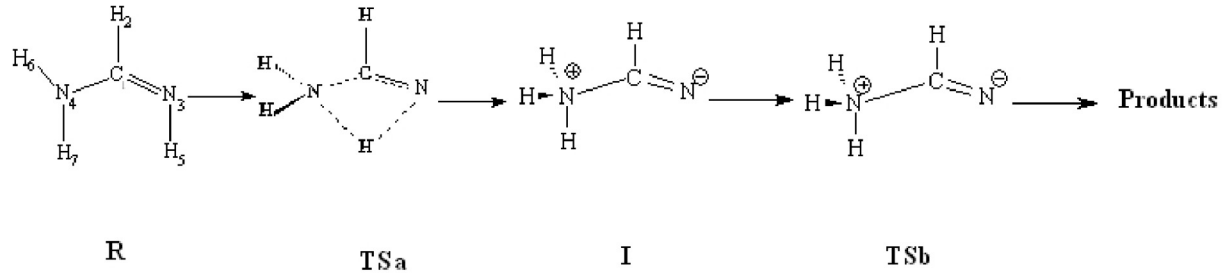


Fig. 1. The C_s and C_1 structures of formamidine.

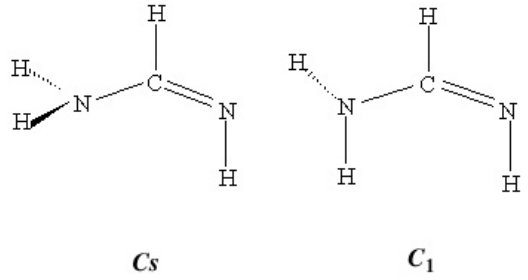
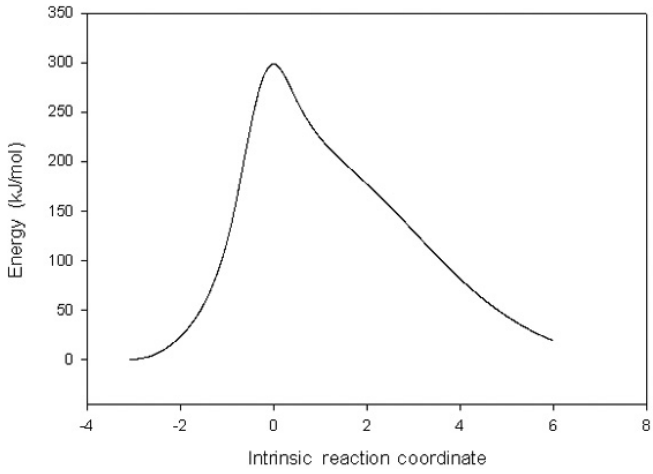


Fig. 2. Energy vs. the IRC for the gas-phase decomposition of formamidine at HF/6-31G(d) with the CalcFC option. Zero energy taken as the reactant.



pared with 128.7° for the reactant. The product is a hydrogen-bonded complex of ammonia with hydrogen cyanide. The activation energy for the unimolecular gas-phase decomposition reaction of formamidine at various levels of theory are listed in Table 2. An activation energy of 333.1 kJ mol^{-1} was reported for this reaction at HF/4-31G(d) (28). In this study, the activation energy is 331.5, 253.5, and 259.1 kJ mol^{-1} at HF/6-31G(d), G1, and G3 levels, respectively. The free energy of activation for the reaction is 315.3, 253.8, and 259.4 kJ mol^{-1} at HF/6-31G(d), G1, and G3 levels, respectively. These values are high and explain why rather extreme conditions are necessary to achieve this reaction experimentally.

Applying the solvent model yields a different mechanism for this reaction from the one in the gas phase. The decomposition reaction in solution involves a two-step mechanism for both the unimolecular and the water-catalyzed decomposition. In solution, the first step involves transfer of a hydrogen from the imino nitrogen to the amino nitrogen forming a zwitterionic intermediate that is stabilized in solution. The transition state (TSa) and the zwitterionic intermediate for this reaction are shown in Scheme 2.

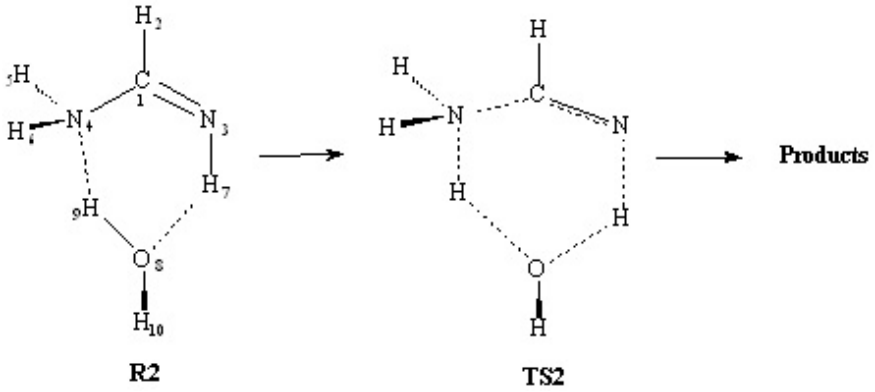
The structures of the reactant and products for the unimolecular decomposition in the gas and solution phases are only slightly different. The first transition state structure for the reaction in solution is similar to the gas-phase structure, but more productlike. For example, the N4—C1 bond length increased from 1.47 Å in the gas phase to 1.53 Å in solution. The zwitterionic intermediate has a slightly longer N4—C1 bond length (1.58 Å), which increases significantly to 1.74 Å in the second transition state, giving a very productlike structure, with a very small activation energy (2.5 kJ mol^{-1}). In solution, the N3-C1-H2 angle of the second transition state (TSb) is 140.3° compared with 132.6° for the first transition state (TSa). The solvent models used in this study predict that the free energy of activation for the unimolecular decomposition would be reduced in aqueous solution. Using the PCM–KLAMT model, $\Delta G^{\ddagger}$ is lowered by 16 and 18 kJ mol^{-1} at HF/6-31G(d) and MP2/6-31G(d) levels, respectively. As given in Table 2, the free energy of activation for the unimolecular decomposition in solution is 237.9 kJ mol^{-1} at the MP2/6-31G(d) level of theory, not that different from the single point value of 236.1 kJ mol^{-1}.

The decomposition of formamidine with one water molecule

Scheme 3 shows the one-step decomposition mechanism for the monohydrated complex of formamidine. This scheme shows that the water molecule catalyses the decomposition by forming a nearly planar six-membered ring with formamidine. In this case, the N3-C1-N4 angle in the transition state TS2 shown in Fig. 3 is 119.4° compared with 106.7° in the unimolecular reaction transition state (TS1, Scheme 1), an increase of 12.7°. The activation energy, the enthalpy of activation, and free energy of activation for this reaction are listed in Table 2. Adding one water molecule significantly relaxes the transition state, reducing the angle strain and consequently reducing the barrier height from 259.1 to 169.4 kJ mol^{-1} at the G3 level of theory. The free energy of activation for this system is 246.3, 178.3, and 182.4 kJ mol^{-1} at HF/6-31G(d), G1, and G3 levels, respectively. These results clearly show that the kinetically difficult reaction takes place more easily when catalyzed by a single water molecule. The IRC analysis of the transition state TS2 for this system is shown in Fig. 4.

© 2005 NRC Canada

Scheme 3.



Scheme 4.

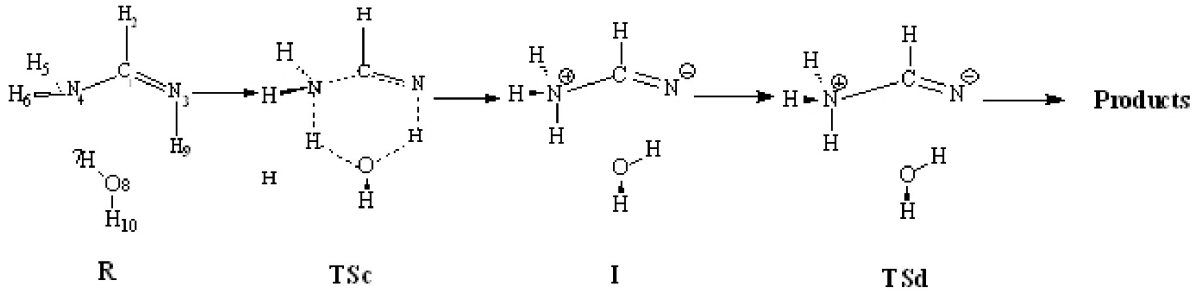


Fig. 3. The transition state structure for the decomposition reaction of formamidine with one water molecule.

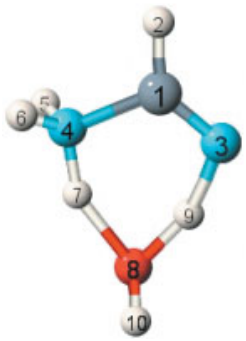
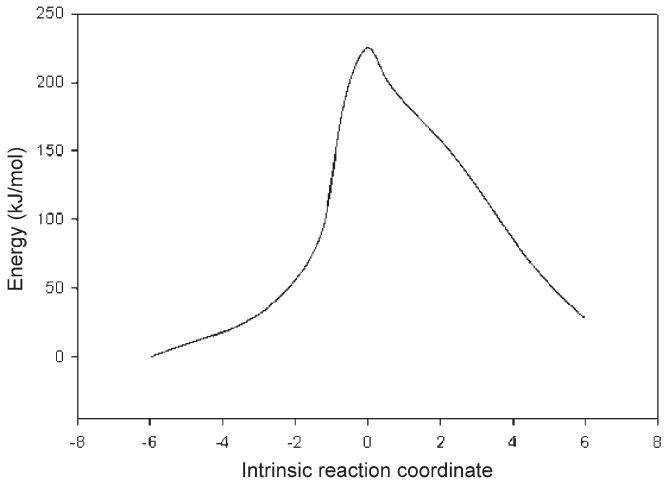


Fig. 4. Energy vs. the IRC for the decomposition of monohydrated formamidine at HF/6-31G(d) with the CalcFC option. Zero energy taken as the reactant.



In solution, the one-water-catalyzed decomposition reaction of formamidine also involves a two-step mechanism forming a zwitterionic intermediate as shown in Scheme 4. The structure of the reactant and products for the one-water-catalyzed decomposition in both gas and solution phases also only differ slightly. As for the unimolecular reaction, the N4—C1 bond increases from 1.50 Å in the gas phase to 1.55 Å in the solution phase in the first step of the reaction. In solution, the N3-C1-H2 angle of the second transition state (TSd) is 141.4° compared with 128.6° for the first transition state (TSc).

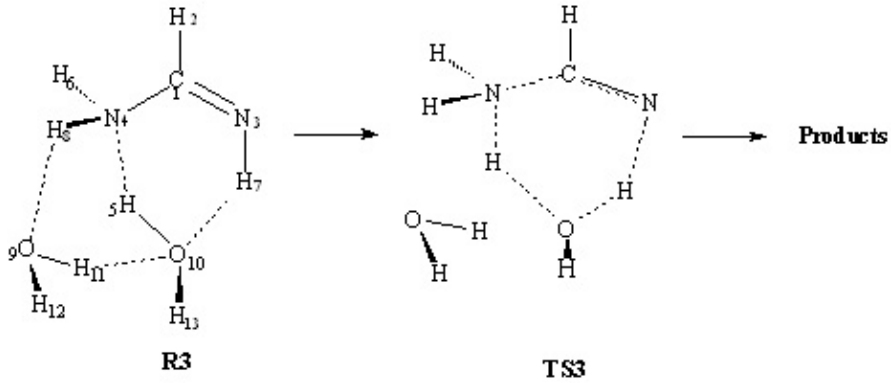
The zwitterionic intermediate has a slightly longer N4—C1 bond length (1.59 Å), which increases significantly to 1.77 Å in the second transition state, giving an even more productlike structure with a very small activation energy (6.0 kJ mol^{-1}). In solution, the free energy of activation would further be reduced by 21 to 42 kJ mol^{-1} (depending on the level of theory used). The free energy of activation for the single water-mediated decomposition in solution is 148.9 kJ mol^{-1} at the MP2/6-31G(d) level, not significantly different from the single point value (157.6 kJ mol^{-1}), although the mechanism changes to a two-step mechanism in solution.

The decomposition reaction of formamidine with two water molecules

Previous research on 1,3-hydrogen shift tautomerization reactions (20) has identified transition state structures in which two water molecules participate in the hydrogen

© 2005 NRC Canada

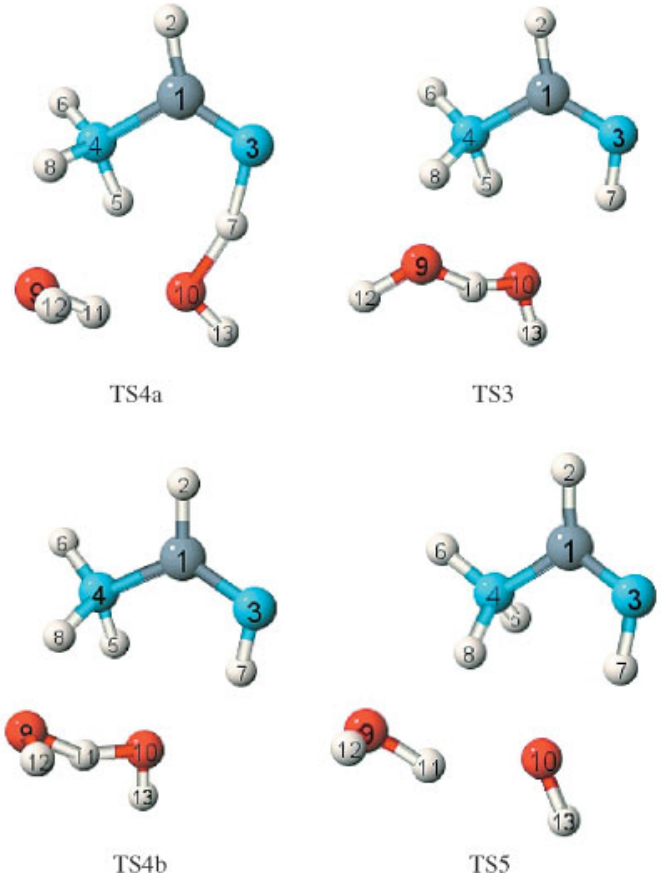
Scheme 5.



transfer by forming an eight-membered ring. Addition of the second water molecule further relieves angle strain, lowering the activation energy for the reaction. However, all attempts to optimize the cyclic eight-membered dihydrated formamidine transition state structure failed. This investigation did, however, lead to four different transition state structures containing a six-membered ring as shown in Fig. 5. Scheme 5 shows the only transition state (TS3) that connects the reactants and the products, as determined from the IRC analysis. This transition state is very similar in structure to TS2 for the one-water-mediated decomposition reaction of formamidine. In TS3, one water molecule directly participates in the hydrogen transfer, as shown in Scheme 5. The second water molecule does not directly participate in hydrogen transfer, but further stabilizes the transition state by hydrogen bonding to both an N4 hydrogen and O10.

Activation energies, enthalpies of activation, and free energies of activation are listed in Table 2 for the decomposition of dihydrated formamidine. Adding the first water molecule reduces the activation energy by 89.7 kJ mol^{-1} at the G3 level. Adding the second water molecule reduces the activation energy of the formamidine decomposition to a much smaller extent, further decreasing the activation energy by only 18.3 kJ mol^{-1}. This is because the first water molecule catalyses the reaction, whereas the second water molecule simply stabilizes the transition state by "solvation". Thus, the water can both stabilize the transition state and act as a catalyst for these reactions. The present results support a single water-mediated decomposition mechanism and that a two-water-mediated transition state does not appear to exist, in the gas phase or in aqueous solution, for this reaction.

Fig. 5. The transition state structures for dihydrated formamidine.



Intermolecular hydrogen-transfer transition states

Three additional transition states were found (TS4a, TS4b, and TS5), which represent intermolecular hydrogen transfer between formamidine and either one or two water molecules and do not result in product formation. Activation energies, enthalpies of activation, and free energies of activation for these intermolecular hydrogen transfers are listed in Table 3. TS4a and TS4b are rotational isomers, differing from each other for the most part with respect to the orientation of H12 (Fig. 5). These two transition states involve the exchange of a hydrogen between formamidine and the two hydrogen-bonded water molecules through a six-membered cyclic structure. The IRC confirms that these transition states lead to the reactant in both directions. TS5 has the highest activation energy among the transition states, and involves a hydrogen (H5) transfer from a single water to N4 of formamidine followed by rotation about the C—N bond and transfer of a hydrogen (H8) back to water (Fig. 5). The IRC confirms that this transition state goes to the reactant in both directions.

IRC analysis

IRC analysis was carried out for all transition states. The IRC analysis for the gas-phase transition state (TS1, Fig. 2) and the monohydrated transition state (TS2, Fig. 4) confirmed that these transition states connected the expected reactants and products. However, the IRC analysis of the

© 2005 NRC Canada

Fig. 6. Energy vs. the IRC for the decomposition of dihydrated formamidine (TS3). Zero energy taken as the reactant.

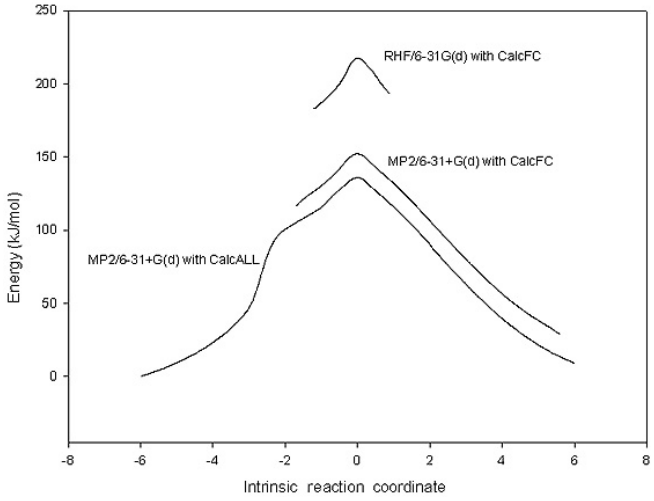


Fig. 7. Energy vs. the IRC for water–formamidine hydrogen exchange (TS4). Zero energy taken as the reactant.

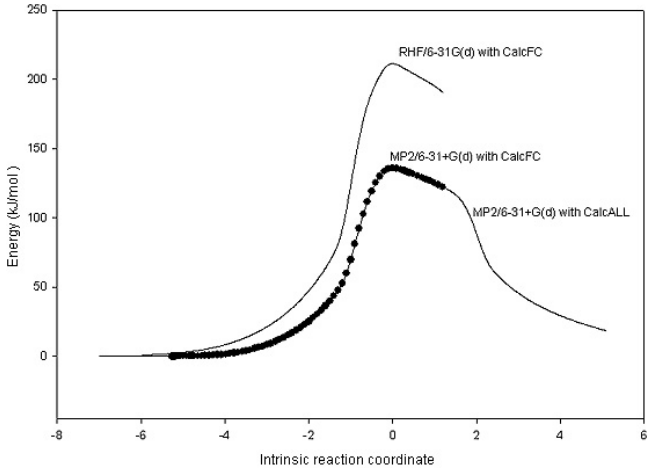
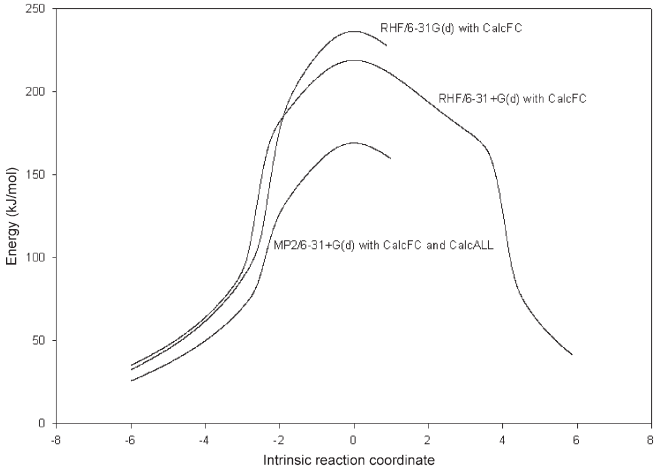


Fig. 8. Energy vs. the IRC for water–formamidine hydrogen exchange (TS5). Zero energy taken as the reactant.



dihydrated transition states (TS3, TS4, and TS5), using the CalcFC option, did not give the complete reaction pathway in several cases, stopping prematurely as shown in Figs. 6–8. Initially, this suggested the existence of an intermediate. Further analysis was carried out using the CalcFC or CalcALL options with structures optimized at different levels of theory and basis set. None of these options consistently gave a complete reaction pathway. In each of the cases in which the complete reaction pathway was obtained, shoulders are found to exist, as can be seen in Figs. 6–8. Such shoulders for some of the options listed above may be indicative of zwitterionic species, unstable in the gas phase but stable in solution phase.

Conclusions

The high degree of stability of formamidine toward decomposition to ammonia and hydrogen cyanide is confirmed by this investigation. We have performed ab initio calculations on water-mediated hydrogen transfer in the decomposition reaction of formamidine. We found that a single water molecule can act as a catalyst, stabilizing the transition state, and thus lowering the barrier height for the gas-phase decomposition reaction. At the G3 level of theory, the one-water-catalyzed mechanism lowers the barrier to 169.4 kJ mol^{-1} from the gas-phase value of 259.1 kJ mol^{-1} for the decomposition reaction of formamidine. Addition of a second water, which simply acts as a solvent molecule, further lowers the barrier to 151.1 kJ mol^{-1}. A two-water-mediated transition state has not been found despite a thorough investigation.

The decomposition reaction of formamidine in solution involves a two-step mechanism for both the unimolecular and the water-catalyzed decomposition. The solvent model predicts a significant lowering of the free energy of activation (16–42 kJ mol^{-1}, depending on the level of theory) for the reaction in aqueous solution relative to the gas phase.

Intrinsic reaction coordinate (IRC) analysis was carried out for all transition state structures to obtain the complete reaction pathway. Thermodynamic properties were calculated for each reaction. The activation energies and the heats of reaction calculated at the Gaussian-n theories agree to within 10 kJ mol^{-1}.[2]

Acknowledgments

We thank the Natural Sciences and Engineering Research Council of Canada (NSERC) for financial support and gratefully acknowledge the Memorial University of Newfoundland Advanced Computation and Visualization Centre for computer time. The authors are grateful for the helpful comments made by the reviewers.

References

1. R.J. Grout. *In* the chemistry of amidines and imidates. *Edited by* S. Patai. Wiley, New York. 1975. Chap. 6. pp. 255–281.

[2] Supplementary data for this article are available on the journal Web site or may be purchased from the Depository of Unpublished Data, Document Delivery, CISTI, National Research Council Canada, Ottawa, ON K1A 0R6, Canada. DUD 4070. For more information on obtaining material refer to http://cisti-icist.nrc-cnrc.gc.ca/irm/unpub_e.shtml.

© 2005 NRC Canada

2. T. Yamabe, K. Yamashita, M. Kaminoyama, M. Koizumi, and A. Tachibana. J. Phys. Chem. **88**, 1459 (1984).
3. S. Scheiner and C.W. Kern. J. Am. Chem. Soc. **101**, 4081 (1979).
4. V. Hrouda, J. Florian, M. Polaasek, and P. Hobza. J. Phys. Chem. **98**, 4742 (1994).
5. V. Hrouda, J. Florian, and P. Hobza. J. Phys. Chem. **97**, 1542 (1993).
6. K.A. Nguyen, M.S. Gordon, and D.G. Truhlar. J. Am. Chem. Soc. **113**, 1596 (1991).
7. T.J. Zielinski and R.A. Poirier. J. Comput. Chem. **5**, 466 (1984).
8. R.A. Poirier, D. Majlessi, and T.J. Zielinski. J. Comput. Chem. **7**, 464 (1986).
9. R.A. Poirier, D. Yu, and P.R. Surjan. Can. J. Chem. **69**, 1589 (1991).
10. Y. Kim, S. Lim, H.-H. Kim, and Y. Kim. J. Phys. Chem. A, **103**, 617 (1999).
11. M. Pecul, J. Leszczynski, and J. Sadlej. J. Phys. Chem. A, **104**, 8105 (2000).
12. K.B. Wiberg and P.R. Rablen. J. Am. Chem. Soc. **117**, 2201 (1995).
13. J. Czernek. J. Phys. Chem. A, **107**, 3952 (2003).
14. X.-C. Wang, J. Nichols, M. Feyereisen, M. Gutowski, J. Boatz, A.D.J. Haymet, and J. Simons. J. Phys. Chem. **95**, 10419 (1991).
15. P. Dziekonski, W.A. Sokalski, Y. Podolyan, and J. Leszcynski. Chem. Phys. Lett. **367**, 367 (2003).
16. Y. Podolyan, L. Gorb, and J. Leszczynski. J. Phys. Chem. A, **106**, 12103 (2002).
17. N.U. Zhanpeisov and J. Leszczynski. J. Phys. Chem. A, **103**, 8317 (1999).
18. L. Shimoni, J.P. Glusker, and C.W. Bock. J. Phys. Chem. **100**, 2957 (1996).
19. Y. Kim, S. Lim, and Y. Kim. J. Phys. Chem. A, **103**, 6632 (1999).
20. Q. Zhang, R. Bell, and T.N. Truong. J. Phys. Chem. **99**, 592 (1995).
21. J.-H. Lim, E.K. Lee, and Y. Kim. J. Phys. Chem. A, **101**, 2233 (1997).
22. M. Nagaoka, Y. Okuno, and T. Yamabe. J. Am. Chem. Soc. **113**, 769 (1991).
23. J. Tortajada, E. Leon, A. Luna, O. Mo, and M. Yanez. J. Phys. Chem. **98**, 12919 (1994).
24. Y. Kim. J. Phys. Chem. A, **102**, 3025 (1998).
25. R.L. Bell and T.N. Truong. J. Phys. Chem. A, **101**, 7802 (1997).
26. C. Flinn, R.A. Poirier, and W.A. Sokalski. J. Phys. Chem. A, **107**, 11171 (2003).
27. L.A. Frederico, T.A. Kundel, and B.R. Shaw. Biochemistry, **29**, 2532 (1990).
28. J. Andres, J. Krechl, M. Carda, and E. Silla. Int. J. Quantum Chem. **XL**, 127 (1991).
29. J. Andres, A Beltran, M. Carda, J. Krechl, J. Monterde, and E. Silla. J. Mol. Struct.: THEOCHEM, **254**, 465 (1992).
30. (*a*) R.A. Poirier. MUNgauss (Fortran 90 version) [computer program]. Chemistry Department, Memorial University of Newfoundland, St. John's, Newfoundland, A1B 3X7, Canada. With contributions from M. Brooker, S.D. Bungay, A. El-Sherbiny, T. Gosse, D. Keefe, C.C. Pye, D. Reid, M. Shaw, Y. Wang, and J. Xidos; (*b*) F. Colonna, L.-H. Jolly, R.A. Poirier, J. Angyan, and G. Jansen. Comput. Phys. Commun. **81**, 293 (1994).
31. M.J. Frisch, G.W. Trucks, H.B. Schlegel, G.E. Scuseria, M.A. Robb, J.R. Cheeseman, V.G. Zakrzewski, J.A. Montgomery, Jr., R.E. Stratmann, J.C. Burant, S. Dapprich, J.M. Millam, A.D. Daniels, K.N. Kudin, M.C. Strain, O. Farkas, J. Tomasi, V. Barone, M. Cossi, R. Cammi, B. Mennucci, C. Pomelli, C. Adamo, S. Clifford, J. Ochterski, G.A. Petersson, P.Y. Ayala, Q. Cui, K. Morokuma, N. Rega, P. Salvador, J.J. Dannenberg, D.K. Malick, A.D. Rabuck, K. Raghavachari, J.B. Foresman, J. Cioslowski, J.V. Ortiz, A.G. Baboul, B.B. Stefanov, G. Liu, A. Liashenko, P. Piskorz, I. Komaromi, R. Gomperts, R.L. Martin, D.J. Fox, T. Keith, M.A. Al-Laham, C.Y. Peng, A. Nanayakkara, M. Challacombe, P.M.W. Gill, B. Johnson, W. Chen, M.W. Wong, J.L. Andres, C. Gonzalez, M. Head-Gordon, E.S. Replogle, and J.A. Pople. Gaussian 98. Revision A.11.3 [computer program]. Gaussian, Inc., Pittsburgh, Penn. 2002.
32. M.J. Frisch, G.W. Trucks, H.B. Schlegel, G.E. Scuseria, M.A. Robb, J.R. Cheeseman, J.A. Montgomery, Jr., T. Vreven, K.N. Kudin, J.C. Burant, J.M. Millam, S.S. Iyengar, J. Tomasi, V. Barone, B. Mennucci, M. Cossi, G. Scalmani, N. Rega, G.A. Petersson, H. Nakatsuji, M. Hada, M. Ehara, K. Toyota, R. Fukuda, J. Hasegawa, M. Ishida, T. Nakajima, Y. Honda, O. Kitao, H. Nakai, M. Klene, X. Li, J.E. Knox, H.P. Hratchian, J.B. Cross, C. Adamo, J. Jaramillo, R. Gomperts, R.E. Stratmann, O. Yazyev, A.J. Austin, R. Cammi, C. Pomelli, J.W. Ochterski, P.Y. Ayala, K. Morokuma, G.A. Voth, P. Salvador, J.J. Dannenberg, V.G. Zakrzewski, S. Dapprich, A.D. Daniels, M.C. Strain, O. Farkas, D.K. Malick, A.D. Rabuck, K. Raghavachari, J.B. Foresman, J.V. Ortiz, Q. Cui, A.G. Baboul, S. Clifford, J. Cioslowski, B.B. Stefanov, G. Liu, A. Liashenko, P. Piskorz, I. Komaromi, R.L. Martin, D.J. Fox, T. Keith, M.A. Al-Laham, C.Y. Peng, A. Nanayakkara, M. Challacombe, P.M.W. Gill, B. Johnson, W. Chen, M.W. Wong, C. Gonzalez, and J.A. Pople. GAUSSIAN 03. Revision B.05 [computer program]. Gaussian, Inc., Pittsburgh, Penn. 2003.

© 2005 NRC Canada

α- and β-Cyclodextrin [2]rotaxanes with (diethylenetriamine)platinum(II) stoppers

Victor X. Jin, Donal H. Macartney, and Erwin Buncel

Abstract: A series of dinuclear platinum(II) complexes, $[(dien)Pt(NH_2(CH_2)_nNH_2)Pt(dien)]Cl_4$ (dien = diethylenetriamine, n = 8, 9, 10, and 12) and their corresponding [2]rotaxanes with α-cyclodextrin (α-CD), $[(dien)Pt\{NH_2(CH_2)_nNH_2{\cdot}\alpha\text{-}CD\}Pt(dien)]Cl_4$, have been synthesized and characterized by ^1H, ^{13}C, and ^{195}Pt NMR spectroscopy and electrospray mass spectrometry. The rotaxanes were prepared by reacting the $\{NH_2(CH_2)_nNH_2{\cdot}\alpha\text{-}CD\}$ pseudorotaxanes with [Pt(dien)]Cl, to stopper the included linear α,ω-diaminoalkane chains with the inert Pt(II) end groups. The kinetics of the self-assembly and dissociation of the β-CD rotaxane, $[(dien)Pt\{NH_2(CH_2)_{10}NH_2{\cdot}\beta\text{-}CD\}Pt(dien)]^{4+}$, were investigated by using ^1H NMR and are indicative of a *slippage* mechanism, owing to the comparable sizes of the β-CD cavity and the $[Pt(dien)]^+$ end group. A relatively weak inclusion of the end group in the β-CD cavity precedes a thermally promoted passage of the β-CD over the $[Pt(dien)]^+$ end group onto the hydrophobic polymethylene chain of the bridging ligand of the thread.

Key words: rotaxanes, pseudorotaxanes, cyclodextrin, platinum complexes, slippage mechanism.

Résumé : On a synthétisé une série de complexes binucléaires du platine(II), de formule générale $[(dien)Pt(NH_2(CH_2)_nNH_2)Pt(dien)]Cl_4$ (dien = diéthylènetriamine; n = 8, 9, 10 et 12), ainsi que les [2]rotaxanes correspondants avec la α-cyclodextrine (α-CD), de formule générale $[(dien)Pt\{NH_2(CH_2)_nNH_2{\cdot}\alpha\text{-}CD\}Pt(dien)]Cl_4$ et on les a caractérisés par spectroscopie RMN du ^1H, du ^{13}C et du ^{195}Pt et par spectrométrie de masse avec électronébulisation. On a préparé les rotaxanes en faisant réagir les pseudorotaxanes $\{NH_2(CH_2)_nHN_2{\cdot}\alpha\text{-}CD\}$ avec du [Pt(dien)]Cl pour bloquer les chaînes linéaires α,ω-diaminoalcanes incluses avec des groupes terminaux Pt(II) inactifs. Faisant appel à la RMN du ^1H, on a étudié la cinétique de l'autoassemblage et de la dissociation du β-CD rotaxane, $[(dien)Pt\{NH_2(CH_2)_{10}NH_2{\cdot}\beta\text{-}CD\}Pt(dien)]^{4+}$ et les résultats suggèrent l'existence d'un mécanisme de glissement en raison des tailles comparables de la cavité de la β-CD et du groupe terminal $[Pt(dien)]^+$. Une faible inclusion du groupe terminal dans la cavité de la β-CD précède un passage favorisé par la chaleur de la β-CD par-dessus le groupe terminal $[Pt(dien)]^+$ et sur la chaîne polyméthylène hydrophobe du ligand qui assure le pont du filament.

Mots clés : rotaxanes, pseudorotaxanes, cyclodextrine, complexes du platine, mécanisme de glissement.

[Traduit par la Rédaction]

Introduction

Cyclodextrins (CD) (1) are a homologous family of cyclic oligosaccharides that are constructed of α-(1→4)-linked glucopyranose units (1–5). The three most common cyclodextrins consist of six (α-CD), seven (β-CD), and eight (γ-CD) monosaccharide subunits, and in terms of molecular architecture can be viewed as toroidal baskets. This intrinsic cyclic nature enables them to function as hosts in the formation of inclusion complexes, and thus they have found widespread medicinal applications as carriers of pharmaceuticals and biochemicals (6). Cyclodextrins are also widely employed as the cyclic component in the syntheses of rotaxanes (7, 8), which are supramolecular complexes (9) in which this cyclic bead is threaded by a linear chain that is terminated by bulky organic or transition-metal-complex stopper groups to prevent dissociation. Several mechanisms for the formation of metal-complex-stoppered [2]rotaxanes of cyclodextrins ($[L_5M\{L—L{\cdot}CD\}ML_5]^{2n+}$) have been identified. The *threading* process involves the attachment of bulky metal complexes (ML_5^{n+}) to donor atoms on each end of the linear thread (L—L) of a preassembled pseudorotaxane (10–14). Alternatively, if the bond between the metal center and the thread donor atom is sufficiently labile, the dissociation of one metal center of a bridged dimer complex ($[L_5M\{L—L{\cdot}CD\}ML_5]^{2n+}$), followed by inclusion of the bridging ligand in the CD cavity, would yield a semirotaxane species ($[L_5M\{L—L{\cdot}CD\}]^{n+}$). The recomplexation of the terminal donor atom by the metal center would yield the [2]rotaxane. We have reported the employment of both methods in the self-assemblies of a series of stable α-cyclodextrin rotaxanes of the types $[(NC)_5Fe\{R(CH_2)_nR{\cdot}\alpha\text{-}CD\}Fe(CN)_5]^{4-}$ (R = 4,4′-bipyridine and (or) pyrazine, and 3- and 4-cyanopyridine) (15–18) and $[[(NC)_5Fe\{pyRpy{\cdot}\alpha\text{-}CD\}Fe(CN)_5]^{6-}$ (pyRpy is a neutral bis(4-pyridyl) ligand such as 4-azopyridine) in aqueous solution (19, 20).

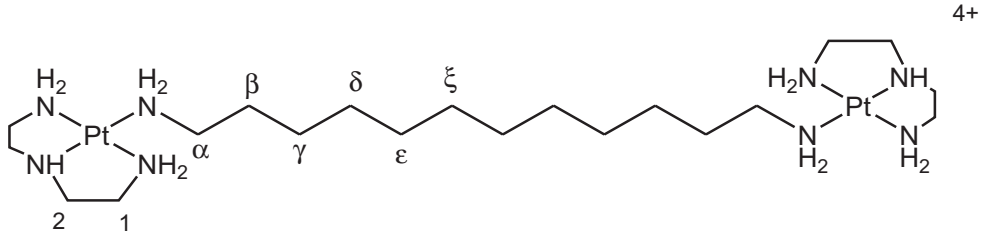
Received 17 August 2005. Published on the NRC Research Press Web site at http://canjchem.nrc.ca on 7 February 2006.

V.X. Jin, D.H. Macartaney,[1] and E. Buncel. Department of Chemistry, Queen's University, Kingston, ON K7L 3N6, Canada.

[1]Corresponding author (e-mail: donal@chem.queensu.ca).

 doi: 10.1139/V05-226 © 2005 NRC Canada

Scheme 1. Structure and proton labeling scheme for $[(dien)Pt(NH_2(CH_2)_{12}NH_2)Pt(dien)]^{4+}$.



When the cavity of the cyclodextrin and the diameter of the metal complex are closely matched in size, the threading of the cyclic component may only occur efficiently at elevated temperatures (21, 22), using a method of preparing rotaxanes termed *slippage* (23). We have used this mechanism for the assembly of a number of α-cyclodextrin rotaxanes with dicationic organic threads $R(CH_2)_nR^{2+}$ (R = NR_3^+, $P(CH_3)_3^+$, 4-*tert*-butylpyridinium, and 4-(α-alkyl-α-methanolpyridinium), and n = 8–12) (24–26). The application of this method to the synthesis of a cyclodextrin [2]rotaxane of β-cyclodextrin, for example, would require an end unit that is comparable in size to the 7.0 Å diameter of the β-cyclodextrin cavity. While octahedral metal centers, such as substituted pentacyanoferrate(II), are typically too large to pass through β-CD, a square-planar coordination geometry at the metal center, such as platinum(II), might permit a slippage process to occur. Cyclodextrin inclusion complexes with mononuclear platinum(II) complexes such as $Pt(P(CH_3)_3)(NH_3)Cl_2$ have been reported by Stoddart and co-workers (27, 28). Dinuclear platinum complexes with bridging α,ω-diaminoalkane linkers, $[\{cis\text{-}PtCl(NH_3)_2\}_2\{\mu\text{-}NH_2(CH_2)_nNH_2\}]^{2+}$, constitute a class of compounds displaying novel DNA-binding properties and high activity in vitro and in vivo against tumor cell lines resistant to cisplatin (29). This activity, however, is accompanied by high toxicity. Other cyclic molecular hosts, such as cucurbiturils, have been proposed (30) and investigated (31, 32) for the encapsulation of dinuclear platinum antitumor agents, to reduce toxicity through slow release and hindered access. Based on the potential medical applications of cyclodextrins for platinum complexes and on an interest in expanding the library of metal complex rotaxane stoppers with different coordination geometries, we have been investigating the syntheses and the kinetics and mechanisms of the assembly and dissociation of cyclodextrin [2]rotaxanes with α,ω-diaminoalkane threads and platinum(II) stoppers with different spectator ligands. We have shown that with a stopper such as (ethylenediamine)(pyridine)platinum(II), the pyridine can act as a "hook" in preventing the dissociation of the cyclodextrin [2]rotaxanes.[2] In this paper, the (diethylenetriamine)platinum(II) center has been employed to stopper α- and β-cyclodextrin [2]rotaxanes, using $NH_2(CH_2)_nNH_2$ (n = 8, 9, 10, and 12) bridging ligands as the threads (Scheme 1).

A series of dinuclear platinum(II) complexes, $[(dien)Pt(NH_2(CH_2)_nNH_2)Pt(dien)]Cl_4$ (**1**–**4**), and their corresponding [2]rotaxanes with α-cyclodextrin (α-CD), $[(dien)Pt\{NH_2(CH_2)_nNH_2\cdot\alpha\text{-}CD\}Pt(dien)]Cl_4$ (**1**α–**4**α), have been synthesized and characterized by ^1H, ^{13}C, and ^{195}Pt NMR spectroscopy and electrospray mass spectrometry. The results of a kinetic investigation of the thermally promoted self-assembly and dissociation of the β-cyclodextrin [2]pseudorotaxane with the $[(dien)Pt(NH_2(CH_2)_{10}NH_2)\text{-}Pt(dien)]^{4+}$ ion are described in terms of a *slippage* mechanism.

Experimental section

Materials

α- and β-Cyclodextrins (Aldrich) were dried at 80 °C under reduced pressure for at least 10 h prior to use. Potassium tetrachloroplatinate(II), diethylenetriamine, 1-adamantanecarboxylic acid, 1,8-diaminooctane, 1,9-diaminononane, 1,10-diaminodecane, and 1,12-diaminododecane (Aldrich) were used as received. Chloro(diethylenetriamine)platinum(II) chloride, [Pt(dien)Cl]Cl, was prepared by literature methods (33, 34).

Preparation of dinuclear platinum complexes

[(dien)Pt(NH$_2$(CH$_2$)$_n$NH$_2$)Pt(dien)]Cl$_4$ (1–4)

The complexes were prepared by stirring a mixture of 1 mmol of the appropriate α,ω-diaminoalkane and 2 mmol of chloro(diethylenetriamine)platinum(II) chloride in 15 mL of distilled water for 4 h at 50 °C. The solutions were reduced in volume to less than 5 mL and cooled. The products were precipitated by adding 15 mL of ethanol, and white crystals were obtained upon recrystallization from 95% ethanol.

[(dien)Pt(NH$_2$(CH$_2$)$_8$NH$_2$)Pt(dien)]Cl$_4$ (1)

Yield: 0.758 g (86%). ^1H NMR (D_2O, ppm) δ: 3.2–2.6 (m, 16H, $H_{1,2}$), 2.56 (t, 4H, H_α), 1.53 (m, 4H, H_β), 1.24 (m, 8H, $H_{\gamma-\delta}$). ^{13}C NMR (D_2O, ppm) δ: 53.65 (C_1), 50.80 (C_2), 47.26 (C_α), 31.07 (C_β), 28.75 (C_γ), 26.15 (C_δ). ^{195}Pt NMR (D_2O, ppm) δ: –2936.

[(dien)Pt(NH$_2$(CH$_2$)$_9$NH$_2$)Pt(dien)]Cl$_4$ (2)

Yield: 0.744 g (83%). ^1H NMR (D_2O, ppm) δ: 3.2–2.6 (m, 16H, $H_{1,2}$), 2.50 (t, 4H, H_α), 1.48 (m, 4H, H_β), 1.17 (m, 10H, $H_{\gamma-\varepsilon}$). ^{13}C NMR (D_2O, ppm) δ: 53.31 (C_1), 50.46 (C_2), 46.93 (C_α), 30.74 (C_β), 28.58 (C_γ), 28.43 (C_ε), 26.15 (C_δ). ^{195}Pt NMR (D_2O, ppm) δ: –2932.

[(dien)Pt(NH$_2$(CH$_2$)$_{10}$NH$_2$)Pt(dien)]Cl$_4$ (3)

Yield: 0.791 g (87%). ^1H NMR (D_2O, ppm) δ: 3.2–2.6 (m, 16H, $H_{1,2}$), 2.56 (t, 4H, H_α), 1.53 (m, 4H, H_β), 1.22 (m, 12H, $H_{\gamma-\varepsilon}$). ^{13}C NMR (D_2O, ppm) δ: 53.56 (C_1), 50.72 (C_2), 45.57 (C_α), 31.06 (C_β), 29.01 (C_γ), 28.85 (C_ε), 26.15 (C_δ). ^{195}Pt NMR (D_2O, ppm) δ: –2937.

[2] V.X. Jin, D.H. Macartney, and E. Buncel. Submitted for publication.

© 2005 NRC Canada

[(dien)Pt(NH$_2$(CH$_2$)$_{12}$NH$_2$)Pt(dien)]Cl$_4$ (4)

Yield: 0.750 g (80%). ^{1}H NMR (D_2O, ppm) δ: 3.2–2.6 (m, 16H, $H_{1,2}$), 2.57 (t, 4H, H_α), 1.53 (m, 4H, H_β), 1.22 (m, 16H, $H_{\gamma-\xi}$). ^{13}C NMR (D_2O, ppm) δ: 53.18 (C_1), 50.34 (C_2), 46.81 (C_α), 30.67 (C_β), 28.74 (C_γ), 28.47 (C_ε), 25.80 (C_δ), 20.97 (C_ξ). ^{195}Pt NMR (D_2O, ppm) δ: –2937.

Preparation of α-CD rotaxanes of dinuclear platinum complexes

[(dien)Pt{NH$_2$(CH$_2$)$_n$NH$_2$·α-CD}Pt(dien)]Cl$_4$ (1α–4α)

The rotaxane complexes were prepared by mixing 1 mmol of the α,ω-diaminoalkane with 2 mmol of α-CD in 20 mL of distilled water for 30 min at 40 °C, followed by adding 2 mmol of chloro(diethylenetriamine)platinum(II) chloride and stirring for at least 4 h. The volume of the solution was reduced to less than 5 mL, and the product was precipitated by adding 20 mL of ethanol to the cooled reaction solution. Pale yellow crystals were obtained upon recrystallization from 95% ethanol.

1α, n = *8*

Yield: 1.39 g (75%). ^{1}H NMR (D_2O, ppm) δ: 5.01 (d, 6H, H_1(CD)), 3.90–3.75 (m, 24H, H_3, H_5, H_6(CD)), 3.65–3.50 (m, 12H, H_2, H_4(CD)), 2.9–2.7 (m, 16H, $H_{1,2}$), 2.57 (t, $H_{\alpha'}$), 2.50 (t, H_α), 1.59 (t, $H_{\beta'}$), 1.47 (t, H_β), 1.39 (m, $H_{\gamma-\delta}$). ^{195}Pt NMR (D_2O, ppm) δ: –2942. ES-MS *m/z*: 428.2 ([M]$^{4+}$, 100), 582.3 ([M + Cl]$^{3+}$, 20), 890.9 ([M + 2Cl]$^{2+}$, 10).

2α, n = *9*

Yield: 1.36 g (73%). ^{1}H NMR (D_2O, ppm) δ: 5.00 (d, 6H, H_1(CD)), 3.90–3.75 (m, 24H, H_3, H_5, H_6(CD)), 3.65–3.50 (m, 12H, H_2, H_4(CD)), 2.9–2.7 (m, 16H, $H_{1,2}$), 2.60 (t, $H_{\alpha'}$), 2.50 (t, H_α), 1.62 (t, $H_{\beta'}$), 1.50 (t, H_β), 1.37 (m, $H_{\gamma-\varepsilon}$). ^{195}Pt NMR (D_2O, ppm) δ: –2940. ES-MS *m/z*: 431.9 ([M]$^{4+}$, 95), 587.7 ([M + Cl]$^{3+}$, 65), 899.4 ([M + 2Cl]$^{2+}$, 10).

3α, n = *10*

Yield: 1.43 g (74%). ^{1}H NMR (D_2O, ppm) δ: 5.00 (d, 6H, H_1(CD)), 3.90–3.75 (m, 24H, H_3, H_5, H_6(CD)), 3.65–3.50 (m, 12H, H_2, H_4(CD)), 2.9–2.7 (m, 16H, $H_{1,2}$), 2.60 (t, $H_{\alpha'}$), 2.51 (t, H_α), 1.60 (t, $H_{\beta'}$), 1.50 (t, H_β), 1.37 (m, $H_{\gamma-\varepsilon}$). ^{195}Pt NMR (D_2O, ppm) δ: –2943. ES-MS *m/z*: 435.1 ([M]$^{4+}$, 100), 592.0 ([M + Cl]$^{3+}$, 20), 905.7 ([M + 2Cl]$^{2+}$, 10).

4α, n = *12*

Yield: 1.35 g (71%). ^{1}H NMR (D_2O, ppm) δ: 4.98 (d, 6H, H_1(CD)), 3.90–3.75 (m, 24H, H_3, H_5, H_6(CD)), 3.65–3.50 (m, 12H, H_2, H_4(CD)), 2.9–2.7 (m, 16H, $H_{1,2}$), 2.58 (t, $H_{\alpha'}$), 2.50 (t, H_α), 1.57 (t, $H_{\beta'}$), 1.45 (t, H_β), 1.34 (m, $H_{\gamma-\xi}$). ^{195}Pt NMR (D_2O, ppm) δ: –2942. ES-MS *m/z*: 442.4 ([M]$^{4+}$, 100), 601.2 ([M + Cl]$^{3+}$, 20), 919.5 ([M + 2Cl]$^{2+}$, 10).

Physical measurements

The ^{1}H NMR kinetic measurements and chemical shift titrations were performed on Bruker Avance-400 and Avance-500 instruments in D_2O (the residual solvent proton signal served as the reference), with the NMR probe temperature maintained to within ±0.5 °C. The ^{195}Pt NMR spectra were recorded on the Avance-400 instrument in D_2O, using K_2PtCl_4 as the external reference at –1620 ppm. In the kinetics experiments on the formation of the [2]rotaxane, a weighed amount of dried β-CD (1–10 mg) was directly added to a 5 mm NMR tube containing a thermostatted solution of the dinuclear [(dien)Pt(NH$_2$(CH$_2$)$_{10}$NH$_2$)Pt(dien)]$^{4+}$ complex (1.0 mmol/L) in D_2O (0.05 mol/L NaCl). Spectra were collected at fixed time intervals for at least four half-lives and then again after 10–15 half-lives until an equilibrium was reached. The concentration of the threaded molecules [L·CD] formed from the guest (L) and host (CD) was determined by integrating the H_β resonances of the alkyl chain of the guest. The plots of $\ln\{([L\cdot CD]_e - [L\cdot CD]_0)/([L\cdot CD]_e - [L\cdot CD]_t)\}$ against time were linear for at least 3 half-lives, with the slopes from the linear regressions yielding rate constants with error limits in the range of 3%–7%. For the kinetics of dissociation of the [2]pseudorotaxane, a weighed amount (11.5 mmol/L) of a competing guest, 1-adamantanecarboxylic acid (35), was added to the equilibrated solution of the [2]pseudorotaxane [(dien)Pt{NH$_2$-(CH$_2$)$_{10}$NH$_2$-β-CD}Pt(dien)]$^{4+}$ (prepared by equilibrating a mixture of 1.0 mmol/L [(dien)Pt{NH$_2$(CH$_2$)$_{10}$NH$_2$}Pt-(dien)]$^{4+}$ and 3.0 mmol/L β-CD). The H_β resonance was again employed to monitor the release of the platinum(II) dimer from the CD cavity.

The mass spectrometry measurements were obtained on a VG Quattro quadrupole mass spectrometer, with an atmospheric pressure electrospray source. The samples, as solutions in distilled water, were introduced into the source at a flow rate of 5 mL min^{-1}.

Results and discussion

Syntheses

The dinuclear platinum complexes, [(dien)Pt(NH$_2$(CH$_2$)$_n$-NH$_2$)Pt(dien)]$^{4+}$, were prepared by the reaction of 2 equiv. of the monomeric chloro(diethylenetriamine)platinum(II) ion with the appropriate α,ω-diaminoalkane bridging ligand. The α-cyclodextrin [2]rotaxanes were synthesized by first mixing the α-CD with the α,ω-diaminoalkane to form pseudorotaxanes (eq. [1]).

[1] $$NH_2(CH_2)_nNH_2 + \alpha\text{-CD} \underset{}{\overset{K_{CD}}{\rightleftharpoons}} \{NH_2(CH_2)_nNH_2\cdot\alpha\text{-CD}\}$$

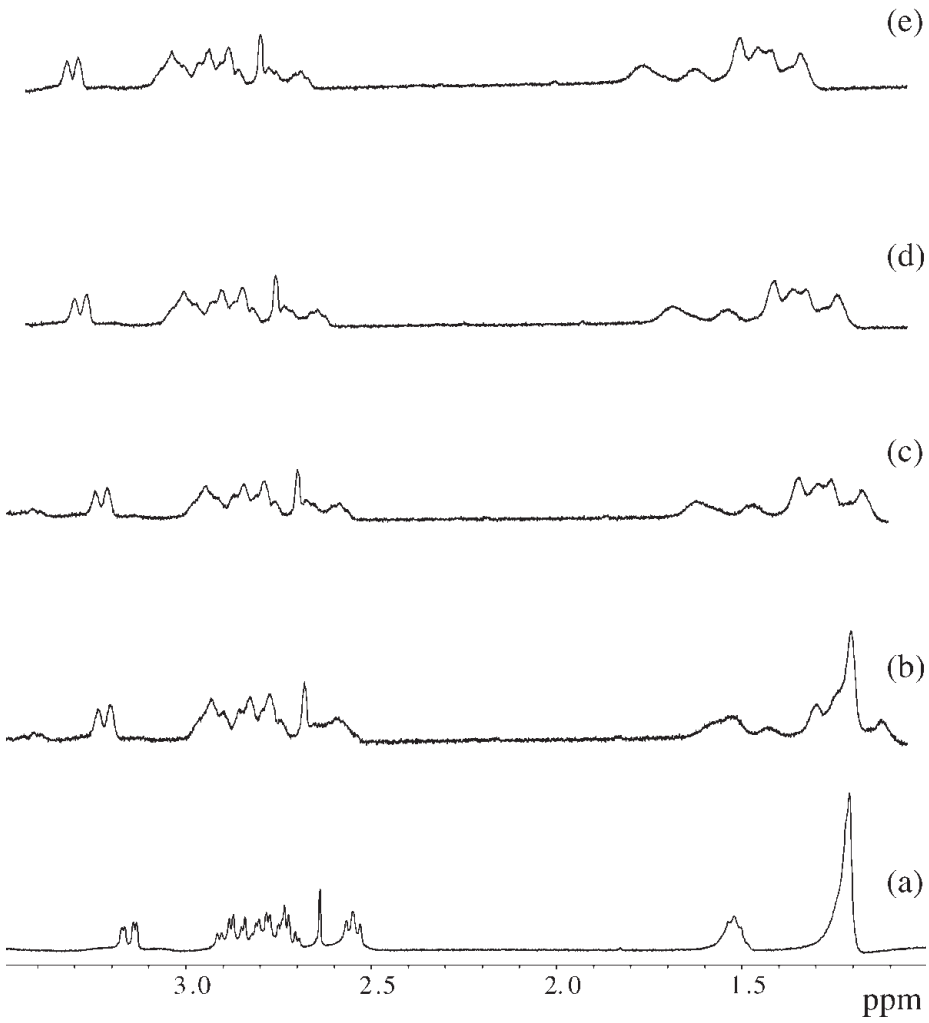
Stability constants for $\{NH_2(CH_2)_nNH_2\cdot\alpha\text{-CD}\}$ of $\log K_{CD}$ = 2.83 (n = 8), 4.13 (n = 10), and 3.85 (n = 12) have been reported previously (36). Adding 2 equiv. of the chloro(diethylenetriamine)platinum(II) ion to the pseudorotaxane at room temperature yielded the following rotaxane (eq. [2]).

[2] $$2[Pt(dien)Cl]^+ + \{NH_2(CH_2)_nNH_2\cdot\alpha\text{-CD}\} \rightarrow [(dien)Pt\{NH_2(CH_2)_nNH_2\cdot\alpha\text{-CD}\}Pt(dien)]^{4+} + 2Cl^-$$

To minimize the production of non-rotaxane dinuclear platinum complexes, it was necessary to carry out the reaction at room temperature. Purification was achieved by recrystallization from a mixture of water and ethanol. All of the complexes were characterized by ^{1}H NMR, ^{13}C NMR, ^{195}Pt NMR spectroscopy, and electrospray mass spectrome-

© 2005 NRC Canada

Fig. 1. ^{1}H NMR spectra of the formation of the [2]rotaxane [(dien)Pt{$NH_2(CH_2)_{10}NH_2$·β-CD}Pt(dien)]$^{4+}$: (*a*) the dimer [(dien)Pt(NH_2-$(CH_2)_{10}NH_2$)Pt(dien)]$^{4+}$ (1.0 mmol/L) and (*b*) 2 min, (*c*) 6 min, (*d*) 19 min, and (*e*) 345 min after mixing with β-CD (10 mmol/L) in D_2O (0.05 mol/L NaCl) at 25 °C.



try. The elemental analyses were consistent with the formation of the rotaxanes with some solvent (water or ethanol) of crystallization. The ^{195}Pt NMR resonance of all of the complexes is found at about –2942 ppm, indicating that a complex with a PtN_4 environment is formed (37, 38).

The presence of the [2]rotaxanes, [(dien)Pt{NH_2-$(CH_2)_nNH_2$·α-CD}Pt(dien)]$^{4+}$ (n = 8–10, 12), in solution were confirmed by electrospray mass spectrometry (ES-MS). In the ES-MS spectra of [(dien)Pt{$NH_2(CH_2)_nNH_2$·α-CD}Pt(dien)]$^{4+}$, signals were observed for the parent molecular ion and for the chloride adducts [(dien)Pt{$NH_2(CH_2)_n$-NH_2·α-CD}Pt(dien)]Cl^{3+} and [(dien)Pt{$NH_2(CH_2)_nNH_2$·α-CD}Pt(dien)]Cl_2^{2+}.

Slippage mechanism

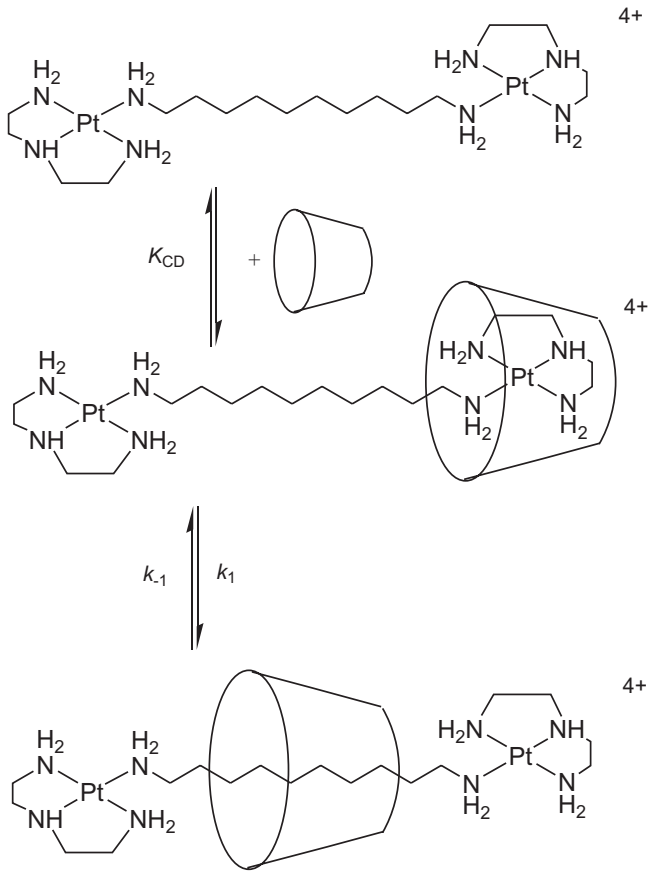
The slippage mechanism was investigated with the dinuclear platinum compound [(dien)Pt{$NH_2(CH_2)_{10}NH_2$Pt-(dien)]$^{4+}$. The threading of linear components of the α,ω-diaminoalkane chain through the β-CD cavity to form [2]rotaxane may be followed by ^{1}H NMR spectroscopy, as the symmetry-related proton resonances of the polymethylene chains of the bridging ligand are split into pairs of peaks upon inclusion in the asymmetric cyclodextrin host. The addition of an excess of β-CD to the [(dien)Pt($NH_2(CH_2)_{10}$-NH_2)Pt(dien)]$^{4+}$ ion results in the very slow, spontaneous threading of the host by the guest molecule, as illustrated by the spectra in Fig. 1, with the splitting of the α (2.6 ppm) and β (1.6 ppm) methylene protons easiest to observe.

The slippage process may be envisaged as occurring by, first, weak and reversible inclusion of the Pt(dien)$^{2+}$ group by the β-CD cavity (Scheme 2), followed by a very slow passage over the Pt(dien)$^{2+}$ to finally position the β-CD over the hydrophobic decamethylene chain to yield the [2]rotaxane. Upon initial addition of β-CD, the resonances for the α and β protons of the methylene chain exhibit small downfield shifts. These induced chemical shifts support an inclusion preequilibrium prior to the slippage process.

The formation of the [2]pseudorotaxane, [(dien)Pt{NH_2-$(CH_2)_{10}NH_2$·β-CD}Pt(dien)]$^{4+}$, is also indicated by electrospray mass spectrometry. An aqueous solution of an equimolar (1.0×10^{-3} mol/L) mixture of two compounds exhibited three signals at m/z 475.9, consistent with

© 2005 NRC Canada

Scheme 2. Slippage mechanism for the formation of the [(dien)Pt{$NH_2(CH_2)_{10}NH_2$·β-CD}Pt(dien)]$^{4+}$ [2]rotaxane.



[(dien)Pt{$NH_2(CH_2)_{10}NH_2$·β-CD}Pt(dien)]$^{4+}$, *m/z* 646.3 for [(dien)Pt{$NH_2(CH_2)_{10}NH_2$·β-CD}Pt(dien)]Cl^{3+}, and *m/z* 987.2 for [(dien)Pt{$NH_2(CH_2)_{10}NH_2$·β-CD}Pt(dien)]Cl_2^{2+}.

The observed first-order rate constants for the slippage process increase with increasing β-CD concentration, with plots of k_{obs} vs. [β-CD] displaying curvatures towards rate saturation at high [β-CD]. Assuming that k_{-1} (Scheme 1) is negligible with respect to k_1, the observed first-order rate constant may be fit to eq. [3].

$$[3] \qquad k_{obs} = \frac{k_1 K_{CD}[\beta\text{-CD}]}{1 + K_{CD}[\beta\text{-CD}]}$$

Double reciprocal plots of k_{obs}^{-1} against $[\beta\text{-CD}]^{-1}$ have been constructed for the rate constants measured at 25, 30, 35, and 40 °C (Fig. 2), with the slopes providing the values of k_1 (Table 1) and activation parameters of $\Delta H^{\ddagger}$ = 97 ± 4 kJ mol^{-1} and $\Delta S^{\ddagger}$ = +44 ± 11 J K^{-1} mol^{-1}. The inclusion stability constant K_{CD}, determined from eq. [3], was relatively constant, ranging from 28 to 38 (mol/L)$^{-1}$ for the temperatures investigated. The kinetic and thermodynamic parameters associated with the self-assembly of the [2]pseudorotaxanes are listed in Table 1.

The kinetics of the dissociation (eq. [4]) of [(dien)Pt{$NH_2(CH_2)_{10}NH_2$·β-CD}Pt(dien)]$^{4+}$ rotaxane (0.5 mmol/L) were investigated (using ^{1}H NMR spectroscopy) in the presence of an excess (11.5 mmol/L) of a competing guest, 1-adamantanecarboxylic acid (ADCOOH).

$$[4] \qquad [(\text{dien})\text{Pt}\{NH_2(CH_2)_{10}NH_2\cdot\beta\text{-CD}\}\text{Pt}(\text{dien})]^{4+} + \text{ADCOOH} \underset{k_1}{\overset{k_{-1}}{\rightleftharpoons}} [(\text{dien})\text{Pt}(NH_2(CH_2)_{10}NH_2)\text{Pt}(\text{dien})]^{4+} + \{\text{ADCOOH}\cdot\beta\text{-CD}\}$$

Rapid and efficient capture of the released β-CD by the 1-adamantanecarboxylic acid guest (K_L = 7.8 × 10^4 (mol/L)$^{-1}$ at pH 6.5 (39)) is expected (eq. [4]) such that the observed first-order rate constant corresponds to the rate-limiting dissociation of the [(dien)Pt{$NH_2(CH_2)_{10}NH_2$·β-CD}Pt(dien)]$^{4+}$ rotaxane. At 25 °C, k_{-1} was determined to be (2.14 ± 0.3) × 10^{-5} s^{-1}, with $\Delta H^{\ddagger}$ = 93 ± 9 kJ mol^{-1} and $\Delta S^{\ddagger}$ = –23 ± 17 J K^{-1} mol^{-1}, calculated from measurements between 25 and 40 °C (Table 1).

The stability constant, K_1, for the [2]rotaxane with respect to its dissociated linear and cyclic components may be calculated from $K_1 = k_1 K_{CD}/k_{-1}$. The values are approximately 1.5 × 10^4 (mol/L)$^{-1}$ (Table 1) and exhibit little dependence on temperature. The stability constant may be compared with those for β-CD rotaxanes of the type {3CNpyr-$(CH_2)_{10}$3CNpyr·β-CD}$^{2+}$ (3CNpyr = 3-cyanopyridine, 810 ± 160 (mol/L)$^{-1}$) and {4CNpyr$(CH_2)_{10}$4CNpyr·β-CD}$^{2+}$ (4CNpyr = 4-cyanopyridine, 2020 ± 160 (mol/L)$^{-1}$) (18). The larger value for the dinuclear platinum(II) thread may be due to the higher positive charge on the end units and possible hydrogen bonding of the dien ligand with the cyclodextrin hydroxyl groups.

The result of this study indicates that the complementary sizes of the square-planar (diethylenetriamine)platinum(II) center and the cavity of the β-cyclodextrin result in a very slow threading of the cyclic component by the linear guest. The enthalpies of activation for the threading (97 ± 4 kJ mol^{-1}) and dethreading (93 ± 9 kJ mol^{-1}) processes in this study are very similar to one another, suggesting that the required distortions in the cyclodextrin and the Pt(dien)$^{2+}$ in these two slippages are nearly the same. The differences in the rates of these processes, therefore, may be related to the entropies of activation. The positive entropy of activation for the threading (k_1) of β-CD (+44 ± 11 J K^{-1} mol^{-1}) likely results from the desolvation of the cationic Pt(dien)$^{2+}$ group as it passes through the β-CD cavity. The unfavourable entropy of activation (–23 ± 17 J K^{-1} mol^{-1}) associated with k_{-1} would correspondingly result from the net resolvation of the end group as it emerges from the β-CD cavity.

The dissociation of the dinuclear platinum rotaxane com-

© 2005 NRC Canada

Fig. 2. Plots of k_{obs}^{-1} against $[\beta\text{-CD}]^{-1}$ for the formation of the $[(dien)Pt\{NH_2(CH_2)_{10}NH_2{\cdot}\beta\text{-CD}\}Pt(dien)]^{4+}$ [2]rotaxane at (●) 25 °C, (○) 30 °C, (▲) 35 °C, and (△) 40 °C.

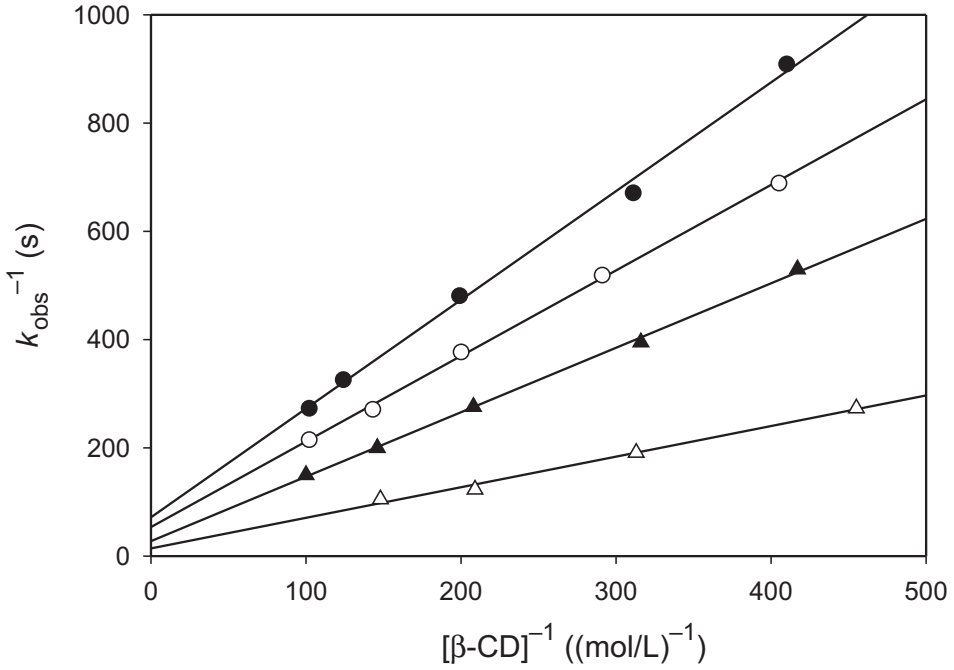


Table 1. Kinetic and thermodynamic parameters for the self-assembly and dethreading of the [2]pseudorotaxane $[(dien)Pt\{NH_2(CH_2)_{10}NH_2{\cdot}\beta\text{-CD}\}Pt(dien)]^{4+}$.

T (°C)	$10^2\ k_1$ (s^{-1})	K_{CD} ((mol/L)$^{-1}$)	$10^5\ k_{-1}$ (s^{-1})	$10^{-4}\ K_1$ ((mol/L)$^{-1}$)
25	1.05±0.10	38±4	2.14±0.20	1.8±0.2
30	1.85±0.04	34±3	3.42±0.10	1.5±0.3
35	3.71±0.08	28±5	6.12±0.30	1.7±0.1
40	7.13±0.10	29±5	13.7±0.6	1.5±0.2
$\Delta H^{\ddagger}$ (kJ mol^{-1})	97±4		93±9	
$\Delta S^{\ddagger}$ (J K^{-1} mol^{-1})	44±11		–23±17	

Note: In D_2O (I = 0.05 mol/L NaCl).

plexes may be prevented by increasing the bulk of the platinum end groups with respect to the diameter of the β-CD cavity. We are currently investigating the use of (*a*) bulkier ligand(s) on the square-planar platinum(II) center and (*b*) oxidization of the square-planar platinum(II) center to octahedral platinum(IV). In view of the demonstrated antitumor activity of platinum(IV) complexes (40), a dinuclear platinum(IV) β-CD rotaxane analogous to those described in this paper would be more inert to dissociation until its reduction to the square-planar platinum(II) oxidation state.

Acknowledgements

The authors thank the Natural Sciences and Engineering Research Council of Canada (NSERC) for financial support in the form of Discovery and Equipment Grants (DHM and EB) and Queen's University and the Ontario Ministry for Training, Colleges and Universities for graduate fellowships (VXJ). We also thank Dr. F. Sauriol for NMR technical assistance and helpful discussions.

References

1. M.L. Bender and M. Komiyama. Cyclodextrin chemistry. Springer-Verlag, Berlin. 1978.
2. J. Szejtli. Cyclodextrins and their inclusion complexes. Akademiai Kiado, Budapest. 1982.
3. J. Szejtli and T. Osa. *In* Comprehensive supramolecular chemistry. Vol. 3. *Edited by* J.L. Atwood, J.E.D. Davies, D.D. MacNicol, F. Vogtle, J. Szejtli, and T. Osa. Pergamon, Oxford. 1996.
4. K.A. Connors. Chem. Rev. **97**, 1325 (1997).
5. J. Szejtli. Chem. Rev. **98**, 1743 (1998).
6. J. Szejtli. Med. Res. Rev. **14**, 353 (1994).
7. G. Schill. Catenanes, rotaxanes, and knots. Academic Press, New York. 1971.
8. J.-P. Sauvage and C. Dietrich-Buchecker (*Editors*). Molecular catenanes, rotaxanes, and knots. Wiley-VCH, Weinheim. 1999.
9. S.A. Nepogodiev and J.F. Stoddart. Chem. Rev. **98**, 1959 (1998).
10. H. Ogino. J. Am. Chem. Soc. **103**, 1303 (1981).
11. H. Ogino and K. Ohata. Inorg. Chem. **23**, 3312 (1984).
12. H. Ogino. New J. Chem. **17**, 683 (1993).
13. R.B. Hannak, G. Farber, G. Konrat, and B. Krauter. J. Am. Chem. Soc. **119**, 2313 (1997).

© 2005 NRC Canada

14. N. Nakashima, A. Kawabuchi, and H. Murakami. J. Incl. Phen. Mol. Recogn. Chem. **32**, 363 (1998).
15. R.S. Wylie and D.H. Macartney. J. Am. Chem. Soc. **114**, 3136 (1992).
16. R.S. Wylie and D.H. Macartney. Supramol. Chem. **3**, 29 (1993).
17. C.A. Waddling and D.H. Macartney. Inorg. Chem. **33**, 5912 (1994).
18. A.P. Lyon and D.H. Macartney. Inorg. Chem. **36**, 729 (1997).
19. A.J. Baer and D.H. Macartney. Inorg. Chem. **39**, 1410 (2000).
20. V.X. Jin, D.H. Macartney, and E. Buncel. Can. J. Chem. **83**, 185 (2005).
21. I.T. Harrison. J. Chem. Soc. Chem. Commun. 231 (1972).
22. I.T. Harrison. J. Chem. Soc. Perkin Trans. 1, 301 (1974).
23. F.M. Raymo and J.F. Stoddart. Pure Appl. Chem. **69**, 1987 (1997), and refs. cited therein.
24. D.H. Macartney. J. Chem. Soc. Perkin Trans. 2, 2775 (1996).
25. A.P. Lyon, N.J. Banton, and D.H. Macartney. Can. J. Chem. **76**, 843 (1998).
26. A.C. Smith and D.H. Macartney. J. Org. Chem. **63**, 9243 (1998).
27. D.R. Alston, A.M.Z. Slawin, J.F. Stoddart, D.J. Williams, and R. Zarzycki. Angew. Chem. Int. Ed. Engl. **27**, 1184 (1988).
28. J.F. Stoddart and R. Zarzycki. R. Recl. Trav. Chim. Pay-Bas, **107**, 515 (1988) and refs. cited therein.
29. N. Farrell. *In* Platinum-based drugs in cancer therapy. *Edited by* L.R. Kelland and N.P. Farrell. Humana Press, Towowa, N.J. 2000. pp. 321–328.
30. S.Y. Jon, N. Selvapalam, D.H. Oh, J.-K. Kang, S.-Y. Kim, Y.J. Jeon, J.W. Lee, and K. Kim. J. Am. Chem. Soc. **125**, 10186 (2003).
31. N.J. Wheate, A.I. Day, R.J. Blanch, A.P. Arnold, C. Cullinane, and J.G. Collins. Chem. Commun. 1424 (2004).
32. Y.J. Young, S.-Y. Kim, Y.H. Ko, S. Sakamoto, K. Yamaguchi, and K. Kim. Org. Biomol. Chem. **3**, 2122 (2005).
33. J.H. Price, A.S. Williamson, R.F. Schramm, and B.B. Wayland. Inorg. Chem. **11**, 1280 (1972).
34. G. Annibale, M. Brandolisio, and B. Pitteri. Polyhedron, **14**, 451 (1995).
35. R.S. Wylie and D.H. Macartney. Inorg. Chem. **32**, 1830 (1993).
36. L. Avram and L.J. Cohen. J. Org. Chem. **67**, 2639 (2002).
37. T.G. Appleton, J.R. Hall, and S.F. Ralph. Inorg. Chem. **24**, 4685 (1985).
38. P.S. Pregosin. Annu. Rep. NMR Spectroscopy. **17**, 285 (1986).
39. R.I. Gelb, L.M. Schwartz, and M.R. Eftink. Bioorg. Chem. **9**, 450 (1980).
40. L.R. Kellend. *In* Cisplatin: Chemistry and biochemistry of a leading anticancer drug. *Edited by* B. Lippert. Verlag Helvetica Chimica Acta, Zurich and Wiley-VCH, New York. 1999. pp. 497–521.

© 2005 NRC Canada

Fluorinated 9-borafluorenes vs. conventional perfluoroaryl boranes — Comparative Lewis acidity

Preston A. Chase, Patricio E. Romero, Warren E. Piers, Masood Parvez, and Brian O. Patrick

Abstract: Perfluorinated 9-phenyl-9-borafluorene, **1**, is an antiaromatic analog of the well-known tris(pentafluorophenyl)borane. Spectroscopic, structural, and electrochemical studies have been performed on **1** and its Lewis base adducts with MeCN, THF, and PMe_3 with a view to assessing its comparative Lewis acid strength relative to $B(C_6F_5)_3$. For the sterically undemanding Lewis base MeCN, **1** and $B(C_6F_5)_3$ have comparable LA strengths, while for more sterically prominent THF, **1** is clearly the stronger Lewis acid (LA) based on competition experiments. We conclude that steric factors, rather than antiaromaticity, are the most important determinants in the LA strength differences between **1** and $B(C_6F_5)_3$.

Key words: boranes, Lewis acids, fluorinated compounds, heterocycles.

Résumé : Le 9-phényl-9-borafluorène perfluoré (**1**) est un analogue antiaromatique du tris(pentafluorophényl)borane bien connu. Afin d'évaluer son acidité relative à celle du $B(C_6F_5)_3$, on a effectué des études spectroscopiques, structurales et électrochimiques sur le composé **1** et sur les adduits qui résultent de sa réaction avec les bases de Lewis MeCN, THF et PMe_3. Sur la base d'expériences de compétition, on a observé que dans le cas de la base de Lewis MeCN qui n'impose pas de demandes stériques spéciales, les forces des acides de Lewis du composé **1** et du $B(C_6F_5)_3$ sont comparables alors que, avec le THF qui impose des contraintes stériques plus grandes, l'acidité de Lewis du composé **1** est nettement plus grande. On en conclut que les facteurs stériques, plutôt que l'antiaromaticité, sont plus importants dans la détermination des différences des forces d'acidité de Lewis entre le composé **1** et le $B(C_6F_5)_3$.

Mots clés : boranes, acides de Lewis, composés fluorés, hétérocycles.

[Traduit par la Rédaction]

Introduction

Highly fluorinated aryl boranes are an important class of Lewis acids because of their high thermal stability, resistance to hydrolysis, and Lewis acid strength (1). Although they have been known for many years (2), their application as activators for single-site olefin polymerization catalysts (3) has sparked interest in defining other applications in areas as diverse as organic synthesis (4), weakly coordinating anion development (5), and cationic polymerization initiation (6). Since Lewis acid strength is related to the effectiveness of the boranes in many of these applications (7), efforts to modulate the Lewis acid properties of the parent tris(pentafluorophenyl)borane have utilized several strategies, including the use of larger, more fluorinated aryl groups (8) and the replacement of one C_6F_5 group with poorly π-donating but electronegative substitutents like $-NC_4H_4$ (9). In some instances, weakening the Lewis acid strength by substitution with nonfluorinated aryl groups is beneficial for a given application (10). It is thus clear that the ability to modulate Lewis acid strength is beneficial for the applications of this family of boranes.

One intriguing strategy for increasing the Lewis acid strength of $B(C_6F_5)_3$ without drastically elevating the steric imposition of the aryl groups about boron is to incorporate the boron center into an antiaromatic ring framework. Using this strategy, we and Marks and co-workers (11) independently prepared the perfluorinated 9,10-diboraanthracene Lewis acid shown in Chart 1. Marks found it to be an exceptionally strong Lewis acid (12), eclipsing $B(C_6F_5)_3$ in competition experiments with low-steric-demand Lewis bases like acetonitrile. In fact, the second boron center is also highly Lewis acidic in these compounds, often performing independently from the first. Taking a cue from early work on boroles by Eisch et al. (13), we developed a second family of antiaromatic perfluoroaryl boranes, the 9-borafluorene compounds **1** and **2** (14) (Chart 1), a closer structural analog of the parent $B(C_6F_5)_3$. A detailed study on the coordination chemistry of compounds **1** and **2** with the unusual Lewis base "Cp*Al^I" showed that they exhibit chemical behavior that is more borane-like than borole-like (15); that is, compounds **1** and **2** coordinate the aluminum Lewis base in an η^1 fashion, rather than undergoing two-electron reduction to give higher hapticity π complexes. Here we show that these reactivity patterns can be extended to more conventional Lewis bases and discuss the relative LA strength of **1** relative to the parent borane $B(C_6F_5)_3$. Structural, competition,

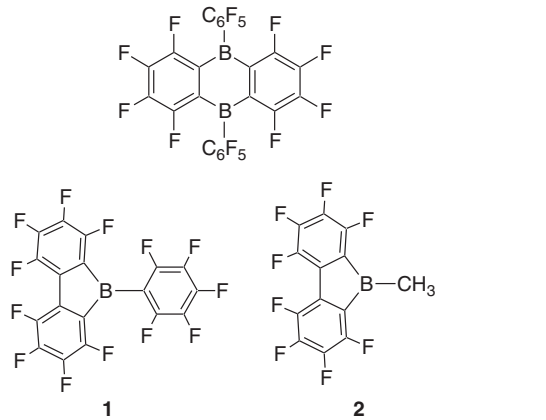
Received 11 August 2005. Published on the NRC Research Press Web site at http://canjchem.nrc.ca on 10 February 2006.

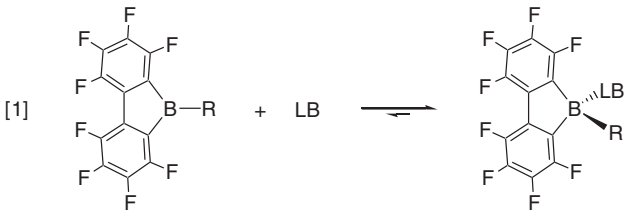
P.A. Chase, P.E. Romero, W.E. Piers,[1] and M. Parvez. Department of Chemistry, University of Calgary, 2500 University Drive N.W., Calgary, AB T2N 1N4, Canada.
B.O. Patrick. Department of Chemistry, University of British Columbia, 2036 Main Mall, Vancouver, BC V6T 1Z1, Canada.

[1]Corresponding author (e-mail: wpiers@ucalgary.ca).

 doi: 10.1139/V05-240 © 2005 NRC Canada

Chart 1.





and electrochemical studies suggest that steric factors dominate in determining the relative Lewis acidity in these compounds and that the antiaromaticity of **1** is not a significant progenitor of its high Lewis acidity.

Results and discussion

The pentafluorophenyl (**1**) and methyl (**2**) 9-borafluorene derivatives were prepared as previously reported (14) and reacted with the sterically differentiated but comparably basic (16) Lewis bases acetonitrile (MeCN) and tetrahydrofuran (THF) and the stronger base trimethylphosphine (PMe_3) to form 1:1 Lewis acid – Lewis base adducts (eq. [1]). In the case of MeCN and THF, an excess of base was used, while for PMe_3 near stoichiometric amounts were employed. In all cases, the compounds **1·LB** and **2·LB** were isolated in good yields as solids simply by removal of the solvent in vacuo. Immediately upon introduction of the Lewis base (LB), orange solutions of **1** and lime green solutions of **2** decolorized, as coordination of the Lewis base disrupted the strong π–π transition involving the low-lying boron-based LUMO, which is responsible for the colors in **1** and **2**. Lewis base coordination fills this orbital, and the LUMO is now a higher energy formally π* orbital; the increase in the energy gap causes the absorption to shift out of the visible range. Similar behavior has been observed in unfluorinated 9-borafluorenes, which have been employed as colourimetric sensors for fluoride ions (17). Although labile (vide infra), the equilibria strongly favor the adducts **1·LB** and **2·LB**; for the stronger Lewis acid **1**, adducts **1·LB** do not relinquish their Lewis bases even with gentle heating under vacuum. All were formed as analytically pure, colorless solids that could be fully characterized using standard methods.

Upon complexation, resonances in the ^{1}H NMR spectra for the coordinated bases in **1·LB** shift downfield significantly; for example, the resonance for the methyl group of the MeCN base in **1·MeCN** shifts to 2.66 ppm vs. 2.10 ppm for free MeCN (18) as electron density is removed by the Lewis acid. For **2·MeCN**, the opposite trend is observed for the B–Me signal, which shifts upfield by 0.7 ppm upon complexation. In the ^{19}F NMR spectra of **1·LB**, similar effects to those observed in the adducts of $B(C_6F_5)_3$ are exhibited: namely, a contraction of the chemical shift difference between the *para*- and *meta*-fluorines ($\Delta\delta_{p,m}$) (19). In $B(C_6F_5)_3$, this value is approximately 18 ppm in noncoordinating solvents, but upon treatment with acetonitrile a value of 8.4 ppm is found (20). The changes observed in **1·MeCN** vs. free **1** indicate that the $\Delta\delta_{p,m}$ value in the -C_6F_5 ring goes from 14.7 to 6.4 ppm upon complexation of MeCN. Upfield shifts of varying severity are also observed in the fluorines of the borafluorene framework and analogous patterns are revealed in the THF and PMe_3 adducts.

The ^{11}B NMR spectra also show a distinct difference between the tricoordinate, base-free Lewis acids and the tetracoordinated adducts (21). In the case of the free acids, the ^{11}B NMR chemical shift for the synthesized 9-borafluorene derivatives ranges from δ 56.0 to δ 67.3. In general, the range in ^{11}B chemical shift for tetrahedral boron occurs at much higher field than related tricoordinate systems. The ^{11}B NMR chemical shifts for the adducts of **1·LB** and **2·LB** occur between δ 8.6 and δ –15.2 ppm. Both **1·PMe$_3$** and **2·PMe$_3$** exhibit coupling in the ^{11}B NMR spectra (δ –14.2 and –11.4, $^1J_{B\text{-}P}$ = 87 and 66 Hz, respectively).

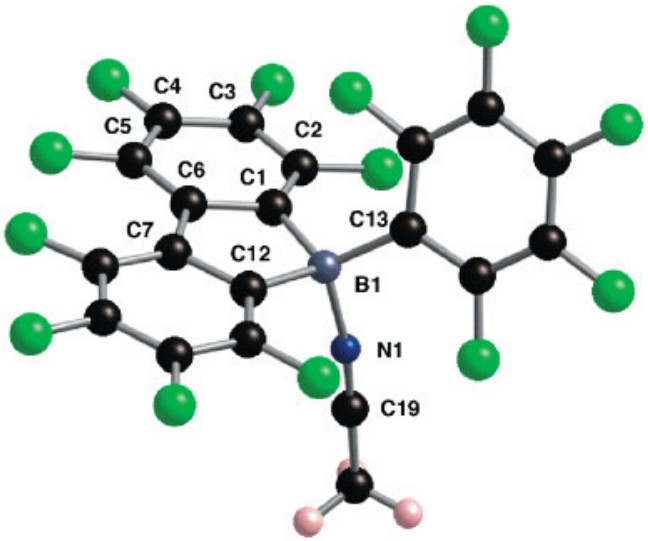
The IR spectra of both **1·MeCN** and **2·MeCN** were recorded, and a diagnostic band for the C≡N stretching mode was observed at 2361 and 2364 cm^{-1}, respectively, similar to that observed for the $B(C_6F_5)_3$ adduct ($\nu_{C\equiv N}$ = 2367 cm^{-1}). The frequency of the C≡N stretching mode for the free base is found at significantly lower wavenumbers ($\nu_{C\equiv N}$ = 2253 cm^{-1}), indicative of a weaker carbon–nitrogen bond compared with that in the adducts. As the donor orbital of MeCN has slight antibonding character with respect to the CN linkage, complexation will remove some of the electron density from this orbital, which will strengthen the CN bond and result in the observed shift in $\nu_{C\equiv N}$ (20).

A crystal structure of **1·MeCN** was obtained, and a view with selected metrical data is presented in Fig. 1 (see also Table 1).[2] Compared to the structure of **1**, there is elongation

[2] Supplementary data for this article are available on the journal Web site (http://canjchem.nrc.ca) or may be purchased from the Depository of Unpublished Data, Document Delivery, CISTI, National Research Council Canada, Ottawa, ON K1A 0R6, Canada. DUD 4074. For more information on obtaining material refer to http://cisti-icist.nrc-cnrc.gc.ca/irm/unpub_e.shtml. CCDC 280874, **1·MeCN** and 280873, $[Cp^*_2Co]^+[\mathbf{1{\cdot}Cl}]^-$ contain the crystallographic data for this manuscript. These data can be obtained, free of charge, via www.ccdc.cam.ac.uk/conts/retrieving.html (Or from the Cambridge Crystallographic Data Centre, 12 Union Road, Cambridge CB2 1EZ, UK; fax +44 1223 336033; or deposit@ccdc.cam.ac.uk).

© 2005 NRC Canada

Fig. 1. Crystalmaker model of the molecular structure of **1·MeCN** with atom labeling scheme. Selected bond lengths (Å): B(1)—N(1) 1.581(3), B(1)—C(1) 1.620(3), B(1)—C(12) 1.612, B(1)—C(13) 1.617(3), N(1)—C(19) 1.133(3), C(1)—C(2) 1.366(3), C(1)—C(6) 1.413(3), C(2)—C(3) 1.384(3), C(3)—C(4) 1.364(3), C(4)—C(5) 1.384(3), C(5)—C(6) 1.389(3), C(6)—C(7) 1.481(3). Selected bond angles (°): C(1)-B(1)-N(1) 106.5(2), C(1)-B(1)-C(12) 98.8(2), B(1)-N(1)-C(19) 171.0(2), C(1)-C(6)-C(7)-C(12) 1.6(2).



of the B—C bonds in both the C_6F_5 ring and the 9-borafluorene fragment. In **1·MeCN**, B(1)—C(1), B(1)—C(12), and B(1)—C(13) are 1.620(3), 1.612(3), and 1.617(3) Å, respectively (cf. 1.555(4) and 1.547(3) Å, respectively, for the analogous bonds in **1**). This is the result of the rehybridization of the boron from sp^2 to sp^3 and the increase in coordination number. The N(1)-B(1)-C(1) and N(1)-B(1)-C(13) angles are 106.5(2)° and 110.2(2)°, respectively, indicative of a distorted tetrahedral environment about boron. The internal angle in the 9-borafluorene is even more compressed than in the free acid; the C(1)-B(1)-C(12) angle is 98.8(2)°, compared with 103.5(2)°. The MeCN base has remained linear (N(1)-C(19)-C(20) = 179.1(2)°) and is bonded in an essentially linear orientation with the boron center. The B(1)-N(1)-C(19) angle is 171.0(2)°, and the acetonitrile methyl group is oriented slightly over the 9-borafluorene ring. The B(1)—N(1) distance (1.581(3) Å) and the C≡N triple bond (N(1)—C(19) = 1.133(3) Å) are quite close to those observed in the MeCN adduct of $B(C_6F_5)_3$ reported by Erker and co-workers (20) (for the equivalent bonds, the B—N and C—N distances are 1.616(3) and 1.124(3) Å, respectively). The same group has performed an accurate determination of the crystal structure of free acetonitrile using a Laser zone melting apparatus (22). From this, the bond length of the C≡N triple bond (α phase, T = 208 K) was found to be 1.141(2) Å. Thus, there is a measurable contraction of the C≡N bond upon complexation in both cases. This correlates with the observed bond strengthening in the IR spectra of **1·MeCN** as the $\nu_{C\equiv N}$ band shifts to considerably higher wavenumbers.

In the case of the structure of base free **1**, Marks and co-workers (12) noted a small but statistically relevant elongation of one of the aryl C=C bonds in the 9-borafluorene framework, namely the C=C bond of the five-membered core ring. This result was also noted in the structures of perfluorinated 9,10-diphenyl-9,10-diboranthracene (11) and 1,2-bis[bis(pentafluorophenyl)boryl] tetrafluorobenzene (11*b*, 23). This effect is also apparent in the adduct, **1·MeCN**. The bond lengths for C(1)—C(6) and C(7)—C(12) are 1.413(3) and 1.415(3) Å, respectively, while the average of the remaining bonds is 1.376(3) Å. The difference in the bond lengths is similar to those observed in the aforementioned cases.

Table 1. Summary of data collection and structure refinement details for **1·MeCN** and **$[Cp^*_2Co]^+[1\cdot Cl]^-$**.

	1·MeCN	**$[Cp^*_2Co]^+[1\cdot Cl]^-$**
Formula	$C_{26}H_9BF_{13}N$	$C_{38}H_{30}F_{13}BClCo$
fw	593.15	838.83
Temperature (K)	198.2	170.15
Crystal size (mm^3)	0.006 3	0.028
λ (Å)	0.710 69	0.710 69
Crystal system	Triclinic	Triclinic
Space group	$P\bar{1}$(#2)	$P\bar{1}$(#2)
a (Å)	8.967 5(9)	13.597(3)
b (Å)	11.599 8(8)	13.678(3)
c (Å)	12.026 4(8)	9.927 5(11)
α (°)	108.632(3)	90.641(15)
β (°)	102.337(3)	90.757(13)
γ (°)	92.938(5)	103.348(16)
V ($Å^3$)	1148.2(2)	1796.0(6)
Z	2	2
Reflections	8855	6647
Unique reflections	3822	6357
No. of variables	370	487
R_1	0.035	0.050
wR_2	0.050	0.049
GoF	1.18	2.09

In our original communication, we noted that **1** exhibits LA strength comparable with that of $B(C_6F_5)_3$ by both the Childs method (24) and that of Laszlo and Teston (25), which uses the relative energies of the π* orbital of LA-complexed crotonaldehyde to assess LA strength. Furthermore, in a competition experiment for the sterically undemanding MeCN, we found a slight preference for **1·MeCN** over MeCN·$B(C_6F_5)_3$, the equilibrium constant being 1.3 at 25 °C. This preference is further emphasized when the sterically more bulky base THF is used in this experiment. Thus, when a 1:1:1 mixture of **1**, $B(C_6F_5)_3$, and THF in d_8-toluene was analyzed by ^1H and ^{19}F NMR spectroscopy, it was found that the equilibrium lies completely towards **1·THF** within the detection limits of NMR spectroscopy. Remarkably, even though $B(C_6F_5)_3$ is known to form a stable, isolable complex with THF, in a competitive situation, **1** dominates the competition for this Lewis base. That this is a thermodynamic preference is illustrated by the fact that identical results are obtained when equilibrium is approached from either side of the equation and by EXSY NMR experiments in the MeCN system, which show that the acetonitriles coordinated to both Lewis acids are exchanging with each other on this timescale. Unfortunately, similar competition experiments using PMe_3 were precluded by the

© 2005 NRC Canada

nearly total insolubility of the $Me_3P{\cdot}B(C_6F_5)_3$ adduct in common solvents (1).

The rather marked dependence of the relative LA strength on the steric properties of the Lewis base employed suggests that the differences in Lewis acidity observed between **1** and $B(C_6F_5)_3$ are grounded in steric factors, rather than the fact that **1** exhibits antiaromaticity. Indeed, a comparison between the bond lengths associated with the borafluorene moiety in **1** vs. **1·MeCN** shows that little change in the C—C distances is observed upon complexation of the base. This suggests that the π character of the ring framework is not perturbed significantly, i.e., the system does not become more aromatic (or less antiaromatic) as the base coordinates the boron center. Accordingly, the Julg *A* values (26) (a measure of aromaticity based on metrical bond distances (27)) for both the five- and six-membered rings do not change significantly in **1·MeCN** vs. **1**. In fact, while the *A* values for the flanking six-membered rings remain essentially the same, at 0.96 and 0.97 in **1** and **1·MeCN**, respectively,[3] the *A*(5) value for **1·MeCN** is actually less (0.89) than that for uncomplexed **1** (0.92). The *A*(5) value in **1·MeCN** is comparable to that of 0.88 observed by West and co-workers (27*b*) for the neutral 9-sila- and 9-germa-fluorenyl systems, which also contain pyramidal atoms in the 9 position.

Given this discussion, we conclude that the reason 9-borafluorene **1** is a Lewis acid of competitive or superior strength to $B(C_6F_5)_3$ (despite being less fluorinated) stems from the greater steric accessibility of the boron center and the lowered back strain encountered upon the pyramidalization of the boron center, which occurs upon complexation of a Lewis base. The flatness of the borafluorene ring substitutent is the main reason for the relaxing of these steric factors; further, the pyramidalization of boron in going from **1** to **1·LB** likely relieves strain in the C-B-C moiety of the five-membered ring. Although long a matter of debate, it has been recently acknowledged that steric factors, particularly the onset of back strain, dominate in determining the relative Lewis acidity of the boron trihalides BX_3 (28, 29).

Although antiaromaticity is likely not playing a strong role in determining the relative Lewis acidity of **1**, given the propensity of boroles to undergo two-electron reduction to form aromatic borollides (30), it seemed reasonable to presume that **1** could be reduced more readily than $B(C_6F_5)_3$. Norton and co-workers (31) have reported on the difficulties associated with reduction of $B(C_6F_5)_3$, but estimate an E_{red} of –0.9 V vs. SCE based on measured E_{red} values for Mes_3B, $Mes_2B(C_6F_5)$, and $MesB(C_6F_5)_2$ (Mes = 2,4,6-$Me_3C_6H_2$) (31*c*). While the electron-withdrawing pentafluorophenyl groups make the boranes easier to reduce from a thermodynamic perspective, the lack of steric protection afforded by the C_6F_5 groups (as opposed to the Mes substitutent, for example) renders the radical anion extremely reactive, even with the surfaces of electrodes.

Cyclic voltammetry (CV) studies were performed on **1** in a variety of solvents using tetrabutylammonium tetrakis(pentafluorophenyl)borate (32) as the supporting electrolyte. Experiments in the noncoordinating solvents CH_2Cl_2 and α,α,α-trifluorotoluene were unsuccessful, so THF was employed. Model experiments on the unfluorinated analogue of **1**, 9-phenyl-9-borafluorene, show that, at scan rates of 500 mV s^{-1} (33), a reversible reduction and oxidation process occurs with a reduction potential of –2.16 V vs. ferrocene (Fc), a similar value to that found for BPh_3. From the available data, it is not possible to determine if the CV of 9-phenyl-9-borafluorene is indicative of a one- or a two-electron process. Under the same conditions, the CV of **1** revealed an irreversible process with a reduction potential at –2.42 V vs. Fc. The very negative potential obtained for **1** in THF was puzzling since it implies that **1** is more difficult to reduce than the unfluorinated analog and runs counter to the expected trend evidenced in the $Mes_nB(C_6F_5)_{3-n}$ series. On the other hand, the value for the reduction potential of **1** in THF is similar to those reported by Campbell (34) on the electrochemistry of simple aromatic fluorinated compounds. Although not directly comparable, since they are determined in different solvents, pentafluorobenzene and decafluorobiphenyl showed a first reduction wave at –2.84 and –2.20 V, respectively. These observations suggest the possibility that the reduction process does *not* actually take place at the boron center, but at the fluorinated aromatic framework, i.e., we are observing the reduction of **1·THF** rather than **1** under these conditions. Campbell also detected the presence of species arising from the rupture of aromatic C—F bonds, which suggests that a similar decomposition pathway might be operating in our case, i.e., via Ar—F scission. Alternatively, the high negative potential for the onset of reduction of **1** may be due to a large kinetic barrier to its reduction, as was observed for $B(C_6F_5)_3$ (31).

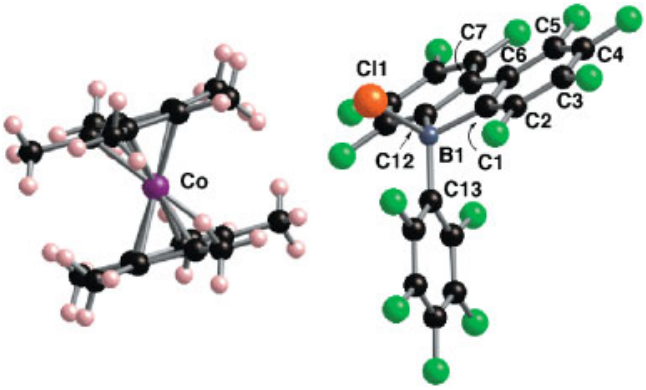
Since attempts to generate $\mathbf{1}^{2-}$ via electrochemical means failed, chemical reduction of **1** was attempted. Given that an earlier study indicated that Al(I) reagents were not sufficiently reducing (15), harsher reducing agents (C_8K, Li, Na, or K) were employed in a variety of solvents (Et_2O, THF, toluene, benzene, bromobenzene, or α,α,α-trifluorotoluene). Unfortunately, these invariably produced ill-defined mixtures. Not surprisingly, reactions involving alkali metals in nondonor solvents proved extremely slow, and after work up, the main products recovered were unreacted **1** and decomposition by-products. Furthermore, attempts to stabilize the putative $\mathbf{1}^{2-}$ by addition of crown ethers were also unsuccessful; only coordination of one of the ether oxygen atoms to the boron center was observed in the ^{19}F NMR spectrum. Given the slow kinetics associated with heterogeneous reductants, we sought a reducing agent that would allow the process to be carried out under homogeneous conditions.

Norton and co-workers (31) have shown that Cp^*_2Co is an effective reductant for $B(C_6F_5)_3$. Reaction between **1** and 2 equiv. of Cp^*_2Co in benzene or toluene led to the precipitation of an oily phase with recovery of 2 equiv. of unreacted Cp^*_2Co from the supernatant. Analysis of the oily material by ^{19}F NMR spectroscopy showed an extremely complex pattern arising from decomposition. However, this oily material was diamagnetic in nature, as judged by its silent EPR spectrum, even at low temperatures (ca. –50 °C). The presence of one remaining equivalent of reducing agent suggests

[3] These values are slightly depressed from the expected values near 1.00 because of the observed lengthening of the C—C bond that the six- and five-membered rings share compared with the other C—C bonds in the flanking six-membered rings observed in these and other systems. Despite the slightly lower *A* value, these rings are essentially fully aromatic.

© 2005 NRC Canada

Fig. 2. Crystalmaker model of the molecular structure of $[Cp^*_2Co]^+[\mathbf{1}\cdot\mathbf{Cl}]^-$ with atom labeling scheme. Selected bond lengths (Å): B(1)—Cl(1) 1.910(9), B(1)—C(13) 1.618(11), B(1)—C(1) 1.617(10), C(1)—C(2) 1.381(10), C(2)—C(3) 1.373(10), C(3)—C(4) 1.350(11), C(4)—C(5) 1.397(11), C(5)—C(6) 1.368(9), C(6)—C(7) 1.491(10). Selected bond angles (°): C(1)-B(1)-C(12) 97.9(6), C(1)-B(1)-C(13) 113.1(7), C(12)-B(1)-C(13) 114.9(6), C(1)-B(1)-Cl(1) 109.8(5), C(12)-B(1)-Cl(1) 106.9(6), C(13)-B(1)-Cl(1) 113.1(6).

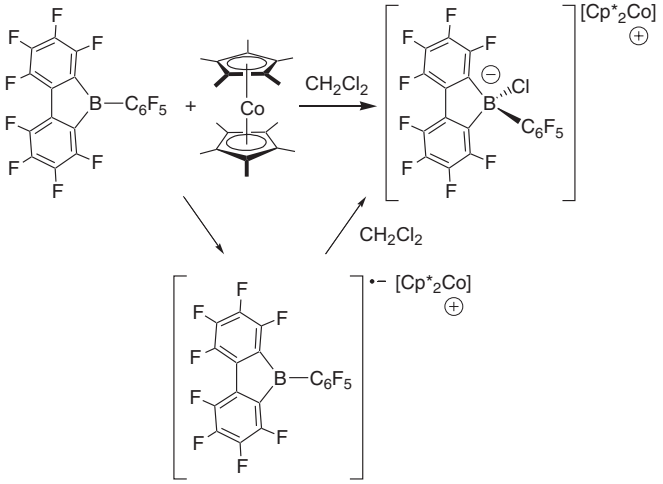


that the initially formed radical anion is highly reactive and that Cp^*_2Co is not sufficiently reducing to produce $\mathbf{1}^{2-}$. In accord with this postulate, the reaction of Cp^*_2Co and **1** in CH_2Cl_2 took place cleanly within seconds, as judged by NMR spectroscopy. The ^1H NMR spectrum showed only a singlet at δ 1.70, corresponding to the expected hydrogen resonances for the Cp* units of the diamagnetic $Cp^*_2Co^+$ cation. ^{19}F NMR spectroscopy clearly revealed a pattern of seven different well-defined signals in the expected range. The difference in chemical shift between the *meta*- and *para*-fluorines of the C_6F_5 ring ($\Delta\delta_{m,p}$ 4.7 ppm) was indicative of borate formation and a significant degree of charge separation. The negative value obtained by $^{11}B\{^1H\}$ NMR spectroscopy of δ –14 is also consistent with formation of a borate center.

Single crystals of the product of this reaction were obtained by slow diffusion of hexanes into a CH_2Cl_2 solution of the compound, generated as described above. The molecular structure of the salt $[Cp^*_2Co]^+[\mathbf{1}\cdot\mathbf{Cl}]^-$ is shown in Fig. 2 and is in accord with all the spectral data. There are no unusual contacts in the structure, and the ions are well separated with a boron—cobalt distance of 7.556(59) Å. The B(1)—Cl(1) distance of 1.910(9) Å is in the expected range for chloroborates, and the boron center in $[Cp^*_2Co]^+[\mathbf{1}\cdot\mathbf{Cl}]^-$ shows a distorted tetrahedral environment with a C(1)-B(1)-C(12) angle of 97.9(6)°, also within the expected range by comparison with related compounds.

The outcome can be rationalized in terms of chloride abstraction from the CH_2Cl_2 solvent, the sole possible source of chloride in the reaction (Scheme 1). A potential direct abstraction of Cl^- by **1** is negated, since **1** is an indefinitely stable species in CH_2Cl_2, as well as in most chlorinated solvents. Thus, the first step may involve the direct reaction between **1** and Cp^*_2Co. Based on the previous observations for the reaction of **1** with Cp^*_2Co in less polar solvents, where only 1 equiv. of Cp^*_2Co was found to react with **1**, a plausible mechanism might involve the intermediacy of a highly reactive, monoanionic radical species. The radical

Scheme 1.



anion rapidly abstracts $Cl^\cdot$ from solvent to form $[Cp^*_2Co]^+[\mathbf{1}\cdot\mathbf{Cl}]^-$. Alternatively, the CH_2Cl_2 solvent may mediate this reaction by electron transfer from Cp^*_2Co to the solvent, which then gives up a chloride ion to **1**. Although this option is not depicted in the scheme, our data do not exclude this as a possibility.

Taken together, the observations garnered from the experiments aimed at two-electron chemical and electrochemical reduction of **1** suggest that this compound behaves more similarly to its perfluoroaryl borane brethren than its nonfluorinated 9-borafluorene analogs. While one-electron reduction is fairly facile, the resulting radical anion is extremely reactive, abstracting atoms from solvent and (or) undergoing dimerization processes.

In conclusion, we find the antiaromatic perfluorinated 9-phenyl-9-borafluorene **1** to be of comparable or greater Lewis acid strength than the noncyclic parent borane $B(C_6F_5)_3$, mainly because of the lesser back strain engendered in adducts upon pyramidalization of the boron center, owing to the flat $C_{12}F_8B$ ring system. The antiaromaticity associated with this function does not appear to play a significant role in determining the Lewis acidity of the system. The high Lewis acidity of **1** contributes to the difficulty in carrying out two-electron reduction chemistry that is facile in unfluorinated analogs.

Experimental section

General procedures

An Innovative Technologies or Vacuum Atmospheres argon-filled glove box was employed for manipulation and storage of oxygen and moisture-sensitive compounds. Reactions were performed using a double manifold argon/vacuum line and modified Schlenk line techniques. Matheson Oxisorb-W gas purification cartridges were used to remove residual oxygen and moisture in the argon stream. Glassware was dried overnight (80–110 °C) and then assembled warm and evacuated on the vacuum line or placed in the glovebox antechamber while hot. Glassware consisted of swivel frit apparatus and line connectors equipped with Kontes valves and round-bottom flasks equipped with ground glass joints. Unless otherwise noted, the introduction of solvent in all

© 2005 NRC Canada

manipulations using the argon/vacuum line was via vacuum transfer with condensation at –80 °C (acetone – dry ice bath). Solvents were purchased from Aldrich and dried and deoxygenated before use in the following procedures. Hexanes, toluene, and THF were dried and deoxygenated via passage through a Grubbs/Dow purification system (35) and were stored in evacuated bombs over titanocene (36) (hexanes and toluene) or sodium – benzophenone ketyl (THF). Benzene was deoxygenated by bubbling argon through the solvent and was dried over sodium and stored over the sodium – benzophenone ketyl. Diethyl ether and methylene chloride were predried over $LiAlH_4$ and CaH_2, respectively, and subsequently stored over sodium – benzophenone ketyl and CaH_2, respectively. All deuterated solvents for NMR experiments were purchased from Cambridge Isotopes. Deuterated benzene, toluene, and THF were dried over 4 Å molecular sieves, stored over sodium – benzophenone ketyl, and distilled prior to use. Deuterated methylene chloride and bromobenzene were dried over 4 Å molecular sieves, stored over CaH_2, and distilled prior to use. After distillation, the deuterated solvents were stored in the glove box, in glass bombs equipped with Kontes valves. NMR spectra were obtained on Bruker AC 200 MHz (^{1}H), AMX 300 MHz (^{1}H, ^{19}F, ^{11}B{^{1}H}), DRX 400 MHz (^{1}H, ^{13}C{^{1}H}), or Varian 200 MHz (^{11}B, ^{11}B{^{1}H}, ^{31}P{^{1}H}) spectrometers. All NMR spectral data are reported in ppm, and NMR spectra of ^{1}H and ^{13}C were internally referenced to the residual solvent peak. The other nuclei were referenced externally with the following standards: ^{11}B ($BF_3{\cdot}OEt_2$, δ 0), ^{19}F (C_6F_6, δ –163.0), ^{31}P (H_3PO_4, δ 0). For all air- and (or) moisture-sensitive compounds and reactions, NMR samples were prepared in the glove box and the NMR tubes were capped with rubber septa. Temperature calibration for the NMR spectra was achieved by monitoring the ^{1}H NMR spectrum of methanol or ethylene glycol (37).

Cyclic voltammetry studies were carried out in a three-electrode cell using a PerkinElmer EG & G instrument (Princeton Applied Research) potentiostat, model 283, connected to a drybox and equipped with a PowerCV™ PowerSuite cyclic voltammetry software. A platinum disk electrode (1.6 mm diameter) and a platinum wire were used as the working electrode and the counter electrode, respectively. A silver wire was employed as a pseudoreference electrode. All the electrodes were purchased from BAS, Inc. All cyclic voltammetry experiments and handling of solids were performed in an argon-filled drybox at room temperature. THF (5 mL, previously dried and degassed) was syringed into an electrochemical cell containing [*n*-Bu_4N][$B(C_6F_5)_4$], and the mixture was stirred until complete dissolution to give a solution of concentration 0.1 mol L^{-1}. A background test was run, and in cases where traces of oxygen were detected, the system was additionally degassed by blowing argon through the solution with the aid of a Pasteur pipette. The samples (0.01 mol L^{-1}) were then run at 50, 100, 200, 500, and 1000 mV s^{-1} using Cp_2Fe (0.01 mol L^{-1}) as an internal standard. Electrochemical grade [*n*-Bu_4N][$B(C_6F_5)_4$] was synthesized according to literature procedures (32) and dried overnight at 130 °C.

Elemental analysis was performed by Dorothy Fox or Roxanna Smith within the department using a Control Equipment Corporation (CEC) 440 elemental analyzer. IR spectral samples were analyzed as KBr plates using a NEXUS 470 FT-IR ESP spectrometer. Electron paramagnetic spectra (EPR) were recorded on a Bruker EMX spectrometer at –50 °C, referencing externally against diphenylpicrylhydrazyl (DPPH, g = 2.0036) as a standard. $C_6F_5BC_{12}F_8$ (**1**), $CH_3BC_{12}F_8$ (**2**), $C_6H_5BC_{12}H_8$, and $B(C_6F_5)_3{\cdot}$MeCN were synthesized via literature procedures. $B(C_6F_5)_3$ was purchased from Boulder Scientific and purified by reaction with $Me_2SiH(Cl)$ in hexanes followed by vacuum sublimation (120 °C, dynamic vacuum). Reagent quantities of PMe_3 and MeCN were dried using 4 Å molecular sieves and CaH_2, respectively, then freshly distilled before use or vacuum transferred directly into reaction vessels. All other reagents were purchased from Aldrich Chemicals and used as received.

Preparation of $C_{12}F_8BC_6F_5(CH_3CN)$ (1·MeCN)

$C_{12}F_8BC_6F_5$ (0.081 g, 0.17 mmol) was placed in a round-bottom flask, and the flask was evacuated and cooled to –78 °C. Methylene chloride (10 mL) was condensed onto the solid, and the solution was stirred. CH_3CN (excess) was then condensed onto the stirred solution. Immediately on exposure to the CH_3CN vapours, the green colour of the 9-borafluorene discharged. The reaction was warmed to room temperature and stirred for 30 min. The solvent was removed in vacuo, and a white powder was obtained. Yield: 0.088 g, 99%. IR (KBr, cm^{-1}) ν: 2361 (C≡N stretch). ^{1}H NMR (CD_2Cl_2) δ: 2.66 (s, 3H, *Me*CN). ^{11}B{^{1}H} NMR (C_6D_6) δ: –8.7 (br). ^{19}F NMR (CD_2Cl_2) δ: –134.6 (m, 4F, overlapped 2F *o*-C_6F_5), –136.3 (m, 2F), –155.6 (m, 2F), –156.9 (m, 2F), –157.7 (m, 1F, *p*-C_6F_5), –164.1 (m, 2F, *m*-C_6F_5). Anal. calcd. for $C_{16}H_3BF_{13}N$: C 46.64, H 0.59, N 2.72; found: C 46.25, H 0.85, N 2.71.

Preparation of $C_{12}F_8BC_6F_5$(THF) (1·THF)

Synthesis was identical to the method employed for $C_{12}F_8BC_6F_5(CH_3CN)$ using $C_{12}F_8BC_6F_5$ (0.084 g, 0.18 mmol). Yield: 0.097 g, 100%. ^{1}H NMR (CD_2Cl_2) δ: 4.24 (m, 4H, THF), 2.15 (m, 4H, THF). ^{11}B{^{1}H} NMR (C_6D_6) δ: 4.1. ^{19}F NMR (CD_2Cl_2) δ: –126.2 (m, 2F, *o*-C_6F_5), –132.6 (m, 2F), –133.7 (m, 2F), –134.5 (m, 2F), –154.6 (m, 2F), –157.1 (m, 1F, *p*-C_6F_5), –163.7 (m, 2F, *m*-C_6F_5). Anal. calcd. for $C_{18}H_8BF_{13}O$: C 48.39, H 1.48; found: C 48.19, H 1.27.

Preparation of $C_{12}F_8BC_6F_5(PMe_3)$ (1·PMe_3)

Synthesis was identical to the method employed for $C_{12}F_8BC_6F_5(CH_3CN)$ using $C_{12}F_8BC_6F_5$ (0.082 g, 0.17 mmol). Yield: 0.094 g, 99%. ^{1}H NMR (CD_2Cl_2) δ: 1.31 (d, 9H, $^2J_{H\text{-}P}$ = 11.0 Hz). ^{11}B{^{1}H} NMR (C_6D_6) δ: –15.2 (d, $^1J_{B\text{-}P}$ = 87 Hz). ^{19}F NMR (CD_2Cl_2) δ: –130.4 (m, 2F, *o*-C_6F_5), –133.4 (m, 2F) –133.7 (m, 2F), –156.0 (m, 2F), –156.6 (m, 2F), –157.8 (m, 1F, *p*-C_6F_5), –163.7 (m, 2F, *m*-C_6F_5). ^{31}P{^{1}H} NMR (C_6D_6) δ: –14.2 (m). Anal. calcd. for $C_{17}H_9BF_{13}P$: C 45.85, H 1.65; found: C 45.57, H 1.60.

Typical conditions for competition experiments

1·THF (0.008 g, 15 μmol) and $B(C_6F_5)_3$ (0.008 g, 16 μmol) were weighed into an NMR tube and d_8-toluene (~0.5 mL) was added. The signals in the NMR spectra were identified by comparison to authentic samples. Equilibrium

© 2005 NRC Canada

constants were evaluated by integration of the ^{19}F NMR spectra of all peaks that were baseline separated.

Preparation of $[Cp^*_2Co]^+[\mathbf{1}\cdot Cl]^-$

Cp^*_2Co (35 mg, 0.11 mmol) was dissolved in ca. 3 mL of CH_2Cl_2 in a vial and added dropwise to a solution of **1** (50 mg, 0.11 mmol), also dissolved in ca. 3 mL of CH_2Cl_2. The brown solution was stirred for 20 min and then layered with hexanes. After cooling overnight at –35 °C, brown crystals of $[Cp^*_2Co]^+[\mathbf{1}\cdot Cl]^-$ were obtained. Yield: 45 mg, 53%. ^1H NMR (CD_2Cl_2) δ: 1.70 (s, 15H, $C_5(CH_3)_5$). $^{13}C\{^1H\}$ NMR (C_6D_6) δ: 94.0 (s, $C_5(CH_3)_5$), 7.1 (s, $C_5(CH_3)_5$). $^{11}B\{^1H\}$ NMR (C_6D_6) δ: –14.0. $^{19}F\{^1H\}$ NMR (CD_2Cl_2) δ: –130.2 (2F, *o*-F), –136.5 (2F), –137.2 (2F), –158.5 (2F), –159.9 (2F), –161.0 (1F, *m*-F), –165.7 (2F, *p*-F). Anal. calcd. for $C_{38}H_{30}F_{13}BClCo$: C 54.36, H 3.58; found: C 54.21, H 3.35.

Preparation of $C_{12}F_8BMe(CH_3CN)$ (2·MeCN)

$C_{12}F_8BMe$ (0.053 g, 0.16 mmol) was weighed into a round-bottom flask, which was evacuated and cooled to –78 °C. Methylene chloride (10 mL) was condensed onto the solid, and the solution was stirred. CH_3CN (~2 mL, excess) was then condensed onto the stirred solution. Immediately on exposure to the CH_3CN vapors, the green colour of the 9-borafluorene discharged. The reaction was warmed to room temperature and stirred for an additional 30 min. The solvent was removed in vacuo, and a white powder was obtained. Yield: 0.058 g, 97%. IR (KBr, cm^{-1}) ν: 2364 (C≡N stretch). ^1H NMR (CD_2Cl_2) δ: 2.42 (s, 3H, *Me*CN), 0.38 (s, 3H, B*Me*). $^{11}B\{^1H\}$ NMR (C_6D_6) δ: –5.1. ^{19}F NMR (CD_2Cl_2) δ: –135.5 (m, 2F), –138.4 (m, 2F), –157.6 (m, 2F), –158.1 (m, 2F). Anal. calcd. for $C_{15}H_6BF_8N$: C 49.87, H 1.67, N 3.86; found: C 49.54, H 1.37, N 3.57.

Preparation of $C_{12}F_8BMe(THF)$ (2·THF)

Synthesis was identical to the method employed for $C_{12}F_8BMe(CH_3CN)$ using $C_{12}F_8BMe$ (0.057 g, 0.18 mmol). Yield: 0.069 g, 99%. ^1H NMR (CD_2Cl_2) δ: 4.04 (m, 4H, THF), 2.04 (m, 4H, THF), 0.40 (s, 3H, B*Me*). $^{11}B\{^1H\}$ NMR (C_6D_6) δ: 8.6. ^{19}F NMR (CD_2Cl_2) δ: –135.0 (m, 2F), –136.2 (m, 2F), –156.9 (m, 2F), –157.5 (m, 2F). Anal. calcd. for $C_{17}H_{11}BF_8O$: C 51.81, H 2.81; found: C 51.65, H 2.65.

Preparation of $C_{12}F_8BMe(PMe_3)$ (2·PMe_3)

Synthesis was identical to the method employed for $C_{12}F_8BMe(CH_3CN)$ using $C_{12}F_8BMe$ (0.053 g, 0.17 mmol). Yield: 0.060 g, 92%. ^1H NMR (CD_2Cl_2) δ: 1.20 (d, 9H, $^2J_{H\text{-}P}$ = 11.0 Hz, P*Me*$_3$), 0.36 (d, 3H, $^3J_{H\text{-}P}$ = 19.0 Hz, B*Me*). $^{11}B\{^1H\}$ NMR (C_6D_6) δ: –14.0 (d, $^1J_{B\text{-}P}$ = 66 Hz). ^{19}F NMR (CD_2Cl_2) δ: –134.5 (m, 2F), –134.7 (m, 2F), –158.1 (m, 2F), –158.3 (m, 2F). $^{31}P\{^1H\}$ NMR (C_6D_6) δ: –11.4 (m). Anal. calcd. for $C_{16}H_{12}BF_8P$: C 48.28, H 3.04; found: C 48.20, H 2.47.

Acknowledgements

Funding for this work was provided by the Natural Sciences and Engineering Research Council of Canada (NSERC) through a Discovery grant to WEP and postgraduate scholarships (PGSA&B) to PAC.

References

1. W.E. Piers. Adv. Organomet. Chem. **52**, 1 (2005).
2. A.G. Massey, A.J. Park, and F.G.A. Stone. Proc. Chem. Soc. 212 (1963).
3. E.Y.-X. Chen and T.J. Marks. Chem. Rev. **100**, 1391 (2000), and refs. cited therein.
4. (*a*) K. Ishihara and H. Yamamoto. Eur. J. Org. Chem. 527 (1999); (*b*) H. Yamamoto (*Editor*). Lewis acid reagents. Oxford University Press, Oxford. 1999.
5. (*a*) S.J. Lancaster, A. Rodriguez, A. Lara-Sanchez, M.D. Hannant, D.A. Walker, D.H. Hughes, and M. Bochmann. Organometallics, **21**, 451 (2002); (*b*) J. Zhou, S.J. Lancaster, D.A. Walker, S. Beck, M. Thornton-Pett, and M. Bochmann. J. Am. Chem. Soc. **123**, 223 (2001); (*c*) R.E. Lapointe, G.R. Roof, K.A. Abboud, and J. Klosin. J. Am. Chem. Soc. **122**, 9560 (2000); (*d*) see ref. 1 and refs. cited therein.
6. (*a*) S.P. Lewis, N.J. Taylor, W.E. Piers, and S. Collins. J. Am. Chem. Soc. **125**, 14686 (2003); (*b*) S.P. Lewis, L.D. Henderson, M. Parvez, B.D. Chandler, W.E. Piers, and S. Collins. J. Am. Chem. Soc. **127**, 46 (2005).
7. (*a*) Z. Xu, K. Vanka, and T. Ziegler. Organometallics, **23**, 104 (2004); (*b*) K. Vanka, Z. Xu, and T. Ziegler. Can. J. Chem. **81**, 1413 (2003); (*c*) Z. Xu, K. Vanka, T. Firman, M. Michalak, and T. Ziegler. Organometallics, **21**, 2444 (2002); (*d*) K. Vanka, M.S.W. Chan, C.C. Pye, and T. Ziegler. Organometallics, **19**, 1841 (2000); (*e*) G. Lanza, I.L. Fragala, and T.J. Marks. Organometallics, **21**, 5595 (2002); (*f*) G. Lanza, I.L. Fragala, and T.J. Marks. Organometallics, **20**, 4006 (2001).
8. (*a*) Y.-X.E. Chen, M.V. Metz, L. Li, C.L. Stern, and T.J. Marks. J. Am. Chem. Soc. **120**, 6287 (1998); (*b*) L. Li, C.L. Stern, and T.J. Marks. Organometallics, **19**, 3332 (2000); (*c*) L. Li and T.J. Marks. Organometallics, **17**, 3996 (1998).
9. G. Kehr, R. Fröhlich, B. Wibbeling, and G. Erker. Chem. Eur. J. **6**, 258 (2000).
10. D.J. Morrison and W.E. Piers. Org. Lett. **5**, 2857 (2003).
11. (*a*) M.V. Metz, D.J. Schwartz, C.L. Stern, P.N. Nickias, and T.J. Marks. Angew. Chem. Int. Ed. **39**, 1312 (2000); (*b*) V.C. Williams, W.E. Piers, W. Clegg, M.R.J. Elsegood, S. Collins, and T.B. Marder. J. Am. Chem. Soc. **121**, 3244 (1999).
12. M.V. Metz, D.J. Schwartz, C.L. Stern, T.J. Marks, and P.N. Nickias. Organometallics, **21**, 4158 (2002).
13. J.J. Eisch, J.E. Galle, and S. Kozima. J. Am. Chem. Soc. **108**, 379 (1986).
14. P.A. Chase, W.E. Piers, and B.O. Patrick. J. Am. Chem. Soc. **122**, 12911 (2000).
15. P.E. Romero, W.E. Piers, S.A. Decker, D. Chau, T.K. Woo, and M. Parvez. Organometallics, **22**, 1266 (2003).
16. They have similar proton affinities: W.G. Mallard (*Editor*). NIST Chemistry WebBook [online]. National Institute of Standards and Technology, Gaithersburg, Md. Available from http://webbook.nist.gov/chemistry/pa-ser.html [accessed 2 August 2005]. 2005.
17. S. Yamaguchi, T. Shirasaka, S. Akiyama, and K. Tameo. J. Am. Chem. Soc. **124**, 8816 (2002).
18. H.E. Gottlieb, V. Kotlyar, and A. Nudelman. J. Org. Chem. **62**, 7512 (1997).
19. A.D. Horton, J. de With, A.J. van der Linden, and H. van de Weg. Organometallics, **15**, 2672 (1996).
20. H. Jacobsen, H. Berke, S. Doring, G. Kehr, G. Erker, R. Frohlich, and O. Meyer. Organometallics, **18**, 1724 (1999).
21. R.G. Kidd. *In* NMR of the newly accessible nuclei. Vol. 2. *Edited by* P. Laszlo. Academic, London. 1983. pp. 49–77.
22. (*a*) T. Brackenmeyer, G. Erker, R. Frohlich, J. Prigge, and U.

© 2005 NRC Canada

Peuchert. Chem. Ber. **130**, 899 (1997); (*b*) D. Brodalla, D. Mootz, R. Boese, and W. Osswald. J. Appl. Crystallogr. **18**, 316 (1985).
23. (*a*) V.C. Williams, C.Y. Dai, Z.M. Li, S. Collins, W.E. Piers, W. Clegg, M.R.J. Elsegood, and T.B. Marder. Angew. Chem. Int. Ed. **38**, 3695 (1999); (*b*) V.C. Williams, G.J. Irvine, W.E. Piers, Z.M. Li, S. Collins, W. Clegg, M.R.J. Elsegood, and T.B. Marder. Organometallics, **19**, 1619 (2000); (*c*) L.D. Henderson, W.E. Piers, G.J. Irvine, and R. McDonald. Organometallics, **21**, 340 (2002).
24. (*a*) R.F. Childs, D.L. Mulholland, and A. Nixon. Can. J. Chem. **60**, 801 (1982); (*b*) R.F. Childs, D.L. Mulholland, and A. Nixon. Can. J. Chem. **60**, 809 (1982).
25. P. Laszlo and M. Teston. J. Am. Chem. Soc. **112**, 8750 (1990).
26. A. Julg and P. Francois. Theor. Chim. Acta, **8**, 249 (1967).
27. The Julg *A* value is calculated according to the equation $A = 1 - (225/n)\Sigma(1 - r_i/r)^2$, where n = No. of C—C bonds in the cyclic system, r_i = C—C bond length, r = average C—C bond length. For recent examples where this analysis has been used in similar heterocycles, see (*a*) P.v.R. Schleyer, P.K. Freeman, H. Jiao, and H.B. Goldfuss. Angew. Chem. Int. Ed. Engl. **34**, 337 (1995); (*b*) Y. Liu, D. Ballweg, T. Muller, I.A. Guzei, R.W. Clark, and R. West. J. Am. Chem. Soc. **124**, 12174 (2002).
28. (*a*) P. Cassoux, R.L. Kuczkowski. and A. Serafini. Inorg. Chem. **16**, 3005 (1977); (*b*) K. Iigima, N. Adachi, and S. Shibata. Bull. Chem. Soc. Jpn. **57**, 3269 (1984); (*c*) A.C. Legon and H.E. Warner. J. Chem. Soc. Chem. Commun. 1397 (1991); (*d*) A.G. Avent, P.B. Hitchcock, M.F. Lappert, D.-S. Liu, G. Mignani, C. Richard, and E. Roche. J. Chem. Soc. Chem. Commun. 855 (1995).
29. (*a*) V. Branchadell and V. Oliva. J. Mol. Struct. (THEOCHEM), **236**, 75 (1991); (*b*) V. Branchadell, A. Sbai, and V. Oliva. J. Phys. Chem. **99**, 6472 (1995); (*c*) P. Fowler. Nature (London), **355**, 586 (1992); (*d*) K. Morokuma. Acc. Chem. Res. **10**, 294 (1977); (*e*) V. Jonas, G. Frenking, and M.T. Reetz. J. Am. Chem. Soc. **116**, 8741 (1994).
30. (*a*) R.J. Wehmschulte, M.A. Khan, B. Twamley, and B. Schiemenz. Organometallics, **20**, 844 (2001); (*b*) R.J. Wehmschulte, A.A. Diaz, and M.A. Khan. Organometallics, **22**, 83 (2003).
31. (*a*) C.J. Harlan, T. Hascall, E. Fujita, and J.R. Norton. J. Am. Chem. Soc. **121**, 7274 (1999); (*b*) R.J. Kwaan, C.J. Harlan, and J.R. Norton. Organometallics, **20**, 3818 (2001); (*c*) S.A. Cummings, M. Iimura, C.J. Harlan, R.J. Kwaan, I. Vu Trieu, J.R. Norton, B.M. Bridgwater, F. Jäkle, A. Sundararaman, and M. Tilset. Organometallics. In press.
32. R.J. LeSuer and W.E. Geiger. Angew. Chem. Int. Ed. **39**, 248 (2000).
33. D. Astruc. Electron transfer and radical processes in transition-metal chemistry. VCH Publishers Inc., New York. 1995.
34. B.H. Campbell. Anal. Chem. **44**, 659 (1972).
35. A.B. Pangborn, M.A. Giardello, R.H. Grubbs, R.K. Rosen, and F.J. Timmers. Organometallics, **15**, 1518 (1996).
36. R.H. Marvich and H.H. Brintzinger. J. Am. Chem. Soc. **93**, 2046 (1971).
37. C. Ammann, P. Meier, and A.E. Merbach. J. Magn. Reson. **46**, 319 (1982).

© 2005 NRC Canada

Theoretical, dynamic, and structural studies of the phenyl rotation in bispentafluorophenyl palladium complexes with scorpion-type ligands

M. Carmen Carrión, Félix A. Jalón, Isabel López-Solera, Blanca R. Manzano, Francisco Sepúlveda, Lucía Santos, Ana María Rodríguez, Miquel Moreno, and Martín Martínez-Ripoll

Abstract: A theoretical study at a DFT level has been carried out on the pentafluorophenyl rotation in the compounds $[Pd(C_6F_5)_2(bpzmPh)]$ (**1**) and $[Pd(C_6F_5)_2(bpz*mPh)]$ (**2**) (bpzm = bis(pyrazol-1-yl)phenylmethane and bpz*mPh = bis(3,5-dimethylpyrazol-1-yl)phenylmethane). The orientation of one C_6F_5 with respect to the coordination plane was forced to adopt specific values to simulate ring rotation and several parameters, such as the disposition of the other C_6F_5 group, the energy of the system, and the skeletal conformation of the bpz′m ligand, were analysed. The maximum energy value was found when the C_6F_5 ring was nearly coplanar with the coordination plane. In both complexes the minimum energy corresponds to a situation where the two rings are nearly parallel. A number of distortions that mainly affect the NPdN bite angle were predicted for the complex containing the bpz*mPh ligand (methylated pyrazoles). Four structures of complexes from this family were determined by X-ray diffraction and the same types of distortion were found. The differences in the free energies of activation for the pentafluorophenyl rotation in complexes containing methylated and non-methylated ligands were theoretically calculated. The calculated values were consistent with the data experimentally determined by NMR spectroscopy. The origin of the difference was attributed to the aforementioned distortions of the complexes containing the bpz*mPh ligand, which were more remarkable in the configuration of maximum energy.

Key words: N ligands, palladium, theoretical studies, DFT calculations, dynamics.

Résumé : Nous présentons les résultats d'une étude théorique de calculs DFT sur la rotation des groupes pentafluorophényles dans les composés $[Pd(C_6F_5)_2(bpzmPh)]$ (**1**) et $[Pd(C_6F_5)_2(bpz*mPh)]$ (**2**) (bpzm = bis(pyrazol-1-yl)phénylméthane et bpz*mPh = bis(3,5-diméthylpyrazol-1-yl)phénylméthane). L'orientation d'un groupe C_6F_5 par rapport au plan de coordination a été forcée à adopter des valeurs spécifiques pour simuler la rotation du cycle et nous avons analysé plusieurs paramètres comme la disposition de l'autre groupe C_6F_5, l'énergie du système et la conformation du ligand bpz′m. La valeur maximale d'énergie a été trouvée quand le cycle C_6F_5 est presque coplanaire avec le plan de coordination. Pour les deux composés l'énergie minimale correspond à une situation où les deux cycles sont presque parallèles. Nous avons prédit un nombre de distorsions qui affectent principalement l'angle de chélatation NPdN pour le composé portant le ligand bpz*mPh (pyrazoles méthylés). Nous avons déterminé par diffraction de rayons X quatre structures de composés de cette famille et nous avons trouvé les mêmes types de distorsion. Nous avons calculé théoriquement les différences d'énergie libre d'activation pour la rotation des groupes C_6F_5 dans les composés portant des ligands méthylés et non-méthylés. Les valeurs calculées sont cohérentes avec les donnés expérimentales déterminées par spectroscopie RMN. L'origine de la différence a été attribuée aux distorsions des composés contenant le ligand bpz*mPh explicitées plus haut, lesquelles sont plus importantes dans la configuration d'énergie maximale.

Mots clés : ligands N, palladium, étude théorique, calculs DFT, dynamiques.

Received 11 February 2005. Published on the NRC Research Press Web site at http://canjchem.nrc.ca on 11 February 2006.

M.C. Carrión, F.A. Jalón, I. López-Solera, B.R. Manzano,[1] and F. Sepúlveda. Departamento de Química Inorgánica, Orgánica y Bioquímica, Facultad de Químicas, IRICA Universidad de Castilla-La Mancha, Avda. C. J. Cela, 10, 13071 Ciudad Real, Spain.
L. Santos. Departamento de Química-Física, Facultad de Químicas, Universidad de Castilla-La Mancha, Avda. C. J. Cela, 10, 13071 Ciudad Real, Spain.
A.M. Rodríguez. Departamento de Química Inorgánica, Orgánica y Bioquímica, Escuela Técnica Superior de Ingeniería Industrial, Universidad de Castilla-La Mancha, Avda. C. J. Cela, 3, 13071 Ciudad Real, Spain.
M. Moreno. Departament de Química, Facultat de Ciències, Universitat Autónoma de Barcelona, 08193 Bellaterra, Barcelona, Spain.
M. Martínez-Ripoll. Instituto Rocasolano del CSIC, Serrano, 119, 28006 Madrid, Spain.

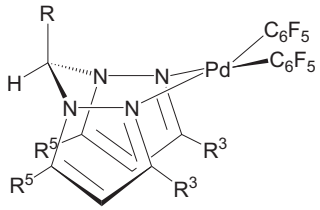
[1]Corresponding author (e-mail: Blanca.Manzano@uclm.es).

 doi: 10.1139/V05-232 © 2005 NRC Canada

Introduction

The chemistry of polyfluorophenyl derivatives of Pd and Pt has been extensively developed in organometallic chemistry (1). In contrast to other metal–aryl groups, the polyfluorophenyl ligands stabilize the metal–carbon bond because of their special electronic properties (2). Far from being simply spectator ligands, there are several examples in which the polyfluorophenyl groups have been shown to be reactive. For instance, it has been possible to study processes of insertion into Pd—C_6F_5 bonds (3), the activation of C—F bonds (4), aryl exchange (5), and other reactions (6, 7). Another aspect worth highlighting here related to polyfluoroaryl palladium and platinum complexes is the rotation of the aryl group around the M—C bond. Examples of both free (8, 9) and restricted rotation of the polyfluorophenyl groups have been described (9, 10–19). Kinetic activation parameters have been calculated for some cases (11, 18–21). Of particular interest is the use of the 3,5-dichlorotrifluorophenyl ligand, whose presence simplifies the ^{19}F NMR spectra (22–24). When bulkier groups are present, such as 2,4,6-tris(trifluoromethyl)phenyl (Fmes), the rotation is quenched because of severe steric hindrance (25). The presence of a larger atom, such as a bromo substituent, in the ortho position also increases the energy barrier of the polyhalophenyl rotation (26). It is important to note that a mirror plane coincident with the coordination plane can exist either in a static situation or because of fluxional processes (15, 18, 27, 28) involving the ancillary ligands. In this case the rotational process cannot be studied unless atropisomers are formed because of the presence of two (or more) asymmetrically substituted polyhalophenyl groups (haloaryls with C_s local symmetry) (18, 26, 29, 30). It has been demonstrated that in certain examples the rapid rotation takes place in a contact ion pair formed by halide dissociation (21), where the decrease in the steric hindrance facilitates the rotation around the metal–carbon bond. In other examples, it has been found that the rotation takes place in square-planar derivatives (11), and a case with a dual mechanism involving four- and three-coordinate species (30) has even been reported. The use of heteroscorpion-type ligands with the formula bis(pyrazol-1-yl)Rmethane (bpz′mR) (see Scheme 1) as ancillary ligands in bispentafluorophenyl palladium complexes gives rise to systems that are appropriate for studying the pentafluorophenyl rotation process. Such complexes do not have a symmetry plane coincident with the coordination plane and the process of boat-to-boat inversion (see Scheme 2) has never been observed when the spacer carbon situated between the pyrazole rings is substituted with a relatively bulky R group (31–34). The isomer in which the R group is situated in an axial orientation in the metallacycle is the only one that has been observed in these derivatives (31–34). In any case, the presence of only one R group would prevent the existence of a "dynamic plane" even if the boat-to-boat process were operating because this process would induce the change of the unique R group from an axial to an equatorial disposition. The use of bis(pyrazol-1-yl)Rmethane ligands offers the possibility of introducing different R substituents with distinct characteristics and sizes. Equally, the pyrazole rings can be substituted differently. In a previous study (34) we observed restricted rotation of the C_6F_5 groups

Scheme 1.

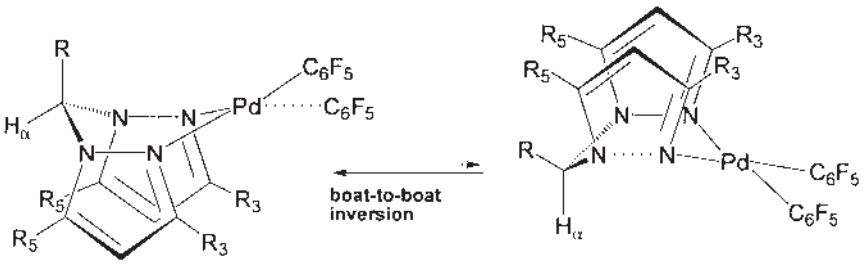


$R^3 = R^5 = H$	R = phenyl	[Pd(C_6F_5)$_2$(bpzmPh)]	**1**
$R^3 = R^5 = Me$	R = phenyl	[Pd(C_6F_5)$_2$(bpzm*Ph)]	**2**
$R^3 = R^5 = H$	R = anisol-2-yl	[Pd(C_6F_5)$_2$(bpzmArOMe)]	**3**
$R^3 = R^5 = H$	R = phenol-2-yl	[Pd(C_6F_5)$_2$(bpzmArOH)]	**4**
$R^3 = R^5 = Me$	R = anisol-2-yl	[Pd(C_6F_5)$_2$(bpzm*ArOMe)]	**5**
$R^3 = R^5 = Me$	R = cyclohexyl	[Pd(C_6F_5)$_2$(bpzm*Cy)]	**6**
$R^3 = R^5 = Me$	R = ferrocenyl	[Pd(C_6F_5)$_2$(bpzm*Fec)]	**7**
$R^3 = R^5 = Me$	R = pyrid-2-yl	[Pd(C_6F_5)$_2$(bpzm*py)]	**8**

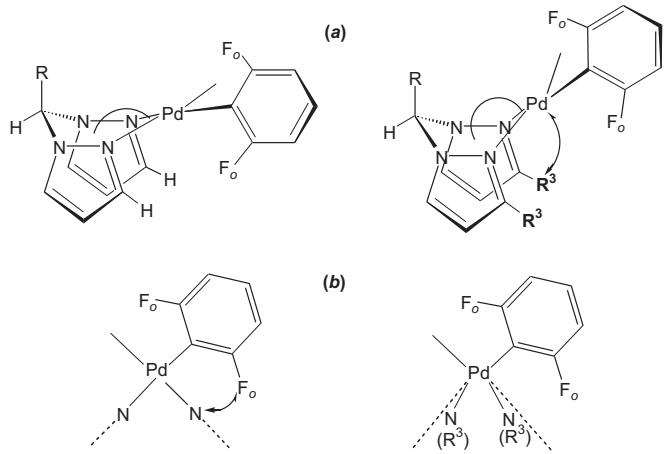
in the complexes depicted in Scheme 1 (except **1**, which is described here for the first time), all of which contain this type of ligand. The free energies of activation were calculated at the coalescence temperature. The absence of dissociative processes and a negligible influence of the R groups were demonstrated in this work. On studying this family of complexes, we unexpectedly found that derivatives where the bpz′mR ligands incorporate unsubstituted pyrazoles showed higher energy barriers than those with 3,5-dimethylated pyrazoles. A similar case, concerning the effect of the substituents on pyrazolate bridges cis to the polyhaloaryl rings, has also been recently reported (24). However, at first sight, a higher level of steric hindrance in the region close to the aryl group would be expected to hinder aryl rotation. In an attempt to explain this apparent contradiction we proposed the existence of a structural deformation when substituents are present on the pyrazole groups that would facilitate the fluoroaryl rotation (34). Indeed, comparison of the X-ray structures of similar complexes that differ in the presence of substituents in the 3-position of the pyrazole ring show that such substituents produce a significant distortion in the boat metallacycle, thus reducing the N-Pd-N/N_4 dihedral angle and also the bite angle of the N-donor ligand (32, 35) (see Scheme 3). This effect was more marked when a *tert*-butyl group was present in the 3-position of the pyrazole ring (35). In our complexes, this deformation would push away the Pd(C_6F_5)$_2$ moiety from the Me^3 pyrazole substituents and decrease the steric hindrance. The closure of the N-Pd-N angle would facilitate the rotation of the C_6F_5 groups by opening the C-Pd-N and (or) the C-Pd-C angles and decrease the steric crowding between the F_{ortho} and the atoms in the cis disposition. In fact, in previous works, higher energy barriers were found for the aryl rotation when the size of the donor atoms flanking the polyhaloaryl group in the coordination plane was increased (11, 23, 26), more so when the rotation took place in square-planar species. On the basis of these ideas, we decided to perform a theoretical study at a DFT level of the whole process of pentafluorophenyl rotation in two systems of this type containing the ligands bis(pyrazol-1-yl)phenylmethane (complex **1**) and bis(3,5-dimethylpyrazol-1-yl)phenylmethane (complex **2**). Our goals in this study were: (*i*) to determine

© 2005 NRC Canada

Scheme 2.



Scheme 3. (*a*) Distortion in the boat metallacycle owing to the steric hindrance of the substituent in position 3 of the pyrazole ring (R^3). The N-Pd-N/N_4 angle is reduced. (*b*) The distortion indicated in (*a*) decreases the N-Pd-N angle and consequently, the steric hindrance decreases between the pyrazole N-donor atom and the C_6F_5 groups.



whether the deformations observed in some X-ray structures can be predicted by theoretical calculations; (*ii*) to analyse the energy and the conformations of the systems in the different steps of the pentafluorophenyl rotation. We were particularly interested in determining whether the aforementioned deformations also occur in the situation of maximum energy in the rotation process. Finally, (*iii*) to establish if a higher energy barrier is theoretically predictable for the complexes containing unsubstituted pyrazoles and to analyze whether the origin of this difference is the aforementioned deformation. To the best of our knowledge, this type of study has never been performed and only a brief paragraph concerning molecular mechanics calculations has previously been published (36). This reference indicated that the most stable conformation of a Pd(II) complex containing a substituted phenyl ligand is that in which the aryl ring is approximately perpendicular to the coordination plane. We believe that these studies and the methodology used can be useful when applied to other types of systems in connection with the rotation of different types of aryl rings that may influence, for example, the enantioselectivity in catalytic processes. In fact, several examples of enhancement of the enantioselectivities (up to 40%–50%) (37, 38) in different catalytic processes when substituents are introduced in an aryl ring present in the asymmetric ligand have been described. This fact has recently been attributed to the restricted rotation of this ring, which gives rise to a more rigid chiral pocket (39). The formation of chiral conformations has also been reported for pentachlorophenyl derivatives that exhibit restricted ring rotation (40).

We have also synthesized and studied the fluxional behaviour of complex **1** (Scheme 1) to complete this family of complexes. The molecular structures of several derivatives of this type were also determined by X-ray diffraction to ascertain whether the stated deformations can be considered a general trend.

Experimental

Methods

All manipulations were carried out under an atmosphere of dry, oxygen-free nitrogen using standard Schlenk techniques. Solvents were distilled from the appropriate drying agents and degassed before use. Elemental analyses were performed with a PerkinElmer 2400 CHN microanalyzer. IR spectra were recorded on a Nicolet Impact 410 spectrophotometer as KBr pellets. NMR spectra were recorded at room temperature (≈25 °C) on a Varian UNITY-300 (300 MHz for ^{1}H, 75.4 MHz for ^{13}C) spectrometer. ^{1}H and ^{13}C NMR shifts were recorded using the residual proton or carbon signal of the solvent as internal standard. A ^{1}H–^{13}C correlation experiment (gHMQC) was used to assign the ^{13}C NMR resonances (Varian INOVA 500 MHz spectrometer). Free energies of activation were calculated (20) from the coalescence temperature (T_c) and the frequency difference between the coalescing signals (extrapolated at the coalescence temperature) with the formula $\Delta G_c^{\ddagger} = aT_c[9.972 + \log(T_c/\delta\nu)]$ ($a = 1.914 \times 10^{-2}$). The estimated error in the calculated free energies of activation is ±0.2 kcal/mol (1 cal = 4.184 J). The probe temperature (±1 K) was controlled by a standard unit calibrated with a methanol reference.

Materials

$[Pd(C_6F_5)_2(cod)]$ was prepared according to the literature procedure (41). Preparation and structural information of complexes **2–8** have been previously reported (32, 34). bpzmPh was prepared according to the literature method (42).

Theoretical calculations

Calculations have been performed using the Gaussian 98 series of programs (43). Density functional theory (DFT) was applied with the B3LYP functional (44, 45). Effective core potentials (ECPs) were used to represent the innermost electrons of the palladium atom. The basis set for the Pd atom was that associated with the pseudopotential (46), with a standard double-ξ LANL2DZ contraction (43). All calcula-

© 2005 NRC Canada

tions were done with the split-valence 6-31G basis set for the hydrogen, carbon, nitrogen, and fluoride atoms (47). Within this basis set, the total number of basis functions was already high for complex **1** where 397 basis functions were needed, whereas complex **2** required 449 basis functions at this level of calculation. The equilibrium geometries were also localized with the higher 6-31G(d) basis set that includes polarization functions on heavy atoms.

Full geometry optimization and direct location of equilibrium geometries were carried out by means of the Schlegel gradient optimization algorithm (48) by using redundant internal coordinates as implemented in the Gaussian 98 package (43). Diagonalization of the energy second-derivative matrix was performed to provide the vibrational harmonic frequencies that were used for evaluating the thermodynamic corrections at 1 atm (1 atm = 101.325 kPa) and 298.15 K to the initially obtained electronic energy. As per usual, we made the approximations of the rigid rotor and the harmonic model for the rotational and the harmonic degrees of freedom, respectively (49).

Preparation of $[Pd(C_6F_5)_2(bpzmPh)]$ (1)

$[Pd(C_6F_5)_2(cod)]$ (100 mg, 0.18 mmol) was dissolved in CH_2Cl_2 (20 mL) and bpzmPh (40.9 mg, 0.18 mmol) was added. The solution was stirred at room temperature for 16 h. Complex **1** was obtained as a white powder after evaporation of the solvent to dryness and washing with pentane (2 × 10 mL). Yield: 89% (106.1 mg). Complex **1**, thus obtained, is spectroscopically pure, but it can be crystallized from dichloroethane–hexane. Monocrystals suitable for analysis by X-ray diffraction were obtained in this way. IR (KBr, cm^{-1}): 956, 1633, 1058 (C_6F_5). ^1H NMR (300 MHz, 1,1′,2,2′-$CDCl_2CDCl_2$, 25 °C, ppm) δ: 6.42 (t, $^3J_{H,H}$ = 2.4 Hz, 2H, H^4_{pz}), 6.60 (d, $^3J_{H,H}$ = 7.3 Hz, 2H, H_{ortho}), 7.25 (d, $^3J_{H,H}$ = 2.0 Hz, 2H, H^3_{pz}), 7.44 (t, $^3J_{H,H}$ = 7.3 Hz, 2H, H_{meta}), 7.50 (t, $^3J_{H,H}$ = 7.3 Hz, 1H, H_{para}), 7.52 (s, 1H, H_α), 7.85 (d, $^3J_{H,H}$ = 2.4 Hz, 2H, H^5_{pz}). ^{13}C NMR (75 MHz, 1,1′,2,2′-$CDCl_2CDCl_2$, 25 °C, ppm) δ: 76.1 (s, 1C, C_α), 107.3 (s, 2C, C^4_{pz}), 125.3 (s, 2C, C_{ortho} Ph), 129.2 (s, 2C, C_{meta} Ph), 130.1 (s, 1C, C_{para} Ph), 132.6 (s, 2C, C^5_{pz}), 135.2 (dm, $^1J_{C,F}$ = 248 Hz, 4C, C_{meta}, C_6F_5), 137.0 (dm, $^1J_{C,F}$ = 248 Hz, 2C, C_{para}, C_6F_5), 144.0 (s, 2C, C^3_{pz}), 147.0 (dm, $^1J_{CF}$ = 248 Hz, 4C, C_{ortho}, C_6F_5). Anal. calcd. for $C_{25}H_{12}F_{10}N_4Pd$ (664.8): C 45.17, H 1.82, N 8.43; found: C 44.90, H 1.96, N 8.18.

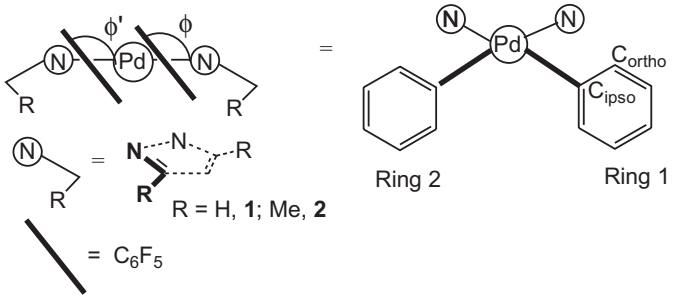
Preparation of monocrystals for X-ray diffraction studies

Monocrystals of **1** were obtained by a slow evaporation of hexane over a concentrated solution of 1,2-dichloroethane. Monocrystals of **2** were obtained by a slow evaporation of acetone-d_6 in an NMR tube. Monocrystals of **3·$C_2H_4Cl_2$** were obtained by slow vaporization of pentane over a 1,2-dichloroethane solution of this complex. A sample of monocrystals of **8** was obtained by slow evaporation of pentane over a solution of this complex in acetone.

X-ray structure determinations for compounds 1, 2, 3·$C_2H_4Cl_2$, and 8

For **1** the intensity data were collected on a Bruker SMART CCD diffractometer using MoKα radiation (λ = 0.710 73 Å) at 23 °C. The data were collected with a frame width of 0.3° in ω and a counting time of 25 s per frame at a crystal-to-detector distance of 4 cm. The diffraction frames were integrated using the SAINT (50) package and corrected for absorption with SADABS (51). For **2** and **3** the intensity data were collected on a NONIUS-MACH3 diffractometer equipped with a graphite monochromator MoK_α radiation (λ = 0.710 73 Å) using an ω/2θ scan technique at room temperature. For **8** the intensity data were collected on a Seifert XRD3000-S diffractometer equipped with a graphite monochromator CuK_α radiation (λ = 1.541 78 Å) at room temperature. The final unit cell parameters were determined from 25 well-centered reflections and refined by the least-squares method. The space group was determined from the systematic absences and this was vindicated by the success of the subsequent solutions and refinements. The structures were solved by direct methods using SHELXS (52) (for **1**, **2**, and **3**) and SIR92 (53) (for **8**) computer programs and refined on F^2 by full-matrix least-squares (SHELXL-97) (54). All nonhydrogen atoms were refined with anisotropic thermal parameters. The hydrogen atoms were included in calculated positions and were refined with an overall isotropic temperature factor using a riding model. Weights were optimized in the final cycles. Complex **3** crystallizes as a solvate with a molecule of 1,2-dichloroethane.

Scheme 4.



Results and discussion

The complexes $[Pd(C_6F_5)_2(bpzmPh)]$ (**1**) and $[Pd(C_6F_5)_2(bpz*mPh)]$ (**2**) have been theoretically analyzed by a DFT study. A number of different parameters that depend on the dihedral angle ϕ have been analyzed for each complex. The dihedral angle ϕ is defined by the torsion angle N-Pd-C_{ipso}-C_{ortho} as shown in Scheme 4. This angle was forced to adopt specific values (in the range from 0° to 180°) and the energy of the structure was minimized until convergence (see Tables 1 and 2). Only the data that correspond to ΔE = 0 in the tables have not been forced (ϕ = 63.5° for complex **1** (Table 1) and ϕ = 83.4° for complex **2** (Table 2)). In these cases, the system was allowed to adopt the structure of lower energy without any restrictions. We have performed some calculations with the SCF=TIGHT keyword. We have seen that the energies are totally unaffected and the geometries are almost equal (differences are less than 1° or 0.01 Å).

The dependence on ϕ of different parameters that are directly or indirectly related with the rotation of the perfluorophenyl groups of the complexes will be discussed in the following sections.

© 2005 NRC Canada

Table 1. Different parameters obtained after the theoretical calculations for complex **1**.

ϕ^a (°)	ϕ'^a (°)	ΔE (kcal/mol)	<N-Pd-N (°)	<N-Pd-N/N_4 (°)
10.0	71.2	9.4	81.6	145.2
20.0	70.2	8.1	82.7	146.9
30.0	68.3	5.4	83.5	148.9
40.0	67.8	3.5	84.2	150.8
50.0	67.2	2.4	84.8	152.0
63.5	66.9	0.0	85.1	153.4
80.0	67.9	0.6	85.1	152.4
85.0	68.8	2.8	85.0	151.9
88.0	69.7	3.1	84.9	151.6
90.0	113.8	1.8	85.6	154.9
100.0	117.0	0.7	85.4	154.9
110.0	117.1	0.04	85.2	153.6
120.0	118.4	0.3	84.9	152.2
130.0	117.6	1.3	84.6	151.3
140.0	117.1	3.3	84.0	149.5
150.0	118.2	6.4	82.8	146.6
170.0	119.5	13.4	80.7	144.6
180.0	110.1	12.7	81.0	147.3

[a]See Scheme 4.

Table 2. Different parameters obtained after the theoretical calculations for complex **2**.

ϕ^a (°)	ϕ'^a (°)	ΔE (kcal/mol)	<N-Pd-N (°)	<N-Pd-N/N_4 (°)
10.0	95.2	9.7	79.6	138.4
20.0	88.3	7.4	80.7	139.8
30.0	84.9	4.8	81.6	141.3
50.0	84.8	1.6	83.5	145.1
70.0	86.3	0.4	84.1	146.8
80.0	90	0.06	84.1	146.4
83.4	91.5	0.0	84.1	146.1
90.0	97.8	0.08	84.0	145.8
100.0	100.5	0.4	83.9	145.4
120.0	120.4	3.7	81.8	138.8
140.0	129.4	7.2	79.3	133.5
160.0	127	9.9	78.7	134.1
170.0	117.1	10.8	78.9	136.4
180.0	104.6	10.3	79.4	138.1

[a]See Scheme 4.

Mutual dependence of the rotation of the two C_6F_5 rings — ϕ vs. ϕ'

It is expected that the rotation of the two C_6F_5 rings will be mutually dependent and, as a consequence, the dependence of the dihedral angle ϕ' with ϕ was first studied. The angle ϕ' was defined according to Scheme 4 and its dependence on ϕ in **1** and **2** is indicated in Tables 1 and 2 and represented in Fig. 1. It is noteworthy that the two graphics of Fig. 1 are not symmetrical, e.g., the ϕ' values for small and large ϕ values are different. This is due to the asymmetry of the nitrogen donor ligand so that the coordination plane is not a plane of symmetry (see Scheme 1). Consequently, small or large ϕ values represent different situations of the pentafluorophenyl ring in the complex (see Scheme 4). Finally, note that $\phi = 0°$ and $\phi = 180°$ correspond to the same structure.

For complex **1**, two values of ϕ' are clearly preferred. For values of ϕ between 10° and 88°, the values of ϕ' are from 67.2° to 71.2°, but for values of ϕ between 90° and 180°, ϕ' is slightly below 120°. ϕ' suddenly changes when ϕ changes from 88° to 90°. In complex **2** the behaviour is different, although some similarities are observed. In this case, a more gradual variation in ϕ' is observed as ϕ is changed. However, two limiting values also exist. A minimum of 84.8° when ϕ is 50° and a maximum of 129.4° when ϕ is 140°. It is noticeable that the minimum value of ϕ' is higher in **2** than in **1**. This can likely be attributed to the higher steric repulsion expected between the F_{ortho} of ring 2 and the methyl group in the 3-position of the pyrazole ring when this angle is small. It is also noticeable that ϕ' does not adopt values that are too low or too high in either of the two complexes, very likely because of the repulsions of the second C_6F_5 ring when it is nearly coplanar with the complex coordination plane.

The mutual dependence found between ϕ and ϕ' can be understood in terms of the second C_6F_5 ring adapting to the rotation of the first, with ϕ' values within the allowed range.

ϕ vs. energy

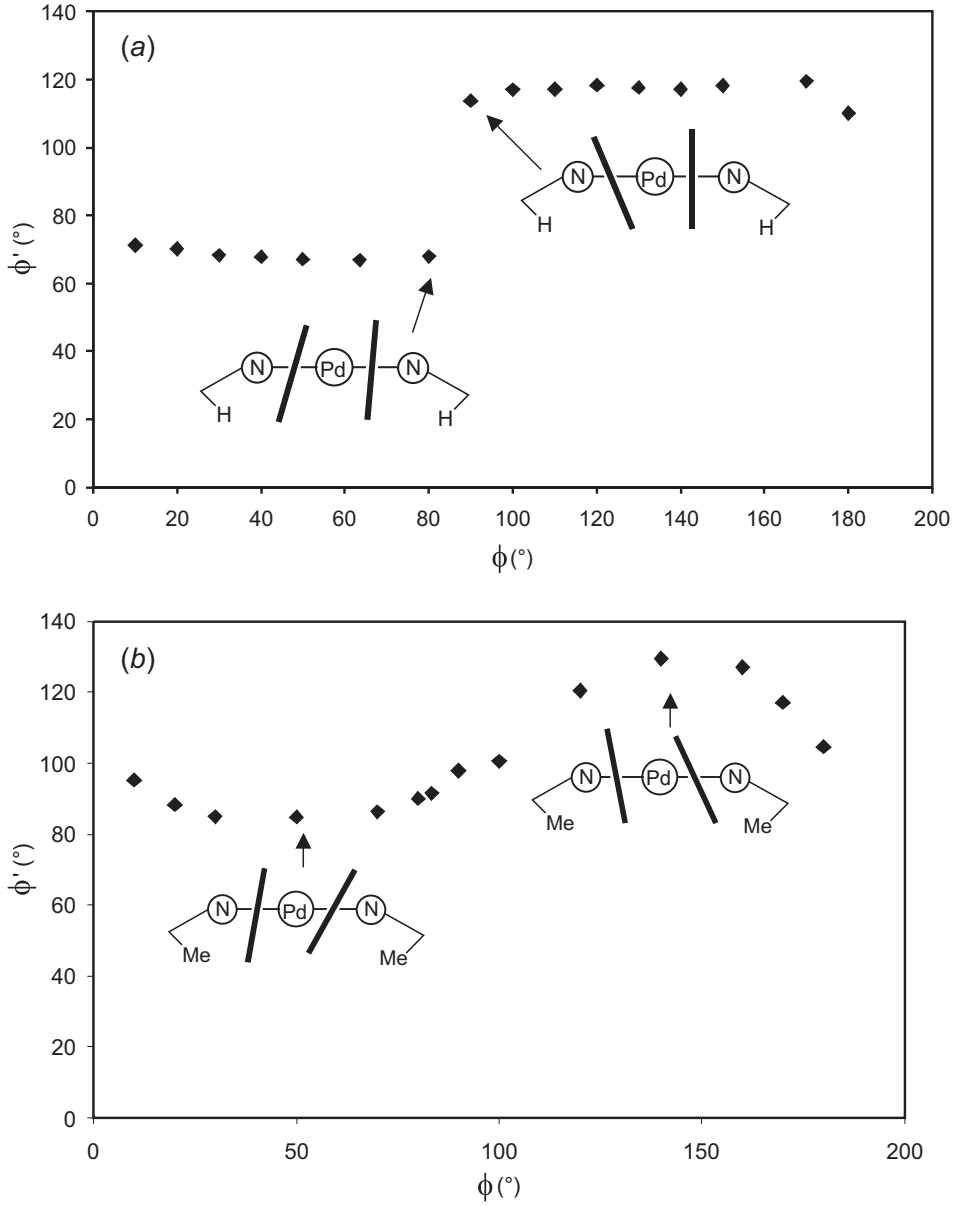
The dependence of the relative energy of the structures of complexes **1** and **2** as a function of ϕ is indicated in Fig. 2 (see also Tables 1 and 2).

As expected, in both cases the maximum energy value is achieved when ϕ is near 180°. This value corresponds to a situation where a C_6F_5 ring is nearly coplanar to the coordination plane and leads to the highest steric repulsion between the F_{ortho} of the rotating ring and the vicinal coordinated atoms (N and C). Comparison of the two diagrams in Fig. 2 shows that the conformations of the C_6F_5 rings are similar for the two complexes in the maximum energy configurations. However, in both complexes the minimum of energy corresponds to conformations with different values of ϕ and ϕ'. For complex **1**, two states of minimum energy (0 and 0.04 kcal/mol) are found. It is outstanding that in these conformations the two C_6F_5 groups are not perpendicular to the coordination plane, but they are nearly parallel ($\phi = 63.5°$, $\phi' = 66.9°$ and $\phi = 110°$, $\phi' = 117.1°$) leading to a hypothetical minimum steric hindrance between the F_{ortho} of both rings. For complex **2**, the minimum of energy is found when both rings are nearly parallel and approximately perpendicular to the coordination plane ($\phi = 83.4°–90.0°$, $\phi' = 91.5°–97.8°$). In this complex the conformation of the rings found in **1** would probably involve considerable steric hindrance between the F_{ortho} of one C_6F_5 ring and the Me substituent of the pyrazole ring cis to it. For this reason such an arrangement cannot correspond to an energy minimum. In an effort to provide evidence for this proposal, the values $\phi = 63.5°$ and $\phi' = 66.9°$ were imposed on the structure of **2** and the energy was then minimized until convergence. A value of 2.4 kcal/mol above the minimum was calculated for this conformation of **2**, thus showing its relative lack of stability with respect to the minimum energy situation.

For a better comparison with the data obtained from the NMR studies, we also calculated the free energy of activation for the higher energy situation for both complexes in the gas phase. The value obtained for complex **1** is

© 2005 NRC Canada

Fig. 1. Plot of the values (obtained from the theoretical calculations) of ϕ′ (°) vs. ϕ (°) for the rotamers of complexes (*a*) **1** and (*b*) **2**.



13.0 kcal/mol and that for complex **2** is 12.2 kcal/mol. These values imply that the methylated complex has a lower free energy activation barrier with a difference of 0.8 kcal/mol.

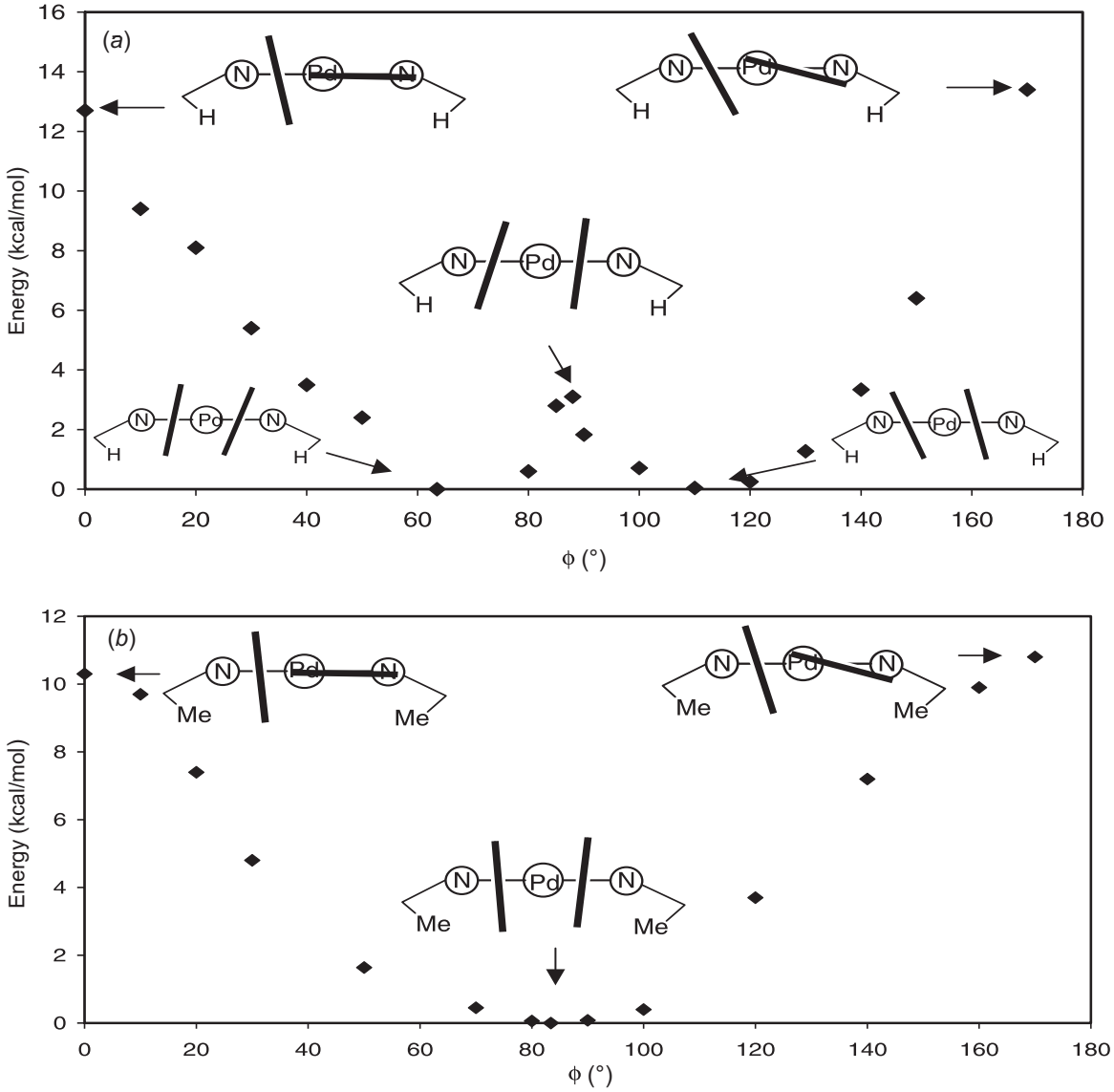
ϕ vs. the skeletal conformation of the coordinated bpz′m ligand — N-Pd-N bite angle and N-Pd-N/N_4 dihedral angle

The skeletal conformation of the bpz′mR ligands must be affected by the rotation of the C_6F_5 groups in the sense that the ligand should adapt its conformation to facilitate this rotation. Bearing in mind our previous proposal concerning the distortions observed in complexes with substituted pyrazoles, we considered two skeletal parameters for the coordinated N-donor ligand (see Scheme 3): (*i*) the bite angle N-Pd-N and (*ii*) the dihedral angle between the coordination plane (N-Pd-N) and the averaged plane of the four pyrazolic nitrogens atoms (NNNN = N_4).

An overview of Fig. 3 shows that these two parameters are linearly related in the sense that the dihedral angle increases as the bite angle N-Pd-N opens. Given this mutual relationship between these parameters, we chose the N-Pd-N bite angle to report the conformation of the N-donor ligand in the different steps of the C_6F_5 rotation. The effect on the bite angle is due to both C_6F_5 groups and, to estimate how much both rings deviate from normality (with respect to the coordination plane), we defined the parameter $\alpha + \alpha'$ as $\alpha = |\phi - 90°|$ and $\alpha' = |\phi' - 90°|$ (absolute values in both cases) and studied its relation with the bite angle. One must also take into account that the situation in which the two rings are orthogonal (α and $\alpha' = 0°$) is the state of minimum energy for complex **2**, but in the case of complex **1** this disposition does not correspond to the minimum state but is not far from it. The variation of the bite angle with $\alpha + \alpha'$ for **1** and **2** is represented in Fig. 4. The whole set of values fits

© 2005 NRC Canada

Fig. 2. Plot of the relative energy (kcal/mol) as a function of the ϕ angle for the rotamers of complexes (*a*) **1** and (*b*) **2**.



well in a branch of a quadratic parabola. Then, it is clear that an inverse relationship exists between these two parameters. In the case of **2**, the variation in the value of the bite angle is reasonably gradual, whereas for **1** it changes very slightly for small α + α′ values (e.g., when the pentafluorophenyl rings are near the normal position), but decreases quite markedly when higher α + α′ values are reached. Considering the relationship previously established, one would expect that the dihedral angle N-Pd-N/N_4 would also be reduced when α + α′ is higher (this has been confirmed). In conclusion, when one C_6F_5 ring is near coplanar with the coordination plane (high value of α + α′), the bpz′mR facilitates, as far as possible, the rotation of the C_6F_5 groups by reducing the N-Pd-N angle.

When comparing both complexes it can be seen that the theoretical values found for the N-Pd-N angle are smaller for the methylated complex for all values of α + α′. The same applies to the N-Pd-N/N_4 angle (see Tables 1 and 2 and Fig. 4). In other words, the methylated complex **2** has more favourable structures for ring rotation in all steps of the process. This situation is consistent with our proposal concerning the distortions induced in the complexes owing to the presence of substituents in the 3-position of the pyrazolyl rings (see Scheme 3).

X-ray structures of [Pd(C_6F_5)$_2$(bpzmPh)] (1), [Pd(C_6F_5)$_2$(bpz*mPh)] (2), [Pd(C_6F_5)$_2${bpzm(2-C_6H_4OMe)}]·$C_2H_4Cl_2$, 3·$C_2H_4Cl_2$, and [Pd(C_6F_5)$_2$(bpz*mPy)] (8)

To complete the family of complexes we synthesized complex **1** in a similar way to the complexes previously reported (33). The corresponding analytical and spectroscopic data are given in the Experimental section.

As previously stated, we were interested in evaluating whether the distortions previously found in complexes of this type with substituted pyrazoles were also present in the solid state. With this aim in mind, we tried to obtain crystals of several derivatives to determine their X-ray molecular structures. Fortunately, suitable crystals could be obtained for complexes **1** and **2** — on which the theoretical calcula-

© 2005 NRC Canada

Fig. 3. Linear plot of the dihedral angle N-Pd-N/N_4 vs. the bite angle N-Pd-N for **1** (◆) and **2** (■) (see Scheme 3, data from the theoretical calculations).

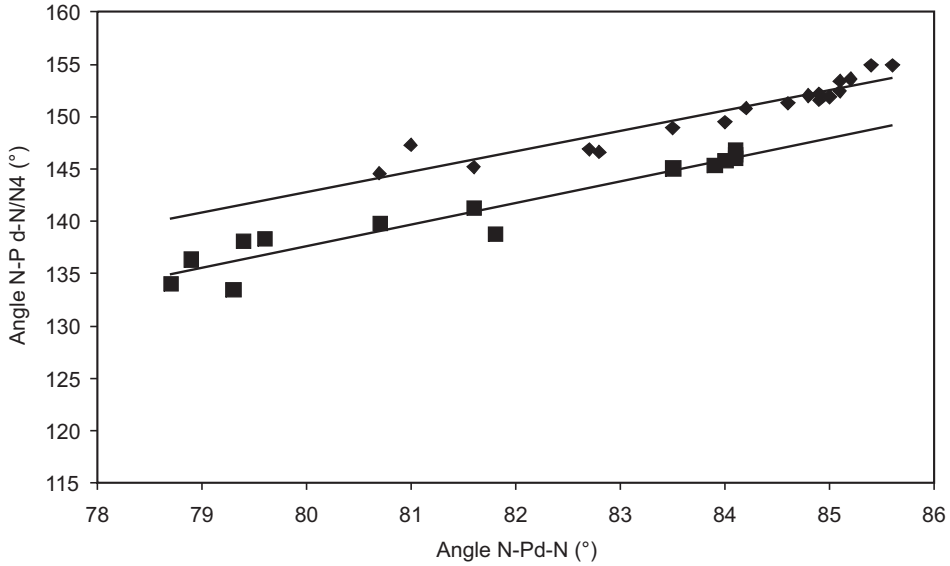
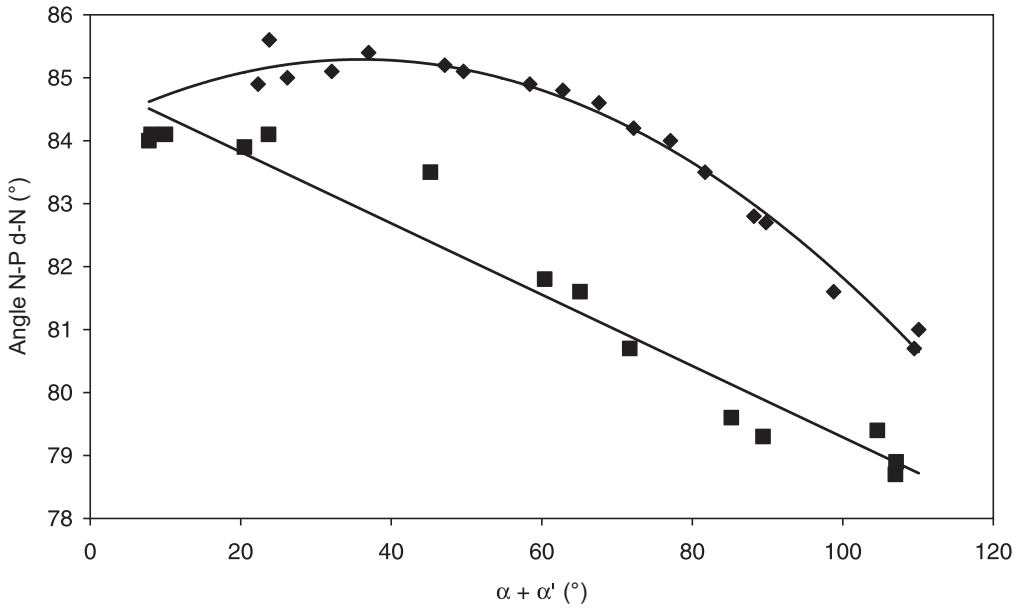


Fig. 4. Plot of the bite angle N-Pd-N vs. the function (α + α′), as defined in the text, for complexes **1** (◆) and **2** (■).



tions were performed for the isolated molecules — and two other complexes previously reported (**3** and **8**). The ORTEP plots of the molecules are shown in Figs. 5–8. The crystallographic data (Table 3) and a list of selected bond distances and angles (Tables 4 and 5) are given. Two molecules are present in the asymmetric unit of complex **1**. These two molecules are quite similar except for the orientation of the phenyl ring of the CHR group (see the following). The data corresponding to only one molecule are given in Table 4. A comparison of experimental data (from X-ray studies) and the calculated equilibrium geometries for **1** and **2** is also given in Table 4. To see whether the 6-31G basis set is good enough to study this system, we have also performed calculations with the larger 6-31G(d) basis set that includes polarization functions on heavy atoms. Comparison of results show that no major improvement emerges from the use of the larger basis set. In fact, the bond length distances involving the palladium are better described by the 6-31G basis set (probably because of cancellation of errors). In general we see quite a good agreement between the X-ray and calculated geometries within both basis sets as the bond lengths differ by less than 0.1 Å and angles agree within an error no larger than 4° (less than 0.07 rad).

For all the complexes, the geometry around the palladium atoms is approximately square-planar, with two coordinated pyrazole nitrogens and the carbons of the pentafluorophenyl rings. The distances of the Pd—N coordination bonds are comparable to those of other bis(pyrazol-1-yl)methane complexes (31–35, 55). Significant differences concerning the Pd—N bond distances were not found on changing the

© 2005 NRC Canada

Table 3. Crystallographic data for complexes **1**, **2**, **3**·$C_2H_4Cl_2$, and **8**.

Complex	**1**	**2**	**3**·$C_2H_4Cl_2$	**8**
Empirical formula	$C_{25}H_{12}F_{10}N_4Pd$	$C_{29}H_{20}F_{10}N_4Pd$	$C_{28}H_{18}Cl_2F_{10}N_4OPd$	$C_{28}H_{19}F_{10}N_5Pd$
Formula weight	664.81	720.89	793.76	721.9
Temperature (K)	291(2)	290(2)	290(2)	292(2)
Wavelength (Å)	0.710 73	0.710 73	0.710 73	1.541 78
Crystal system	Monoclinic	Monoclinic	Monoclinic	Monoclinic
Space group	*P*2(1)/*n*	*P*2(1)/*n*	*P*2(1)/*c*	*P*2(1)/*n*
a (Å)	17.169(6)	11.161(3)	14.321(1)	19.517(2)
b (Å)	14.018(5)	15.714(3)	14.664(1)	15.976(1)
c (Å)	21.491(8)	16.118(8)	15.415(1)	9.0688(6)
β (°)	103.458(9)	103.35(4)	111.3(1)	100.178(9)
Volume (Å^3)	5030(3)	2750(2)	3015.5(4)	2783.3(4)
Z	8	4	4	4
D_{calcd} (g cm^{-3})	1.756	1.741	1.748	1.723
Absorption coefficient (cm^{-1})	8.35	7.71	8.85	6.26
F(000)	2608	1432	1568	1432
Color, habit	Colorless, prismatic	Colorless, block	Colorless, prismatic	Colorless, block
Crystal size (mm)	0.15 × 0.15 × 0.14	0.2 × 0.2 × 0.1	0.3 × 0.3 × 0.3	0.3 × 0.2 × 0.2
θ range for data collection	1.37–25.00	2.02–27.95	2.06–27.97	3.6–66.74
Limiting indices	$-20 \le h \le 17$	$-14 \le h \le 14$	$-18 \le h \le 17$	$-23 \le h \le 22$
	$-16 \le k \le 12$	$0 \le k \le 20$	$0 \le k \le 19$	$0 \le k \le 19$
	$-25 \le l \le 25$	$0 \le l \le 21$	$0 \le l \le 20$	$0 \le l \le 10$
Observed reflections	4243	3355	4801	3797
Independent reflections	8780 (*R*(int) = 0.091 4)	6587 (*R*(int) = 0.065 2)	7247 (*R*(int) = 0.047 0)	4669 (*R*(int) = 0.028)
Data/restraints/parameters	8780/0/722	6587/0/401	7247/0/458	3794/0/471
Goodness-of-fit on F^2	0.964	0.978	1.016	1.008
Final *R* indices ($I > 2\sigma(I)$)	*R*1 = 0.074 9	*R*1 = 0.057 2	*R*1 = 0.046 3	*R*1 = 0.029
	*wR*2 = 0.159 2	*wR*2 = 0.108 5	*wR*2 = 0.139 7	*wR*2 = 0.032
R indices (all data)	*R*1 = 0.170 3	*R*1 = 0.179 1	*R*1 = 0.098 1	*R*1 = 0.040
	*wR*2 = 0.203 9	*wR*2 = 0.137 2	*wR*2 = 0.200 2	*wR*2 = 0.037
Largest diff. peak and hole (e Å^{-3})	0.927 and –0.824	0.885 and –0.605	0.566 and –0.594	0.491 and –0.387

Fig. 5. ORTEP plot with atom numbering of **1** (30% probability ellipsoids).

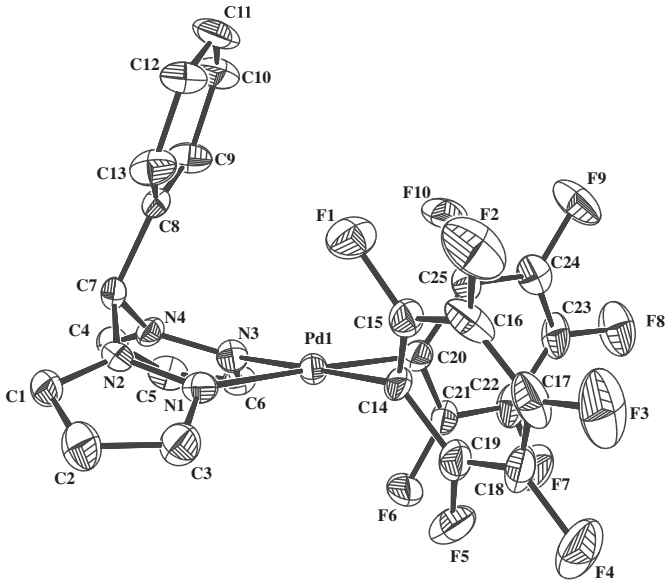
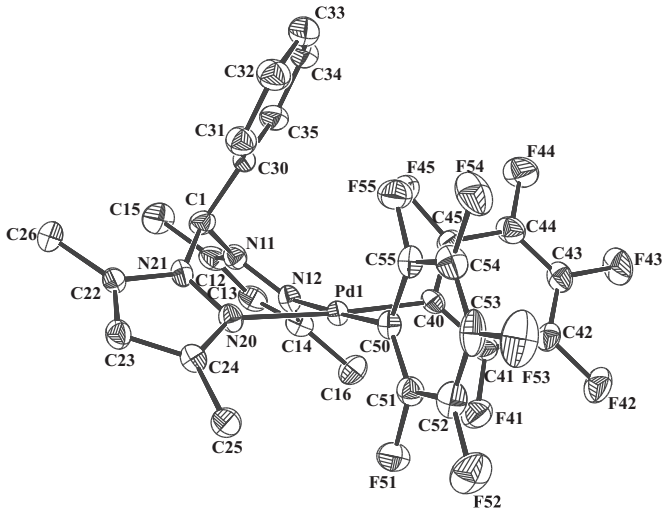


Fig. 6. ORTEP plot with atom numbering of **2** (30% probability ellipsoids).



substituent in the pyrazolyl ring. If a plane is defined containing the palladium atom, the carbon of the CHR group and the C_{ipso} of the R ring, then the plane of the phenyl or pyridine rings in **1**, **2**, and **8** is not far from orthogonal (dihedral angles of 92.0(5)° and 102.7(5)° for the two molecules of the asymmetric unit of **1**, 100.7(2)° for **2**, and 102.8(1)° for **8**). However, in complex **3** the plane of the anisole ring is partially twisted (dihedral angle of 141.3(1)°).

© 2005 NRC Canada

Fig. 7. ORTEP plot with atom numbering of **3** (30% probability ellipsoids).

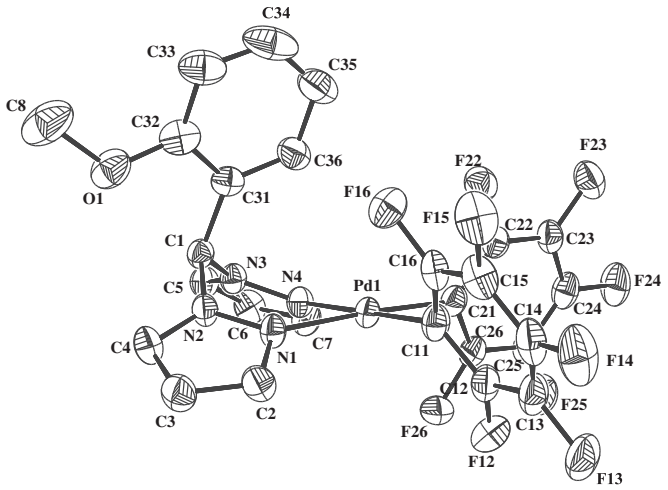


Fig. 8. ORTEP plot with atom numbering of **8** (30% probability ellipsoids).

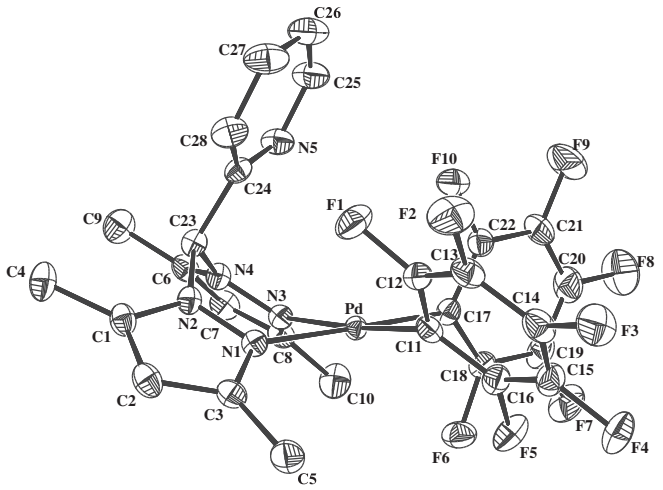


Table 4. Selected geometric parameters (in angstroms and degrees) of complexes **1** and **2** optimized at the B3LYP level in the gas phase and experimental values from the X-ray structure determinations.

	1				**2**		
Geometrical feature	Exp. values	6-31G	6-31G*	Geometrical feature	Exp. values	6-31G	6-31G*
Bond lengths (Å)							
Pd(1)—N(1)	2.066(9)	2.160	2.191	Pd(1)—N(12)	2.094(5)	2.164	2.206
Pd(1)—N(3)	2.093(8)	2.151	2.179	Pd(1)—N(20)	2.127(5)	2.181	2.218
Pd(1)—C(14)	2.01(1)	2.025	2.020	Pd(1)—C(40)	2.023(6)	2.030	2.023
Pd(1)—C(20)	1.99(1)	2.025	2.018	Pd(1)—C(50)	2.016(6)	2.032	2.023
N(2)—C(7)	1.45(1)	1.465	1.460	C(1)—N(11)	1.468(8)	1.464	1.458
N(4)—C(7)	1.45(1)	1.467	1.462	C(1)—N(21)	1.450(8)	1.463	1.459
C(7)—C(8)	1.55(1)	1.528	1.528	C(1)—C(30)	1.526(8)	1.528	1.528
N(1)—N(2)	1.37(1)	1.380	1.360	N(12)—N(11)	1.363(6)	1.389	1.366
N(3)—N(4)	1.36(1)	1.380	1.360	N(20)—N(21)	1.369(6)	1.392	1.367
Bond angles (°)							
C(20)-Pd(1)-C(14)	86.2(4)	86.6	86.4	C(50)-Pd(1)-C(40)	86.2(2)	85.0	84.2
C(20)-Pd(1)-N(1)	177.4(4)	175.5	175.2	C(50)-Pd(1)-N(12)	178.1(2)	179.1	179.7
C(14)-Pd(1)-N(1)	91.6(4)	95.3	96.1	C(40)-Pd(1)-N(12)	93.3(2)	95.1	96.1
C(20)-Pd(1)-N(3)	94.1(4)	93.1	93.3	C(50)-Pd(1)-N(20)	95.4(2)	96.0	96.5
C(14)-Pd(1)-N(3)	179.4(4)	177.3	177.8	C(40)-Pd(1)-N(20)	175.8(2)	176.8	178.1
N(1)-Pd(1)-N(3)	88.2(3)	85.1	84.4	N(12)-Pd(1)-N(20)	85.1(2)	84.1	83.2
N(2)-C(7)-N(4)	109.5(8)	109.7	110.0	N(21)-C(1)-N(11)	110.7(5)	110.3	110.9
N(2)-C(7)-C(8)	113.4(8)	112.9	112.9	N(21)-C(1)-C(30)	113.5(5)	114.6	114.3
N(4)-C(7)-C(8)	112.7(8)	114.3	114.2	N(11)-C(1)-C(30)	114.4(5)	114.0	114.0

This difference probably arises because of the presence of the OMe group, which lies almost in the anisole plane and points away from the molecule. The disposition of the anisole ring is similar to that found in an allylpalladium complex containing the same N-donor ligand (33).

A selection of the structural parameters related to our previous discussion is compiled in Table 6. The data obtained from the theoretical calculations for complexes **1** and **2** have also been included in brackets (for **1** the values for the minimum of ΔE = 0.04 kcal/mol are given). The parameters for the structure of the previously reported ferrocenyl complex **7** are also included (33). A clear difference can be observed between the data for complexes **1** and **3**, where the pyrazole rings are unsubstituted, and complexes **2**, **7**, and **8**, which contain 3,5-dimethylated rings. Both N-Pd-N and N-Pd-N/N_4 angles are higher in compounds **1** and **3** and lower and quite similar for the other three compounds. The difference in the stated angles that depends on the type of pyrazole present in the ligand is in accordance with previous observations (33, 35) and with our theoretical predictions. The values of the two C-Pd-N angles are also reflected in Table 6. It is possible to see that these angles are larger in the methylated complexes, a fact that should facilitate the C_6F_5 rotation. As far as ϕ and ϕ' are concerned, in complexes **1** and **3** these angles are comparable, far from the orthogonal position and very similar to those calculated for the minimum

© 2005 NRC Canada

Table 5. Selected bond lengths and angles for complexes **3**·$C_2H_4Cl_2$ and **8** from the X-ray structures.

3·$C_2H_4Cl_2$		**8**	
Bond lengths (Å)			
Pd(1)—C(11)	2.002(5)	Pd(1)—N(1)	2.092(3)
Pd(1)—C(21)	2.010(5)	Pd(1)—N(3)	2.140(3)
Pd(1)—N(1)	2.085(4)	Pd(1)—C(11)	2.012(4)
Pd(1)—N(4)	2.094(4)	Pd(1)—C(17)	2.013(3)
N(1)—N(2)	1.363(6)	N(1)—N(2)	1.363(4)
N(2)—C(1)	1.463(6)	N(3)—N(4)	1.337(5)
N(3)—N(4)	1.371(6)	N(2)—C(23)	1.448(4)
N(3)—C(1)	1.457(7)	N(4)—C(23)	1.451(5)
O(1)—C(8)	1.434(9)	C(23)—C(24)	1.518(5)
O(1)—C(32)	1.349(9)		
C(1)—C(31)	1.501(8)		
Bond angles (°)			
C(11)-Pd(1)-C(21)	87.7(2)	N(1)-Pd(1)-N(3)	85.2(1)
C(11)-Pd(1)-N(1)	91.1(2)	C(11)-Pd(1)-C(17)	85.5(1)
C(21)-Pd(1)-N(1)	176.7(2)	C(11)-Pd(1)-N(1)	92.7(1)
C(11)-Pd(1)-N(4)	178.6(2)	N(1)-Pd-C(17)	177.8(1)
C(21)-Pd(1)-N(4)	93.7(2)	N(3)-Pd-C(11)	174.6(1)
N(1)-Pd(1)-N(4)	87.5(2)	N(3)-Pd-C(17)	96.4(1)
C(32)-O(1)-C(8)	118.9(7)	N(2)-C(23)-N(4)	111.8(3)
N(2)-C(1)-N(3)	109.6(4)	N(2)-C(23)-C(24)	114.2(3)
N(2)-C(1)-C(31)	112.3(4)	N(4)-C(23)-C(24)	113.6(3)
N(3)-C(1)-C(31)	115.2(4)		

energy structure of 0.04 kcal/mol. In the methylated complex **2**, one of the C_6F_5 rings is not too far from the orthogonal position (according to calculations), whereas the second ring is tilted. For this ϕ' value, less agreement with the theoretical results is observed. To analyze this point the values of ϕ and ϕ' were fixed according to the X-ray structure of **2** and the rest of the structure was minimized using the same theoretical basis as in the preceding discussion. The energy value for this hypothetical structure was 0.8 kcal/mol above the minimum of this system. Perhaps the observed differences in the values of these angles with respect to the gas-phase minimum can be ascribed to the effect of packing in the solid state.[2]

Dynamics of the C_6F_5 rotation in [$Pd(C_6F_5)_2$(bpz′mR)] complexes in solution

The dynamics of the restricted rotation of C_6F_5 groups directly bonded to the square-planar Pd(II) centres for complexes **2**, **8** (32), and **3**–**7** (34) have been previously studied in solution by ^{19}F NMR spectroscopy. The corresponding study for new complex **1** was also carried out in 1,1′,2,2′-$CDCl_2CDCl_2$. At 253 K, one F_{para}, one F_{meta}, and two F_{ortho} signals were observed. The coalescence temperature was reached at 338 K and the free energy of activation was calculated. The data for all complexes are gathered in Table 7.

A plot of the free energies of activation vs. the coalescence temperatures is given in Fig. 9. Two straight lines for methylated and non-methylated derivatives can be plotted. The fact that the points fit approximately to a straight line independently of the solvent used ($CDCl_3$ or 1,1′,2,2′-$CDCl_2CDCl_2$) indicates that this is not an important factor governing the C_6F_5 rotation. Furthermore, the nature of the R groups in the ligands does not seem to have a clear influence either. It is evident from the data that higher values are obtained in complexes with scorpion-type ligands that do not contain substituents in the pyrazole groups than in those with 3,5-dimethylated rings. If we compare the corresponding two straight lines at room temperature, it can be estimated that the free energy of activation is about 2.3 kcal/mol higher for the non-methylated derivatives. The difference in the free energies of activation between complexes **1** and **2** obtained in the theoretical calculations is 0.8 kcal/mol. Although the two results are not quite close, in both cases lower energy barriers are found for the methylated complexes. At this point it is important to stress the fact that theoretical free energy calculations imply assuming that the system behaves as an ideal gas and that the rotational and vibrational degrees of freedom are well-described through the rigid rotor and harmonic approximations, respectively. Besides, the theoretical calculations of free energy of activation are referred to the gas phase and the experimental data correspond to the complexes in solution. As stated, the values of the bite and the N-Pd-N/N_4 dihedral angles are higher for **1** than for **2**. This is also true for the states of maximum and minimum energy. It is remarkable that the differences between the two complexes are higher in the maximum than in the minimum of energy. Consequently, one origin of the different experimental values obtained for the free energy of activation in the two types of complex could lie in the fact that the methylated complexes are more able to adapt the nitrogenated ligand to the ring rotation steric requirements that are more important in the maximum state of energy. In the higher energy structure, the rotating C_6F_5 ring lies approximately in the coordination plane of the complex. In this conformation it is reasonable to assume that the steric hindrance with the substituent in position 3 of the pyrazole could be neglected and then the bite angle N-Pd-N is the main factor to consider. Let us finally emphasize that our calculations have allowed comparison of the structures in the maximum energy situation and not only structures that should correspond approximately to the minimum of energy, such as those obtained from the X-ray determinations.

Conclusion

The rotation of a C_6F_5 group around the Pd—C axis in the complexes [$Pd(C_6F_5)_2$(bpz′mPh)] (bpz′mPh = bis(pyrazol-1-yl)phenylmethane (**1**) and bpz′mPh = bis(3,5-dimethylpyrazol-1-yl)phenylmethane (**2**)) has been theoretically stud-

[2] Supplementary data for this article are available on the journal Web site (http://canjchem.nrc.ca) or may be purchased from the Depository of Unpublished Data, Document Delivery, CISTI, National Research Council Canada, Ottawa, ON K1A 0R6, Canada. DUD 4071. For more information on obtaining material refer to http://cisti-icist.nrc-cnrc.gc.ca/irm/unpub_e.shtml. CCDC 252030 ([$Pd(C_6F_5)_2$(bpzmPh)]) and 244833–244835 ([$Pd(C_6F_5)_2$(bpz*mPh)], [$(Pd(C_6F_5)_2$(bpzmArOMe)·$C_2H_4Cl_2$], and [$Pd(C_6F_5)_2$(bpzmpy)], respectively) contain the crystallographic data for this manuscript. These data can be obtained, free of charge, via www.ccdc.cam.ac.uk/conts/retrieving.html (Or from the Cambridge Crystallographic Data Centre, 12 Union Road, Cambridge CB2 1EZ, UK; fax +44 1223 336033; or deposit@ccdc.cam.ac.uk).

© 2005 NRC Canada

Table 6. Selected structural parameters deduced from the X-ray structures of **1**, **2**, **3**·$C_2H_4Cl_2$, **7**, and **8** (values in brackets correspond to data from the theoretical calculations with the 6-31G basis set).

R (complex)	3,5 pz Substitutent	ϕ (°)	ϕ′ (°)	<N-Pd-N (°)	<N-Pd-N/N_4 (°)	<C-Pd-N (°)
Ph (**1**)	H	105.3	110.6	88.2(3)	159.6	91.6(4), 94.1(4)
		[110.0]	[117.1]	[85.2]	[153.6]	[95.3], [93.1]
2-Anis (**3**)	H	107.6	114.8	87.5(2)	158.9	91.1(2), 93.7(2)
Ph (**2**)	Me	62.3	88.2	85.1(2)	144.9	93.2(2), 95.4(2)
		[83.4]	[91.5]	[84.1]	[146.1]	[95.1], [96.0]
Fec (**7**)	Me	92.5	126.3	84.22(13)	144.0	92.26(15), 95.13(15)
Py (**8**)	Me	96.7	126.5	85.2(1)	145.5	92.7(1), 96.4(1)

Fig. 9. Linear plot of $\Delta G_c^{\ddagger}$ (kcal/mol) vs. T_c for the F_{ortho}–$F_{ortho'}$ exchange (Pd–C_6F_5 rotation) in [Pd(C_6F_5)$_2$(bpz′mR)] complexes. pz′ = 3,5-dimethylpyrazole (■) and pz′ = pyrazole (◆). The numbers near the points refer to the specific complex.

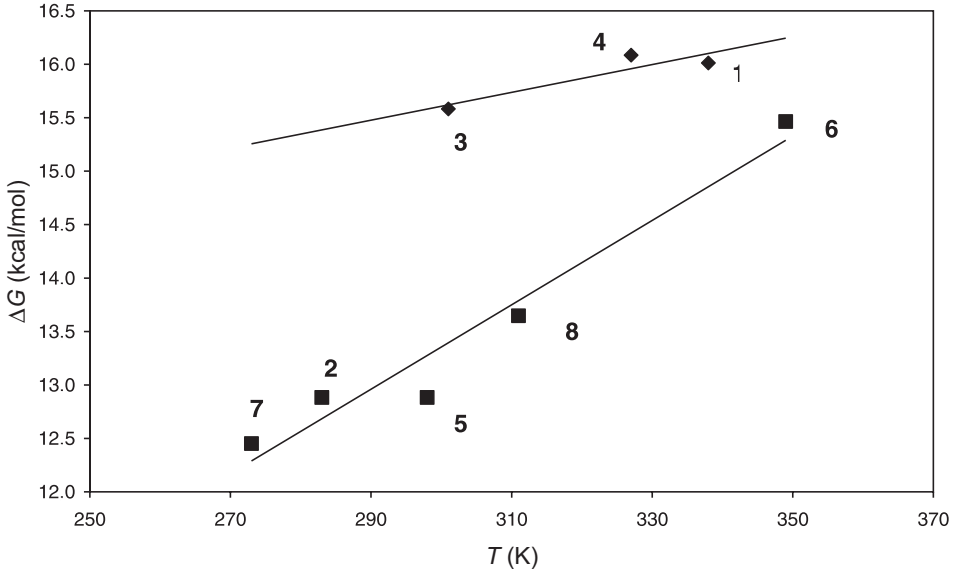


Table 7. Coalescence temperatures (T_c) and free energies of activation at the coalescence temperature ($\Delta G_c^{\ddagger}$) for the F_{ortho}–$F_{ortho'}$ exchange (C_6F_5 rotation).

Complex	3,5 pz Substituent	T_c (K)	$\Delta G_c^{\ddagger}$ (kcal/mol)
1[a]	H	338	16.0
3[b]	H	301	15.6
4[a]	H	327	16.1
2[b]	Me	283	12.9
5[b]	Me	298	12.9
6[a]	Me	349	15.5
7[a]	Me	273	12.5
8[b]	Me	311	13.6

[a] 1,1′,2,2′-$CDCl_2CDCl_2$.
[b] $CDCl_3$.

ied at a DFT level. Results have been compared with experimental information obtained in solution (free energies of activation determined by NMR) and in the solid state (X-ray diffraction studies). Different structural parameters such as the perfluorophenyl ring orientation, energy of the system, and conformation of the nitrogenated ligand have been analyzed. It has been found that when one ring is forced to rotate, the other ring adapts its disposition. The most stable structure for both complexes involves the two pentafluorophenyl rings at a nearly parallel position. In the minimum energy structure of complex **2**, these rings are approximately orthogonal to the coordination plane. This is not the case for complex **1**. Two skeletal parameters related with the coordination of the nitrogenated ligand, namely the bite angle and the N-Pd-N/N_4 dihedral angle, have also been analyzed. Both angles are smaller when the pentafluorophenyl rings deviate more from orthogonality with respect to the coordination plane. The values for these parameters are always smaller in the case of the methylated complex **2**, the effect being more noticeable in the maximum energy geometry.

Lower free activation energies at the coalescence temperature ($\Delta G_c^{\ddagger}$) for the ring rotation process have been found both theoretically and experimentally for the methylated derivatives when compared with the complexes containing unsubstituted pyrazolyl ligands. The origin of the energy differences found in solution for the C_6F_5 rotation may be found in the smaller values obtained from our theoretical calculations for the N-Pd-N bite angle and for the skeletal N-Pd-N/N_4 dihedral angle in **2** as compared with **1** in the state of maximum energy. This finding is consistent with previous proposals that one important effect in the aryl rotation was the "in-plane" hindrance of the donor atoms cis to

© 2005 NRC Canada

the polyhaloaryl group. According to our theoretical and experimental results, the direct steric repulsion of the Me^3 of the pyrazole groups with the pentafluorophenyl rings does not have a clear effect over the C_6F_5 rotation.

Several X-ray structure determinations have been performed for complexes **1**, **2**, and other derivatives of this family. It has been found that the values of the bite angle and the N-Pd-N/N_4 dihedral angle are always smaller in the methylated derivatives, in accordance with theoretical predictions.

Acknowledgments

We are grateful to the Spanish Ministerio de Educación y Ciencia (Project Nos. CTQ2005-01430 and BQU-2002-00301) and the Consejería de Ciencia y Tecnología of the Junta de Comunidades de Castilla-La Mancha (PBI-05-003) for financial support and the computational service of the Universidad de Castilla-La Mancha.

References

1. R. Usón and J. Forniés. Adv. Organomet. Chem. **28**, 219 (1988).
2. A.J. Canty. Comprehensive organometallic chemistry. Vol. 9. *Edited by* E.W. Abel, F.G.A. Stone, and G. Wilkinson. Pergamon Press, Oxford. 1995. Chap. 5; P.M. Maitlis, P. Espinet, and M.J.H. Russell. Comprehensive organometallic chemistry. Vol. 6. *Edited by* E.W. Abel, F.G.A. Stone, and G. Wilkinson. Pergamon Press, Oxford. 1982. Chap. 38.4.
3. R. Usón, J. Forniés, P. Espinet, E. Lalinde, P.G. Jones, and G.M. Sheldrick. J. Chem. Soc. Dalton Trans. 2389 (1982); R. Usón, J. Forniés, P. Espinet, and E. Lalinde. J. Organomet. Chem. **254**, 371 (1983); A.C. Albéniz, P. Espinet, Y. Jeanning, M. Philoche-Levisalles, and B.E. Mann. J. Am. Chem. Soc. **112**, 6594 (1990); A.C. Albeniz and P. Espinet. Organometallics, **10**, 2987 (1991); A.C. Albéniz, P. Espinet, and Y.-S. Lin. Organometallics, **14**, 2977 (1995); A.C. Albéniz, P. Espinet, and Y.-S. Lin. J. Am. Chem. Soc. **118**, 7145 (1996); I. Ara, J. Forniés, A. García, J. Gómez, E. Lalinde, and M.T. Moreno. Chem. Eur. J. **8**, 3698 (2002).
4. S. Park, M. Pontier-Johnson, and D.M. Roundhill. J. Am. Chem. Soc. **111**, 3101 (1989).
5. A.L. Casado, J.A. Casares, and P. Espinet. Organometallics, **16**, 5730 (1997).
6. A.L. Casado and P. Espinet. Organometallics, **17**, 954 (1998).
7. A.L. Casado and P. Espinet. J. Am. Chem. Soc. **120**, 8978 (1998).
8. See, for example: R. Usón, J. Forniés, M.A. Usón, M. Tomás, and M.A. Ibañez. J. Chem. Soc. Dalton Trans. 401 (1994); I. Ara, J. Forniés, E. Lalinde, M.T. Moreno, and M. Tomás. J. Chem. Soc. Dalton Trans. 2735 (1994); L.R. Falvello, J. Forniés, R. Navarro, V. Sicilia, and M. Tomás. J. Chem. Soc. Dalton Trans. 3143 (1994); A.C. Albéniz, P. Espinet, Y.-S. Lin, A.G. Orpen, and A. Martín. Organometallics, **15**, 5003 (1996); J. Ruiz, V. Rodríguez, G. López, P.A. Chaloner, and P.B. Hitchcock. Organometallics, **15**, 1662 (1996).
9. L.R. Falvello, J. Forniés, R. Navarro, A. Rueda, and E.P. Urriolabeitia. Organometallics, **15**, 309 (1996); I. Ara, J.R. Berenguer, J. Forniés, E. Lalinde, and M. Tomás. Organometallics, **15**, 1014 (1996); I. Ara, L.R. Falvello, S. Fernández, J. Forniés, E. Lalinde, A. Martín, and M.T. Moreno. Organometallics, **16**, 5923 (1997); L.R. Falvello, J. Forniés, C. Fortuño, A. Martín, and A.P. Martínez-Sariñena. Organometallics, **16**, 5849 (1997).
10. See, for example: J.M. Casas, J. Forniés, A. Martín, B. Menjón, and M. Tomás. J. Chem. Soc. Dalton Trans. 2949 (1995); I. Ara, E. Delgado, J. Forniés, E. Hernández, E. Lalinde, N. Mansilla, and M.T. Moreno. J. Chem. Soc. Dalton Trans. 3201 (1996); J. Forniés, M.A. Gómez-Saso, A. Martín, F. Martínez, B. Menjón, and J. Navarrete. Organometallics, **16**, 6024 (1997); J. Forniés, F. Martínez, R. Navarro, E.P. Urrialobeitia, and A.J. Welch. J. Chem. Soc. Dalton Trans. 2805 (1995); J. Forniés, R. Navarro, V. Sicilia, and M. Tomás. Inorg. Chem. **32**, 3675 (1993).
11. J.A. Casares, P. Espinet, J.M. Martínez-Illarduya, and Y.-S. Lin. Organometallics, **16**, 770 (1997).
12. G.B. Deacon, B.M. Gatehouse, and K.T. Nelson-Reek. J. Organomet. Chem. **359**, 267 (1989).
13. J. Ruiz, M.T. Martínez, C. Vicente, G. García, G. López, P.A. Chaloner, and P.B. Hitchcock. Organometallics, **12**, 4321 (1993).
14. A.C. Albéniz, J.C. Cuevas, P. Espinet, J. de Mendoza, and P. Prados. J. Organomet. Chem. **410**, 257 (1991).
15. E.W. Abel, K.G. Orrell, A.G. Osborne, H.M. Paint, V. Sik, M.B. Hursthouse, and K.M. Abdul Malik. J. Chem. Soc. Dalton Trans. 3441 (1994).
16. A. Gelling, M.D. Olsen, K.G. Orrell, A.G. Osborn, and V. Sik. Inorg. Chim. Acta, **264**, 257 (1997); K.G. Orrell, A.G. Osborne, V. Sik, and M.W. da Silva. J. Organomet. Chem. **530**, 235 (1997).
17. F. Gómez-de la Torre, F.A. Jalón, A. López-Agenjo, B.R. Manzano, A. Rodríguez, T. Sturm, W. Weissensteiner, and M. Martínez-Ripoll. Organometallics, **17**, 4634 (1998).
18. M.C. Carrión, A. Guerrero, F.A. Jalón, B.R. Manzano, A. de la Hoz, R.M. Claramunt, V. Milata, and J. Elguero. Inorg. Chem. **42**, 885 (2003).
19. K. Marshall, K. Rosmarion, O. Sklyut, N. Azar, R. Callahan, and R. Rothchild. J. Fluorine Chem. **125**, 1893 (2004).
20. J. Sandström. Dynamic NMR spectroscopy. Academic Press, London. 1982.
21. J.A. Casares, S. Coco, P. Espinet, and Y.-S. Lin. Organometallics, **14**, 3058 (1995).
22. J.A. Casares and P. Espinet. Inorg. Chem. **36**, 5428 (1997).
23. M.A. Alonso, J.A. Casares, P. Espinet, J.M. Mártinez-Ilarduya, and C. Pérez-Briso. Eur. J. Inorg. Chem. 1745 (1998).
24. R. de la Cruz, P. Espinet, A.M. Gallego, J.M. Martín-Alvárez, and J.M. Martínez-Ilarduya. J. Organomet. Chem. **663**, 108 (2002).
25. C. Bartolomé, R. De Blas, P. Espinet, J.M. Martín-Alvárez, and F. Villafañe. Angew. Chem. Int. Ed. **40**, 2521 (2001).
26. A.C. Albeniz, A.L. Casado, and P. Espinet. Organometallics, **16**, 5416 (1997).
27. J. Forniés, F. Martínez, R. Navarro, and E.P. Urrialobeitia. Organometallics, **15**, 1813 (1996); J. Forniés, M.A. Gómez-Saso, E. Lalinde, F. Martínez, and M.T. Moreno. Organometallics, **11**, 2873 (1992); J.R. Berenguer, J. Forniés, E. Lalinde, F. Martínez, E. Urriolabeitia, and A.J. Welch. J. Chem. Soc. Dalton Trans. 1291 (1994); J. Forniés, F. Martínez, R. Navarro, E. Urriolabeitia, and A.J. Welch. J. Chem. Soc. Dalton Trans. 2147 (1993); U. Amador, E. Delgado, J. Forniés, E. Hernández, E. Lalinde, and M.T. Moreno. Inorg. Chem. **34**, 5279 (1995); S. Coco and P. Espinet. J. Organomet. Chem. **484**, 113 (1994).
28. J.A. Casares, P. Espinet, K. Soulantica, I. Pascual, and A.G. Orpen. Inorg. Chem. **36**, 5251 (1997).
29. F. Gómez-de la Torre, A. de la Hoz, F.A. Jalón, B.R. Manzano, and A.M. Rodríguez. Inorg. Chem. **39**, 1152 (2000).

© 2005 NRC Canada

30. A.C. Albeniz, A.L. Casado, and P. Espinet. Inorg. Chem. **38**, 2510 (1999).
31. P.K. Byers, A.J. Canty, and R.T. Honeyman. J. Organomet. Chem. **385**, 417 (1990); P.K. Byers and A.J. Canty. Organometallics, **9**, 210 (1990).
32. N. Arroyo, F. Gómez-de la Torre, F.A. Jalón, B.R. Manzano, B. Moreno-Lara, and A.M. Rodríguez. J. Organomet. Chem. **603**, 174 (2000).
33. M.C. Carrión, A. Díaz, A. Guerrero, F.A. Jalón, B.R. Manzano, A. Rodríguez, R.L. Paul, and J.C. Jeffery. J. Organomet. Chem. **650**, 210 (2002).
34. M.C. Carrión, A. Díaz, A. Guerrero, F.A. Jalón, B.R. Manzano, and A. Rodríguez. New J. Chem. **26**, 305 (2002).
35. S. Tsuji, D.C. Swenson, and R.F. Jordan. Organometallics, **18**, 4758 (1999).
36. G.K. Anderson, R.J. Cross, L. Manojlovic-Muir, K.W. Muir, and M. Rocamora. Organometallics, **7**, 1520 (1988).
37. Y. Crameri, J. Foricher, U. Hengartner, C. Jenny, F. Kienzle, H. Ramuz, M. Scalone, M. Schlageter, R. Schmid, and S. Wang. Chimia, **51**, 303 (1997); E.A. Broker, W. Burkhart, M. Hennig, M. Scalone, and R. Schmid. Tetrahedron: Asymmetry, **9**, 4043 (1998); T.V. Rajanbabu, T.A. Ayers, and A.L. Caasalnuovo. J. Am. Chem. Soc. **116**, 4101 (1994).
38. G. Trabesinger, A. Albinati, N. Feiken, R.W. Kunz, P.S. Pregosin, and M. Tschoerner. J. Am. Chem. Soc. **119**, 6315 (1997); M. Tschoerner, P.S. Pregosin, and A. Albinati. Organometallics, **18**, 670 (1999).
39. P. Dotta, P.G. Anil Kumar, P.S. Pregosin, A. Albinati, and S. Rizzato. Organometallics, **23**, 2295 (2004).
40. S. Alvarez, P. Alemany, and D. Avnir. Chem. Soc. Rev. **34**, 293 (2005); P.J. Alonso, J. Forniés, M.A. García-Monforte, A. Martín, B. Menjón, and C. Rillo. Chem. Eur. J. **8**, 4056 (2002).
41. P. Espinet, J.M. Martínez-Ilarduya, C. Pérez-Briso, A.L. Casado, and M.A. Alonso. J. Organomet. Chem. **551**, 9 (1998).
42. L.K. Peterson, E. Kiehlmann, A.R. Sanger, and K.I. The. Can. J. Chem. **52**, 2367 (1974); K.I. The and L.K. Peterson. Can. J. Chem. **51**, 422 (1973).
43. M.J. Frisch, G.W. Trucks, H.B. Schlegel, G.E. Scuseria, M.A. Robb, J.R. Cheeseman, V.G. Zakrzewski, J.A. Montgomery, Jr., R.E. Stratmann, J.C. Burant, S. Dapprich, J.M. Millam, A.D. Daniels, K.N. Kudin, M.C. Strain, O. Farkas, J. Tomasi, V. Barone, M. Cossi, R. Cammi, B. Menucci, C. Pomelli, C. Adamo, S. Clifford, J. Ochterski, G.A. Petersson, P.Y. Ayala, Q. Cui, K. Morokuma, D.K. Malick, A.D. Rabuck, K. Raghavachari, J.B. Foresman, J. Ciolowski, J.V. Ortiz, B.B. Stefanov, G. Liu, A. Liashenko, P. Piskorz, I. Komaroni, R. Gomperts, R.L. Martin, D.J. Fox, T. Keith, M.A. Al-Laham, C.Y. Peng, A. Nanayakkara, C. Gonzalez, M. Challacombe, P.M.W. Gill, B.G. Johnson, W. Chen, M.W. Wong, J.L. Andrés, M. Head-Gordon, E.S. Replogle, and J.A. Pople. Gaussian 98 [computer program]. Gaussian Inc., Pittsburgh, Penn. 1998.
44. A.D. Becke. J. Chem. Phys. **98**, 5648 (1993); A.D. Becke. J. Chem. Phys. **96**, 2155 (1992).
45. C. Lee, W. Yang, and R.G. Parr. Phys. Rev. B, **B37**, 785 (1988).
46. P.J. Hay and W.R. Wadt. J. Chem. Phys. **82**, 299 (1985); W.R. Wadt and P.J. Hay. J. Chem. Phys. **82**, 284 (1985).
47. R. Ditchfield, W.J. Hehre, and J.A. Pople. J. Chem. Phys. **54**, 724 (1971); R. Ditchfield, W.J. Hehre, and J.A. Pople. J. Chem. Phys. **56**, 2257 (1972); P.C. Hariharan and J.A. Pople. Mol. Phys. **27**, 209 (1974); M.S. Gordon. Chem. Phys. Lett. **76**, 163 (1980); T. Clark, J. Chandrasekhar, G.W. Spitznagel, and P.v.R. Schleyer. J. Comput. Chem. **4**, 294 (1983).
48. C.Y. Peng, P.Y. Ayala, H.B. Schlegel, and M.J. Frisch. J. Comput. Chem. **17**, 49 (1996).
49. A.D. McQuarrie. Statistical thermodynamics. University Science Books, Mill Valley, Calif. 1973.
50. Bruker AXS. SAINT. Version 6.26 [computer program]. Bruker Analytical X-ray Systems, Inc., Madison, Wis. 2000.
51. G.M. Sheldrick. SADABS empirical absorption program. Version 2.03 [computer program]. Bruker Analytical X-ray Systems, Inc., Madison, Wis. 2000.
52. G.M. Sheldrick. Acta Crystallogr. Sect. A, **46**, 467 (1990).
53. A. Altomare, G. Cascarano, C. Giacovazzo, and A. Guagliardi. J. Appl. Crystallogr. **26**, 343 (1993).
54. G.M. Sheldrick. SHELXL-97 [computer program]. University of Göttingen, Göttingen, Germany. 1997.
55. G. Minghetti, M.A. Cinellu, A.B.G. Banditelli, F. Demartin, and M. Manassero. J. Organomet. Chem. **315**, 387 (1986); A.J. Canty, N.J. Minchin, L.M. Engelhardt, B.W. Sketton, and A.H. While. J. Chem. Soc. 645 (1986).

© 2005 NRC Canada

Glycosides from the sea cucumber *Cucumaria frondosa*. IV. Structure of frondosides A_2-4, A_2-7, and A_2-8, three new minor monosulfated triterpene glycosides

Alexandra S. Silchenko, Sergey A. Avilov, Alexandr S. Antonov, Anatoly I. Kalinovsky, Pavel S. Dmitrenok, Vladimir I. Kalinin, Carl Woodward, and Peter D. Collin

Abstract: Frondosides A_2-4 (**1**), A_2-7 (**2**), and A_2-8 (**3**) are new monosulfated triterpene glycosides isolated from the sea cucumber *Cucumaria frondosa*. Their structures have been elucidated on the basis of spectral data (2D NMR and MS). Frondosides A_2-7 (**2**) and A_2-8 (**3**) are isomers and differ from each other only by the position of a double bond in their non-holostane-type aglycones.

Key words: Cucumaria frondosa, sea cucumbers, frondosides, triterpene glycosides.

Résumé : Les frondosides A_2-4 (**1**), A_2-7 (**2**) et A_2-8 (**3**) sont de nouveaux glycosides de triterpènes monosulfatés qui ont été isolés du concombre de mer *Cucumaria frondosa*. Leurs structures ont été élucidées sur la base de données spectrales (spectrométrie de masse et RMN 2D). Les frondosides A_2-7 (**2**) et A_2-8 (**3**) sont des isomères qui ne diffèrent l'un de l'autre que par la position d'une double liaison dans leurs aglycones de type nonholostane.

Mots clés : Cucumaria frondosa, concombres de mer, frondosides, glycosides de triterpène.

[Traduit par la Rédaction]

As a continuation of our studies of triterpene glycosides from the Atlantic sea cucumber *Cucumaria frondosa* (1–3) we report herein the isolation and structure elucidation of three new monosulfated glycosides. The fraction of monosulfated glycosides of the A_2 group consists of a complex mixture of minor glycosides that differ from each other by the structure of aglycones and have identical pentasaccharide-branched carbohydrate moieties.

Sea cucumbers were collected in the Gulf of Maine, Penobscot Bay, Maine. The ethanolic extract of *C. frondosa* was sequentially submitted to column chromatography on polychrom-1 (powdered Teflon) and silica gel to give the fraction of monosulfated frondosides of the A_2 group (3). Separation of the A_2 fraction by HPLC on the reverse-phase column yielded three individual glycosides (frondosides A_2-4 (**1**), A_2-7 (**2**), and A_2-8 (**3**)).

The signals of the carbohydrate moieties in the NMR spectra of isolated glycosides (**1**–**3**) were coincident to each other and also with the corresponding signals in the spectra of frondosides A_2-1, A_2-2, A_2-3, and A_2-6, isolated earlier from *C. frondosa* (3). All these data indicated an identity of the pentaoside branched carbohydrate chains of these compounds having one sulfate group. Indeed, the presence of five characteristic doublets (J = 6.6–7.8 Hz) in the ^{1}H NMR spectra of **1**–**3** and corresponding signals of anomeric carbons in the ^{13}C NMR were indicative of a pentasaccharide chain and β configuration of all glycoside bonds (4). The characteristic chemical shift (75.75 ppm) of C-4 of the first xylose residue in the ^{13}C NMR spectra of glycosides **1**–**3** demonstrated the binding of a sulfate group to this position. Positions of interglycosidic bonds were elucidated from the corresponding carbon resonances (taking into account the effects of glycosylation (4)) and were also confirmed by corresponding NOESY and HMBC correlations (Table 1). The structures of carbohydrate chains of **1**–**3** were also confirmed by MALDI TOF MS.

The HR MALDI TOF MS (positive ion mode) of glycoside **1** showed the pseudomolecular ion peak $[M_{Na} + Na]^+$ at m/z 1327.5271, calculated for $C_{59}H_{93}O_{28}SNa_2$ as 1327.5368 m/z, which allowed the determination of a molecular formula of $C_{59}H_{93}O_{28}SNa$ for glycoside **1**.

The MALDI TOF MS of glycoside **1** exhibited the pseudomolecular ion peaks at m/z 1327 $[M_{Na} + Na]^+$ and 1343 $[M_{Na} + K]^+$, and fragmentation ion peaks at m/z 1225 $[M_{Na} - SO_3Na + Na + H]^+$, 1207 $[M_{Na} - OSO_3Na + Na - H]^+$, 1195 $[M_{Na} - Xyl + Na + H]^+$, 1151 $[M_{Na} - 3\text{-O-Me-Glc} + Na + H]^+$, and 1093 $[M_{Na} - SO_3Na - Xyl + Na + 2H]^+$ in the positive ion mode, as well as a pseudomolecular ion peak at

Received 25 July 2005. Published on the NRC Research Press Web site at http://canjchem.nrc.ca on 17 February 2006.

A.S. Silchenko, S.A. Avilov, A.S. Antonov, A.I. Kalinovsky, P.S. Dmitrenok, and V.I. Kalinin.[1] Pacific Institute of Bioorganic Chemistry, Far East Division of the Russian Academy of Sciences, Vladivostok, 690022, Russia.
C. Woodward and P.D. Collin. Coastside Bio Resources Inc., P.O. Box 151, Stonington, ME 04681, USA.

[1]Corresponding author (e-mail: kalininv@piboc.dvo.ru).

 doi: 10.1139/V05-243 © 2005 NRC Canada

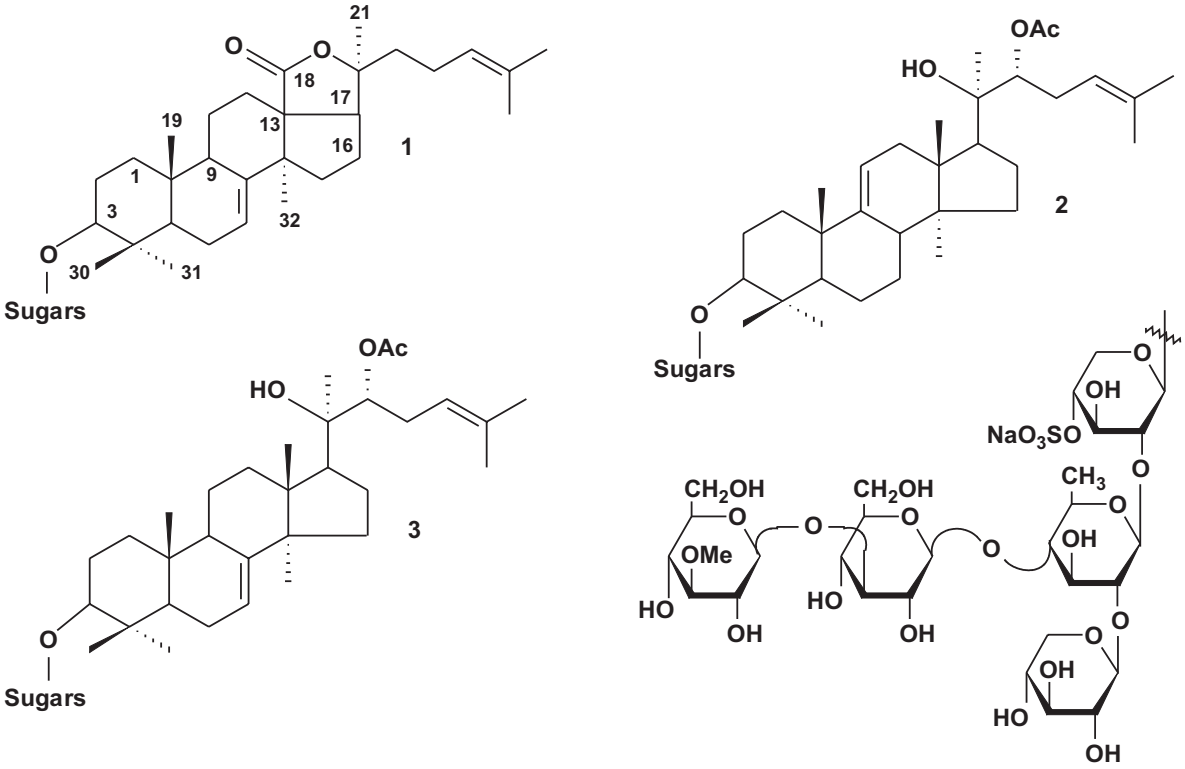


Table 1. ^{13}C and ^{1}H NMR chemical shifts and selected HMBC and NOESY correlations of the carbohydrate moiety of glycosides **1–3**.

Position	δ_C[a,b,c]	δ_H mult. (*J* in Hz)[d]	HMBC	NOESY[e]
Xyl1 (1→C-3)				
1	104.77	4.79 d (7.1)	C: 3	H-3,5-Xyl1, H-3, H-31
2	**81.54**	4.03 m	C: 1-Qui	H-1 Qui
3	75.62	4.45 t (9.0)	C: 2, 4-Xyl1	H-1,5 Xyl1
4	*75.75*	5.18 m		
5	64.40	4.80 dd (12.0, 5.3)	C: 4-Xyl1	
		3.88 m		
Qui (1→2Xyl1)				
1	102.30	5.31 d (7.2)	C: 2-Xyl1	H-3, 5 Qui
2	**82.25**	4.10 m	C: 1,3 Qui	
3	75.47	4.10 m	C: 2 Qui	H-1, 5 Qui
4	**86.63**	3.62 m		H-6 Qui, H-1 Glu
5	70.90	3.62 m		H-1, 3 Qui
6	17.90	1.68 d (5.5)	C: 4,5-Qui	
Glu (1→4Qui)				
1	104.63	4.93 d (7.8)	C: 4-Qui	H-4 Qui, H-3,5 Glu
2	73.60	4.01 m		
3	**87.73**	4.26 m	C: 2,4 Glu, 1-MeGlu	H-1 MeGlu, H-1 Glu
4	69.56	4.07 m	C: 5,6 Glu	
5	77.72	3.99 m		
6	61.84	4.47 m		
		4.18 dd (6.0, 11.5)		
MeGlu (1→3Glu)				
1	105.43	5.32 d (7.8)	C: 3-Glu	H-3 Glu, H-3,5 MeGlu
2	74.92	4.00 m	C: 1,3 MeGlu	
3	87.86	3.73 t (8.9)	OMe	H-1,5 MeGlu
4	70.47	4.11 m	C: 3,5,6, MeGlu	
5	78.20	3.99 m		H-1,3 MeGlu
6	62.02	4.47 m		
		4.26 m		

© 2005 NRC Canada

Table 1 (*concluded*).

Position	δ_C[a,b,c]	δ_H mult. (*J* in Hz)[d]	HMBC	NOESY[e]
OMe	60.66	3.87 s		
Xyl 2 (1→2 Qui)				
1	105.43	5.39 d (6.6)	C: 2-Qui	H-3,5 Xyl 2, H-2 Qui
2	74.92	4.05 m		
3	76.38	4.12 m	C: 2,4 Xyl 2	H-1 Xyl2
4	70.33	4.11 m		
5	66.41	4.39 dd (4.6,11.5)		
		3.67 m	C: 1,3,4 Xyl 2	

[a]Recorded at 125 MHz in C_5D_5N.
[b]Values of δ_C in bold indicate interglycosidic positions.
[c]Value of δ_C in italics indicates a sulfate position.
[d]Recorded at 500 MHz in C_5D_5N.
[e]Mixing time in NOESY is 460 ms.

Table 2. ^{13}C and ^{1}H NMR chemical shifts and selected HMBC and NOESY correlations of the aglycon moiety of glycoside **1**.

Position	δ_C[a]	δ_H mult. (*J* in Hz)[b]	HMBC	NOESY[c]
1	36.07	1.43 m		
2	26.90	1.85 m (a), 2.06 m (e)		
3	89.08	3.25 dd (4.0, 11.6)		H-1, H-5, H-31, H-1 Xyl1
4	39.50			
5	47.96	1.05 m		
6	23.25	2.08 m	C: 7, 10	H-19, H-30, H-31
7	119.84	5.73 m		
8	146.63			
9	47.25	3.51 br d (13.7)		H-1, H-12, H-19
10	35.46			
11	22.78	1.54 m, 1.78 m		
12	30.24	1.96 m, 2.04 m	C: 9, 13, 14, 18	
13	58.54			
14	51.24			
15	34.19	1.65 m, 1.81 m	C: 13	
16	24.45	1.89 m, 2.02 m		
17	53.07	2.21 dd (4.5, 14.5)	C: 13, 18	H-21, H-32
18	179.94			
19	23.90	1.22 s	C: 1, 5, 9, 10	H-1, H-2
20	83.85			
21	25.92	1.42 s	C: 17, 20, 22	H-17
22	39.23	1.71 m, 1.79 m		
23	23.00	2.00 m		
24	123.92	5.17 m		
25	131.71			
26	17.45	1.61 s	C: 24, 25, 27	
27	25.50	1.69 s	C: 24, 25, 26	
30	17.32	1.14 s	C: 3, 4, 5, 31	H-2, H-6 Qui
31	28.63	1.29 s	C: 3, 4, 5, 30	H-1 Xyl1
32	30.75	1.17 s	C: 8, 13, 14, 15	H-15, H-17

[a]Recorded at 125.77 MHz in C_5D_5N.
[b]Recorded at 500 MHz in C_5D_5N.
[c]Mixing time in NOESY is 460 ms.

m/z 1281 $[M - Na]^-$ along with peaks at *m/z* 1149 $[M - Na - Xyl + H]^-$ and 1105 $[M - Na - 3\text{-O-Me-Glc} + H]^-$ in the negative ion mode. MS data confirmed the presence of a sulfate group, xylose, and 3-*O*-methylglucose residues as terminal monosaccharide units in the carbohydrate chain of **1**.

The aglycon moiety of glycoside **1** was found by extensive NMR spectroscopy (^1H and ^{13}C NMR, DEPT, HSQC, HMBC, COSY, and NOESY) (Table 2) to have a holostane-type aglycon. Actually, the signal of the carbonyl group belonging to 18(20)-lactone at 179.94 ppm and the signals at

© 2005 NRC Canada

Table 3. ^{13}C and ^{1}H NMR chemical shifts and selected HMBC and NOESY correlations of the aglycon moiety of glycoside **2**.

Position	δ_C[a]	δ_H mult. (*J* in Hz)[b]	HMBC	NOESY[c]
1	36.26	1.39 m, 1.78 m		
2	26.83	1.87 m, 2.12 m		H-19
3	88.77	3.18 dd (4.5, 16.0)	C-1Xyl1, C-30	H-1, H-5, H-31
4	39.76			
5	52.86	0.92 t (7.5)		
6	21.29	1.47 m, 1.72 m		
7	28.28	1.38 m, 1.65 m		
8	41.29	2.25 m		H-15, H-19
9	149.43			
10	39.19			
11	114.82	5.32 m	C: 10, 13	H-1, H-19
12	37.88	2.13 m, 2.24 m	C: 13, 18, 21	H-21
13	49.59			
14	47.06			
15	33.73	1.42 m, 1.57 m		
16	22.06	1.85 m, 2.43 d (9.5)		
17	50.06	2.22 m		H-32
18	16.40	1.21 s	C: 12, 13, 14, 17	H-12, H-19
19	22.24	1.09 s	C: 1, 5, 9, 10	H-2, H-12, H-30
20	75.81			
21	21.10	1.59 s	C: 17, 20, 22	H-12, H-23
22	79.35	5.40 brd (3.9)	C: 20, 23, 24, OAc	H-16
23	30.13	2.40 m, 2.52 m	C: 22, 24, 25	
24	121.36	5.39 brd (4.2)	C: 23, 26, 27	
25	133.06			
26	17.67	1.71 s	C: 24, 25, 27	
27	25.61	1.71 s	C: 24, 25, 26	H-16
30	16.66	1.11 s	C: 3, 4, 5, 31	H-6, H-6 Qui
31	27.97	1.26 s	C: 3, 4, 5, 30	H-1Xyl1, H-5
32	18.68	0.86 s	C: 8, 13, 14, 15, 19	H-7, H-15, H-16
O*C*OCH$_3$	170.58			
OCO*C*H$_3$	20.98	2.02 s		

[a]Recorded at 125.77 MHz in C_5D_5N.
[b]Recorded at 500 MHz in C_5D_5N.
[c]Mixing time in NOESY is 460 ms.

119.84 (C-7) and 146.63 (C-8) ppm in the ^{13}C NMR spectrum, as well as the signal at 5.73 (m, H-7) ppm in the ^{1}H NMR spectrum, showed that the aglycon of **1** has the same pentacyclic skeleton system as in the aglycon of cucumarioside A_7-3 from *C. japonica* (5) and frondosides A_2-2 and A_2-3 from *C. frondosa* (3). However, the signals of the side chains in the NMR spectra of these substances were different. ^{13}C NMR and DEPT spectra of frondoside **1** demonstrated the signals of a tertiary carbon at 123.92 (C-24) ppm and a quaternary carbon at 131.71 (C-25) ppm. The corresponding proton signal at 5.17 (m, H-24) ppm was observed in the ^{1}H NMR spectrum. These data indicated that there is a 24(25)-double bond in the side chain of **1**. The cross-peaks between the protons of terminal methyl groups H_3-26 (δ 1.61 ppm, s) and H_3-27 (δ 1.69 ppm, s) and C-24 and C-25 in the HMBC spectrum of **1** confirmed the structure of the aglycon side chain. Hence, frondoside A_2-4 (**1**) is 3-*O*-{3-*O*-methyl-β-D-glucopyranosyl-(1→3)-β-D-glucopyranosyl-(1→4)-[β-D-xylopyranosyl-(1→2)]-β-D-quinovopyranosyl-(1→2)-4-*O*-sodium sulfate-β-D-xylopyranosyl}-3β-hydroxyholosta-7,24-diene.

In the HR MALDI TOF MS (positive ion mode) of glycoside **2** the pseudomolecular ion peak $[M_{Na} + Na]^+$ at *m/z* 1373.5874 was observed, calculated for $C_{61}H_{99}O_{29}SNa_2$ as 1373.5786 *m/z*, which allowed the determination of a molecular formula of $C_{61}H_{99}O_{29}SNa$ for glycoside **2**.

The MALDI TOF MS (positive ion mode) of glycoside **2** exhibited a pseudomolecular ion peak at *m/z* 1373 $[M_{Na} + Na]^+$ and characteristic ion peaks at *m/z* 1271 $[M - SO_3Na + Na + H]^+$, 1139 $[M - SO_3Na - Xyl + Na + 2H]^+$, and 1095 $[M - SO_3Na - 3\text{-O-Me-Glc} + Na + 2H]^+$, demonstrating the loss of a sulfate group and terminal monosaccharide residues, along with the characteristic ion peak at *m/z* 1231 $[M - 141 + Na - H]^+$, owing to the cleavage of the C-20–C-22 linkage in the aglycon side chain. The pseudomolecular ion peak at *m/z* 1327 $[M_{Na} - Na]^-$, along with fragmentation ion peaks at *m/z* 1195 $[M_{Na} - Na - Xyl + H]^-$ and 1151 $[M_{Na} - Na - 3\text{-O-Me-Glc} + H]^-$ (owing to the loss of terminal monosaccharide residues), were revealed in the negative ion mode.

The NMR spectra (^{1}H and ^{13}C, DEPT, HSQC, HMBC, COSY, and NOESY) (Table 3) of glycoside **2** indicated the

© 2005 NRC Canada

Table 4. ^{13}C and ^{1}H NMR chemical shifts and selected HMBC and NOESY correlations of the aglycon moiety of glycoside **3**.

Position	δ_C[a]	δ_H mult. (*J* in Hz)[b]	HMBC	NOESY[c]
1	35.67[d]	1.41 m, 1.83 m		H-19
2	27.09	1.85 m, 2.07 m		
3	88.97	3.23 dd (4.0, 15.5)	C: 1Xyl1, 4, 30, 31	H-1, H-5, H-31
4	39.58			
5	49.41	0.99 dd (3.5, 14.5)		H-1, H-31
6	23.21	1.98 m, 2.05 m		
7	121.46	5.74 brd (7.3)		H-15, H-32
8	148.94			
9	48.31	2.41 m		H-18, H-19
10	35.57			
11	23.05	1.55 m, 1.78 m		
12	35.67[d]	1.94 m		
13	45.17			
14	53.09			
15	33.58	1.68 m, 1.78 m		
16	22.49	1.91 m, 2.49 m		
17	52.27	2.08 m	C: 13, 18	H-32
18	25.04	1.48 s	C: 12, 13, 14, 17	H-15, H-19
19	24.55	1.05 s	C: 1, 5, 9, 10	H-1, H-9
20	75.60			
21	21.91	1.59 s	C: 17, 20, 22	H-12
22	79.50	5.38 d (3.8)		
23	30.15	2.41 m, 2.53 m	C: 22, 24, 25	
24	122.16	5.40 d (6.7)		
25	133.15			
26	17.72	1.70 s	C: 24, 25, 27	
27	25.65	1.70 s	C: 24, 25, 26	
30	17.43	1.15 s	C: 3, 4, 5, 31	H-6 Qui, H-6
31	28.66	1.29 s	C: 3, 4, 5, 30	H-1 Xyl1, H-3, H-5
32	30.70	1.18 s	C: 8, 13, 14, 15	H-15, H-16, H-17
$OCOCH_3$	21.06	2.05 s		
$OCOCH_3$	170.70			

[a]Recorded at 125.77 MHz in C_5D_5N.
[b]Recorded at 500 MHz in C_5D_5N.
[c]Mixing time in NOESY is 460 ms.
[d]The signals are interchangeable.

absence of a 18(20)-lactone cycle (lacking the corresponding signal of a C-18 carbonyl group at 180 ppm and the presence of the signal of a C-18 methyl group at 16.40 ppm in the ^{13}C NMR spectrum). Therefore, the presence of a nonholostane aglycon having a 9(11)-double bond (signals at 149.43 (C-9), 114.82 (C-11), and 5.32 (m, H-11) ppm in the ^{13}C and ^{1}H NMR spectra, correspondingly) was detected in **2**.

There were also signals at 121.36 (C-24) and 133.06 (C-25) ppm in the ^{13}C NMR spectrum indicating the presence of a 24(25)-double bond. The signals at 170.58 and 20.98 ppm demonstrated the presence of an acetate group attached to C-22 (79.35 ppm). The signal of a quaternary carbon (C-20) bonded with a hydroxyl group was found at 75.81 ppm.

The comparison of the aglycon parts of the NMR spectra of **2** and known frondoside C isolated from *C. frondosa* (2) revealed the identity of the aglycons of these compounds. Hence, frondoside A_2-7 (**2**) is 3-*O*-{3-*O*-methyl-β-D-glucopyranosyl-(1→3)-β-D-glucopyranosyl-(1→4)-[β-D-xylopyranosyl-(1→2)]-β-D-quinovopyranosyl-(1→2)-4-*O*-sodium sulfate-β-D-xylopyranosyl}-3β,20(*R*)-dihydroxy-22(*R*)-acetoxylanosta-9,24-diene.

In the HR MALDI TOF MS (positive ion mode) of glycoside **3** the pseudomolecular ion peak $[M_{Na} + Na]^+$ at *m/z* 1373.5881 was observed, calculated for $C_{61}H_{99}O_{29}SNa_2$ as 1373.5786 *m/z*, which permitted the determination of a molecular formula of $C_{61}H_{99}O_{29}SNa$ for frondoside **3a**.

The MALDI TOF MS of glycoside **3** exhibited pseudomolecular ion peaks at *m/z* 1373 $[M_{Na} + Na]^+$ and 1389 $[M_{Na} + K]^+$, along with a fragmentation ion peak at *m/z* 1271 $[M - SO_3Na + Na + H]^+$ (demonstrating the loss of a sulfate group) in the positive ion mode and a pseudomolecular ion peak at *m/z* 1327 $[M_{Na} - Na]^-$, along with fragmentation ion peaks at *m/z* 1195 $[M_{Na} - Na - Xyl + H]^-$, 1151 $[M_{Na} - Na - 3\text{-O-Me-Glc} + H]^-$ (owing to the loss of terminal monosaccharide residues), 1185 $[M - Na - 141 - H]^-$ (owing to C-20 – C-22 cleavage of side chain), and 1285 $[M - Na - 43 + H]^-$ (demonstrating the loss of an acetyl group) in the negative ion mode.

The analysis of NMR spectra (^{1}H and ^{13}C, DEPT, HSQC,

© 2005 NRC Canada

HMBC, COSY, and NOESY) (Table 4) along with MS data (**2** and **3** having the same molecular formulas) showed that glycoside **3** is an isomer of glycoside **2**, differing from it only by the position of the double bond in the lanostane nucleus of the aglycon. In fact, the NMR spectra of these compounds were very similar to each other, but there were the signals of a 7(8)-double bond in the ^{13}C NMR spectrum of **3** (at 121.46 (C-7) and 148.94 (C-8) ppm) instead of the signals corresponding to the 9(11)-double bond in the spectrum of glycoside **2**. Hence, frondoside A_2-8 (**3**) is 3-*O*-{3-*O*-methyl-β-D-glucopyranosyl-(1→3)-β-D-glucopyranosyl-(1→4)-[β-D-xylopyranosyl-(1→2)]-β-D-quinovopyranosyl-(1→2)-4-*O*-sodium sulfate-β-D-xylopyranosyl}-3β,20(*R*)-dihydroxy-22(*R*)-acetoxylanosta-7,24-diene.

Glycosides **1**–**3** are new natural products. Lanostane-type aglycons (without a lactone) having "nonshortened" side chains, as in the glycosides **2** and **3**, are rare for sea cucumber glycosides. So far, only three glycosides with this type of aglycon structure have been found in sea cucumbers, namely frondoside C, a trisulfated pentaoside from *C. frondosa* (2), and penaustrosides A and B from *Pentacta australis* (6). It is important to note that glycosides **2** and **3** were obtained as native substances; in contrast to frondoside C and penaustrosides A and B, which were obtained as desulfated derivatives of natural compounds. Glycosides **2** and **3** differed from each other only by the location of a double bond in the aglycon nucleus. This is of special interest because, in most cases, sea cucumbers accumulate glycosides having one type of polycyclic system: either with a 7(8)- or 9(11)-double bond. To date, similar pairs of isomers (disulfated cucumariosides A_3-2 and A_3-3 and trisulfated koreoside A and isokoreoside A) have been found only in one species of sea cucumber, namely, *C. conicospemium* (7).

Experimental section

General experimental procedures

All melting points were determined with a Kofler–Thermogenerate apparatus. Specific rotation was measured on a PerkinElmer 343 polarimeter. NMR spectra were recorded on a AMX Bruker 500 spectrometer at 500.12 MHz for ^1H and 125.67 MHz for ^{13}C and a Bruker DPX 300 spectrometer at 300 MHz for ^1H and 75 MHz for ^{13}C in C_5D_5N with TMS as an internal reference (δ 0). The MALDI TOF MS (positive and negative ion modes) were recorded using a Bruker apparatus, model BIFLEX III, with impulse extraction of ions on an α-cyano-4-hydroxycinnamic acid matrix. HPLC was performed using an Agilent 1100 chromatograph equipped with a differential refractometer on a Diasphere-110 C_{18} column.

Animal material

The sea cucumber *C. frondosa* (family Cucumariidae; order Dendrochirotida) was collected in Penobscot Bay (Gulf of Maine, Maine) in September 2000 by commercial dragging. Taxonomic identification was carried out by Dr. E.N. Gudimova. A voucher specimen is on deposit in the collection of the Murmansk Marine Biological Institute of the Kolsky Scientific Center of the Russian Academy of Sciences, Murmansk, Russia.

Extraction and isolation of the fraction of glycosides belonging to the frondosides A_2 group

Body walls of the sea cucumbers were separated, cut and lyophylized to dryness, then extracted twice with refluxing ethanol (dry weight of the residue was 943 g). The combined extracts were evaporated to dryness and chromatographed on a polychrom-1 column (powdered Teflon, Biolar, Olaine, Latvia) previously loaded in EtOH and washed with water. The glycoside fraction was loaded in H_2O, and inorganic salts and polar impurities were eluted with H_2O. The fraction containing glycosides was eluted with 50% acetone. This glycoside fraction was then chromatographed on silica gel columns eluting with $CHCl_3$–EtOH–H_2O (100:100:17 and 100:75:10) solvent systems to obtain a homogenous (on TLC) crude subfraction of frondosides of the A_2 group (500 mg).

Isolation of glycosides 1–3

The subfraction was subsequently subjected to HPLC on a Diasphere-110 C_{18} (4 mm × 250 mm) column, using solvent systems (MeOH, water, $Na_2HPO_4 \cdot 12H_2O$ (540 mg in 100 mL of water), 72:25:3 and 65:33:2) as the mobile phase followed by desalting on a Teflon column as described previously to give 9.5 mg of glycoside **1**, mp 235–237 °C. $[\alpha]_D^{20}$ –90 (*c* 0.1, pyridine). (See Tables 1 and 2 for NMR data). MALDI TOF MS (positive ion mode) *m/z* (rel. intensity): 1327 ($C_{59}H_{93}O_{28}SNa_2$ $[M + Na]^+$, 1.0), 1343 ($C_{59}H_{93}O_{28}SNaK$ $[M + K]^+$, 0.23), 1225 ($[M - SO_3Na + Na + H]^+$, 0.3), 1207 ($[M - OSO_3Na + Na - H]^+$, 0.06), 1195 ($[M - Xyl + Na + H]^+$, 0.06), 1151 ($[M - 3\text{-O-Me-Glc} + Na + H]^+$, 0.07), 1093 ($[M - SO_3Na - Xyl + Na + 2H]^+$, 0.08). MALDI TOF MS (negative ion mode) *m/z* (rel. intensity): 1281 ($C_{59}H_{93}O_{28}S$ $[M - Na]^-$, 1.0), 1149 ($[M - Na - Xyl + H]^-$, 0.05), 1105 ($[M - Na - 3\text{-O-Me-Glc} + H]^-$, 0.05). Yield: 9.5 mg of glycoside **2**, mp 216 to 217 °C. $[\alpha]_D^{20}$ –10 (*c* 0.1, pyridine). (See Tables 1 and 3 for NMR data). MALDI TOF MS (positive ion mode) *m/z* (rel. intensity): 1373 ($C_{61}H_{99}O_{29}SNa_2$ $[M + Na]^+$, 1.0), 1389 ($C_{61}H_{99}O_{29}SNaK$ $[M + K]^+$, 0.2), 1271 ($[M - SO_3Na + Na + H]^+$, 0.07), 1139 ($[M - SO_3Na - Xyl + Na + 2H]^+$, 0.07), 1095 ($[M - SO_3Na - 3\text{-O-Me-Glc} + Na + 2H]^+$, 0.08), 1231 ($[M - 141 + Na - H]^+$, 0.02). MALDI TOF MS (negative ion mode) *m/z* (rel. intensity): 1327 ($C_{61}H_{99}O_{29}S$ $[M - Na]^-$, 1.0), 1195 ($[M - Na - Xyl + H]^-$, 0.05), 1151 ($[M - Na - 3\text{-O-Me-Glc} + H]^-$, 0.05). Yield: 4 mg of glycoside **3**, mp 224–226 °C. $[\alpha]_D^{20}$ –33 (*c* 0.1, pyridine). (See Tables 1 and 4 for NMR data). MALDI TOF MS (positive ion mode) *m/z* (rel. intensity): 1373 ($C_{61}H_{99}O_{29}SNa_2$ $[M + Na]^+$, 1.0), 1389 ($C_{61}H_{99}O_{29}SNaK$ $[M + K]^+$, 0.3), 1271 ($[M - SO_3Na + Na + H]^+$, 0.07). MALDI TOF MS (negative ion mode) *m/z* (rel. intensity): 1327 ($C_{61}H_{99}O_{29}S$ $[M - Na]^-$, 1.0), 1195 ($[M - Na - Xyl + H]^-$, 0.05), 1151 ($[M - Na - 3\text{-O-Me-Glc} + H]^-$, 0.05), 1185 $[M - Na - 141 - H]^-$, 0.03), 1285 ($[M - Na - 43 + H]^-$, 0.03).

Acknowledgements

The authors acknowledge financial support from CRDF RB1-557-VL-02, Grants of the Presidium of the Russian Academy of Sciences "Molecular and Cell Biology" and "Basic Research to Medicine", Grant of the President of the

© 2005 NRC Canada

Russian Federation No. NSH-725.2003.4, and a grant of FEB RAS for young scientists No. 05-III-G-05-040, NATO Grant LST.NR.CLG. 981098 and Grant RFBR No. 06-04-96016. C. Woodward and P.D. Collin also acknowledge the Maine Technology Institute (Gardiner, Maine) for partial support.

References

1. S.A. Avilov, V.I. Kalinin, O.A. Drozdova, A.I. Kalinovsky, V.A. Stonik, and E.N. Gudimova. Khim. Prir. Soedin. **2**, 260 (1993).
2. S.A. Avilov, O.A. Drozdova, V.I. Kalinin, A.I. Kalinovsky, and V.A. Stonik. Can. J. Chem. **76**, 137 (1998).
3. A.S. Silchenko, S.A. Avilov, A.S. Antonov, A.I. Kalinovsky, P.S. Dmitrenok, V.I. Kalinin, V.A. Stonik, C. Woodward, and P.D. Collin. Can. J. Chem. **83**, 21 (2005).
4. A.S. Shashkov and O.S. Chizhov. Bioorg. Khim. **2**, 437 (1976).
5. O.A. Drozdova, S.A. Avilov, A.I. Kalinovsky, V.A. Stonik, Y.M. Milgrom, and J.W. Rashkes. Khim. Prir. Soedin. **2**, 242 (1993).
6. T. Miyamoto, K. Togawa, R. Higuchi, T. Komori, and T. Sasaki. J. Nat. Prod. **55**, 940 (1992).
7. S.A. Avilov, A.S. Antonov, A.S. Silchenko, V.I. Kalinin, A.I. Kalinovsky, P.S. Dmitrenok, V.A. Stonik, R. Riguera, and C. Jimenes. J. Nat. Prod. **66**, 910 (2003).

© 2005 NRC Canada

Reactions of β-alkoxyvinyl trifluoromethyl ketones with terminal alkynes — Reagent-controlled regioselectivity addition reactions

Shizheng Zhu, Guifang Jin, and Huiling Jiang

Abstract: Reactions of β-alkoxyvinyl trifluoromethyl ketones ROCH=CHCOCF$_3$ (**1**, R = Et, Me$_2$CHCH$_2$), and their cyclic analogues 4-trifluoroacetyl-2,3-dihydrofuran (**2a**) and 5-trifluoroacetyl-3,4-dihydro-2*H*-pyran (**2b**), with terminal alkynes R-C≡CH (**3**, R = Ph, PhCH$_2$, HOCH$_2$, C$_5$H$_{11}$) mainly gave the 1,2-addition products (carbonyl alkynylation) in the presence of *n*-BuLi. However, promoted by ZnCl$_2$–Et$_3$N, the reaction of **1** or **2** with equivalent alkyne predominately provided 1,4-addition products.

Key words: β-alkoxyvinyl trifluoromethyl ketones, alkynes, 1,2-addition, 1,4-addition, catalysts.

Résumé : En présence de butyl lithium, les réactions des β-alcoxyvinyl trifluorométhyl cétones de formule générale ROCH=CHCOCF$_3$ (**1**; R = Et, Me$_2$CHCH$_2$) et de leurs analogues cycliques, tels le 4-trifluoroacétyl-2,3-dihydrofurane (**2a**) et le 5-trifluoroacétyl-3,4-dihydro-2*H*-pyrane (**2b**) avec des alcynes vrais de formule générale R-C≡CH (**3**; R = Ph, PhCH$_2$, HOCH$_2$, C$_5$H$_{11}$) conduisent principalement à des produits d'additions 1,2 (alcynylation du carbonyle). Toutefois, lorsque la réaction est catalysée par du ZnCl$_2$ en présence de Et$_3$N, les réactions des composés **1** et **2** avec un équivalent d'alcyne conduisent principalement aux produits d'additions 1,4.

Mots clés : β-alcoxyvinyl trifluorométhyl cétones, alcynes, addition 1,2, addition 1,4, catalyseurs.

[Traduit par la Rédaction]

Introduction

The present strongly developed interest in organofluorine chemistry has led to considerable studies of trifluoromethyl ketones (1) and, in particular, α,β-unsaturated trifluoromethyl ketones (2). Such ketones have been used as intermediates in heterocyclic synthesis (3) and have also been viewed as synthetic targets owing to their possible pharmacological interest (4). β-Alkoxylvinyl trifluoromethyl ketones (ROCH=CHCOCF$_3$, **1**) are potential fluorinated 1,3-dicarbonyl compounds. Since they were first prepared in 1967 (5), their preparations and chemical transformations have been extensively investigated (6). Our group and others have studied the reactions of acyclic β-alkylvinyl trifluoromethyl ketones with Grignard reagents derivated from alkyl and aryl halides. Generally, acyclic β-alkoxyvinyl trifluoromethyl ketones and the cyclic analogues **2a** and **2b** reacted with Grignard reagents gave the corresponding α,β-unsaturated trifluoromethyl ketone as the sole product, which arose from 1,4-addition on the β-position of the double bond and was followed by β-elimination of alkoxyl group (7). In contrast, the organic zinc compounds prepared in situ reacted with β-alkoxyvinyl trifluoromethyl ketones giving only the 1,2-addition products (Scheme 1) (6*d*, 8).

The factors determining the selectivity between 1,2- and 1,4-additions to a wide range of α,β-unsaturated carbonyl compounds have received much attention and, in particular, asymmetric conjugate additions have been developed (9). The hard acid – soft base concepts have been used to permit the generalizations that among organometallic reagents, organolithiums, which are hard nucleophiles, react by 1,2-addition, and organocopper reagents, which are softer ones, react by 1,4-addition (10). Grignard reagents were seen to lie somewhere between them. Since then there have been major advances in explaining the selectivity of these additions. In reactions that proceed by kinetic control with organometallic reagents having a highly localized negative charge, a charge-controlled 1,2-addition can be expected. In contrast, in additions of nucleophiles having charge dislocalization where the reaction is frontier orbital controlled, a 1,4-addition is expected. However, other factors, notably steric and solvent effects and the nature of the nucleophile, disturb these simple generalizations.

During our continuous study on the fluorinated push–pull

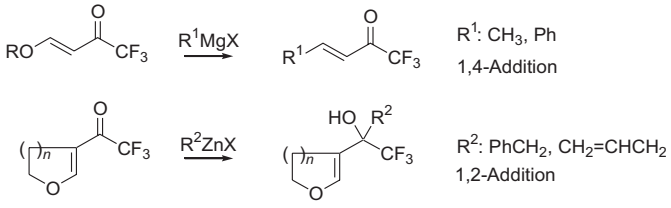
Received 14 June 2005. Published on the NRC Research Press Web site at http://canjchem.nrc.ca on 21 February 2006.

S. Zhu.[1] Key Laboratory of Organofluorine Chemistry, Shanghai Institute of Organic Chemistry, Chinese Academy of Sciences, 354 Fenglin Lu, Shanghai 200032, China.
G. Jin and H. Jiang. Key Laboratory of Organofluorine Chemistry, Shanghai Institute of Organic Chemistry, Chinese Academy of Sciences, 354 Fenglin Lu, Shanghai 200032, China.

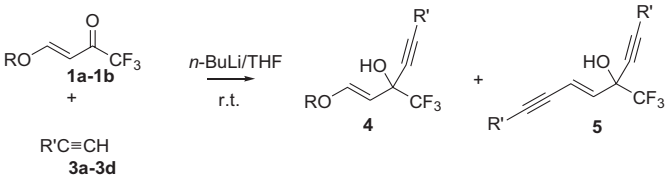
[1]Corresponding author (e-mail: zhusz@mail.sioc.ac.cn).

 doi: 10.1139/V05-247 © 2005 NRC Canada

Scheme 1.



Scheme 2.



R: C_2H_5 (a); $CH_2CH(CH_3)_2$ (b); R': Ph (a); $PhCH_2$ (b); $HOCH_2$ (c); C_5H_{11} (d)

ethylene compounds (11), we investigated the alkynylation of β-substituted unsaturated trifluoromethyl ketones **1** and **2** with terminal alkynes in detail. We found that the reaction products mainly depend on the promoted reagents. *n*-Butyl lithium promoted addition reactions gave 1,2-addition products, a process favored by charge control. $ZnCl_2$–Et_3N promoted addition reactions provided 1,4-addition products, a process favored by orbital control. Herein we report these results.

Results and discussion

Reaction of β-alkoxyvinyl trifluoromethyl ketone **1a** with PhC≡CH **3a** proceeded smoothly at room temperature in the presence of 1 equiv. of *n*-BuLi in THF and finished in 2 h (monitored by TLC). Flash chromatographic purification on silica gel (*n*-hexane – ethyl acetate) gave two products, 1-ethoxy-5-phenyl-3-trifluoromethyl-1penten-4-yne-3-ol (**4a**, 41%) and 1,7-diphenyl-3-trifluoromethyl-4-heptene-1,6-diyn-3-ol (**5a**, 20%), which is an over addition product. When 2 equiv. of *n*-BuLi and **3a** were used, the yield of **5a** increased to 52% (See Scheme 2, Table 1).

The proton NMR spectra of **4a** and **5a** showed that both of them are *trans*-alkenes. The coupling constants between the two alkene's protons were 13 Hz in **4a** and 15 Hz in **5a**, and the chemical shifts of the two alkene's protons in **4a** were 7.12 and 5.00 ppm owing to the presence of the ethoxyl group on the double bond; while in compound **5a** they were 6.56 and 6.31 ppm. Under the same reaction conditions, the reaction of β-isobutoxyvinyl trifluoromethyl ketone (**1b**) with **3a** gave the same results as **1a**.

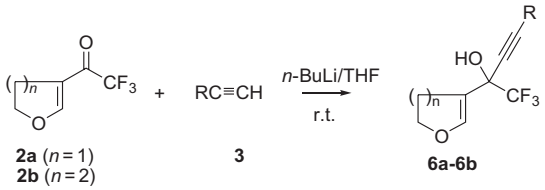
Interestingly, terminal alkynes **3b**–**3d** reacted with **1** affording only 1,2-addition products. No further addition products were detected or isolated even when excessive equivalents of alkynes **3** and *n*-BuLi were used or by prolonging the reaction time to 24 h. When reacted with ketones **1a** and **1b**, the terminal alkynes **3** have excellent regioselectivity except for **3a**. The selectivity could be explained by the structures of the nucleophiles. The phenylacetylene ion is charge delocalized owing to its conjugation structure, therefore, it gave both 1,2-addition and 1,4-addition products. The alkynes **3b**–**3d** only gave 1,2-addition products because their ions have highly localized negative charges without conjugation structures.

Table 1. Reactions of β-alkoxyvinyl trifluoromethyl ketone with alkynes promoted by *n*-BuLi.

Entry	Reactants	Mol. ratio	Time (h)	Products and yields (%)[a]
1	**1a**, **3a**	1:1	2	**4a** (41), **5a** (20)
2	**1a**, **3a**	1:2	2	**4a** (18), **5a** (52)
3	**1b**, **3a**	1:1	2	**4b** (39), **5a** (28)
4	**1b**, **3a**	1:2	2	**4b** (23), **5a** (59)
5	**1a**, **3b**	1:1	4	**4c** (68)
6	**1b**, **3b**	1:1	4	**4d** (65)
7	**1a**, **3c**	1:1	24	**4e** (64)
8	**1b**, **3c**	1:1	24	**4f** (61)
9	**1b**, **3d**	1:1	24	**4g** (67)
10	**2a**, **3a**	1:1	4	**6a** (81)
11	**2a**, **3a**	1:2	4	**6a** (84)
12	**2b**, **3a**	1:1	4	**6b** (81)

[a]The yields are calculated on the ketones.

Scheme 3.



R: Ph (a); $PhCH_2$ (b); $HOCH_2$ (c); C_5H_{11} (d)

In contrast, the cyclic analogues, 4-trifluoroacetyl-2,3-dihydrofuran (**2a**) and 5-trifluoro-3,4-dihydro-2*H*-pyran (**2b**) are less reactive. In the presence of *n*-BuLi, the reactions between **2** and **3a** needed a longer time period (typical 4 h) and only 1,2-addition products **6a** and **6b** were obtained in good yields (Scheme 3). With 2 equiv. of **3a** and *n*-BuLi, no further reaction product was observed. These results indicated the considerable difference between the phenylacetylene lithium reagent and the Grignard reagents that gave exclusively the 1,4-addition products, carbon–carbon double bond attacking products (7, 8).

Recently, considerable progress has been developed in the alkynylation of carbonyl compounds using Lewis acids in combination with bases (12). For example, Jiang and Si (13) prepared a series of propargylic alcohols by treatment of the aromatic aldehydes with terminal alkynes promoted by zinc chloride and triethyl amine. In the subsequent studies on the alkynylation of the β-substituted unsaturated trifluoromethyl ketones **1** and **2**, we also used the $ZnCl_2$–Et_3N system as the promotor. Thus, a mixture of **3a** (1.5 mmol), anhydr. $ZnCl_2$ (2.25 mmol), and Et_3N (2.25 mmol) in toluene was stirred at room temperature for 1 h, then **1a** (1.5 mmol) in 10 mL THF was added. After it was stirred overnight, TLC analysis showed that the reaction was finished, and chromatography purification gave the ketone **7a** (14) in 81% yield. When 2 equiv. of **3a** was used, this reaction gave two products, **7a** (58%) and the double-alkylated product **5a** (25%) (Scheme 4).

Under the same reaction conditions, the reaction of equivalent **3a** to **2a** afforded product **8a** (53%) (Table 2). How-

© 2005 NRC Canada

Scheme 4.

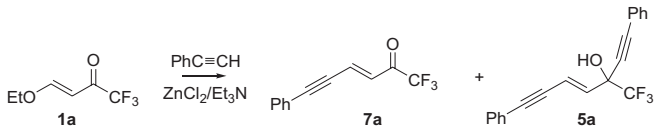


Table 2. Reactions of β-alkoxyvinyl trifluoromethyl ketone with alkynes promoted by $ZnCl_2$–Et_3N.

Entry	Reactants	Mol. ratio	Time (h)	Products and yields (%)[a]
1	**1a**, **3a**	1:1	24	**7a** (81)
2	**1a**, **3a**	1:2	24	**7a** (58), **5a** (25)
3	**2a**, **3a**	1:1	24[b]	**8a** (53), **9a** (7)
4	**2a**, **3b**	1:1	24[b]	No reaction
5	**2b**, **3a**	1:1	36	**8b** (44)

[a]The yields are calculated on the ketones.
[b]The reactions were carried out at 80 °C, the other reactions were at room temperature.

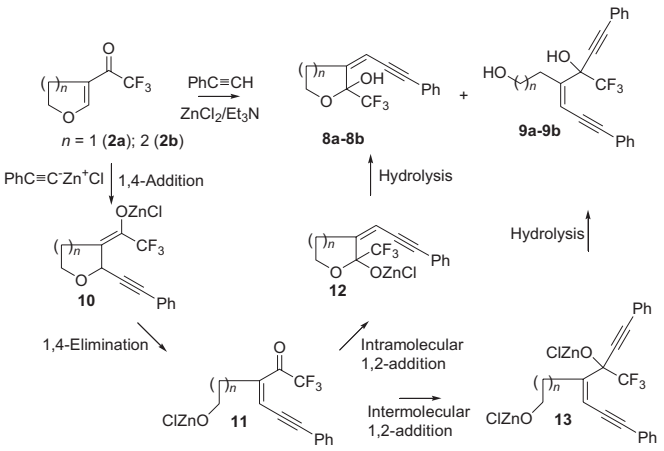
ever, for the reaction of **2b** with **3a**, the alkynylation only occurred at the double bond carbon atom giving the product **8b**. The final product was obtained from a rearrangement of 1,4-addition intermediate **10**, followed by an 1,4-elimination of the alkoxyl group to produce intermediate **11**, then an intramolecular 1,2-addition occurred and gave the final stable product (Scheme 5). The driving force for the rearrangement might be the conjugation of the double bond with the triple bond. Since the intermediate **11** has a ketone functional group, the intermolecular 1,2-addition gave the double addition intermediate **13**, which was hydrolyzed and produced product **9**. It is noteworthy that five-membered **2a** produced two addition products **8a** and **9a**, while six-membered ketone **2b** only afforded **8b**. This difference is aroused from the intermediate **11**. When n = 1 (**2a**), the ethoxyl **11a** is not as flexible as the propoxyl chain **11b** (n = 2, **2b**). Therefore, **11b** can occur through an intramolecular 1,2-addition reaction exclusively, and **11a** can proceed to both intra- and inter-molecular 1,2-addition reactions. Unfortunately, the ketones did not react with 3-phenylpropyne (**3b**) under several different reaction conditions, even at high temperature. The possible reason is that 3-phenylpropyne is not as active as phenylacetylene and $ZnCl_2$–Et_3N could not promote the addition reaction.

In summary, we have studied the reaction and regioselectivity of terminal alkyne addition to β-alkoxyvinyl trifluoromethyl ketone, which is very sensitive to the promoted reagents and ketone structure. Promoted by n-BuLi, the addition of terminal alkynes gave 1,2-addition products in high yields, in marked contrast to the 1,4-additions promoted by $ZnCl_2$–Et_3N. The high regioselectivity and its tenability of the terminal alkynes to enones and the accessibility of fluorine-contained adducts may be useful in the application of these reactive compounds for the effective synthesis of bioactive fluorine-containing substances.

Experimental

Solvents were purified and dried before use. Melting points were determined on a Mel-Temp apparatus and are

Scheme 5.



uncorrected. ^{1}H NMR and ^{19}F NMR spectra were recorded on Varian-360 or Bruker AM-300 instruments with Me_4Si and $CFCl_3$ (with upfield negative) as internal and external standards, respectively; NMR spectra were recorded in chloroform-*d* unless otherwise stated. IR spectra were obtained with a PerkinElmer 983G spectrophotometer using KBr disks of the compound. Low- and high-resolution mass spectra were obtained on HP 5989a and Finnigan MAT instruments, respectively. This institute performed the elemental analyses.

General procedure for the reaction of the alkyne with ketone in the presence of *n*-BuLi

A solution of n-butyl lithium – THF (3 mL, 4.8 mmol) and 10 mL THF was added dropwise to a 50 mL three-necked flask containing phenylacetylene (0.49 g, 4.8 mmol) in 15 mL THF, after stirring at room temperature for 15 min, β-alkoxylvinyl trifluoromethyl ketone (**1a**) (0.806 g, 4.8 mmol) in 10 mL THF was added. The solution was stirred for 2 h and TLC analysis showed the reaction was completed, and then 40 mL of a satd. NH_4Cl solution was added and extracted with ether (3 × 20 mL). The organic layer was washed with brine (30 mL), dried over Na_2SO_4, and concentrated in vacuum. The residue was purified by flash chromatography by using n-hexane–EtOAc as eluent to give two products, **4a** (26%) and **5a** (51%).

1-Ethoxy-5-phenyl-3-trifluoromethyl-1-penten-4-yn-3-ol (4a)

Yield: 41%. FT-IR (KBr, cm^{-1}) ν: 3423 (s), 2984 (w), 2239 (s), 1655 (s), 1491 (s), 1189 (vs). ^{1}H NMR ($CDCl_3$) δ: 7.43 (m, 5H, Ph), 7.12 (d, 1H, J = 12.6 Hz, CH), 5.00 (d, 1H, J = 12.6 Hz, CH), 3.84 (q, J = 7.5 Hz, 2H, OCH_2), 2.90 (s, 1H, OH), 1.32 (t, J = 7.5 Hz, 3H, CH_3). ^{19}F NMR ($CDCl_3$): –81.73 (s, CF_3). MS (70 eV) m/z (%): 270 (M^+, 7.13), 241 (M^+ – Et, 14.11), 225 (M^+ – OEt, 2.72), 201 (M^+ – CF_3, 100.00), 173 (M^+ – CF_3CO, 37.16), 102 (PhC≡CH, 8.40), 77 (Ph^+, 14.85). HR-MS (EI) M^+ calcd. for $C_{14}H_{13}F_3O_2$: 270.0893; found: 270.0865.

1-Isobutoxy-5-phenyl-3-trifluoromethyl-1-penten-4-yn-3-ol (4b)

Yield: 39%. FT-IR (KBr, cm^{-1}) ν: 3423 (s), 2961 (s), 2235 (s), 1651 (w), 1491 (m), 1191 (vs). ^{1}H NMR ($CDCl_3$) δ: 7.51 (m, 5H, Ph), 7.18 (d, 1H, J = 12.6 Hz, CH), 5.01 (d,

© 2005 NRC Canada

1H, J = 12.6 Hz, CH), 3.55 (d, J = 6.6 Hz, 2H, OCH_2), 2.82 (s, 1H, OH), 2.04 (m, 1H, $CH(CH_3)_2$), 0.98 (d, J = 6.9 Hz, 6H, $2CH_3$). ^{19}F NMR ($CDCl_3$): –81.99 (s, CF_3). MS (70 eV) *m/z* (%): 299 (M^+H, 0.41), 298 (M^+, 2.11), 229 ($M^+ - CF_3$, 45.04), 173 ($M^+ - CF_3 - {}^+CHCH(CH_3)_2$), 100.00), 102 (Ph≡CH, 12.11), 77 (Ph^+, 7.08). HRMS (EI) M^+ calcd. for $C_{16}H_{17}F_3O_2$: 298.1186; found: 298.1181.

1-Ethoxy-6-phenyl-3-trifluoromethyl-1-hexen-4-yn-3-ol (4c)

Yield: 68%. FT-IR (KBr, cm^{-1}) ν: 3423 (s), 2983 (s), 2237 (m), 1656 (s), 1183 (vs). ^1H NMR ($CDCl_3$) δ: 7.35 (m, 5H, Ph), 7.03 (d, 1H, J = 12.6 Hz, CH), 4.96 (d, 1H, J = 12.6 Hz, CH), 3.81 (q, J = 6.9 Hz, 2H, OCH_2), 3.78 (s, 2H, Ph*C*H_2), 2.81 (s, 1H, OH), 1.31 (t, J = 6.9 Hz, 3H, CH_3). ^{19}F NMR ($CDCl_3$): –82.21 (s, CF_3). MS (70 eV) *m/z* (%): 284 (M^+, 0.97), 267 ($M^+H - H_2O$, 22.38), 215 ($M^+ - CF_3$, 100.00), 187 ($M^+ - CF_3CO$, 10.43), 115 ($PhCH_2C{\equiv}C^+$, 24.41), 91 ($PhCH_2^+$, 16.55), 77 (Ph^+, 5.62). Anal. calcd. for $C_{15}H_{15}O_2F_3$ (%): C 63.38, H 5.28; found: C 63.63, H 5.55.

1-Isobutoxy-6-phenyl-3-trifluoromethyl-1-hexen-4-yn-3-ol (4d)

Yield: 65%. FT-IR (KBr, cm^{-1}) ν: 3427 (s), 2962 (s), 2240 (m), 1672 (s), 1655 (vs), 1181 (vs). ^1H NMR ($CDCl_3$) δ: 7.36 (m, 5H, Ph), 7.07 (d, 1H, J = 12.6 Hz, CH), 4.95 (d, 1H, J = 12.6 Hz, CH), 3.73 (s, 2H, $PhCH_2$), 3.51 (d, J = 6.6 Hz, 2H, OCH_2), 2.75 (s, 1H, OH), 1.96 (m, 1H, $CH(CH_3)_2$), 0.96 (d, J = 7.2 Hz, 6H, $2CH_3$). ^{19}F NMR ($CDCl_3$): –82.20 (s, CF_3). MS (70 eV) *m/z* (%): 312 (M^+, 1.84), 243 ($M^+ - CF_3$, 100.00), 187 ($M^+ - CF_3 - {}^+CHCH(CH_3)_2$), 85.68), 115 ($PhCH_2C{\equiv}C^+$, 24.83), 91 ($PhCH_2^+$, 19.01), 77 ($Ph^+$, 5.62), 57 ($CH_2CH(CH_3)_2$, 61.2). Anal. calcd. for $C_{17}H_{19}O_2F_3$ (%): C 65.38, H 6.09; found: C 64.99, H 6.48.

6-Ethoxy-4-trifluoromethyl-5-hexen-2-yn-1,4-diol (4e)

Yield: 64%. FT-IR (KBr, cm^{-1}) ν: 3392 (vs), 2983 (s), 2235 (m), 1727 (s), 1186 (vs). ^1H NMR ($CDCl_3$) δ: 7.00 (d, J = 12.6 Hz, 1H, CH), 4.92 (d, J = 12.6 Hz, 1H, CH), 4.36 (s, 2H, CH_2), 3.82 (q, J = 6.9 Hz, 2H, OCH_2), 3.10 (m, 1H, OH), 2.19 (m, 1H, OH), 1.31 (t, J = 6.9 Hz, 3H, CH_3). ^{19}F NMR ($CDCl_3$): –81.82 (s, CF_3). MS (70 eV) *m/z* (%): 225 (M^+H, 1.81), 224 (M^+, 0.83), 207 ($M^+H - H_2O$, 46.76), 179 ($M^+ -$ OEt, 6.89), 155 ($M^+ - CF_3$, 100.00), 109 ($M^+ - CF_3 -$ HOEt, 49.74), 69 (CF_3^+, 17.44). Anal. calcd. for $C_9H_{11}O_3F_3$ (%): C 48.21, H 4.91; found: C 48.51, H 5.23.

6-Isobutoxy-4-trifluoromethyl-5-hexen-2-yn-1,4-diol (4f)

Yield: 61%. FT-IR (KBr, cm^{-1}) ν: 3398 (vs), 2963 (s), 2234 (m), 1727 (s), 1653 (s), 1194 (vs). ^1H NMR ($CDCl_3$) δ: 7.01 (d, J = 12.6 Hz, 1H, =*CH*), 4.93 (d, J = 12.6 Hz, 1H, =*CH*), 4.51 (d, J = 6.6 Hz, 2H, OCH_2), 4.35 (s, 2H, CH_2), 2.19 (s, 2H, 2OH), 2.01 (m, 1H, C*H*$(CH_3)_2$), 0.95 (d, J = 6.6 Hz, 6H, CH_3). ^{19}F NMR ($CDCl_3$): –82.08 (s, CF_3). MS (70 eV) *m/z* (%): 252 (M^+, 3.17), 234 ($M^+ - H_2O$, 1.75), 183 ($M^+ - CF_3$, 76.91), 127 ($M^+ - CF_3 - CH{\equiv}CCH_2OH$, 100.00), 109 ($M^+ - CF_3 - H_2O - CH{\equiv}CCH_2OH$, 47.73), 69 ($CF_3$, 12.71), 57 ($CH_2CH(CH_3)_2$, 96.42). HR-MS (EI) M^+ calcd. for $C_{11}H_{15}F_3O_3$: 252.0979; found: 252.0973.

1,7-Diphenyl-3-trifluoromethyl-4-heptene-1,6-diyn-3-ol (5a)

Yield: 20%. FT-IR (KBr, cm^{-1}) ν: 3404 (s), 2976 (m), 2236 (s), 1655 (m), 1491 (vs), 1191 (vs). ^1H NMR ($CDCl_3$) δ: 7.40 (m, 10H, 2Ph), 6.56 (d, 1H, J = 15.6 Hz, CH), 6.31 (d, 1H, J = 15.6 Hz, CH), 3.01 (s, 1H, OH). ^{13}C NMR (75.3 MHz, $CDCl_3$) δ_C: 134.7 (C-4), 132.1, 132.0, 129.7, 128.9, 128.8, 128.5 (ArC), 122.7 (q, $^1J_{C\text{-}F}$ = 280 Hz, CF_3), 122.7 (ArC-1), 120.7 (ArC-1), 116.3 (C-5), 93.7 (C-7), 89.0 (C-2), 86.0 (C-1), 81.8 (C-6), 71.9 (q, ^1J = 48 Hz, C-3). ^{19}F NMR ($CDCl_3$): –80.48 (s, CF_3). MS (70 eV) *m/z* (%): 326 (M^+, 15.73), 257 ($M^+ - CF_3$, 100.00), 226 ($M^+H -$ PhC≡C^+, 20.70), 127 (PhC≡CCH=CH^+, 14.24), 101 (PhC≡C^+, 10.57), 77 (Ph^+, 14.85). HR-MS (EI) M^+ calcd. for $C_{20}H_{13}F_3O$: 326.0895; found: 326.0919.

2-(4,5-Dihydrofuran-3-yl)-1,1,1-trifluoro-4-phenyl-3-butyn-2-ol (6a)

Yield: 81%. FT-IR (KBr, cm^{-1}) ν: 3407 (s), 2971 (m), 2234 (s), 1656 (s), 1490 (s), 1173 (vs). ^1H NMR ($CDCl_3$) δ: 7.40 (m, 5H, Ph), 6.76 (s, 1H, CH), 4.50 (m, 2H, OCH_2), 3.35 (s, 1H, OH), 2.83 (m, 2H, C*H*$_2$). ^{19}F NMR ($CDCl_3$): –79.52 (s, CF_3). MS (70 eV) *m/z* (%): 268 (M^+, 8.56), 251 ($M^+ -$ OH, 10.52), 199 ($M^+ - CF_3$, 100.00), 97 ($M^+ - CF_3 -$ PhC≡C^+, 38.99). Anal. calcd. for $C_{14}H_{11}O_2F_3$ (%): C 62.69, H 4.10; found: C 62.92, H 4.22.

2-(5,6-Dihydro-4H-pyran-3-yl)-1,1,1-trifluoro-4-phenyl-3-butyn-2-ol (6b)

Yield: 81%. FT-IR (KBr, cm^{-1}) ν: 3412 (s), 2955 (m), 2232 (s), 1658 (s), 1491 (s), 1167 (vs). ^1H NMR ($CDCl_3$) δ: 7.41 (m, 5H, Ph), 7.08 (s, 1H, CH), 4.04 (m, 2H, OCH_2), 2.97 (s, 1H, OH), 2.27 (m, 2H, CH=C-C*H*$_2$), 1.90 (m, 2H, CH_2). ^{19}F NMR ($CDCl_3$): –79.24 (s, CF_3). MS (70 eV) *m/z* (%): 282 (M^+, 6.91), 213 ($M^+ - CF_3$, 100.00), 111 ($M^+ - CF_3 -$ PhC≡CH, 5.67), 83 ($OCH_2CH_2CH_2C{=}CH^+$, 8.40), 77 (Ph^+, 10.85). HR-MS (EI) M^+ calcd. for $C_{15}H_{13}F_3O_2$: 282.0893; found: 282.0868.

General procedure for the reaction of acetylene with ketone in the presence of $ZnCl_2$–Et_3N

Phenylacetylene (0.153 g, 1.5 mmol) was added under an argon atmosphere at room temperature to a solution of anhydr. $ZnCl_2$ (0.306 g, 2.25 mmol) and triethylamine (0.32 mL, 2.25 mmol) in dried toluene (10 mL). After stirring for 1 h, β-alkoxylvinyl trifluoromethyl ketone (0.252 g, 1.5 mmol) was added dropwise. The mixture was stirred overnight and TLC analysis confirmed that the reaction was finished, then the mixture was washed with 40 mL of a satd. NH_4Cl solution, followed by extraction with ether (3 × 20 mL). The organic layer was washed with brine (30 mL), dried over Na_2SO_4, and concentrated in vacuum to give a residue, which was purified by flash chromatography by using *n*-hexane–EtOAc as eluent to give the product.

1,1,1-Trifluoro-6-phenyl-hex-3-en-5-yn-2-one (7a)

Yellow liquid; yield: 58%–81%. FT-IR (KBr, cm^{-1}) ν: 2195 (s), 1722 (s), 1602 (s), 1582 (s), 1205 (s), 1148 (s). ^1H NMR ($CDCl_3$) δ: 7.42 (m, 5H, Ph), 7.25 (d, J = 15.3 Hz, 1H, CF_3COCH=), 6.85 (d, J = 15.0 Hz, 1H, C*H*=C). ^{19}F NMR ($CDCl_3$): –77.80 (s, CF_3). MS (70 eV) *m/z* (%): 224 (M^+, 90.95), 155 ($M^+ - CF_3$, 100.00), 127 ($M^+ - COCF_3$,

© 2005 NRC Canada

66.73), 77 (Ph^+, 14.43). Anal. calcd. for $C_{12}H_7OF_3$ (%): C 64.29, H 3.15; found: C 64.29, H 3.16.

3-(3-Phenylprop-2-ynylidene)-2-hydroxy-2-(trifluoromethyl)tetrahydrofuran (8a)

White solid; mp 72–74 °C; yield: 53%. FT-IR (KBr, cm^{-1}) ν: 3361 (s), 2913 (s), 2200 (m), 1650 (s), 1193 (vs). ^1H NMR ($CDCl_3$) δ: 7.40 (m, 5H, Ph), 6.18 (s, 1H, CH), 4.19 (m, 2H, OCH_2), 3.07 (m, 2H, CH_2), 2.95 (m, 1H, OH). ^{13}C NMR (75.3 MHz, $CDCl_3$) δ_C: 132.2 (*C*=CH), 131.6 (ArC-4), 128.9 (ArC-3, ArC-5), 128.2 (ArC-2), 122.3 (ArC-1), 122.6 (q, $^1J_{C\text{-}F}$ = 280 Hz, CF_3), 109.4 (C=*C*H), 100.7 (*C*-CF_3), 97.1 (C=CH-*C*≡C), 88.3(C=CH-C≡*C*), 68.3 (OCH_2), 31.3 (CH_2). ^{19}F NMR ($CDCl_3$): –83.53 (s, CF_3). MS (70 eV) *m*/*z* (%): 268 (M^+, 27.41), 251 (M^+ – OH, 3.01), 199 (M^+ – CF_3, 100.00), 181 (M^+ – CF_3 – H_2O, 3.03), 91 (PhC≡C^+, 5.45), 77 (Ph^+, 19.36). HR-MS (EI) M^+ calcd. for $C_{14}H_{11}F_3O_2$: 268.0692; found: 268.0711.

3-(3-Phenylprop-2-ynylidene)-2-hydroxyl-2-(trifluoromethyl)tetrahydropyran (8b)

White solid; mp: 56–58 °C; yield: 44%. FT-IR (KBr, cm^{-1}) ν: 3397 (s), 2999 (m), 2204 (m), 1658 (m), 1443 (s), 1185 (vs). ^1H NMR ($CDCl_3$) δ: 7.48 (m, 5H, Ph), 6.24 (s, 1H, CH), 3.98 (dd, *J* = 4.8, 7.5 Hz, 2H, OCH_2), 3.14 (s, 1H, OH), 3.04 (m, 1H, CH_2), 2.60 (m, 1H, CH_2), 2.03 (m, 1H, CH_2), 1.85 (m, 1H, CH_2). ^{19}F NMR ($CDCl_3$): –82.43 (s, CF_3). MS (70 eV) *m*/*z* (%): 282 (M^+, 19.72), 213 (M^+ – CF_3, 100.00), 195 (M^+ – CF_3 – OH, 3.10), 185 (M^+ – $COCF_3$, 30.70), 77 (Ph^+, 10.47). Anal. calcd. for $C_{15}H_{13}O_2F_3$ (%): C 63.83, H 4.61; found: C 64.09, H 4.67.

4-(2-Hydroxyethyl)-1,8-diphenyl-3-trifluoromethyl-4-heptene-1,6-diyn-3-ol (9)

Yield: 7%. FT-IR (KBr, cm^{-1}) ν: 3317 (s), 2233 (m), 1640 (m), 1491 (s), 1444 (m), 1186 (vs). ^1H NMR ($CDCl_3$) δ: 7.52–7.31 (m, 10H, 2Ph), 7.30 (m, 1H, CH), 5.18 (d, *J* = 6 Hz, 1H, CH), 4.07 (m, 2H, OCH_2), 3.32 (s, 1H, OH), 3.09 (d-q, *J* = 6.3, 8.4 Hz, 1H, OH), 2.25 (m, 2H, CH_2). ^{13}C NMR (75.3 MHz, $CDCl_3$) δ_C: 132.1 (C-4), 131.9, 129.7, 128.5, 128.2, 128.2, 125.7 (ArC), 125.1 (q, $^1J_{C\text{-}F}$ = 280 Hz, CF_3), 123.2 (C-5), 88.9 (C-7), 88.4 (C-1), 85.5 (C-6), 81.6 (C-2), 73.9 (C-3), 70.3 (*C*H_2OH), 51.6 (CH_2). ^{19}F NMR ($CDCl_3$): –79.34 (s, CF_3). MS (70 eV) *m*/*z* (%): 370 (M^+, 19.72), 301 (M^+ – CF_3, 100.00), 284 (M^+ – CF_3 – OH, 3.10), 269 (M^+ – PhC≡C^+, 30.70), 77 (Ph^+, 10.47). Anal. calcd. for $C_{22}H_{17}O_2F_3$ (%): C 71.35, H 4.59; found: C 71.21, H 4.69.

Acknowledgment

This work was supported by the National Natural Science Foundation of China (NNSFC) (Grant Nos. 20372077 and 20532040).

References

1. (*a*) R.E. Banks, B.E. Smart, and J.C. Tatlow (*Editors*). Organofluorine chemistry, principles and commercial application. Plenum, New York. 1994; (*b*) R. Filler, Y. Kobayashi, and L.M. Yagupolskii (*Editors*). Organofluorine compounds in medicinal chemistry and biomedical applications. Elsevier, Amsterdam. 1993; (*c*) J.P. Begue and D. Bonnet-Delpon. Tetrahedron, **47**, 3207 (1991).
2. (*a*) W.S. Huang and C.Y. Yuan. J. Chem. Soc. Perkin Trans. 1, 741 (1995); (*b*) A.V. Sanin, V.G. Nenajdenko, K.I. Smolko, D.I. Detrisenko, and E.S. Balenkova. Synthesis, 842 (1998); (*c*) V.G. Nenajdenko, A.L. Krasovsky, M.V Lebedev, and E.S. Balenkova. Synlett, 1349 (1997); (*d*) S.Z. Zhu, C.Y. Qin, G.L. Xu, Q.L. Chu, and Q.C. Huang. J. Fluorine Chem. **99**, 141 (1999).
3. (*a*) V.G. Nenjdenko, A.V. Sanin, and E.S. Balenkova. Russ. Chem. Rev. **68**, 437 (1999); (*b*) M.W. Walter, R.M. Adlington, J.E. Baldwin, and C.J. Schofield. J. Org. Chem. **63**, 5179 (1998).
4. (*a*) M. Kawase, H. Harada, S. Satio, J.M. Cui, and S. Tani. Biorg. Med. Chem. Lett. **9**, 193 (1999); (*b*) D.L. Boger, H. Sato, A.E. Lemet, B.J. Austin, J.E. Patterson, M.P. Patricelli, and B.F. Cravatt. Biorg. Med. Chem. Lett. **9**, 265 (1999).
5. N.P. Gambaryan, L.A. Simonyan, and P.V. Petrovskii. Izv. Akad. Nauk SSSR Ser. Khim. 918 (1967).
6. (*a*) M. Hojo, R. Masuda, Y. Kokuryo, H. Shioda, S. Matsuo, and I.I. Gerus. Chem. Lett. 499 (1976); (*b*) M.G. Gorbunova, S.I. Vdovenko, Y.L. Yagupolskii, and V.P. Kukhar. Zh. Org. Khim. **26**, 1877 (1990); (*c*) S.I. Vdovenko, I.I. Gerus, and M.G. Gorbunova. J. Chem. Soc. Perkin Trans. 1, 559 (1993); (*d*) M.G. Gorbunova, I.I. Gerus, and V.P. Kukhar. J. Fluorine Chem. **65**, 25 (1993); (*e*) H.G. Bonacorso, I.S. Lopes, A.D. Wastowski, N. Zanatta, and M.A.P. Martins. J. Fluorine Chem. **120**, 29 (2003).
7. R.J. Andrew and J.M. Mellor. Tetrahedron, **56**, 7261 (2000).
8. S.Z. Zhu, G.L. Xu, C.Y. Qin, Q.L. Chu, and Y. Xu. Monatsh. Chem. **130**, 671 (1999).
9. I.S. Kruchok, I.I. Gerus, and V.P. Kukhar. Tetrahedron, **56**, 6533 (2000).
10. S.J. Coles, J.M. Mellor, A.H. El-Sagheer, E.E.M. Salem, and R.N. Metwally. Tetrahedron, **56**, 10057 (2000).
11. (*a*) Q.L. Chu, L.P. Song, G.F. Jin, and S.Z. Zhu. J. Fluorine Chem. **108**, 51 (2001); (*b*) S.Z. Zhu, G.F. Jin, W.M. Peng, and Q.C. Huang. Tetrahedron, **59**, 2899 (2003).
12. M. Yamaguchi, A. Hayashi, and M. Hirama. Chem. Lett. 2479 (1992); N.K. Anand and E.M. Carreira. J. Am. Chem. Soc. **123**, 9687 (2001).
13. B. Jiang and Y.G. Si. Tetrahedron Lett. **43**, 8323 (2002).
14. M.A.R. Martins, D.J. Emmerich, C.M.P. Pereira, W. Cunico, M. Rossato, N. Zanatta, and H.G. Bonacorso. Tetrahedron Lett. **45**, 4935 (2004).

© 2005 NRC Canada

Structural analysis of acetylated hardwood lignins and their photoyellowing properties

Yunqiao Pu and Arthur J. Ragauskas

Abstract: Lignin was isolated from aspen bleached chemithermomechanical pulp by employing a mild acid hydrolysis procedure, and the extracted material was acetylated with acetic anhydride. Nuclear magnetic resonance analyses indicated that the relative ease of acetylating lignin hydroxyl groups was phenolic >> γ-side chain > α-side chain. Non-acetylated and acetylated lignins were impregnated onto cellulosic test sheets, and the photo-behavior of the lignins was examined under irradiation with two light sources, a fluorescent lamp and a black lamp. Optical reflective studies indicated acetylation efficiently inhibited the photodiscoloration of aspen bleached chemithermomechanical pulp lignin under visible and near-UV light irradiation. The photostability of the lignin was correlated to the extent of lignin acetylation. The observed photo-stabilization of acetylated lignin during light irradiation was attributed to the acetylation of phenoxy and aliphatic hydroxyl groups in lignin.

Key words: green chemistry, hardwood lignin, acetylation, photo-stabilization, photoyellowing, NMR.

Résumé : Faisant appel à une méthode d'hydrolyse acide douce, on a isolé la lignine de la pulpe chimique/thermique/mécanique blanchie de peuplier et le produit isolé a été acétylé avec de l'anhydride acétique. Des analyses de résonance magnétique nucléaire ont permis de déterminer que les facilités relatives d'acétylation des groupes hydroxyles de la lignine sont dans l'ordre phénolique >> chaîne latérale γ > chaîne latérale α. Les lignines acétylées et non-acétylées ont été imprégnées sur des feuillets d'essai en cellulose et le photocomportement des lignines a été étudié sous irradiation de deux sources lumineuses, une lampe fluorescente et une lampe noire. Des études de réflexion optique indiquent que l'acétylation inhibe efficacement la photodécoloration de la lignine de la pulpe chimique/thermique/mécanique blanchie de peuplier par des irradiations avec des lumières visible ou du proche UV. La photostabilité de la lignine est directement reliée au degré d'acétylation de la lignine. La photostabilisation observée pour la lignine acétylée lors d'une irradiation à la lumière est attribuée à l'acétylation des groupes phénoxy et des groupes hydroxyles aliphatiques de la lignine.

Mots clés : chimie verte, lignine de bois dur, acétylation, photostabilisation, photojaunissement, RMN.

[Traduit par la Rédaction]

Introduction

The need to develop environmentally compatible industrial processes based on renewable resources is an important societal goal. The conversion of wood into pulp fibers using mechanical energy is an example of an environmental green chemistry process. Unlike most chemical pulps, which largely utilize the cellulose component of wood, mechanical pulps utilize all three of the major wood polymers: cellulose, hemicellulose, and lignin, and are accompanied with +90% yields (1). In comparison, chemical pulping and bleaching technologies usually afford pulp yields in the mid to low 40% range (2). The high conversion of lignocellulosics into mechanical pulp insures minimal generation of waste products and improved environmental performance. In summary, mechanical pulping is an environmentally friendly, efficient method of utilizing wood resources for the purpose of generating value-added materials.

Increased usage of mechanical pulps is limited owing to their well-known tendency to rapidly undergo photoyellowing when exposed to near-UV light sources, such as office lighting and sunlight (3–8). Research studies have demonstrated that the photoyellowing process is initiated by the absorption of 300–400 nm light by several lignin functionalities summarized in Fig. 1, including phenacyl-α-*O*-aryl ethers (9), β-*O*-aryl ethers (10–15), extended conjugated structures (16), stilbenes (15, 17, 18), coniferyl alcohol (19), phenolic phenylpropenol (20), and quinone structures (21, 22). The photoabsorption process generates a series of reactive radical intermediates that result in the oxidation of lignin-yielding chromophoric products, including *ortho*- and *para*-quinone lignin derivatives (14, 22–24).

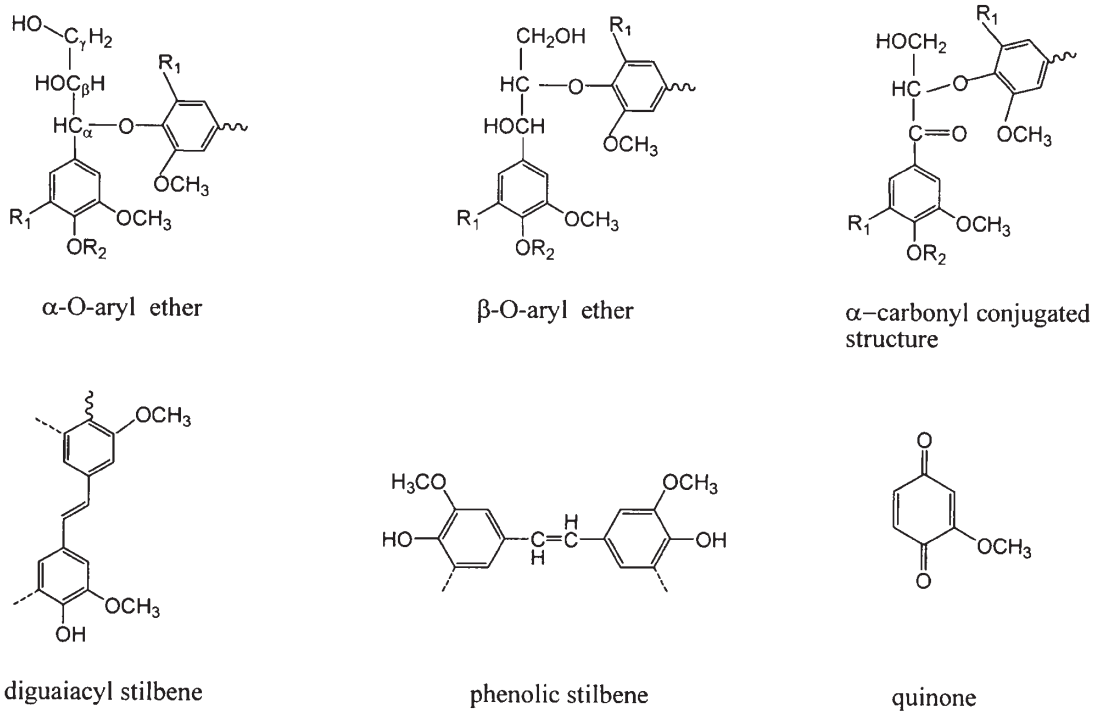
Received 23 August 2005. Published on the NRC Research Press Web site at http://canjchem.nrc.ca on 21 February 2006.

Y. Pu. Institute of Paper Science and Technology, Georgia Institute of Technology, 500 10th St., Atlanta, GA 30332, USA.
A.J. Ragauskas.[1] School of Chemistry and Biochemistry, Institute of Paper Science and Technology, Georgia Institute of Technology, 500 10th St., Atlanta, GA 30332, USA.

[1]Corresponding author (e-mail: arthur.ragauskas@chemistry.gatech.edu).

 doi: 10.1139/V05-231 © 2005 NRC Canada

Fig. 1. Photosensitive HW lignin subunit structures. R_1 = -OCH_3: syringyl unit; R_1 = H: guaiacyl unit; R_2 = H: non-etherified unit; R_2 = C_β: etherified unit.



A number of photostabilization treatments have been pursued to photostabilize high-lignin fibers. These technologies can be broadly described as either additive dependent or fiber modification technologies (25–29). The recent studies by Davidson et al. (26) and Cook and Ragauskas (27) have documented the ability of utilizing binary additive systems to significantly hinder the photoinduced discoloration process. One of the most promising fiber modification methods of halting the photoyellowing process involves acetylation of mechanical pulp, employing acetic anhydride and an acid catalyst (25, 30–32). Model compound studies investigating the chemistry of acid-catalyzed lignin acetylation indicate that phenolics are preferentially acetylated over aliphatic hydroxyl groups when employing structures such as 1-(4-hydroxy-3-methoxyphenyl)-2-(2-methoxyphenoxy)-1,3-propanediol (33). Recently, Pu et al. (34) established that acetylated lignin is the stabilizing component of the softwood acetylated bleached chemithermomechanical pulp.

Argyropoulos and Sun (35) have investigated the structural characteristics of softwood milled wood lignin and lignin model compounds irradiated under nitrogen and oxygen atmosphere. They demonstrated that photoirradiation cleaved β-O-4 ethers present in lignin, with the concomitant formation of new phenolic units, especially C5-related condensed phenolic. Heitner et al. (36) examined the photoreactivity of acetylated softwood milled wood lignin (MWL) in solution and concluded that lignin acetylation decreased the extent of photodegradation by hindering the cleavage of the β-O-aryl ether groups. This stabilization effect hindered the production of phenoxy radicals and lignin chromophores. In our previous study, we examined the photo-oxidative chemistry of the acetylated softwood lignin from chemithermomechanical pulp via a mild acid hydrolysis procedure and found that phenoxy groups were formed during the near-UV light irradiation (37). These previous studies have focused primarily on the photobehavior and chemistry of softwood lignin. Little research effort has been devoted to the hardwood lignin, despite the fact that hardwood mechanical pulps are produced on a substantial scale and known to undergo photodiscoloration when exposed to near-UV light sources. It is well-known that hardwood lignin exhibits differences in structural characteristics in comparison to softwood lignin owing to the presence of syringyl units in the lignin biopolymer (38). These fundamental parameters also influence its photoyellowing properties (39). This paper examines the structural characteristics and photoreactivity of acetylated lignin isolated from hardwood mechanical pulp by NMR.

Experimental

Materials

All chemicals were commercially purchased and used as received, except *p*-dioxane, which was purified by distillation over sodium borohydride before use. A commercially produced aspen bleached chemithermomechanical pulp (BCTMP) was employed in this study. Test sheets (150 g/m^2) were prepared from Whatman filter paper (Qualitative, No. 5), according to standard literature method (40).

Lignin isolation

Lignin was isolated from the aspen BCTMP following the literature method (34, 41). In brief, the pulp was extensively washed, air-dried, and soxhlet-extracted with acetone for 24 h. Air-dried pulp (150 g) was then refluxed in a 0.01 mol/L HCl dioxane–water (3 L, 8.5:1.5) solution under

© 2005 NRC Canada

argon for 1 h. The extracted pulp was filtered and washed with fresh *p*-dioxane (200 mL × 3). The combined aliquots were neutralized with an aqueous saturated solution of sodium bicarbonate and then concentrated under reduced pressure at ≤40 °C. The concentrated solution was added to 700 mL of 0.006 mol/L aq. HCl, and the precipitated lignin was centrifuged, washed with acidic water (pH 2 ~ 3), and freeze dried. The lyophilized lignin was subsequently dried under high vacuum at 40 °C for 24 h. This method produced a low-yield lignin (2.8% yield) with a light-white color.

Lignin acetylation

Lignin acetylation was carried out according to the published method (34), which involved dissolving lignin (0.2000 g) in refluxing dioxane (200.00 mL) and treating this mixture with acetic anhydride (40.00 mL). This mixture was refluxed for selected time periods, then cooled, concentrated, and dried under reduced pressure. The acetylated lignin was dissolved in chloroform and precipitated with the addition of diethyl ether. The precipitated lignin acetate was collected after centrifugation and dried under high vacuum for 24 h (>77% recovery yield).

Photoirradiation

Photoirradiation with fluorescent and black lamps was carried out according to the literature method (37). In brief, non-acetylated lignin (0.0450 g) was dissolved in a 9:1 dioxane–water solution (10.00 mL), uniformly applied onto filter paper test sheets, and subsequently air-dried in the dark. Acetylated lignins were processed in the same manner, except that chloroform was employed as the solvent. The treated test sheets were attached to a merry-go-round apparatus and photolyzed in a Rayonet photochemical reactor (model RPR-100, The Southern New England Ultraviolet Company, Branford, Connecticut, USA) with RPR 5750 UV–vis fluorescent lamps (λ: 350–700 nm) and RPR 3500 UV lamps (black light, λ: 300–400 nm).

The degree of photodiscoloration of the test sheets was expressed as the post-color (PC) values following published method (42). The PC number was calculated according to eqs. [1] and [2],

$$[1] \qquad PC = ((k/s)_{after} - (k/s)_{before}) \times 100$$

$$[2] \qquad k/s = (1 - R_\infty)^2/2R_\infty$$

where k = specific absorption coefficient, s = specific scattering coefficient, R_∞ = reflectance at λ = 457 nm. Reflectance values of the test sheets were determined with a Brightimeter Micro S-5 reflectometer manufactured by Technidyne Corporation (43).

NMR characterization

All NMR spectra were recorded on a 400 MHz Bruker Advance/DMX NMR spectrometer. Quantitative ^{13}C NMR spectra were acquired using DMSO as solvent for non-acetylated and acetylated lignins, with an inverse gated decoupling sequence, 90° pulse angle, 12 s pulse delay, and 10 000 scans (44–46). The integration and carbon content calculation of the functional groups in the ^{13}C NMR spectra were performed in accordance with the literature method (44). The carbon content of a functional group was calculated as the ratio of the integral of the given carbon signal to one-sixth the integral of the aromatic carbons (signals between δ 102 and 156 ppm). Therefore, integration regions can be quantified and reported as the number of carbon atoms per aromatic unit.

The lignin samples were also derivatized with 2-chloro-4,4,5,5-tetramethyl-1,3,2-dioxaphospholane and analyzed by ^{31}P NMR following literature methods (47, 48). Cyclohexanol was used as the internal standard. ^{31}P NMR spectra were recorded using an inverse gated decoupling sequence, 90° pulse angle, 25 s pulse delay, and 150 transients at room temperature. The integration regions for the hydroxyl groups were in accordance with the literature method (47, 48). The signal for the phosphitylated cyclohexanol was separated from the lignin hydroxyl group signals and was integrated and calibrated to 1.0 unit. The content of the hydroxyl group in cyclohexanol was used as the internal standard factor. For various hydroxyl functional groups in lignin, this internal standard factor was multiplied by the integrated intensity and divided by the weight of the lignin sample. The contents of lignin hydroxyl groups were reported as mmol/g lignin.

NMR spectral acquisition and analyses were controlled by Bruker's XWINNMR 2.6 software running on an SGI (Silicon Graphics Indigo) server using the Irix 7.0 operating system. The lignin functional groups characterized by ^{13}C and ^{31}P NMR had standard errors of 3.0% and 1.2%, respectively.

Results and discussion

Structural characteristics of non-acetylated and acetylated lignins

Li and Ragauskas (41) have previously demonstrated the applicability of employing extracted softwood lignin for photochemical studies. Following this procedure, aspen BCTMP lignin was acquired, and this material was subsequently treated with acidic anhydride in *p*-dioxane. Structural changes in lignin during acetylation were monitored by ^{13}C and ^{31}P NMR spectra.

Hardwood lignin is comprised of syringyl and guaiacyl lignin units as summarized in Fig. 1 (38, 44). The changes in acetylated hardwood lignin as determined by ^{13}C NMR are summarized in Figs. 2–4, and the structural assignments are summarized in Table 1. As can be seen in Fig. 2 and Table 1, the acetylation treatment significantly impacts the structure of hardwood lignin. The signal centered at δ 147.1 ppm in non-acetylated lignin has been assigned to C_3/C_5 in syringyl β-O-4 non-etherified unit (44). After acetylation, this signal is shifted downfield to δ 152.2 ppm. The signal centered at δ 145.3 ppm in non-acetylated lignin has been assigned to C_4 in guaiacyl β-O-4 non-etherified unit (44, 51), and this signal is absent in the acetylated lignin. The signal centered at δ 115 ppm in non-acetylated lignin is assigned to C_5-H in guaiacyl unit, and this signal decreases significantly in intensity after acetylation. The corresponding acetylated signal is centered at δ 123 ppm, which is in accord with lignin model compound studies (49). The signal at δ 59.6 ppm has been attributed to the aliphatic C-γ in β-O-4 syringyl and guaiacyl units, and it shifts downfield by 4 ppm after acetylation to δ 63.8 ppm.

© 2005 NRC Canada

Fig. 2. ^{13}C NMR spectra of pre- and post-acetylated (150 min) aspen BCTMP lignins.

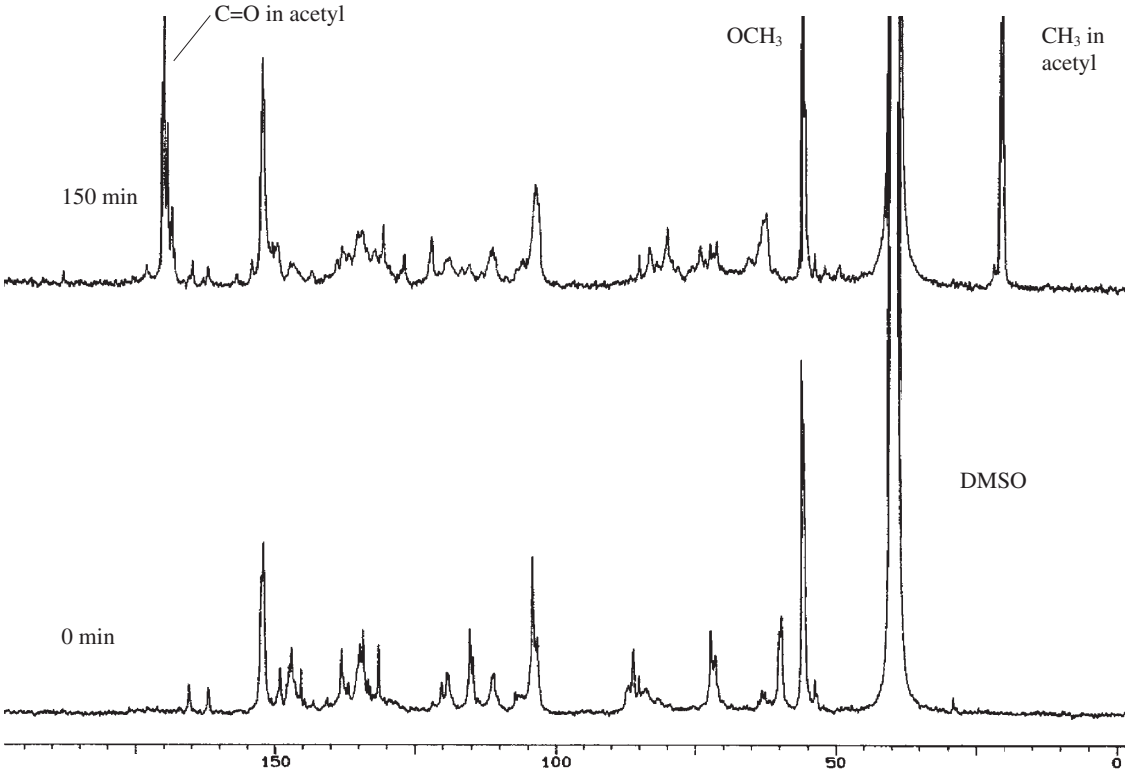


Fig. 3. Acetate methyl group in hardwood BCTMP lignins determined by ^{13}C NMR spectra (expressed as number of C atoms per aromatic ring).

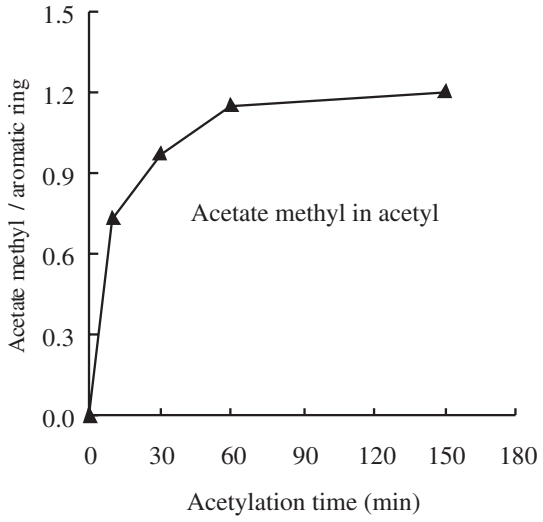
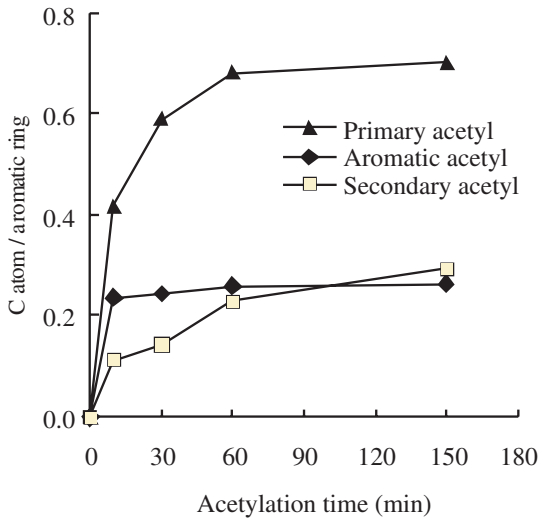


Fig. 4. Carbonyl (C=O) content of acetyl group in hardwood BCTMP lignins determined by ^{13}C NMR spectra (expressed as number of C atoms per aromatic ring).



The acetate methyl group content was calculated by integrating the chemical regions from δ 19.5 to 21.6 ppm. Figure 3 presents the changes of acetate methyl group content in the hardwood lignins at different acetylation times, as determined by quantitative ^{13}C NMR analysis. This result indicates the bulk of the acetylation of lignin is completed within the first 60 min under the reaction conditions employed.

The acetyl carbonyl content was calculated by integrating over the chemical shift regions from δ 168.5 to 169.4 ppm for aromatic acetyl, from δ 169.4 to 170.3 ppm for secondary aliphatic acetyl, and from δ 170.3 to 172.0 ppm for primary aliphatic acetyl. Figure 4 shows the acetyl carbonyl group content in the lignin samples at differing acetylation times. It can be seen in Fig. 4 that the primary aliphatic acetyl content of lignin increases rapidly during the initial 10 min acetylation, and it is higher than the secondary aliphatic acetyl content when lignin was acetylated for the same time. After acetylating lignin for 60 min, the primary aliphatic acetyl content remains almost unchanged, and a

© 2005 NRC Canada

Table 1. ^{13}C chemical shifts and signal assignments for aspen BCTMP lignins (45, 49, 50).

	Assignments	
Chemical shift (ppm)	Non-acetylated lignin	Acetylated lignin
171.0	—	Primary acetyl carbonyl
169.9	—	Secondly acetyl carbonyl
169.0	—	Aromatic acetyl carbonyl
152.2	C_3/C_5 in S β-O-4 etherified	C_3/C_5 in S β-O-4 etherified
149.1	C_3 in G etherified	C_3 in G etherified
147.1	C_3/C_5 in S β-O-4 non-etherified	C_3/C_5 in S β-O-4
145.3	C_4 in G β-O-4 non-etherified	—
139.0	—	C_4 in G β-O-4
138.1	C_1 in S β-O-4 etherified	C_1 in S β-O-4 etherified
134.8	C_4 and C_1 in S β-O-4	C_4 and C_1 in S β-O-4
131.4	C_1 in S β-O-4 non-etherified	C_1 in S β-O-4
127.1	—	C_4 in S β-O-4
122.1	—	C_5 in G units
120.0	C_6 in G units	C_6 in G units
115.2	C_5 in G units	—
111.0	C_2 in G units	C_2 in G units
104~107	C_2/C_6 in S units	C_2/C_6 in S units
86.1	C_β in β-O-4 G and S units	—
80.7	—	C_β in β-O-4 G and S units
71.0–73.0	C_α in β-O-4 G and S units	C_α in β-O-4 G and S units
63.8	—	C_γ in β-O-4 S and G
63.0	C_γ in β-5 and β-O-4 with α–C=O	—
60.0	C_γ in β-O-4 S and G	—
55.9	Aromatic CH_3 in G and S units	Aromatic CH_3 in G and S units
20.4	—	CH_3 in acetyl group

Note: Syringyl unit (S), guaiacyl unit (G).

slow increase of secondary aliphatic acetyl content is observed at 150 min acetylation. This indicates that the aliphatic primary hydroxyl group in lignin is more rapidly, and preferentially, acetylated over the secondary hydroxyl group. This is consistent with the lignin model compounds studies, which have indicated that the γ-hydroxyl group is easily acetylated and the α-hydroxyl group is comparatively resistant toward treatment with acetic anhydride (33). It can also be seen from Fig. 4 that aromatic acetyl content increases rapidly after the first 10 min of the acetylation reaction and then remains relatively unchanged for the remaining 150 min.

Figure 5 summarizes the aliphatic hydroxyl group content from ^{31}P NMR analysis of phosphitylated lignin samples. These results indicate that the aliphatic lignin hydroxyl group content decreases significantly during the initial 60 min acetylation, which could be mostly attributed to acetylation of the aliphatic primary hydroxyl group. For the 60 min acetylation treatment, the aliphatic hydroxy group content was decreased 71.7%, suggesting that 71.7% of the aliphatic hydroxy group was acetylated. For the 150 min acetylation treatment, the aliphatic hydroxy group content was observed to decrease by 73.8%, suggesting that 73.8% of the aliphatic hydroxy group was acetylated. These results also suggest that the lignin biopolymer has a series of residual aliphatic OH groups that are very resistant to acetylation.

Fig. 5. Contents of aliphatic OH group in hardwood BCTMP lignin determined by ^{31}P NMR spectra.

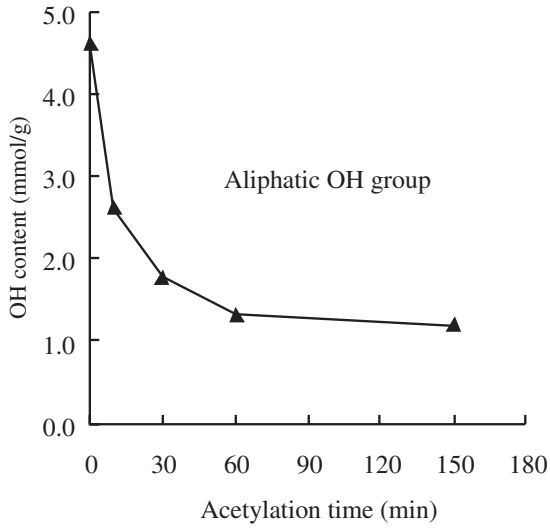


Figure 6 summarizes the phenolic hydroxyl content for the starting and acetylated lignin samples, as determined by ^{31}P NMR analysis. Approximately 93% of guaiacyl phenolic OH groups were readily acetylated in the initial 10 min

© 2005 NRC Canada

Fig. 6. Content of phenolic hydroxyl groups in hardwood BCTMP lignin determined by ^{31}P NMR spectra.

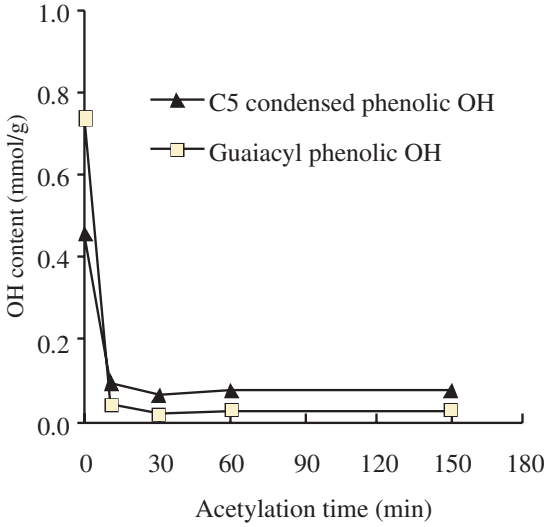
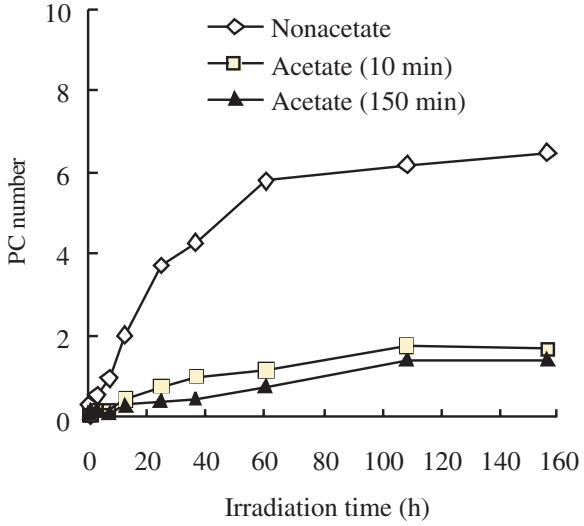


Fig. 7. PC number of filter paper test sheets applied with non-acetylated and acetylated lignins during office light irradiation.



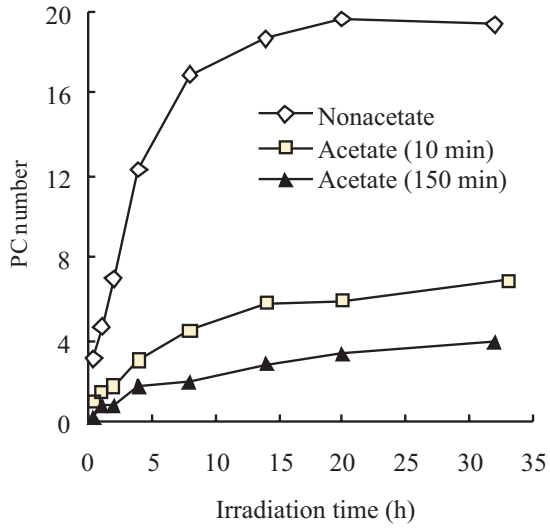
treatment, compared with 80% for the syringyl and C_5-condensed phenolic groups, indicating that the syringyl and C_5-condensed phenolic hydroxyl groups are slower to acetylate. After 10 min acetylation, 88.0% of the total aromatic OH were acetylated, while at 150 min acetylation, 91.1% of the total aromatic OH were acetylated. The ^{31}P NMR results confirm the trends observed by ^{13}C NMR analyses: that the bulk of the phenolic hydroxyl groups in lignin are readily acetylated in the acid-catalyzed acetylation procedure studied.

Photobehavior of non-acetylated and acetylated lignins

To examine the photobehavior of hardwood lignin and the corresponding acetylated samples in the solid state, samples were dissolved in an organic solvent and applied onto cellulose test sheets. The effect of acetylation on the photobehavior of lignin was evaluated by employing a slightly acetylated sample (i.e., acetylated for 10 min) and an extensively acetylated sample (i.e., acetylated for 150 min). The test sheets were irradiated with RPR 5750 UV–vis fluorescent lamps (office light, λ: 350–700 nm), and the results are summarized in Fig. 7. As shown in Fig. 7, the non-acetylated lignin has a higher PC number than the acetylated lignins, suggesting that acetylation treatment efficiently inhibits the photoyellowing of hardwood lignin under office light irradiation. After 60 h of irradiation, non-acetylated lignin test sheets exhibited an increase of 5.8 in PC value, while the acetylated lignin test sheets exhibited an increase of only 1.1 in PC value for 10 min acetylation time, and 0.8 for 150 min acetylation time. The smaller increase in PC values for the acetylated lignin samples, in comparison with the nonacetylated lignin samples, demonstrates that the acetylation process retards the photoyellowing of lignin. Lignin with 10 min of acetylated treatment shows a higher PC number than that with 150 min of acetylation, indicating that acetylation at longer acetylation time results in reduced photodiscoloration.

To examine the effects of acetylation on lignin photodiscoloration under accelerated irradiation, cellulose test sheets impregnated with non-acetylated and acetylated lignins

Fig. 8. PC number of filter paper test sheets applied with non-acetylated and acetylated lignins during black light irradiation.

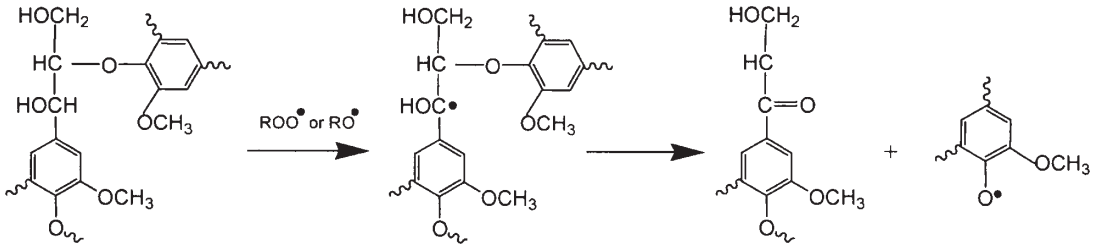


were irradiated with RPR 3500 UV lamps (black light, λ: 300–400 nm). The results in Fig. 8 indicate that the non-acetylated lignin has a higher PC number than acetylated lignin during irradiation. Compared with non-acetylated lignin, acetylated lignin shows a much lower extent of photodiscoloration. After 14 h of irradiation, the treated test sheets exhibit a PC value of 3.2 for lignin acetylated for 150 min, a 5.9 PC value for lignin acetylated for 10 min, and an 18.6 PC value for non-acetylated lignin. This clearly indicates that the acetylation treatment strongly retards the photoreversion of lignin during the accelerated irradiation, and acetylation at longer acetylation time leads to a more pronounced photoyellowing inhibition, which agrees with the observations acquired with the UV–vis fluorescent lamps.

Phenoxy radicals generated from photoreactions during light irradiation have been suggested as a major contributor to the photoyellowing of mechanical pulps (50). The acetylation of hardwood lignin effectively blocks the photo-

© 2005 NRC Canada

Fig. 9. Lignin β-O-4 aryl ether cleavage during photoirradiation.



formation of phenoxy radicals by acetylating these phenolic hydroxyl groups reactive sites, thus inhibiting the photoreversion of lignin. Schmidt and Heitner (12) and Heitner et al. (36) have proposed that cleavage of the β-O-4 group, which produces phenoxy radicals and lignin chromophores, is a main degradation pathway of photoyellowing of mechanical pulps (Fig. 9). The acetylation of side chain α- and γ-hydroxyl groups has been suggested to be, potentially, a means of inhibiting the β-O-4 cleavage, thereby resulting in the photostabilization of lignins (36).

Conclusion

This paper examined the structural characteristics and photobehavior of acetylated lignin extracted from aspen-bleached chemithermomechanical pulp. Analysis of acetylated hardwood lignin demonstrated that the γ-hydroxyl group in the side chain of lignin is easily acetylated and the α-hydroxyl group is comparatively resistant towards acetylation. The phenolic hydroxyl groups of lignin are very easily acetylated, and under the reaction conditions examined, this was accomplished within 10 min. The acetylated lignins exhibit substantially decreased photodiscoloration behaviour under visible and near-UV light irradiation, with enhanced photostabilization being correlated to the overall degree of lignin acetylation. The acetylation of phenolic hydroxyl groups blocks the generation of phenoxy radicals during light irradiation, resulting in the photostabilization of hardwood-acetylated lignin. The acetylation of the side chain α- and γ-hydroxyl groups of hardwood lignin could also inhibit the β-O-4 cleavage, contributing to the observed photostabilization.

Acknowledgments

The authors would like to thank the US Department of Agriculture, Improved Utilization of Wood Program (Grant Nos. 99-35103-8603 and 98-35501-6911) and the member companies of the Institute of Paper Science and Technology for their support of this research.

References

1. G. Smook. *In* Handbook for pulp & paper technologies. *Edited by* M.J. Kocurek. TAPPI press, Atlanta, Ga. 1989. p. 44.
2. S.V. Fleet. *In* Pulp and paper manufacture. *Edited by* M.J. Kocurek, T.M. Grace, and E.W. Malcom. TAPPI press, Atlanta, Ga. 1989. p. 228.
3. G.J. Leary. Tappi J. **50**, 17 (1967).
4. K. Kringstad. Tappi J. **52**, 1070 (1969).
5. J. Janson and I. Forsskåhl. Nord. Pulp Pap. Res. J. **4**, 197 (1989).
6. C. Heitner. *In* Photochemistry of lignocellulosic materials. *Edited by* C. Heitner and J.C. Scaiano. ACS Symp. Ser. No. 531, Washington, D.C. 1993. p. 2.
7. I. Forsskåhl. Trends Photochem. Photobiol. **3**, 503 (1994).
8. M. Paulsson and A.J. Ragauskas. *In* Lignin: Historical, biological, and materials perspectives. *Edited by* W.G. Glasser, R.A. Northey, and T.P. Schultz. ACS Symp. Ser. No. 742, Washington, D.C. 1999. p. 254, 490.
9. J. Gierer and S.Y. Lin. Sven. Papperstidn. **75**, 233 (1972).
10. C. Vanucci, P. Fornier de Violet, H. Bouas-Laurent, and A. Castellan. J. Photochem. Photobiol. A, **41**, 251 (1988).
11. A. Castellan, N. Colombo, C. Cucuphat, and P. Fornier de Violet. Holzforschung, **43**, 179 (1989).
12. J.A. Schmidt and C. Heitner. J. Wood Chem. Technol. **13**, 309 (1993).
13. P.H. Kandanarachchi, T. Autrey, and J.A. Franz. J. Org. Chem. **67**, 7937 (2002).
14. C.M. Felicio, A.E.H. Machado, A. Castellan, A. Nourmamode, D.S. Perez, and R. Ruggiero. J. Photochem. Photobiol. A, **156**, 253 (2003).
15. A. Castellan, N. Colombo, A. Nourmamode, J.H. Zhu, D. Lachenal, R.S. Davidson, and L. Dunn. J. Wood Chem. Technol. **10**, 461 (1990).
16. G. Gellerstedt and L. Zhang. *In* Photochemistry of lignocellulosic materials. *Edited by* C. Heitner and J.C. Scaiano. ACS Symp. Ser. No. 531, Washington, D.C. 1993. p. 129.
17. G. Gellerstedt and L. Zhang. J. Wood Chem. Technol. **12**, 387 (1992).
18. D.S. Argyropoulos, C. Heitner, and J.A. Schmidt. Res. Chem. Intermed. **21**, 263 (1995).
19. U.P. Agarwal and R.H. Atalla. *In* Photochemistry of lignocellulosic materials. *Edited by* C. Heitner and J.C. Scaiano. ACS Symp. Ser. No. 531, Washington, D.C. 1993. p. 26.
20. B. Ruffin, S. Grelier, A. Nourmamode, and A. Castellan. Can. J. Chem. **80**, 1223 (2002).
21. A.J. Ragauskas. *In* Photochemistry of lignocellulosic materials. *Edited by* C. Heitner and J.C. Scaiano. ACS Symp. Ser. No. 531, Washington, D.C. 1993. p. 77.
22. B. Ruffin and A. Castellan. Can. J. Chem. **78**, 73 (2000).
23. S. Barsberg, T. Elder, and C. Felby. Chem. Mater. **15**, 649 (2003).
24. A.J. Michell, P.J. Nelson, and C.P. Garland. Appl. Spectrosc. **43**, 1482 (1989).
25. C. Heitner. *In* Photochemistry of lignocellulosic materials. *Edited by* C. Heitner and J.C. Scaiano. ACS Symp. Ser. No. 531, Washington, D.C. 1993. p. 192.
26. R.S. Davidson, L. Dunn, A. Castellan, and A. Nourmamode. J. Photochem. Photobiol. A, **86**, 275 (1995).
27. C.M. Cook and A.J. Ragauskas. J. Photochem. Photobiol. A, **104**, 217 (1997).

© 2005 NRC Canada

28. B.J.W. Cole, J. Wang, and R.C. Fort. J. Wood Chem. Technol. **20**, 1 (2000).
29. P. McGarry, C. Heitner, J. Schmidt, A. Rodenhiser, R. St. John Manley, G. Cunkle, and T. Thompson. J. Photochem. Photobiol. A, **151**, 145 (2002).
30. M. Ek, H. Lennhom, G. Lindblad, and T. Iversen. Nord. Pulp Pap. Res. J. **7**, 108 (1992).
31. M. Paulsson, R. Simonson, and U. Westermark. Nord. Pulp Pap. Res. J. **10**, 62 (1995).
32. M. Paulsson and A.J. Ragauskas. Nord. Pulp Pap. Res J. **13**, 124 (1998).
33. M. Paulsson, S. Li, K. Lundquist, R. Simonson, and U. Westermark. Nord. Pulp Pap. Res. J. **11**, 109 (1996).
34. Y. Pu, S. Anderson, L. Lucia, and A.J. Ragauskas. J. Pulp Paper Sci. **12**, 401 (2003)
35. D.S. Argyropoulos and Y. Sun. Photochem. Photobiol. **64**, 510 (1996).
36. C. Heitner, R. St. John Manley, B. Ahvazi, and J. Wang. J. Pulp Paper Sci. **10**, 325 (2001).
37. Y. Pu, S. Anderson, L. Lucia, and A.J. Ragauskas. J. Photochem. Photobiol. A, **163**, 215 (2004).
38. C.W. Dence and S.Y. Lin. *In* Methods in lignin chemistry. *Edited by* S.Y. Lin and C.W. Dence. Springer-Verlag, New York. 1992. p. 3.
39. X. Pan and A.J. Ragauskas. J. Pulp Paper Sci. **21**, J25 (1995).
40. TAPPI Test methods 1998 to 1999. TAPPI Press, Atlanta, T 272 sp-97 (1998).
41. C. Li and A.J. Ragauskas. J. Wood Chem. Technol. **19**, 43 (1999).
42. M. Paulsson and A.J. Ragauskas. Nord. Pulp Pap. Res. J. **13**, 132 (1998).
43. TAPPI Test methods 1998 to 1999. TAPPI Press, Atlanta, T 452 om-98 (1998).
44. D. Robert. *In* Methods in lignin chemistry. *Edited by* S.Y. Lin and C.W. Dence. Springer-Verlag, New York. 1992. p. 250.
45. P.M. Froass, A.J. Ragauskas, and J.E. Jiang. Holzforschung, **52**, 385 (1998).
46. T.M. Runge and A.J. Ragauskas. Holzforschung, **53**, 623 (1999).
47. A. Granata and D.S. Argyropoulos. J. Agricul. Food Chem. **43**, 1538 (1995).
48. P.M. Froass, A.J. Ragauskas, and J.E. Jiang. Ind. Eng. Chem. Res. **37**, 3388 (1998).
49. R. Morck and K.P. Kringstad. Holzforschung, **39**, 109 (1985).
50. R. Agnemo, R.C. Francis, T.C. Alexander, and C.W. Dence. Holzforschung, **45**(Suppl.), 101 (1991).
51. H.H. Nimz, D. Robert, O. Faix, and M. Nemr. Holzforschung, **35**, 16 (1981).

© 2005 NRC Canada

A rapid, microwave-assisted, one-pot cyclopropanation reaction to synthesize (4-ferrocenyl)benzoylcyclopropane in the solid state

Juxing Yin, Xiaolong Li, Xiaoli Wu, Baohua Chen, Zenglu Liu, and Qingbao Song

Abstract: Some new (4-ferrocenyl)benzoylcyclopropanes were prepared rapidly via a microwave-assisted, one-pot cyclopropanation reaction in the solid state, directly using 4-ferrocenylacetophenone, aldehyde, and sulfur ylide as the starting materials. The main advantages of this procedure are convenient operation, shorter reaction time, lower environmental pollution, and no need to isolate the intermediate product (chalcone) in a separate step.

Key words: 4-ferrocenylacetophenone, sulfur ylide, microwave-assisted, one-pot, solid state.

Résumé : Faisant appel à une réaction de cyclopropanation monotope, à l'état solide, assistée de micro-ondes et utilisant directement la 4-ferrocnénylacétophénone, l'aldéhyde et un ylure de sulfure comme produits de départs, on a réalisé rapidement la synthèse de nouveaux (4-ferrocényl)benzoylcyclopropanes. Les principaux avantages de cette méthode impliquent son côté pratique, son court temps de réaction, sa faible pollution de l'environnement et le fait qu'il n'est pas nécessaire d'isoler le produit intermédiaire (la chalcone) dans une étape séparée.

Mots clés : 4-ferrocénylacétophénone, ylure de soufre, assistée de micro-ondes, monotope, état solide.

[Traduit par la Rédaction]

Introduction

Ferrocene derivatives have been attracting much interest because of their possible biological activities (1), asymmetric catalytic effects (2), electron transfer features (3) (used as liquid crystals (4) and conductors (5)), and so on. Also, many compounds containing ferrocenyl exhibit good nonlinear optics (NLO) properties in which the ferrocenyl is used as the electron-donating group (6). Carbonyl cyclopropanes containing ferrocenyl are important members of those derivations that may offer a variety of potential applications such as photoactive semiconductors (7) and liquid crystals. They were commonly synthesized by a sulfur ylide reaction in solution (8). However, this method requires high temperatures, harsh reaction conditions, large amounts of solvents, a long reaction time, and tedious workup. In particular, the use of large amounts of solvents leads to the generation of waste as well as environmental pollution. So there is a need to develop a rapid, convenient, and clean method to synthesize this kind of compound.

In the past few years, the utilization of microwave irradiation (9, 10) and solid-state reaction (11, 12) in chemical transformations has attracted considerable interest and is of significant importance in the search for green synthesis (13) and sustainable chemistry. More attractively, many reactions that typically require hours or days to complete full conversion with conventional heating could be realized in several minutes by utilizing microwave irradiation in the solid state. It should be pointed out that the cyclopropanation reaction via the one-pot method, which adopts high-speed microwave techniques in the solid state, was seldom described. In the present work, we will report a microwave-assisted, one-pot cyclopropanation reaction in the solid state to synthesize some (4-ferrocenyl) benzoyl cyclopropanes, which directly used 4-ferrocenylacetophenone (14), aldehyde, and sulfur ylide (15) as the starting materials. This reaction has a series of advantages: (1) it does not require the isolation of chalcones in a separate step; (2) it requires a shorter reaction time; (3) it simplifies the process and handling; and (4) it avoids using large amounts of solvent, reducing waste and pollution. The reaction is shown in Scheme 1.

Received 17 October 2005. Published on the NRC Research Press Web site at http://canjchem.nrc.ca on 21 February 2006.

J. Yin, X. Li, X. Wu, B. Chen,[1] and Z. Liu. State key Laboratory of Applied Organic Chemistry, Lanzhou University, Lanzhou, 730000, P.R. China.
Q. Song. College of Chemical Engineering and Material Science, Zhejiang University of Technology, Hangzhou 310014, P.R. China.

[1]Corresponding author (e-mail: chbh@lzu.edu.cn).

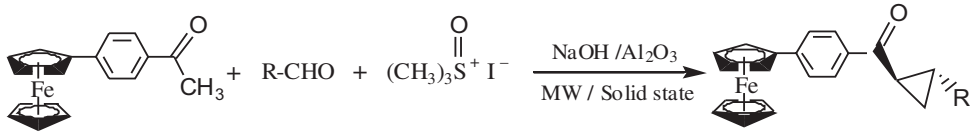
Results and discussion

First we examined the reactivity of different bases for the reaction among 4-ferrocenylacetophenone, liquid benzaldehyde (absorbed on 0.1 g Al_2O_3), and $Me_3S(O)I$ under MW irradiation. The results are shown in the Table 1. It can be seen that the reactivity of NaOH was found to be the best and **2a** was converted to **4a** in high yield. Then, on the basis of these results, we expanded the scope of this transformation to a series of aldehydes, using NaOH as the base. The results are summarized in Table 2.

As expected, a series of (4-ferrocenyl)benzoyl cyclopropanes (**4**) were obtained in high yields. Compound **1** (1.0 mmol) could react completely with aldehyde **2** (1.0 mmol) and some excess sulfur ylide **3** (1.1 mmol) using NaOH as the catalyst. Table 1 shows that both electronic and

 doi: 10.1139/V05-251 © 2005 NRC Canada

Scheme 1. One-pot cyclopropanation.



1 **2** **3** **4**

Table 1. Optimization of reaction conditions.

Entry	Base	Time (min)[a]	Ylide (equiv.)[b]	Yield (%)
1	Na_2CO_3	10	1.1	—[c]
2	KO-*t*-Bu	10	1.1	<5
3	KOH	10	1.1	93
4	KOH	10	1.2	95
5	NaOH	10	1.1	98
6	NaOH	10	1.2	99

[a]Total irradiation time.
[b]Isolated yields.
[c]No product obtained.

steric effects influence the yield obtained. For example, among the substituted benzaldehydes used, the aldehyde bearing the electron-withdrawing group in the para position (Table 1, entry 2) gave a better result. In contrast, unfavorable electronic effects of substituted benzaldehydes (Table 1, entries 5, 7–9) led to some lower yields than for PhCHO. Steric effects of the ortho-substituted aldehyde (Table 1, entry 3) or the aldehyde containing a large group (Table 1, entries 8 and 11) also gave lower yields for the cyclopropanation reaction. For the aldehyde that contains a nitro group, each irradiation period needed to be shortened to 15 s and the frequencies enhanced, otherwise the mixture quickly turned black and only a small amount of the product would be obtained.

In the isolation of the crude product, we obtained a main product, though the other isomers or by-products were difficult to identify, which indicates the high diastereoselectivity of this reaction. The main product is the one we expected, and its 1D NOE spectra of ^{1}H NMR shows that it possesses a trans configuration.

Experimental

General information

4-Ferrocenylacetophenone (14) and trimethylsulfoxonium iodide (15) were prepared as per the literature method, and other reagents were commercial grade and used directly. MW irradiation was carried out with a commercial microwave over Medea WT022J at 2450 MHz in a mortar. ^{1}H NMR and ^{13}C NMR spectra were performed on a Mercury 4N-PFG-300 (**4a**–**4c**, **4e**, **4j**, **4l**) or AVANCE-DRX-200 (**4d**, **4f**–**4i**, **4k**) sensitivity spectrometer in $CDCl_3$ with TMS as an internal standard. Mass spectrometers were obtained by fast atom bombardment (FAB) on a VG ZBA-HS mass spectrograph. IR spectra were recoded in KBr on a Niolet 670FT-IR spectrophotometer. Elemental analyses were carried out on a Carlo-Erba 1106 element analyzer. The melting points reported are uncorrected.

General procedure

A mixture of powdered 4-ferrocenylacetophenone (**1**, 1.0 mmol), NaOH (1.1 mmol, powder), and neutral Al_2O_3 (0.1 g, 200–300 mesh) was ground in a mortar for 2 min, 1.0 mmol aldehyde **2** (liquid aldehyde was absorbed on 0.1 g Al_2O_3) was added in, ground for another 2 min, and the mixture was microwave irradiated six times for 20–25 s each. Then another ground mixture of trimethylsulfoxonium iodide (**3**, 1.1 mmol), NaOH (1.2 mmol), and Al_2O_3 (0.1 g) was added into the former system, and grinding continued for 2 min. All of the mixture in the mortar was irradiated by MW 15–20 times (for 20–25 s each) until the reaction was completed by TLC monitoring. The mixture was washed with EtOH (3 × 10 mL) on a filter funnel by reducing pressure and the EtOH was evaporated. The residue was separated on a flash chromatography column with silica (eluent: petroleum (bp 30–60 °C) – ethyl acetate) and gave the desired products (**4**).

1-(4′-Ferrocenyl)benzoyl-2-phenylcyclopropane (4a)

Orange-red crystals, mp 92–94 °C. IR (KBr, cm^{-1}) ν: 1659 (C=O). ^{1}H NMR ($CDCl_3$, 300 MHz) δ: 1.53 (m, 1H, CH), 1.94 (m, 1H, CH), 2.70 (m, 1H, CH_2), 2.90 (m, 1H, CH_2), 4.06 (s, 5H, cp-ring), 4.43 (s, 2H, cp-ring), 4.75 (s, 2H, cp-ring), 7.20 (d, J = 6.9 Hz, 3H, C_6H_5), 7.34 (d, J = 6.9 Hz, 2H, C_6H_5), 7.50 (d, J = 6.3 Hz, 2H, C_6H_4), 7.94 (d, J = 6.3 Hz, 2H, C_6H_4). ^{13}C NMR ($CDCl_3$, 75 MHz) δ: 198.1, 145.6, 140.9, 135.3, 131.4, 128.8, 128.6, 126.8, 126.0, 70.2, 67.2, 30.1, 29.4, 19.4. MS (FAB) *m*/*z* (%): 407.1 (M^+ + 1, 24), 406.1 (M^+, 36), 289.1 (12), 261.1 (26). Anal. calcd. for $C_{26}H_{22}FeO$ (406.3): C 76.86, H 5.46; found: C 76.79, H 5.48.

1-(4′-Ferrocenyl)benzoyl-2-(4″-bromo)phenylcyclopropane (4b)

Orange-red crystals, mp 145–147 °C. IR (KBr, cm^{-1}) ν: 1648 (C=O). ^{1}H NMR ($CDCl_3$, 300 MHz) δ: 1.54 (m, 1H, CH), 1.93 (m, 1H, CH), 2.67 (m, 1H, CH_2), 2.86 (m, 1H, CH_2), 4.04 (s, 5H, cp-ring), 4.40 (s, 2H, cp-ring), 4.72 (s, 2H, cp-ring), 7.07 (d, J = 7.8 Hz, 2H, C_6H_4Br), 7.44 (d, J = 7.8 Hz, 2H, C_6H_4Br), 7.53 (d, J = 8.1 Hz, 2H, C_6H_4), 7.91 (d, J = 8.1 Hz, 2H, C_6H_4). ^{13}C NMR ($CDCl_3$, 75 MHz) δ: 198.1, 145.9, 140.0, 135.6, 131.8, 128.6, 128.2, 126.0, 120.6, 70.2, 70.1, 67.2, 29.4, 29.3, 19.2. MS (FAB) *m*/*z* (%): 486.3 (M^+, 41), 484.4 (M^+, 41), 289.4 (5), 261.3 (10), 197.3 (7). Anal. calcd. for $C_{26}H_{21}BrFeO$ (485.2): C 64.36, H 4.36; found: C 64.23, H 4.32.

1-(4′-Ferrocenyl)benzoyl-2-(2″-chloro)phenylcyclopropane (4c)

Brown-red solid. IR (KBr, cm^{-1}) ν: 1660 (C=O). ^{1}H NMR ($CDCl_3$, 300 MHz) δ: 1.59 (m, 1H, CH), 1.92 (m, 1H, CH), 2.81 (m, 1H, CH_2), 2.93 (m, 1H, CH_2), 4.06 (s, 5H, cp-ring),

© 2005 NRC Canada

Table 2. Scope of the reaction.

Entry	R	Products (**4**)	Time (min)[a]	Yield (%)[b]	d.r. (trans:cis)[c]
1	C_6H_5-	**4a**	10	98	>95:5
2	4-Br-C_6H_4-	**4b**	10	99	>95:5
3	3-Cl-C_6H_4-	**4c**	10	94	>95:5
4	C_6H_5-CH=CH-	**4d**	10	98	>95:5
5	3,4-OCH_2O-C_6H_3-	**4e**	10	95	>95:5
6	4-O_2N-C_6H_4-	**4f**	12	85	>95:5
7	4-$(CH_3)_2N$-C_6H_4-	**4g**	10	93	>95:5
8	4-Fc-C_6H_4-	**4h**	10	92	>95:5
9	(3-OCH_3-4-OCH_2OCH_3)-C_6H_3-	**4i**	10	94	>95:5
10	Furyl	**4j**	10	97	>95:5
11	Fc-	**4k**	10	93	>95:5
12	CH_3-CH=CH-	**4l**	10	94	>95:5

Note: Fc = ferrocenyl; d.r. = diastereoisomeric ratio.
[a]Total irradiation time.
[b]Isolated yields.
[c]Determined by ^{1}H NMR spectroscopy.

4.42 (s, 2H, cp-ring), 4.74 (s, 2H, cp-ring), 7.23 (br, 3H, C_6H_4Cl), 7.40 (d, J = 7.8 Hz, 1H, C_6H_4Cl), 7.54 (d, J = 8.4 Hz, 2H, C_6H_4), 7.97 (d, J = 8.4 Hz, 2H, C_6H_4). ^{13}C NMR ($CDCl_3$, 75 MHz) δ: 198.1, 145.6, 138.3, 136.2, 135.2, 129.7, 128.7, 128.2, 127.6, 127.0, 126.0, 70.3, 67.3, 28.0, 27.6, 17.8. MS (FAB) *m/z* (%): 442.2 (M^+, 32), 440.2 (M^+, 70), 289.1 (16), 261.1 (21). Anal. calcd. for $C_{26}H_{21}ClFeO$ (440.8): C 70.85, H 4.80; found: C 70.69, H 4.76.

1-(4′-Ferrocenyl)benzoyl-2-phenylvinylcyclopropane (4d)

Brown-red crystals, mp 150–152 °C. IR (KBr, cm^{-1}) ν: 1653 (C=O). ^{1}H NMR ($CDCl_3$, 200 MHz) δ: 1.54 (m, 1H, CH), 1.83 (m, 1H, CH), 2.31 (m, 1H, CH_2), 2.79 (m, 1H, CH_2), 4.09 (s, 5H, cp-ring), 4.45 (s, 2H, cp-ring), 4.78 (s, 2H, cp-ring), 5.83 (dd, J = 9.0, 16.2 Hz, 1H, C=CH), 6.58 (d, 1H, J = 16.2 Hz, C=CH), 7.32 (br, 5H, C_6H_5), 7.50 (d, 2H, J = 8.0 Hz, C_6H_4), 7.92 (d, J = 8.0 Hz, 2H, C_6H_4). ^{13}C NMR ($CDCl_3$, 50 MHz) δ: 198.2, 145.7, 139.2, 136.0, 130.8, 130.5, 128.6, 128.3, 127.3, 127.2 125.9, 70.0, 67.0, 29.4, 22.7, 14.1. MS (FAB) *m/z* (%): 433.3 (M^+ + 1, 27), 432.3 (M^+, 61), 328.2 (16), 289.1 (22), 261.1 (58). Anal. calcd. for $C_{28}H_{24}FeO$ (432.3): C 77.79, H 5.60; found: C 76.65, H 5.58.

1-(4′-Ferrocenyl)benzoyl-2-(3″,4″-methylenedioxy)phenylcyclopropane (4e)

Orange-red crystals, mp 110–112 °C. IR (KBr, cm^{-1}) ν: 1658 (C=O). ^{1}H NMR ($CDCl_3$, 300 MHz) δ: 1.48 (m, 1H, CH), 1.88 (m, 1H, CH), 2.63 (m, 1H, CH_2), 2.81 (m, 1H, CH_2), 4.06 (s, 5H, cp-ring), 4.43 (s, 2H, cp-ring), 4.75 (s, 2H, cp-ring), 5.95 (s, 2H, OCH_2O), 6.67 (s, 1H, C_6H_3), 6.69 (d, J = 7.5 Hz, 1H, C_6H_3), 6.76 (d, J = 7.5 Hz, 1H, C_6H_3), 7.51 (d, J = 8.1 Hz, 2H, C_6H_4), 7.91 (d, J = 8.1 Hz, 2H, C_6H_4). ^{13}C NMR ($CDCl_3$, 75 MHz) δ: 198.0, 145.6, 135.3, 135.0, 128.6, 128.5, 126.1, 126.0, 120.0, 108.5, 106.8, 101.3, 70.3, 67.3, 29.9, 29.3, 19.1. MS (FAB) *m/z* (%): 451.3 (M^+ + 1, 38), 450.3 (M^+, 72), 329.3 (7), 289.2 (15), 261.2 (19), 189.2 (41), 121.1 (100). Anal. calcd. for $C_{27}H_{22}FeO_3$ (450.3): C 72.02, H 4.92; found: C 71.90, H 4.89.

1-(4′-Ferrocenyl)benzoyl-2-(4″-nitro)phenylcyclopropane (4f)

Purple-red solid. IR (KBr, cm^{-1}) ν: 1662 (C=O). ^{1}H NMR ($CDCl_3$, 200 MHz) δ: 1.58 (m, 1H, CH), 2.01 (m, 1H, CH), 2.79 (m, 1H, CH_2), 2.98 (m, 1H, CH_2), 4.04 (s, 5H, cp-ring), 4.42 (s, 2H, cp-ring), 4.73 (s, 2H, cp-ring), 7.33 (d, J = 9.8 Hz, 2H, C_6H_4), 7.58 (d, J = 9.8 Hz, 2H, C_6H_4), 7.91 (d, J = 8.4 Hz, 2H, C_6H_4), 8.19 (d, J = 8.4 Hz, 2H, C_6H_4). ^{13}C NMR ($CDCl_3$, 50 MHz) δ: 199.4, 147.3, 141.2, 135.9, 128.9, 128.4, 126.8, 125.9, 123.9, 69.9, 67.1, 29.7, 28.8, 19.8. MS *m/z* (%): 452.1 (M^+ + 1, 18), 451.1 (M^+, 42), 329.0 (15), 289.0 (37), 261.0 (11). Anal. calcd. for $C_{26}H_{21}FeNO_3$ (451.3): C 69.20, H 4.69, N 3.10; found: C 69.13, H 4.71, N 3.12.

1-(4′-Ferrocenyl)benzoyl-2-(4″-dimethylamino)phenylcyclopropane (4g)

Orange-red crystals, mp 160–162 °C. IR (KBr, cm^{-1}) ν: 1646 (C=O). ^{1}H NMR ($CDCl_3$, 200 MHz) δ: 1.55 (m, 1H, CH), 1.90 (m, 1H, CH), 2.65 (m, 1H, CH_2), 2.83 (m, 1H, CH_2), 2.97 (s, 6H, $2CH_3$), 4.06 (s, 5H, cp-ring), 4.40 (s, 2H, cp-ring), 4.72 (s, 2H, cp-ring), 6.70 (d, J = 9.0 Hz, 2H, C_6H_4), 7.12 (d, J = 9.0 Hz, 2H, C_6H_4), 7.52 (d, J = 8.6 Hz, 2H, C_6H_4), 7.92 (d, J = 8.6 Hz, 2H, C_6H_4). ^{13}C NMR ($CDCl_3$, 50 MHz) δ: 190.3, 132.1, 132.0, 128.3, 127.2, 125.7, 112.9, 111.1, 111.0, 69.8, 66.9, 40.7, 40.1, 40.0, 29.9, 29.2. MS *m/z* (%): 450.2 (M^+ + 1, 25), 449.2 (M^+, 74), 289.1 (8), 261.1 (10). Anal. calcd. for $C_{28}H_{27}FeNO$ (449.4): C 74.84, H 6.06, N 3.12; found: C 74.78, H 6.03, N 3.10.

1-(4′-Ferrocenyl)benzoyl-2-(4′-ferrocenyl)phenylcyclopropane (4h)

Brown-red crystals, mp 80–82 °C. IR (KBr, cm^{-1}) ν: 1657 (C=O). ^{1}H NMR ($CDCl_3$, 200 MHz) δ: 1.56 (m, 1H, CH), 1.94 (m, 1H, CH), 2.68 (m, 1H, CH_2), 2.90 (m, 1H, CH_2), 4.03 (s, 5H, cp-ring), 4.07 (s, 5H, cp-ring), 4.33 (s, 2H, cp-ring), 4.39 (s, 2H, cp-ring), 4.65 (s, 2H, cp-ring), 4.71 (s, 2H, cp-ring), 7.10 (d, J = 7.8 Hz, 2H, C_6H_4), 7.40 (d, J = 7.8 Hz, 2H, C_6H_4), 7.53 (d, J = 8.2 Hz, 2H, C_6H_4), 7.94 (d, J = 8.2 Hz, 2H, C_6H_4). ^{13}C NMR ($CDCl_3$, 50 MHz) δ:

© 2005 NRC Canada

197.7, 138.2, 137.6, 135.1, 128.5, 128.4, 126.2, 126.1, 125.7, 70.2, 69.8, 69.0, 66.9, 66.5, 29.8, 29.1, 19.0. MS (FAB) *m/z* (%): 591.2 (M^+ + 1, 36), 590.2 (M^+, 64), 289.1 (22), 261.1 (27). Anal. calcd. for $C_{36}H_{30}Fe_2O$ (590.3): C 73.25, H 5.12; found: C 73.19, H 5.08.

1-(4′-Ferrocenyl)benzoyl-2-(3″-methoxyl-4″-methoxyl-methoxyl)phenylcyclopropane (4i)

Brown-red solid. IR (KBr, cm^{-1}) ν: 1658 (C=O). ^1H NMR ($CDCl_3$, 200 MHz) δ: 1.55 (m, 1H, CH), 1.92 (m, 1H, CH), 2.69 (m, 1H, CH_2), 2.87 (m, 1H, CH_2), 3.55 (s, 3H, OCH_3), 3.91 (s, 3H, OCH_3), 4.06 (s, 5H, cp-ring), 4.43 (s, 2H, cp-ring), 4.74 (s, 2H, cp-ring), 5.24 (s, 2H, OCH_2O), 6.73 (d, *J* = 8.4 Hz, 1H, C_6H_3), 6.80 (s, 1H, C_6H_3), 7.12 (d, *J* = 8.4 Hz, 1H, C_6H_3), 7.56 (d, *J* = 8.2 Hz, 2H, C_6H_4), 7.95 (d, *J* = 8.2 Hz, 2H, C_6H_4). ^{13}C NMR ($CDCl_3$, 50 MHz) δ: 197.7, 149.9, 145.3, 145.2, 135.1, 128.3, 125.7, 118.0, 116.9, 110.8, 95.7, 83.2, 69.8, 66.9, 56.1, 55.9, 29.6, 29.1, 18.7. MS (FAB) *m/z* (%): 497.3 (M^+ + 1, 14), 496.3 (M^+, 39), 288.8 (11), 261.1 (28). Anal. calcd. for $C_{29}H_{28}FeO_4$ (496.4): C 70.17, H 5.69; found: C 70.07, H 5.71.

1-(4′-Ferrocenyl)benzoyl-2-(2″-furyl)cyclopropane (4j)

Brown-red crystals, mp 78–80 °C. IR (KBr, cm^{-1}) ν: 1661 (C=O). ^1H NMR ($CDCl_3$, 300 MHz) δ: 1.66 (m, 1H, CH), 1.94 (m, 1H, CH), 2.57 (m, 1H, CH_2), 3.12 (m, 1H, CH_2), 4.03 (s, 5H, cp-ring), 4.43 (s, 2H, cp-ring), 4.86 (s, 2H, cp-ring), 5.61 (s, *J* = 1.8 Hz, 1H, furyl), 6.26 (d, *J* = 3.6 Hz, 1H, furyl), 6.36 (dd, *J* = 1.8 Hz, *J* = 3.6 Hz, 1H, furyl), 7.68 (d, *J* = 8.4 Hz, 2H, C_6H_4), 7.99 (d, *J* = 8.4 Hz, 2H, C_6H_4). ^{13}C NMR ($CDCl_3$, 75 MHz) δ: 196.7, 154.2, 146.0, 141.7, 134.8, 128.6, 126.0, 110.8, 105.5, 70.1, 69.9, 67.1, 26.1, 22.1, 16.4. MS (FAB) *m/z* (%): 397.4 (M^+ + 1, 30), 396.4 (M^+, 65), 289.3 (11), 261.3 (19). Anal. calcd. for $C_{24}H_{20}FeO_2$ (396.3): C 72.74, H 5.09; found: C 72.66, H 5.12.

2-Ferrocenyl-1-(4′-ferrocenyl)benzoylcyclopropane (4k)

Brown-red crystals, mp 161 to 162 °C. IR (KBr, cm^{-1}) ν: 1644 (C=O). ^1H NMR ($CDCl_3$, 200 MHz) δ: 1.32 (m, 1H, CH), 1.82 (m, 1H, CH), 2.40 (m, 1H, CH_2), 2.75 (m, 1H, CH_2), 4.03 (s, 5H, cp-ring), 4.11 (s, 4H, cp-ring), 4.18 (s, 5H, cp-ring), 4.40 (s, 2H, cp-ring), 4.72 (s, 2H, cp-ring), 7.54 (d, *J* = 8.2 Hz, 2H, C_6H_4), 7.94 (d, *J* = 8.2 Hz, 2H, C_6H_4). ^{13}C NMR ($CDCl_3$, 50 MHz) δ: 197.8, 147.9, 128.6, 128.3, 125.8, 69.8, 69.1, 68.8, 66.9, 66.7, 29.7, 26.3, 13.7. MS (FAB) *m/z* (%): 515.2 (M^+ + 1, 39), 514.2 (M^+, 47), 328.9 (32), 289.2 (43). Anal. calcd. for $C_{30}H_{26}Fe_2O$ (514.2): C 70.07, H 5.10; found: C 69.97, H 5.08.

1-(4′-Ferrocenyl)benzoyl-2-propenylcyclopropane (4l)

Brown-red solid. IR (KBr, cm^{-1}) ν: 1658 (C=O). ^1H NMR ($CDCl_3$, 300 MHz) δ: 1.13 (m, 1H, CH), 1.60 (m, 1H, CH), 1.75 (d, *J* = 6.6 Hz, 3H, CH_3), 2.13 (m, 1H, CH_2), 2.62 (m, 1H, CH_2), 4.05 (s, 5H, cp-ring), 4.41 (s, 2H, cp-ring), 4.74 (s, 2H, cp-ring), 5.19 (m, 1H, C=CH), 5.66 (m, 1H, C=CH), 7.53 (d, *J* = 7.8 Hz, 2H, C_6H_4), 7.91 (d, *J* = 7.8 Hz, 2H, C_6H_4). ^{13}C NMR ($CDCl_3$, 75 MHz) δ: 199.3, 145.1, 135.3, 131.4, 128.3, 126.2, 125.7, 69.9, 67.0, 29.3, 29.0, 26.4, 18.0. MS (FAB) *m/z* (%): 371.4 (M^+ + 1, 30), 370.4 (M^+, 70), 289.3 (9), 261.3 (28), 109 (70). Anal. calcd. for $C_{23}H_{22}FeO$ (370.3): C 74.61, H 5.99; found: C 74.50, H 5.61.

Acknowledgement

The authors are grateful to the project sponsored by the Scientific Research Foundation for the Returned Overseas Chinese Scholars, State Education Ministry, and the Natural Science Foundation of Gansu Province (No. 3ZS041-A25-008).

References

1. B.E. Maryanoff, S.L. Keeley, and F.J. Persico. J. Med. Chem. **26**, 226 (1983).
2. S.L. You, X.Z. Zhu, Y.M. Luo, X.L. Hou, and L.X. Dai. J. Am. Chem. Soc. **123**, 7471 (2001).
3. S. Fukuzumi, K. Okamoto, and H. Imahori. Angew. Chem. Int. Ed. **4**, 620 (2002).
4. C. Imrie, P. Engelbrecht, C. Loubser, and C.W. McCleland. Appl. Organomet. Chem. **15**, 1 (2001).
5. M. Iyoda, T. Takano, N. Otani, K. Ugawa, M. Yoshida, H. Matsuyama, and Y. Kuwatani. Chem. Lett. 1310 (2001).
6. M.L.H. Green, S.R. Marder, and M.E. Thomson. Nature (London), **330**, 360 (1987).
7. R. Gooding, C.P. Lillya, and C.W. Chiene. J. Chem. Soc. Chem. Commun. 151 (1983).
8. W.M. Horspool, R.G. Sutherland, and B.J. Thomson. J. Chem. Soc. C, 1558 (1971).
9. M. Larhed, C. Moberg, and A. Hallberg. Acc. Chem. Res. **35**, 717 (2002).
10. A.D. Sagar, N.A. Shinde, and B.P. Bandgar. Org. Prep. Proced. Int. **32**, 269 (2000).
11. F.F. Ma, X.L. Li, T. Lan, Y.X. Ma, B.H. Chen, and Q.B. Song. Synthesis, **12**, 1945 (2005).
12. F. Toda, K. Tanaka, and K. Hamai. J. Chem. Soc. Perkin. Trans. 3207 (1990).
13. R.S. Varma. Green Chem. **1**, 43 (1999).
14. G.S. Huang, B.J. Li, W.Y. Liu, L. Shi, and Y.X. Ma. Chem. J. Chin. Univ. **21**, 488 (2000).
15. K.A. Petrov, G.A. Sokolii, and B.M. Polees. J. Gen. Chem. (U.S.S.R.), **26**, 3765 (1956).

© 2005 NRC Canada

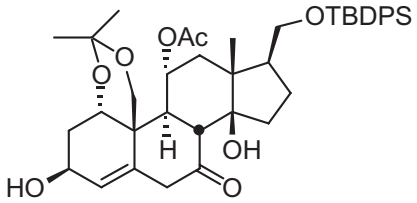
ERRATUM / ERRATUM

Erratum: Studies towards the total synthesis of ouabagenin

Ling Chen and Pierre Deslongchamps

Ref.: Can. J. Chem. **83**: 728–740 (2005).

In the above paper on page 734 (Scheme 6) the structure **33** was incorrectly drawn. It should be replaced by the following structure.



33

Received 6 December 2005. Published on the NRC Research Press Web site at http://canjchem.nrc.ca on 26 January 2006.

L. Chen and P. Deslongchamps.[1] Laboratoire de synthèse organique, Département de chimie, Institut de Pharmacologie de Sherbrooke, Université de Sherbrooke, 3001, 12[e] Avenue nord, Sherbrooke, QC J1H 5N4, Canada.

[1]Corresponding author (e-mail: Pierre.Deslongchamps@USherbrooke.ca).

 doi: 10.1139/V06-004 © 2005 NRC Canada

Canadian Journal of Chemistry

Author Index
Volume 83, 2005

Revue canadienne de chimie

Index des auteurs
Volume 83, 2005

Abd Hamid, S.B., 574
Abdollahi-Alibeik, M., 110
Abiraj, K., 517
Ahmed, N., 1432
Alavi, S., 236
Al-Awadi, N.A., 1543
Al-Bashir, R.F., 1543
Allen, D.P., 943
Al-Marzouqi, A.H., 1833
Almatarneh, M.H., 2082
Aly, A.A., 57
Amani, K., 1808
Amirnasr, M., 2073
Ammal, S.C., 1606
Amyes, T.L., 1536
Anderson, B.G., 574
Andraos, J., 1400, 1415
Andrés, G.O., 1281
Andrews, L.E., 1492
Andurkar, S.V., 37
Ansarian, H.R., 1792
Antonelli, D., 308
Antonov, A.S., 21, 2120
Armstrong, A.F., 1768
Arora, R., 1137
Arseneau, S., 493
Arslan, M., 2039
Asaumi, T., 755
Athimoolam, A., 832
Avila, S., 220
Avilov, S.A., 21, 2120
Aychet, N., 493, 1098
Azizi, N., 146, 505
Babich, J.W., 2060
Babu, G., 716
Bäckvall, J.E., 909
Bae, S.-Y., 1365
Baeg, J.-O., 527
Baerlocher, F.J., 1063, 1158
Bagh, S., 435
Bagheri, M., 146
Bahrami, K., 115
Baik, W., 213
Baines, K.M., 1568
Bajorek, T., 1352
Bakari, S., 1132
Baker, G.A., 1871
Balci, M., 227
Baldwin, J.E., 1510
Bamdad, M., 236
Banerjee, S.R., 2060
Banureka, R., 202
Baradie, B., 553
Barclay, T., 449
Barnett, D.A., 1961
Bartmess, J.E., 2005
Bashir, S., 1124
Baty, J.W., 1516
Beauchamp, A.L., 460
Béguin, C., 37
Behera, J.N., 668
Bélanger-Gariépy, F., 634
Bélec, L., 793
Bencze, L., 882
Berg, D.J., 449
Bernard, G.M., 1721
Berro, C., 220
Berthelot, M., 138
Bhattacharya, S.C., 2067
Bhavani, N., 202
Biswas, A., 2046
Black, D.St.C., 969, 980
Blacquiere, J.M., 2052
Blanco, S.T., 220
Blu, J., 493
Boese, R., 882
Bohle, D.S., 2021
Bohme, D.K., 1839
Bohne, C., 1440
Bombasaro, J.A., 122
Boñaga, L.V.R., 1006
Boreham, D.R., 2060
Borsari, M., 1132
Bouchard, J.-E., 533
Bourque, T.A., 1063
Breen, L.E., 1347
Broczkowski, M.E., 595
Brondani, S., 1171
Brown, R.S., 1268
Buccigross, J.M., 1492
Buncel, E., 195, 1365, 1448, 2091
Burgers, P.C., 1847
Caglioti, L., 882
Cai, X.-h., 273
Camerman, A., 1141
Camerman, N., 1141
Campbell, J.J., 1492
Cannio, M., 1132
Cao, H., 826
Carrión, M.C., 2106
Casey, C.P., 1339
Castellanos, A., 764
Castillón, S., 764
Catellani, M., 741
Ceylan, Z.Ç., 227
Chahma, M., 150
Chakka, N., 929
Chan, A.S.C., 903
Chan, B.K., 1324
Chan, T.H., 693
Chandler, M.K., 93
Chandler, W.D., 1212
Chang, H., 527
Charette, A.B., 533
Chase, P.A., 2098
Chatani, N., 755
Chatterjee, A., 1164
Che, C.-M., 521
Chen, A.C., 943
Chen, B., 2140
Chen, H., 1253
Chen, L., 728, 2144
Chen, S., 1460
Cheng, H., 166
Cherry, J.-P.F., 302
Cheung, W.-H., 521
Chiang, Y., 68, 1202
Chiou, W.-H., 681
Chirik, P.J., 286
Chivers, T., 1768
Cho, C.H., 917
Chruściel, J.J., 508
Church, R., 1071, 1799
Çil, E., 2039
Cimpeanu, V., 244

© 2005 NRC Canada

Ciubotaru, P., 1525
Ciuculescu, C.-A., 244
Claver, C., 764
Clay, M.D., 559
Cobos, J.C., 1812
Coll, F., 1084
Collard, S., 990
Collin, P.D., 21, 2120
Conrad, M.L., 661
Corbi, P.P., 104
Costa-Neto, C.M., 104
Cowie, M., 1043
Cox, R.A., 1391
Cozens, F.L., 1637
Craig, D.C., 174
Cramb, D.T., 1190
Crampton, M.R., 1221
Crudden, C.M., 943
Cummins, C.C., 302
Čuperlović-Culf, M., 2052
Czardybon, W., 1360
D'Alfonso, G., 1017
Dance, I.G., 174
Darkwa, J., 843
Darwish, H.A., 1158
Das, B., 499, 2032
Das, U., 63
Daştan, A., 227
Dawid, M., 443
de Rossi, R.H., 1281
de Souza, E.P., 1483
Deacon, G.B., 969, 980
Dean, P.A.W., 174
Debacher, N.A., 1483
Decken, A., 661, 943, 1063, 1158, 1185, 2052
Deledda, S., 741
Dennett, J.N.L., 862
Derakhshan, M., 1792
Derouane, E.G., 574
Deschamps, N.M., 838
Deslongchamps, P., 728, 2144
Dettwiler, J.E., 793
Diaconescu, P.L., 302
Ding, Z., 1779
Dmitrenok, P.S., 21, 2120
Dong, D., 1741
Dowaidar, A., 1833
Dozol, J.F., 1098
Dragonetti, C., 1017
Drougas, E., 9
Drouin, C., 543
Drouin, S.D., 748
Duffy, S.J., 661
Duncombe, B.J., 1994
Dutta Chowdhury, S.K., 1164
Duval, H., 615
East, A.L.L., 1146
Edmund Tan, C.-H., 1347
Edwards, G.L., 969, 980
Elaridi, J., 875
El-Dusouqui, O.M.E., 1543
El-Hashash, M.A., 251
Ells, B., 1961
El-Soll, A.M.A., 251
Endoh, N., 1178
Enriz, R.D., 122
Evain, K., 138
Evans, W.J., 375
Fallis, A.G., 559
Fan, Q., 903
Fan, X., 16
Fancy, P.D., 1878
Fedorov, A.V., 1561
Fei, X., 449
Feng, J.-K., 166
Feng, L., 903
Feng, S., 449
Ferguson, M.J., 862, 1721
Flinn, C.G., 2082
Flores, A.F.C., 1171
Flores, D.C., 1171
Fogg, D.E., 748
Foucault, H.M., 748
Franzén, R., 266
Freile, M.L., 122
Frenette, M., 869
Frieman, B.A., 606
Frohning, C.D., 1033
Fryzuk, M.D., 315, 652
Fu, X., 1228
Fu, X.B., 485
Fukuyama, T., 711
Gai, X., 990
Galán, J.A., 1124
Galli, S., 1017
Gambarotta, S., 279, 832
García de la Fuente, I., 1812
Garon, C.N., 1063
Gaspar, P.P., 1324
Gaudreault, P., 543
Gavioli, G., 1132
Gesser, J.C., 1629
Gibson, G.T.T., 1268
Gilbert, T.M., 2013
Gill, M.S., 1525
Gillson, A.-M.E., 1492
Glenn, K.M., 2067
Glover, S.A., 1372, 1492
Goikhman, R., 786
Gomaa, M.A.-M., 57
González, J.A., 1812
Görgülü, A.O., 2039
Gossage, R.A., 449, 1185
Gottschling, S.E., 1568
Gowda, D.C., 517
Grabowy, J.A.D., 1864
Green, M.J., 854
Grigg, R., 990
Grossert, J.S., 1878
Groux, L.F., 634
Grushin, V.V., 640
Guevremont, R., 1961
Gullon, T.J., 1063
Güney, M., 227
Gupta, R., 1137
Guthrie, J.P., 1, 1654
Guzei, I.A., 843
Habeck, C.M., 385
Haldar, P., 499
Hammond, G.P., 1492
Hanan, G.S., 1114
Hanessian, S., 801
Hao, C., 2013
Harkins, S.B., 332
Harrington, C.R., 1324
Harrison, A.G., 1969
Harrison, P.H.M., 1253
Hemming, K., 1432
Hempel, A., 1141
Hicks, R.G., 150
Hidai, M., 358
Hillhouse, G.L., 328
Hinde, R.J., 2005
Hirano, K., 937
Ho, C., 403
Holland, P.L., 296
Hollfelder, F., 1629
Hollink, E., 430
Holmes, J.L., 1903
Hook, J.M., 174
Hopkinson, A.C., 1941
Hörner, M., 1171
Hossain, B.M., 1953
Hoz, S., 1448
Hsieh, Y.-H., 769
Hu, X., 16
Hudson, R.H.E., 1731
Humeres, E., 1483
Hung, C.-H., 2021
Huyser, J.J., 854
Huyser, M., 854
Ie, Y., 75
Ihara, H., 1792
Ikeda, G., 1277

© 2005 NRC Canada

Ikemoto, T., 716
Illien, B., 138
Ioachim, E., 1114
Isanbor, C., 1221
Ishar, M.P.S., 260
Ishihara, K., 894
Ishiwata, H., 646
Ivan, M.G., 869
Ivanova, E.V., 1588
Jackson, W.R., 875
Jafarzadeh, M., 1808
Jalón, F.A., 2106
James, B.R., 546
Jana, N.K., 63
Jankowski, C.K., 493, 1098
Jarne, C., 220
Jasiulionis, M.G., 104
Jenkins, H.A., 174
Jenkins, S.I., 1253
Jennings, M.C., 595, 1568
Jiang, H., 2127
Jiang, L., 693
Jin, A.Y., 37
Jin, G., 2127
Jin, V.X., 195, 2091
Jobe, B., 1833
Johnson, J.B., 1339
Johnson, S.A., 315, 652
Johnston, B.D., 929
Jones, N.D., 546
Jones, W.D., 626
Joó, F., 1033
Joshi, B.P., 1826
Juusola, P.M., 46
Kaizuka, T., 646
Kakiuchi, F., 755
Kale, B.B., 527
Kalinin, V.I., 21, 2120
Kalinovsky, A.I., 21, 2120
Kam, K., 1253
Karakuz, T., 786
Karthikeyan, G., 1746
Kayser, M.M., 28
Kazmaier, P.M., 1448
Keep, A., 990
Keirstead, A.E., 1637
Kenne, L., 156
Kerr, M.A., 1752
Keshavarzi, E., 236
Khamnaen, T., 990
Khodaei, M.M., 209
Khosropour, A.R., 209
Kiepek, E., 1448
Kim, B.H., 213
Kim, C.-K., 769
Kim, S., 917
Kindahl, L., 156
King, J.F., 1525
Kirby, A.J., 1629
Kirby, C.W., 174
Kluger, R., 1277
Klys, A., 443, 1360
Kobayashi, S., 937
Koga, Y., 420
Kohn, H., 37
Konermann, L., 1953
Koo, S., 213
Kookhazadeh, M., 209
Korobkov, I., 279, 832
Kosmas, A.M., 9
Kosower, E.M., 1207
Kothakonda, K.K., 801
Kovács, J., 1033
Koyanagi, G.K., 1839
Krafft, M.E., 1006
Krahn, M., 1768
Krasnova, L.B., 1025
Kresge, A.J., 68, 1202
Kundu, U.K., 63
Kurdi, R., 882
Lai, P.H.M., 553
Laitonjam, W.S., 1056
Lam, K.H., 903
Lamouroux, C., 1098
Langer, V., 2073
Laurence, C., 138
Le, X.C., 185
Leandro, L., 1654
LeBel, O., 615
Lee, C.W., 527
Lee, D.G., 1212
Lee, D.S., 375
Lee, H.J., 213
Lee, J.-Y., 1365
Lee, R., 1847
Lee, S.M., 527
Lee, S.-Y., 681
Leger, L.J., 661, 1063
Lehnert, N., 385
Leidens, V.L., 1171
Leigh, G.J., 277
Leigh, W.J., 1324
Leitus, G., 786
Lessard, J., 543
Li, L., 1120
Li, Q., 1146
Li, X., 2140
Liltorp, K., 420
Lin, I.J.B., 812
Lipshutz, B.H., 606
Lipson, R.H., 1891
Little, V.R., 471
Liu, C.B., 485
Liu, Q., 1741
Liu, X.-J., 166
Liu, Z., 2140
Lobato, C.M.L., 1483
López-Solera, I., 2106
Luan, W., 213
Lubell, W.D., 793
Lucenti, E., 1017
Macartney, D.H., 195, 2091
MacBeth, C.E., 332
Macchi, P., 1017
MacKay, B.A., 315
Madkour, H.M.F., 251
Maeder, M., 894
Magusin, P.C.M.M., 574
Mahalanabis, K.K., 1164
Majumdar, K.C., 63, 2046
Makino, K., 1178
Manderville, R.A., 1261
Manzano, B.R., 2106
Mapolie, S.F., 843
Maresca, K.P., 2060
Maris, T., 615
Marshall, W.J., 640
Martínez-Ripoll, M., 2106
Martins, M.A.P., 1171
Marzouk, M.I., 251
Masman, M.F., 122
Mason, J.W., 1063
Massabni, A.C., 104
Mastropaolo, D., 1141
Masuda, J.D., 324, 477
Mauclaire, L., 493
Mawhinney, R.C., 1615
Mayer, P.M., 1864
Mayr, H., 1554
Maziarz III, E.P., 1871
McAuley, A., 894
McDonald, R., 862, 922, 1721
McDonald, R.S., 1253
McFarlane, N., 2060
McMahon, T.B., 1978
Medrano, F.J., 104
Meghdadi, S., 2073
Mehta, G., 581
Mele, G., 674
Memarian, H.R., 115
Milstein, D., 786
Mishra, M., 1164
Mizobe, Y., 358
Mo, G., 1492
Mohammadpoor-Baltork, I., 110, 115

© 2005 NRC Canada

Mony, L., 909
Moon, S.-J., 527
Moore, S.A., 2067
Moore, S.E., 2067
Moreira, A.G., 104
Moreno, M., 2106
Mori, C., 937
Moser, S., 1071
Mosey, N.J., 1752
Moss, R.A., 1228
Motti, E., 741
Moulin, C., 1098
Moura, S., 1171
Mozo, I., 1812
Muchall, H.M., 1588, 1615
Mukhopadhyay, P.P., 2046
Mulder, R.J., 875
Murai, S., 755
Myles, D.J.T., 150
Nagahata, R., 646
Nait Ajjou, A., 702
Najafi, B., 236
Najafian, K., 1561
Nakajima, A., 1178
Narine, A.A., 413
Näther, C., 385
Nelles, M.E., 1063
Neverov, A.A., 1268
Nihan, D.M., 606
Nikolaev, V.A., 68
Nikpour, F., 1808
Nitu, C., 244
Nome, F., 1629
Nongmeikapam, A.D., 1056
Novak, M., 1372
O'Donoghue, A.C., 1536
Ogilvie, K.A., 449
Oh, S.-W., 1721
Ojima, I., 681
Ojwach, S.O., 843
Onyido, I., 68
Orejón, A., 764
Orita, A., 716
Otera, J., 716
Otín, S., 220
Ouellette, R.J., 2052
Ouyang, Y., 1741
Page, M.I., 1432
Pahadi, N.K., 569
Paige, M.F., 435
Pal, P., 574
Palepu, R.M., 2067
Pályi, G., 882
Partanen, J.I., 46
Parvez, M., 1768, 2098
Patil, N.T., 569
Patrick, B.O., 315, 1037, 1460, 2098
Paul, S., 1137
Pavel, C., 244
Pavski, V., 185
Pedrech, A., 1253
Peori, M.B., 1071, 1799
Peressini, S., 1132
Pérez, J.C., 1124
Perumal, P.T., 1746
Perumal, S., 202
Peslherbe, G.H., 1615
Peters, G., 385
Peters, J.C., 332
Phan, T.B., 1554
Piers, W.E., 2098
Pincock, A.L., 1237
Pincock, J.A., 1237, 1287
Pinet, J.-L., 702
Pinto, B.M., 929
Pitchko, V., 1654
Poirier, R.A., 1299, 2082
Pool, J.A., 286
Popik, V.V., 1382
Power, P.P., 244
Priebe, J.P., 1629
Pu, Y., 2132
Puddephatt, R.J., 595
Purves, R.W., 1961
Puškar, L., 1994
Pye, C.C., 1299
Qu, G., 1120
Quartararo, J., 574
Ragauskas, A.J., 2132
Rahimizadeh, M., 1253
Rahman, M.M., 1792
Rajalingam, U., 174
Rajviroongit, S., 990
Ramesh, S.S., 581
Ranieri, A., 1132
Rao, C.N.R., 668
Rasouli, N., 2073
Rauk, A., 1492
Razus, A.C., 244
Reich, H.J., 1577
Ren, A.-M., 166
Riber, D., 559
Richard, J.P., 1536
Richeson, D.S., 958
Ringer, M.K., 1063
Rios, A., 1536
Rivera, D.G., 1084
Riveros, J.M., 1913
Roberto, D., 1017
Roberts, J.D., 1626
Robinson, A.J., 875
Rochon, F.D., 28
Rodopoulos, M., 894
Rodopoulos, T., 894
Rodríguez, A.M., 2106
Romero, P.E., 2098
Roy, B., 63
Rozental, E., 1448
Ruan, J., 903
Ruttink, P.J.A., 1847
Ryu, I., 711
Sadovski, O., 1202
Saidi, M.R., 146, 505
Sakurai, H., 646
Sakurai, T., 1792
Salagre, P., 764
Salehi, M., 2073
Samec, J.S.M., 909
Sánchez, E.E., 1124
Sanchez, M.N.M., 1483
Sandström, C., 156
Sanji, T., 646
Santágata, L.N., 122
Santos, L., 2106
Sauers, R.R., 1228
Saunders, Jr., W.H., 1649
Scaiano, J.C., 869
Schafer, L.L., 1037
Scheffer, J.R., 1460
Schepp, N.P., 1347, 1637
Schrock, R.R., 341
Schröder, D., 1936
Schwarz, H., 1936
Scott, J., 279
Scott, J.M.W., 1667
Scudder, M.L., 174
Sepúlveda, F., 2106
Shaik, S., 1649
Shamrakov, L.G., 1190
Shan, J., 958
Sharma, A., 1826
Shaver, M.P., 652
Shea, S., 1637
Shehatta, I., 1833
Shek, P.Y.I., 1941
Shi, T., 1941
Shi, Y., 1306
Shi, Y.J., 1891
Shi, Z., 769
Shimon, L.J.W., 786
Shoichet, M.S., 553
Shustov, G.V., 93
Sibiya, M.S., 854
Sicora, O., 2052
Sigouin, O., 460

© 2005 NRC Canada

Silchenko, A.S., 21, 2120
Silva, O.F., 1281
Simmons, D.A., 1953
Singer, S.R., 1510
Singh, G., 260
Singh, R., 260
Singh, S., 260
Sinha, A.K., 1826
Sinnott, M.L., 1516
Siu, K.W.M., 1941
Smith, B.D., 2021
Song, Q., 2140
Soolaman, D.M., 403
Speed, A.W.H., 1287
Sridharan, V., 990
Srinivasa, G.R., 517
Stables, J.P., 37
Stace, A.J., 1994
Stanciu, C., 244
Stephan, D.W., 324, 430, 477
Stephan, G.C., 385
Stephenson, K.A., 2060
Stone, J.A., 1921
Stonik, V.A., 21
Stringle, D.L.B., 1473
Stryker, J.M., 922
Su, T., 1921
Sugiura, M., 937
Sun, R., 838
Sunderlin, L.S., 2013
Tachikawa, H., 1597
Tajima, K., 1178
Takafuji, M., 1792
Takats, J., 862
Takeuchi, K., 646
Tanaka, M., 646
Tavagnacco, C., 1132
Teng, A.C.-T., 1268
Tennent, C.L., 626
Terblans, Y.M., 854
Terlouw, J.K., 1847
Thokchom, H.S., 1056
Thompson, L.K., 77, 1195
Thomson, R.K., 1037
Tidwell, T.T., 1197, 1561
Tingley, R., 471, 1799
Trudeau, M.L., 308
Tsang, W.Y., 1432
Tshivhase, M.G., 843
Tuczek, F., 385
Turrini, D., 882
Twamley, B., 449
Ueda, Y., 1178
Uemura, T., 755
Ugo, R., 1017
Um, I.-H., 1365
Unger, J.B., 606
Valliant, J.F., 2060
Van Calsteren, M.-R., 1098
Van Gorp, K.A., 1752
Vasam, C.S., 812
Vasapollo, G., 674
Vaughan, K., 471, 1071, 1799
Védrine, J.C., 574
Velasco, I., 220
Verkerk, U.H., 922
Verraes, V., 46
Vogels, C.M., 661, 1063, 1158, 2052
Vukomanovic, D., 1921
Vukovic, S., 1561
Wakelin, L.P.G., 969, 980
Wan, P., 1306
Wanapun, D., 1752
Wang, F., 28
Wang, H., 185
Wang, J., 16
Wang, R., 943
Wang, R.X., 485
Wang, X., 1903
Wang, Z., 1212
Warkentin, J., 443, 1360
Wasylishen, R.E., 1721
Waterman, R., 328
Weaver, D.F., 37
Webb, J.D., 1158
Wei, P., 430
Weinberg, N., 769
Wender, P.A., 838
Werstiuk, N.H., 1352, 1360
Westcott, S.A., 661, 1063, 1158, 2052
Westh, P., 420
Wheaton, S.L., 1063, 1158
Whelan, A.N., 875
Whipple, W.L., 1577
White, R.L., 1878
Willett, T.C., 1221
Wilson, P.D., 413
Wojciechowski, F., 1731
Wolfe, S., 93, 769
Woo, T.K., 1752
Wood, M., 449
Wood, T.D., 1871
Woodward, C., 21, 2120
Workentin, M.S., 1473
Wright, J.A., 1006
Wright, P.J., 1440
Wu, B., 1994
Wu, R., 1978
Wu, W., 1649
Wu, X., 2140
Wuest, J.D., 615
Wynberg, N.A., 661
Xavier, L.A., 1913
Xiao, W.-J., 826
Xie, Y., 1093
Xu, L., 903
Xu, Y., 266
Yadav, P.N., 1185
Yamamoto, Y., 569
Yamataka, H., 1606
Yamaura, R., 711
Yandulov, D.V., 341
Yang, H.-j., 273
Yang, K., 769
Yang, Q., 1093
Yang, Y., 28
Yap, G.P.A., 748, 958
Ye, F., 716
Yin, J., 2140
Yip, W.-P., 521
Yoo, J.S., 527
Yoon, C.H., 213
Young, D.A., 854
Youssef, A.S.A., 251
Yu, H., 1741
Yu, H.-Z., 403
Yu, W.-Y., 521
Yudin, A.K., 1025
Yue, C., 308
Zamora, M.A., 122
Zanatta, N., 1171
Zargarian, D., 634
Zaworotko, M.J., 894
Zeng, X., 68, 1202
Zhang, D.J., 485
Zhang, F., 595
Zhang, G., 1120
Zhang, G.-l., 273
Zhang, H., 1158
Zhang, L., 990
Zhang, X., 16, 1120
Zhang, X., 1093
Zhao, J., 1941
Zhao, Q., 1093
Zhao, X., 1839
Zhou, C., 449
Zhou, D., 1324
Zhou, X., 166
Zhou, Y., 1448
Zhu, L., 1120
Zhu, R., 1779
Zhu, S., 2127
Zhu, Y., 1202
Zubieta, J., 2060
Zucchi, C., 882

© 2005 NRC Canada

Canadian Journal of Chemistry

Contents
Volume 83, 2005

Revue canadienne de chimie

Sommaire
Volume 83, 2005

January / Janvier

AWARD LECTURE / CONFÉRENCE D'HONNEUR

J. Peter Guthrie 2003 Alfred Bader Award Lecture Predicting the rates of chemical reactions **1**

ARTICLES / ARTICLES

Evangelos Drougas and Agnie M. Kosmas Computational investigation of isomeric and conformeric structures of methyl iodoperoxide **9**

Xuesen Fan, Xueyuan Hu, Xinying Zhang, and Jianji Wang $InCl_3 \cdot 4H_2O$-promoted green preparation of xanthenedione derivatives in ionic liquids **16**

Alexandra S. Silchenko, Sergey A. Avilov, Alexandr S. Antonov, Anatoly I. Kalinovsky, Pavel S. Dmitrenok, Vladimir I. Kalinin, Valentin A. Stonik, Carl Woodward, and Peter D. Collin Glycosides from the sea cucumber *Cucumaria frondosa.* III. Structure of frondosides A_2-1, A_2-2, A_2-3, and A_2-6, four new minor monosulfated triterpene glycosides **21**

Yan Yang, Fengyun Wang, Fernande D. Rochon, and Margaret M. Kayser Synthesis of novel optically pure β-lactams **28**

Albert Y. Jin, Harold Kohn, Cécile Béguin, Shridhar V. Andurkar, James P. Stables, and Donald F. Weaver A quantitative structure–activity relationship study for α-substituted acetamido-*N*-benzylacetamide derivatives — A novel anticonvulsant drug class **37**

Jaakko I. Partanen, Pekka M. Juusola, and Virginie Verraes Re-evaluation of the second thermodynamic dissociation constants of α-alanine, valine, and leucine using potentiometric data measured for aqueous potassium chloride solutions at 298.15 K **46**

Ashraf A. Aly and Mohsen A.-M. Gomaa New cycloaddition of diarylazines with 1,2-dehydrobenzene, 1,1,2,2-tetracyanoethylene, and dibenzoylacetylene — Facile synthesis of acridinones, pyrazolidine, and pyridazine derivatives **57**

K.C. Majumdar, U.K. Kundu, U. Das, N.K. Jana, and B. Roy *N*-Iodosuccinimide — An effective reagent for regioselective heterocyclization of *o*-cyclohex-2′-enylanilines for the synthesis of hexahydrocarbazoles **63**

Y. Chiang, A.J. Kresge, V.A. Nikolaev, I. Onyido, and X. Zeng The 2-oxo-3,3,5,5-tetramethylcyclopentanecarboxylic acid keto–enol system in aqueous solution — Generation of the enol by flash photolytic Wolff rearrangement of 2-diazo-4,4,6,6-tetramethylcyclohexane-1,3-dione followed by hydration of the acylketene thus formed **68**

Author Index / Index des auteurs **AI-1**

February / Février

AWARD LECTURE / CONFÉRENCE D'HONNEUR

Laurence K. Thompson 2004 Alcan Award Lecture From dinuclear to triakontahexanuclear complexes — Adventures in supramolecular coordination chemistry **77**

ARTICLES / ARTICLES

Gennady V. Shustov, Melanie K. Chandler, and Saul Wolfe Stereoselective synthesis of multiply substituted [1,2]oxazinan-3-ones via ring-closing metathesis **93**

Pedro P. Corbi, Antonio C. Massabni, Andréia G. Moreira, Francisco J. Medrano, Miriam G. Jasiulionis, and Claudio M. Costa-Neto Synthesis, characterization, and biological activity of a new palladium(II) complex with deoxyalliin **104**

Iraj Mohammadpoor-Baltork and Mohammad Abdollahi-Alibeik Mild, efficient, and chemoselective dehydrogenation of 2-imidazolines, bis-imidazolines, and *N*-substituted-2-imidazolines with potassium permanganate supported on montmorillonite K-10 **110**

Iraj Mohammadpoor-Baltork, Hamid R. Memarian, and Kiumars Bahrami 3-Carboxypyridinium chlorochromate – aluminium chloride — An efficient and inexpensive reagent system for the selective oxidation of sulfides to sulfoxides and sulfones in solution and under microwave irradiation **115**

© 2005 NRC Canada

Miguel A. Zamora, Luis N. Santágata, Marcelo F. Masman, José A. Bombasaro, Mónica L. Freile, and Ricardo D. Enriz Conformational study of internally retrograde and quasi-retrograde molecules — An ab initio and DFT study **122**

Christian Laurence, Michel Berthelot, Karine Evain et Bertrand Illien Échelles pK_{HB} et enthalpique du pouvoir accepteur de liaison hydrogène de thioéthers, thiols et disulfures **138**

Mojtaba Bagheri, Najmedin Azizi, and Mohammad R. Saidi An intriguing effect of lithium perchlorate dispersed on silica gel in the bromination of aromatic compounds by *N*-bromosuccinimide **146**

M'hamed Chahma, Daniel J.T. Myles, and Robin G. Hicks Synthesis, characterization, and coordination chemistry of phosphines with ethylenedioxythiophene substituents **150**

Lill Kindahl, Lennart Kenne, and Corine Sandström ^{1}H NMR studies on the solution conformation of the [L-Ser^{10}] and [D-Ser^{10}] analogues of contulakin-G **156**

Xiao-Juan Liu, Ji-Kang Feng, Ai-Min Ren, Xin Zhou, and Hong Cheng Theoretical studies on the absorption and luminescent properties of a series of derivatives of 1,3-diphenyl-5-pyrene-2-yl-4,5-dihydro-1*H*-pyrazole **166**

Donald C. Craig, Ian G. Dance, Philip A.W. Dean, James M. Hook, Hilary A. Jenkins, Christopher W. Kirby, Marcia L. Scudder, and Umarani Rajalingam A synthetic, structural, and ^{113}Cd NMR study of cadmium complexes of 1,3-thiazolidine-2-thionate, including the structures of $Cd(C_3H_4NS_2)_2$, $(Cd(C_3H_4NS_2)_2(C_5H_5N)_3 \cdot C_5H_5N$, and $(Ph_4P)_2[I_2Cd(\mu\text{-}C_3H_4NS_2)_2CdI_2]$ **174**

Instructions to Authors **I-1**

Recommendations aux auteurs **R-1**

Notes for authors of papers presenting the results of X-ray crystal structure analyses **I-4**

Recommandations aux auteurs d'articles décrivant la détermination de structures par diffraction des rayons X **R-5**

Author Index / Index des auteurs **AI-1**

March / Mars

AWARD LECTURE / CONFÉRENCE D'HONNEUR

X. Chris Le, Victor Pavski, and Hailin Wang 2002 W.A.E. McBryde Award Lecture — Affinity recognition, capillary electrophoresis, and laser-induced fluorescence polarization for ultrasensitive bioanalysis **185**

ARTICLES / ARTICLES

Victor X. Jin, Donal H. Macartney, and Erwin Buncel Kinetic and spectroscopic studies on α- and β-cyclodextrin rotaxanes with (μ-*N*,*N*′-bis(4-pyridinylmethylene)-α,ω-alkanediimine)bis[pentacyanoferrate(II)] threads **195**

N. Bhavani, S. Perumal, and R. Banureka Stereoselective synthesis and stereochemistry of *r*-2-alkoxycarbonyl-*c*-3-*o*-substituted phenyl-1,4-thiazane 1,1-dioxides **202**

Mohammad M. Khodaei, Ahmad R. Khosropour, and Mehdi Kookhazadeh A novel enamination of β-dicarbonyl compounds catalyzed by $Bi(TFA)_3$ immobilized on molten TBAB **209**

Woonphil Baik, Wanqiang Luan, Hyun Joo Lee, Cheol Hun Yoon, Sangho Koo, and Byeong Hyo Kim Efficient one-pot transformation of aminoarenes to haloarenes using halodimethylisulfonium halides generated in situ **213**

C. Jarne, S.T. Blanco, S. Avila, C. Berro, S. Otín, and I. Velasco Dew points of quaternary ethane + carbon dioxide + water + methanol mixtures — Measurement and modelling **220**

Murat Güney, Zeynep Çelik Ceylan, Arif Daştan, and Metin Balci Substituent effects of the cycloaddition reaction of 7-substituted 5*H*-benzocycloheptenes with singlet oxygen and the chemistry of the benzocycloheptene endoperoxides **227**

Mehrdad Bamdad, Saman Alavi, Bijan Najafi, and Ezat Keshavarzi Investigation of the density dependence of the shear relaxation time of dense fluids **236**

Alexandru C. Razus, Carmen Nitu, Claudia Pavel, Crinu-Anghel Ciuculescu, Valentin Cimpeanu, Corneliu Stanciu, and Philip P. Power Oxidation of 1-(4′-substituted phenyl)-2-(4-methylphenyl)diazene — Benzylic substitution vs. C–azo bond breaking **244**

A.S.A. Youssef, M.I. Marzouk, H.M.F. Madkour, A.M.A. El-Soll, and M.A. El-Hashash Synthesis of some heterocyclic systems of anticipated biological activities via 6-aryl-4-pyrazol-1-yl-pyridazin-3-one **251**

Surinderjit Singh, M.P.S. Ishar, Gajendra Singh, and Rajinder Singh Efficient, microwave-assisted intramolecular 1,3-dipolar cycloadditions of oximes and *N*-methylnitrones derived from *o*-alkenylmethoxy-acetophenones **260**

MINIREVIEW / MINISYNTHÈSE

Robert Franzén and Youjun Xu Review on green chemistry — Suzuki cross coupling in aqueous media **266**

RAPID COMMUNICATION / COMMUNICATION RAPIDE

Xiao-hua Cai, Hai-jun Yang, and Guo-lin Zhang Aromatization of 1,4-dihydropyridines with selenium dioxide **273**

Author Index / Index des auteurs **AI-1**

© 2005 NRC Canada

April / Avril

This issue commemorates the 40th anniversary of the publication of the first report of a dinitrogen complex, namely $[Ru(NH_3)_5N_2]^{2+}$ / Ce numéro souligne le 40e anniversaire de la parution du premier rapport faisant état d'un complexe diazoté, le $[Ru(NH_3)_5N_2]^{2+}$

ARTICLES / ARTICLES

G.J. Leigh Bert Allen and the first complex of dinitrogen **277**

Jennifer Scott, Sandro Gambarotta, and Ilia Korobkov Ligand-assisted reduction of Co(II) to Co(I) and subsequent coordination of dinitrogen **279**

Jaime A. Pool and Paul J. Chirik The importance of cyclopentadienyl substituent effects in group 4 metallocene dinitrogen chemistry **286**

Patrick L. Holland Low-coordinate iron complexes as synthetic models of nitrogenase **296**

John-Paul F. Cherry, Paula L. Diaconescu, and Christopher C. Cummins Portability of the RNNMo(3+) core — Application to the synthesis of dinitrogen-derived trialkoxymolybdenum organodiazenido complexes **302**

Chaoyang Yue, Michel L. Trudeau, and David Antonelli Mesoporous tantalum oxide photocatalysts for Schrauzer-type conversion of dinitrogen to ammonia **308**

Bruce A. MacKay, Samuel A. Johnson, Brian O. Patrick, and Michael D. Fryzuk Functionalization and cleavage of coordinated dinitrogen via hydroboration using primary and secondary boranes **315**

Jason D. Masuda and Douglas W. Stephan Synthesis and structure of a (NacNac)rhodium terminal dinitrogen complex **324**

Rory Waterman and Gregory L. Hillhouse Synthesis and structure of a terminal dinitrogen complex of nickel **328**

Cora E. MacBeth, Seth B. Harkins, and Jonas C. Peters Synthesis and characterization of cationic iron complexes supported by the neutral ligands $NP^{i\text{-}Pr}_3$, $NArP^{i\text{-}Pr}_3$, and $NS^{t\text{-}Bu}_3$ **332**

Dmitry V. Yandulov and Richard R. Schrock Synthesis of tungsten complexes that contain hexaisopropylterphenyl-substituted triamidoamine ligands, and reactions relevant to the reduction of dinitrogen to ammonia **341**

Masanobu Hidai and Yasushi Mizobe Research inspired by the chemistry of nitrogenase — Novel metal complexes and their reactivity toward dinitrogen, nitriles, and alkynes **358**

William J. Evans and David S. Lee Early developments in lanthanide-based dinitrogen reduction chemistry **375**

Gerald C. Stephan, Gerhard Peters, Nicolai Lehnert, Carsten M. Habeck, Christian Näther, and F. Tuczek Bonding, activation, and protonation of dinitrogen on a molybdenum pentaphosphine complex — Comparison to *trans*-bis(dinitrogen) and -nitrile – dinitrogen complexes with tetraphosphine coordination **385**

Author Index / Index des auteurs **AI-1**

May / Mai

AWARD LECTURE / CONFÉRENCE D'HONNEUR

Cassie Ho, Dinah M. Soolaman, and Hua-Zhong Yu 2004 Fred Beamish Award Lecture — Analytical – materials chemistry on old CDs — Beyond self-assembly **403**

ARTICLES / ARTICLES

Arun A. Narine and Peter D. Wilson Synthesis and evaluation of 7-hydroxyindan-1-one-derived chiral auxiliaries **413**

Karin Liltorp, Peter Westh, and Yoshikata Koga Thermodynamic properties of water in the water-poor region of binary water + alcohol mixtures **420**

Emily Hollink, Pingrong Wei, and Douglas W. Stephan Homoleptic magnesium bis-phosphinimide derivatives **430**

Sangram Bagh and Matthew F. Paige Construction and application of a single-molecule fluorescence microscope **435**

Arkadiusz Klys, Malgorzata Dawid, and John Warkentin Synthesis and spectra of aldehyde- and ketone-*O*-(2,5-dihydro-2-methoxy-5,5-dimethyl-1,3,4-oxadiazol-2-yl)oximes — Thermal sources of some methoxy(oximino)carbenes **443**

David J. Berg, Chuanjian Zhou, Tosha Barclay, Xuening Fei, Shengyu Feng, Kevin A. Ogilvie, Robert A. Gossage, Brendan Twamley, and Mark Wood Lanthanide complexes of an oxazoline-phenoxide hybrid chelate **449**

Olivier Sigouin and André L. Beauchamp Oxo-rhenium(V) complexes with 8-hydroxyquinoline derivatives **460**

Vanessa Renée Little, Reid Tingley, and Keith Vaughan Triazene derivatives of (1,*x*)-diazacycloalkanes. Part III. Synthesis and characterization of a series of 1,4-di[2-aryl-1-diazenyl]piperazines **471**

Jason D. Masuda and Douglas W. Stephan Transition metal complexes of a sterically demanding diimine ligand **477**

Dongju Zhang, Xuebing Fu, Ruoxi Wang, and Chengbu Liu Theoretical study of the reaction of titanium ion with ethane — Structure, mechanism, and potential energy surface **485**

© 2005 NRC Canada

Christopher K. Jankowski, Sébastien Arseneau, Jérome Blu, Laurent Mauclaire, and Nicolas Aychet On the synthesis of new amphiphilic entities by the succinic coupling of β-cyclodextrins to calixarenes **493**

Purushottam Haldar and Bijan Das Viscosities of some tetraalkylammonium bromides in 2-ethoxyethanol at 308.15, 313.15, 318.15, and 323.15 K **499**

Najmodin Azizi and Mohammad R. Saidi Solid lithium perchlorate as a powerful catalyst for the synthesis of β-aminoalcohols under solvent-free conditions **505**

Jerzy J. Chruściel ^{29}Si NMR studies on the mechanism of dehydrocoupling of hydrosilanes with hydroxylic reagents in DMF — The role of DMF **508**

RAPID COMMUNICATION / COMMUNICATION RAPIDE

Keelara Abiraj, Gejjalagere R. Srinivasa, and D. Channe Gowda Palladium-catalyzed simple and efficient hydrogenative cleavage of azo compounds using recyclable polymer-supported formate **517**

Author Index / Index des auteurs **AI-1**

June/July / Juin/Juillet

This special issue is dedicated to Professor Howard Alper to honour his outstanding contributions to research in homogeneous catalysis / Ce numéro spécial est dédié au professeur Howard Alper en reconnaissance de ses contributions exceptionnelles dans le domaine de la catalyse homogène

ARTICLES / ARTICLES

Wai-Hung Cheung, Wing-Ping Yip, Wing-Yiu Yu, and Chi-Ming Che Oxidation of anisoles to *p*-benzoquinone monoketals catalyzed by a ruthenium complex of 1,4,7-trimethyl-1,4,7-triazacyclononane with *tert*-butyl hydroperoxide **521**

B.B. Kale, Jin-Ook Baeg, Jin S. Yoo, Sang Mi Lee, Chul Wee Lee, Sang-Jin Moon, and Hyunju Chang Synthesis of a novel photocatalyst, $ZnBiVO_4$, for the photodecomposition of H_2S **527**

André B. Charette and Jean-Emmanuel Bouchard Catalytic asymmetric synthesis of cyclopropylphosphonates — Catalysts' scope and reactivity **533**

Philippe Gaudreault, Christian Drouin, and Jean Lessard First examples of intramolecular addition of primary amidyl radicals to olefins **543**

Nathan D. Jones and Brian R. James Palladium(II) complexes of bis(phosphine)monooxide and bis(phosphine)monosulphide ligands bearing *o*-*N*,*N*-dimethylanilinyl substituents **546**

Bilal Baradie, Patricia H.M. Lai, and Molly S. Shoichet Synthesis and characterization of novel polysiloxane-grafted fluoropolymers **553**

Matthew D. Clay, Ditte Riber, and Alex G. Fallis Competing Diels–Alder intramolecular pathways from cross-conjugated trienes: Fused hydrindenones (bicyclo[4.3.0]nonenones) vs. bridged-ring (bicyclo[3.3.1]nonenones) adducts from a diene-transmissive precursor **559**

Nitin T. Patil, Nirmal K. Pahadi, and Yoshinori Yamamoto Pd(0)–PhCOOH catalyzed addition of oxygen pronucleophiles to allenes and internal alkynes **569**

Prem Pal, Juliette Quartararo, Sharifah B. Abd Hamid, Eric G. Derouane, Jacques C. Védrine, Pieter C.M.M. Magusin, and Bruce G. Anderson A MAS NMR and DRIFT study of the Ga species in Ga/H-ZSM5 catalysts and their effect on propane ammoxidation **574**

Goverdhan Mehta and Senaiar S. Ramesh Polycyclitols — Novel conduritol and carbasugar hybrids as new glycosidase inhibitors **581**

Fenbao Zhang, Michael E. Broczkowski, Michael C. Jennings, and Richard J. Puddephatt Oxidative addition chemistry of dimethyl(dipyridyl ketone)platinum(II) **595**

Bruce H. Lipshutz, Bryan A. Frieman, John B. Unger, and Danielle M. Nihan Thermally accelerated asymmetric hydrosilylations using ligated copper hydride **606**

Olivier LeBel, Thierry Maris, Hugues Duval, and James D. Wuest A practical guide to arylbiguanides — Synthesis and structural characterization **615**

Christine L. Tennent and William D. Jones Kinetics and mechanism of dealkylation of coordinated isocyanide in $Fe(PMe_3)_2(t\text{-}BuNC)_3$ **626**

Laurent F. Groux, Francine Bélanger-Gariépy, and Davit Zargarian Phosphino-indenyl complexes of nickel(II) **634**

William J. Marshall and Vladimir V. Grushin Activation of chlorobenzene with Ni(0) *N*,*N*-chelates — A remarkably profound effect of a minuscule change in ligand structure **640**

Takanobu Sanji, Hiroyuki Ishiwata, Tomoyoshi Kaizuka, Masato Tanaka, Hideki Sakurai, Ritsuko Nagahata, and Kazuhiko Takeuchi An alternative convergent synthesis of silole-core dendrimers **646**

Michael P. Shaver, Samuel A. Johnson, and Michael D. Fryzuk Activation and cleavage of alkynes by the dinuclear tantalum complexes $([NPN]Ta)_2(\mu\text{-}H)_4$ and $([NPN]Ta)_2(\mu\text{-}\eta^1\text{:}\eta^2\text{-}N_2)(\mu\text{-}H)_2$ (where NPN = $PhP(CH_2SiMe_2NPh)_2$) **652**

© 2005 NRC Canada

Natalie A. Wynberg, Lisa J. Leger, Maren L. Conrad, Christopher M. Vogels, Andreas Decken, Stephen J. Duffy, and Stephen A. Westcott Synthesis and catalysed hydroboration of styryl sulfonamides **661**

J.N. Behera and C.N.R. Rao Coordination polymers with Co(II) sulfate layers linked by alkanediamines of varying chain length **668**

Giuseppe Vasapollo and Giuseppe Mele Palladium-catalyzed asymmetric cyclocarbonylation of allyl naphthols **674**

Wen-Hua Chiou, Seung-Yub Lee, and Iwao Ojima Recent advances in cyclohydrocarbonylation reactions **681**

Lu Jiang and Tak Hang Chan Efficient synthesis of the nonamannoside residue of high mannose glycoproteins **693**

Abdelaziz Nait Ajjou and Jean-Louis Pinet Oppenauer-type oxidation of secondary alcohols catalyzed by homogeneous water-soluble complexes **702**

Takahide Fukuyama, Ryo Yamaura, and Ilhyong Ryu Synthesis of acetylenic ketones by a Pd-catalyzed carbonylative three-component coupling reaction in [bmim]PF_6 **711**

Akihiro Orita, Fangguo Ye, Govindarajulu Babu, Tomohiro Ikemoto, and Junzo Otera Double elimination protocol for the synthesis of arylene ethynylenes containing heteroaromatic rings **716**

Ling Chen and Pierre Deslongchamps Studies towards the total synthesis of ouabagenin **728**

Sara Deledda, Elena Motti, and Marta Catellani Palladium-catalysed synthesis of nonsymmetrically disubstituted-1,1′-biphenyls from *o*-substituted aryl iodides through aryl coupling and delayed hydrogenolysis **741**

Samantha D. Drouin, Heather M. Foucault, Glenn P.A. Yap, and Deryn E. Fogg New pseudohalide ligands in Ru-catalyzed olefin metathesis — A robust, air-activated iminopyrrolato catalyst **748**

Naoto Chatani, Takeshi Uemura, Taku Asaumi, Yutaka Ie, Fumitoshi Kakiuchi, and Shinji Murai Rhodium-catalyzed C-H–CO–olefin coupling reactions — A chelation-assisted direct carbonylation at the ortho C—H bond in the benzene ring of 2-arylpyridines **755**

Aránzazu Orejón, Aída Castellanos, Pilar Salagre, Sergio Castillón, and Carmen Claver Oxidative carbonylation of aniline with new cobalt catalytic systems **764**

Yih-Huang Hsieh, Noham Weinberg, Kiyull Yang, Chan-Kyung Kim, Zheng Shi, and Saul Wolfe Hydration of the carbonyl group — Acetic acid catalysis in the co-operative mechanism **769**

Roman Goikhman, Tanya Karakuz, Linda J.W. Shimon, Gregory Leitus, and David Milstein Electron-rich siloxane–platinum complexes — Synthesis, structures, and reactivity **786**

James E. Dettwiler, Laurent Bélec, and William D. Lubell Synthesis and application of L-*N*-Boc-*N*-methyl-β-hydroxyvaline in the preparation of a depsipeptide **793**

Stephen Hanessian and Kiran Kumar Kothakonda Design and synthesis of oxazolidinone ketolide antibiotic segment mimetics **801**

Ivan J.B. Lin and Chandra Sekhar Vasam Review of gold(I) *N*-heterocyclic carbenes **812**

Hong Cao and Wen-Jing Xiao Microwave-accelerated, palladium-catalyzed carbonylative cyclization reactions of 2-iodophenol with alkynes — Rapid and efficient synthesis of chromen-2-one derivatives **826**

Arunachalampillai Athimoolam, Sandro Gambarotta, and Ilia Korobkov Preparation, characterization, and structure of two dipyrrolide thorium homoleptic complexes — Isolation of a dipyrrolide dipotassium salt with an inverted-sandwich type of structure **832**

Paul A. Wender, Nicole M. Deschamps, and Robert Sun Rh(I)-catalyzed cleavage of unactivated C—O bonds — Carbonylative rearrangement reactions of allenyl ethers to 2-carboalkoxy-1,3-dienes **838**

Stephen O. Ojwach, Mmboneni G. Tshivhase, Ilia A. Guzei, James Darkwa, and Selwyn F. Mapolie Furoyl and thiophene carbonyl linker pyrazolyl palladium(II) complexes — Synthesis, characterization, and evaluation as ethylene oligomerization catalysts **843**

Yvette M. Terblans, Johannes J. Huyser, Michelle Huyser, Michael J. Green, Desmond A. Young, and Mike S. Sibiya Aluminium triflate as catalyst for epoxide ring-opening and esterification reactions — Mechanistic aspects **854**

James N.L. Dennett, Michael J. Ferguson, Robert McDonald, and Josef Takats Reaction of [$Fe(CO)_4(\eta^2$-$Me_3SiC{\equiv}CSiMe_3)$] with PMe_3 — CO rather than alkyne substitution **862**

Mathieu Frenette, Marius Gabriel Ivan, and J.C. Scaiano Use of fluorescent probes to determine catalytic chain length in chemically amplified resists **869**

Amanda N. Whelan, Jomana Elaridi, Roger J. Mulder, Andrea J. Robinson, and W. Roy Jackson Metal-catalysed tandem metathesis–hydrogenation reactions for the synthesis of carba analogues of cyclic peptides **875**

Claudia Zucchi, Davide Turrini, Roland Boese, Lajos Bencze, Robert Kurdi, Luciano Caglioti, and Gyula Pályi Alkylcobalt carbonyls. Part XIV. Generation of chiral conformations by centers of chirality in organocobalt complexes **882**

Theo Rodopoulos, Koji Ishihara, Mary Rodopoulos, M.J. Zaworotko, M. Maeder, and A. McAuley Synthesis and reactivity of the macrobicyclic complexes (1,5,8,12-tetraaza-17-oxabicyclo[10.5.2]nonadecane)cobalt(III) perchlorate ([$Co(L_1)(ClO_4)](ClO_4)_2$), [(chloro(1,4,8,11-tetraaza-17-oxabicyclo[9.5.3]nonadecane)cobalt(III) perchlorate ([$Co(L_2)(Cl)](ClO_4)_2$), (4,8-dimethyl-1,4,8,11-tetraaza-17-oxabicyclo[9.5.3]nonadecane)cobalt(III) perchlorate ([$Co(L_3)(ClO_4)](ClO_4)_2$), and (5,8-dimethyl-1,5,8,12-tetraaza-17-oxabicyclo[10.5.2]nonadecane)cobalt(III) perchlorate ([$Co(L_4)(ClO_4)](ClO_4)_2$) — Crystal structure of the L_2 complex **894**

© 2005 NRC Canada

Kim Hung Lam, Lijin Xu, Lichun Feng, Jiwu Ruan, Qinghua Fan, and Albert S.C. Chan Ruthenium catalyzed asymmetric hydrogenation of α- and β-keto esters in ionic liquids using chiral P-Phos ligand **903**

Joseph S.M. Samec, Laetitia Mony, and Jan-E. Bäckvall Efficient ruthenium catalyzed transfer hydrogenation of functionalized imines by isopropanol under controlled microwave heating **909**

Chang Ho Cho and Sunggak Kim β Elimination of a phosphonate group from an alkoxyl radical — Intramolecular acylation using acylphosphonate derivatives as carbonyl group acceptors **917**

Udo H. Verkerk, Robert McDonald, and Jeffrey M. Stryker Coordination chemistry of the tetrakis(2-hydroxyphenyl)ethene support mimic — Polymetallic magnesium, aluminum, and titanium derivatives **922**

Nagasree Chakka, Blair D. Johnston, and B. Mario Pinto Synthesis and conformational analysis of disaccharide analogues containing disulfide and selenosulfide functionalities in the interglycosidic linkages **929**

Masaharu Sugiura, Chieko Mori, Keiichi Hirano, and Shū Kobayashi Direct synthesis of unprotected α-amino acids via allylation of hydroxyglycine **937**

Austin C. Chen, Daryl P. Allen, Cathleen M. Crudden, Ruiyao Wang, and Andreas Decken Synthesis, structure determination, and hydroformylation activity of *N*-heterocyclic carbene complexes of rhodium **943**

Jingning Shan, Glenn P.A. Yap, and Darrin S. Richeson Synthesis, thermal, electrochemical, and photophysical characterization of 1,5-bis(diarylamino)naphthalene derivatives as potential hole transport OLED materials **958**

Gavin L. Edwards, David St.C. Black, Glen B. Deacon, and Laurence P.G. Wakelin Effect of charge and surface area on the cytotoxicity of cationic metallointercalation reagents **969**

Gavin L. Edwards, David St.C. Black, Glen B. Deacon, and Laurence P.G. Wakelin In vitro and in vivo studies of neutral cyclometallated complexes against murine leukæmias **980**

Ronald Grigg, Xinjie Gai, Tossapol Khamnaen, Shuleewan Rajviroongit, Visuvanathar Sridharan, Lixin Zhang, Simon Collard, and Ann Keep Synthesis of *N*-substituted isoindolinones via a palladium catalysed three-component carbonylation – amination – Michael addition cascade **990**

Marie E. Krafft, James A. Wright, and Llorente V.R. Boñaga Pauson–Khand reactions in water **1006**

Giuseppe D'Alfonso, Claudia Dragonetti, Simona Galli, Elena Lucenti, Piero Macchi, Dominique Roberto, and Renato Ugo Surface organometallic chemistry — Carbonyl complexes of Re(I) with silanolates as models of silica anchored rhenium carbonyl species **1017**

Larissa B. Krasnova and Andrei K. Yudin Novel nitrogen containing chelating ligands from aziridines — Preparation, coordination studies, and catalytic application in the cyclopropanation of styrene **1025**

RAPID COMMUNICATIONS / COMMUNICATIONS RAPIDE

József Kovács, Ferenc Joó, and Carl D. Frohning Anion effects in the formation of the active catalyst in the Ruhrchemie – Rhône-Poulenc aqueous biphasic hydroformylation process. Are there any? **1033**

Robert K. Thomson, Brian O. Patrick, and Laurel L. Schafer Synthesis, characterization, and reactivity of the first hafnium alkyl complex stabilized by amidate ligands **1037**

Author Index / Index des auteurs **AI-1**

August / Août

AWARD LECTURE / CONFÉRENCE D'HONNEUR

Martin Cowie 2003 Alcan Award Lecture — Roles of the adjacent metals in the coupling of methylene groups promoted by heterobinuclear complexes of Group 8 and 9 metals **1043**

ARTICLES / ARTICLES

Herojit S. Thokchom, Anita D. Nongmeikapam, and Warjeet S. Laitonjam Synthesis of fused pyrazolo-, isoxazolo-, pyrimido-, and pyridopyrimidines **1056**

Tara A. Bourque, Megan E. Nelles, Teri J. Gullon, Christian N. Garon, Melissa K. Ringer, Lisa J. Leger, Jamie W. Mason, Susan L. Wheaton, Felix J. Baerlocher, Christopher M. Vogels, Andreas Decken, and Stephen A. Westcott Late metal salicylaldimine complexes derived from 5-aminosalicylic acid — Molecular structure of a zwitterionic mono Schiff base zinc complex **1063**

Shasta Moser, Ryan Church, M. Brad Peori, and Keith Vaughan Triazene derivatives of (1,*x*)-diazacycloalkanes. Part IV. Synthesis and characterization of 1-[2-aryl-1-diazenyl]-3-(3-[2-aryl-1-diazenyl]hexahydro-1-pyrimidinylmethyl)hexahydropyrimidines and 1-(5,5-dimethyl-3-[2-aryl-1-diazenyl]hexahydro-1-pyrimidinylmethyl)-5,5-dimethyl-3-[2-aryl-1-diazenyl]hexahydropyrimidines from the reaction of diazonium salts with mixtures of formaldehyde and 1,3-diaminopropanes **1071**

Daniel G. Rivera and Francisco Coll Synthesis and preliminary bioactivity evaluation of new pregnane brassinosteroid-like compounds **1084**

© 2005 NRC Canada

Qingrui Zhao, Xuanjun Zhang, Qing Yang, and Yi Xie One-step synthesis of Sb_2O_3 broom-like belts with controllable morphology **1093**

C.K. Jankowski, M.-R. Van Calsteren, N. Aychet, J.F. Dozol, C. Moulin, and C. Lamouroux Study of the nitration of di-*n*-octylcrown-6 calix[4]arene using LC–MS, NMR, and molecular modelling **1098**

Elena Ioachim and Garry S. Hanan Spectroscopy and electrochemistry of new 6,6′-disubstituted-4,4′-bipyrimidine molybdenum(0) and tungsten(0) tetracarbonyl complexes **1114**

Lingjun Li, Lizhi Zhu, Xinying Zhang, Guisheng Zhang, and Guirong Qu Convenient tetrahydropyranylation of alcohols and phenols by catalytic ferric sulfate hydrate ($Fe_2(SO_4)_3{\cdot}xH_2O$) **1120**

Jacob A. Galán, Elda E. Sánchez, Sajid Bashir, and John C. Pérez Characterization and identification of disintegrins in *Crotalus horridus* venom by liquid chromatography and tandem matrix-assisted laser desorption ionization – quadrupole ion trap time-of-flight (MALDI-QIT-TOF) mass spectrometry **1124**

Souad Bakari, Marco Borsari, Maria Cannio, Giovanna Gavioli, Antonio Ranieri, Silvia Peressini, and Claudio Tavagnacco Role of the solvent in the oxidative process of a Hg electrode in the presence of thiopyrimidine derivatives **1132**

Revika Arora, Satya Paul, and Rajive Gupta A mild and efficient procedure for the conversion of aromatic carboxylic esters to secondary amides **1137**

Andrew Hempel, Norman Camerman, Donald Mastropaolo, and Arthur Camerman Calmodulin antagonists: Structure of *N*-(6-aminohexyl)- 5-chloro-1-naphthalenesulfonamide hydrochloride (W-7) and comparison with trifluoperazine (TFP) — Calmodulin binding **1141**

Qingbin Li and Allan L.L. East Catalyzed β scission of a carbenium ion — Mechanistic differences from varying catalyst basicity **1146**

Jonathan D. Webb, Hanni A. Darwish, Haiwen Zhang, Susan L. Wheaton, Felix J. Baerlocher, Christopher M. Vogels, Andreas Decken, and Stephen A. Westcott Salicylaldimine dimers derived from 2-$H_2NC_6H_4$Bpin (pin = 1,2-$O_2C_2Me_4$) **1158**

A. Chatterjee, M. Mishra, S.K. Dutta Chowdhury, and Kumar K. Mahalanabis One-pot conversion of β-aminocrotononitrile to secondary enaminonitriles including chiral ones — Application to synthesis **1164**

Marcos A.P. Martins, Sergio Brondani, Victor L. Leidens, Darlene C. Flores, Sidnei Moura, Nilo Zanatta, Manfredo Hörner, and Alex F.C. Flores Synthesis and structure of new trichloromethyl-β-diketones — 5-Trichloromethylisoxazole and 5-isoxazolecarboxylic acid derivatives **1171**

Akira Nakajima, Yuto Ueda, Nobuyuki Endoh, Kunihiko Tajima, and Keisuke Makino Electron spin resonance analysis of the oxidation reactions of nitrone type spin traps with gold(III) ion **1178**

Andreas Decken, Robert A. Gossage, and Paras N. Yadav Oxazoline chemistry. Part VIII. Synthesis and characterization of a new class of pincer ligands derived from the 2-(*o*-anilinyl)-2-oxazoline skeleton — Applications to the synthesis of group X transition metal catalysts **1185**

NOTE / NOTE

L.G. Shamrakov and D.T. Cramb Induced structural changes of a supported planar bilayer after exposure to halothane — A real-time atomic force microscopy study **1190**

ERRATUM / ERRATUM

Laurence K. Thompson Erratum: 2004 Alcan Award Lecture From dinuclear to triakontahexanuclear complexes — Adventures in supramolecular coordination chemistry **1195**

Author Index / Index des auteurs **AI-1**

September / Septembre

This issue is focussed on organic reaction mechanisms, particularly to celebrate the distinguished contributions of Canada's physical organic chemists to the study of reaction mechanisms in organic chemistry / Le présent numéro porte principalement sur : les mécanismes des réactions organiques, en particulier pour célébrer l'éminente contribution des spécialistes canadiens de la chimie organique physique à l'étude des mécanismes associés aux réactions en chimie organique

ARTICLES / ARTICLES

Thomas T. Tidwell Physical organic chemistry in Canada 1900–2005 **1197**

Yvonne Chiang, A. Jerry Kresge, Oleg Sadovski, Xiaofeng Zeng, and Yu Zhu Kinetics and mechanism of acid-catalyzed hydrolysis of the diazo functional groups of 1-diazo-2-indanone and 2-diazo-1-indanone in aqueous solution **1202**

Edward M. Kosower The art of discovery in biophysical organic chemistry **1207**

W. David Chandler, Zhao Wang, and Donald G. Lee Kinetics and mechanism of the oxidation of alcohols by tetrapropylammonium perruthenate **1212**

© 2005 NRC Canada

Michael R. Crampton, Chukwuemeka Isanbor, and Thomas C. Willett The remarkable effect of 7-amino substituents on the reactivity of 4-nitrobenzofurazans with nucleophiles **1221**

Robert A. Moss, Xiaolin Fu, and Ronald R. Sauers The fragmentation of 7-norbornyloxychlorocarbene — S_Ni-like transition states **1228**

A.L. Pincock and J.A. Pincock The structure, photochemical reactivity, and photophysical properties of adamantyl X-substituted aryl ethers and a comparison with the alkyl groups, methyl, *tert*-butyl, and allyl **1237**

Karen Kam, Mohammad Rahimizadeh, Robert S. McDonald, Paul H.M. Harrison, Hao Chen, Stephen I. Jenkins, and Adrienne Pedrech Kinetics of glycoluril template-directed Claisen condensations — Effect of thionation of the glycoluril **1253**

Richard A. Manderville Ambident reactivity of phenoxyl radicals in DNA adduction **1261**

Graham T.T. Gibson, Alexei A. Neverov, Allen Chun-Tien Teng, and R.S. Brown Acceleration of the methanolysis of phosphate diesters promoted by $La(OTf)_3$ — The analysis of non-integer $^{s}_{s}$pH/rate profiles resulting from changes in metal ion speciation **1268**

Glenn Ikeda and Ronald Kluger Deuterium labeling as a test of intramolecular hydride mechanisms in the fragmentation of 2-(1-hydroxybenzyl)-N1′-methylthiamin **1277**

Gabriel O. Andrés, O. Fernando Silva, and Rita H. de Rossi Hydrolysis of aryl hydrogen maleate esters mediated by cyclodextrins — Effect on the intramolecular catalysis **1281**

J.A. Pincock and A.W.H. Speed The aromatic character and resonance stabilization energies of substituted cyclopentadienyl and indenyl cations **1287**

Cory C. Pye and Raymond A. Poirier An ab initio study of 1,5-suprafacial shifts in 5-substituted 1,3-cyclopentadienes **1299**

Yijian Shi and Peter Wan Solvolysis and ring closure of quinone methides photogenerated from biaryl systems **1306**

Cameron R. Harrington, William J. Leigh, Bryan K. Chan, Peter P. Gaspar, and Dong Zhou Time-resolved spectroscopic studies of the photochemistry of some diphenylgermylene (Ph_2Ge:) precursors **1324**

Charles P. Casey and Jeffrey B. Johnson Kinetic isotope effect evidence for the concerted transfer of hydride and proton from hydroxycyclopentadienyl ruthenium hydride in solvents of different polarities and hydrogen bonding ability **1339**

Leah E. Breen, Norman P. Schepp, and C.-H. Edmund Tan Photochemical generation and ^{1}H NMR detection of alkyl allene oxides in solution **1347**

T. Bajorek and N.H. Werstiuk Bicyclo[3.2.0]hepta-1,3,6-triene — UV photoelectron spectroscopic and computational studies **1352**

Arkadiusz Klys, Wojciech Czardybon, John Warkentin, and Nick Henry Werstiuk Reactions of acetoxy(methylthio)carbene and *S*-methyl thiopyruvate **1360**

Ik-Hwan Um, Ji-Youn Lee, Sun-Young Bae, and Erwin Buncel Effect of modification of the electrophilic center on the α effect **1365**

Stephen A. Glover and Michael Novak Computational studies of the properties of phenyloxenium ions — A comparison with phenylnitrenium and phenylcarbenium ions **1372**

Vladimir V. Popik The role of molecular geometry in the Wolff rearrangement of α-diazocarbonyl compounds — Conformational control or structural constraints? **1382**

REVIEW / SYNTHÈSE

Robin A. Cox A comparison of the mechanisms of hydrolysis of benzimidates, esters, and amides in sulfuric acid media **1391**

ARTICLES / ARTICLES

John Andraos Scientific genealogies of physical and mechanistic organic chemists **1400**

John Andraos Reaction intermediates in organic chemistry — The "big picture" **1415**

Wing Y. Tsang, Naveed Ahmed, Karl Hemming, and Michael I. Page Competitive endo- and exo-cyclic C–N fission in the hydrolysis of *N*-aroyl β-lactams **1432**

P. John Wright and Cornelia Bohne A temperature-annealing effect on the host–guest complexation with γ-cyclodextrin **1440**

Eric Kiepek, Yuhui Zhou, Shmaryahu Hoz, Ester Rozental, Peter M. Kazmaier, and Erwin Buncel Dissociation of the phenanthroimidazole dimer — A highly delocalized radical — Gomberg revisited **1448**

Shuang Chen, Brian O. Patrick, and John R. Scheffer Photochemistry of 9-methylbicyclo[3.3.1]nonyl aryl ketones — A novel 1,5-disproportionation of 1,4-hydroxy biradicals and asymmetric induction using the solid-state ionic chiral auxiliary method **1460**

Donald L.B. Stringle and Mark S. Workentin Regioselective S—O vs. C—O bond cleavage in sulfenate ester radical anions **1473**

Eduardo Humeres, Maria de Nazaré M. Sanchez, Conceição M.L. Lobato, Nito A. Debacher, and Eduardo P. de Souza The mechanisms of hydrolysis of alkyl *N*-alkylthioncarbamate esters at 100 °C **1483**

© 2005 NRC Canada

Stephen A. Glover, Arvi Rauk, Jeanne M. Buccigross, John J. Campbell, Gerard P. Hammond, Guoning Mo, Luke E. Andrews, and Ashley-Mae E. Gillson The HERON reaction — Origin, theoretical background, and prevalence **1492**

John E. Baldwin and Stephanie R. Singer Deuterium kinetic isotope effects on the thermal isomerizations of deuteriocyclopropane to deuterium-labeled propenes **1510**

John William Baty and Michael L. Sinnott The kinetics of the spontaneous, proton- and Al^{III}-catalysed hydrolysis of 1,5-anhydrocellobiitol — Models for cellulose depolymerization in paper aging and alkaline pulping, and a benchmark for cellulase efficiency **1516**

James F. King, Manjinder S. Gill, and Petru Ciubotaru Benzenesulfonyl chloride with primary and secondary amines in aqueous media — Unexpected high conversions to sulfonamides at high pH **1525**

Ana Rios, AnnMarie C. O'Donoghue, Tina L. Amyes, and John P. Richard Formation and stability of organic zwitterions — The carbon acid pK_as of the trimethylsulfonium and tetramethylphosphonium cations in water **1536**

Rasha F. Al-Bashir, Nouria A. Al-Awadi, and Osman M.E. El-Dusouqui Synthesis of novel sulfonyl-stabilized phosphorus ylides, and the kinetics and mechanism of their conventional and flash vacuum pyrolysis reactions **1543**

Thanh Binh Phan and Herbert Mayr Comparison of the nucleophilicities of alcohols and alkoxides **1554**

Andrei V. Fedorov, Katayoun Najafian, Thomas T. Tidwell, and Sinisa Vukovic Acid enol and dihydropyridine intermediates in pyridylketene hydration — A computational study **1561**

Stephen E. Gottschling, Michael C. Jennings, and Kim M. Baines The addition of alkynes to a tetrasilyldisilene — Evidence for a biradical intermediate **1568**

Hans J. Reich and Wesley L. Whipple Mechanism of the lithium–iodine exchange in an iodothiophene **1577**

Elena V. Ivanova and Heidi M. Muchall Influence of the number of water molecules on the mechanism of *N*-sulfinylaniline hydrolysis **1588**

Hiroto Tachikawa S_N2 and S_N2' reaction dynamics of cyclopropenyl chloride with halide ion — A direct ab initio molecular dynamics (MD) study **1597**

Salai Cheettu Ammal and Hiroshi Yamataka Linear free energy relationship and kinetic isotope effects as measures for the transition-state variation — A case of the neophyl system **1606**

Robert C. Mawhinney, Heidi M. Muchall, and Gilles H. Peslherbe A computational study of the 1,3-dipolar cycloaddition reaction mechanism for nitrilimines **1615**

John D. Roberts Pople, Schneider, and Bernstein — A truly seminal treatise of NMR **1626**

Anthony J. Kirby, José Carlos Gesser, Florian Hollfelder, Jacks P. Priebe, and Faruk Nome Intramolecular general acid catalysis of sulfate transfer — Nucleophilic attack by oxyanions on the SO_3^- group **1629**

Suzanne Shea, Norman P. Schepp, Amy E. Keirstead, and Frances L. Cozens Dynamics of the transient species generated upon photolysis of diarylmethanes within zeolites — Deprotonation and oxidation reactions **1637**

Wei Wu, Sason Shaik, and William H. Saunders, Jr. Valence bond calculations on the transition state for the E2 reaction of fluoride ion with ethyl fluoride — Implications for the More O'Ferrall – Jencks diagram **1649**

J. Peter Guthrie, Leonardo Leandro, and Vladimir Pitchko Elimination reactions — Calculation of rate constants from equilibrium constants and distortion energies by means of no barrier theory **1654**

J.M.W. Scott On the displacement reactions of organic substances in water **1667**

Author Index / Index des auteurs **AI-1**

October / Octobre

ARTICLES / ARTICLES

Se-Woung Oh, Guy M. Bernard, Roderick E. Wasylishen, Robert McDonald, and Michael J. Ferguson A multinuclear solid-state magnetic resonance study of silver nitrate triphenylphosphine **1721**

Robert H.E. Hudson and Filip Wojciechowski The detrimental effect of orotic acid substitution in the peptide nucleic acid strand on the stability of PNA_2:NA triple helices **1731**

Haifeng Yu, Dewen Dong, Yan Ouyang, and Qun Liu Chemoselective thioacetalization with odorless 2-(1,3-dithian-2-ylidene)-3-oxobutanoic acid as a 1,3-propanedithiol equivalent **1741**

Ganesan Karthikeyan and Paramasivan T. Perumal Ionic liquid promoted simple and efficient synthesis of β-enamino esters and β-enaminones from 1,3-dicarbonyl compounds — One-pot, three-component reaction for the synthesis of substituted pyridines **1746**

D. Wanapun, K.A. Van Gorp, N.J. Mosey, M.A. Kerr, and T.K. Woo The mechanism of 1,3-dipolar cycloaddition reactions of cyclopropanes and nitrones — A theoretical study **1752**

Andrea F. Armstrong, Tristram Chivers, Mark Krahn, and Masood Parvez Synthesis and structural characterization of zinc complexes of the imido–amido phosphate anions $OP[(NHR)_{3-x}(NR)]^{x-}$ (R = Me, *t*-Bu; *x* = 1–3) and $EP[(NH\text{-}t\text{-}Bu)_2(N\text{-}t\text{-}Bu)]^-$ (E = S, $NSiMe_3$) **1768**

© 2005 NRC Canada

Renkang Zhu and Zhifeng Ding Enhancing image quality of scanning electrochemical microscopy by improved probe fabrication and displacement **1779**

Mahnaz Derakhshan, Hamid R. Ansarian, M. Mizanur Rahman, Toshihiko Sakurai, Makoto Takafuji, and Hirotaka Ihara A new method for evaluation of the mobility of silica-grafted alkyl chains by suspension-state ^{1}H NMR **1792**

Reid Tingley, M. Brad Peori, Ryan Church, and Keith Vaughan Triazene derivatives of (1,*x*)-diazacycloalkanes. Part V. Synthesis and characterization of 4-ethyl-3-({6-ethyl-3-[2-aryl-1-diazenyl]hexahydro-1-pyrimidinyl}methyl)-1-[2-aryl-1-diazenyl)hexahydropyrimidines from the reaction of diazonium salts with mixtures of formaldehyde and 1,3-diaminopentane **1799**

Mohammad Jafarzadeh, Kamal Amani, and Farzad Nikpour Effective and regioselective iodination of arenes using iron(III) nitrate in the presence of tungstophosphoric acid **1808**

Juan Antonio González, Ismael Mozo, Isaías García de la Fuente, and José Carlos Cobos Thermodynamics of organic mixtures containing amines. IV. Systems with aniline **1812**

Bhupendra P. Joshi, Anuj Sharma, and Arun K. Sinha Microwave- and ultrasound-assisted semisynthesis of natural methoxylated propiophenones from isomeric mixture of phenylpropenes in minutes **1826**

Ibrahim Shehatta, Ali Hassan Al-Marzouqi, Baboucarr Jobe, and Ali Dowaidar Enhancement of aqueous solubility of itraconazole by complexation with cyclodextrins using supercritical carbon dioxide **1833**

Author Index / Index des auteurs **AI-1**

November / Novembre

This issue is dedicated to Professor Paul Kebarle to honour his outstanding contributions to mass spectrometry and its chemical applications / Le présent numéro est dédié au professeur Paul Kebarle en reconnaissance de ses contributions exceptionnelles à la spectrométrie de masse et à ses applications en chimie

ARTICLES / ARTICLES

Xiang Zhao, Gregory K. Koyanagi, and Diethard K. Bohme Gas-phase reactions of atomic lanthanide cations with methyl chloride — Periodicities in reactivity **1839**

Richard Lee, Paul J.A. Ruttink, Peter C. Burgers, and Johan K. Terlouw The water elimination from the ethyl acetate radical cation — Answers from theory to a longstanding mechanistic problem **1847**

Julie A.D. Grabowy and Paul M. Mayer Predicting ion rearrangement reactions — The energetics of the internal S_N2 reaction in gas-phase proton-bound molecular pairs **1864**

E. Peter Maziarz III, Gary A. Baker, and Troy D. Wood Electrospray ionization Fourier transform mass spectrometry of polycyclic aromatic hydrocarbons using silver(I)-mediated ionization **1871**

J. Stuart Grossert, Paul D. Fancy, and Robert L. White Fragmentation pathways of negative ions produced by electrospray ionization of acyclic dicarboxylic acids and derivatives **1878**

Y.J. Shi and R.H. Lipson An overview of organic molecule soft ionization using vacuum ultraviolet laser radiation **1891**

Xian Wang and John L. Holmes A study of the isomerization and dissociation of formal $[acetone–methanol]^{+\cdot}$ ion–molecule complexes **1903**

Luciano A. Xavier and José M. Riveros Gas-phase ion chemistry of $Ti(O\text{-}i\text{-}Pr)_4$ **1913**

John A. Stone, Timothy Su, and Dragic Vukomanovic A collisionally activated dissociation (CAD) and computational investigation of doubly and singly charged DMSO complexes of Cu^{2+} **1921**

Detlef Schröder and Helmut Schwarz Activation of methane by gaseous platinum(II) ions PtX^+ (X = H, Cl, Br, CHO) **1936**

Tujin Shi, Junfang Zhao, P.Y. Iris Shek, Alan C. Hopkinson, and K.W. Michael Siu Carbonate, carbamate, urea, and guanidine as model species for functional groups in biological molecules — A combined density functional theory and mass spectrometry examination of polysodiation and gas-phase dissociation **1941**

Belal M. Hossain, Douglas A. Simmons, and Lars Konermann Do electrospray mass spectra reflect the ligand binding state of proteins in solution? **1953**

Randy W. Purves, Barbara Ells, David A. Barnett, and Roger Guevremont Combining H–D exchange and ESI-FAIMS-MS for detecting gas-phase conformers of equine cytochrome c **1961**

Alex G. Harrison Structural and sequence effects in the fragmentation of protonated tripeptides containing tyrosine **1969**

Ronghu Wu and Terry B. McMahon An investigation of the ion–molecule interactions of protonated glycine with ammonia by high pressure mass spectrometry and ab initio calculations **1978**

Bridgette J. Duncombe, Lijlijana Puškar, Bohan Wu, and Anthony J. Stace Gas-phase experiments on the chemistry and coordination of Zn(II) by aprotic solvent molecules **1994**

John E. Bartmess and Robert J. Hinde The gas-phase acidities of the elemental hydrides are functions of electronegativity and bond length **2005**

© 2005 NRC Canada

Changtong Hao, Thomas M. Gilbert, and Lee S. Sunderlin The bond dissociation energies of SO_3—X^- (X = F, Cl, Br, and I) **2013**

Author Index / Index des auteurs **AI-1**

December / Décembre

ARTICLES / ARTICLES

D. Scott Bohle, Chen-Hsiung Hung, and Bryan D. Smith Theoretical, thermal, and coordination chemistry of the amphoteric thiazate $(NSO^-)^1$ ion **2021**

Bijan Das Thermodynamics of electrolytes in mixed solvent media — Application of the Pitzer ion interaction approach **2032**

Erol Çil, Mustafa Arslan, and Ahmet Orhan Görgülü Synthesis and characterization of alkyl- and acyl-substituted oxime–phosphazenes **2039**

K.C. Majumdar, A. Biswas, and P.P. Mukhopadhyay $SnCl_4$–I_2 mediated regioselective 6-endo- and 5-exo-cyclization of *ortho*-allylenols **2046**

Johanna M. Blacquiere, Oana Sicora, Christopher M. Vogels, Miroslava Čuperlović-Culf, Andreas Decken, Rodney J. Ouellette, and Stephen A. Westcott Dihydropyrimidinones containing boronic acids **2052**

Karin A. Stephenson, Sangeeta Ray Banerjee, Nicole McFarlane, Douglas R. Boreham, Kevin P. Maresca, John W. Babich, Jon Zubieta, and John F. Valliant A convenient solid-phase synthesis methodology for preparing peptide-derived molecular imaging agents — Synthesis, characterization, and in vitro screening of Tc(I) – chemotactic peptide conjugates **2060**

Stephanie A. Moore, Sarah E. Moore, Karen M. Glenn, Subhash C. Bhattacharya, and Rama M. Palepu Fluorescence quenching of Safranine T by inorganic anions in Tween micelles **2067**

Mehdi Amirnasr, Vratislav Langer, Nahid Rasouli, Mehdi Salehi, and Soraia Meghdadi Synthesis, characterization, and single crystal X-ray structures of $[Co^{III}(acacen)(thioacetamide)_2]ClO_4$ and $[Co^{III}((BA)_2en)(thioacetamide)_2]PF_6$ — Solvatochromic properties of $[Co^{III}(acacen)(thioacetamide)_2]ClO_4$ **2073**

M.H. Almatarneh, C.G. Flinn, and R.A. Poirier Ab initio study of the decomposition of formamidine **2082**

Victor X. Jin, Donal H. Macartney, and Erwin Buncel α- and β-Cyclodextrin [2]rotaxanes with (diethylenetriamine)platinum(II) stoppers **2091**

Preston A. Chase, Patricio E. Romero, Warren E. Piers, Masood Parvez, and Brian O. Patrick Fluorinated 9-borafluorenes vs. conventional perfluoroaryl boranes — Comparative Lewis acidity **2098**

M. Carmen Carrión, Félix A. Jalón, Isabel López-Solera, Blanca R. Manzano, Francisco Sepúlveda, Lucía Santos, Ana María Rodríguez, Miquel Moreno, and Martín Martínez-Ripoll Theoretical, dynamic, and structural studies of the phenyl rotation in bispentafluorophenyl palladium complexes with scorpion-type ligands **2106**

Alexandra S. Silchenko, Sergey A. Avilov, Alexandr S. Antonov, Anatoly I. Kalinovsky, Pavel S. Dmitrenok, Vladimir I. Kalinin, Carl Woodward, and Peter D. Collin Glycosides from the sea cucumber *Cucumaria frondosa*. IV. Structure of frondosides A_2-4, A_2-7, and A_2-8, three new minor monosulfated triterpene glycosides **2120**

Shizheng Zhu, Guifang Jin, and Huiling Jiang Reactions of β-alkoxyvinyl trifluoromethyl ketones with terminal alkynes — Reagent-controlled regioselectivity addition reactions **2127**

Yunqiao Pu and Arthur J. Ragauskas Structural analysis of acetylated hardwood lignins and their photoyellowing properties **2132**

Juxing Yin, Xiaolong Li, Xiaoli Wu, Baohua Chen, Zenglu Liu, and Qingbao Song A rapid, microwave-assisted, one-pot cyclopropanation reaction to synthesize (4-ferrocenyl)benzoylcyclopropane in the solid state **2140**

ERRATUM / ERRATUM

Ling Chen and Pierre Deslongchamps Erratum: Studies towards the total synthesis of ouabagenin **2144**

Author Index / Index des auteurs **AI-1**

Contents for Volume 83 / Sommaire pour volume 83 **C-1**

© 2005 NRC Canada

NOTE OF APPRECIATION / NOTE DE RECONNAISSANCE

The quality of the papers in this journal depends a great deal on the efforts of those who agree to act as critical readers of manuscripts. The editors gratefully acknowledge the following who helped us between 1 November 2004 and 31 October 2005:

La qualité des articles publiés dans notre revue dépend beaucoup de ceux qui acceptent de faire une lecture critique des manuscrits. Les directeurs scientifiques expriment leur reconnaissance aux personnes suivantes qui nous ont aidés, du 1er novembre 2004 au 31 octobre 2005 :

Abrahamson, H.
Adams, R.
Ager, D.
Aggarwal, V.
Aiyer, R.
Alcami, M.
Aldabbagh, F.
Alessi, M.
Allcock, H.
Alt, H.
Aquino, M.
Argyle, M.
Armentrout, P.
Arndtsen, B.
Ashcroft, A.
Astruc, D.
Atake, T.
Auclair, K.
Au-Yeung, S.
Auzanneau, F.-I.
Baba, A.
Baer, T.
Bagley, M.
Bain, A.
Baines, K.
Baird, M.
Balahura, R.
Baldwin, J.
Balkus, K.
Ban, F.
Banks, J.
Banwell, M.
Barluenga, J.
Barra, M.
Barriault, L.
Bassani, D.
Battino, R.
Bawendi, M.
Bearne, S.
Bencicn, A.
Bennet, A.
Bernard, G.
Bernd, R.
Bertini, V.
Beyer, M.
Blasko, T.
Boch, R.
Boeré, R.
Boerio-Goates, J.
Bohme, D.
Bohne, C.
Bolm, C.
Bonacorso, H.
Bonin, H.
Bossa, M.
Bottaro, C.
Boukouvalas, J.
Bowie, J.
Boyd, R.
Braese, S.
Braunstein, P.
Brisard, G.
Brodbelt, J.
Brolo, A.
Brown, A.
Brown, S.
Bruce, M.
Brückner, C.
Bryce, D.
Bryce, M.
Bui, V.
Buncel, E.
Burford, N.
Burnell, J.
Butkus, E.
Butler, I.
Cannon, R.
Carpenter, B.
Casado, C.
Castellan, A.
Cavani, F.
Champeney, D.
Chan, B.
Chan, W.
Chandrasekhar, S.
Chang, S.
Chaudret, B.
Chen, E.
Chivers, T.
Choung, S.
Chu, W.
Claver, C.
Clive, D.
Clyburne, J.
Collins, S.
Comba, P.
Connick, W.
Corey, D.
Corrigan, J.
Corti, H.
Cowie, M.
Cox, R.
Cramb, Dr.
Crich, D.
Cross, S.
Crudden, C.
Cuccovia, I.
Cundari, T.
da Costa Ferreira, A.
Danishefsky, S.
Davies, H.
Davis, F.
De, S.
de Lijser, H.
Delhalle, J.
Dénès, G.
Denk, M.
Detellier, C.
Diaz, C.
Ding, Z.
Dolenc, D.
Dondoni, A.
Dunbar, R.
Dupont, J.
Durst, T.
Eaton, S.
Edwards, M.
El Seoud, O.
Ellison, M.
Eltepu, L.
English, A.
Enick, R.
Evans, C.
Evans, D.
Fairbanks, A.
Faller, J.
Fallis, A.
Fang, X.
Field, R.
Fillion, E.
Findlay, J.
Fleming, S.
Flood, T.
Fogg, D.
Forest, E.
Fornies, J.
Foster, N.
Fradin, C.
Frontier, A.
Fryzuk, M.
Fukuzumi, S.
Fürstner, A.
Fyfe, C.
Gagné, M.
Gait, M.
Gambarotta, S.
Garcia, J.
Gates, D.
Gauld, J.
Geiger, W.
Georghiou, P.
Ghiaci, M.
Gibson, V.
Gielen, M.
Girault, H.
Gladiali, S.
Glaser, T.
Goddard, J.
Goltz, D.
Gossage, R.
Goto, K.
Gough, K.
Gould, E.
Goyotsi, Y.
Grainger, D.
Grant, A.
Green, J.
Greene, A.
Grieco, P.
Griffiths, K.
Grigg, R.
Grindley, B.
Gronert, S.
Grubbs, B.
Gubareva, L.
Guldi, D.
Guo, X.
Gupta, R.
Guthrie, P.
Guy, P.
Haines, R.
Hakin, A.
Hall, D.
Hambley, T.
Hanan, G.
Hancock, R.
Hanessian, S.
Hanson, B.
Hanson, G.
Harris, W.
Harrison, P.
Harrod, J.
Hart, D.
Harvey, P.
Hayashi, T.
Heinekey, M.
Hengge, A.
Herring, F.G.
Heyes, D.
Hill, D.
Hillier, I.
Hindsgaul, O.
Hoffmann, T.

© 2005 NRC Canada

Holdcroft, S.
Holmes, J.
Holze, R.
Hopkinson, A.
Hosmane, N.
Houmam, A.
Hu, T.
Hultin, P.
Husson, S.
Iyoda, M.
Jacobsen, E.
Jakeman, D.
James, B.
Janiak, C.
Jaworska, M.
Jenkins, H.
Jessop, P.
Jiang, H.L.
Jiang, J.
Johnston, L.
Jones, C.
Jones, N.
Jones, R.
Jull, T.
Kabalka, G.
Kaboudin, B.
Kaliaguine, S.
Kapantaidakis, G.
Kappe, O.
Kataoka, H.
Katritzky, A.
Katzenellenbogen, J.
Kaur, K.
Kazlauskas, R.
Keay, B.
Keeffe, J.
Keillor, J.
Kevill, D.
King, J.
Kinghorn, A.D.
Kingston, D.
Kinrade, S.
Kirby, A.
Kirk, K.
Kirken, R.
Kiss, T.
Klabunde, K.
Kluger, R.
Knaus, E.
Knochel, P.
Knox, S.
Koch, R.
Kogen, H.
Konermann, L.
Kool, E.
Kotra, L.
Kotsuki, H.
Kovacik, V.
Kraatz, H.-B.
Krafft, M.
Kraus, G.
Kresge, J.
Kroeker, S.
Krol, E.
Kydd, R.
Laasonen, K.
Lai, P.-S.
Lang, H.
Langler, R.
Lapinte, C.
Larock, R.
Lavilla, R.
Lay, P.
Leaist, D.
Lebel, H.
Lee, D.
Lee-Ruff, E.
Legzdins, P.
Leigh, W.
Leighton, J.
Lelj, F.
Lemaire, M.
Lessard, J.
Lever, A.B.P.
Lewars, E.
Leznoff, D.
Lidstrom, P.
Lightstone, J.
Lindoy, L.
Lippert, B.
Lipshutz, B.
Liu, Z.L.
Loeb, S.
Loo, J.
Lopez, S.
Loupy, A.
Low, P.
Lowe, M.
Lubell, W.
Lumsden, M.
Luo, F.-T.
Luzzio, F.
Ma, D.
Macartney, D.
Mackay, B.
MacLachlan, M.
Magee, D.
Maier, M.
Manley, P.
Manos, G.
Mar, A.
Marder, T.
Marino, T.
Marshall, A.
Martin, D.
Martin, V.
Mather, A.
Matta, C.
Mayer, P.
McAuley, A.
McClelland, R.
McGlinchey, M.
McGrady, S.
McIndoe, S.
McMahon, T.
Medarde, M.
Menzinger, M.
Mercier, L.
Merino, P.
Metz, R.
Metzger, J.
Meyers, A.
Michalski, J.
Misaizu, F.
Mitscher, L.
Miura, K.
Moerner, W.
Molina, P.
Montaut, S.
Moriarty, B.
Morin, J.
Morris, R.
Morrow, J.
Mota, C.
Muchall, H.
Mullens, J.
Murphy, S.
Nair, V.
Neckers, D.
Negishi, E.-I.
Nelson, J.
Neumüller, B.
Neves, A.
Nielsen, P.
Nishihara, H.
Nowrouzi, F.
O'Hair, R.
Ohman, L.-O.
Ojadi, O.
Oro, L.
Otter, A.
Overman, L.
Pacey, P.
Palaniappan, S.
Palazzo, G.
Paquette, L.
Parkin, G.
Parvez, M.
Passarelli, V.
Patrick, B.
Pavlik, J.
Pedras, M.S.
Peppe, C.
Perepichka, D.
Perez, M.
Perez-Tomas, R.
Perrin, D.
Peslherbe, G.
Piers, W.
Plaquevent, J.-C.
Pollack, R.
Pomeroy, R.
Pomonis, P.
Poutsma, J.
Power, P.
Power, W.
Pringle, J.
Pruitt, L.
Puddephatt, R.
Pye, C.
Quail, W.
Rademacher, P.
Rajanbabu, T.
Raki, L.
Ratcliffe, C.
Rees, C.
Reimer, K.
Reinhoudt, D.
Reinsborough, V.
Remko, M.
Rempel, G.
Richard, J.
Richeson, D.
Rigby, J.
Riguera, R.
Ripmeester, J.
Risitano, F.
Riveros, J.
Rochon, F.
Rojas-Aguilar, A.
Rosenberg, L.
Rossen, K.
Rosynek, M.
Royer, J.
Russell, C.
Ryabov, A.
Sackus, A.
Sakai, N.
Sappa, E.
Saravanamuttu, K.
Sayari, A.
Scheffer, J.
Scheiner, S.
Schepp, N.
Schiesser, C.
Schlegel, B.
Schleyer, P.
Schmidbaur, H.
Schmitzer, A.
Schofield, C.
Schreiber, D.
Schriemer, D.
Schubert, U.
Schwan, A.
Schweizer, F.
Scott, A.I.
Scriba, G.
Sears, D.
Seeberger, P.
Seger, C.
Seki, M.
Selegue, J.
Shaver, A.
She, X.
Sheardown, H.
Sheridan, R.
Sherman, J.
Shibasaki, M.
Shimizu, G.
Shkurko, O.
Shvartsburg, A.
Simard, B.
Singer, R.
Sinou, D.
Sita, L.
Siu, M.
Slavin, A.
Smith, K.
Snider, B.
Soloshonok, V.
Soltzberg, L.
Spino, C.
Stahl, L.
Stein, A.

© 2005 NRC Canada

Stephan, D.
Stølen, S.
Stone, J.
Storr, T.
Stradiotto, M.
Stretz, H.
Su, D.
Su, M.-D.
Suib, S.
Süss-Fink, G.
Suzuki, N.
Takats, J.
Tanabe, Y.
Taylor, R.
Tee, O.
Terlouw, J.
Tevani, L.
Thakkar, A.
Thibault, P.
Thompson, R.
Thorson, J.
Thull, R.
Tidwell, T.
Tiekink, E.
Timofeeva, M.
Tobe, Y.
Tortajada, J.
Toscano, J.
Tossell, J.
Tremaine, P.
Trionfetti, C.
Tsang, S.c.E.
Tu, S.
Tu, Y.-P.
Tykwinski, R.
Ullrich, T.
Valliant, J.
Van Berkel, G.
Van Brocklin, H.
van der Eycken, E.
van der Rest, G.
van Gaans, P.
van Koten, G.
van Veggel, F.
Vaughan, K.
Vederas, J.
Wachs, I.
Wagner, B.
Wagner, P.
Wan, P.
Wang, A.
Wang, M.
Wang, S.
Wang, W.
Wang, Y.
Ward, D.
Wardell, J.
Warkentin, J.
Warren, S.
Watts, P.
Welton, T.
Wenthold, P.
Wentrup, C.
Werstiuk, N.
Westaway, K.
Westcott, S.
Wetmore, S.
Wharf, I.
White, M.A.
White, R.
Wiberg, K.
Willett, R.
Williams, V.
Wirth, T.
Withers, S.
Wolczanski, P.
Wolf, M.
Wolfenden, R.
Wong, G.
Workentin, M.
Wright, G.
Wroblewski, A.
Wuest, J.
Wuts, P.
Xiao, J.
Yacaman, M.
Yanez, M.
Yang, B.
Yang, D.
Yang, R.
Yip, C.
Young, R.
Zabriskie, M.
Zagorevski, D.
Zanello, P.
Zargarian, D.
Zhao, C.
Zhou, W.
Zubieta, J.

© 2005 NRC Canada